nature

l 287 No 5777 4 September 1980 £1.00 $2.25

St.No-150

(Vol-287)
(No. 5777-5785)
(1-878p)
-66-66-28 [illegible] 3/13
(1980)

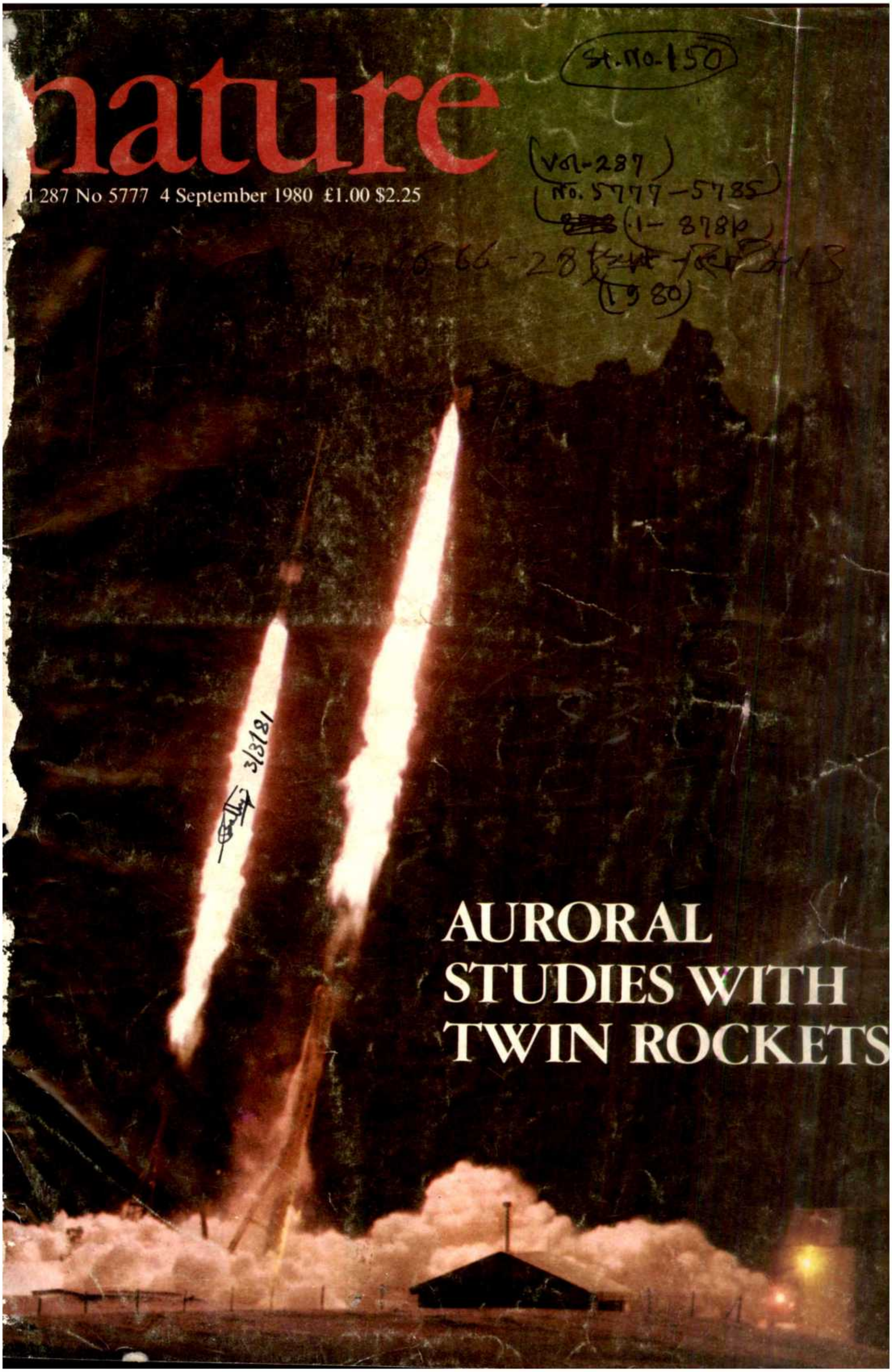

3/3/81

AURORAL STUDIES WITH TWIN ROCKETS

Ion exchangers from Pharmacia Fine Chemicals

The better choice because ion exchangers from Pharmacia Fine Chemicals have excellent capacities, do not have to be decanted, and require the minimum of preparation.

Better results because ion exchangers from Pharmacia Fine Chemicals are bead formed, making them easy to pack and quick to run. Separations can be repeated many times in the same column.

Better information can be found in the NEW handbook "Ion exchange principles and methods" and the Literature Reference Lists, available free on request from Pharmacia Fine Chemicals.

Pharmacia Fine Chemicals AB
Box 175
S-751 04 Uppsala 1
Sweden

Pharmacia
Fine Chemicals

Circle No. 09 on Reader Enquiry Card

nature

Volume 287 No.5777 4 September 1980

NEWS

Future for unprofessional societiés 1
Public-key cryptography muddle 2
Carter pledges support for research 3
Congress falls in line on 1981 funds 3
NIH funding: Congress control 4
Soviet academics: Wasted talent 4
European coal industry: Conversion plans 5
Hunter turned hunted 5
Third World energy: World Bank aid 5
Meat substitutes: Fungal food 6
Culture collections: Fears for fungi 6

NEWS AND VIEWS

Space plasmas: Michael J. Rycroft describes recent experiments on the ionospheric and magnetospheric plasmas 7
Maverick mitochondria: a correspondent describes their unique genetic code and translation machinery 9
Probing the mysteries of seeds: Daphne J. Osborne reports a recent conference 10
Bahamian Atlantis: Marshall McKusick and Eugene A. Shinn examine evidence for the lost continent 11
Retrograde transport in axons: Peter Banks on its mechanism and exploitation 12
The acetylcholine receptor: Charles F. Stevens describes its reconstitution in an artificial bilayer 13
Ultrasensitive mass spectrometry: K. W. Allen on the advantage of using accelerators 14

283

ARTICLES

M.P. Gough, B.N. Maehlum, G. Martelli, P.N. Smith and G. Ventura **Bunching of 8–10 keV auroral electrons near an artificial electron beam** 15
W.S.C. Gurney, S.P. Blythe and R.M. Nisbet **Nicholson's blowflies revisited** 17
R.A. Nicoll, B.E. Alger and C.E. Jahr **Enkephalin blocks inhibitory pathways in the vertebrate CNS** 22

LETTERS

F.A. Cordova and K.O. Mason **A soft X-ray halo around SU UMa** 25
W.H.G. Lewin, L.R. Cominsky, A.R. Walker and B.S.C. Robertson **Simultaneous IR and X-ray burst observation of Ser X-1** 27
E. Ruiz-Hitzky and J.M. Rojo **Intracrystalline grafting on layer silicic acids** 28
V.R.S. Hutton, M.R. Ingham and E.W. Mbipom **An electrical model of the crust and upper mantle in Scotland** 30
G. Davies, R.G. Cawthorn, J.M. Barton Jr and M. Morton **Parental magma to the Bushveld Complex** 33
M.S. Baxter, M.J. Stenhouse and N. Drndarski **Fossil carbon in coastal sediments** 35
P.J. Davies and J.F. Marshall **A model of epicontinental reef growth** 37
K.A. Fanning and V.I. Maynard-Hensley **Oxidative changes to nitrate and boron in marine pore waters** 38
D. Edwards and J. Feehan **Records of *Cooksonia*-type sporangia from late Wenlock strata in Ireland** 41
A. Fiorentini and N. Berardi **Perceptual learning specific for orientation and spatial frequency** 43
D.L. Longo and R.H. Schwartz **T-cell specificity for H-2 and Ir gene phenotype correlates with the phenotype of thymic antigen-presenting cells** 44
G. Dennert **Cloned lines of natural killer cells** 47

Contents continued overleaf

Cover: Simultaneous launch of two Nike Tomahawk sounding rockets from the Andoya Rocket Range, Northern Norway, into an auroral display during a collaborative research programme involving Norwegian, British, USA and Austrian scientists. The bunching of high energy auroral electrons close to an artificially stimulated plasma wave was observed directly and unambiguously for the first time (see page 15). Photograph by Jan Olav Andersen.

Nature® published weekly ISSN 0028-0836
Registered as a newspaper at the British Post Office and the United States Post Office

0028-0836/80/36000C-02$01.00

Buy the quality.

Anti-mouse Thy 1.2
Anti-mouse Thy 1.2, biotin labeled
Anti-mouse Thy 1.2, fluorescein labeled
Anti-mouse Thy 1.1
Anti-mouse Lyt 1.1
Anti-mouse Lyt 2.1
Anti-mouse Lyt 2.2
Anti-mouse Lyb 2.1
Anti-mouse Lyb 2.3
Anti-mouse TL
Anti-human Ia
Anti-human T lymphocyte (Lyt 1)
Anti-murine leukemia virus gp70
Anti-murine leukemia virus p15 (E)

Get the consultation free. (and the coffee cup, too)

When you buy monoclonal antibodies for research from New England Nuclear, you can be sure they are made and tested to the standards of quality traditional in our radiochemicals. These hybridoma-produced immunoglobulins show exceptionally high specificity and titer, confirmed by assay, with results and other technical data included in your shipment.

Then there are the intangible benefits, which you can easily make tangible by calling us toll free. Our technical staff will gladly share with you the experience we have gained in building this major new product line, including the application and behavior of monoclonal antibodies under experimental conditions.

First let us have your name, so we can send you current product information and place you on our mail list, which guarantees that you'll be kept apprised of new developments. We intend to make this the finest and widest line of monoclonal antibodies available for research use. Please circle the inquiry number, or write.

And, oh yes, the coffee cup. It's free when you become a customer (and quite appropriate for use during your dialogue with our staff).

Not for use in humans or clinical diagnosis

NEN New England Nuclear®
549 Albany Street, Boston, Mass. 02118
Call toll-free: 800-225-1572
(In Massachusetts and International: 617-482-9595)

NEN Chemicals GmbH: D-6072 Dreieich, W. Germany, Postfach 401240
Telephone: (06103) 85034. Telex: 4-17993 NEN D
NEN Canada Ltd., 2453 46th Avenue, Lachine, Que. H8T 3C9
Telephone: 514-636-4971. Telex: 05-821808

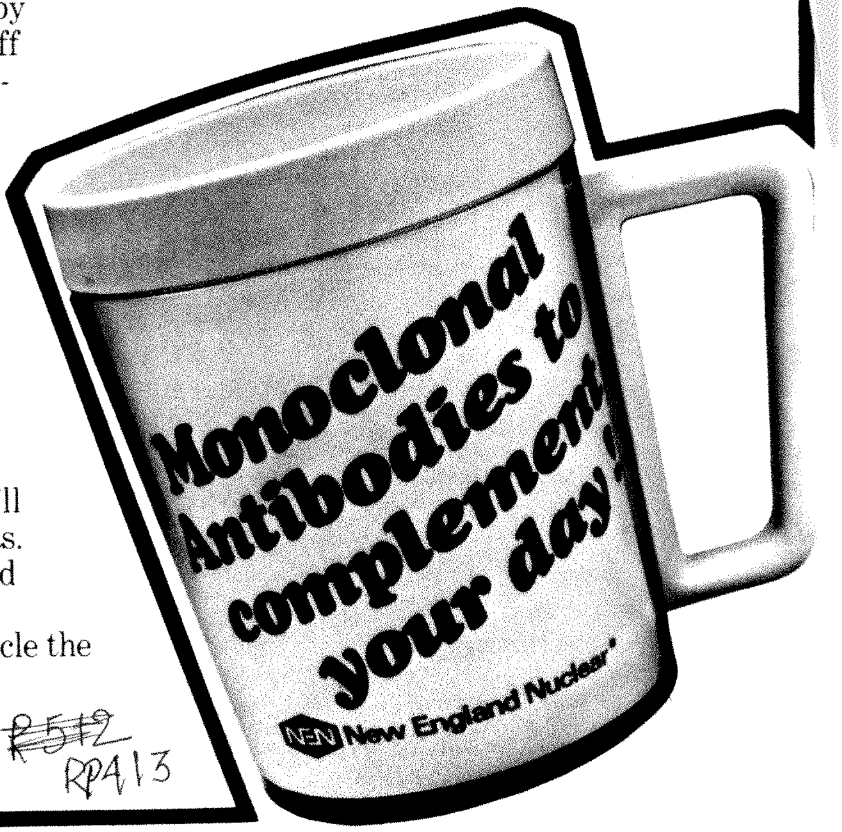

~~R512~~
RP413

Circle No. 19 on Reader Enquiry Card.

LETTERS

P.J. Martin, V. Najfeld, J.A. Hansen, G.K. Penfold, R.J. Jacobson and P.J. Fialkow — **Involvement of the B-lymphoid system in chronic myelogenous leukaemia** 49

B.A. Jakschik and L.H. Lee — **Enzymatic assembly of slow reacting substance** 51

M.R. Kozlowski, S. Sawyer and J.F. Marshall — **Behavioural effects and supersensitivity following nigral dopamine receptor stimulation** 52

J.J. Nordmann and J. Chevallier — **The role of microvesicles in buffering $[\mathrm{Ca}^{2+}]_i$ in the neurohypophysis** 54

F.D. Shaw and J.F. Morris — **Calcium localization in the rat neurohypophysis** 56

H. Al-Khouri and B.D. Greenstein — **Role of corticosteroid-binding globulin in interaction of corticosterone with uterine and brain progesterone receptors** 58

P.D. Evans & J.D. Gee — **Action of formamidine pesticides on octopamine receptors** 60

E. Wanke, E. Carbone and P.L. Testa — **The sodium channel and intracellular H^+ blockage in squid axons** 62

R.G. King and R.M. Marchbanks — **Solubilization of the choline transport system and re-incorporation into artificial membranes** 64

K. Ohtsuki, M. Nakamura, T. Koike, N. Ishida and S. Baron — **A ribosomal protein mediates eIF-2 phosphorylation by interferon-induced kinase** 65

D. Wallach and M. Revel — **An interferon-induced cellular enzyme is incorporated into virions** 68

R. Fontana, P. Canepari, G. Satta and J. Coyette — **Identification of the lethal target of benzylpenicillin in *Streptococcus faecalis* by *in vivo* penicillin binding studies** 70

D.R. Lowy, I. Dvoretzky, R. Shober, M.-F. Law, L. Engel and P.M. Howley — ***In vitro* tumorigenic transformation by a defined sub-genomic fragment of bovine papilloma virus DNA** 72

J.P. Whitlock Jr, R. Augustine and H. Schulman — **Calcium-dependent phosphorylation of histone H3 in butyrate-treated HeLa cells** 74

S.S. Chahal, H.R. Matthews and E.M. Bradbury — **Acetylation of histone H4 and its role in chromatin structure and function** 76

D.K. Ojala, J. Montoya and G. Attardi — **The putative mRNA for subunit II of human cytochrome *c* oxidase starts directly at the translation initiator codon** 79

P.C. Weber and F.R. Salemme — **Structural and functional diversity in 4-α-helical proteins** 82

L.E.M. de Boer — **Do the chromosomes of the kiwi provide evidence for a monophyletic origin of the ratites?** 84

MATTERS ARISING

L.L. Hood — **Cometary collisions on the Moon and Mercury** 86

P.H. Schultz and L.J. Srnka — **Reply to Hood** 87

A.P. Heward and C.R. Fielding — **A braidplain facies model for the Westphalian B Coal Measures of north-east England** 87

R.S. Haszeldine and R. Anderton — **Reply to Heward and Fielding** 88

J. Adams — **High sediment yields from major rivers of the western Southern Alps, New Zealand** 88

G.A. Griffiths — **Reply to Adams** 89

L.M. Van Valen — **Molecular clockwork** 89

D. Dykhuizen and D. Hartl — **Reply to Van Valen** 90

BOOK REVIEWS

Alan Cottrell — **The Nuclear Power Decisions: British Policies, 1953–1978 (Roger Williams)** 91

D. Regan — **Three recent books on current research into evoked potentials** 92

P.J. Ford — **From DNA to Protein: The Transfer of Genetic Information (M. Szekely)** 92

D.W.J. Cruickshank — **X-Ray Analysis and the Structure of Organic Molecules (Jack Dunitz)** 93

MISCELLANY

100 years ago 9

Books received 94

Product review xiii

Classified advertising xix

PHLS

Centre for Applied Microbiology
and Research

Bacterial
Cell Pastes

Escherichia coli MRE 600
The original ribonuclease free strain, buffer washed.
(Minimum quantity 3kg – £420)

Bacillus stearothermophilus NCA 1503
Grown at 60°C the source of many thermostable enzymes.
(Minimum quantity 1·5kg – £480)

Escherichia coli RY 13
Contains restriction endonuclease Eco RI and Eco RI^1.
(Minimum quantity 3kg – £420)

Thermus aquaticus YT-1
Grown at 70°C, the source of thermostable enzymes including restriction endonuclease Taq YI.
(Minimum quantity 0·5kg – £400)

Escherichia coli B
A source of ribosomes, DNA polymerase I, RNA polymerase, DNA ligase and exonuclease III.
(Minimum quantity 3kg – £420)

Micrococcus lysodeikticus NCTC 2665
A source of catalase.
(Minimum quantity 3kg – £420)

All these products can be supplied to overseas customers. 48 other types of cell paste are also available.

The listed products are offered at the quoted sterling prices, subject to availability. Prices include packing in dry ice, and delivery on UK orders, which are subject to VAT at ruling rates. Overseas orders are subject to transport charges at cost. For listed items please send your official order to:

Microbial Products Development
& Production Laboratory, PHLS.
Centre for Applied Microbiology and Research,
Porton, Salisbury, SP4 0JG, Wiltshire, UK.

Circle No. 15 on Reader Enquiry Card.

M

© 1980 Macmillan Journals Ltd
Nature® is published weekly
ISSN 0028-0836
Registered as a newspaper at the
British Post Office

London
4 Little Essex Street, WC2R 3LF
Telephone: (01) 836 6633 Telex 262024
Telegrams: Phusis London WC2R 3LF

Editor: John Maddox
Deputy Editor: Peter Newmark

Editorial Staff
Alun Anderson Naomi Molson
Philip Campbell Sara Nash
Isobel Collins Judy Redfearn
Konrad Guettler Miranda Robertson
Tim Lincoln Robert Walgate
Mary Lindley Charles Wenz
Jonathan Wolfe
Publishing Director: Christopher Paterson
Marketing Director: Ray Barker

New York
15 East 26 Street, New York, NY 10010
Telephone. (212) 689 5900 Telex: 668497

Robert Ubell (American Publisher)
and Sheila Kane

Washington News Bureau
801 National Press Building, DC 20045
Telephone: (202) 737 2355 Telex 64280
David Dickson (Washington News Editor)

International Advertising Manager:
Richard Webb (London) (01) 240 2044

USA Advertising Manager
Henry Dale (New York) (212) 689 5900

Classified Advertising:
4 Little Essex Street, WC2R 3LF
Telephone (01) 240 1101
Classified(USA)
Terence Miller, Suite 832, 50 Rockefeller Plaza,
New York, NY 10020—(212) 765 5758
Display and Classified(Canada)
Peter Drake, 32 Front Street West,
201 Toronto, Ontario M5J 1C5
(416) 364 1623

Advertising Representatives in USA
Display
Nature New York Office—(212) 689 5900
Media Group, Inc (Dallas)—(214) 631 4480
Didier & Broderick, Inc. (Chicago)—
(312) 498 4520
Jobson/Jordan/Harrison/Schulz, Inc.
(San Francisco) (415) 392 6794 (Los Angeles
& Pasadena) (213) 796 9200
Daniel Adams Associates, Inc.
Philadelphia—(215) 353 6191
CEL Associates (Boston)—(617) 383 6136
Brinker & Brinker (Fort Lauderdale)
(305) 771 0064
German Advertising Representative
E. Meckelburg, 6450 Hanau 1, Jahnstrasse 15,
West Germany Tel:— (49) 61 8115343
Japanese Advertising Representative
Orient Echo Inc.
11th Fl, Sankyo Bldg 7-12, Tsukiji 2-Chome,
Chuo-Ku, Tokyo, Japan, Tel: 541-4923.
Annual Subscription including Index

UK		£55
USA & Canada		US$135
Belgium	Airspeed	BF4900
West Germany	Airspeed	DM300
Holland	Airspeed	G325
Switzerland	Airspeed	SF265
Rest of World	Surface	£70
	Airmail	£95

Single copy (post-paid); UK, £1.20, USA & Canada, US$3 50 (surface), US$5.00 (air); Rest of World, £1.15 (surface), £2 (air).

Orders (with remittance) to:
Macmillan Journals Ltd, Brunel Road,
Basingstoke, Hants RG21 2XS
Telephone: Basingstoke (0256) 29242

Nature is published weekly, except the last week in December, by Macmillan Journals Ltd
Second-class postage paid at New York, NY 10010 and at additional mailing offices
US Postmaster, please send form 3579 to:
Nature, 15 East 26 Street, New York, NY 10010.

Vol. 287 No. 5777 4 September 1980

nature

Volume 287 No.5778 11 September 1980

NEWS

More ups and downs for US science 95
Scares about genetic manipulation 96
NSF reorganizes for industrial research 97
Bell Research Labs: Split possible? 98
NPT review conference: No declaration 98
Plutonium: Dounreay loss 99
Academic freedom: Talking shops 99
Marks of reproof 100
Hoyle on life: No dissent 100
Electric vehicles: UK Content 100
US petroleum: Using less 101
Saturn see in Voyager sights 101
Romanian energy: Partners to-be 102
Rural communities: Living now 102

NEWS AND VIEWS

The elementary Universe: M.G. Edmunds reports a workshop on the origin and distribution of the elements 103
Frogs and lizards in tropical forests: Robert M. May explains the density differences between Asia and America 105
Neurotoxicity: M.K. Johnson reports a recent workshop on the organophosphorus esters 105
Laser polarization labelling: Allister I. Ferguson describes how molecular spectra can be simplified 106
Combination chemoprevention of cancer: Michael B. Sporn reports a recent meeting 107
Adenovirus complexities: A report from the EMBO workshop on the molecular biology of the adenoviruses 108
Polymerase III control region: Peter J. Ford on the search for the eukaryote promoter site 109

ARTICLES

F.D. Costantini, R.J. Britten and E.H. Davidson **Message sequences and short repetitive sequences are interspersed in sea urchin egg poly(A)$^+$ RNAs** 111
R. J. MacDonald, M.M. Crerar, W.F. Swain, R.L. Pictet, G. Thomas and W.J. Rutter **Structure of a family of rat amylase genes** 117

LETTERS

R. Ramaty, S. Bonazzola, T.L. Cline, D. Kazanas, P. Mészáros and R.E. Lingenfelter **Origin of the 5 March 1979 γ-ray transient: a vibrating neutron star** 122
P. Mandrou, G. Vedrenne and J.L. Masnou **Low energy γ rays from PSR1822–09** 124
W.-H. Ip **Discussion of the Pioneer 11 observations of the F ring of Saturn** 126
A. Putnis **Order-modulated structures and the thermodynamics of cordierite reactions** 128
K. Rajeshwar, M. Das and J. DuBow **D.c. electrical conductivity of Green River oil shales** 131
M.J.C. Walker **Late-Glacial history of the Brecon Beacons, South Wales** 133
E.H. Lindsay, N.D. Opdyke and N.M. Johnson **Pliocene dispersal of the horse *Equus* and late Cenozoic mammalian dispersal events** 135
W. Wernicke and R. Brettell **Somatic embryogenesis from *Sorghum bicolor* leaves** 138
A. Veerman and M. Vaz Nunes **Circadian rhythmicity participates in the photoperiodic determination of diapause in spider mites** 140
M. Rose and B. Charlesworth **A test of evolutionary theories of senescence** 141
P. Santamaria and M. Gans **Chimaeras of *Drosophila melanogaster* obtained by injection of haploid nuclei** 143
T. Hillensjö and W.J. LeMaire **Gonadotropin releasing hormone agonists stimulate meiotic maturation of follicle-enclosed rat oocytes *in vitro*** 145
G.J. Blackwell, R. Carnuccio, M.Di Rosa, R.J. Flower, L. Parente and P. Persico **Macrocortin: a polypeptide causing the anti-phospholipase effect of glucocorticoids** 147

Contents continued overleaf

Cover: Electron micrograph of a recombination intermediate of two molecules of human adenovirus type 2 DNA with the cross-over point shown enlarged on the right. A study of the molecular mechanism of genetic recombination is described on page 168.

Nature® published weekly ISSN 0028-0836
Registered as a newspaper at the British Post Office and the United States Post Office

0028-0836/80/37000C-02$01.00

from Raven Press

An important series:

Advances in Biochemical Psychopharmacology

SERIES EDITORS:
E. Costa, M.D., and
Paul Greengard, Ph.D.

VOLUME 25

Histochemistry and Cell Biology of Autonomic Neurons, SIF Cells, and Paraneurons

Editors: Olavi Eränkö, Seppo Soinila, and Heikki Päivärinta

SECTION HEADINGS: Phenotypic Plasticity and Development of Sympathetic Cells / Fine Structure of SIF Cells and Modulation of Ganglionic Function / Histochemistry and Experimental Cytology of Adrenal Chromaffin Cells and Glomus Cells / Granular Vesicles and Experimental Cell Biology of Sympathetic Neurons and Paraneurons / Immunohistochemistry of Opioid and Other Peptide Neurons in the Autonomic and Central Nervous Systems / Subject Index.

410 pp., 233 figures, $45.00 (August 1980)
ISBN 0-89004-495-3

VOLUME 24

Long-Term Effects of Neuroleptics

Editors: F. Cattabeni, G. Racagni, P. F. Spano, and E. Costa

This volume examines the molecular mechanisms involved in the therapeutic benefits and untoward side effects of the neuroleptic drugs. Emphasis is on the action of chronic neuroleptics on dopaminergic receptors and on neurotransmitter interaction.

660 pp., $58.00 (1980) ISBN 0-89004-405-8

VOLUME 23

Ergot Compounds and Brain Function—Neuroendocrine and Neuropsychiatric Aspects

Editors: Menek Goldstein, Donald B. Calne, Abraham N. Lieberman, and Michael O. Thorner

This volume describes the pharmacology of ergot compounds. It explores the therapeutic implications of the dopaminergic activity of these compounds in the treatment of parkinsonism, the galactorrhea-amenorrhea syndrome, acromegaly, and several neuropsychiatric disturbances associated with aging. Because of the diversity of the applications of these compounds, this book will be of interest to endocrinologists, neurologists, pharmacologists, and gerontologists.

431 pp., $41.00 (1980) ISBN 0-89004-450-3

VOLUME 22

Neural Peptides and Neuronal Communication

Editors: E. Costa and Marco Trabucchi

This volume reviews recent research on the physiological function of neural peptides. Although emphasis is on the endorphins and enkephalins, chapters also discuss other peptides including substance P, somatostatin, gastrin, bombesin, ACTH, prolactin, corticotrophin and somatotrophin, releasing factors, thyrotrophin, gonadotrophins, growth hormone, β-lypotrophin, α-melanotrophin, and cholecystokinin.

670 pp., $57.00 (1980) ISBN 0-89004-375-2

VOLUME 21

Receptors for Neurotransmitters and Peptide Hormones

Editors: Giancarlo Pepeu, Michael J. Kuhar, and S. J. Enna

This volume discusses the structural and biochemical properties, functions, and ligands of most of the known receptors and identifies their common denominators. Sections include: general and electrophysiological characteristics of receptors; purification and regulation of receptors; monoamine receptors; benzodiazepine and GABA receptors; opioid and neuroendocrine receptors; and receptor alterations in aging and disease.

544 pp., $52.00 (1980) ISBN 0-89004-408-2

Order Form

Please send the following volume(s) of **Advances in Biochemical Psychopharmacology** (indicate quantity):

_____**Volume 25**, $45.00 (Order Code 553)
_____**Volume 24**, $58.00 (Order Code 549)
_____**Volume 23**, $41.00 (Order Code 426)
_____**Volume 22**, $57.00 (Order Code 412)
_____**Volume 21**, $52.00 (Order Code 464)

Please start a Continuation Order beginning with Volume _____.

Prices slightly higher outside the U.S. and Canada.

☐ To save postage and handling charges, I enclose payment (or charge my credit card below). N.Y. residents add 8% sales tax.
☐ Charge my credit card number: _____
Circle one: American Express VISA Diners Club
Master Charge (4-digit interbank number: _____)
Card expiration date: _____
Name (please print) _____
Address _____
_____
Country _____ Postal Code _____

Raven Press 1140 Avenue of the Americas, New York, N.Y. 10036

Na 980

Circle No. 10 on Reader Enquiry Card.

LETTERS

Y. Taché, W. Vale and M. Brown	**Thyrotropin-releasing hormone — CNS action to stimulate gastric acid secretion**	**149**
K. Morita, R.A. North and Y. Katayama	**Evidence that substance P is a neurotransmitter in the myenteric plexus**	**151**
J.E. Smith, C. Co, M.E. Freeman, M.P. Sands and J.D. Lane	**Neurotransmitter turnover in rat striatum is correlated with morphine self-administration**	**152**
W.T. Mason	**Supraoptic neurones of rat hypothalamus are osmosensitive**	**154**
M.R. Ward and C.A.R. Boyd	**Intracellular study of ionic events underlying intestinal membrane transport of oligopeptides**	**157**
U. Otten, M. Goedert, N. Mayer and F. Lembeck	**Requirement of nerve growth factor for development of substance P-containing sensory neurones**	**158**
G.D. Clarke and P.J. Ryan	**Tranquillizers can block mitogenesis in 3T3 cells and induce differentiation in Friend cells**	**160**
S. Fuchs, I. Schmidt-Hopfeld, G. Tridente and R. Tarrab-Hazdai	**Thymic lymphocytes bear a surface antigen which cross-reacts with acetylcholine receptor**	**162**
G.J. Bayliss and H. Wolf	**Epstein-Barr virus-induced cell fusion**	**164**
R.G. Miller	**Do 'lipidic particles' represent intermembrane attachment sites?**	**166**
D.J. Wolgemuth and M.-T. Hsu	**Visualization of genetic recombination intermediates of human adenovirus type 2 DNA from infected HeLa cells**	**168**
S.A. Goueli and K. Ahmed	**Indomethacin and inhibition of protein kinase reactions**	**171**

BOOK REVIEWS

David P. Barash	**Darwinism and Human Affairs (Richard D. Alexander)**	**173**
Maurice Jacob	**Models of High Energy Processes (J.C. Polkinghorne)**	**174**
R.D. Harkness	**Living without Oxygen: Closed and Open Systems in Hypoxia Tolerance (Peter W. Hochachka)**	**175**
B.E. Turner	**Giant Molecular Clouds in the Galaxy (P.M. Solomon and M.G. Edmunds, editors)**	**176**

MISCELLANY

100 years ago	**110**
Product review, blood analysis	**xix**
Classified advertising	xxxii

GUIDE TO AUTHORS

- Review articles should be aimed at a relatively wide readership. Many reviews are invited, but submitted articles may also be accepted; it is advisable to consult us before writing a review article.
- Articles may be up to 3,000 words long with at most six displayed items (figures and tables); they are reports of major research developments.
- Letters are brief reports of original research of unusual and wide interest, not in general longer than 1,000 words; they have at most three or four displayed items.
- 'Matters Arising' permits short discussion (up to 300 words) of papers that have recently appeared in *Nature*.

Articles should be accompanied by an abstract of not more than fifty words. Letters should begin with a paragraph giving the background and main conclusion in terms intelligible to as wide a readership as possible.

Manuscripts may be submitted either to London or New York. Three typed copies should be submitted, each including lettered copies of figures. Typing (including references) should be double spaced. The title should be brief and informative. Pages should be numbered. References, tables and figure legends should start on separate pages. Experimental detail vital to the paper yet which would interrupt the narrative is best placed in the figure legends. Units should be identified in the margin on their first appearance. Equations should occupy single lines if possible: exp(a) is preferred to e^a if 'a' is more than one character.

References are indicated by superscripts in the text. See any contemporary *Nature* for style, but note:

(i) only one reference number need be used if the reference is to several papers by identical authors.

(ii) first and last pages of references should be cited.

Abbreviations should follow the *World List of Scientific Periodicals*, fourth edn (Butterworth, 1963-65). Symposia are often difficult to refer to and only published or soon-to-be-published volumes should be mentioned in references. Their publisher and place of publication should be clearly indicated 'Personal communication' and 'unpublished' should be incorporated in text.

Artwork should be sent with the manuscript and clearly marked with author's name and the figure number. Line drawings should be either photographic prints or in Indian ink on heavy cartridge paper, tracing paper or similar materials. Most figures are reduced to one column width so originals should be about as wide as a page of *Nature*. To enable figures, particularly maps, to be edited in the same style as the text, they should contain only essential material. Ideally, an unlettered original and three lettered copies should be provided; labelling on halftones should, if possible, be avoided entirely. Magnifications quoted should be for the figures as submitted. We are always glad to see artwork for possible use on the cover, but cannot guarantee its return.

In order to save on postal expenses we return only the top copy and artwork of manuscripts that we cannot publish.

Nature's publishing policy is outlined in **258**, 1 (1975) and **264**, v, 11 Nov. (1976).

A no-compromise solution to scanning electron microscopy

The increasing use of scanning electron microscopy in industrial research and product development calls for higher standards and degrees of quantification and improved operational versatility.

Until now however, positional geometry within the specimen environment, along with the many detectors that have to be placed around the specimen, has required an SEM (scanning electron microscope) detector compromise that often produces poor performance in at least one of the operating modes.

So Philips developed a 'no-compromise' scanning electron microscope – the SEM 505 – in which the revolutionary, fibre-optics based, Multi-Function Detector (MFD) interfaces the *detecting elements* with a photomultiplier/pre-amplifier assembly that can be placed outside of the specimen chamber; thus permitting high flexibility in detector placement. The result? Optimum detection performance in all modes because detection geometry is no longer limited by fixed construction or precise port location.

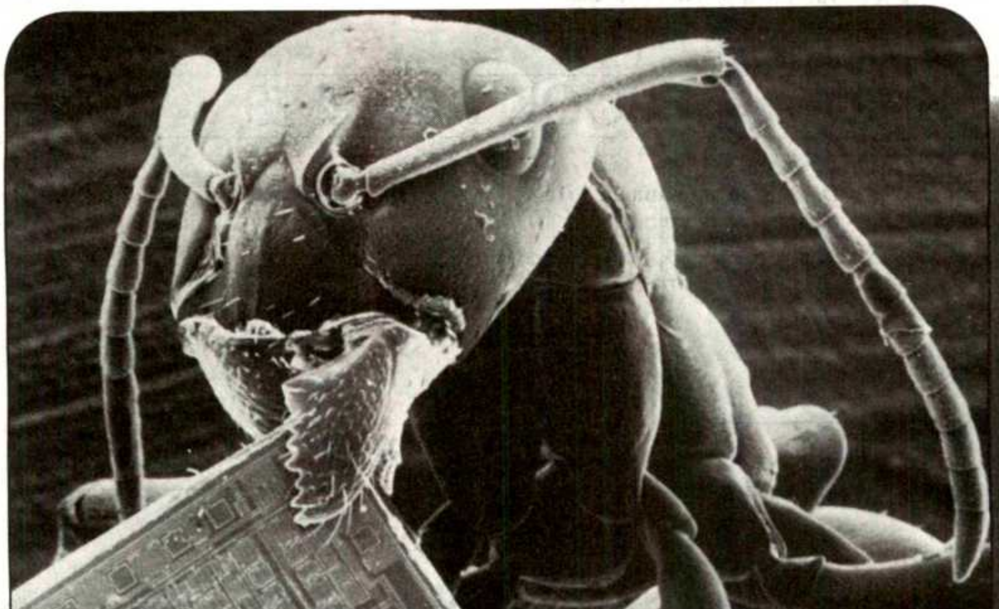

PHILIPS

nature

Volume 287 No.5779 18 September 1980

NEWS

Black sheep slink home from Geneva 177

Dismal science in doghouse once more 178

Polish students form free union 179

DNA recombination forces resignation 179

Uranium enrichment: New French process 180

Fast reactor: UK looks abroad 180

Pakistan uranium: Going ahead alone 181

US science policy: Press under pressure 181

Smallpox inquiry: Union in dispute 182

Law of the sea: Hurdles to jump 183

Overseas students: Some win, some lose 183

Correspondence — Pay as you go; Why examine? (D.A.H. Taylor); Third would matters (Peter Clarke); Felig replies (Philip Felig). 184

NEWS AND VIEWS

What we don't know about pain: P.D. Wall and C.J. Woolf discuss pain, acupuncture and the enkephalins; Shin Ho Chung and Anthony Dickenson comment 185

Hopping and running: R. McNeill Alexander on the energy costs of the different gaits 187

Movable genes: Ron McKay reports a conference on transposable genetic elements 188

The nature of gravitation: A.H. Cook describes experimental tests of the inverse square law 189

Terrestrial heat flow: D.S. Chapman reports a recent conference 190

Myosin phosphorylation: Dixie W. Frederiksen explains the control of contractile systems 191

Bishop Wilberforce and evolution: Richard W. Wrangham on what the Bishop really thought 192

ARTICLES

R. Derynck, E. Remaut, E. Saman, P. Stanssens, E. De Clercq, J. Content and W. Fiers — **Expression of human fibroblast interferon gene in *Escherichia coli*** 193

A.P. Czernilofsky, A.D. Levinson, H.E. Varmus, J.M. Bishop, E. Tischer and H.M. Goodman — **Nucleotide sequence of an avian sarcoma virus oncogene (*src*) and proposed amino acid sequence for gene product** 198

B. Demple and S. Linn — **DNA *N*-glycosylases and UV repair** 203

LETTERS

J.O. Burns and W.A. Christiansen — **Radio jets and bridges in the classical double sources 3C388 and 0816 + 526** 208

K. Doi — **Short-term variability of Cyg X-1 and the accretion disk temperature fluctuation** 210

A.T. Tokunaga, J. Caldwell and I.G. Nolt — **The 20-μm brightness temperature of the unilluminated side of Saturn's rings** 212

D.J. Drewry — **Pleistocene bimodal response of Antarctic ice** 214

D. Sahagian — **Sublithospheric upwelling distribution** 217

J.S. Killingley, W.H. Berger, K.C. MacDonald and W.A. Newman — **^{18}O/^{16}O variations in deep-sea carbonate shells from the Rise hydrothermal field** 218

V.E. Noshkin, K.M. Wong, R.J. Eagle and D.L. Anglin — **Concentrations of ^{113m}Cd in the marine environment** 221

S.D. Thompson, R.E. MacMillen, E.M. Burke and C.R. Taylor — **The energetic cost of bipedal hopping in small mammals** 223

M. deM Fencl, R.J. Stillman, J. Cohen and D. Tulchinsky — **Direct evidence of sudden rise in fetal corticoids late in human gestation** 225

Contents continued overleaf

Cover: The Ferrar Glacier (top) and the snout of the Taylor Glacier (bottom) in McMurdo Sound, Antarctica. The chronology of the Antarctic ice sheet is discussed on page 214.

Nature® published weekly ISSN 0028-0836
Registered as a newspaper at the British Post Office and the United States Post Office

0028-0836/80/38000C-02$01.00

MORE FOR LESS

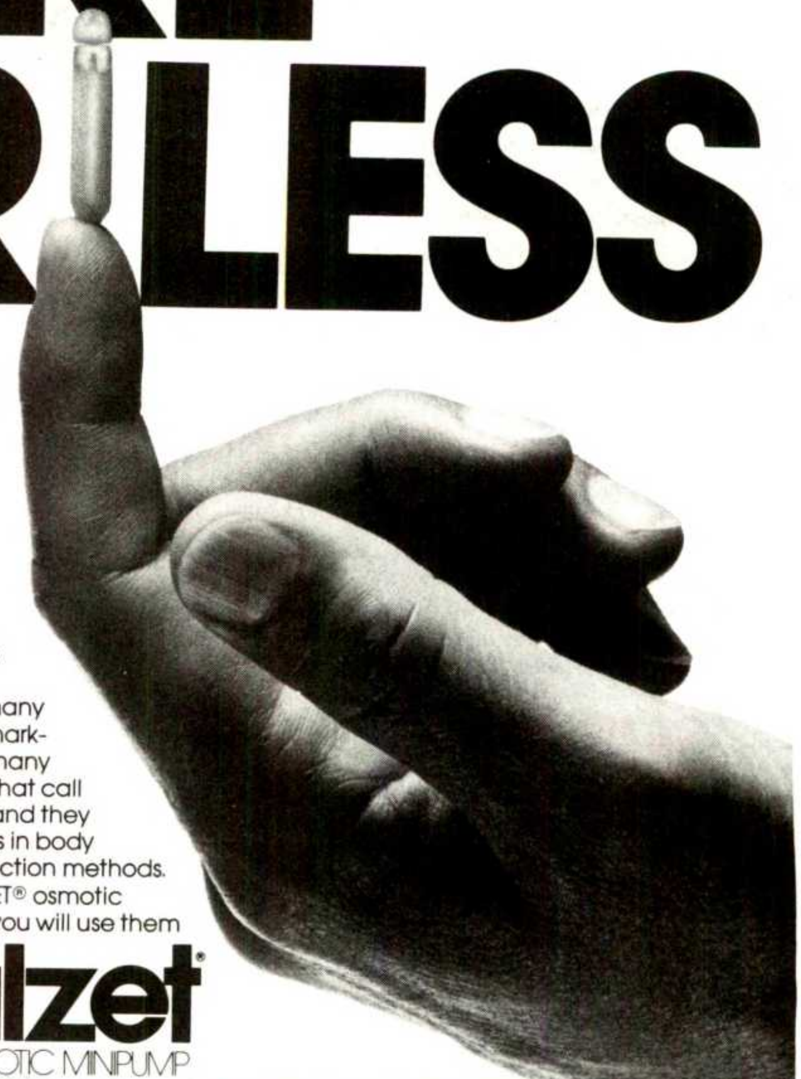

Alza is pleased to introduce the Model 2002 (.5μ l/hr, 14 days) ALZET® osmotic minipump, the latest edition to the ALZET Model 2000 series. The Model 2002 provides a wider temperature range and solvent compatibility for continuous, stress-free, rate-specified administration of bioactive agents in laboratory animals, or in vitro, than our 1700 series minipumps. And at lower cost.

It costs as little as 47¢ per day (in quantities of 100) to attain the kind of control in plasma or tissue concentrations of bioactive agents that was previously possible only with complex systems of expensive infusion pumps.

There are now over 130 published papers in many areas of bioscience based on the use of these remarkable minipumps. Minipumps have made viable many previously impossible or impractical experiments that call for the continuous presence of bioactive agents, and they avoid the large swings in concentrations of agents in body fluids that accompany ordinary pulse/drench injection methods.

You will want to investigate the use of the ALZET® osmotic minipumps, because they are cost-efficient. And you will use them repeatedly because they contribute to better results. To order minipumps or to receive more information, call our toll-free number: 800/227-9953, or send in the coupon below.

alzet®
OSMOTIC MINIPUMP

ALZA, DEPT. Y, 950 Page Mill Road, Palo Alto, CA 94304 Nat.

Please send me information on ALZET® osmotic minipumps:
( ) Current bibliography ( ) Complete technical information ( ) Add my name to your mailing list

Please send me the quantity Model 2001 or Model 2002 minipumps I've circled below.

MODEL 2001			MODEL 2002		
Quantity	Unit Price	Total price	Quantity	Unit Price	Total Price
10	$7.25	$ 72.50	10	$9.75	$ 97.50
50	$6.25	$ 312.50	50	$8.40	$ 420.00
100	$4.95	$ 495.00	100	$6.65	$ 665.00
500	$4.25	$2,125.00	500	$5.70	$2,850.00

I've included my check or purchase order in the amount of ______ (California residents add required sales tax.)
Name ______
Organization ______
Address ______
City ______ State ______ Zip ______ Phone ______

International Orders – Product inquiries, literature requests for ALZET® osmotic minipumps and orders from Europe and Japan may now be directed to: Scientific Marketing Assoc., Ltd., 37 Mildmay Grove, London NI 4RH, England, Telephone: 01-359-5357; Tokai Irika Co., Ltd., Kurihara Building, No. 2-12, 3-chome, Uchi-Kanda, Chuyoda-Ku, Tokyo, Japan, Telephone: 03-254-0052.

©1980 ALZA CORP.

Circle No. 02 on Reader Enquiry Card.

LETTERS

C.L. Uber, R.L. Roth and D.A. Levy **Expulsion of *Nippostrongylus brasiliensis* by mice deficient in mast cells** 226

M.H. Schreier and N.N. Iscove **Haematopoietic growth factors are released in cultures of H-2-restricted helper T cells, accessory cells and specific antigen** 228

S. Gunther, M.A. Gimbrone Jr and R.W. Alexander **Regulation by angiotensin II of its receptors in resistance blood vessels** 230

J.M. Scholey, K.A. Taylor and J. Kendrick-Jones **Regulation of non-muscle myosin assembly by calmodulin-dependent light chain kinase** 233

W.J. Betz, J.H. Caldwell, R.R. Ribchester, K.R. Robinson and R.F. Stump **Endogenous electric field around muscle fibres depends on the Na$^+$–K$^+$ pump** 235

K.L. Kirk, D.R. Halm and D.C. Dawson **Active sodium transport by turtle colon via an electrogenic Na–K exchange pump** 237

J.L. Schnapf and R.N. McBurney **Light-induced changes in membrane current in cone outer segments of tiger salamander and turtle** 239

D.P. Witt and J.A. Gordon **Specific dephosphorylation of membrane proteins in Rous sarcoma virus-transformed chick embryo fibroblasts** 241

J.A. Allen and M.M. Coombs **Covalent binding of polycyclic aromatic compounds to mitochondrial and nuclear DNA** 244

A. Babich, J.R. Nevins and J.E. Darnell Jr **Early capping of transcripts from the adenovirus major late transcription unit** 246

L.M. Van Valen and V.C. Maiorana **The Archaebacteria and eukaryotic origins** 248

M. Kessel and F. Klink **Archaebacterial elongation factor is ADP-ribosylated by diphtheria toxin** 250

P.E. Gisby and D.O. Hall **Biophotolytic H$_2$ production using alginate-immobilized chloroplasts, enzymes and synthetic catalysts** 251

M.J. Connor, J.A. Blair and H. Said **Secondary isotope effects in studies using radiolabelled folate tracers** 253

MATTERS ARISING

E.R.D. Scott and R.S. Clarke Jr **Ordering of FeNi in clear taenite from meteorites** 255

L.A. Sklar and M.C. Doody **Differences in fluidity between bilayer halves of plasma cell membranes** 255

F. Schroeder and D.A. Kinden **Reply to Sklar and Doody** 256

BOOK REVIEWS

Fred Dainton **Higher Education Revisited (Lord Robbins). Higher Education for the Future (Charles Carter)** 257

Peter D. Moore **Grasslands, Systems Analysis and Man (A.I. Breymeyer and G.M. Van Dyne, editors)** 259

C. Pritchet **Photometry, Kinematics and Dynamics of Galaxies (D.S. Evans, editor)** 259

Brian Funnell **The Pre-glacial Pleistocene of the Norfolk and Suffolk Coasts (R.G. West)** 260

MISCELLANY

100 years ago 189

Author index vol. 286 xiii

Books received 261

Classified advertising xxix

***Nature* Indexes:** This week *Nature* includes an Author Index to volume 286, covering July and August 1980. Previous Author Indexes this year appeared in the issues of 20 March (for vol. 283), 22 May (vol. 284) and 24 July (vol. 285).

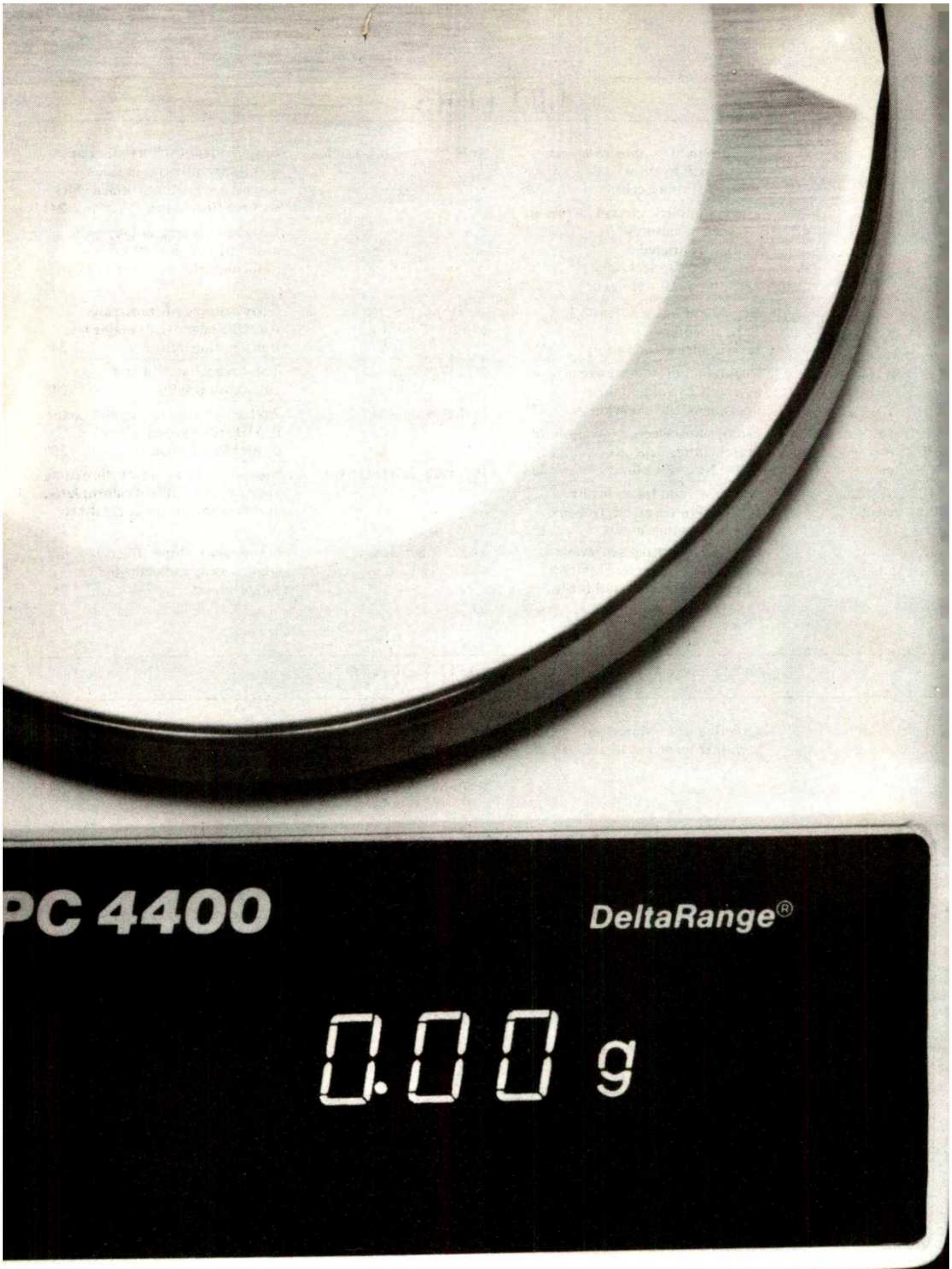
PC 4400
DeltaRange®
0.00 g

nature

Volume 287 No.5780 25 September 1980

NEWS

What future for European reactors? 263
US woos African States with science 265
Still looser UK guidelines 265
Engineering research: Planning for more 266
Electronic publishing: keyboard papers 266
Soviet swindles: Degrees by stealth 267
Space shuttle: Delay costs money 267
Genetic manipulation: Ethics of change 268
German science: Frontier talk 269
French science: Same now, more later 269
Soviet bomb scare 269
Correspondence: Geothermal power (R.V. Harrowell, E.J. Athony); Models of psychosis (G.S. Claridge); Educative computers (Jill Coates); Interferonology (Lee H. Kronenberg); Educating scientists (C.S. Morphet); 270

NEWS AND VIEWS

The last neanderthal in France: A. M. ApSimon discusses the replacement of neanderthal by sapiens man 271
Snakeblennies: Alwyne Wheeler reports the finding of five new species 273
Sexual dimorphism and the evolution of the higher primates: R. D. Martin on the significance of new fossil primate finds 273
Immunological changes in multiple sclerosis: Barry R. Bloom examines the evidence 275
Quantum mechanics and gravitational waves: Bridget Marx on how quantum mechanical effects limit measurement 276
Galileo saw Neptune in 1612: David W. Hughes describes new evidence from Galileo's notebooks 277
Laser annealing for semiconductor devices: I. W. Boyd and J. I. B. Wilson report a recent advanced study institute 278

ARTICLES

P.J. Hamilton, R.K. O'Nions and R.J. Pankhurst **Isotopic evidence for the provenance of some Caledonian granites** 279
J.K. Weissel, R.N. Anderson and C.A. Geller **Deformation of the Indo-Australian plate** 284
D.J. DeRosier, L.G. Tilney and E. Egelman **Actin in the inner ear: the remarkable structure of the stereocilium** 291
Y. Citri and M. Schramm **Resolution, reconstitution and kinetics of the primary action of a hormone receptor** 297
M.-J. Gething, J. Bye, J. Skehel and M. Waterfield **Cloning and DNA sequence of double-stranded copies of haemagglutinin genes from H2 and H3 strains elucidates antigenic shift and drift in human influenza virus** 301

LETTERS

M.C. Begelman, R.D. Blandford and M.J. Rees **Massive black hole binaries in active galactic nuclei** 307
R. Woo and J.W. Armstrong **Spectral broadening measurements of the ionospheres of Jupiter and Saturn** 309
C.T. Kowal and S. Drake **Galileo's observations of Neptune** 311
P.D. Kearney, A.G. Klein, G.I. Opat, and R. Gähler **Imaging and focusing of neutrons by a zone plate** 313
D. Cherns, J.L. Hutchison, M.L. Jenkins, P.B. Hirsch and S. White **Electron irradiation induced vitrification at dislocations in quartz** 314
M. Kennedy, G. Turturro, G.R. Brown and L.E. St-Pierre **Silica retards radial growth of spherulites in isotactic polystyrene** 316
A.J. Kox, J.P.J. Michels and F.W. Wiegel **Simulation of a lipid monolayer using molecular dynamics** 317
R.L. Craig, R.A. Vincent, G.J. Fraser and M.J. Smith **The quasi 2-day wave in the Southern Hemisphere mesosphere** 319
A.A. Burchuladze, S.V. Pagava, P. Povinec, G.I. Togonidze and S. Usačev **Radiocarbon variations with the 11-year solar cycle during the last century** 320
C. Doumas and L. Papazoglou **Santorini tephra from Rhodes** 322

Cover: The arrangement of the acting filament bundle in the stereocilium of the cochlear hair cell is shown in a thin section of the steriocilium (lowerhalf of figure) and in a computer-generated thin section that mimics the true pattern (bottom half). A single-bonding rule which determines how a crossbridging protein links neighbouring filaments accounts for this structure and is discussed on page 291.

Contents continued overleaf

Nature® published weekly ISSN 0028-0836
Registered as a newspaper at the British Post Office and the United States Post Office

0028-0836/80/39000C-02$01.00

Chromatography monitoring as simple as

A

SLIP in a 10 mm or a 3 mm optical path-length cell. These two cells make the UV-1 equally suitable for monitoring in high or low absorbance ranges.

B

SNAP in a 254 nm or a 280 nm filter. The UV-1 provides sensitive and reliable UV monitoring for the detection of proteins, polypeptides and nucleic acids.

C

FLIP a switch for measuring Absorbance or % Transmission. The absorbance setting gives a quantitative linear response at a known sensitivity range and the percent transmission ensures that all peaks remain on scale.

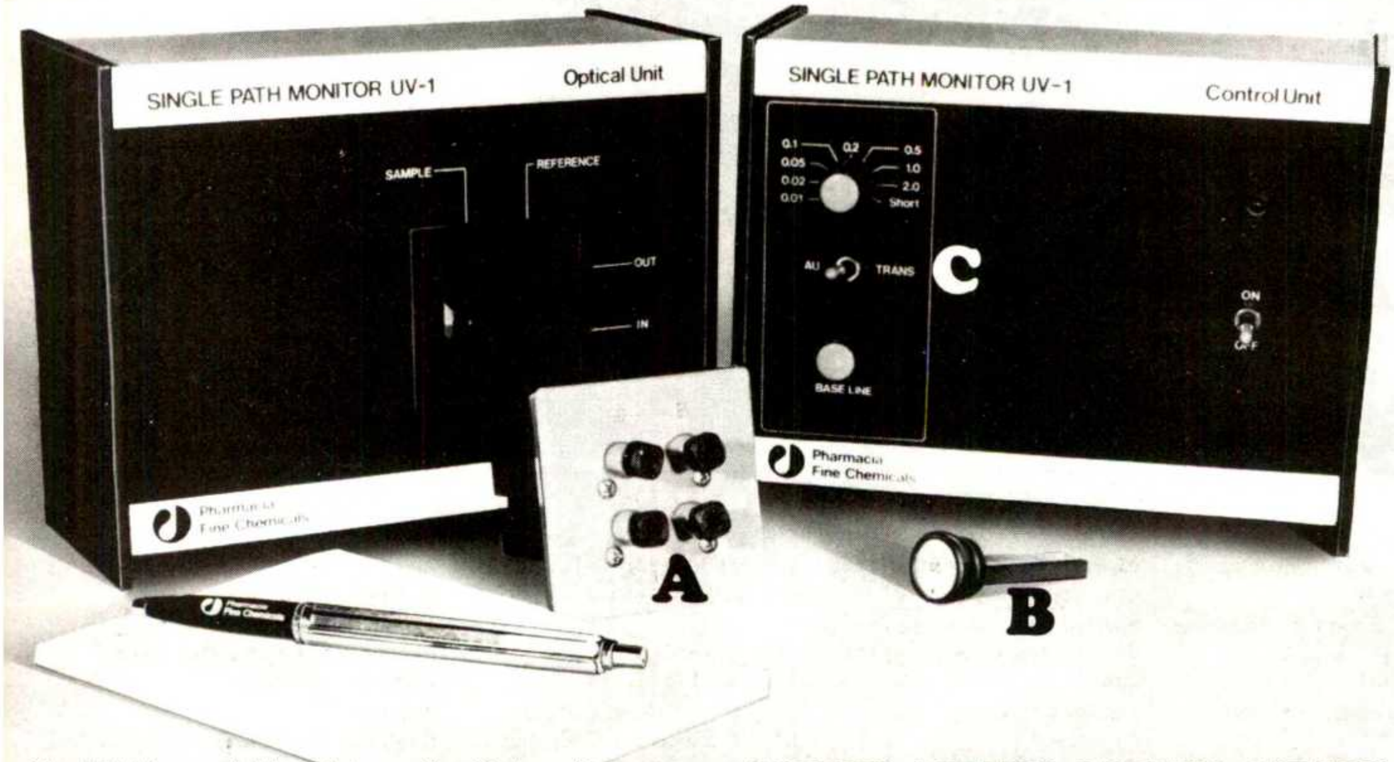

The UV-1 is a reliable, high quality, high performance dual-beam instrument that is ideally suited to your wide range of chromatographic conditions. Ask today for complete specifications on the UV-1 or on the more sophisticated dual sensitivity UV-2 monitor.

NEW! NEW! NEW! NEW!

Now also for monitoring at 214 nm. Available as a complete monitor UV-1/214 or as an optical unit to extend the standard UV-1 to 214 nm.

Pharmacia Fine Chemicals AB
Box 175
S-751 04 Uppsala 1
Sweden

Pharmacia
Fine Chemicals

Circle No. 19 on Reader Enquiry Card.

LETTERS

B.K. Maloney **Pollen analytical evidence for early forest clearance in North Sumatra** 324
R. Karban **Periodical cicada nymphs impose periodical oak tree wood accumulation** 326
J.G. Fleagle, R.F. Kay and E.L. Simons **Sexual dimorphism in early anthropoids** 328
G. Lykkeboe, O. Brix and K. Johansen **Oxygen-linked CO_2 binding independent of *p*H in cephalopod blood** 330
P C.L. Beverley, D. Linch and D. Delia **Isolation of human haematopoietic progenitor cells using monoclonal antibodies** 332
J. Robinson, D. Smith and J Niederman **Mitotic EBNA-positive lymphocytes in peripheral blood during infectious mononucleosis** 334
D.H. Mattson, R.P. Roos and B.G.W. Arnason **Isoelectric focusing of IgG eluted from multiple sclerosis and subacute sclerosing panencephalitis brains** 335
J D. Altringham, P H. Yancey and I.A. Johnston **Limitations in the use of actomyosin threads as model contractile systems** 338
L.K. Johnson, I Vlodavsky, J D. Baxter and D. Gospodarowicz **Nuclear accumulation of epidermal growth factor in cultured rat pituitary cells** 340
B. Ahrén, J. Alumets, M. Ericsson, J. Fahrenkrug, L. Fahrenkrug, R. Hakanson, P Hedner, I. Lorén, A. Melander, C. Rerup and F. Sundler **VIP occurs in intrathyroidal nerves and stimulates thyroid hormone secretion** 343
C.P. VanderMaelen and G.K. Aghajanian **Intracellular studies showing modulation of facial motoneurone excitability by serotonin** 346
J D. Kocsis and S G. Waxman **Absence of potassium conductance in central myelinated axons** 348
T.D. Lamb **Spontaneous quantal events induced in toad rods by pigment bleaching** 349
M. Tsuda, M. Glaccum, B Nelson and T.G. Ebrey **Light isomerizes the chromophore of bacteriorhodopsin** 351
V. Krump-Konvalinkova and K.J. van den Berg **Leukaemia virus infection promotes fibroblast transformation by normal BALB/c mouse DNA** 353
A. Person, F. Ben-Hamida and G. Beaud **Inhibition of 40S-Met-tRNA$_f^{Met}$ ribosomal initiation complex formation by vaccinia virus** 355
S.E. Rognes, P.J. Lea and B.J. Miflin ***S*-adenosylmethionine — a novel regulator of aspartate kinase** 357
L. Willmitzer, M. De Beuckeleer, M. Lemmers, M. Van Montagu and J. Schell **DNA from Ti plasmid present in nucleus and absent from plastids of crown gall plant cells** 359
A De Ronde, A.P.G.M. Van Loon, L.A. Grivell and J. Kohli ***In vitro* suppression of UGA codons in a mitochondrial mRNA** 361
U. Kuhnlein, S.S. Tsang and J. Edwards **Cooperative structural transition of PM2 DNA at high ionic strength and its dependence on DNA damages** 363

MATTERS ARISING

R. Stothers **Giant solar flares in Antarctic ice** 365
D S.P. Dearborn and J.B. Blake **Magnetic fields and the solar constant** 365
D.C. Smith **A tectonic mélange of foreign eclogites and ultramafites in West Norway** 366
L.G. Medaris Jr **Reply to Smith** 367
C. Reavill, N. Leigh, P. Jenner and C.D. Marsden **GABA mediated circling from substantia nigra** 368

BOOK REVIEWS

Jean Berko Gleason **Nim: A Chimpanzee Who Learned Sign Language (Herbert S. Terrace)** 369
Joel A. Eaton **Language of the Stars (Zdeněk Kopal)** 370
Robert Hedges **Archaeological Chemistry (Z. Goffer)** 371
Henry Charnock **Opportunities and Uses of the Ocean (D.A. Ross)** 371
M. Schnitzer **Nature and Origin of Carbohydrates in Soils (M.V. Cheshire)** 372

MISCELLANY

100 years ago 274
Corrigendum 364
Books received 373
Announcements 375
Classified advertising xix

ORION offers the electrodes, meters, and accessories for every pH measurement you will ever want to make... and more.

ORION offers high-quality glass pH electrodes in nine configurations . . . with many connector types . . . four sizes of virtually unbreakable pH electrodes that never need refilling with KCl . . . eight pH meters from low-cost portable models to microprocessor-based systems . . . filling solutions, buffers, and swing-arm holders.

Beyond the excellent hardware, there is your local ORION distributor. He has the expertise and the desire to help you choose the combination of our pH products that is right for your needs. Contact him, or write for more information.

ORION RESEARCH AG Fähnlibrunnenstrasse 5, CH-8700 Küsnacht, Switzerland
Telephone: 01-910 7858/Telex: 57829

Circle No. 08 on Reader Enquiry Card.

A Reliable Low-Cost Incubator
Anaerobic or Aerobic Applications
Ideal for Cell Culture

This Modular Incubator Chamber minimises environmental fluctuations (i.e. temperature, gas and humidity) associated with conventional incubators. Once cultures have been sealed inside the chamber, it may be purged with the required gas mixture and placed in a controlled temperature environment. Each chamber is an isolated system, allowing experimental conditions which were previously impractical or too expensive. Chambers and trays are made from rugged, non-toxic, u-v resistant polycarbonate. The trays hold petri-dishes, test tubes, tissue culture flasks, microtitration plates and multidishes. Now available exclusively from Flow Laboratories and their appointed distributors world-wide.

United Kingdom
Flow Laboratories Ltd.,
P.O. Box 17, Second Avenue Industrial Estate
Irvine KA12 8NB Scotland
Tel: (0294) 72121 Telex: 77231 Flow G

United States
Flow Laboratories Inc.,
7655 Old Springhouse Road, McLean,
Virginia 22102, U.S.A.
Tel: (703) 893-5925
Telex: 234 9030 10 Flowlab MCLN

Companies also in West Germany, France, Sweden, Switzerland, Australia & Singapore.

Circle No. 21 on Reader Enquiry Card.

nature

Volume 287 No.5781 2 October 1980

NEWS

What is wrong with US engineering? 377
Poor outlook for British universities 378
NASA budget falls foul of contracts 379
Einstein observatory in trouble 379
Radiological protection: X-ray survey 380
DNA guidelines: More relaxation 380
Biotechnologys: UK company gells 381
Going and coming 381
French universities: Trouble behind 381
Non-proliferation: India gets fuel 382
Information technology: Cheering on UK 383
Bulgarian science: Reaching out 383
Correspondence: DNA X-ray data (R.A.T. Bates, G.A. Rodley, G.C. McKinnon); Andrei Sakharov (F. Janouch); Preventing plagiarism (Umberto Veronesi); Pesticides as poisons (Thomas H. Jukes, R.A. Davis) 384

NEWS AND VIEWS

Myths, models and human evolution: 385
Infrared astronomy: R.D. Wolstencroft describes the field's first large symposium 386
Hurricane Allen: J.D. Woodley describes the Jamaican coral reefs 387
Industrial biopolymers: Paul Calvert on new applications for biological macromolecules 388
Essential fatty acids and prostaglandins: Michael Crawford explains how a Congress combined the two fields 388
Neural communication and control: Donald MacKay reviews the facts and theories revealed at a recent symposium 389
Chopping and changing in immunoglobulin genes: Miranda Robertson reports the International Congress of Immunology 390

REVIEW ARTICLE

B.K. Chakraverty **Insulating ground state and nonmetal–metal transitions** 393

ARTICLES

J.D. Windass, M.J. Worsey, E.M. Pioli, D. Pioli, P.T. Barth, K.T. Atherton, E.C. Dart, D. Byrom, K. Powell and P.J. Senior **Improved conversion of methanol to single-cell protein by *Methylophilus methylotrophus*** 396
S. Nagata, N. Mantei and C. Weissmann **The structure of one of the eight or more distinct chromosomal genes for human interferon-α** 401
G. Allen and K.H. Fantes **A family of structural genes for human lymphoblastoid (leukocyte-type) interferon** 408
D.V. Goeddel, E. Yelverton, A. Ullrich, H.L. Heyneker, G. Miozzari, W. Holmes, P.H. Seeburg, T. Dull, L. May, N. Stebbing, R. Crea, S. Maeda, R. McCandliss, A. Sloma, J.M. Tabor, M. Gross, P.C. Familletti and S. Pestka **Human leukocyte interferon produced by *E. coli* is biologically active** 411

Contents continued overleaf

Cover: Cell bodies in the buccal ganglion of a mollusc labelled with tritiated 2-deoxyglucose. The technique allows the mapping of the metabolic activity of single neurones and is discussed on page 449.

Nature® published weekly ISSN 0028-0836
Registered as a newspaper at the British Post Office and the United States Post Office

0028-0836/80/40000C-02$01.00

You will have complete control of your collection sequence with the intelligent flexibility of the microprocessor directed Pharmacia fraction collector FRAC-300.

Collect varying fraction sizes in any combination of tubes, scintillation vials and free standing beakers.

FRAC-300 operates in both programmable and conventional modes and can be used in LC or HPLC operations with aqueous solutions or organic solvents.

The FRAC-CC chromatography controller is an accessory to the FRAC-300 which allows you to control valves, peristaltic pumps, and gradient mixers in conjunction with the chromatographic profile to allow automatic sample applications, equilibration of the column, buffer changes, etc.

FRAC-300 and FRAC-CC are integrated components of the total Pharmacia chromatographic system that includes chromatographic columns, a peristaltic pump, UV-monitors, recorders and a wide variety of high performance media for gel filtration, affinity chromatography and ion exchange chromatography.

Make use of this new concept in fraction collection and ask for detailed information today.

Pharmacia Fine Chemicals AB
Box 175
S-751 04 Uppsala 1
Sweden

Pharmacia
Fine Chemicals

Circle No. 10 on Reader Enquiry Card.

LETTERS

E.K. Hege, J.R.P. Angel, R.J. Weymann and E.N. Hubbard **Morphology of the triple QSO PG1115+08** 416
M. Hoppe and C.T. Russell **Whistler mode wave packets in the Earth's foreshock region** 417
K. Krishan **Kinetics of void-lattice formation in metals** 420
M.R. Smith **Influence of modal composition on deformation in garnet lherzolite nodules** 422
G. Schubert, J.M. Straus and M.A. Grant **A problem posed by vapour-dominated geothermal systems** 423
M.S. Steckler and A.B. Watts **The Gulf of Lion: subsidence of a young continental margin** 425
J. Oerlemans **Model experiments on the 100,000-yr glacial cycle** 430
T. Mazany, J.C. Lerman and A. Long **Carbon-13 in tree-ring cellulose as an indicator of past climates** 432
A. Comparini and E. Rodinò **Electrophoretic evidence for two species of *Anguilla* leptocephali in the Sargasso Sea** 435
M. Nabholz, M. Cianfriglia, O. Acutò, A. Conzelmann, W. Haas, H.v. Boehmer, H.R. McDonald, H. Pohlit and J.P. Johnson **Cytolytically active murine T-cell hybrids** 437
A.D. O'Brien, D.L. Rosenstreich and B.A. Taylor **Control of natural resistance to *Salmonella typhimurium* and *Leishmania donovani* in mice by closely linked but distinct genetic loci** 440
M. Steinitz, G. Izak, S. Cohen, M. Ehrenfeld and I. Flechner **Continuous production of monoclonal rheumatoid factor by EBV-transformed lymphocytes** 443
J. Pouysségur, A. Franchi and P. Silvestre **Relationship between increased aerobic glycolysis and DNA synthesis initiation studied using glycolytic mutant fibroblasts** 445
F.J. Sigworth and E. Neher **Single Na$^+$ channel currents observed in cultured rat muscle cells** 447
T.J. Sejnowski, S.C. Reingold, D.B. Kelley and A. Gelperin **Localization of [^{3}H]-2-deoxyglucose in single molluscan neurones** 449
L.A. Chiodo and S.M. Antelman **Repeated tricyclics induce a progressive dopamine autoreceptor subsensitivity independent of daily drug treatment** 451
R.K. Maheshwari, D.K. Banerjee, C.J. Waechter, K. Olden and R.M. Friedman **Interferon treatment inhibits glycosylation of a viral protein** 454
D. Jähner and R. Jaenisch **Integration of Moloney leukaemia virus into the germ line of mice: correlation between site of integration and virus activation** 456
N.S. Yadav, K. Postle, R.K. Saiki, M.F. Thomashow and M.-D. Chilton **T-DNA of a crown gall teratoma is covalently joined to host plant DNA** 458
M. Tsuda, F. Tokunaga, T.G. Ebrey, K.T. Yue, J. Marque and L. Eisenstein **Behaviour of octopus rhodopsin and its photoproducts at very low temperatures** 461
R.F. Hess and A. Bradley **Contrast perception above threshold is only minimally impaired in human amblyopia** 463
K. Alitalo, M. Kurkinen, A. Vaheri, I. Virtanen, H. Rohde and R. Timpl **Basal lamina glycoproteins are produced by neuroblastoma cells** 465
D.K. Smythe, A.G. Skuce and J.A. Donato **Geological objections to an extensional origin for the Buchan and Witchground Graben in the North Sea** 467
P.A.F. Christie and J.G. Sclater **Reply to Smythe, Skuce and Donato** 467
A.R. Williamson **Counting integral numbers of amino acid residues** 468
T.E. Creighton **Reply to Williamson** 468

BOOK REVIEWS

O.L. Zangwill **Wilhelm Wundt and the Making of a Scientific Psychology (R.W. Rieber, editor)** 469
William S. Robinson **Hepatitis Viruses of Man (A.J. Zuckerman and C.R. Howard)** 469
Kenneth Mellanby **Ecology of the English Chalk (C.J. Smith)** 470
A. Ewart **The Geology of New Zealand (R.P. Suggate, chief editor)** 471
J.S. Morley **Steroids and Peptides (J.B. Dence)** 472
C.M. Yonge **British Crabs (R.W. Ingle)** 472

MISCELLANY

Corrigenda 466
Books received xiii
New on the market xiv
Classified advertising xviii

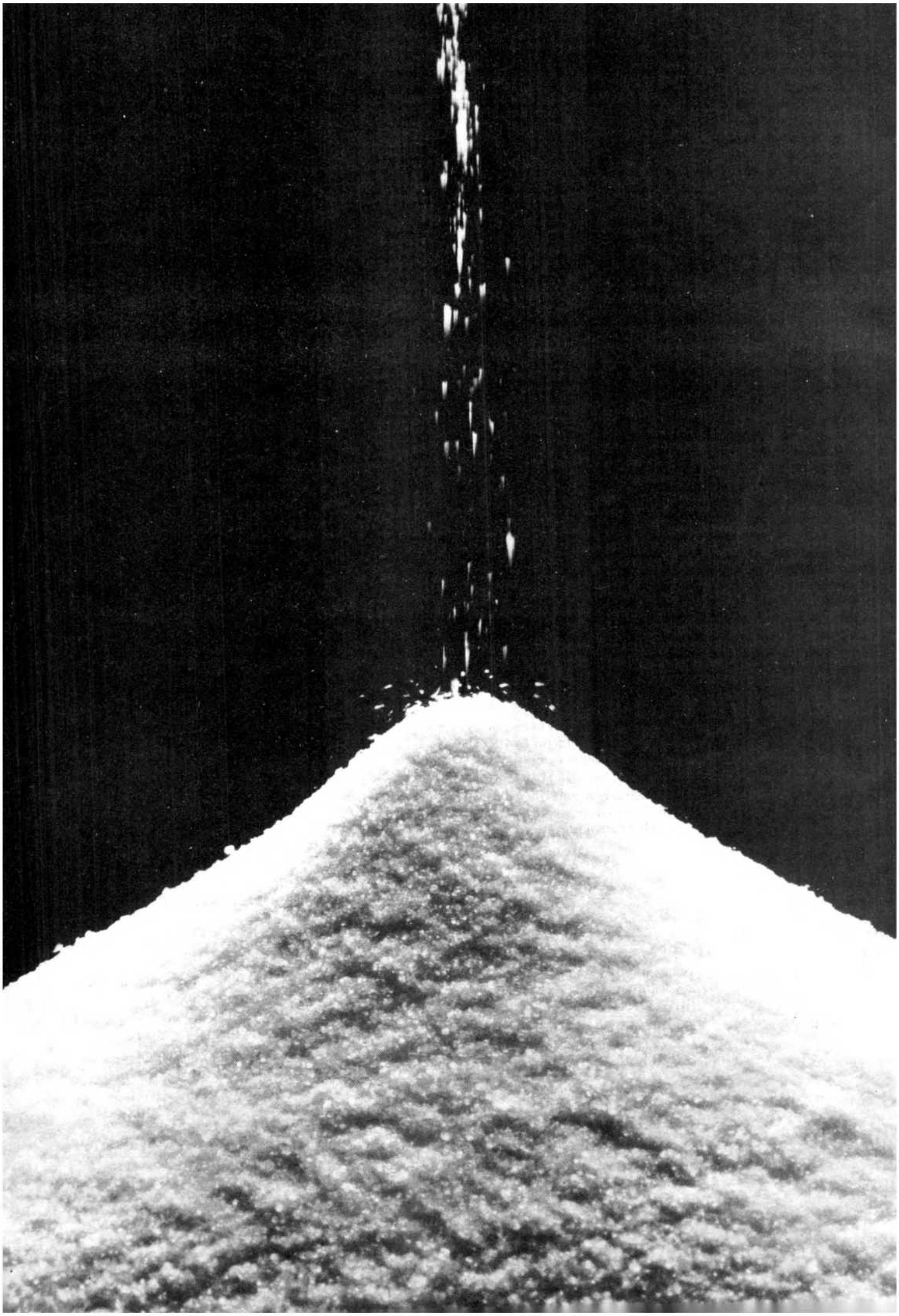

nature

Volume 287 No.5782 9 October 1980

NEWS

Will the DNA guidelines wither away? 473
McNamars's fond farewell to his bank 474
Melanoma increase in radiation labs: Livermore data may be significant 475
EEC worries about veal and hormones 475
EEC hormone law 476
Polish farming: More meat to eat? 476
Kopek interferon 477
Gulf pollution: UN's other worry 477
Nuclear equipment: Secrets lifted 478
European rockets: Range reprieved 478
British PWR: One year back 479
Mining Polish sulphur: Trying harder 479
Correspondence: Hurricane damage (J. Lewis); AChE uses (R. G. Elles *et al.*); Wilberforce and Darwin (F. R. Lucas) 480

NEWS AND VIEWS

Whatever happened to neutrino mass? 481
Nations and numbers, 1980: Robert M. May looks at global population forecasts 482
Towards the conquest of hepatitis B: Arie J. Zuckermann on the first successful vaccine trial 483
Variable stars and galaxies: Julian Osborne and Robert Cole report a recent conference 484
The Tibetan Plateau: Peter Jackson describes the first visit by Western scientists 486
Mycorrhiza and crop production: D. S. Hayman describes a valuable fungus-root association 487
Tales of two accelerators: P. I. P. Kalmus on the death of Nimrod and ZGS 488
Diseases of the motor unit: a report from the Muscular Dystrophy Association meeting 489
Crystallizing membrane protein: Richard Henderson on the first successes 490

REVIEW ARTICLE

Edward B. Ziff **Transcription and RNA processing by the DNA tumour viruses** 491

ARTICLES

B.N. Preston, T.C. Laurent, W.D. Comper and G.J. Checkley **Rapid polymer transport in concentrated solutions through the formation of ordered structures** 499
L. Clarke and J. Carbon **Isolation of a yeast centromere and construction of functional small circular chromosomes** 504
A. Klug, D. Rhodes, J. Smith, J.T. Finch and J.O. Thomas **A low resolution structure for the histone core of the nucleosome** 509

LETTERS

K.O. Mason, J. Middleditch, J.E. Nelson and N.E. White **An optical burst from the star identified with the X-ray source 2S1254--690** 516
D.T. Wickramasinghe and D.A. Allen **The 3.4-μm interstellar absorption feature** 518
D.J. Stevenson **Lunar asymmetry and palaeomagnetism** 520
C.D. Ellyett and J.A. Kennewell **Radar meteor rates and atmospheric density changes** 521
E.C. Zipf **A laboratory study on the formation of nitrous oxide by the reaction $N_2(A^3\Sigma_u^+) + O_2 \rightarrow N_2O + O$** 523
E.C. Zipf and S.S. Prasad **Production of nitrous oxide in the auroral *D* and *E* regions** 525
A. Henderson-Sellers and A.W. Schwartz **Chemical evolution and ammonia in the early Earth's atmosphere** 526
K.A. Whaler **Does the whole of the Earth's core convect?** 528
M.F.J. Flower **Accumulation of calcic plagioclase in ocean-ridge tholeiite: an indication of spreading rate?** 530
J.D. Smith and A.R. Longmore **Behaviour of phosphate in estuarine waters** 532

Cover: High molecular weight polymers may be transported with an unexpectedly high 'diffusion' rate in the presence of a concentrated second polymer due to the formation of organized macroscopic structures. The cover shows these structures forming at a boundary between two polymer solutions (see page 499).

Contents continued overleaf

M
Nature® published weekly ISSN 0028-0836
Registered as a newspaper at the British Post Office and the United States Post Office

0028-0836/80/41000C-02$01.00

New
Vitamin D$_3$
Metabolites

Highest Specific Activities
Widest Range
Highest Quality (HPLC purified)...

For the location and investigation of receptor sites and the assay of circulating levels.

1α,25-Dihydroxy[26,27-*methyl*-^{3}H]cholecalciferol Current batch 163Ci/mmol	TRK.656
✱24R,25-Dihydroxy[26,27-*methyl*-^{3}H]cholecalciferol Current batch 163Ci/mmol	TRK.657
25-Hydroxy[26,27-*methyl*-^{3}H]cholecalciferol Current batch 154Ci/mmol	TRK.655
✱1α,24R,25-Trihydroxy[26,27-*methyl*-^{3}H]cholecalciferol Current batch 163Ci/mmol	TRK.658

✱ Exclusive

Also available, our exclusive range of [23,24(n)-^{3}H]cholecalciferol derivatives.

...from Amersham

The Radiochemical Centre Amersham

Full information is available on request.
The Radiochemical Centre Limited, Amersham, England Telephone 024-04-4444.
In the U.S.A. and Canada
Amersham Corporation, Illinois 60005.
Telephone. 312-364-7100 and
800/323-9750 (Tollfree).
In W. Germany
Amersham Buchler GmbH & Co KG,
Braunschweig. Telephone 05307-4691.

Circle No. 10 on Reader Enquiry Card.

A new journal
to be published by Springer-Verlag

Polar Biology

Managing Editor: G. Hempel

For further information please write to:
Springer-Verlag, Journal Promotion Department, P.O. Box 105 280,
D-6900 Heidelberg, FRG

Springer-Verlag
Berlin Heidelberg New York

Circle No. 15 on Reader Enquiry Card.

LEARNING THROUGH COMPUTERS

D.A. TAWNEY

– an introduction to computer assisted learning in Engineering, Mathematics and the Sciences at tertiary level.

You can teach faster and more thoroughly with the aid of a computer.
This book will tell you how.
Contents: Introduction – CAL in Biology – CAL in Chemistry – CAL in Engineering – CAL in Mathematics – CAL in Physics – CAL in Different Contexts – CAL and Learning Package Design – Computer Aspects – The Cost of CAL – The Evaluation of CAL
This is an essential addition to the standard repertory of teaching methods.
£11.00 0 333 23585 1

For further details contact The Publicity Department, The Macmillan Press, 4 Little Essex Street, London WC2R 3LF.

M MACMILLAN PRESS

P.A. Meyers, M.J. Leenheer, K.M. Erstfeld and R.A. Bourbonniere **Changes in spruce composition following burial in lake sediments for 10,000 yr** 534

A. Tait **Evidence for diploidy and mating in trypanosomes** 536

M. Philipp, R.M.E. Parkhouse and B.M. Ogilvie **Changing proteins on the surface of a parasitic nematode** 538

D.W. Metzger, A. Miller and E.E. Sercarz **Sharing of an idiotypic marker by monoclonal antibodies specific for distinct regions of hen lysozyme** 540

T. Paavonen and P. Häyry **Effect of cyclosporin A on T-dependent and T-independent immunoglobulin synthesis *in vitro*** 542

R.G. Miller **An immunological suppressor cell inactivating cytotoxic T-lymphocyte precursor cells recognizing it** 544

S.W. de Laat, L.G.J. Tertoolen, A.W.C. Dorresteijn and J.A.M. van den Biggelaar **Intercellular communication patterns are involved in cell determination in early molluscan development** 546

M. Dam Trung Tuong, M. Garbarg and J.C. Schwartz **Pharmacological specificity of brain histamine H_2-receptors differs in intact cells and cell-free preparations** 548

Z. Lando, D. Teitelbaum and R. Arnon **Induction of experimental allergic encephalomyelitis in genetically resistant strains of mice** 551

K. Fukada **Hormonal control of neurotransmitter choice in sympathetic neurone cultures** 553

L.H. Lazarus, R.I. Linnoila, O. Hernandez and R.P. DiAugustine **A neuropeptide in mammalian tissues with physalaemin-like immunoreactivity** 555

M.M. Winkler, R.A. Steinhardt, J.L. Grainger and L. Minning **Dual ionic controls for the activation of protein synthesis at fertilization** 558

B.K. Duncan and J.H. Miller **Mutagenic deamination of cytosine residues in DNA** 560

S. Arnott, P.J. Bond and R. Chandrasekaran **Visualization of an unwound DNA duplex** 561

W.E. Rauser and N.R. Curvetto **Metallothionein occurs in roots of *Agrostis* tolerant to excess copper** 563

MATTERS ARISING

S.K. Runcorn, W.F. Libby and L.M. Libby **Superheavy-element fission tracks in iron meteorites** 565

R.K. Bull **Reply to Runcorn *et al.*** 565

V. Canuto and T.B. Tang **Grand unification theories and the large numbers hypothesis** 566

J.D. Barrow **Reply to Canuto and Tang** 566

BOOK REVIEWS

J.S. Bell **Other Worlds: Space, Superspace and the Quantum Universe (Paul Davies)** 567

Roy M. Harrison **Zinc in the Environment (J.O. Nriagu, editor)** 568

Raymond O'Connor **Handbook of the Birds of Europe, the Middle East and North Africa: the Birds of the Western Palearctic. Vol. II. (Stanley Cramp, editor)** 568

Alastair Hay **The Science of 2,4,5-T and Associated Phenoxy Herbicides (Rodney W. Bovey and Alvin L. Young)** 569

Vincent B. Wigglesworth **The Ecology of Vertebrate Olfaction (D. Michael Stoddart)** 570

MISCELLANY

100 years ago 490

Classified advertising xv

GUIDE TO AUTHORS

- Review articles should be aimed at a relatively wide readership. Many reviews are invited, but submitted articles may also be accepted; it is advisable to consult us before writing a review article.
- Articles may be up to 3,000 words long with at most six displayed items (figures and tables); they are reports of major research developments.
- Letters are brief reports of original research of unusual and wide interest, not in general longer than 1,000 words; they have at most three or four displayed items.
- 'Matters Arising' permits short discussion (up to 300 words) of papers that have recently appeared in *Nature*.

Articles should be accompanied by an abstract of not more than fifty words. Letters should begin with a paragraph giving the background and main conclusion in terms intelligible to as wide a readership as possible.

Manuscripts may be submitted either to London or New York. Three typed copies should be submitted, each including lettered copies of figures. Typing (including references) should be double spaced. The title should be brief and informative. Pages should be numbered. References, tables and figure legends should start on separate pages. Experimental detail vital to the paper yet which would interrupt the narrative is best placed in the figure legends. Units should be identified in the margin on their first appearance. Equations should occupy single lines if possible: exp (a) is preferred to e^a if 'a' is more than one character.

References are indicated by superscripts in the text. See any contemporary *Nature* for style, but note:

(i) only one reference number need be used if the reference is to several papers by identical authors.

(ii) first and last pages of references should be cited.

Abbreviations should follow the *World List of Scientific Periodicals*, fourth edn (Butterworth, 1963-65). Symposia are often difficult to refer to and only published or soon-to-be-published volumes should be mentioned in references. Their publisher and place of publication should be clearly indicated 'Personal communication' and 'unpublished' should be incorporated in text.

Artwork should be sent with the manuscript and clearly marked with author's name and the figure number. Line drawings should be either photographic prints or in Indian ink on heavy cartridge paper, tracing paper or similar materials. Most figures are reduced to one column width so originals should be about as wide as a page of *Nature*. To enable figures, particularly maps, to be edited in the same style as the text, they should contain only essential material. ideally, an unlettered original and three lettered copies should be provided; labelling on halftones should, if possible, be avoided entirely. Magnifications quoted should be for the figures as submitted. We are always glad to see artwork for possible use on the cover, but cannot guarantee its return.

In order to save on postal expenses we return only the top copy and artwork of manuscripts that we cannot publish.

Nature's publishing policy is outlined in **258**, 1 (1975) and **264**, v, 11 Nov. (1976).

Compare:
Completeness
Capability
Cost

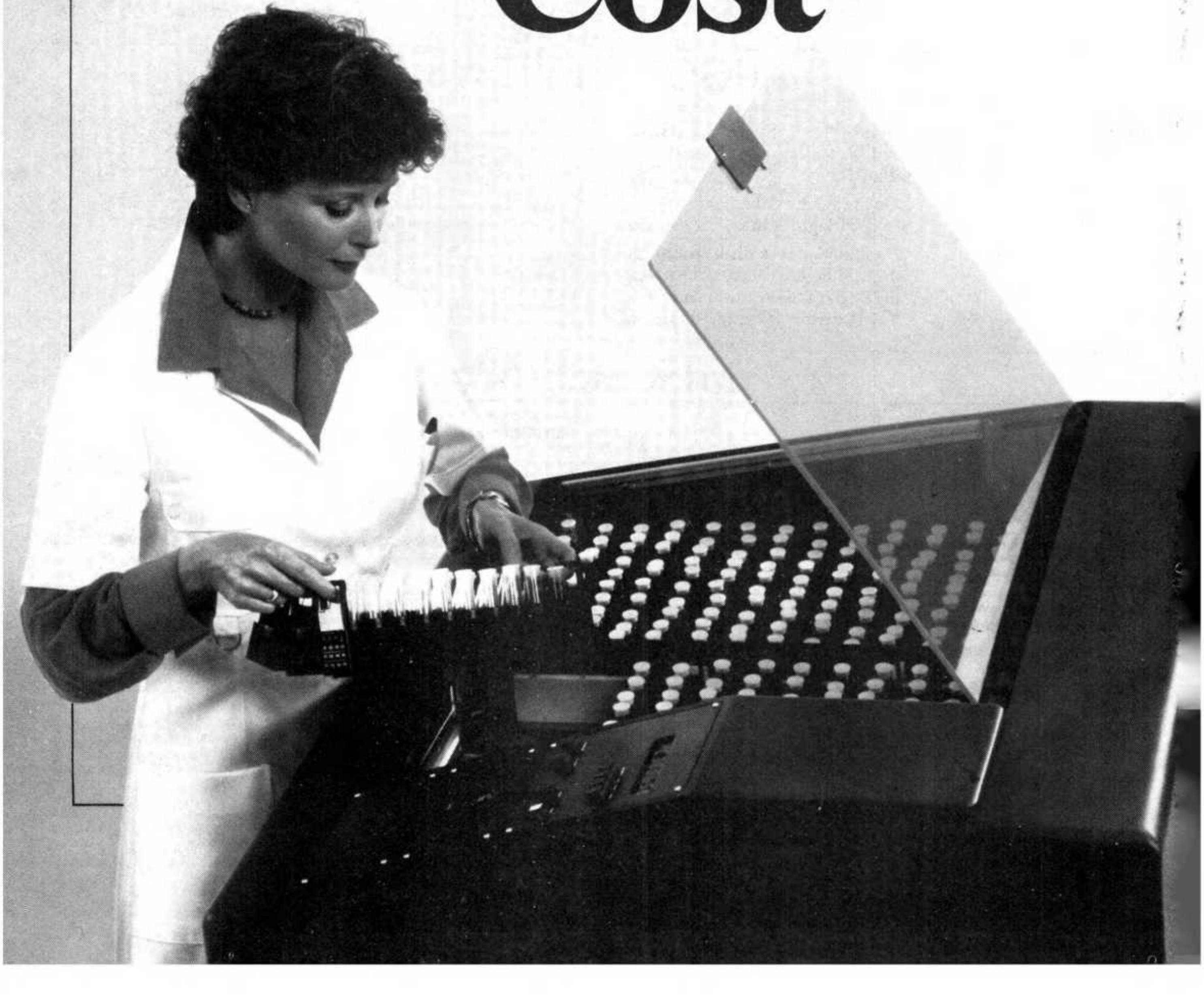

nature

Volume 287 No.5783 16 October 1980

NEWS

Towards less formal arms control? 571
The space agency's neglect of science 572
Another route to fusion to be explored: US looks hard at inertial confinement 573
Canada's uranium with strings attached 573
Swedish guidelines: Cloning committees 574
Academic freedom: Promise for Poles 575
Endangered species: Mediterranean acts 575
Biggest radio telescope in the world 575
Electric cars: Win some, lose some 576
Plates in contact 576
Nuclear wastes: Small disposals 576
Soviet cosmonautics: Cuban went up 577
Forgotten martyrs 577
Correspondence: Non-proliferation (S. Sahin); Technical innocence (R.A. Davis); Read the small print (D. Belasco); Generating costs (F.P. Jenkin) 578

NEWS AND VIEWS

Nutrition and metabolism: Mary Lindley reports a recent conference 579
Scanned image microscopy: I.R. Smith and D.A. Sinclair discuss new scanning microscope designs 580
Ash from Mt St Helens: Robert A. Kennedy describes the effects on plants 581
Gluon fusion: V. Barger on new data from CERN and Fermilab 582
On the Lost Art of Seeing where Things are Going: Simon Heywood on motion perception 583
Optical discs: A.E. Bell describes a new information storage system 583
Neuronal competition: Dale Purves on how nerve cell connections develop 585

ARTICLES

A.D.L. Sharp, P.M. Davis and F. Gray **A low velocity zone beneath Mount Etna and magma storage** 587
H.W. Bergh and D.M. Barrett **Agulhas Basin magnetic bight** 591
E.-M. Mandelkow, A. Harmsen, E. Mandelkow and J. Bordas **X-ray kinetic studies of microtubule assembly using synchrotron radiation** 595
F. Golini, B.L. Semler, A.J. Dorner and E. Wimmer **Protein-linked RNA of poliovirus is competent to form an initiation complex of translation *in vitro*** 600
W. Altenburger, M. Steinmetz and H.G. Zachau **Functional and non-functional joining in immunoglobulin light chain genes of a mouse myeloma** 603
P. Dicker and E. Rozengurt **Phorbol esters and vasopressin stimulate DNA synthesis by a common mechanism** 607

LETTERS

G. Gilmore **Is PKS1921–29 a quasar with correlated radio and optical variations?** 612
A.C. Fabian, P.E.J. Nulsen and G.C. Stewart **Star formation in a galactic wind** 613
M. Ackerman, C. Lippens and M. Lechevallier **Volcanic material from Mount St Helens in the stratosphere over Europe** 614
E.A. Spiegel and N.O. Weiss **Magnetic activity and variations in solar luminosity** 616
D.M. Willis, M.G. Easterbrook and F.R. Stephenson **Seasonal variation of oriental sunspot sightings** 617
T.J. Goreau **Frequency sensitivity of the deep-sea climatic record** 620
M. Magaritz, L. Goldenberg, U. Kafri and A. Arad **Dolomite formation in the seawater–freshwater interface** 622
T.M. Beasley and L.A. Ball **^{243,244}Cm in Columbia River sediments** 624
E.W. Domack, W.W. Fairchild and J.B. Anderson **Lower Cretaceous sediment from the East Antarctic continental shelf** 625

Contents continued overleaf

Cover: Photographs of the Earth's horizon taken during two balloon flights over France before and after the Mt St Helens eruption. Details of the aerosol layer measurements are presented on p.614.

Nature® published weekly ISSN 0028-0836
Registered as a newspaper at the British Post Office and the United States Post Office

0028-0836/80/42000C-02$01.00

Raven Press *announces a major new journal:*

Journal of Molecular and Applied Genetics

A JOURNAL FOR THE RAPID PUBLICATION OF FULL-LENGTH ARTICLES ON STUDIES UTILIZING MODERN GENETIC TECHNIQUES, ESPECIALLY RECOMBINANT DNA METHODS, TO SOLVE BASIC AND APPLIED PROBLEMS IN GENETICS, BIOCHEMISTRY, MEDICINE, AND AGRICULTURE.

Editor-in-Chief:
Howard M. Goodman, Ph.D.
Howard Hughes Medical Institute Laboratory
Department of Biochemistry and Biophysics
University of California, San Francisco
San Francisco, California 94143 U.S.A.

CALL FOR PAPERS

Manuscripts on the synthesis of biologically and medically relevant proteins, genomic organization, chromosomal gene mapping, gene structure, regulation of gene expression, molecular and biochemical studies on genetic diseases, and plant molecular biology are invited for submission. Consistent with the ideals of the International Editorial Board and of the Editor-in-Chief, only papers of the highest scientific merit and originality will be accepted. Publication will begin early in 1981.

The journal will provide generous space for inclusion of figures, and special efforts will be made to avoid excessive reduction. High quality printing on glossy coated paper will assure faithful reproduction of illustrations. The most modern computer typesetting techniques will facilitate rapid publication. The Publisher will be Raven Press, New York. All manuscripts should be submitted to the Editor-in-Chief as noted above. Instructions to contributors are available from either the Editor-in-Chief or from Raven Press, 1140 Avenue of the Americas, New York, N.Y. 10036, U.S.A.

SUBSCRIPTION ORDER FORM

TO: **RAVEN PRESS**
1140 Avenue of the Americas
New York, N.Y. 10036, U.S.A.

Date

Please enter my subscription for Volume 1 (1981) of JOURNAL OF MOLECULAR AND APPLIED GENETICS.
Published bimonthly. **Personal Subscription rates:** U.S. $80; elsewhere $90.
Institutional Subscription Rates: U.S. $135; elsewhere $145.
Air delivery is *included* for European and Mediterranean countries;
for air service *elsewhere* add $15.00.

Name (please print)

Address

Country

Postal Code

Circle No. 06 on Reader Enquiry Card.

MAG/N/10-80

LETTERS

J.E.A. Marshall and D.I. Whiteside **Marine influence in the Triassic 'uplands' 627**

M.R. Clarke, L. Maddock and E. Steurbaut **The first fossil cephalopod statoliths to be described from Europe 628**

M. Game **Best shape for nature reserves 630**

J.S. Jones and R.F. Probert **Habitat selection maintains a deleterious allele in a heterogeneous environment 632**

J.D. Tjepkema, W. Ormerod and J.G. Torrey **Vesicle formation and acetylene reduction activity in *Frankia* sp. CPI1 cultured in defined nutrient media 633**

K.-G. Rau and K. Kalthoff **Complete reversal of antero–posterior polarity in a centrifuged insect embryo 635**

A. Morris and J. Tannenbaum **Cytochalasin D does not produce net depolymerization of actin filaments in HEp-2 cells 637**

O. Mäkelä and G.W. Litman **Lack of heterogeneity in anti-hapten antibodies of a phylogenetically primitive shark 639**

M.T. Chauvet, D. Hurpet, J. Chauvet and R. Acher **Phenypressin (Phe^2-Arg^8-vasopressin), a new neurohypophysial peptide found in marsupials 640**

R.M. Sharpe and H.M. Fraser **HCG stimulation of testicular LHRH-like activity 642**

R.P. Swenson Jr **Gating charge immobilization and sodium current inactivation in internally perfused crayfish axons 644**

H. Bittiger, J. Heid and N. Wigger **Are only α_2-adrenergic receptors present in bovine retina? 645**

I.A. Hendry and C.E. Hill **Retrograde axonal transport of target tissue-derived macromolecules 647**

A.A. Herrera and A.D. Grinnell **Transmitter release from frog motor nerve terminals depends on motor unit size 649**

M. Gavish and S.H. Snyder **Benzodiazepine recognition sites on GABA receptors 651**

M. Yoshida, S. Kawai and K. Toyoshima **Uninfected avian cells contain structurally unrelated progenitors of viral sarcoma genes 653**

J.-P. Hernalsteens, F. Van Vliet, M. De Beuckeleer, A. Depicker, G. Engler, M. Lemmers, M. Holsters, M. Van Montagu and J. Schell **The *Agrobacterium tumefaciens* Ti plasmid as a host vector system for introducing foreign DNA in plant cells 654**

G.M. Cooper and P.E. Neiman **Transforming genes of neoplasms induced by avian lymphoid leukosis viruses 656**

S.H. Northrup, M.R. Pear, J.A. McCammon, M. Karplus and T. Takano **Internal mobility of ferrocytochrome *c* 659**

BOOK REVIEWS

R.C. Lewontin **Farm and Food Policy: Issues of the 1980s (by Don Paarlberg) 661**

K.A. McLauchlan **NMR of Chemically Exchanging Systems (by Jerome I. Kaplan and Gideon Fraenkel) 662**

Susan D. Iversen and Leslie L. Iversen **Chemical Influences on Behaviour (edited by K. Brown and S.J. Cooper) 663**

D.E. Brownlee **Asteroids (edited by Tom Gehrels) 664**

Peter Bryant **Beyond Universals in Cognitive Development (by David Henry Feldman) 665**

MISCELLANY

100 years ago 586

Books received 666

Classified advertising xxvi

PRODUCT REVIEW This week's product review (page xvii) covers lasers, laser components and their applications.

GUIDE TO AUTHORS

- **Review** articles should be aimed at a relatively wide readership. Many reviews are invited, but submitted articles may also be accepted; it is advisable to consult us before writing a review article.
- **Articles** may be up to 3,000 words long with at most six displayed items (figures and tables); they are reports of major research developments.
- Letters are brief reports of original research of unusual and wide interest, not in general longer than 1,000 words; they have at most three or four displayed items.
- 'Matters Arising' permits short discussion (up to 300 words) of papers that have recently appeared in *Nature*.

Articles should be accompanied by an abstract of not more than fifty words. Letters should begin with a paragraph giving the background and main conclusion in terms intelligible to as wide a readership as possible.

Manuscripts may be submitted either to London or New York. Three typed copies should be submitted, each including lettered copies of figures. Typing (including references) should be double spaced. The title should be brief and informative. Pages should be numbered. References, tables and figure legends should start on separate pages. Experimental detail vital to the paper yet which would interrupt the narrative is best placed in the figure legends. Units should be identified in the margin on their first appearance. Equations should occupy single lines if possible: exp (a) is preferred to e^a if 'a' is more than one character.

References are indicated by superscripts in the text. See any contemporary *Nature* for style, but note:

(i) only one reference number need be used if the reference is to several papers by identical authors.

(ii) first and last pages of references should be cited.

Abbreviations should follow the *World List of Scientific Periodicals*, fourth edn (Butterworth, 1963-65). Symposia are often difficult to refer to and only published or soon-to-be-published volumes should be mentioned in references. Their publisher and place of publication should be clearly indicated 'Personal communication' and 'unpublished' should be incorporated in text.

Artwork should be sent with the manuscript and clearly marked with author's name and the figure number. Line drawings should be either photographic prints or in Indian ink on heavy cartridge paper, tracing paper or similar materials. Most figures are reduced to one column width so originals should be about as wide as a page of *Nature*. To enable figures, particularly maps, to be edited in the same style as the text, they should contain only essential material. ideally, an unlettered original and three lettered copies should be provided; labelling on halftones should, if possible, be avoided entirely. Magnifications quoted should be for the figures as submitted. We are always glad to see artwork for possible use on the cover, but cannot guarantee its return.

In order to save on postal expenses we return only the top copy and artwork of manuscripts that we cannot publish.

Nature's publishing policy is outlined in **258**, 1 (1975) and **264**, v, 11 Nov. (1976).

A no-compromise solution to scanning electron microscopy

The increasing use of scanning electron microscopy in industrial research and product development calls for higher standards and degrees of quantification and improved operational versatility.

Until now however, positional geometry within the specimen environment, along with the many detectors that have to be placed around the specimen, has required an SEM (scanning electron microscope) detector compromise that often produces poor performance in at least one of the operating modes.

So Philips developed a 'no-compromise' scanning electron microscope – the SEM 505 – in which a revolutionary, fibre-optics based, Multi-Function Detector (MFD) interfaces the detecting elements with a photomultiplier/pre-amplifier assembly that can be placed outside of the specimen chamber; thus permitting high flexibility in detector placement. The result? Optimum detection performance in all modes because detection geometry is no longer limited by fixed construction or precise port location.

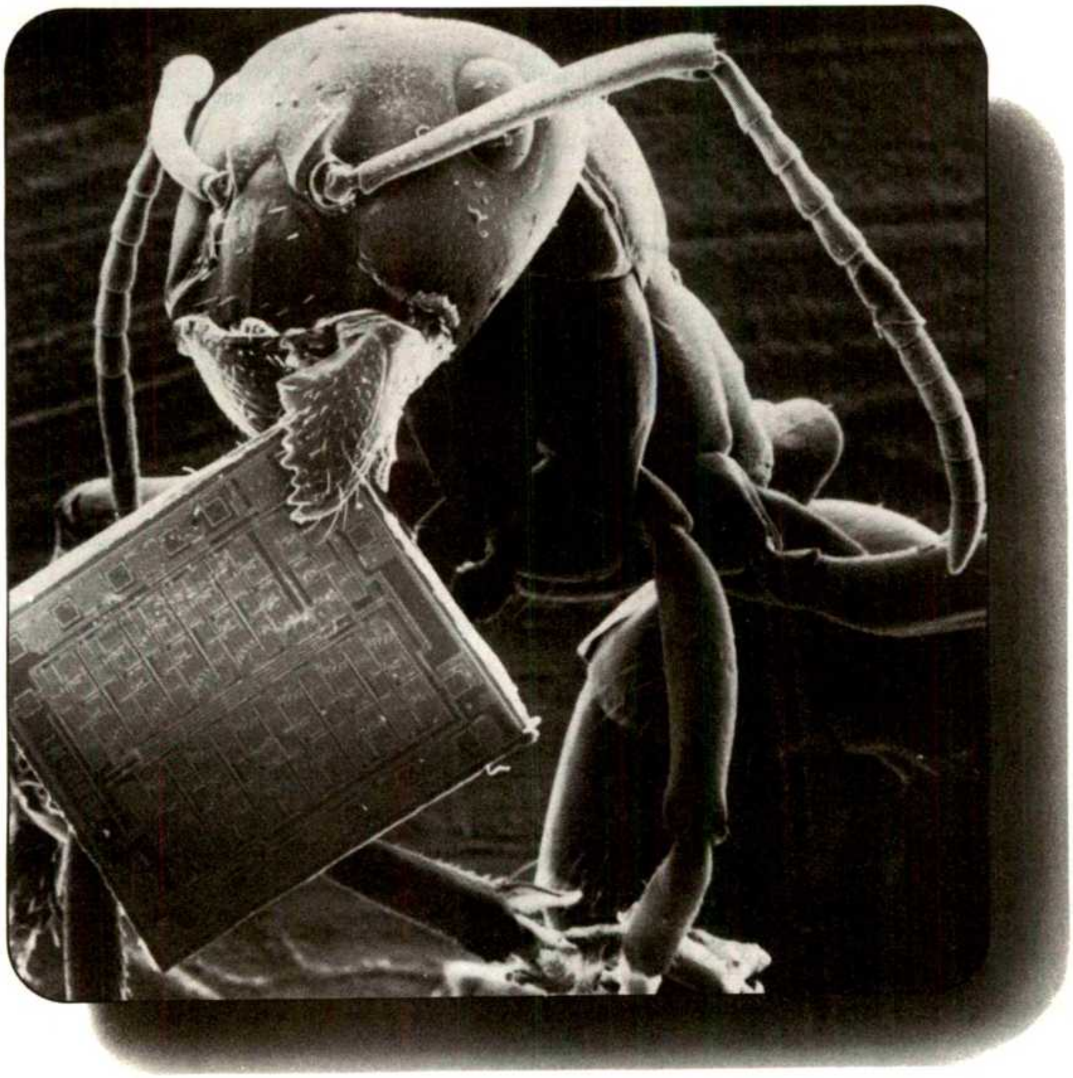

PHILIPS

nature

Volume 287 No.5784 23 October 1980

NEWS

How to change the Nobel Prize rules 667
Making British science policy by stealth 668
Reorganisation of UK medical research 669
Genentech makes splash on Wall Street 669
European universities: no room below 670
Carcinogen regulations: US labs exempt 671
1980 Nobel Prizes 671
Ariane failure known 672
Soviet science: Relations forsworn 672
Baltic oil pollution: Finns fight spill 673
Frosch moves on 673
Correspondence: Science in Spain (A. Garcia-Bellids; Nuclear electricity (J.W. Jeffery) 674

NEWS AND VIEWS

The economics and management of commercial fisheries: Robert M. May analyzes the problems 675
Roles of Rec A revealed: Steve Sedgwick on a protein with many capabilities 676
Charon's diameter: David W. Hughes describes a recent occultation measurement 677
Opioid peptides: Michael J. Brownstein on the search for the precursor molecules 678
Big Eyes: M.J. Disney looks at the problems and costs of massive new telescopes 679

REVIEW ARTICLE

M.F. Land **Compound eyes: old and new optical mechanisms** 681

ARTICLES

T.Y. Shih, A.G. Papageorge, P.E. Stokes, M.O. Weeks and E.M. Scolnick **Guanine nucleotide-binding and autophosphorylating activities associated with the p21^{src} protein of Harvey murine sarcoma virus** 686
J.R. Bedbrook, S.M. Smith and R.J. Ellis **Molecular cloning and sequencing of cDNA encoding the precursor to the small subunit of chloroplast ribulose-1, 5-bisphosphate carboxylase** 692
J. Cooke and D. Summerbell **Cell cycle and experimental pattern duplication in the chick wing during embryonic development** 697

LETTERS

P.S. Butterworth, A.J. Meadows, G.E. Hunt, V. Moore and D.M. Willis **Ultraviolet spectra of asteroids** 701
I.S. McLean and S. Tapia **Discovery of intrinsic linear polarization in SS433** 703
G. Lake and J.W.-K. Mark **Can galaxy warps be used to provide constraints on halo properties?** 705
D.H. Blake, R.M. Crutcher and W.D. Watson **Identification of the anomalous 26.131-MHz nitrogen line observed towards Cas A** 707
G.C. Gaunaurd and H. Überall **Electromagnetic spectral determination of the material composition of penetrable radar targets** 708

Contents continued overleaf

Cover: Interference micrograph of optically inhomogeneous lenses from the eye of the deep-sea crustacean *Phronima*. The optical mechanisms of compound eyes are reviewed on page 681.

Nature® published weekly ISSN 0028-0836
Registered as a newspaper at the British Post Office and the United States Post Office

0028-0836/80/43000C-02$01.00

Chromatography monitoring as simple as

A

SLIP in a 10 mm or a 3 mm optical path-length cell. These two cells make the UV-1 equally suitable for monitoring in high or low absorbance ranges.

B

SNAP in a 254 nm or a 280 nm filter. The UV-1 provides sensitive and reliable UV monitoring for the detection of proteins, polypeptides and nucleic acids.

C

FLIP a switch for measuring Absorbance or % Transmission. The absorbance setting gives a quantitative linear response at a known sensitivity range and the percent transmission ensures that all peaks remain on scale.

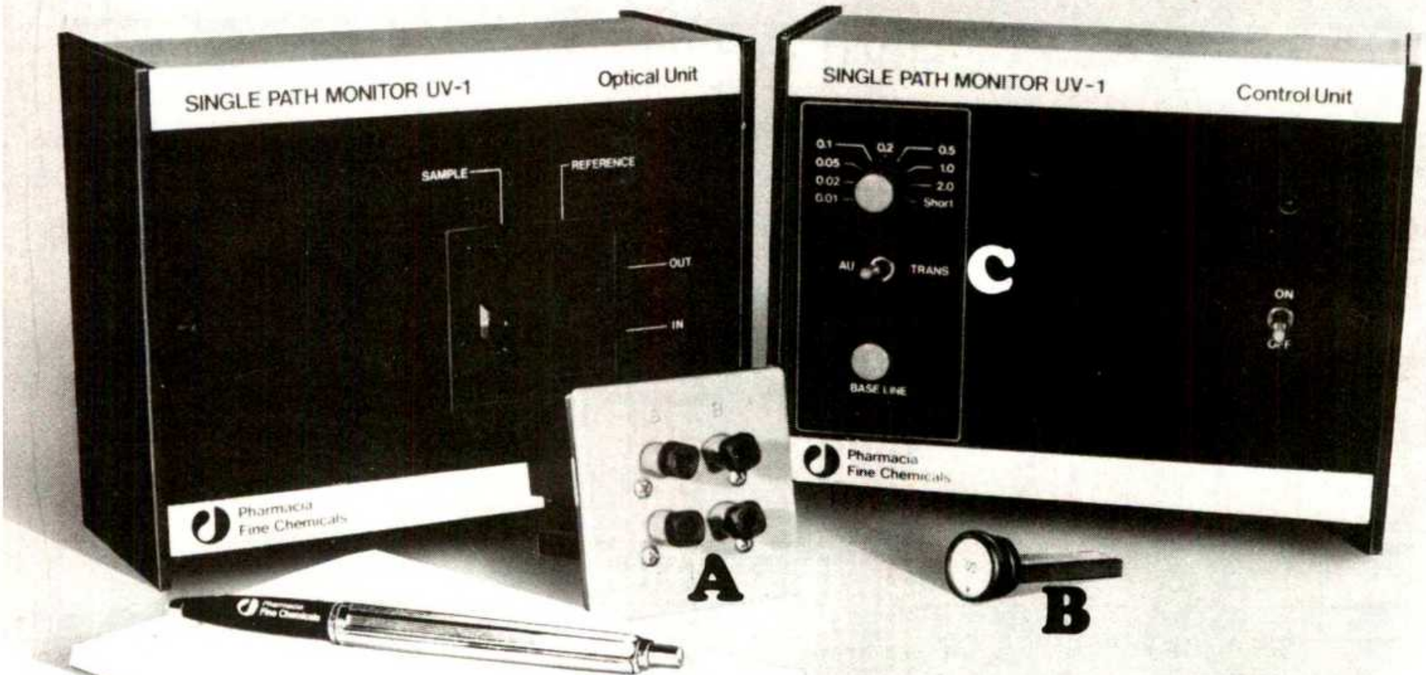

The UV-1 is a reliable, high quality, high performance dual-beam instrument that is ideally suited to your wide range of chromatographic conditions. Ask today for complete specifications on the UV-1 or on the more sophisticated dual sensitivity UV-2 monitor.

NEW! NEW! NEW! NEW!

Now also for monitoring at 214 nm. Available as a complete monitor UV-1/214 or as an optical unit to extend the standard UV-1 to 214 nm.

Pharmacia Fine Chemicals AB
Box 175
S-751 04 Uppsala 1
Sweden

Pharmacia
Fine Chemicals

LETTERS

B.B. McMahon and E.L. Simmons	**Ground-based measurements of atmospheric NO_2 by differential optical absorption**	710
J.A. Pyle and C.F. Rogers	**A modified diabatic circulation model for stratospheric tracer transport**	711
S. Cummings, J.E. Enderby, G.W. Neilson, J.R. Newsome, R.A. Howe, W.S. Howells and A.K. Soper	**Chloride ions in aqueous solutions**	714
I. Ahmad, Y.K. Chau, P.T.S. Wong, A.J. Carty and L. Taylor	**Chemical alkylation of lead (II) salts to tetraalkyllead (IV) in aqueous solution**	716
P.H. Nixon	**Kimberlites in the south-west Pacific**	718
T.J. Palmer, W.S. McKerrow and J.W. Cowie	**Sedimentological evidence for a stratigraphical break in the Durness Group**	720
L.D. Keigwin Jr	**Palaeoceanographic change in the Pacific at the Eocene–Oligocene boundary**	722
D. Kadko and L.H. Burckle	**Manganese nodule growth rates determined by fossil diatom dating**	725
R. Phillips	**Deacidification in a plant with crassulacean acid metabolism associated with anion–cation balance**	727
R.H. Smith and M.R. Shaw	**Haplodiploid sex ratios and the mutation rate**	728
A.A. Fincham	**Eyes and classification of malacostracan crustaceans**	729
M.A. Rogawski and G.K. Aghajanian	**Modulation of lateral geniculate neurone excitability by noradrenaline microiontophoresis or locus coeruleus stimulation**	731
P.A. Liebman and E.N. Pugh Jr	**ATP mediates rapid reversal of cyclic GMP phosphodiesterase activation in visual receptor membranes**	734
R.E. Gordon, P.E. Hanley, D. Shaw, D.G. Gadian, G.K. Radda, P. Styles, P.J. Bore and L. Chan	**Localization of metabolites in animals using ^{31}P topical magnetic resonance**	736
S.R. Stitch, J.K. Toumba, M.B. Groen, C.W. Funke, J. Leemhuis, J. Vink and G.F. Woods	**Excretion, isolation and structure of a new phenolic constituent of female urine**	738
K.D.R. Setchell, A.M. Lawson, F.L. Mitchell, H. Adlercreutz, D.N. Kirk and M. Axelson	**Lignans in man and in animal species**	740
K.A. Gruber, J.M. Whitaker and V.M. Buckalew Jr	**Endogenous digitalis-like substance in plasma of volume-expanded dogs**	743
M.J. Edwards and A.M.R. Taylor	**Unusual levels of (ADP-ribose)$_n$ and DNA synthesis in ataxia telangiectasia cells following γ-ray irradiation**	745
P.J. Smith and M.C. Paterson	**Defective DNA repair and increased lethality in ataxia telangiectasia cells exposed to 4-nitroquinoline-1-oxide**	747
O. Schmidt, J. Mao, R.Ogden, J. Beckmann, H. Sakano, J. Abelson and D. Söll	**Dimeric tRNA precursors in yeast**	750
S. Nakanishi, Y. Teranishi, M. Noda, M. Notake, Y. Watanabe, H. Kakidani, H. Jingami and S. Numa	**The protein-coding sequence of the bovine ACTH-β-LPH precursor gene is split near the signal peptide region**	752
R. Wing, H. Drew, T. Takano, C. Broka, S. Tanaka, K. Itakura and R.E. Dickerson	**Crystal structure analysis of a complete turn of B-DNA**	755

MATTERS ARISING

C.N. Gordon	**Leaping dolphins**	759
D. Au and D. Weihs	**Reply to Gordon**	759
R.H. Thomas, T.J.O. Sanderson and K.E. Rose	**Climatic warming of the West Antarctic ice sheet**	759
D.M. McLean	**Terminal Cretaceous catastrophe**	760
J. Smit	**Reply to McLean**	760

BOOK REVIEWS

Abdus Salam	**The Future of Muslim Civilisation (by Ziauddin Sardar)**	761
Alexander R. McBirney	**Volcanic Activity and Human Ecology (edited by P.D. Sheets and D.K. Grayson)**	762
F.D. Kahn	**Star Formation (by I. Appenzeller, J.L. Lequeux and J. Silk)**	763
R.T. Stewart	**Introduction to Solar Radio Astronomy and Radio Physics (by A. Kruger)**	763
J.T. Enright	**Time in Animal Behaviour (by M. Richelle and H. Lejeune)**	764

MISCELLANY

Corrigenda	758
Errata	758
Books received	765
Classified advertising	xiii

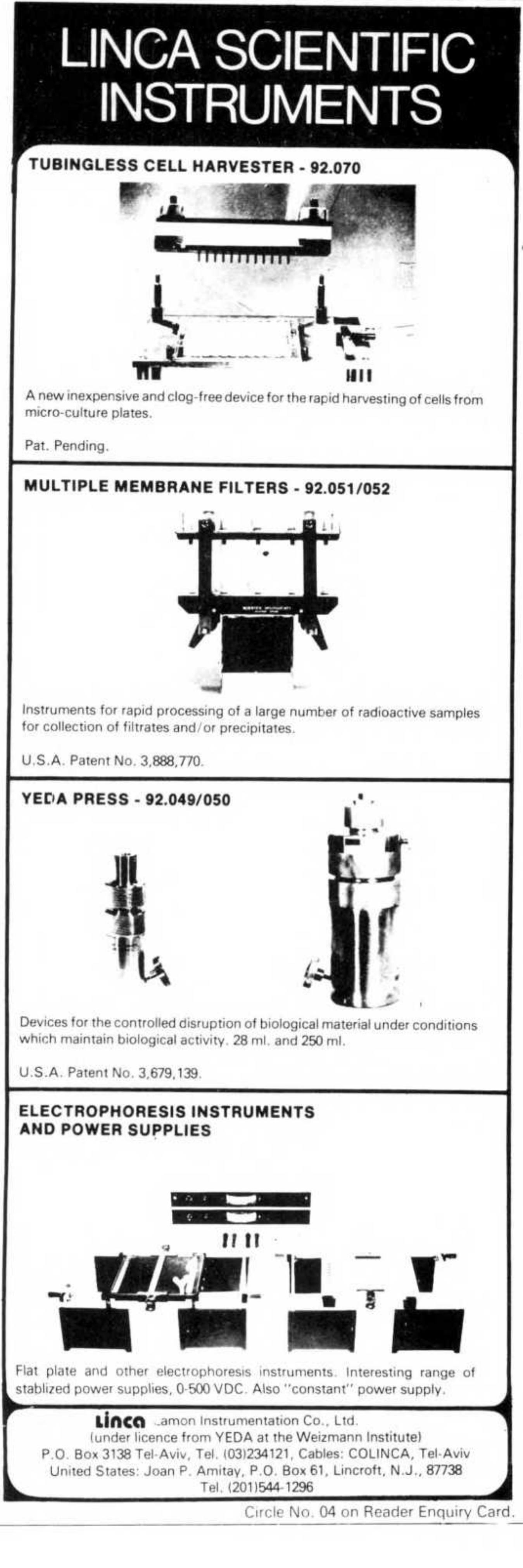

LINCA SCIENTIFIC INSTRUMENTS

TUBINGLESS CELL HARVESTER - 92.070

A new inexpensive and clog-free device for the rapid harvesting of cells from micro-culture plates.

Pat. Pending.

MULTIPLE MEMBRANE FILTERS - 92.051/052

Instruments for rapid processing of a large number of radioactive samples for collection of filtrates and/or precipitates.

U.S.A. Patent No. 3,888,770.

YEDA PRESS - 92.049/050

Devices for the controlled disruption of biological material under conditions which maintain biological activity. 28 ml. and 250 ml.

U.S.A. Patent No. 3,679,139.

ELECTROPHORESIS INSTRUMENTS AND POWER SUPPLIES

Flat plate and other electrophoresis instruments. Interesting range of stablized power supplies, 0-500 VDC. Also "constant" power supply.

Linca Lamon Instrumentation Co., Ltd.
(under licence from YEDA at the Weizmann Institute)
P.O. Box 3138 Tel-Aviv, Tel. (03)234121, Cables: COLINCA, Tel-Aviv
United States: Joan P. Amitay, P.O. Box 61, Lincroft, N.J., 87738
Tel. (201)544-1296

Circle No. 04 on Reader Enquiry Card.

© 1980 Macmillan Journals Ltd
Nature® is published weekly
ISSN 0028-0836
Registered as a newspaper at the
British Post Office

London
4 Little Essex Street, WC2R 3LF
Telephone: (01) 836 6633 Telex: 262024
Telegrams: Phusis London WC2R 3LF

Editor: John Maddox
Deputy Editor: Peter Newmark
Editorial Staff
Alun Anderson
Philip Campbell
Isobel Collins
Konrad Guettler
Tim Lincoln
Mary Lindley
Naomi Molson
Sara Nash
Peta Pickering
Judy Redfearn
Miranda Robertson
Robert Walgate
Charles Wenz
Jonathan Wolfe
Publishing Director: Christopher Paterson
Marketing Director: Ray Barker

New York
15 East 26 Street, New York, NY 10010
Telephone: (212) 689 5900 Telex: 668497
Robert Ubell (American Publisher)
and Sheila Kane

Washington News Bureau
801 National Press Building, DC 20045
Telephone: (202) 737 2355 Telex: 64280
David Dickson (Washington News Editor)

International Advertising Manager:
Richard Webb (London) (01) 836 6633

USA Advertising Manager
Henry Dale (New York) (212) 689 5900

Classified Advertising:
4 Little Essex Street, WC2R 3LF
Telephone: (01) 836 6633

Classified(USA)
Terence Miller, Suite 832, 50 Rockefeller Plaza,
New York, NY 10020—(212) 765 5758

Display and Classified(Canada)
Peter Drake, 32 Front Street West,
201 Toronto, Ontario M5J IC5
(416) 364 1623

Advertising Representatives in USA
Display
Nature New York Office—(212) 689 5900
Media Group, Inc. (Dallas)—(214) 631 4480
Didier & Broderick, Inc. (Chicago)—
(312) 498 4520
Jobson/Jordan/Harrison/Schulz, Inc.
(San Francisco) (415) 392 6794 (Los Angeles
& Pasadena) (213) 796 9200
Daniel Adams Associates, Inc.
Philadelphia—(215) 353 6191
CEL Associates (Boston)—(617) 383 6136
Brinker & Brinker (Fort Lauderdale)
(305) 771 0064

German Advertising Representative
E. Meckelburg, 6450 Hanau 1, Jahnstrasse 15,
West Germany Tel:— (49) 61 8115343

Japanese Advertising Representative
Orient Echo Inc.
11th Fl, Sankyo Bldg. 7-12, Tsukiji 2-Chome,
Chuo-Ku, Tokyo, Japan, Tel: 541-4923.

Annual Subscription including Index

UK & Eire		£75
USA & Canada	Surface only	US$173
Belgium	Airspeed only	BF5695
West Germany	Airspeed only	DM360
Netherlands	Airspeed only	G390
Switzerland	Airspeed only	SF330
Rest of Europe	Airspeed only	£85
Rest of World	Surface	£85
Rest of World	Airmail	£130
(not USA, Canada & Europe)		

Single copy (post-paid); UK, £2.00; USA & Canada, US$6.00 (surface), US$8.50 (air); Rest of World, £2.50 (surface), £3.50 (air).

Orders (with remittance) to:
Macmillan Journals Ltd, Brunel Road,
Basingstoke, Hants RG21 2XS.
Telephone: Basingstoke (0256) 29242

Nature is published weekly, except the last week in December, by Macmillan Journals Ltd. Second-class postage paid at New York, NY 10010 and at additional mailing offices.
US Postmaster, please send form 3579 to:
Nature, 15 East 26 Street, New York, NY 10010.

Vol. 287 No. 5784 23 October 1980

COLLEGE
Circular
CALCUTTA

nature

Volume 287 No.5785 30 October 1980

NEWS

Why bother to rehabilitate Galileo? 767

Solutions for transatlantic universities? 768

More commercial genetic manipulation: Harvard and Biogen establish labs in Cambridge 769

Few complaints on education 769

UK higher education: Commons take stock 770

European Space Agency: Supposing stability 771

Huxley for PRS 771

Indian laboratories: Back to GO 771

NIH research grants: Trying new tricks 772

Polish academy: Flexing muscle 772

No stay for badgers 772

European community: Research without end 773

China plays profit 773

Dangerous pathogens: New UK committee 774

Soviet geophysics: Drilling deeper 774

Uranium deposits: France backs basics 774

NEWS AND VIEWS

Jupiter's magnetosphere: S.W.H. Cowley on the new results from the Voyager spacecraft 775

Iron deprivation as a biological defence mechanism: Thomas Emery describes the role of siderophores 776

The development of animal segments: Gerald Schubiger looks at mutations which affect segment patterns 777

Cosmic spherules: David W. Hughes on their origins 778

The Santorini eruption: Jörg Keller describes the effects on Minoan Crete 779

Global dendroclimatology in sight: A. Barrie Pittock reports a recent conference 780

REVIEW ARTICLE

T.L. Blundell and R.E. Humbel **Hormone families: pancreatic hormones and homologous growth factors** 781

ARTICLES

R. Hutchison, A.W.R. Bevan, S.O. Agrell and J.R. Ashworth **Thermal history of the H-group of chondritic meteorites** 787

D.W. Sears, J.N. Grossman, C.L. Melcher, L.M. Ross and A.A. Mills **Measuring metamorphic history of unequilibrated ordinary chondrites** 791

C. Nüsslein-Volhard and E. Wieschaus **Mutations affecting segment number and polarity in *Drosophila*** 795

J.G. Sutcliffe, T.M. Shinnick, N. Green, F.-T. Liu, H.L. Niman and R.A. Lerner **Chemical synthesis of a polypeptide predicted from nucleotide sequence allows detection of a new retroviral gene product** 801

LETTERS

P.C. Gregory and G.G. Fahlman **An extraordinary new celestial X-ray source** 805

F. Seward, J. Grindlay, E. Seaquist and W. Gilmore **Diffuse X-ray emission from the jets of SS433** 806

O.H.W. Siegmund, P.W. Sanford, I.M. Mason, J.L. Culhane and R. Cockshott **Light from electron avalanches and background rejection in X-ray astronomy** 808

M.R. Issa, P.A. Riley, A.W. Strong and A.W. Wolfendale **Distribution of cosmic-ray electrons in the Galaxy** 810

J.W. Belcher and R.L. McNutt Jr **The dynamic expansion and contraction of the jovian plasma sheet** 813

M.D. Desch **Io control of jovian radio emission** 815

Contents continued overleaf

Cover: The segmental pattern in different mutants of *Drosophila*. The successful identification of the major gene loci affecting segment development is described on page 795.

M

© 1980 Macmillan Journals Ltd

Nature® published weekly ISSN 0028-0836
Registered as a newspaper at the British Post Office and the United States Post Office

0028-0836/80/44000C-02$01.00

Anti hLH Anti hCG Anti hAFP

MONOCLONAL ANTIBODIES

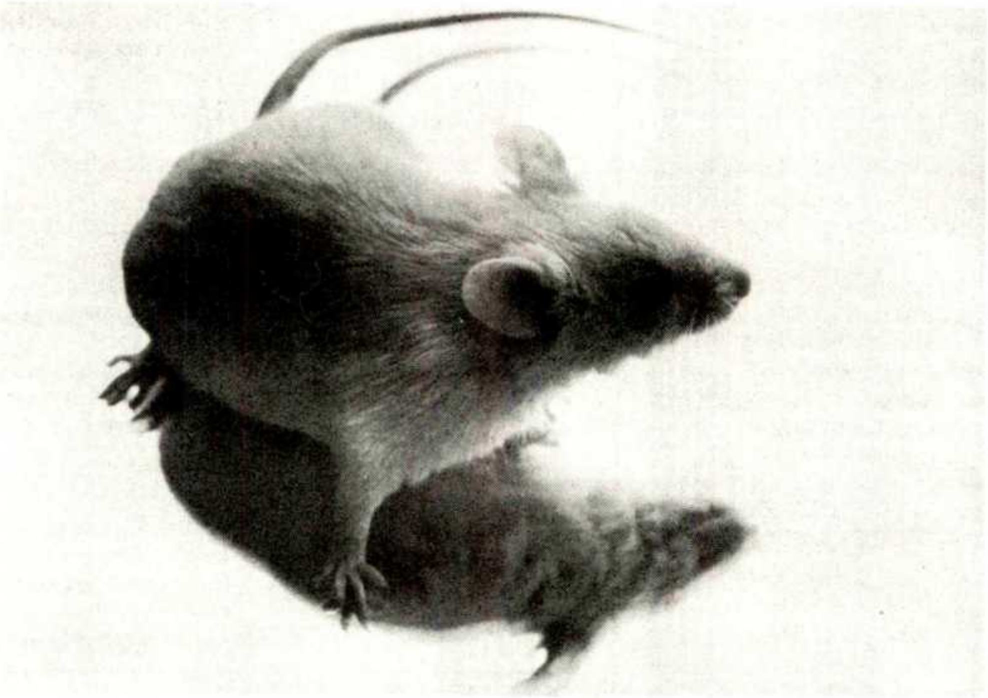

Medix has developed monoclonal antibodies produced by hybridoma cell lines. Our profound experience in these techniques enables us to produce large amounts of truly monoclonal antibodies always having indentical properties.

AVAILABLE
Anti hLH Anti Human Luteinizing Hormone
Anti hCG Anti Human Chorionic Gonadotropin
Anti hAFP Anti Human Alpha-Fetoprotein
Suitable for immunoassays,
affinity chromatography,
immunohistochemistry etc.

Medix is continuously developing new monoclonal antibodies. We are also ready to discuss preparation of special monoclonal antibodies for customers.

For further information:

MEDIX

OY MEDIX AB, PB 819, SF-00101 HELSINKI 10, FINLAND
tel. 358-0-5050155, telex 123367 medix sf

In USA contact:
MONOCLONAL
ANTIBODIES, INC.
719 Colorado Avenue
Palo Alto, CA 94303, USA
(415) 327-2204

Circle No. 10 on Reader Enquiry Card.

LETTERS

E.R. Rambaldi, D.W. Sears and J.T. Wasson	**Si-rich Fe-Ni grains in highly unequilibrated chondrites**	**817**
S. Weiner, Z. Kustanovich, E. Gil-Av and W. Traub	**Dead Sea Scroll parchments: unfolding of the collagen molecules and racemization of aspartic acid**	**820**
K.A. Rahn, E. Joranger, A. Semb and T.J. Conway	**High winter concentrations of SO_2 in the Norwegian Arctic and transport from Eurasia**	**824**
A.J.B. Winter	**The UK wave energy resource**	**826**
P.R. Thompson and N.J. Shackleton	**North Pacific palaeoceanography: late Quaternary coiling variations of planktonic foraminifer *Neogloboquadrina pachyderma***	**829**
P.E. Powell, G.R. Cline, C.P.P. Reid and P.J. Szaniszlo	**Occurrence of hydroxamate siderophore iron chelators in soils**	**833**
J.A. Duddridge, A. Malibari and D.J. Read	**Structure and function of mycorrhizal rhizomorphs with special reference to their role in water transport**	**834**
B.G. Campbell, M.H. Amini, R.L. Bernor, W. Dickinson, R. Drake, R. Morris, J.A. Van Couvering and J.A.H. Van Couvering	**Maragheh: a classical late Miocene vertebrate locality in northwestern Iran**	**837**
K. Sander, M. Lohs-Schardin and M. Baumann	**Embryogenesis in a *Drosophila* mutant expressing half the normal segment number**	**841**
N.S. Krieger and A.H. Tashjian Jr	**Parathyroid hormone stimulates bone resorption via a Na–Ca exchange mechanism**	**843**
P. Grant and E. Rubin	**Disruption of optic fibre growth following eye rotation in *Xenopus laevis* embryos**	**845**
R.W. Baughman and C.D. Gilbert	**Aspartate and glutamate as possible neurotransmitters of cells in layer 6 of the visual cortex**	**848**
C. Holt	**Cell movements in *Xenopus* eye development**	**850**
A. Ruck, S. Kramer, J. Metz and M.J.W. Brennan	**Methyltetrahydrofolate is a potent and selective agonist for kainic acid receptors**	**852**
K.A. Smith, K.J. Gilbride and M.F. Favata	**Lymphocyte activating factor promotes T-cell growth factor production by cloned murine lymphoma cells**	**853**
B. Sredni and R.H. Schwartz	**Alloreactivity of an antigen-specific T-cell clone**	**855**
L.N. Castor	**A G_1 rate model accounts for cell-cycle kinetics attributed to 'transition probability'**	**857**
C.O. Lee, A. Taylor and E.E. Windhager	**Cytosolic calcium ion activity in epithelial cells of *Necturus* kidney**	**859**
L. Samson and J.L. Schwartz	**Evidence for an adaptive DNA repair pathway in CHO and human skin fibroblast cell lines**	**861**
M. Nishikawa, T. Tanaka and H. Hidaka	**Ca^{2+}-calmodulin-dependent phosphorylation and platelet secretion**	**863**
B.B. Aaron and J.M. Gosline	**Optical properties of single elastin fibres indicate random protein conformation**	**865**
S. Marchese-Ragona and M.E.J. Holwill	**Motile flagellar axonemes with a 9 + 1 microtubule configuration**	**867**
A. Jimenez and J. Davies	**Expression of a transposable antibiotic resistance element in *Saccharomyces***	**869**
M.G. Cherian	**Chelation of cadmium with BAL and DTPA in rats**	**871**

BOOK REVIEWS

Patrick D. Wall	**Celestial Lancets: A History and Rationale of Acupuncture and Moxa (by Lui Gwei-Djen and Joseph Needham)**	**873**
C.F. Wells	**Basic Chemical Kinetics (by H. Eyring, S. H. Lin and S. M. Lin)**	**874**
Freda Newcombe	**Neuropsychology of Left-handedness (edited by J. Herron)**	**874**
Arthur T. Winfree	**The Timing of Sleep and Wakefulness: On the Substructure and Dynamics of the Circadian Pacemakers Underlying the Wake-Sleep Cycle (by J. T. Enright)**	**875**
R.J. Tayler	**Theory of Stellar Pulsation (by J. P. Cox)**	**876**

MISCELLANY

100 years ago	780
Errata	872
Books received	877
New on the market	xviii
Classified advertising	xix

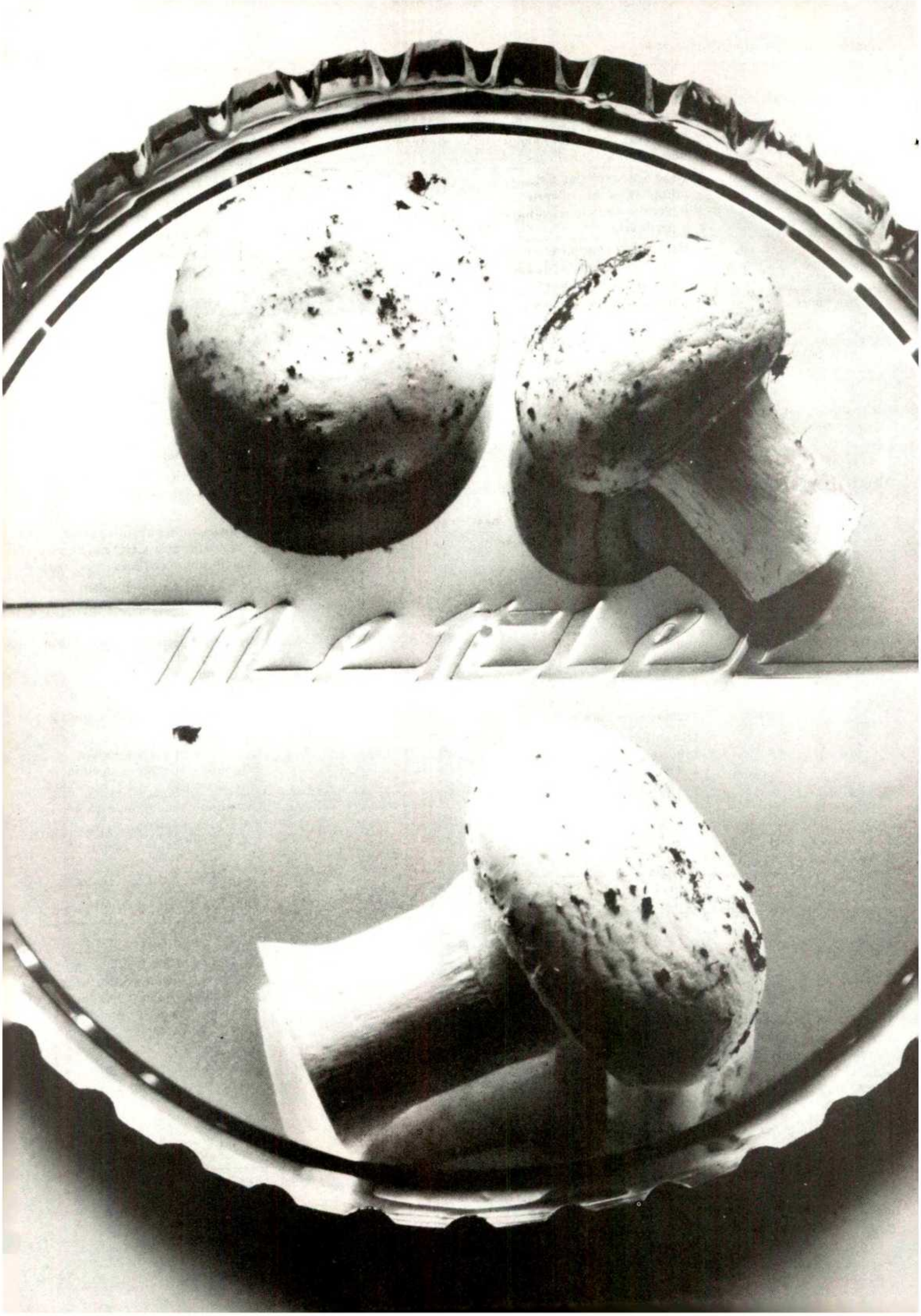

Mettler

nature

4 September 1980

Future for unprofessional societies

One of the curious attributes of the English speaking world is its rich endowment of societies dedicated to advancement of science. The oldest among them have their roots at the end of what the historians call the Age of Improvement, the period spanning the end of the eighteenth century and the beginning of the industrial revolution. People all over the world then imagined prosperity could indeed be wrung from the careful application of technology and that profound social transformation might thus be brought about. The Napoleonic War appeared not to stifle optimists in Britain, while the haunting social dilemmas of the mid-nineteenth century had not been foreseen. What more natural then that people of goodwill should band together in societies for the development of science and technology? The result, still apparent, was the creation of a host of informal scientific societies as different as the Royal Institution (in London) and the American Philosophical Society (in Philadelphia) on the one hand and the British and American Associations for the Advancement of Science on the other. Although, with the passage of time, that part of the original role of these societies concerned with the communication of original science has now been taken over by the professional disciplinary societies that abound, many of them continue and even flourish. Why should this be and what role do they have to play in the decades ahead?

These questions are prompted by the arrival of the season in which the societies for the advancement of science hold their annual conferences. The British Association is meeting this week in the city of Salford (often wrongly called the slummy part of Manchester; the two cities, although contiguous, are constitutionally independent). The American Association will be meeting next January in Toronto, thereby demonstrating that the days have long since gone when members of the British Association would take to ships to hold their annual meetings in distant parts of the British Commonwealth. Instead, the example of the British Association has spawned similar organizations in India, Australasia and South Africa. In the next few months these informal societies will also be holding their annual meetings, somewhat formless gatherings attended by a few thousand people (but the organizers always hope for even more). The perpetuation of these ceremonies, even though they play no significant part in the exchange of information between professional scientists, is a sign that they must serve some purpose. What can that be? How might it be strengthened?

Casual observation, as at Salford this week, suggests several entirely beneficial functions of the unprofessional societies, of which the chief is that they are genuinely unprofessional. They provide the opportunity for people with diverse interests in science to hob-nob with people straight from the laboratory, and thus to learn a little more directly than would otherwise be possible what is happening at at least some parts of what Vannevar Bush called "the endless frontier". To be sure the frontier is covered only patchily at these huge gatherings, which also unhappily provide opportunities for the announcement of "discoveries" that would not filter through the usual refereeing processes by which articles in the scientific journals are judged. On balance, however, the opportunity to learn about science from at least some horses' mouths is much valued by those who attend the meetings and is also a wider public service. Many of the participants are people who teach in schools, or who are similarly isolated from the part of the scientific profession in which they learn their trade; nobody will dispute the importance of any means that helps such people to stay in touch. In recent years, all the unprofessional societies, but the British Association in particular, have also found that young people — students and would-be students — have been the most lively participants at annual meetings. This is yet another sign that the unprofessional societies perform a valuable social function. The suggestion that the annual meetings might also lead to more general enlightenment through the general press is now less true than in the past; most newspapers regard their responsibility with continual seriousness and do not require such meetings to maintain their awareness. Even so, the unprofessional societies obviously render a service both to their members and, in some ill defined way, to the larger public. Why not, in the circumstances, let them get on with what they consider their business in the way they think best?

Unfortunately, that is too much to ask. To the extent that the unprofessional societies ask that public attention should be paid to what they do, public interest in how they set about their work is unavoidable. The case of the British Association is especially difficult, for since the Second World War, the Association has been living from hand to mouth, badly equipped for the job it seeks to do, too dependent on the goodwill and generosity of the cities (and their universities) in which it seeks to hold its annual meetings and on industrial companies and local authorities for the funds to support its regional activities and, most recently, on public funds (administered by the Royal Society) for the cost of running its tiny central office. On the half-a-dozen occasions in the past three decades, on which the cry of threatened bankruptcy has been heard, the Council of the British Association has resolved that radical changes of some kind must be made. And then, perhaps just too soon, funds have appeared from somewhere and have ensured that the changes made are neither radical nor, as it happens, effective. The result is that the British Association stumbles on, from one annual meeting to the next (or, with luck, the next but one) with a part-time Chief Executive Officer and an organization designed to ensure that decisions are made only slowly and half heartedly.

On the face of things, at least, the American Association for the Advancement of Science (AAAS) is in much better shape. Over the years, it has become a successful publisher, first of the distinguished scientific journal *Science* (whose 100th anniversary falls this year) but more recently of the popular journal, *Science 80*. With such a sheet anchor, the AAAS can provide for its own housekeeping and is even strong enough to compete for grants from federal agencies to enquire into matters as different as the renewal of the school science curriculum and the ethical problems (such as they may be) of new techniques in biology and medicine. With this financial symbiosis between its publishing and its public service the AAAS is relatively immune from outside criticism. Yet the organization is not nearly as successful as it might be. Like its British equivalent, the American association is hamstrung by the way in which its organization is built around a notion that there should be different sections of the society for the various disciplines that are from time to time invented. There is, of course, nothing wrong with the concept of disciplines within science but it is especially incongruous that disciplinary interests should be so firmly entrenched in societies claiming that they are essentially interdisciplinary. The fact that the officers of the hosts of sectional committees of the AAAS are elected publically, not nominated by taps on the shoulders from old chums in the British way, does not make the American organization more flexible, but the opposite. The outcome in both cases is that the societies for the advancement of science are usually too slow off the mark in

0028-0836/80/36001-02$01.00

causes that might help to advance science, too inhibited (by their constitution) even from having views on many important matters and yet, paradoxically, whimish — too much inclined to react unpredictably to changing circumstances and changing needs.

This complaint, harsh though it may seem to the devoted people who work hard at making the unprofessional societies function, is, nevertheless, quite fair. For what, in the past few years, have these societies done to help resolve some of the important problems in their declared fields of interest? Issues such as the hazards (if any) of genetic manipulation, public policy on nuclear power and even public policy towards the universities, may have been mentioned at the annual meetings of the British and American societies, but neither organization have used the diversity of its membership hammer out possible solutions. Providing a forum for opposing views on such issues is much easier, but also much less valuable, than attempting to resolve conflicts of opinion in ways that will carry conviction in and outside the scientific profession. Providing opportunities at the annual meetings for well known people to put their well known views on grand subjects such as "Energy", "Population" or "Food" is similarly a largely unproductive enterprise. So how should the unprofessional societies put their houses in order? The most urgent need is that they find a way of tackling problems that at present impede the advancement of science — for one example see below. Organizations that cannot constitutionally have a view on issues such as the organization of research or the safety of nuclear power (and which may not even have studied them) can no longer claim to assist the advancement of science. The unprofessional societies have also been known to make links with their unprofessional constituencies — school teachers, industrial scientists and the like; this, however, is a task that could and should be tackled. (Both the Americans and the British societies will protest that many of their members are teachers, but that is not the same thing.) To accomplish these and other goals will undoubtedly require that the organizations themselves should change, perhaps substantially, but there is no reason to suppose that the change need be so drastic that the valuable aspects of what they do at present would be jeopardized.

Public-key cryptography muddle

The National Science Foundation and the National Security Agency in the United States are making a frightful muddle for themselves by their new policies on academic research in cryptography, made public last week. This is not the first time that there has been trouble between academic cryptographers and the United States Intelligence Agencies. Four years ago there was a minor storm when it turned out that an official of the security agency had written to the (American) Institute of Electrical and Electronic Engineers suggesting that articles on the design of new codes should not be published in the interests of security. Eventually, the row died down only when the official concerned was said to have written in a personal capacity. The latest development is more serious. The National Science Foundation and the National Security Agency have apparently reached an understanding on the processing of future research grant applications in cryptography. The National Security Agency will, it seems, now see all applications in the field that may be sent to the National Science Foundation and will, if it thinks fit, back good projects with its own funds. One consequence may be that more funds are available for research cryptography, which might lift the spirits of the academics in this field. Another is that the National Security Agency may attach to research grants the condition that the results should not be published without prior agreement from the intelligence people, a prospect that will dismay academics.

Is all this, then, a sinister plot to muzzle scientific research in the absence of legal instruments or 'classified' data as in the years immediately after the war? This is one reading of the new arrangement. Whatever the objectives of the National Security Agency the most likely consequence of the Washington agreement will be to make a monkey of the two partners, the National Science Foundation and the National Security Agency. The pace of academic research in this novel field is unlikely to be impeded. Publication, it is hoped, will continue without hindrance. And nobody's national security will be endangered.

What offends the intelligence people is the whole concept of public-key cryptography. They earnestly wish that it had never been invented. The notion is simply that of an unsymmetrical coding system, one in which it is not possible to infer the key for decoding a message in cypher from a knowledge of the rule by which coded messages are themselves produced from ordinary text. Consequently, with these novel codes, instructions for turning messages into codes could be published in the newspapers and it would, nevertheless, be impossible for somebody intercepting a coded message to decipher its meaning. For most people, the difficulty is that of understanding how there can be codes whose writing and reading keys cannot instantly be inferred one from the other. The demonstration theorem required to dispell this scepticism has now been amply proved, most conspicuously by Professor L. J. Adelman of the Massachusetts Institute of Technology. The feasibility of the new coding system depends on the power of their computers now in service, which can use exceedingly complicated rules to turn ordinary text into coded messages. The basis of public-key cryptography is that the unpublished reading key cannot be inferred from the publishable writing key except with such a gigantic commitment of computer power that nobody in his senses would attempt the job.

Plainly, the National Security Agency is unconvinced. How can it be, these men in dark glasses whisper to each other, that a person can write in a code but be unable to decipher his own coded message? Somebody, they suspect, is pulling their legs. And they also appear to have forgotten that unsymmetrical coding systems, like those now being developed, are precisely the instruments needed to make commercial as well as military computer systems private and immune to espionage. Hitherto, there has been no means by which, for example, banks using public telex systems to transmit confidential information can have done so except by the old-fashioned methods of classical cryptography in which the intended recipient of a message is first provided with a secret code book. With the new codes, in principle at least, the writing key can be made freely available and the recipient of coded messages, the only one with access to the reading key, will be the only one able to decipher. The same techniques can and no doubt will be used to safeguard the privacy of personal data stored in central computing systems. The commercial importance of developments such as these is so self evident and so great that now that the potential value of public-key cryptography is appreciated, nothing will prevent the commercial computer companies from working hard towards the development of practical systems. Even if funds for research are not forthcoming from the National Science Foundation, there will no doubt be eager sponsors for academic research in the field of cryptography among the potential commercial users. For many academics however, the commercial sponsorship of research may be as irksome as the possibility that publication could be restricted — as the National Security Agency may choose to do. In practice, however, the sums of money needed in these fields are not large. The importance of free publication is self evident; quite apart from the intrinsic value of the new coded system, this is also a time when interest in the new field of cryptography needs to be stimulated. Is this not eminently a field in which private foundations should step in?

Carter pledges support for research

Washington

Reversing its policies of only a few months ago, the Carter administration has pledged that, if the President is re-elected in November, it will provide sufficient extra funds for basic research to guarantee a real growth of three per cent in both 1981 and 1982.

This would be achieved by requesting from Congress an additional $600 million over the budget request already submitted for the fiscal year 1981 and which it had previously been proposed to request for 1982. The net result, according to Dr Frank Press, director of the Office of Science and Technology Policy (OSTP), will be to generate a real growth in basic research of about 11 per cent between 1978 and 1982.

The proposal to increase support for scientific research came as part of a general package of measures proposed by President Carter last Thursday, designed to revitalize the US economy through stimulating private and public investment.

Eschewing the major cuts in private taxation that have already been proposed by Republican presidential candidate Ronald Reagan, President Carter is proposing a more specifically geared programme that would reduce the tax burden on certain parts of industry and provide selective support for others.

In a speech outlining his general proposals, President Carter said that it was important to promote technological advance through support for research since it provided a large proportion of productivity growth and also "can create literally millions of jobs in the years ahead."

According to Dr Press, the precise distribution of the extra funds — about $225 million of which are expected to go for the extra support of basic research in the fiscal year 1981, which begins in October — will be discussed with leaders of the university and business research communities.

However the initiatives will include:

- Increased support for areas of "targeted" basic research with broad potential applications. Examples provided by Dr Press included the contributions of genetic research to agriculture, and the basic research necessary to support the next generation of microcomputers.
- Increased support for university-based and other "generic technology centres", proposed in last year's domestic policy review of industrial innovation, and already under active consideration in Congress.
- Greater collaboration between government and industry in promoting the long-term growth of particular industries. The model of the Co-operative Automotive Research Project, looking at basic problems in long-term automobile engineering, may be applied to other areas. Possible similar projects under consideration include cooperation with the steel industry on developing new techniques for producing highly specialized forms of steel, and with the mineral extraction industry.
- An additional $50 million will be provided to upgrade research and teaching equipment in universities. A recent report produced by the American Association of Universities showed that in the university sector, the average age of equipment was about twice that in the industrial sector. The new money, some of which was proposed in the President's original January request as part of the National Science Foundation budget but cut out in the March review, will support what Dr Press calls a "long overdue" renovation of research facilities.

Research and development investment in the private sector will also benefit from the new tax incentives which President Carter said that he proposes to introduce next year. In particular, this speeds up and simplifies the depreciation allowance on investment for research and development equipment, part of a general effort to persuade industry to invest more of what it earns in new technology.

"We are really trying to do two things

Congress falls in line on 1981 funds

Washington

With an election coming up, and few pretending that a balanced budget remains either a feasible or a desirable goal, Congress has taken several actions in the past few weeks indicating a general acceptance of the strategy of the Carter administration in support of research.

Indeed in many cases congressional actions on the research budgets of federal agencies have restored funding to the level of the original budget request put forward by President Carter in January, before being cut back in the budget review in March. Recent actions include:

Physics: Following an unsuccessful attempt by the House of Representatives appropriations committee to cut out any increase in support of basic energy sciences in the Department of Energy — which includes high energy and nuclear physics — the equivalent Senate subcommittee has proposed various increases.

In high energy physics, for example, where the administration had requested in March a total of $354 million for operating, equipment and construction costs, the House committee had recommended cutting this to $327 million. The full House, however, subsequently amended this to $343 million; and the Senate subcommittee last week agreed to propose $359 million, the original request in January.

A similar pattern of changes is seen for nuclear physics, where the administration had requested $111 million, the House agreed to $106 million, and the Senate subcommittee is proposing $113 million.

Physicists are optimistic that the Senate's actions will avoid extra delays in the construction of Fermilab's energy-doubler, and any severe cut in operating expenditure next year, both of which had been widely feared. "No one thought we could come close to these figures," said one university lobbyist last week.

Biomedical research: Although its largesse has not been as great as in previous years, the House of Representatives voted last week to raise the administration's proposed 1.7 per cent increase for basic research in the National Institutes of Health to 5.5 per cent, reaching a total of $3,616 million.

The House accepted the administration's argument that a central feature of NIH support should be maintaining the level of competitive research grants at about 5,000 awards a year. However it disagreed that training grants should be cut back in favour of research support, and much of the money added to the NIH budget will go towards postgraduate support.

National Science Foundation: The House voted last month to provide the NSF with the full $1,074 million that had been requested by the administration, although subsequently agreeing to a 2 per cent cut across the board for all the agencies listed in the composite appropriations bill which includes the NSF.

The Senate appropriations subcommittee has also accepted the administration's request recommending a budget of $1,079 million. In addition to shuffling $5 million from basic research to science education (for which the House has allocated an extra $10 million), the Senate subcommittee is proposing to add an extra $5 million to cover the increased fuel cost being experienced by the NSF's Antarctic research programme.

Department of Defense: So far, the House of Representatives has accepted most of the 20 per cent increase in defence support for basic research requested by the administration. However the equivalent Senate committee is still to act; and there are rumours that cuts of the order of $30 to $50 million — which would reduce the growth rate to the expected rate of inflation — are being considered. **David Dickson**

0028-0836/80/360003-02$01.00

with this extra money," said one OSTP official. "Firstly to help underpin the general research base of the private sector. And secondly to support research, orientated towards the products and processes that are likely to be in place in the next few years."

According to Dr Press, the commitment to additional funds will "restore and go beyond the cutbacks proposed last March, which appeared to wipe out any hope of a real growth in support for basic research in the immediate future".

So far the scientific community has given the announcement a cautious welcome, but is waiting until more specific details are announced in the President's budget request next January — if he is re-elected — before passing judgement.

Although the total amount of funds may be small in comparison with the total US research and development effort, their effectiveness will depend on the way they are packaged. According to Dr Jack Crowely of the Association of American Universities "if they are willing to make some difficult decisions and focus funds in high priority areas, then they could achieve quite a bit."

Little direct reference has been made to research funding in the platform statements of the two main political parties. However the Republican statement does refer to the need to increase support for research and development as part of a general effort to increase US military strength.

David Dickson

NIH funding

Congress control

Washington

Despite intense opposition from the biomedical research community, the House of Representatives last week passed a bill which would, for the first time, give it direct responsibility for the budgets and research programmes of nine out of the eleven National Institutes of Health.

At present only two of the institutes — the National Cancer Institute and the National Heart, Lung and Blood Institute — are covered by specific authorizing legislation. The others fall within the broad responsibilities of the Department of Health and Human Resources.

The new bill sets generous budget ceilings for the various institutes, each of which would have its budget authorized by Congress every three years. Overall, the bill recommends a 27 per cent increase in the NIH budget in 1981 to a total of $4,076 million, almost twice the budget increase proposed in the appropriations bill which was also passed last week (see page 3).

However, the implications of the legislation are that Congress will be in a position to exert more direct control over the research programmes of the nine institutes which currently are not controlled by separate legislation. And it is this which has given rise to strong opposition from universities, medical schools and professional associations.

Writing in the *Washington Post* on 25 August, for example, two days before the vote took place on the bill, the past four directors of NIH stated "We are convinced that a long-term federal commitment to research is far and away best served by permanent authority of the type contained in . . . the Public Health Service Act."

The bill has been opposed by the American Association of Medical Colleges, the Association of Professors of Medicine, and the Joint Health Committee of the Association of American Universities. It has also been the source of fierce controversy within the administration. Initially it was opposed by Health Secretary Mrs Pat Harris, who argued that existing legislation was adequate to ensure a high standard of medically important research. Subsequently, however, after various modifications to the bill, the administration agreed to support the new legislation.

NIH administrators, who had previously been among those in opposition, were instructed to hold to the party line (*Nature*, 22 May 1980). And when the bill was introduced last week by Representative Henry Waxman, chairman of the health and environment subcommittee of the House Interstate and Foreign Commerce Committee, he said that both Dr Donald Fredrickson, director of NIH, and Dr Julius Richmond, the Surgeon General, had written giving their support.

Scientists fear that, by giving Congress access to detailed decisions on research priorities, the process could become over-politicized, encouraging short-sighted mandates to explore applied uses of research at the expense of basic research. However, during last week's debate on the bill, a number of congressmen spoke of the need to be in close contact with NIH, programmes.

Despite an intense lobbying campaign by university and medical school scientists, the proposed legislation was passed in the House by 292 votes to 48. It must now be reconciled with a counterpart bill which has been approved by the Senate, promoted by Senator Edward Kennedy.

This does not create authorizing legislation for all NIH institutes, but mandates the creation of a Presidential Commission on Biomedical Research with broad responsibilities to oversee medical research priorities.

David Dickson

Soviet academics

Wasted talent

Soviet planning is still not making sufficient use of the academic potential of the country, according to V. Kirillov-Ugryumov, Chairman of the Higher Attestation Commission (*Vysshaya Atestatsionnaya Komissiya*-VAK) of the Council of Ministers of the USSR. In a *Pravda* article reviewing the work of VAK over the last five years, he pointed out shortcomings not only in VAK's work of awarding higher degrees, but also in the use made of the content of theses. The annual surveys, provided by VAK, of the content of theses and research projects, are not being utilized by the ministries and planning bodies concerned, and the recommendations made to the State Publishing Commission concerning the publication of the most interesting and significant theses are not being implemented. All this, he says, hinders the implementation of research results in the economy. The problem, moreover, is a particularly pressing one now that the country is on the threshold of the Twenty-Sixth Party Congress which will approve the directives for the next five-year plan.

Not, however, that VAK itself escapes without criticism. Six years ago the Central Committee of the Communist Party of the Soviet Union (CPSU) and the Council of Ministers of the USSR approved a resolution which overhauled the whole system of awarding higher degrees, in particular setting up a network of expert councils to assess theses submitted to them. Not all these councils, said Kirillov-Ugryumov, are functioning properly. In 1979 the presidium of VAK had to return no less than 256 works to the relevant councils since the reports on them were "insufficiently clear or well-grounded". Occasionally "ill-will" is creeping into the work of the councils, interfering with objective scientific assessment, and creating a situation resembling a court of law. Kirillov-Ugryumov goes on to decry "subjectivism and red-tape at any stage of the attestation process".

Nowhere in his article does Kirillov-Ugryumov mention a clause in the 1976 Resolution which many Soviet academics found disturbing — the stipulation that the postulants must satisfy VAK not only with the worth of their theses but also with their political record. Indeed, his criticism that certain expert councils have been letting "weak theses" through, and that steps must be taken to remedy this may well be a veiled criticism of councils which look over-leniently on the mediocre efforts of the scions of high party officials. However, a *samizdat* essay by Grigori Freiman recently republished in the West, *"It seems I am a Jew"* contains what is claimed to be a stenographic transcript of an "expert council" meeting, in which remarkable feats of dialectic are produced to find some reason, other than the postulant's Jewishness, to reject a thesis which all participants know in advance cannot be accepted. If Freiman is to be believed — and at the time of writing he was a Professor of the Kalinin State University, and a member of the CPSU — the political clause is apparently being applied under some other guise.

Vera Rich

0028-0836/80/360004-02$01.00

European coal industry

Conversion plans

Plans for commercial coal gasification plants in West Germany will be complete by December, and liquefaction plants by next autumn, the Federal Ministry for Science and Technology has announced. But because German coal is very deep and very expensive, the intention is more to take a lead in the world market for such technology, than to make much use of it in Germany. So, although the construction of 14 coal refining pilot plants costing £3 billion is under study, Research Minister Volker Hauff said last week that oil and gas derived from coal would supply only 3 per cent of Germany's oil and gas needs in 1990.

Germany was forced to develop gasification and liquefaction techniques during the Second World War to provide the country with fuel, and although the technology then became uneconomic compared with cheap Middle East oil, the industry survived through massive exports to South Africa. After a lull in the sixties, German efforts were revived by the oil price rise of 1973. The United States have since spent more on developing new approaches and principles, but Germany appears to be taking a lead with real plant. German spending on research and development of new coal technologies (including remote extraction) is high, taking the lion's share of the non-nuclear energy research programme, which in turn costs some £230 million a year including industrial participation.

In the United Kingdom, investment is nowhere near so great. British Gas has just placed the contract for one pilot gasifier, using a mix of technologies and capable of converting coal dust and lump coal, at a cost of around £14 million; but this can be set against British Gas profits of some £426 million last year alone on retailing North Sea gas. The National Coal Board (NCB) has less to spend, but has recently recommended the construction of two pilot 1 tonne per hour liquefaction plants, one using the liquid solvent extraction process and the other "super-critical gas extraction"; the cost would be £50 million shared between the NCB, British Petroleum, and the Department of Energy.

However, according to an NCB scientist, the British technology is unique in aiming to produce nearly 100% conversion of the coal into high quality transport fuels, plus some liquid petroleum gas and synthetic natural gas. The technology could provide enough impetus to resist penetration of the British market by German or US technology, and might even provide export potential. The world market in sophisticated coal technologies is expected to reach billions of pounds a year in the 1990s, when oil prices rise to a level which would make coal competitive.

Robert Walgate

Hunter turned hunted

According to the Royal Society for the Protection of Birds at least 17 young peregrine falcons were stolen from UK nests this year. With peregrines selling to falconers at up to £1,500 each, nest robbery threatens to reverse the trend towards restoration of the UK breeding population which was severely affected by organochlorine pesticides twenty years ago. Present legislation prohibits the taking but not the keeping of wild birds. But the UK government has just announced plans to legislate against keeping also; it would require all birds of prey in legal captivity to be registered and ringed.

Third World energy

World Bank aid

Washington

Substantial new funds for energy research in developing countries could be one outcome of the proposals announced by the World Bank in Washington last week to help these countries meet their rapidly escalating fuel bills.

The main focus of the Bank's proposals would be the setting up of a new capital investment fund, which would raise money from private banks and lend it to Third World countries for energy projects ranging from nuclear power stations to conservation programmes.

At the same time, however, ideas for sponsoring relevant lines of research are being discussed. One possibility is that an independent fund or institute for research in renewable energy technologies could be established, perhaps taking a cue from the international group of agricultural research centres whose support the Bank currently coordinates.

In addition to the practical problems caused by energy shortages, World Bank officials have been worried that rising energy costs have made it increasingly difficult for many developing countries to pay off their international debts.

In Brazil, for example, the cost of imported petroleum rose from 12 per cent of export earnings in 1973 to 50 per cent last year; in India the increase was from 22 to 60 per cent over the same period.

The result, according to the *World Development Report, 1980* published by the Bank two weeks ago, is that major oil-producing countries will run current account surpluses of about $110 billion in 1980, while the oil-importing, developing countries will have a combined deficit of more than $60 billion. Efforts have been under way for some time to recycle the surpluses to ease the burden on developing countries. The political importance of this was agreed at the economic summit of western leaders in Venice in June.

The World Bank has been watching the situation closely since 1977 and has started making loans for energy projects. This year, following particularly steep price rises, the Bank's president Mr Robert MacNamara asked his staff for a special report on what additional steps might be taken. This report, including sections on conservation and renewable energy sources, was recently made public.

Its main proposal is that the Bank should set up a special affiliate to raise sufficient money on the private capital market to almost double the $13 billion in loans which the Bank itself intends to make over the next five years on energy projects. This should be sufficient to seed an additional $75 billion in bilateral loans, and concessional terms might be arranged for the poorer countries.

The Bank says that many of the projects it already finances show a high return on investment, sometimes up to 30 or 50 per cent. But in many countries difficulty in raising capital has resulted in only superficial efforts to seek oil, and therefore "not enough research and money have been put into the effort to establish whether there are smaller deposits that could make important contributions to their own energy supplies".

Reversing its earlier opinon, the Bank says that it now agrees that conservation programmes offer a substantial potential for cutting back energy needs.

The proposals will be discussed when the World Bank and the International Monetary Fund meet in Washington later this month. However, it is generally believed that Mr MacNamara already has informal commitments that at least part of the money can be raised.

The precise nature of the fund, however, is still open, and so too are details of the way in which money might be used to finance research — although according to World Bank officials one of the biggest needs is the collection and evaluation of performance data about new energy

0028-0836/80/360005-02$01.00

technologies that have already been developed.

The World Bank's report refers to the need to strengthen the national energy research programmes of developing countries, in particular their capacity to adapt developments made elsewhere. And it also says that attention should be given "to the possibility of organizing international programmes on specific renewable energy technologies".

David Dickson

Meat substitutes

Fungal food

Ranks Hovis McDougall (RHM) have received qualified approval from the UK Ministry of Agriculture Fisheries and Food (MAFF) to market, for human consumption, the somewhat processed mycelia of a *Fusarium* fungus. The company has now taken the decision in principle to test whether there is a sufficient market to make a commercial success of the processed mycelia, which goes by the name of mycoprotein.

A pilot plant at RHM Research in High Wycombe, Buckinghamshire, has already produced up to 100 tons per annum of the processed mycelia, sufficient to carry out extensive toxicological and nutritional tests. These have shown that mycoprotein can be fed without ill effects to generations of laboratory animals. It has also passed a number of short-term tests on human volunteers. In nutritional terms mycoprotein compares well with meat, for which it might be a substitute. On a dry weight basis it contains 45 per cent protein — with an acceptable amino acid composition — and has a low fat (10–15 per cent, mostly unsaturated) and cholesterol content. There is also no doubt that it can be made palatable. The only questions now are whether or not its high fibre content (20–25 per cent) is as beneficial as current advocates of fibre would have it, and whether it will meet consumer resistance.

The fungus from which mycoprotein is produced is the A35 strain of *Fusarium graminearum*, a strain which has lost the pathogenicity to plants possessed by its relatives. It is grown in continuous culture at 30°C in 1,300-litre tanks with glucose-syrup as the carbon source and ammonia as the source of nitrogen. A key process follows in which the mycelia are immediately heated up to 64°C for 20 minutes. That treatment kills the mycelia, inactivates their proteolytic enzymes, so that there is no breakdown of protein, but allows the fungal ribonucleases to degrade nucleic acids into products which can be washed out of the cells. In that way the nucleic acid content of the mycelia is reduced from 10 per cent to below the acceptable upper limit of 1 per cent.

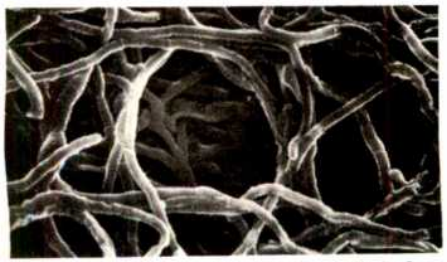

Fusarium mycelia before

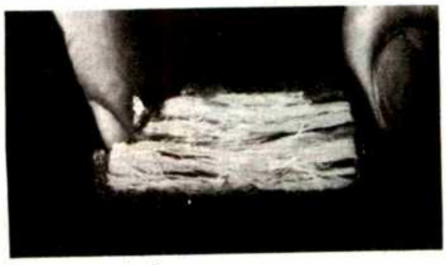

...... and after

Furthermore the rapid heat treatment of the mycelia serves to reduce turgor with the result that mycoprotein has a texture that is not dissimilar to meat fibre. With the addition of flavouring and colouring, it can be made into a passable imitation of fish, chicken, veal or ham. Without any additions it is an unpalatable, colourless, tasteless product.

Human trials of mycoprotein have been very limited so far. Two small-scale and short-term nutritional studies have been carried out by Professor N. S. Scrimshaw at the Massachusetts Institute of Technology and some larger but less rigorous tests have been completed by RHM. The only problem that has emerged is a single case of an allergic reaction to mycoprotein which RHM claim is about par for the course.

On the basis of the human and animal tests MAFF has given permission to RHM to market mycoprotein on a limited scale once a specification has been agreed upon. It has also asked for further animal work to assess the effects of mycoprotein on mineral balance. There are two concerns in that respect. The first is that mycoprotein is lacking in the minerals, particularly iron and zinc, contained in meat. And the second is that the high fibre content of mycoprotein will lead to the retention in the intestine of dietary minerals from other sources — hence a recent recommendation that soya protein for human consumption be fortified with iron

Mycoprotein is the first of its kind. Several other microorganisms are grown and processed world-wide to provide protein supplements to animal feed, but none for human consumption. Also, as Dr J. Edelman, Director of Research at RHM, is at pains to point out, most of the animal feed supplements are the product of bacteria growing on hydrocarbons, and hence classifiable as single cell protein, whereas mycoprotein is produced by a multicellular fungus growing on glucose.

The main question mark still hanging over the future of mycoprotein is whether or not the public will buy it. When the project was started RHM had their eye on the protein gap that was believed to exist in many developing countries. That gap has since been declared a myth. Consequently RHM now have their eye on the UK convenience-food market (plans to seek approval for sale in the US have been put on ice because of the attitude of the Food and Drug Administration). To break into that market with mycoprotein will be no easy matter. Psychological barriers to new foods may be surmountable if the price is right but mycoprotein can only be cheap if produced in large enough quantity. Ten thousand tons per annum (0.25 per cent of annual UK meat consumption) would be realistic for that purpose, claims Dr Edelman; one hundred thousand tons would be "a bonanza" for the "nylon of the food trade".

Peter Newmark

Culture collections

Fears for fungi

The effectiveness of Britain's main collection of non-pathogenic microfungi could be seriously reduced from March next year if £20,000 annual support cannot be found in the meantime. The collection is currently funded to the tune of approximately £60,000 per annum by the Commonwealth Mycological Institute (CMI), which houses it, and £20,000 by the Natural Environment Research Council (NERC), which has said that it will cease to pay its share early next year.

Similar problems were experienced earlier this year by the National Collection of Yeast Cultures (see *Nature*, 24 January), as a result of which an inter-Research Council committee was set up with the aim of observing and monitoring the maintenance of culture collections. The problems of the microfungi collection are the first to be investigated by the new committee. Next week, members of the committee will visit the CMI to make detailed recommendations on how the collection should be continued and whether alternative funds are needed. It will then start looking for new sources of money.

The difficulties with both the yeast and microfungi collections have arisen because they have never been permanently funded. NERC took over the bill for the microfungi collection ten years ago from the then Ministry of Trade and Industry on a temporary basis. The grant was designed to rise with inflation up to a ceiling of £20,000, a level that was reached several years ago. According to the curator of the microfungi collection, Dr Agnes Onions, the collection is already run on a shoestring and if the NERC funds are not replaced it will be impossible to fulfull all the functions of a national collection.

The collection is the main source of non-pathogenic microfungi in Britain for industry, research and educational establishments.

Judy Redfearn

0028-0836/80/360006 01$01.00

NEWS AND VIEWS

SCIENCE COLLEGE
Upper Circular Road
CALCUTTA

Active experiments in space plasmas

From Michael J. Rycroft

SPACE physicists have in recent years been able to plan and conduct 'controlled' experiments in the ionospheric and magnetospheric plasmas. In the experiments, the medium near the space vehicle is deliberately perturbed by the injection of a signal of known characteristics. The signal may be in the form of energetic charged particles; for example, electrons with a particular energy, power and pulse duration injected with an electron gun. Alternatively, the signal may be in the form of electromagnetic waves; an example is the transmitter at Siple Station, Antarctica, injecting VLF waves of known frequency, amplitude and duration. The propagation of the signals can be detected enabling the medium remote from the space vehicle to be investigated.

As a recent conference* showed, the situation is not always as simple as that initially conceived by the experimenters. Soviet Zarnitza and Franco-Soviet Araks experiments of 1975 and recent US and Canadian experiments show that the operation of a high power electron gun aboard a rocket in the upper atmosphere causes complex processes to occur. A Beam Plasma Discharge (BDP) is often initiated; in this, the electron beam develops an instability in which ionospheric electrons are accelerated by plasma (Langmuir) oscillations. If heating to energies > 15 eV occurs, collisions with neutral molecules produce secondary electrons. If the neutral gas density, including the local increase due to outgassing from the rocket body, is high enough, this process cascades. Then a hot plasma halo is formed around the rocket; this is cigar-shaped and aligned along the geomagnetic field. Detectable by a low light level television system, the halo can have a luminosity equivalent to that of a fifth magnitude star. By providing the neutralization current, the enhanced plasma density in this region prevents the rocket potential rising as high as might otherwise have been expected for large electron beam currents.

This halo region is a source of HF (up to ~ 50 MHz) radio waves, at $\sim 2 \times 10^{-20}$ $\mathrm{Wm^{-2}Hz^{-1}}$. These electromagnetic waves are believed to be produced by conversion from electrostatic waves at the large gradients of plasma density existing at the edges of this region. Swept frequency studies show that the radiation is generated preferentially at the electron cyclotron frequency and at the electron plasma frequency, and also at the upper hybrid resonance frequency which is their Pythagorean sum. Radar reflections from the region are also observed. Whistler mode radiation is detected, as are bursts of noise at the lower hybrid resonance frequency which is inversly proportional to the square root of the mean ionic mass of the plasma.

Recently, Norwegian groups have successfully used mother-daughter payloads, with a pulsed electron accelerator being mounted on the daughter and the mother bearing a number of diagnostic instruments. The dimensions of the heated region are found to be two electron Larmor radii across the geomagnetic field and several times that along it. Noise bursts are observed to be generated, not only near the lower hybrid resonance frequency but also at lower frequencies, when the rocket crosses an auroral flux tube in the presence of precipitating energetic electrons. The waves are believed to be produced locally in the region perturbed by the beam and the neutralizing return current. In this issue of *Nature* (p.15) Gough *et al.* present observations, associated with the operation of the electron gun, of 0.8–1.0 MHz electrostatic waves and 8-10 KeV auroral electrons bunched at the same frequency. Waves are excited by the beam when it is injected into the ionospheric plasma; these in turn bunch the electrons in the beam.

A new development is in the use of huge vacuum chambers, such as the 12 m by 26 m chamber at the NASA Johnson Space Center, for laboratory investigation of the behaviour of electron guns before launch. Television recordings show that for low gun currents, the emitted electrons follow helical paths in the magnetic field. As the gun current is increased, a Beam Plasma Discharge is suddenly ignited. This is seen as a spatially broad beam, having a wide distribution in energy and with considerable light output due to the increased plasma production rate. Radiation in the whistler mode and Bernstein modes is recorded, as is noise around the electron plasma frequency and the upper hybrid resonance frequency. Performing experiments related to space plasma physics in the laboratory is a very necessary adjunct to performing laboratory-type active experiments in space plasmas.

Operation of a caesium plasma generator simultaneously with the electron gun in the Araks experiment caused the upper frequency of the HF emissions to increase above 50 MHz. In the West German Project Porcupine, experiments have been carried out involving ~ 200 eV xenon plasma injection. The dynamics of the plasma jet and associated wave processes are studied using instruments on the main rocket and on sub-payloads ejected from it. Particularly interesting are plasma instabilities induced by the xenon injection; sometimes these manifest themselves as electrostatic wave bands whose frequency separation is the cyclotron frequency of protons, but sometimes it is half this frequency. These ion cyclotron harmonic waves, which are detected both as AC electric field and plasma density perturbations, extend in frequency up to at least the twentieth harmonic. The most intense signals are located close to the estimated lower hybrid resonance frequency; of course, this frequency is changed considerably by the ion injection.

With shaped-charge explosive devices aboard rockets, barium has been injected upwards at high velocity. After ionization by solar ultra-violet radiation, the ions move up the geomagnetic flux tubes. Using sensitive optical equipment on the ground, upwards acceleration has sometimes been observed to occur at a height of a few thousand km, presumably by the action of an electric field. Such an electric field would accelerate auroral electrons

---

*A symposium on 'Active experiments in Space Plasmas' was held in Budapest from 11 to 13 June, 1980 as part of the 23rd meeting of COSPAR (the Committee on Space Research) established by the ICSU in 1958. Most of the invited review and contributed papers presented at the Symposium are to be published early in 1981 by Pergamon Press as a volume in the COSPAR Advances in Space Exploration series.

Michael J. Rycroft is Head of the Atmospheric Sciences Division, British Antarctic Survey, Natural Environment Research Council, Cambridge and was a member of the Symposium's Organising committee.

0028-0836/80/360007-02$01.00

downwards.

Project Trigger was a Swedish and US experiment designed to test the response of the auroral ionosphere to the explosive release of a hot, dense caesium plasma. A transient electric field is observed, as are variations of the field aligned fluxes of charged particles from 10 eV to > 300 keV. It is concluded that the field-aligned currents associated with the electric field pulse and cloud conductivity gradient may be responsible for the observed electron acceleration in a manner similar to that leading to the formation of auroral arcs.

Disturbances to the ionosphere are also caused by the explosive release of water from rockets. The ionospheric electrons rapidly recombine, leaving a 'hole' in the ionosphere. Simultaneously the flux of primary auroral electrons decreases by two orders of magnitude, probably because of changes in the auroral 'circuit' caused by the local conductivity decrease. Similar holes in the ionosphere are introduced inadvertently by the highly reactive exhaust gases from rocket engines. The Saturn V vehicle, which launched Skylab in 1973, caused the ionospheric electron content to be halved. The launch, in 1979, of the HEAO-C satellite by an Atlas/Centuar rocket provided confirmation of the effect. The ionosphere was significantly depleted over a horizontal distance of 300 km for some hours.

Ion engine thrusters are now being developed. Using these, ions will be injected into the magnetosphere in the form of a dense, relatively cool plasma beam with a high drift speed. Their effects have not been thoroughly investigated, either observationally or theoretically. Such work is essential because, for example, plans are being made in the US to transfer a Solar Power Satellite, of ~ 10^7 kg, from low earth orbit to geosynchronous orbit using argon ion thrusters. This would deposit ~ 10^6 kg of 3.5 keV argon ions into the magnetosphere. The ~ 10^{31} argon ions would equal the natural content of the magnetosphere, but their energy content would be about a thousand times larger than that present naturally. Such plans are therefore of considerable concern to magnetospheric physicists. It is desirable that preliminary experiments using ion thrusters in the magnetosphere be carried out as soon as possible.

A complementary type of active experiment is the injection of waves into the ionospheric or maganetospheric plasma. Since the launching of the Canadian top-side sounder satellites in 1962, plasma resonances have been stimulated by antennas within the natural space plasma. However, only since 1977, with the advent of the pairs of GEOS and ISEE satellites, and with the Japanese Jikiken (EXOS-B) satellite, have such resonances been studied in the magnetosphere and solar wind. Plasma frequency and upper hybrid resonance frequency signals enable plasmaspheric electron density profiles to be derived; some of these clearly exhibit the plasmapause with attendant fine structure. Bernstein mode electrostatic resonances, the so-called f_{Qn} resonances, plus resonances at harmonics of the electron cyclotron frequency are also observed. The effects of the drifting plasma and of its non-Maxwellian distribution have to be taken into account when interpreting these signals.

In recent years, controlled experiments on the magnetosphere have been carried out using coherent VLF electromagnetic waves injected from Siple Station, Antarctica which are ducted in the whistler mode from one hemisphere to the other. When radiating above a certain power <1W–2kW), these signals exhibit growth rates ranging from 30dB s^{-1}–200 dB s^{-1}. The energy source here is the cyclotron motion of the van Allen radiation belt electrons near the equatorial plane just inside the plasmapause; in the interaction the electrons' pitch angles are reduced and they can be precipitated into the upper atmosphere. The amplified signals can trigger emmisions whose frequency varies with time. Natural emissions are 'entrained', i.e. their frequency-time evolution is dramatically changed when their frequency comes within ~ 50 Hz of that of the coherent Siple signal. Sidebands, with growth evident only in the upper sideband, are generated. Growth of the Siple signals is suppressed either by a whistler mode echo of the signal or by a superposed broadband signal. Growth of natural noise is suppressed at frequencies just less than that of the Siple signal. Unducted signals from the Siple transmitter have been observed on the ISEE and Jikiken spacecraft.Triggering of emissions is evident when the satellite is in the magnetic Northern hemisphere, that is, after the Siple signal has crossed the equatorial plane of the plasmasphere. *In situ* wave-particle interaction studies now become possible, an exciting prospect indeed.

Radiation at harmonics of the fundamental frequency of the electrical power distribution (grid) systems of the industrialised world similarly penetrates the ionosphere and propagates in the whistler mode through the magnetosphere plasma. In principle it can interact with energetic electrons in much the same way as do the Siple signals. There is considerable evidence that it does in fact do so, though more observational studies are required. The significance of this 'pollution' of the magnetosphere remains to be quantified.

There is some controversy too as to whether the occurrence of chorus is affected by power line harmonic radiation. However, studies at Halley, Antarctica, which is geomagnetically conjugate to Newfoundland where there is a mixed 50 and60 Hz power system, show that the intensity of noise of magnetospheric origin at 3.2 kHz is, on average, 0.7 dB less on Sundays than on other days of the week. In a similar vein, but at very much lower frequencies, there is evidence from a century of data that geomagnetic activity is larger, by one standard deviation, at the weekends than during the week. Recent evidence shows that 1 pc pulsations of the geomagnetic field decrease when the DC operated San Francisco Bay Area Rapid Transit train system is operating. Could it be that the growth of ULF coherent waves, by a cyclotron resonance interaction with ions in the magnetosphere, is inhibited by ULF noise of man-made origin?

An HF transmitter, with an effective radiated power > 100 MW, has recently been constructed in northern Norway by West Germany. This powerful heater of the overhead ionosphere can modulate the temperature, and hence the conductivity, of the auroral ionosphere at frequencies between 0.2 and 5 kHz. In the presence of the auroral E-region electrojet, a signal at the frequency of the modulation is radiated. Signals with the appropriate whistler mode dispersion are recorded on the ground. A basically similar phenomenon, but with heating signals propagating obliquely from LF or MF Soviet transmitters, is responsible for the demodulation and radiation of 1 kHz timing pips, which can be received on the ground. More controlled experiments are required in this new field.

The present decade will see the first experiments carried out aboard Spacelab, to be launched by the Space Shuttle. The field of active experiments in space plasmas is well represented here. For example, Canada is proposing an MF/HF transmitter/receiver, with 0.5 kW peak power, using a dipole antenna of up to 300 m length tip-to-tip. Studies are planned of the transmitting antenna itself, ionospheric soundings, electromagnetic and electrostatic wave propagation in magnetoplasmas, parametric decay and plasma instabilities and nonlinearities. VLF wave injection is also proposed using the same antenna, the size being comparable with the whistler wavelength in the ionospheric medium. Waves can thus be injected over a range of wave normal angles (to the geomagnetic field) that are inaccesible from ground-based transmitters. The aim of such experiments is an increased understanding and control of magnetospheric wave-particle interaction mechanisms. Chemical releases, including water produced by fuel cells, from the shuttle are also planned. Finally, on the first Spacelab now scheduled for launch in 1983, Japanese, US and European groups are collaborating on intense (maximum 7.5 kV, 1.6A) electron injection experiments. These are designed to excite artificial aurorae, to study beam-plasma interactions in the ionosphere and to study charging of the Space Shuttle by operation of the gun and its neutralization by both plasma arcjets and neutral nitrogen plumes.□

0028-0836/80/360008-02$01.00

100 years ago

A balloon ascent was made at Cherbourg, on the occasion of the *féte* given by the Municipality to M. Grévy, by MM. Perr and Capt. Gauthier. The general direction of the wind being from the land to the sea, a government steamer was sent out to secure the safety of the aëronants if necessary. Before starting not less than thirty pilot-balloons were sent up to ascertain the superposition of the aerial currents. It was proved that at 40 metres the wind was blowing from the sea. After having travelled for more than an hour in the direction of Portsmouth the aëronauts opened their valve and returned safely on shore. More than a hundred thousand spectators witnessed the experiment. The culminating point of the ascent was an altitude of 1,500 metres, where the travellers could see the English coast, the whole of the Isle of Wight, &c. The scenery is stated to have surpassed description. Some very curious observations were made on the colours of the sea. In the places where the water is very deep it looks quite inky, and the curves of level are so clearly manifested that they bear comparison with equidistance lines worked on ordnance maps. When travelling at so great an altitude ships can be detected with some difficulty; but smoke can be seen even when the smoke-producing steamer can hardly be perceived with the naked eye.

On the evening of July 20, about half-past eight o'clock a remarkable meteor, said to have resembled a comet, apparently about twenty yards in length was observed at Vizimgaum and other places in India, traversing the sky from south to north, and remaining visible for about three-quarters of a minute, during which time the whole sky and country were brilliantly illuminated. The meteor then burst, and some time afterwards a loud sound like distant thunder, which lasted two minutes, was heard.

At a concert given every night in the garden of the Palais Royale, Paris, the orchestra is placed in the vicinity of the fountains which are illuminated by eight splendid Siemens lamps, which work admirably. Two other Siemens lamps have been placed in the shop of a jeweller in the Galleries, and the experiment may eventually lead to the lighting of the whole palace by the electric light.

from *Nature* **22**, 26 August, 401, 1880

Maverick mitochondria

from a correspondent

LAST November, readers of these columns will recollect, the news broke that the genetic code, hitherto thought to be universal, was different in mitochondria. Now, new and startling revelations concerning the machinery that mitochondria use to translate the genetic code are described in three recent papers (*Proc. natn. Acad. Sci. U.S.A.* 77, 1980).

Mitochondria are organelles which exist inside eukaryotic cells where they perform the rites of oxidative phosphorylation. They possess their own DNA which contains genes for the enzymes they require for these rites as well as for their own ribosomal RNA and tRNA. To grasp the importance of the new findings we must first note that the 64 possible codons may be arranged in 16 families. Each family is defined by the first two bases of its codons so that, for instance, GU*N*, where *N* can be U,C,A or G defines the codons of the GU family. It is convenient to refer to the two codons of a family with a pyrimidine (U or C) in the third or 'wobble' position as the prymidine codons and the other two with A or G as the purine codons. In the standard genetic code, eight of the 16 families are unmixed: that is say all four codons in one family code for the same amino acid. In the mixed families several patterns of assignment exist; in six of them the pyrimidine codons signal one amino acid and the purine codons another or, in one family act as termination signals.

In the standard translational machinery, the codons interact one after another with tRNA molecules each bearing an appropriate amino acid. Each tRNA molecule has an anticodon of three bases that interact in an anti-parallel manner with the codon forming three base pairs. The first two base pairings are of the standard Watson-Crick type but the third in the wobble position may be more variable. In this way an anticodon may read from one to three different codons of the same family according to the nature of the base in its wobble position. For instance,an anticodon with U in the wobble position may read both purine codons of a family and one with G may read both pyrimidine codons. With the rules of wobble pairing in mind, it can be shown that a minimum of 31 types of tRNA are required to read the standard genetic code.

The three new papers first of all extend and consolidate our knowledge of the deviations from the standard code that occur in mitochondria from *Neurospera crassa.* (Heckman *et al. Proc. natn. Acad. Sci. U.S.A.* 77, 3159; 1980), from mammals (Barrell *et al. Proc. natn. Acad. Sci. U.S.A.* 77, 3164; 1980) and from yeast (Bonitz *et al. Proc. natn. Acad. Sci. U.S.A.* 77, 3167; 1980). In mitochondria from all three species it now transpires that UGA, instead of acting as a termination signal, codes for tryptophan as does the other purine codon from the UG family. In the AU family the code differs from standard only in mammalian mitochondria where the pyrimidine codons signal isoleucine and the purine codons methionine. Yeast and *Neurospera* abide by the standard pattern in this family. A further change occurs in the unmixed CU family of yeast in which all four codons signal threonine instead of the standard leucine. Apart from these deviations, the other codon assignments in mammals and yeast appear to be standard except for a suggestion that certain codons, normally used for arginine and which have not been detected in portions of the genome translated into protein, may be used as termination signals. In *Neorospera* no further deviants have been detected but the data are still incomplete. It may be noted in summary that the codes used by these three species not only differ from the standard but also differ among themselves. How many other deviations will show up in mitochondria from other species remains to be seen.

These observations, interesting though they may be, do not constitute the major bombshell delivered by these papers. As portents have been seen for some time it is disturbing that nobody has been able to find a full complement of 31 tRNA species in mitochondria, particularly since it has been shown that no extra tRNA is imported from the cytoplasm, at any rate in mammals.

Barrell *et al.* have now shown, by sequencing virtually the entire mitochondrial genome, that there are indeed only 23 tRNA genes in HeLa cell mitochondria. Similarly Bonitz *et al.* have found only 24 in yeast. An examination of the putative anticodons of these genes allows each to be assigned to a codon family. When this is done it is seen that eight are assigned to unmixed families. Invariably in mammals and in 7 cases in yeast these anticodons have a putative U in the wobble position. Since most of the 32 codons involved appear to be used to code for the

0028-0836/80/360009-02$01.00

appropriate amino acid it would appear that in some way these tRNA species can read all four codons of their families by recognising the two non-wobble bases and ignoring the third — a mechanism that I will call super-wobble. This is clearly anomalous but reminiscent of Lagerkvist's two-out-of-three reading scheme (Lagerkvist *Proc. natn. Acad. Sci. U.S.A.* **75**, 2759; 1978). The plot thickens when it is seen that eight further putative anticodons with G in the wobble position must be assigned, one each, to the remaining mixed families and six with a putative U to families requiring them. This makes it possible to read the mixed families according to standard wobble mechanisms.

A grave anomaly remains however. If an anticodon with U in the wobble position is able to read all four codons of an unmixed family, oblivious of the wobble base in the codon, how is it that the anticodons with a U in the third position are able to confine their attentions to the purine codons in the mixed families? To put it another way: why does super-wobble only occur in the unmixed families?

A clue to the answer to this conundrum is to be found in the paper by Heckman *et al.* They show from determinations of the sequence of six tRNA species that the U in those anticodons which must not indulge in super-wobble are modified (precisely how is still unclear) whereas the U in those that may so indulge is not modified. Modification inhibits super-wobble it seems but it remains still to be seen how this is done. Maybe the small and specialised mitochondrial ribosomes play some role in arranging this distinction. Meanwhile two points should be noted: first, most cytoplasmic tRNA species with a U in the wobble position have it in a modified form and second, this clue to the mechanism of the distinction is based on work on *Neurospera*. We must await further developments to see if the U's in mitochondrial tRNA from yeast or mammals are appropriately modified. □

Probing the mysteries of seeds

from Daphne J. Osborne

SEEDS are remarkable things. Each is a precise package enclosing a dry, quiescent and differentiated embryo, with attendant food reserves. Add water and within minutes the seed can be activated to renewed metabolic growth.

Almost every aspect of seed physiology and biochemistry was covered in discussion at the recent International Seed Germination Conference*. Ecologists for example, were assessing germination opportunity by mathematical modelling to include climatic variables and competitive interactions. Dormancy and dispersal of seeds were considered as alternative winning stratagems, depending on the habitat. One interesting model was for 'small patch' survival. In many desert plants, anti-dispersal mechanisms (atelochory) are winners. Seeds are held within the dried up plant until the rains so ensuring that they germinate in already successfully colonized sites.

Although a seed is said to have germinated when the root protrudes, there is no good definition in biochemical terms. The start of DNA replication could be the biochemical marker since imbibed but dormant seeds, although maintaining a continuous metabolic turnover, neither grow nor replicate their DNA and germinating embryos seem not to replicate their DNA until the radicle protrudes.

The depth of dormancy of seeds at shedding depends upon complex combinations of temperature, water availability and photoperiod during seed formation. Some seeds develop what is called secondary dormancy. This can happen if they remain imbibed under conditions in which they will not germinate. Those with a phytochrome-controlled dormancy, broken by exposure to red light may pass into secondary dormancy that is then independent of phytochrome control but broken by chilling. Some weed seeds develop a phytochrome-dependent secondary dormancy when they fail to germinate through lack of oxygen. This may account for successive bursts of germination observed in the field.

The question "do endogenous hormones control dormancy?" was a major talking point. Attempts to relate dormancy directly to either effects of hormone application, or to the levels of endogenous hormones in the seed proved unrewarding. For example, no relationship was established between abscisic acid and secondary dormancy and little understanding emerged for a mechanistic role for abscisic acid from the new, detailed knowledge of its metabolism during seed development and germination. Nor did there appear to be any obvious differences in abscisic acid biochemistry of dormant and non-dormant embryos which might account for their differences in germination. However, added abscisic acid does repress germination, so a role for abscisic acid is not excluded, even though studies of levels and metabolic products seem unlikely to provide the clues. Compartmentation or availability of hormones during particular receptive stages in seed development or germination are more likely to determine their regulatory functions: the precise stage of receptivity presumably depending upon the presence of the appropriate receptor proteins rather than the hormone level.

While control mechanisms of dormancy prove elusive, the mobilization by the embryo of stored protein and carbohydrate reserves at germination are demonstrably under hormonal control from the developing axis.

On seed imbibition in peas and beans, amylolytic or proteolytic activity in the cotyledons with subsequent hydrolysis of stored starch and protein is induced by the presence of the embryo axis (the radicle) or by addition of cytokinins; end-product inhibition or high osmotic concentration in the cotyledon are apparently not the reason for suppression of these enzymes in the absence of the axis. In lettuce, which stores mainly oligomannans, the radicle appears to transmit a stimulus to endosperm cells to produce β-mannanase with further breakdown of the mannans by a β-mannosidase induced in the cotyledons; the whole representing a linked and presumed hormonally regulated sequence. In mung bean cotyledon cells an endopeptidase synthesised on endoplasmic reticulum is transferred to the storage protein bodies during germination; the ensuing hydrolysis of these proteins illustrates the autophagic nature of these bodies and the central role of endoplasmic reticulum in enzyme synthesis. The lighter buoyant density of endoplasmic reticulum of aleurone cells during gibberellin-induced α-amylase production is therefore of considerable interest.

The physical and metabolic effects of seed hydration at germination are critical to seedling establishment. Restraints on water flow to the seed are imposed by the hydraulic properties of the seed-bed and the water energy level of the seed. Again, mathematical modelling based on experimental assays under different water availabilities can now provide predictions of field performance. Saline conditions appear to cause greater reductions of shoot than root growth. Accumulation of abscisic acid in the stressed cotyledons followed by preferential transfer to the shoot may account for this.

Maintaining the water content at a critical level for some while during seed hydration can, however, lead to more uniform germination and convey a greater resistance to sub-optimal temperatures. This is achieved by pretreatments which include an osmoticum such as polyethyleneglycol in the ambient imbibition medium prior to sowing. Such seeds can then be dehydrated and stored before

Daphne J. Osborne is in the ARC Weed Research Organization, Oxford

---

*A Seminar on "Control Mechanisms of and during Seed Germination" sponsored by the Bat Sheva de Rothschild Foundation for the advancement of Science in Israel was held in the Hebrew University, Jerusalem, from March 16th to 29th. The proceedings will be published this year in Volume 28 of the Israel Journal of Botany.

0028-0836/80/360010-02$01.00

sowing. But improvement does not always result. Secondary dormancy occurs if phytochrome controlled seeds are osmotically treated in the dark and there is a critical stage during imbibition before which the germinating seed is tolerant to subsequent dehydration and beyond which, removal of water results in cell death.

Desiccation tolerance of seeds is still poorly understood. It starts during seed formation when synthetic events are shut down. Polysomes are dissociated to monosomes with run-off of mRNA. Within minutes of rehydration at germination, polysomes are re-assembled suggesting that early protein synthesis could be initially independent of new RNA synthesis. But embryogenesis and germination are linked to changing protein patterns and in cotton cotyledons the maternal, constitutive and abscisic acid-induced protein products can be distinguished as well as their associated and different abundancy classes of PolyA-rich RNA messages.

Ageing seeds in the dry state, apparently sustain increasing levels of single stranded breaks in nuclear DNA and an early desiccation-tolerant event at germination is the 'repair' of these lesions with likely restoration of genome fidelity. Such repair capability is important for proper seedling establishment for failure to repair may lead to impaired vigour and low levels of early protein synthesis.

None of the early events of germination are possible without an energy supply. ATP levels are barely detectable in dry seeds. ATP production from inosine mono-phosphate or through an phosphoenol pyruvate-pyruvatekinase generating system are possible but measurements of energy charge favour oxidative phosphorylation. Differing mitochondrial activities may indeed be another factor controlling rates of early protein synthesis.

This meeting identified many problems, exposing the present lack of biochemical understanding of how desiccated cells survive, what makes them dormant and what breaks their dormancy. When knowledge in these areas becomes as far advanced as our current information on the biochemical events of early germination then another seminar will certainly be warranted. □

Bahamian Atlantis reconsidered

from Marshall McKusick and Eugene A. Shinn

During the late 1960s amateur explorers diving in shallow water found tabular limestone blocks which led them to repeatedly publish claims that Bimini Island in the Bahamas was the unsubmerged tip of the lost continent of Atlantis. In 1971, however, Harrison (*Nature* **230**, 287) argued that the supposed stone walls or roads were in fact natural limestone and that some submarine structures described as pillars were hardened concrete originally stored in wooden barrels and dumped overboard in recent times at the harbour entrance.[1] Nevertheless many amateur explorers have ignored the scientific explanation and books and articles that perpetuate this Atlantis myth continue to appear.[2,3] It is our contention that the persistence of the Bimini Island hoax must be explained in sociological rather than geological terms. There is in the US a vigorous cult dedicated to the mystic revelations of a native American prophet, Edgar Cayce (1877-1945), who wrote that lost Atlantis was the centre of all ancient civilization 10,000 years ago and that Bimini was part of that continent. Thus the Bimini affair has become a clash between scientific interpretation and religious dogma.

Geological studies have now gone beyond the 1971 geological reconnaissance of Harrison who wrote that a shell-hash gravel in shallow water was exposed and cemented during the most recent emergence of the Bahamian Banks. In 1978 Shinn's study reported that the so-called 'man-made roadway' was actually submerged beachrock.[4] On the Bimini beaches the high calcium content of the seawater allows the rapid formation of natural limestone beachrock — a fact demonstrated by glass shards, bottle caps, and other beach litter incorporated into the stone. Similar rapid formation of limestone has been shown in coral atolls in the Pacific where World WarII artefacts have been found in the matrix. Beachrock formed by the circulation and evaporation of calcium laden seawater has the following characteristics: (1) tabular fractures, (2) keystone vugs, (3) a surface slope and internal laminations which tend to parallel the beach incline, (4) stratigraphic continuation of sedimentary layers from one tabular block to another, and (5) an overall geometry which reflects tidal zone origin, that is, a narrow band frequently extending a mile or more along the sea front.

Amateur enthusiasts have claimed that the Bimini blocks were quarried by ancient Atlanteans and laid out in an ancient 'Cyclopean, megalithic roadway' which

Beachrock forming on Heron Island, Australia displays just the same features as the "Atlantis Road" in the Bahamas.

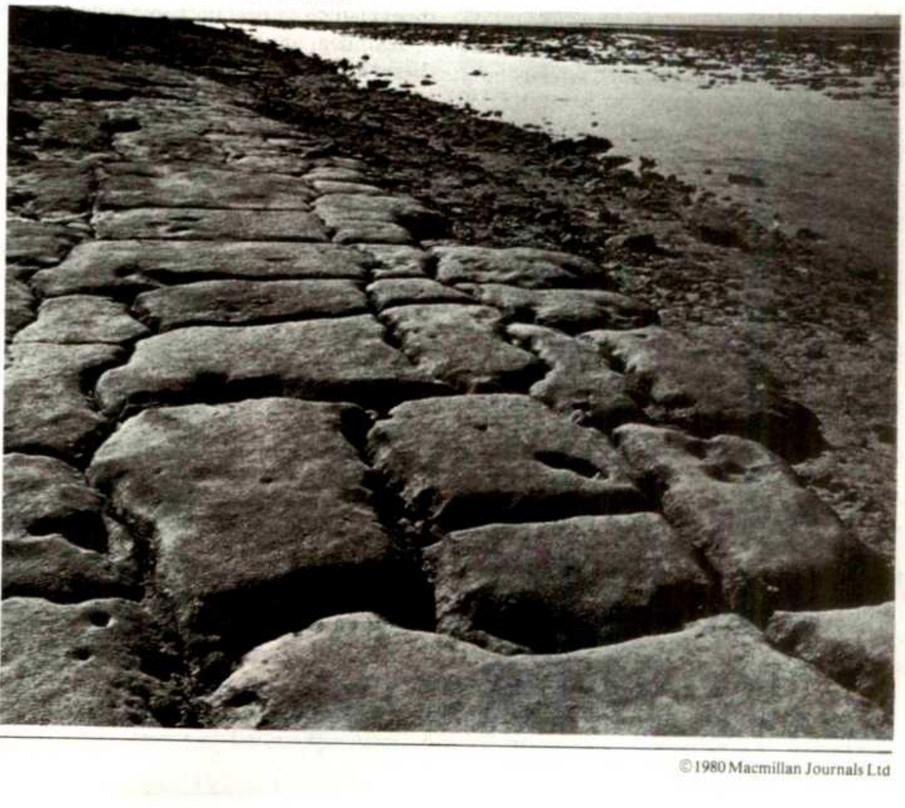

Marshall McKusick is Associate Professor of Anthropology, University of Iowa, Iowa City. Eugene Shinn is a member of the United States Geological Survey, Fisher Island Station, Miami Beach, Florida. His geological study at Bimini reported here was at his own expense and not part of any U.S.G.S. sponsored project.

0028-0836/80/360011-02$01.00

involved using squares and rectangles of various sizes including some 15 feet across. However the limestone structures observed off Bimini in 15 feet of sea have all the features of natural beachrock.[5] The limestone is in a narrow band overlying coral sand and extends for a considerable distance along a former shoreline. The so-called road's hairpin curve is not continuous and parallels the existing headland on shore. The tabular fractures are natural, and the original slope to the sea is present. A sample of 17 oriented cores obtained by Shinn and Tomkins has been examined with X-radiographs. Two areas of the formation were studied, and both show slope and uniform particle size, bedding planes and constant dip direction from one block to the next. If the stones had been quarried and relaid there is no reason to suppose bedding planes would carry stratigraphically from block to block. The sedimentary laminations clearly show that these were not randomly laid stones but a natural, relatively undisturbed formation.

Although under 15 feet of water, the beachrock is of recent geological origin. One ^{14}C date on shell has already been published as 2,200 ± 150 years BP. Jerry J. Stipp (Radiocarbon Dating Lab., University of Miami) has run seven bulk samples from the cores as a class project and gives slightly older dates for the Bimini submerged beachrock.

Laboratory Number	*^{14}C Years BP*
UM - 1363	2745 ± 80
UM - 1364	2770 ± 80
UM - 1359	2780 ± 65
UM - 1365	2835 ± 70
UM - 1361	3355 ± 90
UM - 1360	3500 ± 80
UM - 1362	3510 ± 65

Testing of submerged features in Florida and one test on North Bimini Island shows that the sea level has risen at a rate of about one inch every 40 years for the past 5,000 years. This rate of submergence over 2,200 to 3,500 years would account for 5.58 to 7.22 feet of the 15 feet of sea observed over the beachrock. The remaining 7 to 9 feet of sea may be explained by the undermining of sand allowing the beachrock to gradually settle, an erosive process that is seen in various stages in many parts of the Caribbean. Harrison's map shows that the submerged beachrock is located on the most exposed shore subjected to substantial erosion during winter storms.

The Bimini mystery has been used to promote tourism — "scuba dive over the lost road of Atlantis" — and has been exploited commercially in other ways. During the 1970's an enormous number of books describing ancient Atlantean, Phoenician, Egyptian, Viking, and other mysterious visitors to prehistoric America[6] have been published by both the major and minor New York commercial presses. This science fiction disguised as historical explanation is popular with the reading public and is part of a contempory fad. However, there is more to the Bimini-Atlantis hoax than commercialism. The mystic revelations of the American prophet Edgar Cayce have formed the basis of a successful religious cult with a national membership reported to be 18,000 and a staff of 110 at the Virginia Beach headquarters. The Cayce cult is a religion, and the revelations describe geological catastrophism as the explanation for Atlantis, the lost Pacific continent of Lemuria, and origin of civilization in such mythical lands. The 'sinking' of Atlantis according to Cayce's revelations occurred 10,000 years ago, although the radiocarbon dates of the natural formation show it originated some 7,000 years later.

To explain the rejection of archaeological and geological evidence, it must be said that Bimini is just one of a growing number of archaeological 'shrines' which have become the object of cult worship. Pyramid worship is becoming more common, and in England itself, mystic cults centre upon the alleged religious powers of Stonehenge and other megalithic monuments. Whatever the explanation of these new religious movements, they have led to an unfortunate rejection of the scientific explanation of natural and physical phenomena among a significant segment of the reading public. ☐

---

1 Harrison, W *Nature* 230, 287 (1971)

2 Zink, D D *The Stones of Atlantis* (Prentice-Hall, 1978), *Ancient Stones Speak* (E. P Dutton, New York, 1979)

3 Rebikoff, D *Explorers Jr 57, 122 (1979)*

4 *Shinn, E Sea Frontiers* 24, 130 (1978)

5 McKusick, M *Explorers Jr* 58, 40 (1980)

6. McKusick, M *Antiquity* 53, 121 (1979)

Retrograde transport in axons

from Peter Banks

A novel technique has been developed by Fink and Gainer[1,2] which makes it possible to follow the movements of proteins along nerve axons back towards the cell body. This retrograde movement is of physiological importance because it allows nerve growth factor (NGF) and possibly other materials released by innervated cells to reach the afferent cell bodies to modulate their metabolism. The retrograde axonal path is also taken by tetanus toxin and the neurotropic rabies and Herpes viruses; in the case of tetanus toxin, uptake by the nerve endings depends upon binding to specific sialogangliosides[3]. Recently, the exploitation of retrograde transport has provided an important new tool in neuroanatomical investigations. Horse-radish peroxidase (HRP) injected into the nerve endings can be followed back to the cell body allowing tracing of neuronal circuitry.

The mechanism of fast anterograde transport (50mm per day) from cell body to nerve ending is an energy-dependent process requiring Ca^{2+} ions, intact microtubules and actin[4]. However, the relationship between the smooth endoplasmic recticulum of the axon and neurotransmitter storage vesicles remains unknown. Retrograde transport is much less well understood but there is evidence, based on sensitivity to colchicine, for the involvement of microtubules. Under the electron microscope transported HRP is seen enclosed in membrane-bounded structures suggesting that the smooth endoplasmic reticulum provides the path for transport. However, in a reconstruction of serial sections of optic nerve[4], HRP previously injected into the contralateral optic tectum was never found in recognisable profiles of the reticulum even though, in ten instances, the latter's tortuous course was followed for over $4\mu m$. HRP was found in tubular and oval structures and in multivesicular bodies but none of those displayed any continuity with the endoplasmic reticulum.

Other than following the movement of HRP or of ^{125}I-labelled proteins taken up by nerve endings and direct light microscopy, there are few techniques for studying retrograde transport. Ligation techniques are of value for studying anterograde transport but not for retrograde transport. The distal segment of the nerve, in which retrograde movement towards the ligation is observed, begins to degenerate once contact is lost with the cell body and these changes occur first in the region of the ligation.

Fink and Gainer's new technique[3] enables axonal proteins to be labelled covalently with a radioactive marker (N-succinimidyl [2,3-^{3}H] propionate) following very localised injections into a nerve trunk. The subsequent retrograde and anterograde movements of the labelled proteins can be observed over extended periods of time. Although concentrating on slow transport (1 to 6mm/day), they also showed that the method should be applicable to the study of rapid transport, particularly in the neuro-hypophysial tract. Whilst the proteins transported

---

Peter Banks is Professor of Biochemistry in the University of Sheffield.

1 Fink, D J & Gainer, H *Science* 208, 303 (1980).

2 Fink, D J & Gainer H. *J Cell Biol* 85, 175 (1980)

3 Schwartz, J H *Ann Rev Neurobiol* 2, 467 (1979)

4 LeVail, J.H , Rapisardi, S & Sugino, I K *Brain Res* 191, 3 (1980).

5. Somogyi, P , Hodgson, A J & Smith, A D. *Neuroscience* 4, 1805 (1979)

6 Bentivoglio, M , van der Kooy, D & Kuypers, H G J M *Brain Res* 174, 1 (1979)

0028-0836/80/360012-02$01 00

slowly in the centrifugal direction included the well-known cytoskeletal group, there was a single major centripetal species with a molecular weight of 68,000 which could be serum albumin or a fragment of the neurofilament protein.

The value of the HRP/retrograde transport technique has been greatly extended by some ingenious and very beautiful experiments performed at Oxford by Somogyi, Hodgson and Smith[5]. They combined the tracing of the source of afferent endings by HRP with a modified Golgi stain which enabled tham to identify the cell type acquiring HRP by its shape and dendritic arborization. By coupling the HRP injection with kainic acid, which destroys cell bodies with receptors for glutamic acid but not their afferent endings, and looking for degenerating boutons on the dendrites of Golgi stained cells which contain HRP, they were able to look for neural feed-back loops.

When they made an electrolytic lession in the striatum and injected HRP into the ventromedial nucleus of the thalamus, they found that the distal dendrites of Golgi stained/HRP positive cells in the pars reticularis of the substantia nigra carried degenerating synpatic boutons. They thus demonstrated that a three neurone circuit runs from the striatum and synapses in the substantia nigra and thalamus.

The capriciousness of the Golgi stain also allows the demonstration of stained interneurones synapsing with HRP positive cell bodies and, after placing appropriate lesions, there is also the possibility of detecting degenerating boutons on the interneurones. This multimethodological approach which combines light and electron microscopy, retrograde transport, Golgi staining and placement of lesions is potentially capable of answering many complex neuroanatomical questions.

The organization of efferent projections from the substantia nigra has also been investigated with the aid of the double retrograde fluorescent labelling technique by Kuypers and his colleagues in Rotterdam[6] who obtained evidence that some individual neurones projected to both the thalamus and tectum.

Axonal transport in all its manifestations continues to intrigue and occupy neurobiologists. It is perhaps unfortunate that knowledge concerning its mechanism has not yet matched the explosion of information gained from its exploitation.□

The acetylcholine receptor

from Charles F. Stevens

THE acetylcholine receptor (AcChR) has a a number of important firsts to its credit. As well as using the first neurotransmitter discovered, acetylcholine, it is the first protein of its class to have the conductance of a single open channel measured (25 pS) and to have the distribution of its pore 'open' times determined (the pore stays open an average of about 1 ms). The AcChR pore was also the first in a biological membrane to have the currents flowing through it measured directly (the single channel current is typically about 2.5 pA). Now this protein has chalked up another first: it has been reconstituted in an artificial planar lipid bilayer.

The acetylcholine receptor is very important because it is a representative of a large class of membrane proteins responsible for the electrical activity of the nervous system. These proteins respond to a signal, either a change in concentration of a neurotransmitter present at the membrane surface or a voltage change across the membrane containing the protein, by opening pores that permit ions to pass through the membrane; the ion flows then produce electrical signals which cause or modulate nerve impulse activity or, in the case of AcChR, lead through a chain of events to muscle contraction.

The AcChR is composed of 5 subunits, two smaller ones responsible for binding acetylcholine and three different larger ones whose function has not yet been established. The molecule spans the membrane, protruding about 5 nm from the outer membrane surface and 1.5 nm from the inner surface. Its diameter viewed face-on is about 8.5 nm with a 2.5 nm pit on the outer surface forming a vestibule which narrows to an 0.65 nm ion translocating pore.

A great deal of effort has been devoted to trying to get the isolated molecule to function in an artificial lipid bilayer. Techniques that had been successful in incorporating molecules such as the polypeptide antibiotic gramicidin and some larger but not well characterized molecules like excitability-inducing material into bilayers refused to work for the AcChR. Two technical innovations paved the way for the recent successes. First, Montal and Mueller (*Proc. natn. Acad. Sci. U.S.A.* **69**, 3561; 1972) reported a method of forming bilayers from two separately prepared lipid monolayers: lipid is spread at the interface between solution and air on two sides of a teflon partition that has a small hole in it. When the solution levels on both sides are raised above the hole, a lipid bilayer forms over it. Second, Schindler and Rosenbusch (*Proc. natn. Acad. Sci. U.S.A.* **75**, 3751; 1978) found that when vesicles containing membrane proteins are added to the solution below the monolayer, these vesicles establish an equilibrium with the surface monolayer so that some proteins in the vesicles enter the monolayer. When a bilayer is formed, proteins in the monolayer are then incorporated into the newly formed bilayer. Several methods are available for forming vesicles containing live AcChR molecules.

Two reports of successful reconstitution of the AcChR into bilayers using these techniques have just appeared. Schindler and Quast (*Proc. natn. Acad. Sci. U.S.A.* **77**, 3052; 1980) formed lipisomes containing receptor from *Torpedo* electroplax, the richest source of the AcChR. Nelson, Anholt, Lindstrom and Montal (*ibid* p. 3057) isolated and purified *Torpedo* AcChR, which was first reconstituted in soybean lipid vesicles using a technique developed by Epstein and Racker, and then incorporated the protein into lipid bilayers. The presence of functional AcChRs in the bilayer was detected by measuring an increase in the permeability to cations with applied acetylcholine and by showing that single pores had approximately the same conductance and mean open time as the native AcChR in its natural environment. Further, curare — an agent that is a competitive inhibitor of acetylcholine — blocked the effects of the natural agonist in the reconstituted system.

The next step will be to compare the properties of the reconstituted and native molecules. For example, a considerable change in protein dipole moment accompanies the conformational change at pore opening, and as a result the rates of opening and closing depend on the voltage across the membrane containing the AcChR. The effects of transmembrane voltage, as well as temperature and chemical structure of conformational change inducing ligand, will have to be investigated. Similarly, the alkali metal and alkaline earth cations, as well as a number of small (<.65 nm diameter) positively charged organic ions, pass through the open pore and the relative permeabilities of these ions will have to be determined for the reconstituted AcChR pore. Finally, the effects of the large number of pharmacological agents which alter the AcChR behavior will have to be investigated. In every case differences in the properties of the native and reconstituted molecules will need to be explained in terms of modifications that have occurred either during reconstitution or as result of the altered environment of the reconstituted molecule. When this is done, the advantages of having the reconstituted protein in an easily modifiable environment can be exploited.

As with other multimeric proteins the recently determined partial sequences for the four types of polypeptide chains

---

Charles F. Stevens is Professor of Physiology in the School of Medicine at Yale University, and is currently in residence at Cold Spring Harbor Laboratory, New York.

0028-0836/80/360013-02$01.00

constituting the AcChR show strong homologies, presumably because they evolved through gene duplication. (Raftery, Hunkapiller, Strader & Hood *Science* **208**, 1454; 1980). Many large proteins also have homologies within a peptide chain, again indicating tandem duplications of genetic material. The sequence known for the AcChR amounts to only about 10% of the total, too short to permit the detection of such homologies. However, additional parts of the sequence should be fairly easily obtained by the same techniques. Furthermore, because an estimated 2% of *Torpedo* electroplaque mRNA codes for AcChR, it should be possible to clone and sequence the genes. The base sequence will certainly be helpful in indicating the evolution of the molecule and will be a very important step toward relating the protein structure to its already well described function. The AcChR, then, has a number of chances to add still more firsts in the near future. □

Ultrasensitive mass spectrometry using accelerators

from K. W. Allen

THE detection of long lived radio isotopes such as ^{14}C by mass spectrometric methods using accelerators has a number of important advantages over more conventional methods based on observation of the emitted radiation. First, the sensitivity may be substantially increased, often by several orders of magnitude, so that measurements may be made using milligram samples in a reasonable length of time; second, through the use of a tandem accelerator in which fast negative ions are stripped within the high voltage terminal prior to the second stage of acceleration, discrimination against unwanted stable isobars (for example, N^{14} when detecting ^{14}C) and elimination of molecular ions (for example, ^{13}CH$^-$ which simulates ^{14}C$^-$) by dissociation in the stripper are achieved; and third, the relatively high final energy of the positive ions enables the well established techniques of nuclear particle identification to be employed to advantage.

Ultrasensitive mass spectrometry using the Berkeley 60″ cyclotron was first employed by Alvarez and Cornog in 1939 to show that He^3 rather than ^{3}H was stable, and later (1975) Alvarez and his associates used similar methods to set a very low limit for the natural occurrence of quarks. The need for more sensitive methods of ^{14}C dating in archaeology provided a strong impetus for new developments and in 1977 it was shown independently (see Müller *Physics Today* Feb. 23; 1979) that both cyclotrons and tandem Van de Graaff generators could be used successfully for ^{14}C dating. Within a year or two of these demonstration experiments, approval had been secured for the construction of 3MV tandem generators at the Universities of Arizona, Oxford and Toronto to be dedicated to ^{14}C dating and ultrasensitive mass spectrometry. The first of these new accelerators should be in operation by the end of 1980, but it is likely to be some time before the high accuracy in the ^{14}C/^{12}C isotopic ratio (<0.5%) essential for dating of archaeological samples is achieved on a routine basis.

The importance of accelerator based mass spectrometry increases as the lifetime of the radioisotope studied increases, since the specific activity decreases. Thus it is not surprising that accelerator based methods have already been applied to the detection of the long lived cosmogenic nuclides Be^{10} (1.62×10^6 y), Al^{26} (7.16×10^5 y) and Cl^{36} (3.00×10^5 y). The stable isobar at mass 26, Mg^{26}, does not appear to form negative ions so background is not a problem for Al^{26}. However since both Be^{10} and Cl^{36} have stable isobars, it is necessary to rely on chemical separation and specific ionization measurements to remove the background. At 20 MeV, S^{36} and Cl^{36} ions differ in their specific ionization by about 5%, but at $M = 100$, the difference for neighbouring isobars is only ~ 1%. Thus separation becomes increasingly difficult with increasing mass. In a recent article, Elmore *et al.* (*Nature* **286**, 138; 1980) have shown how a time of flight technique can be used to separate I^{129} (1.6×10^7 years) from I^{127}. Since there are many long lived radionuclides of astrophysical or cosmological interest with $A > 100$, this development is of considerable interest, not only because of the authors' success in measuring I^{129}/I^{127} in meteorites at the 5×10^{-12} level, but also because the experiments exposed the limitations of accelerators designed for nuclear physics research when used for ultra sensitive mass spectrometry of heavy elements.

The half life of I^{129}, although long in absolute terms, is short compared with the age of the solar system (4.55×10^9 years) so that all primordial I^{129} has long ago decayed to its stable daughter, Xe^{129}. There has been much analysis and speculation concerning the role of I^{129} decay in relation to the abundances of the Xenon isotopes in meteorites (see Drozd & Podosek *Earth planet. Sci. Lett.* **31**, 15; 1976) and the abundance of Xe^{129} in old tellurium bearing rocks has been used to set a lower limit of 1.6×10^{25} years to the lifetime of nucleon decay in Te^{130} (Evans & Steinberg *Science* **197**, 989; 1977. Since the decay of a proton or a neutron in Te^{130} leads to I^{129}, there would seem to be advantages in detecting I^{129} rather than its stable isobar Xe^{129} as the primordial background would then be eliminated. It should also be possible by accelerator based negative ion mass spectrometry to obtain greater sensitivity, by a factor $\sim 10^2$ to 10^3, than can be achieved by conventional means. Since the equilibrium yield of I^{129} from nucleon decay, assuming a half life of 10^{30} years, is at most $\sim$ 1300 I^{129} atoms per kilogram of tellurium, improved sensitivity would be very welcome! It will clearly be necessary to obtain tellurium samples from very deep mines to minimise the I^{129} background from radiative neutron capture in Te^{128}, (the neutrons coming from energetic muon interactions), but the occurence of tellurium in association with gold and silver, which both encourages mining and provides neutron shielding for the tellurium, is a helpful factor. While the sensitivity of geochemical methods such as that described above cannot approach that obtainable with the very large cerenkov detectors now under construction for those events in which the entire rest energy of the nucleon is liberated within the detector, the technique is independent of nucleon decay mode and could in principle detect events in which several neutrinos are emitted. Such events are most unlikely to be revealed by direct detection methods.

The detection of nucleon decay is probably the most challenging and difficult application for ultrasensitive mass spectrometry. There are, however, many fields where the technique is likely, after further development, to prove useful. The measurement of the terrestrial abundance of long lived radionuclides such as Pu^{244}, which has a bearing on the origin of the solar system (Hoffman *et al. Nature* **234**, 132; 1971), the detection of solar neutrinos, the search for superheavy elements and the detection of rare stable nuclides at a level of parts per billion are all possible areas of application. The recent work on I^{129} (Elmore *et al.* loc. cit.) emphasizes the value of time of flight techniques and the importance of good resolution at injection to eliminate undesirable negative ions; the heavier the ion, the more important these considerations will be.

It seems likely that, over the next few years, tandem generators which are now too small for effective nuclear physics research will be put to good use as ultrasensitive mass spectrometers. It will be necessary to install high resolution injectors on these accelerators, improve the vacuum systems, and perhaps develop new types of detector, especially for the heavier elements. These improvements are relatively modest however, and it should be possible for small groups working on their own University campuses to make important contributions in many different fields. □

K. W. Allen is Professor of Nuclear Structure at the University of Oxford.

0028-0836/80/360014-01$01.00

Bunching of 8–10 keV auroral electrons near an artificial electron beam

M. P. Gough*, B. N. Maehlum†, G. Martelli*, P. N. Smith* & G. Ventura‡

*School of Mathematical and Physical Sciences, University of Sussex, Brighton BN1 9QH, UK
†Norwegian Defence Research Establishment, Kjeller, Norway
‡University of Florence, Florence, Italy

High frequency modulations (~1 MHz) of energetic (keV) electrons in the auroral ionosphere have been detected unambiguously for the first time using a novel technique. These modulations were induced by an artificially injected pulsed electron beam (8 keV, 4% duty cycle), and were accompanied by electrostatic wave emissions at the same frequency.

IF waves are excited by a charged beam in a magnetoactive plasma, the beam particles should become bunched at or near the frequency of the excited waves. This is also true for the auroral ionosphere, where such bunching effects could be a useful diagnostic technique. Hitherto these effects could not be studied because of the limited bandwidth of rocket telemetry systems. A technique which overcomes this problem was applied here to the semi-controlled conditions provided by a rocket borne 'mother–daughter' experiment incorporating an artificially injected electron beam.

Several experiments have been carried out with electron guns mounted on rocket payloads[1–3]. Emissions created by these electron beams are observed up to frequencies beyond the electron plasma frequency. Cartwright and Kellogg[4], however, noted that most of the radiated beam power goes into waves propagating below the local electron gyro-frequency f_{ce}(~1.4 MHz) as whistler mode waves.

More recently, similar emissions have been observed in natural auroras by receivers operated on the ground[5,6]. Kisabeth and Rostoker[6] further identify the source of the emissions below f_{ce} as field aligned currents with the highest frequencies below f_{ce} associated with electron beams in discrete auroral arcs.

We present here results from an artificial auroral beam experiment in which beam-induced bunching of the energetic auroral electrons is observed at a wave frequency of 0.7 f_{ce}. The only previous attempt[7] to detect bunching or modulation of auroral electrons up to megahertz frequencies yielded an ambiguously low level of modulation around the detection threshold of the instrument.

Observational technique

On 27 November 1978 at 18.55.35 UT, a Nike Tomahawk rocket (Electron 2) was launched from the Andoya Rocket Range, 69° 17′ N, 16° 01′ E, Northern Norway, during natural auroral activity. The main payload or 'mother' was instrumented to measure energetic particles, waves and ambient plasma while a separating sub-payload or 'daughter' contained an electron gun producing at peak current a 100 mA beam of 8-keV electrons. The daughter separated at 70 s (95-km altitude) with a relative forward velocity of 0.5 m before the gun pulse sequence started at 92 s and useful particle measurements were made on the mother between 80 s (108 km on the upleg) and 351 s (108 km on the downleg).

On the mother one of the electrostatic analysers was operated at fixed energy 8–10 keV with near omnidirectional opening angle of 190 × 5°, to monitor both the background and the gun electrons. The channeltron pulses from this detector were analysed as described below to investigate bunching up to frequencies of 5 MHz. Electrostatic and electromagnetic waves measured on the mother by a pair of boom-mounted electrostatic sensors connected to a receiver sweeping between 0.2 and 3.8 MHz (every 30 ms with a bandwidth of 100 kHz) were recorded simultaneously.

The megahertz bunching analysis of the detected 8-keV electrons was performed by on-board processing of the channeltron detector pulses described fully by Gough[8]. The time interval between subsequent pulses produced by 8 keV electrons was measured as the number of cycles of a 10 MHz crystal oscillator. If the electrons arrive randomly at an average rate C s^{-1}, then the probability $P(M)$ of two electrons arriving separated by M cycles of the 10-MHz clock will be given by

$$P(M) = P_0\, e^{-MP_0} \qquad (1)$$

where

$$P_0 = C/10^7 \ll 1$$

Any bunching of the electrons at frequency F (due, for example, to wave–particle interactions) should appear as a cyclic modulation with periodicity $10^7/F$ cycles superimposed on top of the normal non-bunched distribution given by equation (1).

The most probable measurements are those of the shortest time intervals separating two pulses. Given a sufficient accumulation time this makes the technique sensitive to frequencies orders of magnitude greater than the count-rate, but limited by the sampling theorem to a maximum frequency of one half of the crystal clock frequency.

In this preliminary experiment only the time interval between the last two electrons arriving before each telemetry readout was transmitted to the ground. Thus only 400 measurements were available each second, although the average electron arrival rate was between 5×10^3 and 5×10^4 s^{-1}.

If we call $N(M)$ the number of observed pairs of electrons separated by M clock cycles, any bunching at frequency F will produce in the array $N(M)$ maxima around $M = 0$, $M = 10^7/F$, $M = 2\times10^7/F$, and so on. Consequently each data set was searched for the presence of electron bunching at 140 frequency intervals spread linearly between 0.2 and 5 MHz. For each frequency trial, the distribution $N(M)$ was multiplied by a square wave of amplitude ±1 lasting four cycles with phase zero at $M = 0$ (the zero being corrected for electronics dead time).

In the absence of bunching, the distribution of the entries $N(0)$, $N(1)$, $N(2)$, and so on, are approximately poissonian and independent. The difference between the number of counts accumulated in the positive parts of the square wave over those in the negative parts divided by the square root of the total number of counts encompassed by the square wave is expressed as the ratio Z. A 'non-bunched' distribution would give $Z \sim 1$. It follows that the probability of a non-bunched distribution giving $Z > 3$ is 0.0014, and $Z > 2$ is 0.025, for each frequency trial.

0028–0836/80/360015—03$01.00

Experimental results

Figure 1 shows eight sequential data sets of 33.5 s (five spins of the rocket) analysed in the way described above, with Z plotted whenever it exceeded +1.0. The scale is linear and the $Z = +3$ level is given by the base line of the previous data set. This type of frequency analysis enables us to determine fundamental bunching frequencies, although spurious higher harmonics may also appear. The most striking feature of Fig. 1 is a peak which moves down from 1.0 MHz in the data set centred on 99 s to 0.8 MHz in the data set centred on 232 s. The fact that the spectral pattern repeats itself in five consecutive data sets is highly significant.

As in this frequency band the maximum values of Z are 3.5, 4.1, 2.5, 4.0 and 3.4 for the first five spectra respectively, the electrons can be said to have been definitely bunched in the 0.8–1.0 MHz range.

The electrostatic wave sensors on the mother payload were designed to measure waves in this frequency range. Wave bursts associated with the gun pulses were observed in the same narrow frequency band. Unfortunately the booms on which the sensors were mounted did not deploy fully and the data appear to be contaminated by interference, possibly generated within the payload.

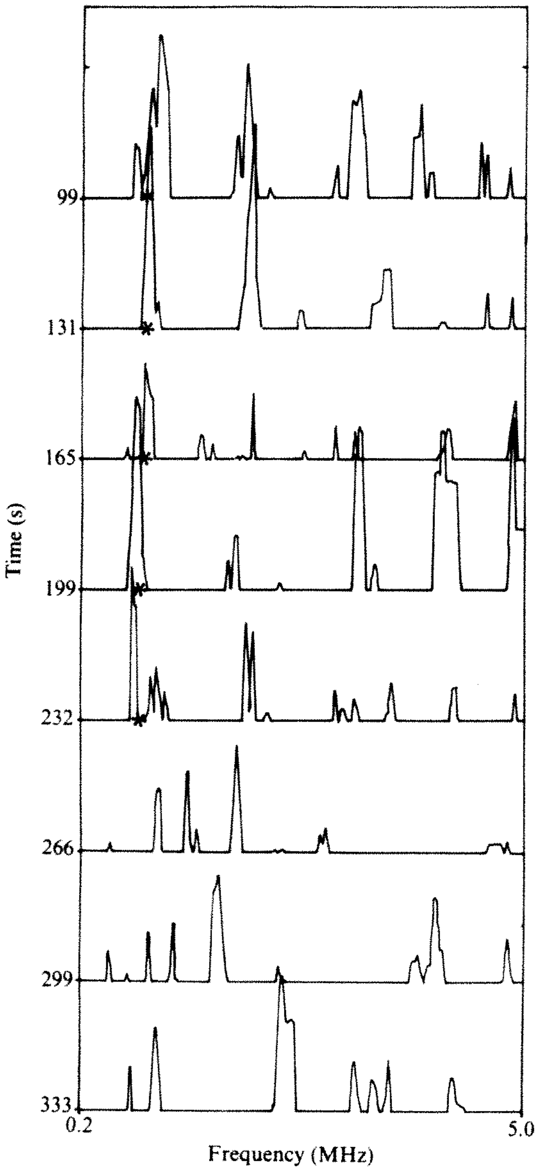

Fig. 1 The observed bunching frequencies of the 8-keV electrons. 33.5 s (five spins) groups of data are presented with Z (see text) plotted against frequency when above $Z = +1$ (baseline) where $Z = +3$ is the baseline of the previous data set.*, Position of the emission observed on the electric field booms. The frequency scale is linear from 200 kHz to 5 MHz.

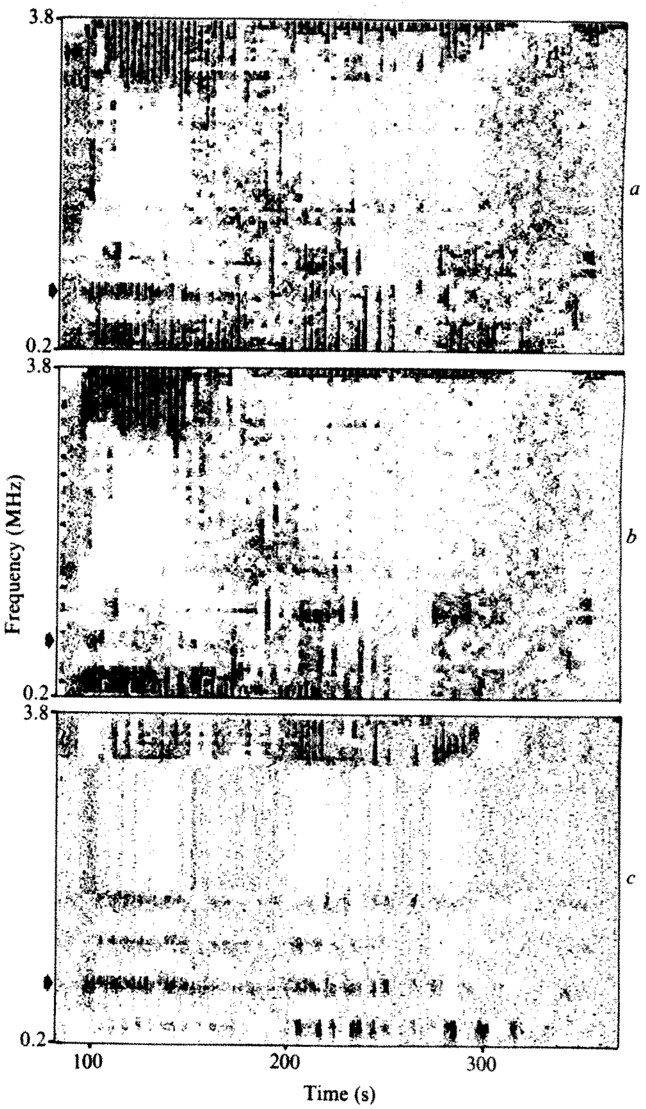

Fig. 2 3.4 s average spectra of electrostatic emissions observed by the electric boom-mounted sensors after subtraction of the average spectrum from 300 to 350 s to remove local interference signals. *a*, All data; *b*, data in between gun pulses; *c*, data during gun pulses. The arrow indicates the position of the emission at $0.7 f_{ce}$. The frequency scales are linear from 200 kHz to 3.8 MHz.

We can assume that towards the end of the flight, the effect of the gun electrons would be much reduced since the mother and daughter reach by then maximum separation, while the interference, if generated in the payload, should not change much. This allows us to correct for interference effects. Figure 2 shows grey scaled 3.4-s average spectra ($\frac{1}{2}$ spin) displayed after subtracting from them the average spectrum for the last part of the rocket flight (300–350 s).

Figure 2*a* shows all the wave data, Fig. 2*b* the wave data recorded in between gun pulses, and Fig. 2*c* the wave data during gun pulses. A distinctive feature of Fig. 2*a* is an emission in the band 0.8–1.0 MHz that persists from 95 s until ~260 s where it disappears in the noise. This emission is much reduced in Fig. 2*b* but enhanced in Fig. 2*c* to be the most distinctive feature in the spectrum. Clearly the emission is directly gun associated and decays rapidly at the end of a gun pulse. The average position of its peak during the 33.5-s data sets of the particle bunching is plotted on the base lines of Fig. 1 as a star for comparison. The close fit clearly shows that the frequency of the electron bunching coincides with that of the observed electrostatic wave. There is no conceivable way in which the two instruments could interfere with each other and we conclude the observed bunching effects are real.

Figure 2 shows clearly that the emission begins soon after 92 s, when the electron gun is switched on. A study of shorter 6.7-s (1 spin) data sets of the electron bunching indicates that no bunching occurred before this time. Similar data sets show that the electron bunching ceases between 250 and 260 s. At this time, the separation between the mother and daughter is ~40 m perpendicular to the geomagnetic field lines. A previous experiment carrying a similar electron gun[9] showed that at this separation the contribution to the observed fluxes by the gun electrons was vanishingly small.

The electron gun was pulsed every 163 ms with a pulse pattern lasting no more than 9.6 ms. The pulse pattern alternated between a single pulse of 9.6 ms, a single pulse of 0.96 ms or a group of six pulses each 1.9 ms. The electron bunching measurements were consequently sorted into three separate data sets for the period 80–260 s into the flight.

The first set contained all measurements made within 54 ms time bins centred on all electron gun pulses (of all three types), the second set corresponds to the next 54-ms time bins and the third set corresponds to the last 54-ms time bins before those containing the next gun pulse pattern. The values of Z of the peak observed around the 1-MHz frequency interval were 3.6, 2.9 and 1.9 respectively, thus showing that the bunching is directly related to the electron gun pulses. However, the measurements are carried out evenly in time but the duty cycle of the gun is much less than unity. Most of the recorded electrons are, therefore, of auroral origin with the observed bunching induced in them by the electron gun pulses.

Discussion

Typical electron plasma frequencies at this altitude are many megahertz, and we would expect to observe electron bunching around the electron plasma and upper hybrid frequencies. However, electron bunching and wave emission occurred at 0.8–1.0 MHz, that is around 0.7 of the local electron gyrofrequency f_{ce}. Several apparently significant peaks ($Z > 2$) occur above 1 MHz in the bunching spectra but, as mentioned above, we have ignored them as they may be spurious artefacts of the method of frequency analysis used here. We have, therefore, limited our discussion to the 0.9-MHz signal.

Jones and Kellogg[10] have provided the theory most relevant to the case of an artificial electron beam in the auroral ionosphere. Using beam-plasma parameters different from those in our case, they have shown that waves will grow in the electrostatic whistler mode but with a small growth rate. Results of calculations using parameters closer to those expected in our experiment show that the electrostatic whistler mode waves (or obliquely propagating electron plasma waves) are unstable in the region of 0.7 f_{ce} (V. K. Jain, personal communication). Maggs[11,12] has shown theoretically that natural electrostatic whistler noise undergoes convective beam amplification if there is a positive slope in the velocity distribution. Such a slope has been seen in natural auroral electron beams associated with waves of this type[6]. As noted above, the measured bunching occurred mainly in the natural auroral electrons, and this effect may have been enhanced or induced by the presence of the beam.

Bunching of naturally occurring intense auroral beams can also be expected, and this technique promises to be a valuable diagnostic tool in advancing our understanding of the processes involved in the aurora.

We thank B. Blackman for building the boom deployment system, B. Narheim for designing the omnidirectional counter, M. Moore and R. White for constructing the bunching electronics, Professor J. A. Bather for advice on statistical interpretation, Dr P. J. Christiansen and T. A. Jacobsen for helpful comments, and P. Rothwell for making available the video records of the aurora.

Received 11 April; accepted 26 June 1980.

1. Winckler, J. R., Arnoldy, R. L. & Hendrickson, R. A. *J. geophys. Res.* **80,** 2083 (1975).
2. Monson, S. J. Kellogg, P. J. & Cartwright, D. G. *J. geophys. Res.* **81,** 2193 (1976).
3. Monson, S. J. & Kellogg, P. J. *Cosmic Phys. Tech. Rep.* 172 (University of Minnesota, 1977).
4. Cartwright, D. G. & Kellogg, P. J. *J. geophys. Res.* **79,** 1439 (1974).
5. Kellogg, P. J. & Monson, S. J. *Geophys. Res. Lett.* **6,** 297 (1979).
6. Kisabeth, J. L. & Rostoker, G. *J. geophys. Res.* **84,** 853 (1979).
7. Spiger, R. J., Murphree, J. S., Anderson, H. R. & Loewenstein, R. F. *J. geophys. Res.* **81,** 1269 (1976).
8. Gough, M. P. *Nucl. Instrum. Meth.* (in the press).
9. Maehlum, B. N., Grandal, B., Jacobsen, T. A. & Troeim, J. *Planet. Space Sci.* (in the press).
10. Jones, T. W. & Kellogg, P. J. *J. geophys. Res.* **78,** 2166 (1973).
11. Maggs, J. E. *J. geophys. Res.* **81,** 1707 (1976).
12. Maggs, J. E. *J. geophys. Res.* **83,** 3173 (1978).

Nicholson's blowflies revisited

W. S. C. Gurney, S. P. Blythe & R. M. Nisbet

Department of Applied Physics, University of Strathclyde, Glasgow G4 0NG, UK

A simple time-delay model of laboratory insect populations which postulates a 'humped' relationship between future adult recruitment and current adult population gives good quantitative agreement with Nicholson's classic blowfly data and explains the appearance of narrow 'discrete' generations in cycling populations.

NUMEROUS elementary ecology texts use as illustrative examples of oscillatory population fluctuations, data drawn from the comprehensive and elegant experiments performed by Nicholson[1,2] on laboratory cultures of the sheep blowfly *Lucilia cuprina*; in these, the population was regulated by the rate of food supply to either the adult population (Fig. 1*a*) or the larval population (Fig. 1*b*, *c*). Notwithstanding their popularity as alleged examples of oscillatory behaviour, the large, quasi-periodic population fluctuations observed by Nicholson are still very imperfectly understood. It is clear from the work of Maynard Smith[3] and May[4] that a combination of high fertility and long development delay must be primarily responsible, and the discrete-time model developed by Varley, Gradwell and Hassell[5] further suggests that a degree of 'overcompensation' in the controlling density dependence may be important. However, beyond these rather generalized insights progress has been slight. Despite a variety of more or less sophisticated attempts[4–6], no theoretical model has yet yielded a truly satisfactory quantitative fit to the time history of even a single culture, still less has it been possible to formulate a comprehensive framework within which the various subtly different experimental results can be systematically inter-related.

In this article, we seek to formulate a model capable of providing such a framework, but as an initially less grandiose target we shall try to answer a number of specific questions about Nicholson's blowfly data. First, we must identify the class of mechanism which produces the quasi-periodic fluctuations; are they self-sustaining limit cycles perturbed by experimental

0028-0836/80/360017—05$01.00

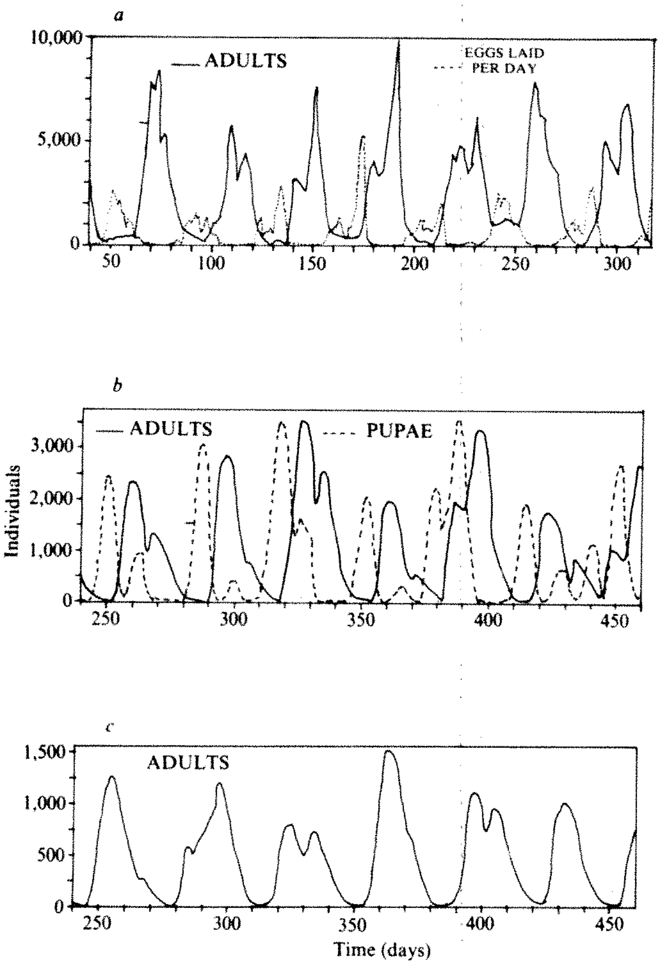

Fig. 1 Quasi-periodic fluctuations in laboratory populations of *Lucilia cuprina*. Population regulated by adult food supply (*a*), larval food supply (50 g per day) (*b*), larval food supply (25 g per day) (*c*). Data from ref. 1.

uncertainty and demographic stochasticity, or are they true quasi-cycles[7] driven by demographic or environmental stochasticity? Second, we wish to know what determines the period and amplitude of the cycles. Lastly and perhaps most interestingly, we wish to understand the observed patterns of breeding activity; specifically, why the two discrete generations per cycle observed in the larval food-limited case (Fig. 1*b*) occur at uneven time intervals, and why in the adult food-limited case (Fig. 1*a*) they merge into a single, almost continuous period of reproductive activity.

The time-delayed logistic model

If it is to be capable of answering questions about the form and timing of generations, our model clearly cannot simply assume that generations are discrete; rather, it must make the initial assumption of overlapping generations and its dynamics must be such as to cause the spontaneous appearance of clearly marked discrete generations in the appropriate conditions. This implies that it must be formulated in terms of a differential, rather than a difference, equation. Probably the simplest single-species continuous time model capable of generating cyclic or quasi-cyclic fluctuations is the time-delayed logistic

$$\frac{dN(t)}{dt} = rN\left[1 - \frac{N(t-T_D)}{K}\right] \qquad (1)$$

May[4] showed that this model gave an acceptable gross fit to the adult population data shown in Fig. 1*a* with a delay time T_D of about 9 days, a value which he argued compared acceptably with the observed delay time. However, there are several serious objections to the time-delayed logistic model both in general and as a specific explanation of Nicholson's data. First, close examination of the life history data[2] shows that the appropriate experimental value of T_D is 14.8 ± 0.4 days, which implies that the discrepancy between 'best fit' and experimental values is worryingly large compared with the confidence interval in the best fit value (±0.5 days). Second, the model "mixes up time-lagged and not time-lagged contributions" (R. M. May, personal communication) in a way which makes it a very poor paradigm for biological phenomena. However, even more serious than either of these objections is the fact that the time-delayed logistic model is entirely incapable of predicting two bursts of reproductive activity per adult population cycle. It is thus structurally incapable of explaining the results obtained by Nicholson in the larval food-limited regime.

A more realistic model

We now formulate an improved continuous time model of an insect population growing in an isolated laboratory culture. As the experimental data which will serve as the primary quantitative test of the model are mainly based on observations of adult population as a function of time, we begin by writing down a balance equation for the population of sexually mature adults, $N(t)$. The experimental conditions clearly preclude any immigration or emigration and thus the rate of change of N must simply be the difference between the total adult death rate (D) and the rate of recruitment to the adult population (R). If we assume that the *per capita* adult death rate has a time- and density-independent value δ, then

$$\frac{dN}{dt} = R - D = R - \delta N \qquad (2)$$

The adult recruitment rate, R, should be evaluated by writing down analogous balance equations for all the life history stages of the species concerned. However, we can evade the resulting complexity (and increase the generality of our model) with the aid of three simplifying assumptions: (1) the rate at which eggs are produced depends only on the current size of the adult population; (2) all eggs which develop into sexually mature adults take exactly T_D time units to do so; (3) the probability of a given egg maturing into a viable adult depends only on the number of competitors of the same age. Together, these assumptions imply that the rate of recruitment at time t can only be a function of the size of the adult population at time $t - T_D$

$$R = R(N(t - T_D)) \qquad (3)$$

so that the entire population dynamic can be expressed by a single delay-differential equation

$$\frac{dN}{dt} = R(N(t - T_D)) - \delta N(t) \qquad (4)$$

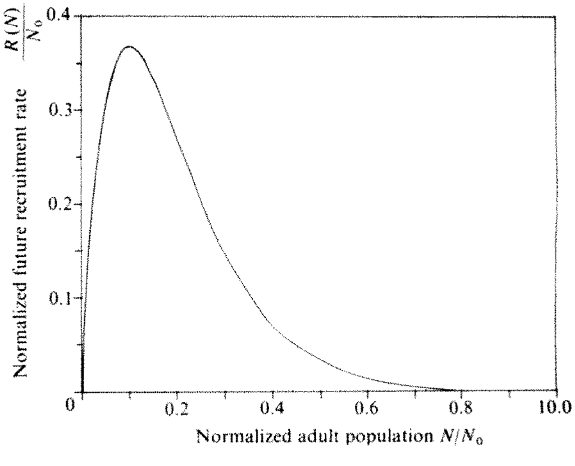

Fig. 2 Assumed dependence of future recruitment rate against present adult population.

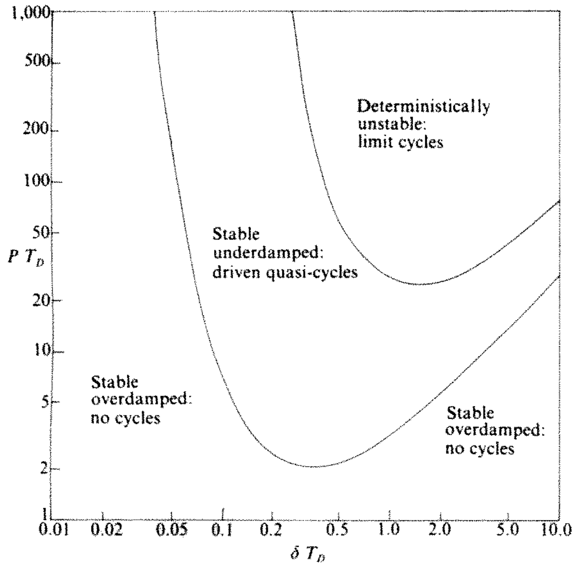

Fig. 3 Qualitative behaviour of the model as a function of the controlling parameters PT_D and δT_D.

Although the recruitment rate function $R(N)$ can in principle be subject to experimental measurement, we wish our model to act as a paradigm for a rather larger class of similar models as well as provide a detailed fit to Nicholson's data, and we therefore seek rather to write down an appropriate algebraic form for $R(N)$. We consider first those experiments in which the only limiting factor is the rate at which food is supplied to the adult population. Here, egg to adult survival may reasonably be expected to be density independent, so that the rate of adult recruitment at time t will be directly proportional to the rate at which eggs were being laid at time $t-T_D$. Provided that the population sex ratio remains reasonably constant, it seems plausible to suppose that, in the presence of excess food, the total rate at which eggs are produced by a population of N adults will be directly proportional to N. However, when food is supplied at a limited rate, intraspecific competition will clearly act to reduce the average *per capita* fecundity of the members of large populations to well below its physiological saturation value. Indeed, where competition is of the 'scramble' type[1], it seems highly likely that very large populations will require the whole of their restricted food intake for physiological maintenance and will thus produce no offspring at all. Clear experimental evidence of such an effect can be found in Fig. 1*a*, which shows that in Nicholson's adult food-limited culture the total egg production rate drops to zero at high populations. Any plausible functional form for $R(N)$ must therefore go to zero as N becomes either very large or very small. In addition, it seems likely that most recruitment curves will display a single maximum (see Fig. 2) at an intermediate population whose size is determined by the available resources. We therefore choose to represent $R(N)$ by a simple function which displays all these properties

$$R(N) = PN \exp\{-N/N_0\} \qquad (5)$$

where P is the maximum possible *per capita* egg production rate (corrected for egg to adult survival) and N_0 is the population size at which the population as a whole achieves maximum reproductive success.

In experiments in which the controlling factor is the rate of food supply to the larval population, the situation is at first sight entirely different. Here, the adults are always provided with excess food and thus always produce eggs at their physiological maximum rate. However, competition among the larvae now makes egg to adult survival highly density dependent, and indeed, Nicholson's batch culture experiments strongly suggest that when an age class is very large, none of its members will actually pupate successfully. Thus, within the limitations of our assumption that egg to adult survival is affected only by competition within a given age class, we can use equation (5) to describe recruitment in both the adult food-limited and the larval food-limited cases.

The dynamics of our model are thus always described by

$$\frac{dN(t)}{dt} = PN(t-T_D)\exp\{-N(t-T_D)/N_D\} - \delta N(t) \qquad (6)$$

which has a single non-trivial stationary state

$$N^* = N_D \ln(P/\delta) \qquad (7)$$

It can easily be shown that the local stability of the steady state and the qualitative properties of the fluctuations about it are entirely controlled by the two quantities PT_D and δT_D, and in Fig. 3 we show the disposition in the $PT_D/\delta T_D$ plane of the various regions of qualitatively different behaviour. Because we seek to understand fluctuations which are at least quasi-periodic, we shall restrict our detailed analysis to the stable/underdamped (damped oscillatory) and locally unstable regions.

If the parameters of our deterministic model are in the stable/underdamped region, we would expect the demographic stochasticity present in a real system to induce quasi-cyclic population fluctuations consisting of bursts of relatively coherent cycles whose period is close to the deterministic natural period, interspersed with short periods of incoherent noise[7]. If we describe the return of an underdamped system to its deterministic equilibrium by a coherence number n_c, defined as the number of cycles over which the amplitude of the transient is reduced by a factor e, then it is found empirically[8] that when such a system is executing driven quasi-cycles, each burst of coherent cycles contains an average of roughly $3n_c$ cycles. Thus, in Fig. 4 we characterize the quasi-cyclic behaviour of our model in the stable/underdamped regime by plotting contours of constant normalized cycle period (T/T_D) and constant coherence number n_c on the appropriate part of the $PT_D/\delta T_D$ plane.

For model parameters in the locally unstable region, the exact solution of equation (6), which can be obtained by numerical integration, takes the form of a self-sustaining oscillation. For some parameter values this is a simple limit cycle, whereas for

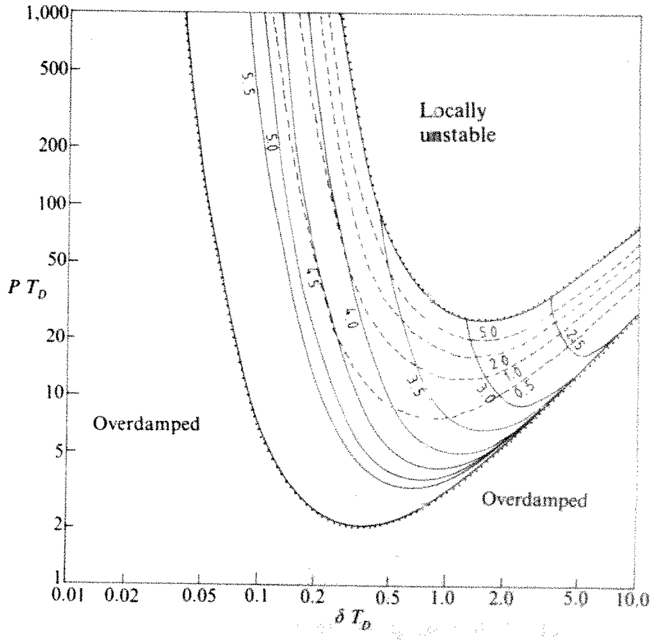

Fig. 4 Characterization of quasi-cyclic behaviour in the stable/underdamped region. Contours of constant normalized period T/T_D (———) and coherence number (– – – –) in the $PT_D/\delta T_D$ plane.

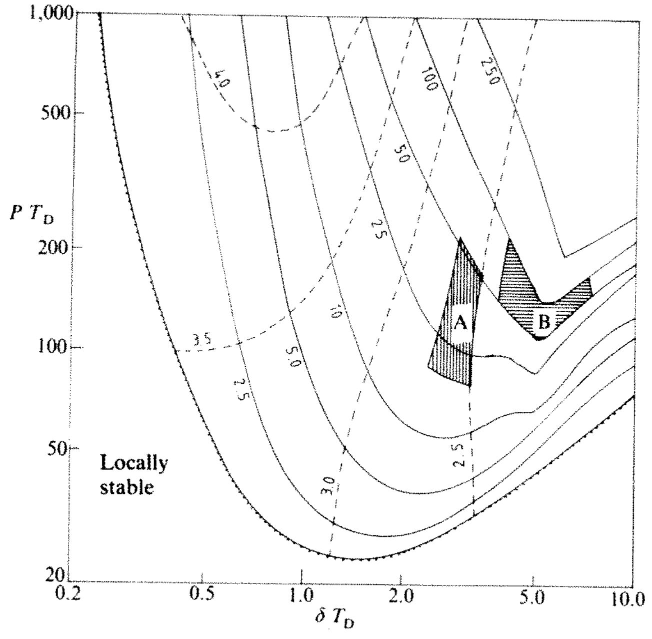

Fig. 5 Characterization of limit cycle behaviour in the locally unstable region. Contour of constant normalized period T/T_D (– – – –) and population ratio $N_{\max}/N_{\min}$ (———) in the $PT_D/\delta T_D$ plane. The area marked A shows the best fit parameters for the data of Fig. 1*a* and the area marked B corresponds to the data of Fig. 1*b*.

others it is a more complex cycle or is even formally aperiodic. In all cases, however, a spectral analysis of the solution reveals a single clearly marked dominant period (T). We have therefore characterized the solutions in this region by the ratio of this dominant period to the development delay (T/T_D) and the ratio of maximum to minimum population observed during the cycle ($N_{\max}/N_{\min}$). In Fig. 5 we plot contours of these quantities in the appropriate part of the $PT_D/\delta T_D$ plane.

An experimental test

As a quantitative test of our model, we now determine the parameter values which give the best fit to the gross characteristics (T/T_D and $N_{\max}/N_{\min}$ or n_c) of the fluctuations in the adult population of Nicholson's blowfly cultures, and then compare these best fit values with independent experimental estimates of the same quantities. We restrict our attention to the adult food-limited case (Fig. 1*a*), because only here do the data allow us to make an accurate independent estimate of the maximum *per capita* fecundity (P).

There is no simple test which will tell us *a priori* whether the fluctuations shown in Fig. 1*a* are self-sustaining limit cycles or driven quasi-cycles, so we must determine the best fit parameters under both hypotheses. If we assume that the fluctuations are of limit cycle type, then our quantitative characterization requires us to measure the maximum to minimum population ratio $N_{\max}/N_{\min}$ and the normalized cycle period T/T_D; quasi-cyclic fluctuations we characterize by $\bar{T}/T_D$ and the coherence number n_c. Examination of Fig. 1*a* combined with our previous identification of the correct value of the delay T_D as 14.8±0.4 days reveals that these quantities lie in the ranges

$$2.5<(T/T_D)<2.7; \quad 29<(N_{\max}/N_{\min})<53; \quad 2<n_c<5 \qquad (8)$$

which enables us to infer from the contour maps given in Figs 4 and 5 that the best fit values of the controlling parameters PT_D and δT_D for the limit-cycle hypothesis are

$$PT_D=150\pm70 \quad \delta T_D=2.9\pm0.5 \qquad (9a)$$

and for the quasi-cycle hypothesis

$$PT_D=23.5\pm4.5 \quad \delta T_D=3.0\pm0.7 \qquad (9b)$$

Although the best fit values of δT_D required under the two hypotheses are essentially indistinguishable, it is clear that the appropriate values of PT_D differ by more than a factor of 6. Thus, an independent estimate of the maximum *per capita* fecundity P will provide a clear *a posteriori* test of the mechanism underlying the observed cycles. We can easily obtain such an estimate from the egg-laying rate data in Fig. 1*a* by recognizing that, because the adult population minima are clearly below the maximum of the total reproduction curve, the value of P is simply given by

$$Pe^{-1}=\frac{\text{Maximum rate of egg-laying}}{\text{population producing maximum reproduction}} \qquad (10)$$

The value of P thus inferred from Fig. 1*a* is in the range 7.4 per day $<P<11.4$ per day, so that our final independent estimate of the controlling parameter PT_D is

$$PT_D=130\pm30 \qquad (11)$$

which is clearly compatible with the value required under the limit cycle hypothesis and absolutely incompatible with the quasi-cycle hypothesis. This, together with the fact that an independent estimate of δT_D is in good general agreement with the values required under both hypotheses, gives us considerable confidence that the fluctuations observed by Nicholson in the adult food-limited case are of limit-cycle type.

Separate generations in cycling populations

Our rather simplistic initial characterization of the non-linear behaviour of equation (6) in the limit-cycle region in fact conceals a wealth of complexity, for the formal repeat period of the cycles can often be many times the empirically observed dominant period. The general pattern is very similar to that seen by Mackay and Glass[9] and May[10] in equations of similar structure; close to the local stability boundary the solution is a simple limit-cycle with period T, but moving deeper into instability produces a number of successive doublings of the repeat time until a region is reached where the solution is formally aperiodic (chaos). Beyond the chaotic region we again see cyclic fluctuations.

These variations in the fine structure of the adult population fluctuations, although mathematically fascinating, are likely to be hard to identify experimentally in the presence of realistic levels of experimental uncertainty. However, the accompanying variations in the predicted pattern of reproductive activity are not only sufficiently dramatic to be easily identified experimentally, but also provide a clear explanation of Nicholson's observation that, in certain experimental circumstances, breeding occurred in quasi-discrete 'generations' but that in others it was much more nearly continuous. The mechanism by which separation of generations can occur in our model is illustrated in Fig. 6. When the minimum adult population in the trough of the cycle ($N_{\min}$) is greater than the population size at which maximum total reproduction occurs, N_0, then breeding activity ($R(N)$) is essentially continuous with one broad peak per cycle (Fig. 6*a*). When $N_{\min}$ is slightly less than N_0 (Fig. 6*b*), the pattern is still much the same but the reproduction rate peak now has a distinctive 'double-humped' shape. However, when $N_{\min} \ll N_0$, the pattern changes dramatically. In simple cases such as Fig. 6*c*, each adult population peak generates two narrow discrete generations, whereas in more complex cases such as Fig. 6*d*, when the adult population variation is only quasi-periodic, the generations are also very variable in size.

We have tested the plausibility of this mechanism as an explanation of Nicholson's observations by comparing the

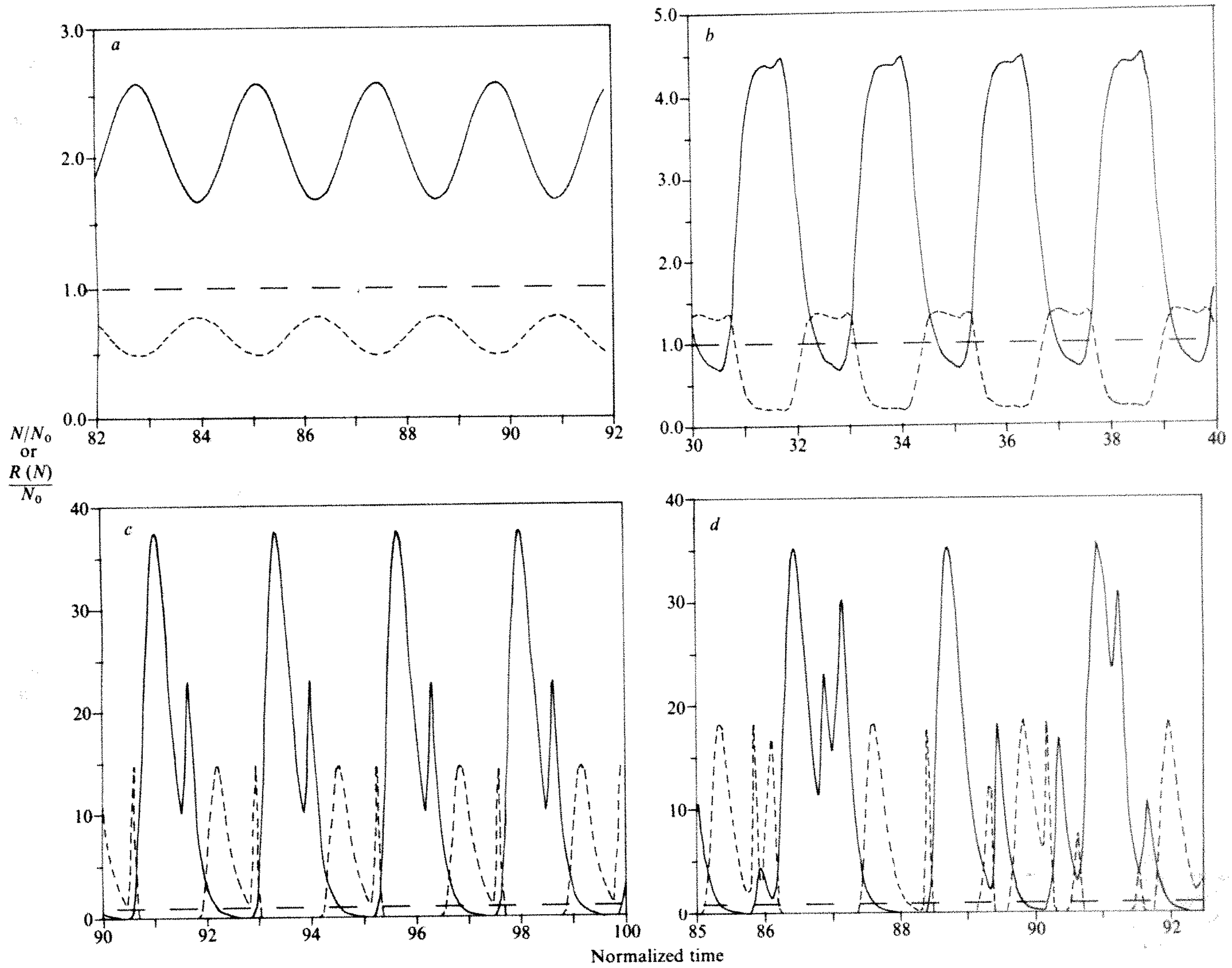

Fig. 6 Separation of generations in a cycling population. Normalized adult population (———) and normalized future recruitment rate (– – – –) as functions of time. *a*, $N_{\min} \gg N_0$: continuous reproduction; *b*, $N_{\min} \sim N_0$: one generation per cycle; *c*, $N_{\min} \ll N_0$: two generations per cycle; *d*, $N_{\min} \ll N_0$ and adult fluctuations aperiodic: complex generation pattern.

patterns of breeding activity predicted by our model with best fit parameters determined from the adult population fluctuations shown in Fig. 1*a* and *b*. For the adult food-limited case (Fig. 1*a*), we predict a single double-humped peak per population cycle, whereas in the larval food-limited case (Fig. 1*b*), we predict that breeding should take place in clearly distinguishable generations occurring at uneven time intervals. It is clear from the egg-laying rate and pupal population data given in Fig. 1*a* and *b*, respectively, that this strongly marked qualitative change is indeed observed experimentally.

Conclusions

The model described above provides a satisfying qualitative fit to Nicholson's blowfly data, and its extreme simplicity thus allows us to deduce that the observed fluctuations arise from the combination of a long development delay with a single-humped total reproduction curve. Moreover, it seems clear that any model containing these two generic features must behave in a generally similar way, so that our picture of the way in which discrete generations may be spontaneously maintained in cycling populations should in fact be rather generally applicable.

This model may thus be the prototype of a family of models which will unify the hitherto diverse 'discrete generation' and 'overlapping generation' views of insect population dynamics and lead to a clearer understanding of the uneven timing of insect generations both in the constant environment of the laboratory and in the variable environments encountered in the field. However, considerable further development will be required before we can fully assess the potential of the framework provided by such models to elucidate the subtle systematic differences in behaviour between various populations. As the range of technically feasible modifications is immense, we strongly believe that further development can only be done efficiently in conjunction with a comprehensive experimental programme.

One of us (S.B.) received an NIED postgraduate grant during this work.

Received 2 May; accepted 20 June 1980.

1. Nicholson, A. J. *Aust. J. Zool.* **2,** 9–65 (1954).
2. Nicholson, A. J. *Cold Spring Harb. Symp. quant. Biol.* **22,** 153–173 (1957).
3. Maynard Smith, J. *Models in Ecology* (Cambridge University Press, 1974).
4. May, R. M. *Stability and Complexity in Model Ecosystems* (Princeton University Press, 1973).
5. Varley, G. C., Gradwell, G. R. & Hassell, M. P. *Insect Population Ecology* (Blackwell, Oxford, 1973).
6. Auslander, D. M., Oster, G. F. & Huffaker, C. B. *J. Franklin Inst.* **297,** 345–376 (1974).
7. Nisbet, R. M. & Gurney, W. S. C. *Nature* **263,** 319–320 (1976).
8. Nisbet, R. M., Gurney, W. S. C. & Pettipher, M. *J. theor. Biol.* **68,** 143–160 (1977).
9. Mackay, M. C. & Glass, L. *Science* **197,** 287–289 (1977).
10. May, R. M. *Proc. Int. Conf. on Nonlinear Dynamics* (New York, 1979).

~~R5P2~~ R413

Enkephalin blocks inhibitory pathways in the vertebrate CNS

R. A. Nicoll, B. E. Alger & C. E. Jahr

Departments of Pharmacology and Physiology, University of California, San Francisco, California 94143

Enkephalin markedly attenuates a variety of GABAergic inhibitory pathways in the CNS, but does not affect the action of GABA. The action of enkephalin is reversed by the specific opiate antagonist, naloxone. Thus, inhibitory interneurones may be primary targets for opioid peptide-containing pathways and disinhibition may be of general importance for opioid peptide action in the CNS.

OPIATE receptors and opioid peptides have been found in a variety of central nervous system (CNS) structures[1]. However, the distribution of these receptors and peptides gives little indication of their possible physiological role. The cellular action of opiates and opioid peptides in the CNS has been the subject of a number of reports (for review see ref. 2). There is considerable evidence of a presynaptic inhibitory role for opioid peptides[3–6] as well as a direct postsynaptic inhibitory action[2,7]. In the CNS, iontophoretic application typically inhibits the firing of sensitive neurones. However, a survey of opioid effects on neuronal activity in several brain regions of the rat revealed naloxone-reversible excitatory effects, and in the hippocampus 90% of the pyramidal cells encountered were strongly excited by enkephalin[7]. Further *in vivo* iontophoretic studies by Zieglgänsberger *et al.*[8] suggested that this excitation may be mediated indirectly by inhibition of neighbouring inhibitory interneurones, resulting in a disinhibition of pyramidal cells. Several recent studies, using primarily extracellular field potential and unit recording in slice preparations, support the proposal that enkephalin depresses the inhibition of pyramidal cells[9–15]. However, a number of questions remain. For instance, different studies have suggested preferential opiate effects on recurrent, or alternatively, on feedforward inhibition, and the site of the opiate effects, whether pre- or postsynaptic, is unknown[11]. Direct effects on excitation have not been ruled out, and there has been some question about the naloxone reversibility of the opiate action[16]. To some extent these difficulties can be attributed to the use of field potential and extracellular unit recording techniques, the results of which may be difficult to interpret. Here, we have used the hippocampal slice preparation and intracellular recording to analyse the cellular actions of enkephalin. In addition, we have extended these results to the *in vitro* olfactory bulb and spinal cord.

Enkephalin blocks i.p.s.ps in hippocampal pyramidal cells

The rat hippocampal slice preparation used in our experiments has been described elsewhere[17]. Stimulating electrodes were placed on the alveus for antidromic activation and in the stratum radiatum for orthodromic activation of pyramidal cells. Pentobarbital (0.1 mM) was added to the perfusate in some experiments, not only to enlarge and prolong the inhibitory postsynaptic potentials (i.p.s.ps), but also to unmask a feedforward, dendritic form of inhibition[17]. The stable enkephalin analogue, D-Ala^2-Met^5-enkephalinamide (DALA), was used in most experiments and was applied by bath perfusion in known concentrations.

We first tested the effects of DALA on field potentials recorded from the stratum pyramidale in response to orthodromic and antidromic stimulation. In the presence of DALA (5 μM), the size of the initial pyramidal population spike increases and additional population spikes appear, although there is no change in the amplitude of the antidromic response (Fig. 1). The facilitation of orthodromic responses is entirely reversed by the addition of naloxone. Concentrations of DALA as low as 10^{-8} M were effective, whereas morphine and Met-enkephalin required 10–100-fold higher concentrations. These findings (see refs 9, 10, 12–15) indicate that opiates, by activating opiate receptors, markedly enhance the excitatory synaptic responses of pyramidal cells, while having no demonstrable effect on antidromic responses.

To determine the mechanism for this profound and selective action, we have used intracellular recording from CA1 pyramidal cells. The left-hand column of Fig. 2 illustrates responses to antidromic stimulation and to two intensities of orthodromic stimulation, recorded with a potassium methylsulphate-filled electrode. The substantial reduction in the deflections caused by hyperpolarizing current pulses indicates that there is a fall in membrane resistance during the i.p.s.p. The i.p.s.p. produced by antidromic stimulation is of short duration and thought to be generated by a collateral feedback, interneuronal circuit mediated by γ-aminobutyric acid (GABA)[18]. The orthodromic i.p.s.p. evoked by high intensity stimuli has an additional depolarizing component which is considered to be generated by a feedforward pathway involving a set of GABA interneurones distinct from those involved in the feedback pathway[17]. DALA has little effect on the membrane potential or resistance of pyramidal cells, and the size of both the orthodromic and antidromic evoked i.p.s.p. is decreased. However, we have consistently found that feedforward inhibitory potentials to orthodromic stimulation are attenuated to a considerably greater extent than the responses to antidromic stimulation

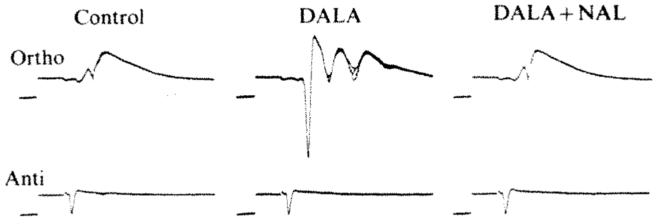

Fig. 1 Effect of opioid peptide (DALA) on field potentials in the hippocampal slice. The left-hand traces show the control responses recorded with an extracellular electrode in the pyramidal cell layer to antidromic (Anti) and orthodromic (Ortho) stimulation. The sharp downward deflections represent the synchronous firing of pyramidal cells and are termed population spikes. The middle traces show that exposure to 5 μM DALA greatly augments the orthodromic population spike and creates later population spikes while having no effect on the antidromic responses. Addition of naloxone (2 μM) to the DALA solution (DALA + NAL) completely reverses the effects of DALA. The calibration pulse at the beginning of each trace is 2 mV and 5 ms.

0028–0836/80/360022—04$01.00

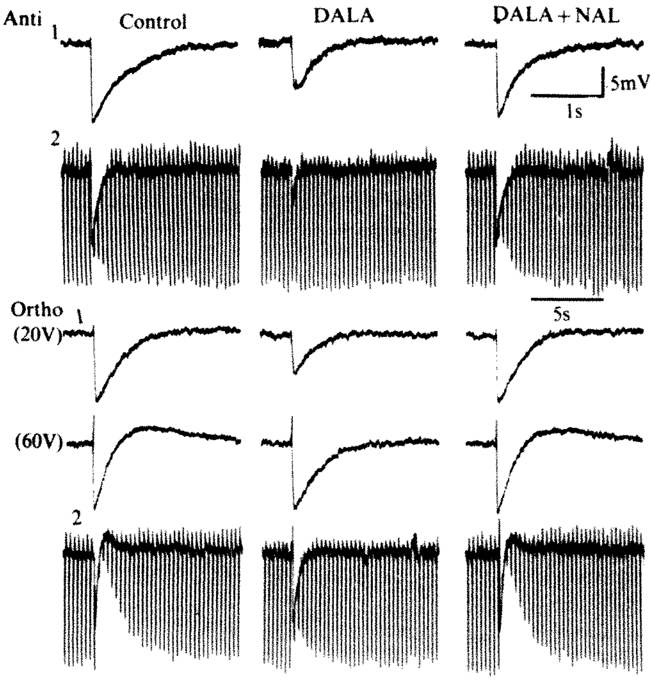

Fig. 2 Opioid peptide (DALA) antagonizes evoked i.p.s.ps in a hippocampal pyramidal cell. The responses to antidromic stimulation are shown at a fast (Anti$_1$) and a slow (Anti$_2$) chart speed with constant current hyperpolarizing pulses. The orthodromic responses are shown at a fast chart speed (Ortho$_1$), and at a low (20 V) and high (60 V) stimulus intensity. Note the late slow depolarization with high intensity stimulation. The response to high stimulus intensity is also shown at a slow chart speed (Ortho$_2$) with constant current hyperpolarizing pulses. The gain is the same in all records. The left-hand column shows the control responses. The records in the middle column were obtained 12 min after switching to 5 μM DALA, and the records in the right-hand column were obtained 15 min after adding 2 μM naloxone to the DALA-containing solution. The bathing medium contained 10^4 M pentobarbital. The resting membrane potential of this cell was −65 mV.

which are generated exclusively by a feedback pathway. In control conditions, orthodromic stimulation elicits a single action potential in pyramidal cells, whereas in the presence of DALA, multiple spikes are usually generated. In all 24 cells examined, DALA attenuated i.p.s.ps and thereby facilitated the ability of an excitatory postsynaptic potential (e.p.s.p.) to fire the cell. These effects of DALA were entirely reversed by naloxone, which by itself had no effect. The attenuation of the i.p.s.p. by DALA was also seen with KCl-filled electrodes, which reversed the i.p.s.ps into large depolarizing potentials (Fig. 3) and resulted in many spontaneous potentials appearing on the baseline (Fig. 4). These depolarizing spontaneous potentials, which are never seen in CA1 pyramidal cells when electrodes are filled with impermeant anions, are blocked by GABA antagonists, prolonged by pentobarbital and abolished by tetrodotoxin[19]. Because true quantal release (release of individual packets of transmitter) is resistant to tetrodotoxin blockade of electrical excitability[20], we conclude that these potentials represent small i.p.s.ps generated by the spontaneous discharge of inhibitory interneurones. With KCl-filled electrodes, cells typically hyperpolarized a few millivolts when exposed to DALA; this resulted from a cessation of spontaneous i.p.s.ps ($n = 7$). The film records in Fig. 4 illustrate this blocking action of DALA on the potentials and its reversal by naloxone.

The present findings indicate that the primary effect of DALA on pyramidal cells is indirect and involves a disinhibition, as proposed previously[8]. Although the effects of GABA antagonists are virtually identical to those reported here for DALA (see also refs 9–15), the DALA antagonism does not occur at the level of the GABA receptor, because the responses to exogenous GABA are not antagonized by DALA (Fig. 3). We consider the blockade of spontaneous i.p.s.ps by DALA to suggest that DALA exerts its effect at the level of the cell body of the inhibitory interneurone, suppressing cell discharge, although a more direct action on GABAergic synaptic terminals[3–6] cannot be excluded by these results. It is interesting that the opiate receptor distribution in the CA1 region determined autoradiographically[21] would agree well with the location of interneurones thought to mediate inhibition[18]. Immunohistochemical studies of the hippocampus[22] suggest that the enkephalin-containing fibres and terminals are present mainly in the very small CA2 field. Perhaps a non-enkephalin, opioid-containing fibre system exists in CA1, or perhaps enkephalin is capable of diffusing from CA2 to the nearby CA1.

Enkephalin blocks dendrodendritic inhibition in the olfactory bulb

We have examined the effects of DALA on other forms of inhibition in the CNS to determine how widespread a phenomenon disinhibition might be. We have recently developed an isolated turtle olfactory bulb preparation to examine dendrodendritic inhibition of mitral cells, using intracellular recording[23]. In all cells tested ($n = 7$), DALA markedly attenuated i.p.s.ps evoked either orthodromically or antidromically, and was particularly effective against those generated at reciprocal synapses by direct depolarization of the mitral cell (Fig. 5, middle column). This effect occurred with little change in the resting membrane properties of mitral cells. Moreover, naloxone could reverse the i.p.s.p. depression (Fig. 5, right-hand column). Because the directly evoked i.p.s.p. is generated solely by dendritic reciprocal synapses, DALA seems to be acting directly on the reciprocal synapses. This site of action agrees with neurochemical and anatomical results. Opiate receptor binding is high in the layers of the bulb in which reciprocal synapses exist[24]. Anatomical studies[25,26] have shown that centrifugal fibres do not make direct contact with mitral cells, but end exclusively on inhibitory interneurones. Of particular interest is the finding that some of the centrifugal fibres synapse directly onto the gemmules of granule cells, the structures which form the reciprocal synapses[25,26]. It will be of interest to see if some of these centrifugal fibres contain enkephalin.

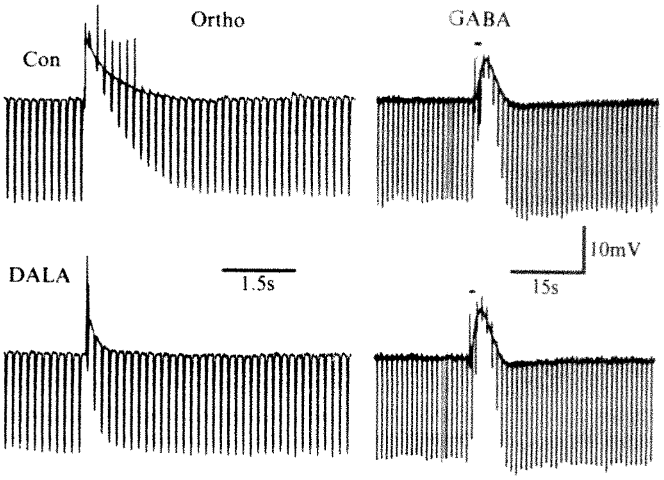

Fig. 3 Opioid peptide (DALA) is not a GABA antagonist. The upper traces show the response to orthodromic stimulation (Ortho) and to an iontophoretic GABA pulse (80 nA) applied to the apical dendrites and recorded from the soma of a pyramidal cell. The lower records were obtained 5 min after switching to a 5 μM DALA-containing solution. The cell hyperpolarized 3 mV, resulting in a slight increase in the GABA responses. The orthodromic response is markedly curtailed. The bathing medium contained 10^{-4} M pentobarbital. The membrane potential was −52 mV. The recording electrode was filled with 3 M KCl.

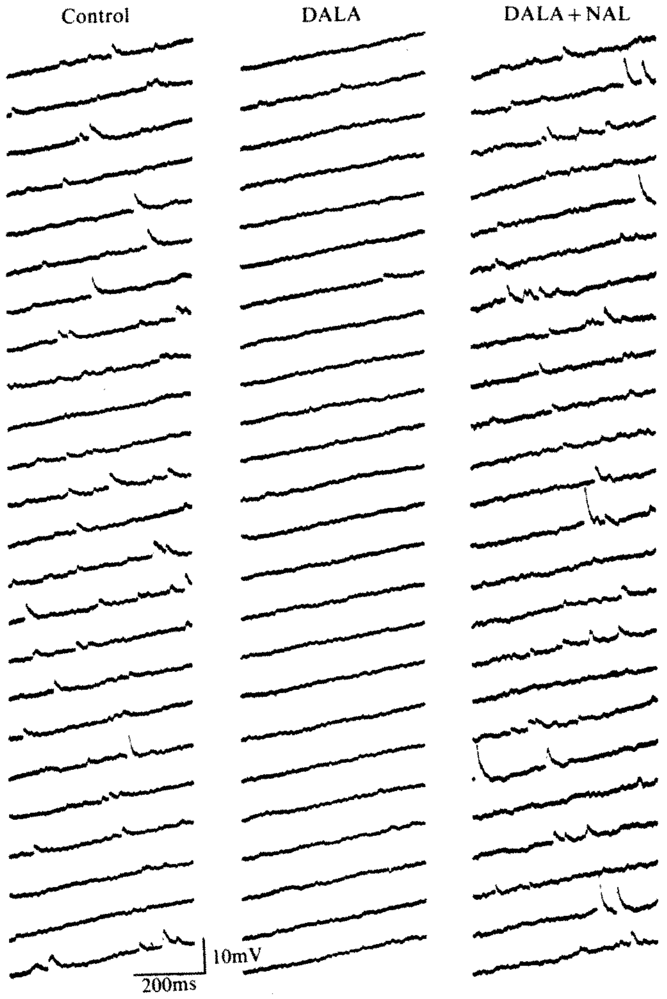

Fig. 4 Opioid peptide (DALA) blocks spontaneous i.p.s.ps in hippocampal pyramidal cell. The responses were recorded on running film with a 3 M-KCl filled microelectrode in the absence of pentobarbital. To block spontaneous action potentials the membrane was hyperpolarized to −69 mV while the film records were obtained. Switching to a solution containing 5 μM DALA for 6 min eliminates the spontaneous depolarizing potentials. Addition of 2 μM naloxone to the DALA-containing solution reverses the depressant action of DALA. The resting membrane potential was −53 mV in control, −56 mV in DALA and −50 mV in DALA+NAL. The faster decay of the potentials in DALA+NAL was due to a fall in membrane resistance resulting from imperfect sealing of the electrode when these records were obtained.

Enkephalin blocks presynaptic inhibition in the spinal cord

Finally, we have tested the effects of DALA on presynaptic inhibition in the isolated spinal cord of the frog in 20 preparations. The techniques used to stimulate and record from this preparation have been described previously[27]. In this preparation, stimulation of the ventral root depolarizes primary afferent terminals. This response can be recorded from the dorsal root with extracellular electrodes and is referred to as a dorsal root potential (d.r.p.)[28,29]. We have found that DALA produces a remarkable and almost complete block of both the d.r.p. (Fig. 6*A*, *B*) and the accompanying inhibition of primary afferent transmission (Fig. 6*C*). This effect is quite selective, for at a time when the d.r.p. is virtually abolished, synaptic excitation by large myelinated primary afferents is either unaffected or actually enhanced. The d.r.p. evoked by stimulating an adjacent dorsal root is less sensitive to DALA. However, both the rising phase of the d.r.p. and the dorsal root reflex (which are considered to be mediated by GABA[30,31]), are depressed by DALA. Although Met-enkephalin and morphine produced effects similar to DALA in the spinal cord, approximately 100-fold higher concentrations were required. A similar depression of d.r.ps by enkephalin and morphine has been observed in the isolated rat spinal cord[32] and intact cat[35,36].

In addition to depressing d.r.ps, DALA hyperpolarizes primary afferents. This effect is due partly to a block of the spontaneously occurring d.r.ps (Fig. 6*A*) and partly to a direct action on the terminals, as the hyperpolarization is not abolished when synaptic transmission is blocked by magnesium or tetrodotoxin. The block of d.r.ps, presynaptic inhibition and the hyperpolarization are all completely reversed by naloxone (Fig. 6*A*). GABA, or a closely related neutral amino acid, is thought to be the transmitter responsible for depolarization of primary afferents[27,29,31]. However, as in the case with hippocampal pyramidal cells, the actions of GABA (Fig. 6*B*) and β-alanine on primary afferents is unaffected by DALA at a time when the d.r.ps are abolished. Therefore, the action of DALA must occur at some earlier step in this pathway, possibly on cell bodies of presynaptic inhibitory interneurones or directly on the axo-axonic synapses.

Concluding remarks

We have found that excitatory opiate effects in various parts of the vertebrate CNS are caused indirectly, and actually occur as the result of disinhibition. These forms of inhibition include feedforward and recurrent inhibition of hippocampal CA1 pyramidal cells, dendrodendritic postsynaptic inhibition of olfactory bulb mitral cells, and presynaptic inhibition of spinal primary afferents. Because enkephalin does not antagonize the action of GABA, the putative neurotransmitter for these inhibitory pathways, a depression of inhibitory interneurone excitability and/or a block in GABA release from nerve terminals are likely explanations for the disinhibition caused by enkephalin. The depression of putative inhibitory neuronal firing by enkephalin, reported by others, would favour the former explanation[8,13].

Such a disinhibitory mechanism at supraspinal sites could help explain the epileptic activity seen following administration of opioid peptides[33,34]. Although morphine is relatively ineffective in blocking i.p.s.ps, generalized seizures have been reported following high systemic doses[37]. Furthermore, the present findings suggest that disinhibition may be an important general mechanism of opioid action in the CNS and that local, GABA-containing, inhibitory interneurones are primary targets of enkephalin-containing fibre systems. Such neurones are thought to have a key role in integrating neuronal information within a given region. Very small changes in the release of enkephalin would, by modifying the spontaneous activity of inhibitory

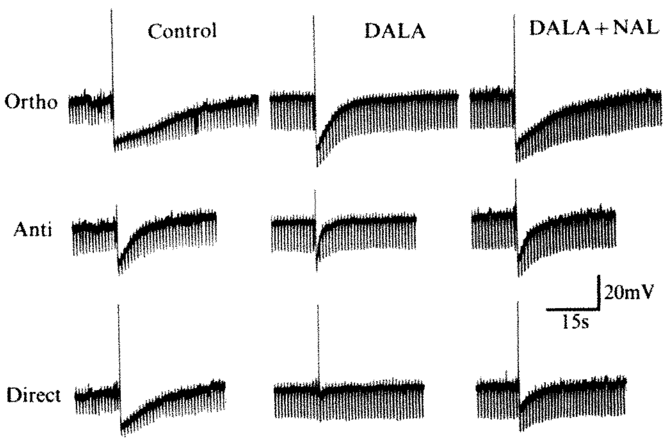

Fig. 5 Opioid peptide (DALA) blocks i.p.s.ps recorded intracellularly from an olfactory bulb mitral cell. The top records were obtained by stimulating the olfactory nerves, the middle records by mitral cell axon stimulation, and the bottom records by direct depolarizing current pulses which discharged the cell. The left-hand column shows the control responses. The middle column shows the responses obtained 20 min after perfusion with a Ringer containing 10 μM DALA. The right-hand column was obtained 40 min after the addition of 7 μM naloxone to the enkephalin-containing Ringer solution. The downward deflections represent responses to constant current hyperpolarizing pulses. The microelectrode was filled with 3 M potassium methylsulphate. The membrane potential of this neurone was −55 mV.

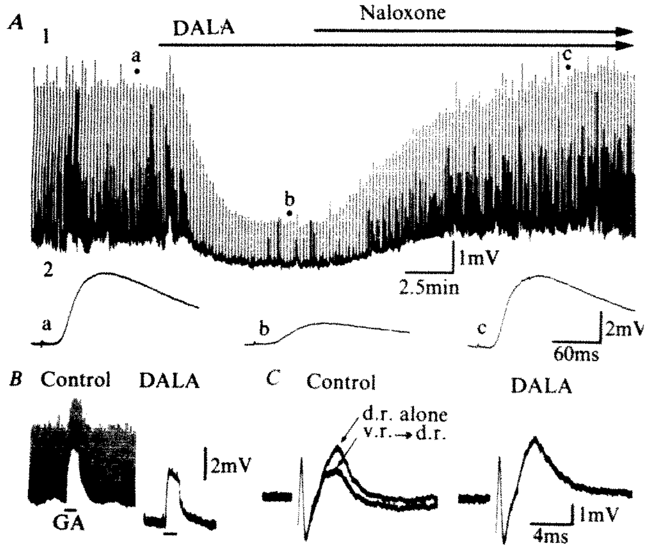

Fig. 6 Opioid peptide (DALA) blocks dorsal root potentials in the isolated frog spinal cord. A_1 shows a continuous recording with sucrose gap from the dorsal root. Dorsal root potentials (d.r.ps) (upward deflections) were evoked by stimulating a ventral root. 5 μM DALA greatly reduced the spontaneous and evoked d.r.ps. Naloxone (2 μM) reverses the effects of DALA. A_2 shows sample film records of the d.r.p. evoked at the times indicated by the small letters. *B* shows that DALA (10 μM) has no effect on the GABA sensitivity of the primary afferents at a time when it abolishes d.r.ps (upward deflections). The time scale is the same as in A_1. *C* shows superimposed film traces recorded with an extracellular electrode positioned in the dorsal horn. Stimulation of the dorsal root elicits a fast presynaptic fibre spike followed by a slow postsynaptic response (d.r. alone). Stimulation of the dorsal root 40 ms after a conditioning ventral root stimulus, at the peak of the d.r.p., results in a decreased postsynaptic response (v.r.→d.r.). DALA (10 μM) which completely abolished the d.r.p. in this preparation also blocks the decrease in the postsynaptic response.

interneurones, result in profound changes in the propagated output of principal cells.

In general, we can conclude that the cellular localization of neurotransmitter receptors may be more meaningful than their overall density in determining the relative importance of the neurotransmitter in a particular CNS region. In the present case, opioid peptides have physiological effects which would at first glance seem to be disproportionately large in comparison with the modest concentration of endogenous peptides or opiate receptors. These effects can be accounted for by the findings that opiate receptors occur at strategic sites for the control of neuronal activity in the structures investigated. This emphasizes the importance of considering transmitter effects in the context of the intrinsic neuronal circuitry of a given CNS region rather than assessing the drug responsiveness of single neurones.

This work was supported by PHS grant GM-23478, RCDA NS-00287 (R.A.N.), NIH Postdoctoral Fellowship 9F32 NS-05744-03 (B.E.A.) and a Chancellor's Fellowship from UCSF (C.E.J.).

Received 6 May; accepted 25 June 1980.

1. Snyder, S. H. *Harvey Lect.* **79,** 291–314 (1979).
2. North, R. A. *Life Sci.* **24,** 1527–1546 (1979).
3. Jessell, T. M. & Iversen, L. L. *Nature* **268,** 549–551 (1977).
4. Mudge, A. W., Leeman, S. E. & Fischbach, G. D. *Proc. natn. Acad. Sci. U.S.A.* **76,** 526–530 (1979).
5. Bornstein, J. C. & Fields, H. L. *Neurosci. Lett.* **15,** 77–82 (1979).
6. Konishi, S., Tsunoo, A. & Otsuka, M. *Nature* **282,** 515–516 (1979).
7. Nicoll, R. A., Siggins, G. R., Ling, N., Bloom, F. E. & Guillemin, R. *Proc. natn. Acad. Sci. U.S.A.* **74,** 2584–2588 (1977).
8. Zieglgänsberger, W., French, E. D., Siggins, G. R. & Bloom, F. E. *Science* **205,** 415–417 (1979).
9. Corrigal, W. A. & Linseman, M. A. *Can. J. Physiol. Pharmac.* **57,** 1457–1459 (1979).
10. Dunwiddie, T., Mueller, A., Palmer, M., Stewart, J. & Hoffer, B. *Brain Res.* **184,** 311–330 (1980).
11. Gähwiler, B. H. *Neurosci. Abstr.* **5,** 282 (1979).
12. Jensen, R. A. *et al. Neurosci. Abstr.* **5,** 530 (1979).
13. Lee, H. K., Dunwiddie, T. & Hoffer, B. *Brain Res.* **184,** 331–342 (1980).
14. Robinson, J. H. & Deadwyler, S. A. *Neurosci. Abstr.* **5,** 281 (1979).
15. Stanley, J. C., DeFrance, J. F., Taber, K. & Dafny, N. *Neurosci. Abstr.* **5,** 282 (1979).
16. Fry, J. P., Zieglgansberger, W. & Herz, A. *Brain Res.* **163,** 295–305 (1979).
17. Alger, B. E. & Nicoll, R. A. *Nature* **281,** 315–317 (1979).
18. Andersen, P., Eccles, J. C. & Løyning, Y. *J. Neurophysiol.* **27,** 608–619 (1964).
19. Alger, B. E. & Nicoll, R. A. *Brain Res.* (in the press).
20. Katz, B. & Miledi, R. *Proc. R. Soc.* **B167,** 8–22 (1967).
21. Atweh, S. F. & Kuhar, M. J. *Brain Res.* **134,** 393–405 (1977).
22. Sar, M., Stumpf, W. E., Miller, R. J., Chang, K.-J. & Cuatracasus, P. *J. comp. Neurol.* **182,** 17–38 (1978).
23. Jahr, C. E. & Nicoll, R. A. *Science* **207,** 1473–1475 (1980).
24. Nadi, N. S., Hirsch, J. D. & Margolis, F. L. *J. Neurochem.* **34,** 138–146 (1980).
25. Halasz, N., Ljungdahl, A. & Hokfelt, T. *Brain Res.* **154,** 253–271 (1978).
26. Price, J. L. & Powell, T. P. S. *J. Cell Sci.* **7,** 125–155 (1970).
27. Barker, J. L., Nicoll, R. A. & Padjen, A. *J. Physiol., Lond.* **245,** 521–536 (1975).
28. Schmidt, R. F. *Ergebn. Physiol.* **63,** 20–101 (1971).
29. Nicoll, R. A. & Alger, B. E. *Int. Rev. Neurobiol.* **21,** 217–258 (1979).
30. Nicoll, R. A. *J. Physiol., Lond.* **290,** 113–128 (1979).
31. Levy, R. A. *Prog. Neurobiol.* **9,** 211–267 (1977).
32. Suzue, T. & Jessell, T. *Neurosci. Lett.* **16,** 161–166 (1980).
33. Frenk, H., Urca, G. & Liebeskind, J. C. *Brain Res.* **147,** 327–337 (1978).
34. Henriksen, S. J., Bloom, F. E., McCoy, F., Ling, N. & Guillemin, R. *Proc. natn. Acad. Sci. U.S.A.* **75,** 5221–5224 (1978).
35. Krivoy, W. A. & Huggins, R. A. *J. Pharmac. exp. Ther.* **134,** 210–213 (1961).
36. Pomeranz, B. & Gurevich, N. *Eur. J. Pharmac.* **60,** 307–313 (1979).
37. Corrado, A. P. & Longo, V. G. *Archs int. Pharmacodyn. Thér.* **132,** 255–269 (1961).

LETTERS

A soft X-ray halo around SU UMa

F. A. Cordova* & K. O. Mason†

* The University of California, Los Alamos Scientific Laboratory,
Los Alamos, New Mexico 87545
† Space Science Laboratory and the Astronomy Department,
The University of California, Berkeley, California 94720

The dwarf nova SU UMa was observed with the imaging proportional counter (IPC) detector[1] on the Einstein X-Ray Observatory on 4 October 1979 at 4 h UT for ~3,000 s. An X-ray source was detected at the position of the star. It had a flux of 1.3×10^{-11} erg cm^{-2} s^{-1} (0.6 counts per s) in the 0.1–4.5 keV energy range of the IPC, assuming a spectral temperature of ~10 keV (ref. 2). In addition, several areas of weaker emission were observed which form a ring that is symmetrically disposed about the position of the dwarf nova. This latter emission is detected only at energies below 0.7 keV. We discuss here the possibility that it arises in material that has been ejected from the star in a nova-like event.

An X-ray map of the SU UMa field is displayed in Fig. 1: the contours of equal X-ray intensity that are plotted show the relatively bright central source surrounded by a patchy distribution of enhanced X-ray emission. The mean radius of this 'ring' is ~14 arc min. The apparent knots of emission in the ring, of scale size ~1 arc min, are typically ~7 ± 3 counts above background. Additional structure may be present within the confines of the ring, particularly to the north-west of the dwarf nova. An examination of a large number of IPC fields demonstrates that this ring-like structure is unique to SU UMa and is not an instrumental effect.

To investigate the structure and luminosity of this feature further, we have summed the counts as a function of radius from the position of the central source in two energy bands. This is plotted in Fig. 2 which shows the counts accumulated in channels 1–4 and 5–14 of the 15 channel pulse-height analyser. Using the detector gain calculated from calibrations performed on the day of the observation, these channels encompass energy bands of 0.09–0.72 and 0.72–4.31 keV. The expected decrease of the counts as a function of radius from the centre of the field of view, caused by vignetting of the telescope, is shown by the dashed lines. The data in the higher energy band are distributed in a manner consistent with this function. However, at low energies

0028–0836/80/360025—03$01.00

there is an excess above the vignetting curve at a radius of $\sim$14 arc min, attributable to the ring. This feature thus seems to be most prominent at low energies.

The total number of counts in the knots comprising the ring (including the north-west filament) is $\sim$13% that of the central source. This actually represents a lower limit to the ring intensity as much of the halo emission could come from extended regions whose surface brightness is too low to appear significant in the present data. Based on the lack of detection of the ring above $\sim$0.7 keV, we estimate its temperature to be of the order of 10^6 K. Using this temperature we calculate the integrated flux from the ring to be $\sim 6\times10^{-13}$ erg cm^{-2} s^{-1}, with an estimated uncertainty of 30%.

The symmetrical distribution of the ring around SU UMa suggests that it might be emission from material ejected by that object. It is unlikely that this material is radiatively excited by emission from the central star, as is the case in planetary nebulae, for example. The calculations of Tarter *et al.*[3] allow us to estimate the temperature of a spherically symmetric, optically thin gas cloud irradiated by a central point source of X rays as a function of the parameter $\xi = L/nr^2$, where L is the luminosity of the central source, n is the gas density and r is the distance of the gas from the central star. At an assumed distance of 100 pc, $L \sim 1.5\times10^{31}$ erg s^{-1} and $r \sim 0.4$ pc. Thus for SU UMa, $\xi \sim 1\times10^{-4}[(0.1\ \text{cm}^{-3})/n]$. This implies a temperature $<10^4$ K, clearly inconsistent with the soft X-ray temperature observed in this observation.

Alternatively, we consider a mechanism analogous to that which gives rise to X-ray emission from Supernova remnants, that is, a blast wave from a nova explosion propagating through the interstellar medium (ISM) and shock heating the ambient material. If the density of the ISM is 0.06 cm^{-3}, which is appropriate for the galactic latitude of SU UMa[4] ($b = 33°$), the total amount of material swept up by a shock of radius 0.4 pc is $\sim 4\times10^{-4}\ M_\odot$. This is larger than the mass typically ejected in a nova explosion[5] ($\sim 10^{-4}\ M_\odot$), so that it is reasonable to assume that the blast wave is in the adiabatic phase (see ref. 6). Adopting $T \sim 10^6$ K and a 0.2–2.0 keV luminosity of $\sim 10^{30}$ erg s^{-1} for the ring, the standard adiabatic solution gives a shock velocity, $V_s \sim 300$ km s^{-1}, an initial explosion energy, $E_0 \sim 10^{45}$ erg, a density for the ISM, $n \sim 0.1$ cm^{-3}, and an expansion age, $t \sim 500$ yr. The explosion energy required by the adiabatic model is similar to the energy liberated in a nova outburst[7], while the ISM density derived is compatible with the expected value of 0.06 cm^{-3} (ref. 4). This interpretation of the X-ray ring is thus self-consistent.

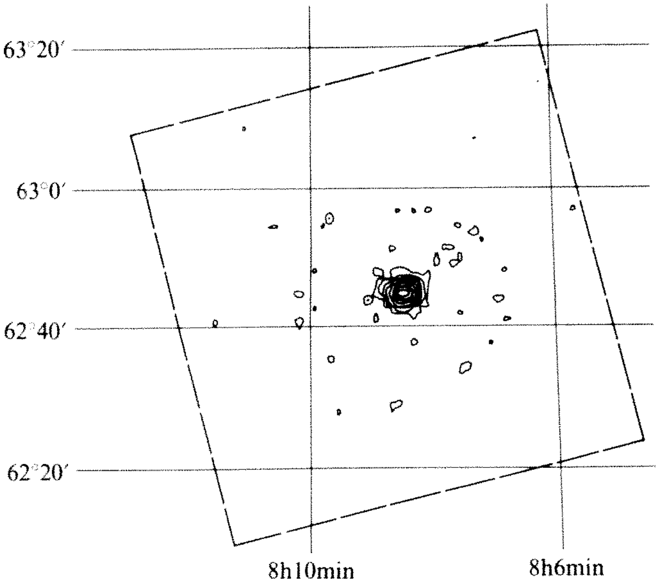

Fig. 1 The isointensity X-ray contour map of the $\sim1°\times1°$ IPC field (delineated by the dotted line boundary) centering on SU UMa. The size of the central object is consistent with the IPC spatial response to a point source (FWHM $\sim$2.3 arc min). Centred approximately symmetrically around the central star at a radius of $\sim$14 arc min is a nonuniform ring of emission.

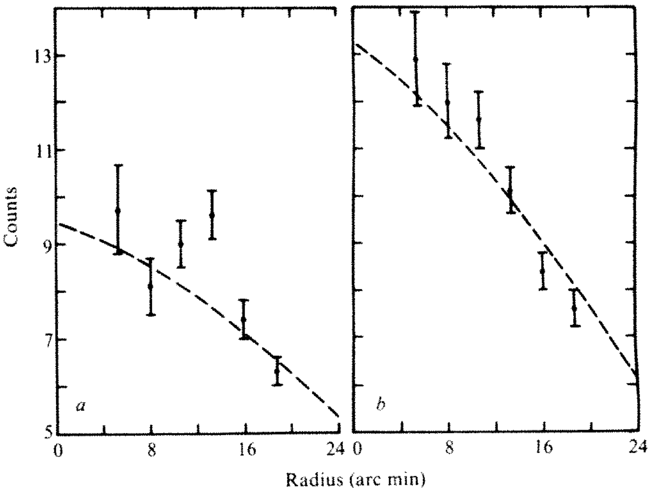

Fig. 2 The radial distribution of the intensity of the SU UMA field. The counts were integrated over radial rings in increments of 2.67 arc min extending outwards from the central source; the counts shown here have been normalized to a 2.67×2.67 arc min area: *a*, for the soft X-ray band of 0.1–0.7 keV and *b*, for the hard X-ray band of 0.7–4.3 keV. (The central source is not depicted as its count rate goes off scale.) The dashed lines represent the normalized effective area function of the IPC field (which depends on energy as well as spatial distribution); it also includes the vignetting function of the Einstein focusing telescope. Only in the soft X-ray band (*a*) is an enhancement above this function evident at the location of the ring.

A visual inspection of the region around SU UMa using the Palomar Sky Survey prints reveals no evidence for optical filamentary structure. The optical filaments associated with Supernova remnants are believed to be low temperature emission from relatively dense interstellar clouds[8,9]. The lack of such emission is to be expected in the present case if the halo resides entirely in the intercloud medium, as is likely given its small size compared with the mean diameter and separation of interstellar clouds[4].

The observation of an X-ray ring (that can be interpreted as resulting from a nova-like explosion) around an object that now shows the characteristics of a dwarf nova provides evidence for a connection between novae and dwarf novae. Other evidence that these two subclasses of cataclysmic variables may be related can be found in the fact that nova 1901 (GK Per) now exhibits dwarf nova-like behaviour[10], and Nova Vul 1979 reportedly exhibited similar behaviour for at least 80 yr before its outburst[11]. These findings may have important implications for evolutionary models of cataclysmic variables. As a possible first detection of an X-ray nova remnant, the X-ray ring around SU UMa provides a new parameter regime for exploring, as is done with Supernova remnants, the physical conditions in the interstellar medium and the physics of the nova outburst. A search for X-ray ejecta from other likely sources, including all types of cataclysmic variable stars, should also be made.

We were guest observers on the Einstein X-ray Observatory. We thank Dr F. R. Harnden of Harvard/SAO for invaluable computational assistance and comments regarding the final manuscript. Useful discussions with Drs S. Hatchett, B. Smith, and H. Bond are also acknowledged. This work was supported in part by the Department of Energy and NASA grant 5-25049. K.O.M. acknowledges financial support from the Miller Institute for Basic Research and NASA grant/NAGW-44.

Received 23 April; accepted 2 July 1980.

1. Giacconi, R. *et al. Astrophys. J.* **230**, 540 (1979).
2. Cordova, F. A., Mason, K. O. & Nelson, J. E. *Astrophys. J.* (submitted).

3. Tarter, C. B., Tucker, W. H., & Salpeter, E. E. *Astrophys. J.* **156,** 943 (1969).
4. Allen, C. W. *Astrophysical Quantities* (Athlone, London, 1973).
5. Bath, G. T. & Shaviv, G. *Mon. Not. R. astr. Soc.* **183,** 515 (1978).
6. Culhane, J. L. in *Supernovae* (ed. Schramm, D. N.) 29 (Reidel, Dordrecht, 1977).
7. Robinson, E. L. *A. Rev. Astr. Astrophys.* **14,** 119 (1976).
8. McKee, C. F. & Cowie, L. L. *Astrophys. J.* **195,** 715 (1975).
9. Sgro, A. G. *Astrophys. J.* **197,** 621 (1975).
10. Webbink, R. *V.S.S., R.A.S.N.Z. Circ.* No. M78/5 (1978).
11. Liller, M. H. & Liller, W. *Astron. J.* **84,** 1357 (1980).

Simultaneous IR and X-ray burst observation of Ser X-1

Walter H. G. Lewin & Lynn R. Cominsky

Department of Physics and Center for Space Research, Massachusetts Institute of Technology, Cambridge, Massachusetts 02139

Alistair R. Walker & Bruce S. C. Robertson

South African Astronomical Observatory, PO Box 9 Observatory, 7935 South Africa

It has been suggested[1,2] that the very bright IR bursts[1,3] observed from the Rapid Burster (MXB 1730 − 335) are due to Type I X-ray bursts[4]. When the bright IR bursts were detected, unfortunately there was no simultaneous X-ray coverage. Therefore, it is not known whether the IR bursts are associated with Type I or Type II bursts or with neither one. The suggestion[1,2] is only based on the low recurrence rate of the IR bursts. If the suggestion is correct, similar bright IR bursts may, in general, accompany Type I X-ray bursts[1,2]. This paper investigates this possibility for one specific case. During the 1977 coordinated worldwide burst watch[5], simultaneous X-ray and IR observations were made. On UT June 17, 00 h 00 min 25s, a Type I X-ray burst was observed, which was almost certainly emitted by Ser X-1 (MXB 1837+05, 4U1837+04) (ref. 6). Simultaneous IR observations failed to detect any bursts. We report here on these observations.

Between UT June 16, 20 h 40 min and June 17 02 h 30 min, IR observations were made with the SAAO 30-inch telescope in Sutherland. The field of view was approximately centered on the star which was first identified by Davidsen[7]. It is now known that the actual star is ~ 2.2 arc s away[8], but that is of no consequence here since the radius of the field of view was ~ 35 arc s. A Glass MK2 IR photometer was used in combination with a lead sulphide detector. The observations were made at 2.2 μm using a Johnson K filter (bandwidth ~ 0.48 μm). The output was displayed on a chart recorder running at sufficient speed that the lock-in time constant of 1 s was the dominant smoothing factor. No indication of an IR burst was found. A 3σ signal in a 1-s readout corresponds to a peak K magnitude of ~ 7. Therefore, at a 3σ level of confidence, the IR flux integrated over the 20 s duration of the burst was less than 1.3×10^{-9} erg cm^{-2}.

SAS-3 observed Ser X-1 (MXB 1837+05, 4U1837+04) between UT 1977 June 11.6 and June 17.5. Between June 11.6 and 14.9 the source was observed with the Horizontal Tube (HT) system[9,10]. A total of nine Type I bursts were observed. From June 14.9 to June 17.5 the source was observed with the Center Slat (CS) system[9,10] (field of view $\sim 1.0° \times 30°$ FWHM) and a total of six bursts were observed. When a Type I X-ray burst occurred on June 17 00h 00 min 25 s, Ser X-1 was within a few arc min of the centre line of the CS and 9.8° from the spacecraft equator (elevation). Consequently, at the time of the burst, the collimator transmission function was 0.57 ± 0.03. The rise time of the burst was less than 1 s, the burst decayed gradually and lasted for about 20 s. The integrated burst flux, in the range 1.4–14 keV, was $(9.3 \pm 0.9) \times 10^{-8}$ erg cm^{-2}.

There is a chance that the X-ray burst did not come from Ser X-1; although it is not possible to calculate a formal probability, we believe this chance to be small. The burst was only observed in the CS and not in the HT system[9,10] ($\sim 1.7°$ FWHM). Thus, it could only come from sources viewed by the CS excluding the area of overlap with the HT system. This excludes the burst source Aql X-1 (ref. 11) since it was located near the centre of the HT system. The only known burst source other than Ser X-1 in the field of view of the CS system was Aql MXB (ref. 9). However, only 15% of the error box of Aql MXB was observed by the CS (and not by the HT system) and the burst frequency of Aql MXB is very low; only one burst was observed in 1976 in 12 days of observing[9]. In addition, a reanalysis at MIT of the 1976 SAS-3 data showed that the burst form Aql MXB (ref. 9) could have come from Aql X-1 (L. Cominsky, A. Lawrence and W. Lewin; unpublished data). If the burst sources Aql X-1 and Aql MXB are the same source, as we suspect, then Ser X-1 was the only known burst source in the field of view of the CS and not in the HT system.

There is another reason why we believe that the burst observed in the CS system was emitted by Ser X-1. Ser X-1 was burst active during the observations with the HT system from June 11.6 to 14.9 and the burst observed on June 17 00 h 00 min 25 s with the CS system was very similar to many from Ser X-1 observed a few days earlier with the HT system.

The ratio of the observed IR (2.2 μm, 0.48 μm bandwidth) and X-ray (1.4–14 keV) fluxes for the burst from Ser X-1 is less than 1.4×10^{-2} at a 3σ level of confidence. For stars in the direction of Ser X-1 ($l^{\mathrm{II}} \sim 36°$, $b^{\mathrm{II}} \sim 5°$), the colour excess $E_{\mathrm{B-V}} \sim 0.6$ mag kpc^{-1} (ref. 12). With a scale height of ~ 150 pc (ref. 13), the path through the dust layer along the line of sight to Ser X-1 is ~ 1.8 kpc. Thus, $E_{\mathrm{B-V}} \sim 1.1$ which yields corresponding values for the extinction[13] $A_{\mathrm{V}} \sim 3.3$ mag and $A_{\mathrm{K}} \sim 0.3$ mag. Thus, after correction for extinction, we find for the ratio of IR and X-ray fluxes an upper limit of 1.8×10^{-2} (3σ level of confidence). We will compare this with the flux ratios of IR bursts and Type I X-ray bursts (not observed simultaneously) from the Rapid Burster.

From the work by Kulkarni *et al.*[1] (1.6 μm, bandwidth 0.3 μm) and that of Jones *et al.*[3] (2.2 μm, bandwidth 0.4 μm), we calculated the integrated IR fluxes. The six IR bursts observed by the Indian group had an average duration of ~ 35 s and an average burst flux integrated over the duration of the bursts of $\sim 2.2 \times 10^{-8}$ erg cm^{-2}. Jones *et al.* observed two events and measured burst durations of ~ 20 s and ~ 12 s. The integrated IR flux values were $\sim 8.2 \times 10^{-9}$ erg cm^{-2} and $\sim 5.5 \times 10^{-9}$ erg cm^{-2}.

Using SAS-3 data (not taken simultaneously with the IR observation), we calculated the integrated fluxes of three Type I X-ray bursts of ~ 20 s duration form the Rapid Burster. All three bursts were observed with the HT system (1.7° FWHM) and in all cases, the Rapid Burster was within 0.3° of the centre of the field of view. The average value (corrected for aspect) in the 1.3–18 keV interval is $(1.0 \pm 0.1) \times 10^{-7}$ erg cm^{-2}.

Thus we find that the observed IR/X-ray (Type I) flux ratios are ~ 0.22 using the IR data by Kulkarni *et al.*[1], (H band) and ~ 0.07 (average value for the two events) using the IR data by Jones *et al.*[3] (K band). For the X-ray flux we used the SAS-3 data which were not taken simultaneously. After correction for extinction[13,14] ($A_{\mathrm{H}} \sim 2.0$; $A_{\mathrm{K}} \sim 1.1$), these flux ratios become ~ 1.38 and ~ 0.19 respectively. Thus they are respectively ~ 77 times and ~ 10 times larger than the 3σ upper limit reported in this paper for the Ser X-1 burst.

Optical bursts have been observed simultaneously with Type I X-ray bursts[15–18] from three burst sources, including Ser X-1 (ref. 17). The optical emission is believed to be due to X-ray heating of the accretion disk[16,17,19–21]. The disk is expected to radiate more or less as a black body of different temperatures whose emission reaches a maximum at energies considerably above those of visible photons. An extrapolation of its spectrum to the IR would predict flux levels several orders of magnitude below what would be detectable. Therefore, the fact that IR bursts were detected from the Rapid Burster excludes that they are related to optical bursts as observed in three other burst sources. If they are of thermal origin, the IR brightness temperatures would be in excess of 4×10^{10} K (ref. 3). It has been suggested that the IR fluxes are produced by maser action[2].

0028-0836/80/360027—02$01.00

The purpose of this paper is to see whether unusually strong IR fluxes as detected from the Rapid Burster (whose origin is still uncertain) accompany Type I X-ray bursts from Ser X-1. Our upper limit reported here indicates that the Type I burst from Ser X-1 was not accompanied by a bright IR burst. One could perhaps argue that the IR bursts are highly directional and that in the case reported here, for Ser X-1, the IR burst missed the Earth. However, if the IR beams are highly directional, they could not be associated with Type I X-ray bursts from the Rapid Burster. Since the Type I X-ray bursts from the Rapid Burster, when present, occur on time scales of hours, one would expect to detect IR bursts (if narrowly beamed) at a much lower rate. However, eight (of which six came in pairs) were detected in 7.9 h (refs 1, 3).

We conclude that if the Type I X-ray burst observed on UT June 17, 00 h 00 min 25 s came from Ser X-1, as is very likely, the possibly associated 2.2 μm IR integrated burst flux (K band) was less than 1.3×10^{-9} erg cm^{-2} (3σ level of confidence). This is substantially fainter than IR bursts observed from the Rapid Burster. However, the integrated fluxes observed in Type I X-ray bursts from the Rapid Burster and Ser X-1 are comparable. Thus, if Type I X-ray bursts are associated with the IR bursts, as suggested[1,2] the flux ratio IR/X-ray is substantially (one to two orders of magnitude) lower for the June 17, 1977 burst from Ser X-1 than for the Rapid Burster.

We suspect that Type I X-ray bursts are not associated with bright IR bursts and that the Rapid Burster is unique in producing the IR bursts, as it is unique in many other ways. If the IR bursts are associated with the Type II bursts from the Rapid Burster, the IR bursts must be highly anisotropic since their frequency of occurrence is considerably less than that of the Type II bursts[20,21].

We thank Dr Jan van Paradijs for his useful comments on this manuscript. L. C. was supported by the Zonta International Amelia Earhart Fellowship program. This research was supported in part by a grant from NASA (NAS5-24441).

Received 6 May; accepted 16 July 1980.

1. Kulkarni, P. V., Ashok, N. M., Apparao, K. M. V. & Chitre, S. M. *Nature* **280,** 819 (1979).
2. Apparao, K. M. V. & Chitre, S. M. (in preparation).
3. Jones, A. W. *et al. Nature* **283,** 550 (1980).
4. Hoffman, J. A., Marshall, H. L. & Lewin, W. H. G. *Nature* **271,** 630 (1978).
5. Lewin, W. H. G. *IAU Circ.* No. 3078 (1977).
6. Li, F. K. *et al. Mon.Not.R.Astr.Soc.* **179,** 21P (1977).
7. Davidsen, A. *IAU Circ.* No. 2824 (1975).
8. Thorstensen, J., Charles, P. & Bowyer, S. *IAU Circ.* No. 3253 (1978).
9. Lewin, W. H. G. *et al. Mon.Not.R.Astr.Soc.* **177,** 93P (1976).
10. Buff, J. *et al. Astrophys. J.* **212,** 768 (1977).
11. Oda, M. *IAU Circ.* No. 3481 (1980).
12. Lucke, P. B. *Astr. Astrophys.* **64,** 367 (1978).
13. Allen, C. W. *Astrophysical Quantities* (Athlone, London, 1964).
14. Kleinmann, D., Kleinmann, S. & Wright, E. *Astrophys. J. Lett.* **210,** L83 (1976).
15. Grindlay, J. E. *et al. Nature* **274,** 567 (1978).
16. McClintock, J. E. *et al. Nature* **279,** 47 (1979).
17. Hackwell, J. A. *et al. Astrophys. J.* **233,** L115 (1979).
18. Pedersen, H. *et al. IAU Circ.* No. 3399 (1979).
19. Canizares, C., McClintock, J. E. & Grindlay, J. *Astrophys. J.* **234,** 556 (1979).
20. Lewin, W. H. G. in *X-Ray Astronomy* (eds Baity, W. & Peterson, L.) 133 (Pergamon, Oxford, 1979).
21. Lewin, W. H. G. & Clark, G. W. *Ann. N.Y. Acad. Sci.* **336,** 451 (1980).

Intracrystalline grafting on layer silicic acids

E. Ruiz-Hitzky & J. M. Rojo

Grupo de Físico-Química Mineral, Consejo Superior de Investigaciones Científicas, Serrano 115 dpdo., Madrid-6, Spain

Silanol groups (Si–OH) present at the surface of amorphous silica and microcrystalline silicates can react with organosilicon compounds to form stable organic derivatives[1–3]. The grafting reaction always occurs at the external surfaces of these materials. The present work considers the intracrystalline grafting on internal Si–OH groups in certain layer silicic acids. For the reaction to occur, the silicic acid must have been expanded by the intercalation of appropriate organic polar molecules such as dimethylsulphoxide; in this way, the individual layers of the silicic acid can be separated and the internal Si–OH groups become accessible to the grafting reagents. The resulting grafted products are organosilicic compounds which retain the lamellar structure of the starting silicic acids, but with the interlamellar surfaces covered by organic groups homogeneously distributed. These materials can be thought of as planar silicones.

Starting materials for the reaction are crystalline silicic acids obtained from natural or synthetic alkali layer silicates by acid treatment[4,5]. These silicic acids have a lamellar structure with intracrystalline Si–OH groups covering the interlamellar surfaces. α-$H_2Si_2O_5$, $H_2Si_8O_{17}.nH_2O$ and $H_2Si_{14}O_{29}.nH_2O$ are used in this work. The last silicic acid is called H-magadiite because it was prepared by acid treatment of the mineral magadiite[4]. Reagents used in the present investigation were trimethylchlorosilane (I) and hexamethyldisilazane (II) which react with the Si–OH groups of the mineral substrate to form siloxane bridges (Si—O—Si):

$$\equiv Si{-}OH + Cl{-}Si(CH_3)_3 \rightarrow \equiv Si{-}O{-}Si(CH_3)_3 + HCl \quad \text{(I)}$$

$$2\equiv Si{-}OH + (CH_3)_3SiNHSi(CH_3)_3 \rightarrow 2\equiv Si{-}O{-}Si(CH_3)_3 + NH_3 \quad \text{(II)}$$

Mixtures of both reagents can be also used with positive results.

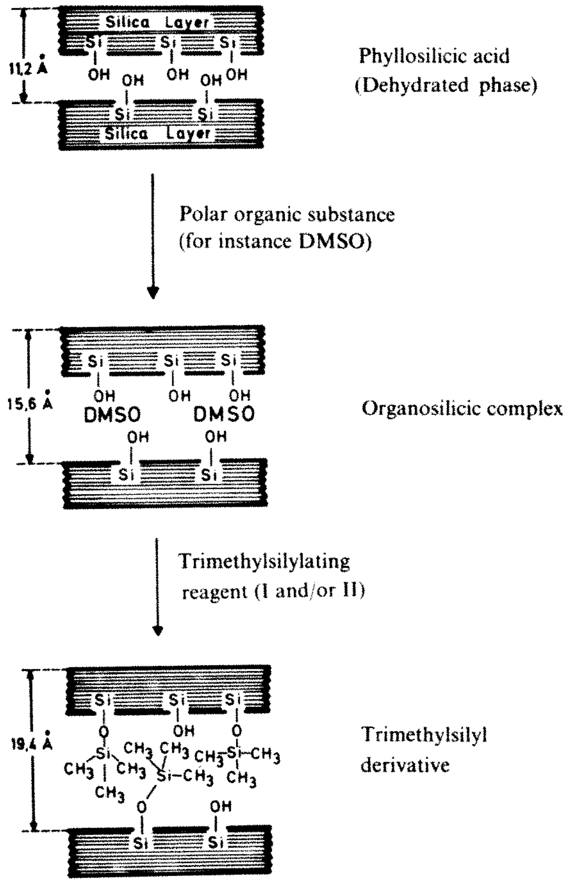

Fig. 1 Interlamellar grafting of $-Si(CH_3)_3$ groups. The synthesis of the trimethylsilyl derivative of the phyllosilicic acids was carried out in two steps: first, the starting silicic substrate (dehydrated phase) was added to an excess of an organic polar substance, as DMSO, and the mixture was stirred continuously for 72 h; excess DMSO was eliminated and the organosilicic complex was recovered. In the second step, reaction between this complex and the trimethylsilylating reagents (I and/or II) was carried out in dioxane for time periods ranging from 24 to 48 h at reflux temperature.

0028-0836/80/360028—03$01.00

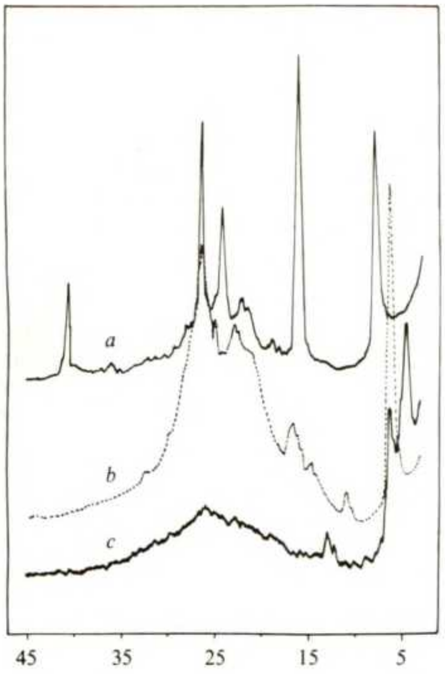

Fig. 2 X-ray diffraction patterns of: *a*, H-magadiite silicic acid, pretreated at 100 °C, 24 h; *b*, H-magadiite (*a*) treated by NMF (intermediate *a*/NMF complex); *c*, trimethylsilyl derivative of *a*, obtained by refluxing the *a*/NMF complex with a mixture of I and II reagents.

If the grafting reaction is carried out by direct treatment of the mineral substrate with organosilanes (I) and/or (II), the resulting product is an organosilicic material with $(CH_3)_3Si$– groups bonded only at the external surfaces of the mineral particles. However, if the silicic acid is previously treated with a polar organic substance such as dimethylsulphoxide (DMSO), *N*-methylformamide (NMF), or *N,N*-dimethylformamide, and subsequently reacted with (I) and/or (II) reagents, then an interlayer grafting on the internal Si–OH groups is produced. The intercalation of the above polar organic substances into the interlayer space of the phyllosilicic acids is a reversible process, as described by Lagaly *et al.*[5]. The swelling produced by these organic molecules makes the internal Si–OH groups accessible to the trimethylsilylating reagents, so that subsequent grafting reaction can occur. Figure 1 explains the different steps in the synthesis of the organosilicic materials.

Evidence of the interlayer grafting of the $-Si(CH_3)_3$ groups was obtained from X-ray diffraction diagrams. The basal spacing (d_{001}) of the phyllosilicic acids increased in all cases, with a mean value of $\Delta d = 8.2$ Å, corresponding to the thickness of two $-Si(CH_3)_3$ groups (Table 1). A disorder in the stacking of the lamellae of the silicic acids is produced during the grafting reaction, as indicated by the broadness of the peaks in the X-ray diffraction pattern (Fig. 2).

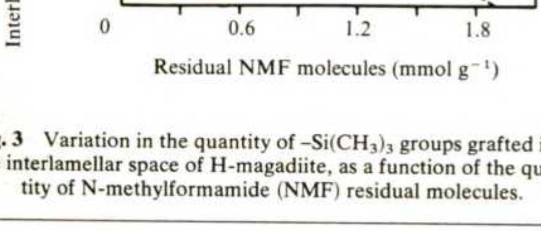

Fig. 3 Variation in the quantity of $-Si(CH_3)_3$ groups grafted into the interlamellar space of H-magadiite, as a function of the quantity of N-methylformamide (NMF) residual molecules.

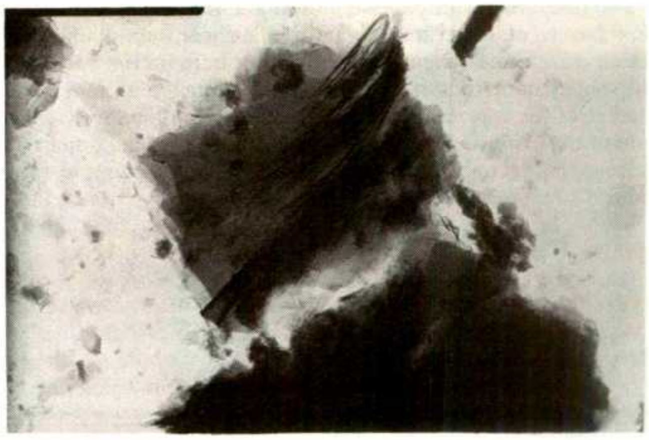

Fig. 4 Microphotograph of a trimethylsilyl derivative of the H-magadiite phyllosilicic acid. Magnification ×75,000.

Chemical analysis and IR spectroscopy show that the progress of the grafting reaction is accompanied by the displacement of the polar organic molecules previously intercalated. The kinetic data show that the rate of grafting reaction of $-Si(CH_3)_3$ groups is equal in absolute value to the rate of desorption of organic polar molecules. Depending on the experimental conditions, a variable quantity of these organic molecules can be trapped in the interlamellar space of the resulting product. The quantity of residual organic molecules (NMF in this case) decreases with the number of $-Si(CH_3)_3$ grafted groups according to a linear relationship (Fig. 3).

The surface covered by grafted $-Si(CH_3)_3$ groups and NMF residual molecules has, in all cases, a constant area equivalent to the calculated area of the interlamellar surface. Chemical analysis and titration of the residual Si–OH groups by NaOH solution can be used to obtain the composition of the resulting materials. For example, in a trimethylsilyl derivative of H-magadiite with a 40% of residual Si–OH groups, the resulting formula can be written as:

$$Si_{14}O_{29}[Si(CH_3)_3]_{1.2}H_{0.8}.0.7\ H_2O$$

where the residual content of organic polar molecules (NMF), as determined by chemical analysis, has been subtracted.

The high thermal stability of these organosilicic materials has been determined by DTA technique. The $-Si(CH_3)_3$ grafted groups remain unaltered until 400 °C.

No important textural changes are observed by electron microscopy when the phyllosilicic acids have been grafted. The planar morphology of the resulting organosilicic materials is shown in Fig. 4, where some corrugation can be seen which could be attributed to the effect of the $-Si(CH_3)_3$ groups grafted on the surfaces of the lamellae.

Table 1 Effect of the interlamellar $-Si(CH_3)_3$ grafting groups on the basal spacing of some typical phyllosilicic acids

Phyllosilicic acid (dehydrated phase)	d_{001} (Å)	Trimethylsilyl derivative d_{001} (Å)	Δd (Å)
α-$H_2Si_2O_5$	7.6	16.2	8.6
$H_2Si_8O_{17}$	16.5	24.4	7.9
$H_2Si_{14}O_{29}$*	11.2	19.4	8.2

* H-magadiite.

The results described above show that it is possible to obtain a new family of macrcmolecular organosilicon compounds, in which the chemical composition depends both on the nature of the starting materials and on the experimental conditions. One feature of these materials is that they maintain the layer structure of the original silicic substrate, but have surface properties corresponding to the organic groups attached, for example, they exhibit a marked organophilic character.

Received 18 February; accepted 20 June 1980.

1. Armistead, C. G. & Hockey, J. A. *Trans. Faraday Soc.* **63,** 2549–2556 (1967).
2. Hair, M. L. & Hertl, W. *J. phys. Chem.* **73,** 2372–2378 (1969).
3. Ruiz-Hitzky, E. & Fripiat, J. J. *Clays Clay Miner.* **24,** 25–30 (1976).
4. Eugster, H. P. *Science* **157,** 1177–1180 (1967).
5. Lagaly, G., Beneke, K. & Weiss, A. *Z. Naturforsch.* **28b,** 234–238 (1973); *Am. Miner.* **60,** 650–658 (1975).

An electrical model of the crust and upper mantle in Scotland

V. R. S. Hutton, M. R. Ingham & E. W. Mbipom

Department of Geophysics, University of Edinburgh, Mayfield Road, Edinburgh EH9 3JZ, UK

Magnetotelluric and magnetovariational studies in southern Scotland[1–4] have been followed by deep electrical soundings at an additional 30 sites. These lie on an approximately linear traverse extending from Kinlochbervie in the Lewisian Foreland to Borthwickbrae in the Scottish Borders (Fig. 1*a*). This traverse crosses the main geological zones of Scotland and follows reasonably closely the line of the LISPB[5] seismic project (Fig. 1*b*). Full details of these geo-electric studies will be published elsewhere. We present here results of two-dimensional modelling of both the magnetotelluric and geomagnetic response functions[6,7] obtained along the traverse.

The model was derived as follows. The digital data from each site were analysed in similar ways to those adopted in refs 8–10. The resulting magnetotelluric response functions, apparent resistivity and phase, were found to be anisotropic at all sites. This indication of lateral variations in conductivity structure was supported by the behaviour of the geomagnetic response functions.

A one-dimensional inversion[11] of the average apparent resistivity and phase data was obtained for each site. These were then used as the basis for applying a two-dimensional modelling programme[12] to each of the sections AA′ and BB′ of the total traverse.

Successive adjustments were then made to the initial two-dimensional models to obtain models which fitted not only both the maximum and minimum apparent resistivity data but also the geomagnetic response functions.

Finally, due to the similarity in the two best-fitting models in the region of overlap to the north of the Highland Boundary Fault, a single geo-electric model was constructed to represent the complete traverse. Observations at Newcastleton and Towhouse[11] have been taken into account to provide a very provisional model across the probable region of the Iapetus suture.

The resulting geo-electric model is given in Fig. 2*a*. This model provides reasonably good agreement between observed and computed response functions for the sites along the traverse marked by arrows in Fig. 1*a*. For traverse AA′, the modelling has been discussed by Mbipom[13] and for traverse BB′ a similar account is in preparation. Here we compare examples of observed and model responses (Figs 3, 4). The model suggests that the electrical structure of the crust and upper mantle in Scotland is, as one might expect from the surface geology, very complex and that there seems to be a distinctive conductivity–depth profile associated with each of the major geological zones along the traverse. For example, the Precambrian fragment to the west of the Moine Thrust is characterized by a resistive crust overlying a less resistive upper mantle, while in the Caledonian metamorphic belt, only the upper 10–15 km of the crust is resistive and the lower crust and uppermost mantle are relatively conducting. The major granitic intrusions are particularly resistive and where the observational density is sufficient the electrical model seems to delineate their form with some success. At the Great Glen, there is a 10 km wide gap in the resistive upper crust where an upper conducting layer connects with the deeper conducting layer of the lower crust and upper mantle. Above average crustal conductivity is also found at shallow depths near the Highland Boundary, Southern Uplands and Stublick Faults. The section of this two-dimensional model covering the south of Scotland confirms and extends the previous one-dimensional interpretation of this region[4]. In the Southern Uplands, the crust is resistive to a depth of ~20 km, and overlies a highly conducting layer, $\sigma \approx 2 \times 10^{-2}\ \mathrm{S\,m^{-1}}$, of poorly defined thickness, 30–70 km. Observational data from the Midland Valley and Northumberland Basin are sparse but in both regions a good conductor exists in the upper crust and it overlies a more resistive layer with the interface between them shelving rapidly near the boundaries of these regions.

This Scottish electrical model can be compared with deep electrical soundings in other countries. Jones and Hutton[4] have already noted the similarity in the conductivity–depth profiles in

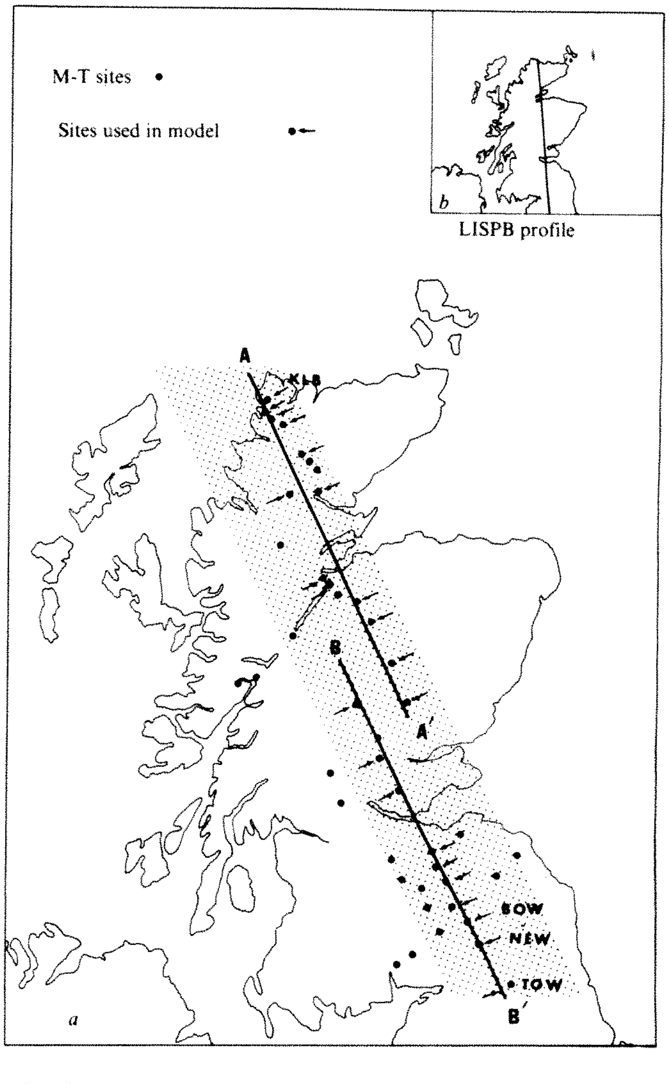

Fig. 1 *a*, Map of Scotland showing the location of the magnetotelluric (M–T) sites. KLB, Kinlochbervie; BOW, Borthwickbrae; NEW, Newcastleton; TOW, Towhouse. *b*, Map of Scotland showing the line of the LISPB study.

0028-0836/80/360030—04$01.00

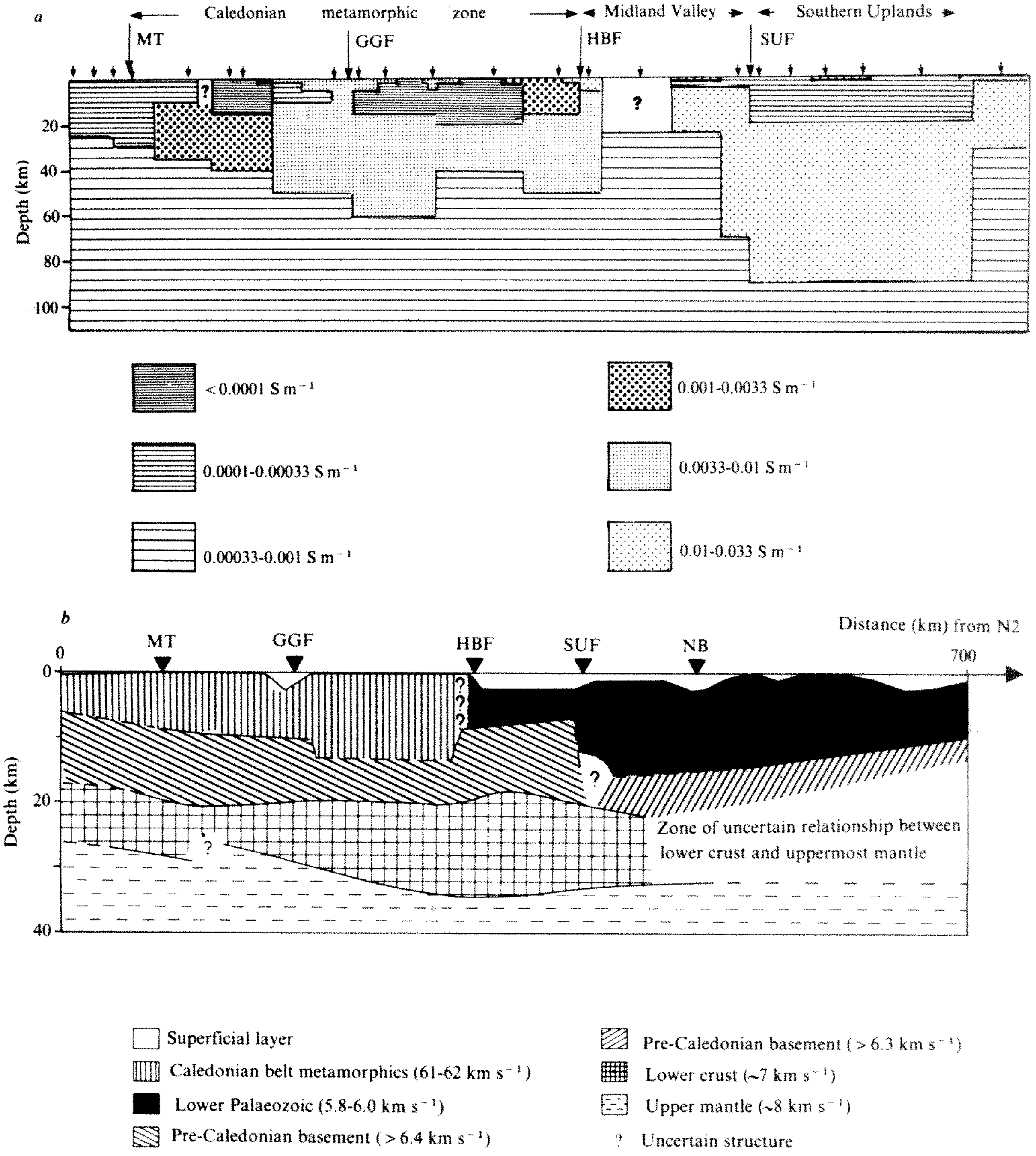

Fig. 2 *a*, The electrical conductivity model of the crust and upper mantle in Scotland for the traverse indicated by the shaded zone in Fig. 1*a*. *b*, Schematic seismic cross-section through the crust and uppermost mantle of northern Britain. MT, Moine Thrust; GGF, Great Glen Fault; HBF, Highland Boundary Fault; SUF, Southern Uplands Fault; NB, Northumberland Basin. (Figure 2*b* from ref. 5.)

the Southern Uplands and in the Canadian Appalachians, regions of common geological history. Further comparison of the Scottish model and that obtained from the Canadian study[14] for a traverse from the Grenville Province of the Canadian Shield to the Appalachians shows another common feature. The electrical conductivity of the lower crust in the neighbourhood of the St Lawrence river, that is the Logan line, where the basement was formed during the Grenville orogeny, is similar to that around the Great Glen, 5×10^{-3} S m^{-1}. In fact, a conductivity–depth profile consisting of a resistive upper crust, a more conducting lower crust and uppermost mantle and a relatively resistive upper mantle seems to be the most common profile in stable continental regions[15–24].

The average conductivity of near-surface continental crustal rocks is generally accepted to be in the range[25] 10^{-5} to 10^{-3} S m^{-1}, as found in the Scottish study along much of the traverse. In some locations, however, the conductivity within the top few kilometres is as high as 10^{-2} to 10^{-1} S m^{-1}. Conductivities of this order of magnitude have been found to be associated with the presence of graphitic schists, geothermal prospects or highly conducting fluids in loosely consolidated sediments.

Thus, in general, all sections of the Scottish model have their counterparts elsewhere. The lateral variation in structure over a distance of only 400 km is, however, probably more striking than in any previous study.

The only published model of the deep structure across Scotland, other than those inferred from studies of surface rocks, is that provided by the LISPB seismic study (Fig. 2*b*).

There is only partial agreement between the geometries of the seismic and electric models. For example, in the Lewisian, the boundary between the resistive crust and more conducting upper mantle occurs at a depth which corresponds well with the Moho as deduced from the seismic study. Further south, however, there is no boundary in the electrical model at Moho depths, but rather a boundary between the resistive upper crust and the more conducting lower crust. This boundary agrees reasonably well with the depth of the Conrad discontinuity. Sharp changes in depth of seismic boundaries, for example, at the Great Glen Highland Boundary and Southern Uplands Faults have their counterparts in the electrical model. The existence of a resistive crust of thickness about 20 km in the Southern Uplands is compatible with the absence of a seismic horizon at 10–15 km depth and a very good conductor in the uppermost mantle is compatible with the absence of a clearly defined signal from Moho depths.

Oxburgh *et al.*[26] have used a schematic crustal model to explain their UK heat flow data. They propose that the variation in heat flow is due to variation in crustal heat production, with the higher heat flow belts including a higher proportion of granites than elsewhere. They require the granites to have a thickness of 16.6 km which is in reasonable agreement with that indicated for the Cairngorm granites in the geoelectric model.

The interpretation of the electrical model will be discussed in detail elsewhere. Here we briefly consider possible explanations of anomalously high conductivity. In the upper crust, it can arise, primarily, as a result of electrolytic conduction in pore fluids, of abnormally high temperature or of intense mineralization. Note that, along the Scottish traverse, the most conducting surface layers coincide with known sedimentary basins in which above average heat flow has recently been reported[26]. The relative contribution of porosity, salinity and temperature in these regions could thus be of interest to the UK geothermal programme. Moreover, similar electrical soundings might be useful to current studies of the deep sedimentary basins in England, especially as pore fluid data are already available from those regions[27].

In the lower crust, the increased pressure and hence crack closure make it unlikely that conduction in electrolytic pore fluids can account for the presence of a conducting zone at this depth. Solid conduction in dry rocks also seems improbable as extremely high temperatures—greater than 700 °C—would be required to provide conductivities of the order of magnitude found in this study. On the other hand, solid conduction through hydrated rocks may be a possibility. Laboratory measurements have also indicated that time-dependent increases in conductivity of up to four orders of magnitude can occur in the solid state due to phenomena such as order–disorder in crystals and rocks[28]. The presence of hydrated rocks with or without associated partial melting has, nevertheless, been the most frequent interpretation for conducting layers in the lower crust[15–24].

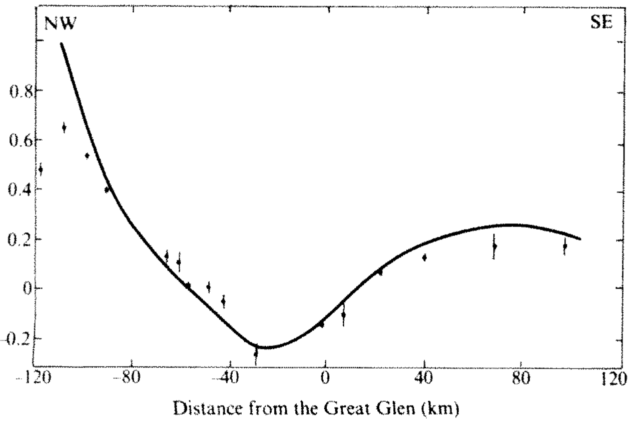

Fig. 3 The variation across the traverse AA′ of the vertical magnetic field transfer function Real (Z/Y), that is the E-polarization case, for a period $T = 95$ s. The solid curve represents the values computed for the model given in Fig. 2*a*. The dots and associated error bars refer to values computed from field data.

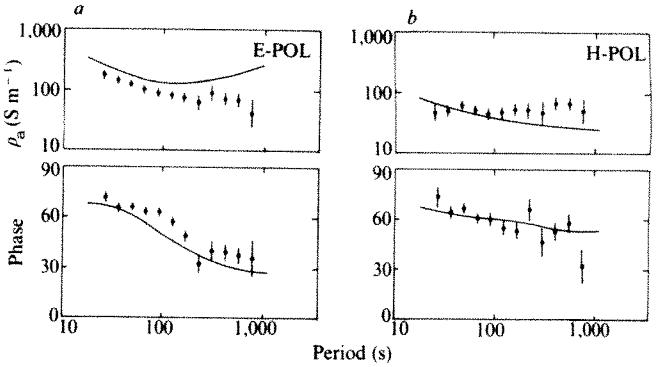

Fig. 4 Apparent resistivity and phase versus period data and associated errors for Yarrow in the Southern Uplands—the station on the traverse BB′ immediately north of BOW in Fig. 1. Curves *a* and *b* correspond respectively to the E and H polarization cases and the smooth curves to the computed values for the model given in Fig. 2*a*.

For example, Berdichevsky *et al.*[18] have discussed the increase in electrical conductivity of granite and other rock types on melting in the presence of water at temperatures of 400–600 °C. They have associated the zone of active granitization and melting with the transition zone between amphibolitic and granulitic facies, that is with the Conrad discontinuity, with the necessary few per cent of water being released as a result of the dehydration at this boundary. Stanley *et al.*[23] have used laboratory results[29–32] to argue that hydrated rocks, such as granite, tonalite, syenite and gabbro, in the upper crust will start melting at 500 °C, especially where the rocks have been subjected to rapid alteration processes. The 500 °C isotherm is, in this case, coincident with a large change in electrical conductivity.

The interpretation of the lower crustal conductor in Scotland in terms of hydrated rocks and partial melting and the other interpretations will be considered elsewhere. However, note that if the granites in Scotland are uranium enriched as in Cornwall and northern England, then a temperature gradient of 30 °C km^{-1} and a depth to the 500 °C geotherm of ~16 km can be expected.

In consideration of Fig. 2*a*, note that: there can be some trade-off between interface depth and conductivity; use of closer station spacing and broader-band electrical soundings may introduce significant changes to the model in some regions; and careful assessment of the validity of laboratory studies is required before further conclusions can be drawn.

It is unfortunate for the tectonic implications of the model that more electrical soundings have not been undertaken in the Midland Valley. If, however, the major boundaries in conductivity structure now suggested to the north and south of this region were confirmed an interpretation of these lateral variations would be possible in terms of former subduction zones as has been suggested in similar studies elsewhere (see refs 33–35). The location of a subsequent subduction zone and the nature of the Iapetus suture[36] may become clearer on the completion of current analyses of geomagnetic and geo-electric observations from northern England.

We thank the NERC for a research grant (GR3/2141) and a studentship for M.R.I., and the Federal Government of Nigeria for a studentship for E.W.M.

Received 2 May; accepted 3 July 1980.

1. Jain, S. & Wilson, C. D. V. *Geophys. J.R. astr. Soc.* **12,** 165–180 (1967).
2. Edwards, R. N., Law, L. K. & White, A. *Phil. Trans. R. Soc.* **270,** 289–323 (1971).
3. Hutton, V. R. S. & Jones, A. G. *J. Geomagn. Geoelec.* (in the press).
4. Jones, A. & Hutton, R. *Geophys. J.R. astr. Soc.* **56,** 329–368 (1979).
5. Bamford, D., Nunn, K., Prodehl, C. & Jacob, B. *Geophys. J.R. astr. Soc.* **54,** 43–60 (1978).
6. Schmucker, U. *Bull. Scripps Inst. Oceanogr.* **13,** 1–165 (1970).
7. Banks, R. J. *Phys. Earth planet. Inter.* **7,** 339–348 (1973).
8. Hermance, J. T. *Phys. Earth planet. Inter.* **7,** 349–364 (1973).
9. Haak, V., *Bayer. Akad. Wissen.* **158,** 1–105 (1978).
10. Rooney, D. & Hutton, V. R. S. *Geophys. J.R. astr. Soc.* **51,** 91–119 (1977).
11. Jones, A. G. thesis, Univ. Edinburgh (1977).
12. Brewitt-Taylor, C. & Johns, P. B. *J. Geomagn. Geoelec.* (in the press).
13. Mbipom, E. W. thesis, Univ. Edinburgh (1980).
14. Kurtz, R. D. & Garland, G. D. *Geophys. J.R. astr. Soc.* **45,** 321–348 (1976).

15. Hyndman, R. D. & Hyndman, D. W. *Earth planet. Sci. Lett.* **4**, 427–432 (1968).
16. Caner, B. *J. Geomagn. Geoelec.* **22**, 113–129 (1970).
17. Dowling, F. L. *J. geophys. Res.* **75**, 2683–2698 (1970).
18. Berdichevsky, M. N., Vanyan, L. L., Feldman, I. S. & Porstendorfer, G. *Beitr. Geophys.* **81**, 187–196 (1972).
19. Edwards, R. N. & Greenhouse, J. P. *Science* **188**, 726–728 (1975).
20. Van Zijl, J. S. V. *The Earth's Crust*, 470–500 (AGU Monograph No. 20, 1977).
21. Nekut, A., Connerney, J. E. P. & Kuckes, A. J. *Geophys. Res. Lett.* **4**, 239–242 (1977).
22. Sternberg, B. K. *J. geophys. Res.* **84**, 212–218 (1979).
23. Stanley, W. D., Boehl, J. E., Bostick, F. M. & Smith, H. W. *J. geophys. Res.* **82**, 2501–2514 (1977).
24. Hermance, J. F. & Pedersen, J. *Geophys. J.R. astr. Soc.* (in the press).
25. Duba, A., Piwinski, A. J., Santor, M. & Weed, H. C. *Geophys. J.R. astr. Soc.* **53**, 583–597 (1978).
26. Oxburgh, E. R. *et al. EEC 2nd int. Seminar on Geothermal Energy* 149–152 (1980).
27. Burley, A. J. *et al. EEC 2nd int. Seminar on Geothermal Energy*, 29–33 (1980).
28. Duba, A. *Acta geod. geophys. Montan.* **11**, 485–495 (1976).
29. Shankland, T. J. & Waff, H. S. *J. geophys. Res.* **82**, 5409–5417 (1977).
30. Wyllie, P. J. *Structure and Physical Properties of the Earth's Crust*, 279–301 (AGU Monograph No. 14, 1971).
31. Zobacki, M. D. thesis, Stanford Univ. (1975).
32. Lebedev, E. B. & Khitarov, N. J. *Geokhimiya* **3**, 195–201 (1964).
33. Law, L. K. & Riddihough, R. P. *Can. J. Earth Sci.* **8**, 1094–1106 (1971).
34. Gough, D. I. *Phys. Earth planet. Inter.* **7**, 379–388 (1973).
35. Garland, G. D. *Phys. Earth planet. Inter.* **30**, 220–230 (1975).
36. Phillips, W. E. A., Stillman, C. J. & Murphy, T. *J. geol. Soc. Lond.* **132**, 579–609 (1976).

Parental magma to the Bushveld Complex

G. Davies*, R. Grant Cawthorn*, J. M. Barton Jr† & Merryl Morton*

* Geology Department, University of the Witwatersrand, 1 Jan Smuts Avenue, Johannesburg 2001, South Africa
† Bernard Price Institute of Geophysical Research, University of the Witwatersrand, 1 Jan Smuts Avenue, Johannesburg 2001, South Africa

The Bushveld Complex of South Africa is a large layered intrusive suite of cumulate rocks for which the parental magma is not directly obtainable. However, we report here indirect evidence from a suite of fine-grained sills in the sediments below the Bushveld Complex. Mineralogical, geochemical and experimental petrological data are consistent with their being representative of the parental magma. They are siliceous picrites ($SiO_2 = \sim 55\%$; $MgO = \sim 12\%$), high in Cr, Ni, Rb and K, and with a high initial Sr^{87}/Sr^{86} ratio, and hence represent a rather unusual magma composition. Crustal contamination may have been important in their evolution.

The layering and mineralogical variation in the Bushveld Complex, shown in Fig. 1, is accepted to be the result of fractional crystallization from a basic magma. However, the exact composition of this magma has been debated. Willemse[1] believed it to be similar to the voluminous metamorphosed gabbroic sills found in the sediments forming the floor to the Bushveld Complex; and suggested contamination of this liquid produced the noritic sills also found in the floor rocks. Typical analyses of these two suites of sills are given in Table 1.

Daly[2] and Wager and Brown[3] studied fine-grained border facies which they believed might be original liquid compositions. Chemically, both are very similar to that proposed as the parental liquid to the Skaergaard Complex (see Table 1), which is surprising as the crystallization sequences and mineral compositions of the two complexes are quite different (Fig. 1).

Vermaak[4] and Hamilton[5] calculated a magma composition using modal proportions from the various zones based on an hypothesis of a new magma injection below the critical zone. Hamilton[5] believed the MgO content of the parental magma exceeded 21% whereas Vermaak[4] regarded it as having komatiitic affinities.

Beneath the Bushveld Complex to the east of Rustenburg, Transvaal, we have identified a suite of micropyroxenitic sills. These intrude the metamorphosed Silverton and Vermont shales and Magaliesberg quartzite of the Transvaal Supergroup[6], and are found from 2 km below to the margin of the complex. They range in thickness from 3 to 10 m. Hopper and branching olivine and abundant bladed to feathery orthopyroxene are present. The matrix is devitrified glass which contains occasional microlites of plagioclase and possibly clinopyroxene (see Fig. 2). These have been described in more detail elsewhere[6]. The crystallization of a small proportion of olivine, followed by a large amount of orthopyroxene, is consistent with the first-formed cumulates of the Bushveld Complex (Fig. 1) and so these sills could represent offshoots of the parental magma.

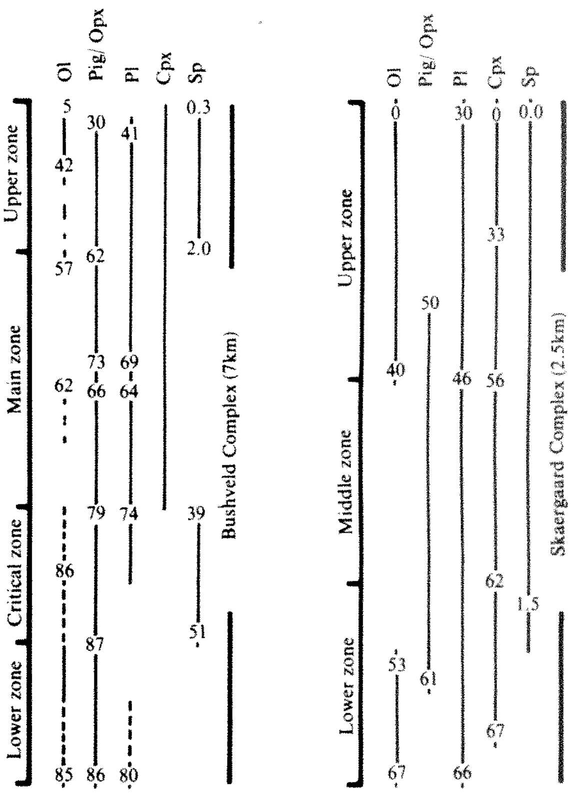

Fig. 1 Crystallization sequences and average mineral compositions in Bushveld and Skaergaard Complexes, from various sources[3,9,16–20]. 100 Mg/(Mg + Fe) ratios for mafic minerals and An content of plagioclase are shown; dashed lines indicate sporadic appearance of cumulus phases. For the spinels, the V_2O_5 contents are shown, except for the minerals near the base of the Bushveld Complex, where numbers refer to the Cr_2O_3 contents.

This suite of rocks is unusual in displaying high SiO_2 content (53–56%) and high MgO (9–13%) and has a Rb/Sr ratio of 0.15–0.20 (Table 1). It also has high K_2O, Ni and Cr.

We have studied several samples experimentally at 3 kbar pressure, one being from the chilled margin of a 3-m sill, occurring 600 m below the Bushveld Complex[7]. It has the second highest magnesium content of the samples analysed (analysis 1, Table 1) but its very fine-grained nature argues against any cumulus enrichment. Phase diagrams at 3 kbar pressure were constructed from our results (Fig. 3*a*, *b*); these are thought to be applicable to the crystallization of the Bushveld Complex. The composition of the chilled margin plots just within the olivine primary phase field in Fig. 3*a* and in the orthopyroxene primary phase volume in Fig. 3*b*.

The likely path it would follow during fractional crystallization is given on Fig. 3*b* by 1–A–B, involving olivine, orthopyroxene, orthopyroxene plus plagioclase, orthopyroxene plus plagioclase plus clinopyroxene. This crystallization sequence is very similar to that observed for the Bushveld Complex (see Fig. 1).

Trace element contents can also be compared with that expected of the parental magma to the Bushveld Complex. Hart and Davis[8] found the partitioning of nickel between liquid and olivine to be dependent on the MgO content of the liquid. For a MgO content of 12.5% a value of $D^{\text{ol}}_{\text{liq}}$ of 9 is obtained. The average NiO content[9] of the lower zone olivine varies between 0.31 and 0.35%. Assuming that those are the first-formed

0028–0836/80/360033—03$01.00

Table 1 Composition of micropyroxenitic sills and some other proposed parental magmas

	1	2	3	4	5	6	7	8	9		10
SiO_2	55.70	56.39	55.78	53.28	55.75	54.57	48.08	50.26	56.10	Q	3.18
TiO_2	0.36	0.34	0.41	0.43	0.44	0.35	1.17	0.91	0.76	Or	6.07
Al_2O_3	12.74	11.65	12.53	13.72	13.67	11.78	17.22	16.26	12.90	Ab	17.06
Fe_2O_3	1.09	1.25	10.11*	10.64*	10.32*	10.04*	1.32	1.99	1.05	An	22.60
FeO	7.80	7.99					8.44	6.83	8.19	Di	9.55
MnO	0.09	0.19	0.19	0.13	0.16	0.16	0.16	0.13	0.18	Hy	39.28
MgO	12.44	13.05	9.71	9.22	9.34	11.36	8.62	6.32	10.12	Mt	1.58
CaO	6.96	6.42	6.50	7.95	7.30	6.25	11.38	9.70	6.38	Il	0.68
Na_2O	2.02	1.73	1.94	1.01	1.83	2.75	2.37	2.58	1.48		
K_2O	1.03	0.96	1.02	0.56	0.96	1.70	0.25	1.20	1.30		
Trace elements											
Ni	292	360	—	309	—	—	112	—	—		
Cr	970	1150	—	900	—	921	430	—	—		
Rb	37	35	—	21	—	54	10	—	—		
Sr	195	186	—	142	—	272	249	—	—		
Ba	439	461	—	—	—	723	—	—	—		
Zr	70	68	—	76	—	69	—	—	—		
Rb/Sr	0.19	0.19	—	0.15	—	0.20	0.04	—	—		

1, Proposed parental magma to the Bushveld Complex, fine-grained margin of a micropyroxenitic sill.
2, Coarser central portion of the same sill as sample 1.
3, Mean of four analyses from a micropyroxenitic sill from the eastern portion of the Bushveld Complex[22].
4, Margin of micropyroxenitic sill intruding Magaliesberg quartzite from which Rb–Sr isotope data were obtained.
5, Margin of micropyroxenitic sill intruding the Silverton shale ~2 km below the Bushveld Complex.
6, Central portion of micropyroxenitic sill intruding the Vermont shale about 700 m below the Bushveld Complex.
7, Proposed parental magma to the Skaergaard Complex[3], revised trace element data from Brooks and Nielsen[21].
8, Typical metamorphosed gabbroic sill[1].
9, Typical noritic sill[1].
10, CIPW normative composition of sample 1.
* Total iron as Fe_2O_3.

minerals, the nickel content for the parental magma should be between 270 and 305 p.p.m., consistent with the data in Table 1.

Chromium partitioning between liquid and orthopyroxene is dependent on temperature and oxygen fugacity[10]. Assuming a value of between 1,350 and 1,300 °C for orthopyroxene crystallization temperature[7] and a $\log f_{O_2}$ of -9, a partition coefficient of between 2.5 and 4 is obtained. The average Cr_2O_3 content[9] of the lower zone orthopyroxene is 0.15%, which requires an original liquid with between 874 and 1,399 p.p.m. chromium. Again the data for these sills fall within this range.

The Rb/Sr ratio of the initial magma to the Bushveld Complex has been calculated from partition coefficients[5] as being in the range 0.15–0.25: this is much higher than most basaltic liquids which vary between 0.01 and 0.05. The data in Table 1 show that these sills have this unusual value for the Rb/Sr ratio. The initial $^{87}Sr/^{86}Sr$ ratio, determined by Hamilton[5], for the parental magma is 0.7056.

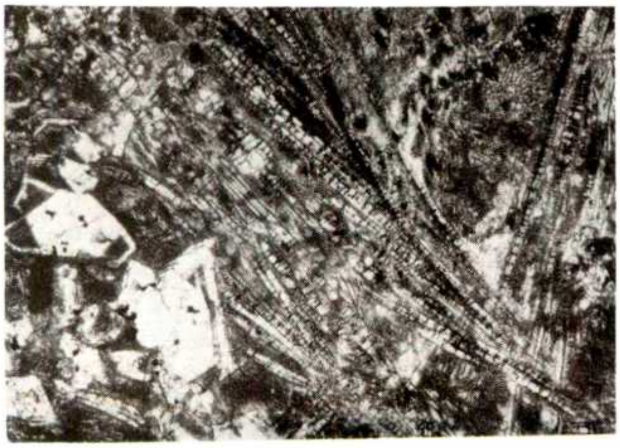

Fig. 2 Photomicrograph of bladed orthopyroxene embedded in very fine-grained matrix of devitrified glass. Hopper olivine crystals present in lower left of photograph. Field of view of the photomicrograph is 0.3 by 0.2 cm.

We have attempted to date an 8-m sill (Table 1, analysis 4) which has a moderate range in Rb/Sr ratios. The data do not define an isochron, but assuming an age[5] of 2,095 Myr, the range in initial $^{87}Sr/^{86}Sr$ ratios is 0.7037–0.7098 with an average of 0.7067. Although more work will be required in this respect it does at this stage support the data of Hamilton[5] and indicates a parental magma anomalously enriched in radiogenic Sr. This, when considered with the high concentrations of SiO_2, K_2O and Rb in such a magnesian magma, suggests that crustal contamination may have been a factor in the genesis of this suite of sills.

The new experimental data[7] mean that previous ideas can now be reassessed. Figure 3 shows a typical gabbro composition (given in Table 1), believed[1] to be the parental magma. The two phase diagrams show the composition plots very close to the

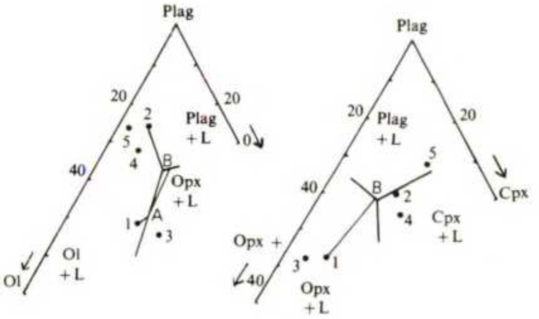

Fig. 3 Phase relationships at 3 kbar pressure from ref. 7 using the projection procedure of Irvine[13]. *a*, Clinopyroxene projection into the system olivine-plagioclase–quartz in cation proportions. *b*, Olivine projection into the system clinopyroxene–plagioclase–orthopyroxene + 4 quartz. The trend 1–A–B in the crystallization sequence is discussed in text. Sample numbers: 1, proposed Bushveld parental magma (analysis 1, Table 1); 2, typical metamorphosed gabbroic sill[1] (analysis 8, Table 1); 3, typical noritic sill[1] (analysis 9, Table 1); 4, proposed parental magma of the Bushveld Complex[3]; 5, proposed parental magma to the Skaergaard Complex[3,21].

olivine, clinopyroxene, plagioclose cotectic and as such will not crystallize the assemblages found for the Bushveld Complex (Fig. 1). Willemse's[1] other contention, that the norite rocks were derived from the gabbro liquid by contamination with siliceous sedimentary material, is questionable as the typical noritic composition (see Table 1) contains higher MgO than the gabbro, and so cannot possibly result from contamination of the latter.

Experimental studies at 1 atm pressure on Wager and Brown's[3] sample gave a different crystallization sequence[11,12] from that found in the Bushveld Complex, and Biggar[12] therefore rejected this as the parental magma. Daly's[2] sample was also studied by Tilley *et al.*[11]: they were dubious about its being the parental magma to the Bushveld Complex as it also gave a different sequence to that observed in the Complex as a whole. Irvine's[13] suggestion that possibly at higher pressures Wager and Brown's[3] sample could produce the right crystallization sequence is not consistent with the phase diagrams in Fig. 3, where the early crystallization of clinopyroxene is implied. The calculations of Vermaak[4] and Hamilton[5] have been questioned by Von Gruenewaldt[14] as the areal extent of the zones is a matter for speculation. Obviously the results of such a calculation would be very dependent on the shape of the complex. If the complex is funnel-shaped as evidence cited by Button[15] and Cameron[9] suggests, then the effect of the lower olivine- and pyroxene-rich (MgO-rich) zones would be overestimated in these calculations. The models of Vermaak[4] and Hamilton[5] are also based on the assumption that there is a new magma influx below the critical zone. Cameron[9] presented detailed mineral analyses across the lower zone–critical zone boundary and concluded there was no evidence for multiple magma injection at this level, at least in the eastern lobe of the Bushveld Complex.

None of the proposed parental magmas of Willemse, Daly, Wager and Brown, Vermaak or Hamilton seem very plausible, while the composition presented here seems in many respects to be consistent with the constraints required for it to be the parental magma to the Bushveld Complex.

Financial support from CSIR (South Africa) towards this research project is acknowledged.

Received 14 February; accepted 2 July 1980.

1. Willemse, J. *Proc. geol. Soc. S. Afr.* **62,** 21–80 (1959).
2. Daly, R. A. *Bull. geol. Soc. Am.* **39,** 703–768 (1928).
3. Wager, L. R. & Brown, G. M. *Layered Igneous Rocks* 588 (Oliver and Boyd, Edinburgh, 1968).
4. Vermaak, C. F. *Econ. Geol.* **71,** 1270–1298 (1976).
5. Hamilton, J. *J. Petrol.* **18,** 24–52 (1977).
6. Cawthorn, R. G., Davies, G., Clubley-Armstrong, A. & McCarthy, T. S. *Lithos* (in the press).
7. Cawthorn, R. G. *et al. Rep. Inst. Geol. Res. on the Bushveld Complex* 18, 27 (University of Pretoria, 1979).
8. Hart, S. R. & Davis, K. E. *Earth planet. Sci. Lett.* **40,** 203–219 (1978).
9. Cameron, E. N. *J. Petrol.* **19,** 437–462 (1978).
10. Schrieber, H. D. & Haskins, L. A. *Proc. 7th Lunar Sci. Conf.* 1221–1259 (1976).
11. Tilley, C. E., Yoder, H. S. Jr & Schairer, J. F. *Yb Carnegie Instn Wash.* **66,** 450–457 (1968).
12. Biggar, G. M. *Contr. Miner. Petrol.* **46,** 159–167 (1974).
13. Irvine, T. N. *Geol Soc. S. Afr., Spec. Publ.* **1,** 441–476 (1970).
14. Von Gruenewaldt, G. *Can Miner.* **17,** 233–256 (1979).
15. Button, A. *Trans. geol. Soc. S. Afr.* **79,** 3–12 (1976).
16. Von Gruenewaldt, G. *Trans. geol. Soc. S. Afr.* **76,** 207–227 (1973).
17. Molyneux, T. G. *Trans. geol. Soc. S. Afr.* **77,** 329–338 (1974).
18. Vincent, E. A. & Phillips, R. *Geochim. cosmochim. Acta* **6,** 1–26 (1954).
19. Lombaard, B. V. *Trans. geol. Soc. S. Afr.* **59,** 59–74 (1956).
20. Molyneux, T. G. *Miner. Mag.* **38,** 863–871 (1972).
21. Brooks, C. K. & Nielsen, T. F. D. *Lithos* **11,** 1–14 (1978).
22. Sharpe, M. R. *Trans. geol. Soc. S. Afr.* **81,** 373–378 (1978).

Fossil carbon in coastal sediments

M. S. Baxter, M. J. Stenhouse & N. Drndarski

Chemistry Department, University of Glasgow,
Glasgow G12 8QQ, UK

Fossil carbon, as present in coal, oil and their derivatives, is free from radioactive ^{14}C and its presence in even small concentrations within sedimentary materials can lead to anomalously old radiocarbon ages. For example, Erlenkeuser *et al.*[1] have noted artificially high ^{14}C ages in the upper 20 cm of Baltic Sea sediments in correlation with enhanced heavy metal concentrations. Both findings are consistent with the growth of industrial activity in this location, and the radiocarbon age increase has therefore in the past been regarded as an approximate measure of the extent of pollution of sediment organics by industrial fossil fuels. The results presented here will indicate that the latter interpretation is not always valid and that in studies of coastal marine sediments the incorporation of natural fossil carbon in the samples can introduce considerable error.

Surface sediments from the Clyde Sea area in south-west Scotland were analysed and their radiocarbon data compared to those reported by other workers (ref. 2 and D. D. Harkness, personal communication) (Table 1). These sediments were brown muds of silt-clay composition and had carbon contents typically around 5% on a dry weight basis. In each case these surface deposits were known to have accumulated during the twentieth century, their radiocaesium and ^{210}Pb contents having been monitored[3]. From each sample, inorganic carbonaceous matter, normally comprising ~1.8% of sediment dry weight, was removed by hydrolysis in hot 15% HCl for 2 hours. It is the residual component—the acid insoluble organic fraction—which is being discussed here. Radiocarbon analysis was performed by either CO_2 gas proportional or C_6H_6 liquid scintillation techniques using conventional methodology[4,5] and the radiocarbon dates are reported in the normal way[6], using the 5,568-year Libby half-life value. For the data presented in Table 1, the standard deviation associated with analysis is normally of minor significance relative to the age differences under discussion but in all cases is less than ±200 yr. The principal observation from the data is that surface ^{14}C ages are extremely large relative to the idealized near-zero values which should apply. There is therefore a significant concentration of fossil carbon present. This in itself is scarcely surprising given that the Clyde marine system receives major inputs of both industrial and domestic organic wastes from the Glasgow connurbation and surrounding regions[7]. While there is some localized variability in ^{14}C age distribution, the general ^{14}C age trend shown in Table 1 can be reasonably interpreted as reflecting the corresponding degree of pollution exposure, with sites nearest industrial releases having oldest ^{14}C ages. At the two extremes in the Table 1 data, ages of 1,595 yr (Loch Etive) and 10,490 yr

Table 1 Radiocarbon ages of surficial sediments

Sample	^{14}C age (yr)	Ref.
Loch Etive*	1,595	‡
Loch Goil, core 1	2,320	This work
Loch Fyne, core 1	2,650	2
Loch Striven	3,255	2
Loch Goil, core 2	3,340	This work
Loch Goil, core 3	3,765	This work
Loch Fyne, core 2	4,405	2
Gare Loch	5,965	This work
Garroch Head†	4,120–10,490	2

*Loch Etive result included for comparison only—this site lies outside the Clyde area on the west coast of Scotland.

†Garroch Head, in the inner Firth of Clyde, is the disposal site for Glasgow's domestic/industrial solid waste. ^{14}C ages decreased from 4,120 yr at the surface to 10,490 yr at 30 cm (ref. 2).

‡D. D. Harkness, personal communication.

0028–0836/80/360035—02$01.00

(Garroch Head) correspond to fossil carbon concentrations (in the organic fraction) of ~18% and 73% respectively. At this stage it was tempting to postulate anthropogenic release of fossil carbon as the sole cause of the observed age anomalies.

The set of results which sheds most light on the issue, however, comes from a 3-m long sediment profile at a sampling site in the Arran Deep trench, a location in the outer Firth of Clyde which is considered relatively natural and far removed from organic waste releases. Here the sediment is very fine-grained brown to grey mud of total carbon content ~2%, approximately one third of which is in carbonate form. The latter fraction was removed by acid hydrolysis as before. The results surprisingly show that erroneously old ^{14}C dates are not confined to post-industrial horizons but occur throughout the profile (Fig. 1). That abnormally high ^{14}C ages are obtained even at depth shows clearly that the contaminant there is of natural origin and suggests that, in the recent sediments considered so far, a combination of both natural and industrial fossil carbon inputs is occurring.

Evidence that the deeper section of the Arran Deep core is pre-industrial and that its ^{14}C chronology is misleading comes first from palaeomagnetic marking of horizons which places the 1.75-m level at ~600 yr before present (R. Thomson and G. M. Turner, personal communication). In addition, the ^{14}C age profile is consistent with a pre-industrial period of constant sedimentation rate (between 170 and 260 cm), which by regression analysis of the data in that interval is assessed at 0.6 ± 0.1 mm yr^{-1} (coefficient of correlation, 0.99). This estimate is in good agreement with a previous assessment of 0.3 to 0.6 mm yr^{-1} for a neighbouring location[2]. To a first approximation, the regression line drawn in Fig. 1 can therefore be regarded as the baseline representing the natural ^{14}C age profile at this site. Extrapolation to zero depth shows that the natural ^{14}C age for surficial deposits is ~3,000 yr, corresponding to a fossil carbon content of ~30%. The explanation of the high natural ages must, in our view, involve the natural erosion and inwash of coal dust from the outcrops of coal seams in the Clyde coast and catchment. This postulate is supported by the result of attempts to totally dissolve deep sediment samples in strong acids. In all cases, a fine black suspension of particulates remains, the carbon content of the dried dust being 60 to 70%. The overall abundance of the coal dust is sufficient to produce the observed age anomalies but would not normally be isolated during conventional pretreatment techniques. Thus when an aliquot of sediment, from 250 cm depth, containing 68 mg of organic carbon was exhaustively treated with HF, the residual particulate material was found to contain 26 mg of organic carbon, corresponding to ~35% of the total acid-insoluble organic fraction. Furthermore, the sediment was shown by microscopic examination to be rich in Carboniferous spores and it therefore seems certain that the high ^{14}C ages in Clyde sediments primarily reflect natural coal erosion in the catchment, a process whose effect has not to our knowledge been reported elsewhere and which could induce major dating errors or be relevant to interpretation of dates from many other areas. Certainly, the magnitude of the effect, the chemical inertness and appearance of the contaminant and the presence of Carboniferous spores combine to rule out the possibility that the observed ^{14}C dilution is caused by soil and blanket peat erosion, a process frequently reported elsewhere[1,8–11], being induced by changes in catchment land use.

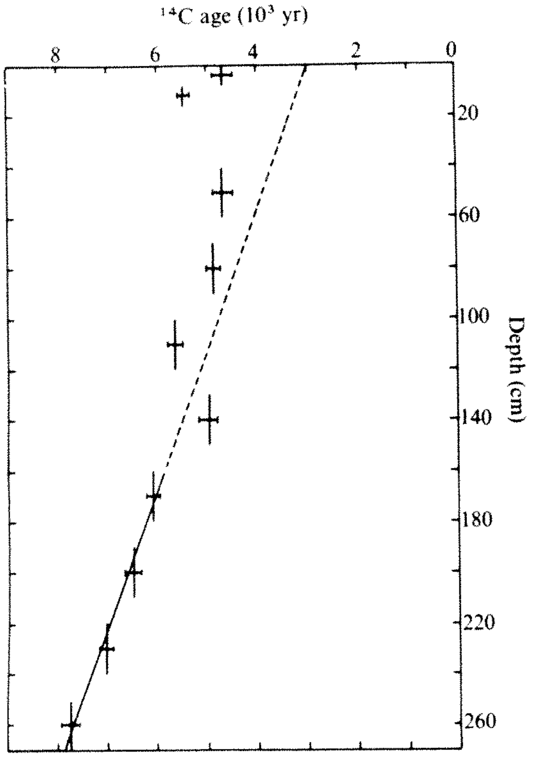

Fig. 1 Radiocarbon age/depth profile in Arran Deep sediments. Horizontal and vertical bars represent the ± 1σ dating errors and sample depth intervals respectively. The straight line is the best fit regression line through the lower data points.

That the upper data points lie to the high-age side of the natural chronology (represented by the straight line) reflects anthropogenic disturbance of the sedimentation pattern. Thus input of fossil carbon by industry and waste dumping further ages the topmost layers and is allied to a much increased deposition rate. While the sampling frequency is insufficient for detailed analysis, it is possible that the uppermost sample is slightly younger through incorporation of artificial ^{14}C released mainly in the 1960s by nuclear weapon tests. In agreement with our interpretation of the ^{14}C profile, ^{210}Pb and radiocaesium analyses (J. Smith-Briggs, personal communication) have shown that the present sedimentation rate is ~20 mm yr^{-1}. The maximum ^{14}C age observed in surface layers (5,450 yr at 15 cm) corresponds to a minimum total fossil carbon contribution of ~50%. Thus at this site the natural fossil carbon contributes 30% and the industrial component 20%.

The results presented briefly here indicate the need to consider natural fossil carbon contamination as a potential and significant source of error in dating sediments. This natural component applies at all sediment depths, and, if constant, does not preclude estimation of deposition rates. In recent surficial samples, however, the natural input is added to and masked by anthropogenic releases. If long cores are not available, the two fossil components cannot be differentiated and considerable errors may arise in evaluating the data. Certainly, in the Clyde Sea area, radiocarbon dating of sediments is dominated by these large fossil carbon effects.

We thank the staff of the Clyde River Purification Board, the Natural Environment Research Council and the crew of the NERC research vessel John Murray for collection of sediment samples. Examination of pollen and spores in the sediment was performed by J. H. Dickson. We also thank D. Thomson and S. Holland for technical assistance.

Received 17 January; accepted 10 July 1980.

1. Erlenkeuser, H., Suess, E. & Wilkomm, H. *Geochim cosmochim. Acta* **38,** 823–842 (1974).
2. Baxter, M. S. & Harkness, D. D. *Proc. I.A.E.A. Symp. Isotope Ratios as Pollutant Source and Behaviour Indicators* 135–141 (1975).
3. Swan, D. S. thesis, Univ. Glasgow (1978).
4. Stenhouse, M. J. & Baxter, M. S. *Radiocarbon* **18,** 161–171 (1976).
5. Campbell, J. A. & Baxter, M. S. *Radiocarbon* **21,** 171–179 (1979).
6. Broecker, W. S. & Olson, E. A. *Radiocarbon* **3,** 176–204 (1961).
7. *Natural Environment Research Council, Clyde Study Group, Report, NERC publ.* ser. C, No. 11 (1974).
8. Pennington, W. *Freshwater Biol.* **3,** 363–382 (1973).
9. O'Sullivan, P. E., Oldfield, F. & Batterbee, R. W. in *Quaternary Plant Ecology* (eds Birks, H. J. B. & West, R. G.) 267–278 (Blackwell, Oxford, 1973).
10. Pennington, W. in *The Effect of Man on the Landscape: The Highland Zone* (res. Rep. Br. Council for Archaeology, 1975).
11. Dickson, J. H. *et al. Nature* **274,** 548–553 (1978).

A model of epicontinental reef growth

Peter J. Davies & J. F. Marshall

Bureau of Mineral Resources, Geology and Geophysics,
Canberra City ACT 2601, Australia

The growth of coral reefs has been a controversial subject ever since Darwin's[1] subsidence theory. Scientists have argued over the major factors affecting growth[2–4], but most have agreed that reefs grow dominantly along their windward margins[5–7], a characteristic displayed in the Permian[8] and Devonian[9] reefs of New Mexico and Western Australia. Recently, however, Adey[10] has indicated that the growth characteristics of windward margins are energy related, such that different growth characteristics are to be expected under different energy regimes. The Great Barrier Reef is a high-energy epicontinental shelf reef system on which it has been suggested[11–13] that, in the prevailing conditions, windward growth has been subordinate to vertical and leeward growth. We present here results from drilling and monitoring studies demonstrating that reef growth in a transgressive epicontinental shelf environment is first vertical and then backwards, especially on the leeward margin, when the reef reaches the stillstand sea level position.

Our main body of data stems from extensive geological studies on and between the reefs of the Southern Great Barrier Reef. Four reefs have been studied in detail, but we report here only the results from One Tree Reef (Fig. 1) where comprehensive and integrated geological[14–17], and biological studies[18–20] have been conducted for 10 yr. Previously reported geological studies on this reef have defined its major physiographical features, relating them to features of the Pleistocene substrate. Thus the present reef rims surmount elevations in the substrate while the present lagoon covers a depression in the Pleistocene surface[16].

The Holocene section of the reef has been cored at six sites (Fig. 1), three near the southern, windward margin (1, 2 and 4), two on the leeward margin (3 and 5) and one on a patch reef in the lagoon (6). The facies variations encountered in four of these holes are shown in Fig. 2, from which the following conclusions are drawn.

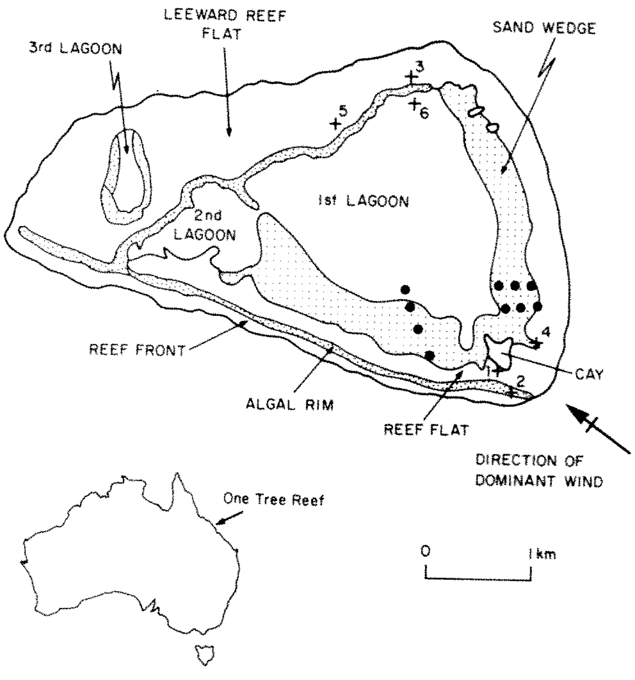

Fig. 1 One Tree Reef: physiographic features and sample sites. +, Drill sites; ●, sediment cores.

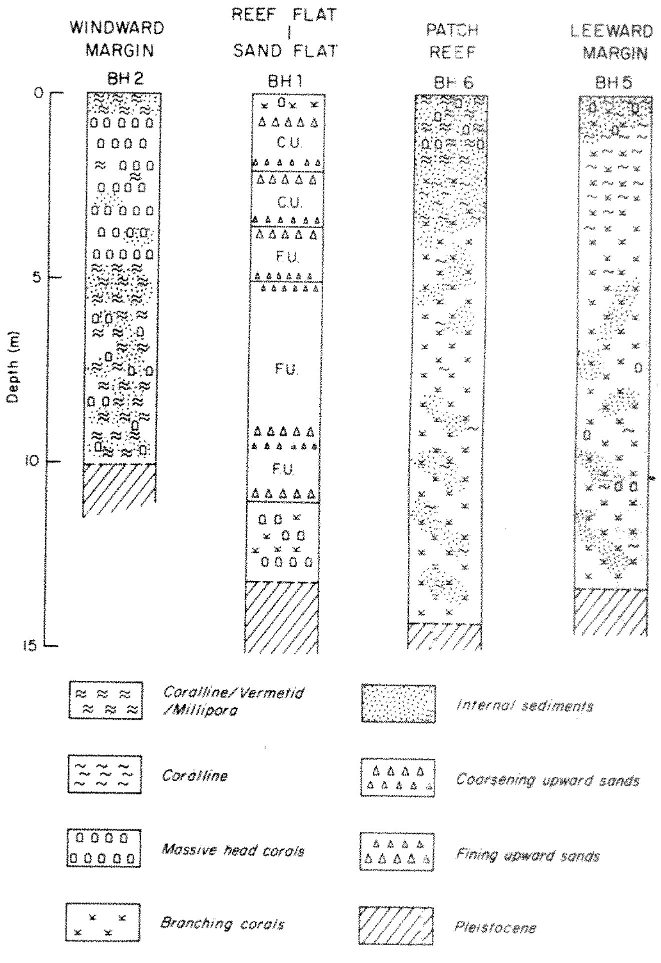

Fig. 2 Stratigraphic sections through Holocene at One Tree Reef, Southern Great Barrier Reef. Drill hole locations are shown on Fig. 1. % recoveries are BH1, 40%; BH2, 95%; BH5, 60%; BH6, 76%.

Growth on the windward margin is dominated by head corals together with a coralline algae/*Millepora*/vermetid assemblage that forms a massive framework (hole 2). The latter assemblage especially dominates the lower section of the drill hole whereas at the surface it forms only thin crusts.

Sands, compositionally identical to and clearly part of the accreting sand wedge (Fig. 1), were encountered to a depth of 11 m in hole 1, drilled at the junction of the reef flat and sand wedge. The lower half of the sand sequences exhibits fining-upward rhythms indicative of episodic storm supply from the reef margin and representing the earliest, deeper subtidal stages of lagoon infill. The upper portions of the sand sequence show a series of coarsening-upward rhythms, representing very shallow subtidal to intertidal accretion. Identical rhythms are seen in vibrocores through the top 5 m of the accreting sand wedge (Fig. 1).

The leeward lagoonal patch reef (hole 6) is surprisingly dominated in the top part of the section by the head coral/coralline algae-*Millepora*-vermetid association, similar to that seen in the windward hole. Porosity is low due to multiple generations of internal sediment. Branching corals predominate throughout the rest of the section.

At leeward sites (hole 5), a much thinner coralline crust with subordinate head corals overlies a dominantly branching coral section forming an open framework.

Radiocarbon dating of corals from three of the boreholes (Fig. 3) shows (1) that growth on windward margins (hole 2) throughout much of the Holocene occurred at a rate of 3.2 m kyr^{-1} except for a short burst in the top part of the section when the rate doubled; (2) that growth on the leeward margins (hole 3) throughout all but the bottom 1.5 m of section was nearly twice as fast as growth on the windward side; (3) that the growing reef reached sea level around 5,000 yr BP on the windward side compared with 1,000 yr BP on the leeward side; and (4) that in hole 1, the slow accretion rate of 1.7 m kyr^{-1} relates to the vertical growth of the accreting sand wedge and correlates well with independent estimates of lagoonal sand accumulation[21,22]. Much of the sand section accumulated only after the windward margin reached sea level, suggesting that little material is shed during the vertical growth phase (Fig. 3).

Growth at the stillstand sea level has been studied by monitoring the relations between calcification and sedimentation. Net calcification estimates at One Tree Reef[18–20] show the windward perimeter zones (algal and coral flat) accreting at a rate of 4 $\mathrm{kg\,m^{-2}\,yr^{-1}}$. Measurements of water and sediment movement show daily losses[23] from the windward algal rim and reef flat of 0.6 and 1.8 kg respectively, this being to leeward, into the lagoon. Similar measurements on the leeward margin indicate differences in sediment transported on neap and spring tides. During neaps, there is a daily excess of 0.6 kg entering the lagoon from the leeward edge whereas during springs, the lagoon water is flushed quickly resulting in an excess of 2.9 kg transported out of the lagoon and over the leeward margin. A conservative estimate would indicate considerably more than 2,000 tonnes of $CaCO_3$ moving over the leeward margin every year. Seismic reflection profiling shows a wedge of sediment, interpreted as Holocene, up to 10-m thick extending 1 km away from the leeward margin (D. Searle, unpublished data).

We conclude that when a reef reaches sea level, growth is markedly influenced by the surface hydrological regime, resulting in lagoonal infill and leeward accretion.

Our data have implications for both growth concepts and reef management. In conditions of sea level rising at a rate greater than the rate of calcification, the dependence of growth on light will give rise to vertically growing structures. These will eventually be drowned if sea-level rise continues to outpace growth. However, if sea-level rise slows or reaches a stillstand position, vertical growth will continue, with little loss through shedding, until such time as the potential accretion exceeds that of sea-level rise. At such time as the hydrological regime imposes its own growth restrictions, accretion will dominate on the leeward margins and the reefs will grow to leeward. That this mechanism also applies to other parts of the Great Barrier Reef is shown by reports from the 1973 Royal Society Expedition to the area[24].

The total growth history of an epicontinental reef system such as the Great Barrier Reef is one of a series of growth phases alternating, during the Plio–Pleistocene at least, with prolonged periods of subaereal exposure. The record will, therefore, consist of a series of reefal and related sediments separated by solution unconformities[25]. If past growth approximates that which has occurred in the Holocene, then the facies patterns produced will resemble those defined in the Holocene, and will differ substantially from those described in the classically accepted models; for example, the windward and leeward directions are reversed. Such a postulate must have important palaeogeographic and mineral exploration significance. Implicit to our model is the understanding that the depth to the Pleistocene substrate determines the time at which the reef reaches sea level and, therefore, the length of time for which changes in the surface zone have occurred. It follows that some reefs may have reached sea level recently, exhibiting few characteristics of leeward accretion: such reefs will contrast with others where lagoons are infilled and where the leeward margin has prograded considerably. We designate reefs which have just reached sea level as juvenile, and those with considerable leeward progradation as senile. One Tree Reef, which is intermediate between senile and juvenile, is described as mature. All reefs in the Capricorn/Bunker Groups of the Southern Great Barrier Reef may be identified in one of these three classes, and we suggest that such a genetically based growth classification may have considerable managerial importance. For example, juvenile and senile reefs may react very differently to environmental perturbations, either natural or man-made.

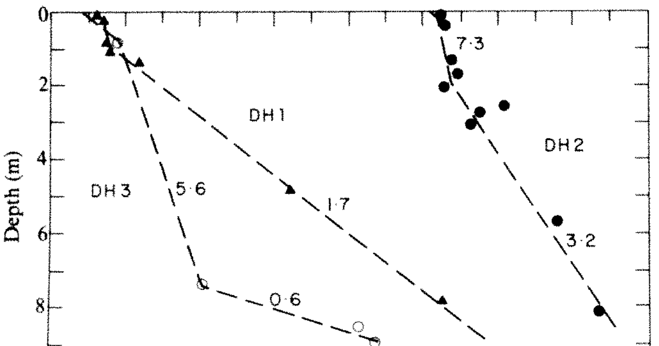

Fig. 3 Rates of reef accretion (m kyr^{-1}) displayed in three boreholes at One Tree Reef. Note that accretion in hole 1 starts only after the perimeter margin (hole 2) has reached sea level around 5,000 yr BP. Only corals in growth position have been dated.

Received 5 February; accepted 2 July 1980.

1. Darwin, C. *The Structure and Distribution of Coral Reefs* (Smith, Elder, London, 1842).
2. Murray, J. *Proc. R. Soc. Edinb.* **10,** 505–518 (1880).
3. Daly, R. A. *Proc. Am. Acad. Arts Sci.* **51,** 157–251 (1915).
4. Davis, W. M. *Am. geogr. Soc. Spec. Publ.* **9** (1928).
5. Holmes, A. *Principles of Physical Geology* (Nelson, Sunbury-on-Thames, 1965).
6. Thornbury, W. D. *Principles of Geomorphology* (Wiley, New York, 1969).
7. Maxwell, W. G. H. *Atlas of the Great Barrier Reef* (Elsevier, Amsterdam, 1968).
8. Newell, N. D. *et al. The Permian Reef Complex of the Guadalupe Mountains Region, Texas and New Mexico* (W. H. Freeman, San Francisco, 1953).
9. Playford, P. E. *Western Australia Geol. Surv. Rep.* 1 (1969).
10. Adey, W. H. *Science* **202,** 831–837 (1978).
11. Davies, P. J. *Proc. 3rd int. Coral Reef Symp.* **2,** 325–330 (1977).
12. Davies, P. J. *et al. Proc. 3rd int. Coral Reef Symp.* **2,** 331–338 (1977).
13. Stoddart, D. *et al. Proc. R. Soc.* **B284,** 149–159 (1978).
14. Davies, P. J., Radke, B. M. & Robison, C. R. *BMR J. Aust. Geol. Geophys.* **1,** 231–240 (1976).
15. Davies, P. J. & Kinsey, D. W. *Mar. Geol.* **24,** 1–11 (1977).
16. Harvey, H., Davies, P. J. & Marshall, J. F. *BMR J. Aust. Geol. Geophys.* **4,** 141–147 (1979).
17. Davies, P. J. & Marshall, J. F. *Search* **10,** 776–779 (1979).
18. Kinsey, D. W. *Proc. 1st int. Coral Reef Symp.* 13–32 (1972).
19. Kinsey D. W. & Davies, P. J. in *Biogeochemical Cycling of Mineral-forming Elements* (eds Trudingar, P. & Swaine, D.) 131–162 (Elsevier, Amsterdam, 1979).
20. Kinsey, D. W. & Davies, P. J. *Limnol. Oceanog.* **24,** 935–940 (1979).
21. Frankel, E. *Proc. 3rd. int. Coral Reef Symp.* **2,** 201–208 (1977).
22. Davies, P. J. *Reef Growth: A Review* (Australian National University Press, in the press).
23. Davies, P. J. & West, B. (in preparation).
24. Orme, G. R., Flood, P. G. & Sargent, G. *Proc. R. Soc.* A**291,** 85–100 (1978).
25. Davies, P. J. *Proc. 2nd int. Coral Reef Symp.* **2,** 573–578 (1974).

Oxidative changes to nitrate and boron in marine pore waters

Kent A. Fanning & Valentine I. Maynard-Hensley
Department of Marine Science, University of South Florida,
St Petersburg, Florida 33701

Reported changes in the composition of marine pore water on contact with air[1–4] led us to investigate whether air-exposure of marine sediment might alter its interstitial concentrations of nitrate and boron. Nitrate should be a good indicator of changes in the oxidation state of marine sediments[5,6], and interstitial boron should reflect changes in the reactivity of sedimentary components because it bonds to clays[7,8] and sediments in a temperature-sensitive manner. We report here that interstitial nitrate concentrations can increase considerably during air exposure of marine sediment and that interstitial boron can be scavenged from some reducing sediment. Sedimentary boron scavenging may affect oceanic boron, but the process may be influenced by interstitial components that prevent the uptake of boron onto freshly formed hydrous ferric oxides.

0028-0836/80/360038—04$01.00

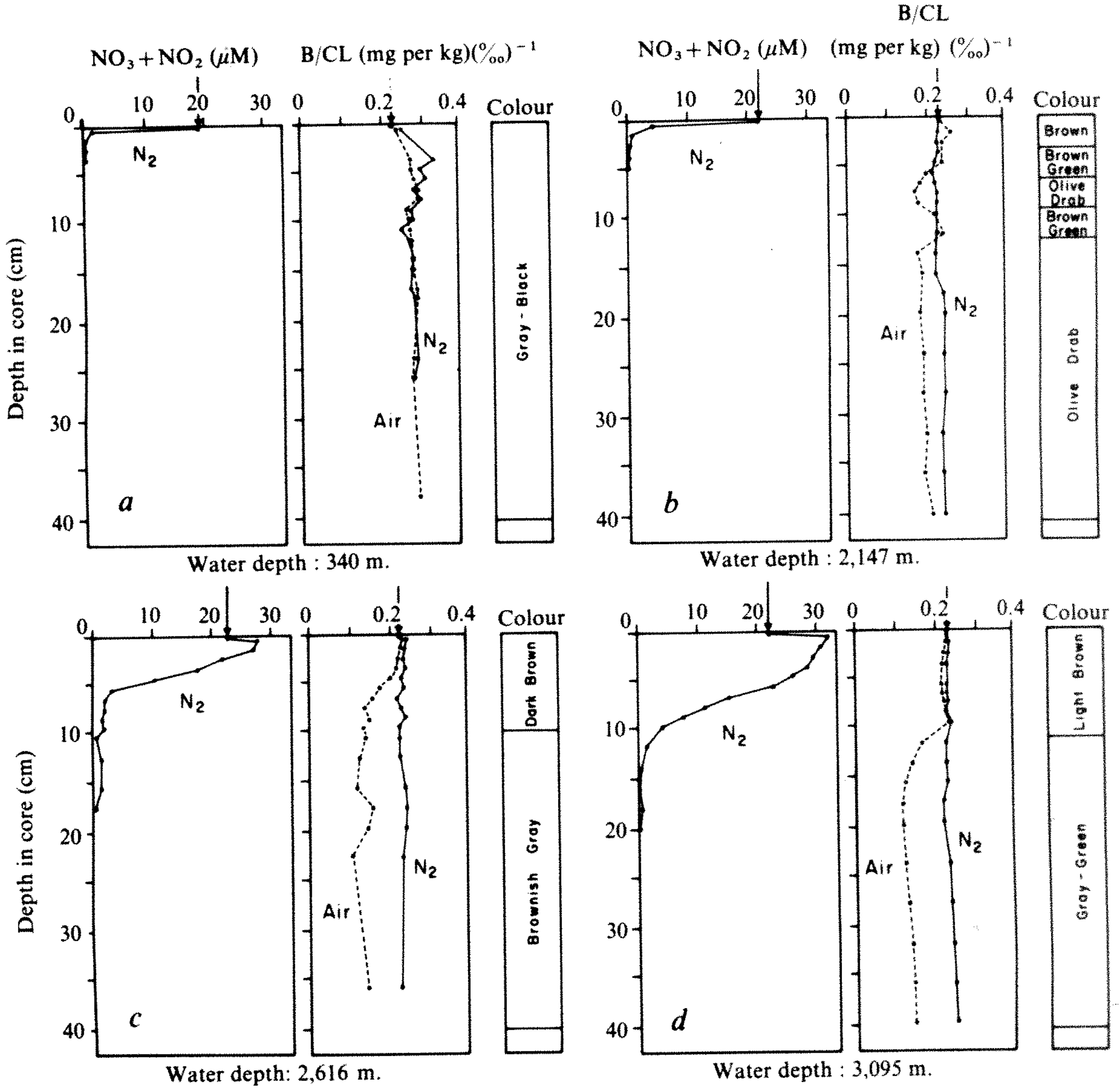

Fig. 1 Air-squeezed (· · · ·) and nitrogen-squeezed (———) profiles of interstitial ratios of boron to chlorinity and interstitial concentrations of nitrate + nitrite in sediments from the delta of the Magdalena River. The arrows indicate values of near-bottom seawater above each core. Colour patterns in the sediment are also shown. A Benthos Model 2171 gravity corer was deployed from the RV Gyre out of Texas A & M University. To minimize disturbance during coring, no cutter, catcher, or barrel was used, and the lowering speed on the winch was less than 20 m min^{-1}. *a*, 340 m water depth; *b*, 2,147 m water depth; *c*, 2,616 m water depth; *d*, 3,095 m water depth.

In August 1977, four 6.5-cm diameter gravity cores were taken from different water depths on the Magdalena River delta near Barranquilla, Columbia (Table 1). Each core was immediately sealed and transferred to a room kept at around the same temperature as that where the core was obtained: 17 °C for the 340-m core and 4 °C for the cores from deeper water (Table 1). Each core was opened and cut into 1-cm slices inside a nitrogen-filled plastic bag at positive pressure. Half of each slice was squeezed to remove its pore water while still inside the bag; the other half was exposed to air for 1–2 h and then squeezed to extract its pore water in oxygenating conditions. For each core, the processing temperature was the same as its storage temperature.

Air-squeezed and nitrogen-squeezed pore waters were analysed for dissolved boron[10], for dissolved nitrate and nitrite[11], and for chlorinity using $AgNO_3$ with dichlorofluorescein as endpoint indicator. Air-squeezed and nitrogen-squeezed profiles for each core were compared to each other and to the core's colour pattern (Fig. 1*a–d*).

Air-exposure of Magdalena sediment produced strong enrichments in interstitial nitrate + nitrite (Table 2). The increases were usually confined to the upper parts of the cores, and the largest were in the upper 4 cm of the core from 2,616 m of water. The zone seemed to be reasonably oxidizing because of its high initial concentrations of nitrate and because of its dark brown colour[12]. Air exposure did not produce large enrichments in sediment which was so reducing that nitrate or nitrite was originally absent. (Possibly the microorganisms whose metabolism might be stimulated by air are not likely to be important in such sediment.) Thus conclusions based on nitrate data from air-exposed sediment may be suspect, even for deeper-water deposits thought to be oxidizing. Also, atmospheric contact may stimulate nitrate production in tidally exposed sediment.

Figure 1 shows only nitrogen-squeezed profiles of nitrate + nitrite for comparison to the profiles of air-squeezed and nitrogen-squeezed interstitial boron. For most of the Magdalena cores, interstitial nitrite concentrations were small (around 0.2 μM), and we will consider only nitrate here.

Figure 1 shows the boron–chlorinity ratios (B/Cl) in the pore-water samples. The conservative nature of oceanic boron means that all results may be compared with the typical value of the ratio: 0.23 (mg B per kg) (‰)$^{-1}$ (see refs 13, 14).

The Magdalena profiles show that interstitial boron can be strongly scavenged from marine pore fluids when atmospheric oxygen penetrates the exposed sediment. In two cores from deeper water (Fig. 1*c*, *d*), interstitial boron–chlorinity ratios were reduced by as much as 50%, indicating a consumption of 210 μM borate or 2.2 mg B per kg of pore water. In the third deeper-water core (Fig. 1*b*), the loss was less. In the shallowest core (340 m, Fig. 1*a*) the ratios were slightly higher than normal, probably because the room in which the 340 m core was processed was a little too warm at 17 °C. Seawater temperature at 340 m was 12 °C, and a 5 °C increase should cause interstitial boron concentrations to rise detectably[9].

No zone showing strong scavenging of boron contained much nitrate. Air-sensitivity of interstitial boron was most likely when the sediments were so reduced that interstitial nitrate was 5 μM or less. When nitrate concentrations were higher, a solid phase capable of removing boron was apparently absent or too oxidized to function.

Actual scavenging phases in reducing zones could have been freshly precipitated forms of Fe(III) which were created when atmospheric oxygen reacted with Fe(II) that was either dissolved in pore water or attached to particle surfaces[1-3]. In cores from water deeper than 2,000 m (Fig. 1*b–d*), zones of sediment that showed no scavenging of interstitial boron had brownish colours, suggesting that Fe(III) dominated over Fe(II) in the solid phases[12]. However, intensity and distribution of boron scavenging varied considerably in the four Magdalena cores. Organic matter in the sediment may influence the degree of scavenging because of the affinity of borate for carbohydrates and other organic compounds with alcohol groups[15,16].

The uptake of oceanic boron by iron compounds was studied by using two laboratory simulations of the action of sedimentary ferrous iron during air exposure at 4 °C. In both, 500 ml of pelagic seawater was enriched with 'scavengeable' nutrients until the initial concentrations were 200 μM silica and 20 μM phosphate—values often found in reducing marine pore waters[3]. Initial boron concentrations were 406 μM (4.29 mg B per kg seawater) in the first experiment and 418 μM (4.42 mg B per kg seawater) in the second. To inhibit the oxidation of Fe(II), the enriched batches of seawater were bubbled with nitrogen for 2 h to remove dissolved oxygen and then acidified to *p*H 3 with concentrated H_2SO_4. $Fe(NH_4)_2(SO_4)_2 \cdot 6H_2O$ was added to each flask to make its acidified seawater 13,000 μM in dissolved Fe(II) so that there was initially a 20 : 1 molar ratio of ferrous iron to total scavengeable solutes (silica + phosphate + boron). In the second experiment, the seawater was also made 20,000 μM in mannitol to see if a large amount of boron-complexing organic matter altered the scavenging of boron. Then, over a 2-h period, oxidative scavenging was induced by adding concentrated NH_4OH dropwise while stirring and bubbling air into the flasks. As the first drops of NH_4OH entered the seawater, a bluish precipitate formed which eventually turned red-brown as air bubbles mixed with it. Towards the end of each experiment, the drops of NH_4OH produced more red-brown precipitate directly with no bluish intermediate. Addition of NH_4OH was stopped when the *p*H passed 8.5 and dissolved iron was less than 3% of its initial value. The reaction flasks were polythene.

Table 1 Data on cores from the Magdalena Delta

Core no.	Water depth (m)	Position
77-G-8, G.C. 2	340	11°08.4′ N, 74°54.8′ W
77-G-8, G.C. 8	2147	11°23.5′ N, 75°25.3′ W
77-G-8, G.C. 7	2616	11°39.5′ N, 75°33.5 W
77-G-8, G.C. 6	3095	11°49.5′ N, 75°38.1′W

Final aliquots were removed from the two batches of seawater, filtered through 0.4 μm Nuclepore membranes, and analysed. The dissolved silica and phosphate initially present in both experiments were at least 98% removed. In the first experiment, the boron–chlorinity ratio was 12% lower after the precipitation of Fe(III) hydroxide was finished. However, in the second experiment, the added manitol apparently restricted the scavenging of boron because the final boron–chlorinity ratio was only 2% less than the initial ratio.

There are two curious features of the Magdalena data (Fig. 1): (1) interstitial nitrate was absent or nearly absent from any sediment in which a sizeable air-induced uptake of interstitial boron occurred, and yet (2) the absence of nitrate did not guarantee an air-induced uptake of boron, for example in most of the 340 m core and in parts of the upper 12 cm of the 2,147 m core.

The laboratory simulations provide partial explanations. Freshly oxidized and precipitated Fe(III) oxide did scavenge boron from seawater along with silica and phosphate. Marine sedimentary Fe(II) that can form fresh Fe(III) oxides is apparently not present until interstitial nitrate has been consumed by reduction reactions[17]. Therefore, air-induced

Table 2 A comparison of concentrations of nitrate + nitrite in nitrogen-squeezed and air-squeezed pore waters from sediment cores from the Magdalena River delta. Concentration units are μmol per litre of pore water

Depth in core (cm)	Core G.C. 2 (water depth, 340 m)			Core G.C. 8 (water depth, 2,147 m)			Core G.C. 7 (water depth, 2,616 m)			Core G.C. 6 (water depth, 3,095 m)		
	N_2	Air	Δ	N_2	Air	Δ	N_2	Air	Δ	N_2	Air	Δ
0–1	1.1	8.2	7.1	4.3	—	—	27.3	72.0	44.7	31.6	30.0	−1.6
1–2	0	2.0	2.0	1.0	20.4	19.4	26.8	45.4	18.6	30.5	31.1	0.6
2–3	0	1.2	1.2	0.8	11.5	10.7	21.4	31.9	10.5	29.3	32.0	2.7
3–4	0	0	0	0.4	—	—	17.2	23.7	6.5	28.2	29.7	1.5
4–5	0	0	0	0	2.5	2.5	10.3	9.5	−0.8	25.9	31.4	5.5
5–6	0	0	0	0	0	0	2.8	2.1	−0.7	22.5	26.4	3.9
6–7	0	0	0	0	0	0	2.0	2.7	0.7	15.3	16.3	1.0
7–8	0	0	0	0	0	0	1.7	1.6	−0.1	11.3	12.7	1.4
8–9	0	0	0	0	0	0	1.3	0.7	−0.6	7.4	9.3	1.9
9–10	0	0	0	0	0	0	1.4	1.5	0.1	4.1	4.3	0.2
11–12	0	0	0	0	0	0	0.4	2.7	2.3	1.4	2.6	1.2
13–14	0	0	0	0	0	0	1.2	2.7	1.5	0.5	1.9	1.4
15–16	0	0	0	0	0	0	1.0	1.3	0.3	0	0.8	0.8
17–18	—	0	—	0	0	0	0	1.5	1.5	0.5	0.5	0
19–20	—	0	—	0	0	0	0	0.7	0.7	0.2	0.5	0.3
23–24	—	0	—	0	0	0	0	0.6	0.6	0	0.3	0.3
27–28	—	0	—	0	0	0	0	0.4	0.4	0	0	0
31–32	—	0	—	0	0	0	0	0.7	0.7	0	0.4	0.4
35–36	—	0	—	0	0	0	0	0.6	0.6	0	0	0
39–49	—	0	—	0	0	0	0	0.3	0.3	0	0	0

boron scavenging and nitrate could be mutually exclusive in sediments. However, our experiments did not display the extensive boron losses found in much of the deeper Magdalena sediment. Perhaps insufficient Fe(II) was used compared with that available in sediments, or the surface area of sedimentary particles may be important. But the lack of boron scavenging in some reducing sediments is more puzzling. The simulations suggest that interstitial organic matter may have been responsible. Although mannitol is not a major organic compound in sediments, it has been reported for marine cores[18], and we found that it hampered the scavenging of boron by Fe(III) oxides. It probably did not drastically alter the surface properties of the Fe(III)–oxide precipitates because silica and phosphate were scavenged with or without mannitol. Therefore, the mannitol may have complexed the boron so that it was not scavenged as effectively. Similar 'protective' complexation between boron and sedimentary organic compounds may occur in natural reducing sediments. In fact, a weak response of interstitial boron to air exposure may be an effective indicator of the presence of such compounds in a sediment.

Marine sediment can encounter elemental oxygen in two forms: an atmospheric gas or an oceanic solute. Our results suggest that this encounter could stimulate reactions which become important parts of the cycles of nitrate and boron in the sea.

We thank Lynn J. Burton and Jabe A. Breland for careful processing of sediment under adverse cold-room conditions. We also thank the office of Naval Research (Contract N00014-75-C-0539) and the NSF (OCE76-82416) for financial assistance.

Received 28 March; accepted 26 June 1980.

1. Bray, J. T., Bricker, O. P. & Troup, B. N. *Science* **180,** 1362–1364 (1973).
2. Troup, B. N., Bricker, O. P. & Bray, J. T. *Nature* **249,** 237–239 (1974).
3. Loder, T. C., Lyons, W. B., Murray, S. & McGuinness, H. D. *Nature* **273,** 373–374 (1978).
4. Lyons, W. B., Gaudette, H. E. & Smith, G. M. *Nature* **277,** 48–49 (1979).
5. Pamatmat, M. M. *Int. Rev. Hydrobiol.* **58,** 345–368 (1973).
6. Bender, M. L., Fanning, K. A., Froelich, P. N., Heath, G. R. & Maynard, V. *Science* **198,** 605–609 (1977).
7. Lerman, A. *Sedimentology* **6,** 267–286 (1966).
8. Couch, E. L. & Grimm, R. E. *Clays Clay Miner.* **16,** 249–256 (1968).
9. Sayles, F. L., Manheim, F. T. & Waterman, L. S. *Init. Rep. DSDP Leg* **20** (1973)
10. Uppström, L. R. *Analyt. chim. acta* **43,** 475–486 (1968).
11. Armstrong, F. A. J., Stearns, C. R. & Strickland, J. D. H. *Deep-Sea Res.* **14,** 381–389 (1967).
12. Sverdrup, H. U., Johnson, M. W. & Fleming, R. H. *The Oceans, Their Physics, Chemistry, and General Biology*, 967–969 (Prentice-Hall, Englewood Cliffs, 1942).
13. Uppström, L. R. *Deep-Sea Res.* **21,** 161–162 (1974).
14. Fanning, K. A. & Maynard, V. *Neth. J. Sea Res.* **12,** 345–354 (1978).
15. Braman, R. S. in *Treatise on Analytical Chemistry, Part II* Vol. 10 (eds Kolthoff, I. M. & Elving, P. J.) 1–101 (Wiley, New York, 1978).
16. Gast, J. A. & Thompson, T. G. *Analyt. Chem.* **30,** 1549–1551 (1958).
17. Froelich, P. N. *et al. Geochim. cosmochim. Acta* **43,** 1075–1090 (1979).
18. Modzeleski, J. E., Laurie, W. A. & Nagy, B. *Geochim. cosmochim. Acta* **35,** 825–838 (1971).

Records of *Cooksonia*-type sporangia from late Wenlock strata in Ireland

D. Edwards

Department of Plant Science, University College, Cardiff CF1 1XL, UK

J. Feehan

Department of Geology, Trinity College, Dublin 2, Ireland

Hitherto the earliest record of a fossil flora containing *Cooksonia* type sporangia was from a mid-Ludlow (Silurian) locality in Wales[1]. The compression fossils illustrated here (Figs 1–4) come from strata assigned to the highest graptolite zone of the Wenlock Series characterized by *Monograptus ludensis*. They were collected (by J. F.) in the Devilsbit Mountain district of County Tipperary, Ireland. But this is not just a record of the first appearance of a genus which extends to the end of the Lower Devonian, because *Cooksonia* has generally been accepted as a vascular plant[2]. Its occurrence at the top of the Wenlock therefore seems to extend the history of vascular plants back to the middle of the Silurian and to indicate that higher plants colonized land surfaces at least 415 Myr ago.

The very fragmentary plant fossils are scattered among numerous irregular patches of coalified material, the rock matrix being a slightly micaceous buff siltstone interlaminated with a grey-green mudstone from which fossils are absent. In marked contrast to later Ludlow records, sterile branching axes of *Hostinella*-type are rare and far outnumbered by the fertile specimens. One of the latter, which exhibits dichotomous branching, is shown in Fig. 1. The sporangia are tangentially extended and oval to irregular in outline. They most closely resemble *Cooksonia pertoni* Lang, but are considerably smaller. We have illustrated the remaining specimens to show some of the range in sporangial morphology, which indicates that more than one morphospecies is represented. As they are subtended by very short lengths of unbranched axis, they do not strictly conform to the generic diagnosis of *Cooksonia*, although one of them (Fig. 4) is similar to *C. hemisphaerica* Lang in sporangial shape.

However, because we have not yet seen tracheids on cellulose acetate film pulls taken from these Irish compression fossils, we cannot be absolutely certain that they were vascular plants. Had they been found in later, for example, Downton (Pridoli) or

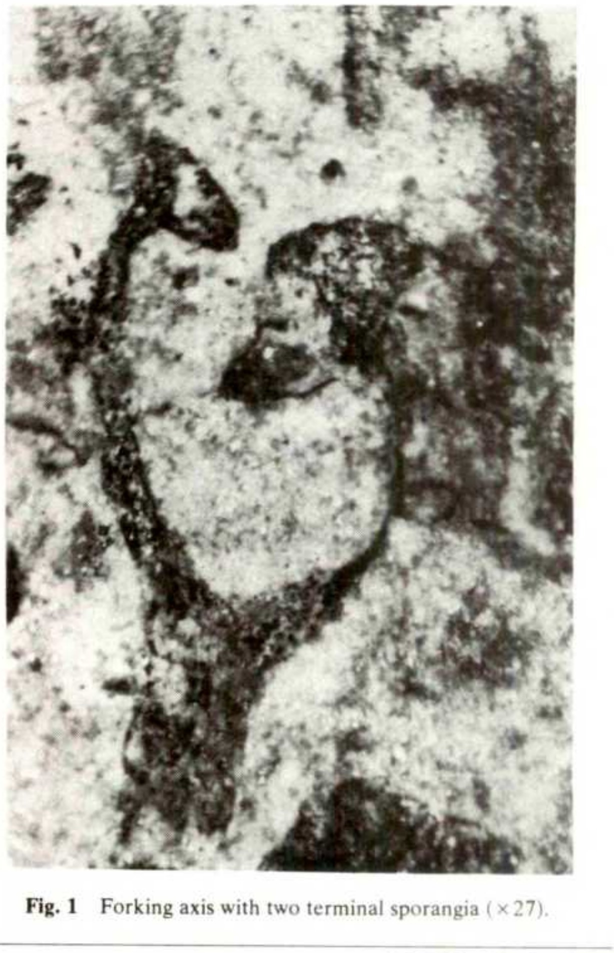

Fig. 1 Forking axis with two terminal sporangia (×27).

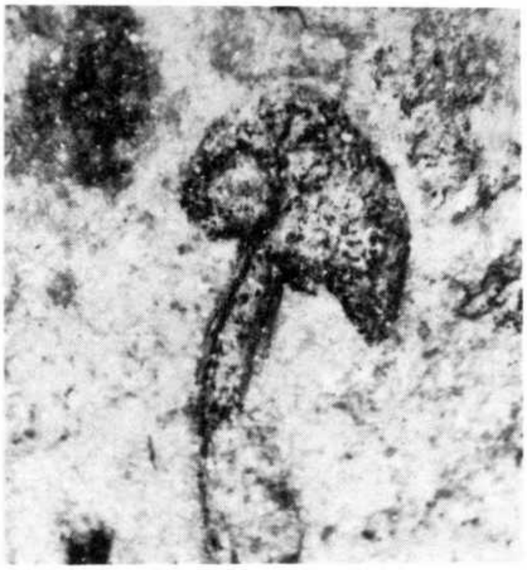

Fig. 2 Terminal sporangium (×25).

Gedinne sediments, such fossils would undoubtedly be assigned to *Cooksonia* and be accepted as vascular plants. In view of their great stratigraphical age and their relevance to such highly controversial issues as the ancestry and origin of vascular plants, the possibility that the Irish fossils had identical morphology to *Cooksonia* but lacked conducting tissues cannot be ignored. Pratt *et al.*[3] described such a level of organization as rhyniophytoid. Sterile branching axes lacking vascular tissues and thought to belong to erect plants have been reported from early Silurian deposits in the United States[4]. The authors of that report suggested that the plants were "representatives of primitively emergent vegetation" (page D71) and "incipient vascular plants" (page D72). In a different physiological approach, Raven[5] argued that the alga-vascular plant intermediate would require a plant body of some size in order to release its meiospores into air currents and that such spores with sporopollenin-impregnated walls would be produced at the apices of parenchymatous axes. Similarly Smith[6] raised the possibility that the parent plants of the simple, smooth-walled spores with triradiate marks which he has isolated from Wenlock strata in County Mayo were non-vascular aquatics (? presumably with emergent sporangia).

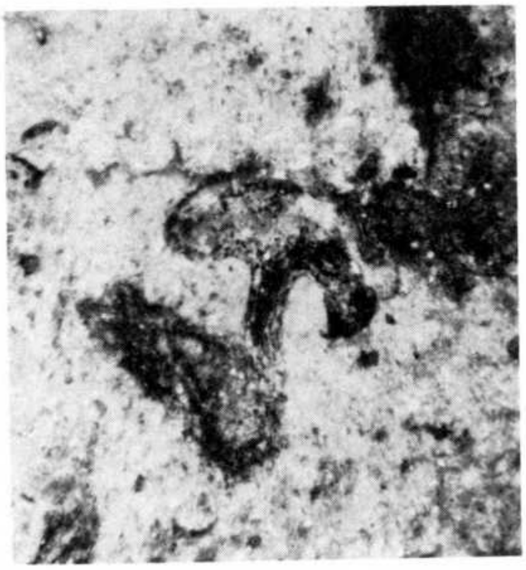

Fig. 3 Reniform terminal sporangium (×25).

Thus practising the caution advised by Banks[7], we can only conclude that the Irish flora certainly contains the earliest known erect fertile land plants and perhaps the earliest fertile vascular plants.

That they are the earliest *Cooksonia*-type sporangia is substantiated by faunal evidence. The necessity for accurate independent stratigraphical dating for any hypotheses relating to the phylogeny of vascular plants, in particular their ancestry and early evolution, has been emphasized elsewhere[1].

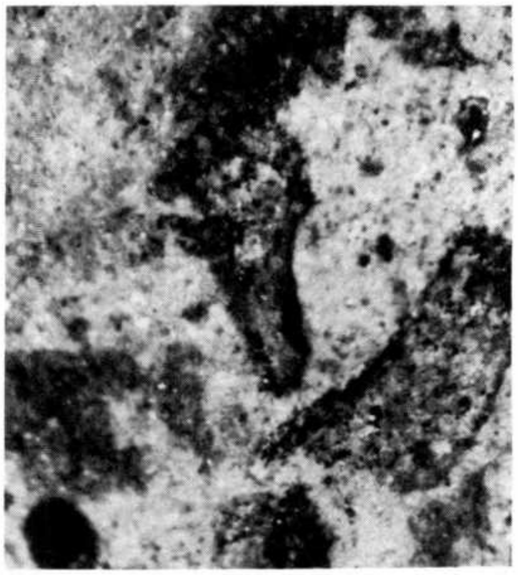

Fig. 4 Globose terminal sporangium (×23).

The rocks of the Devilsbit Mountain area constitute the northeastern end of an extensive inlier of Silurian rocks that extends south-westwards to include Silvermines and Slieve Phelim. The successsion, the overall thickness of which is probably in excess of 2,500 m, comprises a monotonous succession of turbiditic sandstones, laminated siltstones and mudstones, with very rare microconglomerates and volcanic rocks. The siltstones are frequently fossiliferous, yielding a varied fauna of *Cyrtograptus ludgreni* Zone age over much of the inlier[8–11]. To the south-east of Moneygall, near the northeastern end of the inlier, a small area of rocks of *Monograptus ludensis* Zone age is preserved in the core of a syncline in the vicinity of Cloncannon townland. These rocks are characterized by a fauna that includes *M. ludensis* Murchison, which is much the most abundant species present, and *M. auctus* Rickards together with nautiloids, phyllocarids, a small crinoid, occasional small brachiopods and epifaunal bivalves. The plant-bearing lithologies occur near the top of Borrisnoe Mountain, 1.7 km south-east of Moneygall (Grid reference 18 S 052782), near the southeastern edge of the Cloncannon syncline, and towards the base of the *ludensis* sequence, which attains a thickness of around 900 m. The age of the rocks in which the sporangia occur is confirmed by the presence of the two diagnostic graptolite species (identified by Dr R. B. Rickards) both above and below the plant fossils at the locality. Hence these Irish macroplants predate the lower *Baragwanathia* flora of Victoria, Australia even if the early Ludlow age is confirmed[12].

Received 2 June; accepted 18 July 1980.

1. Edwards, D., Bassett, M. G. & Rogerson, E. C. W. *Lethaia* **12,** 313–324 (1979).
2. Banks, H. P. *Bioscience* **25,** 730–737 (1975).
3. Pratt, L. M., Phillips, T. M. & Dennison, J. M. *Rev. Palaeobot. Palynol.* **25,** 121–149 (1978).
4. Schopf, J. M., Mencher, E., Boucot, A. J. & Andrews, H. N. *U.S. Geol. Surv. Prof. Pap.* 550–D, D69–D75 (1966).
5. Raven, J. A. *Adv. bot. Res.* **5,** 153–219 (1977).
6. Smith, D. G. *Geol. Mag.* **112,** 411–414 (1975).
7. Banks, H. P. *Rev. Palaeobot. Palynol.* **20,** 13–25 (1975).
8. Cope, R. N. *Geol. Mag.* **91,** 319–324 (1954).
9. Cope, R. N. *Proc. Roy. Irish Acad.* **60B,** 217–242 (1959).
10. Palmer, D. *Sci. Proc. R. Dubl. Soc.* **A3,** 335–342 (1970).
11. Doran, R. J. P. *Proc. R. Irish Acad.* **74B,** 193–202 (1974).
12. Garratt, M. J. *Alcheringa* **2,** 217–224 (1979).

Perceptual learning specific for orientation and spatial frequency

Adriana Fiorentini & Nicoletta Berardi

Istituto di Neurofisiologia del Consiglio Nazionale delle Ricerche, Pisa, Italy

Several examples of 'perceptual learning' (improvement of some perceptual task with practice) have been reported$^{1-4}$. These studies are of great interest for neurological research because they demonstrate plasticity of the nervous system. Even for apparently basic perceptual tasks, such as visual acuity or vernier acuity^{1,4}, practice can facilitate a neural change which enhances performance. One question in this field is where does this learning occur? Indications about the possible neural site of a learning process may be derived from its specificity for some particular stimulus parameters. For instance, there is a hint that learning in global stereopsis may occur at a stage where visual information is processed by mechanisms selectively sensitive to different stimulus orientations^{3}. We report here an experiment on perceptual learning in the discrimination of gratings of different waveform. Our findings show that learning is specific for both the orientation and the spatial frequency of the practice stimulus.

The aim of the experiment was to evaluate the effects of training on the ability to discriminate gratings of different luminance distributions, to determine whether these effects were retained over time and to ascertain whether the effects would transfer to gratings of different orientations or different spatial frequencies.

The patterns to be discriminated (Fig. 1) were two complex gratings consisting of the sum of two sinusoids of spatial frequency f and $3f$, and contrast 40 and 13%, respectively ($\geqslant 1$ log unit above threshold). The two gratings differed only in the relative spatial phase of the two components. In grating *a* the two sinusoidal components had spatial phase 0°, like the first and third harmonic of a square wave. In grating *b* the spatial phase of the third harmonic was shifted by 90°. The luminance profiles of the two gratings are shown in the inset of Fig. 2.

The gratings were generated on a circular oscilloscope screen (Tektronix 503, 12-cm diameter) by a PDP11/10 computer at the rate of 2 ms per frame and viewed binocularly, with natural pupils. A black fixation dot of 3 mm diameter was superimposed at the centre of the screen. The average luminance of the screen ($10\ \mathrm{cd\ m^{-2}}$) was kept constant during and between grating presentations.

Discrimination of pairs of gratings of the same orientation, contrast and spatial frequency and with the luminance profiles shown in Fig. 2 was assessed with a two-alternative temporal forced-choice procedure. The gratings were presented successively for 16 ms (8 frames) each, with an interval of 500 ms. The order of presentation was varied quasi-randomly from trial to trial. Subjects reported after each trial in which of the two time intervals (indicated by a sound) grating *a* had been presented, and were informed whether their response was correct.

Two experienced and four naive subjects participated in the experiments. All subjects took part in three experimental sessions. In the initial 50–70 trials of each session, the gratings to be discriminated were vertical and viewed from 1.2 m, so that their fundamental spatial frequency was 1 cycle per deg. In the subsequent 80 trials, the gratings were either viewed from the same distance, but orientated horizontally (first experimental session), or orientated vertically and viewed from 60 cm (fundamental spatial frequency 0.5 c/deg, second session) or from 2.4 m (fundamental spatial frequency 2 c/deg, third session).

To evaluate changes in discrimination performance with training, the responses of each subject were grouped in subsequent blocks of 10 trials each. The corresponding blocks of trials of the six subjects were then pooled and the percentage of correct responses evaluated.

The results are presented in Fig. 2, where each point represents the average percentage of correct responses of the six subjects in successive blocks of 10 trials per subject (60 trials per point) relative to the three experimental sessions. The percentage of correct responses in the discrimination trials with vertical gratings of 1 c/deg (full points in Fig. 2) increased progressively during the first session from less than 70% in the first block of trials to more than 90% in the fourth to sixth block, and remained constant thereafter. The effects of trial repetition on discrimination performance with the same pair of gratings were almost completely retained in the second session, run on the next day (Fig. 2, middle left) and completely retained in the third session (Fig. 2, bottom left).

In contrast, the effects of training on discrimination performance with vertical gratings failed to transfer to horizontal gratings (Fig. 2, top right): the percentage of correct responses dropped to levels near chance when the gratings were presented horizontally, and a further 40–50 trials were required for performance to improve to a 90% level.

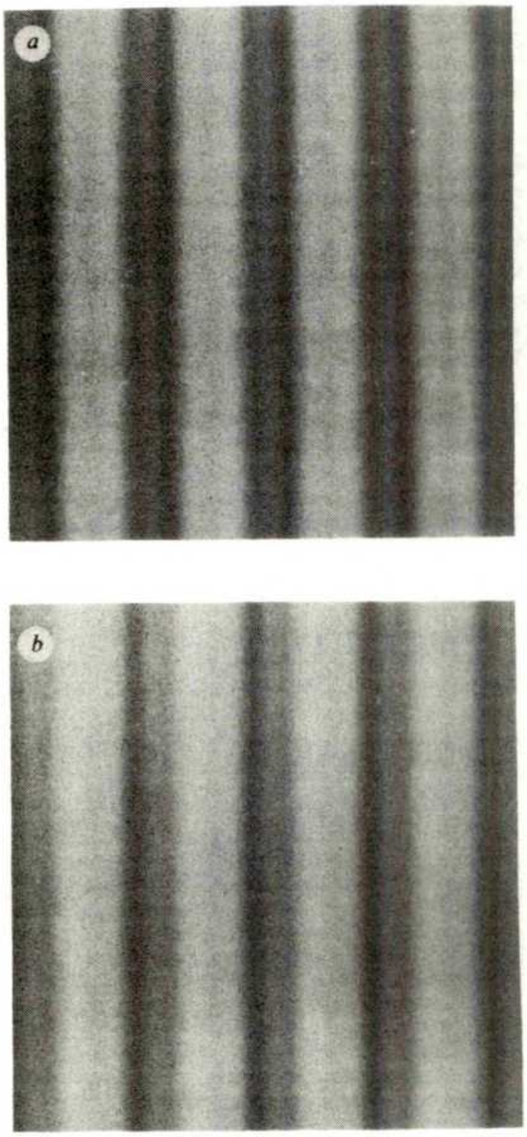

Fig. 1 Patterns to be discriminated: gratings *a* and *b*. The difference between the two patterns is obvious when they are viewed next to each other under steady illumination, but discrimination becomes more difficult when the patterns are presented briefly and in temporal sequence. The reader can appreciate this difficulty by illuminating the figure with a dim light flash.

0028–0836/80/360043—02$01.00

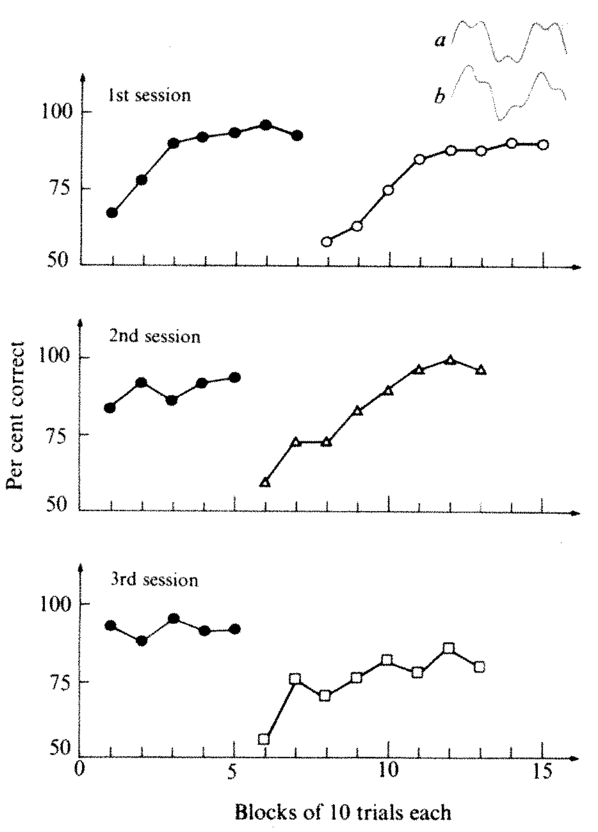

Fig. 2 Percentage of correct forced-choice discriminations of gratings *a* and *b* relative to subsequent blocks of 10 trials each. Data were pooled for the six subjects (60 trials per point). The three graphs refer to three experimental sessions run on separate days. Full points, vertical gratings, fundamental spatial frequency 1 c/deg; open points, horizontal gratings, 1 c/deg (top); open triangles, vertical gratings, 0.5 c/deg; open squares, vertical gratings, 2 c/deg. Insert, luminance profiles of gratings *a* and *b*. In the first session the proportion of correct responses with vertical gratings increased from 0.8 to 1.0 for some subjects and from 0.5 to 0.9 for others. The inter-subject variability was similar in the subsequent runs, whenever a new pair of gratings was used. The changes in the proportions of correct responses from the last block with the practice gratings to the first block with different gratings are all highly significant ($P<0.001$; two-tailed correlated t-test with six pairs of scores).

The same results were obtained in the following two sessions when the viewing distance was changed, so that the fundamental spatial frequency of the gratings varied from 1 to 0.5 c/deg (Fig. 2, middle right) or from 1 to 2 c/deg (Fig. 2, bottom right). In the latter case, performance levelled off at about 80% correct, probably because the third harmonic of the gratings was only slightly above threshold at this viewing distance.

In spite of the relatively small number of trials per point, the regular trend of the curves of Fig. 2 supplies unequivocal evidence that: (1) the ability to discriminate two complex gratings of different luminance profiles rapidly improves with training; (2) the effects of training on the discrimination of a given pair of gratings are retained, at least partially, from one day to the next; (3) the effects of training fail to transfer to gratings orientated at 90° or viewed from a distance differing by a factor of 2 (fundamental spatial frequency differing by 1 octave).

Experiments to be reported in detail elsewhere indicate that smaller changes in grating orientation (±30°) or spatial frequency (±0.5 octave) do not prevent the effects of previous practice from transferring to the new stimuli.

Most observers were able to describe the cues used for discrimination, once they had acquired practice in the task. According to their reports, the patterns were discriminated either on the basis of the apparent sharpness of the bar edges (the bars of grating *a* looking more similar to the black and white stripes of a square wave grating) or because of the detection of narrow dark and bright lines in grating *b* (corresponding to the points of lowest and highest luminance in the grating profile (Fig. 2). These cues, however, were apparently of little use when the orientation of the gratings or the viewing distance was changed. Furthermore, as measurements were made with a forced-choice procedure, the drop in performance cannot have resulted merely from a change in criterion. The improvement in performance with practice is therefore perceptual learning.

The neural mechanism for the learning process remains unknown. However, the present findings unequivocally show that this process must occur at a stage of neural processing at which different orientations (and/or different spatial frequencies) are handled separately.

We thank Professor L. Maffei and Dr D. C. Burr for critical comments on the manuscript. N.B. was supported by the Scuola Normale Superiore, Pisa.

Received 31 March; accepted 18 June 1980.

1. Gibson, E. J. *Psychol. Bull.* **50**, 401 (1953).
2. Gibson, E. J. *Principles of Perceptual Learning and Development* (Appleton-Century-Crofts, New York, 1969).
3. Ramachandran, V. S. & Braddick, O. *Perception* **2**, 371 (1973).
4. McKee, S. P. & Westheimer, G. *Percept. Psychoph.* **24**, 258 (1978).

T-cell specificity for H-2 and Ir gene phenotype correlates with the phenotype of thymic antigen-presenting cells

Dan L. Longo & Ronald H. Schwartz

Laboratory of Immunology, National Institute of Allergy and Infectious Diseases, National Institutes of Health, Bethesda, Maryland 20205

Experiments with chimaeric animals have demonstrated that the H-2 restriction specificity and immune response (Ir) gene phenotype of the T cell is acquired during development in the thymus. The mechanism by which this process occurs is unclear. One level of obligate expression of H-2 and Ir gene products is on the surface of antigen-presenting cells (APCs) which come from bone marrow precursors. We have now examined the turnover of APCs in the thymuses of F_1→parent (P) radiation-induced bone marrow chimaeras and found that APCs of donor phenotype appear at about 2 months after reconstitution. If the peripheral T-cell population is depleted after this time, new T cells emerging from the parental thymus (containing F_1 APCs) behaved like F_1 T cells, suggesting that cells from the bone marrow can influence thymic-directed T-cell differentiation. The thymic APC is an attractive candidate to play such a part in the development of the T-cell repertoire.

Experiments with (responder × nonresponder) $(R\times NR)F_1$ mice[1] and $NR\rightarrow(R\times NR)F_1$ chimaeric mice[2–8] have demonstrated that, for at least one major category of Ir genes, the APC must be of responder genotype to initiate Ir-controlled responses. In contrast, the T cell need not possess the responder allele(s) in its genome as long as it has developed in a responder environment[2–8]. Grafting of nonresponder animals with responder thymus tissue has shown that the thymus is responsible for the phenotypic alteration[9]. Anti-Ia antiserum blocking studies have shown that the genotypic nonresponder T cell becomes a phenotypic responder by learning to recognize Ia molecules of the responder type plus antigen on the surface of the APC[10]. The mechanism by which the chimaeric T-cell population acquires the ability to recognize responder Ia as self in the thymus is unclear, but seems to be a fundamentally different process from tolerance induction or depletion of specific alloreactivity[11]. It is presumed that the maturation of the

Table 1 Most thymic APCs in 1-year-old chimaeras are of bone marrow donor origin

	T cells										
Source of APCs	B10.A			B10.A(18R)			(B10.A×B10.A[18R])F_1				
	Non-pulsed	PPD-pulsed	Δ	Non-pulsed	PPD-pulsed	Δ	Non-pulsed	PPD-pulsed	ΔPPD	GLΦ pulsed	ΔGLΦ
B10.A thymus	2,753 ±290	114,693 ±7,429	111,940	102,315 ±9,120	99,667 ±5,881	−2,648	3,126 ±289	77,364 ±5,929	74,238	5,024 ±611	1,898
B10.A×B10.A[18R])F_1 thymus	73,286 ±4,589	139,221 ±6,722	55,935	58,246 ±4,021	124,694 ±10,755	66,448	3,371 ±410	145,320 ±9,798	141,949	107,446 ±7,420	104,075
B10.A→ (B10.A×B10.A[18R])F_1 chimaeric thymus	7,608 ±575	120,941 ±9,360	113,333	89,437 ±7,349	98,623 ±10,071	9,186	2,916 ±308	86,225 ±6,824	82,309	10,372 ±668	7,456

Lymph node T cells from antigen-primed mice were collected by passage over nylon wool columns. Thymus cells which had been spun in a discontinuous BSA gradient and given 2,000R *in vitro* were used as sources of APCs. The APCs were pulsed with 60 μg purified protein derivative of *Mycobacterium tuberculosis* (PPD) or 100 μg poly-(Glu^{54}-Lys^{36}-Phe^{9})$_n$ (GLΦ) and 10^5 cells were added to 4×10^5 lymph node T cells in flat-bottomed microtitre plates. Antigen-specific proliferation was measured by assessing the ^{3}H-thymidine incorporated into DNA on day 5 of culture by antigen-pulsed versus non-pulsed APCs. The data are expressed as c.p.m. ± s.e.m. for triplicate cultures or as Δ, the difference between antigen-pulsed and non-pulsed cultures. B10.A thymus cells present PPD to B10.A and F_1T cells but not to B10.A(18R) T cells. F_1 thymus cells present PPD to all three types of T cells, and present GLΦ to the F_1T cells. The APCs from the thymus of B10 A→(B10 A×B10.A[18R])F_1 chimaeras present PPD well to B10.A and F_1T cells but poorly to B10.A(18R) T cells. This feature, along with the minimal amount of GLΦ-specific proliferation they induce in F_1 T cells, suggests that most of the APCs in the chimaeric thymus are of B10.A donor origin.

Table 2 Donor type APCs appear in the thymuses of F_1→P chimaeras about 2 months after reconstitution

	T cells						
Source of APCs	B10.A lymph node			(B10.A×B10)F_1 lymph node				
	Non-pulsed	DNP-OVA-pulsed	ΔDNP-OVA	Non-pulsed	DNP-OVA pulsed	ΔDNP-OVA	GLΦ-pulsed	ΔGLΦ
B10.A spleen	1,188±219	41,326±4,008	40,138	2,089±175	33,648±3,161	31,559	2,204±211	115
(B10.A×B10)F_1 spleen	9,745±781	30,998±2,268	21,253	1,957±236	60,523±5,989	58,566	18,762±2,009	16,805
1-week chimaeric thymus (Top BSA fraction)	1,698±267	72,141±1,519	70,443	1,716±242	58,262±6,102	56,546	1,889±310	173
B10.A spleen	2,317±197	62,819±5,583	60,502	4,862±1,010	40,146±3,547	35,284	4,889±526	27
(B10.A×B10)F_1 spleen	12,862±698	44,710±3,972	31,848	5,029±619	72,167±6,739	67,137	29,433±2,579	23,404
2-week chimaeric thymus	2,744±255	121,085±10,126	118,341	5,217±830	108,679±11,044	103,462	5,765±624	548
B10.A spleen	1,814±228	29,487±2,269	27,673	6,914±655	34,926±2,968	28,012	7,475±927	561
(B10.A×B10)F_1 spleen	15,127±1,641	28,889±1,523	13,762	5,792±529	49,611±5,012	43,819	18,267±1,398	12,475
1-month chimaeric thymus	3,168±358	39,607±3,242	36,439	6,345±804	87,431±8,667	81,086	5,831±1,021	0
B10.A spleen	4,276±398	29,657±1,881	25,381	3,724±629	26,717±2,279	22,993	3,998±447	274
(B10.A×B10)F_1 spleen	21,684±1,971	31,804±3,026	10,120	4,024±312	41,618±3,926	37,594	15,066±981	11,042
2-month chimaeric thymus	47,815±4,226	89,762±8,549	41,947	4,256±491	63,295±6,440	59,039	14,311±575	10,055

B10.A animals were immunized with 10 μg DNP-ovalbumin (DNP-OVA) and (B10.A×B10)F_1 animals with the same dose of DNP-OVA and 30 μg GLΦ, all in complete Freund's adjuvant, in both hind footpads. Eight days later, lymph node T cells were obtained by passing lymph node cells over nylon wool columns 4×10^5 cells were plated with 2×10^5 antigen-pulsed or non-pulsed spleen cells or thymus APCs and antigen-specific proliferation was measured by subtracting the ^{3}H-thymidine c.p.m on day 5 of culture of non-pulsed spleen or thymus cells from the counts obtained with antigen-pulsed spleen or thymus cells Pulsing of cells was accomplished by preincubating *in vitro* irradiated (2,000R) spleen or thymus cells (10^7) with 100 μg of GLΦ or 60 μg of DNP-OVA in 1 ml of RPMI 1640 + 10% fetal calf serum for 1 h at 37 °C and washing thoroughly to remove any soluble antigen. Thymic APCs were obtained by taking the cells at the top interface of a discontinuous BSA gradient consisting of 35, 29, 27 and 11% layers which had been spun at 25,000*g* for 30 min. The ability of thymic APCs from (B10.A×B10)F_1→B10.A chimaeras to present GLΦ to F_1 immune T cells was assessed at varying times after reconstitution. The data show that at about 2 months after reconstitution, cells from the thymus of such chimaeras are able to present GLΦ to F_1 immune T cells and elicit an MLR in B10.A T cells, suggesting the presence of donor phenotype F_1 APCs

T cell to self-recognition in the thymus involves the T cell 'seeing' Ia products on the surface of some cell in the thymus. There are two cell types which have been proposed to have this role, thymic epithelial cells[11,12] and thymic macrophages[13]. Some studies have shown Ia molecules on the surface of thymic epithelial cells; however, the cell source of these molecules has not been conclusively demonstrated[14]. Macrophages have been found in the thymus and such cells have been reported to affect *in vitro* T-cell maturation[13]. Recently, we have demonstrated the existence of APCs in the thymus by a functional assay. The ability of such thymic APCs to present antigen can be eliminated by treatment with anti-Ia antiserum plus complement (data not shown). Thus, thymic APCs bear Ia antigens on their surface. We felt that a parsimonious theory of H-2 restriction and Ir gene function might be proposed if APCs in the thymus could be shown to be involved in T-cell maturation. Studies on the APC in spleen[4], peritoneal cavity[4] and skin (Langerhans cells)[15,16] have shown that its precursors originate in bone marrow. Thus, the theories on the cell responsible for exposing the T cell to what is self can be distinguished because, in a radiation-induced bone marrow chimaera, the radioresistant thymic epithelium should be replaced in turnover processes by host genotype epithelial precursors, while old or dying APCs should be replaced by APCs of donor marrow origin, if thymic APCs are similar to APCs in other sites.

To see if thymic APCs are replaced by bone marrow precursors, we examined the phenotype of the thymic APCs in parent (P) low responder→F_1 responder chimaeras. Such chimaeras were made by reconstituting irradiated poly-(Glu^{55}-Lys^{36}-Phe^{9})$_n$ (GLΦ) responder (B10.A×B10.A[18R])F_1 mice with T-cell-depleted GLΦ low responder B10.A bone marrow. Thymic APCs were isolated from B10.A→(B.10.A×B10.A[18R])F_1 chimaeras 1 yr after they were created by fractionating the thymus cells on a discontinuous bovine serum albumin (BSA) gradient (see Table 2 legend)[13]. As shown in Table 1, APCs from such chimaeric thymuses presented GLΦ poorly to F_1 immune T cells but successfully initiated a secondary proliferative response to purified protein derivative of *Mycobacterium tuberculosis* (PPD) in both F_1 and B10.A T cells but not in B10.A(18R) T cells. Also, note the presence of a large mixed lymphocyte reaction (MLR) when B10.A(18R) T cells were used as responders, as well as the negligible MLR made by B10.A T cells in response to the thymic APCs of the B10.A→(B10.A×B10.A[18R])F_1 chimaeras. These data support the notion that donor phenotype B10.A APCs predominate in the thymus, thus suggesting that thymic APCs in

Table 3 T-cell restriction specificity in $F_1 \rightarrow P$ chimaeras is converted from host to donor phenotype by ATS and cortisone treatment

	Medium	DNP-OVA	GLΦ	(T, G)-A--L	Cytochrome *c*
(1) A × B → A	984 ± 106	31,612 ± 2,886	1,123 ± 146	1,076 ± 221	9,751 ± 868
(2) A × B → A 3 months after ATS + cortisone	10,820 ± 3,647	56,724 ± 4,228	26,420 ± 7,156	34,073 ± 686	17,221 ± 535
(3) A × B → B	4,781 ± 1,023	61,811 ± 6,673	5,400 ± 721	51,808 ± 4,782	4,722 ± 562
(4) A × B → B 3 months after ATS + cortisone	2,198 ± 642	28,971 ± 1,777	20,208 ± 2,431	—	—
(5) B6A F_1 → B10.A	5,129 ± 289	81,368 ± 7,249	5,490 ± 671	5,017 ± 1,011	15,894 ± 964
(6) B6A F_1 → B10.A 3 months after ATS + cortisone	7,055 ± 837	90,208 ± 8,266	54,816 ± 4,173	41,725 ± 3,268	20,188 ± 1,863
(7) B10.A 3 months after ATS + cortisone	6,711 ± 278	61,827 ± 3,159	5,682 ± 495	6,653 ± 491	16,922 ± 957
(8) B6A F_1 3 months after ATS + cortisone	4,249 ± 368	81,889 ± 10,218	69,814 ± 5,117	57,431 ± 3,272	14,827 ± 966

Eight months after irradiating parental B10.A (A) and B10 (B) mice with 900–950 R and reconstituting them with T-cell-depleted $(B10.A \times B10)F_1(A \times B)$ or B6A F_1 bone marrow, the $F_1 \rightarrow P$ chimaeras were immunized with 10 μg DNP-OVA, 30 μg GLΦ, 50 μg (T,G)-A-L lot MC6 and 100 μg pigeon cytochrome *c* (gift of Drs E. Margoliash and M. Ultee) in complete Freund's adjuvant in both hind footpads. Eight days later, draining popliteal and inguinal lymph node cells were passed over nylon wool columns and 4×10^5 cells were plated in flat-bottomed microtitre plates with soluble antigen (20 $\mu g\, ml^{-1}$ DNP-OVA, 100 $\mu g\, ml^{-1}$ GLΦ, (T,G)-A--L and pigeon cytochrome *c*). Responses were quantified by incorporation of ^3H-thymidine into DNA on day 5 of culture. Lines 1, 3 and 5 show responses of $(A \times B)\, F_1 \rightarrow B10.A$, $(A \times B)\, F_1 \rightarrow B10$ and B6A $F_1 \rightarrow B10.A$ chimaeras, respectively. F_1 T cells are capable of making responses to all of the antigens tested, but when they develop in a parental environment they are restricted to responses characteristic of that parent. (B10 is a responder to DNP-OVA and (T,G)-A--L and a nonresponder to GLΦ and cytochrome *c*; B10.A is a responder to DNP-OVA and cytochrome *c* and a nonresponder to GLΦ and (T,G)-A--L). However, when cage partners of host restricted $F_1 \rightarrow P$ chimaeras were treated with 0.6 ml of a 1 : 10 dilution of ATS and 5 mg of cortisone acetate, both intraperitoneally, 3 months later their lymph node T cells behave like F_1 cells, that is they are responders to GLΦ, (T,G)-A--L and cytochrome *c* (lines 2, 4 and 6). Lines 7 and 8 show that ATS and cortisone treatment does not alter the phenotype of normal parental or F_1 T cells.

radiation-induced bone marrow chimaeras are ultimately replaced by bone marrow precursors.

The turnover of APCs in the skin and spleen after radiation is markedly different. Splenic APCs disappear within 3–4 days after irradiation and are totally replaced by bone marrow precursors about 7 days after irradiation[4]. Skin APCs, on the other hand, take 65–80 days to be replaced by bone marrow precursors[15,16]. In an effort to determine when thymic APCs in the radiation-induced bone marrow chimaera begin to be replaced by cells of donor origin, we made $(B10.A \times B10)F_1 \rightarrow B10.A$ chimaeras and assayed the antigen presentation function of their thymic APCs at varying times after reconstitution. As shown in Table 2, between 1 week and 1 month after reconstitution, $F_1 \rightarrow P$ thymic APCs were unable to present GLΦ to F_1 immune T cells and no significant MLR was elicited from parental type B10.A T cells. The ability of thymic APCs to present GLΦ to F_1 immune T cells first appeared 2 months after reconstitution, at the same time that a substantial MLR in B10.A T cells was seen. These findings suggested that, at 2 months after reconstitution, donor F_1 APCs were detectable in the thymus of $F_1 \rightarrow P$ chimaeras.

If thymic APCs are important in the development of the T-cell restriction repertoire, then the T cells emerging from a chimaeric thymus after its APCs have become donor genotype should have the donor's restriction specificity. However, T cells, even in 1-year-old chimaeras, behave as though they are restricted to host and not donor phenotype. One possible explanation for this is that the initial T cells maturing in the thymus of a radiation chimaera dominate the peripheral T-cell pool for most of the remainder of the animal's life. If so, new T cells maturing after turnover of APCs in the thymus would make a negligible contribution to the T-cell pool and thus no conversion of the responsiveness of chimaeric T cells would be seen. To test this, we took $F_1 \rightarrow P$ chimaeras 8 months after reconstitution at a time when their T cells were demonstrated to be restricted to cooperative interactions with cells bearing host (parental) major histocompatibility complex (MHC) products, treated them with anti-thymocyte serum (ATS) and cortisone to deplete them of peripheral and thymic T cells, and allowed their parental thymus containing F_1 APCs (Table 2) to repopulate the periphery with T cells. Three months after ATS and cortisone treatment, and 11 months after reconstitution, the mice were immunized and their lymph node T cells assayed. As shown in Table 3, $(B10.A \times B10)F_1 \rightarrow B10.A$, $(B10.A \times B10)F_1 \rightarrow B10$, and B6A $F_1 \rightarrow B10.A$ chimaeric T cells lost their restrictions to host genotype interactions and made substantial proliferative responses to GLΦ, (T, G)-A--L and pigeon cytochrome *c* (lines 1–6). They behaved like F_1 T cells. In control experiments, treatment of normal B10.A or B6A F_1 mice with ATS and cortisone had no effect on the Ir gene phenotype of their T cells 3 months later (lines 7, 8).

The most straightforward interpretation of these data is that self-H-2 is learned in the thymus by T cells upon interaction with MHC products on thymic APCs. The first T cells generated in an $F_1 \rightarrow P$ chimaera encounter parental APCs during maturation and become restricted to parental H-2 specificities. Those T cells emerging from a parental thymus, which has become repopulated with donor F_1 APCs, become restricted to F_1 H-2 specificities. This correlation between the phenotype of the thymic APC and the T-cell restriction repertoire suggests that thymic APCs may be involved in the development of T-cell self-specificity. Alternatively, it is possible that the results demonstrate that in $F_1 \rightarrow P_A$ chimaeras, a suppression mechanism exists[17] which prohibits detection of P_B and F_1-reactive T cells and which is sensitive to ATS and cortisone treatment. Once this suppression mechanism is blocked, P_B and F_1-reactive T cells can be expanded and detected. Our own preliminary experiments have failed to document any suppression of F_1 T-cell function in $F_1 \rightarrow P$ chimaeras. Therefore, we favour the former hypothesis.

The process by which the genome and the developmental milieu interact to produce the exquisitely precise T-cell recognition structure(s) which possesses dual specificities for antigen and MHC products remains an enigma. Evidence has been presented here that suggests that MHC products expressed on the APC in the thymus encountered by the T-cell precursor at a critical stage in its development may be responsible for its subsequent restricted cell interactions.

Received 25 March; accepted 18 June 1980.

1. Yano, A., Schwartz, R. H. & Paul, W. E. *Eur. J. Immun.* **8,** 334–338 (1978).
2. Kappler, J. W. & Marrack, P. *J. exp. Med.* **148,** 1510–1522 (1978).
3. Hodes, R. J., Hathcock, K. S. & Singer, A. *J. Immun.* **123,** 2823–2829 (1979).
4. Longo, D. L. & Schwartz, R. H. *J. exp. Med.* **151,** 1452–1467 (1980).
5. Zinkernagel, R. M. *et al. J. exp. Med.* **148,** 592–610 (1978).
6. Von Boehmer, H., Haas, W. & Jerne, N. K. *Proc. natn. Acad. Sci. U.S.A.* **75,** 2439–2442 (1978).
7. Matsunaga, J. & Simpson, E. *Proc. natn. Acad. Sci. U.S.A.* **75,** 6207–6212 (1978).
8. Billings, P., Burakoff, S. J., Dorf, M. E. & Benacerraf, B. *J. exp. Med.* **148,** 352–359 (1978).
9. Hedrick, S. M. & Watson, J. *J. exp. Med.* **150,** 646–659 (1979).
10. Longo, D. L. & Schwartz, R. H. *Fedn Proc.* **39,** 1127 (1980).
11. Zinkernagel, R. M. *Immun. Rev.* **42,** 224–270 (1978).
12. Jenkinson, E. J., Owen, J. J. T. & Aspinall, R. *Nature* **284,** 177–179 (1980).
13. Beller, D. I. & Unanue, E. *J. Immun.* **121,** 1861–1866 (1978).
14. Rouse, R. V., van Ewijk, W., Jones, P. P. & Weissman, I. L. *J. Immun.* **122,** 2508–2515 (1979).
15. Frelinger, J. G., Hood, L., Hill, S. & Frelinger, J. A. *Nature* **282,** 321–324 (1979).
16. Katz, S. I., Tamaki, K. & Sachs, D. H. *Nature* **282,** 324–326 (1979).
17. Smith, F. I. & Miller, J. F. A. P. *J. exp. Med.* **151,** 246–251 (1980).

Cloned lines of natural killer cells

Gunther Dennert

Department of Cancer Biology, The Salk Institute for Biological Studies, PO Box 85800, San Diego, California 92138

A class of cytotoxic effector cells has recently been discovered[1,2] in normal and immunodeficient nude mice that lyse a wide range of targets of both tumour and non-tumour origin. Unlike other lymphocytes, these natural killer (NK) cells are present at high levels without prior priming and have no immunological memory. Because NK cells act without prior sensitization, they could have a crucial role in immunosurveillance, providing a first defence against arising neoplastic cells. The question of NK-cell specificity is not well understood; results so far suggest that they may recognize specific antigens on their targets. Thus unlabelled competitor cells can inhibit the cytotoxic reaction of NK cells[3]. Furthermore, target–effector binding can be inhibited by isolated target structures[4]. Experiments in which the lysis of mouse and human NK-sensitive targets was competitively inhibited with target suggested that the targets recognized by NK cells are not common ones. To study this important aspect, permanent lines and clones of NK cells have been established *in vitro*. I report here a successful attempt to do this, and show that sublines display the same specificity spectrum as NK cells from normal cells even after recloning. This proves that antigen receptors on NK cells are not clonally distributed but leaves open the two possibilities that NK cells either recognize common structures on NK-sensitive targets or carry many receptors each with a different specificity. Cell-surface markers of NK lines distinguished them from allospecific thymus-derived lymphocyte cell lines through their lack of Lyt-1 and Lyt-2 antigen.

Athymic mice are known to be deficient in functional T cells, yet do not experience a particularly high incidence of tumours. This observation has been attributed to the high NK activity of lymphoid cells from nude mice. These properties made spleen cells from nude mice an appropriate starting material to establish NK cell lines. A number of different supernatants conditioned by spleen cells stimulated with mitogens were tested as tissue culture media. Results showed that media derived from normal spleen cells stimulated with 10 μg ml^{-1} concanavalin A (Con A)[5] were superior to all others tested (data not shown) and supported the survival of effector cells from BALB/c *nu/nu* spleens able to lyse YAC-1 targets (Table 1, expt 1 and ref. 6). Fourteen individual spleen cell cultures were set up in conditioned medium, 12 of which were from BALB/c *nu/nu* mice and 2 from normal BALB/c mice. The cultures were fed weekly by replacing the medium and checked for cell growth. Twelve of the cultures grew progressively and were assayed after 4 months for their cytotoxic activity on YAC-1. Most cultures showed high cytolytic activity in a 6-h assay at attacker-to-target ratios (*a/t*) between 1:1 and 30:1 (Table 1, expt 2).

In subsequent experiments, all cultures were assayed on a panel of target cells, comprising YAC-1 and its relatively NK-resistant derivative, YAC-8 (provided by Drs M. Hansson and R. Kiessling), B10 ME and its relatively NK-resistant parent, BCN (provided by Drs P. Patek, J. Collins and M. Cohn), the C58 lymphoma RIGl and various spleen blast cells induced by bacterial lipopolysaccharide (LPS). There was no detectable difference between the various cultures, culture 11 being a representative example (Table 1, expt 3). There was no lysis on the H-2^k thymic lymphoma RIGl or in LPS spleen blast cells, which are excellent targets for cytotoxic T cells[7]. Strong lysis on YAC-1 and significantly lower lysis on YAC-8 were seen. Similarly to the YAC-1, YAC-8 pair, there was higher lysis on B10 ME than on BCN. Further experiments showed that lysis is independent of Con A because the assays could be performed in the presence of α-methyl mannoside (data not shown). These results showed that these cultures display NK-like activity. Cloning of two of the lines was attempted after they had been in culture for about 4 months. Earlier cloning was not feasible since the cultures seemed to go through a crisis at about 2–3 months after culture initiation. I chose culture 11, derived from a BALB/c mouse and culture 12 derived from a BALB/c *nu/nu* mouse, because they showed somewhat better growth and viability than the others. Both cultures were conditioned to growth at low cell density by seeding 1,000 cells in 0.2 ml into microtitres wells.

Once the cells had grown up they were transferred into bottles and cloning was attempted at 100, 30, 10 and 3 cells per well. Unfortunately, line 12 grew poorly and did not clone below 100 cells per well. In contrast, line 11 showed much better cloning efficiency in that about 30% of the wells with 10 cells per well grew. Individual colonies were grown up and assayed for cytotoxicity on YAC-1 targets. From Table 1, expt 4, it is seen that the sublines have various degrees of cytolytic activity. For instance, subline 11·2 has only 10% cytotoxicity at an *a/t* ratio of 3:1 while sublines 11·5 and 11·13 have 78% and 75% cytotoxicity respectively. Four individual sublines were assayed on four different targets at different *a/t* ratios and compared

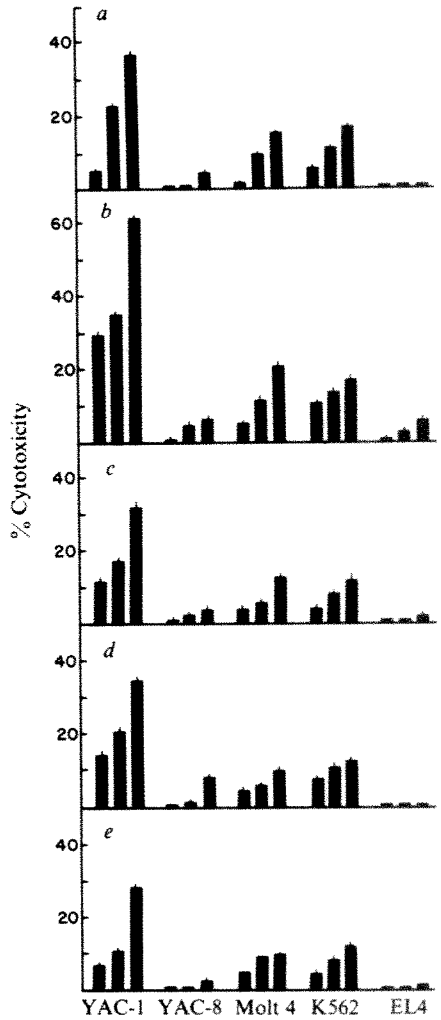

Fig. 1 BALB/c spleen cells (*a*) and the NK sublines 11·1 (*b*), 11·3 (*c*), 11·5 (*d*) and 11·11 (*e*) were assayed for their cytolytic activity on YAC-1 (H-2^a), YAC-8 (H-2^a), Molt 4, K562 and EL4 (H-2^b) targets. Molt 4 and K562 were grown in RPMI 1640 10% FCS and EL4 was grown in D-minimal essential medium plus 10% horse serum. *a/t* ratios were 25:1, 50:1, 100:1 for the spleen cells and 1:1, 2:1, 5:1 for the clones (from left to right). The 8 h time point is given.

0028-0836/80/360047—03$01.00

Table 1 Cytolytic activity of various NK lines and sublines

	Effector cells	Target	% Cytotoxicity at *a/t* ratios 1:1	3:1	4:1	6:1	10:1	20:1	30:1	100:1
Expt 1	BALB/c	YAC-1					21±0.3		36±1.1	54±2.1
(3 h)	*nu/nu*	YAC-1					13±0.4		22±0.2	36±0.9
	nu/nu cultured	YAC-1					20±0.9		40±1.1	62±0.8
Expt 2	Culture 1 *nu/nu*	YAC-1							<1	
(6 h)	Culture 2 *nu/nu*	YAC-1							70±0.5	
	Culture 2 BALB/c	YAC-1					64±2.9			
	Culture 4 *nu/nu*	YAC-1					72±3.1			
	Culture 7 *nu/nu*	YAC-1		14±0.2						
	Culture 8 *nu/nu*	YAC-1					<1			
	Culture 9 *nu/nu*	YAC-1					23±1.1			
	Culture 10 *nu/nu*	YAC-1							5±0.2	
	Culture 11 BALB/c	YAC-1					43±1.2			
	Culture 12 *nu/nu*	YAC-1		18±1.1						
	Culture 13 *nu/nu*	YAC-1		52±2.9						
	Culture 14 *nu/nu*	YAC-1	11±1.1							
Expt 3	Culture 11	YAC-1			86±0.6					
(6 h)	Culture 11	YAC-8			44±0.5					
	Culture 11	B10ME			32±0.3					
	Culture 11	BCN			19±2.9					
	Culture 11	R1·G1			1±0.5					
	Culture 11	C57BL/6			<1					
	Culture 11	SJL			<1					
Expt 4	Cloned subline 11·1	YAC-1					66±1.3			
(5 h)	Cloned subline 11·2	YAC-1		10±0.3						
	Cloned subline 11·3	YAC-1				57±2.9				
	Cloned subline 11·4	YAC-1					60±3.1			
	Cloned subline 11·5	YAC-1		78±1.9						
	Cloned subline 11·6	YAC-1					41±2.5			
	Cloned subline 11·7	YAC-1					61±2.5			
	Cloned subline 11·9	YAC-1						63±2.2		
	Cloned subline 11·10	YAC-1				46±1.0				
	Cloned subline 11·11	YAC-1					63±0.1			
	Cloned subline 11·13	YAC-1		75±0.2						

Effector cells were assayed without prior culture or, spleen cells were cultured for 5 d in RPMI 1640 containing 5% fetal bovine serum (FCS), 5×10^{-5} M β-mercaptoethanol, 40% conditioned medium prepared from Con A stimulated spleen cells as described in ref. 5 for expt 1. For expt 2, cultures were fed with conditioned medium as above on a weekly basis for 4 months, then assayed on targets at one *a/t* ratio. For expt 3; after 4 months, culture 11 was assayed on YAC-1 (H-2^a), YAC-8 (H-2^a) B10ME (H-2^d), BCN (H-2^d), R1·G1 (H-2^k) and C57BL/6 and SJL blast cells induced by culture in bacterial lipopolysaccharide[11]. All target cell lines were grown in RPMI 1640 10% FCS except R1·G1 which was grown in Dulbecco's minimal essential medium plus 10% horse serum. For expt 4, culture 11 was cloned by limiting dilution in Falcon (no. 3040) microtitre wells in conditioned medium as in expt 1 at 1,000 cells per well, grown up and recloned at 10 cells per well. Individual colonies were grown up in Falcon tissue culture tubes (2051), then transferred to Falcon bottles (3013) and fed on a weekly basis. Cytotoxicity was assayed as described in ref. 11 at various *a/t* ratios as indicated. The time of incubation is given for each experiment. % Cytotoxicity = [(experimental ^{51}Cr release − spontaneous ^{51}Cr release)/(maximal ^{51}Cr release − spontaneous ^{51}Cr release)] × 100.

with the cytolytic activity of normal BALB/c spleen cells (Fig. 1). It is seen that BALB/c spleen cells lyse YAC-1 cells very well but YAC-8 and EL4 are not or are very poorly lysed. Both Molt 4 and K562 showed intermediate lysis. Sublines 11·1, 11·5 and 11·11 all showed the same picture comparable to that of BALB/c spleen cells: good lysis of YAC-1, poor lysis on YAC-8 and EL4, and intermediate lysis of Molt 4 and K562. Other sublines which were similarly tested showed the same lytic specificity.

This result could be interpreted in three ways: first, our sublines, if they were true clones, might recognize a common structure on mouse and human NK targets. This conclusion would contradict the previous results obtained with competitive inhibition assays mentioned above[3,4]. Second, NK effectors display more than one receptor each with different specificity on their cell surface. Consequently cloned effectors will lyse different targets using their respective specific receptors. Third, our sublines may not be true clones and consequently there may be different NK effectors with specific receptors in these sublines. Although cloning experiments cannot distinguish between the first two possibilities, the third possibility can be excluded by recloning. Sublines 11·3 and 11·8 were recently recloned at 1 cell per well. Assays on YAC-1, Molt 4, K562 and EL4 of five out of five clones from both sublines showed the same specificity as in Fig. 1 (data not shown). It is therefore likely that we are dealing with true clones. Hence, our NK sublines either recognize a common structure on these targets or display multiple receptors with different specificities. This finding does not exclude the possibility that there is another type of NK effector which expresses specific receptors clonally. In fact, Herberman *et al.*[8,9] recently presented evidence that the NK effectors may be heterogeneous in that both Thy 1^+ and Thy 1^- NK effectors exist. It was therefore interesting to assay our lines and sublines with regard to their cell-surface markers. The original line 11 as well as three sublines were assayed for Thy 1, Lyt 1, Lyt 2 and T200 using monoclonal antibodies and flow microfluorimetry. Table 2 shows that line 11 as well as the three

Table 2 Cell surface markers of NK cell lines

Effector cells	Thy 1	T200	Lyt 1	Lyt 2
Culture 11*	+	+	−	−
Subline 11·3*	+	+	−	−
Subline 11·10*	+	+	−	−
Subline 11·11*	+	+	−	−
C·C3·11·75†	+	+	+	−
BALB/c anti-C3H T killer cells‡	+	+	−	+

The following rat spleen cell–mouse myeloma hybrids producing monoclonal antibodies were used: T24/31.7 specific for Thy 1 (isolated by Dr I. S. Trowbridge); I3/2.3 specific for T200 (ref. 10); 53·7·313 specific for Lyt-1 and 53·6·72 specific for Lyt-2 both (provided by Dr L. Herzenberg).

* NK lines were assayed for cell-surface markers by flow microfluorimetry (FMF) using a rabbit anti-rat immunoglobulin as staining reagent.

† C·C3·11·75 is an allospecific H-2^d anti-H-2^k T cell line established in November 1975 from an MLR culture and maintained since then by allogeneic stimulation[11]. Assay by FMF as for the NK cell lines.

‡ BALB/c anti-C3H T killer cells were raised in a primary MLR and the effects of monoclonal antibodies assayed by complement dependent lysis.

sublines are Thy 1^+, T200$^+$ but Lyt 1^- 2^-. Since Ly 5 is a polymorphism of T200 glycoprotein[10], by inference these NK cells are Ly 5$^+$. The lack of Lyt 1 and Lyt 2 sets these cells clearly apart from allospecific lines of thymus-derived lymphocytes, which can be generated by a mixed lymphocyte reaction (MLR, ref. 11) and propagated by antigenic stimulation. Thus C·C3·11·75, a BALB/c (H-2^d) anti C3H (H-2^k) allospecific line[11], is clearly Lyt 1^+. In control experiments the same anti-Ly reagents were shown to be specific; thus anti-Lyt-1 in contrast to anti-Lyt-2 does not lyse allospecific T-killer cells. The expression of large amounts of Thy-1 antigen on these NK-cell lines, as well as the presence of these NK cells in thymus-deficient nude mice[6], may suggest that these cells do not require differentiation in the thymus for their function. Furthermore, since Thy-1 negative NK cells have been described[9], we may have to search for another class of NK cells, which may have different properties. Our cloned lines of NK cells may be instrumental in analysing the relationship of NK killing and antibody-dependent cell-mediated cytotoxicity. They also provide us with a powerful tool to unravel the nature of these cells and their significance in the immune surveillance against neoplasia.

We thank Susan Yamagata for technical assistance and Dr I. S. Trowbridge for performing the FMF analysis. This work was supported by NIH grants CA 15581 and CA 19334.

Received 17 March; accepted 25 June 1980.

1. Roder, J. C. & Kiessling, R. *Scand. J. Immun.* **8,** 135 (1978).
2. Herberman, R. B. & Holden, H. T. *Adv. Cancer Res.* **27,** 305 (1978).
3. Kiessling, R., Klein, E. & Wigzell, H. *Eur. J. Immun.* **5,** 112 (1975).
4. Roder, J. C., Rosén, A., Fenyö, E. M. & Troy, F. A. *Proc. natn. Acad. Sci. U.S.A.* **76,** 1405 (1979).
5. Rosenberg, S. A., Spiess, P. J. & Schwarz, S. *J. Immun.* **121,** 1946 (1978).
6. Dennert, G. & Hyman, R. *Eur. J. Immun.* (in the press).
7. Dennert, G. & Hyman, R. *Eur. J. Immun.* **7,** 251 (1979).
8. Herberman, R. B., Nunn, M. E. & Holden, H. T. *J. Immun.* **121,** 304 (1978).
9. Mattes, M. J., Sharrow, S. O., Herberman, R. B. & Holden, H. T. *J. Immun.* **123,** 2851 (1979).
10. Omary, B., Trowbridge, I. & Scheid, M. *J. exp. Med.* (in the press).
11. Dennert, G. *Nature* **277,** 476 (1979).

Involvement of the B-lymphoid system in chronic myelogenous leukaemia

Paul J. Martin*, Vesna Najfeld†, John A. Hansen*,
Grace K. Penfold‡, Robert J. Jacobson§‖
& Philip J. Fialkow†

* Division of Medical Oncology, Fred Hutchinson Cancer Research Center, Puget Sound Blood Center, Seattle, Washington 98104 and the Department of Medicine, University of Washington, Seattle, Washington 98195
† Medical Service, Veterans Administration Medical Center, Seattle, Washington 98108 and the Department of Medicine, University of Washington, Seattle, Washington 98195
‡ Department of Hematology, South African Institute for Medical Research and School of Pathology, University of the Witwatersrand, Johannesburg, South Africa
§ Department of Medicine, University of the Witwatersrand and Baragwanath Hospital, Johannesburg, South Africa

Studies with glucose-6-phosphate dehydrogenase (G6PD) isoenzymes have demonstrated that chronic myelogenous leukaemia (CML) is a clonal disorder of pluripotent haematopoietic stem cells which are capable of differentiation to myeloid cells, monocytes, erthrocytes and platelets[1]. It has been observed recently in G6PD heterozygous patients with chronic phase CML that the non-E-rosetting lymphocytes were restricted to a single enzyme type, indicating that some lymphoid cells must also arise from the leukaemic clone[2]. Surface or cytoplasmic immunoglobulin could be detected in up to 46% of the cells of these isolated non-T-lymphocyte populations, which suggested that cells from the CML clone were capable of differentiating into B lymphocytes. To investigate this further, we established Epstein–Barr virus (EBV)-transformed B-lymphoblastoid cell lines derived from patients with CML and studied chromosomes and G6PD to determine whether progenitor B lymphocytes for any of the cell lines had originated from the CML clone. We report here direct evidence that immunoglobulin-synthesizing B lymphocytes can arise from the CML stem cell clone.

Cells for this study were obtained from patient M.K., a woman with Philadelphia chromosome (Ph^1)-positive CML in the chronic phase and known to be heterozygous at the G6PD locus. Peripheral blood leukocytes (PBL) from M.K. were infected with EBV[3] and then dispensed into multiple wells of a microtray (0.5–1.0×10^6 cells per 0.2 ml). Cells from each transformed microculture well were expanded individually as separate cell lines. Preliminary results established that nearly all of the cell lines derived in this fashion from M.K. displayed either A or B G6PD. Furthermore, with some exceptions, a single class of cytoplasmic immunoglobulin heavy chain and light chain were identified in each line. Thus, at the time of study, nearly all of the cell lines were monoclonal. With conventional methods, it is not possible to determine simultaneously the immunoglobulin class, G6PD type and chromosomal composition of a single B cell. With these B-cell lines, however, it was possible to examine the progeny of a single cell for all three markers, and thus infer the phenotype of the progenitor cell for each of the lines.

In nine of the cell lines derived from M.K., 93% or more of the cells were Ph^1–positive (Table 1). In the cells of each of these lines, there was a translocation involving chromosome 7, as well as numbers 22 and 9, the two chromosomes usually involved in the Ph^1 rearrangement, giving the karyotype 46, XX, t(7; 9; 22) (q11 or 21; q34.0; q11.1) (Fig. 1). The same karyotypic rearrangement was present in the patient's unstimulated peripheral blood metaphases for at least 3.5 yr.

Only type B G6PD was detected in each Ph^1–positive cell line, identical to what was found in the blood cell leukaemic clone of this G6PD heterozygous patient[2]. In further studies, the differentiative capacity of the progenitors for four of the Ph^1–positive B-cell lines was examined by identifying the classes of immunoglobulin synthesized by each cell line. The data are presented in Table 1. In these lines, one-third or more of the cells were positive for cytoplasmic immunoglobulin. Moreover, the classes of immunoglobulin differed from line to line. Two cell lines were tested for the expression of Ia antigen and EBV nuclear antigen (EBNA), MK 12.4 and MK 24.6, and each line was positive for both markers.

For unexplained reasons it has not been possible to maintain these cell lines *in vitro* for long periods of time. All of the Ph^1-positive cell lines have lost viability after culture for 3 weeks to 5 months. Ph^1-negative B-lymphoblastoid lines derived from M.K. have been maintained in identical conditions without difficulty, and seem to have the same growth potential as B-lymphoblastoid cell lines derived from normal donors.

Ph^1-positive cell lines have been derived from at least two other CML patients[4,5]. One of these, NALM-1, is a pre-B-lymphoid cell line derived from the peripheral blood of a patient with CML in blast crisis. The other one, K562, was established from the pleural effusion of a patient with CML in blast crisis. K562 is capable of *in vitro* differentiation to haemoglobin-producing erythroid cells[6]. Both of these cell lines are EBNA negative, unlike the MK 12.4 and MK 25.6 cell lines described here.

We have used EBV to derive from a patient with CML a series of B-lymphoblastoid cell lines which originated from the leukaemic clone. A similar approach has been reported recently by Hurley *et al.* for the study of chronic lymphocytic leukaemia

---

‖ Present address: Division of Hematology, Department of Medicine, Georgetown University School of Medicine, Washington, DC 20007.

0028-0836/80/360049—02$01.00

(CLL)[7]. Anti-immunoglobulin idiotype reagents were used to demonstrate that some B-lymphoblastoid cell lines obtained from CLL patients had originated from the CLL clone. In cytogenetic studies, the cell lines which expressed the CLL idiotype were aneuploid, whereas lymphoblastoid cell lines which did not express the CLL idiotype were cytogenetically normal. Thus, EBV infection can transform some progeny of the malignant clone both in patients with CLL and in those with CML.

The finding of Ph^1 in B-lymphoblastoid cell lines derived from our patient directly demonstrates that precursor cells originating from the CML clone are capable of differentiating into immunoglobulin-producing B lymphocytes. Evidence supporting this conclusion has also been provided by the six reported cases of CML in blast crisis in which the majority of blasts were of the pre-B phenotype (cytoplasmic immunoglobulin positive, surface immunoclobulin negative)[8–10]. Although the immunoglobulin synthesis by these cells could reflect the differentiation potential of the original CML clone, the possibility cannot be excluded that immunoglobulin synthesis by a highly malignant (that is, blast phase) CML clone resulted from alterations in the genome that occurred as a secondary consequence of malignancy. Whatever the mechanism that resulted in immunoglobulin synthesis, the cells of these patients represented a monoclonal expansion of malignant blasts, as indicated by studies of the immunoglobulin light chain[8].

The cell lines described here provide evidence that cells of the malignant clone can differentiate into B lymphocytes even during the chronic phase of CML. These cell lines produce different classes of immunoglobulin, indicating further that this differentiation process is not limited to a single immunoglobulin species. This in turn suggests that immunoglobulin restriction is not fixed in stem cells of the CML clone, and that these cells may be responsive to the induction factors which normally regulate B-lymphoid differentiation. The diversity of differentiation seen for the CML clone during the chronic phase, demonstrated here by unrestricted immunoglobulin synthesis in Ph^1-positive stem cells, contrasts with the uniform immunoglobulin expressed by cells during blast crisis. Therefore, immunoglobulin restriction presumably occurs at some stage in differentiation between the pluripotent stem cell involved in the chronic phase of CML and the more differentiated blast cells present in the acute phase of the disease.

Table 1 Ph^1, cytoplasmic immunoglobulin and G6PD analyses of Ph^1–positive cell lines

Line	Ph^{1}* No. of Ph^1–positive cells / No. of cells studied	Cytoplasmic immunoglobulin (% of cells positive) μ	α	γ	κ	λ	G6PD
MK 3.10	70/70	31	0	0	0	33	B
MK 12.4	80/80	20	0	0	57	0	B
MK 12.7	95/95	0	17	0	0	75	B
MK 25.6	110/110	87	0	0	0	82	B

For chromosome studies, Ph^1 was enumerated in conventionally stained metaphases. After screening 30–50 mitoses, an additional 20–60 G–banded metaphases were analysed. More than 93% of cells from each of the B–lymphoblastoid cell lines were 46,XX,t(7;9;22)(q11 or 21:q34.0;q11.1) (see Fig. 1). Cytoplasmic immunoglobulin was stained as described with rhodamine–conjugated F(ab')$_2$ fragments specific for μ, γ, α, κ and λ (ref. 14). These reagents were provided by Dr S. M. Fu. Cells were examined with a Leitz Ortholux Two microscope with a 200 W mercury lamp and Ploemopak two filter system. A minimum of 300 cells were counted. For G6PD determination, cell lysates made by freezing and thawing were subjected to starch gel electrophoresis and the relative activity of the isoenzyme bands was estimated visually. The sensitivity of this technique enables a minor enzyme activity component of 5% to be detected[15].

* The data for the five other Ph^1-positive lines in which immunoglobulin was not studied are 60/60 for line MK-229.1, 78/80 for 12.15, 79/80 for 12.19, 28/30 for 31.2 and 30/30 for 12.23.

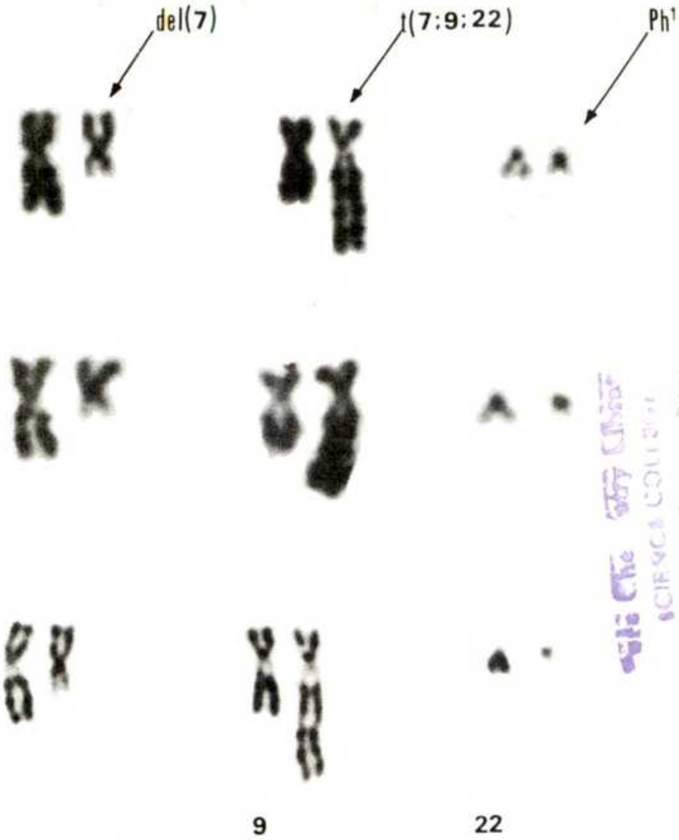

Fig. 1 Partial banded karyotypes of Philadelphia chromosome-positive B-lymphoblastoid cell lines. Colchicine (1 μg ml^{-1}) was added to the cell lines for the final three hours of culture, prior to fixation and staining. Slides were then subjected to a modified 'ASG' banding technique to obtain the banded karyotype of the cells[11]. Paris Conference[12] and its supplement[13] were used for chromosome nomenclature.

The Ph^1-positive B-lymphoblastoid cell lines derived from patient M.K., taken together with previous studies of this and similar patients[1,2], demonstrate that there exists in man a haematopoietic stem cell capable of B-lymphoid, as well as granulocytic, erythrocytic and megakaryocytic differentiation, and that this pluripotent stem cell is involved in CML.

We thank P. Basford, A. Chang, S. Clark, G. Herner, A. Liebling, A. Salo and L. Steinmann for their help. This work was supported by NIH grants CA 18029 and CA 16448 from the NCI, HL 17265 from the National Heart Lung Blood Institute, GM 15253 from the Institute of General Medical Sciences, by Institutional grant no. IN-26U from the American Cancer Society, and by the Veterans Administration, U.S.A. P.J.M. is a Junior Faculty Clinical Fellow of the American Cancer Society.

Received 18 April; accepted 24 June 1980.

1. Fialkow, P. J., Jacobson, R. J. & Papayannopoulou, T. *Am. J. Med.* **63,** 125–130 (1977).
2. Fialkow, P. J., Denman, A. M., Jacobson, R. J. & Lowenthal, M. N. *J. clin. Invest.* **62,** 815–823 (1978).
3. Miller, G. & Lipman, M. *Proc. natn. Acad. Sci. U.S.A.* **70,** 190–194 (1973).
4. Lozzio, C. B. & Lozzio, B. B. *Blood* **45,** 321–334 (1975).
5. Minowada, J., Koshiba, H., Janossy, G., Greaves, M. F. & Bollum, F. J. *Leukaemia Res.* **3,** 261–266 (1979).
6. Anderson, L. D., Jokinen, M. & Gahmberg, C. G. *Nature* **278,** 364–365 (1979).
7. Hurley, J. N., Fu, S. M., Kunkel, H. G., Chaganti, R. S. K. & German, J. *Nature* **283,** 76–78 (1980).
8. Lebien, T. W., Hozier, J., Minowada, J. & Kersey, J. H. *New Engl. J. Med.* **301,** 144–147 (1979).
9. Vogler, L. B., Crist, W. M., Vinson, A. S., Brattain, M. G. & Coleman, M. S. *Blood* **54,** 1164–1170 (1979).
10. Greaves, M. F. *et al. Leukaemia Res.* **3,** 181–191 (1979).
11. Sumner, A. T., Evans, H. J. & Buckland, R. A. *Nature new Biol.* **232,** 31–32 (1971).
12. *Paris Conference: Standardization in Human Cytogenetics* (The National Foundation—March of Dimes BD, OAS VIII, 1972).
13. *Paris Conference (1971) & Suppl. (1975)* (The National Foundation—March of Dimes BD, OAS XI No. 9, 1975).
14. Hijmans, W., Schuit, H. J. R. & Klein, F. *Clin. exp. Immun.* **4,** 457–472 (1969).
15. Fialkow, P. J. *Ann. hum. Genet.* **37,** 39–48 (1973).

Enzymatic assembly of slow reacting substance

B. A. Jakschik & L. H. Lee

Department of Pharmacology, Washington University Medical School,
St Louis, Missouri 63110

When basophils or mast cells are stimulated by a specific antigen they release chemical mediators, including a potent bronchoconstrictor, slow reacting substance of anaphylaxis (SRS-A). The structure of SRS from a mouse mastocytoma[1,2] and rat basophilic leukaemia (RBL-1) cells[3] has been identified as a thioether of arachidonic acid and glutathione[2,3] [not a thioether of cysteine as was originally thought[1]]. SRS has been named leukotriene (LT) C and may be formed by a novel lipoxygenase pathway which also synthesizes 5,6-oxido-7,9,11,14-icosatetraenoic acid (LTA) and 5,12-dihydroxy-6,8,10,14-icosatetraenoic acid (LTB)[1,4]. Homogenates of RBL-1 cells, when incubated with ^{14}C-arachidonic acid, form 5-hydroxy-icosatetraenoic acid (5-HETE) and 5,12-dihydroxy- and 5,6-dihydroxy-icosatetraenoic acid[5]. The latter is the spontaneous breakdown product of the labile intermediate LTA[4]. Formation of both compounds is stimulated by calcium. We have now produced biologically active SRS in a cell-free system generated from RBL-1 cells. Glutathione was essential for SRS synthesis and calcium stimulated its formation.

The experiments were carried out with 10,000*g* supernatant of RBL-1 homogenates[5,6]. The buffer used for the preparation contained 50 mM phosphate *p*H7, 1 mM EDTA, 0.1% gelatin and 14 μM indomethacin. Briefly, RBL-1 cells were washed once with buffer, resuspended at 5×10^7 cells per ml and homogenized on a Tekmar Tissumizer. The homogenate was centrifuged at 10,000*g* for 20 min. The formation of hydroxyacids from ^{14}C-arachidonate was determined by TLC as described previously[5,6]. SRS synthesis was monitored on the isolated, superfused guinea pig ileum[7]. Figure 1 shows the results of a typical SRS experiment. Addition of glutathione proved to be essential for the formation of SRS activity. No such activity was produced when cysteine was substituted for glutathione. The SRS activity was readily blocked by its specific receptor antagonist FPL 55712 (Fig. 1, Table 1). These data confirm earlier reports[2,3] that glutathione and not cysteine is part of the SRS molecule. The incorporation of glutathione rather than cysteine as such into SRS also agrees with our earlier observation with ^{35}S-cysteine[8]. A higher percentage of label was incorporated into SRS when RBL-1 cells were grown for 16 h in the presence of this amino acid as compared to brief exposure (1 h). These experiments had already suggested that cysteine was first incorporated into another compound before utilization in SRS synthesis.

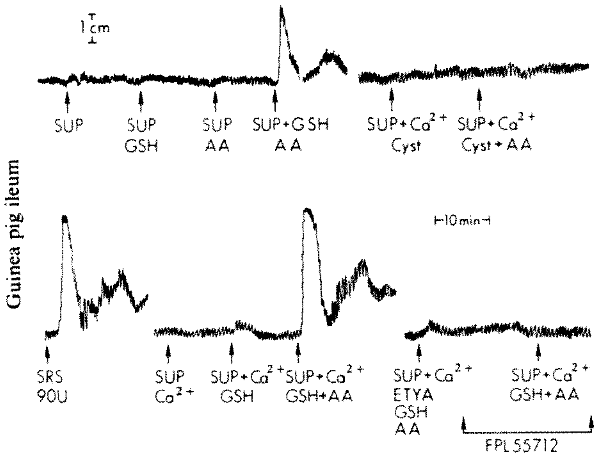

Fig. 1 SRS synthesis by a cell-free system. 10,000*g* supernatant of RBL-1 homogenates was incubated at 37 °C for 15 min with the agents indicated at the following concentrations: reduced glutathione (GSH) 1×10^{-3} M, calcium (Ca^{2+}) 2×10^{-3} M, cysteine (Cyst) 1×10^{-3} M, arachidonic acid (AA) 1.6×10^{-5} M, icosatetraynoic acid (ETYA) 6.7×10^{-5} M. 100 μl of the incubation mixture was tested on the superfused guinea pig ileum[7]. FPL 55712 was applied to the tissue at a concentration of 2×10^{-7} M. The SRS standard was generated from RBL-1 cells as described previously[9].

Table 1 Modulation of leukotrienes

	SRS Activity* (% max)	5,12-DHETE (% c.p.m.)†	5-HETE (% c.p.m.)†
Sup + Ca^{2+} + GSH + AA	100	6.1 ± 1.4	15.0 ± 7.0
Sup + GSH + AA	43.6 ± 8.7	–	–
Sup + Ca^{2+} + AA	0	25.9 ± 4.7	12.1 ± 1.5
Sup + AA	0	1.7 ± 0.5	2.3 ± 1.5
Boiled Sup + Ca^{2+} + GSH + AA	0	–	–
Boiled Sup + Ca^{2+} + AA	–	1.0 ± 0.4	1.2 ± 0.4
	% Inhibition		
ETYA‡	96.5 ± 3.5	90.6 ± 3.5	75.2 ± 2.9
FPL 55712	95.7 ± 2.2	–	–

* The 10, 000*g* supernatant (Sup) from RBL-1 cell homogenates was incubated and tested as in Fig. 1. The size of the contraction was evaluated by determining the area under the curve. The contraction obtained in the presence of Ca^{2+} 2×10^{-3} M, glutathione (GSH) 1×10^{-3} M and arachidonic acid (AA) 1.6×10^{-5} M, was arbitrarily taken as 100% ($n = 5$–7).

† The 10,000*g* supernatant from RBL-1 cell homogenates was incubated as described in Fig. 2 legend. Quantification was achieved by scraping and liquid scintillation counting ($n = 3$ or 4).

‡ Inhibition with icosatetraynoic acid (ETYA) or FPL 55712 was performed as indicated in Figs 2 and 1, respectively. The data are presented as mean ± s.e.m.

However, the addition of glutathione to the incubation mixture reduced the formation of 5,12-DiHETE (Fig. 2, Table 1). This observation suggests the preferential formation of SRS over 5,12-DiHETE. Therefore, the SRS-forming enzyme, probably a glutathione transferase, has a higher affinity for the proposed common intermediate, the 5,6-epoxide, than the enzyme synthesizing 5,12-DiHETE. The production of SRS in the presence of low concentrations of glutathione (Table 1) and lack of SRS formation when boiled supernatant was used, strongly indicate that this SRS formation is enzymatic. These data, therefore, confirm the postulate[1] that SRS is formed by the same enzymatic pathway as LTB with a common intermediate, LTA.

Similar to 5-HETE and 5, 12-DiHETE (Fig. 2, Table 1), SRS synthesis was stimulated by calcium (Fig. 1, Table 1). Therefore, calcium is important for this whole pathway. It is probably necessary for the first step since very little 5-HETE was formed in the absence of calcium (Fig. 2, Table 1). The enhancement of SRS formation by calcium does not appear to be quite as marked as for 5,12-DiHETE and 5-HETE. This may further indicate the preferential formation of SRS over 5,12-DiHETE. As can be seen in Table 1, there was a small, though not significant, increase in counts in the 5-HETE TLC area when no calcium was added to the incubation mixture as compared to incubations with boiled enzyme. Therefore, some hydroperoxide and LTA may be formed in the absence of exogenous calcium. The LTA is then preferentially converted to SRS. This would explain the formation of appreciable amounts of SRS in the absence of added calcium. Icosatetraynoic acid effectively inhibited the synthesis of all the products of the pathway (Figs 1, 2, Table 1).

0028-0836/80/360051—02$01.00

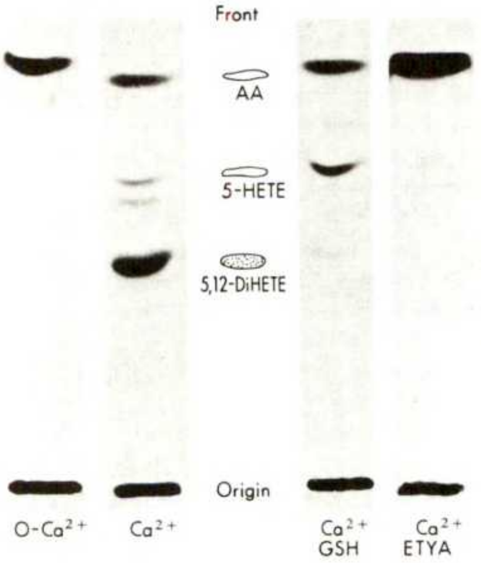

Fig. 2 Effect of glutathione and icosatetraynoic acid on 5,12-DiHETE formation. 10,000*g* supernatant (0.5 ml) was incubated with [1-^{14}C]arachidonic acid (AA) (200,000 c.p.m., specific activity 55 mCi mmol^{-1}) for 20 min at 37 °C, with the agents indicated: calcium (Ca^{2+}) 2×10^{-3} M, reduced glutathione (GSH) 1×10^{-3} M, icosatetraynoic acid (ETYA) 6.7×10^{-5} M. The reaction was stopped by precipitating the proteins with acetone. The *p*H was adjusted to 3.2–3.5 with 2 M formic acid. The mixture was extracted twice with 2 ml of chloroform. TLC was performed in solvent system A9, the organic phase of ethyl acetate/2,2,4-trimethylpentane/acetic acid/water (110:50:20:10; ref.[10]). Radioactive peaks were located by fluorography[11]. Standards were visualized by iodine staining. The identity of 5,12-DiHETE has been established by gas chromatography–mass spectrometry[5].

We are, therefore, now able to assemble SRS and the other LTs enzymatically in a cell-free system. The production of SRS by a cell-free system has not been reported previously despite many attempts. This preparation will enable us to study this pathway and its modulation in greater detail. The data presented here already indicate that in proper conditions SRS (LTC) is synthesized in preference to LTB. It will now be possible to investigate the requirements for each step in the pathway and determine what factors enhance or inhibit the formation of each product. The availability of the enzyme system in a cell-free preparation will allow the determination of substrate specificity for different fatty acids, glutathione analogues and sulphydryl compounds. Therefore, use of this enzyme preparation provides a tool for identifying LT synthesis inhibitors. The discovery of a specific SRS (LTC) inhibitor would be of special significance since SRS is such a potent bronchoconstrictor.

This work was supported by NIH grants 5-R01-HL21874-02 and 5-P30-CA16217-03. Prostaglandin standards were supplied by Dr J. Pike and 5-HETE by Dr R. C. Kelly (Upjohn), FPL 55712 by Fisons and icosatetraynoic acid by Roche.

Received 2 April; accepted 23 June 1980.

1. Murphy, R. C., Hammarström, S. & Samuelsson, B. *Proc. natn. Acad. Sci. U.S.A.* **76,** 4275–4279 (1979).
2. Hammarström, S. *et al. Biochem. biophys. Res. Commun.* **91,** 1266–1272 (1979).
3. Parker, C. W., Huber, M. M., Hoffman, M. K. & Falkenhein, S. F. *Prostaglandins* **18,** 673–686 (1979).
4. Borgeat, P. & Samuelsson, B. *Proc. natn. Acad. Sci. U.S.A.* **76,** 3213–3217 (1979).
5. Jakschik, B. A., Sun, F. F., Lee, L. H. & Steinhoff, M. M. *Biochem. biophys. Res. Commun.* **95,** 103–110 (1980).
6. Steinhoff, M. M. & Jakschik, B. A. *Biochim. biophys. Acta* **618,** 28–34 (1980).
7. Jakschik, B. A., Lee, L. H., Shuffer, G. & Parker, C. W. *Prostaglandins* **16,** 733–748 (1978).
8. Parker, C. W., Jakschik, B. A., Huber, M. G. & Falkenhein, S. F. *Biochem. biophys. Res. Commun.* **89,** 1186–1192 (1979).
9. Jakschik, B. A., Kulczycki, A. Jr., MacDonald, H. H. & Parker, C. W. *J. Immun.* **119,** 618–622 (1977).
10. Hamberg, M. & Samuelsson, B. *J. biol. Chem.* **241,** 257–263 (1966).
11. Bonner, W. M. & Stedman, J. D. *Analyt. Biochem.* **89,** 247–256 (1978).

Behavioural effects and supersensitivity following nigral dopamine receptor stimulation

Michael R. Kozlowski, Steven Sawyer & John F. Marshall

Department of Psychobiology, University of California, Irvine, California 92717

Nigrostriatal dopamine (DA)-containing neurones have the potential to modulate neostriatal output at two levels. First, DA released from the terminals of the DA-containing pars compacta neurones can act on striatal DA receptors. In addition, these pars compacta cells can release DA from their dendrites within the nigra[1–3]. Dendritically released DA could act at receptors located on these same cells ('autoreceptors')[4,5] or at receptors which are located on other nigral elements, especially strionigral afferent fibres[4,6,7]. However, although the stimulation of striatal DA receptors produces clear behavioural effects, no behavioural consequence of nigral DA receptor stimulation has been shown[8,9]. We report here that nigral DA receptor stimulation can produce clear behavioural effects in the appropriate circumstances. Unilateral intranigral injections of the DA receptor stimulant, apomorphine, produce clear contralateral turning in animals that (1) had been previously given intracerebral 6-hydroxydopamine (6-OHDA) injections, which extensively damage the ipsilateral nigral DA-containing cells, or (2) had been pretreated for 1 week with the DA receptor blocker, haloperidol. In addition, the turning produced by intranigral apomorphine in 6-OHDA-treated animals was much greater when the drug was given 14–17 days after the intracerebral neurotoxin than when it was given 4–7 days after, suggesting the development of supersensitivity to apomorphine in the nigra. These results suggest that the nigra must be considered as a site of action for drugs whose main effect is on the dopaminergic system.

Fifty male Sprague–Dawley rats (Simonsen Breeders) weighing 150–200 g had guide cannulae implanted 2 mm dorsal to the left substantia nigra. During the same surgery, 37 of these animals also received an injection of 6-OHDA (8 μg, Sigma) into the left ventral tegmental area (VTA) to destroy the mesotelencephalic DA-containing projection. Desmethylimipramine (15 mg per kg, intraperitoneally (i.p.)) was given 0.5 h before the 6-OHDA injection to protect brain noradrenaline-containing neurones. On days 4–17 postoperatively, all rats were given apomorphine injections through an inner cannula and were then placed in circular bowls where the number of complete rotations was counted for 1-min periods every 5 min for 1 h. After behavioural testing, the location of the cannula tracts was reconstructed from thionin-stained frontal sections of 20-μm thickness.

In agreement with the findings of others[8,9], injections of apomorphine (10 μg) into one substantia nigra of otherwise neurologically intact animals produced little behavioural effect. A small amount of contralateral turning was seen in two of the eight animals tested (Table 1). However, vigorous contralateral rotation occurred when intranigral apomorphine injections were given either 4–7 or 14–17 days after 6-OHDA injections into the ipsilateral VTA (Table 1). These 6-OHDA injections caused extensive ipsilateral DA depletion in both the forebrain (98, 80 and 82% decreases in the neostriatum, nucleus accumbens septi and olfactory tubercle, respectively) and the substantia nigra (90% decrease) when compared with the same structures in the opposite hemisphere. The turning produced by intranigral apomorphine in these DA-depleted animals was elicited in a dose-dependent manner (Fig. 1) and could be

0028-0836/80/360052—03$01.00

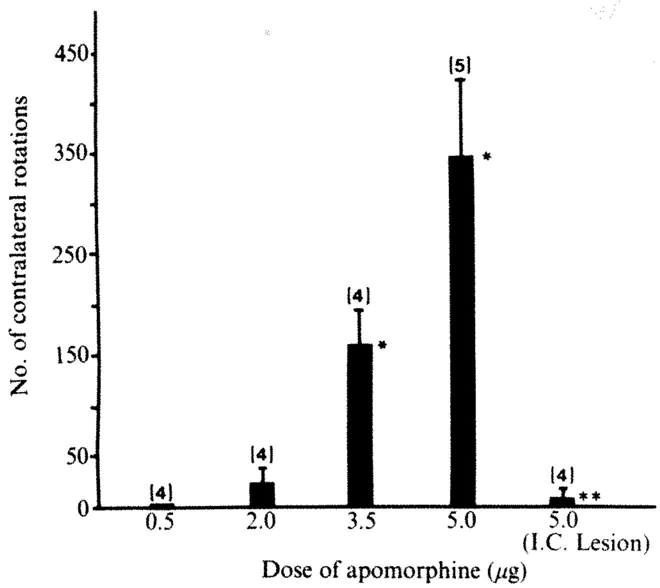

Fig. 1 Dose–response curve for contralateral rotation following intranigral apomorphine given 14–17 days after 6-OHDA treatment. The turning showed a significant dose dependence (*F*-test, $P<0.001$). Numbers in parentheses indicate animals per group. I.C. = internal capsule. 6-OHDA was dissolved in 0.9% saline and 0.1% ascorbic acid (2 μg μl^{-1}) and injected at a rate of 1 μl min^{-1} at the following coordinates: A 2.6, L 1.0, V 7.8. All rats were given desmethylimipramine (15 mg per kg, i.p.) 0.5 h before 6-OHDA. Guide cannulae were implanted at A 2.3, L 2.0, V 5.8–6.3. Apomorphine was dissolved in 0.9% saline and 0.1% ascorbic acid and injected into the substantia nigra in a volume of 0.5 μl at a rate of 1 μl min^{-1} through an inner cannula which extended 2 mm ventral to the tip of the guide shaft. The rats were placed in circular bowls for 1 h following the apomorphine injection, where their rotational behaviour was recorded. Radiofrequency lesions (100 V, 30 s) were made in the internal capsule using a stainless steel dental broach insulated except for 0.6 mm at the tip, positioned at A 4.0, L 2.6, V 8.3. In addition to receiving intranigral apomorphine, the 6-OHDA-treated rats were tested for rotation in response to a low dose (0.25 mg per kg, i.p.) of apomorphine as an index of extensive unilateral DA depletion. Those rats that did not show vigorous contralateral rotation (⩾200 turns) in the subsequent 1 h were not used in the experiment (~17% of the 6-OHDA-treated rats). The DA content (in μg per g wet tissue weight) of the striatum, nucleus accumbens septi, olfactory tubercle and substantia nigra in the right, non-injected hemisphere of 6-OHDA-treated rats were 6.7 ± 0.6, 6.5 ± 1.7, 4.3 ± 0.3 and 1.8 ± 0.5, respectively.
* Significantly more turning than 0.5 μg group, Dunnett's *t*-test, $P<0.05$; ** significantly less turning than 5.0 μg group, Student's *t*-test, $P<0.001$.

blocked by a single systemic injection of the DA antagonist, haloperidol (2 mg per kg, i.p., Table 1). The amount of rotation produced by 5 μg of apomorphine was much greater 14–17 than 4–7 days after the 6-OHDA treatment (Table 1).

Rotation in response to intranigral apomorphine was also seen in animals chronically treated with haloperidol (5 mg per kg, i.p., daily for 1 week followed by a 3-day drug-free period, Table 1). Such chronic haloperidol treatment produces behavioural supersensitivity to systemically administered apomorphine[10,11]. Interestingly, similar amounts of turning resulted from intranigral apomorphine injections iven either after 7 days of haloperidol treatment or 4–7 days after an intracerebral 6-OHDA injection (Table 1).

To investigate the possibility that the turning produced by intranigral apomorphine was mediated by DA receptors located on strionigral or pallidonigral axons, four animals were given small radiofrequency lesions along the course of these fibres in the medial tip of the internal capsule 11 days after an ipsilateral 6-OHDA injection into the VTA. These lesions nearly completely eliminated the rotation in response to intranigral apomorphine (5 μg, Fig. 1) 14 days after the 6-OHDA injection. They also reduced by 75% (*t*-test, $P<0.01$) the turning elicited by the systemic injection of apomorphine (0.25 mg per kg, i.p.). Histological sections showed that the radiofrequency lesions were centred in the medial tip of the internal capsule at a level of A 3.9–A 4.1 (ref. 12). These lesions extended an average distance of 1.0 mm in the antero-posterior plane, 0.6 mm in the medio-lateral plane and 1.2 mm in the dorso-ventral plane. In some brains, slight damage to the immediately adjacent zona incerta, ventral tegmentum and optic tract was found.

The effect of blocking receptors for γ-aminobutyric acid (GABA), a major transmitter in the strionigral and pallidonigral pathways[13,14], with the GABA antagonist, picrotoxin (0.5, 1.0 and 2.0 mg per kg, i.p.), was also examined. At 2.0 mg per kg, pictrotoxin completely blocked the rotation induced by intranigral apomorphine (5 μg, Table 1), but the two lower doses had no effect on turning (data not shown).

Histological examinations confirmed that the cannula tips for apomorphine injection were located in the pars reticulata of the substantia nigra. In a separate group of six 6-OHDA-treated animals in which the cannula tips were placed in the pars compacta, intranigral apomorphine injections produced little or no turning.

The substantia nigra contains at least two types of DA receptor. One type, located on the DA-containing cells of the pars compacta, binds the DA antagonist ^{3}H-spiroperidol with high affinity but does not seem to be linked to an adenylate cyclase[15]. The second type, located predominantly on nigral afferents (strionigral and possibly pallidonigral axons), is linked to adenylate cyclase but fails to bind ^{3}H-spiroperidol with high affinity[13,15]. Three findings indicate that the latter type is important in producing turning after intranigral apomorphine. First, the extensive depletion of forebrain and nigral DA produced by the VTA 6-OHDA injection suggests a massive degeneration of the dopaminergic cells, so that the rotation elicited by intranigral apomorphine is unlikely to be mediated by these neurones. Second, lesions of an area of the internal capsule through which strionigral fibres pass[16] almost completely eliminate this rotation. Third, systemic picrotoxin blocks this rotation, possibly by blocking GABA receptors postsynaptic to the strionigral fibres. However, because a high dose of picrotoxin was needed to block rotation (one-half the dose that is required to produce seizures), a non-physiological action of this drug cannot be ruled out.

Because DA can cause a release of GABA from nigral slices *in vitro*[17], we suggest that the apomorphine-induced turning behaviour is likely to result from a local stimulation of GABA release from strionigral axon terminals within the pars reticulata. This enhanced GABA release should then affect the

Table 1 Effects of 6-OHDA injections and pharmacological treatments on turning behaviour in response to intranigral apomorphine

Treatment	No. of animals	Apomorphine dose (μg)	No. of contralateral turns
1. Intranigral apomorphine only	8	10	1.4 ± 0.9
2. 6-OHDA injections 4–7 d before intranigral apomorphine	9	5	48.2 ± 14.0†
3. 6-OHDA injection 14–17 d before intranigral apomorphine*	5	5	344.6 ± 76.6‡
4. Chronic haloperidol (5 mg per kg, i.p daily on days 5–11 postoperatively) followed by intranigral apomorphine on day 14	5	5	33.6 ± 10.2†
5. 6-OHDA injection 4–7 d before and haloperidol (2 mg per kg, i.p.) 2 h before intranigral apomorphine	5	5	6.8 ± 2.9‡
6. 6-OHDA injection 4–7 d before and picrotoxin (2 mg per kg, i.p.) 10 min before intranigral apomorphine	5	5	0 ± 0

* Results are from Fig. 1.
† Significantly different from group 1, *t*-test, $P<0.05$.
‡ Significantly different from group 2, *t*-test, $P<0.05$.

activity of nigral pars reticulata cells, which have been implicated in the production of rotational behaviour in other experiments[18,19].

In addition to these DA receptors located on pars compacta cells and on strionigral afferents, the nigra may contain additional DA binding sites, as combined lesions of nigrostriatal and strionigral projections do not totally eliminate nigral ^{3}H-spiroperidol binding[15]. An action of apomorphine at these sites may contribute to the behavioural consequences of its intranigral injection, particularly if they are located on nigral output cells. However, the present report offers no evidence for an action of intranigral apomorphine at these sites.

The effects of nigral DA receptor stimulation are strikingly similar to those caused by the stimulation of DA receptors in the neostriatum, a terminal field for the ascending dopaminergic axons. First, although unilateral injections of apomorphine into either the nigra or the striatum produce little behavioural effect in neurologically intact animals (ref. 20 and unpublished findings), injections into either region do produce vigorous contralateral turning following ipsilateral damage of the ascending dopaminergic system, a single injection of reserpine or chronic haloperidol treatment (ref. 20 and unpublished findings). Second, the rotation resulting from both striatal and nigral apomorphine injections seems to be mediated by strionigral fibres (ref. 21 and the present findings). These similarities suggest the intriguing possibility that the axon terminals and dendrites of the dopaminergic pars compacta cells provide a parallel, dual control mechanism for altering the activity of strionigral fibres and, consequently, for controlling the nigral output cells of the pars reticulata.

It is particularly interesting that robust turning in response to intranigral apomorphine occurs in the 6-OHDA- or chronic haloperidol-treated animals, but that only occasional rotations are seen in otherwise untreated animals given the intranigral apomorphine injection. This suggests that the nigra shows enhanced sensitivity to apomorphine following these treatments. The sharply increased rotational response to intranigral apomorphine found between 4–7 and 14–17 days after the 6-OHDA injection parallels the increased behavioural sensitivity to systemically administered apomorphine which develops during this period[22,23].

One process thought to underlie the development of enhanced sensitivity to DA agonists in the neostriatum following damage to the dopaminergic system is a proliferation of postsynaptic DA receptors, as indicated by an increased number of ^{3}H-haloperidol or ^{3}H-spiroperidol binding sites[24,25]. In the nigra, however, no increase in ^{3}H-spiroperidol binding occurs after destruction of the dopaminergic system[24]. This negative finding may reflect the fact that the high affinity ^{3}H-spiroperidol binding sites are largely localized to the DA-containing cells[15]. A possible increase in nigral DA-sensitive adenylate cyclase activity after this lesion has not been investigated. Alternatively, the increased sensitivity to apomorphine may result from changes in the receptors postsynaptic to the strionigral axons. Indeed, chronic treatment with haloperidol increases ^{3}H-GABA binding in the nigra[26,27].

These findings indicate that the nigra must be considered an important potential site of action of systemically administered drugs which act at DA synapses. Part of the contralateral rotation seen in unilateral 6-OHDA-treated rats given systeic apomorphine may be due to a direct nigral action of this drug. In addition, the nigra must be considered as a site of action of antipsychotic and anti-parkinsonian drugs. Finally, the development of an enhanced sensitivity to DA within the nigra may contribute to the behavioural recovery that occurs after subtotal damage to the ascending DA-containing fibres[28,29].

We acknowledge the gifts of haloperidol from McNeill Laboratories, desmethylimipramine from Merrill Laboratories and apomorphine from Dr R. J. Baldessarini. This research was supported by PHS grant MH 31426 and by NSF grant BNS-7914092 to J.F.M. M.R.K. was supported by PHS training grant MH 14599.

Received 13 March; accepted 23 June 1980.

1. Björklund, A. & Lindvall, O. *Brain Res.* **83,** 531–537 (1975).
2. Nieoullon, A., Cheramy, A. & Glowinski, J. *Nature* **266,** 375–377 (1977).
3. Hefti, F. & Lichtensteiger, W. *J. Neurochem.* **30,** 1217–1230 (1978).
4. Groves, P. M., Wilson, C. W., Young, S. J. & Rebec, G. V. *Science* **190,** 522–529 (1975).
5. Aghajanian, G. K. & Bunney, B. S. *Adv. Biochem. Pharmac.* **16,** 433–438 (1977).
6. Gale, K., Hong, J.-S. & Guidotti, A. *Brain Res.* **136,** 371–375 (1977).
7. McGeer, P. L., McGeer, E. G. & Innanen, V. T. *Brain Res.* **169,** 433–441 (1979).
8. Glick, S. D. & Crane, L. A. *Brain Res.* **156,** 380–381 (1978).
9. Kelley, P. Y. & Moore, K. E. *Neuropharmacology* **17,** 169–174 (1978).
10. Gianutsos, G., Drawbaugh, R. B., Haynes, M. D. & Lal, H. *Life Sci.* **14,** 887–898 (1974).
11. Von Voigtlander, P. F. *Fedn Proc.* **33,** 578 (1974).
12. König, J. F. R. & Klippel, R. A. *The Rat Brain: A Stereotoxic Atlas of the Forebrain and Lower Parts of the Brain Stem* (Krieger, New York, 1963).
13. Gale, K., Guidotti, A. & Costa, E. *Science* **195,** 503–505 (1977).
14. Jessell, T. M., Emson, P. C., Paxinos, G. & Cuello, A. C. *Brain Res.* **152,** 487–498 (1978).
15. Quick, M., Emson, P. C. & Joyce, E. *Brain Res.* **167,** 355–365 (1979).
16. Garcia-Munoz, M., Nicolaou, N. M., Tulloch, I. F., Wright, A. K. & Arbuthnott, G. W. *Nature* **265,** 363–365 (1977).
17. Reubi, J.-C., Iversen, L. L. & Jessell, T. M. *Adv. Biochem. Psychopharmac.* **19,** 401–404 (1978).
18. Olianas, M. C., DeMontis, G. M., Mulas, G. & Tagliamonte, A. *Eur. J. Pharmac.* **49,** 233–241 (1978).
19. diChiara, G., Porceddu, M. L., Morelli, M., Mulas, M. L. & Gessa, G. L. *Naunyn-Schmiedebergs Archs Pharmak.* **306,** 153–159 (1979).
20. Ungerstedt, U., Butcher, L. L., Butcher, S. G., Andén, N.-E. & Fuxe, K. *Brain Res.* **14,** 461–471 (1969).
21. Marshall, J. F. & Ungerstedt, U. *Science* **198,** 62–64 (1977).
22. Ungerstedt, U. *Acta physiol. scand.* Suppl. **367,** 69–93 (1971).
23. Thornburg, J. E. & Moore, K. E. *J. Pharmac. exp. Ther.* **192,** 42–49 (1975).
24. Nagy, J. I., Lee, T., Seeman, P. & Fibiger, H. C. *Nature* **274,** 278–281 (1978).
25. Creese, I., Burt, D. R. & Snyder, S. H. *Science* **197,** 596–598 (1977).
26. Gale, K. *Neurosci. Abstr.* **5,** 71 (1979).
27. Gale, K. *Nature* **283,** 569–570 (1980).
28. Stricker, E. M. & Zigmond, M. J. *Progress in Physiological Psychology and Psychobiology* Vol. 6 (eds Sprague, J. M. & Epstein, A. M.) 121–180 (Academic, New York, 1976).
29. Marshall, J. F. *Brain Res.* **177,** 311–324 (1979).

The role of microvesicles in buffering $[\mathrm{Ca}^{2+}]_i$ in the neurohypophysis

Jean J. Nordmann & Jean Chevallier*

INSERM U. 176, rue Camille Saint-Saëns, 33077 Bordeaux, France

* Institut de Biochimie Cellulaire & Neurochimie, 1 rue Camille Saint-Saëns, 33000, Bordeaux, France

It is well established that hormone release from neurosecretory nerve terminals is triggered by an increase of the cytoplasmic ionized calcium concentration which occurs after the arrival of action potentials[1]. For the neurosecretory nerve terminals to recover their basal Ca^{2+} concentration, the calcium which has entered during depolarization must be extruded and/or accumulated in subcellular organelles or bound to some cytoplasmic proteins. Neurosecretory nerve endings are characterized by the presence of hormone-containing granules and microvesicles (earlier referred to as 'synaptoid' vesicles). The role of these microvesicles has been the subject of debate and has recently been reviewed[2]. One of the most attractive hypotheses has been that these organelles represent the retrieved membrane of the granule after exocytosis. However, on stimulation of hormone release, the number of microvesicles does not increase, suggesting that they do not participate in the endocytotic process[3]. Using stereology as a quantifying method, we recently demonstrated a redistribution of microvesicles towards the release site during potassium-stimulated hormone release[3]. It is thus possible that microvesicles in neurosecretory nerve terminals might function as calcium accumulating organelles as suggested for the coated vesicles isolated from the cerebral cortex[4,5]. We report here that a microvesicle-containing microsomal fraction isolated from neurosecretosomes (isolated neurosecretory nerve terminals) possesses an ATP-dependent calcium transporting system. This system enables the fraction to accumulate calcium ions when the external ionized calcium concentration is <1 μM, which is in the physiological range.

0028-0836/80/360054—03$01.00

Bovine neural lobes (40–60 for each experiment) were collected from the local slaughterhouse and kept in ice-cold 0.3 M sucrose buffered with 10 mM HEPES, *p*H 7.2. The glands were carefully dissected out, minced with a pair of scissors and sliced on a MacIlwain tissue chopper at 0.5-mm intervals. The material was then homogenized at 800 r.p.m. in a Teflon homogenizer and the homogenate was centrifuged at $800g_{av}$ for 10 min on a RC-5B Sorvall centrifuge using an HB-4 type rotor. The procedure was repeated with the resulting pellet (P_1) after a further homogenization. The two supernatants were mixed and centrifuged at 1,700*g* for 20 min. The resulting pellet (P_2), which consisted mostly of neurosecretosomes[6], was homogenized in 0.3 M buffered sucrose and the homogenate centrifuged at $26{,}000g_{av}$ for 20 min. The supernatant from this was centrifuged at $100{,}000g_{av}$ for 1 h. The resulting pellet (P_4) was practically devoid of mitochondria and neurosecretory granules, as judged by careful analysis of ultra-thin sections. P_4 was resuspended in 0.15 M KCl, 10 mM HEPES, 5 mM $MgCl_2$, 1 mM EGTA, *p*H 7.2, and its protein content determined using the method of Lowry *et al.*[7]. In one experiment P_4 was fixed by the method described by Shaw and Morris[8]. The pellet consisted primarily of microvesicles an many of them contained precipitate indicating the presence of calcium. Figure 1 shows the time course of calcium uptake by the microvesicle-containing fraction at two different calcium concentrations. This uptake is ATP-dependent and is abolished by addition of the ionophore X537A. The amount of calcium taken up by the microvesicles-containing fraction is higher than that found for a microsomal fraction isolated from pinched-off presynaptic nerve terminals from rat brain cortex[9]. Neither the time course nor the amount of calcium uptake was affected by addition of mitochondrial inhibitors such as ruthenium red (10 μM), antimycin (0.05 μg ml^{-1}) or carbonyl cyanide trifluomethoxyphenyl hydrazone FCCP (0.1 μg ml^{-1}). These results suggest that fragments of mitochondria are not responsible for the ATP-dependent calcium uptake of the microvesicle-containing fraction.

The effect on the Ca^{2+} uptake of the ionophore X537A (Fig. 1) is not due to the influence of an increased membrane permeability to Na^+ ions because (1) the microvesicles were incubated in a sodium-free medium, and (2) addition of sodium (20–40 mM) did not release calcium which had previously been accumulated. The lack of effect of sodium on the calcium accumulated by the microvesicle fraction shows that the preparation used in the present study is unlikely to be contaminated by plasma membranes because a Na^+–Ca^{2+} exchange has been demonstrated in neurohypophyses isolated *in vitro*. Furthermore, the efflux of calcium from preloaded glands does not increase on addition of veratridine, an alkaloid known to increase the sodium conductance in nervous tissue. It thus seems that in neurosecretory nerve endings the release of calcium from the microvesicles is not modulated by the cytoplasmic sodium concentration.

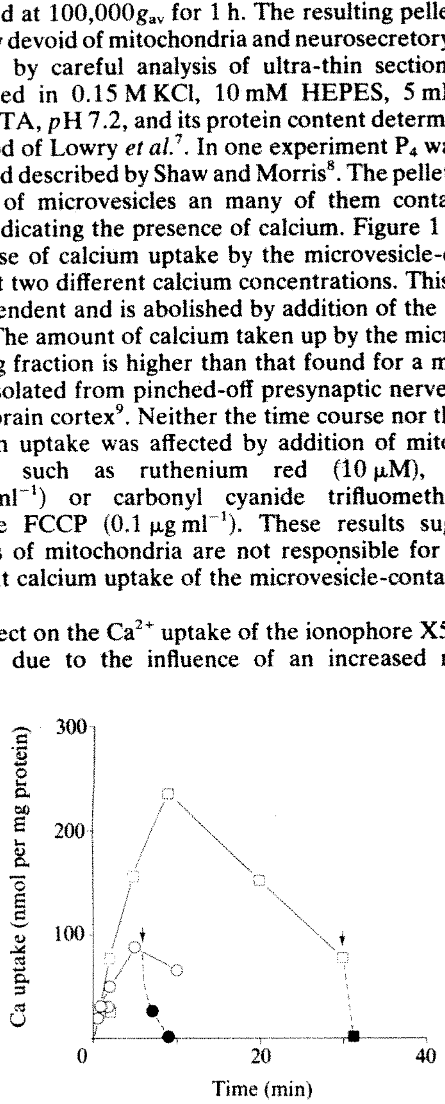

Fig. 1 ATP-dependent Ca^{2+} uptake in microvesicle-containing fraction isolated from bovine neurohypophysis. The preparation (200–300 μg protein ml^{-1}) was preincubated at 37 °C in 5 ml of a medium containing 150 mM KCl, 5 mM $MgCl_2$, 10 mM HEPES, *p*H 7.2, ^{45}Ca-EGTA buffer. After 5 min, 4 mM ATP (final concentration) was added. At different times, 500-μl aliquots were withdrawn and immediately filtered through Millipore filters (0.22 μm pore diameter) as described in ref. 15. 100 μl of the resulting filtrates were counted in a liquid scintillation spectrophotometer. The calcium transport studies were always performed immediately after the isolation of the microvesicle-containing fraction because calcium uptake by the preparation was much lower 16–18 h after the final centrifugation. In some cases, a calcium binding of 10–20 nmol per mg of microsomal proteins was observed in the presence of 4 mM ADP. The ionized calcium concentrations were 0.66 μM (○) and 0.91 μM (□). At the time indicated by the arrow the ionophore X537A (10 μM final concentration) was added (●, ■).

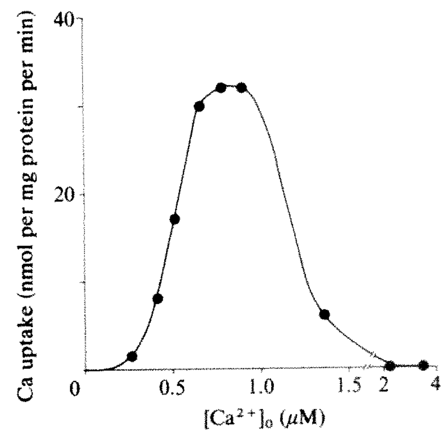

Fig. 2 Effect of free Ca^{2+} concentration on calcium uptake by the microvesicle-containing fraction. Experimental conditions as described in Fig. 1 legend. The calcium in the incubation medium was buffered to the indicated ionized Ca^{2+} concentration with EGTA (1 mM) by taking a Ca-EGTA stability constant of 1.86 × 10^{-7} M. The rate of calcium uptake was obtained from the initial slope of the kinetics illustrated in Fig. 1. The apparent K_m of the Ca^{2+} transport system lies between 0.4 and 0.6 μM. Curve drawn by eye.

The non-mitochondrial ATP-dependent Ca^{2+} transport system described above has a high affinity for calcium. After the calcium has been accumulated into the microvesicle-containing fraction, it can be released passively (Fig. 1). The rate of calcium release is a function of the amount of accumulated calcium. This release of calcium on overloading of the fraction has been observed in other systems[10]. In a series of experiments, aliquots of the microvesicle fraction were incubated in media containing different concentrations of ionized calcium. The rate and the amount of calcium taken up were measured as a function of $[Ca^{2+}]$ in the medium ($[Ca^{2+}]_o$) and the results are illustrated in Fig. 2. The apparent K_m^{Ca} for this transport system is 0.4–0.6 μM. These values lie within the apparent range of cytosolic Ca^{2+} ions, and are similar to those reported for a microsomal fraction isolated from lysed synaptosomes[9]. A pronounced inhibition of the Ca^{2+} transport activity is observed on increasing the free calcium concentration above 1 μM (Fig. 2). This phenomenon can be related to the competition between Ca^{2+} and Mg^{2+} for ATP utilization described in other systems[11].

The present study therefore provides a demonstration that, as suggested earlier[3,12], the microvesicles found in neurohypophysial nerve endings have the capacity to take up calcium and therefore may be involved in controlling the ionized cytoplasmic calcium concentration. The presence of calcium in some microvesicles has been demonstrated previously using the pyroantimonate technique[12]. More recently, Shaw and Morris have been able to demonstrate, using a combined oxalate–pyroantimonate method, the presence of calcium in microvesicles in fixed neural lobes[8]. Microsomal calcium uptake by neurosecretory tissue has previously been shown but the data do not provide information about the origin (nerve cells or pituicytes) of these microsomes[13]. The high affinity (Fig. 2) of the calcium transport system isolated from neurosecretosomes suggests that microvesicles may have an important role in intraterminal Ca^{2+} buffering. Although mitochondria take up calcium, their calcium transport system has a much higher K_m^{Ca} (ref. 14) than the microvesicle fraction. As the arrival of a burst of action potentials is likely to increase the intraterminal ionized calcium concentration from 10^{-7} to 5×10^{-6} M at the most, the microvesicles would buffer the $[Ca^{2+}]_i$ in this range. How the calcium accumulated in microvesicles is released from the nerve terminal is not known. Electron micrographs often show fusion of microvesicles with the plasmalemma and this suggests that the calcium could be released by exocytosis. Alternatively, calcium could be slowly released into the cytoplasm and long-term calcium homeostasis be controlled by some transport system located in the plasma membrane.

This work was supported by grants DGRST 79.7.1057 to J.J.N. and 79.7.0801 to J.C. We thank Fraser Shaw and John Morris for communicating their results to us before publication and for helpful comments concerning the manuscript and Monique Galante and Monique Cazalis for technical assistance.

Received 10 June; accepted 3 July 1980.

1. Douglas, W. W. in *Handbook of Physiology* Sect. IV, 191–224 (Am. Physiol. Soc., Washington, DC, 1974).
2. Morris, J. F., Nordmann, J. J. & Dyball, R. E. J. *Int. Rev. exp. Path.* **18,** 1–95 (1977).
3. Morris, J. F. & Nordmann, J. J. *Neuroscience* **5,** 639–649 (1980).
4. Blitz, A. L., Fine, R. E. & Toselli, P. A. *J. Cell Biol.* **75,** 135–145 (1977).
5. Rahamimoff, H. & Spanier, R. *FEBS Lett.* **104,** 111–114 (1979).
6. Gratzl, M. *et al. Biochim. biophys. Acta* **470,** 45–57 (1977).
7. Lowry, O. H. *et al. J. biol. Chem.* **193,** 265–275 (1951).
8. Shaw, F. D. & Morris, J. F. *Nature* **287,** 56–58 (1980).
9. Blaustein, M. P. *et al. J. gen. Physiol.* **72,** 15–41 (1978).
10. Chevallier, J. *et al. Biol Cell.* **30,** 103–110 (1977).
11. Hasselbach, W. *Prog. Biophys. molec. Biol.* **14,** 167–222 (1964).
12. Stoeckel, M. E. *et al. Cell. Tissue Res.* **157,** 307–315 (1975).
13. Russell, J. T. & Thorn, N. A. *Acta physiol. scand.* **93,** 364–377 (1975).
14. Blaustein, M. P. *et al. Ann. N.Y. Acad. Sci.* **307,** 195–212 (1978).
15. Martonosi, A. & Feretos, R. *J. biol. Chem.* **239,** 648–658 (1964).

Calcium localization in the rat neurohypophysis

F. D. Shaw* **& J. F. Morris†**

* Department of Anatomy, University of London King's College,
London WC2R 2LS, UK
† Department of Human Anatomy, University of Oxford,
Oxford OX1 3QX, UK

Neurosecretory nerve endings in the rat neurohypophysis release their hormones by exocytosis[1] subsequent to an influx of calcium from the external medium[2]. The nerve endings are characterized by the presence of neurosecretory granules, mitochondria, occasional vacuoles, and a population of microvesicles similar in appearance to spherical synaptic vesicles. The function of the microvesicles has, for a long time, been uncertain. In view of evidence that coated microvesicles isolated from cerebral cortex are capable of ATP-dependent calcium accumulation[3], a method has now been developed for the visualization of calcium in the neurohypophysis at the ultrastructural level. With this technique, calcium precipitates are consistently seen in the microvesicles, mitochondria and glial cell (pituicyte) nuclei. In addition, the pituicyte cytoplasm and perivascular space show a diffuse precipitate which can be removed by washing the tissue prior to fixation. The function of the microvesicles might therefore be to sequester calcium within the nerve endings.

The subcellular distribution of calcium in the rat neurohypophysis was studied by a modification of a technique previously described[4]. Adult male rats of the Porton–Wistar strain were anaesthetized with urethane and perfused with a glutaraldehyde fixative containing potassium oxalate, preceded in some cases by a wash with potassium phosphate buffer containing dextran. The posterior pituitaries were dissected out, washed in an oxalate solution, and treated with an osmium tetroxide fixative containing potassium antimonate. The tissue was then washed in distilled water, dehydrated, and embedded for electron microscopy. Control tissue was fixed in solutions lacking oxalate and antimonate. Immersion in osmium/(pyro)antimonate fixatives has been widely used to visualize calcium in nervous and glandular tissue, but it gives relatively poor preservation of fine structure especially in the central nervous system[5–7]. Initial fixation by perfusion with a rapidly penetrating aldehyde, as described here, allows much better preservation[6,7], at the same time immobilizing tissue calcium by precipitation with oxalate.

The neurohypophysis is largely composed of axons and terminals of magnocellular hypothalamic neurones, and of pituicytes. The unmyelinated neurosecretory axons are characterized by numerous dilatations containing neurosecretory granules and mitochondria; neurosecretory nerve endings in addition contain abundant microvesicles, and contact a basement membrane adjacent to a fenestrated capillary[8] (Fig. 1*a*). With the technique used, calcium is indicated by the electron-dense precipitate of antimony (Fig. 1*b–d*). When the neurohypophysis was perfused directly with the oxalate/glutaraldehyde fixative, a striking ultrastructural feature was the presence of abundant precipitates in the cytoplasm and nuclei of the pituicytes, to the extent that their processes were clearly outlined at low power (Fig. 1*b*). A dense precipitate was also present in the perivascular space, and more diffuse deposits were seen over the neurosecretory axons, swellings and terminals. The mitochondria of both neurones and glia were heavily stained; vacuoles usually contained precipitate and virtually every microvesicle contained a single, dense particle of precipitate.

This appearance was significantly altered if the tissue was washed with phosphate buffer solution containing dextran (which facilitates perfusion[9]) for 3–5 min before infusion of fixative. The perivascular space was thereby rendered completely free of precipitate and the diffuse precipitate over neurosecretory elements was also removed. However, precipitate remained localized within the microvesicles, whether they were dispersed (Fig. 1*c*) or in clusters (Fig. 1*d*) and in the vacuoles. Smooth endoplasmic reticulum elements also often contained the stain, and were occasionally seen in intimate association with the microvesicles (Fig. 1*d*). The mitochondria of both neurones and pituicytes (Fig. 1*c*, *d*) retained their precipitates, but the cytoplasmic precipitates in the pituicytes were removed and the precipitate in their nuclei considerably reduced in extent (Fig. 1*d*). Washing with buffer–dextran for 1–2 min produced an intermediate appearance, in which the perivascular space and pituicytes contained a precipitate which was less dense than when fixative was introduced immediately.

Various control experiments suggest that the precipitate visualized was due to calcium in the tissue. Inclusion of 5 mM EGTA in the oxalate wash before osmium/antimonate fixation resulted in the complete absence of deposits when the tissue was subsequently examined, and also demonstrated that they were not an artefact of the fixative procedure itself. Precipitate could also be removed from ultra-thin sections on grids by incubation in 5 mM EGTA at 60 °C for 1 h. This indicates that the deposits do not contain significant amounts of sodium or magnesium (which antimonate will precipitate at higher concentrations[10]).

The diffuse cytoplasmic precipitates seen in tissue exposed to glutaraldehyde/oxalate directly could conceivably be due to *in vivo* ambient levels of free calcium, though it would be difficult to explain their presence in greater amounts in the pituicytes. It seems more likely that they result from the influx of calcium ions from the extracellular space as the tissue dies[11]. However, glial cells can apparently store calcium[12], and pituicytes are capable of taking up radioactive calcium when stimulated with potassium[13]. The presence of gap junctions between pituicytes has led to the suggestion that they might modulate neurosecretory

0028–0836/80/360056—03$01.00

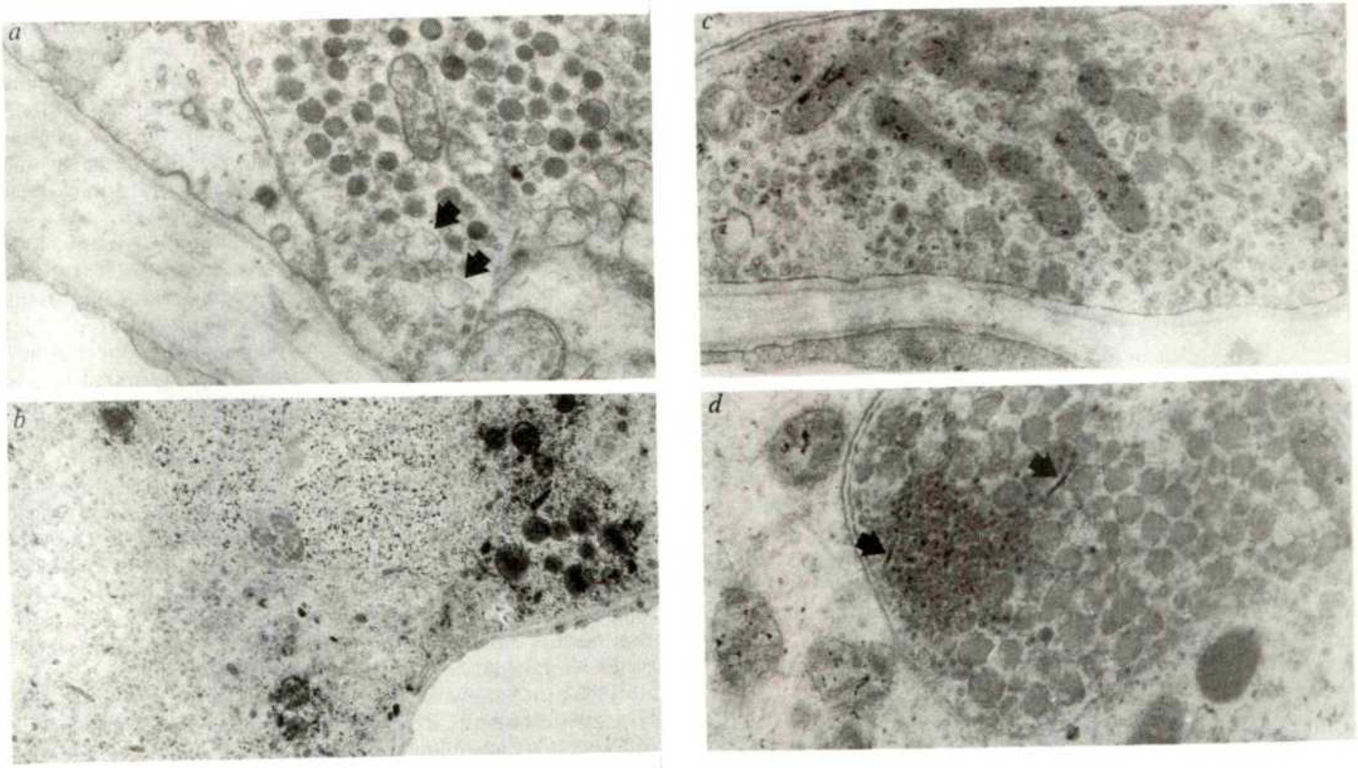

Fig. 1 Electron micrographs of control (*a*) and oxalate/antimonate treated (*b–d*) neurohypophyses. Animals were perfused through an aortic cannula for 10 min with 2.5% glutaraldehyde, 90 mM potassium oxalate, *p*H 7.2. In some cases, this was preceded by 150 mM potassium phosphate buffer and 3.4% dextran (molecular weight 40,000), *p*H 7.2, for 1–5 min. The neurohypophyses were dissected out after 16 h and washed for 30 min in 90 mM potassium oxalate, 7.5% sucrose, *p*H 7.5. The tissue was postfixed for 2 h in 1% osmium tetroxide, 2% potassium antimonate, washed in dilute potassium hydroxide, *p*H 10, for 15 min, dehydrated rapidly in a graded series of alcohol, and embedded in Spurr resin using propylene oxide. Control tissue was fixed in an identical fashion except that potassium chloride replaced oxalate in the prefix and wash, and 100 mM sodium cacodylate replaced antimonate in the postfix. *a*, Neurosecretory terminal, control method. The terminal lies in contact with a basement membrane, separated from a fenestrated capillary endothelium by a wide perivascular space. It contains neurosecretory granules, mitochondria, and microvesicles, some of which are clustered near the basement membrane contact zone; two vacuoles are also present (arrows; ×18,000). *b*, Low power view of tissue fixed directly with glutaraldehyde/oxalate. The nucleus and cytoplasm of a pituicyte (upper region of picture) contain much more precipitate than the surrounding neurosecretory elements; the pituicyte cytoplasm also contains characteristic lipid droplets (×2,700). *c*, Neurosecretory terminal in tissue washed before glutaraldehyde/oxalate fixation. Precipitate is highly localized to mitochondria, microvesicles (in a dispersed configuration here) and a vacuole; it is absent from the perivascular space (×25,000). *d*, Microvesicles in a clustered formation adjacent to a pituicyte in washed tissue. Precipitate is again localized to microvesicles and mitochondria, and also in smooth endoplasmic reticulum associated with the microvesicles (arrows). The pituicyte cytoplasm is almost completely free of precipitate (×25,000).

activity by ionic movements into and through their cytoplasm[14]. The observation of calcium precipitates above background level in the pituicyte cytoplasm could reflect such a function.

The diffuse cytoplasmic precipitate was rapidly washed out of the neural elements but the mitochondria, vacuoles, smooth endoplasmic reticulum and microvesicles appear to be sites of tightly bound calcium. Intracellular binding sites have been proposed to account for the return of the intracellular ionized calcium level to the very low resting value once stimulation has ceased[15]. Localization of calcium in mitochondria was entirely expected in view of their proven calcium-accumulating properties[16], but the available data suggest that the kinetics of brain mitochondrial calcium uptake are not appropriate for dealing with stimulus-induced increases in the level of ionized calcium in nerve terminals[17], when the concentration probably rises from about 10^{-7} to 10^{-5} M at most[18]. Mitochondria may well serve as long-term buffers of neuronal intracellular calcium, however[15]. Deposits in the vacuoles, which are thought to represent membrane endocytosed after hormone release[19], were also to be expected since they would thereby contain extracellular fluid with a calcium content of about 10^{-3} M.

The precipitates observed in smooth endoplasmic reticulum and microvesicles indicate that these organelles may be sites of calcium accumulation. A non-mitochondrial, ATP-dependent calcium accumulation system has been described in brain synaptosomes[17], and coated vesicles isolated from cerebral cortex are capable of calcium uptake[3]. The accompanying letter by Nordmann and Chevallier[20] demonstrates that the subcellular fractions containing predominantly microvesicles isolated from bovine neurohypophyses can accumulate calcium at concentrations appropriate for the post-stimulus recovery phase. The precipitation pattern described here therefore appears to constitute a morphological correlate of the calcium-accumulating function of microvesicles, which are not associated with any known transmitter. This agrees with evidence that the microvesicles do not alter in number with either acute[19,21], or chronic[22] stimulation of hormone release and that membrane is retrieved by vacuoles[19,21] (Fig. 1*a*), rather than by microvesicles as previously suggested[23]. The smooth endoplasmic reticulum appears to share this calcium-sequestering property and has been shown to accumulate calcium in synaptosomes[24].

The increase in microvesicles labelled with horseradish peroxidase after stimulation[25] and the presence of coated microvesicles[23] suggest that these organelles are capable of exocytosis and, indeed, clusters of microvesicles are often seen in 'synaptoid' configurations near the plasmalemma opposite pituicytes or the basement membrane (Fig. 1*a*, *c*). Calcium accumulated by microvesicles might therefore be removed from the nerve ending by exocytosis, the dispersed microvesicles near the membrane being active in this process and the clustered forms (Fig. 1*d*) representing a less active state. During stimulation, the microvesicles appear to move closer to the contact zone of the ending with the basement membrane[19] and thus their exocytosis might be activated when the gland is stimulated.

F. D. Shaw is an MRC Scholar. We thank Drs R. E. J. Dyball and J. J. Nordmann for helpful discussions and also Dr J. J. Nordmann for allowing us to see the accompanying manuscript before submission.

Received 10 June; accepted 7 July 1980.

1. Nordmann, J. J., Dreifuss, J. J. & Legros, J. J. *Experientia* **27,** 1344–1345 (1971).
2. Douglas, W. W. & Poisner, A. *J. Physiol., Lond.* **172,** 19–30 (1964).
3. Blitz, A. L., Fine, R. E. & Toselli, P. A. *J. Cell Biol.* **75,** 135–147 (1977).
4. Borgers, M., de Brabander, M., Van Reempts, J., Anouters, F. & Jacob, W. A. *Lab. Invst.* **37,** 1–8 (1977).
5. Duce, I. R. & Keen, P. *Neuroscience* **3,** 837–868 (1978).
6. Herman, L., Sato, T. & Hales, C. N. *J. ultrastruct. Res.* **42,** 298–311 (1973).
7. Stoekel, M. E., Hindelang-Gertner, C., Dellman, H. D., Porte, A. & Stutinsky, F. *Cell Tissue Res.* **157,** 307–322 (1975).
8. Morris, J. F. *J. Endocr.* **68,** 225–234 (1976).
9. Streit, P. & Reubi, S. C. *Brain Res.* **126,** 530–537 (1977).
10. Klein, R. L., Yen, S-S. & Thureson-Klein, A. *J. Histochem. Cytochem.* **20,** 65–78 (1972).
11. Birks, R. I. *J. Neurocytol.* **3,** 133–160 (1974).
12. Koch, A., Banck, B. & Neuman, B. L. *Expl Neurol.* **6,** 186–200 (1962).
13. Dyball, R. E. J. & Shaw, F. D. *J. Physiol., Lond.* **303,** 60–61P (1980).
14. Dellman, H. D., Stoekel, M. E., Porte, A. & Stutinsky, F. *Experientia* **30,** 1220–1221 (1974).
15. Baker, P. F. *Soc. exp. Biol. Symp.* **30,** 67–88 (1976).
16. Lehninger, A. L., Carafoli, E. & Rossi, C. S. *Adv. Enzym.* **29,** 259–320 (1967).
17. Blaustein, M. P., Ratzlaff, R. W., Kendrik, N. C. & Schwertzer, E. S. *J. gen. Physiol.* **72,** 14–41 (1978).
18. Baker, P. F. *Sci. Prog. Oxf.* **64,** 95–115 (1977).
19. Morris, J. F. & Nordmann, J. J. *Neuroscience* **5,** 639–649 (1980).
20. Nordmann, J. J. & Chevallier, J. *Nature* **287,** 54–56 (1980).
21. Lescure, H. & Nordmann, J. J. *Neuroscience* **5,** 649–659 (1980).
22. Reinhardt, H. F., Henning, L. C. H. & Rahr, H. P. *Z. Zellforsch. Mikrosk. Anat.* **102,** 182–192 (1969).
23. Nagasawa, J., Douglas, W. W. & Schultz, P. A. *Nature* **332,** 241–342 (1971).
24. McGraw, C. F., Somylo, A. V. & Blaustein, M. P. *J. Cell Biol.* **85,** 228–241 (1980).
25. Theodosis, D. T., Dreifuss, J. J., Harris, M. C. & Orci, L. *J. Cell Biol.* **70,** 294–303 (1976).

Role of corticosteroid-binding globulin in interaction of corticosterone with uterine and brain progesterone receptors

H. Al-Khouri & B. D. Greenstein

Department of Pharmacology, St Thomas's Hospital Medical School, London SE1 7EH, UK

The central actions of the steroid hormone progesterone remain an enigma. However, there is no doubt that this hormone has a vital role in the control of sexual function and behaviour in many species, including man. Furthermore, progesterone may be involved in the premenstrual and postpartum syndromes[1]. It would therefore be very useful to know the role and mechanism of action of progesterone in the brain. We now show that there are differences between progesterone receptors in brain and uterus, and possibly in the distribution of the serum progesterone-binding protein, corticosteroid-binding globulin (CBG), which may enter uterine but not brain cells.

Our understanding of the mode of action of steroid hormones was advanced greatly by the discovery of cytosolic receptor proteins which bind the steroid and migrate to the cell nucleus to modify gene expression[2]. Autoradiographic and *in vitro* binding studies have revealed that there are receptors for most classes of steroid hormone in the brain[3–8]. In this respect, progesterone continues to baffle the investigator and studies of progesterone uptake by the brain remain equivocal[6,9–12]. The problem is complicated by the extensive metabolism of progesterone in neural tissues[12] and by the presence in rat serum of CBG, which binds both corticosterone and progesterone avidly[13]. A partial solution to the problem was offered by the discovery of large amounts of highly unstable progesterone-binding components in cytosols from the rat brain, pituitary and uterus[14,15]. The complex dissociated rapidly *in vitro* even at 0 °C, and it was suggested[14] that the rapid dissociation of the complex might account for the failure of previous studies. Recently, a synthetic progestagen, promegestone (R5020, Roussel Uclaf) was introduced; this binds with high affinity to cytosolic proteins in the rat brain, pituitary and uterus[16–18]. The progestagen receptor seems to meet the requirements for a neural progesterone receptor, as it is increased after oestrogen administration in tissues rich in oestrogen receptors[17–19]. The progestagen receptor also seems to occur in the cell nucleus[20,21]. However, several important questions concerning progesterone remain unanswered. Why was the R5020 receptor not discovered using ^{3}H-progesterone? Does R5020 bind to all the progesterone receptors? There is evidence that more than one species of progesterone receptor exists[14]. Perhaps most importantly, does progesterone exert its effect in uterus and brain through the same mechanism?

In an attempt to answer some of these questions, cytosols were first prepared from the hypothalamus, midbrain and uterus of adult intact female rats as described previously[14]. The rats were perfused with 1 l of chilled normal saline before preparation, after which CBG cannot be detected in brain cytosols using sensitive binding studies[14]. After perfusion, the tissues seem normal under light microscopy and the nuclei from these tissues were capable of incorporating ^{3}H-labelled nucleotides into RNA (not shown). The cytosols were then incubated with ^{3}H-progesterone (81 Ci mmol^{-1}, Amersham; 3×10^{-8} mol l^{-1}) for 2 h at 0 °C, when apparent equilibrium between bound and free hormone is attained[14]. The ability of a variety of unlabelled steroids (progesterone, corticosterone, R5020, oestradiol-17β and 5-α-dihydrotestosterone (DHT)) to displace specifically bound ^{3}H-progesterone was tested. The experimental procedures are described fully in the legend to Fig. 1, which shows a typical result, and the results of the series of experiments are given in Fig. 2. The results are summarized as follows: (1) in the hypothalamus and midbrain cytosols, progesterone displaced ^{3}H-progesterone far more rapidly and completely than did any of the other steroids tested, including R5020. The nature of the bound radioactive progesterone remaining in midbrain cytosol after displacement with the unlabelled hormone is unclear but may reflect a very slowly dissociating binding component. (2) In the uterus, progesterone and corticosterone were equipotent in displacing rapidly and virtually completely the specifically bound ^{3}H-progesterone. Corticosterone was very much more potent in this respect in the uterus than in the brain tissues. This pattern of displacement of radioactive progesterone from uterine binding sites was also observed if binding isotherms were prepared (Fig. 1 inset). It has been shown elsewhere[14], using binding isotherms, that in brain cytosols corticosterone is a weak inhibitor of ^{3}H-progesterone binding. (3) Oestradiol-17β and DHT were significantly less potent than progesterone in displacing ^{3}H-progesterone from central and peripheral tissues ($P<0.001$; Student's *t*-test).

The possibility that unlabelled progesterone and corticosterone were displacing ^{3}H-progesterone from plasma CBG, which was not completely flushed from the tissues, was examined by carrying out immunodiffusion studies of cytosols from the rat brain areas, the anterior pituitary and the uterus, using an antibody raised to rat serum. The tissue : buffer ratios and cytosol protein concentrations for the brain areas and uterus were kept as close to each other as possible. Of the tissues tested, only uterine cytosol seemed to react with the antiserum to produce a precipitin line (Fig. 3). Whether the precipitin line shown in Fig. 3 is in fact CBG can only be clarified using the purified protein. The absence of a precipitin line does not mean that no reaction took place using cytosols from the brain, but in view of the equivalence in protein concentrations, this possibility is remote. It is more likely that CBG entered the extravascular compartment in the uterus but not the brain.

Corticosterone caused a total displacement of ^{3}H-progesterone from uterine cytosols. The displacement of ^{3}H-progesterone from uterine cytosols by R5020 must have occurred

0028-0836/80/360058—03$01.00

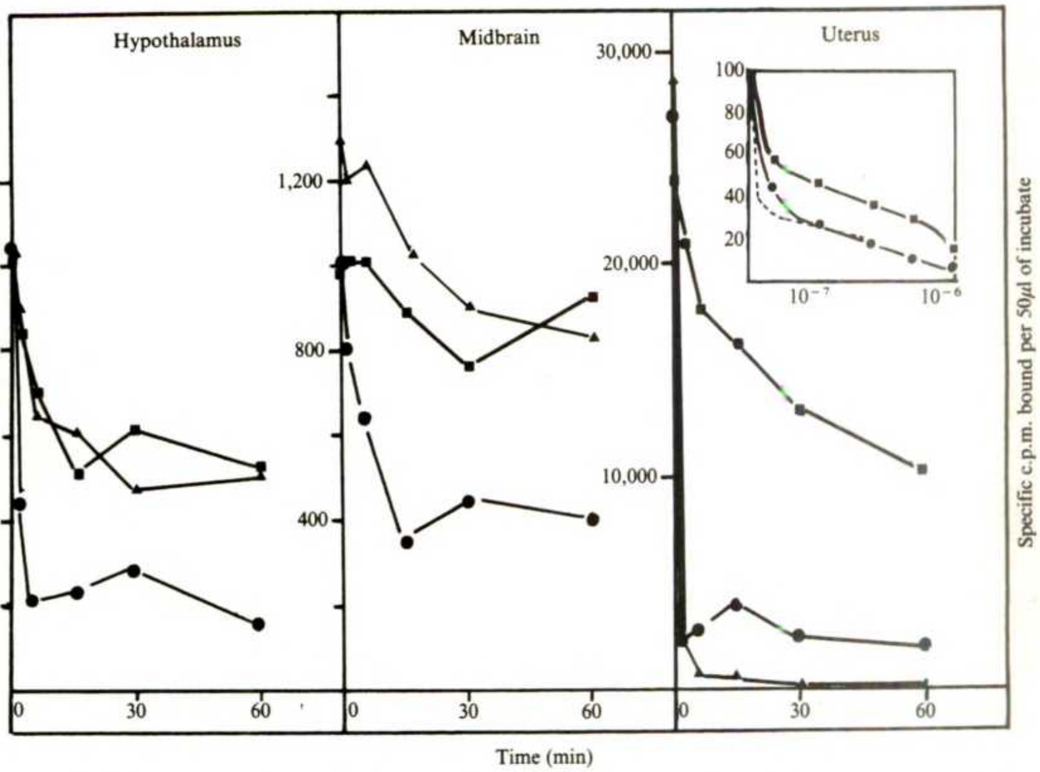

Fig. 1 Exchange of ^{3}H-progesterone and unlabelled progesterone (●), corticosterone (▲) or R5020 (■) in cytosols from the rat brain and uterus. Cytosols were incubated at 0 °C with ^{3}H-progesterone (3×10^{-8} mol l^{-1}) for 2 h, and the bound radioactivity was assessed by rapid gel filtration of 50 μl of the incubate using small columns (10×0.5 cm) of Sephadex LH20 at 1 °C (ref. 14). At time 0 (that is, after 2 h), the unlabelled hormone was added to aliquots of cytosol to give a final concentration of the competitor of 10^{-6} mol l^{-1} and the bound radioactivity was assessed various times later. Results are shown after correction for nonspecific binding of ^{3}H-progesterone. For clarity, results using progesterone, corticosterone and R5020 alone are shown (compare with Fig. 2). Abscissa, time after adding unlabelled steroid; ordinate, specific c.p.m. bound per 50 μl of incubate. Details of the scintillation spectrometry are given elsewhere[14]. Inset: binding isotherms of ^{3}H-progesterone binding in uterine cytosol in the presence of unlabelled progesterone, R5020 or corticosterone (– – – –). Cytosol was incubated with ^{3}H-progesterone (10^{-8} mol l^{-1}) alone or in the presence of varying concentrations of the unlabelled steroid for 2 h at 0 °C. Bound radioactivity was assessed as described above. Abscissa, concentration of unlabelled steroid (mol l^{-1}); ordinate, binding of ^{3}H-progesterone as a percentage of binding in the absence of unlabelled steroid.

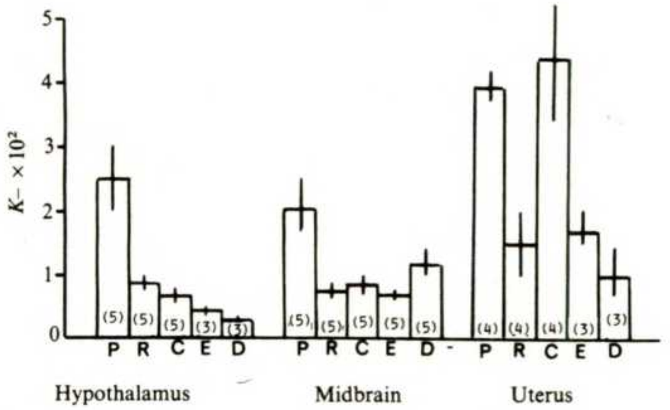

Fig. 2 Displacement of ^{3}H-progesterone from specific binding sites by unlabelled steroids in hypothalamic, midbrain or uterine cytosols. Results are expressed as the dissociation rate constant ($K-$) calculated for each steroid and tissue using the method described in Fig. 1 legend. Results are the mean ± s.e.m. and the numbers of observations are given in parentheses. $K-$ was calculated from the formula: $K- = \ln[(A^0/A)(1/t)]$, where A^0 and A are the specific binding of ^{3}H-progesterone at times = 0 and 60 min, respectively. P, Progesterone; R, R5020; C, corticosterone; E, oestradiol-17β; D, DHT.

exclusively from specific progesterone receptors in the uterus, because this steroid does not bind to CBG[16]. If corticosterone had displaced ^{3}H-progesterone from CBG only, the displacement would have been incomplete. It must be presumed, therefore, that corticosterone does displace ^{3}H-progesterone from specific progesterone receptors in the uterus, to which it apparently binds much more strongly than in the brain. The functional significance of this is unclear, but there is evidence that another glucocorticoid, triamcinolone, binds to progestagen receptors in the human prostate[22].

The importance of these results lies in the clear demonstration that progesterone, the natural hormone, displaces the tritiated steroid from the receptor in brain and uterine cytosols more potently than does R5020. Furthermore, there may be a

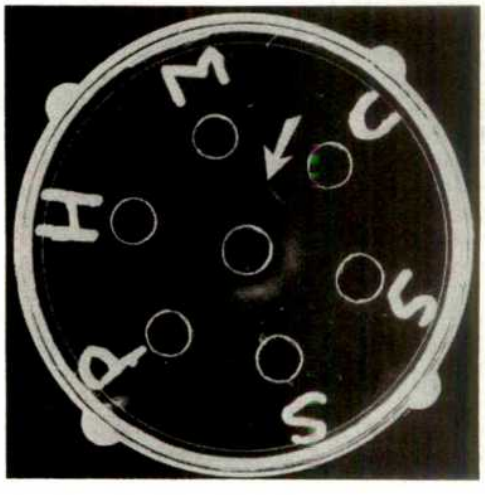

Fig. 3 Immunodiffusion of cytosols from hypothalamus (H), midbrain (M), anterior pituitary (P) and uterine (U) cytosols or rat serum (S) using antiserum raised in a rabbit to whole rat serum (Miles Yeda codes 65-038; lot R134N). To each well 3 μl of protein solution was added and this was allowed to diffuse overnight at 20 °C. The centre well contained the antiserum. The arrow indicates the precipitin line caused by the reaction between antiserum and uterine cytosol. 6.1 μg of midbrain cytosol were applied, 4.5 μg of hypothalamic and 5.0 μg of uterine cytosol.

selective movement of corticosterone carried by CBG to the extravascular and possibly intracellular compartment in the uterus but not the brain. Thus, CBG could act as a carrier receptor for corticosterone into the uterine cell, where corticosterone displaces progesterone from its receptor site. This action would have important implications in, for example, the onset of parturition. Cortisol is known to initiate parturition in the rabbit and this effect is blocked by the administration of progesterone[23]. There are thus grounds for investigating further the interactions between progesterone, corticosterone and their binding proteins in the blood and uterus with respect to the function of this tissue in reproduction.

This work was funded by an MRC project grant to B.D.G. We thank the Special Trustees of St Thomas's Hospital for assistance, Professor G. W. Bisset for reading and commenting on the manuscript, and Mrs Janice Andrews for typing the manuscript. The Ouchterlony plates used were supplied by Miles Laboratories.

Received 4 March; accepted 18 June 1980.

1. Dalton, K. *The Premenstrual Syndrome* (Heinemann, London, 1974).
2. King, R. J. B. & Mainwaring, W. I. P. *Steroid-Cell Interactions* (Butterworths, London, 1974).
3. Stumpf, W. E. *Science* **162,** 1001–1003, (1968).
4. Pfaff, D. W. *Science* **161,** 1355–1356 (1968).
5. Kato, J. & Onouchi, T. *Endocr. jap.* **20,** 429–432 (1973).
6. McEwen, B. S., de Kloet, R. & Wallach, G. *Brain Res.* **105,** 129–136 (1976).
7. Ginsburg, M., Greenstein, B. D., MacLusky, N. J., Morris, I. D. & Thomas. P. J. *Steroids* **23,** 773–792 (1974).
8. Barley, J., Ginsburg, M., Greenstein, B. D., MacLusky, N. J. & Thomas. P. J. *Brain Res.* **100,** 383–393 (1975).
9. Wade, G. N. & Feder, H. H. *Brain Res.* **45,** 525–543 (1972).
10. Luttge, W. C., Wallis, C. J. & Hall, N. R. *Brain Res.* **71,** 105–115 (1974).
11. Sar, M. & Stumpf, W. E. *Science* **182,** 1266–1268 (1973).
12. Karavolas, H. J., Hodges, D. R., O'Brien, D. J. & McKenzie, K. M. *Endocrinology* **104,** 1418–1425 (1979).
13. Westphal, U. in *Biochemical Actions of Hormones* Vol. 1 (ed. Litwack, G.) 209–265 (Academic, New York, 1972).
14. Greenstein, B. D. *J. Endocr.* **79,** 327–338 (1978).
15. Lee, H., Davies, I. J. & Ryan, K. J. *Endocrinology* **104,** 791–800 (1979).
16. Moguilewsky, M. & Raynaud, J.-P. *Steroids* **30,** 99–109, (1977).
17. Kato, J. & Onouchi, T. *Endocrinology* **101,** 920–928 (197).
18. MacLusky, N. J. & McEwen, B. S. *Nature* **274,** 276–278 (1978).
19. Moguilewsky, M. & Raynaud, J.-P. *Endocrinology* **105,** 516–522, (1979).
20. Blaustein, J. D. & Wade, G. N. *Brain Res.* **140,** 360-367 (1978).
21. Seiki, K., Haurki, Y., Imanishi, Y. & Enomoto, T. *J. Endocr.* **82,** 347–360 (1979).
22. Zava, D. T., Landrum, B., Horwitz, K. B. & McGuire, W. L. *Endocrinology* **104,** 1007–1012 (1979).
23. Nathanielz, P. W. & Abel, M. *J. Endocr.* **57,** 47–54 (1973).

Action of formamidine pesticides on octopamine receptors

Peter D. Evans

ARC Unit of Invertebrate Chemistry and Physiology, Department of Zoology, University of Cambridge, Downing Street,
Cambridge, CB2 3EJ, UK

Julian D. Gee

Pfizer Central Research, Pfizer Limited, Sandwich, Kent CT13 9NJ, UK

The formamidines are a structurally novel group of pesticides of growing importance in the control of mites, cattle ticks and certain orders of insects which have become resistant to conventional acaricides and insecticides. Their mode of action is complex with dose-dependent lethal and sublethal effects[1-3]. At sublethal levels they cause behavioural changes in the target pest species (for example in feeding and in mating behaviours), changes which are responsible for the protective effects on crops and livestock. Although many suggestions have been made for the underlying biochemical mechanism, including inhibition of monoamine oxidase activity, uncoupling of respiration and blockade of neuromuscular transmission[1], no direct evidence has been presented. Another possibility is interaction with octopamine receptors in the central nervous system[2,4,5]. We report here that the formamidine acaricide/insecticide, chlordimeform (CDM), and its demethylated derivative can mimic the actions of octopamine at the locust neuromuscular junction. This gives the clearest evidence to date of the site of action of the formamidines and indicates a novel mode of action for these pesticides.

Octopamine is one of several compounds that mimic the action of CDM in exciting certain unidentified neurones in the abdominal ganglia of the larvae of the tobacco hornworm, *Manduca sexta.* The activation of these neurones may be correlated with the increased locomotor activity and uncoordination produced in these animals by sublethal doses of CDM[2]. Octopamine, as well as CDM and some of its derivatives elicit glowing[6], and increase adenylate cyclase activity[7] in the firefly light organ[2,4,5]. Octopamine may be a neurotransmitter in the firefly light organ but in both cases definitive proof for octopaminergic neurones is lacking. However, an identified octopaminergic neurone has been shown to act at the neuromuscular junction of the locust, *Schistocerca americana gregaria*[8,9,10] and the pharmacology of the octopamine receptors has been investigated[11]. This preparation can thus provide a model system in which to study the interaction of the formamidines with identified octopamine receptors.

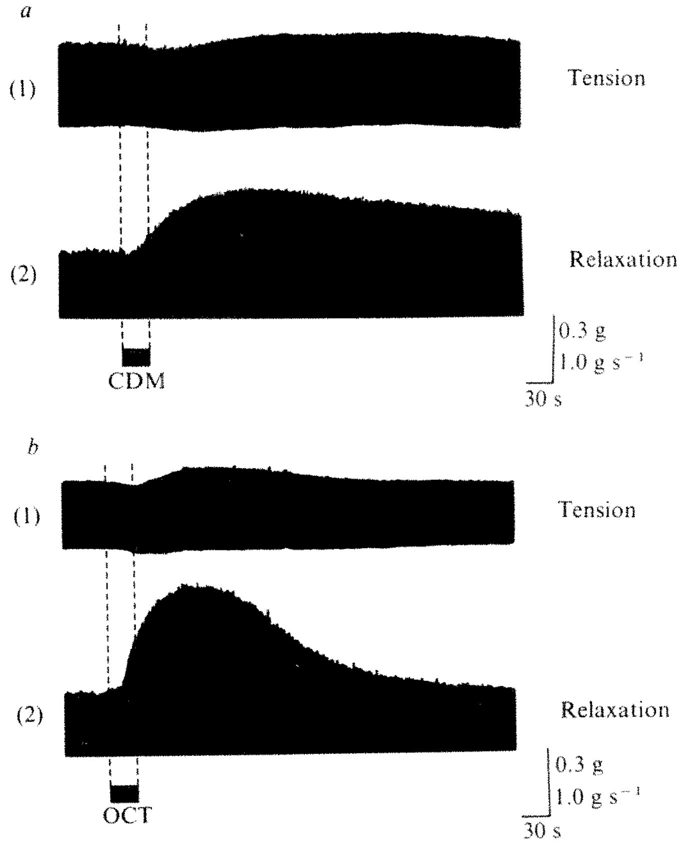

Fig. 1 Comparison of the effects of chlordimeform (CDM) (*a*) and (±)octopamine (OCT) (*b*) on the amplitude of twitch tension and rate of relaxation of twitch tension induced in the extensor tibiae muscle of the hindleg of the locust by stimulation of the slow motoneurone at 1 Hz. Traces *a*1 and *b*1 show the tension responses elicited by application of a 30 s pulse of 10 μM chlordimeform and (±)octopamine respectively. Traces *a*2 and *b*2 show the effects of the respective pulses on the rate of relaxation of twitch tension, the height of each trace being directly proportional to the rate of relaxation. Note the difference in potency and time course of the effects produced by chlordimeform and octopamine.

0028-0836/80/360060—03$01.00

Fig. 2 Dose–response curves for the potentiation of twitch amplitude (*a*) and relaxation rate (*b*) by octopamine (OCT), chlordime- for (CDM) and demethylchlordimeform (DCDM). The results represent the maximum percentage increases obtained at each concentration by application of a 30 s pulse of drug solution to an extensor-tibiae muscle preparation being stimulated at 1 Hz. Each point represents the mean of at least four determinations and the bars represent the s.e.m.

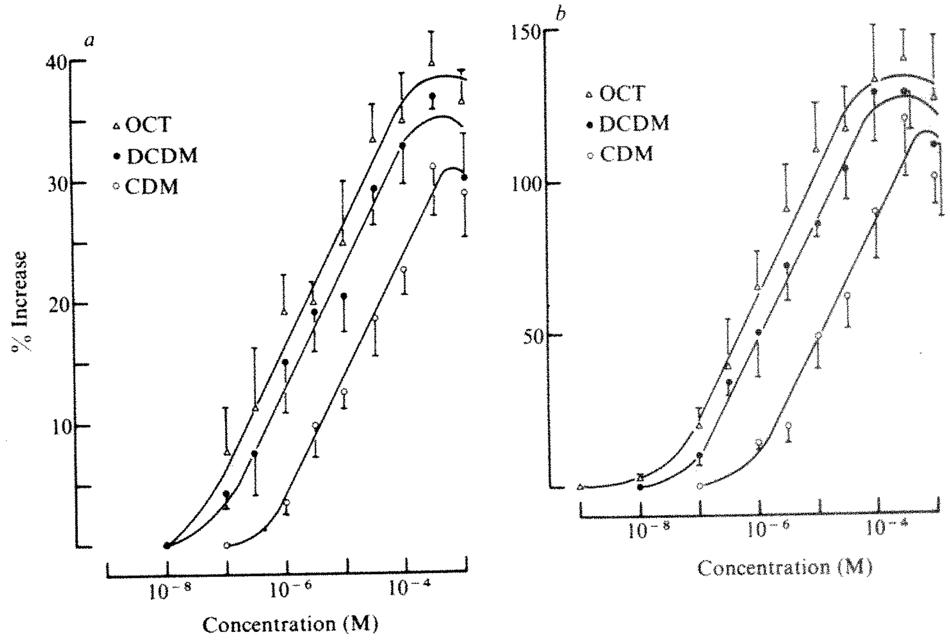

We stimulated repetitively the slow motoneurone (SETi) to the extensor tibiae muscle of the hindleg of *S. americana gregaria* to elicit individual muscle twitches. Using methods described previously, we continuously monitored the amplitude of muscle twitches[8,10] and their rates of contraction and relaxation[12]. Short pulses of known concentrations of the formamidines were introduced into the superfusion fluid bathing the muscle preparation and their effects compared to those produced by comparable pulses of (±)octopamine.

Figure 1 compares the effects produced by a 30 s pulse of 10 μM CDM (Fig. 1*a*) with those produced by a similar pulse of (±)octopamine (Fig. 1*b*). CDM potentiates the size of neurally evoked contractions by 10% and increases the rate of relaxation by 91%. The equivalent pulse of octopamine is more potent and increases the two parameters by 23% and 166% respectively. The time course of the effects of the two compounds differs, the effect of CDM on the relaxation rate, for example, having a half time of decay of 6.7 min whilst that for octopamine is 1.8 min in the particular examples illustrated.

A comparison of the dose–response curves for octopamine, CDM and demethylchlordimeform (DCDM) (Fig. 2*a*, *b*) reveals that the curves are parallel with peak values at 10^{-4} to 10^{-3} M for both the potentiation of twitch amplitude and the increase in relaxation rates. There is no significant difference between the curves for octopamine and DCDM and, the effects of these two compounds at saturating concentrations were not additive (data not shown). As octopamine is the only naturally occurring compound known to be capable of producing these modulatory effects at the locust neuromuscular junction[10] it is likely that CDM and octopamine are acting at the same receptor. Comparing CDM with DCDM (to which CDM is thought to be metabolized to give the lethal toxicant in CDM-poisoned cattle tick larvae[13]) half maximal percentage increases of both twitch amplitude and relaxation rate are obtained at 5×10^{-6} M for DCDM and 5×10^{-5} M for CDM. Thus DCDM is an order of magnitude more effective than CDM. This is in agreement with the rank order of potency of the phenolamines on this preparation where synephrine (the *N*-methylated analogue of octopamine) is more potent than *N*, *N*-dimethyloctopamine[10]. The structural similarities between the formamidines and the phenolamines have been pointed out and the close resemblance between DCDM and synephrine emphasized[4].

Octopamine receptors in insects are selectively blocked by α-adrenergic antagonists, such as phentolamine, in preference to β-adrenergic antagonists such as propranolol[7,9,10,11]. Phentolamine also selectively antagonises the action of CDM at the locust neuromuscular junction. Figure 3 shows an experiment where the effects of 10 μM (±)propranolol and 10 μM phentolamine are compared after an initial potentiation of twitch tension and relaxation rates by exposure of the extensor muscle to a 30 s pulse of 10 μM CDM. Propranolol has no effect, whereas phentolamine brings about a rapid reduction in both responses. Other experiments (not shown) demonstrate that phentolamine, but not propranolol, blocks the effects of CDM applied simultaneously to the extensor muscle.

We have demonstrated that both CDM and DCDM can mimic the actions of octopamine in potentiating twitch tension and increasing the rate of relaxation of tension induced in the extensor tibiae muscle. In both cases the effects are brought about by an interaction with pharmacologically characterized octopamine receptors[11]. In addition to its effects on neurally evoked tension, octopamine inhibits a myogenic rhythm of contraction and relaxation found in a bundle of specialized muscle fibres in the extensor tibiae muscle of the locust hindleg[9,14]. This effect is also mimicked by CDM and DCDM (not shown). The frequency of the myogenic contractions is reduced by 50% by exposure to 10^{-6} M CDM for 10 min.

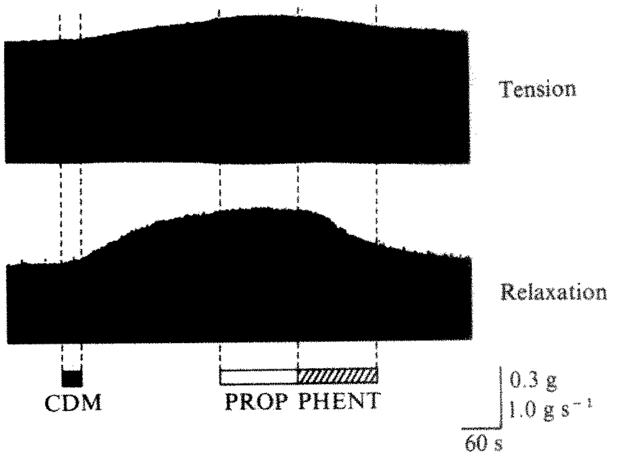

Fig. 3 The effect of blocking agents on the responses of the extensor tibiae muscle to a 30 s pulse of 10 μM chlordimeform (CDM). The top trace indicates the tension responses recorded from the muscle by stimulating the slow motoneurone at 1 Hz and the bottom trace shows the corresponding changes in relaxation rates. (±)propranolol (PROP) 10 μM was applied for a 2-min period indicated by the open bar and 10 μM phentolamine (PHENT) for a 2-min period indicated by the hatched bar.

The effects of the formamidines on neuromuscular transmission in the locust parallel those on the firefly light organ in several respects. In both cases DCDM is more effective than CDM, and their actions are blocked by phentolamine[4]. In the studies on the firefly light organ, however, the exact concentration of the formamidines superfused over the preparation was not reported and the effects of α- and β-adrenergic blocking agents were not compared. The effects of the formamidines are also much longer lasting than those of octopamine in both the firefly and locust preparations. It has been hypothesized that this might be due to a greater tissue solubility of the formamidines which would slow down their penetration to the receptors and maintain an excitatory concentration of the compounds close to the receptors for a longer time than an equivalent dose of octopamine[4]. The longer half-time of decay of the effects of CDM, however, suggests that the formamidines have a longer half-time of receptor occupancy than octopamine.

We thank Dr M. V. S. Siegler for critically reading the manuscript and Drs L. L. Murdock and R. M. Hollingworth for providing a sample of DCDM.

Received 29 January; accepted 20 June 1980.

1. Beeman, R. W. & Matsumura, F. in *Pesticide and Venom Neurotoxicity* (eds Shankland, D. L., Hollingworth, R. M. & Smyth, T. Jr) 179–188 (Plenum, New York, 1978).
2. Lund, A. E., Hollingworth, R. M. & Murdock, L. L. in *Advances in Pesticide Science*, Part 3 (ed. Geissbuehler, H.). 465–469 (Pergamon, Oxford, 1979).
3. Lund, A. E., Hollingworth, R. M. & Shankland, D. L. *Pest. Biochem. Physiol.* **11**, 117–128, (1979).
4. Murdock, L. L. & Hollingworth, R. M. in *Insect Neurobiology and Pesticide Action*, 415–422 (Soc. Chem. Ind., London, 1980).
5. Hollingworth, R. M. & Murdock, L. L. *Science* **208**, 74–76 (1980).
6. Carlson, A. D. *J. exp. Biol.* **49**, 195–199 (1968).
7. Nathanson, J. A. *Science* **203**, 65–68 (1979).
8. Evans, P. D. & O'Shea, M. *Nature* **270**, 275–279 (1977).
9. Evans, P. D. & O'Shea, M. *J. exp. Biol.* **73**, 235–260 (1978).
10. O'Shea, M. & Evans, P. D. *J. exp. Biol.* **79**, 169–190 (1979).
11. Evans, P. D. in *Receptors for Neurotransmitters, Hormones and Pheromones in Insects* (eds Sattelle, D. B., Hall, L. M. & Hildebrand, J. G.) 147–158 (Elsevier, Amsterdam, 1980).
12. Buchan, P. B. & Evans, P. D. *J. exp. Biol.* **85**, 349–352 (1980).
13. Knowles, C. O. & Schuntner, C. A. *J. Aust. ent. Soc.* **13**, 11–16 (1974).
14. Hoyle, G. *J. exp. Zool.* **193**, 425–431 (1975).

The sodium channel and intracellular H^+ blockage in squid axons

Enzo Wanke, Emilio Carbone & Pier Luigi Testa

Laboratorio di Cibernetica e Biofisica del CNR,
16032-Camogli (GE), Italy

Sodium channels in plasma membranes can be blocked by a large variety of toxins[1] and local anaesthetics[2]. This property, however, is not confined to relatively large molecules. For instance, extracellularly applied small ions like hydrogen may also prevent the passive transport of permeant cations across open Na^+ channels[3–6]. A typical feature of this phenomenon[3,5] is that the blocking action of hydrogen is gradually relieved by increasing the voltage applied across the membrane. Although in the frog skeletal muscle there is no clear evidence for a similar intracellular action[7], we report here for the squid giant axon remarkable effects on the ionic permeability of Na^+ channels when the internal perfusate contains an excess of protons. Analysing the action of low pH inside and outside the fibre in terms of a kinetic model[3], we could conclude that Na^+ channels in squid axons are controlled by two independent groups: one with an apparent pK_a of 4.6 and the other with pK_a 5.8, the former feeling one-fifth of the applied membrane potential, the latter three-quarters. As with pharmacological agents[8], we also show that the voltage-dependence of the H^+ blockage is not affected by the presence of the inactivation gate.

Figure 1 shows computer records of Na conductance at normal and low intracellular pH (pH_i) obtained from giant axons of the squid *Loligo vulgaris* perfused and voltage-clamped by the method of Wanke *et al.*[9]. The traces on the right were recorded after 90 s of internal perfusion at pH_i 5.3 and were found to reverse by returning to normal conditions (pH_i 7.2). Applications of low pH_i produce remarkable alterations to both the time course and voltage-dependence of the Na^+-channel conductance. The peak conductance, g^p_{Na}, is strongly depressed below 60 mV while at higher depolarizations the amount of depression is gradually reduced by raising the voltage (Fig. 2*a*). Significantly, at 220 mV the difference of g^p_{Na} at pH_i 7.2 and 5.3 is less than 20% of the control, with a tendency to diminish further at higher potentials. As shown in Fig. 2*a*, lower pH_i has even more marked effects on the shape of $g^p_{Na}(E)$, supporting the idea that the block of g_{Na} by hydrogen ions follows the titration property of an acidic sidegroup. Peak conductance relative to the control at $E = 100$ mV is plotted in Fig. 2*d*.

Figure 1 gives a clear indication that the voltage-dependence of the H^+ block is not related to the action that pH_i has on the gating of both the activation and inactivation processes[10]. This view is supported by the observation that at the end of the g_{Na} records ($t = 4$ ms), when fast Na^+ inactivation is almost complete, the change in g_{Na} with increasing voltage parallels that of g^p_{Na} in the range 140–220 mV. A direct confirmation came from a series of experiments in which the effects of low pH_i were tested in axons treated with the enzyme mixture Pronase[11], which removes selectively the fast inactivation gate of Na^+ channels. As expected, in four trials the effects were similar to those with intact axons (Fig. 2*b*). Several other controls were done to verify that the H^+ blockage was genuine. On a total of more than 30 axons, replacements of the internal ionic composition, type and amount of buffers yielded results analogous to those in Fig. 1.

Although a rigorous treatment of the present data would have required the use of a complete four-barrier model for the Na^+ channel[12], we found it more profitable in our preliminary studies to use the simpler two-barrier model proposed by Woodhull[3]. The model postulates the existence of a receptor site for H^+ ions located part of the way across the Na^+ channel, having the following properties: (1) the rates of hydrogen binding and unbinding are exponential functions of voltage as in Eyring rate theory; (2) an H^+ ion can reach the site from either side of the membrane according to the scheme

$$H_{out} \underset{b_{-1}}{\overset{[H_o]b_1}{\rightleftharpoons}} \text{H-site} \underset{[H_i]b_{-2}}{\overset{b_2}{\rightleftharpoons}} H_{in}$$

where b_i indicate the voltage-independent components of the

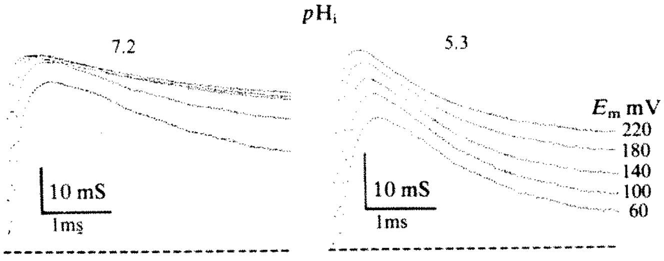

Fig. 1 Time course of Na conductance at neutral (left) and acid (right) pH_i. The membrane was hyperpolarized to −90 mV for 180 s to remove slow inactivation and then depolarized to the test potential indicated. Successive stimuli were separated by 1 s. Positive feedback was used. Data were obtained from current records corrected for TTX-insensitive currents after division by the driving force $E - E_{Na}$. E_{Na} was −26 mV. During stimulation, the periaxonal accumulation of Na^+ ions was controlled by brief hyperpolarizations[9]. In this way E_{Na} was found to increase by less than 3 mV. Internal solutions (mM): 200 Na^+, 117 F^- and $H_2PO_4^-$ (pH_i 7.2) or 200 Na^+, 80 F^- and 45 citric acid (pH_i 5.3). External bath (mM): 109 Na^+, 326 tetramethylamine, 10 K^+, 20 Tris, 10 Ca^{2+}, 40 Mg^{2+}, 555 Cl^- (pH_o 8). Temperature 2 °C.

0028–0836/80/360062—02$01.00

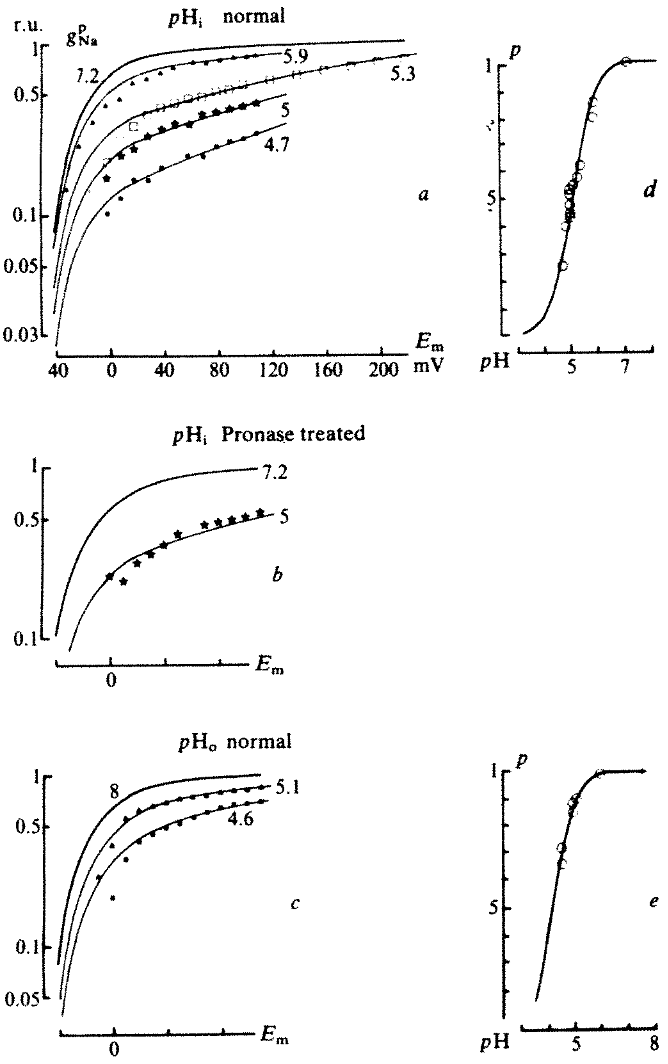

Fig. 2 Action of low pH$_i$ on peak sodium conductance, $g_{Na}^{P}(E)$. *a*, *b* and *c*, symbols indicate experimental data. Solid lines at control pH represent an average from seven axons at pH$_i$ 7.2 and pH$_o$ 8. Continuous lines at test pH are the product of the control curves and the fraction of unblocked channels, *p*, as derived by Woodhull[3]:

$$\left[1+\frac{[H_o]+[H_i]b_{-2}/b_1 \exp FE/2RT}{b_{-1}/b_1 \exp \delta FE/RT(1+b_{-2}/b_1 \exp -FE/2RT)}\right]^{-1} \quad (1)$$

where δ is the fraction of the potential drop crossed on approaching the site from the outside ; b_i are rate constants (see text) and *F*, *R*, *T* have their usual meaning. Solid lines in *c* at pH$_o$ 5.1 and 4.6 were obtained by setting in equation (1): $\delta=0.20$, $b_{-2}/b_1=0.01$ and $b_{-1}/b_1=2.4\times10^{-5}$. Corrected data and standard solutions at pH$_i$ 7.2 and pH$_o$ 8 are the same as those of Fig. 1. Internal solutions of low pH all contained 200 mM Na$^+$ and 45 mM of the following buffers: $H_2PO_4^-$ (pH$_i$ 5.9), citric (5.3, 5 and 4.7). External solutions of low pH had the same ionic content as in Fig. 1 except for the buffer which was 20 mM citric acid for pH$_o$ 5.1 and 4.6. The pronase-treated fibre was perfused for 100 s with a solution containing 2 mg ml^{-1} of enzyme at pH$_i$ 9.9. *d*, *e*, Internal and external pH dependence of the quantity *p* at $E_m=100$ mV. Each dot represents a different axon. Solid lines through data points are derived from equation (1) by setting $E_m=100$ mV.

rate constants and [H$_i$], [H$_o$] the concentrations of protons inside and outside the fibre.

As shown in Fig. 2, the model allows an evaluation of the fraction of unblocked channels, *p*, in terms of three independent parameters: δ, b_{-2}/b_1 and b_1/b_{-1} (see Fig. 2 legend). For the internal block, good fits of the g_{Na}^{P} curves at low pH$_i$ were obtained by setting: $\delta=0.75$, $b_{-2}/b_1=1$ and $b_1/b_{-1}=1.6\times10^{-6}$. Few points at low depolarizations are systematically lower than the theoretical predictions, suggesting the existence of a small unexpected shift of $g_{Na}^{P}(E)$ toward depolarizing voltages. Interestingly, with the same set of parameters we could also fit the pH dependence of the block shown in Fig. 2*d*.

With the view of testing further the validity of the Woodhull's model in squid axons, we reinvestigated the action of low extracellular pH (ref. 13), pH$_o$, on g_{Na}^{P}. As shown in Fig. 2*c*, *e*, low pH$_o$ is apparently less effective in blocking open Na$^+$ channels than a corresponding low pH$_i$ value, suggesting the existence of different titratable groups on each side of the channel: one external with an apparent pK$_a$ of 4.6 and one internal with pK$_a$ 5.8. It is also evident from Fig. 2 that the reduction of g_{Na}^{P} at pH$_o$ 4.6 is smaller than that reported by Carbone *et al.* for unperfused squid axons (probably due to the present improved pH$_i$ control; compare Fig. 3b in ref. 13). Lowering the pH of the external bath is known to decrease the intracellular pH (ref. 14). Thus, it is very likely that in intact fibres the effects of low pH$_o$ superpose partly on those of low pH$_i$, implying that axons with uncontrolled pH$_i$ might be more sensitive to changes of pH$_o$. Although in frog nodes[3] and skeletal muscles[5] the apparent pK$_a$ of the blocking site is systematically higher than the value found here (5.3 against 4.6 for perfused axons), our results indicate a substantial similarity in the external properties of Na$^+$ channels for the three types of membranes.

The presence of an acid group inside the channel accessible from the axoplasmic region is in good agreement with the finding that other pharmacological agents, such as pancuronium[15] and 9-aminoacridine[8] (9-AA), affect open Na$^+$ channels of squid axons in a voltage-dependent manner. Both molecules are positively charged at pH$_i$ 7.2 and have a sufficiently high affinity for their binding site ($K_a=6.2\times10^{-5}$ M and $\delta=0.5$ for 9-AA) to suggest that the acid group in question could be identified with part of their receptor site. Experiments concerning the pH dependence of their rate of action would certainly clarify this theory. Interestingly, the site is hardly accessible to high concentrations of tetrodotoxin (TTX)[16] even when the toxin is applied intracellularly at various pH$_i$ values (own observation). This promptly suggests that the molecular arrays surrounding the internal and the external acid groups might be remarkably different.

To our knowledge there are no other reports indicating the existence of an intracellularly negative group within the Na$^+$ channel. Recently, Nonner *et al.*[7] have shown that in the frog skeletal muscle low pH$_i$ does not produce significant reductions of the peak sodium permeability. They also showed that some inactivation-removing agents previously tested in squid axons have different effects when applied to the muscle membrane. This indicates that we should not make generalizations based on the present findings and suggests that although Na$^+$ channels of various plasma membranes have similar external regions, they might differ substantially in the unexposed internal part.

We thank Drs F. Conti, B. Hille and H. Meves for helpful suggestions on a preliminary version of this work.

Received 22 April; accepted 13 June 1980.

1. Narahashi, T. *Physiol. Rev.* **54,** 813–889 (1974).
2. Hille, B. *J. gen. Physiol.* **69,** 475–496 (1977).
3. Woodhull, A. M. *J. gen. Physiol.* **61,** 687–708 (1973).
4. Schauf, C. F. & Davis, F. A. *J. gen. Physiol.* **67,** 185–195 (1976).
5. Campbell, D. T. & Hille, B. *J. gen. Physiol.* **67,** 309–323 (1976).
6. Ohmori, H. & Yoshii, M. *J. Physiol., Lond.* **267,** 429–463 (1977).
7. Nonner, W., Spalding, B. C. & Hille, B. *Nature* **284,** 360–363 (1980).
8. Yeh, J. Z. *J. gen. Physiol.* **73,** 1–21 (1979).
9. Wanke, E., Carbone, E. & Testa, P. L. *Biophys. J.* **26,** 319–324 (1979).
10. Carbone, E., Testa, P. L. & Wanke, E. *Biophys. J.* (submitted).
11. Armstrong, C. M., Bezanilla, F. & Rojas, E. *J. gen. Physiol.* **62,** 375–391 (1973).
12. Hille, B. *J. gen. Physiol.* **66,** 535–560 (1975).
13. Carbone, E., Fioravanti, R., Prestipino, G. & Wanke, E. *J. Membrane Biol.* **43,** 295–315 (1978).
14. Bicher, H. I. & Ohki, S. *Biochim. biophys. Acta* **255,** 900–904 (1972).
15. Yeh, J. Z. & Narahashi, T. *J. gen. Physiol.* **69,** 293–323 (1977).
16. Rojas, E. & Rudy, B. *J. Physiol., Lond.* **262,** 501–531 (1976).

Solubilization of the choline transport system and re-incorporation into artificial membranes

R. G. King & R. M. Marchbanks

Department of Biochemistry, Institute of Psychiatry,
London SE5 8AF, UK

The carrier-mediated transport of choline has been described in several types of cell[1–3] and at isolated synaptic terminals[4]. The operation of the carrier seems to be a rate-controlling factor for the synthesis of acetylcholine at the synaptic terminals that release this neurotransmitter[5]. The molecular mechansism by which the carrier transports choline is unknown and difficult to investigate because at present it can only be studied in the complex environment of the natural membrane in which it is situated. Furthermore, such studies are hampered by the results of metabolic activity inside the cell itself. The resolution of these difficulties by the separation, purification and examination of carriers in defined systems is hindered by the problem of assaying its activity during the purification procedure. We describe here the separation of the choline carrier from the membrane and its re-incorporation into unilamellar liposomes with retention of its functional activity, thus enabling its purification and examination in isolation to be undertaken.

The starting material used was synaptic plasma membrane of guinea pig cerebral cortex produced from hypo-osmotically shocked synaptosomes (nerve ending particles) by the procedure of Jones and Matus[6]. Membrane material was solubilized with cholate using a modification of the procedure of Kagawa and Racker[7], but as in Racker's original method[8], no urea was present, and 1 mM dithiothreitol was added. Insoluble material was removed by centrifugation at 100,000*g* for 30 min.

A mixture of purified lipids of approximately similar composition to synaptic plasma membrane[9] (40% phosphatidylcholine, 30% phosphatidylethanolamine, 20% cholesterol, 10% phosphatidyl serine w/w) were dispersed by ultrasonication, added to the cholate extract (3 mg ml^{-1} lipids, 2 mg ml^{-1} protein) and dialysed[7]. As dialysis proceeds, unilamellar liposomes are formed and these incorporate proteins and lipids from the original cholate extract. Choline transport was measured by observing the uptake of ^{3}H-choline, the liposomes having been separated from the incubation medium by Millipore filtration followed by two washes.

As shown in Fig. 1, ^{3}H-choline uptake by the liposomes is reduced by the presence of saturating concentrations (10 mM) of nonradioactive choline chloride during the first 4 min of uptake: this effect is not seen after periods of 30 min or more. A comparison with the uptake into liposomes prepared from pure lipid alone cannot be made on a protein basis, but the ratio can be expressed as the fraction of equilibration value or on a phospholipid basis. As Table 1 shows, it is the incorporation of membrane extract into the liposomes that increases the rate of choline uptake and confers saturability. Hemicholinium had no statistically significant effect on pure lipid liposomes.

Table 1 Comparison of ^{3}H-choline uptake by pure lipid liposomes and liposomes made with lipid and cholate-solubilized extract of synaptic plasma membrane

	Fraction of equilibrated value (±s.e.m.(*n*))	
	In 4 min	In 60 min
Lipid alone	0.26±0.05(8)	0.79±0.09(8)
Lipid alone+10 mM choline chloride	0.30±0.04(8)	0.80±0.12(8)
Lipid+extract of s.p.m.	0.49±0.05(6)	0.78±0.08(6)
Lipid+extract of s.p.m.+10 mM choline chloride	0.32+0.03(6)	0.75±0.10(6)

Liposomes were prepared as described in the text, and uptake experiments carried out as described in Fig. 1 legend. Pure lipid liposomes were prepared in the same way with cholate but without the addition of cholate-solubilized extract of synaptic plasma membrane (s.p.m.). Phospholipid content of the liposomes was measured, and the initial rate of uptake expressed on a basis of phospholipid content was 0.46 pmol per mg phospholipid per min (lipid and extract of synaptic plasma membrane) and 0.20 pmol per mg phospholipid per min (lipid alone); both measurements were made at a choline concentration of 1 μM.

To guard against the possibility that ^{3}H-choline is bound to the liposomes, 10 mM choline was present in the washing solution in all experiments. A further check is that trans-activation of influx can be demonstrated in the protein-loaded liposomes. It has been shown in many transport systems, including that for choline[3,5], that preloading with the transported substance actually increases the uptake of that substance. If binding were responsible for the results of Fig. 1, preloading the liposomes with choline chloride would be expected to diminish ^{3}H-choline uptake. However, as shown in Table 2, preloading with cold choline caused completely the reverse. The demonstration in Table 2 that influx is increased by preloading with choline also shows that an important feature of the *in vivo* transport of choline is retained in the artificial membrane system.

Hemicholinium-3 is a specific inhibitor of choline transport[10]. It has an inhibitory effect (Table 2) on choline uptake in protein-containing liposomes, although we found some variability in its effectiveness. Choline transport is known to be sensitive to the Na$^+$ and K$^+$ gradients across the membrane[3,4]. Whether or not this is due to a requirement for sodium co-transport, an inwardly directed negative electrical gradient, or some other mechanism, is unknown. Liposomes were prepared in a predominantly KCl medium and then transferred to a larger volume of predominantly NaCl medium so as to mimic the ion gradient found normally. It was found that liposomes prepared in KCl had

Table 2 Effects of hemicholinium, preloaded choline and valinomycin on uptake of ^{3}H-choline by liposomes prepared with cholate extract of synaptic plasma membrane

	Initial rate as % control±s.e.m.(*n*)
Liposomes+10 mM choline chloride	7±12(8)
Liposomes+100 μM hemicholinium	72±10(8)
Liposomes preloaded with 2 μM choline chloride	132±16(8)
Liposomes preloaded with 10 μM choline chloride	192±24(8)
Liposomes preloaded with 15 μM choline chloride	208±32(8)
Liposomes made in K$^+$ medium and then transferred to Na$^+$ medium:	
Liposomes+10 mM choline chloride	52± 8(10)
Liposomes+8 μM valinomycin	155±22(10)
Liposomes+8 μM valinomycin+10 mM choline chloride	104±18(10)

Liposomes were prepared as described in the text (those made in K$^+$ medium were prepared in the same way, except that 100 mM KCl replaced 100 mM NaCl in all solutions). Uptake over 30 s was measured as in Fig. 1, except that the liposomes were added to a larger volume (360 μl) of NaCl-based dialysis medium containing 2–3 μCi ^{3}H-choline. Preloading was by incubation with choline chloride until equilibrium was reached (control liposomes incubated as well). External choline concentration during ^{3}H-choline uptake was 5 μM (except where 10 mM choline was present). The two control groups of liposomes were in the medium as described above, but with none of the additions, and the rates of uptake were: 1.9 pmol per mg protein per min (upper part) and 3.0 pmol per mg protein per min (lower part), both at a choline concentration of 5 μM.

0028-0836/80/360064—02$01.00

approximately 50% greater initial rate of uptake of ^{3}H-choline than liposomes prepared in a predominantly NaCl medium. Also, valinomycin (which could be expected to produce a potential across the membrane by specifically increasing its permeability to K^+) caused an increased uptake of ^{3}H-choline by the liposomes; this, however, was not inhibited by 10 mM choline chloride. The presence of certain other substances in the external solution, including 2 mM $MgCl_2$, 1 mM $CaCl_2$ and 3 mM MgATP, had no statistically significant effect; however, we have not tested the effects of different concentrations of these substances inside the liposomes.

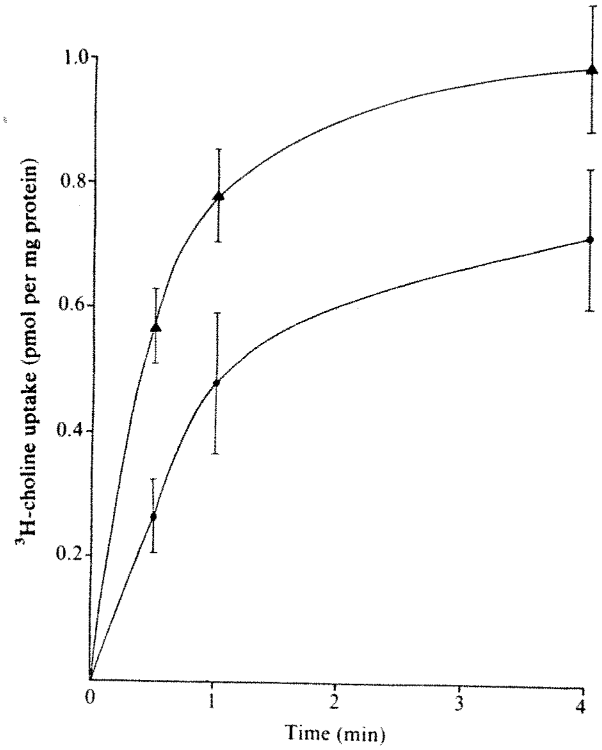

Fig. 1 Time course of uptake of ^{3}H-choline by liposomes containing membrane extract. Liposomes prepared as described in the text were preincubated for 30 min at 37 °C, and then 140-μl samples were added to 70 μl of dialysis fluid (37 °C) containing 1-2 μCi ^{3}H-choline (1 μM). After the required time of incubation (37 °C), 200 μl was placed in 5 ml of ice-cold filtering solution (100 mM NaCl, 10 mM Tris–HCl and 10 mM choline chloride, *p*H 7.4), immediately filtered on Millipore filters (0.22 μm pore diameter) and then washed twice with 10 ml of filtering solution. The order of filtering was randomized because pressure differences in the apparatus affect the blank value. Zero points were obtained by adding the liposome suspension directly to the filtering solution (which already contained ^{3}H-choline) and filtering immediately. Filters were dried, counted in 10 ml of scintillant and uptake of ^{3}H-choline determined from the value of the mean of at least four filtrations, minus the zero value. Protein entrapped on the filters was measured directly[13]. ▲, Without 10 mM choline; ●, with 10 mM choline. Vertical bars show s.e.m of four filtrations.

The effects of varying concentrations of external choline chloride on the uptake of ^{3}H-choline were investigated and it was found that the uptake was saturable, with a half-maximal concentration of 50–100 μM. Double-reciprocal plots of influx against choline concentration showed an inflection at a choline concentration of about 4 μM. Although we cannot explain this phenomenon, it has also been reported[11] in isolated synaptosomes.

In cerebral cortex synaptosomes the initial rate of choline influx at a choline concentration of 1 μM is 10–20 pmol per min per mg protein; the rate in protein-containing liposomes is 0.5–1.0 pmol per min per mg protein, so that only 5–10% of the native activity is retained. This may be because only a fraction of the total carrier has been extracted; alternatively, some may be denatured, some may be incorporated into the membrane in the wrong orientation or, as occurs with erythrocyte glucose arrier[12], only a small proportion of the liposomes contain a functional carrier molecule. The latter proposal would also explain why inhibition of ^{3}H-choline influx by 10 mM choline is only seen during the initial phases of uptake. Whatever the explanation, the solubilized carrier when incorporated into liposomes has retained the important properties of saturability, hemicholinium sensitivity and trans-activation.

R.G.K. was supported by a fellowship from the MRC and the expenses of this research were met by MRC grant G979/507/N to R.M.M.

Received 14 April; accepted 23 June 1980.

1. Sung, C. P. & Johnstone, R. M. *Can J. Biochem.* **43,** 1111–1118 (1965).
2. Hodgkin, A. L. & Martin, K. *J. Physiol., Lond.* **179,** 26–27 (1965).
3. Martin, K. *J. gen. Physiol.* **51,** 497–516 (1968).
4. Marchbanks, R. M. *Biochem. J.* **110,** 533–541 (1968).
5. Marchbanks, R. M. & Wonnacott, S. *Prog. Brain Res.* **49,** 77–88 (1979).
6. Jones, D. H. & Matus, A. I. *Biochim. biophys. Acta* **356,** 276–287 (1974).
7. Bardin, C. & Johnstone, R. M., *J. biol. Chem.* **253,** 1725–1732 (1978).
8. Kagawa, Y. & Racker, E. *J. biol. Chem.* **246,** 5477–5487 (1971).
9. Breckenridge, W. C., Gombos, G. & Morgan, I. G. *Biochim. biophys. Acta* **266,** 695–707 (1972).
10. MacIntosh, F. C. *Fedn Proc.* **20,** 562–568 (1961).
11. Yamamura, H. I. & Snyder, S. H. *J. Neurochem.* **21,** 1355–1374 (1973).
12. Goldin, S. M. & Rhoden, V. *J. biol. Chem.* **253,** 2575–2583 (1978).
13. Schaffner, W. & Weissmann, C. *Analyt. Biochem.* **56,** 502–514 (1973).

A ribosomal protein mediates eIF-2 phosphorylation by interferon-induced kinase

Kenzo Ohtsuki, Masataka Nakamura, Tsuneaki Koike, Nakao Ishida & Samuel Baron*

Department of Bacteriology, Tohoku University School of Medicine, Sendai 980, Japan
*Department of Microbiology, University of Texas Medical Branch Galveston, Texas 77550

We have previously reported that treatment of mouse L cells with interferon (IFN) induces a reduction of initiation factor (eIF-2) activity (ternary complex formation of eIF-2 with Met-tRNA$_f$ and GTP)[1], and that the reduction of eIF-2 activity involves the phosphorylation of eIF-2 by an IFN-induced protein kinase[2]. In addition, we considered that the reduction of eIF-2 activity induced by the kinase (cyclic AMP-independent protein kinase) may be accompanied by the phosphorylation of some intermediary factor(s)[2]. This possibility was supported by early reports that at least two ribosomal proteins (of molecular weights (MWs) 35,000–38,000 and 64,000–67,000) of mouse L cells[3–5] and cellular proteins of Ehrlich ascites tumour cells[6] are highly phosphorylated by IFN treatment. Recently, we and others have purified IFN-induced protein kinases from different cells treated with IFN[2,3,7–9]. These purified kinases show several similarities. The reports suggested that the IFN-induced kinase may be responsible for the phosphorylation of the ribosomal proteins (MWs 35,000–38,000 and 65,000–67,000) and that the phosphorylation of these proteins by the kinase may be associated with the reduced eIF-2 activity in IFN-treated cells[2–4,8,9]. A similar inhibitory mechanism of eIF-2 activity has been demonstrated in rabbit reticulocyte lysates[10–15]. The present study was undertaken to purify a ribosomal protein [MW 65,000 (65K)] from mouse L cells and to examine the effect of the protein on eIF-2 activity, and also on the binding of the ternary complex to the 40S ribosomal subunit. We found that the eIF-2 activity was greatly reduced when both eIF-2 and the ribosomal protein were incubated with IFN-induced kinase *in vitro*. Available evidence suggests that the inhibitory mechanism of eIF-2 activity induced by the kinase *in vitro* may involve phosphorylation of the ribosomal proteins [a small subunit (MW 38,000) of eIF-2 and 65K ribosomal protein] by the IFN-induced kinase.

0028-0836/80/360065—03$01.00

A 65K ribosomal protein was purified from 0.5 M KCl ribosomal extracts of mouse L cells as described in Fig.1. SDS-polyacrylamide gel electrophoresis showed that the purified 65K ribosomal protein was a single polypeptide. Table 1 shows that the 65K ribosomal protein functioned as a phosphate acceptor of IFN-induced kinase *in vitro*; however, the substrate activity of the protein was more than 50% of that of purified eIF (98% pure). About 80 pmol of the ribosomal protein were phosphorylated in these conditions. In addition, double-stranded (ds) RNA (poly(I)·poly(C), 100 ng ml^{-1}) stimulated about 3.2 times the phosphorylation of the ribosomal protein by the kinase *in vitro*. The phosphorylation of the 65K ribosomal protein and eIF-2 was confirmed by SDS-polyacrylamide gel electrophoresis (data not shown). No protein kinase activity in the final preparation of 65K ribosomal protein was detected.

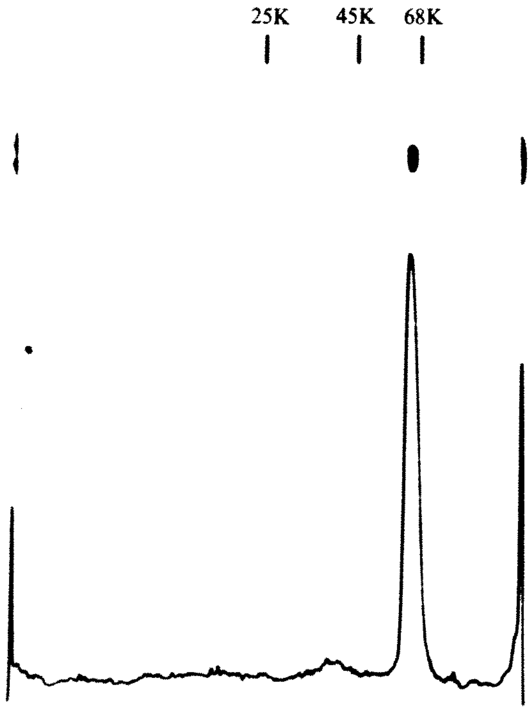

Fig. 1 Purification of the 65K ribosomal protein from 0.5 M KCl extracts of mouse L cells and SDS-polyacrylamide gel electrophoresis of the protein, 0.5 M KCl extracts from ribosomes of mouse L cells were used for the purification of 65K ribosomal protein because early reports showed that at least two proteins (MWs 35,000–38,000 and 64,000–67,000) are highly phosphorylated in the cell extracts of IFN-treated cells and this protein phosphorylation is greatly stimulated by the addition of dsRNA (poly(I)·poly(C), 10–200 ng ml^{-1})[2,3,6]. The 0.5 M KCl extract (about 300 mg crude protein) was passed through a Sephacryl S-200 column (2.2 × 76 cm) previously equilibrated with buffer A [20 mM Tris-HCl (*p*H 7.5) containing 2 mM dithiothreitol, 50 mM KCl and 5% glycerol] to purify a 65K ribosomal protein which was highly phosphorylated by IFN-induced kinase *in vitro*. The column was eluted with buffer A and 1.0 ml of fraction was collected. The fractions (MWs ~60,000–70,000) were pooled and concentrated with solid ammonium sulphate (60% saturation). After dialysis against buffer A (overnight at 4°C), the fraction (~60 mg protein) was further purified by a DEAE-cellulose column (1.4 × 12 cm) previously equilibrated with buffer A. The column was eluted with a linear gradient from 0.05 M to 0.5 M KCl in buffer A (50 ml). DEAE-cellulose column chromatography showed two distinct protein peaks (flow-through fraction and the 0.08 M–0.35 M KCl fraction). Over 70% protein kinase activity of the Sephacryl S-200 fraction was detected in the flow-through fraction, whereas the stimulating effect of dsRNA (poly(I)·poly(C), 100 ng ml^{-1}) on substrate activity for the kinase was detected in the fractions which were eluted between 0.1 M and 0.15 M KCl. Moreover, the activity of cyclic AMP-independent protein kinase was eluted between 0.15 M and 0.2 m KCl. The fractions with substrate activity for the kinase were pooled and immediately concentrated by vacuum dialysis against buffer A to 0.5 ml. Finally, the DEAE-cellulose fraction (total 15 mg protein) was purified by preparative gel electrophoresis. The protein with substrate activity for the kinase in the gel was extracted with 0.5 M KCl extracts from the ribosomes of mouse L cells with a protein yield of less than 1%. SDS-polyacrylamide gel electrophoresis[16] showed that the purified ribosomal protein was a single polypeptide with a MW of 65,000, as estimated from the marker proteins.

We tested the effect of 65K ribosomal protein on eIF-2 activity. Less than a 9% reduction was detected when purified eIF-2 (98% pure) was incubated with the kinase in the absence of the ribosomal protein, whereas the activity was greatly reduced when both eIF-2 and the ribosomal protein were preincubated with the kinase. No reduction of eIF-2 activity occurred when both proteins were incubated without the kinase (Table 2). In addition, no reduction of eIF-2 activity occurred when ATP or Mg^{2+} was omitted from the reaction mixture. The effect of ATP was not substituted by GTP and high levels of Mg^{2+}(>5 mM) prevented the reduction of eIF-2 activity induced by the phosphorylation of these two proteins (eIF-2 and 65K ribosomal protein) by the kinase *in vitro* (data not shown). Low levels of dsRNA stimulated this reduction, but it was prevented by aminopurine which is an inhibitor of the kinase[2,17]. These results showed that the phosphorylation of these two ribosomal proteins by the kinase *in vitro* resulted in the reduction of eIF-2 activity.

Table 1 Effect of dsRNA on phosphorylation of eIF-2 or 65K ribosomal protein by IFN-induced kinase *in vitro*

Additions	[γ-^{32}P] ATP into the substrate (pmol)
None	0.1
eIF-2	15.0
eIF-2 + dsRNA	31.3
65K ribosomal protein	8.9
65K ribosomal protein + dsRNA	28.5
65K ribosomal protein + eIF-2	22.6
65K ribosomal protein + eIF-2 + dsRNA	54.0
65K ribosomal protein + aminopurine	3.8

The reaction mixture (0.1 ml) contained 20 mM Tris-HCl (*p*H 7.5), 4 mM dithiothreitol, 1 mM magnesium acetate, 0.1 mM [γ-^{32}P] ATP (3,000 c.p.m. pmol^{-1}), 10 μg of bovine serum albumin (BSA), 0.5 μg of IFN-induced kinase and a substrate [5 μg of purified eIF-2 (98% pure) or 5 μg of 65K ribosomal protein]. The reaction mixture was incubated for 10 min at 37 °C in the presence or absence of dsRNA (poly(I)·poly(C), 100 ng ml^{-1}) or 1 mM aminopurine. The reaction was stopped by the addition of 0.5 ml of 20% trichroloacetic acid (TCA) and 0.5 ml of 0.2 M sodium pyrophosphate containing 1 mg ml^{-1} of BSA. The radioactivity of the TCA precipitate was determined as previously reported[2].

In the presence of GTP and Met-tRNA$_f$, eIF-2 forms the ternary complex, Met-tRNA$_f$–eIF-2–GTP, which binds to the 40S ribosomal subunit[13,15]. We tested the effect of 65K ribosomal protein on the binding of the ternary complex to the 40S subunit. The complex (ternary complex–40S subunit) formed was analysed by 5–30% (w/v) sucrose density gradient centrifugation. Figure 2 shows that the complex formation was greatly reduced when both eIF-2 and 65K ribosomal protein were preincubated with the kinase in the presence of ATP (0.1 mM) and Mg^{2+} (1 mM). The reduction of the complex formation did not occur if ATP or Mg^{2+} was omitted from the reaction mixture, as described in the reduction of eIF-2 activity induced by the kinase. These results suggested that the phosphorylation of two ribosomal proteins by the kinase results in the reduction of the binding of the ternary complex to the 40S subunit.

The present finding that the reduction of eIF-2 activity involves phosphorylation of both eIF-2 and 65K ribosomal protein by IFN-induced kinase *in vitro* is at least partially consistent with other observations which are: (1) at least two ribosomal proteins (MWs 35,000–38,000 and 64,000–67,000) which are highly phosphorylated by IFN treatment[3–5]; (2) low levels of dsRNA stimulated the phosphorylation of a small subunit (MW 38,000) of eIF-2 and 65K ribosomal protein by the kinase *in vitro*[2,4,17,18]; and (3) in rabbit reticulocyte lysates, the eIF-2 activity is inhibited by a haem regulatory inhibitor (HRI, cyclic AMP-independent protein kinase)[10–12]. However, it has also been reported that no inhibition occurs when highly purified eIF-2 is used[19,20]. In these conditions, HRI phosphorylates only a small subunit of eIF-2, thereby indicating that the phosphorylation of a small subunit of eIF-2 alone is not sufficient to alter the ternary complex forming activity of eIF-2[19,20]. Our data and indirect evidence in the literature on reticulocyte lysates strongly suggest that the 65K ribosomal protein may be the intermediary factor which is responsible for the reduction of eIF-2 activity induced by IFN treatment or IFN-induced kinase *in vitro*. In addition, the recent evidence of a steric difference of a 5′-terminal structure between viral and eukaryotic cell mRNAs suggests that the phosphorylation of ribosomal proteins (eIF-2, 65K ribosomal protein and others) by IFN-induced kinase may be responsible for the discrimination of initiation complex formation between viral and eukaryotic cell mRNAs[21]. We are now carrying out comparative and analytical studies on the biological and physicochemical properties of the 65K ribosomal protein from mouse L cells treated with IFN and the cells infected with viruses.

Table 2 Effect of 65K ribosomal protein on eIF-2 activity

Preincubation	[^{35}S] Met-tRNA into ternary complex (pmol)
Without kinase	
Complete (control I)	23.7
Complete + 65K ribosomal protein (1 μg)	22.5
Complete + 65K ribosomal protein (5 μg)	21.3
With kinase	
Complete (control II)	21.8
Complete + 65K ribosomal protein (5 μg)	12.0
Complete + 65K ribosomal protein (5 μg) + dsRNA (100 ng ml^{-1})	6.3
Complete + 65K ribosomal protein (5 μg) + aminopurine (2 mM)	16.7
Complete + dsRNA (100 ng ml^{-1})	19.7
Complete + aminopurine (2 mM)	20.0

The complete reaction mixture (0.1 ml) contained 20 mM Tris-HCl (*p*H 7.5), 4 mM dithiothreitol, 1 mM $MgCl_2$, 10 μg BSA, 0.1 mM ATP and 5 μg (bound with 23.7 pmol of [^{35}S]Met-tRNA$_f$) of purified eIF-2 (98% pure). The indicated concentrations of the reagent and eIF-2 (5 μg) were incubated for 10 min at 37 °C with 65K ribosomal protein (5 μg) in the presence or absence of IFN-induced kinase (0.5 μg). After incubation, the mixture containing 50 pmol of [^{35}S]Met-tRNA$_f$ (4,500 c.p.m. pmol^{-1}), 0.1 M KCl and 0.1 mM GTP was added to the reaction mixture and then further incubated for 10 min at 0–5 °C. The formed ternary complex of eIF-2 was determined as previously reported[2]. The eIF-2 from ribosomes of mouse L cells and IFN-induced kinase from ribosomes of mouse L cells treated with IFN (500 units for 24 h at 37 °C) were prepared as previously reported[2].

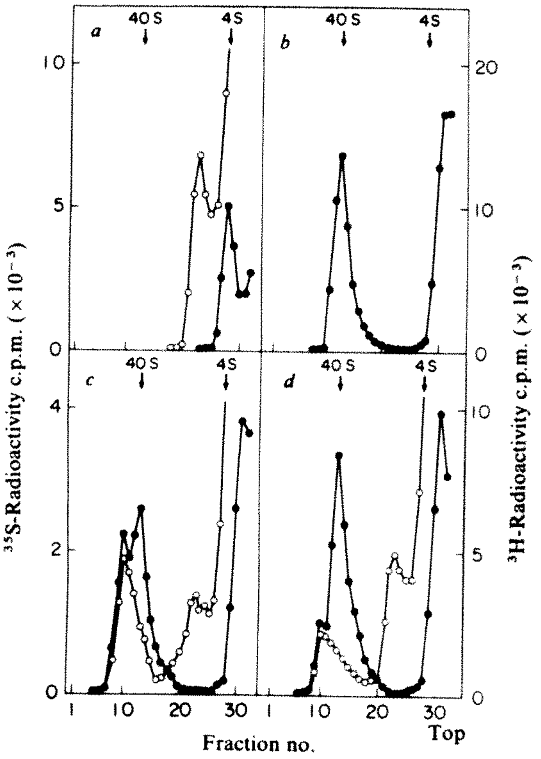

Fig. 2 Effect of 65K ribosomal protein on the binding of the ternary complex to the 40S ribosomal subunit. The reaction mixture (0.1 ml) contained 20 mM Tris-HCl (*p*H 7.5), 0.1 M KCl, 0.1 mM GTP, 50 pmol of [^{35}S]Met-tRNA$_f$ (4,500 c.p.m. pmol^{-1}), 10 pmol of [^{3}H] 40S subunit (0.16 A_{260} units), 1mM $MgCl_2$ and purified eIF-2 (5 μg). Incubation was for 10 min at 37 °C. The reaction mixtures were analysed 5–30% (w/v) sucrose density gradient (4.8 ml) in 20 mM Tris-HCl (*p*H 7.5), 0.1 M KCl and 1 mM $MgCl_2$. Centrifugation was at 45,000 r.p.m. in a Hitachi 50 SW rotor for 3 h at 4 °C. The gradients were divided separately into 10-drop fractions from the bottom of the tube. Radioactivities of ^{3}H and ^{35}S of the fractions were determined in a liquid scintillation spectrometer. *a*, ^{35}S radioactivity of the formed ternary complex ^{35}S-Met-tRNA$_f$–eIF-2–GTP, and ^{3}H-Met-tRNA$_f$ (1,300 c.p.m. pmol^{-1}, 30 pmol) after gel filtration of Sephadex G-25 to remove free ^{3}H-methionine; *b*, ^{3}H radioactivity of ^{3}H-40S subunit; *c*, the binding of the ternary complex to the ^{3}H-40S subunit (10 pmol). A ternary complex was formed in the condition as previously reported[1]. The binding assay was carried out in the presence of 65K ribosomal protein (5 μg) without IFN-induced kinase. *d*, Purified eIF-2 (98% pure, 5 μg) and 65K ribosomal protein (5 μg) were preincubated with the kinase (0.5 μg) in the presence of ATP (0.1 mM). After incubation (10 min at 37 °C), the reaction mixture was added to the binding assay mixture and then incubated for 5 min at 37 °C. ●, ^{3}H; ○, ^{35}S.

This work was supported in part by grants from the MacLaughlin Foundation and from the Ministry of Education, Science and Culture of Japan.

Received 24 March; accepted 4 July 1980.

1. Ohtsuki, K., Dianzani, F. & Baron, S. *Nature* **269,** 536–538 (1977).
2. Ohtsuki, K. & Baron, S. *J. Biochem. Tokyo* **85,** 1495–1502 (1979).
3. Zilberstein, A., Federman, R., Shulman, L. & Revel, M. *FEBS Lett.* **68,** 119–124 (1976).
4. Zilberstein, A., Kimchi, A., Schmidt, A. & Revel, M. *Proc. natn. Acad. Sci. U.S.A.* **75,** 4734–4738 (1978).
5. Gupta, S. *J. Virol.* **29,** 301–311 (1979).
6. Lebleu, B., Sen, G. C., Shaila, S., Cabrer, B. & Lengyel, P. *Proc. natn. Acad. Sci. U.S.A.* **73,** 3107–3111 (1976).
7. Sen, G. C., Taira, H. & Lengyel, P. *J. biol. Chem.* **253,** 5915–5921 (1978).
8. Baglioni, C. *Cell* **17,** 255–264 (1979).
9. Kimchi, A., Zilberstein, A., Schmidt, A., Shulman, L. & Revel, M. *J. biol. Chem.* **254,** 9846–9853 (1979).
10. Datt, A., Haro, C. D., Sierra, J. M. & Ochoa, S. *Proc. natn. Acad. Sci. U.S.A.* **74,** 1463–1467 (1977).
11. Datt, A., Haro, C. D. & Ochoa, S. *Proc. natn. Acad. Sci. U.S.A.* **75,** 1148–1152 (1978).
12. Lenz, J. R. & Baglioni, C. *J. biol. Chem.* **253,** 4219–4223 (1978).
13. Petryshyn, R., Trachsel, H. & London, I. M. *Proc. natn. Acad. Sci. U.S.A.* **76,** 1575–1579 (1979).
14. Ernst, V., Levin, D. H. & London, I. M. *Proc. natn. Acad. Sci. U.S.A.* **76,** 2118–2122 (1979).
15. Haro, D. C. & Ochoa, S. *Proc. natn. Acad. Sci. U.S.A.* **76,** 1741–1745 (1979).
16. Weber, K. & Osborn, M. *J. biol. Chem.* **244,** 4406–4412 (1969).
17. Farrell, P. J., Balkow, K., Hunt, T. & Jackson, R. *Cell* **11,** 187–200 (1977).
18. Ohtsuki, K. *J. clin. Oncol. Hemat.* **10** (in the press).
19. Tahara, S. M. *et al. Proc. natn. Acad. Sci. U.S.A.* **75,** 789–793 (1978).
20. Trachsel, H. & Staehelin, T. *Proc. natn. Acad. Sci. U.S.A.* **75,** 204–208 (1978).
21. Kozak, M. *Cell* **15,** 1109–1123 (1978).

An interferon-induced cellular enzyme is incorporated into virions

David Wallach & Michel Revel

Department of Virology, The Weizmann Institute of Science, Rehovot, Israel

The mechanisms by which interferon inhibits viral growth are only partially understood. Several enzymatic activities increase in cells shortly after treatment with interferon[1–8]. One of these enzymes, oligo-isoadenylate synthetase, synthesizes (2′–5′) isoadenylate oligomers which strongly stimulate the activity of a cellular ribonuclease, RNase F (ref. 7). Interferon also significantly increases the activity of a protein kinase which phosphorylates the initiation factor eIF-2 and can inhibit *in vitro* protein synthesis. Such interferon-induced enzymes, which affect RNA and protein metabolism, might be responsible for many of its effects on viruses. Indeed, inhibition of viral protein and RNA synthesis appears to have a major role in the antiviral state[9]. We have now investigated possible interactions of the two enzymes with viral constituents during the course of infection and found that in two different membrane-coated RNA viruses, vesicular stomatitis virus (VSV) and Moloney murine leukaemia virus (M-MuLV), there is an accumulation of the (2′–5′) oligo-isoadenylate synthetase (E) in the virions. Most of the enzyme is bound to the virion ribonucleoprotein core. The incorporation of E into the virions suggests a direct involvement of the enzyme in regulation of virus functions.

Highly-purified VSV and M-MuLV virions were lysed in NP40, and after mixing with poly(rI):poly(rC)-agarose beads were incubated with [α-^{32}P]ATP. Figure 1 shows the autoradiography of an electrophoretic analysis of the labelled nucleotides formed with VSV virions, grown in BSC-1 monkey fibroblasts and with M-MuLV virions, from chronically infected NIH/3T3 mouse fibroblasts. The nucleotides formed during incubation of ATP with the respective cell extracts are shown in comparison. Equal amounts of proteins were used in the assay of the virions and of the cellular extracts. Before electrophoresis the labelled nucleotides were treated with bacterial alkaline phosphatase so that we analysed the phosphatase-resistant cores of the nucleotides formed by E comprising (2′–5′)ApA; (2′–5′)A(pA)$_2$ and so on.

Figure 1 (lanes 3, 4) shows that purified VSV virions, formed in BSC-1 cells, exhibit a high activity of E. The activity in the virions was proportional to that in the cells. BSC-1 cells which have not been treated with interferon showed low activity of E (Fig. 1, lane 1). Extracts of virions obtained from these untreated cell cultures also formed very little oligo-isoadenylate, but on a protein basis, the activity of E in the virions was about ninefold higher than in the cells (Fig. 1, lane 3). Treatment by 15 U per ml of interferon increased the activity of the enzyme in the cells and in the virions by about 10-fold (Fig. 1, lanes 2, 4). M-MuLV virions, and their host cells (NIH/3T3) showed no activity of E before treatment with interferon (Fig. 1, lanes 5, 7). Following treatment with interferon there was high activity of E in both the cells and the virions (Fig. 1, lanes 6, 8). The length of the oligo-isoadenylate formed by E is proportional to the activity of the enzyme. Thus, only the shortest oligomer, (2′–5′)ApA, is formed in the presence of low concentrations of lysed VSV virions (Fig. 1), while in the presence of higher concentrations of virion lysates there is also formation of (2′–5′)ApApA (Fig. 2*b*, lane 2). Further characterization of the nucleotides formed by VSV virions, is shown in Fig. 2. The products not treated with phosphatase were fractionated on a DEAE-cellulose column, in urea, from which, as shown before[7], dimer and trimer oligo-isoadenylates (2′–5′)pppApA and pppApApA elute sequentially as distinct peaks after the ATP (Fig. 2*a*, peaks I, II). In high voltage paper electrophoresis at *p*H 3.5 the nucleotides of peaks I and II migrated ahead of ADP, as the authentic oligo-isoadenylates[4,7] (not shown). Following treatment by phosphatase, the phosphatase-resistant cores co-migrated in the paper electrophoresis with (2′–5′) oligo A dimer and trimer markers and were clearly distinguished from (3′–5′) oligo A markers and from 5′-AMP (Fig. 2*b*, lanes 3, 4).

Table 1 Fractionation of NP40-treated VSV virions

	E activity (c.p.m. in (2′–5′)ApA)		Protein composition (% of total protein in the fraction)			
	No NP40	+NP40	L	G	N+NS	M
Intact virions	200	2400	2	22	39	35
NP-40 extract	—	230	<1	36	<1	57
NP-40 insoluble cores	1600	1600	3	6	67	25

Purified VSV virions (200 µg protein), labelled *in vivo* by ^{3}H-uridine, were suspended in 100 µl of 0.2% (v/v) NP40, 120 mM KCl, 5 mM MgCl$_2$, 7.5 mM β-mercaptoethanol and 10 mM HEPES buffer, *p*H 7.5. After incubation for 20 min at 4 °C they were applied on a 4-ml cushion of the same solution, but without NP40 and with 20% (w/v) sucrose, and spun for 60 min at 200,000 *g*. The proteins which did not sediment through the cushion were collected and the pelleted ribonucleoprotein cores were resuspended to the original volume of the virion sample in the above solution. Samples (5 µl) of the virions, of virion without NP40, of the non-sedimented proteins and of the NP40-insoluble proteins were assayed for E in the presence of poly(rI):poly(rC)-agarose as described in Fig. 1. The patterns of proteins in the virions and in the two fractions of the detergent-treated virus were analysed by SDS-electrophoresis on 7–18% gradient polyacrylamide gel and quantitated by densitometry. Quantification of the uridine label confirmed that at least 90% of the viral RNA was recovered in the NP40-insoluble pellet.

Although we used no direct visualization technique to confirm the localization of E in the virions, the following arguments eliminate the possibility that the virion activity results from contamination by cellular proteins. As shown in Fig. 1, lane 9, the M-MuLV virions showed very little activity of E unless they were disrupted by detergent. The activity of VSV showed a similar dependence on detergent treatment (Table 1). The enzyme is, therefore, found inside the virion and not just adsorbed on its surface. It is also very unlikely that the enzyme is found inside some cellular sub-particle which would co-purify with the virions, since the density at which VSV virions band is significantly different from the density of M-MuLV. Finally, as shown in Fig. 3, the activity of E fully coincides with the virion peak on sucrose gradient. Three successive sedimentation bandings of purified VSV virions in 20–30% sucrose gradients (between each the virions were dispersed by sonication) did not change the specific activity of E in the virions.

To examine the nature of the association between E and the virus we disrupted VSV virions by NP40 and separated the solubilized proteins from the RNA and its associated proteins (Table 1). The NP40-soluble fraction contained only the membrane-associated G protein and the M protein. Only little E activity was found in this fraction. The majority of the activity of E, originally found in the virions, was recovered in the detergent-resistant fraction (Table 1). This activity, in contrast to the activity of E in the intact virions, was not dependent on the addition of detergent. The detergent-resistant fraction contained all of the RNA-associated proteins L, N and NS, but significantly decreased amounts of the M proteins and very little G protein. Further fractionation of the NP40-insoluble core is necessary to identify the site at which E is bound; E has been shown to bind to double-stranded RNA and its activity is strongly stimulated by double-stranded RNA[6,10]. It seems unlikely that, in the virion, the enzyme is bound to a double-stranded portion of the RNA since the enzyme present in the virion was not active without the addition of the synthetic double-stranded RNA poly(rI):poly(rC). Full activation occurred at concentrations of 1–10 µg ml^{-1} poly(rI):poly(rC) (not shown). Preliminary results suggest that there is a difference between the affinity of virion-associated E and of cellular E for double-stranded RNA. At 0.12 M KCl, E from VSV virion

0028–0836/80/360068—03$01.00

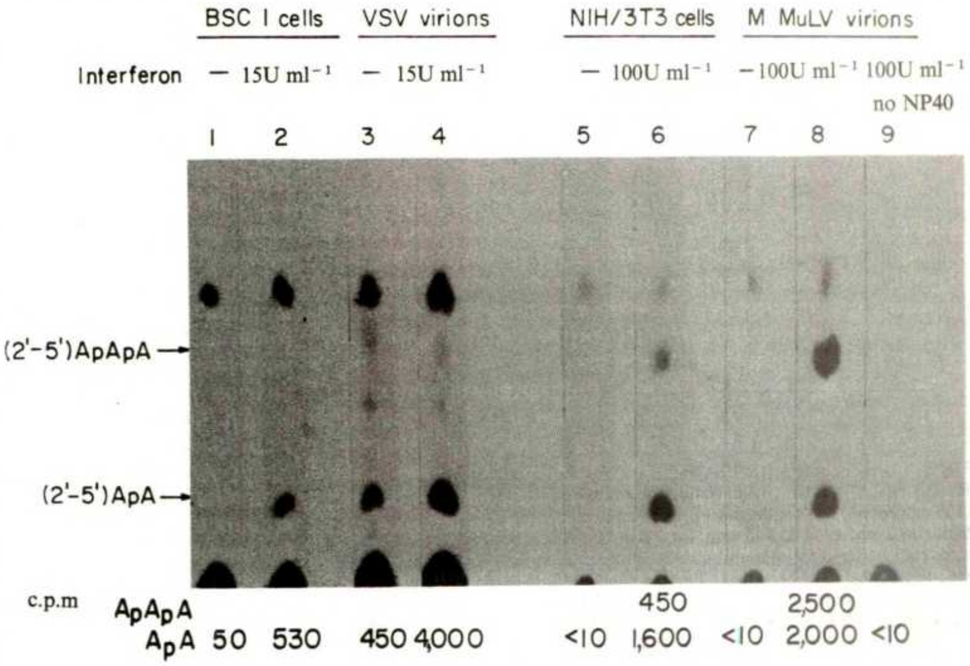

Fig. 1 Electrophoretic pattern of ATP-derived nucleotides formed by disrupted virions and by extracts of the infected cells. VSV (Indiana type, thrice plaque-purified) was collected 12 h after infecting BSC-1 cells with 0.02 plaque forming units (PFU) per cell. Following sedimentation of cell debris at low speed, the virus was sedimented through a cushion of 20% (w/v) sucrose in Dulbecco's phosphate-buffered saline (PBS) and then purified by velocity sedimentation banding in a 20–35% (w/v) sucrose gradient in PBS plus 2 mM EDTA followed by banding in a 20–40% (w/v) tartrate, 20%–0% (w/w) glycerol gradient in 20 mM Tris; 0.5 mM EDTA *p*H 7.4. Following each step the virus was dispersed by brief sonication. The virions formed a single sharp band on the gradients. M-MuLV, released by chronically infected NIH/3T3 cells[18] during a 24-h period, was purified by passing the cell-growth medium through a 0.45 μm Millipore filter, sedimenting the virus on a cushion of 60% sucrose and then banding in a 20–60% (w/v) sucrose gradient which also contained 10 mM Tris–HCl *p*H 7.4, 1 mM EDTA and 100 mM NaCl. Interferon was added to BSC-1 cells 24 h before the infection (15 U ml^{-1} human leukocyte interferon induced by Sendai virus in Namalva lymphoblastoid cells). NIH/3T3 cells were treated with 100 U ml^{-1} mouse interferon (induced by NDV in L929 fibroblasts) and 12 h later the medium was changed and interferon was re-added. Virions were collected 24 h after medium change. Both interferons were purified to about 10^7 U per mg protein. The purified virions were incubated for 20 h at 30 °C, with poly(rI):poly(rC)-agarose beads (PL Biochemicals) in the presence of 0.1% NP40 (except for lane 9), 1.25 mM [α-^{32}P]ATP (100–300 mCi mmol^{-1}), 5 mM magnesium acetate, 120 mM KCl, 1 mM dithiothreitol (DTT), 20 mM HEPES buffer, *p*H 7.5 and 10% glycerol. Following incubation, samples of the labelled products were treated by bacterial alkaline phosphatase and analysed by high-voltage paper electrophoresis at *p*H 3.5 using (2′–5′)ApA and (2′–5′)ApApA markers. E activity in cells was determined in the same conditions using NP40 extracts of cells prepared and pre-adsorbed on poly(rI):poly(rC)–agarose beads as described previously[6]. Equal amounts of viral and cellular proteins were applied on the beads (3 μg VSV and BSC-1 monkey cell proteins and 10 μg of M-MuLV and of chronically infected NIH/3T3 cell proteins). The labelled spots revealed in the autoradiogram given here, were cut out and counted with toluene scintillation fluid. The counts in the (2′–5′)ApA and (2′–5′)ApApA spots are given at the bottom of the figure. A background of 30 c.p.m. was subtracted.

lysates was readily eluted from poly(rI):poly(rC)-agarose beads. In the same conditions the enzyme of the BSC-1 cell extract remained adsorbed to the double-stranded RNA (not shown). The reason for the different behaviour of the virion-associated enzyme is not clear; it raises however the possibility that the interaction of E with viral components interferes with its binding to poly(rI):poly(rC). The mere fact that E is efficiently incorporated into the virions is also suggestive of some association between the enzyme and viral components. Without such an association it is difficult to see how E can be incorporated into

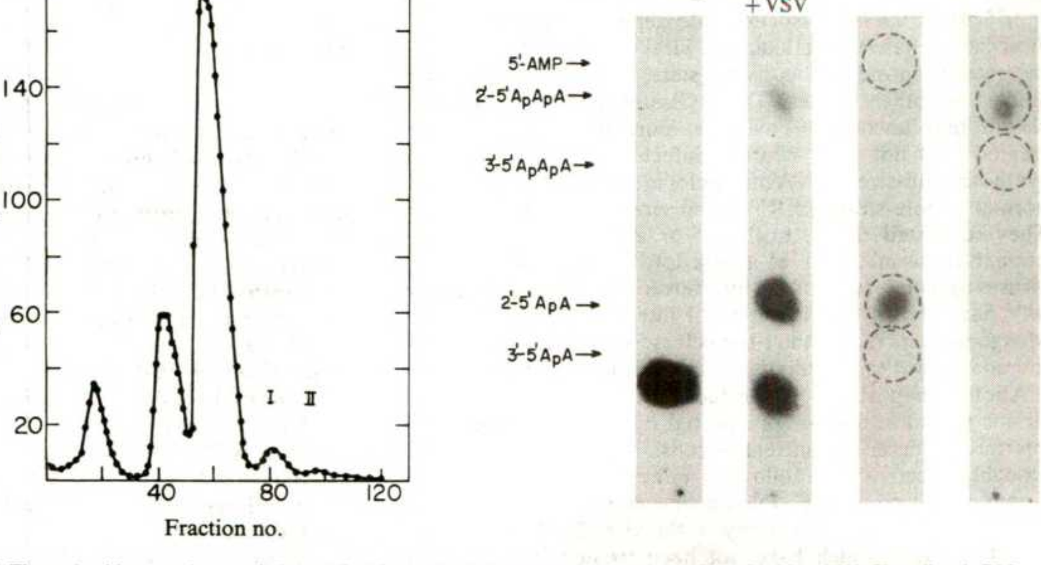

Fig. 2 Characterization of the oligo-isoadenylate synthesized by the disrupted virions. *a*, Chromatography on DEAE-Sephacel, of the nucleotides formed in incubation of lysed virions with [α-^{32}P]ATP. *b*, Electrophoretic analysis, following phosphatase treatment, of the nucleotides formed during the incubation with the virions (lane 2) and of fractions I and II (lanes 3, 4) from the DEAE-Sephacel chromatography. Unlabelled nucleotides, detected by UV light, are indicated by dotted lines [5′-AMP (2′–5′)ApA and (3′–5′)ApA in lane 3 and (2′–5′)ApApA and (3′–5′)ApApA in lane 4]. Lane 1 shows that the slowest migration spot is a contaminant of the [α-^{32}P]ATP preparation. A sample of purified VSV virions (80 μg protein) was incubated with: 100 μg ml^{-1} poly(rI):poly(rC); 1.25 mM [^{32}P]-α-ATP, 5 mM $MgCl_2$; 7 mM DDT, 20 mM HEPES, *p*H 7.5; 50 mM KCl; 10% glycerol and 0.1% NP40 in a final volume of 40 μl for 24 h at 30 °C. The nucleotides were then applied on a 0.7 × 16 cm DEAE-Sephacel column and eluted by a 50–250 mM NaCl gradient in 7 M urea and 50 mM Tris–HCl, *p*H 7.5 buffer. Fractions of 0.5 ml were collected and counted, without scintillation, in the ^{3}H-channel of a scintillation counter (*a*). The fractions in peak I and II were pooled, de-salted and concentrated by adsorption on a small DEAE-Sephacel column and then eluted by 1 M NH_4HCO_3. The nucleotides were treated by bacterial alkaline phosphatase and analysed by high-voltage paper electrophoresis as before[4] (*b*).

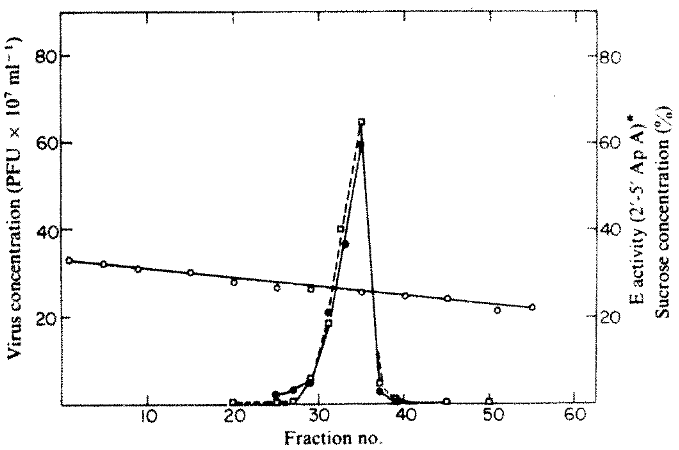

Fig. 3 Co-sedimentation of VSV and E activity. ●, Virus concentration; □, E activity; ○, sucrose concentration. A sample of purified VSV virions (100 μg protein) was applied on a sucrose gradient (13 ml 35%-20% w/v in PBS and 2 mM EDTA) and spun for 1 h at 100,000 *g*. Fractions of 0.3 ml were collected and the amount of virus in each fraction was determined by plaque assay on L929 fibroblasts. Sucrose concentration in the fractions was determined by refractometry. A sample of each fraction was diluted in PBS and spun again for 2 h at 250,000*g*. The pelleted virus was then resuspended in 40 μl of a solution of 120 mM KCl, 5 mM magnesium acetate, 1 mM DTT, 10% glycerol and 20 mM HEPES buffer, *p*H 7.5 and incubated for 18 h at 30 °C with 2.5 mM [α-^{32}P]ATP, 100 μg ml^{-1} poly(rI):poly(rC) and 0.1% NP40. Following phosphatase treatment, a sample was analysed by high-voltage electrophoresis followed by an autoradiography and spectrophotometric scanning of the (2'-5')ApA spots. E activity is expressed as the weight (in mg) of the paper under each scanning peak.

the virions to give activity which exceeds that in the cell, while most other cellular proteins are efficiently excluded from the virions in their assembly.

An interesting implication of the fact that E binds to viral components is that in virus-infected, interferon-treated cells, E is not likely to be evenly distributed but rather to be accumulated in subcellular sites in which there is assembly and synthesis of those viral components to which E can bind. Such uneven distribution of E in the cell might be an important factor in the function of this enzyme, and may result in a stronger effect of E on viral functions. It can also limit the effects of E on the cellular functions since degradation of the oligo-isoadenylate by the 2'-phosphodiesterase[7] might limit their effects [that is, activation of RNase F (ref. 7)] to the site of their synthesis in the cell. As has been pointed out by others, the strong stimulation of E activity by double-stranded RNA, formed during RNA replication of many viruses, might be an important factor in the specificity of the oligo-isoadenylate dependent ribonuclease[11]. Association between cellular and viral components, as part of the interferon-induced antiviral state, was also suggested in studies on other viruses. Thus, Glaster and Lengyel[12] have shown that uncoated reoviruses, purified from interferon-treated (but not from control) infected cells are unable to synthesize full-size mRNA molecules in spite of their apparently normal double-stranded RNA and viral protein composition. They suggested that a nuclease, or a factor which induces premature termination of transcription associates with the viruses upon infection of the interferon-treated cells. Aujean *et al.*[13] have shown that infection of interferon-treated cells by Mengo virus increased the ribonuclease activity in a subcellular fraction known to contain the viral replication complex.

Another implication of the fact that E accumulates in the virions is that E can be transported by the virion itself from interferon-treated to untreated cells. Inside the virion, E is probably inactive but, following infection and uncoating of virions which contain E, the enzyme might synthesize oligo-isoadenylate in close proximity to the viral RNA. Since cells, including those which have not been treated by interferon, contain RNase F which is activated by very low concentrations of oligo-isoadenylate[7], uncoating of the virus which contains E may eventually lead to its own destruction. Virions of MuLVs, formed by interferon-treated cells, have indeed been shown to have reduced infectivity[14,15]. It is possible that the defectiveness of these virions is not due to the alteration of a viral product[16,17], but rather to the incorporation into the virion of an interferon-induced cellular protein which interferes with the normal function of the virus.

So far, the study of the proteins induced by interferon concerned mainly their enzymatic activities. The presence of high amounts of E in virions suggests that besides their activity, the subcellular localization of these proteins and the mode of their interaction with the viral components can be of major importance in determining the way by which they protect cells against viruses.

We thank Mrs Ruth Yaniv for technical assistance, Mr Azriel Schmidt and Dr Edward Simon for helpful discussion, Dr Samuel Salzberg for the NIH/3T3 cells, Mr Gilles Merlin for human leukocyte interferon and Mr Lester Shulman for mouse interferon. This work was supported by GSF (München, FRG) and NCRD (Israel).

Received 31 January; accepted 20 June 1980.

1. Roberts, W. K., Hovanessian, A., Brown, R. E., Clemens, M. J. & Kerr, I. M. *Nature* **264**, 477–480 (1976).
2. Revel, M. *et al.* in *Proc.* 11*th FEBS Meet.* **43**, 47–58 (1977).
3. Kerr, I. M. & Brown, R. E. *Proc. natn. Acad. Sci. U.S.A.* **75**, 256–260 (1978).
4. Zilberstein, A., Kimchi, A., Schmidt, A. & Revel, M. *Proc. natn. Acad. Sci. U.S.A.* **75**, 4734–4738 (1978).
5. Farrell, P. J. *et al. Proc. natn. Acad. Sci. U.S.A.* **75**, 5893–5897 (1978).
6. Kimchi, A. *et al. Proc. natn. Acad. Sci. U.S.A.* **76**, 3208–3212 (1979).
7. Schmidt, A. *et al. FEBS Lett.* **95**, 257–264 (1978).
8. Cooper, J. A. & Farrell, P. J. *Biochem. biophys. Res. Commun.* **77**, 124–131 (1977).
9. Friedman, R. M. & Chang, E. H. in *Interferons and their Actions* (ed. Stewart, W. E. II) 145-152 (CRC Press, Ohio, 1977).
10. Hovanessian, A. G., Brown, R. E. & Kerr, I. M. *Nature* **268**, 537–539 (1977).
11. Nilsen, T. W. & Baglioni, C. *Proc. natn. Acad. Sci. U.S.A.* **76**, 2600–2604 (1979).
12. Galster, R. L. & Lengyl, P. *Nucleic Acids Res.* **3**, 581–598 (1976).
13. Aujean, O., Sanceau, J., Falcoff, E. & Falcoff, R. *Virology* **92**, 583–586 (1979).
14. Pitha, P. M., Rowe, W. P. & Oxman, M. N. *Virology* **70**, 324–338 (1976).
15. Wong, P. K. Y. *et al. Cell* **10**, 245–252 (1977).
16. Chang, E. H. & Friedman, R. M. *Biochem. biophys. Res. Commun.* **77**, 392–398 (1977).
17. Bandyopadhyay, A. K., Chang, E. H., Levy, C. C. & Friedman, R. M. *Biochem. biophys. Res. Commun.* **87**, 983–988 (1979).
18. Salzberg, S., Bakhanashvili, M. & Aboud, M. *J. gen. Virol.* **40**, 121–130 (1978).

Identification of the lethal target of benzylpenicillin in *Streptococcus faecalis* by *in vivo* penicillin binding studies

R. Fontana*, P. Canepari†, G. Satta† & J. Coyette‡

*Istituto de Microbiologia, Università di Padova, Padova, Italy
†Istituto di Microbiologia, Università di Genova, Genova, Italy
‡Service de Microbiologie, Faculté de Médecine, Université de Liège, Liège, Belgium

The mode of bacterial killing by penicillins is still unknown in spite of many studies on the subject. The recent finding of multiple penicillin binding proteins (PBPs) in sensitive bacteria and the possibility of analysing the binding of the antibiotic to exponentially growing cells have provided new directions for investigating this problem[1-3]. Sensitivity to lethal and other effects of penicillin varies very significantly with the conditions of growth of the cells. If PBPs were the penicillin target, changes in conditions of growth causing variations in penicillin sensitivity should be accompanied by changes in these proteins. Furthermore, if one of PBPs could be identified as the killing target, it could possibly be demonstrated to show changes in cells growing in different conditions. We show here that in *Streptococcus faecalis* ATCC 9790 changes in conditions of growth are accompanied by changes in PBPs. Furthermore, in the presence of the minimal dose of ^{14}C-benzylpenicillin causing complete inhibition of cell growth, 100% of the total radioactivity is bound to a single protein (PBP 3).

To study the effect of benzylpenicillin on cells growing in different conditions, we have incubated the cells in the chemically defined medium (CDM) described by Shockman[4] at the

0028-0836/80/360070—03$01.00

temperature optimal for growth (45 °C, generation time 31.5 min) and at a temperature allowing a 1.5-fold lower growth rate (32 °C, generation time 47.27 min).

At 32 and 45 °C, the minimal doses of benzylpenicillin which inhibited cell growth (MIC) were 4 and 0.04 μg ml^{-1}, respectively, thus confirming the apparent direct dependence of penicillin sensitivity of *S. faecalis* cells on the growth rate.

Membranes from cells growing exponentially at 32 and 45 °C were treated with ^{14}C-benzylpenicillin and PBPs detected by polyacrylamide gel electrophoresis and fluorography as described in Fig. 1 legend. As Fig. 1 and Table 1 show, for most of the proteins, the proportion of the total radioactivity bound by the same protein at the two temperatures is clearly different. Note that the various PBPs respond in different ways to the changes of temperature: PBPs 1, 2 and 3 are present in a larger relative amount in membranes from cells grown at 45 than at 32 °C, whereas an increase in the relative amount of PBP 6 is found at the latter compared with the former temperature. This indicates that the changes in PBPs are not due to a nonspecific effect of temperature on these proteins. This was confirmed by the fact that, regardless of growth temperature, binding of penicillin was unaffected by the temperature (32, 37 or 45 °C) used during the binding assay (data not shown). Finally, PBPs of membranes from cells grown at 32 °C in streptococcal broth (SB)[5], a condition allowing a generation time of 35 min, appeared grossly different from those observed in membranes from cells grown at the same temperature in CDM and rather similar to those from cells grown in CDM at 45 °C (Fig. 1). Thus, two different conditions (temperature of incubation and growth medium) associated with changes in growth rate of the cells are also accompanied by changes in the physiological status of PBPs.

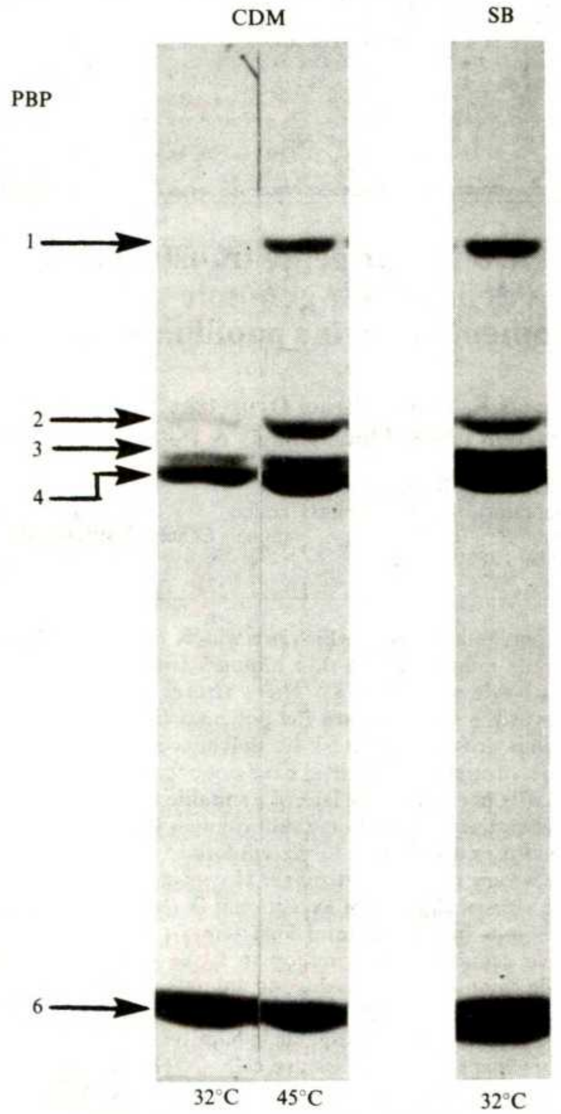

Fig. 1 Penicillin binding proteins of *S. faecalis* grown in different conditions. Membranes were prepared from cells exponentially growing in CDM (chemically defined medium) and in SB (streptococcal broth) and treated with 20 μM ^{14}C-benzylpenicillin (58 Ci mol^{-1}) at 37 °C for 15 min as described in ref. 5. The proteins were then fractionated by SDS-polyacrylamide gel electrophoresis[13] and the PBPs detected by fluorography[14]. PBP 5 has not been detected on these gels; this protein, like the PBPs 7 and 8 of *E. coli*[2], is not consistently observed.

Table 1 Per cent of radioactivity bound to PBPs in *S. faecalis* grown at 32 and 45 °C in CDM

		Per cent of radioactivity bound to				
		PBP 1	PBP 2	PBP 3	PBP 4	PBP 6
Isolated membranes	*A*	1.5	2.7	3.4	24.9	67.2
	B	8.7	11.4	15.7	26.6	37.4
Whole cells	*A*	1.7	1.4	14.2	21.1	57.3
	B	12.4	5.5	25.6	31.3	24.9

The amount of radioactivity bound to PBPs was determined by scanning the fluorograms shown in Figs 1 and 2*Af* and *Bf* with a Joyce-Loebl microdensitometer and calculating the area of the peaks thus obtained. The amount of radioactivity bound to each PBP is expressed as per cent of the total radioactivity bound. *A*, Cells grown at 32 °C; *B*, cells grown at 45 °C.

Cells growing exponentially at 32 and 45 °C were then treated with different concentrations of ^{14}C-benzylpenicillin and PBPs detected by polyacrylamide gel electrophoresis and fluorography. It is evident from Fig. 2 that the relative amount of radioactivity bound to the various PBPs of cells growing at different rates is also different when tested by *in vivo* binding experiments. Note that the differences observed in these conditions, although not similar for all proteins (compare PBPs 1 and 3), were most often of the same type as seen in isolated membranes (see Table 1). The differences between membranes and whole cells could be due to the different accessibility of some PBPs in whole cells and isolated membranes. Alternatively, they could depend on the incomplete saturation of PBPs in whole cells.

Concerning identification of the PBP that could be the lethal target of penicillin, Fig. 2 shows that only PBP 3 binds the antibiotic in cells growing at 45 °C in the presence of 0.04 μg ml^{-1} of ^{14}C-benzylpenicillin, a concentration corresponding to the MIC. In cells growing at 32°C and in the presence of the above concentration of antibiotic, PBP 3 was again the only protein that bound radioactivity. However, in these cells, the radioactivity bound to PBP 3 was approximately fourfold lower

Table 2 Evaluation of the absolute amount of radioactivity bound to PBPs in cells growing in the presence of various ^{14}C-benzylpenicillin concentrations

^{14}C-benzyl-penicillin concentration (μg ml^{-1})		Area of the peak (mm^2) corresponding to				
		PBP 1	PBP 2	PBP 3	PBP 4	PBP 6
0.02	*A*	—	—	43	—	—
	B	—	—	100	—	—
0.04	*A*	—	—	53	—	—
	B	—	—	228	—	—
0.08	*A*	—	11	82	—	—
	B	48	40	252	—	—
0.32	*A*	6	15	112	32	54
	B	72	48	274	—	21
0.80	*A*	32	18	189	297	580
	B	105	57	280	324	63
4.00	*A*	25	20	200	352	804
	B	161	72	332	406	322

The intensities of the bands were measured by scanning the fluorograms shown in Fig. 2*A* and *B* and calculating the area of the peaks thus obtained. *A*, Cells growing at 32 °C; *B*, cells growing at 45 °C.

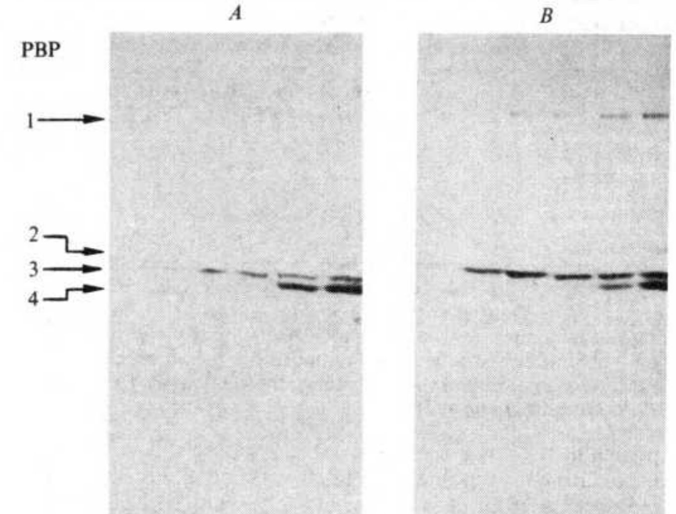

Fig. 2 Penicillin binding to membrane proteins in whole cells of *S. faecalis*. Samples (10 ml) of cells exponentially growing at 32 (A) or 45 °C (*B*) (2×10^8 bacteria per ml) were treated with doses of ^{14}C-benzylpenicillin ranging from 0.02 to 4 μg ml^{-1}. After 5 min, 10 mM cold penicillin was added, the cultures were rapidly chilled and membranes from cells were prepared as described previously[5] with the only exception that lysozyme digestion was carried out by incubating the cells for 30 min at the same temperature as used for growth. No significant breakdown of PBP–penicillin complexes occurred during the preparation of membranes, as only PBP 4 showed a 10% loss of the radioactive label after 30 min of incubation at either temperature (data not shown). Electrophoresis of radioactive membranes and detection of PBPs were carried out as described previously[13,14]. The following concentrations of ^{14}C-benzylpenicillin were used (μg ml^{-1}): *a*, 0.02; *b*, 0.04; *c*, 0.08; *d*, 0.32; *e*, 0.8; *f*, 4.

than that bound in cells growing at 45 °C in the same conditions (Table 2). In the presence of the minimal concentration of benzylpenicillin causing inhibition of cell growth at 32 °C, all PBPs bound radioactivity and the amount of ^{14}C-benzylpenicillin bound by PBP 3 was very close to that bound in the presence of the MIC at 45 °C (Fig. 2, Table 2).

The data presented here clearly indicate that growth of cells incubated at 45 °C could be inhibited through specific binding of penicillin to PBP 3. This protein seems to be the lethal target in *S. faecalis* and sensitivity to the antibiotic seems to depend on the capability of penicillin to bind it. Furthermore, (1) penicillin binds only to PBP 3 in cells growing at 45 °C in the presence of the MIC of the antibiotic; (2) in cells which require a much higher dose of antibiotic for inhibition, a much reduced amount of radioactivity is bound to PBP 3; (3) in the presence of the respective MIC of penicillin at both 32 and 45 °C, the same amount of radioactivity is bound to PBP 3. This could suggest that a minimal dose of penicillin is required to bring about interference with the vital function of PBP 3. Spratt has recently described a mutant of *Escherichia coli* in which resistance to mecillinam is due to the reduced capability of PBP 2 to bind the antibiotic[2]. Similarly, the reduced sensitivity to penicillin of *S. faecalis* observed at 32 °C could be due to the reduced amount of penicillin bound by PBP 3.

Alternatively, the reduced sensitivity observed at 32 °C could be due to the fact that PBP 3 cannot be the lethal target in cells growing in these conditions. This possibility is supported by the fact that the amount of penicillin bound to other PBPs also changes in these conditions. PBPs could perform their functions by interacting in a complex way so that the function of each one (or some of them) depends on the activity of other PBPs (see also ref. 6). In *S. faecalis*, PBP 3 could have an essential role in cell growth at 45 °C, but not at 32 °C, due to changes in the physiological status of this and other PBPs. This could explain different effects observed by various authors and the different mechanisms of bacterial killing proposed[7-12]. Penicillins could have the main property of binding to proteins and interfering with their functions. The effects of penicillins could then depend on the specific function of the bound proteins in a given system and in specific experimental conditions.

This work was supported by a NATO research grant 1683, and by grant 59/78.01874.65 from the Consiglio Nazionale delle Ricerche.

Received 14 April; accepted 23 June 1980.

1. Blumberg, P. M. & Strominger, J. L. *Bact. Rev.* **38,** 291–335 (1974).
2. Spratt, B. G. *Proc. natn. Acad. Sci. U.S.A.* **72,** 2999–3003 (1975); *Nature* **274,** 713–715 (1978).
3. Reynolds, P. E., Shepherd, S. T. & Chase, H. A. *Nature* **271,** 568–570 (1978).
4. Shockman, G. D. in *Analytical Microbiology* (ed. Kavanagh, F.) 567 (Academic, New York, 1962).
5. Coyette, J., Ghuysen, J. M. & Fontana R. *Eur. J. Biochem.* **88,** 297–305 (1978).
6. Giles, A. F. & Reynolds, P. E. *Nature* **280,** 167–168 (1979).
7. Satta, G., Canepari, P., Botta, G. & Fontanna, R. *J. Bact.* **142** (1980).
8. Wise, E. M. & Park, J. T. *Proc. natn. Acad. Sci. U.S.A.* **54,** 75–81 (1965).
9. Tipper, D. J. & Strominger, J. L. *Proc. natn. Acad. Sci. U.S.A.* **54,** 1133–1141 (1965).
10. Hammes, W. P. *Eur. J. Biochem.* **70,** 107–113 (1976).
11. Tomasz, A. & Waks, S. *Proc. natn. Acad. Sci. U.S.A.* **72,** 4162–4166 (1975).
12. Fontana, R., Satta, G. & Romanzi, C. A. *Antimicrob. Ag. Chemother.* **12,** 745–747 (1977).
13. Laemli, U. K. & Favre, M. *J. molec. Biol.* **80,** 575–599 (1973).
14. Bonner, W. M. & Laskey, R. A. *Eur. J. Biochem.* **46,** 83–88 (1974).

In vitro tumorigenic transformation by a defined sub-genomic fragment of bovine papilloma virus DNA

Douglas R. Lowy*, Israel Dvoretzky*, Ralph Shober†, Ming-Fan Law‡, Linda Engel‡ & Peter M. Howley‡

* Dermatology Branch,
† Laboratory of Tumor Virus Genetics,
‡ Laboratory of Pathology, National Cancer Institute, Bethesda, Maryland 20205

The papillomaviruses, which are widely distributed in nature, typically induce benign skin tumours (warts) in their natural hosts (reviewed in ref. 1). These viruses are members of the papovavirus group, as are the polyomaviruses[2]. In contrast to polyomaviruses such as SV40, polyoma and BK (reviewed in ref. 3), the papillomaviruses have not been extensively studied, primarily because of the lack of a suitable tissue culture system. In general, the proliferative skin changes induced by the papillomaviruses are limited to the epidermal cells, and the viruses have a very narrow host range. However, some bovine papilloma viruses (BPV) are exceptional in that they induce fibropapillomas in their natural host (cows); these BPV can also induce cellular transformation in tissue culture[4-6] and fibroblastic tumours in heterologous animals, including hamsters[7], mice[5] and horses[8,9]. BPV DNA from virions can also transform rodent cells and is tumorigenic in hamsters[10]. Recently, a tissue culture focus assay[11] in mouse cells (NIH 3T3 and C127) has been described for those BPV which are the aetiological agents of fibropapillomas in cows. The virally transformed cells, which did not contain infectious virus, grew in soft agar and were tumorigenic in nude (*nu*/*nu*) mice. We[12] have recently molecularly cloned the entire genomes of BPV-1 and BPV-2 (ref. 13) in *Escherichia coli* K12 using the certified plasmid vector pBR322 (ref. 14). We now demonstrate that these cloned DNAs can transform NIH 3T3 and C127 cells. Further, a molecularly cloned fragment which contains 69% of the BPV-1 genome can also induce cellular transformation.

A linear physical map of the 8-kilobase pair closed circular BPV-1 DNA genome (from papilloma 307) is shown at the top of Fig. 1. Restriction endonucleases *Hin*dIII, *Bam*HI, *Eco*RI and *Hpa*I each cleave the viral DNA once, at 0, 0.31, 0.60 and 0.88 map units, respectively[15]. The BPV DNA genome was cloned in pBR322 at the *Bam*HI site (clone 8-2) and also at the *Hin*dIII site (clone 9-1)[12]. After digestion with the enzyme used to insert BPV DNA into the pBR322 vector, the DNA was transfected[16] into C127 and NIH 3T3 mouse cells. Within 2 weeks, foci of transformed cells appeared in each cell line (Fig. 1, expt 1). These foci, which were more distinct on the C127 cells than in the NIH 3T3 cells, were indistinguishable morphologically from foci induced by BPV virions in the same cells. Transfection of NIH 3T3 cells resulted in two to three times more foci than observed in C127 cells with either BPV-1 cloned DNA; this greater sensitivity of the NIH 3T3 cells was also noted following infection with whole virions[10]. In each cell line the two different BPV-1 DNA preparations induced a similar number of foci. BPV-2 DNA, which shows extensive sequence homology with BPV-1 DNA, was cloned in pBR322 at its unique *Hin*dIII site; after digestion with *Hin*dIII, this cloned DNA also induced foci in this transfection experiment (data not shown).

Because BPV-1 DNA linearized at either the *Hin*dIII or *Bam*HI site was equally efficient in transforming these mouse cells, it seemed likely that some BPV-1 sequences might not be required for the induction of cellular transformation. We therefore examined the ability of defined sub-genomic fragments of the cloned viral DNAs to transform the mouse cells. The DNA fragments were prepared by digestion of the *Bam*HI BPV-1 DNA insert with a second restriction endonuclease which cleaved the BPV DNA at a unique site (*Hin*dIII, *Eco*RI and *Hpa*I). The BPV fragments were separated by agarose gel electrophoresis, individually eluted from the gel and transfected into the mouse cells. Of the various cleavage products tested, only the 69% *Bam*HI/*Hin*dIII fragment still induced foci, although its efficiency was lower than that of the complete BPV genome (expt 2). The other sub-genomic fragments tested failed to induce foci.

Table 1 Growth in agar and tumorigenicity of BPV DNA transformants

Transforming agent	Colony formation in agar	Tumour formation in nude mice
Control cells	0	0/4
BPV-1 virus	1.4×10^{3}*	4/4†
*Hin*dIII genome, focus 52	0.6×10^{3}	4/4
*Bam*HI genome, focus 33	2.2×10^{3}	4/4
*Bam*HI genome, focus 43	1.3×10^{3}	4/4
69% Fragment clone 17-6, focus 21	0.8×10^{3}	4/4
69% Fragment clone 17-6, focus 22	1.6×10^{3}	4/4
69% Fragment clone 17-2, focus 24	1.1×10^{3}	4/4
69% Fragment clone 17-2, focus 25	1.9×10^{3}	4/4

Each BPV DNA transformant was isolated from a different dish of C127 cells to ensure that each was separately derived. Each focus of transformed cells was picked 3 weeks after transfection of DNA and propagated separately. Colony formation in 0.35% agar was carried out as described elsewhere[18]. Weanling nude mice were inoculated subcutaneously with 10^6 transformed cells. Tumours were present in all animals by 3 weeks after inoculation. Control animals were observed for 8 weeks.

* No. of colonies per 10^4 cells.

† No. of mice with tumours/no. of mice inoculated with cells.

To eliminate the possibility that the infectivity of the 69% *Bam*HI/*Hin*dIII fragment might be due to the transfection of additional BPV DNA sequences contaminating this DNA in the agarose gel, this fragment and the 31% *Bam*HI/*Hin*dIII fragment were each subcloned in pBR322 from the *Bam*HI BPV clone. Two subclones of each fragment were tested in the C127 mouse cell transfection assay. After separating the BPV DNA from the pBR DNA by digestion with *Bam*HI/*Hin*dIII, both the 69% fragment clones induced foci but the 31% fragment clones failed to do so (expt 3). As noted previously, the specific infectivity of the 69% sub-genomic fragment was lower than that of the complete viral genome. Southern blot analysis of DNA from the transformed cells has indicated that, as expected, the transformants contained BPV DNA sequences from the 69% fragment and no sequences which hybridized with the 31% fragment (M.-F.L. *et al.*, unpublished data).

A good correlation has been noted[17] between anchorage-independent growth of transformed cells and their capacity to be tumorigenic in nude mice. The ability of the BPV-transformed

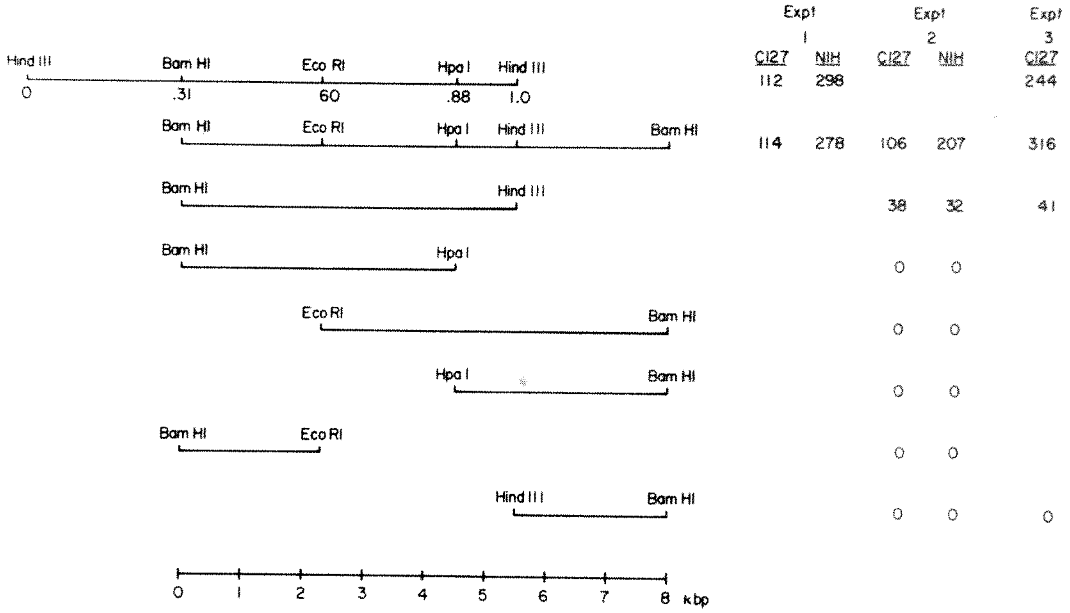

Fig. 1 Duplicate dishes were transfected with restriction endonuclease-digested DNA (0.1 to 0.5 μg per dish) using calf thymus DNA (25 μg ml^{-1}) as carrier[16,24] (similar results were obtained when NIH 3T3 DNA was used as carrier). Foci were counted at 2 weeks for C127 cells and 4 or 5 days later for NIH 3T3 cells. Results are expressed as focus forming units per μg BPV DNA. pBR322 controls were included with each experiment and did not induce foci. A zero means that no foci were observed after testing 1 μg of DNA. In expt 2, the *Bam*HI DNA insert from clone 8-2 was digested with each of the other three enzymes. The DNA was electrophoresed in a 1% agarose gel after restriction endonuclease digestion. The ethidium bromide-stained BPV DNA bands were cut out of the gel and transfected into the cells as previously described[24]. In expt 3, the 69% and 31% *Bam*HI/*Hin*dIII fragments used were clones 17-6 and 16-9, respectively. The DNAs were digested with *Hin*dIII/*Bam*HI, electrophoresed and transfected as in expt 2. kbp, Kilobase pairs.

cells to form colonies in agar[18] and to induce tumours in weanling nude mice has therefore been tested. Transformants derived from individual foci induced in C127 cells by the *Hin*dIII BPV genome, the *Bam*HI BPV genome and the 69% *Bam*HI/*Hin*dIII fragment all grew in soft agar; these cells also induced tumours in the mice after a latent period of 2–3 weeks (Table 1). Mice inoculated with control cells did not develop tumours during 8 weeks of observation.

These observations indicate that not all sequences of the BPV genome are required for cellular transformation. In this regard, the results are similar to those reported for other DNA tumour viruses, such as polyomaviruses and adenoviruses (reviewed in ref. 19). The sequences contained in the 31% *Bam*HI/*Hin*dIII fragment were not essential for the induction of transformation. It is likely that further study may reveal additional BPV sequences which are not required for transformation.

It is not clear why the transforming efficiency of the subgenomic fragment was lower than that of the entire viral genome. It is possible that some of the BPV sequences from 0–0.31 map units may have a specific facilitative role, as has been shown in transformation[20–22] by retroviruses. Alternatively, the smaller size of the fragment or the presence of non-homologous ends may introduce physical constraints which by themselves lower the efficiency of the transfection assay, if circularization of the viral DNA occurs. These or other possibilities may be evaluated by future studies.

The precise relevance of these *in vitro* results to *in vivo* tumours induced by BPV or other papillomaviruses remains to be established. From our data, it may be speculated that *in vivo* transformation of epidermal and fibroblastic cells by BPV does not depend on viral replication. This hypothesis is supported by the observation that the fibroblastic component of BPV-induced tumours does not contain detectable amounts of infectious virus[8]. Some data also suggest that the results obtained with BPV may be relevant to infection with other papillomaviruses. It has recently been demonstrated[23] that BPV DNA (types 1 and 2) contains nucleotide sequences which show homology with human papilloma virus type 1 and with Shope rabbit papilloma virus; this suggests that these viral genomes may be organized similarly. It may further be significant that one of these regions of homology is contained within the transforming 69% *Bam*HI/*Hin*dIII BPV-1 DNA fragment.

Received 7 March; accepted 23 June 1980.

1. Orth, G., Breitburd, F., Favre, M. & Croissant, O. in *Origins of Human Cancer* (eds Hiatt, H. H., Watson, J. D. & Wisten, J. A.) 1043–1068 (Cold Spring Harbor Laboratory, New York, 1977).
2. Melnick, J. L. *et al. Intervirology* **3,** 106–120 (1974).
3. Howley, P. M. in *Viral Oncology* (ed. Klein, G.) 489–550 (Raven, New York, 1980).
4. Black, P. H., Hartley, J. W., Rowe, W. P. & Huebner, R. J. *Nature* **199,** 1016–1018 (1963).
5. Boiron, M., Levy, J. P., Thomas, M., Friedman, J. C. & Bernard, J. *Nature* **201,** 423–424 (1964).
6. Thomas, M., Boiron, M., Tanzer, J., Levy, J. P. & Bernard, J. *Nature* **202,** 709–710 (1964).
7. Friedman, J. C. *et al. C.r. hebd. Séanc. Acad. Sci., Paris* **257,** 2328–2331 (1963).
8. Olson, C., Gordon, D. E., Robl, M. G. & Lee, K. P. *Archs envir. Hlth* **19,** 823–839 (1969).
9. Lancaster, W. D., Olson, C. & Meinke, W. *Proc. natn. Acad. Sci. U.S.A.* **74,** 524–528 (1977).
10. Boiron, M., Thomas, M. & Chenaille, P. *Virology* **26,** 150–153 (1965).
11. Dvoretzky, I., Shober, R., Chattopadhyay, S. K. & Lowy, D. R. *Virology* **103,** 369–375 (1980).
12. Howley, P. M. *et al.* in *Viruses in Naturally Occurring Cancers* (eds Essex, M. *et al.*) (Cold Spring Harbor Laboratory, New York, in the press).
13. Lancaster, W. D. & Olson, C. *Virology* **89,** 372–379 (1978).
14. Bolivar, F. *et al. Gene* **2,** 95–113 (1977).
15. Lancaster, W. D. *J. Virol.* **32,** 684–687 (1979).
16. Graham, F. J. & van der Eb, A. J. *Virology* **52,** 456–461 (1973).
17. Shin, S., Freedman, V. H., Risser, R. & Pollack, R. *Proc. natn. Acad. Sci. U.S.A.* **72,** 4435–4439 (1975).
18. MacPherson, I. & Montagnier, L. *Virology* **23,** 291–294 (1964).
19. Graham, F. L. *et al. Cold Spring Harb. Symp. quant. Biol.* **39,** 637–650 (1974).
20. Andersson, P., Goldfarb, M. P. & Weinberg, R. A. *Cell* **16,** 63–75 (1979).
21. Oskarsson, M., McClements, W. L., Blair, D. L., Vande Woude, G. F. & Maizel, J. V. *Science* **207,** 1222–1224 (1980).
22. Chang, E. H. *et al. J. Virol.* **35,** 76–92 (1980).
23. Law, M.-F., Lancaster, W. D. & Howley, P. M. *J. Virol.* **32,** 199–207 (1979).
24. Lowy, D. R., Rands, E. & Scolnick, E. M. *J. Virol.* **26,** 291–298 (1978).

0028-0836/80/360074—03$01.00

Calcium-dependent phosphorylation of histone H3 in butyrate-treated HeLa cells

James P. Whitlock Jr, Robert Augustine & Howard Schulman

Department of Pharmacology, Stanford University School of Medicine, Stanford, California 94305

Ca^{2+} is prominant in the control of cell proliferation and function[1,2]. However, the biochemical mechanism(s) mediating its effects on nuclear events is unknown. We report here that Ca^{2+}, at physiological concentrations, stimulates the phosphorylation of histone H3 by an endogenous protein kinase in HeLa cell nuclei. Also, pretreatment of cells with Na butyrate, which increases histone acetylation, selectively increases the susceptibility of histone H3 to phosphorylation by the protein kinase. Our results reveal a potential link between histone H3 acetylation and phosphorylation, modifications which are thought to have important effects on chromatin structure and function and suggest a possible mechanism whereby stimuli at the cell surface (such as hormones, mitogens and drugs) may influence biochemical events at the nuclear level; changes in the intracellular Ca^{2+} concentration may influence the phosphorylation of chromosomal proteins, mediated by Ca^{2+}-dependent kinases in the nucleus.

HeLa cells are known to contain a nuclear kinase(s) which phosphorylates histone H3 (ref. 3). We studied histone phosphorylation by incubating HeLa nuclei with [γ-^{32}P]ATP. The nuclei were then washed in 0.3 M NaCl to remove many of the non-histone nuclear proteins. The salt-washed nuclei were extracted with dilute HCl, and the acid-soluble proteins were precipitated and analysed by SDS–polyacrylamide gel electrophoresis and autoradiography. The autoradiogram shown in Fig. 1 indicates that radioactive phosphate is incorporated into an acid-soluble protein which has a mobility identical to that of histone H3. Additional experiments (not shown) indicate that this protein is not removed when nuclei are washed in 0.6 M NaCl but is removed when the NaCl concentration is raised to 2.0 M. Thus, the properties of this protein are identical to those of histone H3 (ref. 4).

Ca^{2+}, at submicromolar concentrations, causes a marked and selective stimulation of ^{32}P incorporation into histone H3 (Fig. 1). In these experiments, the free Ca^{2+} concentration was varied by using a Ca^{2+}-EGTA buffer containing 0.4 mM EGTA (ref. 5). Quantitative densitometry of the autoradiograms indicates that Ca^{2+}, at concentrations of 0.1 μM and 0.5 μM, increases the phosphorylation of histone H3 two- to threefold. Higher Ca^{2+} concentrations (up to 10 mM) produce no further increase in H3 phosphorylation (data not shown). Thus, the phosphorylation of histone H3 is stimulated by Ca^{2+} at concentrations which are presumably physiological. In analogous experiments, we observed that cyclic AMP (10 μM) and cyclic GMP (10 μM) had no effect on H3 phosphorylation (data not shown).

The amino acid residues in histone H3 which are known to undergo phosphorylation are located in the amino terminal region of the protein[6]; this is the same region which undergoes acetylation *in vivo*[6]. We therefore wondered whether one type of histone H3 modification (acetylation) influenced the susceptibility of the protein to a second type of modification (phosphorylation). Cells cultured in the presence of butyric acid accumulate hyperacetylated histones, due to the inhibition of histone deacetylation by butyrate[7–13]. In agreement with the observations of others, we find that exposure of HeLa cells to 5 mM Na butyrate for 16–24 h produces marked acetylation of histones, as judged by the distribution of acetylated forms of

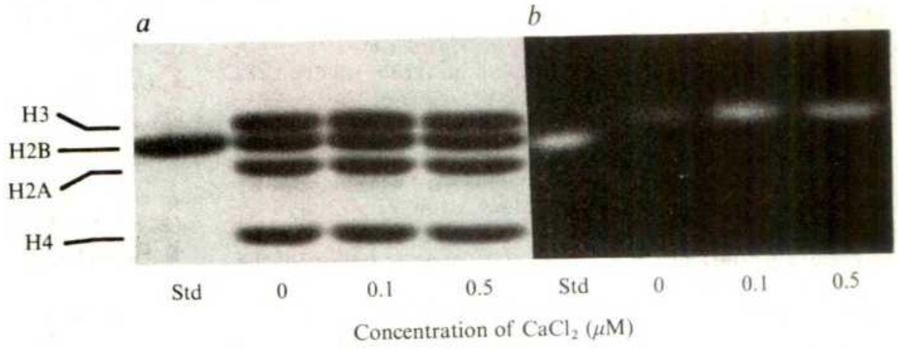

Fig. 1 Calcium-dependent phosphorylation of histone H3 in HeLa cells: *a*, stained gel; *b*, autoradiogram. HeLa cells were grown in monolayers to approximate confluence in Dulbecco's modified Eagle's medium (Gibco). Cells were washed twice with ice-cold phosphate-buffered saline (PBS), collected by scraping into PBS, and pelleted. Nuclei were prepared by Dounce homogenization in the presence of 1% Triton X-100 (ref. 21). Washed nuclei were suspended in a solution of 0.15 M NaCl, 5 mM MgCl$_2$, 5 mM dithiothreitol and 5 mM Na butyrate in 50 mM Tris–HCl, *p*H 7.5 containing the indicated concentration of free Ca^{2+}. The free Ca^{2+} concentration was calculated using an apparent binding constant for Ca^{2+}–EGTA of 7.61×10^6 M^{-1} (ref. 22). The reaction was started by the addition of [γ-^{32}P]ATP (Amersham; 10–50 Ci mmol^{-1}) to a final concentration of 1 μM. Nuclei were incubated at room temperature (22 °C) for 5 min. Preliminary experiments indicated that, under these conditions, the phosphorylation of histone H3 continues to completion. The phosphorylation reaction was stopped by the addition of EDTA to a final concentration of 10 mM. Nuclei were washed following the addition of NaCl to a final concentration of 0.3 M and the salt-washed nuclei were collected by centrifugation. The salt-washed nuclei were extracted for 1 h with ice-cold 0.25 M HCl and centrifuged to pellet the precipitate. The supernatant was removed and precipitated overnight at −20 °C by the addition of 10 volumes of acetone. The precipitate was collected by centrifugation, dissolved in sample buffer and analysed by electrophoresis in discontinuous SDS–polyacrylamide gels[23]. Purified calf thymus histone H2B (Boehringer-Mannheim) was phosphorylated *in vitro*, using [γ-^{32}P]ATP and a purified cyclic AMP-dependent protein kinase and was included in the analysis as a molecular weight standard. The gels were stained with Coomassie blue, destained, and subjected to autoradiography as previously described[23,24]. Electrophoresis was from top to bottom. The positions of the core histones are indicated. Std, H2B standard.

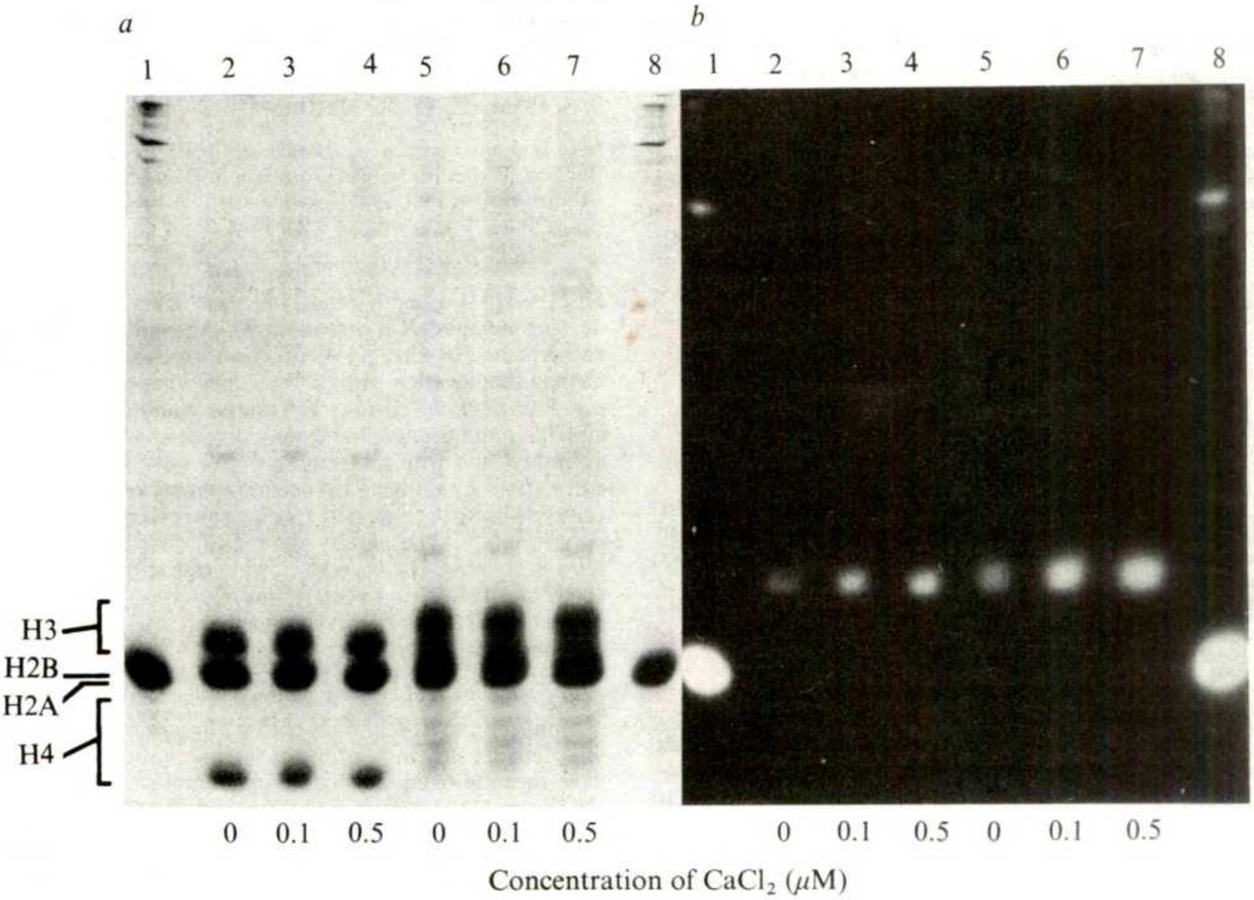

Fig. 2 Histone H3 phosphorylation in butyrate-treated HeLa cells: *a*, stained gel; *b*, autoradiogram. Cells were incubated for 16 h in the absence or presence of Na butyrate (5 mM). Cells were collected and nuclei were prepared as described in the legend to Fig. 1, except that, in the case of butyrate-treated cells, all solutions contained 5 mM Na butyrate. The phosphorylation reaction and isolation of acid-soluble proteins was as described in the legend to Fig. 1. The acetone precipitate was dissolved in sample buffer and analysed by electrophoresis in polyacrylamide gels containing acetic acid and urea[12]. Gels were stained in Coomassie blue, destained, and subjected to autoradiography as previously described[23,24]. Electrophoresis was from top to bottom. The positions of the core histones are indicated. Lanes 1 and 8, H2B standard; lanes 2–4, control (not butyrate-treated); lanes 5–7, butyrate-treated.

histone H4 after electrophoresis in polyacrylamide gels containing acetic acid and urea.

We prepared nuclei from control and butyrate-treated cells (5 mM, 16 h), incubated them in the presence of $[\gamma\text{-}^{32}\text{P}]$ATP, washed the nuclei in 0.3 M NaCl, extracted the nuclei with dilute HCl, and analysed the acid-soluble protein by electrophoresis in acetic acid–urea–polyacrylamide gels, followed by autoradiography. The results (Fig. 2) indicate that histone H3 in butyrate-treated cells is more susceptible to phosphorylation than is histone H3 from control cells. Quantitative densitometry of the autoradiogram indicates that two to three times as much phosphate is incorporated into histone H3 in butyrate-treated cells as is incorporated into histone H3 in control cells (data not shown). In both control and butyrate-treated cells, the phosphorylation of histone H3 is stimulated two- to threefold in the presence of submicromolar concentrations of Ca^{2+} (Fig. 2).

Several kinds of experiments suggest that it is acetylation, *per se*, which renders histone H3 more susceptible to phosphorylation: (1) dose–response experiments (exposure of cells to 0–50 mM Na butyrate for 16 h) and time-course experiments (5 mM Na butyrate for 0–24 h) demonstrate a correlation between increased acetylation and increased phosphorylation; (2) both the hyperacetylation and the increased susceptibility to phosphorylation are rapidly reversed following the removal of butyrate (5 mM) from the medium; (3) exchange experiments (such as incubating kinase-depleted nuclei prepared from butyrate-treated cells with protein kinase activity prepared from control nuclei and vice versa) indicate that the increased phosphorylation is due to an alteration in the histone substrate rather than to a change in the kinase (data not shown).

Our results suggest that an acetylated form(s) of histone H3 is particularly susceptible to phosphorylation and that this event is Ca^{2+}-dependent. The effect of Ca^{2+} presumably reflects a stimulation of protein kinase activity, although we cannot rule out the possibility that its primary effect is to alter the conformation of the histone substrate. The absence of a stained band with a mobility identical to that of the phosphorylated H3 species indicates that it is a relatively small subpopulation of H3 molecules which becomes phosphorylated (Fig. 2). The autoradiogram (Fig. 2) indicates that the phosphorylated form(s) of histone H3 migrates more slowly than the most highly acetylated form(s) of H3 visible on the stained gel. Our findings are consistent with the idea that, in both control and butyrate-treated cells, the most highly acetylated form(s) of H3 is most susceptible to phosphorylation.

In eukaryotic cells, the arginine-rich histones H3 and H4 seem to be of fundamental importance in the folding of nuclear DNA into the nucleoprotein complex known as chromatin[14-16]. The amino acid sequences of both H3 and H4 have been highly conserved throughout evolution[17]; therefore, it is argued that, in principle, chemical modification of a histone(s) could produce important changes in chromatin structure and function. In practice, there is considerable circumstantial evidence to support the view that both acetylation and phosphorylation of the histones have substantial structural and functional effects on the nucleoprotein[6,14,17-19].

Recently, there has been renewed appreciation of the importance of Ca^{2+} in regulating various cellular functions (such as the response to hormonal stimulation and the stimulus-coupled release of neurotransmitters or peptide hormones)[1,2]. It is becoming apparent that Ca^{2+}-dependent protein kinases may mediate some of the intracellular actions of Ca^{2+} and thereby play a central role in regulating the physiological responses of the cell to changes in its external environment[20]. Such Ca^{2+}-dependent kinases have been identified in both membrane and cytosol preparations. Our experiments indicate that such an enzyme(s) may also be present in the nucleus and can utilize a chromosomal protein as a substrate, suggesting a mechanism by which changes in intracellular Ca^{2+} may influence biochemical events in the cell nucleus.

We thank Drs H. Blau, R. Kornberg and G. Ringold for reviews of the manuscript. This work was supported by NIH grant CA 24580, NIMH grant MH 32752 and BRSG grant RR 5353 from the NIH.

Received 24 January; accepted 16 June 1980.

1. Berridge, M. J. in *Advances in Cyclic Nucleotide Research* Vol. 11 (eds Greengard, P. & Robison, G. A.) 1–98 (Raven, New York, 1975).
2. Rasmussen, H. & Goodman, D. B. P. *Physiol. Rev.* **57**, 421–509 (1977).
3. Simpson, R. T. *Nucleic Acids Res.* **5**, 1109–1119 (1978).
4. Hnilica, L. S. *The Structure and Biological Function of Histones* (Chemical Rubber Co., Cleveland, 1972).
5. Schulman, H. & Greengard, P. *Proc. natn. Acad. Sci. U.S.A.* **75**, 5432–5436 (1978).
6. Dixon, G. H. *et al. Ciba Fdn Symp.* **28** (new series), 229–250 (1975).
7. Riggs, M. G., Whittaker, R. G., Newmann, J. R. & Ingram, V. M. *Nature* **268**, 462–464 (1977).
8. Boffa, L. C., Vidali, G., Mann, R. S. & Allfrey, V. G. *J. biol. Chem.* **253**, 3364–3366 (1978).
9. Vidali, G., Boffa, L. C., Bradbury, E. M. & Allfrey, V. G. *Proc. natn. Acad. Sci. U.S.A.* **75**, 2239–2243 (1978).
10. Candido, E. P. M., Reeves, R. & Davie, J. R. *Cell* **14**, 105–113 (1978).
11. Sealy, L. & Chalkley, R. *Cell* **14**, 115–121 (1978).
12. Cousens, L. S., Gallwitz, D. & Alberta, B. M. *J. biol. Chem.* **254**, 1716–1723 (1979).
13. Panyim, S. & Chalkley, R. *Archs Biochem. Biophys.* **130**, 337–346 (1969).
14. Elgin, S. C. R. & Weintraub, H. *A. Rev. Biochem.* **44**, 725–774 (1975).
15. Kornberg, R. D. *A. Rev. Biochem.* **46**, 931–954 (1977).
16. Felsenfeld, G. *Nature* **271**, 115–122 (1978).
17. Isenberg, I. *A. Rev. Biochem.* **48**, 159–191 (1979).
18. Gurley, L. R., D'Anna, J. A., Barkham, S. S., Deaven, L. L. & Tobey, R. A. *Eur. J. Biochem.* **84**, 1–15 (1978).
19. Langan, T. A. *Meth. Cell Biol.* **19**, 127–142 (1978).
20. Schulman, H. in *Handbook of Experimental Pharmacology* (eds Nathanson, J. A. & Kebabian, J. W.) (Springer, Berlin, in the press).
21. Whitlock, J. P. Jr & Simpson, R. T. *Biochemistry* **15**, 3307–3314 (1976).
22. Portzehl, H., Caldwell, P. C. & Reugg, J. C. *Biochim. biophys. Acta* **79**, 581–591 (1964).
23. Whitlock, J. P. Jr *J. biol. Chem.* **254**, 5684–5689 (1979).
24. Simpson, R. T. & Whitlock, J. P. Jr *Cell* **9**, 347–353 (1976).

Acetylation of histone H4 and its role in chromatin structure and function

S. S. Chahal*, H. R. Matthews†‡ & E. M. Bradbury†

* Portsmouth Polytechnic, Biophysics Laboratories, St Michael's Building, White Swan Road, Portsmouth, Hampshire PO1 2DT, UK
† Department of Biological Chemistry, School of Medicine, University of California, Davis, California 95616

Histone H4 is a highly conserved structural component of the nucleosome subunit of chromatin. The activation of chromatin is accompanied by changes in structure which may be caused by histone modification or by interactions of specific non-histone proteins, or both. Histone H4 can be modified by acetylation and this modification has been correlated with chromosome assembly[1] and with transcription[2]. We have now tested these correlations by studying H4 acetate content as a function of the cell cycle using the naturally synchronous cell cycle in *Physarum polycephalum*. The results show two clear correlations: (1) tetra-acetylated H4 correlates with transcription; (2) highly acetylated H4 (2 to 4 acetates per molecule) is inversely correlated with H1 phosphorylation and initiation of chromosome condensation in prophase. The results are consistent with turnover of di-acetylated H4 during chromosome assembly in S phase.

Mohberg and Rusch[3] showed that *Physarum* has histones like other eukaryotes and the bands they identified as H1 and H4 have recently been isolated[4]. The amino acid composition of *Physarum* H4 shows no significant difference from the amino acid composition of calf thymus H4. *Physarum* H4 co-migrates with calf thymus H4 in polyacrylamide gel electrophoresis (PAGE) in acetic acid–urea or SDS or Triton X-100 (Fig. 1).

Physarum H4 splits into five bands on long polyacrylamide gels with acetic acid–urea or Triton X-100 but not with SDS. Only very small amounts of ^{32}P are incorporated into *Physarum* H4 in plasmodia[5]—certainly not enough to account for the observed heterogeneity. By analogy with other H4 histones the heterogeneity was attributed to acetylation and this was confirmed by pulse-labelling experiments and by enhancement

---

‡ To whom correspondence should be addressed.

0028-0836/80/360076—04$01.00

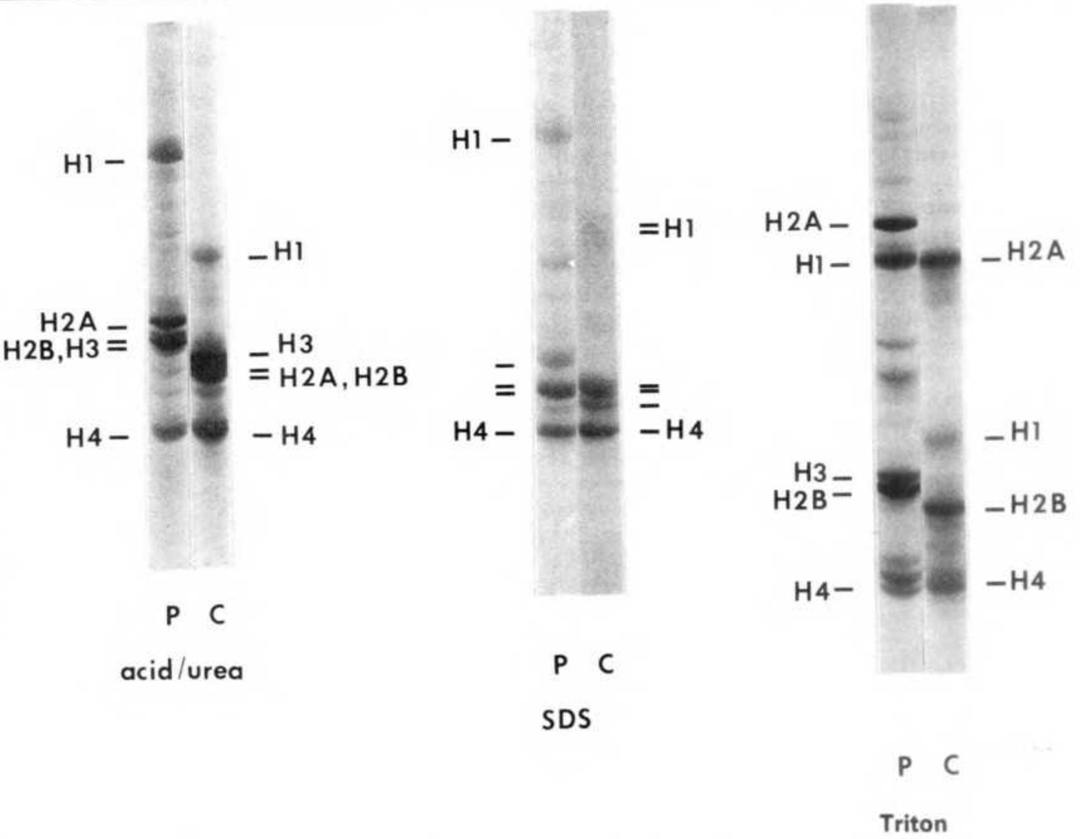

Fig. 1 Comparison of histones from *Physarum* plasmodia and calf thymus by acrylamide gel electrophoresis in the presence of SDS[35]; acetic acid and urea[8]; Triton X-100[36]. C, calf thymus; P, *Physarum*. The labelled bands were identified by electrophoresis of purified histone fractions. Electrophoresis was from top to bottom in 6-mm internal diameter glass tubes, 6 cm long. These gels are not long enough to resolve the H4 species adequately.

of the slower moving bands when butyrate[6] was added to the growth medium (Fig. 2*a*).

The proportion of *Physarum* H4 in each of the five bands was determined by PAGE in acetic acid–urea[7,8]. The H4 was first purified by chromatography on Biogel P10 to reduce the amount of protein loaded on the gels and to remove a minor component that interfered with the measurement of tetra-acetylated H4, Ac_4H4.

Figure 2*b* shows examples of gel scans of *Physarum* H4 from specific stages of the cell cycle. These and others have been analysed in terms of five gaussian peaks and the area under each peak calculated. The areas were thus fully corrected for the overlap between bands. The area corresponding to each species of H4 is plotted in Fig. 3*a* as a function of stage of the cell cycle.

It is clear that at all stages the most abundant species is mono-acetylated H4, Ac_1H4. During G2 phase the proportion of Ac_1H4 rises to ~62% and then falls to ~55%. The fall occurs during the middle part of G2, from 5 h to ~9 h after mitosis in the 11-h cycle. During the 6–9-h period after mitosis there are complementary increases in proportions of Ac_2H4 (16% to 23%), Ac_3H4 (2.5% to 4.3%) and Ac_4H4 (1% to 3%). The data imply an overall increase in acetylation during mid G2 phase. Late G2 is characterized by a sharp drop in Ac_4H4 (3% to 1%), followed in early prophase by a drop in Ac_3H4 (4% to 2%). Ac_2H4 drops sharply through late G2 and prophase (23% to 11%). In early prophase the overall proportion of highly acetylated H4 (2 to 4 acetates per moledule) is at its minimum value (13.5%). During late mitosis and early S phase the increase in proportion of highly acetylated H4 is balanced by drops in both non- and mono-acetylated H4 so that in mid S phase the proportion of highly acetylated H4 reaches its maximum (33.6%). In late S phase the proportion of highly acetylated H4 falls to a plateau level (about 26%) before the minimum (19.4%) in early G2 phase. The most dramatic changes in an individual H4 species occur in Ac_4H4 and these are shown on an expanded scale in Fig. 3*b*. There is a clear minimum (0.4%) in early prophase, a sharp maximum (3.6%) in mid S phase and a second maximum (up to 3%) in mid G2 phase.

Histone H4 is extensively modified in the cytoplasm before entry into the nucleus in duck erythroid cells[7] and in hepatoma cell culture[9]. Figure 3*a* shows a peak of Ac_2H4 in S phase nuclei that is consistent with the notion that newly synthesized H4 enters the nucleus in the di-acetyl form and is then converted to the unmodified form, which shows an increase in late S phase (M2 + 1 h to M2 + 2.5 h) following the increase in Ac_2H4 (M2 to M2 + 1 h). This suggestion is analogous to the situation in HTC cells[9] but pulse-label experiments are required to confirm this interpretation in *Physarum*.

Transcription in *Physarum* during the cell cycle is probably biphasic[10–13] with a very low level in mitosis, a high level in S phase, a low in early G2 and the second high in mid to late G2. Several lines of evidence suggest that the S phase peak is predominantly mRNA synthesis and the G2 phase peak is predominantly rRNA synthesis although the distinction, if correct, is not absolute (for reviews see refs 14, 15). The biphasic pattern correlates closely with the pattern of Ac_4H4 (Fig. 3) supporting the correlation between acetylated histones and transcription. About 2% of *Physarum* DNA codes for rRNA and associated spacer sequences (rDNA)[16,17]. If the G2 phase transcription is predominantly rRNA and is associated with Ac_4H4, then the G2 phase increase in Ac_4H4 from 1% to 3% implies that most of the H4 associated with rDNA would become tetra-acetylated in G2. This prediction can be tested directly.

D'Anna *et al.*[18] found low levels of H4 acetate in mitosis in CHO cells and in the present experiments the lowest values for the proportion of highly acetylated H4 also occur in mitosis, particularly in prophase, where, at M3, the proportion of Ac_4H4 falls as low as 0.4%. The absolute values at M2 are rather different from those at M3 but the direction of change in proportion is the same. The absolute difference may reflect a change in growth pattern as the plasmodium gets larger and the composition of the medium changes. These factors add a slow monotonic change underlying the larger cell-cycle-dependent changes. The amount of highly acetylated H4 in prophase is inversely correlated with phosphorylation of histone H1. As shown in Fig. 3*c*, the phosphate content of H1 reaches its maximum about 20 min before metaphase in *Physarum*[5]. Histone H1 also has a high phosphate content at mitosis in HeLa cells[19] and CHO cells[20].

There is substantial circumstantial evidence linking H1 phosphorylation in late G2 phase and prophase with chromosome condensation (for review see ref. 21). Consequently, it now seems that chromosome condensation may involve the coordinated modification of H1 by phosphorylation and of H4 by deacetylation. It follows that the extension of chromosomes after mitosis would be facilitated by histone acetylation and very rapid acetylation of histone H4 immediately following metaphase is observed.

Acetylation occurs on lysines -5, -8, -12 and -16 of H4 (ref. 1). The N-terminal region of H4 is unstructured in free solution and can be released from a nucleosome core particle by salt[22] or trypsin digestion[23] without a major effect on the integrity of the core particle. Consequently, acetylation of the N-terminal region might be expected to have very little effect on isolated single nucleosomes and preliminary structural studies of acetylated nucleosomes isolated from butyrate-treated HeLa S3 cells support this prediction[24,25]. In the bulk of chromatin, which is transcriptionally inactive, nucleosomes are packed into a higher order structure—the 34-nm coil of Fig. 4 (refs 26–28). It is a reasonable assumption that inter-nucleosomal interactions of the basic N-terminal regions of core histones are involved in generating the 34-nm coil. In this case, acetylation, particularly multiple acetylation of the basic N-terminal, would destabilize the 34-nm coil, causing a transition to a more extended

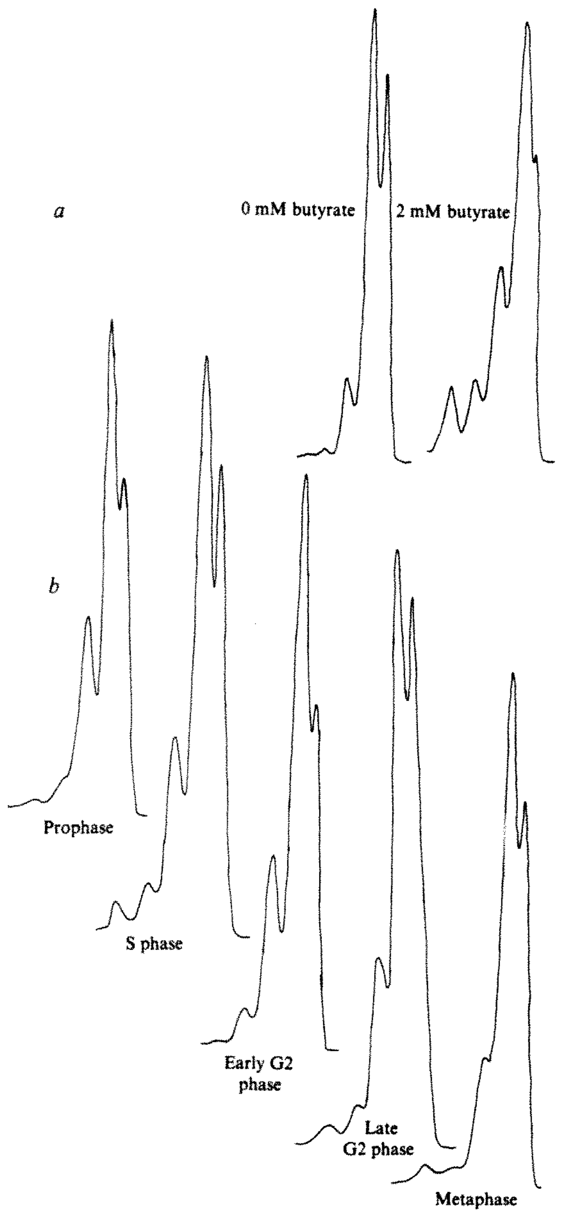

Fig. 2 Polyacrylamide gel electrophoresis of *Physarum* histone H4 in 16-cm long gels. Each profile shows five bands corresponding to 4, 3, 2, 1 or 0 acetates per molecule, reading from left to right in the direction of migration. *a*, H4 from microplasmodia grown in normal medium (left) or in medium containing 2 mM butyrate (right). *b*, H4 from macroplasmodia collected at the following stages of the mitotic cycle (from left to right): mitosis (M2 − 15 min), S phase (M2 + 1.75 h); early G2 phase (M2 + 5 h); late G2 phase (M2 + 7.5 h); and mitosis (M3). Each scan shows the H4 region of a 16-cm long tube gel electrophoresed in acetic acid plus urea[35]. The gels were stained with amido black, destained by diffusion and scanned on a Joyce-Loebl gel scanner. M2 and M3 are the second and third mitosis after fusion, respectively. The cycle time was 11 h.

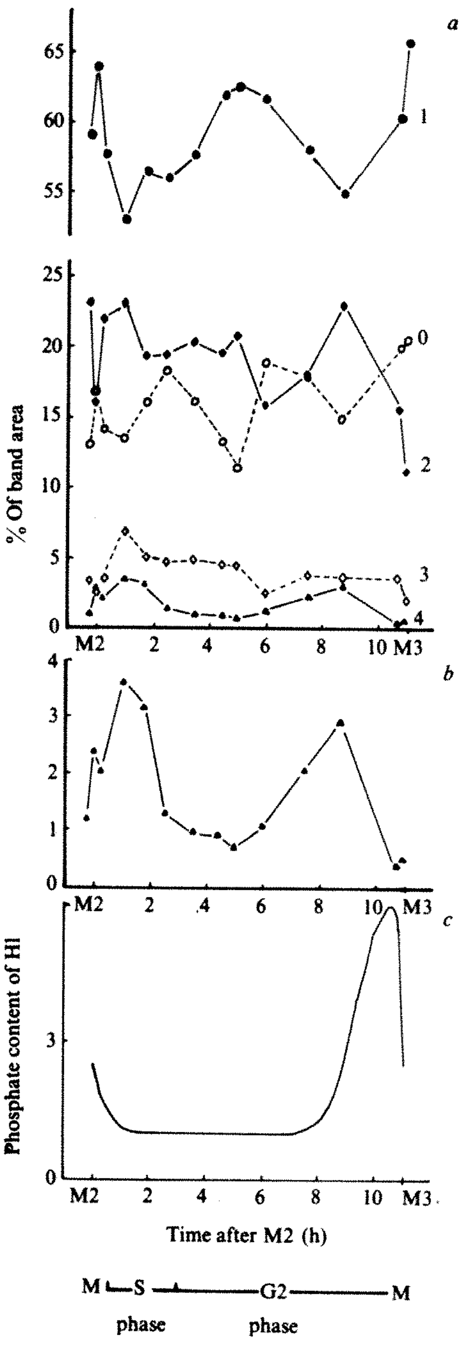

Fig. 3 Acetylated H4 through the cell cycle. *a*, ○--○ Percentage of total H4 in the non-acetylated form; ●—● percentage of total H4 in the mono-acetylated form, Ac_1H4; ◆—◆ percentage of total H4 in the di-acetylated form, Ac_2H4; ◇—◇ percentage of total H4 in the tri-acetylated form, Ac_3H4; ▲—▲ percentage of total H4 in the tetra-acetylated form, Ac_4H4. *b*, Percentage of Ac_4H4, shown on a larger scale. *c*, Relative phosphate content of *Physarum* histone H1 through the cell cycle[5].

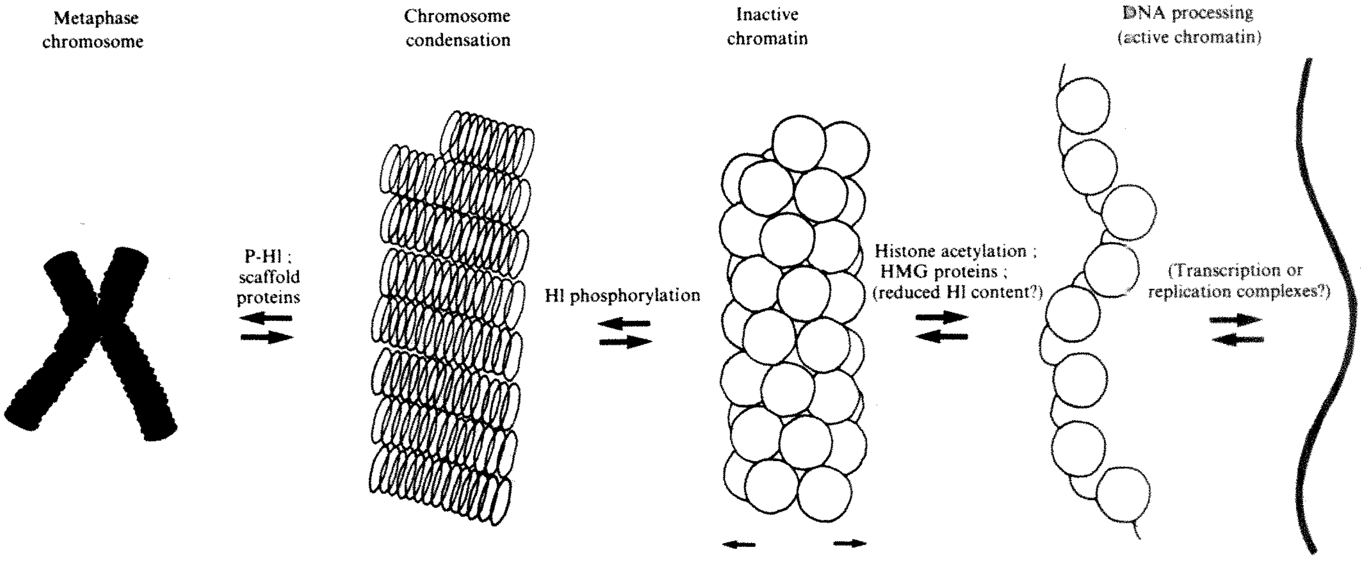
Metaphase chromosome
Chromosome condensation
Inactive chromatin
DNA processing (active chromatin)
P-H1 ; scaffold proteins
H1 phosphorylation
Histone acetylation ; HMG proteins ; (reduced H1 content?)
(Transcription or replication complexes?)

Fig. 4 Model representing the major structural transitions in chromatin. The different structural states are shown in diagrammatic form only.

conformation (Fig. 4). There is substantial evidence that transcriptionally active chromatin is in a more extended conformation than the bulk of chromatin (for example, see ref. 29) suggesting that the role of multiple H4 acetylation is to destabilize the inactive structure of chromatin (Fig. 4). Conversely, deacetylation of H4 would promote the formation of the inactive 34-nm coil and this is observed in mitosis (Fig. 3). Phosphorylation of H1 is probably involved in packing the 34-nm coils into the next order of structure (Fig. 4) and so it is inversely correlated with H4 acetylation. We anticipate one or two further orders of packing, in metaphase, leading to the metaphase chromosome and perhaps involving non-histone 'scaffold' proteins[30]. Other non-histone proteins, particularly HMG proteins[31–34], are also involved in the active chromatin structure and our present understanding of the major structural transitions in chromatin is summarized in Fig. 4.

We thank Miss S. Miller for technical assistance and our colleagues, particularly Dr R. J. Inglis and Mr A. W. Thorne, for help and discussion. The work was supported by the SRC.

Received 14 January; accepted 16 May 1980.

1. Dixon, G. H. *et al. Ciba Fdn Symp.* **28,** 229–258 (1975).
2. Allfrey, V. G. in *Chromatin and Chromosome Structure* (eds Li, H. J. & Eckhardt, R. A.) 167–191 (Academic, New York, 1977).
3. Mohberg, J. & Rusch, H. P. *Archs Biochem. Biophys.* **134,** 577–585 (1969).
4. Corbett, S., Miller, S., Robinson, V. J., Matthews, H. R. & Bradbury, E. M. *Trans. biochem. Soc.* **5,** 943–946 (1977).
5. Bradbury, E. M., Inglis, R. J., Matthews, H. R. & Sarner, N. *Eur. J. Biochem.* **33,** 131–139 (1973).
6. Riggs, M. G., Whittaker, R. G., Neumann, J. R. & Ingram, V. M. *Nature* **268,** 463–464 (1977).
7. Ruiz-Carrillo, A., Waugh, L. J. & Allfrey, V. G. *Science* **190,** 117–128 (1975).
8. Panyim, S. & Chalkley, R. *Biochemistry* **8,** 3972–3977 (1969).
9. Jackson, V., Shires, A., Tanphaichitr & Chalkley, R. *J. molec. Biol.* **104,** 471–483 (1976).
10. Braun, R., Mittermayer, C. & Rusch, H. P. *Biochim. biophys. Acta* **114,** 527–535 (1966).
11. Mittermayer, C., Braun, R. & Rusch, H. P. *Biochim. biophys. Acta* **91,** 387–398 (1964).
12. Grant, W. D. *Eur. J. Biochem.* **29,** 94–98 (1972).
13. Davies, K. E. & Walker, I. O. *J. Cell Sci.* **26,** 267–279 (1977).
14. Sauer, H. W. in *Cell Cycle Regulation* (eds Jeter, J. R. *et al.*) 149–156 (Academic, New York, 1978).
15. Matthews, H. R. in *The Cell Cycle* (ed. Johns, P.) (Cambridge University Press, in the press).
16. Molgaard, H. V., Matthews, H. R. & Bradbury, E. M. *Eur. J. Biochem.* **68,** 541–549 (1976).
17. Vogt, V. & Braun, R. *J. molec. Biochem.* **106,** 567–587 (1976).
18. D'Anna, J. A., Tobey, R. A., Barham, S. S. & Gurley, L. R. *Biochem. biophys. Res. Commun.* **77,** 187–194 (1977).
19. Lake, R. S. & Salzmann, N. P. *Biochemistry* **11,** 4817–4822 (1972).
20. Gurley, L. R., D'Anna, J. A., Barham, S. S., Deaven, L. L. & Tobey, R. A. *Eur. J. Biochem.* **84,** 1–16 (1978).
21. Matthews, H. R. in *Protein Phosphorylation in Regulation* (ed. Cohen, P.) (North-Holland, Amsterdam, 1978).
22. Cary, P. D., Moss, T. & Bradbury, E. M. *Eur. J. Biochem.* **89,** 475–482 (1978).
23. Whitlock, J. & Simpson, R. T. *J. biol. Chem.* **252,** 6516–6520 (1977).
24. Vidali, G., Boffa, L. C., Bradbury, E. M. & Allfrey, V. G. *Proc. natn. Acad. Sci. U.S.A.* **75,** 2239–2243 (1978).
25. Mathis, D. J., Oudet, P., Wasylyk, B. & Chambon, P. *Nucleic Acids Res.* **5,** 3523–3547 (1978).
26. Finch, J. T. & Klug, A. *Proc. natn. Acad. Sci. U.S.A.* **73,** 1897–1901 (1976).
27. Carpenter, B. G., Baldwin, J. P., Bradbury, E. M. & Ibel, K. *Nucleic Acids Res.* **3,** 1739–1746 (1976).
28. Suau, P., Bradbury, E. M. & Baldwin, J. P. *Eur. J. Biochem.* **97,** 593–602 (1979).
29. Johnson, E. M., Allfrey, V. G., Bradbury, E. M. & Matthews, H. R., *Proc. natn. Acad. Sci. U.S.A.* **75,** 1116–1120 (1978).
30. Adolph, K. W., Cheng, S. M. & Laemmli, U. K. *Cell* **12,** 805–816 (1977).
31. Goodwin, G. H. & Johns, E. W. *Eur. J. Biochem.* **40,** 215–220 (1973).
32. Levy-W., B., Wong, N. C. W. & Dixon, G. H. *Proc. natn. Acad. Sci. U.S.A.* **74,** 2810–2814 (1977).
33. Vidali, G., Boffa, L. & Allfrey, V. G. *Cell* **12,** 408–415 (1977).
34. Weisbrod, S. & Weintraub, H. *Proc. natn. Acad. Sci. U.S.A.* **76,** 635–650 (1979).
35. Laemmli, U. K. *Nature* **227,** 680–682 (1970).
36. Borun, T. W., Ajiro, K., Zweidler, A., Dolby, T. W. & Stephens, R. E. *J. biol. Chem.* **252,** 173–180 (1977).

The putative mRNA for subunit II of human cytochrome *c* oxidase starts directly at the translation initiator codon

Deanna K. Ojala, Julio Montoya & Giuseppe Attardi

Division of Biology, California Institute of Technology, Pasadena, California 91125

The gene for subunit II of cytochrome *c* oxidase (COII) in human mitochondrial DNA (mtDNA) is immediately contiguous, on its 5′-end side, to a tRNA^{Asp} gene[1]. Since all eukaryotic mRNAs so far analysed have been shown to have a noncoding stretch, which is presumably used for ribosome attachment[2,3] on the 5′-side of the coding sequence, it was reasonable to ask whether, in the case of the human COII mRNA, the above function is performed by the tRNA^{Asp} sequence or a portion of it, or whether this mRNA lacks a 5′ noncoding stretch. We have sequenced a 5′-end proximal segment of the putative COII mRNA from HeLa cells of about 30 nucleotides and have aligned it with the COII coding sequence in human mtDNA. Our results show that this RNA starts directly at the AUG initiator codon.

Figure 1 shows a region of the *Hpa*II restriction map of HeLa cell mtDNA[4] with the precise positions of the COII gene and of the adjacent putative tRNA genes, as determined from DNA sequencing analysis[1]. Preliminary RNA mapping experiments using the Southern[5] and Alwine *et al.*[6] methods had shown that a single mtDNA heavy (H)-strand coded poly(A)-containing RNA (RNA species 16, in the classification of Amalric *et al.*[7]) maps in correspondence to the COII gene. This RNA, on account of its size (about 800 nucleotides), its abundance, its presence in polysomes and its relatively long half life, is probably the mRNA for subunit II. Recently, using the S_1 protection

0028–0836/80/360079—04$01.00

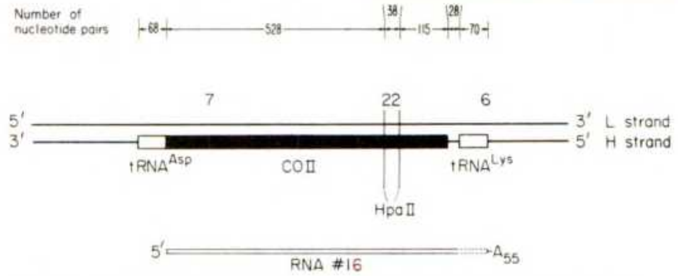

Fig. 1 Region of the *Hpa*II restriction map of HeLa cell mtDNA[4] showing the precise positions of the COII gene and of the adjacent tRNA genes. The positions of the genes were derived from the published DNA sequencing analysis[1]. The mapping position of poly(A)-containing RNA 16 (ref. 10) is shown in the lower part of the figure; the dashed portion indicates the limits of uncertainty in this determination.

technique[8,9], it has been possible to locate the 5′-end of RNA 16 more precisely, and it has been placed at about 540 nucleotides from the *Hpa*II site between fragments 7 and 22; in the same experiments, the 3′-end of the non-poly(A) segment of this RNA has been mapped in the region of the tRNA^{Lys} gene, with indications that it may overlap, in part, or possibly completely the tRNA^{Lys} coding sequence[10] (Fig. 1).

To prepare RNA 16 of high purity and in adequate amounts for sequencing analysis, the micrococcal nuclease procedure for purification of mitochondrial RNA[11] was scaled up as described in the legend for Fig. 2. Lane *a* in this figure shows the electrophoretic pattern in a CH_3HgOH–agarose slab gel, after ethidium bromide staining, of the oligo(dT)-bound fraction of mitochondrial RNA derived from about 2.5×10^9 HeLa cells. The typical pattern of the mtDNA-coded poly(A)-containing RNA species previously described in HeLa cells[7] is clearly recognizable, with the exception of the species known to be relatively short-lived and present in very small amounts (RNA species 1–4 and 6)[12,13]. RNA species 16 was eluted from the gel track shown in Fig. 2*a* and an identical track, treated with RNase-free DNase (to eliminate any contaminating DNA fragments), and re-run on a gel in the same conditions. A sharp band was observed at the expected position (Fig. 2*b*) and the RNA in this band was eluted. Material from about 8×10^9 cells, purified as described above, was labelled at its 5′-end with $[\gamma\text{-}^{32}P]ATP$ and polynucleotide kinase after dephosphorylation with bacterial alkaline phosphatase. The labelled RNA was run on a CH_3HgOH–agarose gel, a band corresponding to intact RNA 16 was observed (Fig. 2*c*) and the RNA in this band was eluted for the sequencing reactions. Mitochondrial 12S rRNA, to be used as a control for the *in vitro* labelling and sequencing technology used in the present work, was purified from the oligo(dT)-unbound RNA fraction of micrococcal-nuclease treated mitochondria and labelled *in vitro* at its 5′-end as described above.

To characterize the 5′-terminus of RNA 16, the *in vitro* 5′-end labelled RNA was subjected to a complete P1 digestion[14] and fractionation on a PEI–cellulose TLC plate. As a control, 5′-end-labelled 12S rRNA was subjected to the same analysis. As shown in Table 1, almost 92% of the radioactivity in the 12S rRNA was found to be associated with pA, the remainder being distributed among the three other nucleotides, in perfect agreement with previous work[11]. In RNA 16, the predominant 5′-terminal nucleotide (~84%) was pA. This result indicated the substantial purity of the RNA 16 used for sequencing in the present work.

Sequencing of the 5′-end proximal segment of RNA 16 and of 12S rRNA was performed by the methods of Donis-Keller *et al.*[15] and Simoncsits *et al.*[16], using base-specific enzymatic

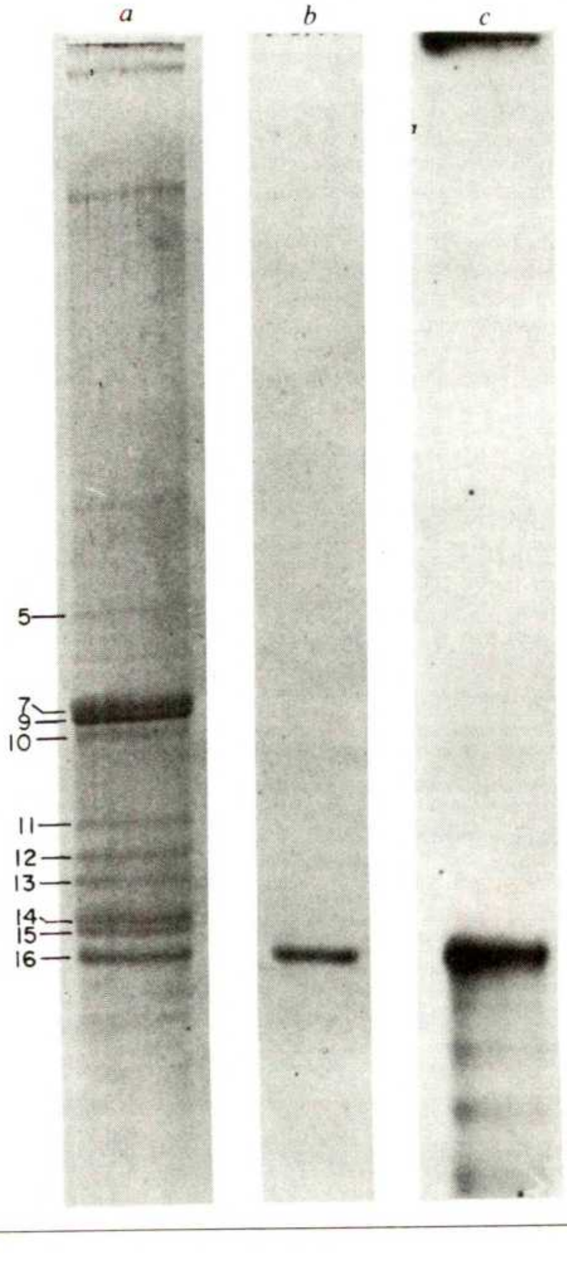

Fig. 2 Isolation and 5′-end labelling of mitochondrial poly(A)-containing RNA 16. *a*, The mitochondrial fraction from 5×10^9 HeLa cells (~30 ml packed cells) was re-suspended in 0.25 M sucrose, 0.01 M Tris–HCl, *p*H 8.0 (25 °C), 0.001 M $CaCl_2$ (1 ml per 1.5×10^8 cells), and treated with 100 units ml^{-1} of micrococcal nuclease (Millipore) at 2 °C for 30 min. EGTA was then added to 2.5 mM and, after 5 min, the suspension was diluted with 0.25 M sucrose, 0.01 M Tris–HCl, *p*H 6.7, 0.01 M EDTA (10 ml per 1.5×10^8 cells), and the mitochondria were pelleted by centrifugation at 10,000 r.p.m. in a SS-34 rotor. The pellet was re-suspended in 0.01 M Tris–HCl, *p*H 7.4, 0.15 M NaCl, 0.001 M EDTA (1 ml per 1.5×10^8 cells), incubated for 5 min at room temperature with 100 µg pronase per ml, then lysed with 1% SDS and incubated for an additional 30 min. RNA was extracted by phenol/chloroform/isoamyl alcohol (25:25:1) as previously described[7],, recovered by ethanol precipitation, denatured by heating at 63 °C for 4 min in 0.01 M Tris–HCl, *p*H 7.4, 0.001 M EDTA and passed through an oligo(dT)-cellulose column. The bound fraction was eluted, heat-denatured again as described above and re-run through the oligo(dT)-cellulose column. The final bound fraction was collected by ethanol precipitation and run through two tracks of a CH_3HgOH–agarose (1.4%) slab gel[7]. *b*, The band in *a* which corresponds to poly(A)-containing RNA 16 was identified by ethidium bromide staining and eluted as previously described[11]. After ethanol precipitation, the RNA was dissolved in 250 µl 0.05 M Tris–HCl, *p*H 6.7, 0.0025 M $MgCl_2$, 0.025 M KCl, incubated with 20 µg ml^{-1} RNase-free DNase (Boehringer Mannheim), pronase–SDS–phenol extracted and re-run through a CH_3HgOH–agarose slab gel. *c*, The RNA 16 band in *b* was eluted, ethanol-precipitated, dissolved in 100 µl of 0.01 M Tris–HCl, *p*H 8.0, and incubated at 65 °C for 15 min with 100 units of bacterial alkaline phosphatase (BRL) per µg RNA (an amount of about 0.17 µg RNA 16 was roughly estimated to be recovered from $\sim5\times10^9$ cells on the basis of its ethidium bromide staining, as compared to that of a known amount of 12S rRNA). Nitrilotriacetic acid was added to 10 mM and, after 15 min at room temperature, 2 µg of closed-circular pBR322 DNA were added as a carrier, and the nucleic acids were extracted with phenol/chloroform/isoamyl alcohol, ethanol-precipitated and dissolved in 15 µl kinase buffer (0.05 M Tris–HCl, *p*H 8.0, 0.01 M $MgCl_2$, 0.005 M dithiothreitol DTT) containing 0.5 nmol of $[\gamma\text{-}^{32}P]ATP$ (8,000 Ci $mmol^{-1}$). After addition of 2 units of polynucleotide kinase (Boehringer Mannheim), the reaction was carried out at 37 °C for 15 min and then stopped by addition of 1.0 M ammonium acetate. Carrier tRNA was then added and the mixture ethanol-precipitated and run on a CH_3HgOH–agarose (1.4%) slab gel.

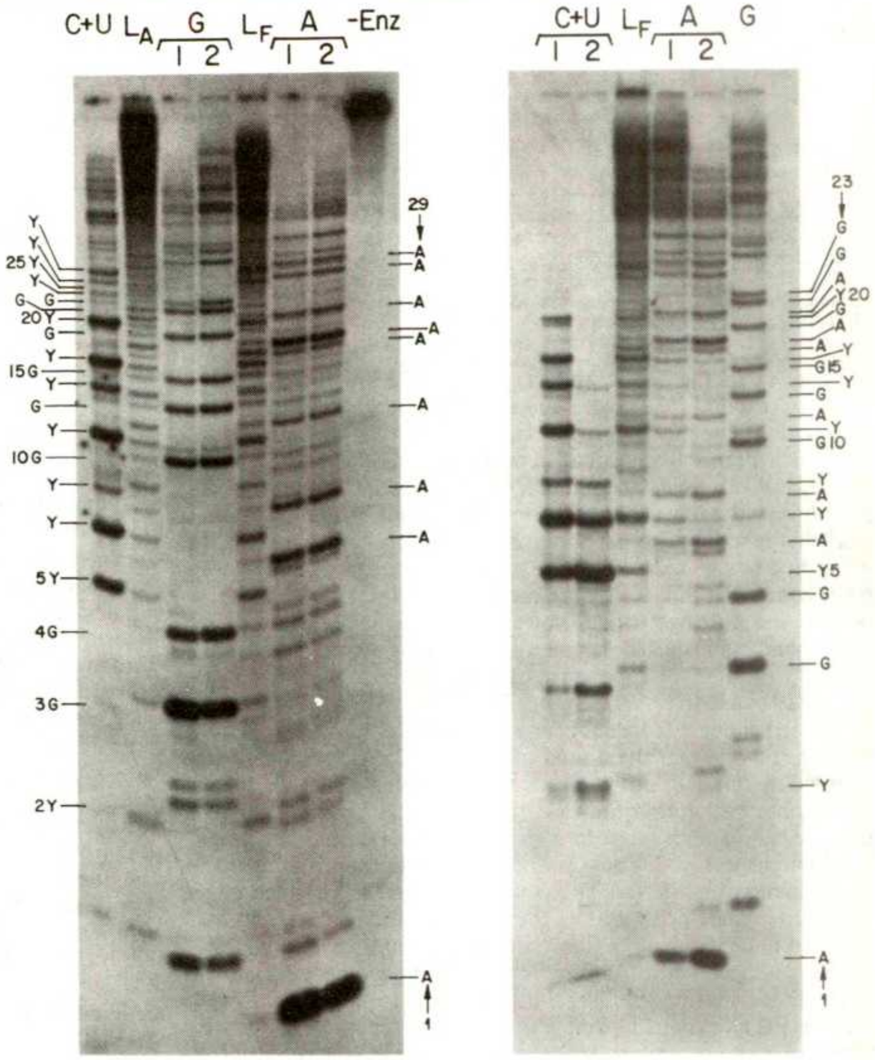

Fig. 3 RNA sequencing of mitochondrial poly(A)-containing RNA16. Autoradiograms of 25% sequencing gels (showing nucleotides 1–29) of partial enzymatic digest of 5′-end labelled RNA 16. Shown at the top of the gel are the cleavage specificities: RNase U2 (A), RNase T1 (G), RNase A (C+U), alkali ladder (L_A), formamide ladder (L_F). The reaction conditions described by Donis-Keller *et al.*[15] were used. The amounts of enzymes used (per ~30 ng RNA 16 and 3 μg yeast tRNA carrier) were, in the left panel: A 0.25 ng; T1 (1, 2), 0.10, 0.05 units; U2 (1, 2), 1.0, 0.5 units; in the right panel: A (1, 2), 0.50, 0.75 ng; T1, 0.02 units; U2, 0.15, 0.5 units. The alkali and hot formamide degradations for the formation of the ladder were performed as described by Donis-Keller *et al.*[15] and by Simoncsits *et al.*[16], respectively. Electrophoresis was carried out on thin (0.5 mm) 25% polyacrylamide (30:1 bisacrylamide)/7 M urea gels in Tris-borate–EDTA buffer at 1,000 V for 6 h.

Palit Chemistry Library SCIENCE COLLEGE 92 Upper Circular R. CALCUTTA

cleavage of the RNA followed by electrophoresis on polyacrylamide/urea gels. The RNases T1 (Sigma) (G-specific), A (Sigma) (C+U-specific) and U2 (Sankyo) (A-specific) were used for this analysis. Since the purpose of this work was the alignment of the RNA sequence with the known DNA sequence, the precise identification of the pyrimidines was considered unnecessary.

The 12S rRNA gel patterns (not shown) yielded a 5′-end-proximal sequence identical to that previously shown for this RNA species[11]. The gel patterns for RNA 16 (Fig. 3) gave a 5′-end proximal sequence which could be read for 29 nucleotides (Fig. 3). The band corresponding to the second nucleotide (a pyrimidine) was very faint in the RNA sample digested with 0.25 ng RNase A (Fig. 3, left panel), but was clearly visible in the sample digested with higher enzyme levels (Fig. 3, right panel). There were a few extra bands in the region corresponding to small oligonucleotides after RNase U2 or T1 digestion (and also after treatment of the sample with the higher levels of RNase A). These bands were in most cases less strong than the *bona fide* specific RNase cleavage products; because of this and because they did not correspond in migration to bands visible in the ladder or corresponded to obviously abnormal ladder steps (like the fairly strong band corresponding to a pyrimidine in the second lane of the right panel), they could in general be recognized as spurious bands. The nature of these extra bands is not clear; they may reflect the presence of contaminating oligo-

```
5'   C C C C C C A A A G C T G G T T T C A A G C C A A C C C C A T G G C C T C C A T G A C T T T T T C A A A A|A G G T A T T
3'   G G G G G G T T T C G A C C A A A G T T C G G T T G G G G T A C C G G A G G T A C T G A A A A A G T T T T|T C C A T A A
     -120                                                                                                              -61

                                          5' ———— tRNA^Asp ————> 3'
     A G A A A A A C C A T T T C A T A A C T T T G T C A A A G T T A A A T T A T A G G C T A A A T C C T A T A T A T C T T A
     T C T T T T T G G T A A A G T A T T G A A A C A G T T T C A A T T T A A T A T C C G A T T T A G G A T A T A T A G A A T
     -60                                                                                                               -1
     5'                   RNA # 16
     A Y G G Y A Y A Y G Y A G Y G Y A A G Y A G G Y Y Y A Y A ————>
     A T G G C A C A T G C A G C G C A A G T A G G T C T A C A A G A C G C T A C T T C C C C T A T C A T A G A A G A G C T T   3' L strand
     T A C C G T G T A C G T C G C G T T C A T C C A G A T G T T C T G C G A T G A A G G G G A T A G T A T C T T C T C G A A   5' H strand
     1                                                                                                                  60
     |———————————————————————————————— CO II ————————————————————————————————>
```

Fig. 4 Alignment of the nucleotide sequence of the 5′-end region of poly(A)-containing RNA 16 with the DNA sequence of the COII gene. The RNA sequence was derived from Fig. 3. The sequence of the 5′-end-proximal region of the COII gene and of the adjacent DNA segment on its 5′-side is reproduced from Barrell *et al.*[1]. Y, Pyrimidine.

Table 1 5′-terminal nucleotide analysis of *in vitro* labelled mitochondrial poly(A)-containing RNA 16 and 12S rRNA

RNA species	Percentage of total ^{32}P radioactivity* AMP	CMP	GMP	UMP
12S rRNA	91.8	1.9	2.0	4.2
Poly(A)-containing RNA 16	83.6	1.3	8.2	7.0

The 5′-terminal nucleotide was determined by exhaustive digestion of the *in vitro* labelled RNAs with nuclease P1 (ref. 14; Calbiochem) and fractionation of the products on PEI-cellulose TLC plates, as previously described[11].

* The values refer to the radioactivity which migrated from the origin. The percentage of the input radioactivity recovered from the origin was, respectively, 1.0 and 1.6% for 12S rRNA and RNA 16.

nucleotides in the RNA 16 preparation, during the 5′-end labelling reaction, or may be due to the formation, during the enzymatic or chemical degradation of the RNA, of oligonucleotides with different phosphate end-groups (2′,3′-cyclic phosphate, 2′ and 3′ phosphate). Similar bands migrating in abnormal position have been observed, previously[11] and in the present work, in the sequencing gel patterns for 12S rRNA. The reading of the first few nucleotides of the sequence near the 5′-end was made somewhat difficult by the presence of these extra bands; beyond the fifth nucleotide, however, the sequence could be read unambiguously. The sequence obtained is shown in Fig. 4, aligned with the DNA sequence of the COII gene region. The entire 29-nucleotide stretch of RNA 16 which has been sequenced appears to be colinear with the DNA sequence. The striking result is that the 5′-end of the RNA corresponds precisely to the first nucleotide of the COII coding sequence.

The observation that the COII mRNA starts directly at the initiator codon raises interesting questions about the mechanism by which the mitochondrial ribosomes attach to this messenger. In all eukaryotic mRNAs analysed so far there is a stretch of variable length which precedes the initiator codon and which is assumed to be involved in ribosome attachment[2,3]. Similarly, in *Escherichia coli* mRNAs there is a 5′-noncoding segment containing a ribosome-binding site[17,18]. A single exception to this rule has been described, namely that of the λ repressor mRNA involved in repressor maintenance[19]. In this case, it was argued that the lack of a strong ribosome binding site could account for the low efficiency of translation of this mRNA. In the case of the mitochondria from human cells (and probably from other animal cells) it is reasonable to think that the special features of their ribosomes make them suitable for binding directly to the initiator codon. It will be interesting to see whether the lack of a 5′-noncoding stretch is a general feature of mitochondrial mRNAs in HeLa cells. Preliminary observations indicate that another mitochondrial poly(A)-containing RNA in these cells, RNA 15, starts with an AUG, which may be the initiator codon for the polypeptide coded by this RNA (unpublished observations).

This work was supported by NIH grant GM-11726. We thank S. Crews for valuable discussions and A. Drew for technical assistance.

Received 23 April; accepted 26 June 1980.

1. Barrell, B. G., Bankier, A. T. & Drouin, J. *Nature* **282,** 189–194 (1979).
2. Hagenbüchle, O., Santer, M., Steitz, J. A. & Mans, R. J. *Cell* **13,** 551–563 (1978).
3. Kozak, M. *Cell* **15,** 1109–1123 (1978).
4. Ojala, D. & Attardi, G. *Plasmid* **1,** 78–105 (1977).
5. Southern, E. M. *J. molec. Biol.* **98,** 503–517 (1975).
6. Alwine, J. C., Kemp, D. J. & Stark, G. R. *Proc. natn. Acad. Sci. U.S.A.* **74,** 5350–5354 (1977).
7. Amalric, F., Merkel, C., Gelfand, R. & Attardi, G. *J. molec. Biol.* **118,** 1–25 (1978).
8. Berk, A. J. & Sharp, P. A. *Cell* **12,** 721–732 (1977).
9. Berk, A. J. & Sharp, P. A. *Proc. natn. Acad. Sci. U.S.A.* **75,** 1274–1278 (1978).
10. Ojala, D. K., Merkel, C., Gelfand, R. & Attardi, G. (in preparation).
11. Crews, S. & Attardi, G. *Cell* **19,** 775–784 (1980).
12. Attardi, G. *et al. ICN-UCLA Symp. molec. cell. Biol.* **15,** 443–469 (1979).
13. Gelfand, R. thesis, California Institute of Technology (1980).
14. Fujimoto, M., Kuninaka, A. & Yoshino, H. *Agr. Biol. Chem.* **38,** 1555–1561.
15. Donis-Keller, H., Maxam, A. M. & Gilbert, W. *Nucleic Acids Res.* **4,** 2527–2538 (1977).
16. Simoncsits, A., Brownlee, G. G., Brown, R. S., Rubin, J. R. & Guilley, H. *Nature* **269,** 833–836 (1977).
17. Shine, J. & Dalgarno, L. *Biochem. J.* **141,** 609–615 (1974).
18. Steitz, J. A. & Jakes, K. *Proc. natn. Acad. Sci. U.S.A.* **72,** 4734–4738 (1975).
19. Ptashne, M. *et al. Science* **194,** 156–161 (1976).

Structural and functional diversity in 4-α-helical proteins

Patricia C. Weber & F. R. Salemme

Department of Biochemistry, New Chemistry Building, University of Arizona, Tucson, Arizona 85721

Protein crystallographic studies show that many structural arrangements appear as common features among proteins which are otherwise unrelated in sequence or function. One of the more recently recognized recurring protein structural motifs is a nearly parallel arrangement of four α-helices to form a sequentially connected left-twisted bundle[1]. We describe here the geometrical properties of these structures and suggest how they relate to the functional and aggregate properties of these molecules.

Currently known proteins which incorporate a 4-α-helical bundle as their dominant structural feature include (1) the haemerythrin subunit and related monomer myohaemerythrin, which are non-haem iron-containing oxygen transport proteins derived from marine worms[2-4], (2) the apoferritin monomer, which associates to form a hollow, 24-subunit cube-octahedral aggregate functioning in iron storage[5], (3) tobacco mosaic virus (TMV) coat protein[6,7], (4) the monomeric haem protein, *Escherichia coli* cytochrome b_{562} (ref. 8), and (5) the dimeric cytochrome *c*′ from *Rhodospirillum molischianum*[9].

Figure 1 schematically compares the known 4-α-helical subunit structures in cylindrical projection. Although the molecules clearly differ in their α-helix, connecting loop, and overall chain lengths, they share a similar overall folding plan in that each is composed of four sequentially joined α-helices (A–D) arranged in a roughly fourfold symmetrical bundle having a net left-handed twist. As shown in recent treatises on helix packing[10,11], individual α-helices can be described, to a first approximation, as twisted parallelepipeds having a square cross-section. It is consequently obvious that the observed arrangement of four nearly-parallel α-helices to form an array having a square cross-section minimizes the accessible surface area of the structure as a whole[12]. Additionally, if it is assumed that these molecules fold from an intermediate state having preformed α-helices[10,13], it can be seen from inspection of Fig. 1 that all sequential helix pairs and intervening connecting loops have a net right-handed superhelical character. This is a well known chiral effect observed in several other protein structural domains[14-23] and is presumed to arise through some intrinsic property of extended polypeptide chains that confers stability on conformations having overall right-handed supercoil characteristics[24,25]. In the present case, these right-handed supercoiled connections provide the most efficient connectivity pattern for the bundle, since alternative left-supercoiled connections would necessitate the formation of a much larger loop passing around the entire molecule (Fig. 1).

Analysis of the available coordinate[26] or literature data[27] shows the helix packing in these molecules to be quite intimate, the mean adjacent interhelix axis distance of closest approach being 9.6 Å, with a standard deviation of 1.4 Å. Interhelix angles are remarkably similar, the mean interhelical angles for adjacent and diagonally related helix pairs being 162.0 ± 5.8° and −158.2 ± 7.0° (mean ± s.d.), respectively[10]. The near constancy of the adjacent pair interhelix axis angle at ~18° (180° − 162°) reflects the fact that the individual helices can only make intimate and extended packing arrangements when their axes are relatively tilted at an angle equal to twice the α-helix pitch angle (~9.0°; ref. 28). Although a detailed description of all the 4-fold symmetric, sterically acceptable 4-α-helical arrangements lies outside the scope of this communication, it can readily be demonstrated that in fact there exists a variety of

0028-0836/80/360082—03$01.00

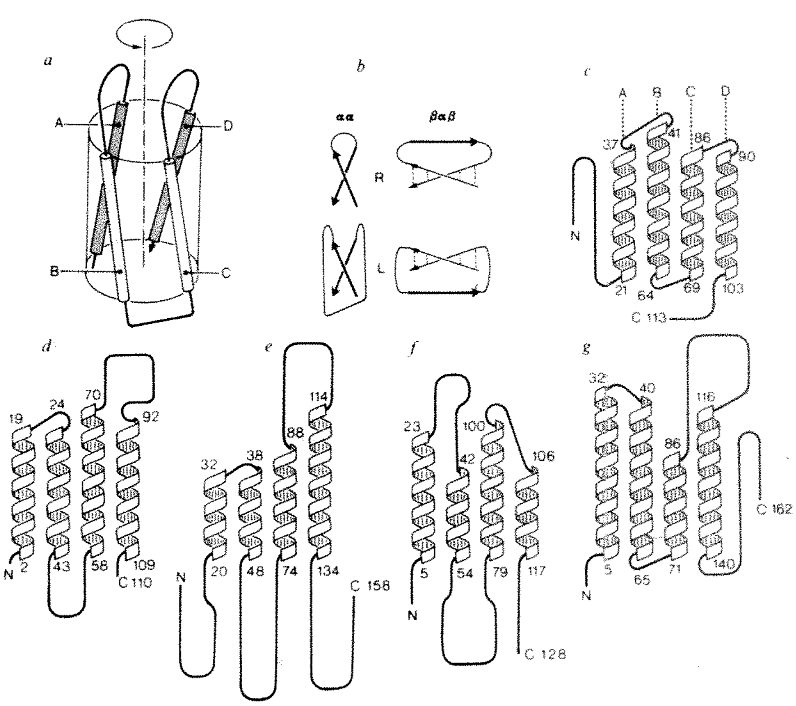

Fig. 1 Schematic representations of the 4-α-helical protein structures. *a*, Schematic representation of helical packing; *b*, schematic representation of chiral connectivity; *c–g*, examples of proteins showing these characteristics: *c*, haemerythrin and myohaemerythrin; *d*, cyctochrome b_{562}, *e*, TMV protein; *f*, cytochrome *c′*; *g*, apoferritin. Note that the connectivity pattern shown here and in Fig. 3 of the apoferritin monomer is one of two possibilities (the alternative being left-handed[5]) either of which appears equally consistent with the current electron density map interpretation (P. M. Harrison, personal communication). Each molecule is illustrated as a cylindrical projection of a common arrangement of four α-helices which are sequentially connected to form a bundle having an overall left-handed twist about the approximate 4-fold bundle axis of symmetry. This arrangement results in a right-handed (R) supercoiled connectivity pattern between adjacent helices, a feature previously observed in several other protein structural domains[14–23]. In *b*, for example, we compare right- and left-hand connected helix pairs with analogous β-α-β domains.

related packing arrangements which are both consistent with the observed geometry and have overall symmetric interactions. Further, as can be shown by an appropriate helix-net representation[28], the interhelix angle of 18° is a value which is uniquely associated with the attainment of regular periodic interactions between all helix pairs in a 4-α-helical bundle. In Fig. 2*a*, we show a packing model[28] of a representative symmetric arrangement which illustrates these points, and a similar representation of the actual packing interactions in cytochrome b_{562} is shown in Fig. 2*b*. These structures are clearly related, and so the previously reported occurrences of high internal symmetry in 4-α-helical structures[27,29] would seem to reflect the symmetrical packing requirements for helices in these bundles.

Because the α-helices in the 4-α-helical bundle structures are straight, they must necessarily diverge from their point of closest interhelix axis approach. Figure 2*c–f* illustrates this behaviour for several 4-α-helical proteins, and demonstrates both that the helical bundles of these structures have been truncated near their points of closest interhelix axis approach, and that the spatial divergence of the helices, which results as a consequence of the helix packing requirements, serves to create the internal binding pocket for the incorporated prosthetic groups.

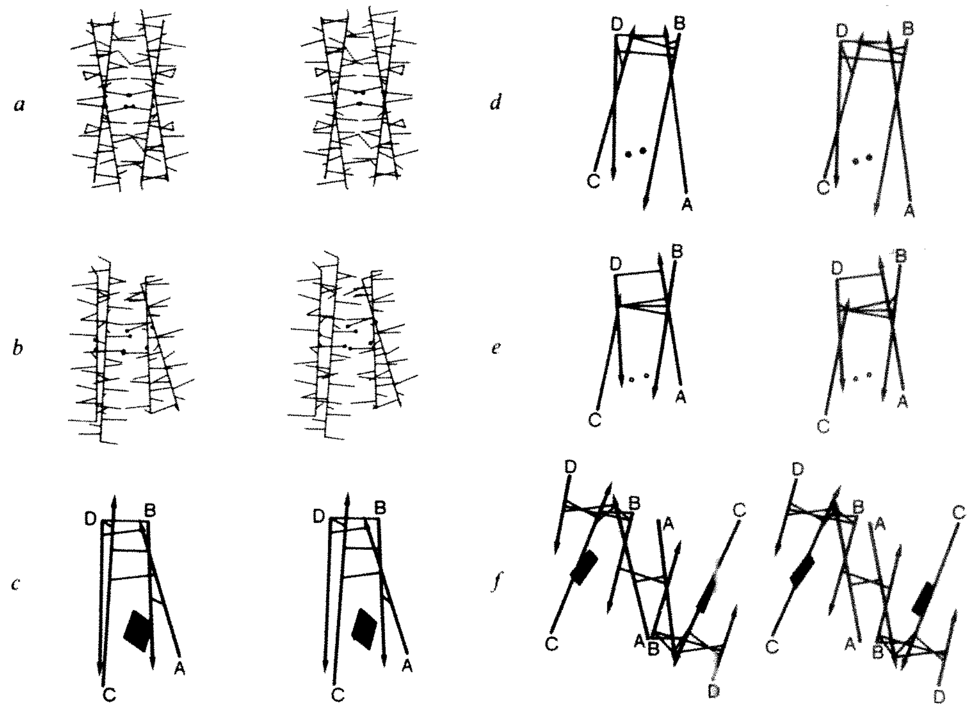

Fig. 2 Packing geometry in 4-α-helical proteins. *a*, A 'broomstick' packing model[28] in which each helix is represented as a helix axis line with 5.6 Å radial vectors[10] passing through Cβ. All adjacent helix pairs have interhelix axis angles of 18° and interaxis close-approach distances of 9.6 Å, so that the structure as a whole has the average geometrical properties of the observed structures. The structure shown has nearly equivalent local packing interactions (for example, dotted connection) which approximately repeat in the direction of the long axis of the bundle. (We note here that the interactions between the residues of straight α-helices can, at best, be only quasi-equivalent along the bundle axis. This situation differs from that observed in superhelical fibrous structures[28].) The arrangement as a whole has 222 point group symmetry, as a consequence of which each face of the bundle presents a packing surface with a diad axis of symmetry. The structure shown is only one of many possible symmetrically related arrangements which share a common overall geometry. *b* Shows a broomstick representation of the helix packing interactions in cytochrome b_{562} (ref. 8). The packing interactions in this molecule are not as regular as the model in *a*, because the residues of the real protein have different packing volumes, and the helical bundle comprising this molecule has been truncated near the region of closest interhelix approach (see *c*), with a concomitant reduction in apparent packing symmetry. Nevertheless, comparison of *a* and *b* clearly shows the helix packing in these structures to be related. *c–f* Show helix axis representations (including close approach interhelix vectors) for several molecules. As shown, all are truncated versions of a generalized 4-α-helical bundle model, which incorporate prosthetic groups in the internal cavity created by the spatial divergence of the individual helices away from their points of closest approach. An arrow indicates the N to C polypeptide chain sense in each helix. *c*, Cytochrome b_{562} (ref. 8). The position of the noncovalently bound haem group is indicated by a solid square. *d*, Myohaemerythrin[2]. Solid circles indicate the location of the bound iron atoms. *e*, Haemerythrin[4]. Iron positions are largely conjectural. *f*, Cytochrome *c′* dimer[9] showing positions of the covalently bound haem prosthetic groups.

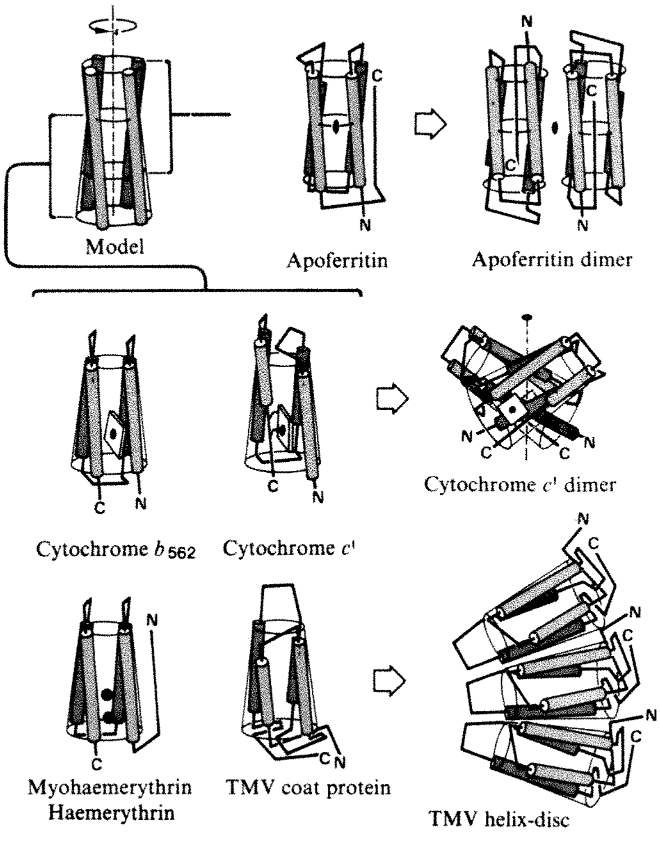

Fig. 3 Schematic representations of the 4-α-helical proteins illustrated as sub-domain arrays of a generalized 4-α-helical divergent bundle model. Broad arrows indicate the relationship between the monomeric and aggregate structural properties of the respective molecules. Details are given in the text.

Figure 3 shows the known proteins of this class illustrated as truncated variations of a generalized 4-α-helical packing model, and summarizes some additional features of their structural and aggregate properties. For example, in addition to the molecules described in Fig. 2, TMV coat protein also clearly appears to be a truncated divergent bundle structure, which instead of incorporating a prosthetic group, has a β-sheet at its divergent end which serves to 'brace' the helices apart[6]. The apoferritin monomer, in contrast, incorporates neither of these features[5] and so its helices pack more symmetrically with an equal extent of interhelical divergence at either end of the bundle. As a consequence, the most extensive pairwise monomer interaction in the cube-octahedral aggregate structure is a symmetrical dimer (Fig. 3) having interhelical interactions which are geometrically similar to those within each monomer[5]. As described in Fig. 2*a*, the symmetrical 4-α-helical packing arrangements which best satisfy the steric requirements of interhelical packing also generate diad axes of symmetry relating surface residues in adjacent helix pairs. As a result, the apoferritin subunits can pack to generate a dimeric structure whose symmetry is similar to that of the monomer.

The truncation of the divergent bundles of the remaining structures precludes the existence of diad symmetry axes on their faces, with a consequent reduction of their aggregate packing symmetry. In cytochrome *c'* for example, the monomers pack about a molecular diad axis which is independent of any symmetry elements of the monomer helix arrangements (Fig. 2).

TMV coat protein differs from the preceding molecules in that it forms aggregates having either 17- or 16.3-fold radial symmetry[6,7] in which each monomer makes different sets of pairwise helical interactions with its neighbours. However, to a good approximation, the interhelical angle between diagonally related parallel helices of the truncated divergent bundle defines the apical angle of a pyramidal prism circumscribing the molecular subunit (Fig. 3). The average observed value for this angle is 22° (180° − 158°, see above), which corresponds closely to the angle subtended by each subunit in both the TMV disk ($360°/17 = 21.2°$) and helix ($360°/16.3 = 22.1°$) structures.

To summarize, it has been shown here that the structural similarity among the 4-α-helical proteins can be attributed to what are basically physical requirements of helix packing and chiral connectivity. Consequently, it is not surprising that this structural arrangement should recur throughout the course of evolution, since it evidently possesses considerable scope for functional and superstructural diversity.

We thank Professor P. M. Harrison for providing apoferritin structural data before publication, and D. W. Weatherford for help with the computer graphics work. This work was supported by NIH grants GM21534 and GM25664, the University of Arizona Computer Center, and a Dreyfus Teacher-Scholar Award to F.R.S.

Received 5 February; accepted 13 June 1980.

1. Argos, P., Rossmann, M. G. & Johnson, J. E. *Biochem. biophys. Res. Commun.* **75**, 83–86 (1977).
2. Ward, K. B., Hendrickson, W. A. & Klippenstein, G. L. *Nature* **257**, 818–821 (1975).
3. Hendrickson, W. A., Klippenstein, G. L. & Ward, K. B. *Proc. natn. Acad. Sci. U.S.A.* **72**, 2160–2164 (1975).
4. Stenkamp, R. E., Sieker, L. C., Jensen, L. H. & McQueen, J. E. Jr *Biochemistry* **17**, 2499–2504 (1978).
5. Banyard, S. H., Stammers, D. K. & Harrison, P. M. *Nature* **271**, 282–284 (1978).
6. Bloomer, A. C., Champness, J. N., Bricogne, G., Staden, R. & Klug, A. *Nature* **276**, 362–368 (1978).
7. Stubbs, G., Warren, S. & Holmes, K. *Nature* **267**, 216–221 (1977).
8. Mathews, F. S., Bethge, P. H. & Czerwinski, E. W. *J. biol. Chem.* **254**, 1699–1706 (1979).
9. Weber, P. C. *et al.*, *Nature* **286**, 302–304 (1980).
10. Richmond, T. J. & Richards, F. M. *J. molec. Biol.* **119**, 537–555 (1978).
11. Efimor, A. V. *J. molec. Biol.* **134**, 23–40 (1979).
12. Richards, F. M. *A. Rev. Biophys. Bioengng* **6**, 151–175 (1977).
13. Ptitsyn, O. B. & Rashin, A. A. *Dokl. Acad. Nauk SSSR* **213**, 473–475.
14. Rao, S. T. & Rossmann, M. G. *J. molec. Biol.* **76**, 241–256 (1973).
15. Rossmann, M. G. & Liljas, A. *J. molec. Biol.* **85**, 177–181 (1974).
16. Rossmann, M. G. & Argos, P. *J. molec. Biol.* **105**, 75–95 (1976).
17. Richardson, J. S., Richardson, D. C., Thomas, K. A., Silverton, E. W. & Davies, D. R. *J. molec. Biol.* **102**, 221–235 (1976).
18. Levitt, M. & Chothia, C. *Nature* **261**, 552–557 (1976).
19. Richardson, J. S. *Nature* **268**, 495–500 (1977).
20. Chothia, C. *J. molec. Biol.* **75**, 295–302 (1973).
21. Sternberg, M. J. E. & Thornton, J. M. *J. molec. Biol.* **105**, 367–382 (1976).
22. Richardson, J. S. *Proc. natn. Acad. Sci. U.S.A.* **73**, 2619–2623 (1976).
23. Sternberg, M. J. E. & Thornton, J. M. *J. molec. Biol.* **110**, 269–283 (1977).
24. Weatherford, D. W. & Salemme, F. R. *Proc. natn. Acad. Sci. U.S.A.* **76**, 19–23 (1979).
25. Ramachandran, G. N., Lakshminarayan, A. V. & Kolaskar, A. S. *Biochim. biophys. Acta* **303**, 8–13 (1973).
26. Bernstein, F. C. *et al. J. molec. Biol.* **112**, 535–542 (1977).
27. McLachlan, A. D., Bloomer, A. C. & Butler, P. J. G. *J. molec. Biol.* **136**, 203–224 (1980).
28. Crick, F. H. C. *Acta crystallogr.* **6**, 689–697 (1953).
29. Hendrickson, W. A. & Ward, K. B. *J. biol. Chem.* **252**, 3012–3018 (1977).

Do the chromosomes of the kiwi provide evidence for a monophyletic origin of the ratites?

Leobert E. M. de Boer

Biological Research Department, Royal Rotterdam Zoological and Botanical Gardens, Rotterdam, The Netherlands

The extensive literature on the origin of the ratites focuses mainly on three questions: are the ratites mono- or polyphyletic, did they evolve from flying ancestors, and are they primitive or advanced? Opinion tends to accept a common descent from flying ancestors for the large ratites (for a summary of ideas see ref. 1). They would have evolved on Gondwanaland some time in the Cretaceous and have become dispersed over the southern continents after its fragmentation[2,3]. However, the position of the small New Zealand kiwis, in many respects the most peculiar of all birds, is still a matter for conjecture[1,4]. The chromosome complements of the large ratites have been found to be remarkably uniform[5–8]. The chromosome set of the kiwi, described here, clearly links up with these, which may be recorded as another indication for monophyly of all ratites. It also indicates that we are dealing here with very ancient karyotypes.

The somatic chromosome complements of the five large ratites previously studied—the ostrich, emu, Australian cassowary and common and Darwin's rhea—proved to be almost identical[5,8]. Minor differences only exist in the third and fifth chromosome pair. This result seems to support a monophyletic origin of this group, and indicates an extreme evolutionary conservatism of their karyotypic morphology, because geographical isolation of their ancestors on the various southern continents caused by the fragmentation of Gondwanaland took place probably 80–90 Myr ago[2,4]. There have been no reports on the chromosomes of the kiwi. Thus, when one of the kiwis (*Apteryx australis*) at the Rotterdam Zoological Gardens recently died unexpectedly, blood and bone marrow were removed posthumously to obtain chromosome preparations (for lymphocyte culturing techniques see refs 9, 10). Possibly as a result of the infectious disease which had killed this specimen (which on postmortem observation was found to be a female), the cultures did not yield optimal results. Thus, chromosome banding studies could not be undertaken, with the exception of C-banding. Nevertheless, the available material permitted a good comparison with the data from the large ratites.

The chromosome set of the kiwi is composed of 80 chromosomes, with 6 pairs of macrochromosomes clearly distinguishable from 34 pairs of microchromosomes (Fig. 1). With the exception of the first and second pairs, all elements have a terminal or nearly terminal centromeric position. The chromosomes of the sixth pair show a weak secondary constriction in the subcentromeric region. The absence of a clearly heteromorphic sex chromosome pair is characteristic in the female specimen studied. In all other birds, with the exception of the ratites, the female is the heterogametic sex in that female individuals possess one Z and one W chromosome (which is generally much smaller) in the sex chromosome pair, whereas males possess two identical Z chromosomes. In the kiwi the fourth chromosome pair is only slightly heteromorphic, one member being consistently slightly smaller than the other. It is therefore possible that these elements represent the sex chromosomes. However, C-banding, a technique used specifically for staining the avian W chromosome, did not indicate the presence of a C-positive element among the macrochromosomes.

This exceptional situation, the absence of a clearly heteromorphic sex chromosome pair and the presence of a slight length difference in the fourth pair of chromosomes, has been found in the ostrich, cassowary, emu and rhea[5–7]. Only in Darwin's rhea have Benirschke *et al.*[8] claimed to have found a normal sex chromosome pair with a large Z and small W chromosome. In all male ratites studied, all chromosome pairs were perfectly homomorphic.

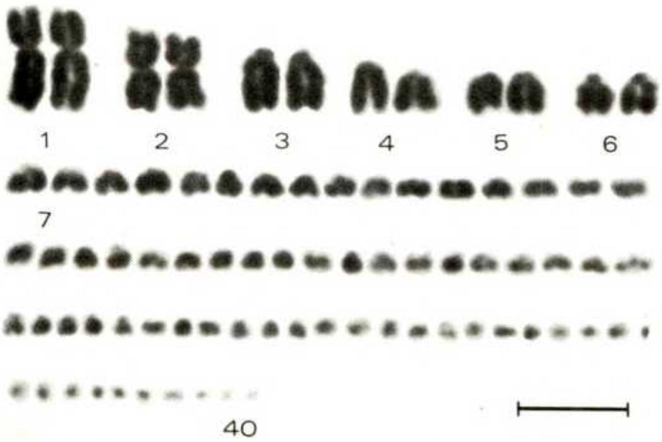

Fig. 1 Representative karyogramme of a female kiwi, *Apteryx australis*, obtained from lymphocyte culture. Note slight difference in length between the members of pair 4. The microchromosomes (pairs 7–40) have not been matched in pairs. Scale bar, 5 μm of absolute length.

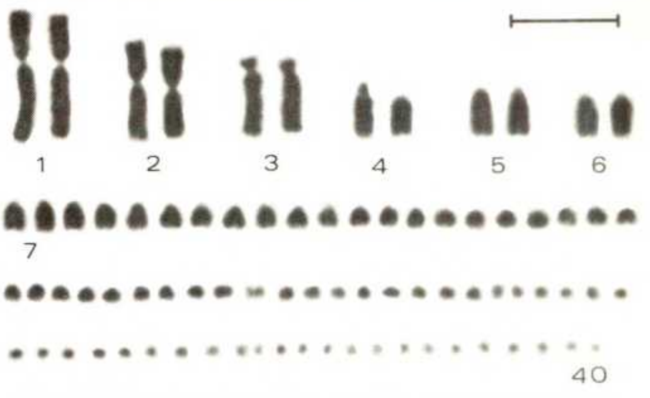

Fig. 2 Karyogramme of a female emu, *Dromaius novaehollandiae* (specifications as in Fig. 1).

The structure of the remainder of the kiwi karyotype also closely resembles those of the large ratites. In fact, the kiwi chromosomes are indistinguishable from those of the emu (Fig. 2) and cassowary. The karyotype of the ostrich differs only in the possible absence of the secondary constriction in the sixth pair and the somewhat smaller short arm in the third pair. The rhea karyotypes differ only by the submedian position of the centromere in the elements of the fifth pair.

Obviously, these gross morphological similarities need to be confirmed by detailed comparisons of chromosome banding patterns based on material from further specimens. Nevertheless, it is obvious that with its karyological characteristics the kiwi perfectly falls within the ratite group. As convergent evolution of karyotype morphology seems improbable, these findings strongly suggest a monophyletic origin of all ratites, including kiwis (and their relatives, the extinct New Zealand moas). However, one problem of this conclusion is that in cladistic[11] terms monophyly can only be concluded on the basis of shared derived characters, not on primitive ones. At present it is impossible to determine whether ratite karyotypic structure is primitive or not. Comparable karyotypes possibly only occur in the unrelated Anseriformes[7], but the sex determining system of the ratites is unique among birds. Further investigation should determine whether this system is primitive, as might be suggested by the fact that clearly heteromorphic sex chromosome pairs are absent in many reptilian groups[12]. Neither can the question of the position of the tinamous, often cited as possibly resembling the flying ancestors of the ratites, be answered from a karyological point of view, because the only report on tinamou chromosomes[13] does not include adequate descriptions or illustrations.

Monophyly or polyphyly apart, there is no doubt of the ancient character of the ratite karyotypic structure. Cracraft[4] places the ostrich–rhea bifurcation, which is generally believed to be the most recent one between the major ratite groups, as far back as 80–90 Myr ago. In the case of monophyly, the branching off of the kiwi and moa ancestors certainly would have been the earliest in ratite history. This would mean that the ratite karyotypes, especially those of kiwi, emu and cassowary, because of their uniformity, have remained practically unchanged during a period of possibly well over 100 Myr. In the case of polyphyly this would have been as long or even longer.

Received 6 May; accepted 9 July 1980.

1. Sibley, C. G. & Ahlquist, J. E. *Bull. Peabody Mus. nat. Hist.* **39,** 1–276 (1972).
2. Fooden, J. *Science* **175,** 894–898 (1972).
3. Cracraft, J. *J. zool. Res.* **169,** 455–545 (1973).
4. Cracraft, J. *Ibis* **116,** 494–521 (1974).
5. Sasaki, M., Ikeuchi, T. & Makino, S. *Experientia* **24,** 1292–1293 (1968).
6. Takagi, N., Itoh, M. & Sasaki, M. *Chromosoma* **36,** 281–291 (1972).
7. Takagi, N. & Sasaki, M. *Chromosoma* **46,** 91–120 (1974).
8. Benirschke, R. J., Sekulovich, R. E. & Risser, A. C. *Chromosome Inf. Serv.* **21,** 13–14 (1976).
9. Boer, L. E. M. de. *Genen Phaenen* **17,** 1–115 (1974).
10. Boer, L. E. M. de. *Genetica* **46,** 77–113 (1976).
11. Hennig, W. *Phylogenetic Systematics* (Urbana University Press, 1966).
12. Gorman, G. C. in *Cytotaxonomy and Vertebrate Evolution* (eds Chiarelli, A. B. & Capanna, E.) (Academic, London, 1973).
13. Lucca, E. J. de. *Revue Bras. Pesquisas méd. Biol.* **7,** 253–263 (1974).

MATTERS ARISING

Cometary collisions on the Moon and Mercury

IT has been proposed that unusual bright and dark swirl-like markings on the Moon and Mercury may be strongly magnetized residues of recent (<100 Myr) collisions of the latter bodies with one or more cometary comas[1]. The photogeological investigations which led to this hypothesis were stimulated, at least in part, by emerging evidence that relatively high-amplitude magnetic anomalies detected with instruments on-board the Apollo subsatellites are concentrated in areas where swirls are found[2,3]. Although we agree that many of the swirls are probably relatively strongly magnetized deposits of impact-generated material, we consider that meteoroid impacts occurring over a span of time comparable to the age of the Solar System can explain their existence at least as well as can recent comet impacts. Our reasons are given below.

First, the inferred sources of medium-amplitude magnetic anomalies on the central near side[2,3] and on the far side[4] are basin ejecta materials. This result is particularly well established on the near side, where anomalies are correlated with exposed segments of primary Imbrium basin ejecta (the Fra Mauro Formation) surrounded by poorly magnetized mare basalt. Both returned sample studies and surface magnetic field investigations support the contention that ejecta materials produced during meteoroid impacts are major sources of magnetic anomalies detected from orbit[5,6]. Therefore, a special explanation for the high-amplitude anomalies involving "high-velocity imprinting of [cometary] coma fine structure" may be *ad hoc*.

Second, there is photogeological evidence that the Reiner Gamma swirl on western Oceanus Procellarum is related in origin to a nearby $3.2 \pm 0.2 \times 10^3$-Myr-old primary impact crater[3] and that some of the larger swirls in Mare Ingenii are associated with the Copernican (1–2×10^3 Myr old) crater O'Day[7]. Thus, a genetic relationship of all the swirls to the late Copernican crater Goddard A caused by a "prograde, incoming split comet system impacting the Moon" as proposed in ref. 1 is arguable. Note also that although there is evidence that many of the more conspicous far side swirls are very young, it is not known whether the young swirls are magnetized.

Third, if both the swirls and the high-amplitude magnetic anomalies are caused by comet impacts, magnetic signatures of more ancient (and more numerous) such impacts should have been detected all over the Moon. Instead, virtually all the high-amplitude magnetic anomalies detected between ±30° of latitude with the Apollo subsatellite magnetometers and charged particle instruments occur in limited selenographic regions where swirl patterns exist. The restricted occurrence of both swirls and high-amplitude magnetic anomalies within particular regions suggests a geological rather than an entirely exogenic control on their origin.

Fourth, the distribution of the largest concentrations of swirl patterns (and magnetic anomalies) on the moon is not random as expected for unusual additions of cometary matter. Specifically, as first pointed out by El-Baz[8], the most conspicuous concentrations of swirls (north of Mare Marginis and within Mare Ingenii) are roughly antipodal to the two youngest large impact basins, Orientale and Imbrium, respectively. As evidence that the antipodal relationship is not fortuitous, the two additional regional concentrations of swirls mapped in Fig. 3*b* of ref. 1 (centred at 165 °W, 23 °S and 125 °W, 20 °S) are within 5° of the Serenitatis and Crisium antipodes, respectively. Each of these four areas is known to be anomalously magnetic[9,10] and at least three of the four areas is marked by the general occurrence of unusual hilly and lineated terrain[11,12]. The latter has been ascribed either to compression at the antipode by body and surface seismic waves generated by the associated basin impacts[13] or to convergence of basin secondaries at the antipode[14]. To explain the concentrations of both swirls and large magnetic anomalies near basin antipodes, a compositional modification of the crust in areas where the hilly and lineated terrain is found has been postulated[15] such that subsequent (meteoroid) impacts on these areas result in crater ejecta which is especially susceptible to magnetization. The necessary compositional modification was proposed to be an increase in metallic iron content, as metallic iron is the ferromagnetic carrier in all sampled lunar materials.

L. L. HOOD

Lunar and Planetary Laboratory,
University of Arizona,
Tucson, Arizona 85721

1. Schultz, P. H. & Srnka, L. J. *Nature* **284,** 22–26 (1980).
2. Hood, L. L., Coleman, P. J. Jr & Wilhelms, D. E. *Science* **204,** 53–57 (1979).
3. Hood, L. L., Coleman, P. J. Jr & Wilhelms, D. E. *Proc. 10th lunar planet. Sci. Conf.* 2235–2257 (1979).
4. Anderson, K. A. & Wilhelms, D. E. *Earth planet. Sci. Lett.* **46,** 107–112 (1979).
5. Strangway, D. W., Gose, W., Pearce, G. & McConnell, R. K. *Nature* **246,** 112–114 (1973).
6. Fuller, M., Cisowski, S. M. & Hale, C. J. *Proc. 10th lunar planet. Sci. Conf.*, 2211–2233 (1979).
7. Schultz, P. H. *Moon Morphology*, 420 (University of Texas Press, Austin, 1976).
8. El-Baz, F. *Trans. Am. Geophys. Un.* (EOS) **52,** 856 (1971).
9. Lin, R. P., El-Baz, F., Hood, L. L., Runcorn, S. K. & Schultz, P. H. in *Lunar Planet. Sci XI*, 626–627 (Lunar and Planetary Institute, Houston, 1980).
10. Hood, L. L., Russell, C. T. & Coleman, P. J. Jr (in preparation).
11. Wilhelms, D. E. & El-Baz, F. *U.S. Geol. Surv. Map*, I-948 (1977).
12. Stuart-Alexander, D. E. *U.S. Geol. Surv. Map*, I-1047 (1978).
13. Schultz, P. H. & Gault, P. E. *The Moon* **12,** 159–177 (1975).
14. Moore, H. J., Hodges, C. A. & Scott, D. H. *Proc. 5th lunar Sci. Conf.*, 71–100 (1974).
15. Hood, L. L. in *Conf. Lunar Highlands Crust*, 72–74 (Lunar and Planetary Institute, Houston, 1979).

SCHULTZ AND SRNKA REPLY—In response to Hood's comments concerning our proposed origin of the bright and dark swirls on the Moon and Mercury, we make the following comments.

First, Hood's proposal that these swirls are strongly magnetized deposits of ejecta from major cratering events is not consistent with available photogeological data. Second, although it has been argued that strongly magnetized material can be generated by an impact event[1–3], it is another matter to transport this material in an ordered fashion over long distances so as to create a magnetic anomaly during its deposition; secondary impact processes and local mixing would be expected to randomize the incoming magnetized material and prevent the building of an anomaly. Rather, the ejecta must come to rest and acquire remanence in the presence of a field; this is difficult to accomplish for impact-generated magnetic fields except perhaps for near-rim basin-sized events[2].

Specific responses to Hood's comments are as follows. First, the existence and possible correlation of medium-amplitude anomalies with the Fra Mauro Formation[4] (Imbrium ejecta deposits) are irrelevant to discussions of the origin of the swirls, other than to note that there are at least three likely processes responsible for lunar magnetic anomalies: impact-induced magnetization preserved in thick ejecta deposits, remanence acquired in the field of a primordial lunar dynamo, and our proposed cometary magnetization[5]. We stated in our report that all three (and likely more) processes have occurred on the Moon during its evolution, but that only cometary magnetization is consistent with the nature of the swirls.

Second, photogeological data do not show that Reiner Gamma is associated with the crater Cavalerius, contrary to the proposal by Hood *et al.*[4]. The swirls are surficial in character and cross a variety of features including secondary craters from Cavalerius. Cavalerius is sufficiently old for craters as large as 10 km to have superposed its ejecta deposits, excavating

0028-0836/80/360086—02$01.00

darker basalts from below. It is crucial to note that such excavations are not present on the Reiner Gamma swirls, indicating that these swirls must be much younger than Cavalerius. Furthermore, the swirls are strong forward light reflectors, in contrast to crater rays, and have a photometric phase dependence unlike any ejecta[6]. Increased forward reflection from lunar soil was observed in areas scoured by the exhaust gases from the Apollo LM descent engine. We point out that the long-term process of impact gardening homogenizes the uppermost regolith in a relatively short time, so that such a photometric effect should have disappeared in the Reiner Gamma Formation if it is an old feature. Finally, a small crater on the rim of O'Day (not the older crater O'Day) was suggested as a possible impact site related to the Ingenii swirls; relation of these swirls to the Goddard-A swirls as part of a single cometary impact event is unimportant for our proposed origin.

Third, Hood comments that if the high-amplitude magnetic anomalies are due to cometary impacts, similar features should be common because presumably many comet impacts have occurred. This is incorrect, as our proposed process affects only the upper regolith (<1 m); magnetization there will be lost comparatively quickly due to impact gardening, and viscous decay[7] of high-field remanence in the altered soil. Thus, only the most recent events, and only those associated with fresh, active comets would be observable as magnetic anomalies.

Fourth, we agree that the apparent connections between swirls, magnetic anomalies and antipodal points of some major basin-forming impacts are intriguing, but we must point out the serious difficulties encountered if these correlations are interpreted as genetically linked. First, the swirls near the crater Goddard A are not at the antipodal point of the Orientale basin, but extend 1,000 km to the east. Hilly and lineated terrains, which may be the result of focussed seismic energy[8] or convergence of secondary ejecta[9], occur at the antipodes of Imbrium and Orientale; the swirls do not. The claimed correlation of swirl positions with the Crisium and Serenitatis antipodes misrepresents the data, as swirls occur in broad bands which pass through these antipodes[5]. We have mapped swirls in these bands where photography permitted their positive identification, but south of this region the photography is extremely poor; the existence of swirls elsewhere on the Moon cannot be excluded. Finally, note that there is no reasonable candidate basin antipodal to Reiner Gamma.

Thus, we reiterate that lunar magnetization is probably the result of a variety of processes. However, the morphology and photometric properties of the light and dark swirls require both their recent origin and confinement to the regolith. They are very young features; this obviates the need to invoke magnetic shielding[10] to preserve the high albedo of their bright components.

P. H. SCHULTZ
L. J. SRNKA*

Lunar and Planetary Institute,
3303 NASA Road One,
Houston, Texas 77058

* Permanent address: Exxon Production Research Co., PO Box 2189, Houston, Texas 7701.

1. Hide, R. *The Moon* **4,** 39 (1972).
2. Srnka, L. J. *Proc. 8th lunar Sci. Conf.*, 785–792 (1977).
3. Srnka, L. J. *et al. Earth planet. Sci. Lett.* **42,** 127–137 (1979).
4. Hood, L. L., Coleman, P. J. Jr & Wilhelms, D. E. *Proc. 10th lunar planet. Sci. Conf.*, 2235–2257 (1979).
5. Schultz, P. H. & Srnka, L. J. *Nature* **284,** 22–26 (1980).
6. Schultz, P. H., Srnka, L. J., Pai, S. I. & Menon, S. *Lunar Planetary Science XI*, 1009–1011 (Lunar and Planetary Institute, Houston, 1980).
7. Tsay, F.-D. *Nature* **246,** 76–78 (1973).
8. Schultz, P. H. & Gault, D. E. *The Moon* **12,** 159–177 (1975).
9. Moore, H. J., Hodges, C. A. & Scott, D. H. *Proc. 5th lunar Sci. Conf.*, 71–100 (1974).
10. Hood, L. L. & Schubert, G. *Science* **208,** 49–51 (1980).

A ?braidplain facies model for the Westphalian B Coal Measures of north-east England

It was proposed by Haszeldine and Anderton[1] that prominent sand bodies in the Westphalian B of north-east England formed as braided river sheet sands following uplift of local sediment source areas. Our studies of uppermost Westphalian A and Westphalian B sediments in the same region support differing conclusions concerning (1) the extent and significance of palaeocurrent variation, (2) petrographic differences between individual sandstones and (3) petrographic evidence that much of the sediment is recycled.

(1) We agree that successive major sandstones have remarkably diverse and sometimes opposed general palaeocurrent trends. However, we find that individual major sandstones often have widely dispersed palaeocurrents at single outcrops and over large areas have complex patterns. Such variability seems contrary to the concepts of Haszeldine and Anderton, in which braided rivers flow down tectonically tilted palaeoslopes.

The same extremely diverse palaeocurrent trends also often apply to sandstones of the interbedded 'coal bearing facies', some of which probably accumulated in the highest energy environment of small shallow water deltas. Minor divergence could be due to crevassing and to th differing orientations of sub-deltas with regard to palaeoslope, but probably not the extremes present.

We suggest that much of this palaeocurrent variability, in the major sandstones and interbedded coal bearing facies, results from minor structural and palaeotopographic control of depositional systems on a coastal plain of almost non-existent palaeoslope. Such conditions pertain over the broad expanse of the modern Mississippi delta plain (through no analogy of delta style is suggested), where river and distributary channels, and delta lobes have diverse orientations with regard to regional palaeoslope[2,3]. Subsidence and continued accumulation of similar deposits should produce the sort of complex sediment body architecture present in the uppermost Westphalian A and Westphalian B of County Durham and elsewhere[4].

(2) We have examined thin sections cut from samples of major sandstones (impregnated with coloured epoxy resin) from County Durham and coastal Northumberland. Varieties and proportions of quartz, feldspars, rock fragments and heavy minerals show few differences that cannot be attributed to grain size[5,6], diagenetic dissolution and replacement[7,8], problems of readily distinguishing small grains of untwinned feldspar from quartz and the presence of intraformational sedimentary rock fragments. The results of our point counting do not substantiate the petrographic differences between major sandstones that might be expected if they were derived from a number of differing source areas.

(3) Only a small proportion of sand within the major sandstones seems to be recycled, direct evidence for recycling being anomalous grain size-rounding relationships, grains with multiple dust rims and overgrowths, half round grains and the presence of extraformational sedimentary rock fragments[6,9,10]. Relatively fresh feldspars, including sodic plagioclases, forming on average 10% of framework grains, are hardly suggestive of recycling from low relief sedimentary source areas in humid tropical climates[6,9,11,12], neither is the original subangular nature of some framework grains. Our preliminary conclusions suggest derivation of these sandstones from a mixed source area containing granitic, low grade metamorphic and sedimentary lithologies. Devonian sediments are probably indicated by occasional rounded recycled grains with haematite dust rims underlying multiple and abraded overgrowths.

Although we welcome the stimulus to Coal Measures sedimentology provided by Haszeldine and Anderton's report, we urge caution over the application of generalized facies models the the Coal Measures, when in many areas of the UK detailed sedimentological knowledge is limited. We intentionally do not provide an alternative model for the major sand bodies within the Westphalian B of north-east England, as each sandstone requires individual consideration, in the context of its surrounding strata. Our experience in County Durham and in other British coalfields also suggests that major sandstones, apparently traceable over wide areas, may have accumulated in a number of depositional environments.

We thank the NCB and their contractors for access to opencast sites. C.R.F. is in receipt of an NERC studentship.

ALAN P. HEWARD
CHRIS R. FIELDING

Department of Geological Sciences,
University of Durham,
Durham DH1 3LE, UK

1. Haszeldine, R. S. & Anderton, R. *Nature* **284**, 51–53 (1980).
2. Fisk, H. N. *Mississippi River Comm., Vicksburg* (1944).
3. Meckel, L. D. *Bull. Am. Ass. Petrol. Geol.* **56**, 639 (1972).
4. Visher, G. S., Ekebafe, S. B. & Rennison, J. *Deltas, Models for Exploration*, 381–397 (Houston geol. Soc., 1975).
5. Odom, I. E., Doe, T. W. & Dott, R. H. *J. sedim. Petrol.* **46**, 862–870 (1976).
6. Blatt, H., Middleton, G. V. & Murray, R. C. *Origin of Sedimentary Rocks*, 2nd edn (1980).
7. Heald, M. T. & Larese, R. E. *J. sedim. Petrol.* **43**, 458–460 (1973).
8. Wilson, M. D. & Pittman, E. D. *J. sedim. Petrol.* **47**, 3–31 (1977).
9. Folk, R. L. *Petrology of Sedimentary Rocks* (Hemphill, Austin, Texas, 1974).
10. Krynine, P. D. *Bull. geol. Soc. Am.* **53**, 1850–1851 (1942).
11. Krynine, P. D. *Am. J. Sci.* **29**, 353–363 (1935).
12. Potter, P. E. *J. Geol.* **86**, 423–449 (1978).

HASZELDINE AND ANDERTON REPLY—Heward and Fielding have highlighted some of the difficulties encountered when attempting to develop a model for the English Westphalian. Our model[1] was not intended as a definitive explanation for the details of the north-east coalfield succession, but as an alternative stratigraphic and sedimentological framework to the 'large delta' model. We proposed a low relief 'coastal plain' depositional environment crossed by many rivers. Heward and Fielding do not disagree with this general idea, but dispute some of the detailed evidence.

Deductions from measured palaeocurrents of the major fluvial facies must be made cautiously, as a wide spread of cross-bedding orientations is expected from any type of fluvial system[2–4]. Only the highest stage indicators, formed when currents are not influenced by lower stage component flows and channel-floor relief, give an accurate measure of the overall river direction[3,4]. Even these high stage current directions, fossilized by bar platform or supraplatform stratification, depend on the type of bar in the river and the method of its accretion to the floodplain[2–4]. Consequently, even from the deposits of one migrating low-sinuosity river, high stage palaeocurrents may easily vary by ±60° from the mean river orientation. These palaeocurrents will still, however, show a vector mean roughly downriver, unless accretion to one bank is dominant[4]. Coal Measures washout directions show good agreement with measured high stage palaeocurrent means, have consistent trends over large areas and have different trends from cycle to cycle. Subsidence resulting from compaction or local faulting may well have produced local palaeolopes, but these were superimposed on the regional drainage pattern. We would expect the sandstones of the coal facies to show a very great palaeocurrent variability, as lakes were probably filled from many directions (ref. 1, Fig. 1).

The sandstones examined by us contain many direct examples of recycled grains. Obviously not all recycled grains will preserve such direct evidence[5]. The apparent lack of extraformational sediment clasts is common in many modern recycled sands[5]. Note also that large quantities of fresh feldspar can survive more than one sediment cycle, and long transport distances in rapidly eroded tropical climates[6,7].

As Heward and Fielding suggest, the differences in sandstone mineralogy are not compelling in isolation, but we think that a greater degree of uniformity would be expected of sands derived from one source. Until a large-scale petrographic examination, combined with an appreciation of the relationships between petrography, the sub-environments within a river and the overall depositional environment shows otherwise, mineralogical differences and grain-size differences between sandstones (such as the anomalous coarse-grained sandstone above the Bensham seam in Northumberland) must suggest heterogeneous sediment sources.

We do not imply that all this sediment was supplied from adjacent areas, and would consider such areas as Ireland, the present North Sea and the Caledonides also contributed significantly. Any other more distant source would not account for the increasing marine influence, decrease in sediment grain size and change in river type from Northumberland towards the thickest Coal Measures in the Southern Pennine coalfields. Palaeocurrent trends of major sandstones from the east, west, south-west and north are thus in accord with our model and the overall palaeogeographical context[8].

R. S. HASZELDINE
R. ANDERTON

Department of Applied Geology,
University of Strathclyde,
Glasgow G1 1XJ, UK

1. Haszeldine, R. S. & Anderton, R. *Nature* **284**, 51–53 (1980).
2. Bluck, B. J. *Scott. J. Geol.* **7**, 93–138 (1971).
3. Bluck, B. J. *Trans. R. Soc. Edinburgh* **70**, 181–221 (1979).
4. Bluck, B. J. *Trans. R. Soc. Edinburgh* **69**, 425–456 (1976).
5. Blatt, H., Middleton, G. V. & Murray, R. C. *Origin of Sedimentary Rocks* (Prentice-Hall, Englewood Cliffs, 1972).
6. Krynine, P. D. *Am. J. Sci.* **29**, 353–363 (1935).
7. Milliman, J. D., Summerhayes, C. P. & Barretto, H. T. *Geol. Soc. Am. Bull.* **86**, 610–614 (1975).
8. Anderton, R. *et al. A Dynamic Stratigraphy of the British Isles* (Allen & Unwin, London, 1979).

High sediment yields from major rivers of the western Southern Alps, New Zealand

GRIFFITHS has recently estimated[1] erosion rates in the Southern Alps of New Zealand. His presentation, however, takes too little heed of published data, and has under-reported the suspended load data available.

(1) Griffiths reports suspended sediment yields from four east-coast and 10 west-coast rivers. In contrast, I have given yields[2,3] for 28 east-coast and 18 west-coast rivers, Thompson and Adams[4] have given yields from 23 of the same east-coast rivers and discussed their calculation and results in detail, and I have given yields[5] from 40 North Island rivers that have comparably high yields.

(2) Griffiths applies a traditional approach to his calculation of suspended loads. The water flow records presently available are generally good, and are quite adequate for suspended load calculations. However, I have expressed some reservations about the suspended load concentration data[4,5]. For flows less than the mean, the data are numerous (see Fig. 2 of ref. 1), but inconsequential as their contribution to the long-term mean load is slight. It is unfortunate that the sampling of flood flows is inadequate. Taking the Haast River data[1] as an example, there are 16 samples taken at less than mean flow, but only six at flows greater than the mean.

For many South Island rivers, half the suspended load is carried at flows greater than 3–8 times mean flow[4]. Because the highest flow sampled for the Haast River is only about twice the mean, considerable extrapolation of any concentration–flow relationship is required to calculate loads. Griffiths seems to have used linear regression for the relation, an approach Thompson and I rejected because of the nature of the data. Our reasons and an alternative method are given elsewhere[4,5]. This method gave the "earlier crude estimates" mentioned by Griffiths[1].

For all rivers except the Cleddau (see below) estimates by our method average 70% higher than Griffiths'. As there are no independent measurements of load in these rivers (note that both Griffiths and I used essentially the same data), and because estimates of load from point concentration samples may be in error by +100% and −50% (ref. 6), the importance of the difference is uncertain.

(3) I do not know on what additional data Griffiths' estimate of 13,000 tonnes km^{-2} yr^{-1} for the Cleddau is based, as I[2,3] estimated 275 tonnes km^{-2} yr^{-1} from concentration and flow data available up to 1977, and showed that the rate of sedimentation in adjacent Milford Sound represented erosion of about 200 tonnes km^{-2} yr^{-1}. This discrepancy of a factor of 50 is remarkable and needs to be resolved.

(4) Griffiths comments briefly on the

importance of bed load. I have derived[2,3] a bed load transport formula, checked it against some measured transport rates in New Zealand rivers, and applied it to many South Island rivers. The value of this (as of any bed load equation) is open to question, but it does estimate the bed load of the Waimakariri River as given by Griffiths[7] to within 15%. Dissolved loads have also been estimated in a general way[2,3] and, taken with the bed and suspended loads, suggest that for the Southern Alps the suspended load is 93%, the bed load 3%, and the dissolved load 4% of total river load.

(5) Griffiths neglects to mention that sampled river loads need not represent long-term average erosion rates. Some sparse New Zealand data[2,3] and observations in New Guinea[8] led me to conclude that in the northern part of the South Island, infrequent, earthquake-caused landslips could double the short-term erosion rate when averaged over hundreds of years.

(6) The obvious relationship between erosion rate and rainfall in the Southern Alps has been widely recognized. My thesis[2] contains data and discussion, showing that Fournier's[9] 2.65 power relationship between erosion rate and rainfall fits the estimates of erosion rate of the eastern slopes of the Southern Alps acceptably well. In contrast to the catchment averages used by Griffiths, the integral of local values of erosion and rainfall rate were used[4]. McSaveney[10] deduced a 2.92 power relationship and observed "rainfall is overwhelmingly the dominant influence on present erosion rates", a result later shown by Griffiths' multiple regression analysis.

(7) Griffiths' work is in general agreement with the published work cited above, and with the exception of the value for the Cleddau, I consider his estimates reasonable. There is an overall balance between rates of crustal shortening, tectonic uplift, river erosion, and deposition offshore for the South Island of New Zealand that indicates contemporary uplift and erosion of the Southern Alps[3]. The balance implies long-term erosion rates of up to 48,000 tonnes km^{-2} yr^{-1}, perhaps half of which occurs as catastrophic landslips. There seems little doubt that quite large catchments in the Southern Alps presently have erosion rates greater than 15,000 tonnes km^{-2} yr^{-1}.

JOHN ADAMS

2-71 James Street, Ottawa,
K1R 5M2, Canada

1. Griffiths, G. A. *Nature* **282,** 61–63 (1979).
2. Adams, J. thesis, Victoria Univ., Wellington (1978).
3. Adams, J. *Bull. geol. Soc. Am.* **91,** 2–4; 1–114 (1980).
4. Thompson, S. M. & Adams, J. *Physical Hydrology—New Zealand Experience* (eds Murray, D. L. & Ackroyd, P.) 213–229 (New Zealand Hydrological Society, Wellington, 1979).
5. Adams, J. *J. Hydrol. N.Z.* **18,** 36–48 (1979).
6. Walling, D. E. *Erosion and Solid Matter Transport in Inland Waters*, 34 (IAHS Symposium, Paris 1977).
7. Griffiths, G. A. *J. Hydrol. N.Z.* **18,** 6–28 (1979).
9. Pain, C. F. & Bowler, J. M. *Z. Geomorph.* **18,** 92–104 (1973).
9. Fournier, F. *Climat et Erosion* (Presses Universitaires de France, 1960).
10. McSaveney, M. J. *Proc. Conf. Erosion Assessment and Control in New Zealand*, 7–24 (1978).

GRIFFITHS REPLIES—In considering Adams' points (1) and (2) the relevant work is that of Thompson and Adams[1]. These authors assert that most of the scatter in New Zealand suspended sediment concentration versus water discharge ratings results from sediment exhaustion effects. They specifically assume that for a given river discharge the concentration on the rising stage of a flood is always higher than on the falling stage. Thompson and Adams[1] support this with results[2] from a single flood on Mararoa River. Because most concentration data have been collected on the falling stage, the authors compensate for sediment exhaustion by fitting straight lines "drawn midway between the scatter of the points" so as to give equal weight to the limited amount of rising stage data. Among the more serious deficiencies in the justification and application of this methodology are: first, on nearby Shotover River[1] scatter limits in the suspended sediment concentration rating are controlled mainly by seasonal effects. Rising and falling stage data are fairly evenly distributed (D. M. Hicks, personal communication). Second, Thompson and Adams did not identify the latter data. On Waimakariri and Forks Rivers, for example, all measurements were made on falling flood stages or at low flows: yet the ratings still are drawn midway through the scatter of the points[1]. Third, Thompson and Adams[1] do not always follow their rating definition prescription. For instance, on Acheron, Ahuriri, Clarence and Rakaia Rivers their ratings do not bisect the data scatter.

Thompson and Adams have made little use of the data: the positions of their rating lines are arbitrary; their results are not repeatable. Consequently, in this context, the relevant works[1,3] were not considered as serious references. At some sites, however, the rating definition is not too sensitive and there is the stated agreement of results[5].

Referring to his point (3) for Cleddau River suspended sediment rating, Adams uses a rating line slope of 1.7, without justification[3], whereas at his other 45 sites he assumes a value of 2.3. Even using his rating equation I cannot duplicate his yield of 275 tonnes km^{-2} yr^{-1}: instead I obtain some 2,000 tonnes km^{-2} yr^{-1}, which reduces the discrepancy to a factor of 6.5. The residual discrepancy is accounted for by his arbitrary definition of the suspended sediment rating. Similar wide discrepancies arise at other sites for the same reason. For example, in Mangatu, Waingaromia and Waipaoa Rivers, Adams[5] lists yields of 28,000, 20,000, 14,000 tonnes km^{-2} yr^{-1} respectively, whereas I calculate, using the same data, values of 7,000, 17,000, 5,000 tonnes km^{-2} yr^{-1}. Adams[3] supports his Cleddau River yield estimate with sedimentation data obtained from a single borehole in Milford Sound. He assumes suspended sediment deposition, age and areal extent of deposit and size of contributing area. This does not, in my view, constitute adequate scientific evidence.

My comments on points (4) and (5) would be too lengthy; my conclusions are similar to point (3).

With regard to point (6) Fournier's[6] relationship as applied by Thompson and Adams[1] does not fit the estimates of erosion rate acceptably well. In fact, the constant E_0, in their modified equation varies from 2,000 to 160,000 tonnes km^{-2} yr^{-1} (see Table 1 in ref. 1).

On Adams' point (7), McSaveney (personal communication) estimates a long-term yield in excess of 50,000 tonnes km^{-1} yr^{-1} in Cropp River, a tributary of Hokitika River[5]. Erosion in this catchment occurs by natural fluvial processes including frequent landslips under high intensity storms.

Finally, the units of suspended sediment concentration used in Fig. 2 and in the calculation of the coefficients in my first paragraph[5] are given incorrectly as kg m^{-3} instead of g m^{-3}. This error, however, does not enter into the results or conclusions.

GEORGE A. GRIFFITHS

Water and Soil Division,
Ministry of Works and Development,
PO Box 1479, Christchurch, New Zealand

1. Thompson, S. M. & Adams, J. *Physical Hydrology—New Zealand Experience* (eds Murray, D. L. & Ackroyd, P.) 213–229 (New Zealand Hydrological Society, Wellington, 1979).
2. Christian, R. & Thompson, S. M. *J. Hydrol. N.Z.* **17,** 50–53 (1978).
3. Adams, J. thesis, Victoria Univ. Wellington (1978).
4. Adams, J. *J. Hydrol. N.Z.* **18,** 36–48 (1979).
5. Griffiths, G. A. *Nature* **282,** 61–63 (1979).
6. Fournier, F. *Climat et Erosion* (Presses Universitaires de France, 1960).

Molecular clockwork

THE results of the very interesting experiment of Hartl and Dykhuizen[1] can be interpreted differently. There are three statistical problems with their conclusion that response by *Escherichia* to natural selection occurs as rapidly with generations of 5 h as with those of 2.5 h.

First, in their Table 2, basing an analysis on the last 200 h instead of the last 300, as equally justified by their own argument on the duration of the later periodic selection, would reverse the conclusion, the rate of evolution being much greater in the

0028-0836/80/360089—02$01.00

chemostats with shorter generation time. Second, non-significant differences are taken to be zero in averaging in Table 2. Using all information (ignoring significance because zero differences in fitness are not really expected and 10 of 11 non-significant differences are ostensibly positive, as expected) gives mean fitness increments of 1.78 per 100 h for shorter-period chemostats and 1.18 for longer-period ones, using the last 300 h, and 2.33 and 0.55, respectively, using the last 200 h. Again, faster evolution with more rapid generations is suggested.

Third, in competition between the same strains grown in each of the two kinds of chemostats, interstrain selection coefficients in both conditions can be compared (their Fig. 2). The trend line summarizing the results seems, however, to be an ordinary regression rather than a co-regression[2], even though the two variables depend equally on each other and there is no asymmetrical prediction involved. A co-regression would be steeper and thus suggest that elimination of weaker strains is more rapid per unit time with short generations than with longer generations; even the regression given is significant in this direction at the 0.05 level. One might want to modify the statistics of their Table 2 by this result, but alternatively, it can itself be taken as another indication of faster change with faster turnover. I do not want to imply that the results suggest a proportionality between generation number and evolutionary rate, merely a positive relationship.

Conceptually, the experiment is interpreted (even in the title) as showing that a constant evolutionary rate per unit time can be caused by natural selection. However, even if the data gave clear support to the conclusions drawn (and I think they suggest the opposite), what would be shown is that generation time does not influence evolutionary rate even under strong selection pressure. The rates of change observed were far from constant even though (perhaps because only three time intervals are involved) not significantly more uneven than rates of molecular evolution. There is no evidence to suggest a long-term approximate constancy in mean rate, as there is for molecular evolution, and an independence of evolutionary rate and generation time has long been advocated[3] from palaeontological evidence. Such an independence, to the extent it exists, is easily explained if evolutionary rate is caused largely by changes in the total environment. A stochastically constant rate of evolution is a much more difficult phenomenon to explain. This gives it power in a genetically based view of evolution; only neutralism predicts it more or less adequately in that context. However, if we take ecology seriously with respect to evolutionary change, a natural (but still unproved) explanation for the observed degree of constancy emerges[4]. It is quite consistent with the observed large short-term differences[5-7] in evolutionary rates, as neutralism may not be[7].

LEIGH M. VAN VALEN

Biology Department (Whitman),
University of Chicago,
915 East 57th Street,
Chicago, Illinois 60637

1. Hartl, D. & Dykhuizen, D. *Nature* **281**, 230–231 (1979).
2. Van Valen, L. *J. theor. Biol.* **45**, 235–247 (1974).
3. Simpson, G. G. *The Major Features of Evolution* (Columbia University Press, New York, 1953).
4. Van Valen, L. *J. molec. Evol.* **3**, 89–101 (1974).
5. Kurtén, B. *Cold Spring Harb. Symp. quant. Biol.* **24**, 205–215 (1960).
6. Van Valen, L. *Evol. Theory* **4**, 45–80 (1978).
7. Lessios, H. A. *Nature* **280**, 599–601 (1979).

DYKHUIZEN AND HARTL REPLY—Before discussing the particular points raised by Van Valen, we wish to emphasize that the molecular clock is sloppy[1], so exactitude should not be expected. It would be wonderful to carry out such experiments for 500 years (or, better yet, 500 Myr). In such a long time span, different results might very well be obtained. We have achieved only 500 h. Nevertheless, our data have remarkable internal consistency for experiments of this sort, and the formal congruence between the characteristics of our results and of the molecular clock are too striking to ignore. Also, we do not suggest that the environment is unimportant to the rate of evolution. The chemostat is a novel environment for *E. coli* K2, and it is likely that the large initial selection is due to this change of environment. It is also possible that the average rate of selection would decrease over time in the constant environment of the chemostat. Chemostats could be run for 2,500 h to see if this supposition is true. If true, it implies that environmental change is required to keep the selective clock wound.

Van Valen has questioned why we chose to analyse the last 300 h rather than the last 200 h. Most of our argument is actually based on the full 500 h as evidenced by the statement "The overall [that is, 500 h] average fitness increment per 100 h is 2.99 in the 2.5 h chemostat and 3.00 h in the 5.0 h chemostat"[2]. (Incidentally, if one treats all fitness differences as if they were significant, as Van Valen suggests, the corresponding averages are 3.28 and 3.05.) We presented the averages for the period 200–500 h only to show that we were not being misled by the large fitness increments that occur in the first 200 h. Van Valen points out that if only the last 200 h are taken for analysis, then it looks as if the 2.5 h strain is evolving faster. But this ignores more than half of the experimental measurements, and it contradicts the conclusion from the entire data set. By using a selected subset of any data, one can contradict any conclusion whatsoever.

There is, however, a better way to settle the issue, which is by direct competition between strains that have evolved for long periods at either a 2.5-h or a 5.0-h generation time. For strains that had evolved for the full 500 h, the largest fitness difference is observed when the experimental test is carried out in a 2.5-h chemostat; the 2.5-h strain is favoured, to be sure, but the fitness difference is a mere 5%. This amount of genetic divergence over 500 h is very small indeed. Moreover, when tests are carried out in a 5.0-h chemostat, selection actually favours the 5.0-h strain. These observations are difficult to reconcile with a presumed more rapid rate of evolution at a 2.5-h generation time[3].

The data in our[2] Fig. 2 are not relevant to the issue of rate of increase in fitness; they pertain to whether measured selection coefficients depend on the conditions of measurements. If the slope of the line in Fig. 2 is truly greater than 1.0, as Van Valen suggests, then we have actually overestimated the rate of increase in fitness in 2.5-h chemostats by about 25%, so our original conclusion receives additional support. Moreover, Van Valen's suggestion of co-regression is well taken. The co-regression line[4] has a slope of 1.5, which, if taken literally, calls for a correction of about 35%, so our original conclusion is more forcefully justified by Van Valen's own technique.

In short, our results indicate that the rate of increase in fitness is related to the amount of time spent in the chemostat rather than the number of generations. The issue is clearly an important one, and we hope that this exchange with Van Valen will encourage more of such experiments to be undertaken.

D. DYKHUIZEN
D. HARTL

Purdue University,
Department of Biological Sciences,
West Lafayette, Indiana 47907.

1. Fitch, W. M. in *Molecular Evolution* (ed Ayala, F. J.) 160–178 (Sinauer, Sunderland, Massachusetts, 1976).
2. Hartl, D. & Dykhuizen, D. *Nature* **281**, 230–231 (1979).
3. Dykhuizen, D. & Hartl, D. *Evolution* (in the press).
4. Sokal, R. and Rolf, F. J. *Biometry* 526–532 (Freeman, San Francisco, 1969).

Matters Arising

Matters Arising is meant as a vehicle for comment and discussion about papers that appear in *Nature*. The originator of a Matters Arising contribution should initially send his manuscript to the author of the original paper and both parties should, wherever possible, agree on what is to be submitted. Neither contribution nor reply (if one is necessary) should be longer than 300 words and the briefest of replies, to the effect that a point is taken, should be considered.

BOOK REVIEWS

Certainty into doubt: 25 years of nuclear debate

Alan Cottrell

The Nuclear Power Decisions: British Policies, 1953–78. By Roger Williams. Pp.365. (Croom Helm: London, 1980.) £19.95. Available from Biblio Distribution Centre, Totowa, New Jersey, $49.

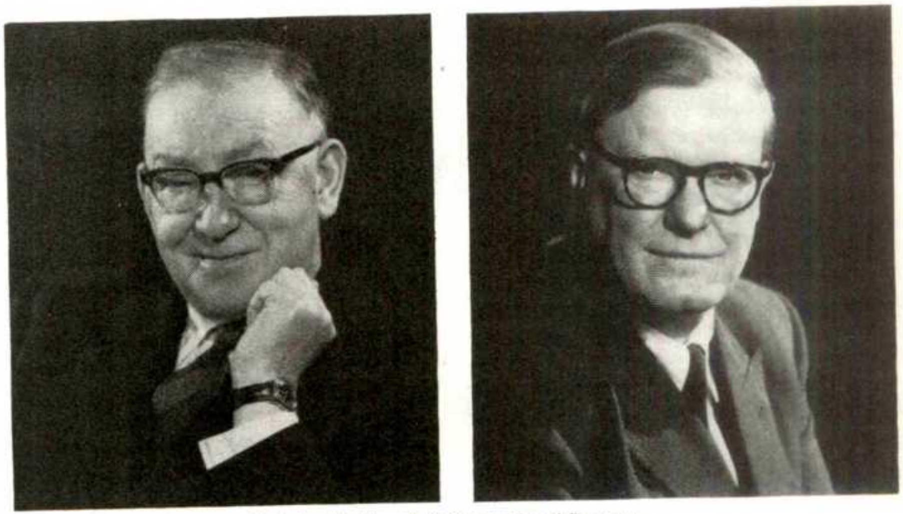

Sir John Cockcroft (left) and Lord Penney — "heroes" of the 1950s and 60s.

THERE IS a saying in the nuclear industry that the reactor you choose is always the best one. It becomes the best one because you work on it, solve its problems, improve it, develop and adapt a whole technology to it, all of which gives it an edge over its rivals. There are certainly grains of truth in this, but the irony is that different countries have different 'best' reactors and hang on to their choices grimly through thick and thin. Today we have each of the three original reactor-producing countries firmly entrenched in its own concepts of thermal reactors: the gas-cooled types, Magnox and AGR, for the British; the light-water ones, PWR and BWR, for the Americans; and the heavy-water one, CANDU, for the Canadians.

It is interesting to follow these deep, insurmountable, trenches back in time to their earliest beginnings in the 1940s as slight traces across the smooth face of the then infant nuclear era. There were the Americans using light-water cooling in their early Hanford reactors, choosing it for its simplicity and because they had the empty spaces in which to site these possibly dangerous plants. From this early background they went on to light-water pressurized reactors for propelling submarines, out of which grew the modern pressurized-water and boiling-water civil reactors. Again there were the British, with their lack of large rivers for coolant in very remote and unpopulated regions, choosing gas-cooling for their early Windscale military reactors, which likewise set them firmly in their own groove; and yet again there were the Canadians, keen to make the best use of natural uranium and so being led to heavy-water, to which they became equally heavily addicted. Only the French, in switching from gas cooling to light-water cooling, dared to jump over into another trench.

Much of this is brought out in Roger Williams's splendid book, *The Nuclear Power Decisions,* which discusses the major British decisions in the civil nuclear field, and the way they were made, between 1953 and 1978. Mostly, the book deals with the history of the Advanced Gas-cooled Reactor (AGR) — of how, despite its various imperfections and vicissitudes, it successfully fought off all threats from every water-cooled rival, basically because it was a gas-graphite reactor, a British concept with British technology and expertise, a direct descendant of the Windscale, Calder Hall and Magnox reactors. Williams takes the reader carefully and clearly through the history of this, giving full weight to all the technical, economic, political and, not least, personal factors involved in the decisions. The sound of those old debates of the 1950s and 60s, now half-forgotten, comes thundering back with the reminders of the great speeches by the heroes of that period — Hinton, Penney, Cockcroft, Plowden, Sherfield, Coleraine, Stanley Brown and others; as well as the clash of argument between the AEA and the CEGB. We are also reminded of the amazing surefootedness of that early period, of the launching in the mid-1950s of a huge programme of Magnox reactors even though their prototype, Calder Hall, was still one year away from completion. Contrast that with the snail-like approach we are making today towards the Fast Breeder Reactor. How did we lose our nerve? Williams is too polite to say but he does make a vigorous plea in his final chapter for a system of public accountability that would make civil nuclear energy as acceptable to the general public in the 1980s as it so obviously was in the 1950s.

Perhaps the difficulties of the AGR had something to do with it, causing us to doubt whether our 'best' really was the best of bests. Williams takes the reader through the dense jungle of AGR politics with immense skill and clarity, especially in regard to the economic and political factors. Despite the intentionally non-technical nature of the book, more could perhaps have been made of the technical differences between AGR and the water reactors, and their significance, particularly from the point of view of safety, for these factors do have important weight in the decision-making. Nevertheless, the account is a very fair and well-balanced one, which is no mean feat in a field where emotions run so high that one distraught civil servant felt impelled to complain that it was impossible for anyone to remain impartial where the choice of reactors is concerned.

The final section of the book deals with the 1978 Windscale decision. This is not only a change of subject — the expansion of the nuclear reprocessing plant — but even more a reflection of the change of mood since the 1950s. No longer is there the gung-ho approach of the early White Papers on reactor programmes. Instead we are in the era of doubt, of public enquiries, of Mr Benn's hesitations, of the cautionary remarks of the Flowers Report, and of the campaigns by the Friends of the Earth and other anti-nuclear groups. So much has the native hue of nuclear resolution been sicklied o'er by the pale cast of thought. And this leads to Williams's final chapter on public accountability and his "conviction that Britain can have a much more successful industrial future than she has had an immediate past, especially where nuclear power is concerned". A book strongly to be recommended. □

Sir Alan Cottrell is Master of Jesus College, University of Cambridge.

Advances in research on evoked potentials

D. Regan

Evoked Potentials. Edited by C. Barber. Pp. 614. (MTP Press: Lancaster, UK, 1980.) £29. *Clinical Uses of Cerebral, Brainstem and Spinal Somatosensory Evoked Potentials.* Edited by J.E. Desmedt. Pp. 354. (Karger: Basel, 1980.) SFr 138, $82.75. *Cognitive Components in Cerebral Event-Related Potentials and Selective Attention.* Edited by J.E. Desmedt. Pp. 322. (Karger: Basel, 1979.) SFr 118, $70.75.

IT HAS been known for almost 100 years that the human brain continuously generates an electrical oscillation called the electroencephalogram (EEG) that can be recorded from electrodes held onto the scalp. The EEG can reach an amplitude of 100 μV, so that the brain's 0.1-10 μV responses to auditory, visual, tactile or olfactory stimulation are usually hidden in the EEG. Consequently, these electrical responses to sensory stimulation, called evoked potentials, were almost unexplored until automatic signal-processing devices, developed in the 1950s, were used to separate evoked potentials from the brain's background activity. Part A of Barber's book is an excellent, concise survey of these signal-processing techniques and evoked potential methodology.

The three books reviewed here together cover all the main directions of current evoked potential research. Many contributors emphasize the present clinical value and future promise of evoked potential recording as an effectively risk-free means of objectively testing hearing, vision and spinal cord function. Clearly, a battery of objective sensory tests would meet a need, particularly with neonates and young infants, where the available methods for testing sensory function are imprecise. In adults, evoked potential tests can distinguish between organic and psychogenic disorders, and practical successes with adult patients are described by authors in all three books. In particular, short-latency evoked potentials recorded from auditory brainstem structures have proved their worth both in the neurological clinic and in assessing hearing disorders, and evoked potentials produced by visual patterns are widely used as an aid to diagnosing multiple sclerosis. Auditory brainstem responses are a promising means of testing infants' hearing, and a technically difficult method for recording from electrodes over the spinal cord has been successfully used with infant patients, but so far visual evoked potentials seem to have had comparatively little impact on the visual testing of infants and the management of amblyopia. Part A of Barber's book identifies limitations in our understanding of visual evoked potential generation that must be overcome if the method is to fulfil its exciting promise in paediatric neuro-ophthalmology.

Evoked potential recording is the only widely available, risk-free means of objectively exploring the activities of normal human brains (analysis of the brain's magnetic field is still at an early stage of development). Consequently, evoked potential recording has a special appeal to scientists interested in aspects of brain activity that may be peculiar to the human species. Rather than studying evoked potentials generated by sensory stimuli, a second line of research explores scalp potentials produced or modified by thinking processes. Several authors in Desmedt's book on cognition show how evoked potentials can be used not only to study the brain activities associated with mental evaluation of incoming sensory information, but also how to study cognitive aspects of brain function including selective attention.

All three books are collections of contributions by different authors, each of whom focuses chiefly on his own research area. Although this style of book can be assembled more quickly and with less individual toil than is the case when the writing is undertaken by only one or two authors, there are disadvantages for the reader. These include greater difficulty in following a coherent thread through successive chapters, and some unevenness in the standard of different authors' contributions. Since each of the books edited by Desmedt addresses a restricted topic these drawbacks are less evident than in Barber's book. Desmedt's two books provide researchers and clinicians with summaries of current research in cognitive evoked potential studies and in somatosensory evoked potentials that are as useful as any available. However, it is a pity that substantial linking commentaries were not incorporated, since these would have made both books more effective as introductory texts. Although its inclusion may have delayed publication, the edited discussion on pattern responses in Barber's book adds considerably to the value of the text. Several more such discussions could have been added with advantage.

Barber's book is based on the 1978 evoked potential conference held in Nottingham, and resembles in some ways a book based on the 1974 Brussels conference (*Visual Evoked Potentials in Man.* Edited by J.E. Desmedt. Clarendon: Oxford, 1977). Some impression of progress in evoked potentials research can be obtained by comparing these two volumes. What emerges is that the relation between cognition and long-latency evoked potentials is more complex than was thought to be the case in 1974; it now seems that several late waves exist, differing from one another in their brain origins and psychological correlates. Our basic understanding of visual evoked potentials advanced substantially before 1974, but progress seems to have slowed since then. The few researchers attempting to develop evoked potentials as much-needed objective measures in psychiatry have continued to encounter formidable problems including the broadness of clinical diagnostic classifications. In contrast, the use of visual evoked potentials in the neurology clinic, a research technique in 1974, is now routine in a large number of hospitals. Perhaps the major new thrusts in basic research and in clinical applications have been in auditory brainstem and somatosensory evoked potentials, and these topics are well covered both by Barber and by Desmedt. □

D. Regan is I.W. Killam Research Professor in the Department of Physiology and Professor of Ophthalmology at Dalhousie University, Halifax, Nova Scotia.

Protein synthesis from start to finish

P. J. Ford

From DNA to Protein: The Transfer of Genetic Information. By M. Szekely. Pp. 284. (Macmillan Press: London, 1980.) Hardback £18, $35.95; paperback £9.95.

From DNA to Protein is an up-to-date (early 1979) account of that fascinating but ill-defined area of biology comprising some genetics, some biochemistry and some macromolecular structure. The book has been written for advanced undergraduates and postgraduate students, but is also intended for research workers wishing to keep up with molecular biology.

My initial reaction to the contents pages was very favourable since the book is logically ordered, starting with a description of DNA structure and replication, followed by transcription and messenger RNA structure and leading into a discussion of translation. There is also a chapter on methods of nucleotide sequence determination which, for some undergraduate teaching purposes, might be too specialized. Such detailed attention nevertheless does indicate the overwhelming role of technology in forcing advances in this area, a point which I think cannot be made too often.

Reading the book in more detail I found that descriptions of particular systems were generally easily followed although there are many places where more careful editing would have improved communication. Some more obvious errors might also have been removed such as the "thousands (of ribosomal RNA genes) in *Drosophila*" (p. 16) or more seriously the suggestions that satellite DNAs are small molecules (p. 28) and that yeast has a single chromosome (p. 34).

On p. 41 there is the ambiguous statement that "In higher organisms in which the enzyme patterns of the different cells are fairly constant, the protein genes are not part of operons. They are dispersed in the chromosome, transcribed separately and their expression is in most cases individually controlled". This is the point at which the author comes nearest to discussing the fundamental problem in eukaryotic gene regulation, which is how an apparently constant genome manages to produce such a diversity of cellular structure and function during development and differentiation. However, the theme of coordinate gene regulation in eukaryotes is not pursued. Nor is any attempt made to rationalize known genetic linkage maps in terms of gene regulation. The passage also serves to illustrate a general weakness of the text, which shows a preoccupation with minutiae and failure to state basic problems clearly and extract a useful synthesis of ideas from the welter of information. In particular I had expected a discussion of gene structure on the basis of the discoveries of overlapping and split genes, since this is promised on the dust cover. Although overlapping and split genes are mentioned on several separate occasions, there is no single passage which attempts to draw together all the observations and to deal with their consequences for the control of messenger RNA synthesis and for the evolution of protein structures.

Some specific topics which I would have liked to see mentioned are transposition and insertion elements as model mechanisms for moving DNA within and between chromosomes; a more detailed treatment of lambda phage as a model for switching between two alternate (lytic or lysogenic) types of development; a treatment of gene numbers in terms of rate limits to transcription; consideration of immunoglobulin genes in relation to specific reorganization of DNA during differentiation; and some discussion of secretion which involves a hydrophobic amino-terminal signal peptide enabling proteins for secretion to cross membranes.

For students the reviews of DNA replication, transcription and translation should be useful and are well referenced up to 1978. Although these chapters relate almost exclusively to prokaryote systems they do give comparisons with eukaryote translation mechanisms, eukaryote RNA polymerases and eukaryote DNA replication mechanisms. The other chapters on the structure of messenger RNA, the structure and function of ribosomes and on transfer RNA are perhaps too specialized for all but the devotee of macromolecular structure and function. □

P. J. Ford is a Lecturer in the Department of Molecular Biology at the University of Edinburgh.

1937, 1951, 1976 — progress in crystallography

D.W.J. Cruickshank

X-Ray Analysis and the Structure of Organic Molecules. By Jack Dunitz. Pp. 514. (Cornell University Press: 1980.) $55, £36.

THIS BOOK has developed out of the Baker Lectures given by Jack Dunitz at Cornell University in the fall of 1976. Once again the publication of a set of the Lectures allows them to be appreciated by a far wider audience than the chemists of Cornell. This volume immediately brings to mind Linus Pauling's influential Lectures of 1937, "The Nature of the Chemical Bond and the Structure of Molecules and Crystals", and J.M. Robertson's notable contribution of 1951, "Organic Crystals and Molecules". Crystallography and organic chemistry have developed enormously in the last quarter century, so that whereas in 1951 Robertson could discuss a large proportion of the 200 or so organic crystal structures then known, in 1976 it would have been impossible for Dunitz to survey 16,000 structures in like fashion.

Dunitz's book is in two parts: "Crystal Structure Analysis" and "Molecular Structure". The first part is a fairly complete guide to current methods of determining the crystal structures of small or medium-size molecules (not proteins). A score or two of books must have been written on crystal structure analysis, but Dunitz's volume is more attractive than most of the others. This is because of the flowing informal style and the penetrating insights and asides of a master of the craft. I suspect his treatment will prove somewhat too professional for most of those chemists he wants to help read the crystallographic literature, but it will be invaluable for young (or not-so-young) crystallographers seeking an overview of the main parts of the subject.

Among the interesting features is a discussion of the frequency of occurrence of particular space groups and Kitaigorodsky's explanation of this in terms of possible molecular packing arrangements. On p.136 we learn of the caesium salt of boromycin, the absolute configuration of which was established before its structural formula. On p.143 we read of the flurry caused in 1972 by Tanaka's claim that all absolute configurations determined by X-ray analysis were wrong and should be changed into their antipodes. Tanaka's claim proved ill-founded, but his error was a happy one for it led to new and independent proofs of the correctness of the Bijvoet method. There is a helpful and well-titled section on hazards of oblique coordinate systems. Both this and the section on thermal motion analysis contain useful worked examples.

Unfortunately the treatment of Fourier transforms is marred by a misprint at a critical point on p.30, and by a failure to make clear whether the inverse transform relates to the minus sign in the exponential argument or to the transformation from **R** space to **r** space. Dunitz is a Lewis Carroll fan and he concludes his summary of simple theorems about Fourier transforms with a quotation from *Alice*:

> "What *is* the use of repeating all that stuff", the Mock Turtle interrupted, "if you don't explain as you go along? It's by far the most confusing thing I have ever heard!"

Dunitz must have had a premonition of trouble on the printed page!

The second part on molecular structure contains four chapters, of which the first, "Crystal Structure Analysis and Chemistry", is both the most substantial and the one of greatest general interest. Dunitz first traces the explosive growth of information on molecular structures and stresses the utility of the computer-based files of structural data collected by the Cambridge Crystallographic Data Centre. He reminds us of the triumphs of classical organic chemistry in the determination of structural formulae, but uses patchouli alcohol as an example of an unexpected contradiction. He reports on conformational analysis, solid-state chemistry and reaction intermediates — the latter illustrated by the remarkable structure of $CO_2(CO)_4(H_2CBu^t)(C_2H_2)$ determined by Mills and Robinson in 1964. Then comes a discussion of molecular potential energy surfaces, which leads on to Dunitz's structural correlation principle whereby the numerous slightly differing 'still' pictures of the same structural fragment in different crystals are used to infer a chemical reaction path. Nucleophilic addition to carbonyl groups is used as one of the examples of this principle.

The remaining chapters include a good account of investigations into the electron-density distributions in molecules, a very clear exposition of the geometrical aspects of the closure constraints in cyclic molecules and an elegant discussion of symmetry in conformational maps.

Dunitz learnt his crystallography in Glasgow and Pasadena. Robertson and Pauling can be well satisfied with the volume their former protégé has now placed alongside their own in the Baker Lecture series. □

D. W.J. Cruickshank is Professor of Chemistry (Theoretical) at the University of Manchester Institute of Science and Technology, and was formerly General Secretary and Treasurer of the International Union of Crystallography.

BOOKS RECEIVED

Mathematics

BEAUMONT, G. P. Intermediate Mathematical Statistics. Pp. 248. Flexi ISBN 0-412-15480-3. (Chapman & Hall: 1980.) flexi £5.95.

CHAKRAVARTI, I. M. (ed.). Asymptotic Theory of Statistical Tests and Estimation. The Proceedings of an Advanced International Symposium held at the University of North Carolina, April, 1979. Pp. 350. ISBN 0-12-166650-6. (Academic: 1980.) $25.

KINDERLEHRER, D. and STAMPACCHIA, G. An Introduction to Variational Inequalities and Their Applications. Pure and Applied Mathematics Series. Pp. 313. ISBN 0-12-407350-6. (Academic: 1980.) $35.

MATSUMURA, H. Commutative Algebra. 2nd Edn. Mathematics Lecture Note Series. Pp. 312. Flexi ISBN 0-8053-7026-9. (Benjamin/Cummings: Reading, Massachusetts, 1980.) $19.50.

SNEDDON, I. N. Special Functions of Mathematical Physics and Chemistry. 3rd Edn. Longman Mathematical Texts. Pp. 182. Flexi ISBN 0-582-44396-2. (Longman: 1980.) £5.95.

WILSON, A. G. and KIRKBY, M. J. Mathematics for Geographers and Planners. 2nd Edn. Pp. 408. Hbk ISBN 0-19-874114-6; pbk ISBN 0-19-874115-4. (Clarendon/Oxford University Press: 1980.) Hbk £12.50; pbk £6.95.

Astronomy

BATTRICK, B. and MORT, J. (compiled by). Proceedings of the 2nd European IUE Conference, Tübingen, Germany, March 1980. Pp. 368. Flexi ISBN 0379-6566. (European Space Agency: Paris, 1980.) F.Frs. 125.

BURKE, W. L. Spacetime, Geometry, Cosmology. Pp. 329. ISBN 0-935702-10-6. (University Science Books: Mill Valley, California, 1980.) NP.

BURKE; W. R. Photovoltaic Generators in Space. Proceedings of the 2nd European Symposium on the Photovoltaic Generators in Space, Heidelberg, Germany, April 1980. Pp. 249. Flexi ISBN 0379-6566. (European Space Agency: Paris, 1980.) F.Frs. 80.

DIXON, R. T. Dynamic Astronomy. 3rd Edn. Pp. 524. Flexi ISBN 0-13-221267-6. (Prentice/Hall: 1980.) £9.70.

DOHERTY, P. Atlas of the Planets. Pp. 143. ISBN 0-600-30439-6. (Hamlyn: Feltham, UK, 1980.) £6.95.

LEVITT, I. M. and MARSHALL, R. K. Star Maps for Beginners. A Fireside Book. Pp. 64. Flexi ISBN 0-671-25422-7. (Simon and Schuster: New York, 1980.) NP.

WALKER, J. (introduction by). Light from the Sky. Readings from Scientific American. Pp. 78. Flexi ISBN 0-7167-1222-9; hbk ISBN 0-7167-1221-0. (W. H. Freeman: 1980.) Flexi £3.30; hbk £7.10.

GRIBBIN, J. The Strangest Star. A Scientific Account of the Life and Death of the Sun. Pp. 184. ISBN 0-485-11207-8. (Athlone: London, 1980.) £6.95.

Applied Biology

BATTISTIN, L., HASHIM, G. and LAJTHA, A. (eds). Neurochemistry and Clinical Neurology. Progress in Clinical and Biological Research Vol. 39. Pp. 500. ISBN 0-8451-0039-4. (Alan R. Liss: New York, 1980.) $38. Available in Europe and the Middle East from European Book Service, Flevolaan 36-38, P.O.B. 124, 1380 AC Weesp, Holland.

BOON, M. E. and TABBERS-BOUMEESTER, M. L. Gynaecological Cytology. A Textbook and Atlas. Pp. 192 + 144 atlas. Hbk ISBN 0-133-26117-8; flexi ISBN 0-333-26117-6. (Macmillan: London, 1980.) Hbk £25; flexi £14.

BRENNAN, M.J., McGRATH, C.M. and RICH, M.A. (eds). Breast Cancer: New Concepts in Etiology and Control. Pp. 406. ISBN 0-12-131150-3. (Academic: 1980.) $31.50.

BRIDGES, J. W. and CHASSEAUD, L. F. (eds). Progress in Drug Metabolism Vol. 4. Pp. 333. ISBN 0-471-27702-9. (Wiley-Interscience: 1980.) £25.

CALABRESE, E. J. Nutrition and Environmental Health. The Influence of Nutritional Status on Pollutant Toxicity and Carcinogenicity. Vol. 1 The Vitamins. Pp. 585. ISBN 0-471-04833-X. (Wiley-Interscience: 1980.) £32.70.

CIBA FOUNDATION SYMPOSIUM 74 (New series). Drug Concentrations in Neuropsychiatry. Pp. 266. ISBN 90-219-4080-9. (Excerpta Medica: 1980.) $45.75, Dfl. 94.

CONDORELLI, L., TEODORI, U., ANGUISSOLA, A. B. and SANGIORGI, M. (eds). Internal Medicine. Proceedings of the XIV International Congress of Internal Medicine ISIM Rome, October 1978. Parts 1 and 2 pp. 1532. ISBN 90-219-0438-1. (Excerpta Medica: 1980.) Parts 1 and 2 $195, Dfl. 400.

COON, M.J. *et al.* (eds). Microsomes, Drug Oxidations, and Chemical Carcinogenesis Vol. 4th International Symposium on Microsomes and Drug Oxidations held at Ann Arbor, Michigan, July 1979. Pp. 618. ISBN 0-12-187701-9. (Academic: 1980.) $39.50.

COON, M. J. *et al* (eds). Microsomes, Drug Oxidations, and Chemical □Carcinogenesis. Vol. II. 4th International Symposium on Microsomes and Drug Oxidations held at Ann Arbor, Michigan, July 1979. Pp. 1258. ISBN 0-12-187702-7. (Academic: 1980.) $41.

COUNCIL FOR INTERNATIONAL ORGANIZATIONS OF MEDICAL SCIENCES (CIOMS). International Nomenclature of Diseases. Vol. III, Diseases of the Lower Respiratory Tract. Pp. 128. Flexi ISBN 92-9036-001-1. (CIOMS: Geneva, 1979.) Sw.fr. 25.

DANIELS, S., HALSEY, M. J. and SMITH, E. B. (eds). Techniques for Diving Deeper than 1,500 feet. UMS Publication No. 40 WS (DD) 6-30-80. The 23rd Undersea Medical Society Workshop. Pp. 159. (Undersea Medical Society: 9550 Rockville Pike, Bethseda, Maryland 20014, 1980.) Pbk np.

DE BOER, J. and BAILLIE, T. W. (eds). Disasters; Medical Organization. Pp. 110 ISBN 0-08-025491-8. (Pergamon: 1980.) £6.50, $14.50.

DOSMAN, J. A. and COTTON, D. J. (eds). Occupational Pulmonary Disease; Focus on Grain Dust and Health. Proceedings of the International Symposium on Grain Dust and Health held in Saskatoon, Canada, November 1977. Pp. 615. ISBN 0-12-221240-1. (Academic: 1980.) $42.

ENGLISH, M. P. Medical Mycology. Pp. 57. Flexi ISBN 0-7131-2795-3. (Edward Arnold: London, 1980) £2.50.

FAGLIA, G., GIOVANELLI, M. A. and MACLEOD, R. M. (eds). Pituitary Microadenomas. Proceedings of the Serono Symposia, Vol. 29. Pp. 566. ISBN 0-12-248150-X (Academic: 1980.) £30, $69.

FRASER, F. C. *et al.* Le Diagnostic Prénatal. Cahiers de Bioéthique Vol. 2. Pp. 281. Flexi ISBN 2-7637-6914-4. (Les Presses de L'Université Laval, Quebec: 1980.) $14.

GIORDANO, C, (ed.). Sorbents and Their Clinical Applications. Pp. 503. ISBN 0-12-285280-8. (Academic: 1980.) $55.

GLENNER, G., COSTA, P. P. E. and de Freitas, A. F. (eds). Amyloid and Amyloidosis. Proceedings of the Third International Symposium on Amyloidosis, Póvoa de Varzim, Portugal, September 1979. Pp. 629. ISBN 90-219-0426-8. (Excerpta Medica: 1980.) $109.75, Dfl. 225.

GUTHRIE, F. E. and PERRY, J. J. (eds). Introduction to Environmental Toxicology. Pp. 484. ISBN 0-632-00659-5. (Blackwell Scientific: 1980.) £16.50.

HAERER, A. F. (ed.). Self-assessment of Current Knowledge in Neurology. 3rd Edn. Pp. 226. (Medical Examination Publishing: New York, 1980.) $17.

HERSOM, A. C. and HULLAND, E. D. Canned Foods. Thermal Processing and Microbiology. 7th Edn. Pp. 380. ISBN 0-443-02122-8. (Churchill Livingstone: 1980.) £14.

HUFFSTADT, A. F. C. Congenital Malformations. The Jonxis Lectures. A series of post-graduate medical courses. Vol. 4 . Pp. 360. ISBN 90-219-6004-4. (Excerpta Medica: 1980.) $44, Dfl. 90.

INTERNATIONAL COMMISSION ON MICROBIOLOGICAL SPECIFICATIONS FOR FOODS. Microbial Ecology of Foods. Vol. 1. Factors Affecting Life and Death of Microorganisms. Pp. 332. ISBN 0-12-363501-2. (Academic: 1980.) $29.50.

JENNER, P. and TESTA, B. (eds). Concepts in Drug Metabolism Part A. Drugs and the Pharmaceutical Sciences Vol. 10. Pp. 109. ISBN 0-8247-6906-6. (Dekker': 1980.) Sw.fr. 98.

KLEIN, G. and WEINHOUSE, S. (eds). Advances in Cancer Research Vol. 32–1980. Pp. 361. ISBN 0-12-006632-7. (Academic: 1980.) $36.

LATNER, A. L. and SCHWARTZ, M. K. (eds). Advances in Clinical Chemistry Vol. 21. Pp. 254. ISBN 0-12-01321-4. (Academic: 1980.) $29.

LEIGH, H. and REISER, M. F. The Patient. Biological, Psychological, and Social Dimensions of Medical Practice. Pp.351. ISBN 0-306-40207-6. (Plenum Medical: 1980.) $19.50.

LEIGH, J. H. The Timber Trade; An Introduction to Commercial Aspects. 2nd Edn. Pp. 115. Flexi ISBN 0-08-024916-7; hbk ISBN 0-08-024917-5. (Pergamon: 1980.) Flexi £4.20, $9.50; hbk £8, $18.

LEUNG, A. Y. Encyclopedia of Common Natural Ingredients Used in Food, Drugs and Cosmetics. Pp. 409. ISBN 0-471-04954-9. (Wiley-Interscience: 1980.) £26.60.

LEVITT, P. M. and GURALNICK, E. S. The Cancer Reference Book. Direct and Clear Answers to Everyone's Questions. Pp. 271. ISBN 0-440-51353-7. (Delta Books, Dell Publishing Co. Inc. 1 Dag Hammarskjold Plaza; 245 East 47 Street, New York, N.Y. 10017:1980.) Flexi $4.95, $5.75 Canada.

OLTON, D. S. and NOONBERG, A. R. Biofeedback. Clinical Applications in Behavioral Medicine. Pp. 437. ISBN 0-13-076315-2. (Prentice/Hall: 1980.) £13.65.

OOTA, K., MAKINODAN, T., IRIKI, M. and BAKER, L. S. (eds). Aging Phenomena; Relationships among Different Levels of Organization. Advances in Experimental Medicine and Biology Vol. 129. Pp. 317. ISBN 0-306-40460-5. (Plenum: 1980.) £37.50.

OWEN, O. S. Natural Resource Conservation; An Ecological Approach. 3rd Edn. Pp. 883. ISBN 0-02-390020-2. (Collier Macmillan: 1980.) £12.95.

PEBERDY, J. F. Development Microbiology. Pp. 230. Hbk ISBN 0-216-91018; pbk ISBN 0-216-91018-8; pbk ISBN 0-216-91019-6. (Blackie: 1980.) Hbk £17.50; pbk £8.50.

PRESTAKO, A. W., CROOKE, S.T. and CARTER, S.K. (eds). Cisplatin; Current Status and New Developments. Papers presented at a symposium sponsored by the University of Alabama in Birmingham Comprehensive Cancer Centre and Bristol Laboratories September 1979, in Atlanta, Ga. Pp. 527. ISBN 0-12-565050-7. (Academic: 1980.) $30.

RAINS, D. W., VALENTINE, R. C. and HOLLAENDER, A. (eds). Genetic Engineering of Osmoregulation; Impact on Plant Productivity for Food, Chemicals, and Energy. Basic Life Sciences Vol. 14. Pp. 381. ISBN 0-306-40454-0. (Plenum: 1980.) $39.50.

RICHTER, G. W. and EPSTEIN, M. A. International Review of Experimental Pathology Vol. 21–1980. Pp. 303. ISBN 0-12-364921-8. (Academic: 1980.) $34.50.

ROBERTS, P. J. (ed.). Biochemistry of Dementia. Based on a Workshop on Biochemistry of the Dementias, held at University of Southampton, March 1979. Pp. 272. ISBN 0-471-27698-7. (Wiley-Interscience: 1980.) £16.

ROSSOF, A. H. and ROBINSON, W. A. (eds). Lithium Effects on Granulopoiesis and Immune Function. Advances in Experimental Medicine and Biology Vol. 127. Proceedings of the Workshop held at Rush University, Wisconsin, June 1979. Pp. 475. ISBN 0-306-40359-5. (Plenum: 1980.) $47.50.

Psychology

ARONSON, E. The Social Animal. 3rd Edn. Pp. 377. Flexi ISBN 0-7167-1230-X; Hbk ISBN 0-7167-1229-6. (W. H. Freeman: 1980.) Flexi £4.30, Hbk £9.50.

CRAIG, G. J. Human Development. Pp. 560. ISBN 0-13-444984-3. (Prentice/Hall: 1980.) £11.65.

HARDIN, G. Promethean Ethics; Living with Death, Competition, and Triage. Pp. 82. ISBN 0-295-95717-4. (University of Washington Press: 1980.) $7.95, £4.80.

PERRET-CLERMONT, A. N. Social Interaction and Cognitive Development in Children. European Monographs in Social Psychology 19. Pp. 206. ISBN 0-12-551950-8. (Academic: 1980.) £14.80, $34.

TURNER, R. R. and REESE, H. W. (eds). Life-Span Developmental Psychology. Intervention. Pp. 346. ISBN 0-12-704150-8. (Academic: 1980.) $24.50.

General

DEPARTMENT OF NATIONAL DEFENCE. Defence 1979. Pp.118. Flexi ISBN 0-660-50455-3. (Department of National Defence: Ottawa, Canada, 1980.) Flexi $3 Canada; other countries $3.60.

DRINKWATER, P. and SELF, E. A Passion for Garlic. Pp.128. Hbk ISBN 0-7156-1404-5; pbk ISBN 0-7156-1405-3. (Duckworth: London, 1980.) Np.

HERBERT, S. The Red Notebook of Charles Darwin. Pp.164. Bulletin of the British Museum (Nat. Hist.) Historical Ser. Vol.7. Pbk ISSN 0068-2306; hbk ISBN 0-8014-1226-9. (British Museum (Natural History)/Cornell University Press: 1980.) Pbk £9; hbk £10.

LASZLO, E. and KURTZMAN, J. (eds). The Structure of the World Economy and Prospects for a New International Economic Order. Pergamon Policy Studies on the New International Economic Order. Pp.118. ISBN 0-08-125119-6. (Pergamon: 1980.) £7.50, $15.

MOHTADI, M.F. (ed.). Man and His Environment Vol.3. Proceedings of the Third International Banff Conference on Man and His Environment held in the Banff Springs Hotel, May, 1978. Pp.152. ISBN 0-08-025792-5. (Pergamon: 1980.) $37, £16.50.

MURPHY, E.F. Energy and Environmental Balance. Pergamon Policy Studies on Energy and Environment. Pp.281. ISBN 0-08-025082-3. (Pergamon: 1980.) £16.25.

TALMOR, E. Descartes and Hume. Pp.174. ISBN 0-08-024274-X. (Pergamon: 1980.) $7, £7.50.

URQUHART, J. Living off Nature. Pp.396. ISBN 0-7139-1229-4. (Allen Lane: London, 1980.) £7.95.

WHITLOCK, R. Rare Breeds: The Vulnerable Survivors. Pp.160. ISBN 0-904727-87-4. (Prism: Dorchester, UK, 1980.) £8.95.

WORLD HEALTH ORGANIZATION. The Work of WHO, 1978–1979. Biennial Report of the Director-General. Pp.264. Flexi ISBN 92-4-156063-0. (World Health Organization: Geneva, 1980.) Flexi SwFr. 18. Also available in Arabic, Chinese, French, Russian and Spanish.

nature

11 September 1980

More ups and downs for US science

Like the Grand Old Duke of York (the one who marched his men to the top of the hill and then down again), President Carter seems bent on making those who depend on his administration for financial support survive successive spells of euphoria and depression. This, at least, is how the chopping and changing on the budget for the coming year (which starts at the beginning of next month) must seem. The tale, chronicled at length in the past few months, is especially bewildering for the research community, which is aware both of the need to be able to plan ahead and of the attempts by Congress (at the urging of the Administration) to devise some way in which the basic research budget can be made less vulnerable to annually changing fashions.

The tale goes like this. In January, the President's budget request to the Congress, in aggregate unbalanced and therefore a disappointment to those who had taken Mr Carter's election promises seriously and also disappointing to foreign exchange dealers, provided for a substantial growth of real support for research and development. The total cost of research and development to federal agencies was to grow rather more quickly than inflation, but basic research was to be treated even more generously with an extra 3 per cent in real terms between the two financial years. The word went out that these provisions were a measure of the Administration's commitment to the importance of basic research. Spirits soared at the National Science Foundation and the National Institutes of Health, which were to be dealt with especially generously.

These spirits did not last for long. Before Congress had time to buckle down properly to its annual and needlessly tedious scrutiny of the proposals, economic crisis was the order of the day. With the prospect of increased inflation, people took to borrowing from the banks to buy goods on tick, with the result that the money supply increased dramatically. Professor Milton Friedman's followers were no doubt kept awake at night with worry, and the dollar slumped on the international exchanges. So the White House itself took a knife to the budget. In total, the discretionary parts of the budget were reduced by some 8 per cent, credit was restricted and interest rates raised. The word went out that these steps were a proof of the Administration's commitment to the battle against inflation. Fair play, research and development did relatively well. Basic research was especially well favoured, but the prospect of growth melted away. Some were brave enough to suggest that this relative leniency was a proof of the Administration's belief in the importance of research and development.

Now the troops are back at the top of the hill again (see *Nature*, 4 September), or are at least half way there. At the end of last month, President Carter announced his "Economic Program for the Eighties" which is a complicated mixture of tax cuts, incentives to further industrial investment, provision for helping people adjust to rapidly changing economic circumstances and — here comes the surprise — more money for research and development, especially for basic research. For practical purposes, the new proposals put the science budget where it was in January, but also give Dr Frank Press, the President's Science Advisor, an extra $255 million to allocate to new projects. Moreover, the President has said that there will be a further increase of 3 per cent on basic research expenditure in the following financial year (beginning on 1 October 1981). So, predictably, the word has gone out that the Administration's commitment to the importance of research and development, and to basic research in particular, has been demonstrated once again. The only fly in the ointment is that much of this promise will not become reality until next January, when President Carter hopes to introduce his next budget resolution to Congress. There is as yet no sign of what Mr Reagan would do if he had the responsibility.

Several questions arise from this curious tale, not the least of which is whether the Administration is really serious in its protestations that the interests of research and development, particularly of basic research, lie close to its heart. The issue is complicated because the President's motives for the timing of his announcement of the new programme of economic recovery are dubious, to say the least. At the beginning of an election campaign, and with his chief opponent calling for a substantial tax-cut across the board, it would be asking too much of flesh and blood to stick to an austere programme of economic restraint. Moreover, the package of measures now announced will win some votes. Salary-earners will benefit from the proposed reduction of social security taxes (although the US Treasury will have to borrow from the market to meet the obligations of the years ahead). Business (especially small business) will benefit from the increased depreciation allowances on capital expenditure. But is it realistic to suppose that there are votes in the promise that the budget for basic research should be restored to that first asked for last January, especially when the decision is for now only a promise? On balance, this part of the package appears as disinterested as anything of the kind could be in an election year. Whatever next January may bring, the Administration's protestations must be taken seriously. No doubt a large part of the credit lies with Dr Press.

The question therefore arises as to whether the Administration is going about its intended task in the best way. Protestations and promises, after all, do not make programmes. The chief novelty in the plan for spending the extra £255 million is that the Administration intends deliberately to stimulate industrial research and development. The first thing to say is that the new commitment derives from an idealistic view of the place of research and development as the root of industrial innovation and productivity. (Idealistic, it should be remembered, does not necessarily mean näive.) Next to the question as to whether it will be possible to vote with a good grace for either of the principal candidates in the coming election, Americans now appear to be mostly preoccupied with the decelerating growth of industrial productivity in the United States. Germany, and even Austria, are becoming more productive faster, and nobody can hold a candle to Japan. The fact that countries such as Britain and Italy are doing even worse than the United States is not a comfort but a warning. But it is also known that the decline of the rate of growth of productivity has been accompanied by a decline of industrial spending on research and development. But is not industrial research the fount from which innovation and productivity spring? And if industry lags, can the government not make good the deficiency by spending public funds on research and development linked with industrial needs?

The calculation is straightforward, familiar and good-hearted. The fact that governments in most other industrialized nations have, in the past thirty years, come to the same conclusions, turned them into policies and then been disappointed in the results does not necessarily imply that the new American initiative will fail. The framework of research is more vigorous and more flexible than elsewhere, and in any case there are lessons to be learned from overseas. No doubt the Administration (if it gets the

0028-0836/80/370095-02$01.00

chance) will avoid the trap of thinking that research and development will enable inherently uneconomic industries to survive. At this stage, the most important need is that the attempt to reinvigorate American industry by research and development should be openly regarded as an experiment, not as a sure-fire remedy. American governments have some experience of the support of industry by directly financed research programmes, but the conspicuous successes are in fields such as agriculture. The most serious danger is that, presented with the opportunity to help shape the pattern of public support for industrial research and development, Congress will fail to resist the temptation to play pork-barrel politics with a programme that deserves a fair chance.

The record of Congress in the past six months has, after all, been no better than that of the Administration. Chopping and changing is bad for all public programmes where continuity is essential, and especially for research and development. By amending its budget for the coming financial year almost as frequently as the British budget was amended by Mr Denis Healey in his heyday as Chancellor of the Exchequer (between 1974 and 1976), the Administration has inevitably damaged confidence and continuity among researchers. Congress has a right, even a duty, to scrutinize the way in which public funds are spent — that is a large part of its constitutional role. On technical matters, however, Congress is inclined to make judgements of budget proposals on the basis of their declared objectives. Feasibility matters less. This year, no doubt because it is an election year, Congress has been unusually trying. One result is that the budget for the coming financial year beginning in a few weeks is still far from settled. Is it not time that the US government as a whole found a less chancy (and costly) way of deciding how funds should be spent on research and development? As things are, there can be no certainty that the brave schemes the Administration has been hatching will be given a fair trial.

That the schemes themselves are adventurous, nobody will dispute. Apart from the restoration of the March cuts of the January budget, which will mean that agencies such as the National Science Foundation and the National Institutes of Health will have more to spend on research grants, there are plans to re-equip university laboratories, to set up "generic technology centres" in partnership with industry and to foster relationships between industry and universities. Sensibly, there are to be consultations between the Administration and the interested parties — universities, industry, and professional and scientific societies — before final decisions are made. In other words, the Administration seems anxious to avoid the trap of imposing a theoretical framework of its own ideas on the pattern of its new spending. That is a sign of grace but also one of the best ways of avoiding obvious pitfalls.

In the long run, however, success will also be determined by broader considerations, many of which have been overlooked in the design of Mr Carter's economic recovery package and the subsequent discussion of it. Whatever may be the merits of the individual components in the package, there is no doubt that the overall effect will be to increase the government's deficit by between $30 billion and $50 billion a year. New expenditure, as on research and development, is tiny compared with the cost of the proposed tax concessions and depreciation allowances. Paradoxically, all this has come about when figures suggest that money supply is increasing again, and rapidly. Neither Keynesians nor monetarists would think this a time when the American economy needs further stimulation by deficit financing. Indeed,the consequence of the economic recovery package (if enacted) may be more inflation and more of the damaging consequences for innovation and investment which have become apparent in the past few years. In short, the underlying problems of American industry may be the problems now unhappily familiar elsewhere.

Scares about genetic manipulation

One of the hopes, perhaps unrealistic, of this new decade was that the arguments about the hazards of this or that new scientific development would be couched in more moderate language than used to be the fashion in the 1970s, when Dr George Wald was one of those given to drawing analogies between would-be genetic manipulators and Hitler's would-be eugenicists. And it is true that, for the most part, the argument about genetic manipulation has taken a turn for the rational, partly because experience has shown that the hazards are less serious than some had fairly thought but also because it has become clear that many of the problems thrown up by the practice of genetic manipulation are different in kind from those originally foreseen — problems occasioned by commercial links between academic scientists and industrial companies, for example (see *Nature* 24 July). Yet, it appears, the old Adam lives on, as can be told from a statement put out last week by the Peoples (*sic*) Business Commission, a pressure group in the Nader mould and based in Washington.

The latest declaration from 1346 Connecticut Avenue is, however, such a travesty of the truth that it deserves to be even more widely known than to those on the commission's mailing list. On Wednesday last week, the *New York Times* carried an account of how Dr Francis H. Ruddle and his colleagues at Yale University have been able to incorporate adenovirus and SV-40 genes into the DNA of mouse embryos. The newspaper quite properly quoted the investigators as saying that they had been able to demonstrate the presence of viral genes in somatic cells of mice developed from the manipulated embryos, but emphasizing that they knew nothing as yet of the physiological function (if any) of the genes concerned. They also pointed out that they have not been able to check whether the exogenous genes survive from one generation to the next, but that they hope to do so when their mice are sexually mature. The occasion for the appearance of this newspaper report was the imminence of a meeting in Berlin at which the work will be described; it is said to be due for publication in the journal *Cell*.

Plainly, last Wednesday was a black day at the Peoples Business Commission. The statement issued later in the week says that the report "marks the beginning of a eugenics program for America". Messrs Jeremy Rifkin and Dan Smith, described as directors of the commission, say that the development represents "the greatest potential technological threat to the sanctity of life since the beginning of human history". The statement goes on to say that "a few people and institutions now have it within their power to irreversibly alter the biological structure of millions of other men and women and their descendants for all time".

Many will say that foolishness of such a plainly exaggerated form is best ignored. That is too tolerant a view. For small though its direct influence may be, the Peoples Business Commission is well placed to help keep the pot of anxiety about genetic manipulation boiling unnecessarily. It should therefore be widely known that the commission's statement is, put simply, a misstatement of the truth, born possibly of ignorance. For Rifkin and Smith, diligent readers of the *New York Times* though they may be, do not read the scientific literature as carefully. For then they would know that the phenomenon in which endogenous virus genes are naturally incorporated into mammalian genomes is now familiar, and biologically important; that techniques similar to those attributed to Ruddle *et al.* have previously been used with other viruses (and not always in the United States); and that the investigation of this phenomenon may be of the utmost importance in the understanding of diseases such as leukaemia. No doubt the time will come when the *New York Times* reports the incorporation of a human gene into a human genome, but even when that happens it will be hard to justify such an intemperate statement as that put out last week. Is it not high time that the commission's sponsors, whatever their sympathies, found a more level-headed vehicle for prosecuting the case against genetic manipulation?

0028-0836/80/370096-02$01.00

NSF reorganizes for industrial research

Washington

The great White House hope that scientific research can be harnessed to the cause of industrial innovation has evoked a quick response elsewhere in the United States government. Other agencies are understandably keen to share in the action. At the National Science Foundation, the most immediate result will be to precipitate the reorganisation over which the National Science Board has been agonizing for several months.

Reorganization will dominate the agenda for a public meeting between the acting director of the Foundation, Dr Donald N. Langenberg, some members of the National Science Board, and the chairmen of the foundation's advisory committees which has been arranged for Saturday this week (13 September). The meeting will be open to members of the public, who will be able to chip in.

The National Science Board is hoping to have completed these and other consultations in time to make a final decision at its meeting in October. Failure to do so would mean that the proposed reorganization could not be built into the federal budget cycle, which might mean that some changes could not be carried out until October 1982.

The most obvious effect of the proposed reorganization will be to rename the Directorate of Engineering and Applied Science the Directorate of Engineering. More than nomenclature is involved, however — it is intended that each of the existing directorates of the NSF should be more directly concerned with the needs of applied science, while the new Engineering Directorate should vigorously support engineering research in universities.

Novel and explicit mechanisms for fostering industrial innovation are thus not a part of the proposed reorganization. Rather, the NSF is relying on the authority it already has to support industrial research. The scheme for funding joint industry–university projects is doing well. The NSF is also proud of the cooperative research centre in polymer science established at Massachusetts Institute of Technology (and now entirely supported by industrial companies). The analogous research centre for the furniture industry in North Carolina has been less successful.

These proposals are likely to win support. There will be more dispute about the proposal, part of the same package, to set up a Social Science Directorate even though the chief effect would be a repackaging of existing divisions (including the new programme in "decision and management" science). One objection is almost certain to be that "neural sciences", linked with "behavioural science", should not be separated from the rest of biology.

Under the new scheme, the foundation's existing rag-bag directorate (for Scientific, Technological and International Affairs) would take over responsibility for programmes such as those for supporting small business research and affirmative action of various kinds.

By Saturday's meeting, NSF will no doubt have been spurred on by Congressman George Brown's congressional subcommittee, to which Dr Lewis Branscombe (Chairman of the National Science Board) and Dr Langenberg are due to give evidence. Mr Brown is using his bill to set up a National Technology Foundation (unlikely ever to become law) as a way of urging on everybody in sight the importance of research as a spur to industrial innovation and production.

Meanwhile, the Department of Commerce has stolen a march on other potential competitors for the new funds that may become available in January by announcing its plans to set up three cooperative industrial research centres dealing with welding, lubrication and powdered metal processing. The Department of Commerce will spend $5.2 million of its own money on the projects, for which proposals are being sought, and hopes that its own contributions to the cost of the centres will shrink to 20 per cent after five years.

Appointments and elections ahead

Washington

After several nail-biting weeks, it now seems that the US Senate will confirm the nomination of Dr John B. Slaughter as Director of the National Science Foundation some time during the week beginning 15 September. It is now thought that the differences, political and procedural, which have arisen over Dr Slaughter's nomination as NSF director (originally announced early in July), will be found to have melted away (or to have been buried) at a meeting of the Senate Committee on Labor and Human Resources due to be held tomorrow, 12 September.

The first stumbling block to Dr Slaughter's confirmation was ironically the reinvocation by Republicans in the Senate of a principle first mentioned by Democrats in the closing months of the first Nixon Administration in 1972 – the doctrine that fixed-term presidential appointments should not be confirmed as soon as this before a presidential election.

Formally, the directorship of the NSF is a six-year appointment, although the statutes allow the President to remove a director from office at any time. In practice, however, a president following such a course would have to contend with the scientific community's view that the directorship of the NSF is not a political appointment in the ordinary sense. Dr Slaughter, when his appointment is confirmed, will be especially hard to dislodge, for he would be the first black American to head an important agency.

Technically, Dr Slaughter's confirmation as NSF director awaits only the vote of the US Senate as a whole, having been recommended ("reported out") by Senator Edward Kennedy's subcommittee on Health and Scientific Research. In practice, the recommendation is flawed by the way in which Democratic members of the subcommittee carried it without a proper quorum. Nobody wants the issue to be debated by the Senate as a whole. The emollient now discovered is a full meeting of the Committee on Labor and Human Relations at which Dr Slaughter's nomination will be on the agenda but (it is hoped) not discussed. The White House has no doubt been reminded of the quip, usually an ethnic slur, "with friends like that, who needs enemies?".

Dr Slaughter's problems (and the NSF's) may melt away, but Dr Al Carnesale, the putative chairman of the Nuclear Regulatory Commission, is certain to have a rougher ride. Carnesale's nomination, the confirmation of which is in the gift of a subcommittee of the Senate Committee on Environment and Public Works, is frankly acknowledged to be political, and for a specific reason. Carnesale, now a tenured professor at the Kennedy Institute at Harvard University, is committed to the view that breeder reactors are economically irrelevant while the price of uranium is as low as at present. Mr Ronald Reagan, the Republican presidential candidate, disagrees. The chances are that in the circumstances Dr Carnesale will have to bide his time until after the election.

Speculation about other post-election changes is already rife, and the odds are shortening on the proposition that Dr Frank Press, now the President's Science Advisor and Director of the Office of Science and Technology Policy, will finish up next spring as president of the National Academy of Sciences. A spokesman of the NAS confirmed last week that Dr Press is a "leading candidate" to succeed Dr Philip Handler, whose second six-year term ends next June.

Procedurally, however, there is a long way to go before this appointment will be decided. Proposals by the nominating committee have to be approved by the Council of the Academy in October.

The by-laws of the academy require that the nominating committee should "assure itself that each proposed nominee will be

0028-0836/80/370097-02$01.00

willing and able to serve if elected", which presumably implies a detailed discussion of the terms on which a "proposed nominee" would take the job.

Thereafter the council of the academy will inform the members, who have until 1 December to make alternative nominations (which must be supported by at least fifty members' signatures). If necessary, ballot papers are distributed by 15 December and must be returned by 15 January 1981. In principle, the council can put more than one name to the membership, but it has not in recent years done so. The present procedure, devised only in the 1960s, appears in the 1980s to be calculated to maximize the embarrassment of the "proposed nominee" and of the academy as a whole.

Bell Research Labs

Split possible?

Washington

There is much consternation at the Bell Telephone Laboratories at the unexpected announcement last week that the parent company, American Telephone and Telegraph (AT&T), is to split into two quite separate operating companies. This move, which has been prompted by a decision of the Federal Communications Commission (FCC) made public in May, may be followed at some later stage by a decision that Bell Labs itself should be split in two.

Scientists working at Bell Labs fear that such a development would impair the quality of the organization's research. For the time being, however, uncertainty rather than anxiety rules. No decision has been made as yet about the consequences of the split in the parent company for the research organization.

The crucial decision of the FCC (known as the Final Decision on the Second Computer Inquiry) is the latest stage in the FCC's decade-long attempt to adjust the rules for regulating the public telephone networks to meet new technical needs. Since 1968, the FCC has held that companies such as AT&T should not enjoy the exclusive right to supply terminal equipment for their telephone lines and other channels of communication.

More recently, the difficulties of regulating the common carrier networks have increased with the development of data processing networks, domestic satellite communications and the prospect of other technical developments. For the past four years, the FCC has been searching for a definition that would allow the networks to supply some kinds of equipment but prohibit them from supplying other items.

In its latest ruling, the commission has abandoned this exercise in semantics and opted for a more radical solution. In future, it says, large common carriers of electronic signals must be concerned only with the development and management of the network. If they wish to supply terminal equipment as well, they must do so through a separately constituted company with a distinctive board of directors, separate premises and so on.

Although the same rule would apply in principle to all telephone companies in the United States, for the time being the FCC has ruled that it should apply only to AT&T and to General Telephone and Electronics, which operates some 8 per cent of the American telephone network in locations scattered from Florida to California.

The response of AT&T to this radical proposal has been equally surprising. Although the company argued strongly against separation in its evidence to the FCC, on the grounds that vertical integration is beneficial, it announced last week that it would go ahead with the formation of two separate companies to be responsible respectively for the operation of the telephone network and the supply of terminal equipment (telephones included).

It is not yet clear whether the separation of the two parts of AT&T will be as complete as the FCC requires. Moreover, the move does not imply that AT&T accepts the commission's ruling — indeed, AT&T is one of thirty objectors who are threatening to carry their case to the courts if the decision is not modified.

The complication for Bell Labs is that the research organization is a jointly owned subsidiary of AT&T and of Western Electric, itself the subsidiary of AT&T responsible for manufacturing terminal and network equipment. The FCC ruling is vague on the implications of the proposed split in AT&T for research and development, saying only that affiliated companies would be required in future to buy research and development services from other affiliated companies at a fair valuation.

One obvious development, that most feared at Bell Labs, is that AT&T may in the end be required to divide both Western Electric and Bell Labs itself into parts separately responsible for communications networks and for terminal equipment. AT&T is also alarmed at the prospect that even separation of activities on which it has now embarked will impede the free flow of ideas between operations and research and development.

If there were to be a split of Bell Labs, the chances are that the largest part would go to the network side. Of the 1980 budget of $1,255 million, more than 45 per cent was exclusively concerned with network operations. The remainder may be considered relevant to both sides of the telecommunications business.

How soon the future of AT&T and of Bell Labs will be decided is a matter for conjecture. The FCC has set a deadline for the complete separation of AT&T by March 1982, but will now be required to comment on the objections to its ruling, most probably in October or soon afterwards. If the courts accept that the objectors to the ruling have a case, several further months may elapse before the regulations have the force of law, in which case the deadline would no doubt be put back. Excessive delay is likely, however, to breathe life into the bills now languishing in Congress that aim more directly to regulate the public communications networks.

NPT review conference

No declaration

The Second Review Conference of the Non-Proliferation Treaty ended on Sunday (two days later than originally planned) with a smack in the face for the three sponsoring nuclear powers, the Soviet Union, the United Kingdom and the United States. Although the nuclear powers had been expecting trouble at the conference, largely on the grounds that they had been less diligent than required by the treaty in the pursuit of strategic disarmament and the fostering of civil nuclear developments elsewhere in the world, they were apparently taken aback also to find themselves criticized on the grounds that either Israel (not a signatory of the treaty) or West Germany (which is) had been helping with the development of nuclear weapons in South Africa.

The most immediate cause of trouble was the failure of the conference to agree on a report of the past month's proceedings at Geneva. The drafting process came to a fruitless end in the early hours of Sunday morning, and the conference was concluded later in its day.

By all accounts, the review conference has been rought going ever since the opening speeches were made in public during the first ten days. The government of Mexico appears to have taken the lead in asking that the nuclear powers should agree to a package of demands on arms control, including a declaration that they would abide by Salt II while awaiting ratification of that treaty, impose on themselves a moratorium on nuclear testing and allow the negotiations on the Comprehensive Test-Ban Treaty (conducted up to now between the three nuclear power signatories of the treaty) to be carried on with the UN Committee on Disarmament. For the nuclear powers, the sticking-point last weekend was this demand that such a declaration should be included in the final report of the review conference.

The overriding question now is whether the failure to produce an agreed report will be followed by mass defections from the treaty. The closing speeches at Geneva, including that from the Iraqi chairman, were variations on the theme that nuclear proliferation remains a serious danger, and that the conference had served to draw attention to many of the beneficial aspects of the treaty.

The discovery by several of the

0028-0836/80/370098-02$01.00

signatories that the quinquennial review conferences offer a means of twisting the arms of the nuclear powers on arms control may paradoxically help to keep some states loyal to the treaty. Others, however, will no doubt be able to use the failure to produce an agreed report as an excuse for withdrawing from the treaty, even though those tempted to take such a step will no doubt be impelled in that direction by separate political considerations.

In the wake of the Geneva conference, the meeting of the Committee on Assurances of Supply of the International Atomic Energy Agency, planned for the end of this month at Vienna, assumes greater importance. It is thought unlikely that the nuclear powers will be spurred to further negotiations on strategic disarmament at least until after the American presidential election.

Plutonium

Dounreay loss

Only a few weeks before the British government is due to make an announcement on the future of the fast breeder reactor, the BBC television programme *Panorama* alleged on 8 September that a total of 35 gram of plutonium from the prototype fast reactor at Dounreay was lost in 1973 and 1976. The United Kingdom Atomic Energy Authority admits that the plutonium has never been accounted for, but says that it could not have left the fuel cycle and was most probably reprocessed or even dumped in a waste repository.

The first case of missing plutonium occurred in 1973 when a routine accountancy check revealed that 10 gram of the element was missing from a can containing the remnants of several spent fuel pins. The pins, originally about 0.2 inches in diameter and 2 feet long, had been irradiated in the reactor core for one year and then chopped up for analysis by chemists and metallurgists. The shortfall in plutonium was equivalent to one fuel pin.

The second case concerned a fuel pin which had been irradiated in the reactor core for one day in 1966. It had then been treated in the same way as the first pin and the can containing it had been stored in a cooling pond. It contained 25 gram of plutonium. In 1977, the can that was thought to contain the remains of the fuel pin was found to contain another type of spent fuel.

The UKAEA says that it investigated the losses and reported the second to Euratom, of which Britain was then a member. A driver of a mechanical digger was hired to uncover all the material in a dump of low-activity waste in the hope that the second lot of missing plutonium would be discovered. The contents of the dump were analysed, but the missing spent fuel was not found.

The UKAEA says that each case was investigated thoroughly, and that the to missing irradiated fuel pins must either have been reprocessed or dumped in a depository for highly radioactive wastes, examination of which would be too hazardous to undertake. It says the plutonium could not have been removed from the fuel cycle. Its conclusion is that there must have been an error in the system of keeping records of the movement of plutonium. Since the incidents, the UKAEA says, it has tightened up on its procedures for monitoring the movement of radioactive materials around the plant.

The *Panorama* programme was also critical of operations at Dounreay on health and safety grounds. It claims that the driver of the mechanical digger, a deaf-mute, was not properly aware of the hazards of what he was doing and was not given adequate protective clothing. It also cites another incident in 1979 when eight men were exposed to plutonium after handling radioactive waste. None of them was aware that the waste contained plutonium and at the end of their shift it was discovered that they had been exposed to radiation.

About this incident, the UKAEA says that the waste handled by the men contained only one gram of plutonium and that none of the men was later found to have significant amounts of plutonium in his blood or urine. The incident had not been reported because the level of alpha radiation in the air in which the men were working was well below the level at which notification to the authorites is obligatory. An attempt was made, says the UKAEA, to inform the deaf-mute driver of the hazards of what he was doing. He was told to stay in his cab and air samples were monitored for radiation. The levels found were within the safety limits.

The uncovering of the incidents has provoked a strong reaction from Mr David Steel, leader of the Liberal Party, who has called for a ministerial statement on the affair. Even before the showing of the film, the AEA had issued a statement that *Panorama* had exaggerated the significance of these incidents, and had also charged the BBC with having declared an interest in making a film about this achivements

Judy Redfearn

Academic freedom

Talking shops

The Hague

Three papers by Dr Andrei Sakharov, written since his exile to Gor'kii, *Eksperimental'noi i Teoreticheskoi Fiziki* (*ZhETF*), the most prestigious physics journal in the Soviet Union. This remarkable development was announced by Nobel Laureate Philip Anderson to last week's Conference of the International Sakharov Tribunal of Conscience and Peace.

According to Professor Anderson, the Editor of the *ZhETF* had initially accepted the papers, which deal respectively with time-reversal, quark/gluon interaction and mass formulae for muons and baryons. At a late stage, however, the censors stepped in to stop publication. The matter, said Professor Anderson, was finally "adjudicated" by the Central Committee of the Politbureau, who decided that publication could go ahead.

The story which amplified by Professor Edward Lozansky, Chairman of the International Sakharov Committee, New York, and a former member of the Moscow Sunday Seminar for Jewish "refusnik" scientists. He told the conference how he had brought the three Sakharov papers to the meeting of the American Physical Society (APS) in April, which decided that if the papers were turned down for political reasons by the Soviet journals the APS would be delighted to consider them. This, thought Lozansky, had probably swung the balance in Sakharov's favour.

Ironically, this revelation of how much Western academic pressure can achieve on behalf of a harassed Soviet colleague was announced at a conference which, in the opinion of several campaigners for academic freedom, should not be taking place at all. One of these is Mrs Tamara Yankielevich, Sakharov's stepdaughter-in-law, now resident in the United States. The main grounds for opposing the conference have been the veiled hints from the Soviet side that vociferous action might jeopardize a plan to allow Sakharov quietly to return to Moscow. "Six months after being exiled" was the first date promised for his return; this has now however become "six months after the end of the Olympics".

Unlike the various other "Sakharov" human rights conferences in the past few years, the Hague conference was a human rights conference specifically focused on Sakharov's own plight. As several speakers pointed out, this is a relatively mild plight. For example, Sakharov still has access to a scientific library just across the street from his Gor'kii apartment. Because all the scientific institutes in Gor'kii are involved in classified work, however, there is no possibility of his having any contact with fellow scientists in his place of banishment.

In his presentation to the conference, Professor John Ziman of the University of Bristol suggested that one of the reasons scientists are particularly concerned with Sakharov's case is that his involvement with problems of academic freedom and human rights generally grew out of his disillusionment with a career in nuclear weaponry — what Ziman called "black science" — like black magic, "the application of knowledge in the power of evil".

His "pilgrimage", as Ziman called it, is therefore of particular concern to all scientists, "hard put to it these days to defend our traditional norms — the universality, the disinterestedness, the openness of a transnational community bringing beneficial knowledge to all".

0028-0836/80/370099-02$01.00

Coincidentally with the Hague conference, two other meetings concerned with the political repression of scientists also took place last week. In Amsterdam, there was the annual meeting of the International Council of Scientific Unions (ICSU) and of its specialist committees, including the Committees on the Free Circulation of Scientists and Safeguards of the Pursuit of Science. This committee, which compiles a register of cases of scientists subjected to unwarranted restriction, is less well known than it should be. During the past year, only some seventeen such cases were added to the register.

The particular roles of scientific and learned societies were stressed at the other meeting last week — the half-day session on scholarly freedom and human rights at the Salford meeting of the British Association.

Marks of reproof

What follows is a summary of Dr Leslie Cohen's suggestions as to how learned societies may help colleagues elsewhere whose academic freedom or human rights are restricted (see text).

1. Statement by the President of the Society.
2. Formal protest by Officers of the Society (published in the Society's bulletin).
3. Provision of facilities for protest meetings, press conferences.
4. Official letter of protest to head of State Party/Academy.
5. Dissemination of information on individual cases to members.
6. Advising members to refuse to
   (a) attend meetings in offending country;
   (b) invite scientists from offending country to conferences;
   (c) allow visits of scientists from offending country, to scientific establishments/laboratories;
   (Note in special cases, visits may be made contingent on discussion of human rights issue in question).
7. Organization of petitions by members on specific case.
8. Granting of recognition and/or publicity to "alternative" meetings and seminars organized by banned scientists.
9. Organizing and/or supporting meetings relating to the work of one particular scientist suffering repression.
10. Sending delegation to investigate cases and intervene if possible.
11. Providing journals free to banned scientists.
12. Providing financial support to exiled scientists.
13. Severing formal relations with academies/societies in offending countries.
14. Causing expulsion of academies/societies of offending country from international organizations.

At such conferences, the question of how to translate concern into concrete action is usually answered only vaguely. On this occasion, Dr Louis Cohen, secretary of the Physical Society (London), put forward a fourteen-point scheme of progressively more severe responses that learned societies might make (see below).

By way of demonstrating what may be achieved by pressure from professional colleagues, Professor John Charap of Queen Mary College, London, was able to announce at the BA meeting an unprecedented success in the case of Yurii Gol'fand, his fellow researcher on supersymmetry. Gol'fand, who was dismissed some years ago from his post as senior researcher at the Lebedev Institute of Physics in Moscow following his application to emigrate to Israel, was, a few weeks ago, reinstated.

Vera Rich

Hoyle on life

No dissent

It would be hard to imagine an event more like that of Daniel entering the lion's den than last week when Sir Fred Hoyle, brandishing his theory that influenza epidemics are caused by extraterrestrial viral material, gave a seminar at the National Institute for Biological Standards and Controls in Hampstead, London. In the event, Sir Fred escaped almost as unscathed as Daniel, although perhaps for different reasons.

Hoyle has evolved his theory in conjunction with Professor N.C. Wickramasinghe of University College, Cardiff, with whom he has recently collaborated on a series of papers on the occurrence of biochemicals in intersteller space. The theory that viruses might also be present in space is a natural extension of that line of work. It is worth postulating, according to Hoyle, because of some anomalies in the epidemiology of influenza which defy the conventional explanation that the virus is passed from person to person, with animals acting as a reservoir.

The anomalies to which Hoyle points are few but striking. He cites, for example, outbreaks of influenza in boarding schools where the great majority of cases occur simultaneously quite unlike the expected, progressive spread from one or a few initial cases. More strikingly he points to reports of the simultaneous outbreak of influenza in the USA and India during the 1918 pandemic. What better explanation for such phenomena than that a space-borne factor descends to trigger the influenza in all cases at the same time? And, in support of that notion, Hoyle marshalls plenty of evidence of atmospheric events that could account for the odd incidence of influenza.

A version of Hoyle and Wickramasinghe's theory that has been circulating in preprint form proposed that individuals carry as part of their own genes the genetic information for each of the many types of influenza virus and that there was a separate space-derived, activating factor for each.

Now, however, he is persuaded that this version of the theory is inadequate in part because of overlooked evidence and in part because biological systems have a good deal more slack than he, as a physicist, had been aware of. As a result the theory has become more complex and now involves a coincidence of three virus-related components, two of them space-derived, for infection to occur.

In becoming so complex, the credibility of the theory has undoubtedly been stretched more than ever. There is also the question of whether or not the basis of the theory — the anomalous epidemiology — is sound. Thus in the discussion that followed Hoyle's talk, Dr A. J. Smith of the Influenza Research Unit at St Luke's Hospital, Guildford, outlined his unit's study of the spread of influenza in a school. Unlike the evidence cited by Hoyle, Smith's data fitted the classical progressive spread of the disease, from a single person, to all those who finally succumbed.

That, however, was the only criticism of substance put to Hoyle in the discussion period. One respected influenza expert was prepared to venture the view in private that whereas he and others had no time for Hoyle's theory they were too polite to say so; "in the USA he would have been eaten alive".

And so it came to pass that, for reasons perhaps more British than biblical, Sir Fred survived the tame lions of Hampstead.

Peter Newmark

Electric vehicles

UK content

Government and industrial support for British research and development on electric vehicles should continue at its present level even though it is likely to be many years before electric vehicles become commercially viable. This is the main recommendation of the first report of the House of Lords Select Committee on Science and Technology, published last week.

The technical problems of developing advanced batteries suitable for use in private cars and of building an infrastructure for overnight recharging are identified as the main obstacles to the early success of the all-electric car. Another problem is that most of the advantages accrue to society and the electricity generating industry and most of their disadvantages fall on their owners. Their commercial success is therefore unlikely much before the petrol-run car becomes exceedingly expensive to run, probably towards the end of the century.

0028-0836/80/370100-02$01.00

The Lords committee warns that there is a danger of Britain becoming complacent about the need to develop alternatives to the internal combustion engine because the availability of North Sea oil might make petrol-run cars economic in Britain after they have ceased to be so in other countries. The committee recommends that the government encourage electric vehicle manufacturers to continue their research at least at the present level, which it finds satisfactory, by continuing to give financial support matched in some way to the manufacturers' own investment. Government should also be prepared to make product-launch money available "to get over the volume-production lump in the next few years". The committee does not, however, suggest that electric vehicle research be centrally planned, finding the present system of manufacturers applying for grants on an *ad hoc* basis satisfactory. It has seen no evidence of any overlap of research.

There is one area, however, in which the Lords say that more work could be done. Hybrid vehicles, propelled by a combination of battery and internal combustion engine, are being vigorously explored in Japan and the USA, but have so far received little attention in Britain. They offer the most promising prospects for private use by overcoming the pure electric car problem of short range, typically 50-70 miles. They also do not necessarily depend on the development of new advanced batteries. A major disadvantage, leading to high capital cost, is that incorporating two different propulsion systems in one vehicle is technically very difficult. Nevertheless, the government should be prepared to make a "small" amount of public money available for testing them, says the committee.

The future of electric vehicle development lies with large companies prepared and able to invest heavily in research and development and not with small businesses set up to build one or two specialized vehicles, says the report. So far, the manufacturers of batteries and components, such as Lucas and Chloride, have invested much more than the major car manufacturers. A possible reason, put to the committee by BL Technology, a subsidiary of British Leyland, is that vehicle manufacturers add only 30 per cent of the final value of an electric vehicle, the electrical component manufacturers standing to win the biggest reward.

The committee hopes that the car manufacturers will eventually be enticed to invest in electric vehicle development by the prospect of major markets in countries which, unlike Britain, cannot rely on a steady supply of oil into the 1990s. It would be a pity, it says, if Britain were to lose its lead in electric vehicle technology now, only to be forced later into buying from abroad because it had been lulled into a false sense of security in the 1980s.

Judy Redfearn

US petroleum

Using less

Washington

Officials at the Department of Energy appear to share with the superstitious the view that to talk about good luck is to ensure that it will disappear — "don't count your blessings" and all that. Accordingly, not much is being made of the dramatic reduction of crude oil imports to the United States in the past year, which in the first eight months are down by 17.2 per cent between 1979 and 1980.

According to the Department of Energy's *Weekly Petroleum Status Report* for 29 August, imports of crude oil and refined products averaged 6,907 million barrels a day in the first 234 days of 1980, compared with a total of 8,341 million barrels a day in 1979. If this keeps up, President Carter's promises at the Venice summit on oil imports will be amply fulfilled.

The diffidence of the statisticians responsible for the weekly statistics is partly technical. The weekly *Status Report,* although admirably up to date, is based on returns from oil companies and crude oil refiners, and is therefore not a direct measure of actual consumption. Perhaps, it is said, the reduction of imports reflects reduced inventories in the distribution network. The rapid attritition of gasoline service stations certainly implies that many retailers' gasoline tanks have been emptied for the last time. The statisticians appear not to dare to take heart from the supposition that most retailers going out of business are doing so because they are selling less.

The statisticians are also diffident because they do not understand why the most recent round of price increases for petroleum products should have demonstrated, after a decade of apparent price inelasticity, that even Americans will buy less gasoline and fuel oil if the price goes up sufficiently. Could it even be that some non-quantifiable consideration, such as the continued presence of American hostages in Iran, has changed people's buying habits?

Whatever the truth, the facts are clear. Between the first eight months of 1979 and the corresponding period this year, gasoline production for the US market has declined by 6.8 per cent, to an average of 6.6 million barrels a day (still more than a third of total volumetric production of 17.6 million barrels a day of all oil products). Distillate fuel oil is also down by 14.2 per cent, partly because householders and commercial consumers have turned down their thermostats, partly because oil companies are chafing at state and even more local price restrictions. Already there are fears that if the coming winter is cold, it may also be hard.

During the same period, stocks of crude oil and of petroleum products have soared. Primary commercial stocks have increased by more than ten per cent in the past year. Gasoline is in especially good supply. Fuel oil is, however, short.

The most obvious disappointment in the statistics so far available for 1980 is that US oil production has hardly changed since

Saturn seen in Voyager sights

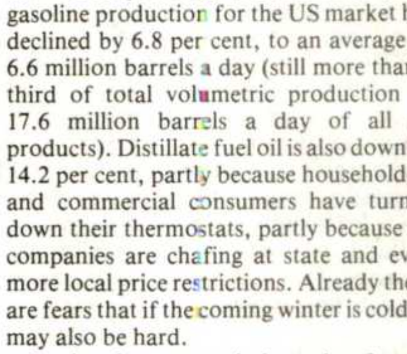

Saturn from Voyager 1 on 24 August, 1980. The dark band on the equator is the shadow of this rings. The three bright specks are satellites.

The accompanying photograph, released at the end of August from the Jet Propulsion Laboratory in California, is one of the first to have been gathered from the spacecraft Voyager 1, now on its way from Jupiter to Saturn. Between 22 August, when the first photographs were obtained, and 24 October, visual observation from Voyager 1 will consist entirely of single-frame photographs. Thereafter, the narrow-angle camera on the spacecraft will be used to collect mosaic photographs of the visible surface of Saturn and of the rings and to search for satellites at present unknown.

The closest approach to Saturn will occur on 12 November, when the spacecraft will also come closest to the satellites Tethys, Mimas and Enceladus. The closest approach to Titan, one of the principal targets for the cameras, will occur on 11 November. Visual observation of Saturn will continue at least until 18 November.

Visual observations are, of course, merely the most memorable of the observations made by planetary spacecraft. Voyager 1 is also equipped with magnetometers, infrared sensors (which will, in particular, produce a map of the surface of Saturn) and devices for recording the interplanetary particle flux and for measuring the size and density of material particles in the rings of Saturn.

0028-0836/80/370101-02$01.00

1979, increasing by only 2 per cent. One explanation of this curious price insensitivity is that potential oil producers are waiting until the price of "new" oil is decontrolled towards the second half of 1981.

The economic consequences of this changing pattern of consumption are plain to see. The three major automobile manufacturers are in the throes of launching their newest small cars — Ford unveiled its new Escort last week — with apprehension and despondency. It the cars do not sell, consumers will buy imported cars and the auto industry will collapse still further. But the profitability of small cars is not nearly as great as that of the old gas-guzzlers.

Using the standard relationship but on the assumption that coal production will continue rapidly to increase, the American Petroleum Institute is now guessing that by 1990 oil consumption in the United States will decline to an average 8-9 million barrels a day, with rather less than half of this imported. Even this estimate may be conservative, for the impending decontrol of petroleum prices may be an unexpected stimulus to drilling. Since the decontrol of natural gas prices during 1979, proven reserves of natural gas have increased more quickly than in the previous decade.

Romanian energy

Partners to-be

Romanian President Nicolae Ceausescu has found the answer to current and future problems of the development, efficient and economic use of raw materials and energy resources, according to the leading Party newspaper *Scinteia.* Reviewing the latest volume in the series "From the Economic Thinking of President Nicolae Ceausescu", *Scinteia* points out that the President was interested in the problem even before the energy crisis. This is, perhaps, not surprising as Romania, once so oil-rich that an oil-rig was depicted on the state coat of arms, has now sunk to the status of a net oil importer.

Judging from the review Ceausescu's book *Energy and Raw Materials Resources* (not yet available in the West) seems to reiterate the draft directives for the 1981–85 five-year plan and the long-term guidelines till 1990, recently accepted by the Joint Plenary Meeting of the Central Committee of the Romanian Communist Party and the Supreme Council of Economic and Social Development.

These guidelines provide for a multilateral energy strategy, to include: the expansion of geological prospecting throughout the country and the Black Sea continental shelf, the speeding up of hydroelectric projects, so that the 30 per cent exploitation of hydroelectric potential of 1980 will reach 45 per cent in 1985, 65 per cent in 1990 and 100 per cent in the year 2000, utilization of low grade and less accessible fuels such as shale, and the expansion of the nuclear energy programme (660 MW capacity by 1985, 3,960 MW by 1990 and 10,000 MW by 2000).

Considerable emphasis is also to be placed on conservation, recycling and what looks remarkably like energy rationing — described by official policy hand-outs as "fixing rational ceilings on heating and lighting". Finally, Romanian scientists, whose work has been more firmly harnessed to the needs of the economy than in any other socialist country, will take part in wide-ranging interdisciplinary research to capitalize on the country's geothermal, Sun, wind and tidal resources, as well as biomass conversion. According to the directives, by the year 2000 these resources should account for some 20 per cent of Romania's energy production (by then nuclear energy will have reached 17 per cent).

Vera Rich

Rural communities

Living now

What sort of society could the future inhabitants of rural areas find themselves living in? A recent idea for a rural community for the future has come from the Dartington Hall Trust in South Devon, England in the form of a model village built on a scale of 1:250. Recognizing, no doubt, that the future can never be planned by the past, the Dartington model has been designed more as an "exercise in the imagination" than as a blueprint for a real village.

Thinking about the future of rural communities fits well into the work of the Dartington Trust, which was set up in the 1920s with the wealth of Leonard and Dorothy Elmhirst to bring back life to rural communities which has been depleted during the industrialization of the nineteenth and twentieth centuries. Most of Dartington's work consists of encouraging small industries, not necessarily associated with rural life, and cultural and educational activities in the countryside of Devon. Its latest venture, however, is more theoretical. According to Maurice Ash, the Trust's chairman, the model village is an attempt to "speak a new language" by thinking differently about the world in terms of qualities rather than quantities.

Dream in balsa wood

That is not to say, however, that the "high" technology of the industrialized world has been ignored. The idea, according to Andrew Page, the brains behind the model, is to achieve a marriage of the microelectronics and green (ecological) revolutions. The model is for a community of about 2,000 people which aims to be as self-sufficient as possible by making use of both "low" and "high" technologies, the emphasis being on energy saving and preserving the quality of the environment. Electricity is supplied mainly from hydro and aerogenerators, transport within the village is by bicycle, horse and cart or on foot, as much local produce as possible is grown around the periphery of the village using labour intensive methods and waste recycling is done on site to produce clean water supplies and methane and other biogases. The village medical centre is designed to offer "alternative therapies" as well as modern medicine.

High-technology services come into their own when the village has to communicate with the rest of the world. Hence a community transport depot houses cars, lorries and vans for those needing to travel outside the village. But the most significant feature is the "cottage office" which houses a "resource centre" offering not only telephones, telexes, photocopying machines and secretarial and accounting services for local businesses, but also television with teletext, Viewdata and other link-up services for worldwide electronic communication. This acknowledgement of the microelectronics age also means that the village can offer educational facilities for all age groups.

Small-scale industry, for producing goods for sale outside the community as well as within it, is based on a mixture of high and low technologies. Few inhabitants would have only one job, the idea being to create job fulfilment by blurring the distinction between work and leisure and engaging people in different tasks at different times. Most people, for example, would spend quite a bit of time farming the green belt surrounding the village or digging their allotments, in addition to their main job. One of the main criteria for using high, labour-saving technology would be the elimination of boring and repetitive tasks.

It is unlikely that the model village will ever become a reality. But some of the ideas and detailed design work that have gone into creating it may be useful in less ambitious projects to build real futuristic societies. The Town and Country Planning Association and Greentown Group, for example, are currently looking for a site to build a small futuristic community of houses and small businesses. And Milton Keynes has already shown an interest in building such a community on a 25 acre site just outside the town. **Judy Redfearn**

0028-0836/80/370101-02$01.00

NEWS AND VIEWS

The elementary Universe

from M.G. Edmunds

SINCE nearly every object in the Universe contains more than one chemical element, it is perhaps not surprising that the experimental determination and theoretical explanation of the abundances of the elements is a rich field of research. The relevance of abundance studies to the whole of astrophysics was very evident in this summer's Santa Cruz Workshop*.

The initial Big-Bang left only isotopes of the very lightest elements, and everything from carbon onwards must have been built up during the evolution of the Universe out of hydrogen inside stars. The synthesis of most elements has been assumed to occur by nuclear reaction chains in the extreme temperatures and densities which occur when a star explodes as a supernova. Although there was much indirect evidence for this basic assumption, it is only recently that direct observational evidence has been found. The analysis of the optical spectra of remnants from such explosions in our own Galaxy (the remnant Cas A) and from a remnant in an irregular galaxy (NGC 4449) by R.P. Kirshner (University of Michigan) does at last provide a clear demonstration that synthesis reactions have occured. The debris of the explosions can be seen streaming out at some thousands of kilometers per second, and has a composition dominated by freshly-synthesized heavy elements (particularly oxygen) with very little unprocessed hydrogen remaining.

Supernovae divide up into two main classes — Type I and Type II — on the basis of the way their phenomenal light emission fades in the first few months after explosion. The exact nature of the stars which give rise to the two different types remains uncertain, but Type II may originate from massive stars (perhaps larger than twelve solar masses). Type I might originate from single stars of somewhat lower masses, or (as originally suggested by J. Whelan & I. Iben *Astrophys. J.* **186**, 1007; 1973) from a binary system of stars when matter is transferred from one component of the system to the other, more condensed star. Models of this second kind were particularly popular at Santa Cruz. Both T. Weaver (Livermore Laboratory) and K. Nomoto (Goddard Space Flight Center) investigated a version in which the gradual transfer of helium onto a white dwarf star results in conditions which give a sudden detonation of nuclear reactions. The exponential pattern of the decay of light output from the resulting explosion gives a fairly direct indication of nuclear syntheses, since the energy output originates in the radioactive decay of freshly synthesised ^{56}Ni which decays to ^{56}Co in a few hours, and then to stable ^{56}Fe in a few months. Models presented by T. Axelrod (Livermore Laboratory) suggest that up to one solar mass of decaying nickel may be involved in a typical Type I supernova, and he claimed that spectral lines of ionised cobalt can be seen in the optical spectrum with a strength and time variation consistent with the decay of large amount of ^{56}Co.

Exactly how the supernovae explode, and how much of the parent star is neutronised and left behind as a highly condensed stellar remnant, remains uncertain — although everyone seemed to agree that the amount of rotation present is likely to be very important in determining the dynamics of the explosion. A particularly intriguing possibility is that, if the pre-supernova star sheds enough of its outer layers for non-explosive mass loss, then a nuclear runaway might occur without a violent release of optical radiation (although there would probably be copious X-ray emission). Thus it may be possible to form neutron stars without an obvious optical supernova event, although a recent lowering of the estimate of the birthrate of pulsars in the Galaxy to one every hundred years (M. Arnaud & R. Rothenflug *Astron. & Astrophys.* **87**, 196; 1980) indicates that optical supernovae may, in fact, provide sufficient neutron stars to account for the observed population.

Supernovae also provide one of the best means of establishing the distance scale to external galaxies, and D. Branch reported work by himself and others at the University of Texas on a supernova in the galaxy M100 which suggests a Hubble constant near 60 km s^{-1} Mpc^{-1}. The result was greeted with relief by many participants because some recent higher values had implied an age of the Universe much smaller than that estimated from radioactive isotope ratios and from ages of old star clusters suggested by stellar evolution theory.

The relative contribution of Types I and II supernovae to the overall heavy element abundances in the Universe is also uncertain, (see, for example, B.M. Tinsley *Astrophys. J.* **229**, 1046; 1979). The observation that oxygen seems more abundant relative to iron in very old stars (which are a sample of early Galactic history) than it is in young stars, prompted S. Woosley (Lick Observatory) to propose on the basis of nucleosynthesis calculations by himself and T. Weaver that oxygen is predominantly synthesised in Type II supernovae and that there were relatively more of these massive stars early on. The major source of iron in the Galaxy would then be subsequent Type I supernovae.

On a galactic scale, the existence of abundance gradients in our own and other large spiral galaxies appears to be well established, in the sense that the central regions have more heavy elements per unit mass than do the outer parts. The best indicators so far are the photoionised HII gas regions, whose spectra have been extensively observed by American, British, French and Mexican groups over the past few years. For our own Galaxy, dust extinction in the Galactic plane makes optical observation difficult, but P. Shaver

---

*The Santa Cruz Workshop in Astronomy and Astrophysics on "The Origin and Distribution of the Elements" was held from July 6 to July 18 at the University of California, Santa Cruz.

M.G. Edmunds is in the Department of Applied Mathematics and Astronomy, University College, Cardiff.

0028-0836/80/370103-02$01.00

(European Southern Observatory) presented radio recombination-line data which show a definite gradient in the electron temperatures of the gas regions as a function of their position in the Galaxy. This may be directly interpreted as an abundance gradient since the temperatures are largely determined by the cooling of the nebula by radiation from the heavy atoms — if abundances vary, then so will the temperatures. For other galaxies there is some indication that the gradients may be flatter in earlier Hubble types, but this correlation of gradient with morphology is unclear, particularly as M. McCall (University of Texas) presented evidence for very different gradients in two galaxies (M101, NGC 6946) which have been classified as exactly the same morphological type.

Even more problematic was P. Wannier's (Caltech) conclusion that the isotope rations ^{12}C/^{13}C, ^{16}O/^{18}O, ^{14}N/^{15}N (as accurately determined from radio molecular line spectra) do not vary significantly across the disk of our own Galaxy, except right in the Galactic Centre. This result is very surprising since the production and destruction rates for the rarer isotope of each of these pairs would be expected to vary considerably if there exists an overall abundance gradient across the Galaxy. Although there may remain some uncertainty in the correction of the molecular line data for fractionation effects in the clouds where the molecules are found, it seems that a radical re-think of the production mechanisms (particularly of ^{18}O, ^{15}N) may be required. Why the Galactic Centre should be different is anyone's guess, but M. Peimbert (University of Mexico), with his discovery of a small Seyfert-like nucleus in M81, reinforced the idea that perhaps all galactic nuclei in spirals are peculiarly active.

The peculiar variation in abundance ratios observed between different stars in some globular star clusters remains something of a mystery. Some of the variations can be ascribed to nuclear processing during the normal evolution of the stars, but variation in other elements seems to force acceptance of the view that there were considerable (and peculiarly selective) inhomogeneities in the initial composition of the gas cloud out of which the clusters formed. But even the anomalies explicable by nuclear processing are not well understood, because according to existing theory many of the stars have not reached a sufficiently advanced evolutionary stage for the products of nuclear reactions in the core of the star to be mixed up by mass motions and reach the surface where they are observed.

The possible inadequacy of mixing theory in stars was stressed by S.E. Persson (Mount Wilson Observatories) for the so-called 'carbon' stars in the Magellanic Clouds, where again there is clear evidence of nuclear processing and mixing at luminosities well below theoretical predictions. Evolved stars undergoing mixing are also a site for synthesis of elements which are formed by repeatedly capturing neutrons at a rate which will allow each successive product of the reaction to β-decay (if it is unstable) before the addition of another neutron. A rather nice demonstration of the occurrence of this reaction chain under different conditions was given by H.E. Bond (Louisiana State University) in his differentiation between 'classic' and 'marginal' Barium stars. In the 'classic' stars the flux of neutrons in the stellar interior has been high enough to add sufficient neutrons to the iron group elements (atomic number A $\sim$ 56) to synthesize considerably heavier elements, giving the characteristic observed over-abundance of Barium (A = 138). The 'marginal' stars show evidence of only a small amount of neutron addition, giving over-abundances of Strontium and Yttrium (A = 88, 89) but insufficient addition to build up a large excess of Barium. Here is concrete evidence of different amounts of nuclear processing during the normal life of stars.

The study of such systematic variations in abundances is of vital importance in sorting out the theory of mixing, and hence tightening up the (still very real) uncertainties in stellar evolution models.

Typical of the spin-off from abundance studies is the discovery by B. Carney (Carnegie Institution of Washington) that there exist some old stars near the Sun with space velocities very much in excess of the velocity of escape from the Galaxy which would be calculated on the assumption that the Sun is near the edge. The continued retention of such stars in the Galaxy strengthens the case for the existence of a large amount of unseen mass outside the Sun's Galactic radius.

The improvements in mass and charge resolution of cosmic ray experiments over the past few years are now beginning to bear fruit. After the observed fluxes have been corrected for reaction during the propagation from their source to Earth, there are no major differences between comic-ray heavy-element composition and that observed in the interstellar medium.

This suggests the origin of Galactic cosmic rays is accelerated interstellar material, rather than freshly-synthesized particles thrown out from the interior regions of a supernova explosion. With present resolutions, one anomaly does seem definite; this is the greater abundance of ^{22}Ne relative to ^{20}Ne in comparison to that observed in most solar system material. Numerous models were invented to explain this, but perhaps the most attractive was the suggestion (S.E. Woosley) that material which had undergone reactions involving the fusion of helium in stars (a product of which would be ^{22}Ne) is preferentially accelerated into cosmic rays. The acceleration would presumably act on this matter after it had been lost from the star. Both the cosmic-ray and gamma-ray observers were quick to point out the serious dilemma facing them — more statistics are needed, and their next generation detectors will have much superior capability, but the number of flights on which they can launch their equipment into orbit is dwindling rapidly.

Another aspect of this widely-ranging workshop was discussion of the isotopic anomalies found in certain discrete regions (or 'inclusions') in meteorites, the anomalies contrasting with a remakable uniformity of isotopic composition (apart from some well-understood fractionation effects) in most solar system material. The anomalies may result from large inhomogeneities in the isotopic composition of the early solar system nebula, although H. Norgaard (Niels Bohr Institute) outlined a scheme for synthesising ^{26}Al (which decays into ^{26}Mg, one of the principal anomalous isotopes) in red giant stars and hoped that dust condensing in the giant stars' atmospheres would provide suitable transport to the early solar system for the radioactive aluminium and its decay product. But the anomalies occur in many different elements, for example G. Wasserburg (Caltech) had found a huge 200% anomaly in ^{107}Ag/^{109}Ag. Confusion is added by the lack of some anomalies which would be expected on nuclear production explanations for other isotopes. Although much beautiful experimental work has been done in discovering these anomalies, their origin remains obscure and must rank as one of the major cosmochemical puzzles.

There was, however, at least one area in which good agreement was reached. This was an estimate of the pre-galactic (i.e. Big-Bang produced) helium abundance. Work by several groups (particularly Peimbert and his collaborators) based on the analysis of spectra of HII regions in irregular galaxies, gave a primordial helium mass fraction of $Y = 0.225 \pm 0.015$. This is in excellent agreement with an estimate of $Y = 0.23 \pm 0.01$ which V. Castellami (University of Rome) made for the helium abundance in a particular type of globular cluster which could be rather well constrained on the basis of stellar pulsation and evolution theory. Since the synthesis of helium in the Big-Bang is influenced by the overall density of the Universe and the details of particle physics, G. Steigman (Bartol Research Foundation) gave an impressive argument that this low value (which is significantly lower than the often-adopted $Y = 0.25$) places constraints on particle physics if a density for the Universe can be assumed. In particular, it may limit the allowed number of neutrino types (whose flavours had been threatening to outnumber those available at the local ice-cream parlour) to only two or three.

Many other problems were discussed at Santa Cruz, and if the function of a good workshop is to raise more questions than it answers, then this one certainly succeeded! □

0028-0836/80/370104-02$01.00

Why are there fewer frogs and lizards in Southeast Asia than in Central America?

from Robert M. May

It has long been suspected that the densities of floor-dwelling amphibians and reptiles are lower in the rainforests of Southeast Asia than in those of Central America.

The first quantitative analysis, however, was made by Scott (*Biotropica* **8**, 41; 1976), who compared his data from two Costa Rican forests with that of Lloyd *et al.* (*Am. Nat.* **102**, 497; 1968) from Nanga Tekalit in Borneo. Inger (*Am. Nat.* **115**, 761; 1980) has recently widened the scope of such comparisons, combining his own additional data from Bornean, Malayan and Thailand forests with Heatwole and Sexton's (*Am. Midl. Nat.* **75**, 45; 1966) results for Panamanian rainforests. The main results are summarized in the Table.

By and large, the numbers in the Table are for floor-dwelling creatures, omitting arboreal and riparian-terrestrial animals (though the Panamanian study includes some lizards captured on trees). Inger notes that turtles and snakes were found too rarely for it to matter whether they are included; similarly, the Costa Rican numbers are little affected by adding in salamanders (as Scott did).

Inger presents further data on the daily catch of frogs and lizards in two other rainforest sites in Borneo, and in three sites (rainforest, logged forest, rubber planting) in Malaya. Although absolute estimates of individuals per m^2 are not available for these sites, the number of catches per day in the rainforest sites were so similar to those in the Old World sites listed in the Table that it is reasonable to assume the densities would also have been similar. On the other hand, the catch per day in the two disturbed sites (logged forest and rubber plantings in Malaya) were more than twice the rates in undisturbed Old World rainforests. Inger suggests this may be due to environmental factors, or to the abundance of species that might be called commensals of man; it could alternatively be due to the enhanced abundance often associated with the 'r-selected' species that characterize disturbed habitats.

The Table shows a consistent pattern, with the total density of frogs and lizards in rainforests in the New World being an order of magnitude higher than those in Southeast Asia. This overall pattern conceals some interesting details. One such is the reversal of the preponderance of frogs over lizards as one goes from Borneo to Thailand; Inger and Colwell (*Ecol. Monogr.* **47**, 229; 1977) attribute this to the relatively dry, harsh seasonal climate of the Thailand sites, which would favour reptiles over amphibians.

What is the explanation for the striking differences revealed in the Table? In terms of ecological roles, species of frogs and lizards dwelling on the floors of tropical forests are very similar; in both Old and New Worlds, the majority feed on arthropods and other invertebrates, and both groups inhabit the same kind of microhabitat. The total number of species of frogs and lizards (species richness) is not significantly different between the two hemispheres. The abundance of snakes or other important predators of frogs and lizards does not show systematic differences.

Comparison of densities of floor-dwelling amphibians and reptiles in lowland (<500m) forests of Old and New World tropics.

Place	Individuals per 100 m^2		
	Frogs	Lizards	Combined
Borneo: Nanga Tekalit	1.31	0.25	1.56
Thailand: Sakaerat			
evergreen forest	0.12	1.03	1.15
deciduous forest	0.27	1.22	1.49
Costa Rica: Rincon de Osa	11.6	3.9	15.5
Costa Rica: La Selva	14.7	2.8	17.5
Panama: Silugandi	29.8	15.4	45.2

Scott attributes the difference in density to there being less production of litter in Bornean forests. But Inger shows some of the estimates of litter production in Bornean forests used by Scott are inappropriate (coming from impoverished heath forests), while others have been revised upward by later work. It does not now seem that production of litter varies much among the major tropical rainforests.

Inger's explanation begins with the observation that a high proportion of the trees in Indo-Malayan rainforests are members of one family, the Dipterocarpaceae. Dipterocarps are noted for their synchronized mast fruiting, which often involves more than 100 species over thousands of square kilometers; the intervals between such reproductive explosions exceed one year. This phenomenon has, however, not been reported for trees in Neotropical forests. Inger suggests that "Mast fruiting should lead to reduction in abundance of an entire class of arthropod primary consumers during non-mast years. In turn, this reduction should affect the total size of the insect population and, therefore, the numbers of insectivorous secondary consumers, such as frogs and lizards. Since ripe dipterocarp seeds do not hang but fall to the ground, it is likely that a reduction in the numbers of seed-eating insects and their arthropod predators would have its greatest effect on the food supply of terrestrial rather than arboreal frogs and lizards."

Inger notes that his hypothesis is susceptible to several tests. If his ideas are correct, both the total number of insects, and the proportion comprising fruit and nut eating insects, should be lower on the floors of Southeast Asian forests than in the Neotropics. Similarly, we would expect to find fewer insectivorous birds feeding on or near the ground.

If Inger's suggestions survive these tests, the problem will have been pushed back one notch. We will then need to understand whether it is historical accident or systematic environmental differences that have produced spectacularly synchronized mast fruiting in Southeast Asian forests and not in the New World. ☐

Robert M. May is Class of 1877 Professor of Zoology at Princeton University.

Neurotoxicity: Mechanisms explored and exploited

from M.K. Johnson

New knowledge of the mechanism of delayed neurotoxicity of some organophosphorus esters is enabling realistic assessment of hazardous levels of exposure. Tri-aryl and mixed alkyl-aryl phosphate esters are widely used as hydraulic fluids, flame retardants and plasticisers and, in both agriculture and disease vector control programmes, organophosphorus pesticides are now used in preference to the persistent halogenated hydrocarbons. Some, but not all, of these esters cause delayed neuropathic effects when tested in sensitive species such as hens or cats and similar neuropathies have occurred in man after ingestion of organophosphates. There is an interval of 10-15 days between ingestion of a neuropathic ester and the onset of clinical signs and, until recently, clinical observation has been the most sensitive tool of the neurotoxicity tester.

At a recent conference* the primary causal molecular changes were presented and the ways in which this knowledge could

M.K. Johnson is in the MRC Toxicology Unit, Carshalton, Surrey, UK.

0028-0836/80/370105-02$01.00

be applied in design and safety evaluation were discussed. M.K. Johnson (MRC Toxicology Unit, UK) showed that many macromolecular sites in nervous tissue are phosphorylated within a few hours of dosing hens with a radio-labelled neuropathic organophosphate. These sites have been dissected into sets and sub-sets by selective use of inhibitors and the delayed neurotoxicity protein phosphorylation site identified unambiguously in one sub-set. The initiation mechanism comprises a phosphorylation of the target protein followed by a bond-fission to form a charged monosubstituted phosphoryl group bound to this site.

Reports at the Round-Table focussed on the fact that the phosphorylation site can hydrolyse phenyl valerate and that toxic attacks on the site can therefore be assessed using the 'neurotoxic esterase' (NTE) as a biochemical monitor. Even at doses producing no clinical or histological effects during the critical 10-15 day period after dosing a response of NTE inhibition at 1-2 days can be observed and quantified. This provides a means to grade the toxic response in a way superior to the previous yes-or-no evaluations.

M. Lotti (Padua University) has studied autopsy samples of human nervous tissue. He finds that *in vitro* the inhibition characteristics of acetylcholinesterase (AChE) and NTE from man are similar to those from the hen. In both species organophosphate poisoning causes cholinergic death only if AChE is highly inhibited. Further, in hens neuropathy is caused only if the maximum inhibition of NTE is greater than 70–80%. To evaluate the hen further as a model we need to know whether equally high inhibition of human NTE is a prerequisite of neuropathy in man. Autopsy material is required from cases of poisoning by compounds which are known to be able to cause neuropathy in sub-lethal doses. The degree of NTE inhibition in the lethal cases should give some guide to the threshold associated with neuropathy. Appeal was made for both NTE and AChE assays to be made whenever deaths occur from organophosphate poisoning; the causative agent should also be proven by tissue analysis and not presumed.

Lotti has carried out such an assay for a case of poisoning by the insecticide omethoate. Although AChE was highly inhibited there was no inhibition of NTE suggesting that neuropathic consequences are not to be expected from survivors of poisonings by omethoate in man. Lotti also showed that doses in excess of the LD_{50} of omethoate did not inhibit brain NTE or cause neuropathy in hens either, again suggesting the hen may be a useful model.

Neural biopsies are obviously unsuitable for monitoring but R. J. Richardson (Ann Arbor) showed that the accessible blood lymphocytes contain an esterase identical to NTE in a variety of its biochemical properties. Provided that the natural fluctuation of lymphocyte levels can be allowed for, routine assay of lymphocyte NTE in potentially exposed persons such as spraymen may allow a neuropathy monitoring system analogous to the assay of blood AChE for acute poisoning.

At the LD_{50} dose diethyl phosphates are always more likely to cause neuropathy than the analogous dimethyl esters. This can be rationalised by analysing effects on NTE independently of all other factors such as metabolic disposal. Study of structure/activity relationships for inhibition of NTE *in vitro* provides a basis for design of non-neuropathic anticholinesterase pesticides. For instance it has been found that esters with hydrophilic or heterocyclic leaving groups have comparatively little affinity for NTE in the test tube and low neuropathic potential *in vivo* and that insecticidal carbamates have no neuropathic potential.

In vivo phosphorylation of the neurotoxicity protein site by neuropathic esters occurs within a period ranging from a few minutes to two days after dosing depending on the route of administration and on whether they require metabolic activation. The secondary bond-cleavage is very rapid in most cases studied but there is then a silent period of about one week before axonal degeneration begins. A. Bischoff (University of Berne) reported that the earliest morphological changes are swellings of some rounded synaptic vesicles at excitatory nerve terminals. These changes were seen at a time when no such changes occurred in the flattened (inhibitory) vesicles although clinical signs of neuropathy were already apparent.

Toxicity testers are already reaping benefit from the understanding of the earliest events. As understanding is extended to the events in the silent period it is hoped that the processes by which axons are maintained may become clearer. Such understanding may be relevant to the modes of action of a wider range of neuropathic chemicals than only the organophosphorus esters. □

---

*A symposium on "Recent Developments in Mechanisms of Neurotoxicity" and a Round-Table discussion on "Delayed Neurotoxicity Testing of Organophosphates" were linked during the Second International Congress of Toxicology in Brussels, 6th — 11th July 1980.

Laser polarization labelling

from Allister I. Ferguson

'A diatomic molecule is a molecule with one atom too many'. This definition, which was coined by Arthur L. Schawlow reflects the kind of despair most spectroscopists encounter when attempting to unravel the complexities of molecular spectra. Even the simplest molecules have such a complicated structure that identifying and assigning quantum numbers to spectral lines is a major task. However, using a laser polarization labelling technique Schawlow and his colleagues at Stanford University have been able to simplify molecular spectra so that the spectra they obtain are more typical of atoms than of molecules. They have been able to identify new highly excited electronic states in a simple diatomic molecule and there are now good prospects for the application of the method to much more complicated molecules.

The factor which complicates molecular spectroscopy is that in addition to the electronic energy levels, which gives rise to atomic spectra, a molecule can vibrate and rotate. These vibrations and rotations add to the electronic energy levels changing a series of isolated levels into a complicated picture of overlapping bands. However, the Stanford group's technique enables a particular level within a band to be 'labelled' so that transitions from this 'labelled' level can be observed and a tremendous simplification in the spectrum be obtained.

The latest research has been reported by Nils Carlson, Toni Taylor and Arthur Schawlow (*Pys. Rev. Lett.* **37**, 683; 1980). They studied the sodium dimer, Na_2, a widely studied diatomic molecule which, like the sodium atom in atomic physics, is much used for testing new techniques before they are applied to more complicated situations. Previously, only six electronic states of Na_2 were known but they have already reported the discovery of some fifteen new states and are confident of discovering even

Fig. 1*a*. A small portion of the absorption spectrum of Na_2. *b*. A larger portion of the same spectrum showing the simplification due to polarization labelling.

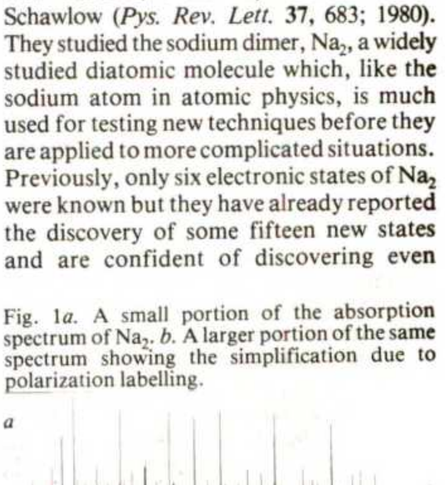

Allister I. Ferguson is in the Department of Physics, Clarendon Laboratory, University of Oxford.

0028-0836/80/370106-02$01.00

more in the near future. With a method powerful enough to find so many new states in such a well understood and highly studied molecule it is tantalising to speculate on the kind of discoveries which might be made on more exotic and less well understood molecules.

The technique that they use was first developed by Richard Teets, Richard Feinberg, Theodor Hänsch and Arthur Schawlow (*Phys. Rev. Lett.* **17,** 683; 1976) and they called it laser polarization labelling. The method uses as a light source a narrowband tunable laser which can excite molecules from isolated vibrational-rotational levels of the ground electronic state to an electronically excited state. If the intensity of the laser is sufficiently large a significant proportion of the population of molecules in the lower level will be transferred to the upper level. By choosing the polarization of the laser appropriately it is possible to orient the levels of the transition in such a way as to create an optical anisotropy in the medium. These levels are said to be 'labelled'. This anisotropy will be experienced by light which is resonant with one of the 'labelled' levels and some other level. Now if broadband light is passed through the medium most of the light will be transmitted without change in polarization. However those light frequencies which do resonate with one of the 'labelled' levels and another level will suffer a depolarization. This depolarization can easily be detected by passing the light through a crossed polarizer. Only those frequencies which interacted with the 'labelled' levels will be transmitted and the spectrum of the this light can be recorded with a spectrograph.

The number of levels that can be reached from a particular 'labelled' level is quite limited due to the quantum mechanical selection rules. In fact, for each 'labelled' level there are at most three rotational levels which can be accessed for each vibrational state. Further selection rules often reduces this number to two.

A typical polarization labelled spectrum in shown in Fig. 1. This shows a small part of the spectrum of Na_2. The pairs of lines in Fig. 1 *b* correspond to the two allowed transitions from each 'labelled' level for each vibrational state. These are the P and R branch transition in the terminology of molecular spectroscopy. Each pair of lines correspond to transitions to different vibrational levels of the excited electronic state. By scanning a wide enough spectral region it is possible to identify the lowest vibrational level and the vibrational and rotational quantum numbers can be found. Given these the molecular constants for the electronic state can then be easily calculated. The classification of the electronic state is determined by selection rules. Also shown in figure 1 *a* for comparison is a traditional absorption spectrum of a much smaller portion of the Na_2 spectrum. Clearly identification of particular electronic states and vibrational and rotational quantum numbers from such a spectrum is extraordinarily difficult.

Carlson *et al.* have scanned wide regions of the Na_2 spectrum and have managed to identify no fewer than fifteen new electronic states. Ten of these states are characterised as being $^1\Delta_g$ and five as $^1\pi_g$. The energies of these new states have been found to follow the well known Rydberg formula, with small corrections due to molecular symmetry. The states are found to correspond to principal quantum numbers of n = 6–15 for the $^1\Delta_g$ states and n = 4–8 for the $^1\pi_g$ states. It should be possible to also find new Σ states and the Stanford group have begun the search for these.

The study of highly excited molecules (Rydberg molecules) has been severely hampered by the very complex structure of the closely spaced Rydberg molecular levels. At the same time studies of Rydberg atoms have been very fruitful (Metcalf *Nature* **284,** 127; 1980) — so much so that Rydberg spectroscopy is now a sub-branch of atomic physics. The work of Carlson *et al.* is a breakthrough in unravelling and interpreting the Rydberg molecule and is the first step to a new and fuller understanding of highly excited molecules which should open the way to Rydberg molecular spectroscopy. □

Combination chemoprevention of cancer

from Michael B. Sporn

THE current use of cytotoxic drugs for treatment of invasive cancer in man depends largely on combination chemotherapy — the combined use of several drugs which exert synergistic effects to achieve the goal of total tumour cell kill. Several papers presented at a recent meeting* suggest that for similar reasons 'combination chemoprevention' might be of importance in the future development of non-cytotoxic drugs for prevention of cancer, that is, for the arrest or reversal of the development of neoplasia in its premalignant stages. Recent advances in the under-standing and control of tumour progression (promotion) have been particularly striking. Using the classical two stage model of mouse skin carcinogenesis (the hydrocarbon, DMBA, as initiator, and the phorbol ester, TPA, as promoter), A.K. Verma and R.K. Boutwell (University of Wisconsin) reported that the combinations of either retinoic acid plus the steroid, dexamethasone, or retinoic acid plus the protease inhibitor, TLCK, exert marked synergistic preventive effects. Their results suggest that retinoic acid, dexamethasone, and TLCK inhibit skin tumour promotion by independent mechanisms. Similar conclusions were reached recently by T.J. Slaga *et al.* (Oak Ridge National Laboratory; *Proc. natn. Acad. Sci. U.S.A.* **77,** 2251; 1980) who have shown that the promotion stage in this system can be further divided into two stages, with the first stage caused by limited application of TPA, and the second caused by the related weak diterpene promoter, mezerein. Slaga *et al.* suggest that low doses of TPA induce formation of primitive skin stem cells, while mezerein induces formation of polyamines and resultant cell proliferation. The TPA effect can be blocked by the protease inhibitor, TPCK, while the mezerein effect is blocked by retinoic acid; glucocorticoids apparently inhibit both stages of promotion. In other studies, Verma, Ashendel, and Boutwell (*Cancer Res.* **40,** 308; 1980) have shown that retinoic acid and indomethacin, an inhibitor of prostaglandin synthesis, exert a synergistic effect to block the induction of ornithine decarboxylase (ODC) caused by TPA; ODC activity has been previously implicated as a key step in formation of polyamines. Whether retinoids and inhibitors of prostaglandin synthesis are synergistic for prevention of skin tumours in the mouse is currently being studied.

Another important area for studies of initiation and promotion is mammary carcinogenesis, in which the internal hormonal milieu of the organism is believed to provide the required promotional stimulus for development of cancer. In the female rat, one or two doses of the alkylating carcinogen, nitrosomethylurea, suffice to initiate carcinogenesis. In new studies, C.W. Welsh (Michigan State University) and R.C. Moon (IIT Research Institute) reported that the combined use of a suppressor of prolactin secretion (2-bromo-α-ergocryptine) together with the retinoid, retinyl acetate, was distinctly superior to either treatment alone in preventing mammary cancer after rats were treated with the carcinogen. Prolactin has long been suspected as a promoting agent in human mammary carcinogenesis, and suppression of its secretion has an obvious rationale. The molecular mechanism of action of the

Michael B. Sporn is Head of the Laboratory of Chemoprevention, National Cancer Institute, Bethesda, Maryland

---

*Annual Meeting of the American Association for Cancer Research, San Diego, California, May 28-31, 1980.

0028-0836/80/370107-02$01.00

retinoids in this system is not known, although it has been shown (Moon *et al.* *Cancer Res.* **39,** 1339; 1979) that they have an anti-proliferative effect on mammary epithelium.

Combination chemoprevention also is applicable to inhibition of the initiation of cancer, as was reported by P.W. Dion, W.R. Bruce *et al.* (Ontario Cancer Institute). It had previously been shown by Bruce's group that mutagenic substances (assayed by the Ames test) are found in human faecal material, and they have been suggested as possible endogenous causative agents for colon cancer. Since it is suspected that these mutagenic substances may be N-nitroso derivatives of intestinal lipids, Bruce *et al.* have fed ascorbic acid and α-tocopherol (known inhibitors of nitrosamine formation) to human volunteers. They reported that the combination of ascorbic acid and tocopherol reduced the median level of faecal mutagen to 25% of control values; the rationale for the combination is to achieve an effective level of anti-oxidant in both the aqueous and hydrophobic phases of the intestinal contents. Another important observation relating to ascorbic acid and cancer prevention was reported by W.F. Benedict and P.A. Jones (University of Southern California), who have shown that levels of ascorbic acid as low as 1 μg per ml can inhibit malignant transformation of mouse fibroblasts caused by methylcholanthrene in cell culture. They found that ascorbic acid was effective in blocking transformation when given as late as 3 weeks after exposure of cells to the carcinogen. Previously, ascorbic acid had been considered to be of chemopreventive use only as an anti-initiating agent. Benedict and Jones' new studies (see also *Cancer Res.* **40,** 2796; 1980) suggest that ascorbic acid may also function as an anti-promoting agent, and will undoubtedly add further interest to the already controversial area of the use of this compound in treatment and prevention of malignancy.

Whatever may be the outcome of these studies, the field of combination chemoprevention appears to be developing rapidly. In other areas of pharmacology the use of multiple drugs to achieve synergistic action and to diminish toxicity is well established. At present, it cannot be predicted how successful such methods might be for applied chemoprevention in man. However, as interest in pharmacological prevention of cancer increases (and as concern about the possible toxic effects of some of the preventive agents, particularly the retinoids, also increases), combination chemoprevention will undoubtedly attract further attention. □

Adenovirus complexities

from correspondents

Two years ago splicing was the hottest subject of discussion at the EMBO workshop on the molecular biology of adenoviruses but the latest meeting* showed that many of the details of complex splicing patterns have already been untangled. Now, the control of virus transcription and DNA replication remain to be elucidated and there has been a clear trend to the development of *in vitro* systems to dissect further the intricacies of eukaryotic cellular control mechanisms.

In vitro transcription systems derived from uninfected KB or HeLa cells with purified RNA polymerase have been used to define the requirements for specific *in vitro* initiations of viral transcription (Lee, University of St. Louis and Corden, University of Strasbourg). Lee used cloned viral DNA fragments as templates to show that the major late promoter is used to initiate RNA products in the correct direction and of the size predicted from the size of the DNA fragment used. All other *in vivo* promoters are also active *in vitro* with the notable exception of the E2 promoter at 75 map units; it is known from sequence analysis that this site lacks a recognisable 'TATAA' box. The promoters vary in strength in the *in vitro* system over a tenfold range, with the major late promoter being most active and early E1A the least active. By using as template a DNA fragment that included the whole of the polypeptide IX transcription unit (the sequence of which is known and which is not spliced *in vivo*), Lee also showed that in his system at least, termination does not occur at a specific site. Transcription continues through the known poly A addition site and very large RNA products are obtained.

Corden, using a similar *in vitro* system, has introduced specific deletions into the DNA template in the region of the major late promoter, to define the sequence requirements for specific initiation of transcription. Removal of bases more than 31 positions upstream from the cap site, or after the site of initiation, did not inhibit *in vitro* transcription, but removal of bases at -31 or -30 resulted in a five-hundred fold reduction in initiation. Similar experiments defined the 5'' promoter boundary at -12 relative to the cap site. In analagous experiments using cloned conalbumin promotor DNA, Corden showed that changing T to a G in the TATAA box lying within the promoter region also reduces the rate of initiation substantially.

Mathews (Cold Spring Harbor) concluded from the hybridization experiments that the non-coding Ad-2 VA RNAs may play a role in virus messenger RNA splicing. Flint (Princeton University) using antibodies from patients with systemic lupus erythmatosus which immunoprecipitate different classes of human ribonucleoproteins reported that some of these antisera inhibit the splicing of Ad-2 early RNA in nuclei isolated from cells infected for 8 hours in the presence of cytosine arabinoside.

Another *in vitro* system that continues to yield intriguing information is that for DNA synthesis. Kelly (Johns Hopkins University), Stillman (Cold Spring Harbor) and Winnacker (München University) showed that nascent DNA chains initiated *in vitro* have terminal protein covalently attached to the 5′ end. Kelly further showed that the polypeptide attached *in vitro* has a molecular weight of 80K in contrast to the 55K product seen on mature virion DNA. However, pulse chase experiments *in vivo* suggest that the 80K form may be a precursor of the 55K protein. Furthermore, they give the same patterns of partial proteolysis with chymotrypsin and are attached to the DNA by the same linkage; a phosphodiester bond between the ß-OH group of serine and the 5′-OH of the terminal deoxycytidine in the DNA.

By stringently inhibiting host cell protein synthesis with anisomycin Lewis (Cold Spring Harbor) reported that his group have identified a new class of 'immediate early' Ad-2 proteins. One of these proteins, which is encoded between 17.0 and 21.5 map units, was clearly shown to be synthesised independent of 'early' region 1A.

Evidence was presented by a number of groups that the Ad-2 major late promoter (co-ordinate 16.4) functions 'early' after infection in permissive cells. Ziff (Rockefeller University) demonstrated by RNase T-1 finger printing that the capped undecanucleotide and promotor proximal spots 1-4 could be clearly identified in cycloheximide treated cells 2-4 hours post infection. Lewis and Akusjarvi (Uppsala University) both identified *in vitro* synthesised proteins (52K and 55K) using Ad-2 m-RNA transcribed from the major late promoter in drug blocked infected cells. Akusjarvi also reported that both of these proteins are synthesised *in vivo* in infected cells blocked for DNA synthesis using cytosine arabinoside.

This meeting produced no definitive data to clarify which adenovirus gene(s) or products are responsible for transformation or malignancy. Past failure to isolate adenovirus conditional lethal mutants defective for transformation has encouraged several groups (Williams, University of Pittsburgh; Ginsberg,

---

*The meeting was held at Peebles, Scotland, June 14-18, 1980.

0028-0836/80/370108-02$01.00

Columbia University and Jones, Purdue University) to use molecular biology techniques and/or *in vitro* mutagenesis to create new mutants. Williams described a 'cold sensitive' mutant which apparently lacks transforming ability. He also reported that the ability of a virus to stimulate host cell DNA synthesis was not alone sufficient to induce transformation. Jones reported studies on an Ad-5 mutant that lacked a single transcript from early 1A which they had generated by inserting an octanucleotide (GGAATTCC) into the Sma I site at 2.85 map units. Preliminary data suggest that this insertion affects transformation.

A number of papers were presented which clearly show that adenovirus DNA is integrated into rodent DNA by illegitimate recombination events. Sambrook (Cold Spring Harbor) Ad-2, Visser (Utrecht University) Ad-5 and Stabel (Cologne University) Ad-12, provided data that for each transformed cell line studied viral integration had occurred at different sites in the host genome. Van den Elsen (University of Leiden) reported that the oncogenicity of Ad-5 and Ad-12 transformed baby rat kidney cell lines in nude mice required the expression of the entire 'early' regions 1A and 1B. Cell lines not expressing 1B 65K protein (Ad-5) or 1B 60K protein (Ad-12) were found to be non-tumourigenic. Graham (McMaster University), reporting on similar experiments using baby hamster kidney cells, concluded that in this system tumourigenic cell lines could be obtained by transfection of Ad-5 DNA which represented early region 1A, but only part of early region 1B (HIND III G fragment).

Raska (CMDNJ — Rutgers) using both serum and cell mediated cytotoxic techniques *in vitro* demonstrated that Ad-12 'early' region 1 codes for a membrane associated antigen. This may be the bonafide virus specific transplantation antigen. However, it is also known that some transformed rat cell lines have a membrane glycoprotein bound to the major histo-compatability antigens. The precursor virus protein of the membrane bound glycoprotein is 16K and is encoded in early region 3.

In conclusion, it seems likely that the next two years of adenovirus research will be dominated by molecular engineering and *in vitro* systems with *in vitro* mutagenesis providing the geneticists with a powerful tool to define more clearly which gene(s) is responsible for malignant transformation and which proteins are involved in transcriptional control of this complicated unit of genes. □

Polymerase III control region defined

from Peter J. Ford

RECENT experiments show that in at least one class of eukaryote genes — 5S ribosomal RNA genes transcribed by RNA polymerase III — control of RNA synthesis is quite different from that found in prokaryotes. In a typical prokaryote gene a promoter site, which binds RNA polymerase, is situated about 10 base pairs upstream (to the 5′ side) from the site at which transcription begins. Mutations in the promoter site alter the level of gene expression but do not affect the actual control of expression. A second site, the operator, overlapping the polymerase binding site is found about 20 base pairs downstream (to the 3′ side) of the initiation site. The operator binds a repressor molecule which prevents polymerase from binding to promotor. Control is exercised by the interactions of small molecules which facilitate either the removal or the binding of the repressor to the operator site. Thus the prokaryote gene consists of a regulatory site overlapping a polymerase binding site located at or just upstream from the point at which transcription begins.

In prokaryotes all genes are transcribed by a single RNA polymerase. In eukaryotes, however, there are at least three structurally and functionally distinct RNA polymerases. Polymerase I transcribes only ribosomal RNA, polymerase II transcribes heterogeneous nuclear RNA (mRNA precursors) and polymerase III trancribes a variety of low molecular weight RNAs including transfer RNAs, 5S ribosomal RNA, low molecular weight RNAs and viral-associated low molecular weight RNAs. The small size of the Polymerase III primary transcripts makes their identification easy and this coupled with their lack of post-transcriptional processing has made genes transcribed by Polymerase III the first choice for studies of regulation.

The somatic 5SRNA gene of *Xenopus borealis* was chosen by Sakonju, Bogenhagen and Brown (*Cell* **19**, 13; 1980) in their search for the eukaryote promoter site. A single 5S gene copy cloned in pBR322 can promote faithful transcription (correct initiation and termination) of 5S RNA in an *in vitro* and an *in vivo* (oocyte injection) assay. By an *in vitro* genetic engineering procedure regions flanking both 5′ and 3′ ends of the gene were deleted and the deleted genes recovered after reinsertion into pBR322. Deletion end points were determined by sequencing the DNA and were numbered from the transcription initiation site (position + 1), base pairs downstream (within the gene) being numbered +2, +3, . . . and base pairs upstream being numbered -1, -2 -3 and so on.

Genes with deletions extending into them from the 5′ end were tested for transcription activity in an *in vitro* transcription assay (Birkenmeier, Brown & Jordan *Cell* **15**, 1977; 1978). It was shown that genes with all 5′ flanking sequences deleted up to the intiation site are actively transcribed but begin at an incorrect site a few nucleotides into the gene, suggesting that the 5′ flanking sequence is required for correct initiation but does not control transcription. Deletions were made extending further into the gene but not until 50 base pairs had been removed was there a drop in transcription efficiency. Remarkably, the size of the transcripts remained about 120 nucleotides, the size of normal 5SRNA. Thus polymerase III is recognizing a sequence starting at least 50 base pairs into the gene from the normal initiation site and is beginning transcription on any appropriate base pair in the region where the normal initiation site should have been put even though this is now replaced by vector pBR322 DNA.

Two points are evident — polymerase binding and transcription depend on a site within the gene itself while the exact point of initiation is influenced by the sequence surrounding the initiation site. To test the relative importance of these two effects Sakonju *et al.*, constructed two 'maxigenes' which had an extra 6 or 20 base pairs inserted between positions +40 and +41 of the gene sequence. Maxigenes are transcribed to give 5S sized transcripts which have begun transcription at sites within the gene. For the +6 maxigene the initiation point is at +10 or +11 base pairs and for the +20 maxigene the initiation point is at either position +21, +22, +23 or +24 within the normal gene sequence. Thus the site within the gene is dominant over the sequence at the normal initiation site, and acts to promote initiation at any convenient site at a loosely fixed distance (about 50 base pairs) upstream from that site, the precise initiation point being determined by the local sequence(s) surrounding potential initiation sites.

Transcription experiments were also carried out with genes deleted progressively from the 3′ end (Bogenhagen, Sakonju & Brown *Cell* **19**, 27; 1980). Since deletions of the 3′ end lack a correct termination site a technique for identifying correct initiation in the absence of correct termination had to be used. Cordycepin triphosphate (3′ dATP) was included in the *in vitro* assay mix serving to terminate a proportion of transcripts at each A residue in the gene sequence. Correct initiation generates a defined set of molecules (analogous to a sequencing ladder) which can be

Peter J. Ford is in the Department of Molecular Biology, University of Edinburgh.

0028-0836/80/370109-02$01.00

100 years ago

PHYSICS WITHOUT APPARATUS

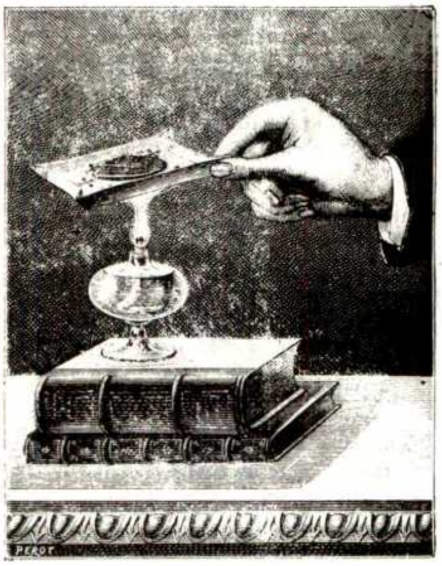

Melting lead on a playing card

A pretty experiment which is easily performed is that of boiling water in a sheet of paper. Take a piece of paper and fold it up, as schoolboys do, into a square box without a lid. Hang this up to a walking-stick by four threads, and support the stick upon books or other convenient props. Then a lamp or taper must be placed under this dainty cauldron. In a few minutes the water will boil. The only fear is lest the threads should catch fire and let the water spill into the lamp and over the table. The flame must therefore not be too large. A small taper will give a flame quite large enough. The paper does not burn, because it is wet; and even if it resisted the wet it still would not burn through, because the heat imparted to it on one side by the flame would be very rapidly conducted away by the water on the other. Another experiment of a similar nature, but perhaps even more striking, is as follows: — Twist up the edges of a common playing-card or other bit of eardboard, so as to fashion it into a light tray. On this tray place a layer of small shot or bits of lead, and heat it over the flame of a lamp. The lead will melt, but the card will not burn. It may be charred a little round the edges, but immediately below the lead it will not be burned, for here again the lead conducts off the heat on one side as fast as it is supplied on the other. Lastly, we give an experiment which, like the two preceding, proves that a good conducting substance may protect a delicate fabric from burning by conducting away the heat rapidly from it. Lay a piece of muslin quite flat upon a piece of metal. A live coal placed on the muslin will not burn it, for the metal takes away the heat too fast. If the muslin is however laid on a bad conductor, such as a piece of wood, it will not be protected, and the live coal will kindle the muslin.

A certain way to obtain an electric spark we have found with what we may call a *Tea-tray Electrophorus.* A common tea-tray of metal is supported on two dry glass tumblers. A piece of common brown paper cut so as to be a little smaller than the tray, and with rounded corners, is warmed, laid on the table and rubbed briskly with a piece of indiarubber, or with a clothes-brush. It is then laid down for an instant on the tray and the tray is touched with the hand. The brown paper is then lifted a few inches above the tray. If at this juncture some person presents his knuckle to the tray he will receive a birght spark, which under favourable circumstances may be a couple of inches long. By simply putting the paper down, touching the tray, and again lifting up the paper the tray is again charged: and a large number of sparks may be thus drawn one after the other in rapid succession. The paper may be lifted by the hands, but it will be found better if a couple of ribbons or strips of paper be fixed on with wax to serve as handles, as shown in our figure.

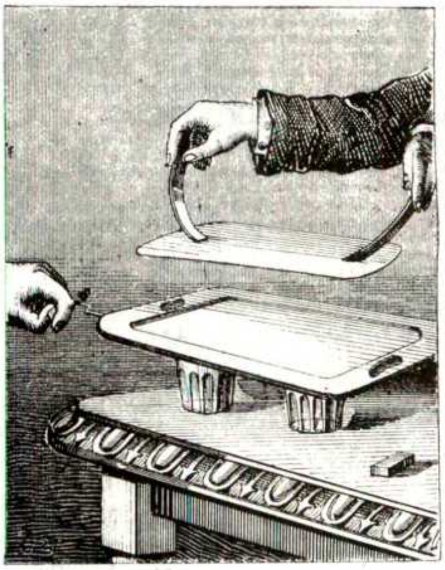

The Tea-tray Electrophorus.

From *Nature* **22,** 9 & 16 September, 440 & 464, 1880.

recognized by their electrophoretic mobility in acrylamide gels. By such means the 3′ end of the gene could be deleted to between +80 and +83 of the gene sequence before correct initiation failed. Together with the previous result this defines the region in *X. borealis* somatic 5S DNA which is required for transcription as lying between positions +50 and +83 of the gene sequence.

An internal promoter is certainly unexpected and different in location from the 5′ flanking promoters of bacterial genes, but is it a general rule for all polymerase genes? The answer is probably yes since there is significant homology of a sequence AGCAGGGT found between base pairs +55 and +62 of the 5S gene and a similarly (±2 base pairs) located sequence in other polymerase III genes — Adenovirus VA I gene and *Bombyx mori* tRNA^{tyr}.

Moreover, similar deletion and transcription studies on tRNA genes (Telford *et al. Proc. natn. Acad. Sci. U.S.A.* **76,** 2590; 1979) show that deletion of 5′ flanking sequences to within −20 base pairs of the transcription initiation site does not impair transcription of the *Xenopus laevis* $\text{tRNA}_1^{\text{met}}$ gene. However, a mutation (Ad5d1309, a dimer deletion) occuring outside the gene between pairs −21 and −24 of the 5′ flanking sequence of adenovirus 5 VA I gene does prevent synthesis of one of the two alternate VA I RNAs (Thimmappaya, Jones & Shenk, *Cell* **18,** 947; 1979). The two VA I RNAs are both transcribed from the same gene but differ by three nucleotides at the 5′ end, VA IA begins with pAGCG . . . while VA IG begins at the second G. The Ad5d1309 mutant produces only the VA IG RNA. The two base pair deletion thus alters the 5′ flanking sequence sufficiently to suppress initiation at A but not at G, demonstrating, in an *in vivo* situation, that local sequences influence the exact site at which transcription begins.

Clearly if the same polymerase III enzyme transcribes a wide variety of genes some of which are independently regulated there must be other factors interacting with the gene–polymerase complex to regulate transcription. One such factor has recently been purified from soluble extracts of *Xenopus* ovaries (Engelke, Ng, Shastry, & Roeder *Cell* **19,** 717; 1980). It had been noticed that 5S genes in chromatin from oocytes were transcribed by a purified polymerase III preparation but a cloned 5S gene was not (Ng, Parker & Roeder *Proc. natn. Acad. Sci. U.S.A.* **76,** 13; 1979). Activity could be restored to the purified polymerase III/cloned 5S gene system by addition of an ammonium sulphate fraction of soluble ovary proteins. Such restoration assays made it possible to purify a 37,000 molecular weight protein which allows faithfull transcription of both *Xenopus* somatic and oocyte cloned 5S genes in a defined reconstituted transcription system using purified polymerase III. The factor, which appears specific for 5S genes, has no activity on a cloned *Xenopus* $\text{tRNA}_1^{\text{met}}$ gene. The factor binds independently of polymerase III to a region of the 5S gene between +45 and +96 base pairs completely overlapping the region identified by deletion mapping as essential for transcription in 5S DNA. Thus there is a possibility that this factor acts in a positive way by directing polymerase III to the 5S gene. It seems certain that this is the first of many factors which will be found to specifically modify the interaction between polymerase III and its genes.

Thus the dogma generated by studies of gene regulation in prokaryotes is breaking down with the demonstration of an internal promoter and regulatory sites for 5S RNA transcription in *Xenopus*. These studies have not yet defined the nature of developmental regulation of these genes, but they have gone a long way towards that goal. □

0028-0836/80/370110-02$01.00

Radiopharmaceuticals

for
diagnostic and
therapeutic
applications

high radiochemical purity
sterilization according to DAB 7

comprehensive range
favourable delivery terms

isocommerz

GmbH · Binnen- und Außenhandelsunternehmen
für radioaktive und stabile Isotope
DDR – 1115 Berlin, Lindenberger Weg 70
German Democratic Republic

Circle No. 27 on Reader Enquiry Card.

The
Fraction Collector
for the '80s is here.

It's FOXY.™

FOXY, the Fraction-Optimizing X-Y fraction collector from ISCO. Microprocessor control permits collection by uniform or mixed time intervals, counted drops, pump revolutions, or ISCO Volumeter discharges. FOXY rejects void volumes and isolates peaks identified by elution times or detected by an ISCO UV monitor. And, it stops flow between tubes and at the end of the run.

FOXY takes practically any size test tube, 28 mm scintillation vials, and even 500 ml bottles. It holds up to 288 tubes in minimal bench space—the keyboard is only 21 cm wide.

To learn more about ISCO's smart generation fraction collector, write ISCO, P.O. Box 5347, Lincoln, Nebraska 68505 U.S.A.

ISCO

Instruments with a difference

Circle No. 07 on Reader Enquiry Card.

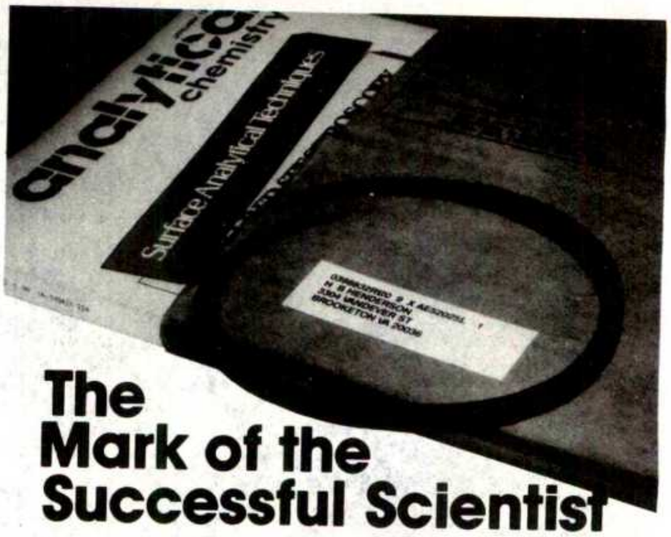

The Mark of the Successful Scientist

An individual subscription to analytical chemistry

Join the successful scientists and receive your *own* subscription to *Analytical Chemistry* so you can use it when—and how—you want!

There are fifteen important reasons why you need your individual subscription:

Twelve monthly issues filled with the latest peer-reviewed research

plus

The April Review Issue (a reference supplement alternating between applications and fundamentals)

and

Lab Guide (a purchasing directory covering instruments, equipment, chemicals and services)

The fifteenth reason? You get all of this vital professional input for just $16.00 a year ($12.00 if you are a member of ACS)!

Guaranteed!
The American Chemical Society will refund the unused portion of your subscription fee at any time you are not satisfied!

Join the Analytical Chemist VIP set!
Call toll free or use the coupon to order your *individual* subscription now!

American Chemical Society
1155 Sixteenth Street, N.W.
Washington, D.C. 20036

1980

Yes! Please send me *Analytical Chemistry* at the following subscription rate:

ACS Members*	U.S.	Canada	Foreign
1-Year	☐ **$12.00**	☐ **$24.00**	☐ **$24.00**
3-Years	☐ **$30.00**	☐ **$66.00**	☐ **$66.00**
Nonmembers			
1-Year	☐ **$16.00**	☐ **$28.00**	☐ **$36.00**
3-Years	☐ **$42.00**	☐ **$78.00**	☐ **$98.00**

CALL TOLL FREE:
800-424-6747
(Credit Cards Only)

Name ____________________

Address ____________________

City ________ State/Country ________ Zip ________

☐ Bill me ☐ Payment enclosed** *(payable to American Chemical Society)*

Charge my ☐ Master Charge ☐ VISA

Card # ________ Interbank # ________ (Master Charge Only)

Exp. Date ________ Signature ________

*Subscription at ACS Member Rates are for personal use only.
**Payment must be made in U.S. Currency, by international money order, UNESCO coupons, U.S. bank draft, or through your subscription agency.

Please allow 60 days for your first copy to be mailed. 0948B

Circle No. 08 on Reader Enquiry Card.

Message sequences and short repetitive sequences are interspersed in sea urchin egg poly(A)$^+$ RNAs

Franklin D. Costantini*, Roy J. Britten & Eric H. Davidson

Division of Biology, California Institute of Technology, Pasadena, California 91125

At least half of the mass and most of the different single-copy maternal mRNA sequences in the egg are covalently associated with transcripts of short repetitive sequences. Only a restricted group of the diverse genomic repeat families are significantly represented. The messages fall into several hundred sets, each containing transcripts from a different repeat family.

THE sea urchin genome includes over 10^5 short repetitive sequence elements interspersed among the single-copy DNA regions[1]. Renaturation kinetics[1,2], as well as primary sequence data[3], indicate that the genomic repeats belong to several thousand distinct sequence families, which in general share little or no homology. Although the biological role of these sequences is unknown, recent studies have shown that almost all of the diverse repeat families are represented in a tissue-specific manner in sea urchin nuclear RNAs[4] and in unfertilized egg RNA[5]. The present work was undertaken to determine the nature of those repeat transcripts stored in the egg. We found that many of these transcripts are covalently associated with RNAs which have the characteristics of egg maternal messengers. Thus, repetitive sequences are interspersed in egg poly(A)$^+$ RNA [p(A)$^+$ RNA] and are included in a large majority of the diverse species of egg message.

Repeated sequence transcripts are included on many egg poly(A) mRNA molecules

According to earlier studies[5] most of the transcripts of short interspersed repetitive DNA sequences in the sea urchin egg are present on RNA molecules several thousand nucleotides long. The possibility thus arose that the repeat sequence transcripts are located on maternal message molecules. The egg of *Strongylocentrotus purpuratus* contains about 50 pg of maternal mRNA (about 1.5% of the total egg RNA) bearing poly(A) tails sufficiently long to promote binding to oligo(dT)-cellulose columns[6–8]. We refer to the egg RNA collected on such columns as the 'p(A)$^+$ RNA', although the flowthrough or 'p(A)$^-$ RNA' fraction apparently includes an approximately equal mass of maternal message, much of which is terminated by short 3' oligo(A) tails which bind to poly(U)-Sepharose and not to oligo(dT)-cellulose[6–9]. Isolation of the p(A)$^+$ fraction of the egg RNA provides a convenient experimental enrichment for at least a large subclass of the maternal message. In addition, use of this fraction minimizes the contribution of known repetitive gene transcripts such as the histone mRNAs, which, in the sea urchin, do not co-purify with p(A)$^+$ RNA[10].

The p(A)$^+$ RNA of the egg was isolated and purified by successive rounds of oligo(dT)-cellulose chromatography. The denatured weight-average length of the p(A)$^+$ RNA was about 5,000 nucleotides, in general agreement with previous measurements[7,11]. This was determined by electron microscopy and gel electrophoresis as described below. The concentration of repetitive sequence transcripts was examined in the p(A)$^+$ RNA and the p(A)$^-$ RNA fractions. Figure 1*a* and *b* displays titration reactions with two cloned repetitive sequences, CS2109B and CS2108, shown earlier to be represented by prevalent egg transcripts[5]. The cloned probes were labelled and strand-separated, and one strand of each was reacted with increasing amounts of egg p(A)$^+$ RNA or p(A)$^-$ RNA[4]. Transcripts complementary to the CS2109B sequence (Fig. 1*a*) are 32-fold more concentrated in p(A)$^+$ RNA than in p(A)$^-$ RNA, and a similar degree of concentration, 38-fold, is observed for the CS2108 sequence (Fig. 1*b*). Given that 1.5% of egg RNA is included in the p(A)$^+$ RNA fraction, these results require that at least a third of the RNA molecules reacting with the two cloned repeats contain long poly(A) tracts.

To determine whether these two cloned repeats are representative, we measured the kinetics of the reaction of a ^{3}H-DNA genomic repetitive sequence tracer with excess egg p(A)$^+$ RNA, p(A)$^-$ RNA and total egg RNA. As shown in Fig. 1*c*, all three reactions were heterogeneous in rate, due to variation in the prevalence of different repeat trancripts[5]. However, it is clear that transcripts of most repeat families detectable in egg RNA are concentrated in the p(A)$^+$ RNA fraction. Considering the initial 30% of each reaction, which represents the more prevalent repeat transcripts, the reaction with p(A)$^+$ RNA occurs about 33 times more rapidly than with unfractionated egg RNA. Hybridization with p(A)$^-$ RNA is not detectably slower than with total egg RNA, so not all repeat-containing molecules are included in the p(A)$^+$ RNA fraction. It can be calculated from these data that about 50% of the transcripts of each average prevalent repeat species co-purifies with the p(A)$^+$ RNA fraction. For comparison, the distribution of single-copy sequence transcripts in the p(A)$^+$ RNA and p(A)$^-$ RNA of the egg is shown in Fig. 1*d*. The tracer in this experiment is a fraction of single copy ^{3}H-DNA selected by prior reaction with egg RNA ('egg DNA', or 'eDNA')[12]. Analysis of the kinetics shows that roughly half of the diverse species of single-copy sequence transcript present in the egg are heavily represented in the p(A)$^+$ RNA fraction. That is, an average of about 75% of the molecules of each RNA species in this class is recovered as p(A)$^+$ RNA. The other half of the mRNA species is mainly found in the p(A)$^-$ RNA fraction, though a small percentage of these molecules is included in the p(A)$^+$ RNA fraction, so that the two reactions ultimately terminate together. Of course, many RNA species may have

---

* Present address: Department of Zoology, University of Oxford, Oxford, OX1 3PS, UK.

0028-0836/80/370111—07$01 00

intermediate degrees of polyadenylation. Additional evidence has been obtained with cloned single-copy DNA probes. As reported elsewhere[13], about 50% of the prevalent transcripts of cDNA clone SpG30 are found in the egg $p(A)^+$ RNA fraction. Similarly, about 35% of the rare transcripts of the cloned Sp88 single copy sequence are recovered as $p(A)^+$ egg RNAs[14].

The distribution of repeat-sequence transcripts in $p(A)^+$ and $p(A)^-$ RNA fractions is consistent with the view that the repeats are found on $p(A)^+$ mRNA molecules. Thus, at least for those repeat families which are represented by prevalent egg RNA transcripts, about half of the molecules bearing each repeat sequence are recovered in the $p(A)^+$ RNA fraction. Furthermore, note that all the diverse repeat transcripts appear to be relatively concentrated in the $p(A)^+$ RNA fraction, while only about half of the different species of single-copy sequence transcript are recovered to a large extent as $p(A)^+$ RNAs.

Electron microscopy of renatured egg $p(A)^+$ RNA

A dramatic visualization of the interspersed sequence organization of egg $p(A)^+$ RNA is presented in Fig. 2. These electron micrographs illustrate the multi-stranded branched structures formed when $p(A)^+$ RNA molecules are renatured. The RNA was first fully denatured, then incubated to an equivalent C_0t of 600 M s in a buffered formamide medium and spread for electron microscopy, as described in the legend to Fig. 2. Almost no complicated structures, such as those shown, were observed in control samples spread immediately after denaturation ($C_0t < 2\times10^{-3}$ M s).

Interpretation of the structures shown in Fig. 2 is greatly assisted by the previous observation[5] that both complements of each repeat sequence are represented in sea urchin egg RNA, as in nuclear RNAs[4]. This is almost certainly not due to symmetrical transcription but to the presence of RNA molecules deriving from different transcription units orientated oppositely with respect to the repeat sequence. In contrast, all single-copy sequences so far analysed in sea urchin egg or nuclear RNAs are asymmetrically represented. This includes a number of specific sequences complementary to cloned probes (ref. 15 and unpublished data), as well as the total single-copy sequence sets of nuclear RNA[16]. With this background, it is clear that the multi-stranded structures shown in Fig. 2 are networks consisting of several individual long $p(A)^+$ RNA molecules held together by renatured complementary short repeat duplexes. The structures shown bear a strong resemblance to the structures formed when DNA from an animal displaying short-period repetitive sequence interspersion is renatured at low C_0t (ref. 17). RNA networks held together by renatured interspersed repeats were described previously by Federoff *et al.*[18], who observed them in HeLa cell nuclear RNA.

About 65% of the total contour length of the $p(A)^+$ RNA in a random sample studied (1.2×10^6 nucleotides) is included in branched structures displaying four or more ends, and apparently composed of two or more molecules. This should approximately estimate the mass fraction of $p(A)^+$ RNA-bearing repeats, since most of the RNA contour length appears to consist of single-stranded regions. Although it is impossible to interpret most of the RNA complexes unambiguously, some qualitative implications follow from their general structure. The presence of complementary repeat sequence transcripts previously observed in total egg RNA is seen to be a property of the $p(A)^+$ RNA. Over two-thirds of the molecules participating in intermolecular duplexes were present in structures displaying six or more ends, and therefore consisting of at least three

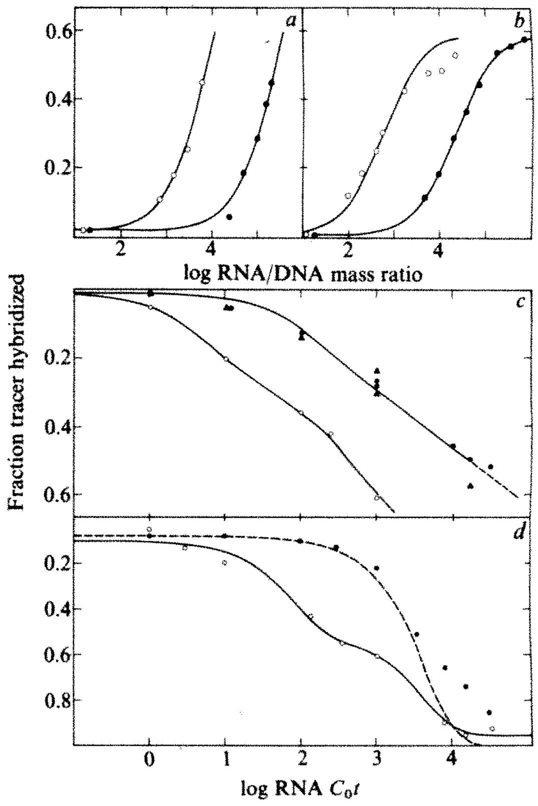

Fig. 1 Distribution of repetitive and single-copy sequences in egg $p(A)^+$ RNA and $p(A)^-$ RNA fractions. Total egg RNA was isolated[35] and fractionated on oligo(dT)-cellulose[40]. The RNA which bound consecutively on three passes was the $p(A)^+$ RNA fraction (1.5% of total egg RNA). RNA which repeatedly failed to bind was the $p(A)^-$ RNA fraction (98%). All RNAs were partially hydrolysed with alkali to about 1,000 nucleotides before hybridization. *a*, Titration of $p(A)^+$ and $p(A)^-$ RNA with the cloned repetitive-sequence, CS2109B[24]. The repetitive sequence cloned in plasmid CS2109B was excised with *Eco*RI, 5′ end-labelled with ^{32}P and strand separated[4]. Excess lower strand tracer was hybridized to termination with increasing amounts of $p(A)^+$ (○) or $p(A)^-$ (●) RNA. All hybridization reactions described here were assayed by hydroxyapatite binding, unless otherwise noted. The curves represent least-squares solutions to the form for the titration reactions given in equation (2) of Scheller *et al.*[4]. The specific fraction of $p(A)^+$ RNA consisting of CS2109B transcripts was 1.3×10^{-4}, and for $p(A)^-$ RNA the fraction was 4.1×10^{-6}. *b*, Titration of $p(A)^+$ RNA and $p(A)^-$ RNA with the upper strand of the cloned repetitive sequence CS2108[23]. The specific RNA fractions measured are 1.8×10^{-3} for $p(A)^+$ RNA and 4.7×10^{-5} for $p(A)^-$ RNA. *c*, Hybridization of excess $p(A)^+$ RNA (○), $p(A)^-$ RNA (●) or total egg RNA (▲) with repetitive ^3H-DNA tracer representing most of the short repeats in the genome. This tracer was prepared, as previously described[5], by reassociating sea urchin ^3H-DNA fragments of average length 3,300 nucleotides to C_0t 40 M s, digesting with S_1 nuclease, binding to hydroxyapatite, and fractionating according to molecular size on a Sepharose CL-2B column. The resulting short-repeat tracer displayed a weight-average length of 300 nucleotides. Hybridization was at 50 °C in 0.12 M phosphate buffer, *p*H 7.0. The data were fitted assuming second-order kinetics[4,5] with two kinetic components, but since the reactions are not terminated, only the faster component of each reaction, representing the more prevalent repeat transcripts, is meaningful. A fast component terminating at 30% hybridization was arbitrarily selected for analysis. The observed rate constants for this component are: $p(A)^+$ RNA, $k = 1.54\times10^{-1}\ M^{-1}\ s^{-1}$; total egg RNA or $p(A)^-$ RNA, $k = 4.6\times10^{-3}\ M^{-1}\ s^{-1}$. *d*, Hybridization of excess $p(A)^+$ RNA (○) or $p(A)^-$ RNA (●) with ^3H-labelled eDNA tracer. The eDNA tracer was prepared by enriching for the fraction of total single-copy ^3H-DNA that hybridizes with total egg RNA (about 3%). This particular eDNA tracer hybridized to an extent of 45% with total egg RNA and was thus about 15-fold purified relative to the starting single-copy DNA. Reactions with $p(A)^+$ and $p(A)^-$ egg RNAs have been normalized to the 45% terminal value. The dashed line indicates the kinetics of the reaction of eDNA with total egg RNA, that is, a single pseudo-first-order kinetic component with a rate constant of $2.3\times10^{-4}\ M^{-1}\ s^{-1}$. This rate was previously determined with several eDNA preparations[12] (see also Fig. 6*a*). The reaction with $p(A)^+$ RNA is heterogeneous and is fitted by two components (solid line), a fast component representing 41% of the tracer, with a rate constant of $1.2\times10^{-2}\ M^{-1}\ s^{-1}$, and a slow component representing 43% of the tracer, with a rate constant fixed at $2.3\times10^{-4}\ M^{-1}\ s^{-1}$. Comparing these rate constants to the rate constant for total egg RNA, we calculate that the fast component represents sequences 75% of whose transcripts are recovered in the $p(A)^+$ RNA fraction, while the slow component represents sequences that are mainly (>95%), though not exclusively, confined to the $p(A)^-$ RNA fraction. Note that the sequence concentration of almost half of the single-copy species is lower in the $p(A)^-$ RNA than in total egg RNA. These are presumably the species predominantly found in the $p(A)^+$ RNA fraction.

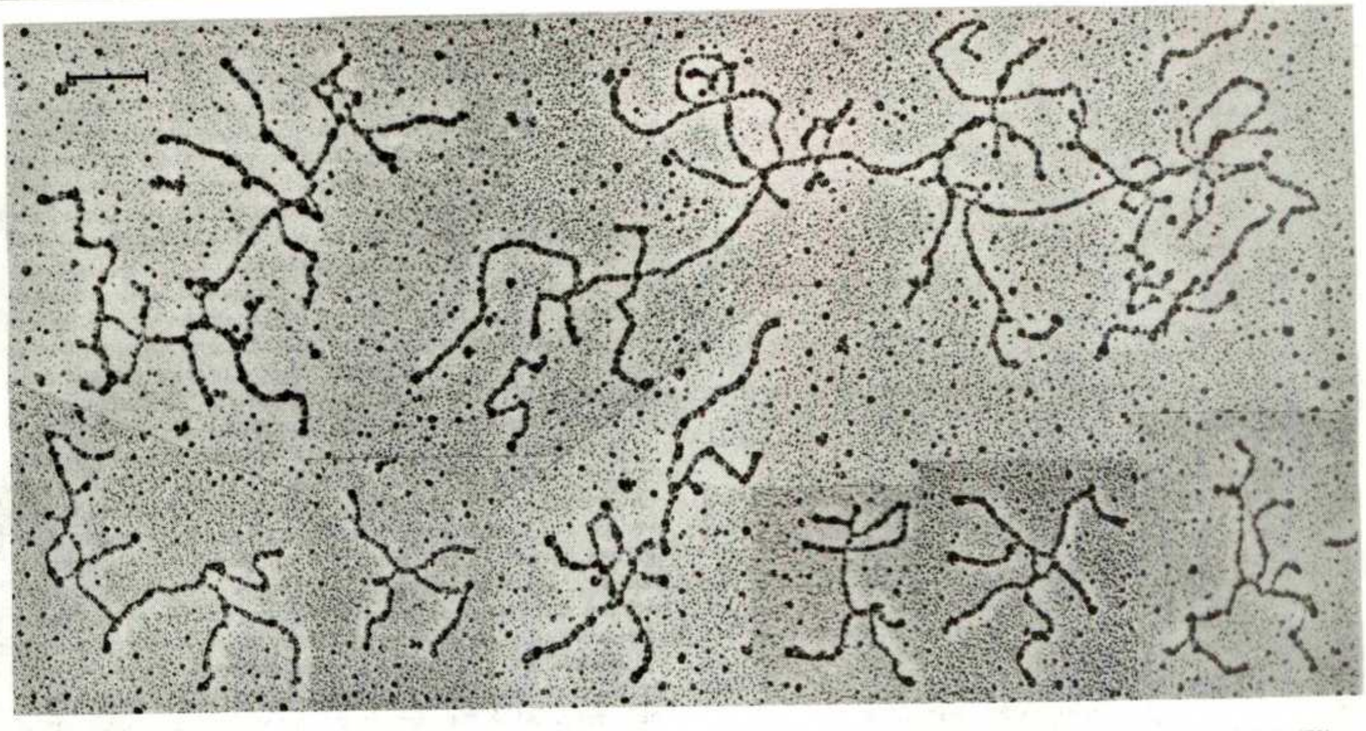

Fig. 2 Electron microscopy of multimolecular structures formed by renaturation of egg p(A)$^+$ RNA. Total p(A)$^+$ egg RNA was denatured at 70 °C in 67% formamide, 0.3 M NaCl, 0.01 M PIPES (*p*H 6.5), 10^{-4} M EDTA for 1 min, then incubated at 30 °C in 58% formamide, 0.75 M NaCl, 0.025 M PIPES (*p*H 6.5), 10^{-4} M EDTA, to equivalent C_0t 600 M s. The RNA was then diluted and spread for electron microscopy[41] from a hyperphase of 80% formamide, 0.1 M Tris (*p*H 8), 5 mM EDTA and 100 μg ml^{-1} cytochrome *c*, at 24 °C. Many multimolecular RNA structures, including large networks, were observed. The montage shown includes several relatively simple examples of such structures. The bar represents a single-strand RNA length of 1,000 nucleotides, estimated from circular single-stranded ΦX174 DNA included on the same grids, and including a 10% correction for the difference in linear densities of single-stranded RNA and DNA in these spreading conditions[42]. To estimate the fraction of RNA in multimolecular structures, random areas of the grid were photographed, and the total contour length of each structure was measured. The structures measured had a total contour length of 1.2×10^6 nucleotides, of which 65% was contained in structures having four or more discernible ends and judged to consist of two or more RNA molecules. Sea urchin rRNA did not form networks when incubated to the same C_0t and spread in identical conditions. When the p(A)$^+$ RNA was spread in the same conditions following denaturation ($C_0t < 2 \times 10^{-3}$ M s), no networks were observed, and less than 4% of the RNA length was in structures containing possible intermolecular duplexes. The denatured p(A)$^+$ RNA had a weight-average length of 5,000 nucleotides, and a number-average length of 3,400 nucleotides, based on a sample of 187 randomly selected molecules. Size determinations by agarose gel electrophoresis in the presence of methyl mercuric hydroxide[43] were consistent with these values.

molecules. It follows that many p(A)$^+$ RNA molecules bear more than one repeat sequence element. Otherwise, almost all renatured structures would include only two molecules and very large networks such as some of those shown in Fig. 2 would never have formed. Another general implication is that most of the length of those p(A)$^+$ RNA molecules which contain repetitive sequence elements consists of single-copy sequence transcript. This is demonstrated directly in the next section.

Interspersion of repetitive and single-copy sequences in egg p(A)$^+$ RNA

To examine the sequence organization of p(A)$^+$ RNA molecules containing repeat transcripts, it was necessary to purify these molecules with respect to the remainder of the RNA. The following strategy proved effective. Egg p(A)$^+$ RNA was labelled *in vitro* with ^{125}I (refs. 19–21), and hybridized with excess repetitive DNA which had previously been mercurated (Hg-DNA)[22]. Details are given in the legend to Fig. 3. Excess non-mercurated sea urchin ribosomal DNA (rDNA) was added to compete out the hybridization of contaminating ^{125}I-rRNA, which amounted to 1–5% of the various ^{125}I-p(A)$^+$ RNA preparations. After denaturation, the reaction mixtures were incubated to C_0t 50 M s with respect to the repetitive Hg-DNA, and fractionated on a sulfhydryl–agarose (SH–agarose) column. RNA molecules hybridized to the repetitive DNA are bound to this column, while non-hybridized RNA flows through. When mixed with the Hg-DNA (denatured or native) but not permitted to anneal, less than 1% of the ^{125}I-p(A)$^+$ RNA bound to the SH–agarose column. This background is somewhat lower than is obtained with the urea–phosphate hydroxyapatite-binding procedure[23] for trapping RNA hybrids formed with excess DNA. Control experiments showed that the same amount of hybrid was recovered with the SH–agarose Hg-DNA procedure, as by the urea–phosphate hydroxyapatite-binding method.

The kinetics of the hybridization reaction between the ^{125}I-p(A)$^+$ RNA and the repetitive Hg-DNA are illustrated in Fig. 3. To provide relative kinetic standards, Fig. 3 includes reactions of a genomic ^{3}H-DNA repeat tracer and of a single-copy ^{32}P-DNA tracer with the same Hg-DNA driver. The reaction of the ^{125}I-p(A)$^+$ RNA occurs at approximately the same rate as the reaction of the repeat DNA tracer. As expected, single-copy sequences are more than 10-fold reduced in concentration in the repetitive Hg-DNA driver compared to whole DNA. There is no reaction whatsoever of the ^{32}P-DNA single-copy tracer until $C_0t > 10^2$. Therefore, the ^{125}I-p(A)$^+$ RNA molecules which hybridize with the Hg-DNA at C_0t 10^{-2}–C_0t 10^2 M s (Fig. 3) must contain repeat sequences. The kinetics exclude the possibility that the trapped RNA molecules were bound by virtue of hybridization with residual single-copy sequences contaminating the repetitive Hg-DNA driver. Furthermore, when the bound RNA is eluted and again reacted with the repetitive Hg-DNA driver, the kinetics observed are consistent with those in the initial reaction.

Although binding the p(A)$^+$ RNA–Hg–DNA hybrids to SH–agarose effectively isolates molecules which include repeat transcripts, the yield of the procedure is low. After hybridization, only 16–19% of the ^{125}I-p(A)$^+$ RNA binds to the SH–agarose column. In the presence of excess sea urchin rDNA, the fraction of ^{125}I-RNA bound falls slightly, to 11–16%. Several factors suggest that this value seriously underestimates the true fraction of p(A)$^+$ RNA molecules which include repeat-sequence elements: (1) The repetitive DNA driver was prepared by incubation of the starting DNA to C_0t 50 M s resulting in under-representation of repeat sequences whose frequency of occurrence is less than 10–20 copies per genome. (2) The

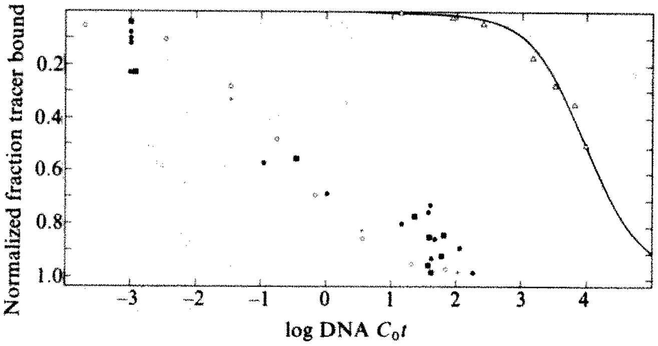

Fig. 3 Kinetics of hybridization of ^{125}I-p(A)$^+$ RNA with excess mercurated repetitive DNA. ^{125}I-p(A)$^+$ egg RNA was hybridized with a 100- to 1,000-fold excess of mercurated repetitive sea urchin DNA and hybridization was assayed by binding to SH–agarose. To facilitate kinetic comparisons, hybridization values are normalized to the maximal extent of reaction in each curve. All reaction mixtures were denatured in 65–75% formamide, 0.3 M NaCl at 75–80 °C, then incubated in 50% formamide, 0.75 M NaCl, 0.025 M PIPES (*p*H 6.5), 10^{-4} M EDTA, 0.1% SDS and 5×10^{-5} M NaCN, at 30 °C. Binding to SH–agarose[44] was performed in 0.5 M NaCl, 0.01 M Tris (*p*H 7.5), 10^{-3} M EDTA, 0.05% SDS, and the bound nucleic acids were eluted with the same buffer containing 0.1 M β-mercaptoethanol. Repetitive sea urchin DNA was prepared by S_1 digestion of total DNA after reassociation to C_0t 50 M s (refs 45 and 46), and the repetitive DNA was covalently mercurated[22]. 85–90% of native or denatured mercurated DNA could be bound to SH–agarose. The abscissa indicates equivalent C_0t values[45], including an estimated 2.5-fold rate retardation due to hybridization in 50% formamide[47]. ■, hybridization of ^{125}I-p(A)$^+$ RNA in the presence of excess non-mercurated rDNA competitor (normalized from a 13% terminal value); ●, the same, but without rDNA competitor (normalized from a 20% terminal value); +, re-reaction of hybridized ^{125}I-p(A)$^+$ RNA with more repetitive Hg-DNA driver, plus rDNA competitor (normalized from a 35% terminal value). For comparison the hybridization kinetics of short repetitive ^{3}H-DNA (○) (normalized from a 90% terminal value), and single-copy ^{32}P-DNA tracer (△) (normalized from a 95% terminal value obtained with unfractionated DNA driver) are shown, with the same repetitive Hg-DNA driver. The latter two reactions were assayed by binding to hydroxyapatite.

reaction criterion (50% formamide, 0.75 M NaCl at 30 °C) probably precludes duplex formation within the less closely related classes of repeat sequences found in the sea urchin genome[24]. (3) The p(A)$^+$ RNA was unavoidably subjected to some strand scission during iodination. The weight-average length of the total iodinated p(A)$^+$ RNA was about 1,400 nucleotides, as measured on denaturing formaldehyde–sucrose gradients[25]. ^{125}I-p(A)$^+$ RNA which had been hybridized with Hg-DNA, bound to SH–agarose, and eluted displayed the same length distribution. While the hybridization procedures thus result in no further strand scission, the fragment length of the p(A)$^+$ RNA after iodination is less than one-third its starting length. Unless all repeat sequences in the RNA are distributed less than 1,400 nucleotides apart, this amount of breakage would have resulted in a decrease in the fraction of p(A)$^+$ RNA bound after hybridization with the repetitive Hg-DNA. (4) The SH–agarose column binds only about 40% of the available repetitive RNA–DNA duplexes. As shown in Table 1, when RNA that fails to bind after reaction with Hg-DNA is re-hybridized, another 8–13% can be bound. When once-bound RNA molecules, all of which must contain a hybridizable repeat sequence, are eluted and re-hybridized, only 40% bind to a second SH–agarose column. A probable explanation, according to experiments not shown here, is that duplexes between mercurated and non-mercurated nucleic acids bind with less than 50% efficiency to SH–agarose. This phenomenon was also reported earlier by Nguyen-Huu *et al*[26]. Using the data of Table 1, we estimate that about 35% of 1,400 nucleotide p(A)$^+$ RNA fragments actually contained recognizable RNA–DNA hybrids (that is, 15% initial binding normalized for a 40% SH–agarose binding efficiency). This estimate is still two-fold below that obtained from our electron microscopic observations. The most likely explanation is the difference of over threefold in RNA fragment length in the two experiments. In addition, more repeat duplexes may have survived the conditions of the electron microscope experiment than could be recovered as Hg-DNA–RNA hybrids, due to the relatively high stability of RNA–RNA duplexes in formamide media.

The repetitive and single-copy sequence content was measured in a sample of ^{125}I-p(A)$^+$ RNA which had been twice reacted with the repeat Hg-DNA driver, in the presence of rDNA competitor, and bound to SH–agarose (preparative data are shown in Table 1). After elution, the RNA was hybridized with excess whole sea urchin DNA, and the ribonuclease resistance of the ^{125}I-RNA was determined as a function of DNA C_0t (refs 23, 27). Data are shown in Fig. 4. Least-squares analysis of this reaction indicates that 85–90% of the mass of the selected ^{125}I-RNA is single-copy sequence transcript. However, these single-copy sequences must be linked to repetitive sequences, since every RNA molecule in the selected ^{125}I-RNA fraction contains at least one repeat-sequence element.

The repetitive sequences in the bound p(A)$^+$ RNA are generally short, although a small fraction of the RNA could consist entirely of repeat transcripts. Figure 4 suggests that the average 1,400-nucleotide ^{125}I-RNA fragment bound to SH–agarose includes less than 200 nucleotides of repetitive sequence. In other experiments ^{125}I-p(A)$^+$ RNA was reacted with the Hg-DNA, bound to SH–agarose and the hybrid molecules were eluted and digested directly with ribonuclease. Only 8–12% of the ^{125}I-RNA was resistant, again indicating that there are no more than 170 nucleotides of repeat sequence on the average RNA fragment in this fraction. It is unlikely that a significant amount of hybridized repetitive RNA was rendered soluble in trichloroacetic acid (TCA) by the ribonuclease digestion since the amount of resistant RNA was the same when the assay was carried out at 0 °C as at 37 °C. It is nonetheless

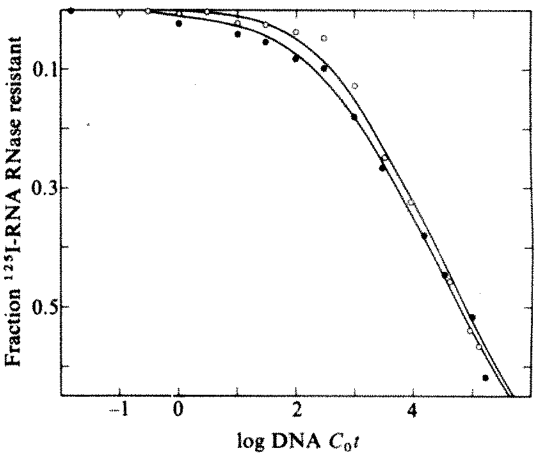

Fig. 4 Repetitive and single-copy sequence content of repeat-containing egg p(A)$^+$ RNA. A fraction of p(A)$^+$ RNA, consisting of transcripts containing repeated sequences, was selected by hybridization with repetitive Hg-DNA and chromatography on SH–agarose (see text). Hybridization of contaminating ^{125}I-ribosomal RNA was blocked by competition with non-mercurated cloned sea urchin ribosomal DNA. This selection procedure was then repeated to assure purity (see Table 1). The final selected ^{125}I-RNA (●), or total ^{125}I-p(A)$^+$ egg RNA (○), was then reacted with a 10^5–10^6-fold excess of total sea urchin DNA. Hybridization was assayed by digestion with 10 μg ml^{-1} ribonuclease A for 1 h at 37 °C in 0.24 M phosphate buffer (*p*H 6.8), 10^{-3} M EDTA, followed by precipitation with cold 10% TCA and collection on Whatman GF/C filters. Hybridized RNA sequences are resistant to digestion in these conditions, while single-strand regions are hydrolysed. To estimate the fractions of ^{125}I-RNA hybridizing with repetitive or with single-copy sequences in the driver DNA the data were fitted using a function that takes into account the retarded hybridization of RNA tracers[48], as well as the effects of a nuclease-resistance assay on the observed kinetics[49–51]. The fraction of the selected ^{125}I-RNA hybridizing as a repetitive component appears to be between 10% and 15%, depending on the allowed average repetition frequency. A reasonable estimate, assuming an average frequency of 100 copies per genome, suggests that 89% of the selected RNA fraction consists of single-copy sequence transcript, and 11% of repeated-sequence transcript, while the total p(A)$^+$ RNA is 93% single-copy sequence transcript and 7% repeated-sequence transcript. These solutions are indicated by the solid lines shown. The total ^{125}I-p(A)$^+$ RNA preparation contained about 1% ribosomal RNA measured by hybridization with cloned ribosomal DNA.

Table 1 Fraction of ^{125}I-p(A)$^+$ RNA binding to SH–agarose after hybridization with excess mercurated repetitive DNA

	% bound			
		Re-reaction of bound fraction		Re-reaction of unbound fraction
Experiment	First reaction +rDNA	+rDNA	−rDNA	+rDNA
1	15	42	40	8
2	16	30,35	40	13

Hybridization and assay conditions are described in the legend to Fig. 3. All hybridizations were carried out at DNA C_0t 50 M s. In each experiment, egg ^{125}I-p(A)$^+$ RNA was hybridized with a 100-fold mass excess of mercurated repetitive DNA, in the presence of a large sequence excess of non-mercurated cloned sea urchin rDNA[39]. The reaction mixtures were then chromatographed on an SH–agarose column. Aliquots of the bound fraction were denatured and re-reacted with additional mercurated repetitive DNA, plus or minus rDNA competitor, as indicated. The unbound fraction was similarly re-reacted in the presence of rDNA competitor.

possible that the average length of the repeat sequences could be somewhat greater than 170–200 nucleotides. In any case we conclude that at least 35% (and perhaps twice this fraction) of sea urchin egg p(A)$^+$ RNA has an interspersed sequence organization, in which short repetitive sequences are covalently associated with longer single-copy sequence transcripts.

Complexity of single-copy sequences linked to repeats in egg RNA

In this section, we demonstrate that the interspersed egg RNAs include most of the diverse species of single-copy sequence transcript found in the egg, and therefore, most of the diverse maternal mRNAs. To measure the complexity of the single-copy sequence transcripts associated with repeats in the egg RNA, we prepared a selected fraction of total egg RNA in which the interspersed RNA molecules were relatively concentrated. We then hybridized this fraction with an eDNA tracer. Hough-Evans *et al.*[12] showed earlier that at least 75% of the single copy sequence represented in total egg RNA is included in the mRNA of early embryo polysomes. The eDNA tracer is therefore a probe for the complex assemblage of single-copy sequences comprising the maternal message set stored in the sea urchin egg.

The RNA fraction required for this complexity measurement was obtained by hybridizing total egg RNA with repetitive Hg-DNA, followed by chromatography on SH–agarose. The egg RNA/Hg-DNA mass ratio was sufficient to permit hybridization of most of the diverse repeat transcripts, but very little of the egg rRNAs or tRNAs (see legend to Fig. 5). After hybridization, 2.2% of the total egg RNA bound to the SH–agarose column. The Hg-DNA was eliminated by DNase treatment, and a measurement was made of the enrichment for repeated sequence transcripts actually obtained in the fractionation. Thus, the concentration of transcripts complementary to two cloned repetitive sequences was determined by titration with the selected RNA fraction. Figure 5 shows that transcripts complementary to the repeat sequence of clone CS2109B are present at an 11-fold higher concentration in this RNA fraction than in total egg RNA. Similarly, the repeat sequence of clone CS2111 (ref. 24) is nine times more concentrated in the selected RNA fraction. We expect, therefore, that single-copy sequence transcripts linked to repeats will also be concentrated in the selected RNA fraction by a factor of about 10, with respect to total egg RNA.

The kinetics of reactions between a ^{32}P-eDNA tracer and the selected RNA fraction, as well as the reaction of the ^{32}P-eDNA with total egg RNA, are shown in Fig. 6*a*. This tracer contained no detectable repetitive-sequence component (data not shown). Both of the eDNA hybridization reactions in Fig. 6*a* terminate at about 85% of the tracer bound. Therefore, the selected RNA fraction includes essentially all the diverse single-copy sequences in total egg RNA. The experiment clearly shows that the single-copy sequence transcripts driving the eDNA reaction are concentrated in the selected RNA fraction. Least-squares solutions to the kinetic data indicate that 70–80% of the reaction is accelerated 10-fold compared to total egg RNA, while the remaining 20–30% is accelerated 2-fold. It follows that at least 70–80% of the diverse single-copy sequences in egg RNA exist on transcripts also containing repeated sequences. Since the large majority of the same single-copy sequences are represented in polysomal mRNA after fertilization, most, if not all, of the interspersed egg RNAs are maternal messages. Furthermore, interspersed transcripts are the major form of these maternal mRNA species, rather than a minor variant. If, for example, only 25% of the transcripts of a particular single-copy sequence contained a repeat sequence, a 10-fold enrichment for that repeat would result in only a 2.5-fold enrichment for the single-copy sequence. It is possible that the 20–30% of single-copy sequences that appear to be less enriched in the selected egg RNA fraction reside on transcripts which lack repeats. Alternatively, these sequences might simply represent regions of transcripts that are relatively distant from repeats and are often separated from them by a strand scission.

Interspersed repetitive sequences exist in prevalent as well as rare or complex-class maternal messages. This was shown by titration experiments with a cloned cDNA fragment, SpG30, which represents a highly prevalent egg p(A)$^+$ mRNA. There are about 2×10^5 molecules of this RNA per egg. The cloned SpG30 fragment is about 700 nucleotides long and consists entirely of single-copy sequence[13]. Figure 6*b* illustrates titration measurements of the sequence concentration of transcripts complementary to the strand separated SpG30 probe in total egg RNA, and in the repeat-enriched selected RNA fraction. Like most rare single-copy transcripts, this highly prevalent single-copy sequence is also about 10-fold more concentrated in the repeat-enriched RNA fraction. A repetitive sequence therefore must be located somewhere on the SpG30 transcript.

Discussion

We have shown that a substantial fraction of the heterogeneous RNA in the sea urchin egg, including the p(A)$^+$ RNA, consists of short repetitive sequence transcripts covalently linked to longer single-copy sequences. While these interspersed transcripts have many properties that identify them as maternal messages, we have not demonstrated that they actually function as messages. However, most of the diverse message sequences in the egg are found on molecules which display an interspersed sequence organization. In addition, essentially all of the mass of the heterogeneous repeat-sequence transcripts in the egg[5] can

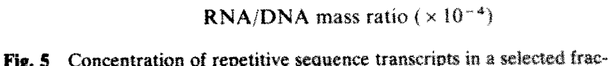

Fig. 5 Concentration of repetitive sequence transcripts in a selected fraction of egg RNA. To yield a fraction enriched for transcripts containing repeated sequences, 1 mg of unlabelled total egg RNA plus 8µg of ^{125}I-labelled total egg RNA was hybridized with 1 mg of repetitive Hg-DNA. This is a sufficient DNA/RNA ratio to provide a DNA sequence excess for any repeat present in more than 20 copies per genome and contained on fewer than 2×10^5 transcripts per egg. The reaction mixture was incubated to Hg-DNA C_0t 50 M s, then fractionated on an SH–agarose column, as described in Fig. 3. The bound fraction was eluted with 0.1 M β-mercaptoethanol, and the repetitive Hg-DNA was completely removed by DNase digestion. Two ^{32}P-labelled cloned repetitive sequences were then titrated with total egg RNA and with the selected RNA fraction. *a*, Titration of the repeat sequences from clone CS2109B, lower strand (■), and clone CS2111, lower strand (●) with total egg RNA. *b*, Titration of the same two repeat sequences with the selected repeat-enriched RNA. The complementary RNA fractions are: CS2109B, 2.1×10^{-6} of total egg RNA and 2.3×10^{-5} of repeat-enriched RNA; CS2111, 1.5×10^{-5} of total egg RNA and 1.4×10^{-4} of repeat-enriched RNA.

be accounted for as interspersed RNA molecules. The precise physical organization of these maternal RNAs is not yet apparent. This will require further analysis of individual transcripts using cloned DNA probes. We know, however, that the repetitive sequence elements are relatively short, averaging only 150–200 nucleotides. According to primary sequence data, six out of eight cloned repeat elements contain translation stop codons in all reading frames[3], and this observation suggests that the repeats may be located elsewhere than in translated regions of the message. It is also likely that more than one repeat-sequence element exists on many RNA molecules. A possibility not yet excluded is that the repeat-sequence elements are removed by cytoplasmic processing events before polysomal translation. It is also possible, if unlikely, that only the minor fraction of egg transcripts which lack repeats serve as maternal messages.

Is interspersed sequence organization a feature peculiar to sea urchin maternal RNAs? Earlier studies on the newly synthesized polysomal mRNA of gastrula stage sea urchin embryos failed to reveal a significant fraction of message containing linked repetitive and single-copy sequences[23,28]. There have been several reports on the sequence organization of messages from other animal cell types (see, for example, refs 29–32). With the aid of cloned probes, Firtel and his associates recently clearly demonstrated that short repeat-sequence elements exist on certain predominantly single copy *Dictyostelium* mRNAs[33,34]. Re-examination of sea urchin gastrula mRNA by the methods described here, as well as those previously used reveals a small fraction of polysomal mRNAs which contain interspersed repeats (unpublished data). However, a major distinction exists in the amount of repetitive-sequence transcript in egg maternal RNA as opposed to gastrula polysomal mRNA. While the egg contains many highly prevalent repeat transcripts[5], the gastrula mRNA seems to contain few if any repeat-sequence transcripts of equally high prevalence. The only highly prevalent interspersed repeat transcripts observable in the sea urchin gastrula are found in the nucleus, as concluded earlier by Scheller *et al.*[4]. The process by which this intracellular distribution of repeat transcripts is achieved during development is unknown, as is its functional significance.

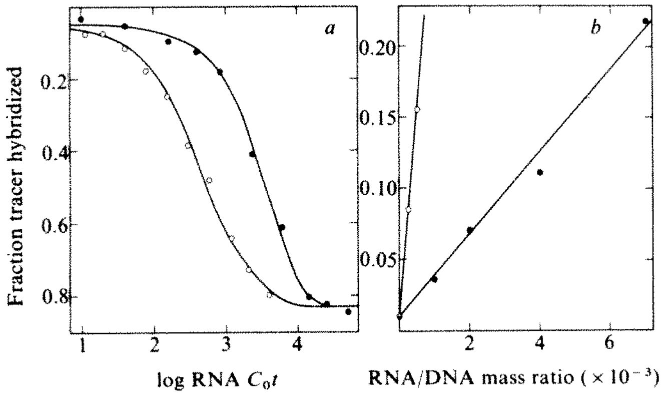

Fig. 6 Complexity of single-copy sequence transcripts included in the selected repeat-enriched RNA fraction. *a*, Hybridization of an eDNA ^{32}P-labelled tracer containing all the single-copy sequences represented in total egg transcripts with excess total egg RNA (●) or with the selected repeat-enriched egg RNA fraction (○) described in Fig. 5. The ^{32}P-labelled eDNA tracer was prepared, as previously described[12], by hybridizing total single copy ^{32}P-DNA with total egg RNA and purifying the hybridized fraction. The eDNA preparation used in this experiment was about 30-fold enriched for egg RNA sequences relative to the starting single-copy ^{32}P-DNA preparation. Hybridization was dependent on added RNA, and hybrids were sensitive to RNase digestion in low salt[52]. The curve shown for the total egg RNA reaction describes a single pseudo-first-order kinetic component with a rate constant of $2.3\times10^{-4}\ M^{-1}\ s^{-1}$. In the kinetic solution shown here for the reaction with the repeat-enriched RNA fraction two components were assumed. The rate constant for the faster component was fixed at $2.3\times10^{-3}\ M^{-1}\ s^{-1}$ or 10 times the rate constant obtained with total egg RNA so as to estimate the fraction of single-copy sequences enriched to the same extent as repeats. This component included 70% of the reaction, while 30% displays a rate constant of $4.1\times10^{-4}\ M^{-1}\ s^{-1}$. *b*, Titration of the ^{32}P-labelled single-copy DNA sequence of clone SpG30, upper strand, with total egg RNA (●) or with the repeat-enriched egg RNA fraction (○). The complementary fraction of total egg RNA was 3.0×10^{-5}, while the complementary fraction of repeat-enriched RNA was 2.9×10^{-4}.

Our most important conclusion pertains to the sequence organization of the sea urchin genome and its possible function. We found earlier[28] that the single-copy sequences represented in embryo mRNA tend to be located non-randomly, close to interspersed repetitive sequences in the genome. Our present data require the further conclusion that most of the structural genes represented in egg RNA belong to sets, each of which is defined by the presence of homologous sequences of a given repeat family. This can be seen as follows: According to previous measurements, transcripts of 10–20% of the diverse repetitive sequence families in the genome, or 500–1,000 different sequence families, are prevalent in the egg RNA[5]. About 10^5 transcripts represent each of these prevalent repetitive sequence families per egg, and together these account for ⩾90% of the mass of interspersed repeat transcripts. No more than a few per cent of the mass of the repeat transcripts are accounted for by rare repeat sequences, that is, those represented in only 10^3–10^4 copies per egg[5]. On the other hand, 60–80% of the maternal mRNA in the egg consists of rare, complex-class single-copy sequence transcripts (refs 7, 12 and unpublished data). Most of these complex-class transcripts are covalently linked to repeats, according to the experiment of Fig. 6*a*, and most of the repeats must belong to the prevalent repeat-transcript class[5]. Since the complexity of the egg single-copy sequence set is 3.7×10^7 nucleotides[12,35], whereas there are only a few hundred kinds of prevalent repeat transcripts, a majority of these repetitive-sequence families must be represented on many (probably between 10 and 50) different rare messages. It follows that the prevalent repeat transcripts belonging to each family must have derived from many distinct transcription units, each including a different single-copy gene (or a few such genes). Thus, both the structural genes expressed during oogenesis and the many thousands of mRNA species produced by their transcription are distributed among several hundred sets, according to the particular repetitive-sequence family represented on each mRNA molecule. A similar organization has been observed in *Dictyostelium*[33,34], where two prevalent repeat transcripts each appear to be associated with 50–100 different rare mRNAs.

The organization of structural genes in sets or 'gene batteries', each associated with a specific repeat family (or families), has been proposed in models for regulation of gene expression[36,37]. It was envisioned that the shared repeats of each battery provide the physical basis for coordinate control of its expression. It is easy to see that the distribution of only 10–20% of the different repeat sequences in the genome among the more than 10^4 single copy message species in the egg implies a non-random arrangement of certain repetitive sequences among those genes which are expressed during oogenesis. However, there is no evidence regarding the actual function, if any, of the transcribed interspersed repeats. Their presence in the maternal RNA provides an unexpected opportunity for further examination of the physiological meaning of genomic sequence interspersion. Among the functions which might be envisioned for these repeat transcripts are suppression of mRNA utilization before fertilization, translational control affecting the timing of utilization of specific mRNA sets following fertilization, control of the differential distribution of maternal mRNAs to various regions of the early embryo, or sites for specific RNA processing events before translation. Alternatively, they might be remnants of transcriptional or post-transcriptional regulatory signals[36,37], incompletely removed from germinal vesicle precursors. A different possibility is that some of the maternal repeat transcripts could serve in a regulatory capacity in early embryo nuclei, where they might be involved in imposing initial patterns of gene expression which are similar to those in effect during oogenesis[12,35,38].

We thank Drs William H. Klein and Richard H. Scheller for their assistance and Drs Richard Axel and Norman Davidson for critical reviews of the manuscript. This research was supported by NIH Grant HD-05753. R. J. B. is a staff member of the Carnegie Institution of Washington.

Note added in proof: The characteristics of sea urchin egg p(A)$^+$ RNA described here pertain as well to the p(A)$^+$ RNA of *Xenopus*, an anuran vertebrate. When p(A)$^+$ RNA from the unfertilized egg of *Xenopus* (obtained by Dr L. Dennis Smith) was renatured and spread for electron microscopy under the exact conditions of Fig. 2 (by M. E. Chamberlin), the following results were obtained. (1) RNA which was not permitted to anneal after denaturation displayed only occasional intrastrand foldback structures. (2) RNA renatured to C_0t 60 was largely involved in structures containing two to four molecules bound by short duplex regions. And (3), RNA renatured to C_0t 600 was largely included in complex multimolecular aggregates often containing more than 10 molecules.

Received 13 March; accepted 20 June 1980.

1. Graham, D. E., Neufeld, B. R., Davidson, E. H. & Britten, R. J. *Cell* **1,** 127–137 (1974).
2. Davidson, E. H. & Britten, R. J. *Q. Rev. Biol.* **48,** 565–613 (1973).
3. Posakony, J. W., Anderson, D. M., Scheller, R. H., Britten, R. J. & Davidson, E. H. (in preparation).
4. Scheller, R. H., Costantini, F. D., Kozlowski, M. R., Britten, R. J. & Davidson, E. H. *Cell* **15,** 189–203 (1978).
5. Costantini, F. D., Scheller, R. H., Britten, R. J. & Davidson, E. H. *Cell* **15,** 173–187 (1978).
6. Reviewed in Davidson, E. H. *Gene Activity in Early Development* (Academic, New York, 1976).
7. Wilt, F. H. *Cell* **11,** 673–681 (1977).
8. Ruderman, J. V. & Pardue, M. L. *Devl Biol.* **60,** 48–68 (1977).
9. Dubroff, L. M. & Nemer, M. *Nature* **260,** 120–124 (1976).
10. Ruderman, J. V. & Pardue, M. L. *J. biol. Chem.* **253,** 2018–2025 (1978).
11. Slater, I. & Slater, D. W. *Proc. natn. Acad. Sci. U.S.A.* **71,** 1103–1107 (1974).
12. Hough-Evans, B. R., Wold, B. J., Ernst, S. G., Britten, R. J. & Davidson, E. H. *Devl Biol.* **60,** 258–277 (1977).
13. Lasky, L. A., Lev, Z., Xin, J.-H., Britten, R. J. & Davidson, E. H. *Proc. natn. Acad. Sci. U.S.A.* **77** (in the press).
14. Lee, A. S., Thomas, T. L., Lev, Z., Britten, R. J. & Davidson, E. H. *Proc. natn. Acad. Sci. U.S.A.* **77,** 3259–3263 (1980).
15. Lev, Z. *et al. Devl Biol.* **76,** 322–340 (1980).
16. Hough, B. R., Smith, M. J., Britten, R. J. & Davidson, E. H. *Cell* **5,** 291–299 (1975).
17. Chamberlin, M. E., Britten, R. J. & Davidson, E. H. *J. molec. Biol.* **96,** 317–333 (1975).
18. Federoff, N., Wellauer, P. K. & Wall, R. *Cell* **10,** 597–610 (1977).
19. Commerford, S. L. *Biochemistry* **10,** 1993–2000 (1971).
20. Orosz, J. M. & Wetmur, J. G. *Biochemistry* **13,** 5467–5473 (1974).
21. Chan, H.-C., Ruyechan, W. T. & Wetmur, J. G. *Biochemistry* **15,** 5487–5490 (1976).
22. Dale, R. M. K., Martin, E., Livingston, D. C. & Ward, D. C. *Biochemistry* **11,** 2447–2456 (1975).
23. Goldberg, R. B., Galau, G. A., Britten, R. J. & Davidson, E. H. *Proc. natn. Acad. Sci. U.S.A.* **70,** 3516–3520 (1973).
24. Klein, W. H. *et al. Cell* **14,** 889–900 (1978).
25. Fenwick, M. L. *Biochem. J.* **107,** 851–859 (1968).
26. Nguyen-Huu, M. C., Sippel, A. A., Hynes, N. E., Groner, B. & Schutz, G. *Proc. natn. Acad. Sci. U.S.A.* **75,** 686–690 (1978).
27. Melli, M., Whitfield, C., Rao, K. V., Richardson, M. & Bishop, J. O. *Nature new Biol.* **231,** 8–12 (1971).
28. Davidson, E. H., Hough, B. R., Klein, W. H. & Britten, R. J. *Cell* **4,** 217–238 (1975).
29. Klein, W. H., Murphy, W., Attardi, G., Britten, R. J. & Davidson, E. H. *Proc. natn. Acad. Sci. U.S.A.* **71,** 1785–1789 (1974).
30. Campo, M. S. & Bishop, J. O. *J. molec. Biol.* **90,** 649–663 (1974).
31. Dina, D., Meza, I. & Crippa, M. *Nature* **248,** 486–490 (1974).
32. Darnell, J. E. & Balint, R. *J. cell Physiol.* **76,** 349–356 (1970).
33. Kimmel, A. R. & Firtel, R. A. *Cell* **16,** 787–796 (1979).
34. Kindle, K. L. & Firtel, R. A. *Nucleic. Acids Res.* **6,** 2403–2422 (1979).
35. Galau, G. A. *et al. Cell* **7,** 487–505 (1976).
36. Britten, R. J. & Davidson, E. H. *Science* **165,** 349–357 (1969).
37. Davidson, E. H. & Britten, R. J. *Science* **204,** 1052–1059 (1979).
38. Davidson, E. H. & Britten, R. J. *J. theor. Biol.* **32,** 123–130 (1971).
39. Blin, N. *et al. J. biol. Chem.* **254,** 2716–2721 (1979).
40. Aviv, H. & Leder, P. *Proc. natn. Acad. Sci. U.S.A.* **69,** 1408–1412 (1972).
41. Davis, R. W., Simon, M. & Davidson, N. in *Meth. Enzym.* **21,** 413–428 (1971).
42. Wellauer, P. K. & Dawid, I. B. *J. molec. Biol.* **89,** 379–395 (1974).
43. Bailey, J. M. & Davidson, N. *Analyt. Biochem.* **70,** 75–85 (1976).
44. Dale, R. M. K. & Ward, D. C. *Biochemistry* **14,** 2458–2469 (1975).
45. Britten, R. J., Graham, D. E. & Neufeld, B. R. in *Meth. Enzym.* **29**E 363–418 (1974).
46. Eden, F. C., Graham, D. E., Davidson, E. H. & Britten, R. J. *Nucleic. Acids Res.* **4,** 1553–1567 (1977).
47. Hutton, J. R. *Nucleic. Acids Res.* **4,** 3537–3555 (1977).
48. Galau, G. A., Smith, M. J., Britten, R. J. & Davidson, E. H. *Proc. natn. Acad. Sci. U.S.A.* **74,** 2306–2310 (1977).
49. Morrow, J. thesis, Stanford Univ. (1974).
50. Smith, M. J., Britten, R. J. & Davidson, E. H. *Proc. natn. Acad. Sci. U.S.A.* **72,** 4805–4809 (1975).
51. Britten, R. J. & Davidson, E. H. *Proc. natn. Acad. Sci. U.S.A.* **73,** 415–419 (1976).
52. Galau, G. A., Britten, R. J. & Davidson, E. H. *Cell* **2,** 9–21 (1974).

Structure of a family of rat amylase genes

Raymond J. MacDonald*, Michael M. Crerar†, William F. Swain,
Raymond L. Pictet‡, Gilles Thomas‡ & William J. Rutter||

Department of Biochemistry and Biophysics, University of California, San Francisco, California 94143

The sequences of two cloned rat pancreatic amylase cDNAs comprising 95% of the mRNA sequence are reported. Analysis of cloned rat genomic DNA fragments using cloned cDNA probes indicates that the rat genome contains multiple closely related amylase genes in which the cDNA sequences are distributed within a region 9 kilobases in length and are interrupted by at least seven intervening sequences.

α-AMYLASE confers on the cell or organism producing it the capacity to use polyglucosides with α-1,4 linkages (such as starch) as energy and carbon sources. The rat genome, like other mammalian genomes, contains multiple closely related amylase genes which are selectively expressed in a number of differentiated cells. Amylase is a major product of the pancreas and parotid glands, accounting for approximately 20% of the total protein[1,2], and is associated with the digestive functions of these tissues. Liver also produces amylase but in relatively low quantities[3]; it is a prominent source of serum amylase in the normal animal[3].

Because of its prominent functional role amylase has served as a specific marker of differentiation[4–9]. The synthesis of amylase is initiated in parotid and pancreas cells at different periods of embryological development according to the differentiative programmes of these cells[10]. The synthesis of amylase in pancreatic acinar cells is apparently dependent on insulin[11], and can be induced fourfold by glucocorticoids so that it represents more than 70% of the total protein synthesis[12]. The difference in amylase levels in pancreas, parotid and liver parallel the relative abundance of amylase mRNA in the tissue[13]. Thus it appears that amylase synthesis is largely regulated at the level of mRNA synthesis or degradation.

The results of a variety of studies suggest the amylases of pancreas, parotid and liver, though similar, are distinct proteins and are the products of at least three distinct genes. The amylases isolated from the pancreas and parotid are immunologically distinguishable and have clearly different peptide maps[14,15]. Immunological studies also suggest differences in the parotid and liver enzymes[16]. The melting profiles of complementary (c)DNA·RNA hybrids formed with pancreatic amylase cDNA indicate greater than 90% sequence homology between pancreatic, parotid and liver amylase mRNAs but also clearly distinguish the pancreatic mRNA from the parotid and liver mRNAs[13]. Preliminary evidence suggests differences between parotid and liver amylase mRNAs as well[13].

Present addresses: * Department of Biochemistry, University of Texas Health Science Center, 5323 Harry Hines Blvd, Dallas, Texas 75235; † BioLogicals, Inc., Department of Biology, York University, Downsview, Ontario, Canada M35 1P3; ‡ Institut de Biologie Moleculaire, Université Paris VII, Tour 43, 75221 Paris Cedex 05, France.

|| To whom correspondence should be addressed.

0028–0836/80/370117—06$01.00

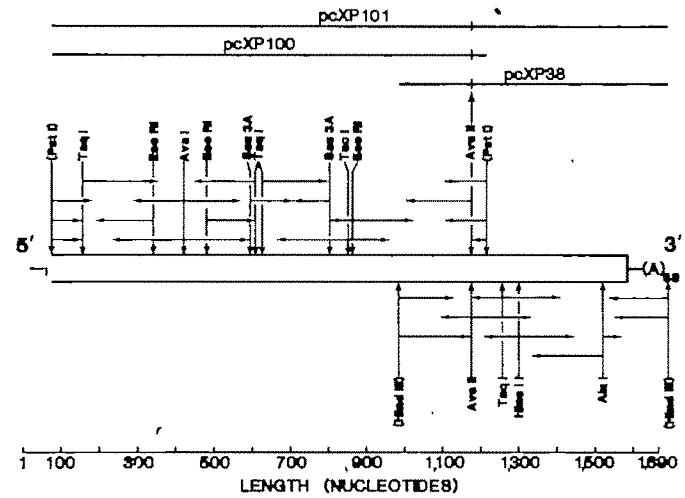

Fig. 1 Sequencing strategy for rat pancreatic amylase mRNA. The extent of the two double-stranded cDNA cloned sequences is discussed in the text. The direction of each sequencing reaction is shown by the horizontal arrows, starting at the restriction sites shown. (The number of bases determined in each reaction is indicated by the length of the arrows.) The 5′ end-labelled restriction fragments for sequencing were prepared from double-stranded cDNA separated from the pBR322 sequences. The internal *Hin*dIII site was derived from the *Hin*dIII restriction site linker added to the pcXP38 insert during the double-stranded cDNA cloning. The dotted line at the 5′ end indicates the uncloned portion of the mRNA.

In view of their common ancestral origin and their selective expression in differentiated cells, the amylase genes present an unusually favourable opportunity for analysis of structure–function relationships in eukaryotic genes. We describe here the nucleotide sequence of amylase mRNA derived from a nearly full-length cDNA cloned in bacteria. From this nucleotide sequence we have deduced the amino acid sequence of pancreatic amylase and certain characteristics of the amylase molecule.

Using the cDNAs as probes we have isolated genomic DNA fragments containing amylase genes. We present here the overall structure of the several amylase genes present in the rat genome.

Sequence of amylase cDNA

The details of molecular cloning of the population of predominant rat pancreatic mRNAs as cDNA and the identification of cloned sequences for a number of secretory enzyme mRNAs including amylase will be described in detail elsewhere[17]. Approximately 220 recombinant clones containing pancreatic amylase cDNA sequences have been identified among approximately 1,400 recombinant bacterial transformants. Restriction endonuclease analysis revealed two overlapping cDNA clones, designated pcXP38 and pcXP100, which contain cDNA inserts of 702 and 1,176 base pairs, respectively. These were sequenced by the method of Maxam and Gilbert[18], according to the sequencing strategy shown in Fig. 1. The sequence is given in Fig. 2. The pcXP38 cDNA insert contains a terminal poly(A) stretch of 68 residues and therefore encodes the 3′ end of the mRNA. The pcXP100 insert overlaps with 227 nucleotides at the 5′ end of the pcXP38 insert (Fig. 1); thus the total length of the mRNA sequence contained in the two plasmids is 1,615 nucleotides. The length of pancreatic amylase mRNA, estimated by agarose gel electrophoresis in the presence of methyl mercury[19], is 1,690±30 nucleotides[17] (average of 12 determinations) including an average poly(A) length of 65 nucleotides[8]. The sequence contained in the two cloned cDNAs therefore represents greater than 95% of the total mRNA sequence and lacks 75±30 nucleotides at the 5′ end of the mRNA.

The nucleotide sequence of the 227-base pair overlap common to both cloned cDNAs is identical at all positions except position 1,139 (Fig. 2) which is unambiguously T in pcXP38 and A in pcXP100. This discrepancy may have been introduced by the cloning procedures[20], or may reflect the cloning of two closely related, perhaps allelic, pancreatic amylase mRNAs.

Organization of the amylase mRNA sequence

The amino acid sequence of rat pancreatic amylase, derived solely from the nucleotide sequence of the mRNA, is given in Fig. 2. The amino acid sequence of the protein has not yet been determined, so comparison of independent amino acid and nucleotide sequences is not possible; however, the authenticity of the proposed reading frame and the consequent amino acid sequence is supported by the following criteria: (1) the reading frame shown is the only one without multiple termination codons; (2) the calculated molecular weight of the proposed amylase sequence, including amino-terminal residues, which probably correspond to a portion of the prepeptide, is 56,570. This is similar to the 58,000 molecular weight estimate for the rat pancreatic amylase precursor synthesized *in vitro*[5]; (3) the amino acid composition of the deduced sequence coincides with that reported for rat pancreatic amylase[17,21]. The fractions of aspartate plus asparagine (17%) and tryptophan (3.5%) are characteristically high for amylase[21] compared with the average for 314 proteins compiled by Dayhoff *et al.*[22]. The amino acid compositions of the multiple potential polypeptides predicted by each of the other two reading frames are dissimilar; (4) digestion of purified rat pancreatic amylase with phenylmethylsulphony fluoride (PMSF) treated carboxypeptidase A in the conditions described by Ambler[23] releases only leucine (data not shown), consistent with the carboxyl terminal dipeptide, Lys-Leu, predicted by the proposed coding sequence[24]; (5) the amino acid sequence is 76% homologous with the amino acid sequence of a number of unordered peptides that account for approximately 75% of the total sequence of porcine pancreatic amylase (provided by L. Paseno, B. Alandie, Y. Mazzei, D. Moinier, J. P. Bizzozero, M. Fougereau, Y. Chickeportiche and G. Marchis-Mouren). It is significant that porcine pancreatic amylase has a lower molecular weight than the rat enzyme by 3,000–5,000 (ref. 25) and has an isoelectric point of 5.4 (ref. 25), compared with 8.8–9.0 for rat pancreatic amylase[15]. Despite these differences the sequence homology between the two enzymes is high.

The amino-terminal portion of the predicted amino acid sequence for rat pancreatic amylase (Fig. 2) can be uniquely aligned with the partial amino-terminal sequence of rat parotid preamylase[26] so that seven of the nine identified residues in a region 27 residues long are congruent. This alignment suggests that the cDNA sequence lacks four-and-one-third codons or 13 coding nucleotides including the initial AUG but contains the carboxyl-terminal portion of the prepeptide. The entire coding region of rat pancreatic amylase mRNA is thus probably 1,551 nucleotides long, encoding 517 amino acids. The exact carboxyl terminus of the prepeptide, that is, the point of cleavage by a signal peptidase[27], cannot be located at this time because the amino terminus of the mature enzyme is acetylated and consequently has not been identified.

The single nucleotide discrepancy within the overlapping sequences of pcXP38 and pcXP100 (position 1,139) is silent with respect to the amino acid sequence since both of the alternative codons, AUA and AUU, specify Ile 379.

The length of the 5′-untranslated region, estimated to be 60±30 nucleotides, is within the range of other reported 5′-untranslated regions, that is, from 32 nucleotides in mouse β-globin mRNA[28] to greater than 112 nucleotides in the ACTH β-lipotropin mRNA[29]. In contrast, pancreatic amylase mRNA has a very short 3′-untranslated region relative to other eukaryotic mRNAs which have been characterized. The 3′-untranslated region of pancreatic amylase mRNA is only 35 nucleotides long whereas the reported lengths of 3′-untranslated regions in other mRNAs range from 57 nucleotides for rat insulin[30] mRNA to 950 nucleotides for mouse dihydrofolate reductase mRNA[31]. A short 3′-untranslated region is not a

```
    1                                   10
    leu leu ser leu ile gly phe cys trp ala gln tyr asp pro his
UG  CUG CUU UCC CUC AUU GGG UUC UGC UGG GCU CAA UAU GAC CCA CAC

                    20                                      30
thr ala asp gly arg thr ala ile val his leu phe glu trp arg trp
ACU GCG GAU GGG AGG ACU GCU AUU GUC CAC CUG UUC GAG UGG CGC UGG

                                    40
ala asp ile ala lys glu cys glu arg tyr leu ala pro lys gly phe
GCU GAU AUU GCC AAG GAA UGU GAG CGG UAC UUA GCA CCU AAG GGA UUU

        50                                      60
gly gly val gln val ser pro pro asn glu asn ile ile ile asn asn
GGA GGG GUG CAG GUC UCU CCA CCC AAU GAA AAU AUU AUA AUU AAU AAU

                        70
pro ser arg pro trp trp glu arg tyr gln pro ile ser tyr lys ile
CCA UCA AGG CCU UGG UGG GAA AGA UAU CAA CCA AUC AGC UAC AAA AUU

80                                      90
cys ser arg ser gly asn glu asn glu phe lys asp met val thr arg
UGC UCA AGG UCU GGA AAU GAA AAU GAA UUC AAA GAC AUG GUG ACG AGG

                100                                     110
cys asn asn val gly val arg ile tyr val asp ala val ile asn his
UGC AAC AAU GUU GGU GUC CGG AUU UAU GUG GAU GCU GUC AUU AAU CAC

                                    120
met cys gly ser gly asn ser ala gly thr his ser thr cys gly ser
AUG UGU GGC UCG GGC AAU AGU GCA GGA ACA CAC AGU ACC UGU GGA AGU

        130                                     140
tyr phe asn pro asn asn arg glu phe ser ala val pro tyr ser ala
UAC UUC AAU CCU AAU AAC AGG GAA UUC UCA GCA GUU CCA UAC UCU GCU

                        150
trp tyr phe asn asp asn lys cys asn gly glu ile asn asn tyr asn
UGG UAU UUU AAC GAU AAU AAA UGU AAU GGA GAA AUU AAU AAC UAC AAU

160                                     170
asp ala asn gln val arg asn cys arg leu ser gly leu leu asp leu
GAU GCC AAU CAG GUC AGA AAU UGU CGU CUG UCU GGC CUU CUG GAU CUU

                180                                     190
ala leu asp lys asp tyr val arg thr lys val ala asp tyr met asn
GCA CUC GAU AAA GAU UAU GUU CGA ACC AAG GUG GCU GAC UAU AUG AAC

                                    200
asn leu ile asp ile gly val ala gly phe arg leu asp ala ala lys
AAU CUC AUU GAC AUU GGU GUA GCA GGG UUC AGA CUU GAU GCU GCU AAG

        210                                     220
his met trp pro gly asp ile lys ala val leu asp lys leu his asn
CAC AUG UGG CCU GGA GAC AUA AAG GCA GUU UUG GAC AAA CUA CAU AAU

                        230
leu asn thr lys trp phe ser gln gly ser arg pro phe ile phe gln
CUA AAU ACA AAA UGG UUC UCC CAA GGA AGC AGA CCU UUC AUU UUC CAA

240                                     250
glu val ile asp leu gly gly glu ala ile lys gly ser glu tyr phe
GAG GUC AUU GAU CUU GGU GGU GAA GCA AUU AAA GGU AGU GAG UAC UUU

                260                                     270
gly asn gly arg val thr glu phe lys tyr gly ala lys leu gly thr
GGA AAU GGC CGC GUG ACA GAA UUC AAG UAU GGU GCA AAA CUU GGC ACA

                                    280
val ile arg lys trp asn gly glu lys met ser tyr leu lys asn trp
GUU AUU CGC AAA UGG AAU GGA GAG AAG AUG UCU UAC UUA AAG AAC UGG

        290                                     300
gly glu gly trp gly phe val pro thr asp arg ala leu val phe val
GGA GAA GGU UGG GGU UUU GUG CCU ACU GAC AGA GCC CUU GUG UUU GUG

                        310
asp asn his asp asn gln arg gly his gly ala gly gly ala ser ile
GAC AAC CAU GAC AAU CAG CGA GGA CAU GGU GCU GGA GGA GCA UCC AUC

320                                     330
leu thr phe trp asp ala arg met tyr lys met ala val gly phe met
CUG ACA UUC UGG GAU GCU AGA AUG UAU AAA AUG GCA GUU GGA UUU AUG

                340                                     350
leu ala his pro tyr gly phe thr arg val met ser ser tyr arg arg
UUG GCU CAU CCU UAU GGA UUC ACC AGA GUA AUG UCA AGU UAC CGA AGG

                                    360
thr arg asn phe gln asn gly lys asp val asn asp trp ile gly pro
ACA AGA AAU UUC CAG AAU GGA AAA GAU GUG AAU GAC UGG AUU GGA CCA

        370                                     380
pro asn asn asn gly val thr lys glu val thr ile asn pro asp thr
CCU AAU AAC AAU GGA GUA ACA AAA GAA GUG ACC AUU AAU CCA GAC ACU

                        390
thr cys gly asn asp trp val cys glu his arg trp arg gln ile arg
ACU UGU GGC AAU GAC UGG GUC UGU GAA CAU CGA UGG CGU CAA AUC AGG

400                                     410
asn met val ala phe arg asn val val asn gly gln pro phe ala asn
AAC AUG GUU GCC UUC AGG AAU GUA GUC AAC GGU CAG CCU UUU GCA AAC

                420                                     430
trp trp asp asn gly ser asn gln val ala phe ser arg gly asn arg
UGG UGG GAU AAU GGC AGC AAC CAA GUG GCU UUU AGC AGA GGA AAC AGA

                                    440
gly phe ile val phe asn asn asp asp trp ala leu ser ser thr leu
GGA UUC AUU GUC UUU AAC AAU GAU GAC UGG GCU UUG UCA AGC ACU CUA

        450                                     460
gln thr gly leu pro ala gly thr tyr cys asp val ile ser gly asp
CAG ACU GGU CUU CCU GCU GGC ACA UAC UGU GAU GUC AUU UCA GGA GAU

                        470
lys val asn gly asn cys thr gly leu lys val asn val gly ser asp
AAA GUC AAU GGC AAU UGC ACU GGA CUU AAA GUA AAU GUU GGC AGU GAU

480                                     490
gly lys ala his phe ser ile ser asn ser ala glu asp pro phe ile
GGC AAA GCU CAC UUC UCU AUU AGU AAC UCU GCU GAA GAC CCA UUC AUU

                500         503
ala ile his ala asp ser lys leu OC
GCA AUC CAU GCC GAC UCA AAG UUG UAA GAGUCAAAUUAAAGAGAUUUAGAUUCA

GCACCA
```

Fig. 2 The nucleotide sequence of rat pancreatic amylase mRNA. The sequence was determined from the double-stranded cDNA inserts of pcXP38 and pcXP100 (Fig. 1) by the method of Maxam and Gilbert[18]. The predicted amino acid sequence is indicated. The divergent heptanucleotide sequence AAUUAAA is underlined. The single nucleotide discrepancy between the double strands of pcXP38 and pcXP100 is circled.

general feature of mRNAs encoding the pancreatic secretory proteins because the 3′-untranslated region of proelastase mRNA is 289 nucleotides long[17]. The short 3′-untranslated region requires that functionally important sequences near the 3′ end of amylase mRNA be either less than 35 nucleotides or contained in the coding region. The heptanucleotide, AAUUAAA is present in this region centred 23 nucleotides from the poly(A). This sequence appears to be the first detected variant of the hexanucleotide sequence, AAUAAA, found approximately 20 nucleotides from the poly(A) in every polyadenylated RNA sequenced to date. The variation of this sequence probably reflects a flexibility in the sequence requirement at this site rather than a modulation of some aspect of the metabolism of exocrine mRNAs since the hexanucleotide, AAUAAA, is conserved in proelastase mRNA[17]. Interestingly, the heptanucleotide AAUUAAA has also recently been found in anglerfish pancreatic somatostatin mRNA[32].

Structural domains in amylase

Several experimental observations suggest that the amylase molecule is arranged in two similar domains. Mammalian amylase can bind two molecules of the substrates glycogen[33] and maltotriose[34] and at least two molecules of the substrate analogue β-cyclodextran[35]. An endogenous protease[36,37] cleaves amylase into two polypeptides of approximately equal size

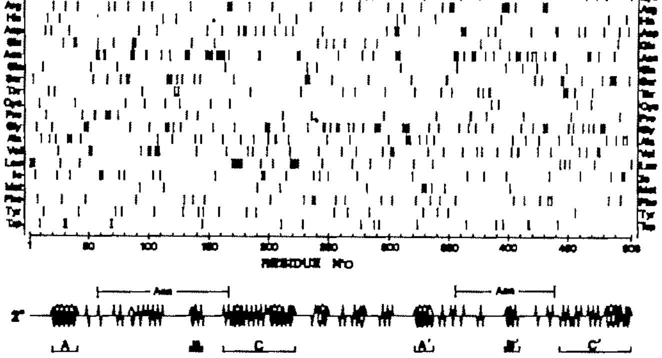

Fig. 3 The amino acid distribution and predicted secondary structure of amylase. Vertical bars indicate the sequence position of each amino-acid residue. Regions of α-helix (-▇-) and β-sheet (┼┼╫╫) were predicted using the methods of Garnier et al.[42] and Chou and Fasman[43]. The former method also predicts β-turns and random coil; however for clarity these have not been included.

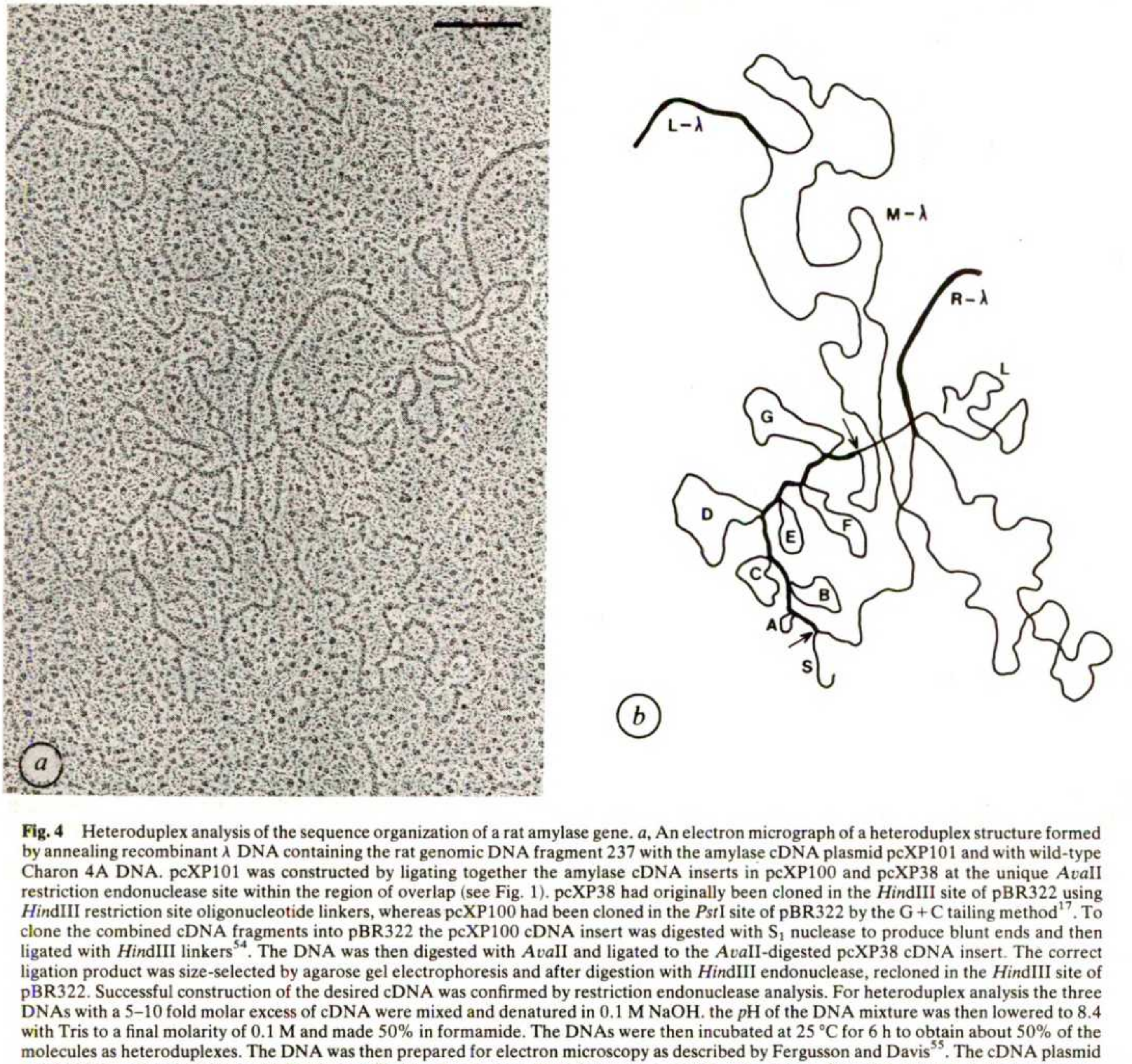

Fig. 4 Heteroduplex analysis of the sequence organization of a rat amylase gene. *a*, An electron micrograph of a heteroduplex structure formed by annealing recombinant λ DNA containing the rat genomic DNA fragment 237 with the amylase cDNA plasmid pcXP101 and with wild-type Charon 4A DNA. pcXP101 was constructed by ligating together the amylase cDNA inserts in pcXP100 and pcXP38 at the unique *Ava*II restriction endonuclease site within the region of overlap (see Fig. 1). pcXP38 had originally been cloned in the *Hin*dIII site of pBR322 using *Hin*dIII restriction site oligonucleotide linkers, whereas pcXP100 had been cloned in the *Pst*I site of pBR322 by the G + C tailing method[17]. To clone the combined cDNA fragments into pBR322 the pcXP100 cDNA insert was digested with S_1 nuclease to produce blunt ends and then ligated with *Hin*dIII linkers[54]. The DNA was then digested with *Ava*II and ligated to the *Ava*II-digested pcXP38 cDNA insert. The correct ligation product was size-selected by agarose gel electrophoresis and after digestion with *Hin*dIII endonuclease, recloned in the *Hin*dIII site of pBR322. Successful construction of the desired cDNA was confirmed by restriction endonuclease analysis. For heteroduplex analysis the three DNAs with a 5–10 fold molar excess of cDNA were mixed and denatured in 0.1 M NaOH. the *p*H of the DNA mixture was then lowered to 8.4 with Tris to a final molarity of 0.1 M and made 50% in formamide. The DNAs were then incubated at 25 °C for 6 h to obtain about 50% of the molecules as heteroduplexes. The DNA was then prepared for electron microscopy as described by Fergusson and Davis[55]. The cDNA plasmid pcXP101 as well as the Charon 4A DNA arms flanking the genomic DNA insert were used as size markers. Scale bar, 0.2 μm. *b*, An interpretive drawing of the heteroduplex structure in *a*. Intervening sequences are designated A–G in the direction of transcription of the gene. Arrows delimit the region of homology between the genomic fragment and the cDNA. Single-stranded DNA tails present at the ends of the gene sequences marked S and L represent the short and long tails of pBR322, respectively. The double-stranded DNAs situated at the ends of the heteroduplex structures marked L-λ and R-λ represent the left and right arms of Charon 4A DNA, respectively, and M-λ represents the middle region of the wild-type Charon 4A DNA.

which exhibit undiminished enzyme activity and nearly identical tryptic peptide maps. Hydrodynamic and low angle X-ray scattering measurements[38] as well as preliminary X-ray crystallographic data[39,40] indicate a molecule consisting of two similar but non-identical lobes separated by a cleft. Although in need of confirmation by X-ray crystallography, significant structural homology between the halves of the proposed amino acid sequence (divided between residues 270 and 271) is suggested by comparison of the halves of the sequence according to the method of McLachlan[41] and by the secondary structure predicted from the proposed sequence according to the methods of Garnier *et al.*[42] and Chou and Fasman (ref. 43 and Fig. 3). Predicted regions of α-helix and β-sheet designated A, B and C (Fig. 3) in the amino-terminal half of the sequence are repeated as similar but non-identical regions A′, B′ and C′ in the carboxyl-terminal half. Asparagine-rich clusters are present in each half and are located symmetrically between regions A and C and A′ and C′. A Pro-Pro sequence is present in each half of the sequence (positions 54–55 and 367–368) located similarly with respect to regions A and A′. A glycine-rich region (21% glycine residues extending from position 245 to 316) separates the two putative domains. The sequence Arg-Lys is present at positions 274 and 275 in the approximate middle of the molecule, and may correspond to the protease-hypersensitive site observed by Robyt *et al.*[36].

A comparison of the two putative domains reveals no significant sequence homology between these regions at either the amino acid or nucleotide level. Conservation of intramolecular structural homology despite retention of little or no amino acid sequence homology has been observed in penicillopepsin[44] and rhodanese[45]. In view of the lack of nucleotide sequence homology between the putative domains the origin of the two domain structure, which could be via fusion of tandemly duplicated primordial genes[46], remains an open question.

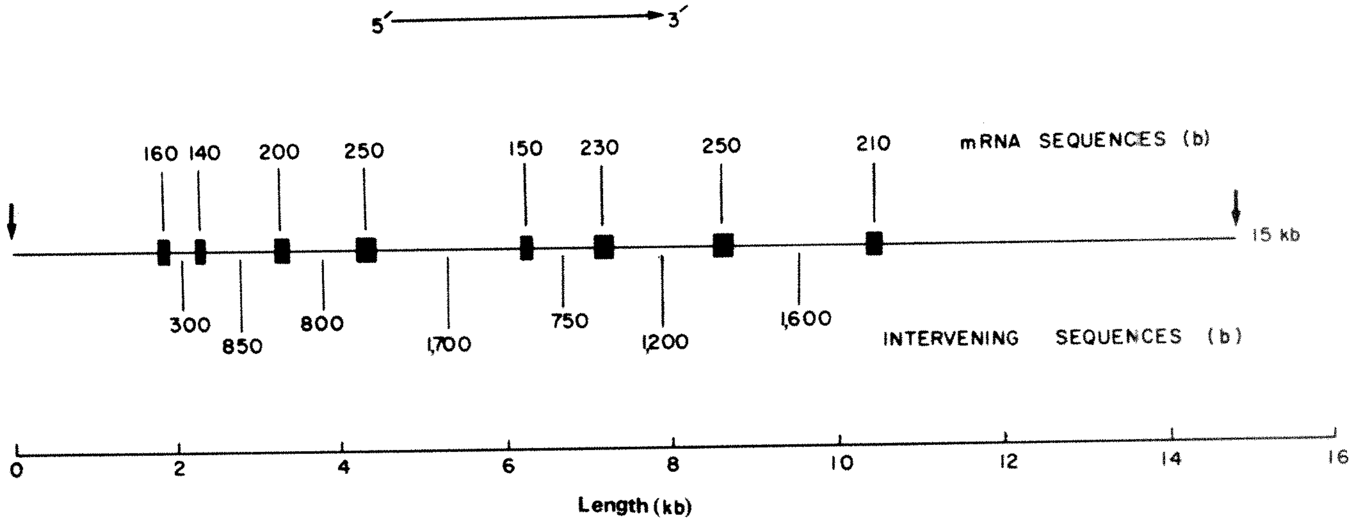

Fig. 5 A schematic representation of the organization of amylase gene sequences in the genomic DNA fragment 237. The lengths of the mRNA (cDNA) and intervening sequences are mean values derived from measurements of at least four heteroduplex structures. Standard deviations range from ±5% for the larger to ±20% for the smallest measurements. λ Charon 4A DNA sequences are not shown here and the arrows indicate the ends of the genomic fragment. kb, kilobases.

Amylase gene structure

Using the cDNA inserts of pcXP100 and pcXP38 as probes, we have screened a rat genomic DNA-lambda Charon 4A DNA library (provided by T. Sargent, R. B. Wallace and J. Bonner[47]) for phage containing rat amylase gene sequences by the method of Benton and Davis[48]. Thirty-nine positive recombinant phage were obtained from 2×10^6 plaques and were subsequently purified and analysed.

The organization of amylase gene sequences within these fragments was determined by restriction endonuclease analysis and electron microscopic examination of heteroduplexes formed by annealing the DNA of the recombinant phage with the amylase cDNA plasmid designated pcXP101. This plasmid was constructed by joining the cDNA inserts in pcXP100 and pcXP38 at a common, unique restriction endonuclease site as detailed in the legend to Fig. 4. The combined cDNA was recloned in pBR322 and its 5′ to 3′ orientation within the plasmid was determined by restriction endonuclease analysis. On digestion of pcXP101 with *Sal*I, a linear molecule with a short strand of pBR322 sequences (0.6 kilobase pairs) at the 5′ end and a long strand (3.7 kilobase pairs) at the 3′ end of the cDNA insert is formed. Amylase genomic sequences could then be orientated after hybridization to this probe by measuring the pBR322 tails present at the ends of the genomic DNA·cDNA hybrid. Wild-type Charon 4A DNA was also included in the heteroduplex mixture to delimit the left and right λ arms which flank the genomic DNA fragments. Genomic sequences flanking the amylase gene sequences could then be identified.

The 39 positive fragments obtained from the library appear to represent nine distinct amylase genes. However, the overall sequence organization as determined by heteroduplex analysis suggests that these genes are all related to a common amylase gene motif. Figure 4*a* and *b* show, respectively, an electron micrograph and the corresponding interpretative drawing of a heteroduplex structure of a gene which exhibits the structural features found in the other gene fragments. This genomic fragment contains cDNA sequences that are interrupted by seven detectable intervening sequences; 5′ and 3′ flanking regions are also present. Estimates of the lengths of these regions are given in Fig. 5. Amylase cDNA sequences are present within a region of 9 kilobases and range in length from approximately 140 to 250 bases. The correspondence of the aggregate lengths of these sequences (1,600 ± 100 bases) with the length of the cDNA probe (1,547 bases), suggests that the entire length of the cDNA is hybridized to the genomic fragment in the heteroduplex. The lengths of the intervening sequences range from approximately 300 to 1,700 bases. Flanking regions extend 2 and 4 kilobases from the 5′ and 3′ ends, respectively, of the amylase gene sequence. We emphasize that the present experiments do not detect sequences at the extreme 5′ end of the mRNA since these sequences are missing in the cDNA probe; intervening sequences have been observed in this region in a number of eukaryotic genes[20,49–53]. Since the 5′ flanking region is 2 kilobases long it is likely that sequences corresponding to the 5′ end of the mRNA are present in this genomic fragment. More extensive 5′ flanking regions, up to 12 kilobases long, are present in other genomic fragments. A sequence analysis of this region should prove useful in analysing tissue-specific gene expression.

Since the library used for this analysis was constructed from a single rat[47], the nine cloned amylase sequences must represent at least five non-allelic genes or pseudogenes. In fact, the nine sequences can be arranged into four closely related pairs by the patterns of restriction endonuclease digestion. With this isolation and characterization of the cDNA and genes it is now possible to envisage a more penetrating analysis of their selective expression in various differentiated cells.

We thank William Nikovits for helping with the electron microscopy, Drs Robert Fletterick and David Agard for help in analysing the proposed amino acid sequence of amylase, Dr G. H. Swift for critical discussions and help with DNA sequencing, Dr H Martinez for computer programs for DNA sequence analysis, Drs T. Sargent, R. B. Wallace and J. Bonner for supplying the recominant DNA library of rat nuclear DNA, Dr G. Marchis-Mouren for sending us the partial amino acid sequence of pig pancreatic amylase, and Dr H. Boyer and F. Blattner for providing the cloning vectors pBR322 and λ Charon 4A, respectively. This research was funded by NIH grant AM21344.

Received 16 June; accepted 17 July 1980.

1. Sanders, T. G. thesis, Univ. Illinois (1970).
2. Loyter, A. & Schramm, M. *Biochim. biophys. Acta* **65,** 200 (1962).
3. Arnold, M. & Rutter, W. J. *J. biol. Chem.* **238,** 2760–2765 (1963).
4. Rutter, W. J., Wessells, N. K. & Grobstein, C. *Natn. Cancer Inst. Monogr.* **13,** 51–65 (1964).
5. Kemp, J. D., Walther, B. T. & Rutter, W. J. *J. biol. Chem.* **247,** 3941–3952 (1972).
6. Sanders, T. G. & Rutter, W. J. *J. biol. Chem.* **249,** 3500–3509 (1974).
7. Van Nest, G. A., MacDonald, R. J., Raman, R. K. & Rutter, W. J. *J. Cell Biol.* (in the press).
8. Harding, J. D. *et al. J. biol. Chem.* **252,** 7391–7397 (1977).
9. Przbyla, A. E., MacDonald, R. J., Harding, J. D., Pictet, R. L. & Rutter, W. J. *J. biol. Chem.* **254,** 2154–2159 (1979).
10. Rutter, W. J., Ball, W. D., Bradshaw, W. S., Clark, W. R. & Sanders, T. G. in *Secretory Mechanisms of Salivary Glands* (eds Schneyer, L. H. & Schneyer, C. A.) 238–253 (Academic, New York, 1967).
11. Palla, J. C., Abdeljlil, A. B. & Desnuelle, P. *Biochim. biophys. Acta* **158,** 25–35 (1968).
12. Rall, L. B., Pictet, R., Githens, S. & Rutter, W. J. *J. Cell Biol.* **75,** 398–409 (1977).
13. Harding, J. D. & Rutter, W. J. *J. biol. Chem.* **253,** 8736–8740 (1978).
14. Malacinski, G. M. & Rutter, W. J. *Biochemistry* **8,** 4382–4390 (1969).
15. Sanders, T. G. & Rutter, W. J. *Biochemistry* **11,** 130–136 (1972).
16. McGeachin, R. L. & Reynolds, J. M. *J. biol. Chem.* **234,** 1456–1400 (1959); *Biochim. biophys. Acta* **39,** 531–500 (1960).

17. MacDonald, R. J. *et al.* (in preparation).
18. Maxam, A. & Gilbert, W. *Proc. natn. Acad. Sci. U.S.A.* **74,** 560–564 (1977).
19. Bailey, J. M. & Davidson, N. *Analyt. Biochem.* **70,** 75–85 (1976).
20. Lomedico, P. *et al. Cell* **18,** 545–558 (1979).
21. Vandermeers, A. & Christophe, J. *Biochim. biophys. Acta* **154,** 110–129 (1968).
22. Dayhoff, M. O., Hunt, L. T. & Hurst-Calderone, S. in *Atlas of Protein Sequence and Structure* Vol. 5, Suppl. 3 (ed. Dayhoff, M. O.) 363 (National Biomedical Research Foundation, Washington DC, 1978).
23. Ambler, R. P. *Meth. Enzym.* **25,** 262–272 (1972).
24. Petra, D. H. *Meth. Enzym.* **19,** 460–503 (1970).
25. Cozzone, P., Pasero, L., Beaupoil, B. & Marchis-Mouren, G. *Biochim. biophys. Acta* **207,** 490–504 (1970).
26. Gorecki, M. & Zeelon, E. P. *J. biol. Chem.* **254,** 525–529 (1979).
27. Blobel, G. & Dobberstein, B. *J. Cell Biol.* **67,** 835–851 (1975).
28. Baralle, F. E. & Borwnlee, G. G. *Nature* **274,** 84–87 (1978).
29. Nakanishi, S. *et al. Nature* **278,** 423–427 (1979).
30. Ullrich, A. *et al. Science* **196,** 1313–1319 (1977).
31. Nunberg, J. H., Kaufman, R. J., Chang, A. C. Y., Cohen, S. N. & Schimke, R. T. *Cell* **19,** 355–364 (1980).
32. Hobart, P., Crawford, R., Shen, L.-P., Pictet, R. & Rutter, W. J. *Nature* (in the press).
33. Levitzki, A., Heller, J. & Schramm, M. *Biochim. biophys. Acta* **81,** 101–107 (1964).
34. Loyter, A. & Schramm, M. *J. biol. Chem.* **241,** 2611–2617 (1966).
35. Mora, S., Simon, I. & Elodi, P. *Molec. Cell Biochem.* **4,** 205–209 (1974).
36. Robyt, J. F., Chittenden, C. G. & Lee, C. T. *Archs. Biochem. Biophys.* **144,** 160–167 (1971).
37. Lehrner, L. N. & Malacinski, G. M. in *Isozymes* Vol. 4 (ed. Market, C. L.) 727–743 (Academic, New York, 1975).
38. Simon, I., Mora, S. & Elodi, P. *Molec. Cell Biochem.* **4,** 211–216 (1974).
39. Fitzgerald, P. M. D., Stankiewicz, P. J., Smith, S. C. & McPherson, A. *J. molec. Biol.* **135,** 753–756 (1979).
40. Payan, F., Haser, R., Pierrot, M., Frey, M. & Astier, J. P. *Acta crystallogr.* **B36,** 416–421 (1980).
41. McLachlan, A. D. *J. molec. Biol.* **61,** 409–424 (1971).
42. Garnier, J., Osguthorpe, D. J. & Robson, B. *J. molec. Biol.* **120,** 97–120 (1978).
43. Chou, P. Y. & Fasman, G. D. *Biochemistry* **13,** 222–245 (1974).
44. Tang, J., James, M. N. G., Hsu, I. N., Jenkins, J. A. & Blundell, T. L. *Nature* **271,** 618–721 (1978).
45. Ploegman, J. H., Drent, G., Kalk, K. H. & Hel, W. G. J. *J. molec. Biol.* **123,** 557–594 (1978).
46. McLachlan, A. D. *J. molec. Biol.* **128,** 49–79 (1979).
47. Sargent, T. D. *et al. Proc. natn. Acad. Sci. U.S.A.* **76,** 3256–3260 (1979).
48. Benton, W. D. & Davis, R. W. *Science* **196,** 180–182 (1977).
49. Breathnach, R., Benoist, C., O'Hare, K., Gannon, F. & Chambon, P. *Proc. natn. Acad. Sci. U.S.A.* **75,** 4853–4857 (1978).
50. Dugaiczyk, A. *et al. Nature* **274,** 328–333 (1978).
51. Cordell, B. *et al. Cell* **18,** 533–543 (1979).
52. Bell, G. I. *et al. Nature* **284,** 26–32 (1980).
53. Tsujimoto, Y. & Suzuki, Y. *Cell* **18,** 591–600 (1979).
54. Goodman, H. M. & MacDonald, R. J. *Meth. Enzym.* **68,** 75–79 (1979).
55. Fergusson, J. & Davis, R. W. in *Advanced Techniques in Biological Electron Microscopy* (ed. Koehler, J. K.) 123–171 (Springer, Berlin, 1978).

LETTERS

Origin of the 5 March 1979 γ-ray transient: a vibrating neutron star

R. Ramaty, S. Bonazzola, T. L. Cline, D. Kazanas & P. Mészáros*

Laboratory for High Energy Astrophysics, NASA/Goddard Space Flight Center, Greenbelt, Maryland 20771

R. E. Lingenfelter

Physics Department and Center for Astrophysics and Space Sciences, University of California, San Diego, La Jolla, California 92093

An unusual γ-ray transient was observed on 5 March 1979, with 12 different instruments on 9 different spacecraft[1–4]. Most of these instruments are incorporated into an interplanetary γ-ray burst network. The source position of the 5 March transient, determined by this network to an accuracy[4] of $\sim 1\times 2$ arc min, is consistent with the direction of the supernova remnant N49 in the Large Magellanic Cloud (LMC). Subsequent analysis[5] of the data, by narrowing the source error box to an area of about 6 by 30 arc s inside the supernova remnant, considerably strengthens this identification. We propose that a vibrating neutron star in the LMC is the source of the 5 March transient. This may be both the first detection of a vibrating neutron star and indirect evidence for gravitation radiation.

In addition to its identification, the 5 March transient has several unique characteristics that set it apart[3,6] from the general class of γ-ray bursts: the peak flux of $\sim 10^{-3}$ erg cm^{-2} s^{-1} in the impulsive phase of the event is an order of magnitude greater than that of any other γ-ray burst. At the distance of the LMC (55 kpc), this implies a luminosity of $\sim 3\times 10^{44}$ erg s^{-1}. The duration of the impulsive phase, $\sim$0.15 s, is also shorter than that of most γ-ray bursts which last for several seconds. The 5 March impulsive energy release, $\sim 5\times 10^{43}$ erg, would thus be larger by more than five orders of magnitude than typical γ-ray burst energies, whose probable galactic origin[7] requires energy releases of only $\sim 10^{38}$ erg.

The exceedingly short rise time of this impulsive phase, $<2\times 10^{-4}$ s, suggests that the size of the emission region does not exceed $\sim$60 km, the light travel distance for this time. That the source may in fact be a neutron star is implied by the energy spectrum[1] of the impulsive phase (Fig. 1) which shows a broad feature centred at $\sim$0.4–0.43 MeV probably due to the gravitational redshift of 0.511 MeV electron–positron annihilation radiation. This radiation should be produced close to the surface of a neutron star with $z=(1-2GM/Rc^2)^{-1/2}-1\cong 0.19$ to 0.28 where M and R are the mass and radius of the star. Similar redshifts have been reported for at least one other γ-ray burst[8,9] and longer duration γ-ray transients[10,11].

A neutron star origin for the 5 March event is also suggested by the observed[1–3] pulsations which follow the impulsive phase for at least 3 min. The pulse period is 8.0 ± 0.05 s, and the average pulsed flux, $\sim 10^{-5}$ erg cm^{-2} s^{-1}, decreases exponentially with a characteristic time of $\sim$50 s. These pulsations could be due to rotation, although the period seems to be too long for a young ($\lesssim 10^4$ yr) neutron star in N49. Such pulsations have not been seen from any other γ-ray burst. The 5 March transient was also followed by three other outbursts[9], apparently from the same source direction, on 6 March, 4 April and 24 April. The peak intensities of these outbursts, however, were much lower than that of the 5 March event, and decreased with each burst.

The energy spectrum of the 5 March event is much softer than that of typical[12] γ-ray bursts. In fact, the bulk of the emission of the 5 March event is in the lower energy ($\lesssim 0.2$ MeV) part of the spectrum which is significantly steeper than that of other γ-ray bursts[13,14] in this energy range.

Although the burst source position strongly suggests association with N49, there are several problems if the source were a neutron star in the LMC. These concern the origin and rapid release of the observed energy, and the very high efficiency of the radiation mechanism. The required mechanism apparently violates the black-body limit in that it must provide a very large luminosity at relatively low photon energies from a small emitting area. Indeed, several authors, using arguments based on the Eddington limit for accretion models[1], on the opacity of γ rays to Compton scattering and pair production[15,16], and on the slow diffusion of photons to the neutron star surface[17], have concluded that the source of the 5 March transient should be closer than a few hundred parsec.

Here we consider that the source of the 5 March transient is in the LMC, based on the rather convincing positional identification with N49. The arguments against an LMC origin based on radiation mechanisms are removed by the e^+–e^- synchrotron cooling and annihilation model presented elsewhere[18] and briefly discussed here. Regarding the energy source, its very large magnitude requires that it be interior to the star, most likely of gravitational origin. The transport of this energy cannot be by photon diffusion. We propose instead that

---

* Permanent address: Max Planck Institute for Astrophysics, Garching, FRG.

0028–0836/80/370122—03$01.00

neutron star vibrations could, in a coherent and rapid fashion, communicate the internal energy to the upper crust and atmosphere. Decay of these vibrations by gravitational radiation[19] would then account for the duration of the impulsive phase, ~0.15 s. An LMC origin for the 5 March transient is not in conflict[6,20] with a galactic origin for the more common γ-ray bursts, as these probably belong to a different class of transients than does the 5 March event.

The basic source of energy in the 5 March transient is not clear, but it could be gravitational energy released by a phase transition[21] in the interior. In this case, the energy should be communicated to the surface in a time comparable to the sound-wave crossing time through the neutron star. As the speed of sound in neutron star matter is[22] of the order c, this time is less than the upper limit in the rise time of the burst. The released gravitational energy could be much larger than observed in γ rays, but the bulk of this energy is not expected to be emitted as electromagnetic radiation. A large fraction of the released energy could in fact be in vibrations[22], $E_{\text{vib}} \cong 10^{53}$ erg $(\delta R/R)^2$, where δR is the vibrational amplitude. For example, if $\delta R/R \sim 10^{-3}$, $E_{\text{vib}} \sim 10^{47}$ erg, in which case conversion of only a small fraction (10^{-3}) of this energy into γ rays would be sufficient to account for the observations.

The strong magnetic fields that are tied to the neutron star play an important part in this conversion. As these fields oscillate together with the surface, they should produce wave motions which would accelerate particles in the atmosphere. In particular, the bulk motions may be converted into magnetoacoustic waves, the high frequency portions of which dissipate in the atmosphere and heat it. Because of the relatively small number of ambient atmospheric particles, this heating would rapidly raise the temperature to a value ($\lesssim 10^9$K) at which e^+-e^- pair production sets in. Further heating increases the radiation density, and the atmosphere becomes radiation dominated. In this case, the density of pairs which coexist with the radiation greatly exceeds that of the ambient matter. As this hot pair plasma attempts to escape from the neutron star, it pushes the magnetic field outwards. But the field, being tied to the star, is compressed, and in the resulting strong field regions the pairs are rapidly cooled by synchrotron radiation.

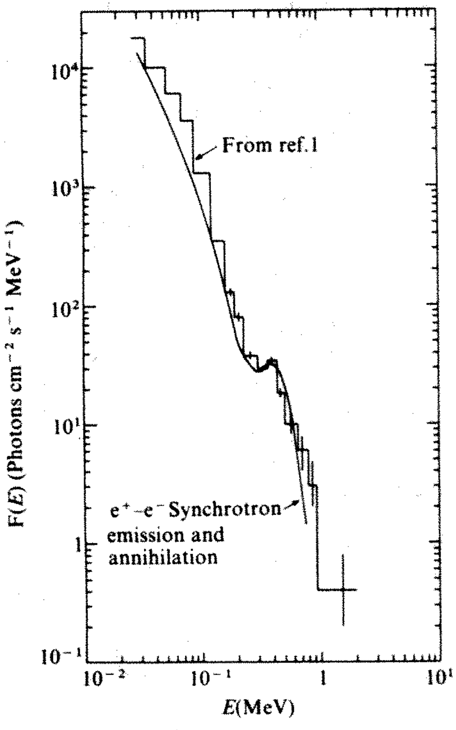

Fig. 1 Energy spectrum of the impulsive phase of the 5 March transient measured[1] during the first 4 s of the event. The photon flux of the impulsive phase is larger than that shown in the figure by a factor of 4/0.15, where 0.15 s is the duration of the impulsive phase. The curve is the calculated[18] spectrum in the e^+-e^- synchrotron cooling and annihilation model.

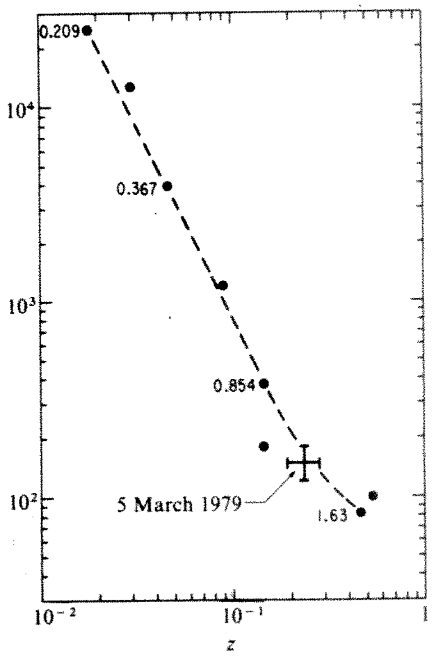

Fig. 2 The calculated[26] (●) quadrupole gravitational radiation damping time versus gravitational redshift for neutron stars. The dashed curve connects cases having the same equation of state and the numerical values are neutron star masses in units of $M_\odot$. The datum point is from γ-ray observations of the 5 March transient[1-3].

The e^+-e^- synchrotron cooling and annihilation model[18], which we now briefly describe, can account (see Fig. 1) for the observed impulsive spectrum. The essential feature of this model is the radiation dominated e^+-e^- pair plasma. Even though its annihilation time is very short ($\sim 10^{-12}$s for the parameters[18] of the 5 March transient), this plasma can maintain itself because the annihilation photons have enough energy to produce new pairs. The energy spectrum of the coexisting radiation, however, is much harder than the observed spectrum. But in regions of strong magnetic field, the pairs can lose their kinetic energies before they annihilate and this converts the hot (~MeV) photon-pair plasma into cooler radiation (~tens of keV) that is devoid of pairs. This conversion takes place in a layer whose thickness does not exceed the photon–photon pair production mean free path. This outer skin layer is also the effective radiating volume of the star. The magnetic field, the pair density and the thickness of the layer are $\gtrsim 10^{11}$ G, $\sim 2 \times 10^{26}$cm^{-3}, and 0.1 mm, respectively[18]. The curve in Fig. 1 is the calculated[18] spectrum produced in the layer: the low energy part ($\gtrsim 0.2$ MeV) is the synchrotron radiation of the pairs, while the high energy part is their annihilation radiation.

The stability and confinement of the radiating layer is an essential requirement of the model, because its absence would lead to relativistic outward expansion that would result in blueshifted radiation rather than the redshifted emission needed to account for the observations. We believe that the magnetic field does play a major role in the confinement, as the energy density in the field is at least as large as that of the e^+-e^- plasma. In particular, confinement may be achieved in the highly compressed magnetic field ahead of the pair plasma. The positive (outward) gradient of the field should exert an inward confining force on the plasma. Possible instabilities, such as the exchange instability, and a radiation-pressure driven Rayleigh–Taylor instability, may be stabilized by the continuous transformation of particles into photons and vice versa, as well as by the strongly sheared field.

The conversion of the neutron star vibrational energy into γ rays should go on as long as the star continues to vibrate. The principal damping mechanism of the vibrations should be gravitational radiation[19]. Neutrino emission[23] is an important damping mechanism only for very young hot neutron stars, while viscous effects (the Urca process and a process[24] involving Σ^- hyperons) are slower[22] than gravitational radiation damping. Escaping shock waves can also damp the vibrations[22], but the loss rate due to shocks should not exceed the observed electromagnetic emission which in our model constitutes only a small fraction of the vibrational energy.

Gravitational radiation is expected to damp the quadrupole and higher mode vibrations on time scales ranging from about 0.1 to 10 s, depending on the properties of the neutron star[25,26]. Using the calculations of Detweiler[26], we plot in Fig. 2 the damping time τ as a function of redshift z, where the dashed curve connects points obtained from the same equation of state. The numerical values next to these points are the corresponding neutron star masses in units of $M_\odot$. The 5 March 1979 datum point shows the observed[1–3] duration of the impulsive phase (120–180 ms) versus the approximate redshift[1]. The implied neutron star mass is ~1–1.3 $M_\odot$, its radius ~10 km, and its quadrupole vibrational frequency ~0.4 ms. The sensitivities of the present gravitational wave detectors were insufficient to observe the expected gravitational radiation (J. A. Tyson, personal communication), and the time resolution of the γ-ray instruments were insufficient to resolve the expected vibrational period in the impulsive emission.

Although gravitational radiation is very effective in damping the quadrupole and higher mode vibrations, it will damp the radial oscillations more slowly[19,22]. The Σ^- process[24], however, could damp the radial vibrations on a time scale of ~50 s, the characteristic decay time of the pulsed phase of the 5 March transient. Thus, the energy source for this phase as well could be neutron star vibrations. The observations would, therefore, imply that the γ-ray luminosity produced by the radial oscillations is smaller than that of the higher modes. This could result from asymmetric excitation of the vibrations which would put more energy into nonradial vibrations. Also, due to its small scale height, the atmsphere is expected to couple better with the higher modes than with radial oscillations. The 8-s period of the pulsed emission, however, is not likely to be a vibrational period. It may be caused by the rotation of the neutron star, although neutron star precession is an alternative explanation (K. Brecher, personal communication). The subsequent weaker bursts, which seem to come from the same source on 6 March, 4 and 24 April, may be aftershocks of the 5 March burst if it indeed results from a major quake in the neutron star interior.

There are, of course, several unresolved aspects of the model that clearly need further study. These include the more precise description of the source of energy of the burst, the nature and efficiency of vibrational heating, the stability of the thin emission region, and the origin of the 8-s pulsed emission. The present general outline of a model for the 5 March transient can account for both the enormous luminosity and the complex temporal and spectral features of the burst by emission form a neutron star in the LMC.

D. K. is an NAS/NRC resident research associate; P. M. was supported by NASA grant NGR 21-002-316; R. E. L. was supported by NSF grant AST79-11987.

Recieved 18 April, accepted 15 July 1980

1 Mazets, E. P, Golenetskii, S V, Il'inskii, V. N, Aptekar', R L & Guryan, Yu A *Nature* **282**, 587–489 (1979).
2 Barat, S. *et al* *Astr Astrophys* **79**, L24–L25 (1979).
3 Cline, T L. *et al* *Astrophys J Lett* **237**, L1–L6 (1980)
4. Evans, W D *et al. Astrophys J Lett* **237**, L7–L10 (1980)
5 Cline, T L. *et al* *Bull Am phys. Soc* **25**, 527–527 (1980).
6 Cline, T L *Comments Astrophys.* (in the press)
7 Fishman, G J, Meegan, C. A, Watts, J W. Jr & Derrickson, J. H *Astrophys. J. Lett* **223**, L13–L15 (1978)
8 Teegarden, B J. & Cline, T. L *Astrophys. J Lett* **236**, L67–xxx (1980)
9. Mazets, E. P & Golenetskii, S. V. *Astrophys. Space Sci* (in the press)
10. Jacobson, A S, Ling, J C, Mahoney, W A. & Willett, J. B. *Gamma Ray Spectroscopy in Astrophysics* (eds Cline, T. L & Ramaty, R) 228–251 (NASA TM79619, 1978).
11 Leventhal, M, MacCallum, J C & Watts, A C. *Astrophys J* **216**, 491–502 (1977)
12 Cline, T. L & Desai, U D. *Astrophys J. Lett* **196**, L43–L46 (1975)
13. Wheaton, W A *et al* *Astrophys. J. Lett* **186**, L57–L61 (1973)
14 Metzger, A E., Parker, R. H., Gilman, D, Peterson, L. E. & Trombka, J I *Astrophys J Lett* **194**, L19–L25 (1974)
15. Helfand, D. J. & Long, K S *Nature* **282**, 589–591 (1979).
16 Aharonian, F A & Ozernoy, L. M *Astronomicheskii tsirkulyar* No 1072, 1–4 (1979).
17 Petschek, A G & Colvin, J D. Preprint (Los Alamos Scientific Laboratories, 1979)
18. Ramaty, R, Lingenfelter, R E. & Bussard, R W *Astrophys. Space Science* (in the press).
19 Wheeler, J A *A Rev. Astr. Astrophys* **4**, 393–432 (1966)
20 Cline, T. L, Desai, U D & Teegarden, B J *Astrophys Space Sci* (in the press).
21 Hartle, J B., Sawyer, R F & Scalapino, D J *Astrophys J.* **199**, 471–481 (1975).
22 Zeldovich, Ya B & Novikov, I. D *Relativistic Astrophysics* Vol 1, (University of Chicago Press, 1971)
23 Kazanas, D & Schramm, D N *Astrophys. J* **214**, 819–825 (1977)
24 Langer, W D & Cameron, A G W. *Astrophys Space Sci* **5**, 213–253 (1969)
25. Thorne, K S *Astrophys J.* **158**, 1–16 (1969)
26. Detweiler, S. L *Astrophys J* **197**, 203–217 (1975).

Low energy γ rays from PSR1822−09

P. Mandrou & G. Vedrenne

Centre d'Etude Spatiale des Rayonnements–CNRS–UPS BP 4346,
31029 Toulouse Cedex, France

J. L. Masnou

CEA, CEN–SEP Saclay BP 2, 91190 Gif sur Yvette, France

Pulsed γ-ray emission in the MeV range (80 keV–6 MeV) has been clearly established[1–4] for the Crab pulsar PSR0531+21 ($P = 33$ ms). The energy spectrum of the pulsed component follows a power law from the X-ray (100 keV) to the high energy γ-ray range (2. GeV) with an index close to 2.1 (ref. 5). Positive detection of pulsed γ ray emission from the Vela pulsar PSR0833−45 ($P = 89$ ms) has been claimed in the 10–30 MeV region by Albats *et al.*[6], and clearly established[6] in the high energy range 50 MeV–3 GeV with a power law index of 1.9. This pulsar was also observed in the X-ray range but with apparently conflicting results (ref. 7 and refs therein), some authors reporting positive detection while other have upper limits below the reported values. Other radio pulsars, especially PSR1822−09, and PSR1747−46 have been investigated at energies above ~50 MeV by the satellites SAS 2[8,9] and COS B[10]. We report here observations of PSR1822−09 ($P = 769$ ms) between 80 keV and 6 MeV at balloon altitudes.

The equipment used, which is described in detail elsewhere[11], consisted of a 10-cm diameter CsI(Tl) crystal (78.5-cm^2 area), 2.5-cm thick, shielded against background by an active NaI(Tl) well 5-cm thick and 8-cm high blocked off at the bottom by 2 NaI(Tl) disks, a total of 10-cm thick whose diameters were the same as the outside diameter of the well (20 cm). The detector field of view, defined by the anticoincidence well, is a cone of half angle 45°. A plastic scintillator 0.5-cm thick was placed against the CsI(Tl) detector to block out charged particles entering the aperture. In the absence of an anticoincidence signal, the CsI(Tl) pulses were analysed by two 128 channel ADCs[12] covering the energy ranges of 80–1,126 keV and 1.5–6 MeV. All events detected during the flight were dated with a ground based clock to within 0.1 ms. The stability of the datation process was checked using a simultaneous recording of a 10^5 Hz oscillator. Gain variations, checked in flight by the observation of the atmospheric 511-keV line, are <1%.

The response of the detector in both energy and angle with respect to the viewing axis was determined in the laboratory using 14 calibrated radioactive sources whose energies covered the range 80 keV–8 MeV. This calibration gives a response matrix for the detector which is used to find the incident photon spectrum using the detected electron spectrum[13].

The telescope, mounted vertically, was launched from Guaratinguetà, Brazil (latitude 22°48′ S, rigidity 11.7 GV) on 12 February 1977. During this flight, which lasted 5 h at a ceiling altitude of 2.4 g cm^{-2}, the galactic disk was observed[14]. As the pulsar PSR1822−09 was also in the field of view, the data were analysed to see whether the pulsar signature could be detected.

We have divided the data into three energy intervals. The pulsar light curve in each energy range, was constructed by folding the data, consisting of all the events, modulo the

0028–0836/80/370124—03$01 00

apparent period, into 10 phase bins, each event being placed in one of the bins as a function of its arrival time. The apparent period was found from the radio values of P and $\dot{P}$ given by Taylor and Manchester[15] after extrapolation to the date of the flight (JD = 2443187.0), and correction for the Doppler effect due to the movement of the Earth; the source was taken to be at the right ascension given by Manchester *et al.*[16] and the declination given by Taylor and Manchester[15]. Only the data taken between zenith angles 13° and 33° were used, which correspond to times between 10:45 and 14:00 UT; the effective exposure at 1 MeV was 3.9×10^5 cm^2 s^{-1}.

Figure 1 shows the light curve obtained between 454 and 1,126 keV. The χ^2 value for this distribution is 16 for 9 d.f., corresponding to a probability $P(\chi^2 \geq 16)$ of 0.07. A Monte Carlo simulation was used to evaluate the overall probability resulting from the three phase histograms obtained using the energy ranges: 80–454 keV ($P = 0.4$); 454–1,126 keV ($P = 0.07$); and 1.5–6 MeV ($P = 0.15$). An overall probability of <1% was obtained. The light curve in the energy range 454–1,126 keV has two characteristic peaks separated by a phase of 0.5 ± 0.1. This structure is also found for PSR0531+21 and for PSR0833–45, above a γ-ray energy of 50 MeV. From this comparison, the two peaks labelled A and B in Fig. 1 have been chosen as pulsed bins in the light curve. The background level is defined using the six remaining bins. With respect to this level, the number of pulsed events (in A and B) is at a 3.4 standard deviation above this background level. Peak A is ~230 ms wide; peak B is 77 ms wide. The intensity ratio between peaks A and B is ~3.

The energy spectrum of the pulsed events was constructed by distributing equally all the data (80 keV–6 MeV) into four energy channels. The incident photon spectrum, corrected for atmospheric absorption, is shown in Fig. 2. A positive detection is observed only for the two channels: 300–530 keV ($(3.1 \pm 1.2)10^{-3}$ photons cm^{-2} s^{-1} MeV^{-1}) and 530–1,126 keV ($(3.8 \pm 1.2)^{-3}$ photons cm^{-2} s^{-1} MeV^{-1}). The pulsar was not detected either between 80 and 300 keV (3 σ upper limit 4.4×10^{-3} photons cm^{-2} s^{-1} MeV^{-1}) or between 1.5 and 6 MeV (3 σ upper limit 6.7×10^{-4} photons cm^{-2} s^{-1} MeV^{-1}). Figure 2 also shows 3 σ upper limits for these two channels, as well as the upper limit between 30 and 80 MeV tacking the upper limit of the flux above 35 MeV (2.7×10^{-6} photons cm^{-2} s^{-1}), from SAS 2[8], and assuming an $E^{-2.4}$ spectrum.

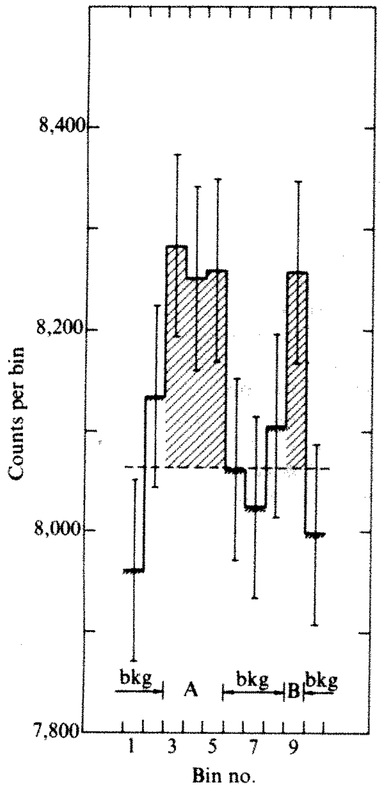

Fig. 1 Light curve observed for PSR1822 – 09 in the energy range 454–1,126 keV. $P(\chi^2 \geq 16/9 \text{ d.f.}) = 0.07$. The dashed line represents the background level.

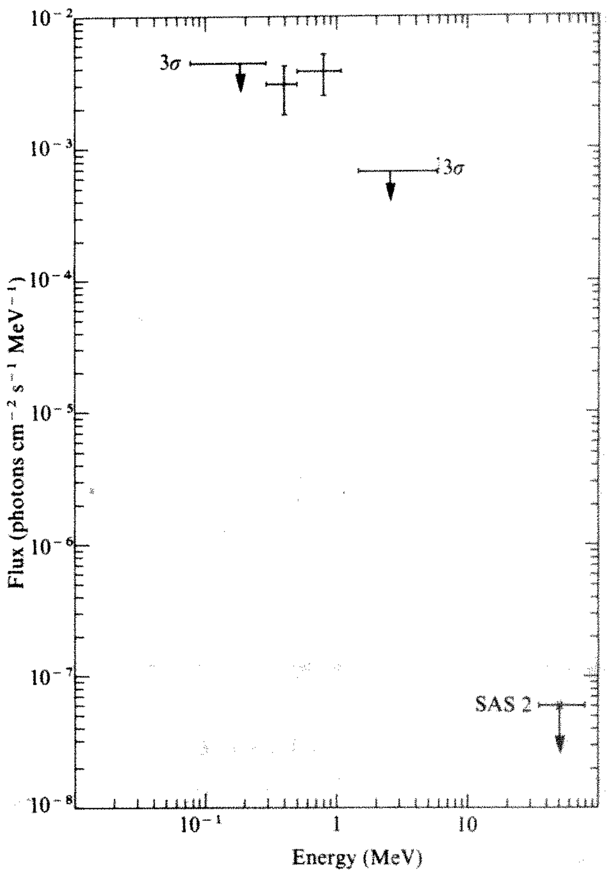

Fig. 2 Energy spectrum for PSR1822 – 09 using the pulsed events in the two peaks (see text).

This spectrum is very different from that observed in the case of the Crab pulsar which is a power law equal to –2.1. It shows a remarkable break around 1 MeV, the index being smaller than –2 above this energy taking into account the SAS 2 upper limit, and close to zero below 1 MeV, if we consider the upper limit between 80 and 300 keV.

Various theories have been invoked to explain pulsar emission. Some of them consider that this emission is localized near the crust of the neutron star[17,18] and others, at the light cylinder[19,20]. In the first model, the high energy particles are accelerated near the crust of the neutron star and propagate along the open magnetic field lines. These particles produce high energy photons by curvature radiation. The primary γ photons can be absorbed by pair production when they cross the magnetic field lines. The secondary particles created by this process emit instantaneously a flux of γ-ray photons by the synchrotron process. The resulting spectral shape depends on the pulsar period, the Lorentz factor of the primary electrons (positrons) and the intensity of the magnetic field at the neutron star pole. Above 1 MeV, the observed spectral index is then consistent with a Lorentz factor for the primary particles of $\simeq 10^7$ or less.

Around 1 MeV our data show a clear break in the spectrum: this could be due to a synchrotron self-absorption process or to a pair-production absorption process. Our results imply that the most important part of the energy emitted by PSR1822 – 09 is emitted in the MeV region. Other observations in this energy range are necessary to confirm this result and to understand better the geometry of the γ emission for this pulsar.

We thank Professors J. Heyvaerts and L. Scarsi for helpful discussions. This work was supported by CNES contract BA 011 02 F.

Received 18 April; accepted 13 July 1980.

1. Kurfess, J. D. *Astrophys. J. Lett.* **168,** L39 (1971).
2. Wilson, R. B. *et al. Proc. 15th int. Cosmic Ray. Conf.* Plovdiv **1,** 24 (1977).
3. Penningsfeld, F. P., Eraser, U. & Schönfelder, V. *Proc. 16th int. Cosmic Ray Conf.* Kyoto (in the press).
4. Orwig, L. E., Chupp, E. L. & Forrest, D. J. *Nature phys. Sci.* **231,** 171 (1971).
5. Bennett, K. *et al. Astr. Astrophys.* **61,** 279 (1977).
6. Albats, P., Frye, G. M. Jr & Thomson, G. B. *Nature* **251,** 400 (1974).
7. Kanbach, G. *et al. Astr. Astrophys.* (in the press).
8. Ögelman, H., Fichtel, C. E., Kniffen, D. A. & Thompson, D. J. *Astrophys. J.* **209,** 584 (1976).
9. Thompson, D. J., Fichtel, C. E., Kniffen, D. A., Lamb, R. C. & Ögelman, H. B. *Astrophys. Lett.* **17**, 173 (1976).
10. Kanbach, G. *et al. Proc. 12th ESLAB Symp.* ESA-SP-124, 21 (1977).
11. Mandrou, P., Vedrenne, G. & Niel, M. *Astrophys. J.* **230,** 97 (1979).
12. Mandrou, P., Niel, M., Narbonne, J. & Sabaud, C. *Nucl. Instrum. Meth.* **133,** 553 (1976).
13. Dupont, A., Giordano, G., Mandrou, P. & Niel, M. *Nucl. Instrum. Meth.* **151,** 233 (1978).
14. Mandrou, P., Bui-Van, A., Vedrenne, G. & Niel, M. *Astrophys. J.* **237,** 424 (1980).
15. Taylor, J. H. & Manchester, R. N. *Astr. J.* **8,** 794 (1975).
16. Manchester, R. N. *et al. Mon. Not. R. astr. Soc.* **185,** 409 (1978).
17. Heyvaerts, J. & Signore, M. *Astr. Astrophys.* (in the press).
18. Salvati, M. & Massaro, E. *Astr. Astrophys.* **71,** 51 (1979).
19. Holloway, N. J. Preprint (1979).
20. Mestel, L., Phillips, P. & Wang, Y. M. *Mon. Not. R. astr. Soc.* **182,** 527 (1979).

Discussion of the Pioneer 11 observations of the F ring of Saturn

W.-H. Ip

Max-Planck-Institut für Aeronomie,
D-3411 Katlenburg-Lindau 3, FRG

The photopolarimetric and charged particle data from the Pioneer 11 Saturn encounter were used as diagnostic tools in a preliminary analysis of the physical nature of the F ring of Saturn. It is argued that the F ring may have two components, with the outer one composed of solid particles of centimetre-diameter and the inner one of micrometre-sized dust particles. Also, the outer component as scanned by the charged particle detectors may have two rings instead of one. The double-ring option, if verified, could have interesting implications for the dynamical origin of the planetary ring systems.

Among the many exciting new results from the recent Pioneer 11 flyby of Saturn[1,2] one of the major findings is the discovery of a new (F) ring located at 2.33 R_s (Saturn radius) just outside the A ring by the Imaging Photopolarimeter (IPP) team[3]. The absorption effects of trapped charged particles by this ring were subsequently detected by the particle experiments[4–7]. According to the IPP observations, the F ring has a width of no more than 800 km and an optical depth of $\leqslant 2\times10^{-3}$. In comparison with the whole saturnian ring system the F ring is very narrow indeed. Interestingly, there may be structures of even smaller scale in the F ring. First, the IPP team found indication of clumpiness in the ring. Second, the charged particle absorption features (the electron data, in particular) displayed distinct variations between 2.34 R_s and 2.36 R_s (refs 4, 5). These structures, if reflecting the condensation of matter around the F ring, would mean the presence of one or more rings (or satellites) with dimensions between 100 and 200 km.

Clearly, the particulate distributions are basic to the understanding of the F ring structure and the charged particle absorption taking place there. While some considerations on the nature of the F ring have been given by the Pioneer 11 experimenters[4,5,7], and by Dermott *et al.*[8]) in connection with their theoretical study of the narrow rings of Jupiter and Uranus, a more detailed ring model will be constructed here taking advantage of the published IPP and charged particle results. As planetary ring absorption is likely to play an important part in the budget of trapped radiation in the magnetospheres of Jupiter and Uranus as well as that of Saturn, we take the F ring as an example to outline some of the essential points of interaction between the planetary rings and the magnetospheric plasma. In particular we will explore the possibility of deducing the physical nature of the planetary rings from a combination of the optical and charged particle observations.

The most interesting F ring absorption features concern the sharp minima at 2.340 and 2.355 R_s observed in both of the inbound and outbound passes together with a central dip in the electron flux of 10 MeV energy range, which was detected only in the inbound pass[4,5]. Briefly, such absorption structures could be produced by three different (idealized) combinations of the ring system:

(1) One single circular ring in a dipole field with certain equatorial offset ($\Delta r \approx 0.01\ R_s$);
(2) One single elliptical ring in a dipole field with negligible equatorial offset ($\Delta r \ll 0.01\ R_s$);
(3) Two circular rings in a dipole field, again, with negligible equatorial offset.

The first two cases are essentially similar and the actual situation may be intermediate between them (that is, one single elliptical ring in a dipole field slightly offset with $\Delta r \leqslant 0.01\ R_s$, see Dermott *et al.*[8]) and this class of ring models will be illustrated by considering case (2). As shown in Fig. 1, charged particles drifting at different L shells would traverse different lengths of the ring material and hence experience varying degrees of reduction in particle flux[9]. As a result of such a longitudinal sampling effect, a radial profile of the absorption feature would be quite non-uniform with absorption minima formed at the inner and outer edges of the sweeping corridor of the ring. If we assume that the absorption profiles (such as locations and widths of the absorption dips) should have a certain correspondence with the radial variation of the integrated mass density or effective optical thickness, some physical parameters of the F ring may be derived. For instance, a plausible choice in which case the ring particles are bound by two orbits with $a_1 = 2.3500\ R_s$, $a_2 = 2.3479\ R_s$, $e_1 = 0.00468$, $e_2 = 0.00415$, and that the lines of apsides of these two orbits are aligned, could give a reasonable fit to the Chicago data[4]. Note that the maximum width of the F ring is about 200 km and the minimum only 50 km here, while the absorption effect extends over a region of 1,400 km. Such a ring configuration resembles the ϵ ring of Uranus[10–13], and by the same token this narrow ring is most likely maintained by a small satellite[8]. Whilst the double absorption minima flanking the ring are caused by the effect of longitudinal sampling of the charged particles, a sharp drop in the particle flux due to local absorption would also be observed if the spacecraft is situated in the near vicinity of the satellite or the main body of the ring (as may be the case for the inbound pass).

Some estimate for the optical thickness of the absorbing particles may be obtained by examining the two absorption minima. As outlined before[7,14–16], the cumulative reduction effect as the charged particles diffuse inward across a radial distance ΔL can be expressed by the survival probability given as:

$$P = \exp(-2N_b\tau) \tag{1}$$

Where N_b is the total number of bounces executed by the charged particles and τ the effective optical depth of the absorbing particles with diameter larger than the absorption range R (~ 5 cm). Defining the radial diffusion time scale as:

$$t_d = \frac{(\Delta L)^2}{4D} \tag{2}$$

(D is the radial diffusion coefficient), and the bounce period t_b is taken to be 2.4 s as appropriate for the 10 MeV electrons. Then with the relation $N_b = t_d/t_b$ plus using $\Delta L \approx 200$ km we find

$\tau \leqslant 3.4 \times 10^6 D$ as $P \approx 5 \times 10^{-2}$ at the outer absorption minimum observed in the outbound pass[4]. Since no more than 20% of the ring material will be sampled in one drift the actual relation should read: $\tau \leqslant 0.8 \times 10^7 D$.

Only upper limits of D have been given [$D < 10^{-8}\ R_s^2\ s^{-1}$ at $3.1\ R_s$, or $D < 6 \times 10^{-7}\ R_s^2\ s^{-1}$ at $3.1\ R_s$ and $10^{-7}\ R_s^2\ s^{-1}$ at $2.5\ R_s$ (ref. 7)]. Consider that the radial diffusion coefficient in the saturnian magnetosphere might have a very steep L-dependence as in the case of the Earth's magnetosphere ($D \propto L^{10}$, see ref. 17), it is possible that $D \leqslant 10^{-9}\ R_s^2\ s^{-1}$ at the position of the F ring; thus $\tau \leqslant 0.8 \times 10^{-2}$. This value is compatible with the value of $> 5 \times 10^{-5}$ as derived from using a somewhat different method[7], and with the IPP result of $\leqslant 0.8 \times 10^{-2}$ if the width of the ring is taken to be 200 km.

Although these values appear to be in satisfactory agreement, the diffusion time scale (t_d) as determined by equation (2) is probably too short in comparison with the drift period of the 7–17 MeV electrons in question (that is, 3×10^3 s compared with 7×10^4 s). In other words, two narrow rings with complete coverage at all longitudes [that is case (3)] might be required instead of just one with partial longitudinal coverage which allows rapid refilling of the absorption dips. To this binary ring system we should add another satellite orbiting between them with semimajor axis $a \approx 2.35\ R_s$ and eccentricity $e \approx 0.004$.

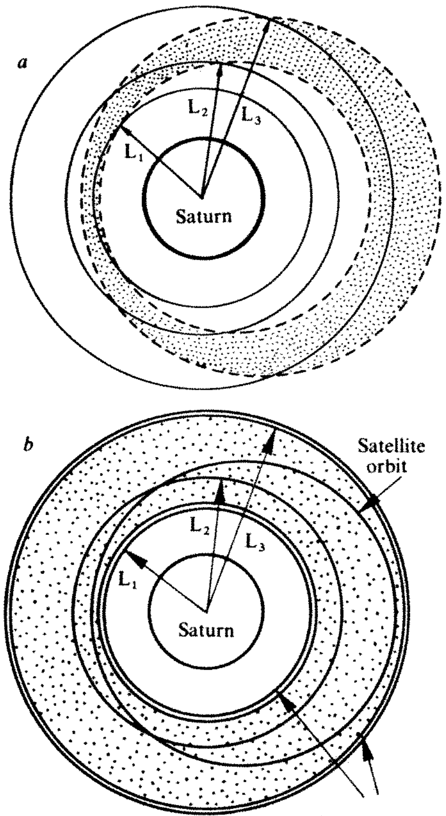

Fig. 1 Sketch of two possible ring configurations to interpret the observed charged particle absorption effects. *a*, One single ring with certain eccentricity and varying width. The charged particles drifting in different L shells would penetrate through different mass of ring material resulting in the formation of sharp absorption minima near perihelion and aphelion. If the diffusion time scale across the ring width is too short the absorption dips due to such longitudinal sampling effect could be refilled at certain positions. *b*, Two circular rings flanking the orbit of a small satellite in elliptical orbit. Two absorption minima would always be imprinted at all longitudes in the charged particle fluxes. If the spacecraft passes directly above or below the ring or satellite, an absorption spike would be observed as well as the inner and outer dips. Also the dipole offset, assumed to be zero here, could actually have a value like a fraction of $0.1\ R_s$.

The physical basis for the formation of such a system may be depicted as follows. After the fragments are ejected from the satellite surface at low speeds as a result of meteoritic bombardment or tidal stress, they would first follow trajectories approximating that of the parent satellite. However, they will be gradually cleared away within the sweeping corridor of the satellite, because of recapture by the satellite, or inward and outward diffusion due to inelastic collision with the satellite or with other small particles. The process of orbital dispersion, in any case, cannot continue forever as it is limited by the collisional frequency and mass density distribution of the interacting medium. It can be easily seen then there will be material piled up at the regions just bordering with the perihelion and aphelion of the satellite. As the particles injected into these edges would all have near circular orbits as a result of prior inelastic collisions, no further orbital dispersion could occur[18]; in this way two narrow rings of dense matter would be formed confining a wider zone of more diffuse nature. Note that such an orbital equilibrium configuration has been discussed before by Hénon[19] but in a somewhat different context.

A clear choice of the F ring configuration is difficult, but the possibility of a binary ring system is emphasized here as it has the potential of shedding new light on the structures of the rings of Uranus and Jupiter.

Another apparent puzzle in the Pioneer data may have some implication on the structure of the F ring—there is no signature of absorption of charged particles at the central position ($2.33\ R_s$) of the F ring as identified by the IPP team. Barring systematic error in the spacecraft position by a margin of 0.01–$0.02\ R_s$ for this moment, we would have to conclude that the F ring detected by the imaging experiment was not responsible for the charged particle absorption. This has several interesting implications about the F ring system.

First, in order to reduce its absorption power but amplify its cross section for light reflection the optical component of the F ring must consist mainly of tiny dust particles of submillimetre size if not smaller. To check this point let us note that the survival probability for charged particles diffusing across a belt of dust particles with average diameter $d \ll R$ can be written as:

$$P = \exp(-2N_b X/R) \qquad (3)$$

where $X = 2d\tau/3$. Now, with $P \gtrsim 0.95$ as judged from the electron data[4,5,7] we have immediately $d \leqslant 5.2 \times 10^{-3}$ cm if the ring width ΔL is about 800 km and $d \leqslant 2.1 \times 10^{-2}$cm if $\Delta L \approx 200$ km. In the above calculation we have assumed $D \approx 10^{-9}\ R_s^2\ s^{-1}$ and $\tau \approx 2 \times 10^{-3}(800/\Delta L)$. If the albedo α of these particles is smaller than unity d would be even smaller. In the extreme case of $\alpha \approx 0.05$, as was found for the uranian ring particles[20,21], we have $d \leqslant 3 \times 10^{-4}$–$10^{-3}$cm. From this point of view, the F ring identified by the IPP experiment may be in fact a dust belt of micrometre-sized particles similar to the jovian ring[22,23].

Second, to boost the absorption power but limit the cross section for light reflection to a small value the ring particles between $2.34\ R_s$ and $2.36\ R_s$ must be of centimetre size if not larger. Also, to explain the absence of this ring in the optical observation a low albedo must be invoked. In this way an optical thickness of $\leqslant 3 \times 10^{-3}$ (for $\alpha \approx 0(1)$) as required to interpret the absorption feature would be reduced to be $\leqslant 2 \times 10^{-4}$ if $\alpha \approx 0.05$. Such a value of optical depth may be below the limit of optical detection. On dynamical grounds, particles of metre size or so are required to maintain the stability of the narrow ring configuration against Poynting-Robertson effect[24]. But is there reason for such a low albedo? Presumably so, as whatever volatile ices on the particle surface would be sputtered away by the energetic ions exposing the (carbonaceous chondritic?) core material of low albedo[25]. [A similar thing can be said of the particles at the outer edge of the A ring in which case there is a difference of about $0.02\ R_s$ between the IPP result and the charged particle data[3–7].]

Finally, that the dust belt of micrometre-sized particles should be located inside of the narrow ring of larger particles is consistent with its being of fragmentation origin—as proposed for the jovian ring[26–29]. Note that the rings of both Jupiter and Uranus have been suggested to be the fragments of small satellites which are spiralling inwards towards the central planets. According to Dermott *et al.*[30], for instance, the reason for such orbital decay is basically that the synchronous orbits of both Jupiter and Uranus are outside the Roche limits, so satellites formed between these two positions would be pulled inward as a result of planetary tidal action. For Saturn, the synchronous orbit at 1.8 R_s is inside of the Roche limit at 2.3 R_s, so a reverse process might take place there—with small satellites accreted from condensations in the A ring being gradually pushed away from the planet. The F ring and its parent satellite are then manifestations of just such a process[26].

We have discussed here the possibility that the F ring may have two components: (1) the inner one mainly consisting of micrometre-sized dust particles (detected by the IPP experiment), and (2) the outer one of centimetre- to metre-sized bodies emitted from a small satellite (observed by the charged particle detectors). This scenario makes interesting comparison with the discovery of the ring system of Jupiter[22,23,31,32]. We have also investigated the possibility of deducing the ring configuration capitalizing on the radial profiles of the observed absorption features of the charged particles. Besides the more conventional configuration of one single narrow ring we find that a double-ring system is also a possibility—if not strictly required by the particle data. Detailed intercomparison of the Pioneer IPP, particles and fields observations may allow us to narrow down some of the uncertainties. Also, the Voyager I flyby in November, which follows essentially the same trajectory, should provide another set of valuable data. From analysis of charged particle experimental data, Simpson *et al.*[33] have concluded that the symmetric pair of the F ring absorption dips observed both inbound and outbound, is caused by two separate narrow rings; Gehrels[34] has found that the high colour index of the optical F ring is consistent with the idea that it is made of micrometre-sized dust particles.

I thank Drs W. I. Axford, W. Fillius and C. K. Goertz for useful discussions on the single ring option, and Drs J. A. Simpson and T. Gehrels for sending me preprints prior to publication.

Received 6 June; accepted 9 July 1980.

1. Dyer, J. W. *Science* **207,** 400 (1980).
2. Opp, A. G. *Science* **207,** 401 (1980).
3. Gehrels, T. *et al. Science* **207,** 434 (1980).
4. Simpson, J. A. *et al. Science* **207,** 411 (1980).
5. Van Allen, J. A. *et al. Science* **207,** 415 (1980).
6. Trainor, J. H., McDonald, F. B. & Schardt, A. W. *Science* **207,** 421 (1980).
7. Fillius, W., Ip, W.-H. McIlwain, C. E. *Science* **207,** 425 (1980).
8. Dermott, S. F., Murray, C. D. & Sinclair, A. T. *Nature* **284,** 309 (1980).
9. Fillius, W. *et al. IAU Coll.* 57 (May 13–16, Kailua-Kona, Hawaii, 1980).
10. Elliot, J. L., Dunham, E. & Mink, D. *Nature* **267,** 330 (1977).
11. Millis, R. L., Wasserman, L. H. & Birch, P. V. *Nature* **267,** 331 (1977).
12. Bhattacharyya, J. C. & Kuppuswamy, K. *Nature* **267,** 332 (1977).
13. Nicholson, P. D. *et al. Astr. J.* **83,** 1240 (1978).
14. Van Allen, J. A. *Highlights of Astronomy* Vol. 4, 195 (1977).
15. Thomsen, M. F. & Van Allen, J. A. *Geophys. Res. Lett.* **6,** 893 (1979).
16. Ip, W.-H. *Nature* **280,** 478 (1979).
17. Schulz, M. & Lanzerotti, L. J. *Particle Diffusion in the Radiation Belts* (Springer, Berlin, 1973).
18. Ip, W.-H. *Proc. 8th Lunar Science Conference*, 67 (1977).
19. Hénon, M. *Science* **199,** 692 (1978).
20. Smith, B. A. *Nature* **268,** 32 (1977).
21. Sinton, W. M. *Science* **198,** 503 (1978).
22. Owen, T. *et al. Nature* **281,** 442 (1979).
23. Smith, B. A. *et al. Science* **204,** 951 (1979).
24. Pollack, J. B. *Space Sci. Rev.* **18,** 3 (1975).
25. Cheng, A. F. & Lanzerotti, L. J. *J. geophys. Res.* **83,** 2597 (1978).
26. Ip, W.-H. *Space Sci. Rev.* **26,** 97 (1980).
27. Morfill, G. E., Grün, E. & Johnson, T. V. Preprint (Max-Planck-Institut für Kernphysik, Heidelberg, 1980).
28. Smoluchowski, R. *Nature* **280,** 377 (1979).
29. Prentice, A. J. & ter Haar, D. *Nature* **280,** 300 (1979).
30. Dermott, S. F., Gold, T. & Sinclair, A. T. *Astr. J.* **84,** 1225 (1979).
31. Acuna, M. H. & Ness, N. F. *J. geophys. Res.* **81,** 2917 (1976).
32. Fillius, W. in *Jupiter* (ed. Gehrels, T.) (University of Arizona Press, Tucson, 1976).
33. Simpson, J. A. *et al. J. geophys. Res.* (in the press).
34. Gehrels, T. *J. geophys. Res.* (in the press).

Order-modulated structures and the thermodynamics of cordierite reactions

A. Putnis

Department of Earth Sciences, University of Cambridge,
Downing Street, Cambridge CB2 3EQ, UK

The determination of palaeo pressures and temperatures (*P, T*) in metamorphic belts is of fundamental importance to our understanding of large-scale physical processes in the Earth. Such determinations are made by comparing observed mineral assemblages with experimental data on their *P, T* stability fields[1], thus assuming that the experiments are an adequate model for the natural reaction. The characterization of the structural state of natural and experimental materials is particularly important in this context. This note demonstrates the effect of the state of cation order on the *P, T* slopes of metamorphic reactions involving cordierite, $(Mg, Fe)_2Al_4Si_5O_{18}$, an indicator phase in metamorphism. Particular emphasis will be placed on the mechanism of Al, Si ordering in cordierite in so far as it relates to the characterization of the degree of cation order and hence the configurational entropy contribution to the thermodynamics of cordierite reactions.

Mg-cordierite occurs in two polymorphic forms. In the high temperature hexagonal structure, stable above ~1,450 °C (refs 2, 3), the Al and Si atoms are distributed over two sets of tetrahedral sites—three T_1 and six T_2 sites per formula unit $Mg_2Al_4Si_5O_{18}$ (Fig. 1). The Al, Si distribution involves two Al and one Si atom disordered over the T_1 sites and two Al and four Si atoms disordered over the T_2 sites[4]. In the slightly distorted low temperature orthorhombic form the T_1 sites are split into two non-equivalent sites T_11 and T_16, while the T_2 sites are split into a set of three non-equivalent sites T_21, T_26 and T_23. Within this new structure the Al, Si atoms are able to form a completely ordered distribution (see Table 1).

Experiments carried out on the mechanism and kinetics of the hexagonal–orthorhombic transition in anhydrous Mg-cordierite confirm that the polymorphism is due to Al, Si ordering and furthermore demonstrate that in equilibrium conditions the ordering transformation is first order involving the discontinuous transformation from a disordered to a well ordered phase at temperatures below ~1,450 °C (refs 3, 5).

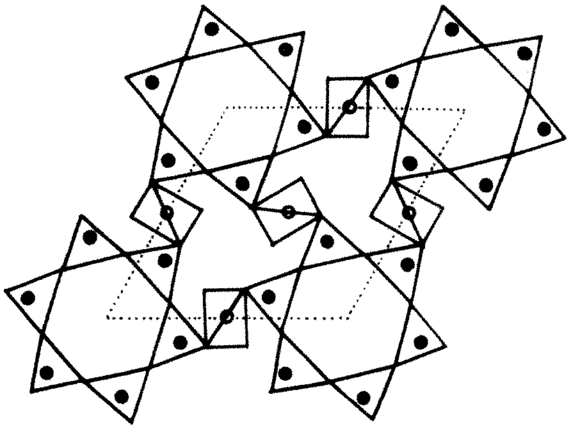

Fig. 1 The structure of hexagonal cordierite showing only the tetrahedral linkages. The tetrahedra in the ring sites (●) are designated T_2, while those outside the ring (○) are designated T_1 in Table 1. The dotted line is the hexagonal unit cell.

0028–0836/80/370128—04$01.00

This polymorphism has been generally characterized by a distortion index Δ, based on the degree of splitting of the peaks derived from the 211 hexagonal peak in an X-ray diffractometer trace[6]. In the hexagonal form Δ is zero, while in the fully ordered orthorhombic form of anhydrous Mg cordierite $\Delta \approx 0.25°$. In nature, however, cordierites of intermediate Δ values are common[7] and although various compositional effects have been proposed to account for this[8-10], the occurrence of these intermediate states in anhydrous Mg-cordierite[2] has yet to be explained. The strongly first order nature of the transformation precludes the formation, in equilibrium conditions, of intermediate structural states. As intermediate cordierites are formed from hexagonal cordierite at temperatures substantially below the equilibrium ordering temperature (that is, in the stability field of fully ordered cordierite), it is pertinent to examine the mechanism of Al, Si ordering in non-equilibrium conditions.

Isothermal annealing experiments were carried out on stoichiometric Mg-cordierite glass at temperatures between 1,150 and 1,430 °C for periods of 0.5–400 h. The preparation and characterization of the starting material and experimental details are given elsewhere[3]. The products of the annealing runs were studied by X-ray diffractometry and transmission electron microscopy.

The first phase to crystallize from the glass is invariably homogeneous hexagonal cordierite, which eventually transforms on annealing to homogeneous orthorhombic cordierite, the stable phase. The mechanism of the transformation in metastable conditions, however, does not involve the direct nucleation and growth of the orthorhombic phase. The transformation proceeds by the formation of a modulated structure in which two orthogonal distortion waves produce a 'tweed' microstructure in transmission electron micrographs (Fig. 2). The average structure as observed by X-ray diffractometry is hexagonal, whereas locally the structure consists of a sinusoidal variation in the degree of distortion towards two twin-related orthorhombic variants. The overall structure may be described as order-modulated, in which the short-range order may be high, while the long-range order, as measured by X-ray diffraction, is zero.

Continued annealing results in a gradual overall coarsening of the microstructure although the unequal development of one or other variant may lead to regions in which the distortions become unbalanced. This manifests itself as a slight departure from the average hexagonal state, and an apparently continuous range of Δ values is obtained by the increasing heterogeneity and growth of the microstructure. The first signs of peak splitting in the X-ray diffractometer traces must already be equated with a considerable degree of coarsening of the microstructure, on a scale of thousands of angstroms. Full details of the coarsening mechanisms will be published elsewhere, but there are two principal conclusions which can be drawn from these results. First, a mechanism which involves the formation of a metastable order-modulated structure will not be detected by methods such as X-ray powder diffractometry which measure long-range effects, and hence any assessment of the structural state obtained by such methods may be in error. Second, the mechanism described here is quite different in character from the temperature-dependent ordering models used by workers currently dealing with the thermodynamics of cordierite reactions[11-13].

Table 1 Tetrahedral sites in the cordierite polymorphs

Nine sites per formula unit $Mg_2Al_4Si_5O_{18}$

Hexagonal form	Orthorhombic form	Site content
3 T_1 sites	2 T_11 sites	2 Al
	1 T_16 site	1 Si
6 T_2 sites	2 T_21 sites	2 Si
	2 T_23 sites	2 Si
	2 T_26 sites	2 Al

Table 2 Volumes and entropies of minerals at 700 °C and 1 atm (ref. 12)

	Volume (cm^3 gfw)	Entropy (cal °C gfw)
Cordierite $2MgO.2Al_2O_3.5SiO_2$ gfw = 584.97	234.01	264.58
Sapphirine $2MgO.2Al_2O_3.SiO_2$ gfw = 344.63	100.55	151.38
Quartz SiO_2 gfw = 60.085	23.72	27.34

One major assumption in the experimental determination of the *P*, *T* stability field of anhydrous cordierite has been that the configurational entropy contribution of Al, Si order is not large[12,13]. This assumption is based on several lines of evidence all of which depend on an interpretation of the limited data provided by X-ray powder diffraction. First, measured heats of solution of Mg-cordierite with Δ values of 0.10, 0.20 and 0.25 prepared in metastable conditions are not significantly different[11,12]. As Al, Si disorder is normally accompanied by considerable enthalpy effects, the conclusion is that all of the samples were similar and had a high degree of order. While this conclusion is in itself valid, it is interpreted in terms of a model in which the degree of order is assumed to be related to a continuously changing Δ value with temperature. Hence the observation that a considerable change in Δ value corresponds to a small inferred change in cation distribution is extrapolated to suggest that hexagonal cordierite with a Δ value of zero must have a high degree of Al, Si order.

However, the order-modulated mechanism described here suggests a different interpretation of the same observations. Ordering via an order-modulated structure results in a high degree of short-range order without any change in symmetry. Thus calorimetric measurements of order-modulated material would be expected to produce results very similar to that of fully ordered orthorhombic cordierite, and subsequent increases in Δ on annealing would have little further enthalpy effects. However, the essentially discontinuous nature of the ordering processes on a local level in the transition from homogeneous hexagonal cordierite (that is disordered) to order-modulated hexagonal cordierite does not allow extrapolation of intermediate Δ values to zero.

Conventional single crystal X-ray structure analysis is not able to distinguish between a completely disordered hexagonal cordierite (Table 1) and the order-modulated state described here, and although the Bragg–Williams order parameter seems to be the same in each case[4], the configurational entropy of the two states may be radically different, as discussed below.

The extent to which the configurational entropy contribution to the total entropy change in a metamorphic reaction affects the *P*, *T* slope may be calculated from the Clapeyron relation $dP/dT = \Delta S/\Delta V$. Although the volumetric effects of cation disorder are negligible, the configurational entropy may be the dominant term, particularly in solid–solid reactions where the overall entropy changes are small. This is well illustrated by the reaction:

$$\text{Anhydrous cordierite} \rightarrow \text{sapphirine} + \text{quartz}$$

$$2MgO.2Al_2O_3.5SiO_2 \rightarrow 2MgO.2Al_2O_3.SiO_2 + 4SiO_2$$

Table 2 shows the volume and third law entropy data from which dP/dT may be calculated. To evaluate the effect of configurational entropy of cordierite alone, the configurational entropy of sapphirine will be taken to be fixed at +4.2 cal per °C gfw as suggested by Newton *et al.*[12]. The validity of this assumption will be discussed below.

The entropy change for the reaction involving fully ordered cordierite ($S_{\text{config.}} = 0$) is therefore given by tabulated third law entropies:

$$\begin{aligned}\Delta S_{\text{reaction}} &= S_{\text{sapph}} + 4S_{\text{qtz}} - S_{\text{cord}} \\ &= (151.38 + 4.2) + (4 \times 27.34) - 264.58 \\ &= 0.32 \text{ cal per °C gfw} \\ \Delta V_{\text{reaction}} &= -38.3 \text{ cm}^3 = -0.915 \text{ cal bar gfw}\end{aligned}$$

Therefore

$$\frac{dP}{dT} = -0.35 \text{ bar per °C}$$

To calculate the slope for this reaction when the cordierite is completely disordered, the configurational entropy of the cordierite must be evaluated. Taking four Al and five Si atoms disordered over the nine T_1, T_2 sites taken together,

$$\begin{aligned}S_{\text{config.}} &= -9R\left(\frac{4}{9}\ln\frac{4}{9} + \frac{5}{9}\ln\frac{5}{9}\right) \\ &= 12.0 \text{ cal per °C gfw}\end{aligned}$$

For the hexagonal structure described in Table 1 with two Al and one Si atoms disordered over T_1 sites and two Al and four Si atoms disordered over T_2 sites

$$\begin{aligned}S_{\text{config.}} &= -3R\left(\tfrac{2}{3}\ln\tfrac{2}{3} + \tfrac{1}{3}\ln\tfrac{1}{3}\right) - 6R\left(\tfrac{2}{6}\ln\tfrac{2}{6} + \tfrac{4}{6}\ln\tfrac{4}{6}\right) \\ &= 11.34 \text{ cal per °C gfw}\end{aligned}$$

Thus, although the Bragg–Williams order parameter of this state[4] may suggest that it is partially ordered, its configurational entropy is very high. In contrast, an order-modulated state with the same apparent long-range order parameter would have a very small configurational entropy.

The dP/dT for the reaction involving hexagonal disordered cordierite with the cation distribution shown in Table 1 is

$$\frac{dP}{dT} = \frac{0.32 - 11.34}{-0.915} = 12 \text{ bar per °C}$$

The P, T slopes for the breakdown of ordered and disordered cordierite to sapphirine + quartz are shown in Fig. 3. The lines necessarily intersect at the order–disorder transition temperature (1,450 °C). The position of this intersection on the pressure axis is defined by reversed experiments and calorimetric data[12,14] in which the equilibrium for the reaction using well ordered cordierite ($S_{\text{config.}}$ assumed to be 1.22 cal per °C gfw) was found to occur in the range 8.2 ± 0.4 kbar at 1,300–1,400 °C with a slope of about 1 bar per °C. This reaction line (dotted in Fig. 3) must also pass through the order–disorder transition temperature for Mg-cordierite.

Thus, while Newton's calorimetric and experimental data are internally self consistent, they represent only one solution for a cordierite with a particular state of order. The fact that the cation disorder in cordierite cannot be dismissed as insignificant stresses the importance of carrying out thermochemical measurements, and experimental high P, high T reactions, on materials in which the state of order has been characterized. Routine transmission electron microscopy combined with X-ray diffraction of such materials can provide considerably more information on short-range order as well as on the mechanism of the ordering process. This latter point is particularly important in relation to the estimation of the relevant configurational entropy corrections.

In the above treatment the effect of disorder in cordierite has been evaluated by assuming a fixed entropy for sapphirine. However, the situation with regard to assumptions of cation order in sapphirine poses even greater problems than in cordierite. The occurrence of two polymorphs and their intimate intergrowths[15,16], and the possibility of a relationship between the polymorphism and Al, Mg and/or Al, Si disorder suggests the need for considerable caution over estimates of configurational entropy. Further, calorimetric measurements on synthetic and natural sapphirines[17] disclose differences which have been attributed to different structural states; hence the synthetic material is not a good model for its natural counterpart. The sensitivity of P, T slopes of dry reactions to configurational entropy corrections, coupled with the structural variations present in natural sapphirines, further underlines the inadequacy of assumptions of $S_{\text{config.}}$ made on the basis of a single X-ray structure analysis of a sample.

Finally, it remains to consider the relevance of a discussion of disordered phases in experimental reactions to natural assemblages. The crystallization of a disordered phase within the stability field of the ordered polymorph is frequently observed where the starting material is in a highly metastable state, such as a glass. This may be a readily understood in terms of the large overall free energy change in the reactions involved with the formation of either phase, in which case the discrimination in favour of the metastable disordered phase is on kinetic grounds, its crystallization having a higher entropy of activation.

In a metamorphic rock, conditions are generally nearer to equilibrium. Consider the prograde formation of a phase with ordered and disordered polymorphs at a temperature below its order–disorder temperature. At constant pressure, the equilibrium temperature (T_1) for any reaction producing the ordered phase will necessarily be lower than the metastable equilibrium temperature (T_2) for the same reaction producing the disordered phase. Above T_2 the enhanced kinetics would favour the nucleation of the disordered phase. Thus, the formation of disordered phases in prograde reactions requires a measure of overstepping of the stable equilibrium temperature, a nearly universal phenomenon in dry rocks.

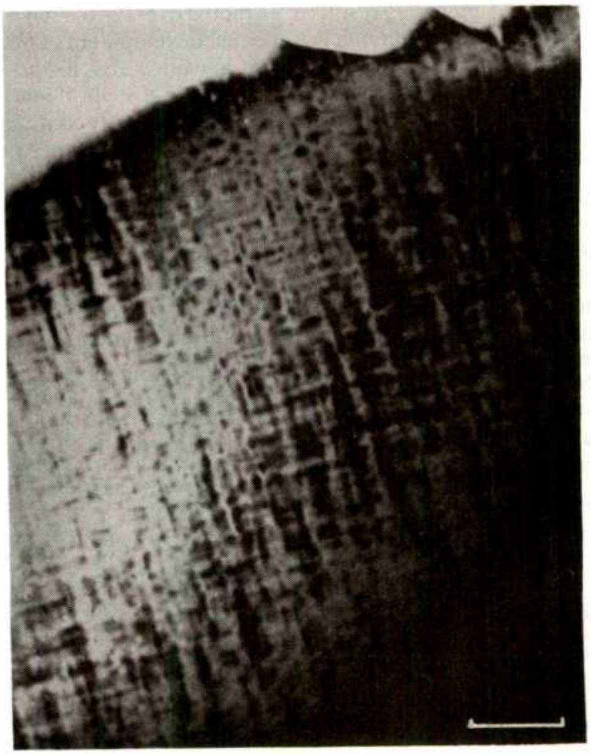

Fig. 2 Transmission electron micrograph of the order-modulated microstructure of cordierite, showing two orthogonal distortion waves normal to (100) and (1$\bar{2}$0) planes of the hexagonal cell. Scale bar, 0.2 μm.

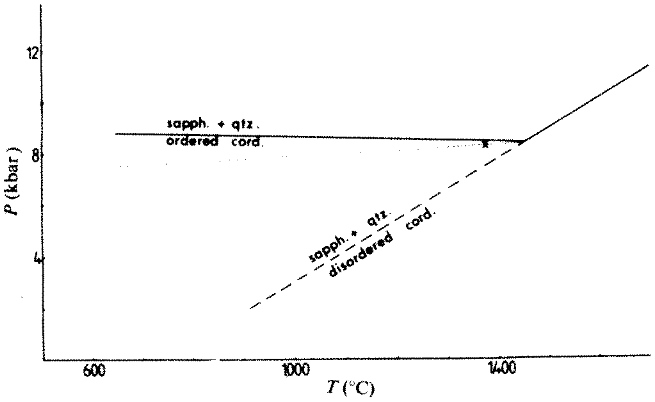

Fig. 3 Pressure–temperature equilibria for the reaction cordierite → sapphirine + quartz for ordered and disordered cordierite. The dotted line and the point X represent the slope and experimental point, respectively, determined for this reaction by Newton *et al.*[12] using a cordierite with assumed $S_{\text{config.}}$ of 1.22 cal °C gfw.

The extent to which disorder plays a major role in the growth of a mineral during metamorphism must be assessed for each individual occurrence. Furthermore, the structural state of a mineral exposed at the Earth's surface is not necessarily the same as that during its growth, and depends on the relative kinetics of the mineral reaction and the ordering process. In this respect the relict microstructure may indicate whether an ordered phase was nucleated directly or has been produced from a disordered phase subsequent to growth. The formation of intermediate structural states in cordierite strongly suggests that ordering occurs via an order-modulated structure.

The microstructures of natural cordierites have not yet been studied. However, in an investigation of the distortion indices of 128 natural cordierites[7], the whole range of Δ values from 0 to >0.25 has been found, and these show characteristic frequency distributions for various geological environments. Notwithstanding the possible compositional effects on Δ values[8–10], this supports Schreyer's hypothesis that the observed Δ values indicate an evolution from an initially disordered high cordierite[7] similar to the process in the experiments described here.

Clearly many of these implications to the *P*, *T* slopes of natural metamorphic reactions remain to be tested. The evidence suggests the need for calorimetric measurements on phases with well characterized microstructures, for repeating experiments on metamorphic reactions using both ordered and disordered reactants, and finally for the characterization of the structural states of the natural assemblages to which experimental studies are applied.

I thank T. J. B. Holland, J. D. C. McConnell and G. D. Price for discussions. Financial support from the NERC is gratefully acknowledged.

Received 7 May; accepted 10 July 1980.

1. Richardson, S. W. *Fortschr. Miner.* **47,** 65–76 (1970).
2. Schreyer, W. & Schairer, J. F. *J. Petrol.* **2,** 294–406 (1961).
3. Putnis, A. *Contr. Miner. Petrol.* (in the press).
4. Meagher, E. P. & Gibbs, G. V. *Can Miner.* **15,** 43–49 (1977).
5. Putnis, A. *Phys. Chem. Miner.* (submitted).
6. Miyashiro, A. *Am. J. Sci.* **255,** 43–62 (1957).
7. Schreyer, W. *Neues Jb. Miner. Abh.* **105,** 211–244 (1966).
8. Stout, J. H. *Am. Miner.* **60,** 229–234 (1975).
9. Schreyer, W., Gordillo, C. E. & Werding, G. *Cont. Miner. Petrol.* **70,** 421–428 (1979).
10. Sellkregg, K. R. & Bloss, F. D. *Geol. Soc. Am. Abstr.* **11,** 513 (1979).
11. Navrotsky, A. & Kleppa, O. J. *J. Am. ceram. Soc.* **56,** 198–199 (1973).
12. Newton, R. C., Charlu, T. V. & Kleppa, O. J. *Contr. Miner. Petrol.* **44,** 295–311 (1974).
13. Newton, R. C. & Wood, B. J. *Contr. Miner. Petrol.* **68,** 391–405 (1979).
14. Newton, R. C. *J. Geol.* **80,** 398–420 (1972).
15. Merlino, S. *Contr. Miner. Petrol.* **41,** 23–29 (1973).
16. Higgins, J. B. thesis, Virginia Polytechnic Institute, Blacksburg (1978).
17. Charlu, T. V., Newton, R. C. & Kleppa, O. J. *Geochim. cosmochim. Acta* **39,** 1487–1498 (1975).

D.c. electrical conductivity of Green River oil shales

K. Rajeshwar, M. Das & J. DuBow

Department of Electrical Engineering, Colorado State University,
Fort Collins, Colorado 80523

The recent interest in the kinetics and mechanistic aspects of the thermal decomposition of oil shale kerogen[1] derives largely from its importance as an alternative energy source to petroleum. In spite of considerable research effort, how oil shale kerogen decomposes to gaseous and liquid hydrocarbon fuels is still not fully understood[1]. The present study considers the d.c. electrical conduction behaviour of Green River oil shales. The observed trends in the electrical behaviour of these materials are correlated with a two-step decomposition model in which the rate-determining processes are shown to be (1) breakdown of an outershell polar bridge structure with an activation energy of 15 ± 2 kcal mol^{-1} (180–350 °C) and (2) cleavage of an inner core naphthenic structure also involving polar groups with an activation energy of 35 ± 3 kcal mol^{-1} (350–500 °C). These structural changes are shown to correspond to the chemical transformation of kerogen to liquid and gaseous hydrocarbons through a bitumen intermediate. Although the present data pertain to Green River oil shales in particular, the observed trend of charge transfer mechanisms in the thermal decomposition behaviour of thermally unstable materials may be indicative of how thermal and electrical properties of all solid materials in general are closely coupled. The common mechanistic origin identified in the present study for the processes of thermal decomposition and electrical conduction, offers the possibility of improving the thermal stability characteristics of a solid by appropriate changes in the electric field surrounding it.

Electrical conductivity (σ) measurements were carried out in the temperature range 25–500 °C, on right circular cylindrical disks of oil shales of diameter ~2.4 cm and thickness of 0.25 cm. The direction of the electric field was perpendicular to the shale stratigraphic planes in all the cases reported below. A nominal field strength of 110 V cm^{-1} was applied across the shale sample and the currents were measured using a conventional operational amplifier circuit. Silver electrodes were used for the measurements; the opposite faces of the sample disks were also coated with silver paint to minimize contact resistance. In a typical 'run', the sample was heated in an atmosphere of dry pre-purified N_2 at a heating rate of ~2 °C min^{-1}. The required d.c. voltage was then imposed across the shale sample. Because of polarization effects, the currents slowly decayed with time at a given temperature—the values finally attaining a steady-state. This steady-state conductivity σ_∞ was recorded at various temperatures and the data displayed in the form of conventional $\ln \sigma_\infty$ versus $1/T$ plots[2].

Figure 1 shows the variation of d.c. conductivity with temperature for a Utah shale, a Colorado oil shale sample and a Wyoming shale[3]. The organic content of these samples was estimated from specific gravity measurements[4] and is expressed in terms of an equivalent Fischer assay as the volume of oil in litres that can be extracted per unit mass (tonne) of the shale. The σT versus $1/T$ plots can be broken up into approximately three segments with activation energies (slopes) E_1, E_2, and E_3 respectively. These values for the different samples and the corresponding temperature intervals are shown in Table 1. The E values within each temperature interval are seen to be comparable for the different samples within the limits of experimental error. More significantly, the slopes are also seen to be relatively insensitive to the amount of organic matter in the shale (Fig. 2 and Table 1). This evidence strongly supports the

0028–0836/80/370131—03$01.00

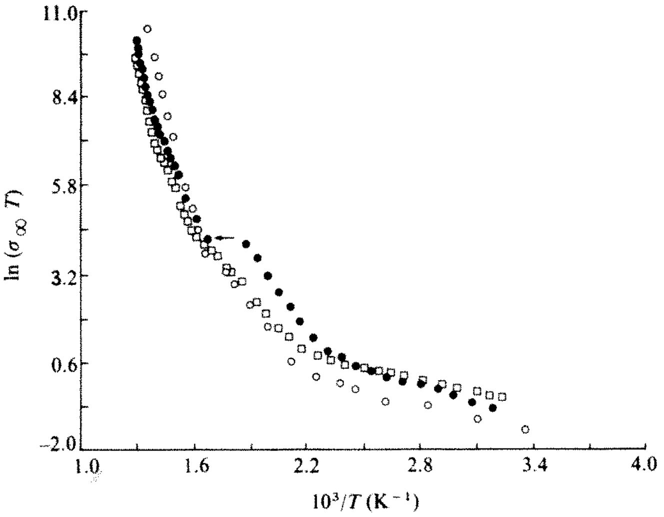

Fig. 1 Variation of steady-state conductivity with temperature for Green River oil shales: □, Wyoming oil shale (135 l tonne^{-1}); ○, Utah oil shale (344 l tonne^{-1}); ●, Colorado oil shale (140 l tonne^{-1}). The arrow denotes a set of isothermal conditions for approximately 10 min followed by resumption of the heating program (2 °C min^{-1}, see text).

linking of the observed E values to an intrinsic charge transfer process whose energetics are independent of the amount of organic matter in the shale. A dependence of the E values on the organic content of the shale would have precluded a straightforward explanation of the observed trends in terms of charge transfer processes. Chemical effects such as decomposition are expected to bring about changes in the magnitude of E with organic content in such a case. The magnitude of the measured σ values, however, do show pronounced time-dependent effects, especially at elevated temperatures (>400 °C, compare with the values denoted by arrows in Figs 1 and 2). These irreversible effects are attributed to thermal decomposition of the indigenous organic matter in the shale. Further evidence is the pronounced hysteresis in σ_∞ values that are observed after heating to ~500 °C and cooling back to room temperature. The σT versus $1/T$ plots show completely different activation behaviour in the cooling cycle. A second heating does not significantly bring about further changes and the conductivity behaviour now reflects charge migration in the residual carbon and in the inorganic mineral matrix in the shale.

Table 1 Activation energies* obtained from d.c. electrical conductivity measurements on Green River oil shales

Sample (oil yield) (l tonne^{-1})	Activation energy† (kcal mol^{-1}) (approximate temperature interval)
Utah oil shale (344)	$E_1 = 38$ (350–500 °C) $E_2 = 15$ (180–350 °C) $E_3 = 3$ (25–180 °C)
Wyoming oil shale (135) H	$E_1 = 36$ (350–500 °C) $E_2 = 14$ (180–350 °C) $E_3 = 3$ (25–180 °C)
Colorado oil shale (140)	$E_1 = 32$ (280–500 °C) $E_2 = 16$ (180–280 °C) $E_3 = 3$ (25–180 °C)
Colorado oil shale (244)	$E_1 = 34$ (350–500 °C) $E_2 = 17$ (180–350 °C) $E_3 = 2$ (25–180 °C)

* Measured values include contribution from migration enthalpies as well as carrier formation energies especially at elevated temperatures (see ref. 2).

† Nominal error in measured values, ±2 kcal mol^{-1}.

The observed trends in the electrical conductivity behaviour are consistent with a two-step decomposition process for oil shale kerogen[1]:

$$\text{Kerogen} \xrightarrow[180\text{–}350\,^\circ C]{E_1} \text{pyrobitumen}$$

$$\xrightarrow[350\text{–}500\,^\circ C]{E_2} \text{oil} + \text{gas} + \text{char} \qquad (1)$$

We propose that the two high-temperature regions in $\ln(\sigma_\infty T)$ versus $1/T$ plots (Figs 1 and 2) refer to the above reactions with activation energies E_1 and E_2 respectively, This interpretation is strongly supported by the good correlation of the present activation energies E_1 and E_2 with those measured recently in this laboratory for the thermal decomposition of Green River oil shale kerogen[5]. Using a non-isothermal thermogravimetry technique, activation energies of 14.53 kcal mol^{-1} and 36.49 kcal mol^{-1} were obtained for the low-temperature thermal decomposition of kerogen and the high-temperature decomposition of pyrobitumen respectively[5]. These values are in excellent agreement with those for E_1 and E_2 in Table 1. The close correspondence of activation energies obtained from two widely disparate techniques—one electrical and the other thermal—underlines a common origin for the processes of charge carrier migration and thermal decomposition in Green River oil shales. As only charged species contribute to the d.c. conductivity, the primary bond-breaking step must involve polar molecules in both stages of reaction (1). A previous structural model[6,7] for oil shale kerogen, involves a non-uniform three-dimensional network wherein the major components (such as isoprenoids, steroids, and terpenoids) are linked by bridges to form the kerogen matrix. Based on the present data, we propose that rupture of cross-linking bridges, most of which are polar in nature (disulphides, ethers and ester groups), is the rate-determining step in both pyrolysis as well as in charge migration. Two types of polar bridges are envisaged: (1) the first 'outershell' group which interlinks the major components and is broken first in the first stage of decomposition and (2) a second 'core' type which holds together the carbon skeletal chain (predominantly naphetenic) within each individual component and is ruptured in the second stage of pyrolysis[7]. The proposed mechanism is consistent with the increased solubility observed for kerogen at the end of the first pyrolysis step; the reduced

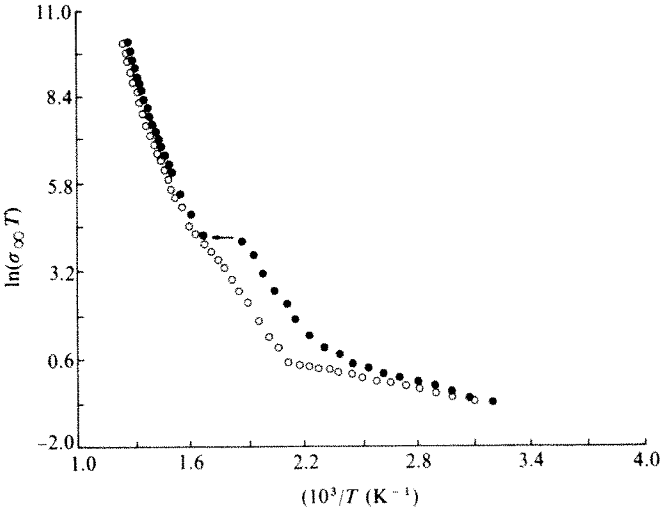

Fig. 2 Comparison of d.c. electrical conductivity behaviour for Anvil Points (Colorado) oil shales containing two different levels of organic content: ●, 140 l tonne^{-1} (same sample as in Fig. 1); ○, 240 l tonne^{-1}.

degree of cross-linking as a result of the breakdown in the bridge structure is expected to enhance the solubility of kerogen markedly.

The conductivity in the low-temperature region is expected to arise mostly from the indigenous moisture in the shale. This process is assigned an activation energy, E_3 (compare with Table 1). The water molecules are presumably trapped within the kerogen macromolecular network. The extremely low E_3 values observed at low temperatures imply a chain mechanism for conduction presumably of the Grotthus-type[8].

Finally, although the present conductivity data have highlighted the importance of charge transfer in the thermal decomposition of oil shale kerogen, further measurements are necessary to elucidate the exact nature of these charged species. Note that similar conductivity measurements on a variety of solid fuels (such as coals) could yield a unified picture of the mechanistic aspects of charge migration and thermal instability in these materials.

We thank the US Department of Energy and the Laramie Energy Technology Center for financial support.

Received 9 April; accepted 8 July 1980.

1. Rajeshwar, K., Nottenburg, R. & DuBow, J. *J. mater. Sci.* **14,** 2025–2052 (1979).
2. Lidiard, A. B. in *Encyclopedia of Physics—Electrical Conductivity* Part 2, Vol. 20 (ed. S. Flugge) 246 (Springer, Berlin, 1957).
3. Rajeshwar, K., DuBow, J. & Rosenvold, R. *Ind. Eng. chem. Prod. Res. Devel.* (in the press).
4. Smith, J. W. *U.S. Bur. Mines Rep.* **7248** (1969).
5. Rajeshwar, K. & DuBow, J. (submitted).
6. Yen, T. F. *ACS Div. Fuel Chem. Preprints* **19,** 109 (1974); in *Oil Shale* (eds Yen, T. F. & Chilingarian, G. V.) 129–147. (Elsevier, Amsterdam,1976).
7. Young, D. K. & Yen, T. F. *Geochim. cosmochim. Acta* **41,** 1411–1417 (1977).
8. Bockris, J. O. M. & Reddy, A. K. N. *Modern Electrochemistry* Vol. 1, 470–476 (Plenum, New York, 1970).

Late-Glacial history of the Brecon Beacons, South Wales

M. J. C. Walker

Department of Geography, Saint David's University College,
Lampeter, Dyfed SA48 7ED, UK

In the uplands of the Brecon Beacons, Black Mountains, Fforest Fawr area of South Wales, small arcuate moraines and/or protalus ramparts are found below steep escarpments and in glacial cirques[1–3]. The freshness and distinctive morphology of many of these features have led to the suggestion that they are not a product of the late Devensian ice sheet, but may have been formed during the Loch Lomond Stadial of the Late-Glacial period (Fig. 1), the last occasion when glaciers existed in the British Isles. I present here pollen-stratigraphic evidence and radiocarbon dates which form the basis for the first Late-Glacial chronology for this area of South Wales, and which prove that the features described above developed during the Loch Lomond Stadial (approximately equivalent with the Younger Dryas of Scandinavia[4–6]).

Within the catchment of Glyn Tarell, on the northern side of the Brecon Beacons escarpment (Fig. 2), two distinctive end moraines occur. Beneath the north-east-facing scarp of Craig-y-Fro (grid ref. SO 972208), an arcuate ridge extends for about 0.75 km down the western slope and crosses the valley floor at ~365 m OD, while in the cirque of Craig Cerrig-gleisiad (grid ref. SO 964220), the innermost of a complex of glacial depositional landforms (some of which may be the product of the late Devensian ice sheet) is a prominent boulder-strewn, arcuate moraine at a height of ~425 m OD. Both moraines enclose infilled kettle-hole basins in which Flandrian limnic and terrestrial sediments have accumulated. The subsurface contours of the two basins were established by sounding the infills along a grid pattern[7] and the deepest points were located. In this way, the oldest sediments in the basins could be sampled. Overlapping cores were then removed with a piston corer for pollen analyses and radiocarbon dating.

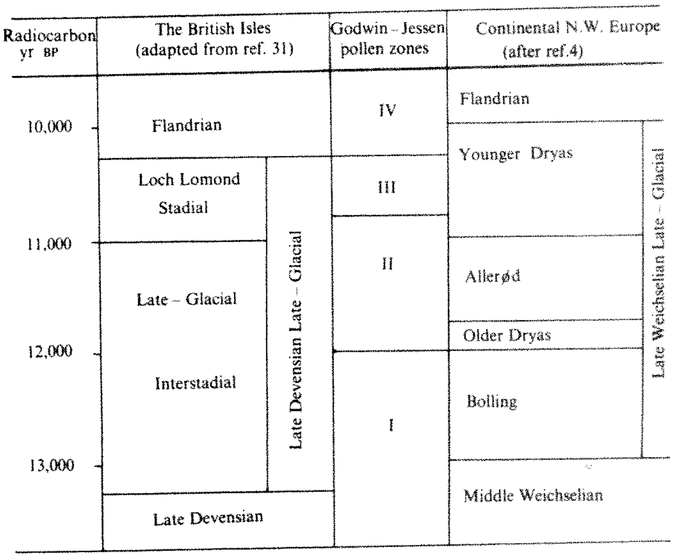
Radiocarbon yr BP
10,000
11,000
12,000
13,000
The British Isles (adapted from ref. 31)
Flandrian
Loch Lomond Stadial
Late – Glacial Interstadial
Late Devensian Late – Glacial
Late Devensian
Godwin – Jessen pollen zones
IV
III
II
I
Continental N.W. Europe (after ref.4)
Flandrian
Younger Dryas
Allerød
Older Dryas
Bolling
Late Weichselian Late – Glacial
Middle Weichselian

Fig. 1 The Late-Glacial period.

At Traeth Mawr (grid ref. SO 967257), some 3.5 km north of Craig Cerrig-gleisiad (Fig. 2), a large dead-ice hollow at ~330 m OD contains a typical Late-Glacial sequence[8] comprising organic muds between minerogenic sediments, and these deposits are, in turn, overlain by Flandrian muds and peats. Cores were removed from a deep part of the basin for pollen analyses, and samples for radiocarbon dating were obtained by bulking material from comparable stratigraphic horizons in six of the cores. As at the sites within the moraines, this procedure was made possible by the clearly defined stratigraphy of the basin sediments. The full stratigraphic sequences at the three sites, the pollen assemblage zones and the dated horizons are shown in Fig. 3. The radiocarbon dates are presented in Table 1.

Three dates were obtained from the Late-Glacial profile at Traeth Mawr, the earliest of which, 11,660 ± 140 BP (SRR-1562), was from the basal organic sediments. The pollen spectra from those horizons show marked upward trends in the curves for *Betula* and *Juniperus*, increases in aquatic taxa and declining values for open-habitat herbs such as *Artemisia* and *Rumex*. The radiocarbon date is, however, over 1,000 yr younger than age determinations from comparable Late-Glacial Interstadial deposits in Scotland[9–12], the Lake District[13–15], North Wales[16] and Cornwall[17]. One reason for this is that initially low productivity within the lake during the early Late-Glacial Interstadial could have led to a very slow rate of sediment accumulation, and as deposition probably increased with the development of the lacustrine ecosystem, it would be extremely difficult to obtain a true age for the basal organic sediments from a 2-cm thick sample of material. This problem may have been exacerbated by the compaction of the unconsolidated organic sediments, a process that can result in several hundred years of sedimentary

Table 1 Radiocarbon dates from the Brecon Beacons

Sample no.	Site	Depth below surface (cm)	Date (yr BP)	δ^{13}C value
SRR-1560	Traeth Mawr	287–289	9970 ± 115	−16.9‰
SRR-1561	Traeth Mawr	369–371	10,620 ± 100	−17.8‰
SRR-1562	Traeth Mawr	397–399	11,660 ± 140	−16.4‰
SRR-1563	Craig-y-Fro	442–444	10,030 ± 100	−29.0‰
SRR-1564	Craig Cerrig-gleisiad	550–552	10,860 ± 70	−25.6‰

0028–0836/80/370133—03$01.00

history becoming compressed into a few centimetres[18]. A third possibility is that the date has been affected by the incorporation of younger carbon, either during the sampling process or through sediment mixing on the former lake floor. Any of these factors, either singly or in combination, could have produced the date of 11,660 ± 140 BP which, in the context of other age determinations from Highland Britain, would seem to be anomalous.

The uppermost Interstadial deposits at Traeth Mawr yielded a date of 10,620 ± 100 BP (SRR-1561). At that level in the profile there is a marked decline in percentages of woody plant pollen, particularly *Betula* and *Juniperus*, the virtual disappearance of the thermophilous herb *Filipendula* cf. *ulmaria*, and a pronounced increase in percentages of taxa indicative of open habitats, notably *Rumex*, *Artemisia* and species of Caryophyllaceae and Cyperaceae. SRR-1561 agrees closely with the date of 10,590 ± 185 BP obtained from a similar biostratigraphic horizon at a site in south-east Ireland[19] (although that assay was made on a 10-cm thick sample), but is markedly younger than the age of 11,000 BP assigned to the beginning of the Younger Dryas Chronozone in north-west Europe[4]. In Scotland and parts of northern England, the onset of cold climatic conditions and the build-up of Loch Lomond Advance ice seem to have begun before 11,000 BP (refs 5, 20), and thus the dates from Traeth Mawr and south-east Ireland, if correct, reflect the later onset of Stadial conditions and subsequent glacier development. This, in turn, might have been caused by time-transgressive southward movement of the oceanic Polar Front[21], but additional dates are required from other areas of western Britain to test this hypothesis.

The end of the Loch Lomond Stadial at Traeth Mawr is dated at 9,970 ± 115 BP (SRR-1560). These early Flandrian horizons are characterized by high Gramineae frequencies, a rising *Juniperus* curve and low arboreal percentages. The radiocarbon date agrees well with dates of 10,080 ± 320 BP, 10,060 ± 380 BP and 10,170 ± 220 BP obtained from basal Flandrian sediments in infilled pingo basins in south Cardiganshire[22–24], and a date of 10,200 ± 220 BP from the base of the Flandrian sequence in Tregaron Bog in west Wales[25], although the large standard errors on these latter dates mean that the true ages of the dated samples could be somewhat earlier. If correct, however, the radiocarbon determination from the Brecon Beacons and from adjacent regions seem to be slightly younger than the conventional age of 10,300 BP which is generally accepted as marking the close of the Late-Glacial period in Britain, and are also younger than dates which have recently been obtained for the wastage of Loch Lomond Advance ice from Rannoch Moor in western Scotland[7,26–28]. Collectively, they imply continued minerogenic inwash into lake basins (possibly associated with periglacial activity) for some time after such processes had ceased to operate in other areas of Britain. The reason for this is unclear, for it would be expected that the effects of climatic amelioration, particularly vegetational development and the trend towards soil stability, would have been experienced first in the more southern and western areas of the British Isles. Further research is clearly needed to resolve this paradox.

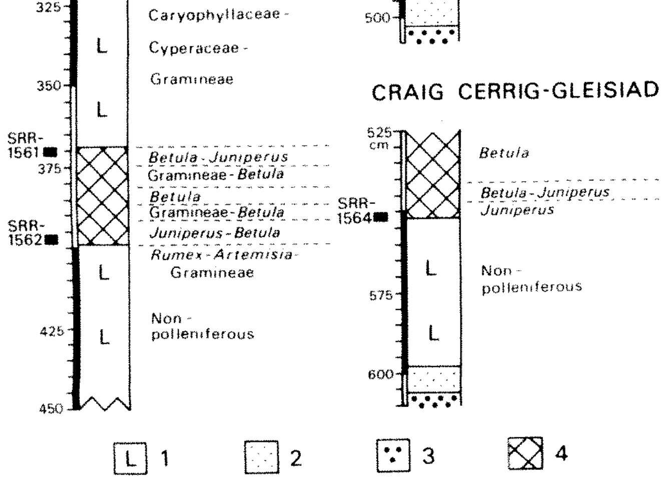

Fig. 2 The Brecon Beacons. Contour interval 100 m. The morainic areas are shown by heavy stipple-shading.

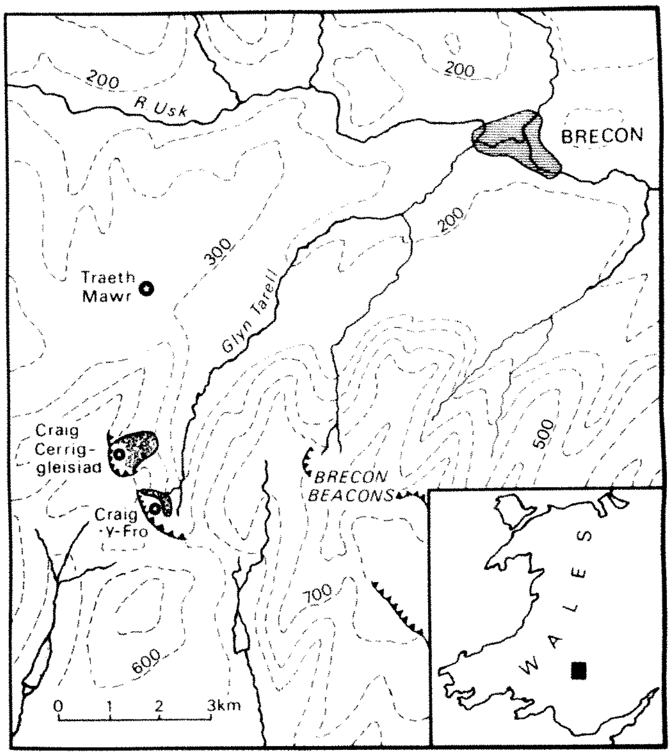

Fig. 3 Stratigraphies, pollen assemblage zones and radiocarbon-dated horizons at the three sites. 1, Fine silt/clay; 2, coarse silt/sand; 3, gravel; 4, gyttja.

At the two sites within the moraines, only Flandrian sediments are present. Lithostratigraphically, the sites are very similar (Fig. 3), the absence of Late-Glacial Interstadial sediments clearly implying that both basins contained glacier ice during the Loch Lomond Stadial. The lowermost organic muds at Craig-y-Fro are characterized by high frequencies of Gramineae and *Juniperus* pollen, and by a rising curve for *Betula*. Similar pollen assemblages are found in the basal sediments at Craig Cerrig-gleisiad, except that low values for *Juniperus* are initially recorded in that profile. The lowermost organic deposits at the two sites within the moraines can therefore be correlated biostratigraphically with the early Flandrian sediments at Traeth Mawr.

A radiocarbon date of 10,030 ± 100 BP (SRR-1563) was obtained from the basal organic sediments at the deepest point in the Craig-y-Fro basin, a date which agrees well with SRR-1560 at Traeth Mawr. At Craig Cerrig-gleisiad, however, the lowermost gyttja deposits were dated at 10,860 ± 70 BP (SRR-1564). This is over 800 yr older than dates obtained from comparable stratigraphic horizons at the other two sites, and is also much older than dates on the Late-Glacial–Flandrian boundary from elsewhere in Britain. The bedrock around Craig Cerrig-gleisiad is old red sandstone, and there are no known outcrops of calcareous bedrock on the northern side of the Brecon Beacons escarpment. The $\delta^{13}C$ value for the dated sample (Table 1) lies within the 'normal' range for gyttja material currently observed from European localities[29], and thus the possibility of contamination by older carbon would seem to be remote. On the other hand, all rocks are known to contain some elementary carbon which can become incorporated into, and concentrated in, gyttja sediments which are accumulating in areas of newly deglaciated terrain[18]. Moreover, it has recently been argued that the $\delta^{13}C$ value on radiocarbon dates from lake muds can no longer be regarded as a reliable indicator of 'hard water error' in view of the polygenetic nature of gyttja material[18,30]. Clearly, therefore, the possibility of a hard water factor in the basal date from Craig Cerrig-gleisiad cannot be excluded, although it is unclear why this should be so when a seemingly 'reliable' date was obtained from a comparable biostratigraphic horizon in the nearby Craig-y-Fro profile (a site located on the same bedrock and with a very similar glacial history).

With the exception of the date from Craig Cerrig-gleisiad, the pollen-stratigraphic and radiocarbon evidence suggests the following sequence of Late-Glacial events. Wastage of the late Devensian ice sheet left the large dead-ice hollow of Traeth Mawr which accumulated organic sediments throughout the mild Late-Glacial Interstadial. Climatic deterioration at ≃10,600 BP led to the break-up of the Interstadial vegetation cover, minerogenic inwash into the Traeth Mawr basin and the recrudescence of small glaciers in the lee of the Brecon Beacons which built moraines beneath Craig-y-Fro and in the cirque of Craig Cerrig-gleisiad. Climatic amelioration at, or shortly before, 10,000 BP prompted the rapid disappearance of these glaciers, the cessation of minerogenic inwash at Traeth Mawr, the onset of organic sediment accumulation in all three basins and the beginnings of Flandrian plant succession.

This research was financed by the British Geomorphological Research Group, and the radiocarbon dates were provided by the Natural Environment Research Council. I thank Dr D. D. Harkness for processing the radiocarbon samples, and Mr A. P. Donald, Mr D. John, Dr D. A. Kirby, Mrs G-M. Kirby, Mr A. Tolley and Mrs M. A. R. Walker for assistance with the fieldwork.

Received 2 June, accepted 9 July 1980

1 Lewis, C A *Brycheiniog* **14**, 97–120 (1970)
2 Lewis, C A in *The Glaciations of Wales and Adjoining Regions* (ed Lewis, C A.) 147–173 (Longmans, London, 1970)
3 Ellis-Gruffydd, I D *Cambria* **4**, 46–55 (Longmans, London, 1977)
4. Mangerud, J , Andersen, S T , Berglund, B E & Donner, J. J *Boreas* **3**, 109–126 (1974)
5 Sissons, J. B *Nature* **280**, 199–203 (1979)
6 Lowe, J J & Gray, J. M. in *Studies in the Lateglacial of North-West Europe* (eds Lowe, J J , Gray, J M & Robinson, J E) 157–175 (Pergamon, Oxford, 1980)
7 Walker, M. J. C. & Lowe, J J. *J. Biogeogr* **4**, 333–351 (1977)
8 Sissons, J. B., Lowe, J. J , Thompson, K. S R. & Walker, M J C *Nature Phys Sci* **244**, 75–77 (1973)
9. Kirk, W & Godwin, H. *Trans R Soc Edinb* **65**, 225–249 (1963)
10 Bishop, W W *Trans. J. Proc Dumfries Galloway nat Hist Antiq. Soc* **40**, 117–132 (1963)
11 Sissons, J B. & Walker, M J C *Nature* **249**, 822–824 (1974)
12. Lowe, J J *Pollen Spores* **20**, 367–397 (1978)
13 Pennington, W & Bonny, A P. *Nature* **226**, 871–873 (1970)
14. Pennington, W *Boreas* **4**, 157–171 (1975)
15. Pennington, W *Phil Trans R. Soc.* B**280**, 247–271 (1977)
16 Coope, G R & Brophy, J A *Boreas* **1**, 97–142 (1972).
17 Brown, A P *Phil. Trans R Soc* B**276**, 251–320 (1977)
18 Sutherland, D. G. in *Studies in the Lateglacial of North-West Europe* (eds Lowe, J J , Gray, J M & Robinson, J E.) 139–149 (Pergamon, Oxford, 1980)
19 Craig, A J *J. Ecol* **66**, 297–324 (1978).
20. Sissons, J. B. *Scotland* (Methuen, London, 1976)
21 Sissons, J B. *Nature* **278**, 518–521 (1979)
22 Shotton, F. W. & Williams, R E G *Radiocarbon* **15**, 451–468 (1973).
23 Shotton, F W , Williams, R. E G & Johnson, A. S *Radiocarbon* **17**, 255–275 (1975).
24 Handa, S & Moore, P D. *New Phytol* **77**, 205–225 (1976)
25. Hibbert, F A & Switsur, V R *New Phytol* **77**, 793–807 (1976)
26 Lowe, J J & Walker, M. J. C. *Nature* **264**, 632–633 (1976).
27 Walker, M J C & Lowe, J J *J Biogeogr* **6**, 349–362 (1979)
28 Walker, M J C & Lowe, J. J in *Timescales in Geomorphology* (eds Cullingford, R A , Davidson, D A & Lewin, J.) 247–259 (Wiley, New York, 1980)
29. Oeschger, H , Riesen, T & Lerman, J. C *Radiocarbon* **12**, 358 (1970)
30 Lowe, J J & Walker, M J C in *Studies in the Lateglacial of North-West Europe* (eds Lowe, J. J , Gray, J M & Robinson, J E) 123–137 (Pergamon, Oxford, 1980).
31 West, R G *Pleistocene Geology and Biology* (Longmans, London, 1977)

Pliocene dispersal of the horse *Equus* and late Cenozoic mammalian dispersal events

Everett H. Lindsay*, Neil D. Opdyke† & Noye M. Johnson‡

*Department of Geosciences, The University of Arizona, Tucson, Arizona 85721
†Lamont-Doherty Geological Observatory, Columbia University, Palisades, New York 10964
‡Department of Earth Sciences, Dartmouth College, Hanover, New Hampshire 03755

The Cenozoic history of land mammals is marked by brief periods of intercontinental dispersal, termed dispersal events[1,2]. One of these dispersal events includes the horse *Equus*, that evolved in North America, dispersed to the Old World in the Pliocene, and became a prominent member of Old World Pleistocene communities. *Equus* was derived from a species of the single-toed horse *Pliohippus*, known only from North America[3]. Timing for the Pliocene dispersal of *Equus* into Europe was questioned[4] following resolution for the appearance of *Equus* into the Siwalik sequence of Pakistan[5]. It seems that there were at least three major dispersal events of large mammals during the Pliocene (at 1.9, 2.6 and 3.7 Myr). We now report new data that limit the time of *Equus*' dispersal and into Europe to the 2.6 Myr dispersal event.

Development of the magnetic polarity time scale[6,7] and its application in magnetostratigraphy[3,8,9] has provided an independent and world-wide time frame for comparison of land mammal dispersal events, and their placement relative to geological events. Figure 1 shows the magnetic polarity time scale for the last five million years, with several North American late Cenozoic biostratigraphic faunal datum events. These biostratigraphic faunal datum events mark the earliest known records for these mammals (such as *Equus*) that dispersed between North America and Eurasia during the late Cenozoic.

Magnetostratigraphic work in Idaho[3] and Washington[10] documents the first occurrence in North American deposits of at least five genera of land mammals (*Trigonictis*, *Satherium*, *Parailurus*, *Ursus* and *Bretzia*) whose ancestry and/or an earlier record occurs in Palaearctica[11–15]. These immigrants are first recorded in North America during the interval of 3.5 to 4.0 Myr during the upper part of the Gilbert magnetic chron. The appearance of this diverse group of Palaearctic immigrants suggests this interval was a major period of land mammal dispersal between North America and Eurasia.

Early Villafranchian faunas lacking *Equus* and *Elephas* (actually the genus *Mammuthus*) are recognized as chronologically significant[16]. Villafranchian land mammal age includes mammal zones MN 16 and 17 (ref. 23) and a pre-E-L-E Villafranchian interval (mammal zone MN 16a) has recently been established[17]. Previous divisions of early Villafranchian faunas[18] tended to include faunas with *Equus* and *Mammuthus* for example, Montopoli in Italy and Malusteni in Romania with faunas lacking those genera (for example, Triversa in Italy and Etouaires in France). The Etouaires and overlying Roccaneyra faunas of France are placed in mammal zone MN 16b by Mein[17]. *Equus* occurs in the Roccaneyra fauna, but is absent from the Etouaires fauna. The early Villafranchian Vialette fauna in France is comparable to that of Etouaires[19], with both *Equus* and *Mammuthus* absent. The Vialette fauna is overlain by a basalt dated 2.6 Myr (ref. 20) and is underlain by a basalt dated 3.3 Myr. Radiometric results from Etouaires, Roccaneyra and Vialette suggest that the European E-L-E fauna datum (the beginning of mammal zone MN 16b) approximates 2.5 Myr, near the Gauss/Matuyama magnetic chron boundary.

To resolve the correlation of faunas in mammal zone MN 16, and to clarify the European E-L-E faunal datum, we collected palaeomagnetic samples during the summer of 1979 from stratigraphic sections in Italy yielding the Montopoli and Triversa faunas. Each locality was sampled at five sites, with three samples per site. The samples from the Montopoli section span 32 m, those from the Fornace RDB (Triversa fauna) section span only 13 m. All samples were subjected to both alternating field and thermal magnetization to remove secondary components of magnetization.

The section at Montopoli is very sandy and exposures are poor. Strata suitable for palaeomagnetic sampling were found only after diligent search. Calcareous concretions were sampled at the stratigraphically higher sites. All samples gave natural remanent magnetization (NRM) directions of normal polarity, and a.f. demagnetization did not produce any change in the polarity. Partial thermal demagnetization was attempted on the upper three sites, and pilot samples from the upper two sites changed to reversed polarity very suddenly between 550 and 600 °C. The intensities of these samples were very low, approaching the limits of sensitivity of the magnetometer. Then all remaining samples were thermally demagnetized at 500 °C, at which point the other samples from the upper two sites changed to reversed polarity (although the intensity was very low) with polarity of remaining samples unchanged. The resulting polarity zonation (Fig. 2) is weak because of limitation imposed by the available lithology. However, it is the most reasonable polarity interpretation likely to become available from that section.

The section at the Fornace RDB quarry at Villafrance d'Asti provided finer grained lithologies and stronger magnetic properties but the section available for sampling is shorter. Poorly indurated sandstones occur above and below the sampled section at the Fornace RDB quarry. After a.f. and thermal demagnitization, four of the five sites gave unquestionable reversely magnetized polarity (Fig. 2). The directions from the second highest site gave normal polarity after thermal demagnetization to 500 °C. This site apparently records a normal event within an otherwise reversely magnetized section (Fig. 2).

The Montopoli section is interpreted to represent the upper Gauss and lower Matuyama magnetic chrons, with the boundary occurring about 25 m above the base of the section, 7 m below the top of the section which is the level of the Montopoli fauna. The quarry that yielded the Montopoli fauna was relocated by A. Azzaroli with the help of residents of Montopoli. Our highest palaeomagnetic site is from the level of the quarry, 15 m distant along strike.

The Fornace RDB section is interpreted to represent the middle of the Gauss magnetic chron, with a record of the Mammoth and Kaena events, separated by a normal magnetozone. The level of mammals recovered from the Fornace RDB quarry approximates the middle of our section. The Arondelli quarry is about 1.5 km distant across the Triversa valley at the same level as the upper part of our section. Azzaroli[21] correlated the Arondelli and Fornace RDB sections as approximately equivalent. Lithology at the top of our Fornace RDB sampled section is similar to that at the Arondelli quarry. Therefore, the Triversa fauna (based on the Fornace RDB and Arondelli quarry assemblages) is placed in the middle to upper half of our Fornace RDB section, which we correlate with the middle of the Gauss magnetic chron. The polarity zonation of the Fornace RDB section is not definitive for that specific chronological interval; it could represent the Gilbert magnetic chron or the lower Matuyama magnetic chron. Both of those interpretations are rejected, based on faunal similarity of the Triversa fauna with the Etouaires and Vialette faunas of France, and radiometric dates associated with those faunas.

Correlations of the Montopoli and Fornace RDB sections with the magnetic polarity time scale are made with reservation. Interpretations are insecure due to low magnetic intensity of samples from Montopoli, and shortness and non-definitive polarity of the Fornace RDB section. Placement of these sections (and faunas) relative to the magnetic polarity time scale is based as much on biochronological correlation of the faunas as on magnetic polarity zonation.

Magnetic polarity zonation of the Fornace RDB section could have been correlated with the lower Matuyama magnetic chron, which would place the Triversa fauna approximately at the Olduvai event. This correlation is rejected because the Triversa fauna should be earlier than the Montopoli fauna which we correlate with the base of the Matuyama magnetic chron. Faunal similarity of the Montopoli and Triversa faunas is strong, the most significant difference between these faunas is the presence of *Equus* and *Mammuthus* in the Montopoli fauna and their absence from the Triversa fauna. The Triversa fauna is rich and diverse; it includes large mammals like *Tapirus*, *Dicerorhinus*, *Mammut*, and *Anancus*[21,22], which are distinct from but comparable in size to *Equus* and *Mammuthus*. If those latter genera had lived in the Po Valley of Italy during the time the sediments that yielded the Triversa fauna were deposited, they would surely be recorded in the fauna.

The Fornace RDB section could also have been correlated with the Gilbert magnetic chron. This correlation is rejected because of an unpublished palaeomagnetic section from the Pichegu quarry about 30 km south of Nimes, France, that supports a correlation of mammal zone MN 14 (earlier than MN

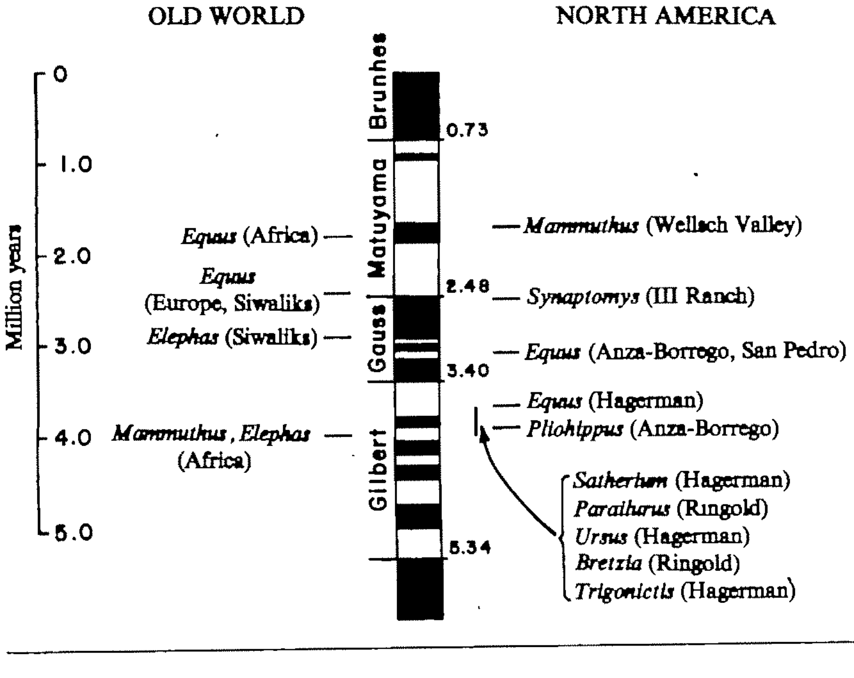

Fig. 1 Important mammalian faunal datum events relative to the dispersal of *Equus*. The central column represents the magnetic polarity time scale (black equals normal polarity and white equals reversed polarity); the Olduvai event is the normal polarity interval at about 1.9 Myr, the Kaena and Mammoth events are the reversed polarity intervals above and below the 3.0 Myr normal polarity event. North American datum events are given for the lowest stratigraphic record of that taxon at the location given in parenthesis. With the exception of *Pliohippus* at Anza-Borrego and *Equus* at Anza-Borrego and San Pedro, the North American faunal data probably represent the earliest North American record for those genera. Old World faunal datum events are believed the earliest known record for those genera on that continent. All faunal datum events are dispersal events with the exception of *Equus* at Hagerman and *Mammuthus* plus *Elephas* in Africa, which are probably evolutionary events. The European E-LE-E (*Equus-Leptobos-Elephas*) faunal datum is placed at the *Equus* faunal datum for Europe and the Siwaliks, at the base of the Matuyama magnetic chron, about 2.5 Myr.

16) with the Gilbert magnetic chron. Suc[24] showed that the palynological extinction of plants of the group Taxodiaceae occurs in southern France during the Pliocene, between the small mammal subzones of Hautimagne and Sete. This chronological interval is approximately at the boundary between mammal zones MN 14 and 15. Suc identified the extinction of Taxodiaceae near the top of the Pichegu section (personal communication), which means the main part of that section is correlative, more or less, with mammal zone MN 14. The Pichegu section, which lacks mammals as it is dominantly marine, is reversely magnetized through an interval of more than 50 m stratigraphically below the extinction of Taxodiaceae. We interpret this long magnetozone of reversed polarity, that corresponds broadly with mammal zone MN 14, as part of the Gilbert magnetic chron. Only the Gilbert magnetic chron in the interval of Ruscinian land mammal age (mammal zones MN 14 and 15) has a monotonously uniform reversed polarity zone of that thickness. Therefore, it seems unlikely that the Fornace RDB fauna, in mammal zone MN 16a, is correlative with part of the Gilbert magnetic chron.

These preliminary results, and our interpretations, support a correlation of mammal zone MN 16 with the late Gauss and early Matuyama magnetic chrons, and suggest the division of MN 16a and 16b approximates the Gauss/Matuyama boundary, 2.48 Myr.

Azzaroli[21] believes that the record of *Equus* and *Mammuthus* from Montopoli is the most primitive and probably earliest record of these mammals in Europe. Thus the appearance of *Equus* and *Mammuthus* in Europe is approximately coincident with their appearance in southern Asia[5] at about 2.5 to 3.0 Myr. Several early Villafranchian faunas in eastern Europe also have early records of *Equus* and *Mammuthus*, and might be as early as, or earlier than, the Montopoli fauna[25,26]. Biochronological-palaeomagnetic sequence studies[27] of the Ponto-Caspian Basin show the beginning of the *Archidiskodon* Superzone (equivalent to the appearance of *Mammuthus*, and possibly *Equus*) at the Mammoth event (about 3.1 Myr) in that area. Extensive Plio-cene–Pleistocene palaeomagnetic studies have been undertaken in southern Tajikistan (near the Russian-Afghanistan border[28] where the Navrukho fauna includes the elephant *Mammuthus* (*Archidiskodon*) *gromovi* (also recorded from Montopoli) and *Equus*. The Navrukho fauna is from rocks with reversed magnetic polarity correlated with the lower Matuyama magnetic chron, and is therefore similar in age to the Montopoli fauna.

Our work in Pakistan[5] demonstrated the appearance of *Equus* and *Mammuthus* in the Oriental zoogeographic region in the late Pliocene (see Fig. 1). We questioned the appearance of these immigrant genera in Europe about one million years before their arrival in southern Asia, but found no definitive data to reject this hypothesis[4]. Results and interpretations given above suggest the coincident appearance of *Equus* and *Mammuthus* in Europe no earlier than about 2.5 Myr.

Equus could not have dispersed before about 3.7 Myr when it evolved from *Pliohippus*; its population density and distribution were probably not sufficient to disperse to Eurasia during the interval 3.7–4.0 Myr, when several Eurasian mammals dispersed to North America. *Equus* became widespread and prominent in the North American faunas after about 3.3 Myr but conditions for dispersal to Asia were apparently not favourable until about 2.6 Myr, shortly before the lemming *Synaptomys* appeared in North America. *Synaptomys* is considered an immigrant to North America and its North American appearance is near-coincident with the south Asian and European appearance of *Equus* (2.5 Myr). Thus, the dispersal history of *Equus* and *Synaptomys* suggest dispersal between North America and Asia about 2.6 Myr.

The discontinuous, sudden, and short duration of these late Cenozoic dispersal events suggests they may be controlled by geological and climatic factors rather than by biological factors. The dispersal history of elephants is similar and supports the concept of more or less widespread and short dispersal events. Elephants evolved in Africa where *Elephas* and *Mammuthus* (*Archidiskodon*) evolved from *Primelephas* at ~4 Myr. *Elephas* dispersed to southern Asia at ~2.9 Myr, slightly before the appearance of *Equus* in southern Asia[5] and the appearance of *Mammuthus* (*Archidiskodon*) in Europe is approximately coincident with the European appearance of *Equus*. The earliest known record[29] of *Mammuthus* in North America is approximately 1.8 Myr. Apparently *Mammuthus* did not enter North America and *Equus* did not enter Africa during the 2.6 Myr dispersal event, because these immigrant populations were too small to warrant further dispersal during that dispersal event. About 1.9 Myr ago, geological and climatic conditions were right for another dispersal event. At that time *Mammuthus* dispersed to North America and *Equus* dispersed to Africa.

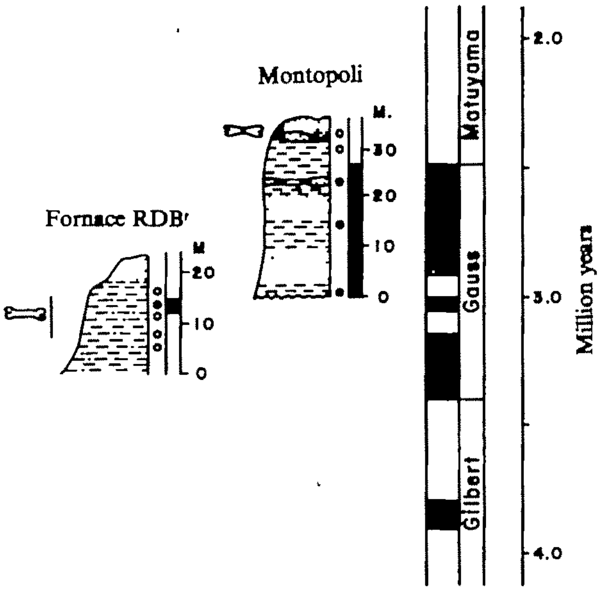

Fig. 2 Magnetic polarity zonation for sections at Montopoli and Fornace RDB quarry (Villafranca d'Asti) in Italy, and correlation of these sections with the magnetic polarity time scale. The Kaena and Mammoth events occur above and below the 3 Myr normal polarity interval. Palaeomagnetic sample sites are shown adjacent to lithologic sections; black circles indicate normal polarity, white circles indicate reversed polarity sites. Location of the Montopoli and Triversa (at Fornace RDB) faunal levels are indicated by bone symbols. The Montopoli fauna is a principal reference for mammal zone MN 16b, with *Equus* present. The Triversa fauna is a principal reference for mammal zone MN 16a, with *Equus* absent.

The earliest datable occurrences of *Equus* in Africa[30] are below the KBS Tuff in the Koobi Fora Formation in Kenya and in member G of the Shungura Formation in Ethiopia. The revised date for the KBS Tuff is 1.81 Myr (ref. 31). The palaeontological evidence (primarily stage of evolution in several lineages of suids) indicates a strong correlation between the KBS Tuff level of the Koobi Fora Formation, member G or H of the Shungura Formation, and Bed 1 of Olduvai Gorge[32–36]. There is a strong palaeontological and radiometric correlation of these units in the interval of 1.8–2.0 Myr. Thus, the appearance of *Equus* in Africa and the appearance of *Mammuthus* in North America may be coincident. We regard the proximity of these appearances as a significant mammal dispersal event, at about 1.9 Myr.

In summary, it appears the horse *Equus* and the elephant *Mammuthus* evolved at approximately the same time in North America and Africa, respectively, and their dispersal to Eurasia was approximately at the same time. Neither is definitely recorded from Europe or Asia prior to about 3.0 Myr, and both are commonly recorded in fossil deposits of both continents younger than 2.5 Myr. Each genus later dispersed to the continent where the other evolved, but is not recorded on that continent until about 1.9 Myr. Additional data are needed to resolve their appearance in Europe in the interval 2.6–3.0 Myr. The dispersal records and timing of dispersal for these two genera serve as a model for late Cenozoic intercontinental dispersal of land mammals. They suggest that the history of mammals during that interval is marked by infrequent, widespread, and comparatively short intervals of intercontinental dispersal. Timing for three of these major dispersal events is approximately 1.9, 2.6, and 3.7 Myr. The nature and timing of these major dispersal events suggest they may be triggered by geological or climatic factors.

This research was supported by a grant from the National Geographic Society and by NSF grant EAR 74-13860. We also acknowledge the counsel and field assistance of A. Azzaroli, M. Mazzini, and C. de Giuli of Italy; of L. Thaler, J. Michaux, and J. P. Suc in France. Lamont-Doherty Geological Observatory publication number 3003.

Received 2 April; accepted 10 July 1980.

1. Simpson, G. G. *Bull. geol. Soc. Am.* **58,** 613–687 (1947).
2. Repenning, C. A. *The Bering Land Bridge* (ed. Hopkins, D. M.) 288–311 (1967).
3. Neville, C., Opdyke, N. D., Lindsay, E. H. & Johnson, N. M. *Am. J. Sci.* **279,** 503–526 (1979).
4. Lindsay, E. H., Opdyke, N. D. & Johnson, N. M. *Proc. Int. Conf. Field-workshop on the Stratigraphy of Loess and Alluvial Deposits IGCP Project 128* (in the press).
5. Opdyke, N. D. *et al. Palaeogeog. Palaeoclimatol. Palaeoecol.* **27,** 1–34 (1979).
6. Cox, A. *Science* **163,** 237–245 (1969).
7. LaBrecque, J. L., Kent, D. V. & Cande, S. C. *Geology* **5,** 330–335 (1977).
8. Johnson, N. M., Opdyke, N. D. & Lindsay, E. H. *Bull. Geol. Soc. Am.* **86,** 5–11 (1975).
9. Opdyke, N. D., Lindsay, E. H., Johnson, N. D. & Downs, T. *J. Quat. Res.* **7,** 316–329 (1977).
10. Neville, C. *et al.* (in preparation).
11. Bjork, P. R. *Trans. Am. phil. Society* **607,** 1–54 (1970).
12. Gustafson, E. P. *Bull. 23, Mus. Nat. Hist. Univ. Oregon* 1–62 (1978).
13. Bjork, P. R. *Trans. Kansas Acad. Sci.* **76,** 24–38 (1974).
14. Repenning, C. A. *J. Res. U.S. Geol. Survey* **4,** 305–315 (1976).
15. Tedford, R. H. & Gustafson, E. P. *Nature* **265,** 621–623 (1977).
16. Hurzeler, J. *Coll. International C.N.R.S.* **163,** 633–636 (1967).
17. Mein, P. *Ann. Geol. Pays Hellenica, extra ser.* **3,** 1367–1372 (1979).
18. Tobien, H. *Palaeogeogr. Palaeoclimat. Palaeoecol.* **8,** 77–93 (1970).
19. Heintz, E., Guerin, C., Martin, R. & Prat, F. *Mem. B.R.G.M.* **78**(1), 169–182 (1974).
20. Bandet, Y., Donville, B. & Michaux, J. *Bull. Soc. géol. Fr.* **20,** 245–251 (1978).
21. Azzaroli, A. *G. Geol.* **41,** 61–79 (1977).
22. Savage, D. E. & Curtis, G. H. *Geol. Soc. Amer. Spec. Pap.* **124,** 207–231 (1970).
23. Fahlbusch, V. *Newsl. Stratigraphy* **5**(2/3), 160–167 (1976).
24. Suc, J. P. *Geobios* **9,** 741–771 (1976).
25. Macarovici, N. *Studies on Cenozoic Paleontology and Stratigraphy* Vol. 3 (ed. Hibbard, C. W.) 39–95 (1975).
26. Benda, L., Meulenkamp, J. E. & Van de Weerd, A. *Newsl. Stratigraphy* **6,** 117–130 (1977).
27. Kochegura, V. V. & Zubakov, V. A. *Palaeogeog. Palaeoclimatol. Palaeoecol.* **23,** 151–160 (1978).
28. Nikiforova, K. V. & Dodonov, A. Y. *Guidebook, International Symposium on the Neogene-Quaternary Boundary,* 173–176 (1977).
29. Harington, C. R. *Syllogeus* **15,** 1–32 (1978).
30. Maglio, V. J. *Nature* **239,** 379–385 (1972).
31. Drake, R. E., Curtis, G. H., Cerling, T. E., Cerling, B. W. & Hampel, J. *Nature* **283,** 368–372 (1980).
32. Curtis, G. H. & Hay, R. L. *Calibration of Hominoid Evolution* (eds Bishop, W. W. & Miller, J. A.) 289–302 (Scottish Academic, Edinburgh, 1972).
33. Cooke, H. B. S. *G. Geol.* **41,** 243–256 (1977).
34. White, T. D. & Harris, J. M. *Science,* 198, 13–21 (1977).
35. Harris, J. M. & White, T. D. *Trans. Am. phil. Soc.* **69,** 1–128 (1979).
36. Cooke, H. B. S. *Science* **201,** 460–463 (1978).

Somatic embryogenesis from *Sorghum bicolor* leaves

Wolfgang Wernicke & Richard Brettell

Friedrich Miescher-Institut, PO Box 273, CH-4002 Basle, Switzerland

Plant regeneration from totipotent cultured cells or protoplasts is a prerequisite for the often proposed genetic modification of plants through somatic cell genetics, and has been achieved in many species. The cereals (and the rest of the Gramineae) have, however, proved to be extremely unresponsive to *in vitro* culture techniques[1]. The most convenient source of plant protoplasts is the leaf tissue because it allows the isolation of a large, relatively uniform cell population without the necessity of killing the plant. However, despite considerable efforts, sustained cell division has never been obtained from cereal leaf blade protoplasts[2]. Thus, a crucial question arises of whether leaf cells from cereals are actually totipotent and consequently, whether they can be useful for somatic cell genetics. We now report that young leaf tissue of a cereal can express totipotency even to the extent of forming somatic embryos. However, the ability to respond is rapidly lost during leaf maturation. We think that this phenomenon can explain many difficulties faced in cereal tissue culture. Moreover, the leaf culture we describe may help to ascertain whether mature cereal cells are merely no longer competent (in the sense of Halperin[3]) to respond to tested *in vitro* conditions or whether they actually lose their totipotency.

Sorghum bicolor (L.) Moench was chosen for the experiments. (So far, only the variety G522 (Funk Seeds International) found to be responsive in immature embryo and inflorescence culture[4,5] has been tested.) Plants were grown from seed in test tubes in aseptic conditions for 10 days. Leaves of grasses grow from the base, thus exhibiting a gradient in maturation from base to top. Starting about 0.5 mm above the apical meristem (1.5 mm above insertion of the first foliage leaf), leaves were dissected under a stereo microscope into 1.5-mm long sections. The leaf sections were unrolled and cultured individually on MS

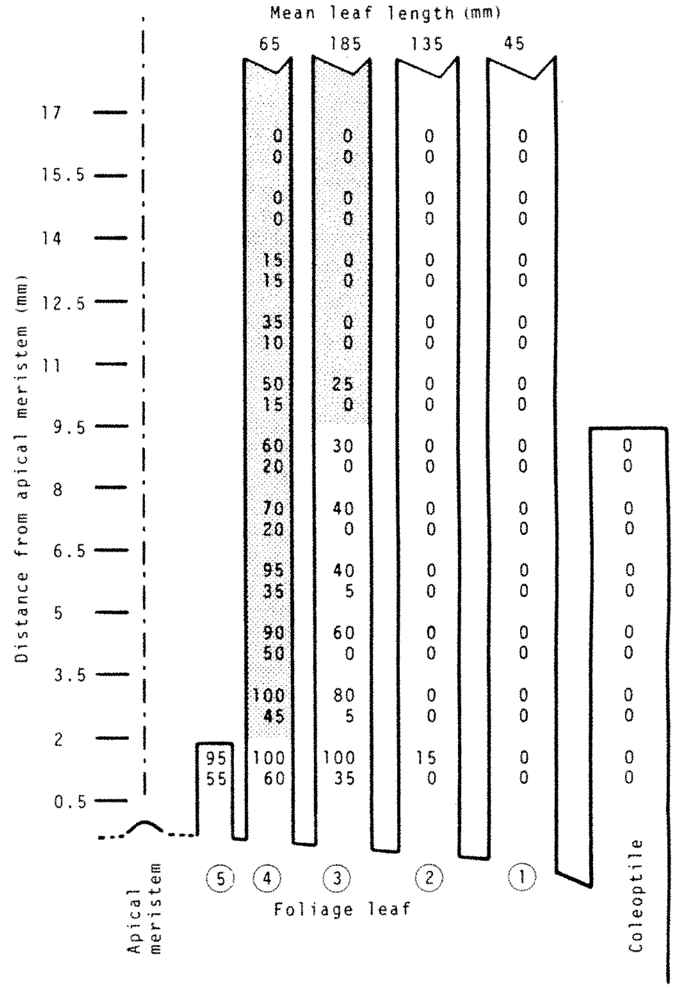

Fig. 1 Diagram of the leaf culture system in *Sorghum bicolor,* showing the response of leaf pieces cultured in the dark at 25 °C. Donor plants were grown from surface sterilized seeds for 10 days on MS medium[6] with 20 g l^{-1} sucrose under 16-h days (light provided by fluorescent tubes, 1,500 lx). Twenty equally sized plants were selected. The lower parts of the plants were cut into 1.5-mm long segments and the leaf pieces were placed individually on MS medium supplemented with 2 mg l^{-1} 2,4-D, 0.1 mg l^{-1} kinetin and 40 g l^{-1} sucrose. The leaf blade was clearly distinguishable from the sheath in the first four foliage leaves and is denoted by the shaded area. The experiments were evaluated after 5 weeks culture. In each segment, upper value: % leaf pieces giving rise to callus; lower value: % leaf pieces with macroscopically visible embryogenic tissue.

0028–0836/80/370138—02$01.00

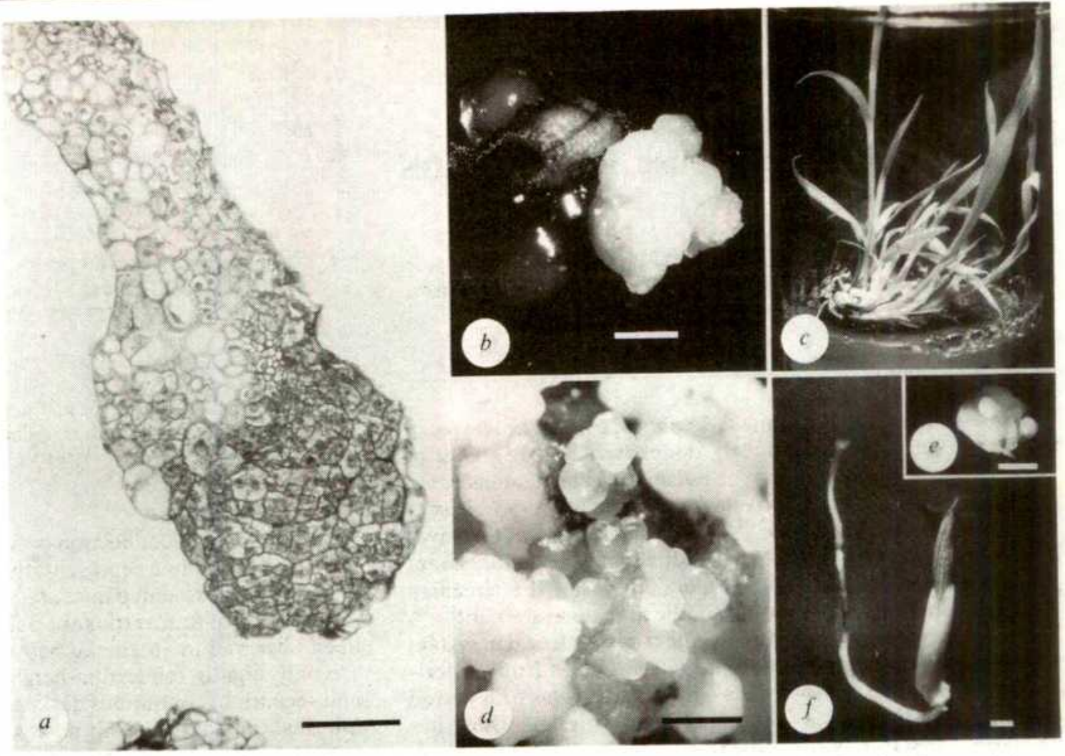

Fig. 2 *a*, Cross-section through a leaf piece (fourth foliage leaf, ~6 mm above the apical meristem) cultured for 5 days on nutrient medium. Note the cell proliferation underneath a region which has been damaged during excision. Scale bar, 100 µm. *b*, Callus growing from a leaf piece (fourth foliage leaf, 14 mm above the apical meristem). The non-proliferating tissue produced a dark pigment. *c*, Plant regeneration in the light (800 lx) from white callus tissue after transfer to auxin-free medium. Shoot growth could be accelerated by addition of 0.1 mg l^{-1} kinetin. *d*, Embryogenic tissue derived from callus shown in *b* after transfer of white compact tissue to a culture medium with reduced 2,4-D concentration. The white globular bodies were able to germinate like zygotic embryos. *e*, Isolated somatic embryo with scutellum, coleoptile and primary root breaking through coleorhiza. Leaf culture origin. *f*, Germinating somatic embryo. In *b*, *d*, *e* and *f*, scale bar, 1 mm.

medium[6]. The youngest leaf that was cultured (fifth foliage leaf) had reached a length of about 2 mm (Fig. 1). In the presence of 2,4-D (1–3 mg l^{-1}) the young leaf pieces proliferated to form a subculturable callus, which consisted for the most part of proliferating yellowish root primordia covered with slimy rootcap-type cells; the roots elongated when 2,4-D was omitted from the medium[7]. In many cases, however, macroscopical examination revealed the presence of a folded, compact, white tissue which, after transfer to auxin-free medium, formed shoots and plantlets (Fig. 2*a*–*c*). Various additions to the medium such as coconut water, casamino acids, cytokinins, different auxins and gibberellic acid (GA_3), were tested. These modifications gave no significant improvement in growth or were even inferior, although the addition of 0.1 mg l^{-1} kinetin seemed slightly to increase the relative proportion of the white tissue. After prolonged culture (~5 weeks), especially after transfer to a culture medium with reduced 2,4-D concentration (0.5 mg l^{-1}), the white tissue formed globular structures (Fig. 2*d*). Many of these structures resembled zygotic embryos in having a scutellum and a clearly defined root–shoot axis. After transfer to a medium without auxin, optionally supplemented with 0.1 mg l^{-1} kinetin, the structures were able to germinate like zygotic embryos (Fig. 2*e*, *f*). In this respect, the leaf cultures did not differ from cultures derived from the scutellum of immature embryos[4].

The response of different leaf pieces is summarized in Fig. 1. It can be seen that the further the 'distance' (spatial and temporal) from the apical meristem, the less responsive the tissue became. This pattern of response correlated with the pattern of leaf blade and leaf sheath maturation described by plant morphologists[8,9].

Cytological examination of cultured immature leaf pieces derived from the fourth foliage leaf revealed that developing mesophyll, bundle sheath and occasionally epidermal cells close to lesions caused by excision were prone to proliferate (Fig. 2*a*). In explants taken from the third foliage leaf, proliferation was more restricted to cells closely associated with the vascular bundles, and resulted in less white, compact tissue (Fig. 1). It seems, therefore, that the embryogenic tissue is formed by mesophyll and/or epidermal cells.

The calluses which have been obtained from immature leaf pieces consist of a mass of proliferating primordia (shoot–embryo and/or root primordia). Full expression of morphogenesis is inhibited by the hormone (2,4-D in this case) essential for stimulation of callus growth, but the primordia can be released by reduction and omission of the hormone. The occurrence of similar responses in morphogenetic cultures of dicots has also been recently discussed[10]. Our findings suggest that the grasses differ from dicots in that the cells have to come from a very immature tissue. In our experiments, totipotent cells were clearly part of the growing leaf blade as well as the leaf sheath, but only in the two least mature leaves. (Root-type callus cultures have been induced from basal (immature) parts of rice leaf sheaths[11].) The recent finding of Saalbach and Koblitz[12], who in a single experiment obtained shoots from a cultured barley leaf, could be explained by proliferation of cells from a leaf that happened to come from close to the apical meristem.

Competence *in vitro* may be correlated with continuing meristematic activity *in vivo*. In fact, in grasses, cell proliferation *in vitro* has only been observed in tissues that are close to an undifferentiated state[13]. Thus, the process which in research on dicots has been termed 'dedifferentiation' has most critical implications for cereal tissue culture. The use of the leaf culture system may enable us to define more precisely the step in differentiation leading to loss of competence (if not totipotency) and thereby possibly overcome the barrier which prevents the mature cells from responding *in vitro*.

We thank Brigitte Bolliger and Stefan Eberhard for technical help and our colleagues for valuable discussions.

Received 17 April; accepted 20 June 1980.

1. Thomas, E., King, P. J. & Potrykus, I. *Z. PflZücht.* **82,** 1–30 (1979).
2. Potrykus, I. in *Advances in Protoplast Research* (eds Ferenczy, L. & Farkas, G. L.) 243–254 (Pergamon, Oxford, and Akademiai Kiado, Budapest, 1980).
3. Halperin, W. *A. Rev. Pl. Physiol.* **20,** 395–418 (1969).
4. Thomas, E., King, P. J. & Potrykus, I. *Naturwissenschaften* **64,** 587 (1977).
5. Brettell, R., Wernicke, W. & Thomas, E. *Protoplasma* (in the press).
6. Murashige, T. & Skoog, F. *Physiol. Pl.* **15,** 473–497 (1962).
7. King, P. J., Potrykus, I. & Thomas, E. *Physiol. Veg.* **16,** 381–399 (1978).
8. Sharman, B. C. *Ann. Bot.* **6,** 245–284 (1942).
9. Kaufmann, P. B. *Phytomorphology* **9,** 277–311 (1959).
10. Thomas, E., Brettell, R. & Wernicke, W. in *Advances in Protoplast Research* (eds Ferenczy, L. & Farkas, G. L.) 269–273 (Pergamon, Oxford, and Akademiai Kiado, Budapest, 1980).
11. Wu, L. & Li, H. W. *Cytologia* **36,** 411–416 (1971).
12. Saalbach, G. & Koblitz, H. *Pl. Sci. Lett.* **13,** 165–169 (1978).
13. O'Hara, J. F. & Street, H. E. *Ann. Bot.* **42,** 1029–1038 (1978).

Circadian rhythmicity participates in the photoperiodic determination of diapause in spider mites

A. Veerman & M. Vaz Nunes

Laboratory of Experimental Entomology, University of Amsterdam, Kruislaan 302, 1098 SM Amsterdam, The Netherlands

The role of circadian rhythmicity in photoperiodic processes in plants and animals is still poorly understood. Involvement of circadian rhythmicity in photoperiodism has been demonstrated for a number of plants[1,2], two mammals[3,4], a number of birds[5,6], and some species of insects[7–11]. Three theoretical alternatives have been suggested with regard to the form this involvement may take, with emphasis on the possibility that the circadian system is concerned with photoperiodic time measurement[12–14]. Most of the evidence for the involvement of the circadian system in both plant and animal photoperiodism comes from experiments with nondiel photoperiods—light/dark cycles with period lengths other than 24 h. The experimental design which has been used most frequently is the so-called resonance technique, in which the light component of a light/dark cycle is held constant and the dark component is varied over a wide range in successive experiments, to provide cycles with period lengths up to 72 h or more. Rhythmic variations in the photoperiodic response with peaks about 24 h apart are evidence for the involvement of circadian rhythmicity in the photoperiodic process studied. However, in some plants[1], a reptile[15], and a number of insect species[16–20], the resonance technique failed to demonstrate any influence of circadian rhythmicity on photoperiodism. Using the same technique we have now found a rhythmic response in the incidence of diapause in the common spider mite, *Tetranychus urticae*, thus showing that in mites also, circadian rhythmicity is involved in the photoperiodic reaction.

Diapause in *T. urticae* is of the facultative type and occurs normally in adult females which have experienced short-day photoperiods during their larval and nymphal stages of development[21]. The most conspicuous characteristic of the diapause state in *T. urticae* is the deeply orange colour of the diapausing females, as compared with the greenish-yellow of the 'summer' females. Other features of the diapause are arrest of oviposition, cessation of feeding, voiding of the intestinal tract and changes in behaviour. For the experiments, the mites were kept on detached leaf cultures of beans (*Phaseolus vulgaris*). Resonance experiments were performed at 19 °C; photoperiodic cycles consisted of a fixed light phase of 8 h duration and dark phases which were varied over 4–84 h, the duration of darkness being increased in steps of 4 h in the repetitions of the experiment. Approximately 250 mites were used in each photoperiodic treatment and each photoperiodic regime was sustained throughout the complete development of the mites.

The results presented in Fig. 1 clearly show that, with a fixed duration of the light phase, the incidence of diapause in *T. urticae* is a rhythmic function of the duration of darkness. Peaks of high diapause incidence recur with cycle lengths (duration of light plus dark) of about 24, 44, 64 and 84 h. Diapause induction is completely averted in photoperiodic cycles consisting of 8 h light combined with dark phases of 4–9, 24–28, 44–48 and 60–64 h. Apart from the cycles with night lengths of 4–9 h, in all photoperiodic regimes the duration of darkness exceeded the critical nightlength, which is 10 h in the strain of mites used. The conclusion from these experiments is that in *T. urticae* circadian rhythmicity is somehow involved in the photoperiodic determination of diapause. Thus we demonstrate here, for the first time, a functional connection between the circadian system and photoperiodism in a representative of the Acarina or mites.

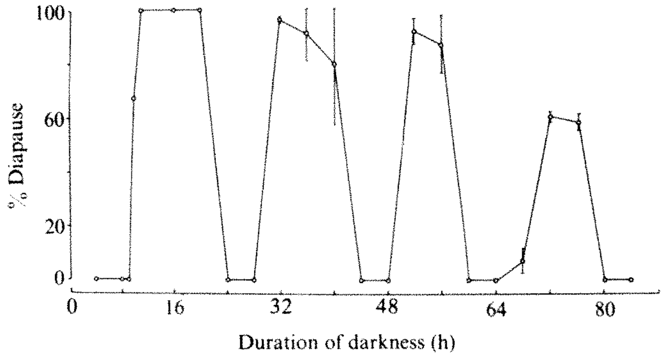

Fig. 1 Diapause incidence in *T. urticae* in cycles of 8 h of light and (abscissa) different durations of darkness. Vertical lines represent ±1 s.e.m.

The results presented here are remarkable in several respects. A sequence of four resonance peaks as shown in Fig. 1 has not been observed in an animal before. The third and fourth peak are only slightly reduced in height in comparison with the first and second. In continuous darkness diapause incidence in these mites is 0% (ref. 21). This means that photoperiodic induction still takes place in cycle lengths of over 80 h. Of these long cycles at 19 °C, only three or four are perceived by the mites during the photoperiodic sensitive larval and nymphal stages. However, previous experiments with *T. urticae* have shown that the summation of photoperiodic information may already be saturated with three photoperiodic cycles[21], which might explain the presence of a fourth resonance peak in the experiments presented here.

Another divergence from the results obtained with other organisms is the fact that the resonance peaks in the experiment with *T. urticae* as shown in Fig. 1 are only about 20 h apart. Resonance experiments with plants, mammals, birds, and insects have shown peak intervals of about 24 h (refs 1–6, 22, 23). If we assume that the peaks of diapause incidence in Fig. 1 result from an influence of the circadian system on the photoperiodic reaction in these mites, the circadian rhythm involved may have a free-running period of only about 20 h. This value is exceptionally low when compared with the values of the periods of all known kinds of free-running circadian rhythms, which tend to be closer to 24 h and normally vary over ~22–27 h (refs 22, 23).

Earlier experiments with *T. urticae*, such as experiments with temperature cycles in continuous darkness[21], with light interruptions in various long nights, and with two light pulses of equal duration in each photoperiodic cycle, could be explained on the assumption that circadian rhythmicity is not involved in photoperiodic time measurement in these mites[24,25]. In work on the fruit tree red spider mite, *Panonychus ulmi*, Lees[26,27] found no indication for the participation of circadian rhythms in the photoperiodic reaction. The divergent results with the two spider mite species are difficult to explain in terms of a mechanism of photoperiodic time measurement. A full account of the results presented here, with considerations on photoperiodic time measurement in spider mites, must await further experiments with nondiel photoperiods in *T. urticae*, which are now under way, and will be published elsewhere.

We thank Miss C. van Ruth and Mr G. van de Berg for technical assistance. This work was supported by a grant to M.V.N. from the Netherlands Organization for the Advancement of Pure Research (ZWO).

Received 9 May; accepted 9 July 1980.

1. Vince-Prue, D. *Photoperiodism in Plants* (McGraw-Hill, London, 1975).
2. Bollig, I., Chandrashekaran, M. K., Engelman, W. & Johnsson, A. *Int. J. Chronobiol.* **4**, 83–96 (1976).

0028-0836/80/370140—02$01.00

3. Elliott, J. A., Stetson, M. H. & Menaker, M. *Science* **178**, 771–773 (1972).
4. Grocock, C. A. & Clarke, J. R. *J. Reprod. Fert.* **39**, 337–347 (1974).
5. Gwinner, E. in *Avian Biology* (eds Farmer, D. S. & King, J. R.) 221–285 (Academic, New York, 1975).
6. Gwinner, E. & Eriksson, L.-O. *J. Orn., Lpz.* **118**, 60–67 (1977).
7. Saunders, D. S. *J. Insect Physiol.* **19**, 1941–1954 (1973).
8. Saunders, D. S. *J. Insect Physiol.* **20**, 77–88 (1974).
9. Beach, R. F. & Craig, G. B. Jr *J. Insect Physiol.* **23**, 865–870 (1977).
10. Dumortier, B. & Brunnarius, J. *C. r. hebd. Séanc. Acad. Sci., Paris* **285**, 361–364 (1977).
11. Thiele, H. U. *Oecologia* **30**, 331–348 (1977).
12. Bünning, E. *Ber. dt. bot. Ges.* **54**, 590–607 (1936).
13. Pittendrigh, C. S. *Proc. natn. Acad. Sci. U.S.A.* **69**, 2734–2737 (1972).
14. Pittendrigh, C. S. in *The Neurosciences Third Study Program* (eds Schmitt, F. O. & Worden, F. G.) 437–458 (MIT, Massachusetts, 1974).
15. Underwood, H. *J. comp. Physiol.* **125**, 143–150 (1978).
16. Peterson, D. M. & Hamner, W. M. *J. Insect Physiol.* **14**, 519–528 (1968).
17. Pittendrigh, C. S. & Minis, D. M. in *Biochronometry* (ed. Menaker, M.) 212–250 (National Academy of Sciences, Washington, 1971).
18. Lees, A. D. *J. Insect Physiol.* **19**, 2279–2316 (1973).
19. Skopik, S. D. & Bowen, M. F. *J. comp. Physiol.* **111**, 249–259 (1976).
20. Bonnemaison, L. *Z. ang. Ent.* **86**, 178–204 (1978).
21. Veerman, A. *J. Insect Physiol.* **23**, 703–711 (1977).
22. Saunders, D. S. *Insect Clocks* (Pergamon, Oxford, 1976).
23. Bünning, E. *Die physiologische Uhr* (Springer, Berlin, 1977).
24. Vaz Nunes, M. & Veerman, A. *J. comp. Physiol.* **134**, 203–217 (1979).
25. Vaz Nunes, M. & Veerman, A. *J. comp. Physiol.* **134**, 219–226 (1979).
26. Lees, A. D. *Ann. appl. Biol.* **40**, 449–486 (1953).
27. Lees, A. D. *Ann. appl. Biol.* **40**, 487–497 (1953).

A test of evolutionary theories of senescence

Michael Rose* & Brian Charlesworth

School of Biological Sciences, University of Sussex, Falmer,
Brighton BN1 9QG, UK

Senescence is the post-maturation decline in survivorship and fecundity that accompanies advancing age. Two main evolutionary theories have been proposed to account for senescence. (1) The mutation-accumulation theory. Deleterious mutations exerting their effects only late in life would tend to accumulate, because of their minimal effects on fitness[1,2]. More precisely, exclusively late-acting deleterious mutations will attain higher equilibrium frequencies under mutation–selection balance than will mutations that act early, resulting in lower mean values for fitness components late in life (ref. 3, p. 218). Medawar[1] emphasized the possibility that this effect would be enhanced by selection of modifiers that postpone the age of onset of genetic diseases. (2) The pleiotropy theory. Williams[4] suggested that many of the genes with beneficial effects on early fitness components have pleiotropic deleterious effects on late fitness components, but are nevertheless favoured by natural selection. (These theories are based on the decline with age in the effect of age-specific fitness-component changes on total fitness[3] (ref. 3, pp. 206–214 and refs 4, 5). Either or both of these theories could apply in any particular population.) Selection experiments in *Drosophila*[6] and *Tribolium*[7] support the pleiotropy theory, although one such experiment gave results that only bordered on significance[8], but the mutation–accumulation theory has never been tested. The present results provide evidence for the pleiotropy theory, but do not support the mutation–accumulation theory.

Tests of evolutionary theories with randomly breeding laboratory populations, as in the present case, require that they be maintained without significant inbreeding after sampling from a long-standing natural population. In August 1975, 400 *Drosophila melanogaster* adults were sampled from the Amherst, Massachusetts, population studies by Ives[9]. There is good evidence that this population has been continuously endemic in the Amherst area since about 1930 (ref. 9). The flies were maintained in the laboratory at 25 °C in 10–16 one-third-pint milk bottles containing Lewis medium and powdered yeast. Discrete generations were used, with 13–15 days from oviposition to adult egg laying. Population size bottlenecks did not occur.

Female phenotypes were assayed as follows. Egg laying counts (24 h) and longevity were recorded from the fourth day of adult life. One male and one female were kept in plastic tubes, under constant illumination at 25 °C, with high-agar charcoal-coloured medium. The surface of the medium was prepared with a yeast paste and a small amount of acetic acid. Daily transfers were performed using CO_2 anaesthesia.

The additive genetic variance (V_A) of a fitness component such as daily egg lay should increase with age if the mutation-accumulation theory is correct. (This is because the additive genetic variance contributed by a di-allelic locus with one allele close to fixation increases with the frequency of the rare allele (ref. 10, p. 135 and ref. 11). The equilibrium frequency of a deleterious allele maintained in the population by recurrent mutation will be higher the later its age of action, if its expression is limited to certain ages[1–3].) Unfortunately, there is a difficult problem concerning the scale on which daily egg lay should be measured so as to test the hypothesis of an increase in V_A with age. Mean daily egg lay shows a senescent decline, from around 70 eggs per day for the first day of assay to about 30 eggs per day

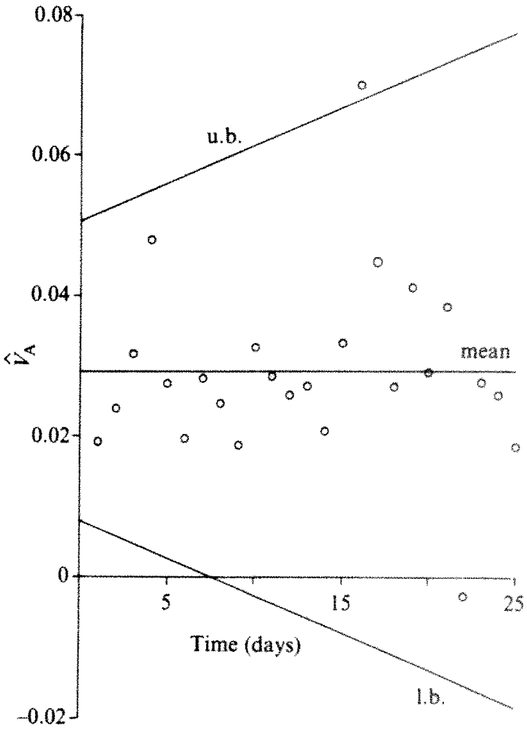

Fig. 1 Estimates of additive genetic variance ($\hat{V}_A$) for egg laying over 24 h. Only data from females which survived the 24 h and laid at least one egg during this period were used, since approximate normality of the data is required for analysis of variance. The data were transformed using the function $x' = \ln(x + 23.81)$, so as to remove the scale effects arising from the fall in egg laying during the 25-day period of assay[12]. The estimates were obtained using a sibling analysis of variance with unbalanced cell allocation (ref. 13, p. 459). The total number of individuals scored falls from 1,099 on day 1 to 396 on day 25. The overall mean for $\hat{V}_A$ during the assay period is 0.02925, which is plotted. The least squares linear regression slope for $\hat{V}_A$ on age has a slope of -0.00002 ± 0.00072, with 95% confidence, which has a t value of -0.0599, with 23 degrees of freedom. This is not significant at any reasonable level of probability. The best estimate for V_A over the period is its mean value. Because of a confounding design variable, confidence intervals for this estimate had to be estimated on an *ad hoc* basis using the normal equations for the unbalanced design[14], giving the upper and lower bounds (u.b. and l.b.) for daily estimates of V_A shown.

---

* Present address: Laboratory of Genetics, University of Wisconsin, Madison, Wisconsin 53706.

0028-0836/80/370141—02$01.00

for the last day of assay shown in Fig. 1. V_A for untransformed daily egg lay shows a parallel decline. This presumably reflects the fact that a gene with a given effect on fecundity, expressed as a proportion of the population mean, will have a higher absolute effect when the mean is high than when it is low. This suggests the use of a logarithmic transformation of the data. We chose to use the transform $x' = \ln(x + 23.81)$, which removes the relationship between mean and gross phenotypic variance in daily egg lay[12].

Figure 1 shows estimates of V_A on the transformed scale, plotted as a function of age. The upper 95% confidence limit for the regression slope of V_A on age is only 0.0070, whereas the mean of V_A is about 0.0292. There is thus little scope for a substantial increase in V_A with age on the basis of these data. Although the method of transformation used here is a standard procedure in quantitative genetics[12], it is open to the objection that it may disguise a relationship between V_A and age on some other, 'true' scale of measurement. A detailed model of the mutation-accumulation theory, to be presented elsewhere, shows that a roughly threefold rise in V_A on our scale, between first and last day of assay, would be needed to account for the observed decline in mean fecundity. This assumes that the effects of mutations (expressed as proportions of mean fecundity) are similar at different ages. Our results therefore imply either that the mutation-accumulation theory is false, or that the late-acting mutations have much smaller proportional effects on fecundity than early-acting ones.

A test of the alternative theory of pleiotropic gene effects[4] was based on the principle[6–8] that selection for increased reproductive output at later ages should result in decreased fertility at early ages. Figure 2 and Table 1 give the results of an experiment which was contrived so that the effects of selection for late reproduction could be detected at any age. These results show that increases in later reproductive output are associated with decreases in early reproductive output, lowered overall reproductive rate, and increased longevity. This concurs with the predictions of the pleiotropy theory of senescence. Comparable results have been obtained in other experiments on *Drosophila* (see refs 7, 15 and Fig. 7 of ref. 16), although the latter authors favoured an interpretation in terms of maternally transmitted, non-mendelian 'ageing factors'. The increase in late fecundity of flies bred from older parents observed in all three experiments, and the increased longevity of such flies that we have detected, are difficult to reconcile with such an interpretation. The only experiment designed as a critical test for the existence of non-mendelian ageing factors in *Drosophila* (using an inbred line to eliminate genetic variability) yielded negative results[17]. Our data provide two lines of evidence in favour of a conventional mendelian interpretation. First, the analysis of variance of the sibling experiment showed similar values for the between-dam and between-sire components of variance (ref. 10, p. 173) in daily fecundity, so that there was no evidence for maternal inheritance[18]. Second, analysis of the additive genetic correlations between fecundity at different ages, and between fecundity at various ages and longevity, gave several high negative values, broadly consistent with the results of the selection experiments[18]. Thus, there seems little reason to think that our selection responses were due to causes other than selection acting on pre-existing, mendelian variability.

Table 1 Significant differences between samples from the E and L populations of Fig. 2*

Character	L mean	E mean	d.f.	Results of t-test
Five-day total egg laying:				
Assay days 1–5	421.91	551.30	201	−12.364
Assay days 11–15	392.19	323.37	190	4.044
Assay days 16–20	286.69	238.78	165	2.431
Assay days 21–25	182.85	136.79	110	2.515
Longevity in assays days	30.25	26.79	200	2.283
Rate of laying during assay	68.61	76.93	200	−3.327

* $P < 0.05$.

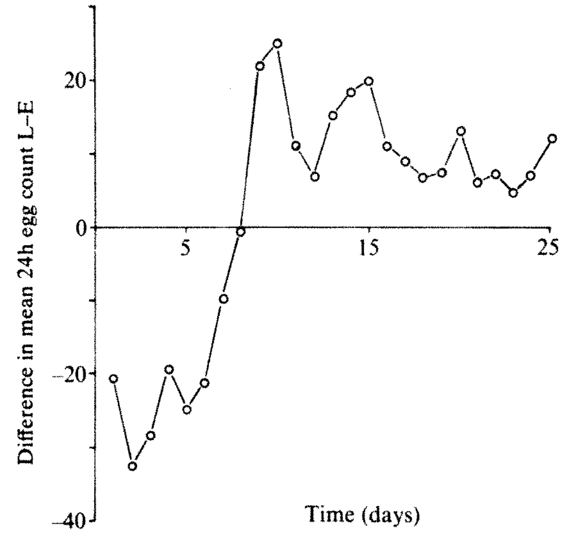

Fig. 2 The ordinate is the difference in mean 24 h egg counts between a sample from a population reproduced at late ages, L, and a sample from a population reproduced at early ages, E. The E population was the base population, maintained as described in the text. The L population was obtained from eggs laid by one generation of the E population. It was then maintained for 12 generations in the same conditions as the E population, but using eggs laid by adults surviving at least 21 days from pupal emergence. Samples of about 100 females were then obtained from each population, and assayed as described in the text. Many of the differences in daily egg-laying shown are statistically significant. Table 1 gives other significant differences between the samples.

We conclude, therefore, that there is genetic variability in female life-history components in *Drosophila*, of the sort postulated by Williams' pleiotropy theory of senescence[4]. This does not, of course, necessarily mean that the established pattern of senescence in *Drosophila* females has been evolved as the result of selection acting on such genes, but this seems likely unless the present properties of genetic variation in *Drosophila* differ radically from those in the past. It therefore seems reasonable to suggest that senescence in *Drosophila* is due to the late-acting deleterious effects of genes which are favoured by natural selection because of beneficial effects at early ages. It does not necessarily follow from this that senescence in all species is due to such pleiotropy. However, that hypothesis is definitely worth testing, in view of the results given here. Articles presenting these experiments in greater detail will appear elsewhere[18].

M.R. was supported by a scholarship from the Association of Commonwealth Universities. We thank Professor John Maynard Smith for reading the manuscript.

Received 8 February; accepted 20 June 1980.

1. Medawar, P. B. *An Unsolved Problem of Biology* (Lewis, London, 1952); *The Uniqueness of the Individual* (Methuen, London, 1957).
2. Edney, R. B. & Gill, R. W. *Nature* **220,** 281 (1968).
3. Charlesworth, B. *Evolution in Age-Structured Populations* (Cambridge University Press, 1980).
4. Williams, G. C. *Evolution* **11,** 398–411 (1957).
5. Hamilton, W. D. *J. theor. Biol.* **12,** 12–45 (1966).
6. Wattiaux, J. M. *Evolution* **22,** 406–421 (1968).
7. Sokal, R. R. *Science* **167,** 1733–1734 (1970).
8. Mertz, D. B. *Physiol. Zool.* **48,** 1–23 (1975).
9. Ives, P. T. *Genetics* **30,** 167–196 (1945); *Evolution* **24,** 507–518 (1970).
10. Falconer, D. S. *Introduction to Quantitative Genetics* (Oliver & Boyd, Edinburgh, 1960).
11. Mukai, T., Cardellino, R. A., Watanabe, T. K. & Crow, J. F. *Genetics* **78,** 1195–1208 (1972).
12. Wright, S. in *Quantitative Inheritance* (eds Waddington, C. H. & Reeve, E. C. R.) 5–41 (HMSO, London, 1952); *Evolution and the Genetics of Populations* Vol. 1, 232 (University of Chicago Press, 1968).
13. Kempthorne, O. *An Introduction to Genetic Statistics* (Wiley, New York, 1957).
14. Mahumunulu, D. M. *Ann. math. Statist.* **34,** 521–527 (1963).
15. Lints, F. A. *Genetics and Ageing* (Karger, Basel, 1978).
16. Lints, F. A. & Hoste, C. *Evolution* **31,** 387–404 (1977).
17. Comfort, A. *Nature* **172,** 83 (1953).
18. Rose, M. R. & Charlesworth, B. *Genetics* (in the press).

Chimaeras of *Drosophila melanogaster* obtained by injection of haploid nuclei

P. Santamaría & M. Gans

Centre de Génétique Moléculaire, CNRS, 91190 Gif sur Yvette, France

Since the observation by Bridges[1,2] of a few mosaics containing haploid tissue in *Drosophila*, specimens supposedly haploid have rarely been found[3-5]. A technique for the easy production of haploid animals or tissues could have important applications. We have now successfully designed such a technique by the production of chimaeras obtained by transplantation of haploid nuclei from a maternal effect mutant that produces haploid embryos. We have used this technique to test the proposal of Jack and Judd[6] that the *zeste* locus of *Drosophila melanogaster* cannot repress the activity of unpaired alleles at the *white* locus.

The mutation 1182 described by M.G. *et al.*[7] and by Zalokar *et al.*[8] produces by a maternal effect haploid embryos that never develop into complete larvae. Recently[9], Debec obtained permanent haploid cell cultures from these embryos and also recovered a mutant stock that is fully penetrant at any temperature. We have again checked the characteristics of eggs of this new strain renamed here *maternal haploid* (*mh*). The technique of fixation and staining is as described by Zalokar *et al.*[10]. In 25 young eggs examined (stages 1–4 of Zalokar and Erk[11]), the 3 polar nuclei were found in their normal place in the anterior part of the cortex. Thirteen other eggs were suitable for a karyotypic analysis (stages 9–13) and all showed a set of haploid chromosomes with an X chromosome. From 200 untreated eggs, 183 developed to blastoderm; gastrulation was abnormal and only 22 differentiated further to form embryos with some muscular movements and abnormal segments.

To obtain the chimaeras, two to six nuclei from eggs at stages 10–14 of Zalokar and Erk[11] laid by homozygous *mh* females crossed to $Ki\ e^{11}$ males, were injected into $y\ f^{36a}$; *mwh jv* host eggs at stages 2–8. We used the transplantation technique of Zalokar[12] as described in Santamaría[13]. From 1,046 injected eggs, 429 adults developed, of which 44 had patches of tissue phenotypically $y^+ f^+$; $mwh^+\ jv^+ Ki^+\ e^+$. Twelve more chimaeric larvae died before imaginal differentiation, and were recognized by black mouth parts and bigger, black intersegmental hooks. The fact that all these chimaeras were neither *kinked* nor *ebony* implies that the initiation of mitosis can be triggered by the entrance of the spermatozoon (virgin eggs from *mh* mothers never develop) and that the haploid nuclei can support development at least until the gastrula stage. The phenomenon differs from that in known parthenogenetic *Drosphila* species[14-17] in which a female pronucleus becomes diploid or the products of meiosis fuse and afterwards undergo normal development.

In 24 chimaeras out of the 44, neither cells nor organs of wild-type phenotype were obviously smaller than those of homozygous *mh* females, indicating that the injected nuclei probably diploidize. In fact, in the permanent cell cultures produced by Debec[9] from haploid embryos, some cells diploidize. Moreover, in the Subtenly experiments[18] involving transplantation of nuclei from haploid blastulae into enucleated eggs of *Rana pipiens*, some of them develop into typical haploids and others into homozygous diploids.

Of the 44 chimaeras, 17 showed reduced cell size in all of the donor tissue. In four the organ was smaller than in controls, and in eight the *mh* organ carried more bristles than controls. Some examples are given in Table 1 and Fig. 1. These three modifications were generally found in the same mosaics, but in small patches the size of the organ or the number of pattern elements could not always be distinguished from those of controls.

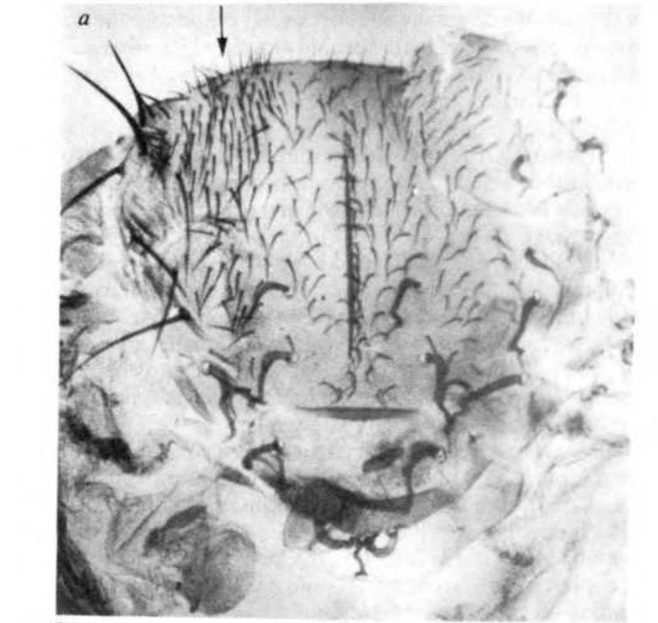

Fig. 1 *a*, Patch of haploid tissue, marked with arrows, in the notum, showing increase in the number of bristles. The host was y, f^{36a}; *mwh jv*. *b*, Normal first leg basitarsus of a *mh* female. *c*, *d*, The first legs of haploid tissue. The basitarsus shows shortening and an increase in the number of bristles. Both were female. *e*, Chimaeric medial triple row formed by reduced, marked with arrows, and normal bristles, both *mh*.

In three more chimaeras in which the size of most of the *mh* cells was normal, a clone also of *mh* cells differentiated in which the bristles were clearly smaller (Fig. 1*e*).

The reduced size of haploid cells and the reduction of organ size are generally found in plants and animals[19], including *Drosophila*[1,2]. However, we believe the variation in the number of elements in the pattern to be new. In *Drosophila*, Held[20] observed a reduction in the number of pattern elements in triploid flies. It is therefore likely that haploid organs woul produce more bristles. As we found chimaeras with the expected characteristics of haploid tissue, it seems reasonable to assume that we are really dealing with haploid differentiation. Moreover, we can argue that the observation of chimaeras with

0028–0836/80/370143—02$01.00

mh tissue in which some cells are normal in size an others small, indicates that some of them became diploid while others did not, therefore excluding the possibility that the small size could be due to other mutations arisen in the strain.

All cuticular regions can be formed by supposedly haploid *mh* cells. However, the fact that complete haploid embryos die implies either that not all embryonic processes can be supported by the *mh* haploid nuclei, or that a maternal effect prevents this development.

Eight chimaeras were formed by *mh* cells in the region of the sex comb. All the chimaeras in the first leg basitarsus were female, but only two had indications of haploidy. Three more chimaeras had a seventh tergite, which is a female characteristic. Our of five *mh* chimaeric genitalia, two were clearly haploid and female, one probably diploid and female, one half male and half female and another one completely male.

Three possible explanations for the maleness are: (1) the formation of X/O; 2A cells, (2) the formation of intersexes 2X; 3A, (3) an ambiguity in the possibilities of differentiation of haploid cells. The well established law of sex determination as a function of the ratio of X to A[21], the fact that X/O males appear in parthenogenetic species[14–17] and the lack of indications of haploidy or triploidy in these chimaeras indicate that the first hypothesis is the most plausible.

If monoploidy of an X is possible, this suggests that monoploidy of a 4th chromosome is also possible in otherwise diploid cells. Haplo-4 tissue would be *Minute* and produce small organs which might be difficult to distinguish from haploid regions. However, haplo-4 individuals never show an increase of pattern elements; also, Minute tissue should either disappear by cell competition[22] or fill an entire compartment when all the cells of the original anlage are of donor origin[23]; this is not the case in most of our haploid chimaeras. Thus, the results presented here indicate that haploid cells can probably develop and differentiate in all the adult cuticular tissue.

Table 1 Comparison between some parameters obtained from 10 homozygous *mh* females and some individual chimaeras

	Control	Chimaeras
Bristles in FLB	105.2 ± 7.7	175, 156
Wing hairs	18.5 ± 2.2	26.4 ± 5.8
Length bristle AP	105.3 ± 4.2	71
Acrosticals	134.3 ± 4.8	156, 195
Bristles in the MTR	93 ± 1.5	77, 73

FLB: first leg basitarsus. Hairs per wing are counted in a square placed in the ocular and between veins L II and L III. Length of the biggest bristle of the anal plate (AP) was measured with an ocular grid. Acrosticals were counted on photographs of the flies. The number of bristles in the medial triple row (MTR) is always reduced in reduced organs probably due to the continuity of elements and as a consequence of the shortening of the wing. In the rest of the organs in which the bristles are interspersed between hairs the phenomenon is the reverse, as in the FLB.

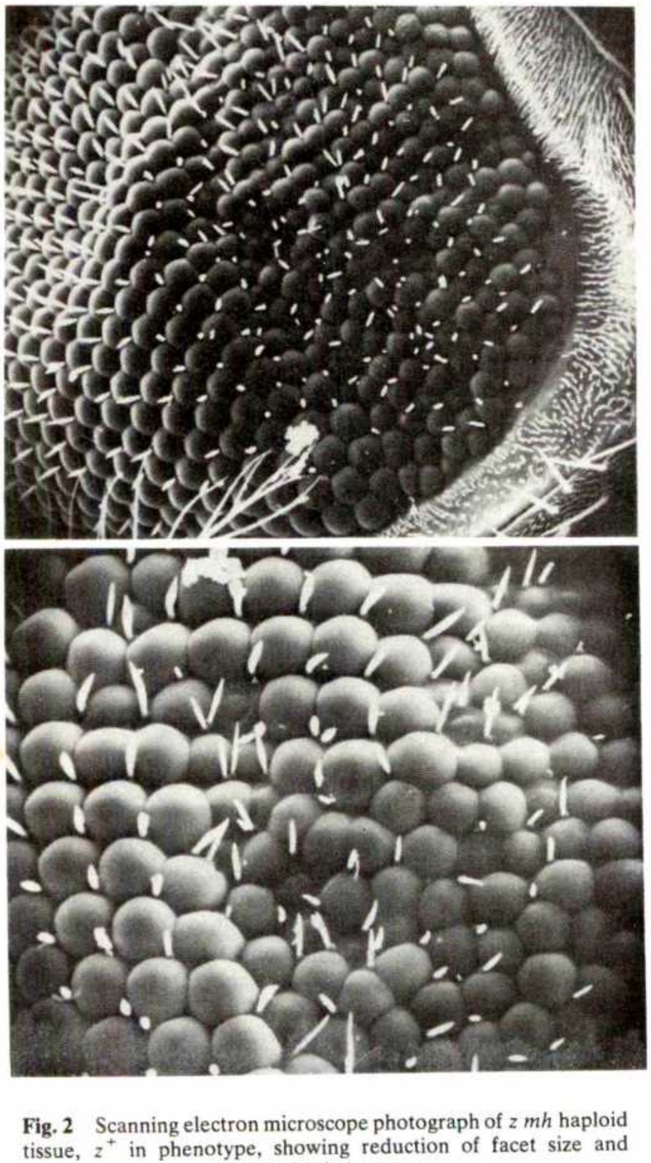

Fig. 2 Scanning electron microscope photograph of *z mh* haploid tissue, z^+ in phenotype, showing reduction of facet size and disturbed bristle pattern.

We hope this technique will prove useful in the analysis of such genetic phenomena as transvection effect, variegation and cis regulation. We have used it to provide new evidence in favour of the thesis of Jack and Judd[6]: in a *zeste* individual, paired *white*$^+$ alleles fail to be expressed while unpaired *white*$^+$ alleles are expressed normally. The repression of *white*$^+$ alleles by *zeste* appears (according to Jack and Judd[6]) to be similar to the transvection described by Lewis[24]. According to this hypothesis, one would predict that haploid *zeste* cells must be *zeste*$^+$ in phenotype. Twenty-two chimaeras were obtained from injection of nuclei from eggs laid by *mh z* females crossed to *Ki e*[11] males into *y w sn* eggs. Eleven of these showed a $y^+\ w^+\ sn^+;\ Ki^+\ e^+$ patch in the eye region: six were *zeste*, four were *zeste*$^+$ and one was *zeste* and *zeste*$^+$. All of the z^+ mosaic areas had reduced cell and organ size (Fig. 2), whereas the *z* areas were normal; therefore, the possibility that the *zeste*$^+$ phenotype is due to the lack of an X chromosome seems unlikely. The fact that the tissue with normal cell size was *zeste* and that tissue with small cells was *zeste*$^+$ provides further support in favour of the haploid nature of the *zeste*$^+$ patches.

We thank Mrs Inge Erk for technical assistance, Drs A. Debec and N. Prud'Homme for criticism and Drs M. Zalokar and P. Simpson for discussions.

Received 1 May; accepted 11 July 1980.

1. Bridges, C. B. *Proc. natn. Acad. Sci. U.S.A.* **11,** 706–710 (1925).
2. Bridges, C. B. *Science* **72,** 405–406 (1930).
3. Waletzky, E. *Drosoph. Inf. Serv.* **8,** 82 (1937).
4. Sturtevant, A. H. *Z. wiss. Zool.* **125,** 323–356 (1929).
5. Hinton, C. W. & McEarchen, W. *Drosoph. Inf. Serv.* **37,** 90 (1963).
6. Jack, J. W. & Judd, B. H. *Proc. natn. Acad. Sci. U.S.A.* **76,** 1368–1372 (1979).
7. Gans, M., Audit, C. & Masson, M. *Genetics* **81,** 683–704 (1975).
8. Zalokar, M., Audit, C. & Erk, I. *Devl Biol.* **47,** 419–432 (1975).
9. Debec, A. *6th Eur. Drosoph. Res. Conf.* (Abstr.) (1979).
10. Zakolar, M., Erk, I. & Santamaría, P. *Cell* **19,** 133–141 (1980).
11. Zalokar, M. & Erk, I. *J. Microsc. Biol. cell.* **25,** 97–106 (1976).
12. Zalokar, M. *Proc. natn. Acad. Sci. U.S.A.* **68,** 1539–1541 (1971).
13. Santamaría, P. *Wilhelm Roux Arch. Entw. Mech. Org.* **178,** 89–98 (1975).
14. Stalker, H. D. *Genetics* **39,** 4–34 (1954).
15. Doane, W. *Science* **132,** 677–678 (1960).
16. Carson, H. L. *Proc. natn. Acad. Sci. U.S.A.* **70,** 1772–1774 (1973).
17. Carson, H. L. *Univ. Tex. Publs* **6205,** 55–62 (1962).
18. Subtenly, S. S. & McLoughlin C. *Anat. Rec.* **125,** 623 (1956).
19. Frankhauser, G. in *Analysis of Development* (eds Willier, B. H., Weiss, P. A. & Amburger, H.) 126–150 (Hafner, New York, 1955).
20. Held, L. I. *Wilhelm Roux Arch. Entw Mech. Org.* **187,** 105–127 (1979).
21. Bridges, C. B. in *Sex and Internal Secretions,* 15–63 (Williams & Wilkins, Baltimore, 1932).
22. Morata, G. & Ripoll, P. *Devl Biol.* **42,** 211–221 (1975).
23. Simpson, P. *Devl Biol.* **54,** 100–115 (1976).
24. Lewis, E. B. *Am. Nat.* **88,** 225–239 (1954).

Gonadotropin releasing hormone agonists stimulate meiotic maturation of follicle-enclosed rat oocytes *in vitro*

T. Hillensjö & W. J. LeMaire*

Department of Physiology, University of Göteborg,
S-40033 Göteborg, Sweden

Although the principal function of gonadotropin releasing hormone (GnRH) is to stimulate the pituitary gland to release luteinizing hormone (LH) and follicle-stimulating hormone (FSH), there is evidence that agonistic analogues of GnRH directly inhibit steroidogenesis in the testis[1] and ovary[2–5]. On the other hand, Clark *et al.*[6] have demonstrated that GnRH and two agonists have a marked stimulatory effect on prostaglandin synthesis by granulosa cells isolated from immature rats treated with pregnant mare's serum gonadotropin (PMSG). Stimulation by these compounds was distinct from that by LH in that no changes in cyclic AMP production were detected. Thus it seems important to investigate the effect of these peptides on other aspects of ovarian function, for example oocyte maturation. Mammalian oocytes are arrested in the dictyate stage of the first meiotic prophase, and meiosis (oocyte maturation) normally resumes in preovulatory follicles as a consequence of the surge of LH and FSH. This maturation can also be initiated *in vitro* by the addition of gonadotropins to isolated preovulatory follicles[7,8], and is accompanied by an increase in the production of lactate[8]. We now report that GnRH and two potent agonists[9] stimulate meiosis *in vitro* in follicle-enclosed oocytes in a dose-dependent and specific manner, and also cause an increase of lactate accumulation during incubation.

Immature, 26-day-old female rats were injected subcutaneously with 10 IU PMSG (Sigma). After 48 h we isolated the intact preovulatory follicles (8 to 14 from each rat) by microdissection. We incubated them (4 to 7 follicles per flask) in 0.7 ml modified Krebs bicarbonate buffer, with and without test substances, at 37 °C for 2–10 h as described earlier[8]. Following incubation, the medium was frozen for later analysis of lactate content[10], and the oocytes were recovered to determine their stage of meiosis. We examined the living oocytes by Nomarski interference contrast microscopy and in certain cases fixed and stained them according to Donahue[11]. Oocytes were put into one of three categories: (1) immature, with germinal vesicle (GV); (2) maturing, with GV breakdown (GVB); (3) mature, with first polar body (PB). The following test substances were added, as indicated, directly to the incubation media: ovine LH(NIH-LH-S18); synthetic GnRH (LHRH batch 750125, Ferring); [D-Ala^6, des-Gly-NH$_2$]GnRH ethylamide (analogue I, Beckman); [D-Leu^6, des-Gly-NH$_2$]GnRH ethylamide (analogue II, Abbott); TRH Roche (Hoffman-LaRoche); oxytocin (Syntocinon, Sandoz) and somatostatin (batch RAA 14511, Kabi).

In control media, the follicle-enclosed oocytes remained immature, whereas LH, used as a positive control, induced maturation with 99% GVB after 4 h incubation (Table 1). Preliminary experiments failed to show any influence of analogue I on the LH response. Somewhat unexpectedly, GnRH as well as the GnRH agonists added alone were potent stimulators of meiosis (Fig. 1). With GVB as an endpoint, the ED$_{50}$ was 492 ng ml^{-1}, 0.588 ng ml^{-1} and 0.898 ng ml^{-1} for GnRH, analogue I and analogue II, respectively. The time course of maturation induced by analogue I was similar to that induced by LH (Table 1). Analogue I caused complete maturation during 10 h incubation as evidenced by PB formation (Table 1). Synthetic TRH, oxytocin and somatostatin did not stimulate meiosis, indicating the specificity of the effect of GnRH and the agonists (Table 2).

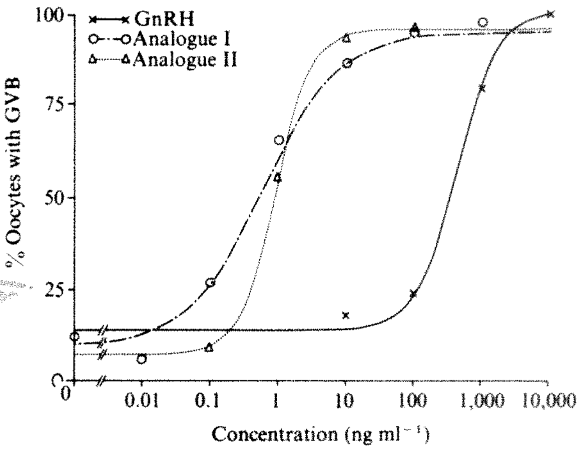

Fig. 1 Dose-response curve of GnRH, analogues I and II on germinal vesicle breakdown (GVB) of follicle-enclosed oocytes incubated for 4 h. The percentage of oocytes with GVB of the total number examined was determined as described in the text. The total number of oocytes analysed were 82, 142, 261 and 141 for control, GnRH, analogues I and II, respectively. Dose–response curves were fitted to the data by computer program using a nonlinear least-squares regression[20].

Although not studied quantitatively, it was clear that GnRH and both analogues also produced dispersal and mucification of the cumulus oophorus, as was previously described for LH and FSH[12].

We also found that lactate accumulation was markedly stimulated by LH (Fig. 2) as reported earlier[8,10]. GnRH, analogue I and II, but not TRH, also enhanced lactate accumulation. The maximal response, however, was considerably less than the maximal response produced by LH. When we tested LH together with analogue I, we did not find any significant additivity.

These data clearly show that GnRH has a stimulatory effect on meiotic maturation of follicle-enclosed rat oocytes. When we initiated these experiments we did not know what results to expect, as GnRH and agonistic analogues have been shown to have both direct inhibitory[2–5] and direct stimulatory[6] effects on different parameters of ovarian function. In our first experiments we found that these substances did not inhibit spontaneous maturation of isolated rat oocytes, nor did they inhibit

Table 1 Time course of meiotic maturation induced by analogue I and LH

	Per cent with GVB		Per cent with PB
	2 h	4 h	10 h
Control	8 (50)	16 (110)	12 (43)
Analogue I	22 (50)	98 (110)	75 (44)
LH	26 (38)*	99 (78)	63 (75)*

Follicle-enclosed oocytes were incubated for the times indicated in absence or presence of analogue I (1 μg ml^{-1}) or LH (1 μg ml^{-1}). Percentage of oocytes with germinal vesicle breakdown (GVB) or first polar body (PB) of the total number examined (in parentheses) was determined as described in the text.

* Data from ref 8.

---

* Permanent address: Department of Obstetrics and Gynecology and the Endocrine Laboratory, University of Miami, School of Medicine, Miami, Florida 33124.

0028-0836/80/370145—02$01.00

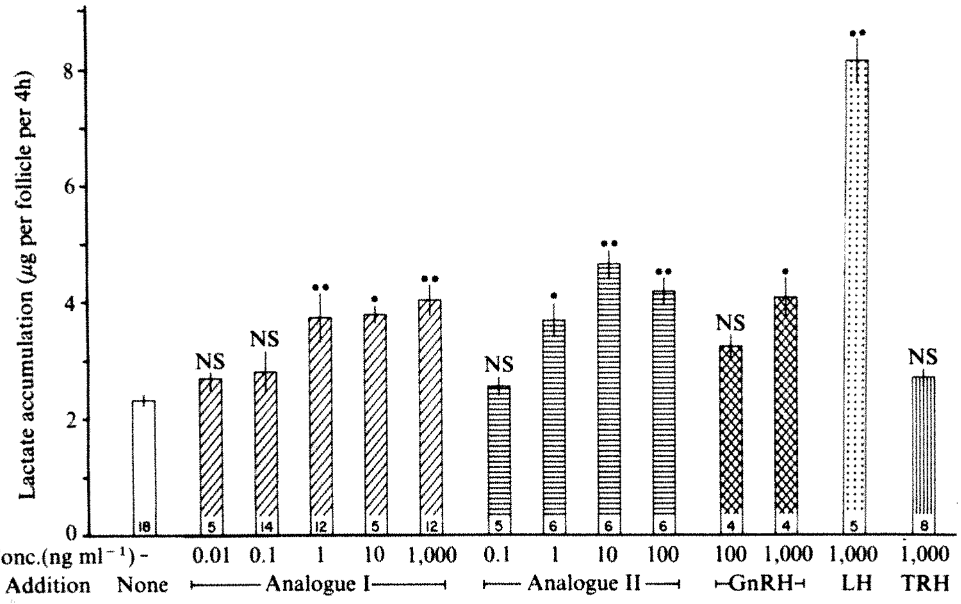

Fig. 2 Effect of LH, TRH and various concentrations of GnRH, analogues I and II on follicular lactate accumulation (μg per follicle) during 4 h incubation. Incubations and lactate measurement were carried out as described in the text. Bar heights represent the means and vertical lines the s.e.m. The number of samples in each group is indicated at the bottom of each bar. Statistical differences between groups were calculated by analysis of variance followed by Student–Newman–Keul's multiple range test. ☐ * $P < 0.05$; ** $P < 0.01$; NS, not significant.

the stimulatory effect of LH on follicle-enclosed oocytes. It was reported recently that GnRH and an agonist produced meiosis and parthenogenetic-like cleavage when injected repeatedly into hypophysectomized diethylstilboestrol-treated rats[13]. Whether the stimulatory effect by GnRH on oocyte maturation has a physiological role, remains to be determined.

Oocyte maturation is normally triggered by LH, but this hormone seems to stimulate meiosis only indirectly through a primary effect on the follicle cells. Although LH stimulates production of follicular cyclic AMP, prostaglandins, steroids and lactate, none of these substances seem to act as meiosis stimulating factors on the oocyte itself[14]. It has been suggested that meiosis is regulated by an intra-follicular inhibitor, the action of which is terminated by LH. An oocyte maturation inhibitor (OMI) has been partially purified from pig follicular fluid and was found to be a peptide with a molecular weight in the order of 2,000 (ref. 15).

The minimal effective dose of GnRH on oocyte maturation in our experiments (0.1 μg ml^{-1}) seems to be far above the possible physiological circulating levels of endogenous GnRH[16]. However, the possibility has been raised that GnRH might be produced locally in tissues other than the hypothalamus, such as placenta[17] and ovary itself[4,18]. If this is the case, then the process of oocyte maturation might be determined partly by a balance of locally formed peptides that may be stimulatory (GnRH) and inhibitory (OMI) in nature.

The mechanism by which GnRH and these two analogues stimulate oocyte maturation also remains to be determined. Clayton *et al.* have shown the presence of specific GnRH receptors in dispersed cells and membrane fractions of luteinized rat ovaries corresponding to a direct action on hormonal stimulation of progesterone and cyclic AMP production[5,19]. The mechanism of stimulation for these peptides may, however, be different from that for LH, as was shown for the stimulation by GnRH of prostaglandin synthesis in rat granulosa cells[6]. Such a concept seems to be supported by our observation that the maximal stimulation of lactate accumulation, obtained by any test dose of GnRH or its two analogues, was well below the maximal stimulation caused by LH. Further detailed studies of the effect of these peptides on other parameters in our incubation of follicle-enclosed oocytes, such as cyclic AMP accumulation and steroidogenesis, might shed light on this problem.

We thank Dr W. F. White (Abbott) for the gift of analogue II, Dr K. Ahrén for support and advice, S. Rosberg for help and advice with the statistical analysis, Mrs H. Thelander for technical assistance and Mrs A-L. Dahl for preparation of the manuscript. This work was supported by grants from the Swedish MRC (No. 05650), and Magnus Bergvalls Stiftelse (to T.H.) and by the NIH (HD08747, to W. J. LeM.). NIH LH-S18 was supplied by NIAMDD. W. J. LeM. is in receipt of a Fogarty Senior International Fellowship (TW00318) and a Visiting Scientist research grant from the Swedish MRC (No. 5732).

Received 23 April; accepted 26 June 1980.

Table 2 Specificity of meiosis-inducing effect of GnRH

Compound added	Concentration (μg ml^{-1})	Per cent GVB	*n*
None	—	12	162
TRH	1	14	44
Oxytocin	0.1	0	20
Somatostatin	0.1	0	19
	1.0	17	42
	10	6	18
GnRH	1	80	45
	10	100	41

Follicle-enclosed oocytes were incubated for 4 h in the presence or absence of various synthetic peptides. The percentage of oocytes with GVB of the total number examined (*n*) is given.

1. Hsueh, A. J. W. & Erickson, G. F. *Nature* **281**, 66–67 (1979).
2. Rippel, R. H. & Johnson, E. S. *Proc. Soc. exp. Biol. Med.* **152**, 432–437 (1976).
3. Hsueh, A. J. W. & Erickson, G. F. *Science* **204**, 854–855 (1979).
4. Ying, S-Y. & Guillemin, R. *Nature* **280**, 593–595 (1979).
5. Clayton, R. N., Harwood, S. P. & Catt, K. J. *Nature* **282**, 90–92 (1979).
6. Clark, M. R., Thibier, C., Marsh, J. M. & LeMaire, W. J. *Endocrinology* (in the press).
7. Tsafriri, A., Linder, H. R., Zor, U. & Lamprecht, S. A. *J. Reprod. Fert.* **31**, 39–50 (1972).
8. Hillensjö, T. *Acta endocr.* (Kbh). **82**, 809–830 (1976).
9. Vale, W., Rivier, C. & Brown, M. A. *A. Rev. Physiol.* **39**, 473–527 (1977).
10. Nilsson, L. *Acta endocr.* (Kbh) **77**, 540–558 (1974).
11. Donahue, R. P. *J. exp. Zool.* **169**, 237–250 (1968).
12. Hillensjö, T., Dekel, N. & Ahrén, K. *Acta physiol. scand.* **96**, 558–568 (1976).
13. Erickson, G. F. & Hsueh, A. J. W. *Soc. gynec. Invest. 27th A. Meet.*, Denver, Abstr. 371 (1980).
14. Lindner, H. R. *et al. Recent Prog. Horm. Res.* **30**, 79–127 (1974).
15. Tsafriri, A., Pomerantz, S. H. & Channing, C. P. *Biol. Reprod.* **14**, 511–516 (1976).
16. Aksel, S. & Glass, R. *Am. J. Obstet. Gynec.* **134**, 619–623 (1979).
17. Siler-Khodr, T. M. & Khodr, G. S. *Am. J. Obstet. Gynec.* **130**, 216–219 (1978).
18. Ying, S-Y & Guillemin, R. *C. r. hebd. Séanc. Acad. Sci. Paris* **289D**, 943–946 (1979).
19. Harwood, J. P., Clayton, R. N. & Catt, K. J. *6th Int. Cong. Endocr.*, Melbourne, Abstr. 813 (1980).
20. Rodbard, D., Moyle, E. & Ramanchandran, J. *Curr. Topics molec. Endocr.* **1**, 79–87 (1974).

Macrocortin: a polypeptide causing the anti-phospholipase effect of glucocorticoids

Geoffrey J. Blackwell*, Rosa Carnuccio, Massimo Di Rosa, Roderick J. Flower*, Luca Parente* & Paola Persico

Institute of Experimental Pharmacology, Faculty of Pharmacy, University of Naples, Via L. Rodino 22, 80138 Naples, Italy
* The Wellcome Research Laboratories, Langley Court, Beckenham, Kent BR3 3BS, UK

Anti-inflammatory glucocorticoids inhibit prostaglandin (PG) biosynthesis by preventing arachidonic acid release from phospholipids rather than inhibiting the cyclooxygenase[1–16]. As in other cells[17–19], this steroid action depends on receptor occupation and *de novo* protein/RNA biosynthesis[12–16]. We have previously shown in guinea pig perfused lungs and rat peritoneal leukocytes that the effect of steroids on PG generation is mediated by an uncharacterized 'second messenger'[13,16]. Now, we report that this factor (which we have named 'macrocortin') is an intracellular polypeptide whose release and synthesis are stimulated by steroids. Macrocortin derived from rat peritoneal leukocytes is very similar to that released from guinea pig lungs.

Steroids prevent PG generation by rat peritoneal leukocytes[14,16,20] and we established that this was due to the release from the cells of a non-dialysable 'second messenger'[14,16]. In these experiments we found that macrocortin release from leukocytes was induced by hydrocortisone in 'physiological' concentrations (Fig. 1*a*) and that the amount released in the presence of a fixed concentration of hydrocortisone was proportional to the number of cells present (Fig. 1*b*). Analysis of the time course of macrocortin release (Fig. 1*c*) showed that 30 min after adding hydrocortisone, approximately half the total inhibitory activity was released into the medium. By 90 min most inhibitory activity was extracellular, and by 150 min release was virtually complete. Leukocytes incubated with 1 μg ml^{-1} cycloheximide or without hydrocortisone did not release the inhibitor. Steroids release other factors from leukocytes[21]; was macrocortin synthesized *de novo* in response to the hydrocortisone, was it stored and secreted by a steroid dependent process, or did both mechanisms operate? To answer these questions we lysed untreated rat peritoneal leukocytes by repeated (4 times) freeze-thawing and heated them to 70 °C for 5 min to provide some protection from proteolysis. Dilutions of these lysates possessed high inhibitory activity suggesting that at least some macrocortin was stored in cells. Pretreatment of cells with hydrocortisone reduced intracellular macrocortin by 90%.

In further experiments, groups of 20 male Wistar rats (200–250 g) were treated with dexamethasone (Decadron, Merck; 1.5 mg per kg subcutaneously in the flank) or with saline. The amount of macrocortin contained in a known number of peritoneal leukocytes after collection was determined each hour for 4 h (five rats for each time point) and compared to saline-treated controls. One hour after steriod treatment macrocortin was undetectable in the leukocytes ($n = 3$). After 2 h, the macrocortin content of the cells had returned to control levels ($n = 2$), and increasing amounts (2–3 times control levels) of the material were found 3 and 4 h after treatment ($n = 3$). These experiments indicate that in addition to a steroid-induced depletion of macrocortin, there is a further phase of re-synthesis and that this increases the amount of inhibitor above control levels.

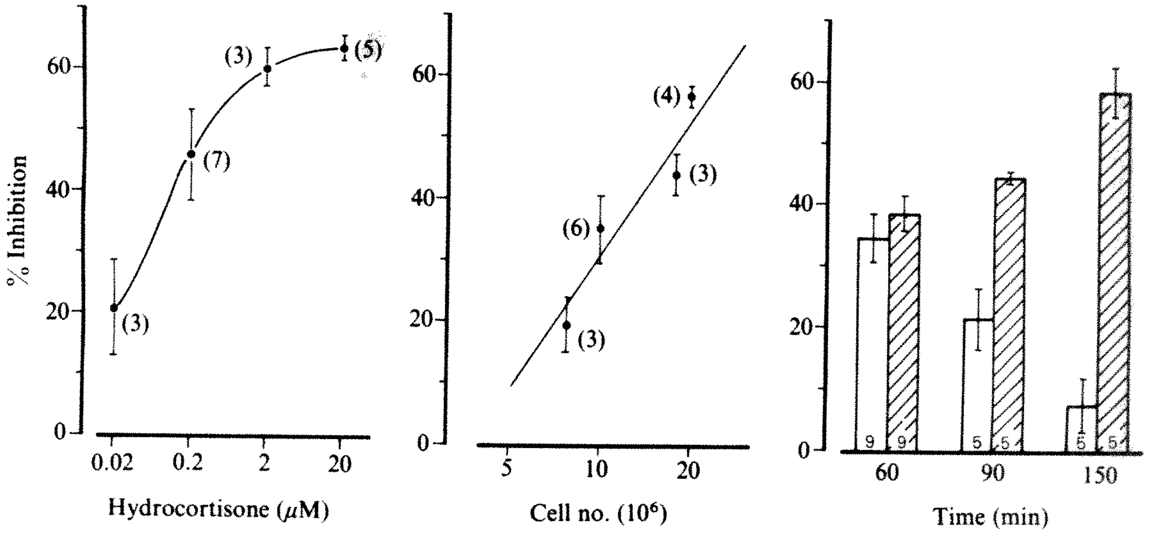

Fig. 1 Male Wistar rats (150–200 g) were killed by exposure to ether. The peritoneal cavity was washed with 20 ml of heparinized Krebs solution and the cell-rich fluid (80% mononucleate and 20% polymorphonucleate) was removed and centrifuged (500 *g*). The cells from 10–15 animals were pooled and washed twice by resuspending in Krebs solution enriched with bovine serum albumin (BSA, 100 μg ml^{-1}). *Release of macrocortin*: The final suspension, usually containing 1×10^7 cells ml^{-1} ('generator leukocytes'), was divided into two samples: hydrocortisone sodium phosphate was added to one sample. No drug was present in the other sample. Both samples were incubated at 37 °C in a metabolic shaker. After incubation, the cells were removed by centrifugation and the supernatants were dialysed overnight against 300 vol Krebs solution at 4 °C. *Assay of macrocortin*: A second pool of freshly collected leukocytes ('test leukocytes') was suspended in Krebs–albumin. A series of 3-ml samples were prepared by mixing 1 ml of cell suspension with 2 ml of dialysed supernatant and incubated for 120 min at 37 °C with killed bacteria (*Bordetella pertussis*) in a ratio of 800–1,000 bacteria per cell. After the incubation the cells were removed by centrifugation and the amount of PGs in the supernatant was determined by bioassay over rat stomach strips using synthetic PGE_2 (Upjohn) as reference standard. Test leukocytes incubated with supernatants collected from steroid-free generator leukocytes released on average 10–12 ng PG (in terms of PGE_2) per 10^6 cells in 120 min. The release was inhibited when the incubation was carried out in presence of dialysed supernatants collected from generator leukocytes treated with hydrocortisone. Results are expressed as mean per cent inhibition (± s.e.m.) of the PG formation by test leukocytes exhibited by various supernatants from steroid-treated generator leukocytes, compared with the PG formation in presence of supernatants from steroid-free generator leukocytes. For other experimental details see refs 14, 16. *a*, Macrocortin release by cells incubated for 90 min with increasing concentrations of hydrocortisone (figures in parentheses indicate numbers of experiments). *b*, Relationship between macrocortin release and number of cells (generator leukocytes) incubated with 20 μM hydrocortisone for 90 min. *c*, Time course of macrocortin release. Cells were incubated with hydrocortisone (20 μM) for different times. At the end of incubation the inhibitory activity present in the Krebs solution as well as within the cells were separately determined. After removing the cells by centrifugation, Krebs solution was collected, dialysed and tested as above (hatched columns). The centrifuged cell pellet was resuspended in an equivalent volume of Krebs solution, disrupted by repeated (4 times) freeze-thawing and centrifuged (100,000 *g* for 60 min). The supernatants were tested for the inhibitory activity as above (open columns). Figures in columns indicate numbers of experiments.

0028-0836/80/370147—03$01.00

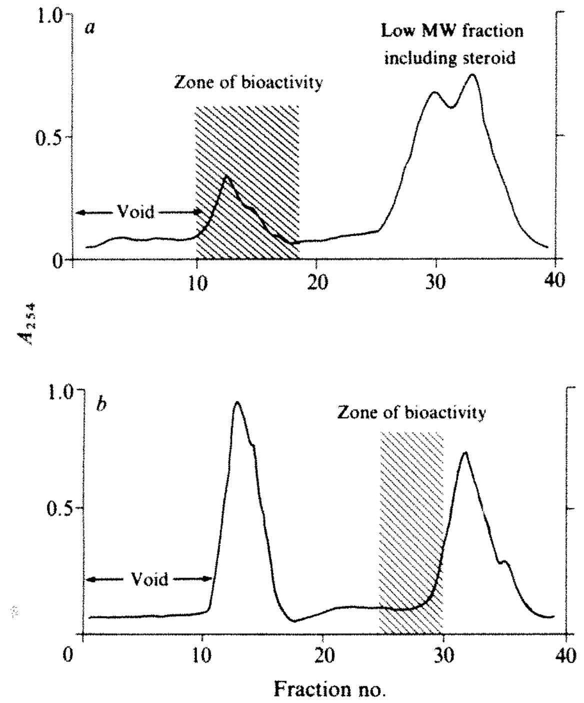

Fig. 2 Partial purification of guinea pig lung macrocortin by Sephadex chromatography. Both columns were 100 × 1 cm, the equilibrating and eluting buffer used in each case was 0.1% ammonium bicarbonate adjusted to *p*H 7.5. The flow rate was 0.8 ml min^{-1} and fractions were collected automatically every 5 min. The UV absorbance at 254 nm was continuously measured with a Uvicord flow cell monitor. For isolation of the lung-derived material, batches of the Krebs solution effluent from steroid-treated lungs were processed in an ultrafiltration chamber fitted with a 500 or 1,000 MW filter. The effluent was concentrated to 100–200 ml and then lyophilized. The residual material was dissolved in 10 ml of buffer and applied to the G-25 (medium) column. Fractions were collected and lyophilized. The biological activity was estimated using lungs treated with cycloheximide (5 μg ml^{-1}) to prevent the effects of the steroid. *a* Shows the results of such an experiment; several UV absorbing peaks were seen; those associated with fractions 10–20 were compounds with a MW greater than the nominal cut-off point of this gel (in this case, 5,000). The UV absorbing peaks which appeared in fractions 25–40 were low MW compounds including the steroid. In one experiment, in which radioactive dexamethasone was added to the crude effluent, all the radioactivity was subsequently recovered in fractions 30–40. There was no trace of radioactivity in the high MW fractions. In contrast, all of the steroid-like bioactivity was recovered close to the void volume. These preparations were free of steroid and buffer salts and could be conveniently lyophilized. This material was rechromatographed on Sephadex G-50 (medium). In this case however, the biological activity was retained by the column and did not emerge until fractions 21–28. Compounds moving with this mobility would have a MW of ~15,000. V_e (ml) BSA, 38.5; trypsin inhibitor, 76.5; macrocortin, 84; cytochrome *c*, 86; dexamethasone, 122.5. Macrocortin production by the lungs was variable. Of all lungs tested, ~15% did not respond to the steroid at all. The inhibitory response to the steroid (thus the production of macrocortin) was enhanced when the glucose concentration in the Krebs solution was increased from 1 g l^{-1} to 2 g l^{-1}. A striking improvement (~twofold) in inhibitory activity was observed when a mixture of 21 amino acids (final concentration of each, ~1 nM) was included in the Krebs solution. Leukocyte-derived macrocortin was prepared as follows: sometimes macrocortin released from cells stimulated by hydrocortisone was used as a starting material, in other instances crude lysates of unstimulated cells were used. In the former case, the medium when separated from the cells was dialysed overnight against 300 vol of Krebs solution at 4 °C before column chromatography. In the latter case, the crude, heat-treated lysates were centrifuged at 100,000 *g* for 1 h to remove coarse debris and precipitated protein. In either case the resulting material was first passed over a Sephadex G-25 column. As with the lung-derived material, bioactivity was found in the void volume and this was rechromatographed on Sephadex G-50. Again, macrocortin activity was retained by the column and eluted with a position indicating a MW of ~15,000. The steroid-induced release of macrocortin from leukocyte incubations was sensitive to the glucose concentration (the amount used here (2 g l^{-1}) is essential for complete release). Vigorous gassing of buffers for more than about 5 min apparently prevented release at the cell density used. The amount of macrocortin found in crude lysates of leukocytes was variable and ~10–20% of preparations contained no detectable material, or very small amounts. At the moment, we cannot gauge the influence of endogenous steroids on the macrocortin content of leukocytes and this could well be a source of variation.

Partially purified macrocortin has been isolated from two sources—the effluent from steroid-stimulated guinea pig lungs, and rat peritoneal leukocytes—see Fig. 2 legend for method. Macrocortin from both sources has an apparent molecular weight (MW) of 15,000 and also has a number of properties in common: both preparations are stable at 70 °C for up to 30 min but are destroyed by boiling. Acidification of the factor to *p*H 2 for 20 min resulted in less than 15% loss of activity. Macrocortin seems to be a protein because lung-derived material lost substantial (40–70%) activity after being stirred overnight at 4 °C with trypsin (10 μg ml^{-1}) or papain (10 μg ml^{-1}). The biological activity of partially purified (ex G50) leukocyte-derived macrocortin was also reduced (60–70%) by incubation for 1 h at 37 °C with 2.0 U of immobilized trypsin (Pierce).

Simple experiments with crude lung or leukocyte macrocortin demonstrated a considerable similarity in their biological activity: phagocytosing rat leukocytes produced less PGs when incubated in effluent from steroid-treated lungs than in effluent from control lungs (3.86 ± 0.53 and 5.63 ± 0.69 ng PGE$_2$ per 10^6 cells; *n* = 7). Krebs solution, in which leukocytes and steroid had been incubated together, inhibited PG synthesis by fresh leukocytes and thromboxane release from the lung[13]. Macrocortin from leukocyte lysates inhibited strongly in both systems. In each type of experiment, boiling abolished, and arachidonate reversed, the inhibition indicating that the inhibitor was heat labile and did not act at the cyclo-oxygenase level. The inhibition was cycloheximide-resistant and could not therefore be due to residual steroid.

Leukocyte-derived macrocortin also inhibited phospholipase activity in the lung as estimated by a radiochemical technique (see Fig. 3). The inhibitory activity was of rapid onset and was abolished by boiling.

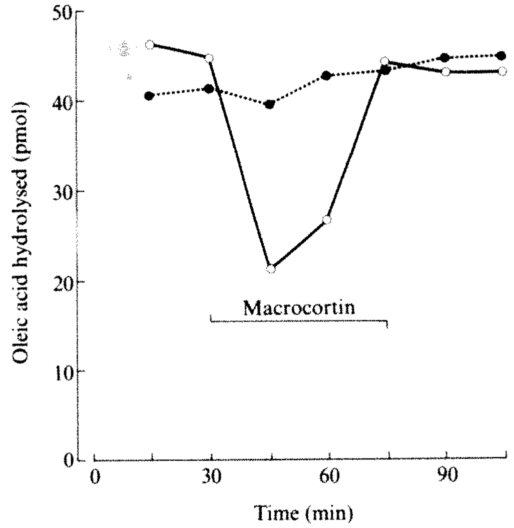

Fig. 3 Inhibition of guinea pig lung phospholipase A$_2$ activity by leukocyte-derived macrocortin. The assay depends on a specifically labelled molecule 1-palmitoyl, 2-^{3}H-oleic phosphatidylcholine. The rationale of the assay, preparation of the isotope and further methodology are described in ref. 11. Briefly, a mixture of the tritiated phosphatidylcholine and ^{14}C-labelled oleic acid (0.1 μCi total), dissolved in Tris buffer (*p*H 7.5), was injected into the Krebs solution entering the pulmonary artery. The effluent was collected for 5 min, 5 ml of Tris buffer (*p*H 7.5; 100 mM) was added to stabilize the *p*H, and the labelled fatty acids were extracted into 5 ml hexane by 1 min vortex mixing. An aliquot of the hexane was transferred into scintillation vials and the solvent evaporated with a gentle stream of nitrogen. Liberation of the ^{3}H-oleic acid from the phosphatide by phospholipase A$_2$ increases the ^{3}H/^{14}C ratio of the extracted fatty acids, enabling percentage hydrolysis to be estimated. The ratio of the two isotopes in a small aliquot of the aqueous solution was also determined: this gave a value for the 'total hydrolysis' and the actual hydrolysis was then calculated. ○, Normal macrocortin (ex G25); ●, boiled material. Lungs had been perfused for 1 h at time '0 min' on the graph. The inhibitory activity was of rapid onset without the latency seen with the corticosteroids.

Arachidonate-derived products such as PGs[22] and 12-hydroxy-5, 8, 10, 14 eicosatetraenoic acid[23] (12-HETE) are involved in the pathogenesis of inflammation. The aspirin-like drugs block the cyclooxygenase[24–26] and this probably explains their therapeutic efficacy. Steroids are without activity on the cyclooxygenase enzyme but potently inhibit PG biosynthesis in viable cells. An important link was established between phospholipase inhibition and steroid action by Gryglewski's group[3] and Danon and Assouline were the first to propose that this was due to an action on the genome[12]. We took this concept further and provided indirect evidence for a second messenger which mediates the anti-phospholipase effects of steroids[13,16]. Here we provide the first direct evidence for such a factor (macrocortin) and have determined that it is a polypeptide of approximately 15,000 MW. In leukocytes steroids cause both a release and re-synthesis of macrocortin—both effects are blocked by inhibitors of RNA/protein synthesis.

Most aspirin-like drugs block only the cyclooxygenase pathway and may potentiate the formation of other arachidonate-derived substances, such as the chemotactic 12-HETE[27] and the bronchoconstrictor slow-reacting substance of anaphylaxis[28]. The steroids differ in this respect and block the formation of all products as they restrict substrate (arachidonate) availability. This may explain why they are able to block cell migration and allergic bronchoconstriction whereas the aspirin-like drugs cannot. In view of the work reported here, we propose that the most likely effector of steroid action on the arachidonate cascade is macrocortin.

Received 6 March; accepted 7 August 1980.

1. Herbaczynska-Cedro, K. & Staszewsa-Barczak, J. *Congr. Hungarian Pharmac. Soc.* Abstr. II, Budapest 19 (1974).
2. Lewis, G. P. & Piper, P. J. *Nature* **254,** 308–311 (1975).
3. Gryglewski, R. J., Panczenko, B., Korbut, R., Grodzinska, L. & Ocetkiewicz, A. *Prostaglandins* **10,** 343–355 (1975).
4. Kantrowitz, F., Robinson, D. C., McGuire, M. B. & Levine, L. *Nature* **258,** 737–739 (1975).
5. Tashjian, A. H., Voelkel, E. F., McDonough, J. & Levine, L. *Nature* **258,** 739–741 (1975).
6. Hong, S-CL. & Levine, L. *Proc. natn. Acad. Sci. U.S.A.* **73,** 1730–1734 (1976).
7. Nijkamp, F. P., Flower, R. J., Moncada, S. & Vane, J. R. *Nature* **263,** 479–482 (1976).
8. Floman, N. & Zor, U. *Invest. Ophthal. visual Sci.* **16,** 69–73 (1977).
9. Tam, S., Hong, S-CL. & Levine, L. *J. Pharmac. exp. Ther.* **203,** 162–168 (1977).
10. Parente, L., Ammendola, G., Persico, P. & Di Rosa, M. *Pol. J. Pharmac. Pharm.* **30,** 141–155 (1978).
11. Blackwell, G. J., Flower, R. J., Nijkamp, F. P. & Vane, J. R. *Br. J. Pharmac.* **62,** 79–89 (1978).
12. Danon, A. & Assouline, G. *Nature* **273,** 552-554 (1978).
13. Flower, R. J. & Blackwell, G. J. *Nature* **278,** 456-459 (1979).
14. Di Rosa, M. & Persico, P. *Br. J. Pharmac.* **66,** 161–163 (1979).
15. Russo-Marie, F., Paing, M. & Duval, D. *J. biol. Chem.* **254,** 8498–8504 (1979).
16. Carnuccio, R., Di Rosa, M. & Persico, P. *Br. J. Pharmac.* **68,** 14–16 (1980).
17. Buller, R. E. & O'Malley, B. W. *Biochem. Pharmac.* **25,** 1–12 (1976).
18. Chan, L. & O'Malley, B. W. *New Engl. J. Med.* **294,** 1372–1379 (1976).
19. Baxter, J. D. & Tomkins, G. M. *Proc. natn. Acad. Sci. U.S.A.* **68,** 932–937 (1971).
20. Bray, M. A. & Gordon, D. *Br. J. Pharmac.* **57,** 466P (1976).
21. Stevenson, R. D. *Clin. exp. Immun.* **17,** 601–606 (1974).
22. Flower, R. J. *Naunyn-Schmiedebergs Arch. Pharmak.* **297,** S77–S79 (1977).
23. Turner, S. R., Tainer, J. A. & Lynn, W. S. *Nature* **257,** 680–681 (1975).
24. Vane, J. R. *Nature new Biol.* **231,** 232–235 (1971).
25. Ferreira, S. H., Moncada, S. & Vane, J. R. *Nature new Biol.* **231,** 237–239 (1971).
26. Smith, J. B. & Willis, A. L. *Nature new Biol.* **231,** 235–237 (1971).
27. Eakins, K. E., Higgs, G. A., Moncada, S., Mugridge, K. G. & Vane, J. R. *Br. J. Pharmac.* **69,** 270P–271P (1980).
28. Burka, J. F. & Flower, R. J. *Br. J. Pharmac.* **65,** 35–41 (1979).

Thyrotropin-releasing hormone—CNS action to stimulate gastric acid secretion

Yvette Taché, Wylie Vale & Marvin Brown

Peptide Biology Laboratory, The Salk Institute, PO Box 85800,
San Diego, California 92138

Much physiological and pharmacological evidence has accumulated to suggest that the autonomic nervous system has an important role in the peripheral modulation of gastric secretion[1], although the neurochemical mediators in the brain which initiate or modulate autonomic input are poorly understood[1–4]. Recently, the demonstration that some oligopeptides present in mammalian brain act in the central nervous system (CNS) to influence profoundly glucoregulation[5], thermoregulation[6,7], blood pressure[8,9], sympathetic outflow[9–11], muscular activity of gut[12,13] and stress-induced gastric haemorrhagic lesions[14] have led us to examine a possible role for some of these endogenous brain oligopeptides as chemical messengers involved in the CNS modulation of gastric secretion. We report here that thyrotropin-releasing hormone (TRH) acts within the CNS to elicit a vagus-dependent stimulation of gastric acid secretion.

In this study we used male Sprague–Dawley CD rats (250–300 g) maintained *ad libitum* on Purina Laboratory Chow and tap water, and housed in conditions of controlled temperature and illumination (from 06 : 00 to 22 : 00 h). All experiments were performed according to the same time schedule in 24-h food-deprived rats with free access to water up to the beginning of treatment. Saline or test materials were injected intracisternally (i.c.) or intravenously (i.v.) via the jugular vein under light ether anaethesia, then the pylorus portion of the stomach was ligated. In some experiments, immediately before peptide injection and pylorus ligature, subdiaphragmatic vagotomy or sham operation was performed using the general method described by Martin *et al.*[15]. Conscious animals were decapitated at various intervals following pylorus ligature and gastric content was collected. Gastric volume and pH were measured and samples (0.5 or 1 ml) analysed for gastric acidity by titration with 0.01 M sodium hydroxide to a pH of 7.0.

Peptides, synthesized by Dr J. Rivier using solid phase methodology[16], and atropine sulphate were freshly dissolved in 0.9% saline before use and injected i.c. in 10 µl or i.v. in 0.2 ml volume. Following analysis of variance, differences between groups were determined by the multiple range test of Dunnett and Duncan using the computer program EXBIOL.

TRH given i.c. induced a marked elevation in the volume, titratable acid concentration and output of gastric secretion (Table 1). The time course of gastric response to TRH (expressed as percentage of changes compared with control decapitated at the same time period and taken as 100% change) indicated that the stimulatory effect of TRH reached a maximum within

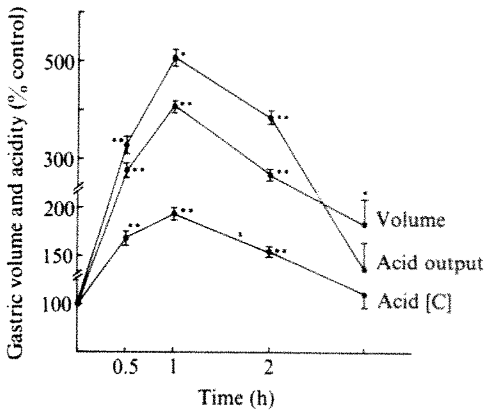

Fig. 1 Temporal effect of TRH (1 µg, i.c.) on gastric secretion. Twenty-four-hour fasted rats were injected with saline or TRH, then the pylorus was ligated and groups of saline and TRH-treated rats were decapitated at 30 min, 1, 2, or 3 h post-treatment. Each curve represents changes in gastric secretion induced by TRH injection, expressed as percentage compared with control groups taken for each time period as 100% change. $*P<0.05$; $**P<0.01$ as compared with saline-treated group decapitated at the same time period post-injection.

0028–0836/80/370149—03$01.00

Table 1 Gastric secretory response to i.c. injection of TRH and TRH analogues

Peptide	No. of rats	Volume (ml per rat)	*p*H	Gastric secretion Titratable acidity Concentration (mequiv. l^{-1})	Output (μequiv.)
Saline	7	2.1±0.5	1.87±0.09	61±9	154±65
TRH	7	5.3±1.0*	1.51±0.05†	95±9†	551±134*
[^{3}Me-His^2]-TRH	7	4.9±0.8*	1.51±0.03†	88±8†	464±111†
[^{1}Me-His^2]-TRH	8	1.6±0.4	1.71±0.11	69±7	130±44

24-h fasted rats under light ether anaesthesia were injected i.c. with saline (10 μl) or peptides (1 μg per 10 μl) and the pylorus was ligated. After 2 h, the animals were decapitated and gastric secretion collected.
* $P<0.001$; † $P<0.05$ as compared with saline-treated rats.

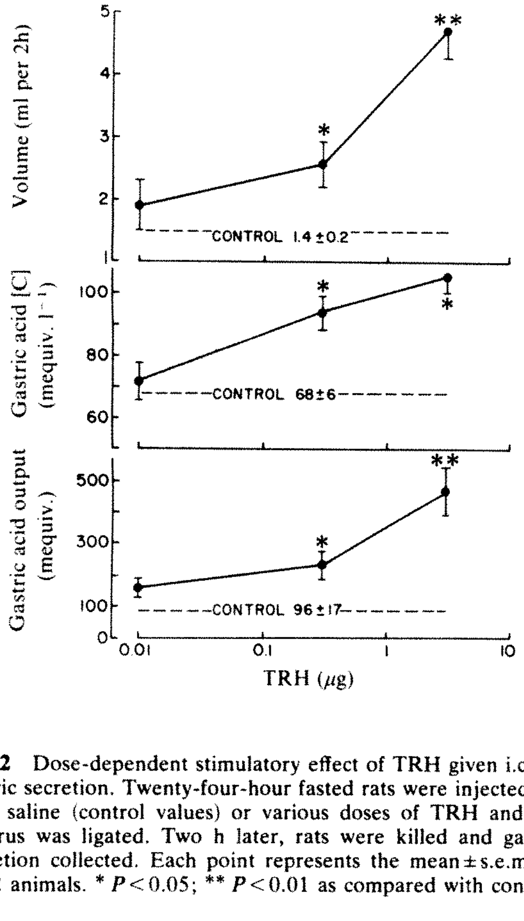

Fig. 2 Dose-dependent stimulatory effect of TRH given i.c. on gastric secretion. Twenty-four-hour fasted rats were injected i.c. with saline (control values) or various doses of TRH and the pylorus was ligated. Two h later, rats were killed and gastric secretion collected. Each point represents the mean±s.e.m. of 5–12 animals. * $P<0.05$; ** $P<0.01$ as compared with control.

1 h, thereafter it returned to the level of control group (Fig. 1). A significant dose-related stimulatory effect is observed following i.c. injection of TRH in doses ranging over 0.3–3 μg as measured 2 h after peptide injection and pylorus ligature (Fig. 2). TRH given i.v. at 10 or 100 μg dose per animal exerted no effect on gastric secretion (data not shown). Using a different experimental design, Morley *et al.* have observed in dogs that TRH inhibited gastric acid secretion stimulated by tetragastrin[17] for the first 15 min. The activity of TRH given i.c. and its ineffectiveness given i.v. strongly support the concept that TRH initially acts through the brain to elicit the stimulation of gastric secretion. The tripeptide has already been shown to have a broad spectrum of CNS-mediated actions unrelated to its neuroendocrine activity, including modification of behavioural[18] and hormonal[19-21] effects of narcotics, or biogenic amines, alteration of thermoregulation[22], blood pressure[23], food intake[24] and muscular activity of gut[12,13]. The stimulatory effect of TRH on gastric secretion appears long-acting, dose-dependent, reversible and specific. The specificity is demonstrated by the inactivity of TRH analogue [^{1}Me-His^2]-TRH (Table 1) which likewise has been found ineffective in other bioassay systems[19,22,25], whereas the active analogue [^{3}Me-His^2]-TRH (ref. 25) mimicked the stimulatory effect of TRH on gastric secretion. Antimuscarinic compounds have been shown to antagonize several CNS-mediated effects of TRH including those on eye pupil[18] and gut muscular activity[12,13]. The effectiveness of vagotomy (data not shown) or atropine (Table 2) in inhibiting the stimulatory effect of TRH on gastric secretion supports the concept that vagus-dependent cholinergic mechanisms could participate in the expression of the gastric response to TRH. However, the exact neuroanatomic site, as well as the CNS and peripheral neuronal/humoral circuits involved, remain to be further identified. On the basis of stimulation and lesion experiments, the hypothalamus (mainly the lateral and ventromedial regions) has been demonstrated in rats to participate in brain control of gastric secretion[26,27]. The fact that high concentrations of TRH are present in the hypothalamus[28] supports the possibility that endogenous TRH may have physiological significance as a CNS chemical messenger involved in brain modulation of gastric secretion.

We thank Millie Newberry and Ron Kaiser for technical assistance, and Susan McCall for manuscript preparation. Research was supported by NINCDS grant NS-14263, NIAMDD grant AM-20917 and the March of Dimes Birth Defects Foundation, and was conducted in part by the Clayton Foundation for Research, California Division. W. V. is a Senior Clayton foundation Investigator, M. B. is a Clayton Foundation Investigator, and Y. T. is the recipient of a Canadian MRC Centennial Fellowship.

Table 2 Blockade by atropine of TRH-induced stimulation of gastric secretion

Group	Treatment	No. of rats	Volume (ml per rat)	Gastric secretion Titratable acidity Concentration (mequiv. l^{-1})	Output (μequiv.)
1	Saline + saline	13	1.1±0.2	61±10	88±2
2	Saline + TRH	9	3.3±0.3*	107±6*	364±35*
3	Atropine + saline	5	0.3±0.1†	30±10†	18±10†
4	Atropine + TRH	5	0.4±0.2† (*)	28±5† (*)	8±4† (*)

24-h fasted rats under light ether anaesthesia were injected i.v. with saline (0.2 ml) or atropine (2 mg per kg) and i.c. with saline (10 μl) or TRH (1 μg 10 μl^{-1}) and the pylorus was ligated. One h later, the amimals were decapitated and gastric secretion collected. * $P<0.01$; † $P<0.05$ as compared with group 1 and in parentheses with group 2.

Received 28 February; accepted 4 July 1980.

1. Soll, A. H. & Walsh, J. H. *A. Rev. Physiol.* **41,** 35–53 (1979).
2. Brodie, D. A., Lotti, V. J. & Bauer, B. G. *Am. J. dig. Dis.* **15,** 111–120 (1970).
3. Osumi, T., Aibara, S., Sakae, K. & Fujiwara, M. *Life Sci.* **20,** 1407–1416 (1977).
4. Yamaguchi, I., Hiroi, J. & Kumada, S. *J. Pharmac. exp. Ther.* **203,** 125–131 (1977).
5. Brown, M., Rivier, J. & Vale, W. *Life Sci.* **21,** 1729–1734 (1978); *Endocrinology* **104,** 1709–1715 (1979).
6. Brown, M., Rivier, J. & Vale, W. *Science* **196,** 998–1000 (1977).
7. Nemeroff, C. B., Osbahr, A. J., Manberg, P. J., Ervin, G. & Prange, A. J. *Proc. natn. Acad. Sci. U.S.A.* **76,** 5368–5371 (1979).
8. Weitzman, R. E., Firemark, H., Riviczky, A. & Nelson, J. C. *Endocrinology* **104,** A292 (1979).
9. Fisher, D. & Brown, M. *Soc. Neurosci. Abstr.* **5,** A136 (1979).
10. Brown, M., Taché, Y. & Fisher, D. *Endocrinology* **105,** 660–665 (1979).
11. Brown, M. & Fisher, D. *Endocr. Soc.* **61,** 125 (1979).
12. Smith, J. R., LaHann, T. R., Chestnut, R. M., Carino, M. A. & Horita, A. *Science* **196,** 660–662 (1977).
13. Tonoue, T. & Nomoto, T. *Eur. J. Pharmac.* **58,** 369–377 (1979).
14. Taché, Y., Simar, P. & Collu, R. *Life Sci.* **21,** 1719–1726 (1979).
15. Martin, J. R., Rogers, R. C., Novin, D. & Vanderwelle, D. A. *Bull. Psychol. Sci.* **10,** 291–294 (1977).
16. Rivier, J., Vale, W., Monahan, M., Ling, N. & Burgus, R. *J. med. Chem.* **15,** 479–482 (1972).
17. Morley, J. E., Steinback, J. H., Feldman, E. J. & Soloman, T. E. *Life Sci.* **24,** 1059–1066 (1979).
18. Yarbrough, G. G. *Prog. Neurobiol.* **12,** 291–312 (1979).
19. Brown, M. & Vale, W. *Endocrinology* **97,** 1151–1156 (1975).
20. Taché, Y., DuRuisseau, P., Ducharme, J. R. & Collu, R. *Eur. J. Pharmac.* **45,** 369–376 (1977).
21. Taché, Y., Lis, M. & Collu, R. *Life Sci.* **21,** 841–846 (1977).
22. Brown, M., Rivier, J. & Vale, W. *Life Sci.* **20,** 1681–1688 (1977).
23. Horita, A. & Carino, M. A. *Proc. west. Pharmac.* **20,** 303–310 (1977).
24. Vijayan, E. & McCann, S. M. *Endocrinology* **100,** 1727–1730 (1977).
25. Vale, W., Grant, G. & Guillemin, R. in *Frontiers in Neuroendocrinology* (eds Martini, L. & Ganong, W.) 375–413 (Oxford University Press, 1973).
26. Misher, A. & Brook, F. P. *Am. J. Physiol.* **211,** 403–406 (1966).
27. Davis, R. A., Brook, F. P. & Steckel, D. C. *Am. J. Physiol.* **215,** 600–604 (1968).
28. Brownstein, M. J., Palkovits, M., Saavedra, J. M., Bassiri, R. & Utiger, R. D. *Science* **185,** 267–269 (1974).

Evidence that substance P is a neurotransmitter in the myenteric plexus

Kiichiro Morita*, R. Alan North* & Yoshifumi Katayama†

* Neurophysiology Laboratory, Department of Pharmacology, Loyola University Stritch School of Medicine, Maywood, Illinois 60153
† Department of Physiology, Kurume University Medical School, 67 Asahi-machi, Kurume-shi 830, Japan

Substance P (SP) is an undecapeptide originally isolated from the gut[1] and since shown to occur within neurones in several parts of the peripheral[2,3] and central[4] nervous systems. Immunohistochemical studies indicate an exceedingly dense network of SP-containing nerves within the myenteric plexus of the guinea pig ileum[5,6]. These nerves are intrinsic to the gut wall[5,7] and can release SP to contract the longitudinal muscle layer[8,9]. We have previously shown[10,11] that SP directly depolarizes myenteric neurones and that this depolarization has a time course and ionic mechanism similar to the slow excitatory postsynaptic potential (e.p.s.p.) which can be produced by electrical stimulation of presynaptic nerves within the myenteric ganglia. We wondered whether SP might mediate this slow synaptic potential[10]. We report here that the SP depolarization and the slow e.p.s.p. are reversibly depressed by chymotrypsin, an enzyme which degrades SP, although the responses to acetylcholine, serotonin and an unknown hyperpolarizing transmitter are unaffected. The results provide direct evidence that a peptide can mediate chemical transmission between neurones in the mammalian nervous system.

Intracellular recordings were made from neurones in myenteric ganglia which had been dissected from the ilea of adult guinea pigs[12]. These ganglia were perfused *in vitro* with warm (37 °C) Krebs solution to which known concentrations of SP or chymotrypsin could be added. The neurones could be seen using Nomarski optics and this allowed placement of the tips of iontophoresis electrodes containing SP or serotonin close to the soma membrane of the impaled cell[11,12]. Focal stimulation of the ganglion surface evoked fast cholinergic synaptic potentials in one class of cells (type 1 (ref. 12), S cells[13]) and sometimes caused a much slower depolarization[14] in both types of cell (also type 2 (ref. 12), AH cells[13]). Perfusion of SP depolarized both types of myenteric neurones and also reversibly blocked the slow e.p.s.p. and the depolarizing response to SP iontophoresis; it did not block the fast cholinergic e.p.s.p. This finding at least suggested that the perfused SP may desensitize the myenteric neurones to the transmitter released by nerve stimulation.

Perfusion of the preparation with chymotrypsin (200 μg ml^{-1}) reversibly abolished the responses to SP applied by either perfusion (Fig. 1*a*) or iontophoresis (Fig. 2). The response to SP iontophoresis could be restored in the presence of chymotrypsin by increasing the amplitude or duration of the ejecting current, arguing against a destruction or inactivation of postsynaptic sites and in favour of enzymatic degradation of SP between the time of its release from the iontophoresis pipette and its action on the cell membrane. Chymotrypsin (200 μg ml^{-1}) reversibly abolished the slow e.p.s.p. (Fig. 1*b*). When the synaptic potential was depressed by chymotrypsin, it could sometimes be restored by increasing the frequency or duration of the stimulating train of pulses. Chymotrypsin usually did not change the membrane potential, input resistance, action potentials or fast e.p.s.p.; nor did it affect the slow hyperpolarizing synaptic potentials which were occasionally observed in response to nerve stimulation[14]. Higher concentrations of chymotrypsin (300–1,000 μg ml^{-1}) depolarized myenteric neurones, often irreversibly. Chymotrypsin (200 μg ml^{-1}) did not block either the depolarizing or the hyperpolarizing responses to iontophoretic application of serotonin (Fig. 2). Carboxypeptidase (200 μg ml^{-1}), which does not cleave the amidated C terminal of SP (ref. 15), had no effect on membrane potential, the fast e.p.s.p., the slow e.p.s.p. and the

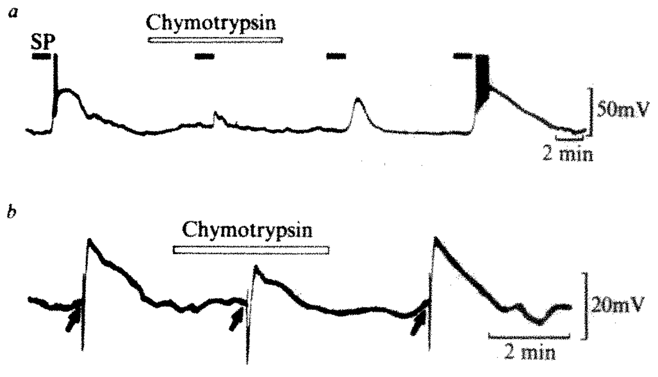

Fig. 1 Recordings of membrane potential from two myenteric neurones. *a*, Substance P depolarization is abolished by chymotrypsin. The perfusion solution contained SP (100 nM) during the four periods (90 s) indicated by the solid bars. The perfusing solution also contained chymotrypsin (200 μg ml^{-1}) where indicated by the open bar. The apparent delay in the onset of the depolarizing action of SP is due entirely to the time taken for the changed solution to flow through the perfusion system before entering the bath (80 s). SP caused a prominent depolarization which initiated action potentials. Chymotrypsin reversibly prevented this action. *b*, Slow e.p.s.p. is depressed by chymotrypsin. The surface of the myenteric ganglion was stimulated with a focal stimulating electrode (10 Hz, 3 s) at the times indicated by the arrows. This caused a short-lasting hyperpolarization followed by a prolonged depolarization (slow e.p.s.p.). Perfusion of chymotrypsin reversibly depressed the slow e.p.s.p. without changing membrane potential or the hyperpolarizing response (which is, presumably, due to a different transmitter).

0028–0836/80/370151—02$01.00

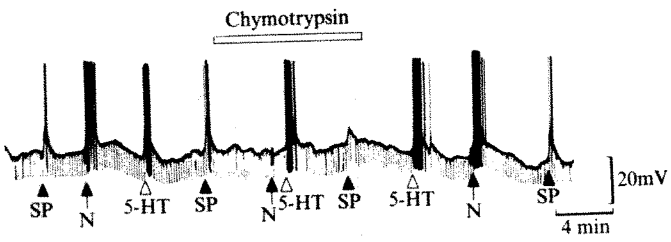

Fig. 2 Membrane potential of a myenteric neurone. Downward deflections are anelectrotonic potentials caused by constant current pulses. SP (100 nA, 5s) and serotonin (5-HT, 20 nA, 10 s) were applied at the times indicated by ▲ and △, respectively. Presynaptic nerves were stimulated (30 Hz, 3 s) at the times indicated by the arrows (N). Both SP and serotonin mimicked the effects of nerve stimulation in this neurone, causing it to depolarize and fire action potentials (full amplitude not recorded). Perfusion with chymotrypsin (200 μg ml^{-1}) did not change membrane potential or resistance but abolished the response to nerve stimulation and greatly reduced the response to SP iontophoresis. The response to serotonin iontophoresis was not depressed.

depolarizing responses to iontophoretic application of either SP or serotonin. Higher concentrations of carboxypeptidase depolarized myenteric neurones, often irreversibly.

In the present experiments, chymotrypsin did not depress the serotonin response in the same cell in which it depressed the slow e.p.s.p. It seems unlikely that serotonin makes a major contribution to the slow e.p.s.p., as has been proposed[16]. It is undetectable in the myenteric plexus of the adult guinea pig ileum without precursor loading and the proportion of cells which contain aromatic amino acid decarboxylase is very low. Furthermore, serotonin either depolarizes or hyperpolarizes myenteric neurones[17], and a substantial proportion of those which are hyperpolarized have ony depolarizing slow e.p.s.ps (Johnson, Y.K., K.M. and R.A.N., in preparation).

The results indicate that a chymotrypsin-sensitive peptide mediates the slow depolarizing potential; the great density of nerve terminals which contain SP make this peptide a likely candidate. At other sites in the mammalian nervous system, evidence for 'peptidergic' transmission remains largely inferential. Enzymatic degradation of released peptide transmitters, although lacking the specificity of pharmacological antagonists, may offer an as yet untested means of establishing the functional role of peptides within the nervous system.

This work was supported by DA01730, NS06672 and the Schweppe Foundation.

Received 24 March; accepted 7 July 1980.

1. Von Euler, U. S. & Gaddum, J. H. *J. Physiol., Lond.* **72,** 74–87 (1931).
2. Nilsson, G. *et al. Histochemistry* **43,** 97–99 (1975).
3. Pearse, A. G. E. & Polak, J. M. *Histochemistry* **41,** 373–375 (1975).
4. Hokfelt, T. *et al.* in *Substance P* (eds Von Euler, U. S. & Pernow, B.) 117–145 (Raven, New York, 1977).
5. Costa, M., Cuello, C., Furness, J. B. & Franco, R. *Neuroscience* **5,** 323–331 (1980).
6. Schultzberg, M. *et al. Neuroscience* **5,** 689–744 (1980).
7. Franco, R., Costa, M. & Furness, J. B. *Naunyn-Schmeidebergs Archs Pharmak.* **307,** 57–63 (1979).
8. Franco, R., Costa, M. & Furness, J. B. *Naunyn-Schmeidebergs Archs Pharmak.* **306,** 185–201 (1979).
9. Rosell, S. *et al.* in *Substance P* (eds Von Euler, U. S. & Pernow, B.) 83–88 (Raven, New York, 1977).
10. Katayama, Y. & North, R. A. *Nature* **274,** 387–388 (1978).
11. Katayama, Y., North, R. A. & Williams, J. T. *Proc. R. Soc.* **B206,** 191–208 (1979).
12. Nishi, S. & North, R. A. *J. Physiol., Lond.* **231,** 471–491 (1973).
13. Hirst, G. D. S., Holman, M. E. & Spence, I. *J. Physiol., Lond.* **236,** 303–326 (1974).
14. Johnson, S. M., Katayama, Y. & North, R. A. *J. Physiol., Lond.* **301,** 505–516 (1980).
15. Chang, M. M. & Leeman, S. E. *J. biol. Chem.* **254,** 4784–4790 (1971).
16. Wood, J. D. & Mayer, C. J. *Nature* **276,** 836–837 (1979).
17. Johnson, S. M., Katayama, Y. & North, R. A. *J. Physiol., Lond.* (in the press).

Neurotransmitter turnover in rat striatum is correlated with morphine self-administration

James E. Smith, Conchita Co, Mark E. Freeman, Michael P. Sands & John D. Lane

Psychiatry Research Unit, Department of Psychiatry, Louisiana State University Medical Center, Shreveport, Louisiana 71130

Drugs of abuse probably exert their reinforcing effects through 'reward' pathways in the central nervous system (CNS)[1,2]. Neuronal systems mediating opiate reinforcement have been investigated using pharmacological and electrolytic lesion procedures. Drugs that interfere with catecholaminergic[3–6] and cholinergic[7] neuronal activity decrease intravenous (i.v.) morphine self-administration in monkeys and rats. Electrolytic lesion procedures in rats have demonstrated that the medial forebrain bundle[8] and caudate nucleus[9] are important in maintaining i.v. morphine self-administration. We have now carried out a direct investigation of striatal (caudate nucleus, putamen and globus pallidus) neuronal systems. We show here that striatal catecholaminergic systems are important in mediating opiate reinforcement, and present direct evidence for the involvement of neurotransmitter systems in morphine reward.

The turnover rates of dopamine (DA), noradrenaline (NA), aspartate (Asp), glutamate (Glu), γ-aminobutyric acid (GABA) and glycine (Gly) were determined in rats self-administering morphine i.v. (condition 1) and in yoked-morphine infused (condition 2) and yoked-vehicle infused (condition 3) littermates. This design was chosen to elucidate the neurochemical effects of the drug alone (conditions 2 and 3) and the effects of the drug self-administration milieu (conditions 1 and 2).

Eleven litters of three (conditions 1–3) adult male Fisher 344 rats were implanted with chronic jugular catheters using a previously described procedure[10,11] and housed together in a large experimental chamber in three separate self-administration cages. Two rats in each litter were made physically dependent over an 8-day period by automatic hourly infusions of morphine in increasing concentrations (2 days each of 1.25, 2.5, 5.0 and 10.0 mg per kg); the third rat received yoked-vehicle (saline) infusions. Each infusion (morphine or saline) was paired with a tone and light stimulus of 30 s duration. Levers were then introduced and one of the physically dependent rats was allowed to self-administer morphine i.v. (10 mg per kg in 0.1 ml saline) by lever pressing. This animal had 24 h access to morphine from that time and could take an infusion on demand by fulfilling the response requirement, which was initially one

Table 1 Content of dopamine, noradrenaline, serotonin (5-HT), aspartate, glutamate, GABA and glycine concurrently measured in the striatum of rats i.v. self-administering morphine and in yoked-morphine and yoked-vehicle infused littermates

	Content						
	pmol per mg protein			nmol per mg protein			
	DA	NA	5-HT	Asp	Glu	GABA	Gly
Morphine self-administration	524.5 ±77.5	34.2 ±9.6	45.6 ±5.9	20.1 ±3.6	86.8 ±10.5	25.3 ±4.9	6.0 ±1.3
Yoked-morphine infused	524.1 ±76.5	35.5 ±7.4	44.9 ±5.7	22.2 ±3.4	93.8 ±10.3	29.8 ±5.8	6.8 ±1.4
Yoked-vehicle infused	549.8 ±85.0	36.1 ±8.2	45.8 ±5.0	21.4 ±4.3	88.0 ±8.0	27.1 ±7.1	6.5 ±1.5

Values are means ± s.d. for $n = 11$ in each treatment condition. Student's t-test for differences between means showed no significant changes.

0028-0836/80/370152—03$01.00

lever press. Eventually, 10 lever presses were required for each injection (fixed ratio 10 schedule of reinforcement). The yoked-morphine and yoked-vehicle injected animals in each litter received simultaneous infusions whenever the self-administration animal earned an infusion. Lever presses from these yoked littermates were recorded. However, such responses were infrequent.

After stable baselines of self-administration had been obtained, the cumulative records for the 3 days before death were used to determine an average inter-injection interval for each litter. On the day of pulse-labelling, at 60 ($n = 5$ litters) and 90 min ($n = 6$ litters) before a predicted injection, 0.5 mCi [U-^{3}H]tryptophan (NEN, specific activity 7.1 Ci mmol^{-1}), 1.0 mCi [2,6-^{3}H]tyrosine (Amersham Searle, specific activity 34 Ci mmol^{-1}) and 0.2 mCi D-[U-^{14}C]glucose (ICN, specific activity 210 mCi mmol^{-1}) were injected through the jugular catheter. The three littermates were killed at the calculated injection time by total immersion in liquid nitrogen. The heads were allowed to warm to −20°C, the brain removed, cut into 1-mm coronal sections, and the striata discretely removed from the frozen sections. The striata were individually pulverized in a stainless steel mortar in liquid nitrogen and the content, specific radioactivity and turnover values for DA, NA, Asp, Glu, GABA and Gly were concurrently determined using previously described procedures[12–14].

Stable morphine self-administration usually developed within 3–4 weeks (27 ± 16 days) (all values are mean ± s.d.), the average inter-jection interval being 122 ± 35 min for the 11 self-administering animals. During the pulse-label interval, neither morphine nor vehicle was delivered to the litter even if the self-administering animal responded appropriately for an injection. However, the stimulus light and tone were presented, resulting in conditioned morphine-like stereotypical behaviour (weaving, bobbing, circling) in both morphine-dependent rats in each litter during the pulse-label interval. Self-administering animals responded for an average of 5 ± 4 injections (~50 responses) during the pulse interval, with most responses occurring near the predicted injection time. These non-reinforced lever presses were a small percentage of the total motor activity occurring during the pulse interval so that neurochemical differences between the morphine self-administering rat and the yoked-morphine injected animals would be unlikely to result from the purely motor effects of these non-reinforced lever presses but may well partially result from the motivational effects of non-reinforcement (extinction).

The striatal content of the putative neurotransmitters and amino acids did not differ in any of the treatment conditions (Table 1), whereas turnover rates were very different in the yoked-morphine infused and self-administering animals (Table 2). Passive morphine infusions alone (yoked-morphine group compared with yoked-saline infused group) resulted in an increase in the turnover rates of DA, Glu, Gly and GABA and a decrease in NA utilization. The effects of the contingent administration of morphine were sometimes even greater. Turnover rates of DA, NA, Asp, Glu and GABA were almost twice and Gly almost half as high in the self-administering rats as in the yoked-morphine infused animals.

The differences between the self-administering and yoked-morphine infused animals are important for several reasons. First, these data demonstrate that the contingent effects of drug self-administration behaviour result in changes in the utilization rates of putative neurotransmitters in the striatum that are sometimes greater than the effect of the drug itself. The interaction between the drug and the environmental context of its abuse, as reflected in this study by the conditions of contingent compared with non-contingent administration, is an important factor in abuse potential that has been recognized in the clinical setting. Humans receiving opiates in a passive fashion (for example, hospitalized individuals receiving opiates for pain) are less likely to self-administer the drug after it has been withdrawn or to engage in drug-seeking behaviour than are addicts who self-administer and are subsequently withdrawn. Self-administration sometimes results in greater changes in striatal neurotransmitter turnover than does passive infusion of the drug into yoked littermates, and seems to have marked neurochemical consequences. Second, these differences demonstrate for the first time a neurochemical correlate of drug self-administration behaviour. Our data indicate that the milieu in which a drug is administered cannot be ignored in basic studies of drug action.

Table 2 Turnover rates for dopamine, noradrenaline, aspartate, glutamate, GABA and glycine concurrently measured in the striatum of rats i.v. self-administering morphine and in yoked-morphine and yoked-vehicle infused littermates

	Turnover rates					
	pmol per mg protein per h		nmol per mg protein per h			
	DA	NA	Asp	Glu	GABA	Gly
Morphine	287.0*	21.6*	32.2*	112.8*	33.9*	1.1*
self-administration	±42.6	±6.3	±5.7	±13.7	±6.6	±0.2
Yoked-morphine	117.8*	10.8*	17.8†	55.7*	12.9*	3.0*
infused	±17.6	±2.2	±2.7	±6.1	±2.5	±0.6
Yoked-vehicle	46.6	45.5	13.9	35.9	3.2	1.5
infused	±7.7	±10.3	±2.8	±3.3	±0.9	±0.3

Turnover rates were measured after administration of ^{3}H-tryptophan, ^{3}H-tyrosine and ^{14}C-glucose. Values are means ± s.d. for $n = 11$ in each treatment group and were calculated as the product of the fractional rate constants (k) and the content values from Table 1. Turnover$_A = k$ (content$_A$). Any measure of neurotransmitter turnover is an approximation, but represents relative rates of metabolism of transmitters and amino acids. Thus, two time points on the linear decay portion of temporal specific activity plots were used to calculate apparent fractional rate constants based on assumptions such as steady state and one open pool, which are obviously not entirely valid and consistent with current concepts of putative neurotransmitter compartmentation. Nevertheless, to obtain a measure of transmitter utilization, the fractional rate constants were calculated as $k = \ln 2/t_{1/2}$, where $\ln 2 = 0.693$ and the $t_{1/2}$ is obtained from a semilogarithmic plot of the specific radioactivities determined at 60 ($n = 5$ litters) and 90 ($n = 6$ litters) min after i.v. injection of 0.5 mCi of ^{3}H-tryptophan, 1.0 mCi ^{3}H-tyrosine and 0.2 mCi ^{14}C-glucose. The turnover rate of serotonin was too low for reliable measurement.

*$P < 0.001$; †$P < 0.01$: the significance of the difference between means as determined with Student's t-test. The self-administration group was compared with the yoked-morphine infused group (effects of self-administration) and the latter was compared with the yoked-vehicle infused group (effects of morphine).

The role of CNS neurotransmitters in opiate action has been extensively investigated[12–19]. Also, several lines of evidence indicate that opiate reinforcement may be mediated by central reward pathways[20–23]. This is further supported by the increase in DA turnover in the striatum of self-administering animals seen in the present study. Furthermore, changes in the turnover rates of the amino acids are consistent with their role as putative transmitters released at a large number of CNS synapses[24]. The interaction of multiple systems during contingent opiate self-administration is now being assessed.

This research was supported in part by USPHS research grant DA–01999–04.

Received 20 March; accepted 7 July 1980.

1. Stein, L. *Fedn Proc.* **23,** 836–850 (1964).
2. Marcus, R. & Kornetsky, C. *Psychopharmacology* **38,** 1–13 (1974).
3. Pozuelo, J. & Kerr, F. W. L. *Mayo Clin. Proc.* **47,** 621–628 (1972).
4. Hanson, H. M. & Cimini-Venema, C. A. *Fedn Proc.* **31,** 503 (1972).
5. Smith, S. G. & Davis, W. M. *Psych. Res.* **23,** 215–221 (1973).
6. Glick, S. D. & Cox, R. D. *Res. Commun chem. Path. Pharmac.* **12,** 17–24 (1975).
7. Davis, W. M. & Smith, S. G. *Life Sci.* **16,** 237–246 (1975).
8. Glick, S. D. & Charap, A. D. *Psychopharmacology* **30,** 343–348 (1978).
9. Glick, S. D., Cox, R. D. & Crane, A. M. *Psychopharmacology* **41,** 219–224 (1975).
10. Weeks, J. R. *Science* **138,** 143–144 (1962).
11. Pickens, R. & Dougherty, J. *Rep. Res. Labs Dep. Psychiat., Univ. Minn,* PR-72-1 (1972).
12. Lane, J. D., Co, C. & Smith, J. E. *Life Sci.* **21,** 1101–1108 (1977).
13. Smith, J. E., Co, C., Mote, T. R. & Lane, J. D. *Trans. Am. Soc. Neurochem.* **10,** 118 (1979).
14. Freeman, M. E., Co, C., Lane, J. D. & Smith, J. E. *Analyt. Biochem.* (in the press).
15. Johnson, J. C., Ratner, M., Gold, G. J. & Clouet, D. H. *Res. Commun. chem. Path. Pharmac.* **9,** 41–53 (1974).
16. Bhargava, H. N. & Matwyshyn, G. A. *Eur. J. Pharmac.* **44,** 25–33 (1977).

17. Iwamoto, E. T. & Way, E. L. *Adv. Biochem. Psychopharmac.* **20,** 357–407 (1979).
18. Brase, D. A. *Adv. Biochem. Psychopharmac.* **20,** 409–428 (1979).
19. Bläsig, J. *Mod. Pharmac. Tox.* **14,** 279–356 (1978).
20. Maroli, A. N., Tsang, W-K. & Stutz, R. M. *Pharmac. Biochem. Behav.* **8,** 119–123 (1978).
21. Belluzzi, J. D. & Stein, L. *Nature* **266,** 556–558 (1977).
22. Atweh, S. F. & Kuhar, M. J. *Brain Res.* **134,** 393–405 (1977).
23. Wise, R. A. *Brain Res.* **152,** 215–247 (1978).
24. Krnjevic, K. *Physiol. Rev.* **54,** 418–540 (1974).

Supraoptic neurones of rat hypothalamus are osmosensitive

W. T. Mason

ARC Institute of Animal Physiology, Babraham,
Cambridge CB2 4AT, UK

It has been found that cells in the region of the supraoptic nucleus (SON) of the hypothalamus are sensitive to osmotic stimuli in a physiological range, and have studied the mechanism by which the osmotic sensitivity arises. An *in vitro* hypothalamic brain slice preparation has been used to make intracellular recordings from the SON. Cells lying in the SON respond to small increases (9–40 mosmol l^{-1}) in the osmolarity of their external environment with a marked increase in firing rate. They respond to NaCl and mannitol although not to glucose. The osmotic sensitivity of SON neurones has a complex origin at both a pre- and a postsynaptic level, being composed first of depolarization of the primary SON neurone by an increase of extracellular osmolarity and second by an increased rate of occurrence of excitatory synaptic events which markedly augment firing rate. These results are consistent with Jewell and Verney's suggestion[1,2] that osmoreception in the mammalian brain occurs in the region of the anterior hypothalamus, and extends this localization by indicating that the SON neurones are themselves both directly osmosensitive and part of an osmoreceptive complex.

Hypothalamic neurones in the mammalian SON are known to control the secretion of oxytocin and vasopressin from the posterior pituitary into the systemic circulation. Jewell and Verney[2] originally proposed that the osmoreceptors regulating vasopressin secretion lay outside the blood–brain barrier in the region of the anterior hypothalamus, and they suggested the SON as one possible site at which osmoreception might occur. Consistent with this, Sladek and Knigge[3] concluded from work with hypothalamo-neurohypophysial explants that the osmoreceptors lay near to the SON. This proposal, however, has generated considerable controversy, centering on three points. First, several workers have disagreed as to whether neurosecretory cells in the SON are themselves osmoreceptors or whether they receive synaptic input from osmoreceptors more distant from the SON[4–6]. Second, is the osmoreceptor really osmotically sensitive, or can the responses observed *in vivo* be accounted for by a sodium receptor[4,5,7–9]? A final area where conflicting results have emerged has been generated by recent work using extracellular recording from the slice preparation by Hatton *et al.*[10] and Wakerley and colleagues[11,12], which found little spontaneous activity and little or no osmosensitivity in the SON, results which conflicted in turn with Leng's finding[6] that direct 'microtap' application of hyperosmolar NaCl *in vivo* excited SON neurones directly. These controversies were thus examined with the potentially powerful *in vitro* slice technique. This technique has several advantages, including: (1) anaesthetics are unnecessary, (2) the preparation is continuously superfused so that known concentrations of substances of interest can be applied, (3) the SON can be identified unambiguously by its proximity to the optic chiasm, (4) the blood–brain barrier is effectively absent, and (5) stable, long-term intracellular records can be obtained.

Coronal or sagittal slices, 300–400 μm thick, of rat hypothalamus were prepared on a vibratome and maintained in oxygenated Yamamoto[14] medium (*p*H 7.5) at 37 °C. The slices were supported on lens tissue/acrylic mesh and O_2/CO_2 (95/5%) moistened with medium blown over them. Perifusion from beneath was accomplished with an LKB peristaltic pump operated at 0.6–1.0 ml min^{-1} in a chamber volume of about 1.5 ml. Renewal of medium in the chamber was 95% complete

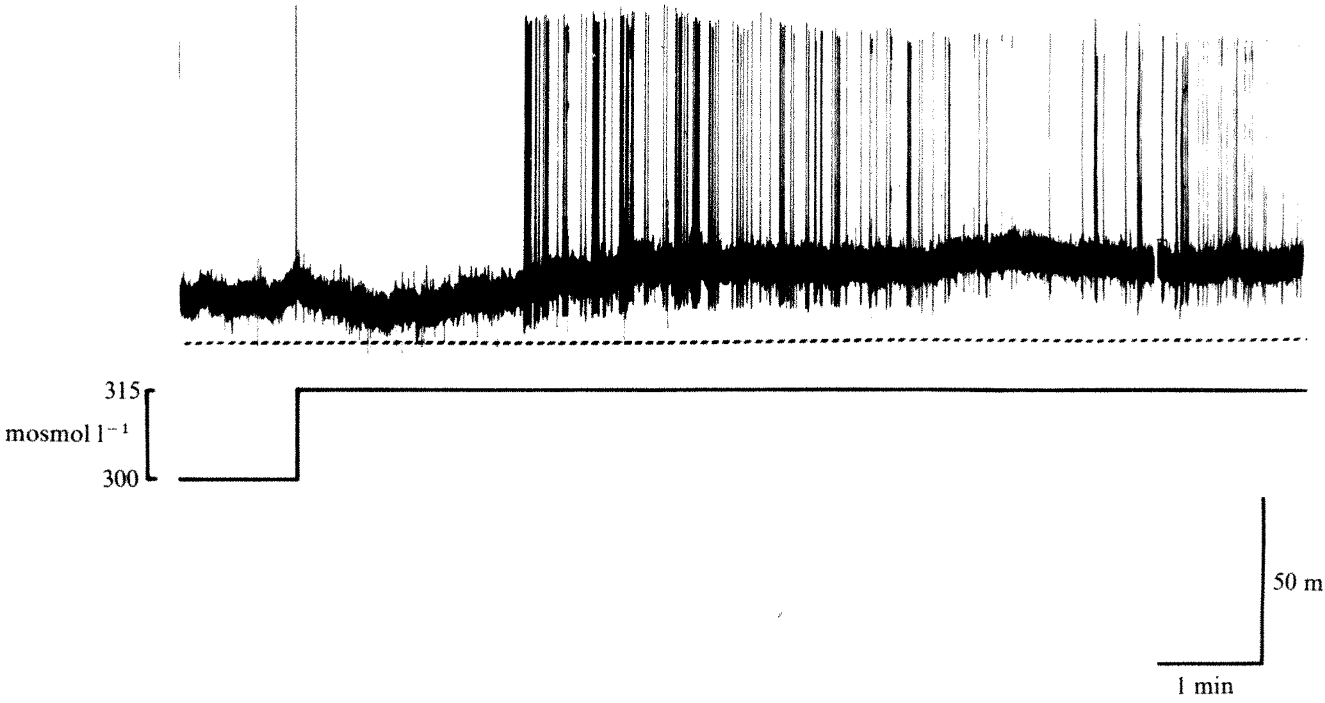

Fig. 1 Intracellularly recorded response from a neurone in the SON of the rat hypothalamus, recorded from a 400-μm slice maintained *in vitro*. Resting membrane potential (V_m) at the start of the record was −61 mV, and membrane resistance (R_m) measured with the bridge balance technique was 140 MΩ. The perifusing medium was changed where indicated to one of higher osmolarity by addition of mannitol, although similar results were obtained with NaCl in other experiments (as in Fig. 2). This cell responded with a clear increase in firing rate, accompanied by a depolarization of V_m of about 12 mV.

0028-0836/80/370154—04$01.00

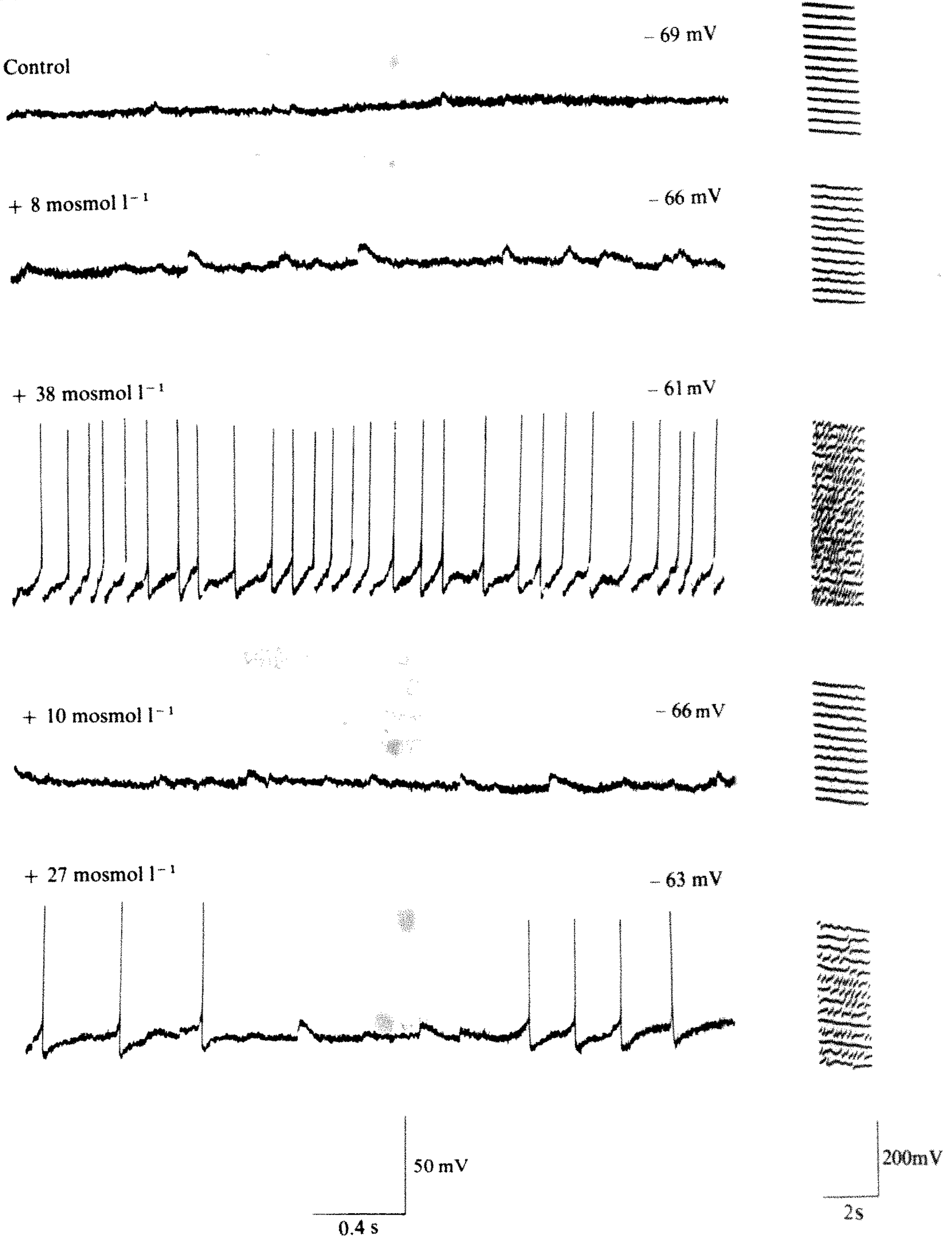

Fig. 2 Osmotic response of a supraoptic neurone recorded intracellularly over a period of 80 min ($R_m \sim 210$ MΩ). In these records, the time scale has been expanded to show the presence of baseline synaptic activity. On the top left of each record is given the presence of baseline synaptic activity. On the top left of each record is given the measured osmolarity change, elicited for this cell by addition of NaCl, with the control value before the start of the osmolarity change being 298 mosmol per kg. The baseline membrane potential for each cell is given on the top right. The records in the main body of the figure were reproduced by a Datalab transient recorder, and spikes have been retouched to represent their accurate height, which had been attenuated by the recorder. Records to the right of the figure are continuous traces photographed from the oscilloscope to show the longer-term baseline spontaneous activity of the same cell, and necessarily, the spike tops in these records have been lost. This cell has been illustrated to show the wide variation in activity which is elicited by osmolarity increase. While this cell would have been classed as a 'quiet' cell due to the lack of cell firing and low frequency of synaptic activity, it is apparent that a small and physiological osmolarity increase modifies both of these properties in a graded manner. Likewise, for a cell exhibiting spontaneous activity when impaled, osmolarity increase amplifies both the frequency of synaptic input and the firing rate of the cell. For this cell, it was possible to effect several changes of the bathing medium, such that a response to osmolarity could be observed, and reversed by returning to the control medium, followed by return to a medium of raised osmolarity about 10 mosmol per kg less than the first test. Resultant spiking was graded with the increase in osmolarity, being 9.2 Hz in the +38 mosmol per kg test and 2.4 Hz in the +28 mosmol per kg test (averaged over 5 min). The response to osmolarity consisted of depolarization of membrane potential, increased firing rate, and an increased frequency of synaptic events. As can be further seen, the initial increase in e.p.s.p. frequency occurred without resultant spiking, action potentials being observed only when V_m allowed the e.p.s.ps to approach threshold, which for this cell was about −50 mV. I.p.s.ps were also observed, although not as frequently as e.p.s.ps in this cell.

in 4–7 min. Osmolarity of the medium was measured with a Knauer semimicro-osmometer. Standard intracellular recording techniques were used, using electrodes filled either with 4M K acetate or 2M Na methylsulphate (resistance 70–250 MΩ). Cells were occasionally marked intracellularly with the fluorescent dye Lucifer CH and examined in wholemount to confirm the recording site as being the supraoptic nucleus.

Some of the basic properties of intracellularly recorded neurones from this preparation have been described previously[13]. SON neurones recorded in slices of hypothalamus showed spike patterning similar to that observed *in vivo*[8,15], and, contrary to earlier reports on hypothalamic slices[10–12], considerable spontaneous activity. In isotonic medium, both phasic and continuous patterns of firing were noted, characteristic of vasopressin- and oxytocin-secreting cells, respectively[8].

When the isotonic perifusion medium (290–295 mosmol per kg) was changed to one of increased osmolarity (305–340 mosmol per kg, with NaCl or mannitol), 19 of 23 cells responded with an overall increase in firing rate (Fig. 1). The increase in spike frequency was superimposed on a slow depolarization of membrane potential (V_m) (13±3 mV (mean±s.d.) for a 35 mosmol per kg increase) graded with osmolarity over a range of 9–45 mosmol per kg. Of the cells responding in this way, three distinct response patterns were observed: (1) 'silent' cells (<0.5 Hz) began to fire (1–10 Hz); (2) slow continuously firing cells (0.5–2.0 Hz) fired more rapidly, firing rate being graded with increase in osmolarity; (3) 'silent' cells and some phasic firing cells began to fire phasically and to fire with an increased burst length, respectively, some eventually firing in a continuous pattern.

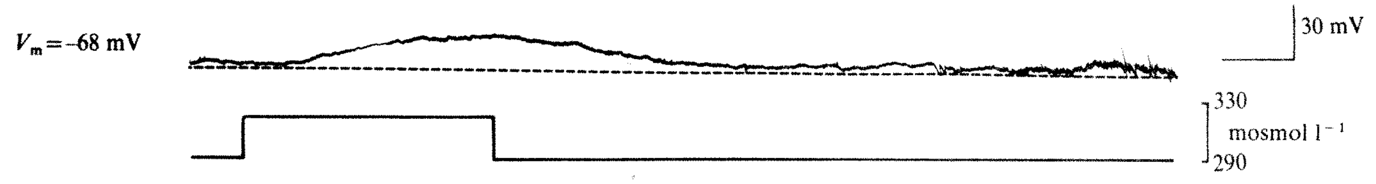

Fig. 3 The effect of increased osmolarity on a supraoptic neurone which had been blocked by increasing the Mg^{2+} content of the bathing medium. R_m was 165 MΩ, measured at the start of the record. Before the beginning of the experiment, after the cell had been impaled, 15 mM $MgSO_4$ was added and an equivalent amount of NaCl removed from the normal medium to maintain the isotonicity at 294 mosmol per kg. This treatment had no discernible effect on V_m. Following this, NaCl was added to raise the osmolarity as shown, and this resulted in a pronounced depolarization of V_m, but without a concomitant increase in firing rate as in Figs 1 and 2. Similarly, as synaptic input to the cell had been largely abolished by Mg^{2+} addition, synaptic potentials were not observed before, during or after increased osmolarity. However, the cell could be driven to fire by intracellular passage of depolarizing current such that V_m was brought above threshold (suprathreshold stimulation for this cell in the presence of Mg^{2+} elicited firing at about 50 Hz). Similar results were obtained where Mg^{2+} was added without removing NaCl, that is, where osmolarity was increased before a test by Mg^{2+} addition. This result indicates that the V_m depolarization resulting from increased osmolarity is a direct action on the primary neurone within the supraoptic nucleus, and not synaptically mediated or requiring synaptic input to the cell.

The firing patterns and depolarization of membrane potential induced by increased osmolarity were completely reversible when cells were restored to isotonic medium. Four 'silent' cells which did not respond to osmotic stimulus with increased firing did, however, depolarize in a manner comparable to responsive cells, but this depolarization did not, at the stimulus used, carry V_m sufficiently close to threshold for activation of firing. Current injected intracellularly through the recording electrode sufficient to depolarize the 'silent' cells beyond threshold elicited rapid firing, as observed in all cells.

During and preceding osmotically induced firing of SON neurones, significant changes in baseline voltage noise were observed. The magnitude of these changes varied from cell to cell and was graded with the measured change in osmolarity. The origin of this noise was a large increase in frequency of synaptic input to the cell, a property previously observed for more peripheral neurones[16–21]. This was analysed to study the correlation between membrane potential, cell firing rate, synaptic events and external osmolarity. Figure 2 shows that increased osmolarity has multiple and synergistic actions on both pre- and postsynaptic properties of SON neurones, in turn leading to an accelerated firing rate. These are increased synaptic input [excitatory postsynaptic potentials (e.p.s.ps) and inhibitory postsynaptic potentials (i.p.s.ps)], depolarization of the postsynaptic cell, and spike generation. For one typical cell, an osmolarity increase of 32 mosmol l^{-1} (w/NaCl) elicited (1) a peak depolarization of 14 mV; (2) increase in frequency of synaptic events (measured postsynaptically) from 3 s^{-1} to 34 s^{-1} (averaged over 5 min) and (3) increase in spike frequency from 1.4 Hz to 6.8 Hz. This observation of increased synaptic input to SON neurones, associated with a change in external osmotic pressure, raised the question of whether osmotically induced depolarization of membrane potential may also have been mediated by slower acting synaptic events, perhaps distant to the SON nucleus.

As demonstrated in Fig. 3, four SON neurones were tested for response to osmolarity increase (three with NaCl, one with mannitol) when they were bathed in 15 mM $MgSO_4$ solutions such that synaptic input was abolished. In three of these experiments $MgSO_4$ was added without removing NaCl and in a fourth experiment $MgSO_4$ replaced NaCl isotonically. The osmotic stimulus was then applied and in all cells a substantial depolarization of V_m resulted, but in the absence of e.p.s.ps/i.p.s.ps and without firing. All cells continued to respond to injected depolarizing current with firing. These results were thus consistent with osmotically induced depolarization being a property of the primary neurone itself rather than a secondary, synaptically mediated event originating either within or outside the SON region.

Finally, the source of the presynaptic input to osmosensitive SON neurones remains a central question as these elements appear to be characterized by osmosensitive properties in their own right. To clarify this question, islands of SON were made from hypothalamic slices previously used for recordings. Not only did nine intracellularly recorded neurones display spontaneous firing and synaptic input as in the intact slice, but also both of two cells tested showed an osmotic response similar to that described above. These observations, coupled with the similarity of response of neurones in coronal and sagittal sections, suggest that both the osmosensitive neurones themselves and the synaptic elements driving these cells lie near to and probably within the SON. The experiments do not of course rule out the possibility that more complex afferent pathways may exist *in vivo*. Inasmuch as the rat SON may not contain interneurones, these results could suggest a functional interaction between excitable SON neurones. In the light of reports that two-thirds of the synaptic input to SON neurones is of intranuclear origin, this might not be surprising[22].

These findings conflict with earlier reports of extracellular recording from hypothalamic slice preparations, in that significant spontaneous activity as well as firing in response to osmolarity changes of the external medium is observed in cells recorded from the SON region. Many features of the spontaneous activity and osmotic responses in these intracellular records closely parallel those observed *in vivo* by means of extracellular recording from anaesthetized animals. These results must therefore strongly support the tentative suggestions of Jewell and Verney[2] as to the siting of the osmoreceptor in the anterior hypothalamus, in confirming that oxytocin- and vasopressin-secreting neurones lying within the SON are part of an excitable osmoreceptive complex. Furthermore, that the osmoreceptive complex as a whole (the pre- and postsynaptic element) lies within or near the SON is indicated by these results, although it cannot be excluded that the osmosensitive presynaptic element is a cut nerve ending of a more distant perikaryon. Whether the basic neuronal properties thus far observed for these osmosensitive cells distinguish them from other central neurones is open to speculation and will require a wide-ranging comparison with cells from other brain regions, but the siting of SON neurones within a dense capillary bed must make them well placed to detect and respond quickly and efficiently to changes in the osmolarity of the blood.

I thank Drs B. A. Cross, R. G. Dyer and G. Leng for helpful discussion and criticism of the manuscript.

Received 9 May; accepted 11 July 1980.

1. Verney, E. B. *Proc. R. Soc.* B**135,** 25–106 (1947).
2. Jewell, P. A. & Verney, E. B. *Phil. Trans. R. Soc.* B**240,** 197–324 (1957).
3. Sladek, C. D. & Knigge, K. M. *Endocrinology* **101,** 1834–1838 (1977).
4. Schrier, R. W., Berl, T. & Anderson, R. J. *Am. J. Physiol.* **236,** 321–332 (1979).
5. Robertson, G. L., Shelton, R. L. & Athar, S. *Kidney Int.* **10,** 25–37 (1976).
6. Leng, G. *J. Physiol., Lond.* **304,** 405–414 (1980).
7. McKinley, M. J., Denton, D. A. & Weisinger, R. S. *Brain Res.* **141,** 89–103 (1978).
8. Brimble, M. J. & Dyball, R. E. J. *J. Physiol., Lond.* **271,** 253–271 (1977).
9. Brimble, M. J., Dyball, R. E. J. & Forsling, M. L. *J. Physiol., Lond.* **278,** 69–78 (1978).
10. Hatton, G. I., Armstrong, W. B. & Gregory, W. A. *Brain Res. Bull.* **3,** 497–503 (1978).
11. Brimble, M. J., Haller, E. W. & Wakerley, J. B. *J. Physiol., Lond.* **278,** 38–39P (1978).
12. Haller, E. W., Brimble, M. J. & Wakerley, J. B. *Expl Brain Res.* **33,** 131–134 (1978).
13. Mason, W. T. *J. Physiol., Lond.* **303,** 56P–57P (1980).
14. Yamamoto, C. & McIlwain, H. C. *J. Neurochem.* **13,** 1333–1343 (1966).

15. Poulain, D. A., Wakerley, J. B. & Dyball, R. E. J. *Proc. R. Soc.* **B196**, 367–384 (1977).
16. Hubbard, J. I., Jones, S. F. & Landau, E. M. *J. Physiol., Lond.* **197**, 639–657 (1968).
17. Fatt, P. & Katz, B. C. *J. Physiol., Lond.* **117**, 109–128 (1952).
18. Blioch, Z. L., Glagoleva, I. M., Liberman, E. A. & Neuashev, V. A. *J. Physiol., Lond.* **199**, 11–35 (1968).
19. Boyd, I. A. & Martin, A. R. *J. Physiol., Lond.* **132**, 61–73 (1956).
20. Furshpan, E. J. *J. Physiol., Lond.* **134**, 689–697 (1956).
21. Shimani, Y., Alnaes, E. & Rahaminoff, R. *Nature* **267**, 170–172 (1977).
22. Léránth, C., Záborsky, L., Marton, J. & Palkovits, M. *Expl Brain Res.* **22**, 509–523 (1975).

Intracellular study of ionic events underlying intestinal membrane transport of oligopeptides

M. R. Ward & C. A. R. Boyd*

Department of Physiology, The University, Dundee DD1 4HN, UK

It is now clear that after a protein meal much of the α-amino nitrogen which is absorbed from the small intestinal tract is transported into the intestinal epithelium across the brush border membrane of the enterocyte in the form of oligopeptides rather than free amino acids[1–3]. We report here the results of electrophysiological experiments using intracellular microelectrodes which allow us to add important information concerning the mechanism of membrane transport which must underlie oligopeptide absorption, in particular with respect to the role of Na^+ in this peptide transport. Such experiments not only reveal the energetics involved in the major pathway for protein absorption from the gastrointestinal tract but may also be important for understanding the mechanism of action of small peptides in quite different cells, such as the Na^+-sensitive binding of the neurohormone oligopeptide enkephalin to the enkephalin receptors in the central nervous system[4,5].

Figure 1 shows the results of a representative experiment in which the potential, V_m, across the brush border membrane of the superfused small intestine of the mudpuppy, *Necturus maculosus*, was recorded by a microelectrode inserted from the mucosal aspect into an epithelial cell[6]. The initial value of $V_m(-45$ mV) is somewhat greater than the mean value we find of 34 ± 2 mV (mean ±s.e.m., $n = 36$), which is almost identical to the mean value found in the same tissue by Garcia-Diaz *et al.*[7]. The cell was exposed initially to the amino acid L-leucine (6 mM), which produced a prompt, marked depolarization of 14 mV which was reversed completely on removal of the amino acid. This confirms previous findings[6,8,9] and strongly suggests an ion-linked co-transport mechanism for entry of this neutral amino acid across the brush border membrane. Subsequent exposure to a higher L-leucine concentration (12 mM) produced a similar reversible depolarization which was almost identical to that found with the lower amino acid concentration, suggesting saturation of the brush border amino acid transport system. The cell was then superfused with a mixture of amino acid (12 mM) and the dipeptide L-leucyl-L-leucine (6 mM). This mixture produced a greater reversible depolarization; also, the rate of depolarization was increased by the presence of the dipeptide in addition to the saturating quantity of monomer. This increase must have been caused by the intact dipeptide rather than the products of extracellular or membrane digestion[10] and therefore shows the existence of a pathway for peptide transport separate from and additional to that for the amino acid. Moreover, it shows that the entry of this neutral dipeptide into the cell via such a pathway is associated with an instantaneous flow of ionic current and thus that peptide transport is electrogenic. Subsequently, the cell was exposed sequentially to 6 mM L-leucine, 12 mM L-leucine and the amino acid and dipeptide mixture (12 mM L-leucine, 6 mM L-leucyl-L-leucine); these solutes were then removed in reverse order. Exposure to the dipeptide produced a prompt 16 mV depolarization of the brush border membrane that was reversed on removal of the solute and was additional to that produced by exposure to a maximal saturating concentration of amino acid.

Ion replacement studies were carried out to elucidate the nature of the current flow induced by the dipeptide, and Fig. 2 shows the result of an experiment in which the effects of the amino acid and of the peptide on V_m were studied in a solution in which Na^+ had been totally replaced by choline. The measured Na^+ concentration in this solution after flow through the bath was 2 ± 1 mM (mean ±s.e.m., 6 observations). In this low concentration of Na^+ the effects on V_m of both amino acid and peptide were not totally abolished; however, the amino acid-induced depolarization was much slower than that seen in the presence of a high external Na^+ concentration (Fig. 1). With the dipeptide there is also a reduction in the rate of depolarization in low compared with high external Na^+, although this reduction is considerably less for the dipeptide than for the amino acid.

These findings may help to resolve the controversy concerning the role of Na^+ in peptide transport. Matthews, Addison and Burston[11] showed that external Na^+ was required for the active accumulation of the poorly hydrolysed dipeptide L-carnosine (β-alanyl-L-histidine) by rings of hamster intestine *in vitro*. Cheeseman and Parsons[12,13], however, found that the trans-epithelial flux of the amino acids glycine and leucine which had entered the tissue as the dipeptides glycyl-L-leucine or L-leucyl-glycine (both of which are hydrolysed intracellularly) was independent of the presence or absence of Na^+ from the intestinal lumen: they suggested that "the non-accumulative entry of the peptides into the epithelium can occur independently of the presence of Na in the lumen". The results shown here clearly demonstrate electrogenic peptide entry for the easily hydrolysed, and therefore non-accumulated, dipeptide L-leucl-L-leucine. The differing sensitivities of the peptide and the amino acid transport systems to a substantial decrease in external Na^+, shown in Fig. 2, is most simply explained on the basis of the driving forces involved, as for any Na^+ co-transport

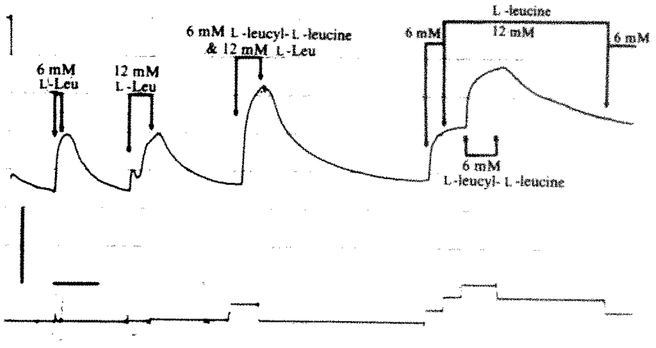

Fig. 1 Pen-recording of the potential across the brush border membrane of an intestinal epithelial cell of the mudpuppy *Necturus maculosus*. A piece of mid-duodenum was superfused at room temperature in a small Perspex chamber (vol. 0.8 ml) at a flow rate of 60 ml min^{-1} with mudpuppy Ringer (Na 115, K 3, Ca 2.7, Cl 116, HCO_3 2.4, PO_4 3.0 mM l^{-1}; pH equilibrated with air, 7.4; osmolarity 220 mosmol l^{-1}). At the start of the trace the cell was impaled from the mucosal aspect under direct visual control with a 24 MΩ glass KCl-filled microelectrode. When a stable recording had been established the composition of the superfusate was abruptly altered as shown (event marker on lower trace). The initial transient observed on exposure to 12 mM L-leucine is due to a small pulse of 6 mM H6W7L-leucine preceding the higher concentration of amino acid. Vertical calibration 20 mV; horizontal calibration 60 s.

---

[*] Present address: Department of Human Anatomy, South Parks Road, Oxford OX1 3QX, UK.

0028–0836/80/370157—02$01.00

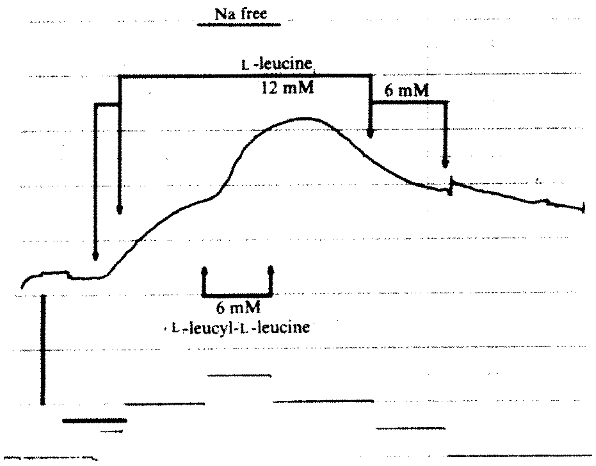

Fig. 2 Pen-recording of the brush border membrane potential of a small intestinal epithelial cell (see Fig. 1). The superfusate was identical to that used in Fig. 1 (except that Na^+ was totally replaced by choline) and its composition was altered as indicated (event marker on lower trace). Initial membrane potential was −47 mV. Vertical calibration, 20 mV; horizontal calibration, 60 s.

system the equilibrium potential[14] is given by

$$V_{\mathrm{equil.}} = \frac{RT}{F} \ln \frac{[\mathrm{Na}^+]_o\,[\mathrm{X}]_o}{[\mathrm{Na}^+]_i\,[\mathrm{X}]_i}$$

where $V_{\mathrm{equil.}}$ is the reversal (equilibrium potential) for that co-transport and $[\mathrm{Na}^+]_o$, $[\mathrm{Na}^+]_i$, $[\mathrm{X}]_o$ and $[\mathrm{X}]_i$ are, respectively, the external and internal Na^+ and co-transported solute activities, and R, T and F have their usual meaning. Clearly, the magnitude of the depolarization observed on exposure to solute will be a function of both the driving force ($V_m - V_{\mathrm{equil.}}$) and the passive membrane resistance[15]. For a readily hydrolysed peptide such as L-leucyl-L-leucine, the intracellular dipeptide activity is kept low because of intracellular peptidase activity; hence, the driving force for Na^+–peptide co-transport will remain high even in solutions with low external Na^+ activity, and peptide transfer coupled to a flow of Na^+ will still occur at an appreciable rate. For both amino acids and poorly hydrolysed peptides in low external Na^+, the driving force will be much reduced because of the intracellular activity of the co-transported substrate, and their uptake will therefore be strongly inhibited.

These experiments show the value of intracellular microelectrode studies in defining the properties and mechanisms of a peptide transport system. By extending the approach to larger oligopeptides it should be possible to classify and map electrophysiologically the peptide transport systems of the brush border membrane. Moreover, the electrogenic nature of peptide transport revealed by such studies may be important with respect to both the evolution[16] and role of small peptides as neurotransmitter and neurohormones in other tissues.

We thank the Wellcome Trust for financial support.

Received 11 June; accepted 9 July 1980.

1. Matthews, D. M. *Physiol. Rev.* **55,** 537–608 (1975).
2. *Ciba Fdn Symp.* **50,** (1977).
3. Gardner, M. L. G. *J. Physiol., Lond.* **253,** 233–256 (1975).
4. Snyder, S. H. *Scient. Am.* **236,** 44–56 (1977).
5. Miller, R. J., Chang, K. H. & Custrecasas, P. in *Centrally Acting Peptides* (ed. Hughes, J.) 195–213 (Macmillan, London, 1978).
6. Boyd, C. A. R. & Ward, M. R. *J. Physiol., Lond.* **285,** 46P (1978).
7. Garcia-Diaz, J. F., O'Doherty, J. & Armstrong, W. McD. *Physiologist* **21,** 41 (1978).
8. Rose, R. C. & Schultz, S. G. *J. gen. Physiol.* **57,** 639–663 (1971).
9. White, J. F. & Armstrong, W. McD. *Am. J. Physiol.* **221,** 194–201 (1971).
10. Parsons, D. S. *Ciba Fdn Symp.* **50,** 373–376 (1977).
11. Matthews, D. M. Addison, J. M. & Burston, D. *Clin. Sci.* **46,** 693–705 (1974).
12. Cheeseman, C. I. & Parsons, D. S. *Biochim. biophys. Acta* **373,** 523–526 (1974).
13. Cheeseman, C. I. & Parsons, D. S. *J. Physiol., Lond.* **262,** 459–476 (1976).
14. Hansen, U-P. and Slayman, C. L. in *Membrane Transport Processes* Vol. 1 (ed. Hoffman, J. F.) 141–154 (Raven, New York, 1978).
15. Philo, R. D. & Eddy, A. A. *Biochem. J.* **174,** 801–810 (1978).
16. Boyd, C. A. R. *J. theor. Biol.* **76,** 415–417 (1979).

0028-0836/80/370158—02$01.00

Requirement of nerve growth factor for development of substance P-containing sensory neurones

Uwe Otten*, Michel Goedert*, Norbert Mayer† & Fred Lembeck†

* Department of Pharmacology, Biocentre of the University, CH-4056 Basel, Switzerland
† Institute for Experimental and Clinical Pharmacology, University of Graz, A-8010 Graz, Austria

The protein nerve growth factor (NGF) is known to be essential for the maturation and maintenance of adrenergic neurones[1] and for the development of sensory neurones during critical stages of embryonic life[2–4]. The investigation of the physiological importance of NGF for the development of sensory neurones has been hampered so far by the lack of biochemical marker substances for these neurones. The demonstration that the undecapeptide substance P(SP) is present in sensory neurones[5,6] suggests that it might be such a marker. SP is synthesized in dorsal root ganglia (DRG)[7] and transported to the terminals of C-fibres located in the dorsal horn of the spinal cord and in the skin[8]. Its release can be demonstrated from the central[9,10] and peripheral endings[11] of sensory nerve fibres which seem to have an important role in pain perception[12,13]. We have investigated the effects of NGF and of purified anti-NGF antibodies on the content of SP in rat DRG and in their respective target organs, namely the spinal cord and the skin. The effects on sympathetic ganglia were included in order to control the effectiveness of both NGF and its antibody. We report here that NGF leads to an increase in SP in spinal ganglia, as previously shown by Kessler and Black[14]. However, in contrast to these authors, we describe that the administration of anti-NGF antibodies produces a marked reduction of the SP content in sensory neurones and in their respective nerve terminals.

2.5S NGF was prepared from submaxillary glands of adult male mice according to Bocchini and Angeletti[15]. Antibodies against 2.5S NGF were raised in goats and purified by affinity chromatography according to Stöckel *et al.*[16]. Two-day old Sprague–Dawley rats received subcutaneous (s.c.) injections of NGF (1 μg per g) during three consecutive days or a single s.c. injection of (50 μg per g) anti-NGF antibodies. Tyrosine hydroxylase (TH) activity was determined according to Mueller *et al.*[17]. Spinal ganglia (ThlO-12), corresponding regions of spinal cord and pieces of skin from the hindlimb were prepared and homogenized in ice-cold 2 M acetic acid (2 ml). The samples were centrifuged, washed twice and the combined supernatants freeze dried. SP immunoreactivity was measured by a radioimmunoassay at a detection level of 6 pg SP according to Mroz *et al.*[18]. Protein concentrations were determined according to Lowry *et al.*[19].

Repeated injections of NGF led to an increase in SP in rat spinal ganglia from 131 ± 20 to 200 ± 14 pg SP per ganglion (Fig. 1). The administration of anti-NGF antibodies caused a gradual decrease in SP up to 17 days, the longest time point studied (Fig. 1). This reduction was paralleled by a decrease in SP content of both the spinal cord and the skin (Table 1). The protein content of the spinal ganglia rose from 17 μg per ganglion at two days of age to 44 μg per ganglion at 19 days. Neither NGF nor its antibody had any significant influence on the protein content of DRG. The total TH activity in the superior cervical ganglion (SCG) showed a threefold increase after repeated administration of NGF, whereas the injection of anti-NGF antibodies produced an almost complete disappearance of TH activity (Table 2), thus indicating optimal effects of NGF[22] and of its antibody[23] on sympathetic ganglia.

The present experiments confirm that postnatal sensory ganglia are responsive to NGF and indicate that they require NGF or a cross-reacting NGF-like protein for their normal development, as evidenced by a decrease in their SP content after the administration of anti-NGF antibodies. Thus the concept that sensory neurones are dependent on NGF only during certain stages of their embryonic development[2] must be extended to the postnatal maturation of these neurones. Postnatal dependence may indicate a physiological function for the retrograde axonal transport of NGF found in sensory neurones[24,25]. Future *in vivo* studies will have to show whether the modulation of SP by NGF is restricted only to defined stages of neuronal development. Our findings do not rule out the possibility that the reduction in SP effected by anti-NGF antibodies is due to neuronal death rather than to an impaired function of sensory neurones. The lack of a decrease in total protein content would, however, suggest that the anti-NGF antibodies only interfere with the functioning of DRG. Future studies will also have to investigate whether other neuropeptides found in sensory ganglia, like somatostatin and cholecystokinin[26], are affected by both NGF and its antibody. Previous studies have shown an effect of NGF on the SP content of DRG in explant cultures[27,28]. Kessler and Black[14] described a significant effect of NGF on the postnatal development of rat sensory neurones, while failing to find an effect of NGF antiserum. The discrepancy between these results and our findings may well be explained by the fact that the antiserum used was less potent than our purified anti-NGF antibodies, as evidenced by the decrease in TH activity in the SCG.

In conclusion, the present results indicate that NGF or a cross-reacting NGF-like molecule is important for the postnatal development of SP-containing sensory neurones. They also suggest that, in addition to the drug capsaicin[29,30], anti-NGF antibodies might be a tool for reducing the SP content of primary sensory neurones.

We thank Mrs M. Burnett for technical assistance and Ms R. Schuligoi for performing the radioimmunoassays. Part of this work was supported by the Austrian Scientific Research Fund (Grant 3506 and 3400).

Table 1 Effects of anti-NGF antibodies on SP content of spinal cord and skin

Spinal cord	
Controls	206 ± 6
Anti-NGF antibodies	126 ± 13*
Skin	
Controls	28 ± 3
Anti-NGF antibodies	15 ± 2*

Two-day old rats were injected with 50 μg g^{-1} anti-NGF antibodies. They were killed 17 d later and SP content (ng per g of tissue) determined. Each value represents the mean ± s.e.m. ($n = 5$ animals).

$*P < 0.01$.

Table 2 Effects of NGF and anti-NGF antibodies (NGF-AB) on TH activity in the rat superior cervical ganglion (SCG)

	Controls	Treated
NGF	134 ± 12.4	388 ± 62.8*
NGF-AB 3 d after injection	122 ± 14.2	32 ± 1.3*
NGF-AB 7 d after injection	178 ± 14.2	21 ± 0.6*
NGF-AB 17 d after injection	242 ± 18.2	11 ± 0.2*

Two-day old animals were treated with either 1 μg g^{-1} NGF or 50 μg g^{-1} anti-NGF antibodies. NGF was injected on three consecutive days and the animals killed one day after the last injection. Anti-NGF antibodies were injected once and the animals killed 3, 7 and 17 d later. The SCGs were rapidly removed and homogenized in 5 mM Tris-HCl buffer, pH 7.4 (0.5 ml), containing 0.1% Triton X-100. TH activity was determined according to Mueller *et al.*[17]. Each value represents the mean ± s.e.m. ($n = 4$–6 animals). Results are expressed as pmol dopa per h per pair ganglia.

$*P < 0.005$.

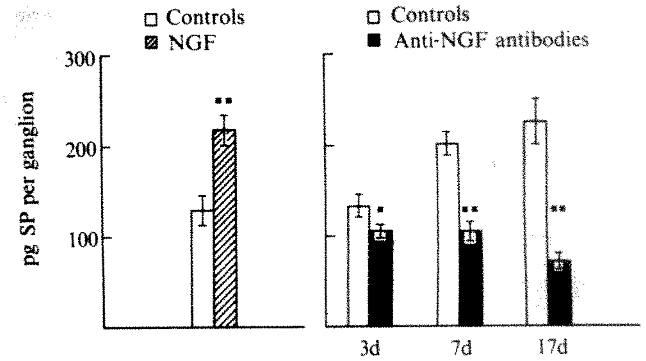

Fig. 1 Effects of NGF and anti-NGF antibodies on content of SP in rat DRG. Two-day old rats were injected s.c. with either 1 μg g^{-1} NGF or 50 μg g^{-1} anti-NGF antibodies. 2.5S NGF was prepared according to Bocchini and Angeletti[15], with the modifications described by Suda *et al.*[20]. The biological activity of NGF was determined according to Fenton[21] and it amounted to 250 biological units per μg of protein. Antibodies against 2.5S NGF were raised in goats and purified by affinity chromatography[16]. Injection of NGF was performed on three consecutive days and SP content in DRG was examined one day after the last injection. Anti-NGF antibodies were injected once. Animals were killed 3, 7 and 17 d after injection and the DRG examined for SP content. Each value represents the mean ± s.e.m. ($n = 4$–6 animals). $*P < 0.01$; $**P < 0.005$.

Received 2 May; accepted 7 July 1980.

1. Mobley, W. C., Server, A. C., Ishi, D. N., Riopelle, R. J. & Shooter, E. M. *New Engl. J. Med.* **297**, 1096–1104, 1149–1158, 1211–1218 (1977).
2. Levi-Montalcini, R. & Angeletti, P. U. *Physiol. Rev.* **48**, 534–569 (1968).
3. Herrup, K. & Shooter, E. M. *J. Cell Biol.* **67**, 118–125 (1975).
4. Barde, Y. A., Edgar, D. & Thoenen, H. *Proc. natn. Acad. Sci. U.S.A.* **77**, 1199–1203 (1980).
5. Hökfelt, T., Kellerth, J. O., Nilsson, G. & Pernow, B. *Science* **190**, 889–890 (1975).
6. Hökfelt, T. *et al. Neuroscience* **1**, 131–136 (1976).
7. Harmar, A., Schofield, J. G. & Keen, P. *Nature* **284**, 267–269 (1980).
8. Takahashi, T. & Otsuka, M. *Brain Res.* **87**, 1–11 (1975).
9. Gamse, R., Molnar, A. & Lembeck, F. *Life Sci.* **25**, 629–636 (1979).
10. Theriault, E., Otsuka, M. & Jessell, T. *Brain Res.* **170**, 209–213 (1979).
11. Bill, A., Stjernschantz, J., Mandahl, A., Brodin, E. & Nilsson, G. *Acta physiol. scand.* (in the press).
12. Nicoll, R. A., Schenker, C. & Leeman, S. E. *A. Rev. Neurosci.* **3**, 227–268 (1980).
13. Henry, J. L. *Brain Res.* **114**, 439–452 (1976).
14. Kessler, J. A. & Black, I. B. *Proc. natn. Acad. Sci. U.S.A.* **77**, 649–652 (1980).
15. Bocchini, V. & Angeletti, P. U. *Proc. natn. Acad. Sci. U.S.A.* **64**, 787–794 (1969).
16. Stöckel, K., Gagnon, C., Guroff, G. & Thoenen, H. *J. Neurochem.* **26**, 1207–1211 (1976).
17. Mueller, R. A., Thoenen, H. & Axelrod, J. *J. Pharmac. exp. Ther.* **169**, 74–79 (1969).
18. Mroz, E. A., Brownstein, M. J. & Leeman, S. E. in *Substance P* (eds von Euler, U. S. & Pernow, B.) 147–155 (Raven, New York, 1976).
19. Lowry, O. H., Rosebrough, N. H., Farr, A. L. & Randall, R. J. *J. biol. Chem.* **193**, 265–275 (1951).
20. Suda, K., Barde, Y. A. & Thoenen, H. *Proc. natn. Acad. Sci. U.S.A.* **75**, 4042–4046 (1978).
21. Fenton, E. L. *Expl Cell Res.* **59**, 383–392 (1970).
22. Thoenen, H., Angeletti, P. U., Levi-Montalcini, R. & Kettler, R. *Proc. natn. Acad. Sci. U.S.A.* **68**, 1598–1602 (1971).
23. Goedert, M., Otten, U. & Thoenen, H. *Brain Res.* **148**, 264–268 (1978).
24. Stöckel, K., Schwab, M. & Thoenen, H. *Brain Res.* **99**, 1–16 (1975).
25. Brunso-Bechtold, J. K. & Hamburger, V. *Proc. natn. Acad. Sci. U.S.A.* **76**, 1494–1496 (1979).
26. Hökfelt, T., Johansson, O., Ljungdahl, Å., Lundberg, J. M. & Schultzberg, N. *Nature* **284**, 515–521 (1980).
27. Schultzberg, M., Ebendal, T., Hökfelt, T., Nilsson, G. & Pfenninger, K. J. *Neurocytology* **7**, 107–117 (1978).
28. Schwartz, J. P. & Costa, E. *Brain Res.* **170**, 198–202 (1979).
29. Jessell, T. M., Iversen, L. L. & Cuello, A. C. *Brain Res.* **152**, 183–188 (1978).
30. Gamse, R., Holzer, P. & Lembeck, F. *Br. J. Pharmac.* **68**, 207–213 (1980).

Tranquillizers can block mitogenesis in 3T3 cells and induce differentiation in Friend cells

G. D. Clarke & P. J. Ryan

Cell Proliferation Laboratory, Imperial Cancer Research Fund,
PO Box 123, Lincoln's Inn Fields, London WC2A 3PX, UK

Compounds of diverse structure induce murine Friend erythroleukaemia (MEL) cell[1] differentiation[2–5]. Seeking a common property[6], Bernstein[7] reported that the relationship between activity and octanol/water partition coefficients for inducers resembled that reported for anaesthetics[7]; moreover, anaesthetics inhibited induction. Since anaesthetics were known to increase membrane fluidity, they suggested that inducers might decrease it. Reporting evidence against unitary theories of anaesthesia[9], Richards *et al.*[10,11] suggested that lipophilic drugs competed, according to their individual structure, with membrane lipids for hydrophobic regions on membrane proteins. The antagonism between pairs of anaesthetics[10,11], anaesthetics and inducers[7,8] and pairs of inducers[5], might thus be explained economically by Richards' anaesthesia model, inducers and lipophilic drugs acting by similar rather than contrary mechanisms. Lipophilic drugs should, therefore, induce differentiation. We report here that some tranquillizers do so. As reported elsewhere for classical inducers[12], they also block non-differentiating 3T3 cells in pre-S. These findings may have application in cancer chemotherapy.

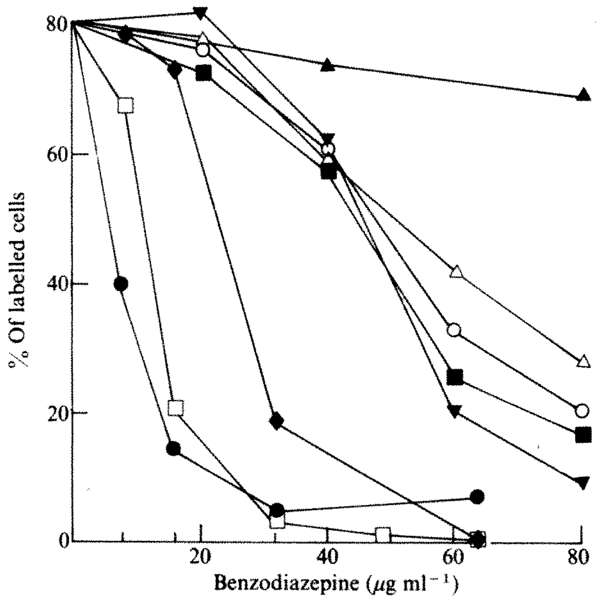

Fig. 2 Swiss 3T3 (4A recloned[27]) cells were maintained in Dulbecco Eagle's medium containing 10% calf serum. Cultures with 2.5×10^4 cells in 2 ml of medium containing 0.5% serum were incubated in 3 cm plastic Petri dishes (Nunc) for 3 days at 37 °C. Medium was then replaced with 6% serum medium containing 30 μM inosine, 2 μC ml^{-1} of tritiated thymidine (Radiochemical Centre, 21 Ci mmol^{-1}) and indicated concentrations of benzodiazepines: ■, chlordiazepoxide from 20 mg ml^{-1} in normal saline; ●, diazepam; ○, flurazepam; ◆, lorazepam; □, medazepam; △, nitrazepam; ▼, oxazepam; and ▲, temazepam, each from 100 mg ml^{-1} solutions in dimethyl sulphoxide. After 26 h incubation, cultures were fixed in formol saline and prepared for autoradiography[16]. The percentage of labelled cells was calculated from differential counts of 300 cells each on duplicate dishes. Cultures with 0.02–0.08% dimethyl sulphoxide did not differ from controls.

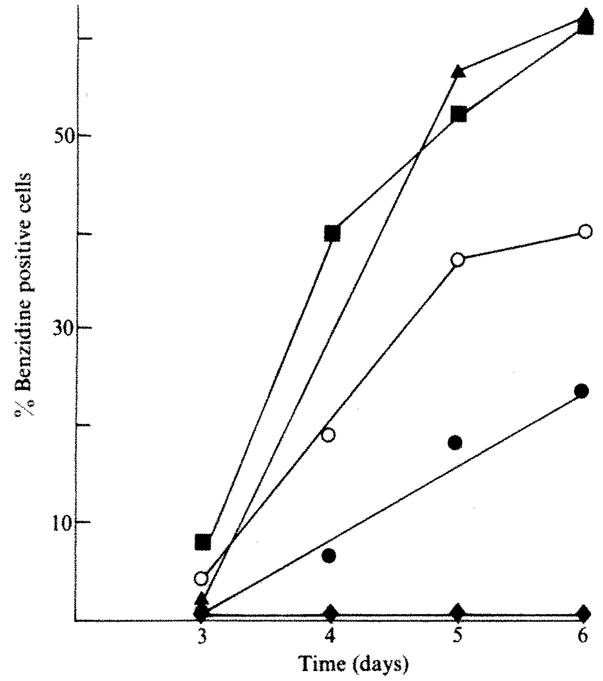

Fig. 1 MEL cells were seeded (as in Table 1 legend) at 3×10^4 ml^{-1} at 0 (◆), 8 (●), 16 (○) and 32 μg ml^{-1} (■) diazepam (dissolved directly into media) and 2.5% dimethyl sulphoxide (▲). Cultures were incubated at 37 °C and duplicates removed daily and stained (Table 1 legend).

The benzodiazepines are a group of tranquillizers which induce anaesthesia in man on intravenous injection[13], yet produce few toxic symptoms when high doses are administered orally or intraperitoneally to mice. We incubated MEL cells for 5 days with concentrations of eight benzodiazepines and stained with benzidine reagent[14] to determine the proportion of the cell population which had accumulated haemoglobin (B+ benzidine positive). At up to lethal concentrations, three of the drugs induced differentiation (Table 1). Diazepam (Valium) and temazepam (Euhypnos) were highly active, giving rise to >50% B+ cells at 40 μg ml^{-1}. Figure 1 shows a time course indicating that 32 μg ml^{-1} of diazepam was as active as 2.5% dimethyl sulphoxide.

We report elsewhere[12] that a wide range of known inducers (dimethyl sulphoxide, hexamethylene bisacetamide, butyrate, ouabain and hypoxanthine) also inhibit the mitogenic effects of serum on 3T3 cells at inducing concentrations. Moreover, volatile anaesthetics such as halothane and nitrous oxide are known to inhibit cell proliferation[15]. We therefore tested the eight benzodiazepines for similar activity.

When 3T3 cells are incubated in medium with 0.5% serum they become quiescent with a low thymidine labelling index[16]. Incubation in medium with 6% serum for 26 h raised this index to 88% and this was reduced to below 35% by 16–80 μg ml^{-1} of seven of the benzodiazepines (Fig. 2). Diazepam was the most active but temazepam, an active inducer at 10 μg ml^{-1}, had little inhibitory effect at 80 μg ml^{-1}. The reduction in the 26-h labelling index was not the result of a brief delay in entry into S phase. In a 5-day growth experiment (Fig. 3), control cultures increased 18-fold but no proliferation occurred in diazepam (64 μg ml^{-1}). Time lapse cinematography showed that only 15% of cells

0028-0836/80/370160—02$01.00

Table 1 Percentage of benzidine positive (B^+) cells induced by benzodiazepines in MEL cell population

Drug	Drug concentration (μg ml^{-1}) 10	20	40	80
Chlordiazepoxide	<0.3	<0.3	3.4	D
Diazepam	18.5	37.4	52.9	D
Flurazepam	<0.3	<0.3	<0.3	D
Lorazepam	<0.3	<0.3	D	D
Medazepam	<0.3	<0.3	D	D
Nitrazepam	<0.3	<0.3	7.2	D
Oxazepam	<0.3	<0.3	0.7	D
Temazepam	24.1	ND	54.2	ND
None	2.7			

Cells of MEL subline F4[26] were maintained in equal parts of Dulbecco Eagle's and Hams F12 medium containing 7.5% fetal calf and 5% calf serum. Duplicate 1-ml volumes of medium, with no addition or with benzodiazepines, were seeded with 3×10^4 cells each in multidishes (Linbro). Chlordiazepoxide was dissolved initially to 20 mg ml^{-1} in normal saline, the other drugs to 100 mg ml^{-1} in dimethyl sulphoxide. After incubation at 37 °C for 5 days, 200-μl aliquots were stained with benzidine reagent[14] and the percentage B^+ (blue) calculated from counts in a haemocytometer. Cultures with dimethyl sulphoxide at 0.02–0.08% did not differ from controls. Diazepam and temazepam dissolved directly into medium were equally active. D, Dead; ND, not determined.

divided and 10% died. When cells were changed to control medium after 48 h in diazepam, 99% divided in 31 h and an 18-fold increase occurred in 5 days (Fig. 3). Thus, diazepam is cytostatic rather than cytotoxic at this concentration.

Induction of differentiation by two tranquillizers supports the view that lipophilic drugs and inducers are a single group, active by virtue of membrane solubility. Our finding that five known inducers[12] and now diazepam, inhibit 3T3 cells at concentrations at which they induce differentiation in Friend cells, is compatible with a hypothetical inverse relationship between the probabilities of proliferation[17] and terminal differentiation[18,19]. This relationship is also suggested by the differentiation in medium with reduced growth potential of normal muscle[19] and adipose[20] cells. We have recently found that 5 of 16 further benzodiazepine derivatives tested induce differentiation in Friend cells. There is no correlation between this activity of the total of seven such inducers and their reported degree of inhibition of ^{3}H-diazepam binding to rat brain membranes[28].

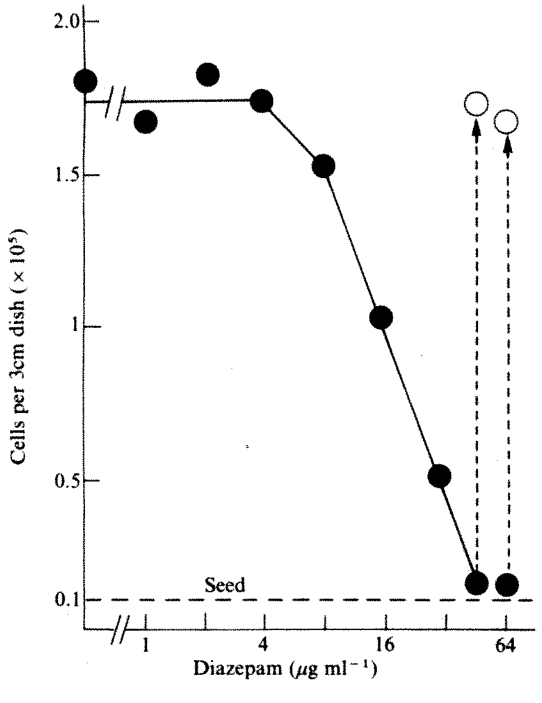

Fig. 3 Control cultures and those containing indicated concentrations of diazepam dissolved directly in 2 ml volumes of medium (Fig. 2 legend) containing 10^4 cells in 3-cm Petri dishes were incubated at 37 °C for 5 days (●). Mean cell counts on duplicated dishes were made with an electronic Coulter counter. Duplicate cultures containing 48 and 64 μg ml^{-1} of diazepam were incubated for 48 h and medium then replaced with drug-free medium for a further 5 days incubation (○) before cell counts.

These findings may have applications in cancer chemotherapy. Agents which hold normal, but not malignant, cells in pre-S have been shown *in vitro* to protect them preferentially against S phase-specific anticancer drugs[21–23]. Benign lipophilic drugs like Valium could conceivably do so *in vivo* (Fig. 3), thus increasing the therapeutic index of such drugs as antifolates, cytosine arabinoside, hydroxyurea and vinca alkaloids. They might also increase differentiation in tumours (see Table 1). Preisler *et al.*[24] have reported that an inducer of Friend cell differentiation may, in some situations, reduce tumour growth rate in mice. Many existing anticancer drugs are lipophilic and it seems possible that their action may not entirely conform with the antimetabolic roles for which they were originally tested. Screening of lipophilic CNS drugs used in man in tumour-bearing mice alone and as protective agents with other anticancer drugs could be worthwhile.

Gifts of drugs, diazepam, chlordiazepoxide, flurazepam, nitrazepam amd medazepam (Roche), lorazepam and oxazepam (Wyeth), and temazepam (Montedison) are acknowledged. Dr Peter Riddle carried out the microcinematography and its analysis and Phil Whitehead assisted in some experiments. We thank Drs Robert Bürk and Ugo Rovigatti for helpful advice and discussion.

Note added in proof: A recent paper by Fehér and Gidali[30] describes the protective effect, for cycling cells of bone marrow against hydroxyurea, of actinomycin D, a lipophilic inducer of Friend cell differentiation[30]. This paper has also drawn our attention to earlier reports of similar specific blocking of normal cell *in vivo* by halothane and nitrous oxide[31–33].

Received 31 March; accepted 4 July 1980.

1. Friend, C., Patuleia, M. C. & de Harven, E. *Natn. Cancer Inst. Monogr.* **22,** 505–522 (1966); Tanaka, M. *et al. Proc. natn. Acad. Sci. U.S.A.* **72,** 1003–1006 (1975).
2. Reuben, R. C. *et al. J. biol. Chem.* **253,** 4214–4218 (1978).
3. Bernstein, A., Hunt, M., Crichley, V. & Mak, T. W. *Cell* **9,** 375–381 (1976).
4. Gusella, J. F. & Housman, D. *Cell* **8,** 263–269 (1976).
5. Leder, A. & Leder, P. *Cell* **5,** 319–322 (1975).
6. Marks, P. A. & Rifkind, R. A. *A. Rev. Biochem.* **47,** 419–448 (1978).
7. Bernstein, A., Boyd, A. S., Crichley, V. & Lamb, V. in *Biogenesis and Turnover of Membrane Macromolecules* (ed. Cook, J. S.) 145–159 (Raven, New York, 1976).
8. Lyman, G. H., Preisler, H. D. & Papahadjopoulos, D. *Nature* **262,** 360–363 (1976).
9. Seeman, P. *Pharmac. Rev.* **24,** 583–655 (1972).
10. Richards, C. D. *Int. Rev. Biochem.* **19,** 157–220 (1978).
11. Richards, C. D. *et al. Nature* **276,** 775–799 (1978).
12. Clarke, G. D. & Ryan, P. J. in *Second International Symposium Tissue Culture in Medical Research* (ed. Richards, R.) (Pergamon, London, in the press).
13. McClish, A. *Can. Anaesth. Soc. J.* **13,** 562–575 (1966).
14. Orkin, S. H., Harosi, F. I. & Leder, P. *Proc. natn. Acad. Sci. U.S.A.* **72,** 98–102 (1975).
15. Sturrock, J. & Nunn, J. F. *Anaesthesiology* **45,** 413–420 (1976).
16. Clarke, G. D., Stoker, M. G., Ludlow, A. & Thornton, M. *Nature* **227,** 798–800 (1970).
17. Brooks, R. F., Bennett, D. C. & Smith, J. A. *Cell* **19,** 493–502 (1980).
18. Gusella, J., Geller, R., Clarke, B., Weeks, V. & Housman, D. *Cell* **9,** 221–229 (1976).
19. Konigsberg, I. R., Sollmann, P. A. & Mixter, L. O. *Devl Biol.* **63,** 11–36 (1978).
20. Green, H. & Kehinde, O. *Cell* **7,** 105–113 (1978).
21. Pardee, A. B. & James, L *Proc. natn. Acad. Sci. U.S.A.* **72,** 4994–4998 (1975).
22. O'Neill, F. J. O. *Cancer Res.* **35,** 1311–1315 (1975).
23. Rozengurt, E. & Po, C. C. *Nature* **261,** 701–702 (1976).
24. Preissler, H. D., Bjornson, S., Mori, M. & Lyman, G. H. *Br. J. Cancer* **33,** 634–645 (1976).
25. Fico, R. M., Chen, T. K. & Canellakis, E. S. *Science* **198,** 53–56 (1977).
26. Oestertag, W., Melderis, H., Steinheider, G., Kluge, N. & Dube, S. *Nature New Biol.* **239,** 231–234 (1972).
27. Brooks, R. F. *Cell* **12,** 311–317 (1977).
28. Squires, R. F. & Braestrup, C. *Nature* **266,** 732–734 (1977).
29. Terada, M. *et al. Proc. natn. Acad. Sci. U.S.A.* **75,** 2795–2799 (1977).
30. Fehér, I. & Gidali, J. *Cell Tissue Kinet.* **13,** 415–424 (1980).
31. Bruce, D. L. & Taurig, H. H. *Anaesthesiology* **30,** 401–405 (1969).
32. Bruce, D. L., Lin, H-S. & Bruce, W. R. *Cancer Res.* **30,** 1803–1805 (1970).
33. Evenwel, R. F., Keizer, H. J. & van Putten, L. M. *Cancer Res.* **36,** 3156–3159 (1976).

Thymic lymphocytes bear a surface antigen which cross-reacts with acetylcholine receptor

Sara Fuchs, Ilana Schmidt-Hopfeld, Giuseppe Tridente & Rebeca Tarrab-Hazdai

Department of Chemical Immunology, The Weizmann Institute of Science, Rehovot, Israel

Acetylcholine receptor (AChR) is a major antigen in the neuromuscular disease myasthenia gravis and it is clear today that the basic defect in this disease is brought about by an autoimmune attack on acetylcholine receptors at the neuromuscular junctions[1,2]. The involvement of the thymus and its role in myasthenia have been widely investigated but are still poorly understood. A high incidence of thymic abnormalities is observed in patients with myasthenia[3] and thymectomy is beneficial in many cases[4]. Immunological studies have demonstrated the presence of humoral as well as cellular immune responses towards thymic tissues in myasthenic patients[5-7]. There were also some reports that animals immunized with thymic extracts develop a partial defect in neuromuscular transmission[8]. In spite of all these observations, the nature and origin of the association between the thymus and the neuromuscular junction in myasthenia gravis are still not known. We have previously demonstrated an immunological cross-reactivity, both humoral and cellular, between a thymic component and AChR[9]; such a cross-reactivity could provide a molecular explanation for the involvement of the thymus in myasthenia gravis. In this study, we demonstrate, by using immunofluorescence and radioimmunological techniques, that thymic lymphocytes bear a surface antigen which binds specifically to antibodies against nicotinic AChR and is thus defined as an 'AChR-like' antigen. A preliminary report of this study has been published[10].

Thymuses from normal mice (C57BL/6 or SJL, 5–7 weeks old) were dispersed to cell suspensions in a phosphate-buffered saline containing 2% bovine serum albumin and 0.02% sodium azide (diluent). The cells were washed, centrifuges for 7 min at 1,200 r.p.m. and resuspended to a concentration of 10^7–10^8 cells ml^{-1}. Anti-AChR sera were obtained in various animal species by immunization with *Torpedo californica* purified AChR[2,11]. For the immunofluorescence studies, 100 μl of the tested antiserum, immunoglobulin or purified antibodies were incubated for 30 min in the cold with 100 μl of thymic cell suspension (10^6–10^7 cells in the diluent) and the mixtures were centrifuged to remove the unbound proteins. The cells were washed twice and then reacted for an additional 30 min at 4 °C in the dark with the appropriate fluorescent reagent. The labelled washed cells were observed in the fluorescence microsope or were analysed in the fluorescence activated cell sorter (FACS)[12]. For the radioimmunological measurements, the binding of anti-AChR antibodies to thymocytes was quantified by ^{125}I-protein A (Table 1)[13].

As depicted in Fig. 1, thymocytes of normal C57BL/6 mice were specifically labelled by treatment with anti-*Torpedo* AChR immunoglobulins, followed by fluorescein- or rhodamine-conjugated goat anti-rabbit immunoglobulins. A large number of the reacted thymocytes (at least 80%) were fluorescently labelled (Fig. 1*a*, *d*). The fluorescence was evenly distributed on the cell surface in minute patches (Fig. 1*a*). Capping of the patches was observed following removal of sodium azide and further incubation at 37 °C (Fig. 1*b*). Immunoglobulins or serum from normal rabbit or anti-ovalbumin immunoglobulins did not result in any staining (Fig. 1*c*, *f*).

The microscopic findings were verified by quantitative analysis of the same samples in the FACS. Specific fluoresence peaks were obtained following labelling with anti-AChR serum, immunoglobulins or purified antibodies (Figs 2 and 3). The labelled cells were shown to be the size of lymphocytes according to their light scattering. Increasing the amounts of the specific rabbit immunoglobulins added resulted in a shift of the peak towards higher relative fluorescence intensity (Fig. 2). It should be noted that C57BL/6 thymocytes were fluorescently labelled also with anti-*Torpedo* AChR sera prepared in monkey or even C57BL/6 mice (Fig. 3*a*, *b*). The reaction with mouse (C57BL/6) anti-AChR serum was of lower intensity than those obtained with rabbit or monkey sera and could be detected only in the higher sensitivity of the FACS (660 V, Fig. 3*b*). Specific binding of anti-AChR sera or immunoglobulins to mouse thymocytes was also observed by radioimmunoassay measurements (Table 1).

Several experiments were performed in order to verify the specificity of the binding to thymocytes. Thus, it was shown that purified anti-AChR antibodies (purified on an AChR-Sepharose adsorbent) bound specifically to thymocytes (Fig. 3*c*, Table 1). Absorption of anti-AChR antibodies on an AChR-Sepharose adsorbent[14] abolished the ability to bind to thymocytes. These two experiments provide direct proof that the reacting antibodies are indeed anti-AChR antibodies and rule out the possibility that antibodies of other non-AChR specificities which could be present in the immunized animals, due to additional autoimmune responses, could react with the thymocytes. Moreover, immunoglobulins or purified antibodies from non-myasthenic rabbits immunized with denatured AChR

Table 1 Binding of anti-AChR to mouse thymocytes

Thymocytes	Sample	Binding (c.p.m.) (dilution)		
	Sera	1/2	1/4	
C57BL/6	Rabbit anti-AChR	46,420	37,310	
	Rabbit anti-RCM-AChR	49,140	47,420	
	Rabbit anti-(T, G)-A-L	16,250	10,200	
	Rabbit normal serum	20,100	N.D.	
C57BL/6	Monkey anti-AChR	75,210	68,420	
	Monkey normal serum	20,210	19,460	
C57BL/6	Mouse (C57BL/6) anti-AChR	46,320	22,470	
	Mouse (C57BL/6) normal serum	19,200	9,720	
			(μg)	
	Immunoglobulins	750	375	180
C57BL/6	Rabbit anti-AChR	51,250	35,720	12,910
	Rabbit anti-ovalbumin	7,870	9,000	8,840
			(μg)	
	Purified antibodies	24	18	
C57BL/6	Rabbit anti-AChR	10,510	4,950	
	Rabbit anti-RCM-AChR	N.D.	4,610	
	Rabbit anti-ovalbumin	1,950	40	
SJL	Rabbit anti-AChR	8,720	2,920	
	Rabbit anti-ovalbumin	1,130	230	

Thymocytes (10^5–10^6 suspended in 50 μl of diluent) were added to aliquots, (100 μl) of the tested sera or immunoglobulins, in wells of microtitre plates. Following an incubation at 4 °C for 30 min, the plates were centrifuged and washed twice with the diluent. ^{125}I-protein A[13] was added (100 μl per well, approximately 150,000 c.p.m.) and the plates were incubated in the cold for an additional 60 min. The plates were centrifuged and washed twice and the wells were separated and counted. Each dilution or immunoglobulin sample was assayed in triplicate and the amount of binding was determined after subtraction of the background radioactivity obtained by incubation of the thymocytes with the diluent instead of the tested serum or immunoglobulin. The background values were about 3,500 c.p.m. and 1,000 c.p.m., respectively, for the two different preoparations of ^{125}I-protein A used for these experiments. The first preparation was utilized in the experiments with sera and immunoglobulins and the second one in the experiments with purified antibodies.

0028-0836/80/370162—03$01.00

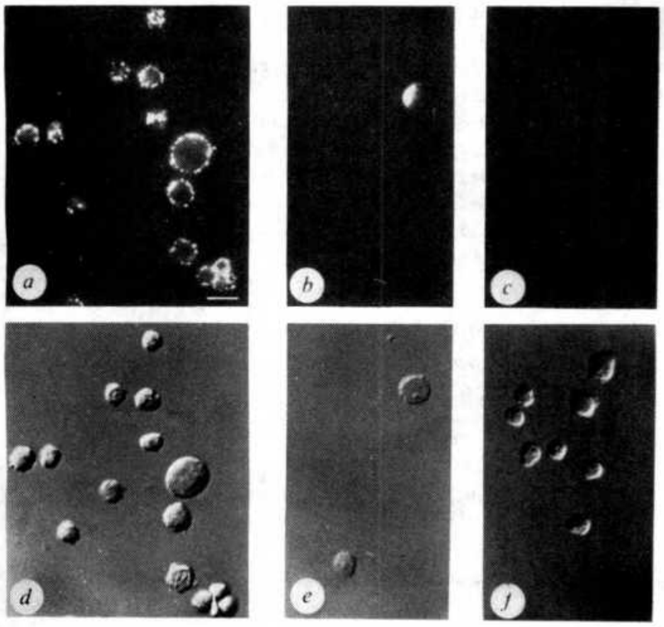

Fig. 1 Immunofluorescent staining of C57BL/6 thymocytes with anti-AChR antibodies. *a*, *b*, Epifluorescence of cells incubated with rabbit anti-AChR IgG followed by rhodamine-goat anti-rabbit IgG. *d*, *e*, Same fields photographed with Nomarski optics. Cells were incubated at 4 °C in the presence of 10 mM NaN_3 (*a*, *d*) and at 37 °C in the absence of azide (*b*, *c*). *c*, *f*, Control: cells were incubated with rabbit anti-ovalbumin IgG instead of anti-AChR. Other conditions are as in *a*, *d*, respectively. Scale bar, 10 μm.

preparation (reduced carboxymethylated AChR, or RCM-AChR[15]) also bound to thymocytes (Fig. 3*d*, Table 1).

In all the experiments described so far, thymocytes from C57BL/6 mice were tested. This mouse strain was shown to be susceptible to experimental autoimmune myasthenia gravis (EAMG)[16]. Similar experiments were performed with thymocytes from a non-susceptible strain[16] in order to test whether the non-susceptibility to EAMG in the latter mice could result from the absence of the 'AChR-like' antigen on their thymocytes. Experiments performed with thymocytes of SJL mice also demonstrated a specific binding of rabbit and monkey anti-AChR sera and of rabbit anti-AChR purified antibodies (Table 1), similar in intensity to that obtained with C57BL/6 thymocytes. These results indicate that the non-susceptibility of SJL mice to EAMG is not associated with a lack of the 'AChR-like' antigen in the thymus.

The results reported here suggest that the component in thymocytes which cross-reacts with anti-AChR antibodies is a surface antigen. The fluoresence studies also demonstrate that the 'AChR-like' antigen on thymic lymphocytes is homogeneously distributed on the cell surface and that a similar number of antibody molecules are bound per cell under a given antibody concentration. It seems that the amount of antibodies reacting with thymocytes in anti-AChR sera is probably rather low or, alternatively, of very low affinity because the cross-reactivity could be observed only by using relatively high amounts of anti-AChR specific sera. We are attempting now to isolate by specific immunoadsorption and to identify the AChR cross-reacting material from the thymus.

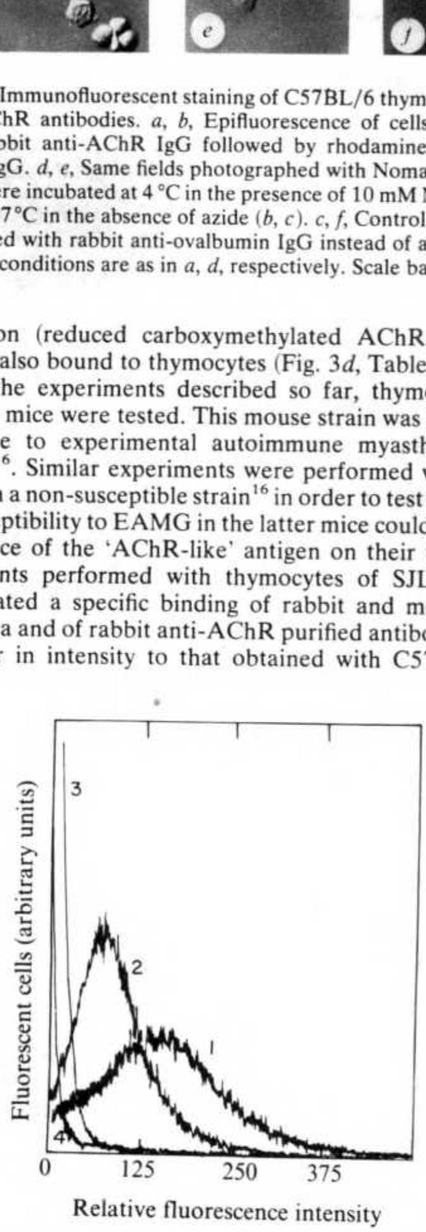

Fig. 2 Immunofluorescence profile of C57BL/6 thymocytes labelled with rabbit anti-AChR immunoglobulins (1, 2, 600 and 200 μg, respectively) and with rabbit anti-ovalbumin (3, 4, 600 and 200 μg, respectively). Fluorescein-conjugated goat anti-IgG was used for staining.

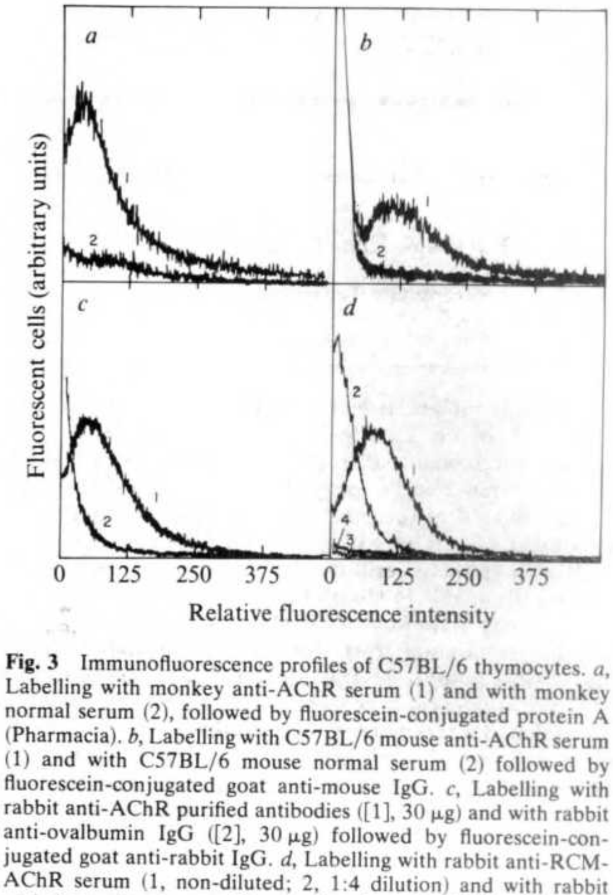

Fig. 3 Immunofluorescence profiles of C57BL/6 thymocytes. *a*, Labelling with monkey anti-AChR serum (1) and with monkey normal serum (2), followed by fluorescein-conjugated protein A (Pharmacia). *b*, Labelling with C57BL/6 mouse anti-AChR serum (1) and with C57BL/6 mouse normal serum (2) followed by fluorescein-conjugated goat anti-mouse IgG. *c*, Labelling with rabbit anti-AChR purified antibodies ([1], 30 μg) and with rabbit anti-ovalbumin IgG ([2], 30 μg) followed by fluorescein-conjugated goat anti-rabbit IgG. *d*, Labelling with rabbit anti-RCM-AChR serum (1, non-diluted; 2, 1:4 dilution) and with rabbit anti-ribonuclease serum (3, non-diluted, 4, 1:4 dilution) followed by fluorescein-conjugated goat anti-rabbit IgG.

It should be pointed out that we did not succeed in demonstrating any significant toxin-binding activity in thymocytes or thymic extracts. This is also in agreement with the finding that antibodies against a pharmacologically inactive RCM-AChR cross-react with thymus (Fig. 3*d*). These results suggest that the immunologically cross-reacting material on thymocytes is probably not an active nicotinic receptor. Nevertheless, an immunological cross-reactivity by itself could explain the association between the thymus and the neuromuscular junction in myasthenia, where the thymic antigen or a modified form of it could be the primary antigen in the spontaneous disease, or alternatively could be damaged by a cross-reactive autoimmune attack by anti-AChR antibodies. Previous reports have suggested that the immunological cross-reactivity between AChR and thymus could stem from myoid cells which were shown to develop to striated muscle fibres in cultures of thymus reticulum under selective medium conditions[17,18], or from some thymic epithelial cells which were shown to contain acetylcholine receptor[19].

The presence of anti-thymus antibodies has been demonstrated in a high percentage of myasthenic patients[7] and we could also detect binding of sera from myasthenics to mouse thymocytes. However, in the spontaneous disease, there is no direct evidence whether the immune response to thymus is a separate independent reaction or whether autoantibodies to AChR cross-react with the thymus. The present study provides direct evidence that anti-AChR antibodies can cross-react with the thymus.

We thank Mr Avigdor Petrank for his assistance in the FACS studies, and Dr Benjamin Geiger and Mr Daniel Bartfield for their help and discussions. G. T. was a visiting scientist from the University of Padova, Italy. This research was supported by grants from the Muscular Dystrophy Association of America, The United States–Israel Binational Science Foundation and the Los Angeles Chapter of the Myasthenia Gravis Foundation.

Received 11 February; accepted 7 July 1980.

1. Drachman, D. B. *New Engl. J. Med.* **298,** 136–142 (1978).
2. Fuchs, S. *Curr. Topics Microbiol. Immun.* **85,** 1–29 (1979).
3. Castleman, B. *Ann. N.Y. Acad. Sci.* **135,** 496–504 (1966).
4. Papatestas, A. E., Alpert, L. J., Osserman, K. E., Osserman, R. S. & Kark, A. E. *Am. J. Med.* **50,** 465–474 (1971).
5. Van der Geld, H. R. W. & Strauss, A. J. L. *Lancet* **i,** 57–60 (1966).
6. Field, E. J. *et al. Lancet* **ii,** 675–676 (1973).
7. Huang, S. W., Rose, J. W. & Mager, R. F. *J. Neurol. Neurosurg. Psychiat.* **40,** 1053–1059 (1977).
8. Goldstein, G. *Lancet* **ii,** 119–122 (1968).
9. Abharonov, A., Tarrab-Hazadai, R., Abramsky, O. & Fuchs, S. *Proc. natn. Acad. Sci. U.S.A.* **72,** 1456–1459 (1975).
10. Schmidt-Hopfeld, I., Tarrab-Hazdai, R., Tridente, G. & Fuchs, S. *Israel J. med. Sci.* **15,** 882 (1979).
11. Aharonov, A., Tarrab-Hazdai, R., Silman, I. & Fuchs, S. *Immunochemistry* **14,** 129–137 (1977).
12. Herzenberg, L. A. & Herzenberg, L. A. in *Handbook of Experimental Immunology* (ed. Weir, D. M.) 22.1–22.21 (Blackwell, Oxford, 1978).
13. Dorval, G., Welsh, K. I. & Wigzell, H. *J. immun. Meth.* **7,** 237–250 (1975).
14. Fuchs, S. & Sela, M. in *Handbook of Experimental Immunology* (ed. Weir, D. M.) 10.1–10.6 (Blackwell, Oxford, 1978).
15. Bartfeld, D. & Fuchs, S. *Proc. natn. Acad. Sci. U.S.A.* **75,** 4006–4010 (1978).
16. Fuchs, S., Nevo, D., Tarrab-Hazdai, R. & Yaar, I. *Nature* **263,** 329–330 (1976).
17. Wekerle, H., Paterson, B., Ketelsen, U. P. & Feldman, M. *Nature* **256,** 493–494 (1975).
18. Kao, I. & Drachman, D. B. *Science* **195,** 74–75 (1977).
19. Engel, W. K., Trotter, J. L., McFarlin, D. E. & McIntosh, C. L. *Lancet* **i,** 1310–1311 (1977).

Epstein–Barr virus-induced cell fusion

Gary James Bayliss & Hans Wolf

Max von Pettenkofer Institute, Pettenkoferstr. 9a,
8000 München 2, FRG

Serological and molecular biological studies[1–3] have shown an association between Epstein–Barr virus (EBV) and nasopharyngeal carcinoma. Although it has been shown that the epithelioid tumour cells carry EBV genomes[4], they are apparently devoid of receptors for EBV (H.W., unpublished observations). Others have suggested that fusion of EBV carrying cells with epithelial cells may be the mode of entry of the virus into cells unable to absorb the virus and that this may be mediated by one of the known syncytium-forming viruses which inhabit the respiratory tract (for example, members of the paramyxovirus group). de Thé and colleagues suggested that intercellular bridges could be seen in NPC tumour material[5]. We have developed a technique which permits the preparation of stable monolayers of viable human lymphoblastoid cell lines[6]. Using this technique we have now demonstrated that EBV can induce fusion between EBV-superinfected lymphoblastoid cells and cells devoid of EBV receptors.

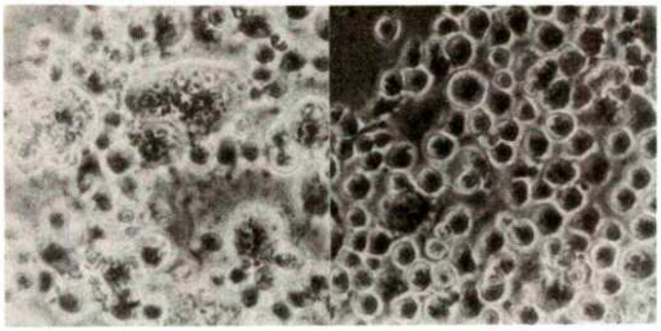

a *b*

Fig. 1 The formation of polykaryocytes in cultures of immobilized superinfected Raji cells. A stock of EBV prepared from P3HR1 cells was used to superinfect Raji cells as previously described[8]. After shaking at room temperature for 1 h, the cells were applied to plastic Petri plates coated with ALG. The infected, immobilized cultures were incubated at 37 °C. *a*, Raji cells superinfected with concentrated virus, 4 h post-infection. *b*, As *a*, but virus diluted 1 : 100. ×650.

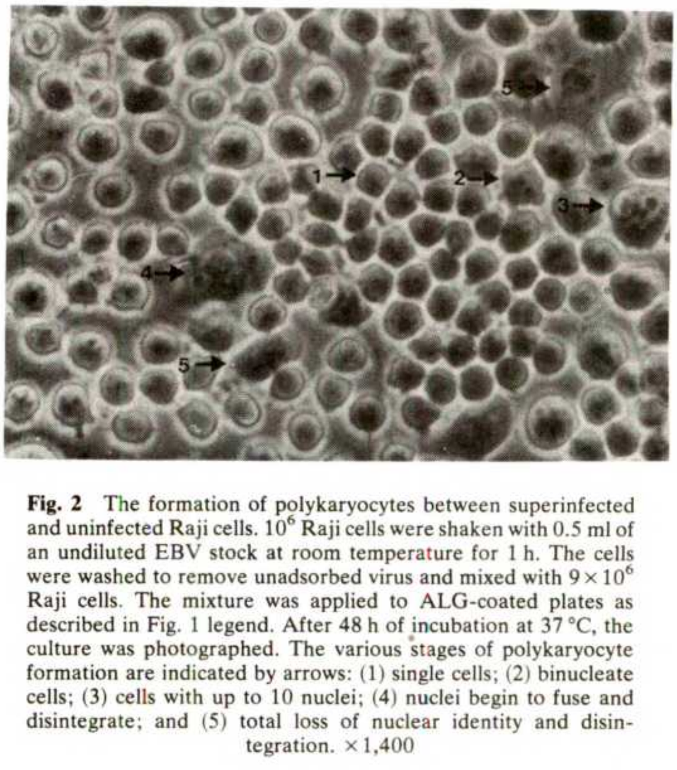

Fig. 2 The formation of polykaryocytes between superinfected and uninfected Raji cells. 10^6 Raji cells were shaken with 0.5 ml of an undiluted EBV stock at room temperature for 1 h. The cells were washed to remove unadsorbed virus and mixed with 9×10^6 Raji cells. The mixture was applied to ALG-coated plates as described in Fig. 1 legend. After 48 h of incubation at 37 °C, the culture was photographed. The various stages of polykaryocyte formation are indicated by arrows: (1) single cells; (2) binucleate cells; (3) cells with up to 10 nuclei; (4) nuclei begin to fuse and disintegrate; and (5) total loss of nuclear identity and disintegration. × 1,400

Raji cells, which carry the EBV genome but do not express early or late viral antigens, are susceptible to superinfection with EBV derived from the EBV-producing cell line P3HR1. Superinfected cells enter an abortive or productive cycle of virus replication depending on the multiplicity of infection. Productively infected cells synthesize viral DNA[7] and several virus-specified polypeptides[8] including early antigen (EA)[9] and viral capsid antigen (VCA)[10]. This superinfection system was used as a model to study the interaction of EBV-infected B-lymphoblastoid cells with one another and with unrelated cells. The response of uninfected Raji cells to immobilization on plastic surfaces coated with antilymphocyte globulin (ALG) has been described elsewhere[6]. When superinfected Raji cells were applied to ALG-coated plates in sufficient numbers to yield a confluent monolayer, polykaryocytes were observed within 2 h of immobilization (4 h after addition of the virus to the cells). Figure 1*a* shows a phase contrast photomicrograph of such a culture. Dilution of the virus stock used to superinfect the Raji cells leads to a diminution of the number of polykaryocytes

0028–0836/80/370164—02$01.00

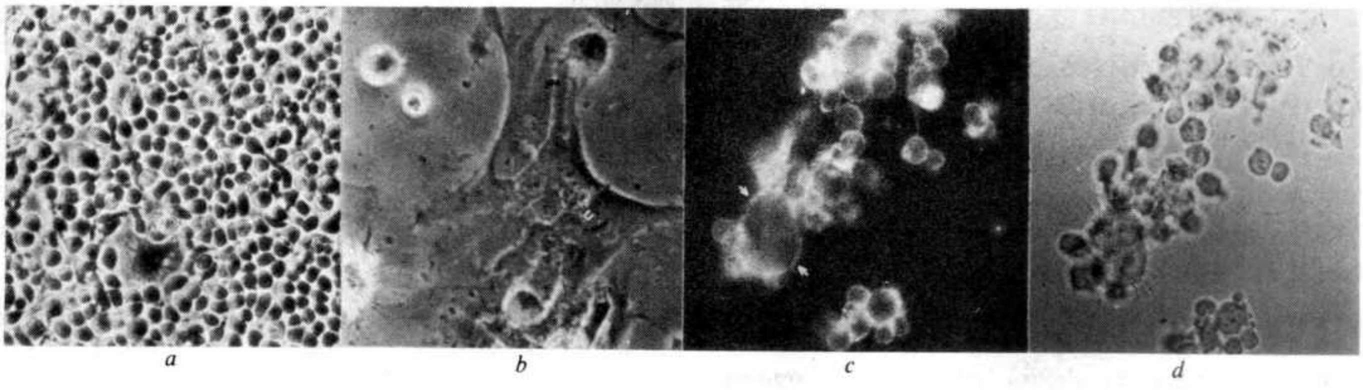

Fig. 3 The formation of polykaryocytes between infected Raji cells and cells devoid of EBV receptors. Raji cells were applied to ALG-coated plates to yield very sparse monolayers (approximately 10% confluent). After the cells had attached, virus was added and 1 h later either Jurkat (T-lymphoblastoid cells; *a*, *c*, *d*) or human embryo fibroblasts (*b*) were added to give a subconfluent monolayer. The cultures were incubated at 37 °C and photomicrographs prepared 20 h after infection. The cultures in *c* and *d* were stained with anti-T-cell serum. *c* Shows a polykaryocyte with T-cell membrane fluorescence. The arrows indicate areas where the polykaryocyte is free of adherent cells (see *d*) and shows clear membrane fluorescence. *d* Is a photograph of the same group of cells taken under normal light. At least three nuclei can be identified within the polykaryocyte. *a*, *b*, ×650; *c*, *d*, ×1,000.

observed (Fig. 1*b*; virus diluted 1:100). Immobilization of Raji cells without addition of exogenous EBV does not induce polykaryocyte formation. With minor modifications this technique can be used to titrate stocks of EBV. A similar series of experiments, in which infected cells were treated with sodium azide or cycloheximide, or in which cells were infected with UV-ray inactivated virus or virus treated with neutralizing antiserum, indicated that at least partial expression of EBV is required to induce cell fusion.

The high multiplicities of infection necessary to induce a full or partial virus reproductive cycle prevents observation of the interaction between infected and uninfected cells. To obviate this problem, superinfected Raji cells were washed to remove unadsorbed virus and mixed with uninfected Raji cells in a ratio of 1:10. The mixture of cells was applied to ALG-coated plates and the cells were allowed to attach as described above. After 48 h, numerous multinucleate cells could be observed and in some of the syncytia the nuclei had begun to disintegrate or coalesce. Figure 2 illustrates the various stages of syncytium formation.

These experiments show that EBV can induce fusion between cells having receptors for EBV, but not whether EBV can induce fusion between receptor-positive and -negative cells. We studied the interaction of superinfected Raji cells with human T-lymphoblastoid cells (Jurkat) or human embryo fibroblasts (HEF). Raji cells were applied to ALG-coated plates to give very sparse monolayers with a cell density of less than 10% of confluency. These cells were infected *in situ* by adding a stock of EBV; after the virus had been adsorbed by the Raji cells, Jurkat or HEF cells were added. After incubation at 37 °C for 20 h, the cultures were photographed (Fig. 3*a*, *b*). From these photographs it is apparent that the cells had fused giving rise to polykaryocytes. Fluorescent antibody staining of the cultures showed that the polykaryocytes contained EBV antigens (EA and VCA) and that the polykaryocytes formed between superinfected Raji cells and Jurkat cells had T-cell membrane determinants on their surface (Fig. 3*c*, *d*).

Our observations suggest that close cell-to-cell contact, as it occurs in closely packed monolayers, is necessary for the development of multinucleate cells. A close contact between epithelial cells and lymphocytes (which may carry EBV genomes) has been observed in the lymphoepithelium of Waldeyer's ring of the throat[11]. The exceptionally close contact between the lymphocytes and epithelial cells in this unique tissue may provide the necessary conditions for EBV-induced fusion between the two cell types. For further considerations of this aspect, and the relationship of EBV to other lymphoepithelial and undifferentiated carcinomas of the Waldeyer's ring see ref. 12.

In situ hybridization studies[13] with NPC tumour material indicate that the cancerous cells carry a heavy load of viral genomes. This could be achieved in one of two ways: either the virus is activated, enters into a lytic cycle and replicates independently of the host cell using virus-specified DNA polymerase[14] or, as in cell lines which carry the genome but cannot enter a lytic cycle, the viral DNA can be replicated using host replicative machinery (for example, see ref. 15). Lymphoblastoid cells in a lytic cycle which contain several thousand copies of the viral genome[16] could fuse with epithelial cells transferring its entire viral load. Tumour cells contain large quantities of viral DNA, the near diploid or near triploid karyotype and chromosomal abnormalities[17] fusion of EBV-carrying lymphocytes with epithelial cells could generate such abnormal cells. In addition the hybrid cell could then eliminate most of the genetic material originating from the lymphoblastoid cell and regain a near normal chromosome number. The efficiency with which EBV can induce cell fusion in tissue culture supports the hypothesis that EBV-induced cell fusion may be important in the infection of epithelial cells, which are normally refractory to infection by this virus, provided that certain conditions of virus activation and close cell contact are met.

We thank Mrs G. Deby for technical assistance and Dr Rodt for supplying the sera. The work was supported by a grant from the Deutsche Forschungsgemeinschaft (DFG Wo 227/2) and from the Sonderforschungsbereich 51.

Received 21 April; accepted 25 July 1980.

1. Old, J. *et al. Proc. natn. Acad. Sci. U.S.A.* **56,** 1699–1704 (1966).
2. Henle, W. *et al. J. natn. Cancer Inst.* **44,** 225–231 (1970).
3. Wolf, H., Werner, J. & zurHausen, H. *Cold Spring Harb. Symp. quant. Biol.* **39,** 791–796 (1974).
4. Wolf, H. *et al. Med. Microbiol. Immun.* **161,** 15–21 (1975).
5. Gazzolo, L., de Thé, G., Viullaume, M. & Ho, H. C. *J. natn. Cancer Inst.* **48,** 73–86 (1972).
6. Bayliss, G. J. & Wolf, H. in *Advances in Comparative Leukemia Research* (eds John, D., Lapin, B. & Blakeslee, J.) 381–382 (Elsevier, New York, 1979).
7. Yajima, Y. & Nonoyama, M. *J. Virol.* **19,** 187–194 (1976).
8. Bayliss, G. J. & Nonoyama, M. *Virology* **87**, 204–207 (1978).
9. Henle, W. *et al. Science* **169,** 188–190 (1970).
10. Seigneurin, J-M., Vuillaume, M., Lenoir, G. & de Thé, G. *J. Virol.* **24,** 836–845 (1977).
11. Döhnert, G. in *Sitzungsbericht der Heidelberger Akademie der Wissenschaften Vol.* 3 96–168 (Springer, Berlin, 1977).
12. Wolf, H., Wilmes, E. & Bayliss, G. J. in *Modern Trends in Leukemia Vol.* 4 (Springer, Berlin, in the press).
13. Wolf, H., zurHausen, H. & Becker, V. *Nature new Biol.* **244,** 245–257 (1973).
14. Ooka, T., Lenoir, G. & Daille, J. *J. Virol.* **29,** 1–10 (1979).
15. Hampar, B. *et al. Nature new Biol.* **244,** 214–217 (1973).
16. Nonoyama, M. & Pagano, J. S. *Nature new Biol.* **233,** 103–106 (1971).
17. Finerty, S. *et al. Br. J. Cancer* **37,** 231–239 (1978).

Do 'lipidic particles' represent intermembrane attachment sites?

Rodman G. Miller

Institute of Histology and Embryology, University of Geneva Medical School, 1211 Geneva 4, Switzerland

Although freeze-fracture electron microscopy is normally analysed with the presumption that particles represent proteins embedded within the membrane, particles which appeared to represent inverted lipid micelles within membranes have been reported[1-4]. I have now confirmed the occurrence of particles in protein-free liposomes, but have found that they behave like intermembrane attachment sites rather than structures within a membrane.

Pits and particles have recently been described on freeze-fracture replicas of liposomes containing an equimolar ratio of cardiolipin and phosphatidylcholine[1]. Furthermore, several lipids which are capable of forming a hexagonal II phase will also form pits and particles on freeze-fractured membranes[2,3]. The interpretation of these results has been that these lipids are able to form inverted micelles, which have a similar organization to the hexagonal II phase, sandwiched between the leaflets of the membrane[1,2,4]. It has also been suggested that some of the particles seen in freeze-fractured biological membranes may also represent inverted lipid micelles in the centre of the membrane[1,2,4]. This is a serious suggestion since, thus far, freeze-fracture replicas have been analysed with the consideration that particles represent proteins (with or without a layer of adsorbed lipids and/or condensate) intercalated in the plane of the membrane. I have now studied a cardiolipin–phosphatidylcholine liposome system to define better the nature of the particles and pits in these membranes.

Multilamellar liposomes were prepared as follows: an ethanol solution of cardiolipin (Sigma) and phosphatidylcholine (egg yolk, Sigma) was dried under a stream of dry nitrogen and hydrated with buffer (100 mM NaCl, 10 mM Tris (*p*H 7.5) with 10% glycerol). The resulting suspension was vigorously shaken for 10 min and sonicated in a bath type sonicator for 10 min. Similar results to those presented have been obtained without glycerol in the buffer and by using the injection method of liposome preparation (see ref. 1 for example). Addition of calcium was performed by addition of an appropriate aliquot of the same buffer containing 10 mM $CaCl_2$ and mixing. Liposomes were quenched in partially solidified freon and freeze-fractured in a Balzers freeze-fracture device.

Multilamellar liposomes formed with an equimolar ratio of cardiolipin and phosphatidylcholine are spherical, smooth and do not contain particles or pits (Fig. 1*a*). The addition of calcium (2 mM final concentration) induces the appearance of particles and pits on some of the liposomes. In most of the liposomes which showed particles or pits, the fracture face exposed was that of the external membrane of the liposome, and contained either particles (Fig. 1*b*) or pits (Fig. 1*c*) but not a mixture of the two. In each case, the leaflet which contained the particles was the external leaflet (E-face) and the leaflet which contained the pits was the internal leaflet (P-face). No fractures which apparently represented the external membrane of a liposome contained pits on the E-face or particles on the P-face. Less than 5% of the liposomes were fractured such that internal membranes of the liposome were revealed. On those that were, I found fracture faces with either particles or pits, and on some occasions a mixture of both (Fig. 1*d*). Consistent with the report that calcium induces fusion in cardiolipin-containing liposomes[3], many liposomes were found that appeared to be partially fused. These will be the subject of a subsequent report from this laboratory (work in progress).

The location of the pits and particles on these membranes was not random: typically they appeared in linear arrays, the individual particles or pits being separated from each other by 12–40 nm. This indicates that long-range interactions are responsible for the location of the pits and particles. Linear arrays of particles occurred along the top of slight ridges on the fracture face, while linear arrays of pits occurred at the bottom of complementary valleys. This effect creates the quilt-like pattern seen in Fig. 1*b–d*. In preparations where the calcium concentration was increased to 6–10 mM, few liposomes remained intact and under the dissecting microscope, massive precipitation of the liposomes was observed. In replicas, the central region of the precipitate no longer appeared as individual bilayer membranes. However, at the edges of the precipitate, regions could be found which appeared to retain the bilayer configuration and which were characterized by high densities of either particles or pits (Fig. 1*e*).

Several observations must be reconciled in a hypothesis which attempts to explain the data: (1) the highly asymmetrical distribution of the particles and pits. In all cases, the outer membrane E-face contained particles while the P-face had pits; (2) the arrangement of the pits and particles into linear arrays; (3) the occurrence of the pits in valleys and particles on ridges of membrane contour; and (4) the absence of particles or pits on many membranes in the preparations. In Fig. 1*g–j*, I present several hypotheses which have been considered: in *g* the model of an inverted micelle in the centre of the membrane is symmetrical with respect to the membrane and cannot be expected to have long-range interactions to alter the contour of the membrane. In *h*, the membrane is distorted to produce a particle–pit pair which is asymmetric but does not have the potential for long-range interactions any further than the diameter of the pit and would not be expected to occur in valleys or ridges of membrane contour. In *i*, a variant of *h*, the production of a pit–particle pair is accompanied by a larger deformation of the membrane contour of a diameter, *x*. This model is asymmetrical, it could provide long-range interactions between the pits or particles up to a distance *x* (minimization of surface energy is expected to aggregate such particles), and the distribution of particles and pits on ridges and valleys, respectively, could be accounted for. That the particles do not appear on all regions of the membrane is not, however, accounted for. Finally, in *j*, the particles and pits are proposed to be attachment sites between two membranes. This model reconciles all the observed data: (1) Such attachments between two membranes necessitate the proximity of another membrane. An observed leaflet would demonstrate pits if the membrane to which it is attached is beneath the fracture plane, and particles if it is above the fracture plane. Both pits and particles would be seen only if the observed membrane is attached to membranes both above and below it. (2) If the attached points are mobile within the plane of the membranes, distension of the spaces between two such membranes can be expected to aggregate the points into a line or, in the extreme case, a cluster. (3) A row of points would be expected to alter the local contours of the membranes such that particles would appear at the tops of ridges and pits at the bottoms of valleys. This would produce the quilt-like pattern which is typical of these preparations; and (4) Although specific lipids (for example, cardiolipin in the presence of calcium) may be a necessary condition for the formation of these pits and particles, the ability to make contact (or maintain contact) with another membrane may be the limiting factor in the production of pits and particles.

Among morphologists, concern has arisen that many of the particles which have been presumed to be indicative of proteins may be purely lipidic. However, the present analysis suggests that lipidic particles may represent sites of membrane contact; this should greatly decrease occasions for concern in biological systems.

A more crucial question arising from the present analysis is

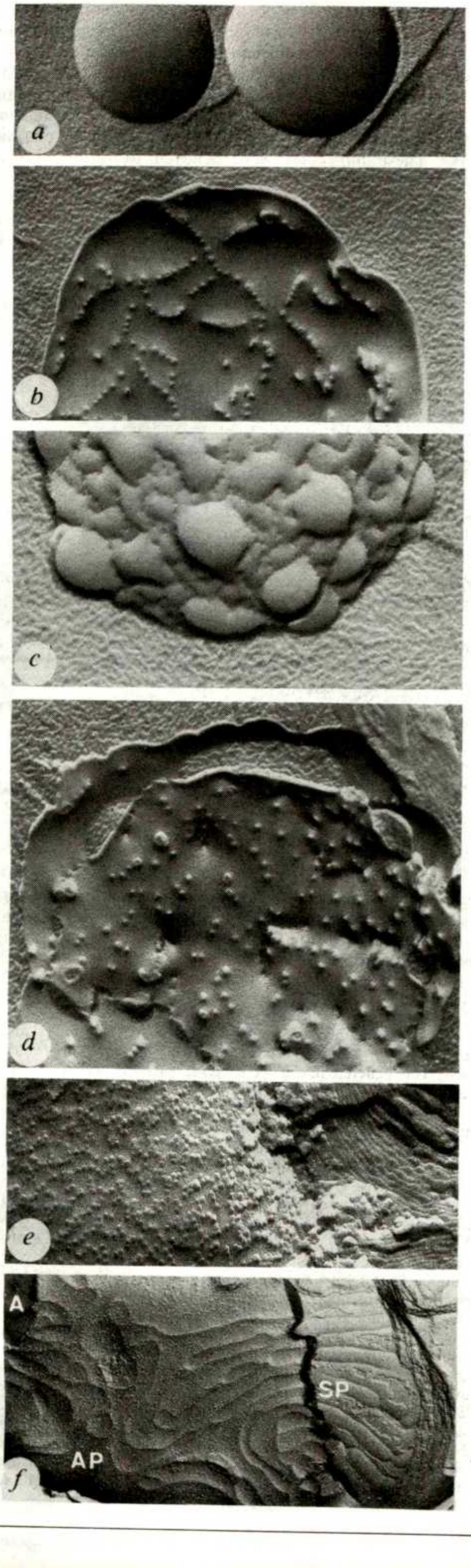

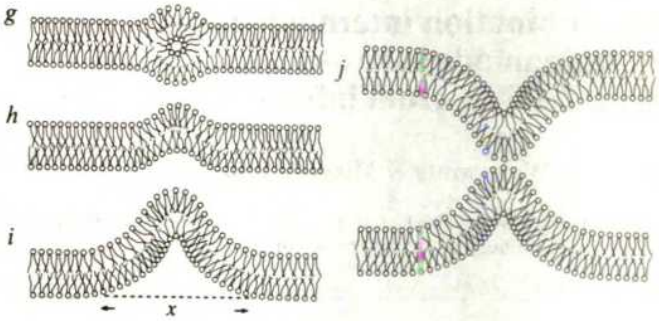

Fig. 1 *a*, Liposomes of 1:1 molar mixtures of cardiolipin:phosphatidylcholine before addition of calcium have membranes which are smooth and uninterrupted by pits or particles: ×80,000. *b*, Addition of calcium to a final concentration of 2 mM induces the appearance of particles on the outer leaflet of the liposome: ×60,000. From the same preparation as *b*: *c*, the inner membrane leaflet of the outer membranes of these liposomes show pits: ×80,000. And *d*, occasionally fractures expose membranes which are not the outer leaflet of the liposome. In these cases, pits, particles or mixtures of the two (as shown here) are present: ×65,000. *e*, When the concentration of calcium is increased to between 6 and 10 mM, precipitation of the liposomes is apparent. At least two phases are present, one with bilayer conformation and many pits or particles, and the other lamellae with no visible aqueous layer between the lamellae: ×80,000. *f*, Freeze fracture of a rat sciatic nerve frozen immediately after removal from the animal. A, axoplasm; AP, axolemmal P-face; SP, Schwann cell P-face: ×25,000. *g–j*, Several hypothetical models which may be considered to explain 'lipidic particles'. *g* and *h* are redrawn after ref. 2. See text for further details.

whether structures (of any material) which attach two membranes together are susceptible to relocation within the plane of the membranes when the membranes in which they are embedded are mechanically pulled apart (for example, by osmotic or freezing effects). In my work, I have found instances where such effects appear to be operating. Figure 1*f* is a particularly striking example of unfixed and non-cryoprotected myelinated nerve where it is believed that growth of ice has created quilt-like arrays of particles on the axolemmal P-face. These arrays are not seen in material which has been fixed. Arrays of this sort are believed to be indicative of structures which are visible in the plane of fracture and which link two membranes together. The location of tight junctions, gap junctions and other structures which link two membranes together may also be susceptible to relocation into clusters and quilt-like patterns as proposed.

I thank the members of this Institute for their help, and, in particular, D. Brown, E. Hooghe-Peters and P. Meda for help with the manuscript, and L. Orci for continuing encouragement. This work was supported by a grant from the Swiss NSF (3.120.77).

Received 8 April; accepted 9 July 1980.

1. Verkleij, A. J., Mombers, C., Leunissen-Bijvelt, J. & Ververgaert, P. J. J. Th. *Nature* **279**, 162–163 (1979).
2. De Kruijff, B. *et al. Biochim. biophys. Acta* **555**, 200–209 (1979).
3. Verkleij, A. J., Mombers, C., Gerritsen, W. J., Leunissen-Bijvelt, L. & Cullis, P. R. *Biochim. biophys. Acta* **555**, 358–361 (1979).
4. De Kruijff, B., Cullis, P. R. & Verkleij, A. J. *Trends biol. Sci.* **5**, 79–81 (1980).

Visualization of genetic recombination intermediates of human adenovirus type 2 DNA from infected HeLa cells

Debra J. Wolgemuth & Ming-Ta Hsu

Department of Molecular Cell Biology, The Rockefeller University,
1230 York Avenue, New York, New York 10021

The study of recombination in prokaryotes has been facilitated by the availability of recombinational mutants and simple genetic elements such as phages and plasmids. These small but defined molecules of DNA have been especially useful for electron microscopic analysis of structural detail of molecules undergoing recombination both *in vivo* and *in vitro*[1–3]. A limitation in the structural analysis of plasmid recombination is the absolute number of recombining molecules which can be identified and analysed amidst a background of nonrecombining molecules[3]. This limitation would be of even greater consequence in studies of genetic recombination in animal cells. We therefore chose virus-infected animal cells as a model system for the study of the molecular mechanism of genetic recombination in higher organisms. HeLa cells infected with adenovirus serotype 2 (Ad-2) offer several advantages for studying recombination: (1) the virus contains a small and well characterized genome of about 35 kilobases; (2) a large amount of Ad-2 DNA is accumulated during lytic infection and host DNA synthesis is suppressed[4]; (3) Ad-2 recombines at a very high frequency[5,6]; and (4) similar to phages, animal viruses and Ad-2 in particular are believed to use many of the host cell's enzymes in necessary metabolic processes, presumably including recombination. In this study we used electron microscopic techniques to visualize the structures of *in vivo* Ad-2 DNA recombination intermediates. Molecules were observed with structures at putative cross-over points which were consistent with the molecular mechanism of recombination proposed by Holliday[7]. In addition, we observed Ad-2 DNA molecules engaged in recombination which were simultaneously serving as templates for replication and/or transcription. To the best of our knowledge, this is the first visualization of *in vivo* recombination intermediates of discrete DNA molecules isolated from eukaryotic cells.

Nucleoprotein complexes were isolated from Ad-2 infected HeLa cells late in infection (20–25 h), a time when viral DNA synthesis and unpackaged viral DNA are maximal[4]. To minimize the cellular DNA background, Ad-2 nucleoprotein complexes were selectively extracted from purified nuclei by the procedures of Wilhelm *et al.*[8] as described in the legend to Fig. 1 and in ref. 9. Aliquots from the sucrose density gradient-fractionated Ad-2 nucleoprotein complexes were prepared for electron microscopy as described by Davis *et al.*[10]. At 20 h post-infection the majority (~70%) of the molecules observed were found to be duplex unit-length Ad-2 DNA. Molecules engaged in viral DNA replication, transcription, and simultaneous replication and transcription were observed and are discussed in detail elsewhere[9].

A small fraction (<1%) of molecules were observed which were characterized by the intimate association of what appeared to be two complete molecules of Ad-2 DNA. Such molecules were followed along their entire lengths under high magnification (~45,000×), photographs were made, and lengths measured to determine the nature of this association. Typical molecules are shown in Fig. 1. Two unit length molecules of Ad-2 DNA are joined at a region of sequence homology (as judged by position in the genome) wherein a cross-over structure can be seen (Fig. 1, inset). Such structures, clearly distinguishable in ~10% of the identified recombination intermediates, were most probably generated by a local denaturation in the region of cross-over[3] allowing visualization of the configuration of the participating strands. This configuration would be predicted from a Holliday-type model of recombination[7] and has been visualized previously with plasmid DNAs[3]. These molecules were believed to represent true

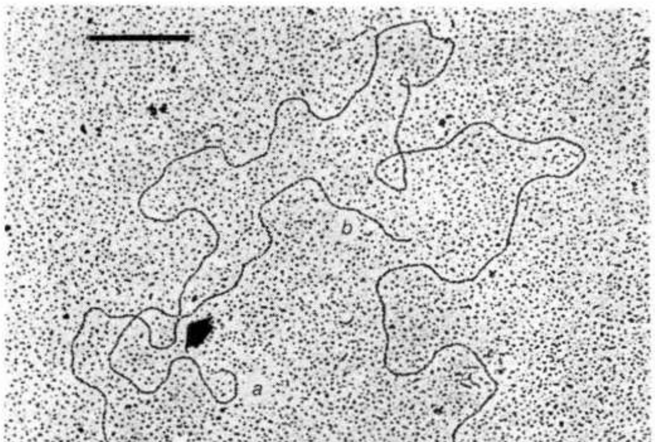

Fig. 1 Electron micrograph of a recombination intermediate of two molecules of Ad-2 DNA. Ad-2 nucleoprotein complexes were selectively extracted from Ad-2 infected HeLa cell nuclei by a modified procedure[9] of Wilhelm *et al.*[8]. Twenty to 24 h post-infection, the cells were pelleted and resuspended in TITE buffer (20 mM Tris, 100 mM NaCl, 0.02% Triton X-100, 2 mM EDTA *p*H 7.4) and homogenized in a tight fitting dounce at 0 °C. The homogenate was layered on 10% sucrose in TITE buffer and centrifuged for 5 min at 500 r.p.m. in a Damon IEC–6000 centrifuge. The pelleted nuclei were resuspended in TEAD buffer [20 mM Tris, 2 mM EDTA, 50 mM $(NH_4)_2SO_4$, 0.1 mM dithiothreitol, *p*H 7.9] and lysed by adding, drop by drop, 2 M $(NH_4)_2SO_4$ to a final concentration of 0.2 M. The lysate was allowed to stand for 10 min on ice and then was centrifuged for 10 min at 10,000*g*. The resulting supernatant or S200 was either layered directly onto 10–60% sucrose gradients in TEAD buffer[8] or was treated with 0.25% sarkosyl and resolved in a 15–30% sucrose gradient containing 10 mM potassium phosphate, *p*H 7.9, 2 mM EDTA, a 0.25 to 0% sarkosyl gradient and 0.25% glutaraldehyde[9]. Centrifugation was in an SW40 rotor at 4 °C for 17 h at 25,000 r.p.m. Various fractions from the sucrose gradient were analysed by electron microscopy. This particular preparation was spread in 50% formamide as described previously[10]. The cross-over point in the recombining molecules (large arrowhead) is enlarged in the inset on the lower right. The thin curved arrow in the inset indicates an overlap between strands which is clearly distinguishable from the Holliday-type structure indicated by the large arrowhead. The length of arm *a* (1.65 μm) is equal to arm *b* (1.64 μm), and *c* (10.68 μm) is equal to *d* (10.60 μm). The sum of *a*, *b*, *c* and *d* is 24.57 μm which is equal to two unit-length Ad-2 genomes (the average length of the intact Ad-2 DNA molecules illustrated in this study is 11.82 ± 0.41 μm). Scale bars, 0.5 μm large micrograph and 0.05 μm inset.

0028-0836/80/370168—04$01.00

Fig. 2 Electron micrographs of Ad-2 molecules with Holliday-type structures at various distances along the genomes. Each photograph shows a close-up of the Holliday structure (arrow) and one of the two pairs of equal length arms. In (*A*), arm *x* is equal to *y* and represents 8.5% of the genome length, a distance closer to the ends than in the molecules shown in Fig. 1 where the Holliday structure lies about at 13.5% of the genome length. In (*B*), *x* is equal to *y* and the Holliday structure is located at a point about 29.8% from an end of AD-2 genome. Preparations were made as described in Fig. 1 legend. Scale bars 0.2 μm (*A*) and 0.4 μm (*B*).

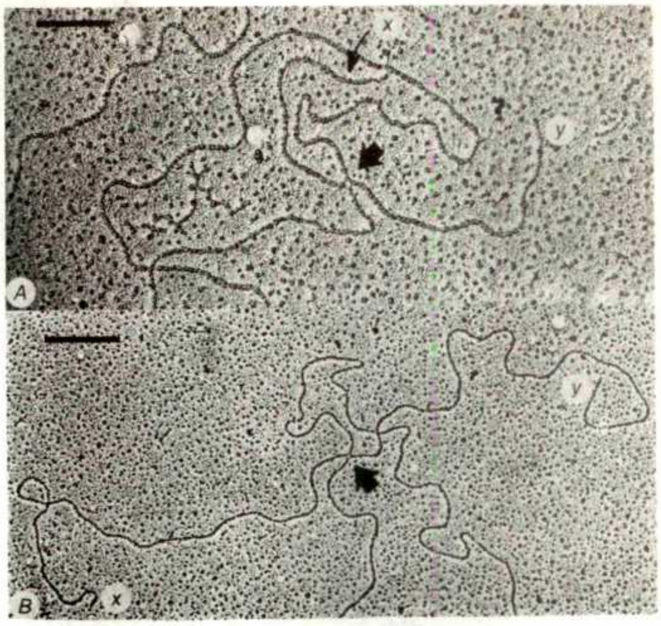

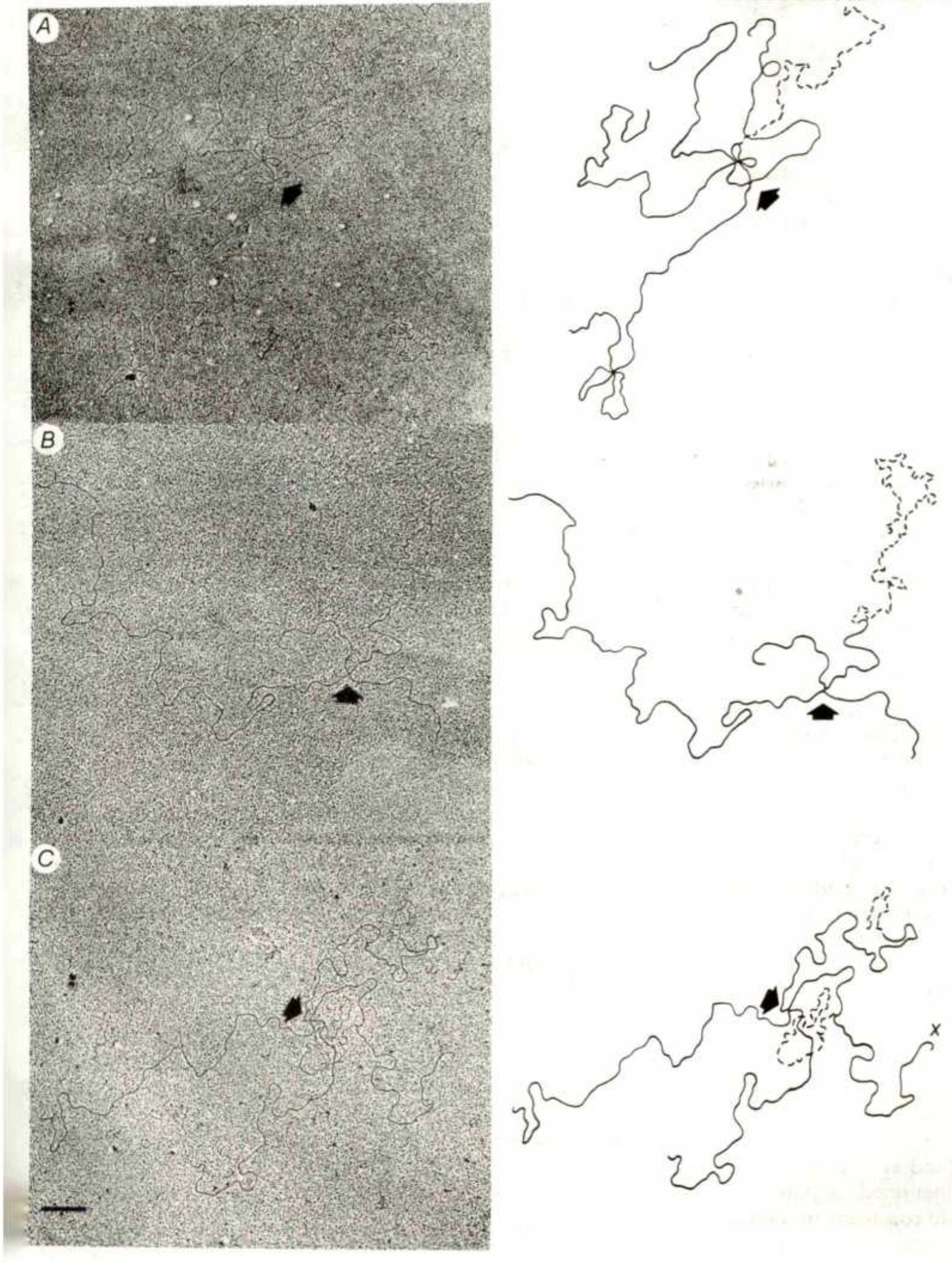

Fig. 3 Electron micrographs and interpretive tracings of Ad-2 recombination intermediates simultaneously engaged in DNA replication. The large arrowhead in each photograph and tracing indicates the point of putative cross-over. Double-stranded DNA is indicated by the solid black line; single-stranded DNA by the dashed line. *A*, Recombination involving an intact double-stranded unit length genome and a type I replication intermediate. The single-stranded displaced parental strand (dashed line) can be seen in the upper right. The sum of the four double-stranded arms is equal to two complete Ad-2 genomes. *B*, Recombination between an intact double-stranded Ad-2 molecule and a presumptive type II intermediate which is partially single-stranded and partially double-stranded. The cross-over point is between double-stranded regions of the two molecules. *C*, Recombination between two molecules containing both type I and type II replicative molecules. The sum of the three completely double-stranded arms and the one double-stranded and single-stranded arm is equal to two Ad-2 genome lengths. The single-stranded branch in the centre of the photograph represents the displaced parental strand complementary to one of the strands in the arm indicated as *X*. Cross-over junctions are located 41%, 16% and 46% along the genome lengths in *A*, *B* and *C*, respectively. The Holliday-type structure is visible in *A* but not in *B* or *C*. Scale bar, 0.5 μm.

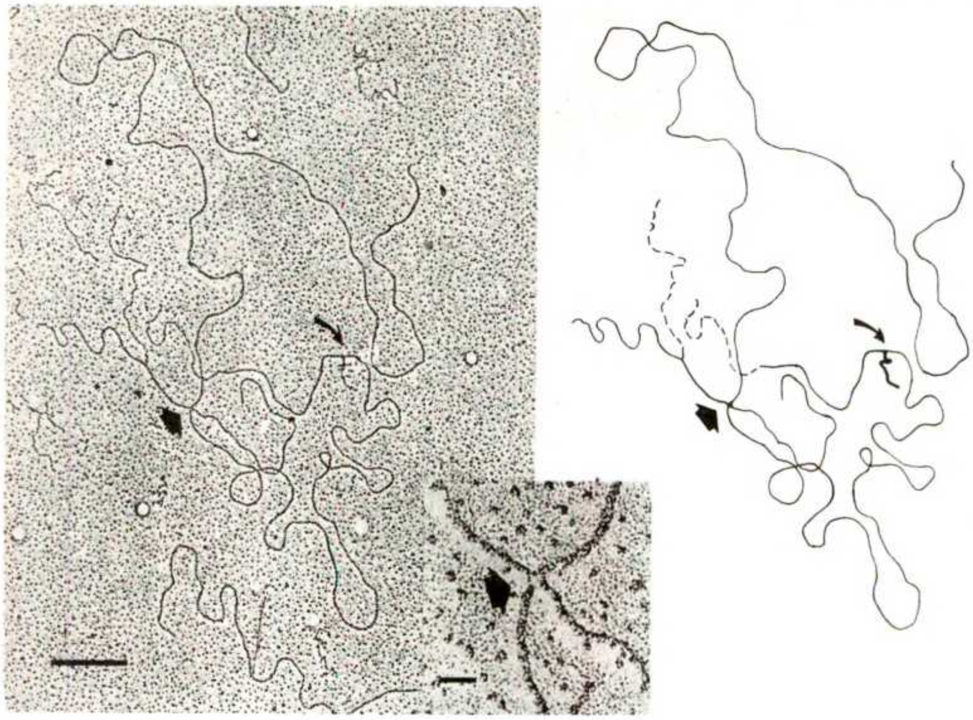

Fig. 4 Electron micrographs and interpretive tracing of recombination intermediate between replicative and transcriptionally active Ad-2 DNA molecules. The putative cross-over point shows a Holliday-type structure (indicated by the large arrowhead and enlarged in the inset). The curved arrow and heavy black line indicate a nascent RNA transcript (discussed in detail in ref. 9). Both type I and type II replication intermediates are seen. The single-stranded portions of these molecules are indicated by dashed lines; the double-stranded portions by the solid lines. Scale bars 0.5 μm large photomicrograph, and 0.05 μm inset.

recombination intermediates according to the following criteria: (1) the structure contained two sets of arms of equal length ($a = b$ and $c = d$ in Fig. 1) from the point of cross-over; (2) the sum of the lengths of the four arms was equal to two unit-length Ad-2 genomes; (3) the highly characteristic appearance of the strands of the molecules at the recombination juncture was observed and these structures were clearly distinguished from mere overlaps (curved arrow, inset to Fig. 1); and (4) such structures were never observed between molecules of purified SV40 DNA added to the preparation. As further illustrated in Fig. 2, these points of putative cross-over were found at various regions of the genome.

Recombination intermediates in which portions of the recombining Ad-2 genomes were apparently replicating were also observed (Fig. 3). The structure of replicating molecules of Ad-2 DNA has been described previously (reviewed in ref. 11). Briefly, Ad-2 DNA replication proceeds in a 5′ to 3′ direction from either end of the duplex molecule, displacing one of the parental strands. The resulting replicating intermediate (type I intermediate) contains two double-stranded branches and one or more single-stranded branches equal to the length of one of the double-stranded branches. For the replication of the displaced parental strand, the predominant mode of synthesis involves initiation at the 3′ end, generating an intermediate with single-stranded portions at one end of the molecule (type II intermediate). As can be seen in Fig. 3 (*A–C*), both types of replicative intermediates were found to be engaged in the recombination process. The recombination intermediate in Fig. 3*A* involves a unit-length double-stranded molecule and a type I replicating molecule with its characteristic fork and displaced parental strand. In Fig. 3*B*, a type II molecule and an intact unit length double-stranded molecule are involved in recombination. Both type I and type II replicating molecules are involved in the recombination event depicted in Fig. 3*C*. An additional category of recombining and replicating molecules was identified which was comprised of more complex structures consisting of recombination intermediates with single-stranded branches at the cross-over point. Analysis of these molecules, which may represent recombination events involving the displaced parental strand, analagous to the model for recombination proposed by Meselson and Radding[12], is under way. One further template activity was identified in molecules undergoing recombination: in addition to consisting of replicating molecules of both type I and type II, one of the recombining molecules shown in Fig. 4 also carries an RNA transcript. It is clear that the recombination event does not involve a sequestered group of molecules in these animal cells as they are simultaneously available to DNA and RNA polymerases.

These observations constitute direct structural evidence for the physical associations between recombining molecules predicted from the model of genetic recombination proposed by Holliday[7] and previously observed in prokaryotes[3]. A feature of this model is a reciprocal exchange between the two genomes with no requirement for DNA synthesis other than a repair-type. Our observation of recombination between non-replicating Ad-2 molecules (Figs 1 and 2) and between replicating molecules but not involving the displaced parental strand (Figs 3 and 4) lends further support to the Holliday-type model of recombination as one possible mechanism for accomplishing genetic recombination during Ad-2 lytic infection. We believe that this is the first time such *in vivo* recombination intermediate molecules have been visualized after isolation from animal cells. The formation of recombinant DNA intermediates between exogenous plasmid molecules in the presence of an extract from unfertilized *Xenopus laevis* eggs reported by Benbow and Krauss[13] was generated totally *in vitro*. Since animal virus genomes are limited in the amount of genetic information they can carry, they are believed to utilize a variety of cellular products to accomplish metabolic events. Elucidation of the molecular mechanisms of recombination in animal viruses in somatic cells should yield information on the genetic recombination process that occurs during meiosis in germ cells.

We thank Dr James E. Darnell Jr for continued support, Dr Selina Chen-Kiang for helpful discussion, Ho-Yun Yu for technical assistance and Lois Cousseau for help in preparing the manuscript. This work was supported by NCI grant CA19073-3. D.J.W. is a Fellow in Cancer Research of the Damon Runyon-Walter Winchell Cancer Fund.

Received 19 May; accepted 24 July 1980.

1. Broker, T. *J. molec. Biol.* **81,** 1–16 (1973).
2. Valenzula, M. & Inman, R. *Proc. natn. Acad. Sci. U.S.A.* **72,** 3024–3028 (1975).
3. Potter, H. & Dressler, D. *Proc. natn. Acad. Sci. U.S.A.* **73,** 3000–3004 (1976); *Cold Spring Harb. Symp. quant. Biol.* **43,** 969–985 (1978).
4. Philipson, L. & Lindberg, U. in *Comprehensive Virology* Vol. 3 (eds Fraenkel-Conrat, H. & Wagner, R. F.) 143–227 (Plenum, New York, 1974).
5. Grodzicker, T., Williams, J., Sharp, P. & Sambrook, J. *Cold Spring Harb. Symp. quant. Biol.* **39,** 439–446 (1974).

6. Young, C. H. S. & Silverstein, S. J. *Virology* **101,** 503–515 (1980).
7. Holliday, R. *Genetics* **78,** 273–287 (1974).
8. Wilhelm, J., Brison, O., Kedinger, C. & Chambon, P. *J. Virol.* **19,** 61–81 (1976).
9. Wolgemuth, D. J. & Hsu, M.-T. *J. molec. Biol.* (submitted).
10. Davis, R. W., Simon, N. & Davidson, N. *Meth. Enzym.* **21**D, 413–428 (1971).
11. Winnacker, E. L. *Cell* **14,** 761–773 (1978).
12. Meselson, M. S. & Radding, C. M. *Proc. natn. Acad. Sci. U.S.A.* **72,** 358–361 (1975).
13. Benbow, R. M. & Krauss, M. R. *Cell* **12,** 191–204 (1977).

Indomethacin and inhibition of protein kinase reactions

Said A. Goueli & Khalil Ahmed

Toxicology Research Laboratory, Department of Laboratory Medicine and Pathology, University of Minnesota, VA Medical Center, Minneapolis, Minnesota 55417

Indomethacin, an inhibitor of prostaglandin biosynthesis, is useful in studies aimed at understanding the metabolism and physiological function of prostaglandins[1]. A recent report[2] showing that indomethacin at 10^{-7} M potently inhibits the cyclic AMP-dependent protein kinases (cAMP-PrK) from ileal mucosa in the presence or absence of cyclic AMP, suggests how indomethacin may antagonize prostaglandin action on ileal mucosa. It also suggests that indomethacin might be useful in studying the properties and functions of protein kinase reactions. Inhibitors of prostaglandin biosynthesis, such as sodium salicylate and acetylsalicylate, at concentrations near 10^{-2} M, have been shown to inhibit bovine diaphragm protein kinase only in the presence of cAMP, while stimulating it in the absence of cAMP[3]. We report here that complete inhibition of cAMP-PrKs by indomethacin requires a concentration of 10^{-3} M and is not tissue-specific, and that the effect of indomethacin is concentration dependent above 2×10^{-4} M for the cAMP-dependent, and above 10^{-3} M for cAMP-independent PrKs. These results contrast previous ones[2].

Cyclic AMP-dependent protein kinase was purified from rabbit ileal mucosa and rat liver cytosol by a modification of methods described earlier[4,5]. Rabbits (~4 kg) were used as the source of ileal tissue. Ilea were rinsed with cold distilled water, and the mucosa was isolated by stripping it off the muscle tissue. Sprague–Dawley rats (weighing 250–300 g, from ARS/Sprague Dawley) were used as the source of liver tissue. Protein kinases I and II, and their catalytic subunit, were purified through DEAE-cellulose and hydroxyapatite steps. Peak I was eluted from DEAE-cellulose at less than 0.1 M NaCl, and peak II at 0.15–0.2 M NaCl. The activity ratios (minus cAMP/plus cAMP) of peaks I, II and the catalytic subunit in the presence of 2 μM cAMP were 0.4, 0.5 and >0.9, respectively, for the rabbit ileum preparation, and 0.17, 0.33 and >0.95, respectively, for rat liver preparations. The ratio of peak I to peak II was 15:85 and 45:55 for rabbit ileum and rat liver, respectively. Each of the three activities was inhibited by the classical cytosol cAMP-PrK inhibitor[6]. A cAMP-independent liver nuclear protein kinase was purified using DEAE-Sephadex and partially (30%) dephosphorylated phosvitin (DPV) affinity chromatography (unpublished work). The enzyme had insignificant activity toward lysine-rich histones, but was very active towards DPV, casein and liver nuclear endogenous non-histone proteins (NHP) as substrates. It was neither stimulated by cAMP nor inhibited by the cAMP-PrK inhibitor. Indomethacin solution was prepared by titration with 0.1 M NaOH of an aqueous suspension of indomethacin until the solution was clear (final *p*H 9.0). The extinction coefficient of this solution was 16,200 and 6,300 at 260 and 319 nm, respectively. This suggests that indomethacin was stable in these experimental conditions. Experiments were also carried out with indomethacin dissolved in ethanol; in this case an appropriate amount of ethanol was added in control reactions. The results obtained were not dependent on the method of preparing the indomethacin solution.

As shown in Fig. 1, indomethacin at 10^{-4} M had no significant effect on any of the rabbit ileum mucosa cAMP-PrKs in the presence or absence of cAMP. Concentrations below 10^{-4} M were equally ineffective (data not given). The same result was

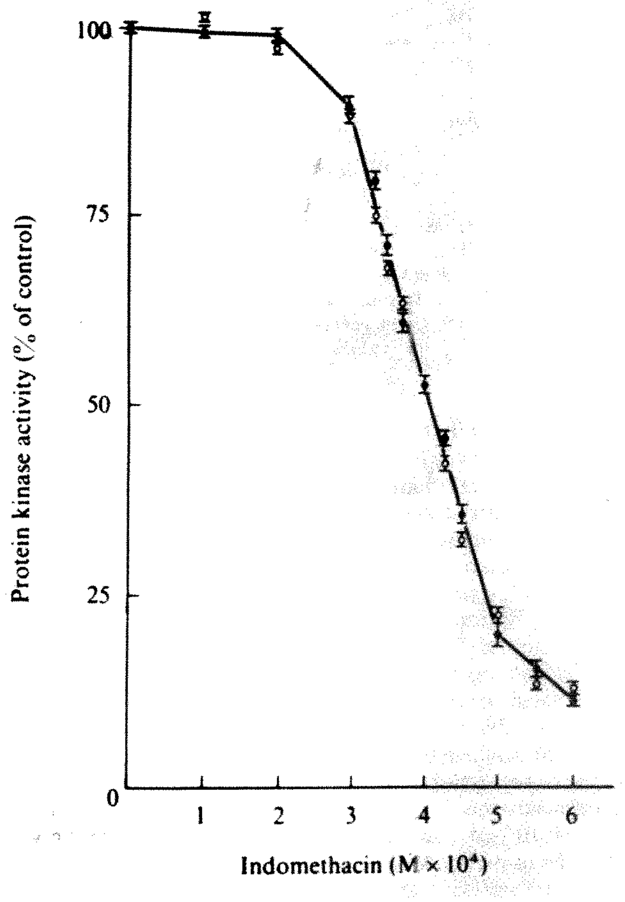

Fig. 1 Effect of varying concentrations of indomethacin on cAMP-PrKs from rabbit ileum mucosa, in the presence or absence of cAMP. The standard reaction medium for assaying cAMP-PrK was Tris-HCl, *p*H 7.45 (30 mM, 37 °C); LRH or protamine sulphate (1–5 mg ml^{-1}); $MgCl_2$ (10.0 mM); [γ-^{32}P]ATP, (0.2 mM, 30–50 μCi μmol^{-1}); with or without cAMP (2 μM); and, enzyme protein (0.04–0.2 mg ml^{-1}) in a final volume of 0.25 ml. The enzyme was allowed 20–45 min prior contact at 37 °C with all the reactants except $MgCl_2$ and [γ-^{32}P]ATP which were added together to initiate the protein kinase reaction, following which aliquots (40 μl) were removed at 0, 4, 8 and 12 min. This material was rapidly spotted on P-81 paper, and the radioactivity incorporated in protein substrates was determined as described by Corbin and Reimann[12]. The assay medium for cAMP-independent nuclear protein kinase consisted of Tris-HCl, *p*H 7.45 (30 mM, 37 °C); DPV (2 mg ml^{-1}); $MgCl_2$ (4 mM): [γ-^{32}P]ATP (3 mM, 2–5 μCi μmol^{-1}), in a final reaction volume of 0.25 ml. The details of incubation were the same as described above. The amount of radioactivity incorporated in DPV was determined as described by Goueli *et al.*[13]. Each data point represents a mean of 10 experimental values ± s.e.m. for each tested enzyme; ●, plus cAMP; ○, minus cAMP. Statistical analysis using Student's *t*-test between activity values in the presence of 0, 10^{-8}, 10^{-7}, 10^{-6}, 10^{-5} and 10^{-4} M indomethacin showed no significant differences at 1% level. All protein determinations were according to Bensadoun and Weinstein[14] using BSA, DPV and lysine-rich histones as standards. In some experiments α-glycerophosphate (*p*H 7.4, 37 °C) was used in place of Tris-HCl (*p*H 7.45, 37 °C) as buffer in protein kinase assays in the presence or absence of indomethacin. Change of buffer did not alter the results described above.

0028–0836/80/370171—02$01.00

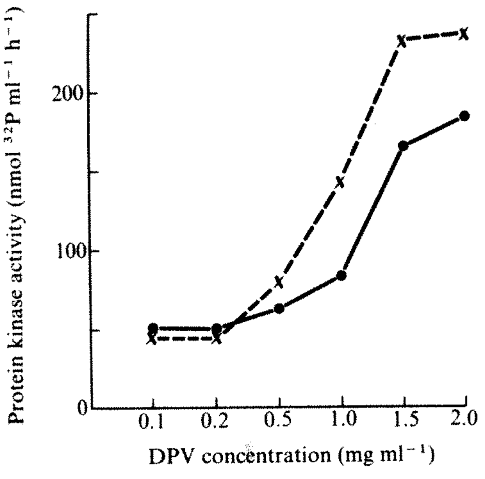

Fig. 2 Effect of varying concentrations of DPV on cAMP-independent nuclear protein kinase activity in the absence or presence of 10^{-3} M indomethacin. The details of assay were as described in Fig. 1 legend. ●, No indomethacin; x, 10^{-3} M indomethacin. Each point represents a mean of three different values ± s.e.m.

obtained with a number of different enzyme preparations, for example liver protein kinase peaks I, II and the catalytic subunit, bovine heart protein kinase peak II (data not shown). Also, the order of addition of various reactants, or the duration of prior contact of the enzyme with the drug, was without effect: the incubation of enzyme with the drug for up to 45 min at 30°C, or 20 min at 37°C, gave the same results as when no prior contact between drug and enzyme was allowed. Addition of 1 mM dithiothreitol had no effect on the protein kinase activity either in the presence or absence of indomethacin. When indomethacin concentration was increased to 10^{-3} M, all of the cAMP-dependent enzymes tested were inhibited, in the presence or absence of cAMP. These findings are in contrast to the previous report[2] which showed that inhibition by indomethacin was time dependent and maximal at a concentration of 10^{-7} M. Only at concentrations of indomethacin of 2×10^{-4} M or higher was there an inhibition of the ileal mucosa enzyme, as well as enzymes from other tissues. The concentration of the inhibitor required for 50% inhibition of the enzyme[7], ID_{50}, for the ileal mucosa enzyme was 6×10^{-4} M, and similar values of ID_{50} were obtained when enzymes from other tissues were tested. We also examined the endogenous incorporation of ^{32}P into cAMP-PrKs. Again, at concentrations of indomethacin above 10^{-4} M, the pattern of inhibition was similar to that noted when protamine or lysine-rich histones were used as substrates (data not given). Thus, our results suggest that indomethacin is not a potent inhibitor of cytosol protein kinase reaction and that the inhibitory effect is not specific for any of the kinases examined. This is similar to the observation that sodium salicylate at 10^{-2} M inhibited the kinase activity by 50% but was without effect at 10^{-3} or less[3].

The effect of indomethacin on a nuclear cAMP-independent protein kinase active toward DPV was also studied. We found that indomethacin did not inhibit this particular reaction, even at a concentration of 5×10^{-4} M; rather, a small stimulation (20–25%) of the kinase activity was observed in these conditions (data not shown). However, at higher concentrations (for example at 10^{-3} M), a small inhibition (25%) of the enzyme activity became apparent. Thus, it appears that this cAMP-independent kinase activity is even more insensitive to indomethacin than that dependent on cAMP. Furthermore, when liver chromosomal NHP was used as substrate for the cAMP-independent PrK reaction, the pattern of inhibition by indomethacin was similar to that observed with DPV as substrate (about 25% inhibition was noted at 10^{-3} M indomethacin).

To determine whether or not substrate concentration modified the indomethacin effect in this reaction, we tested the action of the drug on nuclear protein kinase activity at different concentrations of DPV in the reaction. Figure 2 shows that in the presence of 10^{-3} M indomethacin, this protein kinase reaction was only slightly inhibited in the presence of DPV at a concentration of about 0.2 mg ml^{-1}. However, at higher substrate concentrations (0.5–2.0 mg ml^{-1}) a stimulation of the kinase activity was noted. The above results suggest that indomethacin binds to DPV (a model acidic protein substrate) and lysine-rich histones or protamine (basic protein substrates) in a manner that influences their activity as substrates. It appears that the drug renders a more favourable conformation to DPV and a less favourable conformation to histone or protamine in the respective protein kinase reactions. This is somewhat analogous to the observed *in vitro* effects of polyamines on various protein kinase reactions in the presence of acidic or basic protein substrates[8]. However, note that binding of the drug to the enzyme itself (presumably with low affinity) to produce these changes cannot be excluded. The avid binding of indomethacin to plasma proteins has been reported; over 90% of indomethacin in the blood is bound to plasma proteins and only 10% is free for therapeutic effect[1]. To test whether or not indomethacin binding to proteins in the reaction was reversible, we added 2–10 mg ml^{-1} of bovine serum albumin (BSA) to the reaction in the presence and absence of indomethacin. BSA had no effect on the activity in the absence of indomethacin, but in its presence it completely reversed the inhibitory effect of 10^{-3} M indomethacin on cAMP-PrKs, suggesting that the indomethacin inhibition was reversible (data not shown). This is also in contrast with the previous conclusion[2] on the nature of indomethacin interaction with the enzyme.

The reason for marked differences between our results and those of Kantor and Hampton[2] is not clear. However, we have used a number of different sources of the kinases which have yielded similar results. The general properties of these enzymes are analogous to those reported in the literature. It is well known that cytosol protein kinases from a variety of cells behave similarly; the only variation is demonstrated in the ratio pf peaks I and II without any significant differences in enzymatic properties between peak I enzymes isolated from different tissues[9,10]. Thus, our results indicate that the indomethacin effect is not specific for any of the cAMP-PrKs, regardless of their source, and that complete inhibition of all of the enzymes requires 10^{-3} M concentration of the drug. Similarly, a variety of other enzymes is also known to be inhibited by indomethacin at concentrations in the range of 10^{-5}–10^{-4} M (ref. 11). Such effects of indomethacin, apparent only at higher concentrations, may contribute to the toxic manifestations of indomethacin, rather than reflecting a mechanism of therapeutic action *in vivo*[11].

This work was supported in part by funds from the Veterans Administration Medical Research Fund and from research grant CA-15062 from the D.H.E.W. We thank Mr Alan T. Davis and Miss C. Allison Hughes for their help. Bovine heart cAMP-PrK was from Sigma.

Received 22 October 1979; accepted 23 July 1980

1. Ferreira, S. A. & Vane, J. R. *A. Rev. Pharmac.* **14,** 57–73 (1974).
2. Kantor, H. S. & Hampton, M. *Nature* **276,** 841–842 (1978).
3. Dinnendahl, V., Peterson, H. D. & Schönhöfer, P. S. *Biochem. Pharmac.* **22,** 2223–2228 (1973).
4. Kuo, J. F. & Greengard, P. *Adv. Cyclic Nucleotide Res.* **2,** 41–50 (1972).
5. Kumon, A., Nishiyama, K., Yamamura, H. & Nishizuka, Y. *J. biol. Chem.* **247,** 3726–3735 (1972).
6. Walsh, D. A. *et al. J. biol. Chem.* **246,** 1977–1985 (1971).
7. Job, D., Coheti, C., Dhien, A. & Chambaz, E. M. *Analyt. Biochem.* **84,** 68–77 (1978).
8. Ahmed, K., Wilson, M. J., Goueli, S. A. & Williams-Ashman, H. G. *Biochem. J.* **176,** 739–750 (1978).
9. Corbin, J. D., Keely, S. L. & Park, C. J. *J. biol. Chem.* **250,** 218–225 (1975).
10. Nimmo, H. G. & Cohen, P. *Adv. Cyclic Nucleotide Res.* **8,** 145–266 (1977).
11. Flower, R. J. & Vane, J. R. *Biochem. Pharmac.* **23,** 1439–1450 (1974).
12. Corbin, J. D. & Reimann, E. M. *Meth. Enzym.* **38,** 287–290 (1974).
13. Goueli, S. A., Slungaard, R., Wilson, M. J. & Ahmed, K. *J. pharmac. Meth.* **3,** 235–242 (1980).
14. Bensadoun, A. & Weinstein, D. *Analyt. Biochem.* **70,** 241–250 (1976).

BOOK REVIEWS

Human behaviour: do the genes have it?

David P. Barash

Darwinism and Human Affairs. By Richard D. Alexander. Pp. 317. (University of Washington Press/Pitman: 1980.) $14.95, £9.50.

In his collected *Letters,* John Keats once wrote:

> I go amongst the fields and catch a glimpse of a stoat or a field mouse peeping out of the withered grass. The creature hath a purpose and its eyes are bright with it. I go amongst the buildings of a city and I see a man hurrying along — to what? The creature hath a purpose and its eyes are bright with it.

We may derive two inferences from Keats's poetic prose: (1) living things have a purpose, and (2) purpose is shared by human beings and animals. Unlike poets, who delight in it, scientists typically are trained to run the other way when 'purpose' rears its head. Nonetheless, this seemingly unscientific djinn keeps popping up in modern evolutionary biology. And, thanks to W.D. Hamilton's updating of Darwin, we are finally groping toward an understanding of that purpose: maximization of inclusive fitness. It is becoming increasingly clear that living things go about their business in a way that projects a maximum number of their genes into succeeding generations. Better yet, that *is* their business — and hence their purpose. (Alternatively, Richard Dawkins has emphasized that perhaps it is really the genes who are running the show.)

Like Wilson's *On Human Nature,* this book by Richard Alexander argues that inclusive fitness maximization is a philosopher's stone for understanding human behaviour. It fits well into the current sociology of sociobiology. For some reason, sociobiology has emerged primarily as a US–Britain concord, while continental Europe still contributes largely to ethology rather than its neo-Darwinian cousin. In addition, the British school has maintained a deafening silence on *Homo sapiens,* whereas the Americans are increasingly turning their attentions to the human species. Both groups, however, admire inclusive fitness. Indeed, sociobiology seems to have passed the stage of Thomas Kuhn's paradigmatic revolution and entered into the more extended phase of 'puzzle solving' or 'normal science'.

Alexander's book has its quirks: in 317 pages the word sociobiology is not once volunteered (signs of alpha male–male competition within the field). His prose is often turgid, and his presentation elaborate and convoluted. For example, we are served up Alexander's critique of anthropologist Marshall Sahlins's denial of Alexander's interpretation of Sahlins's work on reciprocity in primitive societies. Sometimes, however, he rises to near-poetry:

> Happiness . . . is eating and sex and parenthood and warmth and touching and ownership and giving and receiving and loving and being loved; it is the cessation of pain and the onset of pleasure; it is finding a way to win; it is having a magnificent idea or a grandchild.

But Alexander isn't Keats, and biology is never far away: "Happiness is a means to reproduction".

Human sociobiology is more than just inclusive fitness theory, but regrettably, we find no mention of male–female differences and parental investment theory, or of parent–offspring conflict. Even sexual selection, a current rage among most sociobiologists, receives short shrift. Although he is at pains to clarify that sociobiology does not imply genetic determinism, Alexander seems naively untouched by the vigorous and specific political objections that others have raised. In the conclusion of his *Origin of Species,* Darwin rather diffidently suggested that "light will be shed" on human beings as well. With light often comes heat. Some of the recent heat deserves considering, if only to refute it: for example, because of its emphasis on the biological unity of *Homo sapiens,* human sociobiology is a potentially potent antidote to racism.

Alexander has steeped himself in anthropology and the results are rewarding: both data and theory on cross-cousin marriage as an adjunct to incest avoidance, more original material on the mother's brother phenomenon, documentation on the overwhelming importance of kin and the curious phenomenon of self-deception, which the author suggests may help explain the reluctance of many to accept the findings of sociobiology applied to themselves. In many ways, this work is a *tour de force,* repeating and elaborating Alexander's many cogent arguments and original presentations of the past few years. He suggests a provocative view of justice, in which "laws function to place limits on reproductive striving", and an ingenious if somewhat disillusioning approach to right and wrong. His usually tight reasoning is less convincing, however, in a concluding treatment of the rise of nation-states, a subject to which evolutionary biology seems to offer little beyond debatable, *post hoc* interpretations.

Homo sapiens is undoubtedly the best-known and most widely studied species on our planet. And yet, ironically, the data base from which sociobiological propositions can be tested is extraordinarily unsatisfying. Alexander relies heavily on G.P. Murdoch's cross-cultural samples and upon the Human Relations Area File. As one who desires to paint in broad strokes on a world-wide canvas, he has no alternative, although anthropologists are (or should be) painfully aware that the HRAF especially is a nightmarish potpourri, ranging unpredictably from careful, quantitative documentation to mere anecdote. It is all we have, however, and therefore its use is justified. But nonetheless, numbers gleaned from such a source derive a reified exaltation that they only rarely merit. In human sociobiology, as in any other science, conclusions are only as robust as the data and, except in recent studies (often conducted specifically to test evolutionary hypotheses), these data tend to be woefully inadequate.

Nonetheless, human sociobiology comes to upgrade social science, not to replace it. Julian Huxley once warned biologists against "nothing butism", the notion that because we are animals we are necessarily nothing but animals. The warning is well taken, but can be turned around with equal force: just because human behaviour is largely the product of social learning and cultural tradition, we should not assume that our behaviour derives from "nothing but" these experiences. We are special, but we are also animals nonetheless, and as in most dichotomies the truth doubtless lies somewhere in between.

Critics are justified in rejecting "just so stories", and to his credit Alexander is especially adroit at establishing falsifiable hypotheses. Animal studies should not be uncritically extrapolated between species, and certainly this includes human beings. However, research on animals can provide propositions about the manner in which natural selection appears to act upon

New and recent Biology titles from Edward Arnold

Ancient Woodland its history, vegetation and uses in England
Oliver Rackham
'Oliver Rackam has produced a masterpiece.' *Arboricultural Journal*
Starting from a picture of the prehistoric wildwood, derived from many sources, he shows how the species composition of woodland has changed, often as a result of management, and how the variety of woodland types still relates to the original mosaic of the wildwood.
Boards £50 416 pages

Environmental Biology
E.J.W. Barrington, F.R.S.
Resource and Environmental Sciences Series
A remarkably unified text which shows how plants and animals have responded to the problems of life in diverse environments — both marine and terrestrial — in different manners. While using a wide variety of plant and animal species to illustrate particular biological principles, Professor Barrington also considers each topic in relation to the success of the organism in coping with its environment.
Paper £5.95 256 pages

Quaternary Palaeoecology
H.J.B. Birks and Hilary H. Birks
This book describes the study of past ecosystems, using a variety of methods to reconstruct the past flora and fauna and, by careful inference, the environment. Special emphasis is placed on pollen analysis since pollens are the most abundant organic remains preserved in Quaternary sediments.
Boards £28 304 pages

Plant Taxonomy and Biosystematics
Clive A. Stace
Contemporary Biology Series
A concise and up-to-date view of the theory and practice of present-day plant taxonomy. It emphasises the dynamic, multi-variate nature of the subject which results from taxonomy being both a basic biological discipline and a synthesis of all biological knowledge.
Paper £8.95 256 pages
Publication October

Edward Arnold
41 Bedford Square,
London WC1B 3DQ

Circle No. 25 on Reader Enquiry Card.

behaviour, even complex social behaviour. Then these predictions — based ultimately on fitness maximization — can be tested cross-culturally. Thus, the world's human societies constitute a global experiment, with many varying cultures and one constant: our biology. The occurrence of universals such as nepotism and incest avoidance therefore suggests some biological underpinnings. Moreover, if these universals coincide with the predictions of fitness maximization, then social scientists ought to take notice. If biology seems arrogant in seeking to include human behaviour within its view, then what of the greater arrogance of those claiming no such help is needed, or wanted?

As the work of Alexander and others is increasingly showing, much of what human beings actually do accords remarkably well with the prediction of what we expect them to do if they are maximizing their inclusive fitness. But what in turn does this mean? It seems unlikely that we possess genes 'for' discrete cultural phenomena, but equally unlikely that culture and biology are totally uncoupled. Accordingly, new and productive directions may well emerge from current work such as that described in the forthcoming book, *Gene–Culture Evolution* (Harvard University Press), by C. Lumsden and E. O. Wilson.

The real question is not: Does evolution say anything about our behaviour?, rather: How much does it say? Since evolutionary theory is 'right', then human sociobiology cannot possibly be wrong — but it can be misleading. Maybe non-adaptive evolution has had a larger say than most sociobiologists typically assume — maybe fitness is only rarely maximized and optimality theory is just a convenient mythology. Whereas Darwin's message seems indisputable, Hamilton's is less so, although it certainly seems correct. And much of sociobiology (and nearly all of Alexander's work) relies on Hamilton's inclusive fitness theory. Finally, maybe human behaviour is just too dependent on complex non-genetic processes of social learning and cultural experience to be much elucidated by selfish DNA molecules jousting with each other to get ahead. But we owe it to ourselves to find out.

Physicist Jean Perrin once wrote that the goal of science was "to explain the complicated visible by some simple invisible", and Einstein suggested similarly that "the ground aim of all science is to cover the greatest number of empirical facts by logical deductions from the smallest possible number of hypotheses". Our own behaviour is a complicated visible, providing an overwhelming array of empirical facts. Sociobiology employs a simple and powerful invisible (evolution by natural selection), based on a seductively unitary hypothesis (differential reproduction of individuals and their genes). When the wife of the bishop of Worcester first heard of Darwin's scandalous new theory, she is reported to have cried "Descended from monkeys? My dear, let us hope that it isn't true! But if it is true, let us hope that it doesn't become widely known!" By contrast, let us hope that the implications of evolution do become widely studied, for *Homo sapiens* no less than any other species. □

David P. Barash is Professor of Psychology and Zoology at the University of Washington, Seattle.

Inspiration for particle physicists

Maurice Jacob

Models of High Energy Processes. By J. C. Polkinghorne. Pp. 131. (Cambridge University Press: 1980.) $24.95, £11.

HIGH energy physics is a fast-moving field, and the paucity of specialized textbooks bears witness to the fact that any detailed exposition of a particular topic runs the risk of becoming rapidly obsolete or of covering a field which drops from the forefront of research. This slim volume cleverly avoids such a predicament. Its discussion of specific techniques will make it a useful tool for many years to come. Indeed, the detailed consideration of how Feynman diagram techniques can be used to obtain asymptotic properties and specific behaviours of model amplitudes covers topics which were of great interest to particle physicists in the 1960s (Regge behaviour) and 1970s (parton model and perturbative quantum chromodynamics) and which are likely to relate to important new developments. The book should be a source of inspiration to the graduate student in theoretical physics and also rewarding to the more knowledgeable reader, for whom it provides access to the wide range of applications of Feynman graph techniques. A combination of heuristic arguments and detailed mathematical treatment makes it easy reading, for reference or as a textbook.

It should be mentioned, however, that, despite its title, this book does not provide a full survey of models of high energy processes. The selective list of topics covered clearly reflects the research interests of the author and his preferred lines of approach. At the same time, many topics are not introduced or discussed as thoroughly as many readers, and in particular students, might wish to see. Mere reference to specialized books will often be inadequate for subjects which are no longer well known to the newcomer, such as Regge behaviour. A more detailed discussion of some topical questions (in particular those involving perturbative QCD) would have been useful to bring the reader fully abreast of present applications. One should, however, mention a detailed presentation of the parton model in a field theoretic language which has recently provoked much interest.

Despite its being too short to meet all requirements, this little book should certainly provide the reader with ideas and with a better understanding of present approaches to high energy interactions. ☐

Maurice Jacob is a senior scientist in the Theoretical Study Division of CERN and a corresponding member of the French Académie des Sciences.

Hypoxia as a way of life

R. D. Harkness

Living without Oxygen: Closed and Open Systems in Hypoxia Tolerance. By Peter W. Hochachka. Pp. 181. (Harvard University Press: 1980.) $17.50, £10.50.

THE thing that strikes you immediately about this book is that the author is an enthusiast. And not simply an enthusiast, but one whose enthusiasm has led him to bring together a great diversity of material to make a coherent story. There is a point in everything he has written, and that, is an unusual achievement for a work that is primarily about biochemistry, a subject prone to accumulation of disconnected facts.

The book is concerned with the ways in which animals obtain energy when they have limited or no access to oxygen. For some this is part of their way of life (intestinal parasitic worms, deep-sea fishes); for others it is a temporary state (fishes wintering in stagnant water, lungfishes sealed in dried mud, bevalve molluscs with their shells shut, seals and other marine mammals when diving). The same sources can provide, for rapid movement, a short-lived burst of energy at a higher rate than could be achieved with the use of oxygen alone (vertebrate and cephaloped muscle). This latter mechanism by degradation of carbohydrate (glycogen) to lactic acid, will be familar to many who would, like myself, be ignorant of other things dealt with in this book. However, the production of lactic acid has snags — its acidity which can adversely affect other tissues. The effect is reduced in diving mammals by use of the acid in organs privileged to have what little oxygen is available, principally the brain and heart (and also, curiously, the adrenals). The problem can also be solved by the production of less awkward end-products, such as by creatures with particular adaptation. One, curiously, is alcohol, produced by goldfish under conditions where little oxygen is available. The fish make ethanol by using in reverse the same set of enzymes as we do to destroy it. how much they enjoy their grog we don't know, but it is nice to think of them quietly solacing themselves as they lie in winter in the mud at the bottom of a cold pond waiting for the spring; and maybe solace others too as they get rid of the alcohol into the surrounding water.

There is much more like this on the curious adaptations which have evolved to enable animals to operate in unusual environments made interesting by the fact that the author is not only a biochemist but also a zoologist. This is what really makes this book so fascinating — he puts the biochemistry into the whole picture of the physiology and life-style of the animals.

So this is a good book which should certainly be in any library that caters for degree students. Is there, then, nothing wrong or the lack of something that would make it better? The approach is primarily biochemical, and the reader needs to be familiar with both the general concepts and the facts of biochemistry. For example, no chemical formulae of compounds are given, only names; enzymes are shortened to abbreviations, explained it is true at the first mention, but not easy to find if you want to check; there is no glossary. Yet the book will interest many who are unfamiliar with biochemical terms, and a short general summary of the biochemical background would be of great value to the non-specialist. To argue that the information is available elsewhere is to miss the point that it is not available when and where it is wanted. Written by Professor Hochachka, at the start of the book, it would not only be in the right place but also probably clearer and more pertinent than anything one could easily find elsewhere.

In one of my excursions into history I came across William Robertson, a most readable 18th century man, who habitually started you off a few hundred, if not thousands, of years earlier. So it would be nice if this book could start in the same sort of way to make it more easily understandable, possibly not to historians, but to a range of people who would find it very interesting but at the moment rather a struggle. So, in summary, an alpha now, and every prospect for an alpha plus for the next edition. ☐

R. D. Harkness is Professor of Physiology at University College London, whose main interest has been in connective tissue with a bias towards comparative physiology.

CALL FOR PAPERS
INTRODUCING THE FIRST RAPID PUBLICATION JOURNAL FOR THE INTERNATIONAL EYE RESEARCH COMMUNITY

CURRENT
EYE
RESEARCH

Monthly
Commencing January 1981

Executive Editors
C. A. Paterson and
N. A. Delamere
University of Colorado,
Health Sciences Center,
4200 E. Ninth Ave. Denver,
Colorado 80262 USA

Editorial Board
The following have provisionally accepted the invitation to join the editorial board

S. K. Brahma
Netherlands
G. H. Bresnick
USA
R. P. Burns
USA
G. D. Cagle
USA
O. A. Candia
USA
H. Cheng
England
R. L. Church
USA
C. Cintron
USA
S. Dikstein
Israel
H. F. Edelhauser
USA
K. E. Eakins
England
P. N. Farnsworth
USA
R. F. Fisher
England.
K. Green
USA
S. Iwata
Japan
P. L. Kaufman
USA
Y. Kikkawa
Japan
S. D. Klyce
USA
H. Maisel
USA
J. McAvoy
Australia
G. Maraini
Italy
S. A. Miller
USA
J. Obenberger
Czechoslovakia
E. S. Perkins
USA
R. R. Pfister
USA
J. L. Rae
USA
M. Reim
West Germany
M. V. Riley
USA
T. O. Wood
USA
T. J. Zimmerman
USA

The principal aim of **Current Eye Research** is to provide rapid publication of full papers, short communications and minireviews, each of high quality.

To ensure rapid publication, accepted articles will be printed directly from camera-ready typescripts prepared by the authors.

Current Eye Research will consider articles encompassing all the areas of eye research. The subject areas include: clinical research, anatomy, physiology, biophysics, biochemistry, pharmacology, developmental biology, microbiology and immunology.

Specially ruled typing sheets and detailed instructions to Authors' can be obtained from either the editors or the publishers.

IRL Press Ltd

Suite 815, Fisk Building,
250 West 57th Street,
New York, NY 10019, USA.

P.O. Box 1,
Eynsham, Oxford OX8 1JJ. UK

Free sample issue available on request.

Circle No. 34 on Reader Enquiry Card.

SCIENTIFIC BOOKSHOP

H. K. LEWIS can supply works in all branches of Pure and Applied Science. Catalogues on request. Please state interests.

SCIENTIFIC LENDING LIBRARY

Annual Subscription from £7.50.
(Available in U.K. only)

Reduced rates for multiple subscriptions.

Prospectus post free on request.

Quarterly List of New Books and new editions added to the Library sent post free to subscribers regularly.

H. K. LEWIS & Co. Ltd.

136 GOWER STREET,
LONDON, WC1E 6BS

Telephone: 01-387 4282
Telegrams: "Publicavit, London, WC1E 6BS."

Circle No. 15 on Reader Enquiry Card.

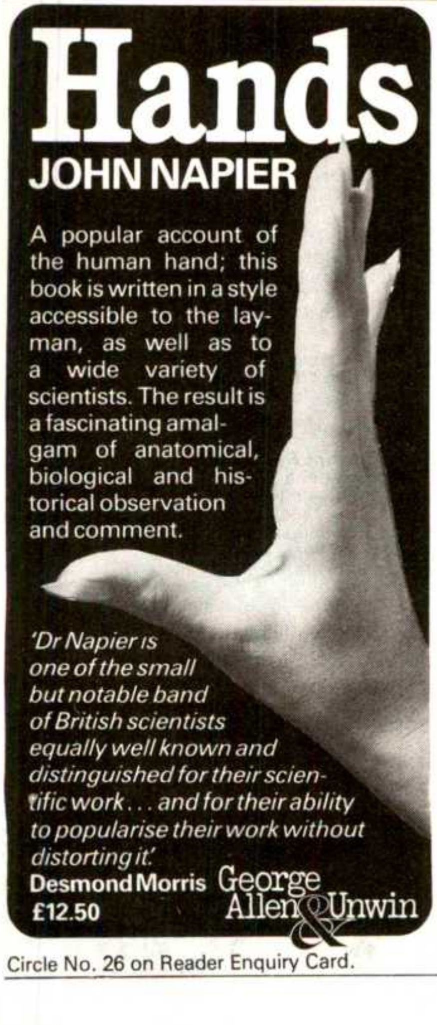
Hands

JOHN NAPIER

A popular account of the human hand; this book is written in a style accessible to the layman, as well as to a wide variety of scientists. The result is a fascinating amalgam of anatomical, biological and historical observation and comment.

'Dr Napier is one of the small but notable band of British scientists equally well known and distinguished for their scientific work... and for their ability to popularise their work without distorting it.'
Desmond Morris

£12.50

George Allen & Unwin

Circle No. 26 on Reader Enquiry Card.

Clouds in the interstellar medium

B. E. Turner

Giant Molecular Clouds in the Galaxy. Edited by P. M. Solomon and M. G. Edmunds. Pp. 300. (Pergamon: 1980.) £18, $41.

THE distribution and physical properties of the neutral interstellar gas in our galaxy have been major subjects of investigation since the discovery of interstellar atomic hydrogen in 1951. With the discovery 12 years ago of interstellar molecules as a new investigative tool, these studies have been extended to the molecular component with the undertaking of two major surveys of galactic carbon monoxide (CO) in 1975. The present volume is a collection of papers on this and related subjects as they stood in mid-1977 at the Third Gregynog Astrophysics Workshop, held at the University of Wales.

As with much of astrophysics, our perceptions of the interstellar medium vary on a timescale rather short compared with that of the publication of this volume. Even the title suffers as a result. It refers to one of two main topics covered, namely the properties of the molecular cloud ensemble that is generally agreed to comprise by mass at least 75% of the total gas of the galaxy interior to the Sun. The principal question is whether the cloud ensemble is dominated by relatively few 'giant molecular clouds' (GMCs) or by a larger number of smaller clouds. Curiously, the title belies the fact that only one of the two survey groups (Solomon and his collaborators) subscribe to the notion of GMCs, while the other group (Burton and Gordon) find that smaller clouds dominate. Loosely, GMCs may be defined as having masses in excess of 10^5 $M_\odot$ (diameters > 40 pc) as distinct from the many smaller clouds (10^2–10^4 $M_\odot$) seen optically near the Sun. Whether or not GMCs dominate (the question is one of interpretation, not of differences in survey data by the two groups) is important to our understanding of galactic structure, because relatively few GMCs affect the distribution of stars and their motions much more than does the same quantity of gas residing in more numerous, smaller clouds. In the past year, extensive modelling of galactic cloud distributions by Liszt and Burton has shown that the observations are consistent with an ensemble of numerous, smaller clouds with at most only about 4% of the clouds by number being GMCs. Although the title of the book may therefore describe only the minority component, it must be emphasized that GMCs are known observationally, the dozen or so examples being discussed in the first two papers.

Star formation, and its association with molecular clouds, is the other principal topic of this book. Where stars may be directly observed, it has been clear for some time that massive OB stars form in or at the edges of the larger molecular clouds (mass of 10^4 $M_\odot$ or larger) while only low-mass stars (including T Tauris) form in small clouds. Observational examples of each of these cases are given in two papers. Other articles discuss various mechanisms for the onset of massive star formation, such as density wave implosions, sequential formation by O star radiation, supernova inducement, cloud-cloud collisions and so on. Doubts about the applicability of any of these mechanisms to at least one object (CRL961) are discussed by L. Blitz, who contributes much of the observational material in this book not available in the open literature. The probable association of OH and H_2O masers with massive protostellar objects is set forth in three observational papers, and the relation of HII regions and molecular clouds is the topic of two papers. On the theoretical side, magnetic fields (the *bête noire* of any model of star formation) are discussed with originality if inconclusion in two papers.

In addition to the above two topics, this volume includes several articles on peripherally related subjects: some outdated work on the galactic centre (two papers); two works on highly specific aspects of interstellar chemistry (on nitrogen chemistry and interstellar biochemicals — the latter is notably speculative and has appeared in journals several times); and finally, even an entertaining paper on the search for planetary systems.

As might be judged from such a plethora of topics, the book is not intended, nor does it succeed, as a synthesis of any aspect of interstellar clouds. Unfortunately, there are no discussion sessions which might have tied the various viewpoints together; thus the forum of a workshop is not reflected in the book. The introduction by the editors serves as a (rather one-sided) overview, but not more.

The belated publication of this volume has limited the usefulness of much of it; no fewer than 21 of the 31 papers, and parts of some others, have appeared in journals. Nevertheless, some valuable material has not been published elsewhere. Examples are the beautiful colour maps of the Solomon *et al.* CO survey, the large-scale CO maps of the Cygnus X, Taurus and Perseus regions in the paper by Blitz, and several of the theoretical discussions.

The book is handsomely produced on high-quality paper, with fine illustrations and a well-thought-out index. Overall, it is certainly to be recommended as a reference book for institutional libraries, and at the price it may well find a place in the personal collections of serious students of the interstellar medium. It is less suitable for a more general audience. ☐

B. E. Turner is at the National Radio Astronomy Observatory, Charlottesville, Virginia.

nature

18 September 1980

Black sheep slink home from Geneva

On the principle that one man's victory is another's defeat, last week's proceedings at Geneva of the second review conference of the Non-Proliferation Treaty (NPT) were not a simple failure. The nuclear powers, it is true, are understandably crestfallen at having failed to persuade their fellow signatories that they have done their best to keep their side of the bargain, especially in strategic disarmament and assistance with civil nuclear technology. But many among the non-nuclear power signatories are correspondingly cock-a-hoop at having stuck to their subversive guns during the Geneva meeting, insisting that the record of the nuclear powers in the past five years does not justify a clean end-of-term report. The non-nuclear powers insisted at Geneva that, if the nuclear powers really wanted a consensus declaration, they would have to agree on the spot to behave as if the Salt II treaty had been ratified, and embark on multilateral negotiations on tactical nuclear weapons and other steps judged unacceptable (see *Nature* 11 September). The failure to reach agreement is also, however, a failure in a broader sense. The signatories of the Non-Proliferation Treaty are loosely held together by a variety of pressures. Some have a genuine conviction that the NPT is a valuable instrument of arms control. Others have been persuaded to sign through coercion by nuclear powers. Others hope that they will have an inside track in nuclear assistance. The most immediate danger now is that this conglomerate of signatories will begin to fall apart. Only a few defections from the treaty (which includes a provision for giving three months' notice) could do a great deal of damage. How likely is such a course of events? What would be the consequences? And what now should the nuclear powers do to make up for the disappointment of Geneva?

Whatever the fall-out, rapid defection is unlikely. Indeed, even the most disaffected signatories will probably stay in the club, at least for the time being. The opportunity to tweak the lions' tails that Geneva provided may after all recur. Political pressures will also persist, as will the tangible threat that withdrawal from the treaty, and from the system of safeguards operated by the IAEA at Vienna, would deprive many states of much-needed nuclear supplies. And a great many signatories will know that they may jeopardize the whole non-proliferation system if they now rock the boat by walking out in a huff. Defections will come, if at all, only much later and for different reasons. No government now a signatory of the NPT is going to embark on the manufacture of nuclear weapons lightly, and without a careful assessment of the political as well as strategic risks of such a step. For most countries interested in such calculations, the political risks of resigning from the NPT are likely to be much smaller than the other risks. Accordingly the failure of the review conference to agree on a final statement cannot be decisive in any present signatory's calculations of the future. The consequences are most likely to be that governments which have so far held out against signing the NPT will now be even more reluctant. In short, the setback at Geneva last week does not, of itself, imply the end of the NPT system as it is.

What the ructions at Geneva do imply, however, is that the non-nuclear powers are much more fierce in their discontent with the past five years' progress in arms control than the nuclear powers had expected. To be sure, the nuclear powers (especially the superpowers) went to Geneva expecting trouble. They expected to be hauled over the coals, told that their performance (and especially their failure to ratify Salt II) was inexcusable and warned that they would have to do much better in the future. In the event, they were not let off the hook as easily as they had expected. Indeed, they were not let off the hook at all. The demand that the signatories of Salt II should behave as if they had ratified it was plainly unacceptable to the Soviet Union. (Although the United States government has often said it would behave as if Salt II had been ratified, President Carter's representatives at Geneva would have been acutely aware that a President Reagan might think differently.) Both superpowers would have shrunk from the demand that Salt III (which is supposed to be concerned with tactical weapons) should be thrown into the Committee on Disarmament, and perhaps with reason.

In a quite dramatic way, however, the NPT review conference has been a psychological shock to the nuclear powers and indirectly to the non-nuclear members of NATO and the Warsaw Pact. Hitherto, it has been possible for the nuclear powers to excuse the slow pace of their arms control negotiations on a variety of grounds — trouble in Afghanistan, uncertainty in the Middle East, presidential elections here or there. What the non-nuclear powers told them at Geneva is that they must make progress whatever the circumstances. This will be a hard prescription to follow. They are, for example, being required seriously to contemplate the completion of the Comprehensive Test-Ban Treaty negotiations and then of giving up all nuclear tests for good (see *Nature* 14 August). The prescription is all the more authoritative because the dissidents at Geneva were not just disaffected developing countries — Sweden and (less openly) countries such as the Netherlands had unkind things to say about the nuclear powers.

How, then, will the black sheep respond? It is tempting to think that Mr Edmund Muskie's statement last week that the US government is now prepared to talk to the Soviet Union about nuclear missiles in Europe is one reaction to what happened at Geneva. Certainly that is a step forward, and one that will bring some good cheer in West Germany as well as elsewhere in Western Europe. But the connection is unfortunately too indirect. There is very little evidence that the Secretary of State has yet had time to consult other interested European states about the form negotiations of this kind should take — yet the European members of NATO are anxious that the next Salt treaty should not be an exclusively Soviet–American deal. Mr Muskie also studiously avoided mentioning the Committee on Disarmament in this context. And he (like everybody else) knows that he will not be able to deliver on his promise if his president is not re-elected. Similarly, the ratification of Salt II must be held up at least until the new Senate assembles in the new year, and may then be just as unlikely as it has been for the past year.

If the nuclear powers seek, as they should, some way of disarming the criticisms they encountered at Geneva on arms control, they have very little choice but to push ahead with the Comprehensive Test-Ban Treaty. The report on these negotiations put out at the end of July was a surprisingly cheerful document, suggesting that much of the technical work has now been done. A little more talking might be enough to do the trick. Indeed, for the past few weeks some of those concerned with the negotiations have been saying that the only missing ingredient in the Comprehensive Test-Ban Treaty is the will of the superpowers to sign on the dotted line. Although plainly an exaggeration (for the Soviet demand that there should be as many remote seismic monitoring sites in the United Kingdom as in the United States remains unresolved), this must be a good approximation to the truth. The question now is whether the drubbing at Geneva will persuade the superpowers to complete the treaty.

The chances are slim. The political inhibitions of the past few months persist. In the circumstances, the nuclear powers should think of taking more seriously the persistent demand of the non-aligned signatories at Geneva — that more of the process of arms control should be entrusted to the Committee on Disarmament in Geneva. It is entirely understandable that the committee has earned itself a bad reputation. For the first decade or so it was a talking shop for the rehearsal of idealistic but also unrealistic schemes for disarmament. Pilloried at regular intervals, the superpowers took care to avoid trouble (and to nullify the committee's work) by the device of their control of the chairmanship of the committee. Since the reorganization (and enlargement) of the committee five years ago, however, its proceedings have been more temperate and more valuable. Moreover, the committee has the virtue of being the only forum of its kind in which both France and China are represented. Because at some stage neither the existing Partial Test-Ban Treaty nor the putative Comprehensive Test-Ban Treaty can survive indefinitely if France and China stay outside, the nuclear powers have everything to gain if questions of French and Chinese adherence to these schemes are seriously taken up. What is needed is a definition of the circumstances in which France and China would sign. The old device of cutting off other people's military production of nuclear explosives is unlikely now to be sufficient. The Geneva black sheep might at least find they were not the only animals of that colour if they used the Committee on Disarmament as a means of exploring such questions.

The nuclear powers have not merely to meet criticisms that they have dragged their feet on strategic arms control (Article VI of the NPT) but also that they have fallen short of their obligations to help with the spread of civil nuclear technology. Here, by good luck, they have an early opportunity to disarm their critics. At the end of this month, the IAEA Committee on Assurance of Supply will meet for the first time in Vienna, chiefly to discover which members of the IAEA have chosen to belong (it is a free-for-all) and to decide when to meet next. Potentially, however, the committee is a means by which the nuclear suppliers (not all of them nuclear powers) could help meet the just criticisms that have arisen of their supply practices. As things are, many governments fear that, after building a nuclear reactor, they may be unable to buy fuel for it on the world market. Only last week, the US Congress finally overrode President Carter's wish to send a consignment of enriched uranium to India; the uranium is contracted for on both sides, but prohibited by the Anti-Proliferation Act of 1968. South Africa is in similar difficulties. Nobody would quarrel with the objectives of this act, which are to require that states supplied with nuclear materials from the United States should agree that all their nuclear installations are covered by IAEA safeguards. The trouble is that the act has demonstrated to all and sundry that arbitrary legislation can always interrupt supply. The result has been to damage confidence. The Anti-Proliferation Act should be repealed, but the IAEA meeting later this month should be used as a means of rebuilding confidence, if necessary by enabling the IAEA itself to become a supplier of nuclear fuel (as its existing statutes allow).

Dismal science in doghouse once more

Economists have often been derided for failing to agree among themselves on the future performance of this or that economy. Now they are in deeper trouble, and are being blamed for having misled the British government. Mrs Thatcher finds herself in serious political difficulties because it now seems that nobody has any clear idea of how much money there is at present in the British economy, or how quickly this money stock is increasing. The issue is important because the government has built its economic policy on an attempt to control both the rate at which the money stock increases and the rate at which the government itself borrows from the public. What has gone wrong?

Part of the difficulty is that the notion of what constitutes the money stock is, to say the least, abstract. It includes not merely the nominal value of the currency in circulation but also the value of borrowing from the commercial banks. This extension of the simplest concept of money makes sense for, in a modern state, bank money far outweighs currency in numerical terms. It is beyond dispute that the money supply is a valuable indicator of economic trends. Broadly speaking, the less money, the less there is to spend on consumption, investment or both. Moreover, governments (or their central banks) can hope to influence money supply by adjusting the interest rate at which they lend to commercial bankers. Monetarists and their critics differ only in their assessments of the importance of this instrument of monetary policy.

The Thatcher government, consistently (to its credit) but some say wrongly, has tried since its election in May last year to follow monetarist policies. In this spirit, it has kept interest rates high, and has tried to cut its own spending. It has been more successful at the first task than at the second — or so it seemed until the money stock was seen to have jumped by five per cent in July and a further three per cent in August.

The reasons for the sudden jump in the British money supply are linked simply with the abolition (in June) of a system whereby the Bank of England sought, two years ago, to limit the growth of money (currency and bank credit combined) by restricting the rate at which individual banks could increase lending. People seeking credit were forced at some cost to go to commercial companies which are not banks and also to banks abroad. Now that the restrictions have been abolished, this informal lending has returned to the banking system, and the money supply has dramatically increased, causing widespread confusion and alarm. It remains to be seen whether the British government will be diverted from its present course by all the fuss, although the British Treasury last week was claiming that nothing had gone wrong, and that the "underlying" growth of the money supply was not excessive.

The Treasury may be right, but should know better than to peddle such facile nostrums. The money supply, although easily defined, is not easily measured. Bank money can be measured simply, but this is not the whole story. If, for example, a manufacturer persuades a supplier to give him an extra month to pay his bills, the money stock has been increased by that amount just as surely as if the manufacturer had borrowed from the bank. So the Bank of England's estimate is that attempts to control the money supply (as measured) will provoke a kind of monetary equivalent of Le Chatelier's principle — there will be compensating (but smaller) adjustments in the opposite direction.

Economists at the Treasury (and their academic colleagues) can be blamed for not having made this much crystal clear to the government, to politicians and to the public. Collectively they must also wear a hairshirt for having failed to emphasize that the control of the money supply is not an end in itself, but rather an index of how monetary policy as a whole is working. The British government's chief objective is to reduce the rate of inflation, to which end high interest rates (and reduced public expenditure) must surely contribute. A fall in money supply would indicate that inflationary pressures are abating. The converse is not however valid, as the past few months have shown. So there is every reason for the British government (if it has the nerve) to stick to its present policies, but with a more intelligent view of what the economic indicators mean. The most urgent need is, however, for a more intelligent (and effective) means of controlling public expenditure. Much of the British government's "saving" so far consists of the requirement that nationalized industries such as the telecommunications network should raise the capital they need for expansion from current users. The consequences are absurd — and inflationary to boot.

0028-0836/80/380178-02$01.00

understand the hazard". The document also criticizes as unwarranted Professor McCarthy's inferences about the production of aerosol particles carrying virus from safety cabinets used in the smallpox laboratory.

Those questioned earlier this week about the ASTMS allegations were unwilling to comment without an opportunity to study the text. Those witnesses at the court hearing who were reached by telephone said, however, that they stood by their evidence.

The coroner at the inquest on Mrs Parker's death had let it be known in advance that he did not wish to go over ground already covered at the court hearing. Mr Clive Jenkins, General Secretary of ASTMS, has nevertheless written to him with a copy of the document. He has also written to Dr Gerald Vaughan, Minister of Health, demanding that the Dangerous Pathogens Advisory Group be reconstituted by including public interest and trades union representatives, and that the government should make clear that it is prepared to spend the monies necessary to make laboratories in universities and hospital pathology departments safe.

Law of the Sea

Hurdles to jump

Washington

Final agreement on international legislation covering deep-sea mining could prove more elusive than suggested by the successful completion of negotiations on a draft United Nations Law of the Sea Treaty in Geneva last month. Even if — as indeed seems likely — a draft treaty is finally agreed and signed by member nations after a final meeting in Caracas early next year, there remains the question of ratification, required of at least sixty states. And this could prove a major stumbling block, particularly in the US Senate.

Member companies and trade associations of the American Mining Congress (AMC) are meeting in San Francisco next weekend to decide their position on the draft treaty which emerged from the Geneva negotiations, the culmination of more than twenty years of talks.

Prior to the Geneva meeting, the congress had expressed strong reservations about some aspects of the US negotiating position, claiming that the chief US negotiator, Ambassador Elliott Richardson, was giving away too much in his eagerness to get the treaty signed.

Many of the companies still express the same reservations. And the AMC's views could be crucial in determining whether the US Congress decides to back the treaty. Earlier this year, following strong pressure from the mining companies, Congress passed a unilateral law defining conditions under which US companies could engage experimentally in deep-sea mining from 1981 unless the UN treaty is in force. Similar actions by Germany, and proposed actions by the United Kingdom and France, are among the factors said to have precipitated the Geneva agreement.

The stakes are high. Total investments of more than $1,000 million are expected to be made by each of the four major consortia now preparing to engage in deep-sea mining, primarily for manganese nodules containing nickel, cobalt and copper. The companies are demanding, above all, a degree of certainty about a reasonable return on their investment.

Among the areas that the mining companies are unhappy about are:

- The lack of guaranteed representation of the United States on the 37-member council of the International Seabed Authority, even though the Soviet Union is given three seats, a position which one executive predicted that the Senate would find difficult to accept.
- The participation as signatories of the treaty of organizations other than UN member states, such as the Palestine Liberation Organization. This could entitle such organizations to share in the profits of deep-sea mining which the US companies are required to provide to the authority for distribution as development aid.
- The requirement that mining companies should make their mining technology available to other countries who demand it.

The major question now facing both US and UN negotiators is whether any movement is possible on these issues before the treaty is signed next year and, if not, whether they are likely to provide a sufficient obstacle to prevent Senate ratification, given the many other advantages to the United States in an international treaty that covers all aspects of nations' rights to the oceans.

None of these reservations is, in itself, expected to be a major stumbling block to the final treaty. Nor, among those who are strong supporters of the treaty, is there any desire to open up discussion again in case the whole package begins to unravel. But claims that "it is all over bar the shouting" may turn out to be a little premature.

David Dickson

Overseas students

Some win, some lose

British universities and colleges appeai to differ markedly in their expectations of numbers of overseas students in the coming academic year. Some universities — a litte to their surprise — expect there will be very little change between last year and this in the numbers of students from overseas. Others expect that numbers will be, by contrast, substantially reduced.

The issue has become a lively topic of conversation among academic registrars because the coming academic year is the first in which the steep increases of student fees decreed by the British government a year ago will begin to bite. The fees apply only to new students, or to students embarking on new courses. Registrars are also quick to point out that at this stage in the academic year, before students have actually registered and paid their fees, estimates of how many will turn up are bound to be provisional.

The universities where there appears to have been very little change in the demand for places include the University of Salford and Loughborough University of Technology. At both institutions (as at most universities) overseas students are now required to produce not merely their fees but a financial guarantee from a bank or some scholarship awarding body, which may require that a student should have £6,500 at his disposal in each of three consecutive academic years.

Elsewhere, the preliminary figures suggest that some kinds of courses are likely to suffer more than others. Applications for places on MSc courses appear to be comparable with last year's at some institutions, which are nevertheless guessing that overseas students will be reduced by ten per cent or more in undergraduate and PhD courses.

One of the difficulties of estimation is that students who have nominally accepted places fail to turn up by the beginning of term, for most British universities early in October. In normal years, it is expected that overseas students will apply to several universities but in the end accept a place at only one of them, which means that a certain amount of double counting is unavoidable at this stage in the academic year. But some also fail to turn up for reasons which are never explained. Some registrars fear that difficulties over finance may increase the numbers in this category in the coming year.

With all these reservations, Imperial College, London says that there has been a "discernible" reduction of the numbers of completed applications from overseas. Portsmouth Polytechnic, one of the largest institutions of higher education in the United Kingdom, is similarly affected — and wonders ruefully whether the explanation may not be the rules which require polytechnics to charge fees laid down by the Department of Education and Science. This year, polytechnic fees for overseas students are nominally some £300 to £400 greater than those in universities.

While registrars at all kinds of institutions agree that the present period is more confusing than any other within living memory, most of them appear to be mildly encouraged that the decline in numbers has not been as dramatic as some of them were fearing earlier this year. Unless there is a sharp deterioration in the next few weeks, overseas student numbers are unlikely to be reduced by anything like the 50 per cent feared by some or by the 30 per cent which appears to have been the base-line for financial planning for the coming year.

CORRESPONDENCE

Pay as you go

Sir—Although far more interesting and important things are now happening in Poland, let me bring to your attention one more Polish subject connected with the Polish regime's abuses of decency or simply the law. Every Polish scientist going abroad for professional purposes, and for a long period, is forced to sign a declaration. ("Long period" means more than eleven weeks. Why just eleven? — Nobody knows.)

The declaration is an obligation to pay some arbitrarily fixed sum of money every month to the so-called "hard currency scholarship fund", created apparently to finance foreign trips for some unspecified persons. The point is that although many Polish scientists were forced to, and did, pay their money *to* the fund, no-one has ever heard of anyone actually getting something *from* this fund. There are rumours that the money is being used to finance "study" trips for Polish journalsts, for example to the United States, where they use the American money to collect materials for painting the American system in black colours. Indeed, the fund in question is under no form of public control, and no-one really knows to what purpose the money is used. The character of the deal comes out most clearly from this paragraph in the declaration:

> "If the currency regulations of the country where I shall be staying would make it impossible to send my contribution to the hard-currency scholarship fund via a bank, I undertake to send the remittance to the nearest agency of the Polish People's Republic abroad."

As you are aware of the political situation in Poland I hope that you will understand my request to keep my name, and address a secret.

Name and address *withheld* — Ed, *Nature*

Nuclear power costs

Sir— The Central Electricity Generating Board (CEGB) is to be congratulated on providing more details of its cost comparisons for the different power station types. As it emphasizes in its report, current relative economic performance of coal and nuclear systems is not an adequate guide to future investment decisions. However, one could argue that operating experience is a guide to future technical (rather than economic) performance. Load factors are one measure of technical performance, and your report made some pertinent observations regarding the reported load factors of power stations operated and planned by the CEGB (*Nature* 21 August, p.753). Obviously the cost per kWh per annum is sensitive to the load factor and it is informative to recalculate the predicted generating costs of possible future nuclear and coal power stations using load factors consistent with those quoted for existing stations. The table summarizes factors on design output given in the CEGB report load.

	Nuclear	*Coal*
Stations (1965–77)	56%	61%
Hinkley B; Drax I	43%	73%
Stations under construction	49%	56%
Future stations	63%	54%

The figures show an unexplained optimism for nuclear systems and a corresponding pessimism for coal systems. Assuming load factors consistent with experience (say 70% for coal and 50% for nuclear) reverses and predicted cost ranking for the fuels in question. Specifically, nuclear comes out some 8% more expensive than coal (2.8 p per kWh compared with 2.6 p per kWh) rather than 35% cheaper as derived by the CEGB.

Richard Marshall

Department of Physics,
University of Keele, UK

Why examine?

Sir—It was interesting to read the article on school examinations (*Nature* 3 July p.2). As one who, although born and educated in the United Kingdom, has spent most of my working life teaching overseas, my usual plaint is that the schools we have to deal with do not teach A levels and that it is so much better in the UK where they do. The main reason why the schools I know do not teach A levels is not choice, but simply lack of qualified teachers.

As in everything else, there are pros and cons and things look different from the other side of the fence. One thing I am convinced of, however, is that good schools are much better at teaching A-level material than are universities. In general, university staff do not make good school teachers.

D.A.H. Taylor

Department of Chemistry,
University of Natal,
Durban, South Africa

Third World matters

Sir—"Pesticides in developing countries" (*Nature* 28 August p.832) was a patronizing editorial on the *New Internationalist*; a journal that is not a "citadel for extreme environmentalists" but a medium for exposing injustice, stimulating debate and campaigning for and on behalf of the poor of the Third World.

Transnational corporations are mostly the villains because it is often their trading practices that accentuate North–South differences. Global profit maximization policies tend not to be compatible with the needs of the people of the Third World. For example, infant mortality rates have increased significantly in areas where advertising has persuaded mothers to abandon breast feeding for Nestle milk powder products. Other cases are more insidious: uncontrolled marketing of harmful products, including cigarettes and pesticides. High blood levels of DDT (30 x that in USA) being the corollary of one aggressive marketing campaign in Guatemala.

New Internationalist is not a scientific journal. It does try to report facts accurately and from an objective stance. This is expected of *Nature*. It was unfortunate that a basic, scientific definition had to be distorted in order to accommodate editorial views: DDT *is* a poison, a poison being a substance that when introduced into or absorbed by a living organism (or ecosystem) destroys life or injures health.

May I reiterate Clive Jenkins' final point (*Nature* 21 August p.754) that *Nature* should abandon prejudice and support quite reasonable crusades to protect people.

Peter Clarke

Department of Genetics,
University of Edinburgh,
Edinburgh, UK

Felig replies

Sir,— Your account of the events surrounding my resignation from Columbia University (*Nature*, 21 August) contains a number of inaccuracies and omissions which may lead the reader to a distorted view of this unfortunate affair.

Firstly, my proposal that Dr Soman be considered for a faculty appointment at Columbia occurred in January rather than February 1980, *before* the first audit which revealed data falsification by Dr Soman. Secondly, the letter by Soman in February 1980, declaring his responsibility for the similarities to the paper from the Roth laboratory and for "fudging" data, was not written at my request but was his own effort to "set the record straight" at the time of his resignation. Dr Soman had, in fact, admitted in March 1979 that he had retained a copy of the Wachslicht–Rodbard manuscript and had used parts of it to prepare his own manuscript. At that time he was severely reprimanded and steps were taken to assure Roth's priority.

Thirdly, the delay in obtaining the first audit was a result of the failure of the agreed upon auditor (Dr Edward Rall) to follow through with his offer to come to Yale and review the original data. Fourthly, while Dr Roth is quoted as considering it "careless" for us to allow publication of our paper pending an audit, he had in fact written to us on 5 March 1979 that "I hope you will go on to have your fine and original piece of research published appropriately". Fifthly, those papers which were considered questionable after the second audit involved studies for which original data were not available for audit because Dr Soman (by his written admission) had destroyed the original notebooks. Sixthly, in addition to informing Dean Tapley on 27 February 1980, I met with five of the senior faculty in the Department of Medicine at Columbia in May 1980, prior to my assuming the Chairmanship, and informed them of Soman's data falsification and that I would be sending letters of retraction to journals.

Finally, your article fails to take note of the fact that at the time the paper on anorexia nervosa was submitted for publication by Soman and myself, Soman was in his third year of a faculty appointment at Yale, had extensive independent grant support, was responsible for his own laboratory and was highly regarded by all his colleagues. Any retrospective analysis of the handling of his wrongdoing in using the Wachslicht–Rodbard manuscript to prepare his own must be viewed in that context.

Philip Feli

Department of Internal Medicine,
School of Medicine, Yale University,
New Haven, Connecticut 06510

injury. Therefore we are also convinced that we must possess an isolated private alarm system which inevitably links injury to pain. The failure of this concept to explain the observed clinical and experimental facts has been discussed extensively and led to the gate control theory[33] and its extensions[34]. Chung and Dickenson use gate theory[33] as though it applied only to a 'pain system'. An acceptable pain theory would have to incorporate an explanation of at least the following clinical facts: (1) the bizarre coupling of the amount of injury to the amount of pain, (2) the triggering of pain by innocuous stimuli to normal tissue (tenderness, referred pain and trigeminal neuralgia), (3) the sensation of pain in missing limbs, (phantom pain), (4) the failure of narcotics to influence some pains, (brachial plexus avulsions), (5) the success and failure of the various counter-stimulation methods (acupuncture, transcutaneous stimulation).

Undoubtedly for lack of space Chung and Dickenson have concentrated on only one particular 'pain' inhibitory system, which is said to operate via noxious inputs and the nucleus raphe magnus to modify the activity of spinal cord nociceptive cells. However, as Chung and Dickenson point out this is only one example of many such inhibitory systems[35]. The brain has many reasons, tactics and strategies for selecting and modifying the incoming information it receives. Each of the different neural systems responsible for such 'controls' offers explanations for particular pain states, and opportunities for therapy. Some of the control systems are located in the spinal cord. For example, stimulation of large low threshold sensory fibres produces a striking inhibition of the response of spinal cord cells to peripheral injury[36]. Other control systems act via the brain[37] and there is good reason to suspect that some of these inhibitory effects are mediated by the small cells of the substantia gelatinosa[38]. Therefore the activity of all nociceptive cells is controlled by a balance of excitatory and inhibitory mechanisms mediated by many neural circuits, some local within the spinal cord and some with long arcs extending from cord to brain.

Experimental investigations of the functional profiles of neurones responding to noxious inputs and of their 'controlling' influences have been performed either in isolated parts of the nervous system such as the spinal cord or in highly unphysiological preparations such as anaesthetized or decerebrate animals. These experimental preparations represent a study of the nervous system locked at one extreme of its functional repertoire. While defining limits is a responsible scientific pusuit, it is difficult to establish the validity of these data in speculating about the operation of the system in the behaving organism. Having studied the functional reportoire of cells in these artificial states, it is clearly necessary to return to a study of their behaviour in the intact behaving organism before we can label cells as 'pain' cells. We are a long way from that step. How best to approach it? One way is to return to the animal and human patient to define the input-output nature of their problems rather than to force them to conform with ancient theory of how they ought to behave. We are emerging from a necessary era of physiology in which attention was concentrated on sudden stimuli and the consequent surge of impulses which ran through the nervous system over the subsequent 100 milliseconds. These volleys are travelling over neural circuits whose transmitting qualities have been set by much slower processes. These began in the embryo and obviously depend on a relatively fixed anatomy but it is now becoming apparent that there are also plastic physiological and biochemical processes which shape the responsiveness of nerve cells. It may well be that the huge newly discovered family of peptides including the enkephalins and endorphins have more to do with setting the mode of operation of the nervous system's analysis mechanisms than with the incoming messages which are to be analysed. □

---

1. Chung & Dickenson *Nature* **283**, 243 (1980).
2. Murphy & Bonica *Arch. Surg.* **112**, 896 (1977).
3. Mendelsohn *Aust. N.Z.J. Med.* **7**, 642 (1977).
4. Spoerel & Leung *Canad. Anaesth. Soc. J.* **21** 221 (1974).
5. Murphy *Adv. in Pain Res. & Ther.* **1**, 811. (Raven Press, New York, 1976).
6. Lee *et al. J. Am. Med. Ass.* **232**, 1133 (1975).
7. Tan, Tan & Veith, *Acupuncture Therapy* (Routledge & Keegan Paul, London, 1975).
8. Andersson *et al. Brian Res.* **63**, 393 (1973).
9. Chapman *et al. Pain* **3**, 213 (1977).
10. Wall & Sweet *Science* **155**, 108 (1967).
11. Sjolund & Eriksson *Brain Res.* **173**, 295 (1979).
12. Melzack *Pain* **1**, 357 (1975).
13. Woolf, *Pain* **7**, 115 (1979)
14. Hokfelt *et al. Proc. natn. Sci.* U.S.A. **74**, 3081 (1977).
15. Markowitz *et al. J. Pharmacol. Exp. Ther* **199**, 385 (1976).
16. El Sobky *et al. Nature*, **263**, 783 (1976).
17. Grevert & Goldstein *Science* **199** 1093 (1978).
18. Jacob & Ramabradran *Europ. J. Pharmacol.* **46**, 393 (1977).
19. Woolf *Brain Res.* **189**, 593 (1980).
20. Sewell & Spenser *Neuropharmacology* **15**, 683 (1976).
21. North *Life Sci.* **22**, 295 (1978).
22. Lindblom & Tegner *Pain* **7**, 31 (1979).
23. Mayer *et al. Brain Res.* **121**, 368 (1977).
24. Hosobuchi *et al. Science* **197**, 183 (1977).
25. Pert & Walter *Life Sci.* **19**, 1023, (1976).
26. Yaksh *et al. Life Sci.* **18**, 1193 (1976).
27. Woolf *et al. Pain* **8**, 237 (1980).
28. Fitzgerald & Woolf *J. Physiol.* In the press.
29. Levine *et al. Nature* **272**, 272, 826 (1978).
30. Lord *et al. Nature* **267**, 495 (1977).
31. Melzack & Wall *Science* **150**, 971 (1965).
32. Wall *Brain* **101**, 1 (1978).
33. Wall In Pain (Ed. J. J. Bonica) (Raven Press, New York, 1980).
34. Handwerker *et al. Pain* **1**, 147 (1975)
35. Basbaum & Fields *J. Comp. Neurol.* **187**, 513 (1979).
36. Dubuisson & Wall *Brain Res.* In the press.

Chung and Dickenson comment: There are two separate issues concerning acupuncture. First, we must ask if acupuncture analgesia is a reproducible phenomenon that can be studied in the laboratory. This question can be evaluated as we have done[1], from published studies. Second, we must ask if acupuncture is clinically effective. This is more difficult to assess, as there are numerous claims and counter-claims and the arguments are generally construed by carefully selecting one set of reports from the 'western experts' and dismissing the results which do not conform with preconceived opinions. We feel that controversy at present over the validity of clinical data is unproductive. Except for a brief mention that stimulation described by the experimenters as 'acupuncture-like' (as distinct from transcutaneous electrical stimulation) appears to be especially effective in relieving chronic pain in man[2-5], we avoided this issue in our review. There are however, many studies demonstrating that electroacupuncture and similar manoeuvres in animals enhance the threshold to pain and influence the responsiveness of pain cells. For example, cells responding steadily to painful stimuli are silenced when "acupuncture-like electrical stimuli" are delivered elsewhere on the body[6]. How the reduced activity of these cells is related to the subjective intensity of pain is unknown, as are the precise neural mechanisms by which such an inhibitory influence is brought about. Regardless of its ultimate clinical usefulness, the phenomenon deserves further investigation, and much of the current research into pain is indeed aimed at elucidating the mechanisms mediating inhibitory influences.

As Wall and Woolf point out, the involvement of opioids in modulating pain is not fully understood and conflicting evidence exists. It is likely that the role of opiates or endogenous peptides in the perception of pain will turn out to be complex. Of the many levels of the central nervous system at which pain transmission can be modulated, the raphe-spinal system appears to exert the most powerful inhibitory effects. We concentrated on this system mainly because the evidence for its inhibitory role is least controversial. Opiates[7], central electrical stimulation[8,9], acupuncture[10] and, more recently, transcutaneous nerve stimulation[11] have been claimed to act to some extent via this nucleus in producing their analgesic effects.

We have not stated, nor implied, that the pain system is isolated from "feelings and behaviour" or from other sensory systems. There are chains of cells which respond preferentially, and often solely and exclusively, to what the experimenter would consider to be noxious stimuli. These are usually referred to as 'cells which are involved in transmitting nociceptive messages', but to avoid circumlocution, we called them 'pain cells'. □

Shin Ho Chung and Anthony Dickenson are at the National Institute for Medical Research, London.

---

1. Chung & Dickenson *Nature* **283**, 243 (1980).
2. Sjolund & Eriksson *Brain Res.* **173**, 295 (1979).
3. Andersson *et al. Brain Res.* **63**, 393 (1973).
4. Boureau *et al. Elect. Clin. Neurol.* **47**, 322 (1979).
5. Melzack *Pain* **1**, 357 (1975).
6. Department of Physiology, Kirin Medical College, Changchun. *Scientia Sinica* **20**, 485 (1977).
7. Dickenson *et al. Brian Res.* **170**, 95 (1979).
8. Taub *Exptl. Neurol.* **10**, 357 (1964).
9. Oliveras *et al. Brian Res.* **120**, 221 (1977).
10. Du & Chao *Scientia Sinica* **19**, 137 (1976).
11. Woolf *et al. Pain* **8**, 237 (1980).

0028-0836/80/380186-02$01.00

NEWS AND VIEWS

What we don't know about pain

from P. D. Wall and C. J. Woolf

A RECENT article in these columns[1] by Chung and Dickenson discusses the relationship between pain, the enkephalins and acupuncture. We are told that "placing a single needle into a certain point of the body can produce . . . a potent amelioration of pain". It is proposed that acupuncture analgesia acts by the release of endogenous opioids within the brain and that these enkephalins indirectly stop "pain cells" in the spinal cord from transmitting their messages. How one wishes all this were true. If it were so, we would be well on our way to understanding and controlling the chronic pain states which continue to plague so many. We would like to supplement Chung and Dickenson by examining whether acupuncture does produce pain relief, what evidence there is for a role for the endogenous opiods in modifying nociceptive transmission and how the nervous system is organized to transmit and process information about noxious stimuli.

After 2,000 years of continuous use in China and some 350 years of intermittent Western enthusiasm, we still await controlled clinical trials which conclude that acupuncture is effective in treating chronic pain[2]. Innumerable, uncontrolled and anecdotal reports exist[3]. Such 'trials' report success rates of up to 94%[4] but in a controlled trial at the University of Washington Pain Clinic[5], none of a 100 patients showed any objective benefit after three weeks of acupuncture therapy. Another controlled trial found that acupuncture does produce a very transient analgesia, but that this analgesia occurs equally with 'sham-acupuncture' and with needling of the traditional meridian points[6]. For acute pain, we read of the successful application in China of acupuncture in half a million operations[7], but this does not match the experience of an invited team of western experts[2,8], who witnessed operations on highly selected patients, only a small fraction of whom had pain free operations with needles alone. Moreover the use of acupuncture for surgery in China is reported to be steadily declining[2,9]. There is no doubt that powerful analgesia with acupuncture does occur and has to be explained. Unfortunately, it is a rare phenomenon and for the huge majority of patients the needle is a blunt tool. Evidently acupuncture, when it works, acts by some mechanism which does not always operate in the majority of people, unlike the uniform ability to react to narcotic analgesics.

All sensory stimuli interact with each other producing distraction, jamming and specific local and distant interactions. Many have selected special examples of this general phenomenon and called them 'experimental acupuncture' although they usually bore no relationship to traditional acupuncture practice. In healthy volunteers, needling or electrical stimulation can produce a mild rise in the threshold for certain painful stimuli[10,11]. This antinociceptive effect is most marked in the region of the painful stimulus[13] and not at a distance or at 'meridians' as predicted by classical acupuncture. The analgesia produced by such experimental acupuncture is quite feeble and unlikely to be clinically useful, and must not be confused with the rare cases of perfect surgical analgesia produced by acupuncture or with the use of segmental transcutaneous electrical stimuli which have a highly satisfactory effect on certain types of hyperalgesias[12-14] with minimal effects on cutaneous pain thresholds[15].

There is no doubt that the enkephalins and a number of other opioid peptides are highly concentrated in specific regions within the brain and spinal cord[16], but their role, if any, in pain remains an enigma. One attempt to study this problem has been to investigate the effect of naloxone, an opiate receptor antagonist, on a variety of different pain states and analgesic procedures. Naloxone completely reverses the analgesic effects of administered narcotics[17]. If the endogenous opioids were active in normal men or animals one would expect that naloxone would antagonize their action and consequently produce pain or a drop in pain thresholds. Most studies in man have shown that naloxone has no effect[18,19], while in animals naloxone has been found to produce hyperalgesia[20,21], analgesia[22], and no change[23], in the response to noxious stimuli. Patients suffering from chronic pain are unaffected by naloxone although one might expect these patients to be mobilizing whatever anti-pain resources they possess[24].

Naloxone has been reported to produce a partial reduction both of experimental acupuncture analgesia in man[25], and of the analgesia produced by midbrain electrical stimulation[26], but these results need to be confirmed since conflicting reports are found in animal studies[27,28]. There is evidence in the rat that local segmental interactions between sensory inputs in the spinal cord are modified by naloxone[29,30] but it will be difficult to determine whether similar changes occur in man. Recently, in fascinating but highly controversial work, Levine & Fields[31] report that very high doses of naloxone abolish the placebo reaction, suggesting that the 'analgesia' resulting from blank injections may be produced by the mobilization of endogenous opioids.

Whatever function the opioids do perform in pain, it is unlikely to be simple as indicated by the growing list of endogenous peptide compounds with opioid activity and the subdivision of the opiate receptors into numerous functional categories. One of the problems in interpreting studies using naloxone is that it has a greater affinity for some classes of opiate receptors than for others[32]. Nevertheless it is clear that there is no evidence for an internal narcotic dispensing system in the brain automatically controlling the intensity of perceived pain.

In their summary of the anatomy and physiology of the pathways which bring news of injury to the brain, Chung and Dickenson use the most classical model for simplicity and brevity. They refer to pain fibres and pain cells in peripheral nerves and spinal cord as though there is a specialised chain of nerve cells which leads inevitably from the fact of injury to the sensory experience of pain. They further isolate this 'pain system' by saying that "in stark contrast to the other senses it is characterised by elaborate feedback networks" which "ensure that it is fail-safe" and "which, when activated, reduces the intensity of persistent pain". This approach "which implies a distinct anatomical and physiological pain system separate from other sensory systems" represents a definite philosophy which would shape future experiments and have considerable therapeutic implications if true. For example, given a distinct anatomy such as the pain cells described and a distinct feed back control such as the raphe nucleus and distinct chemistry such as the enkephalins, one might reasonably hope to achieve pain control with no influence on other aspects of feeling or behaviour. The concept of a separate pain system originates in our own introspective certainty that pain itself is a clearly discrete category of experience which we are convinced implies

---

P. D. Wall is a Professor of Anatomy and Director of the Cerebral Functions Research Group, University College, London; C. J. Woolf is a lecturer in the Physiology Department of the Middlesex Hospital Medical School and Honorary Research Fellow in the Department of Anatomy, University College, London.

0028-0836/80/380185-02$01.00

Hopping and running on two legs or four

from R. McNeill Alexander

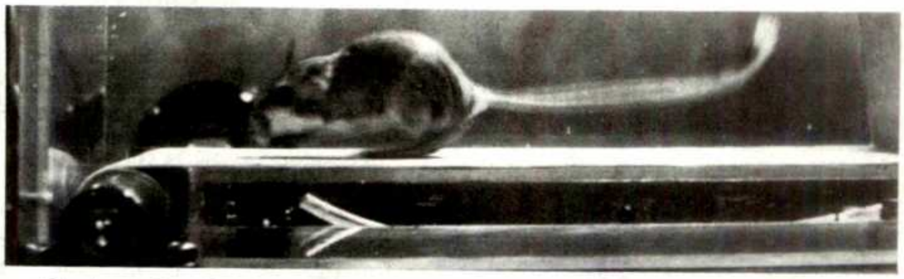

Dipodomys deserti hopping on a moving belt to assess energy consumption. Experimental details are given by Thompson *et al.* on p.223 of this issue of *Nature*.

MOST mammals run on all fours but some run on just two legs (like men) or hop (like kangaroos). Some birds run, some hop and some do both. What are the relative merits of the different gaits? Do they differ in energy cost?

Energy costs of running and hopping can be inferred from measurements of oxygen consumption. Some of the difficulties of physiological experimentation on moving animals can be avoided by training the animal to run on a moving belt as shown. Data has been collected for mammals ranging from mice to horses and lions, and for many birds (summarized by Fedak & Seeherman *Nature* **282**, 713; 1979). Nearly all of it conforms to a simple rule: the power P required for level running at speed u is given by

$$P(u) = P(0) + ku \qquad (1)$$

where k is a constant for the particular animal. $P(0)$ is a little more than the power consumption at rest because it includes a component for maintenance of posture.

Equation (1) implies that the energy required to travel a given distance (in excess of the requirement for standing still) is more or less independent of speed.

This may seem remarkable, but experiments with red kangaroos gave an even more remarkable result (Dawson & Taylor *Nature* **246**, 313; 1973). The power consumption of a hopping kangaroo is independent of speed, or may even fall slightly as speed increases. The energy used by a kangaroo travelling a given distance therefore falls steeply as speed increases. At low speeds a kangaroo uses far more power than (for instance) a gazelle of the same mass, but at 5 m s^{-1} the two animals use about equal powers. It has been suggested that at higher speeds, a kangaroo might travel more economically than a gazelle, but it is difficult to measure power consumption at high speeds because the animals build up oxygen debts.

Various rodents hop like small kangaroos. There are kangaroo rats (*Dipodomys*) in N. America, springhares (*Pedetes*) in Africa and hopping mice (*Notomys*) in Australia. Is power independent of speed for them all? Thompson, McMillen, Burke & Taylor (this issue of *Nature*, p223) find that it is not. Equation (1) holds for many and probably all hopping rodents, with values of k about the same as for quadrupeds of similar mass. The same is true for the rat kangaroo (*Bettongia*, a marsupial). The large kangaroos seem to stand alone in their peculiar energetics.

Though equation (1) holds for a wide variety of animals, the constant k is different for animals of different sizes. Until recently the data seemed to indicate that k was proportional to (body mass)$^{0.6}$ for quadrupeds but to (body mass)$^{0.8}$ for bipeds. Consequently bipedalism was more economical than quadrupedalism for small animals, but less economical for large ones. Why, then, are there small quadrupeds (such as mice) and large bipeds (such as ostriches and, formerly, tyrannosaurs)?

This apparent paradox seems to have been an artefact of the sample of species originally selected for study. Fedak & Seeherman (*Nature* **282**, 713; 1979) showed that though penguins and geese need twice as much power for running as dogs of the same mass, ostriches are as economical as ponies. For any body mass, a wide range of values of k is possible, but the general trend both for quadrupeds and for bipeds is for k to be proportional to (body mass)$^{0.7}$.

It would be satisfying to be able to explain why kangaroos and smaller hoppers have different relationships between power and speed, and why k tends to be proportional to (body mass)$^{0.7}$. This has not yet been achieved. Calculations based on the mechanical work required of the leg muscles provide satisfactory explanations of the power requirements of kangaroos and also of quadrupedal mammals of similar size, and show that slow hopping is more expensive than running because it involves larger fluctuations of potential energy (Alexander & Goldspink *Mechanics and energetics of animal locomotion*, 1977).

Similar calculations grossly underestimate the power requirements of small runners and hoppers, such as mice and quail: indeed they predict that k should be proportional to (body mass)$^{1.0}$. Taylor, Heglund, McMahon & Looney (*J. exp. Biol.* **86**, 9; 1980) have recently tried to resolve this discrepancy, by suggesting that the main metabolic energy cost of running is associated with the generation of muscular force, rather than the performance of work. The forces required are proportional to body mass but smaller mammals need faster muscles, with shorter cross-bridge cycling times, so exertion of force may be more expensive for them. Taylor and his colleagues show for rats, dogs, men and horses, that carrying a load increases k in the same proportion as it increases the forces on the feet. This is consistent with their hypothesis but is not clear evidence for it (as they themselves admit), because the experiment increases forces and work in the same proportion. The hypothesis is unlikely to win general acceptance unless it can be supported by less ambiguous evidence and shown to be quantitatively consistent with our knowledge of muscle physiology. □

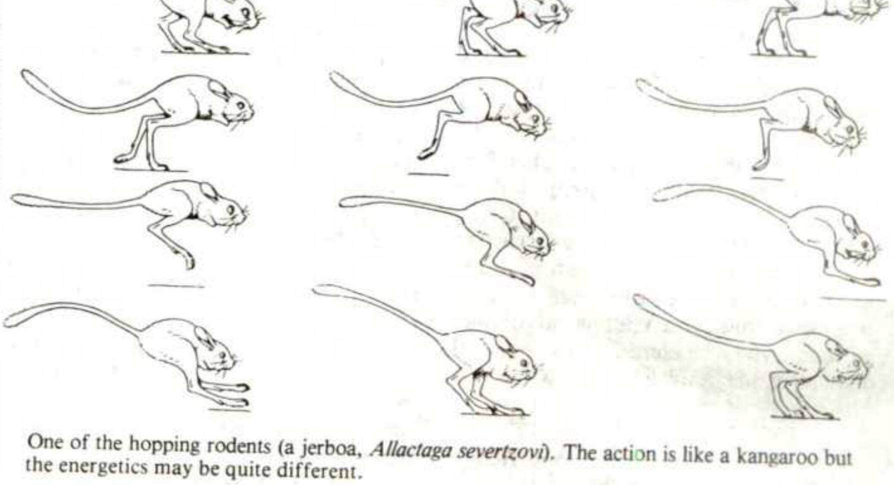

One of the hopping rodents (a jerboa, *Allactaga severtzovi*). The action is like a kangaroo but the energetics may be quite different.

from *How mammals run* Keter Publishing House, Jerusalem, 1974.

R. McNeill Alexander is Professor of Zoology at the University of Leeds.

0028-0836/80/380187-01$01.00

Movable genes

from Ron McKay

BARBARA McClintock's early studies on the breakage- fusion bridge cycle in maize served for many years as a reminder that a major class of genetic change was not explained by the central theories. This year's Cold Spring Harbor Symposium (May 28 — June 4, 1980) showed quite clearly that genetic instability now occupies a central place in our understanding of both heredity and development. The recent rekindling of interest in this field stemmed from observations of the rapid spread of drug resistance markers in bacteria but now extends to eukaryote molecular genetics. In prokaryotes it is clear that there is a class of DNA which promotes its own rapid spread within and between bacterial species. The physical structure of these mobile genetic elements is well understood and current goals are to determine the mechanism and enzymology of this genetic exchange.

One of the best understood of the mobile elements is the bacterial transposon Tn*3*. Transposon Tn*3* confers resistance to the antibiotic ampicillin as it carries a gene which specifies the ampicillin degrading enzyme ß-lactamase. The studies of Heffron, Casadaban and others have shown that as well as this genetic marker Tn*3* carries two genes which function in trans to promote genetic movement or transposition (Fig. *a*). After transposition a new copy of Tn*3* is found at a new integration site but the old copy is still found at the original site — a key feature which distinguishes the movement of transposons from the integration-excision system found in bacteriophage lambda. However, as with phage lambda, transposable elements require certain DNA sequences in cis for transposition. These sequences fall within the inverted terminal repeated sequence which is found at the ends of all mobile genetic elements. The process by which a new copy of a transposable element coding for its own transposase is inserted into another replicon is thought to occur via a fused structure called a co-integrate in which two copies of the transposable element flank the donor molecule (Fig. *b*). Cointegrates from transposons known to code for their own transposases (Tn*3* and Tn*5*) have only been found using mutant transposons. Normally no cointegrates are seen but in some mutations all the transposons are cointegrates. Therefore cointegrates have been proposed as intermediates in transposition. Other transposons which have not been shown to code for transposases but which have IS*1* elements at their ends (for example, Tn*9*) give rise to cointegrates as the end product of wild type transposition. The fused replicon can be resolved, as shown in Fig. *b*, to give the two starting replicons with an additional copy of the transposable function. Heffron (University of California, San Francisco) has shown that the resolution of co-integrates also requires a DNA sequence within Tn*3* in cis. This sequence falls in the central region of Tn*3* and is called by Heffron the internal resolution site (IRS). The DNA sequence of IRS shows some similarity to the terminally repeated DNA sequences but the IRS sequence is unable to substitute for a terminal repeat in transposition. So here we have clear evidence that there is another sequence required in cis for transposition to occur. In addition to IRS there is a resolution function which may be supplied in trans. This function was shown by Sherratt (Glasgow University) to be coded by Tn*3*. Sherratt's studies shows the resolution function to map close to a gene whose product is known to repress transposition. Whether the resolution of co-integrates is another function of the previously defined repressor is not known. Resolution of co-integrates may be a site specific recombination catalysed at a high frequency by two copies of IRS and repressor.

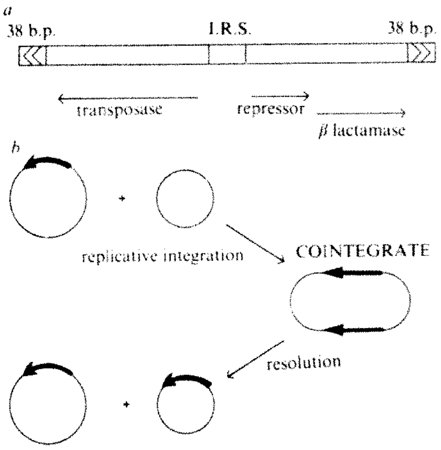

(*a*) *Structure of transposon Tn*3, (*b*) *the transposable element is inserted into another replicon via a cointegrate.*

Genetic studies of Tn*3* have shown that the rate of transposition is influenced by genes carried by Tn*3*. Biek (Utah University) has used transposon Tn*5* to investigate another feature of regulation. In transductional crosses a Tn*5* element in the recipient cell inhibits transposition of the incoming Tn*5*. These results are consistent with a Tn*5* coded repressor of transposition. Genetic mapping localised the inhibition close to the Tn*5* drug resistance marker, neomycin phosphotransferase. However, the two functions are distinct since nonsense mutants of the *neo* gene do not affect transposition. The DNA sequence of Tn*5* has been established (Auerswald, Heidelberg University) and the transcription and translation products identified (Reznikoff, University of Wisconsin), so we can soon expect to know the molecular basis of Tn*5* mediated immunity.

The terminal inverted repeats of Tn*5* are much larger than those of Tn*3* and Reznikoff's laboratory has shown that each arm codes for two polypeptides but the molecular weights of the two proteins coded by each arm differs. Genetic studies have also shown that the two arms are not homologous. Mutations in the repeat proximal to the *neo* gene do not affect transposition but mutation of the distal arm can prevent transposition. The reason for this is apparent now that the DNA sequence of Tn*5* is known. The two arms differ by only a single base in 1,450 base pairs but this generates a stop codon in the coding sequence of the repeat proximal to the *neo* gene so bringing about the altered proteins and the lack of function. Grindley (Yale University) generated variants of the similarly organised transposon Tn*903* which have deletions in one arm. He then mutated the other inverted repeat by inserting 10 base pair Bam HI linkers at suitable restriction sites. This method of *in vitro* mutagenesis, extensively used by Heffron, generates frame shift mutations as the insertion is not an integer multiple of the three base codon. Grindley found that most double mutants of Tn*903* had lost the ability to transpose. The one exception which still transposed had suffered only a 9 base insertion, presumably leaving the distal part of a gene in phase. Although this is good genetic evidence for the expression of a gene in the inverted repeats of Tn*903* no protein has yet been found. How this expression leads to transposition is still not clear.

In Tn*5*, Tn*903*, Tn*3* and in bacteriophage Mu genetic and structural studies have identified genes and in some cases gene products which must mediate and regulate transposition. No *in vitro* assay for transposition is available, nor has enzymatic activity been associated with any of the putative transposases.

How does transposition occur? There may not be a single answer to this question. For example IS*4*, unlike most transposable elements, is site specific. Quite rightly these exceptions do not prevent the search for a single unifying model. As it is generally accepted that a copy of a transposon remains at the original site when transposition occurs, and because replication is actively required for transposition, a phage lambda-like excision-integration system is not favoured. A number of different copy-replication models are available. Harshey and Bukhari (Cold Spring Harbor) have visualized the DNA structures found when the bacteriophage Mu is induced. Mu can only replicate by transposing so a large number of transposition events are found in a single cell. Harshey and Bukhari see DNA structures which can be explained by a 'roll-in' mechanism which can initiate at either end of Mu.

The gene conversion system which controls mating type in yeast may be similar to a transposable system but under careful cellular control. The cassette model for mating type expression holds that

---

Ron McKay is at the Cold Spring Harbor Laboratory, Long Island, New York.

0028-0836/80/380188-02$01.00

information from either of two silent loci is sequentially expressed after transposition to a third (MAT) active locus this transposition is similar to that in prokaryotes as the information remains unchanged at the donor site. The focus of both molecular and genetic studies reported by three groups, Nasmyth (University of Washington), Klar (Cold Spring Harbor) and Haber (Brandeis University), is the cellular control of these three loci. It is not clear how sequences transposed to the *MAT* site become active. The active *MAT* site is a complex locus each *MAT* allele coding for two genes, divergently transcribed from opposite strands (Nasmyth and Klar). Yeast strains carrying recessive mutations in unlinked regulatory genes can express the silent mating type cassettes which shows that the silent copies, normally under negative control in trans, are relieved from this control when the information is switched to the active mating type locus. This rules out a system of the type demonstrated for sarcoma viruses where the cellular *sarc* structural gene and a strong promoter can be brought together to transform cells with high efficiency. Lambda-like independent excision and integration events were ruled out by evidence presented by Klar. He favored a duplicative transposition mechanism where the silent locus physically interacts with MAT since recombinants between MAT and the silent loci have been observed. The genetic studies of Haber (Brandeis University) were also consistent with this view.

Another eukaryotic system where genes are expressed in a mutually exclusive fashion occurs in the protozoan responsible for sleeping sickness. This parasite escapes from the host immune response by altering the dominant surface antigen which constitutes 95% of surface protein. Individuals of the species *Trypansoma brucei* have the ability to express one of many hundreds of special genes as this surface protein and so escape the host immune response. It appears now from work reported by Borst (University of Amsterdam) that at least some genes are moved to special genomic sites to become active. This may be the first generalization of the yeast cassette model and it is intriguing to speculate that other classes of genetic differentiation may be achieved by moving information around the genome.

What are we to make of all this genetic instability? Work on the proteins which mediate genetic recombination: recA, recBC, synaptase and the topoisomerases, emphasizes the ease with which the DNA may be rearranged. At least two conclusions follow: first, where genetic maps are conserved between bacteriophages or between the human and mouse X chromosomes this arrangement must have a selective advantage. Second, there may be systems where widespread genetic rearrangement is favoured over the usual conservative gene arrangement. We known of some of these situations; the recovery of bobbed *Drosophila* and the amplification of *Xenopus* ribosomal genes. A report by Jones (Edinburgh University) suggests that we may no longer be able to relegate these rearrangements to the miscellaneous file. He has found a sequence in the heterogametic W chromosome of female snakes which is conserved in echinoderms, *Drosophila* and mammals. This repeated sequence has at least two dramatic properties. Its sequence arrangement in different tissues of *Drosophila* varies and in mammals, its arrangement in males and females differs. When sex reversed Sxr mice which are phenotypically male but have a female karyotype were tested they exhibited the male pattern. If it is true that Sxr males are not Y autosome translocations but express constitutively the gene normally triggered by a Y chromosome signal, the implication is that the genomic rearrangement is a secondary sexual characteristic. This hypothesis could be tested by examination of another mouse strain Tfm (testicular feminisation) and of bovine freemartins where hormonal regime rather than genetic inheritance is known to mediate altered sexual differentiation. It is a measure of how far our views have changed that Jones' findings were met with interest and not instant disbelief. Of course we are now confident that the clones and blots will tell all. □

100 years ago

The *Philadelphia Record* deserves credit for its successful efforts to break up the sale of bogus medical diplomas. These diplomas were chiefly sold abroad, and it is appalling to learn, that 11,000 of them have been issued during the past few years. "It was well known," the *Times* correspondent writes, "that Dr. John Buchanan, the Dean of 'The American University of Philadelphia,' and several other similar institutions, was engaged in this traffic; but as they were all properly chartered medical schools, and, though disreputable, existing under the sanction of law, the difficulty was to get evidence of the sale of diplomas. Diplomatic complaints about the traffic came from various Governments of Europe, and our people began to be restive under the stigma." By the clever tact of the city editor of the *Record*, however, Buchanan has been brought within reach of the law, and the detectives are on his track. He attempted to put them off the scent by getting a man looking like himself to pretend to drown himself; this bogus case of drowning, however, has deceived nobody.

From *Nature*, **22**, 16 September, 465, 1880

The nature of gravitation

from A.H. Cook

EXPERIMENTAL studies of gravitation have been discouraged by the attitude of many theoreticians who, from the time of Newton, have taken gravitation as something 'given'. Experimenters are not, however, so easily put off by theoretical detachment even though the very small strength of gravitation makes its investigation difficult — the gravitational force between proton and proton is about 10^{-39} of the electrical force which, in practice, means that any laboratory study of gravitation will be bedevilled by all manner of extraneous disturbances.

A simple-minded approach to the experimental study of gravitation is to look at the inverse square law and ask such questions as: what is the 'mass'? Is it always proportional to inertial mass or are there differences from substance to substance? Is there any screening of one body by another, as with electrostatic forces? Is the 'constant' of gravitation constant, or does it depend on velocity, time, position, or the direction of the line joining two attracting bodies, and finally, is the inverse square law strictly obeyed?

We have experimental answers to these questions for the electrostatic force, and they are expressed in the appropriate Maxwell equations. We have some answers for gravitation. Experiments for many years have failed to detect any dependence of gravitation upon material — all hadrons are equivalent gravitationally to within about 1 part in 10^{11}. A few astronomical and geophysical observations have shown the absence of any shielding effect to about the same limit. Geophysical observations of Earth tides show that if there is any dependence of gravitation on direction it cannot exceed 1 part in 10^{8}. These and other effects can be incorporated in certain sorts of theory known as parameterised post-Newton (PPN) gravitation theories, provided sufficient parameters are included. If some of these parameters differ from the values predicted from general relativity, then certain effects in celestial mechanics would occur and might be detectable in refined observations of space craft or the Moon. Although such observations, for example, laser ranging measurements of the orbital motion of the Moon, are now possible, no derivations from the predictions of general relativity have so far been detected.

It should be emphasized that the type of experiment being considered is quite different from attempts to detect gravitational radiation. No one seriously doubts that radiation is entailed by general relativity but the question is whether any object radiates strongly enough to be observed with techniques available on Earth.

With the growth of interest in unified theories of gravitation and other inter-

---

A.H. Cook is Head of the Department of Physics, University of Cambridge.

0028-0836/80/380189-02$01.00

actions, it is natural to suppose that there should be a particle having a finite mass which arises from some broken symmetry in the field theoretic description of gravitation, and it has been suggested that the gravitational potential energy of two masses would not be simply proportional to $1/r$, where r is their separation, but would be given by

$$\frac{G_o M_m (1 + \alpha \exp(-r/\lambda))}{r}.$$

This gives an inverse square law dependence at small distances ($r << \lambda$) and at large distances ($r >> \lambda$) and the ratio of the respective "constants" of gravitation is $(1 + \alpha)$.

Could this , or some other departure from the inverse square law be detected? Long (*Nature* **260**, 417; 1976) claimed to have found such an effect but in a recently published experiment by Spero *et al.* (*Phys. Rev. Lett.* **44**, 1645, 1980) no deviation was detected. As is well known, very delicate tests of the inverse square law of electrostatics can be made using the principle that the field inside a charged sphere vanishes. Construction of a hollow sphere for a gravitational experiment is hardly possible so Spero and his colleagues investigated the gravitational field inside a long tube. Were the tube infinitely long there would be no net internal field but with a finite cylinder there are end effects. The experiment was designed to use a sensitive torsion balance to measure the change in force on a test mass in different radial positions within a long vertical cylinder. A servo-control was applied to the torsion balance to maintain it in a constant position and the restoring force necessary to do so was recorded for different positions of the cylinder relative to a test mass suspended from one end of the balance beam. To attain a useful precision, the experiment had to be very carefully designed. Corrections were determined for the end effects and other stray gravitational fields and precautions were taken against magnetic and convective forces. The experiment depended on the material of the cylinder (which was of stainless steel, 60 cm long, of 6 cm internal diameter and a mass of about 10 kg) being very uniform, and a careful study of the cylinder had therefore to be undertaken. The measured torques were of the order of 5.10^{-13} Nm, showing the extreme delicacy that must be attained in worthwhile experiments on gravitation. The observations agreed with the torque predicted for pure inverse square law attractions to 2.10^{-15} Nm, a result that is inconsistent with Long's earlier study.

It can be said that no deviation of the behaviour of gravitation from the predictions of general relativity has as yet been established experimentally, and one may suspect that none will be. That, however, is not a reason for abandoning experiments such as those mentioned earlier. Gravitation is such a fundamental interaction that it is a worthwhile aim to establish its properties to the very highest precision, particularly since to do so presents a daunting but irresistible challenge to the experimenter. □

Terrestrial heat flux

from David S. Chapman

PRESENT day heat loss through the Earth's crust is approximately 4×10^{13} Joules and as such is of major importance in geodynamic processes. The source of the heat, its mode of transport and its geographical pattern of variation are still questions which remain largely unanswered and they provided the central theme for a recent conference*.

Heat flow measurements have still not been made from many parts of the world so one of the highlights of the conference was the addition of data from China to the global heat flow map. Ji-Yang Wang (Academia Sinica, Beijing) reported that twenty-two values from north China fall into the following patterns: heat flow of 32mW m^{-2} in the Archean crust of central Yanshan; 54 to 75 mW m^{-2} in the neotectonic Huailai and Yanquing basins, and 61 to 84 mW m^{-2} on the block faulted North China Plain (see *J. Volcanol. Geotherm. Res.* in the press) where tectonic activity, according to Wang, "has been strengthening since the Mesozoic era". The Chinese territory also received attention from Anderson (Lamont-Doherty Geological Institute, Columbia) in his report of the first detailed heat flow profile across a continental margin. The demonstration of stable bottom water temperatures on the margin, a prerequisite for shallow marine measurements, will encourage further experiments in spite of the monotony of the results — a uniform 90 mW m^{-2} with one unexplained anomaly in 88 measurements.

In another pioneering effort, Bucher and Decker (University of Wyoming) reported values between 50 and 84 mW m^{-2} in the Ross Island dry valley area of Antarctica. These results significantly extend the coverage of heat flow measurements on the globe. None of the new results depart from the heat flow patterns established elsewhere in the world — heat flow is elevated in young orogenic provinces and decays systematically with increasing geological age — but do allow a better contouring of the global data set.

One issue beginnning to be resolved by the increasing number of heat flow observations is the nature and width of heat flow transitions. That heat flow transitions of 30 mW m^{-2} and greater commonly occur over lateral distances of 10 to 50 km was demonstrated in an analysis of existing data for rift valleys (Morgan, New Mexico State University), by new data from the Southern Rocky Mountains (Decker, University of Wyoming), and by independent new surveys by Stone (University of Arizona) and Chapman and colleagues (University of Utah) of the transition from the Basin and Range to the Colorado plateau physiographic province. In areas where few measurements existed, the transition had been considered to be broad and the source thermal perturbation confined to the asthenosphere. The observations of sharp transitions imply that heat sources must be shallow, within the lithosphere or possibly even within the crust. As the calculation of geotherms, regularly used to predict rheology, mineralogy and partial melting in the lower lithosphere, is critically dependent on the depth distribution of heat sources, modification of much used purely conductive geotherms in certain regions now seems appropriate (as suggested by Lachenbruch & Sass *Geol. Soc. Amer. Memoir* **152**, 209; 1978).

A further caution to those who seek deeper meaning from all heat flow anomalies came from three studies of the role of groundwater in redistributing heat. Heat flow investigators for several years have inferred the role of groundwater in transferring heat, especially in very young oceanic crust, but the direct demonstration of those flows has been difficult. Therefore, the experiments described by D. Abbot and colleagues (Lamont-Doherty) on the simultaneous measurement of excess pore pressure and temperature gradients in sediments covering 22 Myr old crust in the Guatemala Basin is of special significance. The objective was to explain very low observed heat flows of 1 to 20 mW m^{-2} in the region instead of the 105 mW m^{-2} expected on the basis of crustal age. Although measured temperature-depth profiles were linear, usually an indication that convective disturbances are absent, all of the new measurements yielded negative pore pressures within the sediment, indicating downward fluid velocities between 10^{-6} and 10^{-7} cm s^{-1}. Such velocities are sufficient to decrease heat flow by a factor of 10. More important, they confirm the long held suspicion that many subnormal oceanic heat flow areas actually delineate the downgoing side of a sea floor convec-

---

*A Spring American Geophysical Union meeting titled 'Heat flow and crustal properties'' was held in Toronto from May 22 to May 27, 1980.

David S. Chapman is in the Department of Geology and Geophysics, University of Utah.

0028-0836/80/380190-02$01.00

tion system.

On a larger scale of tens of kilometers, groundwater flow was also shown to have major effects on observed heat flow patterns. Lohse, Morgan and Swanberg (New Mexico State University) reported 60 new heat flow determinations from the Rio Grande Rift zone and interpreted the highly variable pattern in terms of ascending warm water in rift fracture zones and intrabasin groundwater flow in the Rio Grande River drainage system. In perhaps the best example of redistribution of crustal heat over lateral distances of hundreds of kilometers, Majorowicz (Warsaw University) demonstrated that a relatively low heat flow of 50-75 mW m^{-2} in the Rocky Mountain foothills of Alberta and an abnormal heat flow of 70-100 mW m^{-2} in the northern Prairies Basin could only be explained by regional groundwater flow.

In contrast to the previous discussions on patterns and mode of transport of the terrestrial heat flux, two papers addressed the source of heat, at least the crustal radiogenic portion now thought to account for about 40% of the continental flux. Our present understanding of this radiogenic heat distribution hinges on the empirical relationship between surface heat flow and surface radioactive heat production first demonstrated in 1968 for plutons by Birch and co-workers, and modeled soon afterwards by Lachenbruch. According to these early models, plutons undergo an upward enrichment in uranium, thorium and potassium, the important heat producing elements. Their combined depth distribution is characterized by the length parameter *b*, the slope of heat flow-heat production line for that pluton. Any of three depth distributions, constant to depth *b*, linearly decreasing to depth 2 *b*, or expotentially decreasing with characteristic decrement *b*, satisfy the heat flow–heat production relationship, although the latter makes the most geological sense.

Now Gosnold (Nebraska University) and Jaupart (University of Paris) have independently suggested modifications to this model and its interpretation. Gosnold has combined fission track, petrographic and oxygen isotope studies on samples from several plutons within the Idaho Batholith. His results suggest, not surprisingly, that heat generation is largely controlled by water–rock interaction in the upper 10 km of the crust. In such a case the overall vertical heat production distribution could be exponential throughout the crust but an inflection in the curve would occur at the lowest depth of meteoric water interaction. Jaupart's modification is more severe. He questioned the assumption that uranium, thorium and potassium have identical depth distributions. He has inferred from his preliminary analysis, although based on surface sampling only, that the three elements have different depth distributions but are similar from one geological province to another. Both these suggestions have interesting geochemical and geophysical implications and it is a pity therefore that the issues may not easily be resolved. The characteristic scale for these processes and the radioactive enrichment is 10 km, and few, if any, geological locations permit sampling over that vertical extent in the igneous crust. ☐

Myosin phosphorylation

from Dixie W. Frederiksen

REGULATION of muscle contraction and cell motility occurs by the control of the interaction of actin and myosin. Primary control is exercised by the intracellular calcium concentration and is modulated at secondary levels by various mechanisms that seem to depend upon the source of the tissue or proteins examined. Myosin phosphorylation plays an important role both in the primary regulation and in the secondary modulation of contraction and motility[1].

In vertebrate striated muscle the binding of calcium to troponin, a protein on the actin filament of the muscle sarcomere, is clearly the event that triggers actin-activation of the MgATPase. Although the direct steric blocking model for this actin-linked regulatory mechanism[2] has been challenged recently[3] there is little debate that troponin and tropomyosin are responsible for primary regulation in vertebrate striated muscles. At the secondary level, phosphorylation of a troponin subunit by cyclic AMP-dependent protein kinase has been shown to result in decreased actin-activated MgATPase activity of striated muscle myosin[4]. Furthermore, although striated muscle myosin phosphorylation was discovered sometime ago by S. V. Perry and his colleagues at the University of Birmingham[5], the function of this modification is still largely unknown. The phosphorylation is presumed to play a secondary role in modulation of the contractile process.

In many smooth muscle and nonmuscle actomyosin systems it seems clear that the calcium-sensitive mechanism responsible for primary regulation is myosin-linked through phosphorylation of one of the small subunits of the myosin molecule. David J. Hartshorne and his collaborators[6] at the University of Arizona and Robert S. Adelstein with his colleagues at the N I H[7] have shown in several elegant experiments that the binding of a calcium-calmodulin complex to myosin light chain kinase and the subsequent phosphorylation of myosin are the initial steps in actin-activation of smooth muscle and some of the nonmuscle myosin MgATPases. The secondary modulation of contraction/motility in these systems seems to include one or more different processes. Cyclic AMP-dependent protein kinase-catalysed phosphorylation of myosin light chain kinase was discovered by the Adelstein group[8] and found to result in decreased activity of the myosin light chain kinase. In addition, direct interaction of calcium with phosphorylated smooth muscle myosin has been reported to modulate the actin-activated MgATPase[9].

The effects of myosin phosphorylation on the contractile apparatus are complex and subtle and reports of the influence of myosin phosphorylation on striated muscle proteins *in vitro* have not been forthcoming. As a result, investigators have turned to the examination of intact muscle for evidence of the effects of phosphorylation. Michael Bárány and his colleagues at the University of Illinois Medical Center[10] have used frog muscle and James T. Stull and his group at the University of Texas Health Science Center[11] have used mammalian striated muscle to monitor the phosphorylation. In these *in situ* studies, phosphorylation of myosin light chain was observed to be correlated with the stimulation of the muscle. Bárány has suggested that the function of the phosphorylation may be to increase the actin-myosin affinity by the formation of a salt-bridge between the phosphoryl group on myosin and the actin-bound calcium on the thin filament. Such an increased affinity would lead to an increased rate of combination of myosin crossbridges with the actin filament.

The phosphorylated myosins of smooth muscle and several nonmuscle systems, unlike their striated muscle counterparts,

Dixie W. Frederiksen is in the Department of Biochemistry, Vanderbilt University, Nashville, Tennessee.

1. Adelstein & Eisenberg *Ann. Rev. Biochem.* **49**, 921 (1980).
2. Bremel *et al. Cold Spring Harb. Symp. quant. Biol.* **37**, 267 (1973).
3. Seymour & O'Brien *Nature* **282**, 680 (1980).
4. Baillin *Am. J. Physiol.* **236**, C41 (1979); Wyborny & Reddy *Biochem. Biophys. Res. Comm.* **81**, 1175 (1978).
5. Perry *Biochem. J.* **151**, 99 (1975).
6. Hartshorne *et al. Biochem.* **17**, 253 (1978).
7. Adelstein *et al. Proc. natn. Acad. Sci. U.S.A.* **76**, 1563 (1979).
8. Adelstein *et al. J. Biol. Chem.* **253**, 8347 (1978).
9. Chacko *et al. Proc. natn. Acad. Sci. U.S.A.* **74**, 129 (1977); Rees & Frederiksen *J. Biol. Chem* in the press.
10. Bárány *et al. J. Biol. Chem.* **254**, 3617 (1979); *Fed. Proc.* **39**, 1547 (1980).
11. Biochem *Biophys. Res. Comm.* **90**, 164 (1979); *Fed. Proc.* **39**, 1552 (1980).
12. Adelstein & Conti *Nature* **256**, 597 (1975); Sobieszek & Bremel *Eur. J. Biochem.* **55**, 49 (1975); Sherry *et al. Biochem.* **17**, 4411 (1978).
13. Suzuki *et al. J. Biochem* **84**, 1529 (1978).

0028-0836/80/380191-02$01.00

Bishop Wilberforce: Natural Selection and the Descent of Man

from Richard W. Wrangham

Samuel Wilberforce, Bishop of Oxford, was the man who played into T.H. Huxley's hands at the British Association's meeting in 1860. They were debating the merits of Darwinism, and the atmosphere in the crowded room was highly charged. Wilberforce was a fine speaker — "Like an olive, his nature secretes his own oil", wrote *Punch*[1] — and he ended his well-prepared attack on evolutionary theory by asking if his opponent were prepared to admit apes to his own ancestry. The reply was deadly. An ape, said Huxley, would be a preferable grandfather to an intelligent man who used his skills to bring ridicule to science.[2] It won the audience and silenced the Bishop, who never spoke again on evolution.

Huxley went on to build a career out of promoting Darwinism, while Wilberforce returned to ecclesiastical matters. But how did he come to feel about evolution? His only published opinion was a review of the *Origin of Species*, written before the debate with Huxley.[3] There he denied unambiguously that evolution was tenable, though he approved of natural selection. He understood the arguments well and used them to maintain that selection acted to keep species constant, not to change them[4].

Now a clue to his subsequent feelings has emerged. The poem below was found earlier this year in his private papers, and is undated. Its theme, "degradation by natural selection", is from Richard Owen's review of the *Origin.*[5] Wilberforce saw all too well the clash between evolutionary theory and his religious beliefs, and in 1860 he had come out in attack. But in this poem he side-stepped the conflict and retreated to comedy. It implies a man too committed to accept the evolutionary argument, yet too honest in the end to deny it. Who knows? Darwin may have had one more convert than he knew.

"Lines written on hearing that Professor Huxley had said that 'he did not care
whether his grand-father was an Ape'."

Oft had I heard, but deemed the tale untrue,
That man was cousin to the Kangaroo;
That he before whose face all nature quailed,
Was but the monkey's heir, though unentailed;
And that the limber Ape, whose knavish ways
And tricks fantastic oft our laughter raise,
Was just what *we* were in some previous state,
Ages ere Noah shipped his living freight.
But now a learn'd Professor, grave and wise,
Stoutly maintains what I supposed were lies;
And, while each listening sage in wonder gapes,
Claims a proud lineage of ancestral Apes.
Alas! cried I, if such the sage's dreams,
Save me, ye powers, from these unhallowed themes;
From self-degrading science keep me free,
And from the pride that apes humility!
But O should fate bring back these dreams accursed,
And shuddering Nature find her laws reversed;
Should this, the age of wonders, see again
Men sunk to monkeys, monkeys raised to men:
Be mine the lot, on some far-distant shore,
Where Science wearies not nor savants bore —
Where no learn'd Apes our fallen race may scorn,
Nor point the moral which our tails adorn —
To shun the sight of metamorphosed friends,
Till time again shall shape their altered ends,
To soothe each fond regret, howe'er I can;
And, at the least, to dream myself a Man!
S. Wilberforce

1. Anon *Punch* **25**, 206 (1853).
2. Foskett, D.J. *Nature* **172**, 920 (1953).
3. Wilberforce, S. *Quarterly Review* **180** (215), 225 (1860).
4. Wrangham, R.W. *New Scientist* **83** (1167), 450 (1979).
5. Owen, R. *Edinburgh Review* **111** (226), 487 (1860).

Richard W. Wrangham is in King's College, Cambridge.

---

have properties that are readily observed *in vitro* and are clearly distinct from those of the unphosphorylated protein. The influence of phosphorylation on the potentiation of the actin-activated myosin MgATPase has been the major focus of attention. Upon phosphorylation of the myosin light chain, the MgATPase activity of the protein in the presence of actin is increased ten- to twentyfold[12].

A third manifestation of the effect of myosin phosphorylation has now been observed *in vitro* with myosin from smooth muscle and nonmuscle cells. Working with myosins from thymus, platelets and gizzard, John Kendrick-Jones *et al.* show in this issue of *Nature* (p.233) that bipolar thick filaments are formed under physiological conditions only if the myosins are phosphorylated. These synthetic thick filaments are stable in the presence of millimolar concentrations of MgATP. Shorter filaments are formed of unphosphorylated myosins *in vitro* at low ionic strength, but these are completely dissociated well below physiological concentrations of MgATP. These results are a striking extension and confirmation of the work by Hiroshi Suzuki and his collaborators at the Tokyo Institute of Technology[13] who first observed that the state of gizzard myosin phosphorylation has a profound effect upon the ability of the protein to form extended aggregates.

The observations of Suzuki and of Kendrick-Jones are particularly important because they resolve some puzzles and raise some interesting questions. If smooth muscle and non-muscle myosin must be phosphorylated in order to form thick filaments *in vivo,* then the absence of such filaments in many electron micrographs of smooth muscle and nonmuscle cells might be explained by the absence of phosphorylated myosin. Furthermore, another possible function of phosphorylation in striated muscle becomes clear — phosphorylated, striated muscle myosin may constitute thick filaments more stable and/or more ordered than the unphosphorylated myoisin.

The questions are intriguing. How does filament formation contribute to the observed actin-activation of the smooth muscle and nonmuscle MgATPase? Is actin-activation due to an increased order in the myosin array and, therefore, to an increased accessibility of myosin to actin? Another very important question raised by Kendrick-Jones has to do with how modification of the head portion of myosin might influence the association and packing of the opposite, tail portion of the molecule. No doubt subsequent studies by these and other investigators will address these problems and will shed even more light upon the nature of the finely tuned control in the contractile protein complex. □

0028-0836/80/380192-02$01.00

Nature Vol. 287 18 September 1980

ARTICLES

Expression of human fibroblast interferon gene in *Escherichia coli*

Rik Derynck*, Erik Remaut*, Erik Saman*, Patrick Stanssens*, Erik De Clercq†, Jean Content§ & Walter Fiers*

* Laboratory of Molecular Biology, State University of Ghent, Ledeganckstraat 35, B-9000 Ghent, Belgium
† Rega Institute for Medical Research, Katholieke Universiteit Leuven, Minderbroedersstraat 10, B-3000 Leuven, Belgium
§ Institut Pasteur du Brabant, rue du Remorqueur 28, B-1040 Brussels, Belgium

The human fibroblast interferon gene was inserted in a thermoinducible expression plasmid under control of the phage lambda P_L promotor. The primary translation products predicted on the basis of the plasmid constructions were hybrid proteins starting with β-lactamase or phage MS2 polymerase information followed by the total preinterferon. On induction, antiviral activity, whose physico-chemical, immunological and biological characteristics closely corresponded to those of authentic human fibroblast interferon, was synthesized. Processing to a size compatible with mature but unglycosylated authentic product was observed.

ON exposure to viruses or other specific inducers most vertibrate cells secrete protein(s) with broad antiviral action known as interferons. Human interferons are being intensively studied for their antiviral[1], anticellular[2] and immunomodulating[3] activities. Clinical trials have been carried out mainly with leukocyte interferon but also with fibroblast interferon, and some promising results have been obtained with both types in the treatment of viral diseases and cancer[1,4–9]. Tests with fibroblast interferon have been severely restricted by its very limited availability.

In a previous report[10], we described the construction and characterization of chimaeric plasmids containing human fibroblast interferon (HF–IF) cDNA. Two other groups have constructed plasmids containing either human leukocyte[11] or human fibroblast[12] interferon cDNA and in the former case, interferon-related polypeptides, as judged by biological and immunological criteria, were detected in *E. coli* strains harbouring the chimaeric plasmids. We have now inserted the HF–IF coding sequence derived from our original clones into appropriate sites on specifically constructed expression vehicles which contain the strong leftward promoter (P_L) of bacteriophage λ. The functioning of the promoter could be controlled by using host strains which synthesize a temperature-sensitive repressor (cI-ts). We describe here how plasmids containing P_L in front of the HF–IF coding sequence direct the synthesis of polypeptides with human fibroblast interferon activity in *E. coli*.

Construction of plasmids allowing expression of HF–IF

Construction of the different plasmids containing HF–IF DNA under the control of lambda P_L is schematically represented in Fig. 1. The formation and use of acceptor plasmids pPLa2311, pPLa8 and pPLc24 will be published in detail elsewhere (E. Remaut *et al.*, in preparation).

None of the chimaeric plasmids previously described contains an uninterrupted HF-IF gene[10]. A complete and continuous coding sequence for HF–IF was reconstituted by inserting an *Eco*RI-*Pst*I fragment from pHFIF-6 and a *Pst*I-*Hae*II fragment from pHFIF-7 into the plasmid pPLa2311. From the resulting plasmid, designated pPLa-HFIF-67-1, a *Bgl*II fragment was excised and ligated into the *Bam*HI site of the β-lactamase region of pPLa8 in the sense orientation with respect to the P_L promoter. The known nucleotide sequence around the *Bam*HI-*Bgl*II junction in this plasmid, pPLa-HFIF-67-12, predicts that a polypeptide initiated at the AUG of the β-lactamase part will terminate on a double amber stop codon in the 5′-untranslated region of the HF–IF gene, 23 nucleotides before the HF–IF initiating AUG (data not shown).

pPLa-HFIF-67-12Δ19 was derived from pPLa-HFIF-67-12 by deleting a *Hin*dII fragment starting within the β-lactamase gene and extending up to three nucleotides before the HF–IF initiating AUG (Fig. 1). From the known nucleotide sequence of the β-lactamase gene (as determined on the progenitor pBR322)[13] and of the HF–IF gene[10], a continuous reading frame starting at the initiating AUG of the β-lactamase gene and running up to the terminating UGA of the HF–IF gene is predicted. The expected fusion polypeptide consists of 82 amino acid residues of the β-lactamase protein, one amino acid coded for at the fused *Hin*dII site, and the complete polypeptide (including the putative signal sequence) specified by the HF–IF gene. The predicted sequence around the junction is: β-lactamase gene moiety-GUU.AAC. AUG-HFIF gene, where the GUU triplet codes for amino acid 82 of the β-lactamase protein.

Alternatively, a hybrid plasmid with the controllable lambda P_L promoter in the clockwise orientation was constructed. The acceptor plasmid was pPLc24, which contains the P_L promoter followed by an *Eco*RI-*Bam*HI fragment (derived from pMS2-7 [ref. 14]) containing the ribosome binding site and part of the MS2 polymerase gene. The pPLa-HFIF-67-1 *Bgl*II fragment containing the HF–IF gene was inserted into the *Bam*HI site of pPLc24, resulting in loss of *Bam*HI and *Bgl*II sensitivity but formation of *Sau*3AI sites at the joints (Fig. 1). In this new plasmid, pPLc-HFIF-67-8, a continuous reading frame starting at the initiating AUG of the MS2 polymerase gene and terminating at the UGA of the HF-IF gene, can be predicted on the basis of the known nucleotide sequences of the MS2 polymerase gene[15] and of pHFIF-6 and pHFIF-7 (ref. 10). The expected fusion protein consists of the N-terminal 98 amino acids of the MS2 polymerase moiety, 27 amino acids coded for by sequences between the *Bgl*II site and the initiating AUG of the HF-IF gene, followed by the complete HF–IF coding region,

0028-0836/80/380193—05$01.00

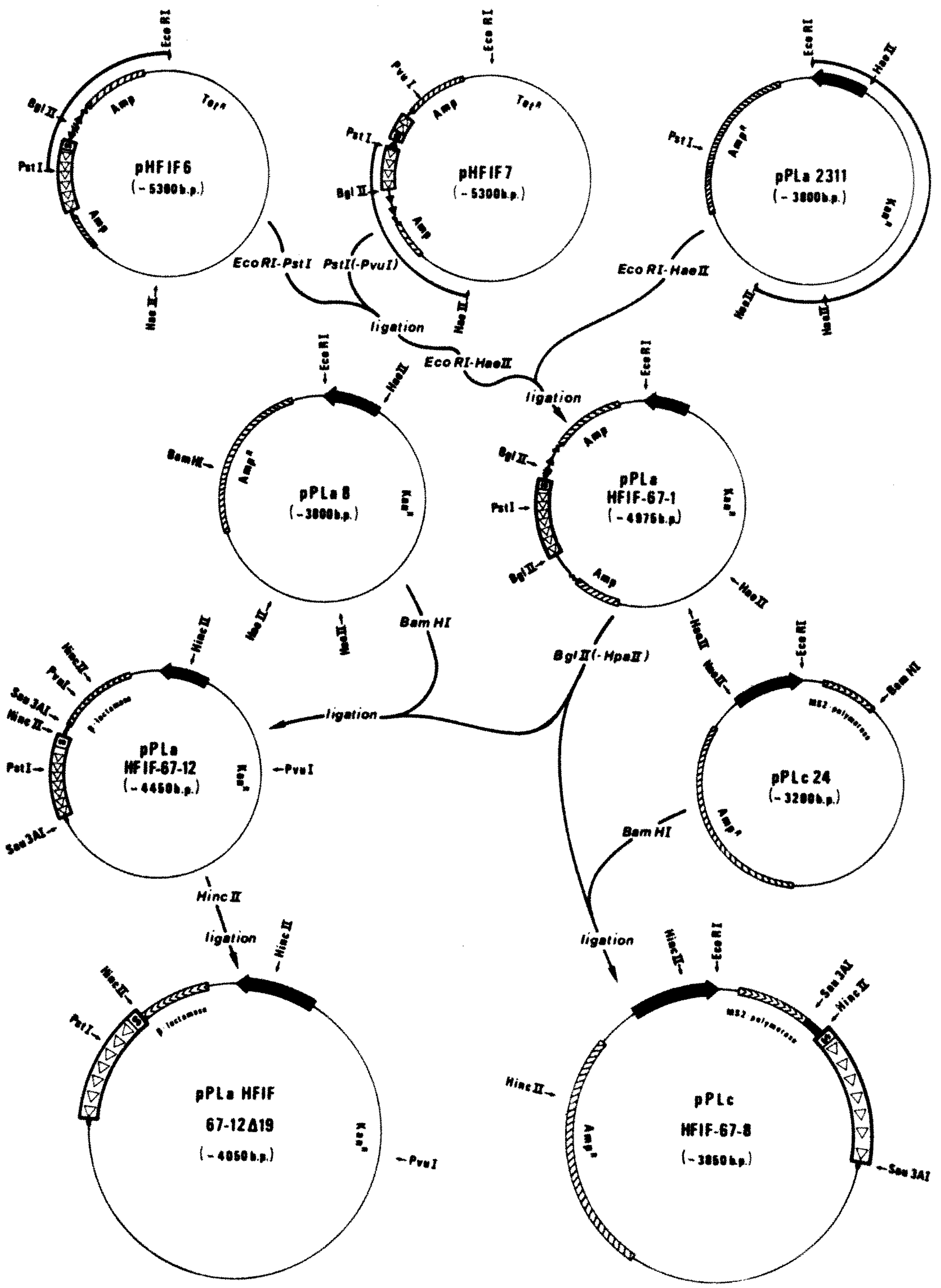

Fig. 1 Schematic outline of the construction of the different plasmids. The HF–IF DNA is indicated by a heavy line, the boxed area being the coding region with the putative signal peptide (S); the triangles indicate the 5'→3' direction of the insert. The heavy arrow indicates the lambda P_L-promoter control element. The ampicillin-resistance region is shown as a shaded area. An interruption of the base line in the insert shows the cross-over region of the inversions of our original HF–IF cDNA-containing plasmids[10]. dA·dT tails are indicated by a wavy line. Amp, β-lactamase region coding for resistance to ampicillin and carbenicillin; Kan, region coding for kanamycin resistance. To construct pPLa-HFIF-67-1, pHFIF-6 DNA was cleaved with *Eco*RI and *Pst*I and ligated to pHFIF-7 which had been cleaved with *Pst*I and *Pvu*I. Following ligation, the mixture was digested with *Eco*RI and *Hae*II and ligated to pPLa2311 which had been digested with *Eco*RI and partially with *Hae*II. The segments of the outer circles indicate the fragments retained in the pPLa-HFIF-67-1 construction: only those restriction sites relevant to the constructions are indicated. Transformants were obtained in $C600r_K^-m_K^+(\lambda)$ with selection for kanamycin resistance and screened for sensitivity to carbenicillin. The structure of a representative plasmid, pPLa-HFIF-67-1, was confirmed by digestions with *Eco*RI, *Pst*I, *Bgl*II and *Hin*cII (=*Hin*dII). To construct pPLa-HFIF-67-12, the HF–IF gene was excised from pPLa-HFIF-67-1 with *Bgl*II, followed by fragmentation of the remaining part of the plasmid with *Hpa*II, which does not cut the HF–IF gene. The DNA was ligated to pPLa8, which had been opened with *Bam*HI. After ligation, the mixture was redigested with *Bam*HI to eliminate recircularized pPLa8 acceptor plasmids. Transformants were obtained in $C600r_K^-m_K^+(\lambda)$ by selection for kanamycin resistance. The structure of pPLa-HFIF-67-12 was examined by analysis with *Pst*I and *Hin*cII. To construct pPLa-HFIF-67-12Δ19, pPLa-HFIF-67-12 was partially digested with *Hin*cII and ligated at a low DNA concentration (0.01 μg ml^{-1}). The mixture was then digested with *Xor*II, an isoschizomer of *Pvu*I producing 3'-protruding ends[26], and religated at low DNA concentration, thereby substantially reducing the probability of religation of the original pPLa-HFIF-67-12 plasmids. The structure of pPLa-HFIF-67-12Δ19 was examined by digestion with *Hin*cII and *Pvu*I. To construct pPLc-HFIF-67-8, the DNA of pPLa-HFIF-67-1 was digested with *Bgl*II and ligated into the *Bam*HI-opened pPLc-24 DNA. The ligation mixture was redigested with *Bam*HI to eliminate religated parental pPLc-24 plasmids. Transformants were selected for resistance to carbenicillin. The insertion and orientation of the *Bgl*II HF–IF fragment was established by *Hin*cII digestion. Restriction enzymes (Biolabs, Boehringer or BRL) were used according to the manufacturer's specifications. Ligations were carried out at 22 °C with T4 DNA ligase in Tris-Cl (50 mM, *p*H 7.6), $MgCl_2$ (5 mM), β-mercaptoethanol (7 mM), ATP (50 μM), (ref. 27). All plasmids were subsequently transferred into *E. coli* M5219 (K12 M72 lac_{am} trp_{am} Sm^R [λCI857ΔHI bio 2521])[16]. Enzymatic reactions were stopped by heating at 65 °C for 10 min.

including the signal peptide. The predicted sequence around the junction is

```
                               -Trp-Asp-Leu-Gln-Phe-Arg-Arg-Gln-Pro-
MS2 polymerase gene moiety-UGG.GAU.CUU.CAG.UUU.CGG.AGG.CAA.CCU.

Phe-Glu-Ala-Phe-Ala-Leu-Ala-Gln-Gln-Val-Val-Gly-Asp-Thr-Val-Arg-
UUC.GAA.GCC.UUU.GCU.CUG.GCA.CAA.CAG.GUA.GUA.GGC.GAC.ACU.GUU.CGU.

Val-Val-Asn-Met-
GUU.GUC.AAC.AUG-HFIF coding region
```

The first amino acid, tryptophan, corresponds to position 98 of the MS2 polymerase.

All constructed chimaeric plasmids were transformed into *E. coli* C600$r_K^-m_K^+$(λ) and, after characterization, transferred into *E. coli* M5219 (ref. 16), allowing the temperature-dependent controlled expression of the lambda P_L (E. Remaut *et al.*, in preparation).

Detection of IF activity in bacterial extracts

Transcription from the P_L promoter on the plasmids can be turned on by shifting the growing culture from 28 to 42 °C. The synthesis of IF-related product(s) was examined by assaying an S100 extract of the bacteria for antiviral activity (Table 1). The cells were lysed either by lysozyme treatment followed by freeze-thawing or by heating in 1% SDS, 1% β-mercaptoethanol, 5 M urea. The extracts of temperature-induced *E. coli* M5219 containing pPLa-HFIF-67-12Δ19 or pPLc-HFIF-67-8 showed a clear antiviral activity, which was reproducibly higher with the latter plasmid. The same non-induced strains as well as induced M5219 containing a reference plasmid (pPLa8) did not show any detectable activity. In M5219 containing pPLa-HFIF-67-12, trace amounts of antiviral activity were occasionally detected after temperature shift (data not shown), presumably due to a rare reinitiation event. The much higher activity obtained after lysis with the SDS, β-mercaptoethanol, urea mixture indicates a possible nonspecific sticking of the antiviral product(s) to bacterial components, for example, cell membranes or nucleic acids. In parallel experiments in which authentic HF–IF was added to a control bacterial extract obtained by lysozyme treatment, only 10–40% of the activity was recovered.

Low but significant amounts of antiviral activity were detected in the supernatant after osmotic shock of induced M5219 transformed with pPLc-HFIF-67-8 (Table 1). When a more severe method of periplasmic extraction was used (that is, spheroplast formation), some activity was also detected with induced M5219 transformed by pPLa-HFIF-67-12Δ19. These results suggest that at least some of the bacterial HF–IF may be secreted into the periplasmic compartment, perhaps concomitantly with the removal of the signal peptide; other explanations, however, cannot be excluded.

Characterization of the bacterial IF activity

The antiviral activity detected in the above-mentioned extracts of induced bacteria was tested for several biological and physical properties characteristic of HF–IF (Table 2). First, the antiviral activity was non-dialysable; after dialysis for 16 h at neutral *p*H the antiviral activity was retained, albeit often at reduced levels (which was also the case for authentic HF–IF preparations). The observed decrease is presumably due to nonspecific sticking to the dialysis membranes, as HF–IF is known to be rather hydrophobic[17], and the unglycosylated bacterial form may be even more so. The antiviral activity could be recovered after precipitation with 67% saturated ammonium sulphate, a concentration known to precipitate HF–IF[18].

When tested for stability at *p*H 2, a common property of fibroblast and leukocyte interferon[1], bacterial HF–IF proved to remain active (Table 2), although again there was often partial loss of activity, but this was also the case with reconstituted authentic HF–IF controls.

The sensitivity of the bacterial HF–IF activity to protease was tested by treating the diluted bacterial extracts with increasing amounts of trypsin. The activity was abolished at the same concentration of trypsin that abolished the activity of authentic HF–IF added to an inactive control lysate.

HF–IF, in contrast to leukocyte interferon, is stable after heating in 1% SDS, 1% β-mercaptoethanol, 5 M urea[19], although we only obtained 10–20% recovery of activity with authentic HF–IF, either alone or in the presence of an inactive bacterial extract (data not shown). The bacterial HF–IF activity remained active in these conditions, as lysis of induced bacteria in this solution resulted in extracts with the highest antiviral titre (Table 1).

The antigenic properties of the *E. coli* IF activity were compared with those of authentic HF–IF. Serial dilutions of goat anti-HF–IF antiserum were incubated with diluted extracts containing bacterial HF–IF activity and with control HF–IF preparations in the presence or absence of an inactive bacterial lysate. The bacterial IF activity was neutralized by the specific antiserum, but some differences were noted in the neutralizing antibody titres for bacterial IF and authentic HF–IF (Table 2). Small differences in neutralization titre were also reported for bacterial leukocyte IF when compared with authentic leukocyte IF[11]. This can be explained by a difference either in antigenicity or in specific IF activity of these bacterial proteins relative to authentic IF.

Table 1 Interferon activity in extracts of *E. coli* M5219 transformed by expression plasmids containing the HF–IF coding sequence

		Interferon activity (units per ml extract) in			
Plasmid	Temperature	S100 extracts after lysis by lysozyme and freeze–thawing (I)	S100 extracts after lysis with SDS, β-mercaptoethanol, urea (II)	Periplasmic fraction: osmotic shock (III)	Periplasmic fraction: spheroplast formation (IV)
pPLa-HFIF-67-12Δ19	28 °C	<3; <2	<30; <100	<2	2
	42 °C	200; 20	200; 2000	<2	10
pPLc-HFIF-67-8	28 °C	<3; <2	<100; <100	<2	<2
	42 °C	200; 50	2,000; 3,000	30	30
pPLa8	42 °C	<3; <2	<100; <100	<2	<2

LB medium (150 ml) was inoculated with 1/500 volume of a fresh seed culture, saturated at 28 °C, and maintained with vigorous shaking at 28 °C until a cell concentration of 2×10^8 ml^{-1} was reached. Induction was by shifting the temperature to 42 °C and incubation of the cultures for 3 h to a final concentration of $4\text{–}6 \times 10^8$ cells ml^{-1}. The cells were collected and washed with Tris-HCl (50 mM, *p*H 7.4), NaCl (30 mM) and repelletted. Several different extraction procedures were used: I, the bacterial pellet was resuspended in a final volume (4 ml) with HEPES-NaOH (50 mM, *p*H 7.0), NaCl (30 mM) 3% calf serum, β-mercaptoethanol (3 mM), to which lysozyme (Sigma) was added to 1 mg ml^{-1}. After incubation at 0 °C for 30 min, the suspension was subjected to one or two freeze–thawing cycles. The S100 fraction was prepared by ultracentrifugation at 60,000 r.p.m. for 1 h in a Beckman SW60 Ti rotor. II, The cells were resuspended as in I and lysed in HEPES-NaOH (50 mM, *p*H 7.0), NaCl (30 mM), 3% calf serum, 1% SDS, 1% β-mercaptoethanol, urea (5 M) at 90 °C for 1–2 min. Clearing by ultracentrifugation was as in I. III, Osmotic shock procedure[21]: the bacterial cell pellet was resuspended in 20% sucrose, EDTA (100 mM), Tris-HCl (100 mM, *p*H 7.4), to a cell concentration of 1×10^{10} ml^{-1}. After 10 min at 0 °C, the suspension was centrifuged for 10 min at 10,000 r.p.m. The pellet was resuspended in water to a cell concentration of 1×10^{10} ml^{-1}. After 10 min on ice, the suspension was again cleared for 10 min at 10,000 r.p.m. To this osmotic shock supernatant was added HEPES-NaOH (50 mM, *p*H 7.0), NaCl (30 mM), β-mercaptoethanol (3 mM) and 3% calf serum. IV, Cells were resuspended in 3.6 ml of 0.1 M Tris-HCl, *p*H 8.0, 20% sucrose, to which 0.4 ml of lysozyme (5 mg ml^{-1} in EDTA [20 mM]) was added. After incubation for 30 min at 0 °C, the suspension was centrifuged for 10 min at 10,000 r.p.m. The supernatant was adjusted to 3% calf serum. IF activity was measured by a cytopathic effect (CPE)-inhibition assay on human fibroblasts trisomic for chromosome 21 in microtitre trays. The cells were challenged with vesicular stomatitis virus (Indiana strain) and the CPE was recorded at 24 h. All assays included an internal HF–IF reference which was calibrated against the NIH HF–IF reference G023-902-527. The limit of detection, normally 1 unit ml^{-1}, was often elevated due to toxicity of certain samples (for example, for the samples obtained with method II, the limit of detection was 30–100 units ml^{-1}). The titres are expressed in units ml^{-1}, although it should be noted that they were obtained by 0.5 $\log_{10}$ dilutions.

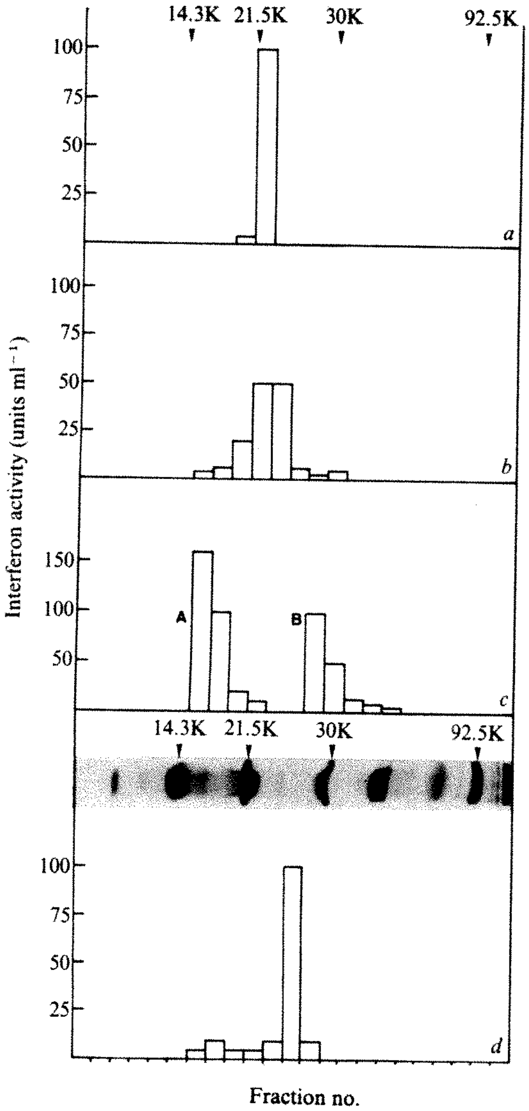

Fig. 2 Polyacrylamide gel patterns of bacterial HF–IF and authentic HF–IF. The following 100-μl samples were loaded on slots of 2 cm width: *a*, authentic HF–IF in Eagle's minimal essential medium, 10% calf serum; *b*, authentic HF–IF in control bacterial extract of M5219/pPLa8 (42 °C); *c*, bacterial extract of M5219/pPLc-HFIF-67-8 (42 °C); *d*, bacterial extract of M5219/pPLa-HFIF-67-12Δ19 (42 °C). ^{14}C-labelled protein markers electrophoresed in an equivalent amount of bacterial extract of M5219/pPLc-HFIF-67-8 (42 °C) are shown as an insertion in *d*. Bacterial extracts were prepared by treatment with SDS, β-mercaptoethanol, and urea (compare with procedure II in legend to Table 1). All samples were boiled for 1 min before electrophoresis, which was run according to Laemmli[28] in 12.5% polyacrylamide gel. IF activity profiles (*a*, *b*, *c*, *d*) were obtained after elution of successive 0.5 cm gel slices for 15 h in 500 μl of 0.5% bovine serum albumin in Tris (0.0125 M), glycine (0.096 M), 0.05% SDS followed by the antiviral IF assay (compare with legend to Table 1). Arrows with molecular weight corresponding to ^{14}C-labelled markers are indicated on top.

HF–IF is largely species specific, exhibiting little (if any) antiviral effect on heterologous cells[1]. Consistent with this property, bacterial IF showed no detectable antiviral protection on cells of monkey, feline, rabbit or mouse origin (Table 3). With respect to the feline cells, bacterial and authentic HF–IF behave differently from human leukocyte interferon.

Further evidence substantiating the presence of active HF–IF in induced *E. coli* extracts was provided by demonstrating the induction of 2', 5'-oligoadenylate (2–5A) synthetase. Kerr *et al.*[20] first reported that interferon increases the level of this enzyme in susceptible cells. As shown in Table 4, appropriate bacterial extracts were able to enhance the incorporation of [α-^{32}P]ATP in ppp5'A2'p5'A2'p5'A. The 2–5A synthetase-inducing activity of the bacterial extracts was proportional to their antiviral activity. This bacterial IF activity was likewise neutralized by anti-HF–IF antiserum.

Size estimations of bacterial HF–IF

To estimate the molecular weight of the bacterial IF activity in comparison with authentic HF–IF, bacterial extracts were fractionated by polyacrylamide gel electrophoresis in denaturing conditions and the antiviral activity determined for eluates from successive gel slices (Fig. 2). Whilst authentic HF–IF showed a single peak of activity after electrophoresis, the bacterial IF activity appeared in two different peaks. Very accurate molecular weights could not be assigned because of insufficient resolution of the gel; this was mainly due to an overloading effect

Table 2 Characterization of the bacterial HF–IF activity

	Interferon titre (units ml^{-1})	
a, Dialysis at neutral *p*H:	Before	After
M5219/pPLc-HFIF-67-8 (42 °C) (I)	200	200
(II)	1,000	200
(III)	30	20
M5219/pPLa-HFIF-67-12Δ19 (42 °C) (I)	200	20
Control HF–IF in M5219/pPLa8 (42 °C) (I)	200	100
	200	10
b, Precipitation with $(NH_4)_2SO_4$ at 67% saturation:		
M5219/pPLc-HFIF-67-8 (42 °C) (I)	100	100
	100	200
M5219/pPLa-HFIF-67-12Δ19 (42 °C) (I)	100	100
Control HF–IF in M5219/pPLa8 (42 °C) (I)	20	20
	30	20
c, *p*H 2 treatment:		
M5219/pPLc-HFIF-67-8 (42 °C) (I)	100	20
(II)	5	5
M5219/pPLa-HFIF-67-12Δ19 (42 °C) (I)	100	10
Control HF-IF in M5219/pPLa8 (42 °C) (I)	1,000	100
d, Heat treatment in 1% SDS, 1% β-mercaptoethanol, 5 M urea (see Table 1)		
	Inactivating end point concentration (mg ml^{-1})	
e, Trypsin digestion:		
M5219/pPLa-HFIF-67-12Δ19 (42 °C) (II)	0.03	
M5219/pPLc-HFIF-67-8 (42 °C) (II) (1,000 units ml^{-1})	0.03	
Control HF–IF in M5219/pPLa8 (42 °C) (II) (1,000 units ml^{-1})	0.03	
M5219/pPLc-HFIF-67-8 (42 °C) (III) (30 units ml^{-1})	0.03	
Control HF–IF in M5219/pPLa8 (42 °C) (III) (30 units ml^{-1})	0.03	
	Neutralization titre (units ml^{-1})	
f, Neutralization by antiserum		
pPLc-HFIF-67-8 (42 °C) (I)	$10^{5.2}$	
(II)	$10^{5.0}$	
(III)	$10^{5.3}$	
pPLa-HFIF-67-12Δ19 (42 °C) (I)	$10^{4.5}$	
Control HF–IF in extract of M5219/pPLa8 (42 °C)	$10^{5.7}$	
pPLc-HFIF-67-8 (42 °C) (II): elution peak A	$10^{4.5}$; $10^{4.2}$	
elution peak B	$10^{4.5}$; $10^{4.7}$	
Control HF–IF eluted from polyacrylamide gel	$10^{5.0}$	
Control HF–IF	$10^{5.7}$	
Control leukocyte IF	<10	
g, Anti-viral activity in heterologous cells (see Table 3)		
h, 2–5A synthetase induction (see Table 4)		

The following experimental methods were used for the characterization: *a*, dialysis at neutral *p*H took place overnight at 4 °C against phosphate buffered saline (PBS). *b*, Two volumes of a saturated $(NH_4)_2SO_4$ solution were added to one volume of extract. After 30 min on ice, the pellet was centrifuged at 12,000*g* for 10 min and redissolved in PBS. *c*, The bacterial extracts were either dialysed for 15 h against glycine-HCl (50 ml, *p*H 2.2), followed by dialysis against PBS for 3 h, or acidified with HCl, followed by neutralization with NaOH. After removal of the precipitate the antiviral activity was determined. *e*, Trypsin digestion was for 1 h at 37 °C with serial dilutions of the enzyme added to the diluted extract. The lowest trypsin concentration that completely abolished the antiviral activity is indicated. *f*, The antibody neutralization assays were carried out essentially as described by Havell *et al.*[22]. About 10 IF units ml^{-1} of the preparations were incubated for 1 h at 37 °C with serial dilutions of goat anti-HF–IF antiserum, after which the residual antiviral activity was determined. Values are presented as neutralizing titres, that is, the highest dilution of antiserum which neutralized the protective effect of IF by 50% multiplied by the interferon titre of the sample assayed. Roman numerals in parentheses refer to the extraction methods described in Table 1.

Table 3 Antiviral protection of bacterial IF activity and authentic interferons

	Interferon activity (units per ml), assayed on					
	Human T-21	Human VGS	Monkey BSC-1	Rabbit primary kidney	Feline lung	Mouse L-929
M5219/pPLc-HFIF-67-8 (42 °C) (II)	3,000	300	<100	<100	<100	ND
(III)	30	<10	<10	<10	<10	ND
M5219/pPLc-HFIF-67-8 (42 °C) (II) elution peak A	2,000	200	<10	<10	<10	<10
M5219/pPLc-HFIF-67-8 (42 °C) (II) elution peak B	2,000	500	<10	<10	<10	<10
Human fibroblast interferon	3,000	500	30	30	<3	<2
Human leukocyte interferon	5,000	500	30	10	1,000	30
Human immune (type II) interferon	3,000	1,000	10	<3	<3	<2
Mouse L-929 interferon	<2	<2	<2	<2	<2	500

The antiviral activity was assayed as described in the legend to Table 1, except that the titres were directly determined from the dilution end points. T-21 are human fibroblasts trisomic for chromosome 21; VGS are normal human diploid fibroblasts[23]. Feline lung cells were obtained from Flow Laboratories (cat. no 0-10907). ND, not determined.

which resulted in a different migration of the proteins, as revealed by internal ^{14}C-labelled protein markers. Both peaks were neutralized to the same extent with anti-HF–IF antiserum (Table 2) and did not show detectable IF activity on heterologous cells (Table 3). The first peak, corresponding to an approximate molecular weight (MW) of 15,000–18,000, may have arisen by haphazard proteolytic cleavage of the fusion protein, or by limited *bona fide* processing at the now internal signal peptide, or by a combination of both processes. As shown previously, the absence of the carbohydrate moieties results in a protein which migrates in polyacrylamide gel to a position of about 4,000 MW below the authentic glycosylated HF–IF[10]. The 15,000–18,000-MW component, clearly present in *E. coli* M5219/pPLc-HFIF-67-8 extract, could also be detected at low but still significant levels in M5219/pPLa-HFIF-67-12Δ19 extracts. The second peak, with an apparent higher molecular weight, could correspond to the fused prokaryotic HF–IF polypeptide, or a slightly processed form. The tentative identification of the slower moving HF–IF activity peak as the fusion protein is strengthened by a different migration of the activity in the extract of M5219/pPLa-HFIF-67-12Δ19 (with a predicted fusion protein of about 28,000 MW) compared to the M5219/pPLc-HFIF-67-8 extract (with a predicted fusion protein of about 33,000 MW) (Fig. 2). The fusion proteins may themselves have some activity or be processed to an active product at the time when the bacterial extract (or gel eluate) is applied onto the human cells for the antiviral assay.

Table 4 2–5A synthetase inducing activity of bacterial lysates and its neutralization by anti-HF–IF antiserum

	^{32}P incorporation (in c.p.m.) into the 2–5A trimer (background subtracted)
a, M5219/pPLc-HFIF-67-8 (42 °C) (III) (30 units ml^{-1})	3,618
Control HF–IF added to M5219/pPLa8 (42 °C) (III) (30 units ml^{-1})	3,695
M5219/pPLa8 (42 °C) (III) (<2 units ml^{-1})	(−1,360)
Control HF–IF (18 units ml^{-1})	1,120
(60 units ml^{-1})	4,338
(180 units ml^{-1})	10,273
(600 units ml^{-1})	21,698
b, Control HF–IF (100 units ml^{-1})	12,468
M5219/pPLa8 (42 °C) (I)	1,011
M5219/pPLa-HFIF-67-12Δ19 (42 °C) (I)	42,193
plus 1 n.u. per ml anti-HF–IF	29,260
plus 100 n.u. per ml anti-HF–IF	727
M5219/pPLc-HFIF-67-8 (42 °C) (I)	17,478
plus 1 n.u. per ml anti-HF–IF	12,115
plus 100 n.u. per ml anti-HF–IF	7,992
plus 10000 n.u. per ml anti-HF–IF	2,517

All samples were diluted sixfold (*a*) or tenfold (*b*) before assay. Antiviral titres (before dilutions) are given in parentheses. Neutralization with goat anti-HF–IF antiserum was at 37 °C for 1 h; n.u. neutralizing units. Roman numerals in parentheses refer to the extraction methods described in Table 1 legend. The obtained values are listed after subtraction of the endogenous background activity: 3,342 c.p.m. in *a* and 2,073 c.p.m. in *b*. The 2–5A synthetase assay was modified from Kimchi *et al.*[24] and Minks *et al.*[25]. Confluent monolayers of HeLa cells in microtitre plates (96 wells) were treated with the diluted bacterial extract or with control HF–IF for 20 h. After cooling and washing with NaCl (140 mM), Tris-HCl (35 mM, *p*H 7.5), the cultures were lysed in 5 μl (*a*) or 10 μl (*b*) of 0.5% NP40, PMSF (1 mM), NaCl (140 mM), Tris-HCl (35 mM *p*H 7.5). After shaking vigorously for 20 min at 0 °C, the lysates were collected and centrifuged for 20 min at 10,000*g*. 3.5 μl of the supernatant was incubated for 2 h at 31 °C in 6 μl of KOAc (100 mM), $Mg(OAc)_2$ (25 mM), HEPES-KOH (10 mM, *p*H 7.4), ATP (5 mM), fructose-1,6-bis-phosphate (4 mM), DTT (1 mM), poly I·C (20 μg ml^{-1}) and 2 μCi of lyophilized [α-^{32}P]ATP (400 Ci mmol^{-1}). The reaction was stopped by heating for 3 min at 95 °C and the samples were treated with 150 units ml^{-1} of calf intestine alkaline phosphatase (Boehringer) at 37 °C for 1 h. After clearing, 1 μl was spotted on PEI-cellulose thin-layer plates and chromatographed in 1 M acetic acid for 2–3 h. The plates were autoradiographed and the incorporation of ^{32}P in the 2–5A trimer was determined.

Conclusion

We have demonstrated the expression of HF–IF activity in *E. coli*. This synthesis depends on the presence of the HF–IF cDNA gene in the appropriate orientation and of the controlled induction of transcription from the P_L promoter. The antiviral activity obtained from *E. coli* is due to the presence of polypeptide(s) which for all physicochemical, biological and immunological characteristics tested closely resembles authentic HF–IF. Polyacrylamide gel electrophoresis resolved the bacterial IF activity into two different size classes; the smaller component presumably resulted from a post-translational cleavage of the fusion proteins.

The HF–IF produced in *E. coli* is still low in titre (about 100 units per 5×10^8 cells ml^{-1}), but undoubtedly this can be improved by better plasmid constructions. Thus, we hope to produce sufficient quantities of bacterial HF–IF to compare its biological and pharmacological properties with those of authentic glycosylated HF–IF and of bacterial leukocyte IF, and perhaps to evaluate its potential clinical applications.

We thank W. Zeegers, A. Van Lierde-Van Lierde, L. De Wit, M. Borremans-Bensch, C. Seurinck-Opsomer and E. De Vleeschouwer for technical assistance. This research was supported by Biogen N. V.

Received 8 July; accepted 28 July 1980.

1. Stewart, W. E. II *The Interferon System* (Springer, Berlin, 1979).
2. Gresser, I. & Tovey, M. G. *Biochim. biophys. Acta* **516,** 231–247 (1978).
3. Bloom, B. R. *Nature* **284,** 593–595 (1980).
4. Desmyter, J. *et al. Lancet* **ii,** 645–647 (1976).
5. Horoszewicz, J. S. *et al. Cancer Treat. Rep.* **62,** 1899–1906 (1978).
6. Sundmacher, R., Cantell, K., Skoda, K., Hallermann, C. & Neumann-Haefelin, D. *Albrecht v. Graefes Arch. Klin. exp. Ophthal.* **208,** 229–233 (1978).
7. Dolen, J. G. *et al. Am. J. Med.* **67,** 127–131 (1979).
8. Treuner, J. *et al. Lancet* **i,** 817–818 (1980).
9. Gutterman, J. U. *et al. Ann. int. Med.* (in the press).
10. Derynck, R. *et al. Nature* **285,** 542–547 (1980).
11. Nagata, S. *et al. Nature* **284,** 316–320 (1980).
12. Taniguchi, T. *et al. Proc. Jap. Acad.* **55,** Ser B, 464–469 (1979).
13. Sutcliffe, J. *Cold Spring Harb. Symp. quant. Biol.* **49,** 77–90 (1978).
14. Devos, R., Van Emmelo, J., Contreras, R. & Fiers, W. *J. molec. Biol.* **128,** 595–619 (1979).
15. Fiers, W. *et al. Nature* **260,** 500–507 (1976).
16. Greer, H. *Virology* **66,** 589–604 (1975).
17. Davey, M. W., Sulkowski, E. & Carter, W. A. *J. biol. Chem.* **251,** 7620–7625 (1976).
18. Knight, E., Jr *Proc. natn. Acad. Sci. U.S.A.* **73,** 520–523 (1976).
19. Stewart, W. E. II, De Clercq, E. & De Somer, P. *Nature* **249,** 460–461 (1974).
20. Kerr, I. M., Brown, R. E. & Hovanessian, A. G. *Nature* **268,** 540–542 (1977).
21. Neu, H. C. & Heppel, L. A. *J. biol. Chem.* **240,** 3685–3692 (1965).
22. Havell, E. A., Vilcek, J., Falcoff, E. & Berman, B. *Virology* **63,** 475–483 (1975).
23. Billiau, A., Joniau, M. & De Somer, P. *J. gen. Virol.* **19,** 1–8, (1973).
24. Kimchi, A. *et al. Proc. natn. Acad. Sci. U.S.A.* **76,** 3208–3212 (1979).
25. Minks, M. A., West, D. K., Benvin, S. & Baglioni, C. *J. biol. Chem.* **254,** 10180–10183 (1979).
26. Wang, R., Shedlarski, J., Farber, M., Kuebbing, D. & Ehrlich, M. *Biochim. biophys. Acta* (in the press).
27. Sgaramella, V. & Ehrlich, S. *Eur. J. Biochem.* **86,** 501–537 (1978).
28. Laemmli, U. K. *Nature* **227,** 680–682 (1970).

Nucleotide sequence of an avian sarcoma virus oncogene (*src*) and proposed amino acid sequence for gene product

A. P. Czernilofsky, A. D. Levinson, H. E. Varmus & J. M. Bishop

Department of Microbiology and Immunology, University of California, San Francisco, California 94143

E. Tischer & H. M. Goodman

The Howard Hughes Medical Institute Laboratories, Department of Biochemistry and Biophysics, University of California, San Francisco, California 94143

The transforming gene (src) *of avian sarcoma virus (ASV) and adjacent regions of the viral genome have been isolated by molecular cloning of viral DNA. Their nucleotide sequence encompasses the whole of* src *and the portion of the gene* env *that encodes gp37, one of two glycoproteins found in the viral envelope.* Src *encodes a single, hydrophobic protein with structural features that conform to previous descriptions of the gene product (pp60*^{src}*). It appears that a single viral protein is responsible for both the initiation and maintenance of neoplastic transformation by avian sarcoma virus. Neither* src *nor its product bear any obvious structural relationship to several other viral oncogenes and their encoded proteins.* Src *is flanked by a repeated nucleotide sequence that may facilitate frequent deletion of the gene from the viral genome.*

VIRAL oncogenesis takes two general forms. Infection by some tumour viruses is apparently one of several successive events that combine to produce the neoplastic phenotype[1]. The precise role of the virus in this setting is an enigma. Other viruses bear genetic loci ('transforming genes' or 'oncogenes') whose expression may be wholly responsible for the transformation of infected cells[2]. Successful studies of both forms of viral oncogenesis have been carried out, but we owe much of the recent advance in our understanding of neoplastic transformation to the exploration of viral oncogenes—their action on the cell is swift and direct; they can be mutated to obtain useful conditional defects; the nucleic acids of which they are composed can be isolated and sequenced; and they act by means of proteins whose properties must underlie the mechanism of transformation.

Avian sarcoma virus (ASV) is a retrovirus that induces fibrosarcomas in infected hosts and transforms fibroblasts in culture. The genome of ASV carries a genetic locus (*src*) whose action is required for both the initiation and maintenance of neoplastic transformation[3]. Previous work has identified one product of *src*—a phosphoprotein of molecular weight 60,000 (refs 4–6) that is anchored to the cytoplasmic aspect of the plasma membrane of infected cells[7,8]. Both crude[9] and purified[10,11] preparations of pp60^{src} phosphorylate tyrosine exclusively in protein substrates, and cells transformed by ASV contain more phosphotyrosine than do uninfected cells[9,12]. These findings have engendered the hypothesis that phosphorylation of tyrosine in one or more cellular proteins is central to the mechanism by which *src* transforms cells. Important issues remain unresolved, however. Can the action of *src* alone induce neoplastic transformation? Is pp60^{src} the sole protein encoded by *src*? What is the nature of the association between pp60^{src} and the plasma membrane? Where are the phosphoamino acids located in pp60^{src}, and what is their role in the enzymatic activity of the protein? Does the phosphotransfer carried out by pp60^{src} *in vitro* reflect the activity of the protein in the infected cell? Might pp60^{src} possess functional properties other than protein kinase activity? As a step towards the resolution of these issues, we have determined the nucleotide sequence of *src* and regions adjacent to it in the ASV genome, and we have used these data to deduce a possible amino acid sequence for pp60^{src}. Inspection of the derived protein sequence permits some speculations on possible relationships between structure and function of pp60^{src}.

Experimental approach

The RNA genome of retroviruses is transcribed into duplex DNA during the early hours of infection[13]. Circular forms of retrovirus DNA can be isolated from infected cells and cloned into prokaryotic vectors[14,15]. We have described previously the use of molecular cloning to isolate a 3.1-kilobase *Eco*RI fragment of DNA (see Fig. 1) that contains the entirety of *src*, all but 65 nucleotides of c (an untranslated region that lies to the right of *src* on the genetic map of ASV; see ref. 16), and about 1.0 kilobases to the left of *src*[15,17]. We subcloned this DNA into the single-stranded DNA phage M13mp2 (ref. 16) to facilitate sequence analysis by the chain termination technique developed by Sanger and colleagues[18]. Clones representing both the positive and negative strands of viral DNA were isolated and sequenced so as to ensure the accuracy of the results. We also

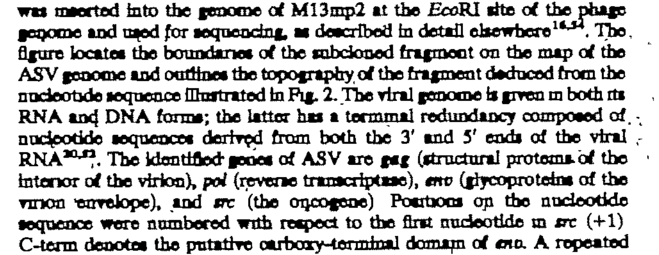

Fig. 1 The genome of ASV and the topography of the subclone used for nucleotide sequencing. A 3.1-kilobase *Eco*RI fragment of cloned ASV DNA was inserted into the genome of M13mp2 at the *Eco*RI site of the phage genome and used for sequencing, as described in detail elsewhere[16,34]. The figure locates the boundaries of the subcloned fragment on the map of the ASV genome and outlines the topography of the fragment deduced from the nucleotide sequence illustrated in Fig. 2. The viral genome is given in both its RNA and DNA forms; the latter has a terminal redundancy composed of nucleotide sequences derived from both the 3' and 5' ends of the viral RNA[20,22]. The identified genes of ASV are *gag* (structural proteins of the interior of the virion), *pol* (reverse transcriptase), *env* (glycoproteins of the virion envelope), and *src* (the oncogene) Positions on the nucleotide sequence were numbered with respect to the first nucleotide in *src* (+1) C-term denotes the putative carboxy-terminal domain of *env*. A repeated sequence described in the text is denoted as d.r., this repeat is direct, that is, it occurs in the same orientation at each position (see Fig. 3). A domain that apparently separates *env* from *src* is denoted i for intercistronic, and an untranslated region at the 3' end of the viral genome is denoted c (refs 16, 17). A possible component of the ribosome-binding site for *src* (see Fig. 3) is designated r.

0028-0836/80/380198—06$01 00

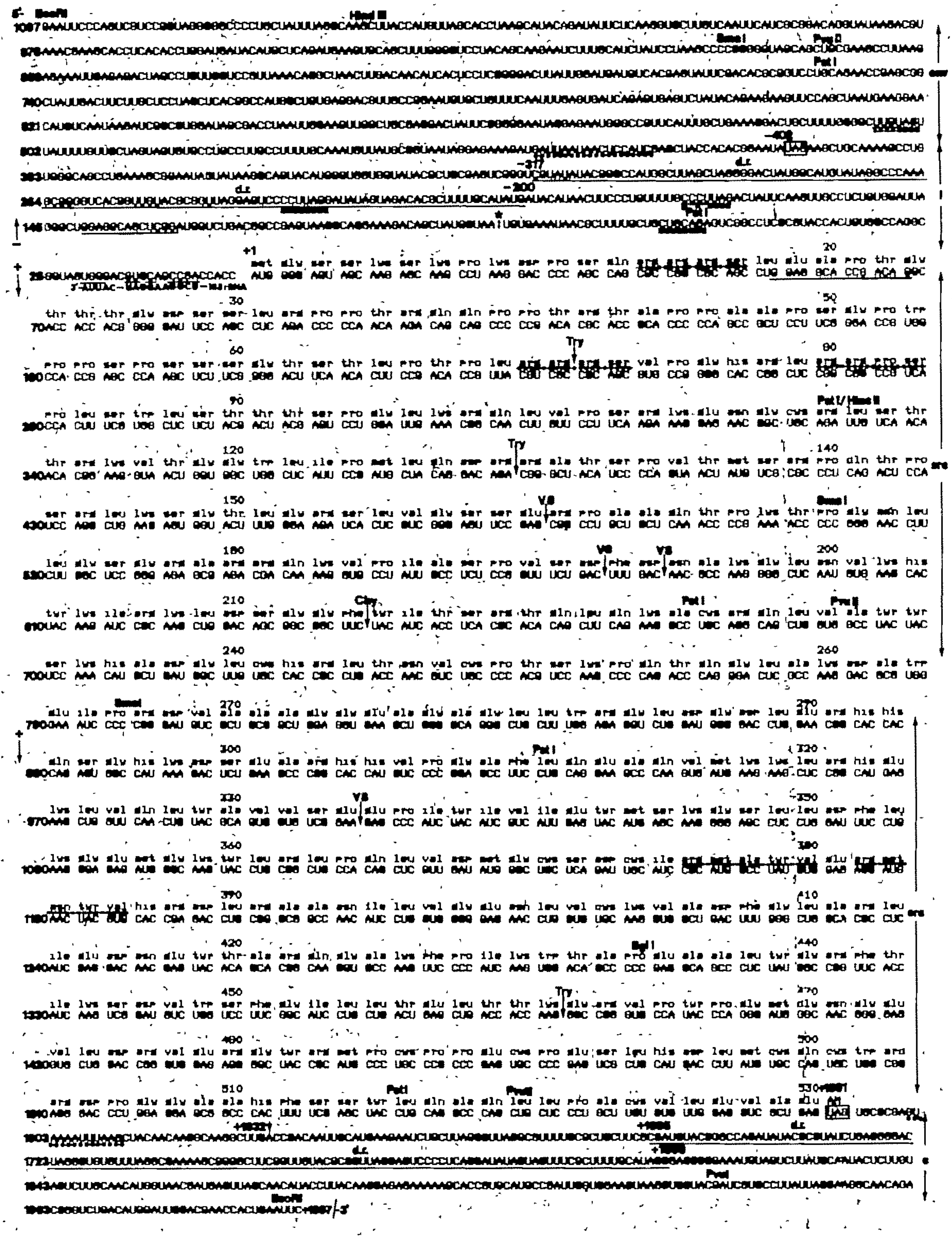

Fig. 2 The nucleotide sequence of *src* and its environs. The chain-termination technique of Sanger and colleagues[18] was used to obtain the entire sequence of both strands of the 3.1-kilobase *Eco*RI DNA fragment described in Fig. 1. Supplementary data were obtained with the procedure of Maxam and Gilbert[19]. Details have been described elsewhere[14]. We used 60 different restriction fragments derived from within the 3.1-kilobase DNA fragment as primers in the chain-termination procedure. The sequence of the DNA is displayed as the plus (sense) strand of viral RNA and is numbered according to the convention explained for Fig. 1, with position 1 being the first nucleotide in the translated frame (or frame 1); frame 2 begins with position 2, frame 3 with position 3. Ts are substituted by Us. An unidentified nucleotide at position −84 is designated by an asterisk. Position −14 is either C or T and position −353 to −352 is either AC or AGC. Also given are: the amino acid sequence encoded by the translatable frame in *src*; possible sites of cleavage by proteases predicted from previous work (ref. 53, and unpublished results of A.D.L. and S. Courtneidge) (Try, trypsin; V8, *Staphylococcus aureus* V8 protease; Chy, chymotrypsin); the locations of sites of cleavage by several widely used restriction endonucleases (all of the identifiable restriction sites can be provided on request); the location of two nearly identical amino acid sequences that each contain a residue of tyrosine (+−−−); the location of the repeated sequence noted in Fig. 1 and described in detail in Fig. 3 (———); the location of prospective phosphoserines in the amino-terminal domain of pp60^{src}, identified as described in the text (••••••); a possible component of the ribosome-binding site for *src*, identified as described by Hagenbuchle *et al.*[25]; two oligonucleotides identified previously in maps of the ASV genome[22–24] (· · · ·); possible splice-acceptor sites (= = = = =); regions homologous to sequence related to the *Alu* family[26] (— — — —); and suggested terminator codons for *env* and *src* (UAG). Numbers preceded by + or − give positions in the nucleic acid sequence; all other numbers indicate the positions of amino acids within the proposed protein sequence of pp60^{src}.

used the procedure of Maxam and Gilbert[19] to obtain supplementary data. The complete strategy for the sequencing and all data are available on request.

Authentication of the nucleotide sequence

Figure 2 illustrates the entire sequence of the 3,094 nucleotides that comprise the 3.1-kilobase pair *Eco*RI DNA fragment, displayed as the sense strand of the viral RNA. Positions within the sequence are numbered with respect to the first nucleotide in *src* (+1) (see below). The nucleotide composition of the fragment is 21.1% T, 25.7% dC, 23.4% dA, and 29,8% dG. We have a variety of reasons to believe that our nucleotide sequence for *src* and its environs is correct:

(1) We have shown elsewhere that the cloned *Eco*RI DNA fragment inserted into M13 for purposes of sequencing contained a functionally competent *src* gene[20]; hence, the structure of *src* (and by inference, the remainder of the DNA fragment) was apparently undisturbed by cloning and propagation in prokaryotic vectors.

(2) The ASV DNA from which we prepared our molecular clones has been mapped extensively by site-specific cleavage with restriction endonucleases[15,21]. The sequence illustrated in Fig. 2 contains all the sites located previously by this means. During the preparation of more than 60 primers for sequencing with the terminator technique, we identified a number of additional restriction sites; these also appear at appropriate positions in the final sequence. Figure 2 summarizes the locations of cleavage sites for several widely used restriction endonucleases. A complete catalogue of restriction sites within the 3.1-kilobase *Eco*RI fragment is available from the authors on request.

(3) The boundaries that we propose for *src* and *env* are in accord with previously developed physical maps of the ASV genome (see below).

(4) Previous analyses of the ASV genome have identified a number of T1 oligonucleotides that also appear in the nucleotide sequence reported here. Moreover, our data are in general agreement with previous, less precise efforts to locate these oligonucleotides on the ASV genome. For example, the oligonucleotide at positions −436 to −420 is contained within the carboxy-terminal domain of *env*, as suggested previously[22], and the oligonucleotide at positions +1,601−+1,612 lies just beyond the 3′ boundary of *src*, rather than within the gene[23]. Other correlations with our data include: six large oligonucleotides within *src* that were identified previously in the genome of SR-A ASV[23], and four oligonucleotides in the vicinity of the carboxy-terminus of *env*, three of which occur in the genome of the Prague-B strain of ASV, the fourth in the genome of the endogenous chicken virus, RAV-0 (ref. 24). The details of these correlations are omitted here but will be supplied on request.

(5) The proposed nucleotide sequence of *src* encodes a protein with structural features that conform to previous descriptions of pp60^{src} (see below).

Structural domains within the nucleotide sequence

Computer-assisted analysis of the sequence allowed us to identify several structural domains, which are discussed below and outlined in Fig. 1.

Positions +1−+1,590 contain a single open reading frame, initiated by AUG and terminated by an amber codon (UAG, (positions +1,591−+1,593)). We deduce that this sequence constitutes *src*: it is located in the appropriate position on the physical map of the ASV genome[17], and translation from the open frame would generate a protein with structural features that conform to previous descriptions of pp60^{src} (see below). Translation from the other two reading frames in the ^{src} domain is blocked principally by opal codons (UGA; 11 of 13 terminators in frame 2, 12 of 15 terminators in frame 3), an unusual feature not encountered in other portions of the DNA fragment. In the unlikely event that all of the 11 opal terminators were to be suppressed, a protein with a molecular weight of ~44,000 could arise from positions +599−+1,805; we have no reason to believe that this ever happens in the infected cell. Of the 16 nucleotides between positions −21 and −6, 10 can base-pair with the nucleotide sequence at the 3′ terminus of 18S ribosomal RNA (see Fig. 3). Hagenbuchle *et al.* have suggested that base-pairing of this sort may be a general feature of the sites at which translation initiates in eukaryotic cells[25]. A similar structure can be formed near the 3′ terminus of *src* (positions +1,341−+1,357), but we cannot yet attribute any specific function to this location.

Positions −1,097 to −401 also contain a single open reading frame that begins at the third base at the left end of the DNA fragment (position −1,095) and terminates with an amber codon (position −402 to −400). The other reading frames are blocked by a mixture of termination codons. We presume that this domain represents the carboxy-terminal portion of the *env* gene that encodes the glycoproteins of the ASV envelope[26]. The location of this domain on the viral genome is appropriate for *env*[17,21], and the amino acid sequence deduced from the open reading frame conforms to available information on the amino acid sequence of a protein (gp37) encoded by *env* (see below).

Positions −399−−1 are closed to translation in all reading frames and apparently constitute an intercistronic region (i in Fig. 1) that separates *src* from *env*. Notable features of this region will be discussed below.

Positions +1,594−+1,997 comprise an apparently untranslated domain previously designated as c[16,17]. We have described the sequence of this domain in detail elsewhere[16].

Miscellaneous aspects of the nucleotide sequence

Several nucleotide sequences are repeated in the untranslated regions on either side of *src*. The most striking of these is a sequence of 126 nucleotides (designated d.r. in Figs 1–3) that is repeated directly (that is, in the same orientation) with 79% fidelity at positions −317−−200 and +1,685−+1,808, and that can be extended to positions −377 and +1,632 with a fidelity of 63%.

A purine-rich sequence of 13 nucleotides occurs juxtaposed to the 3′ end of d.r. Other work has implicated this sequence in the initiation of 'plus strand' DNA synthesis by reverse transcriptase[27,28]. Similar purine-rich sequences are found 11 times at fairly regular intervals (~100–250 nucleotides) throughout the 3.1-kilobase fragment. Perhaps some of these sequences are also involved in the synthesis of plus strand viral DNA, which apparently initiates at multiple sites along the viral genome[29,30].

The 3.3-kilobase mRNA for *src*[31] is formed by joining approximately 0.36 kilobases from the 5′ end of the viral genome to a point located to the left (to the 5′ side) of the *src* gene[32,33]. From the size of the mRNA and the length of the spliced leader, we compute that the splice junction should lie about 0.5 kilobases to the 5′ side of *src*—possibly within the carboxy-terminal domain of *env*[34]. We therefore searched the appropriate regions of the 3.1-kilobase DNA fragment and found four sequences that resemble the proposed prototype (5′-PyPyNPyAG-3′) for splice acceptor sites[35]: TTGTAG at positions −509−−504 (apparently within the carboxy-terminal domain of *env*), CCTTAG at positions −232−−227 and −177−−172, and CTGCAG at positions −62−−57 (located within the i region). We have no means of implicating any of these sequences in splicing. Direct analysis of viral mRNA will be required for definitive identification of the splice junction.

Positions −140−−128 and +54−+67 resemble sequences found within the *Alu* family[36] of interspersed repeated sequences in mammalian DNA and at the origins of replication for several viral DNAs (Fig. 3). The function of these widely distributed nucleotide sequences is not known. One hypothesis suggests that they may serve as origins of DNA replication in the mammalian genome[36]. If so, their presence in the nucleotide sequence of the ASV genome may be gratuitous: retrovirus DNA probably does not function as an independent replicon and may therefore have no need for a replication origin[37,38]. Alternatively, the *Alu* sequences might participate in the

Table 1 Distribution of individual amino acids within the deduced sequence of pp60^{src}

Position	Phe	Leu	Ile	Val	Trp	Pro	Ala	Gly	Met	Cys	Tyr	Ser	Thr	Asn	Gly	His	Lys	Arg	Glu	Asp	Hph	b-a	OH
1–60	0	2	0	0	1	14	4	4	1	0	0	12	7	0	3	0	3	6	1	2	21	6	19
61–120	0	8	0	3	1	7	0	6	0	1	0	8	9	1	1	1	3	10	1	0	19	13	17
121–180	0	7	1	2	1	7	4	6	2	0	0	8	6	2	3	0	2	8	1	1	22	8	14
181–240	2	5	3	4	0	2	5	4	0	1	4	5	2	3	4	2	7	4	0	3	21	10	7
241–300	0	6	1	2	2	3	7	9	0	2	0	3	3	1	3	4	3	4	2	5	21	4	6
301–360	2	7	3	6	0	2	4	4	3	0	4	3	0	0	3	3	6	2	7	1	24	3	3
361–420	1	7	3	6	0	2	5	3	3	3	3	1	1	4	1	1	1	6	4	5	24	−1	2
421–480	3	5	3	4	2	4	5	6	1	0	2	2	5	1	1	0	4	5	4	2	26	3	7
481–530	1	6	0	2	1	6	5	3	2	5	1	3	0	0	3	2	0	3	4	2	21	−1	3
Total no.	9	53	14	29	8	47	39	45	12	12	14	45	33	13	22	13	29	48	24	21	199	—	77
%	1.7	10	2.6	5.5	1.5	8.9	7.4	8.5	2.3	2.3	2.6	8.5	6.2	2.5	4.2	2.5	5.5	9.0	4.5	3.9	37.5	—	14.5

The amino acid sequence illustrated in Fig. 2 was divided arbitrarily into domains of 60 amino acids, beginning at the amino-terminus The table gives, for each domain, the total residues of each amino acid, the sum of the hydrophobic residues (Phe, Leu, Ile, Val, Trp, Pro and Ala; Hph), the predominance of basic over acidic amino acids in each domain (computed as $b-a$; the difference between the sum of His, Lys and Arg and the sum of Glu and Asp), and the sum of the hydrophilic amino acids Ser and Thr (OH).

maturation of mRNAs[36]. We note that three of the candidate splice junctions for *src* mRNA are located in the vicinity of the *Alu*-like sequence at positions −140–−128.

The amino acid sequence of pp60^{src}

We used the nucleotide sequence of the open reading frame in *src* to deduce the sequence of the 530 amino acids contained in the encoded protein. Figure 2 illustrates the deduced amino acid sequence, and Table 1 describes the distribution of individual amino acids within the protein. Several features of the deduced structure conform to previous descriptions of pp60^{src}: the molecular weight is 58,449; the protein is hydrophobic[11]; 9 of the 12 methionines are in the carboxy half of the molecule (ref. 39, and H. Oppermann, personal communication); and the amino acid sequence can account for seven sites of specific cleavage by proteases predicted from previous work (Fig. 2). We conclude that we have probably determined the authentic amino acid sequence for pp60^{src}.

Two separate functional domains have been defined within pp60^{src} (refs 11, 40). One domain (confined to a molecular weight of ~15,000 at the amino-terminus of the protein) anchors the protein to the cytoplasmic aspect of plasma membrane, the other domain protrudes from the membrane and carries the protein kinase activity. These functional domains have apparent correlates in the composition of pp60^{src} (see Table 1): Pro, Arg, Ser and Thr are concentrated in the amino-terminal domain, Cys, Met and Tyr in the carboxy-terminal domain. Most of the protein (and the amino-terminal half in particular) is basic, whereas the carboxy-terminal domain is relatively acidic. We presume that the one-dimensional topography of pp60^{src} described here has its counterparts in the three-dimensional configuration of the protein (which we already know to be a highly elongated molecule—frictional coefficient 1.4; see ref. 5). It seems that the protein was designed on the one hand for tethering to the plasma membrane, and on the other for enzymatic activity beyond the confines of the membrane.

Using conventional procedures[41], we have deduced general features for the possible secondary structure of pp60^{src}. The central portion of the molecule (amino acid residues 221–438) is likely to be in the α-helical configuration; the carboxy-terminal domain seems to be composed of alternating α-helices and β-pleated sheets; and the amino-terminus is probably mainly β-sheet.

The portion of pp60^{src} that is anchored to the plasma membrane contains one (or more) residues of phosphoserine[6,9],

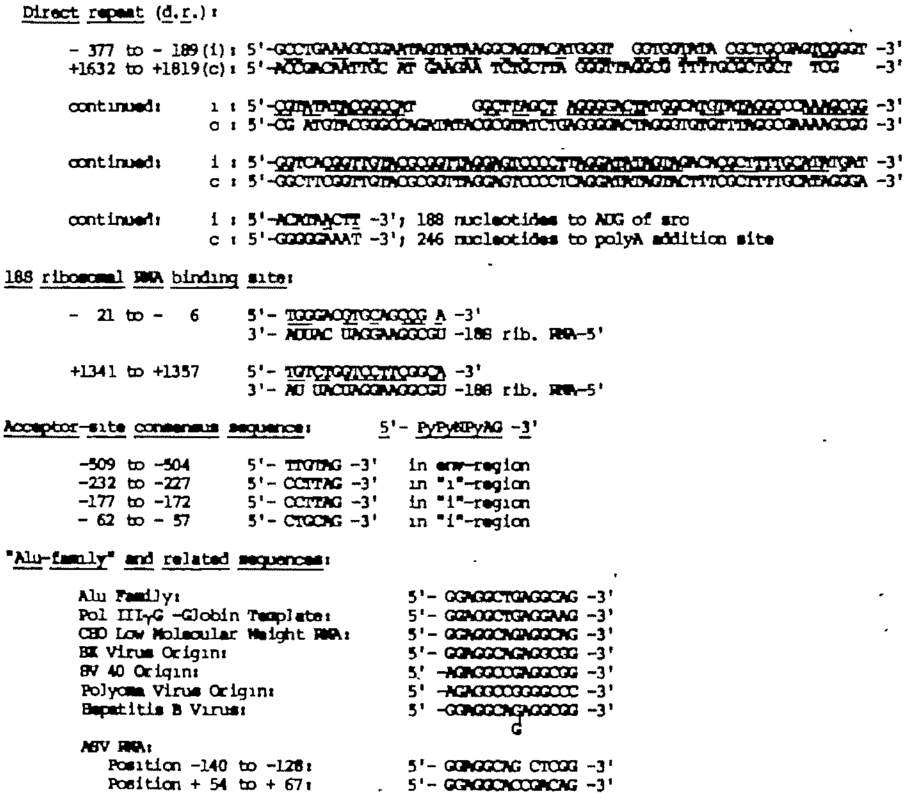

```
Direct repeat (d.r.):

   - 377 to - 189(i): 5'-[illegible] -3'
   +1632 to +1819(c): 5'-[illegible] -3'

   continued:        i : 5'-[illegible] -3'
                     c : 5'-[illegible] -3'

   continued:        i : 5'-[illegible] -3'
                     c : 5'-[illegible] -3'

   continued:        i : 5'-ACATAACTT -3'; 188 nucleotides to AUG of src
                     c : 5'-GGGGGAAAT -3'; 246 nucleotides to polyA addition site

18S ribosomal RNA binding site:

   - 21 to -  6      5'- TGGGACGTGCAGGGG A -3'
                     3'- AUUAC UAGGAAGGCGU -18S rib. RNA-5'

   +1341 to +1357    5'- TGTCTGGTACCTACGGGA -3'
                     3'- AU UACUAGGAAGGCGU -18S rib. RNA-5'

Acceptor-site consensus sequence:        5'- PyPyNPyAG -3'

    -509 to -504     5'- TTGTAG -3'   in erv-region
    -232 to -227     5'- CCTTAG -3'   in "i"-region
    -177 to -172     5'- CCTTAG -3'   in "i"-region
    - 62 to - 57     5'- CTGCAG -3'   in "i"-region

"Alu-family" and related sequences:

    Alu Family:                        5'- GGAGGCTGAGGCAG -3'
    Pol IIIγG -Globin Template:        5'- GGAGGCTGAGGAAG -3'
    CHO Low Molecular Weight RNA:      5'- GGAGGCAGAGGCAG -3'
    BK Virus Origin:                   5'- GGAGGCAGAGGCGG -3'
    SV 40 Origin:                      5' -AGAGGCCGAGGCGG -3'
    Polyoma Virus Origin:              5' -AGAGGCCGGGGCCC -3'
    Hepatitis B Virus:                 5' -GGAGGCAGAGGCGG -3'
                                                 G
    ASV RNA:
      Position -140 to -128:           5'- GGAGGCAG CTCGG -3'
      Position + 54 to + 67:           5'- GGAGGCACCGACAG -3'
```

Fig. 3 Repeated nucleotide sequences within and without *src*. The figure illustrates the various repeated elements identified in the nucleotide sequence of the 3.1-kilobase *Eco*RI DNA fragment The illustrated sequences include: the direct repeat that occurs on both sides of *src*, the consensus sequence from the *Alu* family of interspersed repeats in mammalian DNA and variants of this sequence noted by Jelinek *et al.*[34], a possible component of the ribosome-binding site for *src* and a similar sequence found near the 3' terminus of the gene; and possible splice-acceptor sites located to the 5' side of *src*.

Table 2 Frequency of codons used in the *src* gene

3/UUU/Phe	5/UCU/Ser	2/UAU/Tyr	1/UGU/Cys
► 6/UUC/Phe	8/UCC/Ser	►13/UAC/Tyr	►11/UGC/Cys
1/UUA/Leu	7/UCA/Ser	0/UAA/OC	0/UGA/OP
5/UUG/Leu	8/UCG/Ser	► 1/UAG/AM	8/UGG/Trp
8/CUU/Leu	9/CCU/Pro	5/CAU/His	1/CGU/Arg
►13/CUC/Leu	►15/CCC/Pro	8/CAC/His	►12/CGC/Arg
1/CUA/Leu	10/CCA/Pro	6/CAA/Gln	2/CGA/Arg
►26/CUG/Leu	►12/CCG/Pro	►16/CAG/Gln	►19/CGG/Arg
3/AUU/Ile	7/ACU/Thr	1/AAU/Asn	5/AGU/Ser
►11/AUC/Ile	►11/ACC/Thr	9/AAC/Asn	►12/AGC/Ser
0/AUA/Ile	►11/ACA/Thr	4/AAA/Lys	9/AGA/Arg
12/AUG/Met	4/ACG/Thr	►25/AAG/Lys	5/AGG/Arg
4/GUU/Val	►11/GCU/Ala	8/GAU/Asp	5/GGU/Gly
7/GUC/Val	►16/GCC/Ala	►14/GAC/Asp	►15/GGC/Gly
2/GUA/Val	7/GCA/Ala	6/GAA/Glu	9/GGA/Gly
►16/GUG/Val	5/GCG/Ala	►19/GAG/Glu	►16/GGG/Gly

Relatively abundant codons are indicated by the arrowheads.

the exposed (kinase) domain contains phosphotyrosine[9]. We have attempted to identify the possible locations of these phosphoamino acid sequences in the deduced amino acid of pp60^{src}. Phosphoserines in other proteins are usually found in the following general structure: basic amino acid–basic amino acid–any amino acid–phosphoserine[42]. Three serine residues (17, 73 and 83) in the amino-terminal domain of pp60^{src} satisfy this criterion. Two tyrosine residues in the carboxy half of the sequence (379 and 385) are situated within virtually identical microenvironments (Arg-Met-X-Tyr-Val, where X is either Ala or Asn) that are separated by a single amino acid (Glu). We speculate that this unlikely repetition of amino acid sequence might denote the position(s) of phosphotyrosine in pp60^{src}.

Codon usage in *src*

Table 2 illustrates the prevalence of various codons for each of the amino acids in the translated frame of *src*. Relatively strong biases for particular codons were observed in several instances: CUC and CUG for Leu; UGC for Cys; AUC for Ile; GUG for Val; CAG for Gln; GAG for Glu; UAC for Tyr; CGG and CGC for Arg; and GGC and GGG for Gly; AAG for Lys. U and A are used relatively infrequently in the third position with the exception of the codons for Thr and Pro.

A possible amino acid sequence for the carboxy-terminal domain of viral glycoprotein

The *env* gene of ASV encodes two glycoproteins (gp85 and gp37) which originate from the cleavage of a single polypeptide precursor and remain linked to one another by disulphide bonds[26]. The proteins are arranged 5′-gp85-gp37-3′ on the gene. It seems possible that we have obtained the sequence of 697 nucleotides at the 3′ end of *env*, or 231 amino acids extending leftward from the carboxy-terminus of gp37 (Fig. 4). Hunter and his colleagues have identified eight amino acid residues in the amino-terminal region of gp37 of the Prague-B ASV, a different strain of ASV (E. Hunter, personal communication). Four of the identified residues occur at appropriate positions in the sequence proposed by Fig. 4: Thr at position 43, Asp at positions 47 and 48, and Glu at position 53 (residues 2, 6, 7 and 12, respectively, in the amino acid sequence, from E. Hunter *et al.*, personal communication). The codons for two other residues could be generated by changes in single nucleotides, converting Cys to Gly at position 50 in Fig. 4, and Ser to Ala at position 51. These correlations suggest that the amino acid sequence illustrated by Fig. 4 includes the entirety of gp37, whose amino-terminus would be located at residue 42 in Fig. 4, and whose un-glycosylated molecular weight would be 20,500. The carboxy-terminus of the deduced protein is exceptionally hydrophobic (37 of 43 amino acids, as noted in Fig. 4). This feature might denote a portion of gp37 that is embedded in the lipoprotein envelope of the virus and anchors the entire glycoprotein to the virion[43]. The prevalences of individual codons used to encode this protein are very different from those found for *src* (Table 3). Data presented elsewhere suggest that *src* and *env* had independent and very different evolutionary origins[44,45]. The disparities in codon usage between the two genes may reflect their distinct origins.

Comparison of *src* with other viral oncogenes

Genetic loci responsible for neoplastic transformation of infected cells have been identified within the genomes of Moloney murine sarcoma virus, polyoma virus, SV40 virus and several strains of adenovirus (see ref. 2 for reviews). We have compared the available nucleotide sequences of these loci with the sequence of *src*, and the amino acid sequences of the encoded proteins with pp60^{src}. The nucleotide sequence of *src* bears little resemblance to the sequences of the other viral oncogenes, with the exception of a few oligonucleotides (the largest being nonamers) shared with the gene for the middle T antigen of polyoma virus. We found no appreciable homology among the various amino acid sequences, although pp60^{src}, the T antigen of polyoma, and two proteins encoded in the *E1b* region of adenovirus DNA are all relatively rich in proline (data not shown).

Further comments

Src is frequently deleted during the propagation of most strains of ASV[3]. The mechanism that facilitates this deletion has not been elucidated. We propose that the large repeated nucleotide sequence (d.r.) that flanks *src* might mediate deletion of the gene, for example, by homologous recombination within the viral genome[46]. This proposal can be tested by analysing the sequence that remains at the site of the deletion subsequent to the loss of *src* (work in progress).

The direct determination of amino acid sequence remains a relatively arduous and demanding procedure, despite recent technical advances in sensitivity and convenience[47]. It seems likely that the nucleotide sequence presented here provides the authentic amino acid sequence of pp60^{src} in advance of any direct sequencing of the protein. At least one issue remains controversial, however—the claim that a portion of pp60^{src} (presumably, a terminal 'signal sequence') is removed by membrane-bound protease(s) subsequent to synthesis of the protein[48]. The issue can probably be resolved by identification of a few of the amino acids at the amino-terminus of the mature protein and comparison of these results with the nucleotide sequence of *src*. We note that amino-terminal signal sequences generally have hydrophobic domains rich in leucine[49], features not found in the amino-terminal region of the sequence of *src* (see Fig. 2).

The amino acid sequence deduced here for pp60^{src} suggests that the protein is hydrophobic (average hydrophobicity of 1.1, computed as described in ref. 50). This property is in accord with previous findings that pp60^{src} is an integral protein of the plasma membrane, can be released from the membrane only by treatment with detergents, and is more soluble in aqueous solutions when detergent is present[11]. A more detailed analysis of the

```
                                              ┌►gp 37 ?
  1 - IPSRPVGGPCYLGKLTMLAPKHTDILKVLVNSSRTGIRRKRSTSHLDD -  48

 49 - TCSDEVQLWGPTARIFASILSPGGSSCEALREIERLACWSVKQANLTT -  96

 97 - SLLGDLLDDVTSIRHAVLQNRAAIDFLLLAHGHGCEDVAGMCCFNLSD - 144

145 - QSESIQKKFQLMKEHVNKIGVDSDLIGSWLRGLFGGIGEWAVHLLKGL - 192

193 - LLGLVVILLLVVCLPCLLQMLCGNRRKMINNSIELPHGI          - 231
```

Fig. 4 A possible amino acid sequence for the carboxy-terminal domain of the glycoprotein of ASV. An amino acid sequence was deduced from the nucleotide sequence illustrated in Fig. 2, beginning with position −1,095 and ending before the amber codon at positions −402–−400. The amino acid sequence is given in terms of the conventional single-letter symbols. The underlining demarcates an exceptionally hydrophobic region. The arrow denotes the presumptive amino-terminus of gp37.

Table 3 Codons used in C-terminal domain of the *env* gene

1/UUU/Phe	2/UCU/Ser	1/UAU/Tyr	3/UGU/Cys
4/UUC/Phe	2/UCC/Ser	0/UAC/Tyr	►7/UGC/Cys
5/UUA/Ieu	4/UCA/Ser	0/UAA/OC	0/UGA/OP
►9/UUG/Leu	1/UCG/Ser	►1/UAG/AM	4/UGG/Trp
6/CUU/Leu	►3/CCU/Pro	4/CAU/His	2/CGU/Arg
4/CUC/Leu	►3/CCC/Pro	4/CAC/His	0/CGC/Arg
►8/CUA/Leu	1/CCA/Pro	1/CAA/Gln	►4/CGA6Arg
6/CUG/Leu	1/CCG/Pro	►6/CAG/Gln	1/CGG/Arg
►8/AUU/Ile	0/ACU/Thr	5/AAU/Asn	5/AGU/Ser
4/AUC/Ile	2/ACC/Thr	3/AAC/Asn	5/AGC/Ser
4/AUA/Ile	►6/ACA/Thr	3/AAA/Lys	►5/AGA/Arg
5/AUG/Met	1/ACG/Thr	►8/AAG/Lys	1/AGG/Arg
4/GUU/Val	3/GCU/Ala	►8/GAU/Asp	4/GGU/Gly
4/GUC/Val	4/GCC/Ala	4/GAC/Asp	5/GGC/Gly
3/GUA/Val	3/GCA/Ala	5/GAA/Glu	►7/GGA/Gly
4/GUG/Val	2/GCG/Ala	4/GAG/Glu	5/GGG/Gly

Relatively abundant codons are indicated by arrowheads.

amino acid sequence has revealed two relatively isolated hydrophobic domains at residues 52–57 (average hydrophobicity 2.2) and 121–126 (average hydrophobicity 2.4) (data not illustrated). Both domains are located near the amino-terminus of the molecule where the protein apparently inserts into the plasma membrane[8,40].

The nucleotide sequence reported here substantiates previous assumptions that *src* encodes a single protein. Transfection of the 3.1-kilobase DNA fragment containing *src* into mammalian cells leads to the synthesis of pp60^{src} and the neoplastic transformation of recipient cells[19,51]. Moreover, the transformed cells are tumorigenic in newborn allogeneic animals (unpublished results of H. Oppermann and P. Luciw). We can now rigorously conclude that *src* is the only viral gene required for tumorigenesis by ASV, and that the mechanism of neoplastic transformation by the virus derives entirely from the biochemical properties of pp60^{src}.

Chemical analysis of pp60^{src} and site-specific mutagenesis of *src* will be used to identify the sites of functionally important modifications (such as phosphorylation) within the protein, to locate the active site for phosphotransfer by the protein, and to describe other important features of the protein. These efforts will require the nucleotide sequence of *src* and the amino acid sequence of pp60^{src}.

We thank E. Hunter for his unpublished data on the amino acid sequence of gp37, I. Verma for providing the nucleotide sequence of Moloney murine sarcoma virus *src*, B. Delorbe, R. Parker, P. Luciw and B. Baker for gifts of cloned DNA, J. Messing for providing phage and bacterial strains, H. Martinez for the use of his computer program and for assistance with computerized analysis of nucleotide sequences, J. Shine, R. Swanstrom, J. Majors, L. Levintow, S. Courtneidge and H. Oppermann for helpful discussions and unpublished results, and B. Cook for stenographical assistance. This work was supported by grants from the NCI and the American Cancer Society.

Note added in proof: After preparing this manuscript, we learned of the identification of several new avian sarcoma viruses with transforming genes distinct from *src*. It is now more accurate to designate the virus studied here as Rous sarcoma virus, Schmidt–Ruppin strain—one of several isolates that share closely related *src* genes.

Received 30 June; accepted 16 July 1980.

1. Klein, G. *Proc. natn. Acad. Sci. U.S.A.* **76,** 2442–2446 (1979).
2. Tooze, J. in *The Molecular Biology of Tumor Viruses* (Cold Spring Harbor, New York, 1973).
3. Vogt, P. K. *Comprehensive Virology* Vol. 9 (eds Fraenkel-Conrat, H. & Wagner, R. R.) 341–456 (Plenum, New York, 1977).
4. Brugge, J. & Erikson, R. L. *Nature* **269,** 346–347 (1977).
5. Levinson, A. D., Oppermann, H., Levintow, L., Varmus, H. E. & Bishop, J. M. *Cell* **15,** 561–572 (1978).
6. Collett, M. S., Erikson, E. & Erikson, R. L. *J. Virol.* **29,** 770–781 (1979).
7. Willingham, M. C., Jay, G. & Pastan, I. *Cell* **18,** 125–134 (1979).
8. Courtneidge, S. A., Levinson, A. D. & Bishop, J. M. *Proc. natn. Acad. Sci. U.S.A.* **77,** 3783–3787 (1980).
9. Hunter, T. & Sefton, B. M. *Proc. natn. Acad. Sci. U.S.A.* **77,** 1311–1315 (1980).
10. Collett, M. S., Purchio, A. F. & Erikson, R. L. *Nature* **285,** 167–169 (1980).
11. Levinson, A. D., Oppermann, H., Varmus, H. E. & Bishop, J. M. *J. biol. Chem.* (submitted).
12. Sefton, B. M., Hunter, T., Beemon, K. & Eckhart, W. *Cell* **20,** 807–816 (1980).
13. Weinberg, R. A. *Biochim. biophys. Acta* **473,** 39–56 (1978).
14. Hager, G. L. *et al. J. Virol.* **31,** 795–809 (1980).
15. DeLorbe, W., Luciw, P., Varmus, H. E., Bishop, J. M. & Goodman, H. M. *J. Virol.* (in the press).
16. Czernilofsky, A. P. *et al. Nucleic Acids Res.* **8,** 2967–2984 (1980).
17. Wang, L. H. *A. Rev. Microbiol.* **32,** 561–591 (1978).
18. Sanger, F., Nicklen, S. & Coulson, A. R. *Proc. natn. Acad. Sci. U.S.A.* **74,** 5463–5467 (1977).
19. Maxam, A. M. & Gilbert, W. *Proc. natn. Acad. Sci. U.S.A.* **74,** 560–563 (1977).
20. Luciw, P., Oppermann, H., Varmus, H. E. & Bishop, J. M. *J. Virol.* (submitted).
21. Shank, P. R., Hughes, S. H. *et al. Cell* **15,** 1383–1395 (1978).
22. Wang, L. H., Halpern, C. C., Wadel, M. & Hanafusa, H. *Proc. natn. Acad. Sci. U.S.A.* **75,** 5812–5816 (1978).
23. Wang, L. H. *et al. Cold Spring Harb. Symp. quant. Biol.* **44** (in the press).
24. Tsichlis, P. N. & Coffin, J. M. *J. Virol.* **33,** 238–249 (1980).
25. Hagenbuchle, O., Santer, M., Steitz, J. A. & Mans, R. J. *Cell* **13,** 551–563 (1978).
26. Eisenman, R. N. & Vogt, V. M. *Biochim. biophys. Acta* **473,** 187–239 (1978).
27. Majors, J. E. & Varmus, H. E. (in preparation).
28. Swanstrom, R., DeLorbe, B., Varmus, H. E. & Bishop, J. M. *Proc. natn. Acad. Sci. U.S.A.* (in the press).
29. Varmus, H. E. *et al. J. molec. Biol.* **120,** 55–82 (1978).
30. Kung, H. J., Fung, Y. K., Majors, J. E., Bishop, J. M. & Varmus, H. E. *J. Virol.* (submitted).
31. Weiss, S. R., Varmus, H. E. & Bishop, J. M. *Cell* **12,** 983–992 (1977).
32. Mellon, P. & Duesberg, P. *Nature* **270,** 631–634 (1977).
33. Cordell, B., Weiss, S. R., Varmus, H. E. & Bishop, J. M. *Cell* **15,** 79–91 (1978).
34. Quintrell, N., Hughes, S. H., Varmus, H. E. & Bishop, J. M. *J. molec. Biol.* (in the press).
35. Seif, I., Khoury, G. & Dhar, R. *Nucleic Acids Res.* **6,** 3387–3398 (1979).
36. Jelinek, W. R. *et al. Proc. natn. Acad. Sci. U.S.A.* **77,** 1398–1402 (1980).
37. Shank, P. R. & Varmus, H. E. *J. Virol.* **25,** 104–114 (1978).
38. Bishop, J. M. *A. Rev. Biochem.* **47,** 35–88 (1978).
39. Beemon, K. & Hunter, T. *J. Virol.* **28,** 551–566 (1978).
40. Bishop, J. M. *et al. M. D. Anderson Symp.* (in the press).
41. Chou, P. Y. & Fasman, G. D. *Biochemistry* **13,** 222–249 (1974).
42. Krebs, E. G. & Beavo, J. A. *A. Rev. Biochem.* **48,** 923–959 (1979).
43. Montelaro, R. C., Sullivan, S. J. & Bolognesi, D. P. *Virology* **84,** 1931 (1978).
44. Hughes, S. H. *et al. Cell* **18,** 347–359 (1979).
45. Bishop, J. M. *et al. 12th Miami Winter Symp.* (in the press).
46. Coffin, T. M. *J. gen. Virol.* **42,** 1–26 (1979).
47. Hunkapiller, M. W. & Hood, L. E. *Science* **207,** 523–525 (1980).
48. Kamine, J. & Buchanan, J. M. *Proc. natn. Acad. Sci. U.S.A.* **75,** 4399–4403 (1978).
49. Wickner, W. *A. Rev. Biochem.* **48,** 23–45 (1979).
50. Bigelow, C. C. J. *J. theor. Biol.* **16,** 187–211 (1967).
51. Copeland, N. G., Zelenetz, A. D. & Cooper, G. M. *Cell* **19,** 863–870 (1980).
52. Hsu, T. W. *et al. J. Virol.* **28,** 810–818 (1978).
53. Collett, M. S., Erikson, E., Purchio, A. F., Brugge, J. S. & Erikson, R. L. *Proc. natn. Acad. Sci. U.S.A.* **76,** 3159–3163 (1979).
54. Gronenborn, B. & Messing, J. *Nature* **272,** 375–377 (1978).

DNA *N*-glycosylases and UV repair

Bruce Demple & Stuart Linn

Department of Biochemistry, University of California, Berkeley, California 94720

Repair of some DNA photoproducts can be mediated by glycosylic bond hydrolysis. Thus, Escherichia coli *endonuclease III releases 5,6-hydrated thymines as free bases, while T4 UV endonuclease releases one of two glycosylic bonds holding pyrimidine dimers in DNA. In contrast, uninfected* E. coli *apparently does not excise pyrimidine dimers via a DNA glycosylase.*

DAMAGED bases can arise in DNA by a number of routes. These include spontaneous hydrolysis as in the deamination of cytosine[1] or adenine[2], reaction with such chemical agents as monofunctional alkylating agents[3], and radiation.[4] Two major routes for repair of damaged DNA have been proposed for *Escherichia coli*, initiated by strand breakage near the damage[5], or by specific hydrolysis of the glycosylic bond of a non-conventional base[6]. Using repair of pyrimidine dimers produced in

0028-0836/80/380203—06$01.00

DNA by UV irradiation as a model system, a sequence of repair initiated by phosphodiester bond hydrolysis has been proposed[7]. In this scheme, the initial, perhaps rate-limiting step is endonuclease incision, mediated by enzymes specific for pyrimidine dimers as follows:

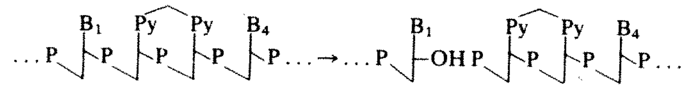

(1)

Excision of the damage is then carried out by an exonuclease, with DNA polymerase and DNA ligase restoring the integrity of the genetic material. Considerable attention has been directed recently toward the alternative pathway initiated by glycosylic bond hydrolysis. Four enzymes have been reported in *E. coli* which remove, respectively, uracil[6], hypoxanthine[2], 3-alkyladenine[8] or formamidopyrimidine[9]. This base excision results in the formation of apurinic or apyrimidinic (AP) sites, which could then be repaired by action of AP endonuclease, DNA polymerase and polynucleotide ligase.

Recently, Grossman and his colleagues presented evidence suggesting that UV endonuclease from *Micrococcus luteus* actually cleaves the phosphodiester bond between the nucleotides of a pyrimidine dimer[10]. This assertion was based on results of gel electrophoresis of a short fragment of UV-irradiated DNA incised by UV endonuclease. Products were observed which appeared to correspond to incision within the pyrimidine dimers. However, when these same fragments were heated at 100°C or exposed to alkali, they exhibited mobility corresponding to a strand cut immediately 5′ to the pyrimidine dimer. This alkali- and heat-lability was similar to that observed for AP sites, and these authors interpreted their results to indicate that UV endonuclease cleavage occurs as follows:

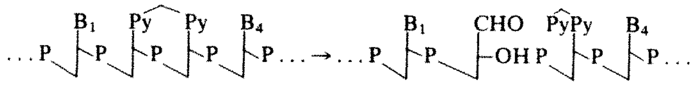

(2)

Thus, an AP deoxyribose is left at the 3′ terminus of the nick and could be removed by heat or alkali to yield a DNA fragment shorter by apparently one nucleotide. This interpretation contrasted with previous models in which phosphodiester bond hydrolysis is the first step in the repair pathway and would result in cleavage 5′ to the dimer rather than within it. We wished to examine which mechanism might apply to the UV endonuclease induced by infection of *E. coli* with bacteriophage T4. Like the *Micrococcus luteus* UV endonuclease, the T4 enzyme appears to be specific for pyrimidine dimers[11] and might well act by a similar mechanism.

In addition, we tested whether *E. coli* endonuclease III acts as a glycosylase followed by an AP endonuclease, since we had previously observed it to cleave two apparently unrelated substrates: DNA containing 5,6-dihydroxydihydrothymine and DNA containing AP sites[12].

T4 UV endonuclease has pyrimidine dimer glycosylase activity

We recently have taken advantage of the requirement of *E. coli* DNA polymerase I for a 3′-hydroxyl nucleotide terminus to probe the structure of endonuclease products[13]. In those experiments it was shown that the UV endonuclease controlled by phage T4 (gene *v*) acts on UV-irradiated DNA to form nicks containing an AP deoxyribose at the 3′ terminus. Such a structure could arise by hydrolysis of the glycosylic bond of the 5′ pyrimidine nucleotide of the dimer, as proposed by Grossman *et al.*[10] for the UV endonuclease from *M. luteus* (see above). The resulting pyrimidine dimer nucleotide at the 5′ terminus would have an important feature: if the cyclobutane bonds of the dimer could be broken by additional UV irradiation (as demonstrated for free thymine dimers in aqueous solution[14]), one pyrimidine would be released as the free base from each such structure. Concomitantly, a normal pyrimidine nucleotide would be left at the 5′ terminus:

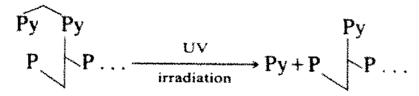

(3)

Thus, photolytic release of pyrimidine bases after treatment of UV-irradiated DNA with UV endonuclease could provide a rapid and specific assay for this unusual structure and for the action of a putative pyrimidine dimer-DNA glycosylase.

As seen in Fig. 1, incubation of UV-irradiated, ^{3}H-thymidine-labelled DNA with T4 UV endonuclease did not of itself result in the release of free thymine. However, secondary irradiation of such enzyme-treated DNA did release free thymine base. The amount of base which could be released was a function of the primary dose to which the DNA was exposed; prolonged incubation with excess UV endonuclease did not increase the amount of free thymine formed. High pressure liquid chromatographic analysis of the products of a limit reaction did not

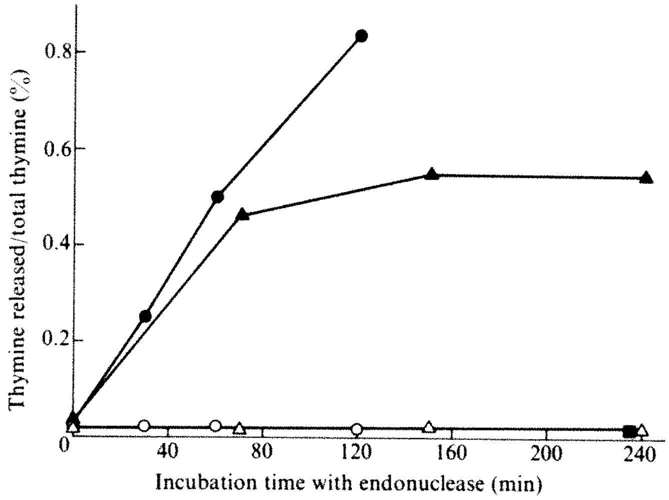

Fig. 1 Generation of photo-releasable thymine by T4 UV endonuclease. T7 ^{3}H-DNA (25,000–29,000 c.p.m. per nmol nucleotide), prepared as described by Richardson[30], was irradiated on ice under a Westinghouse germicidal lamp (G15T8) at a dose rate of $3\ \mathrm{J\ m^{-2}\ s^{-1}}$, as determined by potassium ferrioxalate actinometry[31]. Irradiation was for 0 min (square), 10 min (triangles, 1.35 mM DNA-nucleotide), or 20 min (circles, 0.58 mM DNA-nucleotide). DNAs were then incubated at 37 °C for times indicated in 140 µl reactions containing 25 mM potassium phosphate, *p*H 7.4–1 mM EDTA–0.2 M NaCl–80 µg ml^{-1} BSA, 17 nmol DNA-nucleotide and enzyme [8.4 µl per sample (squares, triangles) or 5.3 µl per sample (circles)]. After chilling, a second 20-min irradiation was carried out under conditions of the primary irradiations (>90% of maximum photorelease) (solid symbols). Samples were then assayed for thymine base by high pressure liquid chromatography (triangles) or by Dowex 1 chromatography (circles). For high pressure liquid chromatographic analysis samples were diluted to 300 µl with water and precipitated by addition of 30 µl of 1 mg ml^{-1} *Bacillus subtilis* DNA and 900 µl 100% ethanol. After 10–30 min at −70 °C samples were spun for 5 min in a Beckman Microfuge. The supernatants were concentrated by evaporation, then mixed with 15 µl of 7.5 mM thymine and water added to a final volume of 350 µl. A 100-µl portion of each sample was then injected into a Waters model ALC/GPC 244 liquid chromatograph with C-18 reverse phase column (25 cm by 4.6 mm internal diameter) equilibrated with 2.5 mM potassium phosphate–2.5% methanol, *p*H 3.0[32]. Flow rate was 2 ml min^{-1} at 1,500 p.s.i. The first 3 ml was collected as a single fraction; subsequent fractions were 0.3 ml. After determining the absorbance of the fractions at 254 nm to identify the thymine location, Triton X-100/toluene-based fluor was added to each and the ^{3}H radioactivity determined. For thymine determination by Dowex 1 chromatography[33], samples diluted to 300 µl with water were precipitated by addition of 100 µl 10 mg ml^{-1} BSA and 500 µl 7% TCA, and centrifugation. The supernatants were extracted twice with 13 vol. cold diethyl ether to remove TCA, and residual ether was removed under a stream of N_2, after which each sample was made to 1,100 µl with water and 11 µl 1 M Tris-HCl, *p*H 7.5. One ml of each sample was then applied to a 1 ml column of Dowex 1-X8 equilibrated with 10 mM ammonium formate, *p*H 4.2. The columns were washed with 5 ml of this same buffer in 1 ml aliquots, and 1 ml fractions were collected directly into scintillation vials and the radioactivity determined. T4 UV endonuclease was prepared as described by Friedberg and King[34], except that the DNA-cellulose fraction was stored at −20 °C in 50% glycerol containing 5 mM potassium phosphate, *p*H 7.0–0.5 mM dithiothreitol–5% ethylene glycol. Enzyme stored in this manner retained full activity after 2 yr.

Table 1 Generation of photo-releasable thymine and nicks by T4 UV endonuclease

Endonuclease incubation (min at 37 °C)	Secondary UV irradiation	Free thymine (pmol)	Total nicks (pmol)
0	–	<1	0.4
	+	<1	0.4
30	–	<1	2.0
	+	2.9	—
60	–	<1	4.2
	+	5.3	3.5
120	–	<1	*
	+	9.6	*

T7 ^{3}H-labelled DNA (0.57 mM, 40,600 c.p.m. per nmol nucleotide) was irradiated with 1,800 Jm^{-2} UV light. Photo-released thymine formed by T4 UV endonuclease was measured by Dowex 1 chromatography as described in Fig. 1 legend. Nicking of the T7 DNA was determined by sedimentation in 5% to 20% sucrose gradients containing 0.25 M NaOH–5 mM EDTA for 210 min at 49,000 r.p.m. in a Beckman SW 50.1 rotor. Average molecular weights were calculated according to Studier[38] and used to determine the average number of nicks per T7 genome. Total nicks of 2 pmol correspond to 9.5 nicks per T7 genome.

* Too numerous to quantify.

detect any labelled base, nucleoside or nucleotide other than thymine with or without the second irradiation (data not shown).

The UV-irradiated DNA was also analysed for the number of nicks produced by UV endonuclease (Table 1). The number of nicks introduced during the enzyme incubation was approximately equal to or somewhat less than the amount of thymine releasable by the secondary irradiation. This near-equality might imply simultaneous action of the DNA glycosylase activity and phosphodiester bond cleavage. However, we have shown previously[13] that, in an enzyme-limited reaction, T4 UV endonuclease acting on UV-irradiated DNA transiently creates sites which are sensitive to AP endonuclease. For T4 UV endonuclease therefore, pyrimidine dimer-DNA glycosylic bond cleavage appears to precede phosphodiester bond cleavage.

Pyrimidine dimers excised *in vivo* by uninfected irradiated *E. coli* are not in the form of pyrimidine dimer nucleotides

We also tested whether the excision of pyrimidine dimers in uninfected *E. coli* cells might be mediated by an *N*-glycosylase activity. Since the literature is unclear with respect to the properties of the enzyme(s) controlled by the *uvr*A, *uvr*B and *uvr*C loci[15,16], we chose to examine the structure of the products excised by this system *in vivo* from the DNA of irradiated cells. Setlow and Carrier[17] and Boyce and Howard-Flanders[18] have shown that pyrimidine dimers removed from the DNA of irradiated *E. coli* are contained in acid-soluble oligonucleotides which are retained in the cells. If this excision process is indeed mediated by hydrolysis of the glycosylic bond of one pyrimidine of the dimer, these oligonucleotides would be expected to contain the pyrimidine dimer nucleotide structure, which could be identified by its UV-dependent release of pyrimidine bases.

We therefore extracted acid-soluble oligonucleotides from cells that had been irradiated and then incubated for 3 h in growth conditions, during which 70% of the dimers were excised from the cellular DNA. Secondary irradiation of these oligonucleotides, however, did not release significant amounts of free thymine (Table 2). If the dimers in this material had each retained but a single glycosylic bond, half of the label measured in dimers should have been released as free thymine—2.2% of the total thymine for the sample shown. Instead, a UV dose which released thymine from essentially all of the dimers acted upon *in vitro* by T4 UV endonuclease yielded less than one-tenth of the 2.2% value. As a control for pyrimidine dimers retaining both glycosylic bonds, oligonucleotides were generated by pancreatic DNase digestion of DNA irradiated *in vitro*. This material (Table 2, sample 3) did not contain significant photoreleasable thymine. On the other hand, irradiated DNA which had been treated with excess T4 UV endonuclease prior to the pancreatic DNase digestion gave rise

Table 2 Test for photo-releasable thymine in excision products of UV-irradiated *E. coli*

Sample	Secondary UV irradiation ($J m^{-2}$)	Thymine in dimers (% total thymine)	Free thymine base (% total thymine)
(1) Acid-soluble fraction from irradiated, non-incubated cells	0	<0.01	0.33
	3,600	ND	0.35
(2) Acid-soluble fraction from irradiated, incubated cells	0	4.4	0.51
	3,600	2.5	0.68
(3) DNase I digest of irradiated T7 DNA, acid-soluble fraction	0	1.8	0.02
	3,600	5.9	0.05
(4) DNase I digest of irradiated, T4 UV endonuclease-treated T7 DNA, acid-soluble fraction	0	2.2	0.09
	3,600	6.2	1.11

E. coli AB1157 was grown for 3 generations to 10^8 cells per ml in 100 ml K medium with 200 μg ml^{-1} deoxyadenosine and 5 μCi ml^{-1} ^{3}H-thymidine (Amersham, 15 Ci $mmol^{-1}$). K medium contains per litre: 1 g NH_4Cl, 6 g Na_2HPO_4, 3 g KH_2PO_4, 10 g glucose, 10 g vitamin-free casaminoacids, 0.2 mg thiamine, 24 mg $MgSO_4$ and 2 mg $CaCl_2$. Cells were collected and washed 5 times by centrifugation using 25 ml 0.1 M NaCl–10 mM Tris, *p*H 7.5 (NT buffer). The final pellet was suspended in 225 ml NT buffer and aliquots of 28 ml were each irradiated at 2 J m^{-2} s^{-1} for 30 s in a 15 cm glass Petri dish with mixing, then returned immediately to ice. Cells were collected by centrifugation and 1/4 of the irradiated cells was suspended in 1 ml 10 mM Tris, *p*H 7.5, and the remainder was suspended in 25 ml NT buffer and added to a flask containing 50 ml K medium. The flask was covered with foil to prevent photoreactivation and incubated for 3 h at 37 °C with shaking. After incubation, the cells were collected by centrifugation, washed twice with 25 ml NT buffer, then suspended in 1 ml 10 mM Tris, *p*H 7.5. An equal volume of cold 10% trichloracetic acid (TCA) was then added to each cell suspension and, after mixing, incubated 10 to 15 min on ice. Acid-insoluble material was removed by centrifugation for 10 min at 10,000 g. The supernatants were extracted 3 times with 5 volumes of ice-cold diethyl ether. Remaining ether was removed with a stream of N_2. Free thymine in the acid-soluble extract of the incubated cells (1–2% of total ^{3}H) was reduced by chromatography on DEAE-cellulose (Brown & Co., Berlin, New Hampshire). A sample (1.2 ml, 2×10^5 c.p.m.) was diluted 5-fold with 10 mM Tris, *p*H 7.9 and applied at about 3 ml per h to a 3-ml column of DEAE-cellulose equilibrated with this same buffer. The column was washed with 5 ml of buffer and eluted with 10 ml of 0.5 M NaCl–9 mM Tris, *p*H 7.9 while 0.5 ml fractions were collected at 2 ml per h. Fractions containing about 98% of the applied radioactivity (3.0 ml) were pooled and evaporated to dryness at 35 °C. This material was redissolved in 300 μl distilled water and applied to a 0.7-cm × 38-cm column of Sephadex G10 equilibrated with 5 mM Tris, *p*H 8.2. Washing with this buffer was continued at 3 ml per h and 0.5-ml fractions collected. Radioactivity in the fractions was determined by scintillation counting, while NaCl was detected by conductivity measurement. More than 90% of the applied material was recovered free of NaCl and used for subsequent studies. Fifty-five μl T7 DNA (0.57 mM-nucleotide, 40,000 c.p.m. per nmol-nucleotide) was irradiated for 300 s at 3 J m^{-2} s^{-1} 254 nm light and 25 μl aliquots made up with stock reagents to 240 μl T4 UV endonuclease cocktail (see legend to Fig. 1). Thirty μl T4 UV endonuclease (33 fmol glycosylic bonds hydrolysed per min per μl) or 30 μl T4 UV endonuclease storage buffer were added and incubation carried out for 6 h at 37 °C. Endonuclease was inactivated by heating for 3 min at 70 °C and glycerol removed from the samples by dialysis against 1 litre of 10 mM Tris, *p*H 7.9. One-twentieth volume of 1 M Tris-HCl, *p*H 7.9 and 0.01 volume of 1 M $MgCl_2$ were then added to each sample, followed by 30 μl of 2 μg ml^{-1} pancreatic DNase (Millipore). Digestion was carried out for 4 h at 37 °C and the reaction mixes chilled on ice. Following this 170 μl 10 mg ml^{-1} bovine serum albumin and 830 μl 7% TCA were added to each sample, followed by mixing and 10–15 min incubation on ice. Acid-insoluble material was removed by centrifugation and the acid-soluble supernatants (containing 65–70% of the total radioactivity) extracted 3 times with 8 volumes of cold diethyl ether. After removal of remaining ether with a stream of dry N_2, 0.01 volume of 1 M Tris, *p*H 8.2 was added to each sample and the samples stored at 0 °C. A secondary irradiation of the extracts was performed as in the legend to Fig. 1. Determination of thymine-containing pyrimidine dimers was by the method of Goldman and Friedberg[39]. Determination of photoreleased thymine by thin layer chromatography was on polyethyleneimine-cellulose plates (Brinkman) in *n*-butanol–acetic acid–water 40:6:15.

to oligonucleotides exhibiting a definite photorelease of labelled thymine (Table 2, sample 4). In uninfected *E. coli*, therefore, excision of pyrimidine dimers is apparently not mediated by a pyrimidine dimer-DNA glycosylase.

The fraction of thymine in dimers decreased during the secondary irradiation of the excision products (Table 2, sample 2), while it increased in the DNase digests (Table 2, samples 3 and 4). Chromatography on DEAE-paper indicated that the label in the digests was mainly in species larger than trinucleotides; in contrast, tritium in the excision products was primarily in the form of dTMP, as originally observed in ref. 17. Since 254 nm light catalyses an equilibrium in which less than one-fourth of the adjacent pyrimidines are dimerized[19], and since in these excision products the adjacent pyrimidines are initially largely dimerized, the proportion of dimers is expected to be reduced by the secondary irradiation. On the other hand, the oligonucleotides of the DNase digests are longer and thus would be expected to have a substantial number of non-dimerized adjacent pyrimidines. In this case, therefore, one expects an increase in the dimer content upon additional irradiation.

5,6-Hydrated thymine residues are removed by DNA glycosylase activity of endonuclease III

Exposure of DNA to UV light or other ionizing radiation produces thymine bases saturated in the 5,6-double bond[20]. Systems for repairing these lesions have been shown to be present in various organisms[20,21], including *E. coli*[22]. An enzyme, endodeoxyribonuclease III, has been isolated from *E. coli* and cleaves DNA which has been heavily UV-irradiated[23]. Characterization of extensively purified endonuclease III indicated that it recognizes lesions other than pyrimidine dimers[12]. Treatment of DNA with osmium tetroxide rendered it especially susceptible to the enzyme, suggesting that the 5,6-dihydroxydihydrothymine residues so formed are the sites of action of endonuclease III. Remarkably, endonuclease III is also highly active in cleaving partially depurinated DNA[12]. A simple hypothesis to explain the varied activities of endonuclease III is that it might contain both DNA glycosylase activity specific for 5,6-hydrated thymine and AP endonuclease activity.

Since UV light produces many lesions in DNA[4], DNA-glycosylase activity of endonuclease III was tested by analysing the products of reaction of the enzyme with ^{3}H-thymine-labelled DNA treated with osmium tetroxide (Fig. 2). Tritium label was recovered as free 5,6-hydrated thymine in amounts dependent upon the level of oxidation. High pressure liquid chromatographic analysis of a sample after extensive incubation showed the presence of tritium only in positions of authentic 5,6-dihydroxydihydrothymine and to a lesser extent in that of 5,6-dihydrothymine (Table 3). Furthermore, analysis of the extent of nicking of the DNA by alkaline sucrose gradient sedimentation indicated that the number of endonucleolytic incisions is equal to or somewhat less than the number of base molecules released by the enzyme (Table 3). At early times the formation of nicks seemed to lag behind the release of damaged bases. Thus it seems that endonuclease III acts first by cleaving the glycosylic bond of a 5,6-hydrated thymidylate residue and then by cutting the phosphodiester chain at the resultant apyrimidinic site. It is noteworthy that the 5,6-dihydrothymine did not appear to be formed by OsO_4 treatment (Table 3). Instead, it may have been introduced during the preparation of the DNA or may have been formed during DNA storage.

Table 3 Comparison of base release and nicking by *E. coli* endonuclease III

DNA treatment	Endonuclease incubation (min at 37 °C)	Free hydrated thymine released (pmol)		Nicks present (pmol)
		Dihydroxy-dihydrothymine	Dihydro-thymine*	
None	0	<0.2	<0.2	1.9
	120	<2.1	3.0	3.1
0.054% OsO_4	0	<2.3	0.2	2.0
	60	16	1.0	11
	120	18	1.3	16
0.52% OsO_4†	0	12.8	<0.02	8.3
	60	120	<0.02	63
	120	130	<0.02	>72

Base release was determined by HPLC and OsO_4 treatment was carried out as described in the legend to Fig. 2. Nicking of the DNA was determined as described in the legend to Table 1. Endonuclease reactions were as described in the legend to Fig. 2.

*Assuming specific radioactivity is that of the DNA thymine, not the undiluted label used during cell growth.

†Values are normalized from 0.27 to 0.48 pmol T7 DNA genomes as used in untreated and 0.054% OsO_4 experiments.

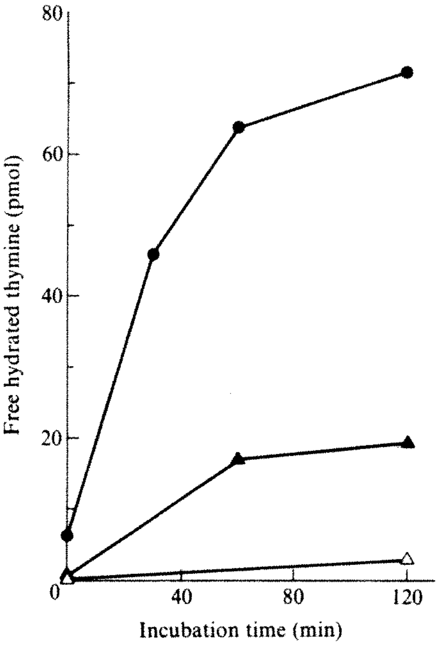

Fig. 2 Release of 5,6-hydrated thymine from OsO_4-oxidized DNA by endonuclease III. Endonuclease III was prepared as described by Gates and Linn[12]. DNA was treated with osmium tetroxide by mixing 190 μl T7 ^{3}H DNA (1.35 mM nucleotide, 25,000 c.p.m. nmol^{-1}) with 255 μl 0.3 M potassium phosphate, *p*H 12.3 and 70 μl 4% aqueous solution of OsO_4 (Polysciences) (circles) or with 190 μl 0.3 M potassium phosphate, *p*H 12.3 and 5 μl 4% aqueous OsO_4 (solid triangles). After 30 min at room temperature 195 μl 1 M potassium phosphate, *p*H 4.0 were added and unreacted OsO_4 extracted twice with 20 vol. of cold diethyl ether[35]. Remaining ether was removed with N_2 and the DNA reannealed as described by Davis and Hyman[36]. The DNA was then dialysed against 10 mM Tris, *p*H 7.5 at 4 °C, EDTA was added to 1 mM, and the solution was concentrated under vacuum. The concentrate was dialysed against 10 mM Tris, *p*H 7.5 and stored frozen at −20 °C for no longer than 2 days before use. Enzyme reaction mixtures contained 20 nmol (circles) or 38 nmol (triangles) of DNA nucleotide in 67 mM Tris, *p*H 8.2–25 mM KCl–0.005% Triton X-100, with enzyme or buffer added to a final volume of 300 μl. After incubation at 37 °C for the indicated times, samples on ice were precipitated and analysed by HPLC as in Fig. 1 legend, except that carrier 5,6-dihydroxydihydrothymine and 5,6-dihydrothymine (Sigma) were added, and 150 μl fractions collected at 1 ml min^{-1} flow rate, 730 p.s.i. Water (150 ml) was added to each fraction and the absorbance at 254 nm determined prior to scintillation counting as for Fig. 1. 5,6-dihydroxydihydrothymine was made by OsO_4-treatment of thymine[35] (Sigma) or by the method of Cadet and Teoule[37]. Open triangles, untreated DNA; solid triangles, DNA exposed to 0.054% OsO_4; circles, DNA exposed to 0.52% OsO_4.

AP endonucleases associated with T4 UV endonuclease and endonuclease III

Given that purified *M. luteus*[24] and T4 UV endonucleases[13] and *E. coli* endonuclease III each contain both DNA glycosylase and AP endonuclease activities, one may ask whether the two activities in some or all of these preparations are properties of a single enzyme. Alternatively, the presence of two activities in such preparations might be an artefact of purification and assay procedures: since endonucleolytic activity was being used as an assay in each case, AP endonuclease needed to be present in order to monitor *N*-glycosylic base removal as strand breakage.

However, there is some evidence against this possibility. With endonuclease III, the ratio of UV to AP endonuclease activity is constant during inactivation of the enzyme by both heat and storage, and the reaction optima for both activities are about the same. Similarly, T4 UV endonuclease loses both UV and AP endonuclease activities at the same rate during storage (data not shown). In addition, attempts to separate AP endonuclease from 5,6-hydrated thymine glycosylase activities have failed, and endonuclease III activity is not altered by isoelectric focusing[23]. Such studies have not been reported for the UV endonuclease of *M. luteus*; nevertheless, the cleavage products of the AP endonuclease activity of that enzyme are like those of endonuclease III and T4 UV endonuclease; that is, nicks containing a 3′-terminal AP deoxyribose[13]. In contrast, cleavage by endonuclease IV (ref. 13), endonuclease VI (ref. 25) and human placental AP endonuclease[26] is on the opposite side of the base-free deoxyribose residues so as to yield nicks containing 5′-terminal deoxyribose-5-phosphate. Thus, the AP endonucleases associated with DNA glycosylase activities are all of the same type and are distinct from those of the AP endonucleases lacking apparent associated DNA glycosylase activity (at least for the limited number characterized to date). It is also possible that the AP endonuclease components of endonuclease III and T4 UV endonuclease are derived from a common source. However, the detergent Triton X-100 stimulates both the AP and UV endonuclease activities of endonuclease III some 5- to 10-fold, but it is without effect on either the AP- or UV-specific endonucleolytic activity present in our preparation of T4 UV endonuclease. In addition, T4 UV endonuclease fails to cleave OsO_4-treated PM2 DNA[13].

In summary, it is possible that the AP endonuclease activities are not fortuitously associated with their respective *N*-glycosylase components, but instead are companion activities in repair complexes or even single polypeptide chains.

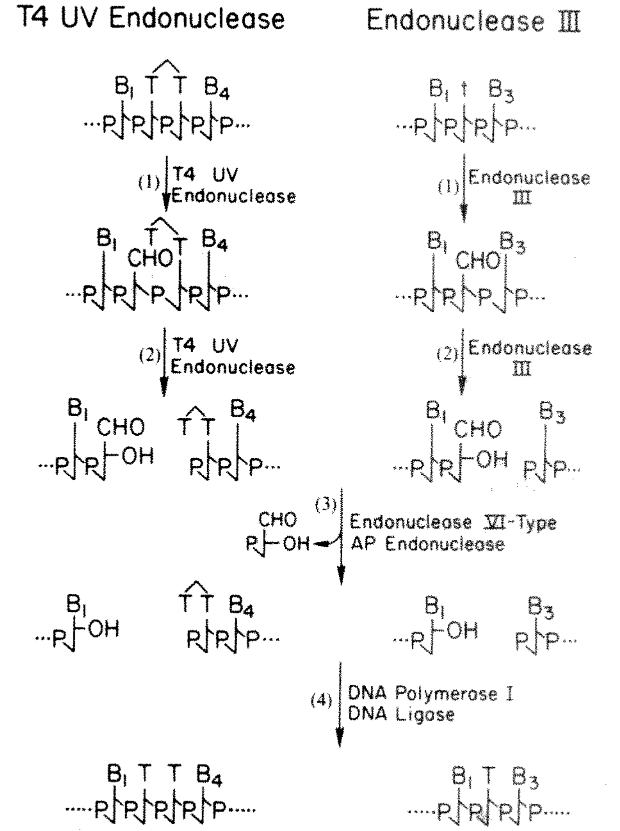

Fig. 3 Excision repair of UV-damaged DNA. The DNA is presumed to be duplex, but for simplicity only one strand is shown. t represents 5,6-hydrated thymine. Endonuclease VI-type refers to AP endonucleases that cleave on the 5′-side of AP sites.

Schemes for UV repair involving DNA glycosylase activities

A scheme for UV repair which extends the base excision studies of Lindahl[6] is emerging from these and related studies[10,13] (Fig. 3). A DNA glycosylase activity specific for pyrimidine dimers (T4 or *M. luteus* UV endonuclease) or 5,6-hydrated thymine (endonuclease III) would first hydrolyse the glycosylic bond of the damaged base. For 5,6-hydrated thymine, the base is completely released from the DNA, as is the case with glycosylase removal of uracil[6], 3-alkyl-adenine[8], hypoxanthine[2] and formamidopyrimidine[9]. For pyrimidine dimers, a structure is formed which retains the dimer in the DNA. It is this pyrimidine dimer attached by only a single glycosylic bond which releases a single pyrimidine when exposed to a secondary dose of irradiation. Judging from the results of Minton *et al.*[27], photoreactivating enzyme *in vitro* would also be capable of acting to cleave dimers at these nicked sites.

Following glycosylase action, two routes are possible for endonuclease incision: hydrolysis of the bond either on the 5′- or on the 3′-side of the AP site. Cleavage on the 3′-side, as has been shown for preparations of endonuclease III and T4 UV endonuclease[13], yields a nick containing a 3′-terminal deoxyribose. Such a structure is an ineffective primer for *E. coli* DNA polymerase I (ref. 13), but can be rendered effective by removal of the 3′-terminal AP site. This removal can be carried out by endonuclease IV or endonuclease VI of *E. Coli*[13], resulting in a gap of one nucleotide at the site of damage (Fig. 3). DNA polymerase I can then excise and resynthesize the damaged region, with DNA ligase restoring the continuity of the DNA to complete the repair. Alternatively, initial cleavage at the AP site arising from glycosylase action might be carried out by an AP endonuclease that leaves a 5′-terminal AP deoxyribose and 3′-OH terminus. As shown previously[13], such nicks directly provide efficient primer termini for *E. coli* DNA polymerase I.

It now seems that in *E. coli*, specific excision repair pathways might proceed via base-excision with specificity for the type of damage lying with DNA glycosylases, while strand incision would occur by virtue of AP endonuclease specificity. Alternatively, apurinic sites might be repaired in a single step by insertion of the appropriate purine base[28]. Endonuclease incision at damaged nucleotide residues would then occur as a back-up mechanism and for cases where no specific glycosylase is available. Such repair would be mediated by enzymes such as endonuclease V, or the *uvr*ABC complex, which appear to recognize many abnormalities in DNA[5,29], rather than by the more specific enzymes such as endonuclease III.

We thank Rufus Day for suggesting the photoreversal experiment; P. Brooks and E. Haeusslein for preparing the T4 UV endonuclease; J. B. Neilands and B. N. Ames for allowing use of HPLC equipment; and Paul Howard-Flanders for helpful discussions. This work was supported by NIH grants GM 19020 and ES 07075 and contract DE-AS03-76-SF34 from the U.S. Department of Energy.

Received 29 April; accepted 3 July 1980.

1. Lindahl, T. & Nyberg, B. *Biochemistry* **13**, 3405–3410 (1974).
2. Karran, P. & Lindahl, T. *J. biol. Chem.* **253**, 5877–5879 (1978).
3. Reiner, B. & Zamenhof, S. *J. biol. Chem.* **228**, 475–486 (1957).
4. Patrick, M. H. & Rahn, R. O. in *Photochemistry and Photobiology of Nucleic Acids* Vol. 2 (ed. Wang, S. Y.) 35–95 (Academic, New York, 1976).
5. Howard-Flanders, P. *A. Rev. Biochem.* **37**, 175–200 (1968).
6. Lindahl, T. *Nature* **259**, 64–66 (1976).
7. Braun, A., Radman, M. & Grossman, L. *Biochemistry* **15**, 4116–4120 (1976).
8. Riazuddin, S. & Lindahl, T. *Biochemistry* **17**, 2110–2118 (1978).
9. Chetsauga, L. & Lindahl, T. *Nucleic Acids Res.* **6**, 3673–3683 (1979).
10. Grossman, L., Riazuddin, S., Haseltine, W. & Lindan, C. *Cold Spring Har. Symp. quant. Biol.* **43**, 947–955 (1978).
11. Yasuda, S. & Sekiguchi, M. *Proc. nat. Acad. Sci. U.S.A.* **67**, 1839–1845 (1970).
12. Gates, F. & Linn, S. *J. biol. chem.* **252**, 2802–2807 (1977).
13. Warner, H., Demple, B., Deutsch, W., Kane, C. & Linn, S. *Proc. natn. Acad. Sci. U.S.A.* **77** (in the press).
14. Beukers, R. & Berends, W. *Biochim. biophys. Acta* **41**, 550–551 (1960).
15. Braun, A. & Grossman, L. *Proc. natn. Acad. Sci. U.S.A.* **71**, 1838–1842 (1974).
16. Seeburg, E. *Proc. natn. Acad. Sci. U.S.A.* **75**, 2569–2573 (1978).
17. Setlow, R. & Carrier, W. *Proc. natn. Acad. Sci. U.S.A.* **51**, 226–231 (1964).
18. Boyce, R. & Howard-Flanders, P. *Proc. natn. Acad. Sci. U.S.A.* **51**, 293–300 (1964).
19. Deering, R. & Setlow, R. *Biochim. biophys. Acta* **68**, 526–534 (1963).

20. Hariharan, P. & Cerutti, P. *J. molec. Biol.* **66,** 65–81 (1972).
21. Nes, I. & Nissen-Myer, J. *Biochim. biophys. Acta* **520,** 111–121 (1978).
22. Hariharan, P. & Cerutti, P. *Proc. natn. Acad. Sci. U.S.A.* **71,** 3532–3536 (1974).
23. Radman, M. *J. biol. Chem.* **251,** 1438–1445 (1976).
24. Tomilin, N., Paveltchuk, E. & Mosevitskaya, T. *Eur. J. Biochem.* **69,** 265–272 (1976).
25. Weiss, B., Rogers, S. & Taylor, A. in *DNA Repair Mechanisms* (eds Hanawalt, P., Friedberg, E. & Fox, C.) 191–194 (Academic, New York 1978).
26. Linsley, S., Penhoet, E. & Linn, S. *J. biol. Chem.* **252,** 1235–1242 (1977).
27. Minton, K., Durphy, M., Taylor, R. & Friedberg, E. *J. biol. Chem.* **250,** 2823–2829 (1975).
28. Livneh, Z., Elad, D. & Sperling, J. *Proc. natn. Acad. Sci. U.S.A.* **76,** 1089–1093 (1979).
29. Gates, F. & Linn, S. *J. biol. Chem.* **252,** 1647–1653 (1977).
30. Richardson, C. *J. molec. Biol.* **15,** 49–61 (1966).
31. Jagger, J. in *Introduction to Research in Ultraviolet Photobiology* 134–139 (Prentice Hall, New York, 1967).
32. Rustum, Y. *Analyt. Biochem.* **90,** 289–299 (1978).
33. Warner, H. & Duncan, B. *J. Virol.* **22,** 835–838 (1977).
34. Friedberg, E. & King, J. *J. Bact.* **106,** 500–507 (1971).
35. Burton, K. & Riley, W. *Biochem. J.* **98,** 70–77 (1966).
36. Davis, R. & Hyman, R. *J. molec. Biol* **62,** 287–301 (1971).
37. Cadet, J. & Teoule, R. *Carbohydrate Res.* **29,** 345–361 (1973).
38. Studier, F. *J. molec. Biol.* **11,** 373–390 (1965).
39. Goldmann, K. & Friedberg, E. *Analyt. Biochem.* **53,** 124–131 (1973).

LETTERS

Radio jets and bridges in the classical double sources 3C388 and 0816+526

Jack O. Burns*

National Radio Astronomy Observatory, VLA Program, Socorro, New Mexico 87801

Wayne A. Christiansen

Department of Physics and Astronomy, University of North Carolina, Chapel Hill, North Carolina 27514

We report on 4885-MHz full synthesis high-resolution (1″) observations [using the NRAO Very Large Array (VLA)] of the 'classical' double radio sources 0816+526 and 3C388. Classical double sources are characterized by strong emission peaks (lobes) at the extremities of a linear structure. Although at lower resolution these sources both appear to have simple double-lobed morphologies, the VLA maps reveal several important new features. 0816+516 was found to have very sharp leading edges indicative of strong deceleration, possibly as a result of encountering a dense extragalactic background gas. The transverse boundaries of the components are also quite steep but still consistent with constant emissivity-filled cylinders rather than limb-brightening. The morphology of 3C388 is dramatically different from 0816+526, since it includes a bright radio jet. Unlike previously observed radio jets which are usually found between the nucleus of the radio galaxy and its extended lobes, the jet in 3C388 is embedded inside the southwestern lobe and a prominent gap in the radio emission exists between the radio nucleus and the beginning of the jet. These observations clearly illustrate that a variety of source substructures, which must be dealt with in theoretical models, exist within radio galaxies which were previously classified simply as classical doubles.

0816+526 and 3C388 were chosen for detailed study with the VLA because their morphologies as seen in lower-resolution maps are typical of classical doubles. 0816+526 is associated with a galaxy in the direction of the cluster Abell 643 (distance class 5), although there is no redshift information to confirm its membership[1]. 3C388 (ref. 2) is identified with a cD galaxy ($z=0.0917$)[3] in the direction of a poor cluster. Both sources are quite luminous with 178-MHz radio powers, P_{178}, of $\gtrsim 3\times 10^{25}\,\mathrm{W\,Hz^{-1}\,sr^{-1}}$ for 0816+526 (assuming $z\sim 0.14$) and 3C388. Furthermore, both radio galaxies meet Fanaroff and Riley's Class II criteria (that is, most of the radio power emanates from the source extremities)[4]. The VLA maps of these radio galaxies have revealed a variety of structures which are as rich and complex as those seen in the lower luminosity doubles[5,6]. Several of these newly discovered features raise some interesting theoretical questions.

3C388 and 0816+526 were observed during a 24-h period on 9–10 July 1979 with the VLA. For these observations, a total of 16 antennas were available in the array with baselines ranging from ~60 m to ~18 km. Although the spacings were distributed non-uniformly (grouped heavily with baselines ≤2 km), the resulting *u*, *v* coverage allowed us to adequately map structures at most position angles in these high-declination sources. A bandwidth of 50 MHz centered on the frequency 4885 MHz ($\lambda=6$ cm) was used. The data were collected, edited and calibrated in a fashion similar to that discussed in Owen *et al.*[7]. 'Dirty' maps were constructed and 'cleaned' using the standard techniques.

Contour maps of the total intensity distribution for 0816+526 and 3C388 are shown in Figs 1 and 2, respectively. The shaded ellipses illustrate the FWHM contour of the elliptical clean beams used in restoring the maps.

The crosses in Figs 1 and 2 mark the positions of optical objects in the fields as seen on the Palomar Sky Surver (PSS) E-prints. The sizes of the crosses represent the formal 1″–2″ error in the optical measurements but they do not reflect the error in locating the galaxy nucleus on the overexposed images of the PSS. It is this second error which is likely to be responsible for the offset of the cross in Fig. 2 from the presumed 'nuclear' radio component in 3C388.

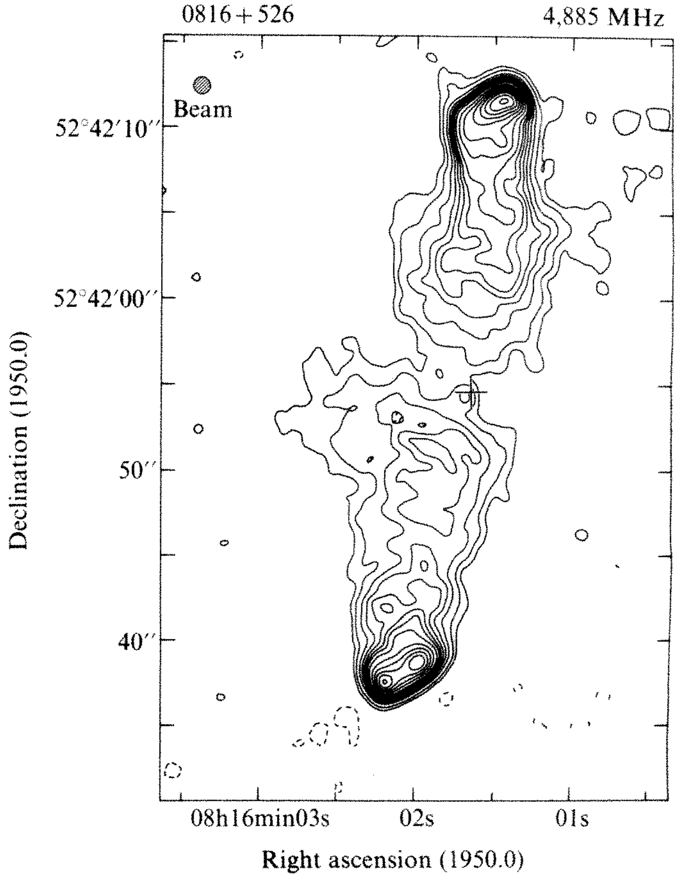

Fig. 1 Total intensity contour map of 0816+526 at 4,885 MHz. The contour levels are 21, 19, 17, 15, 12.6, 10.5, 8.4, 6.3, 5, 4.2, 3.6, 2.5, 1.7, 0.84, 0.42, −0.42, and −0.84 mJy per clean beam area. The shaded circle represents the half-power contour of the VLA clean beam (1″). The cross marks the position of the galaxy identified with 0816+526 as measured from the PSS E-print for this field.

---

*Present address: Department of Physics and Astronomy, University of New Mexico, Albuquerque, New Mexico 87131.

0028–0836/80/380208—03$01.00

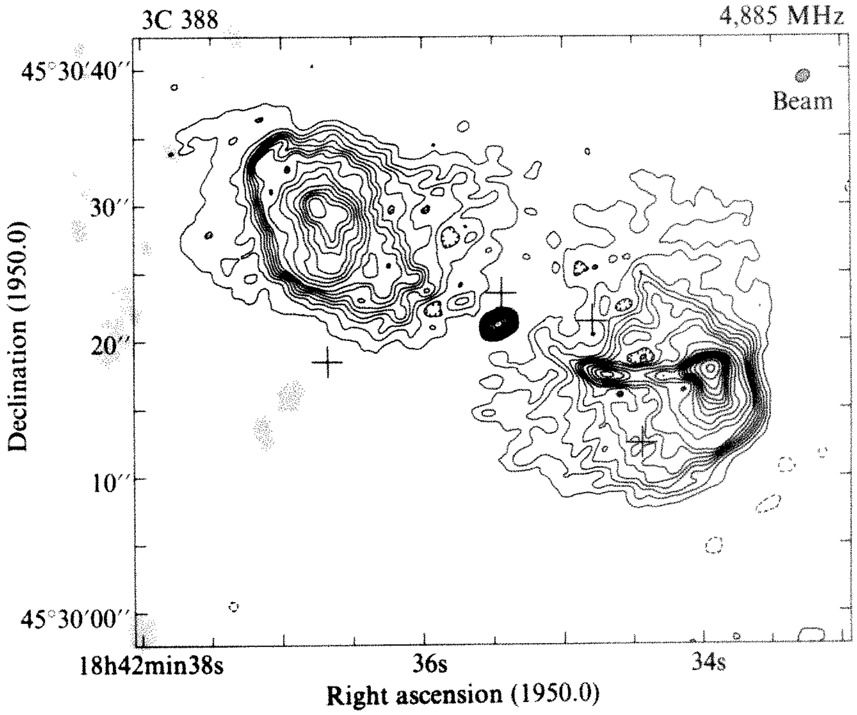

Fig. 2 Total intensity contour map of 3C388 at 4,885 MHz. The contour levels are 62, 50, 37, 25, 19, 13.6, 12.4, 11, 10, 8.7, 7.4, 6.2, 5, 4.3, 3.7, 3.1, 2.5, 1.9, 1.2, 0.6, −0.6, and −1.2 mJy per beam. The peak on this map is 62 mJy. The shaded ellipse represents the half-power contour of the VLA clean beam (1.2" × 0.9", p.a. = −61°). The crosses mark the positions of galaxies in the field of this source as measured from the PSS E-print.

The rich variety seen in the fine structures of both of these sources, in conjunction with high resolution observations of other double sources[6,8-10] indicates that the simple 'classical' double structure previously observed in many radio sources may often be an artifact of insufficient resolution. The new features, such as jets, shells and hot spots which are revealed, may provide the impetus for the testing and development of more detailed theories of radio source evolution. In what follows, since the structures of these two sources are qualitatively different, we shall discuss the structure of each source separately.

Referring to Fig. 1, this source has very sharp leading edges on both the northern and southern extremities. Both of these leading edges are curiously flattened (dense concentration of flux contours) along nearly parallel lines (to within 5°) at position angles of about 57° possibly indicating a large-scale symmetry in the source confinenent mechanism.

The northern component of 0816+526 contains a very intense hot spot ($S_6 = 21.2$ mJy per clean beam area) elongated in p.a. 55°, while the southern component contains a pair of hot spots ($S_6 = 17.2$ mJy per beam and $S_6 = 16.8$ mJy per beam) having nearly equal intensities whose axis lies at p.a. 60°. The strong concentration of the flux contours of both components toward the leading edges implies that steep gradients exist in the internal pressures in both components. This might be expected, if both components are strongly decelerated, possibly as a result of encountering an enhanced background density located well outside the parent galaxy. This dense background gas might be attributed to gaseous remnants from previous activity. An encounter with an enhanced density is also consistent with the sudden reductions in the transverse dimensions of each component observed at declinations of $\delta = 52°41'50"$ and $\delta = 52°42'06"$, respectively. Numerical calculations[11] show that these factors of 2 reductions in transverse radii (as measured from second moments of the one-dimensional strip scans)[12] can be induced by encounters with backgroung media whose densities are enhanced by about a factor of 10.

Another feature of 0816+526 which differs from the structures usually observed in extended doubles is the existence of sharp boundaries along the trailing sides of both components. This is especially noticeable along the sides of the northern component. We have investigated the possibility that trailing regions of this source might be 'limb-brightened' (in the sense that the volume emissivity near the outer boundary of the source exceeds the axial emissivity) by comparing brightness distributions along transverse cuts at declinations between $\delta = 52°41'44"$ and $\delta = 52°42'10"$ with the brightness distributions expected from constant emissivity-filled cylinders whose axes are perpendicular to the line of sight. We find no evidence for limb-brightening since none of these cuts have brightness distributions which rise significantly faster than the constant emissivity case. Even the region in the north component with sharp sides ($52°42'06" < \delta < 52°42'10"$), the brightness distribution can be adequately described by two parameter (radius, peak brightness) least squares fits with filled cylinders ($0.92 <$ correlation coefficient < 0.95; probability that correlation could result from random data in $<0.1\%$). As pointed out by De Young[13], limb-brightening is likely to occur in theoretical models of ram pressure radio sources (whether beams, plasmoids or massive objects) in which relativistic particles are transported and/or accelerated in the sources bow shock. Our failure to detect limb-brightening in this source which has such well-developed hot spots and sharp leading edges seems to indicate that bow shock transport is not likely to be the dominant mechanism for injecting relativistic particles into the trailing regions.

Although the luminosity of 3C388 is roughly comparable to the estimated value for 0816+526, the morphology of this double source is dramatically different as shown by the total intensity map (Fig. 2). Certainly the most interesting feature in this source is the complex jet which is embedded in the south-western lobe. The inclusion of this jet in an extended lobe is remarkable since all radio jets observed previously[5-7] have been located between the galactic nucleus and any extended radio lobes which might be present. In 3C388, however, there is a very noticeable gap in the radio emission between the galactic nucleus and the jet. Furthermore, the jet, which runs almost directly east–west, is definitely not parallel to the double source major axis, having an inclination angle of about 30° with respect to this axis.

The jet (average $S_6 \sim 8$ mJy per beam, percentage polarization, $\pi \leqslant 5\%$) contains two prominent hot spots at opposite extremities (western hot spot: $S_6 = 41.1$ mJy per beam and $\pi \sim 20\%$ polarized, eastern hot spot: $S_6 = 11.2$ mJy per beam and $\pi < 5\%$). The high-intensity contours of the very bright western hot spot are extended toward the south, a direction which is nearly perpendicular to both the jet and the source major axis. Also, extensions in the low-level contours of the eastern hot spot appear to point towards a very intense nuclear radio component ($S_6 = 62$ mJy per beam) located at the centre of the optical galaxy.

The structure of the northeastern lobe of 3C388 contains two interesting substructures. First, this lobe has a sharp 'V'-shaped ridge embedded in an amorphous region of low-level radio emission. (Apex of the 'V' is $\alpha = 18$ h 42 min 37.5, $\delta = 45°30'34''$.) The ridge is highly polarized ($\pi \sim 25$–30%) with a possibly circumferential magnetic field configuration. This polarization structure will be discussed in more detail elsewhere. Second, the rather diffuse hot spot in this component is located well back from the leading edge of the lobe. Both the jet and the 'V'-shaped shell are missing in the 8-GHz map of De Young *et al.*[14], thus raising the possibility that these regions of the source may have steep spectra ($\alpha > 0.8$ where $S_{\nu}\alpha^{-\alpha}$).

Neither of these sources has a structure which appears to be compatible with either of the extremes in the spectrum of ram pressure confined radio source models: namely, simple continuous beam models on the one hand and single injection plasmoid models on the other. Rather, what seems to be called for is some sort of intermittent beam or multiple explosion model; two concepts in which distinctions have become somewhat blurred. A major remaining distinction between these theoretical models does exist in terms of the plasma density assumed to exist inside the observed radio lobes, with the beam models generally invoking a low-density plasma while the plasmoid models invoke high densities.

As mentioned previously, an attractive interpretation for the structure of 0816+526 invokes the penetration of the radio source into an enhanced background density. The intense hot spots in both components of 0816+526 are then attributable to Rayleigh–Taylor instabilities driven by the large deceleration associated with the enhanced background density. In fact, the rapid growth of Rayleigh–Taylor instabilities, along with a general contraction induced by encountering a higher density, may trigger the type of radiative instabilities discussed by Eilek and Caroff[15] and Christiansen *et al.*[16].

For 3C388, physical conditions seem to be quite different. It seems that this source may involve an interaction between an intermittent beam and/or a fresh plasmoid and the boundaries of an evacuated cavity or bubble. The obvious differences in appearance of the major lobes can then be ascribed to the possibility that the two lobes are in different stages of development. That is, in the southwestern component the leading edge of the beam has already impacted on the shell of the cavity creating the observed hot spot. The jet might then be interpreted as being a narrow part of the beam which has not yet reached the shell or perhaps as a reflection jet of plasma which has been focused by and rebounded from the external shell. This latter possibility[17] is particularly intriguing because of the jet's well-collimated structure and lack of polarization.

The northeastern lobe of the source is then interpreted as being in a less well-developed stage in which a new radio component (represented by the diffuse hot spot) is just beginning to make contact with the steep-spectrum shell source. As this plasma rams further into the apex of the shell it should be decelerated and develop a higher surface brightness more closely resembling the structure of the southwestern component.

We thank Frazer Owen, Jean Eilek, and Lawrence Rudnick for critical readings of the manuscript, Roger Blandford and Dave De Young for comments on our interpretations of the source structures, and David Hough for help with data reduction. W.A.C. thanks NRAO for a summer faculty fellowship and the Morehead Foundation at the University of North Carolina for financial support.

Received 19 May; accepted 24 July 1980.

1. Burns, J. O., Owen, F. N. & Rudnick, L. *Astron. J.* **83,** 312 (1978).
2. Pooley, G. G. & Henbest, S. N. *Mon. Not. R. astr. Soc.* **169,** 477 (1974).
3. Mathews, T. A., Morgan, W. W. & Schmidt, M. *Astrophys. J.* **140,** 35 (1964).
4. Fanaroff, B. L. & Riley, J. M. *Mon. Not. R. astr. Soc.* **167,** 31P (1974).
5. van Breugel, W. J. M. & Miley, G. K. *Nature* **265,** 315 (1977).
6. Perley, R. A., Willis, A. G. & Scott, J. S. *Nature* **281,** 437 (1979).
7. Owen, F. N., Burns, J. O., Rudnick, L. & Greisen, E. W. *Astrophys. J.* **229,** L59 (1979).
8. Perley, R. A., Bridle, A. H., Willis, A. G. & Fomalont, E. B. *Astron. J.* **85,** 499 (1980).
9. Burch, S. F. *Mon. Not. R. astr. Soc.* **186,** 519 (1979).
10. Jenkins, C. J., Pooley, G. G. & Riley, J. M. *Mem. R. astr. Soc.* **84,** 61 (1977).
11. Rolison, G. G. & Christiansen, W. A. (in preparation).
12. Burns, J. O., Owen, F. N. & Rudinck, L. *Astrophys. J.* **84,** 1683 (1979).
13. De Young, D. S. *Astrophys. J.* **211,** 329 (1977).
14. De Young, D. S., Hogg, D. E. & Wilkes, C. I. *Astrophys. J.* **228,** 43 (1979).
15. Eilek, J. A. & Caroff, L. J. *Astrophys. J.* **233,** 463 (1979).
16. Christiansen, W. A., Rolison, G. G. & Scott, J. S. *Astrophys. J.* **234,** 456 (1979).
17. Christiansen, W. A., Scott, J. S. & Pacholczyk, A. G. (in preparation).

Short-term variability of Cyg X-1 and the accretion disk temperature fluctuation

Kohsei Doi*

Institute of Space and Aeronautical Science, University of Tokyo,
Komaba, Meguro-ku, Tokyo 153, Japan

Recent thoretical models of Cyg X-1 (refs 1–5) assume that to explain the observed time-averaged spectrum the hard X rays are emitted by inverse-Compton mechanism from an optically thin, hot accretion disk around a black hole. Numerous observations (especially in the energy range$\gtrsim$20 keV) have shown that the source intensity is variable on different time scales[6–17]. Short-term variability on the time scale of ~1 s is especially conspicuous because of its stationary nature and the stability of time scale[6–11]. A balloon observation was carried out to study the variability in the hitherto unknown hard X-ray range ($\gtrsim$20 keV). The results of the analysis, together with those of the former rocket observation, suggest that the variation is essentially spectral, implicating that it originates from temperature fluctuation in an accretion disk. Such a model is discussed here in detail.

Although it has been suggested, along with the shot-noise model, that the variability is caused by local hot spots[9], how such hot spots are generated and decay in an accretion disk with the relevant time scale remains obscure. Moreover, our previous rocket observation (1.5–25 keV) revealed the complete correlation between the variations of different energy bands (that is, the energy independence of the characteristic time scale ~1 s) and energy dependence of the relative amplitude of the variation[11], which presents difficulty to the simple shot-noise model[11,18]. To obtain a wideband picture of the variation, I made a balloon observation in the hard ($\gtrsim$20 keV) X-ray range with a large effective area (~3,000 cm^2) detector comprising pressurized xenon gas proportional counters[19,20]. The balloon flight was carried out on 22 May 1977 in collaboration with the balloon group of ISAS, University of Tokyo.

The coefficient of variation method of analysis[11,19] was applied to the balloon data to compare it with the rocket observation. The coefficient of variation for a data bin-width t_b, $\eta(t_b)$, is defined as the standard deviation of the variation intrinsic to Cyg X-1 normalized to its average intensity; it is a dimensionless measure of the amplitude of variation, and as a function of t_b it carries information on the characteristic time τ($\eta(t_b)$ is constant for $t_b \lesssim \tau$ and decreases monotonously for $t_b \gtrsim \tau$ as the variation is smoothed out).

The results are shown in Fig. 1 for the balloon data in two energy bands (20–35, 35–68 keV) with the previous rocket data in three energy bands. The characteristic time is about the same(~1 s), but there is a striking difference in energy dependence of the amplitude of variation between low (rocket) and high (balloon) energies; for the soft X rays ($\lesssim$25 keV) the lower the energy, the greater the amplitude of variation, while the opposite is true for the hard X rays ($\gtrsim$20 keV).

The relation between the variations observed in different experiments at different times is unknown, so there are

---

*Present address: Shiba High School, 3-5-37 Shiba-koen, Minato-ku, Tokyo 105, Japan.

0028–0836/80/380210—03$01.00

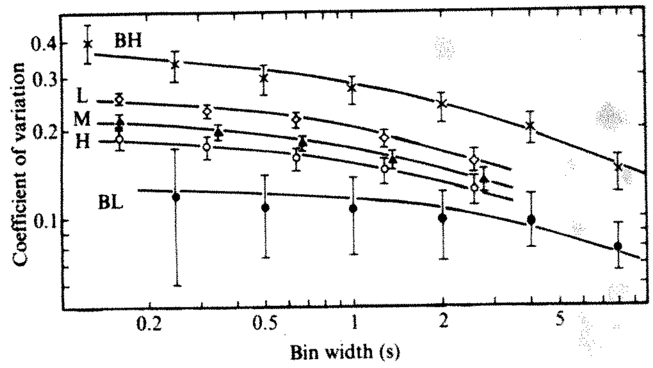

Fig. 1 Coefficients of variation plotted against data bin width for the balloon (BL, 20–35; BH, 35–68 keV) and rocket (L: 1. 5–5; M, 5–10, H; 10–25 keV) data.

difficulties when combining the results to make one picture. The difficulty associated with long-term variation may be alleviated by the average flux data in both experiments being consistent with the normal state spectrum. Assuming that the variation is stationary (which is justified at least in $\lesssim 20$ keV range, because it was observed in virtually all the high time-resolution measurements, deriving essentially the same characteristic time scale ~1 s) there are three possible interpretations: the soft and hard X-ray variations are (1) positively correlated, (2) statistically independent, or (3) anti-correlated. Although none of these can be ruled out by present observational knowledge, note that the third interpretation (which claims that the variation is essentially spectral, keeping the total X-ray luminosity approximately constant although a narrow-band observation indicates intensity variation, see Fig. 2) is consistently accommodated by the accretion disk model. Spectral variation means that the fluctuation of the electron temperature, and a built-in mechanism of such a fluctuation, does exist in the hot disk proposed in the current models.

Energetics in the disk can be summarized as follows. Gravitational energy of accreting matter is absorbed by ions through viscous dissipation and subsequently transfers to electrons through Coulomb collisions. Electrons are cooled by comptonization of low energy (soft) photons, emitting the bulk of energy as hard X rays. The cooling time scale τ_c(~ms) is much shorter than the time scale of Coulomb coupling $\tau_{ei}(\propto n^{-1}T_e^{3/2})$, hence the disk is in the two-temperature state[3,5] ($T_i \gg T_e$; note that $(T_i - T_e)/\tau_{ei} = T_e/\tau_c$ from energy balance). Now if the luminosity of soft photons (L_s) fluctuates, then it will cause the kind of variation suggested from the observations. As the energy supply rate (originally determined by the accretion rate) is considered to be constant ($\sim T_i/\tau_{ei}$) on the time scale of seconds, the energy spectrum has to change to keep the total X-ray luminosity approximately constant. For example, when L_s increases, Compton cooling will lower T_e and a soft (steep) spectrum will result. Stochastic fluctuation of L_s would be expected in the hot disk, which is set up by instabilities and where turbulence is the main source of viscosity.

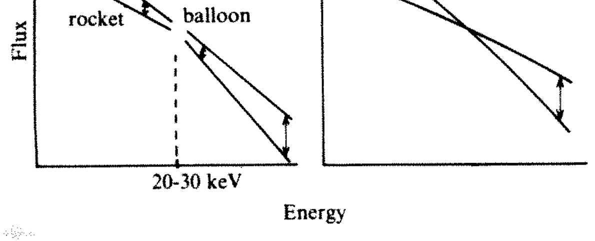

Fig. 2 *a*, Illustration of the energy dependence of the short-term variation derived from the rocket and balloon observation; *b*, a tentative interpretation.

The simplest description of the variation of T_e is

$$\frac{dT_e}{dt} = \frac{T_i - T_e}{\tau_{ei}} - CL_s(t) \tag{1}$$

where the first and second terms in the right hand side represent Coulomb heating and Compton cooling respectively. (The cooling effect is assumed to be proportional to L_s for simplicity; thus $C\langle L_s(t)\rangle = \langle T_e\rangle/\tau_c$ to meet the steady state solution.) Equation (1) is a Langevin equation[18] for stochastic variable $L_s(t)$. Assuming that $L_s(t)$ fluctuates with a time scale τ_s, so that its power spectrum $I_s(\omega)$ is in the form

$$I_s(\omega) \propto \frac{1/\tau_s}{\omega^2 + 1/\tau_s^2} \tag{2}$$

The autocorrelation function of $T_e(t)$ is then,

$$\langle T_e(t)T_e(t+\tau)\rangle \propto \frac{\tau_{ei}\exp(-|\tau|/\tau_{ei}) - \tau_s \exp(-|\tau|/\tau_s)}{(\tau_{ei} - \tau_s)} \tag{3}$$

Note that τ_{ei} is the only long (~1 s) time scale in the inner hot disk, which reflects the high temperature state ($T_i \sim 10^{11}$, $T_e \sim 10^9$ K). τ_s is expected to be much shorter as L_s is considered to originate from cold and dense clumps in the hot disk, where relevant characteristic times (keplerian and hydrodynamic ones) are of the order of milliseconds (ref. 5). Then, equation (3) indicates that the time scale of the variation of T_e (and of X rays) is ~1 s just as observed.

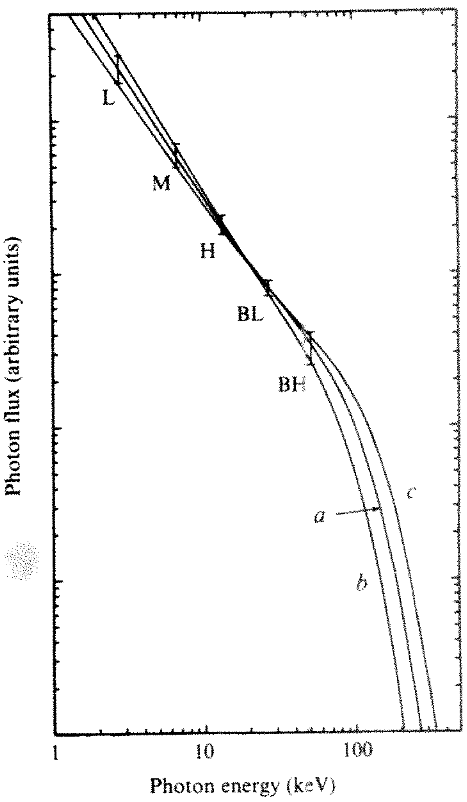

Fig. 3 Theoretical comptonization spectra for *a*, the best-fit parameters $kT_e = 27$ keV and Thomson optical thickness = 5; *b*, $kT_e = 21$ keV; and *c*, $kT_e = 33$ keV, normalized to the total X-ray luminosity (1–300 keV). Vertical bars labelled L, M, H, BL, and BH show ±1 standard deviation of the variations derived from the coefficients of variation at bin-width of 0.5 s (Fig. 1). Each bar is placed at the mean energy of corresponding energy band.

Recently Sunyaev and Trümper[21] have compared the new observational and theoretical results to derive the best-fit disk parameters including a much smaller T_e ($kT_e = 27$ keV) than previously believed. Their theory is based on the (time-averaged) hard X-ray spectrum with high statistical accuracy obtained from balloon observations by the AIT/MPI group and the analytical solution for the comptonization spectrum from a spherical isothermal electron cloud. Their results give more semi-quantitative support to the present model. Figure 3 shows the theoretical spectrum for the best-fit parameters (kT_e = 27 keV, and Thomson optical thickness =5) and the spectra for T_e a little (~20%) higher and lower, normalized to the total X-ray luminosity. The node of the flux variation is indeed at 20–30 keV as suggested from the observation. Figure 3 also shows the ±1 standard deviation of the variations for various energy bands derived from the observational data (Fig. 1) for comparison.

The present model explains the stochastic nature of variability, its characteristic time scale and spectral features at the same time in the context of the conventional accretion disk model for Cyg X-1. Furthermore I suggest that the complex variability of Cyg X-1 over a wide span of time scale may be classified into three categories: (1) non-stationary long-term variation on the time scales from ~10 s (ref. 17) to ~10^6 s (high-low transition[12–15]) due to fluctuations in the outer cool disk and changes in accretion rate[5]; (2) stationary short-term variation discussed here; and (3) millisecond pulsation[16] which presumably reflects the intrinsic time scale to the inner hot disk. A more refined version of extended-range, high time-resolution observation will clarify the nature of the variability.

I thank Professors M. Oda, J. Nishimura, S. Miyamoto and Y.Ogawara for useful discussions.

Received 11 March; accepted 27 May 1980.

1. Thorne, K. S. & Price, R.H. *Astrophys. J. Lett.* **195,** L101 (1975).
2. Eardly, D. M., Lightman, A. P. & Shapiro, S. L. *Astrophys. J. Lett.* **199,** L153 (1975).
3. Shapiro, S. L., Lightman, A. P. & Eardley, D. M. *Astrophys. J.* **204,** 187 (1976).
4. Eardly, D. M. & Lightman, A. P. *Nature* **262,** 196 (1976).
5. Ichimaru, S. *Astrophys. J.* **214,** 840 (1977).
6. Oda, M. *et al. Astrophys. J. Lett.* **166,** L1 (1971).
7. Rappaport, S., Doxsey, R. & Zaumen, W. *Astrophys. J. Lett.* **168,** L43 (1971).
8. Brinkman, A C. *et al. Astrophys. J.* **188,** 603 (1974).
9. Weisskopf, M. C., Kahn, S. M. & Sutherland, P. G. *Astrophys. J. Lett.* **199,** L147 (1975).
10. Rothschild, R. E., Boldt, E. A., Holt, S. S. & Serlemitsos, P. J. *Astrophys. J.* **213,** 818 (1977).
11. Ogawara, Y., Doi, K., Matsuoka, M., Miyamoto, S., & Oda, M. *Nature* **270,** 154 (1977).
12. Heise, J. *et al. Nature* **256,** 107 (1975).
13. Holt, S.S., Boldt, E. A., Kaluzienski, L. J. & Serlemitsos, P. J. *Nature* **256,** 108 (1975).
14. Holt, S. S., Kaluzienski, L. J., Boldt, E. A. & Serlemitsos, P. J. *Nature* **261,** 213 (1976).
15. Sandford, P. W. *et al. Nature* **256,** 109 (1975).
16. Rothschild, R. E., Boldt, E. A., Holt, S. S. & Serlemitsos, P. J. *Astrophys. J. Lett.* **189,** L13 (1974).
17. Canizares, C. R. & Oda, M. *Astrophys. J. Lett.* **214,** L119 (1977).
18. Doi, K. *Nature* **275,** 197 (1978).
19. Doi, K. thesis, Univ. Tokyo (1978).
20. Doi, K. & Fujii, M. *Nucl. Instrum. Meth.* **155,** 305 (1978).
21. Sunyaev, R. A. & Trümper, J. *Nature* **279,** 506 (1979).

The 20-μm brightness temperature of the unilluminated side of Saturn's rings

Alan T. Tokunaga*, John Caldwell† & Ira G. Nolt‡

* Institute for Astronomy, University of Hawaii, 2680 Woodlawn Drive, Honolulu, Hawaii 96822
† Department of Earth and Space Sciences, State University of New York, Stony Brook, New York 11794
‡ Atmospheric Physics and Chemistry Laboratory, NOAA, Boulder, Colorado 80303

The 20-μm brightness temperature of the unilluminated (north) side of Saturn's rings is reported here to be 56±1 K. This measurement, together with previous measurements of the rings at 20 μm, shows that the brightness temperature of the B ring can be approximated by the simple equation $T_B^4 = 56^4 + 1.52 \times 10^8 \sin|B'|$, where B' is the saturnicentric declination of the Sun. We have assumed that emission from the Cassini division is negligible. The constants in this equation may be understood in terms of a two-component heating model for the ring particles—sunlight and radiation from Saturn. We discuss the implications of the IR data for several published ring models.

Table 1 19.8 μm photometry

Ring position flux	$5.75 \pm 0.22 \times 10^{-19}$ W cm^{-2} μm^{-1}
Sky position flux	$3.57 \pm 0.18 \times 10^{-19}$ W cm^{-2} μm^{-1}
Net ring flux	$2.18 \pm 0.40 \times 10^{-19}$ W cm^{-2} μm^{-1}
Ring brightness	$5.88 \pm 1.08 \times 10^{-9}$ W cm^{-2} μm^{-1} sr^{-1}
Corrected ring brightness*	$9.06 \pm 1.66 \times 10^{-9}$ W cm^{-2} μm^{-1} sr^{-1}
Ring brightness temperature	56.0 ± 0.9 K

*See text.

Previous observations showed that the brightness temperature of Saturn's B ring gradually decreased as B' diminished. The current time period is critical because observations at the small values of B' can most effectively distinguish between competing models for the B ring, as shown by Nolt *et al.*[1]. In addition, for several months near the beginning of 1980 the unilluminated side of the rings could be observed from the Earth. This opportunity arises whenever the Earth and the Sun are at opposite sides of the plane of the rings, as can occur during the ring plane crossing[2]. The first IR observations of the unilluminated side of the rings were made with the Pioneer 11 spacecraft, which found a 45-μm brightness temperature of ~55 K (ref. 3). [Ingersoll (personal communication) now considers the Pioneer 11 observation of the unilluminated side of the rings to be a firm detection rather than an upper limit.]

The observations were made with the 3-m IR Telescope Facility (IRTF) at Mauna Kea on Hawaii on 6 January 1980 (UT). A newly developed 2–30-μm liquid helium cooled bolometer system was used for the observations. For the ring observations, a 2-arc s aperture was used with a cooled 19.8-μm filter (Δλ = 6 μm) which defined the wavelength interval. The aperture was centred on the B ring ansa, but the small opening of the rings (the maximum extent of the minor axis was 1.7 arc s) prevented the separation of the A and B rings. The C ring was completely out of our aperture.

The centre of the B ring ansa was only 6 arc s from the edge of the disk of Saturn, and as a result scattered and diffracted radiation from the disk produced a spurious signal (which we call 'sky' signal). We have measured the sky signal at the same radial distance from the limb as the rings but displaced 4 arc s north and south. The signal at the ring position and the adjacent sky is shown in Table 1 (the north and south sky measurements have been combined). As there was no significant difference in the signals at the ring position between the A and B ring ansae, the signals at both ansae have also been combined in Table 1.

The difference in measured flux between the ring and sky positions was $2.18 \pm 0.40 \times 10^{-19}$ W cm^{-2} μm^{-1}. The quoted error is the sum of the errors of the ring and sky positions and is therefore a conservative estimate. The solid angle of the rings within our aperture was determined graphically to be 3.71×10^{-11} sr, using previously published constants[4], so that the surface brightness of the rings is $5.88 \pm 1.08 \times 10^{-9}$ W cm^{-2} μm^{-1} sr^{-1}.

The first dark ring of the Airy diffraction pattern of the telescope has a diameter of 3.4 arc s. Therefore, some of the flux from the ring was diffracted out of the beam. From a two-dimensional convolution of the diffracted ring with our aperture, we estimate that approximately 35±5% of the ring flux was diffracted out of the beam. After adjusting for this we obtain a corrected ring brightness of $9.1 \pm 1.7 \times 10^{-9}$ W cm^{-2} μm^{-1} sr^{-1}, which corresponds to a brightness temperature of 56±1 K at 19.8 μm. This brightness temperature agrees very well with that measured by Pioneer 11 at 45 μm.

It is difficult to correct our result for the emission from the Cassini division because its optical depth and brightness temperature are both very uncertain. The normal optical depth has recently been estimated to be in the range 0.01–0.05 (refs 5–7). For this range of optical depth, the brightness temperature of the Cassini division must be less than 64–71 K for the Cassini division to emit less than 10% of the observed emission. As Nolt *et al.*[1] found that the C ring brightness temperature was 82–85 K at $B' = -6.5°$, a brightness temperature for the Cassini division

0028-0836/80/380212—03$01.00

Table 2 Previous observations of the B ring of Saturn

Saturnicentric solar declination $|B'|$	B ring brightness temperature at 20 μm (K)	Ref.
26.3	94 ± 2	16
26.4	96 ± 3	17
25.8	90.4 ± 1.5	18
16.3	84 ± 2	10
11.8	77.5 ± 3	1
11.5	79.4	19*
6.5	74 ± 3	1
2.83	60–70	3†

*This is based on the higher flux calibration adopted by Sinton *et al.*[19].

†Range of 45-μm brightness temperature from Pioneer 11.

of ≤ 70 K at the time of our observations ($B' = -0.881°$) is plausible. In the following we assume that the emission of the Cassini division is neglible, pending more precise estimates of the optical depth and brightness temperature of the Cassini division.

The ring brightness temperature must be very close to the actual temperature of the unilluminated side of the rings, as the rings are opaque in the line of sight. From the B ring normal optical depth of ≈ 1 at visual wavelengths[8], we estimate the visual line of sight transmission in the direction of the Earth to be $1/\exp(1/\sin 1.72°) \approx 10^{-15}$, where 1.72° is the saturnicentric declination of the Earth. Therefore, with unit emissivity, the physical and brightness temperatures would be identical. For all plausible emissivities, the difference will be very small. For example, at 20 μm, an emissivity of 0.8 would result in an underestimate of the physical temperature of less than 1 K.

We further suggest that our result for the dark side provides a measure of the A and B ring brightness temperature in the absence of solar heating, the condition achieved when $B' = 0°$. Direct solar heating certainly does not influence our observation, as the line of sight transmission for sunlight is even less than the transmission as viewed from the Earth. Heating of the dark side by scattered sunlight is possible[9], but we ignore it for the present. A qualitative explanation of the observed ring brightness of the unilluminated side as discussed below does not require additional heating by scattering.

Our measurement is shown in Fig. 1 along with previous 20-μm observations of the B ring that are listed in Table 2. No correction for the distance of Saturn from the Sun has been applied. Such a correction, as applied by Nolt *et al.*[10], results in a change of brightness temperature of ≤ 1 K, which is less than the uncertainty in the measurements. A very good fit to the data can be obtained using the empirical formula

$$T_B^4 = T_0^4 + C \sin |B'| \qquad (1)$$

where T_0 and C are constants. The first term on the right accounts for the heating from the disk of Saturn that results from reflected solar radiation and IR emission from Saturn. The second term in equation (1) accounts for solar heating as a function of B', a parameterization which has been suggested previously by Murphy[11] and by Pollack *et al.*[12] for various simplified ring models.

Our observations give $T_0 = 56$ K because this is the expected value of the B ring temperature for $B' = 0$ as discussed above. We have neglected here any difference in the A and B ring temperature, because we do not have sufficient information for a two-parameter fit. We find that a value of $C = 1.52 \pm 0.17 \times 10^8$ K^4 gives the best fit to the data, as shown in Fig. 1.

Can the ring temperature of 56 K be explained only from heating by the disk of Saturn? We assume that an idealized ring particle is illuminated by Saturn on only half of its northern hemisphere. Radiation from Saturn from the other side of the ring plane is assumed to be blocked by other ring particles. We then obtain the following simple radiation balance equation

$$(1 - A)f = 4\,\alpha e \sigma T_0^4 \qquad (2)$$

where A is the Bond albedo, f is incident flux from Saturn (W m^{-2}), e is the particle emissivity, σ the Stefan–Boltzmann constant and T_0 the physical temperature of the ring particle. α is a constant which is 1 if the particle radiates into 2π sr and 2 if the particle radiates into 4π sr. The Bond albedo is very uncertain, but a value of 0.6 seems reasonable[13].

For $A = 0.6$ and $T_0 = 56$ K, we obtain from equation (2) the following expression for the incident flux from Saturn

$$f = 5.58\,\alpha e \text{ W m}^{-2} \qquad (3)$$

This can be compared with the expected incident flux at the centre of the B ring resulting from the reflected solar radiation from the disk of Saturn and the IR radiation of Saturn. Assuming an effective temperature of 94.4 K (ref. 3), we find that the incident flux at the centre of the B ring to be 1.4 W m^{-2}. In addition, for an albedo of Saturn's disk of 0.45 (refs 3, 14), we find that the reflected solar radiation (into 2π sr) contributes an additional 1.1 W m^{-2}. The total amount of incident flux is therefore 2.5 W m^{-2}. This is in good agreement with equation (3) if $\alpha e \approx 0.5$. Both α and e are unknown, but for $e = 0.5 \rightarrow 1.0$—a possible range of emissivity—the particle may radiate into $\approx \pi \rightarrow 2\pi$ sr ($\alpha \approx 0.5 \rightarrow 1$) in this simple model. We conclude that the measured brightness temperature of 56 K can be understood qualitatively in the context of single particle radiation balance. The more realistic multi-particle, multilayer model is discussed below.

The second term in equation (1) can also be understood in terms of a simple model. Following Pollack *et al.*[12], the radiation balance of the rings with sunlight is

$$(131.8\text{ K})^4 \sin |B'|(1 - A - T_r) = \alpha e T^4 \qquad (4)$$

where T_r is the transmissivity of the rings and T is the ring physical temperature due to solar heating. B', A, e and α have the same definitions as before. The constant 131.8 K is the temperature of a black disk in equilibrium with the solar radiation at Saturn's distance from the Sun. As discussed above, the transmissivity of the rings is negligible for small B'. Assuming $A = 0.6$ and $T_r = 0$, we obtain from equation (4)

$$T = \frac{1.21 \times 10^8}{\alpha e} \sin |B'| \qquad \text{K}^4 \qquad (5)$$

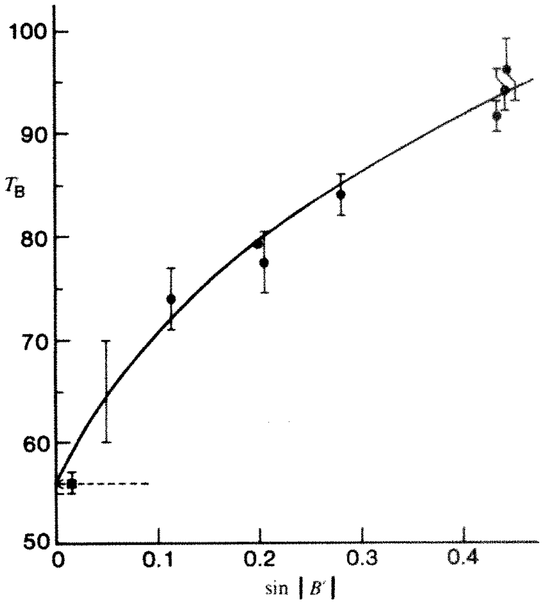

Fig. 1 B ring brightness temperature at 20 μm as a function of sin B'. The solid curve shows the fit achieved with the expression $T_B^4 = 56^4 + 1.52 \times 10^8 \sin |B'|$. The dashed arrow indicates that our measurement of the unilluminated side at $\sin |B'| = 0.015$ is assumed to represent the ring brightness temperature for $B' = 0$, as discussed in the text. All other points are taken from Table 2 and refer to observations of the side of the rings which is illuminated directly by the Sun.

Comparing this expression with the second term in equation (1) with the best-fitting value for the constant C, we see that a reasonable agreement is achieved if $\alpha e \approx 0.8$. Note that the fit is not strictly valid for $B' = 26°$ where $T_r \approx 0.1$.

It is encouraging that roughly the same value for the product αe is obtained in two cases. This increases the possibility that the various parameters have been estimated reasonably well above. However, there are so many areas of uncertainty that we cannot preclude the possibility of fortuitous cancellation for more than one inaccuracy.

The most sophisticated ring model with a prediction for the thermal emission is that by Kawata and Irvine[15]. As shown by Nolt *et al.*[1], this model systematically predicts higher brightness temperatures than observed for $\sin|B'| \sim 0.2$. In addition, this model predicts that $T_0 \sim 50$ K, lower than our observed value. Nolt *et al.*[1] also present the predicted brightness temperature for a two-component model of the rings which fitted the data for $\sin|B'| > 0.1$. This model also fails because it predicted T_0 to be ~ 69 K.

In conclusion, the ring IR brightness temperature on the unilluminated side of the rings has been found to be 56 ± 1 K. The decrease of the B ring brightness temperature is apparently proportional to $\sin|B'|$. These characteristics are not explained by any published detailed ring model, but it can be understood on the basis of single particle radiation balance considerations. These results need to be re-examined if the optical depth and brightness temperature of the Cassini division are found to be outside the limits assumed here.

We thank the staff of the IR Telescope Facility for maintaining the telescope, C. Telesco for providing technical support with the bolometer, and J. Cuzzi for pointing out the possible importance of the Cassini division. J.C. acknowledges the support of NASA contract NSG 7320 during this work. A.T.T. is a Staff Astronomer at the IRTF Facility which is operated by the University of Hawaii under contract from the National Aeronautics and Space Administration. J.C. was a Visiting Astronomer at the IRTF.

Received 3 April; accepted 1 August 1980.

1. Nolt, I. G. *et al. Nature* **283,** 842 (1980).
2. Bobrov, M. S. in *Surfaces and Interiors of Planets and Satellites* (ed. Dollfus, A.) (Academic, New York, 1970).
3. Ingersoll, A. P., Orton, G. S., Münch, G., Neugebauer, G. & Chase, S. C. *Science* **207,** 439 (1980).
4. *The American Ephemeris and Nautical Almanac* (U.S. Naval Observatory, Washington, DC, 1980).
5. Ferrin, I. R. *Icarus* **26,** 45 (1975).
6. Fountain, J. W. *Bull. Am. astr. Soc.* **9,** 463 (1977).
7. Lumme, K. & Reitsema, H. J. *Bull. Am. astr. Soc.* **9,** 463 (1977).
8. Pollack, J. B. *Space Sci. Rev.* **18,** 3 (1975).
9. Gehrels, T. *et al. Science* **207,** 434 (1980).
10. Nolt, I. G., Tokunaga, A., Gillett, F. C. & Caldwell, J. *Astrophys. J. Lett.* **219,** L63 (1978).
11. Murphy, R. E. in *The Rings of Saturn* (eds Palluconi, F. D., & Pettengill, G. H.) (NASA SP-343, 1974).
12. Pollack, J. B., Summers, A. & Baldwin, B. *Icarus* **20,** 263 (1973).
13. Cook, A. F., Franklin, F. A. & Palluconi, F. D. *Icarus* **18,** 317 (1973).
14. Erickson, E. F., Goorvitch, D., Simpson, J. P. & Strecker, D. W. *Icarus* **35,** 61 (1978).
15. Kawata, Y. & Irvine, W. M. *Icarus* **24,** 472 (1975).
16. Murphy, R. E. *Astrophys. J. Lett.* **181,** L87 (1973).
17. Morrison, D. *Icarus* **22,** 57 (1974).
18. Rieke, G. H. *Icarus* **26,** 37 (1975).
19. Sinton, W. M., Macy, W. W., Good, J. & Orton, G. S. *Icarus* **42,** 251 (1980).

Pleistocene bimodal response of Antarctic ice

David J. Drewry

Scott Polar Research Institute, University of Cambridge,
Lensfield Road, Cambridge CB2 1ER, UK

Extent and volume of the Antarctic ice sheet have important roles in modulating global atmospheric and oceanographic processes and have significant implications for world sea levels[1]. The history of ice sheet variations in Antarctica has mainly been founded on studies in the ice free (Dry) valleys of southern Victoria Land (Fig. 1). A detailed glacial chronology by Denton and co-workers[2–4] is based on the premise that Taylor Glacier and neighbouring Wright Upper Glacier are outlets of the East Antarctic ice sheet and that, "the extent of Taylor Glacier reflects the height of this ice sheet, and, since it terminates on land, records of its former positions provide one of the few indications of former heights of the ice sheet"[5]. That the East Anarctic ice sheet reached its maximum dimensions during each of the last four world-wide interglacials is an important conclusion of this work[2]. New geophysical data from Taylor Glacier and the adjacent ice sheet in Victoria Land, Antarctica are presented here which challenge these suppositions.

Between 1967 and 1978 six seasons of airborne geophysical sounding have completed an extensive network of flight lines over East Antarctica[6–8]. Ice thickness profiling has enabled compilation of detailed contour maps of the ice sheet surface to an accuracy[9–11] of ±30 m. Flow lines orthogonal to the contours[12] have been constructed (Fig. 2). In 1974–75 a closely spaced series of Radio Echo Sounding (RES) flight lines was completed over the ice sheet inland of the Dry Valleys (Fig. 3)[13]. These two surveys have defined the pattern of ice flow out of central East Antarctica through the Transantarctic Mountains into the Ross Sea embayment.

In the sector inland of Victoria Land the ice sheet exhibits a wide and prominent ridge which drives ice into the clearly marked catchments of David and Mulock-Byrd Glaciers (Fig. 2). Within 100 km of the western edge of the Transantarctic Mountains, just inland of Taylor Glacier, the ridge terminates in a small dome. The ice sheet drops by more than 100 m into a saddle between this dome and the main part of the ridge. Altitudes determined by barometry along a single traverse line ~30 km south of the dome by Crary during the IGY intimated at a similar elevation distribution[14]. Calkin[15], using less reliable radar results, also suggested the possibility of a dome in this vicinity.

RES surface contours establish a flow pattern in which the now well-defined dome and ridge system effectively blocks ice

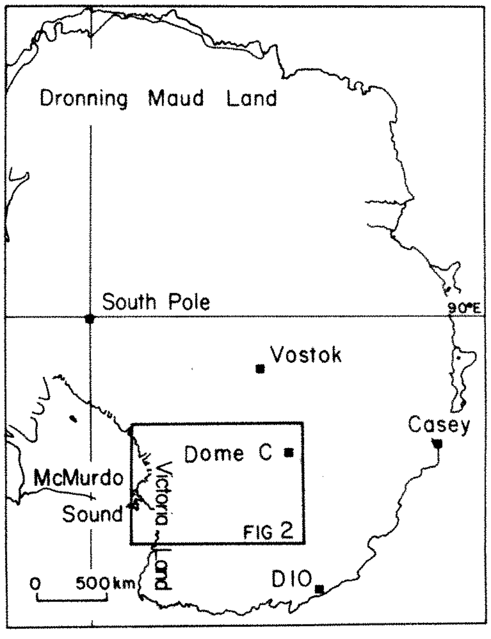

Fig. 1 Antarctic location map (principal places mentioned in text and Fig. 2).

0028-0836/80/380214—03$01.00

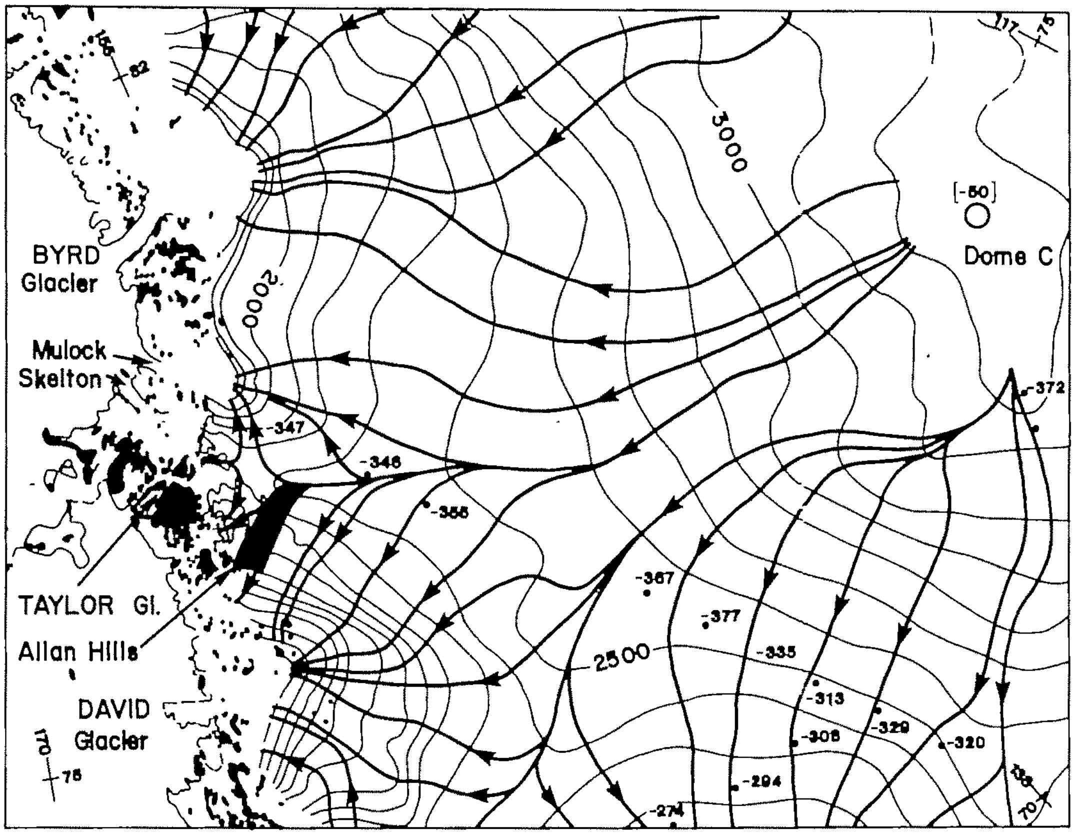

Fig. 2 Ice surface contours and derived flow lines for part of the East Antarctic ice sheet, based on radio echo sounding data[10,11]. Note diverging ice flow from dome inland of Taylor Glacier. Catchment area of ice flowing towards Allan Hills meteorite site is shown shaded. Selected δ^2H and ^{18}O values for surface accumulation are shown[31–33,38].

penetration into the Dry Valleys from central regions of East Antarctica. The catchments, therefore, of small outlet glaciers in southern Victoria Land (for example, Ferrar, Wright Upper, Victoria Upper, Mackay and possibly Skelton) are severely restricted and that of Taylor Glacier is less than 5,000 km^2.

RES results suggest only a local origin for ice in Taylor and adjacent glaciers. To test this hypothesis ice provenance studies, using stable isotope techniques, were performed in January 1978 and January 1979[16].

Five horizontal 1-m ice core samples were taken from the lowermost 1.5 m of exposed ice at the snout of Taylor Glacier in 1978 (Fig. 3). The following season an ice core, 4 m long, was extracted close to the summit of the dome inland of the glacier (Fig. 3). The average accumulation rate in this area is 140 kg m^{-2}yr^{-1} and average snow density in the upper 4 m is 437 kg m^{-3} (refs 14, 17). The core thus sampled 12 yr precipitation and the resulting mean isotopic values are considered representative of surface accumulation at Taylor dome.

Stable isotope results are given in Table 1. Values of δ^2H at Taylor Glacier snout range between −327‰ and −341‰ (the lowermost sample), bracketing similar determinations by other workers[18]. At Taylor dome (the ice divide) δ^2H measurements lie between −341 and −344‰. They correspond closely with those to be expected theoretically[19] given mean annual surface temperature (−43 °C) and elevation (2,400 m). Table 1 also lists isotopic values for ice accumulating in the central parts of East Antarctica. The ice here has a significantly lighter isotopic signature than from southern Victoria Land.

The equivalence of δ^2H ratios at Taylor Glacier snout and at the dome (the difference between the two sets of measurements (3‰) is negligible) strongly suggests that the glacier has been in near isotopic equilibrium for the lifetime of oldest ice sampled, and that the preceding conclusions are valid for several thousand years. Integration with respect to time of maximum surface velocities measured by New Zealand workers[20] gives an estimated minimum period of ice throughput from dome to snout of 10.5 kyr. Corrections applied to particle paths through Taylor Glacier for zones of basal sliding[20] and reduction of velocity with depth[21] give a more realistic throughput time of 15–16 kyr. If these dates are approximately correct we attribute the absence of more isotopically negative ice at the base of Taylor Glacier snout (representing the end of Wisconsin cooling) principally to basal melting upstream. Although ice transit calculations are based on the steady-state assumption they, nevertheless, corroborate glacial geological[3] and geochemical[5,22] conclusions that Taylor Glacier did not expand appreciably during the Wisconsin maximum, and provide no evidence for intrusion of 'cold' East Antarctic ice. Post-Wisconsin advance reported by Denton is attributed to increased local precipitation.

The discovery of meteorites[23] on bare ice at the edge of the Transantarctic Mountains at Allan Hills (100 km north of Taylor Glacier dome) also corroborates the notion of ice sheet stability in southern Victoria Land (Fig. 2). The meteorites have ages between 30 and 800 kyr[24,39] and have been concentrated at

Table 1 Isotopic results from Victoria Land and adjacent ice sheet, Antarctica

Location	Elevation (m)	‰ δ^{18}O	SMOW δ^2H	Ref.
Taylor Glacier snout				
(77° 43.6′ S 162°16.5′ E)				
Lowermost ice 20 cm above bed	NA	$\underline{-42.8}$	−341.3	This work
Mean of lowermost 1.5 m snout ice		$\underline{-41.6}$	−332.0	This work
		−42.5	−330.0	18
Taylor Glacier dome (77°44′ S 158°22′ E)	2,400	−43.4	−342.6	This work
Victoria Land plateau				
78°02′ S 154°06′ E	2,280	$\underline{-43.5}$	−347.4	38
77°02′ S 152°19′ E	2,440	$\underline{-43.3}$	−345.5	38
Dome 'C'				
(74°39′ S 124°10′ E)	3,240	−50.0	$\underline{-401.0}$	33
Vostok				
(78°27′ S 106°48′ E)	3,490	$\underline{-51.4}$	−412.0	38
South Pole	2,825	$\underline{-49.4}$	−396.0	38

Underlined values determined from $\delta^{18}O = 0.12\delta^2H + 1.26$ obtained from 58 ice and snow analyses from Victoria Land.

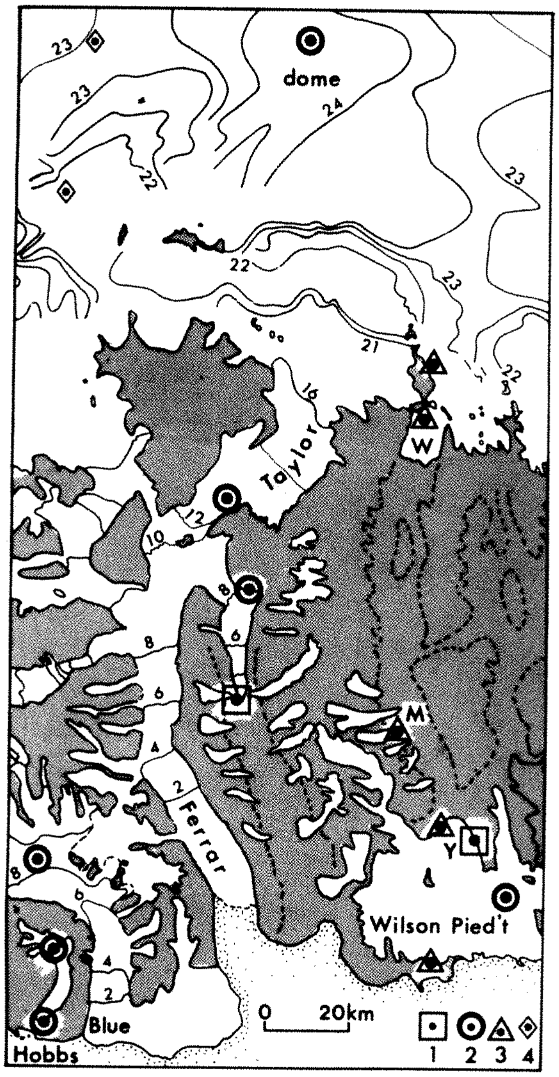

Fig. 3 Taylor and neighbouring glaciers in southern Victoria Land (W, Wright Upper; M, Meserve). Ice sample sites for isotopic analyses: □, 1978; △ ○, 1979. ◇, Oversnow traverse stations[14]. Dome defines limit of Taylor Glacier catchment. Elevation contours are in 10^2 m (after ref. 13).

this locality by flow from the surrounding ice sheet and surface ablation[25]. As Allan Hills presents only a low topographical barrier to the ice sheet any significant thickening in this area (>100 m) would effectively flush-out the meteorites into Mawson Glacier. Assuming that the meteorite infall rate in polar areas is $\sim 1\times10^{-6}$ km^{-2} yr^{-1} (refs 26, 27, 40) we calculate for that part of the ice sheet draining towards Allan Hills ($\sim$1,500–3,000 km^{-2}, Fig. 2) the time to accumulate the $\sim$50 'parent' meteorite new finds[23] is 17–33 kyr. We conclude that the ice sheet in the vicinity of Allan Hills cannot have thickened substantially during this period.

The pattern of fluctuations exhibited by local ice in Victoria Land during the last and possibly earlier glacials is out-of-phase with the bulk of the East Antarctic ice sheet where seaward expansion of continental ice during full glacial periods has been established[28–33]. We explain antiphase behaviour as a result of differing glacio-climatic controls. On the high plateau accumulation is relatively low (50–100 kg m^{-2} yr^{-1})[17] due to steady inland water-vapour depletion of precipitation-bearing air masses that penetrate the continent[34]. In contrast snow-fall reaching Taylor Glacier and neighbouring ice masses comes primarily from air advected over the Ross Sea, regulated by seasonal ice cover, degree of open water, cyclogenesis and orographic effects[35,36].

I suggest that during glacial episodes Northern Hemisphere ice build-up results in a major depression of global sea level causing a modest expansion and thickening of the 'stable' East Antarctic ice sheet. Ice in West Antarctica, however, grounded below sea level, expands dramatically across the Ross Sea continental shelf[28,37]: the zone of seasonal pack ice and open water is moved northwards by several hundred kilometres, reducing precipitation to those glaciers with limited catchments. Stability or even recession of the ice sheet margin in Victoria Land ensues.

During Northern Hemisphere interglacials rising sea level will trigger inland retreat of the ice sheet. With incursion of open water into the Ross Sea embayment, however, enhanced water vapour flux over Victoria Land results in modest expansion of the ice sheet edge and associated minor glaciers.

Widespread use of the detailed glacial chronology of the Dry Valleys area requires caution. The relationship of local 'outlet' glaciers to the glaciological regime of the East Antarctic ice sheet is clearly complex and often independent. Such conclusions may apply to similar locations along the inland edge of the Transantarctic Mountains (for example, Queen Maud Mountains and Reedy Glacier areas). Sites for future investigation of continental glacial fluctuations in the Transantarctic and other mountainous areas will require careful assessment and interpretation. The most suitable may be the margins of the premier outlet glaciers whose catchments lie deep within the ice sheet (for example, David, Byrd, Jutalstraumen, Shirase, Lambert and Minnesota Glaciers).

This work was supported by the NERC under grant GR3/2291 and the NSF Division of Polar Programs. I thank C. Lorius for arranging isotopic determinations, and A. Bath (NERC) for similar analyses in the UK, and my colleagues at the Scott Polar Research Institute for fieldwork assistance.

Received 28 April; accepted 10 July 1980.

1. Radok, U. *Climatic Roles of Ice* (UNESCO, Paris, 1978).
2. Denton, G. H., Armstrong, T. L. & Stuiver, M. in *Late Cenozoic Glacial Ages* (ed. Turekian, K. K.) 267–306 (Yale University Press, 1971).
3. Denton, G. H., Armstrong, T. L. & Stuiver, M. Rev. *Geogr. Phys. Geol. Dyn.* **11,** 265–278 (1969).
4. Calkin, P. E., Behling, R. E. & Bull, C. B. *Antarctic J. U.S.* **5,** 22–27 (1970).
5. Hendy, C. H., Healy, T. R., Raynor, E. M., Shaw, J & Wilson, A. T. *Quat. Res.* **11,** 172–184 (1979).
6. Robin, G de Q., Evans, S., Drewry, D. J., Harrison, C. H. & Petrie, D. L. *Antarctic J. U.S.* **5,** 229–232 (1970).
7. Drewry, D. J. & Meldrum, D. T. *Polar Rec.* **19,** 267–73 (1978); **20,** 43–51 (1980).
8. Robin, G de Q., Drewry, D. J. & Meldrum, D. T. *Phil. Trans. R. Soc.* **B279,** 185–196 (1977).
9. Drewry, D. J. *Polar Rec.* **17,** 359–74 (1975).
10. Steed, R. H. N. & Drewry, D. J. in *Antarctic Geoscience* (ed. Craddock, C) (University of Wisconsin Press, in the press).
11. Steed, R. H. N. thesis, Univ. Cambridge (1980).
12. Budd, W. F. *ANARE Sci. Rep.* Ser A (Glaciology) No. 108, 216 (1969).
13. Drewry, D. J. in *Antarctic Geoscience* (ed. Craddock, C) (University of Wisconsin Press, in the press).
14. Crary, A. P. *IGY Glaciol. Rep.* No. 7, 144 (1963).
15. Calkin, P. E. *Antarctic J. U.S.* **9,** 236–38 (1974).
16. Drewry, D. J. *Antarctic J. U.S.* **14** (1979).
17. Bull, C. B. in *Research in the Antarctic* (ed. Quam, L) 367–421 (American Association for the Advancement of Science, Washington, 1971).
18. Matsubaya, O., Sakai, H., Torii, T., Burton, H. & Kerry, K. *Geochim. Cosmochim. Acta* **43,** 7–25 (1979).
19. Dansgaard, W., Johnsen, S. J., Clausen, H. B. & Gunderstrup, N. *Meddr Grønland* **197,** No. 2 (1973).
20. Robinson, P. *N.Z. Antarctic J.* **1,** 51–57 (1979); thesis, Victoria Univ., Wellington (1979).
21. Paterson, W. S. B. *Physics of Glaciers* (Pergamon, Oxford, 1969).
22. Wilson, A. T. *Tuatara* **15,** 152–164 (1967).
23. Cassidy, W. A. *Antarctic J. U.S.* **13,** 39–40 (1978).
24. Fireman, E. L., Ranticelli, L. A. & Kirsten, T. *Science* **203,** 453–455 (1979).
25. Nishio, F. & Annexstad, J. O. in *Proc. 4th Symp. on Antarctic Meteorites* (ed. Nagata, T) 13–23 (Mem. National Institute of Polar Research, Spec. Issue No. 15, 1979).
26. Brown, H. *J. geophys. Res.* **66,** 1316–1317 (1961).
27. Hawkins, G. S. *Astr. J. R. Soc.* **65,** 318–322 (1960).
28. Hollin, J. T. *J. Glaciol.* **4,** 173–195 (1962).
29. Cameron, R. L. in *Antarctic Snow and Ice Studies* (ed. Mellor, M) 1–36 (American Geophysical Union, Antarctic Res. Ser. no. 2, 1964).
30. Hollin, J. T. & Cameron, R. L. *J. Glaciol.* **3,** 833–843 (1961).
31. Robin, G de Q. *Phil. Trans. R. Soc.* **B280,** 972, 143–68 (1977).
32. Reynaud, D., Lorius, C., Budd, W. F. & Young, N. W. *J. Glaciol.* **24,** 103–116 (1979).
33. Lorius, C., Merlivat, L., Jouzel, J. & Pourchet, J. *Nature* **280,** 644 (1979).
34. Gow, A. J. in *Antarctica* (ed. Hatherton, T.) 221–258 (Methuen, London, 1965).
35. Bull, C. B. in *Studies in Antarctic Meteorology* (ed. Rubin, M. J.) 177–194 (American Geophysical Union, Antarctic Research Ser. no. 9, 1966).
36. Mayewski, P. A., Attig, J. W. & Drewry, D. J. *J. Glaciol.* **22,** 53–65 (1979).
37. Drewry, D. J. *J. Glaciol.* **24,** 231–244 (1979).
38. Lorius, C., Merlivat L. & Hagermann, R. *J. geophys. Res.* **74,** 7027–7031 (1969).
39. Nishiizumi, K. *et al. Earth planet. Sci. Lett.* **45,** 285–292 (1979).
40. Millard, H. T. Jr. *J. geophys. Res.* **68,** 4927–4303 (1963).

Sublithospheric upwelling distribution

Dork Sahagian

Department of Geological Sciences, Rutgers University,
New Brunswick, New Jersey 08903

Hot spots have been defined[1] as centres of volcanism not associated with plate boundaries. Some authors[2,3] have regarded them as surface expressions of upwellings of relatively high temperature material in the mantle. These upwellings, either deep mantle plumes[2,4], or shallow convection cells[5], create a hot spot on the surface of the Earth only where they have molten and broken their way to the surface. I suggest here that there is a uniform sublithospheric upwelling distribution, and that the ability of upwellings to make themselves evident on the surface, and, therefore, the difference in surface hot spot density among the various plates, depends on the velocity and thickness of each lithospheric plate. From these characteristics and the rate of magma entry into the lithosphere, a normalization of the areal hot spot density can be made to calculate the distance between sublithospheric upwellings.

The major effect of the motion of a plate over a mantle upwelling is to limit the time available for the transfer of heat through the lithosphere. Although the process of lithospheric thinning operates on moving plates[6,7], only a fraction of the sublithospheric upwellings are able to penetrate to the surface.

Lithospheric thickness determines the amount of time necessary for an upwelling to penetrate the lithosphere. The thickness depends primarily on the dynamic history of the plate involved, and in particular, its age, which for oceanic regions is related to the distance from the spreading centre[8,17].

The rate of intrusion is important in thinning the lithosphere. This determines the rate of ascent of the lithosphere–aesthenosphere boundary.

The sublithospheric upwelling density (expressed as area per upwelling) can be calculated from the above parameters for each plate using the following equation:

$$K = \frac{A}{S \exp{(VT/R)}} \qquad (1)$$

where K is the sublithospheric area per upwelling, A is the area of a particular plate, S is the number of observed hot spots on the plate, V is the velocity of the plate with respect to a fixed mesospheric frame, $T = t/g$ is the thickness of the plate divided by the global average lithospheric thickness, and R is the rate of ascent of the lithosphere–aesthenosphere boundary.

The values of the above parameters are listed in Table 1. The number of hot spots on each plate is as observed by Burke and Wilson[1]. Hot spots at or very near plate boundaries were omitted, however, because it would be unclear to which plate they belong, and because the lithosphere becomes very thin at rifts and mid-ocean ridges, giving a great penetration advantage to any upwellings underneath. Although other hot spot lists exist[18], this one was chosen as it is the most comprehensive and adheres most closely to the definition of hot spots used here. The velocities of the plates are as calculated by Minster and Jordan[19,20], and agree with other studies[21,22]. Plate thicknesses, as calculated from heat flow considerations of Sclater *et al.*[8] have been averaged over the area of each plate. These average values are in agreement with those calculated from other models[9–14,16]. The global average lithospheric thickness used was 120 km. The rate of ascent of the lithosphere–aesthenosphere boundary is as calculated by Withjack[6] as 2×10^{-8} cm s^{-1}, corresponding to basaltic magma, assumed constant throughout the Earth as hot spots are generally basaltic[1] worldwide. (If all of the magma entering the lithosphere is extruded[23] or otherwise accounted for[24], the basalt represents the bulk composition of the magma, and the above rate is to be used. If, however, the basalt does not represent the bulk composition of the magma, but is only a portion of the magma which is preferentially pushed through the lithosphere, R is greater, 1.5×10^{-7} cm s^{-1} for 5% basalt[6].) It is assumed here that regardless of the value chosen (or any intermediate), the average over the area of each plate remains constant throughout the Earth, and that this value will affect the normalization of the average distance between hot spots, $K^{1/2}$, but not the relative values of K for the various plates.

There are three anomalous plates. The Cocos plate is very small, and has one hot spot, making its hot spot density extremely high. However, so small a plate cannot present a statistically valid distribution, and so can be discounted. The Arabian plate is also very small and has several hot spots which may be associated with the rift system, and as such, cannot be used in this consideration.

The African plate has a large number of hot spots (31), and some authors[1,3,25] have claimed that it has been stationary with respect to the mantle convection pattern for the past 25 Myr. Minster *et al.*[19,20] have found the African plate to be moving only slowly about a rotation pole located within the plate. This rotation about an internal axis manifests itself as a velocity of zero at the pole, increasing with distance from the pole.

When $\ln{(A/S)}$ is plotted against Vt/R, a straight line is obtained, indicating the exponential dependence on Vt/R (Fig. 1). (Here, t is used rather than T for convenience. As they are proportional, the constant of proportionality, g, can be included in the axis scale, and still maintain a true representation of equation (1).) This dependence can be further verified by examining the limiting cases of velocity, thickness, and R. As $V\rightarrow0$, or $t\rightarrow0$, or $R\rightarrow\infty$, the lithosphere is effectively stripped away, and what remains is the sublithospheric area per upwelling, K. To be able to observe any of these limiting cases on the existing lithospheric plates would be an ideal test of equation (1). Clearly, $V\rightarrow0$ would be the most likely possibility. On Fig. 1, this would correspond to the y-intercept, at 3.3×10^6 km^2.

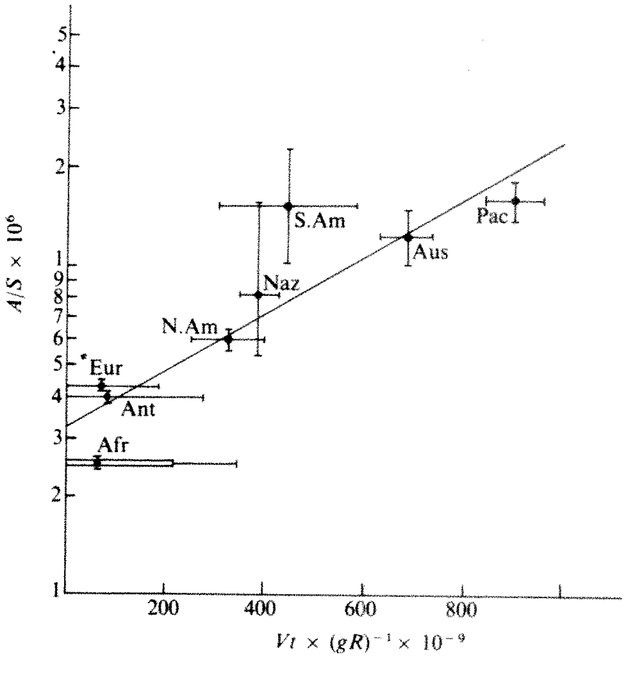

Fig. 1 Semi-logarithmic plot of (plate area/number of hot spots) versus (plate velocity × plate thickness). Horizontal error bars are minimum error associated with each plate from velocity and thickness errors. Vertical error bars represent ±1 hot spot on each plate. The double bar for Africa indicates the true range of Vt, as its pole of rotation lies within the plate. The line was plotted using a least squares fit, yielding an intercept at 3.3×10^6 km^2, with a correlation coefficient of 0.89, yielding a high degree of confidence (99.8%)[29,30] that a correlation exists.

0028-0836/80/380217—02$01.00

Table 1 Values of parameters in equation (1)

Plate	Hot spots	Plate area ($\times 10^{12}$ m^2)	Velocity ($\times 3.2 \times 10^{-10}$ m s^{-1})	Average thickness (km)	Vt	A/S ($\times 10^{12}$ m^2)
Eurasia	16	68.0	0.5	156	78	4.25
Australia	5	61.0	6.0	115	690	12.2
Pacific	7	113.0	9.0	100	900	16.1
North America	10	58.8	2.5	136	340	5.9
South America	3	46.2	3.1	144	446	15.3
Nazca	2	16.4	6.0	65	390	8.2
Africa	31	78.4	0–1.5	144	0–216	2.5
Antarctica	15	59.9	0.6	133	80	4.0

Africa's rotation pole lies within the plate. This causes significant variations in the velocity within the plate. These variations are represented by the double line on Fig. 1. If Africa had a uniformly zero velocity, it would plot as a point on the y-axis, close to the intercept of the line described by all of the plates (except Arabian and Cocos).

The penetration ability of upwellings depends exponentially on Vt/R because as a magma loses heat to the lithosphere, its temperature falls exponentially with respect to time[26] from its initial temperature to the ambient temperature of the lithosphere. If the time necessary for the magma to penetrate the lithosphere is longer than it takes to cool and solidify, there will be no hot spot on the surface. There will, however, be volcanism if the magma reaches the surface more quickly. Plate movement reduces the time available for penetration, while incremental increase of the thickness and magma entry rate increases, and decreases the time necessary for penetration to the surface, respectively. The statistical number of upwellings that reach the surface is proportional to ΔT (see Fig. 2), which decreases exponentially as time necessary to penetrate the lithosphere is increased. Note that as upwellings under any plate are not likely to be all of the same strength (radius, temperature), but are distributed about an average, a plate with characteristics putting it at τ_c will allow half of its upwellings to reach the surface. Plates which lie further to the right will allow less than half, those to the left will allow more.

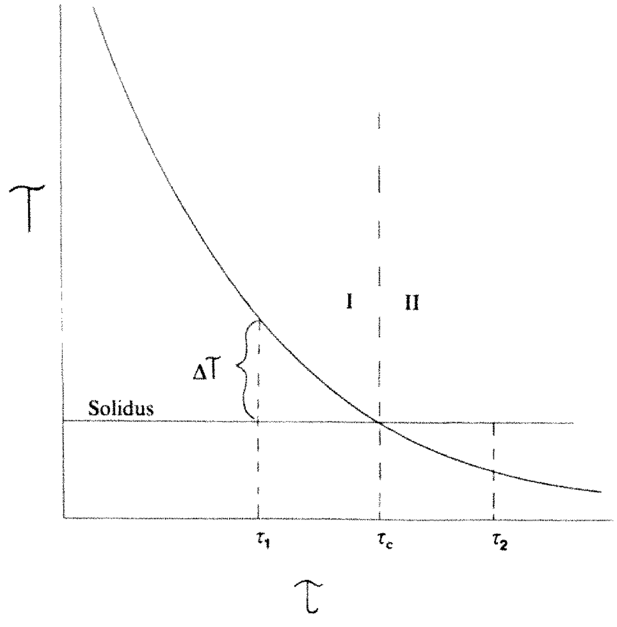

Fig. 2 Plot of temperature versus time for cooling magma. At points to the left of τ_c (region I), for example τ_1, the plate is thin and/or slow enough to allow penetration to the surface of an average upwelling. In region II, for example τ_2, average upwellings will not fully penetrate. At τ_c, half of the upwellings under the lithosphere will reach the surface. The statistical fraction of upwellings greater (I) or less (II) than 1/2 which reach the surface is proportional to ΔT.

The results show the sublithospheric area per upwelling to be 3.3×10^6 km^2, or 1,800 km between adjacent upwellings. The uniformity of the sublithospheric upwelling density may have implications regarding the origin of hot spots. It would seem to indicate a periodic physical[27], rather than random chemical[28], driving mechanism, making a model such as a stratified fluid instability plausible[27].

I thank Jason Morgan, Tom Crough, Eric Christofferson and Michael Carr for criticisms.

Received 14 April; accepted 14 July 1980.

1. Burke, K. & Wilson, J. T. *Sci. Am.* **235,** 46–57 (1976).
2. Morgan, W. J. *Nature* **230,** 42–43 (1971).
3. Thiessen, R., Burke, K. & Kidd, W. S. F. *Geology* **7,** 263–266 (1979).
4. Morgan, W. J. *Bull. Am. Ass. petrol. Geol.* **56,** 203–213 (1972).
5. Richter, F. & Parsons, B. *J. geophys. Res.* **80,** 2529–2541 (1975).
6. Withjack, M. *J. geophys. Res.* **84,** 3008–3022 (1979).
7. Detrick, R. S. & Crough, S. T. *J. geophys. Res.* **83,** 1236–1244 (1978).
8. Sclater, J. G., Jaupart, C. & Galson, D. *Rev. Geophys. Space Phys.* **18,** 269–311 (1980).
9. Kanamori, H. & Press, F. *Nature* **266,** 330–332 (1970).
10. Dziewonski, A. M. *J. geophys. Res.* **76,** 2587–2601 (1971).
11. Okal, E. *Geophys. J.* **49,** 357–370 (1977).
12. Yoshii, *Earth planet. Sci. Lett.* **25,** 305–312 (1975).
13. Chapman, D. & Pollack, H. *Geology* **5,** 265–268 (1977).
14. Pollack, H. & Chapman, D. *Sci. Am.* **237,** 60–76 (1977).
15. Parson, B. & Sclater, J. G. *J. geophys. Res.* **82,** 803–827 (1977).
16. Crough, S. T. *Nature* **256,** 388–390 (1975).
17. Crough, S. T. & Thompson, G. A. *J. geophys. Res.* **81,** 4857–4862 (1976).
18. Frazier, K. *Sci. News* **116,** 202–206 (1979).
19. Minster, J. B. & Jordan, T. H. *J. geophys. Res.* **83,** 5331–5354 (1978); *Ann. Geophys.* Coulomb Vol. (in the press).
20. Minster, J. B., Jordan, T. H., Molnar, P. & Haines *Geophys. J. astr. Soc.* **36,** 541–576 (1974).
21. Solomon, S. C., Sleep, N. H. & Jurdy, D. M. *J. geophys. Res.* **82,** 203–212 (1977).
22. Solomon, S. C. & Sleep, N. H. *J. geophys. Res.* **79,** 2557–2567 (1974).
23. Swanson, D. A. *Science* **175,** 169–170 (1972).
24. Bodvarsson, G. & Walker, G. P. L. *Geophys. J.* **8,** 285–300 (1964).
25. Briden, J. & Gass, J. *Nature* **248,** 650–653 (1974).
26. Jaeger, M. C. in *Poldervaart Treatise on Rocks of Basaltic Composition* (eds Hess, H. H. & Poldervaart, A.) 503 (Wiley-Interscience, New York, 1968).
27. Ramberg, H. *J. geophys. Res.* **77,** 877–889 (1972).
28. Anderson, D. L. *Bull. geol. Soc. Am.* **86,** 1593–1611 (1975).
29. Bevington, P. *Data Reduction and Error Analysis for the Physical Sciences* (McGraw-Hill, New York, 1969).
30. Young, H. *Statistical Treatment of Experimental Data* (McGraw-Hill, New York, 1962).

---

^{18}O/^{16}O variations in deep-sea carbonate shells from the Rise hydrothermal field

J. S. Killingley, W. H. Berger, K. C. MacDonald & W. A. Newman

Scripps Institution of Oceanography, La Jolla, California 92093

Active hydrothermal vents have recently been discovered[1] on the East Pacific Rise near 21° N (Fig. 1). Exotic benthic communities similar to those at the Galapagos vents[2] thrive around many of the vents. Some of these animals have calcium carbonate shells which presumably contain a temperature record in the oxygen isotopes of the carbonate. These provide an opportunity to investigate the temperature preferences of the organisms and, perhaps, the history of temperature variation near the vents. We report here stable oxygen and carbon isotope measurements made on clam shells and on a barnacle collected near the RISE vents from the submersible Alvin at a water depth of ~2,600 m (Fig. 1).

0028-0836/80/380218—04$01.00

The spreading centre here opens at a rate of 6 cm yr^{-1}, intermediate in the spectrum of spreading rates[3,4]. The rise crest consists of an uplifted axial zone 5-km wide and 80-m high[5]. The zone of most recent volcanism is between 600 and 1,400 m wide[6], and the hydrothermal vents occur within a strip only 300–500 m wide. They were mapped over a distance of 6.2 km along the spreading axis[1,7]. Three types of vents were observed. The first kind have low temperatures (10–20 °C), with clear to slightly milky hydrothermal fluids oozing out at rates of a few cm s^{-1} (ref. 8). The second ('white smokers') have plumes of hydrothermal fluids clouded by white precipitates issuing from distinct chimneys at rates of tens of cm s^{-1}. Temperatures[1] are between 100 and greater than 300 °C. The third ('black smokers') show the most vigorous activity ever observed at a sea floor hydrothermal vent. Waters blackened by sulphide precipitates jet out at rates of 1–5 m s^{-1} and at temperatures of at least 350 °C.

MacDonald and others[9] estimate that the heat loss associated with a single black smoker chimney is 2–8 times the total theoretical heat loss for a 1-km segment of ridge out to 1 Myr age to either side. This underlines the importance of hydrothermal circulation in the heat budget of mid-ocean ridges, but also requires that vents of this type be very short-lived. There was, therefore, considerable interest as to whether the isotopic composition of the carbonate shells might provide an indicator of temperature history.

The principal complication in attempting to link shell growth history to vent history is that some animals live several tens of metres away from the highest temperature vents, and that the lateral thermal gradients are extremely high. Water temperatures only 5–10 m away from the vents may be within 5 °C of ambient (2 °C), because the rapid discharge of low density ($\rho \sim 0.62$ g cm^{-3})[9] vent water draws in ambient water at a high rate.

We measured $^{18}O/^{16}O$ ratios on two shells from a new species of the vesicomyid clam, *Calyptogena*[10], and on scales from a new genus and species of stalked barnacle, *Neolepas zevinae*[11]. Clam shell valve ALV 909B-1 was empty, while ALV 914B-1 was from a living specimen (see Fig. 2). The clam shells were recovered from near a 'cool vent' in which water temperatures between 5 and 20 °C were measured. The barnacle was one of six removed from a rock (ALV 915) situated about 28 m from a 'black smoker'. Temperatures in this vent were not recorded because of instrument malfunction, but by analogy with similar vents the temperature of the actual water flow could reach 350 °C.

Samples for isotopic analysis, each about 0.5 mg, were removed with a 0.5 mm drill from points along the growth direction of a valve from each clam at approximately every 2 mm, starting at the shell lip and extending a few centimetres back to include all of the prismatic layer still present in each shell. In the older parts of the shells, this absent layer had presumably dissolved. A few samples were drilled from the nacreous layer towards the hinge. We expected that such sampling of the original prismatic layer, across growth bands, would reveal any extensive temperature fluctuations experienced by the mollusc, at least during the last few years of its life. The samples from the barnacle consisted of single scales removed at ~5 mm intervals along the peduncle, beginning at the base of the capitulum. The clam shells were found to be aragonite by X-ray diffraction, and *N. zevinae* hard parts are reportedly calcite[11].

All samples were heated at 250 °C for 30 min in vacuum, before being isotopically analysed for $\delta^{18}O$ and $\delta^{13}C$ (isotopic ratios are expressed as δ values (PDB) by the usual procedure[12]). The analytical precision was 0.07%.

Figure 3 shows the results of the isotopic measurements on the three specimens. We first consider the $\delta^{18}O$ ranges observed. The $\delta^{18}O$ (PDB) values for clam A (909B1 empty) range from 3.2 to 4.3‰; those for clam B (914B1 live) from 3.0 to 4.3‰; and those for the barnacle from 3.8 to 4.4‰. (Only the ranges of values measured on the clam prismatic layers are considered here because of possible non-equilibrium precipitation of the nacreous layer.)

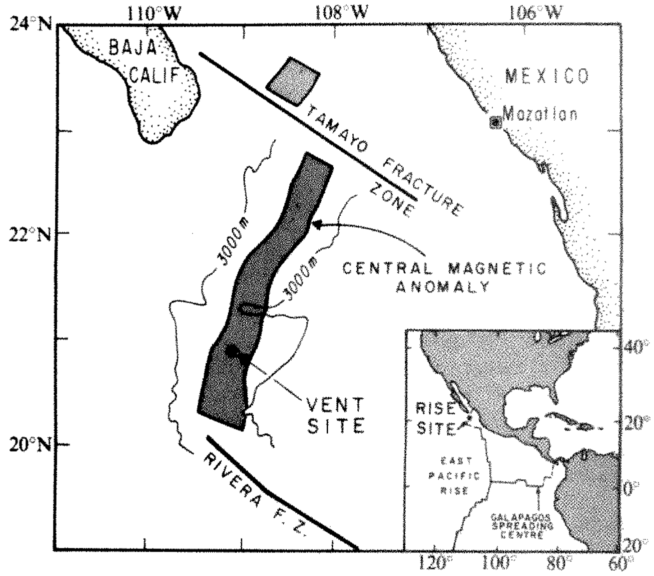

Fig. 1 Regional map.

The measured $\delta^{18}O$ maxima from each shell are essentially the same, which suggests that they correspond to the temperature minimum (the ambient seawater temperature). Although a temperature corresponding to the maximum $\delta^{18}O$ value can be calculated, there are three sources of error: (1) there is disagreement of about 0.5° at near-zero temperatures between different palaeotemperature equations; (2) the difference between the isotopic fractionation behaviour of calcite (on which palaeotemperature equations are based) and that of aragonite is not known; and (3) the isotopic composition of the ambient seawater is not known exactly.

The empirical palaeotemperature equation has the form[13,14]:

$$T(°C) = A - B(\delta^{18}O_c - \delta^{18}O_w) + C(\delta^{18}O_c - \delta^{18}O_w)^2$$

where A, B, C are constants. The isotopic value of calcite is $\delta^{18}O_c$ and $\delta^{18}O_w$ is the isotopic composition of the water from which the calcite precipitated. We assumed a value for $\delta^{18}O_w$ of −0.3‰ for the water in which the clams grew[15] (vent-water composition is not important in this context) and found for the maximum $\delta^{18}O_c$ value (4.3‰) that the calculated temperature (0 °C ± 0.3) was ~2 °C lower than ambient. (Tarutani *et al.*[16] experimentally determined the fractionation between inorganically precipitated calcite and aragonite as 0.6‰ at 25 °C which, if applicable at low temperatures, would lead to a calculated minimum value of 1.8 °C ± 0.4, which is a more reasonable value.) In spite of uncertainties in the actual temperatures, a good estimate can be made of the temperature difference corresponding to the $\delta^{18}O$ range from 3.0 to 4.3‰. This difference is ~4.5 °C, so that if the coldest temperature is 2 °C, then the clams record a range from 2 to 6.5 °C. It has been observed that the clams and some other animals found in similar vent regions of the Galápagos Rift occur some distance from the actual vent, apparently living in water close to ambient temperature[17]. From our data, it seems that the clams experience periods when the water is warmed by geothermal activity to at least 4 °C above ambient temperature. This represents a minimum estimate, for we do not know the upper temperature limit at which the animal ceases to grow shell. A statistical study of shell rim material from a large number of clams might, however, provide clues to the upper tolerance limits for growth.

Five of the $\delta^{18}O$ values measured on the calcitic scales from the barnacle are in the range 4.2±0.2. Ignoring the palaeotemperature equation, this suggests that 4.2‰ corresponds to the ambient water temperature of 2 °C as before, implying that the water/carbonate ^{18}O fractionation is similar for calcite and aragonite at these low temperatures. However, coincidental agreement of maximum δ^{18}values for the two taxa, resulting from different vital fractionation effects, cannot be ruled out.

Besides the ranges of the δ^{18}O values, the nature of the sequences is of interest. It seems that the progression of values in the clam shells shows coherence over a distance of some 10 mm, which presumably corresponds to a period of the order of one year (see below). There may be an indication of cyclicity in clam B, reminiscent of seasonal variations. It is perhaps not entirely unreasonable to expect some types of cyclicity in vent activity. Earth tides have shown to be important in triggering earthquake activity on Galápagos[18] and elsewhere[19-21]. Thus one might expect that the strain produced by Earth tides could affect any diverted flow through cracks by changing the size and linkage of such cracks. Lunar temperature cycles could result from such a mechanism, and the growth lines observed in the clams (Fig. 2) might be profitably studied under this aspect.

We next consider the carbon isotope values. Expected δ^{13}C values for equilibrium precipitation at this site are between 1 and 1.5‰ (ref. 22) if we assume an ambient δ^{13}C of close to 0‰ (refs 23, 24). Observed ranges are −0.5 to −2‰ for the barnacle calcite, 3.5–5‰ for the prismatic layer of clam A and 1–2‰ for that of clam B. The nacreous 'repair' material in both clams is isotopically lighter than the prismatic layer.

Only the clam B record seems to show near-equilibrium values, although, in fact, equilibrium values for aragonite are not well established. Rubinson and Clayton[25] report a fractionation between aragonite and calcite at 25 °C of 1.8‰, which if similar at 2 °C, would suggest that the δ^{13}C value should be ~3‰ at equilibrium. Hence, the clam A record may be closer to equilibrium. In either case, the pronounced difference between the δ^{13}C value of clam A and clam B is puzzling. One might suspect interference from organic matter in the analysis. However, both clams were treated in the same way, and it is not clear how a difference would be introduced through treatment.

If clam A values are near equilibrium, the lighter clam B values could be due to metabolic ^{12}C enrichment or vent-carbon effects, or both. Vent-carbon is expected to be depleted in ^{13}C compared to ambient bottom water, in analogy to volcanogenic carbon. The light values of the barnacle calcite must be considered in the same light.

To interpret the isotopic record in terms of history, we need a time scale. An estimated age of 6.5 yr from radionuclide ratios has been reported for a vesicomyid clam from the Galápagos Rise hot spring field[26]. Presumably, this estimate yields the correct scale for our clam samples. However, the fact that these clams are aragonitic may lead to erroneously young ages if substantial dissolution has occurred.

A valve of clam B (collected live) was cut in the growth direction to expose a cross-section (Fig. 2*a*). The shell structure from the lip (most recent growth) to approximately half way to the hinge consists of the sequential growth bands typical of molluscan prismatic growth. The remainder of the shell is a nacreous layer and is all that remains of the older portion of the shell where the prismatic layer has been dissolved away, due to the fact that the shells grow below the aragonite compensation depth for this region[27].

The mass of the nacreous growth is estimated to be roughly one-half of the mass of the remaining original growth. The nacre presumably also suffered attack and is likewise partly missing, being in turn made up for from below. Thus, a straight radiometric age determination on this specimen could be approximately half the true age. We have measured the average

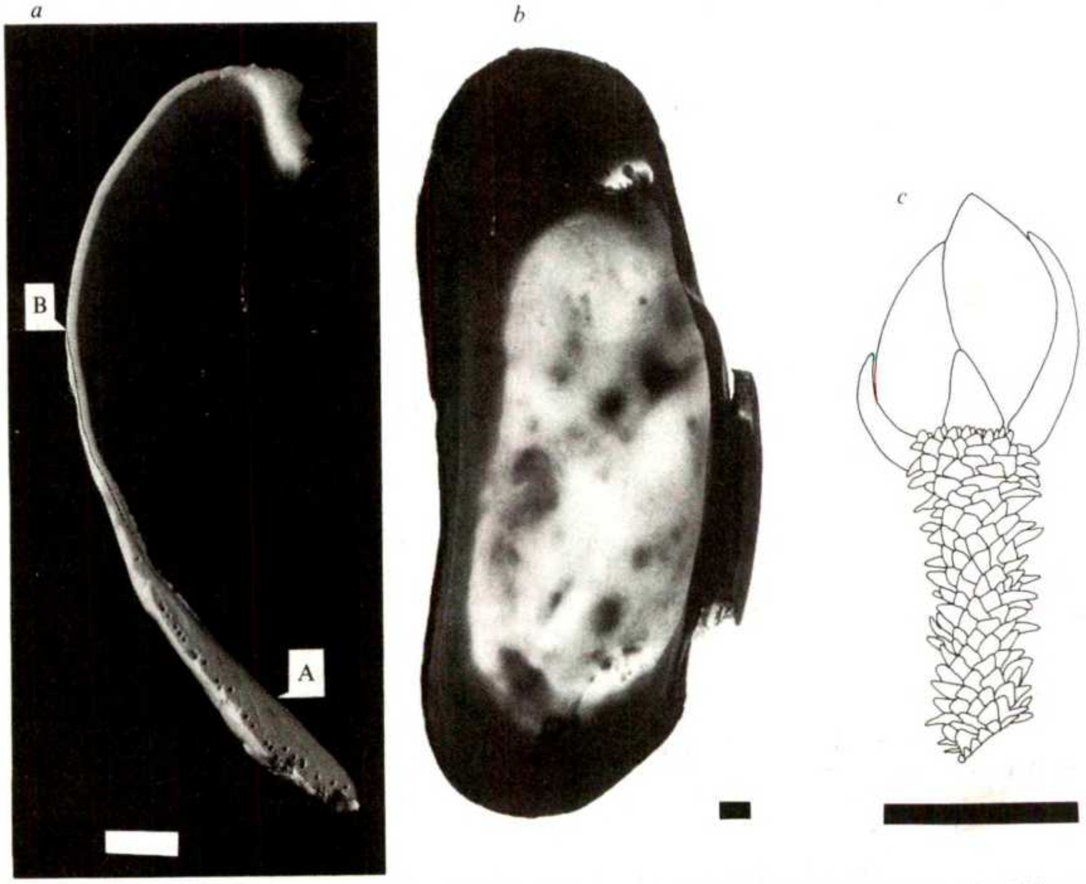

Fig. 2 *a*, Cross-section of clam shell (dorsal margin up) from a living *Calyptogena*, ALV 914 B-1 showing the decreasing thickness of the outer, prismatic, layer until none remains, dorso-laterally beginning at B. The inner secretion of nacre extends from A and increases in thickness until at B it constitutes the whole of the shell wall. Scale bar, 1 cm. (Some of the sample drill holes are apparent in the photograph.) *b*, Shell (dorsal margin to right) of a dead *Calyptogena*, ALV 909 B-1 illuminated with strong light from below. The light area represent secondary, nacreous, structure, while the opaque area indicates regions where all or part of the upper prismatic layer remains. Scale bar, 1 cm. *c*, Lateral view of the barnacle, *Neolepas zevinae*, ALV 915-rock 4 (first paratype, British Museum (Natural History) reg. no. 1979·209). Note that the peduncle is clad with irregular whorls of scales. New whorls are added at the junction between the capitulum and the peduncle so that scales grade in age from the oldest at the point of attachment to the youngest immediately below the capitulum. Scale bar, 1 cm long.

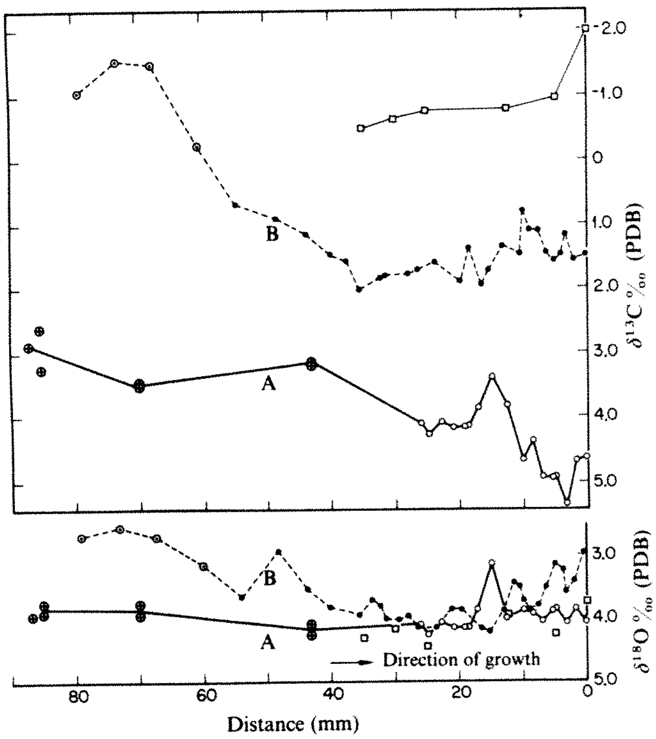

Fig. 3 $\delta^{18}O$ and $\delta^{13}C$ variations as a function of shell growth. Dead clam (A) Calyptogena (ALV909B-1); ○, prismatic growth; ⊕, nacreous growth. □, Barnacle *N. zevinae* (distances for scales analysed are from capitulum to the point of attachment): holotype USNM cat. no. 172581. Living clam (B) (ALV914B-1): ●, prismatic growth; ⊙, nacreous growth. Distances are from the margin of the shell (clam) and from the base of the capitulum (barnacle).

rate of dissolution (about 15 mg cm^{-2} yr^{-1}) of clam fragments by suspending them at a depth of 2,700 m (lat. 0.0°0.2′ N, long. 152°13.0′ W) for 4 months. This rate of dissolution implies that an empty whole shell would dissolve in ~25 yr in the vent region.

Reactivation of a vent after dormancy might be indicated by clam assemblages in various states of preservation. Incidentally, the fact that vesicomyid clams have not been reported from the North Atlantic Ridge crest area, despite the excellent conditions for aragonite preservation there[27], may be in accord with the more slowly spreading rates, which would not be able to support the enormous heat loss associated with high-temperature, high-velocity RISE-type vents.

Our results show that the clams and the barnacle analysed grew at ambient to slightly higher-than ambient temperatures.

Hydrothermal leaks in the vicinity of the vents may influence the stable isotope record of the shells, as well as their growth, and organic carbon of chemosynthetic origin[28] may do likewise. Future work might focus on parallel examination of live-collected clams and other shelled organisms, to separate ambient from individual variations. The possibility of cyclicity in ambient conditions seems worth investigating; if cyclicity exists, it would provide instant age scales for carbonate-secreting organisms.

We thank F. N. Spiess and R. R. Hessler for samples and for encouragement, also R. A. Knox for arranging the dissolution experiment, and M. Kastner for criticisms. This work was supported by the NSF, Oceanography Section: grant OCE78-25587.

Received 11 April; accepted 26 June 1980.

1. Spiess, F. N. *et al. Science* **207,** 1421–1433 (1980).
2. Corliss, J. B. *et al. Science* **203,** 1073–1083 (1979).
3. Larson, R. L. *Bull. geol. Soc. Am.* **82,** 823 (1971).
4. Macdonald, K. C., Miller, S., Kuestis, S. & Spiess, F. N. *J. geophys. Res.* (in the press).
5. Normark, W. *Geology* **4,** 681 (1976).
6. CYAMEX *Mar. geophys. Res.* (in the press).
7. Ballard, R., Francheteau, J., Porgin, C., Juteau, T. & Normark, W. (in preparation).
8. Francheteau, J. *et al. Nature* **277,** 523–528 (1979).
9. Macdonald, K. C., Becker, K., Spiess, F. N. & Ballard, R. *Earth planet. Sci. Lett.* (in the press).
10. Boss, K. & Turner, R. (in preparation).
11. Newman, W. A. *Trans. San Diego Soc. nat. Hist.* **19,** 153–167 (1979).
12. Craig, H. *Geochim. cosmochim. Acta* **12,** 133 (1957).
13. Epstein, S., Buchsbaum, R., Lowenstam, H. A. & Urey, H. C. *Bull. geol. Soc. Am.* **64,** 1315–1326 (1953).
14. Craig, H. in *2nd Conf. Stable Isotopes in Oceanographic Studies and Paleotemperatures* (ed. Tongiorgi, E.) 161–182 (Consiglio Nazionale delle Richerche, Rome, 1965).
15. Craig, H. & Gordon, L. I. in *2nd Conf. Stable Isotopes in Oceanographic Studies and Paleotemperatures* (ed. Tongiorgi, E.) 9–130 (Consiglio Nazionale delle Richerche, Rome, 1965).
16. Tarutani, T., Clayton, R. N. & Mayeda, T. K. *Geochim. cosmochim. Acta* **33,** 987–996 (1969).
17. Galápagos Biology Expedition Participants *Oceanus* **22,** 2–10 (1979).
18. Filson, J., Simkin, T. & Leu, L .K. *J. geophys. Res.* **78,** 8591–8622 (1973).
19. Tamrazyan, G. P. *J. geophys. Res.* **73,** 6013–6018 (1968).
20. Shaw, H. R. *Science* **168,** 1084–1087 (1970).
21. Shaw, H. R., Kistler, R. W. & Evernden, J. F. *Bull. geol. Soc. Am.* **82,** 869–895 (1971).
22. Emrich, K., Ehhalt, D. H. & Vogel, J. C. *Earth planet. Sci. Lett.* **8,** 363–371 (1970).
23. Kroopnick, P. *Deep-Sea Res.* **21,** 211–227 (1974).
24. Kroopnick, P., Deuser, W. G., Craig, H. *J. geophys. Res.* **75,** 7668–7671 (1970).
25. Rubinson, M. & Clayton, R. W. *Geochim. cosmochim. Acta* **33,** 997–1002 (1969).
26. Turekian, K. K., Cochran, J. K. & Nozaki, Y. *Nature* **280,** 385–387 (1979).
27. Berger, W. H. *Deep-Sea Res.* **25,** 447–452 (1978).
28. Karl, D. M., Wirsen, C. O. & Jannasch, H. W. *Science* **207,** 1345–1347.

Concentrations of ^{113m}Cd in the marine environment

V. E. Noshkin, K. M. Wong, R. J. Eagle & D. L. Anglin

Environmental Sciences Division, Lawrence Livermore Laboratory, University of California, Livermore, California 94550

Reports on the detection of ^{113m}Cd in any type of environmental sample have been rare. The 113 mass chain yield is small relative to other longer-lived fission products, such as ^{90}Sr and ^{137}Cs, produced from uranium, plutonium and thorium fissions[1]. Also, only a small fraction of the 113 chain yield decays to ^{113m}Cd (ref. 2). Salter[3] estimated that the ^{113m}Cd/^{90}Sr activity quotient in thermonuclear fission should be 0.003. He stated that "this ratio is in good agreement with data from a few samples measured in the northern hemisphere prior to 1962 which have no ^{109}Cd". This, to our knowledge, was the first report of the detection of fission-produced ^{113m}Cd in the environment. Salter[3] also calculated that 0.062 MCi of ^{113m}Cd and 0.25 MCi of ^{109}Cd were produced by activation during the atmospheric detonation of the 1.4-megaton Starfish device on 9 July 1962 over Johnston Atoll. As both ^{109}Cd and ^{113m}Cd are produced during neutron activation of stable cadmium, and ^{109}Cd is not a fission product, the last part of Salter's statement is significant. The absence of ^{109}Cd in samples collected before 1962 indicates that all nuclear testing before this time, which included all tests conducted at Enewetak and Bikini Atolls in the Marshall Islands, could have generated ^{113m}Cd only as a fission product. It is therefore important to recognize that ^{113m}Cd could be present in other environments contaminated with fission product wastes discharged to the aquatic environment from other nuclear facilities. ^{113m}Cd has a half life[4] of 14.6 ± 0.1 yr and decays predominantly by beta-particle emission. We present here a preliminary report of ^{113m}Cd concentrations measured in sediment and tissue samples of marine organisms collected around different atolls in the Marshall Islands.

A series of pooled and individual fish liver and sediment samples were selected for analysis. It has been well documented that stable cadmium is concentrated by the liver of fish[5,6]. Liver analysis offered the most sensitive test for presence of ^{113m}Cd in the marine environment, especially at those atolls where only global fallout background concentrations could be anticipated in the environment. Gamma spectrometry was used to measure ^{113m}Cd ($E\gamma = 263.7 \pm 0.3$ keV; branching intensity 2.3×10^{-4})[7] in large samples of ashed liver when activity levels were high, otherwise ^{113m}Cd was measured on low-background beta counters following radiochemical separation of cadmium from other radioelements in the samples. The methods used to identify and detect ^{113m}Cd in these samples are reported elsewhere[8].

Concentrations of ^{113m}Cd and other radionuclides detected in the samples are shown in Table 1. Some ^{113m}Cd measurements were made during the 1972–73 radiological survey of Enewetak Atoll. As the relevance of these results has been overlooked,

0028-0836/80/380221—03\$01.00

Table 1 Radionuclide concentrations in fish liver samples from the Marshall Islands

Atoll	Scientific (common) name	Collection date†	pCi per g dry wt (%σ)* ^{60}Co	^{113m}Cd	^{137}Cs	^{155}Eu	^{207}Bi	$^{239+240}$Pu	^{241}Am
Bikini									
Island B-13	*Crenimugil crenilabis* (mullet)	10/78	20(1)	18.5(1)	NA	NA	NA	0.84(2)	NA
Island B-13	*Mulloidichtys samoensis* (goatfish)	10/78	14.2(4)	21.7(1)	ND	ND	1.1(9)	0.17(3)	NA
Island B-5	*Crenimugil crenilabis* (mullet)	10/78	33(1)	15.2(1)	0.72(12)	ND	ND	1.81(2)	NA
Lagoon	*Gymnosarda nuda* (tuna)	6/79	12.8(1)	105(29)	0.18(4)	ND	2.00(2)	NA	NA
Lagoon	*Carcharhinus menisorrah* (grey shark)	11/72	10.4(1)	413(1)	0.67(2)	0.13(2)	5.4(1)	0.147(2)	0.13(3)
Lagoon	*Triaenodon obesus* (white tip shark)	11/72	24(1)	230(8)	0.12(19)	0.04(56)	2.5(4)	0.61(6)	0.36(12)
Lagoon	*Lutjanus bohar* (snapper)	10/78	32.2(2)	1,243(17)	0.066(27)	<0.2	0.67(17)	NA	NA
Enewetak									
Island E-7	*Carcharhinus menisorrah* (grey shark)	12/79	0.30(1)	10.4(13)	0.026(3)	ND	0.11(2)	NA	NA
Island E-7	*Carcharhinus menisorrah* (grey shark)	12/79	0.21(1)	12.9(9)	0.020(5)	ND	0.18(1)	NA	NA
Island E-7	*Carcharhinus menisorrah* (grey shark)	12/79	0.27(1)	8.3(10)	0.016(4)	ND	0.24(1)	NA	NA
E-43	*Carcharhinus menisorrah* (grey shark)	12/79	0.11(1)	3.5(26)	0.003(19)	ND	0.36(1)	NA	NA
E-43	*Carcharhinus menisorrah* (grey shark)	12/79	0.31(3)	10.0(30)	0.020(8)	ND	1.6(8)	NA	NA
E-43	*Carcharhinus menisorrah* (grey shark)	12/79	0.76(1)	24.4(20)	0.030(4)	ND	2.6(3)	NA	Na
E-1	*Carcharhinus menisorrah* (grey shark)	12/79	0.14(1)	7.2(20)	0.024(3)	ND	0.47(1)	NA	0.012(30)
E-1	*Carcharhinus menisorrah* (grey shark)	12/79	0.34(1)	12.2(19)	0.037(3)	0.006(46)	4.05(2)	NA	0.06(18)
E-44	*Carcharhinus menisorrah* (grey shark)	12/79	0.57(1)	19.2(11)	0.024(9)	0.006(22)	1.28(2)	NA	0.037(18)
E-44	*Carcharhinus menisorrah* (grey shark)	12/79	5.61(1)	28.2(7)	0.057(3)	0.017(23)	0.67(3)	NA	0.076(24)
E-44	*Carcharhinus menisorrah* (grey shark)	12/79	0.45(1)	4.5(32)	0.014(7)	ND	0.68(2)	NA	0.021(42)
E-9	*Triaenodon obesus* (whitetip shark)	5.12(1)	95(20)	0.19(7)	0.09(27)	57(2)	NA	1.33(9)	
Rongelap									
Island F-13	*Crenimugil crenilabis* (mullet)	9/78	ND	30.0(2)	0.57(2)	ND	ND	1.56(4)	NA
F-13	*Scarus sordidus* (parrot fish)	9/78	ND	6.0(2)	ND	ND	ND	0.24(4)	NA
Bikar									
D-1	*Crenimugil crenilabis* (mullet)	9/78	0.54(14)	0.30(12)	<0.06	ND	ND	0.036(6)	NA
D-1	*Neomyxus chaptalii* (mullet)	9/78	ND	0.24(15)	ND	ND	ND	0.033(7)	NA
Ujelang									
J-22	*Crenimugil crenilabis* (mullet)	11/78	ND	0.21(40)	ND	ND	ND	0.012(23)	NA
Uticik									
I-1	*Mulloidichthys samoensis* (goatfish)	9/78	ND	0.19(14)	ND	ND	ND	0.003(26)	NA
Jemo									
S-1	*Acanthurus triostegus* (convict surgeon)	10/78	ND	0.41(11)	ND	ND	ND	0.143(3)	NA
Bravo Crater sediment		11/72	29(1)	2.7(1)	7.3(3)	44(3)	63(1)	78(2)	42(3)

NA, Not analysed. ND, Not detected.
* To convert pCi g^{-1} to mBq g^{-1}, multiply values by 37. %σ, Per cent standard deviation of the counting error.
† Activity as of date of collection.

Table 2 Radionuclide concentrations in marine organisms from Enewetak Atoll

Scientific (common) name	Island	Sample	pCi per g dry wt (%σ)* ^{55}Fe	^{60}Co	^{90}Sr	^{113m}Cd	^{137}Cs	^{155}Eu	^{207}Bi	$^{239+240}$Pu	^{241}Am
Invertebrates											
Tridacna gigas (giant clam)	E-2	Kidney	108(4)	477(2)	0.52(40)	4.57(7)	<0.6	<2	19.7(3)	0.42(7)	0.41(5)
Tridacna gigas (giant clam)	E-8	Kidney	101(8)	1,570(1)	0.16(32)	100(2)	<1.3	<1	22.8(5)	0.21(5)	<0.2
Tridacna gigas (giant clam)	E-1	Kidney	87(1)	513(1)	1.09(16)	6.31(7)	<0.5	<0.5	17.5(3)	0.28(13)	0.23(7)
Tridacna gigas (giant clam)	E-2	Viscera	35(3)	108(1)	0.71(18)	1.16(17)	<0.2	0.9(30)	9.2(3)	7.43(1)	0.68(5)
Vertebrates											
Chaetodon auriga (butterfly fish)	E-9	Viscera†	1.67(1)	444(2)	0.98(7)	11.6(3)	<0.7	<0.4	<0.5	1.55(5)	0.23(6)
Crenimugil crenilabis (mullet)	E-9	Viscera	276(4)	104(1)	<0.02	3.07(2)	9.84(5)	25.3(2)	2.23(11)	24.2(2)	11.4(4)
Acanthurus triostegus (convict surgeon)	E-9	Viscera	201(7)	227(2)	17.7(6)	12.9(5)	6.12(7)	6.75(5)	1.10(20)	15.3(10)	3.56(5)
Acanthurus triostegus (convict surgeon)	E-2	Viscera	254(1)	17.8(2)	2.1(6)	13.0(2)	1.60(13)	0.67(21)	1.28(13)	2.23(12)	0.83(5)
Scarus sordidus (parrot fish)	E-2	Viscera	183(3)	151(8)	5.5(6)	5.90(6)	2.57(18)	1.42(50)	<0.3	2.89(3)	1.48(6)
Euthynnus affinis (bonito)	E-36	Light muscle	87(2)	1.3(13)	0.1	0.26(19)	0.68(13)	0.1	6.15(2)	<0.004	<0.3
Euthynnus affinis (bonito)	E-36	Dark muscle	572(1)	16.8(2)	0.1	0.50(14)	0.78(13)	<0.1	3.81(3)	<0.004	<0.1
Euthynnus affinis (bonito)	E-36	Liver	3,130(1)	20.9(2)	0.9	95.5(1)	2.8(8)	0.87(11)	1.66(10)	0.022(29)	<0.1
Euthynnus affinis (bonito)	E-31	Liver	649(1)	14.8(5)	0.4	32.3(1)	0.61(33)	<0.2	0.45(30)	<0.012	<0.009

* To convert pCi g^{-1} to mBq g^{-1}, multiply value by 37. %σ, Per cent standard deviation of the counting error. Abstracted from data in ref. 8; activity as of 11/72.
† Viscera sample includes all internal organs and gut contents which contain undigested sediment. Concentrations are biased by higher concentrations of transuranics, ^{55}Fe and others in sediment.

they are abstracted from the survey report[9] and shown in Table 2.

^{113m}Cd was detected in all samples collected between 1972 and 1979 from Bikini and Enewetak Atolls and in fish liver samples from other atolls in the Marshall Islands, some of which were in the paths of close-in fallout debris from the nuclear tests conducted at Bikini and Enewetak. Radionuclides persist in these environments 21 yr after the last nuclear explosion at the atolls in 1958. ^{113m}Cd concentration was found to be lower in the surface sediment layer compared to ^{60}Co, ^{137}Cs, $^{239+240}$Pu, ^{241}Am and ^{207}Bi, but it exceeds the concentrations of these radionuclides in the liver samples of Bikini tuna, shark and snapper by at least one order of magnitude. In the liver samples of Bikini reef species, ^{113m}Cd concentrations are at present comparable to ^{60}Co and greatly exceed the concentrations of the other radionuclides we have measured so far. The concentrations of ^{113m}Cd in the liver samples of mullet, a herbivore, are much less than the concentrations detected in the pelagic carnivores at Bikini. This comparison suggests the concentration of ^{113m}Cd is greater in representative species from higher trophic levels. Fish from Bikini seem to contain more ^{113m}Cd in the liver than fish from Enewetak lagoon. Concentrations in the flesh of bonito from Enewetak Atoll are much lower than concentrations in the liver samples of the fish. This finding would have been predicted from the studies of stable cadmium distributions in fish. In 1979 grey reef sharks were taken from different quadrants of Enewetak lagoon (distinguished by the different island numbers in Table 1). Very different levels of radionuclides are associated with the lagoon sediments in each quadrant. There seems to be no significant relationship between

^{113m}Cd concentrations in the liver and the geographical region from which the sharks were caught. Although sharks in local regions of the lagoon may encounter very different levels of radioactivity, they appear to act more as 'averagers' as they probably travel into and out of the more or less radioactive parts of the lagoon continuously during their life.

Close-in fallout contamination is still evident in the marine environment at Rongelap Atoll, where concentrations of ^{113m}Cd in mullet liver samples are even higher than the levels detected in mullet collected from the eastern half of Bikini Atoll. The lowest concentration of ^{113m}Cd measured was ~0.2 pCi per dry weight in the liver of reef species from the atolls of Utirik, Ujelang and Bikar. ^{137}Cs activities in the flesh of these fish were in the range of fallout concentrations detected in the flesh of mullet samples collected in 1979 from North Carolina, USA (unpublished data). Therefore, the ^{113m}Cd concentrations in the atoll samples are probably representative of the levels expected at these latitudes from global fallout deposition.

It is not clear at this point if the current absence of reports of ^{113m}Cd concentrations indicates this radionuclide was measured but not detected, or that insufficient effort has so far been made to evaluate this radionuclide in environments receiving fission product wastes. Although production of ^{113m}Cd during the fission event may be low, we have found that this radionuclide persists in the environment and is significantly concentrated in the liver of fish at the atolls. Concentrations presently exceed the levels of most other long-lived man-made radionuclides in liver by orders of magnitude. We have not yet generated sufficient data to evaluate its radiological significance in major dietary items at the Marshall Islands but these analyses are one of our main priorities. Stable cadmium is known to be concentrated by man in the kidney and liver[7]. As ^{113m}Cd will follow stable cadmium through the food chain—it decays by emitting energetic beta particles ($E_{max} = 0.58$ MeV)—and has a relatively long half life, the integrated radiological dose to man from ^{113m}Cd ingestion will be carefully assessed at the Marshall Islands and should also be assessed at other sites where contamination by this radionuclide may be suspected.

We thank Dr D. R. Nelson for samples of shark caught during November–December 1979 at Enewetak Atoll. D.L.A. was a summer participant supported by the Associated Western Universities. This work was performed under the auspices of the US Department of Energy, contract number W-7405-ENG-48.

Received 18 April; accepted 28 July 1980.

1. Nethaway, D. R. & Barton, G. W. *Lawrence Livermore Laboratory Rep.* UCRL-51458 (1973).
2. Wahl, A. C. *J. inorg. nucl. Chem.* **10,** 1–3 (1959).
3. Salter, L. P. *Radioactive Fallout from Nuclear Weapons Tests* (ed. Klement, A. W. Jr) 694, 409–421 (CONF-765, AEC 5 Symp.Series, 1965).
4. Wahl, A. C. *J. inorg. nucl. Chem.* **34,** 1767–1768 (1972).
5. Pentreath, R. J. *J. exp. mar. Biol. Ecol.* **30,** 223–232 (1977).
6. Yamagata, N. *Cadmium Studies in Japan: A Review* (ed. Tsuchiya, K.) 19–43 (North-Holland Biomedical Press, Amsterdam, 1978).
7. Mateosian, E. D. & Goldhaber, M. *Phys. Rev.* **186,** 1285–1288 (1969).
8. Wong, K. M., Noshkin, V. E. & Anglin, D. L. *Hlth Phys.* (submitted).
9. US Atomic Energy Commission, Nevada Operations Office *Enewetak Radiological Survey* Rep. NVO-140, I-III (1973).

The energetic cost of bipedal hopping in small mammals

Steven D. Thompson*, Richard E. MacMillen*, Elaine M. Burke† & C. Richard Taylor†

*Department of Ecology and Evolutionary Biology, University of California at Irvine, Irvine, California 92717
†Museum of Comparative Zoology, Harvard University, Cambridge, Massachusetts 02138

Recent studies of locomotion in red kangaroos (*Megaleia rufa*, 18–28 kg)[1] and Australian hopping mice (*Notomys cervinus*, 36.6 g)[2] have indicated that over a certain range of speeds the energetic cost of bipedal hopping locomotion may become independent of speed. As much as 70% of the decrement in kinetic energy which takes place when the kangaroo lands may be stored in elastic elements and used to propel the kangaroo upwards and forwards as it takes off (leaving only 30% to be added by the muscles)[3,4]. Presumably, this same phenomenon could be exploited by all bipedal hopping mammals and it seems possible that at high speeds this specialized mode of locomotion could result in large energetic savings when compared with the costs incurred by a similarly sized quadruped running at the same speed. This hypothetical lower cost of locomotion has been invoked as an explanation for the rather common occurrence of bipedal hoppers among desert and plains dwelling mammals, as it might substantially reduce the energetic cost of foraging, or travelling, for animals utilizing widely dispersed resources[5–7]. The purpose of the present study was to extend the assessment of the metabolic expense of bipedal hopping to a broader range of body sizes and mammalian taxa. Using indirect calorimetry we measured the cost of locomotion for three bipedal hopping eutherians (0.03–3.0 kg) and one bipedal hopping marsupial (1.1 kg). When properly trained for sustained running, none of the three species deviated from the expected quadrupedal pattern relating cost of locomotion to running speed, even while running fully bipedally. Bipedality must therefore be associated with benefits other than those related to the energetic costs of locomotion.

We trained two spring hares (*Pedetes capensis*, Rodentia; Pedetidae, average weight 3.0 kg), two rat kangaroos (*Bettongia penicillata*, Marsupialia; Macropodidae, average weight 1.1 kg), eight desert kangaroo rats (*Dipodomys deserti*, Rodentia; Heteromyidae, average weight 104 g) and one Merriam's kangaroo rat (*Dipodomys merriami*, 32 g) to hop on a treadmill while we measured their oxygen consumption. We considered the animals 'trained' when they would sustain one gait and position on the treadmill—5 min for the smaller *Dipodomys* and 20 min for the larger species—over a range of speeds. Naive and poorly trained animals would oscillate forwards and backwards along the treadmill at all but a few preferred speeds; these animals also frequently altered their gait when moving from the back to the front of the tread.

Rates of oxygen consumption were measured by enclosing the animal in a Plexiglas chamber which either slid along the tread (*Pedetes* and *Bettongia*) or enclosed it (*Dipodomys*). Air was metered through the box (170 l min^{-1} STP for *Pedetes* and *Bettongia* and 7 l min^{-1} STP for *Dipodomys*). The difference in oxygen concentration (ΔO_2) between dry air entering and leaving the box was measured using an oxygen analyser (Applied Electrochemistry S-3A for the *Pedetes* and *Bettongia* and Taylor Servomex 0–272 for the *Dipodomys*). Rate of oxygen ($\dot{V}O_2$) consumption was calculated assuming a respiratory quotient of 0.8 by multiplying flow through the chamber by ΔO_2 and dividing by 0.9581 as described by Tucker[8] for a similar system. The chambers were checked for leaks of exhaled air by decreasing the flow by 30% as the $\dot{V}O_2$ was monitored. This procedure should increase the magnitude of any loss of exhaled air: no difference was found between $\dot{V}O_2$ measured at either flow rate. In *Pedetes* and *Bettongia*, the rate of anaerobic glycolysis was determined by measuring the change in blood lactate concentration (using a Boehringer-Mannheim lactate test kit) over the timed interval of the run; comparison of resting to running levels of lactate production revealed no significant increase over the range of speeds for which $\dot{V}O_2$ was measured. Anaerobic glycolysis was not assayed in *Dipodomys* due to the adverse effect of blood sampling procedures on treadmill behaviour.

Rates of oxygen consumption increased linearly with speed in all four species of hopping mammals over a wide range of speeds which included the transition from completely quadrupedal to

0028-0836/80/380223—02$01.00

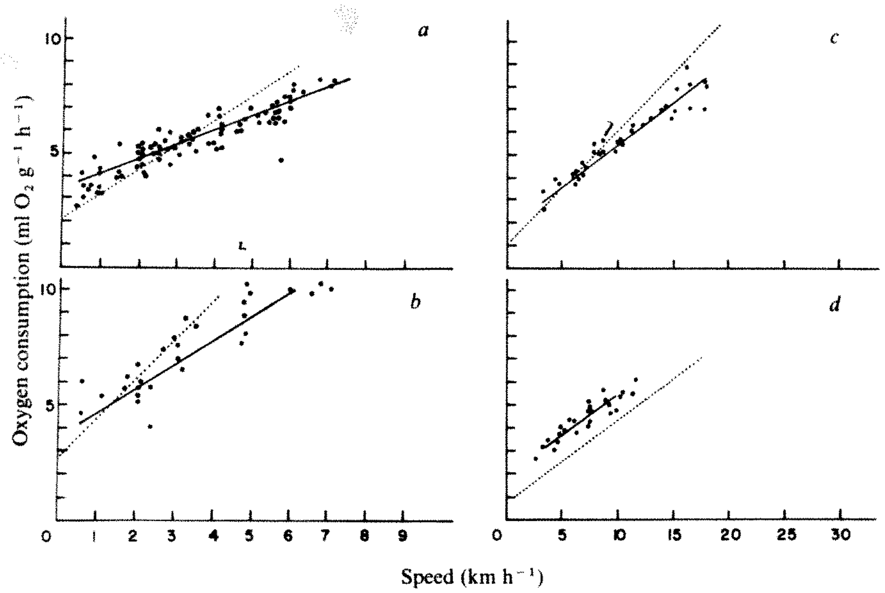

Fig. 1 Rate of oxygen consumption as a function of speed for four small species of bipedal hopping mammals. All values are for fully trained animals (moving at a constant gait and speed, that is, they used one gait and kept their position on the tread constant). Solid lines represent the least squares regression for the linear portion of each graph, where

$\dot{V}O_2$ (ml O_2 per g h) = slope × speed (km h^{-1}) + y intercept

(*a*) *D. deserti*, 104 g, $N = 8$. $\dot{V}O_2 = 0.66 \times \text{speed} + 3.25$. $r^2 = 0.85$, $n = 95$, $P < 0.001$

(*b*) *D. merriami*, 32 g, $N = 1$. $\dot{V}O_2 = 1.1 \times \text{speed} + 3.67$. $r^2 = 0.50$, $n = 25$, $P < 0.005$

(*c*) *B. penicillata*, 1.1 kg, $N = 2$. $\dot{V}O_2 = 0.39 \times \text{speed} + 1.74$. $r^2 = 0.88$, $n = 33$, $P < 0.001$

(*d*) *P. capensis*, 3.0 kg, $N = 2$. $\dot{V}O_2 = 0.34 \times \text{speed} + 2.04$. $r^2 = 0.67$, $n = 26$, $P < 0.001$

Dotted lines represent the predicted oxygen consumption for a running quadrupedal mammal of the same body size using the equation of Taylor, Schmidt-Nielsen and Raab[15]. Slopes of all four empirical regressions are not significantly different from those predicted (*t*-tests, $P < 0.05$).

completely bipedal locomotion (transition speeds were 3–5 km h^{-1} for both *Pedetes* and *Bettongia*, 2–3 km h^{-1} for *D. deserti* and 1.5–2.5 km h^{-1} for *D. merriami*). These speeds also encompassed the normal foraging speeds of both *D. merriami* (average 3.2 km h^{-1}) and *D. deserti* (6.33 km h^{-1})[9]; foraging speeds of *Pedetes* and *Bettongia* are unknown. This rate of increase was very similar to that predicted for a quadrupedal mammal of the same mass (dotted lines in Fig. 1). Although at higher speeds the predicted values are greater than those observed for hopping bipeds (Fig. 1*a–c*), those slight differences are not statistically significant and it seems unlikely that they would confer any biological advantage to bipeds. Plots of $\dot{V}O_2$ against speed for untrained animals gave a sigmoidal relationship similar to that reported by Dawson[2] for a 36.6-g hopping mouse. However, as training proceeded, our animals began to maintain a constant gait and eventually they would remain at the same tread location (near the front of the tread) throughout the run. In the latter conditions, the relationship between $\dot{V}O_2$ and speed was linear (Fig. 1), not sigmoidal. Apparently, the sigmoidal relationship between $\dot{V}O_2$ and speed was an artefact of the fore and aft motion of poorly trained animals; these animals were probably not in a steady state.

We conclude that hopping is not an energetically cheaper way to move for small hoppers (<3 kg) than quadrupedal locomotion. As the locomotory costs of small marsupial and rodent hoppers are similar to those of quadrupedal mammals of comparable body mass, we are left with two questions, one functional and one evolutionary. First, we have no immediate explanation for the differences in locomotory energetics of small (this study) and large (red kangaroos) hoppers; however, it is apparent that those differences do exist. Of the six species of small bipedal hoppers for which the energetic cost of locomotion has now been determined, only one, *Notomys cervinus*, shows any tendency towards an independence of cost and speed. Moreover, because a congener, *Notomys alexis*[10], fails to show any evidence of an uncoupling of speed and energetic cost, it seems plausible that the unique pattern shown by *N. cervinus* may reflect training problems similar to those encountered in the present study. The red kangaroo data, on the other hand, do not seem to be methodological artefacts, and therefore the differences between large and small hoppers seem valid. Second, if there is no energetic advantage for small animals to hop, why do they do so? The majority of bipedal hopping mammals are much smaller than *Megaleia*, and presumably would have locomotory costs qualitatively similar to the four species reported here. Thus, it would seem that the advantage of bipedal hopping locomotion does not, at least for most species, lie within the realm of locomotory energetics.

Our findings do not support models of small mammal foraging behaviour and resource partitioning based on the assumption that the locomotory energetics of small hopping bipeds differ appreciably from those of small quadrupeds. Small hopping bipeds display a wide variety of behavioural traits (for example, vertical leaping, rapid changes in direction) which suggest that the chief benefit of this mode of locomotion is related to enhancement of abilities to escape predation[11,12]. These traits are accompanied by enlargement of both the visual and auditory apparatus; this further suggests that the morphology of small hopping bipeds has been moulded by their increased exposure to predation when foraging in the open areas of habitats with sparse vegetation[13,14]. Thus, it seems most likely that the bipedal hopping mode of locomotion in small mammals has evolved as a result of its advantages for the avoidance of predatory attacks and not as an energetic strategy associated with foraging on dispersed resources.

This study was supported in part by NSF grant DEB76-20116 to R.E.M. and NSF grant PCM 75-22684 to C.R.T.

Received 19 March; accepted 26 June 1980.

1. Dawson, T. J. & Taylor, C. R. *Nature* **246**, 313 (1973).
2. Dawson, T. J. *Nature* **259**, 305 (1976).
3. Cavagna, G. A., Heglund, N. C. & Taylor, C. R. *Am. J. Physiol.* **233**, R243–R261 (1977).
4. Alexander, R. McN. & Vernon, A. *J. zool. Res.* **177**, 265 (1975).
5. Reichman, O. J. & Oberstein, D. *Ecology* **58**, 636–643 (1977).
6. Reichman, O. J. in *Mechanisms of Optimal Foraging* (Garland, New York, 1979).
7. Price, M. V. *J. Mammal.* **59**, 624 (1978).
8. Tucker, V. A. *J. exp. Biol.* **48**, 55 (1968).
9. Thompson, S. D. thesis, Univ. Calif., Irvine (1980).
10. Baudinette, R. V., Nagle, K. A. & Scott, R. A. D. *Experientia* **32**, 583 (1976).
11. Eisenberg, J. F. *Univ. Calif. Publs Zool.* **63**, 1 (1960).
12. Bartholomew, G. A. Jr & Caswell, H. H. Jr *J. Mammal.* **32**, 155 (1951).
13. Webster, D. B. *Physiol. Zool.* **35**, 248 (1962).
14. Eisenberg, J. F. in *Rodents in Desert Environments*, 189–224 (Junk, The Hague, 1975).
15. Taylor, C. R., Schmidt-Nielsen, K. & Raab, J. L. *Am. J. Physiol.* **219**, 1104–1107 (1970).

Direct evidence of sudden rise in fetal corticoids late in human gestation

Montserrat deM Fencl, Robert J. Stillman, Jane Cohen & Dan Tulchinsky

Department of Obstetrics and Gynecology, Harvard Medical School, and the Endocrine Laboratory, Boston Hospital for Women, Boston, Massachusetts 02115

Glucocorticoids accelerate fetal lung maturation in all mammals studied[1], and in some species, such as goat and sheep, concentrations of fetal cortisol increase sharply before term, bringing about a train of events leading to parturition[2]. Studies of cortisol in the umbilical cord blood have revealed no such increase at the end of human pregnancy. But information obtained in that way is difficult to interpret because much of the fetal cortisol is of maternal origin[3,4] and its concentration, if sampled at delivery, is affected by maternal stress[5]. These problems can be avoided to some extent by studying other fetal corticoids. Corticosterone sulphate (once called compound B, and abbreviated to BS) is produced by fetal adrenal glands[6] and is present in greater concentrations in human fetal plasma than in maternal plasma[7]. It is not hydrolysed by the placental sulphatases and is a poor substrate for placental 11 β-hydroxysteroid dehydrogenase[8]. We report here confirmation that the bulk of maternal BS originates from the fetus, and that its concentration increases suddenly at term.

We measured BS in maternal and fetal fluids of normal pregnant women, women carrying anencephalic fetuses and a pregnant woman whose adrenals had been removed 5 yr earlier because she had Cushing syndrome. Samples of plasma, urine and amniotic fluid were assayed for BS after solvolysis and chromatography as before[9]. Student's *t* test was used for statistical evaluations. As Fig. 1 shows, the mean (±s.e.) concentration of BS in the plasma of non-pregnant women was 2.8 ± 0.3 ng ml^{-1}; at mid-pregnancy (21–32 weeks) it increased to 6.7 ± 0.5 ng ml^{-1}, and at term (38–40 weeks) it was about three times greater at 16.0 ± 3.2 ng ml^{-1} ($P < 0.01$). A further increase was observed in women in labour (26.4 ± 6.3 ng ml^{-1}). During labour, those carrying anencephalic fetuses had a significantly lower plasma BS than normal (8.3 ± 0.4 ng ml^{-1}; $P < 0.02$). In the pregnant woman with no adrenals, the concentration of BS in the plasma, which was monitored throughout pregnancy, increased gradually during the second and third trimester, the most pronounced increase occurring in the last week before spontaneous labour began. Before delivery, her plasma BS was within the range seen at term in a normal pregnancy, and there was no further increase during labour.

Quantities of BS in 24-h urine collections of non-pregnant and pregnant women are shown in Fig. 2. The pattern of increase in urinary excretion of BS during pregnancy was similar to that in maternal blood. Serial measurements of BS in the urine of the pregnant woman with no adrenals increased sharply during the week preceding delivery. Excretion of BS by this patient at term reached the range seen in normal pregnancies. Figure 3 shows that in deliveries at mid-pregnancy there was only slightly less BS in umbilical cord blood than at term (54.5 ± 2.9 compared with 62.7 ± 6.7 ng ml^{-1}; $P > 0.1$). In the cord plasma of the infant of the woman with no adrenals, BS was normal (60 ng ml^{-1}). However, in anencephalic fetuses at term, the mean concentration of BS in cord blood (15.9 ± 3.0 ng ml^{-1}) was one quarter of that in normal infants at term ($P < 0.001$). In the woman without adrenals, the amniotic fluid, sampled at vaginal delivery, contained BS within the range of normal pregnancies (42.6 ng ml^{-1}), whereas in two women carrying anencephalic fetuses, BS was abnormally low in the amniotic fluid (3.9 and 6.2 ng ml^{-1}).

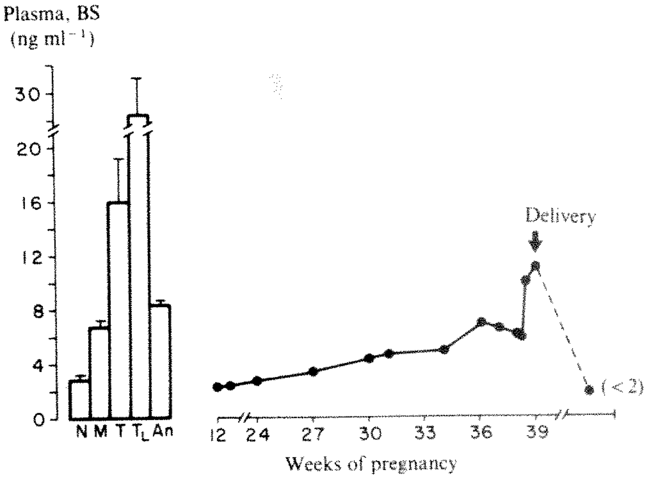

Fig. 1 Corticosterone sulphate (BS) concentrations in the maternal plasma of a woman with no adrenals at various stages of her pregnancy (●). Bars indicate concentration (mean ±s.e.) of BS in plasma of normal non-pregnant (N), and pregnant women at mid-pregnancy (M), term (T), and term in labour (T_L); and in women carrying anencephalic fetuses in labour at term (An). Replacement therapy with fludrocortisone (0.1 mg d^{-1}) and prednisone (7.5 mg d^{-1}) was given to the patient with no adrenals throughout pregnancy. BS was measured after solvolysis as corticosterone by radioimmunoassay (RIA), using an antibody prepared against cortisol-21-hemisuccinate-BSA; the antibody cross-reacted with cortisol (150 %), cortisone (2%), deoxycorticosterone (17%), prednisone (12%), prednisolone (19%), and 17α-hydroxyprogesterone (24%). All these compounds were separated by chromatography before RIA[9]. There was less than 1% cross-reactivity with all other steroids tested. Blank values were always undetectable (<20 pg). The interassay coefficient of variation was less than 15%. Recoveries after extraction and chromatography were 77.7 ± 10.4 (s.d.). In calculating the concentration of BS, corrections were made for differences in molecular weight between conjugated and unconjugated steroids. No. of subjects: N, 8; M, 14; T, 8; T_L, 5; An, 7.

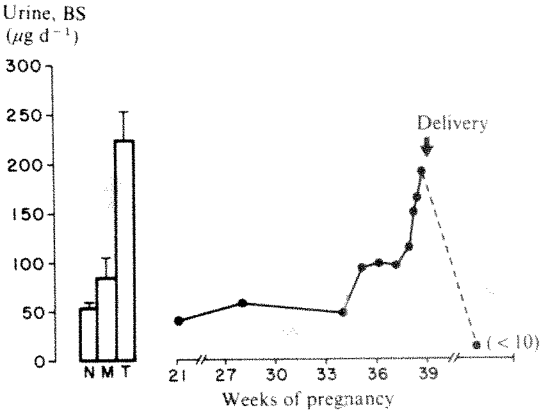

Fig. 2 Corticosterone sulphate (BS) concentrations in the urine of a woman with no adrenals at various stages of her pregnancy (●). Bars indicate values (mean ±s.e.) of BS in the urine of normal non-pregnant (N), and pregnant women at mid-pregnancy (M), and at term (T). No. of subjects: N, 6; M, 3; T, 6.

These data indicate that at least two thirds of BS in the maternal compartment at term is derived from the fetus: in women carrying anencephalic fetuses, concentrations of plasma BS at delivery were one third, and in umbilical cord plasma one quarter of that in normal pregnancies. Because the placenta cannot produce or metabolize BS, the increase in urinary
plasma BS throughout pregnancy indicates increased
tion by the fetal adrenal. This was confirmed because
with no adrenals had normal concentrations of
plasma BS which increased during the last

0028-0836/80/380225—02$01.00

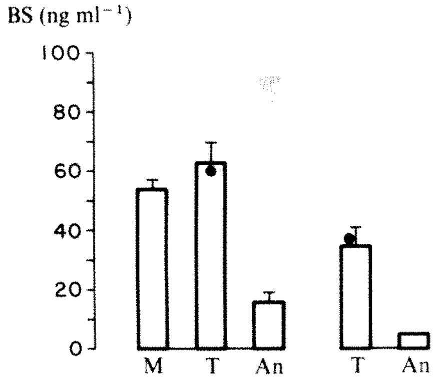

Fig. 3 Corticosterone sulphate (BS) concentrations in umbilical cord plasma and amniotic fluid of a pregnant woman with no adrenals (●). Bars indicate concentrations (mean ±s.e.) of BS in umbilical cord plasma (left) and amniotic fluid (right) of normal women at mid-pregnancy (M), and term (T), and in women carrying anencephalic fetuses in labour (An). No. of subjects umbilical cord: M, 7; T, 8; An, 6. No. for amniotic fluid: T, 8; An, 2.

most pronounced increase during the week preceding spontaneous labour.

The data obtained from the pregnant woman without adrenals, as well as the normal pregnant women, suggest that the production of BS by the fetal adrenals increases markedly near term. These results are compatible with the ultrastructural changes observed in the outer definitive zone of the fetal adrenal at term[10], and the increase in the size of the human fetal adrenal towards term[11]. Furthermore, conjugated cortisol also rises in amniotic fluid towards term[12], possibly a consequence of an increase in urinary excretion of this steroid by the fetus[9]. Thus, it is likely that the increased output of the fetal adrenal near term is not limited to BS but includes other corticosteroids. The fact that concentrations of BS in the umbilical cord plasma of normal infants at term were insignificantly higher than at mid-term, similar to results reported for other corticosteroids, does not exclude an increase in fetal adrenal production near term, for the rate of fetal metabolic clearance of BS into the maternal circulation is likely to be greater in late than in mid-pregnancy.

In humans, corticosteroids have not been implicated in the mechanisms leading to labour; however, they may well have a role in initiating other physiological changes, among them fetal lung maturation. In some species, such as the rabbit, the time of augmented surfactant production is preceded by an increase in fetal circulating unbound cortisol[13], together with an enhancement in the capacity of the lung to convert cortisone to cortisol[14]. Unconjugated corticosterone is a potent glucocorticoid that binds to specific lung receptors in the human[1], and in the rabbit it induces production of lung surfactant[15]. However, it is not known whether corticosterone in its conjugated form binds directly to lung receptors, or whether it can be hydrolysed by lung sulphatases, thus becoming biologically active. Further studies are necessary to clarify whether there is a direct association between increased fetal adrenal corticoid output, as determined by maternal concentrations of BS, and the status of fetal lung maturation, determined by analysis of concentrations of surfactant in the amniotic fluid.

Received 24 March; accepted 30 July 1980.

1. Giannopoulos, G. & Tulchinsky, D. in *Maternal-Fetal Endocrinology* (eds Tulchinsky, D. & Ryan, K.) 310–329 (Saunders, Philadelphia, 1980).
2. Liggins, G. C. *et al. Rec. Prog. Horm. Res.* **29,** 111–159 (1973).
3. Migeon, C. J. *et al. Rec. Prog. Horm. Res.* **17,** 207–243 (1961).
4. Osinki, P. A. *Nature* **187,** 777 (1960).
5. Ohrlander, S., Gennser, G. & Eneroth, P. *Obst. Gynec.* **48,** 381–386 (1976).
6. Goodyer, C. G. *et al. Acta Endocr.* **81,** 774–786 (1976).
7. Klein, G. P. *et al. J. clin. Endocr. Metab.* **36,** 944–950 (1976).
8. Hall, C. St. G. & Giroud, C. J. P. *Can. J. Biochem.* **49,** 1384–1387 (1971).
9. Fencl, M. deM, Koos, B. & Tulchinsky, D. *J. clin. Endocr. Metab.* **50,** 431–436 (1980).
10. Johannisson, E. *Acta Endocr. Suppl.* **130,** 7–107 (1968).
Winters, A. J. *et al. J. clin. Endocr. Metab.* **39,** 269–273 (1974).
hy, B. E. P. *J. clin. Endocr. Metab.* **47,** 212–215 (1978).
15. Toroa., Giannopoulos, G. & Solomon, S. *Endocrinology* **93,** 1342–1348 (1973).
Olson, E. B. & First, N. L. *Steroids* **27,** 869–880 (1976).
h, T. B. & Giroud, C. J. P. *Endocrinology* **96,** 1462–1467 (1975).

0028-0836/80/380226—03$

Expulsion of *Nippostrongylus brasiliensis* by mice deficient in mast cells

Cynthia L. Uber*, Richard L. Roth† & David A. Levy†

Department of Epidemiology* and Department of Biochemistry†, The Johns Hopkins University, School of Hygiene and Public Health, 615 North Wolfe Street, Baltimore, Maryland 21205

Expulsion of the intestinal helminth, *Nippostrongylus brasiliensis*, occurs spontaneously about 2 weeks after a primary infection of rats[1] and mice[2]. Cellular changes in the small intestine coincident with the period of expulsion have suggested several mechanisms by which this 'self-cure' may be effected. Local anaphylaxis was proposed as a possible means of parasite clearance; this hypothesis has been supported by the demonstration of specific reaginic antibody production[3] and jejunal mast cell accumulation[4] in infected animals. In addition, increased mucus secretion[5] and more recently, goblet cell proliferation in the jejunal mucosa of rats[6] have been noted and considered as potentially important in mediating the self-cure reaction. The data presented below indicate that in the absence of demonstrable mast cells, the course of a primary infection with this parasite is unchanged; however, they are supportive of a role for goblet cells in the self-cure reaction.

We have taken advantage of the availability of mast cell-deficient mice to examine the relative contribution of mast cells and goblet cells to the expulsion of *N. brasiliensis*. Either of two mutant alleles at the dominant-spotting locus of the mouse genome, *W* or W^v, when homozygous, is associated with a defect in a pluripotential stem cell precursor[7]. The hybrid W/W^v mouse, resulting from a cross between WB/Re-*W*/+ and C57Bl/6-W^v/+ parents, is grossly deficient of tissue mast cells, as documented by Kitamura *et al.*[7]. The immunological status of these mice with respect to thymus-derived and bone marrow-derived lymphocytes, however, seems to be normal[8]. W/W^v mice, their sex-matched littermates without the mutant alleles (+/+ mice) and C57Bl/6 mice (a background strain), were used in this study.

Kitamura *et al.*[7] demonstrated the mast-cell deficiency of W/W^v mice in histological studies of toluidine blue-stained sections of numerous tissues, including skin and gastrointestinal tract. We confirmed their findings, and obtained the following additional functional and biochemical evidence. First, we found no mast cells in the jejunal mucosa of W/W^v mice. Mast cells were quantitated histologically by removing the entire small intestine and fixing immediately in Carnoy's solution. Sections 2 cm in length were taken from the jejunum and dehydrated in an ascending ethanol series and cleared in α-terpineol. They were then embedded in paraffin and 8-μm sections were cut with a standard microtome. Slides were prepared and stained with astrablau- safranin to demonstrate mast cells[9]. In examining a total of 800 villus-crypt units (VCU) from four W/W^v mice, no mast cells were found. In contrast, there was an average of 0.7 ± 0.13 mast cells per 10 VCU in each of four +/+ controls. This number was somewhat less than that reported in mice of other strains; for example, Swiss–Webster mice may have 25 mast cells/10 VCU (ref. 10). Next, the absence of a passive cutaneous anaphylactic reaction in five 8-week-old male W/W^v mice, tested in the same way as three +/+ controls who were consistently reactive recipients in this assay, provided functional evidence for the mast cell deficiency in their skin. Finally, peritoneal cells from W/W^v mice were shown to lack mast cells, as well as histamine, a biochemical marker for mast cells. Thus, a 20-μl aliquot of an aspirated peritoneal cell suspension from each of five W/W^v mice was consistently negative for histamine using a radioenzymatic technique[11], while a similar aliquot taken from each of three +/+ controls contained an average of 3.6±0.8 ng histamine. (The lower limit of detection of histamine by this method is 0.1 ng per 20 μl.) Examination of samples of the aspirated cells, stained according to Mota's technique[12], confirmed that equal numbers of cells were present in all of the suspensions assayed, although mast cells comprised 11.2±3.6% of the cells from +/+ mice whereas no mast cells were detected among the cells obtained from W/W^v mice. Observations of the profound mast cell deficiency in the W/W^v mouse are thus supported and extended.

In normal mice, infection with *N. brasiliensis* is associated with a marked (at least tenfold) increase in mast cells in the jejunal mucosa[10]. Not surprisingly, this was not the case in W/W^v mice. After infection by the subcutaneous injection of 500 third-stage larvae of *N. brasiliensis*, no mast cells appeared in the jejunum of W/W^v mice up to day 21 after infection, whereas mast cells numbers did increase in +/+ mice (Fig. 1). Of 24 W/W^v and 24 +/+ mice, equal numbers of randomly selected animals were killed immediately before and on days 7, 10, 14, 17 and 21 post-infection, and their intestines prepared as described above. It was not until after day 7 post-infection that the number of mast cells began to increase in mice of the +/+ genotype. Mast cell accumulation continued up to day 21 in this control group.

The course of worm infection, however, determined by killing mice and counting the number of adult worms in the small intestine, was found to be parallel in W/W^v and control mice (Table 1). The course in all three groups of mice was similar to that reported with C3H mice[2]. On day 7, adult worms were found predominantly in the first third of the intestine (measured from the pyloric sphincter) in each group of mice. On day 14, no worms were found in any mouse except one, a C57Bl/6 mouse, which had retained a single worm.

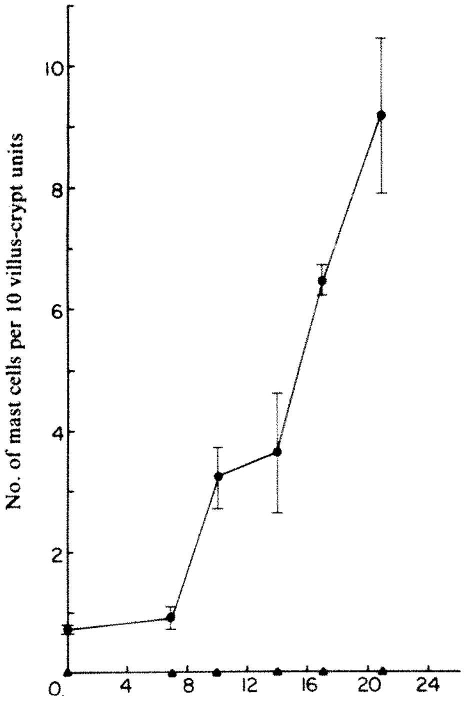

Fig. 1 Intestinal mast cell counts of W/W^v (▲) and +/+ (●) mice during the course of primary infection with *N. brasiliensis*. Twenty-four mice of each genotype were infected on day 0, each with 500 infective third-stage larvae; four of each group were sacrificed on each of the indicated days. A minimum of two sections from each mouse was examined at 400× magnification to identify and count mast cells in the villus-crypt units (VCU). At least 40 VCU in each tissue sample were examined; in sections from W/W^v mice, at least 100 VCU were examined. Standard errors are indicated by vertical bars.

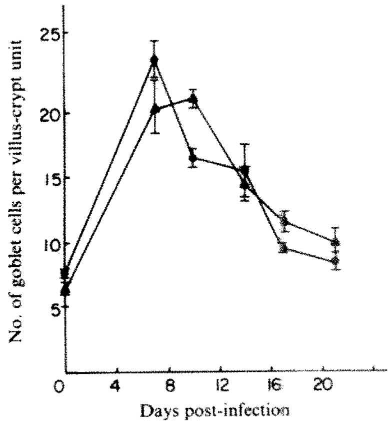

Fig. 2 Intestinal goblet cell counts of W/W^v (▲) and +/+ (●) mice during the course of a primary infection with *N. brasiliensis*. Sections contiguous with those stained for mast cells (refer to Fig. 1) were stained with alcian blue-periodic acid Schiff's[6] and examined for goblet cells (400×). At least 40 VCU in each tissue sample were examined. Standard errors are indicated by vertical bars.

At the same time, increases in goblet cell numbers were apparent in both groups of infected mice, as seen in Fig. 2. Before infection, W/W^v mice appeared to have fewer goblet cells than +/+ mice. On day 7 post-infection, there was a 2–4-fold increase in the number of goblet cells in the jejunal epithelium in both groups of mice. By day 10, the number of goblet cells had already begun to decline, approaching the pre-infection level by day 21. These observations are supported by the appearance of increased mucus content in the jejunum in the regions containing the most worms, particularly evident on day 7. It is noteworthy that intestinal goblet cell numbers and mucus secretion during the course of *N. brasiliensis* infection in these animals more closely paralleled the intestinal worm burden than did the number of intestinal mast cells. These observations are comparable to those made in rats infected with the same parasite[4,6].

Mast cell infiltration of the intestinal mucosa in the presence of specific IgE antibodies has long been taken to suggest that a local anaphylactic-like mechanism is involved in the expulsion of *N. brasiliensis* from the rodent intestine. Nevertheless, involvement of these cells has been questioned[13]. As demonstrated in the present experiment, expulsion in the absence of intestinal mast cells is strong evidence that mast cells and an anaphylactic-like reaction are not necessary for the effective clearance of intestinal worms after a primary infection. Furthermore, the maximum accumulation of intestinal mast cells in normal mice and rats occurs post-infection, which suggests that these cells may have some other role in this process. For example, they may serve a regulatory function[14].

The hypothesis that intestinal goblet cells play a part in the host response to helminthic parasites, suggested as early as

Table 1 Worm burden found in the small intestines of mice of different genotypes on days 7 and 14 post-infection

	Mean worm burden	
Genotype	Day 7	Day 14
WBB6 F_1-W/W^v	132±19*	0±0.0
WBB6 F_1-+/+	128±22	0±0.0
C57Bl/6	105±11	0±0.25

Groups of eight W/W^v, eight +/+ and eight C57Bl/6 mice were infected by the injection of 500 third-stage larvae. Four per group were killed on the indicated days; the small intestine was removed and plac in saline solution. Under direct microscopic observation (10× intestine was opened longitudinally in 1 cm segments and [illegible]70). worms identified and counted. Values are means ±s.e.m.

* Differences on day 7 are not statistically significa

1939[15], was later invoked in *N. brasiliensis* infections[5] and is reinforced by the current data. The apparent increase in the secretion of mucus, much of which might be due to the increased numbers of goblet cells, could provide a means for the mechanical expulsion of the worms as well as being a vehicle for the delivery of host antibody and cells to the site of parasite attachment. The roles of goblet cells, mast cells and their products in immunity to helminths is deserving of further investigation.

We thank Dr Saul Sharkis for supplying W/W^v and $+/+$ mice, and Steven Guarnaccia for technical assistance. This work is supported by grants from the US PHS (AI 07057 and AI 14480).

Received 15 May; accepted 18 June 1980.

1. Taliaferro, W. H. & Sarles, M. P. *J. infect. Dis.* **64,** 157–192 (1939).
2. Love, R. J. *Parasitology* **70,** 11–18 (1975).
3. Ogilvie, B. M. *Immunology* **12,** 113–131 (1967).
4. Miller, H. R. P. *Lab. Invest.* **24,** 339–347 (1971).
5. Wells, P. D. *Expl Parasit.* **12,** 82–101 (1962).
6. Miller, H. R. P. & Nawa, Y. *Expl Parasit.* **47,** 81–90 (1979).
7. Kitamura, Y., Go, S. & Hatanaka, K. *Blood* **52,** 447–452 (1978).
8. Mekori, T. & Phillips, R. A. *Proc. Soc. exp. Biol. Med.* **132,** 115–119 (1969).
9. Enerback, L. *Acta path. microbiol. scand.* **66,** 303–312 (1966).
10. Olson, C. E. & Levy, D. A. *Fedn Proc.* **35,** 491 (1976).
11. Taylor, K. M. & Snyder, S. H. *J. Neurochem.* **19,** 1343–1358 (1972).
12. Prouvost-Danon, A., Lima, M. S. & Javierre, M. Q. *Life Sci.* **5,** 289–297 (1966).
13. Ogilvie, B. M. & Parrott, D. M. V. *Ciba Fdn Symp.* **46,** 183–201 (1977).
14. Bourne, H. R., Lichtenstein, L. M. & Melmon, K. L. *J. Immun.* **108,** 695–705 (1972).
15. Ackert, J. E., Edgar, S. A. & Frick, L. P. *Trans. Am. Microsc. Soc.* **58,** 81–89 (1939).

Haematopoietic growth factors are released in cultures of H-2-restricted helper T cells, accessory cells and specific antigen

M. H. Schreier & N. N. Iscove

Basel Institute for Immunology, Postfach CH 4005 Basel, Switzerland

Colony formation by mammalian haematopoietic cells in culture depends on specific glycoprotein growth factors. 'Colony-stimulating factors' for granulocytic[1,2] and macrophage[3,4] precursors (G- and M-CSFs), as well as for pluripotential and early committed erythroid cells ('burst promoting activity, or BPA[5]) are released in cultures of stimulated spleen, lymph node or peripheral blood cells[5–8]. In such systems the induction stimulus has been either allogeneic cell antigens, or lectins which stimulate T cells, such as pokeweed mitogen, concanavalin A (Con A) or phytohaemagglutin[6] and both T cells and adherent cells are implicated in the process[7,8]. The complexity of the spleen cell populations used in earlier *in vitro* studies has made it difficult to establish the cellular source of the factors and the mechanisms leading to their release. Pure populations of continuously growing cell lines of either monocytic/macrophage[1] or T-cell[10,11] character have already been shown to release haematopoietic activities constitutively. However, such evidence cannot prove that these functions are also expressed by the normal counterparts of these lines. We have reduced the complexity of the spleen cell system by supplying helper T cells in the form of pure clonal populations of known physiological function and antigenic specificity, and demonstrate here that activity is released when helper T cells are cultured with specific antigen, and that release depends on H-2 (I-A region) restricted interaction with accessory cells present in spleen or normal peritoneal cavity.

Table 1 indicates that activities stimulating granulocytic, macrophage and large erythroid colonies are released during in[illegible]dary immune responses by mouse spleen cells in culture. In [illegible]periment, C57BL/6J mice were immunized [illegible] with 10^7 sheep or horse red blood cells. After 3 weeks, spleen cells were cultured in serum-free medium with or without added antigen. Immunological reactivity was monitored by enumerating antibody-producing (plaque-forming) cells (PFC) specific for the challenging antigens after 5 days of culture. The supernatant culture medium was collected after 5 days and assayed for growth-promoting activity in methylcellulose cultures of mouse bone marrow. In these culture conditions, unstimulated spleen cells spontaneously released a background level of activity. However, factor release rose above this background when the cultures contained antigen, correlating positively with the immune responses indicated by PFC. Factor release was most marked when the cells were challenged in culture with the same antigen to which they had been immunized *in vivo*. As also indicated in Table 1, when the spleen cells were treated with an anti-Thy-1 antiserum plus complement before incubation with antigen, no induction of activity above background occurred.

Such experiments documented that recognition of antigen by normal T cells could result in release of haematopoietic factors. However, interpretation of data from this system is complicated by the complexity of the spleen cell population, and the high background levels of factor release even in the absence of homologous antigen. For this reason, we turned to a system in which the functional T-cell component was represented by pure cloned antigen-specific helper T cells. Such cells were derived from immunized spleen cells selectively enriched in culture by repeated antigenic stimulation and finally cloned out in the presence of T-cell growth factor (IL-2)[12–14]. As seen in Table 2, significant haematopoietic factor activity was released in cultures of T-helper-cell clones, but only when both appropriate antigen and syngeneic 'accessory cells' were also present. The latter were provided either by spleen cells (10^6 ml^{-1}) from nude mice devoid of functioning T-helper cells, or more efficiently on a per cell basis by resident peritoneal cells (5×10^4 ml^{-1}).

Function of helper T cells in immune responses is known to involve cellular interactions. These include recognition of major histocompatibility antigens on B cells and 'accessory' cells[15] by the T cells. In the mouse, these antigens are the I–A antigens of the H–2 complex. We accordingly investigated whether the induction of haematopoietic factors in this system would also be H–2 'restricted'. Pure cloned antigen-specific helper T cells were cultured with appropriate antigen, and with accessory cells from congeneic mouse strains recombinant at various points in the H–2 region. The accessory cells were supplied in the form of irradiated spleen cells from which mature T cells had been eliminated by treatment with anti-Thy-1 antiserum and complement. The results, also shown in Table 2, indicate that induction of factor release depends on identity of genotype between the T-helper cell donor and the accessory cells to the left of the I–B subregion of H–2. In a control experiment of the type shown in Table 1, the negative accessory cell donors (B10A.4R and B10A) were comparable to C57BL/6J in their capacity to release CSFs and BPA in response to antigen. Appropriate congeneic strains were not available at the time of these experiments for distinguishing between K- or I–A-region restriction. However, the action of T-helper cells in immune responses *in vivo* has been demonstrated to involve restriction only at I–A[15].

Our experiments indicate that haematopoietic factors are released during immune responses to red cell antigens in culture. The experiment in Table 1 documented such release with normal freshly explanted spleen cell populations. Experiments using pure clonal helper T-cell populations reproduced this phenomenon, providing an additional point of resemblance in function between these clones and their normal counterparts in spleen. In addition, the experiments showed that such release requires both recognition of the antigen by antigen-specific helper T cells, and an interaction, restricted most probably at I–A, between these T cells and Thy-1-negative accessory cells present in spleen or peritoneal cavity. Factors stimulating T (ref. 14) and B (ref. 16) cell growth have already been shown to be released in the same system with similar requirements.

0028–0836/80/380228—0

Table 1 Induction of haematopoietic factor release in spleen cell cultures during a specific antibody response*

Antigen exposure		Treatment before culture	PFC† against:		Colonies induced by supernatant‡ (% of control)		
In vivo	*In vitro*		SRC	HRC	MΦ	G	E
No conditioned medium					5 ± 2	0	3 ± 2
control stimulant§					100 ± 7	100 ± 28	100 ± 13
—	—	—	0	0	55 ± 5	48 ± 16	18 ± 5
—	SRC	—	2,020	0	67 ± 5	48 ± 16	30 ± 6
—	HRC	—	0	965	71 ± 5	48 ± 16	42 ± 7
SRC	—	—	16	0	70 ± 5	43 ± 15	31 ± 6
SRC	SRC	—	68,800	20	100 ± 6	96 ± 23	102 ± 1
SRC	HRC	—	400	1,390	91 ± 6	68 ± 19	62 ± 9
HRC	—	—	72	8	65 ± 5	21 ± 11	26 ± 6
HRC	SRC	—	2,820	10	72 ± 5	48 ± 16	23 ± 5
HRC	HRC	—	70	79,900	92 ± 6	80 ± 21	74 ± 10
SRC	SRC	α-Thy-1 + C′‖	5,520	0	35 ± 4	5 ± 5	7 ± 3
SRC	SRC	C′	52,200	0	100 ± 6	80 ± 21	91 ± 11
HRC	HRC	α-Thy-1 + C′	120	6,030	84 ± 6	7 ± 7	21 ± 6
HRC	HRC	C′	128	71,400	130 ± 7	120 ± 25	98 ± 11

* 1 ml cultures contained 2.5 × 10^6 C57BL/6J spleen cells and 5 × 10^6 red cells where indicated, in serum-free IMDM containing albumin, transferrin and soybean lipids[17,18,20]. They were incubated in 10% CO_2, 8% O_2 and 82% N_2 on a rocking platform[18]. SRC, Sheep red cells; HRC, horse red cells.

† Direct plaque-forming cells per culture against specific red cell antigen[19].

‡ 1 ml methylcellulose cultures contained 1 × 10^5 C57BL/6J bone marrow cells, 4% fetal bovine serum, albumin, transferrin and soybean lipid 20, 2 units of human urinary erythropoietin 20, and 0.08 ml of supernatant from the immune response cultures. Colonies were counted after 9 d of culture. Results are pooled from three independent assays. Colony numbers are expressed as per cent of control ± the s.e.m. expected of Poisson-distributed counts. MΦ, macrophage and mixed neutrophil/macrophage colonies; G, large disperse granulocytic colonies of the type identified by Metcalf and co-workers as eosinophilic[21,22]; E, erythroid or mixed myeloid/erythroid bursts. Mixed myeloid/erythroid bursts comprised about one-third of the erythroid colonies.

§ Conditioned medium from pokeweed mitogen stimulated mouse spleen cells; partially purified by adherence to Con A–Sepharose followed by chromatography on Sephadex G-150 (ref. 5). Absolute counts were: MΦ, 68; G, 5; E, 21 per 10^5 marrow cells.

‖ Incubation with AKR anti-Thy-1.2 antiserum + rabbit serum complement.

Table 2 Antigen-specific and H–2-restricted induction of factor release in cultures of helper T cells and accessory cells

T-cell specificity	Accessory cells				Antigen	Colonies induced by supernatant (% of control)		
	Source	H–2 haplotype						
		K	I ABJEC	D		MΦ	G	E
No conditioned medium						0	0	0
control stimulant						27 ± 3	17 ± 10	70 ± 11
HRC	*nu/nu* spleen*	b	bbbbb	b	HRC	100 ± 5	100 ± 20	100 ± 10
—	*nu/nu* spleen	b	bbbbb	b	—	0	0	3 ± 2
HRC	—				HRC	0	0	2 ± 2
HRC	*nu/nu* spleen	b	bbbbb	b	—	15 ± 2	15 ± 8	18 ± 4
HRC	*nu/nu* spleen	b	bbbbb	b	SRC	6 ± 1	8 ± 5	23 ± 5
HRC	Peritoneal cells†	b	bbbbb	b	HRC	76 ± 4	96 ± 19	95 ± 10
SRC	*nu/nu* spleen	b	bbbbb	b	SRC	78 ± 4	85 ± 18	91 ± 10
SRC	—				SRC	0	0	18 ± 5
SRC	*nu/nu* spleen	b	bbbbb	b	—	22 ± 2	4 ± 4	23 ± 5
SRC	*nu/nu* spleen	b	bbbbb	b	HRC	22 ± 2	12 ± 7	15 ± 4
HRC	C57BL/6J spleen‡	b	bbbbb	b	HRC	72 ± 4	142 ± 23	51 ± 7
HRC	B10.A(4R) spleen‡	k	kbbbb	b	HRC	1 ± 1	0	1 ± 1
HRC	B10.A(5R) spleen‡	b	bbkkd	d	HRC	62 ± 4	131 ± 22	85 ± 10
HRC	B10.A spleen‡	k	kkkkd	d	HRC	0	0	4 ± 2
SRC	C57BL/6J spleen‡	b	bbbbb	b	SRC	39 ± 3	65 ± 16	47 ± 7
SRC	B10.A(4R) spleen‡	k	kbbbb	b	SRC	6 ± 1	12 ± 7	11 ± 3
SRC	B10.A(5R) spleen‡	b	bbkkd	d	SRC	64 ± 4	85 ± 18	64 ± 8
SRC	B10.A spleen‡	k	kkkkd	d	SRC	14 ± 2	23 ± 9	10 ± 3

Cultures (0.2 ml) contained 3 × 10^3 helper T cells (C57BL/6J), accessory cells and 5 × 10^5 red cells where indicated. Serum-free medium and incubation as in legend to Table 1, except that cultures were not rocked. Supernatant medium was collected after 5 d of culture and assayed in methylcellulose cultures of 7 × 10^4 bone marrow cells ml^{-1} as in Table 1. Colony counts, pooled from two independent assays, are expressed as per cent of the counts (MΦ, 200; G, 12; E, 45 per 10^5 marrow cells) in the first experimental group (HRC, *nu/nu* spleen, HRC).

* 2 × 10^5 per culture.

† 1 × 10^4 per culture.

‡ Congeneic spleen cells were irradiated (3,000 rads) and treated with α-Thy-1 serum plus complement before addition (2 × 10^5 cultures.

While it is easy to understand the usefulness of production of lymphopoietic factors under these circumstances, and perhaps of activities stimulating monocyte/macrophage and granulocyte production, the significance of BPA production is less obvious. Perhaps it serves to increase the supply of early committed myeloid and lymphoid precursors[5]. There is an indication that T cells may play a role in stimulating haemopoietic cell growth in the whole animal: Thy-1-bearing cells appear to be required for successful growth of haemopoietic cell grafts in genetically defective W/W^v mice[9]. Since the T-cell deficient nude mouse does not show any gross defect in haematopoiesis, we would suggest that antigen recognition is unlikely to represent the only available pathway to haematopoietic factor production. Perhaps both immunological and non-immunological signals impinge on a cellular system present in the accessory cell population and able to release factors in response to either signal. The presence of a functioning accessory cell population in *nu/nu* spleen is documented in Table 2. The view would predict that haematopoiesis in *nu/nu* mice will prove defective in relation to their normal counterparts only when comparisons are performed during immune reactions.

The experimental system described here, which makes use of pure cloned helper T cells in combination with T-cell-depleted accessory cell populations, provides a basis for specific assay both of the accessory cells and of the signals exchanged between them and helper T cells. Because the culture system contained a source of accessory cells in addition to the helper lymphocyte clones, it is not possible to draw conclusions about the cellular source of the haematopoietic factors from our results. It therefore remains for future experiments to determine the identity of the accessory cells, the cellular source of the factors, and the nature of the I–A-restricted interaction.

We thank R. Tees and M. Schweizer for technical assistance.

Received 28 February; accepted 16 July 1980.

1. Williams, N., Eger, R. R., Moore, M. A. S. & Mendelsohn, N. *Differentiation* **11,** 59–63 (1978).
2. Burgess, A. W. *Biochem. J.* **185,** 301–314 (1980).
3. Stanley, E. R., Cifone, M., Heard, P. M. & Defendi, V. *J. exp. Med.* **143,** 631–647 (1976).
4. Stanley, E. R. *Proc. natn. Acad. Sci. U.S.A.* **76,** 2969–2973 (1979).
5. Iscove, N. N. in *Hematopoietic Cell Differentiation* (eds Golde, D. W., Cline, M. J., Metcalf, D. & Fox, C. F.) 37–52 (Academic, New York, 1978).
6. Metcalf, D. in *Biology of the Lymphokines* (eds Cohen, S., Pick, E. & Oppenheim, J. J.) 515–540 (Academic, New York, 1979).
7. Metcalf, D. & Johnson, G. R. *J. cell. Physiol.* **96,** 31–42 (1978).
8. Nathan, D. G. *et al. J. exp. Med.* **147,** 324–339 (1978).
9. Jedrzejczak, W. W., Sharkis, S. J., Ahmed, A., Sell, K. W. & Santos, G. W. *Science* **196,** 313–315 (1977).
10. Howard, M., Burgess, A., McPhee, D. & Metcalf, D. *Cell* **18,** 993–999 (1979).
11. Schrader, J. W., Arnold, B. & Clark-Lewis, I. *Nature* **283,** 197–199 (1980).
12. Schreier, M. H. & Tees, R. *Int. Arch. Allergy appl. Immun.* **61,** 227–237 (1980).
13. Tees, R. & Schreier, M. H. *Nature* **283,** 780–781 (1980).
14. Schreier, M. H., Iscove, N. N., Tees, R., Aarden, L. & von Boehmer, H. *Immun. Rev.* **51,** 315–336 (1980).
15. Sprent, J. *Immun. Rev.* **42,** 108–148 (1978).
16. Schreier, M. H., Andersson, J., Lernhardt, W. & Melchers, F. *J. exp. Med.* **151,** 194–203 (1980).
17. Iscove, N. N. & Melchers, F. *J. exp. Med.* **147,** 923–933 (1978).
18. Schreier, M. H. *J. exp. Med.* **148,** 1612–1619 (1978).
19. Jerne, N. K. & Nordin, A. A. *Science* **140,** 405 (1963).
20. Iscove, N. N., Guilbert, L. J. & Weyman, C. *Expl Cell Res.* **126,** 121–126 (1980).
21. Johnson, G. R. & Metcalf, D. *Expl Hemat.* **8,** 549–561 (1980).
22. Metcalf, D., Parker, J., Chester, H. M. & Kincade, P. W. *J. cell. Physiol.* **84,** 275–289 (1974).

Regulation by angiotensin II of its receptors in resistance blood vessels

Stephen Gunther, Michael A. Gimbrone Jr & R. Wayne Alexander

Departments of Medicine and Pathology, Peter Bent Brigham Hospital and Harvard Medical School, Boston, Massachusetts 02115

The sensitivity of blood vessels to the vasoconstrictor effects of the hormone angiotensin II appears to be modulated by the activity of the renin–angiotensin system. Elevation of circulating angiotensin II levels by sodium depletion or renal artery stenosis is associated with a diminished pressor response to infused angiotensin II (refs 1–3). Conversely, the vasoconstrictor response to the hormone is enhanced when endogenous angiotensin II levels are reduced by sodium loading[1,4] or nephrectomy[5]. The mechanisms of these varying effects are not known, but physiological and pharmacological experiments suggest involvement of the vascular smooth muscle receptor for angiotensin II (refs 5–8). Modification of the interaction between angiotensin II and its vascular receptor, resulting in altered responsiveness to the hormone, could occur either via 'prior occupancy' of receptors by elevated levels of endogenous angiotensin II resulting in fewer free receptors available to respond to circulating angiotensin II (ref. 5), or, elevated levels of angiotensin II could result in a decrease in receptor affinity for the hormone[7] or a decrease in total receptor number in the vascular smooth muscle cell[8]. We now report the first direct evidence, by radioligand binding assay, that angiotensin II regulates the number of its own receptors in resistance vasculature.

We have recently characterized, in a particulate fraction from rat mesenteric arteries, ^{125}I-angiotensin II binding sites which have the high affinity (equilibrium dissociation constant, K_d = 9.1 nM), low capacity (54 fmol per mg protein), and specificity ed of the physiological angiotensin II receptor[9]. In the dy we have used this system to characterize the vascular angiotensin II receptor in rats in which circulating angiotensin II levels were normal, chronically elevated in response to sodium depletion[10], or depressed by inhibition of angiotensin I converting enzyme[11].

Male Sprague–Dawley rats (300–325 g) were obtained from Charles River Breeding Labs. Control rats ($n = 160$) were maintained on a normal sodium diet (0.29% Na; Ralston Purina) and tap water. Sodium-depleted rats ($n = 160$) were fed a low-sodium diet (<0.05% Na; Hartroft Formula, ICN Life Sciences Group) and distilled water for one to three weeks. A third group of rats ($n = 40$) was also fed the low-sodium diet and distilled water for three weeks, but during the final three days of the diet, the angiotensin converting enzyme inhibitor SQ-14,225 (2-D-methyl-3-mercaptopropanoyl-L-proline; Squibb), 100 mg kg^{-1} day^{-1}, was added to the drinking water. At weekly intervals, 40 control and 40 sodium-depleted rats were killed and plasma renin activity[12] and ^{125}I-angiotensin II binding to mesenteric artery particulate fractions determined as previously described[9]. Similar assays were performed in the sodium-depleted, SQ-14,225-treated rats following the third day of drug administration. Mesenteric artery ^{125}I-angiotensin II binding site capacity and affinity were estimated by Scatchard analysis of binding data. Statistical significance was determined by unpaired, 2-tailed *t*-test, comparing the results of each treated group with those of the simultaneous controls.

In control rats, plasma renin activity averaged 3.1 ± 0.3 (s.e.m.) ng ml^{-1} h^{-1}, and mesenteric artery particulate fractions contained 56.9 ± 1.2 fmol per mg protein of angiotensin II receptors. Neither plasma renin activity nor angiotensin II receptor density varied significantly during the three weeks on the normal sodium diet. In rats maintained on the low-sodium diet alone, plasma renin activity was increased significantly at one week, and by three weeks had reached 5.2 ± 0.5 ng ml^{-1} h^{-1} ($P < 0.05$ compared to control, see Fig. 1). This activation of the renin–angiotensin II system was associated with a significant decrease in ^{125}I-angiotensin II binding capacity in mesenteric artery particulate fractions ($P < 0.01$ compared to control, weeks 1–3; see Fig. 1). After three weeks of sodium depletion, ^{125}I-angiotensin II binding capacity was reduced to 76% of control (41.5 ± 3.3 vs 54.3 ± 3.8 fmol mg^{-1}). In the rats given the

0028-0836/80/38023 1.00

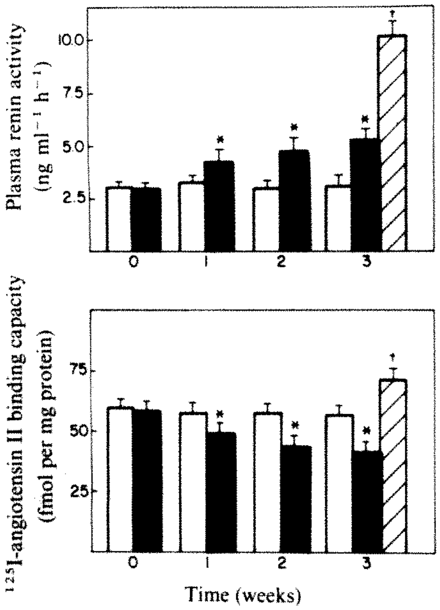

Fig. 1 Changes in plasma renin activity (upper panel) and ^{125}I-angiotensin II binding capacity of mesenteric artery particulate fractions (lower panel) at weekly intervals in rats fed a normal sodium diet (open bars), a sodium-deficient diet alone (solid bars), and a sodium-deficient diet plus 3 days of converting enzyme inhibitor SQ-14,225 (striped bars). Values represent mean ± s.e.m. of four experiments. For each experiment, ten control and ten treated rats were decapitated 15 min after the intraperitoneal administration of heparin, 100 U, and blood collected into iced Vacutainer® tubes containing EDTA for measurement of plasma renin activity[12]. Particulate fractions from mesenteric artery homogenates were prepared from the same animals, as previously described[9]. ^{125}I-angiotensin II binding was determined by incubating aliquots of the particulate fraction (80–100 μg protein) with 0.1–2.0 nM concentrations of ^{125}I-angiotensin II (specific activity 900–1,400 Ci mmol^{-1}) in 0.20 ml assay buffer (50 mM Tris, 5 mM $MgCl_2$, 0.25% bovine serum albumin, *p*H 7.2). After steady-state binding was achieved (90 min at 22 °C), bound and free radioactivity were separated by rapid filtration through Whatman GF/C filters and trapped radioactivity counted in a well-type gamma counter (Searle). Specific binding, defined as (total binding) − (binding in the presence of 1 μM unlabelled angiotensin II), averaged 90% of total counts bound. * = $P < 0.05$ compared to simultaneous controls (normal diet). † = $P < 0.01$ compared to both control and sodium-deficient diet groups.

converting enzyme inhibitor SQ-14,225, during the final three days of the three-week sodium-deficient diet, plasma renin activity was significantly higher, 10.1 ± 0.6 ng ml^{-1} h^{-1} ($P < 0.01$ compared to third week levels in both control rats and rats sodium depleted only). The inhibition of angiotensin II formation in this group of rats, however, resulted in a significant increase in mesenteric artery ^{125}I-angiotensin II binding capacity, to 69.0 ± 4.3 fmol mg^{-1} (an increase of 66% compared to the third week levels in rats sodium depleted only, $P < 0.01$, and of 27% compared to control rats, $P < 0.01$). The changes in ^{125}I-angiotensin II binding capacity produced by sodium depletion or converting enzyme inhibition were not accompanied by a significant change in receptor affinity (Fig. 2).

Our results suggest that the number of angiotensin II receptors in rat mesenteric arteries responds to circulating angiotensin II levels. Increased levels of hormone induced by sodium depletion resulted in a significant decrease in receptor number, whereas inhibition of angiotensin II formation by SQ-14,225 had the opposite effect. That the observed changes in receptor number correlated directly with variations in circulating angiotensin II levels is supported by the following facts: (1) ^{125}I-angiotensin II binding to mesenteric artery particulate fractions is independent of sodium and potassium concentrations from 0 to 100 mM (ref. 9); changes in intra- or extracellular electrolyte composition during sodium deprivation therefore could not affect the binding assay used; (2) ^{125}I-angiotensin II binding is likewise unaffected by bradykinin concentrations as high as 10^{-5} M (ref. 9); the increase in binding capacity following SQ-14,225 administration thus cannot be attributed to an accumulation of endogenous bradykinin resulting from SQ-14,225 inhibition of vascular kininase II activity[13]; (3) renin itself does not appear to play a role, as the increase in plasma renin activity in sodium-depleted rats was associated with a decrease in receptor number, while an even greater increase in plasma renin activity in rats sodium depleted and given SQ-14,225 (due to loss of feedback inhibition of renin release by endogenous angiotensin II (ref. 11)) was accompanied by an increase in receptor number; and finally, (4) an artefactual change in apparent receptor binding capacity due to diet-induced changes in cellular membranes is excluded because both groups of treated rats were maintained on the same low-sodium diet, yet had opposite changes in ^{125}I-angiotensin II binding capacity.

A potential explanation for the results observed in these studies is that receptor-associated endogenous angiotensin II carried over into the *in vitro* binding assay could account for the decrease in binding capacity observed with sodium depletion. To provide insight into this possiblity, we perfused the mesenteric arteries of control rats *in situ* for 15 min with supraphysiological (2 nM) concentrations of ^{3}H-angiotensin II, a radioligand possessing the full biological activity of the native hormone[14], and followed the amount of radioactivity remaining associated with the tissue during the usual preparation of the particulate fraction. As shown in Table 1, immediately following *in situ* perfusion, 68.4 fmol of mesenteric artery receptors were occupied by ^{3}H-angiotensin II, yet less than 2% of the total radioactivity initially present, and essentially none of that which was specifically associated with receptors, was still detectable in

Table 1 *In vivo* labelling of mesenteric artery angiotensin II receptors by perfusion with ^{3}H-angiotensin II

	Crude homogenate		Particulate fraction		
Perfusate	Total radio-activity* (d.p.m.)	^{3}H-angio-tensin II (fmol)	Total radio-activity (d.p.m.)	^{3}H-angio-tensin II (fmol)	Total protein content (mg)
^{3}H-angiotensin II	14,600	257.0	122	2.1	1.44
^{3}H-angiotensin II + antagonist	10,710	188.6	194	3.4	1.40
(Difference)	(3,890)	(68.4)	(0)	(0)	

The mesenteric arteries of three ether-anaesthetized rats (normal diet) were perfused *in situ* at a rate of 0.38 ml min^{-1} with Krebs–Ringer phosphate buffer (*p*H 7.4) for 30 min at 38 °C. During the final 15 min of perfusion, ^{3}H-angiotensin II (specific activity 25.6 Ci mmol^{-1}; NEN) was added to the perfusate at a final concentration of 2 nM. At the end of the perfusion period, the mesenteric arteries from all three rats were excised and washed in ice-cold phosphate-buffered saline (*p*H 7.4). The combined vessels then were homogenized in 10.0 ml ice-cold 0.25 M sucrose as described in ref. 9. An aliquot of this homogenate (1.0 ml) was counted in a liquid scintillation counter (Beckman) to determine the total amount of radioactivity initially present in the vessels from the three rats ('crude homogenate'); the remaining 9.0 ml of the homogenate were then used to prepare a particulate fraction in the same manner as for the radioligand binding assay. The resultant particulate fraction from the three rats (104,000*g* pellet) was resuspended in 0.5 ml water; duplicate 50-μl aliquots were taken to measure total protein content (Lowry method) and the remaining 0.4 ml were counted as above to determine the amount of radioactivity still present in the purified particulate fraction. To determine what fraction of the radioactivity observed at each of these steps represented ^{3}H-angiotensin II specifically associated with receptor, identical experiments were repeated in three additional rats including the angiotensin II antagonist (Sar_1, Ile_8)-angiotensin II (1 μM) in the perfusate for the entire 30-min perfusion period ('^{3}H-angiotensin II + antagonist'). As this dose of the competitive antagonist is sufficient to block the binding of 2 nM angiotensin II to vascular receptors completely[9,15], the radioactivity present in the tissue from these animals presumably reflects ^{3}H-angiotensin II nonspecifically bound or trapped in extracellular fluid. The difference in the amounts of ^{3}H-angiotensin II present in the crude homogenates of the two groups (68.4 fmol) therefore represents ^{3}H-angiotensin II specifically bound to receptors. On the basis of an average ^{125}I-angiotensin II binding capacity of 56.9 fmol per mg protein in the particulate fraction from control animals (Fig. 1), and the total protein contents of the particulate fractions in this experiment (1.40–1.44 mg), the most conservative estimate of the total number of angiotensin II receptors in each of the cr homogenates is ≈81 fmol. Thus, the observed value of 68.4 fmol ^{3}H-angio specifically bound is not excessive. *None of this specifically bound* ^{3}H- II was detected in the final particulate fraction.

* Corrected for counter efficiency and quenching.

the final particulate fraction. Thus, in the experimental conditions of this study, any angiotensin II bound to receptor, after relatively brief exposure *in vivo*, seems to be readily dissociable. Endogenous angiotensin II bound in this state therefore could not account for the observed changes in binding capacity.

The apparent inverse relationship between ambient hormone concentration and angiotensin II receptor density in vascular smooth muscle is similar to that observed with other peptide hormones, such as insulin[16], glucagon[17] and growth hormone[18]. In contrast, angiotensin II seems to regulate its receptors in the adrenal gland in a different manner[19]. In this tissue, angiotensin II-stimulated aldosterone production is potentiated when circulating levels of angiotensin II are chronically elevated, as during sodium depletion[20,21]; *in vitro* binding studies have shown that this increased sensitivity is accompanied by an increase in adrenal angiotensin II receptors[21,22]. Although the regulation by endogenous angiotensin II concentrations of end-organ responsiveness of adrenal and vascular tissues to angiotensin II is directionally opposite, both effects appear to be mediated, at least in part, by hormone-induced changes in receptor number.

Previous direct studies of the regulation of angiotensin II receptors in smooth muscle have used uterine membrane fractions. These studies have yielded conflicting results. Bilateral nephrectomy has been shown to increase both the contractile response of uterine smooth muscle to angiotensin II (ref. 23) and the angiotensin II binding capacity of uterine membranes[24]. The effects of sodium depletion on uterine smooth muscle, however, are contradictory. While Aguilera *et al.*[21] found that sodium depletion for seven days in rats decreased uterine angiotensin II-binding capacity by 40%, Devynck *et al.*[22] reported that sodium depletion for four weeks resulted in an increase in binding capacity. Although the reasons for this discrepancy are not clear, the difficulties in extrapolating binding data from the uterus, a tissue which does not respond to physiological concentrations of angiotensin II, to vascular smooth muscle have been discussed[22].

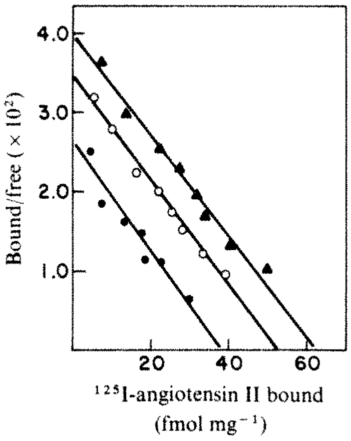

Fig. 2 Representative Scatchard plots of ^{125}I-angiotensin II binding to mesenteric artery particulate fractions from control rats (○), rats sodium depleted for 3 weeks (●), and from sodium-depleted rats given SQ-14,225 (▲). Particulate fractions from ten rats were used in each experiment. Mean equilibrium dissociation constants (K_d) for control (1.04 ± 0.19 nM), sodium-depleted (0.79 ± 0.07 nM), and SQ-14,225-treated (0.94 ± 0.12 nM) groups were not significantly different.

The changes in vascular angiotensin II receptors directly demonstrated in this study, during chronic sodium depletion and converting enzyme inhibition, are consistent with the hypothesis that receptor regulation can modulate vascular responsiveness angiotensin II. At the cellular level several possible sms could contribute to these hormone-induced alter- ptor number. As the *in vivo* receptor labelling experiment indicates, readily reversible binding of hormone to its receptor, *per se*, should not directly influence binding capacity. However, association of hormone with a high-affinity, slowly reversible state of its receptor could result in a transient decrease in binding capacity, through reduction in the number of available receptors. This form of receptor occupancy, if accompanied by uncoupling from secondary biochemical events, might lead to diminished physiological responsiveness. Alternatively, fluctuations in ambient hormone concentration might influence the rates of receptor degradation and/or synthesis, thus changing total receptor number. The relative contributions of these two mechanisms cannot be determined by current techniques *in vivo*. However, preliminary data from our laboratory, in cultured vascular smooth muscle cells suggests that both processes may be involved in regulating the number of angiotensin II receptors available for interaction with hormone. Exposure of cultured rat mesenteric artery smooth muscle cells to 3×10^{-8} M angiotensin II for up to 6 h results in a time-dependent decrease in ^{125}I-angiotensin II binding capacity. The decrease in binding capacity resulting from brief exposure (5 min) is completely reversible within 30 min after removal of angiotensin II from the medium. With longer periods of exposure to angiotensin II (up to 6 h), ^{125}I-angiotensin II binding capacity decreases progressively and recovery requires 4–5 h. Unlike the recovery after short angiotensin II exposure, complete recovery of binding capacity after 6 h of angiotensin II exposure requires new protein synthesis, implying that receptor degradation has occurred. Thus, readily reversible alterations of the angiotensin II receptor may contribute to the relatively rapid changes in vascular responsiveness seen *in vivo* during acute manipulations of the renin–angiotensin system[25,26]. On the other hand, chronic changes in the activity of the renin–angiotensin system may be associated with changes in the kinetics of receptor turnover in vascular smooth muscle cells. These forms of hormone-induced receptor regulation may be important determinants of vascular responsiveness to the vasoconstrictor effects of angiotensin II.

SQ-14,225 was kindly provided by Dr Z. P. Horovitz. We thank Dr Gordon Williams for the measurements of renin activity and Ms Rae Caravaty for technical assistance. This work was supported by grant HL20054 and Biomedical Research Support from the NIH. S.G. is a Clinician Scientist of the American Heart Association, M.A.G. an Established Investigator of the American Heart Association and R.W.A. a recipient of a NIH Career Development Award.

Received 28 January; accepted 16 June 1980.

1. Reid, W. D. & Laragh, J. H. *Proc. Soc. exp. Biol. Med.* **120,** 26–29 (1965).
2. Hollenberg, N. K., Solomon, H. S., Adams, D. F., Abrams, H. L. & Merrill, J. P. *Circulation Res.* **31,** 750–757 (1972).
3. Kaplan, N. M. & Silah, J. G. *J. clin. Invest.* **43,** 659–669 (1964).
4. Healy, J. K., Suszkiw, J. B. & Schreiner, G. E. *Nephron* **3,** 329–343 (1969).
5. Swales, J. D., Tange, J. D. & Thurston, H. *Circulation Res.* **37,** 96–100 (1975).
6. Thurston, H. *Am. J. Med.* **61,** 768–778 (1976).
7. Brunner, H. R., Chang, P., Wallach, R., Sealey, J. E. & Laragh, J. H. *J. clin. Invest.* **51,** 58–67 (1972).
8. Devynck, M. A. & Meyer, P. *Am. J. Med.* **61,** 758–767 (1976).
9. Gunther, S., Gimbrone, M. A., Jr & Alexander, R. W. *Circulation Res.* **47,** 278–286 (1980).
10. Powell-Jackson, J. D. & MacGregor, J. J. *Endocrinology* **68,** 175–176 (1976).
11. Rubin, B. M., Antonaccio, M. J. & Horovitz, Z. P. *Prog. cardiovasc. Dis.* **21,** 183–194 (1978).
12. Emanuel, R. L., Cain, J. P. & Williams, G. H. *J. Lab. clin. Med.* **81,** 632–640 (1973).
13. Erdös, E. G. & Yang, H. Y. T. in *Handbook of Experimental Pharmacology* (ed. Erdös, E. G.) 289–323 (Springer, New York, 1970).
14. Morgat, J. L., Hung, L. T. & Fromageot, P. *Biochim. biophys. Acta* **207,** 374–376 (1970).
15. Regoli, D., Park, W. K. & Rioux, F. *Pharmac. Rev.* **26,** 69–123 (1974).
16. Kahn, C. R., Meville, D. M. & Roth, J. *J. biol. Chem.* **248,** 244–250 (1973).
17. Srikant, C. B., Freeman, D., McCorkle, K. & Unger, R. H. *J. biol. Chem.* **252,** 7434–7436 (1977).
18. Lesniak, M. A. & Roth, J. *J. biol. Chem.* **251,** 3720–3729 (1976).
19. Catt, K. J., Harwood, J. P., Aguilera, G. & Dufau, M. L. *Nature* **280,** 109–116 (1979).
20. Hollenberg, N. K., Chenitz, W. R., Adams, D. F. & Williams, G. H. *J. clin. Invest.* **54,** 34–42 (1974).
21. Aguilera, G., Hauger, R. L. & Catt, K. J. *Proc. natn. Acad. Sci. U.S.A.* **75,** 975–979 (1978).
22. Devynck, M. A. *et al. Clin. Sci. molec. Med.* **55,** 171s–174s (1978).
23. Meyer, P., Papadimitriou, S. & Worcel, M. *Br. J. Pharmac.* **51,** 435–439 (1974).
24. Devynck, M. A., Rouzaire-Dubois, B., Chevillotte, E. & Meyer, P. *Eur. J. Pharmac.* **40,** 27–37 (1976).
25. Thurston, H. & Laragh, J. H. *Circulation Res.* **36,** 113–117 (1975).
26. Oliver, J. A. & Cannon, P. J. *J. clin. Invest.* **61,** 610–623 (1978).

Regulation of non-muscle myosin assembly by calmodulin-dependent light chain kinase

J. M. Scholey, K. A. Taylor* & J. Kendrick-Jones

MRC Laboratory of Molecular Biology, Hills Road,
Cambridge CB2 2QH, UK

The presence of actin and myosin in non-muscle cells suggests that they may be involved in a wide range of cellular contractile activities[1]. The generally accepted view[2] is that interaction between actin and myosin in these cells[3-5] and in vertebrate smooth muscle[6,7], is regulated by the level of phosphorylation of the 20,000-molecular weight (MW) light chain. In the absence of calcium, this light chain is not phosphorylated and the myosin cannot interact with actin. Calcium activates a specific calmodulin-dependent kinase[8-11] which phosphorylates the light chain, initiating actin–myosin interaction. Although most studies on the role of phosphorylation have concentrated on the regulation of actin-activated myosin Mg-ATPase activity, phosphorylation of the light chain also seems to control the assembly of smooth muscle myosin into filaments[12,13]. Using purified smooth muscle light chain kinase, we have confirmed this observation. We report here studies of myosins isolated from the two non-muscle sources, thymus cells and platelets. We observed that these myosins are assembled into filaments at physiological ionic strength and Mg-ATP concentrations, only when the 20,000-MW light chain is phosphorylated.

We initially compared the stability of myosin filaments prepared from non-phosphorylated calf thymus myosin and rabbit skeletal myosin as a function of the Mg-ATP concentration (Fig. 1). The turbidity measurements and electron micrographs show that the filaments from thymus myosin (bipolar filaments, average length 3,380 ± 560 Å) are disassembled completely at a molar ratio of less than 5 mol Mg-ATP per mol myosin, suggesting that Mg-ATP acts at an approximately stoichiometric ratio. Similar results were obtained with myosins isolated from pig platelets and chicken gizzard muscles. These results differ from those of earlier work[14] which indicated that myosin isolated from human platelets formed short bipolar filaments which were stable in a wide range of conditions, including the presence or absence of Mg-ATP at physiological ionic strength.

Filaments prepared from phosphorylated thymus or gizzard myosins were stable at millimolar concentrations of Mg-ATP. Similarly, thymus and gizzard myosin rod subfragments (the tail fragment which contains the self-assembly properties of the myosin) formed filaments which were not disassembled at the Mg-ATP concentrations used in these experiments (up to 10 mM). Mg-pyrophosphate would not substitute for Mg-ATP in disassembling non-phosphorylated thymus or gizzard myosin filaments. These observations suggest that Mg-ATP acts at a specific high-affinity binding site in the subfragment-1 (myosin head) portion of the molecule, which may be the Mg-ATPase active site.

Myosins isolated from rabbit and scallop striated muscles form filaments which are stable at millimolar concentrations of Mg-ATP. In this case, the lack of effect of Mg-ATP must be due to differences in the subunits of these myosins compared with those of vertebrate smooth muscle and non-muscle myosins. These experiments were carried out in conditions roughly comparable to those that are expected to exist inside a 'resting' cell, namely 0.15 M KCl, 1 mM Mg-ATP and the absence of Ca^{2+}. We therefore predict that '*in vivo*', the myosin in resting

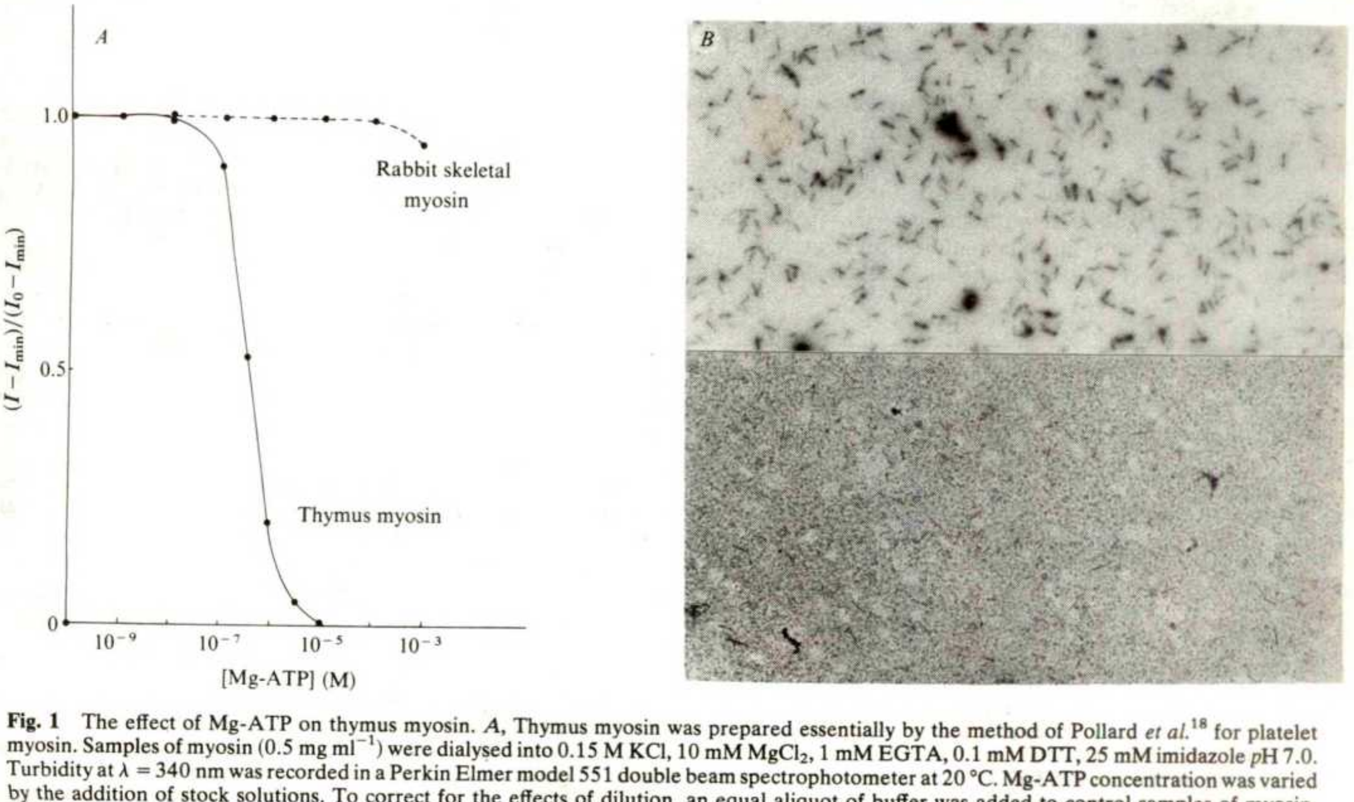

Fig. 1 The effect of Mg-ATP on thymus myosin. *A*, Thymus myosin was prepared essentially by the method of Pollard *et al.*[18] for platelet myosin. Samples of myosin (0.5 mg ml^{-1}) were dialysed into 0.15 M KCl, 10 mM $MgCl_2$, 1 mM EGTA, 0.1 mM DTT, 25 mM imidazole *p*H 7.0. Turbidity at $\lambda = 340$ nm was recorded in a Perkin Elmer model 551 double beam spectrophotometer at 20 °C. Mg-ATP concentration was varied by the addition of stock solutions. To correct for the effects of dilution, an equal aliquot of buffer was added to control samples of myosin. Background turbidity was corrected by plotting $(I - I_{min})/(I_0 - I_{min})$. I is turbidity measured at 340 nm, I_0 the turbidity in the absence of Mg-ATP, and I_{min} the minimal level of turbidity attained during the experiment. Typical values are $I_0 = 0.4$ and $I_{min} = 0.15$. It must be stressed that turbidity measurements should always be used in conjunction with electron microscope observations so as to 'estimate' the degree of filament assembly–disassembly. *B*, Electron micrographs of thymus myosin before (top) and after (bottom) addition of 50 μM Mg-AT
Specimens were prepared by placing 10 μl of the myosin solution to be examined on to carbon-coated 400-mesh grids, allowing the drop to
for exactly 30 s, then washing with 13 drops of buffer (−ATP) and 10 drops of 1% uranyl acetate. Micrographs were examined on
EM400 operated at 80 kV. ×5,000.

---

* Present address: Department of Anatomy, Duke University Medical Center, Durham, North Carolina 27710.

0028–0836/80/380233—03$01.00

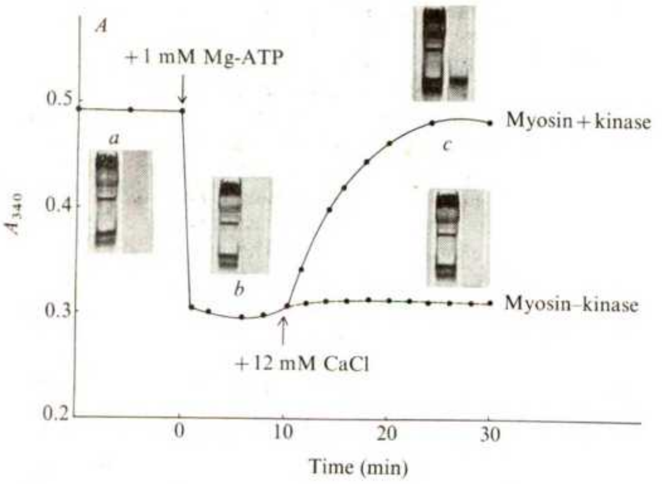

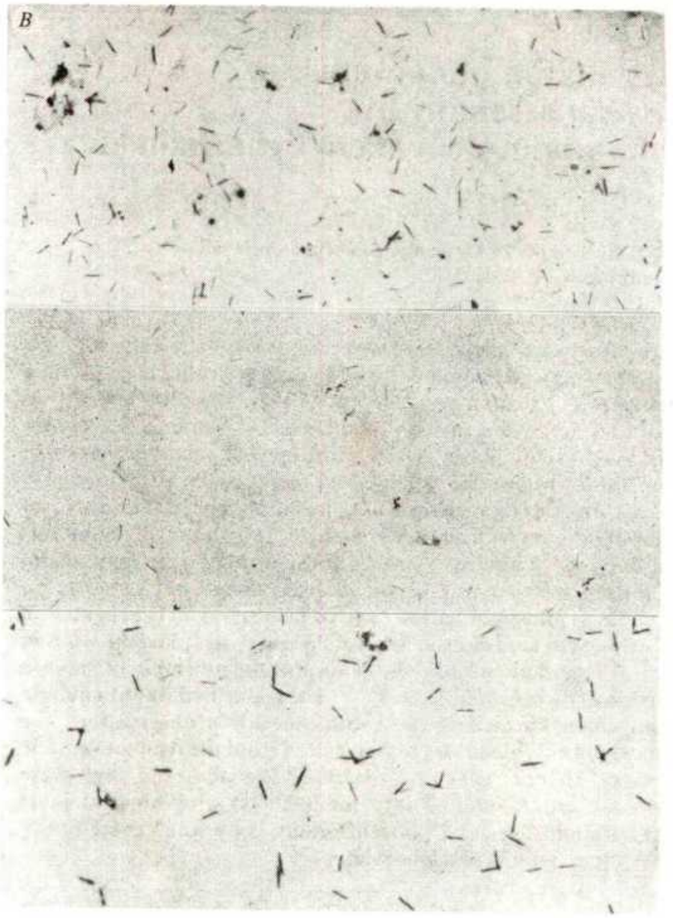

Fig. 2 Induction of thymus myosin filament assembly by phosphorylation of the 20,000-MW, light chain. *A*, Non-phosphorylated myosin filaments (0.46 mg ml^{-1}) were incubated with 25 μg ml^{-1} brain calmodulin in 0.15 M KCl, 10 mM $MgCl_2$, 1 mM EGTA, 0.1 mM DTT and 25 mM imidazole *p*H 7.0. Myosin light chain kinase purified from either chicken gizzard or thymus by calmodulin affinity chromatography[19] was included where indicated. Turbidity was recorded as in Fig. 1. 1 mM [$\gamma^{32}P$]-ATP was added and samples were taken at time points *b* and *c* and the level of myosin phosphorylation determined (Table 1). The specificity of phosphate incorporation into the myosin 20,000-MW light chain was determined by SDS-polyacrylamide gel electrophoresis (PAGE) and subsequent autoradiography (shown in the insets are the 10% acrylamide/SDS gels together with their autoradiograms). The specificity of incorporation was further checked by 8 M urea-PAGE (data not shown). The addition of Mg-ATP caused a rapid drop in turbidity, which remained low until the kinase was activated by addition of $CaCl_2$ to a concentration of 2×10^{-4} M free Ca^{2+}, whereupon a steady increase in turbidity was observed to accompany light chain phosphorylation. In the absence of kinase, there was no light chain phosphorylation or turbidity increase on addition of $CaCl_2$. *B*, Electron micrographs of thymus myosin taken at three critical time points, *a*, *b* and *c* in the assembly assay. Specimens prepared as described in Fig. 1. Top, non-phosphorylated myosin filaments in the absence of ATP; middle, after addition of Mg-ATP to 1 mM, myosin filaments completely disappear, and in their place, a high concentration of dissolved protein is observed on the grid; bottom, after addition of calcium, filaments reappear. ×5,000.

non-muscle and smooth muscle cells exists in a disassembled state, whereas in relaxed vertebrate and invertebrate striated muscles, myosin retains its filamentous organization, in agreement with direct observations on relaxed skeletal muscles[15].

Table 1 Correlation of light chain phosphorylation and actin-activated Mg-ATPase of thymus myosin with filament assembly

Time point during 'assembly assay' (see Fig. 2*A*)	−Kinase mol phosphate per mol light chain	Mg-ATPase (nmol per min per mg)	+Kinase mol phosphate per mol light chain	Mg-ATPase (nmol per min per mg)
1 mM EGTA (Fig. 2*b*)	0.1	4.0	0.25	7.0
2×10^{-4} M Ca^{2+} (Fig. 2*c*)	0.2	4.0	0.75	26.0

Light chain phosphorylation and actin-activated Mg-ATPase activities were determined in conditions identical to those used in the assembly assay at the time points marked *b* and *c* in Fig. 2*A*. The conditions were 25 °C, 0.15 M KCl, 10 mM $MgCl_2$, 0.1 mM dithiothreitol (DTT) and 25 mM imidazole *p*H 7.0. At time point *b*, 1 mM EGTA was present in the buffer, and at time point *c*, 1 mM EGTA and 1.2 mM $CaCl_2$ were present. Myosin phosphorylation was determined by a Millipore filtration method similar to that of Sherry *et al.*[7]. Mg-ATPase activity was determined according to the method of Seals *et al.*[17], after addition of [illegible] actin to a 10-fold weight excess over myosin. At time point *c* the [illegible] phosphorylated the myosin light chain, promoting inter-[illegible] in addition to inducing myosin filament assembly.

Phosphorylation of the 20,000-MW light chain of thymus myosin, disassembled in the presence of Mg-ATP, induces myosin filament assembly. Using calmodulin-dependent light chain kinase purified from either chicken gizzard or calf thymus cells, we have monitored the effect of phosphorylation on the assembly of thymus myosin filaments (Fig. 2). Addition of 1 mM Mg-ATP to non-phosphorylated myosin filaments incubated in the presence of light chain kinase, calmodulin and EGTA, caused a rapid drop in turbidity (Fig. 2*A*). In the electron microscope, the short bipolar filaments which were present before ATP addition are now absent (Fig. 2*B*). The myosin filaments remained disassembled until the kinase–calmodulin complex was activated by the addition of calcium. A steady increase in turbidity and the appearance of bipolar filaments were then observed (average length 5,000±640 Å). The reassembly of the myosin filaments accompanies the phosphorylation of the 20,000-MW light chain (Table 1). In the absence of kinase or calcium, there was no light chain phosphorylation or filament formation. We have observed similar effects with human platelet myosin. These results raise the question of whether phosphorylation regulates myosin filament assembly in all non-muscle cells. Transient assembly of smooth muscle myosin, regulated by light chain phosphorylation, has also been suggested by Suzuki *et al.*[12]. Our results using chicken gizzard myosin are in total agreement with their data. We believe that these findings may be very relevant to the unresolved controversy surrounding the state of myosin in 'relaxed' smooth muscles[16].

Our results suggest that the assembly of myosin filaments may be a crucial step in the pathway leading to non-muscle myosin activation by calmodulin-dependent light chain kinase. However, is it the only step involved in activation, for what contribution does filament assembly make to the observed stimulation of the actin-activated myosin Mg-ATPase activity controlled by light chain phosphorylation (Table 1)? Experiments are in progress to answer this question. Several other important questions remain to be resolved. If myosin filament assembly mediated by phosphorylation is involved in activation, one would predict that relaxation is controlled by dephosphorylation of the myosin and filament disassembly. Experiments are being carried out to test whether the process of filament assembly can be reversed by dephosphorylation of the myosin. How does phosphorylation of a light chain associated with the subfragment-1 region of the myosin modulate the assembly of myosin into filaments, which is generally assumed to be due to interactions between the light meromyosin (LMM) portions of the molecules? To answer this question, we need to know the position of the light chain on the myosin head, the changes that occur when it is phosphorylated or dephosphorylated, and how these changes affect the packing of the myosin molecules in the filament.

In conclusion, we propose that in 'resting' vertebrate non-muscle cells, myosin filaments are absent and are formed transiently during periods of contractile activity. Our observation that the activation process—phosphorylation—generates bipolar myosin filaments provides circumstantial evidence that some type of sliding-filament interaction[15] between actin and myosin may operate in vertebrate non-muscle cells.

We thank Drs H. E. Huxley and P. Wagner for discussion, and Mr P. J. Tooth for preparing gizzard myosin. J.M.S. is a recipient of an MRC studentship, and K.A.T. is a recipient of a post-doctoral fellowship from the Muscular Dystrophy Association.

Received 14 April; accepted 26 June 1980.

1. Pollard, T. D. & Weihing, R. R. *CRC Crit. Rev. Biochem.* **2,** 1–65 (1974).
2. Adelstein, R. S. & Eisenberg, E. *A. Rev. Biochem.* (in the press).
3. Adelstein, R. S. & Conti, M. A. *Nature* **256,** 597–598 (1975).
4. Yerna, M-J., Aksoy, M. O., Hartshorne, D. J. & Goldman, R. D. *J. Cell Sci.* **31,** 411–429 (1978).
5. Trotter, J. A. & Adelstein, R. S. *J. biol. Chem.* **254,** 8781–8785 (1979).
6. Small, J. V. & Sobieszek, A. *Eur. J. Biochem.* **76,** 521–530 (1977).
7. Sherry, J. M. F., Gorecka, A., Aksoy, M. O., Dabrowska, R. & Hartshorne, D. J. *Biochemistry* **17,** 4411–4418 (1978).
8. Dabrowska, R., Sherry, J. M. F., Aromatorio, D. & Hartshorne, D. J. *Biochemistry* **17,** 253–258 (1978).
9. Yerna, M-J., Dabrowska, R., Hartshorne, D. J. & Goldman, R. D. *Proc. natn. Acad. Sci. U.S.A.* **76,** 184–188 (1979).
10. Hathaway, D. R. & Adelstein, R. S. *Proc. natn. Acad. Sci. U.S.A.* **76,** 1653–1657 (1979).
11. Scholey, J. M. & Kendrick-Jones, J. *J. Muscle Res. Cell Motility* (in the press).
12. Suzuki, H., Onishi, H., Takahashi, K. & Watanabe, S. *J. Biochem.* **84,** 1529–1542 (1978).
13. Shoenberg, C. F. & Stewart, M. *J. Muscle Res. Cell Motility* **1,** 117–126 (1980).
14. Niederman, R. & Pollard, T. D. *J. Cell Biol.* **67,** 72–92 (1975).
15. Huxley, H. E. *Science* **164,** 1356–1366 (1969).
16. Shoenberg, C. F. & Needham, D. M. *Biol. Rev.* **51,** 53–104 (1976).
17. Seals, J. R., McDonald, J. M., Bruns, D. & Jarett, L. *Analyt. Biochem.* **90,** 785–795 (1978).
18. Pollard, T. D., Thomas, S. M. & Niederman, R. *Analyt. Biochem.* **60,** 258–266 (1976).
19. Watterson, D. M. & Vanaman, T. C. *Biochem. biophys. Res. Commun.* **73,** 40–46 (1976).

Endogenous electric field around muscle fibres depends on the Na^+–K^+ pump

W. J. Betz, J. H. Caldwell* & R. R. Ribchester†

Department of Physiology, University of Colorado Health Science Center, Denver, Colorado 80262

K. R. Robinson‡ & R. F. Stump‡

Division of Molecular and Cellular Biology, National Jewish Hospital, Denver, Colorado 80206

We describe here experiments which reveal a new physiological specialization in the endplate (synaptic) region of skeletal muscle fibres. Using a vibrating microelectrode[1] which can detect small currents flowing in extracellular fluid, we have found that the membrane in the endplate region behaves as though a steady positive current is generated in this location. Current re-enters the fibre in the extrajunctional region. Further experiments show that this current is dependent on the activity of the sodium pump. The electric field created by this current may be important for long-term interactions between muscle and nerve.

Most experiments to be described were performed on small (lumbrical and flexor digitorum brevis) muscles of the rat hind foot, although similar results were obtained in a few experiments with mouse soleus and frog sartorius muscles. Experiments were performed *in vitro* at room temperature (23 °C). Muscles were bathed in Krebs solution buffered to pH 7.4 with bicarbonate/CO_2 or HEPES.

The vibrating microelectrode works as follows: a metal-filled glass micropipette with a platinum ball (10–15-μm diameter) electroplated on its tip is attached to a piezoelectric bender, which is driven at a constant frequency (about 260 Hz). Excursion distance of the electrode tip is about 35 μm. The input signal is led to a lock-in amplifier (Princeton Applied Research), which filters (with bandpass equal to the vibration frequency), rectifies and then averages the signal over many cycles to reduce noise further (response time constant was 1–10 s). Thus, the output provides a measure of the peak-to-peak potential difference between the electrode tip at its excursion limits. Each electrode is calibrated with a known current source. Peak-to-peak input voltages were calculated by multiplying d.c. output values by 2/0.707; all values presented in text and figures are peak-to-peak. Potential differences of 0.1 μV can be readily detected. Krebs solution resistivity is 75 Ω cm; thus 0.1 μV corresponds to a current density of about 1 μA cm^{-2}. The electrode vibration was oriented perpendicular to the long axis of the muscle; thus, when adjacent to a muscle fibre, it provided a measure of membrane current at that point. Baseline values were obtained with the electrode vibrating far (several mm) from the muscle.

The spatial distribution of current was mapped along the lateral margin of whole muscles (Fig. 1*a*). Outward current was detected near the middle of the muscle, and the maximum outward current was invariably located at the endplate zone, which was identified by subsequent staining for acetylcholinesterase. In the flanking regions, membrane current reversed direction and flowed inward (Fig. 1*a*; *b*, filled circles). This pattern is drawn schematically in Fig. 1*c*, which also illustrates relative dimensions of the electrode and fibre.

To gain further information about the spatial distribution of current sources and sinks, experiments were repeated on single isolated muscle fibres. Flexor digitorum brevis muscles were incubated in Krebs containing 0.1–0.3% collagenase for 2–3 h, and then triturated to release hundreds of single, intact fibres[2]. The current pattern around single fibres was like that obtained for whole muscles (see Fig. 1*b*, open circles). The peak outward current occurred at the endplate, which could be visually identified on the living cells. In some cases it appeared that the nerve terminals had been completely removed by the isolation procedure. Such fibres still generated an outward current in the endplate region; this identifies the muscle membrane as a source of the current. The amplitude of the signal fell off rapidly as [illegible] electrode was moved away from the muscle fibre, be[illegible]ents, undetectable when the electrode was a few hundred [illegible] the fibre. This suggests that, in the whole muscle

---

Present addresses: *Division of Molecular and Cellular Biology, National Jewish Hospital, Denver, Colorado 80206; †Institute of Physiology, University of Oslo, Karl Johans Gate 47, Oslo, Norway; ‡Department of Physiology, University of Connecticut Health Center, Farmington, Connecticut 06032.

0028-0836/80/380235—03$01.00

only the fibres near the surface contributed to the recorded signal. Maximal outward current at the membrane was estimated to be about 10 μA cm^{-2}, and integration of the current profile around the circumference of the fibre gave a value of total outward current of about 1 nA. In a muscle fibre with an input resistance of 0.5 MΩ, this should produce a hyperpolarization of about 0.5 mV.

Five different kinds of experiments suggest a role for the sodium–potassium pump in the generation of the outward current. In each experiment, whole muscles were used and, after initial spatial mapping, all measurements were made at the site of the maximum outward current density (endplate zone). (1) Effect of potassium removal: when Krebs solution without potassium was perfused through the chamber, the outward current was abolished within 15–30 s (Fig. 2*a*). The effect was readily reversible. The rapidity of these effects suggests again that only fibres near the surface of the muscle contributed to the recorded signal. (2) Effects of temperature: perfusing the chamber with ice-cold Krebs solution caused the current to decrease greatly. Conversely, the signal increased in amplitude when warmed Krebs solution (37 °C) was infused. These results are consistent with the involvement of a pump. (3) Effect of ouabain: the cardiac glycoside ouabain is a specific inhibitor of the sodium pump. When mouse soleus muscle was superfused with Krebs solution containing 0.1 mM ouabain, the current was rapidly abolished. The effect was less clear with rat muscle; 10 mM ouabain reduced, but did not abolish the signal. Rat muscle, however, is known to be relatively resistant to ouabain[3]. (4) Effects of sodium replacement: external sodium was completely replaced by lithium. Lithium ions can enter muscle cells, but are not pumped out by the Na$^+$–K$^+$ pump. The Li solution reversibly abolished the current over a period of several minutes. This effect was probably due to a gradual reduction of internal sodium concentration, so that the Na$^+$–K$^+$ pump was no longer active. (5) Sodium 'loading' in the endplate region (Fig. 2*b*). Intracellular sodium concentration in the endplate region was increased by perfusing with Krebs solution containing acetylcholine (ACh, 5×10^{-4}g ml^{-1}) or carbachol (3×10^{-5}g ml^{-1}). These substances activate ACh receptors, whose distribution is restricted to the membrane in the endplate region, and which, when activated, produce an influx of sodium ions. The presence of these drugs changed the current recorded in the endplate region from outward to an extremely large inward current, reflecting the entry of sodium ions. When the preparation was subsequently perfused with Krebs solution containing curare (1×10^{-5}g ml^{-1}) or α-bungarotoxin (4×10^{-6}g ml^{-1}) and no ACh or carbachol, the ACh receptors were blocked, and the recorded current reversed again, becoming about four times larger than normal. (Control experiments showed that curare, α-bungaro-

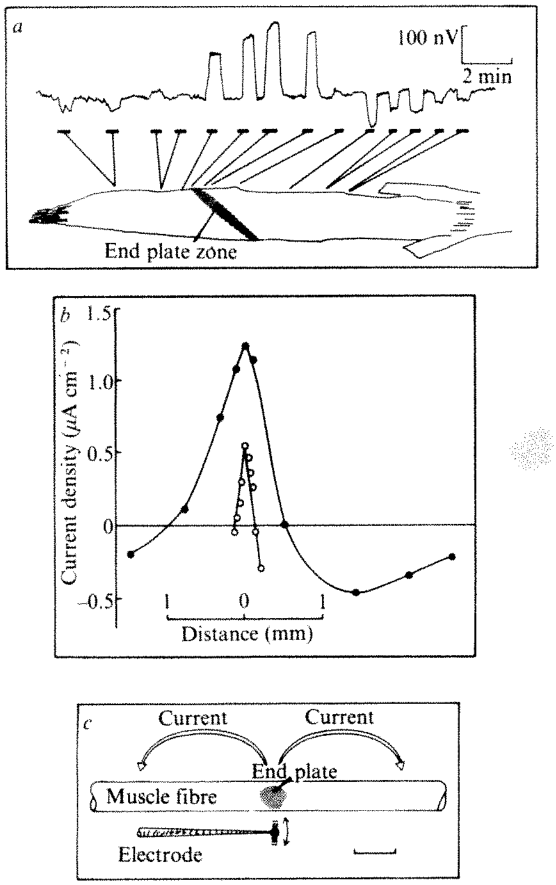

Fig. 1 *a*, Current pattern around whole muscle. The electrode, vibrating continuously, was alternately moved close to the muscle (marked by bars) and then away to a remote reference position in the bath. Recording positions near the muscle are shown by lines connecting the bars to the drawing of the muscle; the stippled area in the drawing marks the endplate zone. The current was largest when the electrode was at the endplate zone, and reversed sign in the flanking regions. Upward deflection represents outward current. The electrode was vibrated perpendicular to the long axis of the muscle (see *c*). *b*, Amplitude of the current (recorded near the muscle) is plotted as a function of distance from the endplate region. Results from ●, an experiment on a whole muscle, and ○, an isolated muscle fibre. *c*, Schematic diagram of a single muscle fibre depicting endogenous current pattern. The electrode tip and le fibre are drawn to illustrate approximate scale (bar ≃ 50 μm).

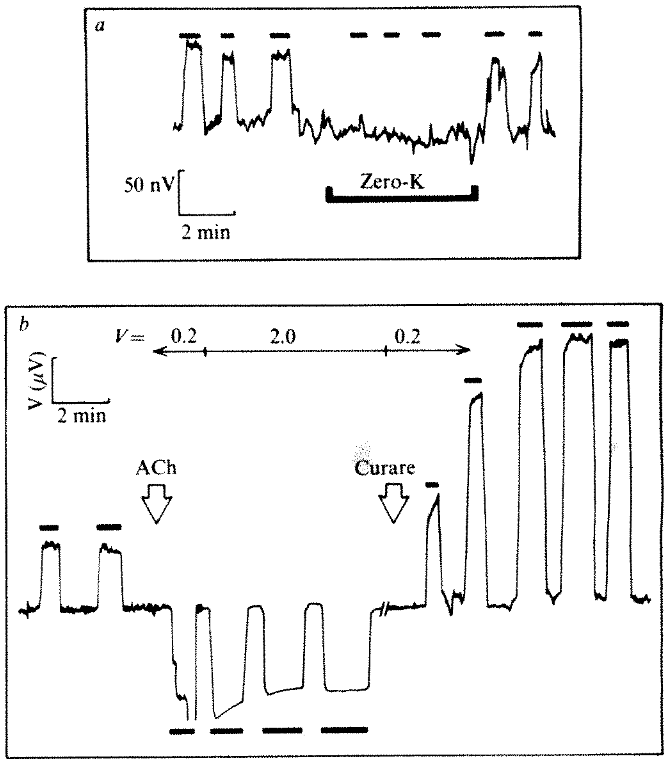

Fig. 2 *a*, Continuous recording obtained during an experiment to test the effect of removal of external potassium ions. During the times marked by the bars, the electrode was close to the muscle, at the endplate zone. Note that the endogenous current was abolished in zero-K Krebs (upward deflection = outward current). *b*, Experiment to test the effect of 'sodium loading' of the endplate region. Recordings near the muscle (marked by bars), were made at the endplate region. After the first two control readings, the chamber was perfused with Krebs containing ACh (plus prostigmine), and the current reversed sign, becoming inward and very large (note 10-fold gain change). When the chamber was later perfused with Krebs containing curare, the current again became outward, and was about fourfold larger than control. All solutions contained tetrodotoxin; the time break represents about 20 min.

toxin, and tetrodotoxin by themselves had no effect on the normal outward current). The increased amplitude of the outward current is consistent with a more active Na$^+$ pump, due to the increased internal sodium concentration.

The results of these experiments lead to the conclusion that the steady currents which were measured are produced or maintained by the Na$^+$–K$^+$ pump. The existence of such pumps and their electrogenicity in skeletal muscle are known[4]. The new finding reported here is the non-uniform spatial distribution of membrane current sources and sinks. This must reflect either a non-uniform distribution of pumping activity (that is, pumps that are more concentrated, more active, or more electrogenic in the endplate region) or a non-uniform distribution of leakage channels, or both. One hypothesis is that there is a higher concentration of electrogenic Na$^+$–K$^+$ pump sites in the endplate region than elsewhere, reflecting the need for removal of sodium ions that enter the fibre through ACh channels during nerve-evoked excitation. However, the outward current persisted *in vitro* for several hours in the absence of nerve-evoked activity (even after ACh receptors were totally blocked by curare or α-bungarotoxin), suggesting that the currents measured in our experimental conditions were independent of fluxes through ACh channels.

Whatever the distribution of pumps and leaks, their non-uniformity produces an electric current and hence an electric field, whose focus is centred on the endplate region. It is naturally of interest to inquire whether this field might serve other functions. For instance, it has recently been shown that ACh receptor distribution on myotubes[5] and growth of neurites in culture (ref. 6, and McCaig, Robinson and Hinkle, unpublished observations) can be affected by externally applied electric fields. This raises the possibility that the endogenous electric field reported here might be significant for long term interactions between neurones and muscle fibres. The estimated peak value of the electric field we measured around single, isolated muscle fibres is one to two orders of magnitude smaller than the fields required for effects on ACh receptor distribution or neurite growth in the studies cited above. However, those conditions and preparations were considerably different from the ones reported here. Moreover, the electric field which exists deep within an intact muscle may be larger than that measured near an isolated fibre. For instance, both the restricted volume of extracellular space and the presence of many endplates lying in register would serve to increase electric field strength.

Received 4 March; accepted 10 July 1980.

1. Jaffe, L. F. & Nuccitelli, R. *J. Cell Biol.* **63,** 614–628 (1974).
2. Bekoff, A. & Betz, W. J. *J. physiol., Lond.* **271,** 25–40 (1977).
3. Detweiler, D. K. *Fedn Proc.* **26,** 1119–1124 (1967).
4. Thomas, R. C. *Physiol. Rev.* **52,** 563–594 (1972).
5. Orida, N. & Poo, M-m. *Nature* **275,** 31–35 (1978).
6. Jaffe, L. F. & Poo, M.-m. *J. exp. Zool.* **209,** 115–128 (1979).

Active sodium transport by turtle colon via an electrogenic Na–K exchange pump

Kevin L. Kirk, Dan R. Halm & David C. Dawson

Department of Physiology and Biophysics, University of Iowa College of Medicine, Iowa City, Iowa 52240

Active sodium absorption by a variety of epithelia is abolished by ouabain, but the obligatory coupling between the movement of sodium and potassium expected from a basolateral (Na$^+$+K$^+$) ATPase has not been convincingly demonstrated[1]. According to the model of Koefoed-Johnsen and Ussing[2], the asymmetric cation selectivities of the apical and basolateral membranes prevent basolateral Na–K exchange from being expressed as opposing transmural ion flows. An additional consequence of this asymmetry is that the short-circuit current (I_{SC}) cannot be identified with the current through the sodium–potassium pump. We used the polyene antibiotic, amphotericin-B, to reduce the resistance and the cation selectivity of the apical membrane of isolated turtle colon so that the basolateral membrane current could be dissected into two components: one through a barium-sensitive potassium channel and another which represents the current associated with ouabain-sensitive, electrogenic, Na–K exchange. Comparison of cation fluxes and short circuit current indicates that in these conditions active sodium absorption is entirely attributable to an electrogenic Na–K pump with a stoichiometry of approximately 3Na:2K.

The presence of a basolateral membrane potassium channel was established by allowing tissues to attain a steady state I_{SC} and then subjecting them to the following sequence of manoeuvres. The steady-state I_{SC} was virtually abolished with ouabain (10^{-4} M, serosal) and then amiloride (10^{-4} M) was added to the mucosal bathing solution. Subsequently, the potassium concentration of either the mucosal or serosal bathing solution was raised to 10–30 mM by the addition of a small volume of concentrated potassium methyl sulphate or KCl. These additions had virtually no effect on I_{SC} although total tissue conductance (G_T) usually increased slightly, presumably due to an increase in the conductance of the paracellular shunt path[3,4]. Figure 1 shows the results of a representative experiment in which amphotericin-B (6 µM) was added to the mucosal bathing solution in the presence of a mucosal to serosal potassium gradient (M:30 mM, S:3.0 mM). Addition of the polyene produced a prompt increase in I_{SC} and G_T. The steady-state I_{SC} was consistent with net cation flow from mucosa to serosa and, as indicated in the figure, was abolished by the addition of BaCl$_2$ (5 mM) to the serosal bath. The polyene-induced increase in I_{SC} was always consistent with the orientation of the applied potassium e.m.f.

To determine the properties of the ouabain-sensitive active cation transport mechanism, portions of isolated colon bathed by identical solutions containing 102 mM Na and 2.5 mM K were subjected to the following procedure. First amiloride (10^{-4}M) was added to the mucosal side to reduce I_{SC} to near zero

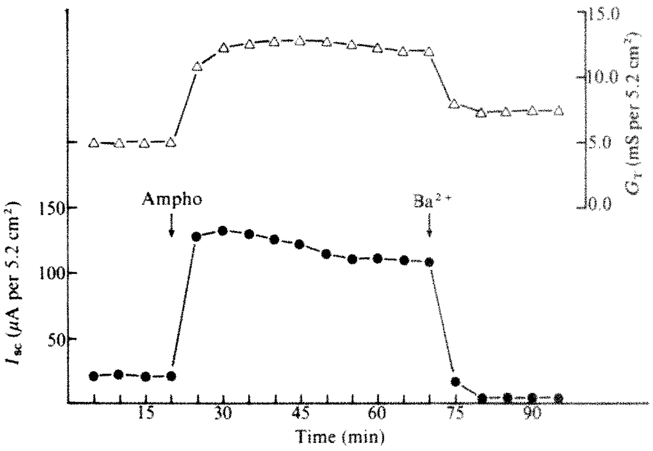

Fig. 1 Portions of stripped turtle colon were mounted in Ussing chambers (area 5.2 cm^2) and bathed on both sides by solutions containing (in mM) sodium benzene sulphonate 100, potassium bicarbonate 2.5, calcium chloride 1.0, sodium pyruvate 2.0, and glucose 5.0. Both solutions were stirred with air so that the *p*H at room temperature was approximately 8.4. Benzene sulphonate was substituted for chloride in an attempt to prevent cell swelling due to net salt movement into epithelial cells in the presence of the polyene[6]. The figure shows short-circuit current (●) and total tissue conductance (△) as a function of time. Active sodium absorption was abolished by adding ouabain (10^{-4} M) to the serosal bath. In the presence of a transmural potassium gradient (M 30 mM, S 2.5 mM) the addition of amphotericin-B (6 µM) increased I_{SC} and G_T. Subsequent addition of BaCl$_2$ (5 mM) to the serosal bath abolished I_{SC} and reduced G_T.

0028-0836/80/380237—03$01.00

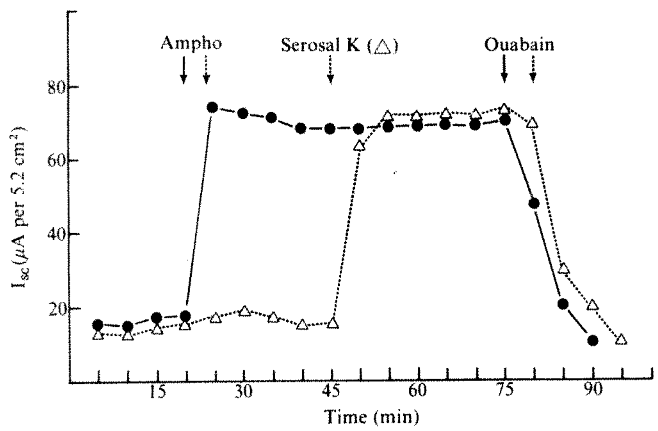

Fig. 2 Short-circuit current as a function of time for colons bathed initially by potassium-containing (●) and potassium-free (△) solutions. I_{SC} was inhibited with mucosal amiloride (10^{-4} M), and $BaCl_2$ (5 mM) was added to the serosal bath. Mucosal amphotericin-B (6 μM) increased I_{SC} only in the presence of serosal potassium. Subsequent addition of potassium to the K-free tissue (△) resulted in a prompt increase in I_{SC}. In both tissues I_{SC} was abolished by ouabain (10^{-4} M).

and abolish sodium absorption[2], then $BaCl_2$ (5 mM) was added to the serosal bath to decrease basolateral potassium conductance. Figure 2 (closed circles) shows the result of a representative experiment in which amphotericin-B (6 μm) was added to the mucosal bath. Addition of the polyene in the absence of electrochemical gradients produced a prompt increase in I_{SC} to a new steady state consistent with net positive charge movement from mucosa to serosa. The polyene-induced I_{SC} was stable for more than 60 min and was abolished by serosal ouabain (10^{-4} M).

The ouabain-sensitive, polyene-induced I_{SC} exhibited an obligatory dependence on serosal potassium. The triangles in Fig. 2 represent a tissue initially bathed on the serosal side by potassium-free, Na benzene sulphonate Ringer's. The addition of amphotericin-B had virtually no effect on I_{SC}; however, subsequent addition of KCl (2.5 mM) to the serosal bath resulted in a prompt increase in I_{SC} to a level virtually identical to that of the control. A further increase in serosal potassium concentration (data not shown) produced an additional increase in I_{SC} suggesting that in these conditions the pump rate is limited by the supply of serosal potassium.

Figure 3 shows the results of a similar experiment designed to evaluate the dependence of the polyene-induced I_{SC} on mucosal sodium. Both tissues were bathed initially on the serosal side by benzene sulphonate Ringer's containing 102 mM Na and 2.5 mM K; and on the mucosal side by Ringer's which was identical except that the sodium benzene sulphonate had been replaced with choline benzene sulphonate containing less than 1 mM sodium. Both mucosal solutions contained amiloride and in one tissue (closed circles) the mucosal sodium concentration was raised to 20 mM by the addition of a small volume of concentrated Na benzene sulphonate. Subsequent addition of amphotericin-B to both tissues produced a prompt increase in I_{SC} only in the tissue exposed to a sodium-containing mucosal solution. Addition of sodium to the second tissue (triangles), however, increased I_{SC} to a level comparable to the first. The amphotericin-induced I_{SC} in both tissues was abolished by ouabain.

Table 1 Amphotericin-induced sodium absorption, potassium secretion and short-circuit current

	ΔI_{SC} (μequiv. cm^{-2} h^{-1})	ΔJ_{net} (μequiv. cm^{-2} h^{-1})	$\Delta J_{net}/\Delta I_{SC}$	n
Sodium	0.67±0.04	2.00±0.16	3.01±0.15	15
Potassium	0.57±0.11	1.14±0.20	2.12±0.14	8

Fluxes of ^{22}Na were measured using mucosal and serosal solutions which were identical Na benzene sulphonate Ringer's in which the potassium concentration had been raised to 14 mM in order to increase I_{SC} in the presence of the polyene. The mucosal bath contained amiloride (10^{-4} M) and the serosal bath contained $BaCl_2$ (5 mM). Net sodium fluxes were obtained by comparing unidirectional fluxes from paired tissues. Preliminary experiments revealed that ^{42}K fluxes significantly underestimated net potassium flux, hence net potassium secretion was determined by using flame photometry to measure the appearance of the ion in a nominally potassium-free mucosal bathing solution which also contained amiloride (10^{-4} M). The serosal solution contained 10 mM potassium and 5 mM $BaCl_2$. Otherwise both solutions were identical sodium benzene sulphonate Ringer's. The values appearing in the table (mean ±s.e.) were corrected for the small diffusional potassium flux which could be estimated by measuring potassium appearance before the addition of the polyene.

In view of the striking dependence of the ouabain-sensitive, amphotericin-induced I_{SC} on serosal potassium and mucosal sodium we measured transmural fluxes of these ions to determine the ionic basis of the current. The results are shown in Table 1 where the amphotericin-induced increases in net sodium absorption and potassium secretion are shown along with the corresponding amphotericin-induced increases in I_{SC}. The results indicate that net Na absorption is approximately three times I_{SC} whereas net potassium secretion is about twice I_{SC}, so that the transepithelial current can be attributed to the difference between the net fluxes of the two cations. Previous studies on lipid bilayers[5], red blood cells[6] and isolated epithelia[7-9] have suggested that the polyene antibiotics can form pores in natural and artificial membranes which are moderately cation selective but do not discriminate appreciably between sodium and potassium. Neilsen[6] recently used the polyene antibiotic, filipin, to reduce the cation selectivity of the apical membrane of frog skin and obtained results consistent with the existence of a sodium–potassium exchange pump. In these experiments, however, the 'pump current' and its relation to active cation fluxes was not clearly defined.

In the presence of mucosal polyene, the transport properties of the turtle colon appear to be dominated by the properties of the basolateral membrane which must contain at least two cation transport elements: a barium-sensitive potassium conductance and an electrogenic sodium–potassium exchange pump. In the presence of serosal ouabain and mucosal polyene the turtle colon is markedly potassium selective, and this potassium

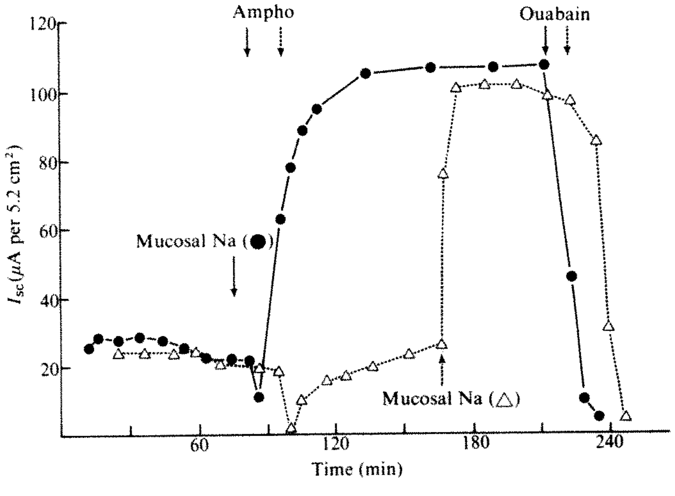

Fig. 3 Short-circuit current as a function of time for tissues bathed initially by sodium-free mucosal solutions and treated with amiloride (mucosal bath) and $BaCl_2$ (serosal bath). After the addition of sodium (20 mM) to the mucosal solution of one (●), amphotericin-B was added to the mucosal solution of both tissues. I_{SC} increased only in the presence of mucosal sodium. Subsequent addition of mucosal sodium to the Na-free tissue (△) resulted in a prompt increase in I_{SC}. In both tissues I_{SC} was abolished by ouabain.

conductance is blocked by serosal Ba^{2+}. This result is consonant with Nagel's report[10] of a Ba^{2+}-sensitive potassium conductance in the basolateral membrane of isolated frog skin. Additional experiments (data not shown) indicate that serosal Ba^{2+} also reduces ^{42}K fluxes across the epithelium in similar conditions. If ouabain is omitted from the serosal bathing solution, amphotericin-B induces a short-circuit current in the absence of transmural cation gradients. This 'active' I_{sc} exhibits an obligatory dependence on mucosal sodium and serosal potassium, is abolished by ouabain, and is numerically equal to the difference between net Na absorption and potassium secretion. These observations suggest that in the presence of serosal Ba^{2+} the polyene-induced I_{sc} represents current attributable to an electrogenic sodium–potassium exchange, where the ratio of sodium to potassium is approximately 3Na : 2K. Thus, sodium absorption by the turtle colon seems to be entirely attributable to the presence, in the basolateral membrane, of a ouabain-sensitive cation exchange pump similar to that which seems to exist in human red blood cells[11,12] and in some excitable membranes[13].

This research was supported by grants from NIH(AM18776) and the Iowa Heart Association (79-G-7).

Received 12 May; accepted 1 July 1980.

1 Schultz, S. G. *Membrane Transport Processes* Vol 1 (ed. Hoffman, J F) 213–117 (1978).
2 Koefoed-Johnsen, V. & Ussing, H H *Acta physiol. scand* **42**, 298–308 (1958)
3. Dawson, D C. *J. Membrane Biol* **37**, 213–233 (1977).
4. Thompson, S. M. & Dawson, D. C *J Membrane Biol* **42**, 357–374 (1978)
5. Marty, A & Finkelstein, A. *J. gen Physiol* **65**, 515–526 (1975).
6 Cass, A & Dalmark, M. *Nature new Biol* **244**, 47–49 (1973)
7 Nielsen, R *J. Membrane Biol* **51**, 161–184 (1979).
8. Lewis, S. A., Eaton, D C, Clausen, C. & Diamond, J M *J. gen Physiol* **70**, 427–440 (1977)
9. Reuss, L *J Membrane Biol* **42**, 65–86 (1978)
10 Nagel, W. *Biochim. biophys Acta* **552**, 346–357 (1979)
11. Post, R L & Jolly, P. C. *Biochim biophys Acta* **25**, 108–128 (1957).
12. Hoffman, J F., Kaplan, J. H. & Callahan, T J. *Fedn Proc.* **38**, 2440–2441 (1979)
13. Thomas, R C *Physiol Rev.* **52**, 563–594 (1972)

Light-induced changes in membrane current in cone outer segments of tiger salamander and turtle

Julie L. Schnapf*

Laboratory of Neurophysiology, NINCDS, National Institutes of Health, Bethesda, Maryland 20014

Robert N. McBurney

Department of Physiology, The Medical School,
Newcastle upon Tyne NE1 7RU, UK

The peak change in membrane conductance of vertebrate photoreceptors in response to the isomerization of a single photopigment has been estimated from recordings of membrane potential to be about 8 pS in rods[1] and 6 pS in cones[2]. For rods the estimate has been largely confirmed by Yau *et al.*[3] by directly recording membrane current responses of rod outer segments to single photoisomerizations. However, no similar measurements have been reported for cone outer segments. Here, we report on direct recordings of membrane currents of single cone outer segments using an extracellular patch electrode. The technique was similar to that described by Yau *et al.*[3] for toad rods. We have measured dark currents of up to 40 pA, and calculate that the conductance change resulting from a single photoisomerization is less than 1 pS.

A portion of the back of the eye of a dark-adapted larval tiger salamander, *Ambystoma tigrinum*, or turtle, *Pseudemys scripta elegans*, was placed vitreal side down on Millipore filter paper. The sclera and pigment epithelium were gently lifted off, leaving the retina, receptor side up, attached to the filter paper. A 300-μm slice of retina and filter paper was submerged in oxygenated Ringer[4] in a superfusion chamber placed side-on under the water-immersion objective of a conventional microscope, and viewed through an IR image converter at ×600 magnification. The outer segment of a single cone was drawn into a Ringer-filled electrode. The resultant high resistance seal made between the electrode interior and the base of the outer segment of a tiger salamander cone, or between the electrode and a red oil droplet of a turtle cone, enabled us to record 50–90% of the membrane current of the outer segment. Measurements of the relative spectral sensitivities of both these receptors in membrane current per incident photon were consistent with cones containing a dehydroretinal-based pigment with an absorption maximum at 620 nm (refs 5, 6). Current was recorded by a virtual ground current-to-voltage converter with a 100 MΩ feedback resistor.

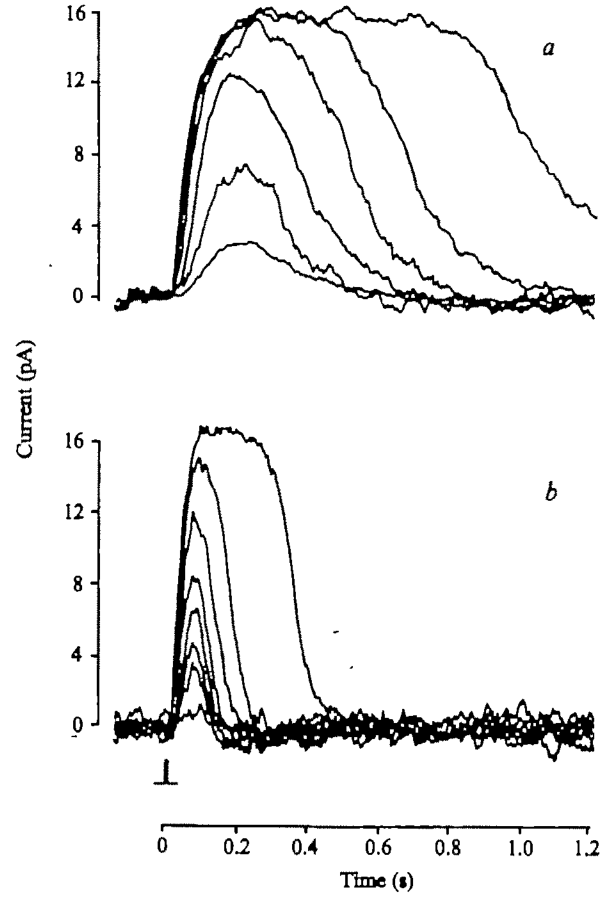

Fig. 1 *a*, Current responses of 'red' cone outer segment of tiger salamander to 10-ms flashes of diffuse white light of increasing intensity; stimulus monitor below. Downward deflection corresponds to inward membrane current, recorded with a d.c. – 10 Hz bandwidth. Average number of effective photoisomerizations per flash, from bottom to top: 3.89×10^2, 1.39×10^3, 3.90×10^3, 1.05×10^4, 3.10×10^4, 3.10×10^5. Stimulus calibration described in Fig. 2. Each trace represents the average of one to nine light responses. The traces shown are uncorrected current records representing, on our estimation, 78% of the true current flowing across the outer segment membrane within the recording electrode. The percentage of membrane current recorded equals the difference in resistance to ground of the electrode with and without the outer segment drawn inside, divided by the resistance of the electrode with the outer segment inside. *b*, Current responses of 'red' cone outer segment of turtle to 10-ms diffuse test flash, bandwidth, d.c. – 10 Hz. Number of effective photoisomerizations estimated per flash, from bottom to top: 1.5×10^2, 6.45×10^2, 1.22×10^3, 1.50×10^3, 2.07×10^3, 4.42×10^3, 1.60×10^4, 1.40×10^5. White light was used for responses 1, 3, 7 and 8; other responses were to red light of $\lambda_{max} = 610$ nm.

Uncorrected current records representing 65% of the true current.

---

* Present address: Department of Ophthalmology, The University of California, San Francisco, California 94143.

0028-0836/80/380239—03$01 00

In the dark, a current of up to 40 pA flowed into the outer segments of cones (about 30 pA averaged over the cones sampled). The current was transiently reduced by a brief flash of light. This is illustrated in Fig. 1*a* for a tiger salamander cone and Fig. 1*b* for a turtle cone. A bright light that elicits a saturating response turns off the dark current completely. The time course of the current response seen in salamander cones was very similar to the voltage response of salamander cones reported by other workers[7], and was also similar in waveform to current responses in *Iguana* cones as measured with pairs of extracellular voltage electrodes[8]. However, current responses of turtle cones to bright flashes lacked the initial transient seen in corresponding voltage responses[2]. We suggest that, as in toad rods[3], the voltage transient seen in turtle cones is due to a voltage-sensitive conductance not located in the outer segment. The relationship between peak change in membrane current, I_p, and light intensity, L, was satisfactorily fitted by a Michaelis–Menten equation of the form $I_p/I_{\max} = (1 + S/L)^{-1}$, where $I_{\max}$ is the maximum change in membrane current and S is the number of incident photons required to produce a half-maximal change in membrane current, as shown in Fig. 2. In six experiments in turtle and tiger salamander, the average number of photoisomerizations needed to elicit a half-maximal response, S^*, was 2,150 (range 1,350–2,750). The method for converting light intensity in incident photons, L, to photoisomerizations, L^*, is given in Fig. 2 legend.

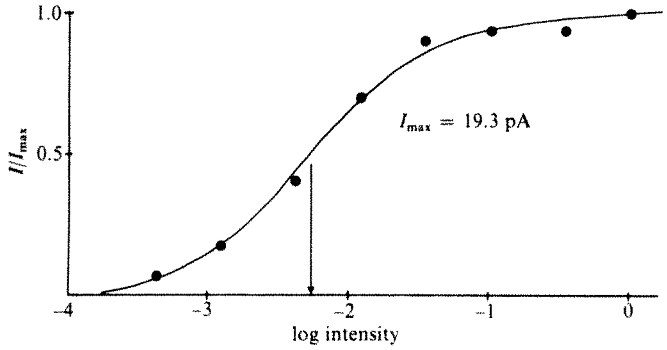

Fig. 2 Peak change in membrane current recorded from a turtle cone outer segment as a function of the intensity of a white, 10-ms test flash. For the cell shown in Fig. 1*a*. Intensity is displayed in log units relative to the maximum unattenuated stimulus. The calculated number of effective photoisomerizations for the unattenuated test light was 3.10×10^5 per flash. The value of the maximum current response, $I_{\max}$, was adjusted to compensate for signal attenuation due to current shunt through the sealing resistance between the electrode and the outer segment. Continuous curve is drawn from a template which described a Michaelis–Menten equation. The arrow, indicating the parameter S, is $10^{-2.26}$ of the unattenuated flash, corresponding to 1.70×10^3 effective photoisomerizations (S^*). From the Michaelis–Menten equation, the response to a single effective photon would be $19.3\ (1 + 1.70 \times 10^3) =$ 0.011 pA. For narrow band spectral stimuli (width at half amplitude = ± 5 nm), the number of photons per μm^2 at all attenuation settings were measured by putting a photodiode (United detector 101A) in place of the retina. The number of effective photoisomerization per test flash, L^*, was estimated by the equation $L^* = 2.3\beta(\lambda)VfLt$, where L is the light intensity in incident photons per μm^2 per s, t is the duration of the test flash, $\beta(\lambda)$ is the specific density of the cone pigment for unpolarized light of wavelength λ (refs 5, 6), V is the volume of the outer cone segment as calculated by measuring the outside dimensions of the cone with an eyepiece micrometer, and f is the fraction of absorbed photons that produced a change in membrane current. The fraction f, estimated as 0.5, was determined by substituting a toad retina for the turtle retina, counting the number of single current 'bumps' (L^*) elicited in a rod by dim light flashes, and dividing by the number of photons absorbed ($2.3\beta(\lambda)VLt$). To calculate photoisomerizations for a 'white' test flash, the intensity of a narrow band stimulus was adjusted so that the current response elicited by this test flash matched that to the white flash. L^* was then calculated from the above equation.

There was no detectable current response to dim flashes where approximately one photoisomerization was elicited per cone. This is not surprising because the substitution of $L^* = 1$ in the Michaelis–Menten equation $I_p/I_{\max} = (1 + S^*/L^*)^{-1}$, with $S^* = 2{,}150$, yielded an average value for the peak change in membrane current per photoisomerization of only 0.013 pA or 0.05% of the maximum current. Our recording system would have been unable to detect such a small change in current. Using a value of 30 mV (refs 2, 7, 9, 10) for the driving force on the membrane current in the dark, we calculate an average decrease in outer segment membrane conductance at the peak of a single photon response of 0.43 pS.

The fraction, B, of channels closed by a single photoisomerization can be determined from the equation $B = (1 + S^*\alpha)^{-1}$, where S^* is as before and α is the ratio of the membrane conductance of a cone during a saturating response and its membrane conductance in the dark[2]. Taking our average value of 2,150 for S^* and an estimate for α of 0.67 (refs 2, 7), for dim flashes each effective photoisomerization blocks 0.07% of the available channels. This is about half the value obtained by Baylor *et al.*[2] based on voltage recordings of turtle cones. The difference may reflect a greater light-adapted state in this preparation. Assuming that this is the case, a single photoisomerization can be expected to elicit approximately a 10–12-μV change in membrane potential[15], and taken with a 0.013-pA current event, this yields an input resistence of an isolated cone of about 800–900 MΩ. This value is close to the value estimated for the input resistance of isolated rods[3,11], but is larger than that previously estimated for turtle cones on the basis of their spatial sensitivity profiles[12].

In response to a step increase in illumination, we observed that the suppression of inward current reached a maximum and then dropped to a plateau in seconds, as shown in Fig. 3 for a light that transiently suppressed all the dark current. The time course of the decay depended on light intensity. Calculations based on those by other workers[13] show that the decrease in quantum catching resulting from photopigment bleaching at these intensities has an insignificant role in the decay of the response to steps of light. On the basis of records obtained with the procedure illustrated in Fig. 3, we suggest that the most likely explanation for the decay in the current response is a reopening of outer segment ion channels that were initially closed during the peak of the response. At about 50 s after the onset of the light, when the current response had decayed and was maintained at a steady plateau level, the light intensity was increased. We observed a further reduction in membrane current. It seems that during the development of the plateau phase a population of unblocked channels had appeared and these were now available to be blocked by a process generated by the arrival of more photons. We suggest that these channels are derived from those blocked during the initial saturating phase of the response.

It has been reported for turtle cones that fluctuations in membrane potential around the mean value in the dark are substantially reduced when the cell is hyperpolarized by bright lights[9]. In weakly coupled cones, a decrease in the standard deviation, σ_v, of membrane voltage fluctuations of as much as 0.66 mV, or 5–6% of the maximum light response, has been observed. We are unable to support the suggestion that this noise is generated in the outer segment. If the voltage fluctuations were due to conductance fluctuations in the outer segment, the reduction in the standard deviation of the current elicited by light should also be 5–6% of the maximum light response, or about 2 pA. Although we have measured some changes in the fluctuations associated with records of outer-segment membrane current between darkness and various levels of illumination, we have not seen a reduction in current noise as large as that predicted from the records of voltage fluctuations of isolated cones. The largest reduction we observed in the standard deviation of the current going from darkness to a saturating light intensity was 0.37 pA in a 38-pA cone, or about 1% of the total current (after compensation for the current shunt through the sealing resistance, bandwidth = d.c. – 10 Hz). As the state of adaptation of the two preparations seem comparable (judging from estimates of S^*), we conclude that a sizeable portion of the reported fluctuations in voltage is not generated in the outer segment.

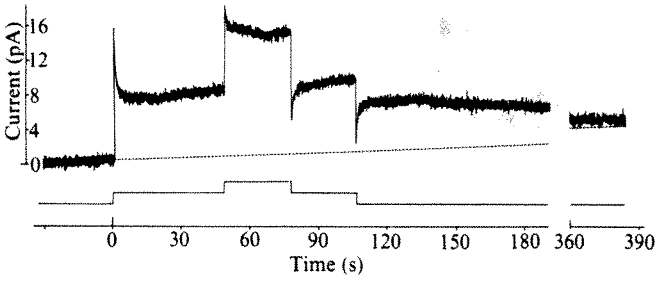

Fig. 3 The current responses of a turtle cone outer segment to steps of light (bandwidth, d.c. – 10 Hz). Uncorrected records representing an estimated 65% of the true current. Stimulus monitor shown below. Steps of illumination correspond to 6.80×10^4 followed by 2.18×10^5 photoisomerizations per s.

We cannot be sure that the current fluctuations we have observed are associated with the phototransduction process. The changes in variance are very small and not measurable in some recordings (especially recordings where the sealing resistance is low and consequently the baseline current noise is high). If the dark current noise that can be abolished in bright light is due to random fluctuations in the number of open ionic channels and these channels can be closed by light, the current i, flowing through each open channel, can be estimated from the equation $i = \sigma_I^2/(\overline{\Delta I}\cdot p)$, where σ_I^2 is the difference between the current variance in the dark and at the peak of a saturating response, $\overline{\Delta I}$ is the mean change in current and p is the proportion of these channels that are already closed in the dark. Using our corrected values $\sigma_I^2 = 0.14$ pA^2 and $\overline{\Delta I} = 38$ pA from one turtle cone and taking $p = 0.3$ (ref. 14), we calculate a single channel current of 0.012 pA. This value is close to estimates of the size of the elementary current event underlying dark noise in rods[1,14]. A comparison between this value and our estimate of the current change produced by a single photoisomerization in dim lights leads us to suggest that if this current noise is generated by fluctuations of light-sensitive channels in the outer segment, a single photoisomerization causes the closure of about one channel.

We thank Sir Alan Hodgkin, Dr D. A. Baylor, Dr T. D. Lamb and Dr D. R. Copenhagen for their comments on the manuscript, and Mrs M. Bragg, Mrs E. Hill and Mrs J. Ansiello for typing versions of the manuscript. This research was supported in part by NIH Postdoctoral Fellowship 5 F32 EY05254 awarded to J.L.S.

Received 25 March; accepted 23 June 1980.

1. Schwartz, E. A. *J. Physiol., Lond.* **272,** 217–246 (1977).
2. Baylor, D. A. Hodgkin, A. L. & Lamb, T. D. *J. Physiol., Lond.* **242,** 685–727 (1974).
3. Yau, K-W., Lamb, T. D. & Baylor, D. A. *Nature* **269,** 78–80 (1977).
4. Brown, J. E. & Pinto, L. H. *J. Physiol., Lond.* **236,** 575–591 (1974).
5. Liebman, P. A. in *Handbook of Sensory Physiology* Vol. VII, Pt 1 (ed. Darnell, H. J. A.) 481–528 (Springer, New York, 1972).
6. Ebrey, T. D. & Honig, B. *Vision Res.* **17,** 147–151 (1977).
7. Lasansky, A. & Marchiafava, P. L. *J. Physiol., Lond.* **236,** 171–191 (1974).
8. Yoshikami, S. & Hagins, W. A. *Ann. N. Y. Acad. Sci.* **307,** 545–561 (1978).
9. Lamb, T. D. & Simon, E. J. *J. Physiol., Lond.* **272,** 435–468 (1977).
10. Baylor, D. A. & Fuortes, M. G. F. *J. Physiol., Lond.* **207,** 77–97 (1970).
11. Bader, D. R., MacLeish, P. R. & Schwartz, E. A. *J. Physiol., Lond.* **296,** 1–26 (1979).
12. Detwiler, P. B. & Hodgkin, A. L. *J. Physiol., Lond.* **291,** 75–100 (1979).
13. Normann, R. A. & Perlman, I. *J. Physiol., London.* **286,** 491–507 (1979).
14. Baylor, D. A., Matthews, G. & Yau, K-W. *J. Physiol., Lond.* (in the press).
15. Baylor, D. A. & Hodgkin, A. L. *J. Physiol., Lond.* **234,** 163–198 (1973).

Specific dephosphorylation of membrane proteins in Rous sarcoma virus-transformed chick embryo fibroblasts

Daniel P. Witt & Julius A. Gordon

Department of Pathology, University of Colorado Health Sciences Center, Denver, Colorado 80262

Chick embryo fibroblasts (CEF) infected with avian sarcoma virus become rapidly transformed as a result of expression of the viral *src* gene[1,2] in the form of a single polypeptide of molecular weight 60,000 (pp60^{src})[3] with protein kinase activity[4] and suggested preferential association with the plasma membrane[5,6]. Studies with normal avian and mammalian cells have revealed the presence of an antigenically related protein[7,8] which seems to have similar kinase activity, but which is present at less than 1% of the levels of virally induced *src* protein found in transformed cells[8,9]. As dynamic protein phosphorylation is important in numerous regulatory processes[10,11], the phenotypic expression of transformation may arise from an imbalance in one or more regulatory mechanisms that are controlled by protein phosphorylation[4,8,12]. The cell membrane is affected during transformation[13], including its phosphotransferase activity[14,15]. The latter has been shown using isolated membrane fractions whose properties may be changed during preparation[16]. Therefore, we have compared the phosphorylation state of individual membrane proteins found in intact normal and RSV-transformed cells and report here the identification of two heavily phosphorylated, acidic membrane proteins in normal CEF which are specifically dephosphorylated on transformation by wild-type and temperature-sensitive Rous sarcoma viruses.

Normal and transformed chick fibroblasts were metabolically labelled with ^{35}S-methionine, and membranes were prepared by the method of Brunette and Till[17] and analysed by two-dimensional gel electrophoresis. Two proteins of molecular weights 57,000 and 55,000 (57 K and 55 K proteins) and similar isoelectric point (~5.1) were identified as being almost exclusively associated with the membrane preparations (Fig. 1). That the membrane association was not an artefact of preparation was supported by the presence of these proteins in membranes prepared by sucrose density centrifugation (Fig. 1*c*, ref. 18). When normal cells (or cells infected with RAV-2, which does not contain the *src* gene) were incubated with ^{32}P-P$_i$, both proteins became heavily labelled within 2 h (Fig. 2*a*). In contrast, transformed cells labelled in identical conditions showed very little net incorporation of phosphate by these proteins (Fig. 2*c*). Quantification of both proteins by ^{35}S-methionine incorporation over 17 h suggested that any apparent net reduction in these proteins following cell transformation was insufficient to account for the dramatic decrease in phosphorylation. Normal cells and cells infected with RAV-2 virus showed no cell density dependence of phosphorylation of these proteins (data not shown).

We examined the turnover of phosphate on these proteins by means of a pulse-chase study (Fig. 2). Normal cells labelled with ^{32}P-P$_i$ for 2 h (Fig. 2*a*) and chased for 4 h (Fig. 2*b*) showed a marked decrease in label associated with intermediate filament protein (IFP) and most other phosphoproteins, some increase in a 87 K protein, but no apparent decrease in the isotope associated with either the 57 K or 55 K proteins. This suggests that phosphatase activity specific for these phosphoproteins is limited in the normal cell or that these proteins are found in a privileged location that is inaccessible to general phosphatase activity. In contrast, little label is detected in these proteins at either time point in RSV-transformed cells (Fig. 2*c*, *d*). Other

0028-0836/80/380241—04$01.00

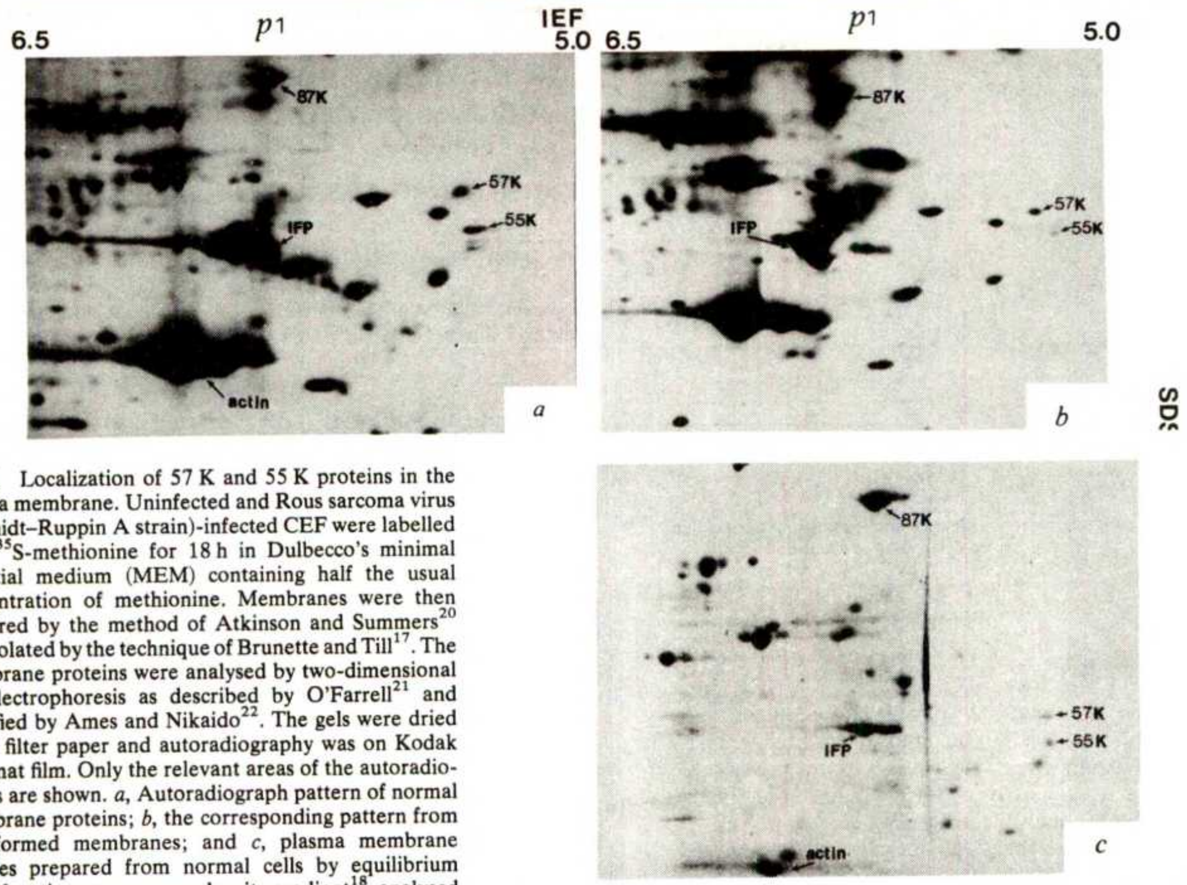

Fig. 1 Localization of 57 K and 55 K proteins in the plasma membrane. Uninfected and Rous sarcoma virus (Schmidt–Ruppin A strain)-infected CEF were labelled with ^{35}S-methionine for 18 h in Dulbecco's minimal essential medium (MEM) containing half the usual concentration of methionine. Membranes were then prepared by the method of Atkinson and Summers[20] and isolated by the technique of Brunette and Till[17]. The membrane proteins were analysed by two-dimensional gel electrophoresis as described by O'Farrell[21] and modified by Ames and Nikaido[22]. The gels were dried on to filter paper and autoradiography was on Kodak X-Omat film. Only the relevant areas of the autoradiograms are shown. *a*, Autoradiograph pattern of normal membrane proteins; *b*, the corresponding pattern from transformed membranes; and *c*, plasma membrane vesicles prepared from normal cells by equilibrium centrifugation on a sucrose density gradient[18], analysed in a similar fashion, and stained with Coomassie blue. It is apparent that there is some degree of association of structural proteins, that is, intermediate filament protein (IFP) and actin, with membranes, particularly those prepared by the Brunette and Till method[17]. The 57 K and 55 K proteins are invariably found to be membrane associated by both techniques. The presence of the 57 K and 55 K proteins could not be detected in the 100,000*g* supernatant from these preparations.

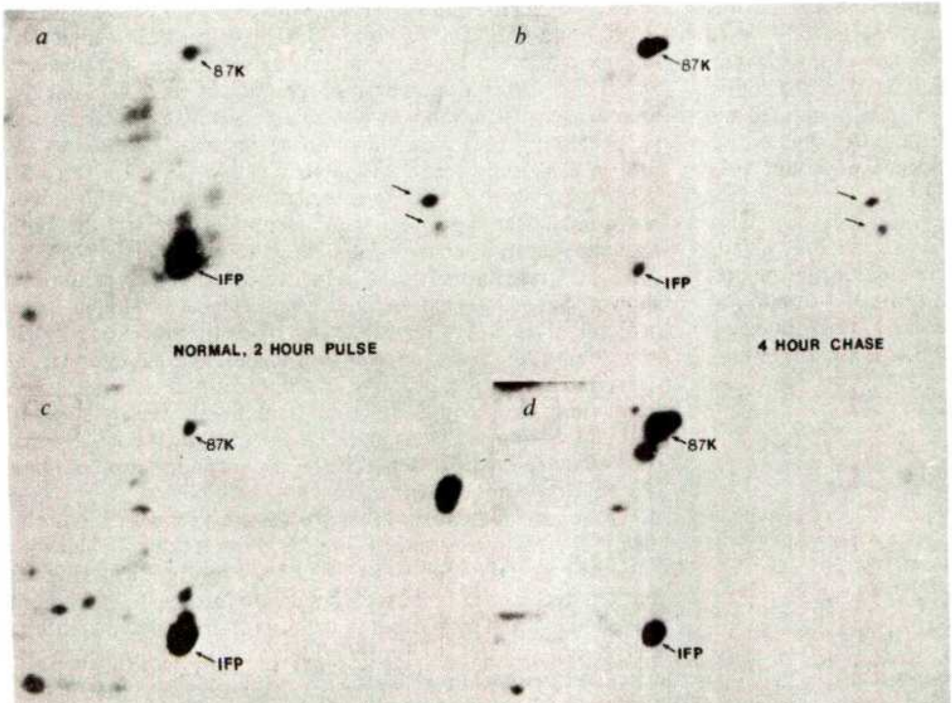

Fig. 2 Relatively slow turnover of phosphate on the 57 K and 55 K proteins. Normal chick fibroblasts (*a*) or Rous sarcoma virus (Prague C strain)-transformed fibroblasts (*c*) were incubated with 1 mCi ^{32}P-P$_i$ in phosphate-free medium for 2 h. The cells were prepared directly for two-dimensional gel analysis by lysis in 2.3% SDS containing 5% mercaptoethanol, heating at 95 °C for 3 min, and adding 2 volumes of 'standard dilution buffer'[22]. Alternatively, following the 2-h pulse, the ^{32}P-labelled normal (*b*) or transformed (*d*) cultures were incubated for an additional 4 h in Dulbecco's MEM (Gibco H-21) with 5% calf serum and 10% tryptose phosphate broth. The samples were prepared as before and whole cell phosphoproteins analysed by two-dimensional gel electrophoresis. In this and following experiments, 10^6 acid-precipitable c.p.m. were loaded per gel. Autoradiography was for 24 h. The 2-h pulse resulted in significant labelling of the 57 K and 55 K proteins in normal cells (*a*, arrows). Although the 4-h chase resulted in loss of label from IFP and most other proteins except protein of molecular weight 87,000 in both normal and transformed cells, there was no significant decrease in label associated with these normal cell phosphoproteins (*b*, arrows) in four successive experiments.

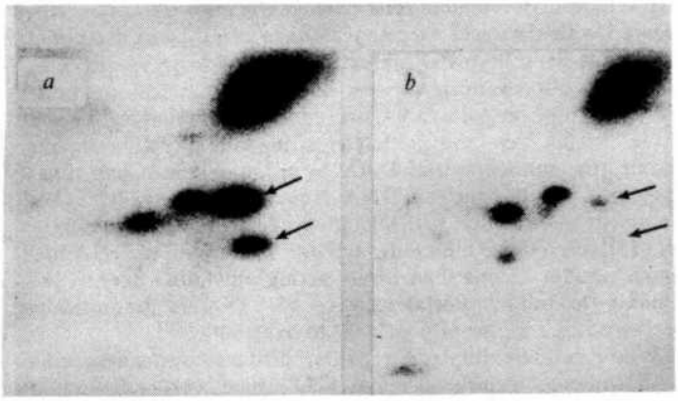

Fig. 3 Effect of growth temperature on phosphorylation of the 57 K and 55 K proteins in cells infected with the temperature-sensitive virus, tsNY68. Chick fibroblasts were infected with tsNY68 virus[19] and incubated at 41 °C (*a*) or 35 °C (*b*). Examination of the cultures by phase microscopy revealed normal cell morphology at a growth temperature of 41 °C (non-permissive temperature) and transformed morphology at a growth temperature of 35 °C (permissive temperature). Cultures at both temperatures were incubated with 1 mCi ^{32}P-P$_i$ per 60-mm plate for 2 h, then lysed in SDS and analysed by two-dimensional gel electrophoresis. Autoradiography was for 72 h. Labelling of the 57 K and 55 K phosphoproteins is seen to be heavy in cells grown at 41 °C, but is almost undetectable in cells grown at 35 °C. Temperature-shift experiments showed that detectable alterations in the phosphorylation state of these proteins occurred within 3–4 h of the temperature change. The two labelled spots seen to the left of the 57 K protein are normal cell phosphoproteins not seen in Figs 2 and 4 because of shorter exposure times.

phosphoproteins in the pulsed and chased transformed cells behaved in a similar fashion to that seen in normal cells.

It was important to determine whether dephosphorylation of the 57 K and 55 K proteins occurred in cells transformed by a temperature-sensitive mutant of Rous sarcoma virus (tsNY68). These cells manifest normal phenotype when maintained at a growth temperature of 41 °C, but show rapid and reversible morphological and biochemical transformation (within 6 h) when shifted to 35 °C (ref. 19).

We found a significant alteration in phosphorylation state of the 57 K and 55 K proteins when comparing cells grown at 41 °C (Fig. 3*a*) with cells grown at 35 °C (Fig. 3*b*). This phosphorylation state is temperature sensitive in both directions within 3–5 h of a shift in temperature, increasing when the temperature is raised and decreasing when the temperature is lowered (data not shown). Thus, it would seem that the dephosphorylation of these proteins is temporally linked to the onset of the transformed phenotype. The slow turnover of the phosphate on these proteins in normal cells (Fig. 2) when considered with these latter data, suggests the existence of a phosphatase activity in transformed cells that is specific for these phosphoproteins. Protein turnover as a significant factor in the dephosphorylation seems less likely, as ^{35}S-incorporation did not show a dramatic decrease in transformed cells and might simply result from some increased susceptibility of the dephosphorylated proteins to degradation.

We considered the possible existence of a specific phosphatase in a mixing experiment. Normal CEF or RSV-CEF were incubated with ^{32}P-P$_i$ and disrupted by nitrogen cavitation. These homogenates were incubated, either mixed (Fig. 4*c*, *d*) or unmixed (Fig. 4*a*, *b*), at 41 °C for 4 h. The phosphoproteins were analysed by two-dimensional gel analysis and autoradiography.

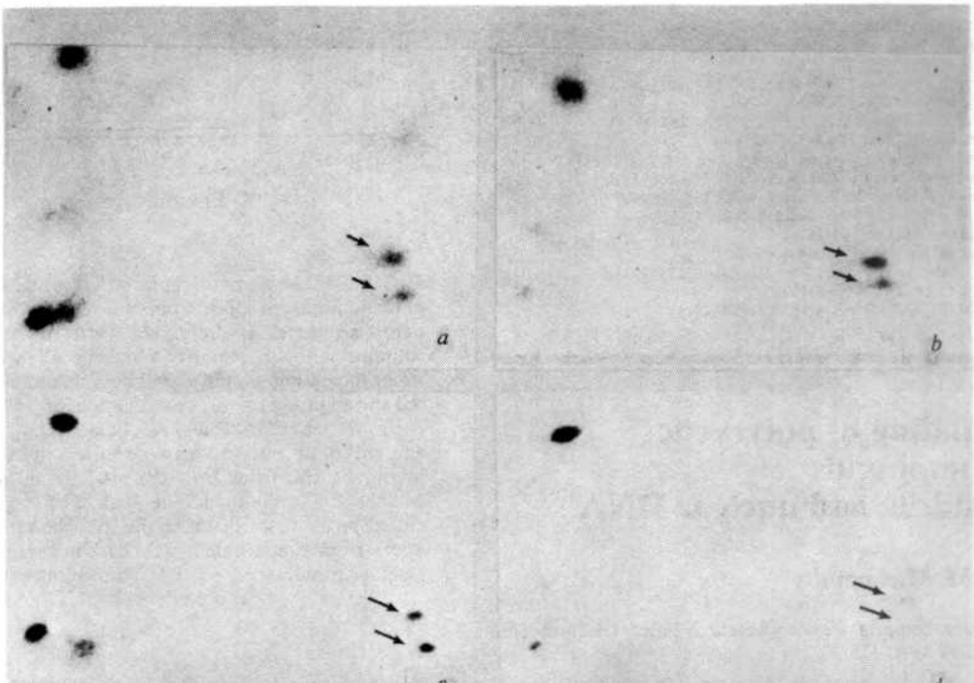

Fig. 4 Specific dephosphorylation of 57 K and 55 K phosphoproteins from normal cells by transformed CEF homogenate. Normal CEF were labelled with ^{32}P-P$_i$ (1 mCi per 100-mm plate) for 2 h and disrupted by nitrogen cavitation (400 p.s.i. in a Yeda cell press) in Tris-Cl buffered saline, *p*H 8.0. Phase microscopic examination of the homogenate showed that fewer than 5% of the cells remained intact. Unlabelled normal cells were also disrupted in the same fashion and mixed with the homogenate derived from an equal number of the labelled cells. An aliquot of this suspension was prepared immediately for electrophoresis (*a*) while the remainder was incubated at 41 °C for 4 h at which time another aliquot was prepared for electrophoresis (*b*). No significant decrease is seen in the level of label in the 57 K and 55 K phosphoproteins although IFP and most other phosphoproteins show marked loss of isotope. The 87 K phosphoprotein is apparently stable to phosphate loss. RSV-transformed (Prague C strain) fibroblasts were disrupted by the same protocol and mixed with the homogenate from an equal number of disrupted ^{32}P-labelled normal CEF. This suspension of mixed homogenates was either prepared for electrophoresis immediately (*c*) or incubated at 41 °C for 4 h (*d*) before SDS solubilization. All samples were analysed by two-dimensional gel electrophoresis. Autoradiography was for 24 h. It is apparent that mixing of transformed cell homogenate with ^{32}P-labelled normal cell homogenate results in the specific dephosphorylation of the 57 K and 55 K phosphoproteins. Note that no decrease in label associated with the 87 K phosphoprotein is detectable in the mixed homogenates (*c* and *d*). These results were verified in three successive experiments.

Only in the mixed homogenate was specific decrease in the activity of these proteins seen (Fig. 4*c*, *d*). The remainder of the autoradiographic pattern obtained with the mixed homogenate was identical to that found with unmixed homogenates. The protein patterns as detected by staining with Coomassie blue remained unchanged in all cases during the 4-h incubation suggesting that general protease activity was not important in these changes.

Our results suggest the presence of a phosphatase activity in transformed cells which appears specific for the 57 K and 55 K phosphoproteins. The function of the 57 K and 55 K proteins is presently unknown although both are membrane associated. The nature of the putative specific phosphatase activity is uncertain although several possibilities come to mind. It is possible that the *src* protein may activate a phosphatase specific for the 57 K and 55 K phosphoproteins. On the other hand, the *src* protein itself may contain an as yet unidentified phosphatase activity.

This work was supported in part by a grant to J.A.G. from the NIH. D.P.W. is the recipient of NIH Research Fellowship grant no. IF32 CA-06380. We thank Eleanor Erikson for providing the virus stocks, for assistance with cell culture techniques and continuing interest in this work. We also thank Kurt Neumann for technical assistance.

Received 21 May; accepted 10 July 1980.

1. Hanafusa, H. in *Comprehensive Virology* Vol. 10 (eds Fraenkel-Conrat, H. & Wagner, R. P.) 401–483 (Plenum, New York, 1977).
2. Vogt, P. K. in *Comprehensive Virology* Vol. 9 (eds Fraenkel-Conrat, H. & Wagner, R. P.) 341–455 (Plenum, New York, 1977).
3. Brugge, J. & Erikson, R. L. *Nature* **269**, 346–347 (1977).
4. Collett, M. S. & Erikson, R. L. *Proc. natn. Acad. Sci. U.S.A.* **75**, 2021–2024 (1978).
5. Rohrschneider, L. R. *Cell* **16**, 11–24 (1979).
6. Willingham, M. C., Jay, G. & Pastan, I. *Cell* **18**, 125–134 (1979).
7. Collett, M. S., Brugge, J. S. & Erikson, R. L. *Cell* **15**, 1363–1369 (1978).
8. Oppermann, H. D., Levinson, A., Varmus, H. E., Levintow, L. & Bishop, J. M. *Proc. natn. Acad. Sci. U.S.A.* **76**, 1804–1808 (1979).
9. Collett, M. S., Erikson, E., Purchio, A. F., Brugge, J. S. & Erikson, R. L. *Proc. natn. Acad. Sci. U.S.A.* **76**, 3159–3163 (1979).
10. Rubin, C. S. & Rosen, O. M. *A. Rev. Biochem.* **44**, 831–887 (1975).
11. Greengard, P. *Science* **199**, 146–152 (1978).
12. Collett, M. S., Erikson, E. & Erikson, R. L. *J. Virol.* **29**, 770–781 (1979).
13. Nicolson, G. *Biochim. biophys. Acta* **458**, 1–72 (1976).
14. Branton, P. E. & Landry-Magnan, J. *Biochim. biophys. Acta* **508**, 246–259 (1978).
15. Branton, P. E. & Landry-Magnan, J. *J. Cell. Physiol.* **100**, 159–168 (1979).
16. Larsson, H., Edstrom, A. & Wallin, M. *J. Neurochem.* **29**, 115–120 (1977).
17. Brunette, D. M. & Till, J. E. *J. Membrane Biol.* **5**, 215–224 (1971).
18. Perdue, J. F. *Meth. Enzym.* **31**, 162–168 (1974).
19. Kawai, S. & Hanafusa, H. *Virology* **46**, 470–479 (1971).
20. Atkinson, P. H. & Summers, D. F. *J. biol. Chem.* **246**, 5162–5175 (1971).
21. O'Farrell, P. H. *J. biol. Chem.* **250**, 4007–4021 (1975).
22. Ames, G. F.-L. & Nikaido, K. *Biochemistry* **15**, 616–623 (1976).

Covalent binding of polycyclic aromatic compounds to mitochondrial and nuclear DNA

J. A. Allen* & M. M. Coombs

Chemistry Laboratory, Imperial Cancer Research Fund, Lincoln's Inn Fields, London WC2A 3PX, UK

Since the pioneering work of the Millers[1] it has become clear that most chemical carcinogens require metabolism to reactive electrophiles and then exhibit their carcinogenic potential by reacting chemically with, and modifying, cellular macromolecules. At first modification of proteins was considered most likely to be of importance in carcinogenesis. Later, Brookes and Lawley[2] demonstrated that the extent of binding of several polycyclic hydrocarbons to DNA, but not to RNA or protein isolated from the skin of mice treated topically with these compounds, correlated with their known carcinogenic potency to this tissue. Mammalian cells, particularly mouse embryo cells, treated with chemical carcinogens have often been used, and DNA has been involved almost exclusively from whole cells. However, mitochondria possess unique DNA which accounts for 0.1–1% of the total DNA present in mammalian cells[3], and three studies have shown that carcinogenic alkylating agents modify the mitochondrial DNA by a factor about five times greater than the nuclear DNA from the same cells[4–6]. We demonstrate here that with six polycyclic aromatic compounds, all of which require metabolic activation and bind to DNA to a much smaller extent than direct-acting alkylating agents, the binding to mitochondrial relative to DNA is dramatically increased by a factor of nearly 50 to over 500.

Whole mouse embryo cells in their third passage from specific pathogen-free Tyler's Original (TO) mice were labelled in culture with [2-^{14}C]thymidine (60 mCi mmol^{-1}) and grown to confluency. Tritium-labelled polycyclic compounds (0.16–1.25 μg ml^{-1}, depending on toxicity) were added as shown in Table 1 and 24–48 h later the cells were collected, washed, and gently disrupted mechanically by hand using a Potter-Elvehjem homogenizer. Nuclei and mitochondria were isolated by the methods of Prescott *et al.*[7] and Miyaki *et al.*[8], respectively, and their purity was checked by light and electron microscopy. Nuclear DNA was extracted using Diamond's modification of the Kirby method[9] which involves isolation of the DNA from SDS lysates by phenol extraction, subsequent treatment with RNase, and a second isolation by phenol extraction. Mitochondrial DNA was obtained basically by the method of Hirt[10]; because mitochondrial DNA was lost during phenol extraction, the latter step and RNase treatment were omitted. The resultant solution of mitochondrial DNA therefore still contained mitochondrial RNA and residual protein which were also labelled

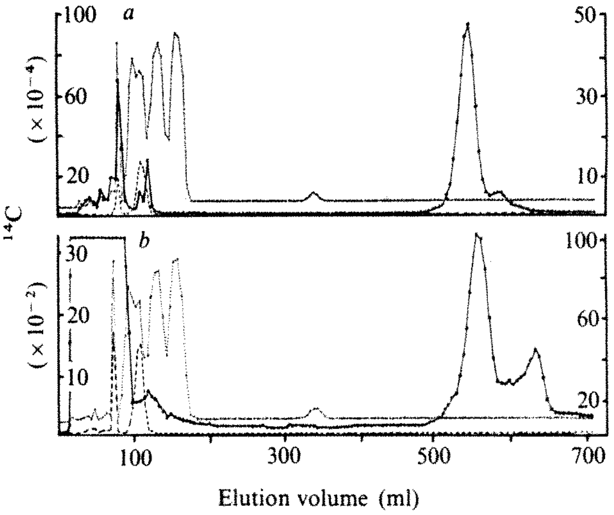

Fig. 1 LH20 chromatography of hydrolysates of nuclear (*a*) and mitochondrial (*b*) DNA from mouse cells treated in culture with benzo[*a*]pyrene. Hydrolysates were run on Sephadex LH20 columns of 90 × 1.5 cm with a linear gradient of 30% methanol in water increasing to 100% methanol. Fractions (5 ml) were collected and aliquots (1.5 ml) were counted for ^{14}C and ^{3}H activities in a LKB Wallac 1215 Rackbeta liquid scintillation counter. The amounts of the nucleosides were corrected for the efficiency of the hydrolysis, calculated from the total ^{14}C in the DNA hydrolysed and the ^{14}C in the thymidine peak. The large amount of tritium eluted in the first 100 ml of the mitochondrial DNA hydolysate arises from the tritiated hydrocarbon bound to the RNA and residual protein. ······, UV absorption at 254 nm; ●—●—●, ^{3}H d.p.m.; – – – –, ^{14}C d.p.m.

---

* Present address: Huntingdon Research Centre, Huntingdon, Cambridgeshire, UK.

0028-0836/80/380244—02$01.00

Table 1 Binding of polycyclic aromatic compounds to nuclear and mitochondrial DNA

				Binding index (μmol of compound bound per mol DNA phosphorous)		
Compound	Specific activity (Ci $mmol^{-1}$)	Dose (μg ml^{-1})	Incubation time (h)	Nuclear DNA (nuc)	Mitochondrial DNA (mt)	Ratio mt/nuc
DMBA	19.6	0.212	24	12.1 ± 2.0	897 ± 63.5	78 ± 18.5*
MCA	9.0	0.496	24	21.9 ± 0.3	1,024 ± 20	47 ± 0.3*
B[*a*]P	18.0, 27.0	0.235	24	7.5 ± 1.9	413 ± 164	53 ± 8.7*
11-MeCPP	13.9	1.250	48	0.53	312	589†
B[*a*]A	5.9	0.644	24	0.44 ± 0.11	104 ± 40.2	230 ± 51.5*
12-MeCPP	27.5	1.250	48	0.28 ± 0.03	26.3 ± 16.2	98 ± 65.5*

All compounds were generally labelled with tritium. DMBA, 7,12-dimethylbenz[*a*]anthracene; MCA, 3-methylcholanthrene; B[*a*]P, benzo[*a*]pyrene; 11-MeCPP, 15,16-dihydro-11-methylcyclopenta[*a*]phenanthren-17-one[24]; B[*a*]A, benz[*a*]anthracene; 12-MeCPP, 15,16-dihydro-12-methylcyclopenta[*a*]phenanthren-17-one[24].

* Duplicate experiments ± s.d.

† Single experiment.

with tritium through binding to the hydrocarbons to these macromolecules.

The amount of nuclear DNA (usually 1–2 mg) was determined by UV spectrophotometry, having calibrated this by phosphorous analysis using the colorimetric method of King and Wotton[11]. Mitochondrial DNA was estimated, following enzymatic hydrolysis and separation of the deoxynucleosides, by relating the ^{14}C d.p.m. in the thymidine peak to the specific ^{14}C activity of the nuclear DNA, and was found to fall into the expected range (about 2 μg). On one occasion this was confirmed by direct estimation of the mitochondrial DNA by the fluorimetric micro method of Hill and Whatley[12] using mithramycin, thus establishing that the ^{14}C specific activities of the nuclear and mitochondrial DNA were similar. After dilution with carrier calf thymus DNA, both samples were hydrolysed enzymatically with DNase which had been carefully checked for absence of RNase activity, and the liberated deoxyribonucleosides were separated by Sephadex LH20 chromatography (Fig. 1). The binding index (μmol of compound bound per mol of DNA phosphorous) was calculated from the total amount of tritium in the modified deoxyribonucleoside peaks which elute after the natural deoxyribonucleosides, assuming the specific activity of the bound compound was unaltered. As Phillips *et al.*[13] have shown, residual protein and RNA do not interfere with this separation because they are eluted in the first 100 ml, immediately before the natural nucleosides. Six polycyclic aromatic compounds were examined in this way, the results of which are summarized in Table 1.

All six compounds modified both nuclear and mitochondrial DNA, and in each case the binding index for the latter was considerably higher than for the former. Although experimental difficulties made the precision of the values rather uncertain, the large differences observed cannot be explained by the small deviations in purine and pyrimidine base ratios known to exist between mammalian nuclear and mitochondrial DNA. These differences in binding index may occur because both the mitochondrial inner[14] and outer[15] membranes contain the enzymes required to metabolize polycyclic aromatic compounds which probably tend to accumulate in these lipophilic membranes[16]. Furthermore, mitochondrial DNA is 'naked', being devoid of the histone and non-histone proteins that are intimately associated with DNA in the nucleus. The highest DNA-binding indices, both nuclear and mitochondrial, are shown by the two most potent carcinogens: 7,12-dimethylbenz[*a*]anthracene (DMBA) and 3-methylcholanthrene (MCA). Benzo[*a*]pyrene and 15,16-dihydro-11-methylcyclopenta[*a*]phenanthren-17-one(11-MeCPP) are similar to each other in potencies[17], but are less active as carcinogens than DMBA and MCA; benz[*a*]anthracene is an extremely weak carcinogen whereas 12-MeCPP is inactive[18]. The nuclear DNA-binding indices of these last four compounds do not reflect this, whereas there is good correspondence with the mitochondrial binding indices. In all cases, the nucleoside adducts seen in the nuclear DNA hydrolysates are also present in the hydrolysates of the mitochondrial DNA, but in addition the latter also exhibit substantial amounts of slower-running adducts. In the case of benzo[*a*]pyrene[19] (shown in Fig. 1) and 11-MeCPP[20], the major nuclear adduct peak is known to represent the compound formed by reaction of the bay-region dihydrodiol epoxide with deoxyguanosine. The slower-running, less polar adducts therefore probably result from reaction of simple non-hydroxylated epoxides, such as K-region or non-K-region epoxides, with a DNA base.

The significance of these findings is not clear. As these cells contain about 1,000 times more nuclear than mitochondrial DNA, the actual amount of compound bound to the former is 2–20 times that bound to the latter. This does not imply that damage caused by this modification will also be in this ratio, because the efficiency of DNA repair may be different at these two sites. However, mitochondrial DNA codes for several essential subunits of ATPase, cytochrome bc_1 and cytochrome *c* oxidase[21], and it is therefore interesting that derangements of energy metabolism often characterize tumours (see ref. 22). Recently Wilkie *et al.*[23] found that most carcinogens they tested caused the cytoplasmic 'petite' mutation in the yeast *Saccharomyces cerevisiae*. Moreover, effects on the cell surface were observed in non-fermentable conditions where mitochondrial function is required for growth. These authors suggest a possible role for mitochondrial mutations in cancer through a heritable disturbance either directly or by modulation of a nuclear gene.

Received 8 April; accepted 23 July 1980.

1. Miller, E. C. & Miller, J. A. *Cancer Res.* **7,** 468–480 (1947).
2. Brookes, P. & Lawley, P. D. *Nature* **202,** 781–784 (1964).
3. Nass, S. *Int. Rev. Cytol.* **25,** 55–129 (1969).
4. Wunderlich, V., Schütt, M., Bottger, M. & Graffi, A. *Biochem. J.* **118,** 99–109 (1970).
5. Wunderlich, V., Tetzlaff, I. & Graffi, A. *Chem.-Biol. Interactions* **4,** 81–89 (1971).
6. Wilkinson, R., Hawkes, A. & Pegg, A. E. *Chem.-Biol. Interactions* **10,** 157–167 (1975).
7. Prescott, D. M., Tao, M. V. N., Evenson, D. P., Stone, G. E. & Thrasher, J. D. in *Methods in Cell Physiology* Vol. 2 (ed. Prescott, D. M.) 131–142 (Academic, New York, 1966).
8. Miyaki, M., Yatagai, K. & Ono, T. *Chem.-Biol. Interactions* **17,** 321–329 (1977).
9. Diamond, L., Defendi, V. & Brookes, P. *Cancer Res.* **27,** 890–897 (1967).
10. Hirt, B. *J. molec. Biol.* **26,** 365–369 (1967).
11. King, E. J. & Wotton, I. D. P. *Micro-analysis in Medical Biochemistry* 3rd edn, 76 (Churchill, London, 1956).
12. Hill, B. T. & Whatley, S. *FEBS Lett.* **56,** 20–23 (1975).
13. Phillips, D. H., Grover, P. L. & Sims, P. *Int. J. Cancer* **22,** 487–494 (1978).
14. Sato, R., Atsuta, Y., Imai, Y., Taniguchi, S. & Okuda, K. *Proc. natn. Acad. Sci. U.S.A.* **74,** 5477–5481 (1977).
15. Raw, I. *Biophys. biochem. Res. Commun.* **81,** 1294–1297 (1978).
16. Graffi, A. *Z. Krebsforsch.* **49,** 477–495 (1940).
17. Coombs, M. M., Bhatt, T. S. & Young, S. *Br. J. Cancer* **40,** 914–921 (1979).
18. Coombs, M. M. & Croft, C. J. *Prog. exp. Tumor Res.* **11,** 69–85 (1969).
19. Sims, P., Grover, P. L., Swasiland, A., Pal, K. & Hewer, A. *Nature* **254,** 326–328 (1974).
20. Coombs, M. M., Kissonerghis, A.-M., Allen, J. A. & Vose, C. W. *Cancer Res.* **39,** 4160–4165 (1979).
21. Borst, P. & Grivell, L. A. *Cell* **15,** 705–723 (1978).
22. Warburg, O. *Science* **123,** 309–314 (1956).
23. Egilsson, V., Evans, I. H. & Wilkie, D. *Molec. gen. Genet.* **174,** 39–46 (1979).
24. Coombs, M. M. *J. labelled Comp. Radiopharm.* **16,** 147–151 (1980).

Early capping of transcripts from the adenovirus major late transcription unit

A. Babich, J. R. Nevins & J. E. Darnell Jr

The Rockefeller University, New York, New York 10021

The various events which result in modification of a primary RNA transcript may have a role in choosing transcripts which are to be processed into mRNA. If there is a stepwise and interdependent nature to each of the modifications then it is important to place the various steps in temporal order. We show here that the formation of a capped 5' terminus seems to be a very early event for adenovirus type 2 (Ad-2) nuclear RNA that is initiated at the major late Ad-2 promoter[1-5]. There is an equally rapid entry of ^{3}H-adenosine into the cap and the first dozen or so adenylate residues in the RNA chain. Taken together with evidence on general mRNA metabolism in Chinese hamster cells[6], it seems unlikely that capping has any differential role in successful RNA processing but rather is an automatic event for all RNA polymerase II products.

Location of the apparent initiation site for the major late adenovirus transcription unit near map position 16 on the genome (refs 3–5); 1 unit = 360 bases; 0 is at the 3' end of the rightward-transcribed strand) followed by the determination of DNA base sequence in this region[7-9] showed that the common late 5' mRNA sequence m^{7}GpppACUCUUCUG occurs only once near position 16 (refs 7–9). It therefore seemed likely that the initiating nucleotide in the primary transcript is the nucleotide which becomes capped during RNA processing. The viral DNA between 16.45 and 18.2 map units contains 536 bases of which 94 are thymidylate residues that are transcribed into adenylate residues in the primary RNA transcript as transcription proceeds from position 16.45 to position 18.2 (ref. 7). Together with the sequence information, an assay of chain length and a measurement of ^{3}H-adenosine in the labelled chains and in the cap, the frequency of capping as a function of chain size can be estimated. For instance, an RNA chain 32 nucleotides long would contain four AMP residues one of which would be in the cap; therefore, 25% of the radioactivity in such a molecule labelled with ^{3}H-adenosine would be in the cap.

Late in adenovirus infection, cells were labelled with ^{3}H-adenosine for 20 min and the total nuclear RNA that sedimented more slowly than 18S was hybridized to *Sma*F DNA (11.6–18.2 map units) that was immobilized on nitrocellulose filters. The hybridized RNA remaining after T1 RNase digestion was then eluted from the DNA. In the first experiment (Fig. 1) the presence of caps in the *Sma*F-specific RNA was determined by digesting the RNA to completion with RNases A and T2 and P$_1$ nuclease followed by treatment with bacterial alkaline phosphatase to release labelled adenosine residues from internal positions in the RNA chain and labelled nuclease-resistant 'cap core' structures[1,6]. Guanosine residues should also be labelled to the extent that ^{3}H-adenosine is converted to guanylate nucleotides. After electrophoresis of the digest (*p*H 3.5) the majority of radioactivity was represented by adenosine (Fig. 1), with also a small amount of guanosine. In addition, there was a peak of labelled, negatively charged material (fractions 38, 39, Fig. 1) that was resistant to the nuclease digestion and that migrated similarly to the appropriate cap core marker (m^{7}GpppAm).

About 2.7% of the total ^{3}H-adenosine radioactivity was in the form of the presumed cap structures (Table 1), suggesting a chain length of about 175 nucleotides if every chain were capped. As the size of the short promoter-proximal chains that were analysed was about 200 nucleotides (see Fig. 2*a*), it seemed that most of the chains must be capped. Because at least some of these molecules represent prematurely terminated transcripts[10,11], these results would indicate that the presence of a cap on an RNA transcript is not sufficient to ensure the completion of the chain.

It remained possible that some of the smallest promoter-proximal chains might be uncapped and contain pppA termini. Therefore the small RNA chains less than 18S were refractionated by sedimentation for a longer time through a second sucrose gradient (Fig. 2*a*). The peak of *Sma*F-specific RNA was in chains about 100–200 nucleotides long with significant hybridizable RNA both larger and smaller than tRNA (80 nucleotides). A 'large pool' from this gradient (fractions 2–7) represented chains longer than about 100 nucleotides, and a 'small pool' (fractions 8–12) contained molecules less than 100 nucleotides long. The promoter-proximal RNA was selected from both the large and small RNA pools by hybridization to the *Sma*F fragment. To detect potential uncapped termini that retained terminal phosphates, the nucleotide analyses were performed differently from those in the first experiment. After selection by hybridization, the RNA was digested only with P$_1$ nuclease and not with bacterial alkaline phosphatase so as to liberate labelled internal A or G residues as 5' nucleotides and leave 5'-terminal adenylate residues intact as either cap structures or uncapped polyphosphate residues[1,6]. After DEAE-paper electrophoresis (*p*H 3.5), both large and small RNA samples yielded pA and pG residues along with material migrating similarly to the cap core marker and the ADP marker (peak C, Fig. 2*b*, *c*). In addition there were two minor peaks (A and B, Fig. 2*b*,*c*) of P$_1$-resistant material that were completely resistant to further digestion by alkaline phosphatase and therefore did not contain terminal phosphates (data not shown).

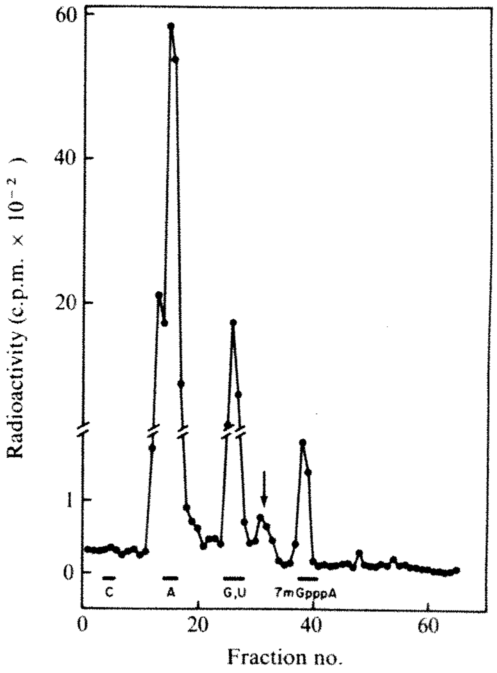

Fig. 1 Analysis of late Ad-2 promoter-proximal RNA for cap content. Adenovirus-infected cells at 16 h post-infection were labelled for 20 min with ^{3}H-adenosine (300 μCi ml^{-1}). The nuclear RNA was prepared and molecules of less than 2,000 nucleotides were isolated by sucrose gradient sedimentation. The promoter-proximal RNA was selected by hybridization to filter-bound *Sma*F DNA (map coordinate 11.6–18.2). After removal of unhybridized RNA and tails by digestion with T1 RNase, the filter was washed with 2 × SSC and then incubated with iodoacetate to inactivate the RNase. The RNA was eluted in H_2O by heating to 100 °C for 2 min. The RNA was first digested with RNase A (200 units ml^{-1}) and T2 (20 units ml^{-1}), followed by digestion with P$_1$ nuclease (200 units ml^{-1}) and then bacterial alkaline phosphatase (20 units ml^{-1}). The digest was analysed by electrophoresis on Whatman 3MM paper at *p*H 3.5. The arrow indicates the origin. The positive electrode is to the right.

0028–0836/80/380246—03$01.00

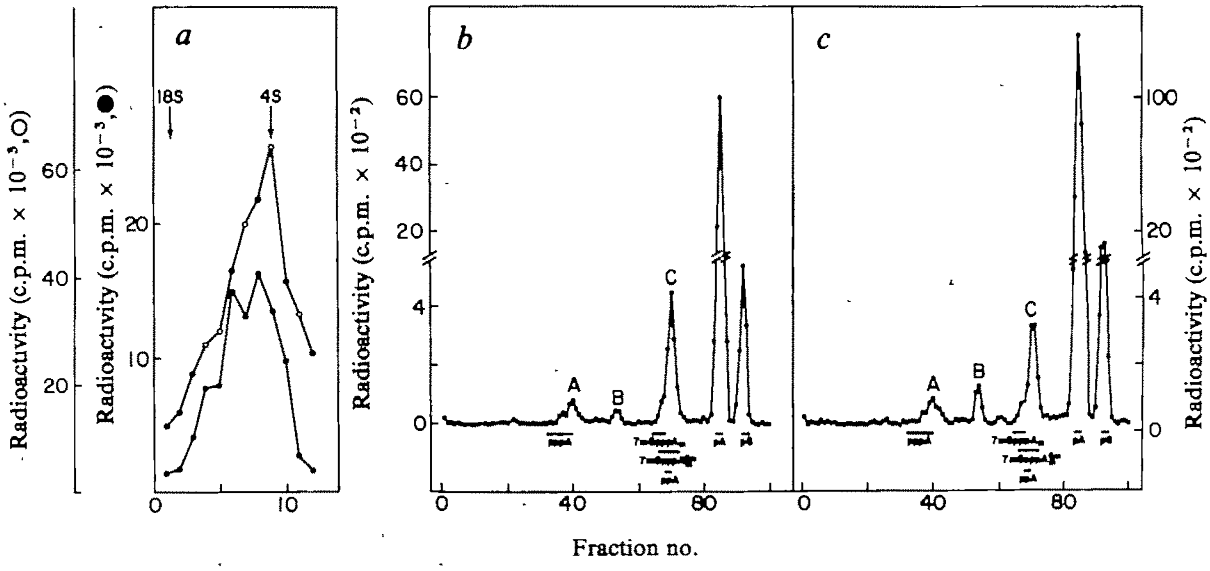

Fig. 2 *a*, Sedimentation profile of small, promoter-proximal late adenovirus nuclear RNA. RNA prepared from infected cells as described in the legend to Fig. 1 was resedimented in a second sucrose gradient (15–30% sucrose, SW41 rotor) at 30,000 r.p.m. for 19 h at 22 °C. Fractions of 1 ml were collected. Aliquots (10 µ1) of each fraction was counted directly in a Triton–toluene scintillant (○) and 50 µl of each fraction was assayed by hybridization to nitrocellulose filters containing the *Sma*F fragment (●). Two pools were made for subsequent analysis. A pool representing large RNA included fractions 2–7; a small RNA pool included fractions 8–12. Analysis of large (*b*) and small (*c*) promoter-proximal RNAs for 5′ termini. The two pools of RNA prepared as described in the legend to Fig. 2 were ethanol-precipitated and then each RNA sample was hybridized to filters containing the *Sma*F fragment. The eluted RNA was digested with P_1 nuclease (200 units ml^{-1}) and then electrophoresed on DEAE-paper at *p*H 3.5. Half of each lane was cut into 0.5-cm wide strips and counted. The other half was eluted and further analysed as described in Fig. 3 legend. The origin is at fraction 0 with electrophoresis towards the positive electrode.

Rather, this material could represent either ring-opened cap structures[12] or an incomplete P_1 digestion product. The major P_1-resistant material (peak C, Fig. 2*b*, *c*), which constituted 70–80% of the non-pA radioactivity, migrated during electrophoresis on DEAE paper as either a cap core (m^{7}GpppAm) or ADP. Treatment of this peak with alkaline phosphatase alone showed that the peak C material from both the large and small pools was resistant to alkaline phosphatase digestion and migrated with the cap core marker (Fig. 3*b*, *d*). The material from peak C was, however, sensitive to a combined pyrophosphatase and alkaline phosphatase digestion yielding labelled adenosine (Fig. 3*a*, *c*), confirming that it was in fact cap core. Thus there was no evidence for terminal phosphorylated structures even in the smallest RNA chains.

Again, in this experiment, the proportion of the radioactivity in caps compared with that in adenylate residues in the RNA chains indicated that all chains were capped. There was a ratio of one A in the cap per 30 As in the chain (or about 160 total residues) for RNA molecules from the larger pool and 1 in 12 (or about 70 total residues) for the smaller pool (Table 1). These estimates of chain length of capped molecules are in good agreement with the sedimentation sizes of the two RNA pools, indicating that nearly every chain possesses a cap, including those transcripts which average only 70 nucleotides and therefore must include many chains considerably shorter than 70 bases. Furthermore, no evidence of uncapped phosphorylated termini could be found even in the short chains. It should be pointed out that free pppA and pppG termini are readily detected in short cellular RNA transcripts that are presumably polymerase I and polymerase III products[6].

A previous analysis of the prematurely terminated transcripts from the major late adenovirus transcription unit demonstrated that in steady-state labelling conditions a prominent species of promoter-proximal RNA of chain length 200–250 nucleotides was detected[11]. Very few prematurely terminated RNA chains in the size range of 80–200 nucleotides were observed. This is not the situation for the promoter-proximal RNA prepared from cells labelled for 20 min with ^{3}H-adenosine where there are many chains in the size range of 100–200 nucleotides. Thus, it is likely that the chains which are less than 100 nucleotides long represent to some considerable degree, growing chains.

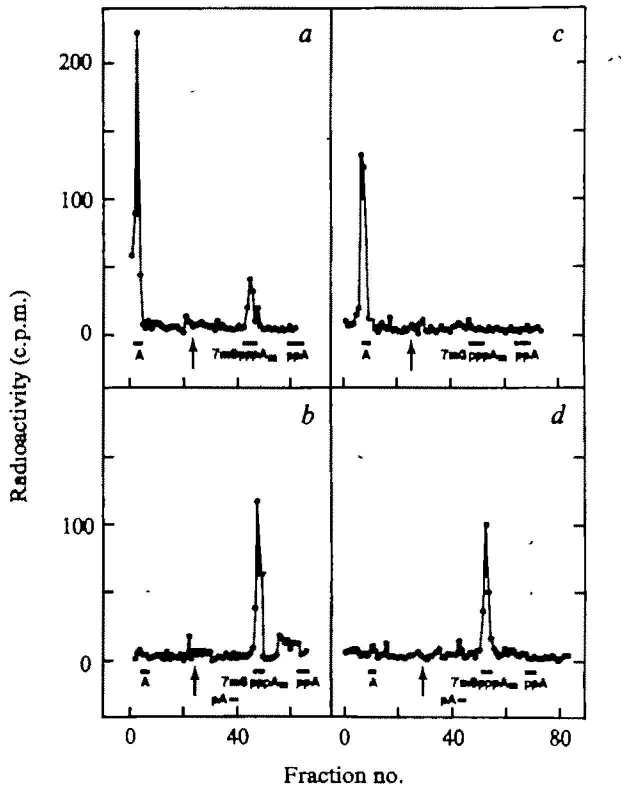

Fig. 3 Analysis of 5′-terminal structures from large and small promoter-proximal RNAs. The material designated as peak C in Fig. 2*b* and *c* was eluted from the DEAE paper in 30% triethylammonium carbonate, *p*H 7.4. The eluted material was lyophilized, dissolved in H_2O and then lyophilized again. The large RNA (*a*, *b*) and the small RNA (*c*, *d*) samples were divided into two parts. One part of each sample was digested with alkaline phosphatase alone. The other part was first digested with pyrophosphatase (1.5 units ml^{-1}) and then with alkaline phosphatase. The digestion products of each sample were then separated by electrophoresis on Whatman 3MM paper at *p*H 3.5. Strips 0.5 cm wide were counted. *a*, *c*, Pyrophosphatase plus alkaline phosphatase. *b*, *d*, Alkaline phosphatase alone. The arrow indicates the origin.

Table 1 Distribution of ^{3}H-adenosine label added late in adenovirus infection

Expt	RNA pool	Radioactivity (c.p.m.) As adenosine	As pA	As cap	% Radio-activity as cap	Predicted chain length
1	—	16,801	—	468	2.7	175
2	Large	—	27,591	978	3.4	153
	Small	—	11,061	1,085	8.9	70

The values for expt 1 are from the data presented in Fig. 1, and for expt 2 from the data presented in Fig. 2*b*, *c*. The predicted chain lengths are based on the location of thymidylate residues in the sequence of Ad-2 DNA between the start site for late transcription at 16.45 map units and the *Sma*I cleavage site at 18.2 map units[7]. For each RNA chain, the cap produced by RNase A and T2 digestion would contain one A residue.

Since these short chains had the highest cap content and did not reveal any pppA termini it is clear that capping occurs soon after synthesis is initiated. Our experiments cannot determine whether the 5′ terminus is capped concomitantly with the initiation of synthesis, although this is a possibility. Furuichi[13] has demonstrated that the formation of a capped 5′ terminus on the cytoplasmic polyhedrosis virus mRNA is a pre-transcriptional event. Weil *et al.*[14] also showed that correct initiation of Ad-2 transcription can be obtained *in vitro* by RNA polymerase II in the presence of a crude cell extract. This crude *in vitro* system produces chains with capped ends. In addition to Ad-2 transcripts, polymerase II cellular transcripts also have caps added early during synthesis[6]. Thus an association of capping enzymes with the initiation complexes for polymerase II transcription is a distinct possibility.

We thank Janet Winkler for technical assistance. This work was supported by NIH grants GM26765-01 and CA09256-04 and ACS grant MV39I. A.B. was supported by Institutional Training Grant T32CA09256 from the NCT.

Received 22 April; accepted 18 July 1980.

1. Shatkin, A. J. *Cell* **9**, 645–654 (1976).
2. Brawerman, G. *Prog. Nucleic Acid Res. molec. Biol.* **17**, 117–148 (1976).
3. Darnell, J. E. *Prog. Nucleic Acid Res. molec. Biol.* **22**, 227–353 (1979).
4. Nevins, J. R. & Chen-Kiang, S. *Adv. Virus Res.* **26**, (in the press).
5. Ziff, E. B. *Nature* (in the press).
6. Salditt-Georgieff, M., Harpold, M., Chen-Kiang, S. & Darnell, J. E. *Cell* **19**, 69–78 (1980).
7. Ziff, E. B. & Evans, R. M. *Cell* **15**, 1463–1475 (1978).
8. Baker, C. C. & Ziff, E. B. *Cold Spring Harb. Symp. quant. Biol.* **44**, (in the press).
9. Gelinas, R. E. & Roberts, R. J. *Cell* **11**, 533–544 (1977).
10. Evans, R. M., Weber, J., Ziff, E. & Darnell, J. E. *Nature* **278**, 367–370 (1979).
11. Fraser, N. W., Sehgal, P. B. & Darnell, J. E. *Proc. natn. Acad. Sci. U.S.A.* **76**, 2571–2575 (1979).
12. Rottman, F., Desrosiers, R. C. & Friderici, K. *Prog. Nucleic Acid Res. molec. Biol.* **19**, 21–38 (1976).
13. Furuichi, Y. *Proc. natn. Acad. Sci. U.S.A.* **75**, 1086–1090 (1978).
14. Weil, P. A., Luse, D. S., Segall, J. & Roeder, R. G. *Cell* **18**, 469–484 (1979).

The Archaebacteria and eukaryotic origins

Leigh M. Van Valen & Virginia C. Maiorana

Biology Dept (Whitman), University of Chicago, 915 E. 57th Street, Chicago, Illinois 60637

Critical analysis of the phylogeny of prokaryotes is in its infancy. Woese and others[1–5] have made the startling proposal that methane-producing bacteria and a few others form a phyletically unified group, the Archaebacteria, as old and as diverse (although not now as numerous) as all other bacteria. The only critique[6] of this proposal is inadequate[7]. Here we present an alternative view, that the Archaebacteria were derived from other bacteria and contain the ancestor of a cell which engulfed others, eventually to become the first eukaryote.

The main evidence used for the relative time of divergence of the Archaebacteria is that their 16S ribosomal RNA is very different from that of other bacteria. However, as Woese recognizes[3], this can be the result of rapid early evolution. The origin of new adaptations often occurs rapidly, as exemplified by the evolution of bats[8], whales[9] and modern placental mammals as a whole[10]. Evolutionary rates vary widely[11], and an attempt[12] to extrapolate the average rate of evolution of cytochrome *c* from vertebrates to angiosperms gave results which contradicted the fossil record[13]. (We do not mean to dispute the usual approximate constancy of protein evolution.) Proteins themselves often evolve unusually rapidly when they undergo a major change in function[14,15]. Even the supposedly nearly invariant histone H4 is very different between ciliates and other eukaryotes[16]. The suggestion[5] that the diversity of Archaebacteria argues against rapid evolution near their origin is a non sequitur; placental mammals are a familiar counter-example in which both phenomena occur. The only studied genomes of archaebacteria are small[17,18], although far from the smallest known for prokaryotes[19].

Our proposal (Fig. 1), based in part on work by Margulis[20], Hall[21] and others, takes the evolution of mechanisms for acquisition of free energy to be central. We discuss the general topic elsewhere[22]. Any phylogeny must be based on a clear recognition of primitive states and derived states, for shared primitive states give no phyletic information[23,24]. A set of differences is not in itself an adequate basis for a phylogeny, in part because the base of the phylogeny can then be anywhere. We take glycolysis alone (as in some lactic-acid bacteria), especially its later stages, to be primitive among surviving organisms because it is almost universally distributed and provides materials for other, presumably derived, processes such as the completed tricarboxylic–acid cycle.

The Archaebacteria are moderately derived prokaryotes in this view, although most surviving prokaryotes are even more derived. Why then should they be so divergent from the others? The answer may be lost in the Archaean, but we can offer an initial suggestion. One of the free-living Archaebacteria, *Thermoplasma*, lacks a cell wall, while the other known Archaebacteria have a wide diversity of cell walls[25] all very different in composition from the walls of all other walled cells. Thus it seems as though the ancestral lineage of Archaebacteria lost its cell wall, possibly for flexibility in locomotion or for energy conservation. Such a change could be related to other changes in adaptation.

Moreover, *Thermoplasma* itself shows several specific and derived similarities with eukaryotes[26]. It has a histone-like protein which produces nucleosome-like condensations of DNA. It has actin- and myosin-like proteins and microbody-like respiration. It can invaginate its plasma membrane, although apparently not with fully developed endocytosis. Such an ability is necessary for a cell which engulfs others.

However, like other surviving Archaebacteria[27], *Thermoplasma* has lipids with branched chains and with ether linkages instead of the esterifications of other prokaryotes and eukaryotes[28]. Unless eukaryote lipids came from another member of the presumptive symbiosis, this suggests that the surviving Archaebacteria evolved their unique lipids and other traits after the ancestral eukaryote diverged.

Halobacterium, a surviving archaebacterium[29] with independently derived light-driven ATP synthesis[18,30], has other specific and derived similarities with eukaryotes. Its light-transducing pigment is almost identical to rhodopsin[18]. Its initiator tRNA resembles that of eukaryotes in some ways[18] and produces a non-formylated methionine[18], as in eukaryotes. The only ribosomal protein studied has a partial amino acid sequence nearly intermediate between those of the bacterium *Escherichia* and the yeast *Saccharomyces*[18]. *Halobacterium* has a ferredoxin rather similar to that of plants[18], and its cell wall is composed of a glycoprotein resembling those of eukaryotic cell walls[18]. It even seems to have more than one non-plasmid chromosome, perhaps several[18]. Another archaebacterium,

0028-0836/80/380248—03$01.00

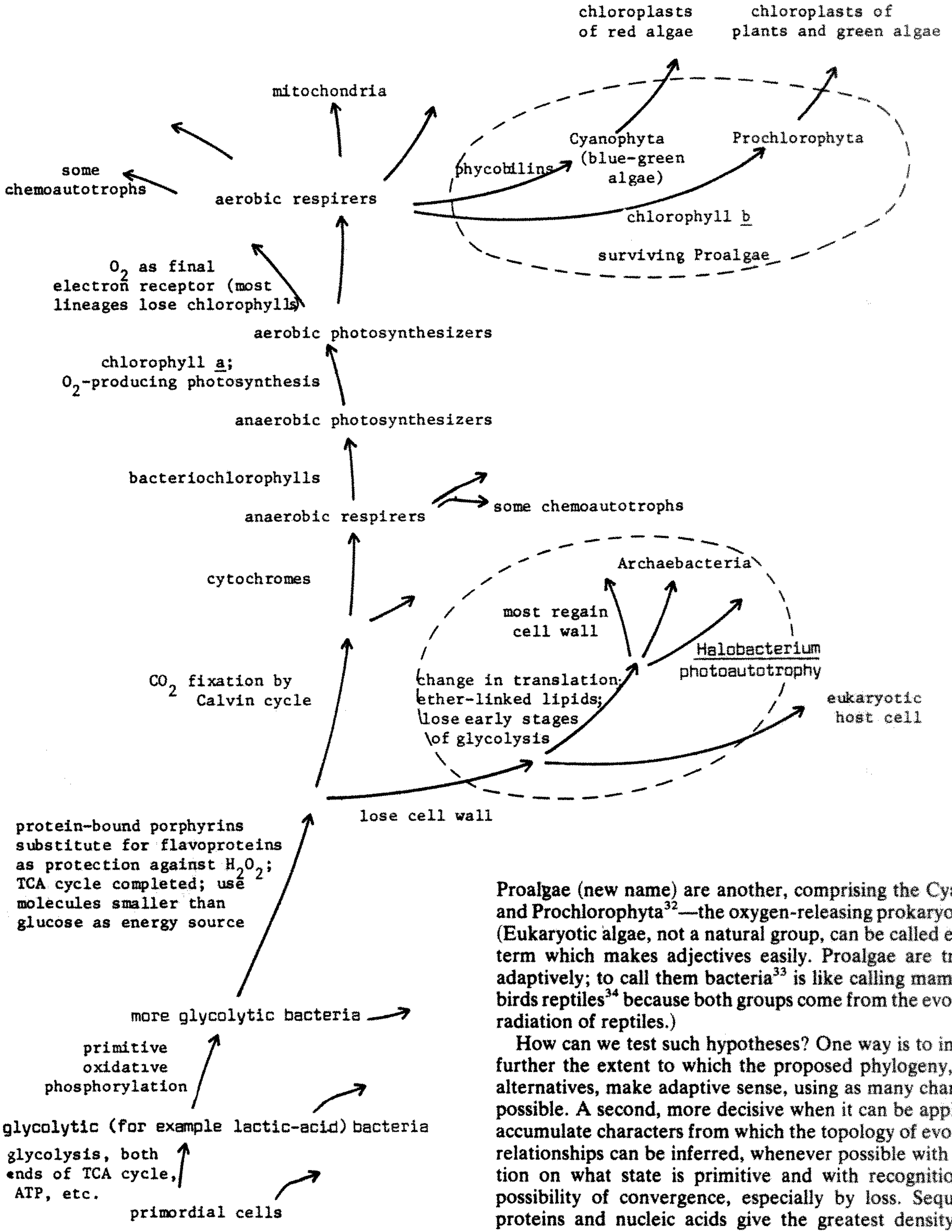
chloroplasts of red algae
chloroplasts of plants and green algae
mitochondria
Cyanophyta (blue-green algae)
Prochlorophyta
phycobilins
some chemoautotrophs
aerobic respirers
chlorophyll b
surviving Proalgae
O2 as final electron receptor (most lineages lose chlorophylls)
aerobic photosynthesizers
chlorophyll a; O2-producing photosynthesis
anaerobic photosynthesizers
bacteriochlorophylls
anaerobic respirers
some chemoautotrophs
Archaebacteria
cytochromes
most regain cell wall
Halobacterium photoautotrophy
CO2 fixation by Calvin cycle
change in translation; ether-linked lipids; lose early stages of glycolysis
eukaryotic host cell
lose cell wall
protein-bound porphyrins substitute for flavoproteins as protection against H2O2; TCA cycle completed; use molecules smaller than glucose as energy source
more glycolytic bacteria
primitive oxidative phosphorylation
glycolytic (for example lactic-acid) bacteria
glycolysis, both ends of TCA cycle, ATP, etc.
primordial cells

Fig. 1 Provisional phylogeny of prokaryotes.

Methanobacterium[17], but not *Halobacterium*[18], may have some repeated DNA.

Perhaps those resemblances to eukaryotes (except probably the cell wall) and those of *Thermoplasma* were present together in an ancestral form (*Thermoplasma* has not been studied for all of these characters) and some have been modified in each lineage. All enzymes of the tricarboxylic-acid cycle occur in archaebacteria, but not all together in the same species[5]. Parasitic mycoplasms also show some specific resemblances to *Thermoplasma*[25,31]; their relation to Archaebacteria needs clarification.

We therefore provisionally regard the Archaebacteria as one of several phyla of prokaryotes, most as yet undefined. The Proalgae (new name) are another, comprising the Cyanophyta and Prochlorophyta[32]—the oxygen-releasing prokaryotic algae. (Eukaryotic algae, not a natural group, can be called eualgae, a term which makes adjectives easily. Proalgae are true algae adaptively; to call them bacteria[33] is like calling mammals and birds reptiles[34] because both groups come from the evolutionary radiation of reptiles.)

How can we test such hypotheses? One way is to investigate further the extent to which the proposed phylogeny, and any alternatives, make adaptive sense, using as many characters as possible. A second, more decisive when it can be applied, is to accumulate characters from which the topology of evolutionary relationships can be inferred, whenever possible with information on what state is primitive and with recognition of the possibility of convergence, especially by loss. Sequences of proteins and nucleic acids give the greatest density of such characters, but the data on rRNA (not sequences because only isolated oligonucleotides have been studied) suggest that so great changes may have occurred in the origins of both archaebacteria and eukaryotes that even such slowly evolving molecules show only random similarity to those of their ancestors. Primitive eukaryotes such as *Eimeria*[35] and *Pelomyxa*[36] also deserve intensive scrutiny.

The translation apparatus of Archaebacteria differs from that of other organisms[4]. Perhaps there is an unbridgeable adaptive valley in this difference[3]. However, we think that this matter cannot be discussed adequately until much more is known about the functioning of existing translation apparatuses, and of potential intermediates, in realistic conditions. Until then we prefer to emphasize other evidence; it is dangerous to claim something is impossible in biology. The same function can be performed very differently in different selective conditions[37].

Nevertheless, Fig. 1 is consistent with existing evidence from macromolecular sequences[38] if primitive aerobic photosynthesizers are now extinct. Reticulate evolution by gene transfer provides an available and plausible excuse for disparities such as the presence in *Halobacterium* of a normal complement of cytochromes in an electron-transport chain[30], but there is a surprising lack of compelling evidence for its importance in any real case.

We thank L. Margulis, P. H. A. Sneath and C. R. Woese for comments.

Received 4 March; accepted 20 June 1980.

1. Woese, C. & Fox, G. E. *Proc. natn. Acad. Sci. U.S.A.* **74,** 5088–5090 (1977).
2. Fox, G. E., Magrum, L. J., Balch, W. E., Wolfe, R. S. & Woese, C. R. *Proc. natn. Acad. Sci. U.S.A.* **74,** 4537–4541 (1977).
3. Woese, C. & Fox, G. E. *J. molec. Evol.* **10,** 1–6 (1977).
4. Woese, C., Magrum, L. J. & Fox, G. E. *J. molec. Evol.* **11,** 245–252 (1978).
5. Balch, W. E., Fox, G. E., Magrum, L. J., Woese, C. R. & Wolfe, R. S. *Microbiol. Rev.* **43,** 260–296 (1979).
6. Steitz, J. A. *Nature* **273,** 10 (1978).
7. Woese, C. R. & Fox, G. E. *Nature* **273,** 101 (1978).
8. Van Valen, L. M. *Evol. Theory* **4,** 103–121 (1979).
9. Van Valen, L. M. *Evolution* **22,** 37–41 (1968); *Bull. Am. Mus. nat. Hist.* **132,** 1–126 (1966).
10. Van Valen, L. M. *Evol. Theory* **4,** 45–80 (1978).
11. Simpson, G. G. *The Major Features of Evolution* (Columbia University Press, 1953).
12. Ramshaw, J. A. M. *et al. New Phytol.* **71,** 773–779 (1972).
13. Van Valen, L. M. *J. molec. Evol.* **3,** 89–101 (1974).
14. Goodman, M. in *Molecular Evolution* (ed. Ayala, F. J.) 141–159 (Sinauer, Sunderland, 1976).
15. Kimura, M. & Ohta, T. *Proc. natn. Acad. Sci. U.S.A.* **71,** 2848–2852 (1974).
16. Glover, C. V. C. & Gorovsky, M. A. *Proc. natn. Acad. Sci. U.S.A.* **76,** 585–589 (1979).
17. Mitchell, R. M., Loeblich, L. A., Klotz, L. C. & Loeblich, A. R. III *Science* **204,** 1082–1084 (1979).
18. Bayley, S. T. & Morton, R. A. *CRC Crit. Rev. Microbiol.* **6,** 151–205 (1978).
19. Schwemmler, W. *Cytobiologie* **3,** 427–429 (1971).
20. Margulis, L. *Origin of Eukaryotic Cells* (Yale University Press, 1970).
21. Hall, J. B. *J. theor. Biol.* **30,** 429–454 (1971).
22. Maiorana, V. C. & Van Valen, L. *Cells: Their Lives and Evolution* (Harper and Row, New York, in the press).
23. Hennig, W. *Phylogenetic Systematics* (University of Illinois Press, 1966).
24. Van Valen, L. M. *Evol. Theory* **3,** 285–299 (1978).
25. Kandler, O. & König, H. *Archs Microbiol.* **118,** 141–152 (1978).
26. Searcy, D. G., Stein, D. B. & Green, G. R. *BioSystems* **10,** 19–28 (1978).
27. Tornabene, T. G. & Langworthy, T. A. *Science* **203,** 51–53 (1979).
28. Tornabene, T. G., Langworthy, T. A., Holzer, G. & Oro, J. *J. molec. Evol.* **13,** 73–83 (1979).
29. Magrum, L. J., Luehrsen, K. R. & Woese, C. R. *J. molec. Evol.* **11,** 1–8 (1978).
30. Lanyi, J. K. *Microbiol. Rev.* **42,** 682–706 (1978).
31. Barile, M. F. & Razin, S. (eds) *The Mycoplasmas* Vol. 1 (Academic, New York, 1979).
32. Lewin, R. A. *Nature* **261,** 697–698 (1976).
33. Stanier, R. Y. & Cohen-Bazire, G. *A. Rev. Microbiol.* **31,** 225–274 (1977).
34. von Huene, F. R. in *Robert Broom Commemorative Volume* (ed. Du Toit, A. L.) 65–106 (Royal Society of South Africa, Cape Town, 1948).
35. Wang, C. C. *Comp. Biochem. Physiol.* **B61,** 571–579 (1978).
36. Bovee, E. C. & Jahn, T. L. in *The Biology of Amoeba* (ed. Jeon, K. W.) 37–82 (Academic, New York, 1973).
37. Ghilarov, M. S. *Zakonomernosti Prisposoblenii Chleneistonogikh k Zhizni na Sushe* (Izdatel'stvo "Nauka", Moscow, 1970).
38. Schwartz, R. M. & Dayhoff, M. O. *Science* **199,** 395–403 (1978).

Archaebacterial elongation factor is ADP-ribosylated by diphtheria toxin

Michael Kessel & Friedrich Klink

Biochemisches Institut, Universität Kiel, Olshausenstrasse 40–60,
D-2300 Kiel 1, FRG

Archaebacteria have been defined as a 'third primary kingdom' of cells in addition to the urkaryotes and the eubacteria[1]. While the latter two correspond approximately to the conventional categories eukaryotes and prokaryotes respectively, the Archaebacteria have up to now comprised four groups of microorganisms: the methanogenic bacteria, the extremely halophilic bacteria and the two thermoacidophilic genera *Sulfolobus* and *Thermoplasma*. Based on ribosomal RNA sequence homologies and lipid composition, they apparently form a distinct group. Furthermore they possess or lack typical biochemical markers of both the eukaryotes and the prokaryotes, as well as having unique properties not found elsewhere[2]. Altogether, this indicates that they are not closer to either one of the classical categories. One clear-cut difference between prokaryotes and eukaryotes is the diphtheria toxin reaction, which catalyses the covalent binding of adenosine diphosphate-ribose (ADPR) to the eukaryotic peptide elongation factor EF2 in contrast to the homologous prokaryotic factor EF-G[3,4]. We report here that diphtheria toxin also catalyses the ADP-ribosylation of archaebacterial elongation factors. In this respect, these factors have to be assigned to the EF2 type; we suppose that the ADP-ribosylatable structure arising so early in evolution is of fundamental importance for the elongation process.

We have investigated crude cytoplasmic fractions of four main representatives of the Archaebacteria: *Halobacterium cutirubrum*, *Methanobacterium thermoautotrophicum*, *Sulfolobus acidocaldarius* and *Thermoplasma acidophilum*. After reaction with diphtheria toxin fragment A and ^{14}C-NAD labelled in the adenine moiety only one protein received a label. This could be demonstrated as radioactivity precipitable by trichloroacetic acid (TCA) and as one radioactive band in SDS–gel electrophoresis (Fig. 1). While *M. thermoautotrophicum*, *S. acidocaldarius* and *T. acidophilum* required the normal conditions[3] for the toxin reaction (neutral *p*H, about 0.05 M K^+, 30 min, 37 °C), high salt (3.8 M K^+ or 2.6 M NH_4^+) and 4 h incubation time were necessary for the extremely halophilic extract to attain maximum labelling. This reflects that the halophilic protein could only react in its native, salt-stabilized conformation, while the toxin fragment A, which has been shown to be remarkably stable to heat[6], extreme *p*H[6] and proteolytic enzymes[4], also tolerates high salt.

For comparison, a number of elongation factors from various eukaryotic sources were ADP-ribosylated in the same manner as the archaebacterial proteins; they showed the same mobility in one electrophoresis system, indicating a molecular weight (M_r) of 96,000. Isotopically labelled proteins from *M. thermoautotrophicum*, *S. acidocaldarius* and *T. acidophilum* were considerably smaller with apparent M_r of 86,000 for *M. thermoautotrophicum* and 83,000 for both the thermoacidophiles. These values are in the range of the M_r reported for the prokarytic, non-ADP-ribosylatable homologue EF-G, which is about 80,000 (ref. 7). The M_r of 111,000 found for the halophilic protein is exceptionally high. The EF-Gs from *Escherichia coli*[8] and *Streptococcus faecalis*[9] as well as mitochondrial factors[10] were shown to be unable to react with NAD and diphtheria toxin. We confirmed this for *Pseudomonas maltophila*, *Bacillus licheniformis*, *E. coli* K 12, *Hyphomicrobium* 526 and *Pedomicrobium* S 122.

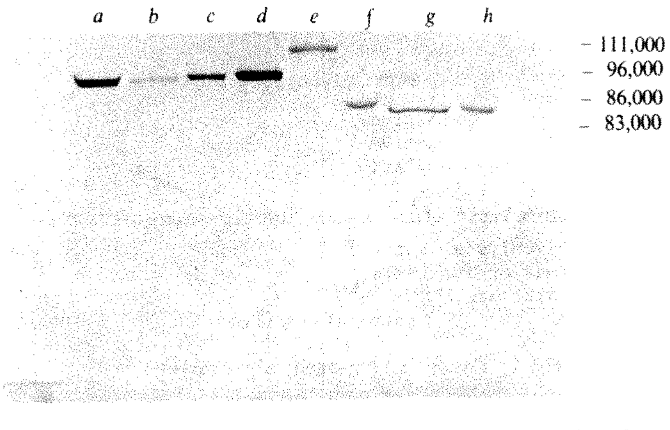

Fig. 1 Products of diphtheria toxin reaction from eukaryotic and archaebacterial sources. Crude fractions of soluble proteins were incubated with mercaptoethanol-reduced toxin (10–20 flocculation units per 75 μl), ^{14}C-NAD (10^{-6} M) and 0.05 M KCl for 30 min at 37 °C. Different conditions were used for the extreme halophile: saturated potassium chloride and incubation time of 4 hours. The reaction mixtures were separated on polyacrylamide gels (7.5%)[5], which were autoradiographed for 6 days. Calibration proteins were phosphorylase b (M_r 94,000), bovine serum albumin (M_r 67,000), catalase (M_r 58,000) and ovalbumin (M_r 43,000). The sources were as follows: *a*, wheat germ; *b*, rabbit liver; *c*, rat thymocytes; *d*, bovine liver; *e*, *H. cutirubrum*; *f*, *M. thermoautotrophicum*; *g*, *S. acidocaldarius*; *h*, *T. acidophilum*. Numbers on the right indicate M_r.

0028-0836/80/380250—02$01.00

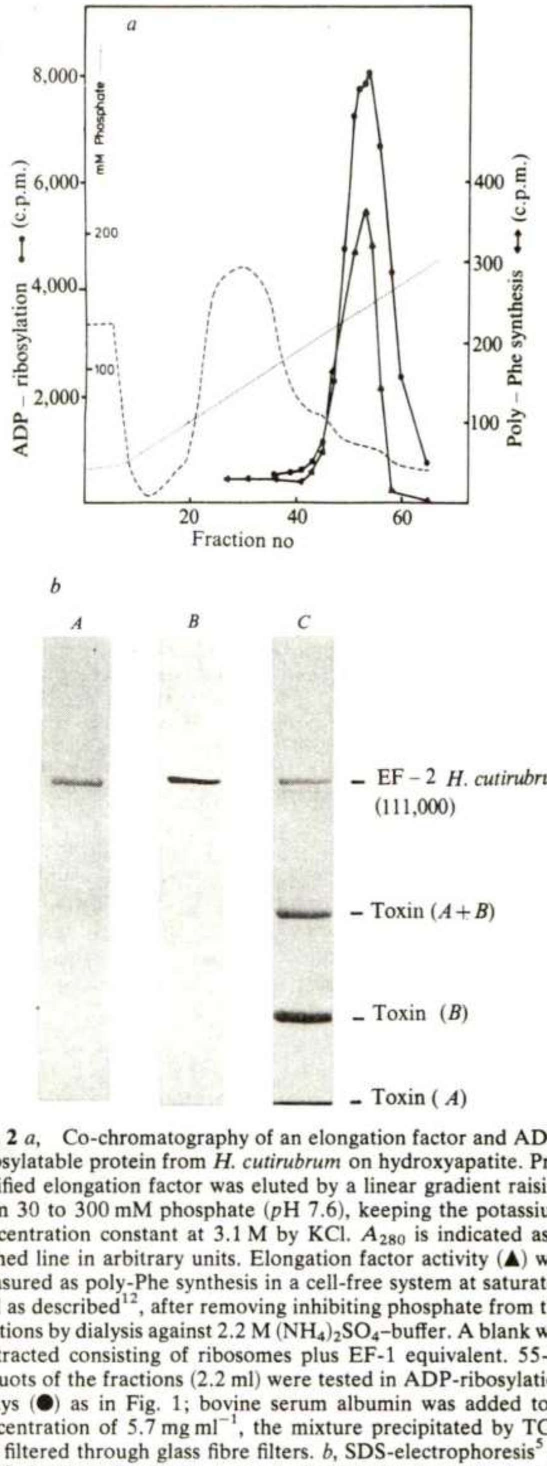

Fig. 2 *a*, Co-chromatography of an elongation factor and ADP-ribosylatable protein from *H. cutirubrum* on hydroxyapatite. Pre-purified elongation factor was eluted by a linear gradient raising from 30 to 300 mM phosphate (*p*H 7.6), keeping the potassium concentration constant at 3.1 M by KCl. A_{280} is indicated as a dashed line in arbitrary units. Elongation factor activity (▲) was measured as poly-Phe synthesis in a cell-free system at saturated KCl as described[12], after removing inhibiting phosphate from the fractions by dialysis against 2.2 M $(NH_4)_2SO_4$–buffer. A blank was subtracted consisting of ribosomes plus EF-1 equivalent. 55-μl aliquots of the fractions (2.2 ml) were tested in ADP-ribosylation assays (●) as in Fig. 1; bovine serum albumin was added to a concentration of 5.7 mg ml^{-1}, the mixture precipitated by TCA and filtered through glass fibre filters. *b*, SDS-electrophoresis[5] of purified elongation factor. Lane *A*, Coomassie blue stain; lane *B*, autoradiography of purified, ADP-ribosylated factor; lane *C*, Coomassie blue stain of lane *B*, containing the toxin bands.

Further investigation of the extremely halophilic archaebacterium *H. cutirubrum* identified the labelled protein with an elongation factor. For the protein synthesis test we modified a test system developed by Bayley[11], using poly(U) as a messenger, tRNA Phe as substrate and an EF-1-equivalent from *H. cutirubrum*[12], which complements with EF-2 to poly-Phe synthesis. The EF-2 co-purified with the ADP-ribosylatable protein using a three-step procedure on Sepharose with a decreasing $(NH_4)_2SO_4$ gradient, gel filtration at 0.9 M KCl/1.1 M $(NH_4)_2SO_4$ and hydroxyapatite (details to be reported elsewhere). The factor elutes from hydroxyapatite at 150 mM phosphate and is nearly homogeneous (Fig. 2*a*). The purified factor reacts with NAD and toxin as described for the crude fraction at high salt conditions. Under modified purification procedures we have also observed a main Coomassie blue band in SDS electrophoresis of M_r about 93,000 (ref. 12), probably due to proteolysis of the factor. The active, ADP-ribosylatable elongation factor from *H. cutirubrum* has a M_r of 111,000 in SDS-electrophoresis (Fig. 2*b*).

The structural basis of the diphtheria toxin reaction in eukaryotic systems is well established: the ADP-ribose residue of NAD is bound covalently to a post-translationally modified histidine[13] (previously called 'X', ref. 14), which only occurs in EF-2. The amino acid sequence of the ADP-ribosylation site has been shown to be highly conserved in yeast, wheat germ, rat and bovine liver[15]. It is obvious that the Archaebacteria also provide the prerequisites for the toxin reaction. Taking into account the high specificity of the toxin for EF-2 and also the evidence from the halophilic system, we conclude that the ADP-ribosylated protein in archaebacteria is an EF-2-type elongation factor. The eukaryotic feature of this elongation factor is a good argument for the separation of Archaebacteria from the prokaryotes as a 'third primary kingdom' (ref. 1). The evolutionary pressure also seems to have worked over the large phylogenetic distance from Archaebacteria to higher vertebrates. This consideration is further strengthened by results about ribosomal proteins, which are probably part of the binding site for the elongation factors on the ribosome[16]. These ribosomal A-proteins (L7/L12-equivalents) show a high degree of N-terminal sequence homology between halobacterial and eukaryotic systems[17]. Thus conservation of these cooperating structures may indicate functional importance for the elongation process in urkaryotes and their possible ancestors.

We thank R. Gehrmann, R. Gebers (Kiel) and K. O. Stetter (Munich) for gifts of bacteria or bacterial extracts, and E. Kaufmann for technical help. Diphtheria toxin was provided by Behring-Werke.

Received 27 May; accepted 23 June 1980.

1. Woese, C. R. & Fox, G. E. *Proc. natn. Acad. Sci. U.S.A.* **74,** 5088–5090 (1977).
2. Woese, C. R., Magrum, L. J. & Fox, G. E. *J. molec. Evol.* **11,** 245–252 (1978).
3. Collier, R. J. *Bact. Rev.* **39,** 54–85 (1975).
4. Gill, D. M. & Pappenheimer, A. M. *J. biol. Chem.* **246,** 1492–1495 (1971).
5. Laemmli, U. K. *Nature* **227,** 680–685 (1970).
6. Drazin, R., Kandel, J. & Collier, R. J. *J. biol. Chem.* **246,** 1504–1510 (1971).
7. Kaziro, Y., Inove-Yokosawa, N. & Kawakita, M. *J. Biochem.* **72,** 853–863 (1972).
8. Tsugawa, A., Ohsumi, Y. & Kato, I. *J. Bact.* **104,** 152–157 (1970).
9. Johnson, W. R., Kuchler, R. J. & Solotorovsky, M. *J. Bact.* **96,** 1089–1098 (1968).
10. Richter, D. & Lipmann, F. *Biochemistry* **9,** 5065–5070 (1970).
11. Bayley, S. T. & Griffith, E. *Biochemistry* **7,** 2249–2256 (1968).
12. Kessel, M. & Klink, F. in *Energetics and Structure of Halophilic Microorganisms* (eds Caplan, S. R. & Ginzburg M.) 453 (Elsevier, Amsterdam, 1978).
13. Bodley, J. W., Van Ness, B. B., Brown, B. A. & Howard, J. B. *Fedn Proc.* **38,** 2059 (1979).
14. Robinson, E. A., Henrikson, O. Z. Maxwell, E. S. *J. biol. Chem.* **249,** 5088–5093 (1974).
15. Brown, B. & Bodley, J. W. *FEBS Lett.* **103,** 253–255 (1979).
16. Hamel, E., Koka, M. & Nakamoto, T. *J. biol. Chem.* **247,** 805–814 (1972).
17. Matheson, A. T., Yaguchi, M., Nazar, R. N., Visentin, L. P. & Willick, G. E. in *Energetics and Structure of Halophilic Microorganisms* (eds Caplan, S. R. & Ginzburg, M.) 481–501 (Elsevier, Amsterdam, 1978).

Biophotolytic H_2 production using alginate-immobilized chloroplasts, enzymes and synthetic catalysts

P. E. Gisby & D. O. Hall

University of London King's College, Department of Plant Sciences, 68 Half Moon Lane, London SE24 9JF, UK

Hydrogen can be produced by illumination of an aqueous mixture of chloroplasts and hydrogenase, in the presence of an electron carrier[1,2]. This system may have potential for development of a solar converter to produce hydrogen from water[3,4] if it can be stabilized or constructed as a completely synthetic system. The immobilization of the chloroplasts, or membrane analogues, would make possible a one-stage reactor with all the components in one chamber, or a two-stage reactor if the electron carrier was passed to another chamber to react with

an immobilized hydrogen-producing catalyst. However, techniques for immobilizing enzymes tend to yield immobilized chloroplasts that are not very active, and other methods must be used[5–8]. We describe here the immobilization of chloroplasts using calcium alginate gels on reinforcing grids of nylon and stainless steel. Chloroplasts thus immobilized are fully active and can be used to produce hydrogen gas. Strengthened films of this sort could provide a good, solid, rigid matrix for a solar converter.

Sodium alginate is a soluble polysaccharide, but calcium alginate is an insoluble gel. If a chloroplast suspension is mixed with a 1 or 2% sodium alginate solution and then brought into contact with 0.1 M calcium chloride, the calcium alginate gel forms immediately. Thus, if the mixture is dropped into calcium chloride from a syringe, the drops solidify on contact and form nearly spherical balls, with the chloroplasts immobilized inside. This approach was used successfully for the immobilization of microbial cells by Cheetham *et al.*[9]. The same method was used in our laboratory and the spheres were found to be active in the hydrogen production system[8] though they tended to disrupt after some time. Further experimentation showed that we could also make flat films of gel inside which the chloroplasts were entrapped; these proved to be much better than the spheres.

The films tended to be rather fragile, and broke up if stirred or shaken for more than 5 min; this problem was overcome by covering a solid grid support with the sodium alginate–chloroplast mixture and dropping calcium chloride on to this mixture with a pipette. The result is that the support becomes embedded in the calcium alginate, giving a flat, rigid structure. The principle is similar to that of reinforced concrete. Muslin was initially used as the strengthening grid but we have also tried nylon and stainless steel. Stainless steel has, in fact, proved to be the best so far, giving strong, easy-to-make films which do not fragment on shaking.

The photosynthetic activity of immobilized chloroplasts was assayed in an oxygen electrode and compared to that of free chloroplasts, using both potassium ferricyanide (oxygen evolution) and methyl viologen (oxygen uptake) as electron acceptors, as shown in Table 1. It was necessary to use only small amounts of chloroplasts for assay because the alginate film was such that it lined the inside of the electrode cavity and the buffer solutions flowed past it. As the illumination of the film was from one side only, that part of the film nearest the light shaded the rest of the film; this was considerable when 100 μg total chlorophyll was immobilized in the film. Stirring would have overcome this problem with free chloroplasts, but this was not possible with immobilized ones. Therefore, it was decided to decrease the amount of chlorophyll present so that the illumination should be saturating over the entire area of the film. Table 1 clearly shows that the photosynthetic electron transport activity of the film-immobilized chloroplasts was not diminished by the immobilization process compared to that of free chloroplasts. However, the spheres only showed 49% of the activity of free chloroplasts.

Table 1 Photosynthetic electron transport activity of immobilized and non-immobilized chloroplasts

	Free chloroplasts	Immobilized chloroplasts	
		Spheres	Films
O_2 evolution rate (μmol O_2 evolved per mg chlorophyll per h)	200	98	198
O_2 uptake rate (μmol taken up per mg chlorophyll per h)	207	107	205

Chloroplasts were isolated essentially as in ref. 13 and resuspended in a solution of 10 mM NaCl, 10 mM HEPES, *p*H 7.5 (2 mg chlorophyll ml^{-1}). Assays were carried out in a Rank oxygen electrode at 25 °C. The reaction mixture contained, in a final volume of 4 ml, chloroplasts containing 25 μg of chlorophyll, 50 mM HEPES, *p*H 7.5, and 10 mM NaCl. For O_2 evolution, the electron acceptor was potassium ferricyanide (3 mM). For O_2 uptake, the electron acceptor was methyl viologen (50 μM)[14]. Both O_2 evolution and uptake were measured in the presence of 2 μM carbonyl cyanide *p*-trifluoromethoxyphenol hydrazone, uncoupling agent. Alginate spheres were made by mixing chloroplasts containing 25 μg chlorophyll with 1 ml of a solution of 1% sodium alginate + 50 mM HEPES (*p*H 7.5) + 1% bovine serum albumin (BSA) and dropping this mixture into 100 ml of 0.1 M $CaCl_2$ + 50 mM HEPES (*p*H 7.5). The films were made by mixing chloroplasts containing 50 μg chlorophyll with 1% sodium alginate + 50 mM HEPES (*p*H 7.5) to final volume of 300 μl. A nylon grid, 1 × 2 cm, mesh 45, aperture size 0.32 mm, was covered in 150 μl of this mixture, and 3 ml of 0.1 M $CaCl_2$ + 50 mM HEPES (*p*H 7.5) were dropped onto the film with a pipette.

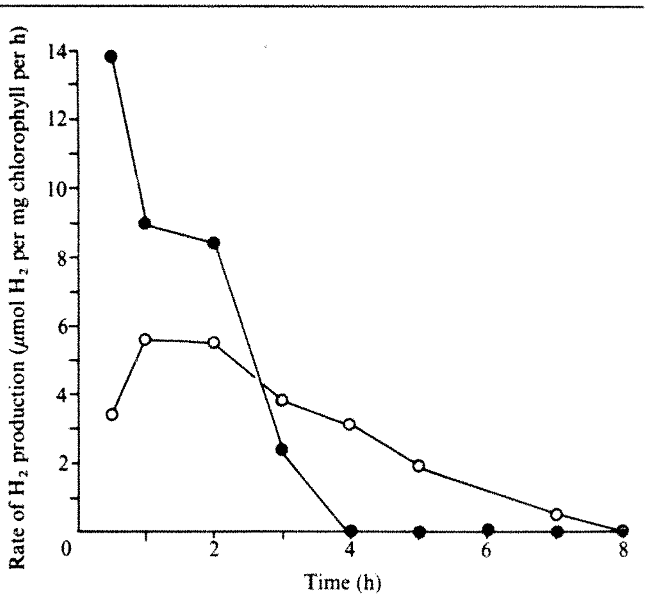

Fig. 1 Rate of hydrogen production against time for system (3)—platinum-polyvinyl alcohol and methyl viologen with spinach chloroplasts. Reaction conditions were as shown for system (3) in Table 2 legend. (Data are from a longevity experiment separate to those shown in Table 2.) ●, No components immobilized; ○, chloroplasts, electron carrier and H_2-evolving catalyst in alginate gel film. Oxygen trap present in both.

Next, we were interested to see if immobilized chloroplasts could be used to produce hydrogen gas, as can free chloroplasts[1,2] using hydrogen-producing catalysts and the appropriate electron carriers. Three catalytic systems were used: (1) *Clostridium pasteurianum* hydrogenase with *Spirulina maxima* ferredoxin as the electron carrier; (2) *Desulfovibrio desulfuricans* (strain Norway) hydrogenase with methyl viologen as electron carrier, and (3) a synthetic catalyst platinum-polyvinyl alcohol[10] with methyl viologen as carrier. The films were made by mixing double the required amount of chloroplasts, electron carrier and catalyst to a final volume of 150 μl. This was then mixed with 150 μl of a solution containing 4% sodium alginate (BDH batch 6097490), 1% bovine serum albumin and 50 mM HEPES, *p*H 7.5, giving a final sodium alginate concentration of 2%. A stainless steel grid (1 × 2 cm, 20 mesh, aperture size 0.99 mm) was covered with 150 μl of the final mixture and then 3 ml of solution containing 0.1 M $CaCl_2$ and 50 mM HEPES, *p*H 7.5, was dropped on to the film from an automatic pipette.

Table 2 shows that hydrogen-evolution was observed using the immobilized chloroplasts, with quite good rates in immobilized systems (1) and (3). However, the percentage of the same reaction system where none of the components are immobilized (figures in parentheses), shows that the rate retained by system (1) after immobilization is 24%, but that for system (3) is 67%. In an immobilized system we have never retained more than 25% of the maximum hydrogen-evolving activity attainable (that is system (1), non-immobilized).

At this stage, the important point is not the absolute rates of hydrogen production (as compared to free chloroplasts) but that the immobilized chloroplasts will evolve hydrogen at reasonable rates. Following work showing the generation of photovoltages and photocurrents[4], it was shown that immobilized chloroplasts and algal cells will produce photocurrents in a three-electrode system when they are coated on an electrode and a suitable potential applied[11]; however, these systems do not produce hydrogen. We have attempted to develop a catalytic solar energy converter which uses water as the source of electrons and protons, and which ultimately gives rise to hydrogen. The system described here is the only one known which fulfils these criteria.

Table 2 Rates of hydrogen production from immobilized and non-immobilized systems

	H_2 evolved (μmol per mg chlorophyll per h)		
	System (1): chloroplasts +*C. pasteurianum* hydrogenase +*S. maxima* ferredoxin	System (2): chloroplasts +*D. desulfuricans* hydrogenase +methyl viologen	System (3): chloroplasts +Pt.PVA +methyl viologen
No components immobilized	21.0 (100%)	7.1 (100%)	7.2 (100%)
Chloroplasts, electron carrier and H_2-evolving catalyst in alginate gel film	5.0 (24%)	1.1 (15%)	4.8 (67%)
No components immobilized, oxygen trap omitted	10.7 (51%)	2.8 (39%)	0 (0%)
Chloroplasts, electron carrier and H_2-evolving catalyst in alginate film, oxygen trap omitted	1.8 (9%)	0.2 (3%)	0 (0%)

Chloroplasts (type C)[15] were prepared essentially as described in ref. 13 and finally suspended in 10 mM NaCl, 10 mM HEPES, *p*H 7.5 (7.5 (2 mg chlorophyll ml^{-1}). Assays for H_2 evolution were carried out in 15-ml glass vials. The reaction mixture (final vol 2 ml in 50 mM HEPES, *p*H 7.5) contained 100 μg chlorophyll, 1% BSA (fraction V powder). When present, the oxygen trap consisted of 100 μmol of glucose, 10 units glucose oxidase, 1,000 units catalase and 20 μl ethanol. System (1) *C. pasteurianum* hydrogenase added to excess; *S. maxima* ferredoxin (25 nmol per vial). System (2) *D. desulfuricans* (strain Norway) hydrogenase, added to excess; methyl viologen was present at 50 μM. System (3) Pt. PVA = platinum-polyvinyl alcohol, containing the equivalent of 125 μg platinum per vial, methyl viologen 50 μM. Hydrogen evolution was assayed over 2 h at 11,000 l and 25 °C using a gas chromatograph as described in ref. 16. Alginate gels were made as described in the text.

The *in vitro* production of hydrogen from reduced substrates, for example EDTA and ascorbate, using dyes as mediators is well established, and efficiencies of 5% conversion of monochromatic light have been reported[4,12]. However, catalytic water-splitting systems have only been substantiated thus far using chloroplast membranes, where the lack of sustained and linear hydrogen production rates over many hours has not allowed the meaningful measurement of solar energy conversion efficiencies.

For the development of a large-scale solar converter, we are investigating the replacement of as many biological components as possible with synthetic compounds, largely because of the instability and expense of the former. System (3) of Table 2 is of particular interest in this respect because in it we have replaced the ferredoxin and hydrogenase used in system (1) with methyl viologen and platinum-polyvinyl alcohol, respectively. In Fig. 1 we show that if calcium alginate-immobilized chloroplasts are used with the two synthetic catalysts of system (3), although the initial rates are lower than for free chloroplasts, we increase the longevity of the system twofold. Preliminary work shows that the inorganic catalysts are not well retained in the gel after initial entrapment, as some leakage occurs. There is, however, no leakage at all of the chloroplasts themselves. Separate immobilization of the synthetic and biological catalysts, and their subsequent incorporation into the alginate gels, supported on a rigid matrix, is the next phase of our work.

We thank Dr K. K. Rao and Miss U. Schleicher for help and the Commission of the European Communities for support. P.E.G. is a British Gas Corporation scholar.

Note added in proof: Initial experiments with free chloroplasts, in collaboration with Dr A. Harriman, have given quantum efficiencies for hydrogen-producing systems (1), (2) and (3) of 0.126 (12.6%), 0.025 (2.5%) and 0.032 (3.2%), respectively (see Table 2).

Received 14 April; accepted 28 July 1980.

1. Rao, K. K. & Hall, D. O. *Photosynthesis in Relation to Model Systems* (ed. Barber, J.) 299–329 (Elsevier, Amsterdam, 1979).
2. Weaver, P. F., Lien, S. & Seibert, M. *Solar Energy* **24**, 3–45 (1980).
3. Porter, G. & Archer, M. D. *Interdisc. Sci. Rev.* **1**, 119–143 (1976).
4. Bolton, J. & Hall, D. O. *A. Rev. Energy* **4**, 353–401 (1979).
5. Keirstan, M. & Bucke, C. *Biotech. Bioengng* **19**, 387–397 (1977).
6. Ochiai, H., Shibita, H., Fujishima, A. & Honda, K. *Agric. biol. Chem.* **43**, 881–883 (1979).
7. Cocquempot, M. D., Thomas, D., Champigny, M. L. & Moyse, A. *Eur. J. appl. Microbiol. Biotech.* **8**, 37–42 (1979).
8. Rao, K. K. *et al. Proc. int. Symp. Biological Applications of Solar Energy* (eds Gnanam, A., Krishnaswamy, S. & Kahn, J. S.) 199–204 (Macmillan, India, 1980).
9. Cheetham, P. S. J., Blunt, K. W. & Bucke, C. *Biotech. Bioengng* **21**, 2155–2168 (1979).
10. Kiwi, J. & Gratzel, M. *Am. chem. Soc. J.* 101–24, 7214–7217 (1979).
11. Ochiai, H., Shibata, H., Sawa, Y. & Katoh, T. *Proc. natn. Acad. Sci. U.S.A.* **77**, 2442–2444 (1980).
12. Kaneko, M., Motoyoshi, J. & Yamada, A. *Nature* **285**, 468–470 (1980).
13. Lilley, R. McC. & Walker, D. A. *Biochim. biophys. Acta* **368**, 269–278 (1974).
14. Reeves, S. G. & Hall, D. O. *Biochim. biophys. Acta* **314**, 66–78 (1973).
15. Hall, D. O. *Nature new Biol.* **235**, 125–126 (1972).
16. Rao, K. K., Rosa, L. & Hall, D. O. *Biochem. biophys. Res. Comm* **68**, 21–27 (1976).

Secondary isotope effects in studies using radiolabelled folate tracers

Michael J. Connor*, John A. Blair† & Hamid Said†

* Department of Biochemistry, Scripps Clinic and Research Foundation, La Jolla, California 92037
† Department of Chemistry, University of Aston in Birmingham, Gosta Green, Birmingham B4 7ET, UK

The use of isotopically labelled compounds as metabolic tracers in *in vivo* and *in vitro* studies is particularly important in folate biochemistry, where the natural coenzyme forms occur in transient and trace amounts. However, during our studies on the whole body metabolism of radioactive folate tracers, we have now observed that some forms of isotopically labelled folate are biologically distinguishable from the unlabelled carrier molecules by an as yet unidentified secondary isotope effect. Folates excreted in the urine of rats dosed previously with mixtures of ^{14}C- and ^{3}H-labelled folate derivatives are apparently ^{3}H enriched, that is contain more ^{3}H than ^{14}C relative to the dosed compound. This apparent ^{3}H enrichment was largely due to the enhanced absorption of ^{3}H-folate from the intestine, confirmed by studies with everted sac preparations of rat jejunum in which it was found that the ^{3}H-labelled folate in the mixture was transported from the mucosal into the serosal compartment at a faster rate than both the ^{14}C-labelled folate and the unlabelled carrier. Secondary isotope effects were also observed on ion-exchange chromatography, ^{3}H-labelled folates with ^{3}H at the C-9 position eluting fractionally earlier than the corresponding unlabelled or [2-^{14}C]folate from DEAE-cellulose, a behaviour similar to that reported earlier for isotopically labelled 2-aminopurine[1] and several amino acids[2]. Such isotope effects may be more widespread and more important than is generally accepted.

Folic acid (Fig. 1) is commercially available (Radiochemical Centre) in three radioactively labelled forms: labelled with ^{14}C (at the C-2 position) or with ^{3}H, either nominally (at the 3′, 5′, 7, 9 positions, with 33.2% at C-9) or generally (at the 7, 9 positions only, with 41% at C-9). Extensive catabolism of the folate molecule occurs *in vivo*[3] and therefore, to facilitate metabolite identification and quantification, we routinely use mixtures of ^{14}C- and ^{3}H-labelled folate tracers in our whole animal studies.

Urine collected 0–48 h after the administration of mixtures of [2-^{14}C]- and [3′, 5′, 7, 9-^{3}H]folate (10–100 μg per kg body weight) to rats contains a large excess of ^{3}H over ^{14}C whereas faecal samples contain more ^{14}C than ^{3}H compared with the dose[4]. Chromatographic analysis on DEAE-cellulose and Sephadex G15 revealed that the catabolites present in the urine that were labelled with ^{3}H only ($^{3}H_2O$, *p*-acetamidobenzoate

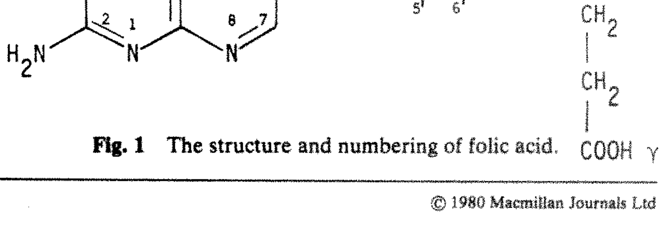

Fig. 1 The structure and numbering of folic acid.

and *p*-acetamidobenzoyl-L-glutamate) accounted for only 50% of the ^{3}H excess, the residue being due to an enhanced ^{3}H to ^{14}C ratio (compared with the dosed compound) of the intact folates excreted (largely 5-methyl-5,6,7,8-tetrahydrofolic acid, 10-formyl-5,6,7,8-tetrahydrofolic acid and unmetabolized tracer). The evidence indicated that either ^{3}H-folate was being absorbed faster or that [2-^{14}C]folate was being absorbed more slowly from the intestine with respect to unlabelled folate. Everted sac preparations of rat jejunum[5] were incubated for 30 min with radiolabelled 10-formyl folic acid, folic acid or pterin-6-COOH and the serosal fluid examined by HPLC. For each of the intact folates examined, an increased serosal ^{3}H to ^{14}C ratio was found compared with the starting material (Table 1). The ^{14}C specific radioactivity of the folate in the mucosal and serosal compartments remained constant. As enhanced ^{3}H-folate absorption was even more pronounced when mixtures of [2-^{14}C]- and [7,9-^{3}H]folate were used compared with mixtures of [2-^{14}C]- and [3′,5′,7,9-^{3}H]folate, the effect was due to the ^{3}H atoms at the 7 and 9 positions. Because the ^{3}H to ^{14}C ratio remained constant in the serosal and mucosal compartments when mixtures of [2-^{14}C]- and [7-^{3}H]pterin-6-COOH (synthesized from a mixture of [2-^{14}C]- and [7,9-^{3}H]folic acid[6]) were used, the important site seems to be position 9, although this assumes that the pterin-6-COOH is transported by a similar mechanism to that of folate.

The isotope effect is not confined to biological situations. When mixtures of [2-^{14}C]- and ^{3}H-folate are eluted from DEAE-cellulose columns, the ^{3}H to ^{14}C ratio decreases across the peak, that is, ^{3}H-labelled molecules elute slightly faster than the ^{14}C-labelled molecules. Similar separations of mixtures of isotopically labelled compounds have been reported previously. We analysed our chromatographic data by the method of Klein *et al.*[7] using the Probit transform to provide the values M (the volume at which 50% of the compound has eluted), ΔM (the difference between the value of M for the unlabelled and labelled compound) and $\Delta M\%$ $[(\Delta M/M)\times 100]$ (Table 2). Graphical plots of the Probit transform of the cumulative percentage of the compound eluted against elution volume gave a series of parallel lines for the unlabelled and corresponding radioactively labelled compounds, demonstrating their homogeneity and absence of co-chromatographing impurities. For all folates examined, the ^{14}C-tracer and the authentic unlabelled compound (measured from its UV absorbance) were well matched, with ΔM values close to zero, whereas the ^{3}H-tracer eluted before both of them (Table 2). We have also observed similar though less marked mismatches on Sephadex G-15 chromatography (data not shown). The chromatographic data confirm the conclusion reached from the everted sac studies that ^{3}H incorporation at the C-9 position is the important factor in the aetiology of the isotope effect, as $\Delta M\%$ for [7,9-^{3}H]folic acid was greater than for [3′,5′,7,9-^{3}H]folic acid and was negligible for [7-^{3}H]pterin-6-COOH in similar conditions (Table 2). The role of the C-9 ^{3}H is also emphasized by the decrease in the size of the isotope effects on formylation at the N-10 position.

Table 1 The relative amounts of ^{3}H-labelled, ^{14}C-labelled and unlabelled pteridines transported into the serosal compartment by everted sac preparations of rat jejunum

Compound and isotope mixture	^{3}H:^{14}C ratio		^{14}C:absorbance ratio	
	Starting compound	Serosal compound	Starting compound	Serosal compound
[2-^{14}C]folic acid, [3′,5′,7,9-^{3}H]folic acid and unlabelled folic acid	1	1.25	1	1
[2-^{14}C]folic acid, [7,9-^{3}H]folic acid and unlabelled folic acid	1	1.29	1	1
[2-^{14}C]10-formyl folic acid, [3′,5′,7,9-^{3}H]10-formyl folic acid and unlabelled 10-formyl folic acid	1	1.10	1	1
[2-^{14}C]pterin-6-COOH, [7-^{3}H]pterin-6-COOH and unlabelled pterin-6-COOH	1	0.98	1	1

Everted rat jejunal sacs were incubated with 1 mM solutions (containing 0.1 μCi each isotope) of the appropriate mixture for 30 min. The combined serosal fluid (from three sacs) was then applied to a Whatman Pastisil 10 SAX Magnum 9 HPLC column (50 cm × 0.94 cm) and eluted with 0.10 M potassium phosphate buffer, *p*H 5.0, at 600–800 p.s.i. to resolve transported unmetabolized starting material from any contaminant metabolites. The isotope content was determined by scintillation counting and unlabelled compound from its UV absorbance at 254 nm. The ^{3}H: ^{14}C ratios in the derivatives found in the tissue at the end of each experiment were similar to those of the serosal compartment.

Table 2 The effect of isotope substitution on elution from DEAE-cellulose ion exchange columns

	ΔM (ml)	$\Delta M\%$
[2-^{14}C]folic acid	No separation detected	
[3′,5′,7,9-^{3}H]folic acid	−4.30	1.59
[7,9-^{3}H]folic acid	−5.10	2.02
[2-^{14}C]10-CHOFA	No separation detected	
[3′,5′,7,9-^{3}H]10-CHOFA	−0.45	0.26
[2-^{14}C]5-MeTHF*	No separation detected	
[3′,5′,7,9-^{3}H]5-MeTHF*	−1.25	0.47
[2-^{14}C]pterin-6-COOH	No separation detected	
[7-^{3}H]pterin-6-COOH	No separation detected	

Mixtures of ^{14}C- and ^{3}H-labelled compounds (0.1 μCi each isotope) and unlabelled carrier (5 mg) were applied to DEAE-cellulose columns (1.5 cm × 30 cm) and eluted with a 0–1.2 M NaCl gradient in 0.05 M sodium phosphate buffer, *p*H 7.0. The ^{14}C, ^{3}H and UV absorbance of each fraction (5 ml) was determined and the degree of isotope fractionation calculated. Values of ΔM are quoted with respect to the elution position (M) of the unlabelled carriers; in the calculation of $\Delta M\%$ the sign is artificially reversed to indicate the displacement of labelled from unlabelled compound in the conventional manner. The approximate elution positions of the carriers are: folic acid, 265 ml; 10-CHOFA (10-formyl folic acid), 175 ml; 5-MeTHF (5-methyl-5,6,7,8-tetrahydrofolic acid), 199 ml; pterin-6-COOH, 208 ml.

* Isolated from rat urine after oral administration of ^{14}C- and [3′,5′,7,9-^{3}H]folic acid.

The C-9 ^{3}H-folate derivatives behaved as if they carried an effective net reduced charge, as they eluted early from anion-exchange columns at neutral *p*H. Several mechanisms have been proposed to explain isotope effects of this type. Gottschling and Freese[1] suggested that an unspecified electronic effect, resulting in a change in the *p*K value of the amino group, was responsible for the chromatographic separation of ^{3}H-labelled 2-aminopurine from unlabelled 2-aminopurine. More recently, Klein and his co-workers[2] have provided evidence that isotope-induced changes in hydrogen bonding and local solvent structure may be important. Similar conclusions have been reported[8] for isotopic separations of a variety of deuterated and unlabelled hydrocarbons by hydrophobic HPLC where differences in C–H and C–D bond perturbation by solvent was considered crucial. Isotope-related changes in solvent/bonding effects would obviously be important in folate–protein interactions, either directly, if, for example, the C-9 position was involved in bonding, or indirectly, by contributing to an effective overall decrease in the net charge of the folate molecule. Because incorporation of a ^{3}H atom at the C-9 position leads to a pronounced effect on the transport of folate across the intestine, careful screening for secondary isotope effects is essential in enzymatic and metabolic studies involving such tracers.

Received 14 April; accepted 26 June 1980.

1. Gottschling, H. & Freese, E. *Nature* **196**, 829–831 (1962).
2. Klein, P. D. & Szczepanik, P. A. *J. Chromatogr.* **42**, 493–502 (1969).
3. Connor, M. J., Pheasant, A. E. & Blair, J. A. *Biochem. J.* **178**, 795–797 (1979).
4. Pheasant, A. E., Connor, M. J. & Blair, J. A. (in preparation).
5. Wilson, T. H. & Wiseman, G. *J. Physiol., Lond.* **123**, 106–125 (1954).
6. Maruyama, T., Shiota, T. & Krumdieck, C. L. *Analyt. Biochem.* **84**, 277–295 (1978).
7. Klein, P. D., Simborg, D. W. & Szczepanik, P. A. *Pure appl. Chem.* **8**, 357–370 (1964).
8. Tanaka, N. & Thornton, E. R. *J. Am. chem. Soc.* **98**, 1617–1619 (1976).

MATTERS ARISING

Ordering of FeNi in clear taenite from meteorites

CLEAR taenite in meteorites[1] contains 48–57% Ni and is optically anisotropic[2], unlike taenite (γ Fe,Ni) which is isotropic. We have proposed[2] that clear taenite is composed of ordered FeNi, a phase first identified in iron meteorites by Albertsen *et al.*[3]. Mehta *et al.*[4] have obtained additional evidence for ordering in clear taenite from their electron-optical studies of a large grain, which one of us (R.S.C.) discovered in the Estherville meteorite. However, they interpret their data to indicate that clear taenite is composed of regions of ordered FeNi, which are 1–3 μm in diameter, in a matrix of disordered γ (taenite) of similar composition. We argue here that this conclusion is in all probability incorrect.

On ordering of FeNi, cubic taenite inverts to the tetragonal CuAu or $L1_0$ structure. Because of this symmetry change, three sets of intergrown crystallites of ordered FeNi, which are oriented in mutually perpendicular directions, form from a single crystal of taenite. These crystallites, which can be observed in reflected light under crossed polars[2], are typically 1–10 μm in diameter.

Mehta *et al.*[4] observed extra superlattice diffraction spots from the $L1_0$ structure in preferentially thinned regions of clear taenite in which the [110] direction was parallel to the electron beam. The thicker regions which did not show extra diffraction spots were interpreted by Mehta *et al.* to be disordered γ. We suggest instead that the thicker regions actually contained sets of ordered crystallites with [101] and [011] directions parallel to the beam. On the original taenite axes, the unit cell of ordered FeNi is C-centered and has dimensions which are very close to those of taenite[3]. Ordered crystallites with [101] and [011] parallel to the beam would therefore show diffraction patterns that are indistinguishable from those of disordered γ. Thus we are confident that Mehta *et al.* misidentified ordered FeNi crystallites as disordered taenite. If we are correct, all regions of {100} sections of clear taenite will show extra superlattice spots, as in this orientation all three sets of crystallites show superlattice diffraction spots.

Although they acknowledge that our interpretation is consistent with their data, Mehta *et al.*[4] strongly emphasize their own conclusion that clear taenite contains ordered FeNi regions in a disordered γ matrix. Other contrary evidence is provided by Mössbauer[3,5] and optical[2] studies of meteoritic metal, which have failed to detect disordered γ of the size, composition and abundance that Mehta *et al.* propose. We still conclude[2,6] that clear taenite is a new mineral, ordered FeNi.

E. S. acknowledges partial support from NASA grant NGL 32-004-064 (K. Keil, Principal Investigator).

EDWARD R. D. SCOTT

Institute of Meteoritics,
Department of Geology,
University of New Mexico,
Albuquerque, New Mexico 87131

ROY S. CLARKE JR

Department of Mineral Sciences,
Smithsonian Institution,
Washington DC 20560

1. Taylor, G. J. & Heymann, D. *Geochim. cosmochim. Acta* **35,** 175–188 (1971).
2. Scott, E. R. D. & Clarke, R. S. Jr *Nature* **281,** 360–362 (1979).
3. Albertsen, J. F., Jensen, G. B. & Knudsen, J. M. *Nature* **273,** 453–454 (1978).
4. Mehta, S., Novotny, P. M., Williams, D. B. & Goldstein, J. I. *Nature* **284,** 151–153 (1980).
5. Danon, J., Scorzelli, R. B., Azevedo, I. S. & Christophe Michel-Lévy, M. *Nature* **281,** 469–471 (1979).
6. Clarke, R. S. Jr & Scott, E. R. D. *Am. Mineral.* **65,** 624–630 (1980).

Differences in fluidity between bilayer halves of plasma cell membranes

ASYMMETRY in the composition of membrane bilayer halves raises the possibility that the individual monolayers have independent physical properties. Recently, Shroeder[1] proposed a method for analysing the fluidity of the individual monolayers of tumour cell plasma membranes. He used an impermeable reagent, trinitrobenzenesulphonic acid (TNBS), covalently linked to outer monolayer amino groups, to quench the fluorescence of *trans*-parinaric acid, a probe which distributes in both monolayers. He contends that the fluorescence of the outer monolayer was quenched and that the elevated polarization of the residual fluorescence reflected a lowered mobility of the *trans*-parinaric acid located in the inner monolayer.

We suggest that TNBS linked to outer monolayer phospholipid amino groups quenches the fluorescence of *trans*-parinaric acid in the two monolayers to a different extent. Because any energy transfer process reduces the donor probe fluorescence lifetime[2], the observed elevation of the polarization of the unquenched *trans*-parinaric acid fluorescence may reflect the impact of the transfer process on fluorescence lifetime[3] rather than probe mobility. Our arguments are based on the following considerations.

(1) The width of membrane lipid bilayers (between opposite polar headgroups) is generally agreed to be less than 50 Å (ref. 4). (2) *trans*-Parinaric acid, 9, 11, 13, 15, all *trans*-octadecatetraeonoic acid is an extended molecule, orientated with its carboxyl group near the polar headgroup. We expect the relatively inflexible tail of *trans*-parinaric acid to be near the middle of the bilayer with the midpoint of its transition dipole (between C-12 and C-13) ~6 Å to either side of the centre of the bilayer. (3) R_0, the distance at which energy transfer between parinaric acid and covalently linked TNBS is 50%, is calculated by standard procedures[5], applicable to membrane bilayer energy transfer to be 23 Å. (4) For a bilayer 48 Å wide, *trans*-parinaric acid chromophores in the outer and inner monolayers will be ~18 Å (0.78 R_0) and 30 Å (1.3 R_0), respectively, from the trinitrophenyl chromophores. (5) With the geometry specified above, we calculate by the method of Wolber and Hudson[6] that, to achieve the 44% reduction of fluorescence of *trans*-parinaric acid by energy transfer between *trans*-parinaric acid and TNBS reported by Schroeder, a TNBS surface density of 0.6 TNBS/R_0^2 is required. The calculations show that ~60% of the outer monolayer and ~27% of the inner monolayer fluorescence are transferred. (6) Fluorescence lifetimes are reduced by energy transfer to an extent similar to the detected change in fluorescence quantum yield[2,5]. For isotropically rotating probes, the Weber–Perrin equation[7] predicts that the lifetime changes in *trans*-parinaric acid caused by the presence of TNBS are alone sufficient to account for the observed elevation of the polarization.

As it seems that the motion of linear probes like *trans*-parinaric acid in membranes is not isotropic[8,9], the extent to which the observed steady-state polarization depends on the probe fluorescence lifetime is a function of both the rate of chromophore motion and its angular extent[3]. These parameters are probably influenced by membrane proteins and cholesterol[10] and can only be extracted by nanosecond polarization measurements[3]. We have, however, observed that the steady-state polarization of parinaric acid probes, confined to the surface monolayer of a serum lipoprotein and quenched by surface-bound energy transfer acceptors, is elevated to an extent comparable to that reported by Schroeder in tumour cell membrane bilayers (L.A.S., unpublished results).

0028–0836/80/380255—02$01.00

We believe that a general validation of Schroeder's method requires absolute proof that only outer monolayer *trans*-parinaric acid is quenched and quenched completely by energy transfer to TNBS. We believe that Schroeder can validate his conclusions about tumour cell bilayers by measuring r_∞, the limiting value of the anisotropy at long times following excitation. Because r_∞ is independent of the fluorescence lifetime and because the residual fluorescence in the presence of TNBS labelling probably arises predominantly from the inner monolayer, an elevated r_∞ in the presence of TNBS would provide good evidence for the difference in the mobility of inner and outer monolayer *trans*-parinaric acid probes.

LARRY A. SKLAR

Scripps Clinic and Research Foundation,
La Jolla, California 92037

MICHAEL C. DOODY

Departments of Medicine and Biochemistry,
Baylor College of Medicine, and the Methodist Hospital,
Houston, Texas 77030

1. Schroeder, F. *Nature* **276,** 528–530 (1978).
2. Forster, T. *Z. Naturforsch.* **4,** 321 (1949).
3. Heyn, M. P. *FEBS Lett.* **108,** 359–364 (1979).
4. Levine, Y. K. in *Mammalian Cell Membranes* Vol 1 (eds Jamieson, G. A. & Robinson, P. M.) 78–96 (Butterworths, London, 1976).
5. Fung, B. K.-K. & Stryer, L. *Biochemistry* **17,** 5241–5248 (1978).
6. Wolber, P. K. & Hudson, B. S. *Biophys. J.* **28,** 197–210 (1979).
7. Weber, G. *Adv. Protein Chem.* **8,** 415–419 (1953).
8. Hudson, B., Wolber, P., Tecoma, E., Morgan, C. C. & Simoni, R. D. *Biophys. J.* **21,** 27a (1978).
9. Kawato, S., Kinosita, K. & Ikegami, A. *Biochemistry* **17,** 5026–5031 (1978).
10. Lakowicz, J. R., Prendergast, F. G. & Hogan, D. *Biochemistry* **18,** 508–519 (1979).

SCHROEDER AND KINDEN REPLY— We thank Sklar and Doody for their comments and appreciate their concern. It is regrettable that these authors treat a complex biological membrane system, the LM cell plasma membrane, as if it were a model membrane. No experimentally determined values for LM cell membranes were presented. In contrast, we have continued our work in this area and substantiated the use of trinitrophenyl (TNP) groups as fluorescence quenchers and asymmetry determination agents in several systems[1–9]. The erroneous assumptions made in the above critique are as follows.

First, comments (1)–(4) of Sklar and Doody assume the width of the LM cell membrane to be less than 50 Å. In contrast, from micrographs obtained with an RCA EMU-36 electron microscope, we have determined the width of the LM cell plasma membrane to be ~80 Å. Thus, half the width of the membrane would be 40 Å, not 23 Å as proposed by Sklar and Doody. The additional width of the LM cell membrane seems to be due to the presence of proteins. This is especially important because at least 10 times more TNP groups were attached to protein amino substituents than to phospholipids. The fluorophore of *trans*-parinaric acid is about 15 Å from the carboxyl end, similar to the distance of the fluorescent anthroyl group in anthroyl-stearate from its carboxyl end[10,11]. Therefore, quenching across the bilayer would be expected to be less than 0.004 times as efficient as in the outer monolayer. Studies of model systems indicate that there is little energy transfer from one leaflet to the acceptor in the opposite one if R_0 is much less than 40 Å (ref. 12).

Table 1 Fluorescence decay of *trans*-parinarate in LM cell plasma membranes

Cell or membrane treatment	$t_{1/2}$ (ns)	
Untreated membranes	5.9	8.9
Membranes + 100 μM TNP-glycine	5.8	9.1
Pretreatment of whole cells with 4 mM TNBS to trinitrophenylate outer monolayer amino groups[1]	6.0	9.1

$t_{1/2}$ Represents the halftime for decay for each decay component. Plasma membrane vesicles were resuspended in phosphate-buffered saline (100 μg ml^{-1}) and *trans*-parinarate was incorporated as described previously[1]. Trinitrophenylated membranes were prepared also as stated previously[1].

Second, our reported increases in polarization were not due to altered fluorescence lifetime. Evidence obtained with an Ortec 9200 nanosecond spectrometer (courtesy of Dr Lynwood Yarbrough, University of Kansas School of Medicine) showed that the fluorescence lifetime of *trans*-parinarate was not altered. Two decay components in unquenched membranes were observed as shown in Table 1. Addition of 100 μM TNP-glycine to plasma membrane vesicles (100 μg protein per ml phosphate-buffered saline, 24 °C, *p*H 7.4) maximally quenched fluorescence but did not alter the halftimes of decay. TNP-glycine has been used as a non-penetrating quencher in very low-density lipoprotein to quench completely the fluorescence of *trans*-parinarate[3–5]. As shown in Table 1, trinitrophenylated membranes also did not show altered halftimes for *trans*-parinarate fluorescence decay. In all cases of maximal quenching by TNP-glycine or TNP groups attached to the membrane, the fluorescence decay curves were superimposable. In addition, similar data were obtained using a second fluorescence probe molecule, 1,6-diphenyl-1,3,5-hexatriene[2]. Lastly, *trans*-parinarate was incorporated into lipid vesicles made from plasma membrane lipid extracts. The quenching agent TNP-glycine showed no differences in polarization between the inner and outer monolayer. This would be expected because lipid vesicles would have a randomized symmetric distribution of lipid molecules across the bilayer.

Thus, our data in no way support the general photophysical artefact alluded to by Sklar and Doody. Indeed, if the quenching data are artefactual, all three probe molecules (*trans*-parinarate, 1,6-diphenyl-1,3,5-hexatriene and *N*-phenyl-1-naphthylamine) and membranes from cells supplemented with choline, *N,N'*-dimethylethanolamine, *N*-monomethylethanolamine and ethanolamine should have given essentially the same data—increased fluorescence polarization in the presence of quenching agent. This was not the case[2]. *N*-phenyl-1-napthylamine did not show differences in polarization in the presence of quenching agents. *trans*-Parinarate incorporated into plasma membranes from *N,N'*-dimethylethanolamine and *N*-monomethylethanolamine-supplemented cells also did not show differences in polarization in the presence of quenching agents.

This work was supported in part by grants from the National Cancer Institute (USPH CA 24339) and from the American Heart Association with funds contributed in part by the AHA Missouri Affiliate (AHA 78 734).

FRIEDHELM SCHROEDER

Department of Pharmacology,
University of Missouri,
School of Medicine,
Columbia, Missouri 65212

DARREL A. KINDEN

Electron Microscopy Facility,
Department of Veterinary Pathology,
University of Missouri,
School of Veterinary Medicine,
Columbia, Missouri 65211

1. Schroeder, F. *Nature* **27,** 528–530 (1978).
2. Schroeder, F. *Eur. J. Biochem.* (in the press).
3. Schroeder, F., Goh, E. H. & Heimberg, M. *FEBS Lett.* **97,** 233–236 (1979).
4. Schroeder, F., Goh, E. H. & Heimberg, M. *J. biol. Chem.* **254,** 2456–2463 (1979).
5. Schroeder, F. & Goh, E. H. *J. biol. Chem.* **254,** 2464–2470 (1979).
6. Fontaine, R. N. & Schroeder, F. *Biochim. biophys. Acta* **558,** 1–2 (1979).
7. Fontaine, R. N., Harris, R. A. & Schroeder, F. *Life Sci.* **24,** 395–400 (1979).
8. Fontaine, R. N., Harris, R. A. & Schroeder, F. *J. Neurochem.* **34,** 269–277 (1980).
9. Schroeder, F. *Biochim. biophys. Acta* **599,** 254–270 (1980).
10. Vanderkooi, J. & McLaughlin, A. in *Biochemical Fluorescence: Concepts* Vol. II (eds Chen, R. F. & Edelhock, H.) (Dekker, New York, 1975).
11. Bulkin, B. J. & Krishnamachari, N. *J. Am. chem. Soc.* **94,** 1109–1114 (1972).
12. Fung, B. K. K. & Stryer, L. *Biochemistry* **17,** 5241–5248 (1978).

BOOK REVIEWS

Higher education: retrospect and prospect

Fred Dainton

Higher Education Revisited. By Lord Robbins. Pp.117. (Macmillan: London/ Holmes and Meier: New York, 1980.) £12, $34. *Higher Education for the Future.* By Charles Carter. Pp.160. (Basil Blackwell: 1980.) £7.50. Available from Biblio Distribution Centre, Totowa, NJ, $15.

IN ONE of his many memorable prose passages Sir Peter Medawar has reminded us that, if a science is really advancing, more and more of the facts are correlated by an intellectual framework comprising "general statements of steadily increasing explanatory power and compass" which relieve us of the burden of remembering every fact — the corollary being that books conveying the essence of the subject should progressively decrease in size. By this token the subject of higher education is either not a science or is retrogressing, for what has been written in the past two decades — and there is much — is often lengthy and devoid of generally accepted unifying ideas.

The largest effort in this field, dinosaurian in size (if not in ultimate fate), is that masterminded by the Carnegie Commission on Higher Education, which has resulted in 21 reports and 64 sponsored studies on the average larger than either of the two books reviewed here. Collectively, and in massive detail, the Carnegie publications take a close look at higher education in the USA, with the aim of recommending a way forward which might suffice to carry 'the system' to the end of this millenium.

These two books are as unlike the Carnegie series as could be. They are short, innocent of graphs, unbuttressed by statistics, and the prose of each is simple, direct, unambiguous and pleasingly free from the polysyllabic jargon of the pundits of education and sociology. Both are written by professional economists, and both are essentially personal statements. But there the resemblance ends.

Lord Robbins's book, as befits the elder statesman and Chairman of the Committee on Higher Education which sat for three years at the beginning of the 1960s — the report of which is undoubtedly the single most important and influential document on higher education ever to be issued in the United Kingdom — is an urbane contemplation of those recommendations which were accepted in 1963 in the light of what has happened since in British universities. Sir Charles, the founding Vice-Chancellor of the University of Lancaster and 20 years Robbins's junior, tells us in pithy prose what the whole British 'system' (if that is not too strong a word) of post-sixth-form education is, what he would like it to become and what he thinks may well happen to it by the time he is Lord Robbins's age.

Lord Robbins

Inevitably, some topics are common to the two books. For instance, both touch on student unrest and show their deep revulsion for the methods and aims of the extremists amongst the student militants of the late 1960s and early 1970s which they see as a denial of the academic values of truthfulness and rationality. I would go further than either and assert that the single most important factor in the diminution in public esteem of the universities was the unacceptable behaviour of that tiny minority of militant students which was given wholly disproportionately magnified coverage by the media. This made it much easier for successive governments to restrict the resources they were prepared to make available to universities.

Robbins poses a severe test for any university subject — "Can it be taught so as to enlarge the general powers of the mind?" I don't think I have ever heard this criterion discussed, let alone applied, at any meeting concerned with science curricula at departmental or faculty level, and I feel that some lecturers and textbook authors are so didactic that their influence is mind-constricting rather than expanding. Many of us will draw some comfort from Robbins's statement of "the desirability of working on something that does not at once arouse spontaneous enjoyment". Scientists should also read, mark and inwardly digest what he says about specialization in undergraduate courses. He acknowledges that advances in arts and science come predominantly from specialists but points out that success for the majority of graduates in the western world rests on their broad educational foundations and their versatility, and he recalls the often forgotten qualification to the expansion explicit in the principle of access to higher education by all who are "able and willing" that there should be many more broader courses.

As a Scot, he frequently looks disdainfully southward at the system in England and Wales which forces irreversible specialization on schoolchildren who are far too immature and inexperienced to make wise choices. For 12 years I have been convinced that a broad span of studies in the sixth form is overwhelmingly advantageous even if it necessitates either a longer academic year or more four-year undergraduate courses. A glorious opportunity to do both now presents itself as the size of the 18-year-old age group declines, but I'll wager it will not be seized. Other reforms advocated by Robbins which would help towards this end are a break of at least a year between school and university and, to contain costs, a system of undergraduate student loans, repayment of which would be required only if the annual income exceeded some stated value, an eminently sane and equitable suggestion which would be easy to administer. However, I most strongly disagree with the notion of loans for postgraduates. Were this to become a reality and Research Council and DES studentships to disappear, much valuable research and trained manpower, especially in the sciences and engineering, would be lost, to the detriment of the country as a whole.

Sir Charles Carter

Robbins has much to say that is wise and thoughtful on the value of research, on its relation to and effects (good and bad) on teaching and on the desirable size of institutions — always a matter of subjective judgement rather than logical argument. But I was surprised that he considers universal tutorial teaching to be generally impracticable. Why ever not? Given that the staff/student ratio is 1/9, this means a tutorial load of only 9 hours per week on a one-to-one basis. Surely this or the 4½ hours per week on a one-to-two basis are not excessive additions to the other duties of academics. Including laboratory demonstrating, I did a 22 contact-hour week in Cambridge in 1949 and was none the worse for it.

Lord Robbins's reflections on internal institutional government, on relations between universities and the state (who am I to dispute his high regard for the University Grants Committee?), on the justification of the twin donnish privileges of tenure and freedom to choose his own work, on why more does not mean and has not meant worse, on the binary system and on many other matters, are full of wisdom and experience. Moreover the book has the peculiar charm that each chapter is cast in the form of a letter to a fictitious correspondent who, one surmises, is highly sceptical of the value of higher education. I am reminded of the dictum of Lord Robbins's fellow Scot, Robert Louis Stevenson, that "Every book is, in an intimate sense, a circular letter to the friends of him who wrote it". The reader cannot fail to respond to the warmth and human kindness which lie behind the adoption of this espistolary device and the manifest benignity of the author, factors which — such is the nature of the human psyche — are more persuasive than the statistical data which Lord Robbins freely admits to be absent.

Sir Charles Carter's approach is entirely different. He epitomizes the rational man and is the natural enemy of cant. His prose is precise, crisp and, in some cases, sharp. His arguments command respect for their cogency even if the premises are sometimes mere assertions. He is prepared to question every assumption, overt or covert, on which he considers the British higher education system to be based — there are no sacred cows for him. Whereas Robbins commands attention by charming the reader, Carter, by deflating many of his readers' preconceptions and ascribing qualities of bravery and foolishness to those who attract his approbation or otherwise, may irritate and repel. I would urge those whose initial reaction takes this form to put aside the irritation and to persist, because this is a stimulating book deserving a wide readership.

He starts with a lucid account of the system as it is. Though as faithful to the subject as a photograph, there are illuminating comments, for example, about "social responsiveness" (words much used in the launching of the polytechnics) as really meaning that "public sector colleges are more easily ordered about" (with which I and, I suspect, many US State College and University Presidents would agree) and about how the UGC allocates resources (with which I do not agree). He then delineates the "needs and desires" of society and of individuals, pointing out that society really needs sufficient people with a range of skills able to learn and to adapt quickly, who can be competent citizens, manage change and yet preserve "culture" — defined as "what is worth remembering" and handing on as a legacy to successive generations. After upbraiding Robbins for "a certain sloppiness of thinking" in assigning a "right" to higher education for all the "able and willing", his chapter on the needs and desires of individuals states that intellectual development is not a sufficient individual need and should be balanced by ethical, social and emotional development. That sentiment is, of course, in praise of virtue and against sin but is imprecise and does not lead to any practical conclusion other than the rather lame one that entry tests should not be restricted to cognitive skill. The next chapter raises the question of the wastefulness and inefficiency of higher education, and the need for better planning. Yet, after a scornful look at the Oakes Committee Report as being weak in its recommendations, he seems to reject planning and to welcome overlap of functions between different types of institution on the ground that planners are "insensitive to the need for variety" and are hostile to new ideas, especially if they did not conceive them — no names, no pack drill!

At this point Sir Charles turns to the future, AD 2000, dealing in turn with the sort of institutions we need, the curriculum, research, and the Government as the (inevitable) paymaster. He gives a high priority to Two-Year Community Colleges (an echo of the USA?) and, believing that scholarship is an essential activity for a good teacher whereas research is not, he therefore wants a differentiation of institutions in higher education according to their research roles, with more inter-institutional mobility for students. The longest chapter deals with the undergraduate curriculum, the inertia of which clearly appals him. He sees the essential elements as a specialist core, related subjects, optional courses (which seem to be directed towards making better citizens) and "the examination of some implications of the specialist studies", though the possible nature of these "implications" is, regrettably in my view, left as an exercise for the reader. He writes much common sense on teaching methods and shares my often-repeated view on the invalid reification into a 'subject' of an area of knowledge divided from the rest for the convenience of the division of labour. Examinations are regarded as necessary but he sees much room for improvement in diagnosing the strengths and weaknesses of candidates.

The word 'research', which he regards as a portmanteau containing many different meanings, next comes under his critical scrutiny. He regards it as being of little value in relation to teaching and as a narrowing activity for many, involving little opportunity for originality and independent critical thought. We all have our views on these matters, but he is surely right when he argues for removing the contractual burden 'to research' from university teachers and for a more positive research policy both nationally (which would carry with it the institutional differentiation mentioned above) and within institutions. But he says nothing about the criteria which such policies should satisfy.

To achieve these reforms Sir Charles proposes new machinery including a Higher Education Grants Committee maintaining contact with institutions through a regionally based inspectorate (*sic!*), a single governing body instead of the usual academic senate and predominantly lay council. The members of the governing body would be chosen more for competence than their representativeness. Twenty-five per cent of the revenue of institutions should come from fees in order to remind everyone that costs should be adjusted to output, though this would in fact provide an unhealthy incentive to maintain student numbers irrespective of quality and reduce the influence of the Grants Committee as a regulatory instrument. He also wants loans for students at least for the third and later years. Finally, after a brief encounter with Illich, a conclusion that technology will not cut the ground from under traditional institutions (which, however, ought to teach for 40 weeks per year rather than 30) and the advocacy of a *right* of access to holders of two GCE A-Level passes, Sir Charles proffers us views of what would happen in the next 20 years.

One wonders why this last chapter was written, for I could find nothing new in it other than a *cri de coeur* for more people "to ask awkward questions" and a means for them to do so. But, if this is the necessary condition for change, and if one cannot invent people to do this or if the present system fails to produce them, does that mean we must endure the inertia he so deplores? I do not believe so, for I have more faith in the institutions and the individuals within them to change, but both need the stimulus of books like these. □

Sir Fred Dainton is a chemist who was Vice-Chancellor of Nottingham University from 1965 to 1970 and Chairman of the University Grants Committee from 1973 to 1978. He is currently Chairman of the National Radiological Protection Board and the British Library Board.

Beyond Tansley's 'ecosystem'

Peter D. Moore

Grasslands, Systems Analysis and Man. Edited by A. I. Breymeyer and G. M. Van Dyne. Pp.950. (Cambridge University Press: 1980.) £65, $140.

IT IS now 45 years since A. G. Tansley coined the term 'ecosystem'. The concept of looking at nature as an integrated whole, with intricate connections between its various component parts, both living and non-living, has now been exploited to an extent which is no doubt far beyond Tansley's wildest dream. The limitations of purely mental models have now been cast aside with the advent of sophisticated computer analogues and precise mathematical analysis. Consequently, the work of the International Biological Programme (IBP) has been designed, carried out and assembled using a systems approach to the ecology of various habitats.

The book reviewed here is a further addition to the various syntheses of IBP data which are currently being published and it is concerned with grassland ecosystems. It differs from the previous volume, *Grassland Ecosystems of the World* edited by R. T. Coupland (reviewed in *Nature* **283**, 317; 1980), in that it is concerned with seeking a description of common processes within grasslands rather than with surveying the variations within the world's grassland types. It is thus a book in which the systems analysis approach to ecosystem study is fully developed and illustrated. Since it has involved 38 different authors from all over the world, it must have been a headache to edit in order to maintain some uniformity of style and approach.

The book is arranged in three parts. In the first, the total system is analysed into its components — abiotic, autotrophic, small and large herbivore, invertebrate and vertebrate predator, and decomposer subsystems respectively. In the second part, the ecosystem is assembled and such total system processes as nutrient cycling, energy flow and trophic structure are considered. Finally, in Part III, the use of the systems approach in the management and exploitation of grassland ecosystems is discussed.

The general approach of editors and authors has been to begin with a simple, easily conceived, low-resolution model of the various systems and subsystems covered and to develop it and elaborate it as necessary. One danger with this is that the initial model can become oversimplified to the extent that it is no longer helpful. This is the case, for example, in the general ecosystem model presented by Breymeyer in the Introduction, in which energy and matter are not separated and both appear to cycle. Hinds and Van Dyne, however, use the same technique very effectively when describing the abiotic subsystem of the grassland ecosystem. Taking water movements, they construct a simple, low-resolution model involving only three components and then expand it to illustrate the complexity of subcomponents within these major divisions and, even more important, the intricacy of likely paths of water movement within such a high-resolution model.

All chapters have strongly developed review components and each is equipped with its own bibliography. Thus, for example, the chapter on the autotrophic subsystem by Singh *et al.* reviews the various models which have been developed to describe the photosynthetic process and its relationship to environmental factors. Particular attention is given to the Waggoner, Chartier and Lommen models of carbon uptake by the leaf.

Among the herbivores, it is evident that there is considerably more information concerning the large herbivores than the small (invertebrates). For the former, a great deal of interesting information is collated, relating not only to energy flow within the large herbivore, but also to food selectivity on the part of many such grazers.

Ecologists concerned with the practicalities of grassland management, rather than the satisfying symmetry of computer-drawn curves, will also find something to interest them in this book. Data are presented from experimental grazing trials in the USA which examine such subjects as the influence of stock density upon floristic composition.

Overall, the book leaves two lasting impressions. One is the value of the systems analysis approach to understanding processes in the ecosystem. The second is the advantages gained by an international approach to the development of such models for habitats with similar structure and life-form composition. In this way one can proceed beyond the high-resolution, complex model to general statements concerning the function of such an ecosystem and the nature of the global variation upon the general theme. This volume, with its predecessor, Vol. 18 in the series, represents a significant step towards this goal. □

Peter D. Moore is Senior Lecturer in the Department of Plant Sciences at King's College, University of London.

Reviews of galactic research

C. Pritchet

Photometry, Kinematics and Dynamics of Galaxies. Edited by D.S. Evans. Pp. 492. (Department of Astronomy, University of Texas: 1980.) $16 + postage.

THIS volume reports on a conference that was held in Austin, Texas, in August 1979. The proceedings of the conference communicate the current excitement over 'nearby' galaxies — a field of research (once considered prosaic by many) that has been transformed by a new generation of technology.

Many of the major scientific results that were presented in Austin are in press, or else have already been published. This of course detracts from the usefulness of the conference proceedings, but nevertheless reflects favourably on the scientific importance of the meeting to participants and their co-workers. Of particular interest are papers (by T.X.Thuan and W. Romanishin, and by R.E. Schild and T.C. Weekes) that purport to show that so-called 'cD' galaxies in poor clusters are simply giant ellipticals. Other exciting new results include the detection of a 'thick-disk' component in SO galaxies (by D. Burstein), and the detection of rotation in the bulges of spiral galaxies (by J. Kormendy and G. Illingworth). This latter finding is in contrast to the (now well-known) non-rotation of elliptical galaxies — a result that is considered at length in this volume. Other topics of extensive discussion include the kinematics of HI and HII in spiral galaxies, and the surface photometry of spirals.

Perhaps the most commendable feature of this volume is the presence of several excellent review papers — by S.E. and K.M. Strom (on the effects of environment on the evolution of elliptical and disk galaxies), by K.C. Freeman (on disk galaxies), by M. Capaccioli (on the kinematics of early-type galaxies) and by J. Kormendy (on component analysis of galaxy luminosity profiles). Two other reviews, on galaxy photometry (by G. de Vaucouleurs and by H. Corwin), provide a historical perspective which may well be instructive to younger astronomers. Though somewhat tersely written, the papers in this compendium maintain an up-to-date and authoritative focus on areas of current interest; all will be of some value to specialists and browsers alike.

Photometry, Dynamics and Kinematics of Galaxies can be recommended to all readers with an interest in modern extragalactic astronomy. The editor, D.S. Evans, and contributors are to be commended for making this volume available sufficiently promptly so as to ensure its immediate scientific value. □

C. Pritchet is a Research Associate at Dominion Astrophysical Observatory, Victoria, Canada.

text books from MACMILLAN PRESS

FROM DNA TO PROTEIN: The Transfer of Genetic Information
MARIA SZEKELY

This is the first textbook which discusses gene structure on the basis of recent discoveries of overlapping and split genes and which genetic information can be encoded into the genetic material and how it can be transferred to other materials.

A perfectly up-to-date account of our present knowledge of the structure and expression of genes in prokaryotic and eukaryotic organisms and the only available text showing the correlation between the structure and function of nucleic acids.

March, £18.00, 0 333 21836 1
£9.95, 0 333 21828 8

HUMAN REPRODUCTION AND DEVELOPMENTAL BIOLOGY
D. J. BEGLEY, J. A. FIRTH and J. R. S. HOULT

An integrated approach to describe the cellular and physiological processes of human reproduction and embryological development in relation to their underlying mechanisms and to their practical applications in medicine. The book combines anatomy, biochemistry, physiology and pharmacology, making it more suitable for modern preclinical and human biology courses.

February, £20.00, 0 333 23423 5
£9.95, 0 333 23424 3

GYNAECOLOGICAL CYTOLOGY
MATHILDE E. BOON and METTE LISE TABBERS-BOUMEESTER

Dr Boon and Dr Tabbers-Boumeester have, over the past ten years, developed the course in diagnostic cytology which was first given in Leiden in 1969.

In this volume they present their insight into both the study of diagnostic cytology, and into the teaching of this increasingly important subject. To illustrate the modern concepts of cytopathology, examples of more advanced approaches are included: as well as scanning and electron microscopy there are details of DNA measurements, morphometry and immunopathology.

June, £25.00, 0 333 26117 8
£14.00, 0 333 26118 6

Macmillan Press books are available from leading booksellers
If you have difficulty obtaining these titles please write to Tony Watson, Macmillan Retail Ltd, Houndmills, Basingstoke, Hants, enclosing purchase price + 70p (p&p).

M MACMILLAN PRESS

The evolution of coastal East Anglia

Brian Funnell

The Pre-glacial Pleistocene of the Norfolk and Suffolk Coasts. By R.G. West. Pp. 300. (Cambridge University Press: 1980.) £40, $84.

ANYONE who has looked down an East Anglian estuary, or across the East Anglian tidal flats and marshes of the present day, will readily appreciate the variety of environments represented there. Assume these environments to have been destroyed and re-created three or four times, under alternately cold and temperate climates, at almost identical topographic levels, and you have some idea of the complexity of the deposits which record the history of the pre-glacial coastlands of East Anglia.

The first comprehensive attempt to interpret these deposits was made by Clement Reid, an officer of the Geological Survey of England and Wales, towards the end of the nineteenth century. For half-a-century afterwards little significant further work was carried out on them until P. Thomson applied modern pollen analytical techniques to the West Runton Freshwater Bed. S. L. Duigan's doctoral thesis of 1954 confirmed Thomson's conclusion that the peat bed at West Runton represented an almost entire interglacial cycle, and at the same time revealed the difficulties that would be encountered by anyone attempting a full interpretation of the whole sequence of Cromer Forest Bed deposits. In 1958 Dr, now Professor, R. G. West started work on a full pollen analytical and environmental interpretation of the Cromer Forest Bed Series and his marathon studies are enshrined in this comprehensive monograph.

The book records for posterity, with faithful care, all the problems, difficulties and complexities of the Cromer Forest Bed deposits as they have revealed themselves to one persistent observer over a period of years. Although it is accompanied by a thorough commentary and separate discussion of some general aspects, such as sea-level changes and environmental interpretation, there are no over-slick summaries that would enable a casual reader to raid the book for quick answers on vertebrate or plant community evolution, stratigraphical correlation or sea-level changes. Each piece of evidence is carefully weighed, considered and recorded, but never forced into a simple framework for the sake of easy conclusions. It thus stands as a record of work that is both complete and still in progress.

Most readers would be well advised to arm themselves with a liberal supply of bookmarks to facilitate cross-reference between the text and the numerous tables, plates and figures (the latter conveniently provided as a separate booklet in a back pocket to the book), as these need to be continuously referred to as the text is read. It is indeed one of the attractions of this book that it is not just a presentation of the author's conclusions but also a complete do-it-yourself kit that will enable readers to reassess and reinterpret the basic data which have been so assiduously collated.

Overall Professor West concludes that the Cromer Forest Bed Formation has accumulated during four main pollen stages. The story starts with an account of the last marine transgression of the Norwich Crag Formation, which extended over the Chalk of north-east Norfolk during the initial substage 'a' of the cool Pre-Pastonian. (There is some reference to the earlier pre-glacial marine deposits of the Ludhamian, Thurnian, Antian and Baventian stages in the text, but only to complete the description of a particular section or borehole or to round off comparisons of floras from later stages.)

The Cromer Forest Bed proper begins with the main Pre-Pastonian (sub-stages 'b' to 'd'), which is represented by freshwater and fluviatile deposits containing cool floras occurring at between −3 and + 5m OD. It is followed by the Pastonian stage, containing temperate pollen, sometimes starting and ending with freshwater deposition, but including a substantial coastal marine phase, at levels between −9 and +8m OD. The succeeding Beestonian stage is again cold, with evidence of frozen-ground conditions, but is also in part coastal–marine in origin. Its deposits occur at between + 2 and + 8m OD in a limited area in north Norfolk. Finally the Cromerian stage *sensu stricto* is temperate, substantially freshwater, but with a significant mid-Cromerian marine or estuarine phase, and occurs at levels of between −7 and +8m OD over a wide area. The sequence concludes with early Anglian arctic peaty muds which are sealed in immediately under the first true glacial deposits on the East Anglian coast.

Correlation of the East Anglian stages with comparable stages identified in the contemporary deposits of the Netherlands is still uncertain, probably owing to the close similarity of successive temperate floras at this period in the Quaternary and to the strong influence of local environments on pollen spectra on both sides of the North Sea at that time. The absence of a definitive correlation does not however detract from the intrinsic interest of the detailed ecological and geographical changes which occurred along the East Anglian coast before the arrival of glaciers.

Professor West is to be congratulated on a major work of scholarship, which certainly matches the contribution of Reid and will undoubtedly become a classic in its own right. □

Brian Funnell is Professor of Environmental Sciences at the University of East Anglia.

BOOKS RECEIVED

Chemistry

ABEL, E. W. and STONE, F. G. A. Organometallic Chemistry Vol. 8. A Review of the Literature Published during 1978. Pp. 547. ISBN 0-85186-690-5. (The Chemical Society: London, 1980.) £44, $115.

ADAMS, D. M. and EBSWORTH, E. A. V. (Senior reporters.) Spectroscopic Properties of Inorganic and Organometallic Compounds Vol. 12. A Review of the Recent Literature Published up to late 1978. P. 406. ISBN 0-85186-920-3. (The Chemical Society: London, 1980.) £32, $84.

BARGON, J. (ed.). Computational Methods in Chemistry. Pp. 331. ISBN 0-306-40455-9. (Plenum: 1980.) $37.50.

BECKER, E. D. High Resolution NMR; Theory and Chemical Applications. 2nd Edn. Pp. 354. ISBN 0-12-084660-8. (Academic: 1980.) $24.

BELL, R. P. The Tunnel Effect in Chemistry. Pp. 222. ISBN 0-412-21340-0. (Chapman & Hall: 1980.) £15.

BRAIBANTI, A. (ed.). Bioenergetics and Thermodynamics: Model Systems. Synthetic and Natural Chelates and Macrocycles as Models for Biological and Pharmaceutical Studies. Proceedings of the NATO Advanced Study Institute held at Tabiano, Parma, Italy, May-June 1979. Pp. 474. ISBN 90-277-1115-1. (Reidel: 1980.) np.

CORBRIDGE, D.E.C. Phosphorus: An Outline of its Chemistry, Biochemistry and Technology. 2nd Edn. Studies in Inorganic Chemistry 2. Pp. 560. ISBN 0-444-41887-3. (Elsevier: 1980.) $95, Dfl. 195.

DYMOND, J. H. and SMITH, E. B. The Viral Coefficients of Pure Gases and Mixtures. A Critical Compilation. Pp. 518. ISBN 0-19-855361-7. (Clarendon/Oxford University Press: 1980.) £25.

ELVIDGE, J. A. and JONES, J. R. (eds). Isotopes: Essential Chemistry and Applications. Lectures delivered at a Review Symposium. Special Publication No. 35. Pp. 400. Flexi ISBN 0-85186-830-4. (Royal Society of Chemistry: Blackhorse Road, Letchworth, UK, 1980.) £12, $32.

FIESER, M. Fieser and Fieser's Reagents for Organic Synthesis. Vol. 8. Pp. 602. ISBN 0-471-04834-8. (Wiley-Interscience: 1980.) £19.60.

LEDNICER, D. and MITSCHER, L. A. The Organic Chemistry of Drug Synthesis. Vol. 2 Pp. 526. ISBN 0-471-04392-3. (Wiley-Interscience: 1980.) £15.25.

MITCHELL, J. Jr and SMITH, D. M. Aquametry Part III. A Treatise on Methods for the Determination of Water. 2nd Edn. Chemical Analysis. A Series of Monographs on Analytical Chemistry and its Applications. Vol. 5. Pp. 851. ISBN 0-471-02266-7. (Wiley-Interscience: 1980.) £41.

NOLEN, J. A. Jr and BENENSON, W. (eds). Atomic Masses and Fundamental Constants 6. Proceedings of the Sixth International Conference on Atomic Masses, held in East Lansing, Michigan, September 1979. Pp. 572. ISBN 0-306-40441-9. (Plenum: 1980.) $59.50.

PENG, C. T., HORROCKS, D. L. and ALPEN, E. L. (eds). Liquid Scintillation Counting; Recent Applications and Development. Vol. II. Sample Preparation and Applications. Proceedings of the International Conference on Liquid Scintillation Counting, Recent Applications and Development, held in the University of California, San Francisco, August 1979. Pp. 538. ISBN 0-12-549902-7. (Academic: 1980.) $32.

SANDLER, S. R. and KARO, W. Polymer Syntheses Vol. III. Organic Chemistry Vol. 29. Pp. 368. ISBN 0-12-618503-4. (Academic: 1980.) $42.50.

SCHNEIDER, M. J. Persistent Poisons. Chemical Pollutants in the Environment. Pp. 67. Flexi ISBN 0-89766-023-4. (New York Academy of Sciences: 1979.) $4.

SISLER, H. H., DRESDNER, R. D. and MOONEY, W. T. Jr. Chemistry; a Systematic Approach. Pp. 902. ISBN 0-19-502630-6. (Oxford University Press: 1980.) £13.50.

SPROKEL, G. J. (ed.). The Physics and Chemistry of Liquid Crystal Devices. Proceedings of the Symposium held at the IBM Research Laboratory, San Jose, California, February 1979. Pp. 348. ISBN 0-306-40440-0. (Plenum: 1980.) $42.50.

SUCKLING, C. J., SUCKLING, K. E. and SUCKLING, C. W. Chemistry Through Models. Concepts and Applications of Modelling in Chemical Science, Technology and Industry. Pp. 321. Flexi ISBN 0-521-29932-2; hbk ISBN 0-521-21661-3. (Cambridge University Press: 1980.) £5.95.

WHISTLER, R. L. and BeMILLER, J. N. (eds). Methods in Carbohydrate Chemistry. Vol. VIII General Methods. Pp. 349. ISBN 0-12-746208-2. (Academic: 1980.) $38.50.

WITTCOFF, H. A. and REUBEN, B. G. Industrial Organic Chemicals in Perspective. Part 1: Raw Materials and Manufacture. Pp. 298. ISBN 0-471-03811-3. (Wiley-Interscience: 1980.) £15.05.

Earth Sciences

BROWN, E. H. (ed.). Geography Yesterday and Tomorrow. Pp. 302. ISBN 0-19-874096-4. (Oxford University Press: 1980.) £10.

COLBECK, S. C. (ed.). Dynamics of Snow and Ice Masses. Pp. 468. ISBN 0-12-179450-4. (Academic: 1980.) $55.

DALMAYRAC, B., LAUBACHER, G. and MAROCCO, R. Géologie des Andes péruviennes. Caractères généraux de l'évolution géologique des Andes péruviennes T.D. n 122. Pp. 501. Pbk ISBN 2-7099-0573-6. (O.R.S.T.O.M: Paris, 1980.) Pbk np.

EMSLIE, R. F. Geology and Petrology of the Harp Lake Complex, Central Labrador: An Example of Elsonian Magmatism. Geological Survey Bulletin 293. Pp. 136. Flexi ISBN 0-660-01544-7. (Geological Survey of Canada: 1980.) Flexi $16.25, other countries $19.50.

JONES, M. J. (ed.). Availability of Strategic Minerals . . . Proceedings of the National symposium on the availability of strategic minerals held in London, November 1979. Pp. 109. Flexi ISBN 0-900488-48-4. (Institution of Mining and Metallurgy: 44 Portland Place, London, UK, 1980.) Flexi £19.

KANDEL, R. S. Earth and Cosmos. A book relating the environment of Man on Earth to the environment of Earth in the cosmos. Pp. 254. Hbk ISBN 0-08-025016-5; flexi ISBN 0-08-023086-5. (Pergamon: 1980.) Hbk $30, £13.50; flexi $14.90, £6.95.

KING, C. A. M. Physical Geography. Pp. 332. Hbk ISBN 0-631-18950-5; pbk ISBN 0-631-11081-X. (Basil Blackwell; 1980.) Hbk £16; pbk £6.50.

LYNCH, D. K. (introductions by). Atmospheric Phenomena. Readings from Scientific American. Pp. 175. Flexi ISBN 0-7167-1166-4; hbk ISBN 0-7167-1165-6. (W. H. Freeman: 1980.) Flexi £4.90; hbk £9.50.

PUTNIS, A. and McCONNELL, J. D. C. Principles of Mineral Behaviour. Geoscience Texts Vol. 1. Hbk ISBN 0-632-00045-3; flexi ISBN 0-632-00583-1. (Blackwell Scientific: 1980.) Hbk £18; flexi £9.80.

REYMENT, R. A. Morphometric Methods in Biostratigraphy. Pp. 175. ISBN 0-12-586980-0. (Academic: 1980.) $32, £13.80.

SCHWAN, W. Shortening Structures in Eastern and Northwestern Himalayan Rocks. Current Trends in Geology Vol. 3. Pp. 62. (Today and Tomorrow's Printers and Publishers; New Delhi, 1980.) Rs. 60, $12.

SCHWIND, J. J. von. Geophysical Fluid Dynamics for Oceanographers. Pp. 307. ISBN 0-13352591-0. (Prentice/Hall: 1980.) £19.45.

SOH, C. T. Korea. A Geomedical Monograph of the Republic of Korea. Pp. 146. ISBN 3-540-09128-9. (Springer: 1980.) DM98, approx. $57.90.

Technology

TURKDOGAN, E. T. Physical Chemistry of High Temperature Technology. Pp. 445. ISBN 0-12-704650-X. (Academic: 1980.) $49.50.

UHLMANN, D. R. and KREIDL, N. J. (eds). Glass: Science and Technology. Vol. 5 Elasticity and Strength in Glasses. Pp. 282. ISBN 0-12-706705-1. (Academic: 1980.) $35.

WARREN, K. Chemical Foundations. The Alkali Industry in Britain to 1926. Oxford Research Studies in Geography. Pp. 208. ISBN 0-19-823231-4. (Clarendon/Oxford University Press: 1980.) £16.50.

WHERRETT, B. S. (ed.). Laser Advances and Applications. Proceedings of the Fourth National Quantum Electronics Conference, 1979. Pp 278. ISBN 0-471-27792-4. (Wiley-Interscience: 1980.) £16.

Computer Science

BRODLIE, K. W. (ed.). Mathematical Methods in Computer Graphics and Design. Based on the proceedings of the conference held at the University of Leicester on September 28th, 1978. Pp. 147. ISBN 0-12-134880-6. (Academic: 1980.) $23, £9.80.

COVVEY, H. D. and McALISTER, N. H. Computers in the Practice of Medicine. Introduction to Computing Concepts. Vol. 1. Pp. 266. ISBN 0-201-01251-0. (Addison-Wesley: 1980.) £13.

COVVEY, H. D. and McALISTER, N. H. Computers in the Practice of Medicine. Issues in Medical Computing. Vol. II. Pp. 205. ISBN 0-201-01249-9. (Addison-Wesley: 1980.) £13.

HOFFMAN, L. J. (ed.). Computers and Privacy in the Next Decade. Proceedings of the Workshop held at Pacific Grove, California, February 1979. Pp. 215. ISBN 0-12-352060. (Academic: 1980.) $16.50.

LAVER, M. Computers and Social Change. Cambridge Computer Science Texts—10. Pp. 125. Hbk ISBN 0-521-23027-6; pbk ISBN 0-521-29771-0. (Cambridge University Press: 1980.) Hbk £8; pbk £2.95.

POSAVAC, E. J. and CAREY, R. G. Program Evaluation. Methods and Case Studies. Pp. 350. ISBN 0-13-729665-7. (Prentice/Hall: 1980.) £11.

Biological Sciences

ALEKSANDROVA, V. D. The Arctic and Antarctic: Their Division into Geobotanical Areas. XXIX Komarov Lecture presented 14 October 1974. Pp. 247. ISBN 0-521-23119-1. (Cambridge University Press: 1980.) £15.

ASANUMA, H. and WILSON, V. J. (eds). Integration in the Nervous System. Symposium held at The Rockefeller University, May 1978. Pp. 357. ISBN 0-89640-033-6. (Igaku-Shoin Medical Publishers: 1979.) $52.50.

ATKINSON, R. Shillay and the Seals. Pp. 167. ISBN 0-00-262763-9. (Collins and Harvill: 1980.) £6.95.

BARRINGTON, E. J. W. Environmental Biology. Resource and Environmental Sciences Series. Pp. 244. Flexi ISBN 0-7131-2788-0. (Edward Arnold: 1980.) £5.95.

BECK, B. B. Animal Tool Behavior: The Use and Manufacture of Tools by Animals. Garland Series in Ethology. Pp. 307. ISBN 0-8240-7168-9. (Garland STPM Press: New York, 1980.) Np.

BECK, S. D. Insect Photoperiodism. 2nd Edn. Pp. 387. ISBN 0-12-084380-4. (Academic: 1980.) $32.50.

BEEZER, A. A. (ed.). Biological Microcalorimetry. Pp. 483. ISBN 0-12-083550-9. (Academic: 1980.) £30, $69.

BERLINER, L. J. and REUBEN, J. (eds). Biological Magnetic Resonance Vol. 2. Pp. 351. ISBN 0-306-40265-5. (Plenum: 1980.) Np.

BOURNE, G. H. and DANELLI, J. F. (eds). International Review of Cytology Vol. 64. Pp. 388. ISBN 0-12-364464-X. (Academic: 1980.) $36.50.

BOURNE, G. H. and DANIELLI, J. F. (eds). International Review of Cytology. Vol. 65. Pp. 380. ISBN 0-12-364465-4. (Academic: 1980.) $39.50.

BROWN, S. B. (ed.). An Introduction to Spectroscopy for Biochemists. Pp. 404. ISBN 0-12-137080-1. (Academic: 1980.) $38.50, £16.60.

BRUSIK, D. Principles of Genetic Toxicology. Pp. 279. ISBN 0-306-40414-1. (Plenum: 1980.) $25.

BUSNEL, R.-G. and FISH, J. F. (eds). Animal Sonar Systems. NATO Advanced Study Institutes Series. Series A: Life Sciences Vol. 28. Pp. 1135. ISBN 0-306-40327-7. (Plenum: 1980.) $75.

CATCHPOLE, C. K. Vocal Communication in Birds. Pp. 68. Flexi ISBN 0-7131-2772-4. (Edward Arnold: London, 1980.) £2.40.

CHRISTENSEN, J. (ed.). Gastrointestinal Motility. Pp. 513. ISBN 0-89004-503-8. (Raven: 1980.) $44.

CIBA FOUNDATION SYMPOSIUMNo. 73 (New series). Trends in Enzyme Histochemistry and Cytochemistry. Pp. 314. ISBN 0-444-90135-3. (Excerpta Medica: 1980.)

CLARKE, G. M. Statistics and Experimental Design. Contemporary Biology Series. 2nd Edn. Pp. 188. Flexi ISBN 0-7131-2797-X. (Edward Arnold: 1980.) £6.50.

CUNHA-VAZ, J. (ed.). The Blood—Retinal Barriers. NATO Advanced Study Institutes Series. Series A: Life Sciences Vol. 32. Pp. 391. ISBN 0-306-40430-0. (Plenum: 1980.) $39.50.

CUSINE, D. and GRANT, J. P. (eds). The Impact of Marine Pollution. Pp. 324. ISBN 0-85664-933-3. (Croom Helm: London, 1980.) £16.95.

DEAG, J. M. Social Behaviour of animals. Pp. 92. Flexi ISBN 0-7131-2770-8. (Edward Arnold: London, 1980.) £3.20.

DE WECK, A. L., KRISTENSEN, F. and LANDY, M. (eds). Biochemical Characterization of Lymphokines. Proceedings of the Second International Lymphokine Workshop. Pp. 622. ISBN 0-12-213950-X. (Academic: 1980.) $39.50.

EL-HINNAWI, E. E. (ed.). Nuclear Energy and the Environment. Environmental Sciences and Applications series Vol. 11. Pp. 300. ISBN 0-08-024472-6. (Pergamon: 1980.) £20, $45.

EVANS, E. A. and SKALAK, R. Mechanics and Thermodynamics of Biomembranes. Pp. 254. ISBN 0-8493-0127-0. (Blackwell Scientific: 1980.) £26.

GOLDSTEIN, L. and PRESCOTT, D. M. (eds). Gene Expression: The Production of RNAs. Cell Biology. Vol. 3. Pp. 684. ISBN 0-12-289503-7. (Academic: 1980.) $65.

GOH, B.-S. Management and Analysis of Biological Populations. Development in Agricultural and Managed-Forest Ecology—8. Pp. 288. ISBN 0-444-41793-1. (Elsevier: 1980.) $75.50, Dfl.155.

GREENE, L. S. and JOHNSTON, F. E. (eds). Social and Biological Predictors of Nutritional Status, Physical Growth, and Neurological Development. Pp. 344. ISBN 0-12-299750-6. (Academic: 1980.) $25.

HAMILTON, P. and MACDONALD, K. B. (eds). Estuarine and Wetland Processes. Marine Science Vol. 11. Pp. 653. ISBN 0-306-40452-4. (Plenum: 1980.) $69.50.

HARE, P. E., HOERING, T. C. and KING, K. Jr (eds). Biogeochemistry of Amino Acids. Papers presented at a conference at Airlie House, Warrenton, Virginia, October 1978. Pp. 558. ISBN 0-471-05493-3. (Wiley: 1980.) £30.50.

HARRIS, H. and HIRSCHORN, K. (eds). Advances in Human Genetics 10. Pp. 394. ISBN 0-306-40386-2. (Plenum: 1980.) $35.

HAYHOE, F. G. J. and QUAGLINO, D. Haematological Cytochemistry. Pp. 320. ISBN 0-443-01974-6. (Churchill Livingstone: 1980.) £32.

HIGGINS, L. G. and RILEY, N. D. A Field Guide to the Butterflies of Britain and Europe. 4th Edn. Pp. 384. ISBN 0-00-219241-1. (Collins: 1980.) £7.95.

HOLÝ, M. Erosion and Environment. Environmental Sciences and Applications Vol. 9. Pp. 225. ISBN 0-08-0244661-1. (Pergamon: 1980.) £22.50, $30.

HUGO, W. B. and RUSSELL, A. D. (eds). Pharmaceutical Microbiology. 2nd Edn. Pp. 352. Flexi ISBN 0-632-00528-9. (Blackwell Scientific: 1980.) £9.50.

JEFFERIES, R. Nature Near London. Facsimile edition. Pp. 242. ISBN 0-906549-15-9. (John Clare Books: 106 Cheyne Walk, London SW10: 1980.) £5.50.

JOHNSON, N. K. Character Variation and Evolution of Sibling Species in the Empidonax difficilis-flavescens Complex (Aves: Tyrannidae). University of California Publications in Zoology Vol. 112. Pp. 158. Flexi ISBN 0-520-09599-5. (University of California Press: 1980.) $9.50.

KABAT, E. A. Sequences of Immunoglobulin Chains. Pp. 185 (US Department of Health, Education and Welfare, Public Health Service, National Institutes of Health: 1979.) Flexi np.

KALTER, S. S. and HENNESSEN, W. (acting eds). Developments in Biological Standardization Vol. 45; The Standardization of Animals to Improve Biomedical Research, Production and Control. Proceedings of a Symposium held at San Antonio, Texas, September 1979. Pp. 248. Flexi ISBN 3-8055-0750-X. (Karger: Basil, 1980). Sfr.65, DM78, $39.

KENNETT, R. H., McKEARN, T. J. and BECHTOL, K. B. (eds). Monoclonal Antibodies. Hybridomas: A New Dimension in Biological Analyses. Pp. 423. ISBN 0-306-40408-7. (Plenum: 1980.) $29.50.

LAMB, J. F., INGRAM, C. G., JOHNSTON, I. A. and PITMAN, R. M. Essentials of Physiology. Pp. 442. Flexi ISBN 0-632-00529-7. (Blackwell Scientific: 1980.) £6.80.

LARSON, R. A. (ed.). Introduction to Floriculture. Pp. 607. ISBN 0-12-437650-9. (Academic: 1980.) $29.50.

LASSEN, U. V., USSING, H. H. and WIETH, J. O. (eds). Membrane Transport in Erythrocytes. Relations between Function and Molecular Structure. Proceedings of the Alfred Benzon Symposium 14 held at the Royal Danish Academy of Sciences and Letters, Copenhagen, August 1979. Pp. 557. ISBN 87-16-08403-9. (Munksgaard: Copenhagen, 1980.) D.Kr.275.

LENCI, F. and COLOMBETTI, G. Photoreception and Sensory Transduction in Aneural Organisms. Lectures presented at the NATO Advanced Study Institute Symposium held in Versilia, Italy, September 1979. Pp. 422. ISBN 0-306-49437-0. (Plenum: 1980.) $45.

LEVINE, L. Biology of the Gene. 3rd Edn. Pp. 542. Flexi ISBN 0-8016-2988-8. (C. V. Mosby: 1980.) Np.

MARTIN, R. M. Cage and Aviary Birds. Pp. 256. Pbk ISBN 0-00-219238-1; hbk ISBN 0-00-219236-5. (Collins: 1980.) Pbk £3.95; hbk £6.50.

MERVYN, L. Minerals and Your Health. Pp. 129. ISBN 0-04-641037-6. (Allen & Unwin: London, 1980.) £5.95.

MORTON, B. (ed.). The Future of the Hong Kong Seashore. Pp. 192. Flexi ISBN 0-19-580425-2. (Oxford University Press: 1980.) £5.50.

MÜLLER-SCHWARZE, D. and SILVERSTEIN, R. M. (eds). Chemical Signals; Vertebrates and Aquatic Invertebrates. Proceedings of the Symposium on Chemical Signals, held at State University of New York College of Environmental Science and Forestry, Syracuse, New York, May 1979. Pp. 445. ISBN 0-306-40339-0. (Plenum: 1980.) $39.50.

MUNSON, P. L., DICZFALUSY, E., GOLVER, J. and OLSON, R. E. (eds). Vitamins and Hormones; Advances in Research and Applications. Vol. 37. Pp. 353. ISBN 0-12-709837-2. (Academic: 1980.) $35.

NADEL, J. A. Physiology and Pharmacology of the Airways. Lung Biology in Health and Disease Vol. 15. Pp. 357. ISBN 0-8247-6382-3. (Dekker: 1980.) SW.Fr.100.

NRIAGU, J. O. Cadmium in the Environment. Part I: Ecological Cycling. Pp. 682. ISBN 0-471-06455-6. (Wiley-Interscience: 1980.) £38.15.

öpik, H. The Respiration of Higher Plants. Pp. 58. Pbk ISBN 0-7131-2801-1. (Edward Arnold: 1980.) £2.50.

PARTSCH, K. J. Die Zoologische Station in Neapel. Modell internationaler Wissenschaftszusammenarbeit. Pp. 369. Flexi ISBN 3-525-42210-5. (Vandenhoeck & Ruprecht: Postfach 77, 3400 Götteningen, 1980.) DM 78.

PECILE, A. and MÜLLER, E. E. (eds). Growth Hormone and other Biologically Active Peptides. Proceedings of the International Symposium held in Milan, September 1979. Pp. 282. ISBN 90-219-0424-1. (Excerpta Medica: 1980.) $53.75, Dfl. 110.

PETERS, H. and McNATTY, K. P. The Ovary. A Correlation of Structure and Function in Mammals. Pp. 175. ISBN 0-236-40158-0. (Granada: St Albans, UK, 1980.) £15.

PETTE, D. (ed.). Plasticity of Muscle. Proceedings of a Symposium held at the University of Konstanz, Germany, September 1979. Pp. 624. ISBN 3-11-007-961-5. (Walter de Gruyter: Genthiner Str. 13, 1000 Berlin 30, 1980.) DM 160.

PICK, E. (ed.). Lymphokine Reports. A Forum for Nonantibody Lymphocyte Products. Vol. 1. Pp. 259. Flexi ISBN 0-12-432001-5. (Academic: 1980.) $28.50.

PIETRO, A. S. (ed.). Methods in Enzymology Vol. 69. Photosynthesis and Nitrogen Fixation. Part C. Pp. 894. ISBN 0-12-181969-8. (Academic: 1980.) $58.

ROBINSON, M. H. and ROBINSON, B. Comparative Studies of the Courtship and Mating Behavior of Tropical Araneid Spiders. Pacific Insects Monographs. Pp. 218. (Bishop Museum Press: Honolulu, Hawaii, 1980.) Flexi np.

RUCKEBUSHE, Y. and THIVEND, P. Digestive Physiology and Metabolism in Ruminants. Proceedings of the 5th International Symposium on Ruminant Physiology, held at Clermont-Ferrand, September 1979. Pp. 854. ISBN 0-85200-315-3. (MTP Press: Lancaster, UK, 1980.) £29.95.

SAN PIETRO, A. (ed.). Biochemical and Photosynthetic Aspects of Energy Production. Pp. 231. ISBN 0-12-618980-3. (Academic: 1980.) $25.50.

SCHEIT, K. H. Nucleotide Analogs. Synthesis and Biological Function. Pp. 288. ISBN 0-471-04854-2. (Wiley-Interscience: 1980.) £16.

SCHMIDT, R. F. and THEWS, G. Physiologie des Menschen. Pp. 798. ISBN 3-540-09446-6. (Springer: 1980.) approx. $57.90.

SCHULTZ, S. G. Basic Principles of Membrane Transport. Pp. 144. Hbk ISBN 0-521-22992-8; pbk ISBN 0-521-29762-1. (Cambridge University Press: 1980.) Hbk £12; pbk £4.25.

SOULÉ, M. E. and WILCOX, B. A. (eds). Conservation Biology. An Evolutionary—Ecological Perspective. Pp. 395. Flexi ISBN 0-87893-800-1. (Addison-Wesley: 1980.) £7.95.

SPIRO, T. G. (ed.). Metal Ion Activation of Dioxygen. Metal Ions in Biology Vol. 2. Pp. 247. ISBN 0-471-04398-2. (Wiley-Interscience: 1980.) £16.

STOKES, F. J. Collins Handguide to the Coral Reef Fishes of the Caribbean and Adjacent Tropical Waters Including Florida, Bermuda and the Bahamas. Pp. 160. ISBN 0-00-219761-8. (Collins: 1980.) £4.50.

SUBTELNY, S. and WESSELLS, N. K. (eds). The Cell Surface: Mediator of Developmental Processes. 38th Symposium of The Society for Developmental Biology. Pp. 374. ISBN 0-12-612984-3. (Academic: 1980.) $26.50.

SUTTON, B. C. The Coelomycetes. Fungi Imperfecti with Pycnidia Acervuli and Stromata. Pp. 696. ISBN 0-85198-446-0. (Commonwealth Agricultural Bureaux: Farnham House, Farnham Royal, Slough, UK, 1980.) UK £28, overseas £33.60.

TSUANG, M. T. and VANDERMEY, R. Genes and the Mind. Inheritance of Mental Illness. Pp. 143. ISBN 0-19-261268-9. (Oxford University Press: 1980.) £5.95.

WALLER, G. R. and DERMER, O. C. (eds). Biochemical Applications of Mass Spectrometry. First Supplementary Volume. Pp. 1279. ISBN 0-471-03810-5. (Wiley-Interscience: 1980.) £81.75.

WAYNFORTH, H. B. Experimental and Surgical Technique in the Rat. Pp. 269. ISBN 0-12-738850-8. (Academic: 1980.) $27.50, £11.80.

WEIBEL, E. R. Stereological Methods. Vol. 1, Practical Methods for Biological Morphometry. Pp. 415. ISBN 0-12-742201-3. (Academic: 1980.) £25, $57.

WHITEHEAD, G. K. Hunting and Stalking Deer in Britain through the Ages. Pp. 304. ISBN 0-7134-2983-9. (Batsford: London, 1980.) £17.50.

WISTREICH, G. A. and LECHTMAN, M. D. Microbiology. 3rd Edn. Pp. 786 + appendix. ISBN 0-02-470910-7. (Collier Macmillan: 1980.) £11.95.

SOHARY, M., HEYN, C. C. and HELLER, D. Conspectus Florae Orientalis. An Annotated Catalogue of the Flora of the Middle East. Fascicle 1. Pp. 107. Pbk ISBN 965-208-020-9. (Israel Academy of Sciences and Humanities: Jerusalem, 1980.) Np.

Applied biology

SANDLER, M. (ed.). Enzyme Inhibitors as Drugs. Biological Council. The Co-ordinating committee for Symposia on Drug Action. Pp. 285. ISBN 0-333-28984-6. (Macmillan: London, 1980.) £25.

SCHWARZ, R. H. and YAFFE, S. J. (eds). Drug and Chemical Risks to the Fetus and Newborn. Proceedings of a Symposium held in New York City, May 1979. Progress in Clinical and Biological Research Vol. 36. Pp. 166. ISBN 0-8451-0036-X. (Alan R. Liss: New York, 1980.) $20.

SELWYN, S. The Beta-Lactam Antibiotics: Penicillins and Cephalosporins in Perspective. Pp. 364. ISBN 0-340-22523-8. (Hodder & Stoughton: Sevenoaks, UK, 1980.) £8.95.

SMITH, R. Biochemical Disorders of the Skeleton. Postgraduate Orthopaedics Series. Pp. 293. ISBN 0-407-00122-0. (Butterworth: 1979.) £19.50.

SPARROW, S. (ed.). Immunodeficient Animals for Cancer Research. MRC Laboratory Animals Centre Symposia. Pp. 245. ISBN 0-333-27550-0. (Macmillan Press: London, 1980.) £20.

STOENNER, H., KAPLAN, W. and TORTEN, M. (eds). Section A: Bacterial, Rickettsial, and Mycotic Diseases Vol. II. CRC Handbook Series in Zoonoses. Pp. 568. ISBN 0-8493-2907-8. (Blackwell Scientific/CRC: 1980.) £50.

STRINGFELLOW, D.A. (ed.). Interferon and Interferon Inducers. Clinical Applications. Modern Pharmacology-Toxicology Vol. 17. Pp. 329. ISBN 0-8247-6931-7. (Dekker: 1980.) Sw.Fr. 92.

TSUANG, M. T. and VANDERMEY, R. Genes and the Mind. Inheritance of Mental Illness. Pp. 143. ISBN 0-19-261268-9. (Oxford University Press: 1980.) £5.95.

TU, A. T. (ed.). Survey of contemporary Toxicology. Vol. 1. Pp. 357. ISBN 0-471-04085-1. (Wiley-Interscience: 1980.) £21.25.

UNESCO/UNEP/FAO. Tropical Grazing Land Ecosystems. Natural Resources Research XVI. Pp. 655. Flexi ISBN 92-3-101611-3. (UNESCO: Paris, 1979.) Np.

Psychology

AJZEN, I. and FISHBEIN, M. Understanding Attitudes and Predicting Social Behaviour. Pp. 278. Hbk ISBN 0-13-936443-9; pbk ISBN 0-13-936435-8. (Prentice/Hall: 1980.) Np.

ALBRECHT, S. L., THOMAS, D. L. and CHADWICK, B. A. Social Psychology. Prentice-Hall Series in Sociology. Pp. 463. ISBN 0-13-817882-8. (Prentice/Hall: 1980.) £11.65.

ALEXANDER, F. and FRENCH, T. M. Psychoanalytic Therapy; Principles and Application. Pp. 353. Hbk ISBN 0-8032-1007-8; flexi ISBN 0-8032-59034. (University of Nebraska Press: 1980.) Hbk £11; flexi £3.

BLAKESLEE, T. R. The Right Brain; A New Understanding of the Unconscious Mind and Its Creative Powers. Pp. 275. Hbk ISBN 0-333-29089-5; flexi ISBN 0-333-29090-9. (Macmillan Press: London, 1980.) Hbk £10; flexi £2.95.

BROWN, T. S. and WALLACE, P. M. Physiological Psychology. Pp 634. ISBN 0-12-136660-X. (Academic: 1980.) $19.95.

BURKE J. J. and WEISS, V. (eds). Risk and Failure Analysis for Improved Performance and Reliability. Sagamore Army Materials Research Conference Proceedings. Pp. 355. ISBN 0-306-40446-X. (Plenum: 1980.) $42.50.

CAPLAN, D. (ed.). Biological Studies of Mental processes. Pp. 414. Pbk ISBN 0-901715-11-5; hbk ISBN 0-901715-12-3. (The British Psychology Society: Letchworth, UK, 1980.) Pbk. £7.50; hbk £12.50.

CLARKE, A. Psychological Models and Neural Mechanisms. An Examination of Reductionism in Psychology. Pp. 206. ISBN 0-19-824422-3. (Clarendon/Oxford University Press: 1980.) £11.50.

GHOLSON, B. The Cognitive-Developmental Basis of Human Learning. Studies in Hypothesis Testing. Developmental Psychology Series. Pp. 250. ISBN 0-12-282350-8. (Academic: 1980.) $19.50.

GUTTENTAG, M., SALASIN, S. and BELLE, D. (eds). The Mental Health of Women. Personality and Psychopathology Vol. 23. Pp. 161. ISBN 0-12-310850-0. (Academic: 1980.) $12.50.

HALLECK, S. L. Law in the Practice of Psychiatry. A Handbook for Clinicians. Pp. 294. ISBN 0-306-40373-0. (Plenum Medical: 1980.) $21.50.

LOCK, A. The Guided Reinvention of Language. Pp. 205. ISBN 0-12-453950-5. (Academic: 1980.) £12.60,$29.

McGUIGAN, F. J., SIME, W. E. and WALLACE, J. M. (eds). Stress and Tension Control. Pp.311. ISBN 0-306-40450-8. (Plenum: 1980.) $29.50.

PLOG, S. C. and SANTAMOUR, M. B. (eds). The Year 2000 and Mental Retardation. Pp. 233. ISBN 0-306-40252-1. (Plenum: 1980.) $19.95.

SANTS, J. (ed.). Developmental Psychology and Society. Pp. 389. ISBN 0-333-21340-8. (Macmillan Press: London, 1980.) £20.

SARASON, I. G. and SARASON, B. R. Abnormal Psychology. The Problem of Maladaptive Behavior. 3rd Edn. Pp. 573. ISBN 0-13-001107-X. (Prentice/Hall: 1980.) £12.95.

STOCKARD, J. *et al.* Sex Equity in Education. Educational Psychololgy Series. Pp. 238. ISBN 0-12-671550-5. (Academic: 1980.) $18.

VALENSTEIN, E. S. (ed.). The Psychosurgery Debate. Scientific, Legal, and Ethical Perspectives. Pp. 594. Hbk ISBN 0-7167-1156-7; pbk ISBN 0-7167-1157-5. (W. H. Freeman: 1980.) Hbk $25; pbk $14.

WEXLER, K. and CULICOVER, P. W. Formal Principles of Language Acquisition. Pp. 647. ISBN 0-262-23099-2. (MIT Press: 1980.) £21.70.

History of Science

KAPITZA, P. L. Experiment, Theory, Practice. Articles and Addresses. Boston Studies in the Philosophy of Science Vol. 46. Pp.429. Hbk ISBN 90-277-1061-9; pbk ISBN 90-277-1062-7. Reidel: 1980.) Hbk Dfl. 90, $47.35; pbk Fgl. 28, z£14.75.

LIVANOVA, A. Landau. A Great Physicist and Teacher. Pp.217. ISBN 0-08-023076-8. (Pergamon: 1980.) £10, $22.50.

RAZZELL, P. Edward Jenner's Cowpox Vaccine: The History of a Medical Myth. 2nd Edn. Pp.133. ISBN 0-904573-41-9. (Caliban: Sunninghill, Ascot, UK 1980.) £10.

TURNER, G. L'E. Antique Scientific Instruments. Pp.168. Hbk ISBN 0-7137-0923-5; pbk ISBN 0-7137-1068-3. (Blandford: Poole, UK, 1980.) Hbk $3.95.

WIGHTMAN, W. P. D. and BRYCE, J. C. (eds). Adam Smith: Essays on Philosophical Subjects. Pp.358. ISBN 0-19-828187-0. (Clarendon/Oxford University Press: 1980.) £14.

nature

25 September 1980

What future for European fast reactors?

Of all the neglected technologies of the past few years, the technology of the fast reactor is the most pathetic. Long gone are the days when governments in the industrialized world were declaring their intention of running up one or two demonstration plants confident in the hope that their electricity utilities would then be able to make limitless (and cheap) electricity without much trouble. As the years have gone by, governments have become more and more hesitant, even pusillanimous. In the United States, fast reactor development is in the doldrums — the demonstration reactor at Clinch River consists largely of a collection of components not yet put together, while all but a few of the small-scale reactors being built or operated ten years ago have now bitten the dust. The trouble at Clinch River is partly financial (the cost of completing the reactor would now be far greater than the original estimate), partly technical (the design leaves much to be desired) and partly political — fast reactors are regarded by the US Administration as the doorway to the "plutonium economy" and the rapid proliferation of nuclear weapons to lie beyond that, while fast reactors have become prime targets for those who go about with "No nukes" on their bumper stickers or tee-shirts.

Outside the United States, the desuetude is less conspicuous even though the brash optimism of the 1950s has largely evaporated. There are substantial prototype fast reactors in France, the Soviet Union, the United Kingdom and West Germany, while a reactor capable of generating 1,200 MW of electricity (and called Super-Phénix) is being built in France with financial support from West Germany and, to a lesser extent, Italy. As the months go by, the prospects improve that, by 1983, this reactor will turn out to be the first full-scale reactor of its kind. The French are already talking of the reductions of capital costs that will come about when the sixth or seventh replicas of Super-Phénix are built. Now, it seems, this talk has wooed the UK Atomic Energy Authority away from its long-standing belief in its own supremacy. This, at least, is one reading of Sir John Hill's welcome last week for the proposal that the United Kingdom might join the European collaboration concerned with Super-Phénix (*Nature,* 18 September). The decision now rests with the British government but will also, no doubt, be influenced by the course of the negotiations on commercial terms which are still to be completed. How sensible is this course of action? What, in any case, are the prospects for fast reactor technology? And does it follow that the nuclear business, in France certainly but perhaps in the rest of Europe, is embarked on what many of its critics consider to be a dangerous path?

The proposal that British interests in fast reactor technology should be met within the framework of some wider collaboration is probably not so much a choice as a Hobson's choice. For several years, it has been obvious that no amount of successful operation of the Prototype Fast Reactor at Dounreay would bring into being the heavy industry that would be needed if fast reactors were ever to be built in earnest. The National Nuclear Corporation (now to be reorganized again, but probably to be made more effective in the process) is having to go through all kinds of gyrations to take on the design and construction of a single pressurized water station on which construction cannot begin for another two years. At the same time, to create the capacity for building fast reactors, especially when the demand for these is entirely unknown, would be impossible. Such an attempt would be a folly. On strictly practical grounds, it is prudent to look for some international arrangement under which the labour of building fast reactors could be divided, together with the profits (if any) in doing so. Wider considerations, European collaboration and all that, reinforce the point. So far, so good.

As always, there are several snags. Is Super-Phénix such a mature fast-reactor design that it will be possible, as the French hope, to use it as the model on which to fashion a whole generation of replicas? Or will it be necessary, after 1983, to build yet another demonstration plant, and to incur the substantial extra costs of doing so? Answers to these questions (which cannot be simple) will no doubt help to determine the British government's response to the Atomic Energy Authority's request. The choice, it will be remarked, is again not an open choice between collaboration and going it alone. Given the government's commitment to a public inquiry before a commercial fast reactor could be built, the Atomic Energy Authority would have to kick its heels for a further five years before the construction of a commercial fast reactor could begin. While scratching their heads over these alarming questions, ministers and the management of the AEA should reproach themselves (and/or their predecessors) for having, aloof and toffee-nosed, scorned the proposals for European collaboration on the development of fast reactors in the decade following the late 1950s.

But why the hurry? And what, in any case, is the objective? If, in the United States, nuclear policy is based (as it has been for the past three years) on the principle that the recylcing of nuclear fuel is economically unnecessary, why should European governments be rushing ahead? The French position is clear and characteristic. Self-sufficiency, or near self-sufficiency, is in itself a legitimate goal. The Commissariat à l'Energie Atomique has calculated that it might be possible to generate a substantial proportion of French electricity production from indigenous uranium, but only with the help of breeder reactors extracting fission energy from uranium-238 (via plutonium-239) as well as from uranium-235. This will not, of course, prevent the French from making deals with Australia for the supply of uranium ore (like that announced last week) — that will be a sensible way of eking out supplies. Elsewhere in Europe, self-sufficiency is less obviously a part of public policy, although few European can take much comfort from American assurances that uranium prices will be relatively low (less than £35 per kilogram of U_3O_8) for the remainder of this century. Prices could leap up, as they have done on several occasions in the past, if (or rather when) there is a revival of confidence in nuclear power in the United States. In most European countries, however, there is no immediate need for a fast-reactor programme on the scale now foreseen in France. The most urgent need is that potential users should become so familiar with this new technology that they will be able to handle it confidently. Much also needs to be learned about the economics of fast reactors, and of the fuel cycles on which they are based. The case for pushing ahead quickly with fast reactor technology is that its long-term importance will be demonstrated only when a number of reactors have been used commercially, by European utilities of all kinds.

If this objective were more clearly recognized, some of the present reactions against the building of fast reactors would, or should, be less intemperate than they are. It must, however, be expected that others will persist. Fears for the safety of fast reactors are rife, but, as commonly stated, are often misplaced. It is in everybody's interests that such anxieties as there are should be widely understood. The fact that a core of a fast reactor

0028-0836/80/390263-02$01.00

contains more than enough fissile material to cause a nuclear explosion does not make every fast reactor a potential bomb.

The most likely sources of potential hazard are, on the contrary, mundane — the apparently devilish capacity of liquid sodium to work its way through leaks and cracks, the formation of vapour bubbles in the circulating sodium which can increase the reactivity of the system (at least if it is physically large enough) and the possibility of chemical interaction between liquid sodium and fuel cans or impurities (such as water). The most likely source of criticality problems is not the formation of a single critical mass of fissile material but, rather, mechanical oscillation within the reactor core which, on paper at least, may be symmetrical enough to set in train a sustained and rapid increase of reactor power. The fact that the nuclear reaction involves fast (1 MeV or so) neutrons rather than thermal neutrons is not in itself a source of potential hazard. The power density of the system (400 W per cm^3 in Super-Phénix) does, however, carry heat-transfer engineering into a novel field, while the use of liquid sodium as a heat transfer medium presents another set of once unfamiliar problems. On balance, however, there is no reason to dispute the claim of the nuclear engineers that individual fast reactors need be no more hazardous than conventional reactors. In Britain, the intended public inquiry, unfortunately now delayed at least until 1985, will provide sceptics a splendid opportunity to test the proposition.

Fears that fast reactors mean a greater risk of proliferation are less substantial, and should now be exorcized. The argument is that if plutonium is separated from spent fuel from thermal reactors, stocks of plutonium will increase as will the oportunities for theft and illicit diversion into bomb-making. In its simplest form, the argument perversely overlooks the simple truth that reprocessing facilities are at present few and far between. The bomb-making states, anxious as they are that the nuclear club should not be enlarged, control the only substantial plants now in operation. Others, even that being built in Brazil, are under international control. India is the exception that proves the rule — its reprocessing facilities are uncontrolled, but their capacity is small. In the past year, and especially in the wake of the International Fuel Cycle Evaluation, there has been much talk of internationally operated reprocessing facilities.

Such schemes, imaginative though they are, are not, however, the most urgent needs in the international effort to control proliferation. Certainly the pace of fast reactor development now on the cards is not going to increase the opportunities of governments to join the nuclear club, at least in the remainder of this century. Moreover, given that such plutonium as fast reactor programmes will produce will accumulate in the stockpiles of well-ordered states (and will also, not doubt, be put back into fast reactors as quickly as possible) there is no reason to think that the chances of illicit diversion will be proportional to the total quantity of plutonium in existence. Safety, in brief, is something to worry about. The risk of proliferation at least for the time being, is not.

Technical innocence in the public service

With much of the British Scientific Civil Service still seething over the pay settlement for this year (*Nature*, 24 July), the Civil Service Commission on Tuesday went some way to acknowledging that scientists in the Civil Service often have a raw deal. The publication of the *Review of the Scientific Civil Service (1980)* (Cmnd 8032, HMSO, £6,10), prepared by a group of officials with Dr Martin Holdgate, Chief Scientist at the Department of the Environment, is not pure emollient, however. The remedies which the review suggests, valuable as far as they go, do not touch the problem which many people (not only scientists in the Civil Service) consider the most serious — the continued separation of scientists (and of other professionals) from the Administrative Group, the body chiefly responsible for the formulation of policy within the British government and within which true mandarins grow up. Although, at the higher reaches of the Scientific Civil Service, a handful of posts are considered as "open" grades, it is inevitable that for most people in the public service the Holdgate review will seem to rub salt in open wounds. So too will the date in parentheses at the end of the title, which is an awkward reminder of how often the question has been considered, and to how little effect.

The case for a merger of scientists (and others) in the public service with the administrators is not to feather the nests of scientists, nor to ensure that each and every one of them can look forward, from the beginning of his career, to being a powerful head of a Department of State, with a briefcase and chauffeur to match. Many scientists would in any case prefer to avoid that path. The need is rather that the public service as a whole should be more able to understand the problems of a technical character with which it has increasingly to battle. The Holdgate review acknowledges this need at the outset of its report. It goes on to record the failure, in the past few years, of the schemes devised to help scientists transfer from their ghetto to the Administrative Group. The explanation is, of course, straightforward. Scientists in early or mid-career do not relish giving up their science to become administrators. Afterwards, it is often too late. The Holdgate remedy is that, in planning people's careers in the Scientific Civil Service, care should be taken that promising people should be given training in the "management skills" supposed essential to administration. The trouble is that without a common understanding throughout the public service that posts as administrators would be found for those wishing to transfer, more training may simply mean more frustration. In any case, for as long as most of those responsible for policy-making persist in their innocence of technical questions, the public service will be less effective than it needs to be. This broad question is outside the terms of reference of the Holdgate review, for reasons which are not necessarily sinister. Nobody should forget that it is the question most in need of answering.

If tinkering with the present system can help, however, Holdgate and his men (*sic*) have some useful things to say, especially on the careers of scientists in the public service. Scientists need to know more clearly than at present what their career prospects are, and to be helped (if they wish) to broaden them. Merit needs to be rewarded, especially in those following less glamorous careers such as the provision of technical services. Decorously, the report skirts round the issue of pay, and also timorously accepts that probationary and fixed-term appointments to the Scientific Civil Service would be impracticable. The truth is that they would be unwelcome, which is another matter. The review comes close to acknowledging the need for a more effective scientific contribution to general policy with its plea (to the administrators) that they should more openly look for and welcome scientific advice within the public service. We shall no doubt see (or not see) what happens

What will happen now? The Civil Service Department (responsible for employing all Civil Servants) will urge everybody in sight to follow the Holdgate recommendations. After a few months, or a few years, this review will join its predecessors in the archives of British public administration. The innocence of the Civil Service as a whole of what the modern world is like will be found to persist. It will be forgotten, then, that the Holdgate review included within its terms of reference the question of what the Sciencitific Civil Service is for; its report dutifully includes a list of the duties scientists in the public service perform. Now and again there is a hint that the committee of officials knew it was avoiding a crucial issue — and the recommendation that research extrablishments might be decentralized may absolve it of some blame. But is it not high time that somebody asked seriously how best 17,000 of the most highly qualified scientists in Britain should serve the public interest? Influencing policy is one thing. Making government research establishments more useful is another.

0028-0836/80/390264-02$01.00

US woos African states with science

Washington

Trade, it seems, no longer follows the flag but the lab. Washington's top science administrators departed for Africa last week for a ten-day trip aimed at stimulating scientific and technical cooperation with four "moderate" African states — Nigeria, Kenya, Senegal and Zimbabwe.

The sixteen-person delegation is headed by Dr Frank Press, director of the Office of Science and Technology Policy (OSTP). Other members include the administrator of the National Aeronautics and Space Administration, the acting director of the National Science Foundation and the director of the National Institutes of Health.

The practical goal of the delegation is to sign a number of agreements with the four countries for programmes of mutual cooperation. These range from setting up an experimental rural telecommunications system based on satellite technology in Senegal to a broad programme of vocational training courses for Nigerian science and engineering students in US universities and technical colleges.

The delegation's visit is also part of a broader strategy to strengthen links with four African countries with which the United States currently has the best relations. The intention is to help these countries to gain economic stability by promoting their technical efforts — and this in turn should provide a basis for their political stability.

In at least one case there are pragmatic reasons for the United States to want to maintain close political links. Nigeria is at present the nation's second largest supplier of petroleum (after Saudi Arabia); and continuation of this supply is important for the nation's security.

Some money is to be made available by the federal government so that agreements reached during the visit can be followed through, for example by arranging for the reciprocal visit of African scientists and policy makers to the United States. But for many countries, additional fiscal resources are less important than access to people and institutions in the United States able to help with their development problems.

OSTP expects agreements for cooperation to be signed in fields such as marine sciences, environmental resources, agriculture, remote sensing, satellite communications, alternative energy sources and the management of scientific research and technical information.

Three of the countries — Senegal, Kenya and Zimbabwe — will be able to benefit from financial and technical assistance offered under the term of US aid policies. In the fourth, Nigeria, the average income is above the limit for concessional terms to be permitted, and the United States will be looking for costs to be reimbursed.

Many of the agreements due to be signed cover areas that would have been the responsibility of the ill-fated Institute for Scientific and Technological Cooperation (ISTC). The setting up of ISTC was proposed by President Carter in 1978 and authorized by Congress last year, but because of a dispute with the Senate over funding is unlikely to come into existence. However, Dr Press said that the scope of the cooperative agreements, which will include feasibility studies of a Nigerian-based tuna industry and a project on ammonia-based synthetic fuels in Zimbabwe, will go beyond the role that had been intended for ISTC. The mission, according to Dr Press, has the full and active backing of President Carter, who had for example discussed it with Dr Robert Mugabe, Prime Minister of Zimbabwe, who visited Washington last month.

One disappointment for US — and possibly African — officials is that the delegation will not include Dr John Slaughter, a black who has been nominated by President Carter as director of the National Science Foundation.

After an inter-party dispute in the Senate over whether Republican members should assent to the appointment of Democrat nominees in the last few months before the Presidential election, Dr Slaughter's nomination was approved by a Senate committee last Wednesday, and is expected to move swiftly through the full Senate with little opposition. The delay has meant that Dr Slaughter will not be on the delegation and his place will be taken by Dr Donald Langenberg, the foundation's acting director. **David Dickson**

Still looser UK guidelines

The Genetic Manipulation Advisory Group (GMAG), responsible in the United Kingdom for the administration of guidelines on recombinant DNA research, has taken a substantial step towards oblivion. From now on, according to the latest revision of its guidelines applicable to university and industrial laboratories, experiments planned for the least stringent of the four categories of safeguards will not be scrutinized in advance by GMAG. Instead, the laboratory safety committee will have to carry through the standard GMAG hazard assessment and assure itself that proposed experiments do indeed belong in Category I. Laboratories will be required to inform GMAG in September each year of all experiments carried out under this licence in the previous year.

Sir William Henderson, chairman of GMAG, estimated last week that this step will relieve GMAG of 90 per cent of its present work. Because of rules which allow much other research to proceed once GMAG has been notified, it is estimated that only some two per cent of the experiments now being planned will have to await formal permission from GMAG.

The proposal that laboratories should be granted an annual licence to carry out experiments in Category I was first considered by GMAG in November 1978, at its first radical revision of the guidelines. The committee then considered that further information was necessary before the matter could be decided.

Sir William and other members of the committee are at pains to emphasize that this most recent revision of the GMAG procedures has been made possible by the accumulation of information in the past two years, and especially by evidence that the capacity of genetically manipulated bacterial cells to produce foreign protein molecules is limited. The assumption is that the production of foreign protein molecules from a single *Escherichia coli* bacterium with a foreign gene at a plasmid site chosen for expression will not exceed 10^6. This, the argument goes, provides ways of quantifying the maximum amount of foreign protein produced in the infection of, say, the human gut by genetically altered bacteria. On this basis, the maximum amount of insulin produced in the gut by *E. coli* carrying an insulin gene could not exceed the equivalent of 0.6 units of the hormone, compared with the 20 or 30 units normally circulating in the body.

Laboratory safety committees will be expected to verify such estimates made by those wishing to carry out experiments, and to adjudicate specific proposals for categorization of the experiments concerned. GMAG itself expects that there will be further revisions of the guidelines, no doubt tantamount to further relaxations, in the not too distant future

GMAG's own concerns are increasingly with proposals for large-scale manufacture — although the volume of applications so far has, apparently, been surprisingly small. Sir William considers, however, that both in respect of what GMAG requires from industrial applicants and more generally, British regulation of genetic manipulation is now less stringent than in the United States.

On large-scale production plants, for example, GMAG has taken the view that it is not feasible to enclose 100,000-litre fermentation vats in completely sealed containers or to operate them under negative pressure. Safety assessment, therefore, turns on an on-the-spot appraisal of the manufacturing plant and proposals for its

0028-0836/80/390265-02$01 00

operation.

Although it is too soon to know whether GMAG will or should go out of business, the recruitment of specialists in genetic manipulation to the committee may now become increasingly difficult. The group, in any case, will have its hands full with the scrutiny of proposals for work in categories II–IV of the guidelines procedures, and with the principles for regulating large-scale manufacture. The reconstitution of the Dangerous Pathogens Advisory Group, expected soon, should, however, help to clarify GMAG's long-term future.

Engineering research

Planning for more

Washington

Federal policy-makers are now in the process of deciding whether the National Science Foundation (NSF) can provide an adequate framework for regenerating the health of the nation's engineering efforts. NSF officials are confident that it can. A prominent component of plans for reorganizing the foundation, formally presented last Thursday to the National Science Board responsible for foundation policy, is the creation of a new engineering directorate (see *Nature* 11 September). Applied science, which shares a directorate with engineering, would be distributed among the other research directorates.

Concern for the health of US engineering research has arisen as part of the wider debate about declining productivity and stagnating innovation. Equally important, however, has been what NSF acting director Dr Donald Langenberg describes as an "upsurge of interest" from engineering societies over the state of their profession and the role of federal support.

Both NSF and its critics agree that US engineering is in poor health. A rapidly escalating demand for engineers for large-scale construction projects in the oil and chemical industries has created a national shortage of engineers. This situation will be exacerbated by the demands of new plants to be financed out of the government's $20,000 synthetic fuels programme.

The shortage is reflected in the high salaries paid to engineering graduates, while another result is that few graduates are tempted to stay on at university to do research once they have completed their first degree. Many postgraduate courses are now largely filled with foreign students and NSF estimates that, overall, there are 2,000 empty positions in university engineering faculties.

Some universities are designing schemes to compensate. Carnegie-Mellon University in Pittsburgh, for example, plans to offer loans of $1,000 a month to PhD candidates, which need not be paid back if the candidate stays on and teaches.

However, there is general agreement that more than a piecemeal approach is needed; the question is the form it should take. Dr Leo Young, president of the Institute of Electrical and Electronic Engineers (IEEE), has proposed a "blue-ribbon commission" — somewhat similar to Britain's Finniston Committee — to look at the problems facing the profession.

In Congress, discussion has focused on a bill introduced by Mr George Brown, chairman of the House science and technology subcommittee, which proposes setting up a National Technology Foundation. Mr Brown admits that his proposal has been put forward chiefly as a vehicle for discussing a range of proposals and that a revised bill is likely to be re-presented to the next session of Congress.

However, many engineers have not lost the opportunity to vent their frustrations at what they consider to be a lack of support from the federal government in general — and the NSF in particular — especially in fields outside space and defence research.

"Those university departments supported by the Department of Defense and the National Aeronautics and Space Administration have fared well, while civilian engineering, such as building technology and machinery design, have been neglected" complained Dr Bruno O. Weinschel, head of a private engineering company and secretary of IEEE.

National Science Board chairman Dr Lewis Branscomb of IBM admitted at congressional hearings on the bill that NSF support for engineering may have been weak in the past, but he insisted that this was now being remedied. He pointed out that for the past two years the board has proposed greater increases in the foundation's support for engineering research than for any other area of science.

NSF is hoping that its planned reorganization will go some way towards meeting its critics and will in particular head off any attempt to set up a new, separate institution (which might, in addition to the organization split, also be in a position to compete for funds). At a public meeting two weeks ago, held to discuss the reorganization proposals, Dr Langenberg said that engineering research could benefit financially from having its own directorate. He also hinted that reorganization plans were likely to be accompanied by a request for a significant increase in funds for engineering research when the foundation's budget request for 1982 goes to Congress in January.

Further financial commitments are likely to result from President Carter's decision about how to embrace science and engineering education in US schools and colleges, a report on which was sent to the White House by NSF and the Department of Education last month, and is expected to be made public shortly. But even if the Administration agrees that there is room for a larger role for engineering in the foundation, Congress may take some convincing. In debating the NSF appropriations in July, the House of Representatives rejected a proposal for a 10 per cent increase in funds for the engineering directorate.

The White House report is likely to have a good deal to say about engineering research in American universities and colleges. Although, elsewhere, engineering graduates tend to stay away from doctoral courses, in its United States the demand is still quite high. There is, however, increasing concern about the willingness of potential faculty members to teach.

Perhaps more significantly, the powerful House Appropriations Committee claimed that its restriction of the use of NSF funds planned for various innovation projects was imposed "to ensure that an unacceptable level of unbudgeted items does not erode funding for basic research programmes which is — and continues to be — the *raison d'etre* of the foundation".

These sentiments find an echo, though somewhat muted, within the scientific community. At the public meeting on 13 September, representatives of several of the NSF's advisory committees expressed concern that too great an emphasis on engineering and applied science could put a further squeeze on basic research. Dr Langenberg replied that he felt basic science was sufficiently robust not to be significantly threatened, but not everyone present was convinced. **David Dickson**

Electronic publishing

Keyboard papers

Those who wish to publish a research article in a journal, who are asked to referee a paper or who simply want to read what their colleagues have been publishing may in future have to turn to a computer terminal. The fully electronic scientific journal is still a few years off, however. But a group of British researchers is already beginning to consider its possibilities, in a project supported to the tune of £256,000 by the British Library.

The aim of the project, which begins in earnest in November, is to investigate whether electronic journals might ever be feasible, how much they would cost the user and the type of problems they would pose to users. The leg work is being done by groups at the University of Birmingham Loughborough University. The Birmingham group, under Professor P. Jarratt, will be providing the central computer facility and hardware and software to other participants in the project at a cost of £122,000. The Loughborough group, under Professor B. Shackel, will coordinate the setting up of an experimental electronic journal using the rest of the funds.

About 35–40 people dotted throughout universities in Britain will be collaborating. Each centre will provide its own terminal linked in to the Birmingham computer. The British Library funds will go towards suggest how agencies could do more. And this would require a response, in particular from the National Institutes of Health (NIH), which have broad responsibility for stimulating the applications of research results through technology transfer.

It will not be easy to develop guidelines on ethical issues comparable to those which exist on safety. The federal government has no jurisdiction over the treatment that a private medical practitioner can offer, while the separation of church and state is paramount.

David Dickson

French Science

Same now, more later

Paris

The French budget for science will grow with inflation next year — but it is not quite the bonanza for science that the Secretary of State for Research, M. Pierre Aigrain, was claiming last week.

At a press conference to launch the proposed budget, which goes before parliament at the end of next month, M. Aigrain boasted of an increase of 20.4 per cent in non-salary research spending in 1981. Inflation is running at 14-15 per cent, however, and some of the increase will be delayed until 1982.

Nevertheless, M. Aigrain's news is good news. In the past two years, the minister has lost most applied research, accounting for about half his budget, to the control of the minister of industry, M. Giraud, and there were fears that one result would be reduced growth in the budget for basic science. But in the event, Aigrain said last week, basic science will grow by four per cent more than applied.

The 1981 budget is highly selective, and some areas of research will shrink in real terms. Space research funded by the Centre National d'Etudes Spatiales, for example, will suffer an increase of only 9 per cent in money terms, while FF535.6 million (£54 million) available to Aigrain's own office, the Délégation Générale à la Recherche Scientifique et Technique, for making direct research contracts with universities in 1980 will actually fall to FF471.7 million in 1981. (It should rise again in 1982.)

Some sleight of hand with the budget conceals these facts. Running costs plus "programme authorizations" will indeed grow by 20.4 per cent next year but authorizations include commitments for future years. Actual cash for basic research is planned to increase from FF3,630 million in 1980 to FF4,200 million in 1981 — a growth of only 15.7 per cent, and of the same order as inflation. Nevertheless, the budget commits the government to more spending in 1982. Some important institutions will even do well in 1981.

The main beneficiaries affecting universities are the three principal research agencies, the CNRS (Centre National de la Recherche Scientifique), INRA (Institut National de la Recherche Agronomique) and CNEXO (Centre National pour l'Exploration des Oceans); the fourth, INSERM (Institut National de la Santé et de la Recherche Medicale) just keeps pace with inflation. One objective is to help to renew ageing equipment and INSERM is judged to have done well in this regard in past budgets. CNRS, which with some 8,700 scientists runs many of the leading laboratories, gains 24 per cent in its "operational" budget, INRA 31 per cent and CNEXO 34 per cent.

Certain big projects also do well. There will be FF48.5 million to cooperate with the Soviet Union on a Venera probe to Venus and a FF64.3 million contribution to the European Space Agency Spacelab programme. The budget also allows for the construction of a submarine and other work (FF21.7 million); a start on construction of a fusion reactor (TORE SUPRA) at Cadarache (FF15.5 million) and a start on a hot dry rock geothermal project (FF1 million). In basic physics, the government will contribute to the "second souffle" at the Institut von Laue Langevin (FF5.4 million), the heavy ion accelerator GANIL (FF6.7 million) and the Franco-German Institut de Radio-astronomie Millimetrique (FF22.6 million).

One tangible benefit of the budget will be the creation of 625 new junior posts, 410 of them for scientists and the rest for technicians, engineers and administrators.

The budget also reveals the French commitment to defence research, spending on which has grown by 23 per cent a year since 1977 to reach a level of FF11,000 million in 1980, accounting for 37 per cent of the national spending for research and development. Of this fraction, some 28 per cent is described as "research" proper but only one per cent of this finds its way to universities.

Robert Walgate

Soviet bomb scare

Washington

Reports of a possible violation by the Soviet Union of a 1974 agreement on underground nuclear tests could prejudice negotiations on a Comprehensive Test-Ban Treaty, now expected to be concluded within a few months.

Officials in the Carter Administration are hurriedly trying to check preliminary seismological data indicating that the 1974 agreement, under which the United States, the Soviet Union and the United Kingdom agreed not to conduct underground tests equivalent to more than 150 kilotons of TNT, may have been violated.

According to a report in the *New York Times*, unnamed security aides claim that an explosion detected on Sunday, 14 September, was the largest that had been registered since the agreement came into effect in 1976. Some said it was close to, but still above, the maximum permissible limit; others that it may have been as large as 650 kilotons.

Data are now being collected from as many detection stations as possible to see if this assessment is correct, or if stories in the press merely reflect attempts to discredit the Administration's arms limitations efforts.

Officials in the Office of Science and Technology Policy said last week that it would be about a month before sufficient data were collected to make a reasonable judgement on the size of the explosion, but the Administration's concern has already been expressed by the State Department to the Soviet ambassador

Current negotiations aimed at securing a comprehensive test-ban have become bogged down over defining the limits beneath which it may be impossible to distinguish a man-made explosion from normal seismic activity. In recent weeks, negotiators in Geneva have been expressing optimism that agreement was close, and that a draft treaty could be ready for signature within a few months.

David Dickson

German science

Frontier talk

An agreement on scientific cooperation between the two Germanies might well be feasible, according to Professor Kurt Hager, Chairman of the Education Committee of the Politburo of the German Democratic Republic (GDR). He was addressing the country's Fifth Conference on Higher Education (4 – 5 September) which was convened to discuss the contribution of universities and other higher educational institutions to strengthening the GDR's economic performance in the 1980s.

The suggestion carried the political proviso that development of relations "would be made easier if the responsible circles in the Federal Republic could bring themselves to abandon their . . . non-recognition of GDR citizenship and disregard for the sovereignty of our state".

The conference was attended by some 4,000 delegates from both academic staff and students, and it was not entirely a political exercise. Educational planners in the GDR have recently been paying considerable attention to the training of young scientists. Earlier this year, a working group from the Education Commitee of the Politburo visited a number of educational establishments throughout the country. Following the presentation of their findings, Professor Hager had stressed that the early training of young scientists was a "vital task of far-reaching importance which would have considerable influence on further economic growth". He advocated that steps should be taken to ensure that "specially talented young people fitted for science" are discovered as early as possible.

Vera Rich

0028-0836/80/390269-02$01.00

CORRESPONDENCE

Geothermal power

SIR—The recent News and Views article by Richardson and White (*Nature* 10 July)[1] and correspondence in your columns[2] have been concerned with the relative merits of two ways of using geothermal energy — district heating and electricity generation — and there does not seem to be much to choose between them. According to Richardson and White, "Neither of the schemes is particularly attractive in absolute terms". Certainly, electricity generation directly from a geothermal source at a temperature below 200°C has previously been considered to be uneconomic[3,4].

It was because of this view that Patscentre, some three years ago, proposed a scheme that allowed the possible exploitation of such low-temperature geothermal sources for economical electricity generation if they coincided with sites for conventional power stations, existing or prospective[5]. Geothermal hot water could be efficiently used for feedwater heating in the power stations. I suggested that such a concidence of sites might be found on the Hampshire (geological) sedimentary basin. The idea was taken up by the Central Electricity Generating Board, and a borehole was sunk last year at Marchwood power station, near Southampton. Earlier this year, you reported that an aquifer had been struck (*Nature*, 8 May)[6]. I understand that the geothermal hot water will probably be used in the Marchwood station as an experimental illustration of the proposed scheme.

It is to be hoped that, if successful, this experiment will be the forerunner of an acceptably efficient method of geothermal electricity generation in the UK and elsewhere.

R.V. HARROWELL

PA Centre for Advanced Studies,
Melbourn, Cambridge, UK

1. Richardson, S.W. & White, A.A.L. *Nature* **286**, 103-104 (1980).
2. Garish, J.D. *Nature* **286**, 326 (1980).
3. Oxburgh, E.R. *Nature* **262**, 526 (1976).
4. Gliddon, B.J. *et al. CEGB Research*, no. 2, 40 (1975).
5. Harrowell, R.V. *Nature* **266**, 299 (1977).
6. *Nature* **285**, 64 (1980).

SIR — The method of evaluation for the district heating option used by Richardson and White in their article on the use of UK geothermal energy resources (*Nature* 10 July, p.103) is not appropriate for UK geothermal resource conditions.

The Department of Energy Geothermal Energy Group have predicted that geothermal energy sedimentary basin resources in the United Kingdom will be most commonly in the range 65 to 80°C. We have recently completed a study for the Department of Energy examining the use of UK geothermal energy resources which concluded that a supply temperature of 65°C will be adequate to meet space and water heating needs. Underfloor heating systems or large natural convectors could operate with a supply temperature of 65°C to satisfy comfort conditions and achieve a return temperature of 30-35°C. We believe, however, that the optimum solution will arise from forced air convection equipment which could reduce the return water temperature to the geothermal source heat exchanger to 20-25°C and furthermore a proposal is in hand directed by W. S. Atkins and Partners and supported by a major UK heating equipment manufacturer to develop a range of such equipment at competitive price levels when compared to standard temperature equipment.

A further important factor to be considered is that the depth of aquifers containing brine at 70°C is such that it could significantly reduce the cost of the geothermal well compared to an aquifer supplying water at 100°C. We suggest therefore that the findings of Richardson and White be reconsidered.

E. J. ATHONY

Environmental Engineering Division,
W. S. Atkins & Partners, Epsom, UK

Models of psychosis

SIR—In a recent News and Views article (*Nature*, 5 June)[1], Snyder expressed the view that phencyclidine — currently all the rage among drug-abusers in the United States — might provide a good pharmacological model of schizophrenia. In the course of his paper he makes a comparison with LSD-25 which, he suggests, is not a good model because it produces perceptual disturbances that are mainly visual in nature, whereas those found in schizophrenia occur primarily in the auditory modality. There is actually no factual basis for that statement; on the contrary, several studies (for example, Young[2]) indicate that the effects of LSD on perceptual, as well as on other psychological, functions, are remarkably similar to the symptoms of schizophrenia. This widely quoted misconception about LSD is only one of many which have led, in my view, to the drug being prematurely rejected as a possible pharmacological model for human psychosis. As I have argued in detail elsewhere[3], I believe a good case can still be made for LSD; though Snyder may be right — phencyclidine may be better.

G.S. CLARIDGE

Department of Experimental Psychology,
University of Oxford, UK

1. Snyder, S.H. *Nature* **285**, 355-356 (1980).
2. Young, B.J. *Br. J. Psychiat.* **124**, 64-73 (1974).
3. Claridge, G.S. *Schiz. Bull.* **4**, 186-209 (1978).

Educative computers

SIR — We were very interested to read your article "Money to spend" (*Nature* 21 August, p.750) about the government's programme on microelectronics in schools and colleges.

One matter of fact, however, we feel should be put right. The estimate of about one hundred schools owning their own computers is a long way off the mark. A survey carried out in the first three months of the year by ourselves and the Schools Council, in which replies were received from 60 out of 104 local education authorities in England and Wales, showed 663 secondary schools with at least one microcomputer. (In Scotland, the figure at the end of August was over 250.)

Even those figures should be taken as very conservative estimates since numbers are growing rapidly from day to day. We know of one local authority, for instance, which is installing a new machine at its schools at the rate of one a week.

If any of your readers would be interested to have a copy of a brief report of our survey referred to above, we should be pleased to send them one.

JILL COATES

Council for Educational Technology,
3 Devonshire Street, London W1N 2BA

Interferonology

SIR — I am writing in response to the note on interferon nomenclature which appeared recently in *Nature* (10 July 1980; **286**, 110).

I recognize that the previous nomenclature is less than ideal because the names ("leukocyte", "fibroblast" etc.) now refer to molecular classes of interferons rather than tissues of origin.

With the foregoing qualification in mind, what is gained by replacing L, F and T with α, β and γ ? If physicists changed the names of the *u, d, s* and *c* quarks, let us say, to *x, y, z* and *t*, absolutely nothing would be gained except the additional complication of memorizing which is which. Fortunately, most physicists, unlike most interferonologists, are aware that such symbols are merely arbitrary denotations for distinct entities and are in themselves meaningless. (As long as there are three interferons, why not Athos, Pothos and Aramis? D'Artagnon would be available if another were discovered.)

Until the structures of interferons are better understood individually and comparatively so that an informative nomenclature can be devised, I fail to see the wisdom in replacing Roman letters with Greek, in substituting one purely arbitrary system with another equally so, and in abandoning a nomenclature which, at least, has the advantage of familiarity.

LEE H. KRONENBERG

San Diego, California

Educating scientists

SIR — I fear that your readers may mistake your report strangely entitled "Subject in search of discipline?" (*Nature* 31 July, p.432) for a factual account of Sir Alec Cairncross's report to the Nuffield Foundation on "Science Studies". *Nature* suggests, not least by the tone of the article, that Cairncross's report is critical of "Science Studies". May I remind you of a major recommendation of the report? Cairncross declares that "There is a continuing need for injecting into most science degrees some provision for minor courses covering up to 15 per cent of the curriculum. These should be examinable".

This is strangely at odds with what *Nature* has to say. *Nature* associates the minor courses to which Cairncross refers with "general chat about the social relations of science", suggests that "Much of what is now provided for students under this heading centres around the much talked of Promethean dilemma" and that "teachers are all too often bent on grinding other axes — political, ideological or religious". These assertions are not drawn from the Cairncross report and neither are they true. They are uncomfortably close to the sorts of uninformed prejudices which many of us involved in serious attempts to serve science education have long struggled to overcome.

Nature expresses itself in favour of the enrichment of science education. I am profoundly sorry that it has not chosen to treat more seriously those who believe that they are making some progress towards this end.

C. S. MORPHET

Science Technology and
Society Association,
Newcastle, UK

0028-0836/80/390270-01$01.00

The last neanderthal in France?

from A.M. ApSimon

THE discovery by Lévêque and Vandermeersch[1] of the fragmentary remains of a skeleton of classic neanderthal type in a Châtelperronian archaeological layer at Saint-Césaire (Charente-Maritime, France), raises once again the problems of the replacement *c.* 34,000 BP of the neanderthal population (*Homo sapiens neanderthalensis)* of western and central Europe by a population of sapiens men (*Homo sapiens sapiens*). Three explanatory hypotheses have been proposed: (1) straightforward evolutionary transformation *in situ* of neanderthal into sapiens; (2) immigration of sapiens leading to the extinction of the neanderthals; (3) sapiens immigration followed by interbreeding in which the distinctive characters of the neanderthals were lost.

Before this new discovery, neanderthal finds from France were exclusively associated with the earlier, Mousterian stone industries (Middle Palaeolithic) characterized by a rich variety of scrapers, knives, spear points and other tools, made mostly on flakes and probably struck using stone hammers. In contrast sapiens were associated with lithic industries (Upper Palaeolithic) in which distinctive long narrow flakes (blades) probably struck off using antler punches played an important role. Although the difference in the industries associated with sapiens and neanderthal suggest they evolved separately, the possibility of *in situ* transformation is not excluded because there are long periods in which the stone industries are without distinctive human remains. In particular, one of the many variants of the Mousterian industries, the Mousterian of Acheulian tradition (MTA) is notorious for its lack of any morphologically distinctive human remains.

Study of the stratigraphic relationships of the different variants of Mousterian industry in SW France[2] suggested that the MTA was relatively late, whereas the known neanderthal remains were relatively early within the earlier part, Würm I–II, of the last glaciation. This would have left a period up to 20,000 years long (c. 55-34,000 BP) from which no human remains were known and during which the transformation to sapiens morphology could have taken place.

Refutation of this argument has come from H. Laville's elucidation[3] of the relative chronology of the sedimentary and climatic phases, as well as of the associated Mousterian industries and human remains, of the early Würmian (Würm I and II) deposits of the caves and rock shelters of the Perigord region of SW France. This has shown that a number of well-known neanderthal finds, including Le Moustier, La Chapelle-aux-Saintes, La Ferrassie and La Quina, date from the later sub-stage (Würm II). Guichard[4] has used this chronology to reassert the coexistence of the four main Mousterian variants, including MTA, during most of the earlier Würmian. F. Bordes[5] had suggested that these variants were the culturally determined markers of distinct ethnic groupings and that evolutionary divergence between these groups could have allowed the emergence of the sapiens lineage, perhaps among the makers of the MTA variant, since this variant showed features foreshadowing Upper Palaeolithic industries. Criticism of Bordes' hypothesis has centred on the extreme improbability of the conservation of separate lineages in an area as small as Perigord through the 40,000 year long early Würmian stage.

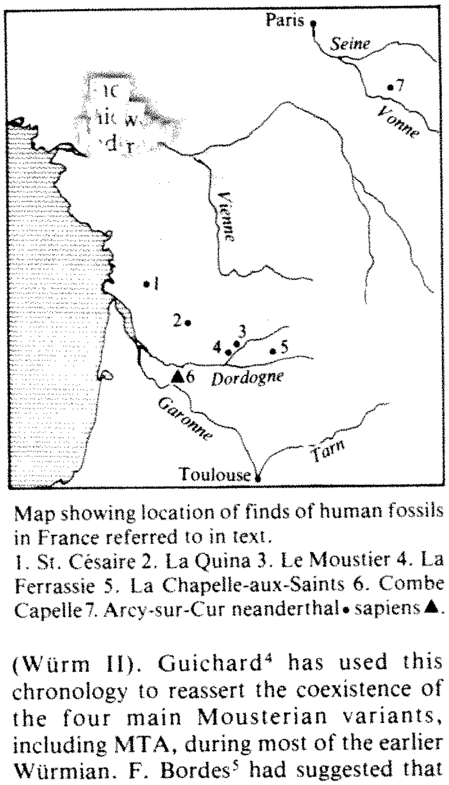

Map showing location of finds of human fossils in France referred to in text.
1. St. Césaire 2. La Quina 3. Le Moustier 4. La Ferrassie 5. La Chapelle-aux-Saints 6. Combe Capelle 7. Arcy-sur-Cur neanderthal • sapiens ▲.

L. and S. Binford[6] attempted to break free from the impasse of ethnic *versus* chronological explanation for variability in Mousterian industries, by suggesting that it might be better explained by adaptation to changing environments and by different tool kits being used for seasonally or functionally different activities. Although the Binfords' hypotheses have been faulted by Bordes[7] and others[8] on grounds that include the unrepresentativeness of the material analysed by them, the over-reductive nature of their analysis, the appearance of similar industries in dissimilar environments, the occurrence of long-maintained year-round occupation and the absence of difference between tool kits from open air and from rock-shelter sites, their work remains of capital importance in calling attention to the potential complexity of causal explanations for artefact variability.

Guichard[4] points a way out of this dilemma through his re-analysis of the diagnostic criteria for the different Mousterian industrial facies. This shows that elements are very rarely entirely absent from a given facies, even though the frequency of particular elements may be very low. This has two consequences: first, it serves to reaffirm the essential unity of the Mousterian tradition and warns against reification of the differences discerned by typologists and, second, it removes the necessary implications of ethnic or functional interpretation, and further weakens the argument for *in situ* transformation.

C.B. Stringer's multivariate metrical study of later Pleistocene hominid cranial material[9] also speaks against the idea of transformation since his results show that the classic neanderthals, including those dated to 'Würm II' in France, were less like the sapiens population of Upper Palaeolithic Europe than were the early neanderthals. His conclusion is that they were probably not the ancestors of modern man.

Although the Châtelperronian is usually treated as the first stage of the Upper Palaeolithic in France, Bordes showed that it probably developed from late Mousterian industries, a possibility hinted

A.M. ApSimon is in the Department of Archaeology, University of Southampton.

0028-0836/80/390271-02$01.00

Climatic Phases	Age BP	Human fossil finds	Industries
Würm III	23,000	Combe Capelle?	Peregordian & Aurignacian
	29,000		
Würm II — III Interstadial	34,000 39,000	St. Césaire? Arcy?	Aurignacian & Châtelperronian & Mousterian
Würm II		La Ferrasie, La Quina La Chapelle-aux-Saints (?) Le Moustier (?)	Mousterian
	55,000		
Würm I — II Interstadial			

Chronological table showing earlier last glaciation phases in SW France (simplified, after Laville[3] and others.

Transition between Middle and Upper Palaeolithic industries

(Châtelperronian is considered the initial stage of Upper Palaeolithic because of blade technology, Aurignacian is marked by bone spear points and specialised flint scrapers and gravers, Perigordian by developed blade technology. Szeletian (see text) uses leaf shaped flint spearheads and is technologically transitional from Middle to Upper Palaeolithic.)

at by cases of direct superposition of the two industries. Thus the Saint-Césaire discovery need come as no surprise in view of previous suggestions that isolated molar teeth possessing very large crowns with complicated relief found in the Châtelperronian deposits at Arcy-sur-Cure, Yonne (Grotte-du-Renne, layer XI), might be neanderthal rather than sapiens. The only other human fossil for which association with Châtelperronian has been claimed is the fully sapiens skeleton from Combe Capelle. However, an objection has been raised by Asmus[10]. Noting that the Châtelperronian layer in which the skeleton lay was very shallow, she suggests that the skeleton could only have been protected from disturbance if, when the burial was made, some at least of the later, overlying Aurignacian layer was already present (for further discussion see ref. 11).

Radiocarbon dates for Châtelperronian lie between *c.* 34,000 and 31,000 BP, so that the Saint-Césaire find is probably very close in time to the appearance of sapiens men. Sapiens remains occur in Aurignacian deposits for which radiocarbon dates of *c.* 32-31,000 BP are available. Rigaud[12] takes cases of interstratification as showing the contemporaneity and separate identities of Châtelperronian and Aurignacian in both their initial and developed stages. If the extant human remains are representative then there was a period during which neanderthal and sapiens men coexisted in SW France. If the rate of morphological change which this situation would require decisively rules out *in-situ* transformation, we are left with the choice between hypotheses two and three.

For indications as to where our choice should lie, we may usefully turn to evidence from recent hunter-gatherer groups. This suggests that both neanderthal[13] and early sapiens may have been organized in small bands, moving within limited but loosely defined territories and operating open, inter-band mating systems. Where bands were moving in areas not fully occupied by defined territories, contacts with previously unknown bands may have happened from time to time. Initial signalling between groups would probably be visual, and if contact behaviour proceeded along simple formalized lines, difficulties in verbal signalling need not have prevented peaceful contacts between strange bands. Châtelperronian — Aurignacian interstratification and possible artefact interchange suggests that peaceful contact may have been the rule, in which case there is no necessity to postulate inhibitions to neanderthal — sapiens mating. As the present chronology is only reliable to within about a 1,000 years the disappearance of the distinctive cranial features of the neanderthals would appear to be virtually instantaneous. The recovery rate of fossil human remains is so low that the chance of being able to document the change is very small.

To suggest that hypothesis three is the preferred one is not to solve all our problems, for despite new evidence of the evolution of *Homo sapiens sapiens* outside Europe[14] there is no good evidence to show how they spread to central and western Europe by *c.* 34-31,000 BP, nor is there evidence of their appearance in east-central Europe earlier than in France. Those sapiens finds from central Europe which by their attribution to Würm II (for example Mladeč, Moravia) have been supposed to provide such evidence, simply reflect differing applications of the Würm I-II-III system in the two areas and it is clear that they belong to what would be called Würm III in SW France.

Nor is there evidence that the Aurignacian complex appears earlier either in central Europe or in the Near East than it does in France. Dates in the range 40,000-35,000 BP quoted for Upper Palaeolithic assemblages in the Mediterranean and Near Eastern region depend on extrapolation of observed sedimentation rates in cave deposits and cannot be taken as a reliable indication of the origins and previous development of 'the Upper Palaeolithic' in that region. Many workers have seen reminiscences of the Mousterian in the Aurignacian, even though in France there is no evidence of interstratification and only very doubtful evidence of end-to-end contact. In central Europe the Szeletian industry appears to evolve from Middle to Upper Palaeolithic status and association with both neanderthal and sapiens remains has been reported. It is uncertain whether the bone spearheads and Aurignacian elements in the evolved Szeletian reflect contact with contemporary Aurignacian bands, or whether, as Hahn[15] suggests, the Aurignacian can be regarded as a logical continuation of the Mousterian and Szeletian tool kits. In his view some features of Aurignacian assemblages were already present at a low frequency in Mousterian assemblages, increasing in Szeletian assemblages, so that these show a crossover between decreasing frequencies of Middle Palaeolithic and increasing frequencies of Upper Palaeolithic elements, in particular the bone tools. The coincidence of the appearance of sapiens men with the Aurignacian in Europe is hard to resist, but it may still be a coincidence, and in the Near East, sapiens men already occur with Mousterian industries[16] as at Skuhl and Qafzeh in Israel. We should be wise to maintain with Maheu[17] "the denial of any causal connection between physical characteristics and industry or culture" and to refuse explanations for the disappearance of neanderthal man which rely on unverifiable assumptions of the inferiority of his intellectual and social capabilities. □

---

1. Lévêque, F., & Vandermeersch, B. *Bull. Soc. Préhist. Francaise* **77**, 35 (1980).
2. Mellars, P. A. *Proc. Prehist. Soc.* **35**, 134 (1969).
3. Laville, H. *La Préhistoire Francaise* **1**, 250 (1976).
4. Guichard, S. R. in *La Préhistoire Francaise* **2**, 1053 (1976).
5. Bordes, F. *The Old Stone Age* (London, World University Library; 1968).
6. Binford, L. R. & S. R. *Amer. Anthrop.* **2**, 68; **2**, 238 (1966).
7. Bordes, F., & De Sonneville Bordes, D. *World Archaeology* **2** (1) 61 (1970).
8. De Sonneville Bordes, D. *Quaternaria* **18**, 9 (1975); Bordes, F. in *Explanations of Culture Change* ed. Renfrew, A. C., 1973); Guichard, S. R. in *La Préhistoire Francaise* **2**, 1053 1976).
9. Stringer, C. B. *J. Archaeol. Sci.* **1**, 317 (1975).
10. Asmus, G. *Eiszeit u. Gegenwart* **15**, 187 (1964).
11. *The Origin of Homo Sapiens* 145 (ed. Bordes, F., UNESCO, Paris, 1972).
12. Rigaud, J. P. in *La Préhistoire Francaise* **2**, 1257 (1976).
13. Trinkhaus, E. & Howells, W. W. *Scientific American* **241**, 6, 94 (1979).
14. Kennedy, G. *Nature* **284**, 11 (1980).
15. Hahn, J. Aurignacien — das ältere Jungpalaolithikum in Mittel — und Osteuropa, *Fundamenta* A 9 (1977).
16. Ronen, A. in *Les sépultures néandertaliennes.* Prétirage, Colloque XII. IX Cong. UISPP, Nice, 27 (1976).
17. R. Maheu in *The Origin of Homo Sapiens* 311 (ed. Bordes, F., UNESCO, Paris, 1972).

0028-0836/80/390272-02$01.00

Snakeblennies

from Alwyne Wheeler

The snakeblennies (fishes of the tribe Ophiclinini within the family Clinidae) are small (up to 16 cm long) and live in shallow water along the cool, southern coasts of Australia. They can be captured in tidal rock pools and in bays at depths of 13 m and several species are known to burrow in mud.

A recent taxonomic study by George and Springer* has made a considerable contribution to our knowledge of these fishes, not least because they name no fewer than five previously undescribed species. They have also revised all the previously named species and produced a clarification of the relationships of these little-known fishes. Thus, the species *Peronedys anguillaris* which was previously assigned to a family on its own, and the genus *Sticharium* which hitherto had been placed in the Notograptidae, are now combined with the Ophiclinidae. These fishes are not, however, considered to be distinct from the members of the family Clinidae, which are widely distributed through the tropical and subtropical oceans. For this reason, these southern Australian fishes are placed in a tribe Ophiclinini within the Clinidae.

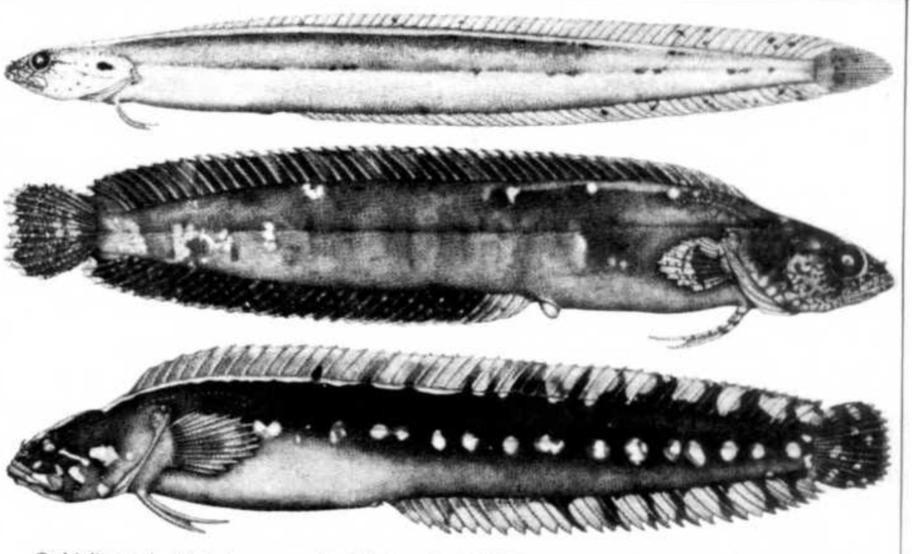

Ophiclinops hutchinsi, new species (89.0 mm); *Ophiclinus pectoralis*, new species (52.0 mm); *Ophiclinus gracilis* (68.0 mm). Drawings by J.R. Schroeder.

One of the pieces of evidence which substantiates the close relationship of *Peronedys* (which was thought to be distinguished by having no pectoral fins) is that several of the species of *Ophiclinops* have very minute pectoral fins, including the newly described *Ophiclinops hutchinsi* from Western Australia.

---

*Anita George & Victor G. Springer: Revision of the clinid fish tribe Ophiclinini, including five new species, and definition of the Family Clinidae. *Smithsonian Contributions to Zoology* 307 (Smithsonian Institution Press, City of Washington, 1980).

Alwyne Wheeler works on fishes at the British Museum (Natural History), London.

Sexual dimorphism and the evolution of higher primates

from R. D. Martin

In this issue of *Nature* Fleagle *et al.* report that three species of primate from Oligocene deposits at the Fayum fossil site show evidence of sexual dimorphism. This discovery has important implications for our understanding of the radiation of monkeys, apes and man as well as enabling us guess something of the social structure of the earliest known Old World anthropoids.

The Fayum fossil site in the Egyptian desert south-west of Cairo is of special significance for the reconstruction of primate evolution. Vertebrate fossils from these Oligocene deposits, dating back some 30 million years, include the first known representatives of the 'higher' primates (monkeys, apes and man). In fact, in the entire African continent, fossil primates from this site provide the only undisputed palaeontological evidence of primate evolution for the first half of the Tertiary epoch (Palaeocene–Eocene–Oligocene). The first fragmentary jaws and teeth of Fayum primates were recorded about 75 years ago and a series of collecting expeditions led by Elwyn Simons (then of Yale University) in 1963–1967 produced a wealth of fossil material from five primate genera (*Apidium; Parapithecus; Oligopithecus; Propliopithecus; Aegyptopithecus*). But soon afterwards events in the Middle East led to suspension of all palaeontological work in the Fayum, and it was not until 1977 that a new programme of joint expeditions was organised by the Geological Survey of Egypt and Duke University. The new initiative has yielded additional material throwing new light on the early evolution of the higher primates.

Interpretation of the initial radiation of the monkeys, apes and man has been thrown into turmoil by new information on continental drift. The traditional view, assuming stable continental positions is that the New World monkeys (platyrrhine) and the Old World monkeys and apes (catarrhines) are two quite distinct branches derived from a prosimian stock spanning the northern continents. The platyrrhines and catarrhines are held to have attained the 'simian grade' independently through parallel evolution. The acceptance of continental drift has, however, generated increasing support for the alternative view that the platyrrhines and catarrhines shared a common ancestor in Africa which had already attained the simian grade. Opponents of this interpretation point out that the first fossil evidence for New World monkeys appears only in the late Oligocene and that the South Atlantic undoubtedly represented a formidable barrier to invasion by terrestrial mammals at that stage. Conversely, reconstructions of continental positions indicate that invasion of South America from North America would have been at least equally unlikely during the Oligocene.

In all of this, the Fayum primates occupy a central position as the earliest relevant fossils. Interestingly, they do show numerous cranial and postcranial similarities to modern New World monkeys, but this is compatible with either monkey or ape origins since the similarities concern primitive features only to be expected in early representatives of the simian grade. It is therefore crucial to determine whether the Fayum primates exhibit specializations specifically linking them to Old World monkeys and apes. On the basis of previous evidence, Simons and his colleagues has already suggested this to be the case. Indeed, Simons proposed that the fossils could be divided into two groups (*Apidium* and *Parapithecus vs Oligopithecus, Propliopithecus* and *Aegyptopithecus*) related to the origins of the Old World monkeys and apes, respectively.

The new primate fossil material from the Fayum deposits has produced no great surprises in taxonomic terms; all of the new specimens can be confidently allocated to four of the five existing genera (*Apidium; Parapithecus; Propliopithecus; Aegyptopithecus*). But the increased sample sizes

R.D. Martin is Reader in Physical Anthropology, University College, London and Visiting Professor in Zoology at Birkbeck College, London.

0028-0836/80/390273-03$01.00

for the dentitions of three species (*Apidium phiomense; Propliopithecus chirobates; Aegyptopithecus zeuxis* have permitted identification of a marked degree of sexual dimorphism (Fleagle, J. G., Kay, R. F. & Simons, E. L. this issue of *Nature* p328). For each of these species, the molar teeth of the lower jaws seem to fall into uniform series, whereas the lower canines and anterior premolars show a bimodal size distribution. (The anterior lower premolar has a facet for occlusion with the upper canine and therefore reflects the degree of development of that tooth.) Of course, one must be wary of inferring sexual dimorphism in fossil material, since two separate but closely related species may be involved, and past controversies over the relationships between gracile and robust australopithecines serve as an object lesson here. Fleagle *et al.*, to their credit, made a separate approach by considering the intraspecific coefficient of variation for the depth of the mandible, which was found to be correlated with the degree of body weight dimorphism in a sample of living primate species. On this criterion, *A. phiomense* and *A. zeuxis* were both found to be comparable to modern sexually dimorphic species such as the howler monkey, the proboscis monkey and the gorilla. It is therefore reasonable to conclude that there is good evidence for sexual dimorphism in at least three of the Fayum primate species.

The phenomenon of sexual dimorphism in body size and development of the anterior dentition in living primates has been examined in detail by several authors in recent years (Gautier-Hion, A. *Mammalia* **39**, 365; 1975; Leutenegger, W. & Kelley, J. T. *Primates* **18**, 177; 1977; Clutton-Brock, T. H. & Harvey, P. H. *J. Zool.* **182**, 1977; Clutton-Brock T. H., Harvey, P. H. & Rudder, B. *Nature* **269**, 797; 1977; Harvey, P. H., Kavanagh, M. & Clutton-Brock, T. H. *J. Zool.* **186**, 475; 1978). The following important generalizations about sexual dimorphism have emerged from these quantitative studies: (1) It is always lacking in species living in monogamous family groups; it may or may not be present in species where males have breeding access to more than one female (polygyny); (2) It tends to increase with increasing body size; (3) It is especially prevalent among terrestrial primate species; (4) It is virtually absent among living prosimian primates, uncommon in New World monkeys and markedly present only among Old World monkeys and apes.

From these generalizations it follows that the three apparently sexual dimorphic Fayum primate species were closer to modern Old World monkeys and apes than to modern New World monkeys. In the New World, notable sexual dimorphism is present only in the large-bodied howler monkeys (*Alouatta* spp:), with males weighing approximately 30% more than females. Yet the Fayum primates span virtually the same body size range as the modern New World monkey Family Cebidae (600 g — 6kg; Kay, R.F. & Simons, E.L. *Int. J. Primatol.* **1**, 21; 1980) and exhibit signs of sexual dimorphism even at the lower end of that size range (*Apidium phiomense*). Kay and Simon (*loc. cit.*) have also inferred from the relatively tall molar teeth of one of the Fayum species *Parapithecus grangeri,* that it might have held terrestrial tendencies, though unfortunately there is insufficient dental material to show whether this species was sexually dimorphic. The prevalence of sexual dimorphism (even at quite small body sizes) and the widespread adoption of terrestrial tendencies among the Old World monkeys and apes are probably linked features, and the Fayum primates seem to fit the general pattern.

Further, it seems highly unlikely that the sexually dimorphic Fayum species lived in monogamous family groups and their social systems probably had a polygynous base, as is typical of modern Old World monkeys. Among modern New World monkeys, by contrast, monogamy is common and it has been suggested that this could have been the ancestral condition for platyrrhines. Thus, the new evidence uniformly suggests that the Fayum primates were an integral part of the evolutionary radiation of the Old World Monkeys and apes, as has been consistently maintained by Simons. One must remember, though that the common ancestor of all monkeys, apes and man must accordingly have antedated the Fayum deposits. Palaeontologists generally tend to date the origin of any group from the first known fossils, whereas incompleteness of the fossil record (particularly for Africa during the first half of the Tertiary) allows for a much earlier date. The earlier the actual date of divergence of the platyrrhines and catarrhines, the greater is the likelihood of an African origin of the higher primates.

An understanding of the the relationship between primate sexual dimorphism and social organization is of considerable interest and enables us to suggest the kind of social groups that fossil primates may have lived in. Explanations of why sexual dimorphism evolved have, hitherto, invoked two male-oriented causative influences: (1) intense male-male competition for females, and (2) defence of the social group against predators by large males. However, sexual dimorphism involves divergent male and female strategies and little attention has been given to factors which might favour small body size in females. In an elegant analysis of dental sexual dimorphism in primates, Harvey *et al.* (1978, *loc. cit.*) used relationships between female tooth size and body size as baselines for assessing male dental development ('relative male tooth size') and were able to analyse more precisely the factors associated with exaggerated development

PHYSICS WITHOUT APPARATUS

Acoustical experiments require, for the most part, the aid of some good instrument or valuable piece of apparatus. Nevertheless a few instructive illustrations of the principles of the science can be improvised without difficuly. Firstly, there is the familiar experiment brought into fashion, we believe, by Prof. Tyndall, of setting a row of ivory billiard balls or glass solitaire marbles along a groove between two wooden boards, and showing how their elasticity enables them to transmit from one to another a wave of moving energy imparted to the first of the row, thus affording a type of the transmission of sound-waves from particle to particle through elastic media. Then we may show how sounds travel through solid bodies by resting against a music-box or other musical instrument, a broomstick, or any convenient rod of wood, at the other end of which we place our ear. A kindred experiment, illustrative of the transmission of sounds through threads, is depicted in the Figure. A large spoon is tied to the middle of a thin silken or hempen thread, the ends of which are thrust into the ears upon the ends of the thumbs. If the spoon be dangled against the edge of the table it will resound, and the tones reach the ear like a loud church bell. The thread telephone or "lover's telegraph," is upon the same principle, the thread transmitting the whispered words to a distance, without that loss by spreading in all directions which takes place in the open air.

From *Nature* **22**, 23 September, 488, 1880.

of the anterior teeth in males of certain species (e.g. terrestrial vs. arboreal species and polygynous vs. monogamous species).

Their data also show that, at any given body size, males often have a shorter row of cheek teeth than females, suggestive of lower energy requirements. Significantly, this applies only to species with polygynous social systems and the divergence between males and female increases with increasing body size. Harvey *et al.* briefly mention the possibility that sexual dimorphism may be related to differential dietary strategies of males and females, and the cheek tooth data indicate that this deserves close examination. It has already been shown, through indirect computations based on activity budgets recorded in captivity, that female Sykes monkeys (*Cercopithecus albogularis*) may consume up to 30% more energy than a male, despite the fact that the latter is some 40% heavier (Coelho, A. M. *Primates* **15**, 263, 1974). It is conceivable that divergent energy strategies of females and males may be the primary factor underlying sexual dimorphism in primates and that male strategies in competition for females and anti-predator defence may be conditional upon this. If this is so, then we have firm evidence that such divergence between female and male energetic strategies was present among early relatives of the Old World monkeys and apes at least 30 million years ago. □

Immunological changes in multiple sclerosis

from Barry R. Bloom

At best one may liken the present state of understanding of multiple sclerosis to that of the blind men and the elephant in the ancient Indian legend. A variety of investigations have each touched a piece of the reality, but no one has been able to integrate the observations into a coherent picture of the disease.

Multiple sclerosis (MS) is an inflammatory demyelinating disease found in a variety of clinical forms, ranging from an exacerbating-remitting course to a chronic progressive disease. Not only is the aetiology unknown, but the variety of clinical patterns and immunological pathological changes seen in different patients are so great that there may be more than a single aetiology — a possibility which provides little comfort to either patients or investigators.

There are two principal hypotheses. The first, based on the induction of inflammatory demyelinating disease in animals immunized with central nervous system tissues or myelin is that MS is an autoimmune disease directed against central nervous system antigens. While the classical animal models of allergic encephalomyelitis (EAE) are not faithful reproductions of the human disease, recent models of relapsing EAE in animals (Raine *et al. Lab. Invest.* **31**, 369; 1974; Wisniewski *et al. Ann. Neurol.* **1**, 144; 1977) suggest that autoimmune mechanisms could well contribute to the pathology. The difficulty with this hypothesis is that no convincing evidence for autoimmunity to CNS antigens or myelin components has been found in patients with multiple sclerosis.

The second hypothesis is that MS is caused or triggered by a persistent virus infection. This is consistent with the epidemiology of the disease, and with the finding of elevated antibodies to measles and other viruses in the cerebrospinal fluid of MS patients. Exacerbations and remissions might be explained by emerging antigenic variants, analagous to those seen in the viral demyelinating disease of sheep (Narayan *et al. Science* **197**, 376; 1977; Bloom *et al. Neurology* **28**, 93; 1978).

Whether triggered by immune reactivity to brain antigens or virus, the histopathologic picture of the demyelinated lesions closely resembles that of cell mediated immune reactions, with lymphocytes and marcrophages predominating. However, the often acute onset of symptoms and rapid clinical remissions suggests that mechanisms which are not characteristic of cell mediated reactions, for example, antibodies, immune complexes or edema, are contributing to the disease.

In trying to understand the immunological basis of multiple sclerosis one encounters a frustratingly large number of clues which do not fit into a coherent picture. In particular, there are elevated levels of immunoglobulins, particularly IgG_1, in the cerebral spinal fluid of the majority of MS patients and elevated titers of antibodies are found to a number of viruses, particularly measles. The immunoglobulins found in brain or CSF of MS patients, when subjected to electrophoresis, show a characteristic discrete or 'oligoclonal' pattern of bands. While similar oligoclonal Ig patterns can be observed in samples from patients with several other diseases, (for example, subacute sclerosing panencephalitis (SSPE), viral encephalitides or meningitides, Guillain-Barré Syndrome and neurosyphilis) the banding patterns in MS patients remain constant over long periods while they vary or disappear with time in other diseases. The oligoclonal electrophoretic patterns of immunoglobulins from CSF or acid eluates of MS brain suggest that they may be derived from a limited number of B-cell clones in the CNS.

In this issue of *Nature*, Mattson *et al.* (p311) report that eluates from individual MS plaques or lesions show limited and discrete patterns of immunoglobulin banding, the sum of which appear to be represented in the pattern of pooled eluates from MS brain. In contrast, electrophoresis of immunoglobulins in SSPE brains shows the same immunoglobulin pattern in different portions of the brain, similar to pooled white matter extracts. Mattson suggests that different immunoglobulin-synthesizing clones are present or expanding in different areas of MS brain, raising the possbility that different antigens may be present in each plaque. In another recent paper, Baird *et al.* (*J. Immunol.* **124**, 2324; 1980) have shown that anti-idiotypic antibodies directed against oligoclonal immunoglobulins in the CSF of one patient with MS crossreacted with immunoglobulins from another, suggesting that two different patients had immunoglobulins with similar, if not identical active sites. The paradox posed by these two results is that different patients may have antibodies directed toward the same antigen, as judged by crossreactive idiotypes; and yet different lesions in the same patients may contain different antigenic determinants, or at least, elicit different antibody clones.

Such sweeping conclusions, however, cannot be accepted without serious reservations. While there may be some cross-reactive idiotypes among immunoglobulins in the CSF of some MS patients, a number of investigations have been unsuccessful in finding crossreactive idiotypes in MS patients. In the case of the discrete electrophoretic patterns derived from different MS plaques, it remains unclear whether the changes in banding are merely quantitative, reflecting, for example, merely different accessibility of old, relative to new lesions to infiltration by B cells, or whether there are real qualitative differences in types of immunoglobulin produced in different plaques. It has been reported by Link and Laurenzi (*Ann. Neurol.* **6**, 107; 1979) that individual oligoclonal bands in CSF may contain both κ and λ light chains. This observation, together with the findings of Mattson *et al.* that a number of the bands from different plaques appeared to have common mobility, raises doubts that meaningful conclusions on the number and nature of B-cell clones can be derived from electrophoretic banding patterns of CSF or brain immunoglobulins. An alternative interpretation suggested by Mattson *et al.* is that a mitogenic effect on B-cells of a CNS breakdown product could polyclonally stimulate proliferation of small numbers of B-cells localized in individual plaques to produce 'nonsense'

Barry R. Bloom is Professor and Chairman in the Department of Microbiology and Immunology, Albert Einstein College of Medicine, New York.

0028-0836/80/390275-03$01 00

antibody. While elevated levels of antiviral antibodies are found in the CSFs of the majority of MS patients, little of the antiviral antibody activity is detected on electrophoresis associated with the oligoclonal bands. It remains unclear to what antigens, if any, the preponderance of the immunoglobulins in MS brains of CSF's are directed.

Another clue that must be considered is the significant genetic association of multiple sclerosis with HLA-D, thought to contain the human counterpart to the murine Ir genes. While the linkage to DW2 is strong among patients in Western Europe and North America, patients in the Middle East and Asia appear to have associations with other HLA-D antigens.

In addition to the relatively unique and stable alterations in immunoglobulin patterns in the CNS of patients with MS, recent observations suggest changes in normal cellular immune parameters as well. Con A- and virus-induced suppressor activity of lymphocytes from MS patients have been found to be significantly diminished (Antel *et al. Ann. Neurol.* **5**, 338; 1978; Neighbour & Bloom. *Proc. natn. Acad. Sci. U.S.A.* **76**, 476; 1979). Santoli *et al. J. Immunol.* **120**, 1369; 1978). Recently Reinherz *et al.* (*N. Engl. J. Med.* **303**, 125; 1980) reported a reduction in total T-cells and in T-cell subsets defined by monoclonal antibodies, particularly the T5 subset, in the blood of MS patients during exacerbations. A number of laboratories have recently found reduced capability of lymphocytes from MS patients to produce IFNα (Type I leukocyte interferon) and IFNγ (Type II or 'immune' interferon) (Neighbour *et al. Neurol.* in the press; Riethmuller *et al. 4th Intl. Cong. Immunol.*) and to have reduced natural killer activity (Benczur *et al. Clin. Exper. Immunol.* **39**, 657; 1980; Neighbour *et al. 4th Intl. Cong. Immunol.*). It is interesting to note that a similar, or even more striking decline in ability to produce interferon or carry out natural cytotoxicity, paralleled by decline in the T5 T-cell subset, is being found in patients with lupus erythematosis, suggesting that these changes are not restricted to multiple sclerosis, but common to several diseases of possible viral aetiology.

It is tempting to infer from these various observations that there is a fundamental defect in immunoregulation in multiple sclerosis. Yet in no instance have the immunological changes been clearly associated with any functional changes in the patients. It is not even known whether the immunoregulatory changes precede attacks of the disease, or whether they follow events, still obscure, which trigger attacks. That there are multiple immunologic changes in MS is clear; but which, if any, are directly related to the disease process remains to be established. ☐

Quantum mechanics and gravitational waves

from Bridget Marx

IT has been said that physics is the science of measurement. The quantum mechanical revolution in the early part of this century threw up many problems and paradoxes concerning measurement and, surprisingly, many of these remain unsolved and little understood. It is true that for the most part physics can progress without a full understanding of the practical and philosophical implications of quantum mechanics but occasionally the full impact of these fundamental problems is felt. The latest group to be left worrying about theories of measurement, post quantum mechanics, comprises those people trying to measure gravitational radiation.

Gravitational waves are predicted by Einstein's theory of general relativity to be ripples in the curvature of spacetime which propagate at the speed of light. What the theoreticians would like the experimentalists to do is, firstly, to demonstrate the existence of these waves, either as a continuous flux or in larger spasmodic bursts, and secondly, to analyse the radiation to give them clues for developing their theories further. However this is no easy task. The effects of gravitational waves are small and not easily detected. Gravitational radiation should be noticeable by its effect on large masses. Experimenters first tried to show its existence by setting up massive antennae and looking for a movement induced by a passing gravitational wave. But the effect predicted by current theory is so small that the sort of displacement one is hoping to measure is of the order of 10^{-19} cm for a resonant bar with a mass of about one ton. When one considers that the Bohr radius of a hydrogen atom is about 5×10^{-9} cm and the 'classical' electron radius is about 3×10^{-13} cm, then the difficulties of measuring 10^{-19} cm can be appreciated. On top of that the experimenters need to make repeated measurements of the same system to look for changes in its position, so the measurement processes must not be such as to cause unpredictable changes of the position of the system. We are not used to treating large objects quantum mechanically, but it is obvious that it must be done in this case. So what limits does the theory of quantum mechanics impose on this measurement scheme?

The quantum theory of measurement warns experimental physicists that no matter how carefully a measurement is made it will always change the system being measured. Consideration of the problems this causes for the detection of gravitational waves has led to the identification of quantum nondemolition (QND) variables (Braginsky, Vorontosova & Thorne *Science* **209**, 547; 1980; Thorne *Rev. Mod. Phys.* **52**, 285; 1980; Caves, Thorne, Drever, Sandberg & Zimmerman *Rev. Mod. Phys.* **52**, 341; 1980; Caves *Phys. Rev. Letts.* **45**, 75; 1980). A quantum nondemolition variable is one for which a sequence of precise measurements can be made, the result of each measurement being completely predictable from the result of the preceding measurements (Caves *et al.* op cit.) The logic of this can be understood by considering the system of a free electron as discussed by Braginsky *et al.* If we measure the electron's position in space and so force it into a well defined position then the Heisenberg uncertainty principle relating the properties of position, x, and momentum, p,

$$\Delta x \Delta p \geqslant h/2$$

ensures that the momentum is changed by an unpredictable amount by the position measurement. That might not bother us much if we don't want to know the electron's momentum, but it does have an effect if we want to make a second measurement of the position. In the time interval, t, between the measurements the electron has moved an amount $x_t = (p/m)t$ where m is the mass of the electron. But as p is uncertain by Δp then x_t is uncertain by an amount $(\Delta p/m)t$, that is

$$\Delta x_t \geqslant \frac{ht}{2m\Delta x}$$

where Δx is the uncertainty of the first measurement. So the more accurate the first measurement the less we can rely on the result of a second measurement of position. Braginsky *et al.* go on to apply the same analysis to a large (10 ton) antenna and show that if the first measurement is made to an accuracy of 10^{-19} cm then a second measurement 10^{-3} second later is uncertain by a least 5×10^{-19} cm. So no subsequent measurement can be compared with the first to the full measurement precision. However, if we had decided to measure momentum rather than position, the second measurement would have been as informative as the first. The position uncertainty would have changed according to the uncertainty principle but this would not have fed back into the momentum unless the electron were in a position-dependent potential. In the situation of a free electron or a freely moving antenna, momentum is a QND observable whereas position is not.

Bridget Marx is in the Division of Mechanical and Optical Metrology, National Physical Laboratory, Teddington, UK.

0028-0836/80/390276-02$01.00

Generally, most observables are not QND observables and there will be 'back-action' from the measurement. This is a problem which must be overcome if such incredibly accurate measurements are to be made. One solution is to find a QND variable to measure and this is the route proposed for the antenna type of gravitational wave detector. As it is not feasible to make sufficiently precise measurements of momentum another variable must be used. Details of how it is proposed to measure the real and imaginary parts of the complex amplitude of a large quantum mechanical harmonic oscillator, both of which are QND variables, are given by Braginsky *et al.* and by Caves *et al.*

Another suggested method for measuring the displacement of masses produced by gravitational waves, is to use a Michelson interferometer. The basic apparatus is shown in the figure. The laser light enters the interferometer, is split by a beam splitter (BS), passes down the two arms to the mirrors mounted on test masses and is reflected back to the beam splitter where it is recombined. The light measured at the detector is a sinusoidal function of the path difference BS1–BS2, and so is sensitive to any differential displacements of the test masses 1 and 2, such as would be produced by a gravitational wave. As the effect of mirror displacement can be amplified by using multiple reflections in each arm of the interferometer this technique is potentially very sensitive. However, this is a position measuring device and so it is subject to the effects of the Heisenberg uncertainty principle just as is the antenna. The problem considered by Caves and earlier by Edlestein, Hough, Pugh and Martin (*J. Phys. E.* **11**, 710; 1978) is how to estimate the measurement limit imposed on this system by quantum mechanics. There is an uncertainty in measuring the light intensity from the interferometer (remember we are looking for a change in intensity to indicate a differential change in BS1, BS2) arising directly from fluctuations in the laser light source. In addition, differential radiation pressure effects from the light on the mirrors could limit the reliability of measurements, especially at high input intensities. This would imply an optimum intensity for an interferometer device.

Do such differential forces exist in real interferometers? The literature on this point is not convincing. Indeed Caves refers to a 'lively but unpublished controversy' on the subject. The problem is fundamental: radiation pressure is a momentum conserving effect due to the particle nature of the light photons, whereas the interference fringes observed with an interferometer are due to the wave nature of light. The wave-particle duality of light, and indeed all particles, has always caused problems. What happens to a photon in the interferometer? An interesting and instructive discussion of this point is given in an article by Frisch (*Contemp. Phys.* **7**, 45; 1965). The important thing to remember is that the problem is very different from the apparently similar experiment of setting up a beam splitter with light detectors in place of the mirrors. In this latter experiment, if a photon were detected at 1 then it certainly wouldn't be detected at 2. So the photon's momentum would be given to either 1 or 2, but not both. However, with the detector placed to monitor the interference pattern — after the beams are recombined — the only assumption that we can make is that each photon goes down both arms of the interferometer, that is that each photon is reflected from both mirrors. If we knew which mirror the photon had been reflected from, we could not observe an interference pattern. This is an experiment directly comparable with the more famous Young's two-slit experiment (see, for example, Bohm *Quantum Theory* Prentice-Hall, 1951), where if we ask which slit the photon came through we can not observe an interference pattern.

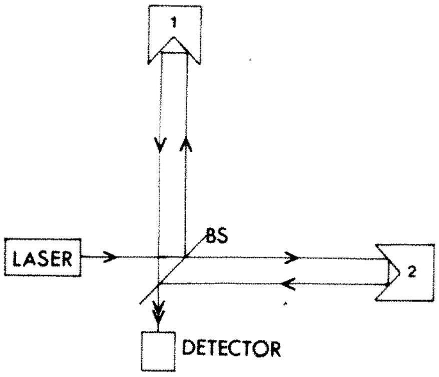

A method for measuring the displacement of masses produced by gravitational waves using a Michelson interferometer.

The discussion of the interferometer problem in some of the literature seems to come uncomfortably close to confusing the two-detector and the two-mirror problems.

The whole field of gravitational wave detection is proving to be full of fascinating problems and will no doubt stimulate physicists in all fields of research. It is particularly interesting to note that these attempts to demonstrate the validity of the last great theory of classical physics, that is general relativity, are being limited by effects which are totally due to the new physics of quantum mechanics. ☐

Galileo saw Neptune in 1612

from David W. Hughes

JOVIAN satellites, lunar mountains, saturnian rings, stars in the Milky Way, Sun spots, phases of Venus — the number of significant observations of astronomical objects made by Galileo Galilei is impressive indeed. The coming together of the invention of the telescope and Galileo's brilliant enquring mind obviously led to a bountiful harvest. Did Neptune slip through his fingers? Galileo saw the planet but recorded it as a star in his notebook. Was the discovery of Neptune in his grasp, almost 234 years before Johnn Galle found it in 1846? I don't think so. The rudimentary star maps of the time, the inadequate telescope mountings and Neptune's distance from the Sun make it nigh on impossible. But still, like all scientists are taught today, Galileo recorded in his observation journal not only what he was specifically investigating but also unusual sightings and events.

That Galileo actually recorded Neptune was discovered recently by Charles T. Kowal of the Palomar Observatory, California Institute of Technology and Stillman Drake, the Professor of the History of Science of the University of Toronto. Their findings are reported in this issue of *Nature* on page 311. Prediscovery observations of planets are common and Neptune is no exception, the famous one being by Lalande in 1795. As people were obviously not looking for Neptune in the seventeenth and eighteenth centuries, the only chance of it being accidentally recorded was if it happened to be in close proximity to something that people were looking at. Extrapolating Neptune's orbit back in time revealed that Jupiter, the brightest and most commonly observed planet, actually passed in front of Neptune both in September 1702 and in January 1613. A search of the records of 1702 is a task for the future. Kowal and Drake decided to start by examining Galileo's 1612–1613 observations of Jupiter.

Now Galileo had discovered the four large Jovian satellites Io, Europa, Ganymede and Callisto in January 1610, and had spent much time observing and analysing the orbital movement of this 'miniature solar system'. On 7 September 1612 Galileo put forward a method whereby observations of the satellites of Jupiter from different places on the Earth's globe could lead to a determination of the longitude of that place to an accuracy of about three degrees. This

David W. Hughes is in the Department of Physics, University of Sheffield.

0028-0836/80/390277-02$01.00

would be very useful for the navigation of ships. The idea was to regard Jupiter as a celestial clock whose 'hands' were the four satellites, their positions gave the local time which could then be compared with Florence time (for example) to give the longitude. Galileo was preparing tables to show the satellite positions and observed Jupiter to this end. Kowal and Drake point out that a star near Jupiter was noted on 28 December 1612 and again on 28 January 1613, in a different position, and this star happens to be Neptune. There are no other bright stars in Virgo anywhere near the position of the Jovian-Neptune conjuction of that year. Galileo thought Neptune was a star because it looked just like one in his telescope. The disk of Neptune subtends about 2.4 arc sec at Earth, way below the 1.24 arc min resolution of Galileo's telescope. Two factors can account for Galileo not noticing the movement of Neptune against the fixed star background. First, there was an absence in that area of the sky of bright stars to form that background and second, the mean daily motion of Neptune is about 22 arc sec, much too small to be detected in those days.

Kowal and Drake's discovery is important because it could lead to an improvement in the accuracy of our knowledge of the orbital parameters of Neptune. Neptune orbits the Sun once every 165 years. As it was only discovered 134 years ago it hasn't been seen to go round once yet. Observations of the orbit over long time periods give clues to the gravitational perturbations the planet suffers and these could lead to the discovery of a planet beyond Pluto. The exact time of the 1702 Jovian occultation of Neptune would be extremely useful in this calculation and this is ample justification for a close scrutiny of the astronimical manuscripts of 1702. Hidden in these might be a record of another historic close encounter between these two planets. □

Laser annealing for semiconductor devices

from I. W. Boyd and J. I. B. Wilson

LASERS are used for cutting, drilling and welding metals and ceramics as well as by surgeons, seismologists and spectroscopists. Now the laser annealing of semiconductors is attracting industrial interest and there have been specialist conferences devoted entirely to this aspect of laser technology[1,2]. A recent NATO Advanced Study Institute in Italy covered both the intriguing physics of the laser irradiation of semiconductors, and some of the technical advances which will be possible in micro-circuit fabrication.

Annealing is the heat-treatment used to restore disordered semiconductor wafers to crystalline perfection, after selected 'dopant' impurities have been implanted into the wafers (as energetic ions) to adjust the electrical conductivity. Conventional furnace annealing uses temperatures of $\sim$ 950°C for $\sim$ 30 minutes but has the unfortunate side effect of allowing the dopant atoms to diffuse into the wafer and to spread out laterally. This negates an important advantage of ion-implantation — the high degree of control over the depth and shape of the implanted (doped) region. Each subsequent thermal treatment causes further spreading of dopant and imposes a restraint on the closer packing of devices within an integrated circuit.

Both electron beams and lasers can be used to apply heat locally to semiconductor wafers, with fine spatial and temporal control, so that only part of a wafer may be heat-treated. Lasers, in contrast to electron beams, have no need for a vacuum enclosure or inert gas cover. The actual temperature reached by a sample will depend both on the laser energy and irradiation time, and on the optical absorption properties of the material and its thermal capacity and conductance.

In silicon, visible laser radiation such as that from a laser ruby (used in the first pulsed laser annealing of ion implanted silicon[3]), is strongly absorbed whereas infrared CO_2 laser radiation is only weakly absorbed (by the free charge carriers) until the sample heats up (producing many free carriers). Both pulsed and continuous (CW) lasers of various types, can recrystalize disordered silicon, but by different mechanisms.

CW laser annealing is similar to the conventional furnace process, for regrowth of the crystal lattice takes place in the solid phase. The high temperatures are, however, only maintained for milliseconds because the laser beam is scanned across the sample and there is insufficient time for dopant to diffuse into the bulk of the wafer. Extended structural defects (such as stacking faults and dislocations) are more effectively removed, and more of the dopant is placed in electrically-active substitutional sites, than by furnace treatment. Pulsed lasers are thought to produce a melted region and this allows dopant atoms to migrate over greater distances before the solid/liquid interface moves back towards the surface. Various modes of regrowth are therefore possible for disordered or polycrystalline layers on crystalline substrates, and in some cases surface ripples remain after the laser treatment. Van Vechten[4] has, however, proposed a theory which places more emphasis on the importance of the electron-hole plasma produced by strong laser pulses. This, he suggests, may sufficiently weaken the covalent bonding of the lattice that rearrangement takes place without formation of a liquid phase. The reflectivity of silicon has been observed to increase sharply during pulsed annealing and although this is generally believed to prove that melting has occurred it is not conclusive. Recent Raman scattering measurements during pulsed annealing of silicon have indicated a lattice temperature of only 300°C (ref.5), well below the melting point of $\sim$ 1,400°C.

There are, then, two alternative laser annealing modes, which either can leave implanted ions in their original region, or can allow them to redistribute. In fact, novel phases and solid solutions may be formed, which are impossible to produce by conventional furnace treatment. It is also possible to form good ohmic contacts on materials such as gallium arsenide and indium phosphide, the surfaces of which will begin to decompose if they are heated to the usual temperatures required for alloying contacts. Further, it is possible to deposit metal, dielectric, and semiconductor films directly from a gaseous compound on to a substrate by laser. The laser beam may either be used to heat the substrate to a temperature at which the impinging vapour can decompose, or be used to directly dissociate the gaseous molecules.

Reports of actual devices formed by laser processing are much fewer than those devoted to more basic studies of the techniques, but laser annealed p-n junctions and MOSFET's can be made from silicon which was originally in the poly-crystalline state. There are problems associated with the ever-present oxide layer on silicon because it may have anti-reflection properties for the laser light at certain thicknesses, and will have different thermal expansivity from the underlying melted silicon. It is essential to use a laser system without hot spots in the beam, and with accurate beam steering to avoid distortion of the beam shape. New specially-designed equipment is now on the market.

Advanced technology lasers may eventually replace furnaces, which are more costly in energy, for annealing ion-implanted silicon devices, but it is the novel applications which are the most exciting, and which may allow the routine use of new semiconductor materials. □

I. W. Boyd and J. I. B. Wilson are in the Department of Physics, Heriot-Watt University, Edinburgh.

1. *Laser-Solid Interactions and Laser Processing — 1978* (American Institute of Physics, Conference Series **50**, 1979).
2. *Laser & Electron Beam Processing of Electronic Materials* (eds Anderson, C.L., Celler, G.K., Rozgonyi, G.A., The Electrochemical Society Inc., 1980).
3. Khaibullin, I.B., Shtyrkov, G.K., E.I. Zaripov, M.M., Galjutdinov, M.F. & Bajazitov, R.M. *Laser Annealing of Implanted Layers* Dep. VINITI N 2061 (1974).
4. Van Vechten, J.A., Tsu, R., Saris, F.W. & Hoonhout, D. *Phys. Lett.* **74A**, 417 (1979).
5. Lo, H.W. & Compan, A. *Phys. Rev. Lett.* **44**, 1604 (1980).

0028-0836/80/390278-02$01.00

ARTICLES

Isotopic evidence for the provenance of some Caledonian granites

P. J. Hamilton*, **R. K. O'Nions*** & **R. J. Pankhurst**†

* Department of Earth Sciences, University of Cambridge, Downing Street, Cambridge CB2 3EQ, UK
† British Antarctic Survey, c/o Institute of Geological Sciences, Grays Inn Road, London WC1X 8NG, UK

A combined Nd- and Sr-isotope study of Caledonian granites in Scotland and northern England demonstrates the importance of continental crust in their petrogenesis and places limits on the involvement of contemporary mantle-derived material.

THE continental crust is generally thought to have been generated over a considerable portion of Earth history through the progressive chemical differentiation of the mantle. Thus, all igneous, metamorphic and sedimentary rocks residing in the continents are ultimately 'mantle derived'. However, petrologists usually reserve the term 'mantle derived' for those igneous rocks derived from primitive mantle melts by magmatic differentiation processes without an intermediate solid stage. If, after a period of residence in the continental crust, such mantle-derived igneous rocks are remelted, the resultant magmas would be designated 'continent derived'. The provenance of granites is an important aspect of the fundamental problem of crustal generation and growth. Granites that are wholly or partially mantle derived make a nett contribution to the mass of the continental crust and are therefore an integral part of crustal growth. In contrast, granites with no mantle-derived component only involve intracontinental differentiation with no concomitant change in continental mass.

To distinguish between mantle and continental derivation in a specific instance, it is necessary to recognize (usually from abundances of radiogenic isotopes) whether or not the precursor material has had a significant residence time in the continental crust. In this context, the main problem has been to find adequate criteria to distinguish between mantle and crustal provenance and in the latter case to quantify the crustal residence time of the precursor material. Hurley and colleagues[1-3] pioneered the application of isotope studies to this particular problem using $^{87}Sr/^{86}Sr$ ratios. Only recently has the Sm–Nd system been exploited as a tracer of granite provenance[4,5]. For example, the Tertiary granites of Skye, north-west Scotland, have much lower $^{143}Nd/^{144}Nd$ ratios than predicted Tertiary mantle values, a feature consistent with a large component of their Nd being derived from Archaean basement[5,6]. A reconnaissance investigation of Sm–Nd isotope systematics in Phanerozoic granites (including the Sierra Nevada batholith, Himalayan granites and Hercynian granites of France) by Allègre *et al.*[4] has revealed the presence of continental-derived components in all cases examined.

It must be emphasized that investigations of granite provenance using the isotopic composition of a particular element (such as O, Sr, Nd) only explicitly refers to the provenance of that element whereas the provenance of other constituents can only be inferred. Ideally, therefore, measurements of the isotopic compositions of several elements exhibiting different chemical behaviour during crustal differentiation and evolution are required to make completely general statements about the provenance of a granite as a whole. The present study uses the combined Nd- and Sr-isotope approach for evaluating the provenance of Caledonian granites occurring in Scotland and northern England and in particular assesses in appropriate situations the possibility of Sm/Nd fractionation attending the differentiation and mobilization of pre-existing continental crust.

Caledonian granite magmatism

The term Caledonian granites encompasses granite (*sensu lato*) rocks that were emplaced into the Caledonides over a period of about 150 Myr, starting ~550 Myr ago and associated with the closure of the Iapetus Ocean[7,8] (Fig. 1). Two of the oldest of these are the Carn Chuinneag and Ben Vuirich granites, dated, respectively, at 555±10 Myr (ref. 9) and 514±7 Myr (ref. 10) using U–Pb chronology of separated zircons. These belong to Read's[11] group of Older granites, and were emplaced before the main Caledonian structural and thermal episodes that occurred ~480–460 Myr ago. The post-tectonic (Newer granites of Read) range in age from ~470 Myr (see ref. 12) to ~390 Myr (refs 12, 13) (Fig. 1). More detailed reviews of the chronology of Caledonian granites can be found elsewhere[12,14-16], and geochronological data pertinent to the granites investigated here are summarized in Table 1. The large variation in initial $^{87}Sr/^{86}Sr$ ratios of Caledonian granites (see Fig. 1 in ref. 17) is noteworthy. Initial $^{87}Sr/^{86}Sr$ ratios ≥ 0.710 are characteristic of the pre-tectonic granites and 475-Myr-old granites of north-east Scotland. It is generally agreed that Proterozoic, or older, crust is involved in their generation[10,18], and that they are S-type granites as defined by Chappell and White[19]. No such consensus exists for the provenance of the remaining post-tectonic Newer granites that have initial $^{87}Sr/^{86}Sr$ ratios ranging down to 0.704.

The U–Pb systematics of Caledonian granite zircons investigated by Pidgeon and coworkers[9,10,12] are particularly relevant to the problems of granite provenance. Several granites, including both pre-tectonic granites (for example, Carn Chuinneag[9] and Ben Vuirich[10]) and post-tectonic granites north of the Highland Boundary Fault (such as Strichen[12] and Foyers[12]) have been shown to contain zircons with $^{207}Pb/^{206}Pb$ and U–Pb ages in excess of the age of granite emplacement. These U–Pb data define reverse discordia which have lower intercepts approximating to, or defining, the age of intrusion and upper intercepts corresponding to ages up to at least 1,000 Myr. Such zircons are considered to predate the magmatic event that produced the granites and to have been inherited as refractory constituents from a crustal percursor to the granites[9,10,12,16]. Therefore, in favourable circumstances they may provide an estimate of the age of some component of the granite.

In addition to studies of radiogenic isotopes, oxygen isotope abundances have been measured by Harmon and Halliday[20] in

0028–0836/80/390279—06$01.00

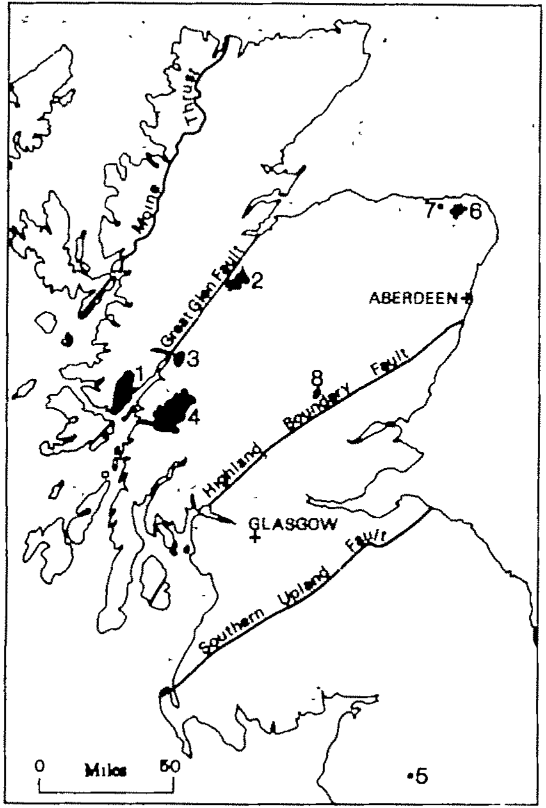

Fig. 1 Map showing the locations of Caledonian granites studied. 1, Strontian; 2, Foyers; 3, Ben Nevis; 4, Etive Complex; 5, Shap; 6, Ben Vuirich; 7, Longmanhill; 8, Strichen.

25 post-tectonic Caledonian granites from both north and south of the Highland Boundary Fault and a more detailed O and Sr isotope study of the Doon, Criffel and Fleet intrusions has also been made[21]. These studies demonstrate the existence of an overall positive correlation between δ^{18}O and ^{87}Sr/^{86}Sr, similar to that previously demonstrated for samples from the Peninsular Ranges Batholith[22]. Harmon and Halliday[20] interpret the correlation in terms of a binary mixing process with one component derived from the mantle or new basic lower crust and the other from a Lower Palaeozoic sedimentary source. Thus, granites possessing low ^{87}Sr/^{86}Sr and δ^{18}O values are considered to be dominated by melts derived from mantle source regions with both negligible crustal residence time and minimal contamination with pre-existing sialic crust (see also ref. 23).

The present study of Rb–Sr and Sm–Nd systematics of selected Caledonian granites includes pre- and post-tectonic examples from north of the Highland Boundary Fault in Scotland and the Shap Granite in northern England (see Fig. 1 and Table 1).

Results

Rb–Sr analyses were carried out at the University of Oxford and the Institute of Geological Sciences, London, and Sm–Nd analyses at the Lamont-Doherty Geological Observatory. The analytical methods used have been described previously[24–27].

New Rb–Sr results for samples measured in the present study are given in Table 2. Initial ^{87}Sr/^{86}Sr ratios (I_{Sr}) (Table 3) have been calculated assuming emplacement ages given in Table 1. I_{Sr} values for the Strontian tonalites and granodiorites exhibit a relatively small range from 0.70534 to 0.70598, whereas that for the biotite granite phase for Strontian is significantly greater at 0.70713. This agrees well with the I_{Sr} value of 0.70700±14 reported by Halliday *et al.*[21] for a sample of this same phase. The Foyers samples in Table 3 exhibit a larger range of I_{Sr} values of 0.70436–0.70819 and were considerably more heterogeneous than the Strontian intrusion at the time of emplacement.

These Rb–Sr data, together with those of Halliday *et al.*[21], are plotted on a Rb–Sr isochron diagram in Fig. 2. The data array for the Foyers granites falls close to the reference line corresponding to the assumed age of emplacement. The remainder of the Foyers' data are also positively correlated but scatter about a line of greater slope. This could reflect mixing between low Rb/Sr–low ^{87}Sr/^{86}Sr and high Rb/Sr–high ^{87}Sr/^{86}Sr components or the inheritance of Rb–Sr systematics from the source region which would correspond to an isotopic event at ~1,000 Myr. Furthermore, the possibility that some of the scatter reflects post-crystallization redistribution of Sr cannot be eliminated at this stage. For Strontian, the Rb–Sr data have been shown to scatter about a line corresponding to an age of 750 Myr (ref. 17), but we note here (Fig. 2) that, relative to a 435-Myr reference line (the emplacement age), it is only the points for the biotite granite which are highly discrepant, perhaps indicating that this unit has a different provenance from the granodiorites and tonalites. It may be relevant that inherited zircon has been reported from the biotite granite phase[16] but not from the other phases in Strontian[12].

Using the emplacement ages given in Table 1, the I_{Sr} values have been computed for the other Caledonian granites studied and are given in Table 3. The total range in I_{Sr} for the granites considered here range from ~0.716 (Strichen, Ben Vuirich, Longmanhill) to ~0.705 (Ben Nevis, Etive).

^{147}Sm/^{144}Nd and ^{143}Nd/^{144}Nd ratios are presented for 19 samples in Table 3, and initial ^{143}Nd/^{144}Nd (I_{Nd}) ratios have been computed using their assumed emplacement ages (Table 1). The I_{Nd} values range from 0.511444 (Longmanhill) to 0.512104 (Strontian). Those intrusions with high I_{Sr} values (Ben Vuirich, Longmanhill, Strichen) have among the lowest I_{Nd} values (Table 3), but there is no other detailed correlation. Note also that in the case of the Foyers intrusion the I_{Nd} values are much less variable than the I_{Sr} values.

The I_{Sr} and I_{Nd} values are also compared in terms of Δ parameters[28] in Table 3. These parameters express the deviations of isotope compositions with the bulk Earth values at the

Table 1 Geochronological data for some Caledonian granites

Intrusion	Age (Myr)	Method	Comments	Emplacement age (Myr)	Ref.
Strontian	435	U/Pb and ^{207}Pb/^{206}Pb	Nearly concordant zircons from granodiorite		12
	1,462 and 381	U/Pb	Reverse discordia for inherited zircons from biotite granite Lower intercept age may reflect Pb loss	435	16
Foyers	Probably predates Lochnagar and Hill of Fare at 415±5 Myr and 413±3 Myr dated by Rb–Sr whole rock. 401±8 Myr K–Ar (biotite)			415	15
Ben nevis	Unpublished Rb–Sr data and 382–399 Myr K–Ar (biotite)			400	15
Etive	Associated with lower old red sandstone lavas				
	390±6	U–Pb	Concordant zircons		12
Shap	394±3	Rb–Sr	Whole rocks and minerals	394	13
	397±7	K–Ar	Micas		13
Strichen	475	U–Pb	Concordant monazite		
	1,000 and 450	U–Pb	Inherited zircon. Lower intercept age may reflect Pb loss	475	12
Longmanhill	Assumed to be the same as Strichen			475	
Ben Vuirich	514±7 and 1,316±26	U–Pb	Reverse discordia for inherited zircon	514	10

Table 2 Rb–Sr data for Caledonian granites measured in the present study

Sample and rock type		Rb (p.p.m.)	Sr (p.p.m.)	^{87}Rb/^{86}Sr	^{87}Rb/^{86}Sr*
Foyers					
PM16	Tonalite	62	1,385	0.1288	0.70682 (5)
PM28	Tonalite	55	1,284	0.1233	0.70691 (4)
PM18	Granodiorite	62	1,070	0.1668	0.70791 (6)
PM21	Granodiorite	73	938	0.2240	0.70765 (5)
PM20	Granodiorite	65	900	0.2079	0.70748 (5)
PM23	Granodiorite	61	837	0.2098	0.70773 (4)
PM19	Granodiorite	70	810	0.2487	0.70764 (5)
PM22	Granodiorite	71	685	0.2982	0.70996 (4)
PM17b	Granodiorite	60	646	0.2673	0.70865 (7)
PM27	Granite	73	378	0.5558	0.70765 (5)
PM24a	Granite	81	350	0.6661	0.70871 (5)
PM26b	Granite	76	332	0.6589	0.70845 (6)
PM25	Granite	75	328	0.6580	0.70848 (4)
PM26a	Granite	85	300	0.8155	0.70943 (6)
PM24b	Granite	91	273	0.9595	0.71026 (6)
Ben Nevis					
P73-3	Granite	95	635	0.4306	0.70701 (7)
Shap					
CCR8	Granite	266	435	1.769	0.71740 (8)
Strontian					
ϕ203	Tonalite	70	1,223	0.1647	0.70700 (5)
ϕ212	Tonalite	51	1,100	0.1334	0.70652 (5)
ϕ200	Tonalite	74	1,036	0.2056	0.70687 (5)
ϕ202	Tonalite	68	877	0.2232	0.70686 (5)
ϕ201	Granodiorite	58	1,186	0.1407	0.70621 (4)
ϕ207	Granodiorite	59	1,172	0.1447	0.70624 (4)
ϕ204	Granodiorite	63	1,084	0.1673	0.70630 (5)
ϕ205	Granodiorite	80	790	0.2916	0.70764 (5)
ϕ209	Granodiorite	81	752	0.3100	0.70758 (5)
ϕ210	Granodiorite	86	628	0.3940	0.70795 (7)
ϕ208	Biotite granite	92	613	0.4317	0.70980 (5)
Etive Complex					
Starav					
Aϕ51	Granite	110	497	0.6402	0.70907 (5)
Aϕ52	Granite	121	739	0.4727	0.70772 (6)
Cruachan					
Aϕ59	Adamellite	128	509	0.7278	0.70897 (5)

* Numbers in parentheses refer to the last digit and is the 2σ error.

appropriate times of emplacement. In Fig. 3 the Δ values are compared with the bulk Earth, for which $\Delta_{Sr} = \Delta_{Nd} = 0$ at all times. Depleted mantle sources, such as represented by mid-ocean ridge basalts (MORB) or the 505-Myr Bay of Islands ophiolite[29], have negative Δ_{Sr} and positive Δ_{Nd} values. In contrast, the continental crust, which is the complement to depleted mantle, has a mean composition with a positive Δ_{Sr} and negative Δ_{Nd} values, although both positive and negative Δ_{Sr} values are known to exist in high grade metamorphic terrains[5,6]. None of the granites analysed as part of this study have Δ values characteristic of depleted mantle; on the contrary, all have negative Δ_{Nd} and positive Δ_{Sr}, similar to much of the continental crust. In this respect, these data are entirely analogous to those reported by Allègre *et al.*[4], and indicate a crustal contribution to all these granite bodies.

The Sm–Nd isotope systematics of Archaean meta-igneous rocks[6,27,30–35] can often be satisfied by simple two-stage models. The first stage can be considered to start some 4,550 Myr ago and end with a crust–mantle differentiation event at t ($t \geq 2{,}500$ Myr). Isotopic evolution in this first stage is characterized by a Sm/Nd ratio indistinguishable from the average chondrite ratio. The second stage extends from t until the present ($t = 0$). This comparatively simple model often seems contradictory to geological considerations that require more complex multistage

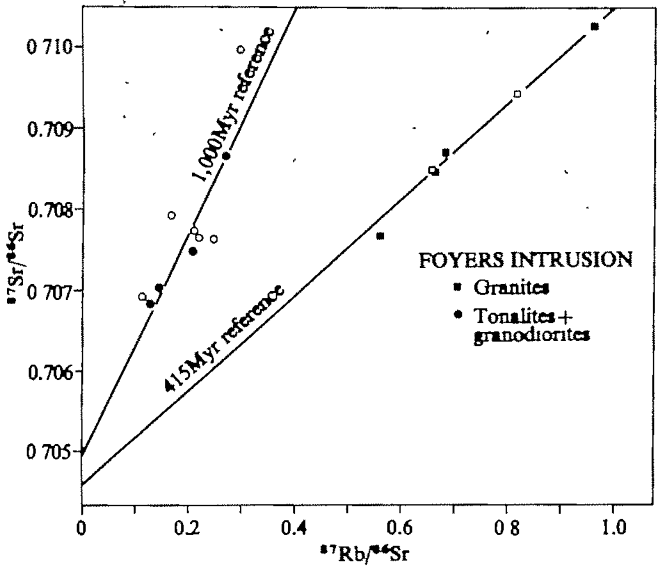

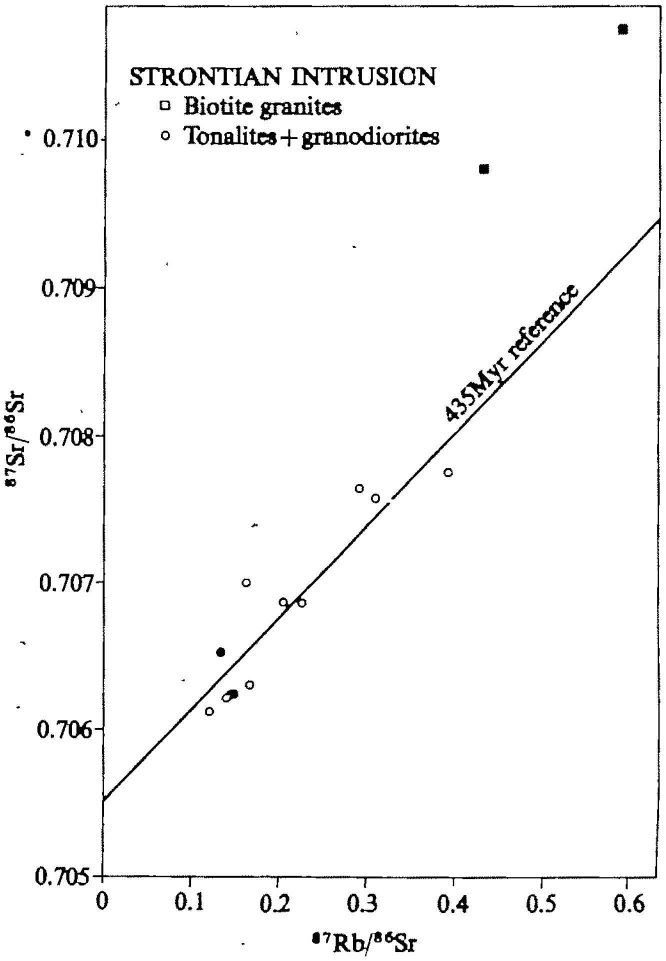

Fig. 2 Rb–Sr isochron diagrams for granite, granodiorite and tonalite phases of the Foyers and Strontian intrusions (Table 2 and ref. 16). The Foyers granites plot close to a 415-Myr reference line (assumed time of emplacement), and the tonalites and granodiorites plot close to a 1,000-Myr reference line. The Strontian tonalites and granodiorites plot close to a 435-Myr reference line (assumed time of emplacement), but the biotite granites do not.

development but merely indicates that the differentiation processes responsible for the production of such rocks occurred over an interval Δt that is not readily resolved from the Sm–Nd isotope systematics.

Model ages (t_{CHUR})[30] have been calculated (Table 3) for each sample assuming such a two-stage evolution. There is no *a priori* reason to assume that these ages should correspond to specific geological events. However, available data indicate that the Sm/Nd fractionation associated with the production of a new crustal segment is likely to be most significant in the history of a given crustal segment, and furthermore suggest that intracrustal differentiation processes involving erosion, sedimentation and metamorphism may have comparatively little effect on Sm/Nd ratios[36–40]. Thus, in some instances t_{CHUR} may provide a reasonable estimate of the time of separation of the Sm and Nd in their precursors from the mantle. t_{CHUR} can be expected to be a minimum age for this event if the mantle reservoir had been previously depleted and had a higher $^{143}\mathrm{Nd}/^{144}\mathrm{Nd}$ ratio than the bulk Earth, or if granitic melt production within the continental crust involved a fractionation of Sm/Nd. Furthermore, if a component derived from the continental crust is mixed with a contemporary mantle-derived component, the t_{CHUR} will not correspond to the provenance age of either component and will, depending on the precise nature of the mixing, usually be a minimum age for the crustal component.

Having noted these limitations, t_{CHUR} model ages range from close to the time of granite emplacement (for example, Shap) to ages much in excess of the emplacement ages (for example, 1,500 Myr for Strichen).

Provenance of Caledonian granites

The presence of inherited zircons and high initial $^{87}\mathrm{Sr}/^{86}\mathrm{Sr}$ ratios have demonstrated that the early Caledonian granites must contain a large component derived from the continental crust[9,10,12,16]. The Sm–Nd isotopic results reported here for the Ben Vuirich, Strichen and Longmanhill granites are entirely consistent with this viewpoint: the Δ_{Sr} and Δ_{Nd} values are very different from those typical of depleted or undepleted mantle, and indicate the existence of a large crustal component. One possible crustal component is the 2,920-Myr (ref. 6) Lewisian basement, which is known from north of the Highland Boundary Fault. Comparison of the Sm–Nd systematics of the Lewisian gneisses[6] with those of these early granites shows that they are not dominated by a Lewisian component. This fact is reflected by the t_{CHUR} ages which, although in some cases considerably greater than the assumed emplacement age, are much younger than the Lewisian. In contrast, the t_{CHUR} ages of the Tertiary Skye granites, which average 2,400 Myr, are considered to contain a large component derived from the Lewisian[5]. U–Pb data reported for inherited zircons in the Ben Vuirich granite define a discordia that intercepts the concordia at 1,316 ± 26 Myr and 514 ± Myr. The upper intercept age is in excellent agreement with the t_{CHUR} age of 1,310 ± 70 Myr. This limits any 'mantle-derived' component in the granite to a negligible proportion and further indicates minimal fractionation of Sm/Nd during remelting of this Proterozoic crustal source. Although less well constrained from zircon data, the same argument may apply in principle to the petrogenesis of the ~475-Myr granites of north-east Scotland.

The origin of the remaining post-tectonic (Newer) granites is more controversial. For example, distribution of inherited zircons (≥ 1,000 Myr old) led Pidgeon and Aftalion[12] to propose a major Proterozoic crustal component in granites north of the Highland Boundary Fault. Caledonian granites south of the fault were ascribed to a Lower Palaeozoic crustal source. In contrast, many other workers[20,23,39–41] have invoked a major involvement, either directly or indirectly, of contemporary (Caledonian) mantle-derived material, with crustal contaminants ranging from Lewisian[39] to Lower Palaeozoic in age.

The Sm–Nd systematics of the Newer Caledonian granites provide some resolution of these possibilities. The Δ_{Nd} and Δ_{Sr} values are compared in Fig. 3*b* with the expected values of depleted mantle source regions in the Caledonian (as represented by the field of mid-ocean ridge basalts computed for 400 Myr ago and by the 505-Myr-old Bay of Islands ophiolite) and the Lewisian gneisses, these being the most extreme compositions likely to be involved. Other potential components, such as Proterozoic or Lower Palaeozoic crustal sources, will be intermediate in isotopic composition. The main question is whether the Δ_{Nd} and Δ_{Sr} values of the granites plotted reflect mixtures between such extreme end-member compositions or whether they are generated from younger continental crust. It is obvious that none of the granites are dominated by Nd and Sr derived from a contemporary depleted mantle source, and even in the case of Strontian granodiorites and tonalites a contribution from

Table 3 Sm–Nd data and initial strontium ratios for some Caledonian granites

Intrusion	Sample	Sm (p.p.m.)	Nd (p.p.m.)	$^{147}\mathrm{Sm}/^{144}\mathrm{Nd}$	$^{143}\mathrm{Nd}/^{144}\mathrm{Nd}$ ($\pm 2\sigma m$)	I_{Sr}	I_{Nd}	ΔNd	ΔSr	t_{CHUR}(Myr)	f*
Strontian											
	ϕ202	4.065	26.00	0.09398	0.512372 (30)	0.70548	0.512104	−0.2 (6)	25 (1)	440 (50)	−0.51
	ϕ203	4.795	27.74	0.1040	0.512292 (30)	0.70598	0.511996	−2.3 (6)	35 (1)	630 (50)	−0.46
	ϕ205	5.231	32.99	0.09537	0.512240 (30)	0.70583	0.511968	−2.8 (6)	32 (1)	650 (50)	−0.51
	ϕ207	6.524	32.06	0.1224	0.512450 (34)	0.70534	0.512101	−0.3 (6)	23 (1)	450 (70)	−0.37
	ϕ210	3.730	19.93	0.1125	0.512320 (24)	0.70550	0.511999	−2.2 (4)	26 (1)	640 (40)	−0.42
	ϕ208	3.112	18.01	0.1039	0.512050 (32)	0.70713	0.511754	−6.8 (6)	57 (1)	1,040 (50)	−0.46
Foyers											
	PM16	9.927	59.90	0.09963	0.512009 (30)	0.70605	0.511738	−7.5 (5)	36 (1)	1,060 (50)	−0.49
	PM18	12.50	72.05	0.1043	0.511963 (24)	0.70692	0.511680	−8.7 (4)	52 (1)	1,190 (40)	−0.46
	PM22	4.482	34.04	0.07919	0.511883 (29)	0.70819	0.511668	−8.9 (5)	77 (1)	1,030 (40)	−0.59
	PM24b	1.769	12.69	0.08394	0.511971 (22)	0.70458	0.511743	−7.5 (4)	7.6 (6)	960 (30)	−0.57
	PM26a	2.416	16.71	0.08695	0.511993 (31)	0.70461	0.511757	−7.3 (6)	8.0 (7)	950 (40)	−0.55
	PM27	1.760	13.06	0.08105	0.512026 (26)	0.70436	0.511806	−6.3 (5)	3.3 (6)	860 (30)	−0.58
Ben Nevis											
	P73-3	3.874	26.51	0.08785	0.511964 (22)	0.70455	0.511734	−8.0 (4)	6.5 (10)	1,000 (30)	−0.55
Etive Complex											
Starav	A051	2.890	19.44	0.08941	0.511870 (30)	0.70542	0.511636	−9.8 (6)	23 (1)	1,160 (40)	−0.54
Starav	A052	3.762	23.72	0.09536	0.511868 (26)	0.70503	0.511618	−10 (1)	16 (1)	1,230 (40)	−0.51
Cruachan	A059	4.851	30.44	0.09585	0.512124 (30)	0.70482	0.511873	−5.4 (6)	12 (1)	840 (40)	−0.50
Shap											
	CCR8	6.525	43.20	0.09080	0.512261 (30)	0.70750	0.512027	−2.6 (6)	63 (1)	590 (40)	−0.54
Strichen											
	P71–17A	8.035	44.67	0.1082	0.511821 (16)	0.7161	0.511484	−11 (1)	ca. 230	1,490 (30)	−0.44
Longmanhill											
	P71–16A	7.474	37.89	0.1186	0.511813 (30)	0.7143	0.511444	−12 (1)	ca. 200	1,720 (60)	−0.39
Ben Vuirich											
	BV–1	8.538	38.70	0.1326	0.512137 (32)	0.7174	0.511691	−6.3 (6)	ca. 260	1,310 (70)	−0.32

* f is the deviation of measured Sm/Nd ratios from the bulk Earth (or CHUR) value[31].

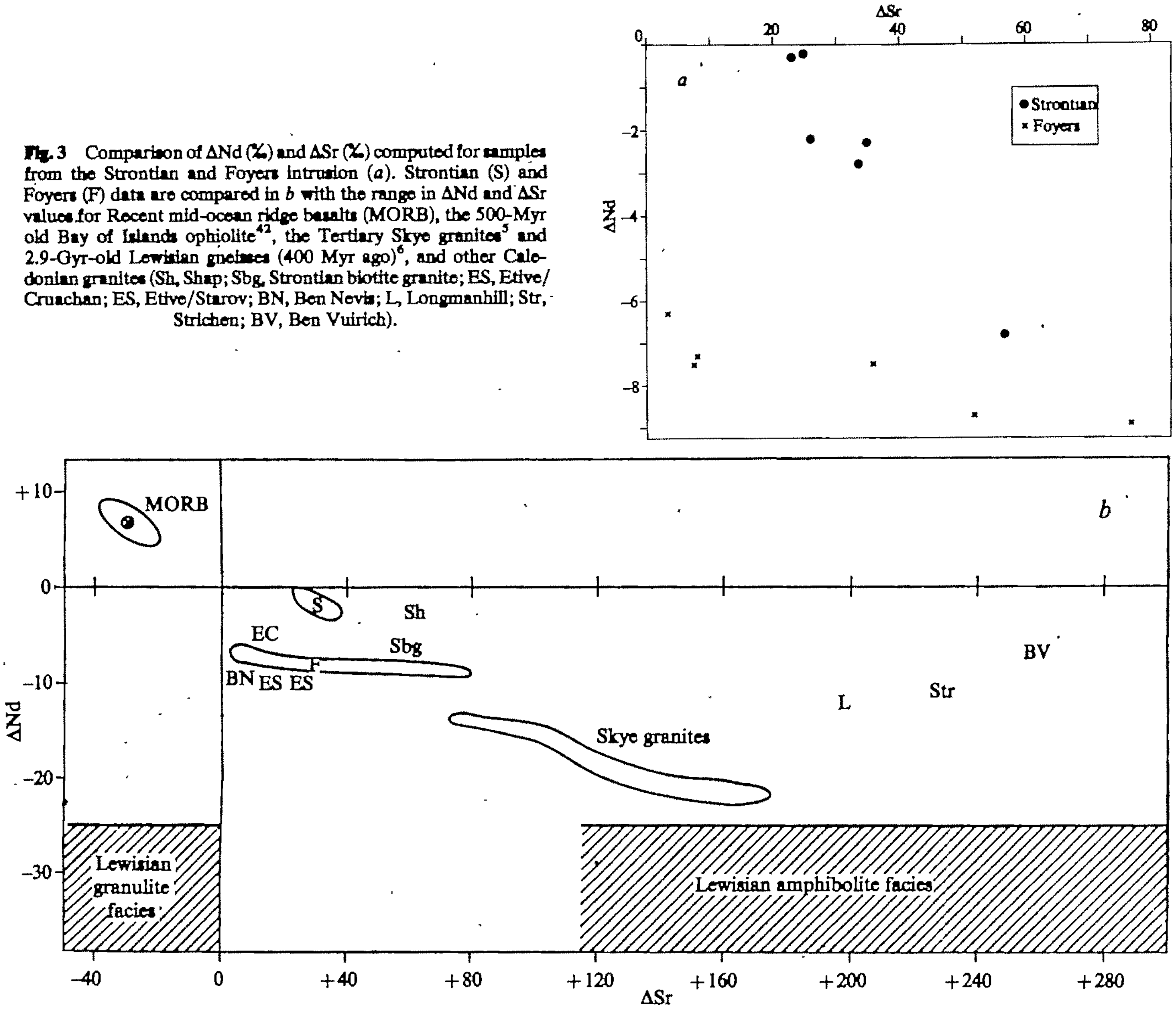

Fig. 3 Comparison of ΔNd (‰) and ΔSr (‰) computed for samples from the Strontian and Foyers intrusion (*a*). Strontian (S) and Foyers (F) data are compared in *b* with the range in ΔNd and ΔSr values for Recent mid-ocean ridge basalts (MORB), the 500-Myr old Bay of Islands ophiolite[42], the Tertiary Skye granites[5] and 2.9-Gyr-old Lewisian gneisses (400 Myr ago)[6], and other Caledonian granites (Sh, Shap; Sbg, Strontian biotite granite; ES, Etive/Cruachan; ES, Etive/Starov; BN, Ben Nevis; L, Longmanhill; Str, Strichen; BV, Ben Vuirich).

this could not exceed ~10‰, although a larger contribution from an undepleted (that is, $\Delta_{Nd} \approx \Delta_{Sr} \approx 0$) source would be permissible. Similarly, the contamination of mantle-derived material with an Archaen crustal source (such as Lewisian) must be restricted to a maximum of ~30% even in the most favourable case (Foyers). However, the trend of Δ_{Nd} and Δ_{Sr} values for the Foyers intrusion (Fig. 3*a*) is incompatible with a simple mixing between mantle and Lewisian endmembers. Rather, the range of Δ values indicates intracontinental differentiation processes, such as sedimentary fractionation of Rb/Sr at relatively constant Sm/Nd, in which case the t_{CHUR} ages (800–1,200 Myr) may give a reasonable estimate of provenance. The broad agreement between the average t_{CHUR} age and the inherited Rb–Sr systematics supports this interpretation, as does the presence of >1,000-Myr-old inherited zircon. For the Strontian intrusion, possible mantle- and continent-derived components are less readily constrained, but the similarity of the Δ_{Nd} and Δ_{Sr} values of the biotite granite to the Foyers samples, together with the evidence for inherited zircon, may indicate a similar Proterozoic crustal provenance at least for this phase.

The Sm–Nd and Rb–Sr data also provide constraints on the provenance of post-tectonic granites that do not contain inherited zircon. The t_{CHUR} ages for the Ben Nevis and Etive granites of ~1,000 Myr are similar to those of the Foyers granite, indicating that their provenance is dominated by Precambrian crust rather than a contemporary mantle source, as has usually been inferred from Sr-isotope data alone. Note, in this respect, that the comparatively low I_{Sr} value for Ben Nevis of 0.7043 in ref. 25 is associated with a δ^{18}O value of 7.8‰, which is at the lower end of the range of δ^{18} values reported by Harmon and Halliday for Caledonian granites[20]. This combination, as interpreted by these authors, reflects a major mantle or new lower crustal component (~70%). However, this conclusion is at variance with the constraint imposed by the t_{CHUR} age of ~1,000 Myr. The interpretation of the I_{Sr}–δ^{18}O correlation for late Caledonian granites as the result of mixing of two components is certainly an oversimplification[42] and low δ^{18}O and low ^{87}Sr/^{86}Sr are not adequate criteria for the recognition of a granite dominated by a contemporary mantle-derived component.

The lack of inherited zircon in the Shap granite[12] and the t_{CHUR} age of 560 Myr suggest that its provenance is not dominated by an old crustal component. It is possible that this intrusion is derived from a contemporary mantle-derived component or from crustal components that have had comparatively short crustal residence times. The Sm–Nd data alone do not favour either of these alternatives, but taken together, the δ^{18}O value of 11‰ and $I_{Sr} = 0.07075$ (ref. 20) suggest a sedimentary rather than a mantle provenance. The tonalites and granodiorites of the Strontian intrusion have both low I_{Sr} values (~0.7056) and low δ^{18}O (~7.2‰)[20]. These parameters, coupled with the t_{CHUR} ages of 400–600 Myr, are quite compatible with a provenance involving a large mantle-derived component. However, in view of the Ben Nevis data, it is not possible to exclude a provenance dominated by a crustal source, albeit one with a comparatively short crustal residence time.

Conclusions

In terms of more general questions of crustal evolution, it is important to ascertain the extent to which granite magmatism (s.l.) reflects intracrustal differentiation in the continents *vis-à-vis* the addition of mantle-derived material to the continents. The results of the present study and previously published isotopic data suggest only minimal, if any, involvement of mantle-derived Sr and Nd components for many of the analysed intrusions. Thus, their formation has involved the recycling of continental crustal materials that have had a prior crustal residence time of $\geqslant 500$ Myr (such as Strichen, Ben Vuirich, Ben Nevis, Etive and Foyers intrusions and the Strontian biotite granite). The Rb–Sr and Sm–Nd isotope data reported here do not directly constrain the provenance of other constituents of the granites present in major, minor or trace proportions: mixing processes can be envisaged whereby the provenance of various elements may indeed differ. However, where indications of provenance using different approaches involving, for example, zircon U–Pb, Rb–Sr and Sm–Nd whole-rock systematics concur (as for Ben Vuirich, Strichen, Foyers), it is more reasonable to assume that all constituents of the granite have the same provenance. Although the isotope systematics of these Caledonian granites indicate a dominance of crustal provenance, it cannot be inferred that the heat required for the melting process was also crustal: this could equally well be supplied from the mantle.

For the remaining intrusions studied there is no unequivocal support for involvement of mantle-derived material that has not had some prior crustal residence. In the case of the Strontian tonalites and granodiorites, involvement of crust with only ~ 100–200 Myr prior residence time is difficult to distinguish from the possibilities or alternatively or additionally involved mantle components. In some cases (such as the Shap granite) a short crustal residence of the precursors is indicated by the comparatively high I_{Sr} and $\delta^{18}O$ values. However, in the case of the Ben Nevis and Etive granites, their t_{CHUR} ages of 800–1,200 Myr suggest that the well documented positive correlation of $\delta^{18}O$ and I_{Sr} for the Caledonian granites may not be simply attributed to mixing of local upper-crustal sediment with a contemporary mantle-derived component.

J. F. Brown and C. Rundles provided some of the samples used in this study. Contribution No. ES 89 of the Department of Earth Sciences, Cambridge. This research has been supported by grants from the NSF and the NERC.

Received 19 May; accepted 30 July 1980.

1. Hurley, P. M., Hughes, H., Faure, G., Fairbairn, H. W. & Pinson W. H. Jr *J. geophys. Res.* **67,** 5315–5334 (1962).
2. Hurley, P. M., Batemen, P. C., Fairbairn, H. W. & Pinson W. H. Jr *Bull. geol. Soc. Am.* **76,** 165–175 (1965).
3. Faure, G. & Hurley, P. M. *J. Petrol.* **4,** 31–50 (1963).
4. Allègre, C. J., Othman, D. B., Polve, M. & Richard, P. *Phys. Earth planet. Inter.* **9,** 293–306 (1979).
5. Carter, S. R., Evensen, N. M., Hamilton, P. J. & O'Nions, R. K. *Science* **202,** 435–438 (1978).
6. Hamilton, P. J., Evensen, N. M., O'Nions, R. K. & Tarney, J. *Nature* **277,** 25–28 (1978).
7. Dewey, J. F. in *The Ocean Basins and Margins 2, The North Atlantic* (eds Nairn, A. E. M. & Stehli, F. G.) 205–231 (Plenum, New York, 1974).
8. Wright, A. E. *Nature* **264,** 156–160 (1976).
9. Pidgeon, R. T. & Johnson, M. R. W. *Earth planet. Sci. Lett.* **24,** 105–112 (1974).
10. Pankhurst, R. J. & Pidgeon, R. T. *Earth planet. Sci. Lett.* **31,** 55–68 (1976).
11. Read, H. H. *Liverpool Manchester Geol. J.* **2,** 653–683 (1961).
12. Pidgeon, R. T. & Aftalion, M. *Geol. J. Spec. Issue* No. 10, 183–220 (1978).
13. Wadge, A. J., Gale, N. H., Beckinsale, R. D. & Rundle, C. C. *Proc. Yorkshire geol. Soc.* **42,** 297–305 (1978).
14. Pankhurst, R. J. & Sutherland, D. in *Igneous Rocks of the British Isles* (ed. Sutherland, D.) (Wiley, New York, 1980).
15. Brown, P. E., Miller, J. A. & Grasty, R. L. *Proc. Yorkshire geol. Soc.* **36,** 251–276 (1968).
16. Halliday, A. N., Aftalion, M., van Breemen, O. & Jocelyn, J. *Geol. Soc. Lond. Spec. Issue* (in the press).
17. Pankhurst, R. J. in *Origin of Granite Batholiths: Geochemical Evidence* (eds Atherton, M. P. & Tarney, J.) 18–33 (Shiva, Copenhagen, 1979).
18. Pankhurst, R. J. *Bull. geol. Soc. Am.* **85,** 345–350 (1974).
19. Chappell, B. W. & White, A. J. R. *Pacific Geol.* **8,** 173–174 (1974).
20. Harmon, R. S. & Halliday, A. N. *Nature* **283,** 21–25 (1980).
21. Halliday, A. N., Stephens, W. E. & Harmon, R. S. *J. geol. Soc. Lond.* **137,** 329–348 (1980).
22. Taylor, H. P. & Silver, L. T. *U.S. Geol. Surv. Open File Rep.* **78–701,** 423–426 (1978).
23. Simpson, P. R., Brown, G. C., Plant, J. & Ostle, D. *Phil. Trans. R. Soc.* A**291,** 385–412 (1979).
24. O'Nions, R. K. & Pankhurst, R. J. *Earth planet. Sci. Lett.* **21,** 13–21 (1973).
25. Pankhurst, R. J. & O'Nions, R. K. *Chem. Geol.* **12,** 127–136 (1973).
26. O'Nions, R. K., Hamilton, P. J. & Evensen, N. M. *Earth planet. Sci. Lett.* **34,** 13–22 (1977).
27. Hamilton, P. J., O'Nions, R. K. & Evensen, N. M. *Earth planet. Sci. Lett.* **36,** 236–268 (1977).
28. O'Nions, R. K., Evensen, N. M., Hamilton, P. J. & Carter, S. R. *Phil. Trans. R. Soc.* A**285,** 547–559 (1978).
29. Jacobsen, S. B. & Wasserburg, G. J. *J. geophys. Res.* **84,** 7429–7445 (1980).
30. DePaolo, D. J. & Wasserburg, G. J. *Geophys. Res. Lett.* **3,** 743–746 (1976).
31. DePaolo, D. J. & Wasserburg, G. J. *Geophys. Res. Lett.* **3,** 249–253 (1976).
32. Hamilton, P. J., O'Nions, R. K., Evensen, N. M., Bridgwater, D. & Allaart, J. *Nature* **272,** 41–43 (1978).
33. Hamilton, P. J., Evensen, N. M., O'Nions, R. K., Smith, H. S. & Erlank, A. J. *Nature* **279,** 298–300 (1979).
34. Hamilton, P. J., Evensen, N. M., O'Nions, R. K., Glikson, A. Y. & Hickman, A. H. *Proc. 2nd int. Archaean Symp.*, Perth (in the press).
35. Taylor, S. R. *Geochim. cosmochim. Acta* **28,** 1273–1285 (1964).
36. Green, T. H., Brunfelt, A. O. & Heiser, K. S. *Earth planet. Sci. Lett.* **7,** 93–98 (1969).
37. Herrman, A. G., Potts, M. J. & Knake, D. *Contr. Mineral. Petrol.* **44,** 1–16 (1974).
38. Smewing, J. D. & Potts, P. J. *Contr. Mineral. Petrol.* **57,** 245–258 (1976).
39. McCulloch, M. T. & Wasserburg, G. J. *Science* **200,** 1003–1011 (1978).
40. Brown, G. C., Plant, J. A. & Thorpe, R. S. in *The Caledonides in the USA* (ed. Wones) (Blacksburg Conf., in the press).
41. Blaxland, A. B., Aftalion, M. & van Breemen, O. *Scot. J. Geol.* **15,** 139–151 (1979).
42. Taylor, H. P. Jr *Earth planet. Sci. Lett.* **47,** 243–254 (1980).

Deformation of the Indo–Australian plate

Jeffrey K. Weissel, Roger N. Anderson & Carol A. Geller

Lamont-Doherty Geological Observatory of Columbia University, Palisades, New York 10964

Intraplate seismicity, deformed oceanic crust and sediments, and local areas of abnormally high heat flow characterize significant internal deformation of the Indo–Australian plate in the northeastern Indian Ocean. The deformation appears analogous to the buckling of an elastic plate with brittle failure at its surface. It is not clear whether the Indo–Australian plate can be resolved into two component parts or whether a new convergent plate boundary is likely to form in the deformed region. The onset of intraplate deformation in the late Miocene seems to be connected to the Himalayan orogenic stage of the collision between India and Asia.

CENTRAL to the concept of plate tectonics are the assumptions that a strong lithosphere overlies a weaker asthenosphere, and that lithospheric plates are undeformed except at their boundaries. Because the evolution of the Earth's surface from the standpoint of plate tectonics has gained widespread acceptance, observations that apparently violate its basic assumptions should be closely examined. Intraplate earthquakes, marine seismic reflection profiling, and heat flow observations delineate an outstanding example of deformation remote from the boundaries of the Indo–Australian plate (which carries both India and Australia, Fig. 1). This article (1) discusses these observations in detail; (2) points to a possible link between deformation in the interior of the Indo–Australian plate and the Himalayan orogeny; (3) speculates on the implications of treat-

0028–0836/80/390284—08$01.00

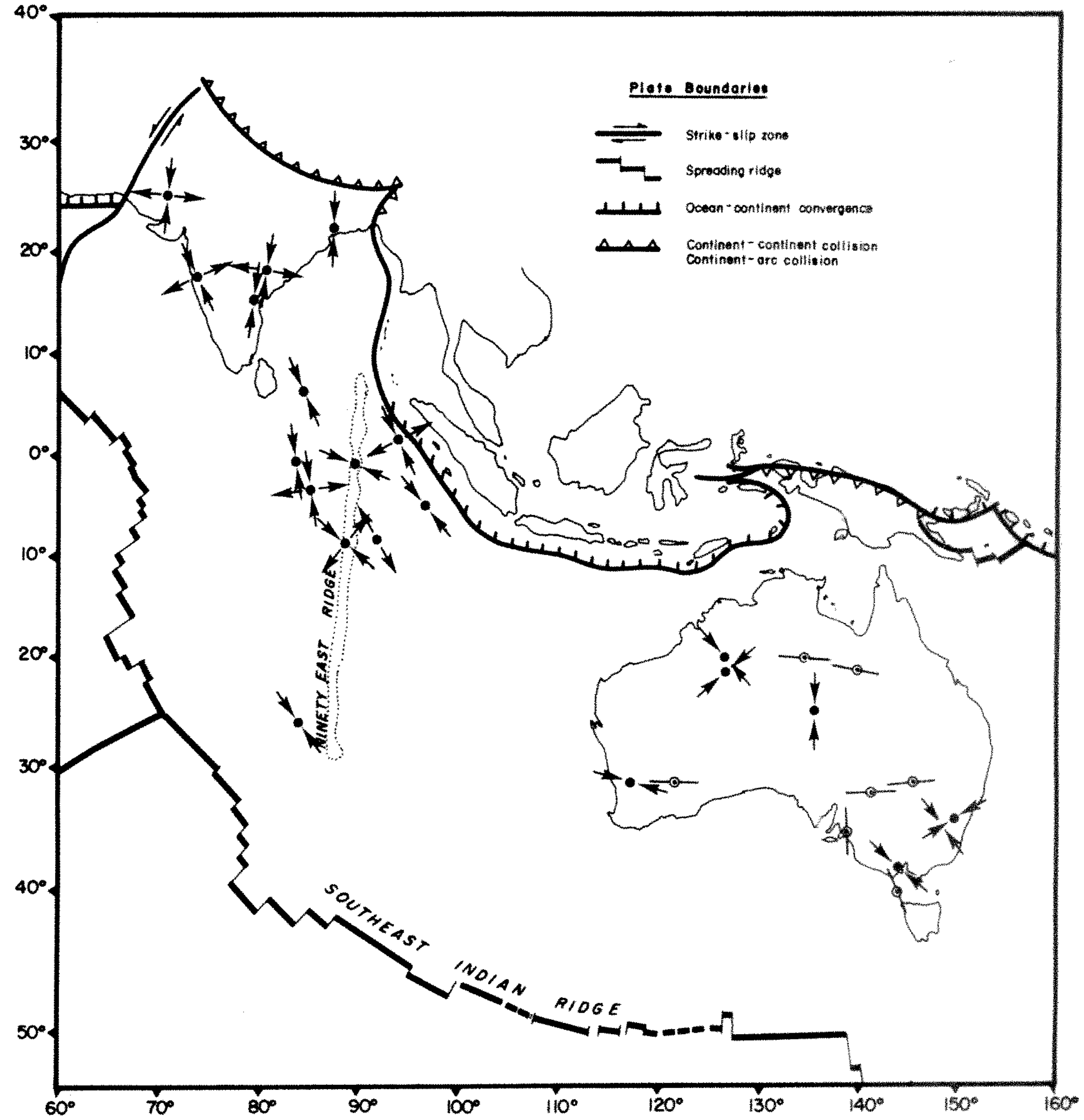

Fig. 1 Directions of principal stress axes for intraplate earthquakes within the Indo-Australian plate[2–8]. Inward-pointing arrows denote the axis of maximum compression; outward-pointing arrows refer to the axis of minimum compression. Also shown (—⊙) are maximum compressional stress directions from *in situ* stress determinations in Australia[9].

ing the deformation as buckling of an elastic plate; and (4) considers whether the intraplate deformation is a precursor of a new convergent plate boundary within oceanic lithosphere of the Indian Ocean.

Intraplate earthquakes and contemporary stress

Seismologists have long noted that the northern part of the Indo-Australian plate displays a high level of intraplate earthquake activity[1–4]. Shallow events occur over a wide band extending from the Indian peninsula through the Australian continent[1–3] and principal stress directions[2,4,5–8] determined for the most significant of these earthquakes are shown in Figs 1 and 2. Except for the single tensional event east of the Ninetyeast Ridge[4] (Fig. 2), principal stress directions and *in situ* stress determinations indicate that the northern part of the Indo-Australian plate is under predominantly horizontal compression. The orientations of the axes of maximum compression change from about N–S in the Indian peninsula to nearly E–W in the Australian continent, a feature predicted by global models in which intraplate stress is determined by assumed plate boundary forces[10].

The significant teleseismicity in this supposedly mid-plate region led Sykes[2] to propose that a new convergent plate boundary may be in the process of forming between Sri Lanka and northwestern Australia. Sykes argued that a new plate boundary would accommodate plate motions that have been resisted by the continuing collision between continental India and Asia. However, Stein and Okal[4] questioned the nascent island arc hypothesis of Sykes[2]. They noted an apparent association between the Ninetyeast Ridge north of about 10° S and several large earthquakes which have occurred since the early part of the century. Stein and Okal[4] proposed that the northern part of the Ninetyeast Ridge is either a plate boundary characterized by left lateral strike slip motion, or that it is the focus of earthquake activity in an area of highly unusual mid-plate tectonics. In either event, the intraplate earthquakes and *in situ* stress measurements (Figs 1 and 2) show clearly that horizontal compression currently characterizes a major portion of the Indo-Australian plate.

Deformation structures

Direct evidence for deformation within the oceanic part of the Indo-Australian plate was found by Eittreim and Ewing[11] from a seismic reflection survey of a small area at the distal end of the Bengal Fan (Fig. 2). The reflection records revealed folding of the sediments and high-angle faulting through to basement along an azimuth of ~100°. Further north in the thicker sedimentary section of the Bay of Bengal, Curray and Moore[12] and Moore *et al.*[13] recognized deformed sediments beneath a prominent unconformity and refracting surface that they could trace throughout the Bay. These previous studies showed that tectonic disturbance of originally flat-lying sediments should be easily seen on seismic reflection records with typical vertical exaggerations of 25 : 1. With this in mind, we examined available seismic records from the northeastern sector of the Indian Ocean (held by Lamont-Doherty Geological Observatory and the National Solar-Terrestrial Geophysical Data Center in Boulder, Colorado) to delineate the geographical extent of permanent deformation within the oceanic portion of the Indo-Australian plate, and to determine the types of structures produced at the surface of oceanic lithosphere deformed under horizontal compression. Clear evidence for intraplate deformation is observed only in seismic reflection records from the southern portions of the Bengal and Nicobar Fans, where deformation of oceanic crust and overlying sediments can be resolved into two parts based on dominant 'wavelengths'.

On a broad scale (100–300 km), acoustic basement (probably oceanic crust) is deformed into 'undulations' with 1–3 km of relief (Fig. 3). Large amplitude (30–80 mGal) free-air gravity anomalies are clearly associated with the broad basement features. Gravity anomalies of such amplitudes and wavelengths will arise if the observed undulations reflect uniform bending of the entire oceanic crust[8]. Sea surface heights measured from numerous GEOS 3 orbital paths across the northern Indian Ocean also reflect the broad-scale basement features interpreted from seismic reflection data and marine gravity data (Fig. 3), although small geoidal undulations with wavelengths 100–300 km are less accurately determined by satellite altimetry than by marine gravimetry[14].

On a smaller scale (5–20 km), seismic reflection data from the southern part of the Bengal Fan and the Nicobar Fan[15] reveal high-angle faulting of acoustic basement (oceanic crust) and overlying sediments, and folding of the sedimentary section. (Note, for example, the faulted basement high 200 km from the left side of Fig. 3 and the general disturbed nature of the sediment cover on this profile.) Two seismic reflection profiles from the southern part of the Bengal Fan, which show typical characteristics of the smaller-scale deformation west of the Ninetyeast Ridge, are shown in Fig. 4.

Of particular importance are the high-angle faults which disrupt the oceanic crust and most of the overlying sedimentary section (Fig. 4*a*, *b*). The involvement of oceanic crust in the faulting precludes movement along a surface of decollement above basement as a cause of the deformation. Spatially, the short-wavelength structures are concentrated at 'deformation fronts' where high-angle faults are particularly closely spaced (see Fig. 4*a*). These deformation fronts, which often form barriers to the southward movement of turbidites over the fan, are separated by less disrupted terrane particularly west of about 86° E.

The seismic profile shown in Fig. 4*b*, which is located between 86° E and the Ninetyeast Ridge, is interesting because it is located very close to the epicentre determined for a $M_s = 6.1$ (ref. 8) strike slip earthquake[5] (Fig. 2). Near the epicentre, high-angle faults which disrupt acoustic basement with throws of the order of hundreds of metres cause little offset of the seafloor (Fig. 4*b*). In fact, 3.5 kHz echosounder data show that these faults offset the sea floor and immediate sub-sea floor reflectors by only 9–18 m. Offsets that increase with depth suggest that the

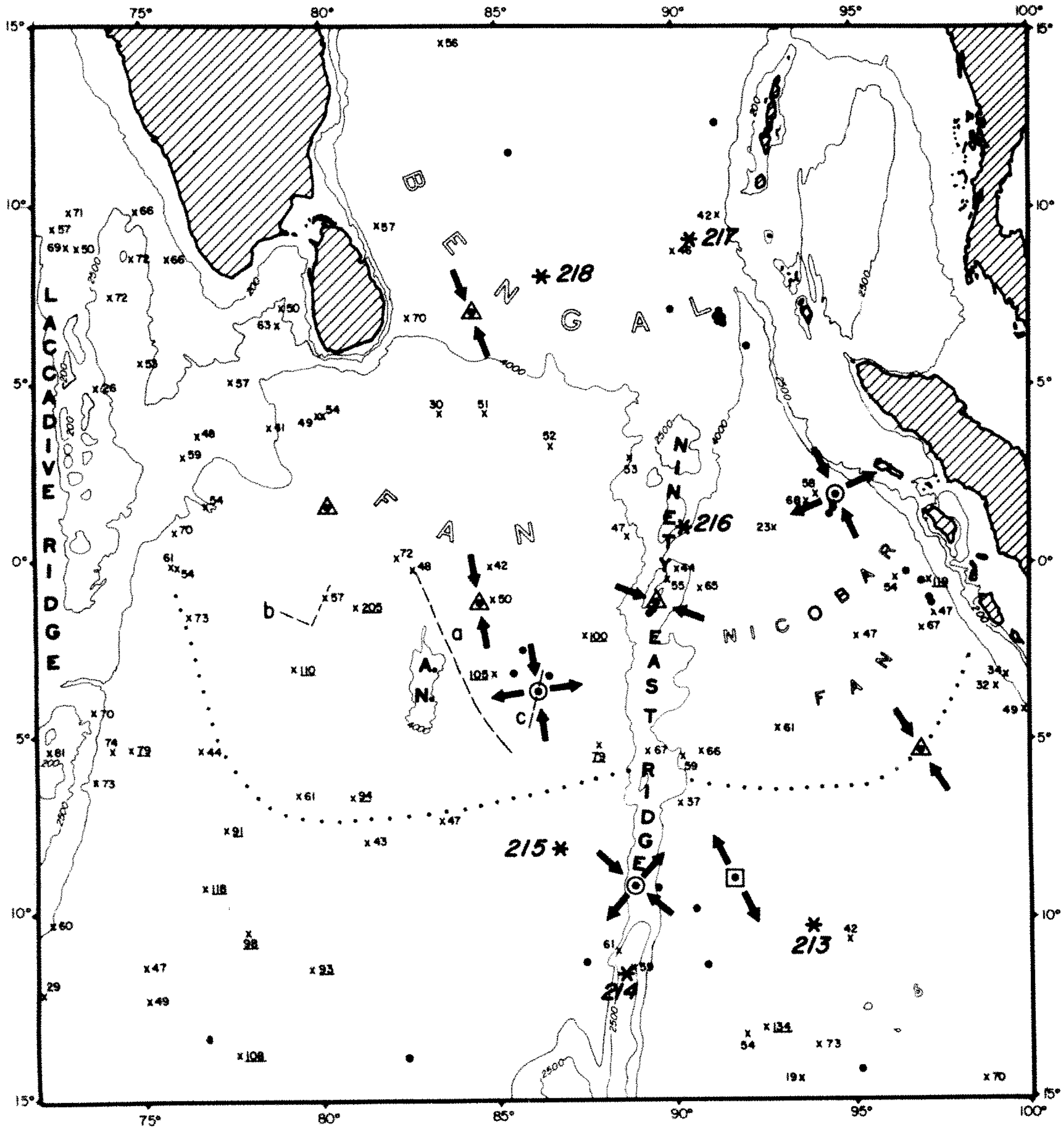

Fig. 2 Directions of principal stress axes for intraplate earthquakes[2–8] and heat flow values[20,34] in mW m^{-2} (numbered crosses) in the northern Central Indian Ocean. [Note that 41.87 mW m^{-2} = 1 HFU (μcal cm^{-2} s^{-1})]. ●, Intraplate earthquakes. ▲, Focal mechanisms with thrust faulting; ⊙, with strike slip faulting; ⊡, normal faulting[4]. Unexpectedly high heat flow values are underlined. *, DSDP sites. The southern limit of fan deposits is shown roughly by the dotted line. Dashed lines locate seismic reflection profiles shown in Figs 3 and 4. AN, Afanazy Nikitin seamount group.

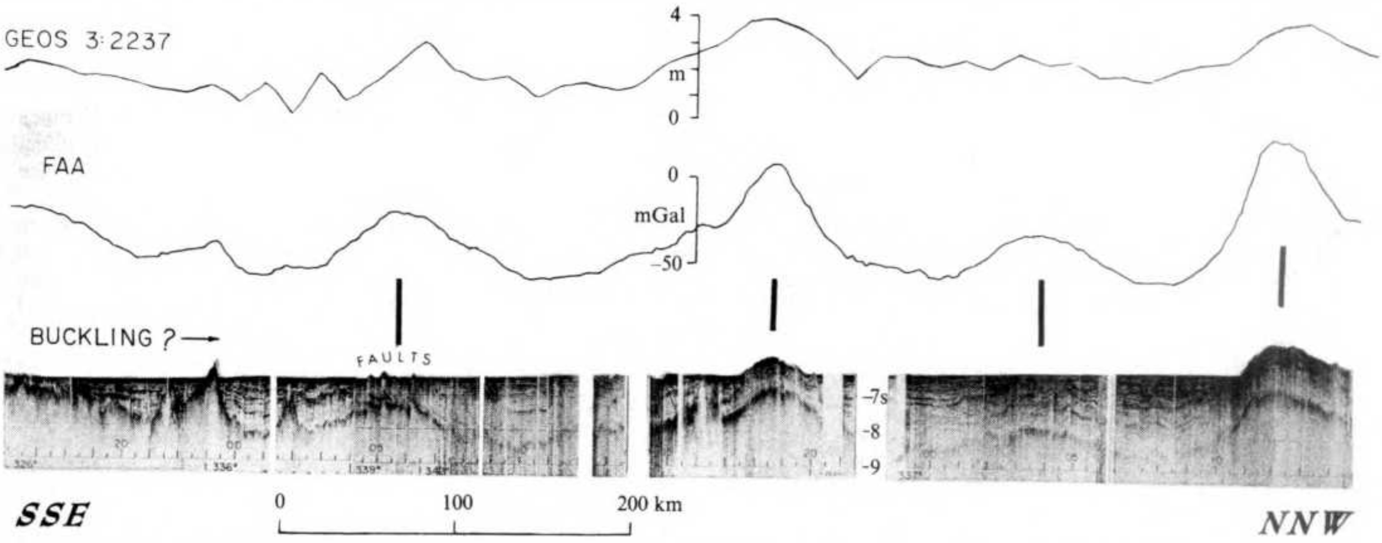

Fig. 3 Broad-scale deformation of the oceanic crust beneath the southern portion of the Bengal Fan (profile a in Fig. 2). Large-amplitude free-air gravity anomalies (FAA) and small-amplitude geoidal undulations (GEOS 3:2237) correlate with the basement deformation.

faults may be growth structures. The small scale structures show a preferred structural asymmetry; the north side is generally upthrown on the high-angle faults and the asymmetric folds, which are likely caused by drag on faults, are generally southward-verging.

Sediments below a prominent unconformity show geometrically conformable structures while above this unconformity the intensity of deformation decreases towards the sea floor (Fig. 4*a*, *b*). At DSDP Site 218, which is further north in the Bay of Bengal (Fig. 2), a widespread unconformity and refracting surface separating locally deformed strata from overlying fan turbidites was found to be uppermost Miocene in age[13,16]. It is likely that this is the major unconformity observed in the seismic reflection records as all Lamont-Doherty piston cores which penetrated the section beneath the unconformity over the southern part of the Bengal Fan contained uppermost Miocene or older faunal groups (ref. 17 and G. Blechschmidt, personal communication). We suggest, from drilling and coring results and the seismic reflection data, that intraplate deformation began in late Miocene time, and that this event is recorded by a prominent unconformity in the sedimentary section of the Bengal Fan.

Both the broad- and small-scale structures provide convincing evidence for deformation remote from the generally accepted boundaries of the Indo–Australian plate. Figure 5 is a map of the broad- and small-scale structures based primarily on single-channel seismic reflection data and gravity data. Several points should be noted. First, the trends of the basement 'undulations' change from ENE–WSW near the Ninetyeast Ridge to E–W or even WNW–ESE in the southwestern part of the Bengal Fan. Second, the basement undulations show culminations and saddles along their trends. Third, the broad structures appear disrupted by the major fracture zone at 86° E which offsets E–W trending magnetic lineations left-laterally by about 850 km (ref. 18). Acoustic basement is shallower on the eastern side of this fracture zone by about 1 km. Fourth, between the 86° E fracture zone and the Ninetyeast Ridge, the trends of the small-scale folds and faults may differ from the trends of the broad basement undulations (Fig. 5). Given the difficulty of tracing individual faults or folds from track to track with the available data distribution, however, this last point should be regarded as tentative.

The available seismic reflection records show that sediment and upper crustal deformation extends from the southern part of the Bengal Fan across the Ninetyeast Ridge into the northwestern Wharton Basin. Compared with the structures observed in the Bengal Fan, deformation of Nicobar Fan sediments in the Wharton Basin appears less severe[15], but seismic reflection coverage is more extensive west of the Ninetyeast Ridge. Seismic profiles over the Ninetyeast Ridge reveal high-angle faulting[19], although the crust of the Ninetyeast Ridge is not as extensively disrupted as the oceanic crust beneath the Bengal Fan. This is unexpected considering the apparent association of relatively large-magnitude earthquakes and the northern portion of the Ninetyeast Ridge[4], and we return to this point below.

Heat flow

The third geophysical parameter which reflects significant tectonic activity within the Indo–Australian plate is heat flow. Presently available geothermal measurements in the northern part of the Indian Ocean (Fig. 2) are mainly random values obtained with the Ewing thermograd (Lamont-Doherty Geological Observatory), or with the Bullard probe (Scripps Institution of Oceanography)[20]. Most heat flow observations lie within the 50–60 mW m^{-2} range predicted for the late Cretaceous through early Eocene crust in the northeastern Indian Ocean[18] by the cooling half-space model for oceanic lithosphere[21]. However, several measurements (that are judged reliable[20]) within the region of deformation delineated by seismic reflection, and some apparently outside that region, yield heat flow values considerably higher than expected (underlined values in Fig. 2). The mean of these high values (107 ± 36 mW m^{-2}) is appropriate for heat flow in lithosphere much younger than the early Eocene–late Cretaceous age established for this region from magnetic lineations[18]. The occurrence of abnormally high values scattered amongst normal values in a mid-plate region is indeed unusual, these are the only excessively high values in old lithosphere in the entire Indian Ocean[20].

Measurement of anomalous heat flow in the oceans is not unusual in itself. Active hydrothermal convection of seawater affects fully one-third of the ocean floor[22]; values lower than the predicted heat loss are expected in such geothermal regimes, as unmeasured heat is being carried from the sea floor by convecting fluids. However, in areas with a thick, uniform sedimentary cover (such as the areas covered by fan deposits in Fig. 2), heat loss by convection is unlikely to occur[23,24]. To explain abnormally high values scattered among expected values, local heat sources in addition to the normal heat flux from the lithosphere must contribute to these values. We believe that the additional heat required is associated with the intraplate deformation and we speculate that heat generated by friction on faults in the crust during earthquakes might be involved. If this is the case, there should be a close spatial correlation between the most

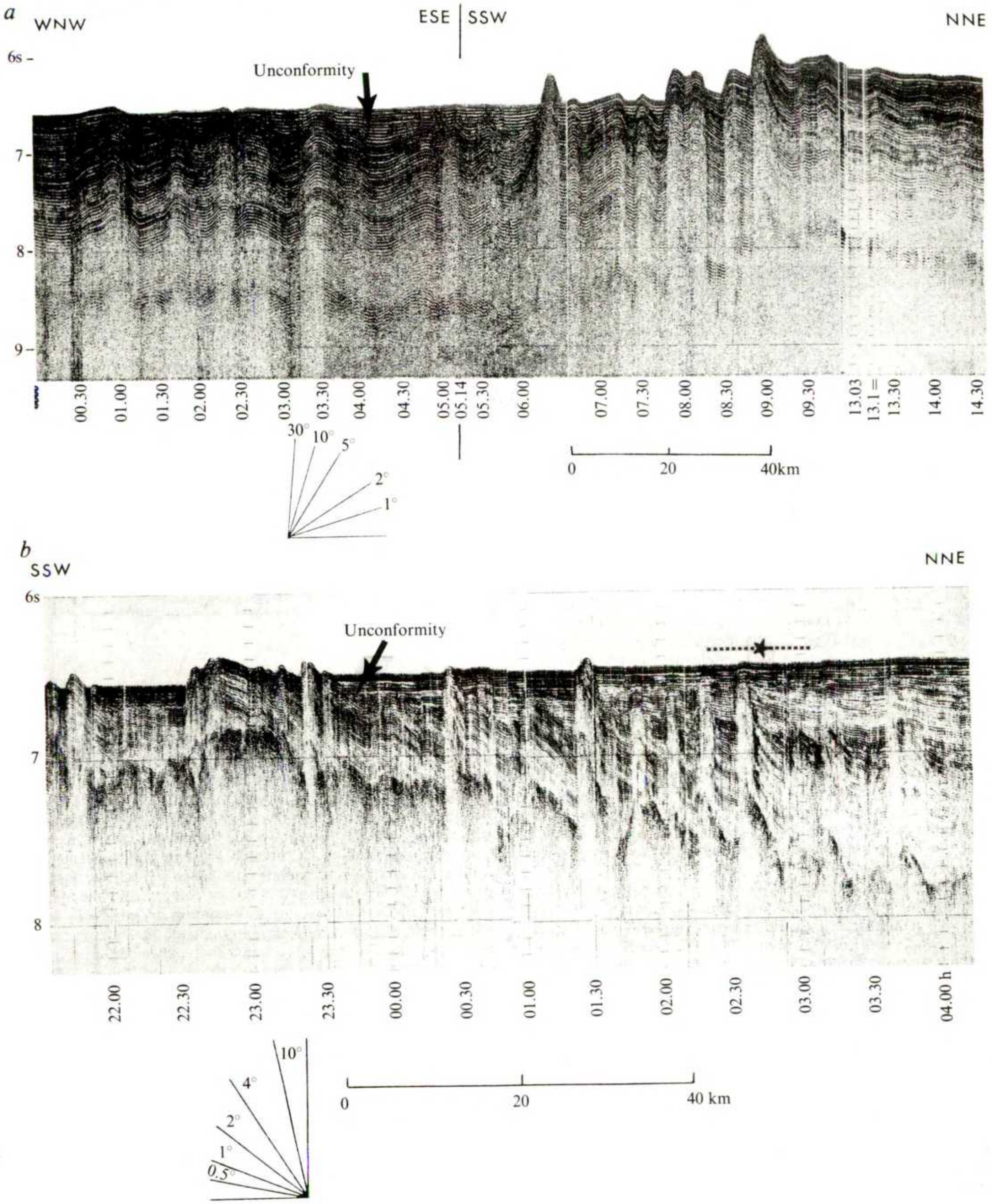

Fig. 4 *a*, Single-channel seismic reflection profile which crosses a promifnt deformation front in the southwestern portion of the Bengal Fan (profile b in Fig. 2). Note the course change near the middle of the profile. On the WNW–ESE track segment, sediment structures have wavelengths that are long compared to those for structures along the SSW–NNE track segment, indicating an approximate E–W structural grain in the area of this profile. The major unconformity marked by the arrow is probably uppermost Miocene in age (refs 13, 16, 17 and G. Blechschmidt, personal communication). VE ~ 20 : 1. *b*, Single-channel seismic reflection profile that passes very close to the epicentre of a strike slip intraplate earthquake (profile c in Fig. 2) denoted by star and broken line. The major uppermost Miocene unconformity is particularly clear on this profile. Note the difference in fault offsets of basement and of the sea floor in the vicinity of the epicentre. VE ~ 22 : 1.

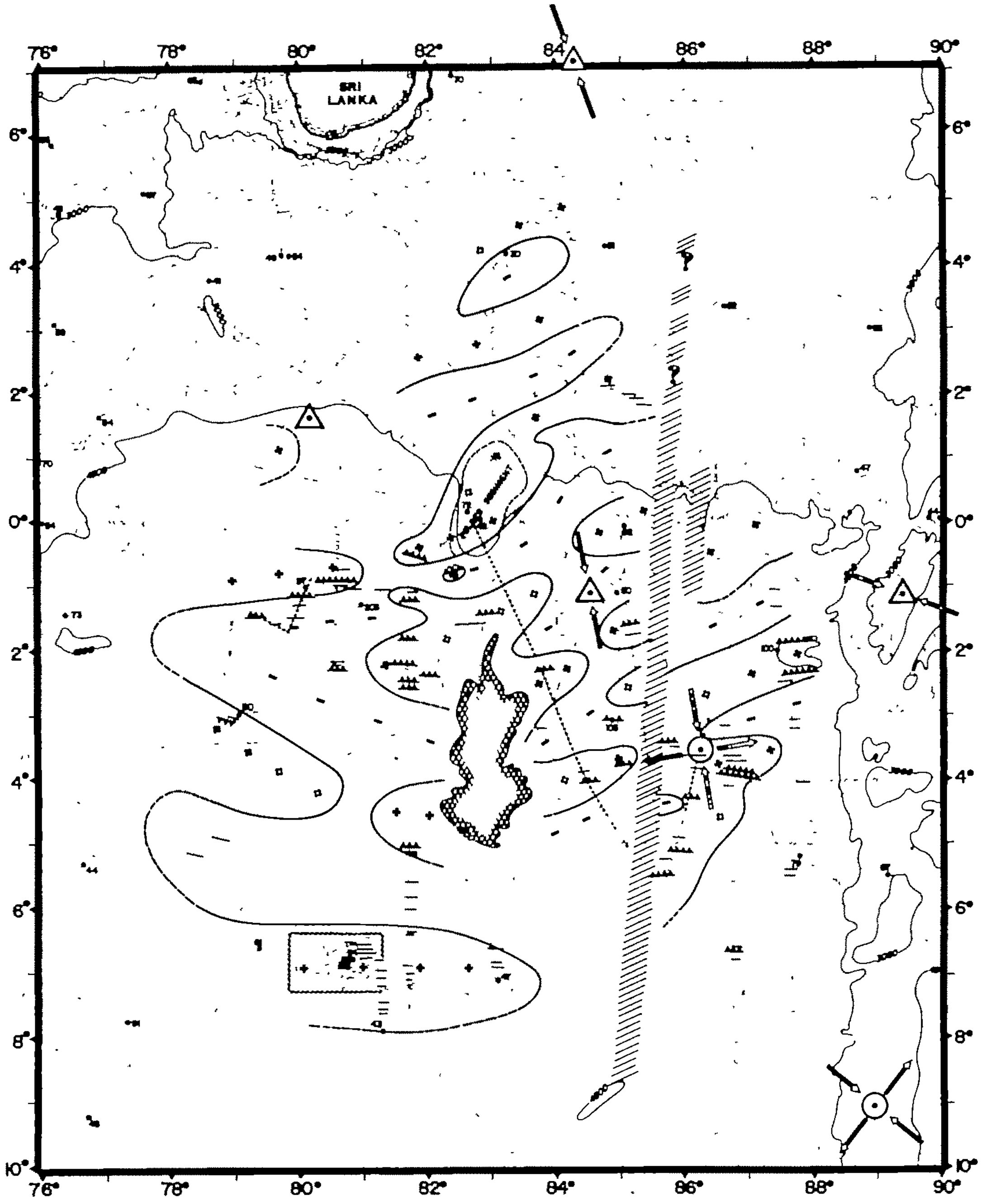

Fig. 5 Broad-scale basement structures are outlined by the heavy lines. Plus signs denote relative highs and minus signs relative lows. Saw-tooth symbols denote outcrop of major high-angle faults with the saw teeth on the upthrown side. Minor high-angle faults are the lighter lines. Numbered dots are heat flow values[20,34] taken from Fig. 2. Principal stress directions for intraplate earthquakes are also from Fig. 2. A major fracture zone at about 85° E with 850 km of left-lateral offset[18] is denoted by the single hatching. The Afanazy Nikitin seamount group is outlined by cross-hatching. Ships' tracks are shown by light dotted lines while the heavy portions denote profiles shown in Figs 2–4. The boxed area at 7° S, 80° E is the survey area of Eittreim and Ewing[11].

tectonically disturbed areas and abnormally high heat flow values. This speculation remains to be tested because available heat flow measurements are too widely spaced (Fig. 2).

Limitations of the data

Because seismicity, seismic reflection data and heat flow define regions of intraplate activity of different geographic extents, an examination of the limitations and special characteristics of these three geophysical parameters is warranted here.

The use of single-channel seismic reflection data to map the geographic extent of deformed oceanic crust and the types of structures produced by tectonic stress is limited by several factors. First, the sound sources used to acquire most of the data available to us were too small to penetrate completely through the thick sedimentary section in the Bay of Bengal. Second, while seismic records with large vertical exaggerations provide a good qualitative picture of the structures developed in response to tectonic stress, a quantitative determination of the dips of the observed high-angle faults is not obtainable. Thus, whether the faults are normal or reverse cannot yet be determined. Third, although the deformation of the Indo–Australian plate recorded in seismic reflection data from the southern part of the Bengal Fan is undoubtedly important, it is possible that other regions of the plate have undergone significant deformation which is not readily apparent in single-channel seismic data. It must be realized that thick stratified sediments provide ideal conditions for examining deformation structures acoustically whereas the same amount of crustal deformation might be difficult to detect in areas devoid of sediment cover or in areas with a thin acoustically transparent pelagic drape.

The time window resolved by each parameter is another factor to be borne in mind when comparing the geographic extents of deformation indicated by earthquake seismology, heat flow, and seismic reflection. Earthquakes have been recorded only for the most recent fraction of geological time. Yet, earthquakes reveal stress information from continental as well as oceanic areas (Fig. 1). Abnormally high heat flow values observed today (Fig. 2) may reflect movements in the crust that occurred long ago compared to the time span of earthquake seismology. Assuming that these anomalous values are expressions at the sea floor of frictional heat generated at the surface of the crust by intraplate earthquakes, we can determine the time taken for conduction of a frictional heat pulse to the sea floor. For a sediment column 1-km thick and an assumed thermal diffusivity of 10^{-2} cm^2 s^{-1}, the peak value of anomalous heat flow reaches the sea floor $\geq 10^5$ yr after generation of the heat pulse in the oceanic crust[25]. The longest time window is resolved by seismic reflection data because seismic profiles portray the entire history of sedimentation and intraplate deformation in the interior of the Indo–Australian plate. As noted above, the disruption of post-Miocene sediments decreases towards the sea floor (Fig. 4*a*, *b*), so that at seismic sound source frequencies, deformation of sediments which have been deposited during the time spanned by historical seismology is not detectable. However, offsets of the sea floor and immediate sub-sea floor reflectors of several metres can be resolved using high frequency (3.5 kHz) sound sources.

Discussion

The evidence presented above for the internal deformation of the Indo–Australian plate allows us to develop a working hypothesis to explain these observations. Several aspects of this have been touched on by previous workers[2-4,11,26].

Intraplate compression capable of causing widespread deformation within the Indo–Australian plate probably arose in late Miocene time, according to DSDP and piston core evidence. Assuming that intraplate stress is sensitive to forces applied at plate boundaries and to the base of the plates[10], we speculate that a major tectonic event could have effected changes in forces acting on the Indo–Australian plate in Miocene time, triggering the observed intraplate deformation. The inception and growth of the Himalayan chain in post-Oligocene time has been cited as a significant change in the collisional tectonics between India and Asia[26-28]. From initial contact in the Eocene until early Miocene, deformation was accommodated along a contact zone between India and Asia, whereas intra-continental thrusting within the Indian block has occurred since the early Miocene[27]. If the second or Himalayan stage of collision between India and Asia greatly increased resistive forces along the plate edge and these were transmitted to the interior of the plate as large horizontal compression, a late Miocene onset of intraplate deformation might reasonably be expected. As suggested originally by Curray and Moore[12], the sedimentation and deformation histories of the deep sea fans of the northern Indian Ocean likely reflect major tectonic events in the collision between India and Asia.

Whatever the history of the intraplate compression, its magnitude has been sufficient to deform oceanic lithosphere into broad undulations (Fig. 3), and produce brittle failure in the oceanic crust (Fig. 4*a*, *b*) over a large area in the northern Indian Ocean (Fig. 5). The general appearance of the deformation is that of a buckled plate (Fig. 3). Assuming that a thin elastic plate of Young's modulus 6.5×10^{11} dyn cm^{-2} is buckled under horizontal compression into a wavelength of 160 km, we determine an apparent elastic thickness for the plate of 12 km and a buckling stress[29] of 24 kbar. However, experiments in rock mechanics indicate that yielding by fracture occurs near the surface of the plate and deformation by flow occurs deep within the lithosphere before such high stresses determined from elastic models are attained[30,31]. The fact that brittle deformation is widely observed in seismic profiles over the region of intraplate deformation suggests that the upper part of the plate has been exposed to stresses in the kbar range. An interesting outcome of the buckling calculation is the anomalously thin effective elastic thickness implied by the wavelength of the undulations. Observations of lithospheric flexure in the oceans have shown that the effective elastic thickness increases with the age of the lithosphere at the time of loading[32]. At the onset of intraplate deformation in late Miocene time, the oceanic lithosphere beneath the southern Bengal Fan would normally have an effective elastic thickness[32] of 20–30 km. This is greater by a factor of ~2 than the 12 km obtained by treating the intraplate deformation as a buckling effect. Assuming that the elastic plate model applies to the real Earth, this discrepancy may indicate either that since the interior of the plate came under large horizontal compression several million years ago the original elastic 'core' of the oceanic lithosphere has been reduced in thickness by yielding at the top and bottom of the plate, or oceanic lithosphere responds to uniform horizontal compression in a way that is different to its response to surface loads.

The large region of permanent strain inferred from seismic reflection data suggests that if the Indo–Australian plate consists of two distinct plates at present, convergence between these plates may be accommodated in a complicated, non-uniform way over a zone several hundred kilometres wide rather than along an obvious plate boundary. This point is important to plate kinematics considerations, as Minster and Jordan[33] found that by treating the Indo–Australian plate as two plates, they could overcome systematic misfits between their model for present-day plate motions (which included a single Indo–Australian plate), and observed Indian Ocean spreading rates and directions. They showed that the observed rates and directions around the Indian Ocean are consistent with about 1 cm yr^{-1} of NW–SE convergence between an 'Indian' plate and an 'Australian' plate along the northern part of the Ninetyeast Ridge[33]. An order of magnitude calculation by Stein and Okal[4] using seismic moments of large events on the Ninetyeast Ridge, produced left lateral slip at a rate of 2.2 cm yr^{-1} along the ridge, consistent with the convergence rate determined by Minster and Jordan[33]. Although both sets of calculations have limitations, the general agreement between them suggests, at first glance, that the northern part of the Ninetyeast Ridge is a resolvable strike-slip plate boundary between the two parts of the Indo–Australian plate. Aside from the question of continuity of this plate boundary, the slip rate along the Ninetyeast Ridge determined by Stein and Okal[4] would relieve all strains predicted from the calculation of Minster and Jordan[33] without any internal deformation of the lithosphere away from the Ninetyeast Ridge. The observations discussed here show that all tectonic displacement between an 'Australian' and an 'Indian' plate is not accommodated by slip along the northern part of the Ninetyeast Ridge, even though strains accumulated through intraplate deformation away from the Ridge are not determinable from the available data.

Finally, do the observations, particularly the seismic reflection data, indicate the impending formation of an intra-oceanic lithosphere subduction zone as suggested by Sykes[2]? While both the broad undulations and the brittle deformation observed in seismic records (Figs 3 and 4) can be attributed to large horizontal compressions within the plate, fracturing of the crust occurs on high-angle faults and not on shallow-angle thrusts that might herald the beginnings of subduction. During our examination of the available reflection data from the north-east Indian Ocean, we found only one example (near 4° S; 87° E) of possible shallow underthrusting (from south to north) throughout the entire region of intraplate deformation within the Indo–Australian plate. We feel that this question cannot be answered at present.

We thank Bhoopal Naini for his contribution to the early phases of this study. John Bodine, Terry Engelder, Dennis Hayes, Klaus Jacob, Lynn Sykes, and Tony Watts critically read the manuscript. This work was supported by NSF grant OCE 79-25070. Lamont-Doherty Geol. Obs. contribution no. 3024.

Received 27 March; accepted 7 July 1980.

1. Stover, C. W. *J. geophys. Res.* **71,** 2575–2581 (1966).
2. Sykes, L. R. *J. geophys. Res.* **75,** 5041–5055 (1970).
3. Fitch, T. J., Worthington, M. H. & Everingham, I. B. *Earth planet. Sci. Lett.* **18,** 345–356 (1973).
4. Stein, S. & Okal, E. *J. geophys. Res.* **83,** 2233–2245 (1978).
5. Fitch, T. J. *J. geophys. Res.* **77,** 4432–4460 (1972).
6. Banghar, A. R. *Bull. seism. Soc. Am.* **62,** 603–649 (1972).
7. Sykes, L. R. & Sbar, M. in *Geodynamics of Iceland and the North Atlantic area,* 207–224 (Reidell, Massachusetts, 1974).
8. Geller, C. A. & Weissel, J. K. (in preparation).
9. Denham, D. *B.M.R. Earth Science Atlas of Australia* (B.M.R., Canberra, 1979).
10. Richardson, R. M., Solomon, S. C. & Sleep, N. H. *Rev. Geophys. Space Phys.* **17,** 981–1019 (1979).
11. Eittreim, S. K. & Ewing, J. I. *J. geophys. Res.* **77,** 6413–6421 (1972).
12. Curray, J. R. & Moore, D. G. *Bull. geol. Soc. Am.* **82,** 563–572 (1971).
13. Moore, D. G., Curray, J. R., Raitt, R. W. & Emmel, F. J. *Init. Rep. DSDP* Leg **22,** 403–412 (1974).

14. Chapman, M. E. & Talwani, M. *J. geophys. Res.* **84,** 3803–3816 (1979).
15. Bowles, F. A., Ruddiman, W. F. & Jahn, W. H. *Mar. Geol.* **26,** 269–288 (1978).
16. Von der Borch, C. C. *et al. Init. Rep. DSDP* Leg **22,** 325–348 (1974).
17. Burckle, L. H. & Opdyke, N. D. *Proc. 1st int. Congr. Pacific Neogene Stratig.* 255–284 (1977).
18. Sclater, J. G. & Fisher, R. L. *Bull. geol. Soc. Am.* **85,** 683–702 (1974).
19. Veevers, J. J. *Init. Rep. DSDP* Leg **22,** 351–368 (1974).
20. Anderson, R. N., Langseth, M. G. & Sclater, J. G. *J. geophys. Res.* **82,** 3391–3409 (1977).
21. Parsons, B. & Sclater, J. G. *J. geophys. Res.* **82,** 803–823 (1977).
22. Anderson, R. N., Hobart, M. A. & Langseth, M. G. *Science* **204,** 828–832 (1979).
23. Anderson, R. N. & Hobart, M. A. *J. geophys. Res.* **81,** 2968–2989 (1976).
24. Sclater, J. G., Crowe, J. & Anderson, R. N. *J. geophys. Res.* **81,** 2997–3006 (1976).
25. Carslaw, H. S. & Jaeger, J. C. *Conduction of Heat in Solids*, 60–61 (Oxford University Press, 1959).
26. Gansser, A. *Geology of the Himalayas* (Interscience, London, 1964).
27. Powell, C. McA. & Conaghan, P. J. *Earth planet. Sci. Lett.* **20,** 1–12 (1973).
28. LeFort, P. *Am. J. Sci.* **275A,** 1–44 (1975).
29. Heiskanen, W. A. & Vening Meinesz, F. A. *The Earth and its Gravity Field*, 318–319 (McGraw-Hill, New York, 1958).
30. Goetze, C. & Evans, B. *Geophys. J. R. astr. Soc.* **59,** 463–478 (1979).
32. Brace, W. F. *J. geophys. Res.* (in the press).
32. Watts, A. B., Bodine, J. H. & Steckler, M. S. *J. geophys. Res.* (in the press).
33. Minster, J. B. & Jordan, T. H. *J. geophys. Res.* **83,** 5331–5354 (1978).
34. Kutas, R. I., Bevsyuk, M. I. & Vygovsky, V. F. *Geothermics*, **8,** 31–36 (1979).

Actin in the inner ear: the remarkable structure of the stereocilium

D. J. DeRosier

Department of Biology and Rosenstiel Basic Medical Sciences Research Center, Brandeis University, Waltham, Massachusetts 02254

L. G. Tilney

Department of Biology, University of Pennsylvania, Philadelphia, Pennsylvania 19104

E. Egelman

Graduate Program in Biophysics, Brandeis University, Waltham, Massachusetts 02254

The actin filament bundle in the stereocilium of the cochlear hair cell has liquid transverse order, but paracrystalline axial order. A single bonding rule, which determines how a cross bridging protein links neighbouring filaments, accounts for this unusual structure. Such liquid order is possible for bundles of other filamentous proteins.

CRYSTALLINE order consists of chemically identical subunits arranged in identical environments. In such an arrangement, we can conclude that the bonding rule for any one subunit is the same as that for all other subunits, even though the details of the atomic interactions between subunits may be unknown. In biological structures the exact equivalence of crystalline bonds is quite often relaxed to a condition of quasi-equivalence[1]. In a quasi-equivalent structure, chemically identical subunits are deformed slightly so that bonds can be formed between subunits which are in almost but not exactly identical environments. In such a structure all subunits make essentially the same specific contacts and thus can be described by a single bonding rule. The concept of the specific bond, which leads to the equivalent or quasi-equivalent arrangement of subunits, has been the basis for understanding the organization of macromolecules in a number of protein-containing structures such as the spherical and rod-shaped viruses, microtubules, and actin filaments.

Biologists, however, do not often find the regular order seen in the examples above. In micrographs of many cellular structures such as the terminal web in the cells of the intestinal brush border[2], the organization is accompanied by great disorder. Compared to such disordered structures, the bundle of actin in the stereocilium of the inner ear of the alligator lizard appears highly ordered. Yet, to the protein crystallographer, who is accustomed to the near perfect regularity of crystals, the most striking feature of this bundle would be its disorder. The stereocilium is an organizational intermediate between the regular order of the icosahedral viruses and the irregular order of the terminal web. It is interesting because it gives us insight into the organization of partially disordered structures.

The stereocilia or hairs of the hair cells, which extend outward from the apical surface, are elongated processes responsible for the transduction of sound; that is, motion of the stereocilia caused by sound produces changes in the membrane potential of the hair cell. Structural studies of the hair cells in the cochlea of the alligator lizard[3,4] show that each hair cell contains about 75 stereocilia of varying size with the largest having a length of 30 μm and a diameter of 0.8 μm. Within each stereocilium is a large polar bundle[5] of more than 3,000 actin filaments which shows an irregular liquid order in transverse section[6] (Fig. 1*a*). Surprisingly some transverse sections show a periodic motif we call festooning, which starts at one edge of the stereocilium and continues to the other (Fig. 1*b*). How can such long-range lateral periodicity arise in a structure with no discernible lateral order? The answer lies in the helical symmetry of the actin and provides insights into the structural principles governing actin bundles and bundles of helical filaments in general.

What is festooning?

The motif seen in the images consists of scalloped rows of actin filaments rather like the folds in drapes pulled to the side of a window. The scalloped rows lie one on top of the other to create the festooned motif. The separation between rows is of the order of 100 Å and seems to be constant in all stereocilia. In contrast, the period of the festooning is large, being of the order of 1,000 Å. In a single section cut through all 75 of the stereocilia that extend from a single hair cell, the direction and period of festooning are generally constant from one stereocilium to the next, but often different for stereocilia from neighbouring hair cells. In an occasional hair cell, however, the stereocilia are disturbed so that, instead of all being exactly parallel to each other, they extend at different angles. In such cells both the period and the direction of the festooning vary considerably. For example, in Fig. 1*c* stereocilium A has a period of 2,400 Å and in a neighbouring stereocilium, B, the direction of the festooning is rotated nearly 90° and the period is 960 Å.

What gives rise to festooning? If the motif simply and directly reflects a corresponding structural organization of the linked actin filaments, then different patterns of festooning would have to correspond to different structural organizations within the stereocilia. Alternatively, we propose that all stereocilia have a single common structure and the different motifs arise from

0028–0836/80/390291—06$01.00

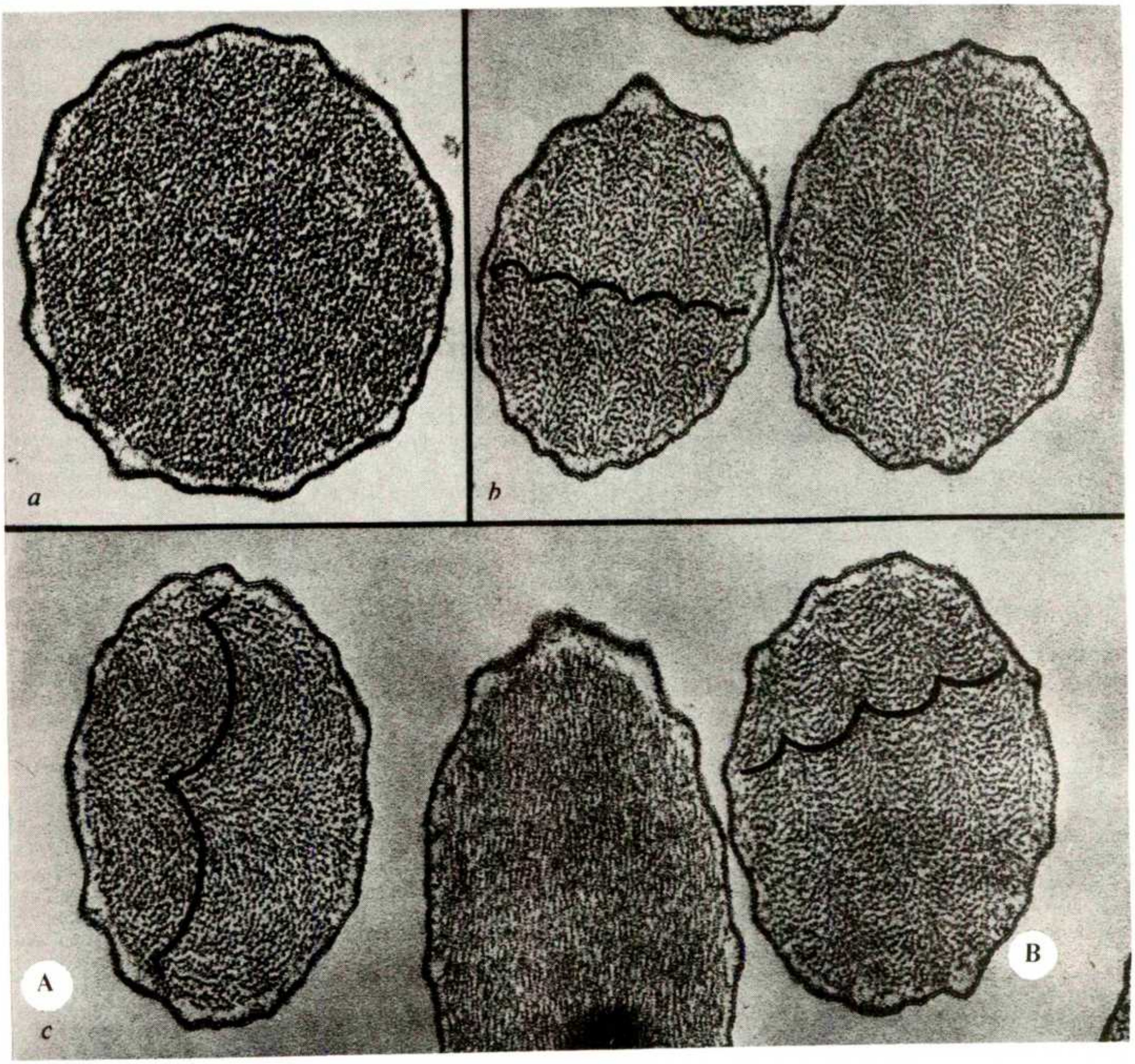

Fig. 1 *a*, Thick transverse section (375 Å or thicker) of a stereocilium from the cochlea of the alligator lizard. Thick sections give no hint of a long-range spatial periodicity but show a liquid arrangement of filaments having a mean interfilament spacing of 100 Å. Optical diffraction patterns of such sections confirm the liquid order showing a pattern consisting of a single diffuse ring. *b*, Thin transverse section of two stereocilia. This section, which is of the order of 200 Å thick, shows a scalloped or festooned pattern with a period of 680 Å. Note that the period and direction of the pattern are the same in both stereocilia. *c*, Thin transverse section of a group of stereocilia. In this cell the orderly and parallel arrangement of stereocilia has been disturbed. As a result the period and direction of festooning are different for different stereocilia. The period in stereocilium A is 2,400 Å and that in B is 960 Å. All magnifications are 120,000.

different orientations of the stereocilia relative to the plane of section. Many features of festooning are explicable as a consequence of taking a thin oblique section through layers of parallel rods, where each successive layer is rotated with respect to the previous layer. This was observed by Bouligand *et al.* for arrangements of chromatin fibres[7]. In the same way, if the crossbridges linking filaments are helically arranged, the axial pattern of crossbridges will be converted into a transverse motif by a slight tilting of the plane of section off a true transverse direction. This is similar to Reedy's discussion[8] of thin sections of insect flight muscle in which a motif having a long period is seen to arise from the periodic crossbridging of myosin to actin. If this explanation is correct for the stereocilium, the period of festooning should depend on the angle of the section relative to the axis of the stereocilium and the direction of the festooning on the direction of the tilt of the stereocilium relative to the knife in the microtome. Differences in the images of different stereocilia then would not indicate differences in structure but rather differences in the magnitude and direction of tilt of the stereocilium relative to the plane of section. Moreover, the festooning should disappear when the section thickness reaches the axial repeat period of the crossbridges.

Bundles with hexagonally arranged filaments

In order to see how these predictions were made, we examined the nature of crossbridges in needles, another bundle of actin filaments formed *in vitro* from sea urchin egg extracts[9,10]. In the needles, actin filaments are linked together by a second protein, fascin. The lattice that describes the positions of the filaments is a hexagonal one. The pattern of crossbridges between filaments, however, cannot be truly hexagonal since the actin filaments to which they are attached do not have hexagonal symmetry. If actin had hexagonal symmetry, it would be possible to construct a crystalline bundle in which all crossbridges are in equivalent, hexagonally related positions. Because actin is helical, however, some of its subunits are in approximately the correct position to make such bonds, so that if 13° of bending is allowed, crossbridges can be formed to link every actin filament to its six nearest neighbours. The resulting structure is thus formed from nearly equivalent or quasi-equivalent bonds.

In the needle, the locations of crossbridges are easily found by finding the positions of pairs of bonding sites on neighbouring filaments in the array. Figure 2*a* shows three filaments taken from a hexagonal array. Let us begin by arranging filaments A and B so that a crossbridge is made at position 2. In the hexagonal array, the bonding rule requires that crossbridged filaments be in axial register and be separated by the appropriate distance (about 85 Å). Using this bonding rule, we find we can also make crossbridges between filaments A and C at position 7 and between filaments B and C at position 11. Some bending of crossbridges is needed to achieve bonding at the different sites, but the amount of bending required, which varies depending on position, is never more than about 13°. The bonding scheme is shown diagrammatically in Fig. 2*b* and from it we see that all neighbouring filaments are linked together. Note that although the diagram is for the first 14 subunits, the crossbridging occurs along the entire length of the bundle so that for any pair of actin filaments, there will be one crossbridge per 375 Å repeat.

How can such a bonding scheme lead to festooning in a bundle? Imagine we cut a thin nearly transverse section through a bundle as is shown diagrammatically for one row of filaments in Fig. 3*a*. The section is thin relative to the axial repeat of the crossbridges, and the plane of section is tilted relative to the bundle axis. At the left-hand edge the crossbridges contained in the section point towards 3 and 9 o'clock. As we progress in the section to the right, the crossbridges included in the section point towards 5 and 11 o'clock. Continuing to the right, the included crossbridges again change direction to 7 and 1 o'clock and then, to complete one repeat of the pattern, to 3 and 9 o'clock. The pattern of crossbridges seen looking down on the section is shown in the top line of Fig. 3*b*. If we extend this pattern from one row to that expected for a hexagonal bundle, we get the festooned pattern shown in Fig. 3*b*. The festooning arises from a conversion of the axial periodicity of crossbridges into a transverse period by the tilt of the almost transverse section. We can make a number of predictions:

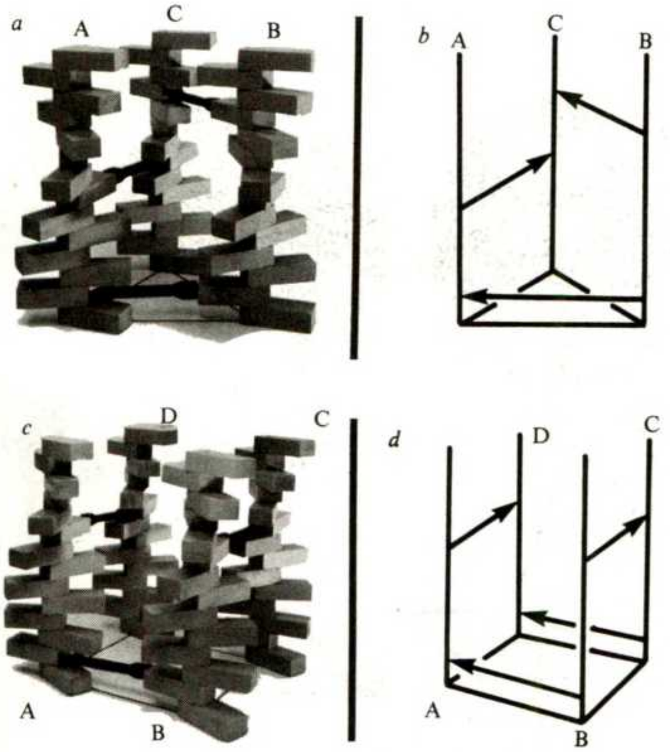

Fig. 2 *a*, Model depicting the arrangement of crossbridges in hexagonally arranged filaments. Three model filaments having the helical symmetry of actin are sitting on three vertices of a hexagonal lattice. The filaments are rotationally set so that the lowest subunit or block on each is pointing in the same direction. The bonding rule, arbitrarily chosen, allows a crossbridge (black arrow) to join the outer end of a subunit on one filament to an inner end on a neighbouring subunit. Such a crossbridge linking filaments A and B is seen at subunit 2, the next to lowest subunit. Because of the helical symmetry of the models, a crossbridge also links filaments C and A at subunit 7 and filaments C and B at subunit 11. The crossbridges which link these three filaments together will link together all the filaments in a hexagonal array. *b*, Schematic drawing of the crossbridging scheme depicted in *a*. *c*, Model depicting the arrangement of crossbridges in tetragonally arranged filaments. Four model filaments identical to those in *a* are sitting on the vertices of a tetragonal lattice. The filaments are rotationally set so that the lowest subunit in each is pointing in the same direction. The bonding rule, which is the same as that in *a*, allows a crossbridge at subunit 2 between filaments A and B and between filaments D and C. Filaments A and D and B and C are crossbridged at subunit 9. With this bonding rule, all the filaments in a tetragonal lattice can be crossbridged. The point of this figure is that the same bonding rule can crossbridge either a hexagonal or a tetragonal array of filaments. *d*, Schematic drawing of the crossbridging scheme depicted in *c*.

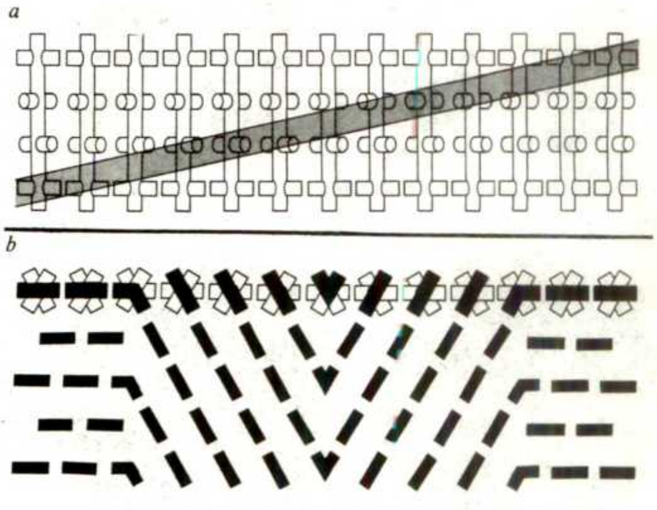

Fig. 3 Scheme showing how festooning arises. *a*, Thin section taken through a single row of filaments—side view. A row of filaments is shown schematically with the crossbridging material drawn in as a series of rods projecting from the cylinder. The portion of the row included in the thin section is indicated by the grey area. *b*, Top view of thin section. If the thin section is viewed from the top, the pattern indicated by blackened bars would be seen. In the upper row the crossbridges not included in the section are drawn in for reference but are not blackened. This row corresponds to the row of filaments in *a*. The remaining rows complete the pattern expected for a hexagonal array of filaments. Thus the second row from the top is shifted left half the interfilament spacing. Row three is a repeat of row one and so on. The result is a festooned pattern.

(1) The pattern should disappear as the section thickness approaches the repeat of 375 Å, since each section will contain crossbridges from one filament to all of its neighbours.

(2) The direction of the festooning depends on the orientation of the knife relative to the axis of the bundle.

(3) In a pair of serial sections of thickness, *t*, the festooned pattern should shift by *t*/375 of its period. Thus if we cut 125-Å sections, the pattern should shift laterally by 1/3 of a festoon in consecutive or serial sections. The period and direction of the motif remain unchanged.

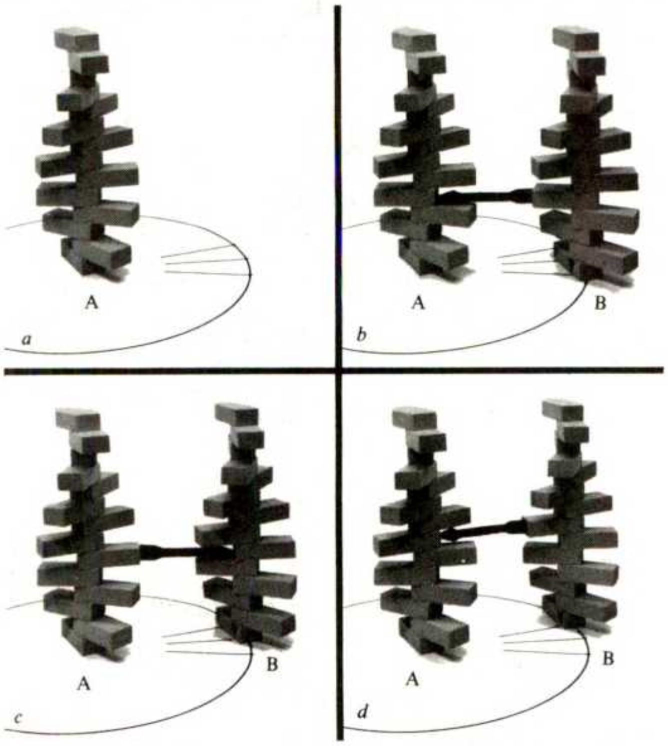

Fig. 4 Model showing the potential of helices to be crossbridged. *a*, Single model filament at the centre of a circle indicating the bonding distance. Three radial lines are drawn to indicate three positions separated by the equivalent of about 10 Å. *b*, Crossbridge formed between a pair of filaments. If a second (outer) filament is placed at the first position and rotationally set so it is in register with the central filament, then, given the bonding rule (see Fig. 2), a crossbridge can be formed at the fifth subunit from the bottom. *c*, Crossbridge formed when the outer filament is moved to second position. If the outer filament is moved around the central filament by the equivalent of 10 Å (or 13°), the most favourable position for a crossbridge is at the sixth subunit from the bottom. Note that the outer filament is moved so that the two filaments remain in register. *d*, Crossbridge expected when the outer filament is in the third position. In the third position, the most favourable subunit for crossbridging is the seventh one from the bottom. Note that as the outer filament moves around the central one in a counter-clockwise manner (as viewed from the top), the most favourable position for a crossbridge rises on the central filament. Continuing this process, we conclude that the outer filament can be crossbridged to the inner one at any position along the circle if a modest amount of crossbridge bending is allowed.

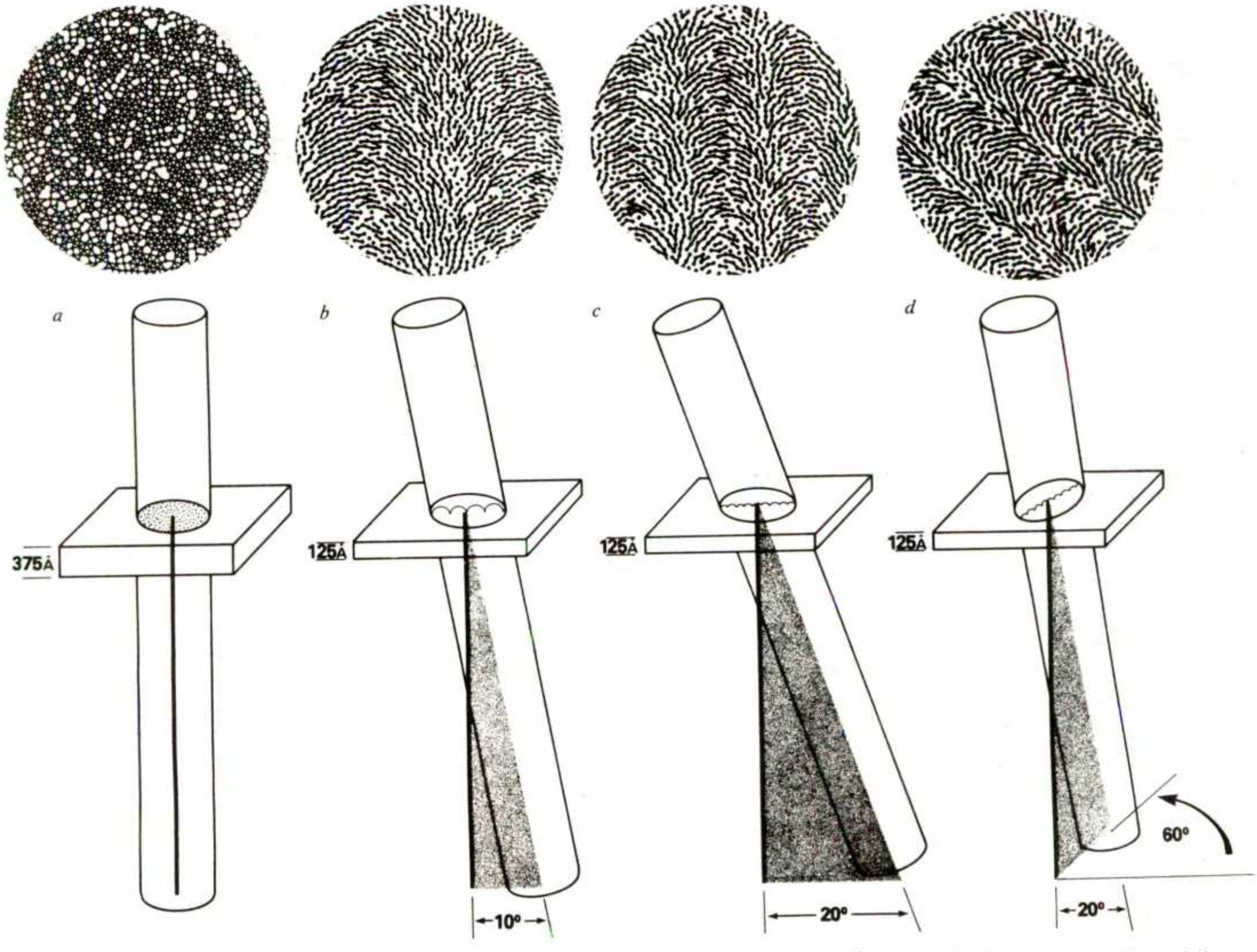

Fig. 5 *a*, Computer simulation of a thick section. If the section thickness is at least the crossbridge repeat of 375 Å, no festooning is seen since crossbridges pointing in all directions from each filament are included in the section. The computer has generated a liquid array of filaments and crossbridges and simulated a 375-Å thick section. *b*, Computer simulation of a thin section cut at a tilt of 10°. The same array of filaments is used as in *a*, but the computer simulated a 125-Å thick section cut at a tilt of 10°. The result is a festooned pattern having a long repeat. *c*, Computer simulation of a thin section cut at a tilt of 20°. Since the tilt is in the same direction the pattern runs in the same direction but has a finer period. *d*, Computer simulation of a thin section cut at 20° tilt but direction of tilt rotated 60°. The effect is to rotate the direction of the pattern 20° but leave the period unchanged.

(4) The period of festooning, *l*, should depend on the tilt of the section relative to the bundle. More specifically, the period should be equal to the axial repeat, *d*, of the crossbridges divided by the sine of the angle by which the bundle is tilted off the normal to the plane of the section, that is, $l = d/\sin\theta$. For actin, $d \simeq 375$ Å and thus a festooning period of 1,000 Å corresponds to a tilt of $\sin^{-1}(375/1{,}000) \simeq 22°$.

(5) The scalloping in the pattern in Fig. 3*c* has its convex side up. If the hand of the helical arrangement of crossbridges is reversed, the pattern would reverse to one with its convex side down. Thus, the asymmetry of the motif can be used to determine the hand of the crossbridges, which depends on the hand of the actin filaments.

In a previous paper[6] we verified these predictions experimentally, but we were unable to understand how the predictions could be valid when the actin filament locations, as seen in transverse section, had no regular order. Although there is no such order in transverse sections, in longitudinal sections we found that actin filaments appeared paracrystalline; that is, they had their cross-over points in register. The question is therefore: how can a bundle of actin filaments maintain itself in perfect longitudinal register yet be disordered in transverse section?

Our key to resolving the paradox came from our study[10] of the bonding rule for the crossbridging of filaments in the hexagonally packed bundles such as the needle from extracts of sea urchin oocytes, in which all filaments are in register. The axial register of the filaments is a requirement because if the filaments were rotated or translated relative to each other, none of the bonding sites, as shown in Fig. 2*a*, would be in the correct orientation and at the correct height to allow crossbridging. Thus, our ability to crossbridge filament A to B, B to C and C to A depends on the cross-over points being in register.

Bundles with tetragonally arranged filaments

What is special about this bonding rule is that we can also make a bundle in which the filaments lie on a tetragonal lattice instead of a hexagonal one. In Fig. 2*c*, the filaments A, B, C and D are placed at the corners of a square. They are arranged so that A is crossbridged to B and C to D at position 2. This is the same crossbridge that is formed at position 2 in the hexagonal bundles. In the tetragonal arrangement we find that at position 9 we can make a crossbridge from A to C and from B to D thus linking together the bundle. The amount of bending of crossbridges is similar to that required in the hexagonal case. Only two crossbridges, however, are made in the first 14 subunits instead of three as is the case in the hexagonal bundle. What we have shown is that the same specific bonds can generate either a tetragonal or a hexagonal bundle.

We can generalize from these two types of bundles by extracting the rules that govern the crossbridging between a pair of filaments. In Fig. 4 the two filaments are placed together so that the cross-over points are in register so that the filaments can be crossbridged. In Fig. 4*b*, a crossbridge can be made at position 5. This crossbridge can still be made if we move filament B about 10 Å along the circle drawn around filament A. At this point less crossbridge bending is required if we change the crossbridge from position 5 to position 6 (Fig. 4*c*). When we again move by 10 Å, the crossbridge changes to position 7 (Fig. 4*d*). The bending of the crossbridges varies depending on the relationship between the two filaments and on the symmetry of the actin, that is the number of subunits per turn. For actin filaments having the symmetry of those in the stereocilium (2.159 units per turn), the crossbridges need be bent no more than 13°, which is the same value found in the fascin crossbridges in the needle. The important point is that two actin filaments can be crossbridged if they are in register and are separated by the length of a crossbridge; or, in other words, if we draw about a filament a circle whose radius is equal to the length of a crossbridge, a second filament put anywhere on the circle can be crossbridged to the first filament provided that the two filaments have their cross-over points in axial register.

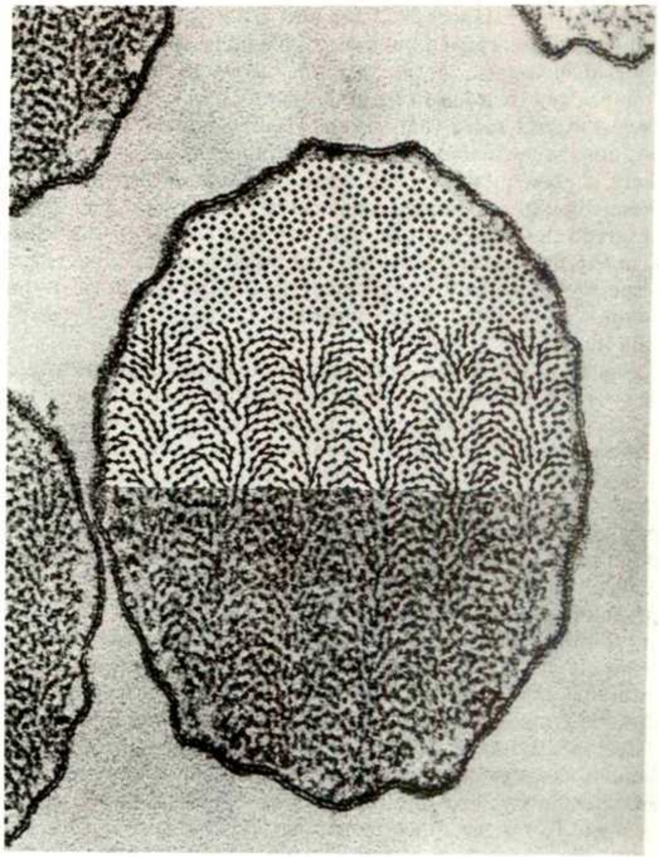

Fig. 6 Composite of the computer-generated array of filaments, filament plus crossbridges, and a thin section of a stereocilium. The top half of the stereocilium has been replaced by a computer-generated thin section that mimics the true pattern. The computer-generated section corresponds to a 150 Å section cut at an angle of 35°. The crossbridges in the upper part of the display are omitted so that the liquid arrangement of filament axes can be easily seen. ×155,000.

Bundles with a liquid arrangement of filaments

With the bonding rule formulated in the preceding sentence, we can generate a liquid-like bundle with specific crossbridges. To demonstrate this, we generated a liquid-like arrangement of filaments using a Monte-Carlo random number generating method. For specifying filament locations, a 512 by 512 element grid, with a scale of 1 grid element = 10 Å, was used. The probability of locating a filament at a given grid position increased as a function of the number of other filaments to which it could be crossbridged. A radial probability function, $P(r)$, was created which incorporated volume exclusion (for $r < 70$ Å, $P(r) = 0$, so no two filaments could be closer than 70 Å apart). $P(r)$ also had a large peak at the crossbridging distance, 100 Å, to reflect the likelihood for two neighbouring filaments to be crossbridged to each other. The grid was scanned, element by element, with the probability of creating a filament at a given grid element equal to P_T, where

$$P_T = 1 - \exp\left[-\sum_i P(r_i)\right]$$

$P(r_i)$ is the radial probability function evaluated for all filaments,

i, located at distances, r_i, from the given grid element. The summation was carried out over all filaments within a radius of 15 grid elements. In the resulting array all filaments were crossbridged to at least one other filament, but, due to volume exclusion, not more than seven. Figures 5*a* and 6 show the positions of the filaments generated by this technique. Note that there is no regularity in the array. The spatial distribution of these computer-simulated filaments is strikingly similar to that observed in the stereocilia. This was true both with regard to filament density and isotropy, and was confirmed by visual inspection as well as comparison of the Fourier transform of the computer-generated array with that of thick sections of stereocilia (Fig. 1*a*).

Figure 5*a* shows the array with all the crossbridges as would be seen in a thick section. These crossbridges are easily drawn in as, according to the scheme illustrated in Fig. 4, all filaments separated by the appropriate distance can be crossbridged. Note how extensively crossbridged the array is. Let us now examine thin sections of the array. The model tells us how the height of a particular crossbridge in the array depends on the direction it points. We set the array so that all crossbridges pointing from 3 to 9 o'clock lie at a height, $h = 0$. If we took a thin section perpendicular to the bundle at $h = 0$, we would find that all the crossbridges which point from 3 to 9 o'clock would lie in this plane. If we look at the next section above the first, we would find that the crossbridges in that section would point in a direction rotated counterclockwise to that in the section at $h = 0$. Thus, in thin sections that are perfectly perpendicular to the bundle, the festooning would not be seen but rather we would see filaments joined into parallel line segments by the crossbridges. If, on the other hand, the sections were cut off the perpendicular, the crossbridge direction would change continuously as the section passes through different heights within the bundle. As we start the section at $h = 0$, the crossbridges would point from 3 to 9 o'clock. As the section moves up, the direction of crossbridges included in the sections shifts in a counterclockwise direction which produces the curved line segments seen in the festooned motif. This effect shows up beautifully in the computer displays. In these displays we varied the angle and direction of tilt of the bundle relative to the plane of the section. Figure 5*b* shows the equivalent of a 125-Å section taken at a tilt of 10°, and Fig. 5*c* shows the same section for a tilt of 20°. Note the change in the period but not direction of festooning. In Fig. 5*d* the direction of tilt is altered by 60° but the tilt is kept at 20°. Note that the direction of festooning, but not its period, changes.

With the computer-generated model we are thus able to produce the festooning seen in electron micrographs of thin sections of the stereocilium (Fig. 6). This model has the following features which mimic the behaviour of the stereocilium on sectioning.

(1) Sections much less than 375 Å in thickness show festooning whereas those about 375 Å lose their festooned motif.

(2) In serial sections the festooning appears to shift laterally by an amount which is proportional to the section thickness.

(3) A change in tilt produces a change in the period of festooning.

(4) In longitudinal sections the filaments are in perfect register.

(5) In Fig. 5*b* the festooned motif has its convex side upward. If the hand of the actin and the crossbridges were reversed, the convex side would be down. Actual tilting of the stereocilia during sectioning, as shown in Fig. 5*b*, shows exactly the convex side-up festooning we predicted. This confirms the hand of the arrangement of crossbridges shown in Fig. 4 (that is, as the filament changes position from that in Fig. 4*b* to Fig. 4*d* the crossbridge moves up rather than down the filament). Thus, the paradox of how one can get crystalline axial order and liquid transverse order is resolved. A liquid-like bundle of filaments with helical symmetry can be crossbridged together with specific bonds, provided that all the filaments are in register. Turning the statement around, we propose that a single crossbridge between any two filaments will force them into register. As this constraint applies to each successive filament in the bundle regardless of their lateral order, the self-assembled bundle must have all its filaments in register. Thus, no external structure is needed to align the filaments; they do it themselves.

What are the biological advantages of a liquid arrangement? Presumably, such a bundle can be put together more quickly than the corresponding hexagonal bundle as the restrictions on placement of filaments in the former are much less than in the latter. For example, the formation of cell extensions such as the actin-containing filopodium[11] can take place much more rapidly because the actin filaments need not make and break connections to become hexagonally packed, a process which takes considerable time. In needle formation, at early times the needles lack transverse order much as the stereocilia of the lizard. On incubation the ordering increases until, after many hours, hexagonally packed filaments are observed[12].

In the hexagonal bundle, the number of crossbridges is a maximum. With increasing disorder in filament position, there will be decreasing numbers of crossbridges. In the limiting case of a very disordered bundle, the paucity of crossbridges will lead to reduced rigidity. This may provide a mechanism for building of bundles of different rigidity or for altering their rigidity after assembly. Exposure to prolonged intense sound produces limp stereocilia, and perhaps this results from alterations in the crossbridges[13].

We have shown that the concept of specific bonding applies to the actin bundles with liquid lateral order in which all crossbridges are in almost identical environments. The potential for such organization is a consequence of the helical symmetry of the actin filaments in which the radial orientation of subunits allows bonding to take place at any angular position around a filament. What is particularly interesting is that the bonding rule for a pair of filaments, at least as we have outlined it here, does not determine the lateral organization. The resulting bundle may be hexagonal as in stereocilia of the chicken (data not shown). Alternatively, using the same bonding rule, the bundle may have only liquid lateral order as in the stereocilia of the alligator lizard. The regularity of filament arrangement would thus not appear to be a consquence of the bonding properties of the actin and its crossbridges. Rather, we suppose that control over this aspect of organization is determined by the conditions at the time of assembly.

Finally, our conclusions about crossbridging between actin filaments can apply equally well to the crossbridging of other helical filaments, for example microtubules or intermediate filaments.

We thank Emma Jean Battles for processing the tissue and cutting sections, Betti Goren for drawing in Fig. 5, and Bill Saunders for photography of the models. We also thank Penny Caponigro and Louise Seidel for help in preparing the manuscript. This work was supported by grants NSF GB22863 to L.G.T. and NSF PCM78-15913 and NIH GM21189 to D.J.D. E.E. is supported by a Dretzin fellowship.

Received 9 June; accepted 31 July 1980.

1. Caspar, D. L. D. & Klug, A. *Cold Spring Harb. Symp. quant. Biol.* **27,** 1–24 (1962).
2. Hull, B. E. & Staehlin, L. A. *J. Cell Biol.* **81,** 67–82 (1979).
3. Bagger-Sjöback, D. & Wersall, J. *J. Neurocytol.* **2,** 329–350 (1973).
4. Mulroy, M. J. *Brain Behav. Evol.* **10,** 69–87 (1974).
5. Flock, Å. & Cheung, H. C. *J. Cell Biol.* **75,** 339–343 (1977).
6. Tilney, L. G., DeRosier, D. J. & Mulroy, M. J. *J. Cell Biol.* **85,** 244–259 (1980).
7. Bouligand, Y., Soyer, M. O. & Puiseux-Dao, S. *Chromosoma (Berl.)* **24,** 251–287 (1968).
8. Reedy, M. K. *J. molec. Biol.* **31,** 155–176 (1968).
9. Kane, R. E. *J. Cell Biol.* **66,** 305–315 (1975).
10. DeRosier, D. J., Mandelkow, E., Silliman, A., Tilney, L. G. & Kane, R. E. *J. molec. Biol.* **113,** 679–695 (1977).
11. DeRosier, D. J. & Edds, K. T. *Expl Cell Res.* **126,** 490–492 (1980).
12. Kane, R. E. *J. Cell Biol.* **71,** 704–714 (1976).
13. Lim, D. J. & Dunn, D. E. *Otolaryngologic Clinics of North America* **12,** 493–513 (1979).

Resolution, reconstitution and kinetics of the primary action of a hormone receptor

Yoav Citri & Michael Schramm

Department of Biological Chemistry, The Hebrew University of Jerusalem, Jerusalem, Israel

The β-adrenergic receptor (R) and the GTP binding protein (G) with which the receptor interacts were obtained in separate soluble fractions. Their recombination produced a hormone responsive system. In the presence of hormone the encounter of R with G in the reconstituted membrane occurs much faster than the subsequent R-induced activation of G.

THE interaction of a hormone or neurotransmitter receptor with the next component along the pathway of signal transmission can be defined as the primary action of the receptor. Resolution of its participating components and subsequent reconstitution are essential to the understanding of the molecular mechanism of receptor function. Unfortunately, this initial step has not been sufficiently characterized even for the much studied insulin[1], acetylcholine[2] and α-adrenergic receptors[3].

There is, however, considerable information about the activation sequence of the β-adrenergic receptor[4,5]: the hormone–receptor complex (R°)[6,7] activates a guanyl nucleotide binding component (G) by introducing GTP into it[8,9]. The activated G (G*) interacts with the catalytic unit (C) of the adenylate cyclase to form the active enzyme (G*C)[10]. Hydrolysis of the bound GTP terminates activation[11]. Replacement of GTP by the hydrolysis-resistant analogue Gpp(NH)p produces a persistently active enzyme complex (G*C)[12]. The process may be described by the following steps:

$$\text{(1)} \qquad R^\circ + G \xrightarrow{k_1} R^\circ G$$

$$\text{(2)} \qquad R^\circ G + \text{Gpp(NH)p} \xrightarrow{k_2} R^\circ + G^* \quad (G^* = G_{\text{Gpp(NH)p}})$$

$$\text{(3)} \qquad G^* + C \xrightarrow{k_3} G^*C$$

Step (1) is the encounter of R° and G in the membrane; step (2) is the R°-induced introduction of Gpp(NH)p into G; and step (3) is the interaction of G* with C to form the persistently active adenylate cyclase. k_1, k_2 and k_3 are the forward rate constants of steps (1)–(3) respectively.

The function of R has so far been investigated only by measuring adenylate cyclase activity in the intact cell membrane. On the basis of such kinetic studies, many models for the action of R in the activation of adenylate cyclase were proposed[4,13–15]. It is, however, extremely difficult to reach definitive conclusions from such studies because the relative amounts of R, G and C in the membrane are fixed and because the function of R is not measured directly in its primary action on G (Steps (1) and (2)), but rather, indirectly, through the action of G* on C (Step (3)).

We have now succeeded in obtaining separate solubilized preparations of R and of G, both free of functional C. Various amounts of the two preparations can be combined to reconstitute functional systems with the desired R to G ratios. When hormone and Gpp(NH)p are added, persistently activated G* is produced. The amount of G* is subsequently measured in a separate system, by its implantation in the membrane of cells which contain an excess of C but no functional G[16–18]. The kinetics of R action on G are found to be first order with respect to R concentration, and zero order with respect to G concentration. The nature of receptor function is discussed in the light of these findings.

Resolution and recoupling of R and G

Solubilization of a functional receptor and its implantation in a cell membrane have been recently reported from our laboratory[19]. Since the solubilized fraction had both R and G activities, we searched for a preparatory step to obtain a membrane preparation which would contain R but no G or C. It was found that treatment with strong alkaline buffer (pH 11.9) eliminated essentially all G and C activity of the membrane, leaving R undamaged. Subsequent treatment of the alkali extracted membrane with deoxycholate produced solubilized R free of G and C. The solubilized G preparation, essentially free of R and C, was obtained by cholate extraction[20]. Mixing of the soluble R preparation with the soluble G preparation, followed by removal of detergents and phospholipid treatment, gave a functional hormone responsive system. The entire procedure of solubilization and reconstitution is shown schematically in Fig. 1. The primary action of the β-adrenergic receptor is studied in the reconstituted system by measuring its product G*. The amount of G* is determined by the proportional enhancement of adenylate cyclase activity in cyc⁻ cells which lack functional G. This activity will be referred to as 'G activated' (Figs 2–5).

Table 1 Specific activities of R in the reconstituted system and in erythrocyte membrane preparations

Systems and treatments	Amount of R* (a)	Rate of G activation† (b)	Specific activity of R‡ (b/a)
I Reconstituted RG, activated by hormone + Gpp(NH)p, fused with cyc⁻	85	12	0.14
II NEM treated membranes activated by hormone + Gpp(NH)p and fused with cyc⁻	169	56	0.33
III Membranes activated by hormone + Gpp(NH)p	72	23	0 32
IV Membranes activated by hormone + Gpp(NH)p fused with each other	72	12	0.17

Systems were activated (2 or 3 min) with 10 μM isoprenaline + 10 μM Gpp(NH)p at 30 °C. Activation was terminated with 10 μM propranolol and after 0 5 min, 10 μM GTP was added. The systems were immediately placed in ice. Adenylate cyclase was measured either directly or after fusion with cyc⁻ cells ('Rate of G activation'). The amount of receptor (R) was determined by binding of ^{125}I-hydroxybenzylpindolol[14] System I: reconstitution was produced by R and G mixing 1 : 1 (v/v) (as described in Fig. 1). System II: membranes were treated with *N*-ethylmaleimide selectively to inactivate the catalytic unit (C)[18,19] After activation, as described above, membranes were treated with phospholipids (40 μl ml^{-1} containing 1 mg protein), pelleted and fused with cyc⁻ cells (Fig. 1). System III. membranes were activated as above, washed once and assayed for adenylate cyclase activity. System IV. membranes activated as in III went through the fusion process, without cyc⁻ cells, and were then assayed for adenylate cyclase

* fmol per system.

† Expressed as G activated per min per system as pmol cyclic AMP min^{-1}.

‡ Expressed as G activated per min per fmol R.

0028-0836/80/390297—04$01 00

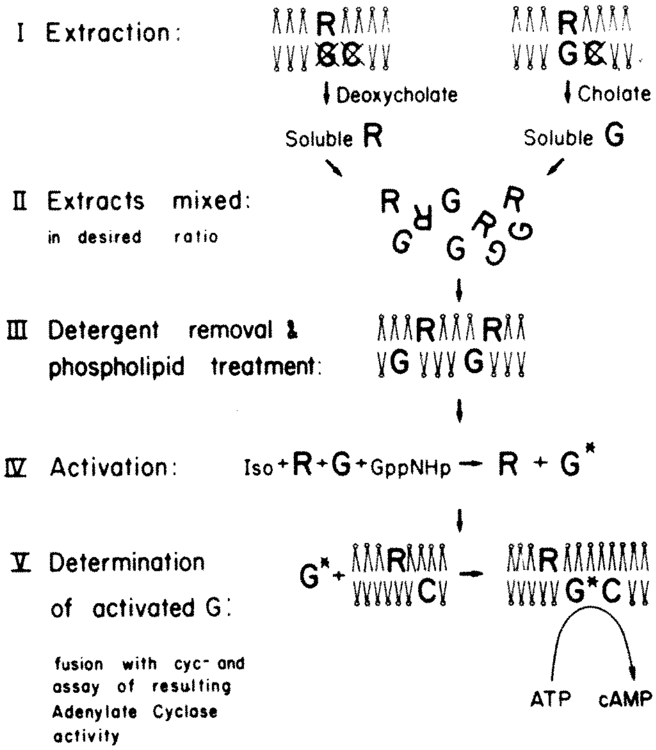

Fig. 1 Scheme describing the differential solubilization and reconstitution of the β-adrenergic receptor and the guanyl nucleotide binding protein. R is the β-adrenergic receptor; G is the guanyl nucleotide binding unit; G* is the Gpp(NH)p activated G unit, and C is the adenylate cyclase catalytic unit. *Receptor extraction*: Turkey erythrocyte membranes[19] were washed with 10 mM MOPS buffer, *p*H 7.5, containing 1 mM mercaptoethanol, and were suspended at 1 mg ml^{-1} in 50 mM phosphate buffer, *p*H 11.9, containing 2 mM EDTA. The suspension was kept for 20 min at 4 °C, centrifuged at 27,000 *g* for 15 min, and resuspended in 20 mM MOPS buffer, 1 mM mercaptoethanol, in half the previous volume. The G unit is lost during this treatment together with 50% of the membrane protein. The alkali extracted membranes, when fused with cyc$^-$ cells, contribute only negligible amounts of G as measured by adenylate cyclase activity. The alkali extracted membranes were treated with phospholipid (10 mg ml^{-1} soybean phospholipid in 10 mM Tris HCl buffer, *p*H 7.5, 1 mM EDTA, sonicated twice for 5 min under N_2), as previously described[19], only that 0.2 ml phospholipid was added per ml of membrane suspension. After incubation at 4 °C in presence of 10 mM $MgCl_2$, 20 μM isoprenaline was added, and the membranes were incubated for 15 min at 30 °C with occasional stirring. The suspension was cooled at 4 °C, centrifuged at 18,000 *g* for 10 min, and resuspended in solubilization buffer[19] at one-ninth the original volume (which served for alkaline extraction). The membranes were solubilized by the addition of one volume of sodium deoxycholate, 12 mg ml^{-1}, in solubilization buffer[19]. The supernatant, after centrifugation at 200,000 *g* for 30 min, served as the soluble R preparation (0.4 mg protein per ml). *G unit extraction*: The procedure was adapted from that of Sternweis and Gilman[20]. Turkey erythrocyte membranes were washed and resuspended at 10 mg protein per ml in cholate solubilization buffer (20 mM HEPES, *p*H 8.0, 2 mM mercaptoethanol, 1 mM $MgCl_2$, 0.2 mM EGTA, 20 μM phenylmethylsulphonyl fluoride). One volume of 20 mg ml^{-1} cholate in the above buffer was added, the suspension was shaken for 30 min at 4 °C, and centrifuged at 200,000 *g* for 30 min. The supernatant served as the G preparation (0.9 mg protein per ml). The procedure apparently inactivated the catalytic unit. *Mixing of solubilized R with solubilized G*: To produce the desired ratio of R:G, the appropriate volumes of the two extracts were mixed. Controls containing only G or only R were mixed with the complementary pure detergent solution instead of the complementary extract. *Detergent removal*: Polystyrene SM-2 beads were added as previously described[19]. The preparations were subsequently treated with phospholipids, 150 μl ml^{-1}, as described above. *Activation*: The phospholipid-treated preparations were incubated at 30 °C with the synthetic hormone isoprenaline (10 μM) or the receptor blocker propranolol (10 μM) plus the non-hydrolysable GTP analogue guanosine 5′-(β, γ-imino)-triphosphate (Gpp(NH)p) (10 μM). After the desired time period, activation was terminated by addition of 10 μM propranolol and 10–100 μM GTP. The mixture was kept at 4 °C for 20 min. After centrifugation at 18,000 g for 10 min, the pellets were frozen in liquid N_2 and stored at −70 °C. These pellets had no detectable adenylate cyclase activity. *Determination of activated G*: Each pellet described above was fused [19,32] with 3×10^7 cells of the mutant cyc$^-$ S49 lymphoma which lacks functional G (refs 16, 17). The resulting increase in basal adenylate cyclase activity was measured in presence of 2 μM propranolol. This activity, referred to as 'G activated', can be attributed solely to the amount of activated G which was transferred by fusion to cyc$^-$ membranes. R of the cyc$^-$ cells (section V above) has no function in this assay. The resulting basal adenylate cyclase activity was directly proportional to the amount of activated G placed in the fusion system. The total amount of G (non-activated plus activated) implanted in the cyc$^-$ membranes was determined by measuring adenylate cyclase activity in presence of 0.1 mM isoprenaline plus 0.1 mM Gpp(NH)p. Adenylate cyclase activity in presence of 10 mM NaF also gave a measure of G units transferred by fusion. These assays were performed at 37 °C for 30 min[33]. *Yield of R and of G*: The β-adrenergic receptor in the R preparation was 0.3 pmol per ml of extract, as determined by binding of ^{125}I-hydroxybenzylpindolol[34] after detergent removal. The G preparation is estimated to contain 2.5 pmol GTP binding sites per ml. The calculation is based on a 50% yield in the cholate extraction, as determined by fusing the extracted turkey erythrocyte membranes with cyc$^-$ cells and assaying adenylate cyclase activity (F^-). The original content of G in the native membrane is taken to be 1 pmol of hormone induced ^{3}H-Gpp(NH)p (ref. 35) or ^{3}H-GTP[9] binding sites per mg of protein.

Hormone activation of the reconstituted R–G system is shown in Fig. 2. Dramatic hormone-induced activation of G is exhibited only by the system which was produced by combining the R and G preparations. The individual preparations of R and of G show only a slight hormonal response. Fluoride activities serve as an independent measure for the amount of G fused into the cyc$^-$ membranes. The R preparation produces no detectable fluoride activity and is therefore considered essentially free of G. The G preparation produces fluoride activity as high as the R plus G system, indicating a similar efficiency for both systems in the transfer of G units to the cyc$^-$ cell membrane by the fusion process. Hence, the only explanation for the very low hormone-induced G activity in the separate preparations of R and of G is the paucity of the G component in the R preparation and the R component in the G preparation.

Efficiency of R–G recoupling

The amount of G activated (G*) per minute by a unit amount of R may be used as a measure of the productive interaction of R with G (specific activity of R). As shown in Table 1, the specific activity of R in the reconstituted system is almost half that of the native turkey erythrocyte membrane (compare systems I and II in Table 1). It is also shown that the specific activity of R measured in the erythrocyte membrane, through its native catalytic unit, is comparable with that measured through the catalytic unit of the cyc$^-$ cells (Table 1, systems II and III). However, this observation should be treated cautiously because the experiments involve the unknown parameters of fusion efficiency with cyc$^-$ cells and the turnover numbers of the catalytic units of cyc$^-$ and turkey erythrocyte membranes. Note also that absolute activities fluctuated considerably in different experiments throughout the present study. The major variables responsible seem to be detergent effects during solubilization and reconstitution, and competence of different batches of cyc$^-$ cells. Therefore, absolute activities are comparable only for different systems within the same experiment.

Kinetics of R–G activation

The availability of separate preparations of R and G presented a unique opportunity to study the kinetics of their interaction as a function of their concentration in the reconstituted membrane.

Figure 3 shows the progress of G activation over an extended time period. It is apparent that the systems containing the larger amount of R exhibit a higher rate. In contrast, the concentration of G does not seem to affect the rate of its activation by R. The cause for the two phases in the kinetics of activation is not yet apparent.

To test the kinetics of the R–G interaction more rigorously, systems with a constant amount of R and different amounts of G were reconstituted. Initial rates of G activation were determined by limiting the activation time to 5 min (see Fig. 1, step IV). Figure 4 clearly demonstrates that the concentration of G had no effect on the initial rate of its activation. The kinetics are zero order with respect to G concentration. The apparent lower initial rate in the two systems containing the lesser amounts of G is due to activation of all the G units within the 5 min incubation period. This is evident from the addition of isoprenaline plus Gpp(NH)p to the final adenylate cyclase assay which does not result in additional activation (Fig. 4, open circles, second activation). The addition of isoprenaline plus Gpp(NH)p in the adenylate cyclase assay also demonstrates that the amounts of G transferred to cyc⁻ cells are directly proportional to the amount in the reconstituted system (Fig. 4, second activation).

Figure 5 shows the effect of R concentration on the initial rate of G activation. The rate is directly proportional to the amount of R and is thus first order with respect to R. Limitations of the system did not permit the R/G ratio to increase to the point of saturation, where the initial rate of G activation might reach a maximum. It is interesting that a similar dependence on R concentration was observed in intact turkey erythrocyte membranes after graded inactivation of R by an affinity label[15].

Analysis of kinetics

In the process of hormone activation of adenylate cyclase R° must meet G, and G* must associate with C (see steps (1)–(3)). If the association of R° with G is rate limiting (step (1)), then the rate of G activation should be dependent on the concentrations of both R and G. On the other hand, if the activation of G by R (step (2)) is rate limiting, then the concentration of RG complex would determine the rate. In the latter case, step (1) must occur much faster than step (2) and, therefore, all R will be in the RG form (when [G] > [R]). Thus, first order kinetics with respect to R concentration and zero order with respect to G concentration are predicted. As shown by the present findings (Figs 4, 5), the latter possibility holds true; step (2) is rate limiting. We therefore conclude that in the reconstituted R–G system, the rate of G activation by R is determined by the step of Gpp(NH)p introduction into the RG complex rather than by the rate of encounter of R with G.

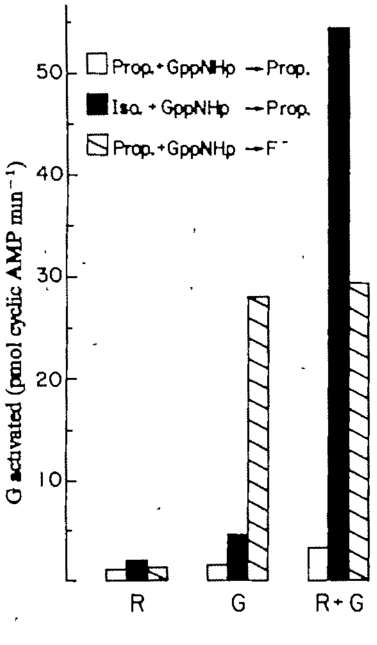

Fig. 2 Hormone-induced activation of G in the resolved and in the reconstituted preparations. Systems were reconstituted as described in Fig. 1 legend. At the mixing stage (step II, Fig. 1) the soluble G extract was combined (1:1 v/v) with deoxycholate, 6 mg ml^{-1} (marked as system G), or with the soluble R (marked as system R+G). The system marked R was prepared by mixing the soluble R extract (1:1 v/v) with 10 mg ml^{-1} cholate. All the systems were then treated as described in Fig. 1 legend, and 0.5-ml portions of each were activated (step IV, Fig. 1) with isoprenaline (black bars) or propranolol (open and crossed bars) for 5 min at 30 °C before addition of Gpp(NH)p for 30 min. Activation was terminated by addition of 10 μM propranolol. After 5 min, 1 ml of ice cold buffer (20 mM MOPS, *p*H 7.5, 1 mM mercaptoethanol, 10 μM GTP, 10 μM propranolol) was added to all systems. The pellets produced by centrifugation were fused with cyc⁻ cells. Adenylate cyclase was determined in presence of propranolol (open and closed bars) or NaF (crossed bars)

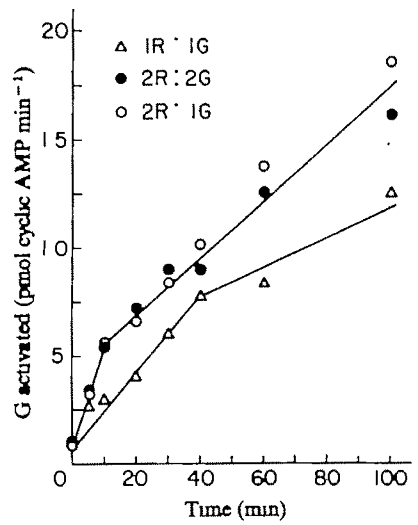

Fig. 3 Kinetics of G activation by the β-adrenergic receptor in reconstituted systems. Preparations (step II, Fig. 1) were mixed in the following ratios: R:G, 1:1 v/v (●); R:G:cholate solution, 2:1:1 v/v/v (○); and R:G:cholate solution:deoxycholate solution, 1:1:1:1 v/v/v/v (△). The systems were treated as described in Fig. 1 legend and activated (step IV, Fig. 1) with isoprenaline plus Gpp(NH)p. At various times 0.5-ml aliquots were taken and added to 1 ml of ice cold buffer (20 mM MOPS, *p*H 7.5, 1 mM mercaptoethanol, 0.1 mM GTP, 10 μM propranolol). The amount of G activated in the samples was determined in presence of propranolol as described in legends to Figs 1 and 2. The relatively low activities in this experiment are due to a low yield of the G preparation used for the reconstitution. This is shown by measurement of total G (determined in presence of Gpp(NH)p plus isoprenaline in the adenylate cyclase assay). Total G activities were (average of all the samples): 10.2 pmol min^{-1} (1R:1G), 20.4 pmol min^{-1} (2R:2G), and 13.2 pmol min^{-1} (2R:1G).

Extrapolating from these experiments with the reconstituted system to the native membrane, either step (2) or (3) could determine the rate of the overall process. An estimate of the apparent rate constant k_2 for step (2) (see legend to Fig. 4) gave a value that was in the same range as the rate constant values calculated for the overall activation process in the native membrane[11,15]. It is therefore possible that step (2) is rate limiting in the overall process of hormonal activation of adenylate cyclase. However, further experiments will be needed to verify this suggestion.

The mobile receptor hypothesis[21] was applied to the β-adrenergic receptor system[13] and it was suggested that the rate of encounter between the receptor and the adenylate cyclase might be the rate limiting step of the activation process. The hypothesis[21] predicted the independent existence of the hormone receptor[6]. However, the RG complex and the rate of G activation were not considered at the time. As these findings indicate that the R–G encounter is not rate limiting in the reconstituted system, a re-evaluation of previous models seems worthwhile.

Experiments on the overall process of adenylate cyclase activation in the native membrane indicated that a small amount of R could activate a larger amount of enzyme[15,22]. The present work shows that R acts catalytically in activating at least 10 times its own amount of G (Figs 2–5). The activation of G by R proceeds in the absence of functional C (ref. 18, legend to Fig. 1). Thus, the catalytic function of the β-adrenergic receptor in the overall process of adenylate cyclase activation seems to be a mere reflection of its primary action on G.

Conclusions

The present study describes the reconstitution of the R–G interaction using solubilized, resolved preparations of R and of G. Kinetic properties of the R–G interaction were revealed which could not be studied in the native membrane where the concentrations of R and G cannot be manipulated and where the concurrent interaction of G with C compounds the analysis. The experiments imply that in the presence of hormone, all R is in

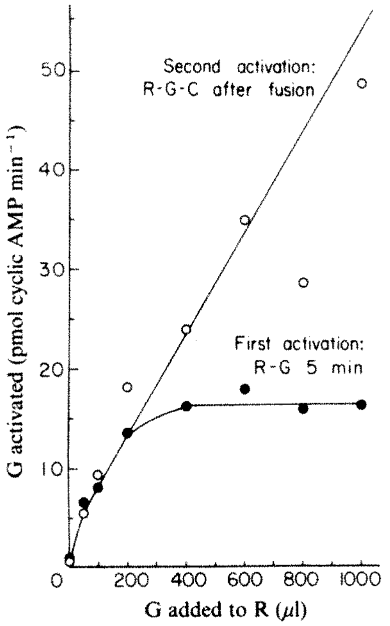

Fig. 4 Initial rates of G activation as a function of G concentration in the reconstituted system. R (0.5 ml) was mixed with different amounts of G (abscissa). In each system the volume of G added was made up to 1.0 ml by addition of 10 mg ml^{-1} cholate. After reconstitution, as described in Fig. 1 legend, 1.0-ml aliquots were activated for 5 min (as in Fig. 3) and fused with cyc$^-$ cells. Systems were assayed with propranolol to show the amount of G which had been activated (first activation) (●). In addition, aliquots from each system were subjected to a second activation with 0.1 mM isoprenaline plus 0.1 mM Gpp(NH)p in the adenylate cyclase assay (○). k_2: The rate constant of step (2) in the text was calculated from the initial rate of G activation shown above, and the yield of G and R in the respective extracts (Fig. 1). R is all in the RG form (see text); therefore $k_2 = 1.4$ min^{-1}.

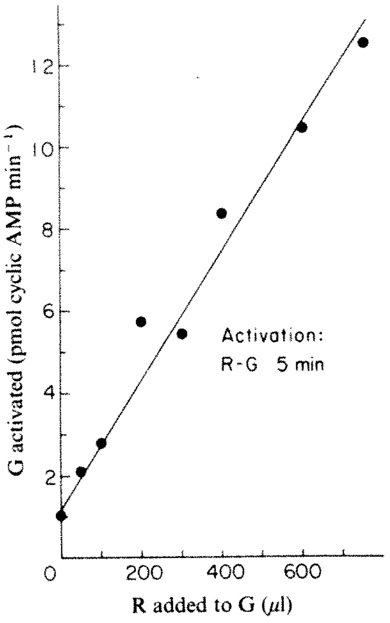

Fig. 5 Initial rates of G activation as a function of receptor concentration in the reconstituted system. A constant amount of G, 750 μl, and increasing amounts of R (abscissa) were mixed and reconstituted. The volume of R was made up to 750 μl with 6 mg ml^{-1} deoxycholate. All other manipulations were as described in Fig. 4 legend.

the RG complex form. This conclusion is supported by recent findings that the hormone induces co-elution of R and G from a gel filtration column[23]. As the R–G interaction has not been studied to date with purified components, the possibility cannot be excluded that unknown additional factors might be involved. It should also be noted that differences between the β-adrenergic receptor of turkey erythrocytes and that of other tissues have been reported[14,24]. However, recent studies suggest that these differences are not fundamental[25,26].

The resolved R and G as well as the reconstituted R–G preparation seem to have considerable potential for future studies on hormone receptor action at the molecular level. A few important questions might be tackled. Are the differences in thermodynamic parameters between the binding of hormone and of blocker[27] due to the hormone-induced primary action of R with G? Does the reconstituted R–G system possess the hormone-induced GTPase activity[28] or is C required for this reaction? What are the specific phospholipid requirements for R and G functions?

The interaction of R with G takes place within a two-dimensional phospholipid bilayer which serves as the solvent. Manipulation of this solvent such as treatment with *cis*-vaccenic acid[29,30] greatly influences the kinetics of adenylate cyclase activation. It is possible, therefore, that more extensive dilution of R and G by phospholipid addition or other manipulations might affect the properties of the system. Unfortunately, there is little information about kinetics of interaction of protein molecules in biological membranes. Rogers and Strittmatter[31] published elegant studies on the interaction of NADH cytochrome b_5 reductase with cytochrome b_5 in native and reconstituted membranes. However, this system may not be a close analogy to the hormone-activated adenylate cyclase. The cytochrome and the enzyme reducing it are anchored in the membrane but the active groups interact in the water phase. In contrast, the β-adrenergic receptor transmits a transmembrane signal and, apparently, interacts with the G unit within, or on, the inner side of the membrane. It is hoped that the approach used in this work will be applicable to the study of other receptor response mechanisms and that the reconstituted R–G system can serve as a paradigm for protein–protein interactions in biological membranes.

We thank Sara Eimerl and Mira Korner for help. The work was supported by NIH grant no. AM-10451-15 and grant no. 2225 from the US–Israel Binational Science Foundation.

Received 2 April; accepted 21 July 1980.

1. Czech, M. P. *A. Rev. Biochem.* **46,** 359–384 (1977).
2. Heidmann, T. & Changeux, J. P. *A. Rev. Biochem.* **47,** 317–357 (1978).
3. Jones, L. M. & Michell, R. H. *Biochem. Soc. Trans.* **6,** 673–688 (1978).
4. Rodbell, M. *Nature* **284,** 17–22 (1980).
5. Ross, E. M. & Gilman, A. G. *A. Rev. Biochem.* (in the press)
6. Orly, J. & Schramm, M. *Proc. natn. Acad. Sci. U.S.A.* **73,** 4410–4414 (1976).
7. Vauquelin, G., Geynet, P., Hanoune, J. & Strosberg, D. *Proc. natn. Acad. Sci. U.S.A.* **74,** 3710–3714 (1977).
8. Rodbell, M., Birnbaumer, L., Pohl, S. L. & Krans, H. M. J. *J. biol. Chem.* **246,** 1877–1882 (1971).
9. Cassel, D. & Selinger, Z. *Proc. natn. Acad. Sci. U.S.A.* **75,** 4155–4159 (1978).
10. Pfeuffer, T. *J. biol. Chem.* **252,** 7224–7234 (1977).
11. Cassel, D., Levkovitz, H. & Selinger, Z. *J. Cyclic Nucleotide Res.* **3,** 393–406 (1977).
12. Schramm, M. & Rodbell, M. *J. biol. Chem.* **250,** 2232–2237 (1975).
13. Cautrecasas, P. & Hollenberg, M. D. *Adv. Protein Chem.* **30,** 251–451 (1976).
14. Maguire, M. E., Ross, E. M. & Gilman, A. G. *Adv. Cyclic Nucleotide Res.* **8,** 1–83 (1977).
15. Tolkovsky, A. M. & Levitzki, A. *Biochemistry* **17,** 3795–3810 (1978).
16. Bourne, H. R., Coffino, P. & Tomkins, G. M. *Science* **187,** 750–752 (1975).
17. Ross, E. M., Howlett, A. C., Ferguson, K. M. & Gilman, A. G. *J. biol. Chem.* **253,** 6401–6412 (1978).
18. Neufeld, G., Schramm, M. & Weinberg, N. *J. biol. Chem.* (in the press).
19. Eimerl, S., Neufeld, G., Korner, M. & Schramm, M. *Proc. natn. Acad. Sci. U.S.A.* **77,** 760–764 (1980).
20. Sternweis, P. C. & Gilman, A. G. *J. biol. Chem.* **254,** 3333–3340 (1979).
21. Cuatrecasas, P. *A. Rev. Biochem.* **43,** 169–214 (1974).
22. Schramm, M. *J. Cyclic Nucleotide Res.* **2,** 347–358 (1976).
23. Limbird, L. E., Gill, M. D. & Lefkowitz, R. J. *Proc. natn. Acad. Sci. U.S.A.* **77,** 775–779 (1980).
24. Minneman, K. P., Weiland, G. A. & Molinoff, P. B. *Molec. Pharmac.* **17,** 1–7 (1980).
25. Lad, P. M., Nielsen, T. B., Preson, S. M. & Rodbell, M. *J. biol. Chem.* **255,** 988–995 (1980).
26. Stadel, J. M., Delean, A. & Lefkowitz, R. J. *J. biol. Chem.* **255,** 1436–1441 (1980).
27. Weiland, G. A., Minneman, K. P. & Molinoff, P. B. *Nature* **281,** 114–117 (1979).
28. Cassel, D. & Selinger, Z. *Biochim. biophys. Acta* **452,** 538–551 (1976).
29. Orly, J. & Schramm, M. *Proc. natn. Acad. Sci. U.S.A.* **72,** 3433–3437 (1975).
30. Rimon, G., Hanski, E., Braun, S. & Levitzki, A. *Nature* **276,** 394–396 (1978).
31. Rogers, M. J. & Strittmatter, P. *J. biol. Chem.* **249,** 5565–5569 (1974); **250,** 5713–5718 (1975).
32. Schramm, M. *Proc. natn. Acad. Sci. U.S.A.* **76,** 1174–1178 (1979).
33. Salomon, Y., Londos, C. & Rodbell, M. *Analyt. Biochem.* **58,** 541–548 (1974).
34. Maguire, M. E., Wiklund, R. A., Anderson, H. J. & Gilman, A. G. *J. biol. Chem.* **251,** 1221–1231 (1976).
35. Cassel, D. & Selinger, Z. *J. Cyclic Nucleotide Res.* **3,** 11–22 (1977).

Cloning and DNA sequence of double-stranded copies of haemagglutinin genes from H2 and H3 strains elucidates antigenic shift and drift in human influenza virus

Mary-Jane Gething*, **Jackie Bye***, **John Skehel**† & **Michael Waterfield***

* Imperial Cancer Research Fund, Lincoln's Inn Fields, London WC2A 3PX, UK
† Division of Virology, National Institute for Medical Research, Mill Hill, London NW7 1AA, UK

Double-stranded DNA copies of the RNA gene coding for the haemagglutinin glycoproteins from human H2 and H3 pandemic strains of influenza virus have been cloned. DNA sequence analysis provides the first reported complete nucleotide sequence of an H2 haemagglutinin gene and a partial sequence (45%) of the H3 gene. The H2 haemagglutinin gene consists of 1,773 nucleotides containing an uninterrupted coding sequence of 1,686 nucleotides specifying a protein of 562 amino acids. Comparison of the amino acid sequences of these haemagglutinins with those of other H3 and avian strains reveals the extent of sequence changes in antigenic shifts and drifts.

THREE main properties of influenza virus haemagglutinins have prompted analyses of their structure. These glycoproteins are responsible for binding virus particles to cells during infection[1] and possibly mediate virus-cell membrane fusion[2-4]; antibodies which react with the haemagglutinin neutralize virus infectivity[5] and, as a consequence, viruses which have the potential to cause new epidemics or pandemics of disease in an immune population have antigenically novel haemagglutinins; and finally, as the major glycoprotein component of virus membranes they share features of biosynthesis, processing and structure with integral membrane proteins of eukaryotic cells and thus serve as models for studying these proteins. Because of these properties, we and others[6-11] have been determining the primary structures of several haemagglutinins. To complete this determination we have synthesized and cloned in a prokaryotic vector complementary DNA copies of haemagglutinin virion RNA. Haemagglutinins used were from strains A/Japan/305/57 (H2 subtype) and X-31 (H3 subtype). We report here the complete nucleotide sequence of the Japan haemagglutinin gene and a partial sequence (45%) of the X-31 gene. Comparison of the derived amino acid sequences with those from other members of the H3 subtype A/NT/60/68/29C[10] and A/Victoria/3/75[9] and with a haemagglutinin from the avian Hav 1 strain A/FPV/Rostock[8] allows correlation of structure and function for the haemagglutinin molecule.

Cloning and DNA sequence of haemagglutinin genes

The influenza haemagglutinins chosen for analysis were from the high-yielding recombinant virus strains A/Japan/305/57: A/Bel/42: A/PR/8/34 (H2N1)[12] and X-31 (H3N2)[13]. These strains contain haemagglutinin genes from the originally isolated strains A/Japan/305/57 (H2) and A/Aichi/2/68 (H3). Total virion RNAs (vRNAs) from the two influenza recombinants were purified and polyadenylated at their 3′ termini using ATP:RNA adenyltransferase[14]. An average of about 50 adenylate residues were added to each RNA molecule. The polyadenylated vRNAs were then used as templates for reverse transcription of single-stranded (ss) DNA copies using oligo(dT)$_{12-18}$ as primer[15]. The products were separated in denaturing conditions on agarose gels into eight discrete bands whose sizes indicated that they were essentially full-length copies of the genomic RNA segments[16] (Fig. 1*a*). In a number of experiments approximately 3-5 μg of cDNA was synthesized using 10 μg of template RNA.

At this point different strategies were chosen for cloning X-31 and Japan nucleic acid sequences. Cloning of X-31 sequences involved direct insertion[17] of poly (dA)-tailed vRNA/cDNA hybrids[18] into the *Pst*I site of plasmid vector pBR322[19] after poly(dT) tailing[18] of the linearized plasmid. However, no full-length cloned copies of the HA gene were obtained. Subsequent experiments with the Japan strain involved the production of double-stranded (ds) DNA copies before insertion into the *Pst*I site of plasmid pAT153 (a derivative of pBR322 with a 622 base pair deletion)[20].

Single-stranded DNA copies of Japan vRNAs were converted to the double-stranded form[21] utilizing the ability of the cDNA to form 3′-terminal hairpin loops[22] to prime DNA polymerase I. Subsequent cleavage of the hairpin loops yields non-covalently joined ds cDNAs. Figure 1*b* shows the resolution on denaturing agarose gels of the ds cDNAs before and after S_1 nuclease treatment. The hairpin-linked ds cDNAs migrated to positions corresponding to approximately twice the molecular weight of ss cDNAs. After S_1 nuclease treatment, most of the ds cDNAs were converted to species which co-migrated with full-length first-strand cDNAs. The ds cDNAs were separated on a sucrose gradient and fractions containing full-length species were selected and tailed with poly(dC) using terminal transferase[18]. The tailed ds cDNAs were inserted into the *Pst*I site of pAT153 after poly(dG) tailing[18] of the linearized plasmid.

Transfection of hybrid plasmids into *Escherichia coli* χ1776 (ref. 23) was by the procedure of Hanahan (personal communication). This method yields $3\text{-}5\times10^7$ transformants per μg of supercoiled plasmid DNA. Transfection with recombinant pBR322 (10 ng vRNA-cDNA insert) or pAT153 (10 ng ds cDNA insert) yielded ~500 tetracycline-resistant bacterial colonies. This corresponds to a transformation efficiency of 2×10^4 transformants per μg of tailed, annealed DNA. The colonies from each transformation were picked and replicated to test ampicillin sensitivity. Approximately 60% of the colonies were Tet^r, Amp^s indicating that they contained recombinant plasmids. These plasmids were grown on nitrocellulose filters and analysed by a modification of the *in situ* colony hybridization procedure[24] using a ^{32}P-cDNA probe for influenza

0028-0836/80/390301—06$01.00

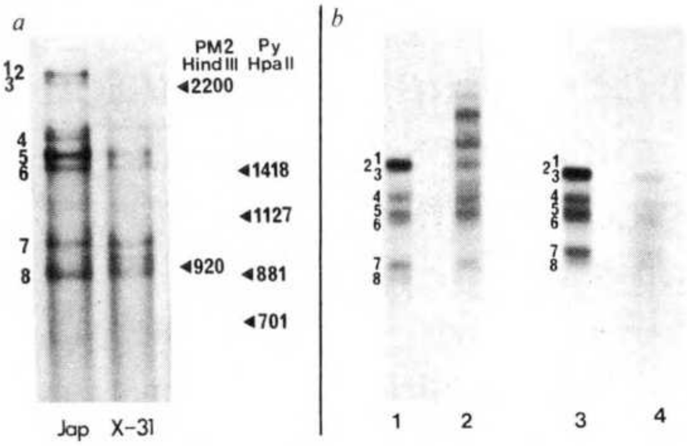

Fig. 1 Characterization of cDNA copies of Japan and X-31 vRNAs. *a*, Separation of cDNA copies of Japan and X-31 vRNAs by agarose gel electrophoresis; polyadenylated vRNAs were reverse transcribed into ss ^{32}P-labelled cDNAs in reaction mixtures containing 50 mM Tris-HCl, *p*H 8.3, 10 mM $MgCl_2$, 140 mM KCl, 30 mM β-mercaptoethanol, 0.5 mM dGTP, 0.5 mM dATP, 0.5 mM TTP, 0.25 mM dCTP (2 μCi μmol^{-1}), 10 μg ml^{-1} oligo(dT) 12–18 (P.-L. Biochemicals), 10 units ml^{-1} rat liver ribonuclease inhibitor (Searle), 50 μg ml^{-1} polyadenylated vRNA and 360 units ml^{-1} AMV reverse transcriptase (a gift from J. Emtage (Searle)). After incubation for 60 min at 42 °C the reaction was terminated by placing the mixture on ice. The cDNAs were separated by electrophoresis on 1.4% agarose gels in 30 mM NaOH, 1 mM EDTA and autoradiographed. The positions of restriction fragments of PM2 (*Hin*dIII) and polyoma (*Hpa*II) virus DNAs are shown as molecular weight markers. *b*, Electrophoretic resolution of Japan ds cDNAs before and after S_1 nuclease digestion. Single stranded ^{32}P-cDNAs prepared by reverse transcription (lanes 1 and 2) were converted to the ds form (lane 2) and digested with S_1 nuclease (lane 4) by the procedure of Wickens *et al.*[21]. Analysis by electrophoresis on agarose gels was as described in *a*.

sequences prepared by reverse transcription of vRNAs using calf thymus primers as random primers[25]. 50–80% of the colonies on nitrocellulose filters contained influenza sequences.

To identify which gene segments were represented in the cloned recombinant plasmids, Japan and X-31 vRNAs were separated in agarose gels, transferred to and immobilized on diazotized paper[25] and probed by hybridization with ^{32}P-labelled recombinant plasmid DNA prepared by nick translation[27]. After autoradiography, clones containing the various vRNA genes were identified (Fig. 2). Restriction endonuclease mapping of plasmids which contained HA sequences indicated that clone 2G10 had an insert corresponding to ~95% of the haemagglutinin gene from the Japan strain and clone 4F12 contained an insert corresponding to ~45% of the X-31 HA gene (Fig. 3).

To obtain a clone containing the missing portion of the Japan HA gene, the *Eco*R1-*Pvu*II restriction fragment from the distal end of the 2G10 insert was used to prime synthesis of a cDNA copy from Japan vRNA template. Using the methods described above, a clone (ExB6) containing the missing sequences was identified and mapped by restriction endonuclease digestion (Fig. 3). Finally, a clone (pJHA) containing the entire Japan HA gene nucleotide sequence (except the last 11 nucleotides) was constructed (Fig. 3). Experiments are in progress to use this cloned gene for expression of haemagglutinin protein in prokaryotic and eukaryotic cells.

Determination of the DNA sequence of the cloned inserts was carried out using the procedures of Maxam and Gilbert[28]. Figure 3 shows the distances sequenced on various restriction fragments. To determine if any of the sequences at the 5′ end of the vRNA were not represented in the clones, or if the cloning procedure had resulted in mutations at this end[8], the 36-base pair *Sau*3A-*Pst*I restriction fragment near the right-hand end of the ExB6 insert was purified, labelled and used as primer for reverse transcription of vRNA template. The single, labelled DNA product was sequenced and the result indicated that only the last 11 nucleotides of the 3′ non-coding region of the Japan vRNA are not represented in the cloned inserts. There were no alterations in the sequence due to the cloning procedure.

Figure 4 provides the completed nucleotide sequences of the complementary RNA strands corresponding to the message coding sequences of the Japan and X-31 genes. Finally, Fig. 6 lists the amino acid sequences derived for the haemagglutinins from Japan, X-31[11], 29C[10], Victoria[9] and Fowl Plague (FP)[8] viruses.

Structure of the haemagglutinin gene

The Japan haemagglutinin gene is 1,773 nucleotides long. The coding region (1,686 nucleotides) begins with an AUG and ends with an UGA terminator. This is followed in the non-coding region by two in phase and one out of phase UAA triplets. Two of the three reading frames contain frequent termination codons so that only one frame is open for translation. The coding portion of the gene exists as a continuous block of nucleotides. The codon usage is similar to that found for the Victoria[9] and FPV[8] haemagglutinin sequences.

There are untranslated regions at both the 5′ (43 nucleotides) and 3′ (44 nucleotides) ends of the haemagglutinin gene (messenger or cRNA strand). The terminal sequences have been determined previously by direct RNA sequencing[29,30] or by sequencing of reverse transcripts[31] and these results confirm that our cloned inserts contain the complete vRNA sequence at the 3′ end and miss only 11 nucleotides at the 5′ end. The first 14 nucleotides at the 5′ end of the HA cRNA and the last 21 nucleotides at the 3′ termini are identical in all the strains that have been sequenced[8–11]. Previous direct RNA sequence analysis of the 5′ ends of vRNA and cRNA transcripts of the eight influenza gene segments from a number of different viral strains showed that, in all cases, the terminal 12–13 nucleotides are closely conserved and that the 5′ and 3′ ends display inverted partial complementarity[29]. This structure may have a role in the process of viral replication. Emtage *et al.*[32] have shown that there is an adventitious prokaryotic-like ribosome binding site near the 5′ end of the cRNA which may be functional during expression of the cloned gene in *E. coli*. This sequence is also

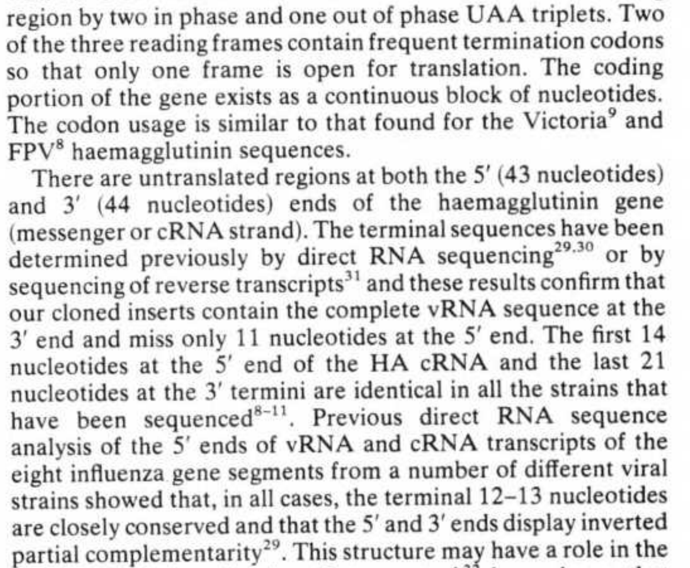

Fig. 2 Assignment of cloned inserts to viral RNA segments. Recombinant plasmid DNA preparations from the numbered clones were labelled with ^{32}P by nick translation[27] and hybridized to fractionated vRNAs immobilized on diazotized paper[26]. The positions of the eight vRNA genes were identified by hybridization with the appropriate ^{32}P-labelled cDNAs prepared by reverse transcription of total X-31 or Japan vRNAs[25].

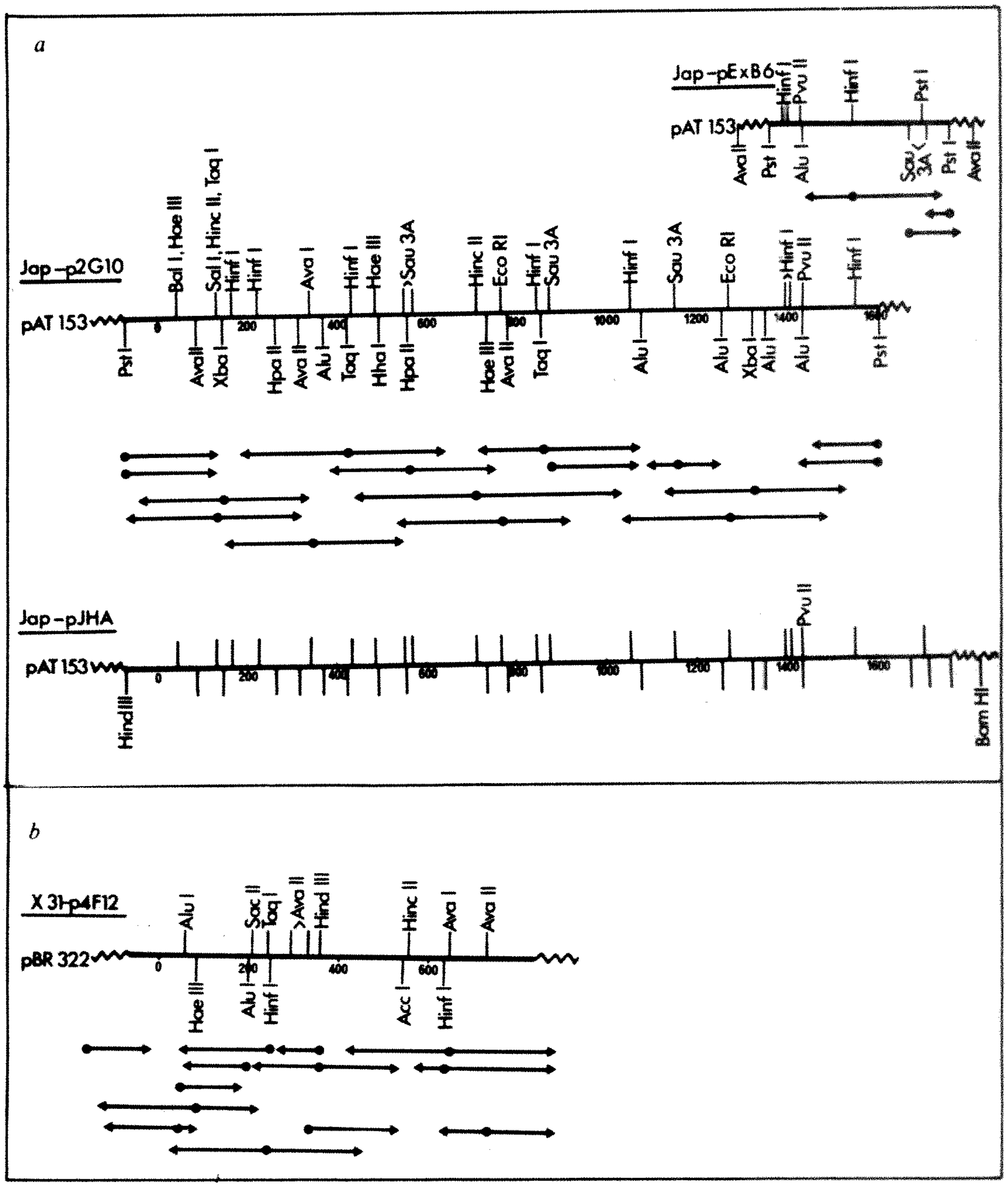

Fig. 3 Restriction enzyme maps of *a*, Japan and *b*, X-31 haemagglutinin gene inserts in recombinant plasmids. The construction of clones p2G10, pExB6 and p4F12 is described in the text. Conditions for all restriction enzyme digestions were as described in the catalogue of New England Biolabs. The distances and directions sequenced on various restriction fragments are shown by arrows. Clone pJHA contains a copy of the entire Japan HA gene except for the last 11 nucleotides of the 5′ non-translated region of the vRNA. It was constructed from the p2G10 and pExB6 clones as follows: the gene insert in p2G10 was excised with *Pst*I and *Hin*dIII linkers were attached to the ends[52]. The *Hin*dIII-*Pvu*II restriction fragment was purified. Similarly the gene insert in pExB6 was excised by cutting the flanking pAT153 sequences with *Ava*II and *Bam*HI linkers were attached to the ends[52] before purification of the *Pvu*II-*Bam* restriction fragment. The *Hin*dIII-*Pvu*II and *Pvu*II-*Bam* fragments were then ligated between the *Hin*dIII and *Bam*HI sites of pAT153 using T4 DNA ligase. After transfection of the ligated mixture into χ1776 a clone pJHA containing the composite full-length insert was obtained and characterized.

present in the human influenza HA genes but the greater distance between it and the AUG codon suggests that it may not function in expression of these genes in bacteria[33]. The remainder of the untranslated regions vary in length and in sequence and show little evidence of common origin or function.

Structure of the haemagglutinin protein predicted from the nucleic acid sequence: cleavage of the polypeptide

The haemagglutinin glycoprotein is synthesized in infected cells as a single polypeptide precursor which is converted by proteolytic cleavage into two disulphide-bonded polypeptides HA1 and HA2[34,35]. The Japan haemagglutinin precursor consists of 547 amino acids and a single arginine residue is removed during formation of HA1 (324 amino acids) and HA2 (222 amino acids)[6]. In this respect Japan haemagglutinin differs from FPV haemagglutinin[8] as at the equivalent site there is a sequence of six charged amino acids which are probably removed during processing. The difference in structure at this site may explain why FPV is susceptible to cleavage activation in a wider range of host cells[36].

Hydrophobic regions of the haemagglutinin

The hydrophobic sequence at the new NH_2 terminus of HA2 which is generated by this cleavage is highly conserved in influenza haemagglutinins[37] and also shows a high degree of similarity to the NH_2 terminus of the F1 subunit of Sendai virus fusion protein[4], which is revealed after cleavage activation of infectivity and fusion activity. Previously we have suggested that these sequences may have a functional role in interaction with and penetration of the cell membrane during infection.

The HA primary translation product contains two additional hydrophobic regions which are present in all the virus strains. These are the signal sequence at the NH_2 terminus and the presumed membrane insertion sequence at the COOH terminus. The nascent Japan HA polypeptide chain contains a hydrophobic signal peptide[6,30,38] which is probably involved in the transport of the polypeptide across the endoplasmic reticulum. This peptide is cleaved off when the process of membrane transfer and insertion is complete. The DNA sequence reported here defines a 15-residue peptide containing 14 uninterrupted non-polar amino acids before the known NH_2 terminus of HA1[6] and agrees with the data of Air[31] and with our previous data from direct RNA and amino acid sequence analyses[30]. The H3 haemagglutinins[9–11] probably also have a signal peptide of 16 amino acids containing 14 uninterrupted non-polar residues since the glutamine residue at position 17 is probably the NH_2-terminal amino acid of the mature protein[7]. Again, although amino-acid sequence data is not available for FPV, homologies at the NH_2 terminus of HA1 suggest that FPV haemagglutinin has an 18 amino-acid signal peptide containing a core of 11 hydrophobic amino acids[8]. It is striking that the proposed signal peptides of the haemagglutinins from the H2, H3 and avian subtypes show no homology with each other, indicating that it is the hydrophobicity and not specific sequence that is important for membrane association. The size and non-polar character of these prepeptides are similar in other membrane or secreted proteins[39].

The third hydrophobic sequence at the COOH terminus of the primary translation product and of HA2 is probably involved in anchoring the protein in the lipid envelope[37]. The haemagglutinins from the H2, H3[9-11] and FPV[8] strains have 41, 27 and 26 non-polar amino acids, respectively, preceding charged amino acids near the COOH terminus. There is some similarity between these sequences but it is significantly less than that found in the rest of HA2. It may be that, as in the case of the signal peptide, it is hydrophobicity and not specific sequence that defines the interaction with the membrane. It is of course not possible to define from these data which amino acids are embedded in the lipid bilayer, but it seems likely that there are no more than 10–12 residues on the inner face of the virus envelope, suggested by the location of charged amino acids at position 10 (H3)[9-11] and 11 (FPV)[8] amino acids from the COOH terminus. The only charged amino acid at the COOH terminus of Japan HA2 is four residues from the end. Similar numbers of hydrophobic amino acids span the lipid bilayer in HLA heavy chain[40] and glycophorin A[41]. However, in these cases the internal hydrophilic tails (approximately 30 residues) are longer.

Conservation of amino acid sequence and location of cysteine or cystine residues

It is now possible to compare the complete amino acid sequence of haemagglutinins from two subtypes of human influenza virus and an avian virus[8-11]. In Fig. 5, the protein sequences have been aligned using a computer program[42] to optimize the homology. The alignment involves only a few small insertions or deletions in the sequences, except at the NH_2 terminus of HA1 where the H3[9-11] haemagglutinins have 10 or 11 extra amino acids and at the cleavage site between HA1 and HA2 where the single arginine residue in the human sequences is replaced by six charged amino acids in the avian FPV haemagglutinin. As shown in Fig. 5 and Table 1, there is considerable sequence homology between the haemagglutinins of all three subtypes (30%). The similarity is even more marked between H2 and Hav1 haemagglutinins (43%), H2 and H3 haemagglutinins (42%) and Hav1 and H3 haemagglutinins (48%). Within the H3 subtype there is 95% sequence homology between the 1968 (X-31) and 1975 (Victoria) isolates. There is a much greater degree of conservation in HA2 than in HA1. Although there can be extensive variation in amino acid sequence (especially in HA1), the results of these observations on the constant size of the haemagglutinins and comparative studies of their secondary structure[43] suggest that all haemagglutinins have a similar three-dimensional structure. This idea is emphasized by the striking conservation of the location of the cysteine residues (Fig. 6) which is probably due to constraints on the folding of the molecule and formation of disulphide bridges. The only portion of the molecule in which there is any variation in the location of the sulphydryl residues is at the COOH terminus where the H3[9-11] and Hav1 haemagglutinins have more cysteines than the H2 protein. Since these residues are probably embedded in the lipid bilayer, their positions may not be constrained by the requirement for formation of disulphide bonds. We have shown that in Japan haemagglutinin all 12 cysteine residues in the external protein spike are involved in disulphide bridges, of which only one (Cys 4-Cys 462) is an interchain link between HA1 and HA2 (unpublished results). The secondary structure formed by the remaining three cysteines, which are either in the lipid bilayer or on the inner side of the membrane, has not yet been elucidated. It is clear, however, that although the COOH terminus, which may be on the inner side of the membrane, could interact with the viral matrix protein, the two cysteine residues at positions 2 and 5 from the terminus of HA2 do not form disulphide bonds linking the two proteins.

Table 1 Conservation of amino acids in haemagglutinin sequences

Amino acids conserved in haemagglutinin sequences of	HA No. (%)	HA1 No. (%)	HA2 No. (%)
All 3 strains (H2, H3, Hav1)	165 (30)	72 (22)	93 (42)
H2 (Japan) and H3 (Victoria)	229 (42)	118 (36)	111 (50)
H2 (Japan) and Hav1 (FPV)	235 (36)	118 (36)	117 (53)
H3 (Victoria) and Hav1 (FPV)	263 (48)	119 (36)	144 (65)
Total	547	325	222

Glycosylation of the haemagglutinins

The haemagglutinin molecule is glycosylated during transport from the endoplasmic reticulum to the plasma membrane of the infected cell[44]. Figure 6 shows the positions of the predicted

```
JAP cRNA   5'-AGCAAAAGCAGGGGUUAUACCAUAGACAACCAAAAGCAAAACA-------------------------------AUG GCC AUC AUU UAU CUC AUU CUC CUG 70
X31 cRNA   5'-AGCAAAAGCAGGGGAUAAUUCUAUUAAUC-AUG AAG ACC AUC AUU GCU UUG AGC UAC AUU UUC UGU CUG GCU CUC GGC CAA GAC CUU CCA

JAP  UUC ACA GCA GUG AGA GGG GAC CAG AUA UGC AUU GGA UAC CAU GCC AAU AAU UCC ACA GAG AAG GUC GAC ACA AAU CUA GAG CGG AAC GUC 160
X31  GGA AAU GAC AAC AGC ACA GAC ACG CUG UGC CUG GGA CAU CAU GCG GUG CCA AAC GGA ACA CUA GUG AAA ACA AUC ACA GAU GAU CAG AUU

JAP  ACU GUG ACU CAU GCC AAG GAC AUU CUU GAG AAG ACC CAU AAC GGA AAG UUA UGC AAA CUA AAC GGA AUC CCU CCA CUU GAA CUA GGG GAC 250
X31  GAA GUG ACU AAU GCU ACU GAG CUA GUU CAG AGC UCC UCA ACG GGG AAA AUA UGC AAC --- AAU CCU CAU CGA AUC CUU GAU GGA AUA GAC

JAP  UGU AGC AUU GCC GGA UGG CUC CUU GGA AAU CCA GAA UGU GAU AGG CUU CUA AGU GUG CCA GAA UGG UCC UAU AUA AUG GAG AAA GAA AAC 340
X31  UGC ACA CUG AUA GAU GCU CUA UUG GGG GAC CCU CAU UGU GAU --- GUU UUU CAA AAU GAG ACA UGG GAC CUU UUC GUU GAA CGC AGC AAA

JAP  CCG AGA GAC GGU UUG UGU UAU CCA GGC AGC UUC AAU GAU UAU GAA GAA UUG AAA CAU CUC CUC AGC AGC GUG AAA CAU UUC GAG AAA GUA 430
X31  GCU UUC AGC AAC --- UGU UAC CCU UAU GAU GUG CCA GAU UAU GCC UCC CUU AGG UCA CUA GUU GCC UCG UCA GGC ACU CUG GAG UUU AUC

JAP  AAG AUU CUG CCC AAA GAU AGA UGG ACA CAG CAU ACA ACA ACU GGA GGU UCA CGG GCC UGC GCG GUG UCU GGU AAU CCA UCA UUU UUC AGG 520
X31  ACU GAG GGU UUC ACU --- --- UGG ACU GGG GUC ACU CAG AAU GGG GGA AGC AAU GCU UGC AAA AGG GGA CCU GGU AGC GGU UUU UUC AGU

JAP  AAC AUG GUC UGG CUG ACA AAG GAA GGA UCA GAU UAU CCG GUU GCC AAA GGA UCG UAC AAC AAU ACA AGC GGA GAA CAA AUG CUA AUA AUU 610
X31  AGA CUG AAC UGG UUG ACC AAA UCA GGA AGC ACA UAU CCA GUG CUG AAC GUG ACU AUG CCA AAC AAU GAC AAU UUU GAC AAA CUA UAC AUU

JAP  UGG GGG GUG CAC CAU CCC AUU GAU GAG ACA GAA CAA AGA ACA UUG UAC CAG AAU GUG GGA ACC UAU GUU UCC GUA GGC ACA UCA ACA UUG 700
X31  UGG GGG AUU CAC CAC CCG AGC ACG AAC CAA GAA CAA ACC AGC CUG UAU GUU CAA GCA UCA GGG AGA GUC ACA GUC UCU ACC AGG AGA AGC

JAP  AAC AAA AGG UCA ACC CCA GAA AUA GCA ACA AGG CCU AAA GUG AAU GGA CAA GGA GGU AGA AUG GAA UUC UCU UGG ACC CUC UUG GAU AUG 790
X31  CAG CAA ACU AUA AUC CCG AAU AUC GGG UCC AGA CCC UGG GUA AGG GGU CUG UCU AGU AGA AUA AGC AUC UAU U 777

JAP  UGG GAC ACC AUA AAU UUU GAG AGU ACU GGU AAU CUA AUU GCA CCA GAG UAU GGA UUC AAA AUA UCG AAA AGA GGU AGU UCA GGG AUC AUG 880

JAP  AAA ACA GAA GGA ACA CUU GAG AAC UGU GAG ACC AAA UGC CAA ACU CCU UUG GGA GCA AUA AAU ACA ACA UUG CCU UUU CAC AAU GUC CAC 970

JAP  CCA CUG ACA AUA GGU GAG UGC CCC AAA UAU GUA AAA UCG GAG AAG UUG GUC UUA GCA ACA GGA CUA AGG AAU GUU CCC CAG AUU GAA UCA 1060

JAP  AGA GGA UUG UUU GGG GCA AUA GCU GGU UUU AUA GAA GGA GGA UGG CAA GGA AUG GUU GAU GGU UGG UAU GGA UAC CAU CAC AGC AAU GAC 1150

JAP  CAA GGA UCA GGG UAU GCA GCA GAC AAA GAA UCC ACU CAA AAG GCA UUU GAU GGA AUC ACC AAC AAG GUA AAU UCU GUG AUU GAA AAG AUG 1240

JAP  AAC ACC CAA UUU GAA GCU GUU GGG AAG GAA UUC GGU AAC UUA GAG AGA AGA CUG GAG AAC UUG AAC AAA AGG AUG GAA GAC GGG UUU CUA 1330

JAP  GAU GUG UGG ACA UAC AAU GCU GAG CUU CUA GUU CUG AUG GAA AAU GAG AGG ACA CUU GAC UUU CAU GAU UCU AAU GUC AAG AAU CUG UAU 1420

JAP  GAU AAA GUC AGA AUG CAG CUG AGA GAC AAC GUC AAA GAA CUA GGA AAU GGA UGU UUU GAA UUU UAU CAC AAA UGU GAU GAU GAA UGC AUG 1510

JAP  AAU AGU GUG AAA AAC GGG ACG UAU GAU UAU CCC AAG UAU GAA GAA GAG UCU AAA CUA AAU AGA AAU GAA AUC AAA GGG GUA AAA UUG AGC 1600

JAP  AGC AUG GGG GUU UAU CAA AUC CUU GCC AUU UAU GCU ACA GUA GCA GGU UCU CUG UCA CUG GCA AUC AUG AUG GCU GGG AUC UCU UUC UGG 1690

JAP  AUG UGC UCC AAC GGG UCU CUG CAG UGC AGG AUC UGC AUA UGA UUAUAAGUCAUUUUAUAAUUAAAAACACCCUUGUUUCUACU-3' 1773
```

Fig. 4 Complementary RNA sequences of haemagglutinin genes derived by sequence analysis of the cloned gene inserts in plasmids 2G10, ExB6 and 4F12.

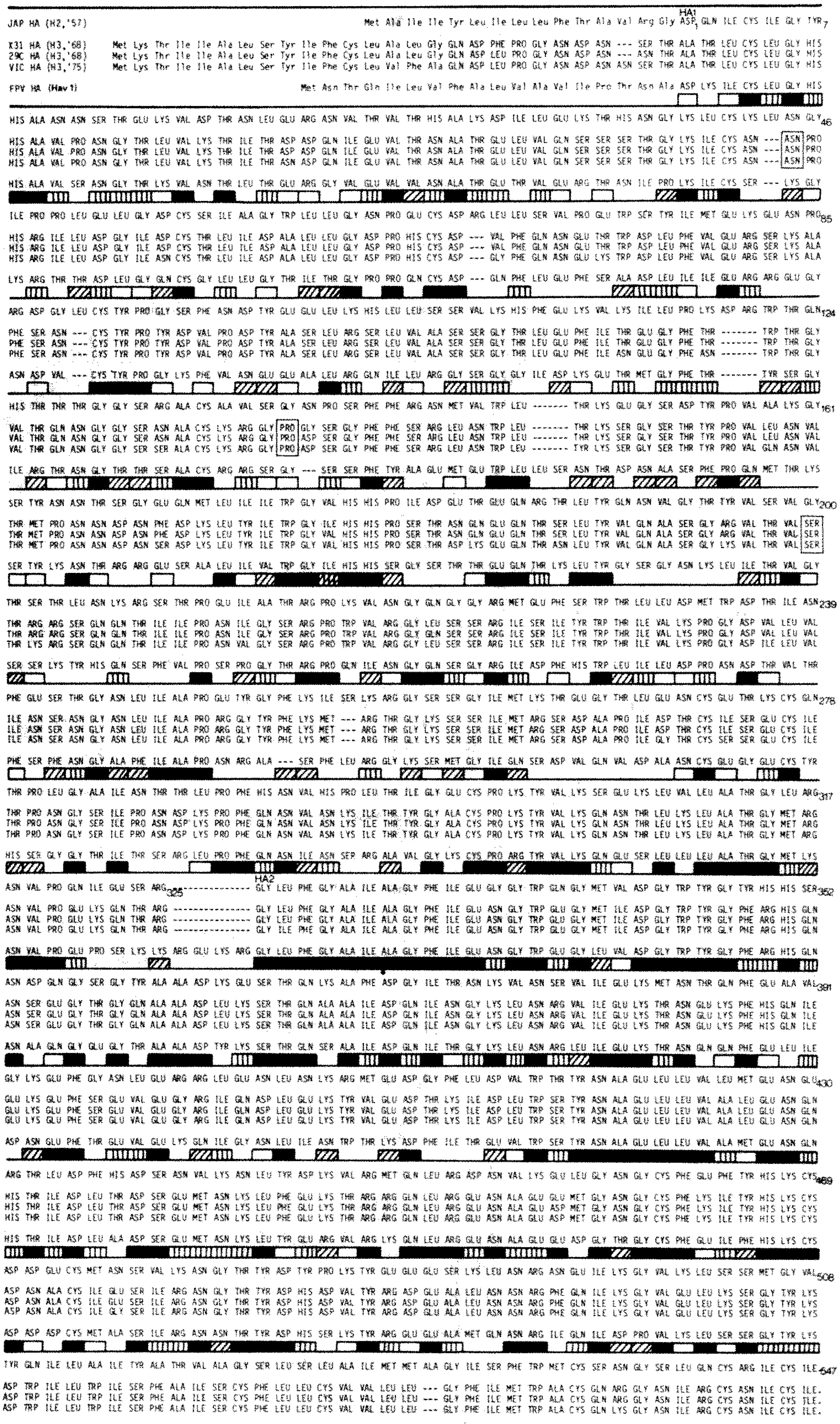

Fig. 5 Amino acid sequences of influenza haemagglutinins. The amino acid sequences of the Japan (H2) and X-31 (H3) haemagglutinins are compared with the sequences from other strains: Victoria (H3)[9] NT60/29C (H3)[10] and Fowl Plague Virus (Hav1)[8]. The COOH terminal amino acid sequence of the X31 haemagglutinin which was not determined by us is from Verhoeyen *et al.*[11]. The sequences have been aligned to maximize homology which is shown between ■, H2, H3 and Hav1 proteins; ▨, H2 and H3 proteins; □, H2 and Hav1 proteins; and ▥, H3 and Hav1 proteins.

carbohydrate attachment sites Asn-X-Ser or Thr[45] in the haemagglutinin sequences. We have confirmed that five of the six possible sites on Japan haemagglutinin are indeed glycosylated (unpublished results). The absence of carbohydrate at the remaining site (Asn$_{139}$-Pro-Ser) is consistent with reports that such a sequence is not glycosylated in other proteins[45]. It remains to establish whether all the other possible sites in the H3 and Hav1 haemagglutinins are in fact glycosylated. Although there is some conservation of the number and position of the carbohydrate residues, there is clearly some latitude for variation in their location. As shown in Fig. 6, there is even variation in the possible attachment sites between haemagglutinins of the H3 subtype. A possible constraint would be a requirement that the carbohydrate should be on the outside of the molecule. Confirmation of such a constraint awaits analysis of the three-dimensional structure of the molecule[46].

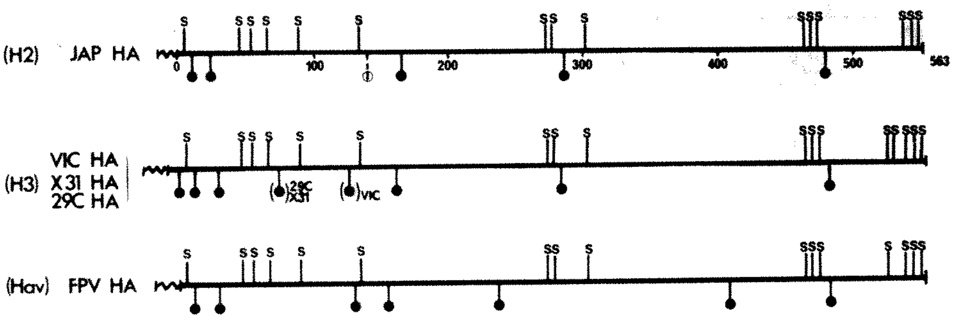

Fig. 6 Schematic representation of the positions of cysteine residues and glycosylation sites in the haemagglutinin amino acid sequences. $\overset{s}{|}$ Cysteine residue; $\overset{\circ}{|}$, carbohydrate side chain;

Antigenicity, shift and drift

The greater degree of variation in HA1 than in HA2 is consistent with the observations[47,48] that the major antigenic sites are located in HA1 and that it is variation in these sites which allows the virus to escape from neutralizing antibody. Between the major shifts in antigenic structure which define the beginning and end of each pandemic era, the haemagglutinin undergoes a series of changes, due to the pressure of increasing antibody prevalence in the population, known as antigenic drift.

The changes responsible for antigenic drift accumulate with time and field strains isolated several years apart from within a single pandemic era (for example, H3 : 1968 to present) show a large number of amino acid changes in peptide mapping studies[49]. In this study we can deduce additional characteristics of the process of antigenic drift by comparing the nucleic acid and protein sequences of the haemagglutinins of the H3 subtype. Clearly, drift occurs by a simple stepwise mutation of the HA nucleotide sequence. There are 65 nucleotide differences between the X-31 (ref. 11) (1968) and Victoria[9] (1975) haemagglutinin genes, resulting in 28 amino acid changes. Although all but one of the amino acid changes could have occurred via single base changes, in five cases double mutations have occurred. The two 1968 isolates (X-31 and the laboratory variant NT60/29C) differ by eight nucleotides and six amino acids. In four cases, the new amino acid is the same as that in the Victoria protein. Similarly, of the 482 amino acids known from the protein chemistry analysis of the haemagglutinin from the 1972 isolate A/Memphis/102/72 (refs 7, 53), 21 amino acids differ in the X-31 protein, although 12 of these amino acids are the same in the NT60 or Victoria haemagglutinins.

It is likely that some of the changes which occur in the haemagglutinin may be antigenically neutral or may cause antigenically significant alterations in distant parts of the protein. So far, it has not been possible to correlate the locations of antigenic sites with the positions of amino acid substitutions. Indeed, the variation within subtypes in a pandemic series is so major that nucleic acid and/or amino acid sequence information from even a large number of field isolates would not provide unequivocal information on the antigenic sites. To simplify this system other workers have used monoclonal antibodies directed against antigenic sites in HA to select variants *in vitro* and thus to mimic antigenic drift[50]. Such studies have so far indicated three or four regions of the HA1 which may constitute antigenic sites. The positions which change in these variants are boxed in Fig. 5.

The more dramatic changes which constitute an antigenic shift are illustrated by a comparison of the amino acid sequences of the H2 and H3 pandemic subtypes (Fig. 5). Clearly the H3 haemagglutinin cannot have arisen by stepwise mutation of the gene of the previous H2 pandemic type and they are so different that it is impossible to map the various antigenic sites by comparing their primary sequences. Furthermore, the fact that the haemagglutinins of the two human strains are no more similar to each other than to that of the avian strain makes it impossible to establish a genealogical tree which would define the evolutionary relationship between them. Recombination or reassortment of haemagglutinin genes between influenza viruses of humans and those of domestic or wild animals has been suggested as the mechanism of antigenic shift[51]. The data presented here are not inconsistent with such a theory.

Hybrid plasmids were transfected into and propagated in *E. coli* χ1776 in containment conditions approved by the British Genetic Manipulation Advisory Group.

Received 28 May; accepted 28 July 1980.

1. Hirst, G. K. *J. exp. Med.* **75,** 49–64 (1942).
2. Klenk, H. D., Rott, R., Orlich, M. & Blödorn, J. *Virology* **68,** 426–439 (1975).
3. Lazarowitz, S. G. & Choppin, P. W. *Virology* **68,** 440–454 (1975).
4. Gething, M. J., White, J. M. & Waterfield, M. D. *Proc. natn. Acad. Sci. U.S.A.* **75,** 2737–2740 (1978).
5. Laver, W. G. & Kilbourne, E. D. *Virology* **30,** 493–501 (1966).
6. Waterfield, M. D., Espelie, K., Elder, K. & Skehel, J. J. *Br. med. Bull.* **35,** 57–63 (1979).
7. Ward, C. W. & Dopheide, T. A. *Br. med. Bull.* **35,** 51–56 (1979).
8. Porter, A. G. *et al. Nature* **282,** 471–477 (1979).
9. Min Jou, W. *et al. Cell* **19,** 683–696 (1980).
10. Both, G. W. & Sleigh, M. J. *Nucleic Acids Res.* **8,** 2561–2575 (1980).
11. Verhoeyen, M. *et al. Nature* **286,** 771–776 (1980).
12. Hay, A. J. *et al. Devl Biol.* **39,** 15–24 (1977).
13. Kilbourne, E. D. *Bull. Wld Hlth Org.* **41,** 643 (1969).
14. Sippel, A. E. *Eur. J. Biochem.* **37,** 31–40 (1973).
15. Buell, G. N., Wickens, M. P., Payvar, F. & Schimke, R. T. *J. biol. Chem.* **253,** 2471–2482 (1978).
16. Sleigh, M. J., Both, G. W. & Brownlee, G. G. *Nucleic Acids Res.* **6,** 1309–1321 (1979).
17. Wood, K. O. & Lee, J. C. *Nucleic Acids Res.* **3,** 1961–1971 (1976).
18. Roychoudhury, R., Jay, E. & Wu, R. *Nucleic Acids Res.* **3,** 863–877 (1976).
19. Bolivar, F. *et al. Gene* **2,** 95–113 (1977).
20. Twigg, A. J. & Sharratt, D. *Nature* **283,** 216–218 (1980).
21. Wickens, H. P., Buell, G. N. & Schimke, R. T. *J. biol. Chem.* **253,** 2483–2495 (1978).
22. Seeburg, P. H., Shine, J., Martial, J. A., Baxter, J. D. & Goodman, H. M. *Nature* **270,** 486–494 (1977).
23. Curtiss, R. III *et al.* in *Molecular Cloning of Recombinant DNA Proc. Miami Winter Symposia, January 1977* (eds Scott, W. A. & Werner, R.) 99–111 (Academic, New York, 1977).
24. Grunstein, M. & Hogness, D. S. *Proc. natn. Acad. Acad. Sci. U.S.A.* **72,** 3961–3965 (1975).
25. Taylor, J. M., Illmensee, R. & Summers, J. *Biochim. biophys. Acta* **442,** 324–330 (1976).
26. Alwine, J. C., Kemp, D. J. & Stark, G. R. *Proc. natn. Acad. Sci. U.S.A.* **74,** 5350–5354 (1977).
27. Maniatis, T., Jeffrey, A. & Kleid, D. G. *Proc. natn. Acad. Sci. U.S.A.* **72,** 1184–1188 (1975).
28. Maxam, A. M. & Gilbert, W. *Proc. natn. Acad. Sci. U.S.A.* **74,** 560–564 (1977).
29. Skehel, L. J. & Hay, A. J. *Nucleic Acids Res.* **5,** 1207–1219 (1978).
30. McCauley, J. *et al. FEBS Lett.* **108,** 422–426 (1979).
31. Air, G. M. *Virology* **97,** 468–472 (1979).
32. Emtage, J. S. *et al. Nature* **283,** 171–174 (1980).
33. Roberts, T. M., Kacich, R. & Ptashne, M. *Proc. natn. Acad. Sci. U.S.A.* **76,** 760–764 (1979).
34. Laver, W. G. *Virology* **45,** 275–288 (1971).
35. Choppin, P. W., Lazarowitz, S. G. & Goldberg, A. R. in *Negative Strand Viruses* Vol. 1 (eds Mahy, B. W. J. & Barry, R. D.) 105–119 (Academic, London, 1975).
36. Rott, R., Klenk, H.-D. & Scholtissek, C. in *The Influenza Virus Haemagglutinin* (eds Laver, W. G., Bachmayer, H. & Weil, R.) 69–81 (Springer, New York, 1978).
37. Skehel, J. J. & Waterfield, M. D. *Proc. natn. Acad. Sci. U.S.A.* **72,** 93–97 (1975).
38. Elder, K. T., Bye, J. M., Skehel, J. J., Waterfield, M. D. & Smith, A. E. *Virology* **95,** 343–350 (1979).
39. Strauss, A. W., Bennett, C. D., Donohue, A. M., Rodkey, J. A. & Alberts, A. W. *J. biol. Chem.* **252,** 6846–6855 (1977).
40. Springer, T. A. & Strominger, J. L. *Proc. natn. Acad. Sci. U.S.A.* **73,** 2481–2482 (1976).
41. Furthmayr, H., Galardy, R. E., Tomita, M. & Marchesi, V. T. *Archs Biochem. Biophys.* **185,** 21–29 (1978).
42. Orr, H. T., Lancet, D., Robb, R., Lopez de Castro, J. A. & Strominger, J. L. *Nature* **282,** 266–270 (1979).
43. Flanagan, M. T. & Skehel, J. J. *FEBS Lett.* **80,** 57–60 (1973).
44. Compans, R. W. *Virology* **55,** 541–545 (1973).
45. Neuberger, A., Gottschalk, A., Marshall, R. O. & Spiro, R. G. in *The Glycoproteins: their Composition, Structure and Function* (ed. Gottschalk, A.) 450–490 (Elsevier, Amsterdam, 1972).
46. Wiley, D. C. & Skehel, J. J. *J. molec. Biol.* **112,** 343–347 (1977).
47. Brand, C. M. & Skehel, J. J. *Nature new Biol.* **238,** 145–147 (1972).
48. Jackson, D. C., Dopheide, T. A., Russell, R. J., White, D. O. & Ward, C. W. *Virology* **93,** 458–465 (1979).
49. Laver, W. G., Air, G. M., Dopheide, T. A. & Ward, C. W. *Nature* **283,** 454–457 (1980).
50. Laver, W. G. *et al. Virology* **98,** 226–237 (1979).
51. Laver, W. G. & Webster, R. G. *Br. med. Bull.* **35,** 29–33 (1979).
52. Scheller, R. H., Dickerson, R. E., Boyer, H. W., Riggs, A. D. & Itakura, K. *Science* **196,** 177–180 (1977).
53. Ward, C. W. & Dopheide, T. A. A. *Virology* **103,** 37–53 (1980).

LETTERS

Massive black hole binaries in active galactic nuclei

M. C. Begelman*, R. D. Blandford† & M. J. Rees‡

* Department of Astronomy, University of California, Berkeley, California 94720
† Theoretical Astrophysics, California Institute of Technology, Pasadena, California 91125
‡ Institute of Astronomy, Madingley Road, University of Cambridge, Cambridge CB3 0HA, UK

Most theoretical discussions of active galactic nuclei (including quasars) attribute their energy production either to an accreting black hole or to a precursor stage—for instance a dense star cluster or a supermassive star—whose inevitable end point is a massive black hole[1]. We explore here the possibility that some active nuclei may contain two massive black holes in orbit about each other. This hypothesis suggests a new interpretation for the observed bending[2] and apparent precession[3] of radio jets emerging from these objects and may indeed be verified through detection of the direct consequences of orbital motion.

There are straightforward reasons for surmising that supermassive binaries exist[4,5]: mergers between galaxies appear to be frequent; cD galaxies in clusters and small groups were quite probably formed in this manner[6–9]; and there is direct evidence that the nearby active galaxy Centaurus A is a merger product[9]. If most galaxies contain massive black holes in their nuclei—relics of earlier activity—then they will settle, under dynamical friction, in the core of a merged stellar system. Many cD galaxies do indeed contain double or multiple cores that may have been formed in this way[10]. There are other scenarios for binary black hole formation. For instance, a rotating super-massive star may undergo bar-mode instability and fission into two components that both collapse[1].

The dynamical evolution of a pair of massive black holes in the violently relaxed core of a newly merged galaxy proceeds through several stages.

(1) The black holes are probably surrounded by dense stellar clusters; that within the less massive galaxy should be denser and will survive intact until the nuclei merge. Dynamical friction is extremely efficient[6] and the cores merge and undergo violent relaxation in a characteristic galactic dynamical time $t_{\rm gal} \sim 10^8$ yr.

(2) The captured hole sinks toward the centre of the stellar distribution on the dynamical friction time scale:

$$t_{\rm df} \sim \frac{6\times 10^6}{\log N}\left(\frac{v_{\rm c}}{300\ {\rm km\ s^{-1}}}\right)\left(\frac{r_{\rm c}}{100\ {\rm pc}}\right)^2 m_8^{-1} \quad {\rm yr} \qquad (1)$$

where the core is presumed to have a central velocity dispersion $v_{\rm c}$, a core radius $r_{\rm c}$ and contain N stars, mass m^*. m_8 is the mass of the smaller black hole, in units of $10^8\ M_\odot$, presumed to be associated with the smaller galaxy. M is the mass of the larger black hole, assumed to be less than Nm^* (the mass of the core). $t_{\rm df}$ is generally longer than the core crossing time and so the merged cores should be fairly relaxed.

(3) When the black hole separation r shrinks to a value $r_{\rm B} \sim (M/Nm_*)^{1/3} r_{\rm c}$, they will become bound to each other with an orbital velocity that is initially smaller than the velocity dispersion of the stars by a factor $(M/Nm_*)^{1/3}$.

(4) The holes continue to spiral together under dynamical friction. As the binary becomes 'harder', the maximum impact parameter for effective energy transfer diminishes as $(r/r_{\rm B})^{3/2} r_{\rm c}$ because a binary cannot lose energy effectively to a field star during an encounter which lasts longer than one orbital period. For longer encounter times, the orbital energy is adiabatically invariant and the energy transfer diminishes exponentially[11]. This affects $t_{\rm df}$ only through the logarithm as long as the binding energy of the binary is small compared with the total kinetic energy of all the stars whose orbits pass sufficiently close to interact effectively.

(5) When $r \leqslant r_{\rm lc} = (m/M)^{1/4}(r_{\rm B}/r_{\rm c})^{9/4} r_{\rm c}$, this condition is violated and further stellar dynamical evolution is controlled by the rate at which stars whose orbits do not come close to the binary can diffuse into more radial 'loss cone' orbits[12] that pass within a radius $\sim r$. Two-body 'star–star' relaxation will repopulate the loss cone in a time ~(solid angle of loss cone) × (two-body relaxation time). The loss cone must be repopulated $(r_{\rm lc}/r)^4$ times to halve the binary orbit. The relevant binary evolution time is then:

$$t_{\rm lc} \sim t_{\rm df} \max\left[1, \left(\frac{m}{M}\right)^{7/4} N\left(\frac{r_{\rm B}}{r_{\rm c}}\right)^{27/4}\left(\frac{r_{\rm lc}}{r}\right)\right] \qquad (2)$$

Collective effects may, however, lead to a more rapid repopulation of the loss cone[13] and evolution on a time closer to $t_{\rm df}$.

(6) The binary becomes 'hard' when its orbital speed reaches $v_{\rm c}$ at a separation $r_{\rm h} \sim (r_{\rm B}/r_{\rm c})^3 r_{\rm c}$. The maximum impact parameter for dynamical friction is now $(rr_{\rm h})^{1/2}$. Each interacting star on average carries off a fraction $\sim m_* m/M^2$ of the binary's binding energy. The binary evolution time scale is now

$$t_{\rm h} \sim t_{\rm df} \max\left[\left(\frac{r_{\rm h}}{r}\right)\ln N, \left(\frac{M}{Nm^*}\right)^2 N\right] \qquad (3)$$

(7) When the binary becomes sufficiently tightly bound, gravitational radiation shrinks the orbit on a time scale $|r/\dot{r}|$ given by

$$t_{\rm GR} \sim 3\times 10^5 \left(\frac{m}{M}\right)^{-1} M_8^{-3} r_{16}^4 \quad {\rm yr} \qquad (4)$$

(8) The evolution now proceeds quite rapidly to coalescence (which takes a time $\sim M_8$ h). This may be accompanied by a powerful burst of electromagnetic radiation, depending on the local gas density and magnetic field strength, as well as a pulse of gravitational radiation[4,5]. Indeed, the final plunge will lead to the emission of net linear momentum and the recoil may be sufficient to eject the combined hole from the core and hence from the galaxy[5].

In addition to these stellar dynamical effects, infall of gas onto the binary can also lead to some orbital evolution. Gas may be flung out of the system, acquiring energy (and angular momentum) at the expense of the binary; alternatively, gas may accrete onto the larger hole, causing orbital contraction as the product Mr is adiabatically invariant. In either case, the evolution time scale is

$$t_{\rm gas} \sim 10^8 M_8 (\dot{M}/1 M_\odot\ {\rm yr}^{-1})^{-1} \quad {\rm yr} \qquad (5)$$

During phases of nuclear activity, gas infall rates $\dot{M}$ of 1–10 $M_\odot\ {\rm yr}^{-1}$ are required for times 10^7–10^8 yr. It is, therefore, quite likely that this process controls the binary evolution when r just exceeds $r_{\rm GR}$ and the stellar dynamical effects are weakest.

These time scales, $|r/\dot{r}|$, are given schematically in Fig. 1. It is clear that the longest evolutionary phase, and therefore the one containing most potentially observable binaries, is that with $r_{\rm h} \gtrsim r \gtrsim r_{\rm GR}$. During this phase a tight binary will persist in a quiescent state with almost constant r, except when it is undergoing fuelling and it becomes a conspicuous source of non-thermal power. The energy dissipated by the material flung out (at the expense of the binary orbital energy) is generally negligible at this time[14]. Slow secular contraction proceeds during active phases and pauses during intervals of quiescence. The details and statistics of observability depend on the time-dependence of $\dot{M}$ (is it intermittent or recurrent?, are the active phases as long as $M/\dot{M}$?). In conditions appropriate to galaxies like M87 ($r_{\rm c} \sim 100$ pc, $v_{\rm c} \sim 300\ {\rm km\ s^{-1}}$, $Nm^* \sim 3\times 10^9\ M_\odot$) it is

028-0836/80/390307—03$01.00

clear that the two-body evolution times given by equations (2) and (3) are much longer than $t_{\rm gas}$. (This may not be true for much less massive cores and small holes, $M \leqslant 10^6 M_\odot$.) If the binary gains mass at a constant rate, then the probability of observing a binary with separation greater than r will fall as r^{-1}. If $\dot{M} \propto M$, then binaries are distributed uniformly in log r. In any case, the separation $r_{\rm GR}$ at which gravitational radiation becomes dominant is insensitive to the values of $t_{\rm h}$ and $t_{\rm gas}$,

$$r_{\rm GR} = 5 \times 10^{16} \left(\frac{m}{M}\right)^{1/4} M_8^{3/4} \times \left[\frac{\min\,(t_{\rm h}, t_{\rm gas})}{10^8\ {\rm yr}}\right]^{1/4} {\rm cm} \tag{6}$$

For $r \leqslant r_{\rm GR}$ the orbital evolution is very rapid and the probability of observing a binary with separation smaller than r will decline as r^4. Most observed binaries will have $r_{\rm GR} \lesssim r_{\rm h}$.

The most direct evidence for a massive black hole binary would be some manifestation of the keplerian motion, which has a period

$$P_{\rm orb} \sim 1.6 r_{16}^{3/2} M_8^{-1/2} \quad {\rm yr} \tag{7}$$

Any eccentricity in the orbit will almost certainly be erased by the frictional drag and so the orbit is assumed to be circular. We generally expect the spin axes of the holes to be misaligned unless thay have both accreted a substantial amount of gas with a fixed angular momentum[15]. The spin axes will then undergo geodetic precession about the total angular momentum. For the more massive hole, the period is,

$$P_{\rm prec} \sim 600 r_{16}^{5/2} (M/m) M_8^{-3/2} \quad {\rm yr} \tag{8}$$

The spin angular momentum will be small compared with that in the binary provided that $(m/M) \geqslant (GM/rc^2)^{1/2}$ and so the spins precess in a cone with the orbital angular momentum as axis.

The beams of plasma which give rise to compact and extended radio structure in active galaxies may be collimated sufficiently near a massive black hole that the Lense–Thirring effect aligns them with the hole's axis[15], irrespective of the original momentum of the inflowing gas. (This requires the collimation scale to be much smaller than the binary separation r in the phases that concern us here.) The beams will then process with period $P_{\rm prec}$. It has been suggested that a scaled-down version of this mechanism causes a pair of jets to precess in SS433 (refs 16, 17).

As $(r_{\rm h}/r_{\rm GR})$ can be as large as 10^4, $P_{\rm orb}$ and $P_{\rm prec}$ can span many orders of magnitude and be made manifest in different ways. We outline below two examples that could correspond to different phases in the evolution of a binary. The observed activity is assumed to be only associated with the more massive component.

Wide binary ($r_{16} \sim 30$, $M_8 \sim 1$, $m_8 \sim 0.1$). In this case the precession time scale is $\sim 3 \times 10^7$ yr—comparable with the inferred lifetime of extended radio components. Precession of the beam axis would then result in an inversion symmetry in the source structure. Such precession has been inferred[3] on phenomenological grounds, but the massive binary seems to be the only way to set this in a dynamical context. (Jet alignment can occur, however, with a lone black hole[15].) Note that the morphology may differ from that associated with a ballistic trajectory, because of gas-dynamical effects, but should nevertheless have the same average symmetry (M.C.B., in preparation).

The orbital period (300 yr) would be too long to be detected directly. However, the broad emission lines may originate in a region around the more massive hole while the narrow lines would come from a much larger system enveloping the binary. The broad lines may then peak at a velocity up to $\sim 10{,}000\, r_{16}^{-1/2} M_8^{-1/2} m_8$ km s^{-1} different from that of the galaxy as determined by the narrow lines. Blue- and redshifts (relative to the narrow lines) should be about equally common.

Close binary ($r \sim r_{\rm GR}$, $t_{\rm gas} \sim 10^8$ yr). In this case $P_{\rm orb} \sim 18(m/M)^{3/8} M_8^{5/8}$ yr, $P_{\rm prec} \sim 3 \times 10^4 (M/m)^{3/8} M_8^{3/8}$ yr. Any extended radio structure associated with jets, built up over many precession periods, will be aligned with the orbital angular momentum; the precession related curvature will be discernible, however, on the scales probed by VLBI or the VLA.

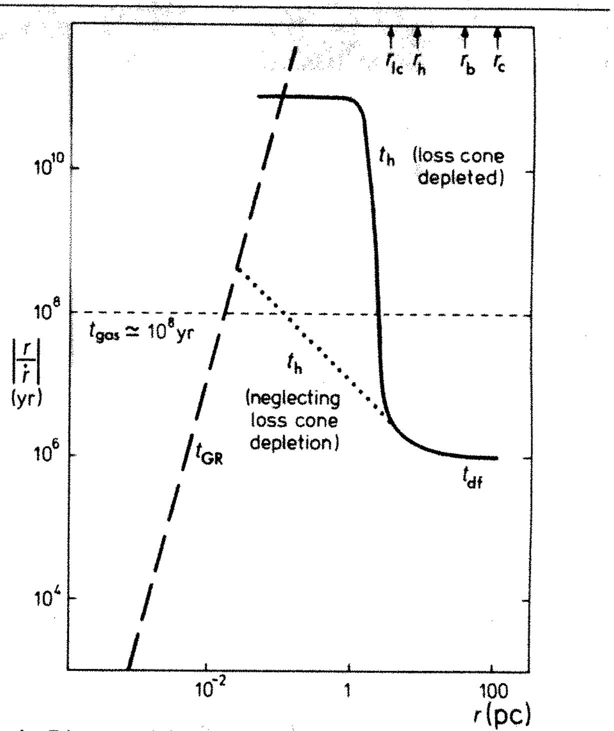

Fig. 1 Diagram of the time scales involved in the approach, and eventual coalescence, of a supermassive binary. The core parameters chosen are those that might be appropriate to a giant elliptical: $r_c \sim 100$ pc, $v_c \sim 300$ km s^{-1}, $N \sim 2 \times 10^9$ and $m_* \sim 1$. The members of the binary are taken to have masses $M_8 = 1$ and $m_8 = 0.3$. For this system, $t_{\rm df} \sim 10^6$ yr. Within $r_{\rm h}$ the evolution time scale would be $(r_{\rm h}/r)t_{\rm df}$ if loss cone depletion could be ignored; however, unless collective effects permit replenishment of the loss cone on much less than the ordinary stellar relaxation time, the evolution within $r_{\rm lc}$ proceeds on a very much longer time scale $\geqslant 10^{11}$ yr (compare equation (3)). Influx of gas into the system at a rate $\dot{M} \sim 1\, M_\odot\, {\rm yr}^{-1}$ would however yield a time scale $\sim 10^8$ yr. Gravitational radiation would take over as the dominant mechanism within $1.3 \times 10^{-2} (t_{\rm gas}/10^8\ {\rm yr})^{1/4}$ pc. The values of the various critical radii are indicated. (Note that in this particular example $r_{\rm lc}$ lies inside $r_{\rm h}$; for the case of two similar masses, as discussed in the text, this ordering is reversed.)

Suppose that the jets precess around a cone of semi-angle ϕ. If the jets were narrow with a non-relativistic speed $V \ll c$, a 'snapshot' would reveal the beam material tracing out a spiral pattern around the core: successive turns would be separated by a fixed distance $vP_{\rm prec}$, the pattern becoming more transverse at larger distances from the apex. However, in the 'superluminal' sources the jet velocity is believed to be relativistic with Lorentz factor $\gamma = (1 - v^2/c^2)^{-1/2}$ in the range 5–10 (ref. 2). What is actually observed from a precessing jet is modified by Doppler boosting and light travel time effects that depend on the observer's orientation. We can readily show that this geometry can account for a large bending and consequent misalignment between fast-moving VLBI features and any extended structure.

Let the observer's line of sight make an angle Ψ with the cone axis. The jet will be observed to be brightest when it makes an angle $\lesssim \gamma^{-1}$ with the line of sight. If $\phi \gtrsim \gamma^{-1}$, this implies that for the strongest sources, the observer direction must lie in the hollow cone, $\phi + \gamma^{-1} \gtrsim \Psi \gtrsim \phi - \gamma^{-1}$. Assuming that the emissivity of the jet decreases away from the apex, the source will again appear brightest when the central region points within an angle γ^{-1} at the observer direction, which it will do for a fraction $\sim (2\pi\gamma\phi)^{-1}$ of each precession period. When observed from this direction, a precessing jet will be brightest and appear to bend through an angle ~ 1 radian. Individual inhomogeneities will, however, appear to move rectilinearly. Superluminal expansion of inhomogeneities convected outwards by the jet with apparent speed $\sim\gamma c$ will occur. Curvature of this order has been reported in a number of superluminal radio sources[2]. For 3C273 and 3C345, continuous bending through an angle ~30° is visible on angular scales θ from ~5 to ~30 m arc s. If the distance of the source is d, we can infer the necessary precession period using the fact that the projected expansion speed is $\sim\gamma c$ to obtain,

$$P_{\text{prec}} \sim 2\pi\phi\theta d/c \qquad (9)$$

For 3C273, we substitute $\phi \sim 60°$, $\theta \sim 30$ m arc s, $d = 800$ *Mpc* to obtain $P_{\text{prec}} \sim 500$ yr. We could obtain this short precessional period if $r_{16} \sim 1.7$, $M_8 \sim m_8 \sim 1$, $t_{\text{GR}} \sim 3\times10^6$ yr. More distant sources require somewhat larger and more probable precessional periods. If, as we have assumed, $\phi \gg \gamma^{-1}$, then at large distance from the nucleus the jet will not be subject to large Doppler shifts.

Orbital motion at the source of a jet is another possible source of jet curvature[18]. However, the maximum transverse displacement in a single wavelength is of order the binary separation r, far too small to account for observed bent superluminal sources, though possibly relevant to small scale bends in sources like NGC6251 (ref. 18) which has a jet 1 pc long, misaligned by 3°. This would be expected from a binary with separation $r \sim 10^{17}$ cm.

We have argued that there are good reasons to expect binary black holes in galactic nuclei and that most observed examples will have separations in the range $10^{16}\text{ cm} \leq r \leq 10^{19}$ cm. Wide binaries may be responsible for inversion-symmetric features in large scale jets. Very close binaries may produce bending and misalignment in VLBI jets through the kinematic consequences of precession. Orbital motion may be reflected in the profiles of permitted emission lines; short orbital periods (~10 yr) may even be detectable photometrically using archival plate libraries.

If the binary hypothesis is correct, then we expect that jets that appear to be orbiting or precessing should be associated with cD or irregular galaxies in clusters or groups with large numbers of close companions. Furthermore, estimating the rate of merging and making an evolutionary correction we can compute the frequency of black hole coalescence events from objects at large redshifts to be in the range 10^{-3}–1 yr^{-1} (refs. 4, 5). These events (hypernovae) would be accompanied by detectable bursts of electromagnetic and gravitational radiation of powers that can, in principle, approach $c^5G^{-1} \sim 10^{59}\text{ erg s}^{-1}$ for a duration of ~1 h. However, as with a supernova, the actual peak electromagnetic power will be moderated by the amount of gas surrounding the explosions, and the strength of the gravitational radiation pulse by a fairly small efficiency factor[5].

Of course the evolutionary properties of binaries could be far richer than we have described. For example, drawing an analogy with stellar evolution, if one of the holes possessed a massive extended disk or envelope in which the inflow time is as long as $|r/\dot{r}|$ then mass transfer between the components could be important and may even account for much of the variability associated with quasars. Also, merging may occur more rapidly than evolution of the binary and three or more black holes may collect in the core. In this case a gravitational sling-shot[19] rather than coalescence will probably occur.

The detection of a stellar cusp around a central mass, as has been claimed for M 87 (ref. 20), implies that this mass is probably not a recently merged binary, because if black holes were brought together by dynamical friction they would have scoured out all the stars passing within r_h and there should actually be a deficit of stars in this region. The cusp may, however, be restored if a large mass of gas has subsequently been accreted thus repopulating the cusp.

We thank Juhan Frank for helpful comments. M.C.B. and R.D.B. thank the Institute of Astronomy, Cambridge for hospitality and acknowledge support under NSF grants AST77-23069 and AST78-05484 respectively.

Received 12 June; accepted 30 July 1980.

1. Begelman, M. C. & Rees, M. J. *Mon. Not. R. astr. Soc.* **185,** 847 (1978).
2. Readhead, A. C. S., Cohen, M. H., Pearson, T. J. & Wilkinson, P. N. *Nature* **276,** 768 (1978).
3. Ekers, R. D., Fanti, R., Lari, C. & Parma, P. *Nature* **276,** 588 (1978).
4. Thorne, K. S. & Braginsky, V. B. *Astrophys. J. Lett.* **204,** 1 (1976).
5. Blandford, R. D. *Sources of Gravitational Radiation* (ed. Smarr, L.) (Cambridge University Press, 1979).
6. Ostriker, J. P. & Tremaine, S. D. *Astrophys. J. Lett.* **202,** 113 (1975).
7. Ostriker, J. P. & Hausman, M. A. *Astrophys. J. Lett.* **217,** 125 (1977).
8. White, S. D. M., *Mon. Not. R. astr. Soc.* **191,** 1p (1980).
9. Tubbs, A. preprint (1980).
10. Wyndham, J. D. *Astrophys. J.* **144,** 459 (1966).
11. Heggie, D. C., *Mon. Not. R. astr. Soc.* **173,** 729 (1975).
12. Frank, J. & Rees, M. J. *Mon. Not. R. astr. Soc.* **176,** 633 (1978).
13. Lynden-Bell, D. in *Relativity Theory and Astrophysics* Vol. 2 (ed. Ehlers, J.) 131 (American Mathematical Soc., 1967).
14. Collins, G. W. *Astron. Quart.* **1,** 39 (1977).
15. Rees, M. J. *Nature* **275,** 516 (1978).
16. Martin, P. G. & Rees, M. J. *Mon. Not. R. astr. Soc.* **189,** 19p (1979).
17. Begelman, M. C. *et al. Astrophys. J.* **238,** 722 (1980).
18. Cohen, M. H. & Readhead, A. C. S. *Astrophys. J.* **233,** L101 (1979).
19. Saslaw, W. C., Valtonen, M. J. & Aarseth, S. J. *Astrophys. J.* **190,** 253 (1974).
20. Young, P. J. *et al. Astrophys. J.* **221,** 721 (1978).

Spectral broadening measurements of the ionospheres of Jupiter and Saturn

Richard Woo & J. W. Armstrong

Jet Propulsion Laboratory, California Institute of Technology,
Pasadena, California 91103

When Pioneers 10 and 11 flew by Jupiter, their 2.3-GHz monochromatic radio signals underwent substantial spectral broadening as they propagated through the planet's ionosphere[1,2]. Although spectral broadening has been observed during radio occultation by the solar corona[3,4], the Pioneer measurements of Jupiter represent the first time it has been observed during radio occultation by a planetary atmosphere. The Pioneer data are also unique in that r.f. spectral broadening, a scattering phenomenon normally associated with strong intensity scintillations ($\sigma_\chi^2 \sim 1$ where σ_χ^2 is the variance of the log-amplitude scintillations), occurred when the intensity scintillations were weak. This unusual opportunity makes it possible to compare the theory for spectral broadening with the more widely used weak intensity scintillation theory[5,6]. We report here that good agreement is found, and present the inferred characteristics of the electron density irregularities for the ionospheres of both Jupiter and Saturn. The Saturn results are based on measurements made during the 1979 Pioneer 11 encounter of Saturn.

The details of the Pioneer 10 radio occultation experiment have been discussed elsewhere[1,2,7]. Figure 1 shows the measured r.f. spectrogram at 2.3 GHz for the lower ionosphere (~200–500 km altitude region designated region C by Woo and Yang[7], where altitude is determined by reference[2] to the atmospheric level at which the neutral gas has a refractivity of 10), measured during exit occultation which took place at 26 °N latitude when the solar zenith angle was about 81°. The electron density irregularities in this region have been found to be isotropic[7]. The inherent linewidth over a comparable integration time as determined from measurements outside the ionosphere is less than 0.5 Hz, and can therefore be ignored when interpreting Fig. 1. The three-dimensional spatial wave number spectrum of the refractive index fluctuations corresponding to a power-law spectrum can be written as[6,7]

$$\Phi(x,\kappa) = \frac{\Gamma(p-1)}{4\pi^2}\sin\left[\frac{\pi(p-3)}{2}\right] c_{no}^2 \exp\left[\left(\frac{x-L}{a}\right)^2\right] \kappa^{-p} \qquad (1)$$

where Γ is the gamma function, κ is the spatial wave number, p is the spectral index, c_{no} is the structure constant of refractive index fluctuations, x is the wave propagation direction, L is the spacecraft to planetary limb distance, and a is the extent of the region of irregularities in the x direction.

Figure 2 shows a plot of the structure wave function $D(\tau)$ divided by 2 (refs 4–6). For the power-law density spectrum, a log–log plot of $D(\tau)$ against τ gives an estimate of the spectral index directly from the slope of a linear fit to the data. We have

0028–0836/80/390309—03$01.00

drawn the dashed line which corresponds to $p = 3.3$, and it can be seen that it represents a very good fit to the data. The power spectrum $W_\chi(f)$ of the log-amplitude scintillations over the same time interval has been studied previously[7] and is reproduced in Fig. 3 with the theoretical fit corresponding to $p = 3.3$. The relevant parameters for the theoretical fit are $v = 3.5 \times 10^4$ m s^{-1} (v is the transverse speed of the line-of-sight path), $a = 1.5 \times 10^7$ m and $L = 2.9 \times 10^8$ m. It is clear that the intensity scintillation and spectral broadening measurements are consistent in showing that the density spectrum is power-law with spectral index about 3.3. Comparison of the structure wave function with W_χ shows that the former is a more sensitive estimator of p. Thus, we conclude that p is 3.3 and not 11/3 (Kolmogorov) as obtained from earlier studies of intensity scintillations alone[7].

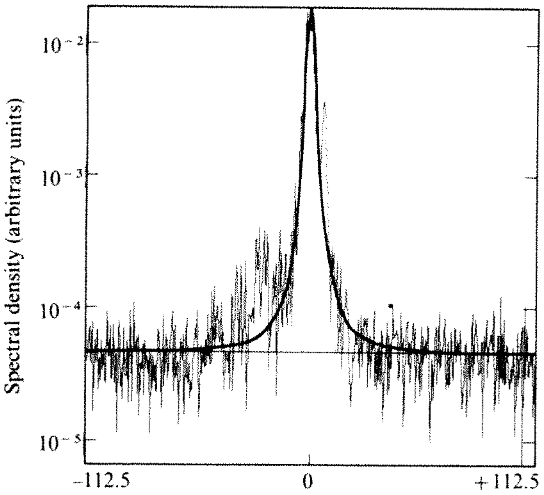

Fig. 1 R.f. spectrogram of Pioneer 10 2.3-GHz signal during Jupiter exit occultation (region C, see text). The heavy solid line is the $p = 3.3$ model discussed in the text, added to an estimate of the system noise (light horizontal line)

For the density spectrum given by equation (1), the variance σ_χ^2 of the log-amplitude scintillations can be obtained[8]

$$\sigma_\chi^2 = \frac{\Gamma(p-1)}{4} \sin\left[\frac{\pi(p-3)}{2}\right] c_{no}^2 \sqrt{\pi}\, a \Gamma\left(\frac{2-p}{2}\right) \cos\left[\left(\frac{2-p}{4}\right)\pi\right] k^{(2-p)/2} L^{(p-2)/2} \tag{2}$$

where k is the free space wave number and equation (2) is valid whenever $\sigma_\chi^2 < 1$. The bandwidth B, which represents the full width between frequencies enclosing half the area under the r.f. spectrum, is related to σ_χ^2 by[8]

$$B = \frac{Av}{2\pi} \sqrt{\frac{k}{L}} \left\{ \frac{4\sigma_\chi^2}{\cos\left[\left(\frac{2-p}{4}\right)\pi\right] \Gamma\left(\frac{p}{2}\right) 2^{p-1}} \right\}^{1/(p-2)} \tag{3}$$

where A is a constant having a value of about 1.95 for $4 \geqslant p \geqslant 3$. Using the measured noise-corrected σ_χ^2 of 0.27 and $p = 3.3$, equation (3) gives $B = 2.5$ Hz. We have superimposed on Fig. 1 the theoretical shape of the spectrum corresponding to these values. As can be seen, the agreement is very good.

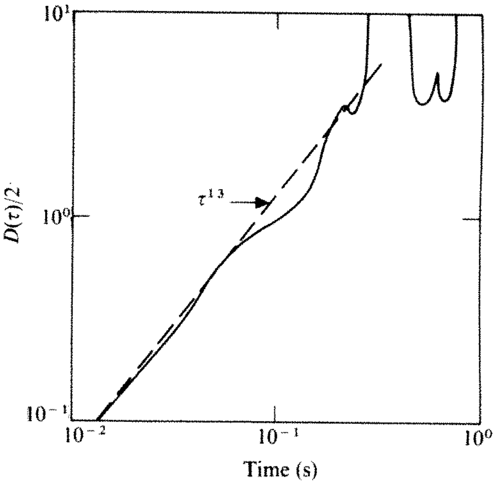

Fig. 2 Structure wave function divided by 2 for spectrum of Fig. 1. The linear fit (dashed line) corresponds to the $p = 3.3$ model.

It is significant that the spectral broadening and intensity scintillation measurements agree so well because this is the first time such a comparison could be made in weak scintillation conditions. When the scintillations become strong, as may be the case when L is large, intensity scintillations become difficult to interpret while the theory for spectral broadening remains valid[5,6]. In this case, spectral broadening becomes the more useful radio observation for measuring the density spectrum. In equation (1) we have assumed that the irregularities are isotropic as is the case for the region C data discussed here. In the upper ionosphere the irregularities are anisotropic because of alignment with the planetary magnetic field[7]. Theoretical results for interpreting spectral broadening measurements taking into account anisotropic irregularities and a general power-law density spectrum are available[9].

Note from equations (2) and (3) that although $\sigma_\chi^2 \sim L^{(p-2)/2}$, B is independent of L but is proportional to v. Thus, like multipath propagation[2], intensity scintillations become more severe when the distance between the planet and spacecraft is increased (as long as $\sigma_\chi^2 \leqslant 1$). On the other hand, the amount of spectral broadening is unchanged as long as v is unchanged. It is also clear from equation (3) that the substantial spectral broadening observed by Pioneers 10 and 11 was due to the very large fly-by velocities, rather than strong intensity scintillations.

The one-dimensional spectrum of the electron density fluctuations is of particular interest because it corresponds to the spectrum measured directly by spacecraft. For the case discussed above, we have $V_{ne}(\kappa) = 2.1 \times 10^{26} k^4 c_{no}^2 \kappa^{-1.3}$. Applying equations (2) and (3) to the results shown in Figs 1–3, we obtain $c_{no} = 8.3 \times 10^{-10}$ m$^{-0.15}$ so that $V_{ne}(\kappa) = 7.8 \times 10^{14} \kappa^{-1.3}$ (el/m^3)^2/m^{-1} for $5 \times 10^{-4} \leqslant \kappa \leqslant 2 \times 10^{-3}$ m^{-1}.

A radio occultation experiment of Saturn was carried out during the recent Pioneer 11 fly-by[10]. We have studied the intensity scintillation and spectral broadening measurements

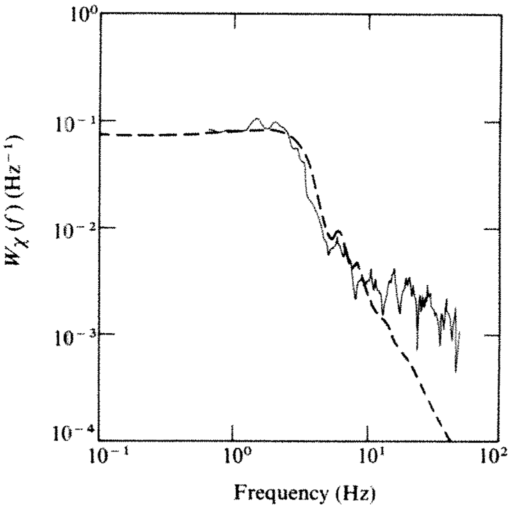

Fig. 3 Fluctuation power spectrum of the log-amplitude scintillations for region C data. Smooth dashed curve is the $p = 3.3$ model. System noise level is about 2.5×10^{-3} Hz^{-1}; the roll-off at high frequencies is due to digital filtering.

made by the ionosphere during exit occultation at latitude 9.5 °S and solar zenith angle 90.6°. Within the instrumental limits of the radio system, neither intensity scintillations nor spectral broadening was detected. Using the relevant parameters for the Saturn occultation ($v = 2.44\times10^4$ m s^{-1}, $L = 1.2\times10^8$ m and $a = 1.6\times10^7$ m) and assuming a density spectrum with $p = 3.3$, we deduce that $c_{no} \leqslant 3.4\times10^{-10}$ m$^{-0.15}$. The corresponding one-dimensional spectrum for the electron density fluctuations is then $V_{ne}(\kappa) \leqslant 1.3\times10^{14}\,\kappa^{-1.3}$ where $\kappa \geqslant 7.8\times10^{-4}$ m^{-1}. The Pioneer 11 measurements, therefore, show that the electron density fluctuations are smaller in the ionosphere of Jupiter. This may not be too surprising because the mean electron densities are higher in the ionosphere of Jupiter[2] than in Saturn[10]. Note that the Pioneer measurements of Jupiter and Saturn represent the observations of only a few locations and that globally these irregularities may vary substantially, as in the case of the Earth's ionosphere[11].

We thank A. Kliore for permitting us to analyse the Pioneer 11 Saturn radio occultation data and for useful discussions, H. Hsu and D. Cheng for help with software development and data analysis, and W. A. Coles for constructive criticism of an earlier version of this report. This report is Jet Propulsion Laboratory Atmospheres Publication 980-7 and presents the results of one phase of research carried out at the Jet Propulsion Laboratory, California Institute of Technology, under contract NAS 7-100, sponsored by the Planetary Atmospheres Program, Office of Space Science, NASA.

Received 25 March; accepted 25 July 1980

1. Kliore, A. *et al. Science* **188**, 474 (1975)
2. Fjeldbo, G., Kliore, A., Seidel, B., Sweetnam, D & Cain, D. *Astr Astrophys* **39**, 91 (1975)
3. Goldstein, R M *Science* **166**, 598 (1969)
4. Woo, R & Armstrong, J W. *J geophys Res.* **84**, 7288 (1979).
5. Tatarskii, V. I. *The Effects of the Turbulent Atmosphere on Wave Propagation* (National Technical Information Service, Springfield, 1971)
6. Ishimaru, A. *Wave Propagation and Scattering in Random Media* Vol 2 (Academic, New York, 1978)
7. Woo, R. & Yang, F C. *J. Geophys. Res* **83**, 5245 (1978).
8. Woo, R., Yang, F. C. & Ishimaru, A. *Astrophys J* **210**, 593 (1976)
9. Woo, R., Yang, F. C & Ishimaru, A *Astrophys* **218**, 557 (1977).
10. Kliore, A *et al. Science* **207**, 446 (1980)
11. Fejer, B G. & Kelley, M C. *Rev Geophys Space Phys* **18**, 401 (1980)

Galileo's observations of Neptune

Charles T. Kowal

Palomar Observatory, California Institute of Technology, Pasadena, California 91125

Stillman Drake

University of Toronto, Toronto, Ontario M5S 1A7, Canada

The planet Neptune was discovered in 1846. As its period of revolution is almost 165 years, Neptune has not yet completed one revolution since its discovery. Largely as a result of this, its orbit is not known with a precision comparable to that of the inner planets. A pre-discovery measurement of Neptune's position by Lalande in 1795 differs from the predicted position by 7 arc s. There is some debate about whether this discrepancy is real or an error of measurement[1]. Clearly, it would be worthwhile to find other pre-discovery observations of this planet. One possible way of finding such observations is to search for close approaches of Neptune to other objects which were frequently observed. Neptune was actually occulted by Jupiter in January 1613 and September 1702 (ref. 2). By 1702 the telescope was in widespread use, and examination of manuscripts of that period should reveal cases where Neptune was seen near Jupiter and mistaken for a star. The abundance of possible material, however, makes a search for such observations lengthy. We have found that Galileo observed the planet Neptune on 28 December 1612 and 28 January 1613. The latter observation may be of astrometric value, and differs by 1 arc min from the predicted position of Neptune. Galileo also detected the motion of Neptune.

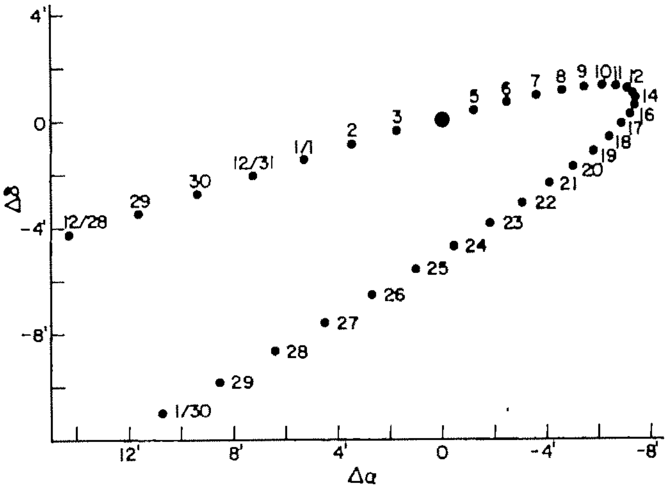

Fig. 1 The positions of Neptune with respect to Jupiter, 28 December 1612 to 30 January 1613. Black dots, Neptune; cross-hatched circle, Jupiter.

We began by examining Galileo's observations of 1612–13. Galileo observed Jupiter almost nightly at that time, and sometimes more than once on the same night. His notebooks have been published in several editions.

Figure 1 shows the ephemeris positions of Neptune with respect to Jupiter for 28 December 1612 to 30 January 1613. The field of view of Galileo's telescope was about 15 arc min, so both planets were within the same field for the entire interval. Jupiter became retrograde in mid-January, and so passed Neptune twice.

Figure 2 shows portions of a page of Galileo's notebooks which cover some of this time interval. In these drawings of Jupiter and its satellites, north is to the upper right, and east to the upper left. The first observation is dated: "1612 December, day 27, hour 15:46 a.m.". This corresponds to 28 December, 0346 a.m., local time. (Galileo considered each day to begin at noon.) A 'fixed star' is marked to the east of Jupiter on this date. The Palomar Sky Survey prints show no bright star in this position. There are, in fact, very few bright stars in that entire region of the sky in the constellation of Virgo. (Galileo was occasionally able to see stars of magnitude 9, but none fainter. Neptune is always brighter than magnitude 8. The galilean satellites have magnitudes of 5 to 6.) We have found that the direction of Galileo's 'star' from Jupiter is almost exactly the direction of Neptune on that night (Fig. 3). It would not have been possible to draw the distance of Neptune to scale, since the planet would have been off the edge of the page, so he put it at the edge of the page and indicated its direction with a dotted line.

Table 1 Mean positions of the objects for 28 January 1613, 2300 UT

Jupiter (from JPL DE 102)	$\alpha = 12$ h 04 min 59.54 s $\delta = +1°02'11.0''$	1950.0
SAO 119234 (includes proper motion)	$\alpha = 12$ h 05 min 27.02 s $\delta = +0°54'10.8''$	1950.0
Neptune (from JPL DE 102)	$\alpha = 12$ h 05 min 33.3 s $\delta = +0°52'24''$	1950.0
Galileo's position of Neptune	$\alpha = 12$ h 05 min 30.5 s $\delta = +0°53'11''$	1950.0

Galileo's position of Neptune with respect to the star is probably accurate to better than 10 arc s as judged from his accuracy in measuring the positions of the satellites. The accuracy of the position of the star itself depends on the accuracy of its proper motion, as listed in the SAO Star Catalog. We have used a total proper motion of 0.13 s in RA, and 11.5″ in declination.

0028–0836/80/390311—03$01 00

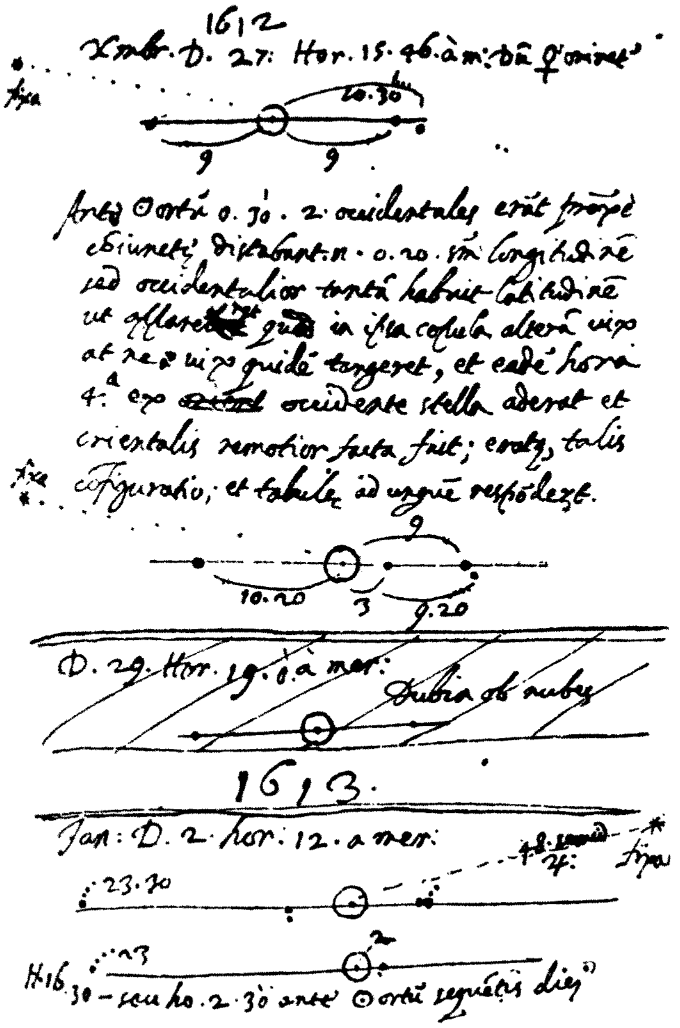

Fig. 2 Portions of a page from Galileo's notebooks, for 27/28 December 1612 to 2/3 January 1613 (ref. 3).

Figure 3 shows the ephemeris positions of the jovian satellites and Neptune for 0300 UT, 28 December 1612, together with the indicated position of Galileo's 'fixed star'. The exact correspondence of the directions and the absence of any bright stars in that area make us confident that Galileo actually saw Neptune on this night—234 yr before that planet was discovered.

Returning to Fig. 2, we see a star marked "48 jovian radii" to the north-west of Jupiter on "1613 January, day 2, hour 12 midnight". This star was easily identified as SAO 119234, visual magnitude 7.1. The star was actually 52 radii from Jupiter at the time. Again, this star would have been off the edge of his notebook paper, so Galileo drew it at the edge of the page.

Galileo must have seen Neptune during each of the following nights. It is puzzling that he did not show the planet in his drawings. Perhaps he did not want to clutter his drawings of the satellites with 'extraneous' objects near the satellite plane.

Figure 4 shows two observations from the end of January 1613. On "day 27" we again find SAO 119234, 20 jovian radii south-east of Jupiter. On the following night, two stars are shown in a separate drawing. The time of this latter observation is given as "day 28, 6 hours after sunset". This corresponds to about 2300 local time on 28 January. A plot of the ephemeris positions of Jupiter, Neptune and the star (Fig. 5), shows immediately that "star 'a'" is SAO 119234, while "star 'b'" is definitely Neptune. Galileo's note in the lower left quarter of this drawing may be translated as follows:

> Beyond fixed star "a", another followed in the same straight line, this is "b", which was also observed on the preceding night, but they (then) seemed farther apart from one another.

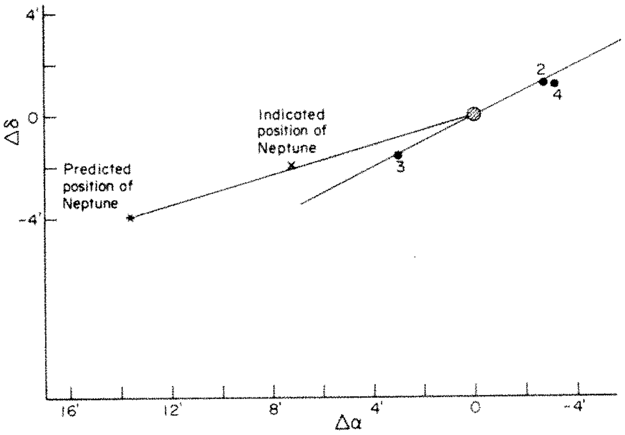

Fig. 3 The positions of Neptune and the jovian satellites, with respect to Jupiter, for 28 December 1612, 0300 UT. All of the positions in this paper are from Development Ephemeris 102, Jet Propulsion Laboratory, Pasadena, California.

Mss. Gal., P. III, T. IV, car. 140r.

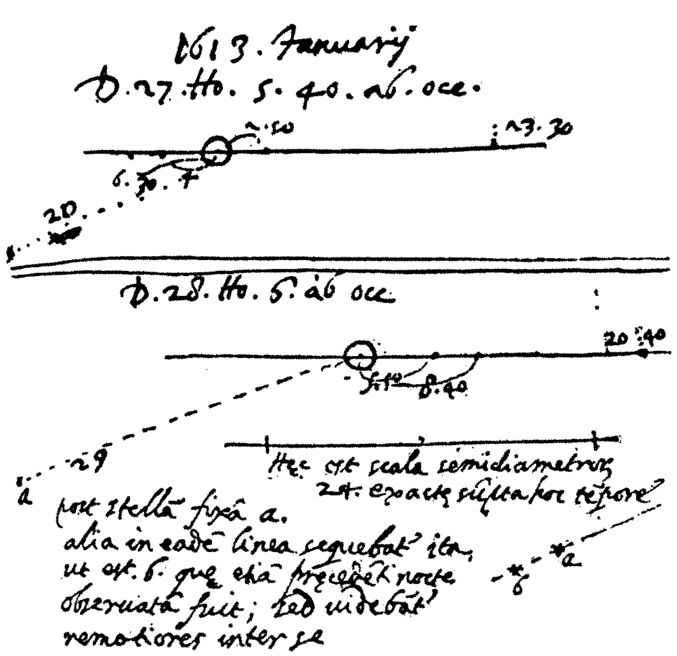
1613. Januarij
a
b

Fig. 4 Galileo's notebook for 26/27 and 27/28 January 1613.

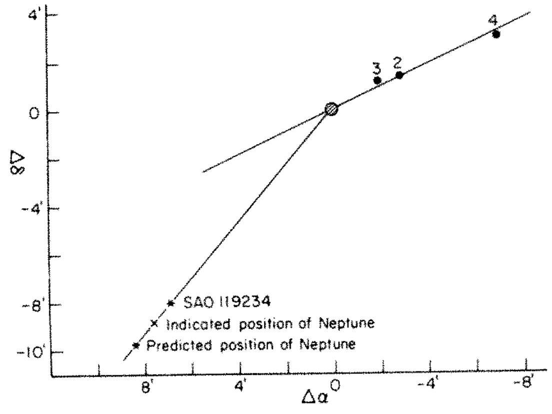

Fig. 5 The positions of Neptune, the jovian satellites and a star, for 28 January 1613, 2300 UT.

In other words, not only did Galileo see Neptune, he also noticed that it had moved with respect to a fixed star. Without an adequate telescope mounting it would have been impossible for him to follow up this observation after Jupiter had moved on, even if he had thought of doing so.

This observation of Neptune may be of astrometric value. Immediately below the drawing of Jupiter and its satellites is a linear scale showing 24 jovian radii. Below this scale is a drawing of the two 'stars'. The drawing indicates that Neptune was 3.75 radii, or just over 1 arc min, from star 'a'. The ephemeris shows that Neptune should have been 2 arc min from the star. It is therefore possible that the ephemeris is incorrect by about 1 arc min—a relatively large amount in celestial terms (see Table 1). We see no reason to doubt that Galileo drew the stars to the indicated scale, although it is surprising that the 'incorrect' ephemeris position still lies on the same straight line from Jupiter and the star. In principle, the error in the ephemeris could be in any arbitrary direction, most likely along the ecliptic, which is not parallel to the line from Jupiter.

We are left, then, with the strong possibility that the ephemeris of Neptune is in error by a significant amount, which would require a revision of the orbital elements of that planet, and suggests the existence of an unknown perturbation. [One of us (S.D.) believes that such revisions may disclose an occasion on which Galileo mistook Neptune for a satellite near Jupiter. Eclipse conditions and an ambiguity in timing one of his observations suggest this as a possibility, even if remote.]

The ephemeris of Neptune used in this work is from Development Ephemeris no. 102 of the Jet Propulsion Laboratory. Other ephemerides will give different results. We hope that this work will help decide which ephemeris is most accurate. It would be most interesting to try to fit the Galileo position and the Lalande positions into a new ephemeris of Neptune.

We thank Drs Jay Lieske and E. Miles Standish for supplying ephemerides of Jupiter, Neptune and the galilean satellites which made this work possible, and Dr Alexander Pogo for help and advice. C.T.K. is supported by grants from the National Aeronautics and Space Administration, and the NSF.

Received 19 May; accepted 5 August 1980.

1. Rawlins, D. *Astron. J.* **75**, 856–857 (1970).
2. Albers, S. C. *Sky Telesc.* **57**, 220–222 (1979).
3. Galilei, G. *Le Opere di Galileo Galilei.* Edizione nazionale (Barbera, Florence, 1890–1909).

Imaging and focusing of neutrons by a zone plate

P. D. Kearney*, A. G. Klein*, G. I. Opat* & R Gähler†

*School of Physics, University of Melbourne, Parkville, Victoria, Australia 3052
†Institut Laue-Langevin, 38042 Grenoble Cedex, France

The use of refractive lenses for long-wavelength neutrons, although possible[1], is severely limited by the fact that the refractive index differs only very slightly from unity (for example, $n-1=2.3\times10^{-4}$ for quartz at $\lambda=20$ Å). However, the fact that only a relatively thin layer of material is needed to produce an optical path difference of half a wavelength (for example, 2.4 μm of Cu at $\lambda=20$ Å) led us to propose[2] previously that neutrons could be focused by diffraction from a phase grating of variable spacing; this is , in fact, a type of zone plate. Zone plates, first described by Soret[3], have been used satisfactorily over a large part of the electromagnetic spectrum[4-6]. We now report the successful focusing and imaging of a slow neutron beam by means of a Fresnel zone plate[8].

Conventional zone plates work by blocking out alternate zones. Constructive interference of the waves diffracted from the remaining zones occurs at specific points which are in an image relationship to their original source. Lord Rayleigh[7] pointed out that phase reversing, rather than absorbing alternate zones, would achieve a focus with greatly enhanced intensity. In the absorbing zone plate, only half the incident amplitude (leading to one-quarter the intensity) is focused; in addition, a 0 order beam of unfocused waves is present. This is not the case with the phase reversal zone plate in which the 0 order is absent and much more of the energy is focused. These facts were experimentally verified by Wood[5].

The geometric pattern of a Fresnel zone plate (see Fig. 1) is precisely that of the interference pattern of two spherical waves of differing radii of curvature. Thus, the zone plate may be regarded as the hologram of a point. This fact suggested our first approach to the construction of zone plates for long wavelength neutrons, along the lines previously used by others[6] in producing zone plates for soft X rays. However, we subsequently found that higher quality zone plates could be produced by the successive photographic reduction of a computer drawn pattern.

Our zone plates, which are of the phase reversal type, were produced in Melbourne by photolithographic techniques close to the limits of resolution used by the microelectronics industry. A thin layer of positive photoresist (Shipley AZ 1350 J) on a silicon wafer substrate was exposed to UV light through a mask carrying the zone plate pattern. After dissolving away the unexposed photopolymer, a layer of copper was electrolytically deposited on to the exposed surface. (Before coating with photoresist, a thin layer of chromium was deposited on the substrate to enhance the adhesion of the copper.) The thickness of the copper deposited was strictly controlled to be equal to $D(\lambda/2)=2.4$ μm, the thickness calculated to give a phase reversal to neutrons of 20 Å wavelength.

$$D(\lambda/2)=\tfrac{1}{2}\lambda/(n-1) \tag{1}$$

where

$$n=1-\lambda^2 Nb/2\pi \tag{2}$$

for a material having N scattering centres per unit volume, each with scattering length b.

The final zone plates produced in this way had the following characteristics: diameter $d=2$ mm, number of zones $\xi=200$, width of outermost zone $\delta=2.5$μm, focal length f (m) $=50/\lambda$ (Å) $=2.5$ m at $\lambda=20$ Å. Note that the width, δ, of the outermost zone, limited by the resolution of our plating technique, determines the quality of the lens in the sense that its F-number (f/d ratio) may be shown to be given by

$$F=\delta/\lambda \tag{3}$$

Thus, our lens has $F=1,250$, which is poor compared with lenses used with visible light but comparable with the performance of lenses used in electron optics. The reasons for this are most easily understood by reference to the holographic aspects of the problem. Regarding the zone plate as a hologram of a point, recorded with light of a given wavelength but reconstructed with waves of wavelength 250 times shorter, it is

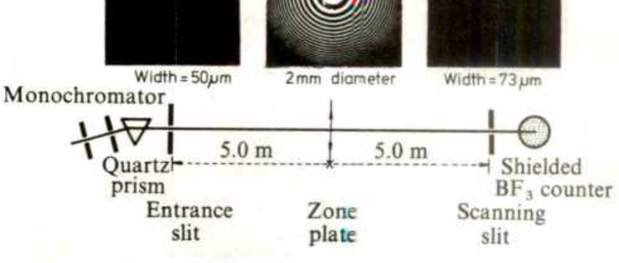

Fig. 1 Schematic layout of neutron focusing experiment.

0028-0836/80/390313—02$01.00

easily shown that the ultimate resolution is still that attainable with visible light. Therefore, better quality zone plate lenses can only be produced by methods avoiding the use of visible light, such as electron beam lithography.

We tested our zone plate on the long wavelength neutron beam, H18, at the High Flux Research Reactor of the Institut Laue-Langevin in Grenoble. The main features of the apparatus are shown in Fig. 1. The monochromator, consisting of a 120° quartz prism with entrance and exit slits, was used to select a 1-Å wide wavelength spread centred on 20 Å. The monochromator exit slit, set to 50 μm width, served as the object to be imaged by the zone plate at 1 : 1 magnification, that is, the object and image distances were both 5 m. The image was scanned in 20-μm steps by a 30-μm wide slit, placed in front of a shielded BF_3 proportional counter. A Polaroid camera with a lithium-loaded ZnS scintillator screen was also used to photograph the beam in the object and image positions, giving the results shown in Fig. 1.

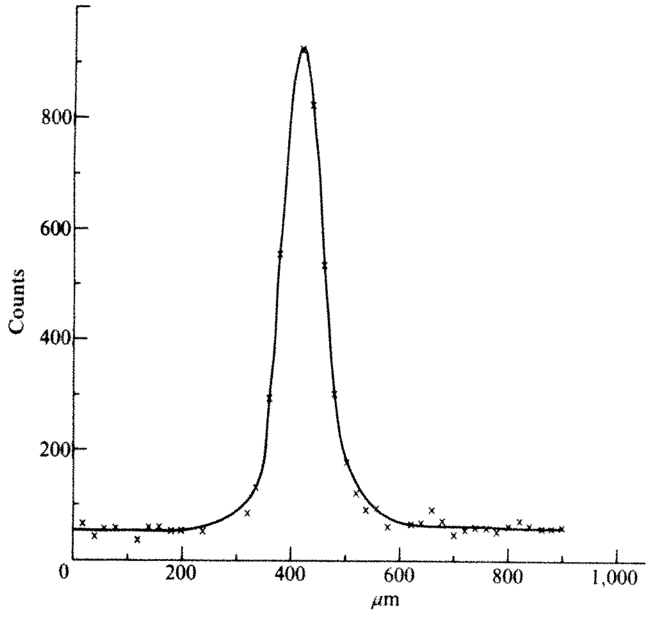

Fig. 2 Neutron intensity in the image plane.

Measurements of the beam detected in the image plane are shown in Fig. 2, and gave FWHM = 73 μm, a value consistent with the instrumental resolution, combined with the calculated chromatic aberration. Because object and image distances were fixed by the lengths of vacuum tanks taking up the flight paths, longitudinal scanning of the focus was not possible with this apparatus. We did, however, verify the calculated focal length by observing the width of the image as the wavelength was varied by rotating the monchromator prism. The image width showed a sharp minimum at 20 Å. An estimate of focusing efficiency (the fraction of neutrons going through the lens aperture that are focused into the image) was obtained by comparing counting rates at the image position with and without the lens. This gave 40 ± 10%, in agreement with theoretical expectations.

The applicability of the zone plate lenses described above is limited by the smallness of their aperture, their inherent chromatic aberrations and the low intensities of available long wavelength neutron beams. Nevertheless, there are several interesting possibilities in the field of neutron optics, some of which we have described previously[2].

We thank the directors and staff of the Institut Laue-Langevin for their hospitality and encouragement, the University of Melbourne for travel grants, Professor J. Kalus of the University of Bayreuth for allowing us the use of his apparatus, R. L. Shaw and P. Francis for their help with the production of holographic zone plates, and D. Sheridan, Siang Tjio and M. Crary for their help with photolithography. A.G.K. thanks the French government for a Senior Fellowship.

Received 1 July; accepted 25 July 1980.

1. Gähler, R., Kalus, J. & Mampe, W. *J. Phys.* **E13**, 546 (1980).
2. Klein, A. G. & Opat, G. I. in *Neutron Interferometry* (eds Bonse, U. & Rauch, H.) (Oxford University Press, 1980).
3. Soret, J. L. *Poggendorff's Annalen* (1875).
4. Andrews, *Optics of the Electromagnetic Spectrum*, 276 (Prentice-Hall, New Jersey, 1960).
5. Wood, R. W. *Phil. Mag.* **45**, 511 (1898).
6. Niemann, B., Rudolph, D. & Schmahl, G. *Optics Commun.* **12**, 160 (1974).
7. Lord Rayleigh. *Encyclopaedia Britannica* 9th edn, Vol XXIV, 421 (Edinburgh, 1880).
8. Benyon, T. D. & Pink, A. G. *Nature* **283**, 749 (1980).

Electron irradiation induced vitrification at dislocations in quartz

D. Cherns, J. L. Hutchison*, M. L. Jenkins & P. B. Hirsch

Department of Metallurgy and Science of Materials,
University of Oxford, Parks Road, Oxford OX1 3PH

S. White

Department of Geology, Imperial College, London SW7 2AZ, UK

Recent observations using the 'weak beam' electron microscopy technique of split images of dislocations in quartz have been interpreted as arising either from dissociation of the dislocations into partials[1], or from a glassy (metamict) phase at the core[2], resulting from irradiation damage. In this letter we describe observations of lattice images of near end-on dislocations in quartz, which enable us to distinguish between these two models.

Quartz, the second most abundant crustal mineral, is important in the study of deformation within the Earth's crust. Plastically deformed quartz has therefore been the subject of numerous studies[3–5] from which two significant findings have emerged: (1) quartz deforms by dislocation creep mechanisms within the deeper crust and (2), trace amounts of lattice-bound OH cause a marked softening of quartz ('water weakening'). The causes of water weakening are not known with certainty but it is thought to arise from increased glide and/or climb velocities[6–9]. Any detailed model for this effect and for the interpretation of stress–strain curves requires a knowledge of the structures of the dislocation cores in quartz. Two different models have been proposed for the commonly encountered *a*-dislocations: Trepied and Doukhan[1] observed a splitting of weak beam images during irradiation in the microscope which they attributed to the movement of partial dislocations bounding a stacking fault composed of a complex twin structure; Cherns *et al.*[2] re-examined the image splitting and proposed an alternative model whereby irradiation damage led to the preferential formation of a metamict region in the vicinity of the dislocation core. The observed widening of the split weak beam images from about 6nm to several tens of nm was then attributed to additional radial displacements around the dislocation, generated by the expansion due to the crystalline–amorphous transition.

We have now attempted high-resolution lattice imaging of deformed quartz to obtain further information about core structures of essentially unirradiated dislocations, and to investigate in detail the development of any metamict phase. We used the naturally deformed quartz from the Cap de Creus shear zones in north-east Spain[10]; detailed textural and electron microscopic studies had been completed on this material, and

---

* To whom correspondence should be addressed.

0028–0836/80/390314—03$01.00

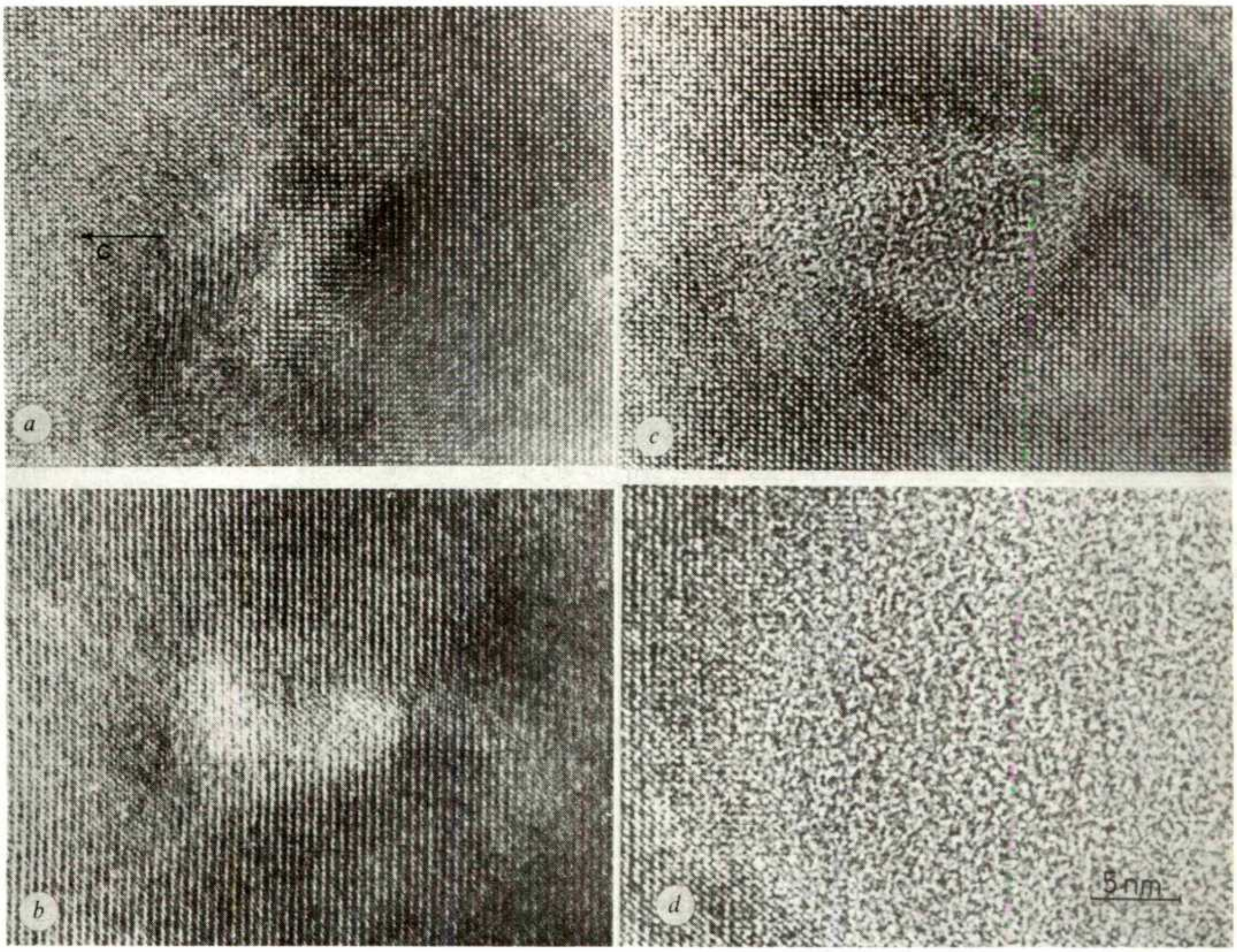

Fig. 1 *a*, $\langle 11\bar{2}0\rangle$ lattice image of a defective region in quartz, before electron beam damage becomes visible. *b*, The same region of crystal, after a further 10 s of exposure to the electron beam. *c*, After another 10 s in the beam a region of 'amorphous' contrast has appeared in the core region. *d*, After a total irradiation time of about 40 s most of the field of view has been replaced by the 'glassy phase'. Magnification, 3×10^6.

consequently it was known to contain *a*-type dislocations lying in the basal (0001) plane. Samples were cut normal to the basal plane and within a few degrees of a $[11\bar{2}0]$ pole. Dislocations of two of the three *a*-types, with Burgers vectors $\mathbf{b}=\frac{1}{3}a[1\bar{2}10]$ and $\frac{1}{3}a[\bar{2}110]$ and with line orientations close to 60°, preferred in these specimens, are close to end-on in a foil oriented at the $[11\bar{2}0]$ pole, if they exhibit dot contrast in diffraction contrast images. Specimens were ion-thinned and examined in a JEOL JEM 200CX electron microscope operating at 200 kV, with a high-coherence LaB_6 electron source and an objective lens with spherical aberration coefficient of 1.1 mm. A minimal exposure technique was used to reduce beam damage effects, photography being carried out on regions adjacent to those used for orientation, stigmation and focusing adjustments. $[11\bar{2}0]$ lattice images were recorded on Kodak 4463 film at a magnification of 4×10^5.

Figure 1 shows an irradiation sequence of an area containing a nearly end-on dislocation, as judged by the dot contrast criterion at lower magnification. The total irradiation time between Fig. 1*a* and *d* was rather less than 1 min. Figure 1*a* shows the earliest stages of the irradiation. In areas well away from the dislocation core the image reflects the quartz structure projected down $[11\bar{2}0]$.

By construction of a Burgers circuit in the undistorted region the presence of a dislocation was confirmed, the Burgers vector being consistent with one of the expected types. In the vicinity of the dislocation core, near the centre of the micrograph, the regular lattice is distorted; direct interpretation in this region is not possible because the dislocation geometry and diffracting conditions are not sufficiently well defined. A slightly later stage of the irradiation is shown in Fig. 1*a*. The strong diffraction contrast at the dislocation has almost disappeared, to be replaced by a lighter region diffracting less strongly than the surrounding area. Within this region the lattice image may still be discerned, but less clearly. In Fig. 1*c*, a central oval-shaped region has developed, displaying 'amorphous' contrast typical of a glass, whereas the regular lattice image is still clearly visible in surrounding regions. In Fig. 1*d* most of the field of view appears amorphous. The contrast between Fig. 1*c* and 1*d* is clearly indicative of a transition from crystalline to metamict quartz, and strongly supports the model proposed by Cherns *et al.*[2]. Vitrification of the dislocation core due to electron irradiation has also been suggested previously by Ardell *et al.*[11]. The metamict region grows with irradiation time in both [0001] and $[1\bar{1}00]$ directions, and is oval with its long axis in the *c* direction.

While the images show no evidence of any pronounced dissociation into partial dislocations on the basal plane, as envisaged by Trepied and Doukhan[1], to be accompanied on their model by displacements along $[1\bar{1}00]$ in the $[11\bar{2}0]$ projection, the possibility of dissociation over a width of less than 1 nm cannot be ruled out. The absence in Fig. 1*a* of evidence for an amorphous region suggests that the image splitting of about 6 nm reported by Cherns *et al.*[2] in the first micrograph of their irradiation sequence is due to the irradiation induced metamict phase. However, we cannot exclude the possibility of the presence of an amorphous region a few tenths of a nanometre in diameter ('colloidal cores' as postulated by Tsinzerling[12]). Finally, note that because of the additional displacements generated by the growth of the metamict phase, great care must be taken in the determination of Burgers vectors of dislocations in quartz.

Received 18 June; accepted 12 August 1980.

1. Trepied, L. & Doukhan, J. C. *J. Mater. Sci.* **13,** 492–498 (1978).
2. Cherns, D., Jenkins, M. L. & White, S. in *Electron Microscopy and Analysis 1979* (ed. Mulvey, T.) 121–124 (Institute of Physics, London, 1980).
3. Nicolas, A. & Poirier, J. P. *Crystalline Plasticity and Solid State Flow in Metamorphic Rocks* (Wiley-Interscience, London, 1976).
4. Carter, N. L. *Rev. Geophys. Space Phys.* **14,** 301–360 (1976).
5. Tullis, J. *Rev. Geophys. Space Phys.* **17,** 1137–1154 (1979).
6. Griggs, D. T. *J. geophys. Res.* **79,** 1653–1661 (1974).
7. McLaren, A. C. & Retchford, J. A. *Phys. Stat. Sol.* **33,** 657–668 (1969).
8. Ball, A. & White, S. *Phys. Chem. Minerals* **3,** 163–172 (1978).
9. Paterson, M. S. & Kekulawala, K. R. S. S. *Bull. Mineral.* **102,** 92–100 (1979).
10. Carreras, J., Estrada, A. & White, S. *Tectonophysics* **39,** 3–24 (1977).
11. Ardell, A. J., Christie, J. M. & McCormick, J. W. *Phil. Mag.* **29,** 1399–1411 (1974).
12. Tsinzerling, D. V. *Zap. Ses. Miner. Obsh.* **93,** 392–397 (1964).

Silica retards radial growth of spherulites in isotactic polystyrene

M. Kennedy, G. Turturro*, G. R. Brown & L. E. St-Pierre

Department of Chemistry, McGill University, Montreal,
Quebec, Canada H3A 2K6

We recently reported the retardation of the rate of crystallization, measured calorimetrically, in isotactic polystyrene (iPS) nucleated with silica (Cab-O-Sil) that had been treated with trimethylsilane[1]. The loading of the nucleant was 5 g per 100 g of polymer or two parts per hundred (p.p.h.) by volume, of polymer. From microscopic observations it was known that the number of nuclei present in the nucleated system was at least double that present in the pure polymer in identical cooling conditions[2]. The only rationale available for the retardation effect seemed to be that the nucleant was inhibiting the growth of the crystals and thus the overall rate of crystallization. However, previous workers have reported spherulitic growth rates to be unaffected by the presence of nucleants in systems with loadings up to 3 p.p.h. (refs 3–6). To clarify this apparent paradox the measurement of the radial growth rates of spherulites in the system iPS–silica by photomicrography was undertaken. Here we confirm that silica does retard the rate of growth of such spherulites.

A Zetopan Reichert research microscope equipped with crossed polarizers and a Nikon 35 mm camera were used in conjunction with a Mettler FP52 hot stage (controlled to ±1°C and calibrated using the melting points of benzoic acid, naphthalene and benzophenone). The samples were prepared by melting 0.1–0.2 mg of iPS between a precleaned microscope slide and a coverglass separated by Pt washers ~20 μm thick. Before observation the samples were premelted at 255 °C for 5 min. Subsequently, they were cooled to the desired crystallization temperature and the growth rates of spherulites was followed by photographing them at regular intervals. The diameters of 15 and 60 spherulites, respectively, for the un-nucleated and nucleated systems were measured at least five times for each photograph and a growth rate for each spherulite was determined, using a linear least squares program, for diameters in the range 15 to 45 μm. An average of the spherulitic growth rates was calculated by taking the average of the growth rates of individual nuclei at a given crystallization temperature.

Figure 1 shows the effect of temperature, in the range 150–200 °C, on the rate of radial growth of spherulites in un-nucleated iPS (viscosity molecular weight approximately 1 × 10^6, equilibrium melting point = 231 °C). The growth rates, G, can be described by a modified form of the Lauritzen–Hoffman equation[7]

$$\ln G = \ln G_0 - \left[\frac{C_1}{R(C_2 + T - T_g)}\right] - \frac{4b_0\sigma\sigma_e T_m^0}{k\Delta H T\Delta T} \qquad (1)$$

where G_0 is a pre-exponential factor which is independent of temperature. The effect of temperature of the rate of transport in a polymer melt is described by the term $[C_1/R(C_2 + T - T_g)]$ where R is the gas constant, C_1 and C_2 are the WLF constants describing viscous flow in polymers, T is the crystallization temperature, and T_g is the glass transition temperature. The remaining term in equation (1) relates to the nucleation energy which depends on the monomolecular thickness b_0, the side and end interfacial energies, σ and σ_e, respectively, the equilibrium melting point, T_m^0, the heat of fusion, ΔH, the Boltzmann constant, k, and ΔT, the supercooling. As shown in Fig. 1, an excellent 'fit' to the growth pattern in the un-nucleated system is obtained when:

$$C_1 = 1.72 \times 10^4 \ \ \text{J mol}^{-1}$$

$$C_2 = 75\ \text{K}$$

$$T_g = 365\ \text{K}$$

and

$$\frac{4b_0\sigma\sigma_e T_m}{k} = 9.25 \times 10^4\text{K}^2 \quad (T_m^0 = 503.8\ \text{K})$$

The addition of 0.8 vol. % fine particle silica (Cab-O-Sil M – 5) caused a decrease in the radial growth rate over the range 170 to 190 °C (Fig. 1). To obtain a fit to the data for this system, equation (1) was modified to include a contribution due to the adsorption of polymer segmers onto the silica with a heat of adsorption (ΔH_{ads}) known[8] to be 2.05 × 10^4 J mol^{-1}, to

$$\ln G = V_2 \ln G_0 - \frac{C_1 + \phi\Delta H_{ads}}{C_2' + T - T_g} - \frac{4b_0\sigma\sigma_e T_m^0}{k\Delta H T\Delta T} \qquad (2)$$

where V_2 is the volume fraction of polymer and ϕ is a constant. Again, an excellent fit is obtained to the data when

$$\phi = 8.27 \times 10^{-2}, \qquad C_2' = 107\ \text{K}$$

The observed increase in C_2 to C_2', that is 75 to 107 K, is in accordance with, but somewhat larger than, directly measured values for the change in T_g in the presence of added silica[9].

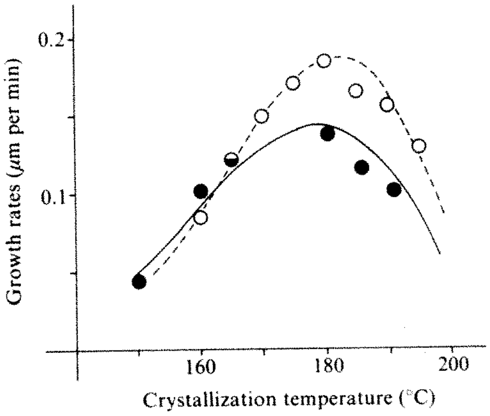

Fig. 1 Effect of crystallization temperature on the spherulite growth rates in un-nucleated (○) and nucleated (●) isotactic polystyrene [– – – – theoretical, equation (1); ——— theoretical, equation (2)].

---

*Present address: Du Pont Research Laboratories, Kingston, Ontario, Canada.

0028–0836/80/390316—02$01.00

Interestingly, as would be expected, a satisfactory account for the retardation in the rate of radial growth in iPS due to added silica can be achieved by considering only the transport term in equation (1).

These results demonstrate a decrease in the rate of radial growth of spherulites in nucleated polymer melts. This effect is probably general but has not been previously recognized because, despite the retardation in the rate of development of the spherulites, the overall crystallization rate will be retarded only in cases where the increase in the number of nuclei is small. The transport limitation has been demonstrated to result from the formation of quasi-crosslinks in the polymer melt as a result of the physisorption of the polymer segments on the nucleant[10].

We thank the Natural Sciences and Engineering Research Council for financial support and Drs Gray and Manley of McGill University for the use of their equipment.

Received 8 April; accepted 17 July 1980.

1. Turturro, G. & St-Pierre, L. E. *J. Colloid Interface Sci.* **67,** 349 (1978).
2. Cole, J. H. & St-Pierre, L. E. *J. Polymer Sci., Polymer Symp.* **63,** 205 (1978).
3. Beck, H. N. & Ledbetter, H. D. *J. appl. Polymer Sci.* **9,** 2131 (1965).
4. Binsbergen, F. L. & de Lange, B. G. M. *Polymer* **11,** 309 (1970).
5. Antwerpen, F. Van & Van Krevelen, D. W. *J. Polymer Sci.* **10,** 2423 (1972).
6. Groeninckx, G., Berghmans, H., Overbergh, N. & Smets, G. *J. Polymer Sci.* **12,** 303 (1974).
7. Hoffman, J. D. & Lauritzen, J. I. *J. Res. natn. Bur. Std.* **A65,** 297 (1961).
8. Yim, A. thesis, McGill Univ., Montreal (1971).
9. Yim, A., Chahal, R. S. & St-Pierre, L. E. *J. Colloid Interface Sci.* **43,** 583 (1973).
10. Chahal, R. S. & St-Pierre, L. E. *Macromolecules* **2,** 193 (1969).

Simulation of a lipid monolayer using molecular dynamics

A. J. Kox*, J. P. J. Michels† & F. W. Wiegel‡

*Institute of Theoretical Physics, University of Amsterdam, Amsterdam, The Netherlands
†Van der Waals Laboratory, University of Amsterdam, Amsterdam, The Netherlands
‡Department of Applied Physics, Twente University of Technology, Enschede, The Netherlands

Numerical simulation is often a useful tool for investigating the behaviour of complex systems with many degrees of freedom. Of the two major methods in this field, the Monte Carlo method and the molecular dynamics method, only the first has been applied to realistic models of lipid monolayers[1–5]. The term lipid monolayer is used here to describe a class of systems consisting of chain molecules on a liquid substrate, the characteristic properties of which can be summarized as follows. (1) The constituent molecules are amphipathic, that is they consist of a hydrophilic (polar) head group and one or more hydrophobic hydrocarbon chains. (2) Due to the amphipathic character of the molecules, the head groups are constrained to the plane of the substrate, whereas the tails are directed outwards from this plane. (3) The collective properties of the molecules are determined by their short-range repulsive and long-range attractive interactions and by the steric repulsion of the tails. We now present what we believe to be the first molecular dynamics simulation of a realistic model of a lipid monolayer. The model system, which has all three properties enumerated above, shows a first order phase transition from an ordered fluid-like state to a disordered, gas-like state.

Cotterill[6] and Toxvaerd[7] have performed numerical dynamics calculations on very rough models of monolayers. Both authors only consider models in which the individual molecules are reduced to purely two-dimensional objects which move in the plane of the monolayer. The influence of the steric interactions of the chains and of their large number of configurations is therefore neglected. Consequently, these calculations are at best a simulation of the crystalline state of a monolayer, with all lipid chains parallel and in the all-*trans* state. Also, the mechanism believed to be responsible for the main phase transition in lipid monolayers—the 'melting' of the tails—is absent in these models. These are rather severe limitations (see ref. 8 for a review of lipid monolayer theory and of some of the terminology used here). To improve this situation we have performed a molecular dynamics simulation of a realistic model of a lipid monolayer. The system consists of 90 chain molecules (lipids), each molecule consisting of seven repeating units (CH_2 groups). The first repeating unit of each chain (the head group) is constrained to move in a plane, thus simulating the interaction between the head groups and the molecules of the substrate. The head groups interact with a 12,6 Lennard-Jones interaction potential with cutoff 2.5σ

$$\begin{aligned} V(r) &= 4\,\varepsilon\{(\sigma/r)^{12}-(\sigma/r)^{6}\} \quad (r<2.5\,\sigma) \\ V(r) &= 0 \quad (r>2.5\,\sigma) \end{aligned} \tag{1}$$

where r denotes the distance between two head groups, and ε and σ are parameters. The geometry of the hydrocarbon chains is simulated in the following way. In each chain, the distance between two neighbouring repeating units is kept fixed, within small fluctuations, by a strong harmonic force, proportional to

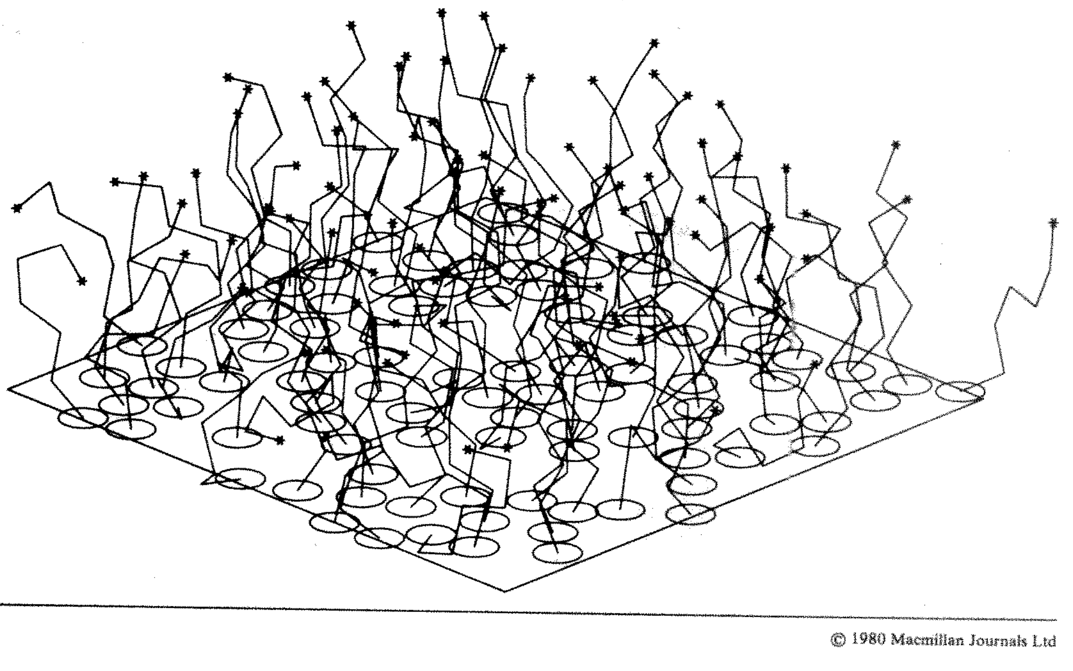

Fig. 1 A typical equilibrium configuration of a lipid monolayer for $T^* = 1$ and $\rho^* = 0.4$. T^* is the reduced temperature: $T^* \equiv kT/\varepsilon$; ρ^* is the reduced number-density: $\rho^* \equiv \rho/\rho_0$ with ρ_0 the close-packed density. The head group of each lipid is indicated by a circle of radius σ and the end of each lipid by an asterisk. Note the clustering of the head groups and the formation of small pores. These pores, which might play a part in membrane permeability, have also been found previously in an exactly solvable membrane model[12–14].

0028-0836/80/390317—03$01.00

$r-\sigma$, which acts to drive the two repeating units back to their equilibrium distance σ. In the same way, a strong harmonic force keeps the distance between any pair of next-nearest neighbours in a chain fixed at the value a. The value of a is chosen in such a way that any two successive C–C bonds in a chain define an angle of 109.5°, in agreement with the experimental value for hydrocarbon chains. With the exception of the head groups, all repeating units in different chains interact with a strong repulsive force proportional to $(\sigma/r)^{20}-1$, with a cutoff σ. The plane to which the head groups of the lipids are constrained acts as a reflecting plane for all other repeating units, through a strong repulsive force.

Clearly, therefore, our model incorporates most of the features quoted in the first paragraph. However there are three exceptions. (1) The attractive part of the interaction between a pair of chains is concentrated in the head groups instead of being distributed over the whole length of the chains. (2) Although the polar forces between the head groups and the molecules of the substrate have been accounted for, the polar interactions between the head groups themselves are neglected. (3) The energy difference of about 0.35×10^{-13} erg between a *trans* and a *gauche* configuration of a C–C bond has not been taken into account, implying that there is no difference between the liquid expanded and liquid condensed phases.

The properties of this system were determined by numerical integration of the equations of motion of the 630 repeating units, using Verlet's algorithm[9]. The calculations were done on the CDC Cyber 73/28 and CDC Cyber 173/8 of SARA in Amsterdam. We used two-dimensional periodic boundary conditions. The initial configuration, for which the all-*trans* state was chosen, tends to equilibrium after a sufficient number of collisions. We used an adjustment procedure[10] to guide the sytem to thermodynamic equilibrium at one particular temperature T. A typical equilibrium configuration is depicted in Fig. 1.

Once the system is in thermodynamic equilibrium, the lateral pressure Π can be calculated from the virial theorem[11].

$$\frac{\Pi A}{NkT} = 1-(2N\langle \mathbf{v}^2\rangle)^{-1}\sum_{i\neq j}(\mathbf{r}_{i,j}\cdot\mathbf{a}_{i,j}). \qquad (2)$$

Here A denotes the area, N the number of repeating units, k is Boltzmann's constant, $\mathbf{r}_{i,j}\equiv\mathbf{r}_i-\mathbf{r}_j$ is the difference between the projections onto the plane of the head groups of the position vectors $\mathbf{r}_i$ and $\mathbf{r}_j$ of two repeating units i and j, $\mathbf{a}_{i,j}$ their relative acceleration in the plane of the head groups and $\langle\mathbf{v}^2\rangle$ the average of the squares of the projected velocities. The time step used in the integration procedure was chosen as $0.005\times\sigma(m/kT)^{1/2}$, with m the mass of a repeating unit. Averages were taken over 24,000 time steps. In this time a repeating unit covered a mean distance of approximately 200 σ. Figure 2 shows a number of points belonging to two isotherms. The isotherm corresponding to the lower temperature shows the characteristic part of the Van der Waals loop which indicates the coexistence region of a system with a first order phase transition. The occurrence of this loop is interpreted to mean that the isotherms of the lipid monolayer are flat in the coexistence region. As this phase transition takes place at rather low densities, it corresponds to the transition between the liquid expanded and gaseous states of the monolayer.

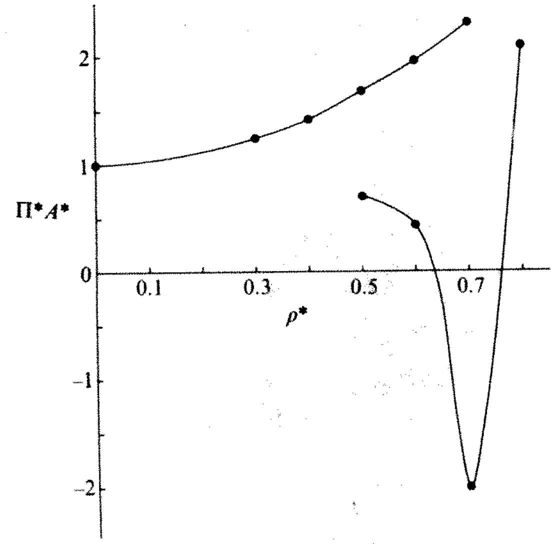

Fig. 2 Lipid monolayer isotherms at temperatures above and below the critical temperature. The upper curve corresponds to $T^*=1$, the lower one to $T^*=1/15$. The product Π^*A^* equals the left hand side of equation (2).

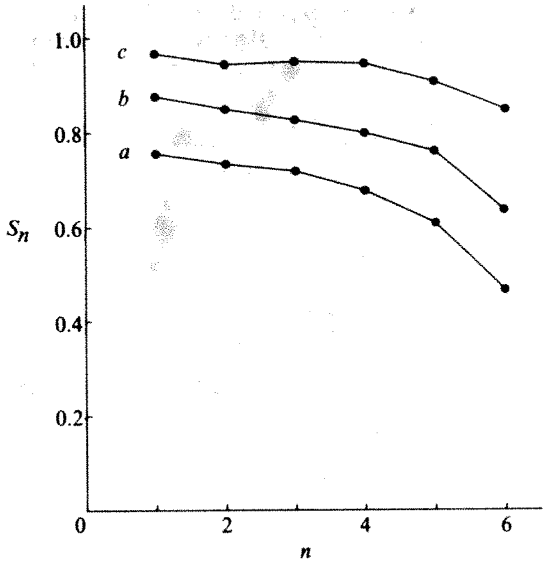

Fig. 3 Lipid monolayer order parameters at $T^*=1$ and $\rho^*=0.3$, 0.5 and 0.7 (curves *a*, *b* and *c*, respectively).

Figure 3 shows the density dependence of a set of important parameters—the order parameters S_n which measure the degree of order in the conformation of a chain. These quantities are defined by the relationship

$$S_n\equiv\frac{3}{2}\langle\cos^2\theta_n\rangle-\tfrac{1}{2} \qquad (3)$$

in which the brackets denote an average over all chains and θ_n the azimuth angle of the nth bond, minus its value in the all-*trans* state, measured with respect to the chain axis in this particular state (see discussion in ref. 8). Both the way in which the order parameters depend on the density and their numerical values agree with the results of Scott[2], who used the Monte Carlo method. Knowledge of the order parameters is important in mean field theories for lipid monolayers of the type discussed by Marcelja[5].

The system discussed here could quite easily be treated numerically. This justifies the expectation that the model can be extended in several ways. We suggest the following possibilities. (1) Extending the number of chains and increasing the number of repeating units per chain. (2) Incorporating the energy difference between a *trans* and a *gauche* configuration, so that it will be possible to study the main phase transition of the monolayer, which separates the liquid-condensed and liquid-expanded states. (3) Adding one or more proteins to the monolayer.

Received 30 April; accepted 28 July 1980

1. Whitttington, S. G. & Chapman, D. *Trans. Faraday Soc.* **62,** 3319–3324 (1966).
2. Scott, H. L. *Biochim. biophys. Acta* **469,** 264–271 (1977).
3. Belle, J. & Bothorel, P. *Biochem. biophys. Res. Commun.* **58,** 433–436 (1974).

4. Bothorel, P., Belle, J. & Lemaire, B. *Chem. Phys. Lipids* **12,** 96–116 (1974).
5. Marcelja, S. *J. chem. Phys.* **60,** 3599–3604 (1974); *Biochim. biophys. Acta* **367,** 165–176 (1974); *Biochim. biophys. Acta* **455,** 1–7 (1976).
6. Cotterill, R. M. J. *Biochim. biophys. Acta* **433,** 264–270 (1976).
7. Toxvaerd, S. *J. chem. Phys.* **67,** 2056–2060 (1977).
8. Wiegel, F. W. & Kox, A. J. *Adv. chem. Phys.* **41,** 195–228 (1980).
9. Verlet, L. *Phys. Rev.* **159,** 98–103 (1967).
10. Michels, J. P. J. *Physica* **90**A, 179–195 (1978).
11. Hoover, W. G. & Alder, B. J. *J. chem. Phys.* **46,** 686–691 (1967).
12. Wiegel, F. W. *J. Stat. Phys.* **13,** 515–530 (1975).
13. Wiegel, F. W. *Phys. Lett.* **57**A, 393–394 (1976).
14. Wiegel, F. W. *Physica* **89**A, 397–407 (1977).

The quasi 2-day wave in the Southern Hemisphere mesosphere

R. L. Craig*, R. A. Vincent*, G. J. Fraser† & M. J. Smith†

*Department of Physics, University of Adelaide, Adelaide,
South Australia 5001
†Department of Physics, University of Canterbury, Christchurch,
New Zealand

We report here preliminary results of a coordinated series of observations made in January and February 1980 to observe the quasi 2-day wave in winds in the Southern Hemisphere mesosphere. The observations were made with the aim of measuring both the vertical and horizontal structure of the wave whose presence has previously been observed at several meteor wind stations in the Northern Hemisphere and at one station (Adelaide) in the Southern Hemisphere[1–3]. Rocket observations also indicate the possible existence of a 2-day wave in the winds near the equatorial stratopause[4]. The observations suggest that the wave is a late summer phenomenon, peaking in late July/early August in the Northern Hemisphere and in late January/early February in the Southern Hemisphere.

Quasi 2-day waves with amplitudes of the order of 10–20 m s^{-1} appear to be typical of both meridional (NS) and zonal (EW) winds in the mid to high latitudes in the Northern Hemisphere[5], although amplitudes nearer 30 m s^{-1} have been quoted for NS oscillations near the Equator[6]. However, an examination of a decade (1966–75) of Adelaide meteor wind data shows amplitudes as large as 50 m s^{-1} in the NS wind component. Further investigations are therefore required to see if the differences in amplitude are due to hemispheric or latitudinal differences or both. Furthermore, more precise measurements of the wave period are required if the source of the wave is to be determined, because many of the previous investigations were for durations of the order of 5 days. Periods in the range 48 ± 6 h have been quoted from the Northern Hemisphere results but a period near 51 h seems favoured[1,7].

Our observations were made from three stations—Townsville (19°40′S, 146°50′E) and Adelaide (34°35′S, 138°30′E) situated in northern and southern Australia, respectively, and Christchurch, New Zealand (43°40′S, 172°40′E). The observations were made using the partial reflection drift technique which enabled both the NS and EW winds to be measured over the 65–100 km height range at either 2 or 2.5 km height intervals (depending on the station) with a time resolution of less than 1 h (refs 8, 9). For the results reported here, hourly mean values were used and only the 80–100 km region is considered because over this height range data are available for both day and night, enabling the tidal wind components to be easily extracted. Observations were made at Christchurch for the whole of January and February, at Adelaide for the period 10 January–12 February and at Townsville for the period 15–31 January. All the data were continuous except for a few occasions when data were lost due to power failures.

Figure 1 shows the hourly mean meridional winds at an altitude of 88 km slightly smoothed by a 3-h running mean, as observed at Adelaide and Townsville. It is apparent that a strong oscillation with about a 2-day period had begun by 10 January at Adelaide, but it did not reach full amplitude at Christchurch (not shown) until 12 January. The oscillation was at its most stable between 10 January and 6 February, and seemed to die out completely by 12 February. At all three stations the NS component of the oscillation was 2–3 times larger in amplitude than the EW component, and maximum amplitudes of up to 50 m s^{-1} occurred in late January. These observations agree well with the previous results from the Adelaide radio meteor winds[3].

As may be seen from Fig. 1, strong 24- and 12-h tidal components were superimposed on the quasi 2-day wave, as expected in view of previous observations at Adelaide. Because of the presence of these strong tidal components the data for each height were analysed with a least squares fitting process to find the mean amplitude and phase of the quasi 2-day wave as well as the period which best fitted the observations. The zonal (u) and meridional (v) wind components were separately represented as a function of time (t) by

$$u(t),\, v(t) = a_0 + \sum_{i=1}^{3} a_i \sin\left(\frac{2\pi}{T_i} t + \phi_i\right)$$

where a_0 is the prevailing wind and a_i and ϕ_i give the mean amplitude and phase for the 12 h ($i = 1$), 24 h ($i = 2$) and the wave of period T_3 which was varied systematically between 46 and 52 h. We found that the best fit occurred for a wave period of 49 ± 1 h.

The amplitude of the 2-day wave seemed to vary with latitude. At Townsville and Adelaide the amplitudes of the meridional component had mean values of 30–35 m s^{-1} in the 85–90 km region and decayed above 90 km. At Christchurch the amplitude was about 18 m s^{-1} at 88 km and increased slowly with height to reach a value of about 25 m s^{-1} at 98 km. The zonal wind components decayed with height at all three stations. The 2-day wave amplitudes were significantly larger than the tidal amplitudes. For example, at Adelaide the mean amplitudes were about 15–20 m s^{-1} in the EW and NS components for both the 24- and 12-h tides. The prevailing winds were typical of a late summer circulation, that is, eastward at heights above 80 km and with a weak equatorward flow.

The time of maximum eastward and northward winds occurred at earlier times at the higher altitudes, implying a downward

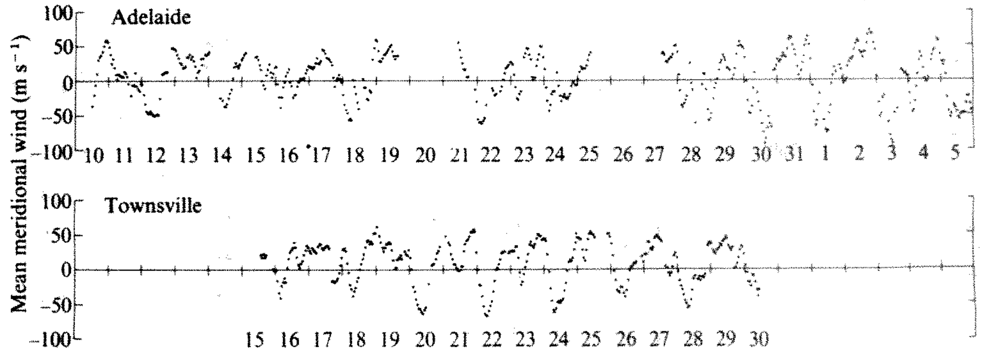

Fig. 1 Hourly mean meridional winds at 88 km observed at Adelaide (35° S) and Townsville (20° S) from 10 January to 5 February 1980, showing the 2-day wave. The values have been smoothed with a 3-h running mean.

0028–0836/80/390319—02$01.00

phase and upward energy propagation. For the meridional component the implied vertical wavelengths were 50 ± 10 km at Townsville and 100 ± 10 km at both Adelaide and Christchurch. The phase of the EW oscillations seemed to lead the NS by 6–12 h. The NS oscillations at Adelaide and Christchurch showed a consistent 15 ± 1 h phase difference, with Christchurch leading. Assuming the phase difference to be due solely to the difference (34°) in longitude, these results are not inconsistent with a westward-propagating planetary wave of zonal wave number 3.

The 2-day wave observed here seemed to persist for ~13–15 cycles, longer than any previous 2-day wave observed at Adelaide. The period was closer to 48 h than the 51–52 h suggested by the Northern Hemisphere results. The amplitude variations with latitude suggest that the meridional velocity amplitude maximizes at low latitudes. It is still not clear whether the wave is larger in the Southern Hemisphere than in the Northern Hemisphere, although the amplitudes at Christchurch do seem to be slightly larger than the results reported from mid to high northern latitudes[5]. However, the inferred zonal wave number agrees with the values found in the Northern Hemisphere[5,10]. Finally, we note that although the phase variations with height indicated that energy was propagating vertically, the little or no growth in amplitude with height indicates that this energy was being dissipated.

We acknowledge the help of A. Didenko and W. K. Hocking in taking the data at Townsville. This research was supported by grants from the Australian Research Grants Committee and the New Zealand Universities Research Committee.

Received 7 June; accepted 25 July 1980.

1. Muller, H. G. *Phil. Trans. R. Soc.* A **271,** 585–598 (1972).
2. Glass, M. & Spizzichino, A. *J. atmos. terr. Phys.* **36,** 1825–1839 (1974).
3. Craig, R. L. & Elford, W. G. *J. atmos. terr. Phys.* (submitted).
4. Coy, L. *J. atmos. Sci.* **36,** 1615–1618 (1979).
5. Muller, H. G. & Nelson, L. *J. atmos. terr. Phys.* **40,** 761–766 (1978).
6. Kal'chanko, B. V. & Bulgakov, S. V. *Geomag. Aeron.* **13,** 955–956 (1973).
7. Muller, H. G. & Kingsley, S. P. *J. atmos. terr. Phys.* **36,** 1933–1943 (1974).
8. Fraxer, G. J. & Smith, M. J. *XVIIth General Assembly I.U.G.G.*, Canberra (1980).
9. Stubbs, T. J. *J. atmos. terr. Phys.* **38,** 979–989 (1976).
10. Glass, M. *et al. J. atmos. terr. Phys.* **37,** 1077–1087 (1975).

Radiocarbon variations with the 11-year solar cycle during the last century

A. A. Burchuladze*, S. V. Pagava*, P. Povinec†, G. I. Togonidze* & S. Usačev†

*Department of Nuclear Physics, Tbilisi State University, Tbilisi, USSR
†Department of Nuclear Physics and Institute of Physics and Biophysics, Comenius University, 81631 Bratislava, Czechoslovakia

As ^{14}C is produced in the atmosphere by interactions between neutrons and nitrogen atoms, changes in the cosmic ray flux associated with the 11-yr solar cycle will produce variations in ^{14}C production with the same period[1]. These variations are difficult to observe because the atmosphere acts as a low-pass filter, greatly attenuating their amplitude[2]. Previous investigations on short-term ^{14}C variations in tree rings either reported no correlation with the 11-yr solar cycle[3–5] or found a correlation with an average amplitude of 1.5 to 3‰ (refs 6–10). However, Baxter *et al.* reported an average amplitude of about 10‰ in tree rings[11,12] and in samples of whiskies, wines and plant seeds[13], and Lavrukhina *et al.*[14] found a 10‰ correlation amplitude in wood samples. However, very precise ^{14}C tree-ring measurements reported more recently[15–17] show only minor short-term ^{14}C variations. A comparison of results obtained by Stuiver[15] and Baxter *et al.*[11] suggests that the larger ^{14}C fluctuations found by the latter group may be due to a lower precision of their ^{14}C measurements. Here we have dated wines from the period 1909–52 and our results show ^{14}C variations with an average amplitude of 4.3±1.1‰ during the 11-yr solar cycle.

Georgian wine samples of known origin (~38° N, ~45° E, altitude ~300 m above sea level), obtained from the Tbilisi Wine Museum, were used for ^{14}C measurements. The ^{14}C concentration of the alcohol fraction of wine should be closely related to the ^{14}C concentration of the grapes from which it was made, and thus to the atmospheric ^{14}C concentration. Our previous investigation of wines from the period 1950–75 showed a very good correlation between ^{14}C levels in the atmosphere and those in wine samples[18]. The use of wines allows an independent determination of the ^{14}C level. Because there is uncertainty regarding possible radial transport of ^{14}C between individual tree rings, the use of wines is preferable for investigating short-term ^{14}C variations during the last century. We also tried to use brandy samples, but found that these were unsuitable because of the special methods used in their preparation.

The methodology of alcohol extraction from wines as well as the method of acetylene and benzene preparation and counting have been described elsewhere[18]. The results are listed in Table 1 and plotted in Fig. 1 as Δ^{14}C values, defined by[19]

$$\Delta^{14}\mathrm{C} = \delta^{14}\mathrm{C} - (2\delta^{13}\mathrm{C} + 50)\left(1 + \frac{\delta^{14}\mathrm{C}}{1{,}000}\right)\text{‰}$$

$$\delta^{14}\mathrm{C} = \frac{A - A_{\mathrm{STD}}}{A_{\mathrm{STD}}} \times 1{,}000\text{‰}$$

where A_{STD} is equal to the product of 0.95 and the activity of NBS oxalic acid, corrected for age to 1950, and A is the activity of the sample, also age corrected to the year of growth. A ^{14}C half life of 5,730 yr has been used in these corrections. Unfortunately, we were unable to carry out mass spectrometric measurements on these samples. However, our previous results[20], obtained with 15 samples of modern wines, showed that δ^{13}C values did not differ by more than ± 1‰ from the mean value of −23.4‰ (1σ error of a single determination was 0.3‰). The results given in Table 1 were corrected for isotopic fractionation using the assumed δ^{13}C value of −23.4‰. The standard deviations quoted (1 σ error) describe only uncertainties associated with the sample, standard and background determinations.

The cyclic trend in the ^{14}C data shown in Fig. 1 is very clear. The gradual decrease in ^{14}C concentration is due to the Suess effect. Our results, when compared with ^{14}C measurements in tree rings for the same period[10,16], are higher by about 5‰. This is perhaps due to the remoteness of the wine growing area from industry and hence a less marked Suess effect.

For a better evaluation of short-term ^{14}C variations, we performed a spectral analysis of our ^{14}C values and compared our results with those of a spectral analysis of sunspot numbers

Table 1 Radiocarbon content of wines calculated with a half life of 5,730 yr

Year of growth	Δ^{14}C in wines (‰)	Year of growth	Δ^{14}C in wines (‰)
1909	+0.4 ± 2.4	1931	−21.1 ± 1.6
1910	+1.0 ± 2.3	1932	−17.3 ± 2.7
1911	−0.1 ± 2.5	1933	−20.5 ± 3.6
1912	−0.9 ± 2.6	1934	−18.0 ± 3.8
1913	−0.4 ± 2.6	1935	−17.3 ± 4.0
1914	+1.8 ± 2.3	1936	−14.6 ± 1.9
1915	+4.6 ± 2.5	1937	−16.9 ± 3.0
1916	+4.3 ± 2.1	1938	−15.9 ± 2.6
1917	−0.3 ± 2.4	1939	−27.9 ± 3.2
1918	−2.5 ± 2.6	1940	−31.1 ± 2.4
1919	−7.6 ± 2.6	1941	−31.1 ± 3.1
1920	−8.7 ± 2.5	1942	−33.3 ± 3.8
1921	−8.8 ± 4.2	1943	−22.5 ± 4.1
1922	−8.5 ± 2.4	1943	−24.3 ± 2.3
1923	−10.1 ± 2.4	1944	−32.4 ± 2.2
1924	−7.3 ± 2.7	1945	−33.3 ± 2.0
1925	−6.8 ± 2.7	1946	−32.2 ± 2.9
1926	−5.2 ± 2.2	1947	−27.3 ± 3.7
1927	−5.5 ± 3.0	1948	−26.5 ± 2.9
1928	−6.5 ± 3.4	1949	−31.0 ± 2.6
1929	−9.7 ± 3.6	1950	−30.5 ± 2.3
1930	−3.6 ± 6.3	1951	−34.8 ± 2.4
1930	−11.1 ± 2.4	1952	−31.8 ± 2.0

Fig. 1 Radiocarbon data of Georgian wine samples (~38° N, ~45° E) for the period 1909–52. The sunspot record has also been included for comparison.

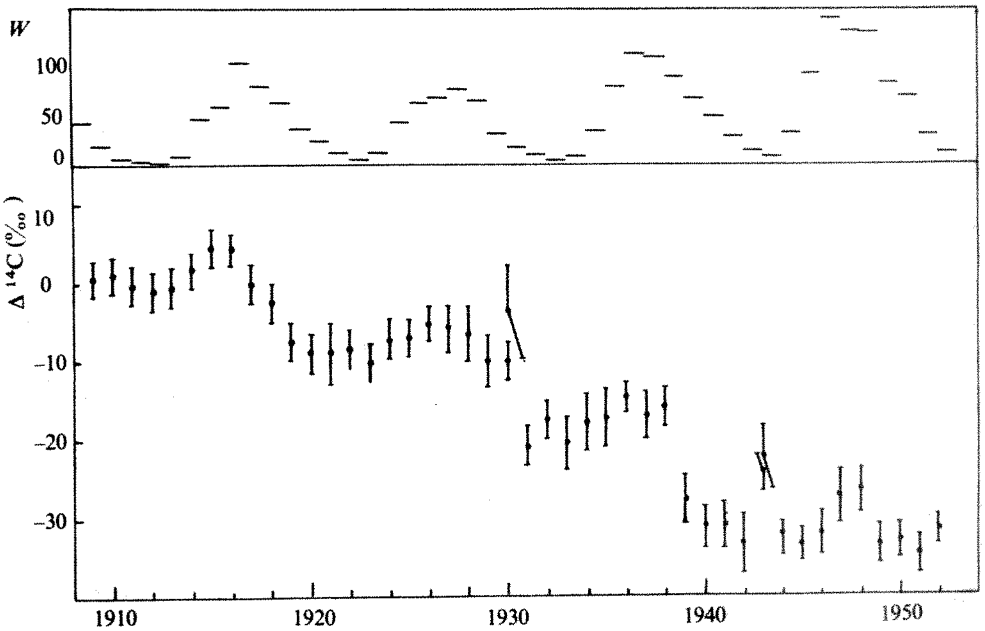

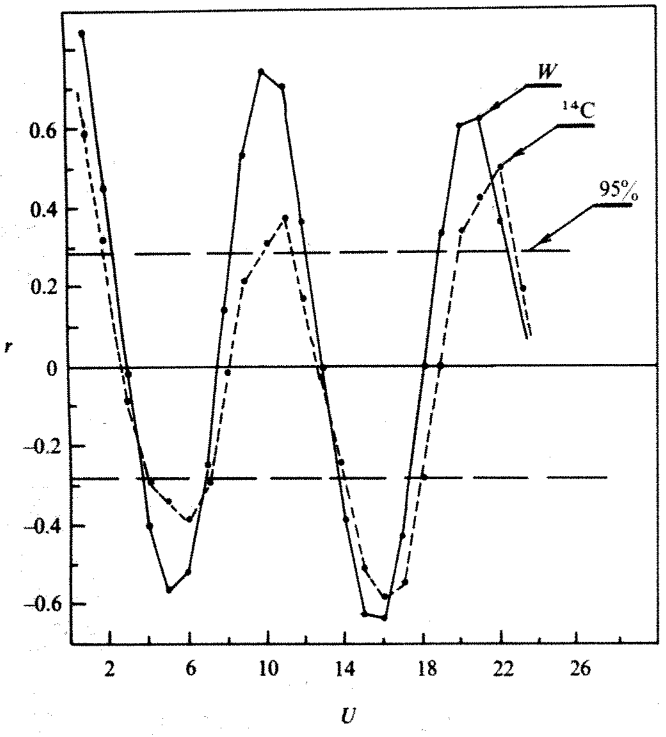

Fig. 2 Autocorrelation functions $r(U)$ of stationary time rows $\Delta^{14}\text{C}(t)$ and $W(t)$ for argument values $U_{^{14}\text{C}} = 11 \pm 1$ yr and $U_W = 10 \pm 1$ yr.

W (Fig. 2). It can be seen that the autocorrelation functions $r(U)$ of stationary time rows $\Delta^{14}\text{C}(t)$ and $W(t)$, for argument values $U_{^{14}\text{C}} = 11 \pm 1$ yr and $U_W = 10 \pm 1$ yr have a quasiperiodical behaviour, with the period of 11-yr at the 95% confidence interval. The 11-yr solar cycle spectra are in both cases very sharp and have a similar shape. The basic power of the spectra is concentrated on the frequency 2.9×10^{-9} Hz, corresponding to a period of 11 yr.

Further, we calculated correlation coefficients for various phase shifts for the different solar cycles. The required phase shifts varied from 3 to 7 yr, with a mean of 4 yr for four solar cycles. The correlation coefficients for optimal phase shifts were 0.67–0.86 for the various solar cycles, and the mean correlation coefficient for the phase shift of 4 yr was −0.58.

As spectral analysis of the ^{14}C data has shown the periodicity of the $\Delta^{14}\text{C}(t)$ row, we also carried out harmonic analysis of $\Delta^{14}\text{C}(t)$ and $W(t)$ rows. Figure 3 shows the first harmonics of $\Delta^{14}\text{C}(t)$ and $W(t)$ rows for different solar cycles. The amplitude of Δ^{14}C variations ranged from 3.3‰ to 5.6‰ for different solar cycles, and the average ^{14}C variation for the investigated time interval was 4.3 ± 1.1‰. The calculated time shift between W and Δ^{14}C maxima was 1–2 yr, and 3.5–5 yr between W maxima and Δ^{14}C minima for the different solar cycles. The harmonic analysis confirms the correlation analysis, especially that ^{14}C values lag behind Wolf sunspot numbers.

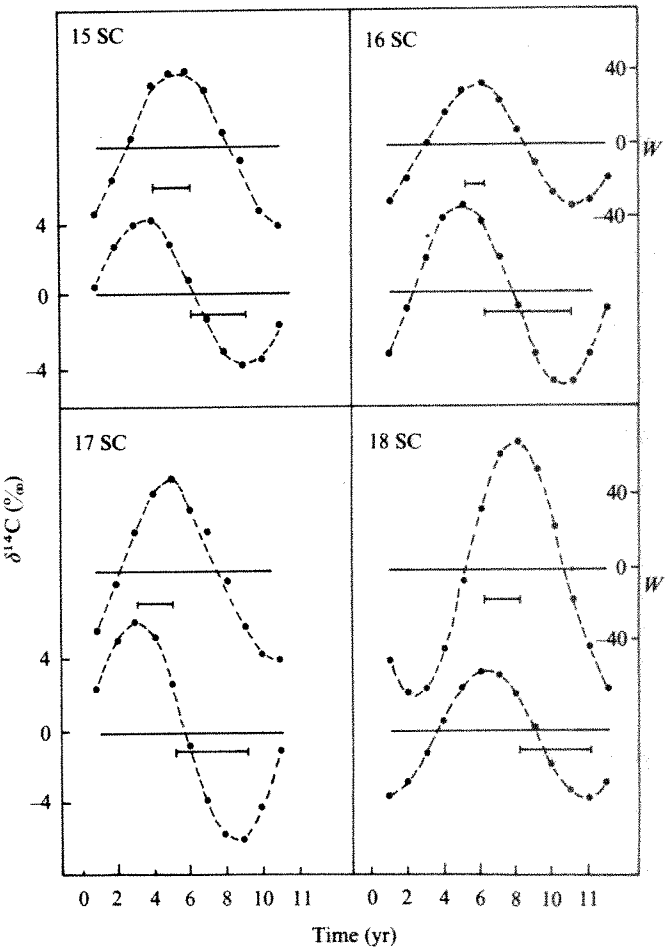

Fig. 3 The first harmonics of $\Delta^{14}C(t)$ and $W(t)$ for the 15th, 16th, 17th and 18th solar cycles (SC).

The amplitude of ^{14}C variations obtained in the present study is about a factor of 2 higher than the results of Damon *et al.*[8] for the 18th solar cycle (3.3 ± 1.1‰ compared with 1.5‰), and 50% higher than our previous results for the 17th and 18th solar cycles[10]. Time shifts in the anticorrelation dependence of Δ^{14}C on W are comparable. The present results only partly cover the time interval investigated by Alekseev *et al.* (1890–1916)[9], but except for the positive correlation, are similar for the years 1890–1900 (3‰ compared with our mean value of 4.3 ± 1.1‰). However, for the time interval 1900–16 the average amplitude obtained by these authors[9,14] is about 10‰ compared with our value of 4.0 ± 1.1‰ for the 15th solar cycle. The reasons for the extreme cycles of 10‰ amplitude found in tree rings by Baxter *et al.*[11] and Lavrukhina *et al.*[14] are poorly understood. Lavrukhina *et al.*[14] found a sharp decrease of 3‰ per yr for the period 1909–16. This decrease may have been caused by an above average fossil fuel contribution.

More precise ^{14}C measurements in tree rings reported recently show only minor ^{14}C fluctuations during the 11-yr solar cycle[15–17]. Furthermore, extensive ^{14}C series of single-year Douglas fir measurements[15] have not shown statistically significant 11-yr periodicity between 1820 and 1950.

Thus, the present investigation has shown the existence of 11-yr ^{14}C variations in wine samples with a mean amplitude of 4.3 ± 1.1‰ over four solar cycles covering the period 1909–52. A comparison of our ^{14}C variations with those of previous investigations has revealed discrepancies which may be due to local variations of stratospheric inputs and the time lag between input and growing season. The observed ^{14}C variations may thus increase dating errors of short-lived samples used for archaeological research.

We thank Dr M. Alaniya for helpful discussions.

Received 18 February; accepted 23 July 1980.

1. Lingenfelter, R. E. & Ramaty, R. in *Radiocarbon Variations and Absolute Chronology* (ed. Olsson, I. U.) 513–537 (Wiley, New York, 1970).
2. Oeschger, H., Siegenthaler, U., Schotterer, U. & Gugelmann, A. *Tellus* **27,** 168–192 (1975).
3. Covan, C., Atluri, C. R. & Libby, W. F. *Nature* **206,** 861–865 (1965).
4. Venkatavaradan, V. S. *Nature* **208,** 772 (1965).
5. Suess, H. E. *J. geophys. Res.* **70,** 5937–5952 (1965).
6. Lerman, J. C., Mook, W. G. & Vogel, J. C. *Nature* **216,** 990–991 (1967).
7. Lerman, J. C. in *Radiocarbon Variations and Absolute Chronology* (ed. Olsson, I. U.) 609–610 (Wiley, New York, 1970).
8. Damon, P. E., Long, A. & Wallick, E. I. *Earth planet. Sci. Lett.* **20,** 300–306, 311–314 (1973).
9. Alekseev, V. A., Lavrukhina, A. K. & Milnikova, Z. K. *Geokhimiya* **5,** 667–675 (1975).
10. Povinec, P. *Acta comen. phys.* **18,** 139–149 (1977).
11. Baxter, M. S. & Farmer, J. G. *Earth planet. Sci. Lett.* **20,** 295–299 (1973).
12. Baxter, M. S., Farmer, J. G. & Walton, A. *Earth planet. Sci. Lett.* **20,** 307–310 (1973).
13. Baxter, M. S. & Walton, A. *Proc. R. Soc.* A**321,** 105–127 (1971).
14. Lavrukhina, A. K., Alekseev, V. A., Galimov, E. M. & Sulerzickii, L. D. *Dokl. Akad. Nauk SSSR* **210,** 941–943 (1973).
15. Stuiver, M. *Nature* **273,** 271–274 (1978).
16. Tans, P. P., de Jong, A. F. M. & Mook, W. G. *Nature* **280,** 826–828 (1979).
17. Stuiver, M. & Quay, P. D. *Science* **207,** 11–19 (1980).
18. Burchuladze, A. A. *et al.*, *Trudy Tbilisi Univ.* 1–28 (TGU Press, Tbilisi, 1979).
19. Broecker, W. S. & Olson, E. A. *Radiocarbon* **3,** 176–204 (1961).
20. Burchuladze, A. A., Pagava, S. V. & Togonidze, G. I. *Proc. Astrofizicheskiye yavleniya i radiouglerod,* 173–176 (TGU Press, Tbilisi, 1976).

Santorini tephra from Rhodes

C. Doumas & L. Papazoglou

Department of Antiquities, National Archaeological Museum,
Tositsa 1, Athens, Greece

The large eruption of the Santorini (Thera) volcano, in ~1500 BC, inspired Marinatos to attribute the decline of the Minoan civilization to this eruption[1]. It is still, however, being debated[2,3] whether tsunamis were actually generated by the eruption of the volcano and whether the ash fall over eastern Crete was sufficient to cause its archaeologically attested desolation. Moreover, the problem of chronology remains unsolved. For, although there is no evidence that the eruption occurred after 1500 BC, the desolation of Crete is accepted as having taken place during the late Minoan IB period, at ~1450 BC (ref. 4). We describe here recent excavations at Ialysos (Trianda) on Rhodes which have produced further evidence of the south-easterly distribution of the Thera tephra. Although a considerable amount of this tephra has been found there, this does not seem to have affected the continuity of life at the settlement, corroborating the view that the ash fall over Crete would have had little, if any, effect.

Confirming the wide distribution of tephra from the late Bronze Age eruption of the Santorini volcano in the south-east Aegean Keller has stated that: "still wanted for our problems is the distinct tephra layer in well defined late Minoan I stratified position"[5]. This tephra layer has now been located in Rhodes near the old Italian excavation at Trianda (Ialysos). We started an excavation on land in May 1978, to examine the possibility of building a new house there. The proximity of this land to the area which Monaco had excavated in 1935 and 1936[6,7], as well as some technical problems, meant that additional care had to be taken causing slow progress and delaying the start of the work. The pottery evidence (Fig. 2) made assigning the first architectural remains (Fig. 1) to the late Minoan settlement an easy task. These remains, at a depth of 1.5 m below the present surface, required careful excavation so that we could study the stratigraphy and thus help to solve the problems already posed by the excavation of the late Bronze Age city of Akrotiri on Thera[8]. As work progressed, to a depth of 1.80 m below the present soil surface, a layer of whitish powdery substance 10 cm thick was

Table 1 Mineralogical analyses* of samples from Rhodes

	Minoan pumice Thera (04)	Minoan tephra Kos (03)	Minoan tephra Rhodes (08)
SiO_2	70.76	71.25	71.26
TiO_2	0.31	0.32	0.31
Al_2O_3	2.06	2.02	1.97
MgO	0.33	0.31	0.31
CaO	1.43	1.37	1.30
Na_2O	4.64	4.42	4.51
K_2O	3.34	3.30	3.4
Cl	0.36	0.36	0.39
Total	96.93	97.13	97.06
H_2O (by difference)	3.0	2.9	3.4

* Analyses performed by J. Keller, Albert-Ludwig Universität, Freiburg.

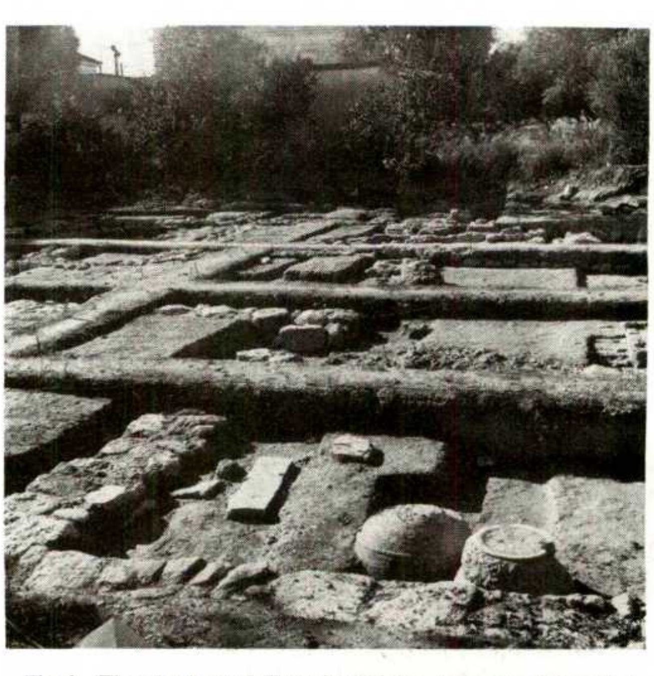

Fig. 1 Theocharis' land, Trianda, Rhodes. A general view of the excavation.

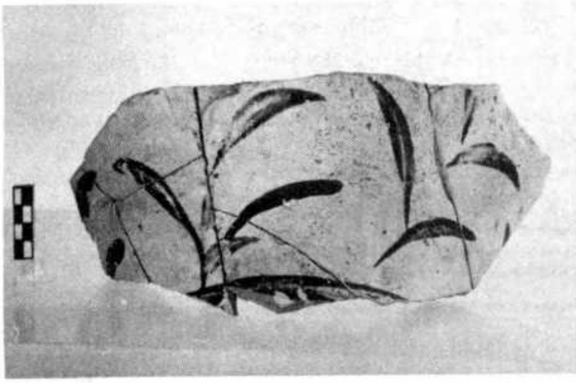

Fig. 2 Pottery fragments from above the tephra layer.

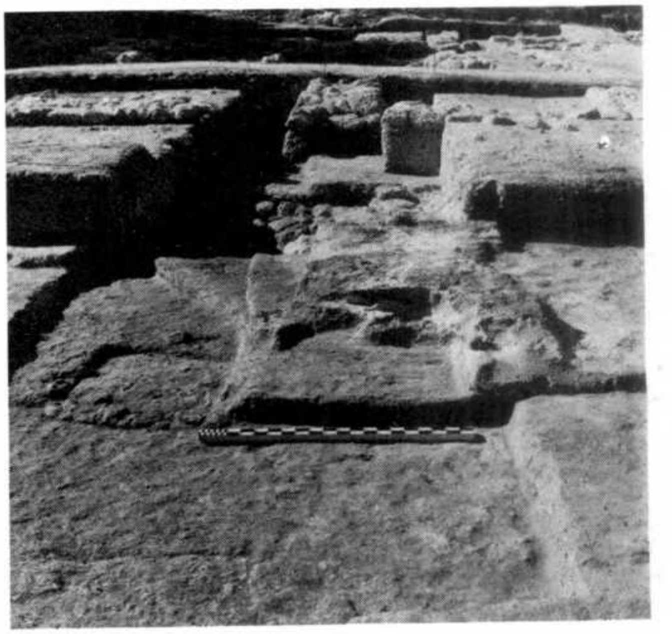

Fig. 3 The tephra layer in square B3.

observed in squares B3–B4 (Fig. 3). The uncontaminated layer of this whitish substance covered ~15 m^2, whereas almost the entire excavated area (~90 m^2) showed patches of this material mixed with earth. The first sample collected was sent to Indiana University, Bloomington, for determination of the refractive index. This material was identified as tephra from Thera on 20 October 1978. Eight more samples were later collected from almost all the excavated area (squares B3–B4: three samples; from just left of square A5 and from squares A6, B5, Γ6 and E3 one sample) and sent to Albert-Ludwig Universität, Freiburg, for mineralogical analysis. These results are shown in Table 1.

Having identified the tephra from Rhodes, it only remained to elucidate when this tephra came to the island. The only pottery evidence from beneath the clear tephra layer consists of sherds belonging to the same vase (Fig. 4). It has been difficult to look for more pottery underneath the pure tephra layer without destroying it. Thus this investigation has been postponed until all problems relating to the tephra layer have been solved. The style and decoration of the above vase place it in the late Minoan I A period[9,10]. All the pottery fragments collected from above the clear tephra layer are mixed, dating from late Minoan I A to late Helladic II B (Fig. 2). Although there is little pottery evidence from under the tephra stratum, note that all the later pottery comes from above the tephra. This location of the later pottery mixed with late Minoan I A suggests that the tephra fall did not cause any significant break in the life of the settlement. This is of paramount importance as far as the eruption of the Santorini volcano and its consequences are concerned. Because if the tephra at Trianda had been airborne, as is suggested by its fine quality and the purity of the layer, then:

(1) A considerable amount of tephra must have fallen over the south-east Aegean region and, anyway, more than that which fell on the eastern part of Crete, where it is estimated to have formed a layer ~1–5 cm thick[11].

(2) It is confirmed that northwesterly winds prevailing during the eruption sent the tephra south-east[11].

(3) It is also confirmed that Rhodes and the south coast of Turkey "have suffered severe tephra-fall"[11].

(4) Despite its thickness, the tephra which fell on Rhodes seems to have had very little if any, influence, on the settlement of Ialysos. This implies that the effect of the tephra fall on Crete was even less. Therefore, the problem of the cause of the desolation of eastern Crete[12–14] remains unsolved, and the disruptive influence of the volcanic eruption of Thera on the development of Aegean civilization more doubtful[15,16].

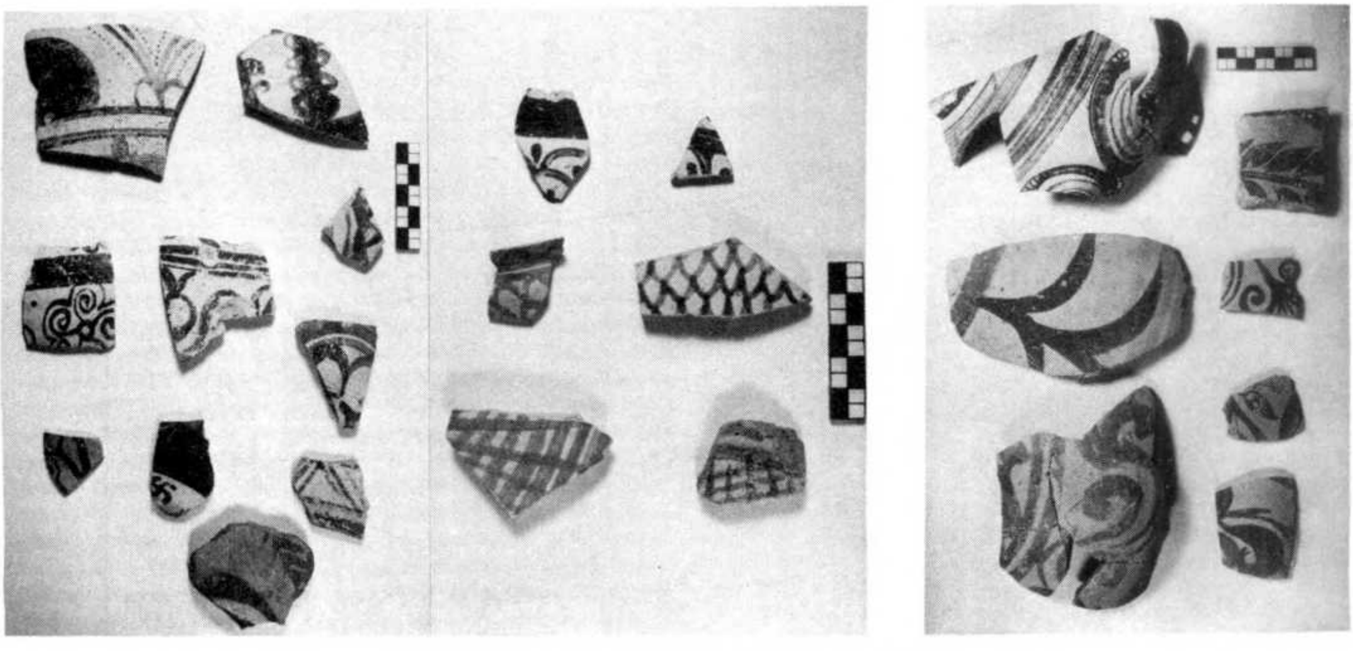

Fig. 4 Pottery fragments from underneath the tephra layer.

We dedicate this paper to the memory of the land owner Mr John Theocharis who died suddenly in the summer of 1979. We thank Professor C. Renfrew and Professor J. Luce for taking care of the first sample when they visited the excavation. We also thank Professor Charles, Dr Dorothy Vitaliano and Professor J. Keller for the examination and analyses of the samples.

Received 3 April; accepted 9 June 1980.

1. Marinatos, S. *Antiquity* **13**, 425–439 (1939).
2. Marinatos, S. (ed.) *Acta int. Scient. Cong. Volcano of Thera*, Athens (1971).
3. Doumas, C. (ed.) *Thera and the Aegean World* Vol. 1 (1978); Vol. 2 (1980).
4. Pichler, H. & Schiering, W. *Archäol. Anzeiger*, 1–37 (1980).
5. Keller, J. *Thera and the Aegean World* Vol. 2 (1980).
6. Monaco, C. *Clara Rhodos* X, 41 ff. (1941).
7. Furumark, A. *Opuscula Archaeologica* VI, 150 ff. (1950).
8. Marinatos, S. *Excavations at Thera* 1 (1967)—VII (1973).
9. Furumark, A. *Mycenaean Pottery: Analysis and Classification* (1941) 282, Motive 16: Grass or Reed.
10. Popham, M. *Annual of the British School of Archaeology at Athens*, 62 (1967).
11. Watkins, N. D. *et. al. Nature* **271**, 122–126 (1978).
12. Pichler, H. & Schiering, W. *Nature* **267**, 821 (1977).
13. Thorarinsson, S. *Thera and the Aegean World* Vol. 1, 270–271 (1978).
14. Platon, N. *Zakros* (1971).
15. Marinatos, S. *Antiquity* **13**, 425–439 (1939).
16. Page, D. *The Santorini Volcano and the Destruction of Minoan Crete* (1970).

Pollen analytical evidence for early forest clearance in North Sumatra

B. K. Maloney

Department of Ethnography, British Museum, London W1X 2EX, UK

Pollen analysis of sediments from the Toba Highlands of North Sumatra, Indonesia reported here suggests strongly that forest clearance by man began ~7,500 yr BP. Less convincing evidence suggests that man may have been disturbing the vegetation perhaps from ~17,800 yr BP, but climate has also changed and isolation of causal factors is, therefore, difficult. No Sumatran archaeological sites have yet been scientifically excavated, nor are ^{14}C dates available[1]. However, megaliths possibly 2,000 yr old occur in the study area[2] and Hindu-Buddhist remains occur further south[2]. Lowland shell-middens may be much older[1,3]. Forest clearance may have begun by 11,000 yr BP on Taiwan[4] and agriculture between 14,000 and 8,000 yr BP in Thailand[5,6] but these conclusions have been disputed[7,9]. Archaeological evidence for agriculture dating from ~9,000 yr BP onwards has been found in Papua New Guinea[10,11] while rice may have been cultivated in Sulawesi[12] by 6,000 yr BP.

Little palynology has been undertaken in Indonesia[13–15]. A 9.76-m long core from Pea Sim-sim swamp (Fig. 1) has yielded a basal ^{14}C date of 18,496 ± 95 (SSR 472). The site is at an altitude of 1,450 m on a plateau (mainly deforested) about 30 km west of an escarpment which falls sharply to Lake Toba at 900 m. Mountains rising above 2,000 m occur 40 km to the north-west, east and south-east. Swamp and limnic sediments have infilled a basin ~100 m in diameter, probably volcanic in origin. Volcanic sediment is absent from the site stratigraphy but the plateau itself is covered with rhyolitic ash at least 75,000 yr old[16] from which the soils are derived.

Climatic data are not available from the immediate locality but readings from Siborongborong[17] nearby indicate a mean annual rainfall of 2,000–2,100 mm for the region. The occurrence of lower montane forest in places demonstrates that the plateau is capable of supporting well developed vegetation in existing conditions. Much of the Toba Highlands, including the area studied, is under wet or dry rice cultivation but millets and, less frequently, taro and sweet potato are also grown.

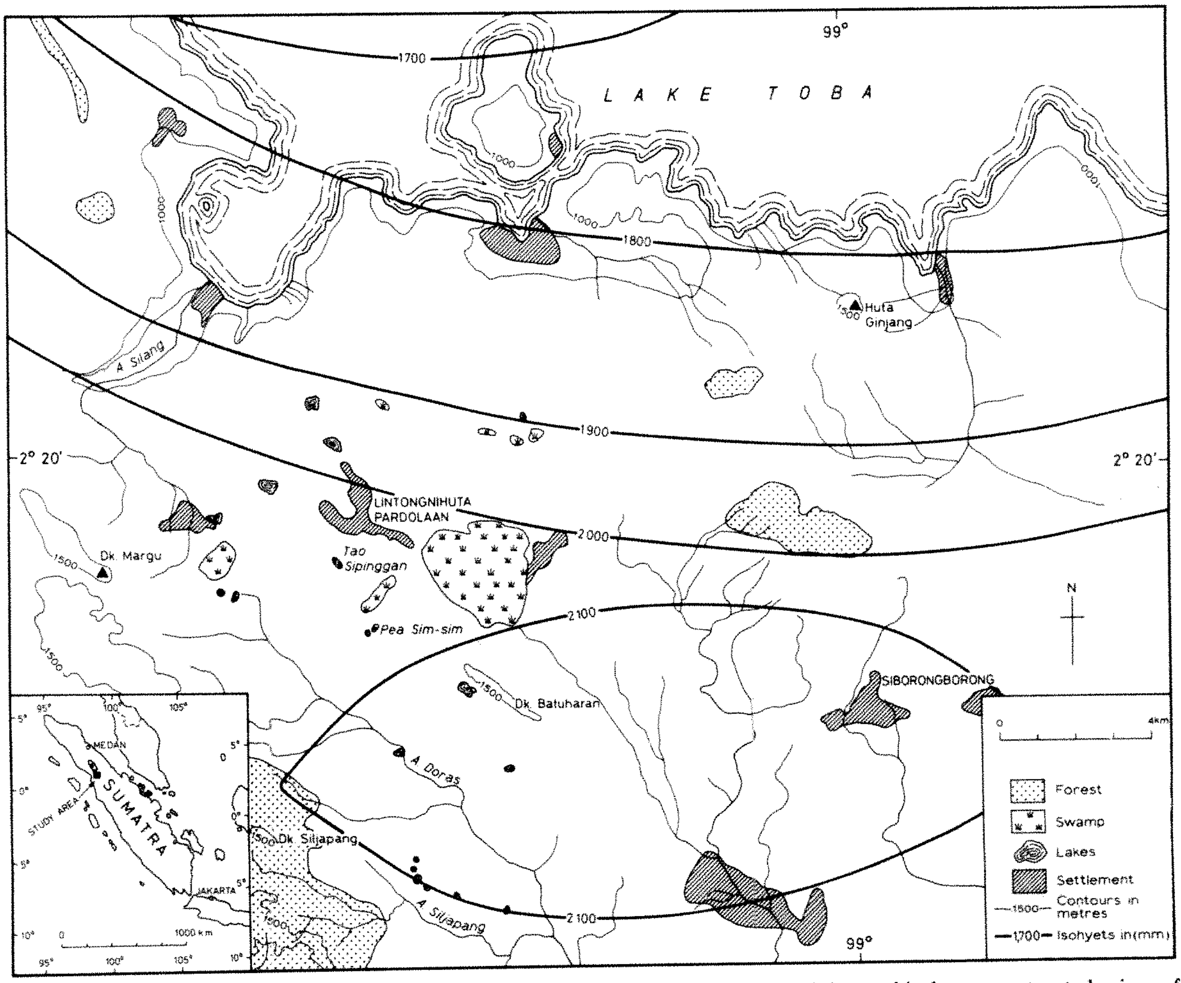

Fig. 1 Location map incorporating topographical data from Hind 1063, sheet 37, third edition and isohyets constructed using ref. 17.

0028–0836/80/390324—03$01.00

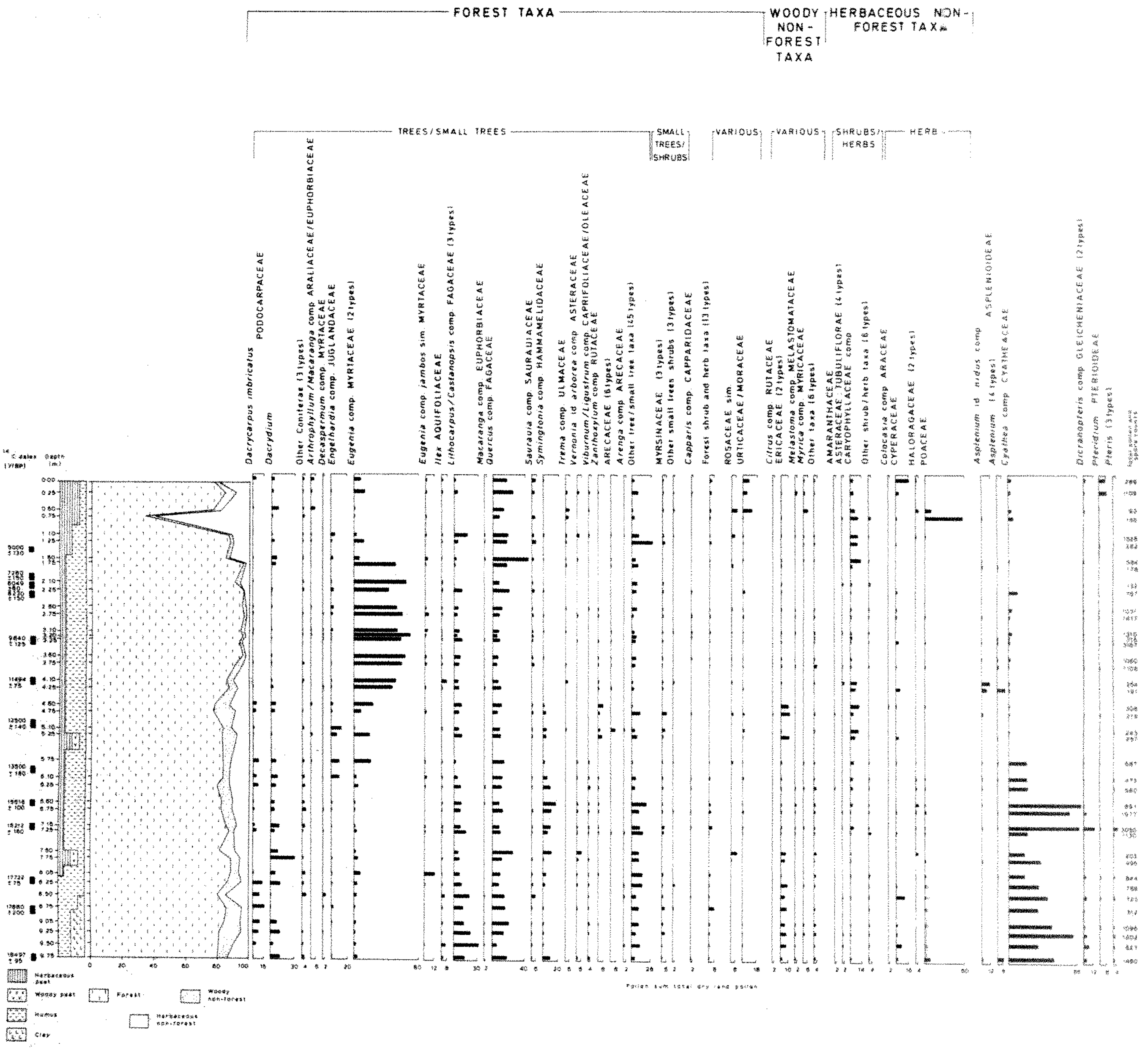

Fig. 2 Pollen diagram and site stratigraphy of the Pea Sim-sim site.

The core analysed was extracted from near the swamp centre. Unfortunately the bottom of the deposit could not be reached. Figure 2 shows a pollen diagram based on an ecological grouping of those pollen taxa which were determined and selected indicator pollens. Radiocarbon dates have been obtained for levels where the biostratigraphy shows important changes and the pollen diagram has been interpreted using spectra from surface sediments, an ecological survey and reference to literature on South-east Asian botany[18–25].

Figure 2 can be divided into four sections. The lowest part, dating between ~18,500 yr BP and an estimated 16,500 yr BP, is dominated by Coniferae and Fagaceae although *Symingtonia* is important in the basal sample. Comparison with the surface sample from the core suggests that forest pollen is over-represented. Indicators of open conditions occur but definite alpine taxa are absent. *Lithocarpus/Castanopsis* pollen is generally deposited within or near the forest but *Quercus* and, particularly, Coniferae pollen seems to be much more widely dispersed. Most of the forest pollen may have been transported in from lower altitudes, however, a mosaic of alpine and upper montane forest vegetation could have been present on the plateau. A brief decline in forest pollen around 17,800 yr BP may relate to climatic deterioration, man's influence, or both: the occurrence of a high percentage of *Cyathea* spores in the lower part of Fig. 2 could be attributed to disturbance by fire while the rapidity of sedimentation supports the view that open conditions existed.

Lithocarpus/Castanopsis or Fagaceae (with *Quercus*)–*Symingtonia* forest became established at ~16,500 yr BP. This persisted until around 12,000 yr BP and may indicate climatic amelioration. *Symingtonia* can grow between 1,000 and 3,600 m above sea level. It is commoner above 1,700 m in Central Sumatra now but its natural lower limit in North Sumatra is not known. Fairly high percentages of taxa which can be significant in secondary forest and swamp forest in addition to primary forest are present and Caryophyllaceae have some of their highest percentages in the core. More ecological data are needed to clarify whether man may have been disrupting the vegetation.

The third part of Fig. 2 dates between ~12,000 and 7,500 yr BP (estimated). *Eugenia* attains large values in many levels. *Lithocarpus/Castanopsis* is quite important but Coniferae and

Symingtonia decline. The change could be attributed to altering climate, with upper montane forest giving way to lower montane forest, but *Eugenia* is often a component of swamp forest and the site stratigraphy indicates that swamp forest probably did exist in the past. As no swamp forest remains in the region it has not been possible to assess the efficiency of the formation in filtering the atmospheric pollen rain. The probability that *Eugenia* pollen especially is over-represented has to be borne in mind while the likelihood that the taxon was growing on dry land and the swamp complicates the interpretation. A *Lithocarpus/Castanopsis–Eugenia* forest may have been present on dry land.

Pollen of well dispersed taxa (*Dacrydium*, *Quercus* and Urticaceae/Moraceae) increases in the top section of the core while *Symingtonia* and *Lithocarpus/Castanopsis* pollen decreases. This suggests an opening out of the forest. *Eugenia* declines abruptly to fairly constant low levels after ~6,500 yr BP; possible disturbance indicators such as *Arthrophyllum/Macaranga* and *Trema* are commoner and the herbaceous non-forest component becomes especially significant. The suddenness of the change suggests that man was probably responsible. Perhaps the swamp forest was the major remaining source of wood? Had swamp forest not been so prominent, earlier dry land forest clearances might have been more strongly shown in the pollen stratigraphy.

Cereals may have been cultivated throughout much of this phase but work on the grass pollens proved to be inconclusive. However, the early literature[26–28] describes a land largely deforested and planted with rice, much as it is now.

Pollen of other possible cultivars (particularly of fruit trees) occurs in numerous samples but the level of pollen identification and statistical considerations make any definite pronouncements unwise.

These findings suggest that agriculture might have been practised in Sumatra for much longer than was previously suspected, but further palaeoenvironmental research is desirable for verification, elaboration and assessment of possible regional interactions.

I thank the NERC and Hull University for funding, the NERC and the University of Zimbabwe for radiocarbon dating, Lembaga Biologi Nasional, Indonesia, for sponsorship and Dr J. R. Flenley for advice and encouragement.

Received 28 May; accepted 8 August 1980.

1. Bellwood, P. *Man's Conquest of the Pacific: the Prehistory of Southeast Asia and Oceania* (Collins, Auckland, 1978).
2. Schnitger, F. M. *Int. Archiv. v. Ethnogr* **35,** Suppl., 1–44 (1938).
3. van Heekeren, H. R. *The Stone Age of Indonesia* (Nijhoff, The Hague, 1972).
4. Tsukada, M. *Palaeogeogr. Palaeoclimatol. Palaeoecol.* **3,** 49–64 (1967).
5. Gorman, C. *Science* **163,** 671–673 (1969).
6. Gorman, C. *World Archaeol.* **2,** 300–320 (1971).
7. Harlan, J. R. & de Wet, J. M. J. *Curr. Ant.* **14,** 51–55 (1973).
8. Vishnu-Mittre in *Evolutionary Studies in World Crops* (ed. Hutchinson, J.) 3–30 (Cambridge University Press, London, 1974).
9. Vishnu-Mittre in *Gastronomy: the Anthropology of Food and Food Habits* (ed. Arnot, M. L.) 13–21 (Nijhoff, The Hague, 1975).
10. Golson, J. in *Sunda and Sahul: Prehistoric Studies in Southeast Asia, Melanesia and Australia* (eds Allen, J., Golson, J. & Jones, R.) (Academic, London, 1977).
11. White, J. P. & Allen, J. *Science* **207,** 728–734 (1980).
12. Glover, I. C. *Indonesia Circle* No. 12, 6–20 (1977).
13. Morley, R. J. thesis, Univ. Hull (1976).
14. Maloney, B. K. thesis, Univ. Hull (1979).
15. Flenley, J. R. *The Equatorial Rainforest: A Geological History* (Butterworth, London, 1979).
16. Ninkovich, D., Shackleton, N. J., Abdel-Monem, A. A., Obradovich, J. D. & Izett, G. *Nature* **276,** 574–577 (1978).
17. Boerma, J. *Kon. Mag. Met. Obs.* Batav., Dl. 1 (1925).
18. Backer, C. A. & Bakhuizen van den Brink, R. C. *Flora of Java* (Noordhoff, Groningen, 1963–68).
19. Bartlett, H. H. *Pap. Mich. Acad. Sci.* **6,** 1–66 (1926).
20. Holttum. R. E. *Flora of Malaya*, Vol. 2 (Government Printer, Singapore, 1954).
21. Ridley, H. N. *J. Malay Brch R. Asiat. Soc.* **S. 1,** 46–115 (1923).
22. van Steenis, C. G. G. J. *Mountain Flora of Java* (Brill, Leiden, 1972).
23. van Steenis, C. G. G. J. (ed.) *Flora Malesiana*, Ser. 1, Vols 4–6 (Wolters-Noordhoff, Groningen, 1948–62); Ser. 2, Vols 6–7 (Wolters-Noordhoff, Groningen, 1959–74).
24. Stein, N. *Die Erde*, **105,** 34–61 (1974).
25. Whitmore, T. C. (ed.) *Tree Flora of Malaya* (Longman, London, 1972–73).
26. Anderson, J. *Mission to the East Coast of Sumatra in 1823* (London, 1826).
27. Burton, R. & Ward, N. *Trans. R. As. Soc.* **1,** 485–513 (1826).
28. von Hügel, A. *Geogr. J.* **7,** 75–82, 175–183 (1896).

Periodical cicada nymphs impose periodical oak tree wood accumulation

Richard Karban

Biology Department, University of Pennsylvania, Philadelphia, Pennsylvania 19104

All deciduous woody tree species of the eastern United States serve as hosts for large numbers of root parasitizing cicada nymphs (*Magicicada* spp.)[1–4]. Periodical cicadas spend their larval lives 6–24 inches underground, feeding on xylem fluid from rootlets and roots[5]. They emerge every seventeenth year in the north or every thirteenth year in the south. Densities of cicadas underground are very great—Dybas and Davis report emergence densities of over 300 nymphs per square yard or about 1,500,000 per acre. This represents the highest reported biomass values of any naturally occurring terrestrial animal[6]. During the adult stage, which lasts 3–4 weeks, cicadas mate and females lay their eggs in twigs of deciduous trees. When the eggs hatch the first instar nymphs fall to the ground to begin their 17-yr development. The damaging effects to twigs by ovipositing adult cicadas is well established[7–13] but the major effect of cicadas may be due to the feeding of nymphs: nymphs are implicated in a reduction in productivity of orchard trees[14–16]. However, no studies have compared growth of parasitized and unparasitized trees in the same environment. I report here that feeding cicada nymphs can reduce tree growth, as measured by growth rings, by as much as 30%.

Fifty scrub oak trees (*Quercus ilicifolia*) were selected randomly on a flat plain of sandy soil, 3 km east of Ridge, New York[17]. Mature periodical cicadas, *Magicicada septendecim* (Brood XIV) had emerged there in 1974 (refs 17–19). All the trees were about 1.5 m tall and grew in a nearly monospecific stand. To minimize environmental variability, trees were selected which did not border trails or roads and were not near runoff channels in the soil. The stems were cut one inch above the ground and annual wood accumulation was measured with a dissecting microscope and ocular micrometer for each year from 1978 to 1971. Although the trees are older than this, 1971 was as far back as it was possible to measure accurately radial wood increment. When cicada eggs hatch the first instars fall into the ground below the egg nest. As cicada nymphs do not travel far during their tenure underground, oviposition scars provide a reliable indicator of the number of nymphs in that immediate vicinity[18,20]. Of the 50 trees selected, 20 had three or more egg nests (oviposition of one set of eggs by one female, mean = 7.20 ± 0.76 nests per plant), 15 had one or two egg nests and 15 had none. A mean of 19 eggs successfully hatch from each nest[21]. Infested and uninfested trees were in a random mixture on the site, precluding the possibility of an environmental cause for differential growth. Infested trees at this site support fewer cicadas than trees at other sites[6]. However, the dwarf oaks at this site are extremely small, are rooted in poor sandy soil and are very slow growing (Table 1).

For each of the three years before the emergence, no significant (0.05 level, Wilcoxon two-sample rank-sum test) difference was found between the trees with three or more egg nests and those with none (Table 1). During the emergence year and each of the four years following it, radial increment of the trees with no cicada eggs was significantly greater ($P<0.05$) than trees with three or more egg nests. Trees with one or two egg

0028–0836/80/390326—02$01.00

Table 1 Annual radial increment (mm) for scrub oak trees (*Quercus ilicifolia*) in Ridge, New York. Results of the Wilcoxon nonparametric two-sample test, the significance associated with each U value and the approximate t_s value are shown.

Year	3 or more eggnests Mean radial growth	Sample size	0 eggnests Mean radial growth	Sample size	U value from Wilcoxon two-sample test	Approximate t_s value	Significance
1978	0.23	20	0.35	15	206	1.87	0.05
1977	0.33	20	0.45	15	202.5	1.75	0.05
1976	0.31	20	0.41	15	212	2.07	0.05
1975	0.28	20	0.41	15	228.5	2.62	0.01
1974*	0.25	20	0.32	15	204	1.80	0.05
1973	0.26	20	0.28	15	165	0.50	none
1972	0.47	20	0.41	15	160	0.33	none
1971	0.78	20	0.58	15	190.5	1.35	none

*The emergence year.

nests were not significantly different than those without nests during any of the years and grew significantly more than trees with three or more nests during 1975 and 1977 only. In this analysis the three years preceding the emergence serve as a control. The fact that there was no difference in growth between the treatments for each of the three years preceding the emergence is evidence that microenvironmental factors, independent of cicadas, are not responsible for the observed growth effect during the years including and following the emergence.

It is difficult to interpret the reduction in growth of trees with egg nests during the emergence year. Cicadas emerge in May and June. The eggs hatch at least six to eight weeks after the emergence so that first instars do not enter the ground until July. It is expected that a large proportion of the annual wood increment would have already been added by this time. However, Phipps presents data showing that seasonal stem enlargement for *Quercus alba* varies considerably from year to year. A substantial fraction of growth may occasionally occur during July and August[22]. Current season wilting, death of branches, epinasty due to differential growth and short, weak shoots caused by oviposition wounds have been noted for *Quercus phellos* and *Quercus palustris*[23]. Thus, oviposition damage or the large energetic demands made by last instar nymphs on their host plant before emergence, rather than feeding nymphs, could reduce radial growth during the emergence year. The data reported here do not allow testing of these hypotheses.

The previous analysis considered differences between trees of the three cicada treatments within each year. Next I examined differences within each treatment and preceding and following the emergence. Total radial increment was summed for the four years following the emergence (1975–78) and for the four years preceding and including the emergence (1971–74) for each tree. Those trees with three of more egg nests grew 43% more during the four years preceding the emergence than during the four years following it ($\chi^2 = 7.20$, $n = 20$, d.f. $= 1$, $P < 0.01$ using Friedman's method for randomized blocks)[24]. No difference was found for the trees without egg nests ($\chi^2 = 0.70$, $n = 15$, d.f. $= 1$) nor for trees with one or two egg nests ($\chi^2 = 0.0$, $n = 14$, d.f. $= 1$). This result is unchanged if the data are analysed without the emergence year, 1974. This analysis shows an inverse relationship between a large number of cicada egg nests and radial incremental growth of *Q. ilicifolia* individuals following the emergence. In this analysis the trees without egg nests serve as controls. The fact that only those trees with three or more cicada egg nests in their canopies show a reduction in wood accumulation and those without cicadas show no effect is further evidence that climatic or other environmental factors are not responsible for the observed reduction in growth of trees with cicadas during the years following the emergence.

The result that cicada nymphs affect tree growth more in years including and following the emergence is in keeping with recent field observations. Periodical cicadas undergo five instars while growing underground. Earlier instars feed on smaller rootlets[25]. Younger nymphs live in short tunnels rather than the more permanent ellipsoidal cells inhabited by older nymphs[25,26]. Young nymphs presumably change feeding sites each time the rootlet they are currently using dies[25]. Older nymphs feeding on larger roots apparently do not kill their host root, resulting in relatively less damage to the tree by older nymphs[5,25].

The greater impact of feeding cicada nymphs in the years immediately following the emergence compared to the years immediately preceding the emergence may also be, in part, the result of a demographic reduction in cicada nymph density. Mortality factors such as predation by moles[27], direct competition[27,28] and starvation[25] reduce the population of cicada nymphs. A schedule of survivorship for developing nymphs is needed.

Periodical cicadas occur in great numbers feeding on all species of deciduous trees in eastern North America. If the growth effect documented here is a general one, cicada nymphs are a serious pest. Feeding cicada nymphs are capable of reducing tree growth by as much as 30%. Because feeding nymphs decrease tree growth more during the years following an emergence than during the years preceding an emergence, they may be inducing a periodical pattern of tree growth.

I thank Timothy Brown for help in preparing and counting growth rings, Chris Simon for logistical help during the study and showing me this forest, Daniel Janzen, James Quinn, Chris Simon, Alan Smith, Truman Young and an anonymous reviewer for comments on the manuscript. I also thank Monte Lloyd and JoAnn White for numerous suggestions and discussions.

Received 19 December 1979; accepted 28 July 1980.

1. Butler, A. W. *Bull. U.S. Dep. Agric. Div. Ent.* **12,** 24 (1886).
2. Dybas, H. S. & Lloyd, M. *Ecol. Monogr.* **44,** 279 (1974).
3. Lloyd, M. & White, J. *J. N.Y. Ent. Soc.* **84**, 148 (1976).
4. White, J. *Am. Nat.* **115,** 1 (1980).
5. White, J. & Strehl, C. E. *Ecol. Ent.* **3,** 323 (1978).
6. Dybas, H. S. & Davis, D. D. *Ecology* **43,** 432 (1962).
7. Riley, C. V. *Bull. U.S. Dep. Agric. Div. Ent.* **8** (1885).
8. Cory, E. N. & Knight, P. *J. econ. Ent.* **30,** 287 (1937).
9. Smock, R. M. & Neubert, A. M. *Apples and Apple Products* (Interscience, New York, 1950).
10. Graham, C. & Cochran, A. B. *J. econ. Ent.* **47**, 242 (1954).
11. Hunter, P. E. & Lund, H. O. *J. econ. Ent.* **53,** 961 (1960).
12. Lloyd, M. & Dybas, H. S. *Evolution* **20,** 133 (1966).
13. Smith, F. F. & Linderman, R. G. *Env. Entom.* **3,** 725 (1974).
14. Banta, E. S. *Proc. Ohio State Hort. Soc.* **118,** 88 (1960).
15. Hamilton, D. W. *Proc. Indiana Acad. Sci.* **71,** 16 (1961).
16. Hamilton, D. W. & Cleveland, M. L. *Proc. Indiana Acad. Sci.* **73,** 167 (1964).
17. Simon, C. M., Karban, R. & Lloyd, M. (in preparation).
18. Marlatt, C. L. *Bull. U.S. Dep. Agric. Bur. Ent.* **71,** (1907).
19. Davis, W. T. *Bull. Brooklyn Ent. Soc.* **19,** 182 (1924).
20. Marlatt, C. L. *Proc. Ent. Soc. Washington* **9,** 16 (1908).
21. Forsythe, H. Y. *Env. Ent.* **5,** 169 (1976).
22. Phipps, R. L. *Ohio Agric. exp. Stn Res. Circ.* 105 (1961).
23. Smith, F. F. & Linderman, R. G. *Env. Ent.* **3,** 725 (1974).
24. Sokal, R. R. & Rohlf, F. J. *Biometry* (Freeman, San Francisco, 1969).
25. White, J. & Lloyd, M. *Am. Midl. Nat.* **94,** 127 (1975).
26. Lloyd, M. & White, J. *Evolution* **30,** 786 (1976).
27. Lloyd, M. & Dybas, H. S. *Evolution* **20,** 133 (1966).
28. Beamer, R. H. *Univ. Kansas Sci. Bull.* **18,** 155 (1928).

Sexual dimorphism in early anthropoids

John G. Fleagle[*], Richard F. Kay[†] & Elwyn L. Simons[‡]

[*] Department of Anatomical Sciences, Health Sciences Center, State University of New York at Stony Brook, Long Island, New York 11794
[†] Department of Anatomy, Duke University Medical Center, Durham, North Carolina 27710
[‡] Duke University Center for the Study of Primate Biology and History, 3705 Erwin Road, Durham, North Carolina 27705

Sexual dimorphism in canine/premolar tooth size and in body size is found among many species of living primates and has been shown to be correlated with social organization. Among extant higher primate species that normally live in nuclear families consisting of a mated pair with their offspring, adult males and females are similar in body size and in the size of canine and anterior premolar teeth. In contrast, higher primate species living in more 'complex' polygynous groups (either single-male harems or multi-male groups) are characterized by sexual dimorphism in the size of canine/premolar teeth and frequently by body size dimorphism as well[1–4]. We provide here the first evidence for sexual dimorphism in three species of primates from the Oligocene of Egypt—*Aegyptopithecus zeuxis*, *Propliopithecus chirobates*, and *Apidium phiomense*. This is the earliest record of sexual dimorphism among higher primates and suggests, by analogy with living species, that the earliest known fossil Old World anthropoids lived in polygynous (either single-male harems or multi-male groups) rather than monogamous social groups.

Four higher primate species have been recovered from the Upper Fossil Wood zone of the Jebel el Qatrani Formation in the Fayum Province of Egypt: two hominoids—*A. zeuxis*[5,6] and *Pr. chirobates*[5–8] and two parapithecids—*Apidium phiomense*[8] and *Parapithecus grangeri*[8]. Until recently, most of these taxa were known from relatively few specimens preserving mainly molar teeth. However, recent cooperative expeditions by the Geological Survey of Egypt and Duke University have recovered more complete dental and cranial remains, as well as additional skeletal material of these early anthropoids[9,10]. Thus, for the first time, there are numerous jaws preserving the lower canines and premolars (Fig. 1)—the teeth that are critical for identifying sexual dimorphism in higher primates[11,12].

The largest species from the Egyptian Oligocene is the early ape, *A. zeuxis*. The molar teeth of specimens assigned to this species are uniform in size; however there is a distinct bimodal distribution in the size of lower canines and premolars similar to that found in sexually dimorphic living species, with the larger canines and premolars presumably belonging to males and the smaller ones to females (Fig. 2*a*,*b*). In both sexes of *A. zeuxis*, the lower canine is a projecting subconical tooth and the anterior lower premolar is sectorial, with a large wear facet on the anterolateral surface where it occludes with the upper canine (Fig. 1*a*, *b*). The lower canines (Fig. 2*a*) and anterior lower premolars (Fig. 2*b*) of presumed females, however, are about 25% smaller than those of presumed males (Fig. 2*a*, *b*).

Propliopithecus chirobates is a smaller ape closely related to *A. zeuxis*. Although this species is known from fewer specimens than *A. zeuxis*, it shows a similar bimodal distribution of canine/premolar dimensions in conjunction with low metric variability in molar dimensions (Fig. 2*a*, *b*). As in *A. zeuxis*, these teeth are very similar in morphology in the two sexes (Fig. 1*c*, *d*), but differ in size.

In *A. phiomense*, a small parapithecid, the canine is not so

the Library
SCIENCE COLLEGE
Upper Circular Road
CALCUTTA

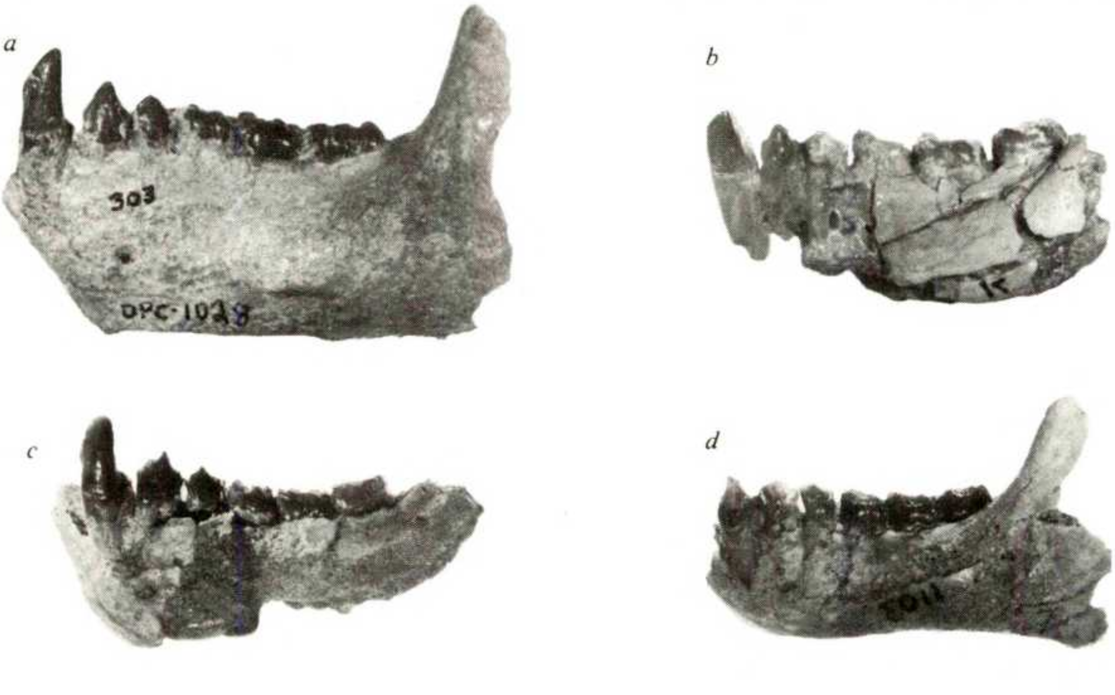

Fig. 1 Lower jaws of early Oligocene Anthropoidea from Egypt. *a*, *A. zeuxis*, male (DPC 1028); *b*, *A. zeuxis*, female (DPC 1042); *c*, *P. chirobates*, male (DPC 1029); *d*, *P. chirobates*, female (DPC 1103); *e*, *A. phiomense*, male (DPC 1089); *f*, *A. phiomense*, female (DPC 1104). All fossils are to the same scale.

0028-0836/80/390328—03$01.00

Table 1 Mandibular depth, body mass ratio of adult males to adult females and social structure of anthropoidea

Species (*N*)		c.v. of mandible depth	Male mass / Female mass	Social structure
Cebus apella	(20)	19.5	1.30^{13}	MM†
Alouatta seniculus	(20)	19.4	1.41^{13}	S or MM†
Nasalis larvatus	(18)	18.3	1.37^{2}	MM^{15}
**Aegyptopithecus zeuxis*	(10)	16.3	*	*
**Apidium phiomense*	(22)	13.6	*	*
Macaca fascicularis	(12)	12.6	1.16^{2}	MM†
Gorilla gorilla	(40)	12.2	1.28^{2}	S or MM^{15}
Pan troglodytes	(26)	9.2	1.04^{2}	MM^{15}
Presbytis rubicunda	(12)	8.3	$1\ 03^{2}$	S^{17}
Hylobates lar	(12)	8.2	1.03^{2}	Mo‡
Saimiri sciureus	(18)	7.5	1.10^{14}	MM†
Pithecia pithecia	(17)	7.4	1.0^{9}	Mo†
Aotus trivirgatus	(17)	7.0	1.04^{2}	Mo^{16}
Hylobates hoolock	(16)	6.9	1.02^{2}	Mo^{18}
Symphalangus syndactylus	(10)	5.9	1.03^{2}	Mo^{16}

Mandibular depth was measured under M_1, sample sizes are to the right of the species. Social structures are categorized as follows: MM, groups with several adult females and several adult males; S, groups usually with one adult male and several adult females; MO, monogamous groups with one adult male and one adult female. All groups with offspring.

† Personal observation.

projecting and the shearing between the upper canine and anterior lower premolar (P_2) is not as well developed as in the hominoids (Fig. 1*e*, *f*). There is, nevertheless, dimorphism in the size of the lower canine relative to molar dimensions (Fig. 2*a*). At present, too little is known of the dental morphology of *Parapithecus grangeri* to determine the extent of sexual dimorphism in this parapithecid.

In addition to dental dimorphism, *A. phiomense* and *A. zeuxis* also show evidence of dimorphism in the depth of the mandibular corpus. (There are not enough jaws of *Propliopithecus chirobates* or *Parapithecus grangeri* to allow statistical comparison of mandibular dimensions.) Among extant higher primates showing sexual dimorphism in body size, the smaller females have relatively shallow mandibles and the larger males have relatively deep mandibles. In species with little sexual dimorphism in body weight, there is no dimorphism in mandible depth. The coefficient of variation ($100\,\mathrm{s.d.}/\bar{x}$) provides an estimate of variability within a species that can be related to dimorphism, but does not require prior identification of the sex of a specimen[11]. There is a very high positive correlation ($r = 0.940$) between the degree of sexual dimorphism in body weight ($\bar{x}$ female mass/$\bar{x}$ male mass) and the coefficient of variation of mandible depth below the first molar (Table 1). *Aegyptopithecus zeuxis* and *Apidium phiomense* show high coefficients of variation for mandible depth suggesting considerable dimorphism in body size.

The correlation of social organization with canine/premolar dimorphism and body size dimorphism among living primates appears to be mainly the result of differences in intra-sexual competition and possibly also predator defense[1–4]. In monogamous species, adults of both sexes appear to be equally active in repulsing same-sex intruders into the group and are often equally active in defense; thus there is little sexual dimorphism. In polygynous species, there is usually much more overt male–male competition for access to females and males often appear to play a greater role in troop defense; therefore males have large canines and anterior premolars and often greater size than females. The canine/premolar dimorphism and mandibular variation exhibited by *A. zeuxis*, *Propliopithecus chirobates* and *Apidium phiomense* are considerably greater than that found among any living monogamous higher primates and suggest that all three extinct species were probably living in polygnous groups characterized by male–male competition.

Among living higher primates, nuclear families and associated sexual monomorphism are found among many of the more primitive New World monkeys and among the lesser apes, suggesting that a monogomous social structure is phylogenetically very old and is possibly the primitive condition for all higher primates[19–21]. The evidence of considerable sexual dimorphism in Oligocene hominoids and parapithecids presented here, however, indicates that more complex, presumably polygynous social structures are definitely very old, probably represent the primitive condition for Old World higher primates, and may well be primitive for all anthropoids.

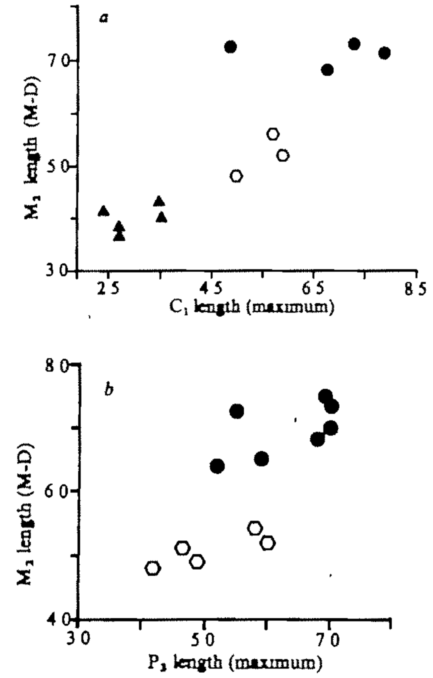

Fig. 2 *a*, Bivariate plot of length of C_1 versus M_2 for *Aegyptopithecus zeuxis* (●), *Propliopithecus chirobates* (○), and *Apidium phiomense* (▲) *b*, Bivariate plot of length of P_3 versus M_2 for *A. zeuxis* (●) and *Propliopithecus. chirobates* (○).

Finally, the finding that sexual dimorphism is typical among Fayum apes has important implications for interpreting the phylogenetic status of *Propliopithecus haekeli*. Since its initial description in the early years of this century[22], the type and sole specimen of this species has been put forth by many scientists as an early human ancestor because of its small canines[23–26]. To the contrary, the similarities between *P. haekeli* and females of *P. chirobates* indicate that *P. haekeli* is not hominid-like but rather is the female of a sexually dimorphic species[5,27]. This invalidates the available evidence for an Oligocene divergence of humans and apes.

We are grateful to the Geological Survey of Egypt for the assistance they provided in all aspects of our field work. This work was supported in part by NSF grants BNS 7683114, BNS 7724921, BNS 7720104 and BNS 79-24149, and Smithsonian Foreign Currency Grant FC 70869600.

Received 14 March, accepted 25 June 1980

1 Clutton-Brock, T H, Harvey, P H & Rudder, B *Nature* **269**, 797–800 (1977)
2 Leutenegger, W & Kelly, J T. *Primates* **18**, 177–186 (1977)
3 Gautier-Hion, A. *Mammalia* **39**, 365–374 (1975)
4 Harvey, P H, Kavanagh, M & Clutton-Brock, T H *J Zool* **186**, 475–485 (1978).
5. Simons, E L *Nature* **205**, 135–139 (1967)
6 Simons, E L. *Primate Evolution* (Macmillan, New York, 1972)
7 Gingerich, P. D *Paläont Z* **52**, 82–92 (1978)
8 Szalay, F. S & Delson, E. *Evolutionary History of the Primates* (Academic, New York, 1979)

9. Fleagle, J. G. & Simons, E. L. *Nature* **276,** 705–707 (1978).
10. Fleagle, J. G. & Simons, E. L. *Folia primatol.* **31,** 176–186 (1979).
11. Pilbeam, D. R. & Zwell, M. *Yb. phys. Anthrop.* **16,** 69–79 (1973).
12. Gingerich, P. D. & Schoeninger, M. J. *Am. J. phys. Anthrop.* **51,** 457–466 (1979).
13. Fleagle, J. G. & Mittermeier, R. A. *Am. J. phys. Anthrop.* **32,** 301–314 (1980).
14. Kay, R. F. thesis, Yale Univ. (1973).
15. Jolly, A. *The Evolution of Primate Behavior* (Macmillan, New York, 1972).
16. Wright, P. C. *Folia primatol.* **29,** 43–55 (1978).
17. Stott, K. Jr & Selsor, C. J. *Mammalia* **25,** 184–189 (1961).
18. McCann, C. H. *Bombay nat. Hist. Soc.* **36,** 395–405 (1933).
19. Eisenberg, J. F. *The Biology and Conservation of the Callitrichidae,* 13–22 (Smithsonian Inst., Washington, 1977).
20. Eisenberg, J. F. in *Primate Ecology and Human Origins* 215–262 (Garland STPM, New York, 1979).
21. Richarz, K. in *Perspectives in Primate Biology* (in preparation).
22. Schlosser, M. *Beitr. Paläont. Geol. Öst.-Ung.* **6,** 1–227 (1911).
23. Gregory, W. K. *The Origin and Evolution of the Human Dentition* (Williams & Wilkins, Baltimore, 1922).
24. Simons, E. L. *Nature* **205,** 135–139 (1965).
25. Kinzey, W. G. *Am. Anthrop.* **73,** 680–694 (1971).
26. Kurtén, B. *Not From the Apes* (Pantheon, New York, 1972).
27. Delson, E. *Actes C.N.R.S. Coll. int.* **28,** 839–850 (1975).

Oxygen-linked CO_2 binding independent of *p*H in cephalopod blood

Gunnar Lykkeboe, Ole Brix & Kjell Johansen

Department of Zoophysiology, University of Aarhus,
DK-8000 Aarhus C, Denmark

The oxygen affinity of the haemocyanin-containing blood of some cephalopods is very dependent on the *p*H of the blood[1,2]. The effect of *p*H on the oxygen affinity is expressed quantitatively as the slope of the function between log P_{50} and *p*H, where P_{50} denotes the oxygen tension at an oxygen saturation fraction of 0.5. This Bohr coefficient, $\Delta \log P_{50}/\Delta pH$, is about −1.8 in the case of *Loligo pealei*[1] and about −1.5 for *Sepia officinalis*[2]. These pronounced Bohr effects are physiologically significant as they should allow the metabolically produced CO_2 in the tissues to promote the dissociation of oxyhaemocyanin and thus facilitate the unloading of oxygen to the tissues. However, the Bohr effect is tantamount to an oxygen-linked hydrogen ion binding to the respiratory pigment and the quantitative parameter of this Haldane effect is the change in the concentration of haemocyanin-bound hydrogen ion ($\Delta cHcH$) accompanying a change in the concentration of haemocyanin-bound oxygen ($\Delta cHcO_2$) at a constant *p*H. According to the linkage equation[3], the Bohr coefficient and the Haldane coefficient are identical: $\Delta \log P_{50}/\Delta pH = (\Delta cHcH/\Delta cHcO_2)_{pH}$. This implies that in a homogeneous system, such as in cephalopod blood, the amount of protons bound to the haemocyanin upon deoxygenation from the fully oxygenated state, at constant *p*H, equals the negative value of the Bohr coefficient times the oxygen capacity. Thus, a Bohr coefficient of <-1 implies that more than 1 mmol of protons will be bound to the pigment per mmol of O_2 unloaded. Since the CO_2 produced in the tissues can maximally yield 1 mmol of protons per mmol of oxygen consumed, at a respiratory exchange ratio of unity, we reinvestigated the reciprocal effects of O_2 and CO_2 on the respiratory properties of cephalopod blood to see whether blood *p*H can decrease during O_2 unloading when CO_2 is the only 'proton source' and the Bohr coefficient is <-1.

A spectrophotometric determination[4] of the oxygen affinity of the blood from *Sepia latimanus* at 25 °C gives the expression log $P_{50} = -1.37 \times pH + 11.83$ in the *p*H range 7.3–7.7 and the Bohr coefficient of −1.37 means that this blood is suitable for our investigation.

The relationship between the CO_2 tension, *p*H and the total content of CO_2 in oxygenated and deoxygenated blood was determined by measuring both *p*H and the CO_2 content[5,6] of blood brought into equilibrium with the appropriate gas mixtures in a tonometer kept at a constant temperature of 25 °C.

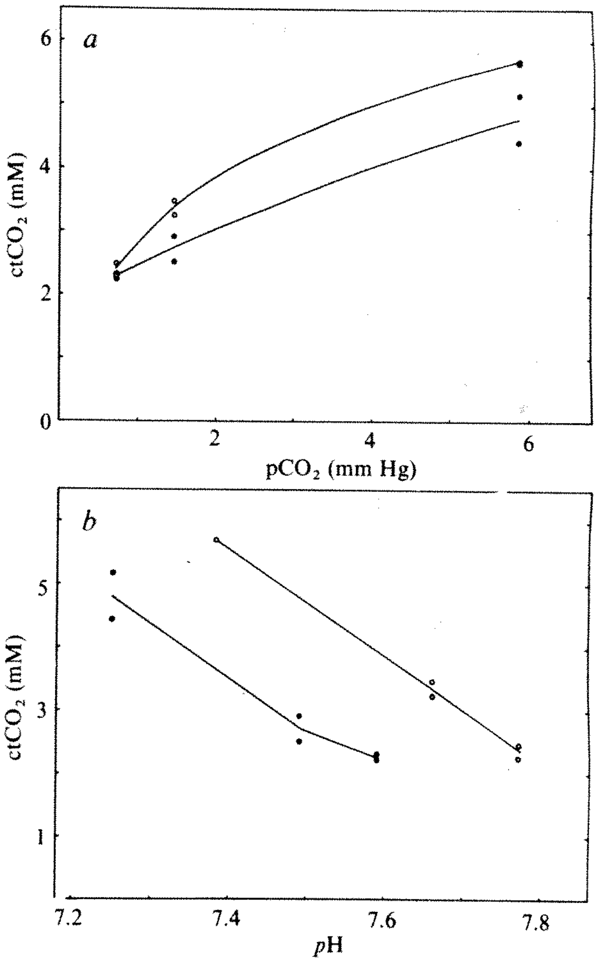

Fig. 1 *a*, CO_2 equilibrium curves of oxygenated and deoxygenated blood. $ctCO_2$ is the total CO_2 content. *b*, The data for total CO_2 content from *a* plotted against the corresponding measured *p*H values. Oxygen capacity = 1.86 mM. ●, Oxygenated; ○, deoxygenated.

Figure 1*a* shows that the deoxygenated blood contains more CO_2 at a given CO_2 tension than the oxygenated blood, except at the lowest CO_2 tension applied where the two curves coincide. As the blood has the same total CO_2 content ($ctCO_2$) at a CO_2 tension of about 0.7 mm Hg, irrespective of the state of oxygenation, one should expect the *p*H to be the same for oxygenated and deoxygenated blood. Figure 1*b* shows that this is not the case, as replotting the values for $ctCO_2$ from Fig. 1*a* against the corresponding *p*H of the blood reveals that a great *p*H difference exists between oxygenated ($pH = 7.59$) and deoxygenated ($pH = 7.77$) blood.

This *p*H difference at a constant CO_2 tension tells us that, as the total CO_2 is nearly unchanged, some of the CO_2 present in the oxygenated blood must have disappeared upon deoxygenation and that it has been replaced by an almost equal amount of bicarbonate.

To investigate this CO_2 component in oxygenated blood, CO_2 washout experiments were performed on oxygenated and deoxygenated blood. Blood tonometered to equilibrium at the lowest CO_2 tension was subjected to a CO_2 pressure of zero. Blood *p*H and $ctCO_2$ were measured repeatedly for about an hour and the results presented in Fig. 2.

The total content of about 2.3 mmol of CO_2 per l is in both cases washed out after 1 h, but both the time course and the total change in *p*H are different. The oxygenated blood shows a change in *p*H from 7.59 to nearly 7.74 and the change is almost fully established after 30 min when the system still contains about 1 mmol of CO_2 per l. By contrast, the deoxygenated blood exhibits a total change in *p*H from 7.77 to 7.99 and this change is complete after 70 min, when the CO_2 content of the blood is

0028–0836/80/390330—02$01.00

reduced to nearly zero. The much smaller *p*H increase in the oxygenated sample compared with the deoxygenated sample and the time course of this change indicate that the CO_2 pool in the oxygenated blood contains a component of CO_2 that is liberated without a simultaneous call for protons, and that the size of this part of the total CO_2 is close to 1 mmol per 1 of blood.

We suggest that this CO_2 component is present in the form of molecular CO_2 bound to the oxygenated haemocyanin and that this CO_2 fraction is oxygen linked such that it is liberated when the oxygen is given off from the haemocyanin.

The size of the oxygen-linked CO_2 component can also be estimated if one assumes that the $ctCO_2$ of the deoxygenated blood, at the two highest CO_2 tensions applied, is composed solely of physically dissolved CO_2 ($cdCO_2$) and bicarbonate. The *p*K′ values of the carbonic acid-bicarbonate system were calculated according to the equation:

$$pK' = pH - \log \frac{ctCO_2 - cdCO_2}{cdCO_2}$$

With the relationship between *p*K′ and *p*H established, *p*K′ values corresponding to the other measured values of *p*H for oxygenated and deoxygenated blood were determined and thereafter the apparent bicarbonate concentrations were calculated. The results of this procedure are represented in Fig. 3.

This plot shows that the calculated amount of apparent bicarbonate plus the physically dissolved CO_2 for oxygenated blood is between 0.7 and 1 mmol less than the measured values for total CO_2. Furthermore, it is now possible to test the identity between the values for the Bohr and Haldane effects. With an oxygen capacity of 1.86 mM (determined as half of the copper content of the blood) and a Bohr coefficient of −1.37, the total ΔcHcH at constant blood *p*H should be about 2.5 mmol per l of blood. When this value is compared with the increase in apparent bicarbonate at constant *p*H—2.7 mM at *p*H 7.38 decreasing to 2.5 mM at *p*H 7.59—a striking resemblance with the predicted value above is apparent. The correspondence of these numbers adds validity to the procedure used concerning the calculation of the apparent bicarbonate concentration and to the estimate concerning the size of the oxygen-linked CO_2 component.

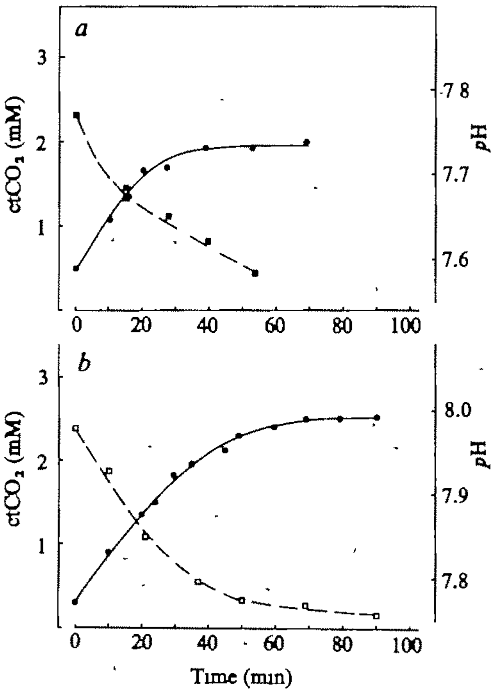

Fig. 2 CO_2 washout curves for *a*, oxygenated and *b*, deoxygenated blood. Squares, $ctCO_2$; circles, *p*H.

The effect of the oxygen-linked CO_2 component is a transformation of the Haldane coefficient to what could be called the functional Haldane coefficient, the latter expressed by the CO_2 binding potential of the system at constant *p*H. The size of this functional Haldane coefficient, in mM CO_2/mM O_2, ranges in *S. latimanus* from about 0.9 at *p*H 7.59 to about 1.1 at *p*H 7.38. This implies that no substantial decrease of the *in vivo* blood *p*H should occur when blood passes the tissue capillaries; on the contrary, small increases in blood *p*H should be more frequent, even at a respiratory exchange ratio of unity.

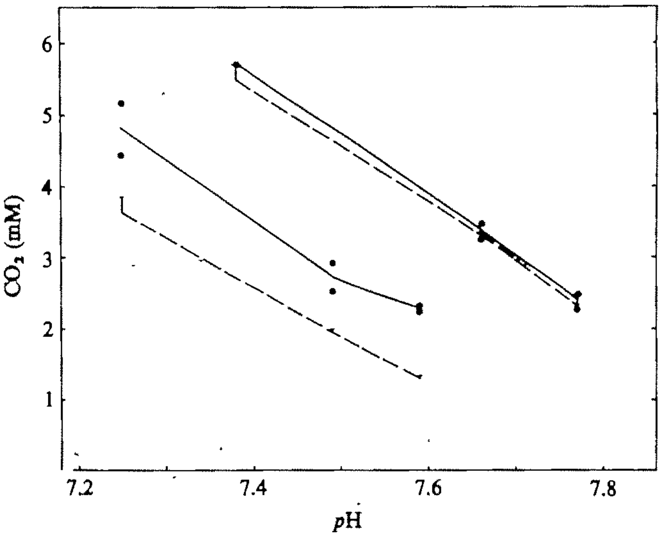

Fig. 3 This shows the same data as Fig. 1*b*, together with the corresponding calculated values for apparent bicarbonate concentration (broken line). Vertical bars (T) indicate the amount of physically dissolved CO_2 (solubility coefficient 0.039 mM l^{-1} $mmHg^{-1}$). Oxygen capacity = 1.86 mM. ●, Oxygenated; ○, deoxygenated; — $ctCO_2$.

The question of whether *p*H can actually decrease during O_2 unloading may be answered affirmatively. A requisite for this answer must, however, be the presence of an oxygen-linked CO_2 component large enough to generate a functional Haldane coefficient: mM CO_2/mM O_2 at constant *p*H, well below unity. This condition is likely to be species dependent and related to metabolic rate and metabolic scope. In *S. latimanus*, a moderately active cephalopod, the condition is marginally present, but in the case of *L. pealei*, a far more active species, it is likely to be more developed.

This study was done on *S. latimanus* blood brought back from the 1979 Alpha Helix expedition supported by NSF grant PCM 77-16269 and the Danish Natural SRC.

Received 10 March, accepted 23 July 1980

1. Redfield, A. C. & Goodkind, R. *J. exp. Biol.* **6**, 340–349 (1929)
2. Wolvekamp, H. P., Baerends, G. P., Kok, B. & Mommaerts, W. F. H. M. *Archs néerl. physiol.* **26**, 203–211 (1942)
3. Wyman, J. Jr *Adv. Protein Chem.* **19**, 224–286 (1964)
4. Lykkeboe, G. & Johansen, K. *J. comp. Physiol.* **104**, 1–11 (1975)
5. Redfield, A. C., Coolidge, T. & Hurd, A. L. *J. biol. Chem.* **69**, 475–509 (1926)
6. van Slyke, D. D. & Plazin, J. *Micromanometric Analyses* (Williams & Wilkins, Baltimore, 1961)

Isolation of human haematopoietic progenitor cells using monoclonal antibodies

P. C. L. Beverley*, D. Linch † & D. Delia‡

* ICRF Human Tumour Immunology Group, University College Hospital Medical School, University Street, London WC1E 6JJ, UK
† Department of Clinical Haematology, University College Hospital Medical School, University Street, London WC1E 6JJ, UK
‡ Imperial Cancer Research Fund, Lincoln's Inn Fields, London WC2A 3PX, UK

Studies of the differentiation of human haematopoietic cells have been greatly advanced by the use of *in vitro* cloning techniques to enumerate the myeloid and erythroid progenitor cells which form colonies in semi-solid medium[1-3]. The granulocytic/monocytic colony-forming cells (CFU-GM) and erythroid burst-forming cells (BFU-E) are thought to be mononuclear cells, similar in size to medium size lymphocytes, but their ontogenetic relationship to other progenitor cells and the putative pluripotential stem cell remains obscure[4,5]. This is partly because elucidation of parent-progeny relationships requires the isolation of precursor cells before they acquire mature phenotypic characters. Physical methods have failed to separate CFU-GM cleanly from other cells because of their heterogeneity, and immunologically specific markers for human progenitor cells have not been reported[6,7]. We report here that a fraction containing all the granulocytic/monocytic and erythroid progenitor cells, as well as cells which may be lymphoid progenitors, can be isolated from bone marrow using a combination of monoclonal antibodies.

The anti-leukocyte antibody (anti-HLe-1) was prepared by hyperimmunization of BALB/c mice with human peripheral blood mononuclear cells. The immune spleen cells were fused using polyethylene glycol to NS-1 myeloma[8] and the anti-HLe-1 clone was isolated by limiting dilution. By indirect immunofluorescence the antibody stains brightly all peripheral thymus-derived (T) and bone marrow-derived (B) lymphocytes and the majority of thymocytes. Peripheral blood monocytes and granulocytes and some bone marrow cells are weakly positive, whereas all other cell types tested, including mature erythrocytes and platelets, are negative[9,10].

The anti-myeloid antibody (TG-1) was derived, by limiting dilution cloning, from a fusion for which BALB/c mice were immunized with a glycoprotein fraction of thymocyte membranes (P.C.L.B. and A. Sullivan, unpublished observations). This antibody recognizes an antigen present on peripheral blood polymorphs and eosinophils but not on T and B lymphocytes and erythrocytes or the surface membrane of thymocytes. In bone marrow it labels predominantly cells of the granulocytic lineage. We do not know why we were able to derive an antibody reacting with granulocytic cells from a mouse immunized with thymocyte glycoproteins.

Samples of human marrow stained by indirect immunofluorescence with anti-HLe-1 were analysed and sorted on a FACS-1. Figure 1*a* shows the cell sorter profile obtained from such an experiment. Three major populations are separable by combinations of light scattering (cell size) and fluorescence intensity. Table 1 shows the cytological characteristics of the three sorted fractions. The unstained cells (fraction 1) are the recognizable precursors of the erythroid lineage. Fraction 2 contains the cells of the granulocytic lineage and fraction 3 contains mainly small and medium lymphocytes whose staining by indirect fluorescence is similar to that of peripheral blood lymphocytes. Table 1 also gives the colony-forming assay data (CFU-GM) for the various fractions and control unsorted marrow. The results show unequivocally that the CFU-GM are in fraction 2, but as this fraction contains approximately 50% of the cells isolated from bone marrow by Ficoll–Hypaque separation, this does not represent a significant enrichment of progenitor activity. However, this result does show that the granulocytic/monocytic progenitors appear on FACS analysis in a zone of cells labelled only weakly with anti-HLe-1 in which there are very few lymphocytes. It was therefore possible to identify the correct zone on the cell sorter profile for isolation of the progenitor cells after removing most granulocytic series cells with anti-myeloid antibody and complement.

Table 1 Differential counts and colony forming cells (CFU-GM) of bone marrow fractions

	Unseparated	Fraction 1	Fraction 2	Fraction 3
Erythrocyte precursors %	13	92	4	0
Blasts and promyelocytes %	0	0	2	0
Myelocytes %	27	4	29	1
Metamyelocytes %	44	3	61	2
Polymorphs %	1	0	3	2
Monocytes %	5	0	0	6
Lymphocytes %	10	1	1	89
CFU-GM per 10^5 cells	39	1.2	89.2	0.6
% Of total nucleated cells	100	17	52	10
% Of total CFU-GM	100	1	117	1

Bone marrow fractions were cytocentrifuged and stained by May–Grünwald Giemsa for differential counting. At least 200 cells were counted in each fraction. Granulocytic and monocytic colonies were grown in semi-solid agar bilayers containing α medium and 25% pre-screened fetal calf serum (FCS)[1]. The feeder layer contained 20% placental conditioned medium as a source of colony stimulating activity[13]. The cultures were incubated for 14 days at 37 °C in 5% CO_2 in humidified air and cell aggregates greater than 40 cells were scored as colonies. Values given are the means of three replicate cultures. This experiment has been repeated many times and the above is a representative sample of the results.

Table 2 Effect of TG-1 and complement on differential count and CFU-GM

	F/H marrow	TG-1+C
Promyelocytes %	1	0
Myelocytes %	10	1
Metamyelocytes %	20	0
Granulocytes %	5.5	0
Lymphocytes %	13	23
Plasma cells %	1	1.5
Monocytes %	5	10*
Erythroid precursors %	35.5	64.5
CFU-GM per 10^5 cells	80	142

* Many of these cells with cartwheel nuclei and ragged cytoplasm are probably degenerating myelocytes and metamyelocytes damaged by the antibody and complement.

In a second series of experiments, therefore, bone marrow cells obtained by Ficoll–Hypaque isolation were treated with TG-1 antibody and complement before staining with anti-HLe-1. The TG-1 antibody kills a significant proportion of bone marrow cells of the granulocytic lineage but spares the CFU-GM (Table 2). The cell sorter profile obtained after this sequential treatment is shown in Fig. 1*b*. Although the erythroid and lymphocyte fractions (fractions 1 and 3) are present, the granulocytic fraction (fraction 2) has been largely removed by the TG-1 treatment. It is still possible, however, to collect the

0028-0836/80/390332—02$01.00

surviving progenitor cells which fall in the band of cells staining weakly with anti-HLe-1. In the experiment detailed in Fig. 1 and Table 3, two different size fractions of this weakly staining population were collected and these represent somewhat different, though overlapping, progenitor cell populations. The majority of the CFU-GM and the more mature GM clusters and CFU-E are found in the large cell fraction. Both fractions, however, contain large numbers of BFU-E, and as BFU-E are thought to be more primitive than CFU-E or CFU-GM[11], it is probable that the smaller cell fraction includes the pluripotential stem cells.

Both fractions contain significant numbers of terminal deoxynucleotidyl transferase (TdT)-positive cells (from 3–15% in different experiments) whereas other sorted fractions do not. The TdT-positive cells in bone marrow are largely Ia (HLA-D) positive and are thought to be lymphoid progenitor cells[12] so that it seems probable that all the bone marrow progenitor cells are included in the weakly HLe-1 stained fraction.

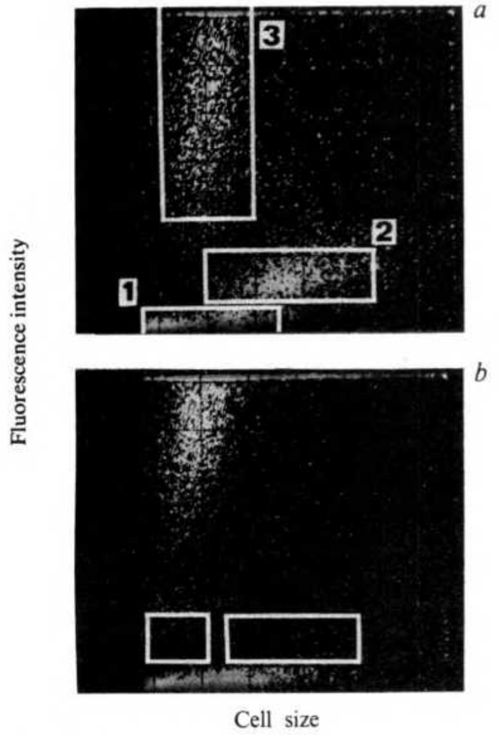

Fig. 1 Bone marrow aspirates were obtained from normal volunteers. The aspirated cells were separated on Ficoll–Hypaque to remove red cells and mature granulocytes and washed in HEPES-buffered RPMI-1640 medium with 5% added fetal calf serum (RPMI-FCS). For analysis or cell sorting, cells were incubated with anti-HLe-1 culture supernatant for 30 min on ice, washed twice with RPMI-FCS and then incubated (30 min on ice) with immunoabsorbent-purified fluorescein-conjugated $F(ab')_2$ sheep anti-mouse immunoglobulin antiserum (100 $\mu g\ ml^{-1}$ in RPMI-FCS), followed by a further two washes. In some experiments both first and second layers were diluted in 10% normal sheep serum to compete for Fc receptors, a procedure which very effectively prevents Fc binding of mouse immunoglobulin by peripheral blood monocytes (P.C.L.B., unpublished observations). This did not significantly change the FACS profile. For removal of mature cells of the granulocytic lineage, aliquots of bone marrow cells were incubated with TG-1 culture supernatant (2×10^7 bone marrow cells per ml) on ice, washed once and incubated at 37 °C for 45 min with undiluted autologous serum as a source of complement (4×10^7 cells per ml). Surviving cells were washed three times by centrifugation through FCS. This procedure killed approximately 50% of the nucleated cells in the Ficoll–Hypaque-isolated bone marrow. Samples were examined for fluorescence and light scattering on a FACS-1. A typical profile of normal bone marrow stained with anti-HLe-1 is illustrated in *a* and windows for collection of unstained erythroid (1), weakly stained myeloid (2) and brightly stained lymphoid fractions (3) are also shown. *b* Shows the effect of treatment of the marrow with TG-1 and complement before staining with anti-HLe-1. The granulocytic fraction is eliminated but cells can still be collected in the windows illustrated.

Table 3 Differential counts and colony forming data of antibody + complement treated and sorted marrow

		F/H marrow	Fraction 1 (small dim)	Fraction 2 (large dim)
Proerythroblasts %		1	5	14
Normoblasts %		16	6	25
Lymphocytes %		25	37	3
Monocytes %		2	1	0
Plasma cells %		1	1	19
Progenitor cells %		1	47	36
Maturing granulocytic cells %		54	3	3
Clusters-GM	per 10^5 cells	169	1,100	8,450
CFU-GM		56	700	2,800
CFU-E		292	3,780	17,130
BFU-E		34	3,333	2,777

Granulocytic/monocytic clusters and colonies were grown as detailed for Table 1. Clusters are smaller cell aggregates (<40 cells) scored at day 7. Erythroid colonies and bursts were grown in 1.8% methylcellulose containing supplemented α medium, 30% pre-screened FCS and 1% deionized bovine serum albumin[14]. Erythroid colonies were grown in the presence of 1 unit ml^{-1} of human urinary erythropoietin, and were scored at day 7 as benzidine-positive aggregates greater than eight cells. Erythroid bursts were grown in the presence of 3 units ml^{-1} of erythropoietin and scored at day 14 as haemoglobin-containing aggregates greater than 64 cells. As BFU-E require addition of feeder cells[15], 5×10^4 Ficoll–Hypaque-separated cells were added to each dish for the assays of fractions 1 and 2. The numbers are therefore derived by subtracting the number of bursts produced by 5×10^4 Ficoll–Hypaque cells from the total in each dish. Similar enrichment of erythroid progenitors has been obtained in two other experiments and of granulocytic monocytic progenitors in four. Progenitor cells are mononuclear cells with a high nuclear/cytoplasmic ratio, immature chromatin, with frequent nucleoli and basophilic cytoplasm. No attempt has been made to classify these as myeloblasts, lymphoblasts or undifferentiated blasts.

In these experiments we have isolated a small fraction of bone marrow (2% of nucleated cells) which contains all the myeloid and erythroid as well as presumptive lymphoid progenitors. The isolation of such a pure population of progenitors should allow detailed investigation of the regulation of progenitors by other cells, will allow a more exact cytological and antigenic phenotype to be assigned to the progenitor cells and may allow identification of pluripotential stem cells. The study also illustrates the usefulness of combinations of monoclonal antibodies in studies of normal differentiation.

We thank Mr W. Verbi for carrying out TdT staining. D. L. is a Wellcome Research Fellow.

Received 30 April; accepted 28 July 1980.

1. Pike, B. L. & Robinson, W. A. *J. cell. Physiol.* **76,** 77–84 (1970).
2. Axelrad, A. A., McLoed, D. L., Shreeve, H. M. & Heath, D. A. *Haemopoiesis in Culture* (ed. Robinson, W.) 226–234 (Washington US Government Printing Office, 1974).
3. Iscove, N. N., Sieber, F. & Winterhalter, K. H. *J. cell. Physiol.* **83,** 309–320 (1974).
4. McCulloch, E. A., Mak, T. W., Price, G. B. & Till. J. E. *Biochim. biophys. Acta* **355,** 260–299 (1974).
5. Metcalf, D. *Clin. Haemat.* **8,** 263–285 (1979).
6. Cline, M. J. & Billings, R. *J. exp. Med.* **146,** 1143–1145 (1977).
7. Janossy, G., Frances, G. E., Capellaro, D., Goldstone, A. H. & Greaves, M. F. *Nature* **276,** 176–178 (1978).
8. Kohler, G. & Milstein, C. *Eur. J. Immun.* **6,** 511–519 (1976).
9. Beverley, P. C. L. *Proc. XI Int. Course Transplantn Clin. Immun.*, 87–94 (Excerpta Medica, Amsterdam, 1980).
10. Bradstock, K. F. *et al. J. natn. Cancer Inst.* **65,** 33–42 (1980).
11. Testa, N. G. *Clin. Haemat.* **8,** 311–333 (1979).
12. Greaves, M. F. & Janossy, G. *Biochim. biophys. Acta* **516,** 193–230 (1978).
13. Burgess, A. W., Wilson, E. M. A. & Metcalf, D. *Blood* **49,** 573–583 (1970).
14. Iscove, N. N. *Cell Differentiation and Neoplasia* (ed. Sanders, G. F.) (Raven, New York, 1978).
15. Nathan, D. G. *et al. J. exp. Med.* **147,** 324–329 (1978).

Mitotic EBNA-positive lymphocytes in peripheral blood during infectious mononucleosis

James Robinson, Douglas Smith & James Niederman

Departments of Pediatrics and Epidemiology and Public Health,
Yale University School of Medicine, New Haven, Connecticut 06510

Infectious mononucleosis (IM) is usually a benign lymphoproliferative disease caused by Epstein–Barr virus (EBV)[1]. Although EBV induces a state of continuous proliferation in infected B lymphocytes *in vitro*[2,3], the most prominent lymphoproliferation during IM is of activated, or atypical, T lymphocytes presumably responding to the virus or virus-infected cells[4]. However, EBV genome-carrying cells are known to be circulating during IM, as cultured peripheral blood leukocytes from patients with the disease give rise to continuous lymphoblastoid cell lines, each cell of which contains the EBV genome and expresses the EBV determined nuclear antigen (EBNA)[5,6]. The proposal that EBV-infected cells in IM blood are not endowed with enhanced growth potential but are merely latently infected[7] is supported by demonstrations that cells infected *in vivo* enter a viral replicative cycle when placed *in vitro* and that most cell lines derived from cultured lymphocytes of IM patients are infected by virus released *in vitro*[8]. However the cells could also be capable of proliferation *in vivo*, since virus production and transformation are not mutually exclusive properties of EBV-transformed cells[9]. Recently, EBNA has been detected in a very small fraction of peripheral blood lymphocytes of IM patients after T cells were first removed[10,11] and this has been interpreted to indicate that cell transformation occurs *in vivo* during IM. The isolation of colonies of EBNA-positive cells from IM blood leukocytes cultures in soft agar suggests that at least some infected cells are capable of direct outgrowth into transformed cells[12]. We report here direct evidence that circulating EBV-infected cells exhibit increased growth properties during IM.

As EBNA is expressed by EBV genome-carrying lymphocytes in IM blood, and this antigen is physically associated with metaphase chromosomes in dividing transformed cells[6], we initially determined whether EBNA-positive cells were capable of entering the mitotic cycle after being placed in culture. When cells were incubated for 18 h after separation and then treated with colcemid, as many as 5% of the EBNA-positive cells were in mitosis (Table 1, Fig. 1*a*). To identify cells which had already entered the mitotic cycle *in vivo* at the time the blood was drawn, cells were treated with colcemid immediately after cell separation was completed. In two patients (Table 1), a small fraction (0.5%) of the EBNA-positive cells were in mitosis (Fig. 1*b*). Cells from one of the patients were examined again for EBNA-positive mitoses after 18 h in culture when there was a six-fold increase in the proportion of EBNA-positive cells arrested in metaphase.

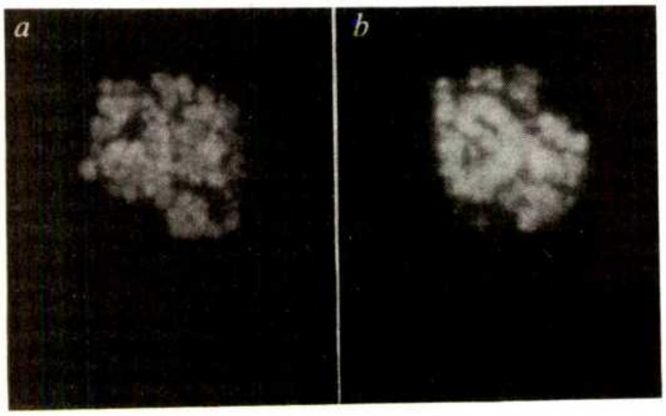

Fig. 1 *a*, EBNA-positive cell in mitosis. T-cell-depleted lymphocytes exposed to colcemid for 2 h after being cultured for 18 h. ×630. *b*, EBNA-positive mitotic cell after 2 h exposure to colcemid beginning immediately after cell separation completed. ×630.

Table 1 Identification of EBNA-positive metaphases in T-cell depleted lymphocytes from patients with IM

Patient	Days of illness	Time (h) cells* in culture	% EBNA	% Of EBNA -positive cells† in mitosis
1	6	18	6.5	5
2	6	18	18	1.0
3	7	2	10	0.5
		18	10	3
4	7	2	12	0.5

Mononuclear leukocytes were isolated on Ficoll–Hypaque gradients[16] from heparinized blood of patients acutely ill with IM. Adherent cells were removed by incubating washed leukocytes in plastic tissue culture flasks for 1 h at 37°C. A population of cells depleted of T lymphocytes and enriched for B lymphocytes was then isolated by separating cells which formed rosettes with neuraminidase-treated sheep erythrocytes (E_N) from non-rosetting cells on a second Ficoll–Hypaque gradient as previously described[3]. The non-T-cell fraction contained less than 4% E_N rosette-forming cells. $0.5\text{–}1 \times 10^6$ cells in 0.4 ml RPMI with 20% fetal calf serum were treated for 2 h at 37°C with $0.1\ \mu g\ ml^{-1}$ of colcemid, either immediately following cell separation, or after the separated cells had been cultured overnight (~18 h) at 37°C. Colcemid-treated cells were swollen in 4 volumes of 1% sodium citrate containing 1 mM $MgCl_2$ and $CaCl_2$ for 10 min at 37°C. Cell smears were then made on a cytocentrifuge, air dried, fixed for 5 min in acetone/methanol (2:1) and stored at −70°C. EBNA-positive cells in the smears were identified by a modification of the anti-complement immunofluorescence test of Reedman and Klein[6]. Gelatin-veronal buffer (GVB)[17] was used as diluent for sera and for washing slides. Smears were incubated with a human serum containing antibodies to EBNA (RM) or a serum lacking EBV antibodies (LH) which had been diluted 1:8 and heat inactivated. After 30 min at 37°C, the sera were aspirated and the smears were immediately covered with a 1:10 dilution of human EBNA-negative serum as a source of complement. The slides were washed three times in GVB and stained for 30 min at 37°C with a 1:30 dilution of rhodamine-conjugated goat anti-human C3 antibodies (Atlantic Antibodies). After three washes in GVB, the slides were mounted in glycerol-PBS, *p*H 9.5, and examined in a Zeiss Universal fluorescence microscope equipped with a Ploem type incident illuminator.

*After cell separation completed.

†100–300 EBNA-positive cells counted.

We detected EBNA in up to 18% of B-cell-enriched IM blood lymphocytes, although other investigators have identified these cells in only 0.1–2% of cells in similar populations[10,11]. However, our patients had been symptomatic for 7 days or less whereas the patients studied in earlier reports were usually in their second or third week of illness. We found that the number of EBNA-positive cells decreased rapidly during the second week of illness to levels comparable to those in earlier reports (data not shown). The low numbers of EBNA-positive cells late in disease precluded the detection of mitotic EBNA-positive cells in these specimens.

Rickinson *et al.*[8] have shown that EBV-neutralizing antibody drastically reduces the outgrowth of transformed cell lines from cultured lymphocytes of IM patients. The antibody presumably acts to neutralize virus released from cells which had been infected *in vivo* but which entered a productive viral cycle *in vitro*. To exclude the possibility that the dividing antigen-positive cells that we detected after 18 h in culture had not been infected by this two-step mechanism, we determined when virus release occurs. We incubated a patient's cells in medium containing EBV-neutralizing antibody at various times after the beginning of culture. As shown in Table 2, EBV-neutralizing antibody did not reduce the frequency of transformation in a quantitive culture assay if it was present only during the first 24 or 48 h. Antibody did reduce the rate of transformation markedly if it was maintained in the cultures for the duration of

0028-0836/80/390334—02$01.00

the experiment or during the second and third day of culture. Thus, virus production and release do not occur during the first 2 days of culture. Even if normal cells could be infected at the time cells were placed *in vitro*, proliferation does not begin immediately. As shown in Table 3, cell division in normal B lymphocytes inoculated with EBV *in vitro* does not begin until 34–46 h after exposure to virus. Thus, our results show that a proportion of cells infected by EBV *in vivo* are capable of cell division after being placed in culture and that some of the antigen-positive cells have already traversed the cell cycle while still in the peripheral blood.

The capacity of the dividing EBNA-positive cells to grow into continuous cell lines is unknown. They may be the same as the cells which form EBNA-positive colonies in soft agar[12]. However, the ability to grow directly into cell lines is not a prerequisite for establishing that transformation occurs *in vivo*. We recently studied a 4-year-old girl who developed a poorly differentiated lymphoplasmacytic malignancy during IM. The tumour cells and the majority of peripheral blood leukocytes contained both EBNA and cytoplasmic immunoglobulins of all heavy and light chain classes[13]. Although in this patient there was unequivocal evidence of viral transformation *in vivo*, her cells either entered a lytic viral cycle or failed to grow in culture; only a few ultimately formed cell lines in soft agar.

During IM, the host immune response to EBV infection, which is usually already evident at the time of diagnosis[14,15], is probably responsible for restricting EBV-induced proliferation to the relatively low levels that we observed *in vivo*. Were it possible to study IM patients before symptoms develop, much higher numbers of dividing EBNA-positive cells might be seen.

Table 2 Time of effectiveness of EBV-neutralizing antibody in reducing the transformation frequency of cultured B-lymphocytes from IM blood

Time period antibody present in cultures				Transformation frequency*
0–24 h	24–48 h	48–72 h	8 weeks	
–	–	–	–	23/24
+	+	+	+	10/24
+	–	–	–	21/42
+	+	–	–	24/24
+	+	+	–	15/24
–	+	+	+	7/24

T-cell-depleted lymphocytes were isolated from a patient with IM on the 6th day of illness as described in Table 1. Replicate cultures of cells containing 5×10^5 cells were incubated at 37 °C for 24-h periods in medium RPMI 1640 supplemented with 15% fetal calf serum and 5% human serum from either an EBV-seropositive (EBV neutralization titre = 1:80) or seronegative individual. Each group of cells was washed three times in RPMI after 24, 48 and 72 h in culture and then resuspended in 0.5 ml of medium with or without antibody. At 72 h, the cells in each treatment group were plated at 10^4 cells per well in microtitre tissue culture plates previously seeded with human placental fibroblast feeder layers as previously described[3]. Cultures were fed weekly by removing half of the medium and replacing it with medium with and without antibody. Cultures were observed for approximately 8 weeks and the number of wells showing transformation in each treatment group were scored. +, Antibody present; –, antibody absent.

*No. of transformed wells/no. of wells plated.

Table 3 Time course of EBV-induced proliferation in B-lymphocytes inoculated with EBV *in vitro*

Time after inoculation (h)	% EBNA	EBNA-positive mitoses per 1,000 cells
10	7	0
22	44	0
34	51	≤1
46	55	16
58	56	94

Lymphocytes depleted of T cells as in Table 1 were isolated from a normal individual and incubated with concentrated EBV (B95-8 strain; multiplicity of infection = 500 physical particles per cell) or medium at 4 °C for 2 h. After three washes, the cells were resuspended in medium at 1.5×10^6 cells ml^{-1}. Aliquots (0.4 ml) of these cells were cultured in 13 × 100 mm stoppered tubes at 37 °C in an atmosphere of 5% CO_2. Beginning 10 h after the cultures were initiated, infected and uninfected cells were treated with 0.1 $\mu\text{g ml}^{-1}$ colcemid at 12-h intervals; smears for EBNA and EBNA-positive mitoses were prepared as described in Table 1.

The increase in the proportion of EBNA-positive cells in mitosis 18 h after being placed in culture suggests a release from the influence of an inhibitory environment. Since no mitotic cells were seen in Giemsa-stained slides prepared from 18-h cultures of T-cell-depleted lymphocytes from four normal individuals, it is more likely that the increased mitotic activity is due to the presence of the EBV genome in the cells than to a nonspecific stimulation of the cells resulting from the absence of T cells or other factors. If adequate host control mechanisms fail to develop *in vivo* during IM, as was likely in our fatal case[13], the EBV-infected cells have the potential for causing a malignant lymphoproliferation.

This work was supported by USPHS grants AI-14741, CA 16038 and CA 12055. We thank D. M. Horstmann and G. Miller for criticisms of the manuscript and J. Nepiarsky for assistance with it. J. R. is a scholar of the Leukemia Society of America.

Received 11 June; accepted 29 July 1980.

1. Henle, G., Henle, W. & Diehl, V. *Proc. natn. Acad. Sci. U.S.A.* **59**, 94–101 (1968).
2. Jondal, M. & Klein, G. *J. exp. Med.* **138**, 1365–1378 (1973).
3. Robinson, J., Andiman, W., Henderson, E. & Miller, G. *Proc. matn. Acad. Sci. U.S.A.* **74**, 749–753 (1977).
4. Sheldon, P., Papamichael, M., Hemsted, E. & Holborow, E. *Lancet* **i**, 1153–1157 (1973).
5. Diehl, V., Henle, G., Henle, W. & Kohn, G. *J. Virol.* **2**, 663–669 (1968).
6. Reedman, B. & Klein, G. *Int. J. Cancer* **11**, 499–504 (1973).
7. Epstein, M. & Achong, B. *Lancet* **ii**, 836–839 (1973).
8. Rickinson, A., Jarvis, J., Crawford, D. & Epstein, M. *Int. J. Cancer* **14**, 704–715 (1974).
9. Miller, G. & Lipman, M. *J. exp. Med.* **138**, 1398–1412 (1973).
10. Klein, G., Svedmyr, E., Jondal, M. & Persson, P. *Int. J. Cancer* **17**, 21–26 (1976).
11. Katsuki, T. *et al. Int. J. Cancer* **23**, 746–750 (1979).
12. Hinuma, Y. & Katsuki, T. *Int. J. Cancer.* **21**, 426–431 (1978).
13. Robinson, J. *et al. New Engl. J. Med.* **302**, 1293–1297 (1980).
14. Niederman, J., McCollum, R., Henle, G. & Henle, W. *J. Am. med. Ass.* **203**, 205–209 (1968).
15. Svedmyr, E. & Jondal, M. *Proc. natn. Acad. Sci. U.S.A.* **72**, 1622–1626 (1975).
16. Böyum, A. *Scand. J. clin. Lab. Invest.* Suppl. **21**, 77–89 (1968).
17. Gershon, A., Kalter, Z. & Steinberg, S. *Proc. Soc. exp. Biol. med.* **151**, 762–765 (1976).

Isoelectric focusing of IgG eluted from multiple sclerosis and subacute sclerosing panencephalitis brains

**David H. Mattson, Raymond P. Roos*
& Barry G. W. Arnason**

The University of Chicago, Chicago, Illinois 60637

Elevated IgG distributed in oligoclonal bands is characteristically observed in the cerebrospinal fluid (CSF) of patients with multiple sclerosis (MS) or subacute sclerosing panencephalitis (SSPE)[1–6]. Similarly, IgG in bands has been detected in neutral saline (NS) and acid eluates of brain material from these two diseases[7–21]. We have now used isoelectric focusing (IEF) to compare IgG eluted from control brain, three plaques and a white matter pool of an MS brain, and three regions of an SSPE brain. A direct peroxidase-conjugated anti-human IgG staining technique was used to stain IgG exclusively and to visualize the minute amounts of IgG obtained from individual MS plaques. Eluates from individual MS plaques have distinct IgG patterns; in contrast, those from separate SSPE brain areas have essentially identical IgG patterns. The identical IgG patterns in three areas of SSPE brain suggest a common response to the same antigen. The different IgG patterns among MS plaques suggest: (1) variable response to the same 'MS antigen' in each plaque, (2) response to different MS antigens in different plaques, (3) synthesis of 'nonsense' antibodies irrelevant to the pathogenesis of MS in each plaque, or (4) some combination of the above.

---

* To whom reprint requests should be addressed.

IgG was eluted by modifications of the techniques of Gilden[21,22] and Weil[14,15] from: the white matter pool (WMP) and three plaques of an MS patient, three discrete brain areas of an SSPE patient, and a WMP of an individual without neurological disease. Although seven NS washes reduced recoverable IgG to nearly zero in all material, subsequent acid elution recovered significant additional IgG (Table 1). The IgG eluted from these tissues, along with serum and CSF from the SSPE case, was then examined by IEF.

NS and acid eluates from each MS plaque had unique overall patterns of IgG bands on IEF despite many shared bands (Fig. 1). The WMP acid eluate contained all the IgG bands found in the acid eluates from the individual plaques plus additional bands. NS eluates had more anodal and fewer cathodal bands than acid eluates. The difference in pattern between acid and NS eluates could not be accounted for by acid exposure because treatment of NS-eluted IgG with acid did not change the IEF pattern. Analysis of three discrete 0.6–1.2 g white matter regions from a second MS case (age 36 yr, with a 13-yr history of chronic progressive MS) has given comparable differences in banding patterns.

The oligoclonal IgG patterns of the NS eluates of all three SSPE brain regions were identical, and similar to the pattern of the CSF. The serum had several bands, identical with bands in the CSF. Acid eluates of the three SSPE brain regions had virtually identical oligoclonal IgG patterns (Fig. 2). When compared with NS eluates and CSF, acid eluates had an additional major cathodal band and other minor differences. A second case of SSPE (age 14 yr, with an 8-month duration of disease and a history of primary measles at age 4 yr) has given similar results.

NS and acid eluates from control WMP showed indistinct bands very different from the sharp bands observed in MS and SSPE eluates (Fig. 3). These bands were more readily discerned in the NS than in the acid eluate. Diffusely distributed cathodal IgG was more evident in the acid than in the NS eluate.

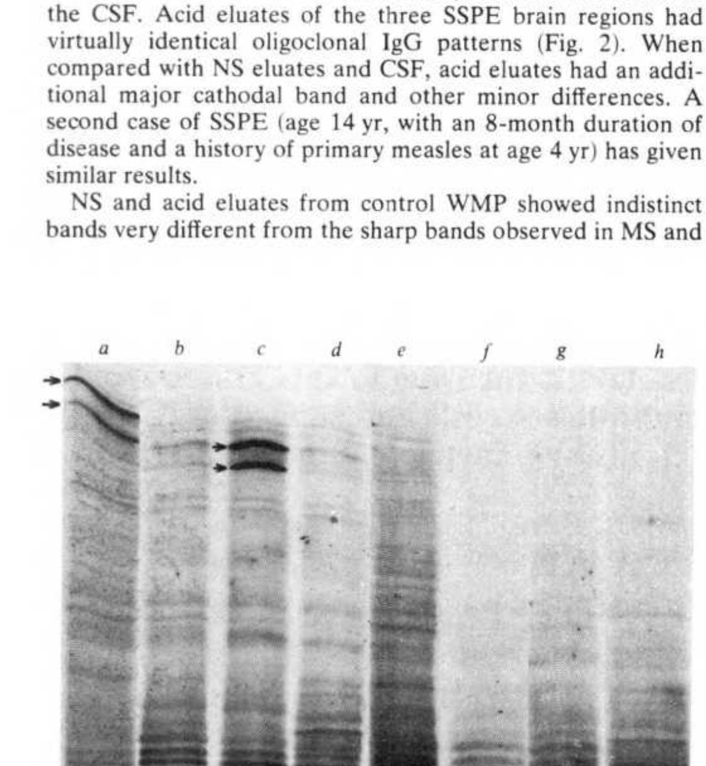

Fig. 1 IEF of MS brain material. *a*, WMP 1st + 2nd NS eluates; *b*, plaque 1 1st + 2nd NS eluates; *c*, plaque 2 1st + 2nd NS eluates; *d*, plaque 3 1st + 2nd NS eluates; *e*, WMP 1st + 2nd acid eluates; *f*, plaque 1 1st + 2nd acid eluates; *g*, plaque 2 1st + 2nd acid eluates; *h*, plaque 3 1st + 2nd acid eluates. The top of the gel is *p*H 7.0 and the bottom is *p*H 9.0. Arrows indicate haemoglobin which stains brown with our peroxidase substrate and is present especially in the 1st + 2nd NS eluates. IEF was carried out using LKB Ampholine PAGplate gels, *p*H 3.5–9.5, on an LKB 2117 Multiphor with an LKB 2103 power supply. The anode solution was 1 M H_3PO_4; the cathode solution 1 M NaOH. Samples containing 2 μg of IgG were applied to the middle of the gel in 5 × 10 mm pieces of filter paper and focused for 2 h at 4 °C and 30 W constant power. Immediately after focusing, gels were fixed for 1 h with trichloroacetic acid (TCA) and sulphosalicylic acid (SSA) (57.5 g TCA and 17.25 g SSA in 150 ml methanol and 350 ml water), and rinsed for 48 h in Tris buffer (0.1 M Tris–HCl, 0.85 M NaCl, *p*H 7.6). A cellulose acetate strip soaked with undiluted peroxidase-conjugated rabbit anti-human IgG (Dako), 40 μl per sample lane, was placed on the gel for 1 h at room temperature in a moist environment. Gels were rinsed with Tris buffer in the dark for 96 h, and developed for 1 h in 30 mg% 3, 3′-diaminobenzidine tetrahydrochloride (Sigma) and 0.06% hydrogen peroxide (in Tris buffer).

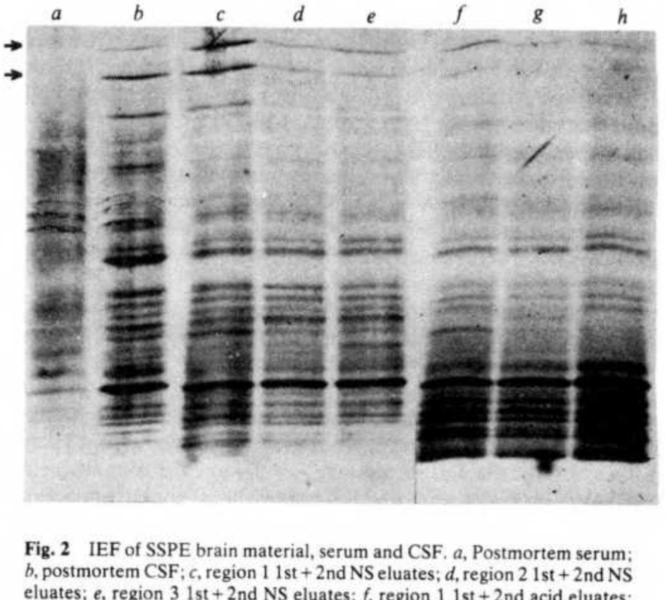

Fig. 2 IEF of SSPE brain material, serum and CSF. *a*, Postmortem serum; *b*, postmortem CSF; *c*, region 1 1st + 2nd NS eluates; *d*, region 2 1st + 2nd NS eluates; *e*, region 3 1st + 2nd NS eluates; *f*, region 1 1st + 2nd acid eluates; *g*, region 2 1st + 2nd eluates; *h*, region 3 1st + 2nd acid eluates. IEF as in Fig. 1.

IgG obtained after acid treatment of normal brain may be nonspecifically bound (through Fc receptors[23,24] or charge affinities), or released from fractured plasma cells. The oligoclonal pattern of this IgG, an observation made previously in NS eluates using agar gel electrophoresis (AGE)[19], may reflect sequestration of certain lymphoid cell clones in normal brain.

Acid elution of SSPE brain is thought to dissociate complexes of anti-measles oligoclonal IgG from measles antigen[14,15,18,20]; NS eluted IgG probably represents antibody in excess of antigen. This view is supported by the observation that most acid- and NS-eluted IgG bands, as well as CSF IgG bands, are absorbable by measles virus[13,17,18]. All three SSPE brain regions we examined had almost identical banding patterns, suggesting a restricted antibody response to the same antigen in each area. CSF and NS eluates, however, contained several IgG bands not apparent in acid eluates of brain. These bands may not be anti-measles antibodies but may instead be the product of nonspecific clones recruited to the brain. SSPE CSF oligoclonal IgG bands not absorbable with measles virus have been reported[13,17,18].

The three MS plaque acid eluates analysed had several bands in common, but each had a unique overall pattern. The acid eluate of MS WMP contained all bands present in the acid eluates of the three plaques plus additional bands, as if patterns from many plaques had been summed. Although some differences in band patterns may be quantitative rather than qualitative, the variation in band pattern from plaque to plaque indicates that different antibody-synthesizing clones are present (or expanded) in different areas of MS brain.

Several explanations for this observation can be advanced. If oligoclonal IgG eluted with acid from MS brain is antibody specifically bound to an MS antigen(s), plasma cell clones producing antibody directed against MS antigen(s) may appear, decline and disappear in different plaques over time. Old, chronic or inactive plaques might then be expected to contain different clones from more recent, active plaques. IgG bands (in serum) are known to change over time in animals chronically stimulated with a well defined antigen[25,26]. Our failure to find any changes in different regions of the brain in SSPE perhaps argues against this interpretation. Although the SSPE cases studied were less than 1 yr in duration, one would have thought that this was sufficient (especially considering an 'incubation period' of at least 10 yr from initial measles infection) for changes to have taken place.

Another explanation, which again would require that all acid-eluted antibody is specifically bound, would be that a different antigen is present in each MS plaque and for this reason antibody-synthesizing clones differ in each plaque. This seems improbable; however, a single agent can undergo antigenic shifts leading to different antibody responses over time. Antigenic shifts have been observed with visna virus in infected sheep brains[27].

A third possibility is that those bands common to all plaques are specific antibody directed against an MS antigen(s), whereas those bands unique to individual plaques are nonsense antibody irrelevant to the pathogenesis of MS. Such nonsense antibody would be the product of plasma cell clones that become localized in the plaque but are not stimulated by any antigen present there. This irrelevant IgG would be released by acid treatment through breakage of nonspecific bonds or rupture of plasma cells. Antibodies to several viruses, such as measles and rubella, are elevated in MS CSF and are oligoclonal in distribution[28]. Although these antibodies do not correspond to the CSF oligoclonal IgG bands seen by AGE, they could appear as bands when CSF or brain eluates are analysed by the more sensitive IEF technique. Of relevance is the observation that mice immunized with several antigens and boosted in a lymph node with one, show recruitment to the node not only of plasma cells specific to the stimulating antigen, but also of lymphoid clones directed against the other antigens[29]. Thus, there is a precedent for the notion that irrelevant plasma cell clones can be recruited in the face of specific antigenic challenge.

Finally, all IgG in MS plaques could be nonspecifically bound, irrelevant to any pathogenic antigen, and represent the product of B-cell clones sequestered randomly during attacks of MS. Bands common to eluates of all plaques would then represent the product of clones constantly maintained by repeated or continuous antigenic exposure whereas bands unique to a plaque would be the product of clones responding to antigens encountered shortly before activation of a plaque by an MS attack.

We believe that resolution of the questions raised by these findings may prove crucial for an understanding of the pathogenesis of MS.

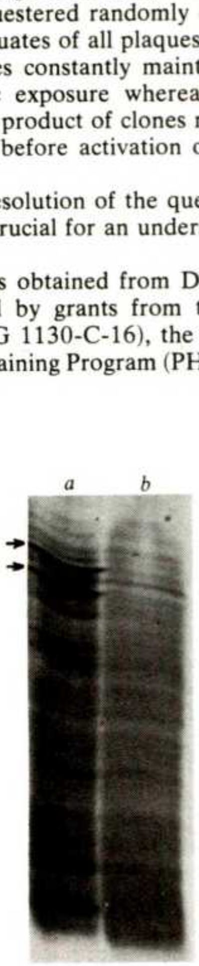

Fig. 3 IEF of control brain material. *a*, WMP 1st + 2nd NS eluates; *b*, WMP 1st + 2nd acid eluates. IEF as in Fig. 1.

Table 1 IgG recovered from MS, SSPE and control brain material on neutral saline and acid elution

	IgG recovered at various elution steps (μg)		
Material (weight)	1st + 2nd NS	7th NS	1st + 2nd acid
MS white matter pool* (6.0 g)	851 (0.142)§	7.7	390 (0.065)§
MS plaque 1* (0.1 g)	57 (0.574)	0	8.9 (0.089)
MS plaque 2* (0.4 g)	113 (0.283)	0.1	18 (0.045)
MS plaque 3* (0.4 g)	131 (0.328)	0.5	20 (0.050)
SSPE cortex region 1† (2.3 g)	1,222 (0.531)	4.1	97 (0.042)
SSPE cortex region 2† (1.8 g)	1,407 (0.782)	0.9	66 (0.037)
SSPE cortex region 3† (2.1 g)	435 (0.207)	1.8	82 (0.039)
Control white matter pool‡ (6.3 g)	641 (0.102)	4.1	41 (0.006)

Sections 8 μm thick were cut on a cryostat and homogenized with 10 strokes of a Dounce homogenizer in a small amount of Dulbecco's phosphate-buffered saline (DPBS) containing 0.02% sodium azide. Each homogenate was rinsed seven times with at least 7 volumes of DPBS containing 0.02% sodium azide at 4 °C, with centrifugations at 100,000*g* for 1 h at 4 °C. Homogenates were then rinsed twice with similar volumes of 0.1 M glycine–HCl buffer at *p*H 2.5 (containing 0.1% bovine serum albumin, 0.005 M ε-aminocaproic acid and 2.8 μg ml^{-1} pepstatin), each time for 1 h at 4 °C with end over end shaking, followed by centrifugations at 100,000*g* for 1 h at 4 °C. Immediately after centrifugation, supernatants from each acid elution were brought to *p*H 7.0 by addition of 1 M Tris(hydroxymethyl)aminomethane (Sigma). The pooled first plus second neutral saline rinses, the seventh neutral saline rinse and the pooled first plus second neutralized acid eluates were concentrated using vacuum ultrafiltration with 25,000 molecular weight cutoff collodion bags (Schleicher and Schuell) against several changes of a 1:10 dilution of DPBS. IgG was quantified in the concentrated eluates by electroimmunodiffusion (Antibodies Incorporated).

* Periventricular white matter and three brain plaques were dissected at autopsy 13 h after death and stored at −70 °C for 2 yr. The patient was a 51-yr-old female with a 9-yr history of chronic progressive MS.

† Three separate areas of cortical white (with adjoining grey) matter were dissected at autopsy 6 h after death and stored at −70 °C for 1 week. Postmortem CSF and serum were also obtained. The patient was a 17-yr-old male with a 10-month history of SSPE. He had a primary measles infection at age 6 yr.

‡ White matter was dissected at autopsy 20 h after death and stored at −70 °C for 2 months. The patient was a 47-yr-old male with lung carcinoma.

§ Values in parentheses are μg per mg IgG recovered from starting material.

SSPE material was obtained from Dr J. H. Webster. This work was supported by grants from the National Multiple Sclerosis Society (RG 1130-C-16), the Kroc Foundation, the Medical Scientists Training Program (PHS 2 T32 GM07281) to D.H.M., by a Basil O'Connor Starter Research grant from the National Foundation March of Dimes (5-162) and a Schweppe Foundation Career Development Award (to R.P.R.).

Received 27 May; accepted 21 July 1980.

1. Kabat, E. A., Moore, D. H. & Landow, H. *J. clin. Invest.* **21,** 571–577 (1942).
2. Bauer, H. in *Encephalidites* (eds van Bogaert, L. *et al.*) 675–680 (Elsevier, Amsterdam, 1961).
3. Laterre, E. C., Callewaert, A., Heremans, J. F. & Sfaello, Z. *Neurology* **20,** 982–990 (1970).
4. Lowenthal, A., Van Sande, M. & Karcher, D. *J. Neurochem.* **6,** 51–60 (1960).
5. Delmotte, P. & Gonsette, R. *J. Neurol.* **215,** 27–37 (1977).
6. Kjellin, K. G. & Vesterberg, O. *J. neurol. Sci.* **23,** 199–213 (1974).
7. Tourtellotte, W. W. & Parker, J. A. *Science* **154,** 1044–1046 (1966); *Nature* **214,** 683–686 (1967).
8. Tourtellotte, W. W., Parker, J. A., Herndon, R. M. & Cuadros, C. V. *Neurology* **18,** 117–121 (1968).
9. Gerstl, B., Uyeda, C. T., Eng, L. F., Bond, P. & Smith, J. K. *Neurology* **19,** 1019–1026 (1969).
10. Link, H. *J. neurol. Sci.* **16,** 103–114 (1972).
11. Vandvick, B. *Ann. clin. Res.* **5,** 308–315 (1973).
12. Norrby, E. & Vandvick, B. *Med. Microbiol. Immun.* **162,** 63–72 (1975).
13. Vandvick, B., Norrby, E., Nordal, H. J. & Degre, M. *Scand. J. Immun.* **5,** 979–992 (1976).
14. Weil, M. L., Leiva, W. A., Heiner, D. C. & Tourtellotte, W. W. *J. Immun.* **115,** 1603–1606 (1975).
15. Weil, M. L. *et al. Infect. Immun.* **24,** 202–210 (1979).
16. Mehta, P. D., Kane, A. & Thormar, H. *J. Immun.* **117,** 2053–2060 (1976).
17. Mehta, P. D., Kane, A. & Thormar, H. *J. Immun.* **118,** 2254–2261 (1977).
18. Mehta, P. D., Kane, A. & Thormar, H. *Ann. Neurol.* **3,** 552–555 (1978).
19. Bollengier, F., Mahler, A., Clonet, G. & Lowenthal, A. *Brain Res.* **152,** 133–144 (1978).
20. Ruth, V., Matikainen, M-T., Salmi, A. & Panelius, M. *Acta neurol. scand.* **57,** suppl. 67, 240 (1978).
21. Gilden, D. & Tachovsky, T. *J. Neurosci. Meth.* **1,** 133–142 (1979).
22. Gilden, D., Devlin, M. & Wroblewska, Z. *Ann. Neurol.* **3,** 403–405 (1978).
23. Aarli, J. A., Aparicio, S. R., Lumsden, C. E. & Tönder, O. *Immunology* **28,** 171–185 (1975).
24. Traugott, U., Snyder, S. & Raine, C. S. *Ann. Neurol.* **6,** 13–20 (1979).
25. Kimball, J. W., Pappenheimer, A. M. & Jaton, J-C. *J. Immun.* **106,** 1171–1184 (1971).
26. Pincus, J. H., Jaton, J-C., Bloch, J. & Haber, E. *J. Immun.* **104,** 1143–1148 (1970).
27. Narayan, O., Griffin, D. E. & Chase, J. *Science* **197,** 376–378 (1977).
28. Nordal, H. J., Vanvick, B. & Norrby, E. *Scand. J. Immun.* **7,** 473–479 (1978).
29. Poskitt, D. C., Frost, H., Cahill, R. N. P. & Trnka, Z. *Immunology* **33,** 81–89 (1977).

Limitations in the use of actomyosin threads as model contractile systems

John D. Altringham, Paul H. Yancey & Ian A. Johnston
Department of Physiology, University of St Andrews, St Andrews, Fife KY16 9TS, UK

Recent studies have suggested that actomyosin threads may provide a useful model for studying the properties of contractile systems[1-3]. The development of highly sensitive positional feedback transducers has enabled the properties of these threads to be measured reproducibly[1]. Potential applications include such systems as ventricle, smooth muscle and non-muscle preparations, from which it is difficult to obtain suitable fibres for mechanical studies. In addition, studies with chemically modified myosins may provide new insights into the relationships between the biochemical and mechanical events in the cross-bridge cycle. However, there are indications that the mechanical properties of actomyosin threads differ from those of intact fibres in several important respects. For example, contraction velocity is proportional to isometric tension in threads[2], but is independent of filament density in intact fibres[4]. We have now determined the force–velocity characteristics of actomyosin threads prepared from muscles with known differences in their physiological contraction velocities. No direct relationships could be found between the velocity characteristics of the threads and those of intact muscle. We conclude that the measured velocities of threads reflect properties of the actomyosins other than cross-bridge cycling times, thus severely limiting the usefulness of this technique for comparative purposes.

Natural actomyosins were isolated from the ventricle and back (fast skeletal) muscles of rabbit, and from the red (slow) and white (fast) myotomal muscles of the dogfish *Scyliorhinus canicula*[5]. Purified actin[6], myosin[7] and tropomyosin–troponins[6] were also prepared from rabbit back muscle. Threads were formed using the method described by Crooks and Cooke[1], involving the extrusion of actomyosin at high ionic strength from a syringe needle moving through a solution of low ionic strength. Isometric contraction was initiated by the addition of ATP or $CaCl_2$ (Fig. 1). Calcium sensitivity (as defined by Lehman and Szent-Györgyi[5]) in the threads was difficult to achieve, even though ATPase activities of the actomyosins were typically >80% calcium sensitive and gel electrophoresis showed the presence of calcium regulatory proteins in the threads. Isotonic contraction velocities were measured in maximally activated threads by release against a series of electronically present loads. The force–velocity curves obtained in this manner are shown in Figs 2 and 3, and the unloaded contraction velocities (V_{max}) and maximal tensions (P_0) are listed in Table 1, together with ATPase activities for the actomyosins.

The data reveal several unphysiological characteristics. First, the velocities are all less than 0.012 lengths s^{-1}, two to three orders of magnitude lower than those of intact muscle fibres. For example, V_{max} values for *Tilapia* adductor operculi white and red fibres are 2.6 and 1.5 lengths s^{-1} at 18 °C (ref. 8); Lännergren reports values of 6.3 and 1.1 lengths s^{-1} for *Xenopus* fast and slow fibres (22.5 °C), and Close gives values of 14.5 and 6.3 lengths s^{-1} for whole extensor digitorum longus and soleus muscles of the rat (35 °C)[10].

Second, the relative velocities of the different thread types do not reflect those of the corresponding muscles (Figs 2, 3, Table 1). Barany[11] has shown a positive correlation between the actomyosin ATPase activity and the contraction velocity of a muscle. However, the velocities of the threads from both animals show a complete reversal of the results predicted from both the ATPase levels and the studies noted above on single fibres and whole muscles from different muscle types. It therefore seems that the measured contraction velocities of actomyosin threads reflect factors other than cross-bridge cycling times. The most important of these is probably related to the geometry and packing of filaments within the threads. Threads lack the polarity and native organization of myofilaments found in intact muscle[12]. As noted above, Cooke and Franks[2] found velocity to be proportional to isometric tension (which is determined by protein concentration) in threads, whereas it is independent of myofibrillar density in intact muscle[4].

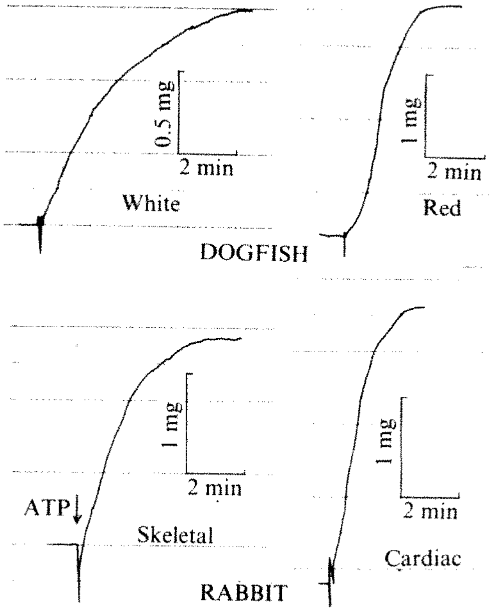

Fig. 1 Development of isometric tension with time in actomyosin threads activated with ATP. Incubation medium contained 50 mM imidazole, 40 mM KCl, 5 mM EGTA, 5 mM $CaCl_2$, 3 mM $MgCl_2$, 0.5 mM $Na_4P_2O_7$ and ATP added to a final concentration of 500 µM. An ATP regenerating system was also present (10 mM creatine phosphate, creatine phosphokinase at >20 units ml^{-1}). Protein purity was examined by SDS-polyacrylamide gel electrophoresis and electron microscopy. Natural actomyosins were used the same day as preparation, purified component proteins directly after purification. Protein concentrations varied from 50 to 65 mg ml^{-1} (determined by a microbiuret method[18]). Tension and force–velocity parameters were measured on a sensitive tensiometer similar in design to that described by Crooks and Cooke[1] (sensitivity in isotonic: 100 mV per 70 µm; in isometric: 135 mV mg^{-1}; drift 0.02 mg h^{-1}; compliance 0.1 µm mg^{-1}). Threads 5 mm long and 240 µm in diameter were attached to the tensiometer using a Plexiglass–acetone glue.

Ultrastructural studies by D'Haese and Komnick[12] have shown that contraction of actomysin threads results in a condensation of the parallel filament system, in cross-section, and increased overlap of filaments in longitudinal section, suggesting that contraction is due to a sliding filament mechanism. These studies also indicate that the conditions of myosin filament formation may determine the properties of the threads. For example, threads prepared by rapid precipitation contain actin filaments decorated with myosin molecules and oligomeric myosin bridges. During isometric contraction, myosin filaments form and, with actin filaments, align themselves along the long axis of the thread. Dialysis of the actomyosin solution before thread extrusion, to give slower myosin precipitation, produces threads with both actin and myosin filaments in the relaxed state. The initial unloaded contraction velocities of these threads is over four times greater than those of rapidly precipitated threads.

Other studies have shown that filament formation by purified myosin depends to a large extent on the conditions of formation

0028-0836/80/390338—03$01.00

Table 1 Unloaded contraction velocity, maximal tension and ATPase activity for actomyosins

Actomyosin source	Mean V_{max} ($L s^{-1} \times 10^2$)	Mean P_0 ($mN cm^{-2} \times 10^3$)	Actomyosin ATPase activity ($\mu m P_i mg^{-1} min^{-1}$)
Rabbit			
Skeletal	0.53±0.05	59.8±17.2	0.51
Cardiac	1.16±0.14	67.1±16.8	0.07
Dogfish			
White	0.18±0.06	26.0±9.7	0.55
Red	0.39±0.12	57.0±4.1	0.18

$L s^{-1}$ = thread lengths s^{-1}; errors indicate ±1 s.d. ATPase activities were determined in an incubation medium of 50 mM imidazole, 40 mM KCl, 0.1 mM $CaCl_2$, 3 mM $MgCl_2$, 2.5 mM ATP and protein concentration 0.1–0.5 mg ml^{-1}; rabbit activities were measured at 37 °C, *p*H 7.0, dogfish activities at 15 °C, *p*H 7.4.

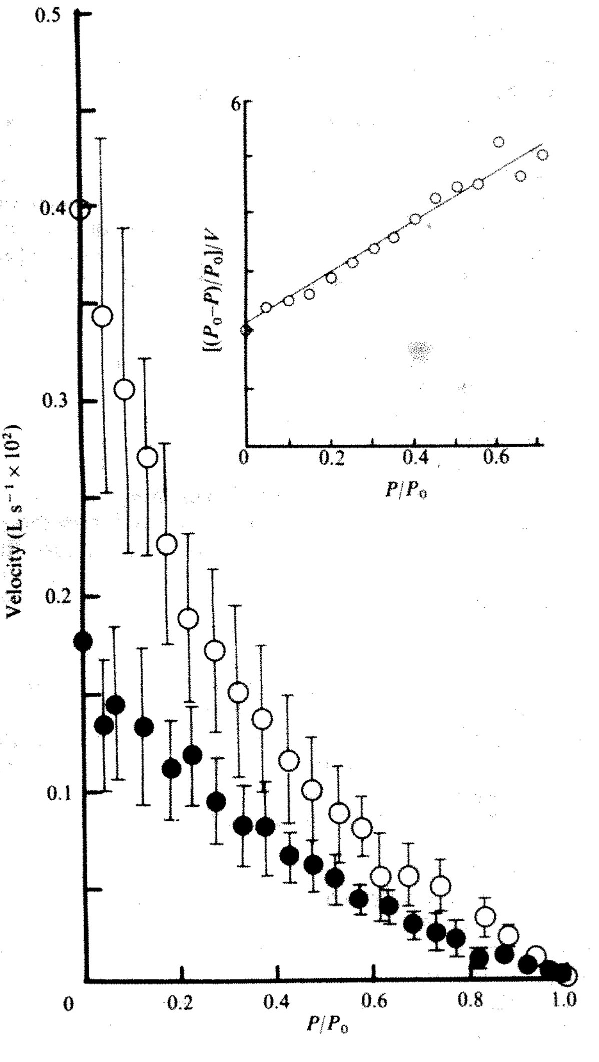

Fig. 2 Force–velocity relationships for dogfish threads at 15 °C, *p*H 7.4. ○, Red muscle; ●, white muscle. Velocities are in thread lengths s^{-1}; P/P_0 = force applied/maximal isometric tension. Error bars indicate ±1 s.d. The data are derived from 6 threads of red actomyosin from 3 animals, and 14 threads of white actomyosin from 6 animals. The inset shows a typical curve for red actomyosin plotted according to the linear form of Hill's equation[19]. Points below 0.7 P_0 lie on a straight line. A similar fit has been described for intact single fibres[9].

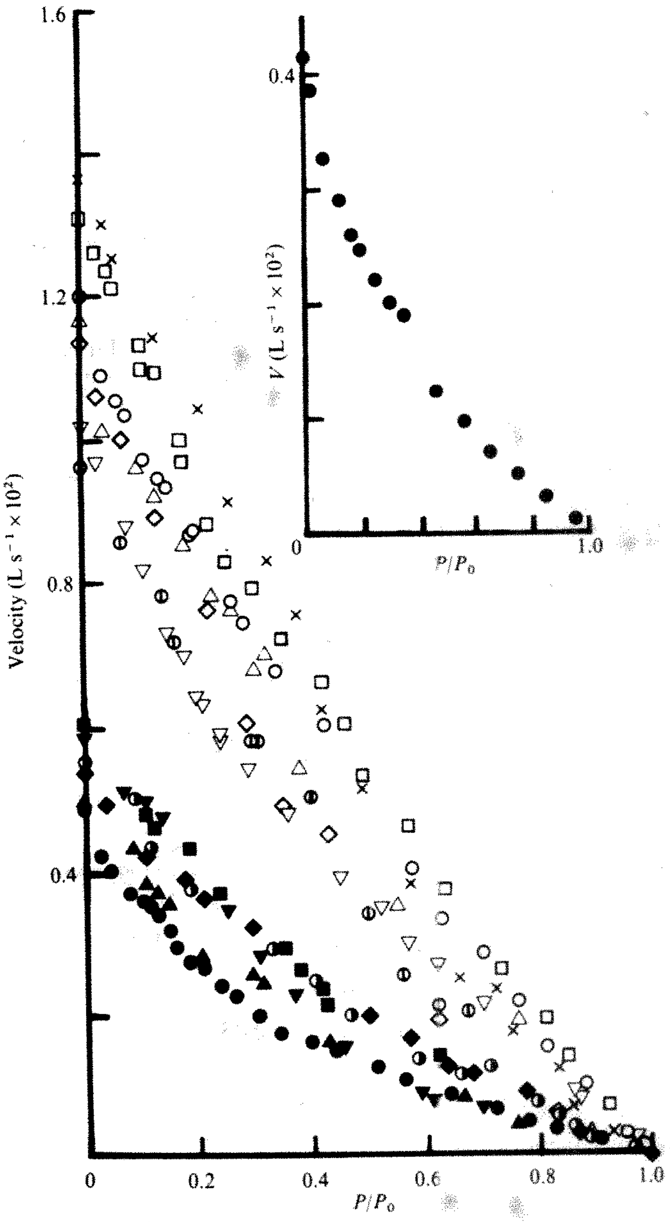

Fig. 3 Force–velocity relationships for rabbit threads at 37 °C, *p*H 7.0. Open symbols represent seven individual threads of cardiac muscle from three animals; solid symbols present six threads of fast skeletal muscle from three animals. The inset shows a typical force–velocity curve for a thread prepared from purified actin, myosin and regulatory proteins of skeletal muscle, demonstrating its similarity to threads of skeletal natural actomyosin.

and the age of the myosin. The length, diameter and shape of synthetic myosin filaments are affected by *p*H (refs 13, 14), ionic strength[14] and the concentrations of ATP, PO_4^{3-}, Mg^{2+} and Ca^{2+} (ref. 15). Specific concentrations of ATP and Mg^{2+} are needed for the formation of filaments with physiological diameters, tapered ends and a central zone of polarity reversal[15]. Storage of myosin in the cold results in the loss of the ability to form these 'physiological' filaments[16]. During storage there is a loss of the LC2 light chain; removal of the LC2 chain from fresh myosin by treatment with dithionitrobenzene (DTNB) mimics this ageing process.

Structural differences among the myosins of fast, slow and cardiac muscles have been well documented[17], and it is possible that these myosins will differ in their abilities to form filaments in the conditions required to prepare and activate threads.

Our results, in conjunction with the above studies, suggest that filament formation, geometry and packing, and not differences in cross-bridge cycling rates, largely determine the observed properties of actomyosin threads. Thus, any physical or chemical manipulation (such as protein concentration, storage time, ion concentrations, DTNB treatment) of the actomyosin that alters its ability to form filaments is likely to result in secondary, unphysiological changes in the contractile properties of threads.

This work was supported by grants from the SRC and the Wellcome Trust. P.H.Y. was in receipt of a NATO Postdoctoral Fellowship and J.D.A. is supported by an SRC Research Studentship. Part of this work was carried out at the Marine Biological Association Laboratories, Plymouth, UK. We thank the Director, Professor E. Denton, for provision of facilities, and Dr Q. Bone for the loan of equipment and for his hospitality.

Received 2 June; accepted 17 July 1980.

1. Crooks, R. & Cooke, R. *J. gen. Physiol.* **69,** 37–55 (1977).
2. Cooke, R. & Franks, K. E. *J. molec. Biol.* **120,** 361–373 (1978).
3. Matsumura, F., Yoshimoto, Y. & Kamiya, N. *Nature* **285,** 169–171 (1980).
4. Josephson, R. K. *J. exp. Zool.* **194,** 135–154 (1975).
5. Lehman, W. & Szent-Györgyi, A. G. *J. gen. Physiol.* **66,** 1–30 (1975).
6. Spudich, J. A. & Watt, S. *J. biol. Chem.* **246,** 4866–4871 (1971).
7. Barany, M. & Close, R. I. *J. Physiol., Lond.* **213,** 455–474 (1971).
8. Flitney, F. W. & Johnston, I. A. *J. Physiol., Lond.* **295,** 49P–50P (1979).
9. Lännergren, J. *J. Physiol., Lond.* **283,** 501–521 (1978).
10. Close, R. *J. Physiol., Lond.* **204,** 331–346 (1969).
11. Barany, M. *J. gen. Physiol.* **50,** Suppl., 197–216 (1967).
12. D'Haese, J. & Komnick, H. *Z. Zellforsch.* **134,** 411–426, 427–434 (1972).
13. Josephs, R. & Harrington, W. F. *Biochemistry* **5,** 3474–3487 (1966).
14. Kaminer, B. & Bell, A. L. *J. molec. Biol.* **20,** 391–401 (1966).
15. Pinset-Härström, I. & Truffy, J. *J. molec. Biol.* **134,** 173–188 (1979).
16. Pinset-Härström, I. & Whalen, R. G. *J. molec. Biol.* **134,** 189–197 (1979).
17. Syrovy, I. *Int. J. Biochem.* **10,** 383–389 (1979).
18. Itzhaki, R. F. & Gill, D. M. *Analyt. Biochem.* **9,** 401–410 (1964).
19. Hill, A. V. *Proc. R. Soc.* **B126,** 136–195 (1938).

Nuclear accumulation of epidermal growth factor in cultured rat pituitary cells

L. K. Johnson*, I. Vlodavsky†, J. D. Baxter* & D. Gospodarowicz†

Howard Hughes Medical Institute Laboratories, * Endocrine Research Division, † Cancer Research Institute and the Department of Medicine, University of California, San Francisco, California 94143

Epidermal growth factor (EGF) is a mitogen for epidermal cells *in vivo*[1,2] and for a wide variety of cells in culture[3–5]. Recently, we and others have reported that EGF can also regulate the cellular levels of various hormones[6] and fibronectin[7] at concentrations which only minimally influence cell division. In addition, EGF treatment of GH$_3$ cells affects chromatin structure such that isolated nuclei from treated cells have an increased capacity to bind bacterial RNA polymerase in initiation site complexes[6]. Thus, the data suggest that various nuclear functions are modulated by EGF in GH$_3$ cells despite its failure to affect DNA synthesis or cell proliferation. Recently, Yanker and Shooter[8] have reported on the nuclear accumulation of nerve growth factor (NGF) in PC12 cells in which NGF does not promote cell division but does influence RNA and protein synthesis while inducing overt differentiation (neurite outgrowth). The similarities between the two systems and the various theories regarding the mechanism by which mitogens exert their growth-promoting and other effects[9,10] led us to investigate whether an interaction between EGF and the cell nucleus can be demonstrated after surface binding and internalization of EGF in GH$_3$ cells. We report here that when its lysosomal degradation is inhibited by chloroquine, EGF accumulates in the nucleus.

Previous studies with GH$_3$ and other cell types have demonstrated that the cell-bound ^{125}I-EGF is rapidly degraded ($t_{1/2}$ = 20 min) to mono-^{125}I-iodotyrosine by lysosomal proteases following endocytotic internalization[6,11,12]. Due to this process, the intracellular amount of intact EGF reaches, within 1–2 h of exposure to EGF, a steady-state concentration which is much lower than the actual amount of internalized EGF and which later decreases even more due to a loss (down regulation) of the cell-surface receptors for the factor. Furthermore, if translocation of EGF into the nucleus does occur, this might require a time longer than the mean half life of the internalized EGF molecules, thereby even further reducing the possibility of detecting significant quantities of nuclear-bound ^{125}I-EGF. Therefore, our approach in probing for nuclear accumulation of EGF in GH$_3$ cells was to use the lysosomal inhibitor chloroquine, which has been shown to inhibit, in this and other cell types, the degradation of EGF and thus allows the intracellular accumulation of EGF[4,6].

In the following experiments, cells were incubated with ^{125}I-EGF in the absence and presence of chloroquine, lysed with buffer containing 0.5% NP40, and tested for the amount of radioactivity associated with the nuclear pellet and cell lysate. As shown in Fig. 1*a*, nuclei isolated from detergent-lysed cells which were exposed to 12.5 ng ml^{-1} ^{125}I-EGF for 18 h contained about 1% of the cell-associated label. In contrast, when cells were incubated with EGF in the presence of increasing concentrations of chloroquine, the amount of nuclear-associated radioactivity increased and reached a plateau of about 14% of the cell-bound counts at a concentration of 75 μM chloroquine. In these conditions, the total amount of cell-associated ^{125}I-EGF (bound plus internalized) was increased sixfold. As shown in Fig. 1*b*, the nuclear accumulation of EGF in chloroquine-treated (75 μM) cells lags significantly behind the rate of internalization of the growth factor. Thus, after a 4-h incubation with EGF, only about 2% of the internalized EGF (measured in the NP40 lysate) was associated with the isolated nuclei, whereas a 24-h incubation resulted in a nuclear accumulation of as much as 12% of the internalized EGF. Such a difference in the kinetics of cytoplasmic accumulation and nuclear binding also suggests that the observed nuclear accumulation of EGF is not due to contamination of the nuclei by membrane- or cytoplasm-bound EGF. This was further documented by electron microscopy of nuclei prepared from control and chloroquine-treated cells (Fig. 1*c*, *d*). In both cases the nuclei were free of the lysosomal vesicles known to accumulate in chloroquine-treated cells. Nuclei were also tested for lysosomal and plasma membrane contamination by assaying the biochemical marker enzymes acid phosphatase and (NA$^+$+K$^+$)ATPase respectively. Acid phosphatase activity in the nuclei measured by the method of Brandenberger *et al.*[13] was less than 0.5% of the total cellular activity in both control and chloroquine-treated cells. Nuclear (Na$^+$+K$^+$)ATPase measured according to Jackson[14] was less than 0.3% of the total cellular activity and similarly was not influenced by chloroquine treatment of the cells.

The possibility that the observed nuclear binding occurred not within the cell but upon lysis in detergent buffer was next examined. Cells were incubated for 18 h with 75 μM chloroquine in the presence or absence of 2 ng ml^{-1} ^{125}I-EGF. After washing the cultures were lysed with the NP40 buffer containing no EGF, 10 μg ml^{-1} unlabelled EGF (in the case of prelabelled cells) or 2 ng ml^{-1} ^{125}I-EGF (in the case of unlabelled cells). Nuclei were then isolated as in Fig. 1 and the bound EGF determined. Nuclei isolated from 10^6 cells prelabelled for 18 h with ^{125}I-EGF contained 5.1 fmol of ^{125}I-EGF while those prelabelled and lysed in buffer containing 10μg ml^{-1} unlabelled EGF contained 4.98 fmol ^{125}I-EGF. However, nuclei isolated with lysis buffer containing ^{125}I-EGF contained only background levels of radioactivity. This suggests that the observed nuclear binding occurs before lysis of the cell. Furthermore, incubation of cells with ^{125}I-EGF and chloroquine at 4 °C rather than 37 °C was not associated with cytoplasmic or nuclear

0028-0836/80/390340—04$01.00

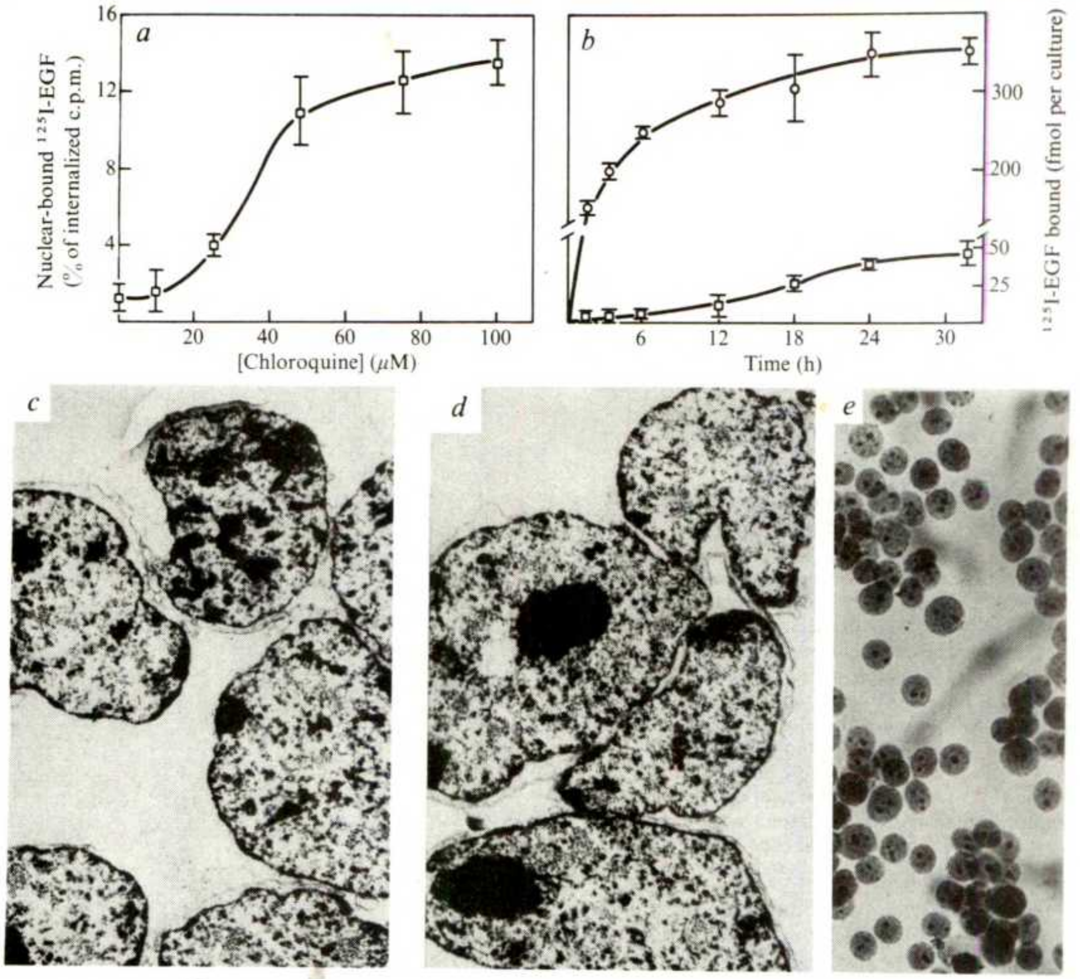

Fig. 1 Nuclear accumulation of ^{125}I-EGF in GH_3 cells. *a*, Effect of chloroquine concentration on the per cent of total cell-associated ^{125}I-EGF found in the nuclear fraction after 18 h. *b*, Kinetics of ^{125}I-EGF accumulation in GH_3 cell lysates and nuclei. 5×10^6 GH_3 cells, maintained as previously described[6], were seeded into 35-mm culture dishes. After 24 h the medium was replaced by 1.0 ml of medium containing 0.5% fetal calf serum and the indicated chloroquine concentrations. One hour later 12.5 ng ml^{-1} ^{125}I-EGF (purified and iodinated as described[4]; specific activity, 460,000 c.p.m. ng^{-1}), was added in the presence and absence of 2.5 μg ml^{-1} unlabelled EGF. After incubation at 37 °C cultures were washed 10 times with phosphate-buffered saline containing 1 mg ml^{-1} BSA and lysed in buffer containing 0.5% NP40 (ref. 6). The initial supernatant after removal of the nuclei (1,000*g*, 5 min) was designated the lysate fraction (open circles) and the nuclei were purified further as described[6] before counting of radioactivity (open squares). The mean and range of triplicate determinations are shown for each experiment. Electron microscopy of nuclear pellets from control (*c*) and chloroquine-treated (*d*) cells. Pellets were fixed on ice in 4% gluteraldehyde, 3.6% formaldehyde, 0.2 M cacodylate buffer (*p*H 7.2). Pellets were postfixed in 1% osmium tetroxide, 0.1 M Na cacodylate (*p*H 7.2), dehydrated in acetone and embedded in epon 812. Sections were stained with uranylacetate and lead citrate and photographed at an initial magnification of 4,500×. *e*, Phase contrast micrograph of nuclei from chloroquine-treated cells. Nuclei were stained with 1% trypan blue and photographed at an initial magnification of 200×.

accumulation of ^{125}I-EGF, demonstrating that the nuclear uptake is dependent on internalization of the growth factor.

Having found conditions for experimentally detecting nuclear-associated ^{125}I-EGF, we next asked if this process strictly paralleled the inhibition of EGF degradation by chloroquine. Alternatively, the nuclear accumulation of EGF could have been due to some other effect of the inhibitor, probably on the outer nuclear membrane. It was found that exposure to chloroquine (75 μM) had no effect on, or increased by at most twofold, the amount of surface-bound ^{125}I-EGF (measured by its release by trypsin). However, chloroquine-treated cultures contained as much as 19.3 times more immunoprecipitable and hence, presumably intact ^{125}I-EGF in their cell lysates than control cells (Table 1). This increase was directly paralleled by a 19-fold increase in the amount of nuclear-associated ^{125}I-EGF. As in the lysate of chloroquine-treated cells, 75% of the nuclear-bound ^{125}I-EGF could be precipitated with anti-EGF after solubilization from the nuclei. The results of these experiments suggest that in control cells, due to rapid degradation of the internalized EGF, only a small percentage (1%) of the internalized growth factor could be detected in the nucleus. In contrast, in chloroquine-treated cultures EGF degradation is greatly diminished, thus allowing a cytoplasmic accumulation of EGF and making a greater proportion of the internalized, intact EGF available for nuclear binding.

The nature of the nuclear sites which interact with ^{125}I-EGF was examined next. Scatchard analysis of the ^{125}I-EGF nuclear accumulation (Fig. 2) shows that the observed nuclear binding is saturable and of high affinity. Two distinct classes of binding affinity are apparent: a high affinity component with a K_d of 0.28 nM and a lower affinity class of sites possessing a K_d of 2.7 nM. The binding capacity of each class of sites estimated from the Scatchard plots is 10^3 and 1.2×10^4 sites per nucleus, respectively. Interestingly, this observation is similar to findings regarding the nuclear binding of NGF in PC12 cells. In that system, two classes of binding sites which differ in affinity by an order of magnitude were also observed[8], although the number of high-affinity sites was two- to fivefold greater than that seen for EGF in GH_3 cells. The NGF nuclear receptor sites in PC12 cells are resistant to extraction with Triton detergents, suggesting that they may be localized at the inner membrane[8]. In that system, both intact nuclei and isolated nuclear membranes retain the ability to bind ^{125}I-NGF. In the case of GH_3 cells, nuclei isolated from either untreated or chloroquine-treated GH_3 cells showed no detectable binding of ^{125}I-EGF when the growth factor was added *in vitro*. Similar negative results were

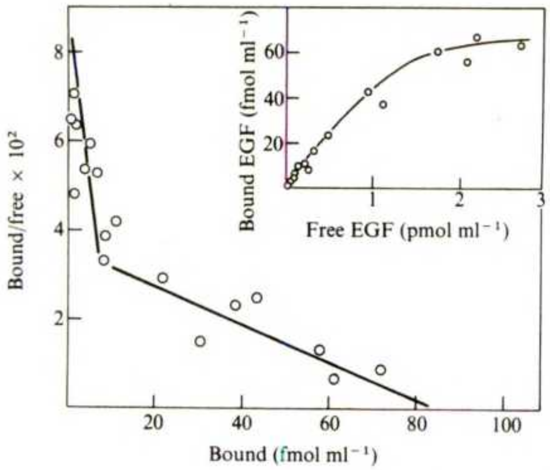

Fig. 2 Scatchard analysis of ^{125}I-EGF binding to GH$_3$ cell nuclei. Cells were seeded and media replaced as described in Fig. 1. Cultures were then incubated for 18 h at 37 °C in the presence of 75 μM chloroquine and increasing concentrations of ^{125}I-EGF (0.05–50 ng ml^{-1}) with or without 2.5 μg ml^{-1} unlabelled EGF. Nuclei were analysed for the amount of specifically bound EGF as described in Fig. 1 legend. The extracellular concentration of free, intact EGF was determined by double immunoprecipitation (rabbit anti-EGF antiserum followed by goat anti-rabbit IgG) of an aliquot (100 μl) of the culture medium before the cultures were washed, as described in Table 1. Plates without cells were used to control for spontaneous breakdown of ^{125}I-EGF during the incubation period at 37 °C. Up to 20% of the total radioactivity was no longer immunoprecipitable, after incubation without cells, as opposed to only 2% in freshly labelled EGF.

obtained with detergent-washed nuclei (nuclei lacking the outer membrane) or with nuclei prepared by mechanical disruption and centrifugation through 2.0 M sucrose[8] (nuclei with an intact outer membrane). We therefore examined the sub-nuclear localization of EGF by subjecting isolated nuclei with bound ^{125}I-EGF to enzymatic fractionation of the chromatin.

GH$_3$ cells were labelled for 24 h with ^{14}C-thymidine followed by a 12-h incubation with ^{125}I-EGF in the presence of chloroquine. The nuclei were then isolated and incubated with micrococcal nuclease at 22 °C. At various times, aliquots were taken and the amount of ^{125}I and ^{14}C released into the supernatant determined. As shown in Fig. 3, micrococcal nuclease solubilized approximately 90% of the labelled DNA within 10 min. The solubilized DNA fragments showed the characteristic nucleosome repeat pattern of chromatin and contained DNA fragment sizes from monomers (180 base pairs) to octamers (Fig. 3*b*). However, no ^{125}I-EGF was released by the nuclease above that which dissociated during the course of the experiment (approximately 9% in the zero time controls), nor was any spontaneous release observed when the EGF-loaded nuclei were lysed with 1.0 mM EDTA. This suggests that the bound EGF is not localized in the chromatin fraction of the nucleus but rather is associated with the inner nuclear membrane or nuclear matrix fraction. The latter contains the so-called 'nuclear scaffolding' (ref. 15), structures thought to participate in the higher-order condensation and packaging of chromatin into metaphase chromosomes before cytokinesis[16]. Direct EGF binding to receptors in the inner nuclear membrane seems unlikely, however, as nuclei isolated by detergent showed no binding when analysed *in vitro* despite their retention of the inner membrane. These findings are in contrast to the sub-nuclear location of two other regulators of growth hormone and prolactin mRNA synthesis, namely the thyroid and glucocorticoid hormone receptors[6]. Both of these receptors are liberated from GH cell chromatin upon DNase digestion[17] and in the case of T$_3$ there may be a preferential localization of the receptor in nuclear fractions more active in RNA synthesis[18,19].

Although a number of common steps appear to follow the initial cell surface binding of various polypeptide hormones and mitogens, the mechanism by which the respective cellular responses are exerted is still far from being understood. Some of these responses require a prolonged exposure to the effector, while others are temporary and occur within minutes. If internalization is a prerequisite, at least for the induction of long-term responses, then an interaction of either the intact polypeptide or its degradation product with the cell nucleus should be considered. Nuclear binding sites for insulin[20] and NGF[8] have been identified in rat liver cells and PC12 cells, respectively. In the case of GH$_3$ cells, although binding to isolated nuclei has not yet been observed, a translocation pathway leading to a nuclear accumulation of EGF can be described in accordance with the present observations.

The nuclear accumulation of EGF in GH$_3$ cells was a small percentage of the total internalized EFG (1%) but increased markedly when the lysosomal degradation of the growth factor

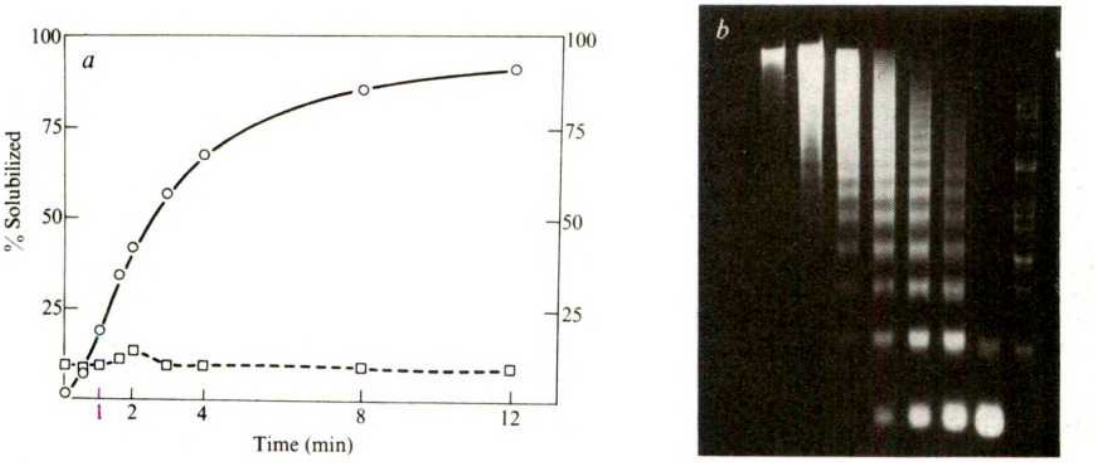

Fig. 3 Influence of micrococcal nuclease on release of ^{125}I-EGF and ^{14}C-thymidine - labelled DNA from isolated GH$_3$ nuclei. Cells (1.5×10^7) were labelled for 24 h with 25 μCi (5 μCi ml^{-1}) ^{14}C-thymidine, followed by an additional 18-h incubation with ^{125}I-EGF (12.5 ng ml^{-1}) in the presence of 75 μM chloroquine. After isolation of the nuclei, aliquots were incubated at 22 °C with 40 units ml^{-1} micrococcal nuclease (Worthington) for the indicated times. The reaction was stopped and nuclei lysed by the addition of a 10-fold volume of 1 mM EDTA and unreleased material was removed by centrifugation (15,000*g*, 5 min). ^{125}I-EGF in the two fractions (pellet and supernatant) was counted first. Each was subsequently brought to 1.0 M perchloric acid, heated to 70 °C for 30 min, and cooled on ice. Precipitated protein was removed by centrifugation and ^{14}C detected by scintillation counting in a Triton–toluene–omniflour cocktail. The per cent of each label released was determined by dividing the amount of label present in the supernatant by the total (supernatant plus pellet) for each time point. The distribution of DNA fragments in the supernatant was examined by subjecting equal ^{14}C c.p.m. to fractionation on a 1% agarose gel (*b*). Outside lanes are marker DNA restriction fragments from plasmid pBR322 while the inside lanes are from the 0.5, 1, 1.5, 2, 3, 4 and 12 min time point supernatants (right to left). ○, Thymidine; □, EGF.

Table 1 Effect of chloroquine on degradation and subcellular distribution of EGF in GH$_3$ cells

Condition*	EGF concentration (fmol per 10^6 cells) Surface†	Lysate‡	Nuclei§
Control	5.07	1.88	0.303
Chloroquine (75 μM)	5.72	36.40	5.78
Increase (-fold)	1.12	19.3	19.0

* 10^6 cells were incubated (18 h, 37 °C) with 2 ng ml^{-1} ^{125}I-EGF, with or without chloroquine, in the presence and absence of 2.5 μg ml^{-1} unlabelled EGF.

† Trypsin-releasable radioactivity. Washed cultures were treated with STV (0.05% trypsin and 0.02% EDTA Gibco) for 5 min at 22 °C, further proteolysis inhibited by adding calf serum (10%), and the radioactivity measured in an aliquot of the supernatant after centrifugation (330*g*, 5 min).

‡ Amount of immunoprecipitable ^{125}I-EGF present in the NP40 lysate minus cell-surface-associated (trypsin-releasable) ^{125}I-EGF. Immunoprecipitation was carried out by incubating (2 h, 37 °C) 1 ml of cell lysate with rabbit anti-EGF antiserum (3 μl) followed by addition (1 h at 37°C and 16 h at 4 °C) of 10 μl goat anti-rabbit IgG antiserum (35% ammonium sulphate cut). Precipitable radioactivity (intact EGF) amounted, after correction for spontaneous breakdown of ^{125}I-EGF (Fig. 2 legend), to about 95% and 50% of the total radioactivity present in the lysates of chloroquine-treated and untreated cells, respectively. When tested in the tissue culture medium the amount of non-precipitable radioactivity did not exceed (in chloroquine-treated cultures) that found in the absence of cells, whereas in untreated cells release of ^{125}I-EGF degradation products, above the 'no cells' control, accounted for up to 90% of the amount of intact EGF accumulated in chloroquine-treated cells.

§ Nuclear pellets were dissolved in 9 M urea, insoluble material removed by centrifugation, and the supernatant (20 μl) subjected to immunoprecipitation as described above after dilution to 1.0 ml with phosphate-buffered saline. The percentage of immunoprecipitable radioactivity in nuclei prepared from chloroquine-treated and untreated cells was similar (65–75%).

was inhibited. This could occur through internalization of EGF by adsorptive endocytosis, followed by fusion of accumulated endocytotic vesicles with the outer nuclear membrane. Release of EGF, either bound or unbound to its surface receptor, into the perinuclear space, inner nuclear membrane or nuclear scaffolding structures could then follow. Such a process may be reflected by findings showing that cytoplasmic vesicles containing fluorescein-conjugated EGF form a perinuclear ring in A-431 cells[21]. In the immature rat uterus, fusion of lysosomal vesicles with the nuclear membrane has been considered as a possible means of introducing oestrogens into the nucleus[22].

No regulatory action of a protein hormone has yet been shown to require hormone degradation. On the contrary, results from our laboratory demonstrate a full induction of thymidine incorporation and cell proliferation by EGF, despite the inhibition of its degradation by either leupeptin or antipain[23]. Whether or not the nuclear accumulation of either intact or modified EGF is in fact responsible for the various nuclear effects exerted by EFG on GH$_3$ cells requires further investigation.

Received 20 March; accepted 22 July 1980

1. Birnbaum, J. E., Sapp, T. M. & Moore, J. B *J. invest Derm* **66**, 313–318 (1976).
2. Savage, C R. & Cohen, S. *Expl Eye Res.* **15**, 361–366 (1973)
3. Rheinwald, J. G. & Green, H. *Nature* **265**, 421–242 (1977).
4. Gospodarowicz, D., Ill, C. R. & Birdwell, C. R. *Endocrinology* **100**, 1108–1115 (1977)
5. Savage, C. R & Cohen, S *J biol Chem.* **247**, 7609–7611 (1972).
6. Johnson, L. K., Baxter, J D., Vlodavsky, I. & Gospodarowicz, D. *Proc natn Acad Sci. U.S A.* **77**, 394–398 (1980)
7. Chen, L. B , Gudor, R. C., Sun, T T , Chen, A. B & Mosesson, M. W. *Science* **197**, 776–778 (1977)
8. Yankner, B. A & Shooter, E M. *Proc. natn. Acad Sci. U.S.A.* **76**, 1269–1273 (1979)
9. Carpenter, G. & Cohen, S *A. Rev. Biochem.* **48**, 193–226 (1979)
10. Das, M. & Fox, F. C *Proc. natn. Acad. Sci U.S A* **75**, 2644–2648 (1978).
11. Carpenter, G., Lembach, K , Morrison, M. & Cohen, S. *J. biol. Chem.* **250**, 4297–4304 (1975)
12. Carpenter, G. & Cohen, S. *J. Cell Biol* **71**, 159–171 (1976).
13. Brandenberger, H. & Hanson, R. *Helv. chim. Acta* **36**, 900–904 (1953).
14. Jackson, P. C. *Biochemistry* **15**, 5641–5651 (1976).
15. Adolph, K. W , Cheng, S. M & Laemmli, U K *Cell* **12**, 805–812 (1977)
16. Laemmli, U K. *et al* *Cold Spring Harb Symp quant Biol* **42**, 351–360 (1977)
17. Levy, B W & Baxter, J D. *Biochem biophys Res Commun.* **68**, 1045–1051 (1976)
18. Charles, M A., Ryffel, G W , Obinata, M , McCarthy, B J & Baxter, J D *Proc natn Acad Sci. U.S A* **72**, 1787–1791 (1975)
19. Samuels, H H , Stanley, F & Shapiro, L *J biol Chem* **252**, 6052–6060 (1977)
20. Gorski, J. A *Biochemistry* **18**, 3674–3678 (1979)
21. Haigler, H , Ash, J F., Singer, S J & Cohen, S *Proc. natn Acad Sci U S A* **75**, 3317–3321 (1978).
22. Szego, C J *Recent Prog Horm Res.* **30**, 171–233 (1974)
23. Savion, N , Vlodavsky, I & Gospodarowicz, D *Proc natn Acad Sci U.S.A.* **77**, 1466–1470 (1980)

VIP occurs in intrathyroidal nerves and stimulates thyroid hormone secretion

B. Ahrén,* J. Alumets, M. Ericsson, J. Fahrenkrug, L. Fahrenkrug, R. Håkanson, P. Hedner, I. Lorén, A. Melander, C. Rerup & F. Sundler

Departments of Pharmacology, Medicine, Surgery, Clinical Pharmacology and Histology, University of Lund, Sweden
Department of Clinical Chemistry, Bispebjerg Hospital, Copenhagen, Denmark
Department of Surgery A, Frederiksborg County Hospital, Denmark

Vasoactive intestinal polypeptide (VIP) is known to have powerful effects on the secretion from several endocrine and exocrine glands[1–3], and occurs in nerves with a ubiquitous distribution in the body[4,5]. This infers that neuronal VIP may be a regulator of such secretion, and there is evidence that it is involved in the regulation of exocrine pancreatic function[3]. Previous studies have shown that adrenergic and cholinergic nerves participate in the regulation of thyroid hormone secretion[6–9]. We describe here combined immunohistochemical and immunochemical studies which show that the thyroid of several species is supplied with VIP-containing nerve fibres that surround blood vessels and run between and along thyroid follicles and that in the mouse neuronal VIP participates in the regulation of thyroid hormone secretion through a mechanism that is mediated by cyclic AMP.

Thyroid tissue specimens from cat, pig and man were fixed by immersion in ice-cold 4% formalin buffered to *p*H 7.0. The human material was obtained at surgery for benign autonomous nodules. Mice, rats and guinea pigs were anaesthetized with sodium pentobarbitone or diethyl ether and perfused via the ascending aorta with large volumes of the fixative solution. The thyroid glands were dissected out and stored in the fixative for 24–48 h and rinsed for 24 h in an ice-cold Tyrode solution containing 5% sucrose. The tissue specimens were frozen in dry ice and sectioned in a cryostat at −15 °C. Sections, cut at 8 μm, were processed for the immunocytochemical demonstration of VIP, using an antiserum (5603) raised against highly purified porcine VIP[10]. The dilution of the antiserum was 1 : 80. The site of antigen–antibody reaction was revealed by the indirect immunofluorescence method of Coons *et al.*[11]. Fluoresceinated goat anti-rabbit IgG was from SBL, Stockholm, Sweden. Controls were sections exposed to VIP antiserum which had been inactivated by incubation with pure porcine VIP (0.3–30 nmol per ml diluted antiserum) for at least 24 h.

The concentration of VIP in the thyroid was determined by radioimmunoassay. Thyroid glands were dissected out from anaesthetized cats, mice, pigs and rats. Normal thyroid gland tissue was also obtained from patients undergoing surgery for thyroid adenoma. The number of specimens are given in Table 1. The tissue was immediately frozen on dry ice, weighed and stored at −20 °C until extraction. VIP was extracted by homogenization at 0 °C in a glass homogenizer containing 5 vol of

---

* To whom correspondence should be addressed.

0028-0836/80/390343—03$01.00

Table 1 Concentration of VIP (pmol per g wet weight) in the thyroid gland of various mammalian species

	Mouse	Rat	Cat	Pig	Man
Mean	25.1	28.6	16.6	0.8	1.8
s.e.m.	2.1	6.2	2.6	0.1	0.4
n	12	6	6	5	6

n, No. of glands analysed in each species.

acidified ethanol (70% ethanol containing 0.74% HCl, w/v). After centrifugation (1,500*g*) at 4 °C for 15 min, the supernatant was decanted and the residues resuspended and homogenized with additional 5 vol of acidified ethanol. After centrifugation, the combined supernatant fractions were evaporated to dryness *in vacuo*. The samples were reconstituted and diluted in assay buffer (sodium phosphate buffer, 0.4 mol l^{-1}, *p*H 7.4, containing 58 μmol human serum albumin (Behringwerke) and sodium chloride (0.1 mol l^{-1}) and assayed in at least three different dilutions. The concentration of VIP in the extracts was measured radioimmunochemically using antiserum no 5603–6 (refs 10, 12).

For studies on the effect of VIP, female mice of the NMRI strain (Anticimex) weighing 20–25 g at the time of experiments, were used. They were fed a standard pellet diet or a low-iodine diet (Astra-Ewos), and tap water *ad libitum*. Porcine VIP, bovine thyrotropic hormone (TSH; Ferring AB) or saline was injected intravenously (i.v.) and the animals were killed after 30 min. The thyroid glands were dissected out, fixed for 18 h at 4 °C in Bouin's solution, dehydrated with ethanol, embedded in paraffin, sectioned at 6 μm and stained by the periodic acid-Schiff (PAS) technique. This technique stains colloid in the follicle lumen as well as colloid droplets in the follicle cells[7]. Radioiodine release from the thyroid was assessed according to McKenzie[13], as modified by Rerup and Melander[14]. The animals were given a low-iodine diet 10 days before experimentation to ensure adequate thyroidal uptake of radioiodine. Each animal was injected intraperitoneally (i.p.) with 16 μCi Na^{125}I (Radiochemical Centre) three days before the experiments, and was given 20 μg L-thyroxine (British Drug Houses Ltd) subcutaneously (s.c.) 72 and 24 h before the experiments. Blood (100 μl) was sampled by orbital puncture before and at specified intervals after the i.v. injection of VIP, TSH and saline, respectively. The injection volumes were 0.1 ml (s.c. and i.p.) or 0.2 ml (i.v.). The radioactivity was measured in an autogamma spectrometer.

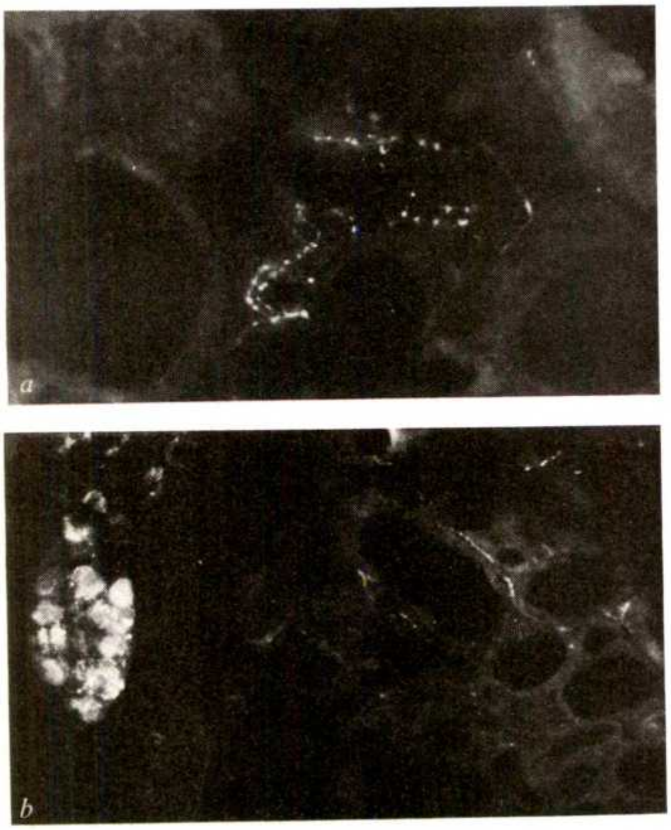

Fig. 1 Immunohistochemical demonstration of VIP nerves in rat (*a*) and mouse (*b*) thyroid. VIP nerves were distributed both around blood vessels (*a*) and between and along thyroid follicles (*b*). In the mouse, VIP immunoreactivity was seen in cell bodies in a local ganglion (left of *b*). Magnification *a*, ×125; *b*, ×190.

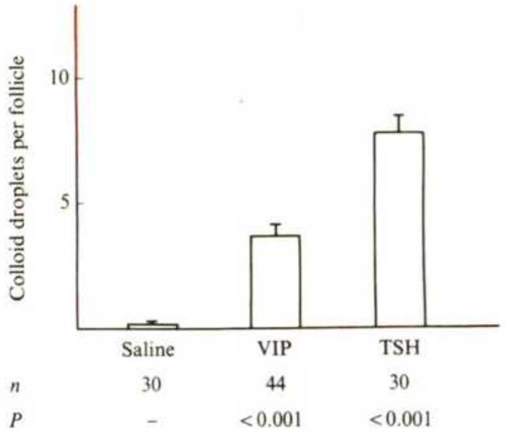

Fig. 2 Colloid droplets in thyroid follicle cells 30 min after an i.v. injection of saline, VIP or TSH. Values are mean ±s.e.m. *P*, Probability level of random difference. *n*, No. of follicles counted.

The influence of VIP and TSH on the production of cyclic AMP in the thyroid was investigated according to Ahrén *et al.*[15], with an ion exchange step included. Briefly, the animals were killed by neck dislocation. The thyroid lobes were dissected out and placed in tubes with 1 ml Krebs–Ringer bicarbonate buffer containing 10 mmol l^{-1} glucose. The preincubation lasted for 30 min and the incubation 25 min. During preincubation and incubation, the medium was bubbled with 95% O_2/5% CO_2 to ensure constant *p*H and oxygenation. To reduce degradation of newly formed cyclic AMP, theophylline (1.0 mmol l^{-1}) was added. Cyclic AMP content was determined in the tissue and in the incubation medium. The tissue was homogenized in ice-cold 10% trichloroacetic acid and centrifuged at 1,500*g* at 4 °C for 30 min. The supernatant was passed through a Dowex-50 column with 1.5 ml bed volume and eluted with distilled water. The eluate was freeze-dried, redissolved in 500 μl distilled water and analysed for its cyclic AMP content by the method of Gilman[16], as modified by Tovey *et al.*[17]. The cyclic AMP content was expressed as pmol per mg tissue protein, determined by the method of Lowry *et al.*[18]. The production of cyclic AMP was calculated as the sum of tissue and medium content. ^{3}H-cyclic AMP was from NEN and cyclic AMP-dependent protein kinase from Sigma. All commercial chemicals were reagent grade.

Immunoreactive nerve fibres were observed in the thyroid of all species examined. They were most frequent in mouse, less frequent in rat and cat and scarce in guinea pig, pig and man. The nerve fibres were thin and beaded, occurred both around blood vessels (Fig. 1*a*) and between and along thyroid follicles (Fig. 1*b*). In the cat and mouse the fibres were rather uniformly distributed within the gland, whereas in the rat they had a characteristically patchy occurrence with areas totally devoid of immunoreactive fibres. In man, single fibres were observed in the stromal tissue surrounding follicles.

In the mouse, a small ganglion containing VIP-immunoreactive nerve cell bodies and fibres was regularly encountered close to the thyroid capsule at the dorso-medial surface of each lobe (Fig. 1*b*). The ganglion was sometimes seen to issue a bundle of immunoreactive fibres projecting into the thyroid parenchyma. This suggests a local origin of at least some of the VIP fibres.

The concentrations of VIP in the thyroid gland of five mammalian species are given in Table 1. Concentrations measured by radioimmunoassay roughly agreed with the relative number of VIP-containing nerve fibres found by immunohistochemistry.

Injection of VIP, like TSH, was associated with formation of numerous intracellular colloid droplets in the mouse thyroid. The increase in the number of colloid droplets was significant compared to saline-injected controls (Fig. 2). VIP, like TSH, raised the blood ^{125}I levels in mice pretreated with ^{125}I and thyroxine. For both VIP and TSH, maximum radioiodine concentrations were reached at 2 h (Fig. 3). Therefore, in subsequent experiments, samples were collected at 0 and 2 h. Figure 3 shows the responses to different doses of VIP or TSH, and to their combination. The dose-response curve for VIP was less steep than that for TSH. The response to 5.0 nmol VIP was roughly equivalent to that to 65 μU TSH. VIP (5.0 nmol) and TSH (50 μU) potentiated the effect of each other. Most, if not all, thyroidal effects of TSH are thought to be mediated[19,20] by cyclic AMP. Like TSH, VIP increased the cyclic AMP production, although to a lesser degree (Fig. 4). VIP has previously been shown to stimulate cyclic AMP formation in several tissues[21–23].

The findings that VIP occurs in nerve fibres in the thyroid and has a stimulatory effect on thyroid hormone secretion suggest that neuronal VIP participates in the regulation of thyroid activity. Earlier studies have revealed that both adrenergic and cholinergic nerves are involved in the regulation of thyroid activity[6–9]. The interaction between the various nervous mechanisms in the control of thyroid function remains to be elucidated.

We thank Prof. V. Mutt for porcine VIP, and Kristine Fogelström, Åsa Gustafson, Anita Hansen, Lena Kvist, Marianne Maxe-Colschen and Lena Poulson for technical assistance. This study was supported by grants from the Swedish MRC (04X-4499), the Medical Faculty, University of Lund, and from P. Carl Petersen's Foundation (J. no B 1093).

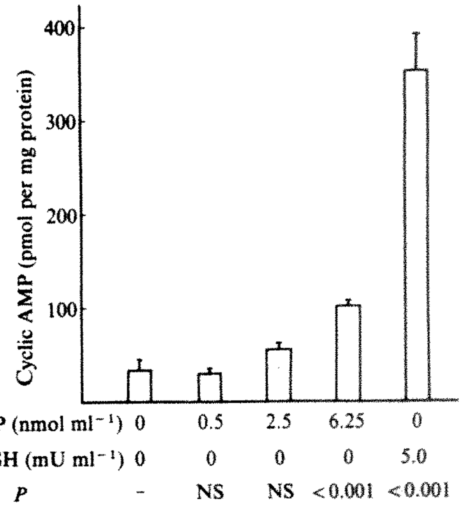

Fig. 4 Thyroidal production of cyclic AMP (pmol per mg tissue protein) *in vitro* during 25 min exposure to VIP or TSH. Four observations per group. *P*, Probability level of random difference. NS, Not significant.

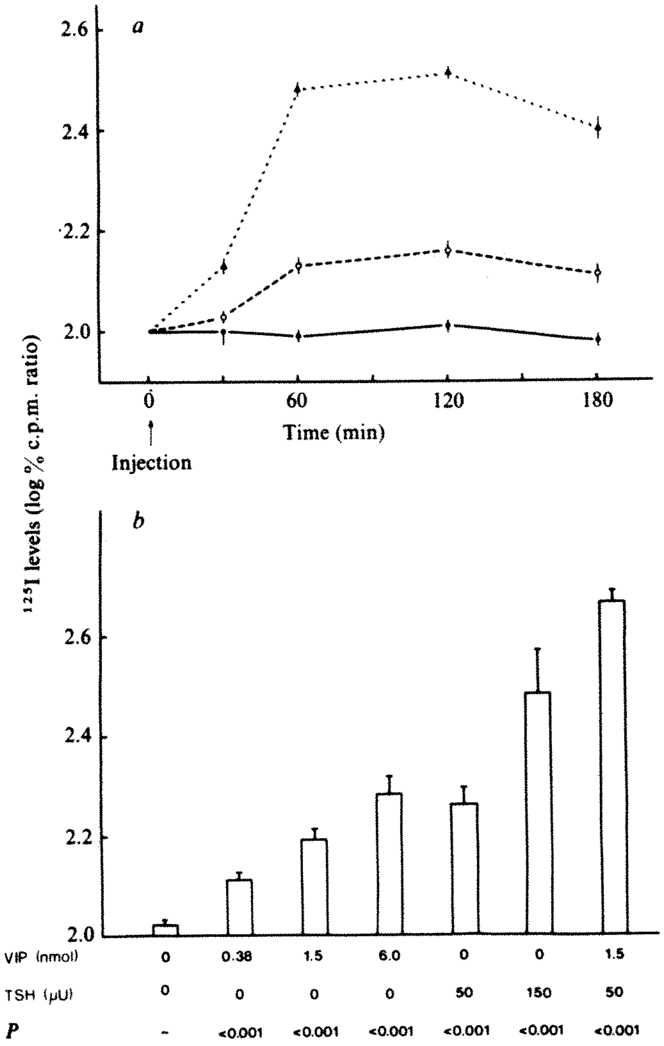

Fig. 3 Changes in blood radioactivity in mice pretreated with ^{125}I and thyroxine following injection of VIP, TSH and saline, respectively. *a*, Time course of the changes. 5–7 mice per group. ▲, TSH (50 μU); ○, VIP (1.5 nmol); ●, saline. *b*, Dose–response relationship. 8–17 mice per group. log% c.p.m. ratio of radioactivity before and 2 h after injection. Values are mean ± s.e.m. *P*, Probability level of random difference.

Received 17 June; accepted 28 July 1980.

1. Schebalin, M., Said, S. I. & Makhlouf, G. M. *Am. J. Physiol.* **232,** E197–E200 (1977).
2. Wu, Z. C., O'Dorisio, T. M., Cataland, S., Mekhjian, H. S. & Gaginella, T. S. *Dig. Dis. Sci.* **24,** 625–630 (1979).
3. Fahrenkrug, J., Schaffalitzky de Muckadell, O. B., Holst, J. J. & Lindkaer Jensen, S. *Am. J. Physiol.* **237,** E535–E540 (1979).
4. Larsson, L. -I. *et al. Proc. natn. Acad. Sci. U.S.A.* **73,** 3197–3200 (1976).
5. Fahrenkrug, J. *Digestion* **19,** 149–169 (1979).
6. Melander, A. *Acta physiol. scand.* Suppl. **370,** 1–31 (1971).
7. Melander, A. & Sundler, F. *Endocrinology* **90,** 188–193 (1972).
8. van Sande, J., Dumont, J., Melander, A. & Sundler, F. *J. clin. Endocr.* (in the press).
9. Melander, A. & Sundler, F. *Endocrinology* **105,** 7–9 (1979).
10. Fahrenkrug, J. & Schaffalitzky de Muckadell, O. B. *J. lab. clin. Med.* **89,** 1379–1388 (1977).
11. Coons, A. H., Leduc, E. H. & Conolly, J. M. *J. exp. Med.* **102,** 49–59 (1955).
12. Fahrenkrug, J. & Schaffalitzky de Muckadell, O. B. *J. Neurochem.* **31,** 1445–1451 (1978).
13. McKenzie, J. M. *Endocrinology* **63,** 372–382 (1958).
14. Rerup, C. & Melander, A. *Acta endocr. kbh* **50,** 177–194 (1965).
15. Ahrén, B., Gustafson, Å., Hedner, P. & Nilsson, H. *Acta endocr. kbh* **89,** 693–700 (1978).
16. Gilman, A. G. *Proc. natn. Acad. Sci. U.S.A.* **67,** 305–312 (1970).
17. Tovey, K. C., Oldham, K. G. & Whelan, J. A. M. *Clin. chim. Acta* **56,** 221–234 (1974).
18. Lowry, O. H., Rosebrough, N. J., Farr, A. L. & Randall, R. J. *J. biol. Chem.* **193,** 265–275 (1951).
19. Dumont, J. E. *Vitams Horm.* **29,** 288–412 (1971).
20. Ketelbant-Balasse, P., van Sande, J. Neve, P. & Dumont, J. E. *Horm. metab. Res.* **8,** 212–215 (1976).
21. Bataille, D., Freychet, P. & Rosselin, G. *Endocrinology* **95,** 713–721 (1974).
22. Laburthe, M. *et al. J. Biochem.* **96,** 239–248 (1979).
23. Frandsen, E. K., Krishna, G. A. & Said, S. I. *Br. J. Pharmac.* **62,** 367–369 (1978).

Intracellular studies showing modulation of facial motoneurone excitability by serotonin

C. P. VanderMaelen & G. K. Aghajanian

Yale University School of Medicine, Departments of Psychiatry and Pharmacology, 34 Park Street, New Haven, Connecticut 06508

The application of serotonin to certain myenteric plexus neurones in the guinea pig small intestine causes a slow depolarization of membrane potential, accompanied by increased neuronal excitability and input resistance[1]. On the other hand, microiontophoretic application of large amounts of serotonin onto mammalian spinal motoneurones is reported to cause membrane hyperpolarization and decreased excitability[2]. However, on the basis of recording spinal reflex activity, serotonin has been reported to enhance net motoneurone activity[3]. Moreover, studies using extracellular single-cell recording techniques indicate that serotonin in small amounts facilitates synaptically or glutamate-induced excitation of mammalian motoneurones in the facial nucleus[4] and spinal cord[5]. It was suggested that these facilitatory actions were modulatory in nature, as serotonin did not induce motoneurone spiking in the absence of extrinsic excitatory input. The study reported here investigated the membrane mechanisms underlying these modulatory effects by obtaining intracellular recordings from rat facial motoneurones during extracellular microiontophoretic application of serotonin, methysergide (a serotonin antagonist) and noradrenaline. Serotonin caused a slow depolarization of membrane potential of about 5 mV which remained subthreshold, accompanied by an increase in electrical excitability of the neurone, and an increase in input resistance. Noradrenaline caused the same changes. Methysergide antagonized the effects of serotonin, but not noradrenaline, indicating that these actions of serotonin are selective and receptor mediated.

Figure 1 illustrates the changes which occurred in a rat facial motoneurone with the iontophoretic administration of a relatively low dose (+25 nA ejection current) of serotonin. Within 32 s, the resting potential shifted from −68 mV to −63.5 mV (Fig. 1*b*), input resistance increased by 32% from an average value of 4.7 MΩ to one of 6.2 MΩ (Fig. 1*c*), and a constant current intracellular depolarizing pulse (1.1 nA, 182 ms duration) which had been adjusted to 73% of rheobase became effective in triggering action potentials (Fig. 1*a*, *d*), indicating an increase in excitability of the neurone.

Increased excitability and slow depolarization in response to iontophoretically applied serotonin were seen in 35 of 41 facial motoneurones analysed. The maximal depolarization seen was 8 mV with 50 nA of serotonin applied for 2 min. The typical amount of depolarization was 3–6 mV with iontophoretic currents of 10–60 nA applied for 0.5–2.0 min. Changes in input resistance were more difficult to detect, due in part to fluctuations in electrode resistance which caused imbalances in the bridge circuit adjustment. However, all changes in input resistance which were clearly seen were increases. No decreases in input resistance were detected in response to iontophoretically applied serotonin. Excitability changes in response to very low doses of serotonin were particularly evident when the amplitude of the long (130–200 ms) depolarizing pulse was adjusted to rheobase so that only one action potential was triggered from it. In such cases, iontophoretic currents of serotonin as low as 5 nA

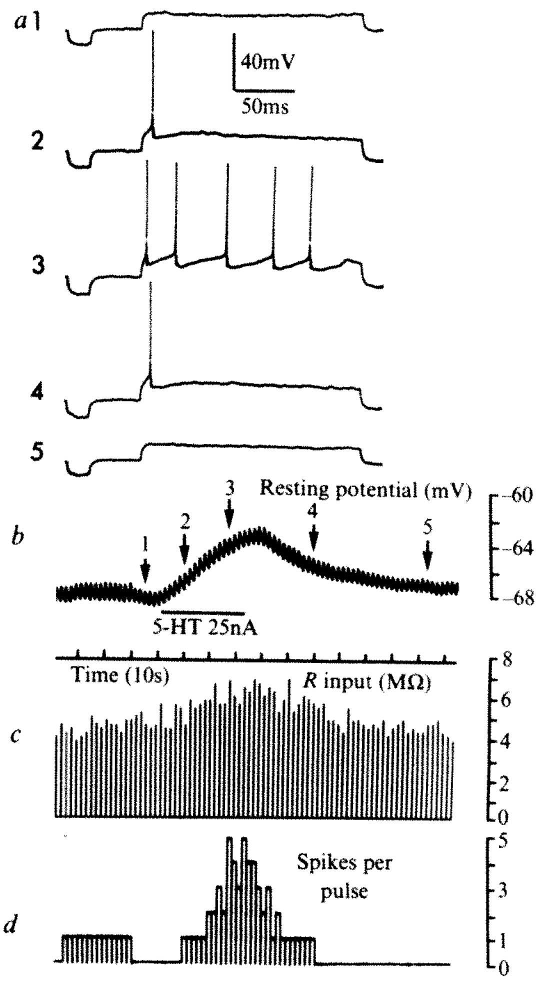

Fig. 1 Effects of iontophoretically applied serotonin (5-HT) on membrane resting potential, input resistance and excitability of a rat facial motoneurone. *a*1–5, Selected sweeps of the oscilloscope taken before, during and after serotonin iontophoresis. Each sweep consisted of a 1.0-nA hyperpolarizing pulse used for input resistance measurement, followed by a longer depolarizing pulse. The depolarizing pulse was set at 1.1 nA, which was 73% of rheobase. Sweeps occurred once every 1.9 s. *b–d*, Simultaneous records of resting membrane potential (*b*), input resistance (*c*) and number of spikes triggered by the depolarizing pulse (*d*). Time marker occurred once every 10 s and applies to *b–d*. The numbered arrows in *b* indicate the points in time at which the numbered sweeps in *a* were taken. The bar in *b* indicates the time during which serotonin (25 nA) was iontophoretically applied. The saw-toothed appearance of the trace in *b* was due to deflections of the pen that remained after filtering, caused by the depolarizing pulse. Input resistance was determined by transferring the stored data from FM tape to a storage oscilloscope where each hyperpolarizing pulse was displayed at high gain and fast time base. The voltage displacement was carefully measured, with compensation for any imbalance in the bridge circuit. Calculated values for input resistance are shown graphically in *c*. The 14 individual spikes in *d* preceding the onset of the serotonin were caused by the depolarizing pulse set at rheobase, before being adjusted to 73% of rheobase. Intracellular recording micropipettes were filled with 2 M KCl and had resistances of 15–25 MΩ. These were affixed with dental acrylic to five-barrel iontophoretic micropipettes, with tip separations between recording and iontophoretic electrodes of 25–60 μm. Iontophoretic barrels were filled with serotonin creatinine sulphate (Regis, 40 mM, *p*H 4.0), methysergide maleate (Sandoz, 5 mM, *p*H 4.0), (−)noradrenaline bitartrate (Regis, 100 mM, *p*H 4.0) and NaCl (2 or 4 M) which was used for the current balance channel such that net current flow from the iontophoretic electrodes was zero at all times. Retaining currents of −15 nA were applied to drug barrels between periods of ejection. The facial nucleus was located in anaesthetized (chloral hydrate, 400 mg per kg, intraperitoneal) male albino rats by the presence of a characteristic antidromic field potential[14] in response to electrical stimulation of the zygomatic branch of the facial nerve.

0028-0836/80/390346—02$01.00

applied for 30 s caused multiple spikes to be triggered from the depolarizing pulse (not shown).

Figure 2 illustrates the selective antagonism by methysergide of the serotonin induced increase in motoneurone excitability. A depolarizing pulse (5.4 nA intensity, 132 ms duration, Fig. 2*a*) was delivered intracellularly to a facial motoneurone once every 2.1 s. This pulse had been adjusted to 90% of rheobase. With the iontophoretic administration (40 nA for approximately 1 min) of either serotonin (Fig. 2*b*1) or noradrenaline (Fig. 2*c*1), excitability was increased, as indicated by the fact that the depolarizing pulses triggered multiple spikes. However, in the presence of iontophoretically applied methysergide (7 nA) and with the same current of serotonin, no spikes were triggered from the depolarizing pulse during 1 min (Fig. 2*b*2), indicating a greatly reduced effect of serotonin on excitability. Methysergide had only a small effect on responses to noradrenaline (Fig. 2*c*2), and this may have been due to a slight decrease in excitability caused by the methysergide itself.

The mechanism for this methysergide-induced decrease in motoneurone excitability was not explored, although we did find that iontophoretically applied methysergide, as well as intravenously administered methysergide or cyproheptadine (another serotonin antagonist), cause decreases in motoneurone excitability, determined by rheobase measurements. It is possible that the serotonin blockers antagonize a tonic facilitatory serotonin input, as facial motoneurones are known to receive a dense serotonin innervation[4,6,7]. A similar explanation has previously been proposed to explain the effects of the serotonin antagonist metergoline on spinal motoneurones recorded extracellularly[5].

Our experiments, using intracellular recording techniques, agree with previous studies using extracellular single unit recording. These showed that microiontophoretically applied serotonin facilitates the excitation of motoneurones caused by stimulation of excitatory afferents or by the microiontophoretic application of glutamate, but that serotonin alone does not elicit action potentials[4,5]. We have shown that this modulatory action of serotonin is associated with a slow, subthreshold depolarization which is accompanied by an increase in both electrical excitability and input resistance. The ionic mechanisms for these serotonin-induced membrane changes are not known, but similar changes in guinea pig small intestine neurones are postulated to be caused by a decrease in Ca^{2+}-dependent potassium conductance (g_{K^+})[8]. Similarly, serotonin causes a depolarization of certain molluscan neurones by decreasing g_{K^+} (ref. 9).

Because we measured excitability directly by means of intracellular injection of depolarizing current, we conclude that serotonin (and noradrenaline) causes a generalized increase in excitability to all types of excitatory input, rather than causing specific increases in receptor sensitivity to a particular neurotransmitter (for example, glutamate). Evidence for selective effects of noradrenaline on γ-aminobutyric acid but not glycine 'postsynaptic mechanisms' in cerebellar Purkinje cells has been reported[10]. Although our data do not rule out possible additional actions of serotonin on various pre- and postsynaptic receptors, the slow depolarization and increased excitability caused by serotonin in facial motoneurones cannot be due to increased tonic release of or increased sensitivity to a conventional excitatory neurotransmitter which would act by increasing ionic conductance to depolarize the membrane. If this were the case, input resistance would decrease rather than increase. Rather, serotonin seems to act via its own receptor to change certain membrane conductances (perhaps g_{K^+}), resulting in a generalized increase in motoneurone excitability. Such a general physiological action is consistent with results from electron microscopic autoradiographic studies which show that ^{3}H-serotonin-labelled terminals form direct axosomatic and axodendritic synaptic junctions on facial motoneurones[11]. A generalized facilitation of excitatory inputs to motoneurones would account for some of the diverse motor components of the excitatory behavioural '5-HT syndrome' seen in animals injected with pharmacological agents which increase stimulation of postsynaptic serotonin receptors[12,13].

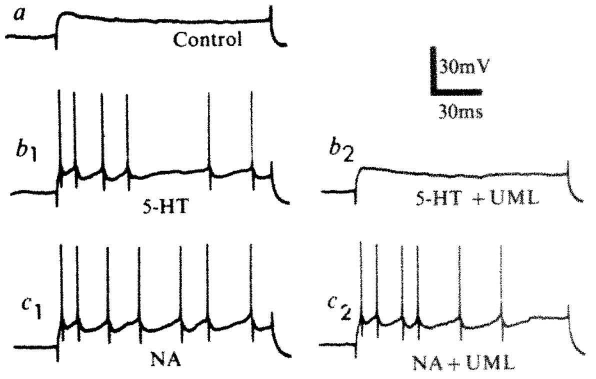

Fig. 2 Selective antagonism of the serotonin (5-HT)-induced increase in excitability by methysergide (UML). *a*, A depolarizing pulse (5.4 nA, 132 ms), which was adjusted to 90% of rheobase, did not elicit any action potentials. *b*1, In the presence of iontophoretically applied serotonin (40 nA for 56.5 s) the depolarizing pulse elicited multiple spikes, indicating increased excitability of the neurone. *c*1, Similarly in the presence of noradrenaline (NA, 40 nA for 55.3 s) multiple spikes were triggered by the depolarizing pulse. Three minutes were allowed for recovery, between the offset of serotonin and onset of noradrenaline. *b*2, After methysergide had been on continuously for 3.5 min (7 nA), iontophoretically applied serotonin (40 nA for 59.5 s) did not cause spikes to be triggered by the depolarizing pulse. *c*2, Iontophoretically applied noradrenaline (40 nA for 56.0 s) still caused multiple spikes to be triggered by the depolarizing pulse, even though the methysergide had been on continuously for 8.5 min. Four minutes were allowed for recovery from the effects of the serotonin before turning on the noradrenaline. To control for changes in methysergide-induced excitability, we ran a second series of tests (data not shown) on the same neurone, in which the depolarizing pulse was adjusted to compensate for changes in rheobase. After 10 min of iontophoretically applied methysergide (7.3 nA), rheobase had increased 13%, indicating decreased excitability. The amplitude of the depolarizing pulse was then adjusted to 90% of the new rheobase, and the effects of serotonin and noradrenaline determined as before. The results were essentially the same as those shown above, except that this time there was not even a small reduction in the effectiveness of the noradrenaline. In fact, the number of spikes triggered was actually slightly more than with noradrenaline alone, probably because of the larger amplitude of the depolarizing pulse. However, the serotonin-induced increase in excitability was strongly antagonized by methysergide, and no spikes were triggered by the depolarizing pulse in the presence of serotonin plus methysergide. Similar findings were obtained in two other neurones in which the depolarizing pulse amplitude was readjusted to compensate for methysergide-induced changes in rheobase.

We thank N. Margiotta and A. Zimnewicz for technical assistance and L. Fields for typing the manuscript. This research was supported by USPHS grants MH-14276, MH-17871 and MH-14459, and the State of Connecticut.

Received 2 June; accepted 2 July 1980.

1. Wood, J. D. & Mayer, C. J. *Nature* **276**, 836–837 (1978); *J. Neurophysiol.* **42**, 582–593 (1979).
2. Phillis, J. W., Tebecis, A. K. & York, D. H. *Eur. J. Pharmac.* **4**, 471–475 (1968).
3. Barasi, S. & Roberts, M. H. T. *Br. J. Pharmac.* **52**, 339–348 (1974).
4. McCall, R. B. & Aghajanian, G. K. *Brain Res.* **169**, 11–27 (1979).
5. White, S. R. & Neuman, R. S. *Brain Res.* **188**, 119–127 (1980).
6. Fuxe, K. *Acta physiol. scand.* **64**, 247, 37–85 (1965).
7. Palkovits, M., Brownstein, M. & Saavedra, J. M. *Brain Res.* **80**, 237–249 (1974).
8. Wood, J. D., Grafe, P. & Mayer, C. J. *Soc. Neurosci. Abstr.* **5**, 749 (1979).
9. Gerschenfeld, H. M. & Paupardin-Tritsch, D. *J. Physiol., Lond.* **243**, 427–456 (1974).
10. Woodward, D. J., Moises, H. C., Waterhouse, B. D., Hoffer, B. J. & Freedman, R. *Fedn Proc.* **38**, 2109–2116 (1979).
11. Aghajanian, G. K. & McCall, R. B. *Neuroscience* (in the press).
12. Green, A. R. & Grahame-Smith, D. G. *Nature* **260**, 487–491 (1976).
13. Jacobs, B. *Life Sci.* **19**, 777–785 (1976).
14. Kitai, S. T., Tanaka, T., Tsukahara, N. & Yu, H. *Expl Brain Res.* **16**, 161–183 (1972).

Absence of potassium conductance in central myelinated axons

Jeffery D. Kocsis* & Stephen G. Waxman

Department of Neurology, Veterans Administration Medical Center
and Stanford University School of Medicine, Palo Alto,
California 94304

Two voltage-dependent changes in ionic permeability are responsible for the action potential in squid giant axon[1]. The depolarization phase of the action potential is due to an initial increase in sodium ion permeability, and repolarization is primarily the result of a later increase in potassium permeability. However, voltage-clamp experiments on mammalian peripheral nodes of Ranvier indicate that potassium conductances (g_k) may be minimal or lacking for intact mammalian peripheral myelinated axons[2–4]. Repolarization for these fibres has been explained in terms of a rapid sodium inactivation and large leakage current[3]. When the myelin around these fibres is acutely disrupted, an immediate and prominent g_k appears[4]. Following demyelination, g_k blocking agents have been shown to reduce late outward currents that are not present in normal myelinated fibres[5]. This suggests that K^+ channels are present in the axonal membrane under the myelin but are 'masked' in normal peripheral myelinated axons. Previous studies have not investigated the presence or role of K^+ channels in central myelinated axons. We here establish that g_k is not detectable in mammalian dorsal column axons.

The effects of superfusion of myelinated axons in the rat dorsal columns (DCs) with the voltage-dependent g_k blocking agents tetraethylammonium hydrochloride (TEA) and 4-aminopyridine (4-AP) were studied. We also recorded intra-axonally from the axons with glass microelectrodes filled with TEA. This allowed us to reach internodal as well as nodal axon membrane in the intact myelinated central axon. Although TEA injection into spinal motoneurones elicited a rapid and powerful prolongation of the motoneurone (soma-dendritic) action potential, the axonal action potential recorded from DC axons remained virtually unchanged even after prolonged TEA injection. In addition, superfusion of the spinal cord with 4-AP or TEA neither changed the action potential waveform nor altered the fibre refractory period.

Extra- and intra-axonal potentials were recorded from the DCs of the rat spinal cord following local DC or sciatic nerve stimulation. The animals were deeply anaesthetized with urethane (1.5 g kg^{-1}) and prepared for acute experimentation. An agar pool was built around the exposed lumbar spinal cord to allow for superfusion of the DC surface with oxygenated and warmed (38 °C) normal Ringer solution (NS) into which 4-AP or TEA could be added[6]. Recordings were confined to within 50 μm of the surface of the spinal cord for the superfusion experiments.

Glass microelectrodes were filled with 3.0 M NaCl for field potential recordings and 2.0 M TEA for intracellular or intra-axonal recordings. Figure 1*a* shows the DC fibre field potential elicited from local surface stimulation of the DC superfused with normal Ringer. The early positive-negative component of the field corresponds to the collective action potential activity of fast conducting myelinated DC axons. The field remains virtually unchanged after introduction of 4-AP (Fig. 1*b*) or TEA (Fig. 1*c*) into the superfusion pool. When the potassium concentration of the NS was increased from 3.0–30 mM, a reversible conduction block occurred promptly, thus indicating the efficacy of the superfusion (Fig. 1*d*). In addition to not affecting the field potential waveform, elicited from a single stimulus, external 4-AP or TEA application also did not alter the refractory period of the fibres as determined from paired stimulation experiments (data not shown). In contrast to the absence of response of the myelinated DC fibres to superfusion with TEA and 4-AP, the compound action potential of nonmyelinated cerebellar parallel fibres is markedly altered by both of these agents[7]. Although 4-AP[8–10], and in some instances TEA[11], have been shown to block voltage-dependent g_k by external application, the accessibility of either 4-AP or TEA to K^+ channel sites following external application is open to question. This is particularly important in view of the recent studies of Chiu and Ritchie[4] showing that K^+ channel distribution may be inhomogeneous, with K^+ channels present at internodal or paranodal membrane regions but not at nodal membrane.

Prolongation of the somatic action potential has been reported[12–14] following intracellular recordings from neuronal cell bodies with TEA electrodes. This effect appears rapidly after diffusion of TEA from the microelectrode or is facilitated by depolarizing currents. Figure 2*a* shows an action potential recorded from a motoneurone immediately after impalement with a TEA microelectrode. The responses shown in Fig. 2*b* and *c* were recorded 4.0 and 12.0 min later, respectively. The action potentials are much prolonged (compare Fig. 2*b* and *c* to *a*), indicating a block of g_k (ref. 12). The same microelectrode was used for recording the intra-axonal responses from DC axons shown in Fig. 2*d–f*. All electrode probes for DC axons were confined to the dorsal 200 μm of the spinal cord, within 300 μm of the spinal cord midline. Intra-axonal impalements were identified by: (1) the presence of negative resting potential; (2) the all-or-none character of the action potential with no underlying synaptic potential; and (3) when possible, collision of directly induced action potentials with those induced from

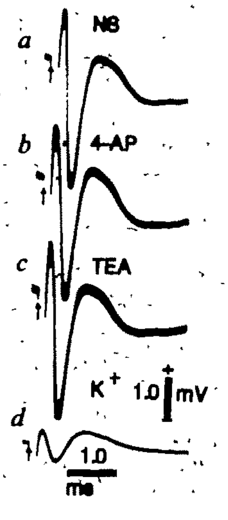

Fig. 1 Field potentials elicited from surface stimulation of the lumbar DC and recorded 3 mm anterior to the stimulation site within 20 μm of the surface. *a*, Responses recorded when the spinal cord was continuously superfused with normal Ringer solution NS. The early positive-negative components of the field correspond to action potential activity of the fast conducting myelinated fibres of the DC. The responses in *b* and *c* were obtained after 30 min of superfusion in 4-AP (3.0 mM) and TEA (10 mM) solutions, respectively. Virtually no change occurs in the waveform of the early positive-negative field component, thus indicating the ineffectiveness of these voltage-dependent g_k blocking agents on these fibres. *d*, A response recorded within 2 min after the K^+ concentration was increased from 3 to 30 mM. A significant reduction in the field occurs at high K^+ concentrations. This effect is reversible within minutes after superfusion with NS. The K^+ blocking action indicates the efficacy of the superfusion system, and shows that the superfusate gains access to the nodal extracellular space. The calibration in *e* pertains to all records.

---

* To whom correspondence should be addressed

0028-0836/80/390348—02$01.00

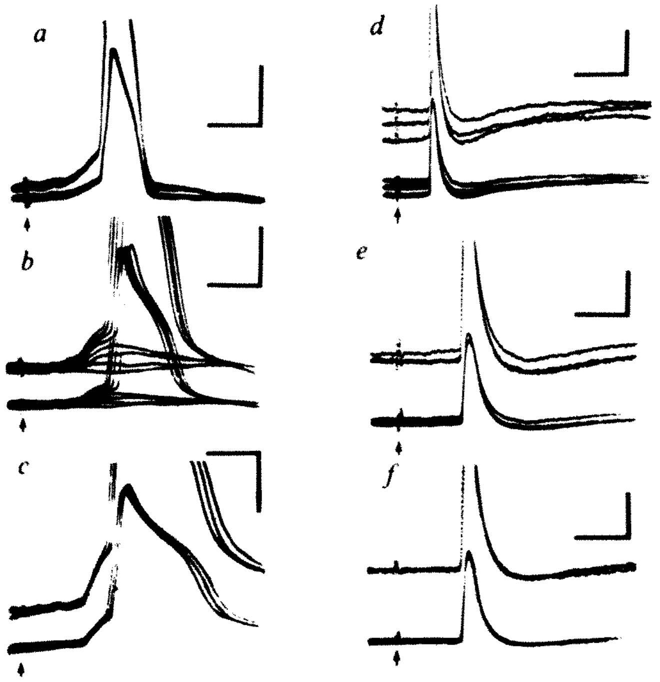

Fig. 2 *a–c*, Intracellular recordings obtained from spinal motoneurones with TEA microelectrodes following stimulation of the ipsilateral sciatic nerve. Orthodromic action potentials can be seen arising from an excitatory postsynaptic potential (EPSP). The upper traces correspond to high gain recordings and the lower traces to low gain recordings. *a*, Records obtained immediately after impalement of the motoneurone. *b*, Records obtained at about 4 min after impalement. Stimulation intensity was varied to demonstrate the graded nature of the EPSP and all-or-none properties of the action potential. Note the broadening of the action potential as the TEA diffuses into the cell. *c*, Records from same cell at about 12 min post-impalement. A marked prolongation of the action potential is evident. *d–f*, Intra-axonal action potentials recorded with same TEA microelectrode as used for *a–c*, from a DC axon near the midline surface of the lumbar cord. *d* and *e* show the axonal action potential at different oscilloscope sweeps, near the time of axonal impalement. *f*, Responses recorded about 25 min after impalement. Depolarizing currents were passed at the time between the records of *e* and *f*. No appreciable prolongation of the axon action potential can be seen after TEA injection. Vertical calibrations indicate 20 mV for lower traces and 10 mV for upper traces for *a–f*. Horizontal calibrations indicate 4 ms in *a–d* and 2 ms in *e* and *f*. Positive voltage deflection is upward.

sciatic nerve stimulation. Conduction velocities for these fibres were greater than 15 m s^{-1}, indicating their myelinated nature. After 25 min of impalement with a TEA microelectrode, virtually no change in the axonal action potential duration can be seen (Fig. 2*f*). We also passed depolarization pulses through the microelectrode to facilitate TEA entry, but still no change in action potential waveform occurred. For five axons, intra-axonal penetrations were held for over 45 min each. No significant change in spike waveform or refractory period was seen in these axons or in 26 other axons held for periods greater than 5 min but less than 45 min. During the passage of depolarization currents, the action potential amplitude was decreased, and hyperpolarization increased the action potential amplitude, thus indicating that the site of impalement was electrotonically close to the site of impulse origin.

The observation here, that external application of either TEA or 4-AP does not prolong the action potential of DC myelinated axons, extends observations made in peripheral nerves to DC axons in the mammalian central nervous system. Also, the lack of action potential prolongation or changes in refractory period after direct intra-axonal injections of TEA into these central myelinated axons suggests that K$^+$ channels contribute little to action potential waveform and recovery for these axons. One might question whether TEA effectively passed from our microelectrode into the axons, and once inside if it diffused sufficiently to present itself to nearby internodal as well as nodal axon surfaces. However, other observations[12–14] and this study show that TEA readily diffuses from electrode to cytoplasm of neurone somata. Although geometrical differences are present between soma-dendritic and axonal regions that could vary diffusion properties, the rapidity of the TEA action on large volume motoneurones, the facilitation of TEA ejection by depolarization pulses, and the relatively long duration impalements of the axons (several over 45 min), suggest that TEA may have passed over a significant axonal length.

Voltage-clamp experiments in mammalian peripheral nerve[4] reveal an immediate appearance of g_k after acute myelin disruption, suggesting that K$^+$ channels are present under the myelin in normal myelinated axons. The absence of demonstrable g_k at intact mammalian peripheral nodes of Ranvier[3] and the lack of effect on the action potential of direct intra-axonal injections of TEA into DC fibres suggest that g_k does not contribute significantly to spike electrogenesis in at least several types of intact mammalian myelinated fibres. Chiu and Ritchie (personal communication) have suggested that potassium channels in the internodal axon membrane may have a normal role in preventing repetitive firing at the node. Although we did not observe repetitive firing after TEA or 4-AP application, our experiments cannot rule this out.

This work was supported in part by the Medical Research Service, Veterans Administration, National Institutes of Health grants RR-5353 and NS-15320, and National Multiple Sclerosis Society grant RG-1231. We thank Professor J. M. Ritchie for helpful discussions.

Received 20 May; accepted 29 July 1980.

1. Hodgkin, A. L. & Huxley, A. F. *J. Physiol., Lond.* **117,** 500–544 (1952).
2. Horakova, M., Nonner, W. & Stämpfli, R. *Proc. int. Un. physiol. Sci.* **7,** 198 (1968).
3. Chiu, S. Y., Ritchie, J. M., Rogart, R. B. & Stagg, D. *J. Physiol., Lond.* **292,** 149–166 (1979).
4. Chiu, S. Y. & Ritchie, J. M. *Nature* **284,** 170–171 (1980).
5. Sherratt, R. M., Bostock, H. & Sears, T. A. *Nature* **283,** 570–572 (1980).
6. Kocsis, J. D., Malenka, R. C. & Waxman, S. G. *Brain Res.* (in the press).
7. Kocsis, J. D., Malenka, R. C. & Waxman, S. G. *Soc. Neurosci. Abstr.* (in the press).
8. Pelhate, M. & Pichon, *J. Physiol., Lond.* **242,** 90–91P (1974).
9. Nicholson, C. G., ten Bruggencate, G. & Senekowitsch, R. *Brain Res.* **113,** 606–610 (1976).
10. Llinás, R., Walton, K. & Bohr, V. *Biophys. J.* **16,** 83–86 (1976).
11. Hille, B. *J. gen. Physiol.* **50,** 1287–1302 (1967).
12. Shapovalov, A. I. & Kurchavyi, C. G. *Brain Res.* **82,** 49–67 (1974).
13. Sugimori, M., Preston, R. J. & Kitai, S. T. *J. Neurophysiol.* **41,** 1662–1675 (1978).
14. Schwartzkroin, P. A. & Prince, D. A. *Brain Res.* **85,** 169–181 (1980).

Spontaneous quantal events induced in toad rods by pigment bleaching

T. D. Lamb

Physiological Laboratory, Downing Street, Cambridge CB2 3EG, UK

Barlow proposed that absolute visual threshold is limited by photon-like noise events in the rod photoreceptors[1], and he later extended the idea to explain the elevation of threshold following bright bleaching lights in terms of increased noise in the photoreceptors[2]. Rushton, on the other hand, has proposed that the threshold elevation during dark adaptation involves changes not within the photoreceptors themselves but rather in the gain of a subsequent 'pool'[3]. I report here measurements of outer segment current in individual rod photoreceptors which demonstrate that spontaneous fluctuations occur at a greatly increased rate following bleaches of around 1%, and that these fluctuations have the form expected for random occurrences of the single photon events. This is consistent with Barlow's ideas but does not indicate whether a gain change subsequent to the receptors also occurs.

The experiments were performed on toad rods using a suction pipette[4–8]. Briefly, a fully dark-adapted animal was pithed and one eye was enucleated under dim red light; then, using IR illumination, the retina was removed and cut into small pieces. With the aid of an IR-sensitive television camera system attached to an inverted microscope the pieces were manipulated under high magnification, and single rod outer segments were drawn into a fine glass pipette by gentle suction, so that membrane current could be measured and the outer segment stimulated with visible light. When recording spontaneous dark events the IR-light was turned off, and stringent precautions were taken to exclude stray light. As in the experiments of Lamb *et al.*[8], two different Ringer solutions were used, one buffered with HEPES[4,5,9–11] and the other with bicarbonate/CO_2 (ref. 12), both at *p*H 7.8. The observed noise increase on bleaching was similar in the two cases, but in HEPES–Ringer the cells gave slower and more sensitive responses which facilitated detection of quantal responses, while the bicarbonate/CO_2–Ringer was probably more physiological but gave faster, less sensitive responses[8].

Figure 1 shows the effect in a cell recorded in HEPES–Ringer, with two traces before the bleach and one trace during recovery. In this Ringer the single photon event is quite large and, as reported by Baylor *et al.*[7], spontaneous occurrences of the quantal events are apparent in the dark-adapted state. Within the 400 s of the first two records, ten such events (marked by arrows) can be seen, in good agreement with the reported mean of 1 per 50 s (ref. 7). The events have an amplitude of almost 1 pA and a time course similar to that of the average flash response to dim light. In the bottom trace, 3 min after a bleach of about 0.4%, the cell showed very marked current fluctuations, even though the flash sensitivity measured at this time had declined slightly from its pre-bleach level. The power spectrum of these fluctuations is shown in Fig. 2, and is compared with the power spectrum predicted for randomly occurring photon-like events. The inset shows the average flash response measured after the bleach, and has been fitted by the independent activation equation[5,6,13] with $n = 4$ stages, and $t_{\text{peak}} = 1.75$ s. The power spectrum associated with this kinetic form consists of the product of $n = 4$ lorentzians:

$$S(f) = S(0) \Big/ \prod_{k=1}^{n} \left[1 + \left(\frac{2\pi f \tau}{k}\right)^2\right], \qquad (1)$$

with $\tau = t_{\text{peak}}/(n-1)$ and is shown by the continuous curve. The vertical position has been chosen to give the best fit by eye, and the broken line is the expected thermal noise. Figure 2 shows that the post-bleach fluctuations have the form expected for randomly occurring single photon events.

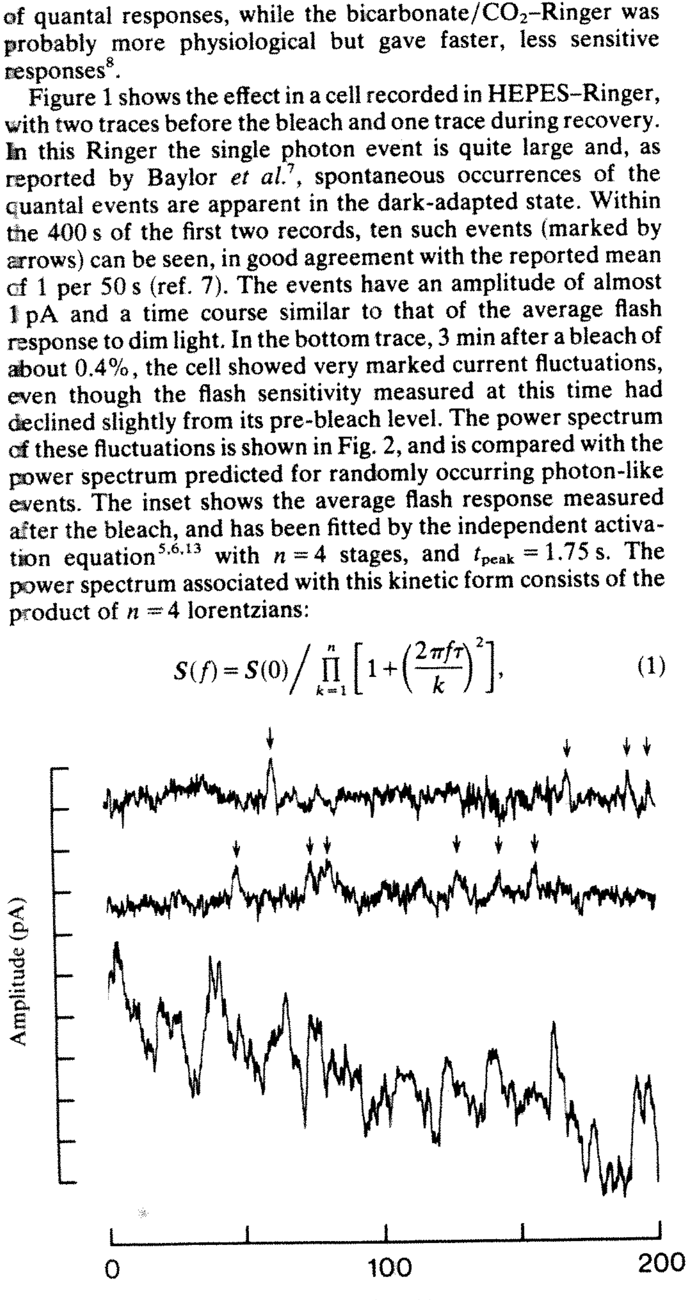

Fig. 1 Increased fluctuations following a bleach. Traces are 200 s records before (upper two traces) and 3 min after a bleach (lowest trace); arrows mark presumed quantal events. Bleach of about 0.4% (3.6×10^5 photons μm^{-2}, calculated to isomerize 9×10^6 rhodopsins); saturating response 18 pA; 23.0 °C; HEPES-Ringer. Each ordinate division represents 1 pA.

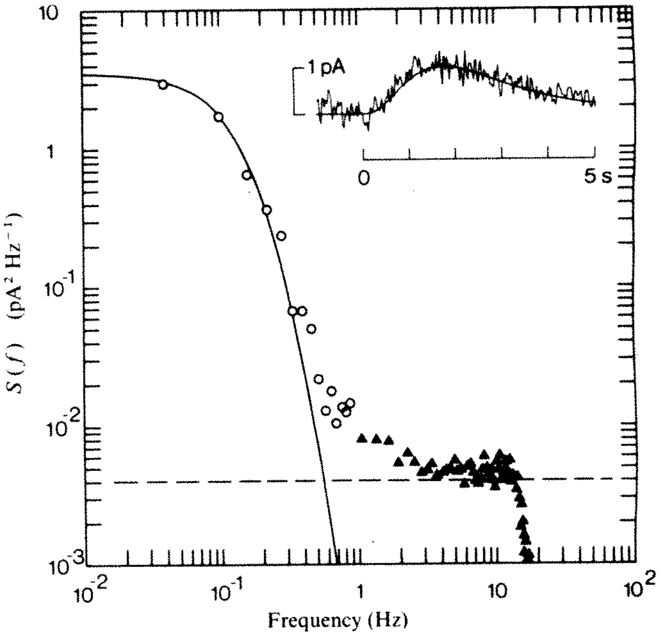

Fig. 2 Power spectrum of post-bleach fluctuations from cell of Fig. 1. Open symbols, averages of 3 raw frequency points; filled symbols, averages of 15. From five records, each 2,048 points at 25-ms intervals (51.2 s); filtered by 15 Hz 6-pole low pass filter and 10 s RC high pass filter. Continuous curve is equation (1) with $S(0) = 3.5$ pA^2 Hz^{-1}; broken line is thermal noise of 4×10^{-3} pA^2 Hz^{-1} for leakage resistance 4 MΩ. Inset shows average flash response determined from six flashes immediately before and six flashes immediately after the lowest record in Fig. 1.

However, the lack of stationarity of the spectral data causes a slight computational difficulty here, as the cell was inevitably recovering during the post-bleach period, and the sensitivity and time course of the flash response changed. Before the lowest record in Fig. 1 the time to peak was 1.5 s, and after the record it was 2.2 s. The averaged response from flashes before and after the fluctuating record is shown in the inset of Fig. 2, and had a time to peak of 1.75 s; it is this averaged response which has been used in computing the expected form of the spectrum. It seems unlikely that this gradual and unavoidable change would significantly affect the form of the predicted spectrum, and the measured fluctuations certainly appear to be explained in terms of spontaneous quantal events.

The rate of equivalent isomerizations may be calculated from the required vertical scaling of the theoretical spectrum. For a random series of identical 'shot' events, the zero frequency asymptote is found from the Fourier transform with $f = 0$, and is simply twice the event rate multiplied by the square of the time integral of the shot event (see, for example, ref. 6). For the case of independent activation kinetics this may be shown to reduce to:

$$S(0) = 5.85 \nu\, t_{\text{peak}}^2 r_{\text{peak}}^2 \qquad (2)$$

where $S(0)$ is the zero frequency asymptote, ν s^{-1} is the rate, and t_{peak} and r_{peak} are the time to peak and peak amplitude of the single photon response respectively. For the cell in Figs 1 and 2, the amplitude of the quantal event in the dark-adapted state averaged about 0.8 pA, but after bleaching the sensitivity was reduced by about 0.12 log units, giving a quantal event amplitude of $r_{\text{peak}} = 0.61$ pA. With $t_{\text{peak}} = 1.75$ s and $S(0) = 3.5$ pA^2 Hz^{-1}, the rate of events is predicted to be $\nu = 3.1$

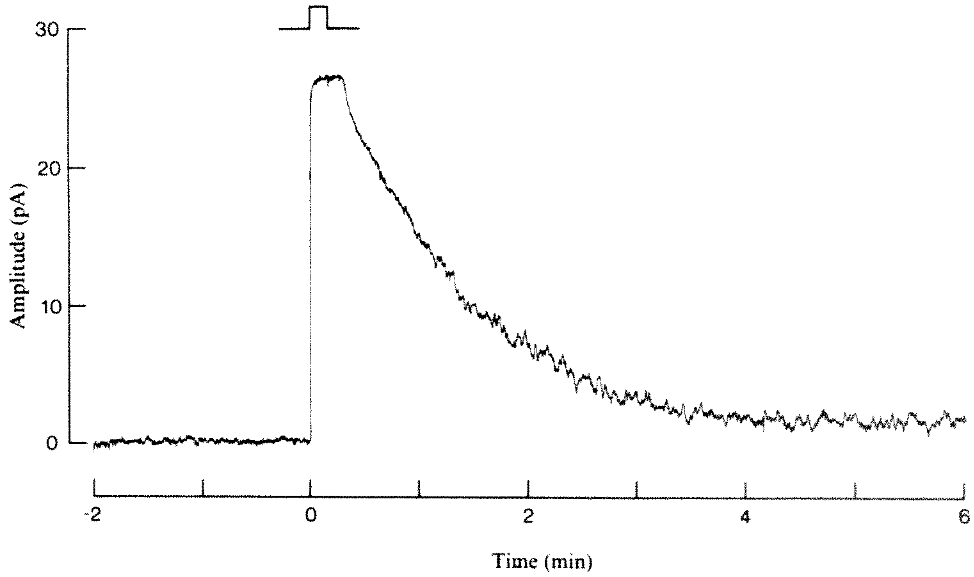

Fig. 3 Response of another cell to a bleach of about 0.7% (7.2×10^5 photons μm^{-2}, calculated to isomerize 1.8×10^7 rhodopsins). Quantal events before the bleach are not visible as the cell was relatively insensitive. Bicarbonate/CO$_2$–Ringer; 23.6 °C; low pass filtered at 5 Hz.

equivalent isomerizations per s. This is about 2.2 log units greater than the spontaneous rate in the fully dark adapted state (0.02 isomerizations per s, ref. 7).

A similar effect from a cell recorded in bicarbonate/CO$_2$–Ringer is shown in Fig. 3. Before the bleach the baseline was relatively quiet, but during recovery the trace became quite noisy, despite a slight reduction in its flash sensitivity. The power spectrum of these fluctuations was again well fitted by the form predicted from the average post-bleach flash response (not shown). This cell was less sensitive than the previous one and the post-bleach quantal event amplitude was estimated to be $r_{\text{peak}} =$ 0.12 pA per isomerization. The zero frequency asymptote $S(0)$ of the spectrum was 0.7 pA^2 Hz^{-1} and substitution in equation (2) gave an estimated mean rate of $\nu = 11$ isomerizations per s for this bleach of 0.7%, about 2.7 log units higher than in absolute dark adaptation.

The conclusion from these results is that, as proposed by Barlow[2], spontaneous photon-like events occur in the rod outer segments at a much higher rate after a bleach than in absolute dark adaptation. This phenomenon seems to explain qualitatively the existence of the psychophysical equivalent background[14] or dark light[1,2] which limits visual detection, and the extent to which it may quantitatively account for dark adaptation behaviour is under investigation (D. A. Baylor and T.D.L.). It is interesting that the situation appears similar in invertebrates, where exposure of a dark-adapted locust retinula cell to intense light causes an increased rate of occurrence of quantal events[15].

I thank Professors H. B. Barlow, D. A. Baylor and A. L. Hodgkin for suggesting the experiment and for helpful discussions. This work was supported by a fellowship from the Wellcome Trust.

Received 7 May; accepted 16 July 1980.

1. Barlow, H. B. *J. opt. Soc. Am.* **46,** 634–639 (1956).
2. Barlow, H. B. *Vision Res.* **4,** 47–58 (1964).
3. Rushton, W. A. H. *Proc. R. Soc.* **B162,** 20–46 (1965).
4. Yau, K.-W., Lamb, T. D. & Baylor, D. A. *Nature* **269,** 78–80 (1977).
5. Baylor, D. A., Lamb, T. D. & Yau, K.-W. *J. Physiol., Lond.* **288,** 589–611 (1979).
6. Baylor, D. A., Lamb, T. D. & Yau, K.-W. *J. Physiol., Lond.* **288,** 613–634 (1979).
7. Baylor, D. A., Matthews, G. G. & Yau, K.-W. *J. Physiol., Lond.* (in the press).
8. Lamb, T. D., McNaughton, P. A. & Yau, K.-W. *J. Physiol., Lond.* (in the press).
9. Brown, J. E. & Pinto, L. H. *J. Physiol., Lond.* **236,** 575–591 (1974).
10. Fain, G. L. *J. Physiol., Lond.* **261,** 71–101 (1976).
11. Bastian, B. L. & Fain, G. L. *J. Physiol., Lond.* **297,** 493–520 (1979).
12. Cervetto, L., Pasino, E. & Torre, V. *J. Physiol., Lond.* **267,** 17–51 (1977).
13. Baylor, D. A., Hodgkin, A. L. & Lamb, T. D. *J. Physiol., Lond.* **242,** 685–727 (1974).
14. Stiles, W. S. & Crawford, B. H. in *Report of a Joint Discussion on Vision* 194–211 (Physical Society of London, Cambridge University Press, 1932).
15. Tsukahara, Y. & Horridge, G. A. *J. exp. Biol.* **68,** 137–149 (1977).

Light isomerizes the chromophore of bacteriorhodopsin

Motoyuki Tsuda*, Moira Glaccum†, Burr Nelson & Thomas G. Ebrey

Department of Physiology and Biophysics, 524 Burrill Hall,
University of Illinois, Urbana, Illinois 61801

The primary photochemical event in the two light-transducing pigments whose chromophore is retinal, rhodopsin or bacteriorhodopsin, is a source of controversy. It was originally proposed that the primary photoevent in the bleaching of rhodopsin is the photoisomerization of the chromophore from 11-*cis* to all-*trans* retinal[1,2]. Photochemical considerations suggested that a photoisomerization is the primary event in both rhodopsin and bacteriorhodopsin[3–7]. However, this description of bacteriorhodopsin's photochemistry has been questioned[8–10]. To elucidate this problem, we determined the isomeric conformation of retinal for two of the photolytic intermediates of bacteriorhodopsin, using a method that enables us to extract chromophores from the photocycle intermediates L and M at low temperatures (−74 °C), and have determined the isomeric conformation of the extracted retinals by HPLC[11,12]. Here we provide direct evidence that isomerization of the chromophore has taken place in two of the early photocycle intermediates (L and M) of bacteriorhodopsin.

The absorption of a photon by light-adapted bacteriorhodopsin (bR$^{\text{LA}}$), the purple membrane protein of the *Halobacterium halobium*, initiates a series of transformations[13], reminiscent of the bleaching sequence of rhodopsin. The primary photochemical product, K, is a bathochromically shifted species; it decays to the photocycle intermediate L and then to M, which eventually returns to bR$^{\text{LA}}$ through the intermediates N and O. bR$^{\text{LA}}$ slowly converts to the dark-adapted bacteriorhodopsin (bR$^{\text{DA}}$). It has been determined that the isomeric form of chromophore of bR$^{\text{LA}}$ is almost completely all-*trans* retinal, whereas bR$^{\text{DA}}$ has a mixture of 13-*cis* and all-*trans* retinals with a ratio of 1:1. The isomeric compositions were

---

*Department of Physics, Sapporo Medical College, Sapporo, Japan; †Department of Genetics, Stanford University School of Medicine, Stanford, California 94305.

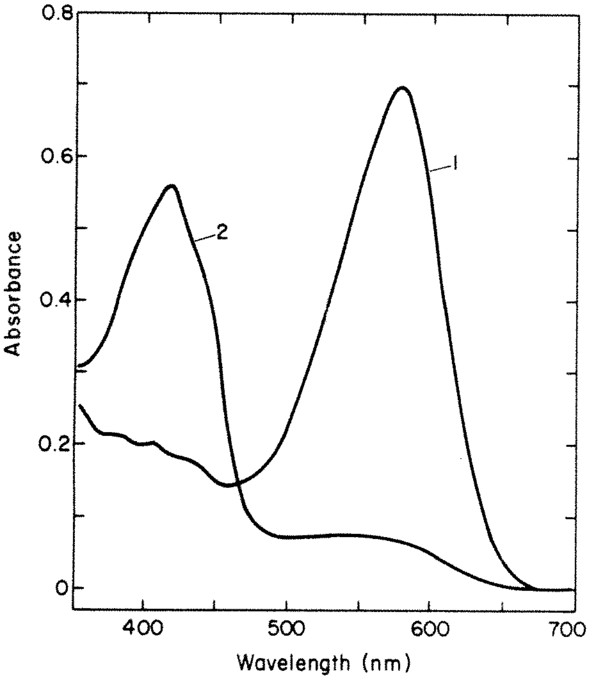

Fig. 1 Photochemical conversion of bR^{LA} to M at −74 °C. Curve 1, bR^{LA} in a 25% NaCl solution adjusted to *p*H 9.5 (0.1 M carbonate buffer) and mixed with glycerol (1 : 2) at −74 °C. Curve 2, the photosteady-state mixture produced by irradiating with $\lambda > 580$ nm light (Corning filter 2–73) for 15 min at −74 °C. The sample was irradiated with the light from a 200-W tungsten lamp using a glass filter. The light was routed to the sample cell through an optical glass fibre (5-mm diameter).

originally determined by chromophore extraction methods[11,14,15]. The validity of determining the isomeric composition by the extraction technique was later verified by several non-destructive spectroscopic techniques[16–19].

To extract chromophores from the L and M intermediates at low temperatures, the extraction solvent should not freeze at low temperatures (−74 °C), it should denature the pigments at the low temperature, and the retinal should not be isomerized by the solvent itself. We found an extraction solvent composed of buffer/glycerol/dichloromethane/hexane (1.6 : 3.3 : 1 : 4) which satisfied the above conditions. The solvent was first emulsified by sonication (30 s). Then a syringe cylinder with the tip blocked by a Teflon plug, containing the bR sample in 67% glycerol was inserted into a test tube containing the solvent. This in turn was immersed in a dry ice–ethanol bath (−74 °C) and the bR irradiated in the syringe with an optical light guide. The plunger was then inserted into the syringe cylinder and the irradiated bR injected into the extraction solvent. Next, the bR sample was mixed thoroughly with the extraction solvent, using a precooled (−74 °C) spatula. The temperature of the sample was monitored with a thermocouple. This procedure denatured the irradiated bR sample at −74 °C as shown by the total fading of the colour to pale yellow. The mixture was then warmed to 0 °C and chromophores extracted by sonication. Extraction by the sonication method gave a substantially greater yield (60 ± 20%) than the syringe method (<10%) and exhibited no preferential extraction of either isomer.

To insure that the isomeric composition of the extracted retinals represented that of the intact pigment and that no isomerization had taken place during our extraction procedure, we extracted the chromophores of bR^{LA} and bR^{DA}. Table 1 shows that isomerization of bR^{LA} and bR^{DA} extracted in our conditions are basically the same as the compositions previously reported. The *p*H, glycerol and temperature we used affected the isomeric composition of the chromophore slightly.

bR^{LA} suspended in a 25% NaCl solution adjusted to *p*H9.5 was mixed with glycerol (1 : 2) to prevent crystallization at low temperatures. The extraction of retinals from bR^{LA} at 0 °C yielded 94 ± 3% all-*trans* retinal and 6 ± 3% 13-*cis* retinal. When bR^{LA} was cooled to −74 °C (Fig. 1, curve 1) and irradiated with light of wavelengths greater than 580 nm ($\lambda > 580$ nm light), the M intermediate was formed (Fig. 1, curve 2). In the dark, the absorption spectrum was stable. Extraction of the chromophores from this preparation yielded 14 ± 3% all-*trans* retinal and 86 ± 3% 13-*cis* retinal. The amount of M, based on the decrease in absorption at 570 nm, was estimated to be 91% (Fig. 1, curve 2). Therefore, our results suggested that the isomeric form of retinal in M was at least 95% 13-*cis* retinal. After making the M intermediate at −74 °C, the sample was warmed to 0 °C, and after waiting for 10 min to ensure that M had returned to bR^{LA}, the chromophores were extracted. This preparation yielded 93 ± 4% all-*trans* retinal and 7 ± 4% 13-*cis* retinal, which corresponds to the composition in bR^{LA} before making M. These results suggested that light isomerized the chromophore in the conversion of bR^{LA} to M and the chromophore was thermally re-isomerized in returning from M to bR^{LA} in the dark.

The intermediate L, which is the precursor of M, is produced as a member of a photosteady-state mixture containing L, M and bR^{LA} when bR^{LA} (in a 25% NaCl solution adjusted to *p*H 7.2) is irradiated with $\lambda > 630$ nm light as shown in Fig. 2, curve 2. Table 1 shows that before making L, bR^{LA} in glycerol contains 92 ± 2% all-*trans* retinal and 8 ± 2% 13-*cis* retinal; after making L and warming the sample to 0 °C for 10 min it contains 92 ± 2% all-*trans* retinal and 8 ± 2% 13-*cis* retinal. Denaturation of the photosteady state formed at −74 °C and extraction of its chromophores yields 53 ± 4% all-*trans* retinal and 47 ± 4% 13-*cis* retinal. The content of L, M, and bR^{LA} in this preparation is difficult to determine precisely because two different extinction coefficients for L have been proposed[20,21]. The amounts of L, M and bR^{LA} in the mixture shown in spectrum 2 of Fig. 1 are calculated to the 57%, 13% and 30%, respectively, assuming $\varepsilon_L = 61{,}000$ (ref. 20) (without consideration of bypass of $L \rightarrow bR^{LA}$) and as 29%, 13% and 58%, respectively, assuming

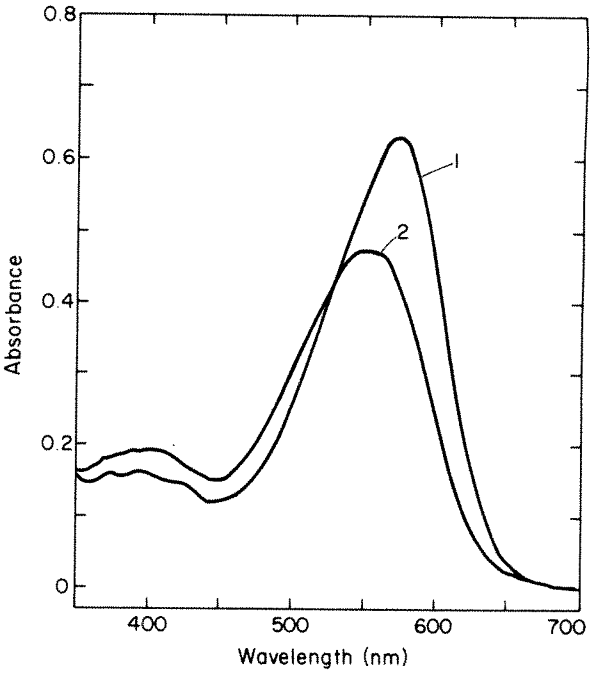

Fig. 2 Photochemical conversion of bR^{LA} to L at −74 °C. Curve 1, bR^{LA} in a 25% NaCl solution adjusted to *p*H 7.2 (0.1 M imidazole-HCl) and mixed with glycerol (1 : 2) at −74 °C. Curve 2, the photosteady-state mixture produced by irradiating with $\lambda >$ 630 nm light (Corning filter 2–59) for 15 min at −74 °C. Irradiation of sample was carried out as shown in Fig. 1.

Table 1 Retinal isomers extracted from bR^{LA}, bR^{DA}, M and L

Species	Conditions	% Composition 13-*cis*	% Composition All-*trans*	Yield (%)
a *p*H 9.5, 25% NaCl				
bR^{D}		55 ± 2	45 ± 2	43 ± 13
bR^{DA} (glycerol)		54 ± 2	46 ± 2	45 ± 9
bR^{DA} (glycerol)	denatured at −74 °C and extracted at 0 °C	54 ± 3	45 ± 3	56 ± 4
bR^{LA}		6 ± 3	94 ± 3	57 ± 8
bR^{LA} (glycerol)		7 ± 4	93 ± 4	45 ± 12
bR^{LA} (glycerol)	denatured at −74 °C and extracted at 0 °C	11 ± 3	89 ± 3	55 ± 9
M (glycerol)	bR^{LA} irradiated with $\lambda >$ 580 nm light for 15 min, denatured at −74 °C and extracted at 0 °C	86 ± 3	14 ± 3	55 ± 15
bR^{LA} (glycerol)	M was warmed up to 0 °C and kept 10 min at 0 °C	7 ± 4	93 ± 4	46 ± 8
b *p*H 7.2, 25% NaCl				
bR^{DA}		52 ± 2	48 ± 2	59 ± 8
bR^{DA} (glycerol)		54 ± 2	46 ± 2	65 ± 20
bR^{DA} (glycerol)	denatured at −74 °C and extracted at 0 °C	56 ± 2	44 ± 2	70 ± 15
bR^{LA}		3 ± 2	97 ± 2	56 ± 10
bR^{LA} (glycerol)		8 ± 2	92 ± 2	53 ± 10
bR^{LA} (glycerol)	denatured at −74 °C and extracted at 0 °C	11 ± 2	89 ± 2	60 ± 8
L	bR^{LA} irradiated with $\lambda >$ 630 nm light for 15 min, denatured at −74 °C and extracted at 0 °C	47 ± 4	53 ± 4	52 ± 10
bR^{LA} (glycerol)	L was warmed up to 0 °C and kept for 10 min at 0 °C	8 ± 2	92 ± 2	60 ± 12

Each experiment was repeated at least five times. Dark adaptation (bR^{DA}) was assured by allowing the bR sample to stand overnight at room temperature for each set of conditions (*p*H, glycerol). Light adaptation (bR^{L}) was accomplished by irradiating the sample with a slide projector for 20 min at 0 °C, followed by immediate extraction. Denaturation and extraction were performed at 0 °C unless otherwise described. An attempt to quantify the efficiency of retinal extraction was made by measuring the A_{365} in hexane solution after extraction. The retinal concentrations in the solution were determined by the retinal composition and using the following extinction coefficients: (4.58×10^4 for all-*trans*, 3.84×10^4 for 13-*cis* at 365 nm)[24]. Separation and analysis of retinals in the extract were carried out by HPLC with micro-Porasil column (Waters Associates). The sample was eluted at a constant flow rate (2 ml min^{-1}) with 4% ether–hexane (v/v). Two well resolved peaks were detected spectrophotometrically (λ = 365 nm). They were identified as the 13-*cis* and all-*trans* isomers of retinal by a comparison of their retention times with those of authentic samples.

$\varepsilon_L = 49{,}000$ (ref. 21) (with consideration of bypass of $L \rightarrow bR^{LA}$). Taking bR^{LA} as all-*trans* and M as 13-*cis* (see above) there is a reasonable correlation between the per cent L and M present spectroscopically from (42–70%) and the per cent of the 13-*cis*isomer present (47 ± 4%) if we assume that chromophore of L is 100% 13-*cis* retinal.

Thus, the present results suggest that light has initiated an event which results in the chromophore of bR^{LA} being isomerized from the all-*trans* to 13-*cis* conformation by the time of the appearance of the L intermediate, and that the 13-*cis* chromophore is thermally re-isomerized to the all-*trans* form in going from M to bR^{LA} in the dark. By far the simplest explanation of our results is the general hypothesis, based on photochemical studies by Rosenfeld *et al.*[3] and Hurley *et al.*[4], that the primary event in bacteriorhodopsin is a photoisomerization requiring that the isomeric conformation of retinal in bR^{LA} be different from its conformation in L and M. Some indications of an isomerization step have also been noticed on the basis of resonance Raman measurements[22,23] although there is still controversy about the interpretation of these spectra.

Our results may be compared with the work of Pettei *et al.*[11], who first suggested the isomerization event was from the all-*trans* to the 13-*cis* isomer. These authors extracted chromophores from 'M-like intermediates' in ether/high salt preparations and guanidinum HCl/high *p*H preparations at 0 °C and concluded that M yields the 13-*cis* isomer, although the correlation between M and the 13-*cis* isomer of the former preparation was rather poor. We find a quite good correlation between the amount of 13-*cis* retinal present and the amount of the M intermediate present. It is possible that the nature of M in ether/high salt and guanidinum HCl/high *p*H at 0 °C is different from M at normal conditions. More likely, as Pettei *et al.* did not actually measure the absorption spectra of their solutions, they had not achieved full photoconversion of bR to M.

We thank Drs Barry Honig, James Hurley and Boryeu Mao for many useful conversations and Beth Ransdell for help. This work was supported by the Japanese Ministry of Education, a Naito Research Grant (1977) to M.T. and by NSF PCM-7911712 and NIH EYO 1323 to T.E.

Received 14 April; accepted 11 July, 1980.

1. Kropf, A. & Hubbard, R. *Ann. N.Y. Acad. Sci.* **74,** 266–280 (1958).
2. Yoshizawa, T. & Wald, G. *Nature* **197,** 1279–1286 (1963).
3. Rosenfeld, T., Honig, B., Ottolenghi, M., Hurley, J. & Ebrey, T. G. *Pure appl. Chem.* **49,** 341–351 (1977).
4. Hurley, J., Ebrey, T., Honig, B. & Ottolenghi, M. *Nature* **270,** 540–542 (1977).
5. Hurley, J., Becher, B. & Ebrey, T. G. *Nature* **272,** 87–88 (1978).
6. Honig, B., Ebrey, T., Callender, R. H., Dinur, U. & Ottolenghi, M. *Proc. natn. Acad. Sci. U.S.A.* **76,** 2503–2507 (1979).
7. Mao, B., Ebrey, T. G. & Crouch, R. *Biophys. J.* **29,** 247–250 (1980).
8. Applebury, M. L., Peters, K. S. & Rentzepis, P. M. *Biophys. J.* **23,** 375–382 (1978).
9. Lewis, A. *Proc. natn. Acad. Sci. U.S.A.* **75,** 549–553 (1978).
10. Warshel, A. *Proc. natn. Acad. Sci. U.S.A.* **75,** 2558–2562 (1978).
11. Pettei, M. J., Yudd, A. P., Nakanishi, K., Henselman, R. & Stoeckenius, W. *Biochemistry* **16,** 1955–1959 (1977).
12. Tsuda, M. & Ebrey, T. G. *Biophys. J.* **30,** 149–158 (1980).
13. Stoeckenius, W., Lozier, R. & Bogomolni, R. *Biochim. biophys. Acta* **505,** 212–278 (1979).
14. Oesterhelt, D. & Hess, B. *Eur. J. Biochem.* **37,** 316–326 (1973).
15. Maeda, A., Iwasa, T. & Yoshizawa, T. *J. Biochem.* **82,** 1599–1604 (1977).
16. Ohno, K., Takeuchi, Y. & Yoshida, M. *J. Biochem.* **82,** 1177–1180 (1977).
17. Sperling, W., Carl, P., Rafferty, Ch.N. & Dencher, N. A. *Biophys. struct. Mech.* **3,** 79–94 (1977).
18. Aton, B., Doukas, A. G., Callender, R. H., Becher, B. & Ebrey, T. G. *Biochim. biophys. Acta* **576**, 424–428 (1979).
19. Tokunaga, F., Iwasa, T. & Yoshizawa, T. *FEBS Lett.* **72,** 33–38 (1976).
20. Becher, B., Tokunaga, F. & Ebrey, T. G. *Biochemistry* **17,** 2293–2300 (1978).
21. Iwasa, T., Tokunaga, F. & Yoshizawa, T. *Biophys. struct. Mech.* (in the press).
22. Aton, B., Doukas, A. G., Callender, R. H., Becher, B. & Ebrey, T. G. *Biochemistry* **16,** 2995–2999 (1979).
23. Stockburger, M., Klosmann, W., Guttermann, H., Massing, G. & Peters, R. *Biochemistry* **18,** 4886–4900 (1979).
24. Hubbard, R. *J. Am. chem. Soc.* **78,** 4662–4665 (1965).

Leukaemia virus infection promotes fibroblast transformation by normal BALB/c mouse DNA

V. Krump-Konvalinkova & K. J. van den Berg

Radiobiological Institute TNO, 151 Lange Kleiweg,
2288 GJ Rijswijk, The Netherlands

All normal cells are thought to carry genetic information for oncogenic transformation, which, on activation to continuous expression, might make the cell cancerous[1]. The presently known transforming retroviruses contain transforming genes which were probably derived by recombination of a slow oncogenic retrovirus with cellular sequences closely related to these genes[2]. It was recently reported[3] that cellular DNA fragments from normal tissue culture cells could transform mouse fibroblasts *in vitro* with a low efficiency. High efficiency of transformation was observed in secondary transfections only when high molecular weight DNA from transformed recipient cells was used as the transforming agent[3]. We observed that DNA isolated from different BALB/c mouse organs can transform both NIH/3T3 and BALB/3T3 cells, although at a low frequency[4]. In attempts to increase the initial efficiency of transformation, we have found that preinfection of recipient 3T3 cells with murine leukaemia viruses markedly enhances focus formation by normal BALB/c DNA fragments.

Table 1 Effect of leukaemia virus preinfection on early transformation of NIH/3T3 fibroblasts with normal BALB/c DNA

Recipient cells	Treatment	Fraction of transformed cultures*	Average no. of foci per dish*	Average frequency of transformation ($\times 10^{-6}$ per μg DNA per cell)
NIH/3T3	BALB/c DNA	0/33	0	0
	Escherichia coli DNA	0/33	0	0
	Transfection buffer	0/33	0	0
NIH/3T3/RMuLV† (Rauscher LV)	BALB/c DNA	3/3	4	2
	E. coli DNA	0/3	0	0
	Transfection buffer	0/3	0	0
NIH/3T3/MoMuLV‡ (Moloney LV)	BALB/c DNA	33/33	18	7
	E. coli DNA	0/33	0	0
	Transfection buffer	0/33	0	0

DNA was isolated from liver, spleen and thymus of 5-week-old germ-free BALB/c mice as previously described[10]. DNA solutions were exhaustively dialysed against 0.1 × SSC (0.015 M NaCl, 0.0015 M trisodium citrate, *p*H 7.0) before use. The transfection experiments were performed by a modification of the Graham and van der Eb method[11]. DNA was dissolved in transfection buffer (*p*H 6.95) to a concentration of 25 μg ml^{-1}, sheared by passing the solutions 20 times through a 0.8-mm needle to a molecular weight of about 10×10^6, as determined by agarose gel electrophoresis, and precipitated with 2.5 M $CaCl_2$ to a final concentration of 125 mM; 0.5 ml of DNA precipitate was added to 2.5 ml of fresh medium on dishes of 3T3 cells seeded 20 h earlier at a concentration of 3×10^5 cells per 60 mm dish. Eighteen hours after the addition of DNA, the cells were trypsinized. Focus formation was evaluated 12–15 days after the DNA treatment.

* Average values from one (NIH/3T3/RMuLV) to four (NIH/3T3/MoMuLV) experiments.

† NIH/3T3 cells were infected with Rauscher leukaemia virus four days before the transfection experiment.

‡ NIH/3T3/MoMuLV is a clonal isolate of NIH/3T3 cells productively infected with Moloney leukaemia virus (gift of Dr H. P. J. Bloemers).

To increase the efficiency of transformation of recipient cells by normal BALB/c DNA fragments, we manipulated the DNA-treated cells using procedures reported to heighten the expression of newly acquired DNA in recipient cells. This involved adjuvant treatment with dimethyl sulphoxide (DMSO) or glycerol[5,6] or the cultivation of DNA-treated cells in the presence of polybrene, insulin and hydrocortisone[7]. However, with none of these procedures did we observe the focus formation directly on DNA-treated cells or soon after the DNA treatment. Instead, DMSO treatment and cultivation of the DNA-treated cells in the presence of polybrene, hydrocortisone and insulin had a toxic effect on the 3T3 cells.

We then investigated whether infection of recipient cells with non-transforming leukaemia viruses had any positive effect, as it has been reported that a similar procedure had a promoting effect on chemical carcinogenesis *in vitro*[8]. The recipient NIH/3T3 cells were productively infected with either Moloney (MoMuLV) or Rauscher (RMuLV) leukaemia virus. The morphology of the 3T3 cells infected with these leukaemia viruses was indistinguishable from that of uninfected controls. The transformation efficiency was greatly enhanced by this procedure. On both MoMuLV- and RMuLV-infected NIH/3T3 fibroblasts, focus formation could be scored as early as 12–15 days after exposure to BALB/c DNA fragments in the cells of the first passage after the DNA treatment (Table 1). In preliminary experiments, supernatants from these transformed cultures showed no transforming activity.

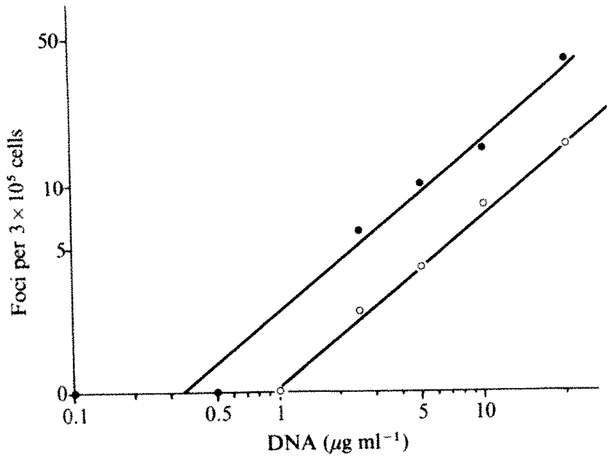

Fig. 1 Kinetics of transformation of NIH/3T3 cells productively infected with Moloney leukaemia virus by fragments of normal BALB/c DNA. The total amount of DNA in each DNA inoculum was adjusted to 25 μg ml^{-1} by the addition of calf thymus DNA before calcium precipitation. ● and ○ represent results of two independent experiments. Three recipient cultures were treated with each dose of DNA. Foci were scored 12–15 days after the treatment with DNA fragments.

The leukaemia virus-infected fibroblasts are transformed by single-hit kinetics (Fig. 1). This indicates that, with the promoting effect of a viral gene, focus formation of fibroblasts is induced by a single BALB/c gene which could be any of the various transforming genes supposed to be present in the mouse genome. The frequency of transformation reached a value of 0.5–1 focus forming units per μg of DNA, which is comparable to that observed for transformation induced with proviral DNA fragments (molecular weight 10×10^6) isolated from Abelson virus-transformed lymphoma cells (V. K.-K. and K. J. B., in preparation).

The nature of the observed enhancement of fibroblast transformation by normal BALB/c DNA fragments after leukaemia virus infection is not clear. The leukaemia virus might provide complementary functions required for expression of endogenous mouse transforming genes[9] such as promoter sites.

We thank Mr. R. H. van Leersum for technical assistance, Dr P. Bentvelzen for suggestions, and Drs P. Bentvelzen and D. W. van Bekkum for their comments on the manuscript. This work was partially supported by the Koningin Wilhelmina Fonds of the National Cancer League.

Received 1 May; accepted 7 August 1980.

1. Huebner, R. J. & Todaro, G. J. *Proc. natn. Acad. Sci. U.S.A.* **64,** 1087–1095 (1969).
2. Stephenson, J. R., Khan, A. S., van de Ven, W. J. M. & Reynolds, F. H. Jr *J. natn. Cancer Inst.* **63,** 1111–1119 (1978).
3. Cooper, G. M., Okenquist, S. & Silverman, L. *Nature* **284,** 418–421 (1980).
4. Van den Berg, K. J., Krump-Konvalinkova, V., Bentvelzen, P. & Van Bekkum, D. W. in *Biological Carcinogenesis* (eds Rich, M. I. & Furmansky, P.) (Dekker, New York, in the press).
5. Stow, N. D. & Wilkie, N. M. *Cancer Res.* **33,** 447–458 (1976).
6. Copeland, N. G. & Cooper, G. M. *Cell* **16,** 347–356 (1979).
7. Hsu, I. & Yang, W. K. *Cancer Res.* **37,** 1704–1714 (1977).
8. Freeman, A. E. *et al. J. natn. Cancer Inst.* **44,** 65–78 (1970).
9. Oscarsson, M., McClements, W. L., Blair, D. G., Maizel, J. V. & Van de Woude, G. F. *Science* **207,** 1222–1224 (1980).
10. Nooter, K., van den Berg, K. J., de Vries, J. B. & Bentvelzen, P. *Eur. J. Cancer* **12,** 633–637 (1976).
11. Graham, F. L. & Van der Eb, A. *J. Virol.* **52,** 456–467 (1973).

Inhibition of 40S-Met-tRNA$_f^{Met}$ ribosomal initiation complex formation by vaccinia virus

Anne Person, Fakher Ben-Hamida & Georges Beaud

Institut de Recherche en Biologie Moléculaire du Centre National de la Recherche Scientifique et de l'Université Paris VII, Tour 43, 2 place Jussieu, F-75221 Paris Cedex 05, France

Infection with vaccinia virus (a poxvirus) quickly[1,2] and efficiently shuts off host protein synthesis in the presence of actinomycin D (refs 3–5) or cycloheximide[6–8]. The cellular messenger RNA apparently remains stable in the infected cells exposed to inhibitors of viral gene transcription[5,9,10]. In some cases vaccinia viral RNA or poly(A) synthesis have been implicated in the establishment of this effect[5,7,11]. However, in the presence of cordycepin (3-deoxyadenosine) which blocks viral gene transcription[12] and cytoplasmic poly(A) synthesis[9], cellular protein synthesis is still efficiently inhibited in vaccinia virus-infected cells[9,12]. This shutoff is also observed *in vitro*, in the corresponding cell-free extracts[13], and in a reticulocyte lysate[14–16]. Therefore the shutoff of host protein synthesis is probably mediated by a factor associated with vaccinia virions. We now report that the formation of the 40S-Met-tRNA$_f^{Met}$ initiation complex is inhibited in cytoplasmic extracts derived from vaccinia virus-infected cells exposed to cordycepin to block viral gene expression. A similar inhibition is found in reticulocyte lysates incubated with purified vaccinia cores, confirming the hypothesis that the factor associated with the viral cores is responsible for the inhibition observed in vaccinia virus-infected cells exposed to inhibitors of transcription.

The binding of initiator Met-tRNA$_f^{Met}$ to 40S ribosomal subunits was measured as previously described[17] after adding either ^{35}S-methionine or purified ^{35}S-Met-tRNA$_f^{Met}$ to cytoplasmic extracts derived from vaccinia virus-infected or uninfected cells. The extracts were pre-incubated with sparsomycin to block the elongation step. Figure 1 shows that 40S-Met-tRNA$_f^{Met}$ initiation complex formation was inhibited to 60% in the infected cell extracts. A similar inhibition was observed when using unwashed ribosomes and post-ribosomal supernatant fractions (S100) instead of the corresponding infected cell extracts; moreover the inhibition was associated with the unwashed ribosomes from the infected cells (data not shown). This reduced amount of ^{35}S-methionine associated with 40S ribosomes indeed represented a reduced formation (or increased dissociation) of the 40S-Met-tRNA$_f^{Met}$ initiation complex as proved by the following results: (1) increasing the incubation time after the addition of ^{35}S-methionine led to a plateau value of 40S-Met-tRNA$_f^{Met}$ complex formation after 30–45 min for control and infected cell extracts; this plateau was 50% lower in the infected cell extracts (data not shown). It is worth noting that the time needed to reach equilibration was much longer in the Ehrlich ascites tumour (EAT) cell-free system than previously observed in the reticulocyte lysate[17]. (2) The addition of purified ^{35}S-Met-tRNA$_f^{Met}$ instead of ^{35}S-methionine to the cytoplasmic extracts from vaccinia virus-infected cells exposed to cordycepin, resulted in a similar inhibition (50–60%) of 40S-Met-tRNA$_f^{Met}$ initiation complex formation. Figure 2*a* shows that the amount of free charged tRNA decreased identically in control and infected cell extracts, probably as a result of degradation or deacylation. Figure 2*b* reveals a plateau value of the ^{35}S-Met-tRNA$_f^{Met}$ bound to the 40S subunit (expressed in ‰ of residual labelled initiator tRNA), reached within 5–10 min for both extracts. This value was 50% lower in the infected cell extract.

The following arguments indicate that this decrease in 40S-Met-tRNA$_f^{Met}$ complex formation is likely to account for the block in initiation of polypeptide chains previously observed in the vaccinia virus-infected cell extracts[13]: (1) the rate of protein synthesis *in vitro* in vaccinia virus-infected cell extracts is inhibited[13] to a similar extent (50–70%) to that of binding of ^{35}S-Met-tRNA$_f^{Met}$ to 40S ribosomes (Fig. 2, Table 1); (2) the inhibition of the 40S-Met-tRNA$_f^{Met}$ complex formation in the infected cell extract was also observed when the corresponding ribosomes and S100 fraction were incubated as described in Fig. 1 but in the absence of sparsomycin; these conditions allow protein synthesis to occur and the ^{35}S-radioactivity associated with the more rapidly sedimenting ribosomal particles was also strongly reduced in the infected cell extract (data not shown); (3) the addition of ribosomal salt wash (RSW) from uninfected cells stimulated three- to five-fold the amount of labelled initiator tRNA bound to 40S particles in the control and infected cell extracts but did not overcome the inhibition of the infected cell

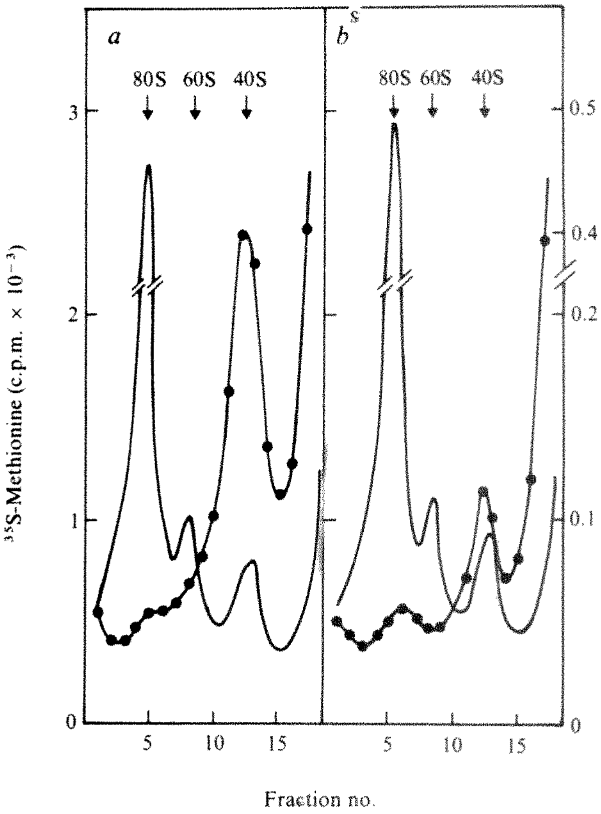

Fig. 1 Binding of ^{35}S-Met-tRNA$_f^{Met}$ to 40S ribosomal subunits in the cytoplasmic extracts from uninfected (*a*) and vaccinia virus-infected (*b*) cells exposed to cordycepin. The lysates prepared from EAT[13] were diluted to 50 A_{260} units ml^{-1} in 3.5 mM Mg acetate, 0.1 M K acetate and all the other components of standard protein synthesis *in vitro*[13]. Incubation (50 µl samples) was at 30 °C for 5 min in the presence of 0.3 mM sparsomycin. Then ^{35}S-methionine was added (800 µCi ml^{-1}) and after a further 10 min incubation, the reaction mixture was diluted with 5 vols cold buffer H: 20 mM HEPES–KOH, *p*H 7.5, 20 mM KCl, 2 mM Mg acetate, 0.1 mM EDTA and centrifuged through 15–30% (w/v) sucrose gradients prepared in buffer H, for 100 min at 49,000 r.p.m. in a Beckman SW 50.1 rotor at 4 °C. The gradients were scanned at 254 nm with an Isco monitor (5 mm path) and collected into 23 fractions. ^{35}S-Met-tRNA (•—•) was measured after cetyltrimethylammonium bromide (CTAB) precipitation[17] and filtration on Whatmann GF/C. The amount of CTAB-precipitable radioactivity was similar for control and infected cell extracts in the top fractions (not shown). About 0.35 molecules of charged initiator tRNA was bound per 40S ribosome particle in the control extract, as estimated from the values of the endogenous methionine pool[13] and from the determination of the free 40S ribosomes based on the optical scans. (Trace of A_{254} shown as continuous lines.)

0028-0836/80/390355—03$01.00

extracts (Table 1). This corroborates a similar effect of these additions on protein synthesis in the corresponding extracts[13].

As protein synthesis is also inhibited at the level of initiation in the reticulocyte lysates incubated with vaccinia cores[14], it was important to measure the 40S–Met–tRNA$_f^{Met}$ initiation complex formation in this *in vitro* system to demonstrate a similar mechanism for the viral core-mediated inhibition. Figure 3 shows that the binding of endogenously labelled ^{35}S–Met–tRNA$_f^{Met}$ to 40S ribosomes is strongly inhibited when the reticulocyte lysate is incubated with purified viral cores. A similar inhibition was observed when adding purified ^{35}S–Met–tRNA$_f^{Met}$ to the reticulocyte lysate preincubated with the vaccinia cores (data not shown). When the concentration of viral cores was varied, the inhibition of 40S initiation complex formation was equal to the inhibition of protein synthesis: adding 3 A_{260} units per ml of cores caused 42% inhibition of 40S–Met–tRNA$_f^{Met}$ complex and 49% inhibition of *in vitro* protein synthesis, whereas adding 9 A_{260} units per ml of cores induced 65 and 66% inhibition respectively. This result confirms the hypothesis whereby the reduced binding of initiator Met–tRNA to 40S ribosomes is indeed responsible for the inhibition of initiation of protein synthesis previously observed[14].

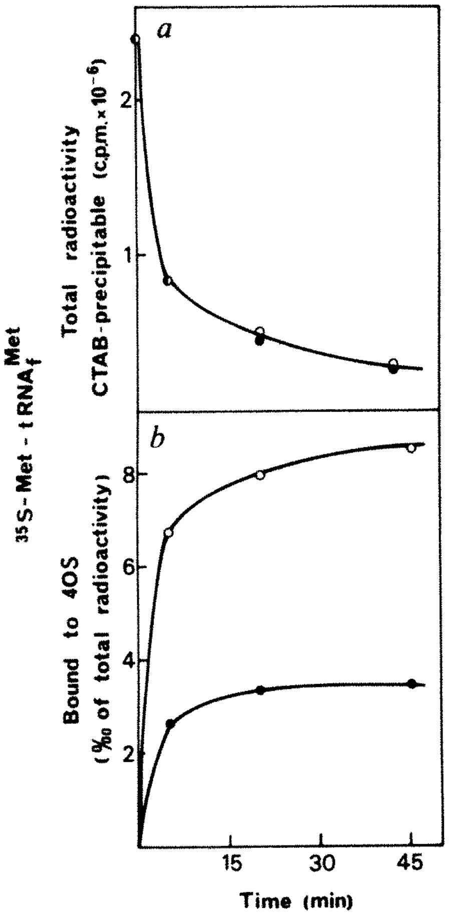

Fig. 2 Kinetics of ^{35}S–Met–tRNA$_f^{Met}$ binding to 40S ribosomal subunits from ribosomes of uninfected and vaccinia virus-infected cells exposed to cordycepin. Ribosomes and supernatant (S100) fractions were prepared by centrifuging cytoplasmic extracts[13] at 198,000*g* for 1 h. The ribosomal pellet was suspended in 10 mM HEPES–KOH, *p*H 7.5, 10 mM KCl, 1.5 mM Mg acetate, 2.5 mM dithiothreitol. The S100 fraction and ribosomes were stored in liquid nitrogen. Ribosomes (40 A_{260} units ml^{-1}) and S100 fraction (7.5 A_{260} units ml^{-1}) were incubated and analysed on sucrose gradients as described in Fig. 1 except that purified ^{35}S–Met–tRNA$_f^{Met}$ (2.4 × 10^6 c.p.m., 30 μg ml^{-1}) was added instead of ^{35}S-methionine. The time of incubation is indicated on the abcissa. Total amount of radioactivity was calculated from the summation of fractions from each gradient. Ribosomes and S100 were from control (○) or infected (●) cells.

Table 1 Effect of RSW addition on the formation of the 40S–Met–tRNA$_f^{Met}$ complex

			^{35}S–Met–tRNA$_f^{Met}$ bound to 40S			
			−RSW		+RSW	
Experiment	Extract from cells	Ribosome concentration (mg ml^{-1})	Radioactivity (c.p.m.)	Inhibition (%)	Radioactivity (c.p.m.)	Inhibition (%)
I	Control	2.7	13,000		42,000	
	Infected	2.9	5,500	58	22,000	47
II	Control	1.4	3,700		16,800	
	Infected	1.5	1,700	54	9,100	46

The binding of ^{35}S–Met–tRNA$_f^{Met}$ to 40S subunits was measured as described in Fig. 2. RSW free of 40S subunits was prepared from uninfected cells[13] and used at 1 mg protein ml^{-1}. Mg acetate was added at 2 mM together with 50 μM spermine when RSW was present[13]. The addition of RSW induces an increase of 38% (expt I) or 57% (expt II) in the amount of native 40S subunits, as measured from the optical scans.

The results presented here reveal that the shutoff of host protein synthesis mediated by vaccinia virus (in the absence of viral gene expression) occurs at the level of Met–tRNA$_f^{Met}$ binding to 40S ribosomes both in reticulocyte lysate incubated in the presence of vaccinia cores and in lysates from vaccinia virus-infected cells exposed to cordycepin. The fact that the same site of lesion is found in both cases strongly suggests a similar mechanism of inhibition. This inhibition in initiation of protein synthesis is generally believed to occur before the binding of mRNA and therefore would result in an inhibition of both cellular and viral mRNA translations. This agrees with previous studies which demonstrated a nonspecific inhibition of cellular and early viral mRNA translation in some experimental conditions[6,10,18]. Presumably a virus-coded protein, synthesized very early in the infection, is involved in releasing the translational block associated with the input virions[6,10,18].

The formation of the 40S–Met–tRNA$_f^{Met}$ complex appears to be an important target for the translational regulation in different physiological systems[19–22] and in most cases, the corresponding inhibition is released by the addition of ribosomal salt wash or purified eIF-2 (refs 23, 24). Although the addition of ribosomal salt wash from uninfected cells stimulated the binding of Met–tRNA$_f^{Met}$ to 40S subunits from infected cells, and also protein synthesis in these extracts[13], it did not abolish the difference between control and infected cells, suggesting the existence of a lesion which may lie in the ribosomes themselves rather than in the initiation factors. This conclusion is reinforced by the finding that addition of purified eIF-2 to reticulocyte lysates inhibited by vaccinia cores produced at best only a partial stimulation of protein synthesis (ref. 14 and R. Kaempfer and E. Katz, personal communication), confirmed the inhibition of protein synthesis by vaccinia cores and did not detect reversal by the addition of 2-aminopurine or purified eIF-2. We must conclude that although the inhibition caused by vaccinia infection superficially resembles the inhibition seen in reticulocyte lysates incubated with double-stranded RNA or in the absence of haemin, where the impairment of 40S–Met–tRNA$_f^{Met}$ complex formation is believed to result from alterations to eIF-2, it must have a different cause. Apparently another mechanism to regulate the level of 40S–Met–tRNA$_f^{Met}$ complexes must exist. The identification of the inhibitor associated with vaccinia cores, now being carried out in the laboratory, may help to elucidate the mechanism of inhibition. A possible role for a vaccinia structural protein in the establishment of the shutoff of host protein synthesis has previously been suggested[25].

We thank Professor F. Chapeville for continuous interest and advice, A. Dru for purifying vaccinia virus, Dr A. L. Haenni for reading the manuscript and Dr H. Trachsel for discussions. Sparsomycin was a gift from Dr J. Douros. Purified tRNA$_f^{Met}$ from beef liver was isolated and provided by O. Kellerman and Professor J. P. Waller. This work was supported by a grant from

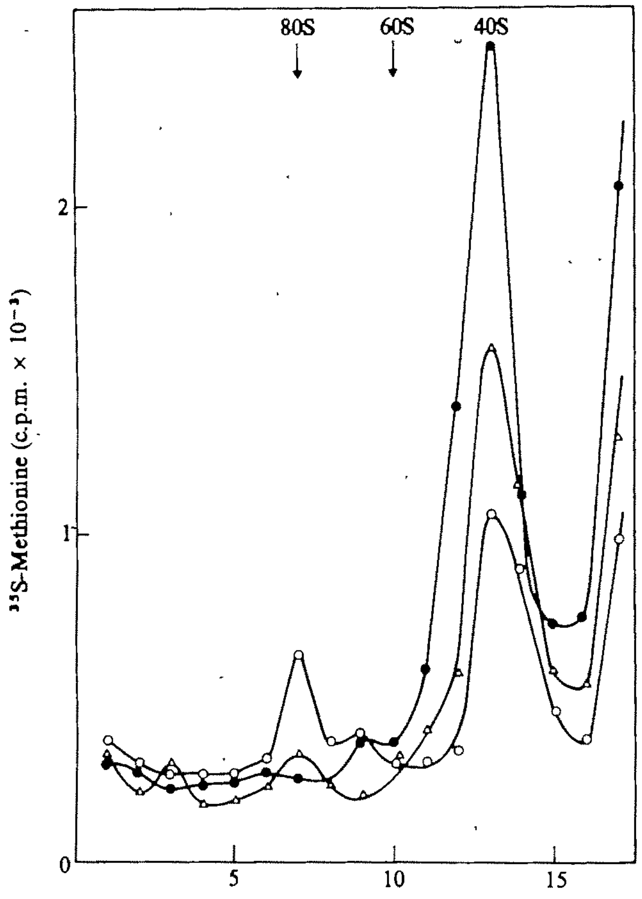

Fig. 3 Inhibition of 40S–Met–tRNA$_f^{Met}$ complex formation by purified vaccinia virus cores. First the reticulocyte lysate (20 μl) was preincubated at 25 °C for 10 min with vaccinia cores (Δ, 3A_{260} units ml^{-1}; 0, g A_{260} units ml^{-1}) or without cores (●) in the presence of 0.33 mM sparsomycin in a total volume of 50 μl of protein synthesis reaction mixture[14]. Then 5 μl of ^{35}S-methionine were added (839 Ci mol^{-1}, 43 μCi) and after a further incubation of 5 min at 30 °C the reaction mixtures were analysed as described in Fig. 1, except for the centrifugation step which was carried out in a Beckman SW 41 rotor for 220 min at 40,000 r.p.m. The amount of CTAB-precipitable radioactivity in the top fractions was similar in the control and in the presence of the cores (not shown).

the Institut National de la Santé et de la Recherche Médicale (ATP 7478). A.P. was the recipient of a fellowship from the Ligue Nationale contre le Cancer.

Received 28 January, accepted 16 July 1980

1. Kit, S. & Dubbs, D. R. *Virology* **18,** 274–285 (1962).
2. Salzman, N. P. & Sebring, E. D. *J. Virol.* **1,** 16–23 (1967)
3. Shatkin, A. J. *Nature* **199,** 357–358 (1963)
4. Moss, B. *J. Virol.* **2,** 1028–1037 (1968)
5. Rosemond-Hornbeak, H. & Moss, B. *J. Virol.* **16,** 34–42 (1975)
6. Moss, B. & Filler, R. *J. Virol.* **5,** 99–108 (1970)
7. Bablanian, R., Esteban, B., Baxt, B. & Sonnabend, J. A. *J. gen. Virol.* **39,** 391–402 (1978)
8. Schrom, M. & Bablanian, R. *Virology* **99,** 319–328 (1979); *J. gen. Virol.* **44,** 625–638 (1979).
9. Person, A. & Beaud, G. *J. Virol.* **25,** 11–18 (1978).
10. Cooper, J. A. & Moss, B. *Virology* **96,** 368–380 (1979)
11. Drillien, R., Spehner, D. & Kirn, A. *J. Virol.* **28,** 843–850 (1978).
12. Esteban, M. & Metz, D. H. *J. gen. Virol.* **19,** 201–216 (1973).
13. Person, A. & Beaud, G. *Eur. J. Biochem.* **103,** 85–93 (1980).
14. Ben-Hamida, F. & Beaud, G. *Proc. natn. Acad. Sci. U.S.A.* **75,** 175–179 (1978)
15. Pelham, H. R. B., Sykes, J. M. M. & Hunt, T. *Eur. J. Biochem.* **82,** 199–209 (1978)
16. Cooper, J. A. & Moss, B. *Virology* **88,** 149–165 (1978)
17. Darnbrough, C., Legon, S., Hunt, T. & Jackson, R. J. *J. molec. Biol.* **76,** 379–403 (1973)
18. Beaud, G. & Dru, A. *Virology* **100,** 10–21 (1980).
19. Lodish, H. F. *A. Rev. Biochem.* **45,** 39–72 (1976).
20. Revel, M. in *Molecular Mechanisms of Protein Synthesis* (eds Weissbach, H. & Pestka, S.) 245–321 (Academic, New York, 1977)
21. Revel, M. & Groner, Y. *A. Rev. Biochem.* **47,** 1079–1126 (1978)
22. Ochoa, S. & de Haro, C. *A. Rev. Biochem.* **48,** 549–580 (1979)
23. Kaempfer, R. *et al.* *Virology* **99,** 170–173 (1979).
24. Lewis, J. A., Falcoff, E. & Falcoff, R. *Eur. J. Biochem.* **86,** 497–509 (1978)
25. Sagot, J. & Beaud, G. *Eur. J. Biochem.* **98,** 131–140 (1979)

S-adenosylmethionine—a novel regulator of aspartate kinase

Sven Erik Rognes*, Peter J. Lea & Benjamin J. Miflin

Biochemistry Department, Rothamsted Experimental Station,
Harpenden AL5 2JQ, UK

Man derives 70% of his dietary requirement of protein directly from the grains of cereals and legumes. These sources are respectively deficient in lysine (and secondarily threonine) and methionine and much effort is being devoted to their improvement[1]. All three amino acids are derived from aspartate via a common metabolic pathway (Fig. 1) in which the first reaction catalysed by aspartate kinase is a key regulatory step limiting their production. In microorganisms, regulation of aspartate kinase occurs by a variety of mechanisms, commonly involving feedback inhibition of one or more isoenzymes by Lys plus Thr, Lys alone or Thr alone[2]. On the other hand, Met control of this step does not seem to conform to a general pattern. Met represses, but does not inhibit aspartate kinase II of *Escherichia coli*; in other species Met can enhance or modify the effects of Lys or Thr[3]. Similarly, varied controls involving Lys and Thr have been reported for the enzymes from higher plants[4] with only one report of an effect of Met[5]. In contrast to these previous results, we suggest here that the methionine derivative (*S*)-*S*-adenosyl-L-methione (AdoMet) is an important regulator of the Lys-sensitive aspartate kinase of higher plants, and that this regulatory mechanism is highly conserved. There is thus a major synergistic interaction of the two nutritionally deficient amino acids Lys and Met to inhibit their own syntheses at the primary regulatory step in the pathway.

Initial studies suggested that plant aspartate kinases may be inhibited by Lys alone[6,7], Thr alone[8] or in a concerted manner by Lys plus Thr[9]. More recent work has shown that certain plants contain two isoenzymes, one sensitive to Thr and one to Lys, the relative proportions of which may vary at different stages of plant development[10–12]. Thr also regulates the activity of homoserine dehydrogenase[4] (Fig. 1(3)). So far the only effect of Met that has been reported in detail is a concerted effect with Lys in which barley aspartate kinase was inhibited 35% by 0.5 mM Lys and 70% by 0.5 mM Lys plus 0.5 mM Met; Met had no effect on its own[5]. Evidence that Met, or a product derived from it, inhibits Met synthesis *in vivo* has been obtained from feeding studies with [^{35}S]O$_4^{2-}$ in *Lemna paucicostata*[13] and barley (S. W. J. Bright, personal communication). Recently it has been found[14,15] that AdoMet regulates the latter part of the pathway by strongly activating Thr synthase (Fig. 1(4)), implying that Thr synthesis may occur only when the cell has made sufficient Met to satisfy its needs for AdoMet. AdoMet has a very important role in plant metabolism, being the predominant biological methyl donor in methyl transfer reactions and a precursor of polyamines and the plant hormone ethylene[13]. AdoMet is rapidly synthesized if Met is fed to intact plants[13,16]. It may thus be that AdoMet rather than Met itself acts as a regulator of Met synthesis. We have therefore investigated its effect on aspartate kinase from a range of higher plants.

Lys-sensitive aspartate kinase was partially purified from barley and muskmelon seedlings, pea and maize leaves and developing seeds of pea and field bean. The effect of various concentrations of Lys and AdoMet on its activity was tested. AdoMet on its own had little effect at concentrations up to 0.4 mM but Lys inhibited the activity from all species studied.

---

* Permanent address Botanical Laboratory, University of Oslo, Blindern, Oslo 3, Norway

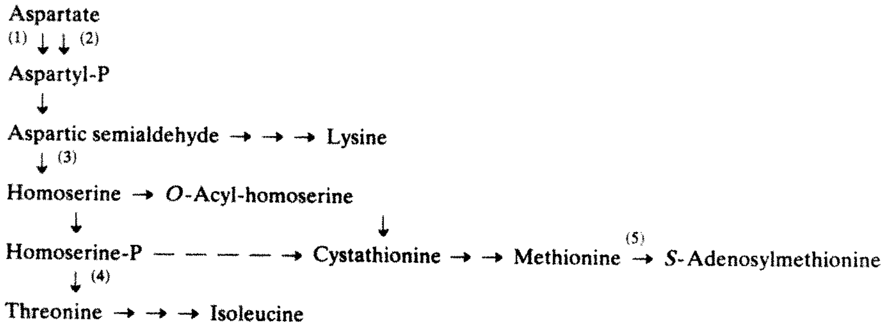
Aspartate
(1) (2)
Aspartyl-P
Aspartic semialdehyde → → → Lysine
(3)
Homoserine → O-Acyl-homoserine
Homoserine-P — — — — → Cystathionine → → Methionine (5) → S-Adenosylmethionine
(4)
Threonine → → → Isoleucine

Fig. 1 Diagram of the biosynthetic pathway for the aspartate family of amino acids. Enzymes: (1) and (2) lysine-sensitive and threonine-sensitive aspartate kinases (EC 2.7.2.4); (3) homoserine dehydrogenase (EC 1.1.1.3); (4) threonine synthase (EC 4.2.99.2); (5) methionine adenosyltransferase (EC 2.5.1.6). The pathway in higher plants (→) differs from that in microorganisms (— — — —→) which synthesize cystathionine via *O*-acetyl- or *O*-succinyl-homoserine rather than *O*-phosphohomoserine.

However, when equal amounts of AdoMet and Lys were added together, a marked synergistic inhibition was observed, with the strongest effect on the barley enzyme (Fig. 2). The AdoMet used was about 90% pure and contained small amounts of *S*-adenosylhomocysteine, 5′-methylthioadenosine and homoserine as detected by TLC. However, inhibition was due to AdoMet since: (1) hydrolysis of the product at *p*H 3 (100 °C, 30 min), which completely breaks down AdoMet to 5′-methylthioadenosine and homoserine[17], reduced the inhibition (by 0.25 mM AdoMet or hydrolysis products) in the presence of 25 μM Lys from 60% to 19%; and (2) *S*-adenosylhomocysteine at 0.25 mM together with 25 μM Lys gave only 9% inhibition. Thr (5 mM) also inhibited part of the isolated aspartate kinase activity from pea leaves (25%) and field bean and pea seed (10%); Thr-sensitive activity was always additive to the (Lys + AdoMet)-sensitive activity. When AdoMet was added to a separate preparation from cotyledons of 4-day-old pea seedlings, which was 90% inhibited by Thr and insensitive to Lys[8], there was no effect on activity either in the presence or absence of Thr. We therefore conclude that AdoMet acts only on the Lys-sensitive aspartate kinase. It is possible that the previously reported effect of Met plus Lys on the barley enzyme[5] was due to the presence of methionine adenosyltransferase (Fig. 1(5)) in the preparation and all the required substrates for AdoMet formation in the assay tube.

Although aspartate kinase can be completely inhibited by Lys alone, the presence of AdoMet greatly enhances its sensitivity toward Lys, decreasing the concentration of Lys required to cause half-maximal inhibition severalfold (Table 1). Conversely, when small amounts of Lys are present, the activity of the enzyme becomes strongly dependent on the AdoMet concentration (Fig. 3). Threonine synthase (Fig. 1(4)) is half-maximally activated by AdoMet within a similar concentration range (60–210 μM)[14,15]; this range corresponds to measured pool sizes

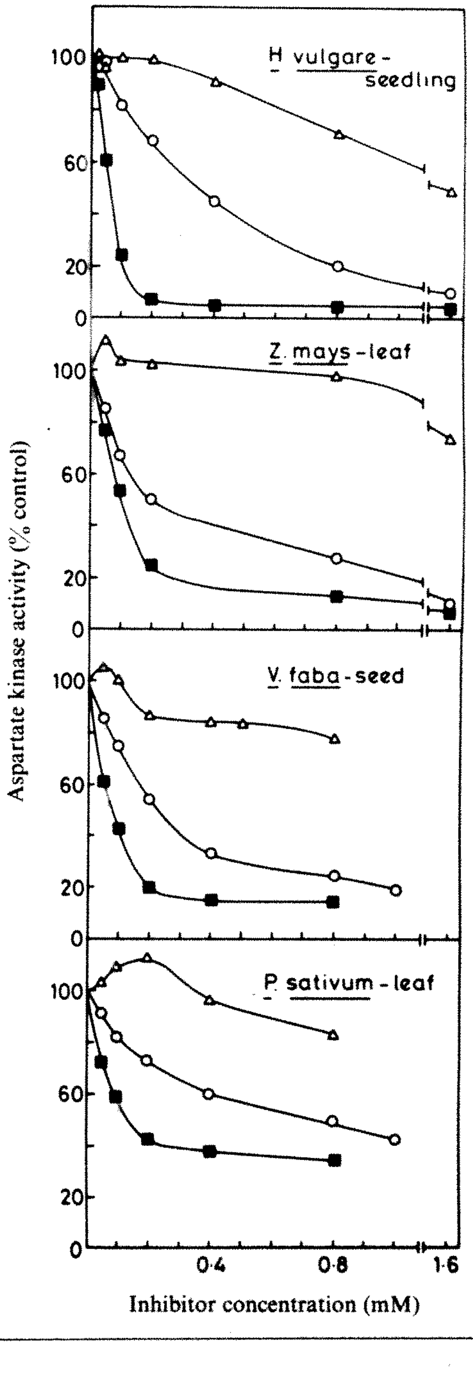

Fig. 2 Synergistic inhibition of higher plant aspartate kinases by Lys and AdoMet. Developing seeds of *Pisum sativum* and *Vicia faba* were collected from pods 18 and 36 days after flowering, respectively. Leaves were collected from light-grown 14-day-old *Zea mays* and 11-day-old *Pisum sativum* seedlings. *Cucumis melo* seedlings were grown in vermiculite for 10 days in light. Excised *Hordeum vulgare* embryos were grown aseptically for 7 days on a sucrose–mineral salts medium. The plant tissues were homogenized and extracted with 50 mM potassium phosphate, *p*H 7.5, containing 100 mM KCl, 2 mM $MgCl_2$, 2 mM EDTA, 15% (v/v) glycerol and 0.2% (v/v) 2-mercaptoethanol (buffer A). Supernatant protein extracts after centrifugation (20,000*g*, 30 min) were fractionated using $(NH_4)_2SO_4$ (0–60% saturation), gel filtration (Sephadex G-75) and ion exchange (DEAE-cellulose). Aspartate kinase (95–100% Lys-sensitive and Thr-insensitive) from *Hordeum*, *Cucumis* and *Zea* was eluted from DEAE-cellulose using buffer A plus 0.4 M KCl. *Pisum* and *Vicia* extracts were treated as described previously[12]. The radioactive aspartate kinase assay[8] was used. Reaction mixtures contained in 100 μl: 12 mM [U-^{14}C]aspartate (purified over a Dowex 1-X8 column, 0.7 Ci mol^{-1}), 25 mM $MgCl_2$, 20 mM ATP, 400 mM NH_2OH-HCl adjusted to *p*H 7.5 with KOH, 1 mM dithiothreitol, 60–200 μg enzyme protein and various concentrations of Lys and AdoMet (Boehringer Mannheim). Labelled aspartylhydroxamate formed after 60–240 min incubation at 30 °C was determined[8]. Control activities (100%) were (in pkat per mg protein): *Hordeum* 58, *Zea* 28, *Vicia* 40, *Pisum* seed 62, *Pisum* leaf 36, *Cucumis* 48. △, AdoMet alone; ○, Lys alone; ■, Lys plus AdoMet (equimolar concentrations).

Table 1 Effect of AdoMet concentration on the sensitivity of plant aspartate kinases to Lys inhibition

	Enzyme source					
	P. sativum leaf	*P. sativum* seed	*V. faba* seed	*Z. mays* leaf	*H. vulgare* seedling	*C. melo* seedling
[AdoMet] (μM)	[Lys] required for half-maximal inhibition (μM)					
0	270	240	180	190	340	250
50	130	120	80	ND	80	125
100	70	90	55	95	48	90
250	30	70	20	ND	22	68

Various concentrations of AdoMet and Lys were added to standard assay mixtures. The concentrations of AdoMet used had no significant effect (activity not less than 95% of control) on the enzyme activities when added alone. ND, not determined. For details of assays see Fig. 2 legend.

in vivo[13]. Our results suggest that the Lys-sensitive aspartate kinase of higher plants also contains a regulatory binding site(s) for AdoMet. Thus the flux through the pathway may be strongly influenced by AdoMet at Lys concentrations of 20 to 200 μM. A potential consequence of this control is that plants could be starved of Thr unless they contained an isoenzyme of aspartate kinase insensitive to AdoMet and Lys. Although a Lys-insensitive, Thr-sensitive enzyme is found in carrot[10,11] and legumes[8,12,18] there is no previous report of such an isoenzyme in cereals. However, our recent but preliminary findings indicate that such an enzyme is present. The likelihood is that, contrary to previous ideas[4,9], the control mechanisms for aspartate kinase in higher plants are remarkably conserved between different species, with two isoenzymes being present: one synergistically inhibited by Lys and AdoMet and the other one inhibited by Thr. Understanding the complex regulatory action of the end products is a prerequisite to devising new selection strategies for obtaining mutants of higher plants that produce enhanced levels of amino acids. Further, it is very important in the analysis of mutants already isolated. For instance a mutant of barley has been selected that has a modified Lys, but not AdoMet, site in its aspartate kinase and contains significantly greater amounts of Thr in the seed[19,20]. The proposed regulation of the aspartate pathway by AdoMet in higher plants differs from that so far reported for microorganisms where Met and/or AdoMet inhibit enzymes specific to the Met branch of the pathway[21]. However, AdoMet may well have regulatory effects, so far unexplored, on other steps of the pathway.

S.E.R. acknowledges the receipt of a Council of Europe Scholarship through the British Council. We also thank J. S. Kueh for growing the barley embryos and S. W. J. Bright for helpful discussion.

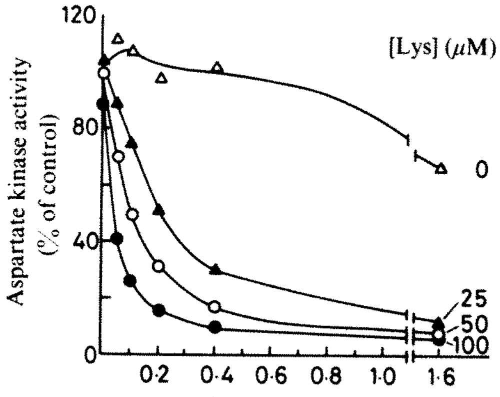

Fig. 3 Effect of Lys concentration on the sensitivity of barley embryo aspartate kinase to AdoMet inhibition. Data obtained as described in Fig. 2 legend.

Received 8 July; accepted 24 July 1980.

1. Miflin, B. J. *Nature* **275**, 483–484 (1978).
2. Truffa-Bachi, P. in *The Enzymes* Vol. 8 (ed. Boyer, P. D.) 509–553 (Academic, New York, 1973).
3. Robert-Gero, M., Le Borgne, L. & Cohen, G. N. *J. Bact.* **112**, 251–258 (1972).
4. Miflin, B. J., Bright, S. W. J., Davies, H. M., Shewry, P. R. & Lea, P. J. in *Nitrogen Assimilation in Plants* (eds Hewitt, E. J. & Cutting, C. V.) 335–358 (Academic, London, 1979).
5. Shrewy, P. R. & Miflin, B. J. *Pl. Physiol.* **59**, 69–73 (1977).
6. Bryan, P. A., Cawley, R. D., Brunner, C. E. & Bryan, J. K. *Biochem. biophys. Res. Commun.* **41**, 1211–1217 (1970).
7. Cheshire, R. M. & Miflin, B. J. *Phytochemistry* **14**, 695–698 (1975).
8. Aarnes, H. & Rognes, S. E. *Phytochemistry* **13**, 2717–2724 (1974).
9. Aarnes, H. *Physiologia Pl.* **32**, 400–402 (1974).
10. Sakano, K. & Komamine, A. *Pl. Physiol.* **61**, 115–118 (1978).
11. Davies, H. M. & Miflin, B. J. *Pl. Physiol.* **62**, 536–541 (1978).
12. Lea, P. J., Mills, W. R. & Miflin, B. J. *FEBS Lett.* **98**, 165–168 (1979).
13. Giovanelli, J., Mudd, S. H. & Datko, A. H. in *The Biochemistry of Plants: a Comprehensive Treatise* Vol. 5 (eds Stumpf, P. K. & Conn. E. E.) Vol. 5, Ch. 12 (Academic, New York, in the press).
14. Madison, J. T. & Thompson, J. F. *Biochem. biophys. Res. Commun.* **71**, 684–691 (1976).
15. Thoen, Å., Rognes, S. E. & Aarnes, H. *Pl. Sci. Lett.* **13**, 113–119 (1978).
16. Davies, D. D. *J. exp. Bot.* **17**, 320–331 (1966).
17. Schlenk, F. & Zydek-Cwick, C. R. *Archs Biochem. Biophys.* **134**, 414–422 (1969).
18. Matthews, B. F. & Widholm, J. M. *Can. J. Bot.* **57**, 299–304 (1979).
19. Bright, S. W. J., Lea, P. J. & Miflin, B. J. *CIBA Fdn Symp.* **72**, 101–114 (1980).
20. Bright, S. W. J., Rognes, S. E., Kueh, T. & Miflin, B. J. (in preparation).
21. Umbarger, H. E. *A. Rev. Biochem.* **47**, 533–606 (1978).

DNA from Ti plasmid present in nucleus and absent from plastids of crown gall plant cells

L. Willmitzer*†, M. De Beuckeleer‡, M. Lemmers‡, M. Van Montagu‡ & J. Schell*‡

* Max-Planck-Institut für Züchtungsforschung, Köln, FRG
† Gesellschaft für Biotechnologische Forschung, Department für Molekularbiologie, Braunschweig, FRG
‡ Laboratory for Genetics, State University of Gent, Belgium

The Gram-negative soil bacterium *Agrobacterium tumefaciens* induces crown gall tumours on most dicotyledonous plants[1,2], its Ti plasmids causing the neoplastic transformation of plant cells[3–5]. Molecular hybridization has shown that transformed cells contain a segment of the Ti plasmid (T-DNA) of molecular weight 8–15 × 10^6 (refs 6–9), of which at least part is transcribed[10,11]. Some copies of the T-DNA are integrated into the plant DNA (unpublished work). In view of the prokaryotic origin of the T-DNA, the possibility of its localization within either mitochondria or chloroplasts must be considered. We present here evidence for the absence of T-DNA from mitochondria and chloroplasts. Our results clearly show its presence within the nucleus.

Two lines of evidence support this conclusion. First, the different organelles were separated and isolated, their DNA was extracted, digested with various restriction endonucleases and hybridized according to the Southern procedure[12] to radioactive probes containing cloned segments of the T-DNA. In the second

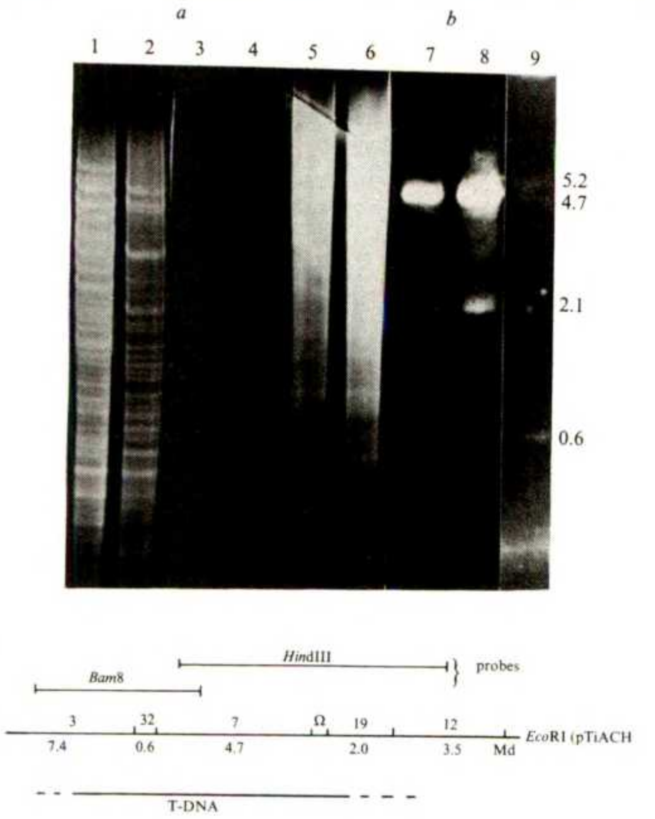

Fig. 1 Hybridization of mitochondrial, chloroplast and nuclear DNA from suspension cultures of *Nicotiana tabacum* variety White Burley transformed by *A. tumefaciens* A6 and B6S3 (both lines originated from the collection of R. A. Schilperoort, University of Leiden) against ^{32}P-labelled fragments of pTiACH5. For isolation of mitochondria and chloroplasts, suspension cultured cells were disrupted by a new cell mill (L. Willmitzer *et al.*, in preparation) in buffer A (ref. 13). The homogenates were filtered through an 80-μm and a 20-μm nylon cloth, centrifuged for 10 min at 1,200*g*, and mitochondria were pelleted by centrifuging the supernatant for 15 min at 12,000*g*. The pellet was redispersed in buffer A and again centrifuged at 12,000*g*. The final pellet was treated with DNaseI (100 μg ml^{-1}) for 30 min at 4 °C. DNase was removed by two washings at 12,000*g* in buffer A, and the dispersed pellet was loaded on a 30–60% sucrose gradient in buffer A, centrifuged for 1h at 22,000 r.p.m. in a SW27 rotor and the mitochondrial band was recovered. Chloroplasts were isolated in the same way but pelleted by two subsequent rounds of centrifugation at 2,000*g* for 5 min. Nuclei were prepared according to Willmitzer[20], substituting 0.5 mM spermidin and 0.15 mM spermin for $MgCl_2$ and incubating the cells overnight with cellulase and pectinase. The purity of the nuclei was checked routinely by phase contrast microscopy, which showed the absence of other subcellular particles. The same result was obtained by electron microscopy. DNA was isolated from the organelles according to Gross-Bellard *et al.*[21] with subsequent iurification on a CsCl gradient. DNA was digested with *Eco*RI in 50 mM, Tris, *p*H 7.5, 100 mM NaCl and 7 mM $MgCl_2$, and the fragments obtained were separated by electrophoresis in 0.8% agarose formed in 40 mM Tris–acetic acid *p*H 8.0, 20 mM NaAc, 1 mM EDTA and ethidium bromide (0.3 μg ml^{-1}), on a horizontal slab gel apparatus at 40 V for 12 h[22]. DNA was then blotted on to nitrocellulose (Schleicher and Schuell) and hybridized against a nick-translated probe of cloned segments of the T-DNA (specific activity 20–40 10^6 c.p.m. μg^{-1}). Hybridization was performed routinely for 36–40 h at 68 °C in 3× SSC, 0.5% SDS, 1 mM EDTA, 0.02% polyvinylpyrrolidone, 0.02% bovine serum albumin and 0.02% Ficoll. After washing filters were exposed for 1–4 weeks. Lanes 1–4, *Eco*RI restriction pattern of mitochondrial (lane 1) and chloroplast (lane 2) DNA and the corresponding autoradiograms obtained after hybridization with nick-translated *Hin*dIII fragment 1 of pTiACH5 (lane 3, mitochondrial DNA; lane 4, chloroplast DNA) 15 μg of DNA was applied each. Lanes 5–8, *Eco*RI restriction pattern of two concentrations of nuclear DNA (lane 5, 15 μg; lane 6, 22 μg) and the corresponding autoradiograms obtained after hybridization with nick-translated *Hin*dIII fragment 1 of pTiACH5 (lane 7, 8). Lane 9, autoradiogram obtained after hybridization of *Eco*RI digested nuclear DNA with nick-translated *Bam* fragment 8 of pTiACH5. The lower intensity of the bands in lane 9 compared with lanes 7 and 8 is due to a lower specific activity of the nick-translated probe. The lower diagram shows a schematic representation of the parts of the Ti plasmid ACH5 (octopine) integrated into nuclear DNA of tobacco cells transformed by *A. tumefaciens* A6 and B6S3. The detailed experiments for the construction of the map will be described elsewhere.

approach, isolated nuclei from transformed cells were incubated in conditions facilitating transcription and the RNA synthesized was analysed for sequences derived from T-DNA.

An efficient method was developed for the isolation of nuclei in plant cell suspension culture, details of which will be described elsewhere (L. Willmitzer, in preparation). Nuclei thus isolated were physiologically active and free from other subcellular particles as revealed by electron microscopy. Standard procedures[13–15] were followed for the isolation of mitochondria and chloroplasts by DNase treatment and sucrose density centrifugation.

Figure 1*a* shows the pattern of mitochondrial and chloroplast DNA from a tobacco octopine tumour line transformed by *A. tumefaciens* A6, after digestion with *Eco*RI and separation of the fragments by electrophoresis on 0.8% agarose gels. Figure 1*a* also shows the corresponding autoradiogram obtained after hybridization with the *Hin*dIII fragment I of the octopine plasmid pTiACH5, which has been shown to be part of the transferred plasmid DNA (T-DNA)[9] (De Beuckeleer *et al.*, in preparation). The chloroplast DNA restriction pattern agrees well with reports of the chloroplast pattern of *Nicotiana* species[16–18]. The mitochondrial DNA shows a higher complexity in comparison with chloroplast DNA as judged by the larger number of distinct bands, in agreement with published data[15,19]. Mitochondrial DNA preparations were characterized by analytical CsCl density gradient centrifugation, exhibiting a distinct peak at the expected density of 1.706 g cm^{-3}. Lack of hybridization was observed consistently in four independently derived chloroplast and mitochondrial DNA preparations of two different tobacco octopine tumours transformed by *A. tumefaciens* A6 and B6S3.

Figure 1*b* shows the pattern of nuclear DNA obtained after digestion with *Eco*RI and separation of the resulting fragments by electrophoresis on 0.8% agarose gels, together with the corresponding autoradiogram obtained after hybridization with *Hin*dIII fragment I and *Bam*HI fragment 8 of pTiACH5. Two bands with molecular weights of 4.7×10^6 and 2.1×10^6 hybridize with the *Hin*dIII fragment I. These fragments correspond, respectively, to the *Eco*RI fragment 7, molecular weight 4.7×10^6, of pTiACH5 plasmid DNA which is therefore an internal fragment of the transferred T-DNA, and to a junction fragment presumably linking the right border of the T-DNA to plant DNA (De Beuckeleer *et al.*, in preparation). When *Bam* fragment 8 was used as hybridization probe, three bands with molecular weights of 0.6×10^6, 4.7×10^6 and 5.2×10^6 emerged, corresponding, respectively, to the internal pTiACH5 *Eco*RI fragments 32 and 7 and the left-hand border fragment (De Beuckeleer *et al.*, in preparation). These data therefore reveal the presence of T-DNA integrated in nuclear DNA.

Hybridization was achieved repeatedly using 11 independently derived preparations of nuclear DNA from two octopine tumour tissues. Because hybridization was achieved with the nuclear DNA, which is enriched by only a factor of 1.1 compared with total cellular DNA, the absence of any hybridization with chloroplast and mitochondrial DNA, which are enriched by a factor of 20 and 100, respectively[23,24], suggests that the T-DNA is not located in plasmids. But there is a possible pitfall: because there is extensive homology between 16S and 23S rDNA of *Escherichia coli* and the rDNA of chloroplasts[25,26] and mitochondria[27], erroneous hybridizations were observed when we used cloned T-DNA probes that were not entirely free of chromosomal *E. coli* DNA.

To substantiate further the presence of the T-DNA within the nucleus, isolated and highly purified nuclei from octopine tumour tissue were incubated in conditions that facilitated active transcription. After a 20-min pulse with α-^{32}P-UTP, labelled RNA was isolated and hybridized to Southern blots of cloned T-DNA fragments. Figure 2*a* shows the stained gel together with the corresponding autoradiogram. The T-DNA appears to be transcribed very actively within the isolated nuclei, providing further strong evidence for the presence of the T-DNA within the nucleus. The autoradiogram indicates that the left as well as the right-hand part of T-DNA are transcribed, for hybridization to the *Hin*dIII fragments 1, 18 and 22 of pTiACH5 is visible. (The nuclear transcription of the T-DNA is under thorough investigation.)

We excluded the possibility that T-DNA is located in the cytoplasm but adsorbs to and penetrates into the nuclei during isolation. To do this, 20 μg of Ti-plasmid (ACH5) representing a 1,000-fold excess over the concentration present in crown gall cells, assuming five copies of T-DNA per transformed cell[28], was added to untransformed plant cells at the onset of nuclear purification. After isolation, nuclei were incubated in conditions facilitating transcription, and ^{32}P-labelled RNA was isolated and hybridized against blots of T-DNA as described above. No hybridization was detectable (Fig. 2*b*).

In summary, this report provides strong structural as well as functional evidence for the presence of the T-DNA within the nucleus of the transformed plant cell.

We thank Professor K. G. Wagner for stimulating discussions; Professor R. Herrmann, for an introduction to the isolation of plasmid DNA, and W. Schmalenbach and G. Simons for technical assistance. This work was supported by the Max-Planck-Gesellschaft, München, and by grants from the Kankerfonds van de ASLK and from the Fonds voor Kollektief Fundamenteel Onderzoek (10.316) to J.S. and M.V.M., M.D.B. and M.L. are indebted for a fellowship to the IWONL.

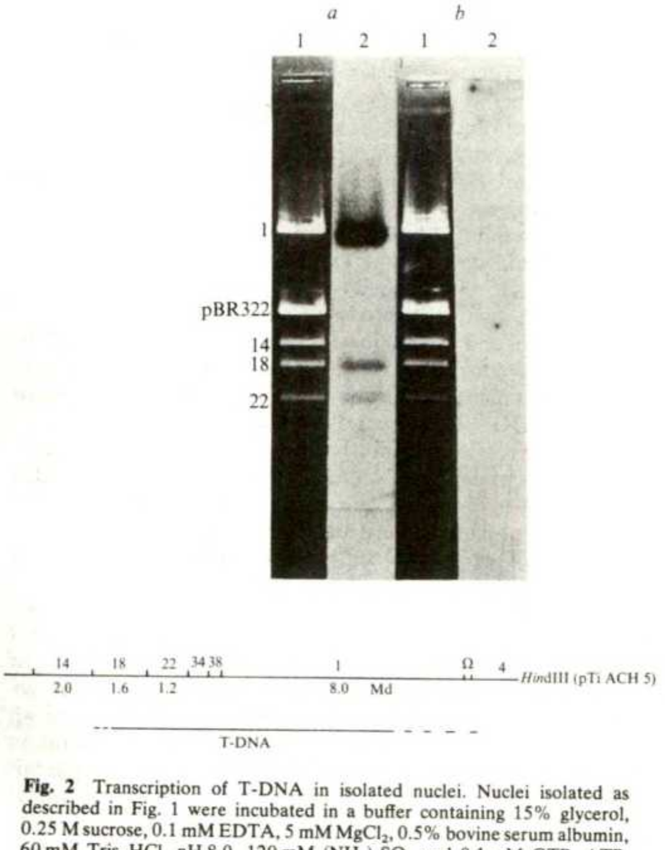

Fig. 2 Transcription of T-DNA in isolated nuclei. Nuclei isolated as described in Fig. 1 were incubated in a buffer containing 15% glycerol, 0.25 M sucrose, 0.1 mM EDTA, 5 mM $MgCl_2$, 0.5% bovine serum albumin, 60 mM Tris–HCl, *p*H 8.0, 120 mM $(NH_4)_2SO_4$ and 0.1 mM GTP, ATP, CTP and 200 μCi α-^{32}P-UTP (specific activity 350 Ci mmol^{-1}) for 20 min at 25 °C. RNA was isolated by two rounds of DNase digestion, proteinase K treatment, phenolization and subsequent chromatography on Sephadex G50. RNA was hybridized against blots of T-DNA clones containing *Hin*dIII fragments 1, 14, 18 and 22 at 68 °C in 3 × SSC, 0.2% SDS, 1 mM EDTA for 40 h. *a*, Hybridization (lane 2) of RNA (10 × 10^6 c.p.m.) transcribed in nuclei isolated from a tobacco crown gall transformed by *A. tumefaciens* A6 to blots of T-DNA clones containing *Hin*dIII fragments 1, 14, 18 and 22. *b*, Autoradiogram (lane 2) obtained after hybridizing RNA (12 × 10^6 c.p.m.) transcribed within the nucleus of untransformed cells where 20 μg of Ti-plasmid (pTiACH5) DNA had been added to the cells at the onset of isolation of the nuclei, representing a 1,000–fold excess over the amount of T-DNA present in transformed cells. The lower diagram shows a schematic representation of the parts of the Ti-plasmid ACH5 integrated into nuclear DNA of tobacco cells transformed by *A. tumefaciens* A6.

Received 8 April; accepted 11 July 1980.

1. Drummond, M. *Nature* **281,** 343–347 (1979).
2. Smith, E. F., Brown, N. A. & Townsend, C. O. *US Dept Agric. Bur. Plant Ind. Bull.* **213,** 1–200 (1911).
3. Zaenen, I. *et al. J. molec. Biol.* **86,** 109–127 (1974).
4. Van Larebeke, N. *et al. Nature* **252,** 169–170 (1974).
5. Watson, B., Currier, T. C., Gordon, M. P., Chilton, M.-D. & Nester, E. W. *J. Bact.* **123,** 255–264 (1975).
6. Chilton, M.-D. *et al. Cell* **11,** 263–271 (1977).
7. Schell, J. *et al. Proc. R. Soc.* B**204,** 251–266 (1979).
8. Schell, J. & Van Montagu, M. *Genome Organization and Expression in Plants* (ed. Leaver, C. J.) (Plenum, Edinburgh, 1980).
9. Tomashow, M. F., Nutter, R., Montoya, A. L., Gordon, M. P. & Nester, E. W. *Cell* **19,** 729–739 (1980).
10. Drummond, M. H., Gordon, M. P., Nester, E. W. & Chilton, M.-D. *Nature* **269,** 535–536 (1977).
11. Gurley, W. B., Kemp, J. D., Albert, M. J., Sutton, D. W. & Callis, J. *Proc. natn. Acad. Sci. U.S.A.* **76,** 2828–2832 (1979).
12. Southern, E. *J. molec. Biol.* **98,** 503–517 (1975).
13. Kolodner, R. & Tewari, K. K. *Biochim. biophys. Acta* **402,** 372–390 (1975).
14. Herrmann, R. G., Bohnert, N. J., Kowallik, K. V. & Schmitt, J. M. *Biochim. biophys. Acta* **378,** 305–317 (1975).
15. Quetier, F. & Vedel, F. *Nature* **268,** 365–368 (1977).
16. Vedel, F., Quetier, F. & Bayen, M. *Nature* **263**, 440–442 (1976).
17. Belliard, G., Pelletier, G., Vedel, F. & Quetier, F. *Molec. gen. Genet.* **165,** 231–237 (1978).
18. Frankel, R., Scowcroft, W. R. & Whitfield, P. R. *Molec. gen. Genet.* **169,** 129–135 (1979).
19. Vedel, F., Quetier, F., Dosba, F. & Doussinault, G. *Plant Sci. Lett.* **13,** 97–102 (1978).
20. Willmitzer, L. *FEBS Lett.* **108,** 13–16 (1979).
21. Gross-Bellard, M., Oudet, P. & Chambon, P. *Eur. J. Biochem.* **36,** 32–38 (1973).
22. Depicker, A., Van Montagu, M. & Schell, J. *Nature* **275,** 150–153 (1978).
23. Tewari, K. K. *A. Rev. Plant Physiol.* **22,** 141–168 (1971).
24. Kung, S. *A. Rev. Plant Physiol.* **28,** 401–437 (1977).
25. Schwarz, Z. & Kössel, H. *Nature* **279,** 520–522 (1979).
26. Schwarz, Z. & Kössel, H. *Nature* **283,** 739–742 (1980).
27. Koncz, Cs. & Sain, B. *FEBS Lett.* **109,** 141–144 (1980).
28. Merlo, D. J. *et al. Molec. gen. Genet.* **177,** 637–643 (1980).

In vitro suppression of UGA codons in a mitochondrial mRNA

A. De Ronde, A. P. G. M. Van Loon & L. A. Grivell

Section for Molecular Biology, Laboratory of Biochemistry, University of Amsterdam, Kruislaan 320, 1098 SM Amsterdam, The Netherlands

J. Kohli

Institut für Allgemeine Mikrobiologie, Altenbergrain 21,
CH-3013 Bern, Switzerland

Although both prokaryotic and eukaryotic messenger RNAs can be easily translated in heterologous protein-synthesizing systems, attempts to achieve correct synthesis of mitochondrial proteins by translation of mitochondrial mRNAs in such systems have failed[1–3]. In general, the products of synthesis are of low molecular weight and presumably represent fragments of mitochondrial proteins[1,2]. These fragments display a strong tendency to aggregate[4]. Explanations have included the use by mitochondria of codons requiring a specialized tRNA population[5] and the fortuitous occurrence within genes of purine-rich sequences resembling bacterial ribosome binding sites[6]. In addition, the long 5′-leader sequences present in many mitochondrial (mt) RNAs may also contribute to difficulties in mRNA recognition by heterologous ribosomes[7]. Recent sequence analysis of human mtDNA[8] suggests that the genetic code used by mammalian mitochondria deviates in a number o respects from the 'universal' code, the most striking of thes being the use of the UGA termination codon to specify tryp tophan. That this may also apply in yeast mitochondria has bee shown by Fox[9] and Macino *et al.*[10], thus providing an obvio and easily testable explanation for the inability of heterologo systems to synthesize full-length mitochondrial proteins. confirm this explanation and describe here the *in vitro* synthe of a full-length subunit II of yeast cytochrome *c* oxidase i wheat-germ extract supplemented with a partially purif mitochondrial mRNA for this protein and a UGA-suppres tRNA from *Schizosaccharomyces pombe*[11].

Our choice of mRNA was based on two considerations. Fi previous cell-free translation experiments had shown that u 27% of the products synthesized under the direction of

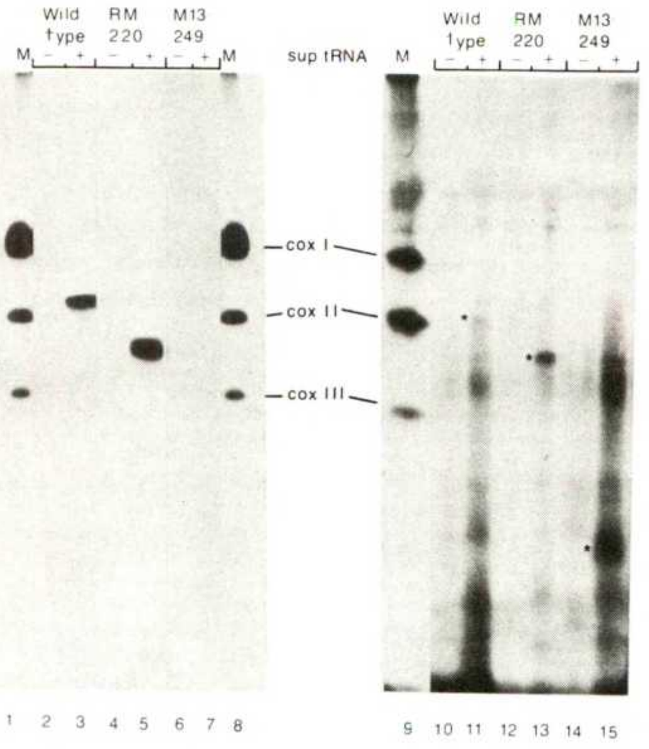

Fig. 1 Autoradiogram of the products synthesized *in vitro* under the direction of mitochondrial mRNA in the presence or absence of $\text{tRNA}^{\text{ser}}_{\text{UGA}}$. Mitochondrial RNA was isolated from the wild-type strain *Saccharomyces carlsbergensis* NCYC74 and from two mutants in the structural gene for subunit II of cytochrome *c* oxidase, *Saccharomyces cerevisiae* M13-249 and RM220 (refs 9, 12). An 11–13S fraction of these RNAs, which is enriched in the mRNA for subunit II, was obtained by sucrose gradient centrifugation[2] and used to programme a wheat-germ cell-free system in the presence or absence of $\text{tRNA}^{\text{ser}}_{\text{UGA}}$ from *S. pombe*[11]. Reaction mixtures (25 μl) contained 12.5 μl wheat-germ extract, prepared as described by Marcu *et al.*[16], 20 mM HEPES (*p*H 7.5), 2.5 mM magnesium acetate, 85 mM potassium acetate, 2 mM dithiothreitol, 0.5 mM spermidine, 0.04 mM of each amino acid, excluding methionine, 3.5 μM [^{35}S]-methionine (260 Ci mmol^{-1}: The Radiochemical Centre, Amersham, UK), 1 mM ATP, 0.03 mM GTP, 4 mM phosphoenol pyruvate, 4 μg pyruvate kinase per ml (Boehringer Mannheim), 5 μM S-adenosylmethionine and 2–3 μg mitochondrial mRNA. Suppressor $\text{tRNA}^{\text{ser}}_{\text{UGA}}$, when present, was added to a final concentration of 40 μg ml^{-1}. Protein synthesis was allowed to proceed for 1 h at 25 °C. 1-μl samples were withdrawn for measurement of incorporation by trichloroacetic acid precipitation and for electrophoretic analysis of total product. The remainder of the reaction mixture was subjected to immunoprecipitation, following the procedure of Maccecchini *et al.*[17]. Immunoprecipitation was carried out in consecutive steps with a pre-immune serum and anti-holo-cytochrome *c* oxidase, using a goat anti-rabbit serum to recover immune complexes in each case. Electrophoresis was performed according to Laemmli[18] on 15% polyacrylamide gels, using subunits I–III of cytochrome *c* oxidase as molecular weight markers. These were prepared by labelling of protoplasts of *S. carlsbergensis* with [^{35}S]-methionine[19] in the presence of cycloheximide (0.6 mg ml^{-1}) after pretreatment with chloramphenicol[20]. Cell lysates were then immunoprecipitated with anti-cytochrome *c* oxidase as described above. After electrophoresis, gels were fixed, impregnated with sodium salicylate[21], dried and autoradiographed for 4–8 days at −70 °C on Kodak XR-1 film with an Ilford tungstate intensifier screen. Lanes 2–7, Samples after immunoprecipitation with anti-cytochrome *c* oxidase; lanes 10–15, the total products of *in vitro* synthesis. Lanes 1, 8 and 9 show subunits I–III of cytochrome c oxidase, labelled *in vivo* before lane 9) and after (lanes 1 and 8) immunoprecipitation as described above. The remaining lanes show the products synthesized *in vitro* under the direction of the various mRNA preparations: wild type, in the absence (lanes 2, 10) and presence (lanes 3, 11) of suppressor tRNA; RM220, in the bsence (lanes 4, 12) and presence (lanes 5, 13) of suppressor tRNA; M13-249, in the absence (lanes 6, 14) and presence (lanes 7, 15) of uppressor tRNA. Due to the low immune reactivity of the subunit II-related olypeptide in M13-249 (ref. 12), the autoradiogram of lanes 6 and 7 was xposed for a slightly longer time to permit better photographic reproduc- on. In the electropherograms of total product, the positions of the various forms of subunit II are marked by *. cox, Cytochrome *c* oxidase.

11–13S fraction of mtRNA is reactive with an antiserum against cytochrome *c* oxidase[1,2]. Transcript mapping shows that the 11–13S fraction contains an 11S RNA which is the major transcript of the gene for subunit II on yeast mtDNA (the *OXI*-1 locus)[2]. Second, since DNA sequence analysis shows that the *OXI*-1 coding sequence is either 753 or 714 nucleotides long[9], depending on the start used, we reasoned that the 11S RNA with a length of only 800–900 nucleotides would be unlikely to contain extensive untranslated regions. Such an RNA may be more readily accepted by eukaryotic ribosomes than one containing a long 5′-leader characteristic of other mitochondrial mRNAs.

Accordingly, an 11–13S mtRNA fraction was prepared by sucrose gradient centrifugation and translated in a wheat-germ extract as described in Fig. 1 legend. To permit unambiguous identification of the *in vitro* product and to rule out possible artifacts resulting from aggregation, translations were performed not only with RNA from wild-type mitochondria, but also with RNA from two well-defined mutants in *OXI*-1. These mutants synthesize characteristically shortened forms of subunit II as a result of frameshifts induced by single base pair insertions or deletions at known sites in the gene[9,12]. Figure 1 shows the results obtained from parallel translations in the presence or absence of $\text{tRNA}^{\text{ser}}_{\text{UGA}}$ (~70% pure) from *S. pombe*. Although there is no significant difference in the total amount of trichloroacetic acid-precipitable counts, the presence of the suppressor tRNA results in the appearance of strong, discrete high-molecular-weight bands. These are evident not only in samples precipitated with anti-cytochrome *c* oxidase (lanes 2–7), but also in samples analysed before immunoprecipitation (lanes 10–15). The latter observation indicates that both translation and suppression must be proceeding extremely efficiently and this is quite remarkable in view of the heterologous nature of the mRNA and the fact that, according to the DNA sequence[9], five UGA stops have to be read through to achieve complete synthesis.

Wild-type subunit II has an M_r of 29,000, while RM220 and M13-249 should yield subunit II-related polypeptides with M_r's of 28,000 and 15,000, respectively, as derived from the DNA sequence[9]. In fact, the products synthesized have M_r's of 31,000, 27,000 and 17,000 in wild type, RM220 and M13-249, respectively. We therefore conclude that full-length cytochrome *c* oxidase subunit II has been synthesized and thus are able to confirm that UGA is translated in yeast mitochondria.

The difference in mobility between the product of *in vitro* synthesis with wild-type RNA and the mature *in vivo* subunit II (2,000) deserves comment. The possibility exists that the *in vitro* product is a precursor form of subunit II. Evidence for the existence of a precursor to this subunit has recently been presented[13]. Furthermore, alignment of the yeast amino acid sequence predicted from DNA sequence analysis[9] with that determined for the beef-heart protein[14], shows that the yeast protein could be larger by up to 27 residues which might represent the non-conserved part of a precursor. However, we cannot formally exclude that this difference merely reflects an altered electrophoretic behaviour arising from the substitution of five tryptophan residues by five serine residues, although this seems unlikely in view of the fact that neither intact subunit II nor the product synthesized in various chain termination mutants shows abnormal behaviour in Ferguson plots of electrophoretic mobility[12,15]. An alternative explanation is that the extra 2,000 results from initiation in the wheat-germ system at a site upstream of the normal initiation codon. Indeed, DNA sequence analysis has revealed two AUG codons separated by 39 base pairs[9] and at present it is not known which of these functions as the normal start. Initiation at the 5′-proximal AUG would generate a protein of M_r approximately 1,300 greater than one initiated at the second site. These three possibilities can be tested. If the existence of a precursor is confirmed, the present *in vitro* system should be valuable in providing sufficient quantities of this protein to permit further characterization and analysis of its mode of processing.

Finally, the present system has great potential for the identification and characterization of other mRNAs in mitochondria, including those with long 5′-leaders. It will be interesting to see whether their correct translation is achieved. Such experiments are now in progress.

We thank Drs R. O. Poyton and D. Deters for gifts of antisera and mutant yeast strains, respectively, Dr T. D. Fox for communicating sequence data before publication and Dr P. Borst for discussions. This work was supported in part by grants to P. Borst and L.A.G. from The Netherlands Foundation for Chemical Research (SON) with financial aid from The Netherlands Organization for the Advancement of Pure Research (ZWO) and to J.K. from the Swiss National Science Foundation.

Received 6 June; accepted 5 August 1980.

1. Moorman, A. F. M., Verkley, F. M., Asselbergs, F. A. M. & Grivell, L. A. in *Mitochondria 1977: Genetics and Biogenesis of Mitochondria* (eds Bandlow, W., Schweyen, R. J., Wolf, K. & Kaudewitz, F.) 385–400 (De Gruyter, Berlin, 1977).
2. Moorman, A. F. M., Van Ommen, G. J. B. & Grivell, L. A. *Molec. gen. Genet.* **160,** 13–24 (1978).
3. Chang, A. C. Y., Lansman, R. A., Clayton, D. A. & Cohen, S. N. *Cell* **6,** 231–244 (1975).
4. Moorman, A. F. M., Grivell, L. A., Lamie, F. & Smits, H. L. *Biochim. biophys. Acta* **518,** 351–365 (1978).
5. Borst, P. & Grivell, L. A. *Cell* **15,** 705–723 (1978).
6. Hensgens, L. A. M., Grivell, L. A., Borst, P. & Bos, J. L. *Proc. natn. Acad. Sci. U.S.A.* **76,** 1663–1667 (1979).
7. Van Ommen, G. J. B., Groot, G. S. P. & Grivell, L. A. *Cell* **18,** 511–523 (1979).
8. Barrell, B. G., Bankier, A. T. & Drouin, J. *Nature* **282,** 189–194 (1979).
9. Fox, T. D. *Proc. natn. Acad. Sci. U.S.A.* **76,** 6534–6538 (1979).
10. Macino, G., Coruzzi, G., Nobrega, F. G., Li, M. & Tzagoloff, A. *Proc. natn. Acad. Sci. U.S.A.* **76,** 3784–3785 (1979).
11. Kohli, J., Kwong, T., Altruda, F., Söll, D. & Wahl, G. *J. biol. Chem.* **254,** 1546–1551 (1979).
12. Cabral, F. *et al. J. biol. Chem.* **253,** 297–304 (1978).
13. Sevarino, K. A. & Poyton, R. O. *Proc. natn. Acad. Sci. U.S.A.* **77,** 142–146 (1980).
14. Steffens, G. J. & Buse, G. *Hoppe-Seyler's Z. physiol. chem.* **360,** 613–619 (1979).
15. Groot, G. S. P., Van Harten-Loosbroek, N. & Kreike, J. *Biochim. biophys. Acta* **517,** 457–463 (1978).
16. Marcu, K. & Dudock, B. *Nucleic. Acids Res.* **1,** 1385–1397 (1974).
17. Maccecchini, M.-L., Rudin, Y., Blobel, G. & Schatz, G. *Proc. natn. Acad. Sci. U.S.A.* **76,** 343–247 (1979).
18. Laemmli, U. K. *Nature* **227,** 680–685 (1970).
19. Côté, C., Solioz, M. & Schatz, G. *J. biol. Chem.* **254,** 1437–1439 (1979).
20. Kreike, J. *et al. Eur. J. Biochem.* **101,** 607–617 (1979).
21. Chamberlain, J. P. *Analyt. Biochem.* **98,** 132–135 (1979).

Cooperative structural transition of PM2 DNA at high ionic strength and its dependence on DNA damages

Urs Kuhnlein, Siu Sing Tsang & Jane Edwards

Environmental Carcinogenesis Unit, British Columbia Cancer
Research Centre, 601 West 10th Avenue, Vancouver,
BC, Canada V5Z 1L3

Pohl and Jovin[1] have shown that poly(dG–dC) · poly(dG–dC) in solution undergoes a cooperative transition at 2.5 M NaCl at neutral *p*H. The two forms of the polymer are structurally different as indicated by a change in ethidium bromide intercalation and in circular dichroism (CD)[1,2]. Wang *et al.*[3] and Davies and Zimmerman[4] have suggested that the low salt form of the polymer might correspond to the B form of DNA (right-handed helix) and the high salt form to the Z form of DNA (left-handed helix). We describe here a salt-induced transition of supercoiled PM2 DNA from a form which passes through nitrocellulose filters to a form which is retained by these filters. The transition occurs between 2.5 and 3.5 M NaCl. The dependence of the apparent equilibrium constant on the salt concentration indicates a cooperative transition. Irradiation of DNA with UV light or alkylation with *N*-acetoxyacetylaminofluorene (AAAF) shifts the transition to lower salt concentrations. The transition can also be observed with linear DNA but requires a much higher salt concentration.

Figure 1 shows the retention of supercoiled PM2 DNA by nitrocellulose filters in dependence of the NaCl concentration. Relatively little DNA is retained below 2.5 M NaCl. However, at higher salt concentrations, DNA binding rapidly increases and at 3.5 M NaCl 80% binding is obtained. When PM2 DNA is irradiated with UV light or reacted with AAAF, the DNA binding profile shifts to lower salt concentrations (Fig. 1).

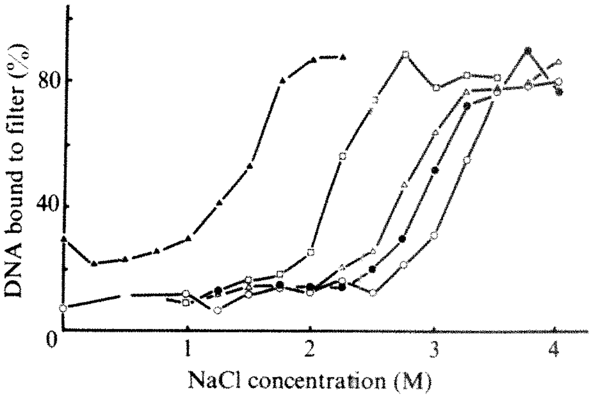

Fig. 1. Retention of supercoiled PM2 DNA by nitrocellulose filters in dependence of the NaCl concentration. ^{3}H-labelled PM2 DNA was isolated as described previously[15]. Aliquots (5 ml) of PM2 DNA at concentrations of 0.25 μM nucleotide in 10 mM Tris-HCl (*p*H 8.0) and various amounts of NaCl were filtered through nitrocellulose filters (Schleicher and Schuell, 0.20 μm pore size). The filters were dried and the radioactivity determined. ○, Untreated DNA; ●, DNA exposed to 60 J m^{-2} of UV light; △, DNA exposed to 120 J m^{-2}; □, DNA exposed to 600 J m^{-2}; ▲, DNA treated with AAAF. UV treatment was carried out at a concentration of 2.5 μM DNA nucleotide in a 10 mM Tris-HCl (*p*H 7.5) on ice. AAAF treatment was at a DNA concentration of 500 μM with 4.5 μg ml^{-1} of AAAF in 2.3% dimethyl sulphoxide and 10 mM Tris-HCl (*p*H 7.5). After incubation at 37 °C for 30 min, the DNA was extracted with ether and dialysed against 10 mM Tris-HCl (*p*H 7.5).

DNA binding could be caused by a salt-induced change of the binding properties of the nitrocellulose filters. However, the influence of DNA damages on DNA binding and the observation that linear DNA binds at a much higher salt concentration than circular DNA (Fig. 4) indicate that binding is caused by a salt-induced structural change of the DNA. This structural transition is reversible. When PM2 DNA is exposed to high salt and diluted to low salt concentrations immediately before filtration, no DNA binding is observed. Glass fiber filters (Whatman GF/C) do not retain DNA exposed to high salt, indicating that the DNA is not precipitated. We propose that high salt induces a transition of G–C rich regions of the DNA helix from a B-type structure to a Z-type structure and that the Z-type structure

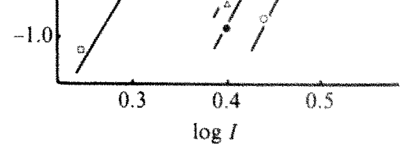

Fig. 2 Double logarithmic plot of the apparent equilibrium constant between the high- and low-salt form of supercoiled PM2 DNA in dependence of the molarity of NaCl (*I*). The values were calculated from Fig. 1 by dividing the amount of DNA bound to the filter by the amount of DNA passing through the filter. The values were corrected for a fraction of DNA (7.5%) which bound to the filters at all salt concentrations. ○, Untreated DNA; ●, DNA exposed to 60 J m^{-2} of UV light; △, DNA exposed to 120 J m^{-2} of UV light; □, DNA exposed to 600 J m^{-2} of UV light. The slopes varied between 13 and 10 with an average of 11.4.

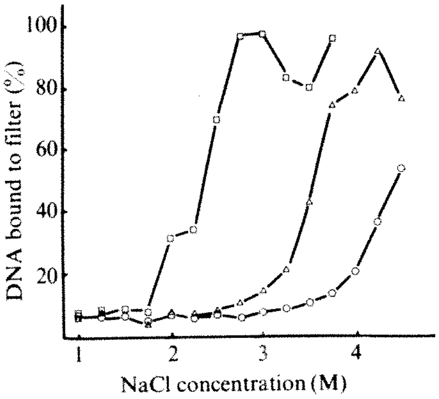

Fig. 3 Dependence of DNA binding on temperature. Aliquots (5 ml) of PM2 DNA at concentrations of 0.25 μM nucleotide in 10 mM Tris-HCl (*p*H 8.0) and various amounts of salt were incubated at 50 °C (□), 23 °C (△) and 0 °(○). They were then filtered through nitrocellulose filters which had been prewashed with 5 ml salt solutions at the same temperatures. The filter speed was 9 s per 5 ml.

itself, or single-strand regions formed in junctions between B and Z segments, bind the DNA to the nitrocellulose filter.

A double logarithmic plot of the apparent equilibrium constant (DNA bound to the filter divided by DNA passing through the filter), according to the equation $\log K = r \times \log(I) + \text{constant}$, where I = molar NaCl, gives approximately straight lines with slopes between 13 and 10 (Fig. 2). The high value of r indicates that the transition is cooperative. The average value of 11 is the same as that reported by Pohl and Jovin[1] for the salt-induced cooperative transition of poly(dG–dC)·poly(dG–dC) with an average length of 34 base pairs.

CD studies indicate that Z DNA segments can also be induced by high salt in naturally occurring DNA[5,6]. Changes of the CD spectrum similar to those induced by high salt have also been observed in DNA or in poly(dG–dC)·poly(dG–dC) alkylated with mitomycin C[7]. This observation and our observation with AAAF- and UV-treated DNA suggest that DNA damages facilitate the transition of the DNA helix from a B form to a Z form.

The Z form in damaged DNA might be favoured for steric reasons. Thus, in oligonucleotides *N*-(deoxyguanosin-8-yl)-acetylaminofluorene, the major adduct in AAAF-treated DNA, assumes the *syn* configuration found in the Z DNA rather than the *trans* configuration found in B DNA[8]. Alternatively, a DNA structure containing B and Z segments might require that the hydrogen bonding between some base pairs is disrupted. DNA damages might therefore favour the Z structure because of interference with hydrogen bonding. Indeed, AAAF treatment and UV treatment lower the melting point of DNA[9,10]. Furthermore, an increase in temperature leads to a transition at a lower salt concentration (Fig. 3). The influence of temperature on the transition is not at the level of the formation of Z form itself (at least in regions with an alternating G–C sequence), as the transition in poly(dG–dC)·poly(dG–dC) is not temperature-dependent[1].

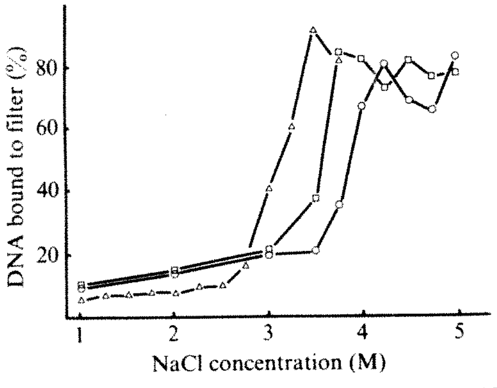

Fig. 4 Retention of native and linear PM2 DNA at 37 °C in dependence of the NaCl concentration. △, Native PM2 DNA; ○, linear PM2 DNA; □, linear PM2 DNA exposed to 600 J m^{-2} of UV light. Linear DNA was prepared by incubating 0.2 mM PM2 DNA nucleotide for 3.5 h with 25 units ml^{-1} of restriction endonuclease *Msp*I (New England Biolabs) in 10 mM Tris-HCl (*p*H 7.5), 10 mM $MgCl_2$, 6 mM KCl and 100 μg ml^{-1} acetylated bovine serum albumin. After incubation, the DNA was extracted with an equal volume of chloroform-octanol (9:1) and dialysed against 10 mM Tris-HCl (*p*H 7.5). Filtrations were carried out as described in Fig. 3 legend.

The transition of segments of the DNA from a B form to a Z form requires unwinding of the DNA helix. In a negatively supercoiled DNA molecule, unwinding of the DNA will remove the supercoils and, depending on the degree of transition, introduce positive supercoils. Since removal of negative supercoils is associated with a considerable decrease in free energy[11,12], one would expect that the B–Z transition is favoured in DNA containing negative supercoils. As shown in Fig. 4, when the negatively supercoiled PM2 DNA is converted to a linear form by treatment with the restriction endonuclease *Msp*I (*Msp*I is an isoschizomer of *Hpa*II which cleaves PM2 DNA at a unique site[13,14]), the transition is induced at a much higher salt concentration.

It will be of interest to demonstrate that Z DNA-like structures also occur at physiological salt concentrations. Indeed, this is the case for DNA damaged extensively with AAAF or with mitomycin C, and, with the appropriate DNA binding proteins present, the transition might also occur with DNA containing fewer lesions. Such Z DNA-like structures might be the trigger for the initiation of DNA repair processes. One would predict from such a mechanism that the presence of negative supercoils is important for DNA repair—it has been demonstrated in *Escherichia coli* that gyrase antagonists which prevent negative supercoiling inhibit the restoration of infectivity of UV-irradiated phage λ DNA[15]. Transitions of DNA segments from a B form to a Z form and vice versa might also be involved in other aspects of regulation of DNA metabolism, a mechanism which would be compatible with the key role of DNA gyrase in *E. coli*[16].

This work was supported by the National Cancer Institute of Canada.

Received 7 March; accepted 23 July 1980.

1. Pohl, F. M. & Jovin, T. M. *J. molec. Biol.* **67,** 375–396 (1972).
2. Pohl, F. M., Jovin, T. M., Baehr, W. & Holbrook, J. J. *Proc. natn. Acad. Sci. U.S.A.* **69,** 3805–3809 (1972).
3. Wang, A. H. J. *et al. Nature* **282,** 680–686 (1979).
4. Davies, D. R. & Zimmerman, S. *Nature* **283,** 11–12 (1980).
5. Tunis, M. B. & Hearst, J. E. *Biopolymers* **6,** 1218–1223 (1968).
6. Maestre, M. F. & Wang, J. C. *Biopolymers* **10,** 1021–1030 (1971).
7. Mercado, C. M. & Tomasz, M. *Biochemistry* **16,** 2040–2046 (1977).
8. Nelson, J. H., Grunberger, D., Cantor, C. R. & Weinstein, I. *J. molec. Biol.* **62,** 331–346 (1971).
9. Fuchs, R. P. P., Lefevre, J. F., Pouyet, J. & Danne, M. P. *Biochemistry* **15,** 3347–3351 (1976).
10. Marmur, J. & Doty, P. *Nature* **183,** 1427–1429 (1959).
11. Depew, R. E. & Wang, J. C. *Proc. natn. Acad. Sci. U.S.A.* **72,** 4275–4279 (1975).
12. Pulleyblank, P. E., Shure, M., Tang, D., Vinograd, J. & Vosberg, H. P. *Proc. natn. Acad. Sci. U.S.A.* **72,** 4280–4284 (1975).
13. Waalwijk, C. & Flavell, R. A. *Nucleic Acids Res.* **5,** 3231–3236 (1978).
14. Wang, J. C. *J. molec. Biol.* **87,** 797–816 (1974).
15. Hays, J. B. & Boehmer, S. *Proc. natn. Acad. Sci. U.S.A.* **75,** 4125–4129 (1978).
16. Cozzarelli, N. R. *Science* **207,** 953–960 (1980).

Corrigendum

In the letter '*β*-Endorphin alters luteinizing hormone secretion via the amygdala but not the hypothalamus' by N. Parvizi and F. Ellendorf, *Nature* **286,** 812–813 in paragraph 2, lines 2/3, the reference to 'Basolateral hypothalamus' is incorrect and it should read 'mediobasal hypothalamus'.

MATTERS ARISING

Giant solar flares in Antarctic ice

ROOD *et al.*[1] have discovered four prominent 'spikes' in a long time record (circa 1150 to the present) of the NO$_3^-$ concentration inside an Antarctic ice core. These four spikes rise 2–3 times higher than the upper envelope of a fluctuating background level of 0–20 μg l^{-1} that has been plausibly attributed to the action of high-energy solar radiation (photons and particles) impinging on the Earth's upper atmosphere and ionizing N$_2$, thereby leading to various chains of chemical reactions that culminate in the formation of NO$_3^-$, some of which is transported, within a few weeks or months, to Antarctica[1]. According to three alternative chronologies provided by Rood *et al.*, the estimated dates of the four NO$_3^-$ spikes lie within the intervals given in Table 1. Three of these dates have been tentatively associated by the same authors with the galactic supernovae of 1604, 1572 and 1181. At the outset, they have rejected energetic particles from the supernova explosion as a possible source of ionization of the terrestial N$_2$ because galactic magnetic fields would have greatly delayed and diffused the particles on their way to Earth. Instead , they have shown that photons of energy $\gtrsim 10$ keV are required. Unfortunately, as they admitted, the total energy requirements are difficult to meet, and the matching of dates with historical supernovae is not perfect.

As an alternative explanation, I suggest that the necessary ionizing radiation could have come from unusually powerful solar flares. These flares would be expected to have occurred preferentially during periods when the Sun was generally most active, that is around the times of the largest maxima in the solar cycle. Two good indices of solar activity are available: for the years elapsed since 1700, there are both sunspot numbers[2] and auroral numbers[3]; for earlier years auroral statistics[3–6] are preferred because the sunspot record (mostly from the Far East) is very sporadic[7]. Despite some incompleteness of the record before 1700, the main trends in the statistics are quite unmistakable (see refs 3 and 5).

The intervals of time in which the largest auroral and sunspot maxima occurred are listed in Table 1, where earlier dates are given only to the nearest half-decade. These intervals of time correlate very well with the known epochs of the NO$_3^-$ spikes. Only in one case is it necessary to recognize that episodes of solar flaring need not occur (as they have not always occurred in modern times) precisely at times of maximum auroral or maximum sunspot numbers. This therefore gives some flexibility in the possible dates of the giant solar flares that is not available in the case of the supernova hypothesis. However, there are no NO$_3^-$ spikes in the years around 1778 and 1957, at which times solar activity was also at a peak. Nevertheless, given the rarity of the proposed flaring events, this absence could simply be a product of statistical fluctuations. Also the Sun may now be somewhat different physically from its state before the long Maunder minimum in 1645–1715 (ref. 2).

According to Table 1, very large solar maxima seem to recur in cycles of ~200 yr, as Schove[4] originally noted. In the background NO$_3^-$ data, there is also some evidence of the Maunder minimum and of the normal 11-yr solar cycle[1]. Bauer[8] estimated that the background concentration could vary by a factor of two during the 11-yr cycle. To extend this further, I consider the largest solar flares in modern times. These have importance class 3+ or 4 and emit $E_{32}\times10^{32}$ erg of high-energy radiation (photons and particles), where $E_{32}\sim1$–2 (ref. 9). The Earth intercepts $4\times10^4\,E_{32}$ erg cm^{-2} of this. According to Rood *et al.*[1], the energy flux needed to produce a NO$_3^-$ concentration of 20 C_{20} μg l^{-1} near the South Pole is ~ $1\times10^5\,C_{20}$ erg cm^{-2} yr^{-1}. Since $C_{20}\lesssim1$, only one or two major flares per year is sufficient to produce all of the background NO$_3^-$. It is therefore not unreasonable to suppose that, every couple of hundred years or so, a giant flare, perhaps 2–3 times more intense than ordinary major flares, erupts on the Sun. An alternative possibility is that a very rapid succession of major flares of the ordinary type takes place. An event of this type may still develop during the current maximum of solar activity.

The Antarctic ice-core measurements are apparently now being pushed to deeper levels than before[1]. Much older NO$_3^-$ spikes may therefore be discovered. One immediate prediction of the solar flare hypothesis is the possibility (though no more than that) of a spike occurring around the year 1000, a time of heightened auroral activity[3–5]. On the other hand, a very bright supernova also appeared in 1006, as Rood *et al.* pointed out. But, fortunately, an *experimentum crucis* to discriminate between the two hypotheses can be made for the middle of the eleventh century, a time of profound auroral quiet but, equally importantly, of a brilliant supernova, the Crab explosion of 1054.

Table 1 Dates of the largest maxima in the Antarctic concentration of NO$_3^-$ and in solar activity indices

Largest NO$_3^-$ maxima	Largest solar maxima
1130–1160	1120–1140
1300–1340	1360–1375
.1590–1600	1565–1585
1610–1620	1605–1630
–	1778–1788
–	1947–1959

RICHARD STOTHERS

NASA Institute for Space Studies,
Goddard Space Flight Center,
2880 Broadway,
New York, New York 10025

1 Rood, R T, Sarazin, C L, Zeller, E J. & Parker, B C *Nature* **282**, 701 (1979)
2 Eddy, J A *Climatic Change* **1**, 173 (1977)
3 Gleissberg, W *Solar Phys* **21**, 240 (1971)
4 Schove, D J *J geophys Res* **60**, 127 (1955)
5 Link, F *Planet Space Sci* **12**, 333 (1964).
6 Siscoe, G L preprint (1980)
7 Clark, D H & Stephenson, F R *Q J R Astr Soc* **19**, 387 (1978)
8 Bauer, E *Nature* **276**, 96 (1978).
9 Talon, R *et al.* in *Solar Gamma-, X-, and EUV Radiation* (ed Kane, S R) 315 (Reidel, Dordrecht, 1975)

Magnetic fields and the solar constant

THOMAS[1] has suggested that changes in the magnetic flux content of the convection zone produces changes in radius. However, his calculations did not include the effect of structural changes in the superadiabatic region on the bulk of the convection zone. Theoretical studies[2–4] have shown that solar luminosity fluctuations can result from small structure adjustments in the convection zone, and can occur on time scales shorter than 1 yr. Such fluctuations are of interest in studies of the terrestrial climate.

The previous calculations have forced these structural changes by assuming a time-dependent mixing length. When the mixing length (physically the convective efficiency) changes, adjustments in the structure occur rapidly in the superadiabatic region, and in turn the bulk of the convection zone adjusts to maintain hydrostatic equilibrium. The result is a temporary luminosity change[3]. Any mechanism which affects the structure of the superadiabatic region will cause such a luminosity fluctuation. The effect of magnetic pressure changes on the superadiabatic region is described here.

We began by including a global magnetic pressure term in a stellar structure code. If the flux is assumed to be concentrated in vertical flux tubes, the pressure at a given radius (r) is given by

0028–0836/80/390365—02$01 00

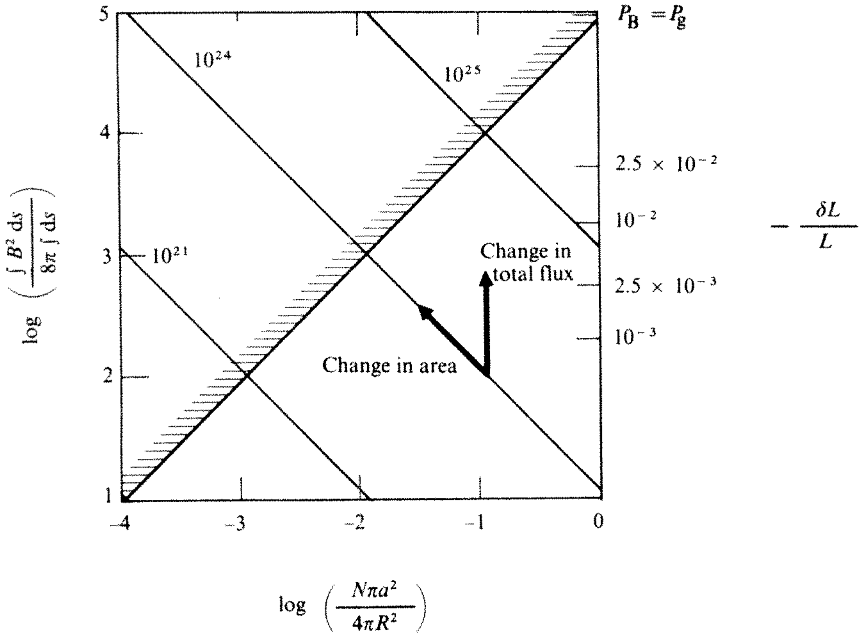

Fig. 1 Global magnetic pressure plotted against the fraction of the solar surface contained in the magnetic flux tubes. The luminosity scale on the right side gives the change resulting from the magnetic pressure change. The oblique lines are contours of constant flux.

$$P_m = \frac{1/8\pi \int B^2 ds}{\int ds} \approx \frac{NB^2 a^2}{32\pi r^2}$$

where N is the number of tubes with flux B and radius a. If the flux in a tube is constant and material is locked to the field lines, then the ratio of magnetic pressure to gas pressure decreases rapidly with depth in agreement with detailed sunspot models by Weiss[6].

The effect of changing the value of the magnetic pressure was explored by changing the surface value through the range $\log P_m = 1$ to 3.8 dyn cm^{-2}. Only in the superadiabatic region (upper few thousand kilometres) was the magnetic pressure term significant. Its gradient results in expansion and decreased density. In response to the lowered density in the superadiabatic region, the bulk of the convection zone begins to expand. The energy for expansion is obtained from the luminosity, and thus increasing the magnetic pressure decreases the solar luminosity.

The magnetic pressure depends on the total magnetic flux present and the area containing that flux. However, there is a minimum area over which a given amount of flux may be distributed that is determined by the requirement that the magnetic pressure in the flux tubes should not be greater than the gas pressure outside the tube.

The surface value of the global magnetic pressure is plotted against the fraction of the solar surface contained in the magnetic flux tubes in Fig. 1. Lines of constant total flux are shown as diagonals and the effect on the pressure of changing the area contained in flux tubes can be seen by moving along one of these lines. The effect on the pressure of changing the total amount of flux contained in the flux tubes is shown by vertical motion in this diagram. The luminosity scale along the right side of Fig. 1 gives the amplitude of the luminosity fluctuation produced by the magnetic pressure change.

The solar budget of magnetic flux is uncertain, but to produce a luminosity change of the order of 0.1% the flux penetrating the superadiabatic region must be $\geq 2 \times 10^{23}$ Mx. The radius change associated with this flux change was found to be $\Delta R/R \leq 10^{-4}$ which is slightly less than the value found by Thomas[1] for two reasons. First, the vertical flux tubes considered here contain less volume through the superadiabatic region than the horizontal flux tubes considered by Thomas. Second, the radius of the upper parts of the superadiabatic region is affected by the luminosity change because energy transport through the outer 1,000 km is partially by radiation[3,4]. Thus reducing the radiative flux causes this region to contract.

While the total amount of magnetic flux in the convection zone is uncertain, the amount of flux required for its pressure to produce a significant luminosity change is apparently high. A 1% luminosity change required a flux change of 2×10^{24} Mx in our model, and resulted in a radius change of $\Delta R/R = 2 \times 10^{-4}$. The action of such large amounts of magnetic flux on convective energy transport may actually dominate the effects discussed here. Unfortunately, although it is well known that strong fields can suppress convection locally (sunspots), the realistic inclusion of the effects of such flux tubes on global convective energy transport is a problem. As the effects of the field on convection have been neglected, the present results should represent the minimum effect of magnetic fields on the solar luminosity and radius.

This work was supported by The Aerospace Corporation on company-financed funds.

D. S. P. DEARBORN

Steward Observatory,
University of Arizona,
Tucson, Arizona 85721

J. B. BLAKE

Space Sciences Laboratory,
The Aerospace Corporation,
Box 92957
Los Angeles, California 90009

1. Thomas, J. *Nature* **280,** 662 (1979).
2. Ulrich, R. *Science* **190,** 619 (1975).
3. Dearborn, D. & Newman, M. *Science* **201,** 150 (1979).
4. Dearborn, D. & Blake, J. B. *Astrophys. J.* (in the press).
5. Parker, E. *Astrophys. J.* **198,** 205 (1975).
6. Sofia, S., O'Keefe, J., Lesh, J. & Endal, A. *Science* **204,** 1306 (1979).

A tectonic mélange of foreign eclogites and ultramafites in West Norway

MEDARIS[1] suggests that eclogites enclosed within the amphibolite-facies country-rock gneisses in the Basal Gneiss Region, West Norway "developed by *in situ* metamorphism of crustal materials"[1]; furthermore he attributes this to an "eclogite-facies metamorphic event"[1]. There are, however, some weaknesses in these hypotheses; also the simple *in situ* hypothesis may detract other geologists, especially geodynamicists, from pondering the genesis of these rocks, some of which are amongst the most exceptional on Earth[2], being the highest-pressure metamorphic rocks in the Caledonide Orogen[3].

Many different kinds of eclogite can be distinguished in the region according to mineralogical, textural, chemical, and pressure (P)-temperature (T) criteria, such that the frequent assumption[1,4–8] of a single origin (the simple *in situ* origin) for all eclogites within country-rock gneiss is difficult to justify. The 'dual' origin of eclogites and ultramafites, with only the ultramafites being foreign, suggested at Lien[1] and elsewhere[7,9], is less credible than my alternative multiple foreign origin[10] of the different eclogite types and also of those meta-igneous rocks (ultramafites, anorthosites, dolerites) for which adequate evidence of igneous intrusion into country-rock gneiss is unavailable (most published examples). A gigantic tectonic mélange is thus envisaged having been created by tectonic introduction of rock fragments from diverse foreign sources of diverse ages of equilibration [for example eclogite-facies eclogites + ultramafites (upper mantle); granulite-facies eclogites + anorthosites + gneisses + autometamorphosed dolerites

0028-0836/80/390366—03$01.00

(lower continental crust); blueschist-facies eclogites (subducting ocean crust); Ulstein-Dimnöy eclogite (subducted ocean crust); Ulstein-Dimnöy "garnet-biotite-gneiss" (subducted argillaceous sediments); marbles (subducted carbonate sediments)] into preserved Precambrian amphibolite-facies country-rock gneisses (also occasionally into each other) by lithospheric interdigitation during two-continent collision[11,12]. The final emplacement event was presumably of Caledonide age[12,13]. Age relationships between the diverse rock types in the Basal Gneiss Region are noted for their complexity[8,12]; the tectonic events deduced here would have produced just such a complexity.

Concerning the Lien locality, of the three rock types described by Medaris[1] (an ultramafite boudin, eclogite boudins, and country-rock gneisses which envelop the boudins), P–T estimates are provided[1] only for the boudins. No evidence is presented for P–T estimates for the country-rock gneisses, although demonstration of the identicalness of P–T and time conditions for equilibration of the eclogites and country-rock gneisses is essential[11,12] to sustain the deduced[1] *in situ* model. The use[1] of assumed co-existing core mineral compositions for geothermobarometry must be suspect when the cores are, by definition, not co-existing, especially when the raw data on zoning patterns is not provided for critical assessment of possible coexistence; confident interpretation of mineral zoning is notoriously difficult, for example in garnet[14].

Low-P estimates[1,6,15] for eclogite equilibration derive mainly from the intersection of iso-$K_{D\,\mathrm{gt/cp}}^{\mathrm{Fe/Mg}}$ P–T dependent lines with iso-$X_{\mathrm{cp}}^{\mathrm{Jd}}$ minimum P-variable T lines yielding minimum P only. Medaris[1] follows Krogh[6,7] in regarding only these minimum P estimates (7–12 kbar[1]) as reflecting the true P. Their trends are thus only consistent[1] in their method of derivation, which would yield a linear positive $\mathrm{d}P/\mathrm{d}T$ trend for any set of eclogites with variable $K_{D\,\mathrm{gt/cp}}^{\mathrm{Fe/Mg}}$ and approximately constant $X_{\mathrm{cp}}^{\mathrm{Jd}}$. Their published data[1,6] are perfectly compatible with any P estimates along the iso-K_{D} lines, easily 10–20 kbar higher than the minima (compare with 15–40 kbar, estimated for other eclogite boudins from the same district[12]). A near-infinite variety of P–T trends is thus possible, including depressurization trends; the supposed "prograde" trend, said[1] to have been "established by Krogh[6]", clearly needs independent corroboration. Medaris[1] claims convergence of his eclogite and ultramafite P–T trends, but they barely converge in his Fig. 2. His inferred eclogite trend[1] lies alongside the basic granulite/eclogite transition[4] based on the low-T linear extrapolation of high-T experimental work[16], an extrapolation inconsistent with other data[17–19] which suggests higher P at low T. Even if the documented[1] prograde eclogite P–T trend at Lien[1], or regionally[6–8], is genuine, it contributes little to support the *in situ* hypothesis if an identical trend is not discernible in the country-rock gneisses, evidence for which is apparently completely lacking. Whilst recognizing the feasibility of generating eclogite iarageneses and granulite- or amphibolite-facies gneisses *in situ* from adjacent basaltic and granitic rocks in certain P–T-composition conditions, I would anticipate the common occurrence of co-existing omphacite + plagioclase in intermediate compositions, but I am not aware of their existence in the country-rock gneisses of this region.

High-P equilibration (> 15 kbar) of at least some eclogite boudins has been implied or specifically estimated by advocates of the foreign tectonic emplacement origin[2,3,11,12,17,20–22,24,25], whilst low P equilibration (<15 kbar) for all eclogite boudins has been implied or specifically estimated for some by advocates of the *in situ* origin[1,4,5,9,15,26–28]. Krogh[6] broke through the <15 kbar threshold by proposing P estimates up to 23 kbar. The significant fact that this estimate[6] lies beyond[11] the known stability field of any plagioclase composition has been bypassed[7] and apparently disregarded[1]. Hence accepting[1,7,8] Krogh's[6] postulated prograde regional P–T trend necessitates the annihilation, kinetics permitting, of each grain of abundant plagioclase in ≈ 4,000 km^2 of country-rock gneisses, yielding ubiquitous eclogite-facies parageneses. The expected evidence for this substantial event is notable for its paucity and dubious validity, apparently being confined[7,8] to depressurization symplectites after omphacite in gneisses around the Ulstein-Dimnöy eclogite[5,15]. Considering published data only, and noting especially: (1) the outcrop of the symplectite-bearing 'garnet–biotite–gneiss'[5,15,29] which occurs only in contact with this eclogite[15,29], and which is "remarkably garnet-rich"[5]; (2) the lack of symplectites reported specifically from the 'dioritic'[5,15,29] typical country-rock gneisses, which are more deformed[29] and migmatitic[15], and (3) the 'uncommon'[5] amphibolitized margins of the eclogite boudin, and its 'welded'[5] contacts, allows, and indeed supports, my alternative interpretation that the so-called 'garnet–biotite–gneiss' is not real country-rock gneiss, but is merely a contiguous layer of amphibolitized K-, Al-and Si-rich quartz-phengite-eclogite tectonically independent of the 'dioritic' real country-rock gneiss. If this is true, then the assertion[15] that this eclogite is a type example of *in situ* metamorphism would be unsubstantiated. Furthermore, taking the absence of plagioclase as one of the essential features of an eclogite-facies group of parageneses[2], the suggested "eclogite-facies metamorphic event"[1] within the country-rock gneisses would be as unfounded as the postulated depression of the country-rock gneisses to depths of ≈ 70 km[1,6,8].

DAVID C. SMITH

Laboratoire de Minéralogie,
Muséum National d'Histoire Naturelle,
61, rue de Buffon,
75005 Paris, France

1. Medaris, L. G. *Nature* **283**, 470–472 (1980).
2. Smith, D. C. *26th int. geol. Congr.*, Paris *Abstr.* 01.3.3, 92 (1980).
3. Smith, D. C. *26th int. geol. Congr.*, Paris *Abstr.* 02.3.1, 145 (1980).
4. Bryhni, I., Green, D. H., Heier, K. S. & Fyfe, W. S. *Contr. Miner. Petrol.* **26**, 12–19 (1970).
5. Green, D. H. & Mysen, B. O. *Lithos* **5**, 147–161 (1972).
6. Krogh, E. J. *Nature* **267**, 17–19 (1977).
7. Krogh, E. J. *Nature* **269**, 730 (1977).
8. Bryhni, I., Krogh, E. J. & Griffin, W. L. *Neues Jb. Miner. Abh.* **130**, 49–63 (1977).
9. Carswell, D. A. *Lithos* **7**, 113–121 (1974).
10. Smith, D. C. thesis, Aberdeen Univ. (1976).
11. Lappin, M. A. *Nature* **269**, 730 (1977).
12. Lappin, M. A. & Smith, D. C. *J. Petrol.* **19**, 530–584 (1978).
13. Lappin, M. A. *J. Petrol.* **15**, 567–601 (1974).
14. Freer, R. *Nature* **280**, 220–222 (1979).
15. Mysen, B. O. & Heier, K. S. *Contr. Miner. Petrol.* **36**, 73–94 (1972).
16. Green, D. H. & Ringwood, A. E. *Geochim. cosmochim. Acta* **31**, 767–833 (1967).
17. O'Hara, M. J., Richardson, S. W. & Wilson, G. *Contr. Miner. Petrol.* **32**, 48–68 (1971).
18. Kennedy, G. C. & Ito, K. *J. Geol.* **80**, 289–292 (1972).
19. Irving, A. J. *J. Petrol.* **15**, 1–40 (1974).
20. O'Hara, M. J. & Mercy, E. L. P. *Trans. R. Soc. Edinburgh* **65**, 251–314 (1963).
21. Lappin, M. A. *Norsk geol. Tidsskr.* **46**, 439–496 (1966).
22. Smith, D. C. *Norsk geol. Tidsskr.* **51**, 141–147 (1971).
23. O'Hara, M. J. *N.E.R.C. Pub. Ser. D*, **6**, 252–253 (1976).
24. Smith, D. C. *Fortschr. Miner.* **54**, 94 (1976).
25. Smith, D. C. *Geolognytt* **10**, 32–33 (1977).
26. Griffin, W. L. & Råheim, A. *Lithos* **6**, 21–40 (1973).
27. Bryhni, I. & Griffin, W. L. *Contr. Miner. Petrol.* **32**, 112–125 (1971).
28. Bryhni, I. *Norsk geol. Unders.* **241**, 1–68 (1966).
29. Mysen, B. O. & Heier, K. S. *Norsk geol. Tidsskr.* **51**, 93–96 (1971).

MEDARIS REPLIES—There is increasing evidence in the Basal Gneiss terrane of western Norway for high-pressure metamorphism due to tectonic thickening of continental crust, probably related to a continent–continent collision of Caledonian age[1–3]. Thus, Smith's suggestion that the Basal Gneiss terrane has originated as a gigantic tectonic mélange due to lithospheric interdigitation during a continent–continent collision deserves evaluation by further field and petrological investigations. Such a model provides a plausible mechanism for emplacement of large ultramafic bodies, such as that at Lien, and would be consistent with the P–T patterns preserved in Norwegian garnet peridotites[4–6].

As Smith has suggested, there may be diverse origins and histories for country-rock eclogites in the Basal Gneiss. Nevertheless, there is now compelling chemical, petrological, textural, and structural evidence[1–3] for *in situ* prograde metamorphism of at least some of the eclogites, and the country-rock eclogites at Lien properly belong in this group.

Unfortunately, I feel that Smith has misrepresented three points in my paper. (1) The garnet-bearing ultramafic rocks and country-rock eclogites are relicts of an earlier eclogite metamorphism that are now surrounded by chlorite peridotite and middle grade gneisses, respectively, and the eclogite-facies rocks themselves have been retrograded to assemblages that are compatible with those in the enclosing rocks. (2) Admittedly, there is no certainty that equilibrium has been preserved between mineral cores. However, mineral cores have relatively uniform compositions within each sample, and different mineral grains within each sample yield consistent core temperatures[6]. (3) I clearly stated that pressure estimates for the country-rock eclogites at Lien, based on the jadeite content of omphacite, are minimum values only. Although many of Kroghs' pressure estimates for eclogites in the Basal Gneiss terrane are minimum values, as he stipulated, others are true estimates, based on the coexistence of orthopyroxene or phengite with garnet and omphacite.

L. G. MEDARIS JR

Department of Geology
and Geophysics
University of Wisconsin
Madison, Wisconsin 53706

1. Krogh, E. J. *Nature* **267,** 17–19 (1977).
2. Bryhni, I., Krogh, E. J. & Griffin, W. L. *Neues Jb. Miner. Abh.* **130,** 49–68 (1977).
3. Griffin, W. L. & Brueckner, H. K. *Earth planet. Sci. Lett.* (in the press).
4. Carswell, D. A. & Gibb, F. G. F. *Lithos* (in the press).
5. Medaris, L. G. *Nature* **283,** 470–472 (1980).
6. Medaris, L. G. *Lithos* (in the press).

GABA mediated circling from substantia nigra

THE dialogue between Waddington[1] and Martin and Haubrich[2] emphasizes the complexity of the interaction between striatal dopamine systems and nigral γ-aminobutyric acid (GABA) mechanisms as recently pointed out by Arnt and Scheel-Kruger[3]. This is particularly true when interpreting behavioural changes in terms of biochemical parameters. The effects of manipulating nigral GABA mechanisms on striatal dopamine release are complex. While nigral application of GABAergic drugs, such as muscimol, increases the firing rate of dopaminergic neurones[4], and the release of dopamine in the ipsilateral caudate nucleus[5-7], GABA itself exerts a biphasic action first stimulating and then inhibiting striatal dopamine release[8]. Furthermore, the nigral application of picrotoxin stimulates dopamine release in the striatum, an effect which is prevented or reversed by diazepam[9], which itself decreases dopamine release in striatum[10] (presumably by facilitation of nigral GABA transmission). Some GABAergic terminals (possibly those projecting to zona compacta) therefore seem to inhibit the activity of nigral dopamine cells, while others (possibly those projecting to zona reticulata) may indirectly activate the same nigral dopamine cells, perhaps via a GABA interneurone. Whether turning behaviour induced by the intranigral administration of muscimol is due indirectly to alteration of dopamine release in the striatum is disputed. In fact, the effect of intranigral injection of GABAergic compounds is critically dependent on the exact site of injection, an issue which has been neglected in the correspondence on this topic.

The initial observation of Tarsy and his colleagues[11] that picrotoxin injected into substantia nigra zona compacta caused contraversive rotation was followed by the discovery of Scheel–Kruger *et al.*[12] that ipsiversive circling resulted from the injection of picrotoxin into a caudal nigral site. Subsequently, James and Starr[13] (and, independently, ourselves[14]) demonstrated that the direction of rotation produced by injection of picrotoxin into rostral nigra is reversed on injection of this compound into caudal nigra, suggesting the existence of separate GABA mechanisms. We obtained similar findings injecting picrotoxin, and also muscimol in caudal and rostral nigra.

The circling produced by the action of muscimol or picrotoxin at each nigral site can be distinguished on the basis of its dependence on intact striatal dopamine mechanisms. Thus, while circling induced by injection of GABA-active compounds into rostral nigra is reduced by 6-hydroxydopamine lesions of the nigrostriatal pathway, or by systemically administered haloperidol, the same treatments are ineffective in inhibiting circling induced by manipulation of GABA mechanisms in caudal nigra[1,13,14]. These findings support Waddington's assertions of non-dopamine-mediated contraversive circling being induced by muscimol injected into substantia nigra zona reticulata[1]. The exact site used by Martin and Haubrich[5] is not clear, but must have involved caudal nigra as muscimol induced contraversive rotation. However, the muscimol perfused into substantia nigra also may have reached GABA receptors in rostral nigra to activate the ascending nigro-striatal pathway so causing increased striatal dopamine release. This would account for the simultaneous occurrence of these phenomena.

The argument as to whether or not the striataldopamine release caused by intranigral muscimol is responsible for contraversive circling is redundant. The circling behaviour initiated by an asymmetry of striatal dopamine function is clearly mediated by strio-nigral fibres and the substantia nigra. Thus, lesioning of the descending strio-nigral pathway prevents contraversive circling behaviour induced by the administration of apomorphine to animals with a unilateral 6-hydroxydopamine lesion of the nigro-striatal pathway[15]. In addition, kainic acid-induced destruction of neurones in substantia nigra zona reticulata, or the injection of picrotoxin or bicuculline into nigra ipsilateral to a 6-hydroxydopamine lesion of the nigro-striatal dopamine pathway, results in reduction, abolition or reversal of the contraversive rotation produced by apomorphine[16]. All these data point to a primary role of a neuronal pathway from caudal nigra independent of dopamine, which is responsible for the mediation of the circling phenomena. The importance of this nigral mechanism is emphasized by the work of Papadopoulos and Huston[17] who showed that spontaneous circling behaviour induced by a unilateral electrolytic lesion of substantia nigra was not influenced by the removal of the telencephalon (including striatum and neocortex). Indeed, we have demonstrated that a hemi-transection rostral to nigra severing all rostral nigral afferents and efferents does not attenuate contraversive circling induced by intranigral administration of muscimol (unpublished observations).

In conclusion, we support Waddington in his assertion that the contraversive circling due to intranigral muscimol administration is not due to striatal events. There can be little doubt as to the importance of a non-dopaminergic nigral output pathway in the mediation of circling behaviour. The nature of this pathway remains unknown as does its target site. It does not seem to involve the known projections of the nigra to the superior colliculus[18] or thalamus[19] and we are now investigating the involvement of nigroreticular pathways.

C. REAVILL
N. LEIGH
P. JENNER
C. D. MARSDEN

University Department of Neurology,
Institute of Psychiatry and King's College
Hospital Medical School,
Denmark Hill, London SE5, UK

1. Waddington, J. L. *Nature* **283,** 696–697 (1980).
2. Martin, G. E. & Haubrich, D. R. *Nature* **283,** 697 (1980).
3. Arnt, J. & Scheel-Kruger, J. *Naunyn-Schmiedebergs Arch. Pharmak.* **310,** 43–51 (1979).
4. Walters, J. R. & Lakoski, J. M. *Eur. J. Pharmac.* **47,** 469–471 (1978).
5. Cheramy, A., Nieoullon, A. & Glowinski, J. *J. Pharmac. exp. Ther.* **203,** 283–293 (1977).
6. Martin, G. E. & Haubrich, D. R. *Nature* **275,** 230–231 (1978).
7. Waddington, J. L. *Br. J. Pharmac.* **60,** 263–264P (1977).
8. Cheramy, A., Nieoullon, A. & Glowinski, J. *Eur. J. Pharmac.* **48,** 281–296 (1978).
9. Cheramy, A., Nieoullon, A. & Glowinski, J. *Life Sci.* **20,** 811–816 (1977).
10. Leviel, V., Cheramy, A., Nieoullon, A. & Glowinski, J. *Brain Res.* **175,** 353–356 (1979).
11. Tarsy, D., Pycock, C., Meldrum, B. & Marsden, C. D. *Brain Res.* **89,** 160–165 (1975).
12. Scheel–Kruger, J., Arnt, J. & Magelund, G. *Neurosci. Lett.* **4,** 351–356 (1977).
13. James, T. A. & Starr, M. S. *Nature* **275,** 229–230 (1978).
14. Reavill, C., Jenner, P., Leigh, N. & Marsden, C. D. *Neurosci. Lett.* **12,** 323–328 (1979).
15. Garcia-Munoz, M., Nicolaou, N. M., Tulloch, I. F., Wright, A. K. & Arbuthnott, G. W. *Nature* **265,** 363–365 (1977).
16. Di Chiara, G., Porceddu, M. L., Morelli, M., Mulas, M. L. & Gessa, G. L. *Naunyn-Schmiedebergs Arch. Pharmak.* **306,** 153–159 (1979).
17. Papadopoulos, G. & Huston, J. P. *Neurosci. Lett.* **13,** 63–67 (1979).
18. Reavill, C., Leigh, N., Jenner, P. & Marsden, C. D. *Expl Brain Res.* **37,** 309–316 (1979).
19. Jenner, P., Leigh, N., Marsden, C. D. & Reavill, C. *Br. J. Pharmac.* **67,** 432P (1979).

0028–0836/80/390368—01$01.00

BOOK REVIEWS

A question of language

Jean Berko Gleason

Nim: A Chimpanzee Who Learned Sign Language. By Herbert S. Terrace. Pp. 384. (Knopf: New York/Eyre Methuen: London, 1980.) $15, £6.50.

WHY would anyone want to try to teach a chimpanzee the sign language used by deaf human beings? For at least two compelling reasons. The first has to do with linguistic questions: is language a strictly human phenomenon, or is it possible that intelligent animals such as chimps, which are physiologically unable to speak, are nonetheless capable of combining symbols in a structured, grammatical way? The second reason is related to what Donald R. Griffin calls "the question of animal awareness": is it possible that we can teach non-human creatures to communicate to us their ideas, thoughts, their world view?

These tantalizing questions about language and cognition are what motivated Herbert S. Terrace, a Professor of Psychology at Columbia University, to adopt an infant male chimpanzee, whom he named Nim Chimpsky (Nim for short) after the linguist Noam Chomsky, a proponent of the view that only humans possess the special innate abilities that make true language possible. According to this view, language is a species-specific capacity, and all human languages share certain grammatical similarities because of the constraints imposed by the human intellect. Thus, all languages are composed of a small number of elements that can be combined in a great variety of utterances, have classes of words that roughly correspond to nouns and verbs, and so on. The fact that only humans possess language and that human infants master the complexities of their native tongue in just three or four years in a fairly effortless way and without extensive tutelage is evidence for the innatist view. By contrast, behaviourists hold that language is not basically different from other behaviours, and that its presence depends primarily on establishing a suitable system of rewards for linguistic behaviour.

Terrace himself has an extensive background in the behaviourist tradition, and in preparation for this project familiarized himself with the literature on language acquisition by children. His plan was to raise Nim in a rewarding human environment, teaching him American Sign Language (ASL), and then to analyse in a rigorous and linguistic way the young chimp's emerging ability to produce one sign at a time and later to combine signs into longer 'utterances'. There are, of course, other apes who have learned sign language, the first and most famous being Beatrice and Allen Gardner's Washoe; and there are apes who have learned to produce certain kinds of messages by manipulating plastic symbols or by striking the appropriate keys on a computer console. Project Nim was to go beyond these by providing a detailed record of Nim's acquisition of ASL, paying special attention to any evidence that he could produce grammatical signed sentences.

While the book gives a good picture of what it is like to live with an ape in New York City, and details the problems the project had in recruiting and keeping the 60 dedicated ASL teachers who worked with Nim, the essence of the book lies in its linguistic argument. The chimp's signed utterances were analysed for evidence of structure in much the same way as is young children's spoken language. By comparison, the chimp was found wanting. Even though he amazed everyone by producing his first ASL sign (*drink*) before the age of four months, his later utterances never went much beyond the two-sign stage. Reviewing the recorded utterances, the author concludes that "his three-sign combinations do not . . . provide new information. Consider, for example, Nim's most frequent two- and three-sign combinations: *play me* and *play me Nim*. Adding *Nim* to *play me* is simply redundant". Since tables of the most frequent combinations are provided, it is possible for the reader to do some armchair analysis, and in this case the conclusion appears to be based on a rather selective view of the data; there are a number of instances listed where a three-sign combination seems to build on earlier two-sign combinations in a way that very much resembles children's language. At the two-sign stage, for instance, Nim said *eat Nim*, while the three-sign list contains elaborations like *more eat Nim* and *banana eat Nim*. This begins to look like structure, but the four-sign combinations are not only very rare, they are all of the redundant *eat drink eat drink* variety. Most of Nim's signing had to do with eating, drinking and playing, but from time to time we are given a glimpse of the young chimp paging through a book and softly signing to himself the names of the things he sees.

Nim at work with one of his teachers

New books from IRL

Nucleic Acids Synthesis: Applications to Molecular Biology and Genetic Engineering.

Proceedings of the International Symposium on Chemical Synthesis of Nucleic Acids. Held May 1980 in Egestorf, West Germany. Nucleic Acids Symposium Series No. 7

In the fields of molecular biology and genetic engineering, synthetic nucleic acids and their constituents have proved to be valuable tools and their uses appear to be infinite. In the present era of 'synthetic biology' it is not surprising that the chemical synthesis of nucleic acids is experiencing a tremendous renaissance. This symposium, which has brought together the experts from all over the world, centres around recent synthetic improvements and their numerous applications.

396 pp ISBN 0 904147 26 6 (Hard)
August 1980 £17.00/US$40.00

Proceedings of the Eighth Symposium on Nucleic Acids Chemistry

Held August 1980 in Sapporo, Japan. Nucleic Acids Symposium Series No. 8.
198 pp ISBN 0 904147 28 2 (Soft)
August 1980 £8.00/US$16.00

Obesity: A Bibliography 1974-1979

The first bibliography, which covered the years 1964-1973, monitored over 100 journals – in this new volume the list has been greatly expanded to include a truly international range of publications. Contains over 4,000 references from a wide range of disciplines.

340 pp ISBN 0904147 17 7 (Hard)
£22.50/US$55.00
Due October 1980

Olfaction and Taste VII

Proceedings of the Seventh International Symposium on Olfaction and Taste and Fourth Congress of the European Chemoreception Research Organisation. Held July 1980 in the Netherlands.

The congress encompassed all work in the field of chemoreception and the proceedings are a near-complete survey of current thinking in the field.

500 pp ISBN 0 904147 20 7 (Hard)
£22.00/US$50.00
Due October 1980

IRL

Information Retrieval

P.O. Box 1, Eynsham,
Oxford OX8 1JJ, England

Suite 815, Fisk Building,
250 West 57th Street, New York,
NY 10019, U.S.A.

Circle No. 17 on Reader Enquiry Card

In the end, the author concludes that there is no evidence that chimps can produce sentences. Moreover, analysis of the project's videotapes indicated that most of his signed utterances were prompted by a teacher and contained major constituents of the teacher's previous utterance. Only 10% of Nim's utterances were spontaneous. Furthermore, he showed little ability to hold a conversation; he tended to interrupt his teachers frequently and to be unaware of the notion of taking turns.

Terrace carried his argument further by analysing films from other ape language projects and arriving at the same conclusions. Like the turn-of-the-century horse prodigy, Clever Hans, who appeared to do sums in his head and tap out the answers with his hoof, the signing apes appear to be responding at least in part to subtle cues from their trainers.

Reports of Terrace's work have been widely disseminated. Understandably, they have added to the ape-language controversy, and counter-arguments from other researchers have begun to appear. The author himself, at the end of the volume, explains why he thinks Nim's full linguistic potential may not have been realized, and he outlines a million dollar plan that he believes would produce greater success in a future project.

Language is the central issue, but the book also offers some rare insights into the personality of a bright young chimp. There are some fine photographs, and an informative appendix devoted to sign language. While the definitive work on language in apes has yet to appear, this is certainly both a scholarly and well-written one. ☐

Jean Berko Gleason is Professor of Psychology at Boston University.

Eclipsing binary light curve analysis

Joel A. Eaton

Language of the Stars: A Discourse on the Theory of the Light Changes of Eclipsing Variables. By Zdeněk Kopal. Pp. 280. (Reidel: 1979.) Hardback Dfl. 120, $63; paperback Dfl. 55, $28.95.

THIS book is written for an exceedingly small audience of specialists, or would-be specialists, involved in eclipsing binary light curve analysis. Contrary to the publisher's claim on the back cover, it is not a suitable book for amateur astronomers — other than those with doctorates in theoretical physics. Likewise, it would be inappropriate as a text for a university course about double stars as its content is too narrowly defined, while the references are almost completely restricted to the work of Kopal and his associates.

Throughout the book, Kopal seems to be re-fighting his traditional battle against the Russell model for calculating light curves. In doing this he has for the most part ignored the important work on the synthesis of light curves in the past decade, in which electronic computers have been used to integrate numerically over the visible surfaces of the components of a model binary system the light received at a distant point. This approach, developed by Leon Lucy, Robert E. Wilson and Graham Hill, to mention but a few of the more important contributors, has practically superseded the Russell model for application to tidally distorted binaries. Yet it rates only a few sentences of disparagement from Kopal.

The subject of this book is a method for determining the geometry of an eclipsing binary star by the Fourier analysis of its light variation, a technique already used extensively by others, Sławek Ruciński for example (*Acta Astronomica* **23**, 79; 1973), in studies of the light curves of W Ursae Majoris binaries. The classical method of analysing such light curves is to calculate a theoretical light curve for an assumed set of geometrical and photometric elements, compare these calculations with the observations of brightness as a function of orbital phase, and modify the elements to produce a better fit.

Kopal has devised a scheme for relating the geometrical elements of the model to certain properties of the Fourier transform of the light variation. Specifically, he has derived complicated algebraic equations relating geometrical elements and certain Fourier coefficients. However, after roundly criticizing the Russell model for basing a light curve solution on only three fixed points on the light curve (as was done in the early days), Kopal goes on to base his Fourier-analysis solutions on the power at only four frequencies in the Fourier transform. Indeed, nowhere in the book does he illustrate the Fourier transform of a light curve. ☐

Joel A. Eaton is a Research Associate at the Dyer Observatory of Vanderbilt University, Nashville, Tennessee, who specializes in studies of eclipsing binary light curves.

Inspec have just published *Ion-Solid Interactions: A Comprehensive Bibliography*, compiled by Walter M. Gibson and Henry H. Teitelbaum. The bibliography, which consists of three volumes — *Bibliography, Permuted title index* and *Author-title index* — and contains more than 12,000 references, is available from Inspec, Nightingale Road, Hitchin, Herts, UK, price £95, $195.

Archaeological chemistry for the curious

Robert Hedges

Archaeological Chemistry. By Z. Goffer. Pp. 376. (Wiley-Interscience: 1980.) £15.20, $33.

THIS book should appeal most to those wishing for a quick canter around the field of applications of chemistry to archaeology. The first 75 pages give a crash course in chemistry — atoms and molecules in one page, analytical techniques in about 30 — so that, having learnt to sit in the saddle and keep his eyes open, the reader is briskly shown all the major 'sights' of archaeological chemistry.

With research in this area flourishing at present, the scenery is rich indeed. Topics range from ancient cement-making to amino-acid racemization dating; from metal corrosion and its conservation to the identification of dyes used in antiquity. As might be expected, most space is reserved for accounts of ceramics and of metallurgy, but room is also found for such less-common subjects as palaeotemperature measurement, soil surveys and authentication. Faced with all this, inexperienced readers will be grateful that the treatment of each topic is, perhaps inevitably, superficial. However, they will obtain a clear idea of the extent to which scientific definition can be imposed on the material with which the archaeologist deals, and a notion of some of the surprising results that can follow from the careful use of analytical techniques. References to original literature are frequently cited, although to benefit from them would demand a deeper knowledge than is provided by this book. The style is relaxed, but never unscientific, and the few mathematical hurdles that have not been avoided are taken easily.

Nevertheless, I doubt that the reader will finish the book with any specific knowledge of the kind of research being conducted now, either in terms of individual work or as more synoptic problems (for example, the geographical exploitation of tin during the Bronze Age, the invention of glazing technologies or the dissemination of iron smelting techniques). Nor would I expect an archaeologist reading this book to be much better able to evaluate critically the results of his colleagues' work. For example, in an area where such cooperation is particularly active — the determination of pottery provenance from the comparison of trace element distributions — the subject is treated in just four pages, has no mention of the statistical problems and only a hint of geochemical difficulties.

The subtitle, *A Sourcebook . . . ,* makes claims that are not lived up to. Important books and journals are omitted in the bibliography, and comparatively few references are given beyond 1975. To cover such a field with authority would require a much more penetrating book. However, no other single volume attempts to cover such wide ground, and this one can be recommended to those whose interest is based on curiosity rather than knowledge. ☐

Robert Hedges is at the Research Laboratory for Archaeology, University of Oxford.

Will we use the ocean wisely?

Henry Charnock

Opportunities and Uses of the Ocean. By D. A. Ross. Pp. 320. (Springer-Verlag: 1980.) DM39.50, $21.80.

ONCE upon a time and a very good time it was oceanography was the profession of a small number of (almost all) men. They devoted their energy, skill and persistence, and sometimes their money, to exploring, measuring and seeking to understand the complicated structure and motion of the sea. Not, one supposes, in the hope of immediate financial gain; apart from pioneers like Maury and Fitzroy, who realized that an understanding of winds and currents could shorten sailing-ship passages and improve their owners' profits, most of the early marine scientists seem to have had only the most general notion that knowledge of the sea would prove useful.

Energy from under the sea — a natural-gas rig in the North Sea

Much more effort has been devoted to marine science since the Second World War, and even more money has been poured in since the great powers decided to deploy their nuclear weapons in submarines instead of aircraft. A vast amount of money is now spent in studying the ocean but with changed and more explicit motives — science is increasingly linked with technology and oceanic exploration has given way to exploitation, to the winning of food, minerals and energy and to the dumping of waste.

Not all of the proposed uses of the ocean are compatible and divergent views are strongly held by a range of interested groups. Dr Ross has set himself the question: "Where is the truth — what are the real problems and opportunities associated with the ocean?" He has attempted "to present some basic information about the ocean in a form that will be understandable to people who are not oceanographers, but who are interested and concerned about the marine environment". So the problems he is concerned with are not so much about the science as about the politics and legalities, while the opportunities are not to understand how the system works but how it can be exploited in a sensible (sustainable?) way.

An objective assessment needs the basic facts, so he gives 30 pages or so on "how the ocean works". It is difficult to compress such a broad subject into so little space — three pages to physical oceanography, for example — so it is not surprising that some of the explanation seems fluent rather than exact.

With finance as the only criterion, the most important users of the ocean are the navies of the world. Figures are hard to come by but it seems clear that a vast sum is spent each year on a range of activity and equipment mainly concerned with the detection of submarines. Anti-submarine warfare is a multi-billion dollar industry.

So the opacity of the ocean to electromagnetic radiation, which makes it dark, cold and mysterious, has led to a huge expenditure of scientists' time and taxpayers' money. Fortunately, perhaps, even though the (mainly acoustic) detection systems are complex the modern submarine is relatively safe in the ocean. Ross quotes a comparison between anti-submarine warfare and a game of baseball with the fielders blindfolded. And it is increasingly a game played between only two players, USA versus USSR, both of whom use the ocean as the location of their major weapon systems, their so-called 'second strike' capability. Because both nations have nearly undetectable submarines with frightening nuclear weapons, Ross argues that the opacity of the ocean deters them from starting a nuclear attack — an optimistic view.

If the opacity of sea water is important to submarines its combination of high density and low viscosity is fundamental to merchant shipping; surface ships remain the only practicable way of transporting heavy and bulky cargo over intercontinental distances. Next to military activity the shipping industry spends most on marine affairs (about 10^{11} dollars/year is said to go on building, maintaining and repairing ships). Ships and shipping have changed a great deal in recent decades: passenger liners are no more and cargo ships have become much more specialized, especially as regards the handling and stowage of their loads. They now need far smaller crews and in spite of much improved navigational aids collisions and other accidents still happen. Such catastrophes may lead to acute pollution of the *Torrey Canyon* type and one sympathizes with Ross's advocacy of "clear and positive control of ships, especially near or within coastal waters". But a comparison of aircraft and marine traffic control shows that this will need significant changes in the education and attitude of seafarers: this is a sociological problem which badly needs study.

The resources of the ocean with which most people are familiar are animal and mineral (it seems unlikely that the vegetable phytoplankton will be harvested in bulk, though seaweed is an important product and its cultivation a new and growing industry). There is much argument about the total amount of fish and related creatures that could be safely harvested — perhaps 2×10^8 tons/year is an optimistic figure. But it seems clear that marine biological resources are not the answer to the basic food problem posed by half the world's population being short of protein. Poorly understood and rather ineffectively controlled, fishing is perhaps the classical example of a non-profit industry. There may be an opportunity to exploit hitherto untaken species (krill is the obvious example); one can improve processing so as to convert trash fish into palatable products; one can develop and improve aquaculture techniques. All these will help supplement the world's protein requirements but seem unlikely to make a major contribution.

Mineral, as distinct from biological, marine resources provide a clearer problem. Most are not renewable so the problem is to find them, extract them and process them, without harming the environment. Here Dr Ross is on home ground, giving a clear account of the probability of exploiting the sediments of the Red Sea brine pools and of the possibility of using the better known manganese nodules. In shallower water offshore hydrocarbons are already a major industry, and will be for decades. Their yearly value (about 4×10^8 dollars) already exceeds that of fisheries.

Marine pollution is a diffuse and ill-defined subject. There is a great lack of information on sources, cycles and sinks of chemicals in the sea. Much of the most objectionable material comes from industrial sources, mainly in developed countries (the degree of marine pollution correlates closely with gross national product). So it would be possible, at a price, to control it at source. This is one of the points made strongly by the developing nations at the UN Conference on the Law of the Sea, and one can readily sympathize with their point of view. Not much interested in the military and shipping aspects, they are concerned to ensure that the industrialized nations do not gain a disproportionately large share of the (perhaps over-stated) marine resources. The scientific study of the ocean comes relatively low on their list of priorities (after agriculture, roads, hospitals, literacy and such) so they see little harm in the pace of marine research being slowed down. Even the so-called developed nations prefer to gain control over as much of the ocean and seabed as possible rather than to make it free for oceanographers to study the basic phenomena.

Ross ends with a chapter "Innovative Uses of the Ocean", including energy from the sea; climate and the ocean; fresh water from the sea; drugs from the sea; disposal of nuclear waste; research on satellite oceanography; the prospects for offshore islands. Again the chapter is too short to do justice to the variety of topics and the author has not been able to polish his writing sufficiently. Altogether the book, though superficially attractive, gives the impression that it would have been much improved by more attention to detail, both in text and illustration. The photographs are good but some of the map projections unfortunate; the text has confusing expressions and rather a lot of minor misprints, even in the prefatory poem (*The Sea and the Hills,* from Kipling's *The Five Nations* — and a good example of his sound and fury style it is).

No one could possibly disapprove of the author's motives — it would be marvellous if politicians and lawyers and admirals and (perhaps especially) multi-national moguls knew and cared more about the sea. But I fear it will need more than a book like this.

Henry Charnock is Professor of Physical Oceanography at the University of Southampton.

Soil sugars for the soil scientist

M. Schnitzer

Nature and Origin of Carbohydrates in Soils. By M. V. Cheshire. Pp. 216. (Academic: 1980.) £15.80, $36.50.

ABOUT 10% of the organic matter in soils occurs as carbohydrates — mainly in the form of polysaccharides comprised of at least seven neutral, two acidic and two basic sugars — which originate from plant and animal remains and from microbial syntheses. From an agricultural point of veiw, their most important functions are to supply microorganisms with readily available food and to bind soil particles into stable aggregates which improve soil aeration, root development and ease of cultivation, and prevent erosion.

The first four chapters of this book deal with the composition and analysis of carbohydrates and polysaccharides in soils. Especially useful are recommended procedures for the hydrolysis and analysis of freed sugars, uronic acids and amino sugars by colorimetric, gas chromatographic and enzymatic methods. A problem in such analyses is that polysaccharides in soils appear to be chemically linked to proteins and humic materials; so far separation from humic materials has been more successful than from proteins.

The next section is concerned with the metabolism of carbohydrates in soils. Incubation experiments with ^{14}C-labelled glucose show that while microorganisms can synthesize soil sugars, the overall composition of microbial polysaccharides differs from that of soil polysaccharides as a whole and can only account for a part of it. It is estimated that the live biomass constitutes only 2.5% of the weight of soil carbohydrates.

The author has made a very useful contribution by bringing together the essence of widely scattered literature published over a period of 85 years. To the best of my knowledge this is the first book to deal with carbohydrates in soil; its appearance will be welcomed by those interested in the chemistry, biology and management of soil organic matter. ☐

M. Schnitzer is Program Leader of soil chemistry and biology research at the Chemistry and Biology Research Institute, Agriculture Canada, Ottawa.

BOOKS RECEIVED

Mathematics

COLLINS, R. and VAN DER WERFF, T. J. Mathematical Models of the Dynamics of the Human Eye. Lecture Notes in Biomathematics Vol. 34. Pp.99. Flexi ISBN 3-540-09751-1. (Springer-Verlag: 1980.) DM 19.50, $11.50.

EASON, G., COLES, C. W. and GETTINBY, G. Mathematics and Statistics for the Bio-Sciences. Pp.578. ISBN 0-85312-175-3. (Wiley: 1980.) £25.

HAWKINS, D. M. Identification of Outliers. Pp.188. ISBN 0-412-21900-X. (Chapman & Hall: 1980.) £10.

REICHL, L. E. A Modern Course in Statistical Physics. Pp.709. ISBN 0-292-75051-X. (University of Texas Press: 1980.) $29.95.

STAHL, S. M. and HENNES, J. D. Reading and Understanding Applied Statistics; A Self-learning Approach. 2nd Edn. Pp.374. Flexi ISBN 0-8016-4754-1. (YB Medical: 1980.) £6.75.

STUMMEL, F. and HAINER, K. Introduction to Numerical Analysis. Pp.282. Flexi ISBN 7073-0130-0. (Scottish Academic Press: 1980.) £9.50.

WÖRZ-BUSERROS, A. Algebras in Genetics. Lecture Notes in Biomathematics Vol. 36. Pp.237. Flexi ISBN 3-540-09978-6. (Springer-Verlag: 1980.) DM 28.50, $16.90.

Astronomy

ABELL, G. O. and PEEBLES, P. J. E. Objects of High Redshift. International Astronomical Union Symposium No. 92. Pp.328. Hbk ISBN 90-277-1118-6; pbk ISBN 90-277-1119-4. (Reidel: 1980.) Hbk Dfl. 80, $42; pbk Dfl. 40, $21.

APPENZELLERS, I., LEQUEUX, J. and SILK, J. Star Formation. Tenth Advanced Course of the Swiss Society of Astronomy and Astrophysics. Pp.222. Flexi ISBN (Geneva Observatory: CH-1290 Sauverny, Switzerland, 1980.) S.Fr. 30.

DYSON, J. E. and WILLIAMS, D. A. Physics of the Interstellar Medium. Pp.194. ISBN 0-7190-0797-6. (Manchester University Press: 1980.) £11.95.

KUNDU, M. R. and GERGELY, T. E. (eds). Radio Physics of the Sun. International Astronomical Union Symposium No. 86. Pp.475. Hbk ISBN 90-277-1120-8; pbk ISBN 90-277-1121-6.) Reidel: 1980.) Hbk Dfl. 115, $60.50; pbk Dfl. 55, $28.95.

PLAVEC, M. J., POPPER, D. M. and ULRICH, R. K. (eds). Close Binary Stars: Observations and Interpretation. International Astronomical Union Symposium No. 88. Pp.598. Hbk ISBN 90-277-1116-X; pbk ISBN 90-277-1117-8. (Reidel: 1980.) Hbk Dfl. 130, $68.50; pbk Dfl. 60, $31.50.

Physics

BERTSCH, G. F. and KURATH, D. (eds). Nuclear Spectroscopy. Lecture Notes of the Workshop held at Gull Lake, Michigan, August 1979. Lecture Notes in Physics Vol. 119. Pp.250. Flexi ISBN 3-540-09970-0. (Springer-Verlag: 1980.) DM 33, $19.50.

EDWARDS, C. (ed.). Gravitational Radiation, Collapsed Objects and Exact Solutions. Proceedings of the Einstein Centenary Summer School held in Perth, Australia, January 1979. Lecture Notes in Physics Vol. 124. Pp.487. Flexi ISBN 3-540-09992-1. (Springer-Verlag: 1980.) DM 52, $30.70.

EISENBURGH, J. M. Theory of Meson Interactions with Nuclei. Pp.403. ISBN 0-471-03915-2. (Wiley-Interscience: 1980.) £21.75.

FAVA, R. A. (ed.). Polymers, Part A: Molecular Structure and Dynamics. Methods of Experimental Physics Vol. 16. Pp.590. ISBN 0-12-471956-5. (Academic: 1980.) $55.

FAVA, R. A. (ed.). Polymers, Part B: Crystal Structure and Morphology. Methods of Experimental Physics Vol. 16. Pp.421. ISBN 0-12-475957-2. (Academic: 1980.) $45.

HAWKING, S. W. and ISRAEL, W. (eds). General Relativity: An Einstein Centenary Survey. Pp.919. Pbk ISBN 0-521-22285-0. (Cambridge University Press: 1980.) £12.50.

HILL, H. A. and DZIEMBOWSKI, W. A. (eds). Nonradial and Nonlinear Stellar Pulsation. Lecture Notes in Physics Vol. 125. Proceedings of a Workshop held at the University of Arizona, Tucson, March 1979. Pp.497. Flexi ISBN 3-540-09994-8. (Springer-Verlag: 1980.) DM 57, $33.70.

HODGSON, P. E. Growth Points in Nuclear Physics Vol. 1. Pp.219. ISBN 0-08-023080-6. (Pergamon: 1980.) $18.

IACOLNITZER, D. (ed.). Complex Analysis, Microlocal Calculus and Relativistic Quantum Theory. Proceedings of the Colloquium held at Les Houches, Centre de Physique, September 1979. Lecture Notes in Physics Vol. 126. Pp.502. Flexi ISBN 3-540-09996-4. (Springer-Verlag: 1980.) DM 57, $33.70.

IOSIFESCU, M. Finite Markov Processes and Their Applications. Pp.295. ISBN 0-471-27677-4. (Wiley: 1980.) £11.75.

MILINE, A. F. and GIACOMO, P. (eds). Metrology and Fundamental Constants. Proceedings of the International School of Physics, Varenna, Italy, July 1976. Pp.815. ISBN 0-444-85467-3. (North-Holland: 1980.) $146.25, Dfl. 300.

NAPOLITANO, L. G. (ed.). Space Developments for the Future of Mankind. Selected Papers from the XXX International Astronautical Congress, Munich, September 1979. Pp.561. ISBN 0-08-025454-3. (Pergamon: 1980.) $100.

PATRA, H. P. and MALLICK, K. Geosounding Principles, 2 Time-Varying Geolectric Soundings. Methods in Geochemistry and Geophysics, 14B. Pp.424. ISBN 0-444-41811-3. (Elsevier: 1980.) $87.75, Dfl. 180.

SUHL, H. and MAPLE, M. B. (eds). Superconductivity in *d*- and *f*-Band Metals. Pp.525. ISBN 0-12-676150-7. (Academic: 1980.) $39.50.

VON OERTZEN, W. (ed.). Deep-Inelastic and Fusion Reactions with Heavy Ions. Proceedings of the Symposium held at the Hahn-Meitner-Institut, Berlin, October 1979. Lecture Notes in Physics Vol. 117. Pp.394. Flexi ISBN 3-540-09965-4. (Springer-Verlag: 1980.) DM 49, $29.

WARD-SMITH, A. J. Internal Fluid Flow. the Fluid Dynamics of Flow in Pipes and Ducts. Pp.566 ISBN 0-19-856325-6. (Clarendon/Oxford University Press: 1980.) £36.

WHITE, C. W. and PEERCY, P. S. (eds). Laser and Electron Beam Processing of Materials. Proceedings of a Symposium held in Cambridge, Massachusetts, November 1979. Pp.769. ISBN 0-12-746850-1. (Academic: 1980.) $40.

WIEGEL, F. W. Fluid Flow Through Porous Macromolecular Systems. Lecture Notes in Physics Vol. 121. Pp.102. Flexi ISBN 3-540-09973-5. (Springer-Verlag: 1980.) DM 18, $10.70.

WUNDERLICH, B. Macromolecular Physics. Vol. 3 Crystal Melting. Pp.363. ISBN 0-12-765603-0. (Academic: 1980.) $42.50.

YARDLEY, J. T. Introduction to Molecular Energy Transfer. Pp.308. ISBN 0-12-768550-2. (Academic: 1980.) $34.

Chemistry

CAMPBELL, I. M. An Examples Course in Reaction Kinetics. An International Case Studies Approach. Pp.163. Hbk ISBN 0-7002-0275-7; pbk ISBN 0-7002-0276-5. (Blackie: 1980.) Hbk £13.50; pbk £6.75.

EMÈLEUS, H. H. and SHARPE, A. G. (eds). Advances in Inorganic Chemistry and Radiochemistry. Vol. 23. Pp.441. ISBN 0-12-023623-0. (Academic: 1980.) $51.

FUKUI, K. and PULLMAN, B. (eds). Horizons of Quantum Chemistry. Proceedings of the 3rd International Congress of Quantum Chemistry held at Kyoto, Japan, October 1979. Pp.296. ISBN 90-277-1105-4. (Riedel: 1980.) Dfl. 75, $39.50.

GOODMAN, C. D. *et al.* (eds). The (p,n) Reaction and the Nucleon-Nucleon Force. Proceedings of the Conference held in Telluride, Colorado, March 1979. Pp.539. ISBN 0-306-40351-X. (Plenum: 1980.) $55.

HARRISON, D. E. F., HIGGINS, I. J. and WATKINSON, R. Hydrocarbons in Biotechnology. Proceedings of a meeting held at the University of Kent, September 1979. Pp.198. ISBN 0-85501-325-7. (Heyden: London, 1980.) $31.50, £14, DM 65.50.

KLABUNDE, K. J. Chemistry of Free Atoms and Particles. Pp.235. ISBN 0-12-410750-8. (Academic: 1980.) $29.50.

LÜSCHER, E. and COUFAL, H. (eds). Liquid and Amorphous Metals. Proceedings of the NATO Advanced Study Institute, Zwiesel, Germany, September 1979. Pp.672. ISBN 90-286-0680-7. (Sijthoff & Noordoff: 1980.) Dfl. 150, $75.

PETRAKIS, L. and WEISS, F. T. (eds). Petroleum in the Environment. Advances in Chemistry Series 185. Pp.371. ISBN 0-8412-0475-6. (American Chemical Society: Washington, DC 1980.) $42.

PETTIT, G. R. Synthetic Peptides Vol. 5. Pp.404. ISBN 0-444-41895-4. (Elsevier: 1980.) $109.75, Dfl. 225.

RICHARDS, E. G. An Introduction to the Physical Properties of Large Molecules in Solution. Pp.266. Hbk ISBN 0-521-23110-8; pbk ISBN 0-521-29817-2. (Cambridge University Press: 1980.) Hbk £18; pbk £5.95.

STONE, F. G. A. and WEST, R. (eds). Advances in Organometallic Chemistry, Vol. 18. Pp.354. ISBN 0-12-031118-6. (Academic: 1980.) $42.50.

THE COMMITTEE ON CHEMISTRY AND PUBLIC AFFAIRS. Chemistry and the Food System. Pp.138. Hbk ISBN 0-8412-0557-4; pbk ISBN 0-8412-0563-9. (American Chemical Society: Washington, DC, 1980.) Hbk $15; pbk. $9.

TIPSON, R. S. and HORTON, D. (eds). Advances in Carbohydrate Chemistry and Biochemistry. Pp.483. ISBN 007237-8. (Academic: 1980.) $49.50.

WALTON, A. G. (ed.). Structure and Properties of Amorphous Polymers. Studies in Physical and Theoretical Chemistry, 10. Proceedings of the 2nd Cleveland Symposium on Macromolecules, Cleveland, Ohio, October 1978. Pp.23[illegible]. ISBN 0-444-51905-5. (Elsevier: 1980.) $53.75, Dfl.110.

WOHLFARTH, E. P. (ed.). Ferromagnetic Materials: A Handbook on the Properties of Magnetically Ordered Substances Vol. 2. Pp. 587. ISBN 0-444-85312-X. (North-Holland: 1980.) $102.50, Dfl. 210.

Technology

HIRVONEN, J. K. (ed.). Ion Implantation. Treatise on Materials Science and Technology Vol. 18. Pp. 502. ISBN 0-12-341818-6. (Academic: 1980.) $55.

RYBCZYNSKI, W. Paper Heroes. A Review of Appropriate Technology ISBN 0-904727-37-8. (Prism Press: Stable Court, Chalmington, Dorset: 1980.) Hbk £7.95; pbk £3.95.

Computer Science

TAYLOR, D. R. F. (ed.). The Computer in Contemporary Cartography. Progress in Contemporary Cartography Vol. 1. Pp. 252. ISBN 0-471-27699-5 (Wiley: 1980.) £15.

Earth Sciences

BANNER, F. T., COLLINGS, M. B. and MASSIE, D. S. (eds). The North-West European Shelf Seas: The Sea Bed and the Sea in Motion. II. Physical and Chemical Oceanography, and Physical Resources. Pp. 338. ISBN 0-444-41693-5. (Elsevier: 1980.) $90.25, Dfl. 185.

EGGINTON, J. The Poisoning of Michigan. Pp. 3[illegible]1. ISBN 0-393-01347-2. (W. W. Norton: 1980.) $13.95.

FORTESCUE, J. A. C. Environmental Geochemistry: A Holistic Approach. Pp. 237. ISBN 3-540-90454-9. (Springer-Verlag: 1980.) DM 69, $40.80.

FRITZ, P. and FONTES, J. Ch. (eds). Handbook of Environmental Isotope Geochemistry. Vol. 1 , The Terrestrial Environment, A. Pp. 532. ISBN 0-444-41780-X. (Elsevier: 1980.) $90.25, Dfl. 185.

HAENEL, R. (compiled by). Atlas of Subsurface Temperatures in the European Community. Pp. 43. (Commission of the European Communities: 1979.) Np.

HOEFS, F. Stable Isotope Geochemistry. 2nd Edn. Minerals and Rocks Vol. 9. Pp. 208. ISBN 3-540-09917-4. (Springer-Verlag: 1980.) DM 59. $34.90.

HOLMQUIET, R. (ed.). Life Sciences and Space Research Vol. XVIII. Proceedings of the Open Meeting of the Working Group on Space Biology of the 22nd Plenary Meeting of COSPAR Bangalore, India, May 1979. Pp. 220. ISBN 0-08-024436X. (Pergamon: 1980.) £20.

MERLA, G. *et al.* A Geological Map of Ethopia and Somalia. Pp.117. Pbk ISBN 0-08-024028-3. (Pergamon: 1980.) $60, £27.50.

OLAUSSON, E. and CATO, I. (eds). Chemistry and Biogeochemistry of Estuaries. Pp.452. ISBN 0-471-27679-0. (Wiley-Interscience: 1980.) £28.50.

POMEROL, C. (ed.). Geology of France with twelve itineries and a geological map at 1:2,500,000. Guides Gèologiques Régionaux. Pp. 256 Pbk ISBN 2-225-67001-3. (Masson: 1980.) Np.

VOWLES, P. D. and CONNELL, D. W. Experiments in Environmental Chemistry: A Laboratory Manual. Pergamon Series on Environmental Science Vol. 4. Pp.102. Hbk ISBN 0-08-024010-0; flexi ISBN 0-08-024009-7. (Pergamon: 1980.) Hbk £9; flexi £4.50.

Biological Sciences

ADAMS, R. L. P. Cell Culture for Biochemists. Laboratory Techniques in Biochemistry and Molecular Biology. Pp.292. Flexi ISBN 0-444-80199-5. (Elsevier/North-Holland: 1980.) $27.75, Dfl. 57.

ANDERSON, E. F. Peyote: The Divine Cactus. Pp.248. Hbk ISBN 0-8165; pbk ISBN 0-8165-0613-2. (University of Arizona Press: 1980.) Hbk $18.50; pbk $6.95.

ANGST, W. Aggression bei Affen und Menschen. Pp.190. Flexi ISBN 3-540-09877-1. (Springer-Verlag: 1980.) DM 32, $18.90.

ASHBURNER, M. and WRIGHT, T. R. F. (eds). The Genetics and Biology of Drosophila Vol. 2d. Pp.702. ISBN 0-12-064943-8. (Academic: 1980.) £54, $124.50.

BADHAM, M. and LAWLESS, M. Chimps with Everything. The Story of Twycross Zoo. Pp.143. Flexi ISBN 0-09-923340-1. (Arrow Books: London, 1980.) £1.25.

BASERGA, R., CROCE, C. and ROVERA, G. Introduction of Macromolecules into Viable Mammalian Cells. Wistat Symposium Series Vol. 1. Pp.357. ISBN 0-8451-2000-X. (Alan R. Liss: New York, 1980.) $26. Available in Europe and the Middle East from European Book Service, Flevolaan 36-38 P.O.B. 124, 1380 AC Weesp, Holland.

BAUER, C., GROS, G. and BARTELS, H. Biophysics and Physiology of Carbon Dioxide. Symposium held at the University of Regensburg (FRG) April 1979. Pp.453. ISBN 3-450-09892-5. (Springer-Verlag: 1980.) DM 86, $50.80.

BES, A. and GERAUD, G. (eds). Cerebral Circulation and Neurotransmitters. Proceedings of the Inernational Congress on Cerebral Circulation, Toulouse, September 1979. Pp.268. ISBN 90-219-0430-6. (Excerpta Medica: 1980.) $48.75, Dfl. 100.

BLOUGH, H. A. and TIFFANY, J. M. Cell Membranes and Viral Envelopes. Vol. 1. pp.456, ISBN 0-12-107201-0. Vol. 2, pp.409, ISBN 0-12-107202-0. (Academic: 1980.) £40, $92. (both vols).

BRODSKY, K. A. Mountain Torrent of the Tien Shan. A faunistic-ecology essay. Monographiae Biologicae Vol. 39. Pp.311. ISBN 90-6193-091-X. (W. Junk: The Hague, 1980.) Dfl. 150, $79.

CHAPMAN, G. The Body Fluids and Their Functions. 2nd Edn. Pp.74. Pbk ISBN 0-7131-2796-1. (Edward Arnold: London, 1980.) £2.75.

CROOKE, S. T. and REICH, S. D. (eds). Anthracyclines. Current Status and New Developments. Proceedings of a workshop on anthracyclines held in Norfolk, Virginia, June 1979. Pp.444. ISBN 0-12-197780-3. (Academic: 1980.) $27.50.

DELRIO, G. and BRACHET, J. Steriods and Their Mechanism of Action in Nonmammalian Vertebrates. Pp.239. ISBN 0-89004-487-2. (Raven: 1980.) $22.50.

ENRIGHT, J. T. The Timing of Sleep and Wakefulness. On the Substructure and Dynamics of the Circadian Pacemakers Underlying the Wake–Sleep Cycle. Studies of Brain Function, Vol. 3. Pp.263. Flexi ISBN 3-540-09667-1. (Springer-Verlag: 1980.) DM 49, $29.

FESTING, M.F.W. (ed.). International Index of Laboratory Animals. 4th Edn. Pp.141. ISBN 0-901053-04-X. (Medical Research Council: 1980.) £5.

HARRIS, C.S. Visual Coding and Adaptability. Pp.332. ISBN 0-89859-016-7. (Lawrence Erlbaum: Hillsdale, New Jersey, 1980.) $24.95.

HEIDEN, U. Analysis of Neural Networks. Lecture Notes in Biomathematics Vol.35. Pp.159. Flexi ISBN 3-540-09966-2. (Springer-Verlag: 1980.) DM 23, $13.90.

HESKETH, J.D. and JONES, J.W. (eds). Predicting Photosynthesis for Ecosystem Models. Vol.I. Pp.273. ISBN 0-8493-5335-1. (CRC, Boca Raton, Florida: 1980.) Np.

HESKETH, J.D. and JONES, J.W. (eds). Predicing Photosynthesis for Ecosystem Models. Vol.II. Pp.279. ISBN 0-8493-5336-X. (CRC, Boca Raton, Florida: 1980.) Np.

HILDEBRAND, R. Nuclear Volume and Cellular Metabolism. Advances in Anatomy Embryology and Cell Biology Vol.60. Pp.54. Flexi ISBN 3-540-09796-1. (Springer-Verlag: 1980.) DM 30, $17.70.

HOLMAN, R.T. (ed.). Progress in Lipid Research, Vol.17. Pp.396. ISBN 0-08-023797-5. (Pergamon: 1980.) £28.

HORECKER, B.L. and STADTMAN, E.R. (eds). Current Topics in Cellular Regulation. Vol.16. Pp.321. ISBN 0-12-152816-2. (Academic: 1980.) $36.

JOHNSON, M.H. and EVERITT, B.J. Essential Reproduction. Pp.356. Flexi ISBN 0-632-00527-0. (Blackwell Scientific: 1980.) £8.50.

KELLMAN, M.C. Plant Geography. 2nd Edn. Pp.181. Hbk ISBN 0-416-73850-8; pbk ISBN 0-416-73860-5. (Methuen: 1980.) Pbk £4.95.

KERKUT, G.A. and PHILLIS, J.W. (eds). Progress in Neurobiology Vol.13. Pp.448. ISBN 0-08-026039-X. (Pergamon: 1980.) Np.

KNOCHE, H. Histologie und Histopathologie. Kurzle für medizinisch-technische Assistenten. Pp.347. Pbk ISBN 3-540-09857-7. (Springer-Verlag: 1980.) DM 58, $34.30.

KORR, H. Proliferation of Different Cell Types in the Brain. Advances in Anatomy Embryology and Cell Biology Vol.61. Pp.72. Flexi ISBN 3-540-09889-2. (Springer-Verlag: 1980.) DM 48, $28.40.

KORYTA, J. (ed.). Medical and Biological Applications of Electrochemical Devices. Pp.331. ISBN 0-471-27678-2. (Wiley-Interscience: 1980.) £27.

LI, C.H. (ed.). Hormonal Proteins and Peptides. Vol.VIII: Prolactin. Pp.231. ISBN 0-12-447208-7. (Academic: 1980.) $29.50.

MILLER, J.H. and REZNIKOFF, W.S. The Operon. Pp.469. Flexi ISBN 0-87969-133-6. (Cold Spring Harbor Laboratory: 1980.) $18 ($21.60 outside US).

MORET, P.R., WEBER, J., HAISSLY, J.-Cl and DENOLIN, H. (eds). Lactate; Physiologic, Methodologic and Pathologic Approach. Pp.257. Flexi ISBN 3-540-09829-1. (Springer-Verlag: 1980.) DM 35, $20.70.

NAPIER, J. Hands. Pp.176. ISBN 0-04-611004-6. (Allen & Unwin: London, 1980.) £12.50.

OLDENDORF, W.H. The Quest for an Image of Brain. Computerized Tomography in the Perspective of Past and Future Imaging Methods. Pp.155. ISBN 0-89004-429-5. (Raven: 1980.) $19.50.

ORR, R.T. and ORR, D.B. Mushrooms of Western North America. California Natural History Guides: 42. Pp.293. ISBN 0-520-03656-5. (University of California Press: 1980.) £7.75.

SCHAFER, W. Fossolien. Bilder und Gedanken zur paläontologischen Wissenschaft. Pp.244. ISBN 3-7829-1075-3. (Im Verlag von Waldemar Kramer: Frankfurt, 1980.) Np.

SCHMIDT-NIELSEN *et al.* (eds). Comparative Physiology: Primitive Mammals. Papers from the 4th International Conference on Comparative Physiology held at Crans-sur-Sierre, Switzerland, June 1978. Pp.338. ISBN 0-521-22847-6. (Cambridge University Press: 1980.) £20.

SHANKS, R.G. (ed.). Cardiovascular Systems. Pp.106. ISBN 0-333-28604-9. (Macmillan Press: London, 1980.) £10.

SOKOLOFF, L. (ed.). The Joints and Synovial Fluid. Vol.II. Pp.561. ISBN 0-12-655102-2. (Academic: 1980.) $55.

SMITH, A.J.E. The Moss Flora of Britain and Ireland. Pp.706. Hbk ISBN 0-521-21648-6; pbk ISBN 0-521-29973-X. (Cambridge University Press: 1980.) Pbk £12.50.

SMYTH, J.D. and SMYTH, M.M. Frogs and Host–Parasite Systems I. An Introduction to Parasitology through the Parasites of *Rana temporaria, R. esculenta* and *R. pipiens.* Pp.112. Hbk ISBN 0-333-28983-8; pbk ISBN 0-333-223535£7. (Macmillan Press: London, 1980.) Hbk £12; pbk £5.95.

SÖLL, D., ABELSON, J.N. and SCHIMMEL, P.R. (eds). Transfer RNA: Biological Aspects. Pp.584. ISBN 0-87969-129-8. (Cold Spring Harbor Laboratory: 1980.) $60 ($72 outside US).

SONESSON, M. Ecology of a Subarctic Mire. Ecological Bulletins No.30. Pp.314. ISBN 91-546-0275-0. (Swedish Natural Science Research Council: Stockholm, 1980.) SwCr.125, $30.

STEC, W.J. (ed.). Phosphorous Chemistry directed towards Biology. Lectures Presented at the International Symposium, Burzenin, Poland, September 1979. Pp.231. ISBN 0-08-023969-2. (Pergamon: 1980.) $60.

SULMAN, F.G. The Effect of Air Ionization, Electric Fields, Atmospherics and other Electric Phenomena on Man and Animal. Pp.398. Hbk ISBN 0-398-03929-1; pbk ISBN 0-398-03930-5. (Charles C. Thomas: Springfield, Illinois, 1980.) Hbk $24.75; pbk $18.75.

Sociology

BENARIE, M. M. Urban Air Pollution Modelling. Pp.405. ISBN 0-333-23391-3. (Macmillan Press: London, 1980.) £30.

EINSTEIN, S. (ed.). Drugs in Relation to the Drug User. Critical Drug Issues. Pp.351. ISBN 0-08-019596-2. (Pergamon: 1980.) £22.50, $45.

EINSTEIN, S. (ed.). The Community's Response to Drug Use. Pp.369. ISBN 0-08-019597. (Pergamon: 1980.) £22.50.

HOWARD-JONES, N. and BANKOWSKI, Z. (eds). Medical Experimentation and the Protection of Human Rights. XIIth CIOMS Round Table Conference. Pp.249. Flexi ISNB 92-9036-002-X. (CIOMS: Geneva, 1979.) SwFr.25.

KIEV, A., MUYA, W. J. and SARTORIUS, N. The Future of Mental Health Services. Proceedings of a Conference on The Future of Mental Health Services, Nairobi, Kenya, August 1979. Pp.257. ISBN 90-219-0429-2. (Excerpta Medica: 1980.) $53.75, Dfl.110.

MARTIN, G. L. and OSBORNE, J. G. (eds). Helping in the Community; Behavioral Applications. Pp.415. ISBN 0-306-40402-8. (Plenum: 1980.) $22.50.

PRICE, R. H. and POLITSER, P. E. (eds). Evaluation and Action in the Social Environment. Pp.235. ISBN 0-12-564650-X. (Academic: 1980.) $18.50.

RANGE, D. G., LAYTON, J. R. and ROUBINEK, D. L. (eds). Aspects of Early Childhood Education. Theory to Research to Practice. Pp.205. ISBN 0-12-580150-5. (Academic: 1980.) $17.50.

RUSHTON, J. P. Altruism, Socialization, and Society. Prentice-Hall series in Social Learning Theory. Pp.244. ISBN 0-13-023408-7. (Prentice/Hall: 1980.) £11.

SHUVAL, J. T. Entering Medicine; The Dynamics of Transition. A Seven Year Study of Medical Education in Israel. Pp.247. ISBN 0-08-024272-3. (Pergamon: 1980.) £15, $33.75.

History of Science

LAVINGTON, S. Early British Computers: The Story of Vintage Computers and the People Who Built Them. Pp.139. Hbk ISBN 0-7190-0803-4; pbk ISBN 0-7190-0810-7. (Manchester University Press: 1980.) Pbk £3.95.

Anthropology

DROOGERS, A. The Dangerous Journey. Symbolic Aspects of Boys' Initiation among the Wagenia of Kisangani, Zaire. Change and Continuity in Africa. Pp.416. Flexi ISBN 90-279-3357-X. (Global Book Resources: London, 1980.) £15.75.

EARLE, T. K. and CHRISTENSON, A. L. (eds). Modelling Change in Prehistoric Subsistence Economies. Studies in Archaeology Series. Pp.261. ISBN 0-12-227850-X. (Academic: 1980.) $24.50.

LYNCH, T. F. (ed.). Guitarrero Cave. Early Man in the Andes. Pp.327. ISBN 0-12-460580-X. (Academic: 1980.) $24.

MIELKE, J.H. and CRAWFORD, M.H. (eds). Current Developments in Anthropological Genetics. Vol. I Theory and Methods. Pp.436. ISBN 0-306-40390-0. (Plenum: 1980.) $45.

THOMPSON, F. H. (ed.). Archaeology and Coastal Change. Papers presented at meetings in London and Manchester on 27th October and 5th November, 1977. Occasional Paper (New Series) I. Pp.154. Flexi ISBN 0-500-99031-X. (Thames and Hudson: 1980.) £12.

General

APOSTOLAKIS, G., GARRIBA, S. and VOLTA, G. Synthesis and Analysis Methods for Safety and Reliability Studies. Pp. 463. ISBN 0-306-40316-1. (Plenum: 1980.) $49.50.

ARDITTI, R., BRENNAN, P. and CAVRAK, S. (eds). Science and Liberation. Pp. 398. Pbk ISBN 0-89608-022-6; hbk ISBN 0-89608-023-4. (South End Press: Box 68, Astor Station, Boston 02123, 1980) np.

ATKINSON, D. Menu French. International Series in Hospitality Management. Pp. 94. Flexi ISBN 0-08-024308-8. (Pergamon: 1980.) Flexi £2.75, $6.

BASSON, M. D. (ed.). Ethics, Humanism, and Medicine Proceedings of Three Conferences held at the University of Michigan, 1978–1979. Progress in Clinical and Biological Research Vol. 38. Pp. 319. ISBN 0-8451-0038-6. (Alan R. Liss: New York, 1979.) $22. Available in Europe and the Middle East European Book Service, Flevolaan 36-38, P.O.B. 124, 1380 AC Weesp, Holland. Dfl. 66.

BLACK, F. L. and REIS, P. J. (eds). Physiological and Environmental Limitations to Wool Growth. Proceedings of a National Worshop, Leura, New South Wales, Australia, April, 1979. Pp. 405. ISBN 0-85834-252-9. (University of New England: Armidale, Australia, 1979.) Aust. $13.50.

BREUER, G. Air in Danger. Ecological perspectives of the atmosphere. Pp. 189. Hbk ISBN 0-521-22417-9; pbk ISBN 0-521-29483-5. (Cambridge University Press: 1980.) Hbk £10; pbk £3.50.

BRODEUR, P. The Asbestos Hazard. Pp. 93. Flexi ISBN0-89766-042-0. (New York Academy of Sciences: 1980.) $4.

CAMPAN, R. L'Animal et Son Univers: étude dynamique du comportement. Pp. 258. Flexi ISBN 2-7089-8700-3. (Éditions Édouard Privat: Toulouse, 1980.) Np.

CARRIERE, D. Solar Houses for a Cold Climate. A detailed study of 26 solar heated houses. Pp. 279. ISBN 0-471-99809-5. (Wiley: 1980.) £10.25.

COMMITTEE OF DISASTERS AND THE MASS MEDIA COMMISSION OF SOCIOTECHNICAL SYSTEMS NATIONAL RESEARCH COUNCIL. Disasters and the Mass Media. Proceedings of the Committee of Disasters and the Mass Media Workshop, February 1979. Pp. 301. Flexi 0 309-03024-2. (National Academy of Sciences: 1980.) $9.75.

CRANE, E. A Book of Honey. Pp. 193. Hbk ISBN 0-19-217657-9. (Oxford University Press: 1980.) Hbkl £6.95. Available in pbk £3.50.

DIN DEUTSCHES INSTITUT FÜR NORMUNG E. V. Catalogue English Translation of Geeman Standards 1980. Completed with December 1979 edition of 'DIN-Mitteilungen + elektronorm'. Pp. 192 (DIN Deutsches Institut für Normung e.v.: 1980.) Flexi np.

DUFTY, W. Sugar Blues. Revised British Edition. Pp. 218 ISBN 0-85626-179-3. (Abacus: Tunbridge Wells, UK, 1980.) £5.95.

FEINBERG, G. and SHAPIRO, R. Life Beyond Earth. The Intelligent Earthling's Guide to Life in the Universe. Pp. 464. Hbk ISBN 0-688-03642-2; pbk ISBN 0-688-08642-X. (William Morrow: New York, 1980.) Hbk £14.95; pbk $7.95.

GASPARINI, I. Giornale Degli Economisti E. Annali Di Economia. Saggi in Onore di Giovanni Demaria. Pp. 948. (Universita Commerciale Luigi Bocconi: 1979.) Np.

GORMAN, J. Hazards to Your Health. The Problem of Environmental Disease. Pp. 70. Flexi ISBN 0-89766-024-2. (New York Academy of Sciences: 1979.) $4.

GORZ, A. Ecology as Politics. Pp. 215. Pbk ISBN 0-89608-088-9; hbk ISBN 0-89608-089-7. (South End Press: Box 68, Astor Station, Boston 02123, 1980.) Np.

HOLLANDS, C. Compassion is the Bugler. The Struggle for Animal Rights. Pp. 201. ISBN 0-904265-35-8. (Macdonald Publishers: Midlothian, Scotland, 1980.) £6.95.

HUETING, R. New Scarcity and Economic Growth. More Welfare Through Less Production? Pp. 269. ISBN 0-444-85400-2 (North-Holland: 1980.) Np.

INFELD, L. Quest — An Autobiography. Pp. 361. ISBN 0-8284-0309-0. (Chelsea Publishing: New York, 1980.) $17.50.

KOREN, H. Handbook of Environmental Health and Safety. Principles and Practices. Parts 1 & 2. Pp. 698. ISBN 0-08-023900-5 (Pergamon: 1980.) £47.50, $95.

LASZLO, E. *et al.* The Obstacle to the New International Economic Order. Pergamon Piolicy Studies on the New International Economic Order. Pp. 144. Hbk ISBN 0-08-025110-2, flexi ISBN 0-80-025110-2. (Pergamon: 1980) Hbk £8.75; flexi £3.55.

MABRO, R. (ed.). World Energy Issues and Policies. Proceedings of the First Oxford Energy Seminar, September 1979. Pp. 367. ISBN 0-19-920119-6 (Oxford University Press: 1980.) £15.

MATURANA, H. R. and VARELA, F. J. Autopoiesis and Cognition. The Realization of the Living. Pp. 140. Hbk ISBN 90-277-1015-5; pbk ISBN 90-277-1016-3. (Reidel: 1980.) Hbk Dfl. 55, $28..95; pbk Dfl. 27.50, $14.50.

ANNOUNCEMENTS

Awards

Three Royal Medals, known also as The Queen's Gold Medals, of the Royal Society are to be awarded to: **Sir Denys Wilkinson** (Vice Chancellor of the University of Sussex); **Professor Henry Harris** (Regius Professor of Medicine in the University of Oxford); **Dr J. P. Wild** (chairman of CSIRO).

The Council of the Royal Society has made the following award of medals: The Copley Medal to **Sir Derek Barton** (L'Institut de Chemie des Substances Naturelles, Gilf-sur-Yvette France); The Rumford Medal to **Professor W. F. Vinen** (University of Birmingham); The Davy Medal to **Professor A. W. Johnson** (University of Sussex); The Darwin Medal to **Professor S. Wright.** (University of Winsconsin); The Hughes Medal to **Dr F. J. M. Farley** (Royal Military College of Science, Shrivenham); The Mullard Prize and Medal to **Sir Edward Abraham** (University of Oxford). The Council has awarded the Royal Society Wellcome Foundation Prize for 1980 to **Dr C. Milstein** (University of Cambridge).

The 1980 Paul-Martini-Prize has been divided between **Dr Winfried Gunselmann** (Institut für Medizinische Dokumentation und Statistik der Universität Erlangen-Nürnberg) and **Professor David Grahame-Smith, Dr Jeffrey Aronson** and **Dr Alan Ford** (University of Oxford).

The recipients of the Wolf prizes — 1980 are: in agriculture, **Professor Karl Maramorosch** (Rutgers University, New Jersey); in mathematics, **Professor Emeritus Henri Cartan** (Université de Paris) and **Professor Andrei N. Kolmogorov** (Moscow State University); in chemistry, **Professor Henry Eyring** (University of Utah); in physics; **Professor Michael E. Fisher** (Cornell University, Ithaca), **Professor Leo P. Kadanoff** (Brown University, Providence) and **Professor Kenneth G. Wilson** (Cornell University, Ithaca); in medicine, **Dr César Milstein** (Medical Research Council), **Professor Leo Sachs** (The Weizmann Institute of Science) and **Dr James L. Gowans** (Medical Research Council).

The Wellcome Trust have awarded the following Senior Lecturerships in medical and veterinary science: **Dr J. K. Aronson** (University of Oxford); **Dr B. Burchell** (University of Dundee); **Dr M. J. Doenhoff** (London School of Hygiene & Tropical Medicine); **Dr S. E. File** (University of London); **Dr S. L. Lightman** (St Mary's Hospital Medical School); **Dr S. Tomlinson** (University of Sheffield); **Dr R. D. Ward,** (Liverpool School of Tropical Medicine); **Dr I. K. Welsh,** (Royal Postgraduate Medical School).

The next prize of the Foundation de Physiopathologie Professeur Lucien Dautrebande for work on human or animal clinical physiopathology, will be awarded during 1982. Further information from: The Office of the Foundation, 35, chaussée de Liège à 5200 Huy, Belgium.

Appointment

Alan R. Katritzky, former Professor of Chemistry in the University of East Anglia, has been appointed from 1 August, to the new Kenan Chair of Organic Chemistry at the University of Florida, Gainesville.

Meetings

20-21 October **Waste Utilization,** Chicago (S. A. Bortz, ITT Research Institute, 10 West 35th St, Chicago, Illinois 60616).

27 October, **Enzyme Mechanisms and the Design of Enzyme Inhibitors,** London (Conference Secretariat, Society of Chemical Industry, 14 Belgrave Square, London SW1, UK).

27-28 October, **Managing Periodicals Profitably,** London (Benn Business Promotions Ltd, Press House, 25 High St, Edenbridge, Kent, UK).

28 October, **The Resources and Resourcefulness of Agriculture,** London (PA to the Director, The Ciba Foundation, 41 Portland Place, London W1, UK).

27-31 October, **1980 Photovoltaic Solar Energy Conference,** Cannes (Mr D. Nicolay, Commission of the European Communities, DGXIII A, Kirchberg, Luxembourg).

29 October, **Food Science and Technology in Developing Countries,** Glasgow (Institute of Food Science and Technology, 105-111 Euston St, London NW1, UK).

29-30 October, **The Manipulation of Genetic Systems in Plant Breeding,** London. (The Royal Society, 6 Carlton House Terrace, London SW1, UK).

2-5 November, **Applications of Accelerators in Research and Industry,** Texas (Conference on Application of Accelerators, PO Box 5368, NTSU Station, Denton, Texas 76203).

4-5 November, **Planetary Exploration,** London (The Royal Society, 6 Carlton House Terrace, London SW1, UK).

6 November, **Is It a Virus?** London (The Royal Society, 6 Carlton House Terrace, London SW1, UK).

7 November, **Nutrition and Diabetes,** Edinburgh (Dr M. I. Gurr, Shinfield, Reading, UK).

11-13 November, **The Food Industry and its Effluents: Treatment and Conservation,** Norwich (Mrs H. Gibbons, AHS, Owles Hall, Buntingford, Herts, UK).

12-13 November, **The Perception and Assessment of Risk,** London (The Royal Society, 6 Carlton House Terrace, London SW1, UK).

20-21 November, **Interaction of the Platelets and the Vessel Wall,** London (The Royal Society, 6 Carlton House Terrace, London SW1, UK).

24 November, **The Physics of Microwave Devices,** London (The Meetings Officer, 47 Belgrave Square, London SW1, UK)

24-28 November, **Combination Processes in Food Irradiation,** Colombo (PO Box 100, Vienna International centre, A-1400 Vienna, Austria).

25 November, **Memory Its Function, Technology and Impact,** London (The Royal Society, 6 Carlton House Terrace, London SW1, UK).

26 November, **Instrumentation and Analysis — Remember the Burette?,** London (Society of Chemical Industry, 14 Belgrave Square, London SW1, UK).

27-28 November, **Gamma ray Astronomy,** London (The Royal Society, 6 Carlton House Terrace, London SW1, UK).

10-12 November, **Automated Instrumentation for the Analytical laboratory,** Central New Jersey (The Centre for Professional Advancement, East Brunswick, New Jersey 08816).

17-19 November, **Practical Mass Spectrometry,** Central New Jersey (The Centre for Professional Advancement, East Brunswick, New Jersey 08816).

2-4 December, **Offshore :Environment in the 80s,** St John's Newfoundland (Information and Public Relations Officer, Killam Labrary, Dalhousie University, Nova Scotia B3H 4HB).

3-5 December, **Practical Colorimetric Chemical Analytical Methododology,** Central New Jersey (The Centre for Professional Advancement, East Brunswick, New Jersey 08816).

9-12 December, **Industrial Membrane Technology,** Central New Jersey (The Center for Professional Advancement, East Brunswick, New Jersey 08816).

15-17 December, **Applied Absorption Technology,** Central New Jersey, The Center for professional Advancement, East Brunswick, New Jersey 08816).

15-19 December, **Genetic Engineering,** Washington (Battelle, Memorial Institute, 505 King Avenue, Columbus, Ohio 43201).

7-9 January, **Plastics Additives,** Central New Jersey (The Center for Professional Advancement, East Brunswick, New Jersey 08816).

27 January, **New Forms of Silicon for Use in Semiconductor Devices,** London (The Meetings Officer, The Institute of Physics, 47 Belgrave Square, London SW1, UK).

3-6 February, **Industrial Membrane Technology,** San Fransisco (The Centre for Professional Advancement, East Brunswick, New Jersey 08816).

8-15 February, **Immunoglobulin Idiotypes and their Expression,** Salt Lake City (ICN — UCLA Symposia, Molecular Biology Institute, University of California, Los Angeles, California 90024).

15-20 February, **Differentiation and Function of Hematopoeitic Cell Surfaces,** Keystone (ICN — UCLA Symposia, Molecular Biology Institute, University of California, Los Angeles, California 90024).

22 February — 1 March, **Mechanisms of Chemical Carcinogenesis,** Keystone (ICN — UCLA Symposia, Molecular Biology Institute, University of California, Los Angeles, California 90024).

1-8 March, **Cellular Recognition,** Keystone (ICN — UCLA Symposia, Molecular Biology Institute, University of California, Los Angeles, California 90024).

8-12 March, **Genetic Variation among Influenza Viruses,** Salt Lake City (ICN — UVLA Symposia, Molecular Biology Institute, University of California, Los Angeles, California 90024).

9-13 March, **Structure and DNA Protein Interactions of Replication Origins,** Keystone (ICN —UNCLA Symposia, Molecular Biology Institute, University of California, Los Angeles, California 90024).

15-20 March, **Development Biology using Purified Genes,** Keystone (ICN — UCLA Symposia, Molecular Biology Institute, University of California, Los Angeles, California 90024).

30 March-3 April, **The Theory and Practice of Solid Dosage Form Manufacture,** London (Mr R. E. Marshall, Dept of Pharmaceutical Sciences, The Pharmaceutical Society of Great Britain, 1 Lambeth High St, London SE1, UK).

30 March-2 April, **Viral Hepatitis, New York** (New York University Postgraduate Medical School, 550 First Ave, New York, New York 10016).

5-11 April, **The Sea in the Service of Man,** Monaco (International Bureau, 16 Regency St, Westminster, London SW1, UK).

5-10 April, **2nd European Congress of Biotechnology,** Eastbourne (ECB2 Secretariat, Society of Chemical Industry, 14 Belgrave Square, London SW1, UK)

6-10 April, **Time and Space in the Emergence of the Atmosphere,** London (R. W. Simms, Dept of Zoology, British Museum (Natural History), Cromwell Road, London SW7, UK).

7-9 April, **Assessment of Imaging Systems,** Reading (Sira Institute Ltd, South Hill, Chislehurst, Kent, UK).

7-10 April, **Properties of Oriented Polymers,** Leeds. (The Institute of Physics, 47 Belgrave Square, London SW1, UK).

8-10 April, **Spring Meeting — Association of Radiation Research,** Dundee (Dr I. V. Chapman, Dept of Medical Biophysics, University of Dundee, UK).

13-16 April, **Electroanalysis in Clinical, Environmental and Pharmaceueutical Chemistry,** Cardiff ((Short Courses Section Electroanalysis Symposium), UWIST, Cardiff, UK).

29 April-1 May, **Energy Storage,** Brighton (BHRA Fluid Engineering, Cranfield, Bedford, UK).

2 June-3 July, **Advanced Training of Foreign Participants in Remote Sensing — Geologic Interpretation,** Flagstaff (John A. Reinemund, US Geological Survey, National Centre — M/S 917, 12201 Sunrise Valley Drive, Reston, Virginia 22092).

7-12 June, **International Leucocyte Culture Conference,** Heidelberg (Dr H. Kirchner, Instiut für Virusforschung, DKFZ Im Neuenheimer Feld 280, D-6900 Heidelberg, FRG).

22-26 June, **Affinity, Chromatography and Related Techniques,** Nijmegen (Dr T. C. J. Gribnau, Kathlieke Universiteit, Nijmegen, The Netherlands).

22-27 June, **3rd European Symposium for Stereology,** Ljubljana (Prof. Dr M. Kalisnik, Institute for Histogy and Embryology, PO Box 10, 61105 Ljuljana, Yugoslavia).

19-24 July, **Chemotherapy,** Florence (Secretariat, 12th International Congress of Chemotherapy, Via della Scala, 10, Florence, Italy).

21-30 July, **General Assembly of IASPEI,** Ontario (Prof. A. E. Beck, Dept of Geophysics, University of Western Ontario, London, Ontario, Canada N6A 5B7).

11-12 August, **Open Symposium on Remote Sensing,** Washington (Dr D. L. Croom, Rutherford and Appleton Laboratories, Ditton Park, Slough, Berks, UK).

17-22 August, **Earth Tides,** New York (J. T. Kuo, Columbia University, New York, 10027).

23-28 August, **Solar World Forum,** Brighton (UK ISES, 19 Albemarle St, London W1, UK).

23-29 August, **7th International Biophysics Congress and 3rd Pan-American Biochemistry Congress,** Mexico City (Cerrada de Popocate-petl, México 13 D.F. Mexico).

31 August-3 September, **Computer Applications in Fermentation Technology,** Manchester (Society of Chemical Industry, 14 Belgrave Square, London SW1, UK).

9-11 September, **Radiopharmacology,** Chicago (Dr L. G. Colombetti, Pharmacology Dept, Loyola University, Stritch School of Medicine, Maywood Ilinois 60153).

Essential information at your fingertips

Every month!

The British Journal of Clinical Pharmacology is the leading authoritative journal presenting results of clinical pharmacological research.

Published monthly on behalf of the British Pharmacological Society the journal:

★ Bridges the gap between medical professions, clinical research and the Pharmaceutical industry.

★ Contains papers and reports on all aspects of drug action in man, in both health and disease.

★ Prints letters and short communications which allow immediate discussion of urgent observations.

Subscribers to British Journal of Clinical Pharmacology receive, free of charge, the proceedings of selected symposia on new methods, new drugs, and new approaches to treatment. Some past symposia have been on narcotic antagonists and antagonist analgesics, labetalol, clobazam mianserin, temazepam and the relationship between angina pectoris and hypertension.

Why not join the growing number of clinical pharmacologists, clinicians and others who rely on the British Journal of Clinical Pharmacology as their information medium.

For a sample copy write to: Frances Roach, Scientific & Medical Division, Macmillan Publishers Ltd., Houndmills, Basingstoke, Hampshire, RG21 2XS.

nature

2 October 1980

What is wrong with US engineering?

To many of those outside the United States, the recent wave of anxiety about the quality of engineering in the United States, and the rate of industrial innovation in American industry, will seem curiously self-indulgent. How can it be, the question will be asked, that the industrial state which, since the turn of the century, has been the dominant source of new technology, and whose people now enjoy unprecedented and unparalleled prosperity largely as a result of past innovation, should so suddenly take fright? Is there something real to worry about? Or is it just another election stunt? What can be learned from experience elsewhere? And what, in any case, can be done?

The speed with which public concern has blown up is breathtaking, almost bewildering. The trigger appears to have been the recognition that the rate at which automobiles imported into the United States, especially those from Japan, may not be halted by the launching of the new indigenous products of the three principal automobile manufacturers, apparently more resolute than before to market vehicles that people are likely to want to buy as gasoline prices keep on increasing. The discovery, or rather the recognition, that the American car industry is less productive, man for man, than its Japanese competitor seems to have helped dramatize more problems of wider long-term significance — the weakness of the dollar, itself dependent on the continuing deficit of overseas trade and, to some extent, on the federal government's own domestic deficit.

In truth, this process of the discovery of crisis in the United States puts the cart before the horse. There have been signs of trouble for much longer than a decade. Since the early 1960s, and before the monetary rot set in, productivity (measured on a man by man basis) has been growing less quickly in the United States than in most other industrialized countries (the United Kingdom and, more recently, Italy excepted). Between 1955 and 1977, the annual growth of productivity in the United States has been an average of 2 per cent per year, only a third of the annual increase of productivity in Japan during the same period. More recently, there have been signs that the rate of investment in manufacturing industry has been declining (as a proportion of national wealth) as consumers have kept on spending, or providing funds for the federal government to spend on their behalf. Where, people are beginning to ask, will it all end?

The first need is not to take fright. There are some respects in which the relatively poor record of recent years is a consequence of earlier success. Thus the displacement of a large part of the labour force from manufacturing industry to the service industries, whose potential productivity is inherently less, implies that the rate of growth of productivity is likely to decline. In this respect, the rate of growth of productivity in the United States has been traded for the availability of health services, education and the like, which Americans have come to think of as essentials, which they would indeed prefer to see improved — and which they are well-heeled enough to afford. The concern in the past decade about environmental quality, and the regulations and restrictions which have followed, have similarly been bought with diminished growth of productivity. (This is not to say that environmental regulations should be swept away but merely that environmental quality is a public purchase; Dr Barry Commoner, the presidential candidate for the People's Party in November, is after all forever saying that "there is no such thing as a free lunch".) Success and prosperity spawn problems in other ways. It is necessarily harder to break new ground, as the United States has been doing for the past century, than to follow a path already trodden. In a world in which international trade is acknowledged to be an important stabilizing influence, and in which attempts to bend the rules are relatively infrequent, it is inevitable that countries at the top, like the United States, will find their industrial supremacy in traditional fields from time to time eroded. Whole industries, footwear for example, have disappeared in the past; others (steel?) will do so in the future. If the automobile industry should find, next spring, that it cannot keep imports at bay, that will not mean that the world has come to an end but merely that the pattern of industrial production is being shared out internationally and economically.

That, at least, is what the textbooks say. The message will bring very little comfort to a Detroit in greater trouble even than at present. But there is a sense in which the pattern of industrial change cannot indefinitely be postponed, or can be forfended only at enormous and increasing cost. Several European countries have learned this lesson the hard way. British shipbuilding is merely the most obvious. In the United States, however, as elsewhere in the industrialized world, the record of the past few years has been confused by the consequences of the curious mixture of deflation and inflation ushered in by the first dramatic increases of the price of oil in the second half of 1973. By now there is ample evidence that, in circumstances like these, industrial investment grinds almost to a halt. The long-term consequences for productivity are plain enough. If worn-out and obsolete machinery is not replaced, and if new kinds of enterprises are not begun, then the growth of productivity must inevitably be diminished. No palliative exists. The only remedy is to avoid inflation and create circumstances in which industries (and people) respond rapidly to changing circumstances.

Last month's package of economic proposals from the White House is in this respect not especially relevant. To the extent that some expected tax revenue is to be forgone, people will have more to spend and some industries may begin to feel cheerful again. But the federal government's deficit and, possibly, the inflation rate, may be increased. By the time that Congress has finished with these proposals, the outcome may not be the stimulus to industrial recovery that President Carter is planning. More directly relevant, but again of dubious consequence, are the proposals that there should be more or less instant tax credits, paid in cash if need be, when manufacturers invest in new equipment. For what it is worth, a very similar proposal is a central part of the French budget for 1981, made public two weeks ago. The objective is laudable, but the results will not necessarily be those intended. If, for example, the chief beneficiaries are those manufacturers who are struggling to preserve industries whose economic foundations have long since disappeared, the cause of productivity will be hindered, not helped.

This is the background against which to judge the concern of the National Science Foundation with research in engineering, and with the training of engineers. The central issue is whether it will be possible, within the $1,200 million budget of the foundation, to make a decisive change in the pace of industrial innovation. For the past several months, the foundation has been searching for a form of internal organization that will enable it to function more effectively in this respect (see *Nature*, 11 and 18 September). It also shares with other federal agencies ambitions to found cooperative research centres that will carry out research on behalf of groups of industries judged to be in need of technological innovation (and prepared to share the cost). The proposed reorganization looks like a leaf out of the book of the

0028-0836/80/400377-02$01.00

UK Science Research Council, which has long since used its Engineering Board as an explicit means of fostering and improving engineering research in British universities. Even the admirers of the Engineering Board acknowledge that it has had an uphill struggle, however. The National Science Foundation may have better luck, given the stronger tradition of research (as distinct from external consultancy) among engineering faculties in the United States. But nobody should think that the cooperative research centres will have a decisive effect. Many will no doubt be useful, but the funds available do not bear comparison with what the mission agencies spend on development contracts.

By the same tests, the proposal that there should be a National Engineering Foundation, with terms of reference similar to those of the National Science Foundation, is likely to fly like a lead balloon. Representative George Brown, the chief sponsor of the scheme, sees it chiefly as a way of goading existing institutions into action. But what action? As long as nobody is sure, a National Engineering Foundation would be simply a cosmetic device, a monument to the common Washington view that any problem can be solved by throwing money at it.

Yet there are constructive things that could be done. In the past twenty years, the character of engineering has changed enormously (especially in the United States), but the engineering schools remain much as they were. The best of them are prestigious places, and have adapted their teaching to changing needs. Elsewhere, teaching and the evolution of the curriculum have been hampered as much by the lack of teachers as money. If the eager beavers in Washington really seek to help, they would be well advised to concentrate on the education of engineers.

The consequences (so far) of the Finniston Inquiry into British engineering education may have been meagre, but the more flexible American university system could well benefit from taking stock of how it educates engineers. Why, for example, should not some engineering schools follow most medical schools in recruiting intending engineers from among people with good first degrees in relevant fields of study? These and other innovations deserve a fair hearing. Some useful ideas are, by all accounts, included in the report of the Secretary of Education and the Acting Director of the National Science Foundation, submitted two months ago but not yet published. Congressmen urging that something should be done about engineering might do worse than demand a sight of that document. But in the long run they must know that the health of the engineering profession depends intimately on the health of the economy, which is Congress's chief responsibility.

Poor outlook for British universities

One thing is certain about the future of the British university system — if it collapses, or if some parts of it collapse, these events will be recorded in the appropriate Annual Survey of the University Grants Committee (UGC) with decorum and gentility. These are the hallmarks of the latest document in this series, published last week (HMSO, Cmnd 8031) and covering the turbulent academic year 1978–79. The UGC records the successive chops and changes of public support for the universities under its wing, and does not in even the mildest language protest that this is not the way in which a motley collection of universities such as the British can be run sensibly, even economically. In the same way, the latest survey tells how the UGC responded to the decision a year ago that the recurrent grant to the universities would be slightly reduced in the academic year now starting by "advising universities . . . that their admission arrangements for 1980 should be so conducted that, if necessary, they could restrict the number of entrants in a way which would restrict the rate of increase in the total numbers of home undergraduates". The survey notes that the UGC "subsequently learned" of the proposals to increase the fees of students from overseas and says that "the unpredictable results of these new arrangements are causing universities much anxiety". The UGC as such stays on the fence, not adding even a mild expression of opinion such as "which we share". They order things differently in France (see page 381).

The truth is that the upshot of government decisions about British university finances in the past two years amounts to the most serious perturbation of the system since the onset of rapid expansion in the early 1960s. The bursars' departments of British universities have become almost as concerned to know what cheques will be in the next post as the most insecure small businesses. The comfortable quinquennial system of financing will not be revived in the foreseeable future, but even the system of rolling budgets offered as a substitute four years ago is vulnerable, from day to day, to quite minor changes of government policy. The UGC itself, in the course of distributing funds to the universities in its charge, frequently finds it necessary to keep back funds for dealing with unexpected problems (a sudden pay award, perhaps). The result is that individual universities sometimes do not learn until towards the end of an academic year whether they will finish up in the black or the red.

The coming academic year will be worse than ever, for the rules have been changed. The UGC's own recurrent grant has been reduced by the estimated cost of educating new students from overseas. Individual universities hope to make good the difference by the increased fees they will recover. It is too soon to known how successful they will be — not all the overseas students offered places have turned up as yet, while it remains to be seen how many will actually have the cash required of them. Some universities, a little surprisingly, seem confident that they will not be much worse off than last year. Others are despondent. It is, however, agreed that total income will decline. The UGC's own reaction is familiar, and understandable. Again it will keep some money up its sleeve, with the intention of helping out universities in trouble. As so often in the past, the successful universities will no doubt be penalized to help those that cannot recruit their expected quota of students from overseas. In the meantime, many university finance officers will be literally unable to make their budgets balance for the coming year. So they will skimp wherever they can, even on the quality of teaching.

Few outside the university system appreciate the debilitating consequences of this way of carrying on. The UGC no doubt regrets the way it has to keep its supposedly autonomous universities on tight and unpredictable purse-strings — but there is not a flicker of regret or even sympathy in the latest annual survey. This omission, tactful though it may be, is important and potentially damaging because there are already many in the universities who question the utility of the long-term survival of the UGC. For several decades, the committee has been held up as a shining example of public administration, a buffer between the government (first the Treasury, now the Department of Education and Science) and the universities. There may be no truth in the suspicion that the UGC is now less staunch a buffer, but its ready compliance with each tiny shift of public policy has given a different impression. That is merely one reason why it should seize what chances come its way to say where it stands. Another is that in the upheavals that lie ahead, some at least among British universities will look to the UGC for protection, not just from penury but from the structural changes there will be if the research councils eventually decide to concentrate their research grants on a smaller number of institutions (as the Merrison committee may well suggest). If the UGC persists in its present passive ways, however, it will be less able to offer help than the circumstances require. The larger and more successful universities will be able to look after themselves — and some would prefer to do so even as things are. There is no unalterable law that all universities must indefinitely survive. The UGC, however, seems well set to let them go without a struggle.

0028-0836/80/400378-02$01.00

NASA budget falls foul of contracts

Washington

The National Aeronautics and Space Administration (NASA) has been caught in crossfire between the US Congress and the Office of Management and Budget (OMB) over whether the federal bureaucracy is spending too much money in employing private consultants to carry out its work. This has resulted in a demand from the Senate that NASA cut $14 million from a budget for consultant services which NASA claims totals only $4.3 million, but which the Senate Appropriations Committee, using a broader definition disputed by both the agency and the OMB, claims to be more than $90 million.

Unless it is reversed during negotiations with the House, the extra cut in NASA's budget, coming on top of a proposed two per cent reduction (approximately $100 million) in its budget request, will mean further pressure on space research projects as efforts are made to protect the space shuttle programme.

The pressures are already beginning to bite. For example, NASA is planning a reduction in the scope of experiments to be carried out by the spacecraft which will take part in the international solar polar mission, due for launch in 1982. Scientists from the European Space Agency, which is providing the second spacecraft in a dual mission, argue that the omission of instrumentation from the US craft could reduce the value of their own findings.

The proposed cuts in NASA's consultancy contracts reflect a general unease in Congress about the way in which federal agencies have come to rely increasingly on outside contractors to meet their responsibilities.

However, the agencies face a dilemma. On the one hand, Congress is continually increasing their work-load while, on the other, the Administration is keen to keep down the cost and size of government. The inevitable result is that the agencies contract work out. This, in turn, provides ample scope for disputes over rigged bidding for contracts, favouritism towards contractors, duplication of work and conflicts of interest.

Several instances of such practices have come to light in the past year. Last week, for example, officials from the Department of Energy admitted before a congressional oversight hearing that they had failed to check up on a consultancy firm employed to help draw up clean air regulations and were therefore unaware that the firm had also been working for companies engaged in a campaign to oppose the Clean Air Act of 1977.

In debating the 1981 budgets for a number of independent federal agencies, the Senate agreed to a proposal from Senator Warren Magnusson, chairman of the Appropriations Committee, to make a 15 per cent cut in the consultancy budgets of three agencies — NASA, the Environmental Protection Agency and the Department of Housing and Urban Development.

In opposing the proposed cuts, NASA complained that the analysis on which they had been calculated did not reflect the difference between narrowly defined contracts for advisory services and service contracts essential to a range of space programmes, including the shuttle.

Strong support for NASA's activities came from Senator Adlai Stevenson and ex-astronaut Senator Jack Schmitt, chairman and ranking minority member of the Senate Science and Space Subcommittee. Mr Schmitt proposed as an alternative that the 15 per cent reduction be according to NASA's own definition of what constitutes a consultant — this would reduce its budget by only $640,000.

However, Mr Magnusson and fellow Appropriations Committee member Senator William Proxmire remained firm. Mr Magnusson quoted a recent report from the General Accounting Office citing OMB's apparent failure significantly to reduce excessive waste, and its abuse of consultants' contracts over a 20-year period, as well as a statement from Admiral Hyman Rickover that "the use of consultants often impedes, rather than facilitates, action by government agencies". Mr Schmitt's amendment was lost by 27 votes to 66.

NASA is not the only agency in trouble about consultants. The Environmental Protection Agency (EPA) announced last Friday the cancellation of a $285,000 contract offered to a research worker at the California Institute of Technology to study the health effects of radon gas because of charges that the contract had improperly been awarded to the university without competitive bidding.

Dr David M. Rosenbaum, head of EPA's Office of Radiation Programs, had offered the contract to the university without seeking other bids on the basis that Caltech was the only contractor qualified to carry out the work involved. However, a university research worker told a Senate committee last Thursday that there were other contractors who could have carried out the same work.

Dr Rosenbaum also justified his actions on the grounds that it would have taken nine months to secure the services of a consultant through competitive bidding, and that because radon was a "serious health problem", fast action was needed.

However, his superior at EPA said that Dr Rosenbaum may have violated the agency's procurement regulations in making the award. And the agency's inspector general said that she had found "serious and troublesome" problems in the contracts procedures used by the radiation office.

David Dickson

Einstein Observatory in trouble

Washington

Equipment problems on board the National Aeronautics and Space Administration (NASA)'s second High-Energy Astronomical Observatory (HEAO 2) — also known as the Einstein Observatory — are causing concern that the mission may have to be brought to a premature end.

Initially the satellite, which was launched in 1978 and has provided the first X-ray telescope as sensitive as ground-based optical telescopes, was planned to operate only for one year. But after its initial success in generating new scientific data, the mission was extended, and until the recent setback NASA scientists hope the satellite would continue to send back data well into next year, when atmospheric drag would take it out of orbit.

How long the satellite goes on operating, however, will now depend on the behaviour of the gyroscopes used to position it. Three weeks ago, the transmission of scientific data had to be temporarily shut down after the failure of two of the six gyroscopes to switch on after a temporary black-out.

The satellite needs three functioning gyroscopes to position itself. One is already dead, and another has been working erratically for some time. The latter, however, has now had to be brought back into service in the hope that its performance will be adequate. If not, NASA officials said last week that they are developing software instructions for a back-up control system which would use the two gyroscopes that are still functioning, as well as either a sun sensor or a star tracker on the satellite.

At Harvard University, whose Center for Astrophysics is responsible for collecting the data transmitted from the Einstein Observatory, scientists also fear that even if the observatory continues to operate satisfactorily — as they are now hoping — the extra fuel consumed during recent manoeuvring to keep solar power cells facing the sun will shorten its lifetime by a couple of months.

The trouble on HEAO 2 started when one of the thrusters on the satellite started to burn for longer than it should during a repositioning manoeuvre. The gyroscopes were subsequently turned off with other equipment, but two failed to start when power was switched back on.

The gyroscopes have given trouble once before at the start of the mission in 1978,

0028-0836/80/400379-02$01.00

but this was resolved by NASA engineers. Ironically, while the problems with HEAO 2 were being worked on, gyroscope problems also developed in its successor HEAO 3, which was intended merely for a six-month mission.

In this case, a command sent to HEAO 3 caused it inadvertently to start drifting from its proper position, leading its control computers to switch the satellite into a "safe" mode. However, this problem is again said by NASA engineers to have been solved.

The HEAO satellites are not the only space activities encountering technical problems. Thus NASA officials are now carrying out an in-depth review of the space telescope programme and are concerned about the possible combined effects of cost overruns and schedule slips.

The critical design review of the telescope has been put back from this summer until January 1981, partly because of the need to redesign the wide-field planetary camera to save weight. In addition, the fine-polishing of the primary mirrors for the telescope is behind schedule; and various contractors for the space telescope project, due to be launched from the space shuttle in early 1984, are complaining that they have been allocated insufficient manpower and funds to keep the programme on schedule.

NASA is soon expected to announce the results of a competition for the location of the Space Telescope Institute, which will collect and analyse data from the telescope. The three main contenders are Johns Hopkins University in Baltimore, Princeton University and the Fermi National Accelerator near Chicago. Two groups — Associated Universities Inc. and Universities Space Research Association — have drawn up separate plans for locating the institute at Princeton. The Baltimore site is being proposed by the Association of Universities for Research in Astronomy and Fermilab by the Universities Research Association Inc., which already operates the laboratory's accelerator for the Department of Energy.

David Dickson

Radiation safety

X-ray survey

A plea for more effective steps to reduce the radiological dose to the gonads of patients from X-ray diagnosis has been put out by the National Radiological Protection Board (NRPB). The board is especially concerned about young adults, and says that if they were protected as well as children usually are, then the genetically significant dose to the British population from diagnostic radiology could be reduced by 40–50 per cent.

The NRPB set out to investigate whether the lessons from a similar study in 1957 under Lord Adrian had been learnt. That study concluded that the dose to the gonads of individuals could be reduced by the use of better radiological techniques, such as narrower beam widths. It also found that gonad dose from the same types of examination varied considerably, sometimes by as much as a factor of three or four between different parts of the United Kingdom.

The new study has found that the genetically significant dose — the average gonad dose per head of population weighted for child expectancy data — has remained approximately the same over the past 20 years despite a 50 per cent increase in the annual number of radiological examinations, suggesting that techniques have indeed improved. But it has also found that local variations in dose for the same examinations are as great as they were in 1957, suggesting that the use of gonad protection varies from place to place.

With this said, the NRPB is not alarmed. The "genetically significant dose" in Britain is still considerably less than in most other industrialized countries and could be responsible for a total of 100 genetic defects a year compared with a rate of 20,000 cases of genetic birth damage each year. Nevertheless, according to one of the reports, a reduction of only 10 per cent in the contribution to the genetically significant dose from diagnostic radiology would be the equivalent of the present contribution from nuclear power. As techniques for reducing the radiological contribution are easily available and relatively inexpensive compared with those needed to achieve a similar reduction from nuclear power, the NRPB says they should be implemented.

The study, based on data about radiological investigations in 1977, measured the gonadal dose in a sample of patients undergoing different types of examinations. The genetically significant dose is inferred from child expectancy data.

A breakdown of examinations into type reveals that most have increased in frequency whereas a few have decreased. A substantial factor in keeping the genetically significant dose down to its 1957 level is the large reduction in the number of obstetric radiological examinations. Their contribution to the genetically significant dose has fallen from 4.5 mrad in 1957 to 0.6 mrad now.

Although the NRPB study claims that there is probably room for further reductions of the genetically significant dose, it has few practical suggestions as to how this might be done. Nor does the NRPB fully understand the large differences of gonadal doses for the same examination in different parts of the country. It also acknowledges that gonad shields cannot be used in all cases, especially where they would obscure organs to be investigated. The plan is to discuss the findings with radiologists later in the year in the hope of finding ways to reduce the genetically significant dose.

Judy Redfearn

DNA guidelines

More relaxation

Washington

The National Institutes of Health (NIH) are expected shortly to reduce the burden of recombinant DNA regulations on research workers. This follows the recommendation of the institute's Recombinant DNA Advisory Committee (RAC) that details of virtually all experiments covered by the current safety guidelines need no longer be submitted to NIH for review.

At the same time, RAC has decided that NIH should limit their attempts to oversee recombinant DNA activities carried out in the private sector. In particular, the committee has proposed a procedure for checking on the biological aspects of large-scale experiments, but is suggesting that it should now restrict itself to general comments on the physical aspects of the fermentation and containment technology rather than reviewing each proposal submitted.

RAC has not gone as far as some would like. At a meeting in Bethesda, Maryland, last week, it decided to defer action on a proposal that clearance from local institutional biosafety committees (IBCs) should no longer be required before a research worker carries out an experiment in containment conditions specified in the guidelines.

The proposals for a procedural change in the guidelines were put to RAC by Dr Maxine Singer, head of the National Cancer Institute's biochemistry laboratory and a prominent participant in the 1973 Gordon conference which first drew attention to the need for caution in recombinant DNA research.

Dr Singer told the committee that many scientists felt that there was unnecessary delay in waiting for the Memoranda of Understanding and Agreement, required by NIH, to be approved by IBCs before research was allowed to begin. Also, there was impatience with the requirement for central review of experiments where the safety procedures to be followed were relatively straightforward.

On the latter point, committee members readily accepted Dr Singer's proposal that central registration be eliminated. Such registration is already no longer required for the bulk of recombinant DNA experiments, those carried out with the disabled K12 strain of the bacterium *Escherichia coli*. The new proposal would chiefly affect experiments being conducted in P2 and P3 physical containment conditions; the status of experiments now requiring the NIH director's explicit approval would not be altered.

More controversial was the proposal to remove the requirement for prior review of experiments by IBCs. Debate on this was coloured by a report presented to the committee on the performance of 19 IBCs

0028-0836/80/400380-02$01.00

studied in the state of California. This revealed, among other things, considerable differences in the rate at which IBCs accepted or rejected proposals for experiments in particular containment conditions, raising questions about the consistency with which research workers are interpreting the guidelines.

The report was prepared by Dr Dianna Dutton of Stanford University School of Medicine, under a grant from the National Science Foundation. She pointed out that IBCs established by private companies in particular had a high acceptance rate of proposals, and also claimed that the fact that none of the IBCs contacted publicized their regular meetings, even though attendance was unrestricted, reflected an apparent reluctance to involve the public in IBC decision-making.

A nationwide study of IBCs is now being planned by NIH, and will be discussed at a meeting of IBC chairmen in November. In the light of this proposed review, and the result of the Stanford study, RAC agreed that consideration of the elimination of pre-review of experiments should be deferred "until the frequency of principal investigator error in selecting containment levels is determined".

In another step designed to lessen the burden of regulation — this time primarily on the private sector — the committee agreed that its review of proposals for large-scale experiments should be focused chiefly on aspects of biological safety.

This decision was the culmination of a lengthy debate over how far NIH should go in regulating recombinant DNA research in the private sector. As there is no legislation, private companies are at present unregulated, although all companies involved have agreed to observe the NIH guidelines voluntarily.

A major stumbling block to this has been disagreement over procedures for evaluating experiments involving more than 10 litres of culture, at present requiring special permission from the director of NIH regardless of the genetic material being used. Some committee members have argued that RAC lacks the technical expertise to evaluate the safety of large-scale fermentation techniques, others that regulation in this area is the responsibility of the Department of Labor's Occupational Safety and Health Administration (OSHA).

Dr Eula Bingham, however, the head of OSHA, has now written to NIH saying that although her agency can act on complaints from workers or on suspicion of a potential hazard, it lacks the statutory powers to require the certification of facilities where no hazard is suspected.

Committee member Dr Sheldon Krimsky of Tufts University proposed that, in the light of OSHA's reply, a subcommittee of RAC should be set up with representatives of other federal agencies to comment on proposed containment procedures for large-scale experiments. He pointed out that although the pre-review of industrial technology might be a radical departure for regulatory agencies in general, it was within the spirit of the scientific and public concern which had originally led to the development of NIH guidelines.

Other committee members, however, were not convinced. Having earlier passed a motion agreeing to procedures for evaluating the biological classification of proposed large-scale experiments — and therefore the level of physical containment that would be required — they amended Dr Krimsky's proposal suggesting a new subcommittee primarily to advise on the proper procedures and design of such operations. The proposed subcommittee would review the effectiveness of local IBCs, including industrial IBCs, but it would not have to approve specific containment procedures for particular experiments; and its creation has still to be approved by the director of NIH.

David Dickson

Biotechnology

UK company gells

Britain's new biotechnology company, Celltech, is beginning to take shape. Sir Michael Stoker, foreign secretary of the Royal Society and former director of the Imperial Cancer Research Fund, has been appointed chairman of the board of directors and it is thought that Norman Carey of G. D. Searle Limited is in line for the scientific directorship. Most of the other members of the board have also been appointed. Offers of senior posts have been made, although it is not yet clear how many of them will be taken up. A full statement is promised later in the month.

Since the National Enterprise Board's announcement in July (*Nature*, 24 July, page 321) that it was to provide 40–50 per cent of the initial £12 million to set up the company, the managing director, Mr G. Fairtlough, has been looking for a site for administrative offices and a laboratory as well as appointing his board and senior posts. The most likely site, as was rumoured earlier, is Cambridge, although other possible sites are also being considered. The plan now is to buy existing offices and laboratories near to each other, which could be adapted easily to the company's needs.

The timing of the start of the company's operations will depend to a large extent on the suitability of the laboratories it acquires, but Mr Fairtlough is hopeful that operations could begin early next year. An older building needing extensive alterations would obviously delay the start.

As soon as the senior post have been filled, Fairtlough plans to start looking for candidates for other posts. The company hopes to build up a staff of 75–100 over the next two years. Initial products will be for medical diagnosis, but the company hopes to expand into other fields later and to cooperate with larger pharmaceutical companies on production of items beyond its scope.

Judy Redfearn

Going and coming

Sir William Henderson, chairman of the Genetic Manipulation Advisory Group (GMAG), responsible for the administration of the UK guidelines on recombinant DNA, will be giving up as chairman at, or soon after, the end of 1980. His original appointment, at the end of 1978, was for a term of two years, but it is understood that he is prepared to stay on for a month or so if his successor cannot take over at the beginning of the year.

In the past few months, there has been some confusion among GMAG members about the future chairmanship of the committee, which has apparently not yet been decided.

GMAG is also in the throes of a debate about its own future. At its next meeting, GMAG will debate a proposal by one of its members that the group should recommend its own demise. The proposal is likely to be resisted by the government departments and agencies concerned, at least until the Dangerous Pathogens Advisory Group (in limbo since the smallpox accident at the University of Birmingham two years ago) is reconstituted.

It has also become known in the past week that the search committee of the European Molecular Biology Organization (EMBO) has nominated as the next director-general of EMBO Dr L. Philipson of the Department of Microbiology of the Biomedium Centre at Uppsala. If appointed by the EMBO council, Dr Philipson will succeed Sir John Kendrew, whose term of office ends next year.

French universities

Trouble behind

Paris

French universities are still recovering from a series of attacks and retreats by the government which have left the universities strictly on the defensive.

In July, the minister for the universities, Mme Saunier-Seïté, vetoed the granting by the universities of the long-standing "engineer PhD", the Docteur-Ingénieur, and cancelled 200 first degree (deuxième cycle) and 600 postgraduate (troisième cycle) courses which were due for reapproval by her ministry.

Last month, the Prime Minister, M. Raymond Barre, intervened in the resulting row, but his action was more cosmetic than real. He restored the freedom to create Docteur-Ingénieurs at 25 of France's 78 universities, and approved a further 22

0028-0836/80/400381-02$01.00

courses at first degree and 39 at postgraduate level, after energetic lobbying by the Conference des Présidents d'Université during the summer.

According to the vice-president of the Conference, Professor Jacques Latrille (president of the Université de Bordeaux II), these concessions are "nothing like enough". Last year some 2,000 Docteur-Ingénieurs qualified and 25 universities cannot cope with the demand, which comes largely from qualified students of the Grandes Ecoles wishing to do research. Although the Grandes Ecoles, sometimes described as the crack training grounds of the French establishment, have a highly selective entry, they offer relatively few opportunities for research.

The scrapping of a net 178 first degree courses will — by government design — chiefly affect the new universities, the score of institutions, such as the universities of Chambéry and Pau, which have been established in the French provinces since the reorganization of 1968 and which tend to have 3,000–5,000 students. The social sciences, educational science, psychology, philosophy, history, geography, foreign languages and the performing arts have all been hit hard, with the result that teaching in these disciplines will be concentrated in the major cities and Paris. There may be further cuts next year, when the other half of the 1,917 undergraduate diplomas will be up for renewal.

The postgraduate cuts, on the other hand, affect mainly the bigger, older universities (15,000 to 20,000 students each), where most research is done; but again the cuts fall mostly in the humanities.

M. Barre, in his recent speech, gave his support to the broad emphasis of Mme Saunier-Seïté's policy — the restoration of "the vigour and quality" of the universities after the "rude shock" of 1968. It was clear, said M. Barre, that an increasing number of postgraduate (troisième cycle) proposals were ill thought-out and sustained by too few professors, libraries and laboratories.

A survey of deuxième and troisième cycle courses by Mme Saunier-Seïté had revealed a single management professor requesting the establishment of three postgraduate courses; six professors of belles lettres proposing ten senior undergraduate courses; and five biology professors proposing three postgraduate courses in life sciences.

M. Barre mentioned the notion of autonomy, but it is unlikely that the state will easily relinquish its vast power to approve all courses as well as appointment of professors and lecturers. On this point, the Prime Minister contrived to sound more like a benevolent dictator, offering democracy to his people "when they were ready", than a man committed to granting independence.

Neither does Mme Saunier-Seïté offer many crumbs of consolation. Although she is president of the Conference des Presidents d'Université, she has attended none of its meetings for more than a year. Academics are not asking for revolution. The government, says Professor Latrille, is entitled to make its own policy for the universities: but the universities should at least be consulted, through existing mechanisms, to give advice on how it is applied.

Robert Walgate

Non-proliferation

India gets fuel

Washington

Last week was a good one for the US nuclear industry, and a disappointment for its critics. On Tuesday, voters in the state of Maine rejected a proposed law which would have banned nuclear power from the state. The next day the US Senate failed to prevent the export of nuclear fuel to the Tarapur nuclear power station in India despite India's continued refusal to submit its nuclear facilities to international inspection.

Both votes had been closely watched as pointers to nuclear policy in the 1980s and both had, in consequence, been the focus of intense lobbying. In the lobbying in Maine, for example, supporters of a bill which would have closed the state's single nuclear power station and forbidden the construction of further nuclear plants were outspent by five to one by pro-nuclear forces, who raised financial support from utility companies around the country.

Although the vote in Maine supports the development of nuclear power, anti-nuclear voters did turn out in strength, and 40 per cent of those voting supported the proposed ban. After the vote, a spokesman for the local utility company admitted that the result demonstrated the substantial public concern that exists about the safety of nuclear power.

In the Tarapur case, the Administration's victory was even closer, and the lobbying even more intense. Shaken by a defeat by three to one in the House of Representatives of its attempts to permit the export of the nuclear fuel and a subsequent defeat in the Senate Foreign Relations Committee, the Carter Administration pulled out all the stops to prevent what was seen as a major challenge to its foreign policy.

Many key senators received telephone calls from the President, and Secretary of State Edmund Muskie even pleaded at length with the Senate Republican Conference. The result was that a resolution to disapprove the export of the fuel was defeated by just two votes, 46 to 48, with a majority of Democrats voting against the resolution and the majority of Republicans — with a significant number of liberal Democrats — voting for it.

India's request for the export of 38 tons of fuel for its Tarapur reactor was the first major test of the Nuclear Non-Proliferation Act of 1978, which forbids the export of nuclear fuel to countries which have not accepted international safeguards on their nuclear facilities.

Earlier this year, the Nuclear Regulatory Commission (NRC) decided unanimously that, since India had not met these requirements, the sale of the fuel could not go ahead. President Carter, however, invoked broader foreign policy considerations to overrule the NRC's decision, and the President's move could only have been overturned by Congress if both houses had voted against it.

The dispute over the export licence resulted from a conflict of strategy about whether non-proliferation objectives should be pursued single-mindedly, as implied by the Non-Proliferation Act, or whether they are as likely to be achieved through more conventional economic and diplomatic channels.

Senator John Glenn, the leading supporter of the resolution opposing the export, said that India, which had conducted a nuclear test in 1974 using components from Canada which had led to the current legislation , had "the worst history of any of our trading partners".

He warned that to back down at this stage would damage the credibility of the whole US non-proliferation policy, and after the result of the vote was known he commented that it would now be "practically impossible" for the United States to try to convince other countries that they should accept nuclear safeguards.

This view, however, was directly challenged by Senator Frank Church, chairman of the Senate Foreign Relations Committee. Reflecting the Administration's own position, Mr Church said that not permitting the export of the nuclear fuel would abrogate an agreement reached in 1963 to supply the fuel. This would permit India to disregard other safeguards built into the agreement and could postpone indefinitely further negotiations with India on nuclear issues.

After the vote, a spokesman for the Carter Administration said that the result would help discussions with India about bringing all India's nuclear facilities under international safeguards, but there was some scepticism in New Delhi. A spokesman for the Prime Minister, Mrs Indira Gandhi, said that her government had not changed its position on comprehensive safeguards, which it still regarded as discriminatory since the major nuclear states — including the United States — were not required to open all civilian and nuclear facilities to international inspection.

This debate is not likely to go away. The Indian Foreign Ministry announced two weeks ago that it had applied earlier in September for a new export licence for 19.8 tons of enriched uranium for the Tarapur plant — a move which could stir up the whole stormy debate again.

David Dickson

0028-0836/80/400382-02$01.00

Information technology

Cheering on UK

The past week has been remarkably active for British thinkers on government policy on information technology, the technology which interfaces computers and telephones, and for some of the designers of the technology itself. The Advisory Council on Applied Research and Development (ACARD), an advisory body to government and counted amongst the thinkers, published a report on the subject; the government announced some changes in the organization of responsibility for it; and British Telecom's research centre at Martlesham Heath, a designer of information technology, opened up its laboratories for more or less public scrutiny.

Central to this activity seems to be an awareness that Britain needs to put more coordinated effort into adopting information technology if it is to be competitive among the industrialized nations not only in the technology itself but also in many aspects of industry and business. This feeling certainly seems to be the basis of the ACARD report, which is more an exercise in publicity for information technology than a detailed analysis of its potential. Written by six industrialists, a trades unionist and a member of ACARD, it is an exhortation to government to take note of information technology rather than a guide to how policies might be implemented.

The report's main recommendation, that one minister and government department should be responsible for coordinating information technology policy, has to some extent been pre-empted by the government's announcement. The former computer systems and electronics divisions of the Department of Industry is to become the information division. It will assume responsibility for government policy formulation on information technology, under one deputy secretary who also has responsibility for the Post Office and satellite communications. In future, responsibility for coordinating government policy will lie with an official committee of the Cabinet Office especially set up for that purpose.

In making an international comparison of the development and uptake of information technology, the ACARD report is not very encouraging for Britain. It finds that the French, West German, Japanese and American governments are spending more than Britain on research, development and promotion. It is particularly nonplussed by the French government which, it says, has succeeded in creating considerable public awareness of information technology through one or two innovative public demonstration projects and at the same time has successfully promoted in other countries the idea that it leads the world in the field on the basis of projects that are not yet operational. This impression has been achieved, says the report, through the skillful use of publicity.

The report does not suggest that Britain should follow suit by committing more public funds to research. However, it does suggest that a leaf could be taken out of France's book by setting up demonstration projects to increase public awareness. Suggestions for doing this include putting telex and facsimile transmision machines in Post Offices, putting Prestel receiving machines in schools and public libraries and providing telephone subscribers with black and white Prestel-like video terminals for directory information.

The government could also help develop information technology industries by buying equipment for its own departments — a move which would need to be carefully implemented to avoid creating artificial markets. The report does not mention this possible pitfall, but it does recommend that the government should help stimulate closer cooperation between users and supplies.

Despite the lack of public funds spent on information technology, Britain is by no means behind on all counts, a fact which was evident at last week's open days at British Telecom's research centre. In such an international business, however, there is strong competition between countries to have their own systems adopted as standard and Britain, says the ACARD report, has been particularly bad at promoting its own interests. It says that Prestel is suffering because extensive negotiations over viewdata standards have failed to get it accepted as an international standard despite its technological lead.

Moves should be taken, it says, to encourage pupils at school to enter this field and to encourage industry to provide its own training schemes. **Judy Redfearn**

Bulgarian science

Reaching out

Varna

An unusual approach to international cooperation lies behind the Third PCITRRA International Colloquium (Physical and Chemical Information Transfer in the Regulation of Reproduction and Ageing), now taking place in Varna, Bulgaria. By presenting the work of young Bulgarian researchers side by side with papers by leading international experts in the field, the organizer, Dr Julia Vassileva-Popova of the Laboratory for Rapid Spectroscopy and Biological Physics of the Bulgarian Academy of Sciences, hopes to stimulate fruitful international working visits.

The theme of PCITRRA, as an international and interdisciplinary colloquium, was selected by Dr Vassileva-Popova in the early 1970s on the grounds that to compete in genetics would be to attempt to break into a very crowded field. She felt there would be more elbow room in the area of non-genetic information transfer, the first stages of hormone action, and bioreceptor and neurotransmitter processes. Since her laboratory is more than self-financing, exporting sophisticated rapid-spectroscopy equipment primarily to the USSR, the funding of basic research is a smaller headache to her than to some other Bulgarian laboratory directors. Accordingly, Dr Vassileva-Popova has been able to gather together a large and keen team. Since East European etiquette normally calls for the laboratory head or research supervisor to be cited as a co-author, this meant that out of the 117 scheduled communications, Dr Vassileva-Popova was named as co-author of 23.

The third PCITRRA colloquium (they have been held at three-year intervals since 1974) was formally part of the celebrations of next year's 1,300th anniversary of Bulgarian statehood, and was in part supported by the State Committee for Culture — the first time apparently that this body has sponsored an international scientific event. Yet Dr Vassileva-Popova is adamant that she is not trying to found a "Bulgarian school" of biophysics/biochemistry. In her opinion, it is scientists and not their countries which matter. Indeed, had it not been for a small organizational error, she said, the participants' badges would not even have shown their countries' names. She even suggested to the international organizing committee that the fourth PSITRRA colloquium might be held outside Bulgaria — a proposal which they emphatically rejected.

Certainly, Dr Vassileva-Popova has been able to attract to Varna an impressive international gathering — including Henry Arnstein and J. R. Tata from the United Kingdom, Oscar Hechter and Elwood Jensen from the United States, Friedrich Jung from the DDR, Rostislav Sovicka from Czechoslovakia, Pushpa Bhargava from India and Andrei Tchernitchin from Chile. And this in spite of the relatively long duration of the colloquium (seven days, with working sessions of up to ten hours a day) — Dr Vassileva-Popova eschews poster sessions, and insists that all papers from her young collaborators which reach the required standard are read in full. In addition, all those foreign visitors who could spare the time were invited to stay on for a new feature of the PCITRRA colloquia, a summer school for young scientists at Burgas, further down the coast.

One notable figure was absent — Sir John Kendrew, who was detained at an EMBO meeting in Heidelberg. His encouragement of Bulgarian biophysics and biochemistry was, however, recognized earlier this year, when he was given the highest award of the Bulgarian People's Republic — the Order of the Horseman of Madara.

Vera Rich

0028-0836/80/400383-01$01.00

CORRESPONDENCE

DNA X-ray data

SIR — We have recently suggested[1] that the available X-ray diffraction data from B DNA are consistent with a model for the structure of DNA which we have called the "side-by-side" model and in which DNA strands are linked together in pairs of the Watson–Crick type but are not wound into a continuous right-handed helix. Our model has however been alluded to[2,3] in terms that suggest that alternatives to the double-helix model have been finally disposed of. We wish now to emphasize that existing X-ray data on B DNA are not in themselves sufficient for an unambiguous decision for or against either model.

Naturally occurring specimens of B DNA do not form single crystals of good quality, and the resolution of available X-ray data is very limited. For these reasons, and because there is rotational disorder in all specimens of B DNA so far reported, the only standard crystallographic quantity that can be immediately calculated from the X-ray data is some cylindrical average of the Patterson function, which must in practice be compared with the corresponding function calculated from molecular models.

We have shown[1] that in the analysis of B DNA data, there are advantages in using what we call the axial Patterson function (essentially the cylindrically averaged Patterson function with the radial coordinate zero) Briefly, the axial Patterson function is less sensitive than the Patterson function itself to imperfections of diffraction data. Of necessity, the axial Patterson function, which averages out much of the fine detail inherent in the observed diffraction patterns, can only be used for preliminary tests of the agreement between model structures and the X-ray data.

The nub of our argument is that the axial Patterson function computed from the data agrees (within the apparent experimental error) with that calculated from the side-by-side model but not with that computed from the double-helix model refined by Arnott and Hukins[4]. We do not of course claim that the double-helix model can therefore be dismissed — the quality of the data is so poor. But in the circumstances one wonders about the value of sophisticated refinements of the double-helix model (for example, ref. 4).

We are also surprised at the recent claim by Greenall *et al.*[5] that the double-helix model is in much better agreement than the side-by-side model with the diffraction patterns measured from paracrystalline B DNA specimens. We find roughly equal disagreement for both models. (We do not wish to make too much of what we feel is an anomaly of the double helix on the tenth layer line, because it could well be an artefact of excessive refinement based on inadequate data.)

For such reasons, it must be concluded that available X-ray data are at best an equivocal means of deciding between alternative DNA models. So much is acknowledged by Crick *et al.*[6]. For X-ray analysis to provide unambiguous distinction between different models of DNA, it will be necessary for much better crystals to be prepared from well characterized polynucleotides. In the meantime, while no doubt the merits of alternative DNA models will be assessed by considerations other than those deriving from X-ray data, it is prudent that the present insufficiency of the latter should be widely and openly acknowledged.

1 Bates, R H T, McKinnon, G C, Millane, R P & Rodley, G A *Pramana* 14, 233 (1980)
2 Arnott, S *Nature* 278, 780 (1979)
3 Cohen, J S *Trends biochem Sci* 5, 58 (1980)
4 Arnott, S & Hukins, D W L *J molec Biol* 81, 93 (1973)
5 Greenall, R J, Pigram, W J & Fuller, W *Nature* 282, 880 (1979)
6 Crick, F H C, Wang, J C & Bauer, W R *J molec Biol* 129, 449 (1979)

R.H.T. BATES
G.A. RODLEY*
G.C. MCKINNON

*Electrical Engineering and *Chemistry Departments University of Canterbury, Christchurch New Zealand*

Andrei Sakharov

SIR— The Olympic games are over; the hopes that Academician Andrei Sakharov might be allowed to leave his internal exile in Gorky and return to Moscow are over now too Professor Sakharov has been exiled for over nine months and has no contact with his scientific colleagues, is not allowed to take part in seminars or lectures, has no access to scientific information so crucial for his research. (Books and journals have to be brought to him by his relatives from Moscow, which usually takes weeks or months. Since January, his colleagues from Lebedev Institute have been allowed to visit him only three times!)

In spite of this, he has managed to write three scientific papers in Gorky, and English translations have been published at SLAC, Stanford University (Estimate of the Quark-Gluon Coupling Constant; Cosmological Models of the University with Rotation of Time's Arrow; Mass Formula for Mesons and Baryons).

I am convinced that it is time now for the world scientific community to escalate the efforts to help our distinguished Soviet colleague. From Andrei Sakharov's last communication it is obvious that he is mainly missing the information about what is going on in physics.

It should be very easy for the physicists to break down this information barrier Let the theoretical institutes, laboratories and groups from all over the world begin sending to Professor Sakharov their preprints, lecture notes, reports. Send them by *registered* mail with the red "Avis de Reception" card to·

Professor Andrei Sakharov
Prospekt Gagarina 214, kv.3
Scherbinka 2, Gorky, USSR

Don't hesitate to ask your local post office to investigate if the red card is not returned to you with Andrei Sakharov's signature within about a month Your local post office is obliged, according to international postal convention, to make the investigation and, if unable to provide proof that the mail was delivered, to pay you compensation

There is no doubt that such world-wide action will not only provide Professor Sakharov with necessary scientific information but will also represent considerable moral support for him. It will be important for Soviet authorities too· they will see that Andrei Sakharov's case is not at all forgotten by the world scientific community

F JANOUCH

*Research Institute for Physics,
Stockholm, Sweden*

Preventing plagiarism

SIR — The article "An outbreak of piracy in the literature" (*Nature* 12 June, p.429) shocked me deeply. In December 1978 Dr Alsabti sent manuscripts to us also, with the headed paper of the M.D. Anderson Tumor Institute. Again, he gave a private address in Houston for correspondence and made acknowledgement to the Jordan Royal Family. Fortunately for us, he grossly overdid it, sending five manuscripts within a month. A call to M.D. Anderson helped us in taking the decision to reject the five manuscripts.

An old custom in the Italian universities called for the approving signature of the professor on the front page of a manuscript. Although I do not agree with a system which may impair scientific freedom, the present incident should teach us how important it is to ascertain directly from the host institution the credentials of an intended author, particularly when complex international relationships are apparent.

UMBERTO VERONESI

*Istituto Nazionale per lo Studio
e la Cura dei Tumori
Milan, Italy*

Pesticides as poisons

SIR— Peter Clarke (*Nature* 18 September p.184) defines a poison, but fails to note that "the dose alone determines the poison" (Paracelsus, 1564), a point that was emphasized correctly in *Nature* 28 August p.832. He says high blood levels of DDT in Guatemala were "the corollary" of an "aggressive marketing campaign" by a transnational corporation, and that cigarettes and pesticides are "harmful products". Cigarettes are harmful to human beings, pesticides to pests The use of DDT in Guatemala was started by the World Health Organization and the United Nations International Children's Emergency Fund to control endemic malaria in 1,500 Guatemalan communities. A reduction in malaria was achieved

THOMAS H. JUKES

*Department of Biophysics and
Medical Physics,
University of California,
Berkeley, California*

SIR — Of necessity, I have had to become something of an "applied toxicologist".

The only still-unfalsified definition of a poison is that of Paracelsus *"Dosis facit venenum"*, the definition offered by your correspondent Peter Clarke (*Nature* 18 September, p.184) contains less of the essential nature of a poison, and therefore fails. *Nature*, consequently, has avoided polemic (unlike your correspondent), and has indeed abandoned prejudice. Dr Clarke's letter is a brilliant piece of special pleading on behalf of a political stance — and I congratulate *Nature*, Sir, on your stand for true objectivity.

I am about to retire from full-time employment as a scientist, but I hope to maintain an attitude of 'informed scepticism'.

R A. DAVIS

*Rodent Research Laboratory
Tolworth Laboratory, Surrey, UK*

NEWS AND VIEWS

Myths, models and human evolution

What on earth can safely be said in public about human evolution? The charitable among those who heard Dr J. R. Durant's Darwin lecture to the British Association this year will have been worrying at this question for the past three weeks. The title of Dr Durant's address — The Myth of Human Evolution — tells the tale sufficiently: the stories that people tell, he argued, and which have been used for various purposes by people as different as Freud and Galton, Lorenz and E.O. Wilson, are but myths; "theories of human evolution have come to embody contemporary hopes and fears about the society in which we live". Specifically, the accusation goes, since the time of Raymond Dart until quite recently, the story told of human evolution has involved a model of human nature which is consistent with the doctrine of Adam and Eve, the Garden and the Fall, the doctrine of Original Sin, the notion that each contemporary human being is a battleground between civility (in the strict sense) and the primitive and powerful Beast within. The notion that primitive men were not merely successful hunters of other species but killers of each other, Durant says, fitted well with contemporary views of society at war within itself. But now, says Dr Durant, the fashion is changing. In making the public legend of human evolution, people have taken to describing primitive humans or hominids as creatures whose survival depended on cooperation between individuals and among groups, whose behaviour was shaped by an implicit recognition of the benefits of the division of labour in a hunter-gatherer society which Adam Smith first clearly described, and whose distinctive attribute — that of language — predisposes towards communality. What view, it might innocently be asked, is right? Neither, said Dr Durant. Each is a myth. Tell us instead, he asked of palaeoanthropologists, palaeoarchaeologists and the rest, the truth. Or at least acknowledge that your data are insufficient to say very much at all.

Stirring stuff like this is certain to evoke some kind of a response. Dr Durant will not have been surprised that, to begin with, the British daily newspapers were hesitant in knowing where he stood. Was he an anti-Darwinist, a Lamarckian or perhaps even a Creationist? When the fine print showed that he is none of these things, the tide of excitement ebbed. Mr Ronald Reagan, running for President of the United States, had in any case captured more attention with his aside in Dallas, Texas on the teaching of evolution in American schools (and may yet capture the Creationist vote in the United States with a sufficiently well-calculated goof.)

Durant's complaint, in any case, was a complaint against a style of argument. His targets were writers such as Lorenz (in the old school) and E.O. Wilson (in the newer fashion). His audience, given its provenance, may not fully have appreciated that Durant had selected pushovers for his attack. "Criticize Lorenz's concept of innate aggression" must now be a standard essay topic in undergraduate biology courses in most universities. Before long it will be joined by topics such as "What is the evidence (if any) for the belief that genetically determined altruism has played a part in human evolution?". He was entirely within his rights to complain that, in much of what passes for a general account of the evolution of human beings and of human nature, people who should know better are too fond of making too much of far too little evidence. Their common error is to take a living primate species as a model for earlier — and even contemporary — human (or hominid) society. Human nature being what it is, it is not surprising that these reconstructions reflect their prejudices or their hopes of wish fulfillment.

So far, so good. Dr Durant must have been well satisfied with his attack on such a variety of false prophets. Yet there is more than this to say and to ask. Why, for example, does the question of human evolution evoke such powerful interest, and such passion? What is to be said with confidence in such a field, where the data are likely always to be insufficient? And how should an account of human evolution be constructed — and made immune to the attentions of the myth-makers?

Nobody should be surprised that these issues excite deep and general interest. Long before Darwin made it possible to talk about the issues in concrete terms, people at large were understandably preoccupied with the subject matter of *Genesis*. All writers on the human condition have found it necessary to tackle the same questions — although it remains a puzzle that the Greeks, typified by Plato in the *Laws*, contemplated a past more or less indistinguishable from their present. For the past century, however, the public interest in human evolution has mostly been guided by Darwin's terms of reference. It would have been charitable of Dr Durant to have acknowledged that that is a step forward, and away from myth. But there is, as he complained, some way to go.

The lack of evidence is the chief stumbling block. The palaeoanthropologists may not really agree, but they are fortunate among those who work on human evolution. They have bones and other objects to measure, but past behaviour has left no fossils, only occasional artefacts from which behaviour must be inferred. In the circumstances, it is remarkable how much has been accomplished with the fossils uncovered in the past half-century. The time-span of human and earlier hominid evolution has been pinned down more accurately than could have been hoped a decade ago: 3.25 million years, give or take the usual ten per cent, will span the earliest australopithecine so far known (*A. afariensis*) and the present. Anatomical evidence appears to make possible the distinction between potential ancestors of hominids and apes among the contemporaries of late-Tertiary *Ramapithecus*. The palaeoanthropologists have been helped along by pieces of unexpected good luck — such as the way in which genetic differences between extant primate species will increasingly be used as evolutionary clocks. Even so, the reconstruction of this relatively tangible part of human evolution is full of uncertainty. Was *Homo habilis* an ancestor, or a dead end? Which of the specific names which the palaeoanthropologists have put into circulation will survive discoveries not yet made? Calculated scepticism — which jibes uneasily both with the temperament of the practitioners and the expectations of the public — is clearly essential.

So how, with such caveats, can progress be made towards a robust understanding of how early people, and hominids, behave? Most of Dr Durant's complaints were levelled at those who have embellished fossils with patterns of behaviour for which there is no evidence. He may have unfairly overlooked the opportunities that do exist for tackling these questions empirically — for example, by constructing models of the coordinated evolution of anatomy and behaviour, using data gathered not merely from the fossil beds but from analyses of the structure of, say, intelligence, observations by psychologists of the acquisition of specified skills in infants and other primate species and even the evolutionary implications of, say, protein biochemistry.

The trouble, of course, is that models are easily misunderstood. The safeguard, in this field as in, for example, cosmology, is that their function should be widely understood. A model is but a hypothesis to be tested. To regard it otherwise is to make a myth of it.

0028-0836/80/400385-01$01.00

Infrared astronomy comes of age

from R. D. Wolstencroft

A recent conference* provided the first opportunity to discuss the contributions to astronomy being made by the new infrared telescopes on Mauna Kea, Hawaii. Infrared observations, both of cool clouds of interstellar gas and of the infrared sources within them, give vital information on the conditions under which star formation occurs. A wealth of new information is being obtained by a range of sophisticated instruments and the first studies are being carried out in regions of star formation outside our Galaxy.

Interstellar clouds exhibit a wide range of size, mass, density and temperature. They are observed over a wide range of wavelengths, from the optical to the radio, and with a variety of techniques which emphasize regions of differing density and temperature in a given cloud. The synthesis of such observations to give an overall picture of a cloud are still at a rather rudimentary stage. Because of this and also because of the continuous nature of the cloud — inter-cloud medium no completely logical classification for clouds has yet been derived. Thus the terms in use such as 'molecular cloud', 'dark cloud' or 'globule' do not necessarily define objects with similar physical properties. R. J. Evans (University of Texas) summarized the properties of molecular clouds and discussed the problems of classification. A typical giant molecular cloud is 100 pc across with a mass, up to half of which may be molecular hydrogen, of about 10^5 solar masses. Stars tend to form in the densest and hottest parts of the cloud, usually in clusters. Massive stars form preferentially in the larger clouds whereas the low mass stars form in clouds of all sizes. The infrared sources found in the molecular clouds may be either embedded stars or protostars; they are very luminous, typically in the range 10^3 to 10^5 times the solar luminosity.

Clouds at the low end of the mass and length scale are the Bok globules which were discussed by A. R. Hyland (Mount Stromlo Observatory). A promising new approach was described for studying the short wavelength infrared extinction by looking at background sources seen through a globule. The technique has been applied to a relatively symmetric globule in the Coalsack dark cloud. From the canonical relation between infrared colour excess, visual extinction and molecular hydrogen column density, a mass of 11 solar masses and a radius of 0.25 pc can be derived. Thermal emission from the dust at far infrared wavelengths can yield the typical temperature (about 15° K) and mass (about 0.1 solar mass) of the dust in a globule. It is probable that most globules are not undergoing gravitational collapse.

The Orion Molecular Cloud (OMC) is a well studied region which received much attention at the symposium. N. Z. Scoville (University of Massachusetts) described a model of an expanding envelope of gas centred on the Becklin-Neugebauer (BN) and Kleinmann-Low complex of infrared sources: the expansion velocity, based on CO mm line measurements, is 50 km sec^{-1} at 0.1 pc from the centre. A quite different view is held by R. Genzel (Center for Astrophysics) who proposed a model based partly on a VLBI proper motion study of maser sources: the source IRC 2, rather than the BN object is the centre of a low velocity (18 km sec^{-1}) outflow with a higher velocity outflow in the surrounding region. IRC 2 is an unusual source: it has a very strong 10µm absorption feature, possibly a greater luminosity than the BN source and it is the only SiO maser in a star-forming region. Other evidence of energetic motions in OMC comes from observations of molecular hydrogen emission in the 2.1µm vibrational quadrupole line and other rotational lines: this emission may be due to shocked gas at a temperature of about 2,000 K.

Results from a variety of sophisticated instruments were presented, notably those in the field of far infrared spectroscopy and speckle interferometry. As an example, infrared speckle interferometry by R. R. Howell and colleagues (Steward Observatory) has shown that the source W3 IRS 5, previously thought to be one source, is in fact a double source with a one arc second separation. If many sources prove to be double or multiple and if the components were to have different temperatures this could significantly affect our interpretation of source temperatures. F. Sibille and P. Lena (Meudon Observatory) have measured upper limits to the angular size of several sources, including 0.08 arc s for BN at 2.2µ. There is a strong possibility that proto-planetary disks will eventually be resolved by this technique.

Evidence for the presence of magnetic fields in molecular clouds comes from recent studies of the polarization of infrared sources in the clouds, a topic reviewed by H. M. Dyck and C. J. Lansdale (University of Hawaii). The generally large linear polarization, the approximately constant ratio of circular to linear polarization and wavelength dependence are consistent with a model of aligned grains in the vicinity of the source. An alternative explanation for the observed polarization in terms of scattering by grains in a bipolar nebula or similar geometrical configuration appears to be ruled out. A twist in the grain alignment along the line of sight near the source is implied by the circular polarization: twists of between 20 degrees and 80 decrees can be deduced for the nine sources so far studied. The grains are most probably aligned by an enhanced Galactic magnetic field permeating the cloud. Questions concerning the strength of the field, the origin of the twists in the grain alignment and the location in the cloud of the polarizing region, are of great interest and should be answered by further careful polarimetric observations in the infrared.

The latest observational results concerning the galactic centre were reviewed by I. Gatley (UKIRT, Hawaii) and E. Becklin (University of Hawaii). Outside the central few parsecs an expanding ring of molecular clouds has been identified from CO mm line measurements. The far infrared luminosity (30 to 100µm) in the region can be explained by thermal emission from dust heated by a large density of late type stars. Within the central few parsecs are a number of 10µm sources which appear to be objects a fraction of a parsec across with about one solar mass and 10^5 solar luminosities. A preliminary analysis of the observations suggests that they may be losing mass at a high rate: the nature of these objects is quite uncertain, but it is tempting to think of them as analogues of the BN object. Another important finding, based on 30 to 100µm observations, is the low abundance of dust within the central parsec. A black hole may be needed to explain the variety of observational results now available.

Star formation in the nuclear region of external galaxies was reviewed by G. H. Rieke (University of Arizona). About 40 percent of galactic nuclei so far studied show a large infrared excess at 10µm: whenever this excess is seen a very large infrared luminosity (10^9 to 10^{10} solar luminosities) is also seen within a few hundred parsecs of the centre. The 10µm silicate feature is also present in these same galaxies. Rieke argues that thermal radiation by dust is the immediate source of the observed radiation with the ultimate origin of the high luminosity being rapid star formation in the nuclear region. The nuclear infrared source is resolved in all cases. For example C. T. Telesco (University of Hawaii) reported that the 10µm emitting region of M51 has a diameter of about 3 kiloparsecs. Rieke posed three important questions which should be addressed in the near future: (1) What is the initial mass function (IMF) for star formation in nuclear regions? From a study of M82 it appears that there may be a bias against the formation of stars with masses below 2 or 3 solar masses relative to

R.D. Wolstencroft is at the Royal Observatory, Edinburgh.

---

*The International Astronomical Union Symposium on Infrared Astronomy was held in Kailua-Kona, Hawaii, June 23-27, 1980 and was sponsored by four organizations operating telescopes on Mauna Kea: NASA (3.0m Infrared Telescope Facility — IRTF), SRC (3.8m UK infrared telescope — UKIRT), the Canada-France-Hawaii Telescope Corporation (3.6m CFHT) and the University of Hawaii (2.2m UHTE).

0028-0836/80/400386-02$01.00

Hurricane Allen destroys Jamaican coral reefs

from J. D. Woodley

HURRICANE Allen, which traversed the Caribbean in early August, was the second strongest ever recorded with wind speeds approaching 300 kph (185 mph). Fortunately, its track was mostly over the sea but, while the islands were spared the impact of extreme winds, they were exposed to enormous storm-generated waves. In the small hours of Wednesday 6th August, Allen passed within 50 km of the north-east coast of Jamaica. Severe wind damage occurred to the forests of the Blue Mountains and the banana plantations of the adjacent lowlands. Huge waves beat upon the eastern and northern shores, claiming several lives. Houses built on cliffs 12m above the sea were destroyed. Beneath sea-level, the spectacular fringing coral reefs suffered considerable damage.

The Discovery Bay Marine Laboratory of the University of the West Indies is at a site is in the middle of the north coast and not in the area hardest hit but, after the hurricane waves subsided, the water was turbid with fine sediment and pulverised tissues; there was a smell of dead corals, gorgonians and sponges. Death and injury to these and other organisms have now been assessed. Branching corals have been smashed, massive corals toppled or split, and plate-like ones fractured or torn off the reef slopes. Gorgonians and sponges have been ripped away or broken, echinoids destroyed and many fishes injured too. Physical damage varies with exposure and submarine profile, but in some places extends below –50m. Tons of sediment have been removed from the reef slopes and terraces. Sand-blasting and flying missiles have caused extensive abrasion, especially in the shallowest zones, where almost total destruction prevails. Before the storm, luxuriant stands of elkhorn coral (*Acropora palmata*) dominated the breaker zone from 0 to –6m (Fig. 1). This species is well able to resist the forces of ordinary breaking waves, but evidently not those generated by a severe hurricane. It has been reduced to rubble (Fig. 2) and some of this flung on to the reef flat, forming islands where none was before.

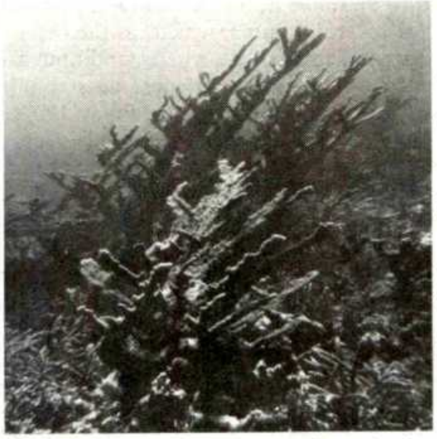

Fig 1 A stand of *Acropora palmata* in the breaker zone before the hurricane.

Photographs by J.W. Porter, University of Georgia

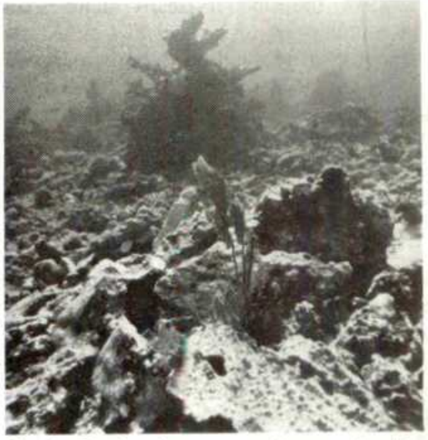

Fig 2 The breaker zone at the same locality after Hurricane Allen.

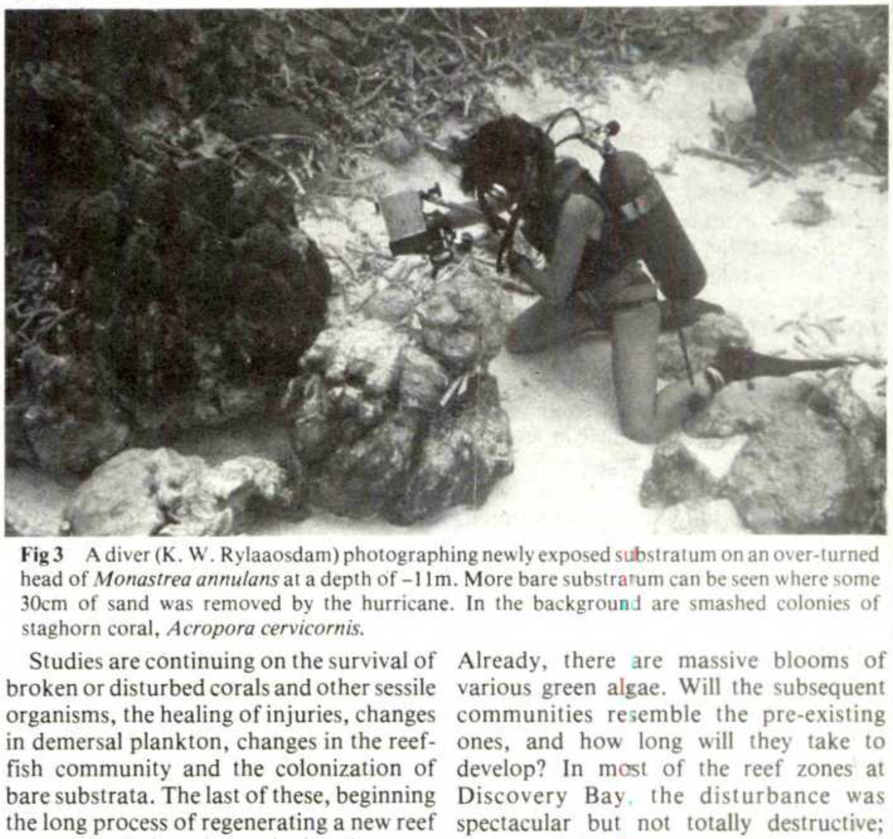

Fig 3 A diver (K. W. Rylaaosdam) photographing newly exposed substratum on an over-turned head of *Monastrea annulans* at a depth of –11m. More bare substratum can be seen where some 30cm of sand was removed by the hurricane. In the background are smashed colonies of staghorn coral, *Acropora cervicornis.*

Studies are continuing on the survival of broken or disturbed corals and other sessile organisms, the healing of injuries, changes in demersal plankton, changes in the reef-fish community and the colonization of bare substrata. The last of these, beginning the long process of regenerating a new reef community, is of particular interest. Abrasion, fracture and sediment removal have exposed large areas of new surface for colonization throughout the reef profile (Fig. 3), but especially in shallow water. Already, there are massive blooms of various green algae. Will the subsequent communities resemble the pre-existing ones, and how long will they take to develop? In most of the reef zones at Discovery Bay, the disturbance was spectacular but not totally destructive; recovery is likely to occur within a few years. Where extreme damage has occurred, that is, in shallow water and progressively deeper on reefs further east, it is possible that 'recovery' will take decades.

J. D. Woodley is Director of the Discovery Bay Marine Laboratory, Discovery Bay, Jamaica.

---

the IMF for the solar neighbourhood. (2) Are there any galaxies intermediate between the high and low infrared luminosity galaxies? (3) What mechanism starts and sustains the star formation activity?

The correlation between neutral hydrogen velocity width and integrated magnitude for galaxies (Fisher–Tully relation) can be used to determine the Hubble flow velocity, H_0, and hence the extragalactic distance scale. M. Aaronson (Steward Observatory) discussed his latest results using infrared magnitudes which give a tighter correlation than the optical magnitudes used in earlier studies. With the exception of galaxies in the Virgo cluster the value of H_0 is 95± 4 km sec^{-1} Mpc^{-1}. Judging from the reaction to Aaronson's talk at the meeting this new value of H_0 is being treated very seriously. Since the canonical value of 55km sec^{-1} Mpc^{-1} by Sandage and Tamman is very much less, it is clear that the origin of the discrepancy between these values must be urgently sought. For Virgo $H_0 = 65$ km sec^{-1} Mpc^{-1} which can be interpreted as an infall of the local group of galaxies towards Virgo at a radial velocity of 480 km sec^{-1}.

The vigorous growth of the subject makes it likely that this first symposium devoted to all major fields of infrared astronomy may well be the last with such a wide compass. The direction this expanding field of research will go in is not easy to predict. However it is clear that infrared observations of redshifted galaxies will play a vital role in the solution of many of the most important cosmological problems, a point stressed by M. Longair (University of Cambridge) at the end of the symposium. □

0028-0836/80/400387-02$01.00

Industrial biopolymers

from Paul Calvert

THE term biopolymers really includes all macromolecules of biological origin but, for industrial application, biopolymers can be divided into two categories: those to be used in aqueous solution and those to be used as solids.

The first category contains a wide range of polysaccharide thickeners, emulsifiers and gelling agents used in the food industry and in a wide range of printing and coating applications. These materials can be extracted from trees, seeds and seaweeds or can be manufactured by modifying starch or cellulose. A variety of microorganisms also produce water soluble extracellular polysaccharides and it was a microbial product — Xanthan gum — that was the centre of attention at a recent meeting in Birmingham*. Xantham gum is produced commercially by Kelco from *Xanthomonas campestris* and consists of a glucose main chain with three-unit side chains (mannose-glucoronic acid-mannose) on every other glucose residue. It was picked for its unusual gelling properties from a survey of microbial polysaccharides carried out by Allene Jeanes at the US Department of Agriculture in the 1950s. It is pseudoplastic, that is it forms a gel or high viscosity solution which thins when the solution is stirred. The viscosity is stable to changes in temperature, pH and salt concentration but can be modified by adding other vegetable gums. This gives it a wide range of uses, for example in 'instant' desserts and in salad dressings that flow out of the bottle but not off the salad.

One very important possible application for water soluble polymers is in the secondary recovery of oil. A normal oil well only produces about 40 per cent of its oil content in the combined processes of primary recovery, where the oil comes out under its own pressure, and secondary recovery where it is forced out by water or gas pumped down a series of holes surrounding the oil reservoir. The extraction is limited by the failure of the water to displace oil from porous rock and by the tendency of the water to follow cracks in the rock directly to the central well rather than sweeping the oil before it. There are a variety of ways to enhance oil recovery (for a review see Arnold, C.W. in *Microbial Polysaccharides and Polysaccharases* ed. Berkeley, Gooday, & Ellwood, SGM/Academic Press, 1979) but a possible new approach is through a combination of surfactants, to allow the water to displace the oil from rock, with water-soluble polymers to increase the water viscosity and prevent it by-passing the oil. The requirements for such a polymer are that it gives a high viscosity increase at low concentrations but is shear-thinning for ease of pumping. It should also be stable at the bottom of an oil well for several months, which, in the case of deep North Sea wells where conditions are most severe, means it must be stable in saline at temperatures of about 120°C. Polyacrylamides have been used successfuly in the US although the cost was high compared to the value of the oil produced. For general use, polyacrylamides are too unstable and too easily absorbed and every known water soluble polymer has been considered as an alternative. Xanthan gum or a similar microbial polysaccharide seem to be suitable but current fermentation methods of production make them expensive. Also, at a rate of one pound of polymer used per barrel of oil produced there may not be sufficient production capacity for the polysaccharides to satisfy the potential demand even if all fermentation plants were employed for this one product.

In the light of the increasing price of oil and the current interest in fermentation methods of producing industrial chemicals it seems natural to seek an industrial plastic made by microorganisms. For a biopolymer to be used as a plastic it should be a linear uncross-linked molecule insoluble in hot water but soluble in organic solvents or, better, capable of melting and processing without decomposition. Given that natural structural polymers like cellulose and collagen tend to be made from polar monomers and derive their insolubility from strong intermolecular hydrogen bonding it is not surprising that suitable examples are rare. One example is poly (β-hydroxybutyrate) which is an optically active thermoplastic polyester with a melting point around 175°C produced as an intracellular storage compound by various bacteria inlcuding *Azotobacter vinelandii* and *Pseudomonas solanasearum*.

If a suitable naturally produced thermoplastic were available it may still not be practicable to manufacture it. Any fermentation process leads to products which must be separated and purified and this may be considerably more expensive than a simple catalytic polymerisation, (for example, ethylene to polyethylene) although it may be competitive with the more expensive condensation processes leading to nylons or polyethylene terephthalate.

Thus while the traditional biopolymers, cellulose and rubber, are still the most important and water soluble biopolymers are in production, a solid polymer, the plastic microbe, has yet to come. □

---

*A symposium on "Recent advances and Industrial Applications in Biopolymers" organised by the Society of Chemical Engineers was held in Birmingham in March

Paul Calvert is in the School of Molecular Sciences, University of Sussex.

Essential fatty acids and prostaglandins

from Michael Crawford

IN 1930 at the University of Minnesota in Minneapolis, George and Mildred Burr made the remarkable discovery that dietary linoleic acid was essential for growth, development and normal function in rats. At this time, pharmacological activity of a group of uncharacterised substances from semen and male accessory glands was also being studied by U.S. von Euler at the Karolinska Institute in Stockholm. He characterized the material as a biologically active hydroxylated unsaturated fatty acid and named it 'prostaglandin'.

World War II interrupted research on the 'essential fatty acids' (EFA) and 'prostaglandins' (PG), and it was not until the 1950s, with the introduction of radioisotopes, gas-liquid chromatography and mass spectrometry that further progress was made. During the 1950s and 1960s EFAs were shown to be required by several species, including man, and linoleic acid was found to be metabolized to longer chain polyunsaturated acids. In 1964 these were established as the precursors for the PGs by Van Dorp and colleagues of Unilever in Holland and by Bergström and colleagues at the Karolinska Institute in Sweden.

In spite of this evidence establishing a link between EFA and the PGs, work in both fields remained separate. Pharmaceutical companies became excited by the potential of PGs, their analogues and inhibitors in the fields of reproductive physiology, inflammation and thrombosis. Meanwhile in the EFA camp, advances were made in establishing the role of EFA in cell membrane function, brain growth and the prevention of atherosclerosis and thrombosis. At the time, however, benefits of high linoleic acid diets to the cardiovascular system were largely attributed to reduction in blood cholesterol. The important role of EFAs and PGs may well be in the integrity of vascular membranes, the stability of platelets and in modulation of vascular tone.

A recent Congress* was held to bring the two fields together. Both Burr and von Euler attended the Congress as guests of honour. The sessions were designed to highlight the precursor-product relationship between EFAs, PGs and other biologically important EFA metabolites.

A number of different speakers independently supported the idea that nutritional management of dietary precursors should affect biosynthesis of PG and other oxygenated products. The practical applications of this include the reduction

Michael Crawford is in the Nuffield Laboratories, London and was one of the Congress program coordinators.

---

*The Golden Jubilee Congress on Essential Fatty Acids and Prostaglandins was held at the University of Minnesota, May 4-7, 1980.

0028-0836/80/400388-02$01.00

of hypertension and of atherosclerosis and the prevention of retinopathy in human diabetics by a diet rich in linoleic acid over a six-year period. In cardiovascular disease also, EFA aspects of nutrition emerged as a positive contribution to health in contrast to the negative effects of saturated fats and cholesterol.

It was suggested that conventional descriptions of EFA deficiency as a scaly skin and an elevated triene/tetraene ratio may be inadequate because different disease states were described in which conversion of linoleic acid to the PG precursors were impaired. Psoriasis is one example of EFA deficiency in which supplies of the linoleic and arachidonic acids are adequate but in which there is a block in the enzyme cyclooxygenase necessary for PG formation. In addition, the conversion of dihomogammalinolenic and arachidonic acids to the spectrum of leukotrienes, thromboxanes and prostacyclins may need to be similarly considered. In this context, present recommendations for linoleic acid intake of 1-2% of dietary energy may have to be revised upwards, especially when one considers our present high consumption of saturated fatty acids and their competition with EFAs for the enzyme systems. It is possible that the health of the vascular endothelium and the prevention of atherosclerosis should be a criterion by which one measured EFA requirements.

New leukotrienes were described bringing to three the families of leukotrienes. Within each family two compounds have pro-inflammatory and bronchoconstrictor roles making them possible mediators of inflammation and asthma. Probably these account for the biological activity of the slow reacting substance in anaphylaxis (SRS-A). There were also reports on chemical synthesis of novel leukotrienes and of the biosynthesis of leukotriene-like substances from 18-carbon fatty acids possessing Δ 5-unsaturation.

In the prevention of thrombosis and control of the immune system, there was renewed speculation that PGE_1 and/or other derivatives of the EFA precursor (8, 11, 14-20:3) may play previously hidden roles. Alteration of PG metabolism induced by the therapeutic use of lidocaine in endotoxin shock in baboons indicated that prostacyclin might be involved in protection against shock. This finding, for the first time, provided a rational link between adequate nutrition and susceptibility to stress and shock.

Columbinic acid proved to be of great importance. Derived from the seeds of the Columbine, its structure is similar to linoleic acid with a *trans* double bond at the five position. This acid was found to express many EFA functions associated with linoleic acid, but it cannot be converted to prostaglandins. Columbinic acid thus provides an experimental tool for separating PG-mediated functions from the structural lipid functions of essential fatty acids. For instance, columbinic acid could restore skin lesions of EFA-deficient rats, but could not normalise the response to inflammation.

Other exciting topics included a report suggesting that arthritis may be alleviated by dietary means involving 6, 9, 12-18:3. This result was found in an animal model of immune-mediated arthritis, the leukocytes from such animals were not able to take part in chemotaxis. With this and the other reported examples from the immune response and cardiovascular areas, the distinct impression was given that we may be on the verge of new and exciting developments in dietary control or prevention of major chronic disease states.

The Congress banquet ended with two historic speeches from two remarkable men — Burr and von Euler — remarkable not only for their work but for their great insight and natural humility. As scientists we were reminded to "expect the unexpected" and to realise that original discoveries often only become important after development by others whose contributions are forgotten.

The unique formula for this Congress worked in a very special way. It was the first meeting of two branches of science which have been distant acquaintances for many years; the knowledge each offered the other fused them into one. It is to be hoped that the new links and friendships it created will help to expand the new and permanent dimension that was added to biology in Minneapolis.

Neural communication and control: facts and theories

from D. M. MacKay

Everyone would agree that the interaction between theory and experiment should ideally take place in one and the same head. This is doubly true in a field such as brain research, where we are often in doubt as to the categories in which our problems should be expressed, let alone resolved. Present-day education being what it is, however, few of those most productive in experimental neuroscience are ideally equipped to do their own theorising; and all too many theorists show a lack of that sense of proportion that comes from long exposure to experimental fact.

Perhaps because of its close kinship with problems of engineering, the study of neural communication and control has enjoyed more than its share of theoretical attention over the past three decades. Can we learn anything from the history of those exceptional theories that have succeeded in catalysing experiments on new lines with useful results? Conversely, which current experimental findings (if any) seem likely to set theoretical speculation off in fresh directions? These were the kinds of question faced at a recent Symposium*.

T. H. Bullock (University of California, San Diego) set us off with an impressive survey of the diversity of physical changes that might serve to represent information or to control function in a single neuron, and therefore should not be overlooked by theorists of neural communication. Field potentials can be causative (for example, at the Mauthner cell axon cap). The relative timing of impulses may be as important as their mean frequency, especially if central 'clocking' occurs. Even physical movement of fibres cannot be discounted. Much of the ensuing discussion sought to narrow the range over which these alarming complications may be significant; but there was general agreement that at least in plexiform tissue the representation of neuronal interaction by means of 'circuits' was too simple to be safe.

Simultaneous recording from multiple microelectrodes, described by G. L. Gerstein (University of Pennsylvania) and others, offers a particularly promising new line of data for theorists of local network function. With tungsten microwire bundles, for example, Gerstein has found much greater similarity in the patterns of coincident firing of a group of visual cortical neurones than in the responses of a single neuron to two successive stimuli. This suggests that sensory information may be represented with lower variance in ensemble statistics than in single-unit histograms. A host of theories of neural network function in other areas may become testable as this technique develops.

A beautiful preparation for the study of neuronal interaction was described by P. Andersen (University of Oslo), who has succeeded in maintaining isolated slices of hippocampal cortex in functional condition for recording *in vitro*. Among many important results, he finds remarkable equipotency of synapses on the inner regions of pyramidal cell dendritic trees, and virtual simultaneity of excitation of a row of pyramidal cells by parallel afferents. Summation of simultaneous EPSPs from neighbouring inputs is perfectly algebraic, with no sign of conductance interference even at synapse separations below 50μm. Andersen's recordings identify GABA-containing interneurones as important modulators of pyramidal function.

D. M. MacKay is Head of the Department of Communication & Neuroscience, University of Keele, UK.

---

*A Satellite Symposium of the 1980 Physiological Congress, co-sponsored by the Commission on Communication and Control Processes of the International Union of Pure and Applied Biophysics, was held between July 20 and 24 at the University of Debrecen in Hungary. The organizers were S. Damjanovich & G Szekely (Hungary), P I Johannesma (Netherlands) and D. M MacKay UK.

An elegant experiment was described by M. Constantine-Paton (University of Princeton), on the tectal innervation from a third eye implanted in the developing frog. This shows that stereotypic segregation into alternating bands of ocular dominance can develop from an initial state of overlap between the two projections, and is superimposed upon a retinotopic representation of visual space. R. M. Gaze (National Institute of Medical Research, Mill Hill), working with compound (double-nasal, double-temporal, double-ventral) eyes in *Xenopus,* reported data supporting the "tea-trade" model of connection-formation developed by Willshaw and von der Malsburg[1].

The cerebellum has long invited theoretical modelling by the regularity of its geometry. Another highlight of the meeting was the study by M. Ito (University of Tokyo) of adaptive changes in the flocculo-vestibulo-ocular system of the alert rabbit, which has for the first time yielded a detailed and nearly complete functional picture of a cerebellar subsystem. Mossy fibre impulses from the labyrinth are transferred across the flocculus and elicit signals from Purkinje cells that adjust the vestibulo-ocular reflex. 'Retinal slip' error signals, sent to climbing fibres via the inferior olive, modify the efficacy of mossy fibre synapses on the Purkinje cells until the adjustment is accurate. Conjoint stimulation of mossy and climbing fibre afferents reduces the efficacy of parallel-fibre synapses. Although the synaptic changes found are opposite to those postulated in Marr's theory[2], being rather in the direction assumed by Albus[3], the general framework of Marr's original conceptualisation of cerebellar function appears to be supported by these findings.

At the theoretical 'whole-brain' level V. Braitenberg (Max-Planck-Institute, Tübingen) challenged us to consider the implications of some neuroanatomical statistics. With pyramidal cells making up perhaps three quarters of the neuronal population, synapses at a density of 10^9 per mm^3, and fibres perhaps 3×10^9 per mm^3, he argued that more than 100 axons must cooperate in order to excite one pyramidal cell. Hence the influence of any one pyramidal cell on another might be relatively small, despite their proximity. He favoured a view of the cerebral cortex as an array of associative cell assemblies rather than of feature-classifying units, with co-operative state–transitions representing specific 'decisions'.

Finally, D. M. MacKay (University of Keele) described recent experiments, based on his earlier information-flow analysis of cognitive agency[4], which gave evidence of goal-conflict between the two 'halves' of split-brain patients only at the executive level. The inference suggested was that the direct physical correlate of cognitive agency is not cortical activity as such, but rather the cooperative activity of a 'supervisory system' whose dominant evaluative level is embodied in diencephalic or other structures not divided by the splitting operation.

One's impression from the meeting as a whole (from which the above are only samples) is that the working relationship between experimentalists and theorists of neural function is entering on a new and remarkably fruitful phase. ☐

---

1. Willshaw, D.J. & von der Malsburg, C. *Phil. Trans. R. Soc. B* **287**, 203 (1979).
2. Marr, D. *J. Physiol. (London)* **202**, 437 (1969).
3. Albus, J.S. *Math. Biosci.* **10**, 25 (1971).
4. MacKay, D.M. in *Brain and Conscious Experience* (ed. J.C. Eccles) 422 (1966); *Cerebral Correlates of Conscious Experience,* (eds. P.A. Buser & A. Rougeul-Buser) 53 (1978).

Chopping and changing in immunoglobulin genes

from Miranda Robertson

A concluding speaker, summarizing one of the 19 themes of the 4th International Congress of Immunology*, remarked that immunological research seems not so much to rush forward like a river, as to advance and retreat by turns like the tide. While there may be some truth in this assessment for cellular immunology, it clearly does not apply to the molecular biology of immunoglobulin genes, which has been advancing with gathering momentum ever since Tonegawa and his colleagues announced the first V region sequence in 1978[1]. Yet even in this field, there were signs at the Congress, if not of a retreat, at least of a significant change in orientation. Many of the molecular biologists who have been seeking an explanation for the diversity of antibody molecules have now clearly shifted their attention from somatic recombination of DNA to somatic point mutations.

The data which have led to the recent emphasis on recombination were reviewed by E. Kabat (Columbia University), and can be recapitulated as follows (see also ref. 2). It is known that the antigen-binding variable region of the immunoglobulin light chain is constructed from two separate genes: a V gene and a J gene. During the differentiation of an immunoglobulin-secreting B cell, one of a set of between 100 and 1,000 germ-line V genes combines at random, and with slight variations in the precise site of recombination, with one of a set of 5 germ-line J genes. The site of recombination coincides with the third hypervariable region. The heavy-chain variable region is constructed by a similar process with one additional complication. The V genes of heavy chains do not join directly to the J genes, but to a third set of genes, the D genes, which join in turn to the J genes. The D region of the heavy chain, which may vary considerably in length, corresponds to the third hypervariable region.

Given that each of the two immunoglobulin chains is constructed by such random recombination of substantial sets of germ-line genes, and that the light and heavy chains assort independently, it has been argued, here[3] and elsewhere, that there are enough germ-line immunoglobulin genes to account for the entire antibody repertoire without any need to postulate further diversification by mutation.

But whether or not these mechanisms could in principle account for all antibody diversity, there was general recognition at the Congress that in practice they do not. Kabat pointed out how little evidence there is that sequence changes brought about by V-J recombination have any effect on antigen-binding specificity, which depends not only on hypervariable region 3 but on hypervariable regions 1 and 2 as well. He himself, on the basis of an extensive survey of amino acid sequence data, adopts the minority view that the entire V region is constructed from mini-genes separately encoding each of the four framework regions and three hypervariable regions — a view that has been partly vindicated by the discovery of the separate D and J genes encoding the third hypervariable and fourth framework regions in the heavy chain. But while it is undeniable that, historically, amino-acid sequences have been rather good predictors of otherwise surprising properties of immunoglobulin genes, the balance of opinion is heavily against the mini-gene hypothesis in its extreme form. This is because of the evidence at the DNA level that only one rearrangement takes place between sperm and adult, and that that rearrangement results in transposition of a continuous sequence of DNA containing all three of the first three framework regions with the first two hypervariable regions *in situ.*

The majority view therefore is that any antibody diversity not generated by known recombination mechanisms cannot be explained by recombination at all; and an accumulation of evidence, some of it by no means new, has led to a pronounced switch in emphasis from recombination to somatic mutation as the main generator of antibody diversity.

Ontogeny and diversity

The data that are now recognized as pointing to somatic recombination are

---

Miranda Robertson is associate editor of Nature

*The 4th International Congress of Immunology was held in Paris on the 21st to 26th July, 1980 and was organized by the Société Française d'Immunologie.

0028-0836/80/400390-03$01.00

those showing that isolated amino-acid substitutions occur not only in the hypervariable regions but also in the framework regions of secreted immunoglobulin chains. Such substitutions were reported in mouse V_L chains some years ago by Weigert *et al.*[4], and were in fact apparent from a comparison of the first sequenced germ-line V_L gene with the myeloma gene which had provided the probe[1]. A more systematic investigation of departures from germ-line sequences is now under way in a collaboration between K. Rajewsky's laboratory (University of Cologne) and A. Bothwell in Baltimore's laboratory, where 10 germ-line genes have been sequenced for comparison with immunoglobulin genes from a panel of hybridomas secreting antibodies against nitrophenol (NP). This comparison is still in progress, but in the meantime both Rajewsky and P. Gearhart (Carnegie Institute) reported a highly suggestive relationship between immunoglobulin diversity and B cell ontogeny.

This relationship is revealed in a comparison of antibodies of different classes directed against the same antigen. The first class of antibodies to be expressed in an immune response is always IgM, followed by IgG and later perhaps by IgA or IgE, the different classes of antibody being defined by the constant region of the heavy chain, which may be μ, γ, δ, or ε. It is believed that the sequential expression of different classes of antibody recognizing the same antigen (the heavy-chain switch) reflects the sequential recombination of a single V-D-J combination with the different C_H genes, by a process known to involve DNA deletion[2].

Gearhart reported an initial comparison of anti-phosphorycholine (PC) antibodies that suggests, indirectly, that the heavy-chain switch may be associated with somatic mutation in the V region. Partial sequences of 15 hybridoma proteins showed that while all four IgM proteins examined had identical N-terminal sequences, those of eight out of nine IgG proteins had amino-acid substitutions. Seven myeloma IgA anti-PC proteins were also partially sequenced and substitutions were found in 5 of those. Rajewsky has found a similar pattern of substitutions in a preliminary comparison of hybridomas secreting anti-NP IgM and IgG. One important incidental point to emerge from these investigations is that the same idiotype was expressed on the different immunoglobulin classes, which invalidates the use of anti-idiotypic antisera for monitoring changes in the V region during B cell ontogeny[3].

At present, the evidence in favour of such changes is necessarily indirect, and there is clearly an urgent need for a B cell clone in which a class switch can be induced so that comparison of V regions is possible within a single cell line. (Cell lines that undergo class switches do exist, but they are tumour cell lines of suspect ploidy.)

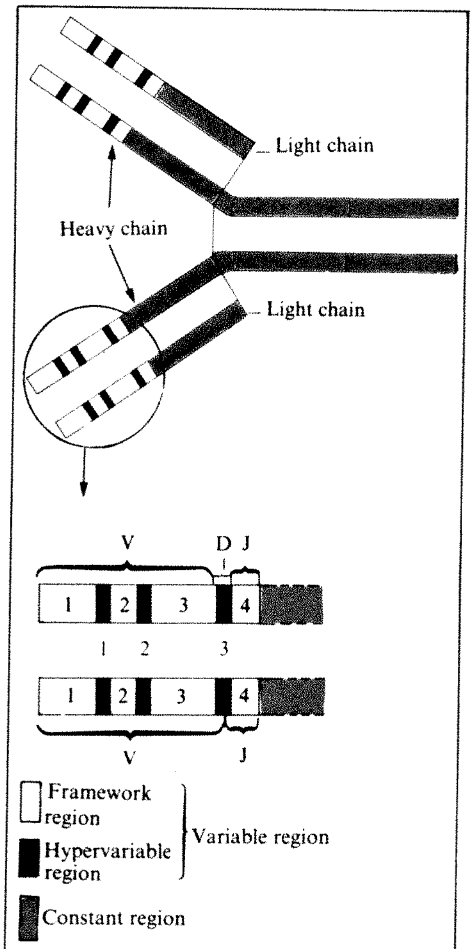

Immunoglobulin molecules are made up of four chains: one pair of heavy chains and one pair of light chains. Each chain is divided functionally into two regions: the variable region, which mediates antigen recognition, and the constant region, which in the case of the heavy chains mediates the effector function of the molecule.

The variable region can be further subdivided into four regions which vary only slightly from one antibody molecule to another, and are known as the framework regions, and three regions (the hypervariable regions) which are very much more variable and in the folded protein form the actual antigen-binding site.

Each light chain is now known to be coded by three separate genes: a C gene coding for the constant region, a J gene coding for the fourth framework region and part of the third hypervariable region, and a V gene coding for the first three framework regions including hypervariable regions one and two and part of hypervariable region three.

Each heavy chain is coded by four separate genes: a C gene coding for the constant region, a J gene coding for the fourth framework region, a D gene coding for the third hypervariable region, and a V gene coding for the first three framework regions including hypervariable regions one and two.

Ig genes of T cells

While the immunoglobulin molecule steadily yields its secrets to the combined onslaught of restriction enzymes and sequencers, the T cell receptor continues to elude molecular and cellular immunologist alike. This is particularly tantalizing in view of the evidence at the cellular level that the antigen binding sites of T cell receptors are encoded by immunoglobulin V_H genes. The original evidence for the expression of V_H genes in the T cell receptor was the demonstration that T cell help in antibody production could be induced or inhibited by anti-idiotypic antibodies[5]. Since then both suppressor (T. Tada, Tokyo University; M. Taussig, ARC Babraham; A. Nisonoff, Harvard University) and helper (E. Mozes, Weizmann Institute) cells have been found to bind anti-idiotype antibodies and to release idiotype-bearing factors which suppress or induce the production of antibodies to a specific antigen.

Progress on the biochemical characterization of these factors has however been slow, and in the meantime the appealing prospect of unifying T and B cell responses to antigen within a regulatory network based on idiotypic determinants of a single repertoire of V_H regions has become fogged with complications. C. Janeway (Yale University), discussing the variable consequences of attempts to manipulate the immune response with anti-idiotypic antibodies, pointed out that there is evidence that T cells have a more restricted repertoire than B cells, since an anti-idiotypic antibody that suppresses only a part of the B cell response to an antigen (the idiotype-positive part) can completely eliminate the T cell response to the same antigen. In the light of recent developments, this could simply mean that T cells use the same germ-line V genes but do not subsequently diversify by mutation. However a more serious problem arises in a result reported by H. von Boehmer (Basel Institute of Immunology) who has used an anti-V_H antiserum raised by D. Givol (Weizmann Institute) and his colleagues to stain cytotoxic T cells. To circumvent the problem of antigen specificity and the T cell repertoire, Givol produced an antiserum directed against common V_H framework determinants. This antiserum has been used successfully to isolate T cell factors but von Boehmer finds that it does not stain cytotoxic T cell clones.

Meanwhile, molecular biology laboratories have been competing in the attempt to by-pass the biochemistry altogether and reach for the receptor DNA with heavy-chain probes. Tonegawa, as reported at the Congress by von Boehmer, has used a J_H probe to explore a cloned cytotoxic T cell line and found V genes either in their germ-line arrangement, or rearranged aberrantly, but never rearranged to produce a V-D-J join as in a differentiated B cell.

In spite of the overwhelming evidence that none of the known immunoglobulin C regions is present on T cells, D. J. Kemp (Walter and Eliza Hall Institute of Medical Research) and T. Rabbitts (MRC Laboratory, Cambridge) have used a C region rather than a V region probe and shown, surprisingly, that the gene encoding the μ chain is rearranged both in T lymphoma cells[6] and in cloned T cells[7]. Kemp's colleagues have however gone on to show that although the μ gene is transcribed it is not translated[8].

What, then, is the significance of the apparently futile rearrangement of immunoglobulin genes in T cells? The answer suggested by Kemp is that they reflect the operation in T cells of the same enzymes that mediate the recombination events accompanying differentiation in B cells; and that T cell differentiation, therefore, is probably dependent on the same enzyme system, not necessarily operating on the same genes.

Abortive rearrangements in B cells

Abortive rearrangement of immunoglobulin genes is in fact an extremely common feature of B myeloma cells, in which it was first reported by Lenhard-Schuller *et al.*[9]. It has since been shown that in a large proportion of immunoglobulin-secreting myelomas, rearrangement of both light and heavy chain genes has occurred on both chromosomes, although only one directs the synthesis of immunoglobulin[10,11]. (The other may however give rise to protein fragments, which have occasionally been reported in biochemical investigations of myeloma cells.)

There are three ways of looking at these rearrangements. One possibility is that they are a peculiarity of myeloma cells and would not be seen in normal B cells if it were only possible to clone one and look at its DNA. This view is increasingly disfavoured. The second, which was emphasized by P. Leder (US National Institutes of Health), is that they may be a part of the price the immune system pays for antibody diversity. For example, one obvious consequence of the variable site of V-J joining is that in some recombined genes the reading frame may be shifted; and detailed investigations at the DNA level have now shown that this indeed accounts for an abortive rearrangement in myeloma MPC 173[12] in which a frame shift resulting from the V-J join on one chromosome produces a stop codon within the J sequence.

Similarly detailed investigations on another myeloma, MPCII, have revealed[13,14] a rather different kind of abortion, in which the V region on one chromosome recombines with a 'pseudo-joining' sequence, closely homologous to the V-J recombination sequence but falling within the intron between the J regions and the C region. This gives rise to a primary transcript from which the J region is missing and in which the splice signals in the RNA are altered in such a way that the V region sequence is spliced out during RNA processing and the final product of translation is a curious little fragment consisting of a hydrophobic leader sequence attached to the constant region of the κ chain. For abortive rearrangements of this sort however M. Weigert (University of Philadelphia) does not accept an explanation in terms of necessary sacrifices to the generation of diversity. He adopts the third possible view of abortive rearrangements, which is that they are the mechanism of allelic exclusion[11].

One of the numerous problems posed by B cells is that of how they contrive to express the immunoglobulin genes on only one of the two homologous chromosomes of a diploid cell. Once it was realized that immunoglobulin gene expression involves rearrangement of the DNA, an obvious possibility was that the DNA remained in the germ-line configuration on the excluded chromosome. However, restriction digest data on that point were conflicting. The conflict is now resolved: in some myelomas the immunoglobulin genes on the excluded chromosome remain in the germ-line configuration, in others they do not; and furthermore rearrangement cannot be the prerequisite for immunoglobulin gene transcription, since C_L (though never V_L) fragments may be transcribed in some myelomas from an unrearranged chromosome[11].

The important point is that in no case has a myeloma cell been shown to express more than one functional chain of each type. Weigert takes the view that this is because immunoglobulin genes have evolved so as to prevent such an occurrence by making functional rearrangements highly improbable. This accounts, he argues, for the survival of the 'pseudo-joining' site described by Leder, and for the conservation of 'pseudo-J' genes, originally described in κ light chains and now for λ light chains and for heavy chains (O. Bernard, Walter and Eliza Hall Institute). 'Pseudo-J' genes are J genes which do not lead to expression after recombination with a V segment. The conservation of such genes in the repertoire of the three different kinds of chain must imply that they have an important function: namely, to ensure that functional rearrangements are so unlikely that they almost never occur on both chromosomes. It follows from this that a large number of B cells probably undergo abortive rearrangements on both chromosomes and die without ever expressing immunoglobulin.

Further support for this general scheme is to be found in recent evidence on the fate of the κ light chain genes in B cells secreting λ light chains. For B cells have to decide not only which of two allelic sets of λ or κ light chains is to be expressed, but whether they are to be λ or κ in the first place. That the two decisions may be made on a similar basis was first suggested by the discovery[9] that, just as the genes for the unexpressed allele have been found to be rearranged, so the genes for the unexpressed κ class are rearranged in myeloma cells secreting λ chains. This discovery has now been confirmed and extended by Alt *et al.*[15] who have shown that in two out of four λ-secreting mouse myeloma cell lines, the κ genes are not only abortively rearranged but transcribed and translated into protein fragments. Similarly, Leder and his colleagues have shown that κ genes are rearranged in human B cell lines secreting λ chains.

These data are consistent with the general idea that abortive rearrangements may be the rule rather than the exception. However, preliminary investigations in Leder's laboratory on the converse question of the fate of λ light chain genes in human B cell lines secreting κ chains casts some doubt on whether light-chain class exclusion is really exactly analogous to allelic exclusion within a light-chain class. For in κ-secreting lines, the λ genes seem to remain in the germ-line configuration. The implication of this is that chromosomal rearrangements may take place in a predetermined order, so that only if recombination of the κ genes fails to produce a functional light chain will the λ genes be rearranged. It is already clear that there is some hierarchy in the rearrangement of genes for different immunoglobulin chains since it is established that heavy-chain genes are expressed before light-chain genes. As soon as a functional light chain is expressed, it can combine with the heavy chain to form a complete cell surface receptor. Alt *et al.* suggest that it is this event that shuts off further rearrangements of immunoglobulin genes so as to exclude the formation of λ chains in cells already expressing κ chains.

According to the evidence so far, then, there is a pecking-order for the DNA-recombining enzyme such that V_H genes are rearranged first, followed by the $V_{L\lambda}$ genes and finally, but only in the absence of existing surface immunoglobulin, the $V_{L\lambda}$ genes.

What is conspicuously missing from this picture is its context. While the ambitions of molecular biologists run to the possibility not only of isolating clones of B cell precursors, but even of dispensing with the cell altogether so as to examine the recombination mechanism without interference, there is on the other hand a real need to understand the events of lymphocyte differentiation in general in the context of the physiological signals that trigger them.

1. Tonegawa, S., Maxam, A.M., Tizard, R., Bernard, O. & Gilbert, W. *Proc. natn. Acad. Sci. U.S.A.* **74**, 3518 (1978).
2. Molgaard, H.V. *Nature* **286**, 657 (1980).
3. See Robertson, M. *Nature* **283**, 332 (1980).
4. Weigert, M. & Riblet, R. *Cold Spring Harb. Symp. quant. Biol.* **41**, 837 (1976).
5. Eichmann, K. & Rajewsky, K. *Eur. J. Immun.* **5**, 661 (1975).
6. Kemp. D.J. Harris, A.W., Cory, S. & Adams, J. *Proc. natn. Acad. Sci. U.S.A.* **77**, 2876 (1980).
7. Forster, A., Hobart, M., Hengartner, H. & Rabbitts, T. *Nature* **286**, 847 (1980).
8. Walker, I.D. & Harris, A.W. *Nature* in the press.
9. Lenhard-Schuller, R., Hohn, B., Brack, C., Hirama, M. & Tonegawa, S. *Proc. natn. Acad. Sci. U.S.A.* **75**, 4709 (1978).
10. Perry, R.P. *et al. Proc. natn. Acad. Sci. U.S.A.* **77**, 1937 (1980).
11. Coleclough, C., Cooper, D. & Perry, R.P. *proc. natn. Acad. Sci. U.S.A.* **77**, 1422 (1980).
12. Altenburger, W., Steinmetz, M. & Zachau, H. *Nature* in the press.
13. Seidman, J. & Leder, P. *Nature* **286**, 779 (1980).
14. Choi, E., Kuehl, M. & Wall, R. *Nature* **286**, 776 (1980).
15. Alt, W. Enea, V., Bothwell, A.L.M. & Baltimore, D. *Cell* **21**, 1 (1980).

REVIEW ARTICLE

Insulating ground state and nonmetal–metal transitions

B. K. Chakraverty

Groupe des Transitions de Phases, CNRS BP 166, 38042 Grenoble Cedex, France

For over a decade there has been intense activity in the field of nonmetal–metal transitions in condensed systems in general and in solids in particular. The object of this review is to pinpoint the nature of the insulating ground state and to outline recent trends in our understanding of the metallic state and related phase transition.

ALL condensed systems can be considered as belonging to essentially three canonical states which in their simple limits are: metals, Mott insulators and covalent insulators (P. W. Anderson, personal communication). It is easy to define the metallic state in the simple limit—here the kinetic energy of the electrons dominates all relevant interactions whether between electrons and electrons or between electron and ion cores. The simple metals from the first columns of the Periodic Table especially those of the second, third and fourth columns are well described by this limit (r_s is small, where r_s is electron–electron distance and is a measure of electron–electron repulsion $\sim 1/r_s$ as well as of their kinetic energy $\sim 1/r_s^2$). As the kinetic energy of the electrons (their bandwidth) becomes smaller as we go away from this limit, two distinct types of symptoms usher the transition to the two other canonical states before the system becomes insulating: the characteristic large susceptibility and specific heat of almost magnetic metals such as Pt (ref. 1) which indicate strong repulsive interaction between electrons (henceforth called Mott–Hubbard U)[2] and on the other hand superconductivity which results from electron–ion interactions (henceforth called λ).

The decreasing bandwidth is achieved in principle by increasing the atom–atom distance which would obviously result if the process is continued until it results in systems of well separated atoms. Individual atoms are in general magnetic when their electrons are in open shells. This limit is represented by the paramagnetic 'Mott' insulators, which include a wide variety of transition metal oxides and sulphides, such as NiO and V_2O_3; their magnetic properties show that these cations retain unpaired spins and in spite of their open shells show no metallic conduction. This is because the repulsive energy U needed to put an extra electron on the same orbit is higher than the kinetic energy (bandwidth W) gained in delocalizing the electron resulting the electron preferring to remain in a localized state on every atom. This is the second canonical limit of $U > W$, which we have designated as 'Mott insulators'. In this limit, the system will permit two classes of excitation: (1) those involving the reversal of a spin in place of the type

$$S_i^+ = C_{i\uparrow}^+ C_{i\downarrow}, \quad Si^- = C_{i\downarrow}^+ C_{i\uparrow}$$

where S_i are the spin-operators on site i and Cs are the creation and annihilation operators. And (2) those involving the actual creation of a free pair of carriers of the form $C_{i\sigma}^+ C_{j\sigma}$, $i - j \rightarrow \infty$. The latter requires the excitation energy U, whereas the former does not (if the spins are not ordered) and for $U \gg W > kT$ we will have a paramagnetic insulator. As long as $W \neq 0$ but remains smaller than U, mixing of the spin-states through electron tunnelling between sites will occur so that the ground state will order antiferromagnetically ($J_{aF} \sim W^2/U$), although we may note that the resulting doubling of the lattice periodicity has nothing to do with the insulating Mott ground state: most Mott insulators remain nonconducting above the Néel temperature. One must point out that the Mott transition to a metallic state at zero temperature is, by definition, a phase transition of first order due to many-electron screening of U (and an electron must necessarily suddenly change from localized to itinerant behaviour) and this has nothing to do with the polemic whether the Hubbard hamiltonian generally used to describe interacting electron system in a narrow band gives a first or a second order phase transition or not.

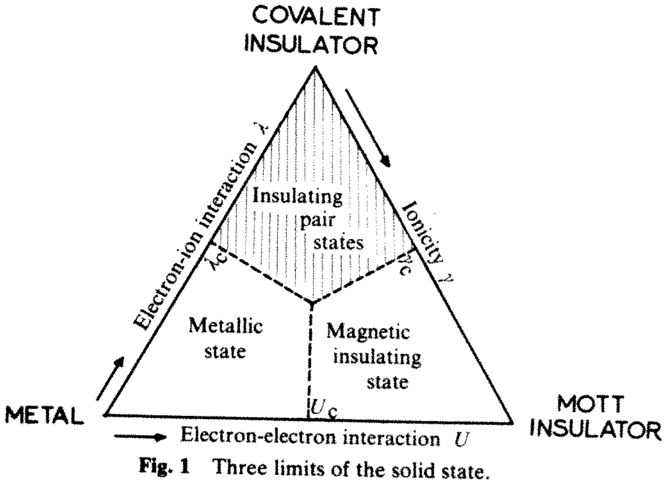

Fig. 1 Three limits of the solid state.

The third canonical limit of the solids is reached when the electron–ion interaction λ far exceeds the electron bandwidth W. As we approach from the side of a perfect metal ($\lambda = 0$, since by definition free electrons do not see the perturbing potential of the ions), a non-zero λ makes itself felt by phonon-induced resistivity $\sim T^5$ in the low temperature region. In the ground state, however, this non-zero λ has two strikingly related behaviours, both related to λ-induced attractive interaction between two electrons: if $\lambda \ll W$, this results in electron pairing and superconductivity, while for $\lambda \gg W$, we find ourselves in localized pair ground states which are diamagnetic singlet states, the covalent insulators being their extreme canonical limit (their essential diamagnetism differentiates them from the Mott insulators) of this class of solids. It is essential to realize that a purely local one electron–ion interaction results in a non-local two-electron attractive interaction sufficiently strong to overcome the repulsive mutual Coulomb interaction so that paired ground state can occur. The tendency to pairing is quite evident as we look into the Periodic Table. The fifth column semimetals provide an excellent example—Bi, As, Sb. These metals have an outer s-shell completely full leaving three electrons in their p-orbitals, along x, y and z directions. In a tight-binding theory of the cubic structure (all these metals at high pressure are cubic) as developed by Labbé and Friedel[3], the dominant hopping

0028-0836/80/400393—04$01.00

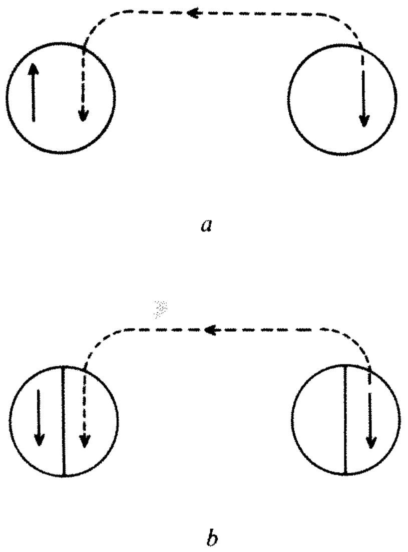

Fig. 2 *a*, Kinetic interaction, antiferromagnetic ground state. *b*, Kinetic interaction, degenerate orbitals, ferromagnetic ground state.

integral is the p_σ-type which gives simply three one-dimensional tight-binding bands each of which will be half filled. The effect of λ would be essentially a lattice distortion, known as 'Peierl's distortion' leading to pairing up of the electrons along x, y and z orbitals and thus one expects a layered structure in which each Bi atom will have three close neighbours in the x, y and z directions, which is what one observes in the actual metals. Note that in these semimetals, the Peierl's distortion leads to a Fermi surface with incomplete gaps, hence very large dielectric constants and small effective mass of the carrier which explain their semimetallic behaviour. The pairing phenomenon leading to Peierl's distortion is a process which competes with superconductivity and if for example Bi or As or Sb can be kept simple cubic, either by pressure or by quenching in impurities, they develop a remarkably high superconducting transition temperature ~10 K. Similarly, the A_{15} high T_c transition metal superconductors are equally subject to the martensitic structural instability often before the superconductive transition. This shows that the effects of λ on the metallic ground state are (1) superconductivity, (2) covalent-pairing leading to incomplete gaps at the Fermi surface in some cases—as in the semimetals or uniform distortion as in the A-15 compounds and (3) for larger λ, the tendency to covalent-pairing becomes so great that we get bipolaronic insulating state[4] (counterpart of the superconducting ground state) and eventually a covalent insulator like Ge or Si, where one can think of the pseudo-potential interaction λ as having eaten up the whole of the Fermi surface making a complete energy gap all around the Brillouin zone. These three canonical states of the solids—metals, Mott insulators and covalent insulators—are depicted in Fig. 1, in an 'alchemical' triangle (at $T=0$) which shows clearly the metal–nonmetal transition boundary to be expected as we move away on U-axis or λ-axis from the simple metal limit. The third axis that ties up the covalent insulator with the Mott insulator is the ionicity parameter γ (Pauling–Phillips–Van Vechten[5]) or the Madelung energy contribution that increases as we approach the Mott-insulation limit. On the Mott insulator side, anions are completely diamagnetic (unlike the cations), filling up the closed rare-gas shells. Approaching the boundary towards covalency, the outermost anionic wave functions spread out into the cationic orbitals. On the other side of the covalent ionic boundary as the ionicity decreases, we start building up the pair states like H_2, O_2 or N_2 or larger groups like benzene, where internally within the molecule we have mobile pair of electrons, but overall a molecular insulating crystal. For the rest of the article, we shall not elaborate any further on this third axis of the alchemical triangle.

Mott insulators

The transition from a metallic to Mott-insulating ground state is by definition accompanied by no change of lattice symmetry. The states on either side of the transition remain paramagnetic (from Pauli to Curie–Weiss behaviour) and is brought about as the lattice parameters are expanded such that diminution of W leads to U/W exceeding some critical value ~1. A rough idea of this critical value can be obtained from elementary arguments. Assume that U is small and the system is in the metallic state with one electron per atom. If we now remove one electron from its site and let it travel around the system, it will on each site have an energy ε_0+U due to repulsive interaction of the electron already sitting there. If the electron on its tour through the crystal happens to catch the hole it left, it will have an energy ε_0 at the side where it happens. This means the electron will recognize the hole as a potential well of depth U (and radius R). We can easily find out when these two body scattering events start to form a bound state. This is an elementary problem in quantum mechanics and gives us the binding condition as

$$\frac{8}{\pi^2}\frac{m^*U}{h^2}R^2>1$$

where m^* is the effective mass of the electron. Fitting the density of states to a rectangular density of states function and a bandwidth W, we can rewrite the bound-state condition as

$$\frac{U}{W}>\frac{\pi}{4}\left(\frac{4\pi}{9}\right)^{1/3}\sim 0.88$$

which is not very different from the Hubbard solution.

Are there any experimental systems that show the Mott ground state? Unfortunately the paramagnetic insulating ground state at $T=0$ is not the lowest energy state due to exchange effect between the electrons and is thus unobservable. This exchange effect can be essentially of two kinds: if the orbitals are non-degenerate and we have one electron per atom, the exchange is a so-called kinetic exchange and is antiferromagnetic, as seen in Fig. 2*a*. The hopping of electron from one site to another is only possible if they have opposite spins; (for identical spins, the Pauli principle prevents all electron transfer) so that the lowest energy state is antiferromagnetic, with a $J_{AF}\sim W^2/U$. Thus in the ground state, we will find an insulating and antiferromagnetic material. On the other hand, suppose the lowest energy orbitals are degenerate (say doubly degenerate) and we have one electron per atom. We expect the system to be metallic as the band will be 1/4 full but it will be a ferromagnetic

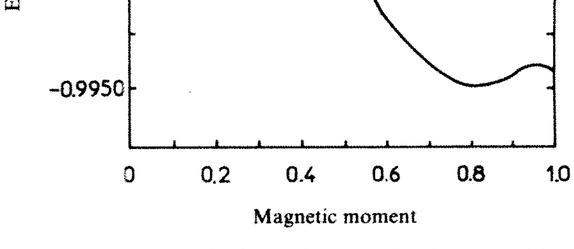

Fig. 3 Total energy at the first order metal–insulator transition as a function of the magnetic moment in the unit cell at $r_s = 2.84$. The inset shows an enlargement of the double-well structure. The arrow indicates that value of M for which the bottom of the upper spin band crosses the top of the lower spin band.

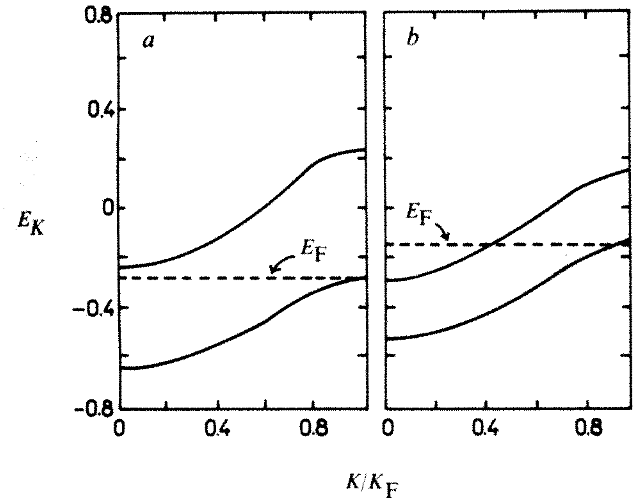

Fig. 4 Spin-split bands at the first order phase transition. *a*, The bands and the existence of an energy gap when the electrons are completely spin aligned ($M=1$). *b*, The overlapping bands which occur at the second energy minimum (see Fig. 3) for $M=0.82$.

metal due to the following simple argument[6] (Fig. 2*b*). If the two electrons on the adjacent sites have identical spins but on different orbitals, they can profit from Hund's rule coupling when one hops, as shown, to give

$$J_{\text{ferro}} \sim -\frac{W^2}{U-J_0}$$

where J_0 is Hund's rule coupling energy, while

$$J_{\text{AF}} \sim \frac{W^2}{U}$$

These two behaviours are very nicely illustrated in the transition metal dichalcogenide crystals of pyrite structure as we go from $CoSe_2$ to NiS_2. In CoS_2, the doubly degenerate e_g orbitals has one electron per atom; CoS_2 is metallic and ferromagnetic. In NiS_2, the same e_g orbitals now have to accommodate two electrons per atom; NiS_2 is insulating and antiferromagnetic. Thus NiS_2 (refs 7, 8) is a very good candidate for a Mott insulator. And under pressure at ~30 kbar, NiS_2 does go to a metallic ground state. A pure Mott transition has also been claimed[9] for V_2O_3 and its Cr-doped alloys, at its high-temperature transition to the insulating paramagnetic state. This is one of the most completely studied system; controversy remains, however, because the paramagnetic insulating state is reached as temperature is increased and the antiferromagnetic insulating ground state is accompanied by lattice symmetry change considerably complicating the implication of correlation 'only' in this system.

Recently, more quantitative calculation of the Mott–Hubbard transition had been performed by Rose *et al.*[10] For the system of one electron per atom, they have obtained as a function of r_s the ground-state energy (Fig. 3) energy dispersion (Fig. 4*a*, *b*) as well as magnetic moment per site (Fig. 5). We see very nicely the first-order metal–nonmetal transition at an $r_s=2.84$ predicted by Mott (this corresponds to Mott's universality criterion of $n^{1/3}a_0=0.22$). The double-well structure of Fig. 3 is the signature of the first-order phase transition. Considering Fig. 4*a* drawn for $r_s=2.84$, we see the band occupation when magnetization per site $M=1$, that is, complete spin polarization of the system. Consider taking a few electrons out of the lower band and putting them in the upper band. We must pay an energy ΔE to do this as Fig. 3 shows. However, there is a second effect which causes this energy increase to stop and leads to the formation of the second minimum at $M=0.82$. This effect results from the fact that the electrons and holes created by the transfer interact and reduce the energy gap between the two bands. In fact this effect is sufficiently large so that when we put enough electrons in the upper band, the bottom of the upper band crosses the Fermi surface of the lower band and energy is gained by transferring electrons to the upper band. The result is the minimum at $M=0.82$ (Fig. 4*b*). The qualitative behaviour is exactly as described by Mott's original arguments for the first order nature of the metal-insulator transition. These calculations also show formation of a spin moment in a second order phase transition at $r_s=2.74$ (Fig. 5).

To conclude this section, we will mention a completely different class of systems that show metal–nonmetal transition and are probably closest to the spirit of the original idea of Mott—that as the atom–atom distance is decreased, the system must go suddenly to the nonmetallic state. These systems are the low-density fluids or dense metallic vapours at high critical temperatures or pressures, and have been studied extensively by Hensel and co-workers[11] over the last decade. The most thoroughly studied is mercury (critical temperature 1,760 °C, critical pressure 1,510 bar for liquid–vapour transition) and it shows a transition to a fluid nonmetal as the pressure is varied. The fluid alkali metals on the other hand like Cs or Rb (ref. 12) show Mott transition at their critical points of gas–liquid transition with anomalous increase of the magnetic susceptibility as the Mott localization limit is approached (for Cs this occurs at around 1,800°C).

Bipolaronic insulators

In complete contrast to the Mott insulators, the bipolaronic insulators are characterized as a ground state of localized pairs of electrons in singlet state. Such an insulator is thus completely diamagnetic and is obtained as we go along the λ axis of Fig. 1, until a critical λ_c is reached at which the Fermi surface is unstable to the formation of these pair states. Unlike Mott insulators, the bipolaronic insulators are actually seen experimentally as a ground state[13] in a wide variety of solids and have opened up quite a new field of investigations.

The idea behind the formation of a bipolaron is really quite simple: in order for two electrons otherwise itinerant in an empty band to come together (either on the same site or on two nearby sites) and stay together localized, the lattice must locally deform to couple these two electrons together through a deformation-induced attractive interaction $\sim g_0^2/M\omega_0^2$ (where g_0 is an electron–lattice interaction term, M the atomic mass, ω_0 a lattice frequency) so as to compensate and exceed the instantaneous Coulomb repulsion $v(\sim e^2/\varepsilon r_0)$ of the underformed lattice. The total energy of the two-electron system is then

$$E_T=\frac{g_0^2}{M\omega_0^2}-v$$

When E_T exceeds $W/2$, the two electrons will emerge from the bottom of the band as a localized bound pair state. This situation is schematically shown in Fig. 6 where E_T is plotted against

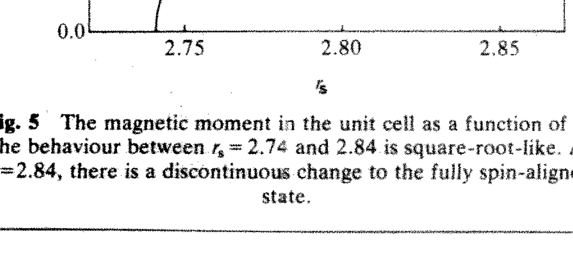

Fig. 5 The magnetic moment in the unit cell as a function of r_s. The behaviour between $r_s=2.74$ and 2.84 is square-root-like. At $r_s=2.84$, there is a discontinuous change to the fully spin-aligned state.

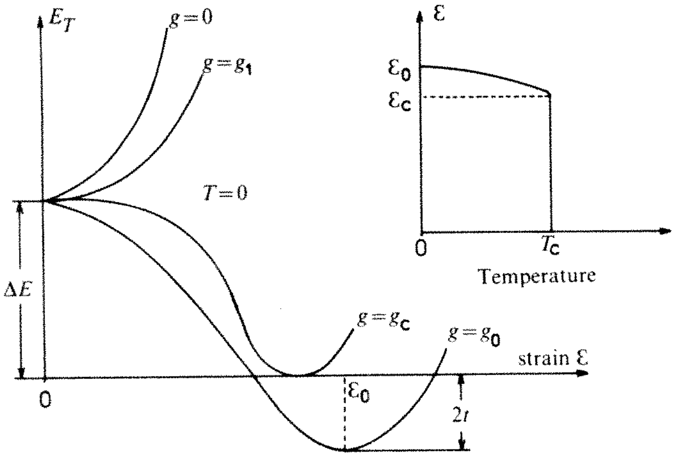

Fig. 6 Total energy of electron pair as a function of lattice deformation.

lattice deformation ε for different values of the coupling constant g_0 and we observe the critical g_0 at which the bound state for the two electrons appears. The transition to the insulating state is sudden and as we raise the temperature, the appearance of the metallic state is characterized by the vanishing of the deformation (insert Fig. 3). Such a pair is called a bipolaron in analogy with polarons. Note, however, that unlike polaronic concepts, bipolaron formation is not necessarily due to optical phonons. Ti_4O_7 (ref. 13) and its alloys remain the most extensively studied bipolaronic insulators. There are several important points that need however to be emphasized:

(1) In nature, it is rare[14] to find a $s = 1/2$ system that does not have a diamagnetic ground state.

(2) The interaction between the two electrons is really between two strain centres (two 'polarons'), that is, elastic interaction and can be long-range, highly anisotropic and oscillating in character.

(3) The bipolarons stand exactly in the same relationship to Bardeen–Cooper–Schrieffer superconducting pairs as does a localized electron to an itinerant one. A phase diagram between superconducting ground state and an insulating bipolaronic ground state has recently been suggested[15] as a function of the coupling strength λ.

(4) Formation of bipolarons is to be distinguished from the Peierl's transition[16]; unlike the latter, there is no lattice symmetry change involved in the former. In this sense, the bipolarons also differ from the insulating ground states of the so-called layer compounds due to charge density wave formation where the lattice periodicity is modulated[7,8].

We have attempted a synthesis between what we called the three simple canonical states of solids—metals, Mott insulators and covalent insulators. No attempt has been made to include all varieties of metal–nonmetal transition—for example the valence transitions[17] in rare-earth compounds, or the transitions in lower dimensionality[18] solids or Anderson transitions[19,20] in disordered systems. Each of these are in a rapidly developing state both theoretically and experimentally and it is quite impossible to include any of them in this short review. The reader is referred to specific articles dealing with these topics. *Note added in proof*: A complete calculation of the Goodenough–Kanamori rules and their relevance to Mott insulators has recently been published[21].

1. Friedel, J. in *The Physics of Metals* (ed. Ziman, J. M.) 382 (Cambridge University Press, 1969).
2. Hubbard, J. *Proc. R. Soc.* A**276**, 238 (1963).
3. Labbé, J. & Friedel, J. *J. Phys. (Paris)* **27**, 153 (1966).
4. Chakraverty, B. K. & Schlenker, C. *J. Phys.* **37**, C4-353 (1976).
5. Pauling, L. *The Nature of Chemical Bonds* (Cornell University Press, New York, 1960).
6. Goodenough, J. B. *Magnetism and the Chemical Bond*, 165 (Interscience, New York, 1963).
7. Wilson, J. A. & Yoffe, A. D. *Adv. Phys.* **18**, 193 (1969).
8. Krill, G. thesis, Univ. Louis Pasteur, Strasbourg (1976).
9. McWhar, D. B., Menth, A., Remeika, J. P., Brinkman, W. F. & Rice, T. M. *Phys. Rev.* **7**, 1920 (1973).
10. Rose, J. H., Shore, H. B. & Sander, L. M. *Phys. Rev.* B**21**, 3037 (1980).
11. Hensel, F., *Liquid Metals 1976*, 372 (Conference Series no. 30, Institute of Physics, Bristol, 1976).
12. Freyland, W. *Proc. J. Phys.* (in the press).
13. Lakkis, S., Schlenker, C., Chakraverty, B. K., Buder, R. & Marezio, M. *Phys. Rev.* B**14**, 1429 (1976).
14. Fazekas, P. & Anderson, P. W. *Phil. Mag.* **30**, 423 (1974).
15. Chakraverty, B. K. *Lett. J. Phys.* **40**, L-99 (1979).
16. Peierls, R. E. *Quantum Theory of Solids*, 108 (Oxford University Press, London, 1955).
17. Parks, R. D. (ed.) *Valence Instabilities and Related Narrow Band Phenomena* (Plenum, New York, 1977).
18. Chaikin, P. M., Garito, A. F. & Heeger, A. J. *Phys. Rev.* B**5**, 4966 (1972).
19. Anderson, P. W., *Phys. Rev.* **109**, 1492 (1958).
20. Mott, N. F., Pepper, M., Pollitt, S., Wallis, R. H. & Adkins, C. J. *Proc. R. Soc.* A**345**, 169 (1975).
21. Feinberg, D. & Ranninger, J. *Phys. Rev.* B**21**, 3366 (1980).

ARTICLES

Improved conversion of methanol to single-cell protein by *Methylophilus methylotrophus*

J. D. Windass*, M. J. Worsey, E. M. Pioli, D. Pioli, P. T. Barth, K. T. Atherton & E. C. Dart
ICI Corporate Laboratory, The Heath, Runcorn, Cheshire, WA7 4QE, UK
D. Byrom*, K. Powell & P. J. Senior
ICI Agricultural Division, Billingham, Cleveland, TS23 1LB, UK

The glutamate dehydrogenase gene of Escherichia coli *has been cloned into broad host-range plasmids and can complement glutamate synthase mutants of* Methylophilus methylotrophus. *Assimilation of ammonia via glutamate dehydrogenase is more energy-efficient than via glutamate synthase, thus the recombinant organism converts more growth substrate, methanol, into cellular carbon.*

A CRITICAL factor in determining the suitability of a microorganism for use in the production of single-cell protein (SCP) is the efficiency with which it converts substrate carbon into cellular carbon[1]. A major reason why the obligate methylotroph *Methylophilus methylotrophus* was selected for use in the ICI process to produce SCP from methanol was its high 'carbon conversion efficiency'. However, we have identified a potential source of methanol wastage due to its mode of ammonia assimilation. Instead of using glutamate dehydrogenase (GDH) to catalyse the conversion of ammonia and 2-oxoglutarate into glutamate, this organism uses a two-stage pathway, dependent

---

* Present address: ICI Joint Laboratory, University of Leicester, Leicester LE1 7RH, UK.

0028–0836/80/400396—06$01.00

on glutamine synthetase (GS) and glutamate synthase (GOGAT), to carry out the same function (Fig. 1)[2]. The latter pathway requires one extra molecule of ATP per molecule of glutamate formed.

M. methylotrophus probably uses the energetically suboptimal pathway for ammonia assimilation because of the environment in which it evolved. GS has a much higher affinity for ammonia than GDH[3] and is therefore more effective in scavenging for low concentrations of ammonia. Since ammonia concentrations are not growth-rate limiting during SCP production, exchanging the ammonia assimilation pathway used by *M. methylotrophus* should result in the organism consuming less energy for this process; correspondingly more methanol should be available for protein synthesis. We have used recombinant DNA techniques to carry out this exchange by introducing the *Escherichia coli* *gdh* gene, which codes for GDH activity, into a mutant of *M. methylotrophus* which lacks GOGAT.

Cloning the *E. coli gdh* gene

The best available strain for screening for a cloned *E. coli gdh* gene was *E. coli* CB100, which is deficient in both GDH (gdh^-) and GOGAT ($gltB^-$) and therefore requires glutamate for growth[4]. Derivatives which have received a *gdh* gene from another source should be readily selectable by virtue of their glutamate independence. However, because CB100 is λ-resistant and a relatively poor transformation host we initially cloned the *gdh* gene by *in vivo* techniques using RP4::Mu (refs 5, 6).

A $gltB^-$ *E. coli* strain (obtained from Dr J. Cole) was lysogenized with Mu *cts* and a derivative of RP4 carrying Mu *cts* was transferred into it. This strain was grown overnight at 37 °C and was then mated non-selectively at 30 °C with a derivative of CB100 which is *rec*A, rif^r and which is lysogenic for Mu *cts* (CL412). Progeny of this mating were transferred to plates of minimal medium deficient in glutamate but containing rifampicin and kanamycin. This should select for progency of CL412 which have received plasmid RP4 derivatives carrying a segment of the donor strain's chromosome containing a functional *gdh* gene (that is, an RP4'*gdh* plasmid). Several methods were used to prove that some of the progeny of this mating and selection did carry authentic RP4'*gdh* plasmids. First, the plasmids could be transferred through an intermediary host (C600 *rec*A) and back into CL412, selecting only for kanamycin resistance, and they still conferred glutamate independence on the latter strain. Second, elimination of the RP4-derived plasmid from CL412 by mating in an incompatible, trimethoprim-resistant (Tp^r), P-group plasmid, R751 (ref. 7), resulted in simultaneous loss of glutamate independence. Finally, enzyme assays showed that when glutamate independence was conferred by these plasmids it led to the acquisition of GDH and not GOGAT activity.

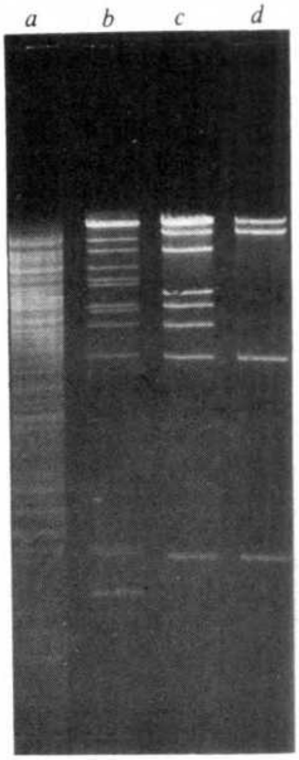

Fig. 2 Comparative *Pst*I restriction endonuclease analysis of RP4' *gdh* DNAs with RP4 and *E. coli* DNAs. RP4' *gdh* plasmid DNAs were prepared from fresh 100 ml overnight cultures of CL412 cells by a Triton X-100 (0.05%)/lysozyme lysis procedure[14], followed by 2 min vigorous vortex mixing and by centrifugation with ethidium bromide and caesium chloride[15], without a preliminary clearing spin. The closed circular DNA was collected dropwise, after preliminary aspiration of the dense linear DNA band, and was then dialysed for 2–3 h against 0.01 M Tris (*p*H 7.5); 1 mM EDTA (TE buffer) before phenol extraction, *n*-butanol extraction, ethanol precipitation and re-dissolving in TE buffer. RP4 DNA was prepared in essentially the same way and was a gift from G. S. Sharpe. *E. coli* C600 DNA was prepared as described by Marmur[16], except that the cells were lysed with lysozyme and Triton X-100. DNAs were digested with *Pst*I (MRE Porton) in 30 μl of 20 mM Tris (*p*H 7.5), 10 mM $MgCl_2$, 50 mM $(NH_4)_2SO_4$ and 100 μg ml^{-1} BSA for 60 min at 30 °C, before incubation at 70 °C for 10 min and electrophoresis on a 40 cm × 0.3 cm 1% agarose gel at 200 V overnight, under the conditions of Sharp *et al.*[17] The gel was stained in 2 μg ml^{-1} ethidium bromide for 30 min, washed in water for 30 min and photographed under UV light. *a*, *E. coli* C600; *b*, RP4' *gdh*3; *c*, RP4'*gdh*4; *d*, RP4.

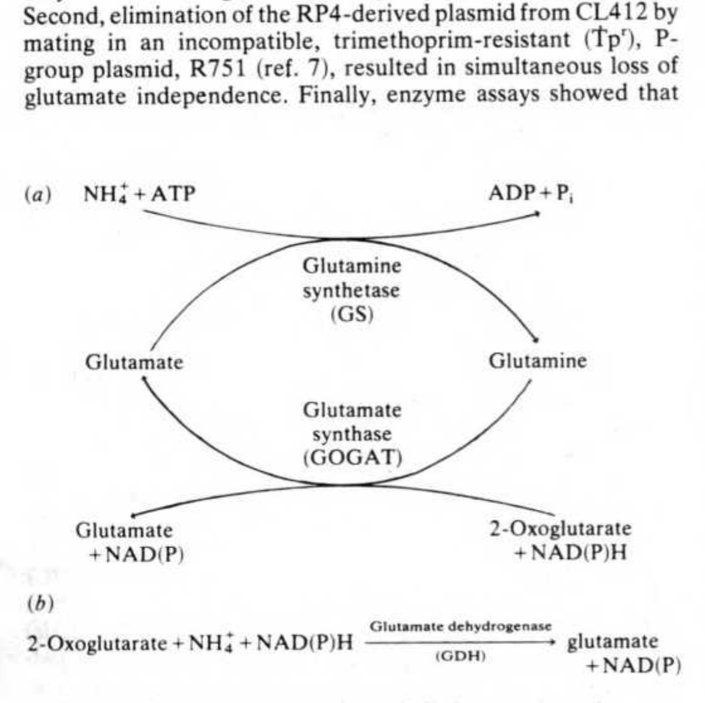

Fig. 1 Pathways of ammonia assimilation by bacteria. *a*, GS/GOGAT; *b*, GDH.

*Pst*I cleavage of plasmid DNA prepared from some of the RP4'*gdh* carrying strains gave the gel electrophoretic patterns shown in Fig. 2. Although fragments common with RP4 are clearly present, the RP4'*gdh* plasmids are much larger and give more complex restriction patterns than RP4 itself. Similarly, the plasmids RP4'*gdh*.3 and RP4'*gdh*.4 have homologous *Pst*I DNA fragments which they do not share with RP4. However, the RP4'plasmids clearly differ from each other, RP4'*gdh*.3 being substantially larger than RP4'*gdh*.4. All of these features might be anticipated because of the method of construction of the plasmids, which should have resulted in the transfer of substantial, but variably sized pieces of the *E. coli* chromosome to RP4, together with two copies of the Mu *cts* phage genome[6]. Following transfer of these RP4'*gdh* plasmids directly from *E. coli* to *M. methylotrophus*, by selection for antibiotic resistances conferred by RP4, we were unable to detect GDH activity; this could be due to the probable instability of plasmids of this structure in a recombination-proficient host[6], or to inefficient transcription of the heterologous DNA.

To isolate a more defined DNA fragment carrying the *E. coli gdh* gene, we cloned DNA from three of the RP4′*gdh* plasmids on to the vector plasmid pACYC184 (ref. 8), using the restriction enzymes *Hin*dIII, *Bam*H1 and *Sal*I. Only with the latter enzyme were substantial numbers of recombinant plasmids obtained which caused CB100 to become chloramphenicol-resistant and glutamate-independent. Plasmid DNA, isolated from four such transformants, contained in each case, a 7.6-kilobase fragment of *E. coli* genomic DNA, flanked by *Sal*I targets (Fig. 3). Enzyme analyses on CB100 strains carrying these pACYC184 derivatives, which confer glutamate independence, show convincingly that this independence is caused by the presence of high levels of GDH (Table 1*a*). The enzyme level apparently reflects the multi-copy nature of the pACYC184 vector plasmid, which indicates that increased gene dosage can cause enhanced GDH production in *E. coli*. Minicell experiments have confirmed that the principal new polypeptide, resulting from the presence of the 7.6-kilobase DNA fragment in the pACYC184 recombinant plasmids, co-migrates with purified *E. coli* GDH on SDS/polyacrylamide gels and is immunoprecipitable with anti-*E. coli* glutamate dehydrogenase antibody (T. C. Hodgman, personal communication). We are therefore confident that the *Sal*I-derived pACYC184 recombinant plasmids we have isolated carry a functional *E. coli gdh* gene and have designated them pACYC184/*gdh* plasmids.

Construction of plasmids to transfer the *E. coli gdh* gene to *M. methylotrophus*

Because pACYC184 is not transferable to *M. methylotrophus*, other plasmid vectors have had to be used to achieve *gdh* gene transfer; these are shown in Fig. 4. pRP301 is a low copy-number conjugative derivative of RP4 which has lost one of the two *Sal*I sites of that plasmid, together with kanamycin resistance (Km^r; ref. 9). Like RP4 it can transfer itself from *E. coli* to *M. methylotrophus* and maintain itself in its new host. pTB70 is a derivative of the multi-copy plasmid R300B (ref. 9), which confers streptomycin resistance (Sm^r) and sulphonamide resistance (Su^r) and into which the Km^r transposon Tn5, together with a small additional piece of DNA, has been inserted. Tn5 gives pTB70 a single *Sal*I site [10]. Like R300B, pTB70 can be mobilized by RP4 to *M. methylotrophus* and is capable of stable maintenance in this organism.

The *E. coli Sal*I *gdh* fragment was readily transferred from pACYC184/*gdh* to the pRP301 and pTB70 vectors. Donor and recipient plasmid DNAs were mixed, cleaved with *Sal*I, ligated and transformed into CB100, selecting for ampicillin-resistant (Ap^r) or Km^r transformants respectively and screening these for glutamate independence. Representative examples of the pRP301/*gdh* and pTB70/*gdh* recombinant plasmids isolated from such glutamate-independent transformants are shown in Fig. 3. Enzyme activities in CB100 cultures carrying such recombinants are consistent with the gene dosage effects noted above (Table 1*a*); pTB70/*gdh* plasmids in particular are of interest as they give rise to the highest levels of GDH in *E. coli* of any plasmids we have constructed so far.

pRP301/*gdh* recombinant plasmids could be transferred directly into *M. methylotrophus* from CB100 by selection for Ap^r. However, unlike RP4, neither pRP301 nor pRP301/*gdh* was found to be stable in *M. methylotrophus*. After growth for 11 generations on ampicillin-free medium, only about 50% of the cells remained resistant to this antibiotic. This phenomenon was not observed with *E. coli* cultures carrying the equivalent plasmid. Nevertheless ampicillin selection was routinely maintained for all strains carrying them. pTB70/*gdh* plasmids can efficiently be mobilized into *M. methylotrophus* from *E. coli* by RP4, selecting for Sm^r transconjugants. Some of these transconjugants stably acquired both RP4 and pTB70/*gdh*, others only acquired the latter plasmid, as judged by their antibiotic resistances. Plasmid DNA isolated from *M. methylotrophus* carrying either pRP301/*gdh* or pTB70/*gdh* was indistinguishable from the corresponding plasmid DNAs isolated from *E. coli* strains, as judged by restriction endonuclease analysis. To determine whether the *E. coli gdh* gene which had been transferred to *M. methylotrophus* on pRP301/*gdh* and pTB70/*gdh* plasmids gave rise to functional GDH, enzyme assays were performed on cultures which had been grown in the presence of 100 $\mu g\ ml^{-1}$ ampicillin or 15 $\mu g\ ml^{-1}$ streptomycin, respectively, to ensure retention of the plasmids in the absence of any means of directly selecting for *gdh* gene retention. As shown in Table 1*b*, *M. methylotrophus* cultures carrying either pRP301/*gdh* or pTB70/*gdh* plasmids produce significant levels of GDH as well as normal levels of GOGAT. *M. methylotrophus* itself produces only GOGAT. The *E. coli gdh* gene therefore appears to be functional in *M. methylotrophus* without further manipulation, although the efficiency of the expression is substantially reduced. The impact of gene dosage is shown in that *M. methylotrophus* carrying pRP301/*gdh* contains substantially lower levels of GDH than when carrying the multi-copy plasmid pTB70/*gdh* (Table 1*b*). The level of GDH in *M. methylotrophus* pTB70/*gdh* cultures is about 45% of that present in gdh^+ *E. coli* strains and this might be expected to be sufficient to allow efficient growth of a glutamate synthase-deficient *M. methylotrophus* strain.

Table 1 GDH and GOGAT activities in strains of *E. coli* and *M. methylotrophus*

		Enzyme	
		GDH	GOGAT
(*a*) *E. coli* strains	Cofactor:	NADPH	NADPH
C600		1010	215
CB100		ND	ND
CB100 (pACYC184/*gdh*)		4880	ND
CB100(pRP301/*gdh*)		1390	ND
CB100(pTB70/*gdh*)		6130	ND
(*b*) *M. methylotrophus* strains	Cofactor:	NADPH	NADH
M. methylotrophus	30	ND	78
M. methylotrophus (pRP301/*gdh*)	30	75	72
M. methylotrophus (pTB70/*gdh*)	30	453	75
M. methylotrophus	37	ND	229
M. methylotrophus (pTB70/*gdh*)	37	835	115
M. methylotrophus 56.2 (pTB70/*gdh*)	37	757	ND

E. coli strains used in enzyme assays were grown in M9 medium[22] supplemented with appropriate amino acids at 40 $\mu g\ ml^{-1}$ and thiamine at 4 $\mu g\ ml^{-1}$. *M. methylotrophus* strains were grown on medium containing (per litre): $(NH_4)_2\ SO_4$, 1·8 g; $MgSO_4 \cdot 7H_2O$, O . 2 g; $NaH_2PO_4 . 2H_2O$, 1 . 4 g; K_2HPO_4, 1.9 g; $FeCl_3$, 0.98 mg; $CuSO_4 . 5H_2O$, 0.02 mg; $MnSO_4 . 4H_2O$, 0.1 mg; $ZnSO_4 . 7H_2O$, 0.1 mg; $CaCO_3$, 1.8 mg. *p*H was adjusted to 6.85 and methanol added to give a final concentration of 0.5% v/v. Aliquots (500 ml) of pre-warmed media were inoculated with 50 ml overnight cultures grown in the presence of 100 $\mu g\ ml^{-1}$ chloramphenicol, 100 $\mu g\ ml^{-1}$ ampicillin or 15 $\mu g\ ml^{-1}$ streptomycin, where appropriate, to ensure selection for plasmid retention. The cultures were grown with shaking aeration at 37 °C to an A_{650} of 0.5, harvested by centrifugation, washed with 10 ml ice-cold buffer (22 mM $KH_2\ PO_4$; 50 mM $Na_2\ HPO_4$; 85 mM NaCl and 0.1 mM $MgSO_4$) and stored overnight on ice as cell pellets. Cell extracts were prepared by resuspending the pellets in 1 ml buffer, sonication and pelleting cell debris by centrifugation at 80,000 *g* for 60 min. Enzyme assays were performed at 30 °C, unless otherwise indicated. The assay mix contained (in a 3 ml cuvette): 50 mM HEPES buffer *p*H 7.5; 1 mM EDTA; 1 mM 2-oxoglutarate; 0.16 mM NAD(P)H; cell extract 0.01–0.1 ml. The reaction was initiated by the addition of substrate to give a final concentration of 10 mM, using NH_4Cl to assay GDH or L-glutamine to assay glutamate synthase. The oxidation of NAD(P)H was followed at 340 nm using a Perkin–Elmer 554 spectrophotometer and a water-jacketed cuvette holder. Enzyme activities are given in nmoles NADH or NADPH oxidized min^{-1} mg $protein^{-1}$, protein concentration being determined by the method of Lowry *et al.*[23]. ND = No detectable activity.

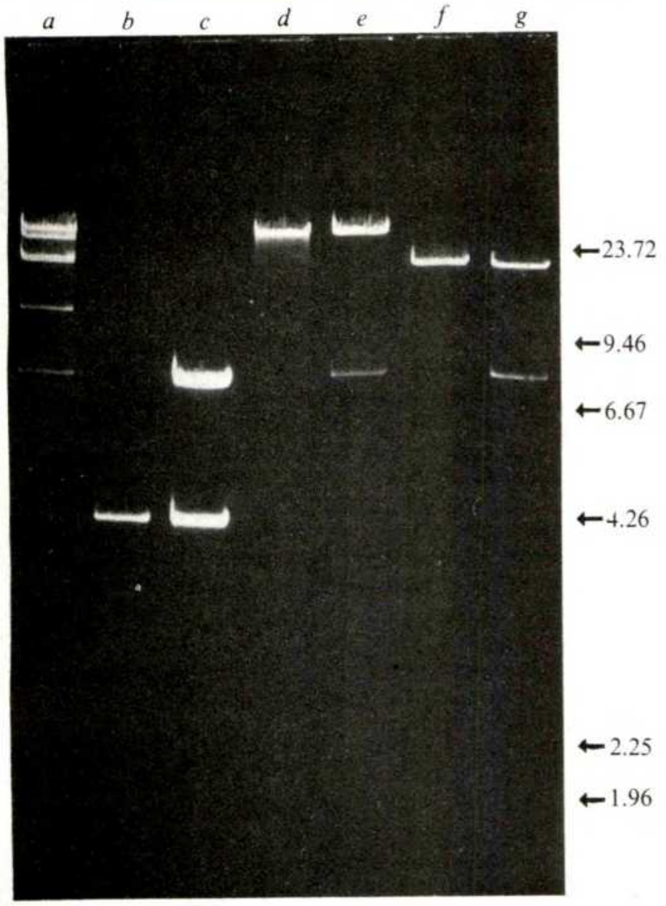

Fig. 3 Comparative *Sal*I restriction endonuclease analysis of RP4′*gdh*4, pACYC184/*gdh*, pRP301/*gdh* and pTB70/*gdh* plasmids. Plasmid DNAs were prepared from suitable CB100 derivatives as described in the legend to Fig. 2. *Sal*I digests were performed in 30 μl volumes with enzyme obtained from Bethesda Research Laboratories, under the recommended conditions. Electrophoresis, staining and photography were also as described in Fig 2. *a*, RP4′*gdh*4; *b*, pACYC184; *c*, pACYC184/*gdh*; *d*, pRP301; *e*, pRP301/*gdh*; *f*, pTB70; *g*, pTB70/*gdh*. The size markers were obtained by running a *Hin*dIII digest of λDNA in a parallel track, and are given in kilobases.

Isolation and characterization of GOGAT deficient mutants of *M. methylotrophus*

To ensure that *M. methylotrophus* carrying the cloned *E. coli gdh* gene was entirely dependent upon the GDH pathway for ammonia assimilation, it was necessary to block the existing GS/GOGAT pathway. Elimination of GS activity would result in a glutamine requirement which would not be supplemented by the presence of GDH activity; it was therefore necessary to block the GS/GOGAT pathway by isolating a mutant deficient in GOGAT.

Since GOGAT functions in the biosynthesis of glutamate (Fig. 1), through which most ammonia is assimilated into the cell, the obvious phenotype of mutants which have lost this activity would be an ability to grow on glutamate but not ammonia as sole nitrogen source[2]. However, *M. methylotrophus* cannot use glutamate as sole nitrogen source; uptake experiments suggest that this is due to impermeability to this compound (J. McNairney, personal communication). Permeability mutants which are able to use glutamate as a nitrogen source can be readily selected from *E. coli* W (ref. 11), which resembles *M. methylotrophus* in poor uptake of glutamate. However, we have been unable to isolate such mutants from the latter organism.

A search was initiated to find alternative nitrogen sources (Table 2), but of the compounds tested only glutamine gave a positive result. However, we have been unable to isolate either glutamine auxotrophs of *M. methylotrophus* or alternatively mutants able to grow on glutamine but not ammonia as sole nitrogen source. Furthermore, experiments with radiolabelled glutamine indicated that it too cannot be taken up by the cell (W. Naylor, personal communication). Since *M. methylotrophus* can grow on extremely low concentrations of ammonia, and as glutamine is rather unstable, it is conceivable that apparent growth on glutamine is due to the presence of ammonium ion impurities. Alternatively, *M. methylotrophus* may have some mechanism for breaking down glutamine extracellularly and growing on the ammonia thus produced.

These results indicated that a mutant which had lost GOGAT activity would not be able to grow on any of the nitrogen sources tested. A strategy was therefore adopted of isolating temperature-sensitive mutants and screening these for strains able to grow at the non-permissive temperature following the introduction of pTB70/*gdh* into them. Out of a total of 550 mutants, isolated after mutagenesis with *N*-methyl-*N*′-nitro-*N*-nitrosoguanidine, four were found which could grow at the non-permissive temperature (37 °C) when they had received this plasmid. However, these mutants failed to grow at 37 °C when pTB70 was transferred into them, indicating that they were complemented by a function encoded by the 7.6-kilobase pair cloned fragment of *E. coli* DNA carried by pTB70/*gdh*. Similarly, when the mutants carried the low copy-number plasmid pRP301/*gdh*, which only gives rise to low levels of GDH in *M. methylotrophus* (Table 1*b*), they grew poorly at 37 °C. Mutants carrying pRP301 alone, failed to grow at this temperature.

Mutants of *E. coli* lacking GOGAT activity and relying on GDH for growth on ammonia are unable to grow on media supplemented with 0.075 mM NH_4^+, although the wild-type organism will grow slowly on such media[2]. This is probably due to the difference in the affinity for ammonia of the enzymes involved[3]. We therefore tested the ability of the putative temperature-sensitive GOGAT mutants of *M. methylotrophus* carrying pTB70/*gdh* to grow on plates containing 0.07 mM NH_4^+ at 30 °C and 37 °C. The results for one such mutant, 56.2, are shown in Table 3. Whereas, at 30 °C, both the wild-type and the temperature-sensitive mutants formed colonies on plates with ammonia concentrations down to 0.07 mM, at 37 °C the temperature-sensitive mutants complemented by pTB70/*gdh* would not grow on 0.07 mM ammonia. The latter strains grew well, however, on both 1 mM and 15 mM ammonia. This strongly suggests that these strains use GDH for growth and are

Table 2 Nitrogen sources for *M. methylotrophus*

Compound	Growth
NH_4^+	+
L-glutamine	+
L-glutamate	−
L-aspartate	−
L-proline	−
L-arginine	−
L-alanine	−
γ-L-glutamyl-L-glutamate	−
L-alanyl-L-glutamate	−
L-pyroglutamate	−
N-acetyl-L-glutamate	−
DL-α-methyl glutamate	−
L-glutamic acid dimethyl ester	−
L-glutamic acid diethyl ester	−
γ-benzyl-L-glutamate	−

Overnight cultures of *M. methylotrophus* were centrifuged, washed in buffer and inoculated into liquid medium of the composition described in the legend to Table 1, except that the compounds to be tested were the sole nitrogen source and were assessed at both 5 mM and 10 mM. Growth was scored after 48 h incubation at 37 °C. + Indicates growth, − indicates no growth.

unable to use GOGAT for ammonia assimilation at 37 °C. Finally, enzyme assays demonstrated that temperature-sensitive mutants complemented by pTB 70/*gdh* and grown at 37 °C lack detectable GOGAT activity but have high levels of GDH synthesized from the plasmid-carried *gdh* gene derived from *E. coli*. The results for mutant 56.2 are shown in Table 1*b*.

Thus *M. methylotrophus* has now been genetically modified so that it can assimilate ammonia via the energetically more favourable GDH route. The resultant organism *M. methylotrophus* 56.2 carrying pTB70/*gdh*, was tested in continuous culture under methanol-limiting conditions at a dilution rate of 0.2 h^{-1}. Subsequent enzyme assays and plasmid analysis showed that the *gdh* gene was stably maintained even in the absence of antibiotic selection and that the modified organism gave 4–7% higher carbon conversion than its unmodified precursor.

Discussion

The isolation of a fragment of *E. coli* DNA containing a functional gene for GDH and the identification of plasmid vectors capable of transferring this DNA fragment by conjugation from *E. coli* to the obligate methylotroph *M. methylotrophus* has enabled temperature-sensitive mutants of the latter organism to be screened for those deficient in GOGAT activity. The resultant transconjugants must use the *E. coli* GDH to synthesize all the glutamate[2] and hence all the organic nitrogen they require for growth at the non-permissive temperature. The use of the energetically more efficient GDH ammonia assimilation pathway results in more methanol being converted into cellular carbon. Thus, using recombinant DNA techniques, we have been able to make a fundamental alteration in the primary metabolism of *M. methylotrophus*, inactivating one function and replacing it with a heterologous one derived from a separate microbial genus. The resulting organism is able to convert significantly more methanol into SCP than the parental strain.

One of the principal problems of gene transfer between organisms which are not closely related has been in the expression of the transferred gene in its heterologous host[12]. Although the *E. coli gdh* gene is expressed in *M. methylotrophus*, the enzyme activity produced per gene copy is 10–20-fold lower than in *E. coli*, as can be seen by comparing enzyme activities in *M. methylotrophus* carrying pRP301/*gdh* or pTB70/*gdh* with those in a *gdh* mutant of *E. coli* carrying the corresponding plasmid (Table 1). In both microorganisms, the amount of GDH activity seems to be determined largely by gene copy number. In *E. coli* the relatively wide ranges of GDH activity which can occur suggests that any mechanism of regulating the level of *gdh* gene transcription can readily be overcome and that no significant deleterious effects accrue from excess *gdh* gene expression. In *M. methylotrophus* the presence of the *gdh* gene on the high copy-number plasmid pTB70 results in an enzyme activity which is sufficient to permit efficient growth under conditions where it provides the sole pathway of ammonia assimilation.

One surprising result of this work is the apparently high frequency with which we were able to detect mutants defective in GOGAT amongst mutants isolated solely on the basis of temperature sensitivity (4 out of 550). However, in both *E. coli* and *Klebsiella aerogenes* GOGAT has been shown to be a complex enzyme consisting of two different large polypeptides[2]. Thus one might expect temperature-sensitive mutations

Table 3 Growth of *M. methylotrophus* and its derivatives on various ammonia concentrations

Incubation temperature (°C)	NH_4^+ concentration (mM)	Growth *M. methylotrophus*	 *M. methylotrophus* 56.2	 *M. methylotrophus* 56.2 (pTB70/*gdh*)
30	0.07	+	+	+
30	1	+	+	+
30	15	+	+	+
37	0.07	+	–	–
37	1	+	–	+
37	15	+	–	+

Growth was tested by streaking to single cells on 1.5% agar plates using the *M. methylotrophus* medium described in the legend to Table 1 except that the $(NH_4)_2SO_4$ concentration was varied as shown. Growth was scored after 48–72 h incubation. + Indicates visible colonies, – indicates no growth.

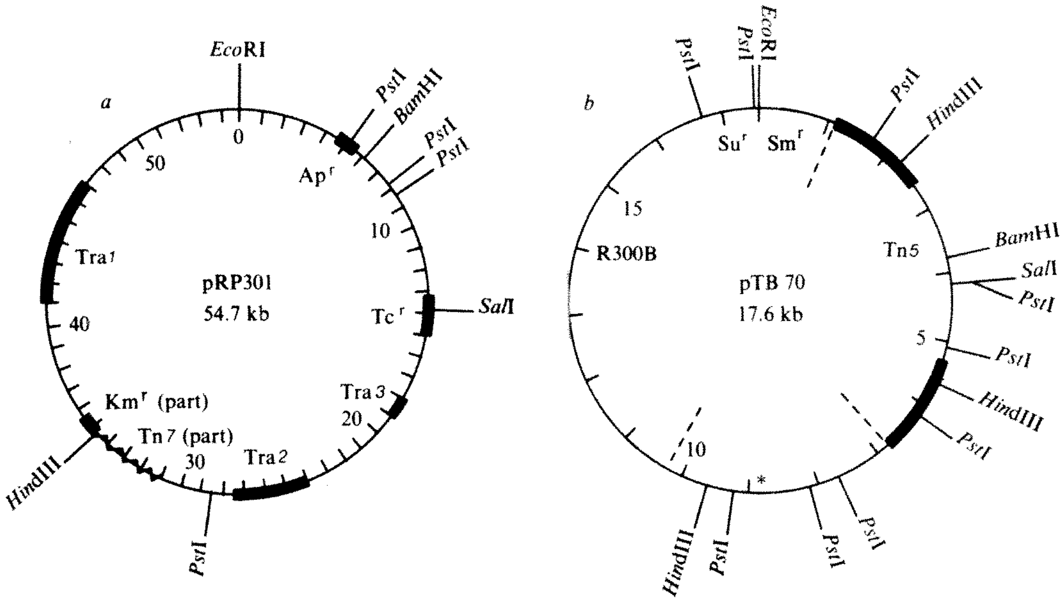

Fig. 4 Maps of the plasmid vectors used in *M. methylotrophus*. *a*, pRP301 was derived, as previously described[9], from an RP4::Tn7 plasmid (pRP3) by excision of the small *Hin*dIII fragments, followed by ligation and transformation into *E. coli*. It has lost the Km^r of RP4 and the Tp^rSm^r of Tn7. Its remaining *Sal*I site is within the gene conferring Tc^r. The blocks represent previously mapped genes on RP4 (refs 9, 18). *b*, pTB70 was derived from R300B which is a wide host-range, multicopy, 8.5-kilobase pair, Sm^r Su^r IncQ plasmid[19,20]. JR66a (*Inc*Ia, Tn5) was used to mobilize R300B from *E. coli* into *Proteus mirabilis* 13, selecting for Km^r on MacConkey agar containing polymyxin B (25 μg ml^{-1}) to counter-select the donor. *Inc*I plasmids cannot be maintained in *P. mirabilis*[21], therefore transconjugants should contain R300B::Tn5 plasmids. The restriction map of pTB70, a plasmid from one such transconjugant, is closely similar to that of R1162::Tn5, derived by Meyer *et al.*[10] (R1162 is very similar or identical to R300B[19]), but shows that it has acquired, in addition to Tn5, a 3.6-kilobase pair piece of DNA (marked *) which may also be derived from JR66a (ref. 22). The heavy lines indicate the inverted repeats in Tn5. Restriction maps were deduced from the plasmid restriction fragments seen on 0.8% and 1.5% agarose gel after electrophoresis, using *Hin*dIII fragments of λDNA as size markers. Sizes given in kilobases (kb).

affecting this enzyme to occur at a relatively high frequency. Furthermore, the genome size of an obligate methylotroph such as *M. methylotrophus* may be relatively small (*Methanobacterium thermoautotrophicum*, an obligate methanogen, only has a genome of molecular weight 1.1×10^9, as compared to the *E. coli* genome, for example, which has a molecular weight of 2.7×10^9 (ref. 13)).

For the purposes of strain improvement and modification, the alteration we have made in *M. methylotrophus* could not have been achieved either by prolonged selection under continuous culture conditions or by a conventional mutagenic approach. It represents the planned adaptation of a microorganism to a man-made environment using a combination of both mutation and intergeneric gene transfer. Effectively we have reversed the consequences of an evolutionary selection pressure which apparently demanded that the organism possessed a highly effective method of scavenging for ammonia in an ammonia-deficient environment. The evolution of many living systems must have been subject to similar pressures from environments deficient in key nutrients. Where the energy source is non-limiting, such deficiencies may be accommodated by using more energy to push equilibria in favour of the synthesis of the desired product. For industrial or agricultural use, however, this form of adaptation is contrary to efficient production and we feel there are potential savings to be made by identification of metabolic features which incur such an 'energy penalty'. It represents a new and exciting area for the application of recombinant DNA techniques.

We thank Dr B. J. Bachman for providing CB100; Dr M. Van Montagu for RP4::Mu *cts*; I. Garner, T. Hodgman and P. Burke for assistance with enzyme assays and communication of unpublished results; Dr G. M. Tonge for helpful discussions and Mr R. B. Vaisey for the fermentation work. pTB70 was isolated while one of us (P.T.B.) was working in the laboratory of Professor N. Datta.

Received 5 June; accepted 9 July 1980.

1. Cooney, C. L. in *Microbial Growth on C_1-Compounds*, 183–197 (Society of Fermentation Technology, Tokyo, 1975).
2. Tyler, B. *A. Rev. Biochem.* **47**, 1127–1162 (1978).
3. Miller, R. E. & Stadtman, E. R. *J. biol. Chem.* **247**, 7407–7419 (1972).
4. Pahel, G., Zelenetz, A. D. & Tyler, B. M. *J. Bact.* **133**, 139–148 (1978).
5. Denarie, J. *et al.* in *DNA Insertion Elements, Plasmids and Episomes* (eds Bukhari, A. I., Shapiro, J. A. & Adhya, S. L.) 507–520 (Cold Spring Harbor Laboratory, New York, 1977).
6. Faelen, M. *et al.* in *DNA Insertion Elements, Plasmids and Episomes* (eds Bukhari, A. I., Shapiro, J. A. & Adhya, S. L.) 521–530 (Cold Spring Harbor Laboratory, New York, 1977).
7. Jobanputra, R. S. & Datta, N. *J. med. Microbiol.* **7**, 169–178 (1974).
8. Chang, A. C. Y. & Cohen, S. N. *J. Bact.* **134**, 1141–1156 (1978).
9. Barth, P. T. in *Plasmids of Medical, Environmental and Commercial Importance* (eds Timmis, K. N. & Puhler, A.) 399–410 (Elsevier, Amsterdam, 1979).
10. Meyer, R., Boch, G. & Shapiro, J. *Molec. gen. Genet.* **171**, 7–13 (1979).
11. Halpern, Y. S. & Umbarger, H. E. *J. gen. Microbiol.* **26**, 175–183 (1961).
12. Atherton, K. T., Byrom, D. & Dart, E. C. *Symp. Soc. gen. Microbiol.* **29**, 379–405 (1979).
13. Mitchell, R. M. *et al. Science* **204**, 1082–1084 (1979).
14. Katz, L., Kingsbury, D. T. & Helinski, D. R. *J. Bact.* **114**, 577–591 (1973).
15. Bazaral, M. & Helinski, D. R. *J. molec. Biol.* **36**, 185–194 (1968).
16. Marmur, J. *J. molec. Biol.* **3**, 208–218 (1961).
17. Sharp, P. A., Sugden, B. & Sambrook, J. *Biochemistry* **12**, 3055–3063 (1973).
18. Barth, P. T., Grinter, N. J. & Bradley, D. E. *J. Bact.* **133**, 43–52 (1978).
19. Barth, P. T. & Grinter, N. J. *J. Bact.* **120**, 618–630 (1974).
20. Grinter, N. J. & Barth, P. T. *J. Bact.* **128**, 394–400 (1976).
21. Datta, N. & Hedges, R. W. *J. gen. Microbiol.* **70**, 453–460 (1972).
22. Miller, J. H. in *Experiments in Molecular Genetics* (Cold Spring Harbor Laboratory, New York, 1976).
23. Lowry, O. H., Rosenbrough, N. J., Farr, D. L. & Randall, R. J. *J. biol. Chem.* **193**, 265–275 (1951).

The structure of one of the eight or more distinct chromosomal genes for human interferon-α

Shigekazu Nagata, Ned Mantei & Charles Weissmann

Institut für Molekularbiologie I, Universität Zürich, 8093 Zürich, Switzerland

The 12 interferon (IFN)-related sequences detected in a human gene bank fall into not less than eight distinct classes, indicating that there are at least eight IFN-related genes. Most, if not all, of these direct the synthesis of an IFN in Escherichia coli. *The sequence of one chromosomal gene and its flanking regions was identical to that deduced for the cDNA corresponding to IFN-α1 mRNA. No evidence was found for the existence of an intron, in either the coding or the non-coding segments of the gene.*

WE recently reported the isolation of cloned hybrid plasmids containing cDNA derived from IFN-producing human leukocytes[1]. Many of these plasmids were capable of directing the synthesis of polypeptides with human leukocyte-type IFN (HuIFN-α [ref. 2]) activity in *E. coli*[1,3]. The cDNA inserts of two such hybrids, Z-pBR322(*Pst*)/HcIFN-2h and -SN206 (Hif-2h and Hif-SN206), have been sequenced[3,4]. The amino acid sequences of the polypeptides IFN-α1 and IFN-α2, encoded by Hif-2h and Hif-SN206, respectively, differ in 17% of their positions; moreover, as deduced from the DNA sequences, IFN-α1 is one amino acid longer than IFN-α2, due to the absence of the codon for Asp 44 in IFN-α2. IFN-α1 and IFN-α2 differ in five and nine of 32 amino-terminal residues, respectively, from IFN isolated from lymphoblastoid cells and partially sequenced by Zoon *et al.*[5], designated IFN-α3.

We concluded that at least three distinct genes for IFN-α (ref. 3) exist in man. It was of interest to find evidence for the presence of several IFN-related genes in the DNA of one individual, as the cDNA clones had been derived from pooled blood samples and might reflect an extreme form of polymorphism. We therefore isolated and characterized cloned human chromosomal DNA fragments that hybridize or cross-hybridize to Hif-2h cDNA.

We report in this article the identification of eight distinct chromosomal DNA fragments which cross-hybridize with Hif-2h cDNA, most of which direct the formation of IFN in *E. coli*. We have identified and sequenced one chromosomal IFN gene which has the same coding sequence as Hif-2h cDNA. This gene for IFN-α1 lacks introns, both in the regions corresponding to the coding and to the non-coding part of the mRNA. Other than the histone genes and certain viral genes, this may be the first instance of a functional gene in higher organisms which codes for a protein and yet contains no introns.

Cloned human chromosomal DNA fragments hybridizing to Hif-2h cDNA

Lawn *et al.*[6] have prepared a collection of hybrid phage derived from fragments of fetal human chromosomal DNA, generated

0028–0836/80/400401—08$01.00

by partial cleavage with *Hae*III and *Alu*I, and joined with *Eco*RI linkers to λ Charon 4A arms. This gene bank was screened by an '*in situ*' procedure[7,8] using as probe the ^{32}P-labelled IFN-α1 cDNA insert excised from the hybrid plasmid Hif-2h[1,4]. Sixteen hybridization-positive phage clones were isolated from 240,000 plaques by repeated plaque purification[8]. Ten of the hybrid phage DNA preparations were cleaved with *Hin*dIII, *Tac*I, *Hha*I, *Bam*HI, *Eco*RI and *Bgl*II, respectively, the fragments separated by agarose gel electrophoresis, traferred to a Millipore membrane[9] and hybridized with the ^{32}P-labelled Hif-2h cDNA insert. Figure 1 shows, as an example, the patterns resulting from the experiments with *Eco*RI, *Pn*dIII and *Bgl*II; Figure 2 summarizes the total data. In each case, the positions of at least a few characteristic restriction sites were established, and the region(s) hybridizing to the IFN probe were delineated.

The hybrid ML-λCh(*Eco*)/Hchr(AH)IFN-10 (chr-10) appears to contain two separate IFN-α1-related genes, because both the 5'- and 3'-terminal Hif-2h cDNA probes (*Pst-Bgl*II fragment, nucleotides 1–315 for 5' probe; *Eco-Pst* fragment, nucleotides 685–910 for 3' probe, see ref. 4) hybridize with the 5.2- and the 20-kilobase *Bgl-Bgl* fragments (data not shown). Chr-16 clearly contains two IFN-α1-related sequences, because the two *Bgl*II fragments comprising the λ arms and part of the insert hybridize to the probe, but two internal *Bgl*II fragments from within the insert do not. Clones chr-1 and chr-23 seem to be independent isolates of the same DNA segment, as they yield identical restriction fragments. Clones chr-3 and chr-26 may represent DNA segments which overlap over much of their length because they have several *Eco*RI and *Hin*dIII fragments in common. The gene in chr-1 and one of the genes in chr-10 might be the same because the *Hin*dIII-*Hin*dIII and *Eco-Eco* fragments which hybridize with the Hif-2h cDNA probe have the same length (3.2 and 0.95 kilobases, respectively). It seems that the 'right-hand' gene of chr-16 may be identical with the gene in chr-35 (orientated in the opposite direction), as each of the two clones yields a 1.4-kilobase *Bgl-Bgl* and a 2-kilobase *Eco-Eco* fragment which hybridize with the Hif-2h cDNA probe. Therefore, the chr-16 and chr-35 inserts probably overlap. As Fig. 2 shows, all other hybridizing segments seem unique. For example, the characteristic features of the putative gene in chr-1 are: (1) *Eco*RI cleavage yields a strongly hybridizing 0.95-kilobase and a weakly hybridizing 7.8-kilobase fragment. Even if one of the hybridizing fragments has an *Eco*RI end generated by the cloning procedure, one of the two fragments must represent the chromosomal gene. (2) *Hin*dIII cleavage yields a weakly hybridizing >20-kilobase fragment, which must comprise the right-hand λ arm, and a strongly hybridizing 3.2-kilobase fragment, which must lie completely within the cloned fragment, and therefore represents the hybridizing region. (3) There is a *Tac*I site outside the hybridizing region, not further from the gene than about 5 kilobases. As mentioned above, chr-23 is identical to chr-1 in all regards, and one of the hybridizing regions of chr-10 contains a 0.95-kilobase *Eco*RI and a 3.2-kilobase *Hin*dIII fragment as does chr-1. The hybridizing *Hin*dIII fragments of chr-3, chr-12, chr-16, chr-30 and chr-35 are all completely contained in the cloned DNA frag-

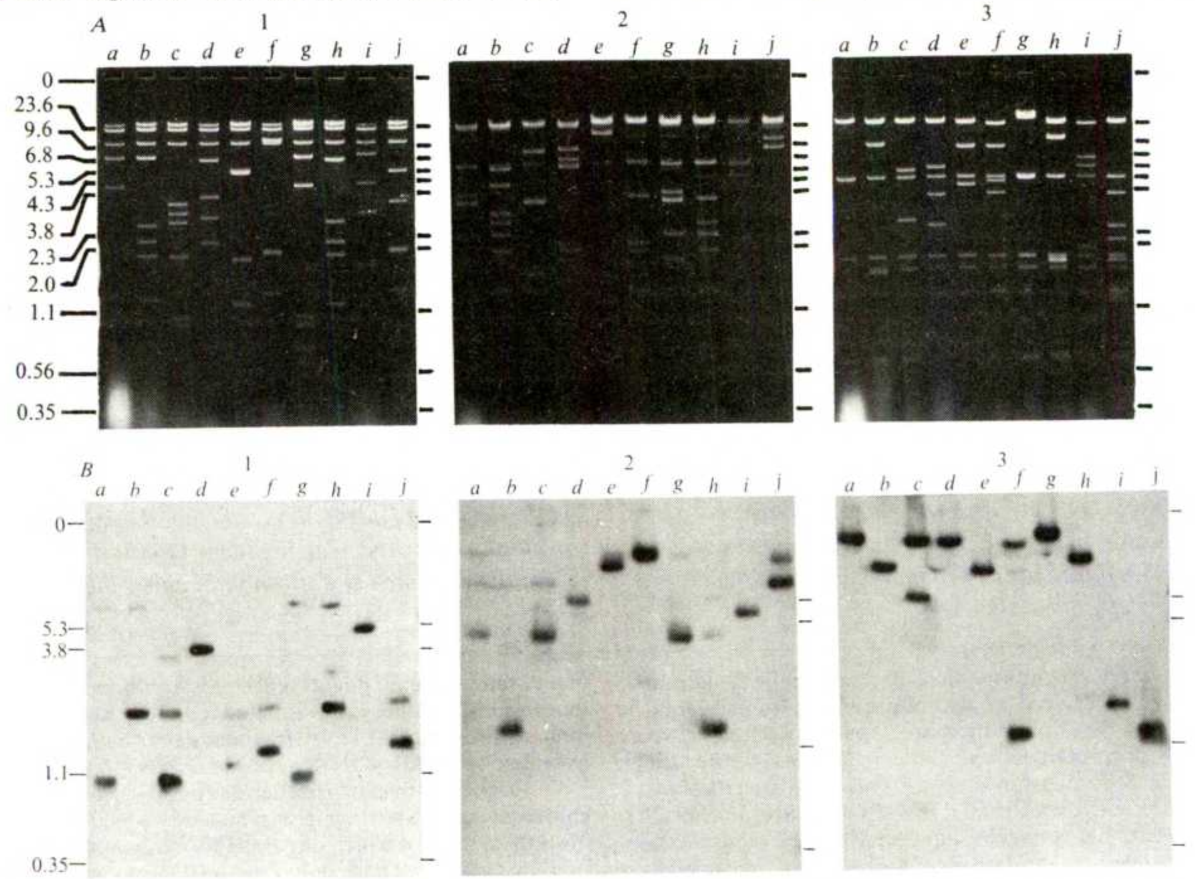

Fig. 1 Restriction and hybridization analysis of cloned human chromosomal IFN-α-related DNA. The IFN-α-related clones were selected from the λ-linked human genome library prepared by Lawn *et al.*[6]. About 240,000 plaques (about 3,000 plaques per 9.5×9.5 cm^2 filter membrane) were processed and screened by hybridization by the technique of Benton and Davis[7] as modified by Maniatis *et al.*[8]. The probe was prepared by cleaving plasmid Hif-2h[1,4] with *Pst*I, isolating the IFN cDNA insert by agarose gel electrophoresis, and labelling it by nick translation ([α-^{32}P]dATP, 250 Ci mmol^{-1}, and [α-^{32}P]dCTP, 200 Ci mmol^{-1} (NEN); specific activity of probe, 1.5×10^8 c.p.m. μg^{-1}) as described[50]. Plaques appearing to give a positive hybridization response were subjected to three cycles of plaque purification[8]. Sixteen hybridization-positive clones were isolated and 10 of these were further examined. DNA was prepared[51,52] and digested with the restriction enzymes indicated. All enzymes except *Bsp*I were purchased from New England Biolabs and used as recommended by the supplier, except that 200 μg ml^{-1} gelatin replaced bovine serum albumin in the buffers. The fragments were separated by electrophoresis in 1% agarose gels, using Tris-acetate-EDTA buffer (*p*H 7.8) containing 1.0 μg ml^{-1} ethidium bromide, and photographed in UV light. The fragments were transferred to Millipore membrane filter as described by Southern[9] and hybridized with the nick-translated Hif-2h cDNA fragment described above. Panels 1, 2 and 3, digestion with *Eco*RI, *Bgl*II and *Hin*dIII, respectively. Hybridization (600,000 c.p.m. per filter) and washing procedures are as given by Maniatis *et al.*[8]. Exposure was for 12 h. *A*, Photographs of ethidium bromide-stained gels in UV light. *B*, Autoradiogram of the hybridized filters. The lanes contain the following samples: *a*, chr-1; *b*, chr-3; *c*, chr-10; *d*, chr-12; *e*, chr-13; *f*, chr-16; g, chr-23; *h*, chr-26; *i*, chr-30; *j*, chr-35. As a marker, *Hin*dIII-cleaved λ DNA and Hif-2h (ref. 4) cleaved with *Eco*RI and *Bgl*II were run in parallel.

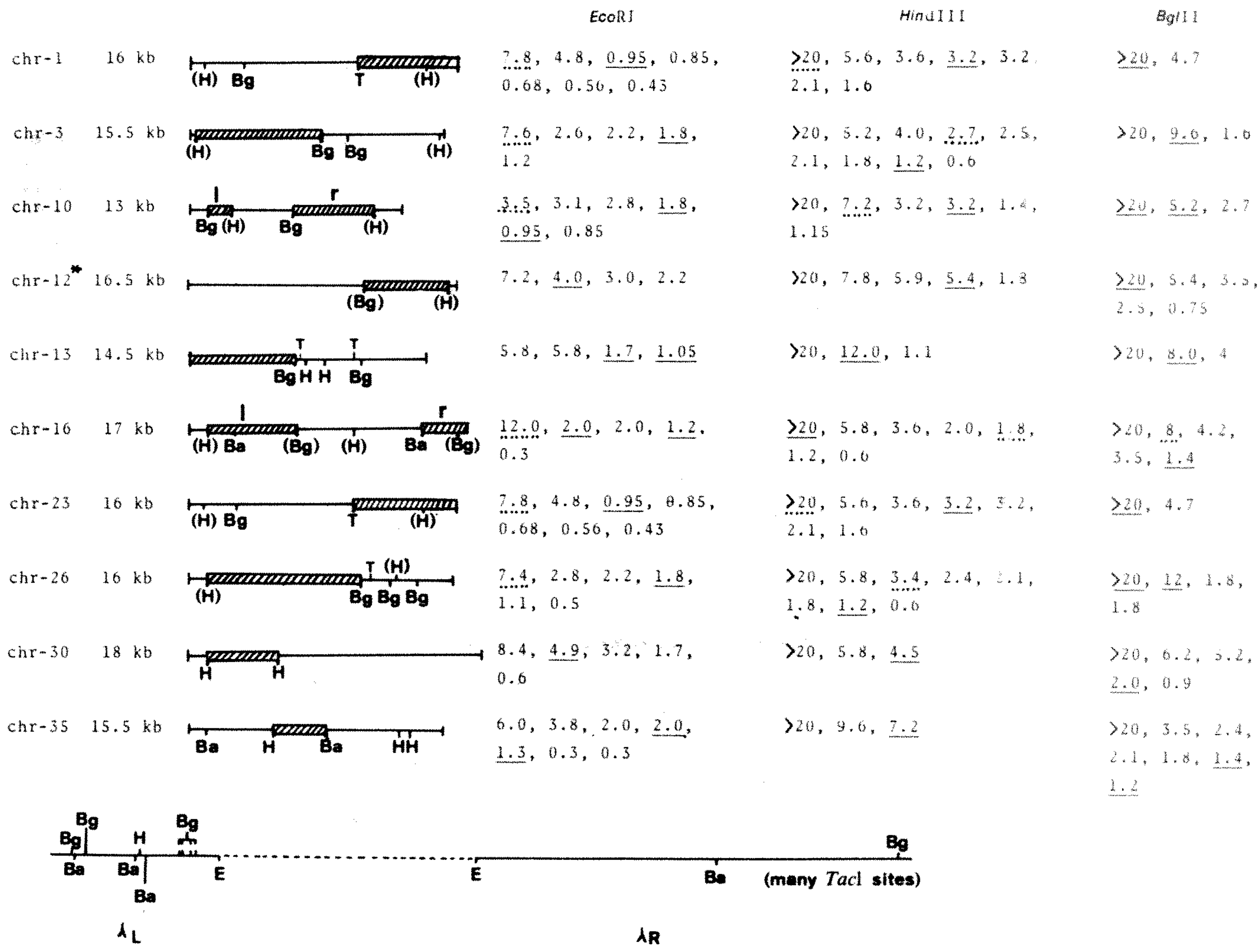

		*Eco*RI	*Hin*dIII	*Bgl*II
chr-1	16 kb	7.8, 4.8, 0.95, 0.85, 0.68, 0.56, 0.43	>20, 5.6, 3.6, 3.2, 3.2, 2.1, 1.6	>20, 4.7
chr-3	15.5 kb	7.6, 2.6, 2.2, 1.8, 1.2	>20, 5.2, 4.0, 2.7, 2.5, 2.1, 1.8, 1.2, 0.6	>20, 9.6, 1.6
chr-10	13 kb	3.5, 3.1, 2.8, 1.8, 0.95, 0.85	>20, 7.2, 3.2, 3.2, 1.4, 1.15	>20, 5.2, 2.7
chr-12*	16.5 kb	7.2, 4.0, 3.0, 2.2	>20, 7.8, 5.9, 5.4, 1.3	>20, 5.4, 3.5, 2.5, 0.75
chr-13	14.5 kb	5.8, 5.8, 1.7, 1.05	>20, 12.0, 1.1	>20, 8.0, 4
chr-16	17 kb	12.0, 2.0, 2.0, 1.2, 0.3	>20, 5.8, 3.6, 2.0, 1.8, 1.2, 0.6	>20, 8, 4.2, 3.5, 1.4
chr-23	16 kb	7.8, 4.8, 0.95, 0.85, 0.68, 0.56, 0.43	>20, 5.6, 3.6, 3.2, 3.2, 2.1, 1.6	>20, 4.7
chr-26	16 kb	7.4, 2.8, 2.2, 1.8, 1.1, 0.5	>20, 5.8, 3.4, 2.4, 2.1, 1.8, 1.2, 0.6	>20, 12, 1.8, 1.8
chr-30	18 kb	8.4, 4.9, 3.2, 1.7, 0.6	>20, 5.8, 4.5	>20, 6.2, 3.2, 2.0, 0.9
chr-35	15.5 kb	6.0, 3.8, 2.0, 2.0, 1.3, 0.3, 0.3	>20, 9.6, 7.2	>20, 3.5, 2.4, 2.1, 1.8, 1.4, 1.2

Fig. 2 Partial restriction maps of cloned, IFN-α-related chromosomal DNA fragments. Features of the vector λ Charon 4A DNA are shown in the bottom line. Derivation of the partial map of the chr-1 insert (*a*) was as follows: the total length of the insert, about 16 kilobases, was determined by summing the lengths of the *Eco*RI fragments. Cleavage with *Bgl*II yielded two fragments not found in the vector arms, with the lengths >20 and 4.7 kilobases. The larger fragment gave a positive hybridization response (compare with Fig. 1). As *Bgl*II cleavage of the λ arms must yield vector fragments of 1.55 (left arm) and 19.55 (right arm) kilobases linked to fragments of the insert, there must be a single *Bgl*II site within the insert, at 3.15 kilobases from the internal (*Eco*RI) end of the left λ arm. *Hin*dIII cleavage gave seven new fragments of >20, 5.6, 3.6, 3.2, 3.2, 2.1 and 1.6 kilobases, indicating six sites within the insert. The 3.2-kilobase fragment(s) gave a strong, and the >20-kilobase fragment a weak, hybridization response. As the (single) *Hin*dIII site on the left λ arm is 4.9 kilobases from the *Eco*RI site and the right arm (20 kilobases) has no *Hin*dIII site, one may conclude that the insert has a *Hin*dIII site at 0.7 kilobases from the internal end of the left arm. As the sum of all *Hin*dIII fragments derived from the insert alone is 13.7, and 0.7 kilobases of the 5.6-kilobase fragment are due to the insert, 14.4 kilobases of the insert are accounted for. Thus, about 1.6 kilobases of the >20-kilobase *Hin*dIII fragment must be due to the insert, which locates a *Hin*dIII site at about 1.6 kilobases from the internal end of the right-hand λ arm. The other four *Hin*dIII sites were not located. *Tac*I digestion of the λ hybrid (data not shown) yielded 9.2- and 5.4-kilobase fragments, the smaller of which hybridized to the IFN-α probe; the λ arms were digested to fragments of ≤0.6 kilobases, except for one 1.1-kilobase fragment which is not derived from an internal end. Therefore, *Tac*I digestion releases the insert with <0.6 kilobases of vector DNA at each end. As double digestion with *Tac*I and *Bgl*II (data not shown) yielded two 5.4-kilobase and one 3.5-kilobase fragments, the *Tac*I site must be located 5.4 kilobases to the right of the *Bgl*II site. Furthermore, the region hybridizing to the IFN probe must be located between the *Tac*I site and the junction with the right-hand λ arm. The partial maps of the other cloned DNAs were derived in similar fashion; data additional to that of Fig. 1 were obtained from digests with *Tac*I or *Bam*HI, and double digests with *Tac*I and *Bam*HI and *Hin*dIII, respectively. The accuracy of the maps is about ±10%. Parentheses around a restriction site indicate that other sites of the same kind exist but were not mapped. Hatched boxes indicate the locations of the DNA segment hybridizing to the probe. The table at the right indicates fragment length (other than those given by the λ arms alone) resulting from the cleavage with the restriction enzyme indicated. The fragments giving hybridization with the IFN-α probe are underlined with a solid line in the case of a strong, and with a dotted line in the case of a weak, response. Bg, *Bgl*II site; *H*, *Hin*dIII site; Ba, *Bam*HI site; E, *Eco*RI site; T, *Tac*I site. kb, kilobases. * Chr-12 has two unmapped *Tac*I sites.

ment and all differ from the 3.2-kilobase fragment of chr-1. The hybridizing *Hin*dIII fragment of chr-13 is 12 kilobases long; 7.1 kilobases lie within the insert, so that here too the 3.2-kilobase fragment of chr-1 cannot be accounted for. With chr-16, two hybridizing regions were delineated (see above). The right-hand putative gene (*r*), which is probably not completely contained in the fragment, is considered identical to that in chr-35. As the hybridizing region of chr-35 has no features in common with chr-1, chr-16 (*r*) is also different from chr-1. The hybridizing *Hin*dIII fragment of chr-16 (*l*) is completely contained in the insert and is far smaller than that of chr-1. We conclude that the putative genes of chr-3, chr-12, chr-13, chr-16, chr-26, chr-30 and chr-35 differ from that of chr-1. The same conclusion is reached from the fact that none of the *Eco*RI fragments of chr-1, hybridizing or not, are present in any of the clones mentioned above except for a 7.6-kilobase fragment of chr-3 which is close in size to the 7.8 kilobases of chr-1. From similar arguments based on the data of Fig. 2 regarding comparisons of the other clones and additional Smith–Birnstiel mapping of chr-3, chr-10, chr-13, chr-26 and chr-35, we conclude that the 12 putative IFN-α genes fall into not less than eight distinct classes.

Hif-chr-35 (and the right-hand segment of Hif-chr-16, to which it is probably identical) is the only DNA with a *Bgl*II site in the putative coding region (compare with table in Fig. 2). As the two different IFN-α cDNAs examined to date, Hif-2h and Hif-206, have one and two *Bgl*II sites, respectively, within their coding sequences, it seems likely that only the chr-35 gene with its single *Bgl*II site is a counterpart to one of the two cloned cDNAs, most likely to Hif-2h. This conclusion was reinforced by observing that when the 3'-terminal Hif-2h cDNA segment, which contains only the 3' non-coding region, was used as a probe, the chr-35 restriction fragments gave a much stronger hybridization response than those of any of the other chromosomal DNAs. As 3' non-coding regions of homologous genes diverge more strongly than their coding sequences[3,10], a 3' probe discriminates between different but related sequences more readily than total probes. The chromosomal counterpart to Hif-206 has not yet been found.

How many of the chromosomal clones contain sequences coding for polypeptides with IFN activity? As the cytopathic effect reduction assay[11] can detect minute amounts of IFN, less than one active molecule per bacterial cell, we tested the lysates of *E. coli* infected with the hybrid λ phages. Eight of 10 phage strains examined (all but chr-10 and chr-12) gave lysates containing IFN activity, ranging from 3 to 50 U ml^{-1}. For chr-10 and chr-12, the hybridizing *Hin*dIII–*Hin*dIII or *Eco–Eco* fragments, subcloned into the *Pst* site of pBR322, expressed IFN activity in *E. coli* (K. Henco and M. Streuli, unpublished results).

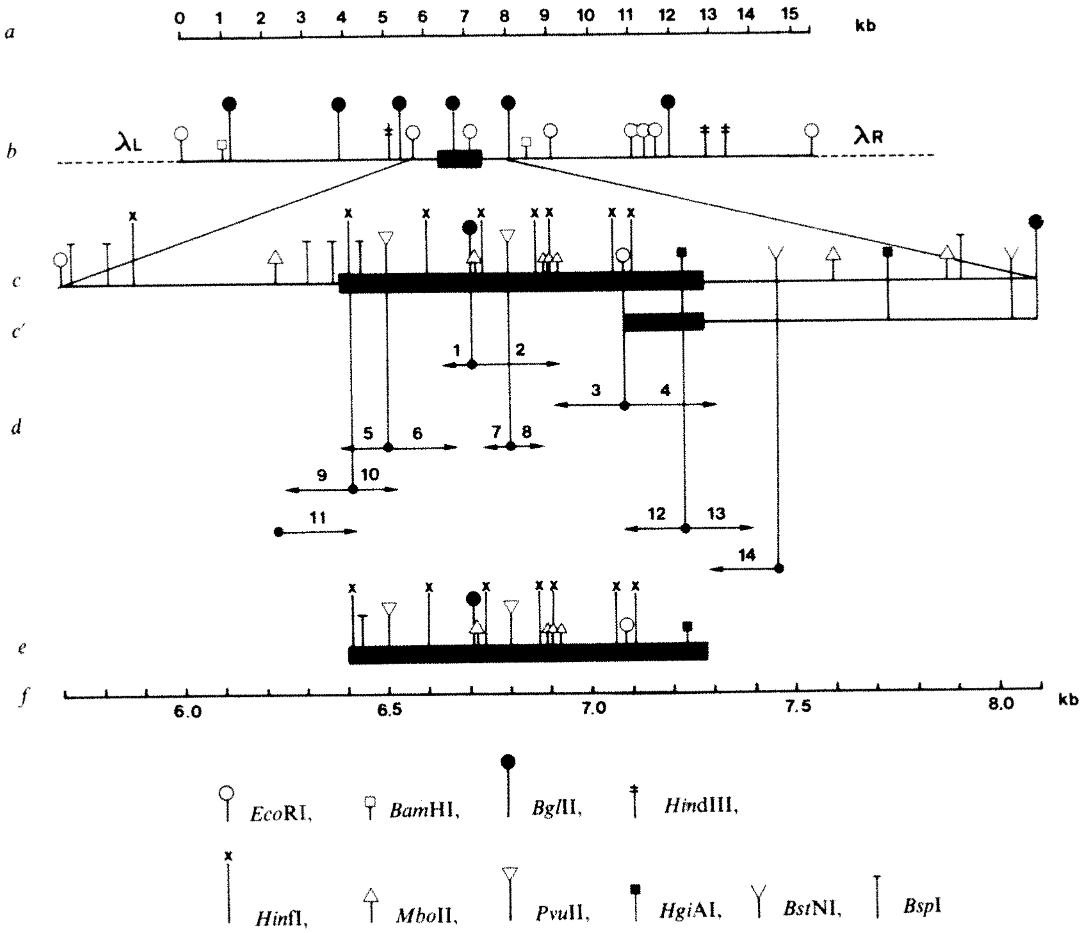

Fig. 3 Restriction map of the cloned human chromosomal DNA fragment chr-35; strategy for the nucleotide sequence determination. The gene-containing region of chr-35 was subcloned: chr-35 was cleaved with *Hin*dIII and *Bam*HI, and the 3.4-kilobase fragment (which contains the region hybridizing to the Hif-2h cDNA probe, compare with Fig. 1) was elongated with dC residues, annealed to pBR322 which had been cleaved with *Pst*I and elongated with dG[13]. Clones of *E. coli* HB101 transformed with the resulting hybrids were screened by *in situ* colony hybridization[53] with the ^{32}P-labelled Hif-2h fragment described in Fig. 1 legend. Plasmids (Z-pBR322(*Pst*)/HchrIF-35HB or HchrIF-35HB) were prepared from the positive clones by method B described by Wilkie *et al.*[54]. The orientation of the insert was established by digesting the plasmid with *Eco*RI and determining the length of the shorter fragment. The orientation coinciding with that of the β-lactamase gene was designated α, the opposite one, β. Restriction sites were determined by Smith–Birnstiel mapping[55]: HchrIF-35HBα was digested with *Eco*RI, labelled at the 5' termini and digested with *Bgl*II (and *Pst*I, to cleave an undesired fragment of about 1 kilobase). The 1.04-kilobase *Eco-Bgl*II (3'-proximal) and the 0.96-kilobase (5'-proximal) *Eco-Bgl*II fragments were isolated by agarose gel electrophoresis as described[56]. Both fragments were partially cleaved with *Hin*fI, *Bsp*I and *Mbo*II, respectively, the products separated on a 1% agarose gel in Tris-acetate buffer (*p*H 7.8) containing 1 μg ml^{-1} ethidium bromide, and radioactive bands were visualized by autoradiography (data not shown). *Bst*NI and *Hgi*AI sites were similarly determined only on the 1.04-kilobase (3'-proximal) *Eco-Bgl*II fragment (*c'*). *a*, Scale in kilobase pairs (kb) for *b*; *b*, restriction map of chr-35 DNA in Charon 4A DNA; *c*, blow-up of restriction site map of the IFN coding sequence and flanking regions determined on HchrIF-35HBα; *e*, map of the cloned cDNA insert of Hif-2h (from Mantei *et al.*[4]); *f*, scale in kilobase pairs applicable to *c–e*. For nucleotide sequence determination, HchrIF-35HBα was cleaved with the restriction enzyme indicated and 5'-terminally labelled as described by Mantei *et al.*[4]. Labelled fragments were cleaved with a second restriction enzyme, the products were separated by electrophoresis through a 5% polyacrylamide gel in Tris-borate-EDTA buffer[57], extracted from the gel and purified as described[56]. The various fragments for sequencing were prepared as follows (the number indicates the nominal fragment chain length in base pairs, the ends are designated by the enzyme which generates them, the labelled end is indicated by an asterisk, and the numbers in parentheses refer to the arrows shown in *d*). (1) and (2), Cleavage of HchrIF-35HBα with *Bgl*II, labelling, cleavage with *Eco*RI and *Pst*I, isolation of (1) *Bgl*-Eco*-940, and (2) *Bgl*-Eco*-360. (3) and (4), Cleavage of HchrIF-35HBα with *Eco*RI, labelling, cleavage with *Bsp*I, isolation of (3) *Eco*-Bsp*-680 and (4) *Eco*-Bsp*-880. (5), (6), (7) and (8), Cleavage of HchrIF-35HBα with *Pvu*II, labelling, cleavage with *Bgl*II and *Eco*RI, isolation of (5) *Pvu*-Eco*-780, (6) *Pvu*-Bgl*-215, (7) *Pvu*-Bgl*-90 and (8) *Pvu*-Eco*-290. (9) and (10), Cleavage of HchrIF-35HBα with *Eco*RI, isolation by 1% agarose gel electrophoresis in Tris-borate EDTA buffer[57] of *Eco-Eco*-1300, cleavage with *Hin*fI, isolation of *Hinf-Hinf*-450 (for [9]) and *Hinf-Hinf*-180 (for [10]), labelling, cleavage with *Mbo*II (for [9]) or *Ava*II (for [10]), isolation of (9) *Hinf*-Mbo*II-190 and (10) *Hinf*-Ava*II-150. (11), Cleavage of HchrIF-35HBα with *Mbo*II, labelling, cleavage of HchrIF-35HBα with *Mbo*II, labelling, cleavage with *Bgl*II, isolation of (11) *Mbo*-Bgl*-465. (12), (13) and (14), Cleavage of HchrIF-35HBα with *Bsp*I and *Bgl*II, isolation by agarose gel electrophoresis as above of *Bsp-Bgl*-1200, cleavage with *Hgi*AI (for [12] and [13]), or *Bst*NI (for [14]), labelling, cleavage with *Mbo*II (for[12] and [13]) or *Eco*RI (for [14]), isolation of (12) *Hgi*-Mbo*II-300, (13) *Hgi*-Mbo*II-360, and (14) *Bst*-Eco*-380.

This shows that all cloned DNA segments contained at least one potentially active IFN gene, and that these genes most likely did not contain introns in their coding regions, as *E. coli* is believed to be incapable of splicing mRNAs[12]. Our data thus suggest that the genome of an individual human contains not less than eight different IFN-coding sequences, supported by the fact that the proportion of IFN-related sequences detected in the clone bank is about one in 16,000. Assuming a value of 3×10^9 base pairs for the haploid human genome, the expected value for a single-copy gene in a bank with an average DNA fragment size of 16 kilobases (the average value found for the 10 clones examined) would be about one in 190,000; thus, the frequency of Hif-2h-related segments is 12 times higher than expected for a single gene. When Lawn *et al.*[6] screened 300,000 plaques from the same gene bank with a β-globin cDNA probe, they identified two clones. The expected value for a single gene should have been 1.6 clones per 300,000 plaques, however the probe could potentially cross-hybridize with two γ and a δ gene as well. We conclude that the number of distinct DNA segments cross-hybridizing with IFN-α1 cDNA may be around 10–15, and that many of these will prove to code for IFN-like proteins.

Identification of a chromosomal gene corresponding to IFN-α1

The cDNA insert of Hif-2h (which codes for IFN-α1) has a single *Bgl*II site within the coding region[4]. The chromosomal IFN-related DNA clone with the same feature was chr-35. This DNA was further characterized by restriction analysis and Southern blotting; Fig. 2 shows that the region hybridizing to the Hif-2h probes lies within a 3.4-kilobase region flanked by a *Bam*HI and a *Hin*dIII site. To facilitate further analysis, this fragment was subcloned into the *Pst*I site of pBR322 using the dC–dG tailing procedure[13]. Several clones of *E. coli* transformed with the resulting hybrids were isolated, cultures were grown to an apparent OD_{650} of 0.8 and the bacteria collected and lysed as described[1]. Seven of 10 clones examined showed IFN activities of 75–500 U per g of cells. One of the IFN-producing clones, Z-pBR322(*Pst*)/Hifchr35-HBα, was characterized by restriction analysis. Figure 3 shows that its restriction map is indistinguishable from that of the cDNA insert of Hif-2h; in particular, there is no indication of introns within the coding sequence, that is, between the *Hin*fI site in the 5′ non-coding region, and the *Eco*RI site in the 3′ non-coding region.

To prove this conclusion, and to determine whether or not the 5′ and 3′ non-coding regions contain introns, it was necessary to compare the nucleotide sequences of Hif-2h cDNA and the relevant segments of the chr-35 DNA.

Nucleotide sequences of the chromosomal gene chr-35 and the cDNA coding for IFN-α1

The nucleotide sequence of Hif-2h cDNA has been reported previously[4]. The coding region, which includes a signal sequence, comprises 567 base pairs and is followed by a 242-base pair 3′ non-coding region. The 5′ non-coding region consists of 56 nucleotides and is probably incomplete, as with all cDNA clones generated by the technique we used[14]. Moreover, it has been found that artifactual sequences can be generated in the process of synthesizing the double-stranded cDNA copy of a mRNA, especially in the 5′ region[15]. We therefore redetermined and extended the 5′-proximal nucleotide sequence essentially as described by Tsujimoto and Suzuki[16]. We prepared a *Pvu*II–*Bsp* minus-strand restriction fragment, extending from nucleotide +44 to nucleotide +5 (see Fig. 3) and labelled at the *Pvu*II end. This fragment was hybridized to poly(A) RNA from IFN-producing leukocytes and reverse transcriptase was used to elongate it with unlabelled deoxyribonucleotides. The denatured product, analysed on a polyacrylamide gel (Fig. 4), showed a major band of about 115 nucleotides. Thus, about 75 nucleotides had been added to the primer, indicating a 5′ non-coding sequence of about 70 nucleotides. The major radioactive band was sequenced by the Maxam–Gilbert procedure[17] and the sequence shown in Fig. 6 obtained. The sequence of the cDNA transcribed directly on the mRNA is identical to that of the cloned cDNA, except for the four 5′-terminal nucleotides; moreover, it is longer by 11 residues. As at least two species of IFN-α are expressed in human leukocytes, the mRNA species which served as template for direct reverse transcription may differ from that which gave rise to the cloned cDNA. However, as shown below, the chromosomal DNA is identical to the cloned Hif-2h cDNA except for the four discrepant nucleotides,

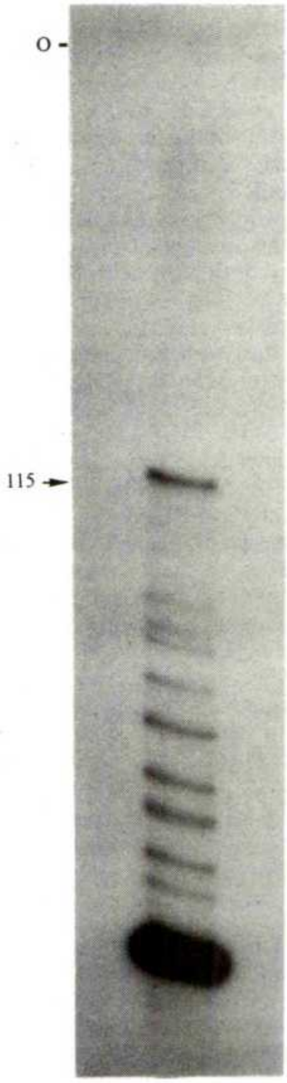

Fig. 4 Determination of the nucleotide sequence of cDNA complementary to the 5′ end of IFN mRNA. Synthesis of cDNA complementary to the 5′ end of IFN mRNA was accomplished as follows: the plasmid Hif-2h, which contains the almost complete cDNA to IFN-α1 mRNA, was cleaved with *Pvu*II and the 5′ termini labelled with ^{32}P-phosphate as described[4], to a specific activity of 1.2 μCi pmol^{-1}. Following cleavage with *Bsp*I, the products were denatured and applied to a 16% polyacrylamide gel for strand separation[17]. The 40-base pair *Pvu*II-*Bsp* minus-strand fragment (which extends from positions 44 to 5, see Fig. 6) was recovered as described[56]. The fragment (0.5 pmol, 0.5 μCi) was mixed with 3 μg 12S poly(A) RNA from virus-induced human leukocytes[1] in 4.5 μl NaCl (6.6 mM), 0.6 mM EDTA, 6.6 mM HEPES (*p*H 7.5). After heating for 90 s to 100 °C, NaCl was added to 0.18 M and the mixture (5 μl) incubated 40 min at 60 °C. After addition of Tris-HCl (*p*H 7.5) to 40 mM, dithiothreitol to 1 mM, $MgCl_2$ to 5 mM, dGTP, dATP, TTP, and dCTP to 0.5 mM each (final volume 30 μl), incubation was carried out with 3.5 U reverse transcriptase for 90 min at 37 °C. The mixture was extracted with phenol, precipitated with ethanol, and the DNA subjected to electrophoresis through a 12% polyacrylamide gel in 50 mM Tris-borate (*p*H 8.3), 1 mM EDTA, 7 M urea, for 5 h at 900 V. Autoradiography was for 21 h. The band with the lowest mobility (corresponding to a fragment about 115 nucleotides long) was eluted and sequenced as described[4,17]. The sequence is given in Fig. 6.

where it agrees with the direct reverse transcript. Thus, the discrepancy is likely due to the type of artefact described by Richards *et al.*[15].

Does the direct reverse transcript extend to the 5′ terminus of the mRNA as Tsujimoto and Suzuki[16] found? The case of IFN-α1 was examined using an S_1 mapping procedure. A 780-base pair *Pvu*II–*Eco*RI restriction fragment of the chromosomal DNA, which extends from position +44 to −740 and comprises the region corresponding to the putative 5′ terminus of the mRNA, was prepared with a 5′-terminal label at the *Pvu*II end, hybridized to poly(A) RNA from IFN-producing leukocytes and digested with S_1 nuclease. As a size marker, a sample of the labelled probe was degraded by the Maxam–Gilbert procedure[17]. Polyacrylamide gel analysis revealed two major protected fragments (Fig. 5) of 115 and 116 base pairs, and a series of minor, shorter fragments. Mouse β-globin mRNA, analysed by this procedure, yields two DNA fragments longer by four and five nucleotides than expected[18], perhaps because the presence of a cap hinders digestion of the DNA probe by S_1 nuclease. We conclude that the position of the 5′-terminal nucleotide of the major portion of the mRNA lies about 67 nucleotides upstream from the first AUG triplet, agreeing with conclusions drawn from the analysis of the direct cDNA transcript. We tentatively assume that the 5′ end of the IFN-α1 mRNA has the sequence AG... and begins at position −67 (Fig. 6); however, it could equally map at the AG two nucleotides further upstream. Most eukaryotic mRNAs start with the sequence AC... (ref. 19), however the rat preproinsulin II mRNA is believed to begin with the sequence AG[20]. A faint set of bands, mapping 98 base pairs upstream (about 5% of the radioactivity of the major bands) was also detected. These are probably due to incompletely digested probe, as similar findings have been noted occasionally with the globin mRNA system; however we cannot yet exclude a longer species of IFN mRNA, perhaps a precursor.

Some restriction sites of the chromosomal IFN subclone Hif-chr35Hbα were mapped, and the nucleotide sequence corresponding to the gene and its flanking regions determined as outlined in Fig. 3 legend. Comparison of the chromosomal and the cDNA sequence (Fig. 6) shows complete identity, from the 5′ end of the cDNA sequence obtained by direct reverse transcription to the last nucleotide preceding the poly(A) tail, as determined from the cloned cDNA. Thus, no intron could be detected in the chromosomal sequence corresponding to mature IFN mRNA.

Is the IFN-α1 gene devoid of introns?

The IFN-α1 primary transcript could initiate upstream from the position corresponding to the 5′ end of the mature mRNA, and an intron could be contained within this segment of the precursor. Maturation of the pre-mRNA would then require splicing, followed by removal of a 5′ segment. It will be interesting to determine whether the weak bands detected by S_1 mapping are due to IFN-α1 precursor transcripts longer than mature IFN-α1, and whether or not mature IFN mRNA is capped: *in vitro* transcription of the chromosomal gene might provide further clarification. Anyway, note that 28 nucleotides upstream from the putative 'cap' site there is a sequence 5′-TATTTAA-3′ flanked on both sides by GC-rich segments, which may correspond to the 'Hogness box' described 23 to 25 nucleotides upstream from the cap site for many chromosomal genes[21]. This suggests that initiation of transcription does occur at the putative cap site, and that there are no introns within the IFN-α1 transcriptional unit. Certainly there are no introns within the IFN-α1 coding sequence, and the fact that most, if not all, chromosomal IFN genes identified so far lead to the synthesis of IFN in *E. coli* suggest that this is generally true for IFN-α sequences. In this regard the IFN-α1 (and possibly all IFN-α) genes seem to resemble the sea urchin histone genes which also have no introns[22], and to differ from all other protein-coding nuclear genes of higher eukaryotes described so far, which have at least one, but frequently many, introns[23–25].

Messenger RNAs of SV40 accumulate in the cytoplasm only if the corresponding primary transcripts contain an intron[26,27]. Moreover, Hamer and Leder[28] have shown that β-globin coding sequences cloned in SV40 DNA only give rise to stable mRNAs if the primary transcript contains an intron, either in the SV40 or in the globin moiety. This cannot be true for all coding transcripts, as neither do histone genes have introns[22], nor does the primary transcript of the polypeptide IX gene of adenovirus type II contain an intron counterpart[29]. Also, much of retroviral RNA is exported from the nucleus without splicing[30,31]. Since 5,6-dichloro-1-β-D-ribofuranosylbenzimidazole (DRB) inhibits the synthesis of most mRNAs, but not that of the adenovirus polypeptide IX mRNA[32], it will be of interest to determine its effect on IFN-α mRNA synthesis.

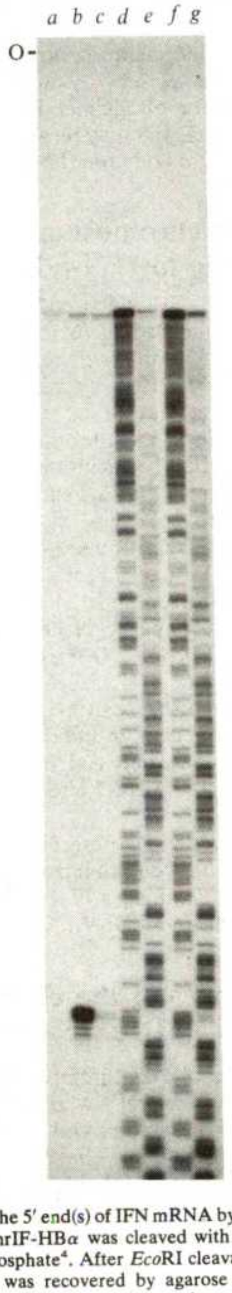

Fig. 5 Mapping of the 5′ end(s) of IFN mRNA by S_1 mapping. The plasmid Z-pBR322(*Pst*)/HchrIF-HBα was cleaved with *Pvu*II and the 5′ termini labelled with ^{32}P-phosphate[4]. After *Eco*RI cleavage, the ^{32}P-labelled 780-base pair fragment was recovered by agarose gel electrophoresis. The fragment (0.03 pmol, 24,000 c.p.m.) was denatured, hybridized in 80% formamide to poly(A) RNA from IFN-producing leukocytes[1], digested with nuclease S_1 (ref. 58), and analysed by polyacrylamide gel eletrophoresis on a 12% gel (18 h, 900 V), all as described in Weaver and Weissmann[18] and Mantei *et al.*[4]. To provide a 'sequence ladder' as length marker, the ^{32}P-labelled fragment described above was subjected to the A+G and C+T degradations described by Maxam and Gilbert[17] and in protocols provided by the same authors. The autoradiogram shown was obtained after a 5-day exposure. Lane *a*, 0.1 μg poly(A) RNA from non-induced leukocytes; lane *b*, 2 μg induced leukocyte RNA; lanes *c*, *f* and g, 0.2 μg induced leukocyte RNA; lanes *d* and *f*, A+G degradation products; lanes *e* and g, C+T degradation products.

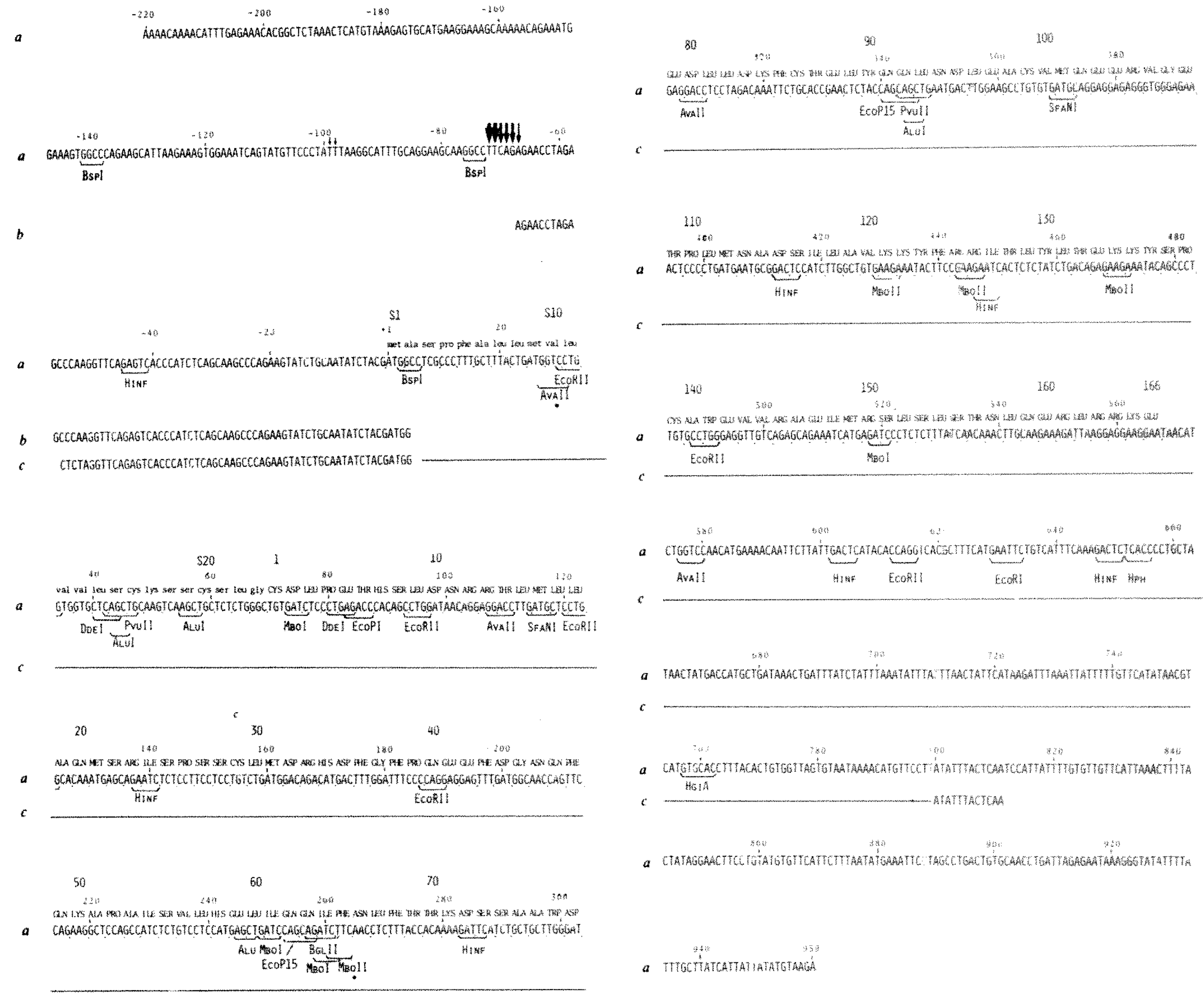

Fig. 6 Nucleotide sequence of the chromosomal IFN-α1 coding segment and its flanking regions. *a*, The 5'-labelled fragments described in Fig. 3 legend were degraded according to Maxam and Gilbert[17] with the modifications described in protocols provided by the same authors in September 1978 and fractionated as described in ref. 4. *b*, The sequence of cDNA complementary to IFN-α1 mRNA determined as described in Fig. 4 legend. *c*, Nucleotide sequence of the cloned IFN-α1 cDNA (Hif-2h, from Mantei *et al.*[4]); the continuous line indicates identity with the sequence in *a*. The vertical arrows indicate the location (±1 nucleotide) of the probe termini generated by the S_1 RNA mapping procedure, as described in Fig. 5 legend.

The multiplicity of interferon genes

We have shown that chromosomal IFN genes isolated from a gene bank derived from an individual embryo fall into at least eight different classes, as judged by restriction site distribution. As there is more than one difference between the classes in almost all cases, the genes probably differ by more than the occasional point mutation, as is commonly found with polymorphic genes[33,34]. As the cloning procedure may introduce deletions into chromosomal DNA[35], a conclusive classification requires confirmation by analysis of independent gene isolates and/or Southern analysis of uncloned chromosomal DNA. We believe that all the genes we have described are of the α (or leukocyte) type because (1) the homologies between α and β (or fibroblast) type IFN are so limited that cross-hybridization is unlikely (ref. 36 and W. Fiers personal communication) and (2) because all IFN-β cDNAs analysed so far contain a *Bgl*II site[37–39], and the only chromosomal IFN gene with a *Bgl*II site in the set analysed (chr-35) is definitely an α-type gene.

The genes we analysed could be derived from at least four different loci assuming that substantial polymorphism exists, but more likely reflect the existence of eight different loci. A linkage map will resolve this question; so far, there is evidence that at least some of the genes are clustered, for example chr-10 and chr-16 each contain two IFN sequences.

Are all IFN genes expressed in eukaryotic cells? As most, if not all, chromosomal IFN genes identified so far give rise to biologically active IFN in *E. coli*, they obviously are potentially expressible and do not resemble the α-globin-like silent gene found by Nishioka *et al.*[40]. Clearly, analysis of the IFN fractions derived from leukocyte IFN preparation by HPLC[41] may reveal the number and nature of IFNs produced by these cells. The heterogeneity of leukocyte IFN preparations[41] often ascribed to varying degrees of glycosylation may reflect the gene multiplicity described here. As an IFN species isolated from lymphoblastoid cells and partially sequenced[5] (IFN-α3) differs from two species of IFNs known to be expressed in virus-treated leukocytes (IFN-α1 and IFN-α2), conceivably different types of cells may preferentially express different IFN α genes. The easiest analyses are probably at the mRNA level, using as probes the 3' non-coding regions of the different IFN-α genes, which seem to differ the most between different genes[3].

We conclude that at least eight but perhaps as many as 10–15 distinct *IFN* genes exist. This gene multiplicity suggests that

IFNs may be functionally heterogeneous. The most striking functionally heterogeneous proteins encoded by a multigene family are the immunoglobulin variable chains, where each gene product probably has a different epitope specificity. The human β-globin family comprises at least five members, some of which differ distinctly in their biochemical properties, and which are synthesized at different stages of development[42,43]. With other families, such as those of the chorion proteins[44,45] or actins[46], it is not clear to which extent the genes code for proteins of different functions. The differences in amino acid sequences of at least some of the IFN genes[3-5] are certainly substantial enough to allow for proteins with quite different properties. As reported elsewhere, one striking functional difference between IFN-α1 and IFN-α2 is their relative virus-protective activity on cells of different species: the ratio of activities on bovine and human cells is 20–50 for IFN-α1 and one or less for IFN-α2 (refs 3, 47). This difference in cross-species reactivity could reflect different specificity for cell receptors, and questions whether different IFN species may be addressed to different target cells within the same host. It will also be of interest to ascertain whether each of the IFN species shows the full range of activities ascribed to leukocyte IFN preparations[39,48].

We thank Dr T. Maniatis for the human gene bank, Dr J. Beard for reverse transcriptase, Dr P. Dierks for $[\gamma\text{-}^{32}\text{P}]$ATP, A. Schamböck for S_1 nuclease, A. Kiss for *Bsp*I and Dr P. Sharp for bringing the experiments with DRB to our attention. The work was supported by the Schweizerische Nationalfonds (3.481.79), the Kanton of Zürich and Biogen S.A.

Received 31 July; accepted 22 August 1980.

1. Nagata, S. *et al. Nature* **284,** 316–320 (1980).
2. Stewart, W. E. II *et al. Nature* **286,** 110 (1980).
3. Streuli, M., Nagata, S. & Weissmann, C. *Science* (in the press).
4. Mantei, N. *et al. Gene* **10,** 1–10 (1980).
5. Zoon, K. C. *et al. Science* **207,** 527–528 (1980).
6. Lawn, R. M., Fritsch, E. E., Parker, R. C., Blake, G. & Maniatis, T. *Cell* **15,** 1157–1174 (1978).
7. Benton, W. D. & Davis, R. W. *Science* **196,** 180–182 (1977).
8. Maniatis, T. *et al. Cell* **15,** 687–701 (1978).
9. Southern, E. M. *J. molec. Biol.* **98,** 503–517 (1975).
10. Kafatos, F., Efstratiadis, A., Forget, B. & Weissmann, S. *Proc. natn. Acad. Sci. U.S.A.* **74,** 5618–5622 (1977).
11. Stewart, W. E. II & Sulkin, S. E. *Proc. Soc. exp. Biol. Med.* **123,** 650–653 (1966).
12. Mercereau-Puijalon, O. & Kourilsky, P. *Nature* **279,** 647–649 (1979).
13. Villa-Komaroff, L. *et al. Proc. natn. Acad. Sci. U.S.A.* **75,** 3727–3731 (1978).
14. Efstratiadis, A., Kafatos, F. C., Maxam, A. M. & Maniatis, T. *Cell* **7,** 279–288 (1976).
15. Richards, R. I., Shine, J., Ullrich, A., Wells, J. R. E. & Goodman, H. M. *Nucleic Acids Res.* **7,** 1137–1146 (1976).
16. Tsujimoto, Y. & Suzuki, Y. *Cell* **18,** 591–600 (1979).
17. Maxam, A. M. & Gilbert, W. *Proc. natn. Acad. Sci. U.S.A.* **74,** 560–564 (1977).
18. Weaver, R. F. & Weissmann, C. *Nucleic Acids Res.* **7,** 1175–1193 (1979).
19. Baralle, F. E. & Brownlee, G. G. *Nature* **274,** 84–87 (1978).
20. Lomedico, P. *et al. Cell* **18,** 545–558 (1979).
21. Goldberg, M. thesis, Stanford Univ. (1979).
22. Schaffner, W. *et al. Cell* **14,** 655–671 (1978).
23. Gannon, F. *et al. Nature* **278,** 428–434 (1979).
24. Cochet, M. *et al. Nature* **282,** 567–574 (1979).
25. Wahli, W., Dawid, I. B., Wyler, T., Weber, R. & Ryffel, G. U. *Cell* **20,** 107–117 (1980).
26. Volckaert, G., Feunteun, J., Crawford, L. V., Berg, P. & Fiers, W. *J. Virol.* **30,** 674–682 (1979).
27. Gruss, P., Lai, C.-J., Dhar, R. & Khoury, G. *Proc. natn. Acad. Sci. U.S.A.* **76,** 4317–4321 (1979).
28. Hamer, D. H. & Leder, P. *Cell* **18,** 1299–1302 (1979).
29. Aleström, P. *et al. Cell* **19,** 671–681 (1980).
30. Parsons, J. T., Coffin, J. M., Haroz, R. K., Bromley, P. A. & Weissmann, C. *J. Virol.* **11,** 761–774 (1973).
31. Bishop, J. M. *A. Rev. Biochem.* **47,** 35–88 (1978).
32. Vennström, B., Persson, H., Pettersson, U. & Philipson, L. *Nucleic Acids Res.* **7,** 1405–1418 (1979).
33. Mandel, J. L. *et al. Cell* **14,** 641–653 (1978).
34. Hardison, R. C., Butler, E. T. III, Lacy, E. & Maniatis, T. *Cell* **18,** 1285–1297 (1979).
35. Lauer, J., Shen, C.-K. J. & Maniatis, T. *Cell* **20,** 119–130 (1980).
36. Taniguchi, T. *et al. Nature* **285,** 547–549 (1980).
37. Taniguchi, T., Ohno, S., Fujii-Kuriyama, Y. & Muramatsu, M. *Gene* **10,** 11–15 (1980).
38. Derynck, R. *et al. Nature* **285,** 542–547 (1980).
39. Houghton, M. *et al. Nucleic Acids Res.* **8,** 2885–2894 (1980).
40. Nishioka, Y., Leder, A. & Leder, P. *Proc. natn. Acad. Sci. U.S.A.* **77,** 2806–2809 (1980).
41. Rubinstein, M. *et al. Proc. natn. Acad. Sci. U.S.A.* **76,** 640–644 (1979).
42. Weatherall, D. J. & Clegg, J. B. *Cell* **16,** 467–479 (1979).
43. Fritsch, E. F., Lawn, R. M. & Maniatis, T. *Cell* **19,** 959–972 (1979).
44. Weldon Jones, C. & Kafatos, F. C. *Nature* **284,** 635 (1980).
45. Spradling, A. C., Digan, M. E., Mahowald, A. P., Scott, M. & Craig, E. A. *Cell* **19,** 905–911 (1980).
46. Kindle, K. L. & Firtel, R. A. *Cell* **15,** 763–778 (1978).
47. Stewart, W. E. II *et al. Gene* (in the press).
48. Masucci, M. G. *et al. Science* (in the press).
49. Stewart, W. E. II in *The Interferon System* (Springer, Vienna-New York, 1980).
50. Jeffreys, A. J. & Flavell, R. A. *Cell* **12,** 429–439 (1977).
51. Blattner, F. *et al. Science* **196,** 161–169 (1977).
52. Fried, M. *et al. Nature* **279,** 811–816 (1979).
53. Hanahan, D. & Meselson, M. *Gene* **10,** 63–67 (1980).
54. Wilkie, N. M. *et al. Nucleic Acids Res.* **7,** 859–877 (1979).
55. Smith, H. O. & Birnstiel, M. L. *Nucleic Acids Res.* **3,** 2387–2398 (1976).
56. Müller, W., Weber, H., Meyer, F. & Weissmann, C. *J. molec. Biol.* **124,** 343–358 (1978).
57. Peacock, A. C. & Dingman, C. W. *Biochemistry* **6,** 1818–1827 (1967).
58. Wiegand, R. C., Godson, G. N. & Radding, C. M. *J. biol. Chem.* **250,** 8845–8855 (1975).

A family of structural genes for human lymphoblastoid (leukocyte-type) interferon

Geoffrey Allen & Karl H. Fantes

Departments of Immunochemistry and Virology, Wellcome Research Laboratories, Langley Court, Beckenham, Kent BR3 3BS, UK

Amino acid sequences of tryptic and chymotryptic peptides from human lymphoblastoid interferon (IFN-α) have been determined. The results show that IFN-α consists of a family of proteins with at least five different, but homologous, primary structures. There appears to be little, if any, glycosylation of the major components of IFN-α.

TWO major classes of human type I interferons (IFNs), leukocyte (IFN-α) and fibroblast (IFN-β), may be distinguished serologically and have been shown to be the products of separate structural genes[1]. Amino-terminal peptide sequences showed no homology[2,3], although there is homology elsewhere in the sequences[4]. Interferon produced by the Namalwa lymphoblastoid cell line after induction by Sendai virus is primarily of the leukocyte type[5]. Human leukocyte (and Namalwa) IFN is heterogeneous, as shown by SDS-polyacrylamide gel electrophoresis[6-10], isoelectric focusing[11-16], high-performance liquid chromatography[17] and affinity chromatography[9]. This heterogeneity has been ascribed to different extents of glycosylation of the molecule[7,9,15,18,19] or partial degradation of a native molecule[8,20]. We show here that IFN-α produced by Namalwa cells consists of a family of proteins with at least five different, but homologous, amino acid sequences, and is therefore the product of several structural genes. No direct evidence for glycosylation has been found, although it cannot, at present, be excluded.

Separation of interferons

Studies on the structures of human IFNs have been limited by the small amounts of pure material available. However, Namalwa IFN, produced on a large scale at Wellcome Research Laboratories[21] and purified by a combination of methods including trichloroacetic acid precipitation, acid ethanol extrac-

0028–0836/80/400408—04$01.00

tion and antibody affinity chromatography, was available in relatively large quantities. About 4 mg was used in the present work. The IFN was separated into two forms by chromatography on a column (10 × 1,980 mm) of Sephadex G-75 (Superfine) in NH_4HCO_3(50 mM)/0.01% thiodiglycol. Each form (IFN-αA and IFN-αB, of apparent molecular weights 22,000 and 18,500, respectively) gave multiple bands upon SDS-gel electrophoresis (Fig. 1).

Sequencing of interferons

Amino acid compositions of IFN-αA and IFN-αB were determined, and were found to be similar to each other, but significantly different from those reported for human leukocyte[17] and one component of lymphoblastoid[22] IFNs. Less than 0.2 residues of glucosamine or galactosamine per molecule were determined in either IFN-αA or IFN-αB. Details of these studies will be reported elsewhere (G. A., manuscript in preparation).

Tryptic peptide maps of performic acid-oxidized IFN-αA and IFN-αB were prepared on cellulose thin-layer plates by electrophoresis at *p*H 4.4 and chromatography in butan-1-ol/acetic acid/water/pyridine (15:3:12:10 by vol). Peptides were detected with ninhydrin and arginine-containing peptides with phenanthrene quinone[23]. The maps were quite different: only free lysine and arginine and one other major spot in each clearly coincided, although some weak spots on the map of IFN-αB corresponded to some of the strong spots on the map of IFN-αA. The number of tryptic peptides from IFN-αA indicated that this fraction of IFN consisted of a single polypeptide of molecular weight about 18,000, with, perhaps, limited microheterogeneity; in contrast, more peptides were present in the tryptic digest of IFN-αB than would be derived from a single polypeptide chain of this size.

Amino-terminal sequences of IFN-αA and IFN-αB (about 3 nmol each) were determined by the method of Chang *et al.*[24], using 4-*N*,*N*-dimethylaminoazobenzene-4′-isothiocyanate. The results for the 14 N-terminal residues were similar:

IFN-αA (–)-Asp-Leu-Pro-Glx-Thr-His-Ser-Leu-Gly-Ser- (–)- Arg-Thr-

IFN-αB (–)-Asp-Leu-Pro-Gln-Thr-His-Ser-Leu-Gly-$\overset{\text{Asn}}{\underset{\text{Ser}}{+}}$-Arg-Arg-Thr-.

The first six steps of the degradation gave very clear results (except that some glutamic acid as well as glutamine seemed to be present at position 5 in IFN-αA), showing that any impurities with a free N-terminal residue were present at less than 5% of the molar amount of IFN. No N-terminal residue was detected for either IFN-αA or IFN-αB. The N-terminal residue was identified as cysteine from the study of peptides from the reduced and [*S*-^{14}C]carboxymethylated protein. As little butyl acetate-soluble coloured material was released upon treatment of the dimethylaminoazobenzene thiocarbamyl proteins with trifluoroacetic acid, the N-terminal cysteine residue in the native protein is probably involved in a disulphide bond.

Tryptic peptides from IFN-αA and tryptic and chymotryptic peptides from IFN-αB were purified from ~1 mg digests of the performic acid-oxidized or reduced and ^{14}C-carboxymethylated proteins by gel filtration followed by thin-layer peptide mapping. Peptide sequences were determined by either the micro-'dansyl–Edman' method[25] or the method of Chang *et al.*[24].

Comparison of interferon sequences

While this work was in progress, a complete amino acid sequence, deduced from the nucleotide sequence of cloned cDNA derived from leukocyte IFN mRNA, was published[26]. Peptide sequences determined here could be aligned unambiguously by homology with the sequence of Mantei *et al.*[26], and a summary of the directly determined peptide sequences is presented in Fig. 2. Many differences between the sequences of IFN-αA, IFN-αB and that presented in ref. 26 are evident. The N-terminal 20 residues determined by Zoon *et al.*[2] are represented among the sequences determined here, except that no N-terminal serine was detected. Residues 72–113 of IFN-αA were isolated as a single tryptic peptide, and only the first 19 residues of this could be sequenced. Sequence information has been obtained for all but five residues of IFN-αB. Several peptides were isolated in yields too low to permit sequencing, and other peptide sequences will probably be identified with further study.

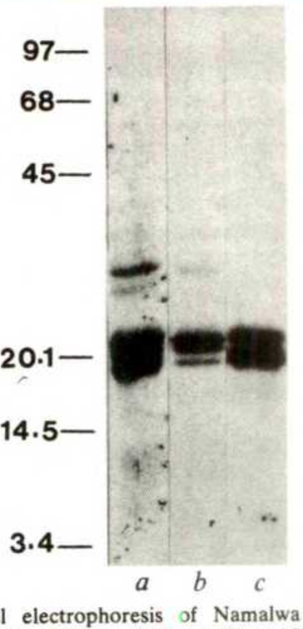

CALCUTTA 700009

Fig. 1 SDS-gel electrophoresis of Namalwa IFN. Samples (~5 μg) of Namalwa IFN (*a*), IFN-αA (*b*) and IFN-αB (*c*) were submitted to SDS-polyacryacrylamide gel electrophoresis (15% acrylamide) using the system of Laemmli[32], but with slab rather than tube gels. The gel was fixed in 15% trichloroacetic acid, stained with 0.1% Coomassie blue R250 in methanol/acetic acid/water (45:10:45 by vol) overnight and destained in 7% acetic acid. The positions of marker proteins run in parallel are shown: 97, phosphorylase; 68, bovine serum albumin; 45, ovalbumin; 20.1, soybean trypsin inhibitor (Kunitz); 14.5, lysozyme; 3.4, insulin B chain.

As predicted from the tryptic peptide map, IFN-αA consists of an almost homogeneous peptide chain, but microheterogeneity was observed at a few positions. IFN-αB is a mixture of at least three different polypeptides (all different from both of those in IFN-αA), as shown most clearly by the isolation of three different tryptic peptides from residues 14–23 and from residues 24–31:

14 23
Thr-Leu-Met-Leu-Leu-Ala-Gln-Met-Ser-Arg,

14 22
Thr-Leu-Met-Leu-Leu-Ala-Gln-Met-Arg,

14 23
Ala-Leu-Ile-Leu-Leu-Ala-Gln-Met-Gly-Arg, and

24 31
Ile-Ser-Pro-Ser-Ser-Cys-Leu-Met-Asp-Arg,

24 31
Ile-Ser-Pro-Phe-Ser-Cys-Leu-Lys,

24 31
Ile-Ser-Leu-Phe(Ser, Cys)Leu-Lys.

High yields of C-terminal peptides were obtained from both IFN-αA and IFN-αB, showing that proteolysis close to the C terminus does not occur during the biosynthesis and isolation of lymphoblastoid IFN.

The total number of different polypeptide sequences cannot be determined from the present work, but the minimum number is five (at least two in IFN-αA and at least three in IFN-αB). The complete separation of the polypeptide components which would be required for the determination of the precise number of different total sequences has been achieved only on a very small scale[10,17], insufficient for sequencing studies by established

```
          1                                   10                                      20
IF-α1     CYS-ASP-LEU-PRO-GLU-THR-HIS-SER-LEU-ASP-ASN-ARG-ARG-THR-LEU-MET-LEU-LEU-ALA-GLN-MET-SER-ARG-ILE-

IF-αA     CYS-ASP-LEU-PRO-GLN-THR-HIS-SER-LEU-GLY-SER-ARG-ARG-THR-LEU-MET-LEU-LEU-ALA-GLX-MET-ARG(ARG)(ILE-


IF-αB     CYS-ASP-LEU-PRO-GLN-THR-HIS-SER-LEU-GLY-ASN-ARG-ARG-THR-LEU-MET-LEU-LEU-ALA-GLN-MET-GLY-ARG-ILE-
                          GLU                 ASP             ALA     ILE                     SER
                                                                                              ARG

                              30                                      40
IF-α1     SER-PRO-SER-SER-CYS-LEU-MET-ASP-ARG-HIS-ASP-PHE-GLY-PHE-PRO-GLN-GLU-GLU-PHE-ASP-GLY-ASN-GLN-PHE-

IF-αA     SER-LEU-PHE-SER-CYS-LEU-LYS-ASP-ARG-HIS-ASP-PHE-GLY-PHE-PRO-GLN-GLU-GLU-PHE- — -GLY-ASN-GLN-PHE-
                                              ARG

IF-αB     SER-LEU-PHE-SER-CYS-LEU-LYS-ASP-ARG-HIS-ASP-PHE-GLY-PHE-PRO-GLN-GLU-GLU-PHE-ASP-GLY-ASN-GLN-PHE-
              PRO SER             MET     HIS ARG         ARG ILE


              50                                      60                                      70
IF-α1     GLN-LYS-ALA-PRO-ALA-ILE-SER-VAL-LEU-HIS-GLU-LEU-ILE-GLN-GLN-ILE-PHE-ASN-LEU-PHE-THR-THR-LYS-ASP-

IF-αA     GLN-LYS)(ALA-GLU-ALA-ILE-SER-VAL-LEU-HIS-GLU-MET-ILE-GLN-GLN-ILE-PHE-ASN-LEU-PHE-SER-THR-LYS-ASP-
                          THR     PRO

IF-αB     GLN-LYS-ALA-GLN-ALA-ILE-SER-VAL-LEU-HIS-GLU-MET-ILE-GLN-GLN-THR-PHE-ASN-LEU-PHE-SER-THR-LYS-ASP-
                  THR PRO                                 LEU                             THR     GLX


                                      80                                      90
IF-α1     SER-SER-ALA-ALA-TRP-ASP-GLU-ASP-LEU-LEU-ASP-LYS-PHE-CYS-THR-GLU-LEU-TYR-GLN-GLN-LEU-ASN-ASP-LEU-

IF-αA     SER-SER-ALA-ALA-   -ASP-GLU-THR-LEU-LEU-ASP-ASP-PHE-TYR-THR-PRO-LEU-TYR-
              GLX

IF-αB     SER-SER-ALA-ALA-TRP-ASP-ASP-ASP-LEU-LEU-ASP-   -PHE-CYS-THR-GLU-LEU-TYR-GLN-GLN-LEU-ASN-ASP-LEU-
                      THR         GLX THR                     SER

                      100                                     110                                     120
IF-α1     GLU-ALA-CYS-VAL-MET-GLN-GLU-GLU-ARG-VAL-GLY-GLU-THR-PRO-LEU-MET-ASN-ALA-ASP-SER-ILE-LEU-ALA-VAL-

IF-αA                                                                           )(GLU-ASP-SER-ILE-LEU-ALA-VAL-

IF-αB     GLU-ALA-CYS-VAL-MET-                      )(VAL-GLY-GLU-THR-PRO-LEU-MET-ASN-ALA-ASP-SER-ILE-LEU-ALA-VAL-
                          LEU

                                              130                                     140
IF-α1     LYS-LYS-TYR-PHE-ARG-ARG-ILE-THR-LEU-TYR-LEU-THR-GLU-LYS-LYS-TYR-SER-PRO-CYS-ALA-TRP-GLU-VAL-VAL-

IF-αA     ARG-LYS-TYR-PHE-GLN-ARG)(ILE-THR-LEU-TYR-LEU-LYS)(GLU-LYS-LYS)(TYR-SER-PRO-CYS-ALA-TRP-GLU-VAL-VAL-

IF-αB     ARG-LYS-TYR-PHE-GLN-ARG-ILE-THR-LEU-TYR-LEU-THR-GLU-LYS-LYS-TYR-SER-PRO-CYS-ALA-TRP-GLU-VAL-VAL-
          LYS             ARG

                              150                                     160
IF-α1     ARG-ALA-GLU-ILE-MET-ARG-SER-LEU-SER-LEU-SER-THR-ASN-LEU-GLN-GLU-ARG-LEU-ARG-ARG-LYS-GLU

IF-αA     ARG-ALA-GLU-ILE-MET-ARG-SER-PHE-SER-LEU-SER-THR-ASN-LEU-GLN-GLU-SER-LEU-ARG-SER-LYS-GLU

IF-αB     ARG-ALA-GLU-ILE-MET-ARG)(SER-LEU-SER-PHE-SER-THR-ASN-LEU-GLN-GLU-ARG)(LEU-ARG)(ARG-LYS-GLU
                                      PHE     LEU                     LYS             SER     ASX
```

Fig. 2 Summary of amino acid sequences identified in Namalwa interferon. The sequences determined in tryptic (and some other) peptides of IFN-αA and tryptic and chymotryptic peptides of IFN-αB are aligned by homology with the complete sequence of leukocyte IFN 1 (IFN-α1) determined by analysis of cDNA (ref. 26). The sequences are written in the standard three-letter notation. In addition, *Ile* denotes Ile or, less likely, Leu; *Leu* denotes Leu or, less likely, Ile (the method of Chang *et al.*[24] does not clearly distinguish between these residues); and *Arg* denotes Arg or Lys (residue 23 of IFN-αA provides a site for tryptic cleavage, and either arginine or lysine could be placed in this position). The numbering system is that of IFN-α1; IFN-αA has a deletion at residue 44 (—). Peptide sequences which have not been shown experimentally to be connected are separated by parentheses. Gaps in the sequences indicate positions for which no residue has been identified. Where more than one residue has been identified at a single position, the alternative residues are written below the line.

methods. Complete sequences of further individual components may well be obtained more readily from the analysis of nucleotide sequences in cloned cDNA, and, indeed, a second species of leukocyte IFN cDNA has recently been detected (M. Streuli, S. Nagata and C. Weissmann, unpublished results quoted in ref. 4).

The sequence of IFN-αA differs from that described in ref.26 in at least 20 positions, whereas peptides in IFN-αB were, on the whole, more closely related to the published sequence. However, Leu 60 and Ile 64 have not been found in peptides isolated from IFN-αB. The analysis of peptide sequences is not yet complete, so the sequence of Mantei *et al.*[26] may be present in purified Namalwa IFN, but probably only as a minor component.

If the sequence of Mantei *et al.* is included, multiple residues have been identified at 41 positions out of 166 (25%). Although this is not the total figure for mismatch, clearly the several leukocyte-type IFNs are much more closely related than are leukocyte and fibroblast IFNs, between which 71% of the amino acid residues differ[4]. A quantitative study of homology is not yet justified, as the data base is incomplete, but note that a highly conserved region, residues 133–151, where no differences have been detected between the various leukocyte-type IFNs, is also a region which shows strong homology between fibroblast and leukocyte IFNs[4]. This suggests a common functional role for this portion of the polypeptide chain.

The low content of aminosugars and the lack of detection of typical glycopeptides (characterized by a lower elution volume from Sephadex G-50 columns and a lower R_F on TLC than would be expected from their amino acid compositions) suggest that the major components of lymphoblastoid IFN are not glycosylated. Also, no sequence of the type Asn-X-(Ser or Thr), generally required for glycosylation of asparagine residues, has been identified. A glycosylation site could, however, be present in residues 91–113 of IFN-αA, which have not been placed in sequence. The neutral sugar content has not been determined, so some O-linked glycosylation, or glycosylation of minor components, cannot be excluded. Several observations[7,9,15,18,19,27] suggest that leukocyte and lymphoblastoid IFNs are glycosylated, although some workers have doubted that leukocyte IFN is a glycoprotein[12,28]. Further study is required before a definite conclusion can be reached.

The total number of different polypeptide sequences constituting human leukocyte IFN (and hence the number of structural genes) may be sufficient to account for all the heterogeneity seen by isoelectric focusing and gel electrophoresis (at least seven components were detected here, as shown in Fig. 1, but it has not been demonstrated that all of these are active as IFNs). If so, the different apparent molecular weights of the different components of IFN as determined by SDS-gel electrophoresis are not related to significant differences in the true molecular weights, but rather to such factors as binding of different amounts of SDS or different conformations of IFN-SDS complexes. The separation by gel filtration into IFN-αA and IFN-αB is also probably not related to significant differences in molecular weights, but to different conformations, IFN-αA being, presumably, more elongated in structure.

Importance of multiple interferon structural genes

The functional significance of multiple structural genes for IFN remains to be elucidated. Multiple genes have been identified for other proteins, such as actin[29-31]. With actin, the proteins are synthesized in large amounts and there are well established differences in functional properties between the different gene products. Possibly, different IFN gene products have different biological activities, or different specificities towards different target cells, and they may be differentially induced by different viruses.

We thank Dr C. Weissmann for making available sequence information before publication.

Note added in proof: The complete sequence of a second species of human leukocyte interferon (IFN-α2), deduced from the nucleotide sequence of cloned cDNA, has recently been determined[33]. IFN-α2 is very similar to, and may be identical with, one of the components of IFN-αA.

Received 28 July; accepted 21 August 1980.

1. Cavalieri, R. L., Havell, E. A., Vilček, J. & Pestka, S. *Proc. natn. Acad. Sci. U.S.A.* **74,** 3287–3291 (1977).
2. Zoon, K. C. *et al. Science* **207,** 527–528 (1980).
3. Knight, E. Jr, Hunkapiller, M. W., Korant, B. D., Hardy, R. W. F. & Hood, L. E. *Science* **207,** 525–526 (1980).
4. Taniguchi, T. *et al. Nature* **285,** 547–549 (1980).
5. Strander, H., Mogensen, K. E. & Cantell, K. *J. clin. Microbiol.* **1,** 116–117 (1975).
6. Stewart, W. E. II & Desmyter, J. *Virology* **67,** 68–73 (1975).
7. Bridgen, P. J. *et al. J. biol. Chem.* **252,** 6585–6587 (1977).
8. Chadha, K. C., Sclair, M., Sulkowski, E. & Carter, W. A. *Biochemistry* **17,** 196–200 (1978).
9. Grob, P. M. & Chadha, K. C. *Biochemistry* **18,** 5782–5786 (1979).
10. Berg, K. & Heron, I. *Scand. J. Immun.* **11,** 489–502 (1980).
11. Fantes, K. H. *Ann. N. Y. Acad. Sci.* **173,** 118–121 (1970).
12. Mogensen, K. E., Pyhälä, L., Törmä, E. & Cantell, K. *Acta. path. microbiol. scand.* **B82,** 305–310 (1974).
13. Törmä, E. T. & Paucker, K. *J. biol. Chem.* **251,** 4810–4816 (1976).
14. Havell, E. A., Yip, Y. K. & Vilček, J. *Archs Virol.* **55,** 121–129 (1977).
15. Stewart, W. E. II, Lin, L. S., Wiranowska-Stewart, M. & Cantell, K. *Proc. natn. Acad. Sci. U.S.A.* **74,** 4200–4204 (1977).
16. Salit, M. G. & Ogburn, C. A. *Archs Virol.* **63,** 133–142 (1980).
17. Rubinstein, M. *et al. Proc. natn. Acad. Sci. U.S.A.* **76,** 640–644 (1979).
18. Bose, S., Gurari-Rotman, D., Ruegg, U. T., Corley, L. & Anfinsen, C. B. *J. biol. Chem.* **251,** 1659–1662 (1976).
19. Stewart, W. E. II, Wiranowska-Stewart, M., Koistinen, V. & Cantell, K. *Virology* **97,** 473–476 (1979).
20. Thang, M. M. *et al. Proc. natn. Acad. Sci. U.S.A.* **76,** 3717–3721 (1979).
21. Finter, N. B., Fantes, K. H. & Johnston, M. D. *Devl Biol. Standard* **38,** 343–348 (1978).
22. Zoon, K. C., Smith, M. E., Bridgen, P. J., zur Nedden, D. & Anfinsen, C. B. *Proc. natn. Acad. Sci. U.S.A.* **76,** 5601–5605 (1979).
23. Yamada, S. & Itano, H. A. *Biochim. biophys. Acta* **130,** 538–540 (1966).
24. Chang, J. Y., Brauer, D. & Wittman-Liebold, B. *FEBS Lett.* **93,** 205–214 (1978).
25. Bruton, C. J. & Hartley, B. S. *J. molec. Biol.* **52,** 165–178 (1970).
26. Mantei, N. *et al. Gene* **10,** 1-10 (1980).
27. Chadha, K. C., Grob, P. M., Hamill, R. L. & Sulkowski, E. *Archs Virol.* **64,** 109–117 (1980).
28. Jankowski, W. J., Davey, M. W., O'Malley, J. A., Sulkowski, E. & Carter, W. A. *J. Virol.* **16,** 1124–1130 (1975).
29. Vandekerkhove, J. & Weber, K. *J. molec. Biol.* **126,** 783–802 (1978).
30. Cleveland, D. W. *et al. Cell* **20,** 95–105 (1980).
31. Fyrberg, E. A., Kindle, K. L., Davidson, N. & Sodja, A. *Cell* **19,** 365–378 (1980).
32. Laemmli, U. K. *Nature* **227,** 680–685 (1970).
33. Streuli, M., Nagata, S. & Weissmann, C. *Science* (in the press).

Human leukocyte interferon produced by *E. coli* is biologically active

David V. Goeddel[*], Elizabeth Yelverton[*], Axel Ullrich[*], Herbert L. Heyneker[*], Giuseppe Miozzari[*], William Holmes[*], Peter H. Seeburg[*], Thomas Dull[*], Laurie May[†], Nowell Stebbing[†], Roberto Crea[‡], Shuichiro Maeda[§], Russell McCandliss[§], Alan Sloma[§], John M. Tabor[§], Mitchell Gross[§], Phillip C. Familletti[§] & Sidney Pestka[§]

Departments of Molecular Biology*, Biology†, and Organic Chemistry‡, Genentech Inc., 460 Pt. San Bruno Blvd,
South San Francisco, California 94080
§ Roche Institue of Molecular Biology, Nutley, New Jersey 07110

A human leukocyte interferon cDNA was enzymatically synthesized, inserted into the vector pBR322, and cloned in Escherichia coli. *The DNA sequence codes for a 23-amino acid signal peptide followed by an interferon polypeptide of 165 amino acids. An expression plasmid was constructed which permits the synthesis in* E. coli *of 2.5×10^8 units of interferon per litre of culture. This LeIF protected squirrel monkeys from lethal encephalomyocarditis virus infection.*

THE interferons (IFNs) are a family of proteins characterized by a potent ability to confer a virus-resistant state in their target cells[1,2]. In addition, IFNs can inhibit cell proliferation and modulate immune response (reviewed in ref. 2). These properties have led to the clinical use of IFN for the treatment of viral infections and malignancies.

The classical, or type I, IFNs consist of at least two distinct gene products which differ antigenically[3,4] and have different target cell specificities[5]. Leukocyte interferon (LeIF) and fibroblast interferon (FIF) are named for the cells from which they are derived. Messenger RNAs for LeIF and FIF have been isolated and translated *in vitro* and in *Xenopus* oocytes[4,6-8].

Both LeIF[9,10] and FIF[11] have been purified to homogeneity; reported molecular weights range from 17,500 to 21,000. The specific activities of these preparations are remarkably high, 2×10^8 to 1×10^9 U per mg protein. Unfortunately the yields from eukaryotic cells have been correspondingly low. Two litres of human blood are required to produce approximately 1 μg of

0028-0836/80/400411—06$01.00

purified LeIF[9]. Nevertheless, advances in protein sequencing techniques have permitted the determination of partial amino acid sequences[11–13].

Recombinant DNA technology provides an alternative method of producing large quantities of IFN using bacterial cells. Human FIF cDNA has recently been cloned[14,15] and biologically active mature FIF expressed in *Escherichia coli*[15]. Likewise, a species of human LeIF cDNA has been cloned in *E. coli* and expressed in an apparent precursor form with a signal peptide attached[16]. We describe here the construction of a plasmid directing the high level expression in *E. coli* of a human LeIF which exhibits *in vivo* antiviral activity.

Construction and identification of clones containing LeIF cDNA sequences

Cells from the human myeloblastoid line KG-1 (ref. 17) were collected 5 h after induction with Sendai virus and the 12S sucrose gradient fraction of poly(A) RNA was isolated as described elsewhere[18]. This mRNA had an IFN titre of 8,000 U μg^{-1} in the *Xenopus laevis* oocyte assay[4]. Five µg of mRNA was used to prepare double-stranded cDNA by standard procedures[19,20]. The cDNA was electrophoresed on a 6% polyacrylamide gel and 110 ng of material from 600 to 1,300 base pairs in length were recovered by electroelution. A 20-ng portion of this cDNA was tailed with deoxyC residues[21], annealed with 100 ng of plasmid pBR322 (ref. 22) which had been tailed with deoxyG residues at the *Pst*I site, and used to transform *E. coli* K12 strain 294 (ref. 23). Approximately 1,000 tetracycline-resistant, ampicillin-sensitive transformants were obtained per ng of cDNA. A rapid plasmid isolation procedure[24] was used to prepare about 1 µg of plasmid DNA from each of 500 individual transformants. Each DNA sample was denatured and aliquots were applied to each of three nitrocellulose filters following a published procedure[25].

The amino acid sequences of several tryptic fragments of human LeIF have been determined (W. Levy, J. Shively and S. P., unpublished results). This information permitted the design of synthetic deoxyoligonucleotides potentially complementary to different regions of LeIF mRNA. The two tryptic peptides T-1 and T-13 were selected because they had amino acid sequences requiring the synthesis of only 12 and four undecamers, respectively, to account for all possible coding sequences (Fig. 1). Four sets of deoxyoligonucleotide probes were synthesized for each sequence, containing either three (T-1A, B, C, D) or one (T-13A, B, C, D) oligonucleotides each.

```
                    Tryptic peptide (T-1)       Tryptic peptide (T-13)

Protein            Ala-Glu-Ile-Met-Arg          ---His-Glu-Met-Ile-Gln---

                         A   A     A                 C   A       A   A
mRNA            5' GCN GA  AUC AUG  GN          5' CA  GA  AUG AUC CA
                         G   U     C                 U   G       U   G
Complementary                A
DNA primers     3'     CTT TAG TAC GC (T-1A)    3' GTA CTT TAC TA (T-13A)
                             T                     --G----------- (T-13B)
                       --C----------- (T-1B)       ------C------- (T-13C)
                       ------------T- (T-1C)       --G---C------- (T-13D)
                       --C---------T- (T-1D)
```

Fig. 1 Synthetic deoxyoligonucleotides designed to prime cDNA synthesis from LeIF mRNA. Amino acid sequences are given for peptide 1 and a portion of peptide 13 derived from a tryptic digest of human LeIF-β1 (W. Levy, J. Shively and S. P., unpublished results). All potential mRNA sequences coding for these peptides are shown. The indicated complementary deoxyoligonucleotides 11-bases long were chemically synthesized by the phosphotriester method[36]. Four individual primers were prepared in the T-13 series. The 12 T-1 primers were prepared in four pools of three primers each using a strategy described elsewhere[15]. ^{32}P-labelled cDNA was prepared from these primers using published reaction conditions[37]. The reactions (60 µl) were performed in 20mM Tris-HC1 (*p*H 8.3), 20 mM KCl, 8 mM $MgCl_2$, 30 mM *β-merceptoethanol*. Reactions included one µg of each primer (that is 12 µg total for T-1 series, 4 µg total for T-13 series), two µg of 12S fraction mRNA from induced cells (or 10 µg of poly(A) mRNA from uninduced cells), 0.5 mM dATP, dGTP, dTTP, 200 µCi [$\alpha^{32}P$]dCTP (2–3,000 Ci $mmol^{-1}$; Amersham), and 60 U reverse transcriptase. Product was separated from unincorporated label by gel filtration on a 10-ml Sephadex G-50 column, treated with 0.3 M NaOH for 30 min at 70°C to destroy RNA, and neutralized with HCl. Hybridizations were performed as described[15,25].

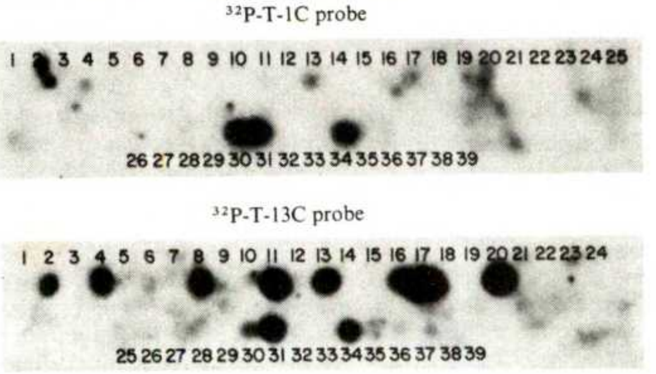
^{32}P-T-1C probe

^{32}P-T-13C probe

Fig. 2 Hybridization of potential LeIF cDNA recombinant plasmids with ^{32}P-labelled synthetic deoxyoligonucleotides. Plasmid DNA from the 39 clones was prepared by a standard cleared lysate procedure[38] and purified by Biorad Agarose A-50 column chromatography. Samples (3 µg) of each preparation were linearized by treatment with *Eco*RI, denatured in alkali and spotted on two separate nitrocellulose filters (1.5 µg per spot)[25]. Individual synthetic deoxyoligonucleotide primers and primer pools were phosphorylated with [$\gamma^{32}P$]ATP as follows: 50 pmol of oligonucleotide and 100 pmol of [$\gamma^{32}P$]ATP (2,500 Ci $mmol^{-1}$; New England Nuclear) were combined in 30 µl of 60 mM Tris-HCl (*p*H 8) 10 mM $MgCl_2$, 15 mM β-merceptothanol. Two units of T4 polynucleotide kinase were added and, after 30 min at 37°C, ^{32}P-labelled primers were purified by chromatography on 10-ml Sephadex G-50 columns. Hybridizations were performed using 10^6 c.p.m. of primer T-13C or 3×10^6 c.p.m. of primer pool T-1C. The hybridizations were performed at 15 °C for 14 h in 6 × SSC, 10 × Denhardt's solution, as described by Wallace *et al.* [28]. Filters were washed for 5 min (three times) at 0 °C in 6 × SSC, dried, and exposed to X-ray film. Results are shown above for primer T-13C and primer pool T-1C.

These synthetic deoxyoligonucleotides were used to prime the synthesis of radiolabelled single-stranded cDNA for use as hybridization probes (see Fig. 1 legend). The template mRNA was either the 12S RNA from KG-1 cells induced with Sendai virus (8,000 U IFN activity μg^{-1}) or total poly(A) mRNA from uninduced leukocytes (<10 U IFN activity μg^{-1}).

The three sets of nitrocellulose filters containing the 500 plasmid samples were hybridized with three different cDNA probes: (1) induced cDNA primed with the T-1 set of primers, (2) T-13-primed induced cDNA, and (3) uninduced cDNA prepared by using both sets of primers. Clones were considered positive if they hybridized more strongly to one or both of the induced cDNA probes (1) and (2) than to the total uninduced probe(3). Thirty clones (pL1–pL30) were selected from the 500 for further analysis.

At this time a partial-length (~750-base pair) LeIF cDNA recombinant plasmid pIFL104, as identified by a mRNA hybridization selection procedure, became available[18]. A unique 260-base pair *Bgl*II restriction fragment isolated from this clone was labelled with ^{32}P (ref. 26) and used as probe to screen another 400 transformants by an *in situ* colony screening procedure[27]. Nine colonies (pL31–pL39) were identified which hybridized to different extents with this probe. Plasmid DNA was prepared from all 39 potential LeIF cDNA clones and rescreened with the same 260-base pair DNA probe using the dot hybridization procedure[25]. Three plasmids (pL4, pL31, pL34) exhibited very strong hybridization signals, four (pL13, pL30, pL32, pL36) hybridized moderately, and three (pL6, pL8, pL14) hybridized weakly with the probe.

The 39 potential LeIF cDNA recombinant plasmids were also screened with ^{32}P-labelled synthetic undecamers (individual T-1 primer pools or individual T-13 primers) directly as hybridization probes. The hybridization conditions were chosen such that perfect base pairing should be required for detectable hybridization signals[28]. Plasmid pIFL104 was found to give significant hybridization with primer pool T-1C and primer T-13C, but no detectable hybridization with the other undecamers. As shown in Fig. 2, several of the 39 potential LeIF plasmids (pL2, 4, 13, 17, 20, 30, 31, 34) also hybridized with both of these probes. Restriction analysis revealed that only one of these plasmids, pL31, also contained a 260-base pair internal *Bgl*II fragment.

Pst I digestion of pL31 showed the size of the cDNA insert to be approximately 1,000 base pairs.

DNA sequence of recombinant plasmid pL31

The entire *Pst*I insert of pL31 was sequenced by both the Maxam–Gilbert chemical method[29] and an enzymatic method[30] using the bacteriophage M13 cloning vector mp7 (P. S., unpublished results). The DNA sequence is shown in Fig. 3. Protein sequence information from LeIF (ref. 13; W. Levy, J. Shively and S. P., unpublished results) permitted the determination of the correct translational reading frame and allowed us to predict the entire LeIF type A (our term for the LeIF encoded by pL31) amino acid sequence, including a precursor segment or signal peptide. The first ATG translational initiation codon is found 60 nucleotides from the 5′ end of the sequence and is followed, 188 codons later, by a TGA termination triplet; there are 335 untranslated nucleotides at the 3′ end, followed by a poly(A) sequence. The putative signal peptide (presumably involved in the secretion of mature LeIF from leukocytes) is 23 amino acids long. The 165-amino acid polypeptide constituting the mature LeIF has a calculated molecular weight of 19,390. The DNA sequence also shows that the tryptic peptides T1 and T13 of LeIF β_1 (Fig. 1) correspond to amino acids 145–149 and 57–61, respectively, of LeIF A. The actual DNA coding sequences found in these two regions are those represented by primer pool T-1C and primer T-13C, as the hybridization data in Fig. 2 had suggested.

The amino acid sequence deduced from the DNA sequence of LeIF type A has only partial identity with the directly determined NH_2-terminal amino acid sequences of LeIFα1 (20 out of 22 positions)[13] and human lymphoblastoid IFN (16 out of 20 positions)[12]. It also differs significantly from the complete amino acid sequence recently deduced from the nucleotide sequence of LeIF I (ref. 31). LeIF I codes for a mature IFN of 166 amino acids, as compared to 165 amino acids for LeIF A. The extra amino acid (aspartic acid) of LeIF I is between amino acids 43 and 44 of LeIF A. Furthermore, only 137 of the remaining 165 amino acids (83%) are identical. The single longest stretch of homology between the two LeIFs is 19 amino acids (residues 132–150), and in one region (residues 100–106) only two out of seven amino acids are identical. The amino acid homology in the signal peptide sequence is 74% (17/23 identical residues). The glycine–cysteine cleavage site between the signal and IFN sequence is the same in both IFNs. In addition, the 3′ untranslated regions of LeIF A and LeIF I mRNAs (335 compared with 242 nucleotides) differ considerably. The explanation for these discrepancies lies in the fact that there is a family of non-identical LeIF genes (including pL4, pL13, pL30, pL32), evidence for which will be reported soon.

Expression of leukocyte pre-interferon A

The precursor form of LeIF A (Le-preIF A) was expressed in *E. coli* by ligating the 1,000-base pair *Pst*I insert into the *Pst*I site of the plasmid pNCV. pNCV is a derivative of pBR322 containing part of the *E. coli* tryptophan operon (extending from the promoter–operator region through the *trp* E gene, with a deletion[32] of a portion of the *trp* leader and *trp* E coding regions) which has been modified to contain a unique *Pst*I site at the C-terminal end of the *trp* E protein coding sequence (H. H., unpublished results). The LeIF A DNA sequence can be inserted into pNCV in either of two orientations. As shown in Table 1, only plasmids having inserts which are orientated correctly with respect to the direction of transcription from the *trp* promoter give detectable IFN activity. Extracts of *E. coli* containing the plasmid pLe-preIF A2 gave approximately 480,000 U of activity per litre of culture, considerably higher than the maximal 20,000 U l^{-1} reported by Nagata *et al.* for Le-preIF D (ref. 16). The Le-preIF A produced by *E. coli* can be visualized by staining and co-migrates with human growth hormone (191 amino acids; molecular weight 22,000) on SDS-polyacrylamide gels (J. Perry, unpublished results). This suggests that the expression of Le-preIF A in pNCV is due to translation initiating at the signal peptide ATG start codon.

```
5'
                                                             S1                                  S10
                                                             met ala leu thr phe ala leu leu val ala
TGAGCCTAAACCTTAGGCTCACCCATTTCAACCAGTCTAGCAGCATCTGCAACATCTACA ATG GCC TTG ACC TTT GCT TTA CTG GTG GCC
                                                50

                                    S20         S23 1                                   10
leu leu val leu ser cys lys ser ser cys ser val gly CYS ASP LEU PRO GLN THR HIS SER LEU GLY SER ARG
CTC CTG GTG CTC AGC TGC AAG TCA AGC TGC TCT GTG GGC TGT GAT CTC CCT CAA ACC CAC AGC CTG GGT AGC AGG
            100                                                             150

                            20                                      30
ARG THR LEU MET LEU LEU ALA GLN MET ARG LYS ILE SER LEU PHE SER CYS LEU LYS ASP ARG HIS ASP PHE GLY
AGG ACC TTG ATG CTC CTG GCA CAG ATG AGG AAA ATC TCT CTT TTC TCC TGC TTG AAG GAC AGA CAT GAC TTT GGA
                                            200

        40                                      50                                      60
PHE PRO GLN GLU GLU PHE GLY ASN GLN PHE GLN LYS ALA GLU THR ILE PRO VAL LEU HIS GLU MET ILE GLN GLN
TTT CCC CAG GAG GAG TTT GGC AAC CAG TTC CAA AAG GCT GAA ACC ATC CCT GTC CTC CAT GAG ATG ATC CAG CAG
                250                                                         300

                            70                                      80
ILE PHE ASN LEU PHE SER THR LYS ASP SER SER ALA ALA TRP ASP GLU THR LEU LEU ASP LYS PHE TYR THR GLU
ATC TTC AAT CTC TTC AGC ACA AAG GAC TCA TCT GCT GCT TGG GAT CAG ACC CTC CTA GAC AAA TTC TAC ACT GAA
                                            350

        90                                      100                                     110
LEU TYR GLN GLN LEU ASN ASP LEU GLU ALA CYS VAL ILE GLN GLY VAL GLY VAL THR GLU THR PRO LEU MET LYS
CTC TAC CAG CAG CTG AAT GAC CTG GAA GCC TGT GTG ATA CAG GGG GTG GGG GTG ACA GAG ACT CCC CTG ATG AAG
        400                                                                 450

                            120                                     130
GLU ASP SER ILE LEU ALA VAL ARG LYS TYR PHE GLN ARG ILE THR LEU TYR LEU LYS GLU LYS LYS TYR SER PRO
GAG GAC TCC ATT CTG GCT GTG AGG AAA TAC TTC CAA AGA ATC ACT CTC TAT CTG AAA GAG AAG AAA TAC AGC CCT
                                            500

        140                                     150                                     160
CYS ALA TRP GLU VAL VAL ARG ALA GLU ILE MET ARG SER PHE SER LEU SER THR ASN LEU GLN GLU SER LEU ARG
TGT GCC TGG GAG GTT GTC AGA GCA GAA ATC ATG AGA TCT TTT TCT TTG TCA ACA AAC TTG CAA GAA AGT TTA AGA
            550                                                             600

        165
SER LYS GLU STOP
AGT AAG GAA TGA AAACTGGTTCAACATGGAAATGATTTTCATTAATTCGTATGCCAGCTCACCTTTTTATGATCTGCCATTTCAAAGACTCATGT
                                     650                                               700

TTCTGCTATGACCATGACACGATTTAAATCTTTTTCAAATGTTTTTAGGAGTATTAATCAACATTGTATTCAGCTCTTAAGGCACTAGTCCCTTACAGA
                                      750                                               800

GACCATGCTGACTGATCCATTATCTATTTAAATATTTTTAAAATATTATTTATTTAACTATTTATAAAACAACTTATTTTTGTTCATATTACGTCATGT
                                      850                                               900

CACCTTTGCACAGTGGTTAATGTAATAAAATATGTTCTTTGTATTTGGTAA
                                      950
                                                          3'
```

Fig. 3 Nucleotide and amino sequences of pL31 (LeIF A). The DNA sequences of both strands of the *Pst*I insert were determined by the Maxam–Gilbert technique and by the dideoxy chain termination procedure[30] after subcloning *Sau*3a fragments of pL31 into the M13 vector mp7 (P.S., unpublished results). Numbers above each line refer to amino acid position (S refers to signal peptide) and numbers below each line to nucleotide position.

Table 1 Interferon activity in extracts of *E. coli*

E. coli 294 transformed by:	Cell density (cells ml^{-1})	IFN activity (U per ml culture)	LeIF molecules per cell
pLe-preIF A2	3.5×10^8	480	120
pLe-preIF A3	3.5×10^8	0	0
pLeIF A25	3.5×10^8	36,000	9,000
pLeIF A25	1.8×10^9	250,000	12,000
pLeIF A118	3.5×10^8	20	5

The 1,000-base pair *Pst*I insert (0.5 μg) from pL31 was ligated to 0.2 μg of *Pst*I-cleaved pNCV and the product used to transform *E. coli* 294. Recombinant plasmids containing inserted LeIF cDNA were identified by colony hybridization[27] using the ^{32}P-labelled 260-base pair *Bgl*II fragment from pL31 as a hybridization probe. Digestion of these plasmids with *Pvu*II identified clones with the LeIF A DNA sequence orientated in the correct orientation (pLe-preIF A2) and in the opposite orientation (pLe-preIF A3). The construction of pLeIF A25 and pLeIF A118 for direct expression of LeIF A is described in Fig. 4 legend. pLeIF A118 has the *trp* promoter orientated such that transcription proceeds away from the LeIF A gene. Extracts were prepared for IFN assay as follows. One-ml cultures were grown in L-broth containing 5 μg ml^{-1} tetracycline to an A_{550} of ~1.0, then diluted into 25 ml of M9 medium containing 0.2% glucose, 0.5% casamino acids and 5 μg ml^{-1} tetracycline. 10-ml samples were collected by centrifugation when A_{550} reached 1.0 and cell pellets were suspended in 1 ml of 15% sucrose, 50 mM Tris-HCl (*p*H 8.0), 50 mM EDTA. One mg of lysozyme was added and, after 5 min at 0 °C, cells were disrupted by sonication. The samples were centrifuged for 10 min at 15,000 r.p.m. in a Sorvall SM-24 rotor. IFN activity in the supernatants was determined by comparison with LeIF standards by the cytopathic effect (CPE) inhibition assay[2]. To determine the number of IFN molecules per cell, a LeIF specific activity of 4×18^8 U mg^{-1} was used[9]. To measure *p*H2 stability, the 250,000 U ml^{-1} extract of *E. coli* 294/pLeIF A25 was diluted 500-fold with MEM giving a concentration of 500 U ml^{-1}. A LIF standard (Wadley Institute) previously titrated against the NIH LIF standard, was also diluted to a final concentration of 500 U ml^{-1}. Aliquots (1 ml were adjusted to *p*H 2 with 1 M HCl, incubated at 4 °C for 52 h, neutralized by addition of NaOH and IFN activity determined by the standard CPE inhibition assay[2]. To measure neutralization by antibody, 25-μl aliquots of the 500 U ml^{-1} samples (untreated) were incubated with 25 μl of rabbit anti-human LeIF (10,000 neutralizing units ml^{-1}) for 60 min at 37 °C, centrifuged at 12,000*g* for 5 min and the supernatant assayed.

Direct expression of mature leukocyte interferon

The procedure followed to express LeIF A directly as a mature IFN polypeptide was a variation of that employed previously for human growth hormone[20]. As shown in Fig. 4, a *Sau*3a restriction endonuclease site is conveniently located between codons 1 and 2 of the LeIF A sequence. Two synthetic deoxyoligonucleotides were designed which incorporate an ATG translational initiation codon, restore the codon for amino acid 1 (cysteine), and create an *Eco*RI sticky end. These oligomers were ligated to a 34-base pair, *Sau*3a–*Ava*II fragment of pL31. The resulting 45-base pair product was ligated to two additional DNA fragments to construct an 865-base pair synthetic–natural hybrid gene which codes for LeIF A and which is bounded by *Eco*RI and *Pst*I restriction sites. This gene was inserted into pBR322 between the *Eco*RI and *Pst*I sites to give the plasmid pLeIF A1.

Next, a 300-base pair *Eco*RI fragment was constructed which contains the *E. coli trp* promoter, operator, and the *trp* leader ribosome binding site but stops short of the ATG sequence for initiation of translation of the leader peptide (D. Kleid and D. Yansura, unpublished results). This DNA fragment was cloned into the *Eco*RI site of pLeIF A1. Transformants carrying plasmids with the *trp* promoter orientated in either possible orientation were assayed for IFN activity (Table 1). Clone pLeIF A25, in which the *trp* promoter was inserted in the desired orientation, gives high levels of activity (2.5×10^8 U l^{-1}). Low levels of activity are obtained even if the *trp* promoter reads away from the LeIF A gene, as in the case of pLeIF A118 (2.0×10^4 U l^{-1}). The IFN produced by *E. coli* 294/pLeIF A25 behaves like authentic human LeIF; it is stable to treatment at *p*H2 and is

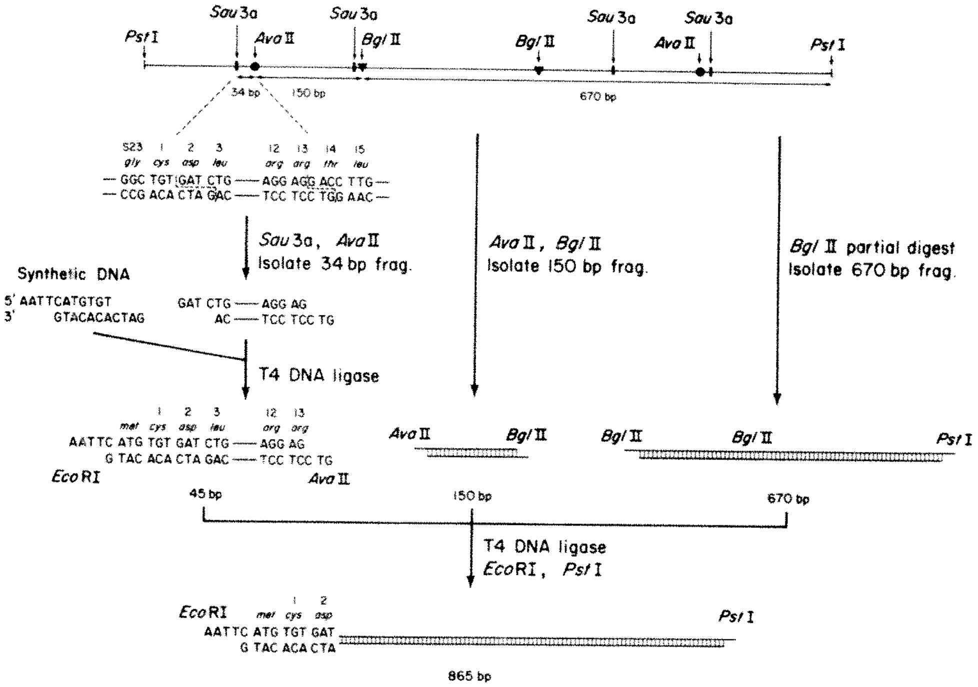

Fig. 4 Construction of a gene coding for the direct synthesis of mature human LeIF A in *E. coli*. 250 μg of plasmid pL31 were digested with *Pst*I and the 1,000-base pair insert isolated by gel electrophoresis on a 6% polyacrylamide gel. Approximately 40 μg of insert were electroeluted from the gel and divided into three aliquots for further digestion. *a*, A 16-μg sample of this fragment was partially digested with 40 U of *Bgl*II for 45 min at 37 °C and the reaction mixture purified on a 6% polyacrylamide gel. Approximately 2 μg of the desired 670-base pair fragment were recovered. *b*, Another sample (8 μg) of the 1,000-base pair *Pst*I insert was restricted with *Ava*II and *Bgl*II. One μg of the indicated 150-base pair fragment was recovered after gel electrophoresis. *c*, 16 μg of the 1,000-base pair piece were treated with *Sau*3a and *Ava*II. After electrophoresis on a 10% polyacrylamide gel, approximately 0.25 μg (~10 pmol) of the 34-base pair fragment were recovered. The two indicated deoxyoligonucleotides, 5′-dAATTCATGTGT (fragment 1) and 5′-dGATCACACATG (fragment 2) were synthesized by the phosphotriester procedure[36]. Fragment 2 was phosphorylated as follows: 200 μl (~40 pmol) of [γ-^{32}P]ATP (5,000 Ci mmol^{-1}; Amersham) was dried down and resuspended in 30 μl of 60 mM Tris-HCl (*p*H 8), 10 mM $MgCl_2$, 15 mM β-mercaptoethanol, containing 100 pmol of DNA fragment and 2 U of T4 polynucleotide kinase. After 15 min at 37 °C, 1 μl of 10 mM ATP was added and the reaction allowed to proceed another 15 min. The mixture was then heated at 70 °C for 15 min, combined with 100 pmol of 5′-OH fragment 1 and 10 pmol of the 34-base pair *Sau*3a–*Ava*II fragment. Ligation was performed for 5 h at 4 °C in 50 μl of 20 mM Tris-HCl (*p*H 7.5), 10 mM $MgCl_2$, 10 mM dithiothreitol, 0.5 mM ATP and 10 U T4 DNA ligase. The mixture was electrophoresed on a 6% PA gel and the 45-base pair product recovered by electroelution. 860,000 Cerenkov c.p.m. were recovered (~30 ng, 1 pmol), combined with 0.5 μg (5 pmol) of the 150-base pair *Ava*II–*Bgl*II fragment and 1 μg (2 pmol) of the 670-base pair *Bgl*II–*Pst*I fragment. The ligation was performed at 20°C for 16 h using 20 U of T4 DNA ligase. The ligase was inactivated by heating to 65 °C for 10 min. The mixture was then digested with *Eco*RI and *Pst*I to eliminate polymers of the gene. The mixture was purified by 6% polyacrylamide gel electrophoresis. 36,000 c.p.m. (~0.04 pmol, 20 ng) of 865-base pair product were isolated. One half (10 ng) of this was ligated into pBR322 (0.3 μg) between the *Eco*RI and *Pst*I sites. Transformation of *E. coli* 294 gave rise to 70 tetracycline-resistant, ampicillin-sensitive transformants. Plasmid DNA isolated from 18 of these transformants was digested with *Eco*RI and *Pst*I. 16 of the 18 plasmids had an *Eco*RI–*Pst*I fragment 865 base pairs in length. One μg of one of these, pLeIF A1, was digested with *Eco*RI and ligated to a 300-base pair *Eco*RI fragment (0.1 μg) containing the *E. coli trp* promoter and *trp* leader ribosome binding site. Transformants containing the *trp* promoter were identified using a ^{32}P-*trp* probe in conjuction with the Grunstein–Hogness colony screening procedure[27]. An asymmetrically located *Xba*I site in the *trp* fragment allowed us to determine recombinants in which the *trp* promoter was orientated in the direction of the LeIF A gene. bp, Base pair.

Table 2 Antiviral effect of various LeIF preparations against EMC virus infection of squirrel monkeys

		Serum PFU ml^{-1}					
Treatment	Survivors	Day 2		Day 3		Day 4	
Control		10	3	3×10^4	10^4	$>10^5$	$>3.4\times10^4$
(bacterial	0/3	0		0		1,200	
proteins)		0		0		0	
Bacterial		0		0		0	
LeIF A	3/3	0		0		0	
		0		0		0	
LeIF standard		0		0		0	
	3/3	0		0		0	
		0		0		0	

All monkeys were male (average weight 713 g) and had no EMC virus antibodies prior to infection. The monkeys were infected intramuscularly with 100 × LD_{50} EMC virus (determined in mice). The control treated monkeys died at 134, 158 and 164 h post-infection. IFN treatments of 10^6 U were intravenously at −4, +2, 23, 29, 48, 72, 168 and 240 h, relative to infection. The bacterial LeIF was a column chromatography fraction (R. Wetzel, unpublished results) from a lysate of *E. coli* 294/pLeIF A25 at a specific activity of 7.4×10^6 U mg^{-1} protein. The control bacterial proteins were an equivalent column fraction from a lysate of *E. coli* 294/pBR322 at twice the total protein concentration. The LeIF standard was Sendai virus-induced IFN from normal human buffy-coat cells, purified chromatographically to a specific activity of 32×10^6 U per mg protein. Survival of the monkeys in the IFN-treated group is significant at the 5% level by a log rank χ^2 analysis[39]. PFU, plaque forming unit.

neutralized by rabbit anti-human LIF antibodies. The IFN has been partially purified and has an apparent molecular weight of 20,000 (R. Wetzel and M. Ross, unpublished results).

In vivo antiviral activity of LeIF A

The *in vivo* efficacy of IFN needs the presence of macrophages and NK cells, and the *in vivo* mode of action seems to involve stimulation of these cells[33–35]. Thus, it remained possible that the IFN produced by *E. coli* 294/pLeIF A25, though having antiviral activity in the cell culture assay, would not be active in infected animals. Moreover, the *in vivo* antiviral activity of the bacterially produced, non-glycosylated LeIF A might be different from the IFN derived from human 'buffy coat' leukocytes. Therefore the biological activity of bacterially synthesized LeIF A (~2% pure) was compared with buffy coat LeIF (~8% pure) in lethal encephalomyocarditis (EMC) virus infection of squirrel monkeys (Table 2). The control monkeys showed progressive lethargy, loss of balance, flaccid paralysis of the hind limbs and watering of the eyes commencing ~8 h before death. The IFN-treated monkeys showed none of these signs; they remained active at all times and developed no viremia (Table 2). The one monkey in the control group which did not develop viremia by 4 days died latest (164 h post-infection) but showed high titres of virus in the heart and brain on post mortem. The IFN-treated monkeys did not develop antibodies to EMC virus as determined 14 and 21 days after infection. These results demonstrate that the antiviral effects of LeIF preparations in the infected animals can be attributed solely to IFN because the contaminating proteins are quite different in the bacterial and buffy coat preparations. In addition, these results indicate that glycosylation is not required for the *in vivo* antiviral activity of LeIF A. The pharmacokinetics and toxic effects of the natural and bacterially produced LeIFs are currently being compared.

Discussion

With 12S poly(A) mRNA from induced human leukocytes, a full length LeIF A cDNA has been synthesized and cloned in the *E. coli* vector pBR322. This particular clone (pL31) was identified by colony screening using a DNA fragment from a shorter LeIF cDNA clone[18] as hybridization probe. pL31 was also found to hybridize to synthetic deoxyoligonucleotide probes whose sequences were based upon LeIF amino acid sequence data. Several additional types of LeIF recombinant plasmids were identified by hybridization to radiolabelled LeIF cDNA probes. These probes were prepared by using the synthetic deoxyoligonucleotides as primers for the synthesis of cDNA using 12S poly(A) mRNA from induced cells as template. This approach should be generally applicable for the identification of recombinant plasmids obtained through cDNA cloning of rare mRNA species, assuming that some protein sequence information is available.

The 961-base pair DNA sequence of pL31 codes for 188 amino acids, 23 of which are probably cleaved during the process of secretion of mature LeIF from leukocytes. The 188-amino acid leukocyte pre-IF A was expressed in *E. coli* under *trp* promoter control and bacterial extracts were found to be biologically active in tissue culture assay. It is not yet known if the IFN activity is associated with the pre-interferon itself, or if a small proportion of Le-preIF A is processed by *E. coli* to a biologically active form. A plasmid was also constructed which codes for high level expression of the 165 amino acid LeIF A preceded only by a methionine. The present yield of 2.5×10^8 U per litre of culture corresponds to about 600 μg of IFN per litre of culture, assuming an LeIF specific activity of 4×10^8 U mg^{-1} (ref. 9).

This bacterially synthesized LeIF A exhibits the *p*H 2 stability and immunological characteristics of authentic human LeIF, and it protects squirrel monkeys against lethal infection with EMC virus when treatments are initiated prior to viral challenge. Studies are under way to determine if bacterially produced LeIF A has therapeutic, as well as prophylactic, value. Additionally, the *in vivo* activity of LeIF A is being compared with the activities of bacterially produced human fibroblast IFN[15], and several other types of bacterially expressed LeIF.

We thank Dr Doug Fodge and Stephen Rowe for help in establishing the CPE inhibition assay and the *Xenopus* oocyte assays at Genentech and for their valuable contributions during this work; Claire Langdon and Eileen Cunningham for performing the oocyte assays; Parkash Jhurani, Martin Struble and Mark Vasser for deoxyoligonucleotide synthesis and purification; Drs Pat Gray and David Leung for performing some of the hybridization experiments; Jim Fenno and George Prender for assistance in the squirrel monkey experiment. We also thank Dr Norwood Hill and Wadley Institutes of Molecular Medicine for leukocytes and LeIF; Dr J. Beard for reverse transcriptase; Drs Kan Agarwal and Bruce Wallace for helpful suggestions; and Drs Warren Levy and Jack Shively for LeIF protein sequence information prior to publication. A sample of the human LeIF standard and the rabbit anti-human LeIF antibody were obtained from the National Institutes for Allergy and Infectious Diseases, Bethesda, Maryland. This work was performed in accordance with current NIH guidelines.

Received 2 July; accepted 13 August 1980.

1. Isaacs, A. & Lindenmann, J. *Proc. R. Soc.* **B147,** 258–267 (1957).
2. Stewart, W. E. II *The Interferon System* (Springer, New York, 1979).
3. Havell, E. A. *et al. Proc. natn. Acad. Sci. U.S.A.* **74,** 3287–3291 (1977).
4. Cavalieri, R. L., Havell, E. A., Vilcek, J. & Pestka, S. *Proc. natn. Acad. Sci. U.S.A.* **7** 3287–3291 (1977).
5. Gresser, I., Bandu, M. T., Brouty-Boye, D. & Tovey, M. *Nature* **251,** 543–545 (1974).
6. Pestka, S., McInnes, J., Havell, E. & Vilcek, J. *Proc. natn. Acad. Sci. U.S.A.* **72,** 3898–39 (1975).
7. Reynolds, F. H. Jr, Premkumar, E. & Pitha, P. M. *Proc. natn. Acad. Sci. U.S.A.* 4881–4885 (1975).
8. Thang, M. N., Thang, D. C., De Maeyer, E. & Montagnier, L. *Proc. natn. Acad. Sci. U.S* **72,** 3975–3977 (1975).
9. Rubinstein, M. *et al. Proc. natn. Acad. Sci. U.S.A.* **76,** 640–644 (1979).
10. Zoon, K. C., Smith, M. E., Bridgen, P. J., zur Nedden, D. & Anfinsen, C. B. *Proc. n Acad. Sci. U.S.A.* **76,** 5601–5605 (1979).
11. Knight, E., Jr, Hunkapillar, M. W., Korant, B. D., Hardy, R. W. F. & Hood, L. E. *Scie* **207,** 525–526 (1980).
12. Zoon, K. C. *et al. Science* **207,** 527–528 (1980).
13. Levy, W. P., Shively, J., Rubinstein, M., Del Valle, U. & Pestka, S. *Proc. natn. Acad. U.S.A.* (in the press).
14. Taniguchi, T. *et al. Proc. Japan Acad.* **55B,** 464–469 (1979).
15. Goeddel, D. V. *et al. Nucleic Acids Res.* (in the press).
16. Nagata, S. *et al. Nature* **284,** 316–320 (1980).
17. Koeffler, H. P. & Golde, D. W. *Science* **200,** 1153–1154 (1978).
18. Maeda, S. *et al. Proc. natn. Acad. Sci. U.S.A.* (in the press).
19. Wickens, M. P., Buell, G. N. & Schimke, R. T. *J. biol. Chem.* **253,** 2483–2495 (1978).
20. Goeddel, D. V. *et al. Nature* **281,** 544–548 (1979).
21. Chang, A. C. Y. *et al. Nature* **275,** 617–624 (1978).
22. Bolivar, F. *et al. Gene* **2,** 95–113 (1977).
23. Backman, K., Ptashne, M. & Gilbert, W. *Proc. natn. Acad. Sci. U.S.A.* **73,** 4174–4178 (19

24. Birnboim, H. C. & Doly, J. *Nucleic Acids Res.* **7**, 1513–1523 (1979).
25. Kafatos, F. C., Jones, C. W. & Efstratiadis, A. *Nucleic Acids Res.* **7**, 1541–1552 (1979).
26. Taylor, J. M., Illemensee, R. & Summers, S. *Biochim. biophys. Acta* **442**, 324–330 (1976).
27. Grunstein, M. & Hogness, D. S., *Proc. natn. Acad. Sci. U.S.A.* **72**, 3961–3965 (1975).
28. Wallace, R. B., Shaffer, J., Murphy, R. F., Bonner, J. & Itakura, K. *Nucleic Acids Res.* **6**, 3543–3557 (1979).
29. Maxam, A. M. & Gilbert, W. *Meth. Enzym.* **65**, 499–560 (1980).
30. Smith, A. J. H. *Meth. Enzym.* **65**, 560–580 (1980).
31. Mantei, N. *et al. Gene* **10**, 1–10 (1980).
32. Miozzari, G. F. & Yanofsky, C. *J. Bact.* **133**, 1457–1466 (1978).
33. Herberman, R. B. *et al. Cancer Treat. Rep.* **62**, 1893–1896 (1978).
34. Gidlund, M., Orn, A., Wigzell, H., Senik, A. & Gressor, I. *Nature* **273**, 759–761 (1978).
35. Stebbing, N., Dawson, K. M. & Lindley, I. J. D. *Infect. Immun.* **19**, 5–11 (1978).
36. Crea, R., Kraszewski, A., Hirose, T. & Itakura, K. *Proc. natn. Acad. Sci. U.S.A.* **75**, 5765–5769 (1978).
37. Noyes, B., Mevarech, M., Stein, R. & Agarwal, K. L. *Proc. natn. Acad. Sci. U.S.A.* **76**, 1770–1774 (1979).
38. Clewell, D. B. & Helinski, D. R. *Biochemistry* **9**, 4428–4440 (1970).
39. Peto, R. & Pike, M. C. *Biometrics* **29**, 579–584 (1973).

LETTERS

Morphology of the triple QSO PG1115+08

E. K. Hege, J. R. P. Angel, R. J. Weymann & E. N. Hubbard

Steward Observatory, University of Arizona, Tucson, Arizona 85721

Weymann *et al.*[1] have reported that two faint unresolved objects located within 3 arc s of the QSO PG1115+08 have also the same spectra. The emission lines of C III λ1,909 and C IV λ1,549 at a redshift of 1.72 have central wavelengths and profiles that are indistinguishable between the objects. It is inferred that the three objects are likely to be images of the same QSO produced by intervening matter acting as a gravitational lens. Only one other example of such an effect is known, that is the double QSO 0957+56A,B. In this case, the two QSO images are of roughly equal magnitude ($V\sim17$) and separated by 6 arc s. A plate obtained in excellent seeing by Stockton[2] shows an intervening galaxy at $z=0.4$ lying about 1 arc s from one of the QSO images. The present observations were undertaken to search for evidence of an intervening galaxy in PG1115+08, appearing either directly in a deep image, or as a difference in colour between components, and also to look for any structure in the three images. A colour difference could arise, as was the case for the double QSO, if a galaxy is nearly coincident with one of the QSO images.

The Multi-Mirror Telescope (MMT) was used for this study because of its consistently excellent seeing, with images of 1 arc s or better for much of its use in the past year. As part of a study of the short-term motion and stabilization of the six images relative to each other, and of interferometry between different mirrors, we have been using Steward's intensified television camera on he MMT. Having very high gain, provided by a plumbicon elevision camera coupled to a four-stage image intensifier, it is deally suited for this study of the QSO.

While the present controls allow six images of the MMT to be -aligned well enough to resolve the QSO components in the mbined image, as was done when the first spectra of the fainter mponents were obtained, the image quality in good seeing is graded. For the present work we used only one of the six -m mirrors. The camera was located directly at the Casse- in focus, where the plate scale is 3.6 arc s mm^{-1}. The camera put (in standard video format with 30 full frames of 480 lines s) was recorded on video tape, with a frame number code ded to the video signal. Recordings of ~10 min duration were de through filters corresponding approximately to the B, V I photometric bands as detailed in Table 1. The telescope s not guided during these recordings. Short integrated images re obtained off-line by first digitizing the frame and co-adding field of 10×10 arc s from 30 successive frames (intervals). Between 50 and 100 of these short integrations were then further co-added after being laterally translated so the peak of the brightest QSO image was always in the same pixel. The fixed pattern of a digitized blank video field was subtracted from each 1-s video integration before co-adding. In this is like precise guiding at 1-s intervals. The resulting for the three colour bands and also for a broad band with no filter are shown in Fig. 1. For photographic processing, the fourth root of image intensity is mapped on the linear grey scale.

The camera was mounted with the elevation axis vertical. Effects of field rotation of the altazimuth telescope are negligible over the short observing intervals. Figure 2 shows an 8-s integration in the broad band, with no centering, over a wider field including a neighbouring object, with celestial coordinates marked. Table 1 summarizes the magnitude differences and separations that are derived from analysis of the three QSO components, labelled A, B and C after Weymann *et al.*[1]. The uncertainties in the mean intensity ratios expressed in stellar magnitude differences, reflected by statistical scatter in the ratios measured, are commensurate with the uncertainty in the flat-field response (≤5% r.m.s.) of the four stages of fibre-optic coupled Varo image intensifiers.

Because of the low declination and early transit of the object at the time of observation, these images were taken at large zenith distances. Elongation due to atmospheric dispersion can be seen in the expected vertical direction in all three images in the broadband exposure (4,100–8,500 Å), shown in Fig. 1*c* at $\sec z=1.5$. The best resolution with negligible degradation due to dispersion is found in the red exposure, Fig. 1*d*, despite the greater zenith distance, $\sec z=2.5$ at the time of exposure. The image profiles for components B and C show a FWHM of 0.6 arc s, and are round. The image of the bright component A is, however, distinctly not round, being apparently elongated by ~0.5 arc s at a position angle of about 20°. We believe that we can rule out the elongation being an artefact of the optics or data reduction, as the centering was done on the A image, and the B

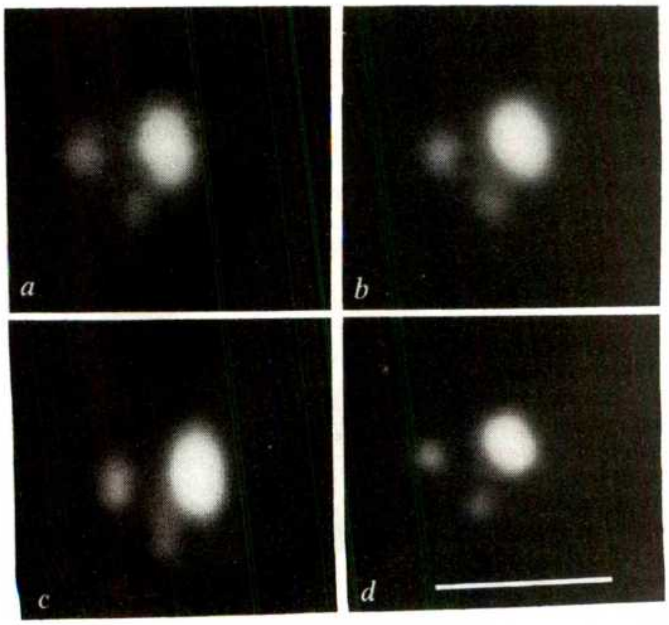

Fig. 1 Single-mirror images of PG1115+08. *a*, Blue; *b*, *V*; *c*, unfiltered; *d*, red. See Table 1 for definition of bandpasses. The images are slightly anamorphic with 13% stretching in the vertical direction. The bar gives the average scale for 5 arc s

0028-0836/80/400416—02$01.00

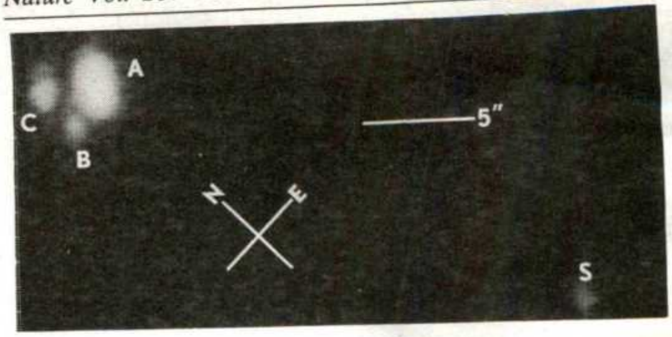

Fig. 2 A wider field image of PG1115+08 in which the celestial coordinates are marked and the components are identified. The object S is at 161°, 23 arc s from component A. The scale and distortion are the same as for Fig. 1.

and C images are indeed round. We have further data at higher magnification which may be able to yield confirmation by the techniques of speckle interferometry.

From the images and analysis above we can make the following observations.

(1) The two companion images each appear like unresolved point sources, seeing limited at the resolution of 0.6 arc s FWHM. The primary image A is not a single stellar object. It would be consistent with two point sources about 0.5 s apart.
(2) The data are consistent with all objects having the same colour, although there is a trend suggesting that C, the further and brighter companion, may be 0.25 mag redder in *B-I* colour.
(3) No other nearby objects brighter than $V \sim 21$ are detected within a radius of 5 arc s from A. If there is an intervening galaxy it must either be fainter than this limit or lying well within 1 arc s of one of the components.

From the observed relative magnitudes and the fluxes measured by R. F. Green and M. Schmidt (personal communication), we can compute fluxes for each of the components. If the slight excess red flux in component C is real and were due to a galaxy similar to the one Young *et al.*[3] measured in 0957+561, we can estimate the galaxy's magnitude by fitting the flux of C by a linear combination of a similar galaxy spectrum and the measured spectrum of A. The best fit is obtained with 15% of A and 17% of such a red galaxy. When the fluxes are recomputed using C = 0.15 A, an estimate of the galaxy flux results which suggests a somewhat fainter and slightly redder galaxy of $m_v \sim$ 20.7. However, we must emphasize that colour differences are not statistically significant, and such a faint galaxy is consistent with but not required by the data.

The research reported here used the Multiple Mirror Telescope Observatory, a joint facility of the University of Arizona and the Smithsonian Institution. We thank J. T. Williams and L. Vaughn for assistance in adapting our instrument to the MMT focal plane and to W. Light for skillful operation of the MMT. We acknowledge use of the image processing facility at Kitt Peak National Observatory in producing the half tone prints. This work was supported in part by the Air Force Geophysical Laboratory.

Table 1 Magnitude differences and separations of the QS components A, B and C

Pair	Magnitude difference* B†	V‡	No filter§	I‖	Separation (arc s)	Angle¶
A–B	2.35	2.34	2.40	2.38	1.9±0.1	263°±5°
A–C	2.00	1.93	1.89	1.78	2.4±0.1	217°±5°
B–C	0.35	0.41	0.51	0.60	2.0±0.1	

* Errors are estimated to be 0.1 mag for A–B and A–C differences, and 0.2 mag for B–C.

† Blue band defined by Hoya B-390 and photocathode cutoff, ~4,100–4,800 Å.

‡ Standard Johnson *V* band.

§ Half-power points with no filter are 4,100–7,600 Å.

‖ Infrared band defined by Schott RG 715 filter and photocathode cutoff, ~7,150–8,500 Å.

¶ Position angles calibrated assuming 161° for position angle of object marked S in Weymann *et al.*[1].

Received 1 August; accepted 27 August 1980.

1. Weymann, R. J. *et al. Nature* **285,** 641–642 (1980).
2. Stockton, A. (in preparation).
3. Young, P., Gunn, J. E., Kirstian, J., Oke, J. B. & Westphal, J. A. *Astrophys. J.* (in the press).

Whistler mode wave packets in the Earth's foreshock region

M. Hoppe & C.T. Russell

Institute of Geophysics and Planetary Physics, University of California, Los Angeles, California 90024

The definit identification of the basic modes of the variety of electromagnetic waves common in the interplanetary medium upstream of the Earth's bow shock has been difficult because of the Doppl shifting which results from their attempts to propagate in the personic solar wind. We have used magnetometer data from dual ISEE-1 and -2 spacecraft, taken when the spacecraft re separated by a few hundred kilometres, to measure the parent velocities of a subset of these waves. This has allowed e first determination of wave phase velocities, rest-frame fruencies, wavelengths, intrinsic polarizations and thus ve modes. We have now applied this technique to the class f upstream phenomena designated the discrete wave pac. These are isolated fairly monochromatic wave packet wi quencies ~0.4 Hz in the spacecraft frame which rotate i th t-handed sense about the magnetic field direction o ed in the spacecraft frame. Our studies of the time dela en the observation of such wave packets at the tw raft demonstrate conclusively that these waves are, in fact, right-handed polarized wav requencies several times greater than the proton ncy, attempting to propagate upstream against the s but being carried towards the Earth by the solar wind fl

resolution of the ambiguity inherent in the study of wa gating in a moving medium requires two point measu . We have approached this problem by using data s the matching UCLA/ISEE magnetometers to attack t lem, using them to time the delay (Δt) between arance of a wavefront at first one, then the second, spa The wave velocity in the spacecraft frame ($v_{s/c}$) can then by dividing the distance travelled by the wave as ates between the spacecraft by the time taken to tra ance. The distance itself is the projection of the spa aration vector (**S**) in the direction of propagation (pparent velocity is thus

$$v_{s/c} = \frac{\mathbf{S}\cdot\hat{\mathbf{k}}}{\Delta t}$$

tion vector is a well determined quantity (±1 k m ISEE mission ephemeris tapes. The direction gation can be determined through eigenval he magnetic field variance matrix[1]. The dete then allows $v_{s/c}$ to be calculated. The velocity in the intrinsic wave phase velocity (onent due to solar wind convection ection of the solar wind velocity (ropagation

$$v_{s/c} = v_{ph} + \mathbf{V}_{sw}\cdot\hat{\mathbf{k}}$$

© 1980 M

Thus, once the solar wind velocity is known, the intrinsic wave phase velocity can be found by substituting the value of $v_{s/c}$ determined from equation (1) into equation (2) and solving for v_{ph}.

We applied this technique to a set of discrete wave packets observed by the ISEE-1 and -2 spacecraft on day 307 of 1977. The general characteristics of this variety of upstream wave were established by Russell *et al.*[2] in a comprehensive study based on single-spacecraft measurements, which we briefly summarize. The wave packets, which are most often found embedded in trains of irregular lower frequency (0.05 Hz) waves, typically grew rapidly in time and decayed more slowly, generally lasting two or three cycles. Wave packets were observed with frequencies throughout the interval chosen for study, 0.14–1.4 Hz with an average frequency of 0.4 Hz, and were left-hand polarized in 90% of the cases. From measurements of wave ellipticity, Russell *et al.* hypothesized that these waves were intrinsically right-hand polarized whistler mode waves of frequencies several times the proton gyrofrequency. Cold plasma theory predicts that such waves should have phase velocities of ~100 km s^{-1}, which is significantly less than the typical solar wind velocity. Thus, if these waves were, as hypothesized, attempting to propagate upstream against the solar wind flow, they would be swept backwards over the spacecraft, resulting in the observed reversal of polarization. We present here direct experimental verification of this hypothesis.

The time period studied was 0200–0300 UT of day 307 of 1977 (Fig. 1). At this time, the spacecraft were in the interplanetary medium, inbound on the dawn side of the Earth at 1030 LT, several Earth radii (R_e) upstream of the final bow shock crossing which occurred at 0600 UT. The interplanetary magnetic field was essentially radial during this time period and the angle between the field and the nominal shock normal was 25°. Bursts of quasiparallel shock structure were encountered hroughout the inbound portion of this orbit, and the studied nterval is characterized by strong irregular magnetic field disrbances with time scales of 30 s, and by the presence of diffuse prathermal ions (D. D. Sentman, personal communicat). agnetic field data used in this study were high-resolu easurements made by the dual UCLA magnetomet nboard ISEE-1 and -2. Data acquisition rate at this time w ctors per s. Solar wind speeds were estimated using data fr e University of Iowa's ISEE LEPEDEA plama analysers.

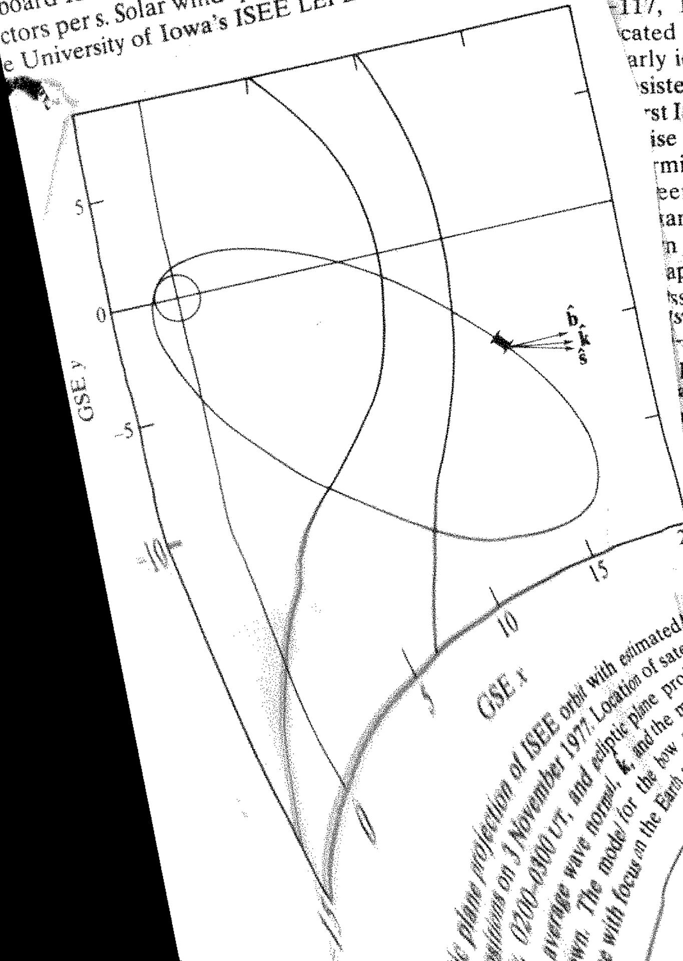

1 Ecliptic plane projection of ISEE orbit with estimated spacecraft positions on 3 November 1977. Location of satellites during od of study, 0200–0300 UT, and ecliptic plane projection of ld, b̂, the average wave normal, k̂, and the model bow shock also shown. The model for the bow shock is an ellipse with focus on the Earth and ellipticity 0.8

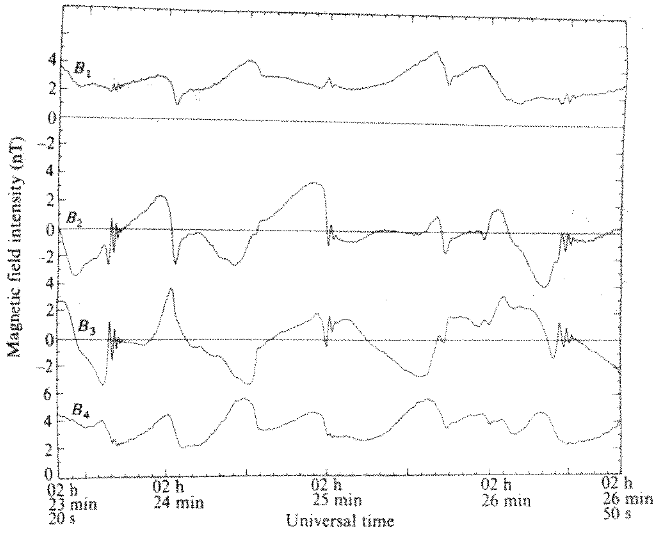

Fig. 2 The three vector components, in GSE coordinates, and the total magnitude of the magnetic field measured by the ISEE-2 magnetometer as the spacecraft was inbound on day 307 of 1977. The spacecraft was at a radial distance of 16.6 R_e, upstream of the bow shock at 1030 LT.

Three typical wave packets are shown in Fig. 2. Note that the amplitude of these waves is a large fraction of the background field. As is the usual case, the packets (seen here beginning 02 h 23 min 39 s, 02 h 24 min 59 s and 02 h 26 min 25 s) are embedded in a train of lower-frequency waves and seen to be intimately related to the low-frequency wave structure, occurring when the field magnitude suddenly returns to low values after a more gradual increase. All the wave packets seen in the studied interval begin at the foot of sharp drops in the field magnitude (B_T), although not all such drops are accompanied by wave packets (for example, sharp decrease in B_T at 02 h 24 min 05 s). The field structure is thus apparently a necessary but not sufficient condition for the development of the packets on this day.

The profiles of the packet which begins at 02 h 23 min 39 s, as seen at the two separate spacecraft, are presented in higher resolution in Fig. 3. The spacecraft separation at this time was −117, 180 and −107 km (GSE coordinates), with ISEE-2 cated upstream and to the west of ISEE-1. The signals are arly identical (the correlation is 0.92) except for a small but sistent time delay between the appearance of the wavefront st ISEE-2 and then, 0.5 s later, downstream at ISEE-1. The ise time delay characteristic of the wave packets was rmined from studies of the behaviour of the correlation een signals from the two spacecraft as a function of lag time, ample of which, for the wave packet shown in Fig. 3*a*, is n in Fig. 3*b*. Correlation coefficients averaged over inter appropriate to the signal duration were calculated for ssive 0.25-s lags, consistent with the magnetometer's sition rate of 4 vectors per s. The correlation averaged over duration of the wave packet peaks at 0.5 s, with secon peaks appearing at 1.5-s intervals, consistent with the ated wave frequency. The time delay expected for a static ure simply convecting with the solar wind flow would have .3 s. The time delay can be determined to within ~ ± 0.1 s uch plots, which at this spacecraft separation allows the ion only of those wave phase velocities ≥70 km s^{-1}. Of wave packets observed in the hour 0200–0300 on day were characterized by velocities too small for us to from the solar wind flow and the measurements on the g 11 cases are presented here.

nination of the second element of the analysis, the velled by the wavefront as it propagates between the equires determination of the direction of propaga ave. This direction can be determined within an

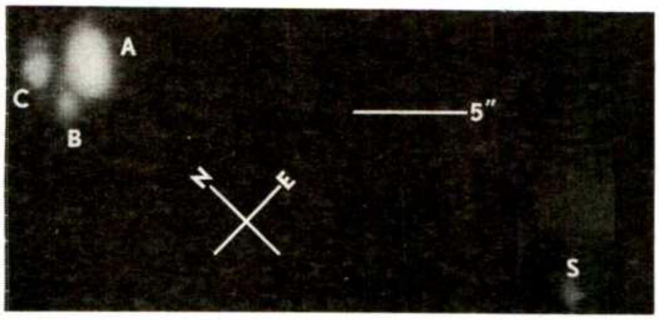

Fig. 2 A wider field image of PG1115+08 in which the celestial coordinates are marked and the components are identified. The object S is at 161°, 23 arc s from component A. The scale and distortion are the same as for Fig. 1.

and C images are indeed round. We have further data at higher magnification which may be able to yield confirmation by the techniques of speckle interferometry.

From the images and analysis above we can make the following observations.

(1) The two companion images each appear like unresolved point sources, seeing limited at the resolution of 0.6 arc s FWHM. The primary image A is not a single stellar object. It would be consistent with two point sources about 0.5 s apart.

(2) The data are consistent with all objects having the same colour, although there is a trend suggesting that C, the further and brighter companion, may be 0.25 mag redder in *B-I* colour.

(3) No other nearby objects brighter than $V \sim 21$ are detected within a radius of 5 arc s from A. If there is an intervening galaxy it must either be fainter than this limit or lying well within 1 arc s of one of the components.

From the observed relative magnitudes and the fluxes measured by R. F. Green and M. Schmidt (personal communication), we can compute fluxes for each of the components. If the slight excess red flux in component C is real and were due to a galaxy similar to the one Young *et al.*[3] measured in 0957+561, we can estimate the galaxy's magnitude by fitting the flux of C by a linear combination of a similar galaxy spectrum and the measured spectrum of A. The best fit is obtained with 15% of A and 17% of such a red galaxy. When the fluxes are recomputed using C = 0.15 A, an estimate of the galaxy flux results which suggests a somewhat fainter and slightly redder galaxy of $m_v \sim 20.7$. However, we must emphasize that colour differences are not statistically significant, and such a faint galaxy is consistent with but not required by the data.

The research reported here used the Multiple Mirror Telescope Observatory, a joint facility of the University of Arizona and the Smithsonian Institution. We thank J. T. Williams and L. Vaughn for assistance in adapting our instrument to the MMT focal plane and to W. Light for skillful operation of the MMT. We acknowledge use of the image processing facility at Kitt Peak National Observatory in producing the half tone prints. This work was supported in part by the Air Force Geophysical Laboratory.

Table 1 Magnitude differences and separations of the QSO components A, B and C

Pair	Magnitude difference*				Separation (arc s)	Angle¶
	B†	*V*‡	No filter§	*I*‖		
A–B	2.35	2.34	2.40	2.38	1.9 ± 0.1	263° ± 5°
A–C	2.00	1.93	1.89	1.78	2.4 ± 0.1	317° ± 5°
B–C	0.35	0.41	0.51	0.60	2.0 ± 0.1	

* Errors are estimated to be 0.1 mag for A–B and A–C differences, and 0.2 mag for B–C.

† Blue band defined by Hoya B-390 and photocathode cutoff, ~4,100–4,800 Å.

‡ Standard Johnson *V* band.

§ Half-power points with no filter are 4,100–7,600 Å.

‖ Infrared band defined by Schott RG 715 filter and photocathode cutoff, ~7,150–8,500 Å.

¶ Position angles calibrated assuming 161° for position angle of object marked S in Weymann *et al.*[1].

Received 1 August; accepted 27 August 1980.

1. Weymann, R. J. *et al. Nature* **285,** 641–642 (1980).
2. Stockton, A. (in preparation).
3. Young, P., Gunn, J. E., Kirstian, J., Oke, J. B. & Westphal, J. A. *Astrophys. J.* (in the press).

Whistler mode wave packets in the Earth's foreshock region

M. Hoppe & C. T. Russell

Institute of Geophysics and Planetary Physics, University of California, Los Angeles, California 90024

The definite identification of the basic modes of the variety of electromagnetic waves common in the interplanetary medium upstream of the Earth's bow shock has been difficult because of the Doppler shifting which results from their attempts to propagate in the supersonic solar wind. We have used magnetometer data from the dual ISEE-1 and -2 spacecraft, taken when the spacecraft were separated by a few hundred kilometres, to measure the apparent velocities of a subset of these waves. This has allowed the first determination of wave phase velocities, rest-frame frequencies, wavelengths, intrinsic polarizations and thus wave modes. We have now applied this technique to the class of upstream phenomena designated the discrete wave packets. These are isolated fairly monochromatic wave packets with frequencies ~0.4 Hz in the spacecraft frame which rotate in the left-handed sense about the magnetic field direction as observed in the spacecraft frame. Our studies of the time delay between the observation of such wave packets at the two spacecraft demonstrate conclusively that in the plasma rest frame these waves are, in fact, right-handed polarized waves with frequencies several times greater than the proton gyrofrequency, attempting to propagate upstream against the solar wind, but being carried towards the Earth by the solar wind flow.

The resolution of the ambiguity inherent in the study of waves propagating in a moving medium requires two point measurements. We have approached this problem by using data sets from the matching UCLA/ISEE magnetometers to attack this problem, using them to time the delay (Δt) between the appearance of a wavefront at first one, then the second, spacecraft. The wave velocity in the spacecraft frame ($v_{s/c}$) can then be found by dividing the distance travelled by the wave as it propagates between the spacecraft by the time taken to travel this distance. The distance itself is the projection of the spacecraft separation vector (**S**) in the direction of propagation ($\hat{\mathbf{k}}$), and the apparent velocity is thus

$$v_{s/c} = \frac{\mathbf{S} \cdot \hat{\mathbf{k}}}{\Delta t} \tag{1}$$

The separation vector is a well determined quantity (±1 km) available from ISEE mission ephemeris tapes. The direction of wave propagation can be determined through eigenvalue analysis of the magnetic field variance matrix[1]. The determination of Δt then allows $v_{s/c}$ to be calculated. The velocity is a combination of the intrinsic wave phase velocity (v_{ph}) and an additional component due to solar wind convection, which is equal to the projection of the solar wind velocity ($\mathbf{V}_{sw}$) in the direction of wave propagation

$$v_{s/c} = v_{ph} + \mathbf{V}_{sw} \cdot \hat{\mathbf{k}} \tag{2}$$

Thus, once the solar wind velocity is known, the intrinsic wave phase velocity can be found by substituting the value of $v_{s/c}$ determined from equation (1) into equation (2) and solving for v_{ph}.

We applied this technique to a set of discrete wave packets observed by the ISEE-1 and -2 spacecraft on day 307 of 1977. The general characteristics of this variety of upstream wave were established by Russell *et al.*[2] in a comprehensive study based on single-spacecraft measurements, which we briefly summarize. The wave packets, which are most often found embedded in trains of irregular lower frequency (0.05 Hz) waves, typically grew rapidly in time and decayed more slowly, generally lasting two or three cycles. Wave packets were observed with frequencies throughout the interval chosen for study, 0.14–1.4 Hz with an average frequency of 0.4 Hz, and were left-hand polarized in 90% of the cases. From measurements of wave ellipticity, Russell *et al.* hypothesized that these waves were intrinsically right-hand polarized whistler mode waves of frequencies several times the proton gyrofrequency. Cold plasma theory predicts that such waves should have phase velocities of ~100 km s^{-1}, which is significantly less than the typical solar wind velocity. Thus, if these waves were, as hypothesized, attempting to propagate upstream against the solar wind flow, they would be swept backwards over the spacecraft, resulting in the observed reversal of polarization. We present here direct experimental verification of this hypothesis.

The time period studied was 0200–0300 UT of day 307 of 1977 (Fig. 1). At this time, the spacecraft were in the interplanetary medium, inbound on the dawn side of the Earth at 1030 LT, several Earth radii (R_e) upstream of the final bow shock crossing which occurred at 0600 UT. The interplanetary magnetic field was essentially radial during this time period and the angle between the field and the nominal shock normal was 25°. Bursts of quasiparallel shock structure were encountered throughout the inbound portion of this orbit, and the studied interval is characterized by strong irregular magnetic field disturbances with time scales of 30 s, and by the presence of diffuse suprathermal ions (D. D. Sentman, personal communication). Magnetic field data used in this study were high-resolution measurements made by the dual UCLA magnetometers[3] onboard ISEE-1 and -2. Data acquisition rate at this time was 4 vectors per s. Solar wind speeds were estimated using data from the University of Iowa's ISEE LEPEDEA plama analysers.

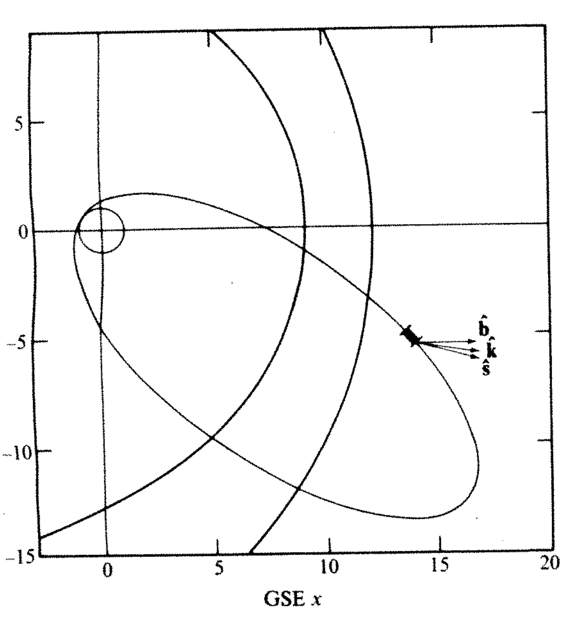

Fig. 1 Ecliptic plane projection of ISEE orbit with estimated shock and magnetopause positions on 3 November 1977. Location of satellites during the period of study, 0200–0300 UT, and ecliptic plane projection of the magnetic field, b̂, the average wave normal, k̂, and the model bow shock normal, ŝ, are also shown. The model for the bow shock used in this calculation is an ellipse with focus on the Earth and ellipticity 0.8.

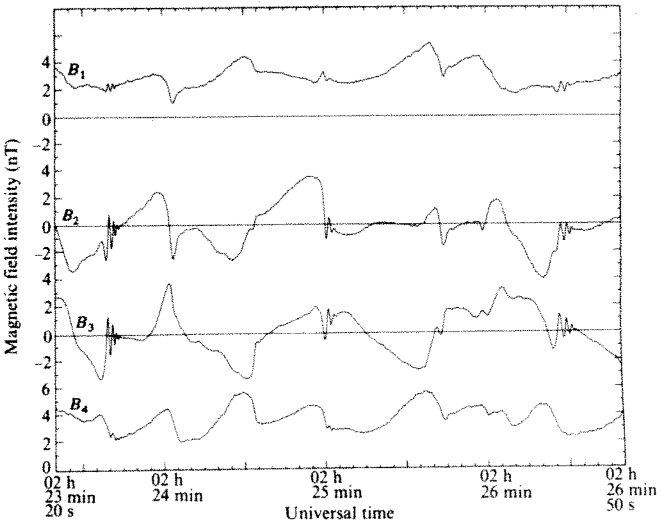

Fig. 2 The three vector components, in GSE coordinates, and the total magnitude of the magnetic field measured by the ISEE-2 magnetometer as the spacecraft was inbound on day 307 of 1977. The spacecraft was at a radial distance of 16.6 R_e, upstream of the bow shock at 1030 LT.

Three typical wave packets are shown in Fig. 2. Note that the amplitude of these waves is a large fraction of the background field. As is the usual case, the packets (seen here beginning 02 h 23 min 39 s, 02 h 24 min 59 s and 02 h 26 min 25 s) are embedded in a train of lower-frequency waves and seen to be intimately related to the low-frequency wave structure, occurring when the field magnitude suddenly returns to low values after a more gradual increase. All the wave packets seen in the studied interval begin at the foot of sharp drops in the field magnitude (B_T), although not all such drops are accompanied by wave packets (for example, sharp decrease in B_T at 02 h 24 min 05 s). The field structure is thus apparently a necessary but not sufficient condition for the development of the packets on this day.

The profiles of the packet which begins at 02 h 23 min 39 s, as seen at the two separate spacecraft, are presented in higher resolution in Fig. 3. The spacecraft separation at this time was −117, 180 and −107 km (GSE coordinates), with ISEE-2 located upstream and to the west of ISEE-1. The signals are nearly identical (the correlation is 0.92) except for a small but consistent time delay between the appearance of the wavefront at first ISEE-2 and then, 0.5 s later, downstream at ISEE-1. The precise time delay characteristic of the wave packets was determined from studies of the behaviour of the correlation between signals from the two spacecraft as a function of lag time, an example of which, for the wave packet shown in Fig. 3*a*, is shown in Fig. 3*b*. Correlation coefficients averaged over intervals appropriate to the signal duration were calculated for successive 0.25-s lags, consistent with the magnetometer's acquisition rate of 4 vectors per s. The correlation averaged over the 6-s duration of the wave packet peaks at 0.5 s, with secondary peaks appearing at 1.5-s intervals, consistent with the estimated wave frequency. The time delay expected for a static structure simply convecting with the solar wind flow would have been 0.3 s. The time delay can be determined to within ~±0.1 s using such plots, which at this spacecraft separation allows the resolution only of those wave phase velocities ≳70 km s^{-1}. Of the 24 wave packets observed in the hour 0200–0300 on day 307, 13 were characterized by velocities too small for us to resolve from the solar wind flow and the measurements on the remaining 11 cases are presented here.

Determination of the second element of the analysis, the distance travelled by the wavefront as it propagates between the spacecraft, requires determination of the direction of propagation of the wave. This direction can be determined within an

180° ambiguity by minimum variance analysis. Values computed by this technique independently from data from each of the spacecraft were in good agreement, and our analysis is based on averaged values. The time evolution of the field of the packet of Fig. 3*a* is shown in Fig. 4, where the variation is presented in the principal axes system. The field variation in the plane of the wavefront is plotted on the left. Note that the field rotates in the left-hand sense about the ambient field direction, which is into the paper in this case. As seen here, the wave packets generally exhibit a nearly perfectly circular polarization. This same sense of rotation, left handed in the spacecraft frame, has been observed in all cases. The planarity of the wave is documented by the linearity of the right-hand plot, which shows the field variation in the plane formed by the direction of maximum variance and the wave normal. The nearly perfect plane circular polarization of this packet is typical and well justifies our identification of the direction of wave propagation with the minimum variance direction, which requires such

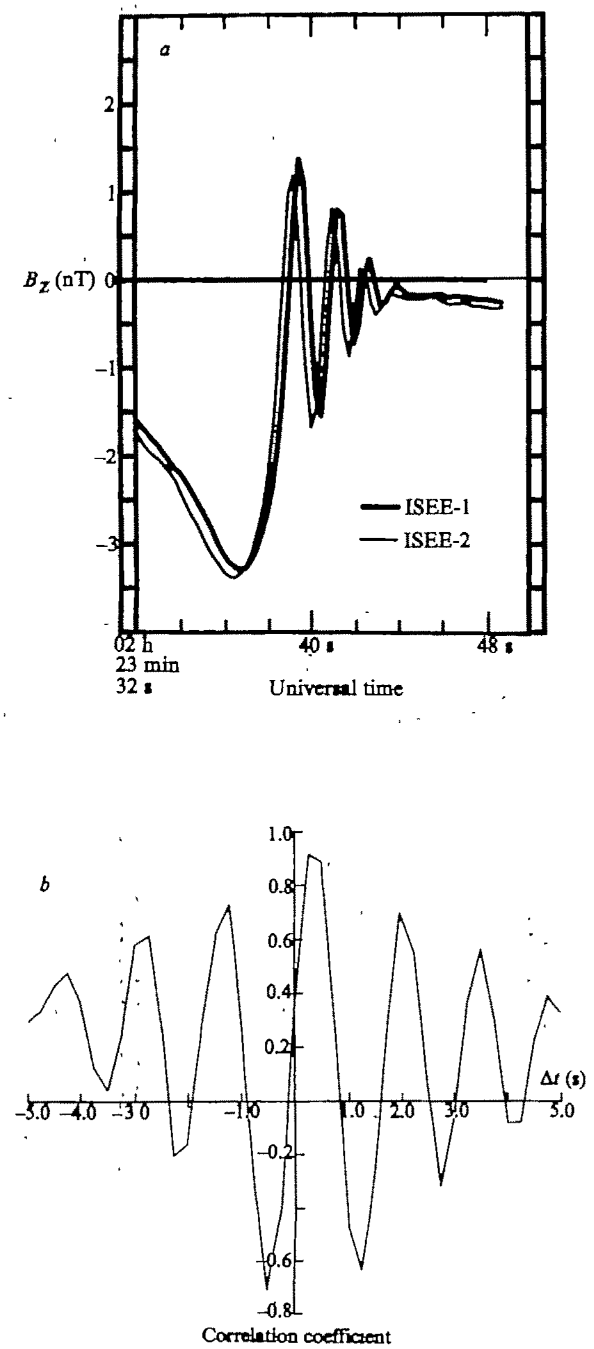

Fig. 3 *a*, Overlay of wave-packet signatures in the *z* component of the field of the two spacecraft for wave packet beginning at 02 h 23 min 39 s. *b*, The weighted correlation coefficient of signals from the two spacecraft as a function of imposed successive 0.25-s lag times (Δt). The correlation coefficient is the average lagged product of the times series on the two spacecraft for each of the three vector components weighted by the variance in that component. The correlation coefficients for each of the three components were quite similar. The correlation has been averaged over the 6-s duration of the 02 h 23 min 39 s wave packet. Positive Δt corresponds to signals which appeared first at ISEE-2.

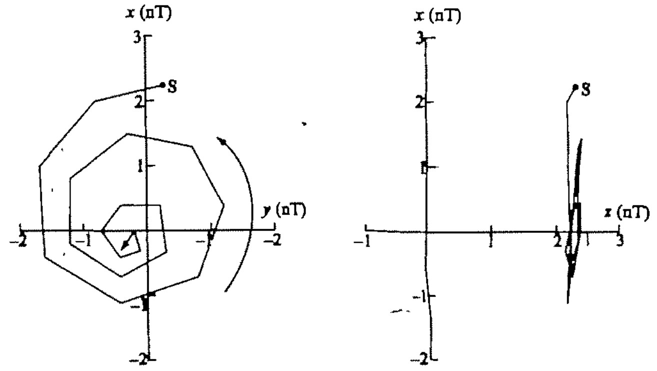

Fig. 4 The time evolution of the field vector of the 02 h 23 min 39 s packet, beginning at point S. The *x*, *y* and *z* axes correspond, respectively, to the directions of the maximum, intermediate and minimum variance eigenvectors

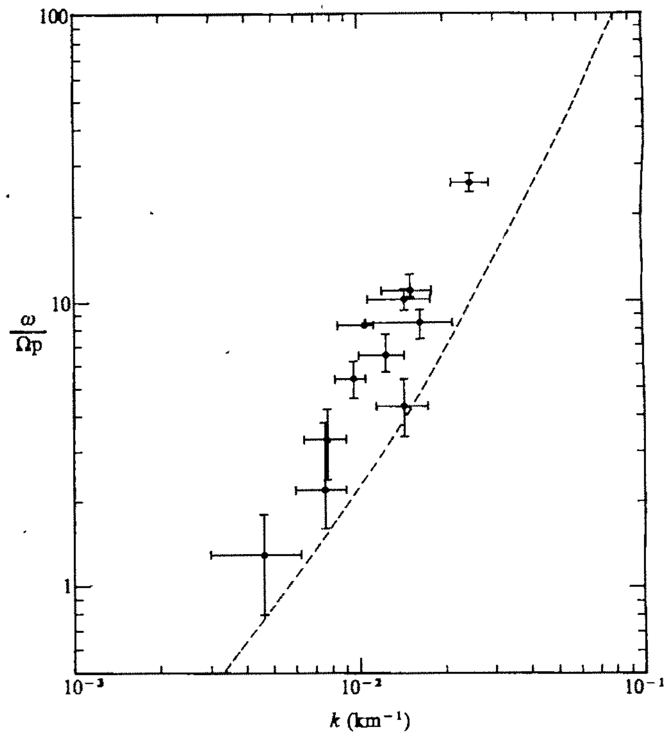

Fig. 5 Experimentally determined rest-frame frequencies, normalized to the local proton gyrofrequency, are plotted against wave number. Error bars represent uncertainties due to an estimated 0 1-s imprecision in Δt, which is the most significant source of error during this time interval. Also plotted (dashed line) is the relation expected from the cold plasma dispersion relation for a solar wind density of 3 cm^{-1}, magnetic field magnitude of 3 nT and propagation angle of 25°, average values typical of this time period

polarization for its validity. The direction of minimum variance is well determined in all cases. Typical ratios of the intermediate to minimum eigenvalue are ~50, indicating that minimum variance directions are generally determined to within at least 1°. This direction tends to lie close to that of the ambient magnetic field with the typical angle between $\hat{\mathbf{k}}$ and **B** being ~25°.

From measurements of the wave frequency in the spacecraft frame (f_0) together with the wave velocity as determined above, one can also calculate the wavelength (λ): $\lambda = v_{s/c}/f_0$. The wavelength divided by the phase velocity then yields the plasma frame frequency (f_r): $f_r = \lambda/v_{ph}$. The results of such determinations for the wave packets studied here are presented in Fig. 5, where the angular frequency, ω, has been normalized to the local proton gyrofrequency, Ω_p, and plotted as a function of wave number k.

For comparison, we have presented the cold plasma dispersion relation for estimated ambient solar wind parameters and the 25° propagation angle typical of these packets, plotted as the dashed line in Fig. 5. The general trend of the data is quite consistent with the theoretical prediction although experimentally determined values tend to lie on the high side of the curve.

Theoretical approaches to these waves have been suggested previously by Wu[4], Hasegawa[5] and Gul'yel'mi and Bondarenko[6] who, respectively, invoke wave-echo phenomena, a two-stream instability between the solar wind and magnetosheath plasma and MHD soliton formation. The extreme turbulence occurring both in the magnetosheath and in the foreshock region during quasiparallel shock conditions as seen here argues against the feasibility of a plasma echo mechanism causing the waves. The present results are also inconsistent with both modes derived from the two-stream instability, which are a right-handed mode with $v_0 \gg \mathbf{V}_{sw}$ and a left-handed mode propagating downstream. The agreement between the predictions of MHD soliton theory and wave packet characteristics found by Gul'yel'mi and Bondarenko is not confirmed by the present work.

In conclusion, the measurements present a consistent general picture of whistler mode plasma waves attempting to propagate upstream against the solar wind flow with phase velocities of the order of several times the Alfvén speed and wavelengths of the order of several hundreds of kilometres. Because the waves are being blown backwards over the spacecraft, their frequencies have been shifted from values several times the proton gyrofrequency in the rest frame to higher values in the spacecraft frame, and their intrinsic right-hand polarizations have become apparent left-hand polarizations at the spacecraft. The wave packets in this interval occur coincidentally with a sharp drop in the field strength which follows a more gradual rise in magnitude. As these structures are being blown downstream, the discrete wave packets are, in fact, on the upstream side of these lower-frequency structures, much like the whistler waves often seen at the foot of the bow shock[7,8]. Thus, the low-frequency structures shown in Fig. 2 seem to be little shocks attempting to stand in the solar wind flow but being too weak and being blown backwards towards the Earth.

This work was supported by the National Aeronautics and Space Administration through grants NAS 5-25772 and NAS 5-20094 through the University of Iowa subcontract no. R 44855. We thank L. A. Frank and D. D. Sentman for the use of the ISEE LEPEDEA data from which the solar wind parameters were derived and the presence of backstreaming suprathermal ions during the period was verified.

Received 18 April; accepted 18 July 1980.

1. Sonnerup, B. U. O. & Cahill, L. J. *J. geophys. Res.* **72**, 171–183 (1967).
2. Russell, C. T., Childers, D. D. & Coleman, P. J. Jr *J. geophys. Res.* **76**, 845–861 (1971).
3. Russell, C. T. *IEEE Trans. Geosci. Electron.* **GE-16**, 239–242 (1978).
4. Wu, C. S. *J. geophys. Res.* **77**, 575–587 (1972).
5. Hasegawa, A. *J. geophys. Res.* **77**, 84–90 (1972).
6. Gul'yel'mi, A. V. & Bondarenko, N. B. *Geomag. Aeronaut.* **18**, 284–286 (1978).
7. Fairfield, D. H. *J. geophys. Res.* **79**, 1368–1378 (1974).
8. Greenstadt, E. W. *J. geophys. Res.* **80**, 502–514 (1975).

Kinetics of void-lattice formation in metals

K. Krishan

Reactor Research Centre, Kalpakkam 603 102, Tamil Nadu, India

Since the discovery[1] that voids form in neutron-irradiated stainless steel and that these could form into a three-dimensional lattice[2], void-lattices have been observed in some b.c.c. metals[2,3] such as Mo, W, Nb, and Ta, and in f.c.c. metals[4,5] such as Al and Ni. The irradiation conditions in which a void-lattice is formed are not understood[6], but several explanations[7–11] of the stability of the void-lattice have been given on the basis of void–void elastic interaction[9–11]. Our present approach regards the void-lattice formation as a phase transition associated with the bifurcation of the homogeneous steady state in the mean field theory[12,13]. The void-lattice is an interesting example of a class of phase transitions manifested by open, nonequilibrium, dissipative structures and have an inherent capability of self-organization. Although void-lattice formation has already been examined on this basis[14,15], we show here that the transition is induced in certain microstructural conditions where vacancy loop dynamics has an important role. The theory generally agrees with experimental features and predicts that another spatially dependent state exists which can influence irradiation-induced phenomena that have important technological implications for the development of fast reactor materials.

In the homogeneous rate theory[12,13] the steady-state vacancy and interstitial concentrations C_V and C_I respectively, jointly represented by a column matrix $\mathbf{C}_P$, are stable against any spatial deviations $\delta\mathbf{C}_P$ produced due to the fluctuations within the grain of size d. The stability[16] is due to the presence of sinks like voids, vacancy loops, interstitial loops and network dislocations whose sink densities are represented by ρ_s, ρ_v, ρ_i and ρ_d respectively. If D_v and D_I are vacancy and interstitial diffusion constants, Z_I the bias, $\beta_V = D_V(\rho_s + \rho_d + \rho_i + \rho_v)$, $\beta_I = D_I\rho_s + Z_I D_I(\rho_d + \rho_i + \rho_v)$ and α the recombination parameter, then the deviations $\delta\mathbf{C}_P$ in a linear approximation close to the steady state are governed by the equation

$$\delta\mathbf{C}_P = (\mathbf{A}_{11} + \mathbf{D}\nabla^2)\delta\mathbf{C}_P \tag{1}$$

where

$$\mathbf{A}_{11} = \begin{pmatrix} -\beta_V - \alpha C_I & -\alpha C_V \\ -\alpha C_I & -\beta_I - \alpha C_V \end{pmatrix} \tag{2}$$

The matrix **D** is diagonal with elements D_V and D_I and the Laplace operator allows for point defect diffusion and the possibility of forming spatially ordered dissipative structures[17]. Using bifurcation analysis we choose a convenient orthogonal basis in terms of which the time and space evolution of any arbitrary deviation $\delta\mathbf{C}_P$ can be studied. We also examine how the basis functions themselves evolve and, therefore, attempt solutions of the type

$$\delta\mathbf{C}_P = \mathbf{f}_P e^{\omega_M t} \sin\left(\frac{m_1\pi x}{d}\right) \sin\left(\frac{m_2\pi y}{d}\right) \sin\left(\frac{m_3\pi z}{d}\right) \tag{3}$$

where m_1, m_2, m_3 are integers $\neq 0$, $\mathbf{f}_P$ is a column matrix for the amplitudes and $\nabla^2\delta C_V = M^2\delta C_V$ with $M^2 = (\pi^2/d^2)(m_1^2 + m_2^2 + m_3^2)$. The boundary condition $\delta\mathbf{C}_P = 0$ at the grain surface has been imposed consistent with the grain boundary being an effective sink. Further, after the bifurcation due to the spatial dependences, flows or currents $j_V = -D_V\nabla\delta C_V$ and $j_I = -D_I\nabla\delta C_I$ in the point defects will develop. These flows must be consistent with the symmetry of the host lattice. This amounts to imposing additional constraints on the indices m_1, m_2 and m_3. If we now substitute equation (3) into (1) we obtain values of the frequencies ω_M which satisfy equation (1) and find that $\omega_M < 0$

0028–0836/80/400420—02$01.00

for all values of sink densities ρ. This means that in this model the original homogeneous state is stable and any arbitrary deviations will decay to zero. In other words no soft mode $\omega_M = 0$ can arise because for no positive value of M^2 is the condition

$$\det|\mathbf{A}_{11} - DM^2| = 0 \qquad (4)$$

satisfied.

In the above analysis the response of the extended defect structure to changes in $\mathbf{C}_P$ has been ignored. This response is important and provides the additional interaction or coupling which leads to the bifurcation of the homogeneous state. This coupling arises mainly through the terms $\beta_V C_V$ and $\beta_I C_I$ which give the rate of loss of point defects to sinks. These terms are nonlinear when one includes the response of the microstructure as β_V and β_I are related through the sink densities to the sizes and concentrations of the extended defects. Let the column matrix $\delta\mathbf{C}_e$ represent the deviations δr_s in the void radius r_s and δN_v in the vacancy loop concentration N_v. These deviations will be functions of the spatial positions of the voids and vacancy loops. The contribution of interstitial loops can be included along with network dislocations under a suitable approximation. The equation of motion within the framework of the linear analysis is given by

$$\frac{d}{dt}\begin{pmatrix}\delta\mathbf{C}_P\\ \delta\mathbf{C}_e\end{pmatrix} = \left\{\begin{pmatrix}\mathbf{A}_{11} & \mathbf{A}_{12}\\ \mathbf{A}_{21} & \mathbf{A}_{22}\end{pmatrix} + \begin{pmatrix}\mathbf{D}\nabla^2 & 0\\ 0 & 0\end{pmatrix}\right\}\begin{pmatrix}\delta\mathbf{C}_P\\ \delta\mathbf{C}_e\end{pmatrix} \qquad (5)$$

where from the BEK theory[13], $\mathbf{A}_{22}$ is diagonal with elements $\dot{r}_v/\bar{r}_v$ and $-\dot{r}_s/r_s$; $\bar{r}_v$ is the initial radius of the vacancy loops. The coupling matrices $\mathbf{A}_{12}$ and $\mathbf{A}_{21}$ are functions of ρ_v and ρ_s. Following our previous arguments we again attempt solutions of the type given by equation (3) for $\delta\mathbf{C}_P$ and similar space dependent solutions for $\delta\mathbf{C}_e$ where the amplitude term $\mathbf{f}_P$ will now be replaced by a column matrix $\mathbf{f}_e$ for the extended defects. It is convenient, however, to partition the 4×4 matrix in equation (5) into two separate equations, one for $\delta\mathbf{C}_P$ and the other for $\delta\mathbf{C}_e$ using the standard partitioning techniques. Examining as before the possibility of a soft mode $\omega_M = 0$ we obtain now in place of equation (4) the condition

$$\det|\mathbf{A}_{11} - \mathbf{A}_{12}\mathbf{A}_{22}^{-1}\mathbf{A}_{21} - \mathbf{D}M^2| = 0 \qquad (6)$$

This equation for certain values of ρ_v and ρ_s, which are the critical values for the transition, has solutions for positive values $M^2 = 3\pi^2/d^2$. This is the first bifurcation and represents the onset of the void-lattice formation.

Several experimentally observed features of the void-lattice formation emerge from this analysis. Figure 1 shows a phase diagram in the ρ_v, ρ_s space with the critical values of the densities obtained from equation (6) showing where the first bifurcation occurs. Whether the system reaches critical density values depends on how the system evolves in time and this has to be obtained by a solution of the BEK equations[13]. After the first bifurcation secondary bifurcations take place together with the ordering of the void-lattice. This introduces coarsening in the void distribution with correlations in void positions gradually emerging as is seen experimentally. The analysis of secondary bifurcations is difficult because of the stability factors coupled with the complex time and spatial dependence of the states involved. Such an analysis may have to be done by computer simulation techniques as in the case of simpler models which show similar self-organization behaviour[17]. Energy considerations as discussed by Malen and Bullough[9] probably influence the final stages of void-lattice formation leading to the high stability of such a lattice. However, preliminary results show that as a function of ρ_v the parameter M^2 saturates at a value of about $10^{15}\ \mathrm{m}^{-2}$ which, for a given grain diameter $d \sim 10^{-5}$ m, gives $m_1 \simeq m_2 \simeq m_3 \simeq 100$, implying a void-lattice spacing of about 1,000 Å in reasonable agreement with experiments. The symmetry of the void-lattice must be the same as the host lattice because of the constraints imposed due to physical considerations on m_1, m_2 and m_3 arising due to the currents which develop after the bifurcation. However, a more fundamental approach, although difficult to analyse, would be to examine the factors which cause only those fluctuations which are consistent with the host lattice symmetry to grow. The phase transition involved is symmetry breaking from a homogeneous to a space periodic one. This explains why voids initially form randomly and only subsequently become ordered. The structure of the matrix $\mathbf{A}_{22}$ shows that $\dot{r}_v < 0$ is a requirement for bifurcation. The instability is therefore related to the vacancy loop formation. This is generally confirmed by experiments as electron-irradiation which produces voids effectively, but not vacancy loops, fails to give rise to regular void arrays. Such arrays are formed in both neutron and charged particle irradiation where vacancy loops are formed due to collapse of cascades. Note that no specific property of the vacancy loops is involved but rather the manner in which they couple with point defects. Such microstructural induced ordering effects can be expected in fairly general conditions in situations involving irradiation, stress or temperature gradients. It is in this context that the partial void ordering in nitrided steel[18] by electron irradiation has to be viewed, where the possible trapping of vacancies by nitrogen gas atoms could produce the same effect as vacancy loops.

These results are interesting both because they explain many features of void-lattice formation, and because the possibility of a phase transition to a new spatially dependent state has important implications for several irradiation-induced phenomena which are of interest in the development of materials for fast reactors.

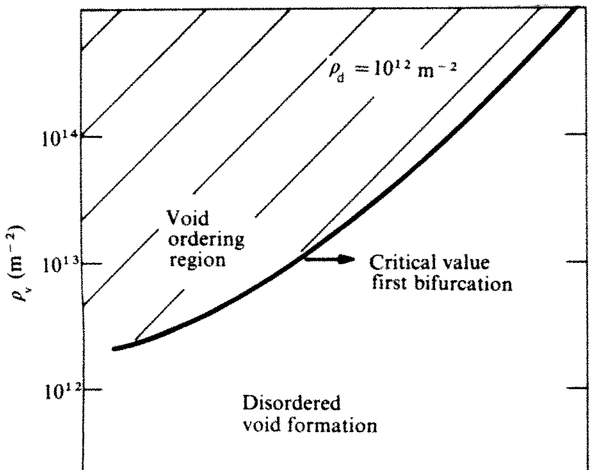

Fig. 1 Phase diagram showing where the first bifurcation appears. A vacancy migration energy of 1.3 eV has been used. For bifurcation and onset of void-lattice formation the system must evolve into the void ordering region.

I thank Drs G. Venkataraman, S. Dattagupta and G. Ananthakrishna for their comments and suggestions.

Received 27 May; accepted 13 August 1980.

1. Cowthorne, C. & Fulton, E. J. *Nature* **216,** 575–576 (1967).
2. Evans, J. H. *Nature* **229,** 403–404 (1971).
3. Wiffen, F. W. in *Radiation-induced Voids in Metals* (eds Corbett, J. W. & Lanniello, L. C.) 386–396 (Albany, New York, 1971).
4. Mazey, D. J., Francis, S. & Hudson, J. A. *J. nucl. Mater.* **47,** 137–142 (1973).
5. Kulcinski, G. L., Brimhall, J. L. & Kissinger, H. E. *J. nucl. Mater.* **40,** 166–174 (1971).
6. Stoneham, A. M. in *Consultant Symposium, The Physics of Irradiation Produced Voids* (ed. Nelson, R. S.) 319–329 (AERE-R7934, 1975).
7. Foreman, A. J. E. *AERE Rep.* R-7135.
8. Lucas, A. A. *Phys. Rev.* **B7,** 3527–3537 (1973).
9. Malen, K. & Bullough, R. in *Voids Formed by Irradiation of Reactor Materials, BNES Conf.* (eds Pugh, S. F., Loretto, M. H. & Morris, D. I. R.) 109–119 (BNES, 1971).
10. Stoneham, A. M. *J. Phys. F* **1,** 778–784 (1971).
11. Tewary, V. K. & Bullough, R. *J. Phys.* **F**2L, 69–72 (1972).
12. Brailsford, A. D. & Bullough, R. *Phil. Mag.* **27,** 49–64 (1973).
13. Bullough, R., Eyre, B. L. & Krishan, K. *Proc. R. Soc.* **A346,** 81–102 (1975).
14. Imada, M. *J. Phys. Soc. Jap.* **45,** 1443–1448 (1978).
15. Benoist, P. & Martin, G. in *Proc. int. Conf. on Fundamental Aspects of Radiation Damage in Metals* Vol. 2 (eds Robinson, M. T. & Young, R. W. Jr) 1236–1243 (CONF-751006, 1975).
16. Krishan, K. *Radiat. Effects* **45,** 169–181 (1980).
17. Nicolis, G. & Prigogine, I. *Self-Organization in Nonequilibrium Systems* (Wiley, New York, 1977).
18. Fisher, S. B. & Williams, K. R. *Radiat. Effects* **32,** 123–124 (1977).

Influence of modal composition on deformation in garnet lherzolite nodules

M. R. Smith

Department of Geology and Mineralogy, University of Oxford,
Parks Road, Oxford OX1 3PR, UK

A textural distinction has been drawn, in peridotites derived from kimberlite pipes, between relatively undeformed granular types and strongly deformed sheared types[1], that corresponds roughly with the absence and presence of large strained olivine grains (porphyroclasts) surrounded by smaller, recrystallized grains (neoblasts). More detailed classifications have also been proposed[2–6]. The textural variety is probably caused by both widespread mantle creep and more localized phenomena connected with kimberlite eruption[7–12]. From consideration of dynamically recrystallized grain size[11] and dislocation densities[12], it seems that nodules that contain neoblasts have been deformed in high stress and strain rate conditions, over short periods of time, before eruption. The formation of the sheared textures and the eruption of the kimberlite are approximately simultaneous. I report here detailed textural observations on 10 garnet lherzolite nodules collected from kimberlite pipes in South Africa and Lesotho. They all have sheared textures, as defined above, showing a range from small amounts of grain boundary recrystallization to almost complete consumption of olivine porphyroclasts. Sections were cut parallel to the foliation and modal analyses were accurately determined by point counting one slide from each sample. The number of olivine porphyroclasts on each slide was then independently counted. The fewer the grains, the greater is the accuracy of estimating their number. Average porphyroclast areas were then calculated (Table 1). The data suggest that modal composition controls the extent of shearing.

Figure 1 shows the relationship between average porphyroclast area and percentage of olivine from the 10 thin sections. It seems that the lower the olivine content, the higher is the degree of deformation as recognized by the smaller areas of olivine porphyroclasts. The range of textures encompassed by the sheared group can be attributed to the range in olivine percentages.

This relationship can be justified by considering that the correlation will still hold if the sum of the other minerals present in the rock (pyroxene and garnet) is plotted along the x-axis. Kohlstedt and Van der Sande[13] have estimated that the climb velocity of dislocations in enstatites is $<0.1\%$ of that in olivine. This behaviour results in a high creep resistance of orthopyroxene compared with olivine[14] in the high temperature, hot working flow regime characteristic of these xenoliths. Despite recovery, strain rates are high enough to increase the strain energy at grain boundaries to a point where olivine begins to recrystallize while orthopyroxene continues to deform by slip and rotation. This is confirmed in natural examples which show that enstatites, diopsides and garnets have a lesser tendency to polygonize and recrystallize[2–5]. Thus these minerals act as relatively rigid material while olivine recrystallization dominates. Where metasomatic philogopite is seen to replace garnet on decompression it can also be included.

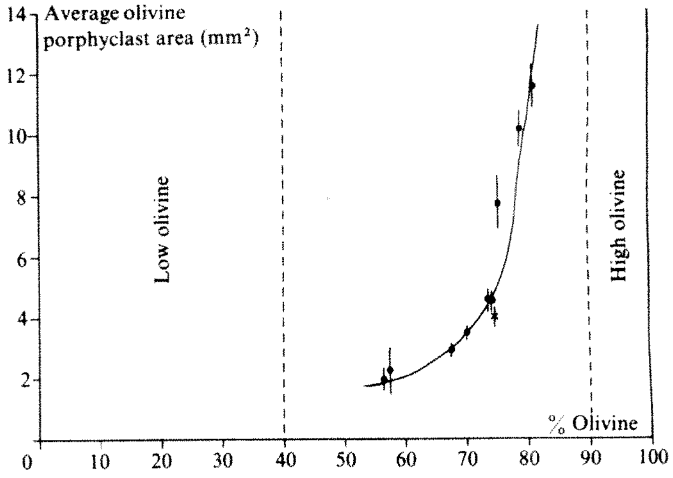

Fig. 1 Dependence of olivine porphyroclast grain size on amount of olivine after onset of recrystallization.

At the onset of deformation, stresses are maximized at porphyroclast grain boundaries as evidenced by recrystallization along them. If strain rates are high enough, concentrations of strain energies along these boundaries eventually cause recrystallization until the olivine porphyroclasts are entirely consumed. Olivine/olivine grain boundaries will be destroyed as neoblasts are produced along them while orthopyroxene/olivine, clinopyroxene/olivine and garnet/olivine boundaries will be relatively preserved. Thus strain energies high enough for olivine recrystallization will be retained at the latter boundaries between the rigid material and the olivine grains. Rigid/olivine boundary lengths will depend on modal percentages, hence percentage rigid material will determine available concentrations of strain energy, the release of which is accomplished by recrystallization.

The cross in Fig. 1 (nodule: BD2501) indicates a lower than expected area value. This sample has a higher percentage of garnet plus clinopyroxene, relative to orthopyroxene, than all the other samples, and optical evidence shows that these minerals are more resistant to recrystallization and disruption than orthopyroxene. Higher strain energies may have persisted at garnet/olivine and clinopyroxene/olivine boundaries while the pyroxenes began to recrystallize and so reduced the areas yet further. Similarly the square in Fig. 1 (nodule: XDB5) has no garnet and little clinopyroxene and has a high area value. The high olivine field ($>90\%$) marks an area where recrystallization cannot continue after the onset of deformation. Indeed the

Table 1 Modal analyses and porphyroclast areas

Nodule	% olivine neophyroclast	% olivine porphyroclast	Slide area (mm^2)	No. olivine porphyroclasts	Porphyroclast area (mm^2)
BD2501	68.52±0.5	5.88±0.5	340	5	3.66–4.34
PHN2762	53.89±1	3.41±1	377	6	1.51–2.77
PHN2761	47.41	25.88	383	22±2	4.13–4.96
KDT11	47.90	8.57	238	11±2	1.57–2.27
KJAG22	0.80	79.85	444	31±2	10.74–12.23
JJG859	54.85	15.05	700	30±2	3.29–3.76
BD2344	48.08	19.23	480	32±2	2.71–3.08
BD2384	15.86	62.59	566	35±2	9.57–10.74
XDB5	0.53	74.68	440	43±5	6.85–8.65
JJG703	2.00	71.71	427	68±5	4.19–4.86

0028–0836/80/400422—02$01.00

nodules showing the largest modal proportion of olivine (nodule: KJAG22) has only 0.8% neoblasts and shows olivine tablets of the type considered[11] to be formed by relief of strain energies during kimberlite eruption.

The existence of sheared dunites (>90% olivine) at Thaba Putsoa and the Frank Smith pipe[8] and at Kampfersdam[15] seems to conflict with the relationship in Fig. 1. The dunites found at Thaba Putsoa, however, are reported as having "porphyroclasts of olivine up to 1 cm in diameter" (very large). At the onset of deformation, and in suitable conditions, olivine/olivine grain boundaries will be destroyed and a certain percentage of recrystallized olivine will, hence, be present to exhibit porphyroclastic textures. The porphyroclast sizes will thus remain at a constant maximum to the right of the second dotted line in Fig. 1.

In contrast, deformation of dunites "to varying degrees"[15] at Kampfersdam and other pipes cannot be explained by the above mechanism. The Kampfersdam dunites have been interpreted to be high temperature nodules due to the coarseness of their olivine groundmass. The recrystallization mechanism involving percentage of rigid material may only dominate within a certain range of conditions which are not, at present, possible to define, although current detailed geochemical studies (S. Beswetherick personal communication) may produce information. On the other hand, there may, in this case, have been a genuine externally imposed gradient in strain which is not evident in the specimens plotted on Fig. 1. The low olivine field (<40%) may indicate complete destruction of olivine porphyroclasts but the increased interaction of rigid/rigid grain boundaries as olivine percentage is reduced may tend to prevent further recrystallization.

An example of the modal compositional effects is shown by the single nodule (KDT11) which shows bands of high and low olivine contents. Figure 2 shows a grain map of this nodule in which the textural range of different samples is seen at the contact zone between bands. Larger olivine porphyroclasts tend to be restricted to the olivine rich bands while only neoblasts are seen in the areas where orthopyroxene predominates.

The above observations have important implications for the origin of the range of sheared textures we see at the surface. An externally imposed strain gradient is apparently not the only factor required to produce the spectrum of sheared textural types seen. The spectrum may be produced, at least partially, by compositional differences in the xenolith source regions. From phase considerations, production of basaltic liquids from garnet lherzolite results from partial melting in the approximate ratio, 1 olivine : 5 orthopyroxene : 10 clinopyroxene : 10 garnet[16]. The high orthopyroxene + clinopyroxene + garnet modal peridotites will correspond roughly with material less depleted in basalt, hence degree of partial melting may determine extent of shearing. Although granular nodules—those that do not contain recrystallized olivine—were not included in this study, note that in the least sheared samples studied the textures become similar to some granular types. The textural contrast between sheared and some granular forms may then be a transition related to extent of depletion. Before onset of deformation olivine grain sizes may have been considerably larger.

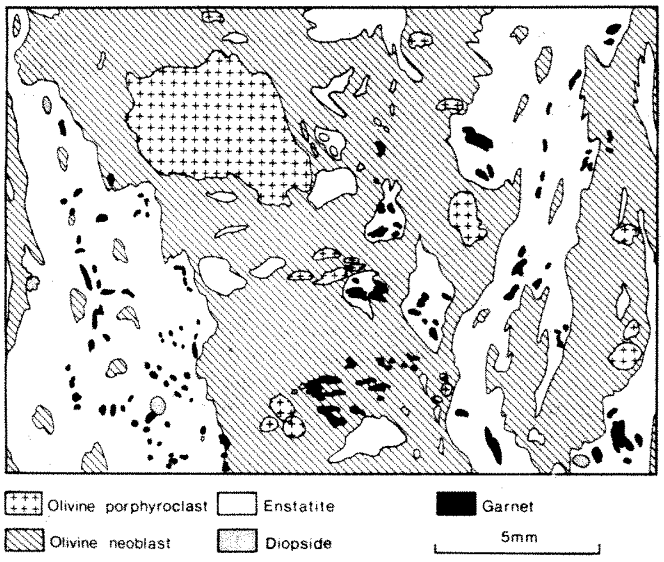

Fig. 2 Grain map of KDTII showing compositional banding with preference of olivine porphyroclasts for olivine bands.

The present data indicate that the factor that controls extent of shearing, as recognized by consumption of olivine porphyroclasts by recrystallization, may be modal composition. From a structural point of view there is a genetic connection between degree of shearing and mechanical properties of the rock. It seems that the observed strain gradient would then be a function of internal compositional factors and not an external stress, temperature or strain rate gradient.

I thank J. B. Dawson, A. J. Erlank, J. J. Gurney and P. H. Nixon for collecting the nodules and K. G. Cox and D. G. Fraser for critically reading the manuscript. This work was supported by the NERC.

Received 10 March; accepted 23 June 1980.

1. Boyd. F. R. & Nixon, P. H. *Yb. Carnegie Instn Wash.* **72,** 431–445 (1973).
2. Boullier, A. M. & Nicolas, A. *Lesotho Kimberlites* (ed. Nixon, P. H.) 57–66 (Lesotho National Development Corporation, Maseru, 1973).
3. Boullier, A. M. & Nicolas, A. *Phys. Chem. Earth* **9,** 97–105 (1975).
4. Cox, K. G., Gurney, J. J. & Harte, B. *Lesotho Kimberlites* (ed. Nixon, P. H.) 76–98 (Lesotho National Development Corporation, Maseru, 1973).
5. Harte, B., Cox, K. G. & Gurney, J. J. *Phys. Chem. Earth* **9,** 477–506 (1975).
6. Harte, B. *J. Geol.* **85,** 279–288 (1977).
7. Boyd, F. R. *Geochim. cosmochim. Acta* **37,** 2533–2546 (1973).
8. Boyd, F. R. & Nixon, P. H. *Phys. Chem. Earth* **9,** 431–454 (1975).
9. MacGregor, I. D. *Phys. Chem. Earth* **9,** 455–466 (1975).
10. Basu, A. R. *Earth planet. Sci. Lett.* **33,** 443–450 (1977).
11. Mercier, J. C. C. *Proc. 2nd int. Kimb. Conf.* **2,** 197–212 (1979).
12. Goetze, C. *Geology* **3,** 172–173 (1975).
13. Kohlstedt, D. L. & Van der Sande, J. B. *Contr. Miner. Petrol.* **42,** 169–180 (1973).
14. Green, H. W. & Radcliffe, S. V. *Geophys. Monogr.* **16,** 139–156 (1972).
15. Boyd, F. R. & Nixon, P. H. *Geochim. cosmochim. Acta* **422,** 1367–1382 (1978).
16. Green, D. H. & Ringwood, A. E. *Contr. Miner. Petrol.* **15,** 103–190 (1967).

A problem posed by vapour-dominated geothermal systems

Gerald Schubert* & Joe M. Straus

Space Sciences Laboratory, The Aerospace Corporation, Los Angeles, California 90009

Malcolm A. Grant

Applied Mathematics Division, Department of Scientific and Industrial Research, Wellington, New Zealand

Vapour-dominated geothermal systems present an apparently extraordinary physical phenomenon—a layer of water lying stably on a body of steam. The first geothermal exploitation at Lardarello, Italy, was in such an area. We present here an analysis of the gravitational stability of water over steam in a porous medium. This shows that the near surface condensate layer of a vapour-dominated geothermal system can be stably maintained above the main steam reservoir by restoring forces associated with the displacement of the phase-change interface. For typical conditions in vapour-dominated geothermal systems, stability can be maintained provided that the permeability of the rocks at the depth of the steam–water boundary does not exceed about 40 nm^2 (0.04 millidarcy). The stability requirement determines the thickness of the condensate layer or the proximity of the top of the steam reservoir to the surface.

---

*Permanent address: Department of Earth and Space Sciences, University of California, Los Angeles, California 90024.

The basic structure of vapour-dominated systems is revealed by pressure measurements in wells drilled to different depths, as shown in Fig. 1 for the Kamojang geothermal field in Indonesia. The water table lies 100–150 m below ground surface. From there to 500 m depth, pressure increases as in normal groundwater, that is, approximately hydrostatically at a rate determined by the density of liquid water. Below 500 m depth, however, pressure increases only very slowly with depth; the rate of increase with depth is approximately that in a static column of steam. Pressure profiles similar to that in Fig. 1 have been published for the Lardarello geothermal field[1].

A section through the Kamojang field[2] (Fig. 2) illustrates the physical structure of a vapour-dominated geothermal system[3–5]. A layer of brine, or very saline water, overlying a magmatic heat source, is presumed to exist at greater depth than shown in Fig. 2. The heat supply boils steam off from the brine, and this steam ascends through the fractured rock. It continues to rise until, at about 500 m depth, it meets the 'condensate layer', the liquid-dominated layer overlying the steam system. In the centre of the field some steam passes through this liquid, much like bubbles rising through water, and gives rise to a surface discharge of steam in fumaroles, steaming ground, acid springs and mud pools. Outside the central area of the field, steam does not escape from the steam reservoir.

Although drilling shows that steam is the pressure-controlling phase in the main reservoir of a vapour-dominated system, various observations demonstrate that the steam in this region must be in contact with some liquid water which is at or near residual saturation. The total production of steam at Lardarello is much greater than could be stored in a steam phase, although it could be accommodated as liquid[6]. At two of the vapour-dominated systems now explored, the geysers in California and Kamojang, although no longer at Lardarello, the fall in pressure caused by exploitation is accompanied by a fall in temperature, consistent with a temperature related to the steam–water saturation curve. Temperatures measured in the main steam reservoir of the Kamojang field (Fig. 1) agree with the saturation temperatures corresponding to the measured pressures. Measurements at the geysers also suggest that temperature increases with depth along the boiling point curve in the steam reservoir[7].

In the liquid-dominated condensate layer, temperatures generally lie on a linear conduction profile[2,7]. This is a consequence of both the surface temperature and the relatively low permeability of the near surface rocks as compared with those in the main steam reservoir. Where the near surface rocks are relatively more permeable, steam rises closer to the surface, and actually reaches it in some locations[2]. In these areas, the temperature profile would lie on the saturation curve at all depths.

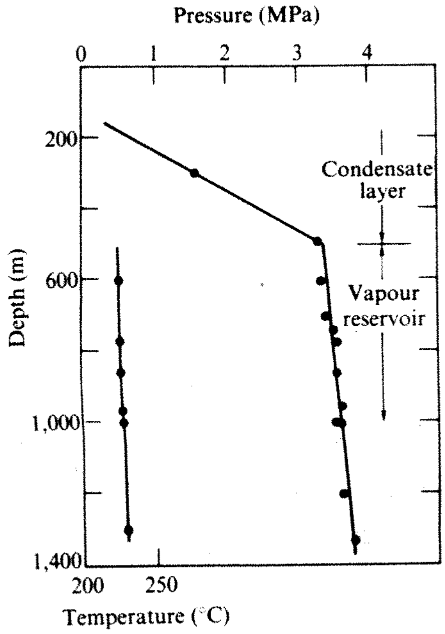

Fig. 1 Measurements of pressure and temperature in the Kamojang geothermal field in Indonesia (excluding the vicinity of well 7).

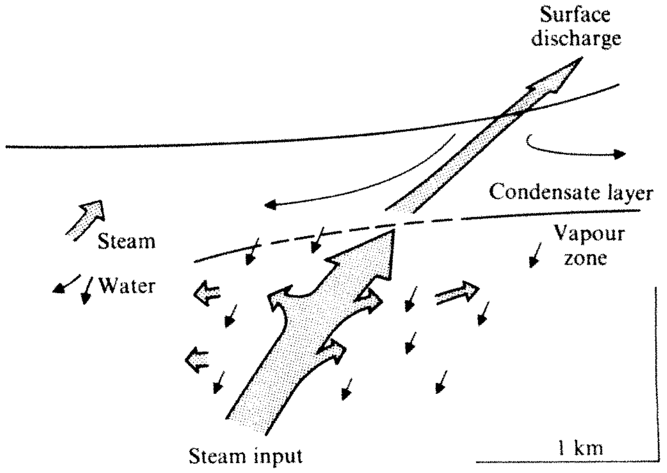

Fig. 2 Inferred structure of the Kamojang field[2].

The major problem posed by the structure of Fig. 2 is why does the water not fall down? A sealed cap cannot separate the condensate layer from the steam reservoir because the natural discharge of the systems indicates that there is continuous permeability, at least in some places, between the mobile steam beneath and the mobile water above. If the water–steam interface behaved as a boundary between immiscible fluids, the configuration of water over steam would be gravitationally unstable for any permeability of the rocks in the vicinity of the interface, no matter how small. This can be understood by imagining a disturbance to the system which resulted in some downward flow of water towards the interface. If the water and steam were immiscible fluids, the boundary between them would be displaced downwards by such a disturbance. As a consequence, a vertical column of fluid in the region of the disturbance would contain more water and thus would be heavier than a column of fluid in the undisturbed quiescent state. The additional weight of the perturbed column provides a downward force tending to reinforce the original disturbance and displace the interface even further. Thus, the configuration is unstable.

A phase-change interface, however, distorts quite differently in response to such a disturbance because the interface must remain on the Clapeyron or equilibrium curve separating the phases. The location of a phase-change boundary is mainly dependent on temperature and pressure, and, unlike the case of the interface between immiscible fluids, flow can occur across a phase-change interface. Downward flow of water towards the steam–water boundary brings fluid to the interface that is colder than the fluid at the undisturbed location of the boundary as a consequence of the natural geothermal gradient. This causes the boundary to be displaced upward to lower pressure because it must remain on the Clapeyron curve. The phase-change interface distorts in a direction opposite to the sense of flow towards it, in striking contrast to the behaviour of the interface between immiscible fluids. As a result of the upward displacement of the phase-change boundary, a vertical column of fluid in the region of the disturbance would contain less water and thus would be lighter than a column of fluid in the undisturbed state. The reduced weight of the perturbed column provides an upward buoyancy force tending to oppose the original disturbance and stabilize the system. Another effect which tends to reinforce the stabilizing tendency of advection of colder water toward the phase change is that when water moves downward towards the phase change and the boundary moves upwards in response, there is a mass flow across the phase change which converts water into steam. This phase transformation requires the absorption of the latent heat of vaporization and results in cooling of the surrounding fluid. As noted immediately above, cooling leads to upward displacement of the phase boundary and stabilization of the system. The cooling produced by the effects of advection and latent heat absorption promotes one destabilizing tendency associated with the thermal contraction of the water—colder water weighs more, and this additional weight of the column tends to drive the system in the same direction as the original downward perturbation.

To assess these effects quantitatively we have analysed the gravitational stability of horizontally infinite superposed fluid layers separated by a phase-change interface in a porous medium. The basic state consists of a motionless layer of water above a static layer of steam. Pressure increases with depth in the undisturbed state according to the hydrostatic law; the liquid and vapour densities govern the slopes of the pressure–depth profiles in the water and steam layers, respectively. Temperature is assumed to increase linearly with depth in the basic state. The stability of this configuration is governed by Darcy's law, which relates velocity and pressure perturbations, the incompressible continuity equation (density changes within each phase are negligible), which relates horizontal and vertical velocity perturbations, and the phase equilibrium equation, which relates pressure perturbations to the distortion of the water–steam interface. The differential equations for the disturbances are linearized and solved subject to the following conditions: (1) isothermal upper and lower boundaries, (2) no flow through the lower boundary, (3) constant pressure on the upper boundary, (4) continuity of pressure, temperature and mass flow at the water–steam interface, and (5) balance of conductive heat flux and latent heat release at the phase-change boundary.

The analysis shows that stabilization of water overlying steam requires

$$K < \frac{2k}{L\left(\frac{\mathrm{d}p}{\mathrm{d}T}\right)_{\mathrm{c}}} \frac{\left(\frac{\bar{\mu}_{\mathrm{l}}}{\bar{\rho}_{\mathrm{l}}}+\frac{\bar{\mu}_{\mathrm{v}}}{\bar{\rho}_{\mathrm{v}}}\right)}{\left(1-\frac{\bar{\rho}_{\mathrm{v}}}{\bar{\rho}_{\mathrm{l}}}\right)} \left\{ \frac{\Gamma\left(\frac{\mathrm{d}p}{\mathrm{d}T}\right)_{\mathrm{c}}}{g\bar{\rho}_{\mathrm{l}}} - \frac{\left(\frac{\bar{\rho}_{\mathrm{v}}}{\bar{\rho}_{\mathrm{l}}}+\frac{\bar{\mu}_{\mathrm{v}}}{\bar{\rho}_{\mathrm{v}}}\frac{\bar{\rho}_{\mathrm{l}}}{\bar{\mu}_{\mathrm{l}}}\right)}{\left(1+\frac{\bar{\mu}_{\mathrm{v}}}{\bar{\rho}_{\mathrm{v}}}\frac{\bar{\rho}_{\mathrm{l}}}{\bar{\mu}_{\mathrm{l}}}\right)} \right\}, \qquad (1)$$

where ρ is density, μ is dynamic viscosity, $(\mathrm{d}p/\mathrm{d}T)_{\mathrm{c}}$ is the slope of the Clapeyron curve, L is the latent heat, Γ is the geothermal gradient, g is the acceleration of gravity, k is the combined thermal conductivity of the fluid and matrix (dominated by the conductivity of the rocks), K is the permeability, and subscripts l and v refer to liquid and vapour, respectively. All the quantities in equation (1) are to be evaluated at the quiescent position of the water–steam interface. Condition (1) is necessary for stability. Although it is not sufficient, an exact analysis[8] shows that the value of permeability given by the right side of equation (1) is a good estimate of the maximum permeability for which stabilization is possible.

The evaluation of equation (1) leaves little uncertainty in the largest value of permeability allowing stabilization of the condensate layer. This is because all the quantities in equation (1), except for k and Γ, depend only on temperature, and there is little temperature variation within and among the steam reservoirs of natural vapour-dominated systems. In addition, the condensate layers are generally several hundred metres thick, precluding any large uncertainty in the value of Γ. Finally, the thermal conductivities of reservoir rocks are known to within factors of 2 or 3. Using a value of 242 °C for the temperature at the condensate layer–steam zone interface (see Fig. 1), $\Gamma = 0.555\ ^{\circ}\mathrm{C\,m^{-1}}$ and $k = 4\ \mathrm{J\,m^{-1}\,s^{-1}\,K^{-1}}$, we find that K must be less than 80 nm^2 (0.08 millidarcy) for the condensate layer to be gravitationally stable [a more exact analysis[8] shows that $K \lesssim 40\ \mathrm{nm}^2$ (0.04 millidarcy) for stability].

A permeability of 40 nm^2 is more than an order of magnitude smaller than permeabilities generally thought to occur in the main reservoirs of geothermal systems. It is not surprising, however, that relatively low permeability is required near the condensate layer–steam zone interface to keep the water from falling down into the underlying region of steam. The significance of our result is the fact that any stabilization is possible for a non-zero value of permeability. The natural discharge of vapour-dominated geothermal fields attests to the through-flow of steam within the system. This could not occur if some impermeable layer were required to seal or cap the main steam reservoir to stabilize the condensate layer. It is the special behaviour of the phase-change interface between water and steam that permits stabilization of the systems with a non-zero permeability; if the interface behaved in a manner similar to the boundary between immiscible fluids the rocks would have to be impermeable to keep the condensate layer from falling down.

The low permeability required for the stability of the condensate layer probably determines the thickness of the layer. During the formation of a wet geothermal system, rising steam from the relatively permeable main reservoir penetrates rocks whose permeability decrease with proximity to the surface. The top of the main reservoir will extend upwards until condensate can be stabilized by rocks of sufficiently small permeability.

We thank Geothermal Energy N.Z. Ltd, managers of the Kamojang Project, acting on behalf of the Indonesian and New Zealand governments, for supplying the data used in Figs 1 and 2. This work was supported, in part, by NSF grant ENG 76-82119.

Received 28 April; accepted 22 July 1980.

1. Celati, C., Squarci, P., Taffi, L. & Stefani, G. C. *Proc. 2nd U.N. Symp. Dev. and Use of Geothermal Resources*, 1583–1590 (U.S. Government Printing Office, 1975).
2. Grant, M. A. *Geothermal Resources Council Trans.* **3**, 271 (1979).
3. White, D. E., Muffler, L. J. P. & Truesdell, A. H. *Econ. Geol.* **66**, 75 (1971).
4. Truesdell, A. H. & White, D. E. *Geothermics* **2**, 154 (1973).
5. D'Amore, F. & Truesdell, A. H. *Proc. 1979 Stanford Geothermal Reservoir Workshop* (1979).
6. James, R., *N.Z. J. Sci. Technol.* **11**, 706 (1968).
7. Ramey, H. J. Jr, submitted as evidence, Reich and Reich vs. Commissioner of Internal Revenue, Tax Court of the United States, 52 T. C. No. 74 (1970).
8. Schubert, G. & Straus, J. M. *J. geophys. Res.* (in the press)

The Gulf of Lion: subsidence of a young continental margin

M. S. Steckler & A. B. Watts

Lamont-Doherty Geological Observatory, and Department of
Geological Sciences of Columbia University, Palisades,
New York 10964

The origin of the subsidence of Atlantic-type continental margins is of much interest to geology and geophysics. The main problem at these margins is in explaining the substantial thicknesses of mainly shallow-water sediments which accumulate soon after rifting and plate separation. We have now used biostratigraphic data from commercial wells to study the subsidence history of a young Atlantic-type continental margin. Backstripping the sediment load reveals that the margin has been subsiding at nearly mid-ocean ridge rates. Geological data indicate that lithospheric stretching alone cannot account for this amount of subsidence and other processes must be involved.

Studies of biostratigraphic data from deep commercial boreholes suggest that the tectonic subsidence of margins is thermal in origin[1–5]. Sleep[1] suggested the subsidence is due to cooling of the lithosphere following uplift and erosion. This model cannot, however, fully explain the amount of tectonic subsidence observed at these margins[3] or the lack of evidence of domal uplift during rifting[6]. McKenzie[7] proposed a model in which the subsidence is due to cooling of the lithosphere following stretching and thinning at the time of rifting. This model seems to explain the tilted and rotated blocks bounded by listric faults which develop during rifting[8,9].

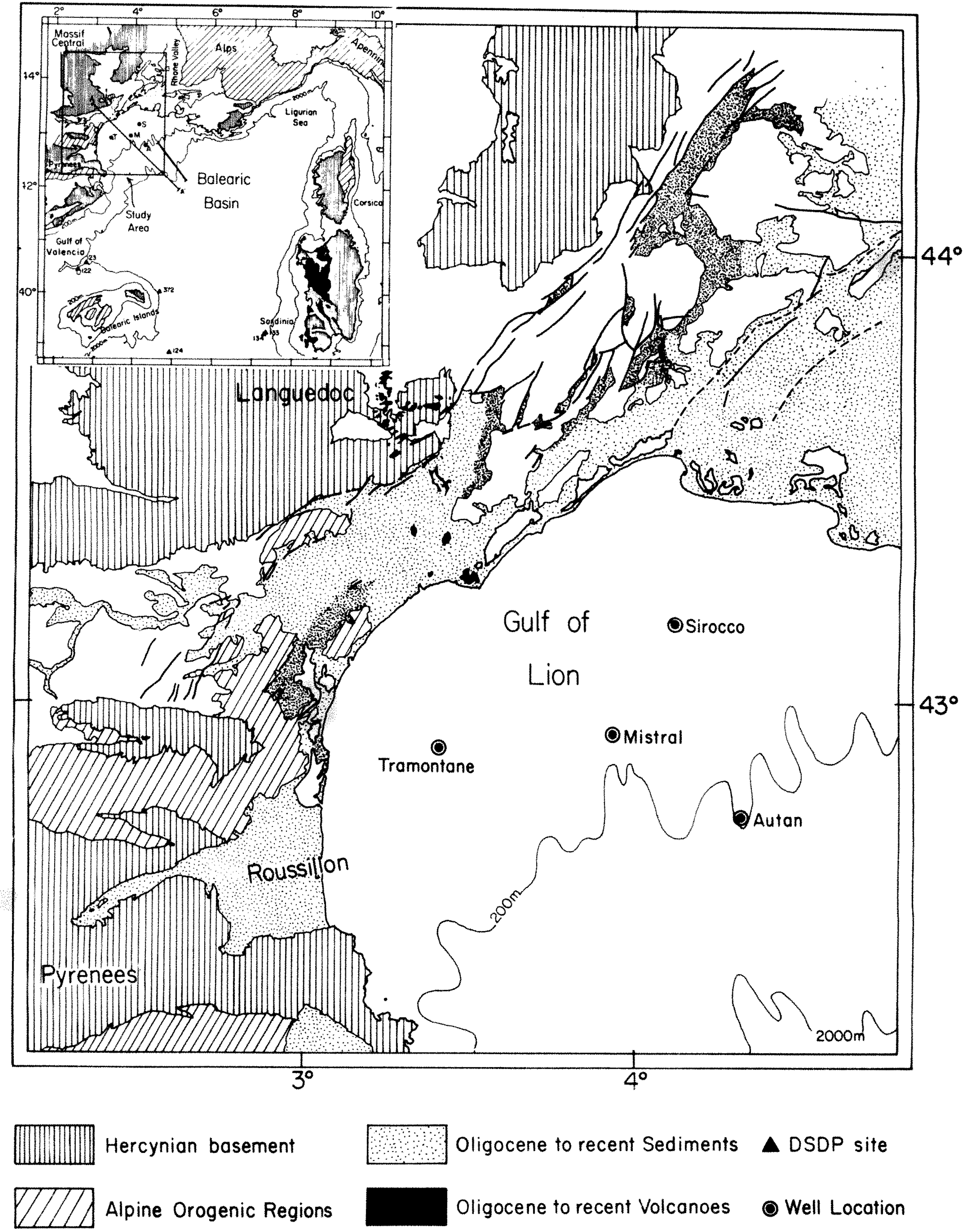

Fig. 1 Geology of the Gulf of Lion. The heavy lines are faults which have been active during the Oligocene, dashed where inferred. The heavier dots show the location of Oligocene red beds. Inset, generalized geology of the regions surrounding the Balearic Basin and location of Gulf of Lion. The heavy line is the location of the 'Christiane' multichannel seismic profile[30,32], A–A' is the location of the profile shown in Fig. 2.

By quantitatively accounting for the effects of sediment and water loading the tectonic subsidence of a margin can be isolated[2–4]. To correct for sediment and water loading, the sedimentary section should be reconstructed at intervals during the development of the margin, taking into account the effects of compaction, changes in water depths and eustatic sea-level changes. The sedimentary section should then be isostatically unloaded, or backstripped[2,3].

Most previous studies have been based on stratigraphic data from the thickly sedimented, relatively old margins, such as eastern North America. The wells in these studies generally did not sample the pre-rift and syn-rift sediments or crystalline basement rocks and therefore do not provide either a complete record of the subsidence history or a reliable age for the opening of the central North Atlantic. A detailed knowledge of the early subsidence history is important in discriminating between different models for the origin of the margin.

A good example of a well sedimented young Atlantic-type continental margin is the Gulf of Lion in the Balearic Basin (Fig. 1). Geophysical data indicate that the Balearic Basin contains up to 6 km of sediments, including over 1 km of Messinian evaporites, overlying a thin oceanic-type crust[10–12]. Geological and palaeomagnetic evidence[11,13–16] suggests the basin formed by Oligocene/Miocene rifting of Corsica–Sardinia from France (Fig. 1). Messinian evaporites had been interpreted[17] as indicating that the western Mediterranean was not a deep basin until post-Miocene time. However, DSDP site 372 east of Menorca[18] established that the western Mediterranean was already a deep basin by the Lower Burdigalian (~20 Myr BP). Although the tectonic setting of the basin is poorly known, it may have formed as a back-arc basin behind a migrating island arc–trench system to the east[16]. Extensive Oligocene through Lower Miocene andestic volcanism related to this arc is found in western Sardinia[19].

Figure 1 summarizes the geological setting of the Gulf of Lion. The Eocene in southern France was a period of overthrusting associated with the Pyrenean orogeny[20,21]. The Oligocene, in contrast, was a period of extension and normal faulting[20,21], much of which seems to have reactivated older fault trends. Continental sediments accumulated in NE–SW trending grabens in Languedoc and Roussillon. Similar extension and graben structures also occurred in Sardinia and along the margins of the Balearic Islands[22,23]. Drainage patterns in southern France during the Eocene and Oligocene were towards the north and west, away from the present Mediterranean[24,25]. Then, in the Lower Miocene (Aquitanian) a major transgression occurred marking the opening of the Balearic Basin[26,27].

The structure and stratigraphy of the Gulf of Lion margin is known from commercial drilling and seismic reflection data. Three of the wells drilled recovered over 3 km of Miocene to Recent sediments overlying Palaeozoic basement[28,29]. In addition, the Autan well (Fig. 1) recovered 244 m of ?Oligocene red beds[29]. The seismic data in the Gulf of Lion[30–33] show a gently dipping Pliocene to Recent sedimentary section unconformably overlying a more steeply dipping Miocene section. Information on the basement structure of the Gulf of Lion is sparse but available data[28,33] indicate the Miocene to Recent sedimentary section overlies horst and graben structures which are infilled by continental sediments of probable Oligocene age (Fig. 2). Thus, the available geological and geophysical data show that the structural evolution of the Gulf of Lion region margin was similar to that of a normal Atlantic-type continental margin[12].

We have used biostratigraphic data from three wells[29] in the Gulf of Lion (Figs 1, 2). The sediments in each well were backstripped[2,3] to obtain the tectonic subsidence of the margin. The wells were corrected for compaction using available sonic, density and porosity logs (L. Montadert, personal communication) and backstripped with the Airy model of isostasy[2,34] and a mantle density of 3.33 g cm^{-3}. The palaeobathymetry for the wells was based on the micropalaeontological studies of Cravatte *et al.*[29]. We did not correct for eustatic sea-level changes as they are not well known in the Neogene due to uncertainties in the timing of Antarctic glaciation.

The sedimentary record in the wells is interrupted by a major erosional unconformity due to the Messinian salinity crisis[30,35] (Fig. 3). The unconformity is observed as a discontinuity in the lithological logs. We backstripped each well using as wide a range of estimates for the magnitude of the erosional event as

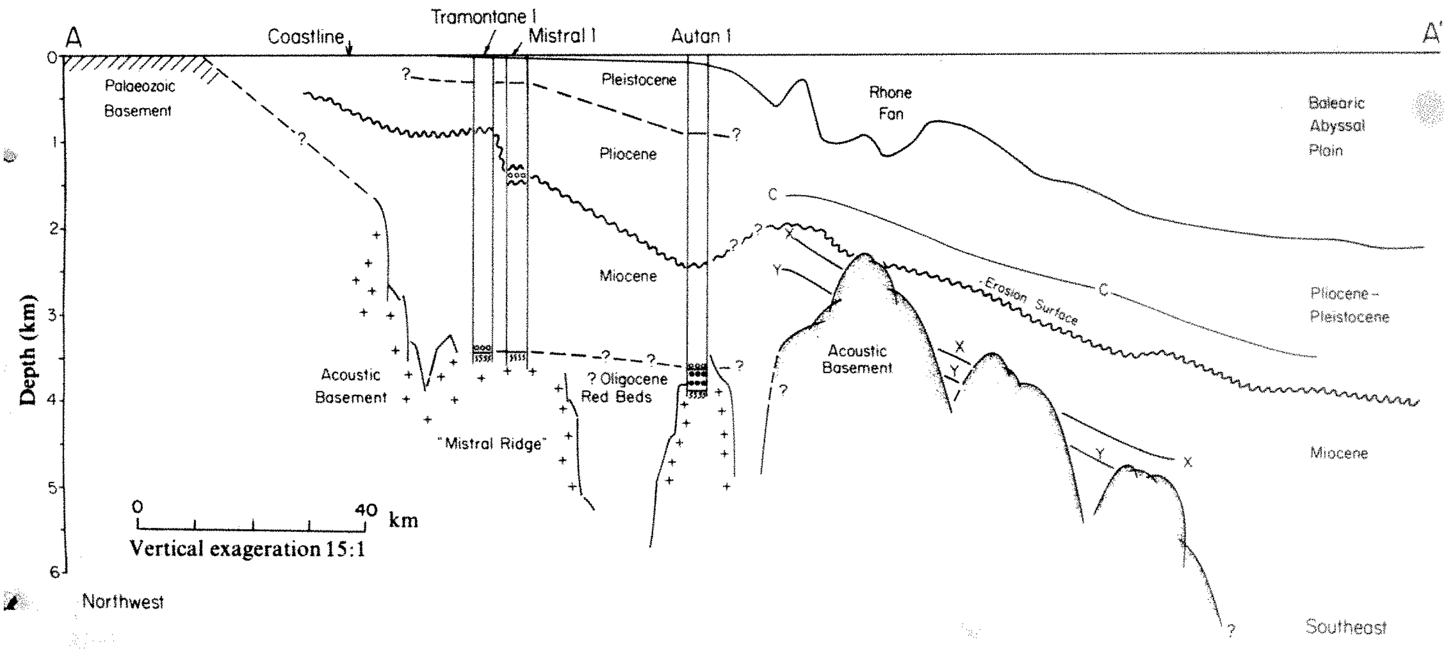

Fig. 2 Profile across the Gulf of Lion margin. Prominent seismic reflectors and acoustic basement are projected from the 'Christiane' profile[30]. In the wells: ○, basal conglomerates; ●, continental red beds. The wells bottomed in Palaeozoic schists[28,29]. The basement structure suggests prominent horsts and grabens infilled by red beds (refs 28, 33 and L. Montadert, personal communication) seaward of a hinge zone.

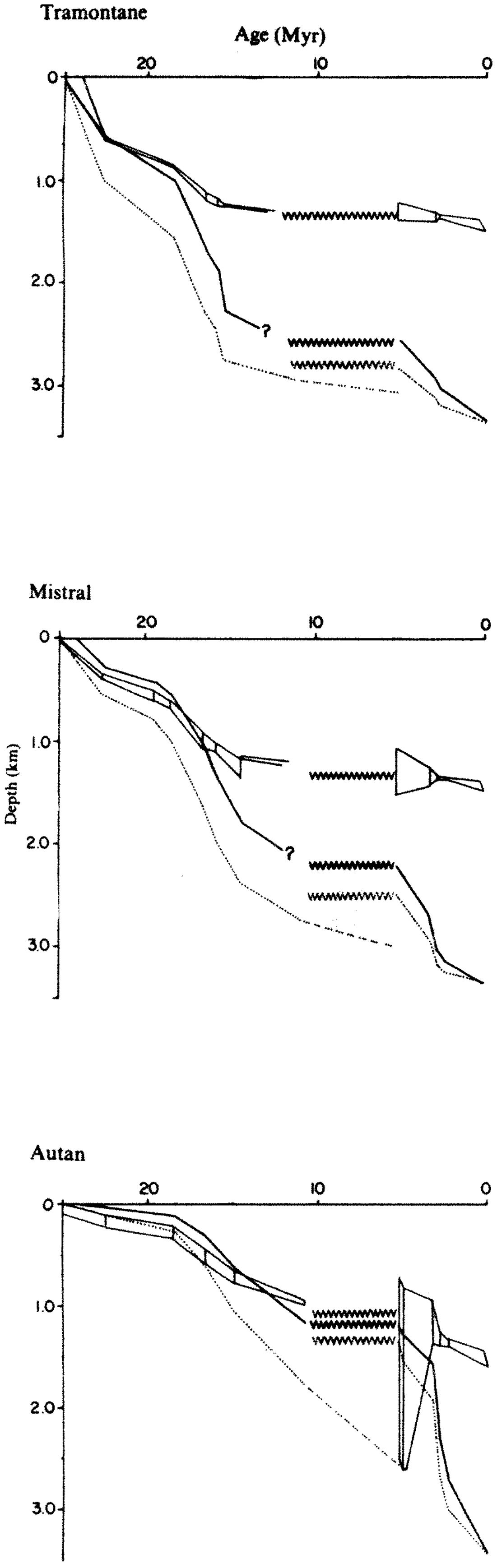

Fig. 3 Subsidence in the three wells studied. The heavy solid lines are the observed sediment thicknesses. The dotted lines represent the reconstructed sediment accumulation after correction for compaction, dashed where later removed by erosion. The double solid line is the subsidence after backstripping. The width of the lines represent the range of estimates for the water depth based on micropalaeontological studies[29].

was compatible with the well logs and found that in each case the trend of the tectonic subsidence (Figs 3, 4) was continuous through the salinity crisis. This agrees with the interpretation of the Messinian event as an evaporitic drawdown[32,35].

Using the observation that the tectonic subsidence was continuous, it is possible to estimate the amount of erosion of the margin during the salinity crisis. We found that 1,200–1,500 m of sediments were eroded at Autan and that much less were eroded at the more landward Mistral (380–600 m) and Tramontane (<320 m) wells. The water depths immediately following the salinity crisis were estimated to be 700–900 m at Autan and correspondingly smaller at the more landward wells, in agreement with those determined from micropalaeontological studies[29]. At the Autan well, however, by using the trend of the tectonic subsidence we can estimate a much smaller range of water depths than that which can be estimated from micropalaeontology (bathyl).

The tectonic subsidence at each well (Fig. 3) constitutes less than half of the total sediment accumulation and continues smoothly through the Messinian event. The tectonic subsidence is similar in form for each of the wells. The main difference occurs in the early subsidence which is larger in a landward direction. Small variations in the rate of the tectonic subsidence appear to correlate from well to well and may be due either to changes in sea-level[36] or to uncertainties in absolute age dating of the sediments.

The most likely cause of the tectonic subsidence is thermal contraction following stretching and thinning of the margin at the time of rifting. A useful way to examine the thermal subsidence of a margin is to plot the tectonic subsidence against $\sqrt{\text{age}}$ (ref. 7). Figure 4 shows the tectonic subsidence for the wells along with that predicted by a lithospheric stretching model[7]. The origin in Fig. 4 is 25 Myr BP which is the best estimate for the age of opening of the basin[13,14,16,27]. The parameter $\beta = \infty$ is equivalent to the subsidence of a mid-ocean ridge.

The total tectonic subsidence at each well is large and seems to exceed $\beta = 10$. The fit of the subsidence data to the model, however, is poor. The tectonic subsidence early in margin history is progressively greater in a more landward direction and at Tramontane exceeds that of a mid-ocean ridge.

Numerical modelling of the continental margin off Norway[37] has shown that lateral transport of heat towards the continent may be important in the early history of the margin. We have, therefore, modified McKenzie's[7] model to include a finite crustal thickness for oceanic lithosphere and the effects of lateral as well as vertical conduction of heat. The subsidence was computed for a two-dimensional model in which β varied across the margin (Fig. 4*b*). The fit to the subsidence data has been greatly improved (Fig. 4*a*) and the estimates of β (2.6 to 6) at the wells reduced. These considerations suggest that thermal cooling, both vertical and lateral, of a hot, thinned lithosphere can explain the tectonic subsidence of the margin.

The magnitude of the tectonic subsidence implies that the continental basement in the Gulf of Lion was greatly extended during rifting. Extension of this magnitude, however, does not seem to be compatible with the geology of the Gulf of Lion. Normal faulting and graben structures containing Oligocene red beds occur both on land[20,21] and off-shore (ref. 33 and L. Montadert, personal communication). However, the volume of these pre-rift and syn-rift sediments is relatively small compared with the volume of the post-rift sediments (Figs 1, 2). All the wells drilled in the Gulf of Lion (Fig. 1) contain little or no Oligocene sediments (Fig. 2) and are located on horsts. If the lithosphere had been stretched by the estimated values of β then the sediment accumulation during rifting should have been in excess of 4 km. Thus, the small observed subsidence associated with rifting precludes large amounts of stretching of continental crust, while the magnitude of the thermal subsidence requires extensive heating of the lithosphere during rifting.

These results suggest that although there was extension during the Oligocene, the passive heating resulting from stretching[7] cannot fully account for the observed tectonic subsidence of the

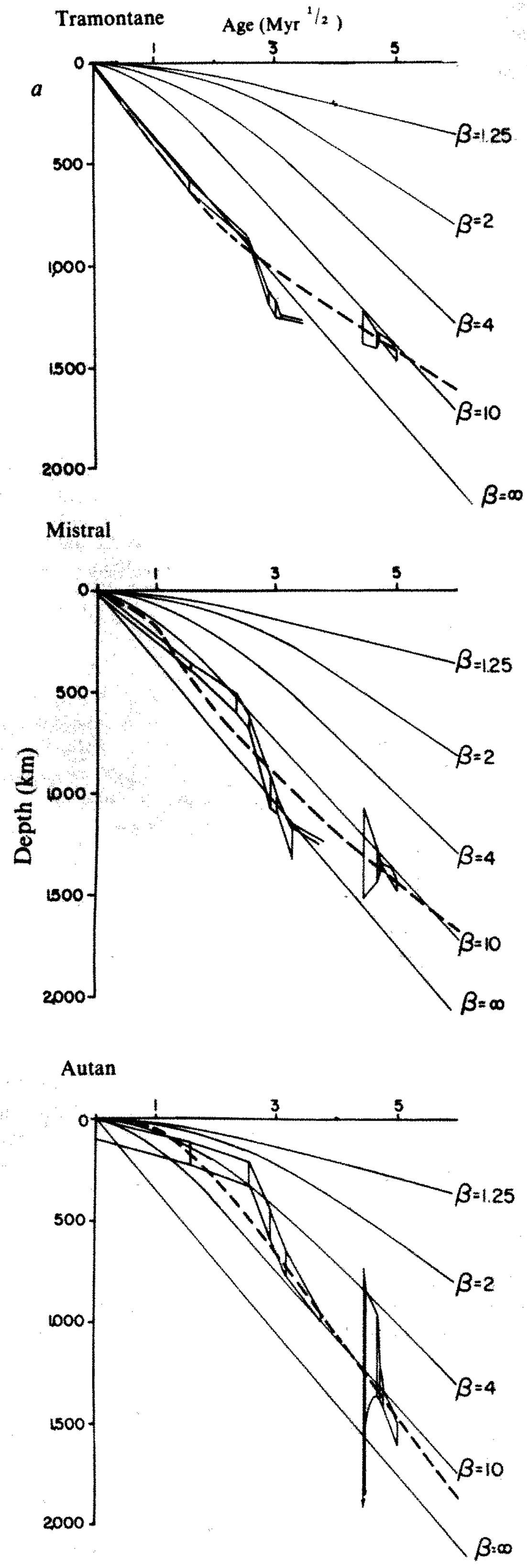

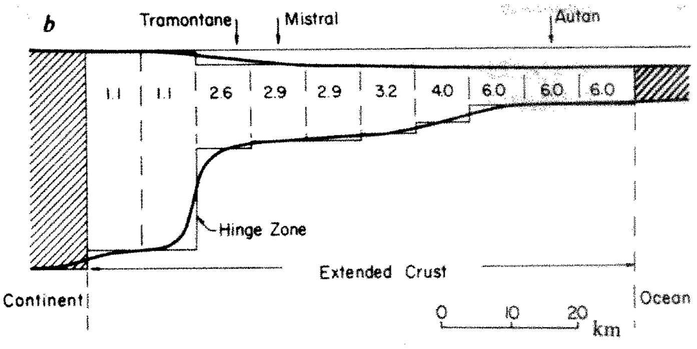

Fig. 4 *a*, Tectonic subsidence plotted against square root of the age. Width of lines represents range of estimates for water depth[29]. Age of opening was assumed to be at 25 Myr BP. Light lines, theoretical subsidence calculations from lithospheric stretching model[7]. $\beta = \infty$ corresponds to mid-ocean ridge subsidence. Dashed lines, subsidence calculations for two-dimensional model illustrated in *b*, Crustal section of the two-dimensional model used to estimate subsidence at the wells. Dashed lines represent boundaries of the blocks used for calculations. The values for each block are the estimates of β. The heavy lines illustrate the crustal thinning that occurred at the margin at the time of stretching (25 Myr BP). Note the large values of initial water depths. No vertical exaggeration.

margin. Thus, other mechanisms of heating the margin at the time of rifting are required. One possibility is that a thick crust and relatively high thermal gradients already existed in the lithosphere before rifting, due to Pyrenean Eocene overthrusting and/or andesitic volcanism in the nearby island arc–trench system. Alternatively, continental rifting may be caused by deep seated processses in the mantle which result in an active heating of the lithosphere at the margin. Further work on other Atlantic-type continental margins is needed to distinguish between these possibilities.

We thank L. Montadert for the sonic, density and porosity logs for the wells. This work was supported by a Phillips Petroleum Company Fellowship to M.S.S. and NSF grant OCE 77-10647. Lamont–Doherty Contribution no. 3036.

Received 14 April; accepted 4 July 1980.

1. Sleep, N. H. *Geophys. J. R. astr. Soc.* **24,** 325 (1971).
2. Watts, A. B. & Ryan, W. B. F. *Tectonophysics* **36,** 25 (1976).
3. Steckler, M. S. & Watts, A. B. *Earth planet. Sci. Lett.* **41,** 1 (1978).
4. Keen, C. E. *Can. J. Earth Sci.* **16,** 505 (1978).
5. Royden, L., Sclater, J. G., & von Herzen, R. P. *Bull. Am. Ass. petrol. Geol.* **64,** 173 (1980).
6. Kent, P. *Phil. Trans. R. Soc.* **A294,** 125 (1980).
7. McKenzie, D. P. *Earth planet. Sci. Lett.* **40,** 25 (1978).
8. de Charpal, O., Guennoc, P., Montadert, L. & Roberts, D. G. *Nature* **275,** 706 (1978).
9. Montadert, L., de Charpal, O., Roberts, D., Guennoc, P. & Sibuet, J. *Maurice Ewing Symp. Ser.* **3,** 154 (1979).
10. Fahlquist, D. A. & Hersey, J. B. *Bull. Inst. oceanogr. Monaco* **67,** 52 (1969).
11. Ryan, W. B. F., Stanley, D. J., Hersey, J. B., Fahlquist, D. A. & Allan, T. D. in *The Sea* Vol. 4, Pt 2, 387 (1971).
12. Hsü, K. J. in *The Ocean Basins and Margins* Vol. 4A, 29 (Plenum, New York, 1977).
13. Argand, E. *C.r hebd. Séanc. Acad. Sci., Paris,* 171 (1924).
14. Alvarez, W. *Nature phys. Sci.* **235,** 103 (1972).
15. Bayer, R., LeMouel, J. L. & LePichon, X. *Earth planet. Sci. Lett.* **19,** 168 (1973).
16. Alvarez, W., Cocozza, T. & Wezel, F. C. *Nature* **248,** 309 (1974).
17. Auzende, J. -M., Bonnin, J., Olivet, J. -L., Pautot, G. & Mauffret, A. *Nature phys. Sci.* **230,** 82 (1971).
18. Hsü, K. J. & Montadert, L. *et al. Init. Rep. DSDP* Leg **42A** (1978).
19. Boccaletti, M. & Guazzone, G. in *Paleogeografia del Terziario Sardo nell'ambito del Mediterraneo Occidentale* (ed. Cherchi, A.) 57 (1974).
20. Gottis, M. *Livre P. Fallot* Vol. 1, 383 (Soc. geol. France, 1962).
21. Ellenberger, F. & Gottis, M. *Rev. géogr. Phys. Géol. Dyn.* **9,** 153 (1967).
22. Cocozza, T. & Schöfer, in *Paleogeografia del Terziario Sardo nell'ambito del Mediterraneo Occidentale* (ed. Cherchi, A.) 145 (1974).
23. Mauffret, A., Montadert, L., Lavergne, M. & Willm, C. *Init. Rep. DSDP* Leg **42A,** 889 (1978).
24. Demangeon, P. *Rev. géogr. Phys. Geol. Dyn.* **3,** 149 (1960).
25. Cornet, C. *Mém. Soc. géol Fr.,* **103,** Nouv. sér 44,2 (1965).
26. Pannekoek, A. J. *Verh. Kongr. Ned. Geol. Mijnbouwk. Gen.* **26,** 53 (1969).
27. Burollet, P. F. & Byramjee, R. S. *C.r.hebd. Séanc Acad. Sci. Paris,* **278**D, 1321 (1972).
28. Burollet, P.-F & DeFaure, P. in *The Mediterranean Sea—a Natural Sedimentation Laboratory* (ed. Stanley, D. J.) 91 (1972).
29. Cravatte, J., DuFaure, P., Prim, M. & Rouaix, S. *Not. Mém. Compagnie Fr. Petrol.* **11,** 209 (1974).
30. Ryan, W. B. F. *Sedimentology* **23,** 791 (1976).
31. Leenhardt, O. *et al. Bull. Centre Rech. Pau—SNPA* **6,** 365 (1972).
32. Biju-Duval, B. *et al.* in *The Geology of Continental Margins* (eds. Burk, C. A. & Drake, C. L.) 675 (Springer, New York, 1974).
33. Biju-Duval, B., Letouzey, J., & Montadert, L. *Init. Rep. DSDP* Leg **42A,** 951 (1978).
34. Watts, A. B. & Steckler, M. S. (AGU, in press).
35. Hsü, K. J. *Scient. Am.* **227,** 27 (1972).
36. Watts, A. B. & Steckler, M. S. *Maurice Ewing Symp. Ser.* **3,** 218 (1979).
37. Zielinski, G. W. *J. geophys. Res.* **84,** 7577 (1979).

Model experiments on the 100,000-yr glacial cycle

J. Oerlemans*

Royal Netherlands Meteorological Institute, De Bilt, The Netherlands

It is believed that during the Quaternary era changes in global ice volume were mainly due to changes in the size of the ice sheets on the Eurasian and American continents. Time spectra of oxygen isotope records from deep-sea cores and of the Earth's orbital parameters are remarkably similar in the 10,000–120,000-yr range[1,2], suggesting that changes in global ice volume are forced by insolation variations. Model studies by Weertman[3,4] and Pollard[5] have confirmed this point to some extent: the 20,000- and 40,000-yr cycles can be reproduced, but the 100,000-yr cycle does not show up. Recently, Imbrie and Imbrie[6] have fitted simple nonlinear mathematical models to δ^{18}O curves. They found that reasonable fits are obtained if the time scale for ice-sheet growth is about 27,000 yr and for decay about 7,000 yr. The present study considers the problem of the 100,000-yr cycle in a similar way. Experiments with a Northern Hemisphere ice-sheet model show that the 100,000-yr cycle and its sawtooth shape may be explained by ice sheet/bedrock dynamics alone. This cycle seems to be an internally generated feature and is not forced by variations in the eccentricity of the Earth's orbit.

First, consider the 'classical' record of core V12-122 (Fig. 1). This core has a comparatively high resolution and spans about the last 500,000 yr. Two features that are immediately evident are that the dominant signal is a periodic one, with a period of about 100,000 yr, and that this cycle is strongly asymmetric, having a sawtooth shape. The strong response of the cryosphere on the 100,000-yr time scale, as compared with those on the 20,000- and 40,000-yr time scales, suggests some kind of resonance. Variations in eccentricity of the Earth's orbit may have combined with the internal dynamics of the climate system to create a strong signal in global ice volume.

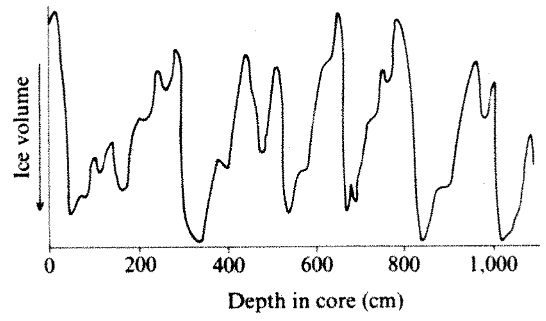

Fig. 1 A plot of the δ^{18}O record of the Carribean core V12-122 (data from ref. 12). According to the 'tune-up' time scale of Hays *et al.*[2], the glacial maximum found at a depth of 840 cm in this core occurred at 430,000 yr BP. The most pronounced features are the 100,000-yr cycle and the asymmetric shape of these cycles.

Figure 1 suggests that the time needed to create full-size ice sheets is 50,000–100,000 yr, considerably more than has been suggested by theoretical studies[4,7]. I will discuss some model results indicating that such a growth time scale is in accordance with bedrock/ice sheet dynamics.

The most dramatic feature of Fig. 1 is the speed with which deglaciations seem to take place ~10,000 yr. Also important is the fact that just before deglaciation starts, the growth rate of the ice volume does not fall, which indicates that during the glacial maxima the Northern Hemisphere ice sheets were far from equilibrium. Also, the difference in δ^{18}O between a glacial minimum and the subsequent maximum is fairly constant, suggesting an inherent instability of the climate system, and probably of the cryosphere.

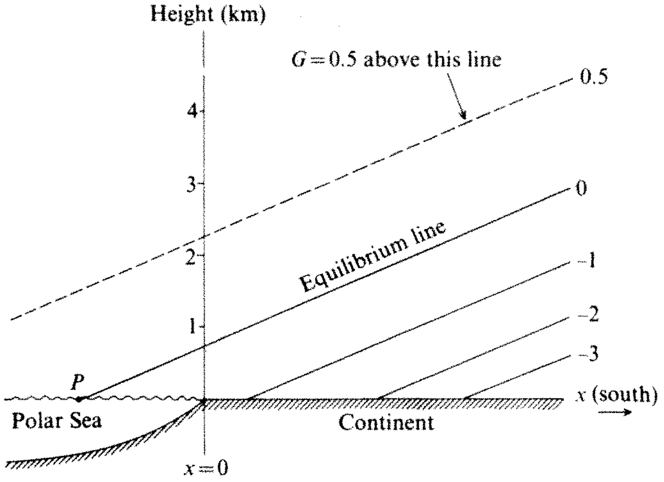

Fig. 2 Mass–balance conditions for a Northern Hemisphere ice sheet, as parameterized in the model. The intersection of the equilibrium line with sea level is called the 'climate point', and is indicated by *P*. Insolation variations are represented by shifting *P* north- and southwards. Values of the constants used are: $a = 0.73 \times 10^{-3}\ \mathrm{yr}^{-1}$, $b = 0.27 \times 10^{-6}\ \mathrm{m}^{-1}\mathrm{yr}^{-1}$, $\chi = 0.65 \times 10^{-3}$. Values for *G* are given beside each line.

A mechanism that might explain this instability is bedrock sinking. Weertman[4] first suggested this as a possible cause for rapid deglaciation in connection with the Northern Hemisphere ice sheets. I will now discuss model experiments which deal with this point.

The Northern Hemisphere ice-sheet model to be used is described by the equations[8]

$$\frac{\partial H}{\partial t} = \frac{\partial}{\partial x}\left[D\frac{\partial(H+h)}{\partial x}\right] + DH/Y^2 + G \tag{1}$$

$$\frac{\partial h}{\partial t} = -\alpha(H+3h) \tag{2}$$

$$G = a(H+h-E) + b(H+h-E)^2 \tag{3}$$

Equation (1) formulates the conservation of ice mass; it is essentially a nonlinear diffusion equation. The diffusivity for ice mass *D* increases monotonically with ice thickness *H* and the slope of the ice surface $\partial(H+h)/\partial x$ (where *h* is the bedrock height with respect to some geopotential level). The *x*-axis points in a southward direction, so the evolution of the ice sheet is explicitly computed along a meridian. The term DH/Y^2 governs lateral ice-mass discharge, where *Y* is a characteristic east–west length scale of the ice sheet. *G* is the mass balance of the sheet, and is a function of height with respect to the equilibrium line [see equation (3)]. The height of the equilibrium line (defined by $G = 0$) is denoted by *E*; it increases linearly with *x* at a rate χ (Fig. 2).

Equation (2) deals crudely with isostatic adjustment of the Earth's crust. In the equilibrium case, $h = -H/3$ corresponds to a rock density of three times that of ice. The time scale of adjustment is given by $1/3\alpha$.

Figure 2 shows in detail the appearance of the mass balance. Insolation variations may be interpreted as shifting the equilibrium line northwards and southwards. During periods with large eccentricity of the Earth's orbit, the amplitude of the 'climate point' *P*, due to precession of the equinoxes, is about 10° in terms of equivalent latitude[9]. Only during such periods does *P* reach the continent; normally, it is located in the Polar Sea.

---

[*] Present address: Institut voor Meteorologie en Oceanografie, State University of Utrecht, Princetonplein 5, 3508 TA Utrecht, The Netherlands.

0028-0836/80/400430—03$01.00

If P lies on the continent for some time, an ice sheet will start to grow. Due to the feedback between surface elevation and mass balance the ice sheet may continue to grow even if insolation increases and P returns to the Polar Sea. Bedrock sinking, however, attempts to cancel this feedback.

I have carried out several numerical integrations of equations (1)–(3). The model was solved on a grid with 70 km spacing, the lateral scale Y being 1,000 km. (For more technical detail, see ref. 8.) In the first experiment, a periodic forcing was imposed by varying the position of the climate point according to

$$P = -140 + 490 \times \sin(2\pi t/T) \text{ km} \qquad (4)$$

Remember that $P < 0$ implies that P is located in the Polar Sea. T was set to 20,000 yr, so equation (4) roughly represents conditions during maximum eccentricity. The precise form of the forcing function seems to be relatively unimportant—once the ice sheet reaches a height of ~500 m, ice-sheet dynamics take over. Thus, the only requirement is that P remains for a sufficient time on the continent. In view of this, our model can be kept simple by using equation (4) as a universal forcing function in this experiment.

Figure 3 shows four model runs with various time scales for isostatic adjustment (T^*). Figure 3*a* ($T^* = \infty$) shows the case without any movement of the bedrock. The ice sheet grows slowly, then more rapidly, and comes into a stable oscillation with quite small amplitude. A huge increase in the height of the equilibrium line would be required to remove the ice sheet.

Figure 3*b* and *c* show what happens if adjustment takes place on time scales of 30,000 and 10,000 yr, respectively. The ice sheet grows at a smaller rate now, and after about 100,000 yr disappears 'spontaneously'. Apparently, the sinking of the bedrock brings a large part of the ice surface beneath the equilibrium line, thus setting the breakdown in motion. Here, significantly, a sawtooth shape appears.

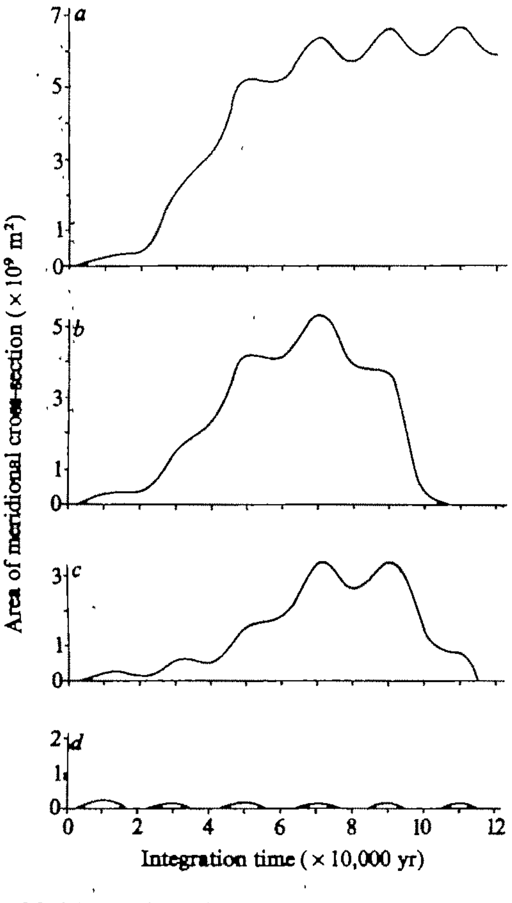

Fig. 3 Model runs with various time scales of isostatic adjustment (T^*). The area of the meridional cross-section through the ice sheet is given along the vertical axis. To obtain the ice-sheet volume, this should be multiplied by a characteristic east–west extent of the sheet. Values for T^* are: *a*, ∞; *b*, 30,000 yr; *c*, 10,000 yr; *d*, 5,000 yr.

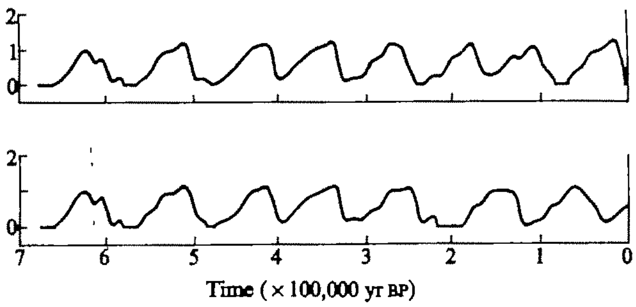

Fig. 4 Two model runs in which the Milankovitch insolation variations are imposed. The vertical axis gives a measure of the ice volume, a value of 1 on the scale corresponds to a meridional ice-sheet size of about 2,000 km and a maximum ice thickness of about 3,000 m. For more details on the parameterization of the mass balance see ref. 9. The only difference between the two runs is the value of T^*, 10,000 and 11,000 yr, respectively, in the upper and lower runs.

Figure 3*d* shows the situation when $T^* = 5{,}000$ yr, so that the isostatic balance is restored very quickly. In this case, the ice sheet cannot grow—the bedrock sinking completely cancels the effect of the height–mass balance feedback.

I next examined the situation in which the model is forced by real insolation variations. These variations were computed from expansions of the orbital parameters given by Berger[10] and translated into mass–balance variations by using an ice/snow melt model[9]. In each of two runs performed, the integration was started at 675,000 yr BP, with initial condition $H(x) = h(x) = 0$.

Figure 4 shows the results. The only difference between the two runs is the value used for the time scale of isostatic adjustment. The agreement in the character of the simulated curves and the δ^{18}O record is striking—a 100,000-yr periodicity and an asymmetric shape of the glacial cycles. However, a different situation is obtained with regard to the phase of the cycles. Although dating of the δ^{18}O record is in fact not accurate enough to verify the model simulation of all glacial cycles, a comparison of the curves shown in Fig. 4 indicates that the phase of the glacial cycles seems to be extremely sensitive to the model parameters. I believe that this property of the model reflects a realistic feature: the global climatic variations of the Pleistocene seem to have been of a stochastic periodic nature. In view of this, it seems unlikely that the present model can produce an 'in-phase simulation' of the observed ice-volume record, but it does provide a physical explanation for the occurrence of the glacial cycles.

One of the implications of the present results is that the 100,000-yr cycle is mainly internally generated by the interaction of the bedrock adjustment and the height–mass balance feedback. This means that the occurrence of a 100,000-yr peak in the power spectrum of the δ^{18}O record[2] is unrelated to variations in eccentricity. Recent work by Kominz and Pisias[11] strongly supports this view: they found that coherence spectra of an oxygen isotope record and the orbital parameters showed no significant peak around a period of 100,000 yr.

Because the present theory deals with two large ice sheets on the Northern Hemisphere continents, it seems unlikely that they can be simulated with exactly the same model parameters. It is possible, however, that the Laurentide ice sheet dominates, and trails the Eurasian one with it through the atmospheric/oceanic teleconnection. Another objection to the theory is the passive role of the Southern Hemisphere. I must stress that the fact that global ice volume seems to lag the Southern Hemisphere sea-ice extent or sea-surface temperature[2] need not imply that events in the Southern Hemisphere initiate glacial cycles. This may be simply a matter of different response times.

Thus, my main conclusion is that the 100,000-yr cycle can be explained by ice sheet/Earth's crust dynamics, as was suggested by Weertman[4]. Due to bedrock sinking, ice sheets grow very slowly. If the bedrock sinking becomes more substantial, a larger part of the ice surface comes below the equilibrium line, setting the breakdown in motion. Another glacial cycle starts if two conditions are fulfilled—summer insolation should be well below 'normal' and the bedrock should have been raised again.

Received 4 June; accepted 1 August 1980.

1. Van den Heuvel, E. P. J. *Geophys. J. R. astr. Soc.* **11**, 323-336 (1966).
2. Hays, J. D., Imbrie, J. & Shackleton, N. J. *Science* **194**, 1121-1132 (1976).
3. Weertman, J. *Nature* **261**, 17-20 (1976).
4. Weertman, J. *J. geophys. Res.* **78**, 4463-4471 (1961).
5. Pollard, D. *Nature* **272**, 233-235 (1978).
6. Imbrie, J. & Imbrie, J. Z. *Science* **207**, 943-953 (1980).
7. Weertman, J. *J. Glaciol.* **38**, 145-158 (1964).
8. Oerlemans, J. *Tellus* (in the press).
9. Oerlemans, J. & Bienfait, J. M. in *Proc. Sun and Climate Conf.* (CNES, Toulouse, 1980).
10. Berger, A. L. *J. atmos. Sci.* **35**, 2362-2367 (1978).
11. Kominz, M. A. & Pisias, N. G. *Science* **204**, 171-173 (1979).
12. Imbrie, J., Van Donk, J. & Kipp, N. G. *Quat. Res.* **3**, 10-38 (1973).

Carbon-13 in tree-ring cellulose as an indicator of past climates

T. Mazany, J. C. Lerman & A. Long

Laboratory of Isotope Geochemistry, Department of Geosciences, University of Arizona, Tucson, Arizona 85721

Following Urey's suggestion[1] that the ^{13}C abundance (usually expressed as a relative ratio: $^{13}C/^{12}C$ or $\delta^{13}C$) fixed in plant carbon may be temperature dependent, several authors have investigated the relationship between $\delta^{13}C$ and climate. These workers searched for a coefficient relating $\delta^{13}C$ variations to temperature variations[2–7]. The results, obtained on field collected samples, failed to yield agreement about the extent of a climatic effect or even its existence. Growth chamber experiments, performed on different plant species in controlled conditions to eliminate environmental factors other than temperature, showed no clear relationship between $\delta^{13}C$ and temperature[8,9]. These various contradictory results suggest that factors other than temperature contribute to determining $\delta^{13}C$ in plants. We now present evidence that the variations of the relative abundance of stable isotopes of carbon in tree rings indicate past climate changes. Thus carbon isotope composition appears to be a proxy indicator that may help to extend the meteorological data base into pre-instrument times.

To gain a better understanding of the relationship between $\delta^{13}C$ values in tree rings and climate, we analysed two dendrochronologically-dated tree sections collected at Chetro Ketl, an archaeological site in Chaco Canyon, New Mexico. These samples, one, of ponderosa pine (*Pinus ponderosa*) dating from AD 810 to 1045 (sample CK-713), the other, a white fir (*Abies concolor*) dating from AD 931 to 1047 (sample CK-857), were provided by the Laboratory of Tree-Ring Research at the University of Arizona. Tree-ring material was chosen for the experiments because it can be absolutely dated, and, in this case, tree-ring width variations provided information on climate variations with which to correlate our isotope data. These variations are derived from the regional tree-ring chronologies for Chaco Canyon, of which there is one for ponderosa pine and one for white fir[10,11]. The dendrochronological record is obtained by standardizing the ring widths of each one of several trees in one region, forming ring-width indices, with a mean value of 1.0 (see refs 10–12). These indices are averaged over the several individual trees to obtain the regional tree-ring chronology, which is given as a time series of mean standardized ring-width indices[12–14]. This filters the growth effects experienced by individual trees, while preserving climatically induced variations. In the Chaco Canyon and similar arid areas, ring-widths generally relate to climate in the following way: wide rings are produced during wet-cool years, and narrow rings during warm-dry years[14–16]. The strength of these qualitative relationships has been discussed in statistical terms in recent work by Fritts *et al.*[17].

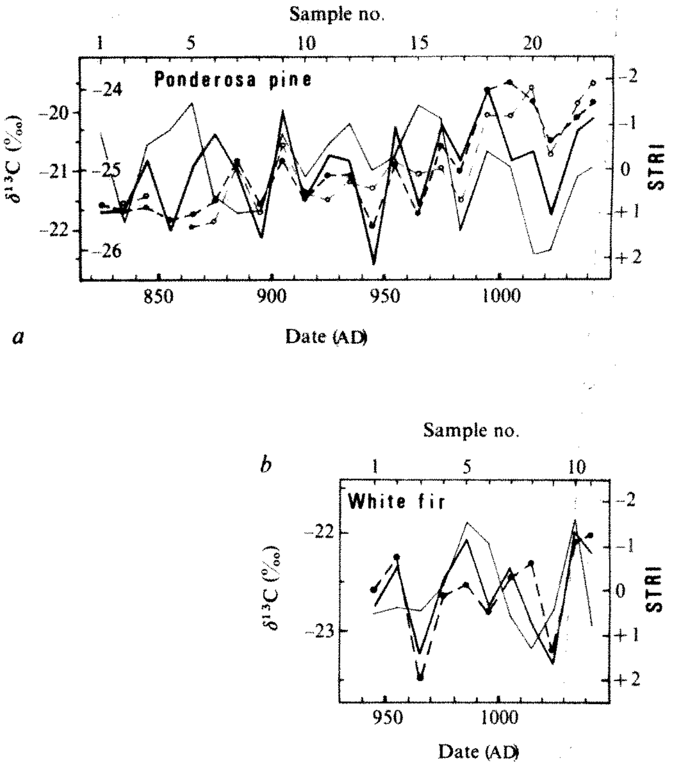

Fig. 1 Time series $\delta^{13}C$ values and tree-ring indices in the three sections from the Chetro Ketl site. All $\delta^{13}C$ values are expressed by reference to the PDB standard. The $\delta^{13}C$ scales and the STRI (standard tree ring index) scales have been normalized by subtracting to each value in a series the mean of each series then dividing it by the corresponding standard deviation. *a*, Thick line: decadal means of the Chaco Canyon regional ponderosa mean STRI. Thin line: decadal means of the individual STRI for the sampled section. Open circles: $\delta^{13}C$ (lignin) decadal values (inner scale). Solid circles: $\delta^{13}C$ (cellulose) decadal values (outer scale). *b*, Thick line: decadal means of the Chaco Canyon regional white fir mean STRI. Thin line: decadal means of the individual STRI for the samples section. Solid circles: $\delta^{13}C$ (cellulose) decadal values.

Before we could ascertain the significance of a time series of carbon isotope values and test the potential of this method for the reconstruction of palaeoclimates, we had first to determine which chemical component of wood—cellulose or lignin—is most sensitive to climate; and second, to assess the uniformity of the isotope record by studying the δ values in different tree species from the same site and by measuring the variations in isotope values of a single set of rings around the tree circumference. We began our experiment by sampling a single radius of the ponderosa pine section. This provided 22 samples of 10 yr each and one of 6 yr, beginning at AD 820. These and later samples were ground into sawdust and extracted with benzene and ethanol in a Soxhlet extractor to remove oils, waxes, resins and other relatively mobile materials which may not be coeval with the corresponding tree ring. The extracted wood was separated into cellulose and lignin using standard chemical procedures similar to those described by Browning[18]. Carbon dioxide obtained from combustion of lignin or cellulose at 800 °C was analysed with an isotope ratio mass spectrometer (Micromass 602C) with an overall precision better than 0.1‰. The results are shown in Table 1 and in Figs 1*a* and 2*a*. (In the discussion that follows we give the correlation coefficients *r* as well as their values adjusted to remove the trends reflected by the first-order autocorrelations. These adjusted values are given

0028-0836/80/400432—04$01.00

within square brackets. The adjustment was done by transforming the values in each measured series using the formula given in ref. 17, p. 21. The figures in parentheses are the 95% confidence limits.)

Results from this analysis show that the $\delta^{13}C$ values of cellulose and lignin strongly correlate with each other, $r = 0.914$ (0.80 to 0.96) [0.858 (0.65 to 0.95)] (Fig. 2*a*). The cellulose, however, has a higher correlation coefficient, $r = -0.653$ (−0.33 to −0.84) [−0.837 (−0.64 to −0.93)] with the ponderosa pine regional tree-ring index than does the lignin $r = -0.497$ (−0.08 to −0.76) [−0.666 (−0.29 to −0.86)] (Figs 1*a*, 2*a*, *b*). Thus, in our second experiment, on white fir samples, we analysed only the cellulose. The white fir section gave 11 samples dated between AD 940 and 1045, coeval with the outer 11 ponderosa pine samples. The $\delta^{13}C$ values for white fir are in general about 1.5‰ lower than the $\delta^{13}C$ values in ponderosa pine and also correlate well with the white fir regional tree-ring indices $r = -0.800$ (−0.38 to −0.95) [−0.761 (−0.25 to −0.94)] (Figs 1*b* and 2*c*).

Studies by other investigators have shown circumferential variations of $\delta^{13}C$ within a tree ring[19,20]. To check for the variations of $\delta^{13}C$ values for different azimuths around our ponderosa pine tree section and their effect on our results we analysed three different sets of rings from four radial cuts other than the original radius samples. Only cellulose was isolated. The results on different radii show circumferential variations of an amplitude of about 1‰, but the relative variations observed between the different sets of rings are almost identical (Fig. 3). However, a sequence of average isotope values composed of $\delta^{13}C$ values from several radii reflects the tree-ring width variations more closely than $\delta^{13}C$ values from a single radius (for example, the one at azimuth = 0°) does.

Our results suggest a valid correlation between carbon isotope values and climate. The $\delta^{13}C$ values for both cellulose and lignin reflect the climatic variations recorded by the regional tree-ring width indices. Of the two wood components, cellulose seems to be the most sensitive to climate. Two facts argue against this relationship being an artefact of ring width as Wigley *et al.*[21] recently suggested. First, our isotope values, which have been measured on each of the sections (of different species), correlate with the regional climatic regime recorded by the regional tree-ring index and, second but most important, the isotope values do not correlate with the tree-ring indices derived from the measurements on the single tree from which the isotope samples were taken. The correlation coefficients between $\delta^{13}C$ and tree-ring indices for each one of our specimens are not significant at the 95% level: $r = 0.256$ (−0.17 to 0.60) [−0.167 (−0.55 to 0.27)] for the ponderosa pine, and −0.072 (−0.64 to 0.55) [0.065 (−0.59 to 0.67)] for the white fir. This indicates that the carbon isotopes reflect mainly regional conditions and are not largely dependent on factors which affect only individual trees, such as tree growth or other metabolic factors. A source of systematic error might be the fact that samples containing groups of rings instead of individual rings are weighted averages of wood (cellulose), thus the δ-values are not the average values for 10 individual years. In our samples the actual ring widths of the ponderosa pine and white fir sections varied by ±30%, therefore, we do not expect that the method introduced large systematic errors. A precise estimate of the weighting error would require the knowledge of a well defined coefficient (δ-value)/(ring-width). Since such a coefficient could only be determined on the basis of many $\delta^{13}C$ analyses of individual single-year tree-rings, we could in our case, only roughly estimate it and we conclude that its magnitude did not affect our interpretation of the analyses. Obviously, single ring samples are to be preferred for palaeoclimatic research.

Several mechanisms could contribute to the observed relationship between $\delta^{13}C$ and climate. A simple but still speculative one, has been described elsewhere[22]. It is based on the fact that $\delta^{13}C$ in plant cellulose depends on the $\delta^{13}C$ value of the atmospheric CO_2 which surrounds the leaves during photosynthesis. The atmospheric $\delta^{13}C$ values vary diurnally as well as seasonally, and are more negative in times and places of greater plant respiration[22–25] because CO_2 contributed by plant respiration is depleted in $\delta^{13}C$ (for example, causing plants grown in the recirculated respired CO_2 atmosphere of very dense forests to have a δ-value as low as −39‰) (see refs 22–25). Consequently, during times when climate favours greater vegetation activity, the local atmosphere $\delta^{13}C$ values would become more negative, a change reflected in the carbon fixed in the plant cellulose[24,25].

Table 1 Cellulose and lignin contents of tree-ring samples

	Pinus ponderosa: sample CK-713				*Abies concolor*: sample CK-857		
Sample date (AD)	Regional index	Specimen index	Cellulose $\delta^{13}C$ (‰)	Lignin $\delta^{13}C$ (‰)	Regional index	Specimen index	Cellulose $\delta^{13}C$ (‰)
820–829	1.178	0.767	−21.60	—	—	—	—
830–839	1.166	1.434	−21.69	−25.43	—	—	—
840–849	0.957	0.844	−21.63	−25.34	—	—	—
850–859	1.259	0.733	−21.85	—	—	—	—
860–869	0.983	0.531	−21.73	−25.69	—	—	—
870–879	0.851	1.234	−21.53	−25.66	—	—	—
880–889	1.010	1.346	−20.83	−24.94	—	—	—
890–899	1.283	1.336	−21.57	−25.56	—	—	—
900–909	0.740	0.768	−20.82	−24.74	—	—	—
910–919	1.081	1.072	−21.45	−25.29	—	—	—
920–929	0.933	0.850	−21.05	−25.37	—	—	—
930–939	0.953	0.686	−21.05	−25.16	—	—	—
940–949	1.420	1.059	−21.95	−25.24	1.0399	1.1293	−22.59
950–959	0.823	0.919	−20.88	−24.91	0.9459	1.1049	−22.22
960–969	1.159	0.556	−21.72	−25.59	1.1498	1.1094	−23.52
970–979	0.808	0.656	−20.60	−25.02	0.9806	1.0013	−22.64
980–989	0.961	1.486	−20.99	−25.38	0.8761	0.6741	−22.50
990–999	0.659	0.898	−19.67	−24.36	1.0415	0.7891	−22.81
1000–1009	0.953	1.046	−19.50	−24.38	0.9460	1.1447	−22.46
1010–1019	0.924	1.666	−19.84	−24.03	1.0803	1.2953	−22.28
1020–1029	1.180	1.636	−20.51	−24.83	1.1723	1.0998	−23.20
1030–1039	0.831	1.101	−20.08	−24.22	0.8637	0.6740	−22.06
1040–1045	0.778	1.015	−19.82	−24.00	0.9115	1.1737	−22.00

No other factors, such as biochemical temperature effects, are necessary to explain the results of our analyses. The time series of Fig. 1*a* also shows an increasing trend in δ with time. This can probably also be ascribed to the local atmosphere existing near the soil, which is fixed by the young tree during its growth[3,5]. The relationship described above between vegetation activity and local atmosphere[22] explains the results of our research on both trees from the Chaco Canyon area (Fig. 1): increased local plant activity produces, (1) wider tree-rings, (2) more negative δ^{13}C values of the local atmosphere CO_2, and, consequently more negative δ^{13}C of plant cellulose. Experimental field work on living junipers was done by Arnold[26]. He compared the δ^{13}C in the leaves with records of close meteorological stations, and found that juniper leaves in a wide area of Arizona have more negative δ-values for years when the temperature during their growth was low and the precipitation high. These conditions are precisely those which determine wide growth rings for trees in these arid areas[12-14].

We should also discuss an apparent contradiction between the results of the present analysis and the model[22]. The model seems to require that trees from the same region should have identical δ^{13}C values, but we evaluated the correlation coefficient between the δ^{13}C values in the cellulose of the ponderosa pine and white fir samples with each other and found it to be only 0.454 (−0.20 to 0.83) [0.518 (−0.17 to 0.87)]. At first this seems to conflict with a model hypothesizing atmospheric CO_2 fluctuations as the mechanism for δ^{13}C fluctuations observed in tree rings. The explanation for this rather low correlation between δ^{13}C values of our two trees from the same region is that these trees inhabit different ecological niches which would have different local atmospheres. Ponderosa pine is found in warm and dry environments while white fir is partial to cooler and wetter environments[27]. More plant growth occurs in the wetter white fir environment, thus CO_2 more locally respired by white fir trees and other plants contributes to a more negative δ^{13}C value for the local atmosphere CO_2. This would not be in equilibrium with the bulk atmosphere, particularly in the early morning, as our field measurements showed for the White Mountains, California[22]. The white fir δ^{13}C values reflect this more negative value. This also may account for the absence of large positive peaks in the δ^{13}C white fir data, peaks which are present in the ponderosa pine data (Fig. 1*a*, *b*). This could explain the lack of a good correlation between δ^{13}C of both trees, while the lack of good correlation between both regional tree-ring chronologies would be due to each species having a different response[14,15] to climate.

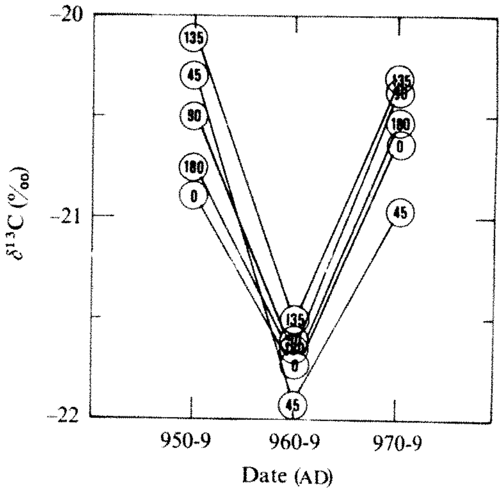

Fig. 3 Radial series: δ^{13}C (cellulose) in the ponderosa pine section at 5 different radii for 3 different decades. The figures indicate the azimuth in degrees. The azimuth 0° samples correspond to the time series of Fig. 1*a*.

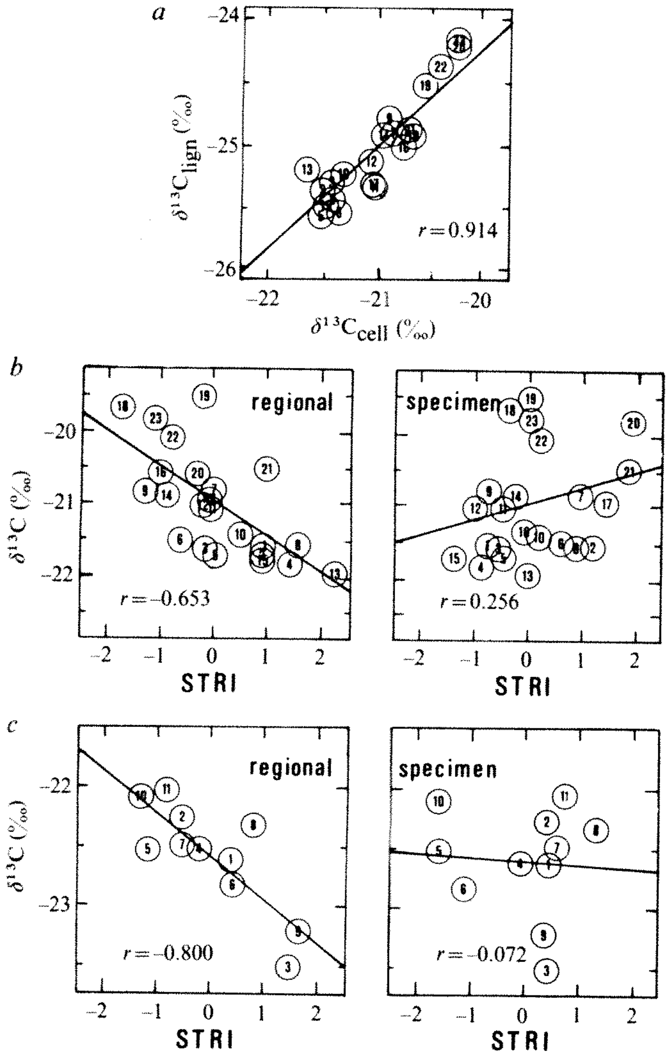

Fig. 2 Linear regressions (the figures within the circles represent sample numbers as given in Fig. 1). The *r* values adjusted for autocorrelations of first order are given in the text. *a*, δ^{13}C (cellulose) versus δ^{13}C (lignin) in ponderosa pine samples. *b*, δ^{13}C (cellulose) in ponderosa pine samples versus regional STRI (standardized tree-ring indices) for ponderosa pine. *c*, δ^{13}C (cellulose) in white fir samples versus regional STRI for white fir.

We have demonstrated a relationship between climate and stable carbon isotope values in tree rings. Cellulose is the most sensitive wood component, and in a single radius the time series variation are representative of climate. Stable carbon isotope analysis in tree rings may thus become an important method for extracting climate data from 'complacent' trees, those in which ring width variations are not responsive to climatic conditions (for example, trees tapping a permanent water source). In such a case, the isotope values of the wood should still record changes in the δ^{13}C values of the atmospheric CO_2 produced by fluctuations of the regional plant biomass. Moreover, from the above results, it seems that a single tree contains climate data equivalent to conventional dendroclimatology which, instead, uses the mean of several trees. Isotope dendroclimatology may thus be the proxy indicator that will help enlarge our data base for large scale climate models or simulations, and be also of benefit to archaeologists for local palaeoclimate reconstructions[28].

This research was funded by the NSF Climate Dynamics Program, and by the State of Arizona. We thank P. E. Damon, B. Bannister, J. Dean, H. C. Fritts and W. Robinson for useful discussions. The tree-ring samples were prepared by T. Harlan, Laboratory of Tree-Ring Research; chemical treatment and mass spectrometer analyses were performed by J. LoFaro and G. Hennington.

Received 10 March; accepted 23 July 1980.

1. Urey, H. C. *J. chem. Soc.* 562–581 (1947).
2. Craig, H. *Science* **119,** 141–143 (1954).
3. Smith, B. N. & Epstein, S. *Pl. Physiol.* **47,** 380–384 (1970).
4. Lerman, J. C. *Coll. Int. CNRS* **219,** 163–181 (1974).
5. Libby, L. M. *et al. Nature* **261,** 284–288 (1976).
6. Pearman, G. I., Francey, R. J. & Fraser, P. J. B. *Nature* **260,** 771–773 (1976).
7. Wilson, A. T. & Grinsted, M. J. *Nature* **265,** 133–135 (1977).
8. Troughton, J. *Yb. Carnegie Inst. Wash.* **73,** 780–783 (1974).
9. Smith, B. N., Oliver, J. & McMillan, C. *Bot. Gaz.* **137,** 99–104 (1976).
10. Dean, J. S. & Robinson, W. J. *Expanded Tree-Ring Chronologies for the Southwestern United States,* 39 (Laboratory of Tree-Ring Research, Univ. of Arizona, Tucson, 1978).
11. Robinson, W. J., Harrill, B. G. & Warren, R. *Tree-Ring Dates from New Mexico, B,* 16–24 (Laboratory of Tree-Ring Research, Univ. of Arizona, Tucson, 1974).
12. Bannister, B. in *Science in Archaeology* (eds Brothwell, D. & Higgs, E.) 191–205 (Thames and Hudson, London, 1969).
13. Stokes, M. A. & Smiley, T. A. *An Introduction to Tree-Ring Dating* (University of Chicago, 1968).
14. Fritts, H. C. *Tree Rings and Climate* (Academic, London, 1976).
15. Fritts, H. C. *Ecol. Monogr.* **44,** 411–440 (1974).
16. LaMarche, V. C. Jr *Science* **183,** 1043–1048 (1975).
17. Fritts, H. C., Lofgren, R. G. & Gordon, G. A. *Quat. Res.* **12,** 18–46 (1979).
18. Browning, B. L. *Methods of Wood Chemistry* (Interstate, New York, 1967).
19. Freyer, H. D. & Wiesberg, L. in *Isotope Ratios as Pollutant Source and Behavior Indicators,* 49–62 (IAEA, Vienna, 1975).
20. Tans, P. P. thesis, Univ. Gröningen (1978).
21. Wigley, T. M. L., Gray, B. M. & Kelly, P. M. *Nature* **271,** 92–93 (1978).
22. Lerman, J. C. & Long, A. in *Short Papers of the Fourth Int. Conf. Geochron. Cosmochron., Isotope Geol.* (ed Zartman, R. E.) 248–250 (USGS, 1978); in *Int. Meeting on Stable Isotopes in Tree-Ring Research, Proc.*, New Paltz, New York, 22–25 May 1979 (in the press).
23. Keeling, C. S. *Geochim. cosmochim. Acta* **23,** 322–334 (1960); **24,** 277–298 (1961).
24. Lerman, J. C. in *Environmental and Biological Control of Photosynthesis* (ed. Marcelle, R.) 323–335 (Jung, The Hague, 1975).
25. Lerman, J. C. & Raynal, *C.r. hebd. Séanc. Acad. Sci., Paris* Ser. D **215,** 1391–1394 (1974).
26. Arnold, L. D. thesis, Univ. Arizona (1979).
27. Preston, R. J. Jr *Rocky Mountain Trees,* 1963 (Dover, New York, 1948).
28. Mazany, T. in *Short Papers of the Fourth Int. Conf. Geochron. Cosmochron., Isotope Geol.* (ed. Zartman, R. E.) 280–282 (US Geological Society, 1978).

Electrophoretic evidence for two species of *Anguilla* leptocephali in the Sargasso Sea

Antonio Comparini & Emanuele Rodinò

Istituto di Biologia Animale, Università di Padova, 35100 Padova, Italy

Schmidt[1,2] produced indirect evidence that in order to reproduce the European eel (*Anguilla anguilla*) migrates to a definite zone of the Sargasso Sea, contiguous and partially overlapping the breeding area of the American eel (*Anguilla rostrata*). The two forms were recognized as distinct species on the basis of differences in meristic characters[3,4]. Later, Tucker[5] proposed that the two Atlantic eel populations originate from the same gene pool and are not distinct species but merely eco-phenotypes, their distinguishing characters being environmentally determined. More recent electrophoretic analysis has favoured the existence of two distinct species[6–9] and of particular significance from a genetic point of view is the very marked difference in malate dehydrogenase (MDH) allele frequencies between samples of American and European eels (refs 8, 10–12, Table 1*a*). However, inferring genetic isolation from genetic differentiation in eels is difficult[13,14], because of the possibility of differential selection. We report here the first observations on variability at four polymorphic loci in young *Anguilla* larvae caught in the breeding area. The observed genotype distribution and allele frequencies, particularly at the MDH-2 locus, definitely confirm the presence of two species of *Anguilla* leptocephali in the spawning zone of the Sargasso Sea.

The aim of the cruise of the FRV 'Anton Dohrn', from 19 March (Bermuda) to 9 May (Bremerhaven) (1979), was to resolve problems of sampling technique and egg and larval identification. During the period 21 March to 15 April, in the middle of spawning[1,4], more than 1,800 leptocephali of *Anguilla* were captured in different stations between 22–29° N and 55–70° W, in and near the spawning areas defined by Schmidt[1,2]. As expected, the captured leptocephali were mainly of the O-group (first year larvae) 7–25 mm in length and no more than a few weeks old[4]. Details of the fishing technique, place of capture and larval distribution are reported elsewhere[15]. Most of the larvae were preserved for myomere counts in the laboratory; 121 individuals of the O-group and five of the I-group (about 40 mm) were analysed on board by starch gel electrophoresis. Myomere counting on board was very rough due to local conditions and was later shown to be not completely reliable (for details, see ref. 16).

Table 1 Observed (and expected) genotype distribution at the MDH-2 locus (see Fig. 1) and relative allele numbers and frequencies in European and American eels (*a*) and *Anguilla* leptocephali from the Sargasso Sea (*b*)

(*a*)				
MDH-2 genotypes	*A. anguilla**		*A. rostrata*†	
aa	3 (1.6)		639 (638.2)	
ac	65 (65.8)		55 (56.5)	
cc	671 (679.1)		2 (1.3)	
Others‡	340 (332.5)		— —	
Total	1,079		696	
Alleles	No.	Frequencies	No.	Frequencies
a	83	0.039	1,333	0.958
c	1,712	0.793	59	0.042
Others§	363	0.168	—	—
(*b*)				
Genotypes	No.	Alleles	No.	Frequencies
aa	72 (45.8)	*a*	152	0.603
ac	8 (53.1)	*b*	5	0.020
cc	35 (15.4)	*c*	88	0.349
Others‖	11 (11.7)	*d*	2	0.008
		e	5	0.020
Total	126		252	

Only genotypes and alleles common to both species are reported in full.

* Totals are obtained by pooling unpublished genotype distributions observed in samples of *A. anguilla*[11,12].

† Pooled data from Williams *et al.*[10].

‡ Observed number of other genotypes also fitted well with Hardy–Weinberg distribution.

§ Frequencies of 'other' alleles: $b = 0.047$; $d = 0.025$; $e = 0.088$; three very rare alleles = 0.009.

‖ 'Other' observed genotypes: $bb = 1$; $bc = 3$; $cd = 2$; $ce = 5$.

For (*b*), $\chi^2_{(3)} = 78.3$, $P \ll 0.01$.

Among enzyme systems reported polymorphic in elvers and older eels[8,10–12], only three showed enough activity or clear enough electrophoretic patterns for a reliable genetic interpretation—MDH, phosphoglucose isomerase (PGI) and lactate dehydrogenase (LDH). Special attention was given to the scoring of MDH because of the previously reported difference in allelic frequencies between the two populations.

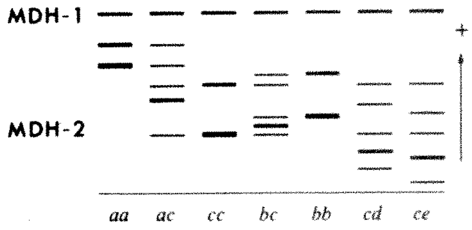

Fig. 1 Schematic representation of the MDH electrophoretic patterns observed in the leptocephali sample and genetic interpretation of variability at the MDH-2 locus. It is assumed that polypeptide products of the two loci randomly assemble to form homodimers and intralocus and interlocus heterodimers of intermediate electrophoretic mobility. Following our previous convention[17], the alleles are indicated by *a*, *b*, *c*, *d*, *e* in the order of the anodic mobility of the respective homodimer bands. Previous laboratory analysis of the MDH pattern in a sample of American eels has shown that the common MDH-2 allele of *A. rostrata* (named *a* by Williams *et al.*[10]) has the same electrophoretic mobility as the fast allele *a* previously reported in *A. anguilla*[11,12,17]; the rare allele *b* of *A. rostrata*[10] corresponds to the common allele *c* of *A. anguilla*[11,12,17].

0028–0836/80/400435—03$01.00

Table 2 Observed (and expected) genotype distribution at PGI-1, PGI-2 and LDH-2 loci in samples of *A. anguilla* and *A. rostrata* leptocephali.

Loci and genotypes*	*A. anguilla*†	*A. rostrata*†
PGI-1		
bb	28 (29.8)	67 (67.1)
ab	9 (7.2)	4 (3.9)
bc	9 (7.2)	1 (0.9)
Others	0 (1.8)	0 (0.1)
Total	46	72
	‡$P<0.001$	
PGI-2		
bb	39 (39.3)	67 (67.1)
ab	2 (1.8)	3 (2.9)
bc	4 (3.7)	2 (1.9)
bd	1 (0.9)	0 (0.0)
Others	0 (0.3)	0 (0.1)
Total	46	72
	n.s.	
LDH-2		
aa	29 (29.4)	50 (50.0)
bb	0 (0.3)	0 (0.0)
ab	7 (6.3)	1 (1.0)
Total	36	51
	$P<0.01$	

* The genetic interpretation of the electrophoretic patterns and the electrophoretic methods are reported in refs 11, 17, 20.

† Species identification on the basis of MDH-2 genotypes.

‡ P values are computed with contingency χ^2 tests on the number of alleles, and with a weighted homogeneity test for allele frequencies[21].

The larval MDH electrophoretic patterns (Fig. 1) correspond closely to those previously described in elvers and adults of *A. anguilla* (Fig. 2) and *A. rostrata*[10]; as in other teleosts[18] they are genetically explicable assuming the presence of two MDH loci, one of which is polymorphic in the *Anguilla* species. The observed and expected genotype distribution and the allele frequencies for the polymorphic locus MDH-2, in the whole larval sample, are reported in Table 1*b*. The observed genotype distribution shows a very strong homozygote excess as compared with that expected according to the Hardy–Weinberg law.

Excluding inbreeding and selection against heterozygotes in a sample consisting mostly of very young larvae, the homozygote excess most probably results from the sampling together of individuals originating from two distinct populations with appreciable difference in allele frequencies (the Wahlund effect). This is consistent with the view that the sample was made up of groups of larvae belonging to both *Anguilla* species having respectively the same, or very similar, allele frequencies to those reported for samples of elvers and older eels 'recruits' and 'residents', respectively[10].

If this is true, then the MDH-2 genotype can also be useful in young leptocephali as a diagnostic character of the species, easier to recognize and more reliable at this stage than the rough myomere count made on board[15,16]. Indeed, in pooled samples of recruits and residents, on the basis of the reported MDH-2 allele frequencies (Table 1*a*), the probability of correct diagnosis of the species is more than 0.998 (as calculated applying the Ayala and Powell[19] statistics) if the *aa* homozygotes are scored as *A. rostrata*, the heterozygotes showing the 'ambiguous' genotype *ac* are not considered and all the other genotypes are scored as *A. anguilla*.

With the use of this parameter and omitting the eight observed *ac* individuals, the remaining 118 leptocephali analysed on board can be separated into 72 *A. rostrata* (*aa* genotypes) and 46 *A. anguilla* (*cc* and other genotypes). Laboratory myomere counts of preserved larvae, now in progress, are indeed showing that in the main batch of leptocephali *A. rostrata* larvae were the more abundant (F.-W. Tesch, personal communication).

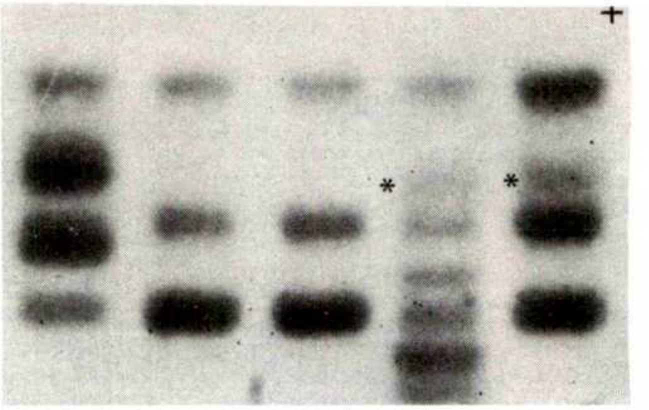

Fig. 2 Photograph of some MDH electrophoretic patterns observed in specimens of *A. anguilla*. The MDH-2 genotypes, from left to right, are: *ac*, *cc*, *cc*, *ce*, *cc*. Asterisks indicate bands corresponding to the mitochondrial MDH activity which appear in frozen specimens. Horizontal electrophoresis in 11.5% starch gel was carried out using electrode buffer 0.18 M Tris-citrate, *p*H 7.5, 1:15 diluted in the gel. The staining solution was: neutralized L-malic acid (10^{-2} M), NAD (10^{-3} M), monotetrazolium salt (10^{-3} M), phenazine methosulphate (10^{-4} M) in 0.05 M Tris-HCl, *p*H 8.

On the basis of the previous assumption, we report in Table 2 the genotype distribution at the PGI-1, PGI-2 and LDH-2 loci for the two larval groups. The observed numbers are in each case near to the expected assuming Hardy–Weinberg equilibrium. Comparison of allele numbers and of allele frequencies with statistical tests showed significant differences at the PGI-1 and LDH-2 loci, supporting the genetic separation of the two groups. Table 3 shows the allele frequencies at the same loci for both groups, in comparison with those observed in pooled samples of *A. anguilla*[11,12] and *A. rostrata*[14], respectively.

In *A. anguilla*, there is no appreciable difference, at these loci, between larvae caught in the spawning zone and eels caught in different European coastal waters[11]. It seems, therefore, that there is no differential selection at these loci during the years of larval drift; this is in accord with our previous observations of a lack of genetic differentiation among samples of recruits from different parts of Europe[11,12,20].

Table 3 Allele frequencies at PGI-1, PGI-2 and LDH-2 loci in samples of *A. anguilla* and *A. rostrata* leptocephali (L). For comparison, data from pooled samples (P) of both eel species are reported.

Loci and	*A. anguilla*		*A. rostrata*	
alleles	L	P*	L	P†
PGI-1	46	1,058	72	
a	0.098	0.083	0.028	
b	0.804	0.822	0.965	No
c	0.098	0.089	0.007	data
Others	—	0.006	—	
	n.s.			
PGI-2	46	1,067	72	2,271
a	0.022	0.008	0.021	0.009
b	0.924	0.941	0.965	0.788
c	0.043	0.049	0.014	0.203
d	0.011	0.002	—	—
	n.s.		(‡ $P<0.001$)	
LDH-2	36	820	51	
a	0.903	0.915	0.990	No
b	0.097	0.085	0.010	data
	n.s.			

* Pooled data from our previous paper[11,12].

† Pooled data for 'recruits' only from Koehn and Williams[14].

‡ P values are computed according to Workman and Niswander test[21].

In *A. rostrata*, comparable data are available only for the PGI-2 locus. There is a very significant difference in allele frequencies between the larval sample and that reported for recruits of the North American shore. Moreover, in resident eels of this species, a latitudinal cline in allele frequencies at this locus was observed, while recruits were genetically homogeneous[10]. This pattern was demonstrated to be temporally constant[14]. The higher frequency of the common allele *b* (>0.9, and close to that found in leptocephali) was obtained in the northern part of the sampled range (Halifax, Nova Scotia; St John's, Newfoundland). It is perhaps premature to make the hypothesis of a temporal or geographical subdivision in the spawning of *A. rostrata* adults coming from different parts of the American coast; however, we note that some doubts still remain about the extension of the spawning place of this species[22].

In conclusion, observation on the genetic variability of some enzyme loci in a sample of young *Anguilla* leptocephali caught in the spawning ground have shown the existence in this zone of larvae from two different gene pools, thus definitively confirming Schmidt's theory of the existence of two distinct Atlantic *Anguilla* species.

The cruise was sponsored by the International Council for the Exploration of the Sea as a preliminary part of the International Eel Expedition[23]. This work was also supported by the Italian National Research Council through funds granted to the Institute of Marine Biology of Venice. We thank Dr F.-W. Tesch (Biologische Anstalt Helgoland, Hamburg) for enabling A.C. to participate in the cruise and for his help, Professor B. Battaglia for discussions and Professor J. A. Beardmore for help with the manuscript and English text.

Received 20 February; accepted 14 July 1980.

1. Schmidt, J. *Nature* **111,** 51–54 (1923).
2. Schmidt, J. *A. Rep. Smithson. Inst. for 1924*, 279–316 (1925).
3. Ege, W. *Dana Rep.* **16,** 1–256 (1939).
4. Tesch, F.-W. in *The Eel* (Chapman & Hall, London, 1977).
5. Tucker, D. W. *Nature* **183,** 495–501 (1959).
6. Sick, K., Bahn, E., Frydenberg, O., Nielsen, J. T. & von Wettstein, D. *Nature* **214,** 1141–1142 (1967).
7. Drilhon, A. & Fine, J. M. *Rapp. P.-v. Réun. Cons. perm. int. Explor. Mer* **161,** 122–125 (1971).
8. de Ligny, W. & Pantelouris, E. M. *Nature* **246,** 518–519 (1973).
9. Jamieson, A. & Turner, R. J. *Biol. J. Linn. Soc.* **13,** 41–45 (1980).
10. Williams, G. C., Koehn, R. K. & Mitton, J. B. *Evolution* **27,** 192–204 (1973).
11. Rodinò, E. & Comparini, A. in *Marine Organisms, Genetics, Ecology and Evolution* (eds Battaglia, B. & Beardmore, J. A.) 389–424 (Plenum, New York, 1978).
12. Rodinò, E. & Comparini, A. *Boll. Zool.* **45,** Suppl. II, 47–61 (1978).
13. Koehn, R. K. *Mar. Biol.* **14,** 179–181 (1972).
14. Koehn, R. K. & Williams, G. C. *Evolution* **32,** 624–637 (1978).
15. Tesch, F.-W., Kracht, R., Schoth, M., Smith, D. G. & Wegner, G. *ICES*, C. M. 1979 M: 6 (in the press).
16. Comparini, A., Kracht, R., Schoth, M. & Tesch, F.-W. (in preparation).
17. Comparini, A., Rizzotti, M., Nardella, M. & Rodinò, E. *Boll. Zool.* **42,** 283–288 (1975).
18. Master, C. J. & Holmes, R. S. *Res. Mon. Frontiers Biol.* **42,** 1–308 (1975).
19. Ayala, F. J. & Powell, J. R. *Proc. natn. Acad. Sci. U.S.A.* **69,** 1094–1096 (1972).
20. Comparini, A., Rizzotti, M. & Rodinò, E. *Mar. Biol.* **43,** 109–116 (1977).
21. Workman, P. L. & Niswander, J. D. *Am. J. Hum. Genet.* **22,** 24–49 (1970).
22. Vladykov, V. D. *J. Fish. Res. Bd Can.* **21,** 1523–1530 (1964).
23. *SCOR Proc.* **14,** 49–50 (1978).

Cytolytically active murine T-cell hybrids

M. Nabholz*, M. Cianfriglia*, O. Acuto*, A. Conzelmann*, W. Haas†, H. v. Boehmer†, H. R. McDonald‡, H. Pohlit§ & J. P. Johnson‖

* Swiss Institute for Experimental Cancer Research, CH-1066 Epalinges, Switzerland
† Basel Institute of Immunology, CH-4058 Basel, Switzerland
‡ Ludwig Institute of Cancer Research, CH-1066 Epalinges, Switzerland
§ Institut Pasteur, Paris, France
‖ Institut für Immunologie, Universität München, D-8000 München, FRG

Following the demonstration that hybrids between normal B-lymphocytes and myeloma cell lines continue to secrete antibodies with the same specificity as those produced by the parental B-cells[1], many groups have tried to use this approach to obtain cell lines expressing T-lymphocyte functions by crossing thymoma lines not expressing any measurable activity with various types of T-cell populations. Although there have been reports that hybrids could be isolated which secrete T-cell products with immunological activity[2–5], efforts to produce functionally active hybrids from cytolytic T-cells have all been unsuccessful (refs 6, 7, and M. N. and H. D. Engers, unpublished). We have fused an established, T-cell growth factor (TCGF)-dependent murine cytolytic T-lymphocyte (CTL) line with a mouse thymoma line and have obtained hybrids with cytolytic activity when we selected the hybrids in TCGF-containing medium, while hybrids isolated in the absence of growth factor showed no detectable cytolytic potential.

Recently, clonable murine T-cell lines with cytolytic activity have been derived from normal CTL populations cultured in medium supplemented with TCGF-containing supernatant from concanavalin A (Con A)-stimulated spleen cells (CS)[8,9]. Such CTL lines remain strictly dependent on CS medium for growth, but share many characteristics with permanent cell lines derived from other tissues[10]. B6.1.2 is a cloned CTL line obtained from spleen cells of a female C57Bl/6 mouse activated against syngeneic male cells. At the time of its isolation, it was cytolytically active against lipopolysaccharide-activated spleen cells (LPS-blasts) from male mice carrying the H–2D^{b} allele as well as from H–2D^{d} mice of either sex[11]. A mutant, TG14.OU5, was derived from this line, which is resistant to both 6-thioguanine (TG^{r}, 10^{-4} M) and ouabain (OU^{r}, 10^{-3} M), by two cycles of mutagenesis with ethyl methane sulphonate, followed by single-step selection with one of the drugs[10]. The resistant phenotype of this mutant has remained stable for 8 months of growth in the absence of either drug. The parental cells and the mutant show comparable lytic activity against the BALB/c myeloma S194, but both lines today display only marginal activity against LPS-blast targets.

B6.1.2 and TG14.OU5 have a near-diploid karyotype with several abnormal metacentric chromosomes[10] (Table 1). The cells have an irregular shape and grow mainly in suspension with only a slight tendency to adhere (Fig. 1). CSP.2 is a CTL line derived from C3H/HeJ (H–2^{k}) cells activated against syngeneic spleen cells haptenated with 3-(p-sulphophenyldiazo)-4-hydroxyphenylacetic acid (SP)[10]. In its lytic activity this line is hapten specific and H–2 restricted (Fig. 4): it will lyse SP-coupled LPS-blasts from B10-A (H–2K^{k}D^{d}) mice but shows no significant activity against hapenated B10.AQR (H–2K^{q}D^{d}) target cells.

B6.1.2, TG14.OU5 and CSP.2 all express the Thy-1.2 alloantigen. The thymoma lines used in the experiments described here, AKR-A (from Dr R. Herberman, NCI) and a TG^{r}OU^{r} BW5147 subline (from Dr. R. Hyman, Salk Institute) express the Thy-1.1 allele. They grow in suspension, in medium with or without CS, and show no detectable lytic activity against S194 or LPS-blasts, even when Con A is added to overcome the requirement for specific target-cell recognition[12]. AKR-A has a near-tetraploid karyotype and most cells carry one characteristic metacentric chromosome (Table 1).

Cells of the parent lines were mixed and fused, and plated out in different media (see Fig. 2 legend for details). Two to three weeks after fusion the plates were scored for growth: no growth was detected in plates with or without CS seeded with PEG-treated cells of only one of the parental lines or with untreated cell mixtures. In plates seeded with mixtures of AKR-A and TG14.OU5 cells treated with 50% polyethylene glycol

0028-0836/80/400437—04$01.00

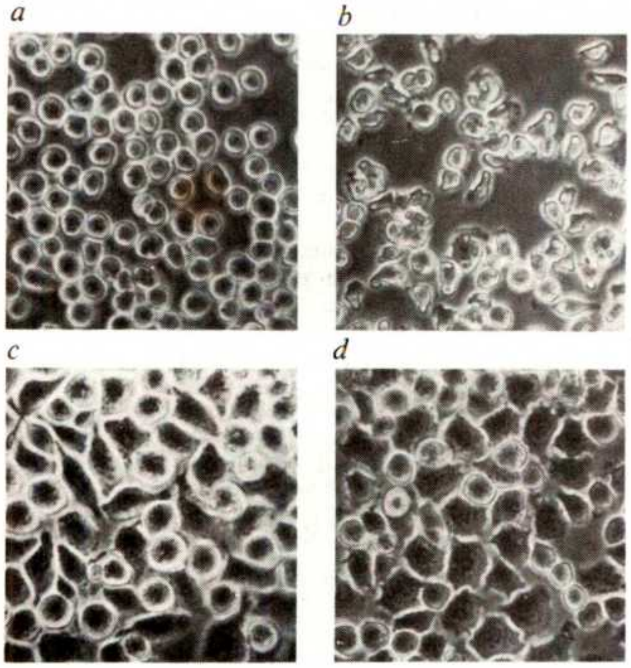

Fig. 1 Morphology of parental cell lines, AKR-A (*a*) and B6.1.2 TG14.OU5 (*b*) and two cytolytically active hybrid clones, MN9.19.7 (*c*) and MN9.20.2 (*d*). Phase-contrast micrographs of living cells.

(PEG), vigorous growth was observed in 70 of 96 wells not containing CS, and in 95 of 96 wells with CS. The cells growing in the absence of CS were round or slightly irregular and resembled the thymoma parent. They showed no tendency to adhere to the plastic surface and piled up to form regularly shaped colonies. The same cell type was found in many wells containing CS, but in addition most of the latter wells contained colonies formed by cells with a morphology quite distinct from that of either parent (Fig. 1): these cells were very large and flat and adhered quite strongly to the plastic surface. Size and shape varied somewhat from colony to colony, and although they clearly showed a strong tendency to adhere they could form multiple layers.

Table 1 Chromosome constitution of parental cells and two hybrid clones

	Total	Biarmed	Markers		
			AKR-A	TG14.OU5	
AKR-A	77.5(71–79) ±2.3	1.8(0–2) ±0.4	9/10	0/10	0/10
TG14.OU5	32.2(28–34) ±1.7	8.1(8–9) ±0.3	0/14	14/14	14/14
MN9.19.7	126.7(93–144) ±15.8	11.4(9–14) ±1.4	8/12	12/12	12/12
MN9.20.2	89.3(81–105) ±21.9	8.1(6/9) ±1.3	10/10	10/10	9/10

Chromosomes were prepared using the ASG-banding technique[17] and classified according to Nesbitt and Franke[18]. Chromosome number (range) ± s.d. was determined and the same metaphases were screened for the presence of marker chromosomes characteristic for the parental cell lines. Almost all MN9.19.7 metaphases contained two copies of each of the TG14.OU5 markers. TG14.OU5 lacks recognizable chromosomes 6, 7 and 8, whilst AKR-A and the hybrids contain several copies of these chromosomes.

We found that none of 34 populations selected in the absence of CS displayed any cytolytic activity whereas 60 of 79 presumptive hybrids selected in the presences of CS gave more than 10% specific lysis in the presence of Con A (Fig. 2). When the morphology of the latter hybrids was scored, it became apparent that all of the populations from the six wells containing only or almost only thymona-like cells gave less than 10% lysis. Ten independent (uncloned) populations, selected in the presence of CS, were expanded and maintained in CS medium containing HAT and ouabain (HOS medium). Their growth rate is comparable to that of the CTL parent line. Two of these populations consisted entirely of cells with the thymoma-like morphology. All 10 populations expressed both parental Thy-1 alleles: more than 90% of the cells were lysed when treated with monoclonal anti-Thy-1.2 or anti-Thy-1.1 antibodies and complement. Background lysis was less than 10%. The cytolytic activity of these hybrids against S194 varied (Fig. 3). The two thymoma-like hybrids had no detectable activity, even in the presence of Con A. The adherently growing hybrids all expressed some activity in the presence of the lectin and all except one showed some lysis also in its absence.

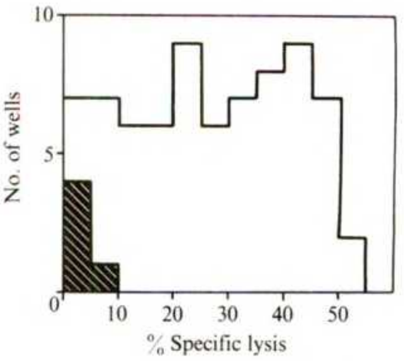

Fig. 2 Cyolytic activity of AKR-A × TG14.OU5 hybrids selected in medium supplemented with Con A supernatant. Before fusion the drug-resistant parents were grown for two passages in medium containing thioguanine and ouabain to eliminate any revertants. 1×10^7 cells of either parent were mixed and fused using 50% PEG (molecular weight 1,000) in a procedure essentially identical to the one described by Galfré *et al.*[14]. The fused cells were plated out at a density of 1×10^4 per cell type per well per 100 μl in flat-bottom microtitre plates (96 wells, Costar) in MLC medium or in MLC medium supplemented with 30% CS[8]. 100 μl of the same medium containing 10^{-4}M hypoxanthine, 5×10^{-7} M amethopterin, 1.6×10^{-5} M thymidine (HAT)[15] and 2×10^{-3} ouabain were added to each well on the next day. (This medium selects for cells in which the codominant ouabain resistance marker of one parent is complemented with the wild-type hypoxanthine phosphoribosyl transferase gene of the other.) One week later about two-thirds of the medium was replaced, keeping the HAT and ouabain concentration constant. 24 days after fusion cells were detached by vigorous pipetting with a multichannel micropipette (Flow) and transferred to round-bottom 96-well microtitre plates (Greiner). They were washed once and 10^4 ^{51}Cr-labelled S194 target cells and Con A (10 μg ml^{-1} final concentration) were added, all in Dulbecco's minimal essential medium with 5% fetal bovine serum. Plates were spun for 1 min at 1,000 r.p.m. and incubated for 6 h at 37°C. Specific isotope release into the medium was determined according to Brunner *et al.*[16]. Spontaneous release was 12%. Hatched bars show activity of populations from wells containing only thymoma-like cells.

Several of the independent cytolytically active hybrids were cloned, by plating cells at limiting dilutions (0.3 cells per well in HOS medium on feeder layers of irradiated peritoneal C3H cells[8]). Two independent clones have now been maintained in continuous culture for three months and are still cytolytically active, although the activity of one of them has declined considerably. Seventy days after fusion these two clones were

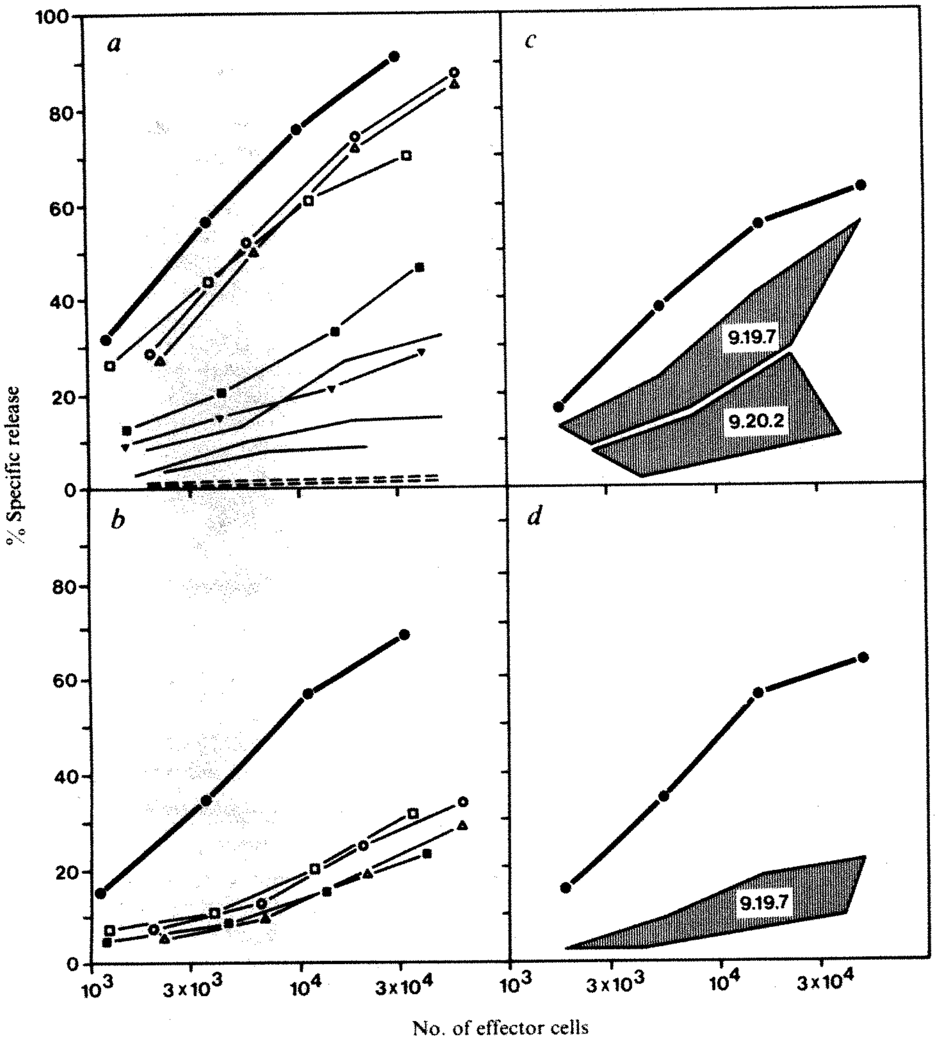

Fig. 3 Cytolytic activity (^{51}Cr release) of independent uncloned populations of AKR-A × TG14.OU5 hybrids (*a*, *b*) and individual clones (*c*, *d*), assayed in presence (*a*, *c*) and absence (*b*, *d*) of Con A. Targets: 10^4 S194 cells. Effector cells were collected during exponential growth. Adherent populations were detached with 0.02% EDTA in phosphate-buffered saline. ●, TG14.OU5. In *a* and *b*: ——, adherently growing hybrids; — — —, thymoma-like hybrids; ■, MN 9.19; ▼, MN9.20. In *c* and *d* the shaded areas indicate the range of activities of subclones derived from two cloned hybrids: MN9.19.7 (five subclones) and MN9.20.2 (four subclones). In *b* and *d* only significant activites are plotted. All subclones of 9.19.7 were active.

subcloned. All of the tested subclones gave significant lysis when tested in the presence of Con A, but most of the clones derived from the weaker line had only marginal activity (Fig. 3). Karyotype analysis of these two lines demonstrates that one of them contains approximately one set of each of the parental chromosomes, whilst the other carries two sets of TG14.OU5 chromosomes and one from the thymoma parent (Table 1).

It is very difficult to determine whether the AKR-A × TG14.OU5 hybrids described above express determinant-specific recognition structures, because, in the absence of Con A, the CTL-line parent as well as the hybrids show significant lytic activity only against tumour cell targets and, as we have argued elsewhere[10], such targets are not adequate for a specificity analysis of established CTL lines.

We therefore crossed the TG^{r}OU^r BW5147 thymoma line with CSP.2 using an essentially identical procedure. The results of this fusion were very similar to those of the AKR-A × TG14.OU5 cross[13], except that the morphological differences between the hybrids selected in the presence and those selected in the absence of CS were less obvious. We tested four hybrid populations selected without CS and seven selected in the presence of CS for expression of parental Thy-1 alleles and specific cytolytic activity. More than 90% of the cells of all populations were lysed by both anti-Thy-1.1 and anti-Thy-1.2 antibodies and complement. None of the CS-independent populations showed any lytic activity whilst all of the populations selected in CS lysed SP-coupled but not unhaptenated H-2^k LPS-blasts. Several of the active hybrids were tested against targets of different H-2 haplotypes and their activity was

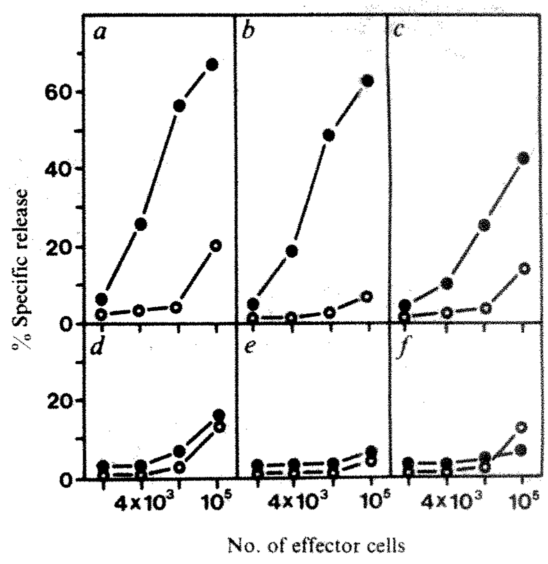

Fig. 4 Specificity and H-2 restriction of hybrids between BW5147 and CSP.2. Targets: LPS-blasts, untreated (○) or haptenated with 50 mM 3-(*p*-sulphophenyldiazo)-4-hydroxyphenylacetic acid (●), from B10.A mice (*a*, *b*, *c*; H-2 haplotype K^{k}I-A^{k}I-C^{d}D^d) or B10.AQR (*d*, *e*, *f*; qkdd). Effector cells: *a* and *d*, CSP.2; *b* and *e*, hybrid MN12.18.17; *c* and *f*, hybrid MN12.7. 3-h assay with 10^4 targets, spontaneous release ranged from 13–15%.

found to be H-2 restricted (Fig. 4). Active clones were obtained by limiting dilution and have maintained their specific activity for several months of continuous culture.

Our findings suggest that the earlier failures to obtain cytolytically active CTL-thymoma hybrids were due to the fact that such hybrids share the requirement for TCGF with their CTL parents and were not detected because all selections were carried out in the absence of CS. However, alternative explanations are possible. Clearly, our results suggest a relationship between TCGF dependence and expression of cytolytic competence. But, at present, we cannot decide whether the cytolytically incompetent, TCGF-independent thymoma-like hybrids are derived from active, growth factor-dependent cells, for example, by segregation of a particular CTL-line chromosome or whether the active hybrids have lost a thymoma chromosome carrying a gene (or genes) suppressing the CTL phenotype in the inactive hybrids. Other, less attractive possibilities have to be envisaged: (1) the two types of hybrids may be derived from different variants co-existing in the thymoma or the CTL lines. This interpretation is made unlikely by the very similar results obtained in three different crosses involving two thymomas and three CTL clones[13]. (2) Alternatively, the manifestation of the CTL phenotype in a hybrid may depend on a single stochastic event occurring early after fusion or it may be determined, for example, by the stage of the cell cycle in which the cells giving rise to a hybrid clone are at the moment of fusion.

Whatever the answers to these questions may be, it appears likely that cytolytic T-cell hybrids will provide us with new efficient tools for a genetic analysis of the control of the expression of T-cell functions.

This work was supported, in part, by grants from the Swiss NSF (to M.N.), the Schweizerische Krebsliga (to M.N. and A.C.) and the Deutsche Forschungsgemeinschaft (Sonderforschungsbereich 37-B9 to J.J.). M.C. is recipient of an EMBO fellowship. We thank Drs F. Fitch and M. Gefter for gifts of monoclonal antibodies.

Received 17 April; accepted 5 August 1980.

1. Köhler, G. & Milstein, C. *Nature* **256,** 495–497 (1975).
2. Taniguchi, M. & Miller, J.F.A.P. *J. exp. Med.* **148,** 373–382 (1978).
3. Kontiainen, S. *et al. Nature* **274,** 477–480 (1978).
4. Watanabe, T., Kimoto, M., Marynama, S., Kishimoto, T. & Tamamura, Y. *J. Immun.* **121,** 2113–2117 (1978).
5. Taussig, M. J., Corvalan, J. R. F., Bims, R. M. & Holliman, A. *Nature* **277,** 305–307 (1979).
6. Hämmerling, G. J. *Eur. J. Immun.* **7,** 743–746 (1977).
7. Köhler, G., Lefkovits, I., Elliot, B. & Coutinho, A. *Eur. J. Immun.* **7,** 758–761 (1977).
8. Nabholz, M., Engers, H. D., Collavo, D. & North, M. *Curr. Topics Microbiol. Immun.* **81,** 176–187 (1978).
9. Baker, P. E., Gillis, S. & Smith, K. A. *J. exp. Med.* **149,** 273–278 (1979).
10. Nabholz, M. *et al. Immun. Rev.* **51,** 125–156 (1980).
11. v. Boehmer, H. *et al. Eur. J. Immun.* **9,** 592–596 (1979).
12. Bevan, M. & Cohn, M. *J. Immun.* **114,** 559–565 (1975).
13. Conzelmann, A. *et al.* in *Proc. XXVIII Annual Coll. on Protides of the Biological Fluids* (ed. Peeters, H.) (in the press).
14. Galfré, G., Howe, S. C., Milstein, C., Butcher, G. W. & Howard, J. C. *Nature* **266,** 550–552 (1977).
15. Littlefield, J. W. *Science,* **145,** 709–710 (1964).
16. Brunner, K. T., Engers, H. D. & Cerottini, J.-C. in *In vitro Methods of Cell-mediated and Tumor Immunity* (eds Bloom, B. R. & David, J. R.) 737–740 (Academic, New York, 1976).
17. Buckland, R. A., Evans, H. J. & Sumner, A. T. *Expl Cell Res.* **69,** 231–236 (1971).
18. Nesbitt, M. N. & Francke, U. *Chromosoma* **41,** 145–158 (1973).
19. Pohlit, H., Haas, W. & v. Boehmer, H. *Eur. J. Immun.* **9,** 681–690 (1979).

Control of natural resistance to *Salmonella typhimurium* and *Leishmania donovani* in mice by closely linked but distinct genetic loci

Alison D. O'Brien,* David L. Rosenstreich† & Benjamin A. Taylor‡

*Department of Microbiology, Uniformed Services University of the Health Sciences, Bethesda, Maryland, 20014
†Department of Medicine and Microbiology, Albert Einstein College of Medicine, New York, New York, 10046
‡Jackson Laboratory, Bar Harbor, Maine, 04609

Inbred strains of mice vary in their sensitivity to infection with both *Salmonella typhimurium*[1,2] and *Leishmania donovani*[3]. In both cases, this differential susceptibility is genetically controlled. Resistance to the intracellular parasite *L. donovani* is determined by a single locus on chromosome 1, designated *Lsh* (ref. 4). The primary regulator of resistance to *S. typhimurium* is a single, dominant autosomal gene, named *Ity* (for immunity to *typhimurium*)[5], and it has also been recently mapped to chromosome 1 (ref. 6). In addition, two other genetic loci regulate resistance to *S. typhimurium* in mice. These genes, *Lps*^{d} and *xid*, are mutant alleles that render C3H/HeJ and CBA/N mice, respectively, salmonella susceptible[7,8]. Both Bradley and his colleagues[3,4], and Plant and Glynn[2,6], noted similar patterns of resistance or susceptibility of inbred strains of mice to *L. donovani* and *S. typhimurium*, and therefore suggested that *Lsh* and *Ity* might be the same gene. Mapping of both genes to the same region of chromosome 1 supported this hypothesis but no linkage studies have been used to test it. Since recombinant inbred (RI) mouse strains are, in effect, permanent segregant populations[9], they are ideal for determining linkage between resistance genes to two different pathogens. Therefore, we determined the *S. typhimurium* susceptibility of five sets of RI mouse strains that had been previously typed for *Lsh*[4] and conclude that *Lsh* and *Ity* are closely linked but distinct genetic loci.

Mice from 25 BXD RI and their salmonella-resistant (DBA/2J)[5] and -susceptible (C57BL/6J)[5] progenitor strains (Jackson Laboratory) were injected subcutaneously (s.c.) with approximately 25 *S. typhimurium* organisms of the virulent TML strain[10]. The actual number of organisms administered was determined by plate count. The cumulative 28-day mortality was then assessed. For each strain at least two separate experiments were performed and progenitor strain controls were always included. In addition, the geometric mean number of *S. typhimurium* per spleen for each RI strain was ascertained[7] at day 9 after s.c. infection of mice with 10^3 TML.

The number of viable organisms per spleen of animals which died from salmonellosis before day 9 was estimated as 10^8 based on spleen counts in highly moribund mice. A comparison of the *Lsh* type, as previously reported by Bradley *et al.*, and the *Ity* types derived from our experiments, is shown in Table 1. RI strains were classified as *Ity*^{s} if $\geq$60% of the animals in a group died and if the $\log_{10}$ geometric mean counts per spleen were >5.0, whereas strains were considered *Ity*^{r} if mortality was $\leq$40% and if the $\log_{10}$ geometric mean counts were <4.50. The viable count limits for assigning an *Ity* type were chosen on the basis of the 99.9% confidence limits on the geometric means of the progenitor control strains. For those RI strains with lethality between 40 and 60% (that is, BXD-22, -19, -29, -25 and -8), *Ity* types were determined by spleen counts only because this single criterion was used by Plant and Glynn[6] for mapping the *Ity* locus. The *Ity* types of two RI strains (BXD-28 and BXD-31) were not designated because >60% of the animals died although their geometric mean spleen counts were in the resistant range. The discrepancy between these two parameters in BXD-28 and BXD-31 mice and the intermediate lethality (40–60%) for five BXD RI strains suggest that another gene(s), distinct from *Ity*, is influencing the outcome of infection. This is supported by our observations that the s.c. LD_{50} of *S. typhimurium* for BXD-28 mice was only 20 (compared with <2 for C57BL/6J mice and 5×10^4 for DBA/2J mice) but the F_1 progeny of BXD-28 and C57BL/6J parents were clearly *Ity*^{r} by spleen counts ($\log_{10}$ geometric mean count for four mice was 2.69). The origin of this hypothetical salmonella sensitivity gene(s) is not clear because progeny from the progenitor strains,

Table 1 *S. typhimurium* susceptibility of BXD recombinant inbred and progenitor strains

Strain	No. dead/total no.	*S. typhimurium* response $\sin^{-1}\sqrt{\text{no. dead/total no.}}$	$\log_{10}$ geometric mean organisms per spleen (no. of mice)	*Ity* type	*Lsh* type*
C57BL/6J	30/30	85±5	6.13 (28)	s	s
BXD-24	11/11	81±8	5.98 (5)	s	s
BXD-12	10/10	81±9	5.46 (4)	s	s
BXD-18	9/9	81±10	5.04 (5)	s	r
BXD-5	8/8	80±10	6.98 (4)	s	s
BXD-20	7/7	79±11	6.33 (3)	s	r
BXD-28	21/22	78±6	4.46 (12)	?	r
BXD-21	6/6	78±12	6.06 (5)	s	s
BXD-31	6/6	78±12	4.28 (7)	?	s
BXD-9	9/10	72±10	7.41 (4)	s	s
BXD-2	10/12	66±8	6.98 (5)	s	s
BXD-14	10/12	66±8	5.80 (5)	s	s
BXD-11	7/9	62±10	5.82 (5)	s	s
BXD-16	7/9	62±10	5.08 (5)	s	s
BXD-22	6/9	55±10	5.10 (5)	s	s
BXD-19	9/14	53±8	6.40 (4)	s	s
BXD-29	7/12	50±8	3.91 (5)	r	s
BXD-25	5/9	48±10	3.37 (5)	r	r
BXD-8	4/8	45±10	2.71 (4)	r	r
BXD-13	3/9	36±10	2.00 (5)	r	r
BXD-15	4/12	36±8	2.28 (5)	r	r
BXD-1	3/12	30±8	2.62 (5)	r	r
BXD-27	2/9	28±10	3.52 (4)	r	r
BXD-23	3/14	27±8	2.26 (5)	r	r
BXD-30	1/12	17±8	4.49 (5)	r	r
DBA/2J	2/25	17±6	3.61 (27)	r	r
BXD-6	0/7	11±11	3.15 (6)	r	r
BXD-32	0/7	11±11	2.20 (5)	r	r

The formula $\phi = \sin^{-1}\sqrt{\text{no. dead/total no.}}$ the arc sin transformation of the raw data, was used for statistical analysis according to ref. 15. The s.e. of ϕ is 828/no tested. r, Resistant; s, susceptible. Values are means ± s.e.

* The *Lsh* types for BXD-1–29 are taken from ref. 4. The *L. donovani* responses of BXD-31 and BXD-32 were obtained through Dr David Bradley (personal communication).

Table 2 *S. typhimurium* susceptibility of LXB6, 58NXL and BRX58N recombinant inbred and progenitor strains

Strain	No. dead/total no.	*S. typhimurium* response $\sin^{-1}\sqrt{\text{no. dead/total no.}}$	$\log_{10}$ geometric mean organisms per spleen (no of mice)	*Ity* type	*Lsh* type†
C57BL/6J	30/30	85±5	6.13 (28)	s	s
LXB6-4	11/11	81±9	7.85 (3)	s	s
LXB6-2	3/3	73±17	7.92 (5)	s	s
LXB6-3	4/10	39±9	3.30 (2)	r	r
C57L/J	1/16	14±7	3.48 (4)	r	r
B10.D2(58N)	4/4	76±14	5.90 (6)	s	s
58NXL-3	11/12	74±8	6.69 (4)	s	s
58NXL-4	11/12	74±8	7.08 (6)	s	s
58NXL-2	6/7	68±11	8.00 (4)	s	s
58NXL-1	4/19	42±9	3.59 (3)	r	r
C57L/J	1/16	14±7	3.48 (4)	r	r
58NXL-8	0/13	8±8	3.68 (4)	r	r
BRX58N-13	11/11	81±9	6.51 (5)	s	s,r‡
B10.D2(58N)	4/4	76±14	5.90 (6)	s	s
BRX58N-12	5/8	52±10	6.34 (5)	s	s
BRX58N-7	6/11	48±9	6.83 (7)	s	s
BRX58N-9	4/9	41±9	3.15 (7)	r	r
BRX58N-3	2/11	25±9	3.74 (2)	r	r
C57BR/cdJ	3/20	23±6	4.11 (4)	r	r
BRX58N-10	1/8	21±10	3.50 (5)	r	r
BRX58N-8	0/6	12±12	3.85 (7)	r	r
BRX58N-1	0/7	11±11	2.50 (6)	r	r
BRX58N-11	0/10	9±9	3.16 (4)	r	r

r, Resistant; s, susceptible.

* The statistical analyses are described in Table 1 legend. Values are means ± s.e.

† The *Lsh* types are taken from ref. 4.

‡ Different *Lsh* types were observed in two separate experiments[4].

that is (C57BL/6J × DBA/2J)F_1 mice, were salmonella resistant (0/4 dead by day 28 when challenged s.c. with 10^3 TML) and were able to restrict early *S. typhimurium* net growth in their spleens ($\log_{10}$ geometric mean count for 10 mice was 3.27). As our criteria for *Ity* typing emphasized spleen counts, the influence of this undefined gene(s) on data interpretation was minimized. Moreover, it is clear that the major gene controlling *S. typhimurium* sensitivity is one closely linked to *Lsh*, since the *Lsh* and *Ity* genotypes were concordant in 21 of the 24 typable BXD RI strains. However, the two genes do not appear to be identical because three strains (BXD-18, -20 and -29) had different responses to *S. typhimurium* and *L. donovani*.

Table 3 *S. typhimurium* susceptibility of LPS-responsive BXH strains and F_1 progeny derived from C57BL/6J and LPS-unresponsive BXH parents

RI strain or F_1 hybrid	No. dead/total no.	*S. typhimurium* response $\sin^{-1}\sqrt{\text{no. dead/total no.}}$	$\log_{10}$ geometric mean organisms per spleen (no. of mice)	*Ity* type of BXH strain	*Lsh* type of BXH strain†
LPS-responsive					
19	4/13	34±8	ND	r	r
14	0/6	12±12	2.65	r	r
F_1 from C57BL/6J × LPS-unresponsive					
BXH 3	34/35	80±5	ND	s	s
4	8/24	35±6	ND	r	r
7	6/37	24±5	ND	r	r
6	3/33	15±4	ND	r	r
8	0/11	9±8	ND	r	r

The responses of BXH strains to LPS are taken from ref. 11. ND, Not determined; r, resistant; s, susceptible.
* The statistical analyses are described in Table 1 legend. Values are means ± s.e.
† The *Lsh* types are taken from ref. 4.

[illegible] Che[illegible] Library
[illegible] COLLEGE
[illegible] Upper Circular Road
[illegible]

Genetic studies were performed to verify the *Ity* types of two of these strains. The progeny of crosses between BXD-18 and C57BL/6J mice were tested for salmonella sensitivity and the extent of *S. typhimurium* multiplication in their spleens. We reasoned that if BXD-18 mice are salmonella susceptible as a consequence of Ity^s expression, then no gene complementation should be observed in (C57BL/6J × BXD-18)F_1 mice. Thus, our findings that these F_1 mice were sensitive to *S. typhimurium* (4/4 deaths after s.c. infection with 25 organisms) and were unable to control early salmonella growth in their spleens (geometric mean count for nine mice was 6.18) confirm the Ity^s genotype of BXD-18 mice. To verify the Ity^r genotype of BXD-29 mice, we assessed the spleen counts of individual mice derived from crosses of (C57BL/6J × DBA/2J)F_1 female mice with BXD-29 male mice. Because Ity^r is dominant[2,5,6], 100% of [(C57BL/6J × DBA/2J) × BXD-29] F_1 mice should be Ity^r if BXD-29 animals are Ity^r, whereas only 50% should be of this genotype if BXD-29 animals are Ity^s. Since all eight of the [(C57BL/6J × DBA/2J) × BXD-29]F_1 mice had spleen counts $<10^5$, the Ity^r genotype of BXD-29 mice was verified. The salmonella responses of the BXD RI strains therefore suggest that *Lsh* and *Ity* are closely linked, but non-identical, genes. Further studies with LXB6, 58NXL, BRX58N and BXH RI strains confirmed this linkage. No crossovers between *Ity* and *Lsh* or discrepancies between lethality and spleen counts were observed among the 17 strains of LXB6, 58NXL and BRX58N mice tested (Table 2). Experiments with BXH RI strains were complicated by the expression of the defective lipopolysaccharide response gene (Lps^d) in some of these strains. As mentioned above, this gene (or one closely linked to it) renders mice susceptible to salmonellae. Moreover, mice homozygous for this allele (Lps^d/Lps^d genotype) are susceptible to murine typhoid regardless of their *Ity* type[7]. Thus, we expected that all BXH mice of the Lps^d/Lps^d genotype would be susceptible to infection, and, in fact, all mice of the BXH-2, -3, -4, -6, -7, 8 and -12 strains, which are LPS unresponsive[11], died following s.c. infection with approximately 25 *S. typhimurium*. Interestingly, Lps^d does not influence the response of mice to leishmaniasis because both Lsh^r and Lsh^s types occur among these strains[4]. To determine the *Ity* type of some of these LPS-low responder strains, we crossed mice of BXH-3, -4, -6, -7, and -8 with LPS-responsive (Lps^n) C57BL/6J mice. As Lps^d is recessive and as C57BL/6J mice are Ity^s, Lsh^s, we were able to use these F_1 mice for *Ity* typing. Such typing was based solely on lethality data because when these experiments were done we did not routinely perform splenic analyses. As indicated in Table 3, the *Ity* and *Lsh* types were concordant in these five hybrid strains. Moreover, the *Ity* and *Lsh* types were also concordant in the two LPS-responsive BXH strains examined (Table 3).

These data provide the first direct evidence for linkage between the chromosome 1 loci, *Lsh* and *Ity*. In only three of 48 *S. typhimurium*-typable strains was there apparent recombination between these markers. Thus, the estimated recombination frequency between *Ity* and *Lsh*, as calculated by the equation of Haldane and Waddington[12], is 0.02 ± 0.01 (s.e. of the estimate). It seems unlikely that the close association of *Ity* and *Lsh* evolved by chance when the 2% recombination frequency is viewed in terms of the entire mouse genome. The advantage of maintaining these loci in close proximity during the evolutionary process is not clear because neither organism appears to be a natural pathogen of feral mice. Nevertheless, the linkage does suggest that the functions of the products of the genes may be related. Since macrophages are critical in the control of both *L. donovani*[12] and *S. typhimurium*[13] infections, it seems reasonable to presume that these gene products are involved in some phase of the uptake or killing of the organisms by macrophages. One may also speculate, based on such analogous genetic loci as the H-2 and HLA complexes of mice and men, respectively, that man too may have genes which regulate his response to intracellular microbial infections. The concept of a human genetic complex analogous to the murine *Lsh-Ity* complex is not only intriguing but would also have far-reaching clinical implications. Since Ity^s mice cannot be protected from murine typhoid by immunization with standard vaccines[14], protection of humans with similar genetic defects may require the development of new vaccines designed specifically to overcome such deficiencies.

This research was supported by the Uniformed Services University of the Health Sciences Research Protocol R07306 and grant GM 18684 from the National Institute of General Medical Sciences. The Jackson Laboratory is fully accredited by the American Association for Accreditation of Laboratory Animal Care. We thank Drs Janet Plant, Jenefer Blackwell and David Bradley for helpful suggestions and Drs Blackwell and Bradley for confirming the *Lsh* type of BXD-28 mice.

Received 29 January; accepted 7 August 1980.

1. Robson, H. G. & Vas, S. I. *J. infect. Dis.* **126,** 378-386 (1972).
2. Plant, J. & Glynn, A. A. *J. Infect. Dis.* **133,** 72-78 (1976).
3. Bradley, D. J. *Nature* **250,** 353-354 (1974).
4. Bradley, D. J., Taylor, B. A., Blackwell, J., Evans, E. P. & Freeman, J. *Clin. exp. Immun.* **37,** 7-14 (1979).
5. Plant, J. & Glynn, A. A. *Mouse News.* **57,** 38 (1977).
6. Plant, J. & Glynn, A. A. *Clin. exp. Immun.* **37,** 1-6 (1979).
7. O'Brien, A. D. *et al. J. Immun.* **124,** 20-24 (1980).
8. O'Brien, A. D., Scher, I., Campbell, G. H., MacDermott, R. P. & Formal, S. B. *J. Immun.* **123,** 720-724 (1979).
9. Bailey, D. W. *Transplantation* **11,** 325-327 (1971).
10. Gianella, R. A., Broitman, S. A. & Zamcheck, N. Z. *Am J. dig. Dis.* **16,** 1007-1013 (1971).
11. Watson, J., Riblet, R. & Taylor, B. A. *J. Immun.* **118,** 2088-2093 (1977).
12. Bradley, D. J. & Kirkley, J. *Clin. exp. Immun.* **30,** 119-129 (1977).
13. O'Brien, A. D., Scher, I. & Formal, S. B. *Infect. Immun.* **25,** 513-520 (1979).
14. Medina, S., Vas, I. & Robson, G. G. *J. Immun.* **114,** 1720-1725 (1975).
15. Taylor, B. A. *Genetics* **83,** 373-377 (1976).
16. Haldane, J. B. S. & Waddington, C. H. *Genetics* **16,** 357-374 (1931).

Continuous production of monoclonal rheumatoid factor by EBV-transformed lymphocytes

Michael Steinitz*, Gabriel Izak*§, Sara Cohen*, Michael Ehrenfeld† & Ianco Flechner‡

* Department of Hematology and † Department of Internal Medicine A, Hadassah University Hospital, Jerusalem, Israel
‡ Department of Medical Bacteriology, Hebrew University, Hadassah Medical School, Jerusalem, Israel
§ Deceased

Human B lymphocytes are immortalized by Epstein–Barr virus (EBV, ref. 1). The virus can be used to establish lymphoblastoid cell lines that produce and actively secrete specific antibodies[2]. The original method, which we have used for various antigens[2–4] is based on selection of the specific surface antigen receptor-positive lymphocytes from the peripheral blood lymphocytes of a donor who was previously sensitized to the corresponding antigen. Furthermore, by cloning the polyclonal anti-NNP cell line we have produced human monoclonal antibodies for the first time *in vitro*[5]. About 5–20 μg ml^{-1} stably produced[5] specific antibody is obtained in the supernatant of the cell lines. This approach can be used for the *in vitro* production of monoclonal human autoimmune antibodies by EBV-immortalized lymphocytes from patients with autoimmune diseases. We demonstrate the continuous production *in vitro* of a monoclonal IgM anti-IgG antibody (rheumatoid factor, r.f.) by a lymphoblastoid cell line established from a patient with rheumatoid arthritis.

Rheumatoid factors that occur in the sera of patients with rheumatoid arthritis are antibodies that react with antigenic determinants on the Fc portion of human IgG. They are heterogeneous with respect to their antigen specificity and can belong to the IgM, IgG or IgA class. In rheumatoid arthritis, rheumatoid factors are usually polyclonal in nature while monoclonal rheumatoid factors have been described in infectious mononucleosis and lymphoproliferative disorders[6].

We have isolated the lymphocytes from a 15-ml blood sample from a patient (A.N.) with classic rheumatoid arthritis. Standard agglutination tests of the patient's serum using sensitized sheep erythrocytes with rabbit amboceptor (Rose Waaler test) and latex suspension coated with human IgG, gave titres of 1:1024 and 1:80 respectively. Selection and isolation of the antigen receptor-positive cells was carried out by rosetting the lymphocytes[7] with a 10-fold excess of human IgG coated on erythrocytes and subsequently separating them on a Ficoll–Isopaque gradient (density 1.077)[5]. The rosette-containing pellet was infected with a B958-derived EBV[1]. The infected cells were incubated in RPMI 1640 in 20% fetal calf serum (FCS) at 37 °C, 5% CO_2. The emerging cell line contained 0.6% cells that rosetted with human IgG-coated erythrocytes. This very low percentage was apparently due to the fact that in the initial selection stage not only antigen receptor-positive lymphocytes were rosetting with the IgG-coated erythrocytes but also non-related B lymphocytes that had Fc receptors. However, lymphoblastoid cell lines have very weak Fc receptors and usually do not form rosettes with IgG-coated erythrocytes[8]. Therefore we re-selected the emerging line by two subsequent re-rosettings. The outcoming cell line (r.f.-A.N.) is 100% EB nuclear antigen positive[9]. It has a 2-day doubling time and has now been maintained in tissue culture for more than 12 months.

The cells are surface and cytoplasmic IgM λ positive, IgA, IgD and κ negative as shown by staining of live and fixed cells with fluorescein isothiocyanate (FITC)-conjugated rabbit anti-human immunoglobulins (Table 1). The nonconcentrated culture supernatant of growing cells (up to 7×10^5 cells ml^{-1}) agglutinated human IgG and rabbit IgG-coated erythrocytes up to 1/128–1/512 dilution; the agglutination was inhibited by 2-mercaptoethanol. A 100-fold concentrated medium of 10^6 cells growing for 24 h in RPMI with 1.25% FCS had a specific agglutination titre of 1:16,000. By indirect staining of rabbit-IgG-coated erythrocytes previously incubated with the cell line supernatant (Table 1) the specific antibody was identified as an

Table 1 Immunoglobulin classes of r.f.-A.N., and of the r.f.s. produced *in vitro* and *in vivo*

r.f.-A.N. cells and erythrocytes stained	Fluorescence staining for human: Ig	IgM	IgG	IgA	IgD	κ	λ
r.f.-A.N. live cells*	+	+	−	−	−	−	+
r.f.-A.N. fixed cells*	+	+	−	−	−	−	+
Rabbit IgG-OxE exposed to culture supernatant†	+	+	−	−	−	−	+
Goat IgG-OxE exposed to culture supernatant‡	−	−	−	−	−	−	−
DNA OxE exposed to culture supernatant§	−	−	−	−	−	−	−
OxE exposed to culture supernatant	−	−	−	−	−	−	−
Rabbit IgG-OxE exposed to A.N. serum¶	+	+	+	+	−	+	+
OxE exposed to A.N. serum¶	−	−	−	−	−	−	−

* 5×10^5 living cells and a smear of ethanol–acetic acid (95:5)-fixed cells[10] were stained for surface and cytoplasmic immunoglobulins respectively.

† Ox erythrocytes (OxE) coated with sub-agglutinating titre of rabbit anti-ox erythrocytes were incubated with r.f.-A.N. cell supernatant or with A.N. serum for 60 min, washed and stained with Dakopatts FITC-conjugated rabbit anti-human (1), IgG, IgA, IgM, κ and λ, (2) anti-IgM specific for μ chains, (3) anti-IgG specific for γ, Fc fragment, (4) anti-IgA, specific for α chains, (5) anti-K (Bence-Jones), (6) anti-λ (Bence-Jones) and (Behringwerke) rabbit anti-human IgD, specific for δ chains.

‡ Goat IgG was coupled to ox erythrocytes by the $CrCl_3$ method as detailed in the legend to Table 2. The coating was tested by specific agglutination with rabbit anti-goat IgG (Meloy).

§ Single-stranded DNA was coupled to ox erythrocytes with $CrCl_3$. The coating was confirmed by specific agglutination of the erythrocytes.

¶ The serum of patient A.N. was absorbed with 2 vol of packed ox erythrocytes before it was used in the assay.

Table 2 Multi-layer cluster formation by r.f.-A.N. cells

Erythrocytes	Cluster formation with rabbit anti-human* Igs (final dilution): None	Ig (10^{-5})	IgM (10^{-3})	IgG (10^{-4})	IgA (10^{-3})	κ (10^{-3})	λ (10^{-3})
H-IgG-Ox†	−	+	+	−	−	−	+
H-IgG-Ox + NaN_3‡	−	−	−	−	−	−	−
Ox	−	−	−	−	−	−	−

* 200 washed r.f.-A.N. cells were mixed in a flat-bottomed microplate with 0.02 ml human IgG-coated 10% ox erythrocytes in 0.2 ml RPMI, 20% FCS, with rabbit anti-human immunoglobulins. The rabbit sera used were the unlabelled reagents listed in the legend to Table I (Dakopatts). The rabbit antisera were so diluted that they did not agglutinate the IgG-coated erythrocytes. Clusters were examined under a low-power inverted microscope after 4 h incubation at 37 °C.

† IgG coating was performed by mixing 1 vol of saline-washed erythrocytes, 2 vol of 2 mg ml^{-1} human gammaglobulins (Pentex) in saline and 2 vol of 'aged' 2.5 mM $CrCl_3$ (ref. 12). The mixture was incubated at room temperature for 5 min followed by three washes with saline.

‡ NaN_3 was used in a final concentration of 0.7 mM.

0028–0836/80/400443—03$01.00

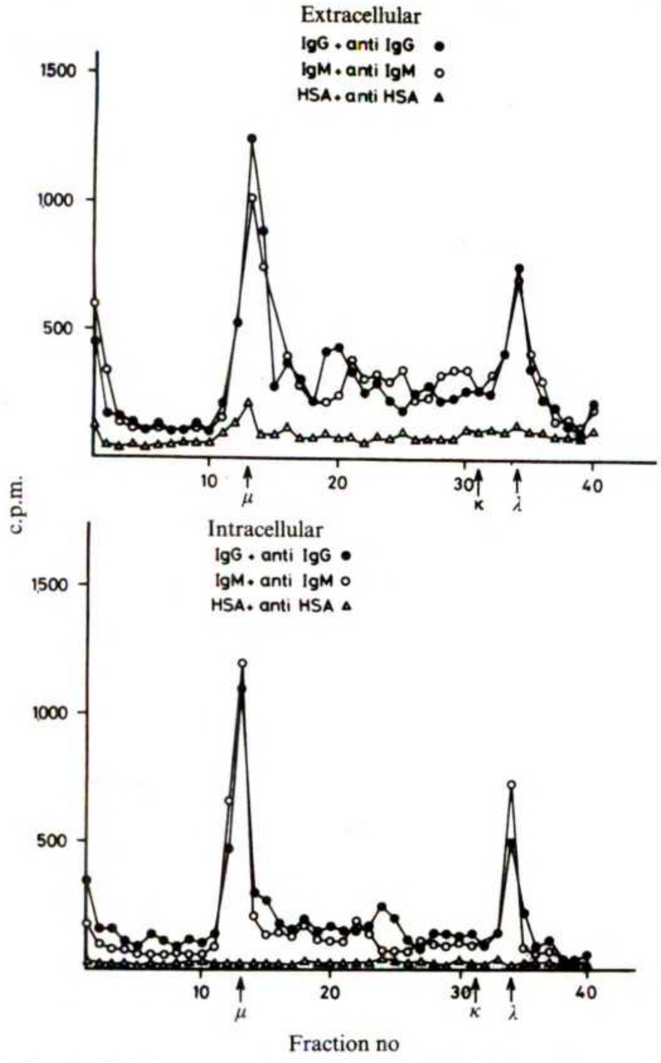

Fig. 1 Gel electrophoresis of immunoglobulins produced by r.f.-A.N. cell line. 12×10^6 r.f.-A.N. cells were incubated in 8 ml of RPMI, amino acid-free medium with 15% dialysed FCS with 40 μCi ml^{-1} of ^{3}H-labelled amino acid mixture (Amersham) for 24 h. Supernatant was collected, and cells were washed twice and lysed in 2 ml Triton 1%. Both supernatant and cell lysate were dialysed. The supernatant was concentrated 10 times. Aliquots (0.1 ml) of each sample were co-precipitated in a final volume of 0.5 ml with the following antisera and the corresponding antigen in the equivalence zone: rabbit anti-human IgG (Dakopatts) and human IgG; goat anti-HSA (Meloy) and HSA; rabbit anti-human IgM (Dakopatts) and human IgM. The precipitate was washed four times, lysed with 0.1 ml of 1% SDS and SDS-PAGE was performed on 12% acrylamide gels for 4 h (4 mA per tube). The positions of the control markers are indicated by arrows. Cell lysate analyses are shown on the left-hand traces; culture supernatant analyses are shown on the right-hand traces.

IgM, λ. The contrast between the polyclonal anti-IgG that characterizes the patient's serum (A.N.) and the monoclonal type of the anti-IgG of the r.f.-A.N. cell line is evident (Table 1). 65 ± 10% of the r.f.-A.N. cells form specific rosettes with human or rabbit but not goat IgG-coated erythrocytes or human IgM-coated erythrocytes. The erythrocytes used were: (1) $CrCl_3$-IgG coated, (2) O, Rh$^+$ coated with human IgG anti-D (Ortho), (3) A, Rh$^+$ and (4) B, Rh$^+$ coated with sub-agglutinating titres of IgM anti-A and anti-B antibody-containing sera.

The high percentage of rosettes is comparable with the specific rosette percentage that characterized the cloned anti-NNP lines[5], which also never reached 100%.

Instead of a plaque assay we developed a method to identify the class of the specific antibody and also the number of cells secreting this antibody, based on the observation of Lubbe *et al.*[11]. These workers demonstrated the formation of a multilayer cluster of antigen-coated erythrocytes around a specific antibody-producing mouse lymphocyte by adding an allogeneic anti-mouse immunoglobulin serum. Table 2 shows that on mixing r.f.-A.N. lymphoblastoid cells with an 100-fold excess of human IgG-coated erythrocytes and diluted rabbit antisera to different classes of human immunoglobulins we detected giant multi-layer clusters. These clusters were formed only in the mixtures containing anti-human total immunoglobulins, IgM or λ chains. No clusters were formed when anti-IgG, -IgA and κ-chains or uncoated erythrocytes were used, and cluster formation was totally inhibited by sodium azide. These results demonstrate that the cells are actively secreting IgM, λ antibodies against human IgG. The significant information this assay provides and the simplicity of its performance make it preferable to the conventional plaque-forming assay.

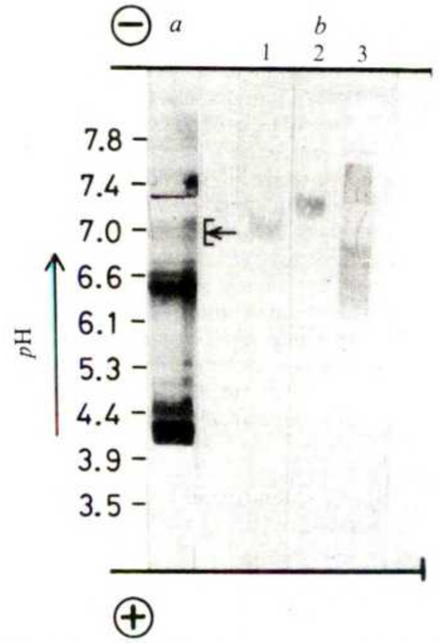

Fig. 2 IEF and immunofixation patterns. *a*, IEF of a concentrated (×1,000) culture supernatant of the cell line r.f.-A.N. Concentration was performed by precipitation with 50% saturated $(NH_4)_2SO_4$ followed by dialysis against H_2O; the resulting euglobulin was dissolved in 1 ml saline. IgM concentration was 150 μg ml^{-1}. *b*, Immunofixation patterns obtained with goat anti-human IgM, μ-chain specific serum (Hyland): lane 1, concentrated culture supernatant of the cell line r.f.-A.N.; lane 2, Waldenström' macroglobulinaemia serum (Meloy A 204; 80, 891) diluted 1 : 75 in saline; lane 3, serum from patient A.N. (undiluted). In all cases 20 μl of the samples soaked into Paratex filter pieces (LKB) were applied on the gel surface. Guiding *p*H values of the gradient are shown. Agarose IEF was performed in Isogel agarose gel 0·5% (Marine Colloids Division; FMC Corp.) in the presence of a 2% final concentration of Ampholine (LKB) *p*H 3.5–9.5, supplemented as required by Ampholines with the *p*H range 2.5–4.0 and 5.0–8.0. The dimensions of the agarose plates were 110 × 125 mm. The runs were performed in an LKB Multiphor at 5 °C. The current was kept at 10 mA for 10 min, then the Paratex pieces were removed and focusing was continued at 6.25 W constant power (1,000 V limiting) for 1 h. Immunofixation was carried out essentially as described by Pedersen and Axelsen[16].

To characterize the cells and their immunoglobulin product further, they were incubated for 24 h with radioactive amino acid mixture. Both the cell lysate and the culture supernatant were assayed for labelled anti-IgG immunoglobulins by co-precipitation in the presence of human IgG and rabbit anti-human IgG (Fig. 1). The radioactivity is clearly restricted to μ and λ chains. In parallel, co-precipitation of another sample of the same culture supernatant and cell lysate in the presence of human IgM and rabbit anti-human IgM was qualitatively and quantitatively identical to the corresponding co-precipitation with human IgG and rabbit anti-human IgG. This indicates that all the IgM secreted into the culture medium has anti-IgG activity and that apparently the line is monoclonal.

No radioactive precipitation occurred when goat anti-human serum albumin (HSA) and HSA were added to samples of the cell lysate and the culture supernatant. This is due to the fact that the *in vitro*-produced antibody does not react with goat IgG (see also Table 1).

The clonality of the immunoglobulin product synthesized by the established cell line has been tested by isoelectric focusing (IEF, Fig. 2) in agarose gels, followed by immunofixation. Since the r.f. antibody studied belongs to the IgM class, agarose gels with negligible sieving effects and minimal electroendoosmosis were used[13].

The pattern obtained using the concentrated culture supernatant showed a limited microheterogeneity characteristic for monoclonal IgM antibodies[13]. The pattern is similar to that obtained when a serum from a patient with Waldenström's macroglobulinaemia has been tested in the same run. This provides additional evidence of the monoclonal origin of the r.f. synthesized by the cell line r.f.-A.N.

The presence of a few closely spaced bands in IEF, when the sample containing the intact antibody was analysed (Fig. 2, *a*, *b* 1) and of a single peak corresponding to the L-chains derived from the same antibody in SDS-polyacrylamide gel electrophoresis (PAGE) (Fig. 1) are stringent criteria for monoclonality[14]. We should mention that the samples tested were crude preparations and that specific procedures to purify the r.f. antibody were not used so as to avoid the selection of a homogeneous population of antibodies.

This is the first time that specific r.f.-producing B cells from rheumatoid arthritis patients have been isolated, immortalized and established as a permanent autoimmune antibody-producing cell line. The availability of such cells can contribute to the understanding of the nature of the cells involved in autoimmune diseases. In addition, this defined product of the cell line is preferable to the unpredictable supply of polyclonal r.f. which is usually used in the radioimmunoassay for detecting immune complexes[15].

Gilliland *et al.*[17] established a cell line with no pre-selection from the synovium of a patient with rheumatoid arthritis that synthesized predominantly IgG, and that had an r.f. activity associated with IgG and IgM. These workers succeeded in establishing such a line after 100 unsuccessful trials from different synovial fluids. Our results suggest an approach to establish autoimmune antibody-producing cell lines that can be extended to other autoantibodies, such as anti-DNA, anti-T.

We have not studied the antigenic specificity of the *in vitro* produced r.f. in relation to the IgG molecule. The *in vitro* produced antibody can be used as an additional tool for understanding the structure and genetics of IgG molecules.

We thank Professor Dov Sulitzeanu for fruitful discussions. This work was carried out with the support of a Volkswagen Stiftung grant Az: I/36 120-121.

Received 5 June; accepted 16 July 1980.

1. Miller, G. & Lipman, M. *Proc. natn. Acad. Sci. U.S.A.* **70,** 190–194 (1973).
2. Steinitz, M., Klein, G., Koskimies, S. & Mäkelä, O. *Nature* **269,** 420–422 (1977).
3. Kozbor, D., Steinitz, M., Klein, G., Koskimies, S. & Mäkelä, O. *Scand. J. Immun.* **10,** 187–194 (1979).
4. Steinitz, M., Seppälä, I., Eichmann, K. & Klein, G. *Immunobiology* **156,** 41–47 (1979).
5. Steinitz, M., Koskimies, S., Klein, G. & Mäkelä, O. *J. clin. Lab. Immun.* **2,** 1–7 (1979).
6. Capra, J. D., Winchester, R. J. & Kunkel, H. G. *Arthritis Rheum.* **12,** 67–73 (1969).
7. Osoba, D. *J. exp. Med.* **132,** 368–383 (1970).
8. Nilsson, K. & Pontén, J. *Int. J. Cancer* **15,** 321–341 (1975).
9. Reedman, B. M. & Klein, G. *Int. J. Cancer* **11,** 499–520 (1973).
10. Kearney, J. F. & Lawton, A. R. *J. Immun.* **115,** 671–676 (1975).
11. Lubbe, F. H., Rossi, G. & Zaalberg, O. B. *J. immun. Meth.* **12,** 131–140 (1976).
12. Goding, J. W. *J. immun. Meth.* **10,** 61–66 (1976).
13. Rosen, A., Ek, K. & Åman, P. *J. immun. Meth.* **28,** 1–11 (1979).
14. Trump, G. N. & Singer, S. J. *Proc. natn. Acad. Sci. U.S.A.* **66,** 411–418 (1970).
15. Cowdery, J. S., Jr., Treadwell, P. E. & Fritz, R. B. *J. Immun.* **114,** 5–9 (1959).
16. Pedersen, N. S. & Axelsen, M. H. *J. immun. Meth.* **30,** 257–262 (1979).
17. Gilliland, B. C., Ford, D. K. & Mannik, M. *Arthritis Rheum.* **21,** 330–336 (1978).

Relationship between increased aerobic glycolysis and DNA synthesis initiation studied using glycolytic mutant fibroblasts

J. Pouysségur, A. Franchi & P. Silvestre

Centre de Biochimie, Université de Nice, Parc Valrose,
06034 Nice, France

Reports from several laboratories have suggested that increased rates of glycolysis play an essential part in the initiation of DNA synthesis. This is based on observations that aerobic glycolysis: (1) occurs at low rate in resting mammalian cells and at very high rate in tumour cells[1–3]; (2) increases rapidly after DNA synthesis is initiated by addition of serum or purified growth factors[4,5], and (3) correlates with the expression of the transformed phenotype[6]. Also, specific inhibitors of aerobic glycolysis prevent the initiation of DNA synthesis[4]. To determine whether the rapid activation of phosphofructokinase—and therefore glycolysis—by purified growth factors[7] is necessary for the initiation of cell proliferation, we have isolated and studied two classes of glycolytic mutants. The first, isolated from Chinese hamster fibroblasts, has a total block in the glycolytic pathway[8]. The second, from hamster and Fisher rat fibroblasts maintains a permanent high rate of glycolysis. We have found that both classes of mutants retain normal control of DNA synthesis in response to serum. This dissociation indicates that growth-factor-stimulated glycolysis is not involved in the control of initiation of DNA synthesis and cell proliferation.

We used two fibroblast lines requiring serum for growth. The first, 023 which can grow in agarose, is a subclone of Chinese hamster lung fibroblasts (CC139 of ATCC). In spite of a spontaneously-transformed phenotype, its DNA synthesis is dependent on the addition of serum (Fig. 1, inset) or purified growth factors[9]. When CC139 cells are deprived of serum, DNA synthesis is arrested. As with normal cells, DNA synthesis and cell division can be reinitiated by addition of serum. A minimum of 8–10 h is required for the first cells to enter S phase (Fig. 1). The cell population doubles 20 h after stimulation by serum.

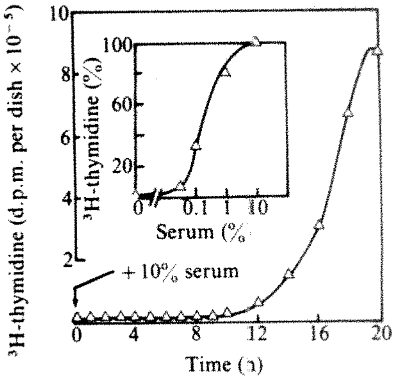

Fig. 1 Re-initiation of DNA synthesis by serum to Chinese hamster fibroblasts. Confluent cultures of Chinese hamster fibroblasts (35-mm dishes) were washed twice with Dulbecco's medium to remove residual serum and then incubated for 29 h in a mixture (1 : 1) of Dulbecco's and F12 medium (Gibco) deprived of serum. DNA synthesis was re-initiated by addition of 10% fetal calf serum (FCS) and its rate was measured as follows. Cells in duplicate dishes were pulsed for 1 h at 37 °C with 1 ml of culture medium containing 10% serum and ^{3}H-thymidine (5 μCi ml^{-1}). The cells were then washed twice with phosphate-buffered saline and fixed (60 min at 0 °C) with 1 ml of trichloroacetic acid 10% containing 1 mM thymidine. Radioactivity of the acid-precipitable fraction was measured after solubilization in 0.1 M NaOH. The inset shows the rates of DNA synthesis to different concentrations of serum, following 29 h of serum starvation. DNA synthesis was measured after incubation for 24 h with ^{3}H-thymidine (0.5 μCi *ml*$^{-1}$). Values are expressed relative to the thymidine incorporation obtained with 10% FCS.

0028–0836/80/400445—03$01.00

Table 1 Glucose transport and glycolysis in Chinese hamster and Fisher rat fibroblasts and mutant derivatives

	Cell line	Origin	Phenotype	Glucose transport (3-*O*-MGlc) (nmolmg^{-1} min^{-1})	Glycolysis (lactate formed) (μmol per mg protein per h)
Chinese hamster fibroblasts	023	CC139 (ATCC)	Wild type	0.110 (100%)	1.4 (100%)
	DS7	023	Glycolysis$^-$ (pgi$^-$)	0.027 (25%)	0.08 (5%)
	GSK3	023	Respiration	0.430 (390%)	3.8 (260%)
Fisher rat fibroblats	FR3T3	(ref. 10)	Wild type	0.17 (100%)	0.65 (100%)
	GSR16	FR3T3	Respiration$^-$	0.35 (200%)	4.0 (610%)
	FR3T3-Py	FR3T3	Transformed by polyoma virus	0.30 (180%)	2.3 (350%)

All cells were grown in Dulbecco's modified Eagle's medium supplemented with 10% fetal calf serum. 023 Is a ouabain-resistant clone derived from the Chinese hamster fibroblasts CC139 (ATCC). DS7 and GSK3 were derived from 023 cells after mutagenesis with ethylmethane sulphonate as described for DS7[8]. The selection of the respiration-deficient mutants, GSK3 and GSR16 has been described elsewhere[13]. Cells were planted in 35-mm dishes, cultured to near confluency in 2–3 days, and assayed for 3-*O*-methyl D-glucose. For 3-*O*-MGlc transport studies, cells were precharged with 50 mM 3-*O*-MGlc before transport and assayed with 50 μM 3-*O*-MGlc. Rates of transport are the average of duplicate determinations with time points of 15, 30 and 60 s. Rates of glycolysis were calculated from the linear kinetic (lactic acid produced into the medium) obtained with time points of 30, 60 and 90 min.

Therefore, as with normal cells, growth-factor deprivation reversibly arrests these Chinese hamster cells in the G_0/G_1 phase of the cell cycle. The second cell line was isolated by Seif and Cuzin[10] from Fisher rat embryo fibroblasts. This diploid line, FR3T3, is anchorage-dependent, non-tumorigenic and dependent on serum for growth.

To analyse the relationship between increased glycolysis and the initiation of DNA synthesis, we searched for a class of mutants in which glycolysis is supressed and another in which it is permanently derepressed. We used tritium 'suicide' to select these mutants. From hamster fibroblasts treated with ^{3}H-labelled 2-deoxyglucose we selected DS7, a mutant lacking phosphoglucose isomerase activity. (Details of the selection are given elsewhere[8].) By a similar method, but using [6-^{3}H]-D-glucose, we isolated GSK3 from hamster cells and GSR16 from rat fibroblasts. Some of the clones surviving ^{3}H-glucose 'suicide' had a specific defect in the oxidation of glucose by the Krebs cycle. This was due to a block in respiration that resulted in a decrease in oxygen uptake. One consequence of this mutation is a decrease in ATP derived from oxidative metabolism; this in turn triggers a permanent activation of glycolysis to compensate for the deficit in energy.

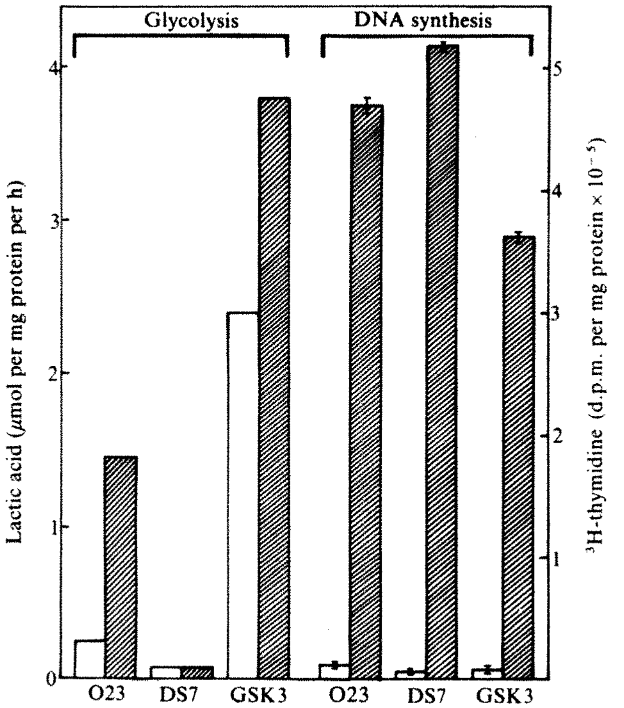

Fig. 2 Rates of glycolysis and DNA synthesis in serum-starved and serum-refed Chinese hamster fibroblasts. Wild type (023) and mutant (DS7 and GSK3) cells were grown for 2 d in media containing 10% FCS (10^6 cells per 35-mm culture dish). The cells were then washed (twice to remove residual serum) and incubated for 29 h in the mixture (1:1) of Dulbecco's and F12 medium. At the end of the starvation period, media were renewed and half of the cells were supplemented with 10% FCS (hatched bars). Rates of glycolysis were measured as the amount of lactic acid produced during the first hour after starvation (see legend to Table 1). Rates of DNA synthesis were determined by the incorporation of thymidine into acid-precipitable material after 24 h of incubation in the presence (hatched columns) or absence (open columns) of 10% serum and ^{3}H-thymidine (0.2 μCi ml^{-1}).

Table 1 summarizes rates of glucose transport and glycolysis in the two cell lines and their mutant derivatives. The rate of glycolysis is decreased 20-fold in DS7, whereas it is increased six-fold in GSR16 (compared with the corresponding parental lines). Interestingly, in conjunction with a block in glycolysis, DS7 has low glucose transport activity, whereas derepression of glycolysis in GSK3 or GSR16 is accompanied by increased glucose transport. The biochemical basis for this co-regulation will be discussed elsewhere[11]. It is also interesting that the respiration-deficient mutation introduced into FR3T3 activates glycolysis and glucose transport to values higher than those observed in the highly transformed polyoma virus derivative, FR3T3-Py (Table 1).

Figure 2 shows that re-initiation of G_0/G_1-arrested wild type 023 cells by serum rapidly stimulates (sixfold) glycolysis. In contrast, as would be expected, serum cannot stimulate glycolysis in the deficient mutant DS7. However, re-initiation of its DNA synthesis is not prevented by the glycolytic defect. Even in conditions of serum starvation, GSK3 sustains levels of glycolytic activity 10 times higher than those in wild-type arrested cells, and even higher than in serum-stimulated 023 cells. Although serum starvation fails to reduce rates of glycolysis and glucose transport to low levels, DNA synthesis is arrested in GSK3 cells (Fig. 2).

Results obtained with the untransformed cell line FR3T3 and its derivatives are shown Fig. 3. As with GSK3, when the respiration-deficient mutant GSR16 is starved of serum for 48 h, its rate of glycolysis is not reduced to low levels: indeed it is slightly higher than in polyoma-virus transformed FR3T3 and 10 times higher than in normal FR3T3. However, Fig. 3 shows that in contrast to FR3T3-Py in which DNA synthesis cannot be arrested, GSR16, like the parent FR3T3 line, has normal control of DNA synthesis and cell division.

Thrash and Cunningham[12] have demonstrated a dissociation of increased transport from initiation of fibroblast proliferation. Our studies extend this dissociation to aerobic glycolysis and support their report because DS7 and GSK3 have a 15-fold difference in glucose transport (Table 1), yet they both show normal control of DNA synthesis.

Zielke *et al.*[13] have reported that human fibroblasts can undergo one to two cell divisions in the absence of glucose, provided that the anabolic function of glucose required for nucleic acid synthesis is substituted by the addition of purines

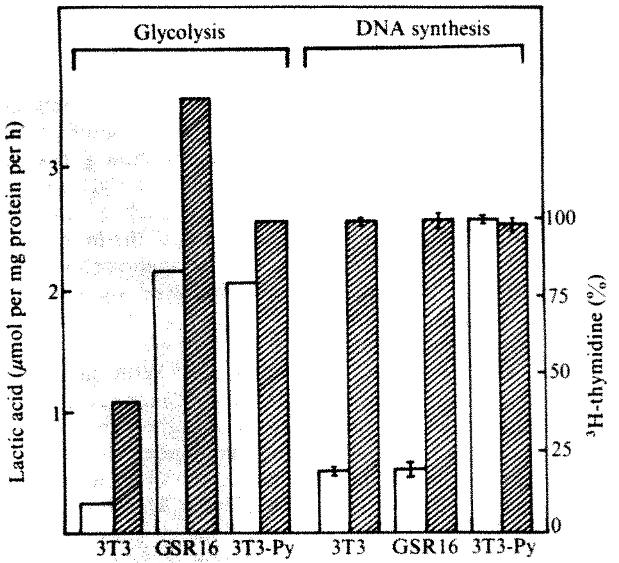

Fig. 3 Rates of glycolysis and DNA synthesis in serum-starved and serum-refed Fisher rat fibroblasts. FR3T3, GSR16 and FR3T3-polyoma transformed cells (10^5 per 35-mm dish) were grown for 2 d in 10% FCS and then starved of serum for 48 h in the mixture (1 : 1) of Dulbecco's and F12 medium. Then half the cells were supplemented with 10% FCS. Rates of glycolysis and DNA synthesis were measured as for Fig. 2. Open columns, cells starved of serum; hatched columns, cells with 10% serum added.

and pyrimidines to the medium. Therefore, one may ask whether a possible role of glucose metabolism in controlling DNA synthesis or cell proliferation *in vivo* has been masked in *in vitro* studies, in which a rich medium (DMEM/F12) containing nucleic acid precursors was used. There are two lines of evidence against this possibility. (1) The results shown in Fig. 2 for 023 and DS7 were also observed when the cells were serum-starved and serum-stimulated in Dulbecco's medium alone (not containing the nucleic acid precursors of the F12 medium). In this situation the anabolic function of glucose is required and the pentose-phosphate shunt, still functional in DS7, facilitates the re-initiation of DNA synthesis. (2) We have shown that the glycolytic block in DS7 cells does not prevent their capacity to form tumours[8] and therefore to proliferate *in vivo*.

In conclusion, the properties of GSK3 and GSR16 indicate that the loss of growth regulation of transformed or tumour cells is not linked to their high glucose metabolism. Also it seems clear from the study of the glycolysis-deficient mutant DS7 that growth factor-activated glycolysis or glycolysis *per se*, is not necessary for the initiation of DNA synthesis and cell division.

We thank Dr Rolando Pêrez for stimulating discussions; Professor Gérard Ailhaud for support; Dr Mary Murphy for reading the manuscript and Mrs Geneviève Oillaux for typing it. This work was funded by CNRS (LP 73-00), DGRST (Membranes Biologiques, no. 77-7-1269) and by INSERM (ATP no. 82-79-114).

Received 27 May; accepted 7 August 1980.

1. Warburg, O. *Science*, **123**, 309–314 (1956).
2. Ramaiah, A. *Curr. Top. Cell Regul.* **8**, 297–345 (1974).
3. Suolinna, E. M., Lang, D. R. & Racker, E. *J. natn. Cancer Inst.* **53**, 1515–1519 (1974).
4. Rubin, H. & Fodge, D. in *Control of Proliferation in Animal Cells* (eds Clarkson, B. & Baserga, R.) **1**, 801–816 (Cold Spring Harbor Laboratory, 1974).
5. Diamond, I., Legg, A., Schneider, J. & Rozengurt, E. *J. biol. Chem.* **253**, 866–871 (1978).
6. Carroll, R., Ash, J., Vogt, P. & Singer, J. *Proc. natn. Acad. Sci. U.S.A.* **75**, 5015–5019 (1978).
7. Schneider, J., Diamond, I. & Rozengurt, E. *J. biol. Chem.* **253**, 872–877 (1978).
8. Pouysségur, J., Franchi, A., Salomon, J. C. & Silvestre, P. *Proc. natn. Acad. Sci. U.S.A.* **77**, 2698–2701 (1980).
9. Pérez, R., Franchi, A. & Pouysségur, J. *Eur. J. Cell Biol.* **22**, 541 (1980).
10. Seif, R. & Cuzin, F. *J. Virol.* **24**, 721–728 (1977).
11. Franchi, A., Silvestre, P., Pérez, R. & Pouysségur, J. (in preparation).
12. Thrash, C. & Cunningham, D. *Nature* **252**, 45–47 (1974).
13. Silvestre, P. thesis, Univ. Nice (1980).
14. Zielke, R., Ozand, P., Tildon, T., Sevdalian, D. & Cornblath, M. *Proc. natn. Acad. Sci. U.S.A.* **73**, 4110–4114 (1976).

0028–0836/80/400447—03$01.00

Single Na^+ channel currents observed in cultured rat muscle cells

Frederick J. Sigworth & Erwin Neher

Max Planck Institut für biophysikalische Chemie,
D-3400 Göttingen, FRG

The voltage- and time-dependent conductance of membrane Na^+ channels is responsible for the propagation of action potentials in nerve and muscle cells. In voltage-step-clamp experiments on neurone preparations containing 10^4–10^7 Na^+ channels the membrane conductance shows smooth variations in time, but analysis of fluctuations[1,2] and other evidence[3] suggest that the underlying single-channel conductance changes are stochastic, rapid transitions between 'closed' and 'open' states as seen in other channel types. We report here the first observations of currents through individual Na^+ channels under physiological conditions using an improved version of the extracellular patch-clamp technique[4–6] on cultured rat muscle cells. Our observations support earlier inferences about channel gating and show a single-channel conductance of approximately 18 pS.

Our cell preparations were myoballs[7,8] prepared from 19–20-day old rat embryos. After fusion to form myotubes the cells were treated for 2 days in 10^{-6} M colchicine, which caused them to assume a spherical shape, and then returned to the normal growth medium (Dulbecco's minimal essential medium with 10% fetal calf serum) for 2–5 days before use. As excitable cells, myoballs were advantageous for several reasons. First, Na^+ channels in frog muscle show longer activation time constants than those in frog nerve, and we observe slower activation in myoballs than in mammalian nerve[9]. The long time constants reduce the time-resolution requirements of the recording system. Second, the absence of connective tissue in the cell culture allows direct access to the sarcolemma without enzyme treatment[5]. And third, the spherical shape of the cells allows the use of a conventional, two-microelectrode voltage clamp for measurement of the whole-cell currents. In contrast to the recent recordings from K^+ channels in squid axons by Conti and Neher[10], we were also able to use physiological ionic solutions for our experiments. We did, however, cool the cells to room temperature (19–22 °C) to slow the channel kinetics.

The recording method (Fig. 1) represents an order-of-magnitude improvement in resolution over previous results from the patch recording technique. The basis of the improvement is an increase from 10^8 to 10^{10} Ω of the seal resistance that electrically isolates a small patch of membrane for current measurement[6]. The higher resistance introduces less thermal noise (which in the past was the predominant noise source) allowing a wider recording bandwidth to be used. It also allows voltage steps to be applied to the patch without the necessity of voltage-clamping the entire cell with microelectrodes. A seal is formed by applying gentle suction in the pipette which is pressed against the cell membrane. In two experiments we estimated the membrane patch area to be 2 and 10 μm^2 from transfer capacitance measurements on cells that were also voltage-clamped with microelectrodes. This area is large in view of the 0.3–0.5 μm diameter of the opening in the pipette tip, and suggests that part of the membrane is drawn into the pipette, forming an omega shape (Fig. 1).

The size of the peak Na^+ currents recorded with the microelectrode clamp in these cells varied from essentially zero to about 1 mA per cm^2 of surface area; this latter current density corresponds to about 10 channels per μm^2 surface area. Capacitance measurements[7] suggest that the total membrane area is much larger than the surface area, as would be expected from transverse tubules or extensive membrane infolding. The

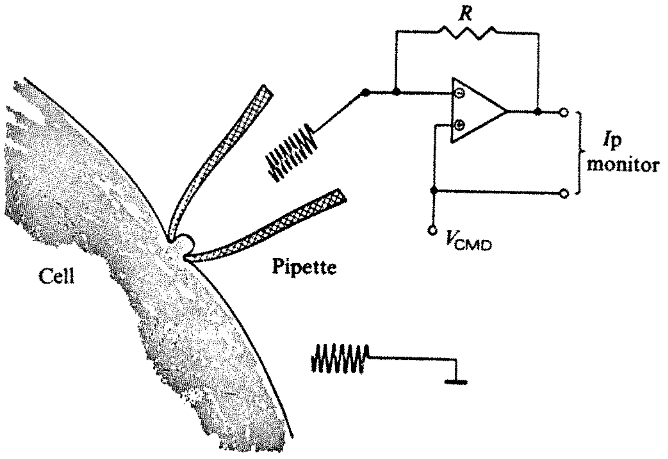

Fig. 1 Recording system. Details of pipette fabrication and use are given in ref. 6. Briefly, a freshly fire-polished glass pipette with inner opening diameter ~0.3–0.5 μm is filled with modified Ringer solution and pressed against a myoball (cell diameter 30–80 μm). Suction (5–50 cm H_2O) is applied to the inside of the pipette for 5–30 s until the sealing resistance, measured as the current response to small voltage pulses at V_{CMD}, suddenly increases to > 1 GΩ. Ag–AgCl electrodes are used in the pipette and for the reference electrode in the bath. The patch clamp circuitry resembles that described previously[5], but was modified to exploit the high seal resistance. The current measuring resistance R was increased to 10 GΩ, and frequency-response corrections were applied in a later amplifier stage to maintain flat response in the current monitor signal to 7 kHz. The operational amplifier is a Burr–Brown 3523J. As the input shunt capacitance ($\simeq 3$ pf) causes the voltage noise of the amplifier to predominate at high frequencies, we coat the pipettes with wax or Sylgard to reduce the wall capacitance. The potential inside the pipette is controlled by V_{CMD}; this also provides very good control of the potential of the membrane patch since the pipette access resistance is < 10 MΩ and the patch currents cause negligible changes in the resting potential of the cell. The bathing Ringer solution contained (in mM): 140 NaCl, 1.4 KCl, 2.0 $MgCl_2$, 1 $CaCl_2$ and 20 HEPES at *p*H 7.4. The pipette solution was the same with 0.2–1 $\mu g\ ml^{-1}$ α-bungarotoxin added to block acetylcholine receptors. Both solutions were filtered (0.2 μm pore size) immediately before use. Occasionally 5 mM TEA Cl (replacing NaCl) was also present to block K^+ channels; this had no obvious effect on the patch current recordings.

small number of channels in a patch—at most 3–5 channels were simultaneously active—is consistent with this. Also, voltage clamp of the cells sometimes showed large, tetrodotoxin (TTX)-sensitive regenerative responses at small depolarizations, characteristic of a large membrane component under poor voltage-clamp control. No responses of this kind were seen in the patch clamp recordings, however.

Figure 2*c* shows a series of current records from a membrane patch, obtained by successive depolarizations to $V = 10$ mV, where V is the displacement from the resting potential. Discrete current pulses of varying duration appear after the start of the depolarizations; inactivation of the currents appears as a reduction in the frequency of appearance later in the depolarizations. In roughly half of the records no channel events were seen; in two records of the 300 taken in this run two overlapping events were seen.

Conditions known to reduce the Na^+ current also affect these current pulses. When two-thirds of the Na^+ in the pipette was replaced with the impermeant substitute tetramethylammonium ion (TMA), the discrete currents were reduced in size (Fig. 2*d*). In other experiments the sensitivity to block by TTX was tested statistically. For these we used two culture dishes of cells 5 days after colchicine treatment because at this later stage the channel density seems to be more uniform[11], as reflected by the fraction of patches that contain channels. In each dish four recordings were made, three with Ringer solution in the pipette and one with 1 μM TTX added. Channel activity was present in all six patches in the absence of TTX, and not present in TTX, showing that TTX blocks at least some of the channels ($P < 0.05$, Fisher test).

Assuming that the Na^+-channels in these cells are identical and function independently, one expects that the sum of many current records from a few channels should show the same properties as the sodium current measured in a conventional voltage-clamp from thousands of channels. Such an average time course derived from 300 depolarizations of the membrane patch is shown in Fig. 2*b*. It shows the typical kinetic behaviour[12] with a rapid ($\tau_m \simeq 0.8$ ms) activation followed by a slower ($\tau_h \simeq 2.6$ ms) inactivation process.

Averages and representative single records are also shown in Fig. 3 for variously sized depolarizations. With increasing depolarization the peak inward current first increases, as the probability that channels are open rises, and then decreases as the single-channel currents become small near the reversal potential. The mean channel open time, τ, shows the qualitative behaviour expected from Hodgkin–Huxley kinetics[12] where $\tau = 1/(3\beta_m + \beta_h)$. At small depolarizations τ increases with depolarization as the closing rate constant β_m decreases. At larger depolarizations the increasing inactivation rate β_h shortens τ. There is, however, a quantitative disagreement, with τ not differing significantly from τ_m in the data of Fig. 2 and in two other experiments at $V = 10$ and 20 mV. At such small depolarizations, where activation is small, τ would be near $\tau_m/3$ in the Hodgkin–Huxley theory. The channel lifetimes are consistent, on the other hand, with the kinetic theory of Armstrong and Gilly[13] in which the final opening step of the channel is rate limiting in channel activation.

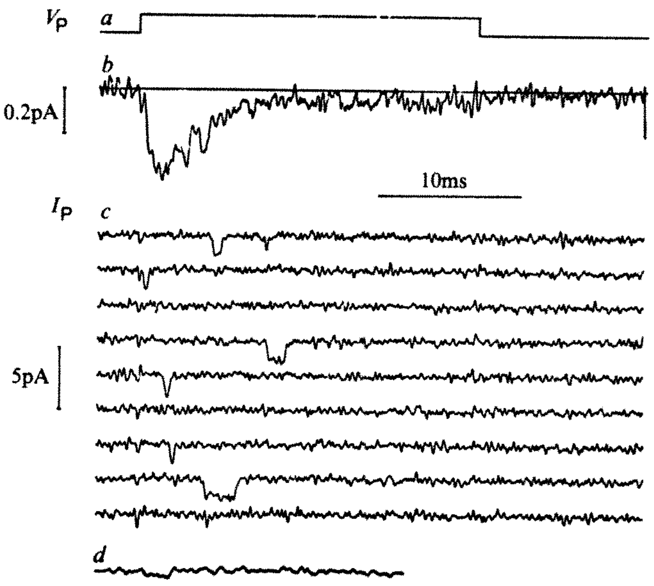

Fig. 2 Single-channel currents during 10 mV depolarizations. *a*, Imposed patch membrane potential. The patch was held hyperpolarized by 30 mV; 40 mV depolarizing pulses were given at 1-s intervals. *b*, Average of a set of 300 current records elicited by these pulses. *c*, Nine successive individual records from this set. The mean channel current was −1.6 pA, and lifetime was 0.7 ms. *d*, Example of a current record obtained in another experiment where two-thirds of the Na^+ in the pipette was replaced with tetramethylammonium ion. The record was plotted on the same scale as *c* but additional filtering was used to reduce the noise level. Leakage and capacitance currents were subtracted in each case using means of responses to symmetrical hyperpolarizing pulses; to remove a residual capacitance artefact in *b* and *c* a mean time course was computed from records in which no channel activity was visible, and this mean was subtracted from individual records. Filtering of the data resulted in effective system risetimes of 300, 180 and 300 μs in *b*, *c*, and *d*, respectively. The patch apparently contained 2–3 active channels, as estimated from responses to larger depolarizations. The solution in the pipette contained 5 mM TEA. Cell 3.1; temperature, 18 °C.

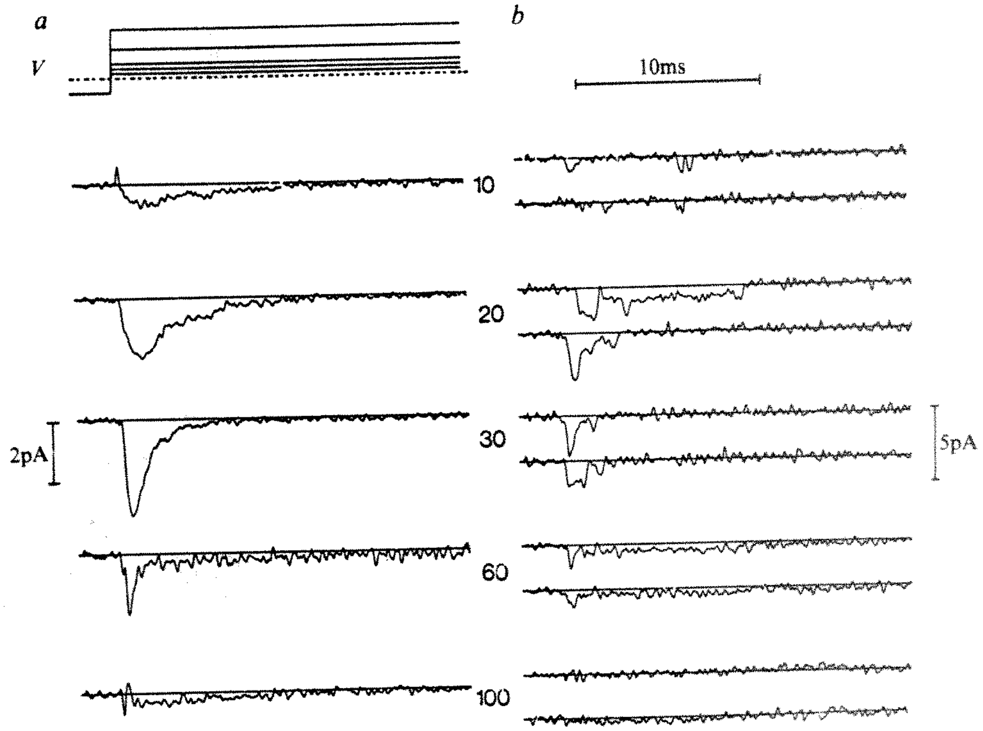

Fig. 3 Patch currents obtained with depolarizations to the various potentials V shown. a, Means calculated from 24–104 current records; b, representative individual records at each potential. Overlapping currents from 2–3 channels can be recognized at $V = 20$ and 30 mV. Note the decrease in current size near the reversal potential (approximately $V = 100$ mV). Leakage and capacitance currents were subtracted with averages from symmetrical hyperpolarizations. Recording system risetime was 220 µs. Cell 7.1, 3 days after colchicine treatment. Temperature, 22 °C.

Estimates of the cell resting potentials allow us to express values of V in terms of absolute membrane potential. Impalements with microelectrodes showed maximum resting potentials in the range −60 to −70 mV. h_∞ curves from averaged patch currents showed $h_\infty = 0.5$ in the range $V = 0$ to −15 mV whereas measurements with the microelectrode voltage clamp showed corresponding absolute potentials of −80 to −95 mV. We conclude therefore that the resting potentials were in the range −60 to −80 mV. This places the apparent reversal potential $V_{Na} \simeq 100$ mV in Fig. 3 in the absolute membrane potential range of +20 to +40 mV.

The size of the single-channel currents corresponds to a single-channel conductance $\gamma = 18$ pS. This value is at first sight surprisingly large, as γ estimates for frog nerve Na^+ channels, based on current fluctuation analysis, are in the range 6–8 pS (refs 1, 2). These values become twice as large, however, when they are corrected to the temperature and higher sodium concentration used in our experiments, assuming[14] $Q_{10} = 1.3$ and a linear concentration dependence of conductance.

The extracellular patch clamp as used in this work promises to be a powerful electrophysiological technique for tissue-cultured cells. The ability to clamp and change the potential in small patches of membrane now allows voltage-clamp studies to be performed on cells that are too small or have unsuitable geometries for microelectrode work.

We thank Drs B. Sakmann and O. Hamill for advice and help in getting the seals to work, and H. Karsten for preparing the myoballs. F.J.S. is a fellow of the Alexander von Humboldt Stiftung.

Received 30 June; accepted 18 August 1980.

1. Conti, F., Hille, B., Neumcke, B., Nonner, W. & Stämpfli, R. *J. Physiol., Lond.* **262,** 699–727; 729–742 (1976).
2. Sigworth, F. J. *J. Physiol., Lond.* (in the press).
3. Hille, B. *A. Rev. Physiol.* **38,** 139–152 (1976).
4. Neher, E. & Sakmann, B. *Nature* **260,** 799–802 (1976).
5. Neher, E., Sakmann, B. & Steinbach, J. H. *Pflügers. Arch. ges. Physiol.* **375,** 219–228 (1978).
6. Neher, E. in *Techniques in Cellular Physiology* (ed. Baker, P. F.) (Elsevier, Amsterdam, in the press).
7. Horn, R. & Brodwick, M. *J. gen. Physiol.* **75,** 297–321 (1980).
8. Godman, G. C. & Murray, M. R. *Proc. Soc. exp. Biol. Med.* **84,** 668–672 (1953).
9. Chiu, S. Y., Ritchie, J. M., Rogart, R. B. & Stagg, D. *J. Physiol.* **292,** 149–166 (1979).
10. Conti, F. & Neher, E. *Nature* **285,** 140–143 (1980).
11. Spector, I. & Prives, J. M. *Proc. natn. Acad. Sci. U.S.A.* **74,** 5166–5170 (1977).
12. Hodgkin, A. L. & Huxley, A. F. *J. Physiol.* **117,** 500–544 (1952).
13. Armstrong, C. M. & Gilly, W. E. *J. gen. Physiol.* **74,** 691–711 (1979).
14. Frankenhauser, B. & Moore, L. E. *J. Physiol.* **169,** 431–437 (1963).

Localization of [^{3}H]-2-deoxyglucose in single molluscan neurones

T. J. Sejnowski*‡, S. C. Reingold*, D. B. Kelley† & A. Gelperin*

*Department of Biology, Princeton University, Princeton,
New Jersey 08544
†Department of Psychology, Princeton University, Princeton,
New Jersey 08544

The glucose analogue 2-deoxyglucose (2-DG) can be used quantitatively to measure metabolic activity[1] and is widely used qualitatively for mapping functional activity in the brain[2–4]. The resolution (meaning the full width at half maximum of the grain density distribution around a line source) of the technique using [^{14}C]-2-DG and X-ray film is limited to about 100 µm[5]. Attempts have been made to improve the resolution using [^{3}H]-2-DG (ref. 6) and cellular resolution has been achieved in the goldfish retina[7] and with cultured mouse neurones[8]. An anatomical technique for mapping the metabolic activity of individual neurones would be useful for studying invertebrate central nervous systems, which are relatively simple and stereotyped compared to vertebrate brains. The [^{3}H]-2-DG technique was applied to an invertebrate in a study of the *Drosophila* visual system[9], though without cellular resolution. We present here modifications of the [^{3}H]-2-DG technique to demonstrate localization of 2-DG in single neurones of *Limax maximus*, a gastropod mollusc, with a resolution of less than 1 µm.

Glucose and 2-DG compete both for transport into and out of a cell and for phosphorylation by hexokinase inside the cell. Once 2-DG is phosphorylated to 2-deoxyglucose-6-phosphate (2-DG-6-P), it is not metabolized further and accumulates in the cell. In the conventional [^{14}C]-2-DG technique[1], the tissue is frozen, sectioned on a cryostat, picked up on a warm coverslip

---

‡Present address: Department of Neurobiology, Harvard Medical School, 25 Shattuck St, Boston, Massachusetts 02115.

0028-0836/80/400449—03$01.00

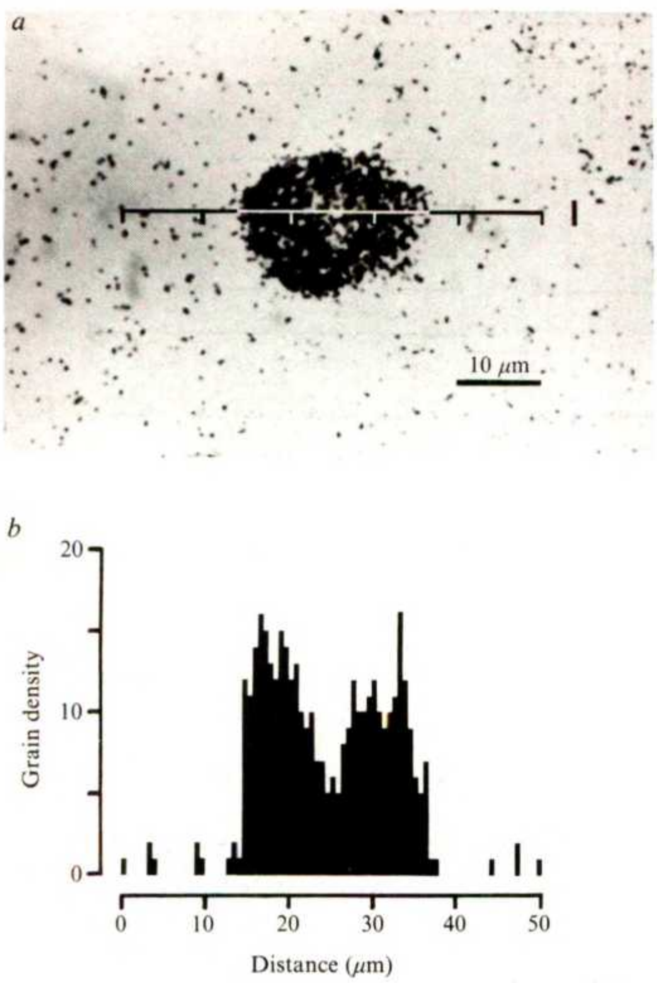

Fig. 1 Measurement of silver grain density over a single cell body in a buccal ganglion. *a*, Light-microscopic autoradiograph from a preparation incubated in [^{3}H]-2-DG for 45 min and freeze-substituted with acetone at −70 °C. During the incubation, a neurone in the buccal ganglion was stimulated with an intracellular electrode to elicit action potentials at the rate of 2 s^{-1}. Several cells in the buccal ganglion were labelled. Scale bar, 10 μm. *b*, A reticle with 100 lines was superposed over the cell at high magnification and the silver grains were counted by focussing through the emulsion of the autoradiograph. The number of silver grains between reticle lines (in a rectangle (0.63×4.6 μm) as shown to the right of the cell) is plotted as a function of distance along the line drawn through the cell body in *a*. The drop in density of silver grains over the centre of the cell occurs over the nucleus. The density of silver grains over the cytoplasm is 4.1 μm^{-2}, which is 40 times the average background density over the tissue surrounding the cell and 290 times the background density in the emulsion.

and dried on a hot plate, during which the 2-DG and 2-DG-6-P can freely diffuse and interfere with the localization of the label within cells. One way to prevent diffusion is to replace the water in the cell with a solvent in which 2-DG and 2-DG-6-P are insoluble and to exclude water from the tissue in all subsequent steps. We have localized [^{3}H]-2-DG using two methods: in the first, the tissue was frozen and freeze-substituted[10] with acetone at −70 °C, and in the second, the tissue was dehydrated in dry acetone at 4 °C.

The buccal ganglion of *L. maximus* innervates the animal's feeding musculature and contains several large identifiable neurones as well as several hundred smaller cells[11,12]. The stereotyped structure of the ganglion, its small size (about 1 mm in diameter) and its accessibility to electrophysiological techniques make it suitable for studying the uptake of 2-DG by single neurones. In each experiment, a pair of buccal ganglia was dissected and placed in saline modified by lowering Ca^{2+} to 0.07 times its normal concentration and raising Mg^{2+} by five times to reduce transmission at chemical synapses. (The composition of the solution was 56 mM Na^+, 4.2 mM K^+, 0.5 mM Ca^{2+}, 23 mM Mg^{2+}, 104 mM Cl^-, 0.2 mM $H_2PO_4^-$, 2.5 mM HCO_3^- and 5 mM dextrose.) Approximately 100 μCi ml^{-1} of 2-[1,2-^{3}H]-deoxy-D-glucose (New England Nuclear NET-549, specific activity 40 Ci mM^{-1}) was added to the bath and the ganglia were incubated for 1 h or less, depending on the experiment. Afterwards, the ganglia were rinsed in five washes of fresh saline over 30 min. For freeze-substitution, the ganglia were then rapidly frozen in Freon 22 cooled to −160 °C with liquid nitrogen, placed in a vial containing 20 ml dry acetone and 1 g of Al_2O_3 (Brockman grade 1), and kept at −70 °C for 48 h. For acetone dehydration, the ganglia were placed in an identically prepared vial and kept at 4 °C overnight. No fixatives were used. (Fixation with glutaraldehyde[6,7] results in a loss of over 90% of the radioactivity from the tissue[7,8].) After either freeze-substitution or dehydration, the tissue was gradually warmed to room temperature and embedded in Araldite to which 1% by weight Dow-Corning silicone fluid[13] had been added. The embedded

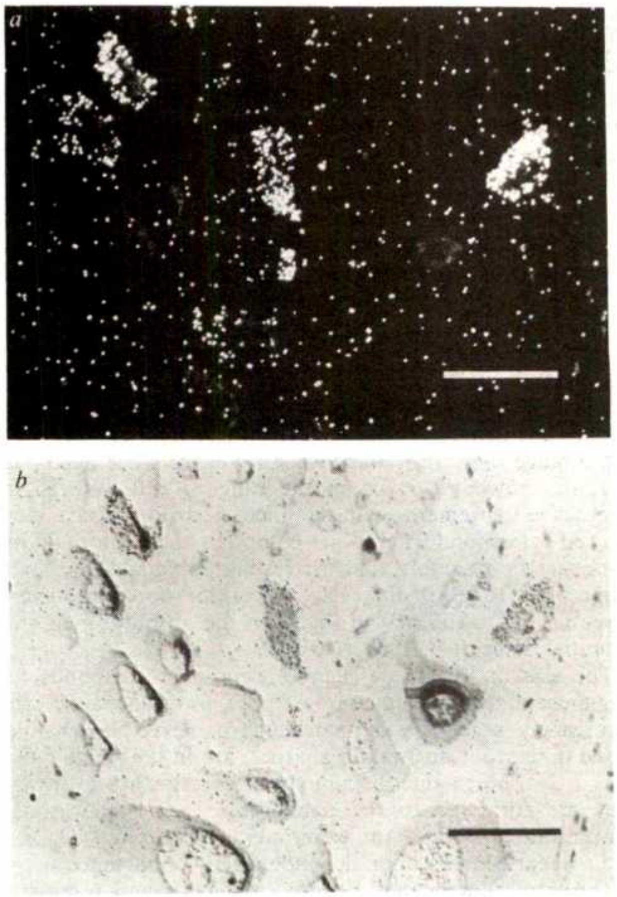

Fig. 2 Light-microscopic autoradiograph of several labelled cell bodies in a buccal ganglion. The ganglion was incubated in [^{3}H]-2-DG for 20 min and dehydrated in dry acetone at 4 °C. During the incubation a neurone was stimulated with an intracellular electrode to elicit action potentials at the rate of 2 s^{-1}. The sections were lightly stained with methylene blue. *a*, Five labelled cells (dark-field illumination). The cell bodies could be traced in serial sections through the ganglion. The nuclei of the two labelled cells on the far left and the cell on the far right were not labelled above background. The average density of silver grains over the labelled cells was 0.1 μm^{-2}–0.5 μm^{-2}, which was approximately 10–50 times the background density over surrounding tissue. *b*, The same section in *a*, photographed using Nomarski differential interference contrast optics. Scale bar, 40 μm.

tissue was then dry-sectioned at 2–4 μm on an ultramicrotome and placed on a slide coated with a thin layer of anhydrous glycerol. The glycerol was evaporated by setting the slide on a hot plate at 110 °C. The slides were then dipped in Kodak NTB-2 nuclear emulsion, dried, exposed at 4 °C for 2–4 weeks, developed in Kodak D-19 at 16 °C for 6 min, washed and stained with either 1% methylene blue or 1% toluidine blue.

Scintillation counting was used to determine the uptake of [^{3}H]-2-DG by ganglia during incubation and the loss of label during subsequent processing. The amount of radioactivity left in the acetone following either freeze-substitution or dehydration was less than 0.5% of the total radioactivity remaining in the ganglion. The loss of label during autoradiography was not quantitatively assessed, but it was probably low because spreading of label around the edges of the section or around discretely labelled structures within the section was never seen.

Autoradiographs of buccal ganglia incubated in [^{3}H]-2-DG revealed labelled individual neurones in all preparations. No cells were labelled in control ganglia incubated without [^{3}H]-2-DG, thus ruling out positive chemography. In seven heavily labelled cells from three preparations, the density of silver grains over cell bodies was between 0.1 μm^{-2} and 4.5 μm^{-2}, which was 10–50 times the mean background density over adjacent tissue. The glucose utilization is therefore 10–50 times greater within some cells than without. The localization of [^{3}H]-2-DG in a single heavily labelled buccal neurone is shown in Fig. 1*a*. The density of silver grains drops sharply at the boundary of the cell body, with the transition from maximum grain density to background occurring in less than 1 μm (Fig. 1*b*). The resolution of the technique appears to be limited by the size of a developed silver grain, which has a diameter of 0.5 μm. Whenever the stained cell membrane of a labelled cell is visible, the grain density drops abruptly at the cell membrane. In some labelled cells, such as those shown in Fig. 2, the grain density also drops abruptly at the nuclear membrane, with much lower labelling over the cell nucleus than the cytoplasm. In addition to labelled cell bodies, labelled structures could also be detected in the neuropil.

The high resolution obtained with this technique is probably the result of removing water from the tissue. During freeze-substitution, the maximum concentration of water at the interface between ice and acetone is 4% at −70 °C (ref. 14). Thus, molecules insoluble in acetone diffuse very little from the site at which they were immobilized during freezing. For example, freeze-substitution has been used to localize Ca^{2+} in subcellular compartments[15]. More diffusion of 2-DG and 2-DG-6-P occurs within the cell with acetone dehydration at 4 °C than with freeze-substitution at −70 °C. However, the labelling of single cell bodies using acetone dehydration had the same resolution as with freeze-substitution. We can therefore conclude that both freeze-substitution and acetone dehydration are effective in localizing [^{3}H]-2-DG within single neurones.

The [^{3}H]-2-DG technique presented here can be used to measure the qualitative change in the distribution of label under different conditions. Preliminary experiments indicate that the labelling of single neurones demonstrated here is correlated with spontaneous and stimulated electrical activity in the ganglion[16]. The technique could be useful in studying networks of neurones underlying behaviour in the isolated central nervous system[17]. In particular, the participation of small neurones, which are difficult to study electrophysiologically, can be monitored as easily as large neurones. It may also be possible to measure the metabolic activity of axon terminals in the neuropil. As the resolution reported here is close to the limiting resolution of light microscopy, further improvement will require the use of electron microscopy.

This investigation was supported by NIH postdoctoral fellowships MH07670 (T.J.S.) and NS05188 (S.C.R.). The Grass Foundation (S.C.R.), NIH grant HD12126 (D.B.K.), NSF grant BNS76-18792 (A.G.), NIH training grant MH13445, and the Whitehall Foundation. We thank Katherine Cross for her assistance with photography.

Received 28 April, accepted 28 July 1980

1 Sokoloff, L *et al* *J Neurochem* **28**, 897–916 (1977)
2 Hubel, D H, Wiesel, T N & Stryker, M P *Nature* **269**, 328–330 (1977)
3 Des Rosiers, M H *et al* *Science* **200**, 447–449 (1978)
4 Kelley, D. B *Science* **207**, 553–555 (1980)
5 Goochee, C., Rasband, W & Sokoloff, L *Ann Neurol* **7**, 359–370 (1980)
6 Des Rosiers, M H & Descarries, L *C r hebd Séanc Acad Sci, Paris* **D287**, 153–156 (1978).
7 Basinger, S F., Gordon, W C & Lam, D. M K *Nature* **280**, 682–684 (1979)
8 Ornberg, R L *et al. J Cell Biol* **83**, 142a (1979)
9 Buchner, E, Buchner, S & Hengstenberg, R *Science* **205**, 687–688 (1979)
10 Feder, N & Sidman, R. L *J biophys biochem Cytol* **4**, 593–600 (1958)
11 Gelperin, A, Chang, J. J & Reingold, S C *J Neurobiol* **9**, 285–300 (1978)
12 Reingold, S C & Gelperin, A *J exp Biol* **85**, 1–19 (1980)
13 Stirling, C E & Kinter, W B *J Cell Biol* **35**, 585–604 (1967)
14 Van Harreveld, A, Crowell, J & Malhotra, S K *J Cell Biol* **25**, 117–137 (1965)
15 Henkart, M P, Reese, T S & Brinley, F J. Jr *Science* **202**, 1300–1303 (1978)
16 Reingold, S C *et al* (submitted for publication)
17 Chang, J. J & Gelperin, A *Proc natn Acad Sci U S A* **77** (in the press)

Repeated tricyclics induce a progressive dopamine autoreceptor subsensitivity independent of daily drug treatment

Louis A. Chiodo & Seymour M. Antelman*

Psychobiology Program, Department of Psychology,
University of Pittsburgh, Pittsburgh, Pennsylvania 15260

Dopamine (DA) has largely been ignored in considering possible mechanisms underlying the therapeutic effects of tricyclic anti-depressants (TCA)[1–3]. Most previous work done has focused on the ability of some TCAs to block the *in vitro* re-uptake of DA[1]—an effect which unfortunately requires very high doses. Recently, however, Serra *et al.*[3] proposed that TCAs may exert their therapeutic effects by inducing a subsensitivity of presynaptic receptors located on the dendrites and soma of DA neurones (DA autoreceptors). This hypothesis was directly tested by examining the influence of TCAs on the demonstrated ability of the DA agonist, apomorphine, to depress selectively the spontaneous activity of single DA cells. We now report that repeated administration of both typical and atypical TCAs induces a progressive subsensitivity of DA autoreceptors, and that this gradual augmentation of DA autoreceptor subsensitivity depends on the passage of time rather than daily TCA administration. The latter finding suggests that daily drug administration may not be therapeutically necessary.

The 53 male albino rats (200–250 g; Zivic Miller) used in these studies were housed two per cage with free access to food and water and maintained on a 12 h light/dark cycle. Animals were handled and weighed daily for 2 weeks before experiments began. All experiments were done in double-blind conditions. After a period of drug treatment (specified below) the animals were anaesthetized with chloral hydrate [400 mg per kg, intraperitoneally (i.p.)], mounted in a stereotaxic apparatus and the spontaneous discharge rates of single DA neurones located within the zona compacta of the substantia nigra (SNC; coordinates: anterior 1,300–2,400 μm, lateral 1,300–2,400 μm [ref. 4]) were monitored as previously described[5,6]. Briefly, extracellular electrical activity was recorded through glass micropipettes filled with 2 M NaCl which was saturated with fast green dye (tip size 1–3 μm, *in vitro* d.c. impedance of 4–12 MΩ). Neuronal signals were fed into a high input–impedence differential amplifier (bandpass filters: 100 Hz and 3 kHz) whose output was led into a window discriminator, a signal integrator and digital frequency meter. The femoral vein was catheterized for the intravenous (i.v.) administration of all pharmacological agents. All drug doses are based on the weight of the salt. At the termination of each experiment the recording

---

*Also at Western Psychiatric Institute and Clinic, Department of Psychiatry, School of Medicine, University of Pittsburgh, Pittsburgh, Pennsylvania 15260

0028-0836/80/400451—04$01 00

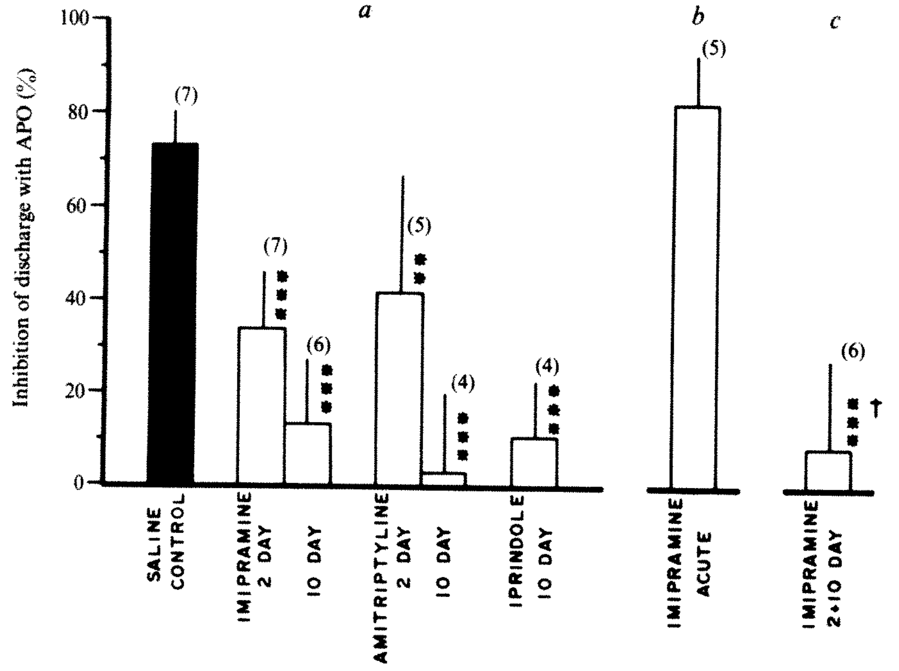

Fig. 1 The effects of various TCA treatments on the apomorphine-induced (APO; 0.004 mg per kg, i.v.) inhibition of the spontaneous activity of zona compacta DA neurones. See text for doses and details. $^{***}P<0.001$, $^{**}P<0.02$; two-tailed *t*-test, $\dagger P<0.05$ relative to 2-day imipramine group. Number tested in parentheses.

site was marked by passing a 40-μA negative current for 10 min which results in the injection of the dye[7]. The animals were then perfused and the brain sliced and stained. All neurones reported in this study were histologically located in the zona compacta region of the substantia nigra.

Single DA neurones were located on the basis of the previously described electrophysiological criteria of Bunney and Aghajanian[8]. That is, DA cells within the SNC spontaneously discharged at rates of 1–9 Hz, had biphasic action potentials (+/−) with amplitudes of 0.4–1.5 mV and typically displayed a train of action potentials or 'burst' on discharge. All cells also met the pharmacological criteria for identifying DA neurones established by these investigators[8,9]. Spontaneous activity was inhibited by the administration of a presynaptic dose of apomorphine and increased by the DA antagonist, haloperidol. To avoid contaminating any of our results, verification of the effects of haloperidol always took place immediately before terminating the recording session.

In the first experiment we investigated whether repeated injections of both typical (imipramine and amitriptyline) and atypical (iprindole) TCAs could alter DA autoreceptor sensitivity. Animals were placed into one of the following treatment groups: (1) 2 days of imipramine; (2) 10 days of imipramine; (3) 2 days of amitriptyline; (4) 10 days of amitriptyline; (5) 10 days of iprindole; and (6) 10 days of saline vehicle. All drugs were administered intraperitoneally in a dose of 10 mg per kg twice daily. Forty-eight hours after cessation of drug treatment the animals were recorded from as described above. Once a DA neurone was located its spontaneous activity was monitored for a minimum of 4 min to establish a reliable baseline rate. Apomorphine was then administered. Since a 0.004 mg per kg (i.v.) dose of apomorphine has been shown to inhibit DA neuronal activity by stimulating only DA autoreceptors located within the SNC[10], we used the degree of inhibition obtained with this dose as our index of DA autoreceptor sensitivity. The present results indicate that repeated TCA injection induces a subsensitivity of presynaptic DA autoreceptors (Figs 1*a*, 3). All TCA treatments resulted in a significant attenuation of the ability of apomorphine to inhibit the spontaneous discharge of DA neurones. Ten days of TCA administration resulted in a greater degree of DA autoreceptor subsensitivity than 2 days of treatment. Although TCA treatment also produced a tendency toward an overall increase in baseline firing rates, relative to saline controls this difference was not statistically significant.

To determine the possible functional significance of TCA-induced DA autoreceptor subsensitivity we examined the responsiveness of subsensitive cells to tail pressure, a mildly activating, non-painful stimulus. We have previously shown that tail pressure induces DA-dependent behaviours and also alters the activity of midbrain DA neurones[5,6]. All TCA treatments increased the ability of tail pressure to alter the spontaneous discharge of DA neurones (Fig. 2). This effect was significantly different from saline controls in both the 2- and 10-day imipramine groups as well as the 10-day amitriptyline group ($P<0.05$ for all three). Interestingly, the 10-day amitriptyline group, which showed the greatest degree of DA autoreceptor subsensitivity, was the group most responsive to tail-pressure induced changes in discharge. The fact that some of the groups (that is, the 10-day iprindole) did not reach statistical significance is probably due to a combination of relatively small group size and a large degree of group variance.

To investigate the possibility that residual TCAs might simply be competing with apomorphine for autoreceptor binding and, in so doing, reduce its effectiveness, we examined the effects of acute administration of imipramine (0.4 mg per kg, i.v.) on the subsequent injection of apomorphine (0.004 mg per kg, i.v.). Acute imipramine had no effect on the ability of apomorphine to inhibit DA neuronal discharge (Fig. 1*b*). It also failed to alter the spontaneous activity or responsiveness to tail pressure of these neurones relative to controls (Fig. 2).

The augmentation of DA autoreceptor subsensitivity seen after 10 days of imipramine and amitriptyline treatment is reminiscent of the progressive behavioural sensitization that can occur following the administration of amphetamine and other stimulants[11,12]. Although stimulant sensitization is usually induced by repeated drug treatment it is not dependent on such treatment and long-lasting effects have been observed following only a single amphetamine injection[13]. These findings raise the question of whether the progressive DA autoreceptor subsensitivity that occurs between 2 and 10 days of TCA treatment actually depends on administering these agents for 10 days.

To answer this question we ran an additional group of animals which received 2 days of imipramine (10 mg per kg, i.p. twice a day) followed by 10 drug-free days. Thus, this group was tested for subsensitivity at the same time as the group receiving 10 days of imipramine followed by 2 drug-free days. This treatment produced the same degree (actually 32% greater) of DA autoreceptor subsensitivity as the 10-day imipramine group

(Fig. 1c). Consistent with these data, 2 days of imipramine followed by 10 drug-free days (2+10 day group) resulted in significantly greater subsensitivity than an equal number of injections followed by only 2 drug-free days (2+2 day group). That is, the administration of the presynaptic dose of apomorphine inhibited the spontaneous activity of DA cells by only 9.2±19.0% in the 2+10 day group but by 34.1±12.4% in the 2+2 day group ($P<0.05$, see Fig. 1). This experiment clearly demonstrates that the TCA-induced progression in DA autoreceptor subsensitivity is not dependent on repeated daily drug treatment. Moreover, these data provide an additional and definitive argument against explaining subsensitivity in terms of direct competition between TCAs and apomorphine. That is, maximal subsensitivity was observed at a time (10 days after cessation of injections) when little if any residual imipramine would be expected in the brain.

The present study provides the first electrophysiological demonstration of DA autoreceptor subsensitivity. Moreover, the fact that both classical and newer TCAs induce progressive subsensitivity within the same time frame as their antidepressant effects suggests that DA autoreceptor subsensitivity must be considered as a possible mechanism underlying the therapeutic effects of these agents. Finally, and perhaps most significantly, we have found that the progressive augmentation of DA autoreceptor subsensitivity induced by TCAs is not dependent on repeated daily drug administration. Thus, short-term drug treatment seems to be sufficient to trigger a subsensitivity which then undergoes a progressive enhancement as a function of time regardless of whether TCAs are again administered. This finding may be clinically relevant in several respects. If presynaptic DA autoreceptor subsensitivity is critical for the therapeutic efficacy of TCAs, then our data suggest that daily treatment with these agents may not be necessary for the amelioration of depression. The same data also provide a possible explanation of the delayed therapeutic onset of TCAs—it may reflect the time necessary for the development of a critical degree of receptor subsensitivity as well as the build-up of TCAs to steady-state therapeutic concentrations[14]. It would be interesting to know whether TCA-induced changes in noradrenaline[15,16] and serotonin[17] receptors are also independent of repeated drug treatment.

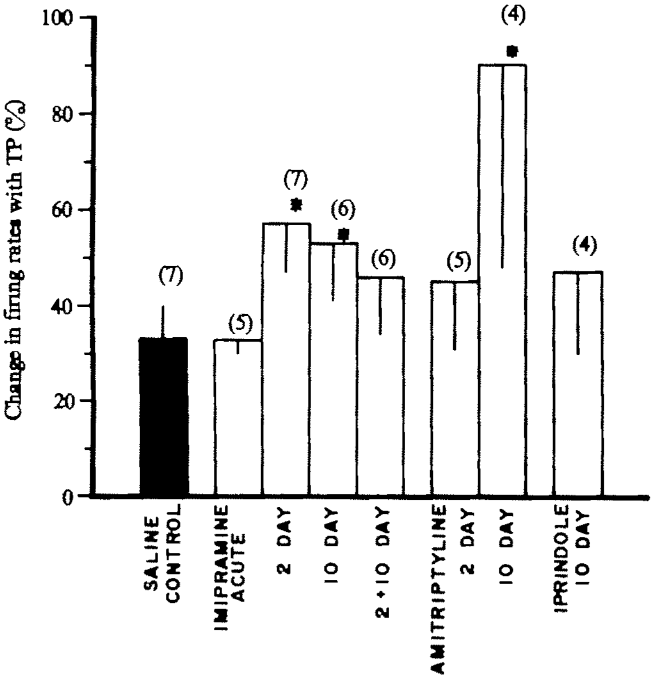

Fig. 2 TCA potentiation of tail-pressure induced (TP) changes in DA neuronal discharge. Data from same animals represented in Fig. 1. *$P<0.05$, two-tailed t-test. Number tested in parentheses.

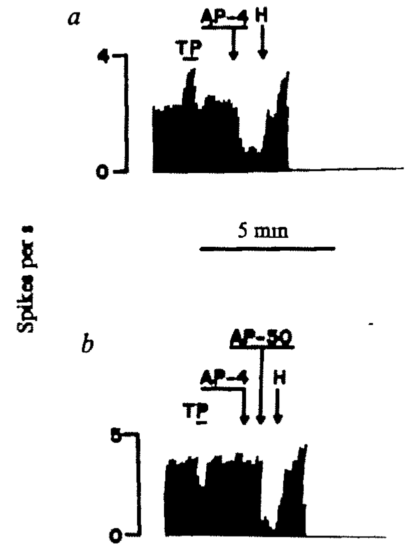

Fig. 3 Cumulative histograms of DA neurones located in the zona compacta demonstrating the effects of repeated TCA treatment on the ability of a presynaptic dose of apomorphine (APO-4; 4 μg per kg, i.v.) to inhibit the spontaneous firing of these neurones. *a*, Saline-treated control cell. A presynaptic dose of apomorphine produced an 81% inhibition of neuronal activity. Haloperidol (HAL; 0.2 mg per kg, i.v.) reversed this effect. *b*, Cell from an animal treated with imipramine for 10 days. A presynaptic dose of apomorphine had no effect on the spontaneous activity of this cell however, the subsequent administration of a postsynaptic dose of apomorphine (APO-50; 50 μg per kg, i.v.) was able to inhibit neuronal discharge by 86%. Haloperidol (0.2 mg per kg, i.v.) again reversed this effect. Horizontal bars represent the duration of the sensory stimulus, mild tail pressure (TP). Arrows indicate the i.v. administration of pharmacological agents.

The possible functional significance of subsensitive DA autoreceptors is reflected in our finding that animals showing such a subsensitivity also demonstrate an enhanced responsiveness to an activating environmental stimulus (tail pressure). Enhanced responsiveness to environmental stimuli is essentially the functional definition of successful TCA treatment.

Although TCA doses used in these experiments are about four times those used clinically this is not likely to explain our findings as preliminary data from our laboratory indicate similar effects with electroconvulsive shock, a non-pharmacological antidepressant treatment. This raises the question of whether our findings are specific to treatments having an antidepressant effect. In this regard, it should be noted that perturbation of DA autoreceptors does not invariably give rise to subsensitivity. Using a similar procedure Gallager *et al.*[18] have shown that repeated treatment with haloperidol induces DA autoreceptor supersensitivity.

We can only speculate about the mechanisms underlying TCA-induced subsensitivity of DA autoreceptors. First, a blockade of dendritic DA uptake[19] would result in overstimulation of DA autoreceptors which might then compensate by the induction of subsensitivity. Second, by analogy to the finding that repeated TCA administration produces a decrease in the number of cortical β-adrenergic receptors[16], it is possible that a similar decrease in the number of DA autoreceptors underlies our effects. Finally, it is important to note that our data are not incompatible with the induction of noradrenergic subsensitivity[15,16] which has been reported to follow repeated TCA treatments. Our noradrenaline–dopamine interaction hypothesis[20,21] indicates that decreased noradrenaline activity actually results in an increase in DA functioning. For instance, interference with noradrenaline activity either by inhibiting synthesis, stimulating presynaptic α-receptors or postsynaptic

α-receptor blockade can reverse the behaviourally suppressive effects of postsynaptic DA receptor antagonists (ref. 20, and unpublished observations).

We thank Dr J. Perel for comments on this manuscript. This work was supported by MH-32306 and RSDA MH-00238 (to S.M.A.), MH-16581, and training grant 5T32-MH-14634.

Received 26 March; accepted 28 July 1980.

1. Halaris, A. E. & Freedman, D. X. in *Biology of the Major Psychoses* (ed. Freedman, D.) 247–258 (Raven, New York, 1975).
2. Randrup, A. & Braestrup, C. *Psychopharmacology* **53,** 309–314 (1977).
3. Serra, G., Argiolas, A., Klimek, V., Fadda, F. & Gessa, G. L. *Life Sci.* **25,** 415–424 (1979).
4. Konig, J. F. R. & Klippel, R. A. *The Rat Brain: A Stereotaxic Atlas* (Williams & Wilkins, Baltimore, 1974).
5. Chiodo, L. A., Caggiula, A. R., Antelman, S. M. & Lineberry, C. G. *Brain Res.* **176,** 385–390 (1979).
6. Chiodo, L. A., Antelman, S. M. Caggiula, A. R. & Lineberry, C. G. *Brain Res.* **189,** 544–549 (1980).
7. Thomas, R. C. & Wilson, U. J. *Nature* **206,** 211–213 (1965).
8. Bunney, B. S. & Aghajanian, G. K. in *Antipsychotic Drugs: Pharmacodynamics and Pharmacokinetics* (eds Sedvall, I. G., Uvnas, B. & Zotterman, Y.) 305–318 (Pergamon, New York, 1976).
9. Bunney, B. S., Walters, J. R., Roth, R. H. & Aghajanian, G. K. *J. Pharmac. exp. Ther.* **185,** 560–571 (1973).
10. Skirboll, L. R., Grace, A. A. & Bunney, B. S. *Science* **206,** 80–82 (1979).
11. Segal, D. S. & Mandell, A. J. *Pharmac. biochem. Behav.* **2,** 249–257 (1974).
12. Stripling, J. S. & Ellinwood, E. H. Jr in *Cocaine and Other Stimulatns* (eds Ellinwood, E. H. Jr & Kilbey, M. M.) 327–352 (Plenum, New York, 1977).
13. Antelman, S. M., Eichler, A. J., Black, C. A. & Kocan, D. *Science* **207,** 329–331 (1980).
14. Glassman, A. H. & Perel, J. M. in *Psychopharmacology: A Generation of Progress* (eds Lipton, M. A., DiMascio, A. & Killam, K. F.) 917–922 (Raven, New York, 1978).
15. Vetulani, J., Stawarz, R. J., Dingell, J. V. & Sulser, F. *Naunyn-Schmiedebergs Arch. Pharmac.* **293,** 109–114 (1976).
16. Banerjee, S. P., Kung, L. S., Riggi, S. J. & Chanda, S. K. *Nature* **268,** 455–456 (1977).
17. de Montigny, C. & Aghajanian, G. K. *Science* **202,** 1303–1306 (1978).
18. Gallager, D. W., Pert, A. & Bunney, W. E. Jr *Nature* **273,** 309–312 (1978).
19. Bjorkland, A. & Lindvall, O. *Brain Res.* **83,** 531–537 (1975).
20. Antelman, S. M. & Caggiula, A. R. *Science* **195,** 646–653 (1977).
21. Antelman, S. M. & Caggiula, A. R. in *Animal Model in Psychiatry and Neurology* (eds Hanin, I. & Usdin, E.) 227–245 (Pergamon, New York, 1977).

Interferon treatment inhibits glycosylation of a viral protein

Radha K. Maheshwari*, Dipak K. Banerjee†, Charles J. Waechter†, Kenneth Olden‡ & Robert M. Friedman*

*Laboratory of Experimental Pathology, NIAMDD, National Institutes of Health, Bethesda, Maryland 20205
†Department of Biological Chemistry, University of Maryland School of Medicine, Baltimore, Maryland 21201
‡Howard University Cancer Research Center, Washington DC 20060

Earlier, we reported[1] a 30–200-fold reduction in the yield of infectious vesicular stomatitis virus (VSV) released from L cells treated with 10–30 reference units ml^{-1} of interferon (IFN); however, in these cultures virus particle production, as measured by VSV particle-associated viral RNA, virus nucleocapsid protein and viral transcriptase, was inhibited less than 10-fold. There was biochemical and morphological evidence of a significant reduction in glycoprotein (G) and membrane protein (M) of VSV particles released from IFN-treated cells[2,3]. We compare here the effects of tunicamycin (TM) and IFN in L cells. Treatment with TM or IFN reduced the production of infectious VSV particles, decreased the amount of G and M proteins in VSV released from treated cells, and inhibited an early step in the formation of asparagine-linked oligosaccharide chains, the incorporation by membrane preparations from treated cells of *N*-acetylglucosamine into glycolipids with the properties of dolichol derivatives.

It is known that G protein of VSV contains two 'complex' type asparagine-linked oligosaccharide chains[4]. The role of polyisoprenoid glycolipid intermediates in the biosynthesis of *N*-glycosidically bound oligosaccharides is well established[5–8], and work by several groups[9–11] has implicated dolichol-linked oligosaccharides in the glycosylation of the G protein of VSV. TM, a glucosamine-containing antibiotic produced by *Streptomyces lysosuperficus*[12], inhibits the lipid intermediate pathway by blocking the transfer of *N*-acetylglucosamine-1-phosphate from UDP-*N*-acetylglucosamine to dolichyl monophosphate (Dol-P)[13–19]. Treatment with TM inhibited the formation of glycosylated G protein in VSV-infected BHK cells[20–22].

The Indiana strain of VSV used in this work was plaque purified and passaged at low multiplicities. Virus titre was assayed as 50% tissue culture infectious doses ($TCID_{50}$) by observation of virus-induced cytopathic effect in Vero cells grown in microtitre plates, or by a plaque titration method as PFU ml^{-1}; the titre was 2×10^9 $TCID_{50}$ ml^{-1}. The mouse L cell (from Dr D. Burke) was very sensitive to the virus growth inhibitory effect of mouse IFN. Mouse IFN was prepared and partially purified on an antibody affinity column[23]. The specific activity of this preparation was greater than 4×10^7 international mouse reference units (r.u.) per mg protein.

Table 1 Effect of IFN and TM on the production of VSV

VSV released from L cells treated with:	Virus titre (PFU ml^{-1})	Inhibition ($\log_{10}$)
Control for IFN (no treatment)	8.0×10^7	—
IFN (30 r.u. ml^{-1})	7.5×10^5	2.1
Control for TM (no treatment)	3.0×10^7	—
TM (0.5 μg ml^{-1})	4.0×10^6	0.90
TM (1.0 μg ml^{-1})	4.0×10^5	1.90

L cells were grown in 150 cm^2 flask (2×10^7 cells) and treated with 0–30 r.u. per ml of interferon for 14 h; the cell monolayers were washed three to four times to remove the residual interferon. All monolayers were then infected with VSV at a multiplicity of five plaque-forming units (PFU) per cells. TM (0.5 or 1 μg ml^{-1}) was added to cells after 1 h of VSV infection. All monolayers were further incubated for 20 h. The supernatant fluids were then collected and sedimented at 10,000*g* to remove cell debris. Virus titre in these supernatant samples were quantified by a plaque titration method.

There was a 200-fold decrease in infectious virus titre in VSV released from L cells treated with IFN (30 r.u. ml^{-1}). TM (0.5–1 μg ml^{-1}) inhibited the infectious virus production in the range of 10–80-fold (Table 1). Purified virus samples with the same amount of protein or radioactivity were applied to SDS-polyacrylamide gel electrophoresis (PAGE) slab gels[24]. After electrophoresis, the gels were stained, dried and exposed to Kodak X-OMAT film. When the incorporation of radioactive precursor was quantified by fluorography[25], three proteins (G, N and M) were clearly visible in samples of virus not treated with TM; however, in VSV released from TM (0.5–1 μg ml^{-1})-treated cells there was a dose-dependent decrease in G protein; also, a faster moving band appeared between G and N proteins. This band could not be labelled by glucosamine, suggesting that this was an unglycosylated G protein (Fig. 1, lane 3); the M protein was also inhibited in samples treated with TM. In VSV released from IFN-treated cells, there were also three proteins (G, N and M) clearly visible; however, the G and M proteins were reduced in amount compared to VSV released from cells not treated with IFN (Fig.1, lane 7). When the G protein was labelled with glucosamine and an equal amount of protein loaded on gels, we observed that in VSV released from IFN-treated cells, there was a very significant inhibition of glucosamine incorporation. Electron microscopic studies revealed that VSV particles released from cells treated with either TM or IFN lacked glycoprotein spikes. These effects of TM on released VSV were very similar to those observed in VSV released from cells treated with IFN (30 r.u. ml^{-1}) and suggested that in VSV released from cells treated with IFN, there was a deficiency in G protein compared to VSV released from untreated cells.

Since lipid-linked oligosaccharides are involved in the glycosylation of VSV glycoprotein G[9–11], we carried out preliminary studies to see if IFN treatment affected the biosynthesis

0028–0836/80/400454—03$01.00

of *N*-acetylglucosaminyl derivatives of dolichol. When membranes from IFN-treated cells were incubated with UDP-*N*-acetyl-[^{14}C]glucosamine, only 18% as much label was incorporated into glycolipid as compared to the preparations from untreated cells (Table 2). When the assays were carried out in the presence of 10 nmol of exogenous Dol-P, the labelling of glycolipid was stimulated in both preparations, but the rate of synthesis of glycolipid was still substantially higher in membranes from untreated cells. This result indicated that the reduction in glycolipid formation by IFN-treated cells was probably not due to a deficit in endogenous acceptor lipid. The direct addition of IFN to the incubation mixture had no effect on the labelling of the glycolipid fraction. The observations that the labelling of *N*-acetylglucosaminyl lipid was stimulated by exogenous Dol-P, was inhibited by TM$^{13-18}$ (data not shown), and that *N,N′*-diacetyl-[^{14}C]chitobiose was released by mild acid (0.01 M HCl, 100 °C, 15 min) treatment of the glycolipid fraction, strongly suggest that the glycolipids labelled in these experiments were *N*-acetylglucosaminyl derivatives of dolichol involved in lipid-mediated protein glycosylation. More detailed studies on the characterization of the glycolipids synthesized by this *in vitro* system are in progress.

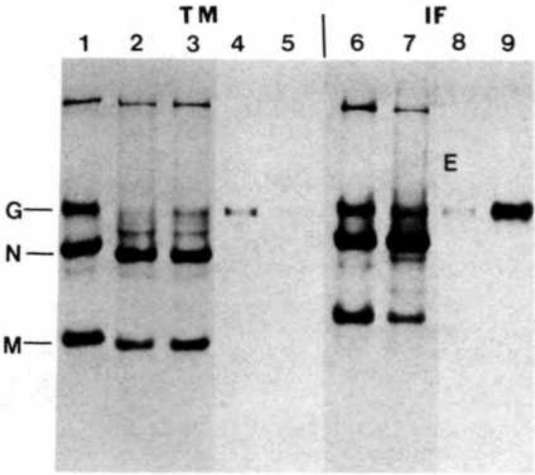

Fig. 1 L cells were treated with IFN or TM as described in Table 1. After virus adsorption and incubation for 2 h, the monolayers were washed with methionine-free medium and then ^{35}S-methionine (20 μCi ml^{-1}, specific activity, 800 Ci mmol^{-1}, Amersham) was added to monolayers in special minimal essential medium (MEM) devoid of cold methionine and supplemented with 2% dialysed fetal calf serum (FCS). After 6 h of incubation, 2 ml of regular MEM supplemented with 5% FCS was added to each culture and cells were incubated overnight. For labelling of glycoprotein (G), monolayers were infected with VSV for 2 h and the cultures were washed with glucose-free MEM. All cultures were refed with 15 ml of special medium (glucose-free MEM) containing 20 Ci ml^{-1} of ^{3}H-glucosamine for 6 h and then 2 ml of regular MEM was added to each culture and cultures were incubated overnight. The supernatant fluids were collected and clarified at 10,000*g* for 15 min to remove cellular debris. The clarified supernatant fluids were centrifuged at 42,000*g* for 2 h. The pellet was resuspended in a small volume of TES (Tris-EDTA-sodium chloride) buffer (*p*H 7.2) and was further purified by banding on 20–50% (w/w) equilibrium sucrose gradients for 16 h at 72,000 *g*. Proteins were analysed by SDS-PAGE^{24}. Purified VSV proteins with equal amount of radioactivity were applied to the gels except those in which G protein was labelled with ^{3}H-glucosamine where equal amounts of protein were added. The gels were subjected to electrophoresis and then stained with Coomassie brilliant blue R. After destaining they were impregnated with 2, 5-diphenyloxazole (NEN), dried, and exposed to Kodak X-OMAT X-Ray film. Phosphorylase B (molecular weight 92,500), bovine serum albumin (molecular weight 69,000), ovalbumin (molecular weight 46,000), carbonic anhydrase (molecular weight 30,000), and cytochrome *c* (molecular weight 12,300) were used as reference protein molecular markers. TM lanes: (1), proteins labelled with ^{35}S-methionine of VSV from cells not treated with TM; (2), proteins of VSV from cells treated with TM (1 μg ml^{-1}); (3), proteins of VSV from cells treated with TM (0.5 μg ml^{-1}); (4), G protein of VSV labelled with ^{3}H-glucosamine and released from cells not treated with TM; (5), G protein of VSV released from cells treated with TM (1 μg ml^{-1}). IFN lanes: (6), proteins labelled with ^{35}S-methionine of VSV from cells not treated with IFN; (7), proteins of VSV from cells treated with IFN (30 units ml^{-1}); (8), G protein of VSV labelled with ^{3}H-glucosamine and released from cells treated with IFN (30 r.u. ml^{-1}); (9), G protein of VSV released from cells not treated with IFN. Three VSV proteins, G, N and M, are visible on gels.

Inhibition of the synthesis of *N*-acetylglucosaminyl lipids with properties of dolichol derivatives, that serve as precursors for the dolichol-bound oligosaccharide lipid intermediates in protein glycosylation, was lower by membrane preparations from IFN-treated cells as compared to membrane preparations from untreated cells and could also be partially responsible for results obtained with VSV released from L cells treated with IFN; such virions were selectively deficient in G and M protein$^{1-3}$. It might also explain results on Moloney murine leukaemia virus (MMLV) from IFN-treated TB cells, where virus with markedly decreased infectivity was produced^{26}. The MMLV virions were also deficient in the viral envelope glycoproteins gp 69/71, so that the decreased amount of glycoprotein may be directly related to a slower rate of synthesis of *N*-acetylglucosaminylpyrophosphoryldolichol (GlcNAc-P-P-Dol) in IFN-treated cells.

Table 2 Effect of IFN treatment on transfer of *N*-acetylglucosamine from UDP-*N*-acetylglucosamine into glycolipid

Treatment of cells	Addition to incubation mixture	*N*-Acetyl-[^{14}C]glucosamine incorporated into glycolipid fraction (c.p.m. per mg membrane protein)
None	None	6,180
None	Dol-P(10 nmol^{-1})	20,700
IFN(30 r.u. ml^{-1})	None	1,130
IFN (30 r.u. ml)	Dol-P(10 nmol)	2,680

L cells were grown in Petri plates to confluency (1 × 10^{7} cells) and were treated with 30 r.u. per ml of interferon overnight. All cell monolayers were washed with saline three times, scraped, and centrifuged at 1,500 r.p.m. for 10 min. The cell pellets were suspended in 4 vol of ice-cold buffer consisting of 0.1 M Tris-HCl (*p*H 7.0), 0.25 M sucrose, 1 mM EDTA and homogenized. After homogenization, the suspensions were clarified by centrifugation at 8,500*g* for 5 min. The supernatant fluids were pelleted at 39,000*g* for 20 min and the pellets (crude particulate fraction) were resuspended in homogenization buffer. The protein content was measured by the Lowry procedure^{28}. Each reaction mixture contained crude particulate enzyme preparation; 50 mM Tris-HCl (*p*H 8.0); 0.125 M sucrose; 0.5 mM EDTA; 15 μM UDP-*N*-acetyl-[^{14}C]glucosamine (620 c.p.m. pmol^{-1}); 10 mM $MgCl_2$ and 0.02% Triton X-100 in a total volume of 0.1 ml. Dolichyl monophosphate was dispersed by ultrasonication in 0.1% Triton X-100 and 10 nmol were added where indicated. Following an incubation at 37 °C for 10 min the amount of *N*-acetyl-[^{14}C]glucosamine incorporated into the glycolipid fraction was assayed as described elsewhere^{17}. Lipid-phosphorous was determined by the Bartlett procedure^{29}. Dol-P, dolichyl monophosphate.

It will be interesting to determine whether the synthesis of GlcNAc-P-P-Dol is generally sensitive to IFN-treatment in a wide variety of animal cells. If glycosylation of asparagine residues in viral membrane glycoproteins is critical for the assembly of infectious particles of some viruses, inhibition of the enzymatic transfer of *N*-acetylglucosamine-1-phosphate from the nucleotide derivative to Dol-P would be an effective means of impeding viral production. The effects on glycosylation may also be pertinent to the varied activities of interferons on cell growth and on the immune system^{27}.

We thank Ms S. Harrell and F. Mottram for technical help, and Dr D. Epstein for many helpful discussions.

Received 20 May; accepted 30 July 1980.

1. Maheshwari, R. K. & Friedman, R. M. *J. gen. Virol.* **44,** 261–264 (1979).
2. Maheshwari, R. K., Jay, F. T. & Friedman, R. M. *Science* **207,** 540–541 (1980).
3. Maheshwari, R. K., Demsey, A. E., Mahanty, S. B. & Friedman, R. M. *Proc. natn. Acad. Sci. U.S.A.* **77,** 2284–2287 (1980).
4. Etchison, J. R., Robertson, J. S. & Summers, D. F. *Virology* **78,** 375–392 (1977).
5. Lucas, J. J. & Waechter, C. J. *Molec. cell. Biochem.* **11,** 67–78 (1976).
6. Waechter, C. J. & Lennarz, W. J. *A. Rev. Biochem.* **45,** 95–112 (1976).
7. Hemming, F. W. *Biochem. Soc. Trans.* **5,** 1223–1231 (1977).
8. Parodi, A. J. & Leloir, L. F. *Biochim. biophys. Acta* **559,** 1–37 (1979).
9. Robbins, P. W., Hubbard, S. C., Turco, S. J. & Wirth, D. F. *Cell* **12,** 893–900 (1977).
10. Hunt, L. A., Etchison, J. R. & Summers, D. F. *Proc. natn. Acad. Sci. U.S.A.* **75,** 754–758 (1978).
11. Tabas, I., Schlesinger, S. & Kornfeld, S. *J. biol. Chem.* **253,** 716–722 (1978).
12. Takatsuki, A., Arima, K. & Tamura, G. *J. Antibiol.* **24,** 215–223 (1971).
13. Takatsuki, A., Kohno, K. & Tamura, G. *Agric. biol. Chem.* **39,** 2089–2091 (1975).
14. Tkacz, J. S. & Lampen, J. O. *Biochem. biophys. Res. Commun.* **65,** 248–257 (1975).
15. Lehle, L. & Tanner, W. *FEBS Lett.* **71,** 167–170 (1976).
16. Struck, D. K. & Lennarz, W. J. *J. biol. Chem.* **252,** 1007–1013 (1977).
17. Waechter, C. J. & Harford, J. B. *Archs Biochem. Biophys.* **181,** 185–198 (1977).
18. Ericson, M. C., Gafford, J. T. & Elbein, A. D. *J. biol. Chem.* **252,** 7431–7433 (1977).
19. Hickman, S., Kulczcki, A., Jr, Lynch, R. G. & Kornfeld, S. *J. biol. Chem.* **252,** 4402–4408 (1977).
20. Leavitt, R., Schlesinger, S. & Kornfeld, S. *J. Virol.* **21,** 375–385 (1977).
21. Gibson, R., Schlesinger, S. & Kornfeld, S. *J. biol. Chem.* **254,** 3600–3607 (1979).
22. Gibson, R., Leavitt, R., Kornfeld, S. & Schlesinger, S. *Cell* **13,** 671–679 (1978).
23. Ogburn, C. A., Berg, K. & Paucker, K. *J. Immun.* **111,** 1206–1218 (1973).
24. Wagner, R. R., Schnaitman, T. C. & Synder, R. M. *J. Virol.* **3,** 395–403 (1969).
25. Bonner, W. M. & Laskey, R. A. *Eur. J. Biochem.* **46,** 83–88 (1974).
26. Friedman, R. M., Maheshwari, R. K., Jay, F. T. & Czarniecki, C. *Ann. N.Y. Acad. Sci.* (in the press).
27. Stewart, II, W. E. *Interferon* **1,** 29–51 (1979).
28. Lowry, O. H., Rosebrough, N. J., Farr, A. L. & Randall, R. J. *J. biol. Chem.* **193,** 265–275 (1951).
29. Bartlett, G. R. *J. biol. Chem.* **234,** 466–468 (1959).

Integration of Moloney leukaemia virus into the germ line of mice: correlation between site of integration and virus activation

Detlev Jähner & Rudolf Jaenisch

Heinrich-Pette-Institut für Experimentelle Virologie und
Immunologie an der Universität Hamburg,
Martinistrasse 52, 2000 Hamburg 20, FRG

Endogenous avian[1–3] and murine[4–9] C-type viruses are genetic elements which are transmitted at several distinct chromosomal loci. Different patterns of virus activation have been observed in a variety of different mouse strains[10–12]. However, because there are multiple copies of closely related endogenous viruses in every mouse strain, the genetic basis of the differential expression of these genes is poorly understood. A new substrain of mice, BALB/Mo, was derived previously[13] carrying the exogenous Moloney leukaemia virus (M-MuLV) genome on chromosome 6 (ref. 14). Virus activation occurs in lymphatic tissues of all BALB/Mo mice soon after birth[12]. We report here the derivation of three new substrains of mice each carrying a single M-MuLV genome on different chromosomal integration sites. Each locus was associated with a distinct phenotype of virus expression. Evidence is presented that apparently identical viral genomes show differences in spontaneous virus activation and that defective viral genomes can be carried in the germ line of mice.

Four to eight cell embryos were isolated from pregnant mice, treated with pronase to remove the zona pellucida and cultivated *in vitro* as described previously[13,15]. For infection with M-MuLV the embryos were co-cultivated overnight with subconfluent Cl 1A cells[16]. They developed into blastocysts and were subsequently transferred into the uterus of a pseudopregnant female. Of 28 mice derived in this way, 12 were viraemic when tested by radioimmunoassay for p30 at the age of 4 weeks. One viraemic male (no. 62) of ICR origin was selected. When mated with normal females, 20 of his 75 offspring were viraemic at 4 weeks of age. This paternal transmission of virus suggests that M-MuLV was integrated into cells of the germ line of male 62. The fraction of viraemic offspring observed (26%) deviates from the mendelian expectations for transmission of a single dominant gene and suggests 'germ-line mosaicism'[13]. Biochemical evidence (Fig. 1) indicates that male 62 was not only mosaic in the germ line but also in somatic tissues (see below). In contrast, his viraemic sons transmitted viraemia to approximately 50% of their offspring. This mendelian transmission indicates that they were heterozygous for a single viraemia-inducing genetic locus and indicates that the exogenous M-MuLV had been converted to an endogenous virus in these mice.

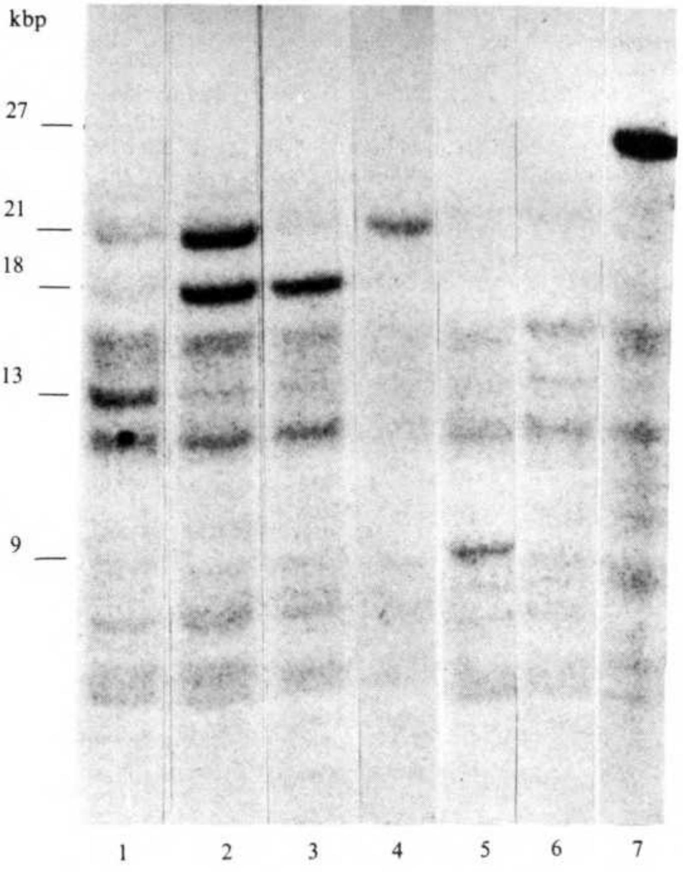

Fig. 1 Restriction enzyme analysis of mouse liver DNA. High molecular weight DNA from liver biopsies was digested with *Eco*RI, separated on agarose gels, transferred to nitrocellulose filters and hybridized to M-MuLV-specific cDNA as described[19]. *Eco*RI-digested λ DNA was used as a size marker. Lane 1, DNA from male 62; lanes 2–5, DNA from individual N-1 animals; lane 6, ICR control; lane 7, BALB/Mo DNA. The size and position of M-MuLV-specific fragments is indicated on the left. kbp, Kilobase pairs.

The integration site of M-MuLV in the DNA of male 62 and his offspring was analysed with the restriction enzyme *Eco*RI using the technique of Southern[17]. This enzyme has no recognition site in the viral genome[18]. M-MuLV-specific sequences were detected above the background of endogenous murine viruses by using an M-MuLV-specific probe[19]. Figure 1, lane 7, shows a single M-MuLV-specific fragment with a molecular weight of 27 kilobase pairs in BALB/Mo liver DNA which was run as a control. This band represents the endogenous M-MuLV copy in BALB/Mo mice[19,20]. Multiple bands with much lower relative intensities than the M-MuLV-specific bands are present in all mouse DNAs and are due to residual cross-homology of our specific probe with endogenous murine viruses. Three new M-MuLV-specific fragments not present in the uninfected control (lane 6) with molecular weights of 21, 18 and 9 kilobase pairs, respectively, were detected in the offspring of male 62 (lanes 2–5). The liver of male 62 (lane 1) carries all three

0028–0836/80/400456—03$01.00

Table 1 Characterization of genetically transmitted M-MuLV sequences and phenotype of mice

Origin	No. of animals	M-MuLV in *Eco*RI fragment (size in kilobase pairs)	No. of M-MuLV copies per diploid genome equivalent	Expression of viraemia	Genetic locus
Male 62	1	21 18 13 9	2	+	–
N-1 of male 62	3	21	1–1.2	–	*Mov-2*
	5	18	0.9–1.2	+	*Mov-3*
	8	21 18	2–2.4	+	*Mov-2* *Mov-3*
	6	9	0.9–1.1	–	*Mov-4*
	8	–	0	–	–
BALB/Mo (heterozygous)	–	27	1	+	*Mov-1*

Backcross animals of the N-1 generation from male 62 were derived as described in the text. Viraemic and non-viraemic offspring were partially hepatectomized[21] and the liver DNA was subjected to restriction enzyme analysis and to quantitative hybridization using specific M-MuLV cDNAs as hybridization probes[19,22]. The size of M-MuLV-specific *Eco*RI fragments (see Fig. 1) and the number of M-MuLV-specific DNA copies per diploid mouse genome equivalent are given[22]. Animals were tested for viraemia at 3 weeks of age[13]. Designation of genetic loci is explained in the text. Data on BALB/Mo mice are taken from previous publications[19,20].

M-MuLV-specific bands found in his offspring and one additional band of 13 kilobase pairs. These band intensities are weaker than the respective bands in DNA of his offspring. Together with quantitative hybridization data (Table 1) detecting only two M-MuLV copies per genome equivalent, these results indicate that M-MuLV sequences were present in only part of the liver cells. Thus male 62 showed mosaicism in somatic tissues as well as in the germ line.

Restriction enzyme analysis of liver DNA revealed five genotypes among his offspring (Table 1). The 21- and 18-kilobase pairs M-MuLV-specific bands segregated independently and were found alone or in combination in individual offspring. This suggests that a single blastomere of male 62 was doubly infected with virus and gave rise to a clone of infected cells. Animals carrying the 9-kilobase pair band presumably originated from germ cells derived from a different infected blastomere. This interpretation is supported by the equal intensities of the 21- and 18-kilobase pair bands as opposed to the unequal intensities of the 13- and 9-kilobase pair bands, respectively, in the liver of male 62 (Fig. 1, lane 1).

Genetic segregation studies showed that the 21- and 18-kilobase pair fragments were transmitted at the expected mendelian ratio of approximately 50% to the N-2 generation (Table 2). Germ-line transmission was also found in animals segregating the 9-kilobase pair copy. Our results define three new genetic loci carrying M-MuLV-specific sequences, designated *Mov-2, Mov-3* and *Mov-4* corresponding to the M-MuLV-specific *Eco*RI fragments of 21-, 18- and 9-kilobase pairs length, respectively. The locus representing the M-MuLV gene in BALB/Mo mice has been designated previously as *Mov-1* (ref. 14).

The structures of the integrated M-MuLV genomes were analysed after digestion of cellular DNA with the restriction enzyme *Pvu*II (Fig. 2). Fragments *a, b, c, d* correspond to the 3′ half, the *pol* region, the *gag* region and the *pol–gag* junction, respectively, of the M-MuLV genome[23]. No difference was observed between the internal M-MuLV fragments generated from *Pvu*II cleavage of DNA from mice of genotype *Mov-1* (lane 2), *Mov-2* (lane 3) or *Mov-3* (lane 4). DNA from mice with genotype *Mov-4*, however, had lost the largest *Pvu*II fragment (lane 5), suggesting that the integrated M-MuLV in these mice contains a deletion in the 3′ half of the viral genome. Further analysis with *Sac*I confirmed this conclusion (data not shown). Our results show that no major rearrangements in the M-MuLV genomes carried in the latter three substrains of mice have occurred and that partially deleted viral copies can be present in the germ line of mice.

Table 2 correlates the genotype of the mice with the status of viraemia. Three different phenotypes were observed: (1) early development of viraemia in animals carrying the *Mov-3* gene; (2) no viraemia at 3 weeks of age but occasional activation of M-MuLV later in life in animals carrying the *Mov-2* gene; (3) no occurrence of viraemia in animals carrying the *Mov-4* gene. Viraemia in *Mov-3* animals occurred at age 3 weeks or younger and was followed by rapid development of fatal leukaemia at 2 to 4 months of age. The genetic transmission of the *Mov-3* gene correlates well with the occurrence of viraemia and supports the conclusion that the presence of this gene induces early virus expression. Mov-2 animals, however, occasionally activate virus later in life. Table 2 shows that 14 out of 150 N-2 animals which were derived from Mov-2 males bred with normal females developed viraemia at 2 to 4 months of age. As only 50% of the offspring are expected to carry the *Mov-2* gene, the incidence of virus activation is approximately 20%. When viraemic N-2 males were bred again with normal females, a similar incidence of viraemia in the N-3 generation was observed. In contrast to Mov-2 animals, none of 60 offspring of Mov-4 animals became viraemic.

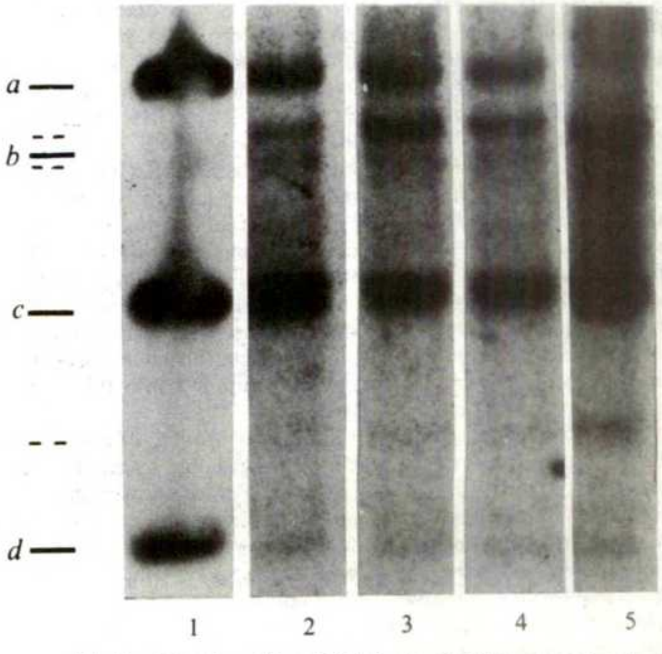

Fig. 2 Digestion of liver DNA by *Pvu*II. DNA was analysed as described in Fig. 1. Lane 1 shows a *Hin*dIII-*Pvu*II double digest of M-MuLV cloned in pBR 322 (provided by S. Goff). Lane 2, BALB/Mo DNA (Mov-1); lane 3, Mov-2 DNA; lane 4, Mov-3 DNA; lane 5, Mov-4 DNA. *a–d* Mark the positions of the M-MuLV fragments after *Pvu*II digestion as published[23].

Table 2 Genetic transmission of M-MuLV sequences and incidence of viraemia in second backcross generation

M-MuLV-specific *Eco*RI fragment in father	Locus	M-MuLV-specific sequences in DNA of N-2 mice/total tested	Viraemic N-2 animals/total tested	Percentage
18 Kbp	Mov-3	14/28	125/255*	49
21 Kbp	Mov-2	6/14	14/147†	9.5
9 Kbp	Mov-4	1/5	0/60	0

N-1 males of genotype Mov-2, Mov-3 and Mov-4 were identified after partial hepatectomy as described in Table 1. They were bred with normal females and some of the offspring were again partially hepatectomized and the presence of M-MuLV-specific sequences in the liver DNA determined by quantitative hybridization[22]. All animals were repeatedly tested for viraemia using the RIA for p30 (ref. 13).

* Animals segregating the *Mov-3* locus were viraemic at the youngest age tested (3 weeks).

† Animals segregating the *Mov-2* locus were non-viraemic at 3 weeks of age; some mice developed viraemia at later ages (between 2 and 4 months of age).

Having become viraemic, Mov-2 animals develop leukaemia quickly. The disease is indistinguishable by histological and molecular parameters from the leukaemia occurring in Mov-3 animals. The host range of the activated virus was determined. The virus grew equally well on NIH 3T3 and BALB 3T3 cells but did not replicate in CCl 64 cells. This phenotype bred true when cloned on either of the permissive cell lines. Thus the virus was NB tropic like the original virus used for infection of the embryos.

The sequence homology of Mov-2 and Mov-3 virus was analysed by molecular hybridization. RNA was isolated from NIH 3T3 cells which were infected with Mov-2 virus and from spleens of viraemic Mov-2 and Mov-3 animals. Each RNA preparation annealed to the same extent (95%) to M-MuLV cDNA at low C_rt values. In contrast, RNA of spleens from non-viraemic Mov-2 animals annealed to the same extent as RNA from control animals (15% annealing at a C_rt value of 10,000). Furthermore, when DNA from NIH 3T3 cells infected with virus activated from Mov-2 animals was digested with *Pvu*II, no differences in the cleavage pattern of integrated viral sequences were observed in comparison to Cl 1A virus, BALB/Mo virus or Mov-3 virus (data not shown). This suggests that Mov-2 animals activate NB tropic Moloney virus integrated into their germ line.

We chose Moloney leukaemia virus as a model system to establish the experimental conditions for integrating genetic material into the germ line of mice. The animal exposed to virus was a mosaic carrying viral genomes in part of his somatic and germ cells and genetically defined mouse strains were only obtained after segregating the genes in the next generation. As preimplantation embryos are not permissive for expression of viral functions[15], our experimental approach can be used to introduce other than viral genetic information into the germ line.

The M-MuLV genome carried at the *Mov-1, Mov-2* and *Mov-3* locus, respectively, was indistinguishable by all criteria used. Virus activation in the respective mice, however, was different. Thus, cellular sequences flanking an integrated viral genome may influence its expression by a *cis*-acting mechanism, as has been suggested[24,25]. The mechanisms by which animals have acquired endogenous viruses and the evolutionary forces that influenced virus expression are not known. Our results indicate that the endogenous viruses of mice may have entered the germ line by infecting early embryos and that the different phenotypes of virus expression observed in inbred mouse strains may depend on the chromosomal integration site of the virus. Our model system should facilitate investigations to understand the regulation of C-type virus expression during cellular differentiation and its possible role in evolution.

We thank Drs S. Goff, E. Gilboa and D. Baltimore for providing us with the M-MuLV clone and Dr J. Bilello and all members of the tumour virus laboratory for constructive criticism. The technical assistance of D. Grotkopp and E. Hoffmann is gratefully acknowledged. This work was supported by a grant from the Deutsche Forschungsgemeinschaft and by Research Contract NOICP 71008 from the NCI. The Heinrich-Pette-Institut is financially supported by Freie und Hansestadt Hamburg and by Bundesministerium für Jugend, Familie und Gesundheit, Bonn. This study was performed as part of the PhD study of D.J. at the University of Hamburg.

Received 6 March; accepted 7 August 1980.

1. Astrin, S. M. *Proc. natn. Acad. Sci. U.S.A.* **75,** 5941–5945 (1978).
2. Hughes, S. H. *et al. Cell* **18,** 347–359 (1979).
3. Frisby, D. P., Weiss, R. A., Roussel, M. & Stehelin, D. *Cell* **17,** 623–634 (1979).
4. Chattopadhyay, S. K., Lowy, D. R., Teich, N. M., Levine, A. S. & Rowe, W. P. *Cold Spring Harb. Symp. quant. Biol.* **39,** 1085–1101 (1975).
5. Rowe, W. *J. exp. Med.* **136,** 1272–1285 (1975).
6. Ihle, J. N., Joseph, D. R. & Domotor, J. J. Jr *Science* **204,** 71–73 (1979).
7. Ihle, J. N. & Joseph, D. R. *Virology* **87,** 298–306 (1978).
8. Kozak, C. & Rowe, W. P. *Science* **199,** 1448–1449 (1978).
9. Cohen, J. C. & Varmus, H. E. *Nature* **278,** 418–423 (1979).
10. Lerner, R., Wilson, C., del Villano, B. C., McConahey, P. J. & Dixon, F. J. *J. exp. Med.* **143,** 151–166 (1976).
11. Strand, M., August, J. T. & Jaenisch, R. *Virology* **76,** 886–890 (1977).
12. Jaenisch, R. *Virology* **93,** 80–90 (1979).
13. Jaenisch, R. *Proc. natn. Acad. Sci. U.S.A.* **73,** 1260–1264 (1976).
14. Breindl, M., Doehmer, J., Willecke, K., Dausman, J. & Jaenisch, R. *Proc. natn. Acad. Sci. U.S.A.* **76,** 1938–1942 (1979).
15. Jaenisch, R., Fan, H. & Croker, B. *Proc. natn. Acad. Sci. U.S.A.* **72,** 4008–4012 (1975).
16. Fan, H., Jaenisch, R. & MacIsaac, P. *J. Virol.* **28,** 802–809 (1978).
17. Southern, E. *J. molec. Biol.* **98,** 503–517 (1975).
18. Verma, J. M. & McKennet, M. A. *J. Virol.* **26,** 630–645 (1978).
19. Jähner, D., Stuhlmann, H. & Jaenisch, R. *Virology* **101,** 111–123 (1980).
20. v.d. Putten, H., Terwindt, E., Berns, A. & Jaenisch, R. *Cell* **18,** 109–116 (1979).
21. Jaenisch, R. & Hoffmann, E. *Virology* **98,** 289–297 (1979).
22. Jaenisch, R. *Cell* **12,** 691–696 (1977).
23. Gilboa, E. *et al. Cell* **16,** 863–874 (1979).
24. Cooper, G. M. & Silverman, L. *Cell* **15,** 573–577 (1978).
25. O'Rear, J., Mizutani, S., Hoffman, G., Fiandt, M. & Temin, H. *Cell* **20,** 423–430 (1980).

T-DNA of a crown gall teratoma is covalently joined to host plant DNA

N. S. Yadav*, K. Postle†, R. K. Saiki†§, M. F. Thomashow† & M.-D. Chilton*

*Department of Biology, Washington University, St Louis, Missouri 63130
†Department of Microbiology & Immunology, University of Washington, Seattle, Washington 98195

***Agrobacterium tumefaciens* strains containing tumour-inducing (Ti) plasmids[1–3] incite cancerous growths called crown galls when inoculated into wounded dicotyledonous plants. Tumour tissue can be cultured axenically *in vitro*, and exhibits a transformed phenotype in the absence of the inciting bacterium. Transformed cells grow autonomously, are auxin and cytokinin autotrophic *in vitro*[4] and synthesize opines[5–8], novel amino acid derivatives dictated by Ti plasmid genetic information[9–11]. A small segment of the Ti plasmid, termed T-DNA is maintained in axenic tumour cells[12–19]. Mitochondrial and chloroplast DNA from a crown gall teratoma are free from T-DNA, whereas nuclear DNA contains T-DNA in amounts similar to that in total tumour cell DNA[20,21]. T-DNA appears to be attached to what is presumably plant DNA in the crown gall tumour cell: Southern blot analysis[22] of tumour DNA digested with restriction endonucleases reveals T-DNA fragments that are not fully homologous to Ti plasmid DNA[14,17,21]. We report here the isolation by molecular cloning of a 'border fragment' T-DNA and flanking plant DNA from the crown gall teratoma BT37 and show that T-DNA is covalently joined to a repeated DNA element of the tobacco nuclear genome.**

---

‡Present address: Department of Microbiology, University of California, Irvine, California 92717.

§Present address: Cetus Corporation, 600 Bancroft Way, Berkeley, California 94710.

0028–0836/80/400458—04$01.00

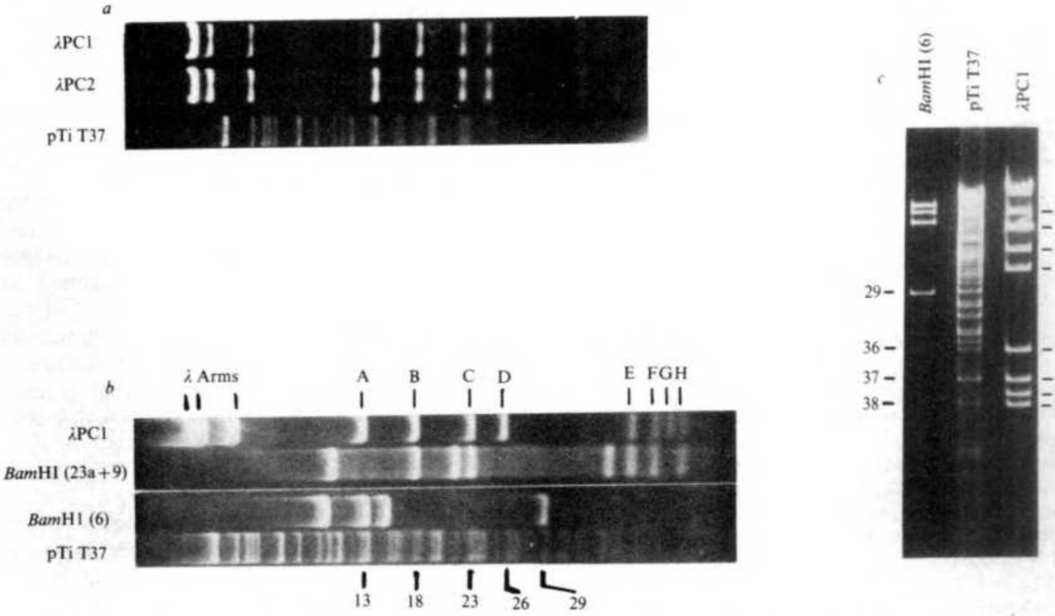

Fig. 1 *Eco*RI digests of DNA from λPC1 and λPC2, pTi T37 and cloned fragments of pTi T37. Charon 4A bacteriophage[30] DNA was digested with *Eco*RI and the vector arms separated from internal fragments by sedimentation through 5–20% NaCl linear gradients. Partial and complete *Eco*RI digests of BT37 tumour DNA, isolated as described in ref. 12, were fractionated in the same manner (F. Blattner, personal communication). Fragments 10–20 kilobases in size (correct for Charon 4A cloning inserts) were pooled. Phage arms (20 μg) and target fragments (7 μg) were incubated with T4 DNA ligase for 16 h at 4 °C (50 μl reaction volume). Packaging was performed by published procedures[23,24]. Phages were plated on 9.2 cm^2 Petri dishes at 20,000 plaques per plate. Lifts were prepared[25] and hybridized with pTi T37 DNA labelled *in vitro* by nick translation[26], in order to detect plaques containing T-DNA inserts. Two positive plaques, λPC1 and λPC2, were detected and purified. *a*, *Eco*RI digests of λPC1 and λPC2 DNA (isolated from CsC1 banded phage particles by phenol deproteinization and dialysis) and of pTi T37 DNA were fractionated by electrophoresis in a horizontal slab gel of 0.7% agarose as described previously[31]. The three largest molcular weight fragments in the phage DNA digests are Charon 4A arms. *b*, *Eco*RI digests of λPC1 DNA, pTi T37 DNA and two recombinant plasmids containing the left end of T-DNA from pTi T37 (see text and Fig. 2) were fractionated as described above in 1% agarose. c, *Eco*RI digests of λPC1 DNA, pTi T37 DNA and (as molecular weight marker) one recombinant plasmid from the left end of T-DNA were fractionated by vertical 1.5% agarose slab gel electrophoresis in TB buffer (10.8 g Tris base, 0.93 g disodium EDTA and 5.5 g boric acid per litre). Fragments of pTi T37 were numbered starting from fragment 29, which is also indicated in *b*. Fragment G is not an internal pT1 T37 fragment.

For molecular cloning of T-DNA fragments from BT37 tobacco teratoma DNA, we used the strategy of F. Blattner *et al.*[23]: shotgun cloning of a mixture of *Eco*RI partial and complete digest fragments of total tumour DNA into Charon 4A bacteriophage. Ligated DNA (see legend to Fig. 1 for details) was packaged *in vitro* into phage coats[23,24] and approximately 10^6 plaque-forming units were plated and screened by hybridization of plaque 'lifts'[25] with Ti plasmid DNA, labelled *in vitro* by nick translation[26] with $[\alpha\text{-}^{32}\text{P}]$deoxynucleotide triphosphates. Two positive plaques were picked and purified. The *Eco*RI cleavage patterns of the resulting two recombinant phage DNAs are presented in Fig. 1*a*. λPC2 possesses six of the eight *Eco*RI insert fragments contained in λPC1; the latter are designated A–H in decreasing order of molecular weight (Fig. 1*b*). To determine how many of the insert fragments were homologous to Ti plasmid DNA, a Southern transfer prepared from them was hybridized with ^{32}P-labelled[26] pTi T37 plasmid DNA. Autoradiography revealed that all insert fragments except the G fragment of λPC1 hybridized strongly (data not shown). Further studies used only λPC1 to determine whether any of its insert fragments were border fragments containing both Ti plasmid and plant DNA sequences.

A map of the part of pTi T37 detected in plant tumour line BT37[16,19–21] is presented in Fig. 2. Part of *Bst*I fragment 6 as well as the whole of 23A, 9 and 14A are detectable in the tumour DNA by Southern blot analysis[21]. Eight intact *Eco*RI fragments of the Ti plasmid are internal to this region and are also detectable by Southern blot analysis of BT37 tumour DNA[19,21]. To compare the insert fragments of λPC1 with the *Eco*RI fragments that map in T-DNA, we compared the single and multiple cleavage products of Ti plasmid fragments with those of λPC1. Because of the complexity of total Ti plasmid DNA, we used two clones of Ti plasmid DNA in the vector pBR322. One contained *Bst*I fragment 6, and the other contained a partial digest product, *Bst*I fragments 9 plus 23A plus the unnumbered small fragment between them. Figure 3 shows that *Eco*RI fragment 13 (cut from the appropriate *Bst*I clone) co-migrates with A, 18 with B, and 23 with C. Also, the two subfragments of D generated by *Bst*I/*Eco*RI double digestion of λPC1 correspond to *Bst*I/*Eco*RI double digest fragments of the appropriate *Bam*HI clones (data not shown). Confirmation of D as *Eco*RI fragment 26 was achieved by recloning D into pBR325 (ref. 27), labelling this recombinant plasmid and hybridizing it to a Southern blot of pTi T37 *Eco*RI fragments as well as λPC1 *Eco*RI fragments. The probe hybridized with D in the phage DNA digest as expected and with fragment 26, of identical electrophoretic mobility, in the Ti plasmid digest (data not shown).

The low molecular weight inserts E, F and H of λPC1 co-migrate with subfragments of the (23A+9) *Bst*I clone (Fig. 1*b*) and in the Ti plasmid *Eco*RI digest, fragment 36 co-migrates with E, 37 with F and 38 with H (Fig. 1*c*). Clearly fragment G is not an intact *Eco*RI fragment of the Ti plasmid: no *Eco*RI fragment of pTi T37 co-migrates with it (Fig. 1*c*).

Fragment G could be either a plant DNA fragment included in the original phage clone by coincidence, or a border fragment abutting A on the left or (less plausibly) F on the right. For DNA hybridization analysis, G was recloned into the *Eco*RI site of pBR325 (ref. 27), and an *Eco*RI digest of this clone, containing vector and G fragments, was used to prepare Southern blots. When duplicate tracks were hybridized with labelled pTi T37 DNA (Fig. 3*a*), fragment G hybridized weakly. G thus

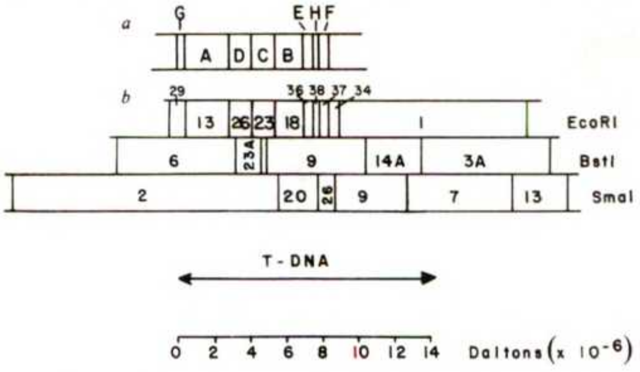

Fig. 2 Map of the T-DNA portion of pTi T37 and of the inserts of λPC1. For the *Sma*I fragment map and evidence see ref. 16. The *Bst*I fragments were mapped hybridizing isolated *Sma*I and *Hpa*I fragments to Southern blots[22] of *Bst*I digest fragments of pTi T37 as described previously[32]. *Bam*HI (a *Bst*I isoschizomer) fragments of partially digested pTi T37 were cloned into the *Bam*HI site of pBR322, and clones containing the following inserts were picked from a bank of 200 clones by colony hybridization[33]: fragment 6, fragments 9 and 23A and the small unnumbered fragment between them, fragment 14A and fragment 3A. Digestion of these recombinant plasmids with *Sma*I, *Hpa*I, *Bst*EII and combinations of these enzymes produced the fragments predicted by the map presented here and the published *Hpa*I and *Bst*EII maps[16]. Digestion of these recombinant plasmids with *Eco*RI alone and in combination with the other enzymes mentioned above allowed us to determine the *Eco*RI fragment map of pTi T37 shown above. The numbers assigned to the small fragments (34–37) were determined by the method described in Fig. 1*c* legend. *a*, The fragment map of the inserts in λPC1; *b*, the fragment map of pTi T37. Evidence for the arrangement of these fragments is based on the identification of their counterparts in the Ti plasmid digest as described in the text. Assignment of G to the left edge of the phage insert is based on its hybridization to Ti plasmid fragments mapping in this region (see text).

appeared to contain a short piece of Ti plasmid DNA. To determine whether G derived from the left edge of T-DNA, we hybridized Southern blots of Ti plasmid fragments generated by four different restriction enzymes (Fig. 3*b*). The G probe hybridized to *Bst*I fragment 6, *Eco*RI fragment 29, *Sma*I fragment 2 and *Hpa*I fragment 5 (see map in ref. 16), evidence that G is indeed from the left edge of T-DNA. *Eco*RI fragment 29 was recloned from *Bst*I fragment 6, and this recombinant plasmid also hybridized with G weakly (Figure 3*a*). We conclude that fragment G has weak homology with the leftmost edge of the T-DNA portion of the Ti plasmid. Much of G is not Ti plasmid DNA, for its hybridization with the Ti plasmid fragments is poor compared with homologous reactions run simultaneously.

Next we tested fragment G for homology with tobacco DNA. Normal tobacco leaf DNA and BT37 tumour DNA were cleaved with *Eco*RI or *Bst*I and the fragments immobilized by Southern blotting[22]. The cloned G fragment in the vector pBR325 was labelled by nick translation and used as probe. Figure 4 shows that this fragment hybridizes to a series of bands in the tobacco DNA digests. Two other fragments of λPC1 (A and D) cloned in the same vector and used as probes in parallel hybridization studies with tobacco DNA did not hybridize to such bands (data not shown). We conclude that fragment G is homologous to a family of repeated DNA sequences in the tobacco genome. The prominent pattern of *Eco*RI fragments of tobacco DNA to which G hybridizes suggests that this family is a 'clustered repeat'[28,29]. The smaller and simpler *Bst*I cleavage products to which G hybridizes suggest that there are *Bst*I sites internal to the repeat element. The role of such repeated DNA sequences in the eukaryotic genome is unknown. We note no significant difference in the intensity or pattern of bands in the tumour DNA digest compared with normal tobacco leaf DNA digest (Fig. 4 and other data not shown). Thus, the organization and copy number of the repeated DNA family to which G hybridizes is not altered grossly during tumorigenesis. Tumour DNA must contain one altered member of this family—the one into which T-DNA is inserted; however this member is not noticeable in Fig. 4, presumably because of the abundance of unaltered family members.

We conclude that the T-DNA found in BT37, a tobacco crown gall teratoma, is covalently joined at its left edge to plant DNA. Apart from this, the T-DNA fragments that we have isolated from this tumour line appear to be colinear with the corresponding region of the Ti plasmid: no noticeable alterations have occurred in this region of T-DNA whilst in the plant cell. Consistent with the location of T-DNA in the nuclear rather than chloroplast or mitochondrial DNA fraction[21], its left border fragment hybridizes to repeated DNA chracteristic of eukaryotic genomic DNA. It is not clear from this study whether T-DNA is an integral part of a tobacco chromosome in the transformed plant cell; it could constitute an extrachromosomal autonomously replicating DNA element. There is, however,

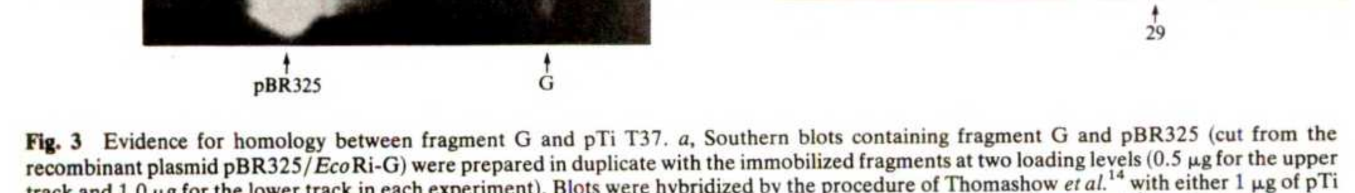

Fig. 3 Evidence for homology between fragment G and pTi T37. *a*, Southern blots containing fragment G and pBR325 (cut from the recombinant plasmid pBR325/*Eco*Ri-G) were prepared in duplicate with the immobilized fragments at two loading levels (0.5 μg for the upper track and 1.0 μg for the lower track in each experiment). Blots were hybridized by the procedure of Thomashow *et al.*[14] with either 1 μg of pTi T37 DNA (2.6×10^7 c.p.m. μg^{-1}) or 0.5 μg of recombinant plasmid pBR325/*Eco*RI-29 DNA (1.66×10^8 c.p.m. μg^{-1}) in 5 ml of reaction medium[14]. Probes were labelled by nick translation[26] with ^{32}P-labelled deoxynucleotide triphosphates. *b*, Southern blots[22] of pTi T37 digests produced by four restriction endonucleases (*Sma*I, *Hpa*I, *Bst*I and *Eco*RI) were hybridized[14] with 0.5 μg of recombinant plasmid pBR325/*Eco*RI-G (1.26×10^8 c.p.m. μg^{-1}). The numbers of the digest fragments to which the probe hybridized are indicated.

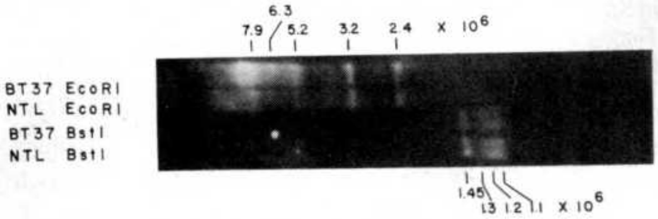

Fig. 4 Evidence for homology between fragment G and tobacco DNA. *Bst*I digests of 2.8 μg of normal tobacco leaf DNA isolated as described elsewhere[34] and of BT37 tumour DNA, in addition to *Eco*RI digests of 5.0 μg of the same two DNAs, were fractionated in horizontal slab gels of 0.7% agarose and blotted by Southern's procedure[22]. The blots were hybridized[14] with 1.5 μg of recombinant plasmid pBR325/*Eco*RI-G (5.4×10^7 c.p.m. μg^{-1}). The autoradiogram shown was exposed for 48 h (with two Dupont Cronex intensification screens) at −80 °C. Molecular weights of the bands in the autoradiogram were estimated from a calibration curve for the original gel based on digest fragments of known molecular weight. NTL, Normal tobacco leaf DNA, BT37, tobacco BT37 tumour DNA.

little precedent for the existence of such an element. Regardless of the physical situation of T-DNA our data make it clear that this foreign prokaryotic DNA element has become joined to eukaryotic DNA. The mechanism and specificity of such novel joining of phylogenetically alien DNAs may be revealed by analysis of DNA sequence at the border regions.

This work was supported by research grant NP194 from the American Cancer Society. M.E.T. was supported by a Damon Runyan–Walter Winchell Cancer Fund postdoctoral fellowship. We thank Drs Fred Blattner and Jerry Slightom for assistance in the cloning experiments.

Note added in proof: Similar results have been obtained for two T-DNA border fragments from an octopine-synthesizing tobacco crown gall tumour[35].

Received 14 May; accepted 28 July 1980.

1. Zaenen, I., Van Larebeke, N., Teuchy, H., Van Montagu, M. & Schell, J. *J. molec. Biol.* **86,** 109–127 (1974).
2. Van Larebeke, N. *et al. Nature* **252,** 169–170 (1974).
3. Watson, B., Currier, T. C., Gordon, M. P., Chilton, M. D. & Nester, E. W. *J. Bact.* **123,** 255–264 (1975).
4. White, P. R. & Braun, A. C. *Cancer Res.* **2,** 597–617 (1942).
5. Menagé, A. & Morel, G. *C. r. hebd. Séanc. Acad. Sci., Paris* **259,** 4795–4796 (1964).
6. Menagé, A. & Morel, G. *C. r. Séanc. Soc. Biol.* **159,** 561–562 (1965).
7. Firmin, J. L. & Fenwick, G. R. *Nature* **276,** 842–844 (1978).
8. Guyon, P., Chilton, M.-D., Petit, A. & Tempé, J. *Proc. natn. Acad. Sci. U.S.A.* **77,** 2693–2697 (1980).
9. Petit, A., Delhaye, S., Tempé, J. & Morel, G. *Physiol. Vég.* **8,** 205–213 (1970).
10. Bomhoff, G. *et al. Molec. gen. Genet.* **145,** 177–181 (1976).
11. Montoya, A., Chilton, M.-D., Gordon, M. P., Sciaky, D. & Nester, E. W. *J. Bact.* **129,** 101–107 (1977).
12. Chilton, M.-D. *et al. Cell* **11,** 263–271 (1977).
13. Chilton, M.-D. *et al. Microbiology 1978,* 136–138 (1978).
14. Thomashow, M. F., Nutter, R., Montoya, A. L., Gordon, M. P. & Nester, E. W. *Cell* **19,** 729–739 (1980).
15. Merlo, D. J. *et al. Molec. gen. Genet.* **177,** 634–643 (1980).
16. Yang, F. *et al. Molec. gen. Genet.* **177,** 707–714 (1980).
17. Schell, J. *et al. Proc. R. Soc.* B**204,** 251–266 (1979).
18. Van Montagu, M. & Schell, J. in *Plasmids of Bacteria of Medical Environmental and Commercial Importance* (ed. Timmis, K.) 71–96 (Elsevier, Amsterdam, 1979).
19. Schell, J. & Van Montagu, M. in *Genome Organization and Expression in Plants* (ed. Leaver, C.) 453–470 (Plenum, New York, 1979).
20. Chilton, M.-D. *et al.* in *Genome Organization and Expression in Plants* (ed. Leaver, C.) 471–450 (Plenum, New York, 1979).
21. Chilton, M.-D., Saiki, R. K., Yadav, N., Gordon, M. P. & Quétier, F. *Proc. natn. Acad. Sci. U.S.A.* **77,** 4060–4064 (1980).
22. Southern, E. M. *J. molec. Biol.* **98,** 503–517 (1975).
23. Blattner, F. R. *et al. Science* **202,** 1279–1284 (1978).
24. Becker, A. & Gold, M. *Proc. natn. Acad. Sci. U.S.A.* **72,** 581–585 (1975).
25. Benton, W. D. & Davis, R. W. *Science* **196,** 180–183 (1977).
26. Maniatis, T., Jeffrey, A. & Kleid, D. G. *Proc. natn. Acad. Sci. U.S.A.* **72,** 1184–1188 (1975).
27. Bolivar, F. *Gene* **4,** 121–136 (1978).
28. Wensink, P. C., Tabata, S. & Pachl, C. *Cell* **18,** 1231–1246 (1979).
29. Eden, F. C. *et al. Biochemistry* (submitted).
30. Blattner, F. R. *et al. Science* **196,** 161–169 (1977).
31. Sciaky, D., Montoya, A. L. & Chilton, M.-D. *Plasmid* **1,** 238–253 (1978).
32. Chilton, M.-D. *et al. Plasmid* **1,** 254–269 (1978).
33. Thayer, R. E. *Analyt. Biochem.* **98,** 60–63 (1979).
34. Chilton, M.-D. *Genetics* **81,** 469–483 (1975).
35. Thomashow, M. F. *et al. Proc. natn. Acad. Sci. U.S.A.* (in the press).

Behaviour of octopus rhodopsin and its photoproducts at very low temperatures

Motoyuki Tsuda*, Fumio Tokunaga*‡,
Thomas G. Ebrey*, Kwok To Yue†, Jeffrey Marque†
& Laura Eisenstein†

* Department of Physiology and Biophysics, 524 Burrill Hall,
University of Illinois, Urbana, Illinois 61801
† Department of Physics, Loomis Laboratory, University of Illinois,
Urbana, Illinois 61801

Many aspects of light energy transduction in photoreceptors are under study[1,2]. One important problem concerns the light-initiated primary event in rhodopsin and the identity of the primary photoproduct. It is usually assumed that the red-absorbing pigment bathorhodopsin[3] is the first photoproduct. In cattle rhodopsin, it is produced within 6 ps of excitation[4] and is stable at 77 K. However, Yoshizawa *et al.*[5–7] have found a blue-absorbing pigment, hypsorhodopsin, in photosteady-state mixtures formed with orange light at liquid helium temperatures (~5 K). On warming the hypsorhodopsin in the dark to liquid nitrogen temperatures (77 K), it converts to bathorhodopsin. These two results suggested that hypsorhodopsin might be a precursor of bathorhodopsin, but that presents difficulties. For example, hypso-type intermediates have not been seen for all visual pigments[6]. Moreover, when cattle rhodopsin was irradiated with blue light at liquid helium temperatures, it was converted to bathorhodopsin without forming detectable hypsorhodopsin[6,7]. Finally, rapid kinetic experiments to determine the time course of formation of bathorhodopsin and hypsorhodopsin have given ambiguous results[4,8–10]; this may be due to the use of rhodopsins from different species. Because squid rhodopsin seemed to have more hypsorhodopsin in photosteady states than cattle rhodopsin[7], we have studied the photo products of another cephalopod rhodopsin at carefully controlled low temperatures (±0.2 K). We report here that octopus rhodopsin has a hypso intermediate that is easily formed on irradiation but that the batho-product appears before significant amounts of the hypso-product accumulates. Moreover, the thermal conversion of hypsorhodopsin to bathorhodopsin must be fitted with two rate constants, and the activation enthalpy of the faster process is almost zero, that is, it is temperature independent over the range studied.

Octopus (Mizudako, *Paroctopus defleini*) microvillar membranes were prepared as previously described[11]. Rhodopsin was extracted from the membranes with a 2% digitonin solution, glycerol was added to the preparation to give a final concentration of 75%, and the samples were stored at −70 °C. The *p*H of the solution was adjusted to 10.5 with sodium carbonate buffer just before the start of an experiment, so that at room temperature any bleached rhodopsin would go to alkaline metarhodopsin ($\lambda_{max} = 376$ nm)[12].

On cooling to 10 K, the λ_{max} of octopus rhodopsin (476 nm at 10 °C) shifted to 486 nm (Fig. 1, curve 1). When the octopus rhodopsin was very briefly irradiated with 480 nm light at 10 K, the spectral change indicated the formation of a bathochromic product (octopus bathorhodopsin) (Fig. 1, curve 2). On further irradiation, the concentration of the bathochromically absorbing product increases (curve 3) and the appearance of a hypsochromically shifted photoproduct (octopus hypsorhodopsin) can also be seen (Fig. 1, curve 4). With further irradiation using 530 nm light, a photosteady state is formed which contains large amounts of hypsorhodopsin (56%), as well as rhodopsin (<4%) and isorhodopsin (>40%), with almost no bathorhodopsin. A detailed analysis of the spectra shows that hypsorhodopsin and bathorhodopsin appear concomitantly. Figure 1 strongly suggests that on irradiation of rhodopsin at

---

‡ Present address: Deparment of Physics, Tohoku University, Sendai, Japan.

0028–0836/80/400461—02$01.00

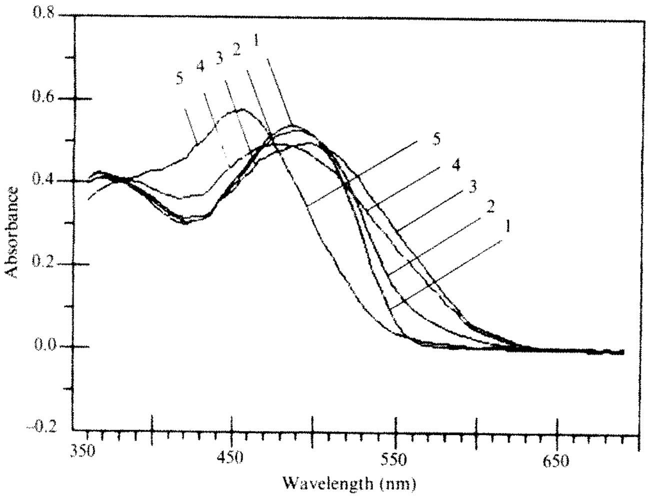

Fig. 1 Spectral changes observed in the conversion of rhodopsin to bathorhodopsin, hypsorhodopsin and isorhodopsin at 10 K. Curve 1, octopus rhodopsin in digitonin (*p*H 10.5) 10 K; curves 2–4, products of irradiation at 480 nm for successive periods of 8, 64 and 2,048 s; curve 5, photosteady state obtained by irradiation at 530 nm for 10 min. Curve 5 represents about 56% hypsorhodopsin, >40% isorhodopsin and <4% rhodopsin. This composition was determined as in ref. 7. All spectra were recorded with a Cary 14 using a Janis 10DT super Varitemp Optical Dewar.

10 K, the stable, blue-absorbing ground state species, hypsorhodopsin, is apparently not the precursor of the bathorhodopsin formed at this temperature.

On slowly warming up from 45 K, the spectrum of the photosteady-state mixture formed by irradiating octopus rhodopsin at 10 K shifted to longer wavelengths with sharp isosbestic points at 479 nm and 374 nm, as shown in Fig. 2. In the insert, the change in absorbance at 540 nm, indicating the formation of bathorhodopsin, is shown as a function of temperature. Judging from the similarity of their absorption spectra, the batho-product obtained by warming is identical to bathorhodopsin produced by irradiation of octopus rhodopsin at 80 K (B. Mao, M.T. and T.G.E., unpublished observations). Thus, the data of the insert show that hypsorhodopsin is converted to bathorhodopsin above 45 K. This transition temperature is much higher than that observed for the bovine[6] and squid[7] or frog[13] hypsorhodopsin → bathorhodopsin transition. There is no evidence of any stable intermediates between hypsorhodopsin and bathorhodopsin.

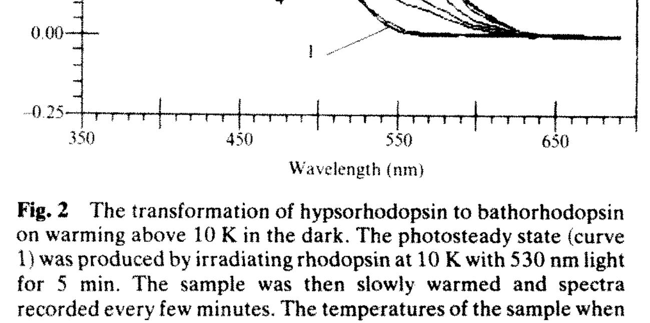

Fig. 2 The transformation of hypsorhodopsin to bathorhodopsin on warming above 10 K in the dark. The photosteady state (curve 1) was produced by irradiating rhodopsin at 10 K with 530 nm light for 5 min. The sample was then slowly warmed and spectra recorded every few minutes. The temperatures of the sample when the spectrum was measured are: (1) 10 K, (2) 40 K, (3) 50 K, (4) 55 K, (5) 60 K, (6), 65 K, (7) 70 K, (8) 80 K. Inset: absorbance at 540 nm (indicating the formation of bathorhodopsin) as a function of temperature.

We attempted to measure the enthalpy of activation in the thermal conversion of hypsorhodopsin to bathorhodopsin. At a given temperature, rhodopsin was irradiated with continuous yellow light ($\lambda > 490$ nm) for 3 min to reach the photosteady state. Immediately after the light exposure, the decay of hypsorhodopsin was monitored by the absorbance at 440 nm and the formation of bathorhodopsin by the absorbance at 550 nm. For temperatures between 53 K and 73 K, we plotted $\ln(A_t - A_\infty)$ as a function of time, where A_t and A_∞ are the absorbance at t min and infinity, respectively. The rates of both hypsorhodopsin and bathorhodopsin are non-exponential; both curves can be fitted fairly well by the sum of two exponentials. The temperature dependence of the two rates is plotted in an Arrhenius manner (ln K against $1/T$) in Fig. 3. The temperature dependence of the decay of hypsorhodopsin gives $\Delta H = 0.87 \pm 0.29$ kcal mol^{-1} and $\Delta H = 0.09 \pm 0.28$ kcal mol^{-1}. A similar pair of values are found for the formation of bathorhodopsin. The non-exponential character of the hypsorhodopsin decay processes implies that hypsorhodopsin is not a single homogeneous species. We are now studying the thermal decay process in more detail, in particular the nature of the component which seems to be almost temperature independent.

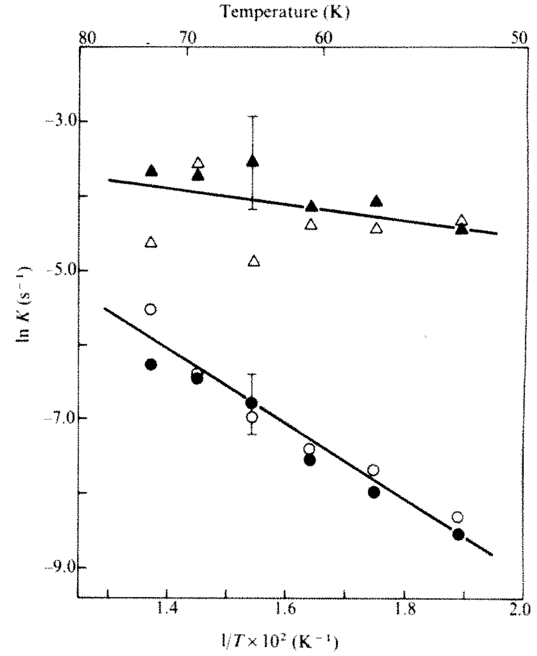

Fig. 3 Arrhenius plot of kinetic data for the decay of hypsorhodopsin (decrease in absorbance at 440 nm) and formation of bathorhodopsin (increase in absorbance at 550 nm). △, Faster phase; ○, slower phase in the decay of hypsorhodopsin. ▲, Faster phase; ●, slower phase in the formation of bathorhodopsin.

This work was supported in part by NIH grants EY01323, EY03142 and GM18051, and NSF grant PCM 79-05072.

Received 17 March; accepted 24 June 1980.

1. Honig, B. *A. Rev. phys. Chem.* **29,** 31–57 (1978).
2. Honig, B., Ebrey, T., Callender, R. H., Dinur, U. & Ottolenghi, M. *Proc. natn. Acad. Sci. U.S.A.* **76,** 2503–2507 (1979).
3. Yoshizawa, T. & Wald, G. *Nature* **197,** 1279–1286 (1963).
4. Peters, K., Applebury, M. L. & Rentzepis, P. M. *Proc. natn. Acad. Sci. U.S.A.* **74,** 3119–3123 (1977).
5. Yoshizawa, T. in *Handbook of Sensory Physiology* Vol. VII, pt 1 (ed. Dartnall, H. J. A.) 146–179 (Springer, Berlin, 1972).
6. Yoshizawa, T. & Horiuchi, S. in *Biochemistry and Physiology of Visual Pigments* (ed. Langer, H.) 69–81 (Springer, Berlin, 1973).
7. Shichida, Y., Tokunaga, F. & Yoshizawa, T. *Photochem. Photobiol.* **29,** 343–351 (1979).
8. Shichida, Y., Kobayashi, T., Ohtani, H., Yoshizawa, T. & Nagakura, S. *Photochem. Photobiol.* **27,** 335–341 (1978).
9. Monger, T. G., Alfano, R. R. & Callender, R. H. *Biophys. J.* **27,** 105–116 (1979).
10. Kobayashi, T. *FEBS Lett.* **106,** 313–316 (1979).
11. Tsuda, M. *Biochim. biophys. Acta* **545,** 537–546 (1979).
12. Tsuda, M. *Biochim. biophys. Acta* **578,** 372–380 (1979).
13. Horiuchi, S., Tokunaga, F. & Yoshizawa, T. *Biochim. biophys. Acta* **503,** 402–404 (1978).

Contrast perception above threshold is only minimally impaired in human amblyopia

Robert F. Hess & Arthur Bradley*

Physiological Laboratory, University of Cambridge,
Cambridge CB2 3EG, UK

Amblyopia is a condition occurring at birth, or in early childhood, which affects up to 5% of the population and is characterized by degraded vision in one eye not able to be corrected by spectacles and having no observable lesion in the eye itself. Its cause is therefore uncertain, yet indirect evidence suggests a neural one, very likely in the visual areas of the brain. Ambyopia is usually associated with either a strabismus (eye misalignment) or anisometropia (unequal refractive error). Investigation into its neural basis has involved two approaches: psychophysical research in humans with amblyopia[1-6] has shown marked contrast deficits for threshold stimuli, suggesting deficient contrast coding at and above threshold in amblyopia. Neurophysiological research on animals deprived in early life with either a surgically induced squint or an optically induced anisometropia has suggested that 'blur' may be the common etiological basis for these two amblyopias[7]. We have investigated here whether amblyopes exhibit contrast deficiencies for other than threshold stimuli. Our measurements show that the threshold deficits measured in amblyopia bear no simple relationship to what happens above threshold. There is no contrast coding abnormality in amblyopia in the high-contrast range typical of everyday vision. We also give suprathreshold evidence for anisometropic and strabismic amblyopia having different neural bases.

Repetitive spatial patterns with a sinusoidal luminance profile were generated independently on each side of a video display. Using a partition and a motor-driven sectored disk (for alternate presentation of stimuli to each eye) an amblyope could be presented with the same pattern of independent contrast to each eye. Care was taken to ensure that all subjects were optically corrected. An experimental session began with the amblyope setting a contrast detection threshold for each eye at a particular spatial frequency. Gratings would then be set at any one of several contrasts above this threshold and presented to the amblyopic eye as the standard. The task was to adjust the contrast of the pattern seen by the good eye (variable) until it was perceptually equated to that seen through the amblyopic eye (standard). In some experiments this experimental protocol was reversed with the normal eye observing the standard contrast stimulus. Five settings were averaged for each contrast match using the method of adjustment.

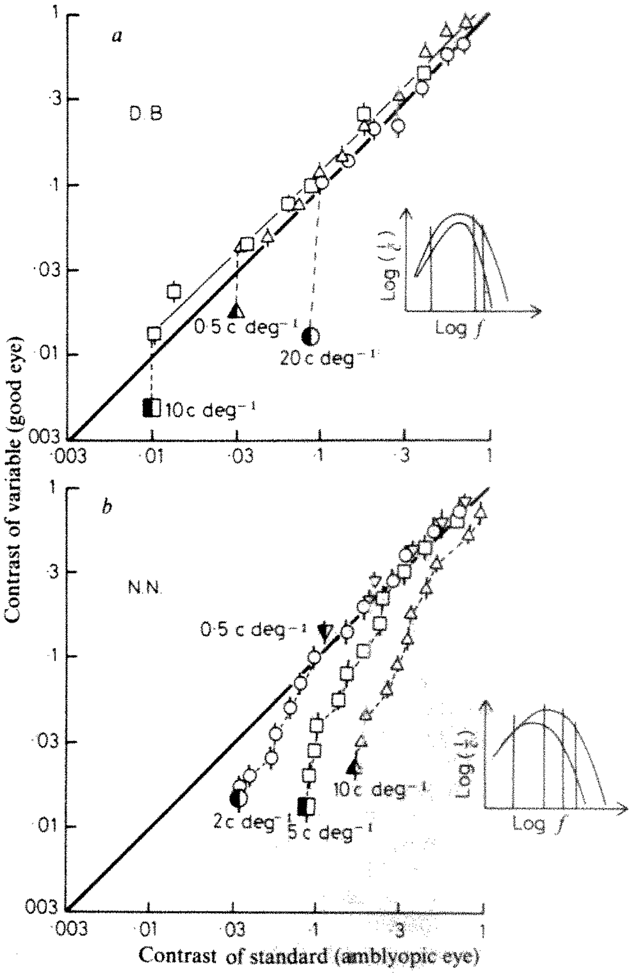

Fig. 1 Contrast matching results are displayed for three different spatial frequencies. The contrast of the standard grating shown to the amblyopic eye was matched by a variable grating of the same spatial frequency shown to the normal fellow eye. Each axis is logarithmic. Contrast thresholds are indicated by half-filled symbols. Inset is the form of the contrast threshold response for the normal and amblyopic eye. Strabismic (*a*) and anisometropic (*b*) amblyopia are compared. The gratings were displayed on a video screen for 500 ms. Field size of the stimulus was 10 deg, its mean luminance was 200 cd m^{-2} and its colour was green (P 36 Phosphor).

In both figures the matching results have been plotted on logarithmic coordinates. If contrast matches between the eyes are set to equality then the results will fit along the diagonal line with a slope of 1. This is true for normal observers. Figure 1*a* and *b* which show contrast matching data for a representative strabismic amblyope and for a representative anisometropic amblyope are very different. For the strabismic amblyope (Fig. 1*a*), once the target contrast is just slightly above its detection threshold it is perceived correctly by the amblyopic eye. This result is independent of the bar size of the target (spatial frequency). However, for the anisometropic amblyope (Fig. 1*b*), contrast perception is degraded over a substantial suprathreshold range (0.5 log unit–1 log unit). This range is dependent on the spatial frequency of the pattern. These results suggest that even if the threshold losses for these two forms of amblyopia look similar, their suprathreshold perception is dramatically different. This finding which has been confirmed for a group of strabismic and anisometropic amblyopes is summarized in Table 1 in terms of the contrast ratio between the eyes at threshold and at a contrast 3dB above threshold. An equivalent result is obtained when the contrast standard is shown to the normal eye. These results strongly suggest that strabismic and anisometropic amblyopes have different perceptual deficits.

These results also allow a better estimation of the type of neural dysfunction in human amblyopia. For example, strabismic amblyopia behaves as though the contrast range had been truncated to a different extent for each spatial frequency, thus maintaining normal suprathreshold contrast perception. Therefore, even though the contrast thresholds are raised in this form of amblyopia, this threshold disturbance has no suprathreshold relevance. It is as if a switch has been inserted somewhere in the amblyopic visual system to restrict the lower range of contrasts available to each set of frequency-specific neurones in the amblyopic visual system. To this extent the strabismic amblyope's system is well modelled by normal peripheral function. Figure 2*a* illustrates how normal contrast perception varies as a function of the position of a target in the peripheral field of vision for a normal subject. These results for normal peripheral viewing are very similar to that of the strabismic amblyope, supporting a more recent suggestion[8] based solely on

---

* Present address: School of Optometry, University of California, Berkeley, California 94720.

0028–0836/80/400463—02$01.00

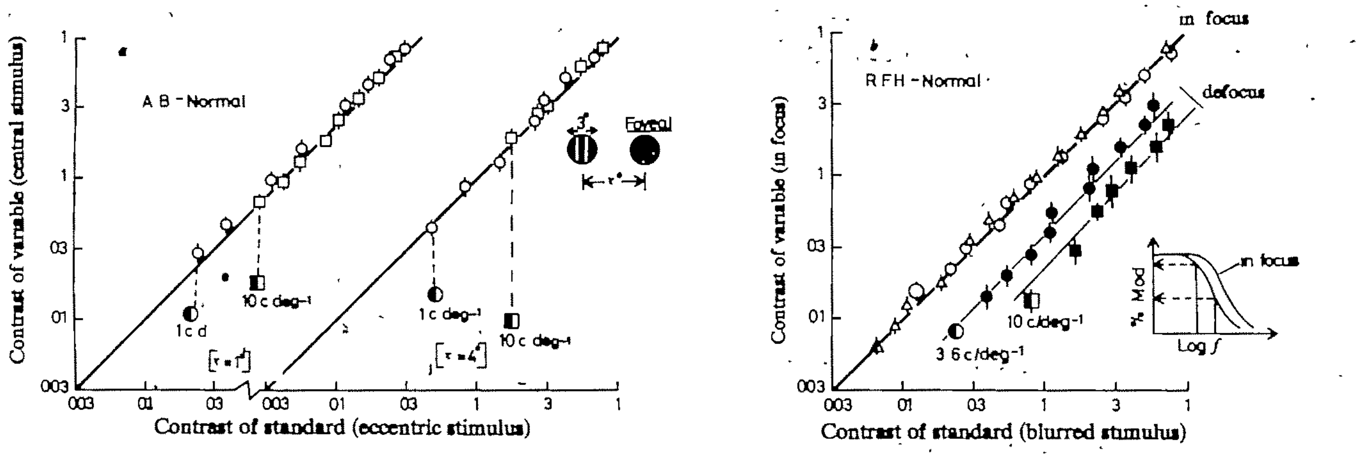

Fig. 2 Contrast matching results are displayed for a range of spatial frequencies. These results are plotted in an identical manner to those in Fig. 1. The contrast loss from two extents of eccentric viewing (1° and 4°) is displayed (*a*) as well as the contrast loss from optical blur (*b*). These should be compared with strabismic and anisometropic amblyopia (Fig. 1) respectively (see text).

threshold measurements that vision in strabismic amblyopia resembles that of the normal periphery.

The contrast matching abnormality is obviously different for the anisometropic amblyope (Fig. 1*b*); however the defective contrast perception does gradually diminish as the absolute contrast of the standard increases. Even for very fine targets (for example 10 c deg^{-1}) the defect at threshold is much larger than at high contrast levels (see also Table 1). It is interesting that the neural contrast deficit does not merely mimic the optical contrast loss due to the restricted (blurred) visual input present in early life. The contrast loss found with optical blur is displayed in Fig. 2*b* and this should be compared with the anisometropic result in Fig. 1*b*. Blur expected from a physical consideration should affect suprathreshold contrast perception as much as threshold perception (parallel displacement of the contrast matching line on log/log axes). Although optical blur (Fig. 2*b*) in early life may have originally produced the amblyopia seen in Fig. 1*b*, it remains possible that substantial neural compensation may have occurred by the amblyopic visual system in the higher contrast range (compare Figs 1*b* and 2*b* in the upper range). This neural compensation may explain why adult amblyopes do not accept that the degraded vision from their amblyopic eye looks like a defocused version of what they see through their fellow normal eye. This compensation is best thought of as a gain change of about a factor of 2 for all spatial frequencies. It is as if an extra stage of amplification is present somewhere in the amblyopic visual system to boost the neural suprathreshold contrast signal in only the upper part of the range. A similar contrast gain change has been reported[9] for the normal eye at high spatial frequencies and for some astigmatic subjects. These findings for contrast perception in subjects with abnormal vision are similar to those for loudness perception in subjects with peripheral damage to the auditory system. Within the auditory domain such a 'gain change' is referred to as 'recruitment'.

Table 1 Comparison of threshold and suprathreshold abnormality (3 dB above threshold) for strabismic and anisometropic amblyopes

Subjects	Spatial frequency (c deg^{-1})	Threshold contrast ratio	Suprathreshold contrast ratio (a contrast 3dB above threshold)
(*a*) Strabismic amblyopes			
D.B.	0.5	0.5	1.25
	10.0	0.65	1.26
	20.0	0.16	1.01
S.C.	0.5	0.11	0.9
	1.0	0.1	0.95
	4.0	0.05	0.85
S.N.	0.25	0.16	1.12
	1.0	0.12	1.20
	3.0	0.05	0.12
F.B.	0.5	0.5	1.13
	1.0	0.61	0.97
	10.0	0.1	0.96
(*b*) Anisometropic amblyopes			
N.N	2	0.40	0.37
	5	0.13	0.25
	10	0.14	0.16
A.H.	6	0.80	0.75
	10	0.45	0.50
	20	0.33	0.41
S.C.	6	0.40	0.50
	10	0.21	0.31
	15	0.15	0.30
	20	0.1	0.18
A.C.	1	0.3	0.5
	2	0.09	0.16
	3	0.017	0.1

In conclusion our results strongly suggest that the contrast coding abnormalities in amblyopia are mostly limited to threshold conditions and also that the neural basis of anisometropic and strabismic amblyopia is different. They also highlight the nature of the suprathreshold contrast deficit in each condition. Although it has been shown that human amblyopes do not exhibit deficits in contrast perception in the mid- to high-contrast range, they do experience difficulty in identifying such stimuli. This is due to a somewhat independent anomaly in spatial perception. They see targets 'distorted'[10], for example a simple black and white stripe pattern appears jumbled and twisted yet, as shown here, the individual components are perceived at their correct contrast. Clearly this spatial distortion is likely to be the main basis of amblyopia. The defining features reported here for the two main forms of human amblyopia should be amenable to neurophysiological assessment in animals which have been either strabismically or anisometropically deprived in the early months of life. Such assessment may indicate the relevance of animal models as well as the possible neural substrate for these human perceptual phenomena.

We thank F. W. Campbell, H. B. Barlow, D. Tolhurst and R. Blake for helpful discussions. R.F.H. was supported by a Meres Senior Studentship from St John's College, Cambridge. We also acknowledge financial support from the MRC and the Wellcome Trust.

1. Gstalder, R J & Green, D. G. *J Pediat Ophthal* 8, 251–255 (1971)
2 Mitchell, D E, Freeman, R. D, Millodot, M & Haegerstrom, K *Vision Res* 13, 535–557 (1973).
3 Rentschler, I, Hilz, R. & Brettel, B *Invest. Ophthal* (*Suppl*) 17, 293 (1978)
4 Levi, D M & Harwerth, R. S. *Invest Ophthal* 16, 90–95 (1977)
5. Hess, R. F & Howell, E R *Vision Res* 17, 1049–1055 (1977)
6 Sjostrand, J *J. metab. Ophthal* 2, 135–140 (1978).
7 Ikeda, H & Wright, M. J *Br J Ophthal* 58, 165–175 (1974)
8 Hess, R F, Campbell, F. W & Zimmern, R *Vision Res* 20, 295–305 (1980).
9 Georgeson, M A & Sullivan, G D *J Physiol, Lond* 252, 627–656 (1975)
10. Hess, R F, Campbell, F W. & Greenhalgh, T *Pflugers Arch ges Physiol.* 377, 201–207 (1978)

Basal lamina glycoproteins are produced by neuroblastoma cells

K. Alitalo*, M. Kurkinen*, A. Vaheri* & I. Virtanen†

*Department of Virology, †Department of Pathology, University of Helsinki, Haartmanikatu 3, SF-00290 Helsinki 29, Finland

H. Rohde & R. Timpl

Max-Planck-Institut für Biochemie D-8033 Martinsried bei München, FRG

Murine neuroblastoma cells have been widely used as a model system for neuronal cells as they can be induced to differentiate in culture by various stimuli, such as dibutyryl cyclic AMP (dbcAMP)[1], prostaglandin[2], and serum starvation[3]. The cells respond with assembly of microtubules, leading to neurite outgrowth[4,5], with increased activity of neuronal-specific enzymes, tyrosine hydroxylase, choline acetyltransferase and acetylcholine-esterase[6,7], and synthesis of neurotransmitters[8]. The differentiated cells lose tumorigenicity[9]. Cell-to-substratum adhesion is evidently crucial for neurone extension *in vitro*[10]. Neurite outgrowth is induced by treatments that increase cell-to-substratum adhesion in some neuronal cell cultures[11,12]. We have now identified the major high molecular weight proteins synthesized and secreted by murine C1300 neuroblastoma cells as fibronectin, laminin and type IV procollagen, of which the latter two were also found to be deposited in pericellular matrix form.

The mouse neuroblastoma cells (C1300, clone NB41A3); American Type Culture Collection, CCL 147) were cultured in Eagle's medium supplemented with 10% fetal calf serum and antibiotics. To induce morphological differentiation, the neuroblastoma cells were plated sparsely and cultured in the presence of 1 mM dbcAMP. The polypeptides secreted into the culture medium by metabolically labelled (^{3}H-proline or ^{14}C-glycine) neuroblastoma cells were precipitated with ammonium sulphate and analysed by SDS-polyacrylamide gel electrophoresis. The major polypeptide as seen on autofluorograms migrated with an apparent molecular weight (MW) of 230,000 (Fig. 1, lanes 2 and 3). In addition, labelled polypeptides were seen with MWs of 400,000 and 170,000. These polypeptides were disulphide-bonded to each other since similar analysis of unreduced samples revealed a major polypeptide band with a MW of 440,000 and larger material (Fig. 1, lane 1). The overall pattern of protein secretion did not appreciably vary over a wide range of labelling times and was not affected by the presence of 1 mM dbcAMP in the cultures (not shown).

Several major bands could be identified as either fibronectin or laminin polypeptides by precipitation from the neuroblastoma cell extracts and culture media with the respective antibodies (Fig. 1, lanes 4 and 5). The fibronectin chains showed an apparent MW of 230,000, while laminin polypeptides could be visualized as a closely spaced doublet with MW of 215,000 together with a higher molecular weight (400,000) component. The radiolabelled laminin polypeptides co-migrated with protein-stained[13] components of authentic laminin purified from the mouse EHS sarcoma[14] (not shown).

Initial analysis of medium proteins produced in the absence of ascorbate failed to identify collagenous protein. Since laminin has so far only been found together with collagen type IV both *in vivo*[14,15] and *in vitro*[16,17], we also examined media of cell cultures labelled in the presence of sodium ascorbate and the cross-link inhibitor β-aminopropionitrile fumarate. Two new disulphide-linked polypeptides MWs 170,000 and 180,000 according to collagenous standards) were now secreted and were sensitive to a highly purified bacterial collagenase (Fig. 1, compare lanes 2 and 3; 6 and 7). These two polypeptides comprised about 16% of protein-bound ^{3}H-proline-derived radioactivity and could be specifically precipitated with antibodies to type IV collagen (Fig. 1, lane 8). Antibodies to interstitial procollagens or collagens did not precipitate protein-bound radioactivity (Fig. 1, lane 9). The type IV procollagen polypeptides were particularly rich in the matrix material attached to the growth substratum (Fig. 2*a*) at the expense of fibronectin polypeptides, which were abundant in the medium (Fig. 2*b*). Indirect immunofluorescence studies using previously described procedures[16] confirmed the presence of all three glycoproteins in the cells and deposition of laminin under the attached cells, as will be reported in detail elsewhere.

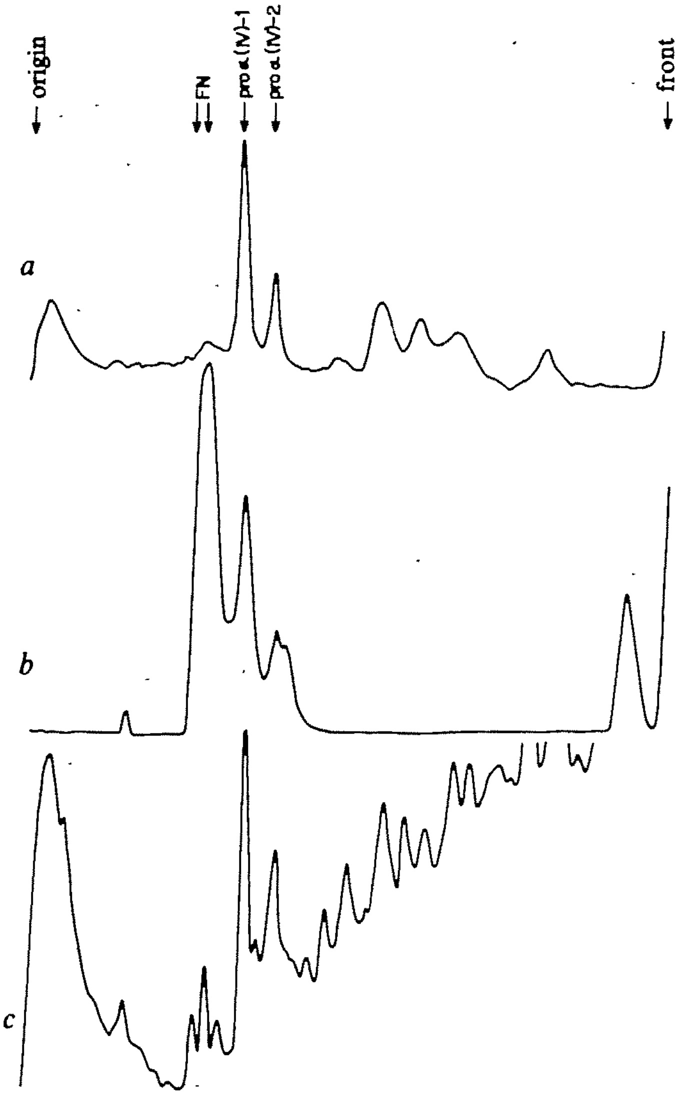

Fig. 1 Electrophoretic analysis[32] of metabolically labelled proteins secreted into the medium by undifferentiated C-1300 neuroblastoma cells. Lane 1 medium, non-reduced; lanes 2, 3 and 7, medium reduced with mercaptoethanol. The medium in lanes 3, 6 and 7 was obtained in the presence of ascorbate (30 μg m^{-1}) and β-aminopropionitrile fumarate (30 μg ml^{-1}); lane 6, medium after treatment with bacterial collagenase. Proteins were precipitated before analysis with ammonium sulphate (281 mg ml^{-1}) in the presence of gelatin carrier (50 μg ml^{-1}) and protease inhibitors[33]. Lanes 4, 5 and 8, identification of proteins by immunoprecipitation[16] with specific antibodies to laminin[14] (lane 4), fibronectin[18] (lane 5) and type IV collagen[34] (lane 8). Control precipitates in lane 9 were obtained either with anti-type II collagen or normal rabbit IgG. The polypeptides were visualized by fluorography[35]; lanes 4 and 5 were exposed for 6 d, the other lanes for 3 d. Except for lane 1 all samples were analysed in reducing conditions. Globular proteins as indicated by their molecular weights (left side) and type I collagen and procollagen chains (right side) were used for calibration.

0028-0836/80/400465—02$01.00

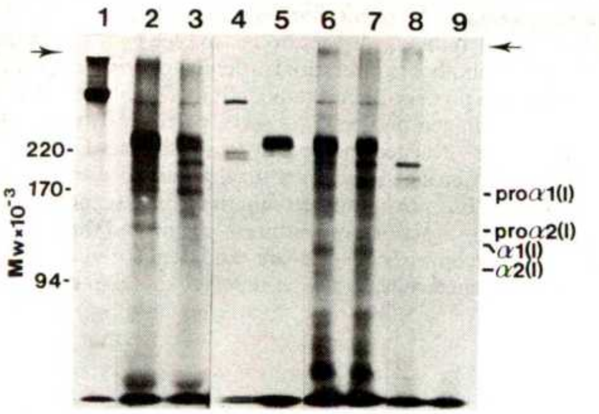

Fig. 2 Comparison of labelled proteins in the matrix (*a*), medium (*b*), and cell layer (*c*), obtained from undifferentiated C-1300 neuroblastoma cultures by densitometric scanning. Cell-free substrate-attached matrix was prepared using sequential extraction of cell layers with 0.5% sodium deoxycholate and hypotonic buffer in the presence of protease inhibitor[36]. Cell layer contained both intracellular and matrix proteins solubilized directly into electrophoresis sample buffer. The positions of fibronectin (FN) and type IV procollagen pro-α1 (IV) and pro-α2 (IV) chains are indicated by arrows. Electrophoresis was carried out in reducing conditions.

No distinct deposits of fibronectin or type IV procollagen could be detected in cultures of either attaching or differentiating cells, but the latter was identified by electrophoresis (Fig. 2*a*). Essentially similar results were obtained with the NB42B clone[5] of C1300 cells.

Several methods of determining the amounts of the major glycoproteins secreted by morphologically undifferentiated and differentiated C1300 cells gave no consistent differences between the two. This was the case when radioactivity in the high molecular weight peptide bands was plotted against cell number or amount of protein in the cell layer. Quantification of medium proteins by radioimmunoassay (RIA) using antibodies directed against human plasma fibronectin[18] or the large, pepsin-resistant fragment of laminin[19] gave similar values for both states, when corrected for the amount of cells in each culture. Nearly identical patterns for radioactive polypeptides were also observed in both cell layers, or isolated pericellular matrix material by electrophoresis followed by autofluorography or by RIA for pepsin-solubilized laminin.

These results show production of fibronectin, laminin and type IV collagen by two clones of a well-characterized line of murine neuroblastoma cells able to differentiate in culture. Cell-surface associated polypeptides of molecular weights similar to that of laminin and antigenically distinct from fibronectin have been detected both in N18 neuroblastoma[20] and in PC12 pheochromocytoma cell clones[21]. Furthermore, both nerve growth factor and dbcAMP have been found to induce alterations in protein secretion and substrate-attached material of PC12 cell structures[22], whereas dbcAMP and subsequent differentiation had no effect on protein secretion in the present study.

The only collagenous protein secreted by neuroblastoma cells was of the basement membrane type. Its polypeptide pattern was very similar to that of type IV procollagen secreted by murine parietal yolk sac cells *in vivo*[23] and tumour cells in culture[17]. Note that secretion of collagen by neuroblastoma cells was detected only in ascorbate-treated cultures. The significance of type IV collagen for neuroblastoma cells remains unknown. Our data demonstrate that neuroblastoma cells in culture produce proteins characteristically found in a wide variety of basement membranes. It is possible that this synthesis pattern is an example of the so-called retrodifferentiation of tumour cells[24] and represent the primitive ectodermal origin of the (neuroblastoma) cells[25]. Currently held views indicate that neurones lack adjacent basal laminae in the central nervous system[26,27] and that Schwann cells are responsible for matrix production in the peripheral nervous system[28,29]. Intraneuronal synaptic clefts[30] and neuromuscular junctions[31], however, contain matrix material. Thus it is also possible that basement membrane production by neuroblastoma cells, particularly in their differentiated state, reflects a similar *in vivo* activity.

We thank Anja Virtanen, Raili Taavela and Hildegard Reiter for assistance. This work was supported by grants from the Finnish Cancer Foundation, NIH (grant no. CA24605), the Finnish Medical Research Council and Deutche Forschungsgemeinschaft.

Pure Chemistry Library
Science College
92 Upper Circular Road
Calcutta

Received 21 May; accepted 28 July 1980.

1. Prasad, N. K. & Hsie, A. W. *Nature new Biol.* **223,** 141–142 (1971).
2. Prasad, N. K. *Nature new Biol.* **236,** 49–52 (1972).
3. Seeds, N. N., Gilman, A. G., Amano, T. & Nierenberg, M. *Proc. natn. Acad. Sci. U.S.A.* **66,** 160 (1970).
4. Marchisio, P. C., Osborn, M. & Weber, K. *J. Neurocytol.* **7,** 751–756 (1978).
5. Augusti-Tocco, G. & Sato G. *Proc. natn. Acad. Sci. U.S.A.* **64,** 311–315 (1969).
6. Richelson, E., *Nature new Biol.* **242,** 175–177 (1973).
7. Schubert, P., Humphreys, S., Baroni, C. & Cohn, N. *Proc. natn. Acad. Sci. U.S.A.* **64,** 316–323 (1969).
8. Amano, T., Richelson, E. & Nierenberg, M. *Proc. natn. Acad. Sci. U.S.A.* **69,** 258–263 (1972).
9. Prasad, N. K., Sahu, S. K. & Sinha, P. K. *J. natn. Cancer Inst.* **57,** 619–631 (1976).
10. Schubert, D. & Jacob, F. *Proc. natn. Acad. Sci. U.S.A.* **67,** 247–254 (1970).
11. Schubert, D., Humphreys, S., Witry, F. & Jacob, F. *Devl Biol.* **25,** 514–546 (1971).
12. Letourneau, P. C. *Expl Cell Res.* **124,** 127–138 (1979).
13. Griffith, J. P. *Analyt. Biochem.* **46,** 402–412 (1972).
14. Timpl, R. *et al. J. biol. Chem.* **254,** 9933–9937 (1979).
15. Foidart, J.-M. *et al. Lab. Invest.* **42,** 336–342 (1980).
16. Alitalo, K., Kurkinen, M., Vaheri, A., Krieg, T. & Timpl, R. *Cell* **19,** 1053–1062 (1980).
17. Alitalo, K., Vaheri, A., Krieg, T. & Timpl, R. *Eur. J. Biochem.* **109,** 247–255 (1980).
18. Vuento, M. & Vaheri, A. *Biochem. J.* **183,** 331–337 (1979).
19. Rohde, H., Wick, G. & Timpl, R. *Eur. J. Biochem.* **102,** 195–201 (1979).
20. Akeson, R. & Hsu, W.-C. *Expl Cell Res.* **115,** 367–377 (1978).
21. McQuire, J. C., Greene, L. A. & Furano, A. V. *Cell* **15,** 357–365 (1978).
22. Schubert, D. *Brain Res.* **155,** 196–200 (1978).
23. Tryggvason, K., Gehron Robey, P., Martin, G. R. *Biochemistry* **19,** 1284–1289 (1980).
24. Uriel, J. *Adv. Cancer Res.* **29,** 127–174 (1979).
25. Prasad, K. N. & Sinha, P. K. in *Cell Differentiation and Neoplasia* (ed. Saunders, G. F.) (Raven, New York, 1978).
26. Shellswell, G. B., Restall, D. J., Duance, V. C. & Bailey, A. J. *FEBS Lett.* **106,** 305–308 (1979).
27. Schachner, M., Schoonmaker, G. & Hynes, R. O. *Brain Res.* **158,** 149–158 (1978).
28. Thomas, P. K. *J. Cell Biol.* **23,** 375–382 (1964).
29. Bunge, M. B., Williams, A. K., Wood, P. M., Uitto, J. & Jeffrey, J. J. *J. Cell Biol.* **84,** 183–202 (1980).
30. Peters, A., Palay, S. L. & Webster, H. (eds) *The Fine Structure of the Nervous System* (Saunders, Philadelphia, 1976).
31. Sanes, J. R. & Hall, Z. W. *J. Cell Biol.* **83,** 357–370 (1979).
32. Laemmli, U. K. *Nature* **227**, 680–685 (1970).
33. Narayanan, A. S. & Page, R. C. *J. biol. Chem.* **251,** 5464–5471 (1976).
34. Timpl, R., Martin, G. R., Bruckner, P., Wick, G. & Wiedemann, H. *Eur. J. Biochem.* **84,** 43–52 (1978).
35. Bonner, W. M. & Laskey, P. A. *Eur. J. Biochem.* **46,** 33–83 (1974).
36. Hedman, K. *et al. J. Cell Biol.* **81,** 83–91 (1979).

Corrigenda

In the letter 'Discovery of a very distant supernova' by M. R. S. Hawkins, *Nature* **286,** 467–469, in Table 1 the epoch of J4394 is 29.7.78. In Fig. 1 the point with the same ordinate as the cross is spurious and in Fig. 3 two of the points in the top left-hand corner are spurious. The sentence in line 44 on p. 468 beginning 'Note that . . .' should read 'In particular, the fit was made without the last two observations, which after galaxy subtraction were the most uncertain.' In line 3 on p. 469, for 'non-expanding Doppler' read 'non-Doppler'.

The following acknowledgement refers to the letter 'Renin-like effects of NGF evaluated using renin-antagonists' by D. B. Avrith *et al.*, *Nature* **285,** 248–250. 'We thank Professor Vernon, Department of Chemistry, University College London, for the gift of immunologically pure β-subunit of NGF'.

MATTERS ARISING

Geological objections to an extensional origin for the Buchan and Witchground Graben in the North Sea

CHRISTIE AND SCLATER'S refraction results[1] corroborate our inference from regional gravity[2] that the crust under the Buchan and Witchground Graben area of the North Sea is anomalously thin (see Fig. 1). However, their mechanism[3] for the development of the grabens, invoking crustal stretching by a factor of ~2 during the late Jurassic to early Cretaceous, raises serious geological problems. (1) The structure of the inner Moray Firth at lower Mesozoic levels[4] precludes both N–S extension of more than a few per cent, and significant later transcurrent movement on the Great Glen fault[5]. How can Christie and Sclater reduce their supposed N–S crustal extension of at least 60 km, along the Greenwich meridian, to zero, 200 km to the west? Our gravity modelling shows that if gross crustal extension occurred at all, it was in a NE–SW to E–W direction below the Viking and Central grabens, and not in a N–S direction across the Moray Firth. (2) The thickening of the Palaeozoic layer from near zero, at either end of their refraction profile, to about 4 km in the centre, implies up to 4 km of pre-late Permian erosion, and/or a Palaeozoic depositional basin. In contrast, their upper crustal layer seems to have an approximately constant thickness. The post-Zechstein, pre-stretching thickness of these two layers together was presumably, therefore, 5 km or less at the ends of the profile, but ~18 km in the centre. Whether or not erosion took place, it is clear that the crust was already highly anomalous by the mid-Permian so that the later, planar, 40-km deep Moho, depicted in Christie and Sclater's Fig. 4*a* as the initial (pre-stretching) crustal structure, is inconsistent with these implications from their own refraction results. (3) The major graben-boundary faults, probably active from the late Carboniferous (Stephanian) to the late Jurassic, are depicted (their Fig. 4*a*) as having had no effect on the Moho, whereas unobserved listric faults are postulated to have thinned the crust (their Fig. 4*b*) by a factor of ~2 shortly afterwards. Also not observed is the extreme rotation, of the order of 60°–80° (ref. 6), of the Jurassic and older sediments required to produce such extension—actual tilts are only a few degrees. Well developed listric faults can now be recognized elsewhere on seismic reflection sections (for example, ref. 7), but can only account for upper crustal extension of ~25%. (4) The effusion of a 3-km thick pile of mildly under-saturated alkali olivine basalts in the centre of the refraction profile[8] apparently pre-dates the initiation of the supposed stretching period by some 10 Myr, whereas rapid extension would probably result first in tholeiitic volcanism (particularly in the form of dyke swarms) before the more alkaline volcanism resulting from deeper partial melting. The only major pre-Tertiary tholeiitic dyke swarm in the region is considerably older, at ~290 Myr, preceding a major period of igneous activity in the Permian. In contrast, magmatism during the late Jurassic and early Cretaceous was trivial[8].

In view of these problems we conclude that rapid extension of the scale required never occurred. Other mechanisms such as loading of an elastic or visco-elastic lithosphere[2,9] can explain the last 120 Myr of North Sea subsidence just as readily as a thermal model, but without requiring such a catastrophic initiating mechanism.

M. J. Russell has suggested that the problem of the thin crust beneath the North Sea may be tackled by rejecting the assumption that the crust was originally of standard continental thickness and composition. The contiguity of the Scottish–Norwegian and North German–Polish Caledonides through the North Sea[10], and the implication, mainly from faunal provinciality, of three widely separated Lower Ordovician continental blocks[11], lead us to propose that the anomalous crust under the North Sea grabens may date back to the closing of a Lower Palaeozoic ocean. We therefore predict a small but significant difference in the seismic structure of the crust on either side of the grabens, as has been observed across the Iapetus suture[12] (Fig. 1). The later major tectonic and magmatic events of north-west Europe can all be ascribed, in principle, to the effects of nearby seafloor spreading in the early Permian[13], early Cretaceous[7] and the Tertiary, without resorting to an *ad hoc* stretching event.

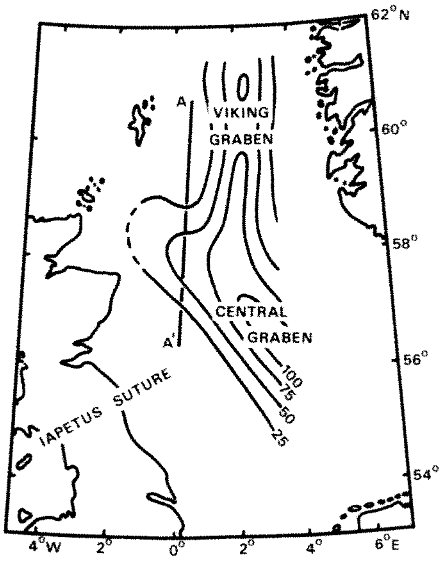

Fig. 1 Residual gravity anomaly (mGal) after removal of the effect of all Upper Palaeozoic and younger sediments (from ref. 2). AA' is refraction profile of ref. 1. Three-dimensional modelling predicts a Moho depth of 25 km below the centre of profile AA', on the lobe of overlap where the 200-km wide zone of thin crust below the Central Graben runs into the 130-km wide zone below the Viking Graben. Minimum Moho depth below the centre of each graben is 20 km, assuming a 'normal' Moho depth of 30 km and a density contrast 0.4 g cm^{-3} across the Moho.

D. K. SMYTHE
A. G. SKUCE
J. A. DONATO

*Institute of Geological Sciences,
19 Grange Terrace,
Edinburgh EH9 2LF, UK*

1. Christie, P. A. F. & Sclater, J. G. *Nature* **283**, 729–732 (1980).
2. Donato, J. A. & Tully, M. C. in *Petroleum Geology of the Continental Shelf of North-west Europe* (ed. Illing, L. V.) (Heyden, London, 1980).
3. McKenzie, D. *Earth planet. Sci. Lett.* **40**, 25–32 (1978).
4. Bacon, M. & Chesher, J. *Norg. geol. Unders.* **316**, 99–104 (1975).
5. Bacon, M. & Chesher, J. *Scott. J. Geol.* **11**, 79–82 (1975).
6. Proffett, J. M. *Bull. geol. Soc. Am.* **88**, 247–266 (1977).
7. Montadert, L., Roberts, D. G., De Charpal, O. & Guennoc, P. *Init. Rep. DSDP* **48**, 1025–1060 (1979).
8. Woodhall, D. & Knox, R. W. O'B. *Bull. geol. Surv. G. Br.* No. 70, 34–56 (1979).
9. Beaumont, C. *Geophys. J. R. astr. Soc.* **55**, 471–497 (1978).
10. Ziegler, P. A. *Geologie. Mijnb.* **57**, 589–626 (1978).
11. Keppie, J. D. *Nova Scotia Dep. Mines Pap.* 77–3 (1977).
12. Bamford, D., Nunn, K., Prodehl, C. & Jacob, B. *Geophys. J. R. astr. Soc.* **54**, 43–60 (1978).
13. Russell, M. J. & Smythe, D. K. in *Petrology and Geochemistry of Continental Rifts* Vol. 1 (eds Neumann, E.-R. & Ramberg, I. B.) 173–179 (Reidel, Dordrecht, 1978).

CHRISTIE AND SCLATER REPLY—We thank Smythe *et al.* for providing the opportunity to elaborate on the extensional model for basin formation[1]. First, it cannot be denied that extension has taken place in the North Sea, and the strong temporal correlations between North Atlantic and North Sea activity[2,3] enable us to refute the suggestion that the model is *ad hoc*.

As noted by us, evidence for the required extension must be found in the North Sea geological record for the model to be acceptable. Concerning the amount and type of extension, we would make the following points.

(1) Although the refraction line is a linear profile, this does not constrain the extension to be parallel to it or even one-dimensional and indeed the model describes areal extension[4]. Clearly, the geometry of the basin requires two-dimensional extension to have taken place in the vicinity of well 3 (ref. 4).

0028–0836/80/400467—02$01.00

(2) Such extension, if azimuthally independent, would require linear extensions of 34 and 26% to produce the locally maximal values of *b* of 1.8 and 1.6 respectively[4].

The amount of extension accommodated by listric faults is debatable. Although Montadert *et al.*[5] suggest that listric-faulted blocks on the north Biscay margin, displaying tilts of 20° to 30°, allow some 15% extension, the same seismic reflection data have been interpreted by X. Le Pichon and J.-C. Sibuet (personal communication) to allow extension of 200% to 300%. Both Montadert *et al.* and Le Pichon and Sibuet cite extension as being the primary cause of crustal attenuation in this area, with post-rift subsidence the result of isostatic adjustment to cooling of the lithosphere.

We agree that magmatism during the Jurassic and early Cretaceous was trivial, justifying our assumption that crustal material was conserved. However, the apparent predating by basaltic effusions of the onset of extension by ~10 Myr seems more to support the placing of the stretching event in the Lower Jurassic than to refute the model.

The noted existence of a Permo–Triassic event in the North Sea may require an explanation of subsidence in terms of the superposition of two main stretching episodes. In this case, we would agree that the North Sea crustal thickness may already have been attenuated by the start of the Jurassic phase of activity, in which event, less Jurassic extension of even a one-dimensional type would be required to produce the seismic cross-section.

However, the good agreement between the seismic and gravity estimates of the depth to the Moho suggests that there is indeed crustal attenuation beneath the North Sea Basin, and 4 km of actual post mid-Cretaceous sedimentation is compelling evidence for something other than simple loading of an elastic lithosphere, which predicts a thickened crust[6]. A loading hypothesis would require the existence of a wide, 1,200-m deep depression at the time of the Aptian–Albian unconformity over a somehow previously thinned crust.

P. A. F. CHRISTIE

Department of Earth Sciences,
Bullard Laboratories,
Madingley Road,
Cambridge CB3 0EZ, UK

J. G. SCLATER

Department of Earth and
Planetary Sciences,
Massachusetts Institute of Technology,
Cambridge, Massachusetts 02139

1. McKenzie, D. *Earth planet. Sci. Lett.* **40,** 25–32 (1978).
2. Ziegler, P. A. *Geologie. Mijnb.* **57,** 589–626 (1978).
3. Christie, P. A. F. thesis, Cambridge Univ. (1979).
4. Christie, P. A. F. & Sclater, J. G. *Nature* **283,** 729–732 (1980).
5. Montadert, L., Roberts, D. G., De Charpal, O. & Guennoc, P. *Init. Rep. DSDP* **48,** 1025–1060 (1979).
6. Beaumont, C. *Geophys. J. R. astr. Soc.* **55,** 471–497 (1978).

Counting integral numbers of amino acid residues

THE method of "counting integral numbers of amino acid residues per polypeptide chain" described by Creighton[1] is not new either in concept or in execution. The idea of using varying ratios of iodoacetamide and iodoacetate to alkylate proteins and then to determine the number of alkylated cysteine residues by gel electrophoresis was first introduced by Feinstein[2] in 1966. In that original paper starch gel electrophoresis was used. Subsequently, Feinstein and Stott[3] used isoelectric focusing to resolve the differently charged proteins. In both of those papers the 'charge-shift' technique was used to determine the number of free thiol groups on partially reduced proteins.

More recently Singer and I[4] have used 'charge-shift' analysis of fully reduced protein to determine the cysteine content. We have therefore used the method in exactly the same manner as that described by Creighton. Extension of the charge-shift method to other amino acid residues is an obvious possibility. However, the data presented by Creighton relate only to the determination of cysteine residues.

I am most surprised that the previous publications on the charge-shift method should have escaped the attention of both Creighton and the *Nature* referees.

A. R. WILLIAMSON

Institute of Biochemistry,
University of Glasgow,
Glasgow G12 8QQ, UK

1. Creighton, T. E. *Nature* **284,** 487–489 (1980).
2. Feinstein, A. *Nature* **210,** 135 (1966).
3. Stott, D. I. & Feinstein, A. *Eur. J. Immun.* **3,** 229–235 (1973).
4. Singer, P. A. & Williamson, A. R. *Eur. J. Immun.* **9,** 224–231 (1979).

CREIGHTON REPLIES—The papers cited by Williamson[1–3] describing the 'charge-shift' method of determining cysteine residues, which has become the same in principle as the method I used[4], were unfortunately unknown to me, the referee of my paper, all the colleagues with whom I discussed this matter, and the authors of all review articles and monographs on the subject of amino acid analysis that I could find. A thorough search through the index of *Amino Acid, Peptide and Protein Abstracts* for papers on amino acid analysis also failed to uncover these papers. This ignorance of the development of Feinstein's original work[2] can be attributed to its publication only as a small part of papers dealing with the biosynthesis of immunoglobulins published in an immunological journal[2,3], with no mention of the method in either the titles or abstracts. This is an instructive example of how care must be taken if the attention of the appropriate audience is to be drawn to published work.

Having now studied these papers in detail, I note that the validity of the charge-shift method was not established at that stage, either by confirming the results with an independent, established method or by demonstrating that it gave the correct results with a well characterized protein. It was also used inappropriately with a protein that was electrophoretically heterogeneous so that the results were ambiguous[3]. Demonstrating the validity of this method is especially important because it depends critically on the completeness and the specificity of the reaction of cysteine thiol groups with iodoacetate and iodoacetamide. I demonstrated this by obtaining single electrophoretic bands of unfolded proteins treated with the limiting cases of just iodoacetamide and just iodoacetate[4]. There was then no uncertainty about where to start and where to stop counting the bands generated by reaction with mixtures of the two reagents. The number of bands generated gave the correct number of cysteine residues for six well characterized proteins. When this procedure is used with a new protein, a well characterized protein should always be included as a control, to ensure the specificity and completeness of the reactions.

It is clear that this general method of determining integral numbers of specific amino acid residues is simple, easy, and can give unambiguous results when properly applied. The general approach should be useful for some amino acid residues other than cysteine; the observations of Anderson and Hickman[5] using carbamylation and of M. Hollecker in this laboratory using succinic anhydride[6] demonstrate that it may readily be extended to lysine residues.

T. E. CREIGHTON

MRC Laboratory of Molecular Biology,
University Medical School,
Hills Road,
Cambridge CB2 2QH, UK

1. Feinstein, A. *Nature* **210,** 135–137 (1966).
2. Stott, D. I. & Feinstein, A. *Eur. J. Immun.* **3,** 229–235 (1973).
3. Singer, P. A. & Williamson, A. R. *Eur. J. Immun.* **9,** 224–231 (1979).
4. Creighton, T. E. *Nature* **284,** 487–489 (1980).
5. Anderson, N. L. & Hickman, B. J. *Analyt. Biochem.* **93,** 312–320 (1979).
6. Hollecker, M. & Creighton, T. E. *FEBS Lett.* (in the press).

Matters Arising

Matters Arising is meant as a vehicle for comment and discussion about papers that appear in *Nature.* The originator of a Matters Arising contribution should initially send his manuscript to the author of the original paper and both parties should, wherever possible, agree on what is to be submitted. Neither contribution nor reply (if one is necessary) should be longer than 300 words and the briefest of replies, to the effect that a point is taken, should be considered.

BOOK REVIEWS

The genesis of experimental psychology

O. L. Zangwill

Wilhelm Wundt and the Making of a Scientific Psychology. Edited by R.W. Rieber. Pp.252. (Plenum: 1980.) £15.44, $24.50.

THIS book was compiled to mark the centenary last year of the establishment of the first laboratory in the world to be devoted exclusively to experimental psychology. Its founder was Wilhelm Wundt, a physiologist with a taste for philosophy, who had worked for many years at Heidelberg under the shadow of the great Helmholtz. After a somewhat undistinguished early career in physiology, Wundt was translated to Leipzig as a professor of philosophy, to which he was undoubtedly better suited, and at Leipzig he remained for the rest of his life.

In 1873, Wundt published the text on which his reputation has been principally based. In a later edition, this was translated into English by his devoted follower, E.B. Titchener, as *Principles of Physiological Psychology*. Of all Wundt's voluminous writings, this is, if not the best, certainly the best known. Wundt's own introductory statement to the original edition on "the task of physiological psychology" is one of the few extracts from his writings to appear in this volume which, however, also includes a fascinating review of the first German edition of the *Principles* by William James.

How did Wundt view experimental psychology? One may note first that whereas he saw physiological and experimental psychology as being virtually synonymous, he was in no doubt whatsoever that the latter warrants acceptance as a distinct and separate department of knowledge. This is well brought out in the second of the two excellent chapters by Kurt Danziger on Wundt's theoretical position. Arising from his exposition of Wundt's theory of human behaviour, Danziger directs special attention to the classical series of experiments on reaction times which were among the earliest fruits of his laboratory. Danziger treats the measurement of reaction times as in no sense a mere adjunct to physiology, as it had hitherto been viewed, but as a coherent manifestation of psychological research in its own right having direct relevance to the explanation of human behaviour.

As Wundt saw it, the most central of the issues underlying reaction time measurements was concerned with human volition. The distinction between "sensorial" and "muscular" reaction times, Wundt believed, had important theoretical implications for an understanding of volitional activity and its relationship to the evolution of higher-order choice and decision processes. Such issues, he considered, lie totally outside the province of physiology, which then even more than now was conceived to be limited to essentially reflex models of involuntary action. Indeed the prolonged neglect of Wundt's work in America was undoubtedly due, in part at least, to the protracted behaviourist hegemony and the reductionist philosophy which it embodied. Even in Germany, the belief that selective attention, so central to Wundtian thinking, lacked explanatory value, became a central tenet of Gestalt psychology and under its influence reaction times, too, ceased for many years to be of more than marginal interest.

Currently, behaviourism is clearly in decline, and cognitive and developmental preoccupations in psychology equally clearly in the ascendant. In consequence, the climate is once again more sympathetic to the Wundtian outlook and this book may itself result in a revival of interest in his work. True, concepts of information processing and control mechanisms have replaced the Wundtian concepts of volition, apperception and creative synthesis, the roots of which lie deep in the *Naturphilosophie* of mid-nineteenth-century Germany. As Danziger rightly points out, present-day psychology is concerned primarily with an understanding of human performance, governed by concepts of selective attention, information processing, and decision and choice. Such a psychology may, in some sense, widen rather than diminish the gap between psychology and the neurosciences, but it leaves unaffected Wundt's insistence on experimental psychology being conceived as an autonomous discipline which stands in symbiotic relationship with physiology. Further, although Wundt regarded social psychology as an historical and cultural rather than as an experimentally based discipline, his emphasis on its pre-eminent importance for psychology in general will find a sympathetic response in many quarters today.

One particularly valuable contribution made by this book is the challenge it provides to the received ideas about Wundt and his work which stem largely from the writings of Titchener and his pupil, E.G. Boring, the celebrated historian of experimental psychology. This challenge emerges particularly clearly in Blumenthal's chapter on Wundt and early American psychology, though it is unfortunate that it was not thought appropriate to reprint his enlightening reappraisal of Wilhelm Wundt which appeared five years ago. Danziger has also some highly relevant things to say about Titchener's many misapprehensions of Wundt's philosophical position. Solomon Diamond contributes a long essay on Wundt's early life and activities as a physiologist, though his somewhat uninhibited personal criticism may be thought to limit its biographical value.

Although inevitably a hodge-podge, this book will be welcomed by many people who are genuinely interested in the origins and development of experimental psychology, even though some of them may still continue to believe, with William James, that psychology is less a science than the hope of a science. ☐

O.L. Zangwill is Professor of Experimental Psychology in the University of Cambridge.

HBV *et al.*

William S. Robinson

Hepatitis Viruses of Man. By A.J. Zuckerman and C.R. Howard. Pp.269. (Academic: 1980.) £16.80, $39.

OCCASIONAL reviews of hepatitis viruses by experts are welcome because knowledge of these viruses has been advancing so rapidly over the past decade that it is sometimes difficult for those in the field, much less outsiders, to keep up and assimilate all of the new findings. Such reviews are most helpful when they are able to provide new insights, bring some order where chaos reigns among conflicting data, evaluate new findings in the context of other relevant and better studied biological systems, or provide a bibliography which makes a body of research literature readily available to readers. The authors of this book are active investigators in the field and have a broad knowledge of recent work. They intended this book to provide "an account of the more important published advances and exciting developments in this field". The book does provide a large amount of recent information about hepatitis viruses. It attempts to cover widely different aspects of such viruses, including their history, ultrastructure, antigenic structure, molecular structure, epidemiology, course of infection, pathology of associated diseases, immunology, laboratory testing, animal and cell culture infection, environmental control measures and management of infected patients, immunization and antiviral treatment. Most of the book by far is devoted to hepatitis B virus (HBV), less to hepatitis A virus and least to the newly recognized non A, non B hepatitis agents; coverage is thus in proportion to the amount of new information about each of the viruses.

Some aspects are more successfully covered than others. The first chapter, "The History of Viral Hepatitis", includes many important findings from the earliest recordings of hepatitis-like disease to recent breakthroughs that have propelled the field forward. This account is well documented with references. After this chapter the presentation changes. As each area is considered, recent findings are almost exclusively given, and older work is omitted or briefly summarized, often without referencing. Frequently statements are presented as fact without documentation. For example, a large part of the chapter "Pathology of the Liver in Acute Viral Hepatitis", is devoted to a near-textbook description of histological features of acute human viral hepatitis without documentation. By presenting only recent findings on epidemiology, only the surface of this subject is covered. Certain important and long-standing epidemiological concepts about these viruses are omitted such as the different epidemic and endemic patterns of infections, the different dynamics of the viruses in human populations and the different factors which are involved in maintenance of each in populations, to name a few. In some places experimental results are given without crediting the investigators, for example on p.26. An experiment in which HBsAg was detected "in 18 out of 24 saliva specimens and in 10 out of 10 samples of semen" is presented without a reference. Similar statements are found throughout the book. This failure to document the source of some recent findings that are given in detail in the book and the almost complete omission of older findings and reference to literature (that before 1975) greatly limit the value of this book as a reference source for investigators in the field, teachers and students. The authors suggest that the earlier literature is fully cited in a previous book by one of them. This, of course, is only partially satisfactory since it requires simultaneous reading of both books to obtain the whole picture and it leaves this book as only a partial account.

The information in the book is usually presented as a sequence of descriptions of the findings of individual studies. Little attention is given to comparison of findings of different investigators, offering explanations of differences in findings, suggesting new approaches which might resolve differences, or organizing and analysing complex subjects. For example, e antigen is such a complex subject and a number of apparently conflicting findings have been reported. Claims suggesting that e antigen is an immunoglobulin, related to lactic dehydrogenase, or that it may represent a virion component, have been published. These different findings are not critically analysed nor is a judgement as to the merit of each offered. No approaches are suggested for resolving the differences. Conflicting data concerning the relationship of e antigen to liver disease are similarly handled.

The chapter entitled "The Nature of Hepatitis B Virus" is similarly a descriptive account of experimental findings about the virion. The reader is given little feeling that HBV is a virus in the modern sense with specific genes whose functions are involved in viral structure, infection and replication. Although few details of virus replication at the molecular level are available for HBV, there is evidence for the identity of some viral gene products, such as HBsAg polypeptides, and evidence for locations of viral antigen synthesis and the structure of viral DNA forms in cells.

Finally it is disappointing that the structural, molecular and biological features of hepatitis B that distinguish it from viruses of other groups were not especially pointed out in order to provide a perspective of this interesting and unique virus. In this regard, the recent finding of a similar virus in woodchucks was not included. The woodchuck virus is important not only because it indicates that HBV may be only one member of a new group of viruses, but because its association with hepatoma in infected animals offers one of the most compelling arguments for an important relationship of viruses with properties like those of HBV to primary liver cancer, an issue with HBV in man.

Thus, although this book provides much recent and important information about several viruses which are of great biological and clinical interest, the choice of material and its presentation limit the book's value as an introduction to these viruses and as a reference work for those already familiar with the field. ☐

William S. Robinson is Professor of Medicine at the Division of Infectious Diseases, Stanford University School of Medicine, California.

In memoriam: the English chalklands

Kenneth Mellanby

Ecology of the English Chalk. By C.J. Smith. Pp. 573. (Academic: 1980.) £23.80, $55.

As a schoolboy I thought of the chalklands of England as a crocodile. A geological map hung on the wall of one of my classrooms, and its most prominent feature appeared to me to resemble a light-blue reptile with the North and South Downs as the upper and lower jaws, the body turning round so that the tail ended up in Norfolk and Lincolnshire. Living in Scotland and the north of England, I never visited my crocodile until, as an undergraduate at Cambridge, I was taken by the botany department to study chalk grassland near Royston. I still remember my first visit, in spring, when the Pasque flower was at its best. This and many subsequent visits to Royston Heath, Salisbury Plain and other chalk grasslands continued to impress me with both the beauty and the scientific interest of these areas. Even when I dropped botany for entomology, the butterflies and other insects sustained my fascination.

For over 100 years naturalists have shared my enthusiasm, for even a cursory glance through the literature shows that more work has been done on chalk grassland than on any other plant and animal habitat. Dr C.J. Smith has performed a notable service in bringing the results of this careful study into one book. He lists well over 700 references, and he is clearly familiar with the information contained in them all.

We are given a description of the chalk's geology and the history of the land use; there are details concerning the plants and animals and their interactions. The result cannot be called light reading: it is far too concentrated for that. But anyone interested in natural history who has visited the chalk will find something of interest, and something to stimulate him to further observation. Serious students will all acknowledge their indebtedness to Dr Smith's singleness of purpose, and this volume will be accepted for many years as the final authority on its subject.

The book makes it clear that the areas of chalk grassland which are of particular interest have all been profoundly affected by human activity. The land was first cleared of trees by our distant ancestors, mainly to grow arable crops. After a few years of declining fertility it was allowed to go down to grass, which was grazed by stock — cattle and sheep. The best turf has existed for centuries. This species-rich grass only persists when it is regularly grazed, otherwise rank growth crowds out the most prized plants, and shrubs develop in the first stage leading to the forest climax. The scrub and woodland have their own interest and beauty, but it is the grass with all its flowers which has the greatest appeal. The sad thing is that it is this old grass which is so rapidly disappearing from England. It remains on only about 3% of the area covered 200 years ago, mainly as small fragmented patches on slopes too steep to cultivate. It is being replaced by fertile arable fields and improved, productive but species-poor grass. The modern farmer obtains many times the yield of former days — in doing so he improves the soil in structure and fertility, but he totally and irreversibly destroys the area from the point of view of nature conservation.

I am less optimistic than Dr Smith about the future of the fauna and flora of the chalk. Some unimproved grass will no doubt remain in nature reserves but, with the rise in land prices, economic pressures will probably affect the rest. So I welcome this book as a memorial to those who have worked on the chalk, and a record of one of the glories which is so surely departing from the English countrvside. □

Kenneth Mellanby was director of Monks Wood Experimental Station, under the British Nature Conservancy, from 1961 to 1974.

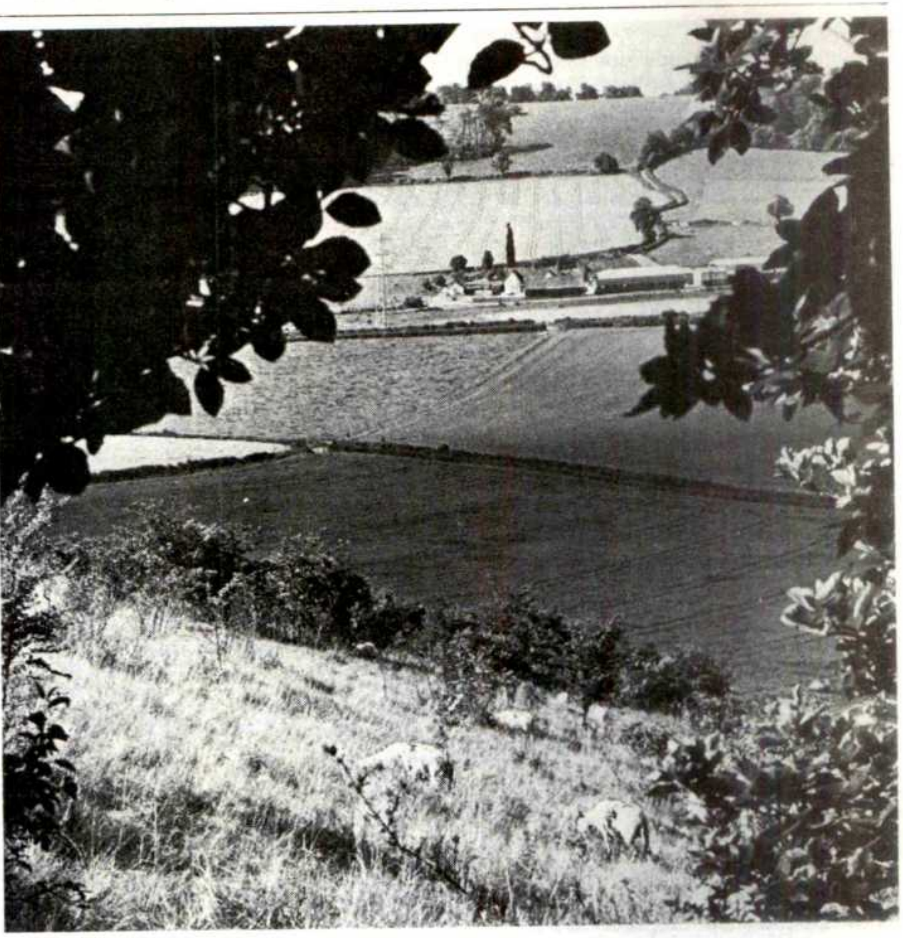

Buttlers Hangings, a Naturalists' Trust Reserve, near West Wycombe in Buckinghamshire. The land here is too steep to cultivate, and represents the last remnant of chalk grassland and scrub between the woodlands of the plateau and arable land of the valley.

A milestone for the geologists of New Zealand

A. Ewart

The Geology of New Zealand. Chief editor R.P. Suggate. (Government Printing Office: Wellington, 1978/79.) Two-volume set NZ$92.50 + postage.

In 1950 the late R. W. Willett, then Director of the New Zealand Geological Survey, instigated an ambitious 1:250,000 mapping programme of New Zealand. Completed in 1968, the programme provided both stimulus and unity to geological research in New Zealand.

Only now, 15 years after the huge task of putting the results into print was started, have the efforts of geologists and editors culminated in the appearance of these two imposing volumes. Based on the contributions of 38 specialist authors, professionally produced and lavishly illustrated, the books represent the compilation and synthesis of a vast amount of data.

The organization of the text emphasizes the three distinctive tectonic phases through which New Zealand has evolved: the Tuhua Orogeny (mid to late Palaeozoic), the Rangitata Orogeny (mid to late Mesozoic) and the Kaikoura Orogeny (Miocene to the present day). The opening chapter provides the framework for the main text with sections on aspects of basic geology, and the following nine systematically treat, in great detail, the geology of New Zealand and its outlying islands, starting with the oldest sequences.

Six of the contributions lay down a descriptive basis. Each is concerned with a specific event and follows through the geological development of the region from the late Precambrian–Devonian to the Quaternary. Thoughtful editorial work is evident in that the format is consistent throughout: in each case an introduction leads on to consideration of the palaeontology, stratigraphy and petrology. Most notable is the profusion of illustrative material — maps, tables, correlation charts, photographs and line drawings litter the text. Interspersed between the descriptive chapters are three devoted to interpretation and synthesis of data on the three main orogenic phases.

The treatise concludes with a consideration of palaeogeographical and palaeoenvironmental evolution, from the early Palaeozoic to Recent, as deduced primarily from the fossil record. This last chapter emphasizes the affinities and palaeogeographical links of the faunas and floras, and attempts to identify the gross climatic patterns and changes through the fossil record and their timing.

Shortcomings of the work are predictable, indeed inevitable, given the extended period of production and the number of authors involved. The contributions vary somewhat in style, objectivity and depth of treatment. In certain chapters overlap of topics is evident, and the material is not always internally consistent (for example the discussions of metamorphism in Chapters 4 and 5). Because the main text was prepared in the early 1970s the interpretations are made largely within the context of the New Zealand region alone, with only sporadic attempts at synthesis in terms of modern concepts of plate tectonics. This problem was recognized by the editors, however, and at the end of Vol. 2 they have provided a supplement to each chapter which consists of a brief review of developments up to about 1976, together with relevant references.

The Geology of New Zealand does not provide an easy introduction to the region and it will undoubtedly be used mainly for reference. However, publication of the volumes is certainly a milestone for geological research in New Zealand. They will provide a firm foundation for future research and should also be of great value to all geologists concerned with the south-west Pacific, indeed to all those whose special interest is Mesozoic and Cenozoic geology. The chapters dealing with the history of these relatively younger rock sequences indicate how much New Zealand has to offer in such studies.

In all, this is an oustanding work. It is a tribute not only to the editors and authors, but also to the strength and enthusiasm of the New Zealand Geological Survey. ☐

A. Ewart is Reader in Geology at the University of Queensland.

Chemistry of steroids and peptides

J. S. Morley

Steroids and Peptides: Selected Chemical Aspects for Biology, Biochemistry, and Medicine. By J.B. Dence. Pp. 418. (Wiley-Interscience: 1980.) £20.85, $47.50.

THE commendable general purpose of the author is to present the background of steroid and peptide chemistry to research workers in biology, biochemistry and medicine. Of the various classes of naturally occurring compounds, steroids and peptides are arbitrarily chosen for discussion (future volumes may deal with carbohydrates, lipids and nucleotides). They are discussed separately in introductory chapters, and in chapters on synthesis and chemical properties.

The opening articles will be the most useful in that they deal with matters (occurrence, structure, nomenclature, physical properties and physiologically active species) of general interest to workers in other disciplines. The introduction to steroids is particularly well written. Even a modest background in chemistry should suffice to understand the clear accounts of seemingly complex topics — conformation, configuration, sequence rules, IR and UV spectroscopy, Woodward–Fieser rules and chirality, for example. Peptides are treated less well, and one is left with the impression that the author's experience of the field is drawn mainly from reading; perhaps this explains the often strange choice of examples. Nevertheless, basic information is well presented, and there is a useful summary of nomenclature rules (blatantly violated in later parts of the book!)

The chapter on steroid synthesis contains useful summaries of biosynthesis and steroid conjugates, but that on peptide synthesis may mislead rather than inform. There is, for example, no mention of protecting groups for C-terminal carboxy, and commonly used techniques are inadequately covered because of over-emphasis on newer, as yet unproven methodology. It is unfortunate that coupling methods are illustrated by reference to an unsatisfactory synthesis of the L,D,L-isomer of thyroliberin; the methods involved, in contrast to those used in a later synthesis, lead to a partly racemic product. If a reader ever "should find himself in a situation where he must synthesise a peptide" he would be well advised to refer to one of the many specialist reviews of peptide synthesis rather than to this chapter.

The discussion of chemical properties cover oxidation, reduction, substitution reactions, derivatization and microbial transformations (steroids), and modifications at the N- and C-terminus and side-chain groups (peptides).

Returning to the aim of the book, the author has, I believe, wrongly assessed the needs of non-chemical research workers. If he had devoted more space to the topics discussed in the introductory chapters, and omitted or curtailed coverage of chemical synthesis, his book could have been more strongly recommended. ☐

J. S. Morley is Head of Peptide Research at the Pharmaceuticals Division of ICI Limited, Alderley Park, Cheshire.

ANNOUNCING
A NEW JOURNAL

ARTERIOSCLEROSIS: A Journal of Vascular Biology and Disease

Published by the American Heart Association

This journal has been designed to provide a forum for the publication of high quality research from a variety of disciplines bearing on the biology, prevention, and impact of vascular diseases relating to arteriosclerosis. We invite papers on:

Vascular biology
Pathology of vascular lesions
Platelets and thrombogenesis
Lipid and lipoprotein metabolism
Connective tissue biochemistry and metabolism
Population and genetic studies
Interplay of risk factors
Arteriosclerosis in the young
Animal models
Evaluation of intervention
Detection and quantification of arterial lesions

Contact the Editorial Office for Guidelines to Authors: 1107 N.E. 45th Street, Room 316, Seattle, WA 98105, Phone: (206) 545-1609. Editor: Edwin L. Bierman, M.D. Associate Editors: Paul Bornstein, M.D., Laurence Harker, M.D., Arno J. Motulsky, M.D., Russell Ross, Ph.D.

Circle No. 25 on Reader Enquiry Card.

Pennant would be proud

C. M. Yonge

British Crabs. By R.W. Ingle. Pp.222 (British Museum (Natural History)/Oxford University Press: 1980.) £16.

WHEN the decapod crustaceans learnt to tuck an increasingly reduced abdomen under a laterally expanding cephalothorax, the crabs had arrived. The well-enclosed gills permitted exploitation of intertidal and, in warmer lands, of terrestrial environments. The lateral scuttling movement proved ideal for seeking widely dispersed food and for insinuation within protective shelter.

Thomas Pennant separated these "crustaceous animals" from the insects where Linnaeus had placed them, and the fourth volume of his *British Zoology* (1777) contains figures of our commoner species. These include the male and female of the Long-clawed Crab, *Corystes cassivelaunus* (Pennant), here reproduced to form a highly suitable frontispiece to a book representing the culmination of later studies initiated by William Elford Leach in his *Malacostraca Podophthalmata Britanniae* (1815–1820; completed by C. B. Sowerby in 1875).

Although less numerous here than in the tropics, there are 67 British crabs. Their long-needed modern description has now been admirably supplied in this authoritative book by Dr R. W. Ingle of the British Museum (Natural History). Initial accounts of early work on geographical and bathymetric distribution, and descriptions of external anatomy illustrated with accomplished line drawings, precede full systematic and descriptive information about all species. This is followed by 34 plates carrying double that number of extremely clear photographs. An exhaustive reference list completes a volume which will be welcomed by all marine biologists. It is a credit alike to author and to publisher, and a notable addition to works on carcinology. ☐

Sir Maurice Yonge is an Honorary Fellow in Zoology at the University of Edinburgh.

nature

9 October 1980

From the Chemistry Library
SCIENCE COLLEGE
[illegible] Upper Circular Road
CALCUTTA

Will the DNA guidelines wither away?

On both sides of the Atlantic, the regulations for the control of recombinant DNA research are being substantially relaxed (see *Nature* 27 September and 2 October). At the present pace of about one major relaxation every two years, it will not be long before the regulations have virtually disappeared. Both in Britain and the United States, the regulatory authorities (the National Institutes of Health and the Genetic Manipulation Advisory Group) have decided that a substantial part of their work shall be in effect delegated to local safety committees, working within institutions (in the United States) or laboratories (in the United Kingdom). The categories of hypothetical hazard into which experiments of different kinds have been slotted in the past five years, have also been changed once again, with the result that a large proportion of the experiments still formally under the control of the regulatory bodies will now be exempt. Is it time that governments began to think of what should be done about recombinant DNA research say two years from now, when there is almost nothing left to regulate?

Some recrimination is unavoidable. Many impatient people, who have regarded the past period of regulation as an intolerable and unnecessary impediment to their work, will make fun of the way in which the guidelines were hardly complete before the process of dismantling them began. Some, alas, will take out their anger on hapless Professor Paul Berg, who is rightly or wrongly thought to have been the instigator of the movement to regulate recombinant DNA research — or to have provided governments with an excuse to do so. Then, no doubt, in other DNA laboratories, there will be some who will continue to complain that the genetic manipulators are being given an even wider licence to pervert the course of human evolution and so on. Both strands of complaint will be misjudged. Both camps should be grateful that the regulatory bodies have somehow kept the peace in the past five years.

The truth is that at the outset, five years ago, a great many serious people, many of them molecular biologists, were genuinely alarmed at the risks that recombinant DNA research might bring. The risks were always conjectural, but they could not be confidently equated with zero. But, in the past five years, solid evidence has accumulated that many of the conjectured risks are insubstantial. *Escherichia coli* K12 does not, after all, survive in the human gut, while the frequency of recombination of K12 with wild-type *E. coli* or other organisms has turned out to be too small to sustain the conjecture that altered genes might become permanent components of the gut flora. The recognition, since the guidelines were first drawn up, that introns are more the rule than the exception in eukaryotic genes has decreased the chance that a plasmid carrying a foreign piece of DNA will actually become a source of foreign and possibly damaging protein. Some of the more fanciful conjectures of the past — the possibility that engineered bacteria or viruses might disturb the immune system, for example — have not been much affected by discoveries in the past few years, but they were always conjectural conjectures, so to speak. In general, the discoveries in the past five years which bear on the safety of genetic manipulation support the argument that genetic manipulation is unlikely to create threats to people, other animals and plants that would not have arisen in the course of evolution. This does not imply that all risks can now be disregarded, but merely that most of the risks originally conjectured are less immediate than was thought.

The systems set up by most governments for regulating recombinant DNA research have served a useful purpose in the past five years. They have provided the general public with a sense that everything possible has been done to avoid or to diminish risk. Most of the committees responsible for administering the guidelines have functioned well. Some of them (the NIH committee, for example) have even functioned publicly. From the public point of view, they have also worked cautiously. Restrictions have been removed, and types of experiments recategorized, only after the wisdom of doing so had been fully substantiated. (The recategorization by NIH of certain animal virus experiments in the summer of 1978 may have been an exception.) One result may be that people have not been able to get ahead with research as quickly as they might. Another has been that there has never been a legitimate cause of complaint by the general public against the practice of genetic manipulation. Such warnings of impending catastrophe as there have been have cut very little ice.

The benefits of this climate of civility in the past five years far outweigh the inconvenience and the delay which some have suffered. The cost of the special laboratories which have been built to contain experiments no longer required to be carried out in such stringent circumstances is a small price to pay for the relative peace and quiet there has been. (The institutions saddled with them may take some comfort from knowing that if they become white elephants, they may also be taken as marks of their prestige in the late 1970s.) There is yet a chance that the case of recombinant DNA research may become a useful model of how new technologies might be introduced.

So what lessons can be learned from the experience of the past few years? And what does the future hold for recombinant DNA research?

The first thing to appreciate is that the time has not yet come to make a bonfire of the regulations. The main result of the most recent relaxation is, in effect, to license laboratories and their safety committees to carry out experiments in the lowest categories of supposed hazard. Categories, and prescribed containment, will remain for others, and it will be some time before further relaxation is possible. Looking ahead, some kinds of recombinant DNA experiments that people wish to carry out would in future (as now) fall within the scope of the guidelines which regulate experiments with dangerous pathogens even if the recombinant DNA guidelines were abolished. Problems of scaling-up from the laboratory to the manufacturing scale also remain, and the regulatory committees are rightly preoccupied with them. (One useful beginning would be to find a better distinction between the first and the second than the entirely arbitrary supposition that 10 litres of any culture constitutes "scaling-up".) Ultimately, however, procedures on an industrial scale will be regulated by the statutes which apply to occupational safety, so that that the withering away of the guidelines for recombinant DNA will not provide manufacturers with an entirely free hand.

Thus there is a prospect that the DNA guidelines may, at some time in the future, be subsumed in other and long-standing sets of guidelines. What about the experiments in the P2 and P3 categories (NIH terminology) that will continue to be regulated by DNA guidelines at least for the next few years. Even here, the regulatory authorities should move as quickly as they can towards some version of a licensing system — one in which laboratories (and their safety committees) take the first responsibility for deciding what degree of containment is appropriate for which experiment, and then provide the regulatory authorities with a

0028-0836/80/410473-02$01.00

report on what they have been doing at least once a year. Apart from the benefits that would follow for DNA researchers, questions of industrial secrecy would also by such a step be simplified enormously. In moving towards such a system, however, the committees should be much more concerned than in the past to coordinate their practice internationally. The unfortunate case of Dr Samuel Kennedy of the University of California (see *Nature* 18 September) may be a vivid illustration of the trouble caused when governments follow different standards. Nobody can know at this stage what part international competition played in the affair, but the German guidelines were at the time less stringent than the American — and Dr Kennedy's chief rivals in the study of the arbovirus genome are in West Germany. Is it not high time that the regulatory committees recognized that such ironies will persist as long as they decline (as they have almost studiously done) to talk to each other directly?

The question remains of how best to deal with problems like those occasioned by genetic manipulation which are certain to arise again. In retrospect, in countries as different as Britain and the United States, the committees set up to hold the ring between the public and the molecular biologists have served reasonably well. If anything, the molecular biologists have been more frustrated than the public, which is only right and proper. On balance, especially in the early days, it would have been helpful if the proceedings of the British group responsible for the guidelines had been carried on in public as, for most of its time, the corresponding American committee has been required to do by the Freedom of Information Act. Many incipient misunderstandings about the functioning of the Genetic Manipulation Advisory Group have been consequences of the secrecy imposed on it under the Official Secrets Act as well as by the conventions of Whitehall. People may rightly ask what kind of public assurance can stem from the proceedings of a secret committee. Even so, the committee has functioned better than many expected.

The most obvious deficiency of the past few years is that, faced with a problem of assessing the safety of a new and unexplored laboratory technique, the responsible committees (and the scientific community itself) did very little to provide the data on which objective assessments of safety might be based. It is true that people have fed each other quantities of *E. coli* from time to time, and there have been a few half-hearted attempts to see whether genes incorporated into bacteria can find their way into the somatics cells of laboratory animals. Few opportunities have been seized for looking into the ways in which bacteria carrying foreign genes might actually damage their adventitious hosts. The customary explanation, during most of the past five years, is that the people most competent to carry out such experiments have been too preoccupied with exploiting the new techniques whose safety was called in question. With a few conspicuous (and honourable) exceptions, those with the most vivid interest in demonstrating that their techniques are as safe as they now appear have been content with arm-waving. They, as well as the rest of us, are lucky that things have turned out as they have, and that the general perception of the risks of genetic manipulation has so quickly, and painlessly, moderated. It could have turned out quite differently.

McNamara's fond farewell to his bank

Who would think that the president of a large automobile manufacturer turned US Secretary of Defense at the height of the Vietnam War would turn out to be a superb president of the World Bank? The credentials, impressive enough, are on the face of things unfitting. Yet the governors of the bank plainly knew what they were doing when they appointed Mr Robert McNamara to his present post nearly fourteen years ago. During that period he has managed both to dramatize the cause of economic development in the poorest countries of the world and then to make the World Bank itself into a powerful instrument for prosecuting that cause. He has, in other words, justly earned the right to make the fierce complaints which marked his valedictory address to the members of the bank last week. And he is right, of course, to note that the cause of development has gone sour in the past few years, right to complain that many industrialized countries (Britain was singled out) are reducing their contributions to overseas aid, right to complain that the OPEC surplus states should carry a much greater burden and right to fear for those who carry the true burden of development:

> "We do not see their faces, we do not know their names, we cannot count their number. But they are there. And their lives have been touched by us, and ours by them."

In retrospect, Mr McNamara's most cheerful memories will no doubt be of the early 1970s, when he was stumping the world urging governments that they should not forget the "poorest of the poor" and at the same time persuading the members of his bank that their funds should be invested as often in social infrastructure as in mammoth capital projects. Even then, however, it was an uphill struggle. With a few rare exceptions (Sweden, for example), most industrialized countries never consistently came near the United Nations target for overseas aid of 0.7 per cent of GNP. Since the increase of the price of oil, performance has worsened — and the World Bank has become even more important as a source of multilateral aid. The explanation is, unfortunately, all too simple. Industrialized governments have become obsessed with domestic problems, many of them caused by the increased price of oil. But at a time when voters are being asked to pay more tax or to do without public services, governments are plainly unwilling to prosecute the cause of development. The Brandt Commission was upbraiding them for their neglect earlier in the year. Mr McNamara has now added his complaints.

The complaints are fair, but they will not be listened to with much care. One trouble is that governments are preoccupied with other things. A more serious difficulty, which both the Brandt Commission and Mr McNamara overlook, is that the cause of development has gone sour because relations between the industrialized states and the rest of the world have themselves gone sour. Although most oil consumers recognize by now that the crude oil prices of the 1950s and 1960s were unfair to the oil producers, they have not enjoyed the humiliations of the past few years, or the economic upheavals that have gone with them. And they will not forget them. In such circumstances however, it is natural enough, if wrong, that the Western oil consumers should be saying that if any group of states should take responsibility for helping with economic development of the poor countries, the OPEC states are the obvious candidates. So (as Mr McNamara says) they are. Unfortunately the OPEC states are even more preoccupied with their own problems than are the industrialized states of the West. Since there is no prospect that the members of the Warsaw Pact and its adherents will produce the kind of help that the developing countries need, it is no wonder that Mr McNamara's speech was so gloomy.

So is all hope lost? Not quite. Or perhaps not yet. There are a few clouds with silver linings. The OPEC states have somehow to manage their surpluses, usually by asking other people to do that on their behalf. There may be some pickings for development there. Better, even the past two sad decades have shown that some developing countries can actually develop, and make good. The example of India is not a joke. Better still, it appears now to have been understood in the West (but also in the developing world) that development assistance is not the provision of capital funds but help with the process of development, "infrastructure" as the saying goes. Sometimes this means teaching businessmen how to do accounts, politicians how to be ministers and children how to read. Building roads is by these standards capital-intensive. If only Mr McNamara had had another fourteen years, he might have been able to demonstrate what many suspect — that the most imaginative development is cheap.

0028-0836/80/410474-01$01.00

Melanoma increase in radiation labs?

Livermore data may be significant

Washington

US Department of Energy officials remain baffled about the cause of an abnormally high incidence of malignant melanoma among employees of the University of California's Lawrence Livermore Laboratory, one of the nation's centres for nuclear weapons research.

An advisory board report released in Washington last week confirmed findings suspected since 1976, and substantiated earlier this year by California's Department of Health Services, that the incidence of skin cancer among laboratory employees was three to four times the national average.

The California study showed that between 1972 and 1977, 19 white workers at the laboratory had developed malignant melanoma, compared with between 4.6 and 6.4 cases expected using national statistics, a result which it said was "very unlikely to have occurred by chance".

At the request of the Department of Energy, the data were reviewed by an advisory board chaired by Dr Arthur Upton, then director of the National Cancer Institute. The board found no flaws in the Californian study and revealed that the increased incidence seems to have continued, with eight more cases of melanoma being reported up to June 1980.

However, the advisory board reports that preliminary efforts to explain the excess have not succeeded in implicating any specific cause. It says that the occupational safety, industrial hygiene and medical programmes of the laboratory appear to be well conceived and well conducted, and that additional protective health measures "appear to be unwarranted".

It also lists a range of possible environmental causes, from occupational exposure to chemicals to details of individual lifestyles, which it says should be studied in more detail to get to the root of the problem.

"Part of the difficulty is that there may be no problem at all. We still don't really know if this thing is real; it may be just a statistical fluke" stated one member of the board last week, pointing out that the continued high incidence could be the result of people looking for — and finding — melanomas many years earlier than they would otherwise be detected.

Although a relatively rare form of cancer, the incidence of malignant melanoma has been increasing faster than almost any other cancer in recent years. In San Francisco, for example, the number of cases rose from 5.8 to 11.2 per 100,000 between 1970 and 1975, and similar figures have been reported for other parts of the country.

One fashionable explanation is that, because the greatest increase has been found among fair-skinned professionals, whose work tends to keep them indoors, it may be caused by intermittent exposure to ultraviolet radiation, for example as a result of excessive sunbathing or other outdoor activity.

Preliminary examination of the occupational histories of those contracting skin cancer has failed to reveal any obvious common pattern of exposure to particular chemicals or forms of radiation, and the board's report points out that although malignant melanomas have been found in an irradiated person, epidemiological studies have failed to produce convincing evidence that tumours may be induced in the skin by ionizing radiation.

However, the possibility that occupational exposure to, for example, internal emitters and ultraviolet radiation may contribute to the aetiology of melanoma is one of several avenues that the laboratory intends to explore further. "It is just possible, because of changes in lifestyle such as improved nutrition, that we have managed to increase our risk of cutaneous melanoma to the point where, although radiation was not a cause in the past, it might have become one today", says Professor John A.H. Lee of the Department of Epidemiology at the University of Washington in Seattle.

In a memorandum submitting the board's report to Energy Secretary Charles Duncan, the Department of Energy's Assistant Secretary for the Environment, Dr Ruth Clusen, suggests that further studies by both the laboratory and the state Department of Health Services should be supported.

The latter has already proposed a major follow-up programme, which is being reviewed by the department that will take a detailed look at the particular social characteristics of the Lawrence Livermore workforce. A parallel study may also be carried out at another Department of Energy site.

The Lawrence Livermore Laboratory is operated by the University of California under contract from the Department of Energy. Its involvement in weapons research — and the resulting need to keep much of the research programme secret — has been the source of sharp controversy over whether its links with the university should be maintained.

Last year the university's board of regents rejected a call from California Governor Jerry Brown that all weapons-related research be moved to the Los Alamos Laboratory, and last month the regents agreed to start negotiations with the Department of Energy for a new management contract for the laboratory. The current contract expires in 1982.

David Dickson

EEC worries about veal and hormones

The massive veal market in Europe, consuming eight million calves a year, was on the verge of collapse this week following scares in France and Italy over the levels of an artificial growth hormone — diethylstilboestrol — in the meat. Diethylstilboestrol (DES) is a synthetic oestrogen which caused vaginal cancers in the daughters of mothers who were prescribed it (in large doses) as a protection against spontaneous abortion in the 1940s and 1950s. Its use is banned in the United States and in most countries of Europe, but a black market has sprung up because this chemical can add 5–15 kg to the weight of a calf and thus double a farmer's profits.

In Italy, the trouble began on 4 September, when the Ministry of Health placed a temporary ban on twenty-two brands of baby foods containing veal. A fairly crude bioassay had shown samples to contain an active oestrogen, probably DES. On 22 September a local magistrate in Latina, south of Rome, used the wide powers of Italian magistrates to impose a nationwide ban on the sale of veal. The Rome laboratory of the Istituto Superiore di Sanita, the technical arm of the Ministry of Health, is now making mass spectroscopic measurements of the hormones isolated from the baby foods to check for DES. In the view of a British scientist, the levels are probably "quite high" or they would be undetectable by the original method.

In France, pressure began independently from the left-wing trades union group, Paysans Travailleurs, whose members had accumulated evidence that French veal producers were using the synthetic hormone. Paysans Travailleurs then recruited help from the consumer group, the Union Fédérale des Consommateurs, which called for a boycott of veal in the September issue of its magazine, *Que Choisir*. Subsequently, in a rare enforcement of French law on the matter, a 29-year-old pharmacist and veal producer was jailed.

Pressure from farmers and other interests has forced the Italian magistrate to relax his ban somewhat, but sales of veal have still fallen by 50–60 per cent in both France and Italy, and the export of calves

0028-0836/80/410475-02$01.00

from Britain — where hormone use is controlled under the 1968 Medicines Act but not banned — has fallen to a trickle in a business normally worth £500,000 a week.

Last Tuesday agriculture ministers of the European Community tried to take a grip in the affair by promising that Commission officials would devise a scheme — within a couple of months — for uniform testing of hormone levels in meat throughout the EEC. Despite great pressure from Italy, however, the ministers drew back from imposing a total ban, but will not easily agree on the directive they have asked for.

EEC hormone law

Belgium, Denmark, France, Italy and the Netherlands already have a total ban on the use of natural or artificial hormones, but avoidance is thought to be commonplace. Belgium, France and West Germany take the view that a partial relaxation of the ban in favour of natural hormones — oestradiol and testosterone — would stop the abuse of the synthetic hormone which can be injected directly into the muscle as an oily, crystalline suspension, and is not easily detected by visual inspection of the meat after the animal is slaughtered; other hormone preparations, however, are administered as pellets implanted prominently in the ear. The ear is discarded at the slaughterhouse, but injected muscle will find its way straight to the table — or the baby food.

West German legislation, at present, distinguishes a list of hormones which may be administered — the positive list — and a list which may not — the negative list. On the latter are those which have an oral oestrogenic activity of more than one-fifth that of DES, so banning DES, the related hexoestrol, and two other artificial oestrogens. On the positive list at less than one-fifth the activity are the natural oestradiol and the artificial agent zeranol.

In Britain, the Medicines Act allows licensing of hormone preparations by the Veterinary Products Committee, under the Ministries of Agriculture and Health. Under these licences zeranol and hexoestrol are on free sale to farmers; and Hoecht's Finaplix (an androgen used in beef production) and Implixa (used for veal) administered by vets. The drugs may not be administered within at least 60 days of slaughter (although the drugs firms are pressing to reduce this period). The Pharmaceutical Society has the statutory authority to police the proper use of the drugs.

DES is no longer used in veal or beef production in Britain, although it is used occasionally in pig farming. One veal producer for the small — 70,000 head a year — British home market, Philip Paxman of Volac Ltd, said last week that he had stopped using hormones at all because of public pressure; and they are rarely used in the 300,000 head export market, he believes, because calves are shipped at 4–6 weeks old for fattening on the continent.

UK specialists in the use of sex hormones in farming argue that any proposed European legislation should distinguish between artificial agents and natural steroids (like oestradiol and testosterone); and that the use of natural steroids should be limited to tissue levels of around 1 in 10^9 — similar to those found in untreated farm animals. For the synthetic anabolic agents, and their frequently unknown residues, they should be shown to be non-toxic and non-carcinogenic before licensing.

European consumers unions, however, represented in Brussels by the Bureau Européen des Unions Consommateurs (BEUC) are pressing hard for all hormone use for meat production to be banned. It is too difficult for a policing authority to distinguish natural from unnatural hormones, says BEUC, so both should go. If agreed, this would have a big impact on beef production in the UK, which in the past few years has come to depend on hormone supplements for its profits, and would cause pressure to increase the use of antibiotics which have a similar effect on weight gain.

And perhaps Italy should worry more about olive oil than veal. According to one pharmaceutical company spokesman, vegetable oestrogens — of one-hundredth or so the bioeffectiveness of oestradiol, are present in olive oil at such a high level that the consumption of 50–100 g of olive oil a day would reverse an ageing woman's post-menopausal changes. But then if Italy can ban veal, it can probably ban olive oil too.

Robert Walgate

Polish farming

More meat to eat?

Agriculture is an extremely sensitive issue in Poland. After all, it was the announcement of increases in the price of meat products on 1 July that led to the recent wave of industrial unrest. Speaking last week at the Olsztyn Agricultural–Technical Academy, the Polish President, Henryk Jablomski, explained that what Polish agriculture needs is a robust, up to date and consistent farm policy, which will take into account the needs of development, technical equipment and the "fullest possible utilization" of scientific achievements. In particular, there is a pressing need for people of "considerable professional qualifications and social dedication" to implement research and guide agricultural development.

Under clause 6 of the Gdansk accords, the Polish government undertook to create "lasting prospects for developing peasant family farms which are the foundation of Polish agriculture". The greater openness of information stipulated by clause 3 of the same accords means that for the first time official figures comparing the performance of state and private agriculture are being made available to the general public. Some 75 per cent of Polish agricultural land is still in private hands — some 3 million family farms of which barely 400,000 exceed 10 hectares. A minimum of 15 –20 hectares is considered necessary for really efficient farming in Polish conditions, hence the large state farms would be expected to have the most advantages particularly because the state sector receives 64 per cent of all investment in agriculture. Yet, according to the official figures for 1979 (quoted by Leszek Chmielowski in *Zycie Warszawy*, 23 September), the state sector uses 2.5 times more chemical fertilizers and 2.6 times more concentrated feedstuffs to give the same amount of produce.

Chmielowski suggested that subsidies to state farms should be reduced, administrative costs minimized and unrealistic plans phased out. The land fund (largely made up of former private farms handed over to the state in return for a pension by elderly farmers without an heir eligible to succeed them) should not, said Chmielowski, simply be used to increase the area of (often unproductive) state farms, but should be made available to all private farmers who wish to expand.

Nevertheless, the members of the new "self-governing" farmers' union feel that Chmielowski's proposals do not go far enough. He stressed, for example, that the state sector, properly organized, still has "an important and growing role to play". But as Wieslaw Kecik, a young intellectual temporarily coopted as an "assistant" to the new union, explained, the greatest deterrent to the ambitious private farmer is his lack of security of tenure. Official policy, since the early 1970s, has aimed at "collectivisation without loss of production". If the state sector is to grow, the private farmers feel, it can only do so at their expense.

Moreover, said Mr Kecik, there are considerable price differentials in favour of the new sector. The private farmer must pay more for all essentials, and receives lower prices for his produce, except for a few "commercial" crops such as rape-seed and flax. Abolition of such inequalities, and the guarantee of land tenure, "must be", said Mr Kecik, "basic postulates of the new self-governing farmers' union".

The day after Chmielowski's article appeared, the Prime Minister, Josef Pinkowski, addressed a meeting of farmers and agricultural workers in terms of apparent reassurance. After calling on all those engaged in agriculture and its ancillaries, including research, to increase their efforts, Pinkowski indicated that the government would raise funds to create favourable conditions for "the whole of agriculture — all productive private farms". "We should like every farmer to feel that his work is secure", he added. "We want him to know that his intentions and production plans, his desire to

0028-0836/80/410476-02$01.00

modernize his farm and to increase its productivity, will meet with continuous support from the State."

Last Saturday, at the meeting of the Party Central Committee, First Secretary Stanislaw Kania was even more forthcoming. "Individual peasants carry the Society", he said. "We shall ensure that every peasant is certain of his ownership and his farming tenure."

The next few months should show how far practical policy implements these assurances. **Vera Rich**

Kopek interferon

Last week, the Soviet news agency TASS announced that interferon can be purchased in any Soviet drug store for 56 kopeks per ampoule. The Soviet Union, said TASS, was the first country to produce interferon commercially, and for more than a decade Soviet doctors have been using interferon to prevent influenza and other virus diseases of the respiratory tract. Soviet doctors, said TASS, also use interferon against leukaemia and viral skin diseases. A patent for interferon production has been purchased from the Soviet Union by Japan.

What the TASS announcement does not make clear, however, is the extremely low dosage in the 56 kopek ampoule. Samples analysed in Western laboratories contained dosages of the order of 1,000 units or less. The market price of Finnish interferon is US $25.00 per million units. At 64.4 kopeks to the dollar, Soviet interferon is therefore by no means competitive.

A careful reading of the TASS interview with Dr Valentin D. Solov'ev, moreover, reveals that studies on leukaemia, skin diseases, and also the veterinary use of bovine and porcine interferon, are still at the experimental stage. It is only the interferon nose-drops, which Dr Solov'ev himself pioneered in 1968, that are in regular use. However, Western experts find it difficult to understand the discrepancy between their results and those of Dr Solov'ev. In the West, interferon has been used successfully to prevent respiratory virus infections, but only at high doses and in patients with little or no natural resistance.

As far as mass prophylaxis is concerned, as the *British Medical Journal* observed recently, since interferon, like any intranasal liquid, has only a short half-life in the nasal cavity, but needs long-term contact with the nasal epithelial cells in order to make them more resistant to virus infection, "it is therefore difficult to understand how . . . nose drops containing a low titre of human leukocyte interferon could cause the degree of protection under epidemic conditions reported by Dr Solov'ev". **Vera Rich**

Gulf pollution

UN's other worry

War is the greatest immediate threat to the Middle East — but the destruction of its fragile water supply, the Gulf itself, must be next. At the end of this month local marine scientists meet in Kuwait, next door to the Iraq/Iran conflict, to pledge research spending of up to $5 million over two years to find out exactly what is happening to the waters of the Gulf.

The long-term development of the region, the Gulf States have recently recognized, depends on proper environmental management of the Gulf and its coastal regions; yet little is known of its ecology, oceanography or meteorology. The water of the Gulf is needed for agriculture, coastal industries, and for drinking, yet the highest density of tankers in any ocean discharges its ballast into it, and many industries such as desalination plants with their associated chloralkali works (using mercury catalysts), aluminium smelters (emitting hydrogen fluoride), fertilizer plants (emitting ammonia), and refineries (sulphur dioxide and hydrocarbons) belch out completely uncontrolled emissions. Already seafood is frequently tainted with oil, and city environments have deteriorated markedly in the past two or three years.

Kuwait Harbour, twentieth century skyline

There are also at least 20 major industrial development regions around the Gulf coast, enjoying the world's greatest rate of development, and populations are flooding to these areas from the interior. Often the legal or institutional mechanisms do not exist to control pollution. And all this is threatening a sea on average only 35 metres deep, which evaporates more water than it receives from river run-off. (The Indian Ocean contributes the balance, through the Straits of Hormuz.)

Sewage is coming under control more rapidly than other pollutants, because of the existence of international contracting companies which are selling systems to Gulf States. Sewerage networks and treatment plants will serve the whole of Kuwait by 1982, Qatar by 1985. But Bahrain's system is not planned to be complete until 2008, and Saudi Arabia's treatment plant on the Gulf is overloaded.

Hence the effort, catalysed by the Regional Seas Programme of the United Nations Environment Programme (UNEP) to undertake research into the sources and impact of pollutants. At present there are relatively few institutes in the region capable of doing the research, but the picture — UNEP estimates — will be "drastically changed" within a year. UNEP, with its experience in the Mediterranean pollution programme, will help with training, but the Gulf States will jealously guard their technical independence: they have no wish for "expert" teams descending from outside.

At Kuwait, seven research projects will be discussed. The most likely to be funded concerns oil: what are the principal sources of oil pollution in the Gulf, how is the oil distributed, and what are its effects on human health and the marine and coastal ecosystems? But to understand this question, the basic physical and chemical oceanography of the Gulf must be studied, and the biological balance of the sea understood.

Meteorology is also important. The "Shamal" winds blow dust which sediments much of the surface oil; Kuwait suffers frequent calms and temperature inversions which trap airborne emmission. Coastal mining is affecting wave erosion and sedimentation patterns, which could in turn affect access by the supertankers; Gulf currents at all depths must be measured. What is the residence time of water in the various regions of the Gulf? This question affects the concentrations that pollutants might be expected to reach.

Other studies would measure the levels of heavy metals in economically important marine organisms; and investigate the distribution and sensitivities of plankton, the lowest level of the food chain.

Robert Walgate

Nuclear equipment

Secrets lifted

Washington

US physicists concerned that their work may become subject to national security restrictions because of its potential military value to foreign powers will soon have a public list to turn to for guidance. The list should also be an invaluable guide to foreign governments wishing to find out what the United States considers sensitive in nuclear technology.

The main purpose of the list will be to provide officials in the Department of Commerce with guidance on what controls should be applied to technology exports in sensitive areas such as nuclear energy. The full list is being drawn up by the Department of Defense, as required by the Export Administration Act of 1979. Last week, as part of this exercise, the Department of Energy (DoE) published in draft form a table of what it calls "energy-related militarily critical technologies".

Details are given of the major components of all technologies related to the exploitation of nuclear energy, from nuclear fuel processing and fusion reactors to security techniques. For each "critical" technology, the department identifies "keynote hardware" necessary for its successful implementation. It describes not only the military and the civilian uses of the technology but also the foreign countries in which there is evidence that the technology is currently available.

The proposed classifications are only preliminary, and are open to public comment so that a more refined list can be produced. The department hopes that the list will be valuable in calling attention to areas of concern, but publication of the list may also prove to be controversial. Some countries, particularly in Europe, have previously argued strongly that as much information as possible about the components of nuclear technology — particularly those relevant to its military applications — should remain secret. They claim that publication could provide a shopping list for non-nuclear countries interested in obtaining nuclear weapons, making the job of limiting proliferation more difficult.

Department officials said last week that all the information in the list had been taken from the open literature. They claim that, although they have indicated where a country has the capability to develop a technology, this does not imply that it has done so, since much of the information was inferred from data reported in the scientific and technical literature.

The table accompanies a broader but less detailed list of militarily-sensitive technologies published in the Federal Register on 1 October by the Department of Defense. Its publication stems from recommendations made four years ago by the Defense Science Board that, if the United States wanted to restrict the export of technologies which might later be used against it, this might be achieved most effectively by shifting the focus of control from end products to the set of "critical technologies" on which the development of these products depended.

To those who might complain that the list is giving away information that could be useful to a potential nuclear power, the department points out that it has not listed many "black arts" or tricks of the trade which cannot be listed as keynote hardware, but may be just as essential to the proper operation or equipment.

The table was compiled in the framework of legislation aimed initially at increasing trade with the Soviet Union and other Eastern European nations: a revised approach was recommended as a way of doing this without sacrificing national security, by placing controls on know-how rather than directly on hardware.

Since then, however, federal policy has been pushed in two other directions. One has resulted from the decision to restrict high technology exports to the USSR following the Soviet occupation of Afghanistan. The other has been fall-out from the *Progressive* case, where a court agreed that once information has been made publicly available it can no longer be considered classified for legal purposes.

The result has been a schizophrenic desire to tighten restrictions in one direction and loosen them in another. The resulting ambiguity caused an overzealous State Department official earlier this year to prevent a postgraduate scientist studying in the United States from travelling to San Diego for a conference on fusion technology. **David Dickson**

Table Critical elements in nuclear fuel cycle technology — DoE

	Critical technology	Military use	Civilian use	Foreign availability
A.	Uranium enrichment	Nuclear weapons	Power reactors, research reactors	—
(i)	Gaseous diffusion	—	—	UK, France, USSR, FRG, Netherlands, China, Sweden, Switzerland
(ii)	Gas centrifuge	—	—	USSR, UK, Netherlands, FRG, Japan, France, Pakistan, Australia, Italy, Switzerland, Sweden, Brazil
(iii)	Laser isotope separation	Separation of fissile isotopes	Purifying materials	Canada, France, FRG, Japan, South Africa, UK, USSR
B.	Reprocessing technology	Nuclear material production	Power reactor fuel cycles	Belgium, France, FRG, India, Italy, Japan, Taiwan, UK, USSR
C.	Heavy water production	—	Power reactors	Canada, France, USSR?, Norway?, India, Argentina
D.	Fuel fabrication	Nuclear propulsion, nuclear materials production	Power reactor fuel	France, USSR, Canada, FRG
E.	UF_6 production	Feed for enrichment plant	Feed for enrichment plant	USSR, France, FRG, Belgium, UK, Japan, China, South Africa, Italy, Canada

European rockets

Range reprieved

The European Space Agency's rocket launching ranges have been reprieved, at least for a further five years. But they will now have to operate on a reduced scale. This was the chief outcome of the meeting last week of the agency's Scientific Programme Committee, at which the representatives of France, West Germany, Norway and Sweden undertook to provide 80 per cent of the cost of operating the two rocket ranges in Sweden and Norway.

The meeting was marked by a further attempt by the United Kingdom to reduce its commitment to the two ranges, at Kiruna (Sweden) and Andoya (Norway), at present estimated to be £1.8 million a year. Although originally a principal partner (with West Germany) to the tune of 40 per cent of the cost, Britain has been reducing its contributions since 1977, largely on the grounds that its need has been reduced since the ending of the Skylark programme.

Last week, the British representatives appear to have startled their partners by suggesting that, from the end of 1980, the British contribution to the total budget of the ranges should be reduced from 20 per cent to roughly three per cent, with a time limit of only three years.

The proposal was not formally accepted at last week's meeting, but will now be put to the Council of the Space Agency for a final determination. Switzerland and the Netherlands also offered last week to continue their contributions at about two per cent of the total, but declined to sign the protocol that would have ensured full operation of the two ranges.

The Science Research Council (SRC)'s position appears to be that its need in the past three or four years has been to launch about six or seven Petrel rockets each year, and that rocket launching facilities in Canada and Alaska can be used on a one-off basis more cheaply than the average cost of the European subscription. Contributing members of the European organization, known as ESRANGE, are required to pay a fee for each rocket launched in addition to their subscription, and neither of these costs includes that of the rocket or of the equipment which it carries. **Judy Redfearn**

0028-0836/80/410478-01$01.00

British PWR

One year back

The announcement last week by Britain's Central Electricity Generating Board (CEGB) that it will be applying for permission to build its first pressurized water reactor (PWR) at Sizewell in Suffolk was not unexpected. That it may also choose to build another reactor, possibly another PWR, on the same site two to four years later, was more of a surprise. The CEGB says, however, that two 1,200-MW reactors on the site would be roughly in line with permission granted in 1974 to build one 2,000-MW advanced gas-cooled reactor alongside the existing 420-MW Magnox station.

The CEGB will be putting in a formal planning application for the first plant, Sizewell B, early next year. That will include a basic reference design drawn up by the National Nuclear Corporation. By the end of next year, the main stage of the design will be put to the Nuclear Installations Inspectorate for fault analysis, well before the public inquiry expected to take place in the summer of 1982.

The form of the inquiry is not yet settled. Past experience, especially that of the Windscale inquiry in 1978, suggests that, if the board is given the go-ahead, it will be mid-1983 at the earliest before construction can begin, putting back the British government's plans for the next generations of nuclear power stations by one year.

The basic design of the British PWR is that of the Westinghouse Corporation, but its adaptation to local conditions, and especially to British safety standards, is a considerable task. According to the industry, the British standards are among the most stringent anywhere, chiefly because of the multiplicity of stand-by systems required. Designing the buildings to house the Westinghouse system for the soft sands of Sizewell will also add time.

About a dozen of the 200 or so engineers now working on the design have come from Westinghouse and the US Bechtel Corporation, an arrangement that has prompted some opposition from those outside the industry who feel that Britain has the expertise to go it alone. The Bechtel Corporation, which has helped to design PWRs throughout the world, has claimed that the cost of building a PWR in the United States is about $850 per kW compared with the estimate of £1,000 per kW in Britain. Apart from differences in the accounting basis of these calculations, much of this difference is said to stem from the present strength of sterling, additional safety requirements, construction problems specific to the Sizewell site and the low productivity of the British construction industry. In any case, according to the generating board, the figures now being talked of are estimates, not contract prices. **Judy Redfearn**

Mining Polish sulphur

Trying harder

Sulphur production in Poland's Tarnobrzeg basin is to be doubled as part of the country's economic recovery plan. The present output of the area is 5 million tonnes per year, one-third of world production, of which 80 per cent is exported, so that this increase could play a major part in paying off Poland's soaring international debts.

Sulphur production is both one of the oldest and one of the newest industries in Poland. In 1415, King Wladyslaw Jagiello granted the miners of Krakow the right to prospect for "sulphurous minerals" in the vicinity. Four hundred years later, in his classic treatise "*On the Resources of the Carpathians and Other Polish Mountains and Plains*" (Warsaw, 1815), the Polish mineralogist Stanislaw Staszic remarked that "Poland stands on sulphur". By the end of the nineteenth century, however, existing mines had been worked out, and in 1921, the last of the old mines, at Posadza, closed down.

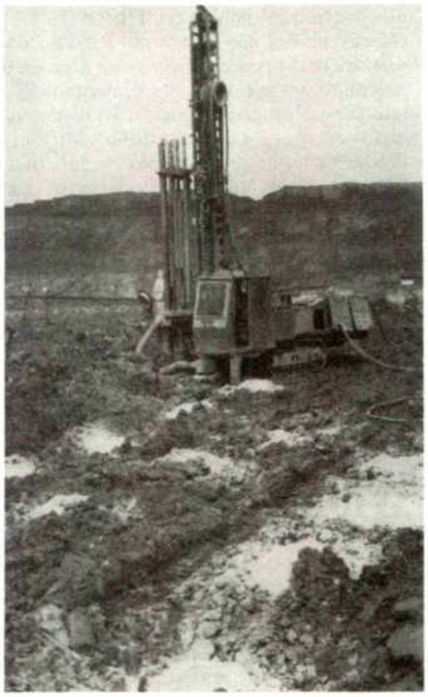

Between the Wars, several geologists suggested that sulphur beds might be located in the Miocene sediments of the Sub-Carpathian foreland, but it was not until 1953 that substantial deposits were located at Tarnobrzeg. Open-cast mining began the following year. Towards the end of the 1960s the Gryzbow and Jeziorko mines were opened; these use a borehole method of underground melting, and some 80 per cent of Polish sulphur is produced by this technique.

The Polish sulphur industry is now backed by a considerable research and development structure. Environmental problems of the industry and the regeneration of worked-out pits were elaborated in the early 1970s by a special team at the Krakow Academy of Mining and Metallurgy, and as the officials of the Tarnobrzeg mine point out, land reclamation begins as soon as a particular sector of the pit is exhausted. Plans are in hand to use closed-cycle water in all borehole mines.

Although Poland is the world's largest sulphur producer, there are, however, occasionally odd shortages on the home market. Earlier this year, Gdansk radio noted that the local epidemiological station, which is responsible for environmental monitoring, had been unable to obtain necessary supplies of sulphuric acid. In 1979, it received only 8 litres, instead of the 200 ordered.

The increased production from Tarnobrzeg, which should remedy such defects as well as boosting exports, should not, in the short term, make serious inroads into Poland's sulphur reserves. According to one expert at Tarnobrzeg, at the current rate of production, Polish mines already in operation hold enough reserves for at least another 75 years, and a similar amount of sulphur is estimated to lie in other natural deposits not yet even broached.

In the Soviet Union the outlook for sulphur production seems less optimistic. Although the Soviet Union has some indigenous sulphur, the deposits are deep and difficult to exploit, and some 10–12 per cent of Poland's sulphur exports go to the Soviet Union. A joint Soviet–US survey also indicates that there will be a world shortage in sulphur by the year 2020, because of soaring demands from the Third World. The promotion of research into cost-effective method of recycling sulphur would help the situation — at present, reclaimed sulphur costs four times mined sulphur.

For the moment, however, the main problem faced by the Polish sulphur industry is how to extract the sulphur fast enough. At the Tarnobrzeg open-cast pit, for example, the stockpile between the mine and the processing plant is virtually zero, and a breakdown in the conveyor belt lasting more than a few hours could bring the processing plant to a halt. The transport/export process is also operating full-tilt. Sulphur is exported either by rail or through the liquid-sulphur terminal at Gdansk (the home port of Poland's three liquid-sulphur tankers). So when, early in September as a kind of postscript to the recent industrial unrest in Poland, the Tarnobrzeg sulphur-workers finally went out on strike — seeking pay and social security parity with miners rather than factory workers — the authorities were quick to ask for the election of a strike committee to keep the disruption as brief as possible. **Vera Rich**

0028-0836/80/410479-01$01.00

CORRESPONDENCE

Hurricane damage

SIR — Not only did hurricane Allen select many small island countries, it did so while affecting their capitals the least. Of the nine island countries directly affected by the hurricane before it struck the Central and North American mainland, seven were most seriously affected in areas which did not include the capital city; Barbados, St Vincent, St Lucia, Dominican Republic, Cuba, Jamaica and the Cayman Islands. In nearly all cases, statements of the hurricane's effects issued from the capitals were qualified by references to isolated areas or "the interior" from which reports had not yet been received, but with the expectation that when they were, figures of dead and damage would rise significantly.

When serious hurricanes occur in provincial and rural areas which are normally remote and inaccessible, the degree of local self-reliance and local self-government may determine the capacity for recovery. Dependence on central national government, usually the case, will only function effectively through country-wide communications systems. It is systems of communication, however, which often suffer most significant hurricane damage, quickly isolating provincial and rural areas from the capital, and from each other. Trees fall, blocking roads and causing telephone and electric power cables to be severed, cable poles and radio antennas to collapse and power supplies to fail. Telephone, radio and telex systems become inoperable, and airports close. Roads are destroyed by sea erosion and landslide, and travel by boat is impossible or extremely dangerous until gales have subsided.

The development of international and regional precautions is principally based on improved international communications systems, but effective precautions have to be implemented and undertaken within and by each country. Effective readiness will depend on political will, personal commitment, local understanding and infrastructural resources. Certainly, improvements to inter-island and international communications are needed, but until more efficient national assessments of disaster impact, and consequential needs, are developed through improved national communication of all kinds, there will be little effective use, in disaster, of the improvements to international communications that are being scheduled. More importantly, the present incoming warnings of hurricanes, whilst receivable by governments in the capitals, may not be available to local communities. Ultimately, effective communication facilitates further decision, action or undertaking, which will be the quicker only if administrative and infrastructural resources are upgraded to enable appropriate responses.

Field research from the University of Bath, supported by the Leverhulme Trust, undertaken in two countries (one of them in the Caribbean) has shown the smallest countries to suffer the greatest national scale, as distinct from magnitude, of disaster damage, and hurricane Allen has seemingly selected many Caribbean small countries for reiteration. Provincial districts are more vulnerable to hurricane damage in terms of damage distribution, than the urban centres. Hurricane Allen has not only selected many of the smallest and poorest countries of the Caribbean, on which to inflict itself, but also the most rural and poorest of those countries. In their experience of hurricane Allen these areas have made manifest a double vulnerabilit which identifies a need for improved preparedness against such eventualities and greater self-reliance before many more hurricanes have passed.

JAMES LEWIS

Project for Natural Disaster Vulnerability Analysis, Centre for Development Studies,
University of Bath,
Bath, UK

AChE uses

SIR — We would like to comment on an advertisement from the US Army in the September 11th edition of *Nature* (p.xxxiii) calling for scientists in the genetic engineering field to submit proposals to "clone" the gene for the human enzyme acetylcholinesterase. Isolating the gene for the enzyme and cloning it in bacteria using genetic engineering techniques will allow large quantities of pure acetylcholinesterase to be prepared for the first time. The US Army may have a number of uses for the enzyme in mind: as an antidote to nerve gases for soldiers in battle, as a test for other antidotes and as a test for the effectiveness of new nerve gas weapons. Many workers in the genetic engineering area see the potential for developing this biotechnology into the basis for an ecologically sound and highly energy efficient industry of the future producing useful products. We deplore the signs that the military/industrial powers are moving into the field to distort the technology into the manufacture of commodities of war.

R.G. ELLES, T.R. SKERN, M.E.E. HILL,
J.E. ARRAND, D.A. WESTAWAY,
C.G.P. MATHEW, A.J. KEELAN,
S.M. DARLING, C. COUTELLE,
J.M. CRAMPTON, J.T. ROGERS,
I.J. JACKSON & R. WILLIAMSON

Biochemistry Department,
St Mary's Hospital Medical School,
London, UK

Willberforce no ape

SIR—Wrangham's publication (*Nature* 18 September)[1] of the hitherto unknown verses of Wilberforce is interesting and valuable. Unfortunately he repeats the story that Wilberforce played into Huxley's hands, and Huxley scored a great victory. Neither of the two journalists present thought he had. Nor did Joseph Hooker, writing to Darwin the following evening; he thought that Huxley had done well but that it was he, Hooker, who had made the case for darwinism[2]. Lyell thought so too[3].

Wilberforce was not an obscurantist. In his review of the *Origins of Species* he was at pains to emphasize that Darwin's theory should be judged only on scientific grounds[4]. Wilberforce allows that Darwin's theory could be true, and "if Mr Darwin can . . demonstrate to us our fungular descent, we shall dismiss our pride, and avow, with the characteristic humility of philosophy, our unsuspected cousinship with the mushrooms" (ref.4, p.231). Wilberforce objected that Darwin had not, in 1860, made out his case, and that there were serious difficulties, in view of the known stability of species, in supposing that one species could be transmuted into another.

These were serious scientific arguments, worthy of a vice-president of the British Association. Darwin acknowledged their cogency[5]. It was not really until the 1940s that they were adequately answered. Although now we can say with confidence that Darwin was right and Wilberforce wrong, Wilberforce was not being wrong-headed. On the evidence available at the time, his was a perfectly reasonable position to take, and the one taken by most scientists[6].

It is doubtful that Wilberforce asked Huxley whether he was descended from an ape. It makes a good story, but Wilberforce had used the *first* person plural in his review, and the use of the first person is borne out by Wilberforce's biography and one — admittedly late — account[7]. What Wilberforce may have asked Huxley in the second person is where he drew the line between human descendants and ape-like ancestors, if, as was generally admitted, the offspring was of the same species as the parents[8]. It is an instance of the Sorites fallacy, of which biologists are impatient, but which has been much discussed by logicians in recent years. Huxley, however, was ready to answer the question he had not been asked. Three months earlier, in the April issue of the *Westminster Review*, he had accused the critics of Darwin of making him out to be no better than an ape himself, and since Wilberforce was now criticizing him for being a darwinian, he must be calling him an ape too.

Wilberforce was, as Wrangham says, both honest enough to see the force of the arguments in favour of evolution and sensitive to some of its implications — not so much theological as human. In 1860 genetic arguments were being adduced in the United States in defence of slavery, and Wilberforce had in his review a witty passage about the colour prejudices of ants, who always have black ants as their slaves (ref. 4, p.253-254). Evolutionary arguments could be used — in our century have been used — to justify the degradation of man. Wilberforce realized, as these verses show, that a theory's being uncomfortable does not preclude its being true, but that its being true does not prevent its being uncomfortable.

One other moral may be drawn. Science cannot flourish without scientific controversy, and in every scientific controversy most of the views canvassed will ultimately be shown to be wrong. Nobody holds it against Einstein that he confessed himself unable to believe in a dice-playing God. Why is not equal charity extended to Wilberforce's contribution to the British Association?

J.R. LUCAS

Merton College,
Oxford, UK

1. Wrangham, R.W. *Nature* **287**, 192 (1980).
2. Huxley, L. *Life and Letters of Sir Joseph Dalton Hooker* Vol.i, 525-527 (1918).
3. Mrs Lyell, *Life of Sir Charles Lyell* Vol.ii, 335 (1881).
4. Wilberforce, S. *Q. Rev.* **180**, 256 (1860).
5. Darwin, F. *Life and Letters of Charles Darwin* Vol.ii, 324-325 (1888).
6. Carter, G.S. *A Hundred Years of Evolution*, 70 (1957); *The Athenaeum*, 1707, 19 (1860).
7. Wilberforce, R.G. *Life of Bishop Wilberforce* Vol.ii, 451 (1881); Tuckwell, W. *Reminiscences of Oxford*, 51-52 (1900); but see Fawcett, H. *Macmillan's* 111, 14, 88 (1860).
8. Huxley, L. *Life and Letters of Thomas Henry Huxley* Vol.i, 185, quoting Vernon Harcourt.

0028-0836/80/410480-01$01.00

NEWS AND VIEWS

Whatever happened to neutrino mass?

Earlier this year, the high-energy physicists and the rest of us were much excited by preliminary reports that neutrinos may not, after all, be devoid of mass. For a few weeks in the spring, people in several disciplines were more than ready to embark on yet another substantial modification of accepted ideas. Cosmologists and astrophysicists as well as the theoretical particle physicists were involved. If neutrinos have mass, that might suffice to hold the universe together, the cosmologists were saying. Astrophysicists were looking for an explanation of the puzzling discrepancy between the measured and predicted fluxes of neutrinos from the sun. But now, the wave of excitement has died down almost as quickly as it blew up. Observers of the scene may be forgiven for suspecting that the whole affair was a consequence of the notoriously fertile imagination of the particle physicists. What is happening? And what lies ahead?

The events of the past few months are easily narrated. From three independent sources there were reports that neutrinos might be more interesting than the massless (and chargeless) particles that Pauli first postulated (in 1932) to explain why electrons from the beta decay of identified isotopes do not carry away all the energy released in the decay. Most attention centred on reports of conference presentations by Dr F.W. Reines, of the University of California at Irvine, that a reactor experiment had provided evidence of the phenomenon called neutrino oscillation (see Rujula and Glashow, *Nature*, 21 August). In this process, one type of neutrino will spontaneously be converted into a mixture of all types.

When the process was first suggested on theoretical grounds by B. Pontecorvo in 1968, there were of course only two types of neutrinos, corresponding to the electron and the mu-meson. (Strictly speaking, just as there is an anti-electron corresponding to the electron, so there is an anti-neutrino corresponding to the ordinary electron neutrino). Now, with the discovery of the tau-lepton, and the supposition that there must be a corresponding tau-neutrino, there is more scope for oscillation.

Reines' experiment (carried out at the power reactor at Savannah River) is acknowledged to be a difficult one. A reactor on power is a prolific source of neutrinos, but the background of neutrinos generated by nuclear processes elsewhere in the universe is also substantial. The trouble is that the experiment is bedevilled with potential uncertainties and errors — too little is known of the energy spectrum of neutrinos from a power reactor and the frequency of nuclear reactions is small (because neutrinos are what they are). It seems to be necessary to look for a 20 per cent effect (the change in the frequency of the reactions stimulated by the neutrinos) with a piece of equipment of poor precision. Only the accumulation of data over time will provide a clear answer.

This, no doubt, is why Reines's experiment has provoked controversy among the particle physicists, most of it well-mannered. Some complain at the statistical treatment of the data, others at the physical interpretation of the observations. All, even Reines, appear to agree that more data (and therefore time) is needed before anybody can be certain. This is why many people see more hope in experiments which are quite different. Some of the difficulties may be overcome by working with energetic beams of neutrinos produced artificially by particle accelerators.

Others, however, think there may be more future in experiments designed to measure directly the mass of the electron neutrino (if, indeed, it should differ from zero). Oscillation and mass are connected by the theories now being designed to unify three of the four natural forces of nature (gravity excluded). If neutrino oscillation, or interconversion of neutrinos takes place, then neutrinos should also have mass — and each of the three types of neutrino should have a different mass. The demonstration of either non-zero mass or of neutrino oscillation would most probably bring comfort to the theorists.

Attempts at the direct measurement of neutrino mass are by no means novel — if, in the old days, the theorists went around saying that neutrinos have no mass, what more natural than that experimentalists should set out to check the assertion. Moreover, there seems very little doubt that the best route to a direct measurement of the neutrino mass is by observation of the electrons emitted by radioactive tritium, one of the least energetic of beta decays and thus one in which the energy-spectrum of the decay electrons will be most sensitive to the mass of the neutrino.

In the late 1960s, measurements like these had set an upper limit to the neutrino mass of 60 electron-volts, itself something like one part in 100,000 of the mass of the electron. More recently, however, a group from the Institute of Theoretical and Experimental Physics in Moscow has announced that measurements of the energy spectrum of decay electrons from tritium gives a mass for the electron-neutrino which is different from zero and somewhere between 14 and 40 electron-volts.

So far, the chief effect of this has been to stimulate others to embark on similar investigations and several tritium experiments are under way. (For example, in Stockholm and in Chalk River, Canada — and no doubt in many other laboratories.) The experimental difficulties are almost bizarre.

The objective is to measure the energy of decay electrons accurately when the energy is a fraction of an electron-volt — and the accuracy that matters most is that when the energy is least and where, in the nature of beta-decay, the number of decay electrons is also least. Tritium must be mounted in such a way that decay does not itself disturb the measurements — in the Moscow experiment, for example, tritium was incorporated into sugar molecules whose disruption after a decay was even in itself a source of experimental confusion. Evidently, the smaller the neutrino mass, the more difficult these experiments will be.

If the upper limit on the neutrino mass gets too small, the cosmologists will of course lose interest. They require a mass of some 30 electron-volts to close the universe. Nothing less will interest them. For accounting for the unexpectedly small neutrino flux from the sun, the mere phenomenon of oscillation will suffice. The mass is comparatively unimportant.

The particle physicists are the most downcast by the cloud now hanging over the non-zero neutrino mass. Their problem is simple. If the unified theories of particles are to work as simpler but apparently successful theories have worked in the past, neutrino oscillations should happen, and the neutrino mass should differ from zero, if only by a very small amount. In other words, there is a now familiar dilemma. A favoured theory predicts some phenomenon whose measurement is inherently difficult. Gravitational waves predicted by the general theory of relativity are an obvious illustration. But these are precisely the circumstances in which, with the best will in the world, people are tempted to make more of their data than is fair.

0028-0836/80/410481-01$01.00

Nations and numbers, 1980

from Robert M. May

THE continuing increase in the global population is such that most of us have difficulty keeping track of the current figure — for 1980 it is 4.4 billion. As noted in previous News and Views articles[2-5], this global number conceals much variation among individual nation states and among regional groupings. Any analysis of population trends and prospects must deal with these variations; a particularly good recent analysis is by Mauldin[6] (in the special 'Centennial Issue' of Science). Over the 30-year span 1950-1980, the population of the world has grown by 70%, from 2.5 billion to 4.4 billion. In this period, Europe underwent a relatively small increase of 23%, the USA and the USSR both had increases of just under 50%, while the developing countries almot doubled their population (from 1.7 billion to 3.3 billion, with increases of 125% in Latin America, 114% in Africa and 85% in Asia).

Looking ahead, Mauldin[6] suggests "the prospects until the year 2000 are for a slowing of growth rates for all areas except Africa, but the numbers to be added will be enormous". The United Nations projections foresee continued decline in the rate of population growth in developed countries; the estimates are for an increase of less then 8% over the next 20 years in Europe, and about 17% in the USA and the USSR, to give an average figure around 12-13% for all developed countires. The so-called developing countries seem likely to increase their population by about 50%, broken down as 76% in Africa, 65% in Latin America, 55% in South Asia and about 24% in East Asia.

All this adds up to a remarkable change in global demographic patterns over the second half of the twentieth century; over this 50-year span the developed countries are likely to have increased their populations by about one-half (from 830 million to 1270 million), while the developing countries are likely to have seen a threefold increase in population (from around 1.7 billion to around 4.9 billion).

These facts and projections are summarized in Figure 1, which shows the age distribution of the total populations of developed and of developing countries in 1980, and the corresponding UN projections for the year 2000. The high proportion of young age classes in developing countries is characteristic of relatively rapidly growing populations. Even though growth rates are likely to slow down over the next 20 years, the large number of people yet to move into their reproductive years in developing countries means that populations will continue to grow. This phenomenon — the "momentum of population growth" — can be expressed most dramatically by noting that even if zero population growth (ZPG — birth rates equal to death rates) could be attained overnight in a developing countries, they would still be committed to a rough doubling of total population before coming to equilibrium; the triangular age profiles on the left in Figure 1 will eventually settle to the more rectangular pattern of the age profiles on the right (characteristic of ZPG populations), but these 'rectangles' must be erected on the large base of the infant cohort.

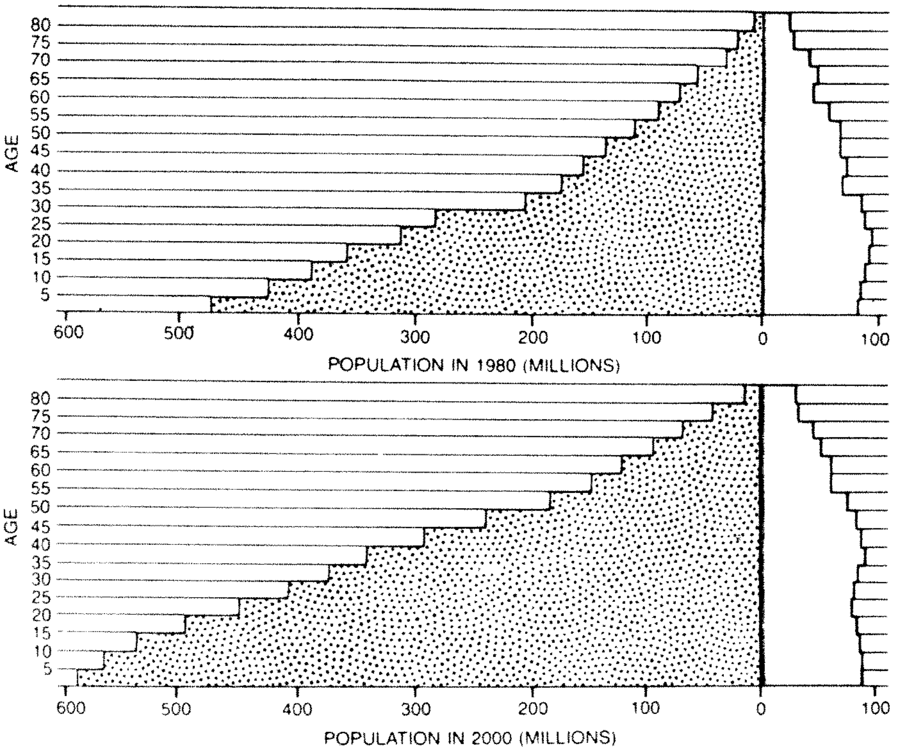

The magnitude and age composition of the total population in developing countries (shaded, on the right) and in developed countries (unshaded, on the left) are shown; the top figure is for 1980, and the bottom represents the UN projection of the year 2,000. The figure is adapted from Mahler[7], who observes "Comparison of the 1980 and 2000 shapes shows how the underdeveloped countries' large population now under 15 will move into laborforce years, exacerbating unemployment, and how baby-boom cohorts of developed countries will have aged."

Observations about the size and growth of the world's population are notoriously subject to many uncertainties[6]. As discussed previously[3], the current population of China, which represents about one-quarter of the global total, is unknown to within 5% or arguably even 10%. The Chinese census planned for 1981 may produce a firmer figure. The most populous African country, Nigeria, is estimated as somewhere in the range 70 to 85 million, but it could be more. The current fuss about the 'undercount' of city populations in the 1980 USA census, and its consequences for Federal aid distributed according to population-based formulae, emphasizes that even the US population is uncertain to within about 2%. As we look to the future, we peer through a glass ever more darkly.

With these caveats, the projections summarized above are based on country-by-country extrapolations of present trends[6-8]. These vary greatly among the developing countries, as can be seen from Table 1. The Table shows the crude birth rates (expressed as births per 1,000 of population) in 1965 and in 1975, for the less developed countries with populations in excess of 35 million (Vietnam is excluded because the information about vital rates is thought to be unreliable. The Table also shows the percentage change manifested in the crude birth rate between 1965 and 1975 (with an asterisk denoting no significant change), along with a qualitative assessment of the strength of family planning programs in the country.

Table 2 represents a more encompassing, but less detailed, version of Table 1. This Table shows the average percentage decline in crude birth rates between 1965 and 1975 in 94 developing countries, grouped according to social setting and the intensity of family planning efforts. Social setting is a variable which combines rankings on 7 socioeconomic scales: adult literacy; school enrollment; life expectancy at birth; infant mortality rate; per capita gross

---

Robert M. May is Class of 1877 Professor of Zoology at Princeton University.

1. Population Reference Bureau, Inc., *World Population Data Sheet*, Washington, D.C. (1980).
2. May, R. M. *Nature* **261**, 12 (1976).
3. May, R. M. *Nature* **265**, 101 (1977).
4. May, R. M. *Nature* **271**, 504 (1978).
5. May, R. M. *Nature* **272**, 491 (1978).
6. Mauldin, W. P. *Science* **209**, 148 (1980).
7. Mahler, H. *Sci. Amer.* **243**(3), 66 (1980).
8. *World Population Trends and Prospects By Country, 1950-2000* (UN, New York, 1979).
9. Mauldin, W. P., Berelson, B *Stud. Fam. Plann.* **9**, 10 (1978).

0028-0836/80/410482-02$01.00

national product; percentage of males employed outside agriculture; and percentage of population living in cities of 100,000 or more[6-9]. Although there continues to be much dispute and uncertainty about the cause of recent fertility declines in developing countries, Table 2 shows that both 'social setting' or degree of development and family planning programs have significant correlation with patterns of declining fertility[9].

Most population estimates for the year 2000 cluster around 6 billion (the 'high, medium and low' UN estimates[8] are 5.9, 6.2 and 6.5 billion), mainly set by the 'momentum' effects discussed above. Any estimate of the eventual steady state global population is necessarily much more uncertain. The momentum of population growth means that populations in developing countries will continue to undergo significant increases until well into the twenty-first century, and there is no consensus as to when, and at what rate, fertility will begin to decline in Black Africa, Bangladesh and Pakistan. Mauldin's[6] assessment is that "if the leaders of the major developing countries view rapid population growth as an impediment to economic development and act accordingly, and if the donor community also continues and perhaps increases assistance to such countries, the population of the world might plateau around 10 billion. But larger numbers are all too possible." And none of the estimates take any explicit account of the problems of feeding these multitudes. □

Table 1: Decline in crude birth rates, 1965-1975, in countries with populations of 35 million or more (after Mauldin[6]).

Country	1980 population (millions)	crude birth rate (per thousand)		percentage decline in crude birth rate, 1965-1975	family planning program
		1965	1975		
China	975	34	22	35	strong
India	694	43	36	16	moderate
Indonesia	152	46	36	22	moderate
Brazil	122	42	33	21	weak
Bangladesh	89	48	48	*	weak
Pakistan	82	47	47	*	weak
Nigeria	77	49	49	*	weak
Mexico	70	44	37	16	weak
Philippines	51	44	34	23	moderate
Thailand	48	44	33	26	moderate
Turkey	45	40	34	16	weak
Egypt	42	41	37	10	weak
Iran	38	45	45	*	moderate
South Korea	38	32	22	29	strong
Burma	35	40	40	*	none
Total	2,523	40	33	20	

Table 2: The average decline in crude birth rates between 1965 and 1975 (expressed as a percentage) is shown for 94 developing countries, grouped according to social setting and the intensity of family planning efforts. The numbers in brackets indicate the number of countries in each particular grouping. (Compiled from data summarized by Mauldin and Berelson[9].)

	family planning effort				
high	30 (9)	29 (5)	9 (4)	* (6)	19 (24)
upper middle	24 (1)	18 (8)	6 (11)	* 4	10 (24)
lower middle	23 (1)	14 (2)	* (8)	* (12)	* (23)
low middle	— (0)	— (0)	* (7)	* (16)	* (23)
Total	29 (11)	21 (15)	* (30)	* (38)	9 (94)

*denotes no significant change

Towards the conquest of hepatitis B

from Arie J. Zuckerman

THE current issue of the *New England Journal of Medicine* (9 October) reports the remarkable success of a carefully controlled trial of hepatitis B vaccine in a high risk population in the United States. This achievement by Wolf Szmuness and his colleagues must be regarded as a milestone in the annals of preventive medicine because hepatitis B virus has not yet been propagated and serially passaged in cell culture. The credit for the development of this unusual vaccine lies with the series of studies conducted between 1970 and 1973 with the MS-2 strain of hepatitis B by Krugman and his colleagues. (*J. Infect Dis.* **122**, 432; 1970; *New Engl. J. Med.* **288**, 755; 1973).

Their studies demonstrated that diluted serum containing hepatitis B virus heated to 98°C for one minute prevented or modified infection in 69 percent of susceptible individuals. These observations provided the stimulus for the preparation of a vaccine using the 22nm small spherical hepatitis B surface antigen particles purified from the plasma of healthy carriers and inactivated with formaldehyde, with our without treatment by heat.

Hepatitis B is of tremendous importance in every field of medical practice; with progression of the infection some patients experience chronic liver disease including cirrhosis, and there is also an association with primary liver cancer. Infection with hepatitis B virus, particularly in early life, may be followed by the persistent carrier state. The world reservoir of carriers at present is estimated to number about 200 million, and they too may suffer liver damage.

The wide range of parenteral and inapparent parenteral routes of transmission of hepatitis B includes the transfusion of blood and certain plasma derivatives, the use of inadequately sterilised syringes, needles and instruments, sexual contact, particularly among promiscuous homosexual men, and possibly transmission by blood-sucking arthropods. In some regions of the world, transmission of hepatitis B to infants may be as high as 50 percent from carrier mothers, or from mothers with acute infection in pregnancy or shortly after delivery.

A vaccine against hepatitis B is urgently required for groups at high risk of infection. These groups include patients requiring multiple transfusions, patients with natural or acquired immune deficiency and patients with malignant diseases; patients and staff of haemodialysis, transplant and oncology units and residents and staff of institutions for the mentally-handicapped. Viral hepatitis is an occupational hazard amongst health care and laboratory personnel. High rates of infection occur in homosexual men, drug addicts and prostitutes. The high rates of perinatal transmission of hepatitis B in some regions may make protective immunisation of susceptible women of child-bearing age and of infants the only practical way of interrupting transmission of the infection. Immunisation must also be considered for

Arie Zuckerman is Professor of Microbiology and Director of the WHO Collaborating Centre for Reference and Research on Viral Hepatitis at the London School of Hygiene and Tropical Medicine.

0028-0836/80/410483-02$01.00

persons living in areas where the prevalence of infection is high.

Szmuness *et al.* chose for the trial a young, healthy population of male homosexuals who are known to be at an unusually high risk of infection (*Ann. intern. Med* **83**, 489; 1975). The cooperation of the participants in this meticulously organised, placebo-controlled, randomised, double-blind clinical trial of the hepatitis B vaccine was excellent: the loss was 15.4 percent of those entered, a rate much lower than the projected 40 percent annual rate of loss. Of the 1,083 susceptible individuals who received the first injection, 96.5 percent received the second injection six months after the primary inoculation. The follow-up was excellent and of the 6,332 scheduled visits and bleedings, 91.2 percent were actually carried out.

Hepatitis B surface antibody developed within one month of the injection in 31.4 percent of recipients of the vaccine; this increased to 77 percent one month after the second injection, to 87 percent within three months and to 90 percent within six months. The booster injection at six months produced a further increase to 96 percent and high titres of antibody persisted, essentially unchanged, for 18 months of follow-up in 65–70 percent of the subjects. There is the possibility, of course, that the vigorous antibody response found in some of the subjects was boosted naturally by repeated exposure to the virus. Nonetheless, the antibody response resulted in a dramatic reduction in the incidence of infection in the vaccinated group. This high protective efficacy was observed in all sub-groups of participants, including those with a large number of different sexual partners who are most at risk.

Much has been written about the possible undesirable side-effects of a vaccine prepared from plasma of persons who are persistent carriers of hepatitis B surface antigen (Zuckerman, *Nature,* **255,** 104; 1975) and guidelines have been proposed by the World Health Organisation for the preparation of such hepatitis B vaccines (WHO *Techn. Rep. Series,* **602;** 1977). Rigorous purification of the 22nm spherical hepatitis B surface antigen particles was undertaken during the preparation of the vaccines used in the trial by Szmuness *et al.* Digestion with pepsin ensured freedom from contaminating host substances, and the purified particles were treated with formaldehyde to inactivate any residual live virus(es). The vaccine was tested for live hepatitis A virus in susceptible marmosets and for live hepatitis B virus in susceptible chimpanzees and it was also tested extensively to ensure the absence of extraneous viruses. There was no evidence that residual hepatitis B virus was present in the preparation and no seroconversion in the vacinees could be attributed to the intact virus. It is gratifying that most of the adverse reactions were relatively minor, rarely more than a sore arm, although rashes, nausea, vomiting, joint pain and fatigue were also reported. Fever occurred in 2.6 percent of those vaccinated and in 2.2 percent of the those receiving the placebo and, indeed, the incidence of all side-effects was similar in the two groups.

Finally, a most important finding was that the development of hepatitis B surface antibody is synonymous with protection against hepatitis B. Therefore, as the authors point out, once immunogenicity has been demonstrated in a particular population which might not respond as well as young, healthy adults, there should be no need to prove efficacy again; indeed such a procedure might be ethically questionable and delay the availability of the vaccine to those who need protection.

Variable stars and galaxies

from Julian Osborne and Richard Cole

The night sky may appear almost unchanging but a closer look reveals that there are many astronomical objects showing some form of variability. The extent and form of this variability was the topic of a recent conference* and, at its close, one might have been forgiven for thinking that there could be no safe standard stars left!

Variability seen in the whole Sun was reviewed by Stenflo (Institut fur Astronomie, Zurich). Of the short timescale variations, only the 5 minute oscillations are well established. Diameter variations with periods between 5 minutes and 1 hour are still controversial and theoretical understanding difficult because of the large number of eigenmodes with periods in this range. Exciting news came with the confirmation of the 160.01 minute period by Fossat and Grec (University of Nice). The period has been seen as a Doppler pulsation since 1974, and although observed by groups in Crimea, Birmingham and Stanford, has remained doubtful because 160.01 minutes is close to one-ninth of 24 hours. The University of Nice group went to the South Pole and obtained an uninterrupted run of data from the full disk lasting 120 hours.

Observations from the South Pole both suppress Earth rotation effects, and make use of the very good sky transparency. All groups report the same period, amplitude and phase but a theoretical explanation awaits identification of the order and mode of the oscillation. Kotov (Crimea Astrophysical Observatory) reported that the amplitude changes at the rotation period of the Sun and that there are small accompanying variations in brightness and cm radio emission.

Very long period variations were reported by Hughes (Queen's University, Ontario; Sterrewacht, Leiden) who was analysing 32 years worth of 10 cm radio data. He noted periodicities at 1,150 days and about 700 days, neither of which were present throughout the data. A 750 day periodicity was seen during 1970-75, as claimed by Sakurai (*Nature* **278,** 146; 1979) for the neutrino flux, and as seen by Shapiro *et al.* (*J. atmos. Sci.* **19,** 506; 1962) in the relative sunspot number. Of course, a relationship between the solar core and the overall activity of the sun would be very interesting. Other periodicities have been seen, all of which are consistent with a 260 day variation.

Ciatti (University of Padua) reviewed our knowledge of the 135 classified supernovae, showing the clear distinction between type I (64%, 3 — 4 $M_\odot$, M-S progenitors from old disk population) and type II supernovae (28%, progenitors greater than 10 $M_\odot$, stars in spiral arms). Hughes reported the discovery of a new SNR (G109.2-1.0) with the Westerbork telescope. The remnant has a good circular shell of 24 arcmin diameter, and is at a distance of 4.7 kpc. It has been seen as an X-ray source by the Einstein satellite.

The 1979 Type II Supernova in M100 was exceptionally well observed, there being data in the radio, IR, optical, UV and X-ray ranges. Evans (University of Keele) showed that only pre-existing circumstellar graphite grains explained the infrared excess seen 260 days after maximum light.

Palumbo (Instito TESRE del CNR, Bologna) reported UV observations which show the existence of an additional slow moving shell (10^3 km s^{-1}) exterior to the expanding photosphere (10^4 km s^{-1}). The shell, which had twice the radius of the photosphere at one week, is thought to be due to the progenitor's stellar wind, which is required to be $10^{-4} M_\odot$ yr^{-1} to provide the 0.2 $M_\odot$ of the shell. Whilst not seen at radio wavelengths 10 days after maximum, it was observed one year later ($S_{6cm} = 5mjy$). So far there is only an upper limit to the X-ray emission. Double structure has also been observed in the Crab Nebula by Danziger (ESO), in that there appears to be two expansion velocities for each spectral line ($\Delta V \sim$ 265 km s^{-1}).

In a review on pulsars, Lyne (Jodrell Bank) said that the recent Molongo survey had increased the number of radio pulsars to over 320, including 3 binary pulsars (of which only 1913 + 16, shows energy loss attributable to gravitational radiation). There are thought to be at least 5 × 10^5 pulsars in the Galaxy. (Taylor, *8th Texas Symp.* 1977 and Davies *et al.* *MNRAS* **179,**

Julian Osborne and Richard Cole are in the Mullard Space Science Laboratory, University College, London.

---

*Fifth European Regional Meeting of the IAU — "Variability in stars and galaxies" was held at the University of Liege, Belgium, on 28 July 1980.

0028-0836/80/410484-02$01.00

635, 1977). These have an average lifetime of 4 × 10^6 years, derived from their characteristic age and migration velocity. Together, these give a pulsar creation rate of about 1 every 8 years, greater than the supernova rate of 1 every 20 to 100 years. Thus, there appears to be more pulsars created than supernovae, although no other birth mechanism for pulsars is known which would provide the high migration velocity (150 km s^{-1}) and scale height (400pc). The problem would be relieved if the Galactic electron density was 0.02 cm^3 instead of 0.03 cm^3, or if pulsars could be created in supernovae that did not create optically visible remnants. However, Hefland's work with the Einstein satellite (*IAU Symp.* **95**, Bonn Aug. 1980) shows that many young supernova remnants do not contain pulsars, thus making the problem worse.

Van Paradijs (University of Amsterdam, MIT) provided a lucid review of X-ray bursters. Dividing the binary galactic X-ray sources according to the ratio of their X-ray and optical luminosities gives two distinct types of X-ray emitters:-
(1) L_x/L_{opt} less than 10; primaries are O,B stars $M_v \sim -5$, hard X-ray spectra, X-ray pulsars, X-ray eclipses common. (2) L_x/L_{opt} greater than 10, primaries are 'Sco type', $M_v \sim +3$, soft X-ray spectra, busters.

A typical burst will have a rise time of 1 second and a decay time of 10 – 60 seconds. There are, however, two types of burst activity. Type I bursts are seen from all bursters, they occur every couple of hours and their spectra soften during decay. Type II bursts are only seen from the 'Rapid Burster' (MXB 1730-335), which also exhibits type I burst activity. The type II bursts occur about every 10 seconds and have spectra which do not soften. The energy of a type II burst is proportional to the time from the previous burst, implying accretion build up and overflow.

The estimate of 1 - 5 $M_\odot$ for the mass of the X-ray emitter and the estimated radius of the emission region (10 km) have given rise to a successful model for type I bursts. In this, the X-ray emission is due to thermo-nuclear flashes in the helium rich material on the surface of a neutron star, this being accreted from a binary companion.

This model describes the bursts well, with the bursts ceasing if the accretion rate is so great as to cause continuous nuclear burning. Until recently there was no evidence for the binary nature of the bursters but, recent spectral observations of the optical counterparts suggest a companion to CenX-4 (*IAU* circ. 3487), and an accretion disk in AO620-00 (Murdin *at al. MNRAS* **192**, 709; 1980). The optical counterparts of these stars, and of A1742-28, are K type stars.

Correlated optical bursts have been seen in three sources so far. (1735-44, 1837 + 05, 1636-53; Van Paradijs). The energy of the optical bursts is 5 orders of magnitude lower than that of the X-ray bursts and are thought to be due to reprocessing of the X-ray flux. There is a 2 second delay between the X-ray and the optical bursts, reprocessing might cause a delay of 0.5s so the implied distance to the reprocessing site is 1.5 light seconds. It is expected that the reprocessing occurs around the edge of an accretion disk, the size of which implies a neutron star companion of 0.4$M_\odot$ consistent with K-type stars.

Pederson (ESO) reported optical and X-ray coverage, noting one slow burst (rise time 3-4 sec) in optical and X-ray from MXB 1636-53, and one fast optical burst (rise time less than 200 msec) from MXB 1735-44, for which there was no X-ray coverage. Infra-red bursts from the 'Rapid Burster' were described by Jones (Imperial College). This group has discovered very bright bursts ($m_k \sim m_h \sim 6$) of $\sim$10 sec duration with fast flashes (some less than 0.3 sec) superimposed. These bursts are only an order of magnitude less intense than the X-ray bursts, but do not follow the known type I or type II behaviour.

Walker (RGO) has been studying the blue light curve of the black hole candidate Cyg X-1 over the past 8 years. He has found that the light curve and period have varied. A periodic change is suggested, such as a third object (period > 18 years) or precession of either of the known components.

His most recent data showed a dramatic change in the light curve. The primary maximum had decreased and the secondary maximum had increased and attained a double structure. This behaviour had been seen once previously, just before an X-ray transition. Evidently, an X-ray transition did take place between mid May and early June of this year (*IAU* Circ. 3491).

Shklovsky (Space Research Institute, Moscow) described his model of the peculiar object SS433, as an O,B super giant with an extreme stellar wind (10^{-4}m yr^{-1}) in a binary system with a neutron star of low magnetic field at the centre of an accretion disk. These are surrounded by an expanding cloud, optically thick to infrared radiation. The moving lines are reproduced by blobs which become optically thin to Hα as they are blown from the accretion disk onto the circum-system cloud. These blobs become shocked and heated to $10^{7\text{-}8}$ K to produce X-rays.

King (University of Leicester) confirmed a previous X-ray iron line detection, and suggested a change of the X-ray continuum; no periods were found in the range 1-200 days, despite considerable X-ray variability. The infra-red flux is also variable ($\Delta M = 1.6$), the IR colours however, remain constant. There is a suggestion of an 11.8 day IR period, but no period was seen at 13 days.

Observations of SS433 reported by Schilizzi (Dwingeloo Radio Observatory, Holland) showed milli arcsec variation within 6 months. At a larger scale, Spencer (Jodrell Bank) described the radio structures as consisting of an unresolved central core (less than 0.3") with a flat spectrum and a 3" halo with a spectral index of —1.1, elongated in the direction of the SNR W50. He noted a 1 week flare in the core which was not seen in the halo.

Ciatti has undertaken a study of moving lines, observing that they vary irregularly in intensity and wavelength, sometimes forming multiple systems. He notes that the velocity and angle of the jets varies night by night whilst following the general precession. His best fit period is 165.5 days, using 200 nights observations over 3 cycles. The intrinsic colours of SS433 lead Firmani (Instituto de Astronomica, Mexico) to conclude that the primary is an early type star intermediate between Of and WN8. These stars are of 15 $M_\odot$ burning helium in

100 years ago

PHYSICS WITHOUT APPARATUS

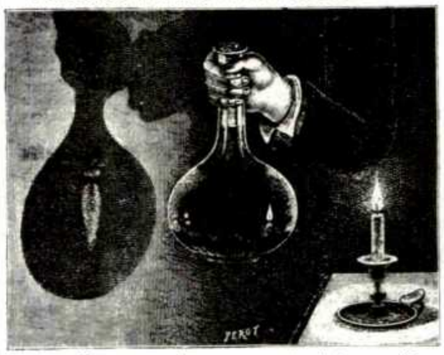

To illustrate the geometrical laws of refraction through lenses, a good reading-glass of large size is a desirable acquisition. Spectacle-lenses, though of smaller size, and therefore admitting less light, are also of service. In the absence of any of these articles, it is generally possible to fall back upon a water-decanter, provided one can be found of a good globular form, and not spoiled for optical purposes by having ornamental work cut upoin the sides of the globe. The figure shows how this decanter, filled with water, is to be employed. It is held a few inches away from a white wall, and a candle is placed at the opposite side, so that its light falls through the decanter on to the wall. The candle is moved towards or away from the decanter until the position is found in which its rays focus themselves upon the wall giving a clear inverted image of the candle flame upon the wall. The experiment may be varied by setting down the candle on the table and then moving the decanter to and fro until a definite image is obtained. If a large hand reading-glass be available, the image will be much clearer than with the improvised water-lens; and a further improvement in the manner of experimenting may be made by using a screen of white paper or card instead of a whitened wall on which to receive the image.

From *Nature* **22**, 7 October, 541 & 537, 1880.

0028-0836/80/410485-02$01.00

their core, with $2 M_\odot$ H envelopes. The time to loose this envelope gives a 20,000 years life time for the SS433 phenomenon. He expects there to be 10 SS433 type systems in the galaxy.

Pauliny-Toth (Max-Plank-Institut) presented interesting pictures of the variations in the milliarcsec structure of active galactic nucleii. He mentioned 3C84, in which 3 bright regions are expanding but not moving apart, the rate of expansion implies that the source 'began' 20 years ago; all regions having the same spectrum. He discussed 4 sources showing apparent super-luminal velocities: 3C273, in which 3 central compact components are separating in the direction of the main jet; 3C345, in which a double component has changed to a core-jet structure; 3C120, in which there were strong outbursts in 1971-74 when the source was double (the central source is now a core-jet and there are no outbursts); and 3C279, which is showing 21c separation of a double source, and 40c separation of a new third component. By contrast, NGC 1275 shows only a slow expansion (0.1c) and no separation of the components. □

On the Tibetan plateau

from Peter Jackson

THE Tibetan Plateau has long fascinated not only romantics and mystics, but also geoscientists. It has been recognised as one of the most interesting areas of the globe particularly in relation to continental drift and tectonics, since it was here that the Indian plate, which broke away from Gondwanaland, crashed into the Eurasian plate about 38 million years ago. The suture line lies along the valley of the Tsangpo river, about 100 kilometres north of the main Himalayan axis.

The area remained generally closed to science although, after the Peoples Republic of China asserted itself in the area in the 1950s, reports filtered through of some activity by Chinese scientists. It was thus with some excitement that geologists and natural scientists received invitations from Academia Sinica to participate in a symposium on the geology and natural history of the Qinghai-Xizang (Tibetan) Plateau. Over 60 scientists from 17 countries gathered in Peking in May for a week of meetings at which the Chinese reported in detail on the results of 20 years of research in Tibet.

Liu Tung-shen, Vice-Chairman of Academia Sinica, told the meeting that the rich fossil beds on the plateau had yielded 3,800 species of over 30 families in recent years, compared with only 300 before 1950. In the Himalaya, fossils of *Glossopteris* and cold water biota were found in late Palaeozoic beds, while north of the Tsangpo fossils of *Gigantonoclea* and warm water biota were uncovered in the Permian formation, indicating the importance of the valley as a palaeontological boundary.

Palaeogeomagnetic study confirmed that areas to the north and south of the river valley belonged to different plates — to the north the crust is about 70 kilometres thick, and to the south about 50 kilometres thick. Isostatic anomaly in the Everest area is + 120mg, and uplift is continuing as the Indian plate still pushes north. For the last 100,000 years since the Pleistocene a rise of 10 mm per yr has been estimated by Chinese scientists.

It is believed that the Himalayan system may have been completed between Miocene and Pliocene, but even in late Tertiary the plateau may not have been more than 1,000 metres in elevation, judging from fossils of the three-toed horses *Hipparion* found during the recent explorations. The Himalayas are considered to have reached great heights in the late Pleistocene, bringing about a climatic change to present conditions when they blocked the warm wet monsoon and made Tibet a cold, arid area.

The week in Peking was an absorbing and active one but was just a preliminary to the real object of interest — a two-week field excursion to Tibet, from Llasa westwards and finally passing through the Himalayas to Kathmandu.

The high altitude physiologists found that the Tibetans,although their capital Llasa is at a height of 3,660m, had the same blood haemoglobin values as lowlanders in, for example, Shanghai, but lowlanders up on the plateau showed a significant increase in haematological values, which became normal only after 10 to 15 years. The surprising revelation was that when lowlanders, whose haematological values had become normal, returned to the lowlands they suffered a period of one to three months of re-adjustment. A high percentage of the lowlanders have to leave the plateau because, after a year or two, they develop chronic mountain sickness with a tremendous increase in red blood cells.

Many of the visiting scientists had taken with them NASA earth satellite imagery of the area through which we passed. Glaciologists noted that studies of the imagery in the United States tied in well with what was actually observed. The surprise in paraglacial geology was that typical phenomena such as the sorting of stones by freezing and thawing on slopes was not as widespread as expected at such high altitudes. It became evident that this was because of the extreme dryness of the air so frost action was almost absent. Characteristic phenomena were found only in moist areas.

Glaciation in Tibet appears to have been little more during the Pleistocene than it is today, and E. Reiter of Colorado State University suggested that this was because the Indian summer monsoon, which brings in moisture and snow, was either very short during the Pleistocene or sometimes even absent. He suggested, on seeing heat shimmer in temperatures of about 9°C on a 5,220 metre pass, that heat from the plateau generates an anti-cyclone and draws in the monsoon from India. During global cold periods, however, such as during the Pleistocene, when the gradient between the equator and the poles is strong and the sub-tropical high pressure belt is drawn towards the equator, the northward pull of the Tibetan plateau may be insufficient to bring in the monsoon.

Most of the valleys had sand dunes, which, in some cases, such as around Lhasa, were shapeless conglomerations resulting from complicated wind patterns. But along the Tsangpo near Xigatse, and further west near Tingri, sickle-shaped dunes were seen, which were the result of a steady up-valley wind. T. Pewe, of the University of Arizona, remarked that silt particles from among the sand had blown up the hills and walked back down forming areas of retransported loess favourable to agriculture. He said that according to Professor Liu, this was the first report of loess in the area.

Scientists of several disciplines commented on signs of over-exploitation and damage to the physical environment, which indicated the need for considerable care in the future economic development of Tibet. Almost every other cart met on the roads carried fuel. Men and women were seen trudging homeward with heavy loads of shrubs, such as *Sophora moorcroftiana*, which had been dragged out by the roots.

Jack Ives, of the University of Colorado, pointed out the conspicuous and recent gulleying and dissection of fans resulting from deforestation and over-grazing, probably combined with the development of a colder and more arid climate in the last 3,000 years. Ives had presented a paper at the symposium on mapping natural hazards, which stressed the dangers of placing settlements on alluvial fans because of floods and rock and mud flows. In Tibet many villages were placed just there, presumably because of the availability of water. It was agreed by both foreign and Chinese scientists that there was a need for collaborative research to pinpoint dangerous trends, to help decision makers improve the welfare of the people of Tibet and to achieve a better ecological balance and effective management of natural resources. It was considered especially important to use new techniques developed in the US for areas where the data base is short — as it is in Tibet — to predict floods and other dangers to settlements on alluvial

Peter Jackson is a writer on nature conservation.

0028-0836/80/410486-02$01.00

fans.

While Chinese experts pointed to some remarkable results in agricultural production and spoke of the potential of Tibet, the visitors stressed the need for caution in view of the short growing season, which could be seriously affected by variability in annual rains, possibly resulting in bad harvests and famine.

Perhaps the least satisfied of the visitors were the zoologists, despite the thrill of collecting lizards, fish, butterflies and small fauna at record altitudes. Brought up on old records of remarkably tame wildlife in Tibet — wild yak, wild ass, blue sheep, antelope, gazelle, geese and duck — they were disappointed to see no large mammals, and birds were generally sparse in numbers. There were only two or three sightings of shy bar-headed geese (*Anser indicus*), which used to be numerous and confiding on the plateau. This seemed to indicate strong hunting pressure in contrast to the former reverence for wildlife. However, Chinese zoologists reported that there were still populations of most Tibetan species on the sparsely inhabitated central plateau, which whetted appetites for further studies.

Collaboration between Chinese and foreign scientists has already begun, and, as a result of the symposium, there is now likely to be a burst of activity aimed at unravelling the secrets of Tibet and applying the knowledge there and elsewhere. □

SCIENCE COLLEGE

Mycorrhiza and crop production

from D.S. Hayman

VESICULAR-ARBUSCULAR mycorrhiza, a symbiotic fungus-root association, can greatly increase the utilization of phosphate present in soil. Recent research suggests that the symbiotic association can be harnessed to achieve more economical use of costly superphosphate fertilizers and better exploitation of cheaper, less soluble rock phosphate.

The vesicular-arbuscular (VA) mycorrhizal fungi infect more plants than any other fungi and are necessary for many plants to grow well, but until recently, they had escaped widespread attention. This is for two reasons: first, the association is so well balanced that young feeder roots show no sign of damage even when densely infected, and second, the fungi themselves cannot as yet be cultured in the absence of a living root and so do not appear on agar plates used to isolate other soil and root-inhabiting micro-organisms.

VA mycorrhizal infections are seen as vesicles and arbuscules borne on the mainly aseptate hyphae occupying the root cortex. Similar structures have been reported in fossil roots some 300 million years old and are present in their modern relatives (ferns, psilopsids and clubmosses), as well as in some gymnosperms and angiosperms colonizing most habitats around the world.

VA mycorrhiza is found in most agronomic species except the brassicas and sugar beet and is widespread in the two major crop families, Leguminosae and Gramineae. Important crops where benefits from mycorrhiza have been shown include pasture and forage legumes (but not lupins), maize, wheat and barley, potatoes, many vegetables, herbaceous and tree fruits, and many tropical plantation crops. Temperate zone plants with thick fleshy roots and few, short root hairs generally benefit considerably from VA mycorrhiza; for example, onions, citrus, grapevine, sweetgum and *Coprosma*. In the tropics, pineapple, *Stylosanthes*, *Centrosema*, coffee, tea, cocoa, oil palm, papaya and rubber all have dense VA infections. Cassava appears to be obligately mycorrhizal which probably explains why it is able to grow in impoverished phosphate-deficient soils (Van der Zaag *et al.*, *Field Crops Res.*, **2**, 253; 1979) while needing high phosphate concentrations in solution culture.

The extent to which particular plants depend on mycorrhiza is largely governed by their root morphology. Generally those with the most limited root-soil contact (coarse, hairless roots) benefit most from the network of mycorrhizal hyphae extending from the mycelium inside the root to the surrounding soil. Ions such as phosphate are fairly immobile and a phosphate-depletion zone often develops around roots in phosphate deficient soils. The hyphae are able to reach beyond this zone and directly translocate nutrients from the soil to the root cortex where transfer to the plant occurs. There is often a dramatic response to mycorrhiza in such soils while, in contrast, there is little effect on the uptake of readily mobile ions such as nitrate. Experiments with ^{32}P-labelled phosphate indicate that VA mycorrhizal hyphae obtain their extra phosphate from the labile pool rather than by dissolving insoluble phosphates. This may account for plant growth responses reported in silos amended with some phosphate fertiliser. The better utilization of sparingly soluble rock phosphates is explained by the hyphae making closer physical contact than roots with the ions dissociating at the particle surface.

Mycorrhizal benefits are not limited to improved phosphorus uptake. Absorption of other elements including zinc and copper can be enhanced. Recent work (see Allen *et al. Can.J.Bot.* **58**, 371; 1980) suggests that growth hormones such as IAA and cytokinins may be present at higher concentrations in plants that are mycorrhizal than in those that are not. There is also some evidence that plants with mycorrhiza may be better equipped to withstand stress conditions such as occur during transplanting or periods of drought, in soils containing toxic levels of aluminium, manganese or salt, or in unstable soils where the hyphae may bring about soil aggregation. In legumes, nodulation and nitrogen fixation have been greatly increased by mycorrhizal innoculation, sometimes beyond that achieved by adding phosphate fertilizer alone. Certain host-fungus combinations may also increase a plant's resistance to some root pathogenic fungi and nematodes. Whether this occurs by direct physical exclusion through competition for sites, or by metabolic changes involving antibiotic production or increased vigour has not yet been clarified. There are situations, however, where the VA fungal drain on host carbohydrate or possible disruption of host metabolism may outweigh the benefits to the plant. This swing from mutalistic symbiosis to parasitism has been shown in some grasses and cereals grown at above optimum phosphate levels.

As the effects of VA mycorrhiza on plant growth are generally positive much research is directed towards harnessing its advantages. This requires an understanding of the physiology and ecology of the association, a knowledge of which crop species or cultivars are most likely to benefit from mycorrhiza, screening and selection of the most efficient fungal endophytes, development of suitable procedures for large-scale innoculum production and innoculation techniques, and an assessment of field situations where mycorrhizal innoculation would be most valuable. Factors that decrease mycorrhiza in the field, for example, pesticides, high fertilizer levels and poor aeration, should also be considered.

Experiments carried out using plants in pots have helped our understanding of mycorrhizal function but they are not always a good guide to responses in the field. Field experiments, however, pose two major problems: how to produce high quality (pathogen-free, high viability) innoculum in quantity (see Menge *et al.*, *Proc.Int.Soc.Citriculture* **1**, 129; 1977) and how to innoculate crops on a field scale (see Mosse & Hayman in *Tropical Mycorrhiza Research* ed. Mikola, Oxford University Press, 1980). Innoculum can consist of infested soil (usually from stock plants and containing spores, mycelium and infected root fragments), clean infected roots (as grown in nutrient-flow culture, see *Rothamsted Report* (1) 188; 1980) or pure fungal cultures (not yet achieved). For

D.S. Hayman is on the Soil Microbiology Department, Rothamsted Experimental Station, Harpenden, UK.

0028-0836/80/410487-02$01.00

annual crops sown over large areas inoculum can be pelleted with the seed or placed in the seed furrow either dry or in a slurry. Such material is bulky, yet enough must be applied to ensure substantial early infection when the crop's demand for phosphate, and hence mycorrhiza, is at a peak. Perennial crops are more easily handled since they can be innoculated in containers to produce vigorous mycorrhizal colonization of the root system by appropriate endophytes before transplantation.

Field situations must be selected where mycorrhizal benefits look most probable; crops already known to be responsive to mycorrhiza should be tested in nutrient-stressed soil at sites where the indigenous population of mycorrhizal endophytes is small or inefficient. Current examples are marginal sites in temperate regions (for example, white clover in hill pastures), ferrolateritic soils which are deficient in and/or 'fix' phosphate as found in huge expanses of the tropics (for example, the Brazilian cerrado), eroded, degraded or unstable sites (for example, coal tips, quarries and sand dunes), and soils fumigated to remove plant pathogens (for example peach and citrus nurseries in California.)

Results so far have shown that growth responses to field innoculation with selected mycorrhizal endophytes can vary from nothing to around threefold. Test crops have included white clover in Britain and New Zealand, lucerne in Spain and Britain, maize and cowpea in Nigeria and cereals in Pakistan. Similar responses have been reported in citrus and up to 84 fold increases in sweetgum in fumigated nurseries in the US. Less dramatic, but nevertheless important responses, are also possible in more standard agricultural soils and techniques to measure these should be refined. In many other situations, however, mycorrhiza may have no discernable effect on crop yield.

At this stage, despite the enormous recent upsurge in mycorrhizal studies, undue faith in mycorrhiza as an agricultural elixir should be tempered by a realistic appraisal of which aspects might best be exploited on a practical scale. □

Tales of two accelerators

from P.I.P. Kalmus

At 17.00 on 6 June 1978, Nimrod accelerated its last particles. The users, a Queen Mary College — Rutherford Laboratory collaboration, recorded their final events in a kaon-nucleon polarization experiment and ended a fifteen year era during which several hundred scientists from the UK and overseas had used the 7 GeV proton synchrotron at the Rutherford Laboratory. Three weeks later a meeting took place where the events surrounding the conception, construction and life of this machine were recalled by a small number of distinguished speakers.

In September of the following year the 12.5 GeV Zero Gradient Synchrotron of the Argonne National Laboratory in Illinois was closed down, and a two-day symposium was held to recall its history and achievements. The proceedings of both these meetings have recently appeared in print. *Nimrod: The 7 GeV Proton Synchrotron,* edited by John Litt, is available from the Rutherford Laboratory and *History of the ZGS,* edited by Joanne Day, Alan Krisch and Larry Ratner, is published by the American Institute of Physics as No. 60 in its conference proceedings.

It is tempting to contrast the two machines, to compare their performance and to look for different styles of conducting high energy physics in the two countries, but I will leave that to some future historian of science. Some sociologist might even read national characteristics into the fact that in Britain we waited three weeks before holding the wake whereas our American colleagues held theirs two weeks before the death of the ZGS! However, to me, the similarities between the stories of the two machines and their user communities are much more striking than their differences.

Nimrod was built to enable UK universities to carry out research in the exciting new field of high energy physics. The concept of a national laboratory with central facilities was, however, a novel one in Britain and was viewed with considerable suspicion and apprehension by some prominent university scientists. Similarly, the main purpose of the ZGS was to provide the universities of the American Mid-West with facilities which would rival those on the East and West Coasts, and the idea of basing academic research at a Government laboratory was viewed with hostility by some universities and, in particular, by the Mid-West Universities Research Association.

However, both machines were authorised in the late 1950s. Both made use of the well-established weak focusing principle. Particles make slow oscillations in the horizontal and vertical planes about the idealised orbit. The oscillations have large amplitudes and require a guiding magnet of large aperture. It was felt that the design was safer for achieving high intensity beams than the newly invented strong focusing principle which was being used in the CERN and Brookhaven machines. These were then under construction and were designed for higher energy but much lower intensity. In fact, the strong focusing machines performed extremely well and their intensities were raised gradually over the years to rival those of the wide aperture machines.

Already during the construction periods the directors of both projects went to considerable efforts to involve members of the university community both in policy making and in the actual design and construction of bubble chambers, beamlines and other facilities. In this both laboratories were highly successful. The fears of university scientists that they would be taken over by Big Brother proved groundless, and in fact Rutherford and Argonne became shining examples of how technologically complex central facilities can serve large user communities. This expertise lives on: the Users Organisation at Fermilab is modelled on that at Argonne and the Rutherford Laboratory (now combined with Appleton) is serving the needs of university scientists and engineers in a variety of fields.

Both accelerators began operation in 1963. Although not the highest energy machines in Europe or America, the range covered by their particles was a particularly fruitful one, the available energy being comparable to the rest mass energy of the stable hadrons and the lower lying unstable particles.

The achievements of the users of Nimrod were primarily in strong interaction physics, in particular, nucleon-nucleon and meson-nucleon interactions. Starting with total and elastic differential cross sections successive generations of experiments measured gradually more complex spin parameters using polarized targets. Much of our present knowledge of hadron spectroscopy stems from this machine. The ZGS, partly because of its higher energy, supported a rather wider variety of experiments including, for example, neutrino interactions in the 12 foot hydrogen bubble chamber. In its final years there was a vigorous programme of physics using an accelerated and extracted beam of polarized protons. The ZGS was the obvious machine for this technique as its uniform magnetic field was likely to cause less beam depolarization than might be the case in other machines.

Well over 200 experiments were conducted at the ZGS and each was a significant research project occupying the effort of perhaps ten physicists for three years. The Nimrod booklet gives a list of 120 PhD theses written on work done with this accelerator.

Both machines were closed prematurely, and both for the same reason — to release funds and support for the new generation of more powerful accelerators at CERN and at Fermilab. The kaon-nucleon experiment that concluded the Nimrod

---

P.I.P. Kalmus is Professor of Physics at Queen Mary College, London. In the first half of the 1960s he was a staff member of Argonne. Since then he has been a user of the Rutherford facilities.

0028-0836/80/410488-02$01.00

programme is now analysed and published. The postgraduate student who worked on it has written his thesis and is embarking on the next stage of his career at CERN. A whole generation of high energy physicists, some of whom are now at the forefront of particle research, received their training at Nimrod or the ZGS. I personally feel privileged to have participated in a small way in both these adventures. ☐

Diseases of the motor unit

from a Correspondent

IT has been estimated that more than one third of neurological hospital admissions can be attributed to neuromuscular disorders. This large group of diseases was the subject of a recent conference* and, perhaps the major message to emerge was that many basic techniques are now being adapted to serve as specific probes in studying both normal and disordered structure, function and interactions of nerves and muscles. Where such probes have been applied, for example in the case of α-bungarotoxin and myasthenia gravis, rapid progress has been made. The newer techniques offer similar promise for understanding of the muscular dystrophies and other neuromuscular disorders.

The Duchenne form of muscular dystrophy (DMD) is the commonest of the muscular dystrophies and is inherited as a sex-linked recessive trait. It produces progressive muscular weakness in boys and culminates in total disability before the teens. Circumstantial evidence suggests a disorder of the plasma membrane manifested by leakage of muscle-specific enzymes into the circulation, minute breaks in the plasma membrane early in the course of the disease, and a large number of biochemical defects in muscle and other cells. Much evidence was added at the meeting for a membrane or membrane-associated abnormality, although the underlying defect was not defined. Using freeze-fracture techniques Bonilla and Schotland (University of Pennsylvania) found decreased intramembranous particles in sarcolemmal membranes of DMD and facioscapulohumeral dystrophy muscles. These changes suggest defects in the sarcolemma but their significance is not understood. Red blood cells of patients with DMD show increased phosphorylation of a specific membrane protein fraction in band II of spectrin (Roses, Duke University). Although he has identified the sub-fraction responsible for this effect there is little enthusiasm for the idea that the spectrin abnormality could reflect the basic biochemical defect in DMD. Other cell types, such as lymphocytes, may also show membrane abnormalities. Gruemer (Medical College of Virginia) reported that there is decreased capping of DMD lymphocytes upon exposure to anti-human immunoglobulin. Despite the inability of several research groups to confirm these results, Gruemer carried out a double-blind study in collaboration with the Johns Hopkins group that correctly identified DMD lymphocytes in over 90 percent of samples. In another leukocyte study, Shay (University of Texas) demonstrated a defect of microtubules in mononuclear cells from DMD patients and carriers, using immunofluorescent techniques. A variety of biochemical abnormalities were reported in DMD tissues, including a decrease in adenyl cyclase in sarcolemmal membranes of cultured muscle (Wilner, Columbia University) and an increase in calcium transport by DMD erythrocytes (Pleasure & Mollman, University of Pennsylvania) These disparate findings continue to provide tantalizing evidence for a cell membrane defect in DMD, but are still far from identifying the nature of the defect, or indeed proving that it bears any important relationship to the disease process.

The mechanisms by which abnormal muscle tissue self-destructs may provide more immediate practical applications. There are two proteolytic enzyme systems in muscle fibers (Goldberg, Harvard University), the lysosomal enzymes which degrade normal proteins before their disposal, and an ATP-dependent enzyme system which degrades defective proteins. By blocking the lysosomal enzyme system with leupeptin and other antagonists, muscle breakdown and the degradation of specific proteins can be prevented. Stracher (State University of New York) has applied this interesting approach by using leupeptin in animals with 'dystrophies', or with denervated muscles, and has found a significant retardation of muscle wasting and histological changes.

The changes that occur in muscle cells after breaching the sarcolemmal membrane (as probably occurs in DMD), can be studied by making multiple micropunctures in skeletal muscles *in vivo* (Karpati, Montreal Neurological Institute). The retraction of myofibrils and dilatation of sarcoplasmic reticulum are similar to the changes seen in early lesions of DMD. Perfusion of the limb with EDTA reduces the severity of the lesions, suggesting that calcium may be involved in the destructive process. W. K. Engel (NIH) visualized calcium in human muscle biopsies by a histochemical method. He reported that both damaged and regenerating fibers appear to have elevated calcium concentrations; thus, calcium may contribute to degenerative and regenerative processes in muscle cells. A. Engel (Mayo Clinic) stained muscle biopsies from a wide variety of disease conditions for activated complement complexes (the 'membrane attack complex'). All muscle fibers undergoing necrosis contained activated complement components regardless of the underlying disease.

These studies all suggest that there are several definable steps between the initial lesion in muscle disorders and the ultimate destruction of the muscle fiber. Therapeutic measures aimed at interfering with these intermediate steps may be able to offer effective treatment.

Developments in the field of myasthenia gravis (MG) have outstripped those in other areas of neuromuscular disease. The availability of α-BuTx (α-bungarotoxin) as a specific probe made possible the indentification of the ACh receptor defect nearly 7 years ago. Since that time, much progress has been made in understanding the pathogenesis and devising treatments for this disease. Drachman (Johns Hopkins University) described the mechanisms by which anti-ACh receptor antibodies produce a reduction of available receptors. They include: (1) accelerated endocytosis and degradation of the ACh receptors, (2) blockade of the receptors' active sites, and (3) antibody-mediated, possibly complement-dependent, damage to the receptors and postsynaptic membranes. The mechanism of endocytosis was further elaborated by Pumplin (University of Maryland) and Drachman, who showed by freeze-fracture techniques that cross-linking of ACh receptors by the antibody causes them to clump and aggregate, before their endocytosis *via* coated pits that form in the muscle membrane. Fuchs (Weizmann Institute) reported that immunization of rabbits with denatured ACh receptor can diminish the severity of experimental autoimmune myasthenia gravis (EAMG), presumably by stimulating the production of antibodies that block the binding of more pathogenic antibodies against the native ACh receptor. Another strategy involved the use of anti-idiotype anti-bodies that appear to protect against EAMG. Such therapeutic approaches may eventually be used in human MG. Lindstrom (Salk Institute) has prepared an extensive collection of monoclonal antibodies against ACh receptor from the electric organs of rays and eels, for the purpose of mapping the structure of the ACh receptors.

Major progress has been made in understanding the 'trophic' interactions between nerves and target cells. ACh transmission may account for the motor nerve's role in regulating the resting membrane potential (RMP) and the extrajunctional ACh receptors of skeletal muscle (Drachman, Pestronk & Stanley, Johns Hopkins University). Post-synaptic blockade of ACh transmission completely reproduces the effects of surgical denervation on the RMP and the extrajunctional ACh receptors, while disuse results in a partial denervation-like effect on these two muscle parameters. The formation of junctions

---

*A conference "Diseases of the Motor Unit" was held at Key Biscayne, Florida, sponsored by the Muscular Dystrophy Association, June 2-6, 1980.

0028-0836/80/410489-02$01.00

between nerves and muscles induces the accumulation of ACh receptors (Fischbach, Harvard University) and a low molecular weight substance from chick spinal cord and brain that produces an increase in ACh receptors of cultured muscle has been extracted. The implication of this and other similar studies is that such substances may play a role in the subsynaptic accumulation of ACh receptors at neuromuscular junctions.

Reverse trophic influences of the innervated target cells on neurons within the chick ciliary ganglion were described by Landmesser (Yale University) & Pilar, (University of Connecticut). During development, an excessive number of nerve cells compete to innervate a limited number of target cells; those neurons that form connections are able to survive and mature, while those that fail to connect undergo cell death. The proportion of cells that die can be greatly increased by ablating the target and conversely, the proportion of survivors can be increased by pruning out some of the ciliary neurons. The same effect is also seen in tissue culture; the maturation and survival of ciliary neurons is enhanced by co-culture with an appropriate target tissue, skeletal muscle.

The regulation of nerve sprouting was analyzed by Pestronk and Drachman. Pharmacological denervation (using blockers of nerve conduction of ACh release) induces sprouting of nerve terminals which branch and enlarge over the surface of each muscle fiber. Extrajunctional ACh receptors appear to play a role in this type of sprouting, since blockade by α-BuTx prevents the formation of terminal sprouts. However, in collateral sprouting occurring when neighboring muscle fibers are denervated little effect is produced by blockade of ACh receptors. Finally, intrinsic factors such as age may greatly effect the nerve's ability to sprout — both terminal sprouting and regeneration after injury are progressively impaired with increasing age.

The basement membrane of the motor endplate may be particularly important in neuromuscular junction formation (McMahan, Harvard University) Even after destruction of skeletal muscle cells, the basement membrane retains its organization, and is capable of serving as a target for regenerating motor nerves. Moreover, the basement membrane appears to act as a scaffold for the reorganization of regenerating muscle. If a muscle is damaged and then allowed to regenerate, new endplates form at their previous sites, as directed by the remaining basement membrane.

Extracellular matrix may also play a role in interactions between Schwann cells and axons. The 'dystrophic' mouse shows a defect in myelination of nerve roots, with some Schwann cells apparently refusing to ensheath the naked axons. Aguayo (Montreal General Hospital) showed that grafting segments of unmyelinated nerve roots from 'dystrophic' mice to normal or even 'dystrophic' mice resulted in correction of the myelination defect. Bunge (Washington University) was able to reproduce the myelination defect in tissue culture of 'dystrophic' mouse dorsal root ganglia, and to correct the abnormality by the addition of fibroblasts or of serum. This suggests that the lack of an extracellular substance normally secreted by Schwann cells results in impaired myelination.

Perhaps the greatest promise for future research in neuromuscular disease lies in the application of a variety of powerful new biological techniques to the eminently workable nerve-muscle system. Among the new techniques described at the conference were monoclonal antibodies to serve as probes of surface membrane components of chick skeletal muscle (Fambrough, Carnegie Institute of Washington) and tissue culture of pathological muscle. Successful culture of skeletal muscle from patients with myotonic dystrophy was demonstrated by Appel (Baylor College of Medicine) and abnormalities in cultured Schwann cells from patients with adrenal leukodystrophy and Issac's syndrome by Askanas (NIH). Finally, the techniques of modern biochemical genetics are just beginning to be applied to skeletal muscle. Recombinant techniques have been used to clone genes for contractile proteins by Yaffe (Weizmann Institute) and Schwartz (Baylor College of Medicine). H. Epstein (Baylor College of Medicine) pointed out the encouraging prospects for identifying the genetic abnormalities in the muscular dystrophies by such methods. □

Crystallizing membrane proteins

from Richard Henderson

After many years of disappointing failures the first succesful attempts to crystallize membrane proteins have recently been reported. Large three-dimensional crystals suitable for X-ray analysis are needed for the resolution of the protein structure in atomic and chemical detail, a level of analysis essential for the understanding of phenomena such as channel selectivity and the mechanism of action of membrane bound pumps and receptors.

In the first paper, Ozawa *et al.* (*Proc. natn. Acad. Sci. U.S.A.* **77**, 928; 1980) describe crystals of the cytochrome c oxidase-cytochrome c complex. These crystals were made from detergent (cholate)-solubilised oxidase almost completely depleted of lipid (<1%). Cytochrome c was added to make a 1:1 complex and crystals obtained by removal of detergent by dialysis. The crystals contained both oxidase and cytochrome c in a 1:1 ratio, but both detergent and lipid were absent. They are thus well-characterised chemically but the extent of crystalline order remains to be determined by X-ray diffraction. At the moment, they are needles rather too small for analysis.

The most successful and promising reports used the detergent, octylglucoside, recently made commercially available. In two exciting reports, crystals were made by precipitation of membrane proteins solubilised in octyl glucoside without removal of the detergent. The crystals thus contained a substantial amount of detergent in addition to aqueous regions, the protein and perhaps also some lipid.

Michel and Oesterhelt (*Proc. natn. Acad. Sci. U.S.A.* **77**, 1283; 1980) used 2.5 — 2.8 M salt to precipitate octyl glucoside-solubilised bacteriorhodopsin, obtaining two crystal forms, one needle-shaped and the other cube-shaped. These crystals are truly three-dimensional and one form (the needle) is ordered to at least 8 Å resolution. The needles have the interesting property of being strongly dichroic and the purple chromophore is oriented almost exactly along the needle axis. Further structural work should therefore be useful to determine the chromophore orientation and if better diffraction patterns can be obtained, the crystals may well be suitable for higher resolution analysis.

Garavito and Rosenbusch (*J. Cell Biol.* **86**, 327; 1980), used polyethylene glycol to precipitate the pore-forming protein, porin that comes from *E. coli.* outer membranes, after solubilising with octyl glucoside. They obtained birefringent rhombic plates and prisms using β-octyl glucoside and non-birefringent but larger, bipyramids using α-octyl glucoside which they had to synthesize themselves. The large bipyramids gave X-ray diffraction spots out to 3.8 Å resolution making them ordered at least to a resolution close to that required to reveal atomic detail.

This recent flurry of successful crystallizations may now mean that membrane proteins are sufficiently purified and characterised, and that detergent development is sufficiently well-advanced, that a substantial effort to crystallize many more membrane proteins should be started. Perhaps these results, exciting in themselves, will provide the impetus for these efforts. It seems that it would now be worthwhile both to try to crystallize other membrane proteins and to develop other detergents like octyl-glucoside, which itself remains in solution while the protein-detergent complex is precipitated. □

Richard Henderson is in the MRC Laboratory of Molecular Biology, University Medical School, Cambridge.

0028-0836/80/410490-01$01.00

REVIEW ARTICLE

Transcription and RNA processing by the DNA tumour viruses

Edward B. Ziff
The Rockefeller University, New York, New York 10021

Messenger RNA synthesis by the DNA tumour viruses proceeds by a complex but versatile series of transcription and RNA processing steps. The major mechanistic features of this pathway are probably very similar to those used by the animal cell host itself. The viruses have, however, evolved intricate arrangements of protein coding sequences and sites for RNA initiation, polyadenylation and splicing which allow them to use their genetic information to maximum advantage.

THE DNA viruses which infect animal cells and transcribe their messenger RNA in the host nucleus provide an attractive and easily manipulated system for studying eukaryotic gene expression. The phenomenon of messenger RNA splicing, now recognized as occurring throughout the eukaryotic kingdom, was first discovered in the human adenovirus. This virus, together with the simian virus 40 (SV40) and the mouse virus, polyoma, which will also be considered in this article, realises the full potential of RNA splicing to assemble a range of different messages from a limited amount of primary genetic information. To maximize the efficiency of their relatively small genomes, they have evolved complex transcription units in which the primary transcripts can be processed in different ways to yield different end products (for a review of transcription unit design see ref. 1). Adenovirus-2 (Ad-2, and the very similar Ad-5) is a member of the group C human adenoviruses, and transcribes its RNA from a 35,000-nucleotide linear DNA genome. SV40 and polyoma are both papovaviruses, with covalently closed circular supercoiled genomes ~5,200 nucleotides long, and closely related genetic organization and mRNA maps. (The closely related human papovavirus BK[2] will not be discussed here.) This review summarizes the arrangement of genes and messenger RNAs within the three viruses, and compares mRNA synthesis pathways to illustrate common mechanistic features. In addition to productive infections, all these viruses can cause neoplastic transformation in certain cell types, but this will not be considered here.

Transcription of adenovirus-2

Ad-2 productive infection of HeLa cells proceeds through a ~36-h infectious cycle which is conventionally divided into early and late stages, separated by the onset of viral DNA replication approximately 8 h after infection (for a review see ref. 3). Ad-2 transcription is by the host RNA polymerase II[4,5] and both DNA strands encode mRNA[6,7].

Transcription during the early stage follows a complex programme. There are at least five early transcription units (shown in Fig. 1) to which mRNA species and proteins have been mapped[8–16]. Each of these, including EIA and EIB, the two tandem transcription units at the left end, has a separate promoter, demonstrated by nascent chain analysis[17], UV transcription mapping[18,19] or 5,6-dichloro-1-β-D-ribofuranosylbenzimidazole (DRB) inhibition of transcription[20]. Structurally distinct capped mRNA 5′ termini[21] are encoded by each of the early regions and have been mapped within sequenced DNA templates[22]. Although unique caps were found for region EIA and EIB[22], the caps for EII[23], EIII, EIV and the protein IX mRNA are heterogeneous, and result from staggered 5′ termini encoded within a 2–6-base region (C. C. Baker and E.B.Z., unpublished results). The staggering is non-random and favours the use of purines rather than neighbouring (or intervening) pyrimidines, reminiscent of the prokaryotic initiation preference for purines (for a review, see ref. 24). The two left-end transcription units EIA and EIB encode functions capable of cell transformation[25–28], and have been partially sequenced in Ad-5 (refs 29, 30). Region EIA products are also implicated in the efficient production of mRNAs from the other early regions (see below)[31]. Mutants in region EIB are complemented by human embryonic kidney cell functions, and this region may encode the Ad-2-specific tumour antigen[32]. Region EII encodes a 72,000 molecular weight DNA binding protein (DBP) which participates in DNA replication[33,34] and may regulate early transcription during the late stage (see below). Region EIII is distinguished by its location wholly within the major late transcription unit and encodes a glycoprotein which appears on the cell surface[35,36]. EIII and EIV yield mRNAs with complex splicing patterns[12,14]; notably, two 3′ termini have been detected for mRNAs with the region EIII 5′ end. Two additional leftward regions which are tentatively allocated to the early class are known. One encodes the IVa2 protein, a minor component of the virion; the second, which maps between map coordinates 19.8 and 23.5, encodes low abundance mRNAs and is the locus of the ts36 DNA minus mutation[37].

Modulation of early mRNA synthesis

Ad-2 early transcription units are not activated simultaneously, EIA being expressed within 1 h of infection, EIB, EIII and EIV somewhat later, and region EII within 2–3 h of infection[38].

The expression of transcription units at the left end of the genome is of particular interest. These encode multiple mRNA species which have common 5′ and 3′ termini but differ in the internal arrangement of their splices[8,12,14–16]. During the early stage of infection, region EIA encodes two 13S species, EIA-a and EIA-b shown in Fig. 1*B*. The donor splice points for these species differ by approximately 200 residues and their DNA sequences have been mapped[39]. The alternative splices change the internal peptides of region EIA proteins without altering the amino or carboxy termini. These EIA transcripts are very rapidly transported to the cytoplasm, and have a short half life[40]. Region EIB encodes two species, EIB-a, a 22S mRNA, and EIB-b, a 13S species[12,14,41]. During the late stage of infection, the proportions of the different left-end mRNAs change to favour the splicing pattern of the shorter species. A new 9S mRNA, EIA-c, appears from EIA, and the amount of EIB-b

0028–0836/80/410491—09$01 00

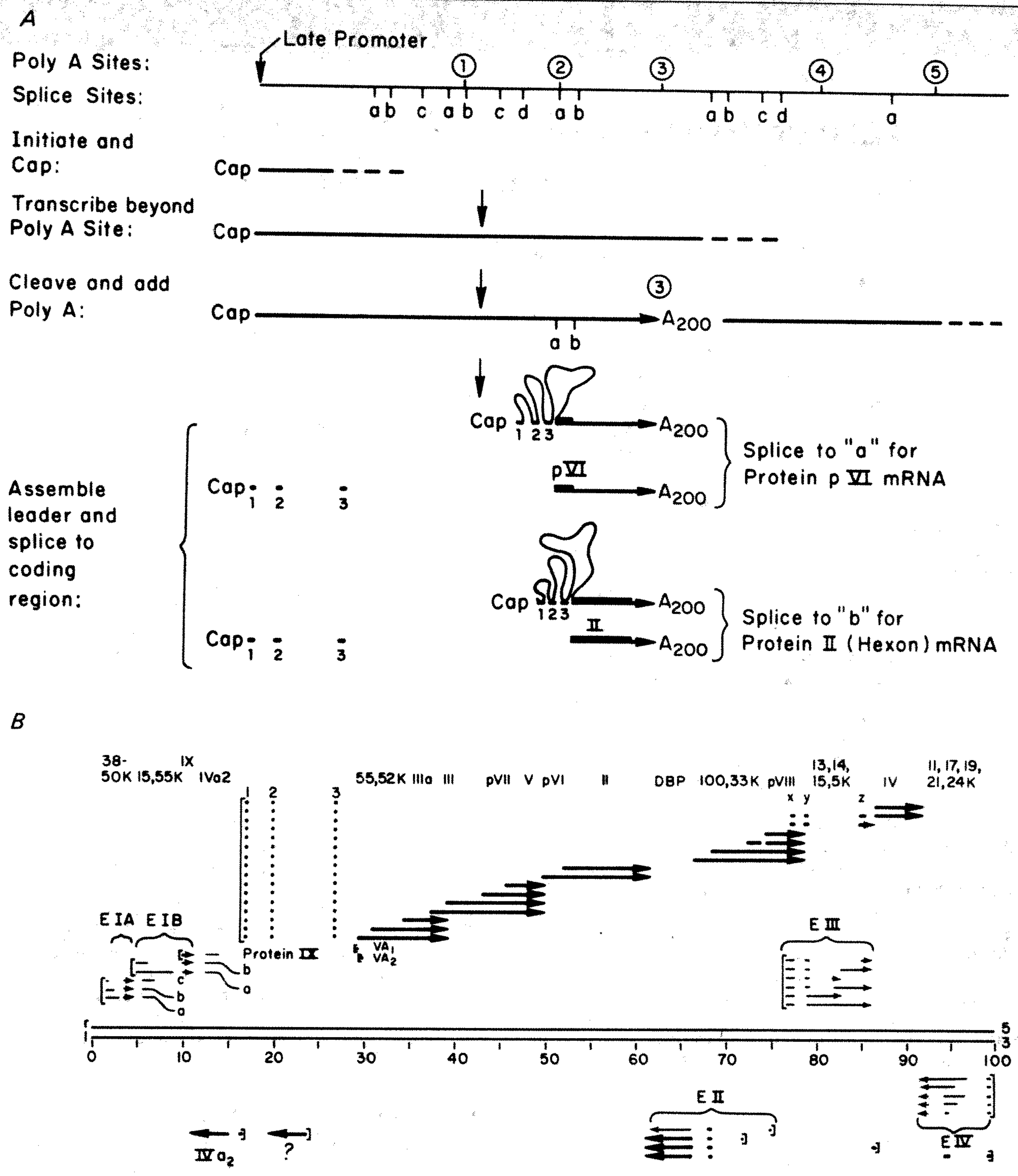

Fig. 1 Synthesis of messenger RNA by adenovirus-2. The physical map of Ad-2 is divided into 100 units, each consisting of ~350 nucleotides. RNAs synthesized from left to right utilize the DNA r-strand as template and are 'rightward' transcripts. Those transcribed in the opposite direction are 'leftward'. *A*, Transcription and processing of late messenger RNA. Precursors to late messenger RNA are rightward molecules initiated at the major late promoter and are capped while nascent RNA, Five sites, ① to ⑤, exist for the polyadenylation of these transcripts. However, only one poly(A) site is used for any given transcript, although on average the five sites are used with approximately equal frequency. RNA polymerase transcribes beyond the functional poly(A) site, ③ in this example, and continues until it reaches the far end of the genome at coordinate 100. Soon after the polymerase passes ③, while the RNA is still a nascent molecule, the transcript is cleaved to expose the poly(A) acceptor. RNA sequences encoded at coordinates 16, 19 and 27 are spliced together to form a non-coding tripartite 5′ leader. This leader is subsequently spliced adjacent to a coding sequence. Several alternatives are possible for this final splicing step when any particular poly(A) site has been utilized, for example joining the leader to *a* or to *b*. In the example shown, splicing to *a* juxtaposes the leader to the coding sequences for the pVI protein, while splicing to *b* splices the leader adjacent to the hexon coding sequence. The mRNA produced by splicing to *a* contains the coding sequences for both pVI and hexon. However, eukaryotic ribosomes do not re-initiate translation at internal positions, and translation of this multicistronic mRNA is confined to the first cistron, pVI. Hexon is translated from mRNA with leader spliced to *b*. Two 'choices', selection of the poly (A)site and the leader splicing site, therefore govern the mRNA species which is produced from the primary transcript. This processing pathway allows 14 or more different proteins to be encoded within a single transcription unit, and places their expression under the control of one promoter. *B*, Adenovirus-2 messenger RNA maps. Early messenger RNAs fall within five separate transcription units, EIA–EIV. Each early transcription unit encodes multiple species which differ in the positions of their internal splices. The mRNAs encoding the proteins IX and IVa2 are expressed at an intermediate stage of infection. Species from the major late transcription unit fall into five 3′ co-terminal families with all members of a given family sharing a common poly(A) site. The mRNAs from this transcription unit also share a common 5′-capped tripartite leader. For mRNAs within a 3′-co-terminal family, this leader is spliced adjacent to different coding sequences. Other leader sequences, *x*, *y* and *z*, appear in some fibre (protein IV) mRNA molecules. The protein translation products of various mRNAs are aligned with their genes. The VA RNAs are RNA polymerase III products described in the text. See text for refs. *B* is redrawn from ref. 16.

accumulating in the cytoplasm increases dramatically by 50–100-fold[12,40,41].

Further evidence for the temporal complexity of transcription comes from the Ad-2 protein IX[42,43]. Its mRNA is synthesized later than the early mRNAs but synthesis still occurs in the presence of cycloheximide or cytosine arabinoside (Ara C), which block late mRNA[44]. The protein IX mRNA is therefore assigned to an 'intermediate' stage of transcription. It is unspliced and has a 3′ terminus that coincides with that of the EIB mRNAs, but its 5′ end is encoded at coordinate 9.7, about 1,800 residues downstream from the EIB cap site[42,43]. Nascent transcripts initiated at 9.7 are not found in the early state nor is the protein IX mRNA detected in the cytoplasm at this time. Both are detected during the late stage[19]. These experiments strongly indicate that these are separate promoters for the protein IX mRNA and the EIB mRNAs, and that the 5′ end of the protein IX mRNA is not formed by cleavage of a larger EIB transcript, thus suggesting transcriptional control.

Ad-2 early proteins may participate in the control of Ad-2 early gene expression. Region EIA mutants yield diminished quantities of early mRNAs from the EIB and EII–IV transcription units[31,45,46], suggesting that a product encoded by EIA may be required for efficient expression of the other early regions. It is noteworthy that transcription from each early region occurs in the presence of a variety of protein synthesis inhibitors[38,47], suggesting that synthesis of an EIA protein is not an absolute requirement for expression of the other early regions.

Early transcription units are also subject to negative regulation. When early RNA synthesis is monitored in the presence of Ara C, a drug which blocks both DNA synthesis and most late mRNA, early viral transcription is shut down approximately 6 h post-infection[48–50]. However, if protein synthesis is blocked by cycloheximide, early mRNA is overproduced (or stabilized) relative to the wild type, suggesting that negative control of early transcription (or mRNA stability) depends on protein synthesis[51].

The pertinent viral regulatory protein blocked by cycloheximide may be the DBP, the translation product of early region EII[52]. The DBP has a single-stranded DNA binding function in viral DNA replication, but also has the capacity to bind to DNA termini or double strands[53]. Several facts suggest a complex role for the DBP in adenovirus gene expression. With ts125, a mutant of Ad-5 that produces a temperature-sensitive DBP, early transcription does not undergo its normal shut-off[48–50]. A detailed analysis of early transcription with cells infected with ts125 shows that the major negative effect of the protein is on region EIV, and that control of the rate of synthesis of region EII is normal in ts125 infection at the non-permissive temperature[54]. The apparent negative regulatory action of the DBP on early region EIV could parallel the proposed SV40 large T antigen autoregulation (see below), which is thought to act at the RNA initiation step. In this connection, it is of interest that the DBP and SV40 T antigen are related by their capacity to change Ad-2 host range. Although Ad-2 expresses both early functions and certain late functions, including replication of its DNA in monkey cells[55–57], a greatly decreased yield of infectious particles is obtained[58]. The cause of the block imposed by monkey cells is unknown, but certain late proteins are synthesized in decreased yield[59], possibly as a result of reduced levels of synthesis of functional mRNAs[60,61]. Simultaneous infection with SV40 overcomes the host range block. Expression of the sequences coding for the proline-rich carboxy-terminal segment of the SV40 T antigen (see below) is implicated as the relevant SV40 function because Ad–SV40 hybrid recombinant viruses which encode this segment of T are also non-defective in monkey cells[62–64]. Also, SV40 mutants with deletions at the 3′ end of the early region that remove C-terminal peptides (Fig. 3*B*) are defective in adenovirus helper function[65]. Microinjection of a related Ad–2–SV40 hybrid protein which contains the C-terminal peptide also overcomes the block[66]. Mutants of Ad-2 which overcome the block have been selected, and marker rescue experiments have mapped the locus of the mutation within the DBP gene[67]. The mutant DBP thus seems to fulfill a function required during monkey cell infection that can also be provided by SV40 T antigen.

The full story of Ad-2 early regulation is likely to be even more complex. During the early stage of infection, the 5′ end of region EII mRNA is encoded near coordinate 75 (ref. 23). However, during the late stage a considerable fraction of the mRNA from region EII has a 5′ leader encoded at either coordinates 72 or at 86 (refs 12, 16). Thus, there is an activation of 'late specific' 5′ ends for transcripts of 'early' region EII DNA. In agreement, synthesis of this early protein continues into the late phase[68].

The early to late switch

The major shift in Ad-2 gene expression is the early to late switch, which is closely coupled to the onset of DNA replication and dramatically increases the abundance of late transcription unit mRNAs. These messengers contain a common tripartite 5′ leader (whose detection marked the discovery of splicing) which is encoded at coordinates 16, 19 and 27 on the genome as shown in Fig. 1*B*[69–74]. The 5′ terminus of this leader is released by T1 RNase as an undecanucleotide[75] which is encoded at coordinate 16.45 (ref. 73). With the onset of the late stage, transport of cell mRNA to the cytoplasm ceases, although synthesis of polyadenylated cellular nuclear RNA continues[68].

Although the mechanism of this shift is not known, it has been established that blockage of DNA replication by chemical inhibitors of DNA synthesis such as Ara C[12] or by DNA minus conditional lethal mutations[76,77] prevents the formation of most late mRNA. Thus, ts125 fails to synthesize late mRNA if placed at the non-permissive temperature during the early stage of infection[77]. It also fails to replicate its DNA[33]. As found for ts mutants of SV40 T antigen at the non-permissive temperature[78], the onset of DNA replication (rather than the maintenance of synthesis) seems to be the critical factor for late mRNA synthesis. If ts125 is shifted to the non-permissive temperature during the late phase, late RNA synthesis continues although DNA replication ceases[77]. Late mRNA synthesis is also dependent (at least indirectly) on protein synthesis, and late mRNA (as well as DNA replication) is blocked if cycloheximide is added early in infection. The block to late mRNA caused by these drugs may not be absolute because the coordinate 16.4 'late' capped 5′ terminus is found in cycloheximide-treated cells early in infection (E.B.Z. and A. Shaw, unpublished results). In the presence of Ara C, late mRNA species with their 3′ end at coordinate 38 are found[12].

Virus promoters and primary transcripts

The precursors to mRNAs from the major late transcription unit are large rightward-transcribed nuclear molecules up to 25 kilobases long[79–81]. The initiation site for late RNA (5′ terminus of the primary transcript) was mapped at coordinates 16.3–16.5 by the nascent chain method applied to isolated nuclei[82] and *in vivo*[73]. The RNA initiation site was mapped more precisely by showing that late nuclear RNA contains marker oligonucleotides encoded just downstream from the late cap site but lacks sequences predicted by the DNA structure immediately upstream[73]. This was confirmed for transcripts synthesized *in vivo* and in isolated nuclei[22,82,83]. Coincidence of the promoter and the cap site implies that the initiating residues of the primary transcript are incorporated into the capped 5′ terminus of late mRNA.

RNA initiation site structures

Many eukaryotic structural genes contain a region of homology[84] which precedes the mRNA cap site by 30 or 31 residues and has the canonical structure TATAAA (the Hogness box). The presence of the Hogness box in the Ad-2 late promoter[73] and at a constant location with respect to cell cap sites, suggests that it is involved in transcription initiation. Other regions of homology are shared between the late promoter and the globin[73,85] and conalbumin genes[86]. The majority of the Ad-2 early cap site sequences also share a Hogness box[22], suggesting that each early cap site is also an RNA polymerase II initiation site. Region EII seems to lack a Hogness box[23], as do the late SV40 and polyoma cap sites (see below), but the significance of this difference is not known.

Regulation of the late primary transcript

Initiation of a capped transcript at the late promoter has been obtained *in vitro* with a soluble system using Ad-2 late promoter DNA, RNA polymerase II from HeLa cells as well as polymerase from various heterologous sources including *Xenopus*, and an S-100 fraction from uninfected cells[87]. 'Fingerprint' analysis of these *in vitro* transcripts gave the pattern of RNase T1 oligonucleotides found *in vivo*, indicating selective and accurate initiation at the cap site *in vitro*. Extracts of whole uninfected HeLa cells also initiate capped late promoter transcripts up to 5,000 nucleotides long, without polymerase supplementation[88]. Moreover, the latter system also initiates at the cap sites for the early promoters EIA and EIB, and the intermediate promoter protein IX.

The fact that for correct initiation *in vitro*, the Ad-2 late promoter (as well as early and intermediate ones) requires no viral component other than the cloned 5′ segment of the transcription unit suggests that no virus-encoded factor is required to activate this promoter, at least when it is present as naked DNA. Late transcription could be negatively controlled at the initiation step by a 'repressor', or the late promoter could be active at all times, with the primary transcript changing from non-productive to productive transcripts. Indeed, late transcripts proximal to the coordinate 16.5 promoter are hypermolar in comparison with downstream (coordinates 30–100) sequences[82]. Thus, a proportion of late transcripts are terminated before they reach the major blocks of late genes. A similar (although not necessarily related) observation has been made for RNA synthesized in the presence of DRB[20,89]. This drug acts at a site downstream from the promoter, and limits transcripts to promoter-proximal (potentially the attenuated) sequences[90].

Processing of late transcripts

The pathway for processing late mRNA is given in Fig. 1*A*. The 3′ ends of mRNAs from the late transcription unit are encoded at five poly(A) sites, each to the right of coordinate 16 (ref. 91). These have been mapped precisely at coordinates 38, 50, 62, 78 and 92 (refs 16, 92–94). Radiolabelling studies indicate that RNA sequences in polyadenylated nuclear molecules adjacent to each of these five poly(A) sites are labelled with equal kinetics in time periods less than required to complete the transcript, implying that nascent RNA is the poly(A) acceptor[95]. The size of the newly polyadenylated RNAs implies that they retain essentially all their intervening sequences, and received their poly(A) before splicing occurred[95]. Unspliced polyadenylated molecules are also observed by electron microscopy[96] and RNase T1 oligonucleotides from the late Ad-2 first intervening sequence are found in nuclear molecules with 3′ poly(A)[73]. However, with such large RNAs it is difficult to exclude the possibility of the excision of short stretches before poly(A) addition occurs. Isolated nuclei also synthesize polyadenylated transcripts with 3′ ends at coordinates 38, 50, 62 and 78, coincident with the *in vivo* poly(A) sites[97]. The nonpolyadenylated fraction of this RNA, however, also includes species with 3′ termini at coordinates 38 and 50, as well as a proportion of large molecules with partially spliced 5′ leaders. Although some splices may occur on nonpolyadenylated RNA, the final splice of the leader to the mRNA main body seems to be confined exclusively to the polyadenylated RNA class.

With early regions EII and EIV, polyadenylated nuclear RNAs are also readily detected with the size and map position expected for unspliced but capped precursors[98–100]. Studies on the production of mRNA from early regions EII and EIV have determined the size of the molecule to which labelled poly(A) becomes attached after brief exposure to ^{3}H-adenosine. Over 90% of the new poly(A) was on unspliced molecules[101]. If the unspliced, polyadenylated precursor to region EII mRNA is labelled *in vivo*, and nuclei are isolated and incubated with cell extracts, this RNA is spliced *in vitro*[102]. The general rule seems to be that poly(A) addition precedes splicing, but it is not known whether this effect is a consequence of rapid poly(A) addition and slow splicing, or whether poly(A) addition is a prerequisite for splicing.

Late in infection, Ad-2 transcription occurs in equimolar amounts along the entire late transcription unit (with the exception of hypermolar transcription near the promoter discussed above)[80,95]. The primary transcripts initiated at coordinate 16 extend beyond the five poly(A) sites, and proceed virtually to the

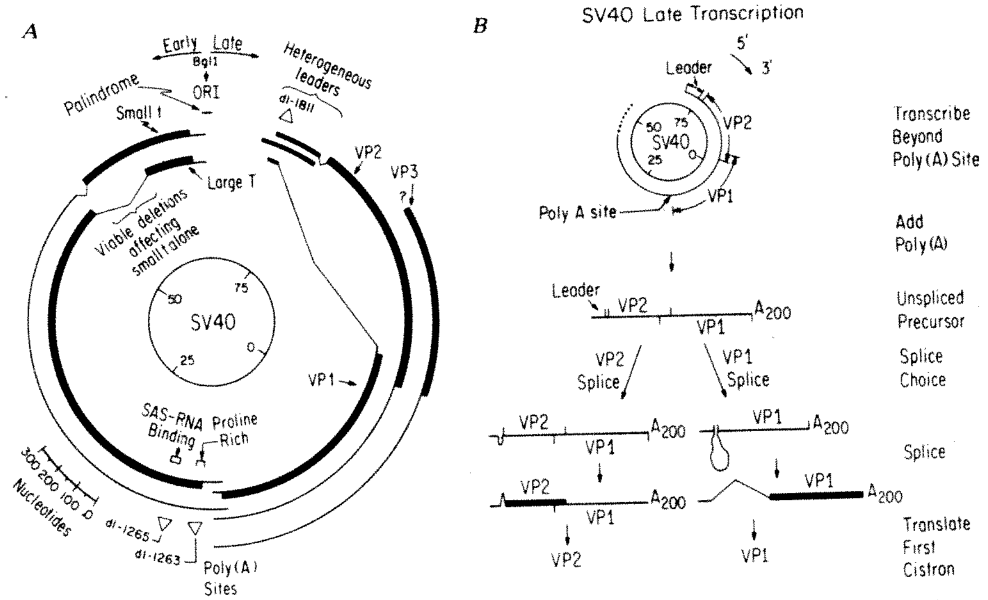

Fig. 2 SV40 messenger RNAs. *A*, Messenger RNA map. The 5′ termini of SV40 mRNAs map near the origin of DNA replication (ORI). ORI contains an inverted repeat palindrome centred on the *BglI* restriction endonuclease cleavage site. The ORI region is shown in detail in Fig. 4. Early mRNA species are transcribed anticlockwise on this map, and late clockwise. The polyadenylated 3′ ends of early and late mRNAs overlap. Two early mRNAs, which differ in the positions of their internal splices, encode, respectively, the SV40 tumour antigens small t and large T, which are amino co-terminal. The T mRNA lacks the translational terminator sequence for the t protein and T translation continues essentially to the 3′ end of the mRNA. Late mRNA species encode the structural proteins VP1, VP2 and VP3. VP2 and VP3 are carboxy co-terminal, and both differ from VP1. A single DNA sequence, however, encodes the amino terminus of VP1 and the carboxy terminus of VP2 and VP3, but two different reading frames are used. The leaders spliced to the coding regions of the late mRNAs are heterogeneous, with multiple 5′ termini. The VP3 splicing pattern is not well established. The effects of DNA deletions, the presence of a SV40 associated small RNA (SAS RNA) and possible functions of the proline-rich carboxy terminus of T are discussed in the text. *B*, Pathway of synthesis of SV40 late mRNAs. Newly formed late nuclear transcripts are molecules which extend from the cap site(s) beyond the poly(A) site, but are shorter than the full length of the genome. These primary transcripts are apparently cleaved and polyadenylated at the poly(A) site to yield unspliced molecules with the 5′ and 3′ ends of mature mRNA. As with Ad-2 late mRNAs (Fig. 1), multiple pathways exist for splicing this precursor to allow synthesis of a family of 3′-co-terminal mRNAs. In the example given here, the alternatives of splicing the leader adjacent to either the VP2 or the VP1 coding sequences are shown. The cistron closest to the cap is translated. See text for refs.

end of the genome at coordinate 100 (ref. 103). At this stage of infection, mRNA 3′ ends are apparently generated by cleavage. Products from both the 5′ and 3′ sides of the cleavage have been detected in isolated nuclei[97]. Although only approximately one-fifth of the RNA mass reaches the cytoplasm[95,104], polyadenylated sequences are transported almost quantitatively[95]. This implies that there are no non-productive polyadenylation events, and that only one poly(A) tract is added per late transcript although all five potential acceptors are transcribed. Thus, polymerases can evidently traverse one poly(A) site non-productively, utilize a second downstream site and avoid non-productive polyadenylation at the remaining positions, although they are transcribed and the acceptor is a nascent RNA. This suggests that the transcription complex actively prevents non-productive poly(A) addition, possibly through a regulated commitment of the polyadenylation machinery to one of the poly(A) receptors to the exclusion of the other four, at the time of initiation[95]. Alternatively, the virus may have evolved a gradient of poly(A) site efficiencies which counterbalances map positions and ensures that each poly(A) site is used with approximately equal efficiency. The Ad-2 late 3′ acceptors contain the AAUAAA homology found near the poly(A) of cell mRNAs even for termini encoded within the transcription unit, for example, at coordinate 50 (ref. 91).

The number of translatable Ad-2 mRNA species from the late transcription unit[105] is greater than the number of 3′ termini. This excess is explained by the existence of messengers which are staggered in sequence at the 5′ end (adjacent to the 5′ leader), overlap at internal positions, and share common 3′-terminal structures[92]. The late mRNAs are organized into five banks of overlapping messengers (see Fig. 1*B*)[91,93,94]. Present evidence suggests that the larger of the 3′ co-terminal species (from a given family) contain coding sequences for more than one protein, but that only the 5′-terminal coding sequence is translatable[92,93,106]. Adjacent sequences, silent in the large mRNAs, are translated from shorter mRNA species belonging to the same 3′-co-terminal message family[92,93,105–107]. This model is supported by the fact that the 5′ leader, sequenced for both the fibre[72] and the hexon[108,109] mRNAs, lacks an AUG, but that translation initiation sites are found within the mRNA main body. These late 3′-co-terminal families parallel the papovavirus late 3′-co-terminal mRNAs described below. The late leader also contains a sequence complementary to the 3′ end of 18S ribosomal RNA which may facilitate ribosome binding[73,108].

If we consider the 3′-co-terminal messengers (and their translation products), the five poly(A) sites divide Ad-2 late protein coding sequences into discrete blocks capable of expressing more than one protein through the formation of 3′-co-terminal mRNAs. With the Ad-2 late transcription unit, two post-transcriptional 'choices' (outlined in Fig. 1*A*) presumably govern which segment of nuclear RNA will be transported to the cytoplasm as mRNA: selection of the poly(A) site from one of five positions within the late transcription unit followed by selection of the site to which the leader is spliced. All these events are nuclear[110]. The actual mechanism for removing the intervening sequences may be quite complex. Late nuclear RNA contains species which have the leader assembled as far as 19.3, 21.6, 24.8, 25.6, 26.0, 26.2, 26.4 and 26.9 coordinate map units and which are colinear downstream[96]. These results suggest that the primary pathway for processing late nuclear RNAs has a sequential polarity for splicing from 5′ to 3′. In some cases incompletely spliced mRNAs are transported to the cytoplasm. With the fibre mRNA, and a related mRNA synthesized by an Ad-2–SV40 hybrid virus, a proportion of the molecules contain up to three extra leader segments, *x*, *y* and *z* of Fig. 1*B*; however, these do not affect translation[111,112]. With infections in monkey cells, a proportion of the fibre mRNAs retain even larger abnormal RNA sequences which are derived from coordinates 66–78 and are normally present only in mRNAs from the fourth co-terminal block[61]. Thus, the monkey cell block (see above) may result from defective splicing or premature transport. Sequences used for both early and late splicing show extensive homology with equivalent cell sequences, implying common sequence recognition for the cell and at least some splices of both early and late viral transcripts[23,73,113].

Although the mechanism of splicing is not established, most models postulate an intramolecular mechanism (see Fig. 1*A*), perhaps with small RNAs bridging the splice junctions and holding the exon sequences in close proximity to allow accurate cleavage and religation[114]. With Ad-2, attractive candidates for this role are the RNA polymerase III-encoded virus-associated (VA) RNAs. Two prominent species, 5.5S and 5.2S (about 156 nucleotides long), are encoded by genes which lie just in front of the late gene block, close to coordinates 29–30 on the Ad-2 map (Fig. 1*B*) and separated by a short spacer[115–118]. Both species of VA RNA appear during early infection, but the 5.2S species levels off and the 5.5S species increases during the late stage[116]. Splicing models have been proposed in which VA RNA base-pairs with splice junctions of late transcripts[119].

In addition to polyadenylation and splicing, late mRNAs are modified by methylation of internal A residues at the N^6 position[120]. These are added in the nucleus before splicing and (in contrast to the bulk of the RNA transcripts) are highly conserved on transport to the cytoplasm, suggesting that they may play a part in designating which sequences from the large transcript are to appear as mRNA.

mRNA arrangement for SV40 and polyoma

As with adenovirus, productive infections of SV40 and polyoma involve the temporal regulation of gene expression, with the synthesis of 'early' and 'late' mRNAs at different stages in infection. The early and late mRNAs of SV40 and polyoma are transcribed with opposite polarity with respect to the DNA physical map, and use opposing DNA strands as templates. Their 5′ termini are, however, clustered within a region of the genome that includes the origin of DNA replication[121–124]. Because the complete DNA sequences of SV40[125,126] and polyoma[127–132] have been determined, precise gene and mRNA mapping is possible.

The arrangement of SV40 genes and transcripts is shown in Fig. 2. During the first 8–10 h of SV40 infection, mRNAs are synthesized for two early proteins, the 90–100 kilodalton large T antigen[133] required for viral DNA replication, and the 15 kilodalton small t antigen[134–137] implicated in cell transformation (for a review see ref. 38). The mRNAs for SV40 T and t have closely mapping or identical 5′ and 3′ termini, but differ in their splicing[139,140]. The RNA encoding t is colinear with the DNA sequence from an AUG at coordinate 66 to a terminator at 55 (refs 140–142), but is followed by a downstream splice which falls completely within the untranslated region. In the T mRNA, the 5′ side of this splice shifts to remove the terminator and allow T translation to continue essentially to the 3′ end at coordinate 17 (ref. 140). The T and t proteins thus share amino-terminal sequences, but differ at their carboxy termini, and the smaller protein is encoded by the larger mRNA[143–145]. As a consequence of the early splicing patterns, deletions in DNA exclusive to t shown in Fig. 2*A* do not affect T synthesis[146]. Recently, a SV40-associated small RNA (SAS RNA) of unknown function, induced late in infection, has been identified that can associate with early viral mRNA near the 3′ end of the coding region (Fig. 3*A*) (ref. 147 and P. Berg, personal communication). If small RNAs indeed mediate splicing, a third splicing arrangement for SV40 'early' messengers may exist.

The messenger RNA map of polyoma is shown in Fig. 3*A*. Initiation of early transcription probably occurs near the beginning of the early region, because a defective genome that contains only tandemly repeated copies of the replication origin is an efficient template for early RNA synthesis[148]. With polyoma, evidence for organization of early genes is provided by alignment of open reading frames in early DNA with known early proteins encoded by the wild type and by deletion mutants. This analysis identifies early coding regions with splices analogous to those for SV40 T and t (refs 138, 149–151) and predicts proteins with highly homologous amino acid sequences^{127,132,152}. As with SV40, deletions in the t gene between coordinates 80 and 85 (hr-t deletions shown in Fig. 3*A*) do not change the apparent size of T^{153}. Downstream from the t gene, two reading frames are open for translation, suggesting that the T gene is overlapped by a second, out of phase, coding sequence. Polyoma encodes a third major early protein, the 55 kilodalton middle T, which shares amino-terminal peptides with T and t but differs at the carboxy terminus$^{154-159}$. Messenger RNA for T is synthesized according to a third early splicing pattern which also removes the t terminator, but joins the coding sequences for the amino terminus to the second large open reading frame, which is shifted with respect to the T frame. The frame-shifted overlap of polyoma middle T and T mRNAs results in differing carboxy termini for the two antigens, encoded by the same DNA segment, and is reminiscent of the cistron *D–E* and *A–B* overlaps in ΦX174 (ref. 158).

Both polyoma and SV40 encode three late proteins, VP1, VP2 and VP3, which are structural components of the virion^{131,159}. Mapping of nascent late transcripts places the start site for the late SV40 transcription a short distance upstream from coordinate 0.735, very near the region of the DNA which encodes the late mRNA 5′ termini, as shown in Fig. 2*B*, and suggests transcription initiation at the cap sites^{160}. The SV40 late messengers have heterogeneous capped 5′ termini encoded in a ~400-residue region adjacent to the replication origin (Fig. 4)$^{161-163}$. As with Ad-2, capped purine 5′ ends predominate greatly over pyrimidines. Two 5′ termini starting with AUU account for the majority of the species^{164,165}. A deletion mutant of SV40, d1-1811, mapped in Fig. 3*B*, which lacks the major cap site is, however, viable and transcribes mRNAs which have 5′ termini that are minor components in a wild-type infection^{166}. Polyoma late mRNAs also have heterogeneous 5′ termini. Three of these have been mapped in the genomes by sequencing and arise from a cluster, again with purines favoured over pyrimidines^{167}.

T antigen function

SV40 T antigen, as well as a protein encoded by the adenovirus–SV40 hybrid D2 which contains the carboxy-terminal sequence of T antigen, binds to the SV40 DNA replication origin, protecting the region shown in Fig. 4^{168,169}. The 5′ end of the early (T antigen) messenger RNA is encoded within the binding site for this antigen^{140}. Thus, T antigen may regulate its own synthesis, possibly through binding to the initiation site for its mRNA. This idea is supported by the overproduction of early mRNA by ts A mutants of SV40 at the non-permissive temperature$^{169-174}$. Post-transcriptional steps may also regulate early mRNA synthesis. In undifferentiated embryonal carcinoma cells, early mRNA is transcribed but it is neither spliced nor transported to the cytoplasm^{176}. However, when these cells are stimulated by retinoic acid to differentiate, early transcripts are processed into early mRNA^{175}.

The replication origin

In binding to the SV40 origin, successive T antigen molecules are added in the direction of the late cap site(s)^{169}. Functional T antigen is required for the initiation of each round of DNA replication^{177,178}, and DNA replication is in turn required for the onset of the late stage of transcription. However, if replication has already commenced, a temperature shift of a ts T antigen mutant which halts DNA replication permits continued transcription of late RNA^{179}. Late RNA sequences are also detected in the nucleus at low levels at early times before DNA replication$^{180-182}$, or when DNA replication has been blocked with ts T antigen mutants^{183}. Similarly, polyoma 'late' sequences may be detected at early times, before DNA replication, at a stage when late mRNA is not yet being synthesized^{184}. These observations imply that late RNA synthesis is not strictly dependent upon DNA replication. SV40 DNA may be isolated as a 'minichromosome' complex which contains histones in a beaded nucleosomal structure^{185}. A short region of this complex which extends from the origin of DNA replication to the late cap sites (coordinates 0.67 to 0.73, Fig. 4) is preferentially cleaved by a variety of nucleases, suggesting that these residues are exposed to the solvent, rather than being masked by the histones of nucleosomal beads$^{186-188}$. This same region contains the proposed SV40 RNA initiation sites, and if this structure is maintained *in vivo*, exposure of the putative promoters to the

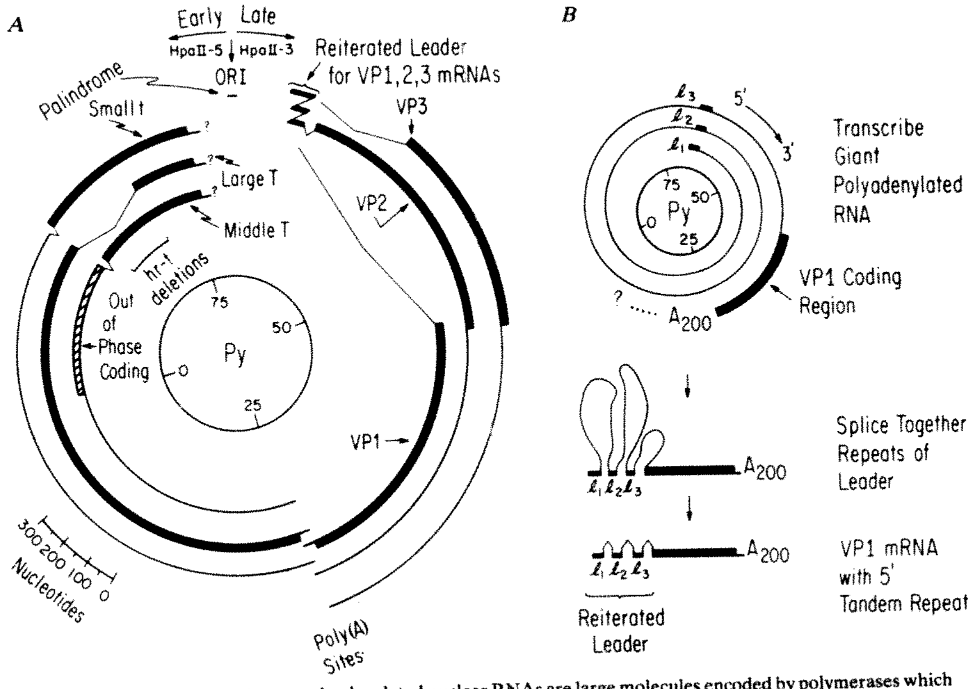

Fig. 3 Polyoma messenger RNAs. *A*, Messenger RNA map. As with SV40 (Fig. 2), the 5′ termini of polyoma mRNAs map near the origin of DNA replication (ORI). The sequence of the ORI contains an inverted repeat palindrome which overlaps the junction of fragments 3 and 5 from *Hpa*II restriction endonuclease digests of polyoma DNA. Early mRNAs are from anticlockwise transcripts, and late from clockwise transcripts. Polyoma synthesizes three early mRNA species which encode the tumour antigens small t, large T, and middle T. Although the exact splice points for the early mRNAs have not been determined, the t and T messengers have splicing patterns comparable to those of the equivalent SV40 mRNAs. With the mRNA for T, splicing allows translation to continue beyond the t gene. Translation enters the region encoding T, however, in a second out of phase reading frame generating a novel carboxy-terminal sequence for T. The arrangement of coding sequences in the polyoma late messengers is analogous to those of SV40 (see Fig. 2) and the polyoma mRNAs also have heterogeneous capped 5′ termini (not shown). The 5′ leader, however, contains a novel tandemly reiterated sequence (see below). The hr-t deletions are discussed in the text. *B*, Polyoma VP1 mRNA synthesis. At the late stage of infection, polyoma polyadenylated nuclear RNAs are large molecules encoded by polymerases which make several transits of the circular genome. These polymerases can transcribe the late poly(A) acceptor sequence without addition of poly(A), on one transit, but use the poly(A) acceptor sequence on a subsequent pass (compare with late Ad-2 in Fig. 1). It is not established whether this 3′ end is formed by RNA cleavage. The mature mRNA contains a 5′ leader with tandem repeats (1_1, 1_2, 1_3) of a sequence that exists only once in the genome. The reiteration results from the splicing together of each occurrence of this sequence within the giant polyadenylated RNA and joining the repeated structure to the VP1 (shown here), VP2 or VP3 coding sequences. See text for refs.

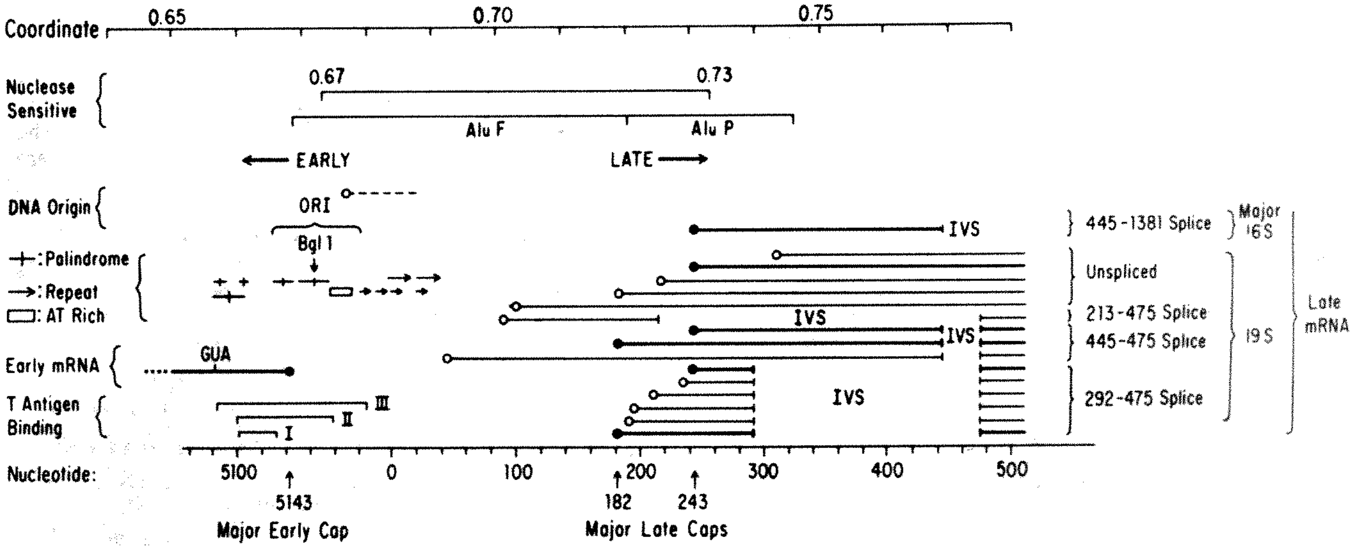

Fig. 4 Organization of transcripts and DNA sequences within the ORI region of SV40. A detailed map of the DNA replication origin (ORI) region of SV40 between coordinates 0.64 and 0.78 is shown (compare with Fig. 2). This region encodes the cap structure (●—, major species; ○—, minor species) of SV40 early (transcribed 5′ to 3′ leftward here) and late (transcribed right) mRNAs. The AUG of early mRNA which encodes the amino terminus of T and t tumour antigens is shown. The limits of ORI defined by deletion mutants are indicated. ORI contains a 27-base inverted repeat sequence centred on the *Bgl*I restriction endonuclease cleavage site, and is flanked by various direct and palindromic inverted repeat sequences and an A+T-rich region. The sequence of one arm of the central palindrome is also highly repeated in several animal cell DNAs. The SV40 T tumour antigen, and related proteins, bind as mono-, di- or trimers to the ORI DNA and protect, respectively, sequences I–III from DNase digestion. Because the cap site for early mRNA lies within this binding site, T antigen may autogenously regulate its synthesis by repressing transcription of its mRNA. The capped 5′ termini of late mRNAs are heterogeneous and encoded within a ~400-nucleotide region adjacent to the ORI. SV40 minichromosomes are sensitive to nuclease in this region. DNase 1 preferentially cleaves between coordinates 0.67 and 0.75 and restriction enzymes such as *Alu*I release the restriction fragments *Alu* F and *Alu* P more rapidly than other fragments. Intervening sequences (IVS) and splice sites for late 19S and 16S mRNAs are shown. See text for refs.

nucleoplasm could facilitate RNA polymerase binding to the DNA.

During bi-directional SV40 DNA replication, if new histone synthesis is blocked by cycloheximide, parental histones distribute themselves asymmetrically, with 80–90% segregating with the 'leading' side of the two DNA replication forks[189]. With SV40, the parental DNA which is the template for the leading side of DNA replication (at both forks) is also the template for mRNA. In the cell, nucleosomes also preferentially associate with DNA template strands which code for stable cell nuclear RNA. Thus, replication origins and RNA initiation sites may have similar arrangements in the cell and the virus[189].

It has recently been shown that a major class of DNA repeat sequences found in animal cells contains a 15-nucleotide sequence which is homologous with a sequence at the SV40 DNA replication origin[190]. The 15-nucleotide sequence forms one half of a palindrome which is centred about the *Bgl*I cut site of the virus at coordinate 67 (Fig. 4). In the cell, these sequences are interspersed between many genes[191], including those of the mouse β-globin gene cluster[190] where, in an *in vitro* transcription system, they are transcribed by RNA polymerase III[192]. The homologous sequence is also found at the DNA replication origins of polyoma, BK virus and hepatitis B virus, and within a small RNA which hydrogen bonds to mRNA[190]. Although it is possible that these repeats in the cell are DNA replication origins interspersed between transcription units, and are cellular targets of T antigen, their function has not been established.

Formation of the polyadenylated 3′ end

The polyadenylated 3′ ends of SV40 early and late mRNA converge at coordinate 17 and overlap[126]. As indicated in Fig. 3*B*, SV40 late transcription continues in an equimolar fashion at least 1,000 residues beyond the poly(A) site of late mRNA, implying that a cleavage event forms the 3′ end[160,193]. With polyoma, polyadenylated late nuclear transcripts are giant RNA molecules (see Fig. 3*B*), two or three times larger than genome length[194,195]. These probably result from multiple transits of the polymerase around the circular genome. Just as polymerases transcribing Ad-2 late RNA can pass five poly(A) sites but use only one, so polymerases may make several passes across the late polyoma poly(A) site before a functional poly(A) receptor is synthesized. For both papovaviruses, the AAUAAA hexanucleotide homology is found adjacent to early and late poly(A) sites[126,131].

Splicing papovavirus late mRNA

The predominant late RNA sequences in the nucleus are unspliced and extend from the cap site(s) to the poly(A) site. This suggests that capping and polyadenylation precede splicing[193]. Splicing of SV40 yields, with approximately equal efficiency[196], two major size classes of mRNA: 18S–19S, which encodes VP2 and VP3, and 16S, which encodes VP1[126,197,198]. At least two alternative forms of 19S mRNA are found which differ in the splicing of the 5′ leader (Fig. 4)[162]. For both forms, the 5′ leader is non-coding, and the same AUG which lies within the main body of the mRNA is utilized for initiation of VP2 translation[162]. To form the VP1 mRNA, a much larger intervening sequence is removed, and the leader is juxtaposed to a second downstream AUG which initiates VP1 translation[199]. In fact, this AUG lies within the VP2 gene, but the VP1 and VP2 gene sequences which overlap are read in different frames. The mRNA for VP3 is not well characterized, but the gene for this third late SV40 protein forms a 3′-co-terminal overlap with the VP2 mRNA, and utilizes an internal AUG codon of VP2 for the start of translation[200]. The choices of splice available for forming SV40 late 3′-co-terminal mRNA shown in Fig. 2*B* directly parallels the Ad-2 splice choice of Fig. 1.

Late mRNA species from SV40 can survive the deletion of large segments of their leaders without loss of function[201,210,211]. Integrity of the splicing sites themselves, however, is a prerequisite for stable mRNA synthesis. If the splice junction on one or both sides of an intervening sequence is deleted, the transcript is destabilized and is degraded in the nucleus[202–205]. The short sequence homologies at splice sites, GU at the donor (5′) side and AG at the acceptor (3′) side, found in cellular genes[206], are also found for SV40 (ref. 162).

Although the arrangement of late genes and mRNAs in polyoma[207,208] is very similar to that in SV40, the existence of the giant polyadenylated polyoma nuclear species apparently permits splicing mechanisms to form mature mRNA leaders with a novel structure. The polyoma late mRNAs contain a sequence which is reiterated in the 5′ leader, but which occurs only once in the DNA[209]. In the processing model which explains this paradox (Fig. 3*B*), giant polyoma transcripts are spliced to join together each occurrence of the repeat sequence in giant RNA to form a reiterated leader structure[209]. SV40 late mRNA also has reiterated leaders, but with a lower frequency, consistent with the shorter average size of nuclear transcripts[212].

Conclusions

Studies of DNA virus transcription suggest a common pathway for the synthesis of many viral mRNAs that includes initiation at the cap site, transcription of the mRNA precursor beyond the functional poly(A) site, cleavage and polyadenylation to form the 3′ end, followed by splicing and transport. Many features of this pathway are likely to be shared with the cell. The viruses have, however, evolved complex arrangements of coding sequences and sites for initiation, splicing and polyadenylation of RNA which use the pathway to maximum advantage. The next task is to identify the steps in these pathways that are regulated, and to identify the viral and cellular components which exert control.

I thank J. Darnell, C. Baker, M. Moore, P. Snyder, A. Shaw, M. Wilson, M. T. Hsu, R. Lamb and P. Deininger for stimulating discussions, T. Broker, L. Chow and J. Lewis for providing Fig. 1*B*, and the American Cancer Society for a Faculty Research Award.

1. Darnell, J. *Prog. Nucleic. Acid Res. molec. Biol.* **22,** 327–353 (1979).
2. Seiff, I., Khoury, G. & Dhar, R. *Cell* **18,** 963–97 (1979).
3. Philipson, L. *Adv. Virus Res.* **25,** 357–405 (1979).
4. Wallace, R. & Kates, J. *J. Virol.* **9,** 627–635 (1972).
5. Price, R. & Penman, S. *J. Virol.* **9,** 621–626 (1972).
6. Sharp, P. A., Gallimore, P. H. & Flint, S. J. *Cold Spring Harb. Symp. quant. Biol.* **39,** 457–474 (1975).
7. Pettersson, U., Tibbetts, C. & Philipson, L. *J. molec. Biol.* **101,** 479–501 (1976).
8. Berk, A. J. & Sharp, P. A. *Cell* **12,** 721–732 (1977).
9. Westphal, R. & Lai, S. D. *J. molec. Biol.* **116,** 525–548 (1977).
10. Lewis, J. B. *et al. Cell* **7,** 141–151 (1976).
11. Buttner, W., Veres-Molnar, Z. & Green, M. *J. molec. Biol.* **107,** 93–114 (1976).
12. Chow, L., Broker, T. & Lewis, J. *J. molec. Biol.* **134,** 265 (1979).
13. Chow, L. T., Roberts, J. M., Lewis, J. B. & Broker, T. R. *Cell* **11,** 819–836 (1977).
14. Berk, A. J. & Sharp, P. A. *Cell* **14,** 695–711 (1978).
15. Kitchingman, G., Lai, S. & Westphal, H. *Proc. natn. Acad. Sci. U.S.A.* **74,** 4392–4395 (1977).
16. Chow, L. T., Lewis, J. R. & Broker, T. R. *Cold Spring Harb. Symp. quant. Biol.* **44** (in the press).
17. Evans, R. M. *et al. Cell* **12,** 733–739 (1977).
18. Berk, A. J. & Sharp, P. A. *Cell* **12,** 45–55 (1977).
19. Wilson, M., Fraser, N. & Darnell, J. *Virology* **94,** 175–184 (1979).
20. Sehgal, P., Fraser, N. & Darnell, J. *Virology* **94,** 185–191 (1979).
21. Hashimoto, S. & Green, M. *Virology* **94,** 254–272 (1979).
22. Baker, C. C. & Ziff, E. B. *Cold Spring Harb. Symp. quant. Biol.* (in the press).
23. Baker, C. C., Herisse, J., Courtois, G., Galibert, F. & Ziff, E. *Cell* **18,** 569–580 (1979).
24. Pribnow, D. in *Biological Regulation and Development* Vol. 1 (ed. Goldberger, R.) 219–277 (Plenum, New York, 1979).
25. Gallimore, P. H., Sharp, P. A. & Sambrook, J. *J. molec. Biol.* **89,** 49 (1974).
26. Graham, F. L. *et al. Cold Spring Harb. Symp. quant. Biol.* **39,** 637 (1975).
27. Flint, S. J., Gallimore, P. H. & Sharp, P. A. *J. molec. Biol* **96,** 47 (1975).
28. van der Eb, A. J., Mulder, C., Graham, F. L. & Houweling, A. *Gene* **2,** 115 (1977).
29. van Ormondt, H., Maat, J., de Waard, A. & van der Eb, A. J. *Gene* **4,** 309 (1978).
30. Maat, J. & van Ormondt, H. *Gene* **6,** 75 (1979).
31. Berk, A. J., Lee, F. Harrison, T., Williams, J. & Sharp, P. A. *Cell* **17,** 935–944 (1979).
32. Harrison, T., Graham, F. & Williams, J. *Virology* **77,** 319–329 (1977).
33. Ginsberg, H., Ensinger, M., Kauffman, R., Mayer, J. & Lundholm, V. *Cold Spring Harb. Symp. quant. Biol.* **39,** 419–429 (1974).
34. van der Vliet, Levine, P. A., Ensinger, M. & Ginsberg, H. *J. Virol.* **15,** 348–354 (1975).
35. Ross, S. & Levine, A. J. *Virology* **99,** 427–430 (1979).
36. Persson, H., Oberg, B. & Philipson, L. *J. Virol.* **28,** 119 (1978).
37. Galos, R. S., Williams, J., Binger, M. H. & Flint, S. J. *Cell* **17,** 945–956 (1979).
38. Nevins, J. R., Ginsberg, H. S., Blanchard, J. M., Wilson, M. C. & Darnell, J. E. *J. Virol.* **32,** 727–733 (1979).
39. Perricaudet, M., Akusjarvi, G., Virtanen, A. & Pettersson, U. *Nature* **281,** 694 (1979).
40. Wilson, M. C., Nevins, J. R., Blanchard, J. M. & Darnell, J. E. Jr *Cold Spring Harb. Symp. quant. Biol.* (in the press).
41. Spector, D. J., McGrogan, M. & Raskas, H. J. *J. molec. Biol.* **126,** 395–414 (1978).
42. Pettersson, U. & Mathews, M. B. *Cell* **12,** 741–750 (1977).
43. Aelstrom, P. *et al. Cell* **19,** 671–681 (1980).
44. Persson, H. V., Pettersson, U. & Mathews, M. B. *Virology* **90,** 67–79 (1978).
45. Jones, N. & Shenk, T. *Proc. natn. Acad. Sci. U.S.A.* **76,** 3665–3669 (1979).
46. Jones, N. & Shenk, T. *Cell* **17,** 683–689 (1979).
47. Eggerding, F. & Raskas, H. J. *J. Virol.* **25,** 453–458 (1978).
48. Blanton, R. & Carter, T. *J. Virol.* **29,** 458–465 (1979).
49. Carter, T. & Blanton, R. *J. Virol.* **28,** 450–456 (1978).
50. Carter, T. & Blanton, R. *J. Virol.* **25,** 664–674 (1978).
51. Craig, E. & Raskas, H. *J. Virol.* **14,** 26–32 (1974).
52. van der Vliet, P. C. & Levine, A. J. *Nature new Biol.* **246,** 170–174 (1973).
53. Fowlkes, D. M., Lord, S. T., Linne, T., Pettersson, U. & Philison, L. *J. molec. Biol.* **132,** 163–180 (1979).
54. Nevins, J. & Winkler, J. *Proc. natn. Acad. Sci. U.S.A.* (in the press).
55. Feldman, L. A., Butel, J. & Rapp, F. *J. Bact.* **91,** 813–818 (1966).
56. Friedman, M. P., Lyons, M. J. & Ginsberg, H. S. *J. Virol.* **5,** 586–597 (1970).
57. Hashimoto, K., Nahajima, K., Oda, K. & Shimojo, H. *J. molec. Biol.* **81,** 207, 223 (1973).
58. Rabson, A. S., O'Conor, G. T., Berezesky, I. K. & Paul, F. J. *Proc. Soc. exp. Biol. Med.* **116,** 187–190 (1964).
59. Eron, L., Westphal, H. & Khoury, G. *J. Virol.* **15,** 1256–1261 (1975).
60. Klessig, D. F. & Anderson, C. W. *J. Virol.* **16,** 1650–1668 (1975).
61. Klessig, D. F. & Chow, L. T. *J. molec. Biol.* **139,** 221–242 (1980).
62. Kelly, T. J. Jr & Lewis, A. M. Jr *J. Virol.* **12,** 643–652 (1973).
63. Lewis, A. M. Jr *et al. J. Virol.* **11,** 655–664 (1973).
64. Morrow, J. F., Berg, P., Kelley, T. J. Jr & Lewis, A. M. Jr *J. Virol.* **12.** 653–658 (1973).
65. Cole, C. N., Crawford, L. V. & Berg, P. *J. Virol.* **30,** 683–691 (1979).
66. Tijan, R., Fey, G. & Graessman, A. *Proc. natn. Acad. Sci. U.S.A.* **75,** 1279–1283 (1978).
67. Klessig, D. F. & Grodzicker, T. *Cell* **17,** 957–966 (1979).
68. Beltz, G. A. & Flint, S. J. *J. molec. Biol.* **131,** 353–373 (1979).
69. Chow, L. T., Gelinas, R. E., Broker, T. R. & Roberts, R. J. *Cell* **12,** 1–8 (1977).
70. Berget, S., Moore, C. & Sharp, P. A. *Proc. natn. Acad. Sci. U.S.A.* **74,** 3171–3175 (1977).
71. Klessig, D. F. *Cell* **12,** 9–21 (1977).
72. Zain, S. *et al. Cell* **16,** 851 (1979).
73. Ziff, E. B. & Evans, R. M. *Cell* **15,** 1463–1476 (1978).
74. Akusjarvi, G. & Pettersson, U. *J. molec. Biol.* **134,** 143–158 (1979).
75. Gelinas, R. E. & Roberts, R. *Cell.* **11,** 533–544 (1977).
76. Berget, S. M., Flint, S. J., Williams, J. F. & Sharp, P. A. *J. Virol.* **19,** 879–889 (1976).
77. Carter, T. H. & Ginsberg, H. S. *J. Virol.* **18,** 156–166 (1976).
78. Cowan, K. P. Tegtmeyer, P. & Anthony, D. D. *Proc. natn. Acad. Sci. U.S.A.* **70,** 1927–1930 (1973).
79. Bachenheimer, S. & Darnell, J. E. *Proc. natn. Acad. Sci. U.S.A.* **72,** 4445–4449 (1975).
80. Weber, J., Jelinek, W. & Darnell, J. E. *Cell* **10,** 911–616 (1977).
81. Goldberg, S., Weber, J. & Darnell, J. E. Jr *Cell* **10,** 617–621 (1977).
82. Evans, R., Weber, J., Ziff, E. & Darnell, J. E. *Nature* **278,** 367–370 (1979).
83. Manley, J., Sharp, P. A. & Gefter, M. *Proc. natn. Acad. Sci. U.S.A.* **74,** 5323–5327 (1979).
84. D. Hogness, Goldberg, M. & Lifton, R. (personal communication).
85. Konkel, D. A., Tilghman, S. M. & Leder, P. *Cell* **15,** 1125–1132 (1978).
86. Cochet, M. *et al. Nature* **282,** 567–574 (1979).
87. Weil, P. A., Luse, D. S., Segall, J. & Roeder, R. G. *Cell* **18,** 469–484 (1979).
88. Manley, J. L., Fire, A., Cano, A., Sharp, P. A. & Gefter, M. L. *Proc. natn. Acad. Sci. U.S.A.* (in the press).
89. Fraser, N. W., Sehgal, P. & Darnell, J. E. *Proc. natn. Acad. Sci. U.S.A.* **76,** 2571–2575 (1979).
90. Fraser, N. W., Sehgal, P. B. & Darnell, J. E. *Nature* **272,** 590–593 (1979).
91. Fraser, N. & Ziff, E. *J. molec. Biol.* **124,** 27–51 (1978).
92. Ziff, E. B. & Fraser, N. *J. Virol.* **25,** 897–906 (1978).
93. Nevins, J. R. & Darnell, J. E. *J. Virol.* **25,** 811–823 (1978).
94. McGrogan, M. & Raskas, H. J. *Proc. natn. Acad. Sci. U.S.A.* **75,** 625–629 (1978).
95. Nevins, J. R. & Darnell, J. E. *Cell* **15,** 1477–1494 (1978).
96. Berget, S. M. & Sharp, P. A. *J. molec. Biol.* **129,** 547–565 (1979).
97. Manley, J. L., Sharp, P. A. & Gefter, M. L. *J. molec. Biol.* **135,** 171–197 (1979).
98. Goldenberg, C. J. & Raskas, H. J. *Cell* **16,** 131–138 (1979).
99. Craig, E. A. & Raskas, H. J. *Cell* **8,** 205–213 (1976).
100. Craig, E. A., Sayavedra, M. & Raskas, H. J. *Virology* **77,** 545–555 (1977).
101. Weber, J., Blanchard, J. M., Ginsberg, H. S. & Darnell, J. *J. Virol.* (in the press).
102. Blanchard, J. M., Weber, J., Jelinek, W. & Darnell, J. E. *Proc. natn. Acad. Sci. U.S.A.* **75,** 5344–5348 (1978).
103. Fraser, N. W., Nevins, J. R., Ziff, E. & Darnell, J. E. *J. molec. Biol.* **129,** 643–656 (1979).
104. Flint, S. J. & Sharp, P. A. *J. molec. Biol.* **106,** 749–771 (1976).
105. Lewis, J. B., Anderson, C. W. & Atkins, J. F. *Cell* **12,** 37–44 (1979).
106. Anderson, C. W., Lewis, J. B., Atkins, J. F. & Gesteland, R. F. *Proc. natn. Acad. Sci. U.S.A.* **71,** 2756–2760 (1974).
107. Paterson, B. M., Roberts, B. E. & Kuff, E. L. *Proc. natn. Acad. Sci. U.S.A.* **74,** 4370–4374 (1977).
108. Akusjarvi, G. & Pettersson, U. *Cell* **16,** 841–850 (1979).
109. Akusjarvi, G. & Pettersson, U. *Proc. natn. Acad. Sci. U.S.A.* **75,** 5822–5826 (1978).
110. Nevins, J. R. *J. molec. Biol.* **130,** 493–506.
111. Chow, L. T. & Broker, T. *Cell* **15,** 497–510 (1978).
112. Dunn, A. R., Mathews, M. B., Chow, L. T., Sambrook, J. & Keller, W. *Cell* **15,** 511–526 (1979).
113. Akusjarvi, G. & Pettersson, U. *J. molec. Biol.* **135,** 171–197 (1979).
114. Roberts, R. *Nature* **283,** 132–133 (1980).
115. Mathews, M. B. *Cell* **6,** 223–229 (1975).
116. Soderlund, H., Pettersson, U., Vennstrom, B., Philipson, L. & Mathews, M. B. *Cell* **7,** 585–593 (1976).
117. Mathews, M. B. & Pettersson, U. *J. molec. Biol.* **119,** 293–328 (1978).
118. Celma, M. L., Pan, J. & Weissman, S. M. *J. biol. Chem.* **252,** 9032–9042 (1977).
119. Murray, V. & Holliday. R. *FEBS Lett.* **106,** 5–7 (1979).
120. Chen-Kiang, S., Nevins, J. R. & Darnell, J. E. Jr *J. molec. Biol.* **135,** 733–752 (1980).
121. Sambrook, J. P., Sharp, A. & Keller, W. *J. molec. Biol.* **70,** 57–71 (1974).
122. Kamen, R., Lindstrom, D. M., Sure, H. & Old. R. *Cold Spring Harb. Symp. quant. Biol.* **39,** 187–198 (1974).
123. Kamen, R., Sedat, J. & Ziff, E. *J. Virol.* **17,** 212–218 (1976).
124. Khoury, G., Martin, M. A., Lee, T. N., Danna, K. J. & Nathans, D. *J. molec. Biol.* **78,** 377–389 (1973).
125. Fiers, W. *et al. Nature* **273,** 113 (1978).
126. Reddy, V. B. *et al. Science* **200,** 494–502 (1978).
127. Soeda, E., Arrand, J. R., Smolar, N. & Griffin, B. E. *Cell* **17,** 357–370 (1979).
128. Soeda, E. *et al. Nucleic Acids Res* **7,** 839–859 (1979).
129. Friedmann, T., Doolittle, R. F. & Walter, G. *Nature* **274,** 291–293 (1978).
130. Friedmann, T., LaPorte, P. & Esty, A. *J. biol. Chem.* **253,** 6561–6567 (1978).
131. Deininger, P., Esty, A., LaPorte, P. & Friedmann, T. *Cell* **18,** 771–779 (1979).
132. Friedmann, T., Esty, A., LaPorte, P. & Deininger, P. *Cell* **17,** 715–724 (1979).
133. Tooze, J. *The Molecular Biology of Tumor Viruses* (Cold Spring Harbor Laboratory, New York, 1973).
134. Prives, C., Gilboa, E., Revel, M. & Winocour, E. *Proc. natn. Acad. Sci U.S.A.* **74,** 457–461 (1977).
135. Crawford, L. V. *et al. Proc. natn. Acad. Sci. U.S.A.* **75,** 117–121 (1978).
136. Sleigh, M. J., Topp, W. C., Hanich, R. & Sambrook, J. F. *Cell* **14,** 79–88 (1978).
137. Bouck, N., Beales, N., Schenk, T., Berg, P. & Di Mayorca, G. *Proc. natn. Acad. Sci. U.S.A.* **75,** 2473–2477 (1978).
138. Rigby, P. *Nature* **282,** 781 (1979).
139. Berk, A. J. & Sharp, P. A. *Proc. natn. Acad. Sci. U.S.A.* **75,** 1274–1278 (1978).
140. Reddy, V. B., Ghosh, P. K., Lebowitz, P., Pintak, M. & Weissman, S. M. *J. Virol.* **30,** 279–296 (1979).
141. Paucha, E. & Smith, A. E. *Cell* **15,** 1011–1020 (1978).
142. Volckaert, G., van de Voorde, A. & Fiers, W. *Proc. natn. Acad. Sci. U.S.A.* **75,** 2160–2164 (1978).

143. Paucha, E., Harvey, R. & Smith, A. E. *J. Virol.* **28,** 154–170 (1978).
144. Paucha, E. *et al. Proc. natn. Acad. Sci. U.S.A.* **75,** 2165–2169 (1978).
145. Simmons, D. T. & Martin, M. A. *Proc. natn. Acad. Sci. U.S.A.* **75,** 1131–1135 (1978).
146. Thimmappaya, B. & Shenk, T. *J. Virol.* **30,** 668–673 (1979).
147. Alwine, J. C., Dhar, R. & Khoury, G. *Proc. natn. Acad. Sci. U.S.A.* **77,** 1379–1383 (1980).
148. Condit, R., Cowie, A., Kamen, R. & Fried, M. *Proc. natn. Acad. Sci. U.S.A.* **75,** 69–73 (1978).
149. Soeda, E. & Griffin, B. E. *Nature* **276,** 294–298 (1978).
150. Hattori, J., Charmichael, G. G. & Benjamin, T. L. *Cell* **16,** 505–513 (1979).
151. Favloro, J., Treisman, R. & Kamen, R. *Meth. Enzym.* (in the press).
152. Friedmann, T., Doolittle, R. F. & Walter, G. *Nature* **274,** 291–293 (1978).
153. Silver, J., Schaffhausen, B. & Benjamin, T. *Cell* **15,** 485–496 (1978).
154. Ito, Y., Brocklehurst, J. R. & Dulbecco, *Proc. natn. Acad. Sci. U.S.A.* **74,** 4666–4670 (1977).
155. Hutchinson, M. A., Hunter, T. & Eckhart, W. *Cell* **15,** 65–77 (1978).
156. Smart, J. E. & Ito, Y. *Cell* **15,** 1427–1437 (1978).
157. Ito, Y. *Virology* **98,** 261 (1979).
158. Barrell, B. G., Air, G. M. & Hutchinson, C. A. III *Nature* **264,** 34–41 (1976).
159. Fried, M. & Griffin, B. *Adv. Cancer Res.* **24,** 67–114 (1977).
160. Ford, J. P. & Hsu, M. T. *J. Virol.* **28,** 795–801 (1978).
161. Groner, Y., Carmi, P. & Aloni, Y. *Nucleic Acids Res.* **4,** 3959–3968 (1977).
162. Ghosh, P., Reddy, V., Swinscoe, J., Lebowitz, P. & Weissman, S. *J. molec. Biol.* **126,** 813–846 (1978).
163. Canaani, D., Kahana, C., Mukamel, A. & Groner, Y. *Proc. natn. Acad. Sci. U.S.A.* **76,** 3078–3082 (1979).
164. Hageman, G. & Fiers, W. *Nucleic Acids Res.* **5,** 2359–2371 (1978).
165. Hageman, G. & Fiers, W. *J. Virol.* **25,** 824–830 (1978).
166. Haegeman, G., van Heuverswyn, H., Gheysen, D. & Fiers, W. *J. Virol.* **31,** 484–493 (1979).
167. Flavell, A. S., Legon, S., Cowie, A. & Kamen, R. *Cell* **16,** 357–371 (1979).
168. Reed, S. I., Ferguson, J., Davies, R. N. & Stark, G. *Proc. natn. Acad. Sci. U.S.A.* **72,** 1605–1609 (1975).
169. Tijan, R. *Cell* **13,** 165–179 (1978).
170. Tegtmeyer, P., Schwarz, M., Collins, J. K. & Rundell, K. *J. Virol.* **16,** 168–178 (1975).
171. Alwine, J. C., Reed, S. I. & Stark, G. R. *J. Virol.* **24,** 22–27 (1977).
172. Reed, S. I., Stark, G. R. & Alwine, J. C. *Proc. natn. Acad. Sci. U.S.A.* **73,** 3083–3087 (1976).
173. Khoury, G. & May, E. *J. Virol.* **23,** 167–176 (1977).
174. Reed, S. I., Stark, G. R. & Alwine, J. C. *Proc. natn. Acad. Sci. U.S.A.* **73,** 3083–3087 (1976).
175. Segal, S., Levine, A. J. & Khoury, G. *Nature* **280,** 335–338 (1979).
176. Segal, S. & G. Khoury, *Proc. natn. Acad. Sci. U.S.A.* **76,** 5611–5615 (1979).
177. Chou, J. Y., Avila, J. & Martin, R. G. *J. Virol.* **14,** 116–124 (1974).
178. Tegtmeyer, R. *J. Virol.* **10,** 591–598 (1972).
179. Cowan, K., Tegtmeyer, P. & Anthony, D. D. *Proc. natn. Acad. Sci. U.S.A.* **70,** 1927–1930 (1973).
180. Salzman, N., Ferdinand, F., Brown, M. & Khoury, G. *Proc. natn. Acad. Sci. U.S.A.* **74,** 5443–5447 (1977).
181. Ferdinand, F. J., Brown, M. & Khoury, G. *Proc. natn. Acad. Sci. U.S.A.* **74,** 5443–5447 (1977).
182. Parker, B. A. & Stark, G. R. *J. Virol.* **31,** 360–369 (1979).
183. Khoury, G. & May, E. *J. Virol.* **23,** 167–176 (1977).
184. Piper, P. W. *J. molec. Biol.* **131,** 399–407 (1979).
185. Griffith, J. D. *Science* **187,** 1262–1203 (1975).
186. Varshavsky, A. J., Sundin, O. & Bohn, M. *Cell* **16,** 453–466 (1979).
187. Scott, W. A. & Wigmore, D. J. *Cell* **15,** 1511–1518 (1978).
188. Walbeck, W., Fohring, G., Chowdhury, A., Gruss, P. & Sawer, G. *Proc. natn. Acad. Sci. U.S.A.* **75,** 5969–5968 (1978).
189. Seidman, M. M., Levine, A. J. & Weintraub, H. *Cell* **18,** 439–449 (1979).
190. Jelinek, W. R. *et al. Proc. natn. Acad. Sci. U.S.A.* **77,** 1398–1402 (1980).
191. Jelinek, W. R. *Proc. natn. Acad. Sci. U.S.A.* **75,** 2679–2683 (1978).
192. Duncan, C. *et al. Proc. natn. Acad. Sci. U.S.A.* **76,** 5095–5099 (1979).
193. Lai, C. J., Dhar, R. & Khoury, G. *Cell* **14,** 971–982 (1978).
194. Acheson, N. H., Buetti, E., Scherrer, K. & Weil, R. *Proc. natn. Acad. Sci. U.S.A.* **68,** 2231–2235 (1971).
195. Birg, F., Favloro, J. & Kamen. R. *Proc. natn. Acad. Sci. U.S.A.* **74,** 3138–3142 (1977).
196. Ford, J., Cozzitorto, J. & Hsu, M. T. *J. Virol.* (in the press).
197. Hsu, M. T. & Ford, J. *Proc. natn. Acad. Sci. U.S.A.* **74,** 4982–4985 (1977).
198. Aloni, Y., Dhar, R., Laub, O., Horowitz, M. & Khoury, G. *Proc. natn. Acad. Sci. U.S.A.* **74,** 3686–3690 (1977).
199. Ghosh, P. *et al. J. biol. Chem.* **253,** 3643–3647 (1978).
200. Contreras, R., Rogiers, R., van de Voorde, A. & Fiers, W. *Cell* **12,** 529–538 (1977).
201. Subramanian, K. N. *Proc. natn. Acad. Sci. U.S.A.* **76,** 2556–2560 (1979).
202. Lai, C. J. & Khoury, G. *Proc. natn. Acad. Sci. U.S.A.* **76,** 71–75 (1979).
203. Cruss, P., Lai, C. J., Dhar, R. & Khoury, G. *Proc. natn. Acad. Sci. U.S.A.* **76,** 4317–4321 (1979).
204. Hamer, D. H., Smith, K. D., Boyer, S. H. & Leder, P. *Cell* **17,** 725–735 (1979).
205. Volkaert, G., Feunteun, J., Crawford, L. V., Berg, P. & Fiers, W. *J. Virol.* **30,** 674–682 (1979).
206. Breathnach, R., Benoist, C., O'Hare, K., Gannon, F. & Chambon, P. *Proc. natn. Acad. Sci. U.S.A.* **75,** 4853–4957 (1978).
207. Kamen, R. & Sure, H. *Cell* **7,** 361–371 (1976).
208. Siddell, S. & Smith, A. E., *J. Virol.* **27,** 427–435 (1978).
209. Legon, S., Flavell, A. J., Cowie, A. & Kamen, R. *Cell* **16,** 373–388 (1979).
210. Shenk, T. E., Carbon, J. & Berg, P. *J. Virol.* **18,** 664–671 (1976).
211. Villareal, L. R., White, R. T. & Berg, P. *J. Virol.* **29,** 209–219 (1979).
212. Reddy, V. B., Ghosh, P. K., Leibowitz, P. & Weissman, S. M. *Nucleic Acids Res.* **5,** 4195–4124 (1978).

ARTICLES

Rapid polymer transport in concentrated solutions through the formation of ordered structures

B. N. Preston, T. C. Laurent*, W. D. Comper & G. J. Checkley

Department of Biochemistry, Monash University, Clayton, Victoria 3168, Australia

Our previous finding that high molecular weight polymers in certain systems can be transported with an unexpectedly high apparent 'diffusion' rate in the presence of a concentrated second polymer has been shown to be due to the formation and movement of organized macroscopic structures in an otherwise convection-free solution. The structures are not formed as part of a normal phase separation but will dissipate with time. Their formation may be understood by recently developed principles of nonlinear nonequilibrium thermodynamics.

OUR studies on the mechanism of macromolecular transport in gels and polymeric networks in solution have been primarily concerned with relating our observations to biological transport and organizational phenomena, in particular to transport phenomena occurring in the extracellular matrices of connective tissues and within passive membranous structures (for reviews see refs 1, 2). We now present results concerning the kinetics and ultimate formation of ordered structures arising from concentration gradients in aqueous multicomponent polymer solutions.

Initial observations of rapid transport of macromolecules in polymer networks

Preston and Snowden[3] observed that polyethylene glycol and polyvinyl alcohol exhibited higher migration rates in polysaccharide solutions than in polysaccharide-free media. Similar experiments with compact globular solutes exhibited reduced transport rates which were explained by hindered diffusion[4–6]. A detailed re-investigation[7] of the ternary polymer–polymer–solvent systems, using a capillary technique[8], confirmed the earlier studies. Some of the results of this investigation have been reported[9,10]. The transport of a linear flexible macromolecule (component 1) in solutions of a polysaccharide (component 2) was found to show a marked dependence on (1) time, (2) molecular weight (MW) and concentration gradient of component 1, and (3) MW and concentration of component 2.

As an example of several systems studied we consider the migration of polyvinylpyrrolidone (PVP) (MW $\sim 3.6\times10^5$; $D = 2.1\times10^{-7}$ cm^2 s^{-1}) as component 1 in a solution of dextran (MW $\sim 10^4$) as component 2. As described previously[7,9,10], at low concentrations of component 2 (C_2), a slight reduction in the transport rate of component 1 was observed. As C_2 was increased, the migration of component 1 increased to a rate 40 times higher than that observed in the absence of component 2,

---

* Permanent address: Institute of Medical and Physiological Chemistry, University of Uppsala, Box 575, S-751 23 Uppsala, Sweden.

0028–0836/80/410499—05$01.00

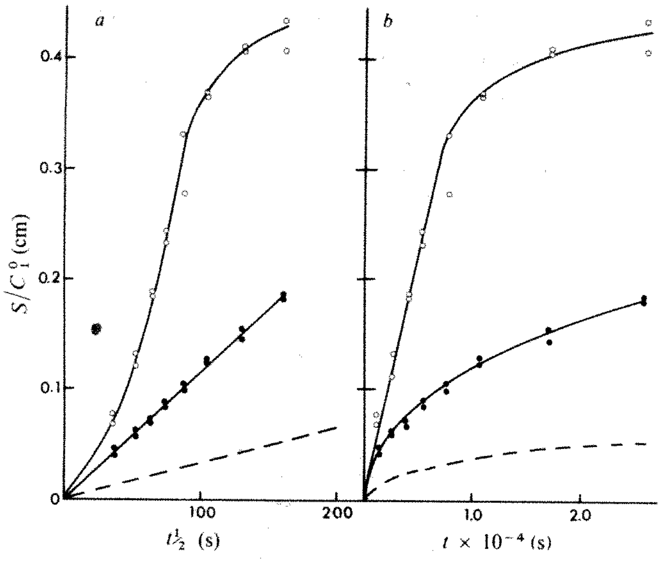

Fig. 1 Transport of ^{3}H-PVP (○) and ^{14}C-sorbitol (●) over a boundary formed by layering 135 mg ml^{-1} dextran (MW ~10^4) over 5 mg ml^{-1} ^{3}H-PVP (MW ~3.6×10^5), 10 mg ml^{-1} ^{14}C-sorbitol and 135 mg ml^{-1} dextran. S is the amount transported per cm^2 of surface area and C_1^0 the initial concentration in the lower compartment. For normal diffusion the transport should be proportional to $(t)^{1/2}$, as shown for sorbitol but not for PVP (*a*). Instead, the PVP transport is directly proportional to time before it levels off (*b*). For comparison, the normal diffusion of ^{3}H-PVP in water is included (– – –). Experiments were carried out at 20 °C.

and then, decreased at still higher values of C_2. When the transport of glucose or sorbitol ($D = 58 \times 10^{-7}$ cm^2 s^{-1}) as a solvent marker was measured simultaneously with the migration of component 1, the behaviour of the low molecular weight solute was normal in that its transport rate was reduced ($D = 39 \times 10^{-7}$ cm s^{-1}) by the presence of component 2. This suggests that gravitational instabilities[11] had not led to macroscopic convectional destruction of the boundary. As ternary polymer–polymer–solvent systems are known to be affected by phase transitions[12], it was possible that the enhanced migration rates were linked to the kinetics of phase transitions. We therefore established[7] that the systems under study were in regions far from phase transitions.

The time dependence of the apparent diffusion rate of component 1 was very marked in the initial stages. The rates reported[10] were those measured after an interval of 41 h, where they exhibited only a slight time dependence. Our qualitative interpretation of these effects was focused on the hydrodynamic and thermodynamic parameters considered important in determining diffusion rates in multicomponent systems[13–15]. This approach has been successful in describing polymer diffusion in binary systems[16–18]. However, we show here the rapid transport of PVP in dextran solutions is not a normal diffusional process.

Time dependence of PVP transport in dextran solutions

When the transport of PVP in dextran solutions was analysed as a diffusional process, it was found that the migration rate was markedly time dependent. However, as the capillary technique used precluded an accurate analysis of transport rates at early times, we used a new technique to investigate time dependence.

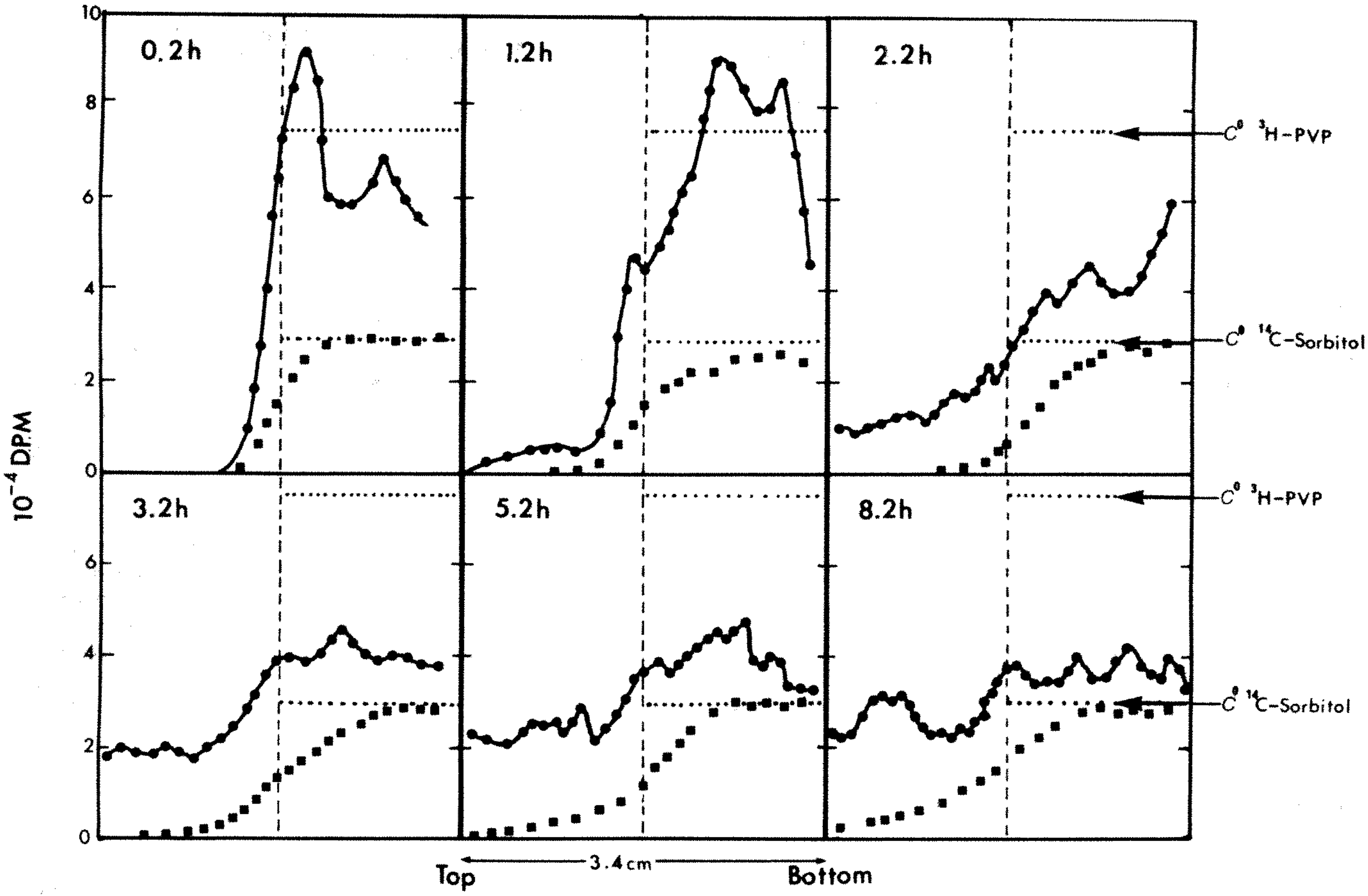

Fig. 2 The solutions described in Fig. 1 were layered in 3.4 cm long plastic tubes. Their contents were fractionated after various times—0.2 to 8.2 h and the distribution of ^{3}H-PVP (●) and ^{14}C-sorbitol (■) determined. The change in concentration of ^{14}C-sorbitol is due to normal diffusion, whereas ^{3}H-PVP spreads more rapidly and exhibits a wave-like distribution. The position of the original boundaries (– – –) and the original concentrations of the components (. . . .) are indicated. The ordinate represents the radioactivity found in each fraction.

The apparatus consists of a diffusion cell (designed by L. -O. Sundelöf) in which a free horizontal boundary is formed by a shearing mechanism between two solutions of comparable volume. Transport of labelled material across the boundary can be directly monitored as a function of time, by using a number of identical cells. For simplicity we will consider the behaviour of the ^{3}H-PVP (component 1) in a dextran (component 2) of concentration, $C_2 = 135$ mg ml^{-1}. This value of C_2 corresponds to a maximal apparent diffusion rate of component 1[10]. Most experiments used a PVP concentration difference of 5 mg ml^{-1} in the presence of a sorbitol concentration difference of 10 mg ml^{-1}, the latter acting as a solvent marker to detect any macroscopic convective flow. Figure 1 shows the time dependence of ^{3}H-PVP and of the ^{14}C-sorbitol flux in this system. The ordinate represents the ratio of the quantity of solute transferred (S) across the boundary per unit cross-sectional area, to the initial concentration of the solute (C_1°) in the lower part of the diffusion cell. When S/C_1° is plotted against (time)$^{1/2}$ ($t^{1/2}$) (Fig. 1*a*), the transport of the ^{14}C-sorbitol follows diffusional kinetics (linear with respect to $(t)^{1/2}$) and corresponds to a diffusion coefficient of $\sim 40 \times 10^{-7}$ cm^2 s^{-1}. The transport of the ^{3}H-PVP follows a sigmoidal pattern, not expected for a normal diffusional process. However, if S/C_1° is plotted against time (Fig. 1*b*), two distinct transport modes are observed for the ^{3}H-PVP. In the first 3 h, about 40% of the polymer moves across the initial boundary, and the transport rate seems to be linearly related to time. At later times, the rate falls to a much smaller value. The striking differences in the behaviour of PVP and ^{14}C-sorbitol confirms the previous results in that no bulk convective flow is occurring in a system in which high rates of ^{3}H-PVP transport are observed. Figure 1 includes comparable data describing the transport of ^{3}H-PVP in the absence of the dextran network.

The linear time dependence of the initial ^{3}H-PVP transport rate suggests that its migration might be mediated by a convectional or gravity-induced process. It is unclear why such movement is not accompanied by a similar behaviour of the solvent marker ^{14}C-sorbitol. However, the diffusion rate of the ^{14}C-sorbitol does increase slightly over that in PVP-free media ($D = 33 \times 10^{-7}$ cm^2 s^{-1}). Although the transport rates increase with temperature, a correction term allowing for the temperature dependence of the viscosity of water makes the rates temperature independent. This indicates absence of any active process in the transport of ^{3}H-PVP, suggesting instead that the transport rate is a function of the viscosity of the system. In agreement with this conclusion, we previously reported[10] that the rapid transport is a function of the molecular weight of the network component, we now relate this to the macroscopic viscosity of the system.

To study the spatio-temporal relationships of the process, the experiment was carried out in a vertical centrifuge tube. After layering the dextran solution onto a solution containing dextran, ^{3}H-PVP and ^{14}C-sorbitol, the tube was allowed to stand for varying periods of time, and was then fractionated by displacement with a dense fluid (tetrabromoethane). The profiles of the distribution of material as a function of time are shown in Fig. 2*a*–*f*. Two features of the time evolution of this system are evident: (1) the migration of ^{3}H-PVP results in a wavelike distribution of material propagating throughout the solution; and (2) ^{14}C-sorbitol shows no comparable behaviour, developing a normal gaussian-like distribution.

Effect of parameters influencing the density differences over the boundary

The direct influence of gravity on PVP transport in dextran solutions was established by monitoring PVP migration in the analytical ultracentrifuge by UV absorption. The boundary conditions (see Fig. 1 legend) were similar to those in experiments performed at unit gravity. We found that the PVP transport rate increased with the centrifugal force acting on the system; however, the relationship was not a simple one. For example, at unit gravity the rate was 1.4 mm h^{-1}, at 1,077 *g* it was 3.8 mm h^{-1} and at 44,000*g* 9.0 mm h^{-1}.

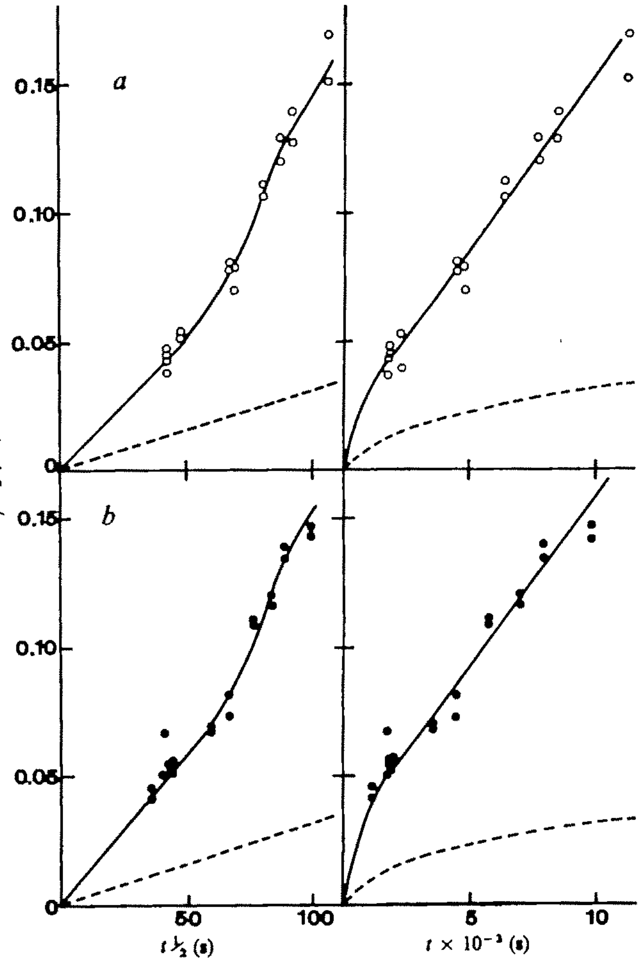

Fig. 3 The upward (*a*) and downward (*b*) fluxes of dextran over a boundary similar to that described in Fig. 1 legend except that PVP is unlabelled and dextran labelled with ^{3}H. For comparison, the normal (trace) diffusion of dextran in a system containing 135 mg ml^{-1} dextran but no PVP has been included (- - -). The dextran fluxes in the presence of PVP are much higher than in normal diffusion and do not obey diffusion kinetics. Experiments were carried out at 20 °C.

Our attempts to stabilize the boundary with density differences by conventional means did not always produce a 'stabilization' in terms of reducing the enhanced PVP transport. The presence of a sorbitol concentration of 10 mg ml^{-1} in the lower solution or the use of D_2O in the lower solution did not affect the magnitude of the PVP transport. These results suggest that the 'instabilities' caused at the boundary are not affected by the macroscopic density of the solutions as derived from low molecular weight solutes or dense solvents.

Conversely, the PVP transport rate seems to depend critically on the concentration gradients of macromolecular species across the boundary. Variation of the PVP concentration gradient markedly affects the subsequent transport rates[7]. At low PVP concentration gradients no anomalous transport was seen.

Dextran flux in the system

The unidirectional transport rates of ^{3}H-dextran were measured in both directions across the PVP boundary, and indicated that dextran was also rapidly transported and, as with PVP transport, was essentially linear with time (Fig. 3*a*, *b*). The unidirectional rates were of similar magnitude; this means there was only a small resultant downward flux of dextran over the boundary. Figure 3*a* and *b* also show the unidirectional transport rates of the dextran in the absence of any PVP gradient; this represents the self (or tracer) diffusion behaviour of dextran at $C_2 = 135$ mg ml^{-1} ($D = 3.6 \times 10^{-7}$ cm^2 s^{-1}).

Direct visualization of the PVP transport

Direct visualization of the fluxes involved was achieved using a blue-labelled PVP obtained by coupling PVP to remazol brilliant blue (see Fig. 4 legend). When a free boundary was formed in either a thermostatted Tiselius diffusion cell or by manual methods in a test tube or glass cuvette, a striking series of events was seen. After an initial period, a number of uniformly spaced blue vertical 'fingers' or spikes appeared at the boundary (Fig. 4*a*). These spikes grew at a rate comparable in magnitude to the PVP transport rates given earlier and were associated with a concomitant development and propagation downwards of colourless fingers. In view of our earlier observations, it is tempting to suggest that the polymeric components of the blue advancing fingers are PVP and dextran and that the descending structures contain only dextran. After 2–3 h, the system seemed to reach a 'stable' state in which a regular pattern of alternate blue and colourless lines extended through the whole volume (Fig. 4*b*). The pattern resembles the salt fingers observed in the double-diffusion system of Turner[19].

To observe the formation of these structured flows from above, the experiments were performed in a Petri dish (32 mm diameter). The dextran solution containing the blue-labelled PVP was layered under a dextran solution of similar concentration but without the PVP. The ensuing series of events was again complex but briefly consisted of the initial formation of needle-like structures of relatively intense blue colour at the perimeter of the dish and directed radially towards the centre (Fig. 5*a*), followed by the formation of several concentric circles of blue colour parallel to the perimeter of the dish (Fig. 5*b*). The two patterns then merged to yield a very complex mosaic-type appearance (Fig. 5*c*). Within 20 min the regular pattern had begun to disperse and within 2 h a homogeneously coloured solution was obtained.

Variants of the two behaviours described above can be created by using D_2O in the lower solution, which seems to prevent the downward growth of structures, or by changing the boundary conditions (different container shapes). The experiments were also carried out in the dark with similar results, indicating that these events were not light induced, arising from absorption effects.

The apparent generalization of these phenomena or closely related events has been suggested by comparable observations in various ternary polymeric systems under similar constraints.

A tentative explanation of the phenomenon

Our physical picture of the phenomenon supposes concentration inhomogeneities occur in the volume proximal to the initial boundary, so that regions of differing densities are formed. Regions of relatively high density would sink and subsequently displace regions of lower densities; conversely, the low density regions may float and displace regions of higher density. Possible mechanisms leading to density inhomogeneities include a net water flux downwards due to osmotic pressure differences across the boundary, or a net movement of dextran upwards due to the chemical potential gradient induced in the uniform dextran matrix by the presence of the PVP[20]. This latter effect would increase the concentration of matrix dextran immediately above the initial boundary with consequent sinking

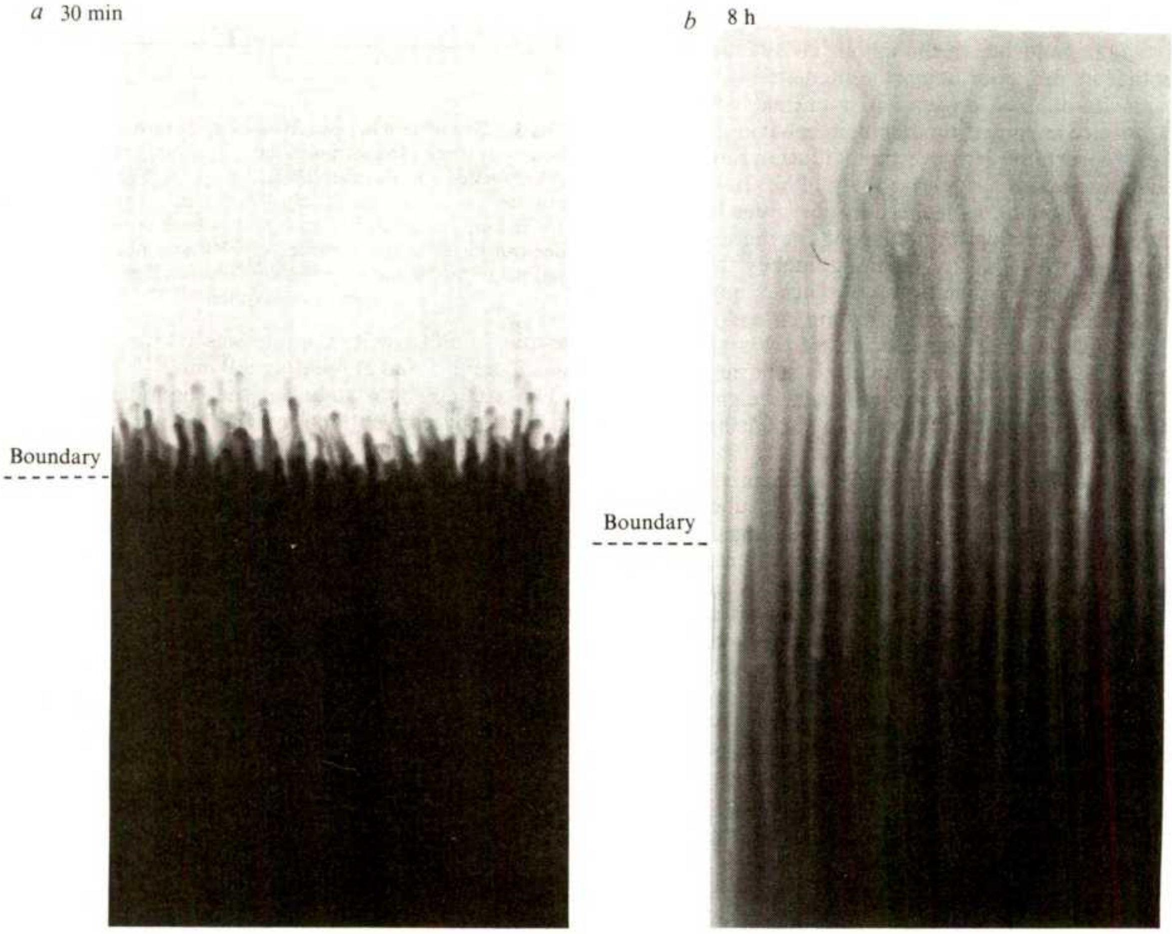

Pure Che sity Library
SCIENCE COLLEGE
Upper Circular Road
CALCUTTA

Fig. 4 The formation of structures at the boundary between 135 mg ml^{-1} dextran (top) and 5 mg ml^{-1} blue PVP, 135 mg ml^{-1} dextran and 10 mg ml^{-1} sorbitol (bottom). Blue PVP was prepared by heating PVP (5 g) and remazol brilliant blue (0.75 g) in NaOH (200 ml, 0.05 M) at 50 °C for 3 days. The coloured polymer was purified by repeated washings with distilled water in Amicon ultrafiltration apparatus equipped with a PM 10 membrane filter, under a pressure of 60 p.s.i. The boundary was formed in the centre of a 6.0 cm long Tiselius cell and photographed 30 min (*a*) and 8 h (*b*) after layering. The structures remained in the cell for at least 24 h. × 3.

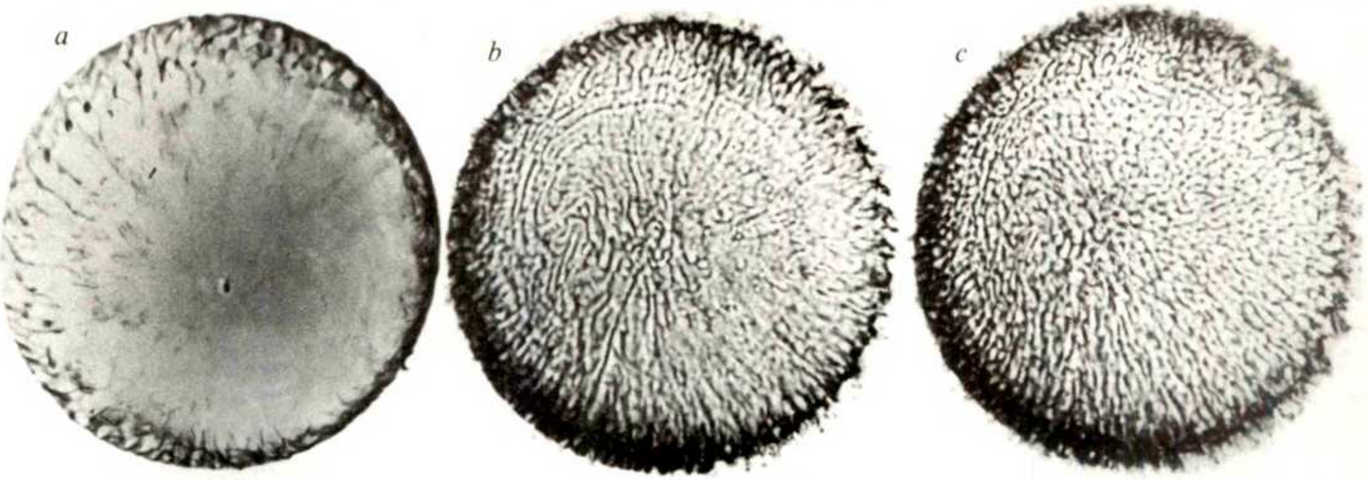

Fig. 5 The formation of structures in a Petri dish seen from above. A boundary between the same solutions described in Fig. 4 legend was formed by layering 1 ml of blue solution under 1 ml of clear dextran solution with a needle. The photographs were taken *a*, 4 min; *b*, 12 min; and *c*, 20 min after the layering. × 2.

of the regions of PVP-free solutions through the layers of solution below the boundary. Alternatively, the intrinsic compositional differences in regions close to the boundary due to thermal fluctuations in polymer concentrations could, without invoking any initial transport across the boundary, create unstable regions which would coalesce and grow—a non-equilibrium nucleation phenomenon of the kind described by Nicolis and Prigogine[21].

Whatever the precise mechanism of formation, the dense regions may start a downward movement of fingers and displace regions of PVP-containing solution upwards. The slow diffusional characteristics of the PVP will retain this polymer in the upward-going structures and its vertical transport rate will be rapid and basically determined by the bulk movement of the structures. Low molecular weight solutes such as sorbitol will, however, undergo a rapid lateral diffusive exchange between the upward- and downward-moving structures and hence the net transport in the vertical directions will be low and governed by the lateral diffusional process. The observation that high concentrations of low molecular weight solutes (sorbitol or D_2O) in the solution below the boundary do not inhibit the rapid transport of the PVP can be understood in terms of a rapid equilibrium of these solutes between regions close to the boundary where initial polymer concentration inhomogeneities exist. Furthermore, these small molecular weight solutes may equilibriate rapidly between the upward- and downward-moving structures, thereby limiting their 'stabilizing' effect.

Are dissipative structures involved in these systems?

Glansdorff and Prigogine[22], through a general formulation of nonequilibrium statistical mechanisms, have concluded that two basic conditions are required for the formation of ordered coherent structures in an open system. First, factors must operate on the system to drive it further from an equilibrium state. Second, nonlinear mechanisms must act between the various elements of the system. When these conditions are met, certain types of fluctuation can be amplified and drive the system to a new regime which differs from the initial reference state. This regime is characterized by the appearance of organizations (called dissipative structures) whose probabilities of occurrence at equilibrium would be negligible. It is important to recognize that nonequilibrium unexpectedly may be the source of order-producing coherent behaviour in space and time.

It seems that the two basic requirements for the formation of self-organizing coherent behaviour are present in our system. First, the PVP concentration gradient will induce a chemical potential gradient in the dextran network, where no actual dextran concentration gradient exists. Such an induced chemical potential gradient would cause the dextran, initially at uniform concentration, to migrate, thus forcing the system further from the equilibrium state. Second, it is well recognized that the thermodynamic parameter describing the interactions occurring in concentrated polymer systems is nonlinear. We thus tentatively conclude that the observed structures in the ternary systems are an example of dissipative structures.

We believe that our demonstration of self-organization occurring merely by intrinsic heterogeneities in polymer concentration is an important concept for an understanding of the organization and transport of high molecular weight solutes in biological systems. Furthermore, similarities exist between the presently described phenomenon and the 'finger' instabilities arising from the penetration of a fluid into a porous medium containing a more viscous fluid[23]. These instabilities are gravity or pressure induced and, when considered in conjunction with our observations, may be particularly relevant to an understanding of the complex transport effects found in the nerve axon.

This project was supported by the Australian Research Grants Committee, Australian Humane Research Foundation and the Swedish MRC.

Received 13 May; accepted 28 July 1980.

1. Comper, W. D. & Laurent, T. C. *Physiol. Rev.* **58,** 255–315 (1978).
2. Preston, B. N., Laurent, T. C. & Comper, W. D. *Biochem. Soc. Meet.* Colworth, 1979 (in the press).
3. Preston, B. N. & Snowden, J. McK. in *Biology of Fibroblast* (eds Kulonen, E. & Pikkarainen, J.) 215–230 (Academic, New York, 1973).
4. Laurent, T. C., Björk, I., Pietruszkiewicz, A. & Persson, H. *Biochim. biophys. Acta* **78,** 351–359 (1963).
5. Preston, B. N. & Snowden, J. McK. *Proc. R. Soc.* A**333,** 311–313 (1973).
6. Ogston, A. G., Preston, B. N. & Wells, J. E. *Proc. R. Soc.* A**333,** 297–309 (1973).
7. Kitchen, R. G. thesis, Monash Univ. (1975).
8. Anderson, J. S. & Saddington, K. *J. chem. Soc. S,* 381–386 (1949).
9. Sundelöf, L.-O. *Ber. Bunsen Ges.* **83,** 329–342 (1979).
10. Laurent, T. C., Preston, B. N. & Sundelöf, L.-O. *Nature* **279,** 60–62 (1979).
11. Brakke, M. K. *Archs Biochém. Biophys.* **55,** 175–190 (1955).
12. Albertsson, P. -Å. *Partition of Cell Particles and Macromolecules* (Wiley, New York, 1960).
13. Laurent, T. C., Preston, B. N., Pertoft, H., Gustafsson, B. & McCabe, M. *Eur. J. Biochem.* **53,** 129–136 (1975).
14. De Gennes, P. G. *J. chem. Phys.* **55,** 572–579 (1971).
15. Ogston, A. G. & Preston, B. N. *Biochem. J.* **183,** 1–9 (1979).
16. Kitchen, R. G., Preston, B. N. & Wells, J. D. *J. Polym. Sci.* **55,** 39–49 (1976).
17. Laurent, T. C., Sundelöf, L. -O., Wik, K. O. & Warmegård, B. *Eur. J. Biochem.* **68,** 95–102 (1976).
18. Roots, J., Nyström, B., Sundelöf, L. -O. & Porsch, B. *Polymer* **20,** 337–346 (1979).
19. Turner, J. S. *Adv. chem. Phys.* **32,** 135–149 (1975).
20. Sundelöf, L.-O. *Chem. Zvesti* **25,** 203–214 (1971).
21. Nicolis, G. & Prigogine, I. *Self-Organization in Non-Equilibrium Systems* (Wiley, New York, 1977).
22. Glansdorff, P. & Prigogine, I. *Thermodynamic Theory of Structure, Stability and Fluctuations* (Wiley, New York, 1971).
23. Saffman, P. G. & Taylor, G. *Proc. R. Soc.* A**245,** 312–329 (1958).

Isolation of a yeast centromere and construction of functional small circular chromosomes

Louise Clarke & John Carbon

Department of Biological Sciences, University of California, Santa Barbara, California 93106

The centromeric DNA (CEN3) *from yeast chromosome III has been isolated on a 1.6 kilobase-pair segment of DNA located near the centromere-linked* CDC10 *locus of* Saccharomyces cerevisiae. *When present on a plasmid carrying a yeast chromosomal replicator,* CEN3 *enables that plasmid to function as a chromosome both mitotically and meiotically. Minichromosomes containing* CEN3 *are stable in mitosis and segregate as ordinary yeast chromosomes in the first and second meiotic divisions.*

In an attempt to isolate and characterize yeast centromeric DNA, the techniques of overlap hybridization[1], complementation of mutations in yeast through transformation[2,3], immunological screening[4,5], and complementation of auxotrophic mutations in *Escherichia coli*[6] have been used in our laboratory to obtain a number of hybrid plasmids containing DNA segments from around the centromere-linked *leu2*, *cdc10*, and *pgk* loci on chromosome III of *Saccharomyces cerevisiae.* A contiguous region of about 25 kilobase pairs of DNA that extends from the *LEU2* gene to the *CDC10* gene has been obtained on a set of overlapping plasmids[1,3]. Among these is the plasmid pYe(*CDC10*)*1*, which contains the yeast *CDC10* gene included on an 8 kilobase-pair segment of yeast DNA[3]. This plasmid was selected by complementation of the *trp1* and temperature-sensitive *cdc10* lesions in strain XSB52-23C from a pool of hybrid plasmid DNAs composed of segments of sheared yeast DNA joined by poly (dA · dT) connectors into the *E. coli*-yeast shuttle vector, pLC544 (ref. 3). This vector contains the yeast *TRP1* gene along with the chromosomal replicator, *ars1* (ref. 7).

Unlike other *ars1* bearing plasmids described by Stinchcomb *et al.*[7], Kingsman *et al.*[8], and below, pYe(*CDC10*)1 is relatively stably maintained through mitotic and meiotic cell divisions in yeast. We have investigated the nature of this stability both biochemically by localization and preliminary sizing of the stabilizing segment of DNA, and genetically by examining the behaviour of pYe(*CDC10*)1 and its derivatives in mitosis, meiosis, sporulation and germination. The stabilizing segment is confined to a 1.6-kilobase pair region on the left (*LEU2*) side of the *CDC10* locus. Its presence on plasmids that also carry a yeast chromosomal replicator [*ars1* (ref. 7) or *ars2* (ref. 9)] permits those plasmids to behave mitotically and meiotically as minichromosomes. Genetic markers on a minichromosome act as linked markers. They segregate in the first meiotic division as centromere-linked genes, are thus present in the two sister progeny of the second meiotic division, and are unlinked to genetic markers on other chromosomes. We conclude that the stabilizing DNA segment from pYe(*CDC10*)1 is a functional centromeric DNA sequence, the centromere of chromosome III (*CEN3*).

Plasmid pYe(*CDC10*)1 is mitotically stable

We have reported previously that in cultures of individual XSB52-23C/pYe(*CDC10*)1 transformants growing at 37 °C in the absence of tryptophan (selective conditions) only about 1–2 cells in 500 examined microscopically have lost the plasmid and express the easily distinguished Cdc10$^-$ phenotype[3]. Using overlap hybridization[1], a number of other plasmids have now been identified from our pLC544(*TRP1 ars1*)-yeast DNA genomic library that carry DNA segments from the *cdc10* region of chromosome III (Fig. 1). One of these, pYe98F4T, carries the *CDC10* locus because it complements the *cdc10* mutation in strain XSB52-23C, and it also contains additional DNA in the direction of *PGK*, but lacks about 3.5 kilobase pairs of DNA in the *LEU2* direction that is found on pYe(*CDC10*)1. Microscopic examination of cultures of individual XSB52-23C/pYe98F4T transformants (growing selectively) reveal that approximately one-half of the cells express the mutant Cdc10$^-$ phenotype, indicating extensive plasmid loss and instability. The degree of mitotic stability of pYe(*CDC10*)1, pYe98F4T, and two other *TRP1 ars1* plasmids containing DNA from near the *CDC10* locus, pYe65H3T and pYe101C3T (Fig. 1), was further examined by growing individual cultures of XSB52-23C transformants containing each of these plasmids on rich medium at 23 °C (nonselective conditions). After approximately 20–30 generations of nonselective growth, individual clones of the original transformants were scored for loss of plasmid (loss of the Trp$^+$ phenotype). As seen in Table 1, 97% of the clones derived from transformants harbouring pYe(*CDC10*)1 retained the plasmid after this extensive period of nonselective growth. Plasmids pYe98F4T, pYe65H3T, and pYe101C3T are completely segregated, however, in the same conditions. The parent vector in the above plasmids, pLC544 (ref. 8), other *TRP1 ars1* plasmids such as YRp7 and YRp7–Sc2604 (ref. 7), plasmids containing the chromosomal replicator (*ars2*; ref. 9), and many plasmids containing 2 μm DNA replicators[10] are also mitotically unstable.

Plasmid pYe(*CDC10*)1 is meiotically stable and segregates as a chromosome

Because stability in mitosis is a predicted property of a replicating unit carrying a functional centromere, the unique mitotic stability of pYe(*CDC10*)1 encouraged us to examine the behaviour of this plasmid through meiosis and sporulation. Strain XSB5223Cα/pYe(*CDC10*)1(*cdc10 leu2 trp1*/*CDC10 TRP1*) was crossed with X2928-30-1*A*a(*trp1 leu1 ade1 met14*), diploids were sporulated and the resulting asci were dissected for genetic analysis. Data from 16 tetrads (cross 1, Table 2) indicate that the plasmid (marked by the wild-type *TRP1* allele) in at least 60% of the asci segregates in the first meiotic division as a chromosome and is thus found in the two sister spores, the products of the second meiotic division. Only parental ditype and nonparental ditype asci were obtained in this cross using as

0028–0836/80/410504—06$01.00

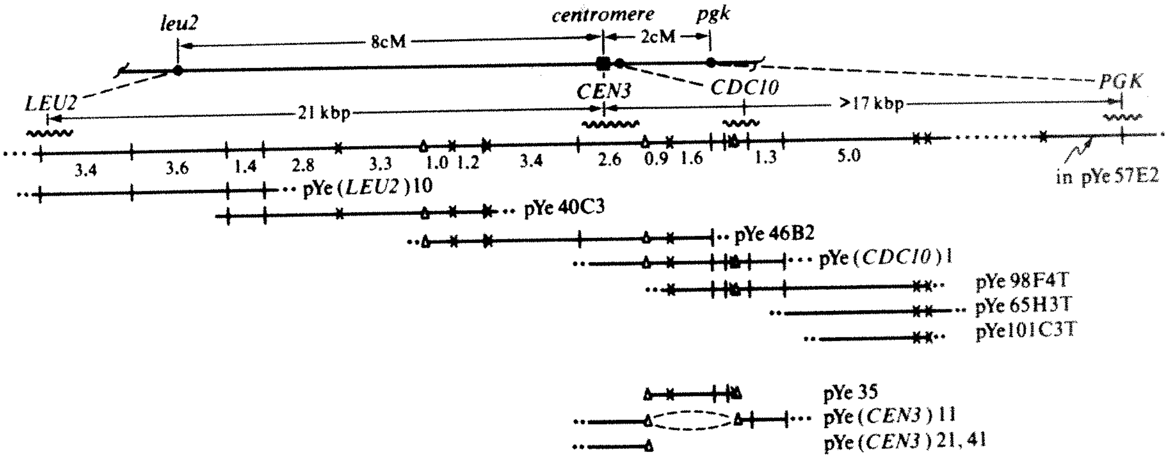

Fig. 1 Genetic and physical maps of the centromere region of *S. cerevisiae* chromosome III. The restriction map gives the location of *Eco*RI (—|—), *Hin*dIII (—×—), and *Bam*HI (-Δ-) sites in the DNA. Numbers denote kilobase pairs (kbp). The order of inserts in various overlapping plasmids is indicated below the restriction map. Small dots at the ends of inserts pertain to those sheared segments of yeast DNA that are joined to their respective plasmid vectors by poly (dA · dT) connectors. The isolation and characterization of plasmids pYe(*LEU2*)10 (ref. 6), pYe40C3 (ref. 1), pYe46B2 (ref. 1), pYe(*CDC10*)1 (ref. 3), and pYe57E2 (ref. 5), have been described. Plasmids pYe98F4T, pYe65H3T, and pYe101C3T were obtained by overlap hybridization and characterized as described by Chinault and Carbon[1], with the modification that a single restriction fragment (from pYe(*CDC10*)1) purified by agarose gel electrophoresis was used as probe in the hybridizations[20]. Plasmids pYe(*CDC10*)1, pYe98F4T, pYe65H3T, pYe101C3T, pYe35, and pYe(*CEN3*)11 all contain the *TRP1 ars1* vector, pLC544 (ref. 8). The vector portion of the remaining plasmids is ColE1.

references the centromere markers *leu1*, *leu2*, *met14*, and *ade1* (complete data not shown). Thus the *TRP1* locus on the plasmid behaves as a centromere-linked marker. The *TRP1* gene on pYe(*CDC10*)1 is unlinked to *ade1*, *cdc10*, *leu1*, *leu2*, or *met14* and is therefore not integrated on chromosomes I, III, VII or XI. The plasmid was completely lost in about 30% of the asci and in one ascus was found in all four spores, but did not segregate either 1+:3− or 3+:1− in any asci analysed in this cross.

A second cross was carried out with one of the progeny of cross 1, SB17*Aa*/pYe(*CDC10*)1(*cdc10 trp1 leu2 ade1*/*CDC10 TRP1*), and strain 6204-18Aα (*cdc10 leu2*). Data similar to that from Cross 1 were obtained (cross 2, Table 2). The plasmid in cross 2 again segregates 2+:2− in the first meiotic division in 92% of the asci and is found in all four spores in one ascus. With *ade1* as the reference centromere marker, again the marker scored on the plasmid (*CDC10* in this cross) is centromere-linked. The plasmid marker, *CDC10*, is unlinked to chromosome IV, because in those tetrads where *CDC10* segregated 2+:2−, *TRP1* (wild-type allele on both the minichromosome and one parental chromosome) segregated both 2+:2− and 4+:0−.

Backcrosses of plasmid-bearing progeny from cross 1 with the original parents XSB52-23C and X2928-3D-1A gave the same pattern of 2+:2− segregation of the wild-type plasmid marker that is independent of the segregation of markers on other chromosomes. In all the above crosses, the two markers on pYe(*CDC10*)1, *CDC10* and *TRP1*, were linked in every ascus scored (data not shown). None of the asci obtained consisted of two viable and two nonviable sister spores. Thus the minichromosome does not appear to pair with any of the other yeast chromosomes.

The centromeric DNA (*CEN3*) is located on the left (*LEU2*) side of the *CDC10* locus

The data presented above indicate that plasmid pYe(*CDC10*)1 contains functional centromeric DNA (*CEN3*) from chromosome III. Making use of the set of overlapping plasmids (Fig. 1) and various reclones from the *CDC10* region, we have attempted to determine the location of *CEN3*. In order to locate the *CDC10* gene on pYe(*CDC10*)1 we had previously constructed two reclones of this plasmid[3]. The first, pYe(*CEN3*)11 (see Fig. 1; referred to as pYe(*CDC10*)1-1 in ref. 3) contains all the yeast DNA in pYe(*CDC10*)1 cloned into pLC544, except the 3.5-kilobase pair *Bam*HI fragment from the middle of the insert. The second, pYe35 (referred to as pYe(*CDC10*)1-2 in ref. 3) contains only this 3.5-kilobase pair *Bam*HI restriction fragment and the vector pLC544 (Fig. 1). Neither plasmid complements the *cdc10* mutation in yeast[3], which indicates that one of the two *Bam*HI sites on pYe(*CDC10*)1 is probably close to or within the *CDC10* gene. Both pYe(*CEN3*)11 and pYe35 DNAs transform Trp$^-$ yeast to Trp$^+$ with high efficiency[3], since

Table 1 Mitotic stability in yeast of various plasmids and minichromosomes containing DNA from the centromere region of chromosome III

	No. of individual transformants tested		Average per cent of Trp$^+$ or Leu$^+$ transformants remaining after nonselective growth	
Plasmid	Strain XSB52-23C	Strain RH218	Strain XSB52-23C	Strain RH218
pYe(*CDC10*)1	5	ND	97	ND
pYe(*CEN3*)11	5	3	95	83
pYe(*CEN3*)41	2	ND	91	ND
pYe35	5	5	<1	7
pYe98F4T	5	ND	<1	ND
pYe65H3T	2	ND	<1	ND
pYe101C3T	2	ND	<1	ND
pYe(*CEN3*)21	4	ND	<1	ND
pYe(*ars1–ars2*)1	ND	8	ND	5

Yeast strains XSB52-23C*a*(*cdc10 gal leu2–3 leu2–112 trp1*) and RH218*a* (*CUP1 gal2 mal SVC trp1*) were transformed with the above plasmid DNAs and in each case several individual transformants were isolated and grown nonselectively overnight on YPD (rich) medium. Each culture was subsequently streaked for single colonies on YPD agar, allowed to grow for 2 days at 23 °C (XSB52-23C) or 32 °C(RH218) and replica-plated onto minimal agar medium with or without tryptophan or leucine, depending on the marker carried by the plasmid. Between 40 and 100 individual clones of each original transformant were scored for plasmid loss after growth at 23 °C (XSB52-23C) or 32 °C (RH218). Preparations of media and transformation of yeast were carried out as described by Hsiao and Carbon[9]. ND, not determined.

they contain a *TRP1 ars1* vector. However, only one, pYe(*CEN3*)11, yields transformants that are all mitotically stable for the Trp$^+$ phenotype (Table 1). When a mating was carried out between XSB52-23C/pYe(*CEN3*)11(*trp1 cdc10*/*TRP1*) and X2928-3D-1A(*trp1 ade1*), data similar to that for crosses 1–4 were obtained (Table 2). In 60% of the asci 2+:2− segregation was observed for the *TRP1* marker on pYe(*CEN3*)11. The minichromosome was lost entirely in 27% of the asci and in 13% was found in all four spores. Again only parental and non-parental ditype asci were obtained with respect to centromere reference markers, indicating centromere linkage of *TRP1*. No linkage of the minichromosome to chromosomes I or III was observed, since pYe(*CEN3*)11 segregated independently of the *ade1* and *cdc10* markers.

Because *trp1* yeast transformants harbouring pYe98F4T are all unstable for the Cdc10$^+$ (and Trp$^+$) phenotype, and those carrying pYe(*CEN3*)11 are all stable for Trp$^+$ (Table 1), the stabilizing or centromeric DNA (*CEN3*) is most probably contained in pYe(*CEN3*)11 (and pYe(*CDC10*)1) on the 1.6-kilobase pair segment which extends from the *Bam*HI site to the end of the insert in the direction of the *leu2* locus (Fig. 1). To test this hypothesis, we recloned the 1.6-kilobase pair yeast DNA segment into the plasmid, pGT12(*LEU2 ars1*)^{11}. The DNA segment was excised from pYe(*CEN3*)11 DNA with the enzymes *Bam*HI and *Hin*dIII. This treatment yields a single *Bam*HI–*Hin*dIII restriction fragment whose *Bam*HI site is derived from the single *Bam*HI site in pYe(*CEN3*)11 and whose *Hin*dIII site is derived from a *Hin*dIII site in the vector (pLC544), located about 400 base pairs from the end of the insert of yeast DNA. The 1.6-kilobase pair segment of interest, which is thus included on a 2.0-kilobase pair *Bam*HI–*Hin*dIII fragment, was then inserted into plasmid pGT12, also cut with a combination of *Bam*HI and *Hin*dIII.

Plasmid pGT12 was constructed by inserting a 1.4-kilobase pair *Eco*RI restriction fragment containing *TRP*1 and *ars*1 (ref. 7) and a 2.2-kilobase pair *Pst*I fragment containing the *LEU2* gene^{11} into the single *Eco*RI and *Pst*I sites of pBR322 (ref. 11). This plasmid also carries resistance to tetracycline. When the 2.0-kilobase pair *CEN3* fragment is inserted into pGT12 cut with a combination of *Bam*HI and *Hin*dIII, both Tet^R and *TRP1* expression are destroyed, but the *ars1* chromosomal replicator is left intact. The resulting plasmid, pYe(*CEN3*)41 (Fig. 2), thus carries both *CEN3* and the replicator *ars1* in addition to the *LEU2* marker.

Plasmid pYe(*CEN3*)41 transforms strain XSB52-23C(*leu2-3 leu2-112*) to Leu$^+$ with high frequency and is stable in the transformants (Table 1). Its behaviour in meiosis (cross 6, Table 2) is essentially the same as that described for pYe(*CDC10*)1 and pYe(*CEN3*)11 in crosses 1–5. Thus the presence of the 1.6-kilobase pair segment (*CEN3*) on a plasmid carrying a yeast chromosomal replicator is all that is required for the plasmid to behave as a chromosome in mitosis and meiosis in the majority of asci analysed.

CEN3 minichromosomes are not integrated into the yeast genome

Genetic data in crosses 1-6 confirm random assortment of *CEN3* minichromosomes with respect to chromosomes I, III, IV, and XI. The possibility that *CEN3*-containing plasmids are integrated near the centromere of one or several other yeast chromosomes was tested both biochemically and genetically. First a mating was performed between two minichromosome-bearing progeny (cross 7, Table 2). In the majority of asci in cross 7, the minichromosomes (both *TRP1*) show the 2+:2− segregation pattern, indicating that the minichromosomes frequently go to the same pole in the first meiotic division and thus do not pair with each other all the time, if at all. This segregation pattern also confirms that pYe(*CDC10*)1 is not integrated into any other single chromosome in the parents in this cross. If it were, all daughter spores should contain plasmid, because the chromosome pair into which the plasmid is integrated would duplicate in meiosis I and go to opposite poles. This point is again confirmed in cross 8 where the minichromosomes are individually marked. In at least two asci both minichromosomes went to the same pole in meiosis I (Tables 2 and 3) and were therefore both found in the same two sister spores.

In addition, biochemical evidence shown in Fig. 3 demonstrates that pYe(*CEN3*)41 is not integrated anywhere in the yeast genome. Crude yeast DNA was prepared from two germinated sister spores that contained the minichromosome

Table 2 Meiotic segregation of the minichromosomes

Genetic cross no.	Minichromosome in cross	Minichromosome marker scored	Distribution in tetrads of genetic marker on minichromosome (%)					Test for centromere linkage of marker on minichromosome			Reference centromere marker (chromosome)
			4+:0−	3+:1−	2+:2−	1+:3−	0+:4−	PD	NPD	T	
1	pYe(*CDC10*)1	*TRP1*	1 (6%)	0	10 (63%)	0	5 (31%)	2	8	0	*met14*(XI)
2	pYe(*CDC10*)1	*CDC10*	1 (8%)	0	11 (92%)	0	0	2	8	1	*ade1*(I)
3	pYe(*CDC10*)1	*TRP1*	1 (7%)	0	11 (79%)	0	2 (14%)	4	7	0	*met14*(XI)
4	pYe(*CDC10*)1	*TRP1*	4 (21%)	0	11 (58%)	0	4 (21%)	ND	ND	ND	—
5	pYe(*CEN3*)11	*TRP1*	2 (13%)	0	9 (60%)	0	4 (27%)	4	5	0	*ade1*(I)
								5	4	0	*cdc10*(III)
6	pYe(*CEN3*)41	*LEU2*	3 (14%)	3 (14%)	13 (62%)	1 (5%)	1 (5%)	7	6	0	*trp1*(IV)
								7	5	0	*cdc10*(III)
7	pYe(*CDC10*)1 × pYe(*CDC10*)1	*TRP1*	6 (35%)	0	9 (53%)	1 (6%)	1 (6%)	ND	ND	ND	—
8	pYe(*CDC10*)1	*TRP1*	10 (24%)	1 (2%)	31 (74%)	0	0	15	16	0	*met14*(XI)
	pYe(*CEN3*)41	*LEU2*	8 (19%)	2 (5%)	24 (57%)	0	8 (19%)	10	14	0	*met14*(XI)
								17	2	0	*TRP1*(mini)

In all the above crosses the marker used to follow the minichromosome was wild type on the minichromosome and mutant in both parents. The crosses were: 1. XSB52-23Cα/pYe(*CDC10*)1(*cdc10 leu2–3 leu2–112 trp1 gal*/*CDC10 TRP1* with X2928-3D-1A*a*(*ade1 gal1 his2 leu1 met14 trp1 ura3*); 2, SB17A*a*/pYe(*CDC10*)1 (*ade1 cdc10 leu2–3 leu2–112 met14 trp1*/*CDC10 TRP1*) with 6204-18Aα(*cdc10 thr4 leu2–3 leu2–112*); 3, SB1C*a*/pYe(*CDC10*)1(*his2 leu1 met14 trp1*/*CDC10 TRP1*) with XSB52-23Cα (*cdc10 leu2–3 leu2–112 trp1 gal*); 4, SB17Bα/pYe(*CDC10*)1 (*ade1 cdc10 leu2–3 leu2–112 met14 trp1*/*CDC10 TRP1*) with X2928-3D-1A*a*; 5, XSB52-23Cα/pYe(*CEN3*)11 with X2928-3D-1A*a*; 6, XSB52-23Cα/pYe(*CEN3*)41 with X3144-1D*a*(*ade2 arg9 can1 his2 his6 leu2 pet8 trp1*); 7, SB14B*a*/pYe(*CDC10*)1 (*ade1 his2 trp1*/*CDC10 TRP1*) with SB17Bα/pYe(*CDC10*)1(*ade1 cdc10 leu2–3 leu2–112 met14 trp1*/*CDC10 TRP1*); 8, SXB52-23Cα/pYe(*CEN3*)41 with SB17A*a*/pYe(*CDC10*)1. Transformation of yeast in the presence of polyethylene glycol^2 results in a high proportion of diploid transformants (a/a or α/α)^8. Diploids are easily recognized by the extremely low spore viability obtained when they are crossed with a haploid, and in this way were eliminated from the group of haploid transformants used in the above crosses. PD, parental ditype; NPD, nonparental ditype; T, tetratype; ND, not determined.

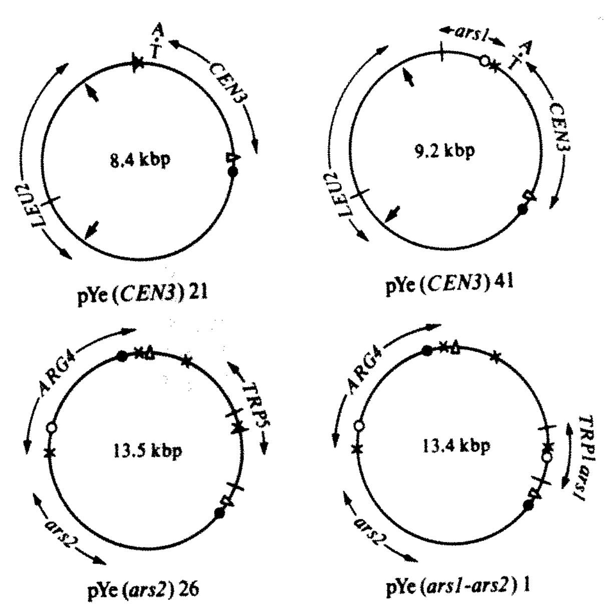

pYe(*CEN3*)21 pYe(*CEN3*)41

pYe(*ars2*)26 pYe(*ars1-ars2*)1

Fig. 2 Physical maps of various plasmid DNAs. The maps show the location of *Eco*RI (—|—), *Hin*dIII (—×—), *Bam*HI (—Δ—), *Pst*I (—┬—), *Sal*I (—●—) and *Bgl*II (—○—) sites in the DNAs and indicate approximate locations of pertinent replicators and genes. The construction and use of these plasmids is described in the text. Their sizes are indicated in kilobase pairs (kbp).

(*LEU2*) and from one of the two sisters in the same ascus that was phenotypically Leu$^-$. This tetrad, in which the minichromosome pYe(*CEN3*)41 segregated 2+ : 2−, was obtained from cross 6 (Table 2). Figure 3 shows an autoradiograph of a Southern blot hybridization[12] in which each of the DNA preparations above was cut to completion with *Sal*I, *Bam*HI, or *Bgl*II. There is a single restriction site for each of these enzymes in the vector portion of pYe(*CEN3*)41 or between the vector and the yeast DNA insert (Fig. 2). In Fig. 3, lanes with DNA from minichromosome-containing progeny (lanes *b* and *c*) show a single band of hybridization to the radioactive probe, [^{32}P]pBR322 DNA. This band has the same mobility regardless of the enzyme used to cut the DNAs, and the mobility is identical to that of linear pYe(*CEN3*)41 generated in the presence of a plasmid-free yeast DNA preparation (lanes *d*) with *Bam*HI or *Bgl*II. The absence of any hybridization bands of sizes other than linear pYe(*CEN3*)41 suggests that this minichromosome is not integrated into yeast genomic DNA. We have not yet attempted to integrate any of the pYe(*CEN3*) plasmids into genomic DNA. Such an event would be expected to lead to dicentric chromosomes and probable mitotic instability[13].

Functional chromosomes require both centromeric DNA and a chromosomal replicator

All the minichromosomes studied and described above contain both *CEN3* and the chromosomal replicator *ars1*. The need for such a replicator with regard to *CEN3* function was tested by inserting the 2.0-kilobase pair *Bam*HI–*Hin*dIII restriction fragment carrying *CEN3* into the plasmid pGT6. Plasmid pGT6 is pBR322 (Tet^r, Amp^r) with a 2.2-kilobase pair fragment carrying the yeast *LEU2* gene inserted into its single *Pst*I site[11]. This plasmid also carries resistance to tetracycline, but not resistance to ampicillin. The 2.0-kilobase pair *Bam*HI–*Hin*dIII *CEN3* fragment was ligated into *Bam*HI–*Hin*dIII cut pGT6 DNA, resulting in the inactivation of Tet^r and yielding the plasmid, pYe(*CEN3*)21, whose structure is shown in Fig. 2.

Somewhat surprisingly, pYe(*CEN3*)21 DNA which contains *CEN3*, but lacks a chromosomal replicator sequence (Fig. 2), also transforms XSB52-23C to Leu+ with a frequency as high as does pYe (*CEN3*)41 DNA. Plasmid pYe(*CEN3*)21 is very unstable mitotically, however (Table 1). When grown under selective conditions in minimal liquid medium without leucine, the doubling time for transformants of pYe(*CEN3*)21 is about 12 hours, as compared to 4 hours for those transformants carrying pYe(*CEN3*)41. In log phase under selective conditions greater than 95% of the cells have segregated pYe(*CEN3*)21, whereas no segregation of pYe(*CEN3*)41 is detected under the same conditions. In general, more than 50% of yeast cells, originally transformed with plasmids carrying chromosomal replicators such as *ars1* (near *TRP1*) or *ars2* (near *ARG4*), lose the plasmid while being grown selectively[7,9]. The high frequency of transformation and high mitotic instability exhibited by pYe(*CEN3*)21 in yeast is perhaps most easily explained by postulating the presence of a weak or partial replication origin on the 1.6-kilobase pair (*CEN3*-containing) segment that permits only enough replication for the plasmid to be transferred to a few daughter cells in the population. It is not known whether this origin plays a role in centromere function.

Plasmids containing two chromosomal replicators are mitotically unstable

Since pYe(*CEN3*)21 DNA does transform yeast with high efficiency in the absence of a chromosomal replicator and seems to have a weak origin of replication of its own, we tested the possibility that any two chromosomal replicators on a plasmid might give mitotic stability to that plasmid in yeast. This notion has been addressed previously by Stinchcomb *et al.*[7], who looked at the behaviour of multimeric forms of *ars1* and found that yeast cultures transformed with monomer, dimer, and trimer *YRp7*(*TRP1 ars1*) were equally unstable mitotically and had identical growth rates.

We have put the *ars1* replicator together on a plasmid with *ars2* (a chromosomal replicator near *ARG4*)[9] in the following way. The plasmid pYe(*ars2*)26 (Fig. 2) contains the yeast *ARG4* and *TRP5* genes and the *ars2* replicator (C. L. Hsiao and J.C., manuscript in preparation). Plasmid pYe(*ars1–ars2*)1 was constructed by treating pYe(*ars2*)26 DNA with *Eco*RI endonuclease and inserting the 1.4-kilobase pair fragment carrying *Trp1* and *ars1* (ref. 7) into the plasmid DNA, thereby partially deleting the *TRP5* gene and replacing it with *TRP1* and ars*1* (Fig. 2). When *trp1* yeast was transformed to Trp$^+$ with pYe(*ars1–ars2*)1 DNA, transformants were as unstable mitotically for the Trp$^+$ phenotype as those transformed with pYe35 which carries only *ars1* (Table 1). In the same experiment, pYe(*CEN3*)11 showed less than 18% loss of the Trp$^+$ phenotype. In addition, the *ars1* replicator segment is in opposite orientations with respect to *CEN3* in pYe(*CDC10*)1 and pYe(*CEN3*)41, and both minichromosomes are equally stable. We conclude that two chromosomal replicators together do not convey mitotic stability upon a plasmid and that *CEN3* is unique

Table 3 Genetic analysis of mating between two haploid parents each carrying an individually marked minichromosome (cross 8)

Distribution in tetrads of markers on minichromosomes		No. of tetrads showing segregation pattern
TRP1(pYe(*CDC10*)1)	*LEU2*(pYe(*CEN3*)41)	(% of total)
4+ : 0−	4+ : 0−	3 (7%)
4+ : 0−	2+ : 2−	4(10%)
4+ : 0−	0+ : 4−	3 (7%)
3+ : 1−	2+ : 2−	1 (2%)
2+ : 2−	4+ : 0−	5(12%)
2+ : 2−	3+ : 1−	2 (5%)
2+ : 2−	2+ : 2−	19(45%)
2+ : 2−	0+ : 4−	5(12%)
	Total no. of asci analysed	42(100%)

Strains in cross 8 are described in Table 2, where the meiotic segregation patterns of the minichromosomes are summarized. Among the 19 asci where both minichromosomes segregated 2+ : 2−, both went to the same pole in the first meiotic division in 2 asci and to opposite poles in 17 asci.

in its stabilizing effect. This conclusion is further verified by the observation that *CEN3*, when isolated on a 5.1-kilobase pair *Eco*RI fragment derived from plasmid pYe46B2 (Fig. 1) and inserted into the *Eco*RI sites at the *TRP5* locus on pYe(*ars2*)26 (Fig. 2), mitotically stabilizes this *ARG4 ars2* plasmid for the Arg$^+$ phenotype (C. L. Hsiao and J.C., unpublished result).

Minichromosomes do not always pair in the first meiotic division

The absence of asci with two viable and two nonviable sister spores in crosses 1–6 indicates that the minichromosomes do not pair at the first meiotic division with any of the 17 yeast chromosomes. Cross 8 (Tables 2 and 3) was performed with two strains, each harbouring a *CEN3 ars1* plasmid marked with either *LEU2* or *TRP1*. Both parents in cross 8 have mutations at both *leu2* and *trp1*, therefore the behaviour of each minichromosome can easily be followed individually. A detailed analysis of this cross is given in Table 3, from which the following conclusions can be drawn. Each plasmid individually exhibited the 2+ : 2− segregation pattern in more than 60% of the tetrads examined. In the 19 asci where both plasmids segregated 2+ : 2−, the minichromosomes went to opposite poles in the first meiotic division in 17 asci, but they did assort to the same pole in 2 asci. These numbers support the notion that the minichromosomes do not always pair, but there is a strong preference for them to go to opposite poles in the first division. Otherwise, they seem to segregate randomly and independently with respect to one another, and all combinations of 4+ : 0−, 2+ : 2−, and 0+ : 4− are seen (Table 3). For example, both minichromosomes were found in all four spores in three tetrads; in five tetrads pYe(*CEN3*)41 was found in all four spores, but pYe(*CDC10*)1 segregated 2+ : 2−; in three asci pYe(*CDC10*)1 was in all four spores, but pYe(*CEN3*)41 was completely lost. Thus two minichromosomes together in the same sporulating diploid show the same meiotic behaviour as either one exhibits alone.

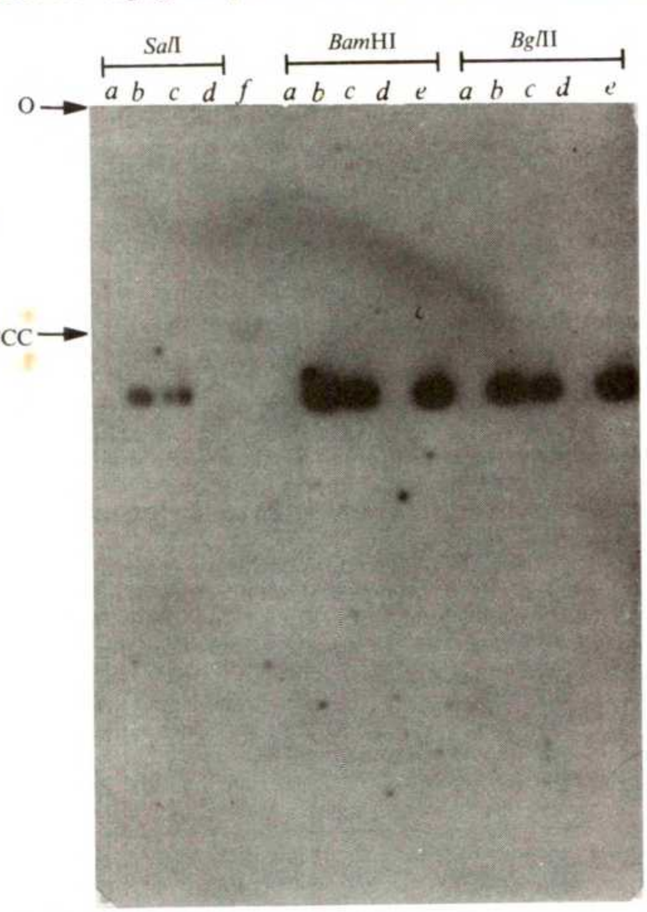

Fig. 3 Southern blot hybridization autoradiograph of total yeast DNAs from pYe(*CEN3*)41-containing strains with $[^{32}P]$pBR322 DNA as probe. Crude yeast DNA was prepared as described by Stinchcomb *et al.*[7] from one Leu$^-$ progeny (lanes *a*) and two Leu$^+$ progeny (lanes *b* and *c*) of a single 2+ : 2− ascus in cross 6 and from a Leu$^-$ progeny of a 3+ : 1− ascus in the same cross (lanes *d*). Approximately 2 μg of each DNA preparation was digested with *Bam*HI, *Sal*I, or *Bgl*II and electrophoresed in 0.75% agarose. Other lanes on the gel contained 2 ng of pYe(*CEN3*)41 DNA mixed with 2 μg of crude Leu$^-$ yeast DNA, either undigested (lane *f*) or digested (lanes *e*) with restriction enzyme. Blot hybridization was carried out according to Southern[12], with the following modifications. The fragments were transferred from the gel to nitrocellulose as described by Wahl *et al.*[21] and hybridization conditions were those of Cameron *et al.*[22]. The probe was pBR322 DNA labelled *in vitro* by nick translation[23] as described by Chinault and Carbon[1]. The origin (O) and position of covalently-closed circular pYe(*CEN3*)41 DNA (CCC) are indicated on the autoradiograph.

Discussion

We have identified a small DNA element (*CEN3*) from *S. cerevisiae* chromosome III that when present on a plasmid with a chromosomal replicator (*ars1* or *ars2*) allows the plasmid to behave as a functional chromosome in yeast. Minichromosomes containing *CEN3* are stable in mitosis, and in most cases segregate as chromosomes in the first meiotic division and are thus found in the two sister progeny of the second meiotic division. The *CEN3* element is therefore capable of controlling copy number, thereby ensuring proper meiotic segregation. In approximately 15% of the tetrads analysed in crosses involving *CEN3* plasmids, the minichromosome is lost completely. Generally, in yeast strains that are aneuploid for one or more chromosomes, the extra chromosomes are also somewhat unstable[14]. Tetrads in which a *CEN3* minichromosome segregates 1+ : 3− are rare, therefore the minichromosome is more stable through the second meiotic division than in the first.

In approximately 20% of the tetrads analysed, the minichromosome is found in all four spores after meiosis. This may be a result of selective diploidization of the *CEN3* plasmid or could indicate a loss of control of minichromosome replication. Inability of minichromosomes to pair may cause a certain instability in their attachment or involvement in the meiotic apparatus. Thus control over plasmid replication may be eliminated in some cases resulting in multiple copies that are distributed to all four spores. The 4+ : 0− tetrads are not a separate class, since the same 4+ : 0−, 2+ : 2−, 0+ : 4− patterns are exhibited by the progeny after further matings. Moreover, data from cross 8 (Tables 2 and 3) show that one minichromosome can segregate 2+ : 2− while another in the same meiotic event is distributed 4+ : 0−.

The genetic data show that minichromosomes do not pair with any of the normal yeast chromosomes, since asci containing two non-viable sister spores are not seen. However, two minichromosomes in the same diploid exhibit a strong preference to migrate to opposite poles in the first meiotic division. To determine exactly how much DNA, or which regions of DNA are involved in pairing of chromosomes at the first meiotic division, increasingly larger segments of DNA may be added *in vitro* to either or both ends of the *CEN3* segment on a plasmid. Pairing could then be assayed by genetic analysis.

Because plasmid pYe98F4T complements the *cdc10* mutation in yeast and plasmids pYe(*CEN3*)11 and pYe35 do not (Fig. 1), we have concluded that the *CDC10* gene is probably located in the region of the single *Bam*HI site in pYe98F4T. The *cdc10* locus had previously been placed directly next to the centromere of chromosome III (refs 15–17). The data presented here indicate that *cdc10* is located about 3 kilobase pairs from the centromere on the right arm of chromosome III. There are approximately 25 kilobase pairs of DNA between the *LEU2* and *CDC10* genes[3]. The genetic map distance between *leu2* and centromere is about 8 cM (refs 3, 16 and 17). Thus there is an average of about 3 kilobase pairs cM^{-1} from *leu2* across the centromere to *cdc10*. This number is close to the 2.7 kilobase pairs CM^{-1} determined by Strathern *et al.*[18] for very large distances on the circular chromosome III, indicating that the centromere does not appreciably distort recombination frequencies in the *leu2–cdc10* region.

We have shown previously that within the limits of a standard Southern blot hybridization, plasmid pYe(*CDC10*)1 contains only unique DNA[3]. By this same criterion, all the DNA between *leu2* and *cdc10* is unique DNA[1]. Work in progress is expected to define further the size of the centromeric DNA segment and its nucleotide sequence. Whether centromeric DNA sequences are unique for each chromosome may eventually be determined by sequencing other centromeres obtained in the same way.

The small circular chromosomes we have constructed around the *CEN3* element have many properties that mimic those of the much larger parental chromosomes. They are stable both in mitosis and through the first and second divisions of meiosis, probably because *CEN3* is providing an attachment site for spindle structures, a site that may be unique for each chromosome. A chromosomal replicator must accompany the *CEN3* segment to permit proper centromere function, but the replicator alone, or a combination of chromosomal replicators, do not stabilize a plasmid. Therefore the minichromosomes, like the larger chromosomes, require both an attachment site and one or more replicators. Unlike the parental chromosomes, the small circular chromosomes do not always pair, but, as is the case in sporulating aneuploid yeast strains, absence of pairing does not prevent the chromosomes from segregating in meiosis. Although we have no evidence that the weak replicator in the *CEN3* region is involved in centromere function, it is intriguing to speculate that it may be a specialized replicator for that region, perhaps serving to drive sister chromotids apart in a final burst of DNA synthesis, as suggested by DuPraw[19].

The *CEN3* minichromosomes are excellent probes for the study of events in mitosis and meiosis, particularly with regard to the protein–nucleic acid interactions occurring between the centromere and the mitotic and meiotic spindle structures. Minichromosomes with a functional centromere will be useful as well for studies of chromatin structure and the organization of DNA-associated proteins in the centromere region.

Finally, the mitotic stability of *CEN3* plasmids make them especially suitable cloning vehicles. Studies of expression of cloned genes on minichromosomes would not be complicated by the variable mitotic stability displayed by other vectors constructed for cloning in yeast. The functional centromeric sequence, *CEN3*, is not altered by propagation in *E. coli*, since all the *CEN3* minichromosomes were originally isolated in that bacterium before being put into yeast, and the absence of any gross alterations in DNA sequence in cloned segments from around the *CEN3* region has been previously confirmed by Southern blot hybridizations to restriction digests of total yeast genomic DNA[1,3]. It will also be of considerable interest to determine if the yeast centromere will function when introduced into other cell types on the appropriate self-replicating DNA vectors.

We thank Dr Terrance G. Cooper for many helpful discussions about the genetic data, Dr Robert K. Mortimer for introducing us to the intricacies of yeast genetics and for constructing strain XSB52-23C, Robert Gimlich for technical assistance and Drs Craig Chinault, Ronald Hitzeman, and Alan Kingsman for isolating many of the overlapping plasmids around centromere-linked loci on chromosome III. This research was supported by a grant (CA-11034) from the NCI, NIH.

Received 19 May; accepted 1 August 1980.

1. Chinault, A. C. & Carbon, J. *Gene* **5,** 111–126 (1979).
2. Hinnen, A., Hicks, J. B. & Fink, G. B. *Proc. natn. Acad. Sci. U.S.A.* **75,** 1929–1933 (1978).
3. Clarke, L. & Carbon, J. *Proc. natn. Acad. Sci. U.S.A.* **77,** 2173–2177 (1980).
4. Clarke, L., Hitzeman, R. A. & Carbon, J. *Meth. Enzym.* **68,** 436–442 (1979).
5. Hitzeman, R. A., Chinault, A. C., Kingsman, A. J. & Carbon, J., *ICN–UCLA Symposia on Molecular and Cellular Biology* Vol. 14, (eds Maniatis, T. & Fox, C. F.) 57–68 (Academic, New York, 1979).
6. Ratzkin, B. & Carbon, J. *Proc. natn. Acad. Sci. U.S.A.* **74,** 487–491 (1977).
7. Stinchcomb, D. T., Struhl, K. & Davis, R. W. *Nature* **282,** 39–43 (1979).
8. Kingsman, A., Clarke, L., Mortimer, R. K. & Carbon, J. *Gene* **7,** 141–152 (1979).
9. Hsiao, C.-L. & Carbon, J. *Proc. natn. Acad. Sci. U.S.A.* **76,** 3829–3833 (1979).
10. Gerbaud, C. *et al. Gene* **5,** 233–253 (1979).
11. Tschumper, G. & Carbon, J. *Gene* **10,** 157–166 (1980).
12. Southern, E. M. *J. molec. Biol.* **98,** 503–517 (1975).
13. McClintock, B. *Proc. natn. Acad. Sci. U.S.A.* **25,** 405–416 (1939).
14. Parry, E. M. & Cox, B. S. *Genet. Res.* **16,** 333–340 (1971).
15. Hartwell, L. H., Mortimer, R. K., Culotti, J. & Culotti, M. *Genetics* **74,** 267–286 (1973).
16. Mortimer, R. K. & Hawthorne, D. C. *Meth. Cell Biol.* **11,** 221–233 (1975).
17. Culbertson, M. R., Charnas, L., Johnson, M. T. & Fink, G. R. *Genetics* **96,** 745–764 (1977).
18. Strathern, J. N., Newton, C. S., Herskowitz, I. & Hicks, J. B. *Cell* **18,** 309–319 (1979).
19. DuPraw, E. J. *DNA and Chromosomes* (Holt, Rinehart and Winston, New York, 1970).
20. Tabak, H. F. & Flavell, R. A. *Nucleic Acids Res.* **5,** 2321–2332 (1978).
21. Wahl, G. M., Stern, M. & Stark, G. R. *Proc. natn. Acad. Sci. U.S.A.* **76,** 3683–3687 (1979).
22. Cameron, J. R., Loh, E. Y. & Davis, R. W. *Cell* **16,** 739–751 (1979).
23. Rigby, P. W., Dieckmann, M., Rhodes, C. & Berg, P. *J. molec. Biol.* **113,** 237–251 (1977).

A low resolution structure for the histone core of the nucleosome

A. Klug, D. Rhodes, J. Smith & J. T. Finch
MRC Laboratory of Molecular Biology, Hills Road, Cambridge CB2 2QH, UK
J. O. Thomas
Department of Biochemistry, University of Cambridge, Tennis Court Road, Cambridge CB2 1QW, UK

Image reconstruction to 22 Å resolution of the histone octamer $(H3)_2(H4)_2(H2A)_2(H2B)_2$ shows it to have a 2-fold axis of symmetry, and the overall shape of a left-handed helical spool on which to wind about two turns of a flat superhelix of DNA in the nucleosome. From this structure and the results of various cross-linking studies, we have deduced the arrangement of the individual histones. We propose that the $(H3)_2(H4)_2$ tetramer forms a dislocated disk which defines the central turn of DNA, while the two H2A–H2B dimers lie one on each face, each associated with about one half a turn.

THE fundamental unit of chromatin structure is the nucleosome[1] which consists of a stretch of DNA wound about a histone core. With the knowledge that the arginine-rich histones H3 and H4 existed in solution as tetramers[2,3], the lysine-rich histones H2A and H2B as dimers[2,4], and that the four histones occur in chromatin in equimolar amounts, Kornberg[5] proposed that the core of the nucleosome was a histone octamer of composition $(H3)_2(H4)_2(H2A)_2(H2B)_2$. Octamers of histones in chromatin were demonstrated by chemical cross-linking, and the octamer was also shown able to exist free in solution in 2 M NaCl, which displaces the DNA[6,7]. The octamer in 2 M NaCl was later characterized by hydrodynamic and other methods[8–10].

While attempting to crystallize the histone octamer we have produced regular fibres at high ionic strength, and have used electron microscopy and the image reconstruction method[11,12] to produce a low resolution three-dimensional density map of the octamer. It has 2-fold symmetry. The nature of the octamer structure suggests its orientation relative to that of the superhelix of DNA in the nucleosome, corresponding with that demonstrated by neutron diffraction studies of nucleosome core particle crystals[13]. We have used the results of Mirzabekov *et al.*[14] on the chemical cross-linking of histones to nucleosome core DNA, and the information on histone–histone proximities given by cross-linking, to assign regions of density in the octamer map to particular histones. This constitutes a proposal for the spatial arrangement of histones in the nucleosome core, from which it can be seen that the $(H3)_2(H4)_2$ tetramer defines the basic fold of the nucleosome DNA and the H2A–H2B dimers continue it.

Preparation and electron microscopy of histone octamer tubes

The histone octamer was prepared from rat liver as described earlier[8], in 2 M NaCl–100 mM Tris Cl, *p*H 7.0, or 2 M NaCl–137 mM sodium borate, *p*H 9.0. When a solution of the octamer is brought to >40% saturation with ammonium sulphate at 4 °C, keeping the NaCl and buffer concentrations constant (final concentration of octamer 2 mg ml^{-1}), a precipiate forms over a period of days that contains all four histones in their original equimolar amounts. Electron micrographs of negatively stained samples of the precipitate fixed with glutaraldehyde show sheaf-like aggregates of a dozen or so hollow tubular structures, of external diameter about 300 Å and several micrometres long. If fixing is omitted, the tubes break down to short lengths, some so short that they lie on the grid end-on to give an annular image (Fig. 1*a* arrow). Specimens more suitable for image analysis may be obtained by adding the stain to the precipitate before applying it to the grid. This dissociates the sheaves but maintains the length of the individual tubes (Fig. 1*b*, *c*). Essentially identical tubes were grown using histone octamer from turkey erythrocytes and beef kidney.

The state of aggregation of the histones in conditions where tubes form was checked by cross-linking with dimethyl suberimidate[6,15] and shown to be octameric, the time course being similar to that described previously for the free octamer in 2 M NaCl[16]; as expected there is also some evidence of octamer–octamer cross-linking. (Because cross-linking of amino groups cannot be carried out in ammonium sulphate, we used instead dipotassium hydrogen phosphate (0.5M)-potassium pyrophosphate (0.615M) which also promotes aggregation into tubes [B. Rushton, J.T.F. & A.K., unpublished results].)

Moreover, comparison of cross-linked dimers at comparable stages of cross-linking shows that the arrangement of histones in the octamer is essentially the same for the octamer in the tubes, the octamer free in solution, and the octamer in the nucleosome; these dimers are those reported previously in the nucleosome[6,7] and H3–H2B. For the tubes, the same dimers are formed at roughly the same relative rates and are present in similar relative amounts, the main differences being consistent with unmasking of a higher proportion of amino groups in H3 and H4 than in H2A and H2B on going from the nucleosome to the octamer in high salt. We therefore believe that extrapolation from the model for the octamer present in the tubes (Fig. 4) to the octameric core of the nucleosome (Fig. 5) is valid.

Image analysis and 3-dimensional reconstruction

The transverse striations, of spacing about 65 Å, across the hollow tubes indicate that they are built from rings of (octamer) units. The annular images are evidently short stacks of rings seen end-on, and sometimes a regular series of protuberances can be seen around the circumference. The number of units per ring cannot be counted unequivocally, but is in the range 10–12. The number can be estimated by viewing the images of the long tubes obliquely from the bottom of the page. At this angle, the units can be seen to lie on long-pitch helices. The number of parallel helices on one side of the tube appears to be five rather than six indicating 10 units per ring. A more reliable estimate is obtained by close inspection of the edge-on views in the long tubes: the succession of superposition patterns seen—and such patterns are not as sensitive to distortions as are quantitative analyses—is characteristic of 10 units per ring. The value 10 was confirmed by the Fourier analysis described below. Another class of tube was occasionally found of slightly larger diameter, containing 11 units per ring, but they were less well ordered than the 10-fold tubes and gave poorer maps.

We have investigated the structure of the octamer tubes by Fourier transform techniques[11,12], using computer programs developed for correlating helical particles[17]. Optical transforms were used initially to select well ordered particles, then the best were processed by computer to give phase information for a quantitative assay of the state of specimen preservation, and again from among these were selected a smaller set of particles which correlated well with one another, after allowance was made for their different orientations. The data from a final set

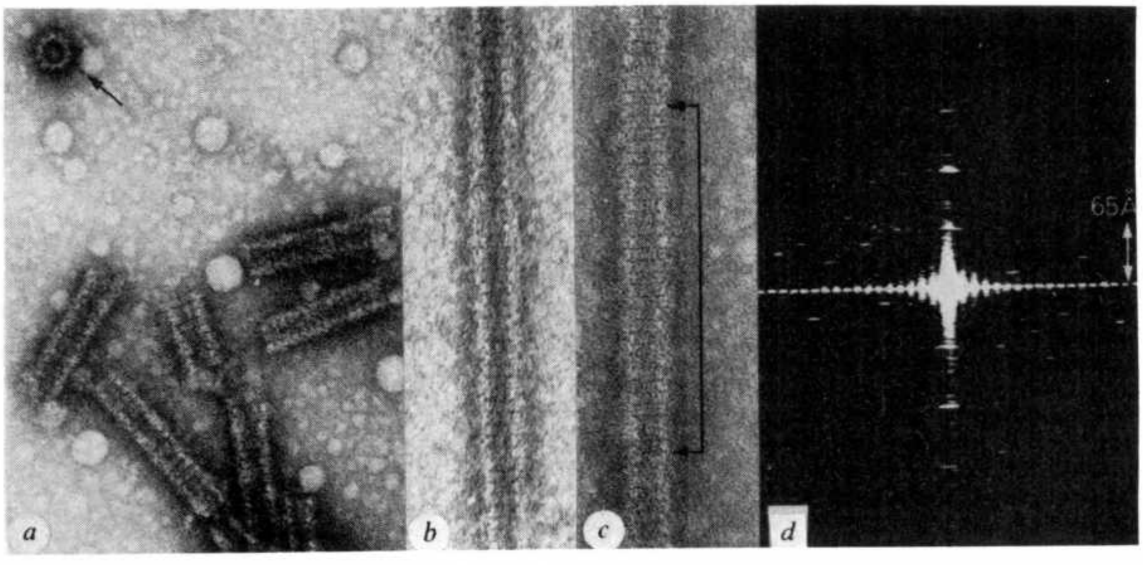

Fig. 1 Electron micrographs of tubes of histone octamers, negatively stained with 0.1% uranyl acetate; in *a*, the stain was applied after the specimen was applied to the grid, and in *b* and *c*, beforehand. Oblique helical lattice lines of pitch about 280 Å can be seen clearly in *b*, in which the contrast of one side of the particle dominates. *d*, Optical diffraction pattern of the length marked in *c*; the first meridional reflection is at an axial spacing of 65 Å. The strong second order of this reflection indicates that the projected density in the rings is roughly divided into two layers, as is evident in the images themselves. Magnifications: *a*, 175,000×; *b*, 236,000×; *c*, 242,000×.

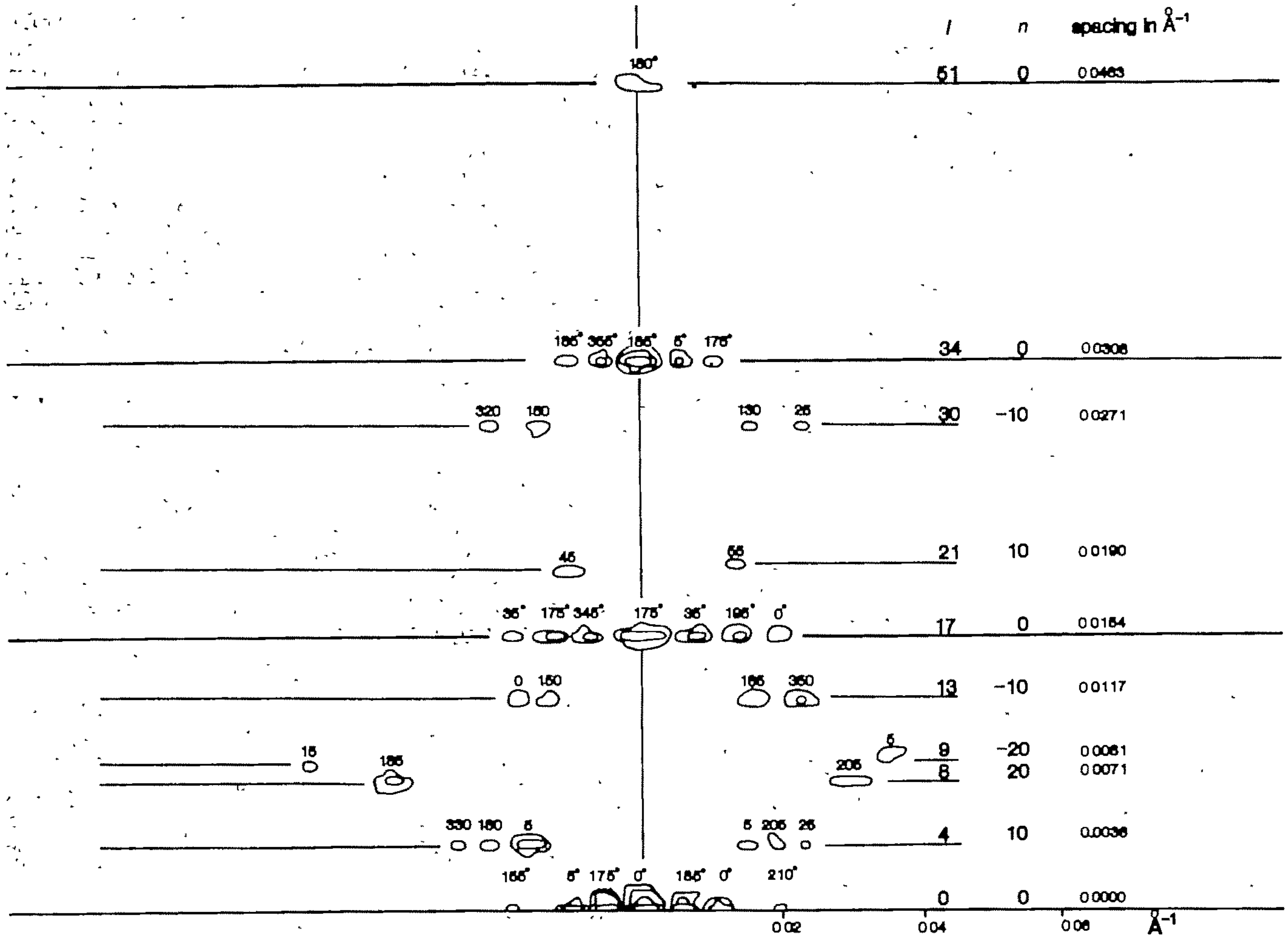

Fig. 2 A map of the amplitudes and phases in the computer Fourier transform of the octamer tube in Fig. 1*c*. The image was densitometered on a raster with a spacing equivalent to about 2.5 Å. The layer lines are marked by an index l corresponding to the simplest rational approximation to the helical repeat. The helical selection rule for the diffraction pattern is $n = 10n'$ where n' is given by $l = 4n' + 17m$; the orders n of the Bessel functions on each layer line are indicated. Because the rotational symmetry is of even order (10-fold), the phases of corresponding peaks on left and right sides should ideally be the same, and the discrepancy between them is a measure of the state of preservation of the specimen. The presence of radial dyads was tested for by searching for the position of putative dyads in the image which make the phases as close as possible to 0° or 180°. The lowest value of the (weighted) residuals found (corresponding to the Q-type of residual (of ref. 17) for the three best particles were individually 41°, 38° and 18°, and 31° for the average, showing that dyads are present. The best particles were found by examining the correlation between the two sides of their transform (near and far sides of the particle) and the correlation between different particles. During this analysis, a radial scale factor is computed to help compensate for variations in magnification and particle shrinkage during drying; most such scale factors varied by less than 10% from the average. When there is no overlap of different helical contributions on the same layer line, as here, each Fourier transform yields two independent data sets, corresponding to the near and far sides of the particles. Separate radial scale factors were used for the two sides to allow for differential shrinkage, the J_0 contributions being omitted for the determination of the scaling factor, but apportioned afterwards, one half to each side.

were combined to calculate Fourier components for a three-dimensional synthesis.

An optical diffraction pattern and computer transform of one of the best tubes are shown in Figs 1*d* and 2 respectively. The axial reflection on a layer line of spacing 65 Å corresponds to the thickness of a ring. Off-meridional intensity occurs on a layer line of spacing about 280 Å, and corresponds to helical lines of pitch 280 Å running obliquely across the particles (Fig. 1*b*). The absolute hand (left) of this helical family, and hence of the whole structure, was found from electron micrographs of shadowed specimens. The relative rotation of successive rings is reflected in the ratio of the spacings of the 280 Å and 65 Å layer lines, which varies between 4.0 and 4.4 for different particles and different regions along the same particle. An average of 4.25 ($=\frac{17}{4}$), corresponding to a rotation of $2\pi/10\times(4/17)$ between successive rings, was adopted as the simplest rational approximation for numbering the layer lines in Fig. 2.

Analysis of the computer transforms of images of the tubes showed that, to the resolution of the micrographs, the histone octamer itself possesses a 2-fold axis of symmetry. Transforms were correlated with each other[17] to bring all the particles into a common registration, to permit data averaging. During this fitting procedure, a phase residual is calculated which gives a measure of how well correlated any two particles are. No significant differences in the residuals were found between the best fits of particles either way up, showing that the tubes were non-polar and so possessed radial dyad axes. The final map (Fig. 3), comprising the average data from three particles, has a nominal resolution of about 20 Å in both axial and radial directions, but all contributions at less than about 30 Å are weak. The three particles chosen were those that correlated best with each other, and also individually showed equally good preservation in their near and far sides.

Description of the structure

The map of the octamer tube reconstructed from the averaged data with imposed 2-fold symmetry is presented in Fig. 3. The rings of the tube are divided into ten distinct units, each presumably representing an octamer; the division between rings is also clear, and thus, except for small boundary regions, the density corresponding to one octamer can be unequivocally dissected from the map. A model of this density is shown in Figs 4*a* and 7*a*: the contour cutoff in constructing the model was

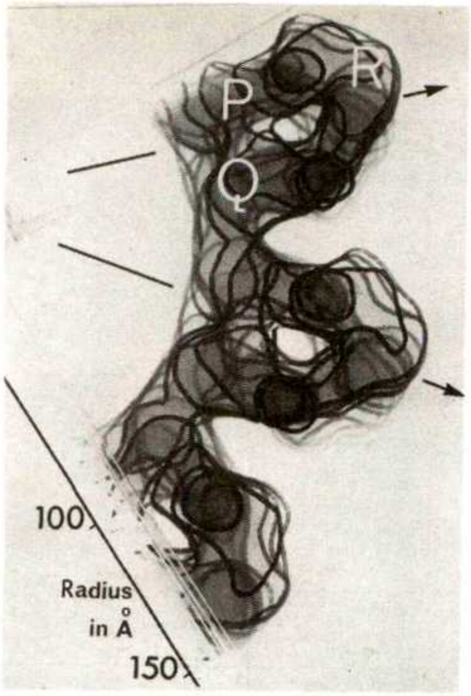

Fig. 3 Three-dimensional reconstruction of the histone octamer tube, plotted as sections through the map. The region shown corresponds to $2\frac{1}{2}$ octamers, that is a 90° sector of the tube of height 65 Å, and is viewed in a direction tilted slightly away from the tube axis. The lowest contour level has been chosen to give the appropriate hydrated molecular volume of the octamer. The dyad axes of symmetry passing through the octamers are marked by arrows.

chosen to give a hydrated molecular volume of 137,000 Å^3, taking $M_r = 110{,}000$ and assuming a density for hydrated protein of 0.8 daltons Å^{-3} (ref.18).

Figure 4*a* shows the wedge-shape appearance of the model, whereas Fig. 7*a* shows that at its broadest aspect the particle has a roughly circular outline of approximate diameter 70 Å. At right angles to this the particle is 56 Å at its thickest point. These are suitable dimensions to form the histone core of a nucleosome core particle of external diameter 110 Å and thickness 55 Å (ref. 19): subtracting the DNA from the outside would leave a cylindrical inner space of about 70×55 Å.

The correspondence goes further. The nucleosome core is a wedge-shaped particle, of bipartite character[19], and the octamer also has a similar wedge shape, split into two and twisted somewhat about its dyad axis. This is best seen in Fig. 3 where the wedge is viewed approximately sideways on. The two ridges at the thick end, marked P and Q, slope up in an opposite direction to the ridge at the thin end, marked R, so that they, together with the ridges on the sides of the wedge, form a rough helical ramp, of pitch about 25 Å, whose course is marked in Fig. 4*b*. The ridges forming the ramp are rather broken up, and there is some variation in individual image reconstructions, but the continuity is not in doubt. The sense of the ramp is left-handed, as expected if the DNA superhelix is to wind around the octamer.

The octamer shape revealed here resembles that found in the density map of the protein moiety of the nucleosome core, produced from a neutron diffraction study of crystals of nucleosome core particles, using the method of contrast variation (Fig. 2*c* of ref.13). That study also gave a map of the DNA, and hence the orientation of the 'wedge' of $1\frac{3}{4}$ turns of DNA[19] relative to the wedge formed by the histone core. This orientation is the same as that shown in Fig. 4*b*. It is thus the octamer that determines the architecture of the nucleosome. The 2-fold symmetry of the DNA superhelix allows it to interact with its octameric histone core along a common twofold axis.

Note that the map identifies the stain-excluding regions, so that the model presumably depicts the hydrophilic surfaces of the particle, which are exposed to the negative stain, and is thus dependent on the way in which the stain actually interacts with (and possibly distorts) the surface of the histone molecules and penetrates the gaps between them. At low resolution, the individual histone molecules are not resolved, yet our map shows protuberances presumably corresponding to exposed portions of the individual molecules making up the oligomer, and channels corresponding to the spaces between them.

Clearly the octamer has fairly large cavities in it accessible to the negative stain. These run irregularly through the structure to a hollow centre, and, together with the overall flat shape, could surely account for the anomalous frictional ratio of about 1.3, found from hydrodynamic observations[8], even without a contribution from any flexible N-terminal tails[20].

When a superhelix (representing the DNA) is wound smoothly at a mean radius of about 45 Å on the helical spool formed by the octamer, as in Fig. 5, it fits snugly at the thick and thin ends of the wedge, but does not hug the sides so well. Although this might be an artefact, it could reflect true disorder arising from flexible N-terminal regions of the histones, which might be lost to view in the stain and would certainly be lost in the averaging procedure. The differential fit may be related to the differential cutting along the DNA of the nucleosome core shown by DNAse I. We noted earlier that the regions of low cutting frequency lie at two diametrically opposite areas, corresponding to the 'sites' −4 and +4 on one side, and −1 and +1 on the other (Fig. 8 of ref. 19). It is likely that this increased protection is associated with tighter contact with the histone core at the two ends of the wedge. Indeed, the distribution of diffuse intensity in X-ray diffraction patterns of the nucleosome core crystals shows that the DNA on these two 'ends' of the nucleosome core is held more rigidly than that at the 'sides' (J.T.F. and A.K., unpublished results). A stiff molecule like DNA wound neatly on to a spool need not have equal contact all along its length; it need only be fixed at a few points and the bending stiffness will do the rest.

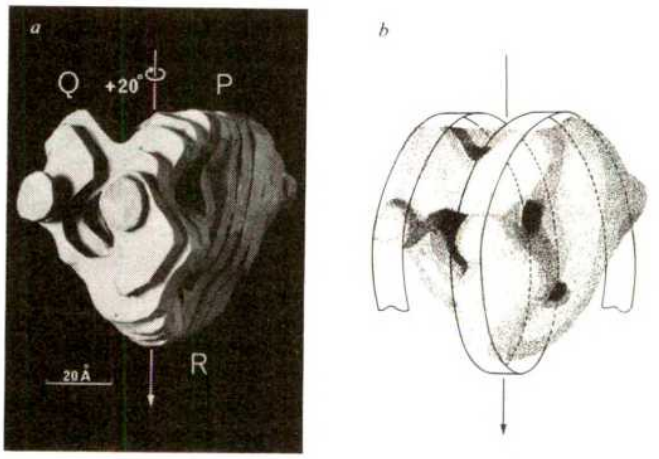

Fig. 4 *a*, Model of histone octamer obtained by cutting out solid sections of the map in Fig. 3. The dyad axis is marked by an arrow, and the view is at an angle of about 20° to that in Fig. 3, as can be seen from the inclination of the sections. *b*, A drawing of *a* showing how the ridges on the periphery of the octamer model form a more or less continuous helical ramp of external diameter about 70 Å and pitch about 27 Å, on which about $1\frac{3}{4}$ turns of a superhelix of DNA of the appropriate dimensions[19] could be wound. In a further reconstruction, not included here, there is a lower density at one of the ends of the ridges P and Q (between the marks $H4^1$ and $H2B^1$ in Fig. 5*a*) but the continuity of the ramp is clear.

Assignment of histones to regions of the map

We have used histone–DNA cross-linking results, which map the sites of interaction of histones relative to the 5′-end of a DNA strand, and information on histone–histone proximities from cross-linking studies, to assign individual histones to particular regions of the density map. Our main assumption is that the histones are too small to be multi-domain proteins, although they could still have flexible N-termini. Others[14,21,22] have suggested three-dimensional arrangements of histones within the nucleosome core, using similar chemical evidence, but an interpretation based on such results alone is ambiguous because neither type of cross-linking study distinguishes between the two copies of each histone present. Our three-dimensional density map restricts the number of possibilities. Thus, for example, the ridge R (Fig. 4*a*) which lies in the region of DNA sites −1 to +1 (Fig. 5*a*) is too narrow to accommodate more than one thickness of a histone molecule, and other models are not compatible with this feature. The proposed arrangement is the only one we can find that both fits the major cross-linking data and is compatible with the shape of the octamer.

Histone–DNA cross-linking

The points of contact of histones along the DNA strands determined by histone–DNA cross-linking studies[14] are not sufficient to fix the spatial arrangement of the histones in the nucleosome core. Using the three-dimensional structure in Fig. 4 we have distinguished between the two copies of each histone as shown in Fig. 5. If the two copies of each histone are designated by superscripts 1 and 2, then the results of Mirzabekov *et al.*[14] may now be written more specifically as shown in Fig. 6. Thus, for example, the H3 that makes contact with the DNA 75 bases from the 5′ end is H3^1, whereas the H3 that lies close to the 3′ end (see also ref. 23) is H3^2.

Note that we do not always assume that the pattern of histone–DNA cross-links observed by Mirzabekov *et al.*[14] directly reflects the linear order of histones along the DNA. Even if the major contact of a histone is with a particular DNA segment, it is entirely possible (because the distance between the two superhelical turns is only about 28 Å, that is, roughly the dimensions of a histone molecule) that a histone may also make a less frequent, or minor, contact with the turn of DNA above or below it. Thus, to reconcile our model with the finding[14] of a contact between H2A and the DNA 75 bases from the 5′-end (between sites 0 and 1 in Fig. 5), we have assigned this contact to H2A^1, which also lies close to the DNA turn above, near the segment 0–20 bases from the end (sites −7 and −6). No histone–DNA cross-link corresponding to this contact is observed[14], but an H2A molecule is required there by symmetry, because of the contact at 135 base pairs (between sites 6 and 7); the absence of a cross-link need not be significant and might arise through lack of suitably disposed lysine side chains in the region of contact.

Recently[24] Mirzabekov and his colleagues have refined their results and have assigned particular histone–DNA contacts to individual DNA strands. However, the weak spots on gels identified in that work need not arise from oscillations of linkages between strands as suggested and can be accommodated into our spatial arrangement with the reasonable assumption that a particular histone can cross-link to either one of the neighbouring DNA strands of the double helix. We attempt here only to associate a histone with a particular region of the DNA double helix, without regard to strand.

If the DNA superhelix in the model (Fig. 5) were unfolded, the linear arrangement of the histones along the DNA would be:

$$\mathrm{H2A^1{-}H2B^1{-}H4^1{-}H3^1{-}H3^2{-}H4^2{-}H2B^2{-}H2A^2}$$
$$(\text{site } -7 \rightarrow \text{site } +7)$$

This might seem to be at odds with the contacts broken when the nucleosome unfolds at low ionic strength, or in urea or urea/2M NaCl[25-27]. However, in the first case [25], although two particular residues (Cys 110 in the C-terminal region of the H3s) move apart, the basic N-terminal regions of the proteins may not behave in the same way; and in the other cases[26,27], loss of particular cross-links generated by 'zero-length reagents' could result from only small local perturbations, because these reagents require very precise contacts and juxtapositions for cross-linking.

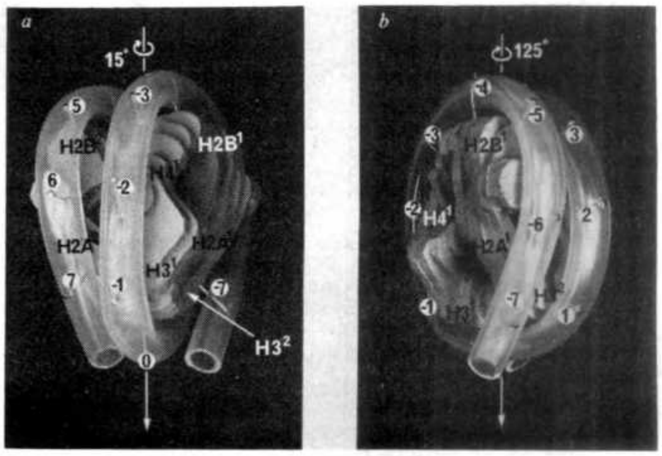

Fig. 5 *a*, The histone octamer structure with two turns of a DNA superhelix wound on it. The assignment of the individual histones to various parts or features of the model is described in the text. (For clarity the DNA double helix is represented by a plastic tube of somewhat smaller diameter than it would actually have.) Distances along the DNA are indicated by numbers −7 to +7 (taking the dyad axis as origin), to mark the 14 repeats of the double helix contained in the 146 base pairs of DNA of the nucleosome core. The positions of the numbers correspond approximately to the sites of attack, that is local maxima in the frequency of cutting by the enzyme DNase I (compare with Fig. 8*b* of ref. 19). The superscripts in the numbering of the histone molecules follows the direction of ordering of the DNA sites, so that the helical ramp of the octamer is formed by the histones in the order H2A^1–H2B^1–H4^1–H3^1–H3^2–H4^2–H2B^2–H2A^2. *b*, Another view of *a*, rotated further by 110°; the direction of view is similar to that in Fig. 7*a*.

Histone–histone cross-linking

Cross-linking of histones indicates proximities between them with limits defined by the lengths of the reagent used and the nature of the residues cross-linked, for example, a cross-link formed with dimethyl suberimidate indicates that ε-amino groups of two lysine residues (each amino group being about 7 Å from the protein backbone) are within about 12 Å of each other. If two histones can be cross-linked with zero-length reagents they must be in contact. Again, the cross-linking results do not distinguish between the two copies of each histone, but in the model in Fig. 5 this distinction is made.

Five cross-linked histone dimers were originally emphasized (together with histone–DNA cross-linking results) in making the histone assignment in Fig. 5, as follows. With dimethyl suberimidate the cross-linked dimers $(\mathrm{H3})_2$, H3–H4, H2A–H2B, H4–H2A and H4–H2B were found[6,7]. Of these, $(\mathrm{H3})_2$ is also formed by mild oxidation[28] showing that the single cysteine —SH groups of the two H3 molecules in the chicken erythrocyte nucleosome are close enough to permit oxidation to the disulphide[53]. H3–H4, H2A–H2B and H4–H2B are cross-linked with zero-length reagents[29-31]; and $(\mathrm{H3})_2$, H3–H4 and H2A–H2B with a short cross-linker (methyl acetimidate)[32]. The four dimers $(\mathrm{H3})_2$, H3–H4, H2A–H2B and H4–H2B formed with both long and short reagents of very different specificities and requirements must reflect major histone–histone interactions: these are clearly accommodated in Fig. 5. The pairs H3/H4, H2A/H2B and H4/H2B were also found to interact strongly in solution by physical studies[33]. The fifth cross-linked dimer, H4–H2A, produced in roughly the same yield as H4–H2B with dimethyl suberimidate[6], and also found in a later study with a different reagent of similar length[34], is also accommodated in Fig. 5.

Figure 5 places the two H3s in contact and represents a strong interaction about the dyad axis as already proposed[25,28,35,36]. The two H2As are placed on opposite faces and on opposite sides of the wedge-shaped particle; the two H2Bs are also on opposite faces but at the same end of the wedge. H2A and H2B are thus placed as heterodimers, H2A–H2B, consistent with the identical rates of cross-linking of H2A and H2B in chromatin[6]. Our assignment brings H2A and H2B into juxtaposition along, rather than across, the helical ramp, and so accommodates the

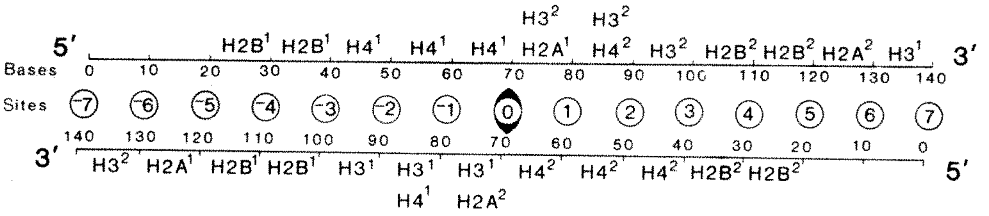

Fig. 6 Assignment of DNA–histone cross-links to individual histone molecules. The diagram is adapted from Fig. 4 of Mirzabekov *et al.*[14] whose results show which histone type can be cross-linked to which location on the DNA, but which cannot distinguish between the two copies of each histone type. Based on the models of the octamer and nucleosome core particles (Figs 4 and 5), we have assigned superscripts 1 and 2 to the pattern of Mirzabekov *et al.*[14] to distinguish the two copies. Note that the action of the overall dyad of the nucleosome is to turn one DNA strand into the other, and to interchange the superscripts on the histones. We have kept the same number in bases along a DNA strand as that used by Mirzabekov *et al.*, although these should be increased by 4% (ref. 66). The diagram incorporates the average stagger of two bases found for the DNAse I cutting sites on the opposite strands of the DNA[67,68].

finding that on UV irradiation H2A and H2B are linked to each other through a short piece of DNA[37]. The two H4s, which interact with the two H3s, but weakly, if at all, with each other (see also below), are placed along the sides of the wedge-shaped particle because they interact with both H2A and H2B. An important cross-linked product accounted for by Fig. 5 is the trimer H2A–H2B–H4 generated by successive treatments of chromatin with UV light and tetranitromethane[38].

Note that, in the histone arrangement proposed, where the linear order is H2A–H2B–H4–H3–H3–H4–H2B–H2A (Fig. 5), the four major dimers $(H3)_2$, H3–H4, H4–H2B and H2B–H2A, are all neighbours along the helical ramp. This would be expected from a bifunctional lysine reagent which would have a high probability of cross-linking lysines abundant on a protein surface. As the major function of the lysines of the histone core is to bind the DNA, we would expect them to be particularly abundant in the surface regions where the DNA is bound. The dimers that appear on cross-linking will therefore, as it were, mark out the path of the DNA.

Our assignments accommodate the five major cross-linked dimers referred to above. We now discuss other dimers that have been found (with the longer reagents, 12–15 Å span). Dimers found in reasonable yields are H3–H2B (refs 22, 34, 39, and J. O. T., unpublished results), H3–H2A[39], and $(H2A)_2$ and $(H2B)_2$[22]. Although H3–H2A is clearly consistent with Fig. 5, the others are less obviously so. However, the histone shapes are not known, and the H3–H2B dimer can be accommodated if the $H2B^1$ and $H3^1$ molecules are elongated to meet each other near the centre of the particle face (see Fig. 5). Likewise H2B molecules of sufficient width could account for an $(H2B)_2$ dimer; and $(H2A)_2$ dimers could arise by cross-linking with long reagents across the central cavities.

In addition to the nine cross-linked dimers discussed above, $(H4)_2$ is also possible in principle, and has been found as 1% of the total dimers generated by formaldehyde[40]. (However, all ten possible dimers are produced with this reagent, and the nature of the cross-linking species is unclear [formaldehyde itself is not bifunctional].) Although $(H4)_2$ does not seem to represent a major contact, it can be accommodated in the model in Fig. 5 if the H4s are elongated (extended into the 'no-man's land' in Fig. 7*b*; see below), or it might arise by transient contacts generated as the structure 'breathes'.

Relation of H1 to the other histones in the nucleosome

Electron microscopy[41], DNase I digestion[42] and UV cross-linking[37] suggest that in the nucleosome H1 'seals' a two-turn 166-base pair[19] nucleosome core by binding to the DNA where it enters and leaves the nucleosome. Consistent with this, Mirzabekov and his colleagues[43] observe strong cross-linking of H1 to 175-base pair DNA over a stretch close to the ends.

By extrapolation from the 146-base pair structure to a complete two-turn particle as in Fig. 5, H1 would bind to the DNA near the $(H3)_2$ dimer region. This location would explain the H1–H3 cross-link reported in nuclei and chromatin[44] (in fact two H3s per H1 are suggested) and also, as H1 is extended, at least in solution[2,45], the H1–H2A cross-link found in mononucleosomes (refs 46, 47, and J.O.T., unpublished results). The extended shape of H1 is also invoked[43] to explain the cross-linking of H1 at intervals along almost the whole length of the DNA in the 175-base pair nucleosome as well as the major interaction at the ends, but it is not easy to imagine the nature of such binding.

Dissection of the octamer into the $(H3)_2(H4)_2$ tetramer and H2A–H2B dimers

The histones assigned as above fall naturally into an arginine-rich tetramer and two lysine-rich dimers, and thus accord with the mode of disproportionation of the free octamer in solution[6,7,9,10], that is:

$$\text{H2A H2B.(H3)}_2\text{(H4)}_2\text{.H2A H2B} \rightleftharpoons$$

$$\text{H2A H2B.(H3)}_2\text{(H4)}_2 + \text{H2A H2B} \rightleftharpoons$$

$$\text{(H3)}_2\text{(H4)}_2 + 2 \times \text{H2A H} \times 2\text{B}$$

The finding of an intermediate hexamer shows that the two H2A–H2B heterodimers can dissociate independently, consistent with their location on opposite faces of our model of the core particle (compare with ref. 48).

If these two heterodimers are removed from the octamer model in Fig. 7*a* the remaining $(H3)_2(H4)_2$ tetramer is revealed as a 'distorted horseshoe' (one H4 being above the plane of the other) or, if the H4s meet, as a 'dislocated disk', the uncertainty being reflected in the no-man's land in Fig. 7*b*. The highly asymmetric shape of the tetramer, if it persists in solution, might explain its anomalously low sedimentation coefficient ($s^{\circ}_{20,w}$ = 2.81S) and resulting high frictional ratio ($f/f_0 = 1.63$)[49]. Others have attributed the slow sedimentation to freely mobile N-terminal regions extending from a more compact globular core[50], and a contribution from such effects cannot be ruled out.

In the dislocated horseshoe model (Fig. 7*b*) the two H4 molecules do not touch, and indeed no $(H4)_2$ is observed on cross-linking the free octamer (J. O. T., unpublished results) or the nucleosome core, except for a few per cent in one study with formaldehyde (see above). However, the $(H3)_2(H4)_2$ tetramer free in solution, on treatment with dimethyl suberimidate, does give some cross-linked $(H4)_2$, in about the same amount as $(H3)_2$ (H3–H4 being the major cross-linked dimer)[2]. This could be due to 'contraction' of the tetramer when the DNA is removed and/or increased possibilities for cross-linking of H4 to itself (and to H3) in the absence of the lysine-rich histones H2A and H2B. As already noted, we do not know where the histone boundaries lie, but probably H4 is elongated since it interacts with the DNA in the nucleosome at three sites about 10 bases apart[14] (see Fig. 6). Whatever the details, the tetramer emerges as a disk-shaped object of approximate thickness 27 Å, consistent with spacings observed in electron micrographs and X-ray patterns of fibres made of H3/H4 histones[51].

The central role of the arginine-rich histone tetramer in the nucleosome

There is now much evidence supporting the proposal of Kornberg[5] that the arginine-rich tetramer $(H3)_2(H4)_2$ is critical in forming the nucleosome. As first shown by Felsenfeld and co-workers[52], and subsequently by others[53–58], H3 and H4, without H2A and H2B, can confer nucleosome-like properties on DNA when assessed by various criteria. These properties were assumed to arise from one tetramer combined with a nucleosome core length of DNA. However, it was subsequently found that H3 and H4 alone can form both tetrameric and octameric complexes with DNA[59,60] and therefore this interpretation has had to be re-examined. Although it has now been shown[61] that tetramers alone, like octamers, can generate folded complexes about the size of nucleosomes, with long DNA, they do not confer complete resistance of 140 base pairs to nuclease digestion[60], and the question of just how much a tetramer contributes to the supercoiling of the DNA is not yet settled[36,53,55,56].

The structure deduced for the tetramer in Fig. 7*b* and its location with respect to the DNA (Fig. 5*b*) explains some of the properties it confers on the DNA in the absence of H2A and H2B. The tetramer spans the diameter of the nucleosome and can be regarded as 'measuring out' the DNA in a turn, agreeing with our earlier suggestion[19]. (In the interaction of the tetramer with the central region of the DNA in a nucleosome, the structure resembles 'model 2' of ref. 52 [their Fig. 13].)

Thus a disk-shaped tetramer (Fig. 7*b*) would be expected to protect the 80 base pairs of DNA in the central turn of the nucleosome from attack by nucleases. This is consistent with the results of Stockley and Thomas[60] who showed that digestion of long chromatin that had been stripped of all histones except H3 and H4 resulted in two classes of nucleoprotein complexes containing protected DNA; one class contained single H3/H4 tetramers associated with DNA about 70 base pairs long, the other containing an octamer of H3 and H4 and about 140 base pairs of DNA. This explained why micrococcal nuclease limit digests of reconstitutes prepared at an H3/H4 : DNA weight ratio of 0.5 : 1 showed a strong pattern of bands up to about 70–80 base pairs, but only weak or fleeting protection between 80 and 140 base pairs[52], as at this histone : DNA ratio the nucleoprotein complexes were mainly tetrameric, with only a little octamer[59]. Moreover, the proposed interaction of the tetramer with a turn of DNA would probably mean that a single tetramer alone could induce a degree of supercoiling in relaxed, closed circular DNA, although an octamer of H3 and H4 may be necessary to develop the full number of superhelical turns characteristic of true nucleosomes containing all four histones[62].

In our model, the tetramer constrains the central 80 base pairs of DNA into one physical superhelical turn, but it can presumably also bind loosely the two additional half-turns in nucleosome-length DNA, because compact tetrameric complexes of nucleosome size and containing about 145 base pairs are formed when $(H3)_2(H4)_2$ tetramers are reconstituted on to SV40 DNA at low histone : DNA ratios[61], these complexes being less dense than their octameric counterparts. Such folded tetrameric complexes may also be intermediates in reconstitution experiments with 140-base pair DNA, in which 'primed' complexes of H3, H4 and DNA bind H2A and H2B at low ionic strength to regenerate nucleosome cores[36,48,52,53,63].

The central role of the $(H3)_2(H4)_2$ tetramer in nucleosome structure as it emerges from this study is to organize the DNA into the central turn of a 'primary particle'. In nucleosome assembly H2A and H2B could then add to this intermediate as two heterodimers, stabilizing it by binding firmly the two extra half-turns of DNA previously bound loosely in the H3/H4–DNA complex, thereby completing the 166-base pair nucleosome core. H1 would then bind to the core to seal the two turns, and also provide a binding site for an adjacent length of linker DNA. The nucleosome would thus be complete. Such a sequence of events would provide a physical rationale for the temporal order of assembly of histones on to newly replicated DNA[64,65].

We thank Dr L. Amos for help and Drs A. D. Mirzabekov and C. W. Carter for sending us preprints of their papers (refs 22, 24 and 43). J. O. T. acknowledges the support of the SRC.

Received 5 May; accepted 15 August 1980.

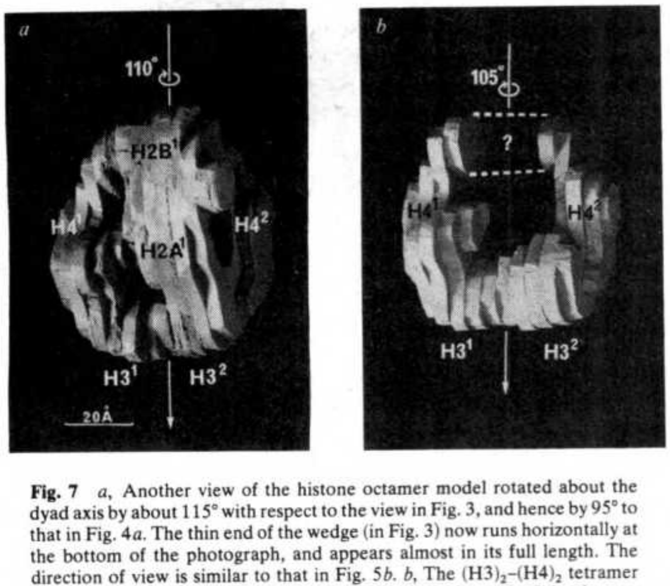

Fig. 7 *a*, Another view of the histone octamer model rotated about the dyad axis by about 115° with respect to the view in Fig. 3, and hence by 95° to that in Fig. 4*a*. The thin end of the wedge (in Fig. 3) now runs horizontally at the bottom of the photograph, and appears almost in its full length. The direction of view is similar to that in Fig. 5*b*. *b*, The $(H3)_2$–$(H4)_2$ tetramer dissected out of the octamer model, the view being about 5° off that in *a*, to show the shape in its broadest aspect. The boundaries between the tetramer and the two dimers of H2A–H2B removed from the front and back of it have been chosen at the regions of slenderest connection so as to give approximately the appropriate volumes. The region marked ? is a no-man's land which cannot be assigned unambiguously to one or other of the H4 and H2B molecules which border it. The tetramer has the shape of a distorted horseshoe or dislocated disk, so that its periphery constitutes about one turn, or somewhat less, of a flat left-handed helix. The stretch of DNA associated with it runs from about sites −4 to +4. The hole in the middle may be exaggerated by the staining (see text).

1. Kornberg, R. D. *A. Rev. Biochem.* **46,** 931–954 (1977).
2. Kornberg, R. D. & Thomas, J. O. *Science* **184,** 865–868 (1974).
3. Roark, D. E., Geoghegan, T. E. & Keller, G. H. *Biochem. biophys. Res. Commun.* **59,** 542–547 (1974).
4. Kelley, R. A. *Biochem. biophys. Res. Commun.* **54,** 1588–1594 (1973).
5. Kornberg, R. D. *Science* **184,** 868–871 (1974).
6. Thomas, J. O. & Kornberg, R. D. *Proc. natn. Acad. Sci. U.S.A.* **72,** 2626–2630 (1975).
7. Thomas, J. O. & Kornberg, R. D. *FEBS Lett.* **58,** 353–358 (1975).
8. Thomas, J. O. & Butler, P. J. G. *J. molec. Biol.* **116,** 769–781 (1977).
9. Eickbush, T. H. & Moudrianakis, E. N. *Biochemistry* **17,** 4955–4963 (1978).
10. Ruiz-Carrillo, A. & Jorcano, J. L. *Biochemistry* **18,** 760–768 (1979).
11. DeRosier, D. J. & Klug, A. *Nature* **217,** 130–134 (1968).
12. Crowther, R. A. & Klug, A. *A. Rev. Biochem.* **44,** 161–182 (1975).
13. Finch, J. T., Lewit-Bentley, A., Bentley, G., Roth, M. & Timmins, P. *Phil. Trans. R. Soc.* (in the press).
14. Mirzabekov, A. D., Shick, V. V., Belyavsky, A. V. & Bavykin, S. G. *Proc. natn. Acad. Sci. U.S.A.* **75,** 4184–4188 (1978).
15. Thomas, J. O. & Kornberg, R. D. *Meth. Cell Biol.* **18,** 429–440 (1978).
16. Thomas, J. O. & Butler, P. J. G. *Cold Spring Harb. Symp. quant. Biol.* **42,** 119–125 (1977).
17. Amos, L. A. & Klug, A. *J. molec. Biol.* **99,** 51–73 (1975).
18. Matthews, B. W. *J. molec. Biol.* **33,** 491–497 (1968).
19. Finch, J. T. *et al. Nature* **269,** 29–36 (1977).
20. Lilley, D. M. J., Pardon, J. F. & Richards, B. M. *Biochemistry* **16,** 2853–2860 (1977).
21. Trifonov, E. *Nucleic Acids Res.* **5,** 1371–1380 (1978).
22. Carter, C. W. Jr, Levinger, L. F. & Birinyi, F. *J. biol. Chem.* **255,** 748–754 (1980).
23. Simpson, R. T. *Proc. natn. Acad. Sci. U.S.A.* **73,** 4400–4404 (1976).
24. Shick, V. V., Belyavsky, A. G., Bavykin, S. G. & Mirzabekov, A. D. *J. molec. Biol.* **139,** 491–517 (1980).
25. Dietrich, A. E., Axel, R. & Cantor, C. *J. molec. Biol.* **129,** 587–602 (1979).
26. Martinson, H. G., True, R. J. & Burch, J. B. E. *Biochemistry* **18,** 1082–1089 (1979).
27. Martinson, H. G. & True, R. J. *Biochemistry* **18,** 1089–1094 (1979).
28. Camerini-Otero, R. D. & Felsenfeld, G. *Proc. natn. Acad. Sci. U.S.A.* **74,** 5519–5523 (1977).
29. Martinson, H. G. & McCarthy, B. J. *Biochemistry* **14,** 1073–1078 (1975).
30. Martinson, H. G. & McCarthy, B. J. *Biochemistry* **15,** 4126–4131 (1976).
31. Bonner, W. M. & Pollard, H. B. *Biochem. biophys. Res. Commun.* **64,** 282–288 (1975).
32. Wyns, L., Lasters, I. & Hamers, R. *Nucleic Acids Res.* **5,** 2345–2358 (1978).
33. D'Anna, J. A. Jr & Isenberg, I. *Biochemistry* **13,** 4992–4997 (1974).
34. Bonner, W. M. *Nucleic Acids Res.* **5,** 71–85 (1978).
35. Olins, A. L. *et al.* in *The Molecular Biology of the Mammalian Genetic Apparatus* Vol. 1 (ed. Ts'o, P. O. P.) 211–237 (North-Holland, Amsterdam, 1977).
36. Klevan, L., Dattagupta, N., Hogan, M. & Crothers, D. M. *Biochemistry* **17,** 4533–4540 (1978).
37. Sperling, J. & Sperling, R. *Nucleic Acids Res.* **5,** 2755–2773 (1978).

38 Martinson, H. G., True, R., Lau, C. K. & Mehrabian, M. *Biochemistry* **18**, 1075–1082 (1979)
39 Hardison, R. C., Zeitler, D. P., Murphy, J. M. & Chalkley, R. *Cell* **12**, 417–427.
40 Jackson, V. *Cell* **15**, 945–954 (1978)
41. Thoma, F., Koller, Th. & Klug, A. *J. Cell Biol.* **83**, 403–427 (1979)
42 Simpson, R. T. *Biochemistry* **17**, 5524–5531 (1978)
43 Belyavsky, A. V., Bavykin, S. G., Goguadze, E. G. & Mirzabekov, A. D. *J. molec. Biol.* **139**, 519–536 (1980)
44 Glotov, B. O., Itkes, A. V., Nikolaev, L. G. & Severin, E. S. *FEBS Lett.* **91**, 149–152 (1978)
45 Edwards, P. A. & Shooter, K. V. *Biochem. J.* **114**, 227–235 (1969)
46 Bonner, W. M. & Stedman, J. D. *Proc. natn. Acad. Sci. U.S.A.* **76**, 2190–2194 (1979).
47 Boulikas, T., Wiseman, J. M. & Garrard, W. T. *Proc. natn. Acad. Sci. U.S.A.* **77**, 127–131 (1980)
48. Jorcano, J. L. & Ruiz-Carrillo, A. *Biochemistry* **18**, 768–774 (1974)
49 Roark, D. E., Geoghegan, T. E., Keller, G. H., Matter, K. V. & Engle, R. L. *Biochemistry* **15**, 3019–3025 (1976).
50 Moss, T., Cary, P. D., Crane-Robinson, C. & Bradbury, E. M. *Biochemistry* **15**, 2261–2267 (1976)
51 Wachtel, E. J. & Sperling, R. *Nucleic Acids Res.* **6**, 139–151 (1979)
52. Camerini-Otero, R. D., Sollner-Webb, B. & Felsenfeld, G. *Cell* **8**, 333–347 (1976)
53. Camerini-Otero, R. D. & Felsenfeld, G. *Nucleic Acids Res.* **4**, 1159–1181 (1977)
54 Boseley, P. G., Bradbury, E. M., Butler-Browne, G. S., Carpenter, B. G. & Stephens, R. M. *Eur. J. Biochem.* **62**, 21–31 (1976)
55. Oudet, P. *et al.* *Cold Spring Harb. Symp. quant. Biol.* **42**, 287–300 (1977)
56 Bina-Stein, M. & Simpson, R. T. *Cell* **11**, 609–618 (1977).
57. Moss, T., Stephens, R. M., Crane-Robinson, C. & Bradbury, E. M. *Nucleic Acids Res.* **4**, 2477–2485 (1977).
58 Burton, D. R. *et al.* *Nucleic Acids Res.* **5**, 3643–3663 (1978)
59 Simon, R. H., Camerini-Otero, R. D. & Felsenfeld, G. *Nucleic Acids Res.* **5**, 4805–4818 (1978).
60 Stockley, P. G. & Thomas, J. O. *FEBS Lett.* **99**, 129–135 (1979)
61 Thomas, J. O. & Oudet, P. *Nucleic Acids Res.* **7**, 611–623 (1979)
62 Germond, J. E., Hirt, B., Oudet, P., Gross-Bellard, M. & Chambon, P. *Proc. natn. Acad. Sci. U.S.A.* **72**, 1843–1847 (1975).
63 Ruiz-Carrillo, A., Jorcano, J. L., Eder, G. & Lurz, R. *Proc. natn. Acad. Sci. U.S.A.* **76**, 3284–3288 (1979).
64 Worcel, A., Han, S. & Wong, M. L. *Cell* **15**, 969–977 (1978)
65. Senshu, T., Fukuda, M. & Ohashi, M. *J. Biochem. (Japan)* **84**, 985–988 (1978)
66. Prunell, A. *et al.* *Science* **204**, 855–858 (1978)
67 Sollner-Webb, B. & Felsenfeld, G. *Cell* **10**, 537–547 (1977)
68 Lutter, L. C. *J. molec. Biol.* **117**, 53–69 (1977)

LETTERS

An optical burst from the star identified with the X-ray source 2S1254 – 690

K. O. Mason*, J. Middleditch†, J. E. Nelson† & N. E. White‡

*Space Sciences Laboratory and Astronomy Department, University of California, Berkeley, California 94720
† Lawrence Berkeley Laboratory, University of California, Berkeley, California 94720
‡ Goddard Space Flight Center, Greenbelt, Maryland and University of Maryland

High time-resolution photometry of the proposed optical counterpart (Star 30)[1] of the X-ray source[2] 2S1254 – 690 is reported here. An event of high statistical significance was observed from the star that has all the temporal characteristics of an X-ray burst (see, for example, ref. 3). 2S1254 – 690 has not previously been identified as an X-ray burst source, but its optical counterpart shows properties in common with this class of objects. We also derive the X-ray spectrum of 2S1254 – 690 using data obtained with the HEAO 1 satellite. The spectrum can be fit in the energy range 0.18–30 keV by a power law of photon index –2.5, modified by interstellar absorption.

2S1254 – 690 Star 30 was observed with the 4-m telescope at CTIO as part of a systematic survey of the photometric properties of X-ray source counterparts. The star was observed in white light with a cooled EMI 9658 R photomultiplier tube with an S 20 photocathode (red extended by prismatic reflection). Data were taken with a 5-arc s diameter aperture and at a time resolution of 10 ms. The observation lasted ~45 min and began at 23.50 UT on 24 June 1979. A total count rate of ~2,400 counts per s (c.p.s.) was recorded on the star, of which ~1,700 c.p.s. were due to the sky background.

At approximately 00.10 UT on 25 June, the total count rate from star plus sky was observed to increase rapidly to ~3,200 c.p.s. on the real time monitor in the 4-m telescope control room. This represents an increase of a factor of two in the stellar count rate. A visual check of the TV guider confirmed that the equipment continued to function normally and the sky conditions were stable. The data collected during this time are plotted in Fig. 1 accumulated in intervals of 0.2 s. The event observed is remarkably similar to the X-ray bursts identified in several galactic sources. It has a rise-time of ~1.7 s and then decays more slowly, having a total duration of ~20 s. The data are consistent with a morphology that has either a relatively flat maximum, or alternatively a second peak in flux that occurs about 5 s after onset. Again, such a multiply peaked, or flat-topped, structure has been observed in X-ray bursts[3]. No other event of this kind was observed during the remainder of the observation of 2S1254 – 690.

Because of the marked similarity in structure between the optical burst we have detected from 2S1254 – 690 Star 30 and X-ray bursts, we believe that we probably observed the optical counterpart of such an X-ray burst from 2S1254 – 690. Optical bursts of lesser statistical quality have been reported from three burst sources, MXB1735 – 44 (ref. 4), MXB1837 + 05 (ref. 5) and MXB1636 – 53 (ref. 6) coincident with X-ray bursts. The observation of burst-like behaviour from 2S1254 – 690 Star 30 is consistent with its identification as the optical counterpart of the X-ray source. No X-ray bursts have been reported from 2S1254 – 690 thus far, and this means that it is the first bursting source to be catalogued in the optical region of the spectrum. However, we note that 2S1254 – 690 does lie within the 12° radius error circle of an X-ray burst observed by Apparao with the SAS-3 rotation modulation collimator, whose position was reported by Lewin and Clark[3].

We have searched for evidence of periodic modulation in the light from 2S1254 – 690 Star 30 by constructing Fourier transforms of the data. No spike due to periodic modulation above the 1.2% pulsed fraction level was observed from 0.02 to 50 Hz in a power spectrum constructed from the entire data-set.

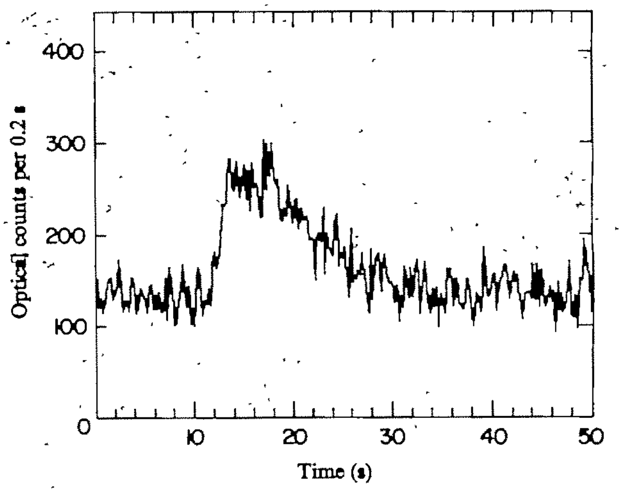

Fig. 1 Time series obtained in white light on the CTIO 4-m telescope in the vicinity of the burst-like event observed from 2S1254–690 Star 30. Data are accumulated in 0.2-s intervals and time is measured on the abscissa in seconds from 25 June 00. 08. 43 UT. The ordinate shows the excess count per 0.2-s bin above sky background registered on the star.

0028–0836/80/410516—03$01.00

Table 1 HEAO 1 0.18–20 keV spectral fits for 2S1254 – 690

Spectral model	α/kT	$\log(N_H)$	Line Energy	 EW	 FWHM	χ^2 min	D.f.
Power law	2.38	21.44	—	—	—	132	71
Exponential + gaunt factor	—	—	—	—	—	363	71
Black body	—	—	—	—	—	~1,000	71
Power law + narrow line	2.46	21.48	6.4	0.4	—	99	69
Power law + broad line	2.47	21.51	6.5	0.6	1.6	92	68

However, when data only from the immediate vicinity of the burst are considered, a peak is found at a frequency of 36.40 Hz that is 12.6 times the average power at neighbouring frequencies. The *a priori* probability that any bin in our 4,000-point transform would have this much power as a result of a random statistical fluctuation is 1%, so that the peak at 36.40 Hz is statistically an unusual event. The periodicity is present in the 20 s of data taken during the burst and also in a data-set that includes the 7-s interval preceding the burst and the 13-s interval following it. The mean pulsed fraction is ~5% of the mean count-rate from the star.

The pulsation is too weak to enable us to determine its properties more precisely although if the effect is confirmed, the implied size of the optical emission is only ≤0.3 light s. Experimenters using the A1 experiment on the HEAO 1 satellite have reported an 83-Hz periodicity in one X-ray burst from MXB1728 – 337 (Sadeh and Wood, personal communication). The period of the pulsation, which was detected both before and during the burst, changed by a significant amount during the time it was observed, and was not seen in three other bursts observed from the same source. High time-resolution observations of bursts to investigate the nature of these pulsations clearly deserve more attention.

The known optical characteristics of 2S1254 – 690 Star 30 are summarized elsewhere[1]. The star ($V = 19.1$) has a UV excess, and may exhibit line emission at λ 4,640 Å corresponding to the C III–N III blend often seen in X-ray sources. These properties are similar to those of several galactic X-ray source counterparts, including several bursters.

We have investigated the X-ray properties of 2S1254 – 690 using scanning data taken with the proportional counters of the A2 experiment[7] on HEAO 1 in August 1977, February 1978 and August 1978. The source was visible for periods of 2.5, 5.0 and 5.0 days respectively on these occasions. The overall flux of 2S1254 – 690 was constant throughout to within ~15% on time scales of ~1 h. The sensitivity of the experiment to short time-scale bursts is, however, low because the source is within the largest field of view of the instrument (6° FWHM) for at most one minute every ~30-min satellite rotation period.

To investigate the X-ray spectral properties of 2S1254 – 690, we have examined the pulse height analyser data taken with the low, medium and high energy detectors (LED, MED and HED respectively) of the A2 experiment. These data have been modelled in turn with power-law, exponential plus gaunt factor and black-body models, allowing for absorption in the interstellar medium in each case using the elemental absorption cross-sections given by Brown and Gould[8].

The results of fitting these models to the combined data from the LED (0.18–2.5 keV) and MED (2.0–20 keV) detectors, which together provide data in 75 energy channels, are summarized in Table 1. The relative normalization of the spectrum in the two detectors is a free parameter in the fits in order to allow for small uncertainties in their relative effective area. Of the three simple models tried, only a power law gave a reasonable fit to the data (minimum χ^2 of 132 for 71 d.f.). This is true also when the MED and HED (2–60 keV) data are analysed separately. The quality of the power law fit was further improved by the addition of an emission line at ~6.5 keV. For the combined LED and MED data, a model that included a narrow line resulted in a minimum χ^2 of 99 for 69 d.f., while the best fit for a power law plus a broad line gave a minimum χ^2 of 92 for 68 d.f. The line had a best-fit energy of 6.5±0.5 keV, an equivalent width of 0.6±0.1 keV, and a FWHM of 1.6±0.5 keV. It may be fluorescent iron line emission similar to that found in some pulsating X-ray sources (see for example ref. 9). The allowed range of power law slope is expressed in Fig. 2 as a function of low energy absorption column density. Figure 2 also shows the best-fit spectral model, which has a photon spectral index of $\alpha = -2.47$ (energy index -1.47) and a column density, N_H, of 3.2×10^{21} equivalent H atoms cm^{-2}.

The HEAO 1 spectral measurements of 2S1254 – 690 are consistent with the work of Jones[10] on this source. The spectrum is similar in overall slope to the X-ray spectra of most burst sources that have been studied[11] (an exception is the burster 2S1916 – 053 which has a hard spectrum[12]). The form of the spectrum, however, a power law, is notable. The HEAO 1 data show that a power law representation of the spectrum of 2S1254 – 690 is clearly preferred over simple exponential or black-body models in the energy range 0.18–20 keV (Table 1). Furthermore, data from the 2–60-keV HED detectors of the A2 experiment confirm that the power law measured from the LED

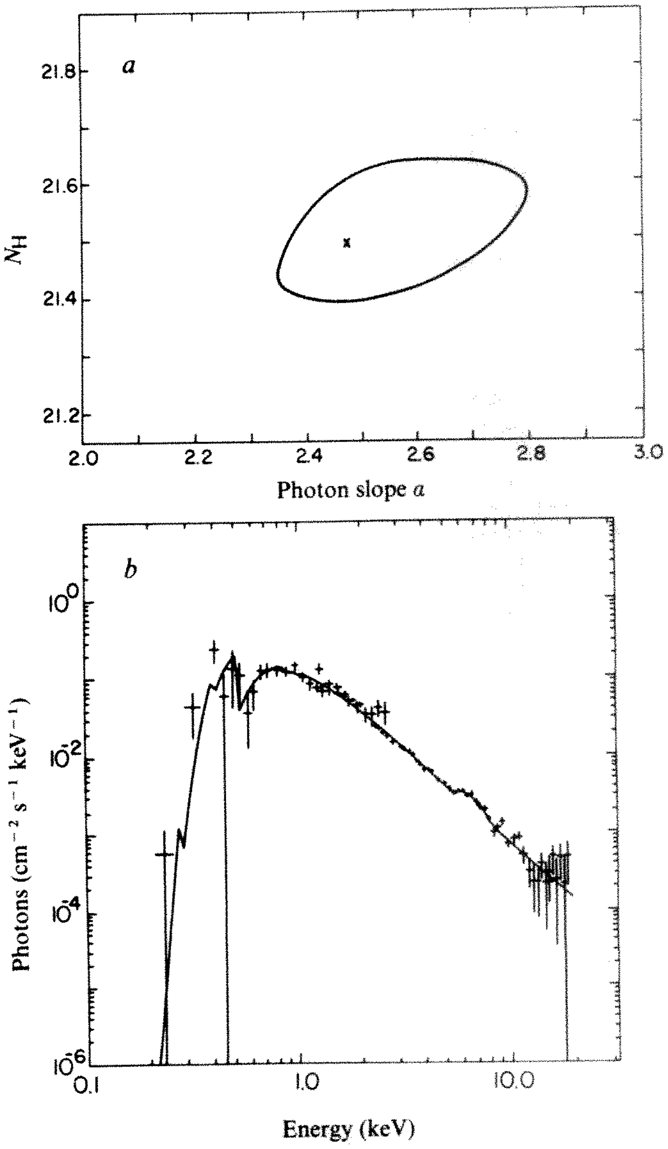

Fig. 2 The 0.18–20-keV spectrum of 2S1254 – 690 derived from data obtained with the HEAO 1 A2 experiment. *a*, Allowed range of photon index and absorption column density for a power law model plus a broad line. The solid line encloses the 90% confidence region. *b*, Best-fit photon spectrum shown relative to the corrected MED and LED data.

and MED data adequately describes the spectrum of 2S1254−690 up to an energy of at least 30 keV. In general, the incidence of power law spectra among the 'population II' X-ray sources that have been studied to date is low (see, for example, refs 13, 14). One X-ray source whose 2–12-keV spectrum sometimes has a power law distribution is 4U0614+09, which is also suspected of being a burster[15]. 4U0614+09 was observed on two occasions by the collimated proportional counter[16] on Ariel V. During the first observation which lasted ~2 days the source was relatively steady, varying by less than 10% on a time scale of ~100 min. The integrated 2–12-keV count spectrum from this observation has been modelled by one of us (K.O.M., unpublished). A power law spectrum, although not statistically acceptable (due in part to systematic uncertainties in the detector response at low energies and in part to a probable excess near ~6.5 keV), yields a minimum χ^2 value which is a factor of three below that obtained by fitting an exponential plus gaunt factor shape. The best-fit power law photon index was $\alpha = -2.6$, close to that found for 2S1254−690. During the second Ariel V observation[16] of 4U0614+09, the source was more active and showed variations in intensity by up to a factor of two. The OSO 8 satellite detected a burst from the vicinity of 4U0614+09 during the same period[15]. The variation in the strength and spectrum of the source precluded addition of data from more than one orbit, but on an orbit by orbit basis, exponential+gaunt factor spectra provided consistently better fits to the Ariel V data than a power law, in contrast to the first observation (see also ref. 14).

Thus we have evidence that at least one optical burst source, 2S1254−690, and a suspected X-ray burst source, 4U0614+09, occasionally emit power law X-ray spectra. Power law X-ray spectra are usually associated with non-thermal mechanisms (for instance, synchrotron radiation) or inverse compton radiation from a hot relativistic accretion disk[17]. If X-ray bursters are accreting neutron stars, this goes against naive expectations that X-ray emission from such stars should be essentially thermal in shape[18–20]. However, it is also possible that a suitable combination of thermal spectra of different temperatures might simulate a power law distribution over a limited energy range. The detailed observation and classification of X-ray source spectra could be a useful way to investigate the nature of these objects, but a better theoretical understanding of emission from compact stars[21] is probably required before such studies can be used to constrain the physical processes occurring there.

K. O. M. and J. M. were visiting astronomers at the Cerro Tololo Interamerican Observatory. We acknowledge support from the Miller Institute for Basic Research, NASA grant NAGW-44 and NSF grant AST78-06873 (K.O.M.) and the US Department of Energy (J. M. and J. E. N.) We thank Dr Kent Wood for discussing the HEAO-1 A1 data on MXB 1728-337, and Drs W. H. G. Lewin and L. Cominsky for discussing SAS 3 burst data.

Received 19 May, accepted 14 August 1980

1 Griffiths, R. E. *et al.* *Nature* **276**, 247 (1978)
2 Bradt, H. V., Doxsey, R. E. & Jernigan, J. G. in *X-ray Astronomy* (eds Baity, W. & Peterson, L.) 3 (Pergamon, Oxford, 1979).
3 Lewin, W. H. G. & Clark, G. W. *Ann. N.Y. Acad. Sci.* (in the press)
4. Grindlay, J. E. *et al.* *Nature* **274**, 567 (1978)
5. Hackwell, J. A. *et al.* *Astrophys. J.* (in the press)
6. Pedersen *et al.* *IAU Circ.* No. 3399 (1979)
7. Rothschild, R. E. *et al.* *Space Sci. Instrum.* **4**, 269 (1979).
8. Brown, R. H. & Gould, R. J. *Phys. Rev. D.* **1**, 2252 (1970).
9 Pravdo, S. H. & White, N. E. *Astrophys. J. Lett.* (in the press)
10. Jones, C. *Astrophys. J.* **214**, 856 (1977)
11. Lewin, W. H. G. & Joss, P. C. *Nature* **270**, 211 (1977)
12. Becker, R. H. *et al.* *Astrophys. J. Lett.* **216**, L101 (1977).
13 Lamb, P. & Sanford, P. W. *Mon. Not. R. astr. Soc.* **188**, 555 (1979).
14 Greenhill, J. G., Coe, M. J., Bell-Burnell, S. J., Strong, K. T. & Carpenter, G. F. *Mon. Not. R. astr. Soc.* **189**, 563 (1979)
15. Swank, J. H., Becker, R. H., Boldt, E. A., Holt, S. S. & Serlemitsos, P. J. *Mon. Not. R. astr. Soc.* **182**, 349 (1979).
16. Mason, K. O. *et al.* *Mon. Not. R. astr. Soc.* **177**, 513 (1976).
17. Shapiro, S. L., Lightman, A. P. & Eardley, D. M. *Astrophys. J.* **204**, 187 (1976)
18. Alme, M. L. & Wilson, J. R. *Astrophys. J.* **186**, 1015 (1973).
19. Shapiro, S. L. & Salpeter, E. E. *Astrophys. J.* **198**, 671 (1975)
20. Gnedin, Y. & Sunyaev, R. *Astr. Astrophys.* **25**, 233 (1973)
21 Lea, S. M. *Proc. Workshop on Compact Galactic X-ray Sources*, Washington (eds Lamb, F. & Pines, D.) 115 (University of Illinois, 1979).

The 3.4-μm interstellar absorption feature

D. T. Wickramasinghe

Royal Observatory, Edinburgh EH9 3HJ, UK

D. A. Allen

Anglo-Australian Observatory, Epping, Australia

Estimation of the organic component of interstellar grains has provoked considerable interest[1,2]. Recently Duley and Williams[2] concluded from an absence of the 3.4-μm CH absorption band in obscured IR sources that organic compounds in grains account for ≤10% of carbon in the interstellar medium. We report here the detection of a 3.4-μm absorption feature in three IR sources and hence argue that an appreciable mass fraction of interstellar grains are predominantly organic in character.

The presence of a possible absorption feature in the wavelength region 3.3–3.5 μm in the published spectra of some highly obscured IR sources was considered by Hoyle and Wickramasinghe[3] to be evidence for the ~3.4-μm stretching vibration band of CH, which is characteristic of most organic molecules. In most cases for which data have been available the 3.4-μm feature is seen in the wing of a broad, strong water-ice band centred at 3.1 μm. Although the difficulty of matching the extended red wing of the 3.1-μm feature by water ice alone has been noted[4], the presence of CH absorption has not been established. In deriving their limit, Duley and Williams[2] used an uncertain upper limit of optical depth $\tau(3.4) \leq 0.05$ for a visual extinction $A_V = 70$ mag which they estimated to be consistent with current astronomical data. We now discuss observations of five IR sources having $10 < A_V < 35$ which lack the 3.1-μm ice absorption band and determine or place strong limits on the strength of the 3.4 μm CH absorption feature.

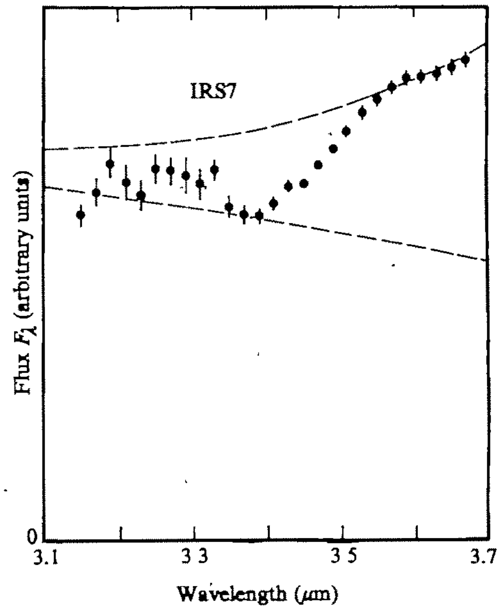

Fig. 1 Spectrum of the galactic centre source IRS7 showing the 3.4-μm absorption band. The upper and lower curves are discussed in the text.

The observations were made in February and April 1980 with the 3.9-m Anglo-Australian Telescope and the IR photometer-spectrometer. The IR sources, all optically invisible, include two in the galactic centre region[5], two in the Coalsack[6], and one recently discovered by Jones and Caswell (personal communication) coincident with an OH source at the 1950 coordinates 17 h 46 min 12.5 s, −27° 41′ 03″. For all sources we acquired photometry at 1.25, 1.65 and 2.2 μm, and spectra with $\lambda/\Delta\lambda \sim 50$ in the wavelength regions 2.0–2.5 and 3.1–3.7 μm. Stellar spectral types were derived from our shorter wavelength spectra, and these were combined with the photometry to derive values of A_V, using the interstellar extinction data of Jones and Hyland[7]. The latter data partly parallel other published values, and the agreement is good except that for the galactic centre sources we find somewhat earlier spectral types (and hence larger extinction) than Neugebauer *et al.*[8]. The longer wavelength spectra were searched for absorption near 3.4 μm. Table 1 details the results. The 3.1–3.7 μm spectrum of IRS 11 has a low signal-to-noise ratio. The limit $\tau(3.4)/A_V \leq 0.004$ for the Ophiuchus dark cloud[9] may be added to the data of Table 1.

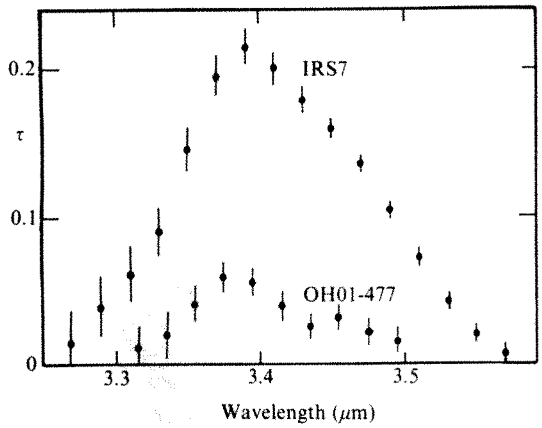

Fig. 2 Band profiles in IRS7 and OH01 − 477. The optical depth τ is calculated as described in text.

Figure 1 shows the 3.4-μm absorption feature in the source IRS7. The lower continuum in Fig. 1 is the expected flux for the M4 supergiant extrapolated from our 2-μm data with the Jones and Hyland reddening law assuming $A_V = 34$ mag. The observed excess is clearly due to circumstellar dust. We estimate the excess in this wavelength region to correspond to a reddened 300 K black body on the basis of the spectrophotometry data of Willner *et al.*[11]. The resulting continuum fitted at 3.6 μm is shown as the upper curve in Fig. 1 and demonstrates that the observed feature is an absorption at 3.4 μm. The residual structure in the first five points of Fig. 1 probably reflects the failure to correct wholly for the strongest of the telluric water vapour bands at 3.2 μm. The presence of a possible absorption feature near 3.4 μm in the spectrum of IRS7 has already been reported[10,11]. Our data provide unambiguous evidence for the existence of this band and define its characteristics.

Figure 2 is a plot of the band shape smoothed to a resolution of 0.08 μm. In deriving the optical depth we have allowed the continuum at the short wavelength region to be lowered to fit our data at 3.2–3.3 μm. This may have artificially steepened the short wavelength edge of the band but the central wavelength is not affected. We find the wavelength of the peak absorption to be 3.99 ± 0.02 μm, the equivalent width to be 330 Å and the intrinsic FWHM to be 0.13 μm. A similar procedure was adopted with OH01 − 477. The band shape included in Fig. 2 is the weighted mean of two observations. We have not attempted to deduce a band shape for IRS11 because the detection of the 3.4-μm feature in this source is at the 3σ level.

Table 1 Derived values of A_V and $\tau(3.4)$ for the programme sources

Source	Spectral type	A_V	$\tau(3.4)$	$\tau(3.4)/A_V$
Coalsack 3-1	M6	11	≤0.06	≤0.005
Coalsack 2-2	M0	15	≤0.06	≤0.004
OH01 − 477	M4	19	0.06	0.003 ± 0.001
GCIRS11	M4	30	0.2:	0.006:
GCIRS7	M4I	34	0.22	0.006 ± 0.001

We believe that the 3.4-μm absorption arises in the general interstellar medium. The main arguments against a circumstellar origin are: (1) The feature is present in the three most highly obscured sources. (2) We find no evidence of 3.4-μm absorption in the M supergiant VX Sgr, nor in M giant stars. Moreover we expect none in oxygen-rich stars such as those we consider here where carbon preferentially forms CO. (3) Becklin *et al.*[12] argued from the similar colours of the bluest galactic centre sources that most of the reddening towards IRS7 is interstellar.

We discount an origin in the dense molecular clouds, where absorption due to other CH and CC bonds is known to arise[13] because: (1) sources known to be obscured by molecular clouds show absorption at 3.1 μm; and (2) The line of sight towards IRS 7 and 11 does not pass through the molecular clouds mapped by Solomon *et al.*[14]. Finally the width of the 3.4 μm absorption feature argues against an origin in the gaseous phase in low temperature diffuse interstellar clouds.

Using laboratory data on the strength of the 3.4-μm CH band in various common organic molecules, Duley and Williams[2] have related the optical depth τ(3.3–3.4 μm) at peak absorption to the total visual extinction A_V assuming that all the carbon is in the form of a particular organic species. We may now use these results and our observations to estimate the fraction of carbon that is required to be organic material. We find that ~10% may exist in alkanes, whereas the unsaturated hydrocarbons (alkenes, alkynes or aromatics) would account for the visual extinction as well as the 3.4-μm absorption with no requirement for any other grain material.

The difficulty of fitting the extinction curve at all observed wavelengths using a distribution of grains of one specific composition is well known. A grain model based entirely on organic molecules is also clearly ruled out on the basis of the high depletions observed for gas phase metals in the interstellar medium. The present observations do, however, suggest that an appreciable fraction of the observed IR and visual extinction may arise from grains that are largely organic in character.

We thank Bob Carswell for permission to take some of the daytime observations, and Harry Hyland and Terry Jones for drawing to our attention OH01 − 477. D.T.W. thanks Professor Chandra Wickramasinghe for pointing out the significance of establishing the presence of a 3.4-μm interstellar extinction feature, and Professors F. Hoyle, P. M. Solomon and K. Nandy for valuable discussions.

Received 6 June; accepted 20 August 1980.

1. Whittet, D. C. B. *Nature* **281,** 708 (1979).
2. Duley, W. W. & Williams, D. A. *Nature* **277,** 40 (1979).
3. Hoyle, F. & Wickramasinghe, N. C. *Nature* **268,** 610 (1977).
4. Merrill, D. M., Russell, R. W. & Soifer, B. T. *Astrophys. J.* **207,** 763 (1976).
5. Becklin, E. E. & Neugebauer, G. *Astrophys. J. Lett.* **200,** L75 (1975).
6. Smyth, M. J. & Sim, M. E. *Nature* **283,** 457 (1979).
7. Jones, T. J. & Hyland, A. R. *Mon. Not. R. astr. Soc.* (in the press).
8. Neugebauer, G., Becklin, E. E., Beckwith, S., Matthews, K. & Wynn-Williams, C. G. *Astrophys. J. Lett.* **205,** L139 (1976).
9. Whittet, D. C. B. & Blades, J. C. *Mon. Not. R. astr. Soc.* **191,** 309 (1980).
10. Soifer, B. T., Russell, R. W. & Merrill, K. M. *Astrophys. J. Lett.* **207,** L83 (1976).
11. Willner, S. P., Russell, R. W., Puetter, R. C., Soifer, B. T. & Harvey, P. M. *Astrophys. J. Lett.* **229,** L65 (1979).
12. Becklin, E. E., Matthews, K., Neugebauer, B. & Willner, S. P. *Astrophys. J.* **220,** 831 (1978).
13. Soifer, B. T. *et al. Astrophys. J. Lett.* **232,** L53 (1979).
14. Solomon, P. M., Scoville, N. Z., Penzias, A. A., Wilson, R. W. & Jefferts, K. *Astrophys. J.* **178,** 125 (1972).

Lunar asymmetry and palaeomagnetism

D. J. Stevenson*

Department of Earth and Space Sciences, University of California at Los Angeles, Los Angeles, California 90024

The compositional asymmetry between the nearside and farside of the Moon and the natural remanent magnetism (NRM) of lunar rocks are poorly understood. The compositional asymmetry is indicated by the 2-km offset towards the Earth of the centre of mass relative to the centre of figure and the concentration of both KREEP and mare basalts on the nearside. Wasson and Warren[1] recently noted that these asymmetries may be better explained by an asymmetric crystallization of a primordial magma ocean than by the often proposed[2-4] greater thickness of farside anorthositic crust. The NRM[5] has been attributed to an ancient lunar dynamo[6,7]. I propose here a model for the early lunar evolution in which the preferred gravitational energy state consisted of an asymmetric accumulation of a liquid iron alloy (Fe–Ni and a small amount of sulphur) which displaces upwards the cold, primordial, undifferentiated core. The resulting depth asymmetry of the outer partially molten zone leads eventually to the subcrustal accumulation of light, magnesium-rich pyroxenes and olivine, preferentially in one hemisphere, sufficient to explain the offset and also indirectly providing a possible explanation for the nearside concentration of KREEP and mare basalt. Meanwhile, slow downward migration of the iron releases gravitational energy sufficient for convection and dynamo generation in an iron layer for about 10^9 yr. The proposed present state of the Moon has a symmetrically placed iron core (radius ≃ 500 km), unlike a previous model for the lunar asymmetry[8].

A crucial assumption in the model is an early Moon consisting of a cold interior region and a hot outer region, consistent with (but not limited to) conventional accretion models[9,10]. The outermost few hundred kilometres are frequently modelled as fully molten (the putative magma ocean) but this is neither geochemically essential nor geophysically plausible. A balance of likely accretional energy input with the outward heat flow suggested by Nusselt–Rayleigh number convection recipes[11] suggests that this region will self-regulate to a viscosity within a few orders of magnitude of 10^{16} P, for which substantial partial melting (essential to explain the anorthosite crust and KREEP) may be needed[12]. For such a viscosity, the convective heat transport is then ~100-fold greater than the present heat output, sufficient to eliminate the excess accretional energy input in about 10^8 yr. Boundary layer theory[13] then predicts a convective overturn time ~10^5 yr, sufficiently smaller than the evolution time scale to ensure lateral homogenization.

The absence of siderophiles in lunar rocks and the low oxygen fugacity of lunar magmas enable metallic Fe-Ni (ref. 14) to be present, although the lunar density, moment of inertia and magnetic measurements[15] limit the amount to ≲5% by mass. Iron droplets (maintained at least partially liquid by a small amount of sulphur) can readily precipitate to form a thin layer above the cold, undifferentiated primordial core. However, this situation is spontaneously unstable because a lower gravitational energy U can be achieved if the iron accumulates on one side, forming a crescent-shaped region and displacing the much less dense primordiel core upwards (Fig. 1). For a displacement h, the change in U is approximately $\Delta\rho_1 g\pi R_c^2 h^2 - \Delta\rho_2 g V_{Fe} h$, where $\Delta\rho_1 \equiv \rho_c - \rho_m$, $\Delta\rho_2 \equiv \rho_{Fe} - \rho_m$, ρ_c is the primordial core density, ρ_m is the (partially molten) mantle density, ρ_{Fe} is the liquid iron alloy density, g is the gravitational acceleration, R_c is the primordial core radius and V_{Fe} is the volume of precipitated iron. As compressional effects are negligible, the preferred h is given by minimizing U and is therefore approximately $1/2(\Delta\rho_2/\Delta\rho_1)V_{Fe}/\pi R_c^2$. More detailed, rigorous calculations change this approximate result by ≲30%.

For $\rho_c = 3.34\ \mathrm{g\ cm^{-3}}$, $\rho_m = 3.15\ \mathrm{g\ cm^{-3}}$ (corresponding to 25% partial melt, an arbitrary choice), $\rho_{Fe} = 7.0\ \mathrm{g\ cm^{-3}}$, $R_c =$ 1,300 km and $V_{Fe} = 3 \times 10^{23}\ \mathrm{cm^3}$ (that is, 5% iron by mass), the predicted value of h (~600 km) exceeds the depth of the mantle. This means that the primordial core could be displaced to the lunar surface. If a true magma ocean were possible ($\rho_m =$ $2.8\ \mathrm{g\ cm^{-3}}$), h would be ≃200 km, still a large effect. This asymmetry would have no lasting consequence if the iron could migrate to the centre in ≲10^8 yr. However, core formation in the Moon was much less rapid than in the other terrestrial bodies because of the low gravity (implying low deviatoric stresses associated with the asymmetry) and the low free iron abundance. The sinking layer[16] and Rayleigh–Taylor (Elsasser droplet[17]) core formation modes are slow (~10^9 yr) because the primordial core is cold and downward transport of heat is inefficient[18]. Stresses associated with the asymmetry are 0.1–1 kbar (limited in part by the low stress level for an $l = 1$ spherical harmonic of the load[19]) but the resulting cold deformation will not eliminate the asymmetry.

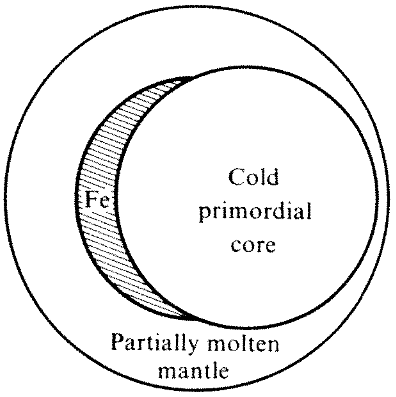

Fig. 1 Schematic representation of the energetically preferred asymmetric arrangement of matter within the early Moon, after precipitation of a liquid iron alloy from the partially molten mantle. The magnitude of the asymmetry is not well known but could be large (see text). The right-hand side is identified with the present nearside of the Moon (but the early orientation is irrelevant because the Moon's orbit has already tidally evolved to a large Earth–Moon separation).

As the asymmetry develops, partially molten mantle will flow into the deep region above the iron layer. Because the mantle adiabat is much less steep than the liquidus or solidus[20], this material will undergo some pressure-induced freezing. Subsolidus, high-viscosity material tends to be stagnant (an analogous situation is observed in convection experiments on fluids with strongly temperature-dependent viscosity[21]) and there will be a tendency for the least fusible solid fraction to accumulate preferentially in the deepest mantle regions. These are the magnesium-rich pyroxenes and olivine[20] (less dense than the average Moon by ~2%, but more dense than the early, partially molten mantle). Subsequently, at about 4,200 Myr BP, when the degree of partial melt in the outer regions has decreased (because of gradual cooling as surface bombardment decreases) and the anorthositic crust has formed, these light crystallites will rise to beneath the farside crust. A layer of thickness $d \lesssim 200$ km on the farside, thinning to zero thickness beneath the nearside crust, gives an offset between centre of mass and centre of figure of about $1/2(\Delta\rho/\rho)d$, about the right amount for a density contrast $\Delta\rho \simeq 0.06\ \mathrm{g\ cm^{-3}}$ between the light crystallites and the rest of the upper mantle. The characteristic time scale for lateral

---

* Present address: Division of Geological and Planetary Sciences, California Institute of Technology, Pasadena, California 91125.

0028–0836/80/410520—02$01.00

spreading of this layer is about $3\mu R^2/\Delta\rho g d^3$ (a generalization of ref. 22), where R is the radius, and this time scale exceeds 5×10^9 yr provided the viscosity $\mu \gtrsim 10^{22}$ P. This constraint should be satisfied as the material has a high solidus temperature and is within the thermal boundary layer, even that of 4×10^9 yr ago[11]. The low stress level for an $l = 1$ spherical harmonic of the load also helps prevent efficient lateral spreading[19]. The upwelling of crystallites may also sweep the last dregs of partial melt (from which KREEP was presumably derived[23]) around towards the nearside, thereby perhaps explaining the asymmetric KREEP distribution. The nearside predominance of mare basalts later in the evolution can be attributed to the presence of primordial, more fusible material and greater radiogenic heating in the nearside mantle[1].

Meanwhile, silicate grains detach from the deep side of the primordial core and float upward through the iron layer. The detachment rate is determined by the slow downward heat transport[18] (the time scale of iron core formation T_c may be as long as 10^9 yr) and the total gravitational energy released is about 1×10^{35} erg (ref. 24). Although insignificant if averaged over the whole Moon, this energy release is important for the iron layer. For an adiabatic temperature gradient of 2×10^{-6} K cm^{-1} and a thermal conductivity of 5×10^6 K^{-1} cm^{-1}, the integrated conductive heat transport along a liquid iron adiabat is 5×10^{25} T_c erg (T_c in yr), less than the energy released provided $T_c \lesssim 2\times10^9$ yr. Superadiabaticity and convection must ensue in the iron layer, and an application of mixing length theory[25] suggests a convective velocity $v \sim 0.1$ cm s^{-1}. The corresponding magnetic Reynolds number $R_M \equiv vd/\lambda \sim 10^2$ for a layer depth $d \sim 10^7$ cm and the magnetic diffusivity $\lambda \sim 2\times10^4$ cm^2 s^{-1} appropriate to liquid iron. Even for the slow rotation of the Moon (angular velocity $\Omega \sim 2\times10^{-6}$ s^{-1}), $v \ll \Omega d$, so the Coriolis force is dynamically important and dynamo generation should be possible[26]. The integrated ohmic dissipation is about $10^{23}H^2T_c$ erg for a characteristic current $\sim H/d$, and as this is of the order of 10^{34}–10^{35} erg, it follows that $H \sim 10$ G (the Carnot efficiency factor being irrelevant for gravitational stirring[27]). This may be the toroidal field, but it is energetically possible to have an external field comparable to that inferred from palaeofield studies, without invoking exotic energy sources such as superheavy elements[28].

Because g and the rate of gravitational energy release decrease as the iron approaches the centre, the field H decreases with time and dynamo generation will cease (for lack of an energy source sufficient to drive convection) once a central iron core forms, at ~3,000 Myr BP. However, several problems remain in relating lunar magnetism to an ancient lunar dynamo[29], and the model presented here does not attempt to resolve them all. More important than the details of the model are the basic ideas: an inevitable asymmetry and the likelihood of an ancient lunar dynamo. The model is testable (in principle) by lunar seismic studies designed to detect nearside–farside mantle variations and the existence (still hypothetical) of an iron core.

I thank D. Shirley and J. Wasson for useful discussions. This work is supported by NASA grant NGL 05-007-002.

Received 16 June; accepted 1 August 1980.

1. Wasson, J. T. & Warren, P. H. *Lunar planet. Sci.* **11,** Abstr., 1220 (1980).
2. Wood, J. A. *The Moon* **8,** 73 (1973).
3. Kaula, W. M. *et al. Proc. 5th Lunar Sci. Conf.*, 3049 (1974).
4. Haines, E. L. & Metzger, A. E. *Proc. Conf. Lunar Highlands Crust* (1980).
5. Fuller, M. *Rev. Geophys. Space Phys.* **12,** 23 (1974).
6. Runcorn, S. K. *et al. Proc. R. Soc.* **A325,** 157 (1971).
7. Strangway, D. W., Pearce, G. W., Gose, W. A. & Timme, R. W. *Earth planet. Sci. Lett.* **13,** 43 (1971).
8. Ransford, G. & Sjogren, W. *Nature* **238,** 260 (1972).
9. Wetherill, G. W. *Proc. 8th Lunar Sci. Conf.*, 1 (1977).
10. Kaula, W. M. *J. geophys. Res.* **84,** 999 (1979).
11. Schubert, G., Stevenson, D. J. & Cassen, P. *J. geophys. Res.* **85,** 2531 (1980).
12. Feigenson, M. D. & Spera, F. *J. geophys. Res. Lett.* **7,** 145 (1980).
13. Turcotte, D. L. & Oxburgh, E. R. *A. Rev. Fluid Mech.* **4,** 33 (1972).
14. Brett, R. *Geochim. cosmochim. Acta* **37,** 165 (1973).
15. Goldstein, B. E., Phillips, R. J. & Russell, C. T. *Proc. 7th Lunar Sci. Conf.*, 3321 (1976).
16. Vityazev, A. V. & Mayeva, S. V. *Izv. Phys. Solid Earth* **12,** 79 (1976).
17. Elsasser, W. M. in *Earth Science and Meteoritics* (eds Geiss, J. & Goldberg, E.) 1 (North-Holland, Amsterdam, 1963).
18. Stevenson, D. J. *Lunar planet. Sci.* **11,** Abstr., 1088 (1980).
19. Lambeck, K. & Pullan, S. *Phys. Earth planet. Interiors* **22,** 12 (1980).
20. Warren, P. H. & Wasson, J. T. *Proc. 10th Lunar Sci. Conf.*, 2051 (1979).
21. Booker, J. R. *J. Fluid Mech.* **76,** 741 (1976).
22. Ramberg, H. *Phys. Earth planet. Interiors* **1,** 63 (1968).
23. Warren, P. H. & Wasson, J. T. *Rev. Geophys. Space Phys.* **17,** 73 (1979).
24. Shaw, G. H. *Phys. Earth planet. Interiors* **20,** 42 (1979).
25. Clayton, D. D. in *Principles of Stellar Evolution and Nucleosynthesis*, 257 (McGraw-Hill, New York).
26. Stevenson, D. J. *Icarus* **22,** 402 (1974).
27. Gubbins, D. & Masters, T. G. *Adv. Geophys.* **21,** 1 (1979).
28. Runcorn, S. K. *Science* **199,** 771 (1978).
29. Daily, W. D. & Dyal, P. *Phys. Earth planet. Int.* **20,** 255 (1979).

Radar meteor rates and atmospheric density changes

C. D. Ellyett & J. A. Kennewell

Department of Physics, University of Newcastle,
New South Wales 2308, Australia

As a way of explaining the evidence linking recorded radar meteor rates with solar activity, it has been suggested that variations of the atmospheric scale height at meteor ablation altitudes, themselves controlled by the Sun, may be responsible. A quantitative examination of a theoretical treatment by Kaiser (personal communication) now shows that the above suggestion is certainly plausible, and details the necessary scale height changes as a function of the meteor mass exponent.

Using observations made in New Zealand, Canada and Sweden, Lindblad[1] and C.D.E.[2,3] have provided evidence suggesting a link between the apparent radar meteor echo rate and the solar cycle. The phase of this correlation is such that the apparent radar meteor rate increases towards the time of solar minimum. Lindblad has also claimed a connection relevant to short-term periodicities[4]. This variation in meteor rate seems to be an atmospheric effect, and the explanation proposed[5] is a Sun-controlled variation of the atmospheric density gradient at meteor ablation heights (80–120 km), probably modulated by solar X-ray flux. However, an anomalous increase in the meteor rate was recorded around 1963, greater than that ascribed to the solar effect[6,7]; this has been ascribed[5] to an abrupt decrease in solar X-ray output. We, however, consider that this anomaly shows a much higher correlation, both spatially and temporally, with an increase of particulate matter in the atmosphere[8]. Nevertheless, we believe that a change in atmospheric scale height must be responsible for the observed change in echo rate.

A decrease of atmospheric scale height (that is, an increase of density gradient) will bring about this ablation of a meteroid of a given size over a shorter path length. (Correlation with path length has in fact been noted[5].) It might thus be reasonably expected that, because the total energy release is (relatively) independent of path length, the shorter path length would be brighter, with a concomitant increase of linear electron density.

With regard to radar observations, however, an increase of linear electron density is offset by the shorter path length, although Lindblad[1] (who was monitoring both trail length and echo amplitude) has not observed this to be the case. The absence of a quantitative treatment of this problem has made some workers sceptical of the suggested link between scale height and observed rate. Baldwin and Kaiser[9] have suggested that variability in D-region ionospheric absorption may be a more important factor. However, our quantitative study shows that, at least for larger values of the mass exponent s, the large variation in observed meteor rate that C.D.E. requires[3] can be accounted for by appropriate changes of density and scale height.

0028–0836/80/410521—02$01.00

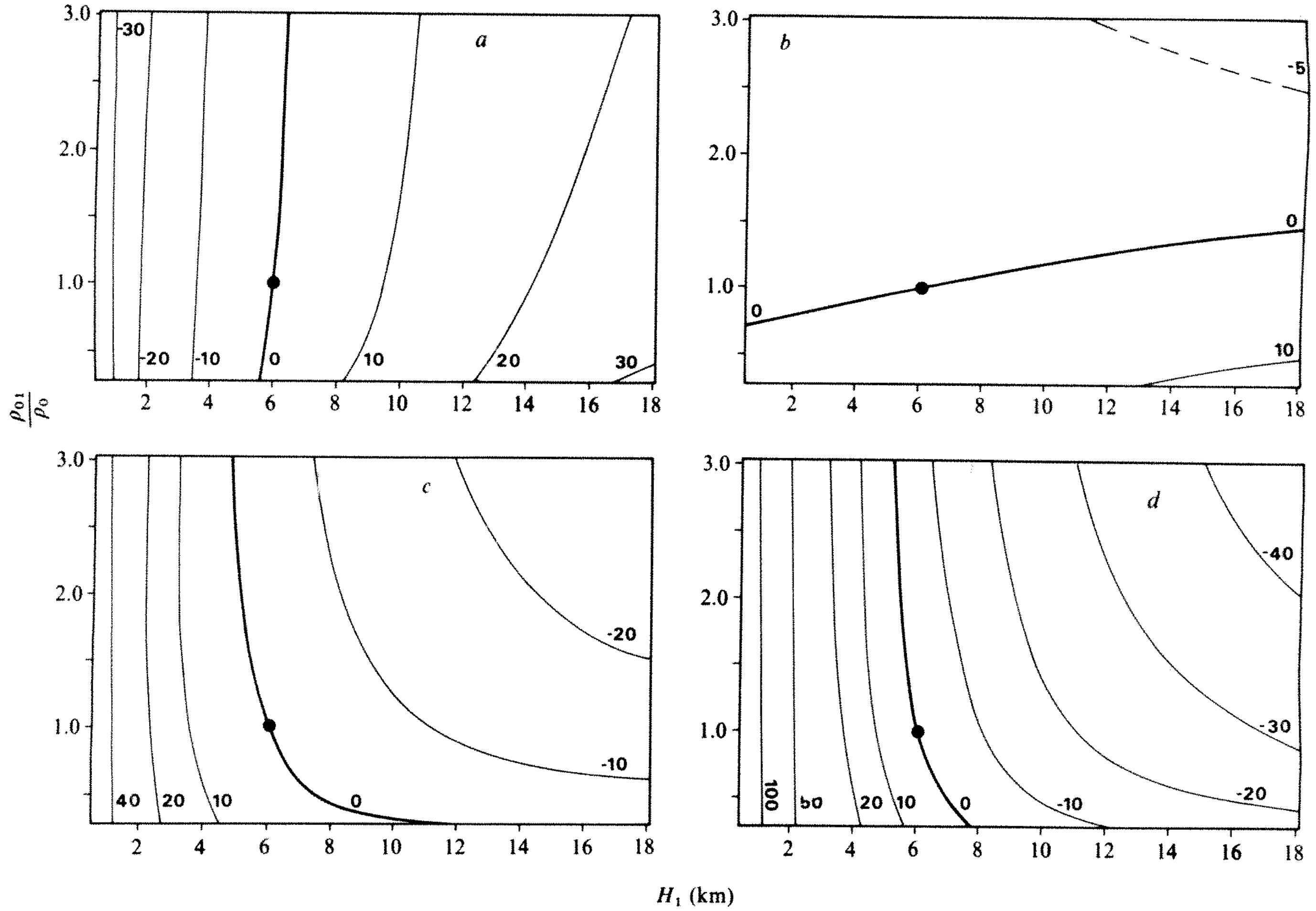

Fig. 1 Percentage change in observed meteor echo rate as a function of atmospheric parameters and meteor mass exponent s where $s = 1.8(a)$, $2.0(b)$, $2.2(c)$ and $2.4(d)$. Change is expressed as $(100(N_1 - N)/N)$ where N is the observed rate at a scale height of 6 km and density ρ_0 at height 100 km, and N_1 is observed rate for a scale height H_1 and density ρ_{01}.

Using classical ablation theory for compact meteoroids[10–14], Kaiser has shown that

$$\frac{N_1}{N} = \left[1 + \left(\frac{5-3s}{2}\right)\left(\frac{H_1}{\bar{h}} \ln\frac{\rho_{01}}{\rho_0} - \frac{H_1}{3\bar{h}} \ln\frac{H_1}{H}\right)\right]\left(\frac{H_1}{H}\right)^{2-s}$$

where N is the observed rate at a density scale height of H, $\bar{h}$ is the mean height (determined by atmospheric parameters) around which the meteor reflection points are distributed, ρ_0 is the atmospheric density at $\bar{h}$ for the rate N, N_1 is the observed rate for a new density scale height of H_1 and a density ρ_{01} at $\bar{h}$, and s is the exponent in the meteor mass distribution curve, which for sporadic meteors has been expermentally determined to lie between about 2.0 and 2.3. (Simek and McIntosh[15] have obtained a value of $s = 2.35 \pm 0.1$ for the radar sporadic background in the magnitude range of interest.)

A computer analysis of this equation has been carried out to ascertain the percentage change in observed meteor rate as a function of the three variables ρ_{01}, ρ_0, H_1 and s. These results are presented graphically in Fig. 1 for values of s between 1.8 and 2.4. The values for $\bar{h}$ and H have been taken to be 100 km and 6 km, respectively.

It is immediately evident from Fig. 1 that the percentage change of observed meteor radar rate is sensitive to s. For $s = 2.0$, no combination of density scale height and absolute density change will produce much more than a 5% change of meteor rate. As might be expected from an inspection of the equation, $s = 2.0$ represents the point about which the graphical contours exhibit a marked change of form. For $s < 2.0$ a decrease of scale height actually results in a decrease of meteor rates, contrary to simple expectation. However, as s increases above 2, the magnitude of the rate increase with decreasing scale height quickly grows.

The maximum rate increase to be accounted for, excluding the abnormal 1963 peak, is about 24%, and for $s \geq 2.2$, such an increase is possible. A halving of scale height from 6 km to 3 km will produce this percentage increase with $s = 2.3$. At this reduced scale height, which corresponds, of course, to a doubling of the air density gradient, the rate is relatively independent of the absolute air density. For $s = 2.5$, only a 30% decrease in scale height is necessary to produce the required increase of meteor rate.

In conclusion, it is possible for change of atmospheric density gradient at meteor ablation heights to have produced the changes noted in the observed radar meteor rate. Further and continuing measurements of the relevant atmospheric parameters in the meteor region are desirable in order to throw further light on this problem.

Received 1 April; accepted 8 August 1980.

1. Lindblad, B. A. *Space Res.* **7,** 1029–1043 (1967).
2. Ellyett, C. D. *ESSA Tech. Rep. ERL-71-ITS61* (US Department of Commerce, Washington, DC 1968).
3. Ellyett, C. *J. geophys. Res.* **82,** 1455–1462 (1977).
4. Lindblad, B. A. *Nature* **273,** 732–734 (1978).
5. Lindblad, B. A. *Nature* **259,** 99–101 (1976).
6. Ellyett, C. D. & Keay, C. S. L. *Science* **146,** 1458 (1964).
7. McIntosh, B. A. & Millman, P. M. *Science* **146,** 1457–1458 (1964).
8. Kennewell, J. A. & Ellyett, C. D. *Science* **186,** 355–357 (1974).
9. Baldwin, J. P. & Kaiser, J. R. *Mon. Not. R. astr. Soc.* **129.** 85–102 (1965).
10. Kaiser, T. R. *Phil. Mag.* Suppl. **2,** 495 (1953).
11. Kaiser, T. R. in *Meteors* (ed. Kaiser, T. R.) 119 (Pergamon, Oxford, 1955).
12. Kaiser, T. R. *Mon. Not. R. astr. Soc.* **121,** 284 (1960).
13. Kaiser, T. R. *Mon. Not. R. astr. Soc.* **123,** 265 (1961).
14. Kaiser, T. R. & Closs, R. L. *Phil. Mag.* **43,** 1 (1952).
15. Simek, M. & McIntosh, B. A. *IAU Symp.* **33,** 362 (1968).

A laboratory study on the formation of nitrous oxide by the reaction $N_2(A^3\Sigma_u^+) + O_2 \rightarrow N_2O + O$

Edward C. Zipf

Department of Physics and Astronomy, University of Pittsburgh, Pittsburgh, Pennsylvania 15260

Metastable $N_2(A^3\Sigma_u^+)$ molecules are produced copiously in auroral substorms by the impact of low-energy secondary electrons on N_2 and by the absorption of cosmic rays and solar X-rays at *E*-region altitudes and below. The major loss process for $N_2(A^3\Sigma_u^+)$ molecules below 100 km is collisional deactivation by O_2. We present here the results of a detailed study of the reaction $N_2(A^3\Sigma_u^+; v' = 0, 1, 2) + O_2 \rightarrow N_2O + O$, and we show that N_2O is formed with an effective yield of 0.6 with a probable absolute error of ±30%.

Harteck and Dondes[1] have shown that the irradiation of air by high-energy neutrons produces N_2O quite efficiently with an energy cost of 33 eV/N_2O molecule. Cylindrical shock wave studies simulating lightning have produced similar results[2]. However, neither of these investigations sheds light on the details of the reaction(s) leading to the synthesis of nitrous oxide. In a recent study in which N_2–O_2 mixtures were bombarded by 14 MeV neutrons, only two products, $N^{13}N$ and $N^{13}NO$, were observed[3]. Malcombe-Lawes[3] suggested that the reaction

$$N_2(A^3\Sigma_u^+) + O_2(X^3\Sigma_g^-) \rightarrow N_2O(X^1\Sigma) + O(^3P) + 3.0\ \mathrm{eV} \quad (1)$$

was the principal source of the observed nitrous oxide.

We have carried out a detailed study of this process, and we find that reaction (1) forms N_2O with a quantum yield of 0.6±30%. As metastable $N_2(A^3\Sigma_u^+)$ molecules are formed efficiently by electron impact with a total cross-section which is quite large[4] ($\sim 1.4 \times 10^{-16}\ \mathrm{cm}^2$ at 15 eV), these energy-rich molecules (and in turn N_2O) will be produced copiously by the low-energy electrons created by cosmic rays in the mesosphere and stratosphere, by solar X-ray and *EUV* absorption in the *D* and *E* regions and by the secondary electrons produced by high-energy particles precipitating into the auroral zone.

A block diagram of the plasma spectroscopy apparatus and a detailed description of the techniques used in this study are given elsewhere[5]. Only a brief summary of these techniques will be presented here. $N_2(A^3\Sigma_u^+)$ molecules were formed inside a cylindrical stainless steel cavity by a periodically pulsed microwave discharge. The behaviour of the $N_2(A^3\Sigma_u^+)$ molecules in the discharge and afterglow period was monitored by measuring the absolute intensity and the three-dimensional spatial distribution of the Vegard–Kaplan bands $[A^3\Sigma_u^+ \rightarrow X^1\Sigma_g^+]$ (see Fig. 1). With a typical power pulse width of 200 μs and a repetition rate of 20 pulses per s, $N_2(A^3\Sigma_u^+)$ concentrations of $>2 \times 10^{11}$ molecules cm^{-3} were produced by the end of the discharge period in a mixture consisting of 6.0 torr argon, 120×10^{-3} mm Hg nitrogen, and 1.0×10^{-3} mm Hg oxygen. Pulse counting and coherent summing techniques were used to observe the temporal behaviour of the *VK* emission during the afterglow period. The experiment was generally allowed to accumulate photon counts until the decay of the *VK* bands originating from each of the $v' = 0$, 1, and 2 vibrational levels that were detectable could be followed over an intensity range of at least three orders of magnitude (Fig. 2). The absolute sensitivity of the entire optical system was determined using standard lamps (both tungsten ribbon and deuterium lamps) calibrated by the National Bureau of Standards and by the Optronics Laboratory. The absolute accuracy of the calibration of the optical system approaches that of the standard lamps themselves (~5%). From the time-dependent data, the quenching coefficients for the depopulation of $N_2(A^3\Sigma_u^+)$ in a specific vibrational level by O_2, $k(v')$, could be evaluated. From these results $[k_0 = 1.9 \times 10^{-12}\ \mathrm{cm}^{-3}\ \mathrm{s}^{-1},\ k_1 = 4.0 \times 10^{-12}\ \mathrm{cm}^{-3}\ \mathrm{s}^{-1}]$ and from the absolute intensity and spatial distribution measurements, the total $N_2(A^3\Sigma_u^+)$ loss rate within the volume of the microwave cavity from reaction with and/or quenching by O_2

$$L(A^3\Sigma_u^+) = \frac{1}{\tau_0} \sum_{v'} k_{v'}\, n(O_2) \int_0^{\tau_0} \int_{\mathrm{volume}} M_{v'}(\vec{r}, t)\, \mathrm{d}t\, \mathrm{d}\vec{r}^3 \quad (2)$$

was determined. In this expression, $M_{v'}(\vec{r}, t)$ is the local $N_2(A^3\Sigma_u^+; v')$ concentration at a specific time during the discharge or afterglow while $n(O_2)$ is the molecular oxygen density, and τ_0 is the power-pulse repetition period.

The buildup of N_2O as the result of reaction (1) was observed by a quadrupole mass spectrometer which sampled the gas

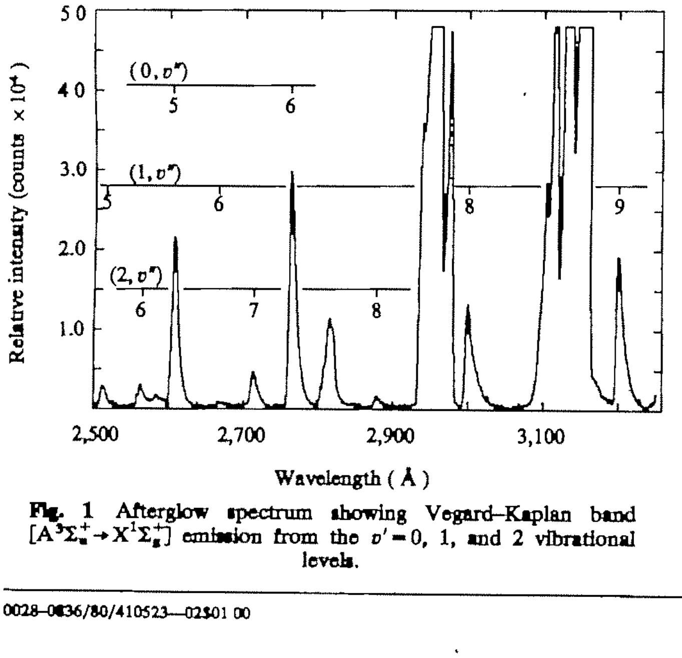

Fig. 1 Afterglow spectrum showing Vegard–Kaplan band $[A^3\Sigma_u^+ \rightarrow X^1\Sigma_g^+]$ emission from the $v' = 0$, 1, and 2 vibrational levels.

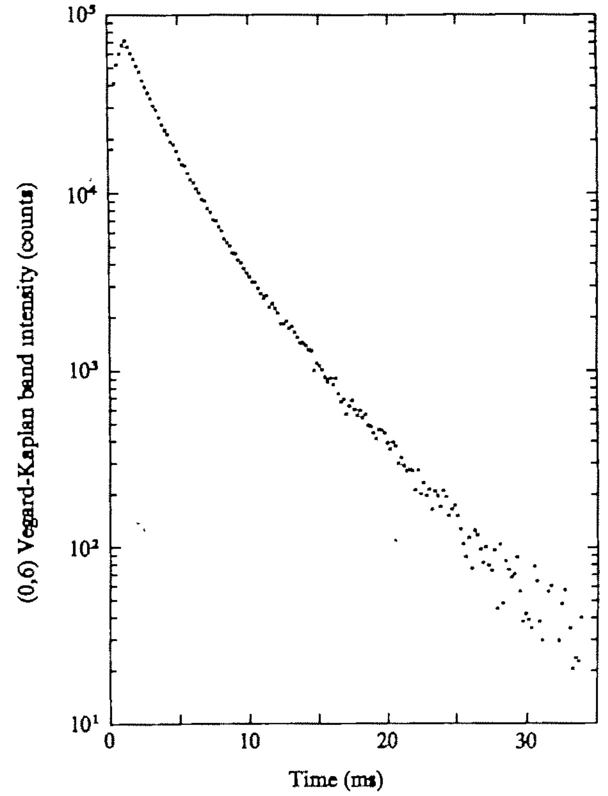

Fig. 2 The temporal behaviour of the (0, 6) Vegard–Kaplan band. The buildup of the $N_2(A^3\Sigma_u^+; v' = 0)$ concentration during the 1.0 ms microwave discharge can be seen readily. From the decay of the (0, 6) band intensity during the afterglow period, the total O_2 quenching coefficient for $v' = 0$ could be evaluated.

0028-0836/80/410523—02$01.00

through a small aperture in the side of the cavity (Fig. 3). Typical N_2O steady-state concentrations of 2×10^{12} molecules cm^{-3} were observed. The limiting sensitivity of the mass spectrometer to N_2O in the conditions of the experiment was $\sim10^9\ cm^{-3}$ so that accurate measurements of the N_2O concentration could readily be made. The N_2O signal was corrected for a small contribution (<10%) due to carbon dioxide whose concentration could be determined accurately from the magnitude of the mass peak at 22 AMU. The later is due almost exclusively to CO_2^{2+} ions and not N_2O^{2+} because the ratio of the effective ionization efficiency for these species in the conditions of the experiment was $CO_2^{2+}/CO_2^+ = 1.29\times10^{-2}$ and $N_2O^{2+}/N_2O^+ < 5\times10^{-5}$, respectively.

In the present work, particular attention was paid to the potentially undesirable effects of impurities either in the gases used or as outgassing by-products from the vacuum system itself. To minimize these difficulties, the vacuum system was constructed entirely of stainless steel using metal gaskets where components were joined, and it was baked until the background pressure was 5×10^{-10} torr, and the virtual leak rate for the entire vacuum system was reduced to less than 10^{-10} torr s^{-1}. The neutral mass spectrometer was also used to determine the actual composition of the gas in the microwave cavity including other oxides of N_2 (NO and NO_2). These measurements showed quite clearly that the local $n(O_2)$ concentration in the microwave cavity was reduced significantly (15–20%) as the result of reaction (1), and it underlines the importance of measuring the absolute, *in situ* concentration of all reactants in a yield measurement.

The N_2O molecules formed by reaction (1) are removed from the microwave cavity chiefly by pump-out through the aperture servicing the mass spectrometer and, to a minor extent, by reactions in the discharge and afterglow periods. The total nitrous oxide loss rate, $(V/\tau_1)N$, when the discharge was on, was determined from the N_2O rise-time data (τ_1), the volume of the microwave cavity, V, and the N_2O concentration, N, measured by the mass spectrometer. The relationship between the steady-state N_2O and $N_2(A^3\Sigma_u^+)$ loss rates is

$$(V/\tau_1)N = \varepsilon L(A^3\Sigma_u^+) \qquad (3)$$

where ε is the efficiency of reaction (1). In conditions where τ_1 is kept constant, equation (3) predicts that the steady-state N_2O concentration will be directly proportional to the total number of $N_2(A^3\Sigma_u^+)$ molecules observed per cycle (equation (2)). This behaviour is shown quite clearly by the data of Fig. 4. By varying τ_0, $n(O_2)$ and the microwave power-pulse width, the N_2O concentrations predicted by equations (2) and (3) were further verified, and the efficiency, ε, was evaluated. The results of this study show that $\varepsilon = 0.6$ with a probable absolute error of ±30%.

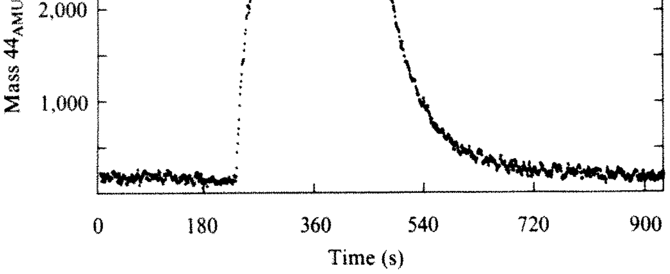

Fig. 3 Mass 44 AMU neutral mass spectrometer signal showing the buildup of nitrous oxide when the periodically pulsed microwave discharge is turned on and its subsequent pump-out when the discharge is turned off.

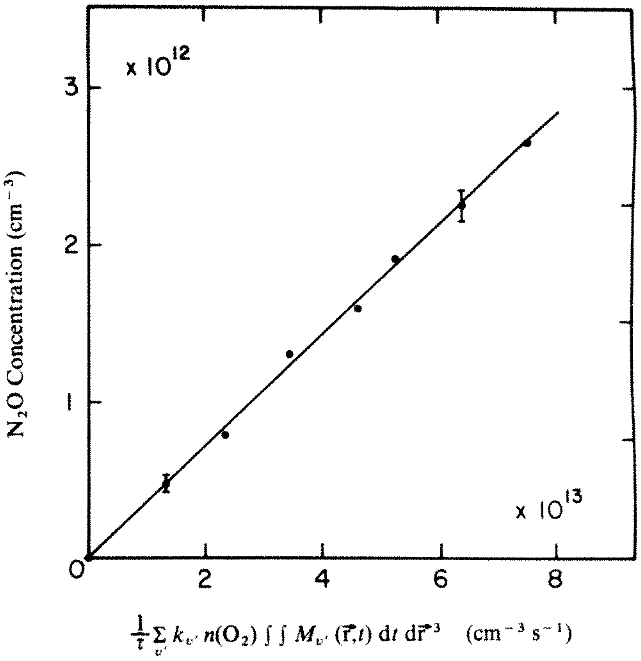

Fig. 4 A plot of the measured N_2O concentration versus the total $N_2(A^3\Sigma_u^+)$ loss rate.

The present study confirms the suggestion by Malcombe-Lawes[3] that N_2O is formed efficiently when metastable $N_2(A^3\Sigma_u^+)$ molecules react with O_2. Some nitric oxide was also observed in our experiment [$NO \sim 0.2\ N_2O$] possibly as the result of the reaction of N_2O with $O(^1D)$ atoms formed in the microwave discharge. The observed NO_2 concentration was less than $10^{10}\ cm^{-3}$ even though NO_2^+ was a major afterglow ion. This suggests that the NO_2 buildup is rate-limited by ion-molecule reactions which rapidly convert NO_2 molecules to NO_2^+ ions that subsequently recombine dissociatively to form NO.

Recent rocket-borne studies of $N_2(A^3\Sigma_u^+)$ excitation in auroral substorms[6–9] indicate that energetic electrons degrading in air at low pressure ($p < 10^{-3}$ torr) form ~0.35 $N_2(A)$ molecules per electron–ion pair. These results, when combined with the present study, indicate a minimum energy cost of ~157 eV per N_2O for $A^3\Sigma_u^+$ molecules in the $v' = 0$ and 1 vibrational levels. The lower energy cost reported by Harteck and Dondes[1] (33 eV per N_2O) may be a consequence of the high pressures used in the neutron experiments. In the conditions of their experiment, many metastable and excited states which are formed copiously by particle bombardment and which relax radiatively in our afterglow experiment would be collisionally deactivated. This process might result in enhanced $N_2(A)$ production (and thus N_2O) at atmospheric pressure or these species [for example, $N_2(a^1\pi_g)$] might react directly with O_2 to form nitrous oxide. Thus, when the A-state is formed by particle precipitation in auroral substorms, an energy cost of ~157 eV per N_2O is probably realistic. But, when the A-state is formed by X-ray and cosmic ray absorption in the stratosphere and below, a yield of one N_2O per electron–ion pair may be a better estimate.

Received 2 April; accepted 14 July 1980.

1. Harteck, P. & Dondes, S. *J. chem. Phys.* **24,** 619 (1956).
2. Zipf, E. C. & Dubin, M. *EOS* **57,** 156 (1976).
3. Malcombe-Lawes, D. J. *Nature* **247,** 540 (1974).
4. Cartwright, D. C. *J. geophys. Res.* **83,** 517 (1978).
5. Zipf, E. C. *Geophys. Res. Lett.* **6,** 881 (1979).
6. Swider, W. *Geophys. Res. Lett.* **3,** 335 (1976).
7. Sharp, W. E. *J. geophys. Res.* **76,** 987 (1971).
8. Sharp, W. E. & Torr, D. G. *J. geophys. Res.* **84,** 5345 (1979).
9. Gerard, J. C. & Rusch, D. W. *J. geophys. Res.* **84,** 4335 (1979).

Production of nitrous oxide in the auroral *D* and *E* regions

E. C. Zipf

Department of Physics and Astronomy, University of Pittsburgh, Pittsburgh, Pennsylvania 15260

S. S. Prasad

Jet Propulsion Laboratory, Pasadena, California 91103

Metastable $N_2(A^3\Sigma_u^+)$ molecules are formed efficiently in auroral substorms by electron-impact excitation of N_2. In the auroral *D* and *E* regions, $N_2(A^3\Sigma_u^+)$ molecules react rapidly with O_2 to form N_2O at a globally averaged rate that could be as high as $2\times10^{27}\ s^{-1}$. We report here that in favourable substorm conditions, the N_2O density at 100 km could be as large as $10^9\ cm^{-3}$.

Metastable $N_2(A^3\Sigma_u^+)$ molecules are produced copiously in auroral substorms by the impact of low-energy electrons[1,2]. Above 120 km, quenching by atomic oxygen

$$N_2(A^3\Sigma_u^+)+O \rightarrow N_2(X^1\Sigma_g^+)+O \qquad (1a)$$

$$N_2(A^3\Sigma_u^+)+O \rightarrow NO+N \qquad (1b)$$

and radiation of the Vegard–Kaplan bands

$$N_2(A^3\Sigma_u^+) \rightarrow N_2(X^1\Sigma_g^+)+h\nu \qquad (2)$$

are the dominant $N_2(A^3\Sigma_u^+)$ loss mechanisms, while below 100 km collisional deactivation by O_2 rapidly becomes the principal depopulation process[3,4]. Because a recent laboratory study[7] shows that the reaction

$$N_2(A^3\Sigma_u^+;\ v'=0,1,2)+O_2 \rightarrow N_2O+O \qquad (3)$$

produces nitrous oxide with an efficiency of 0.6±30%, the auroral borealis will produce significant quantities of N_2O poleward of latitude 55°.

Detailed studies of the excitation of $N_2(A^3\Sigma_u^+)$ molecules in auroral substorms have provided some insight into the maximum N_2O production rate in an auroral arc[1–4]. Although there is some disagreement concerning the absolute magnitude of the pertinent excitation cross-sections and the shape of the auroral secondary-electron flux, the recent work of Sharp *et al.*[1,5,6] shows that the ratio of the $N_2(A^3\Sigma_u^+)$ production rate to the total ion-pair production rate, *q*, is ~0.35. Thus, in view of the $N_2(A^3\Sigma_u^+)$ laboratory results, the N_2O production rate, $P(N_2O)$, could be as much as 0.21 *q*. As the globally averaged energy deposition rate due to particle bombardment during periods of maximum solar activity[8] is $\sim6\times10^{29}\ eV\ s^{-1}$, the maximum N_2O production rate would be $\sim4\times10^{27}$ molecules s^{-1} if reaction (3) was the only A-state loss mechanism.

Table 1 N_2O loss processes and chemical lifetimes at 100 km

	Reaction	Lifetime for IBC I aurora (s)
R(1)	$O(^1D)+N_2O \rightarrow 2NO$ or N_2+O_2	1.1×10^7
R(2)	$N(^2D)+N_2O \rightarrow NO+N_2$	1.3×10^8
R(3)	$O^++N_2O \rightarrow O_2^++N_2$	1.0×10^9
R(4)	$N^++N_2O \rightarrow NO^++N_2$	3.6×10^7
R(5)	$N_2^++N_2O \rightarrow NO^++N_2+N$	1.3×10^7
R(6)	$N_2^++N_2O \rightarrow N_2O^++N_2$	7.1×10^6
R(7)	$e+N_2O \rightarrow N_2O^++2e$	1.2×10^8
R(8)	$e+N_2O \rightarrow$ dissociation products	1.2×10^8
R(9)	$N_2O^++O_2 \rightarrow O_2^++N_2O$	1.1×10^{-3}
R(10)	$N_2O^++e \rightarrow$ dissociation products	6.0×10^{-2}

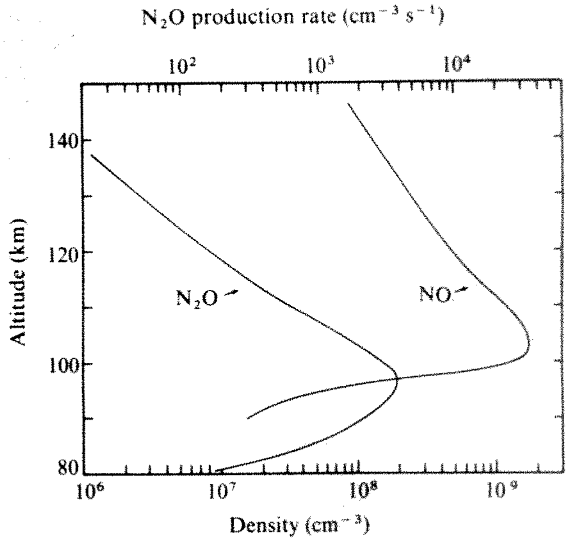

Fig. 1 The N_2O production rate in an IBC I aurora[5] [I(3,914 Å) = 4 kR]. The N_2O density assuming constant energy deposition for 5×10^4 s is compared with the NO values calculated by Gerard and Rusch[11] for the same aurora and equal integration times.

Although reaction (3) does control the $N_2(A^3\Sigma_u^+)$ chemistry below 95 km, most of the energy deposited by precipitating auroral electrons is above 95 km where processes (1) and (2) are also quite important. Thus, the effective N_2O production rate will be somewhat less than the upper limit obtained above. A more realistic assessment can be made from *in situ* measurements of the volume emission rate of the (0, 0) first negative band of N_2^+, η(3,914 Å), in typical IBC I and II⁺ aurora. This emission feature is frequently used to monitor the energy deposited in the auroral ionosphere by precipitating particles because its volume emission rate is directly proportional to the local ionization rate[9,10],

$$\eta(3{,}914\ \text{Å}) = \frac{q}{14.7}\,\frac{0.88[N_2]}{0.88[N_2]+0.5[O]+[O_2]}$$

The local N_2O production rate is related to η(3,914 Å) by

$$P(N_2O) \simeq 6.2\ \eta(3{,}914\ \text{Å})\left\{\frac{\varepsilon k_3[O_2]}{k_1[O]+k_3[O_2]+0.52}\right\} \qquad (4)$$

where [O], $[O_2]$, and $[N_2]$ are the atomic oxygen, O_2 and N_2 concentrations, respectively, ε is the efficiency for producing N_2O by reaction (3), and k_1 and k_3 are the total reaction rate coefficients for $N_2(A^3\Sigma_u^+)$ deactivation by O and O_2, respectively. Figure 1 shows the N_2O production rate calculated from published λ 3,914 Å data for an IBC I aurora[5] with k_1, $k_3(v'=0)$, and $k_3(v'=1)$ equal to $1.2\times10^{-10}\ cm^3\ s^{-1}$, $1.9\times10^{-12}\ cm^3\ s^{-1}$, and $4.0\times10^{-12}\ cm^3\ s^{-1}$, respectively[5,7]. Table 1 lists the principal N_2O loss processes and the effective N_2O chemical lifetime at 100 km for each loss channel in the IBC I aurora studied by Sharp *et al.*[5]. None of these processes is an effective nitrous oxide sink on the time scale of a typical auroral substorm. The N_2O diffusion lifetime is also quite long (days). Thus, the local N_2O buildup in the auroral *D* and *E* regions is determined by source functions such as that shown in Fig. 1 integrated over the total amount of time that the auroral activity lasted (minutes to hours). As an example we have assumed in Fig. 1 that the energy deposition in the IBC I aurora remained constant for 5×10^4 s. The maximum predicted N_2O density, $2\times10^8\ cm^{-3}$, is nearly an order of magnitude smaller than the NO concentration measured by Sharp[12] and estimated by Gerard and Rusch[11] assuming an equal integration period. With still longer integration times, the N_2O density would continue to increase relative to NO because the latters growth is ultimately rate-limited by

0028–0836/80/410525—02$01.00

the reaction $N+NO \rightarrow N_2+O$. Thus, N_2O concentrations greater than 10^9 cm^{-3} could be produced in IBC III aurora or by lower-level activity lasting for many hours, and, in favourable conditions, the N_2O concentration could actually exceed the local nitric oxide density.

The total N_2O column production rate in Fig. 1 is 6.3×10^9 cm^{-2} s^{-1} for an IBC I aurora in which the λ3,914 Å overhead intensity was 4.0 kR. These results imply an effective energy cost of ~330 eV per N_2O molecule in the aurora studied. Thus, a more realistic upper limit on the globally averaged N_2O production rate from auroral activity would be $\sim 2\times 10^{27}$ s^{-1}. Table 1 implies that the chemical lifetime in the auroral *D* region is quite long. Thus, the buildup of N_2O in the polar region is probably rate-limited by transport processes. Although vertical diffusion will carry some of the nitrous oxide into the polar mesosphere, the horizontal winds which were invoked by Cravens *et al.*[13] to explain the longitudinal distribution of NO in the *E* region, would also transport much of the N_2O equatorward where sunlight and reactions with O(^{1}D) would slowly decompose it.

Received 2 April; accepted 14 July 1980.

1. Sharp, W. E. *J. geophys. Res.* **76,** 987 (1971).
2. Shemansky, E. D., Zipf, E. C. & Donahue, T. M. *Planet. Space Sci.* **19,** 1669 (1971).
3. Deans, A. J. & Shepherd, G. G. *Planet. Space Sci.* **26,** 319 (1978).
4. Rees, M. H. & Jones, R. A. *Planet. Space Sci.* **21,** 1213 (1973).
5. Sharp, W. E., Rees, M. H. & Stewart, A. I. *J. geophys. Res.* **84,** 1977 (1979).
6. Sharp, W. E. & Torr, D. G. *J. geophys. Res.* **84,** 5345 (1979).
7. Zipf, E. C. *Nature* **287,** 523–524 (1980).
8. Johnson, R. G. & Sharp, R. D. in *Atmospheric Emissions* (eds McCormac, B. M. & Omholt, A.) 219 (Van Nostrand, New York, 1969).
9. Jones, R. A. & Rees, M. H. *Planet. Space Sci.* **21,** 537 (1973).
10. Vallance-Jones, A. *Can. J. Phys.* **53,** 2267 (1975).
11. Gerard, J. C. & Rusch, D. W. *J. geophys. Res.* **84,** 4335 (1979).
12. Sharp, W. E. *J. geophys. Res.* **83,** 4373 (1978).
13. Cravens, T. E., Gerard, J. C., Stewart, A. I. & Rusch, D. W. *J. geophys. Res.* **84,** 2675 (1979).

Chemical evolution and ammonia in the early Earth's atmosphere

A. Henderson-Sellers

Department of Geography, University of Liverpool,
Liverpool L69 3BX, UK

A. W. Schwartz

Department of Exobiology, University of Nijmegen, The Netherlands

A constraint on research into the evolution of the Earth's atmosphere may have been resolved by recent work on the photochemical reduction of atmospheric nitrogen by a naturally occurring form of TiO_2 (ref. 1). We show here that this source could have provided a small but vital abiological supply of ammonia in the early atmosphere of the Earth. Locally the levels of NH_3 produced by this mechanism satisfy the requirements of origin-of-life biologists whilst global levels do not conflict with chemical and physical constraints on the surface/atmosphere system nor with geological evidence for early Precambrian conditions.

It has become increasingly difficult from the viewpoints of exobiology and astrogeology to harmonize theories on the evolution of the Earth's atmosphere. The problem centres around the existence and/or abundance of reduced constituents in the early atmosphere[2]. Originally both astronomical and biochemical theories[3] supported the hypothesis that the initial atmosphere of the Earth was composed primarily of chemically reduced compounds. However, Rubey's work[4] and more recent geological (the oldest rocks yet discovered, from the Isua belt in West Greenland[5,6], are dated at (at least) 3,800 Myr and imply deposition conditions similar to the present-day) and astronomical[7,8] evidence argue strongly for a scenario in which degassing from a volatile-rich surface veneer leads to atmospheres composed mainly of carbon dioxide and water vapour (with smaller amounts of nitrogen and carbon monoxide) on all the terrestrial planets[9–12]. The origin and subsequent evolution of life on Earth is easier to explain if a small mixing ratio of more reduced compounds such as methane and ammonia existed in the early Earth's atmosphere[2]. Significant amounts of reduced gases could have been produced by the pyrolysis, during this early period of outgassing, of material similar to that still surviving in type I carbonaceous chondrites (survival of large quantities of intact organics during this process seems unlikely). However, a highly reducing atmosphere around the Earth, even if so produced, could not have persisted for any significant length of time[13]. The problem is particularly severe for ammonia. It has been argued that photodestruction of ammonia would have been substantially complete in <1 Myr (ref. 14). Kuhn and Atreya[15] have concluded more recently that a mixing ratio $\leq 10^{-4}$ of ammonia would have been "irreversibly" converted to N_2 in <40 yr. The photodestruction of NH_3 is an important problem as most models of chemical evolution require significant concentrations of NH_3 and NH_4^+ in solution for the synthesis of amino acids and other biochemicals. Bada and Miller[16], for example, estimate that NH_4^+ concentrations must be $>10^{-3}$ M to permit an equilibrium of equal concentrations of amino acids and the corresponding hydroxy acids at *p*H 8.

None of the studies of photolytic NH_3 destruction has considered the possible role of mechanisms for the resynthesis of NH_3. The synthesis of HCN at high efficiency by means of spark discharges in mixtures of N_2 and CH_4 offers an attractive route to biologically important molecules[17,18]. Aside from the question of the possible source and concentration of methane, clearly such syntheses may also involve the participation of NH_3, although it is produced *in situ* through the decomposition of HCN in aqueous solution (always the major process at any reasonable concentration of HCN in water). Consequently, it is not clear whether NH_3 produced by this route alone in bodies of water on the Earth's surface would have escaped ultimate photolytic destruction, although reactions in liquid inclusions in frozen lakes could have been an exception[19]. However, this would not have been the only available pathway for the synthesis of NH_3. Recent work on the direct photolytic reduction of N_2 on natural, semiconductor catalysts suggests a massive process which would have operated to increase steady state concentrations of NH_3 near ground level and, more importantly, in associated sources of ground water.

A systematic study of catalytic mechanisms of nitrogen fixation has established that titanium dioxide is an effective catalyst for the photochemical reduction[20,21] of N_2 to NH_3. A detailed investigation of naturally occurring areas rich in titanium revealed that certain deserts (such as the Imperial Sand Dunes, California) possess an extraordinary activity in the conversion[1] of atmospheric nitrogen to NH_3. It is estimated that one acre (~4,047 m^2) of this type of desert sand generates between 1 and 10 kg of NH_3 in a year. Thus the current global production may be estimated at between 6.8×10^9 and 6.8×10^{10} kg per year. We suggest that this process would provide a significant abiotic source of ammonia on the primitive Earth. This source of NH_3 can only resolve the conflict between astronomers and biochemists if it supplies adequate amounts of this reduced gas to localized areas whilst not perturbing the surface/atmosphere system (especially the surface temperature and chemical nature of the troposphere) beyond the fairly close constraints imposed by geological data. Our results suggest that both these sets of constraints are satisfied by this source of ammonia. The rate of nitrogen reduction is obviously a function of the total area of a suitable catalyst and the type of irradiation that it suffers. It seems reasonable to assume that early in the history of the Earth the level of surface irradiation by UV light was considerably increased. Even if, as has been suggested[22], the oxygen content of the atmosphere was within a factor of 10 of its present level 2,000 Myr ago, the earliest stages of surface/atmospheric

0028-0836/80/410526—03$01.00

Table 1 The greenhouse effect caused by ammonia in the early Earth's atmosphere for the addition of 10^{13} kg NH_3

Time (Myr BP)	p_{CO_2} (mbar)	10^{13} kg NH_3 ΔT (K)
4,250	310	17.2 (327.2)
3,500	70	15.1 (311.1)
2,500	18	13.7 (305.7)

Temperatures (in parentheses) are values from ref. 11 with the NH_3 increment added.

interaction probably included a significant effect of NH_3 fixation by desert sands, particularly as near-UV light is also effective[20]. Note that the measured production rates in these experiments indicate a substantially greater rate for the surface-catalysed production process than for the noncatalytic reverse oxidation. Thus a net accumulation of NH_3 in the vicinity of the catalyst would have been inevitable. We calculate, on the basis of an experiment described by Schrauzer[1], that the ammonia produced would have corresponded to a solution 0.01 M in the absorbed water of the desert sand tested. Thus the minimum requirements for the origin and subsequent evolution of life can be achieved, at least, locally. (The NH_3 mixing ratio in equilibrium with this concentration is *p*H dependent, but could not exceed 10^{-4}.)

However, are likely global levels of NH_3 consistent with the recognized climatological and geological data? We suggest that an upper limit for the global level of NH_3, assuming a production rate enhanced by two orders of magnitude together with a residence time against chemical destruction in the atmosphere of between 10 and 100 yr, is 10^{13} kg in the early atmosphere of the Earth. Higher levels than this seem unlikely for several reasons: (1) ammonia dissolves readily in water and thus a large mixing ratio of NH_3 in an atmosphere known to be in contact with considerable areas of surface liquid water throughout the Precambrian[23] is difficult to sustain; (2) photochemical oxidation of NH_3 rapidly removes it from the bulk atmosphere; (3) surface temperatures are a direct function of the abundance in the atmosphere of any gas which possesses IR absorption bands. Ammonia's strong absorption in the IR, caused earlier speculations concerning the atmosphere of the early Earth to include relatively large mixing ratios of ammonia[24]. There is clearly an important relationship between the likely production rates, the removal by photolysis and global temperatures.

The addition of even small amounts of a gas which possesses strong features in the IR part of the spectrum to atmospheres which are already in equilibrium with a surface at a temperature close to the present-day value (between 285 and 290 K) may pose serious problems to any atmosphere/surface evolution model. This is why we have computed the extra 'greenhouse effect' due to addition of 10^{13} kg of ammonia to the atmosphere. The precise global level of ammonia is extremely difficult to estimate as the destruction rate depends on the ground level mixing ratio, the eddy diffusion coefficient and the opacity of the atmosphere at the appropriate wavelengths[14,15]. However, this new source seems to be of the same order of magnitude as previously computed destruction rates[15] and thus the global budget of NH_3 could be enhanced. Geological evidence pertaining to the ambient surface temperatures[5,23] is now an important source of information. The extra temperature increment has been calculated using computer programmes described in detail elsewhere[25]. The numerical model includes the major regions of NH_3 band absorption (that is, 2.8–3.2; 5.5–7.2; 8.0–15.0 and longwave of 35.0 μm) plus the effects of broadening both by neutral gases and other absorbers. The solution of the radiative transfer equation is approximate but the accuracy and usefulness of the model over evolutionary time scales has been demonstrated[10,26]. Particular attention has to be paid to the regions of overlap between absorption bands (in this case the bands of water vapour and ammonia). We have followed Goody[27] in taking the transmission in regions of overlap as the product of the fractional transmissions of the individual bands. This is more appropriate than the use of an empirical relationship for application to atmospheric evolution over geological time periods. The variation in the solar luminosity, planetary flux factor, albedo and partial pressure of all atmospheric constituents is included. Table 1 lists the 'greenhouse increments' for the addition of 10^{13} kg of ammonia to an evolving atmosphere of CO_2 with the present-day level of water vapour. (The effect of adding this amount of NH_3 to atmospheres more recently than 2,500 Myr ago has not been calculated as there are conclusive geological data against such high levels[28] and the irradiation of the surface by UV light would by this time have decreased considerably, thus reducing the fixation rate.) This carbon dioxide atmosphere is described in detail elsewhere[11]. The resulting surface temperatures (that is, the temperatures of their model plus our calculated increment) are shown in parentheses in Table 1. (There is an interesting feedback effect associated with this mechanism for abiological nitrogen fixation—if surface temperatures rise in response to the addition of NH_3 to the early atmosphere then it is possible that larger areas of desert sands suitable for the catalytic reaction described by Schrauzer[1] may occur, thus producing a positive feedback cycle.) There are, of course, other climatological parameters which could be perturbed by such changes. The most difficult of these to consider is the possible perturbation in cloud cover. It has been suggested[29] that over geological time periods the percentage cloud cover may have remained approximately constant.

The computed average global surface temperatures in Table 1 seem to be rather high. Compare the value at 4,250 Myr ago with the early temperature of Venus calculated from the simple radiation balance equation

$$\frac{S}{f}(1-A)=\sigma T_e^4 \tag{1}$$

where *S* is the solar flux (Wm^{-2}), *f* the planetary flux factor[26], *A* the albedo, and σ the Stefan-Boltzman's constant.

At the time of planetary formation and assuming an increase in solar luminosity of between 40 and 45%, the effective temperature of Venus from equation (1) is between 295 K (for $f=4$) and 350 K (for $f=2$) (ref. 10). It is generally believed that the high early surface temperatures on Venus triggered the runaway greenhouse effect which finally resulted in the present-day massive atmosphere and very high surface temperatures (~750 K). Our results suggest, therefore, that 10^{13} kg of NH_3 in the evolving atmosphere of the Earth could produce surface temperatures too high for the subsequent evolution that is known to have occurred. The question of the possibility of a climate catastrophe has been discussed recently[28,30]. We suggest that the geological data[23,31] do not support any scenario which has either very high early surface temperatures or very large mixing ratios of ammonia. Note, however, that work on oxygen isotope levels in certain cherts suggests higher surface temperatures in the Precambrian[32]. We consider that surface temperature data are a valuable additional source of information. If the primitive atmosphere[28] contained even larger amounts of NH_3 (say through a combination of catalytic fixation and impact degassing of CI type material), the known surface temperature evolution would seem to be impossible. For instance, we have computed the additional greenhouse increment for 10^{15} kg NH_3 in the 4,250 Myr BP atmosphere in Table 1. In this case the value of $\Delta T = 108.3$ K gives a global average temperature of 418.3 K.

The present results suggest that a source of abiological ammonia by fixation of atmospheric N_2 in the presence of TiO_2 may provide enough reduced gas for local conditions (as dissolved NH_3) to be hospitable for the origin and subsequent evolution of life. However, the strong dependence of global surface temperatures on the partial pressure of ammonia indicates that the global mixing ratio is unlikely ever to have been above 1.5×10^{-5} by volume. This mechanism of NH_3 production may have constituted the major source of NH_3 in the prebiotic world, although photochemical destruction clearly restrained the build-up of ammonia levels in the primitive atmosphere.

We thank G. N. Schrauzer for unpublished data.

Received 6 May; accepted 17 July 1980.

1. Schrauzer, G. N. *Chem. Engng News* 7 (1978).
2. Schwartz, A. W. in *Marine Organic Chemistry* (eds Duursma, E. K. & Dawson, R.) 7–30 (Elsevier, Amsterdam, in the press).
3. Oparin, A. I. *The Origin of Life* (Macmillan, New York, 1938).
4. Rubey, W. W. *Bull. geol. Soc. Am.* **62,** 1111 (1951).
5. Moorbath, S., O'Nions, R. K. & Pankhurst, R. J. *Nature* **245,** 138 (1973).
6. Schidlowski, N., Appel, P. W. V., Eichmann, R. & Junge, C. E. *Geochim. cosmochim. Acta* **43,** 189 (1979).
7. Owen, T. in *Evolution of Planetary Atmospheres and Climatology of the Earth*, 1 (CNRS Toulouse, 1978).
8. Henderson-Sellers, A., Benlow, A. & Meadows, A. J. *Q. Jl R. astr. Soc.* **21,** 74 (1980).
9. Morss, D. A. & Kuhn, W. R. *Icarus* **33,** 40 (1978).
10. Henderson-Sellers, A. & Meadows, A. J. *Nature* **270,** 589 (1977).
11. Owen, T., Cess, R. D. & Ramanathan, V. *Nature* **277,** 640 (1979).
12. Benlow, A. & Meadows, A. J. *Astrophys. Space. Sci.* **46,** 293 (1977).
13. Walker, J. C. G. *Evolution of the Atmosphere* (Macmillan, New York, 1977).
14. Ferris, J. P. & Nicodem, D. E. *Nature* **238,** 268 (1972).
15. Kuhn, W. R. & Atreya, S. K. *Icarus* **37,** 207 (1979).
16. Bada, J. L. & Miller, S. L. *Science* **159,** 423 (1968).
17. Toupance, G., Raulin, F. & Buvet, R. *Origins of Life* **6,** 83 (1975).
18. Sanchez, R. A., Ferris, J. P. & Orgel, L. E. *Science* **154,** 784 (1966).
19. Sanchez, R. A., Ferris, J. P. & Orgel, L. E. *J. molec. Biol.* **30,** 223 (1967).
20. Bickley, R. I. & Vishwanathan, V. *Nature* **280,** 306 (1979).
21. Schrauzer, G. N. & Guth, T. D. *J. Am. chem. Soc.* **99,** 7188 (1977).
22. Levine, J. S., Hays, P. B. & Walker, J. C. G. *Icarus* **39,** 295 (1979).
23. Windley, B. F. (ed.) *The Early History of the Earth* (Wiley, London, 1976).
24. Sagan, C. & Mullen, G. *Science* **177,** 52 (1972).
25. Henderson-Sellers, A. & Meadows, A. J. *Planet. Space. Sci.* **27,** 1095 (1979).
26. Henderson-Sellers, A. & Meadows, A. J. *Planet. Space. Sci.* **24,** 41 (1976).
27. Goody, R. M. *Atmospheric Radiation* (Clarendon, Oxford, 1964).
28. Hart, M. H. *Icarus* **33,** 23 (1978).
29. Henderson-Sellers, A. *Nature* **279,** 786 (1979).
30. Schneider, S. H. & Thompson, S. L. *Icarus* **41,** 456 (1980).
31. Miller, S. L. & Orgel, L. E. *The Origins of Life* (Prentice-Hall, New Jersey, 1974).
32. Knauth, I. P. & Epstein, S. *Geochim. cosmochim. Acta* **40,** 1095 (1976).

Does the whole of the Earth's core convect?

K. A. Whaler

Bullard Laboratories, Department of earth Sciences, University of Cambridge, Madingley Road, Cambridge CB3 0EZ, UK

Higgins and Kennedy[1] used data on the behaviour of iron at high temperatures and pressures to infer that the top of the Earth's liquid core is stably stratified. Attempts to confirm this result both thermodynamically[2] and using seismological data[3] have been inconclusive. I present here geomagnetic results which may resolve the controversy. If a stratified region exists there will be no upwelling or downwelling of core fluid at the core–mantle boundary (CMB), so there will be no horizontal divergence of velocity v, that is $\nabla_H\cdot\mathbf{v} = 0$, where

$$\nabla_H = \nabla - \hat{\mathbf{r}}(\hat{\mathbf{r}}\cdot\nabla)$$

$\hat{\mathbf{r}}$ denotes the unit radial vector. This hypothesis can be tested directly, using geomagnetic data, at a few isolated points on the CMB, and local averages of $\nabla_H\cdot\mathbf{v}$ can be examined over the rest of the surface. A statistical treatment of the results strongly suggests that $\nabla_H\cdot\mathbf{v} = 0$, which is a consequence of a stably stratified layer.

The radial induction equation at the CMB, where $\mathbf{v}\cdot\hat{\mathbf{r}} = 0$, is, on the decade time scale[4,5],

$$\dot{B}_r + \mathbf{v}\cdot\nabla_H B_r + B_r\nabla_H\cdot\mathbf{v} = 0 \tag{1}$$

where a dot denotes time differentiation and the subscript r the radial component. This equation cannot be used to calculate the horizontal divergence of velocity directly because of a fundamental ambiguity[4,5]. However, at local extrema of B_r (points at which $\nabla_H B_r = 0$), the second term of equation (1) vanishes, eliminating the unknown **v**. If the horizontal velocity divergence is zero, these extrema must be points at which $\dot{B}_r$ is zero. Roberts and Scott[4] have observed that this condition would hold if the velocity were purely toroidal.

Table 1 Secular variation and horizontal divergence at extrema

Position $(\theta^\circ, \phi^\circ)$	$\dot{B}_r(\times 10^{-3})\gamma\ \mathrm{yr}^{-1}$	$\nabla_H\cdot\mathbf{v}(\times 10^{+3})\ \mathrm{yr}^{-1}$
(9, 329)	−0.78	−17.46
(34, 110)	−0.04	−0.06
(37, 45)	−0.71	5.73
(39, 268)	−0.45	−0.69
(48, 357)	−0.32	−0.99
(52, 164)	0.35	7.63
(65, 59)	−2.10	−4.13
(81, 190)	0.75	2.25
(94, 350)	−0.68	−1.66
(98, 33)	−2.34	−3.87
(103, 84)	2.85	5.53
(110, 267)	1.18	5.04
(118, 176)	0.43	−1.13
(123, 351)	0.09	−15.01
(128, 48)	−0.16	−0.60
(138, 295)	1.21	4.42
(145, 348)	0.95	5.76
(148, 113)	1.00	1.70
(163, 225)	1.76	2.57

The analysis was carried out for the International Geomagnetic Reference Field (IGRF) model[6] of 1965.0, a set of surface spherical harmonic coefficients up to eighth degree and order. The radial component of the field at the CMB ($r = 3{,}485$ km) is shown in Fig. 1. Solid contours indicate positive and zero values and dotted contours are negative, the contour interval is 1 G. The dashed lines are contours of zero $\dot{B}_r$, and in general they pass remarkably close to the extrema of B_r. I have found 19 extrema, marked by crosses in Fig. 1, whose secular variation and horizontal velocity divergence are given in Table 1. It is impossible to construct satisfactory error bounds either for the positions of the extrema or the zero $\dot{B}_r$ contours, so, to check that these numbers are significant, I have compared the mean and standard deviation of these $\dot{B}_r$ values with those from sets of 19 geographically randomly distributed points (see Table 2). None of these sets contained points with an angular separation of less than 15°. Clearly, the random points are more variable: none of the 24 sets had a smaller standard deviation than that of the extremal points. Taking all the random points together (mean 0.26, standard deviation 2.05), I used a one-tailed *F*-test on the ratio of the variances of the random and extremal points. The null hypothesis of the variances being equal can be rejected

Table 2 Means and standard deviations of $\dot{B}_r$ for extremal and random sets of points

Mean $(\times 10^3)$	Standard deviation $(\times 10^3)$
0.157	1.251†
0.442	1.520
0.493	1.522
0.932*	1.527
0.096	1.530
0.053	1.563
1.003*	1.578
0.005	1.582
0.577	1.589
−0.142	1.589
0.467	1.655
0.128	1.667
−0.281	1.815
−0.187	1.820
0.642	1.913
0.414	1.935
0.267	1.992
−0.308	1.997
0.144	1.998
0.468	2.016
0.392	2.020
0.357	2.051
−0.227	2.087
0.235	2.288
0.246	2.312

* The mean is inconsistent with zero at 95% level (using a 2-tailed Student's *t*-test).

† Extremal set; the rest are randomly generated.

0028–0836/80/410528—03$01.00

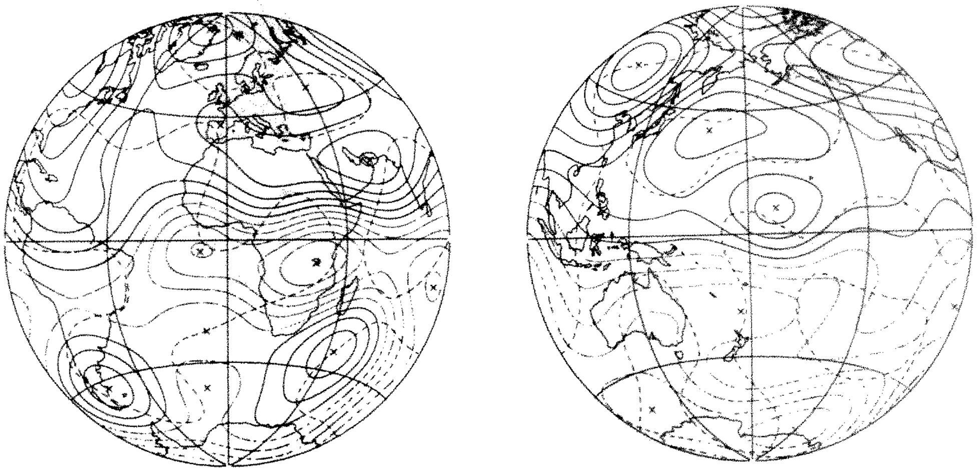

Fig. 1 Radial component of main field for 1965.0 at CMB on a Lambert equal area projection are positive and zero values, dotted contours negative. Dashed lines are contours of zero radial secular variation. Local extrema of the radial main field component are marked by crosses.

at the 99% level. Looking at the means of the individual sets, five have a smaller mean than that of the extremal points, but two others (marked with an asterisk in Table 2) are inconsistent with zero at the 95% level (using a two-tailed Student's *t*-test). Thus the values of $\dot{B}_r$ (and hence $\nabla_H\cdot\mathbf{v}$) at the extrema are significant—they are consistent with zero and less variable than would be expected from purely random sampling.

Backus (personal communication) suggested that $\nabla_H\cdot\mathbf{v}$ over the rest of the core could be estimated by integrating equation (1). The most useful form is shown to be, after some manipulation,

$$\iint_{S_0} \dot{B}_r\,\mathrm{d}S + B_r \iint_{S_0} \nabla_H\cdot\mathbf{v}\,\mathrm{d}S = 0 \qquad (2)$$

where the surface S_0 is bounded by a contour of B_r. Thus an additional necessary (but not sufficient) condition is that integrals of $\dot{B}_r$ over any surface bounded by a contour of B_r must vanish if $\nabla_H\cdot\mathbf{v} = 0$. I have computed surface integrals for the 1965.0 IGRF with 10% accuracy; the corresponding values of $|\iint \nabla_H\cdot\mathbf{v}\mathrm{d}S|/\iint \mathrm{d}S$ are presented in Table 3. Each surface of integration encompasses 1 G variations in the main field (2 G between +1 and −1 G), so the surfaces of integration are independent and together cover the whole core. Again the effect of errors in the spherical harmonic coefficients cannot easily be assessed, so the results were compared with sets of random integrals of $\nabla_H\cdot\mathbf{v}$. The random integrals were generated by rotating the secular variation field, keeping the main field fixed, and then integrating $\dot{B}_r$ over the same surfaces. This preserved the frequency content of the secular variation field.

The absolute values of the integrals of $\nabla_H\cdot\mathbf{v}$ per unit surface area for the rotated secular variation fields are also given in Table 3. The two rotations were through 180° in longitude (the transformation $(\theta, \phi) \rightarrow (\theta, 180° + \phi)$) and North to South Pole inversion $((\theta, \phi) \rightarrow (180° - \theta, 180° - \phi))$. Of both sets of random integrals 60% are larger than for the unrotated $\dot{B}_r$ field, and the mean integral of $\nabla_H\cdot\mathbf{v}$ per unit area, regardless of sign, is 62.3 and 38.8 after rotation, but 30.4 for the original integrals. These results suggest that the average horizontal divergence is less than for a random secular variation field.

The results presented here should be relatively insensitive to errors in the IGRF because a statistical treatment has been adopted, but there are problems associated with the downward continuation of the surface fields. The short-wavelength crustal component of the main field and errors in the secular variation are amplified by extrapolation to radii below the surface. Most secular variation models are dominated by small-scale instabilities at the CMB. A fuller report incorporating techniques for reducing these problems will be given elsewhere[7].

Assuming $\nabla_H\cdot\mathbf{v} = 0$ everywhere, the velocity component perpendicular to contours of B_r can be found everywhere on the CMB. An upper limit for the vertical growth rate of velocity, $\partial v_r/\partial r$, at the CMB is $1.44\times10^{-10}\,\mathrm{s}^{-1}$ (averaging $|\nabla_H\cdot\mathbf{v}|$ from Table 1). Benton and Muth[8] recently obtained $1.23\times10^{-10}\,\mathrm{s}^{-1}$ and $0.95\times10^{-10}\,\mathrm{s}^{-1}$ using independent methods. Benton[9] has developed a method similar to part of that described here. The data say nothing about the region below the CMB and convection may still occur deeper down. An alternative explanation of this result is that the core fluid flow is dominated by rotation (geostrophic) and is uninfluenced by strong magnetic fields.

Table 3 Integrals of $\nabla_H\cdot\mathbf{v}$ over surfaces bounded by contours of B_r for the original and rotated $\dot{B}_r$ field

		$\lvert\iint \nabla_H\cdot\mathbf{v}\,\mathrm{d}S\rvert/\iint \mathrm{d}S(\times10^{+4})$		
B_r (G)	Location	Original field	After 180° ϕ rotation	North to South Pole inversion
>7	Russia	1.54	36.28	42.53
6–7	Russia	3.79	35.78	43.08
>6	North America	5.16	6.13	39.29
5–6	Russia	7.19	35.52	47.48
5–6	North America	2.66	7.48	25.32
>5	Persian Gulf	40.79	523.03	16.20
4–5	Russia	11.72	31.70	44.85
4–5	North America	2.01	11.59	12.33
4–5	Persia	36.10	14.00	1.10
3–4	Asia	23.80	0.32	10.03
3–4	North America	24.06	19.81	9.39
>3	Mid-Pacific	24.84	61.64	6.95
2–3	Northern Hemisphere land masses	6.10	2.69	10.00
2–3	Mid-Pacific	38.00	62.62	110.42
>2	Off South Africa	13.04	217.71	26.79
>2	South America	54.47	33.15	64.76
1–2	Equatorial	74.14	28.50	4.45
1–2	North Pole	8.33	11.37	52.68
1–2	Off South Africa	69.11	292.33	71.80
1–2	South America	105.61	70.22	133.24
<1	North Pole	36.47	62.84	7.65
<1	North Pacific	60.72	53.09	205.58
−1–+1	Equatorial	59.85	81.49	107.66
−1–+1	South Atlantic	76.70	112.54	49.31
−2–−1		13.83	94.55	25.77
−3–−2		14.97	57.89	13.16
−4–−3		1.70	7.65	26.79
<−4	West African Coast	17.21	6.24	9.35
−5–−4	Central Africa	46.50	47.47	18.14
−5–−4	Indian and South Pacific Oceans	3.53	18.18	5.65
<−5	Indian Ocean	55.70	7.46	9.77
−6–−5	Central Africa	40.31	30.55	14.37
−6–−5	Antarctic	4.85	18.08	9.90
<−6	Central Africa	40.54	25.35	12.23
<−6	Antarctic	37.02	38.11	8.88
	Mean	30.37	62.29	38.44

The values of B_r indicate the contours that bound the surfaces of integration.

Received 9 June; accepted 29 August 1980.

1. Higgins, G. & Kennedy, G. C. *J. geophys. Res.* **76**, 1870–1878 (1971).
2. Boehler, Reinhard & Kennedy, G. C. *J. appl. Phys.* **48**, 4183–4186 (1977).
3. Masters, G. *Geophys. J. R. astr. Soc.* **57**, 507–534 (1979).
4. Roberts, P. H. & Scott, S. *J. Geomagn. Geoelect.* **17**, 137–151 (1965).
5. Backus, G. E. *Phil. Trans. R. Soc.* **A263**, 239–266 (1968).
6. Zmuda, A. J. *IAGA Bull.* No. 28 (1971).
7. Whaler, K. A. & Gubbins, D. *Geophys. J. R. astr. Soc.* (in the press).
8. Benton, E. R. & Muth, L. A. *Phys. Earth planet. Interiors* **20**, 127–133 (1979).
9. Benton, E. R. *Phys. Earth planet. Interiors* (in the press).

Accumulation of calcic plagioclase in ocean-ridge tholeiite: an indication of spreading rate?

M. F. J. Flower

Department of Geological Sciences, University of Illinois, Chicago, Illinois 60680

Basaltic magma generated at the Mid-Atlantic Ridge (MAR) appears on eruption to be characterized by the widespread accumulation of calcic plagioclase (An_{70-90}) independently from olivine and clinopyroxene[1–5]. Plagioclase accumulation is curiously absent from basalt formed at faster-spreading ridge axes such as the Eact Pacific Rise (EPR)[6–11], and it is interesting to speculate about the possible relationship of this phenomenon to spreading rate. Recent experiments[12] and studies of thermal regime at ocean-ridge spreading axes as a function of spreading rate[13,14] suggest an attractively simple solution to the problem, and point the way to a useful genetic spreading rate distinction for ophiolite rocks of unknown provenance.

The major-element chemical variation of basalts sampled from the Atlantic and Pacific Oceans is depicted schematically in Fig. 1 showing principal mechanisms of post-genetic fractionation identified from least-squares analysis of rock and glass data (1–4). Trends 1–4 are all encountered in Atlantic basalts, but trend 3 (representing cotectic fractionation of plagioclase + clinopyroxene ± olivine) is the prevalent, if not exclusive, trend in Pacific basalts[7–10], with only one recently reported example of trend 1 (ref. 11). Trends 1 and 2 are rarely encountered in Atlantic basalts, but trend 4 is common. However, it is noticeably absent from the Pacific. This trend reflects accumulation of calcic plagioclase in both primitive (MgO-rich) and evolved (MgO-poor) liquids, and is interesting in view of experimental indications[15–18] that plagioclase is at no pressure the sole anhydrous liquidus phase for tholeiitic basalt. Appeal to hydrous melting and high oxygen fugacity as a means to enrich primary magma in normative plagioclase[2–4,15] is probably not justified in view of the low volatile contents measured in ocean-ridge basalts[19,20] and ubiquitous FeO-enrichment trends in MORB glass[21], and we are led to interpret it as an effect of differential phenocryst distribution under anhydrous conditions.

Density relations at one atmosphere are quite complex. Evolved, FeO-rich, basaltic liquid is more dense than MgO-rich, primitive liquid[22] while CaO-rich plagioclase, typically crystallizing from primitive magma, is denser than NaO-rich plagioclase characteristic of evolved magma[12]. In general, however, most plagioclase varieties will be denser than primitive or moderately primitive magmas at pressures less than about 1 kbar (ref. 12). Slow cooling and crystallization in shallow reservoirs would allow plagioclase to accumulate along with denser mafic phases by gravitative separation from the liquid phase. Fujii and Kushiro[12] demonstrate that with increasing pressure

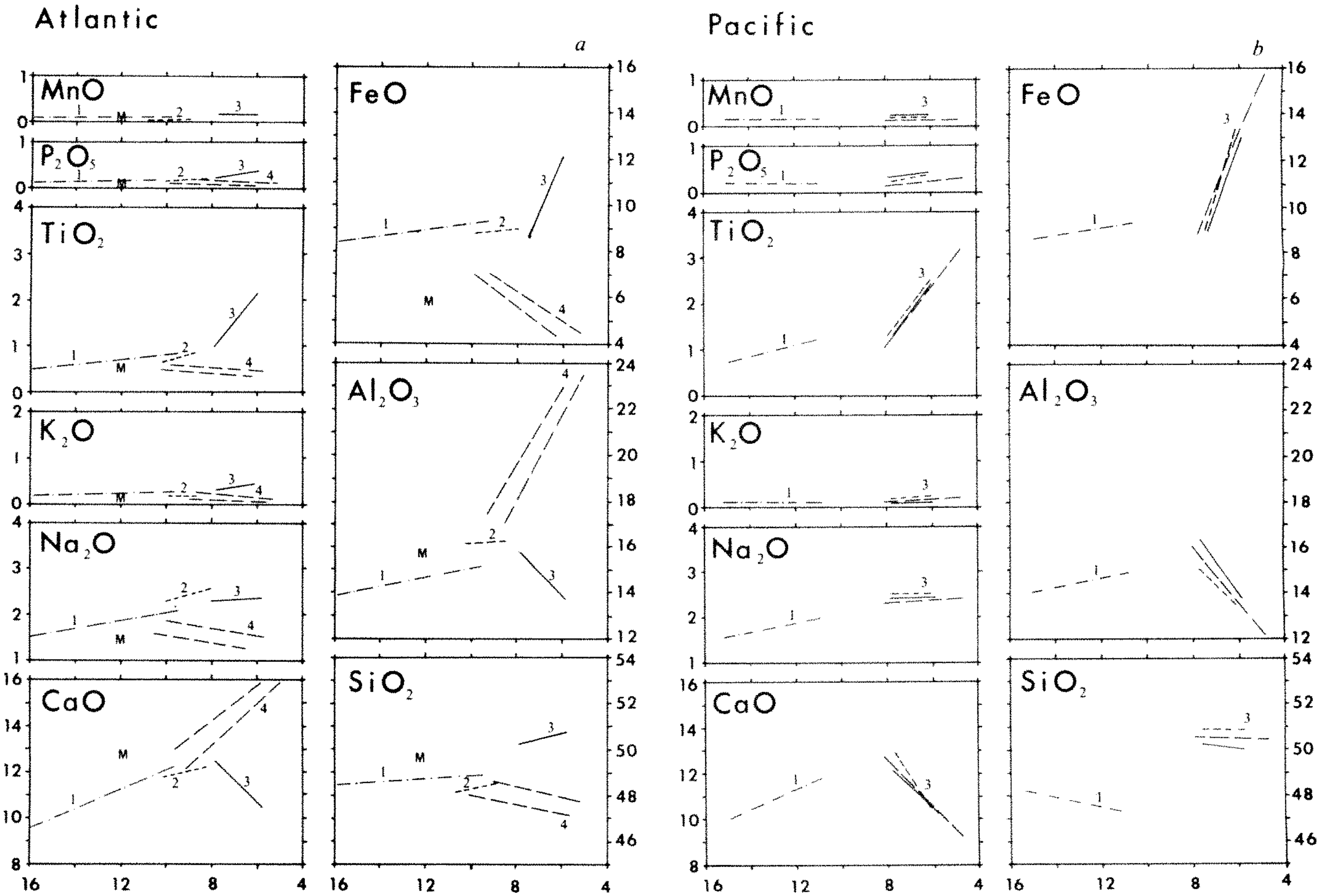

Fig. 1 MgO variation diagrams to illustrate ocean-ridge basalt fractionation, from data cited in *DSDP Initial Report* Vols **34, 37, 45, 46, 51–53, 64** and **65**, and in refs 1–11, 21, 30. Trend lines as follows: (1) olivine control by fractionation or accumulation; (2) olivine + plagioclase fractionation; (3) plagioclase + clinopyroxene ± olivine fractionation; (4) accumulation of plagioclase; (M) accumulation of plagioclase + clinopyroxene + olivine. All types appear in Atlantic basalts; type 4 is rare or non-existent in Pacific basalts.

0028–0836/80/410530—03$01.00

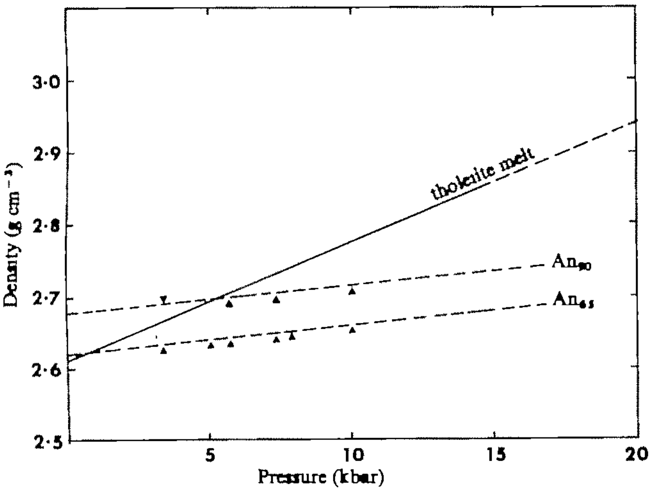

Fig. 2 Density versus pressure relations for Kilauea 1921 olivine tholeiite melt and plagioclase feldspar (after Fujii and Kushiro[12]). Solid lines indicate melt density and broken lines plagioclase density at near-liquidus temperatures. Triangle apices show direction of plagioclase movement.

there is a tendency for plagioclase to float in MgO-rich basaltic liquid, the extent of this tendency depending on plagioclase anorthite content and a significant increase in melt density with pressure. Fujii and Kushiro show that the melt density increase transgresses that of plagioclase (An_{90}) at about 6 kbar (Fig. 2), indicating that pressure is the main requirement for plagioclase flotation. These relations may be confirmed by molar volume calculations[23] and directly through experiment[12].

By implication, therefore, the demonstration of plagioclase flotation independently from mafic phases in erupted basalt may reflect pressure-characteristic fractionation in ocean-ridge magma supply systems. The type and extent of fractionation resulting from the cooling and crystallization of mantle-released magma is determined by the interrelation in *P–T* space of basalt liquidi, ocean-ridge geotherm and magmatic ascent path(s). Experimental evidence[16] and the discovery of both spinel- and plagioclase-lherzolite 'fossil' melt residues[24,25] suggests primary ocean-ridge tholeiite is generated by fairly advanced (15–25%) partial melting, at consistently low water and oxygen fugacities, near the solidus intersection of the plagioclase/spinel-lherzolite transition, that is, at about 1,300 °C and 8–10 kbar pressure. These conditions imply primary liquid compositions with 10–12 weight % MgO, consistent with requirements (for example, olivine compositions of ~ Fo_{90}) for equilibration with common residue lherzolite compositions[26]. More MgO-rich primary compositions[27] would show multiple saturation at about 15 kbar, so that a 'pivotal' region of 10–15 kbar (30–45 km depth) may be defined as a constraint to average ridge axis geotherm configurations (see ref. 28).

Sleep[14] computed isotherm distributions for the upper 10 km of ridge axes in relation to spreading rates and was able to define the relative stability of magma reservoirs. According to Sleep's model, basalt supraliquidus temperatures become increasingly localized along axial geotherms as spreading rate declines. At very slow rates (<1 cm per yr), high-level magma storage appears unlikely and diapiric solid intrusion to the sea floor may occur. These considerations are combined schematically in Fig. 3, and together allow us to postulate:

(1) Two or more stages of crystallization (for example, at 15–25 km and <5 km depth, but depending on model parameters) for magma ascending at slow-spreading (<about 5 cm per yr) axes; and

(2) Exclusively low pressure (for example, < about 3 km depth) crystallization at fast-spreading (> about 5 cm per yr) axes, with direct ascent of superheated primitive magma into shallow axial chambers; as general conditions for the steady-state geotherms depicted.

Although melting and magma uprise are probably episodic (constraints and limitations of this model are discussed in ref. 29), an important qualitative deduction can be made from Fig. 3: that polybaric fractionation, a regime promoting the accumulation of plagioclase in magma, is far more likely at slow-spreading than fast-spreading ridge axes. Further support for the influence of spreading rate on fractionation is provided by the widespread development of phenocryst reaction morphologies in Atlantic, but not in Pacific, basalts[6–10,30–33]. Resorption and oscillatory zoning of plagioclase and clinopyroxene phenocrysts are often attributed to minor variations in P_{H_2O} and/or magma mixing[34], but are equally explicable as due to partial polybaric re-equilibration of higher-pressure liquidus assemblages in cogenetic liquid, during its storage at low pressure.

'Fast-spreading' basalts are invariably aphyric or only sparsely phyric[7–10]. There is no reported occurrence of phenocryst reaction of the type observed in Atlantic basalts, or of plagioclase accumulation. Where present, phenocrysts appear to represent low pressure liquidus crystallization products[7–10]. Interestingly, basaltic crust generated at 'intermediate' spreading rates (for example, at the Gorda Rise, Costa Rica Rift and Gulf of California) shows incipient development of the 'slow-spreading' petrographic tendencies[6]. Finally, intra-flow variation due to plagioclase accumulation during post-eruptive phenocryst movement (flow differentiation) is not significant in comparison to that associated with pre-eruptive fractional crystallization[35], and in any case could not be spreading rate-dependent.

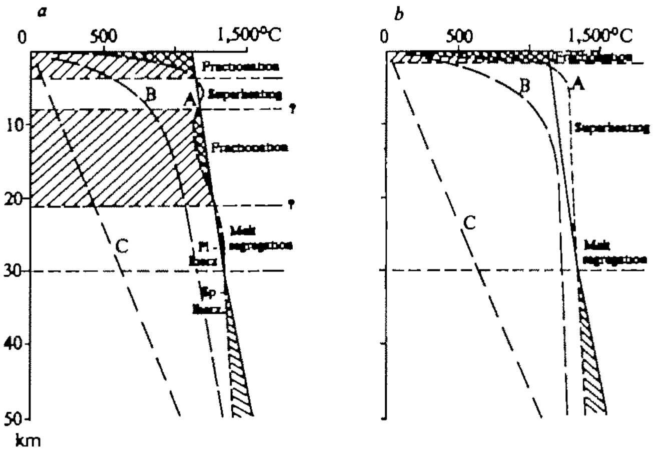

Fig. 3 Thermal gradients interpolated from Sleep's[14] computed isotherm distribution for *a*, a slow-spreading (1 cm per yr) ocean-ridge and *b*, a fast-spreading (5 cm per yr) ridge, and from experimental data for high pressure 4-phase saturation in primitive tholeiite (ref. 16); *a*, at spreading axis, *b*, at 30 km from axis, and *c*, 'average' ocean crust. Schematic depth intervals for fractionation, superheating and melt segregation reflect idealized steady-state spreading. Pl. lherz., plagioclase-lherzolite; Sp. lherz., spinel-lherzolite.

To summarize, I interpret the accumulation of plagioclase in ocean-ridge tholeiite as a comparatively high pressure effect. It is characteristic of slow-spreading axes such as the MAR for which thermal models[13,14] and seismic data[36,37] imply transient, polybaric, fractionation systems, while it is incipient only, or absent, at faster-spreading axes. The oft-cited general enrichment of FeO*, TiO_2 and lithophile elements at the latter (for example ref. 38), attributed to iterative fractionation processes under low f_{O_2} conditions in steady-state magma chambers[39,40], may be in part illusory, and result simply from relative dilution of these components by the accumulated plagioclase in Atlantic basalt. As further confirmation, no systematic chemical distinction of basaltic glass (that is liquid fraction) can be made between fast and slow-spreading axes[21].

Rare earth element and Sr data should be sensitive to plagioclase accumulation. However their interpretation has to consider the combined potential effects of plagioclase and apatite (?) buffering in the melt residue, and removal of plagioclase during fractional crystallization prior to accumulation. It should also be noted that Eu anomalies are comparatively slight for CaO-rich plagioclase in relation to basalt liquid at low f_{O_2} (refs 41, 42). DSDP/IPOD basalts[43-51] show correspondence between coarsely plagioclase-phyric lithologies and small (but significant) positive Eu anomalies, and decreased Rb/Sr, Zr/Sr, Ti/Sr (etc.) ratios as compared to glass or aphyric types.

Evidence for phenocryst-liquid reaction and plagioclase accumulation may be a sensitive indicator of thermal and kinematic conditions at dilating plate margins, and provide important information on the nature of magma supply at ocean ridges. Such petrochemical spreading rate discriminants may be applicable to obducted ocean crust whose conditions of formation at extinct accretionary plate margins are not easily inferred from other criteria.

I thank Bill Melson, Paul Robinson, Hans Schmincke and Tom Wright for useful discussions.

Received 12 March; accepted 16 July 1980

1. Byerly, G. R. & Wright, T. L. *J. Volcanol. geotherm. Res.* **3,** 229–279 (1978).
2. Blanchard, P. *et al. J. geophys. Res.* **81,** 4231–4246 (1976).
3. Flower, M. F. J., Robinson, P. T., Ohnmacht, W., Marriner, G. & Schmincke, H. U. *DSDP Init. Rep.* **51–53,** 939–956 (1980).
4. Staudigel, H., Bryan, W. B. & Thompson, G. *DSDP Init. Rep.* **51–53,** 977–986 (1980).
5. Flower, M. F. J., Robinson, P. T., Schmincke, H. U. & Ohnmacht, W. *Contr. Mineral. Petrol.* **64,** 167–195 (1977).
6. Flower, M. F. J. & O'Hearn, T. *DSDP Init. Rep.* **65** (in the press).
7. Clague, D. A. & Bunch, T. E. *J. geophys. Res.* **81,** 4247–4256 (1976).
8. Byerly, G. R., Melson, W. G. & Vogt, P. R. *EOS* **56,** 469 (1975), abstr.
9. Batiza, R., Rosendahl, B. R. & Fisher, R. L. *J. geophys. Res.* **82,** 265–276 (1977).
10. Mazullo, L. J. & Bence, A. E. *J. geophys. Res.* **81,** 4327–4351 (1976).
11. Schrader, E. L., Rosendahl, B. R. & Furbish, W. J. *Oceanol. Acta* **2,** 238–247 (1979).
12. Fujii, T. & Kushiro, I. *Ann. Rep. Dir. Geophys. Lab.* **76,** 419–424 (1977).
13. Kuznir, N. J. & Bott, M. H. P. *Geophys. J. R. astr. Soc.* **47**, 83–95 (1976).
14. Sleep, N. H. *J. geophys. Res.* **80,** 4037–4042 (1975); *Geophys. Res. Lett.* **5,** 526–528 (1978).
15. Kushiro, I. & Thompson, R. N. *Ann. Rep. Dir. Geophys. Lab.* **71,** 357–362 (1972).
16. Bender, J. F., Hodges, F. N. & Bence, A. E. *Earth planet. Sci. Lett.* **41,** 277–302 (1978).
17. Presnall, D. C., Dixon, J. R., O'Donnell, T. H. & Dixon, S. A. *J. Petrol.* **20,** 3–35 (1979).
18. Fujii, T., Kushiro, I. & Hamuro, K. *DSDP Init. Rep.* **45,** 413–518 (1979).
19. Moore, J. G. *Contr. Mineral. Petrol.* **28,** 272–279 (1970).
20. Delaney, J. R., Meunow, D. W., Graham, D. G. *Geochim. cosmochim. Acta* **42,** 581–594 (1978).
21. Melson, W. G., Vallier, T. L., Wright, T. L., Byerly, G. R. & Nelen, J. in *Geophysics of the Pacific Ocean Basin and its Margin* (American Geophysics Union, 1976).
22. Sparks, R. S. J., Sigurdsson, H. & Meyer, P. *EOS* **60,** 971 (1979).
23. Bottinga, Y. & Weill, D. F. *Amer. J. Sci.* **269,** 169–182 (1970).
24. Menzies, M. A. & Allen, C. *Contr. Mineral. Petrol.* **42,** 273–285 (1973); **45,** 197–213 (1974).
25. Melson, W. G. & Thompson, G. *Phil. Trans. R. Soc. Lond.* A**268,** 423–441 (1971).
26. Frey, F. A., Green, D. H. & Roy, S. D. *J. Petrol.* **19,** 463–513 (1978).
27. Elthon, D. *Nature* **278,** 514–518 (1979).
28. Bottinga, Y. & Allegre, C. J. *Phil. Trans. R. Soc. Lond.* A**288,** 501–524 (1978).
29. Flower, M. F. J. *J. Geol. Soc. Lond.* (submitted).
30. Ayuso, R. A. & Bence, A. E. *J. geophys. Res.* **81,** 4305–4325 (1976).
31. Flower, M. F. J. & Bryan, W. B. *DSDP Init. Rep.* **51–53,** 1557–1562 (1979).
32. Bryan, W. B., Frey, F. A. & Thompson, G. *Contr. Mineral. Petrol.* **64,** 223–242 (1977).
33. Natland, J. H. *DSDP Init. Rep.* **45,** 423–446 (1979).
34. Rhodes, J. M. & Dungan, M. A. *2nd Ewing Vol., Am. Geophys. Un.* 262–272 (1979).
35. Flower, M. F. J. & Robinson, P. T. *J. geophys. Res.* (submitted).
36. Fowler, C. M. R. *Geophys. J. R. astr. Soc.* **47,** 459–591 (1976).
37. Steinmetz, L., Whitmarsh, R. & Moreira, V. *Geophys. J. R. astr. Soc.* **50,** 353–380 (1977).
38. Nisbet, E. G. & Pearce, J. A. *Nature* **246,** 468–469 (1973).
39. Rosendahl, B. R. *et al. J. geophys. Res.* **81,** 5294–5304 (1976).
40. Orcutt, J. A., Kennet, B. L. M. & Dorman, L. M. *Geophys. J. R. astr. Soc.* **45,** 305–320 (1975).
41. Drake, M. J. *Geochim. cosmochim. Acta* **40,** 457–465 (1975).
42. Sun, S. S. & Nesbitt, R. W. *Contr. Mineral. Petrol.* **65,** 301–325 (1978).
43. Dostal, J. & Muecke, G. K. *DSDP Init. Rep.* **37,** 573–576 (1977).
44. Puchelt, H., Emmermann, R. & Srivasta, R. K. *DSDP Init. Rep.* **37,** 581–590 (1977).
45. Schilling, J. G., Kingsley, R. & Bergeron, M. *DSDP Init. Rep.* **37,** 591–598 (1977).
46. Bryan, W. B., Thompson, G., Frey, F. A., Dickey, J. S. & Roy, S. D. *DSDP Init. Rep.* **37,** 695–704 (1977).
47. Hoernes, S. & Friedrichsen, H. *DSDP Init. Rep.* **45,** 541–550 (1979).
48. Rhodes, J. M., Blanchard, D. P., Dungan, M. A., Rodgers, K. V. & Brannon, J. C. *DSDP Init. Rep.* **45,** 447–459 (1979).
49. Flower, M. F. J. *et al. DSDP Init. Rep.* **46,** 179–213 (1979).
50. Wood, D. A. *et al. DSDP Init. Rep.* **49,** 597–656 (1979).
51. Tarney, J., Saunders, A. D., Weaver, S. D., Donnellan, I. C. B. & Hendry, G. L. *DSDP Init. Rep.* **49,** 657–692 (1979).

Behaviour of phosphate in estuarine water

J. David Smith & Andrew R. Longmore

Marine Chemistry Laboratory, School of Chemistry,
University of Melbourne, Parkville, Victoria 3052, Australia

The phosphate load in many rivers has been increased through soil disturbance and discharge of sewage and other wastes. Understanding how much phosphate may be removed from the waters of rivers and estuaries to the sediment would aid waste disposal planning. Phosphate carried through estuaries to coastal waters can increase growth of phytoplankton and macroalgae, with effects on fisheries and fouling of structures and beaches. Removal of dissolved phosphate to the sediment in estuaries has been predicted from indirect evidence[1–3], but measurements of dissolved phosphate in estuaries have shown various patterns of behaviour[4–7]. A constant level of dissolved phosphate over a wide salinity range, observed in some estuaries[6,7], has been attributed to buffering of the phosphate by particulate matter. This implies the release of phosphate from particulate matter in some conditions. Seawater held in contact with large concentrations of sediment in laboratory conditions tends to a steady-state level of dissolved phosphate in the range 3–28 μg P l^{-1} (refs 8–11). Our laboratory studies, using a simple estuarine mixing model system, show that inorganic removal of phosphate is likely to be less than 10% in estuaries fed by rivers of iron content near the world average[12].

Phosphate in waters of the Yarra River estuary (Australia) shows large variations related to river flow (Fig. 1). At low flow (21 February 1977) filtered river water contained 185 μg P l^{-1}, and adjacent seawater in Port Phillip Bay[13] contained 90 μg P l^{-1}, with a major input of phosphate part way along the estuary. After a period of high flow (24 June 1977) phosphate in the filtered river water was 32 μg P l^{-1}, with much of the phosphate in the estuary then being supplied from the seawater. This variability of phosphate distribution in the Yarra estuary made interpretation in terms of phosphate behaviour difficult, and a series of laboratory studies were undertaken to elucidate the effects of some of the non-biological factors.

Reactions in estuaries are strongly influenced by interactions of dissolved species with surfaces of suspended particles, and by aggregation of fine particles as salinity increases. Both types of interaction have the effect of converting 'dissolved' species into 'particulate' form, where the differentiation is by whether or not the species passes through a chosen filter. The ionic strength and *p*H of estuarine waters increase with increasing salinity, and a

Table 1 Starting solutions used in estuarine mixing experiments

No.	Humic acid (mg l^{-1})	Iron (μg Fe l^{-1})	Phosphate (μg P l^{-1})
1	0	0	185
2	9.0	0	184
3	1.2	100	160
4 (*a*)	0	750	124
5 (*b*)	0	750	42
6 (*c*)	9.0	750	174
7 (*d*)	0	750	144

Each solution initially contained 200 μg P l^{-1} added as KH_2PO_4. The results show the concentration of phosphate remaining in solutions that had been aged overnight, then filtered. *a*, P added after Fe. *b*, P added before Fe. *c*, P added after humic acid and Fe. *d*, Fe added 5 days before P. Results of adding seawater to unfiltered solutions *a*, *b* and *c* are shown in Fig. 3.

0028-0836/80/410532—03$01.00

complex sequence of reactions ensues. For this reason we designed a laboratory system to simulate the progressive mixing of river water and seawater, as it occurs in an estuary, rather than using the alternative of batch mixing. The Yarra estuary is stratified[14] with mixing occurring at different rates in the horizontal and vertical directions. A time of 1–2 h for doubling of the salinity was estimated for the horizontal direction, and this was later confirmed by J. Hinwood (personal communication). For estuaries that are much larger, especially if they are also well mixed, the half life for salinity change may be longer by orders of magnitude.

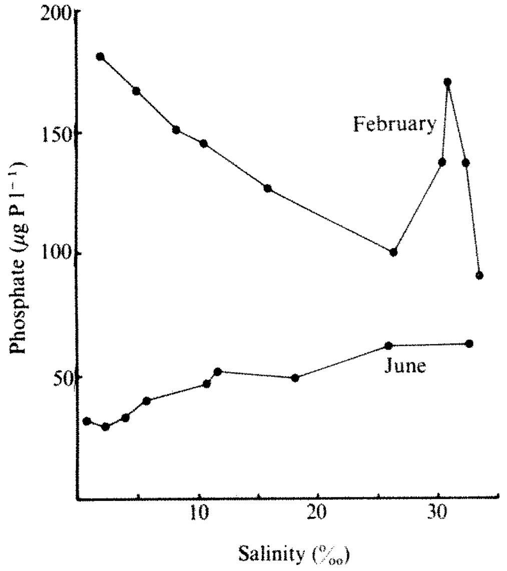

Fig. 1 Variation of dissolved phosphate with salinity in waters of the Yarra River estuary on two occasions in 1977.

In our laboratory model, seawater was pumped at a steady rate into a vessel containing river water, and the mixture pumped out at the same rate to maintain a constant volume. The solution was held at 15 ± 0.1 °C, and stirred at a constant rate to ensure rapid mixing and maintain particulate matter in suspension. The salinity approached that of the seawater exponentially, with a half life for salinity change governed by the rate of flow of the peristaltic pump used and the initial volume of river water. Adding seawater at 3.4 ml min^{-1} to 500 ml of river water gave a half life for salinity of about 90 min. Samples of the outflow were collected for analysis over a period of 5 h. Phosphate was determined colorimetrically[15] on 10-ml samples collected in a graduated syringe and immediately filtered through 0.2-μm pore size Nuclepore filters. All acid-soluble phosphates, including dissolved and colloidal forms, would be included using this method. Iron was determined colorimetrically using ferrozine[16] on filtered samples buffered at pH 5. Humic acid was determined from absorbance at 365 nm, calibrated using humic acid extracted from a large volume of Yarra river water. Salinity was determined to ±0.1‰ from refractive index.

In a laboratory experiment, estuarine mixing was simulated by adding seawater to unfiltered Yarra river water. The seawater from Bass Strait (S = 35.0‰, pH 8.09) contained 4 μg P l^{-1} which was unchanged by filtration. River water collected above seawater influence, contained 26 mg l^{-1} suspended matter and 1.9 mg l^{-1} humic acid and was pH 7.25. The filtered river water contained 99 μg Fe l^{-1} and 124 μg P l^{-1}, compared with 1,800 μg Fe l^{-1} and 214 μg P l^{-1} in the acidified unfiltered water. Thus in the river water sample used, 94.5% of the iron and 42% of the phosphate was associated with the particulate matter. Behaviour of the three components measured during mixing was non-conservative, with iron removal 70% (similar to that reported for other rivers[12,17,18]), humic acid removal 23%, and phosphate removal 6%. The salinity of maximum removal was different for each component (Fig. 2).

A separate series of experiments using synthetic starting solutions allowed the effects of iron and humic acid to be differentiated. When $FeCl_3$ was added to water, the level of Fe detectable after filtration fell very rapidly to less than 5 μg l^{-1}. Iron was stabilized in 'solution' by adding humic acid[19]. We found that 1.2 mg of humic acid per 100 μg of Fe was effective, using a filtered solution of 1.2 mg ml^{-1} Aldrich commercial humic acid in 0.1 M tris(hydroxymethyl)methylamine. The starting solutions listed in Table 1 were allowed to stabilize overnight before use, and the amount of phosphate in a small sample of filtrate was determined immediately before the start of each mixing experiment. The addition of iron after the phosphate caused much greater phosphate removal than occurred when the iron was added before the phosphate. When seawater was added to the unfiltered starting solutions in the estuarine mixing model, dissolved phosphate was essentially conservative in all cases except in the presence of high levels of iron and humic acid. Starting with 9 mg HA, 750 mg Fe and 200μg P l^{-1}, a maximum of 44% of the phosphate was removed from solution (Fig. 3).

The lack of interaction of iron with humic acid is expected as both are anionic. The indifference of iron to dissolved phosphate during estuarine mixing is related to the low concentration of iron in true solution in ionic form, and the chemical stability of hydrated iron oxide colloidal particles after they are formed. When associated with humic acids, iron is present both weakly bound on external surfaces, and as hydrated oxides[20]. The

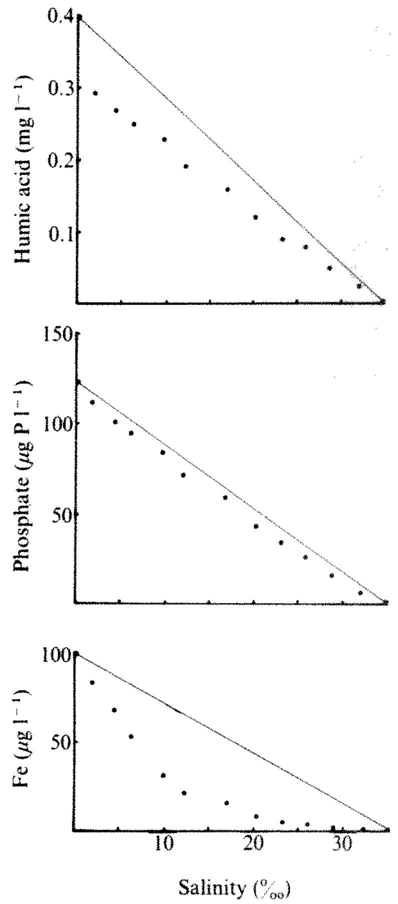

Fig. 2 Changes in concentration of filterable humic acid, phosphate and iron, when seawater was added to unfiltered Yarra River water in a laboratory model system.

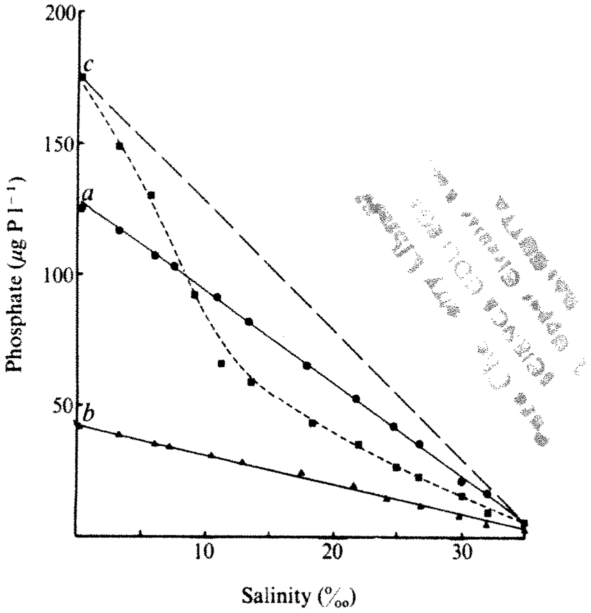

Fig. 3 Concentrations of filterable phosphate observed during addition of seawater to different synthetic solutions in a laboratory model system. Initial solutions were prepared as follows: *a*, phosphate added after iron; *b*, phosphate added before iron; *c*, phosphate added after humic acid and iron. The initial solutions were stirred overnight then used unfiltered.

weakly bound iron seems able to interact with dissolved phosphate. The presence of cations of Na, K, Ca and Mg, which are able to complex phosphate, is expected to increase the stability of dissolved phosphate in real river waters compared with the synthetic starting solutions[21].

A consequence of the observed behaviour of phosphate is that the proportion of phosphate removed from solution in river water, before it enters the sea, will be largely controlled by the sequence and concentrations of the additions of iron, humic acid and phosphate to the river. In rivers exceptionally high in iron and humic acid, up to about half of the dissolved phosphate may be removed by inorganic processes in the estuary. For rivers near the world average concentration of iron[12], dissolved phosphate is likely to show conservative chemical behaviour in the estuary, or removal to only a small degree.

We thank the ARGC and VIMS for financial support.

Received 18 April; accepted 11 August 1980.

1. Jitts, H. R. *Aust. J. mar. Freshwat. Res.* **10,** 7 (1959).
2. Sholkovitz, E. R. *Geochim. cosmochim. Acta* **40,** 831 (1976).
3. Boyle, E. A., Edmond, J. M. & Sholkovitz, E. R. *Geochim. cosmochim. Acta* **41,** 1313 (1977).
4. Mackay, D. W. & Leatherland, T. M. in *Estuarine Chemistry* (eds Burton, J. D. & Liss, P. J.) 185–218 (Academic, London, 1976).
5. Van Bennekom, A. J., Berger, G. W., Helder, W. & De Vries, R. T. P. *Neth. J. Sea Res.* **12,** 296 (1978).
6. Stefansson, U. & Richards, F. A. *Limnol. Oceanogr.* **8,** 394 (1963).
7. Butler, E. I. & Tibbitts, S. *J. mar. Biol. Ass. U.K.* 52, 681 (1972).
8. Pomeroy, L. R., Smith, E. E. & Grant, C. M. *Limnol. Oceanogr.* **10,** 167 (1965).
9. Stirling, H. P. & Wormald, A. P. *Est. Coast. Mar. Sci.* **5,** 631 (1977).
10. Wormald, A. P. & Stirling, H. P. *Est. Coast. Mar. Sci.* **8,** 441 (1979).
11. Lu, J. C. S. & Chen, K. Y. in *Chemistry of Marine Sediments* (ed. Yen, T. F.) 181–222 (Ann Arbor, Ann Arbor, 1977).
12. Figures, G., Martin, J. M. & Meybeck, M. *Neth. J. Sea Res.* **12,** 329 (1978).
13. Smith, J. D. & Longmore, A. R. *Aust. J. mar. Freshwat. Res.* **31,** 119 (1980).
14. Blutstein, H. & Smith, J. D. *Wat. Res.* **12,** 119 (1978).
15. Murphy, J. & Riley, J. P. *Analyt. chim. Acta* **27,** 31 (1962).
16. Stookey, L. L. *Analyt. Chem.* **42,** 779 (1970).
17. Coonley, L. S., Baker, E. B. & Holland, H. O. *Chem Geol.* **7,** 51 (1971).
18. Murray, J. W. & Gill, G. *Geochim. cosmochim. Acta* **42,** 9 (1978).
19. Pickard, G. L. & Felbeck, G. T. *Geochim. cosmochim. Acta* **40,** 1347 (1976).
20. Sinesi, N., Griffith, S. M., Schnitzer, M. & Townsend, M. G. *Geochim. cosmochim. Acta* **41,** 969 (1977).
21. Stumm, W. & Morgan, J. J. *Aquatic Chemistry* 518 (Wiley-Interscience, New York, 1970).

Changes in spruce composition following burial in lake sediments for 10,000 yr

Philip A. Meyers, Mary J. Leenheer
& Karen M. Erstfeld

Department of Atmospheric and Oceanic Science, The University of Michigan, Ann Arbor, Michigan 48109

Richard A. Bourbonniere

National Water Research Institute, Canada Centre for Inland Waters, Burlington, Ontario, Canada L7R 4A6

Organic matter in lake sediments is a mixture of biological materials from a number of modern sources plus variable amounts of recycled detrital material. Hence, it is usually difficult to distinguish input variations over time from the diagenesis of organic matter. Comparison of old material of known biological origin with younger material helps resolve this problem. We have compared the compositions of wood and needles from a modern white spruce (*Picea glauca*) with those from a white spruce buried for 10,000 yr in a lake bottom. Although the tissues are structurally well preserved, some chemical changes are evident in the old samples. Total fatty acid concentrations decrease by over 90%. Sterol and hydrocarbon concentrations are similar in the modern and 10,000-yr-old wood, but the concentration of sterols is lower in the old needles. Cellulose components in the wood have decreased relative to lignin components, although both types of materials remain in high concentration in comparison to other organic components.

The types of chemical alterations which biological materials experience during early diagenesis in geological settings are important to biogeochemistry. A particularly interesting approach which has been used to describe some of these changes has involved chemical analysis of fossil materials, including bones[1], hair[2], corals[3], and marine plankton[4,5]. In addition, fossilized fruit[6], leaves[7] and wood[8,9] have been studied.

We collected samples of wood and needles from a living white spruce (*P. glauca*) at The University of Michigan Matthaei Botanical Gardens near Ann Arbor. Similar samples were obtained from a tree which had been drowned and buried still erect in a lake bottom 10,000 yr ago. This lake was formed by glacial damming near present-day Marquette, Michigan, and was then quickly filled with sediment[10]. Lipid components of wood and needle samples were extracted in a Soxhlet apparatus with benzene–methanol for 48 h and by alkaline hydrolysis of the extracted samples in methanolic 0.5M KOH in benzene. The two extracts are analogous to the unbound and bound lipids released from sediments by a similar treatment[11]. Each extract was fractionated by thin-layer and column chromatography into fatty acid, sterol, and aliphatic hydrocarbon fractions which were analysed by gas chromatography. Cellulose and lignin components of the modern and ancient wood samples were isolated by hydrolysis with 5M NaOH at 170 °C for 12 h followed by extraction of the degradation products with ethyl acetate. These were analysed as their trimethylsilyl derivatives by GC and GC-MS.

As shown in Table 1, the concentrations of all of the needle components and some of the wood components are lower in the 10,000-yr-old samples than in the modern ones. If the biochemical processes of the white spruce have not changed over the past 10,000 yr, then these differences are due to alterations which have occurred in the older samples during burial in the water-saturated sediment.

Fatty acid concentrations show the greatest differences, and these reflect degradation of acids originally present in the wood

0028–0836/80/410534—03$01.00

and needles. The unbound fractions have greater decreases in concentration than do the bound fractions. Because the unbound acids are extracted readily with solvent, it is probable they exist in forms that are vulnerable to both solution and microbial attack in an aqueous environment such as a lake sediment. There are some differences between the distributions in the wood and needle samples. For example, *n*-tetradecanoic acid is abundant in both the modern and old needles, but not in either wood sample. Also, *n*-docosanoic and *n*-tetracosanoic acids are important components of the unbound acids in the needles, but not in the wood. Another major difference is that the bound acid fraction is an order of magnitude more abundant in the needle samples.

Some of the fatty acid changes are shown in Fig. 1. These compositions are of wood samples; comparable changes were observed in the needles. Relative proportions of unsaturated acids are less in the older wood, whereas the contributions of *anteiso* methyl-branched acids indicative of microbial processes increases. Longer-chain *n*-alkanoic acids seem to be degraded less in the bound acids. Similar differences have been found in fatty acids extracted from modern and 12,000-yr-old Lake Huron sediments[12] and evidently are due to diagenesis rather than changes in input.

Unbound sterol concentrations of the needles indicate a time-related loss of the same magnitude as found in the fatty acids. However, the bound sterol concentration increases from essentially zero to 55 $\mu g\, g^{-1}$, suggesting conversion of some unbound sterols to bound forms. A similar conversion has been reported in young sediments[13,14] and also seems to occur in the wood samples. In the wood, this is accompanied by a small increase in the concentration of unbound sterols. Because diagenetic formation of sterols from other wood components is unlikely, the apparent increase in concentration suggests preferential losses of proteinaceous and saccharide materials, with the result that sterols comprise a larger portion of the old wood. Sterols are evidently only mildly reactive in wood. This also appears to be true in sediments[13–15].

Although at lower concentrations than the sterols, aliphatic hydrocarbons behave similarly. The concentration of unbound hydrocarbons is lower in the old needles than in the new, but higher in the old wood than in the modern sample. Unlike the sterols, no conversion of hydrocarbons from the unbound form to the bound form is evident. In view of the lack of reactive functional groups in saturated hydrocarbons, this is not surprising. Normal alkanes from C_{16} to C_{37} are present in these samples, and no major compositional changes are found between the 10,000-yr-old and modern samples.

The changes in the lipid components of the needles suggest that the unbound lipids are easily removed or degraded over geologically short periods of time in sediments. Much of this material may exist as a waxy coating on the needles which is exposed to microbial degradation, chemical weathering and dissolution. Unbound lipids in wood are internal structural components and therefore not as available to similar attack as are the needle-coating lipids. Even so, wood fatty acids are destroyed or converted to non-acid forms relatively quickly. Evidently, preservation of fatty acids in sediments requires special circumstances, such as anoxic conditions and rapid burial.

Table 1 Extractable components of modern and 10,000-year-old wood and needles from the white spruce *Picea glauca*

	Wood			Needles		
Component	Modern	Old	Δ	Modern	Old	Δ
Fatty acids						
unbound	1,414	77	−1,337	2,785	114	−2,671
bound	27	20	−7	362	237	−125
total	1,441	97	−1,344	3,147	351	−2,796
Sterols						
unbound	311	339	+28	2,159	107	−2,052
bound	2	11	+9	0	55	+55
total	313	350	+37	2,159	162	−1,997
Hydrocarbons						
unbound	27	36	+9	146	54	−92
bound	1	1	0	1	1	0
total	28	37	+9	147	55	−92
Cellulose plus lignin	157	192	+35			

Concentrations of fatty acids, sterols and hydrocarbons are given in μg per g dry wood, cellulose plus lignin components are in mg per g. Δ, Difference between modern and old concentrations.

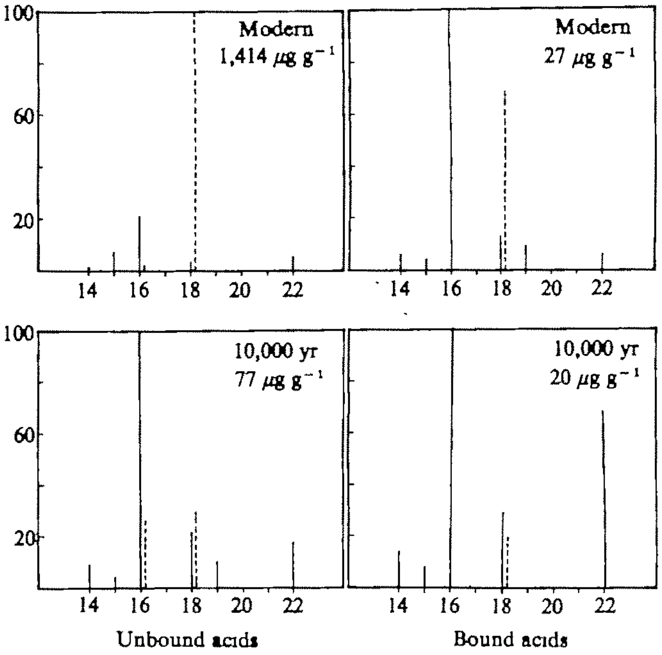

Fig. 1 Comparison of fatty acids extracted from modern and 10,000-yr-old spruce wood. Unbound acids released by Soxhlet extraction; bound acids by alkaline hydrolysis of extracted wood. Compositions are relative to major acid component (100%). Acids are displayed by number of carbon atoms. Solid lines represent *n*-alkanoic acids; dashed lines *n*-alkenoic acids, dotted lines *anteiso* acids.

The cellulose plus lignin component of the old wood is at a higher concentration than in the modern wood. As suggested in the case of wood sterols and hydrocarbons, this indicates less alteration of these materials relative to other, more labile components. Lactic acid is the most abundant compound found in these samples. Oxalic and succinic acids are present as hydrolysis products of cellulose[16]. Their proportions relative to each other are the same in both samples. Vanillic acid and ferulic acid are also found and are derived from lignin[16,17]. The contribution of cellulose components, represented by oxalic and succinic acids, decreases relative to that of lignin components, represented by vanillic and ferulic acids, in the old wood. The ratio of these components changes from 2.2 in the modern wood to 1.2 in the old, indicating a selective loss of cellulose compared to lignin over this 10,000-yr period of burial.

These data give relative rates of degradation of some types of biological compounds buried in lake sediments for short periods of geological time. In woody tissue, the order of alteration is fatty acids $\gg$ sterols $>$ aliphatic hydrocarbons $>$ cellulose $>$ lignin. In spruce needles, the order is fatty acids $=$ sterols $\gg$ aliphatic hydrocarbons. These relative rates can be useful for understanding the cycling of organic matter in young subaqueous sediments. Furthermore, this study describes some woody tissue changes which occur during the early stages of coalification.

We thank Dr W. J. Merry for buried spruce samples, and we acknowledge support from the donors of the Petroleum Research Fund administered by the American Chemical Society and from the NSF (grant EAR 7822432).

Received 19 February; accepted 10 July 1980.

1. Dungworth, G., Schwartz, A. W. & van de Leemput, L. *Comp. Biochem. Physiol.* **53B,** 473–480 (1976).
2. Gillispie, J. M. *Science* **170,** 1100–1102 (1970).
3. Wehmiller, J. F., Hare, P. E. & Kujula, G. A. *Geochim. cosmochim. Acta* **40,** 763–776 (1976).
4. King, K. Jr & Hare, P. E. *Science* **175,** 1461–1463 (1972).
5. King, K. Jr *Nature* **252,** 690–692 (1974).
6. Hohn, M. E. & Meinschein, W. G. *Geochim. cosmochim. Acta* **41,** 189–193 (1977).
7. Dilcher, D. L., Pavlick, R. J. & Mitchell, J. *Science* **168,** 1447–1449 (1970).
8. Giannasi, D. E. & Niklas, K. J. *Science* **197,** 765–767 (1977).
9. Sigleo, A. C. *Science* **200,** 1054–1056 (1978).
10. Traver, R. *Am. Forests* **86,** 32–35, 51–54 (1980).
11. Farrington, J. W., Henrichs, S. M. & Anderson, R. *Geochim. cosmochim. Acta* **41,** 289–296 (1977).
12. Meyers, P. A., Bourbonniere, R. A. & Takeuchi, N. *Geochim. cosmochim. Acta* **44,** 1215–1221 (1980).
13. Lee, C., Gagosian, R. B. & Farrington, J. W. *Geochim. cosmochim. Acta* **41,** 985–992 (1977).
14. Nishimura, M. & Koyama, T. *Geochim. cosmochim. Acta* **41,** 379–385 (1977).
15. Nishimura, M. *Nature* **270,** 711–712 (1977).
16. Bourbonniere, R. A. thesis, Univ. Michigan (1979).
17. Hedges, J. I & Mann, D. C. *Geochim. cosmochim. Acta* **43,** 1803–1807 (1979).

Evidence for diploidy and mating in trypanosomes

A. Tait

Department of Genetics, University of Edinburgh, West Mains Road,
Edinburgh EH9 3JN, UK

The question of whether any sexual process takes place at some stage of the life cycle of the trypanosome has often been raised[1,2] and crosses between different drug-resistant strains[3,4] have provided no convincing answer. Multinucleate forms of trypanosomes have been observed by electron microscopy[5,6] but their significance and origin remain obscure. As part of a study aimed at examining the speciation and genetics of the *Trypanosoma brucei* complex of trypanosomes, a series of isolates from a population of *T.b. brucei* have been screened for electrophoretic variation in 19 enzymes. The results of this survey, reported here, provide strong evidence that trypanosomes are diploid and undergo random mating and recombination.

The population used consisted of 17 stocks of *T.b. brucei*, collected in 1969–70 from Lugala, Uganda, by members of the East African Trypanosomiasis Research Organisation (EATRO). Fifteen of the stocks were obtained by injection of infected tsetse salivary glands into mice and subsequent storage of infected blood in liquid nitrogen. The remaining two stocks were obtained by injection of infected blood from wild game into mice, followed by storage in liquid nitrogen. Samples of these stocks were transferred to the Centre for Tropical Veterinary Medicine in Edinburgh. This material was made available by Dr A. Gray and preparations of trypanosomes were obtained by infecting laboratory mice with these stocks, followed by DEAE-cellulose chromatography[7] of infected blood. Extracts from such purified preparations were then subjected to starch gel electrophoresis and the gels specifically stained for the 19 enzymes listed in Table 1.

Electrophoretic variation was observed in eight of the enzymes, which can be subdivided on the basis of the type of variant banding pattern obtained on gels (Table 1). In type I, with, for example, isocitrate dehydrogenase, some stocks produce a single band of enzyme activity at one position on the gel (1CD-1), others produce a single band at a second position (1CD-2), and a third group of stocks produce three bands, two of which correspond to 1CD-1 and 1CD-2, respectively, the third (of double intensity) lying midway between 1CD-1 and 1CD-2 (Fig. 1*a*). In type II, with, for example, alkaline phosphatase, individual stocks may produce single bands at one of two alternative positions (AP-1 or AP-2), whereas other stocks produce two bands at positions corresponding to AP1-1 and AP-2 (Fig. 1*a*). Of the eight polymorphic enzymes found, three are of type I and five of type II (Table 1). Furthermore, four of the type II enzymes show more than two possible positions at which the bands may appear. The variants observed for the eight polymorphic enzymes are shown in Fig. 1*a* and *b*, together with the nomenclature used for their designation. With all these enzymes multiple-banded types were observed, triple banded in the case of type I and double banded in the case of type II.

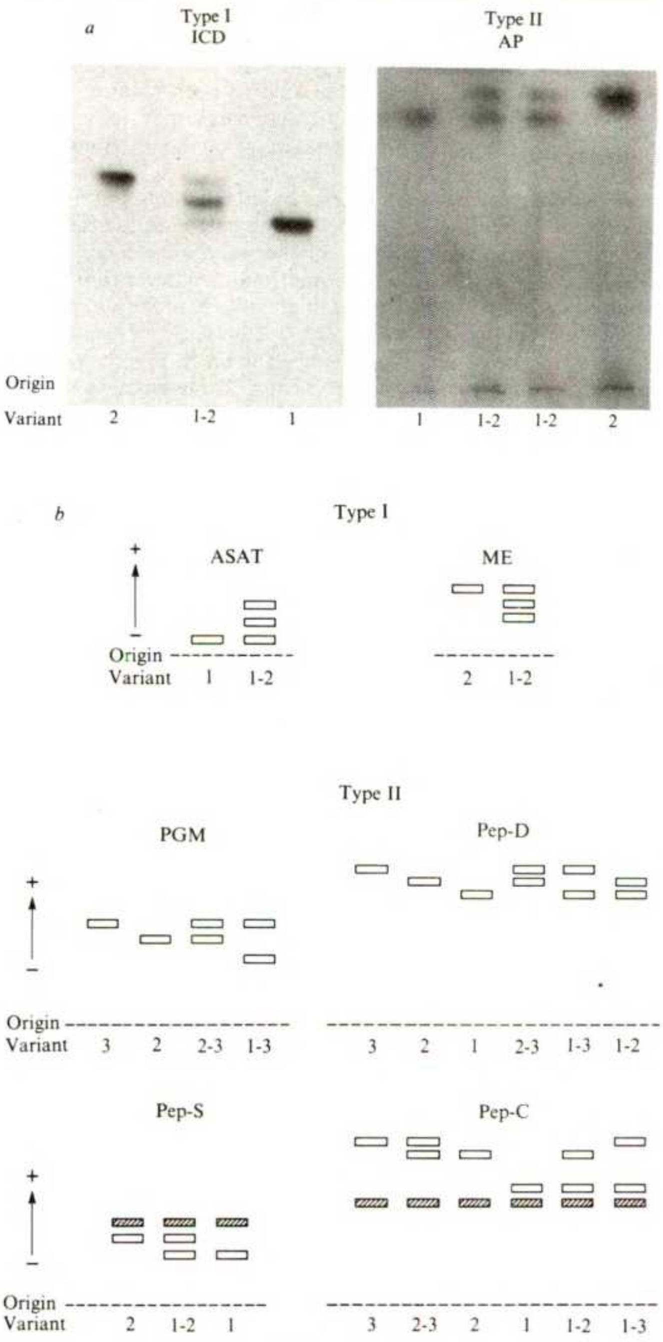

Fig. 1 Electrophoretic enzyme variation in isolates of *T.b. brucei*. *a*, Photographs of starch gel electrophoresis slabs stained for isocitrate dehydrogenase (ICD) and alkaline phosphatase (AP). Samples were run in 9% hydrolysed starch gels in 0.026 M Tris, 0.0033 M citric acid, *p*H 8.6, at 270 V for 3 h. The electrode buffer was 0.66 M Tris, 0.083 M citric acid, *p*H 8.6, and the enzyme activities were stained using published methods[16]. *b*, Diagrams of starch gel electrophoresis slabs stained for aspartate amino transferase (ASAT), malic enzyme (ME), phosphoglucomutase (PGM), peptidase-S (Pep-S), peptidase-C (Pep-C) and peptidase-D (Pep-D). The peptidases are designated on the basis of their di- and tripeptide specificities using the nomenclature described by Harris and Hopkinson[16]; the cross-hatched bands shown on Pep-S and Pep-C gels represent the two invariant peptidases (Pep-A and Pep-B, see Table 1) which overlap in their substrate specificities. Details of the electrophoretic conditions and activity stains will be published elsewhere. The variant bands observed are designated by numbers in order of increasing mobility.

0028-0836/80/410536—03$01.00

Table 1 Electrophoretic enzyme variation in *T.b. brucei*

Enzyme	Abbreviation	Mono-morphic	Poly-morphic	Type	Alleles
Threonine dehydrogenase	TDH	+	–	–	–
6-phosphogluconate dehydrogenase	6PGD	+	–	–	–
Glucose-6-phosphate dehydrogenase	G6PD	+	–	–	–
Mannose-phosphate isomerase	MPI	+	–	–	–
Glucose phosphate isomerase	GPI	+	–	–	–
Malate dehydrogenase	MD	+	–	–	–
Phosphoglyceromutase	PGlyM	+	–	–	–
Heptanoyl esterase	Hest	+	–	–	–
Acetyl esterase	Acest	+	–	–	–
Peptidase-B (prolyl-leucine)	Pep-B	+	–	–	–
Peptidase-A (valyl-leucine)	Pep-A	+	–	–	–
Isocitrate dehydrogenase	ICD	–	+	I	2
Alanine aspartate amino transferase	ASAT	–	+	I	2
Malic enzyme	ME	–	+	I	2
Phosphoglucomutase	PGM	–	+	II	3
Alkaline phosphatase	AP	–	+	II	2
Peptidase-S (tyrosyl-tyrosyl-tyrosine)	Pep-S	–	+	II	2
Peptidase-C (leucyl-alanine)	Pep-C	–	+	II	3
Peptidase-D (phenyl-alanyl-proline)	Pep-D	–	+	II	3

Summary of the results obtained by screening 17 stocks of *T.b. brucei* for electrophoretic enzyme variation. Type I and type II refer to the type of multiple banding observed (see text). Alleles refers to the presumed number of alleles determining each enzyme.

Table 2 Numbers of stocks of *T.b. brucei* showing different enzyme genotypes

Enzyme	Geno-type	Observed	(Expected)	Enzyme	Geno-type	Observed	(Expected)
ICD	1	3	(3.3)	Pep-S	1	6	(5.27)
	1–2	9	(8.38)		1–2	7	(8.33)
	2	5	(5.34)		2	4	(3.23)
PGM	1	1	(0.06)	Pep-C	1	3	(1.77)
	1–2	0	(0.36)		1–2	3	(4.18)
	2	1	(0.53)		2	3	(2.47)
	2–3	4	(4.57)		2–3	4	(3.81)
	3	10	(9.95)		3	2	(1.46)
	3–1	2	(1.58)		3–1	2	(3.23)
ASAT	1	9	(9.9)	Pep-D	1	0	(0.02)
	1–2	8	(6.1)		1–2	3	(1.7)
	2	0	(1.0)		2	4	(2.86)
ME	1	0	(0.39)		2–3	3	(6.46)
	1–2	5	(4.34)		3	6	(7.99)
	2	12	(12.29)		3–1	1	(1.92)
				AP	1	2	(3.7)
					1–2	12	(8.3)
					2	3	(4.7)

Genotypes are designated as described in Fig. 1*a*,*b*. Expected genotype numbers were calculated from the observed allele frequencies assuming that the population was in Hardy–Weinberg equilibrium.

Hybrid banding patterns such as those seen in types I and II enzymes would be expected in a diploid organism in which some individuals are heterozygous for allelic variants of dimeric (in the case of type I) and monomeric (in the case of type II) enzymes. Similar patterns of multiple banding have been shown for many enzymes in, for example, humans[8], *Drosophila*[9] and mice[10], and have been demonstrated to be due to individuals heterozygous for the different alleles. Thus, the observation of both single-banded and hybrid-banded electrophoretic enzyme patterns suggests, by analogy with other organisms, that trypanosomes are diploid and that mating has taken place to generate the 'heterozygous' patterns. Godfrey and co-workers have reported variation in enzyme electrophoretic mobility in several different species and subspecies of trypanosomes[11–13] and with five of the enzymes 'hybrid' band patterns have been reported[14,15] in stocks of the *T. brucei* complex. These results would also support the interpretation of the observations presented here.

An alternative explanation, in the case of the type II enzymes, might be based on the assumption that the two-banded patterns are not due to heterozygotes, but to mixtures of two different clones. It is unlikely, however, that the stocks used in this study were, in fact, such mixtures. Four stocks exhibiting multiple band patterns were cloned by infecting mice with single trypanosomes and the resulting clones examined by starch gel electrophoresis. All four cloned stocks again showed multiple-banded patterns for all eight polymorphic enzymes. Thus, none of the multiple-banded patterns shown by these stocks could have been due to mixtures of clones. Moreover, in the case of the type I enzymes which show three bands of activity, the band of intermediate mobility was only observed in conjunction with the two other bands; nor were there any stocks showing mixtures of the latter without the intermediate band. It is, therefore, assumed that most of the stocks showing multiple-banded patterns were heterozygotes. Based on this assumption, the allele frequencies for these enzyme variants and from them the expected genotype frequencies can be calculated, assuming that the population is in Hardy–Weinberg equilibrium. The observed and predicted genotype proportions are presented in Table 2 for the eight enzymes studied. Clearly, expected and observed proportions are in good agreement and the goodness of fit has been examined using the χ^2 test. The values obtained show that the observed proportions of genotypes do not differ significantly at the 5% level from those predicted by the Hardy–Weinberg equilibrium. This finding, together with the similarity of the banding patterns to those observed with known heterozygotes in other organisms and their occurrence in all variant enzymes examined, provides strong evidence that these trypanosome strains are diploid and undergo random mating.

The data also provide evidence for the occurrence of genetic recombination between genes at different enzyme-determining loci. Classification of the stocks with regard to variants of any two enzymes simultaneously shows (Table 3) that 50 out of a possible total of 90 recombinant types occur, even with the small number of stocks studied. As the number of isolates is small, comparisons have only been made between pairs of enzymes showing two alleles. This strongly suggests that recombination has occurred between the loci specifying these enzymes, as the frequency of possible combinations of variants generated by

Table 3 Combinations of variants of AP, ASAT, ICD, ME and PEP-S

	AP			ASAT			ICD			ME			PEP-S		
	1	1–2	2	1	1–2	2	1	1–2	2	1	1–2	2	1	1–2	2
AP															
1															
1–2															
2															
ASAT															
1	1	7	1												
1–2	1	6	1												
2	0	0	0												
ICD															
1	0	3	0	3	0	0									
1–2	2	7	0	4	5	0									
2	0	3	2	2	3	0									
ME															
1	0	0	0	0	0	0	0	0	0						
1–2	0	5	0	3	2	0	3	0	2						
2	2	8	2	6	6	0	0	9	3						
Pep-S															
1	1	5	0	2	4	0	0	5	1	0	0	6			
1–2	1	4	2	3	4	0	1	2	4	0	3	4			
2	0	4	0	4	0	0	2	2	0	0	2	2			

The numbers of stocks showing the various possible pairwise combinations of enzyme variants. See Table 1 for abbreviations used. A total of 17 stocks was examined.

mutation in the absence of recombination would be expected to be very low.

The present findings provide strong evidence for diploidy, random mating and recombination between different loci in this population of trypanosomes. Conclusive proof that these organisms are diploid and undergo mating would require the demonstration of heterozygotes produced by hybridization of cells showing different variants of the same enzyme. Experiments are under way (using a range of genetic markers) to demonstrate such hybridization.

This work was supported by a Wellcome Trust Fellowship in Tropical Medicine. I thank Drs A. Gray and T. Jones for making available the trypanosome stocks used in this work, Professor G. H. Beale for helpful discussions and J. Wallace for technical assistance.

Received 7 May; accepted 19 August 1980.

1. Walker, P. J. *Int. Rev. Cytol.* **17,** 51–98 (1964).
2. Baker, J. R. *Trans. R. Soc. trop. Med. Hyg.* **72,** 109–112 (1977).
3. Amrein, Y. U. & Fulton, J. D. *J. Protozool.* **6,** 120–122 (1959).
4. Amrein, Y. U. *Expl Parasit.* **17,** 261–263 (1965).
5. Ormerod, W. E. & Venkatesan, A. *Trans. R. Soc. trop. Med. Hyg.* **65,** 736–741 (1971).
6. Evans, D. A. & Ellis, D. S. *Trans. R. Soc. trop. Med. Hyg.* **73,** 126 (1979).
7. Lanham, S. M. & Godfrey, D. G. *Expl Parasit.* **28,** 521–534 (1970).
8. Harris, H. in *The Principles of Human Biochemical Genetics*, 25–35 (North-Holland, Amsterdam, 1970).
9. Prakash, S., Lewontin, R. C. & Hubby, J. L. *Genetics* **61,** 841–858 (1969).
10. Selander, R. K., Smith, M. H., Yang, S. H. & Johnson, W. E. *Univ. Tex. Publs* **7103,** 49–90 (1971).
11. Godfrey, D. G. & Kilgour, V. *Trans. R. Soc. trop. Med. Hyg.* **70,** 219–224 (1976).
12. Miles, M. A. *et al. Nature* **272,** 819–821 (1978).
13. Kilgour, V. & Godfrey, D. G. *Nature new Biol.* **244,** 69–70 (1973).
14. Gibson, W., Mehlitz, D., Lanham, S. M. & Godfrey, D. G. *Tropenmed. Parasit.* **29,** 335–345 (1978).
15. Gibson, W. *J. Protozool.* **26,** 72A (1979).
16. Harris, H. & Hopkinson, D. A. in *Handbook of Enzyme Electrophoresis in Human Genetics* (North-Holland, Amsterdam, 1976).

Changing proteins on the surface of a parasitic nematode

Mario Philipp, R. M. E. Parkhouse* & Bridget M. Ogilvie

Divisions of Parasitology and Immunology*, National Institute for Medical Research, Mill Hill, London NW7 1AA, UK

Most of the organisms of the phylum Nematoda are free living, but some are animal or plant parasites of major importance to man. During their life cycle all nematodes undergo a series of moults in which they shed an external cuticle, consisting of an outermost membrane-like layer of unknown composition and a series of fibrillar layers similar to collagens[1–4]. Because of this structure, the cuticle has been viewed as an acellular exoskeleton[1] with rather inert molecular components. However, observations have shown that it contains enzymes and sometimes haemoglobin[3,4], and that nutrients are absorbed through it in the infective lárvae and adult stages of *Brugia pahangi*[5]. It is bound by complement and antibody, resulting in the adherence of leukocytes[6], and antibody-dependent cell-mediated reactions damage the cuticule of newborn larvae of *Trichinella spiralis*[7–9] and the microfilariae of *Dipetalonema viteae* and *Litomosoides carinii*[10,11]. We report here that the surface of the cuticle of the parasitic nematode *Trichinella spiralis* expresses protein molecules which change qualitatively following the moulting process, and quantitatively during growth of the worms within one stage. Also, surface proteins are released *in vitro* at a rate which depends on the conditions of culture of the worms.

If the cuticle is functional it should have a more dynamic molecular structure than has so far been described. As parasitic nematodes are exposed to very different host environments during their life cycle, we chose to study surface components of one of them—*T. spiralis*.

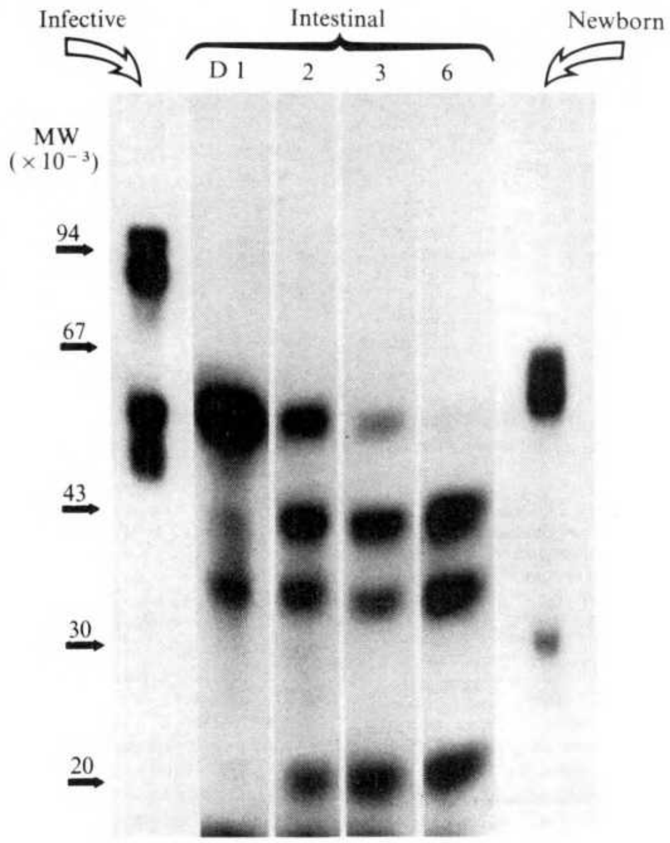

Fig. 1 Radiolabelled surface proteins of the three stages of *T. spiralis*: infective larvae, intestinal worms (removed from small intestines at days 1, 2, 3 and 6 after oral infection), and newborn larvae. About 10^4 infective larvae, 10^4 intestinal worms and 10^5 newborn larvae were washed 10 times in phosphate-buffered saline (PBS) by low-speed centrifugation. To 0.1–0.5 ml of PBS containing the worms and 0.1–1 mCi $Na^{125}I$, chloramine T was added to a final concentration of 0.050 mg ml^{-1}. The mixture was left to react at room temperature for 3 min after which tyrosine was added to react with the uncombined iodine. As judged by mobility, the worms were 90–100% viable after labelling. The worms were washed repeatedly in PBS and then lysed in Tris-P buffer (10 mM Tris-HCl, *p*H 8.3, 50 μg ml^{-1} *L*-1-tosylamide-2-phenylethylchloromethyl ketone, 25 μg ml^{-1} *N*-α-*p*-tosyl-L-lysine-chloromethyl ketone-HCl, 1 mM phenylmethyl sulphonyl fluoride and 2% Na deoxycholate). Intestinal worms and infective larvae were disrupted by homogenization in a glass–glass homogenizer, whereas sonication was used with newborn larvae. The lysates were centrifuged for 30 min at 11,000*g* and the supernatant, containing 90–95% of the total radioactivity (70–80% acid precipitable) was analysed by SDS-polyacrylamide gel electrophoresis (SDS-PAGE). Slab gels containing 7.5% acrylamide were used. The samples were boiled for 5 min in a buffer solution containing 8.3 mg ml^{-1} β-mercaptoethanol and 17.0 mg ml^{-1} SDS. The radiolabelled material has been shown to be located on the worms surface by: (1) Autoradiographs of sections of radiolabelled worms. (2) Absorption of antibodies to the labelled proteins by whole intact worms. (3) Alteration of the rate of turnover of the radiolabelled proteins by neutrophil attachment to the worms' surface (this letter). The SDS-PAGE pattern of the infective larvae was neither altered when the worms were radiolabelled 72 h after the pepsin digestion of rat muscle, nor when radiolabelled worms were incubated with pepsin in similar conditions to the ones used in the digestion process, before homogenization.

0028-0836/80/410538—03$01.00

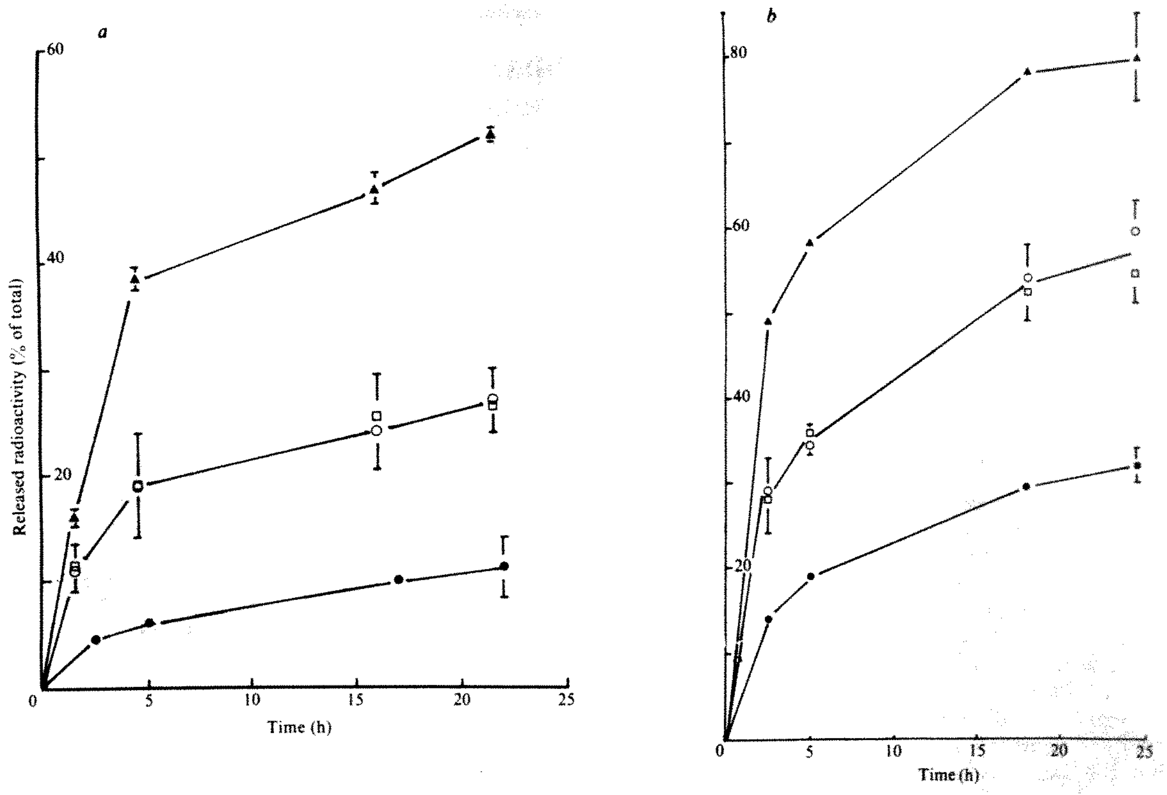

Fig. 2 Release of radiolabelled proteins from the surface of *a*, infective larvae and *b*, intestinal worms (day 2) cultured in RPMI (●), normal rat serum (□), immune rat sera (○), in RPMI and immune rat sera plus rat neutrophils (▲). RPMI 1640 (Gibco) was buffered with $NaHCO_3$ and 20 mM HEPES to *p*H 7.2, and 1×10^5 units ml^{-1} penicillin, 100 μg ml^{-1} streptomycin and 1% glucose were added. About 10 living radiolabelled worms were incubated in 0.4 ml of the above media at 37 °C. Aliquots (5 μl) were taken at intervals and from the measured radioactivity the average released amount was calculated and expressed as per cent of the initial radioactivity of the worms. All data points were determined in triplicate. Error bars represent maximum dispersion of average data points corresponding to duplicate experiments run on two different occasions. Normal rat sera were collected from Sprague–Dawley rats and kept at −20 °C until used. Immune rat sera were taken from Sprague–Dawley rats 21 days after oral infection with 4,000 infective larvae of *T. spiralis* and kept at −20 °C until used. Neutrophils were obtained by peritoneal lavage of Sprague–Dawley rats 4 h after they had been given a peritoneal injection of 10 ml of 1% glycogen (Sigma) in PBS. This yielded about 80% neutrophils. About 2×10^7 cells were used in each experiment.

The life cycle of *T. spiralis* can be reproduced in the laboratory using rodent hosts[12]. The infective larvae, which are found in the striated muscle of vertebrate hosts, can be recovered by enzymatic digestion of the muscular tissue[12]. When such muscle is ingested by another animal, the infective larvae undergo a very rapid series of moults that are completed within 24 h, and the worms become adapted to the small intestine of the host. The intestinal stage worms grow and become sexually mature during the first 5 days after oral infection, and can be recovered from the intestine between days 1 and 6 (ref. 12). The newborn larvae, which are shed from the mature female worms after mating can be recovered by maintaining the 6-day-old intestinal stages *in vitro* overnight[12]. In *in vivo* conditions the newborn larvae make their way through the wall of the small intestine and migrate to striated muscle cells of the new host, thus completing the life cycle.

Infective larvae, intestinal worms and newborn larvae were surface-labelled with ^{125}I-labelled iodine, as described in Fig. 1 legend. The radiolabelled surface components of each stage, including four different phases in the maturation of the intestinal stage, were analysed by electrophoresis on SDS-polyacrylamide slab gels. An autoradiograph of such a slab gel is shown in Fig. 1. All samples are reduced with β-mercaptoethanol.

The infective larvae expressed four main surface proteins of apparent molecular weights (MWs) 47,000, 55,000, 90,000 and 105,000. The intestinal stage presented a qualitatively different pattern of surface proteins. At day 1 after oral infection extracts of labelled worms gave one predominant band of MW 56,000 on the gels. However, unlike the molecule of MW 55,000 seen on infective larvae, this component did not bind to lentil lectin (data not shown). A second fainter band ran at MW ~33,000 (Fig. 1, D1) and traces of radiolabelled protein could be detected at MWs ~40,000 and 20,000 in extracts of 1-day-old intestinal worms.

During maturation of the intestinal worms—days 1 to 6 after infection—an inversion in the relative intensity of the bands took place. Thus, the intensity of the 56,000 MW band decreased, and the 40,000- and 20,000-MW bands became gradually more intense. A slight intensification of the 33,000-MW band could also be seen.

The surface protein pattern of the newborn larvae was qualitatively different compared with the other two stages. There were two bands running at approximate MWs of 58,000 and 64,000, and a pair of comparatively faint bands of MWs 28,000 and 30,000. Thus, whereas the surface proteins changed qualitatively in the transition between any pair of different stages, only quantitative changes took place when the intestinal worms passed through the different phases in their maturation.

Further evidence for a dynamic cuticle came from experiments which showed that the radiolabelled surface proteins of the infective larvae and the intestinal worms may be released by the worms *in vitro*. Worms of either stage were radiolabelled with ^{125}I, as described in Fig. 1 legend, and incubated at 37 °C in four different culture conditions: RPMI, normal rat serum, immune rat serum and immune rat serum plus rat neutrophils. Samples of the culture fluid were taken at intervals and the released radioactivity was expressed as a percentage of the total radioactivity present on the worm's surface at time zero. A plot of the released radioactivity against time for both the infective larvae and intestinal worms is shown in Fig. 2*a* and *b* respectively. Radiolabelled material was released in all four culture conditions. The rate of release was slowest in RPMI. In this medium the infective larvae released the 55,000-MW protein first and then the 105,000-MW component. The other two surface components were not released even after 48 h in culture. The intestinal worms released all four of their radiolabelled surface components in RPMI. The release of proteins was twice as fast when the worms were left in normal rat sera or sera from immune rats (previously infected with *T. spiralis*). This phenomenon cannot be explained in terms of different viability of the worms as they started to die only after 48 h in culture either in RPMI or in rat sera with or without antibody. Antibodies did not seem to affect the rate of protein release although they could be shown to bind to the radiolabelled proteins, in as much as these co-precipitated with immune rat sera and an anti-rat immunoglobulin antiserum.

A marked increase in the rate of release was achieved by co-culturing the worms with rat neutrophils (5×10^7 cells per ml) in the presence of immune rat sera (Fig. 2). Neutrophils adhered to the surface of both the infective larvae and the intestinal worms and began to dissociate from the worms' surface after 3–4 h in culture. Similarly, enhanced release of surface molecules was obtained when the labelled worms were cultured with normal serum and neutrophils (data not shown). These results indicate that the radiolabelled proteins are located on the surface of the cuticle, possibly on the outermost membrane-like layer, as neutrophils can be shown to remove this layer by about 4 h in culture (M. Jungery, personal communication). Furthermore, antibodies which precipitated the radiolabelled proteins also bound to intact worms, and autoradiographs of sections of radiolabelled worms showed that the label was on the cuticle and not on internal organs of the worm (M.P., R.M.E.P. and B.M.O., unpublished observations). The label was not concentrated in any particular region of the cuticle. However, release of protein material from the region of the bacillary pores cannot be ruled out nor confirmed with our present data.

In conclusion, our results indicate that the cuticle of *T. spiralis* is a dynamic organ, the surface of which shows dramatic changes at the molecular level during the moulting process and more gradual modifications during growth within one stage. The qualitative modifications of the surface proteins during a change in stage and antigenic evidence imply that these molecules are stage-specific. The surface proteins are strikingly few in number and are released into the medium when *T. spiralis* is maintained *in vitro*. This suggests that the secretions and excretions of nematodes include proteins shed from the cuticle.

We thank Ms Patricia M. Taylor and Mr N. W. T. Clarke for technical help, and the photography department for assistance. B.M.O. is a member of the Wellcome Trust staff. M.P. is supported by a grant from the Filariasis Component of the UNDP/World Bank/WHO Special Programme for Research and Training in Tropical Diseases.

Received 7 June; accepted 18 August 1980.

1. Lumsden, R. D. *Expl Parasit.* **37,** 267–339 (1975).
2. Bird, A. F. *The Structure of Nematodes* (Academic, New York, 1971).
3. Lee, D. L. *Adv. Parasit.* **4,** 137–254 (1966).
4. Lee, D. L. *Adv. Parasit.* **10,** 347–379 (1972).
5. Chen, S. N. & Howells, R. E. *Parasitology* **78,** 343–354 (1979).
6. Soulsby, E. *Pathology of Parasitic Diseases* (ed. Gaafar, S.) 243–257 (Purdue University Studies, Lafayette, Indiana 1971).
7. Mackenzie, C. D., Preston, P. M. & Ogilvie, B. M. *Nature* **276,** 826–828 (1978).
8. Kazura, J. W. & Grove, D. T. *Nature* **274,** 588–589 (1978).
9. Kazura, J. W. & Aikawa, M. J. *Immunology* **124,** 355–361 (1980).
10. Tanner, M. & Weiss, N. *Acta tropica* **35,** 151–160 (1978).
11. Subrahmanyam, D., Mehta, K., Nelson, D. S., Rao, Y. V. B. E. & Rao, C. K. *J. clin. Microbiol.* **8,** 228–232 (1978).
12. Dennis, D. T., Despommier, D. D. & Davis, N. *J. Parasit.* **56,** 974–977 (1970).

0028-0836/80/410540—03$01.00

Sharing of an idiotypic marker by monoclonal antibodies specific for distinct regions of hen lysozyme

Dennis W. Metzger, Alexander Miller & Eli E. Sercarz

Department of Microbiology, University of California, Los Angeles, California 90024

Idiotypes have been defined serologically as variable-region markers present on unique subsets of antibody molecules. Most studies involving myeloma proteins and antibody responses in inbred mice have indicated that idiotypy is closely related to antigenic specificity. However, indirect evidence[1-7] suggests that idiotypy can sometimes be dissociated from specificity. In the response to the small monomeric protein, hen egg-white lysozyme (HEL), previous results[8,9] demonstrated that 70–95% of the anti-HEL antibody found in sera of primed and boosted mice is specific for a particular region of HEL and bears a predominant idiotype (IdX-HEL). In this report, hybridoma anti-HEL antibodies tested with well-characterized peptide fragments of HEL show that the IdX-HEL marker can be found on antibodies of completely distinct antigen specificities. Thus, a mode of recognition other than antigenic recognition probably plays a major role in the immune response to HEL.

Hybridoma anti-HEL antibodies were obtained by fusing HEL-primed A/J spleen cells with the nonsecreting BALB/c myeloma cell line, S194/5.XXO.BU.1 (Salk Institute). The growing hybrids were cloned by limiting dilution and monoclonality was confirmed by isoelectric focusing of several individual subclones, all of which for a particular hybridoma were indistinguishable with regard to spectrotype. The activity of the monoclonal antibodies was determined in a solid-phase radioimmunoassay[10] by direct binding to HEL and, in addition, this assay was used with peptide fragments that define discrete segments of the HEL molecule (N–C peptide amino acids 1–17, Cys 6–Cys 127, 120–129; mixed disulphide L_{II} peptide amino acids 13–105; and mixed disulphide L_{III} peptide amino acids 106–129) to assess specificity. The N–C peptide overlaps with L_{II} for a small sequence of five amino acids (13–17); L_{II} and L_{III} are non-overlapping peptides. Bovine ribonuclease, a protein of similar size and charge to HEL, was used to assess background levels of binding. As seen in Table 1, the anti-HEL hybridoma antibody, 6D7, recognizes the L_{II} but not the N–C peptide. Conversely, the hybridoma antibody, 5E4, recognizes HEL and the N–C peptide. In other experiments (not shown) the peptides

Table 1 Specificity of hybridoma antibodies 6D7 and 5E4

	Antigen on plate: radioactivity bound (c.p.m. $\times 10^{-3}$)			
Hybridoma	HEL	Ribonuclease	N–C	L_{II}
6D7	19.7	1.8	1.9	13.2
5E4	17.9	0.7	13.9	0.8

Specificity was assessed in a solid-phase radioimmunoassay in which the wells of microtitre plates (Cooke) were coated with 100 µl of 0.5 mg ml^{-1} antigen at 4 °C overnight. The plates were then flooded with a solution of 1% bovine serum albumin in phosphate-buffered saline (1% BSA–PBS) at room temperature for 1 h to saturate the protein-binding capacity of the wells. Next, the hybridoma supernatants (25 µl) were added to the wells at room temperature for 2 h. Binding was assessed using 50 µl of affinity-purified ^{125}I-goat anti-mouse Ig (10^5 c.p.m. per well) at room temperature for 1 h. Between each specific addition, the plates were washed extensively with 1% BSA–PBS. 6D7 is an IgG2bκ monoclonal antibody and 5E4 is an IgGlκ monoclonal antibody as determined by the solid-phase radioimmunassay using rabbit anti-subclass antisera (provided by Drs J. Teale and N. Klinman, Scripps Clinic and Research Foundation) to assess binding to HEL. The results are expressed as c.p.m. bound per well.

Table 2 Competitive inhibition of the binding of hybridoma antibodies 6D7 and 5E4

Inhibitor	Amount of inhibitor (μg)	Inhibition of 6D7 binding (%)		Inhibition of 5E4 binding (%)	
		HEL plate	L_{II} plate	HEL plate	N–C plate
HEL	0.001	16	24	5	0
	0.1	88	78	45	94
	10	92	88	94	92
Ribonuclease	10	0	0	0	0
L_{II}	10	58	90	0	0
N–C	10	0	0	33	72

Inhibition studies were performed using the solid phase radioimmunoassay and a dilution of hybridoma supernatant capable of 40–50% maximal binding to the insolubilized antigen. The supernatants (25 μl) were preincubated with 25 μl of 1% BSA–PBS to determine control binding or with 25 μl soluble inhibitor at 37 °C for 30 min and then at 4 °C overnight. The mixtures were incubated at room temperature for 2 h in wells coated with the target antigen after which the wells were washed and incubated at room temperature for 1 h with 75 μl of ^{125}I-goat anti-mouse Ig (10^5 c.p.m. per well). As much as 1 μg of L_{II} or N–C did not cause significant inhibition of binding of 6D7 or 5E4, respectively.

were coupled to keyhole limpet haemocyanin (KLH) to increase the sensitivity of detection and significant binding to L_{III}–KLH over background was observed with 5E4 but not 6D7. Thus, 5E4 appears to have specificity for a determinant in the C-terminal portion of HEL (amino acids 120–129) whereas 6D7 is specific for an epitope within the middle region of HEL (amino acids 17–105).

These non-overlapping specificities were confirmed by competitive inhibition of the radioimmunoassay in which the hybridoma antibodies were pre-incubated with the soluble peptides and then assayed for binding to insolubilized HEL and its fragments. As seen in Table 2, L_{II} but not N–C competed effectively for the binding of 6D7 to HEL (and L_{II}). On the other hand, N–C but not L_{II} inhibited the binding of 5E4 to HEL (and N–C). Thus, 5E4 and 6D7 recognize distinct epitypes on the HEL molecule. The need to use the peptides in large amounts relative to HEL for inhibition suggests that the antibodies have greater affinity for the native, conformationally restricted, HEL molecule than for the peptides.

The idiotypy of the two monoclonal antibodies was investigated next. It has been found[8] that anti-IdX-HEL antiserum appears to define an idiotypic marker which resides close to the antigen-combining site and is present on the majority of secondary response anti-HEL antibody. Thus, anti-IdX-HEL antiserum, unlike polyvalent anti-Ig, interferes with the binding of HEL to its antibody in a standard Farr-type assay. The presence of IdX-HEL on 5E4 and 6D7 was assessed in a similar manner using a guinea pig anti-IdX-HEL antiserum raised against a third hybridoma anti-HEL, AD2. AD2, although not showing detectable binding to peptide fragments, does exhibit a relatively rare pattern of cross-reactions different from either 5E4 or 6D7 when tested with a panel of related lysozymes. The anti-IdX-HEL antiserum induced with AD2 appears to be similar to anti-idiotype raised against serum anti-HEL in that it interferes with the binding of HEL to most of the secondary anti-HEL serum antibody of B10.A mice. As shown previously[9], such antibody is specific primarily for the N–C peptide. The anti-IdX-HEL antiserum against AD2 does not affect the binding of an essentially non-HEL cross-reactive lysozyme, human lysozyme, to its antibody (D. W. M., unpublished observations). As seen in Fig. 1, the recognition of HEL by 5E4 or 6D7 was in both cases almost completely inhibited by the anti-IdX-HEL antiserum, presumably by interaction with variable region residues not directly within, but close to, the antigen-combining site. In contrast, an anti-HEL hybridoma antibody, 2G3, which appears to lack the IdX-HEL marker, was almost unaffected by anti-idiotype treatment. We have also found that the individual hybridoma product, 6D7 (as well as 5E4), can remove all the activity from an anti-idiotypic antiserum raised against conventional serum anti-HEL antibody[11]. Thus, two monoclonal antibodies that clearly differ in peptide specificity for a multideterminant antigen can both bear the IdX-HEL marker.

Earlier studies from our laboratory demonstrated that the majority of serum antibody produced in secondary responses of mice shared two properties: specificity for the N–C portion of HEL and presence of a common idiotype, IdX-HEL[8,9]. The small amount of L_{II}-specific antibody that was detectable appeared to lack the IdX-HEL marker. Nevertheless, using hybridoma technology we have been able to detect L_{II}-specific, idiotype-positive antibodies.

In previous work[11,12] we found that anti-HEL antibodies displaying the IdX-HEL marker replace an IdX-negative anti-HEL population appearing early after immunization. This replacement, along with the results in this report, indicates that idiotype selection *per se* plays a pivotal role in the predominance of the IdX-HEL marker during the secondary anti-HEL response. This selection is presumably mediated by an idiotype-specific T cell (IdXTh); in recent work it has been demonstrated that such IdXTh cells are necessary to complement antigen-specific T cells (AgTh) for the optimal induction of an *in vitro* anti-HEL response[13]. The activation of AgTh cells of a particular specificity under the influence of the major histocompatibility complex, in concert with antigen-bridging constraints in T–B collaboration, can explain the prevalent epitypic specificity of the B cell response. This combination of potent idiotypic selection by IdXTh cells and specificity selection by AgTh cells would rationalize the common finding of convergence between idiotypy and antigen specificity. Occasional utilization of less common T-helper cell clones could allow idiotypy to be associated with antibody of different specificity, as we have noted here and as observed in the seminal findings of Oudin and his colleagues[1,2].

This work was supported in part by USPHS grants CA-24442 and AI-11183. D. W. M. is a postdoctoral trainee supported by NRSA-NCI 5 T32 CA09120-05.

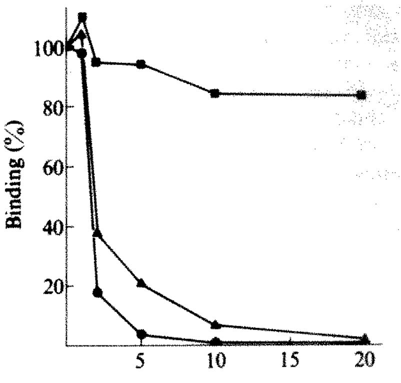

Fig. 1 Inhibition of hybridoma anti-HEL binding to ^{125}I-HEL by anti-idiotype. Anti-IdX-HEL was raised in guinea pigs using affinity-purified monoclonal anti-HEL antibody that was obtained by fusing immune B10.A lymph node cells with the BALB/c myeloma, P3x63Ag8. The resulting antiserum was repeatedly passed over normal (B10.AxBALB/c)F_1 Ig columns. Inhibition curves with anti-IdX-HEL were obtained by adding increasing amounts of anti-idiotype to tubes containing a dilution of hybridoma anti-HEL capable of binding 40–50% of 10ng ^{125}I-HEL. Following incubation, the Ig fraction in each tube was precipitated with 18% (w/v) Na_2SO_4, the precipitates were washed extensively, and the amount of bound ^{125}I-HEL was determined using a Nuclear Chicago γ-counter. Data are presented as the per cent of binding obtained in the absence of anti-idiotype. All values have been corrected for background binding in tubes containing anti-IdX-HEL and ^{125}I-HEL alone. ■ hybridoma antibody 2G3; ▲ hybridoma antibody 6D7; ● hybridoma antibody 5E4.

Received 9 April; accepted 28 July 1980.

1. Oudin, J. & Michel, M. *J. expl Med.* **130,** 619–642 (1969).
2. Oudin, J. & Cazenave, P.-A. *Proc. natn. Acad. Sci. U.S.A.* **68,** 2616–2620 (1971).
3. Cazenave, P.-A. *FEBS Lett.* **31,** 348–354 (1973).
4. Eichmann, K., Coutinho, A. & Melchers, F. *J. expl Med.* **146,** 1436–1449 (1977).
5. Karol, R., Reichlin, M. & Noble, R. W. *J. expl Med.* **148,** 1488–1497 (1978).
6. Enghofer, E. M., Glaudemans, C. P. J. & Bosma, M. J. *Molec. Immun.* **16,** 1103–1110 (1979).
7. Wikler, M. *et al. J. expl Med.* **150,** 184–195 (1979).
8. Harvey, M. A., Adorini, L., Miller, A. & Sercarz, E. E. *Nature* **281,** 594–596 (1979).
9. Benjamin, C. D., Miller, A., Sercarz, E. E. & Harvey, M. A. *J. Immun.*, **125,** 1017–1025 (1980).
10. Pierce, S. K. & Klinman, N. R. *J. expl Med.* **144,** 1254–1262 (1976).
11. Metzger, D. W., Miller, A. & Sercarz, E. E. (in preparation).
12. Metzger, D. W., Miller, A. & Sercarz, E. E. *Fedn Proc.* **39,** 572 (1980).
13. Adorini, L., Harvey, M. & Sercarz, E. E. *Eur. J. Immun.* **9,** 906–909 (1979).

Effect of cyclosporin A on T-dependent and T-independent immunoglobulin synthesis *in vitro*

T. Paavonen & P. Häyry

Transplantation Laboratory, Fourth Department of Surgery, University of Helsinki, Haartmaninkatu 3, SF 00290 Helsinki 29, Finland

An immunosuppressive cyclic polypeptide, cyclosporin A (CyA), isolated originally from two species of fungi[1], prolongs organ allograft survival in several species[2–7]. However, virtually nothing is known about the pharmacokinetics of this substance and its mode of action in man. We have quantified the impact of CyA on T-dependent and T-independent immunoglobulin (Ig) synthesis of human blood leukocytes *in vitro*, and on the proliferating capacity of the interacting lymphoid cell populations—T cells, B cells, Tμ and Tγ cells. CyA inhibited all responses at approximately equal concentrations. The blast cells rather than resting lymphocytes and/or Ig-synthesizing plasma cells were incapacitated by the drug. As the phagocytosis of accessory macrophages was inhibited only at a 100–1,000-fold higher drug concentration, we conclude that CyA has a relatively specific direct effect on human T and B blast cells *in vitro*.

Pokeweed mitogen (PWM) induces a T-dependent Ig-synthesis in human lymphocytes *in vitro*[8], whereas *Staphylococcus aureus* bacteria act in similar conditions as T-independent mitogens[9]. Present fractionation methods enable adequate separation of the participating lymphoid cell populations and the evaluation of the effect of the drug on the different populations separately.

Human mononuclear leukocytes were isolated via Ficoll–Isopaque (FIP, Pharmacia) density centrifugation[10], treated with iron powder plus magnet[11], washed and plated for culture. Microculture conditions in Falcon Microtest II tissue culture plates with 3×10^5 responder cells and 200-μl volume were used. Pokeweed mitogen (50 μg ml^{-1}, Gibco), or heat-killed, formalin-fixed *S. aureus* Cowan I bacteria[9] at a concentration of 100×10^6 organisms ml^{-1}, were used as mitogens. CyA, which is insoluble in water, was first dissolved in absolute ethanol and added to cultures at indicated final concentrations. All cultures containing CyA contained an equal amount (0.13%) of ethanol, and for controls corresponding stimulations in the absence and in the presence of ethanol were used. The proliferative activity in cultures was measured by 6-h tritiated thymidine (^{3}H-TdR) uptake (2 μCi ml^{-1}, specific activity 6.7 Ci mmol^{-1}; NEN) on the fourth culture day, when the peak proliferative response took place. To quantify the viable cell number, the blastogenic response and the rate of intracellular Ig synthesis, 10^4 chicken red blood cells (ChRBC) were added per culture well before terminating the cultures. The cell viability and the blastogenic response were assessed from May–Grünwald–Giemsa-stained cytocentrifuged cell smears[11]. The degree of intracellular Ig synthesis was analysed from similar smears with fluorescein isothiocyanate-conjugated, 1:30 diluted, polyvalent anti-human Ig (anti-IgM, -IgA, and -IgG; Dakopatts) using standard fluorescence technology. The results were expressed as number of blast cells, lymphocytes or cells containing intracellular Ig per 100 (autofluorescent) ChRBC. The release of Ig was quantified by indirect protein A (Pharmacia) plaque assay on the sixth culture day[12], and expressed as plaque-forming cells (PFC) per 10^5 cultured cells.

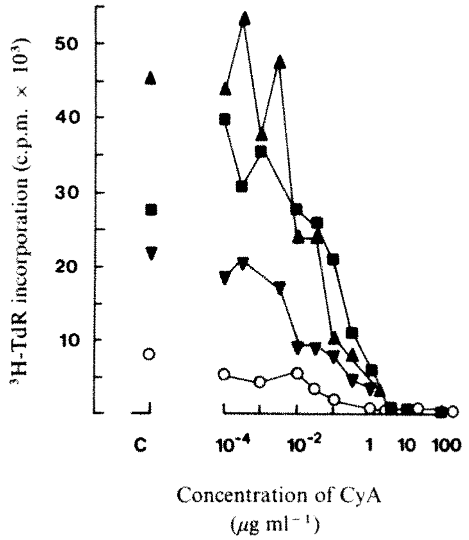

Fig. 1 Effect of increasing concentrations of CyA on the proliferative response of T- (■), Tμ- (▼), Tγ- (▲), and B-enriched (○) blood white cell populations to PWM. C indicates PWM-stimulated control cultures in the presence of 0.13% of ethanol. Mean incorporation in controls containing no mitogen was approximately 1–3 × 10^2 c.p.m.

Fractionation of T and B cells and the Tμ and Tγ subsets of T cells was modified from Moretta *et al.*[13]: FIP-isolated iron powder-treated blood mononuclear cells were rosetted with 2-aminoethyl-isothiouronium bromide-hydrobromide-treated sheep red cells[14] and centrifuged over FIP. The interphase (B-enriched) fraction contained >95% lymphocytes and 1–2% of monocytes. Approximately 80% of the lymphocytes expressed surface Ig. The red cells from the bottom (T-enriched) fraction were lysed[11] and the white cells were rosetted with IgG-coated erythrocytes as described[13]. After another centrifugation over FIP, the Tμ-enriched fraction was collected from the interphase while the bottom fraction was enriched for Tγ. In three separate experiments we found that the B cells, without recombination with T cells, were entirely unable to synthesize Ig after stimulation with PWM. When the B cells were recombined with T cells, the response was reconstituted. Recombination with Tμ cells induced an even higher Ig response, whereas recombination with the Tγ-enriched population was distinctly inferior in helper capacity. This indicates enrichment of helper cells in the former and either lack of helper cells and/or enrichment of suppressor cells in the latter T-cell fraction.

Mononuclear phagocytes were enriched via fractionation over a discontinuous Percoll gradient. Percoll (Pharmacia) was mixed with 10% fetal calf serum (FCS) containing RPMI-1640 medium (Gibco) at the following concentrations (%): 37.5, 40.0, 42.5, 45.0 and 47.5, and layered in five layers. 100×10^6 FIP-isolated blood leukocytes were layered in the RPMI-FCS medium on the top layer, the tubes were centrifuged for 45 min at 267*g* and the fractions from the five interphases were recovered. Mononuclear phagocytes were distributed primarily at the first interphase, where 90–95% of all leukocytes were monocytes according to morphological criteria.

In four experiments we stimulated the blood leukocytes with PWM or *S. aureus* bacteria, and quantified the rate of ^{3}H-TdR incorporation, intracellular Ig synthesis and release of Ig into culture medium (Table 1). CyA suppressed all responses at

0028-0836/80/410542—03$01.00

Table 1 Effect of CyA on PWM- and staphylococcus-induced *in vitro* responses of unfractionated blood cells

Test parameter and (day of assay)	Mitogen	Expt	No eth*	Eth†	Concentration of CyA (μg ml^{-1})					
					10^{-4}	10^{-3}	10^{-2}	10^{-1}	1	10
^{3}H-TdR incorporation (c.p.m. × 10^3) (Day 4)	PWM	1	12.4	14.9	18.0	14.0	12.3	5.7	3.0	0.2
		2	23.2	26.7	23.0	21.9	22.2	16.5	13.2	0.2
	Staphylococcus	1	9.8	10.6	10.5	10.4	8.1	2.9	1.7	0.2
		2	13.9	13.8	13.1	14.6	13.0	9.1	8.0	0.1
	—	1b	0.8	1.3	1.1	0.9	0.8	0.4	0.4	0.1
		2	2.7	2.8	1.5	0 9	0.9	0.7	0.4	0.1
Intracellular Ig-containing cells (per 100 ChRBC) (Day 6)	PWM	3	44	52	62	49	37	17	1	0
	Staphylococcus	3	37	59	42	32	30	7	3	0
	—	3	3	2	1	1	0	4	0	0
Ig-releasing cells (PFC per 100,000 cultured cells) (Day 6)	PWM	1	258	270	285	276	138	60	30	6
	Staphylococcus	1	201	202	216	180	132	54	12	0
	—	1	10	16	12	10	10	4	6	0

* No ethanol present in the control culture.

† 0.13% of ethanol was present in this control culture and in all CyA-containing cultures.

Table 2 Effect of CyA on the viability of lymphocytes and blast cells in PWM- and *S. aureus*-stimulated culture of unfractionated blood cells

Mitogen*	Cell per culture (per 100 ChRBC)	No eth†	Eth‡	Concentration of CyA (μg ml^{-1})					
				10^{-4}	10^{-3}	10^{-2}	10^{-1}	1	10
PWM	Blasts	333	355	225	327	275	120	109	5
	Lymphocytes	886	676	999	786	861	1,010	868	378
Staphylococcus	Blasts	147	176	166	108	65	56	29	0
	Lymphocytes	1,394	996	937	965	755	1,032	1,111	272

* Counts performed on the 6th day of culture.

† Control without ethanol.

‡ 0.13% of ethanol was present in this control culture and in all CyA-containing cultures.

Table 3 Effect of CyA on the phagocytic activity of cultured blood monocytes

Expt	No eth*	Eth†	Concentration of CyA (μg ml^{-1})‡					
			10^{-4}	10^{-3}	10^{-2}	10^{-1}	1	10
1	6.5±0.8	7.0±0.9	6.3±0.8	5.5±0.5	6.7±0.7	4.8±0.6	4.5±0.6	2.8±0.7
2	6.0±0.5	5.0±0.6	5.5±0.5	4.9±0.5	5.0±0.6	4.0±0.4	4.9±0.4	2.0±0.4

* No ethanol present in control culture.

† 0.13% ethanol added to control culture.

‡ Number of ingested staphylococci per cell after culture of the blood monocytes for 48 h in the presence of various concentration of CyA. Mean numbers of triplicate determinations ±s.d. Exposure time of staphylococci, 30 min; CyA present in the culture medium also during phagocytosis.

equal concentrations, regardless of whether PWM or staphylococci were used as mitogen.

Blood leukocytes were then enriched for T and B cells, and the T cells further to Tμ and Tγ cells. The effect of the drug was assessed separately on the proliferative response of the different cell populations. In all three experiments the drug suppressed at equal concentrations the proliferative response of T, Tμ and Tγ and B-enriched cell populations to PWM (Fig. 1). Whereas a distinct suppression of the blastogenic response (Table 2) was observed already at a concentration of 10^{-3}–10^{-2} μg ml^{-1}, the viability of resting lymphocytes was not decreased until a concentration of 1–10 μg ml^{-1} was reached.

Because both mitogens are monocyte-dependent, a possibility still existed that CyA affects through the accessory cells, that is, through the monocytes present in the culture. Blood monocyte-enriched population was therefore cultured for 48 h in the presence of different concentrations of CyA, and 200 × 10^6 staphylococci were added per culture. After an additional 30-min incubation, coverslips were removed from the bottom of the culture vessels, washed, stained and the average number of intracellular staphylococci was quantified (Table 3). Prior culture with CyA has virtually no effect on the phagocytic activity of blood monocytes up to a concentration of 1 μg ml^{-1}. At 10 μg ml^{-1}, the rate of phagocytosis was reduced by ~50%.

Altogether, CyA suppressed at equal concentrations both T-dependent and T-independent Ig production. The distinctly inhibitory concentration *in vitro*, 1 × 10^{-1} μg ml^{-1}, was somewhat smaller than the expected maintenance concentration in the blood after peroral administration at the recommended dose of 17 mg per kg per day (ref. 7). Moreover, all participating populations of lymphoid cells—T helper cells, T suppressor cells and B cells—were equally sensitive to this drug, and the drug suppressed far better the blastogenic response than killed resting lymphocytes in cultures. Because blood monocyte phagocytosis was not affected by previous culture with CyA, we consider it unlikely that the drug effect is mediated through the accessory mononuclear phagocytes[15,16].

Although species differences may exist, our results contradict the finding of White *et al.*[17] on porcine lymphocytes that T cells are more sensitive than B cells to CyA *in vitro* and those of Gordon *et al.*[18] who demonstrated that colony formation by transformed human 'B lymphocytes' is marginally less sensitive to CyA than colony formation by (a fraction of) T lymphocytes. However, our results are compatible with these of Borel *et al.*[2]

who demonstrated that haemagglutinating antibody response in the mouse was suppressed at approximately equal doses compared to skin graft rejection, and with the observation of Allison *et al.* (unpublished, cited in ref. 4) that T and B blastogenic responses of human lymphocytes are affected at equal drug concentrations. The rather selective effect of CyA on T and B blast cells is compatible with the 'decloning' hypothesis suggested for CyA as a possible mode of action in certain species[4,19], though not yet in man.

We thank Dr J. F. Borel and Sandoz Pharmaceuticals for supplying the drug. This study was financed by NIH-NIAID grant no. 1 RO1 AM26882-01.

Received 31 March; accepted August 1980.

1. Dreyfuss, M. *et al. Eur. J. appl. Microbiol.* **3**, 125 (1976).
2. Borel, J. F. *et al. Agents Actions* **6**, 468 (1976).
3. Kostakis, A. J., White, D. J. G. & Calne, R. Y. *IRCS med. Sci.* **5**, 243 (1977).
4. Green, C. J. & Allison, A. C. *Lancet* **i**, 1182 (1978).
5. Calne, R. Y. *et al. Lancet* **i**, 1183 (1978).
6. Vialettes, B. *et al. Transplantation* **28**, 435 (1979).
7. Calne, R. Y. *et al. Lancet* **ii**, 1033 (1979).
8. Gmelig-Meyling, F., UytdeHaag, A. G. C. M. & Ballieux, R. E. *Cell. Immun.* **33**, 156 (1977).
9. Forsgren, A., Svedjelund, A. & Wigzell, H. *Eur. J. Immun.* **6**, 207 (1976).
10. Böyum, A. *Scand. J. clin. Lab. Invest.* **21**, Suppl. 97 (1968).
11. Häyry, P. & Andersson, L. C. *Scand. J. Immun.* **5**, Suppl. 5, 31 (1976).
12. Hammarström, L., Bird, A. G., Britton, S. & Smith, C. I. E. *Immunology* (in the press).
13. Moretta, L. *et al. J. Immun.* **122**, 984 (1979).
14. Pellegrino, M. A., Ferrone, S., Dietrich, M. P. & Reisfeld, R. A. *Clin. Immun. Immunopath.* **3**, 324 (1975).
15. Waldron, J. A., Horn, R. G. & Rosenthal, A. S. *J. Immun.* **111**, 58 (1973).
16. Gehrz, R. C. & Knorr, S. O. *Clin. exp. Immun.* **37**, 551 (1979).
17. White, D. J. G. *et al. Transplantation* **27**, 55 (1979).
18. Gordon, M. Y. & Singer, J. W. *Nature* **279**, 433 (1979).
19. Homan, W. P., Fabre, J. W. & Morris, P. J. *Transplantation* **28**, 439 (1979).

An immunological suppressor cell inactivating cytotoxic T-lymphocyte precursor cells recognizing it

Richard G. Miller

Department of Medical Biophysics, University of Toronto, and the Ontario Cancer Institute, 500 Sherbourne Street, Toronto, Ontario, Canada M4X 1K9

The immune system does not normally react against self components. Originally, it was postulated that self-reactive cells were somehow deleted or blocked[1]. More recent thinking[2,3] is that such cells are suppressed by regulatory networks similar to those limiting the immune response against non-self determinants. Both mechanisms may exist[4,5]. I describe here a type of suppression more closely related to the first postulate. In the *in vitro*, one-way, mixed lymphocyte reaction (MLR), cytotoxic T-lymphocyte precursor cells (CLP) from the responder population give rise to cytotoxic T-lymphocytes (CL) capable of lysing target cells from the stimulator population[6–8]. A subpopulation of cells in the spleen of athymic nude mice can, when added to such cultures, inactivate CLP capable of recognizing either the H-2 antigens or TNP modifications of the nude spleen. Regarding the nude spleen cells, activation of self-react ve cells is being prevented.

Table 1 presents measurements of the cytotoxic activity produced in various MLRs which demonstrate the suppression phenomenon. In experiment 1, line 1, BALB/c ($H-2^d$) lymph node (LN) cells produce a good cytotoxic response against both irradiated RNC ($H-2^k$) spleen cells and irradiated B10 ($H-2^b$) spleen cells. Addition of BALB/c.nu spleen cells to the cultures has little effect on either response (line 2). However, addition of RNC.nu spleen cells leads to a significantly lower cytotoxic response against the RNC spleen cells but not against the B10 spleen cells, that is, suppression is observed when the added nude spleen cells are syngeneic to the stimulator cells (line 3). The ability of the added nude spleen cells to cause suppression is destroyed by subjecting them to one freeze–thaw cycle (line 4), implying that the suppression results from a physiological process. These results confirm previous, more extensive studies[9] in which it was shown that B.nu or $(A \times B)F_1$.nu spleen cells suppress an A anti-B response but not an A anti-C response where A, B and C represent three H-2-different mouse strains.

An anti-TNP-modified self response can also be suppressed. Addition of RNC.nu spleen cells to RNC anti-RNC-TNP cultures suppressed the response if the RNC.nu spleen cells were also TNP-modified (Table 1, expt 2). The same nude cells, whether TNP-modified or not, were equally competent at suppressing a BALB/c anti-RNC response. Similar results have been obtained using B6.nu spleen cells in the B6 anti-B6-TNP response and BALB/c.nu spleen cells in the BALB/c anti-BALB/c-TNP response. Controls established that the effector

Table 1 Suppression of cytotoxic responses by added nude spleen cells

	Added nude spleen cells	Cytotoxic activity	
		BALB/c anti-RNC response	BALB/c anti-B10 response
Expt 1	0	196 ± 28	114 ± 25
	BALB/c	228 ± 65	158 ± 25
	RNC	86 ± 8*	111 ± 23
	RNC (freeze–thaw)†	168 ± 19	NT
		RNC anti-RNC-TNP response	BALB/c anti-RNC response
Expt 2	0	192 ± 22	201 ± 26
	RNC	183 ± 18	38 ± 8*
	RNC-TNP	77 ± 16*	41 ± 7*
		BALB/c anti-BALB/c-TNP response	
Expt 3	0	55 ± 12	
	BALB/c-TNP	15 ± 7*	
	mixture‡	60 ± 10	
		$(RNC \times C57BL/6)F_1$ anti-RNC-TNP response	$(RNC \times C57BL/6)F_1$ anti-B6-TNP response
Expt 4	0	216 ± 47	50 ± 10
	RNC	216 ± 27	54 ± 10
	RNC-TNP	109 ± 16*	27 ± 5*

Each entry is the mean ± s.e.m. cytotoxic activity for a group of eight microcultures, each culture containing LN cells as responder cells, 3×10^5 irradiated (1,500 rad ^{137}Cs γ rays) spleen cells as stimulator cells and 10^5 (expt 1 and expt 3) or 3×10^5 (expt 2 and expt 4) nude spleen cells being tested for their ability to suppress the response of the culture. For the anti-H-2 responses (BALB/c anti-RNC, BALB/c anti-B10), 3×10^4 responder LN cells were used; for the remaining cultures, 2×10^5 responder LN cells were used. When required, TNP-modified cells were produced by the method of Shearer *et al.*[17] as described previously[18]. Each experiment included control groups containing nude spleen cells and stimulator cells but no responder LN cells. None of these control groups developed significant cytotoxic activity. Each culture was in 0.2 ml of α-minimal essential medium supplemented with 10% fetal calf serum, 5×10^{-5}M 2-mercaptoethanol and 10 mM HEPES buffer as described in detail elsewhere[9]. After 5 days of incubation at 37 °C, cultures were assayed for cytotoxic activity by addition of 3×10^3 ^{51}Cr-labelled target cells obtained from a 2- or 3-day culture of spleen cells identical to the stimulator cells incubated with concanavalin A ($2 \mu g \, ml^{-1}$). Fractional specific ^{51}Cr release, p, defined as (observed release − spontaneous release)/(total releasable − spontaneous release) was measured as previously described[9] and re-expressed as cytotoxic activity $= -100 \ln (1-p)$. This transformation re-expresses the ^{51}Cr release so that the cytotoxic activity is directly proportional to the number of CL present rather than the number of target cells destroyed[19]. An entry of 10 corresponds to 10% specific ^{51}Cr release; an entry of 100 to 63% specific ^{51}Cr release. NT, Not tested.

* Response significantly less ($P < 0.05$) than for the corresponding group of cultures not containing added nude spleen cells.

† The RNC.nu spleen cells were frozen and thawed once before addition to the cultures.

‡ Cultures identical to those of the preceding two lines, that is, with and without added BALB/c.nu-TNP spleen cells, were mixed immediately before assaying for cytotoxic activity.

0028–0836/80/410544—03$01.00

cells produced were T-cells that lysed syngeneic cells only after TNP modification.

The suppression produced by adding nude spleen cells could occur at one or more of several levels of the MLR and subsequent cytotoxicity assay: (1) a reduction in the number of CLP activated; (2) a reduction in the number of CL produced per activated CLP; or (3) a reduction in the measured cytotoxic activity per CL either as a result of suppression of the lytic efficiency per CL or as a result of competitive inhibition of the lysis of the labelled target cells by remaining unlabelled nude spleen cells. Experiment 3, Table 1, provides evidence against the last possibility: adding suppressed cultures to non-suppressed cultures just before the assay for cytotoxicity produced no decrease in the measured cytotoxic activity. To distinguish between possibilities (1) and (2), limiting dilution analysis was used to measure both the frequency of CLP (f_{CLP}) and the relative number of CL produced per activated CLP in the presence and absence of nude suppressor cells. In the culture conditions used, the CLP is the least frequent required cell so that failure of a culture to respond indicates that the culture contained no CLP[8,10]. The probability, P, of this happening is, from the first term of the Poisson distribution, given by $P = \exp(-f_{CLP}N)$ where N is the number of LN cells cultured. The cytotoxic activity developed in replicate RNC anti-RNC-TNP cultures containing varying numbers of RNC LN responder cells, fixed numbers of RNC.nu spleen cells with or without TNP modification, and fixed numbers of RNC-TNP stimulator cells, was measured and each culture was scored as responding or non-responding. Figure 1*a* shows the fraction of non-responding cultures and Fig. 1*b* the mean cytotoxic activity per culture, both as a function of N. The values for f_{CLP} determined from Fig. 1*a* are shown in Table 2 (line 1). The value for f_{CLP} is about two and a half times lower when the added nude spleen cells have been TNP-modified. From the slopes of the lines in Fig. 1*b* and from the measured CLP frequency, one can calculate the mean cytotoxic activity produced by the clone of CL from a single CLP (Table 2). It is significantly greater in the presence of suppression. Possibly the suppressor cells can suppress regulator cells, limiting the magnitude of the response[2] as well as preventing CLP activation. Note that this effect tends to reduce the overall observed suppression in cytotoxic activity. Equivalent results were obtained on analysing the BALB/c anti-BALB/c-TNP response (expt 2, Table 2).

The suppression observed in an anti-H-2 response also results from a reduction in the number of CLP activated (expt 3, Table 2). RNC.nu spleen cells were used to suppress a BALB/c anti-RNC response. To obtain a population of nude cells which would not suppress, but at the same time provide the accessory cells required to meet the conditions of the limiting dilution assay[8], use was made of a previous observation[9] that slowly-sedimenting nude spleen cells contain the required accessory cells but are relatively free of suppressive activity, whereas rapidly-sedimenting cells are enriched in suppressive activity. Thus, the CLP frequency measured in the presence of nude spleen cells (line 1) is about half that measured in the presence of slowly-sedimenting (2–4.5 mm h^{-1}) nude spleen cells (line 2). Addition of rapidly-sedimenting (4.5–9 mm h^{-1}) nude cells to the slowly-sedimenting nude cells restores the suppression.

The cytotoxic response against syngeneic target cells which have been virus- or TNP-modified is known to be H-2 restricted, that is, the CL obtained produce preferential lysis of target cells sharing both the modification (virus or TNP) and H-2 with the original stimulator cells[11,12]. I therefore investigated whether TNP-modified nude spleen cells could suppress an anti-TNP response on an H-2-different background. Care was taken to avoid possible allogeneic effects by working only with parent–F_1 strain combinations. In expt 4, Table 1, RNC.nu spleen cells, with and without TNP modification, were added to either an (RNC×C57BL/6)F_1 anti-RNC-TNP response or an (RNC×C57BL/6)F_1 anti-C57BL/6-TNP response. The RNC-TNP-modified nude cells suppressed both responses about twofold. Similar results were obtained on adding RNC.nu spleen cells, with and without TNP modification, to an (RNC×C57BL/6)F_1 anti-(RNC×C57BL/6)F_1-TNP response and measuring the response against RNC-TNP and C57BL/6-TNP target cells. I conclude that the nude spleen suppressor cells show at most a slight preference for suppression of a TNP-modified self response in which the H-2 of the nude cells and stimulator cells is shared. In experiments using the same microculture technique as used here to analyse TNP cross-reactivity at the level of single clones of CL (ref. 18), it was found that at least 40% of clones specific for the TNP-modified stimulator could also lyse a particular H-2-unrelated, TNP-modified target cell. Thus, the apparent lack of H-2 restriction seen here might merely reflect cross-reactivity at the level of the CLP, the presumed site of action of the suppressor.

Table 2 Frequency of CLPs activated in presence and absence of suppressor cells

Expt	Response	Added nude spleen cells	Precursor frequency per 10^6 LN cells	Cytotoxic activity per clone
1	RNC anti-RNC-TNP	RNC	182 (135–246)	5.3 ± 0.5
		RNC-TNP	73 (53–100)	6.7 ± 0.7
2	BALB/c anti-BALB/c-TNP	BALB/c	105 (65–168)	7.1 ± 0.7
		BALB/c-TNP	37 (24–58)	8.7 ± 0.9
3	BALB/c anti-RNC	RNC (unfractionated)	594 (413–853)	11.5 ± 1.2
		RNC (2–4.5 mm h^{-1})	1,140 (877–1482)	5.4 ± 0.5
		RNC (2–4.5 mm h^{-1}) +RNC (4.5–9 mm h^{-1})	468 (348–629)	8.3 ± 0.8

The frequency of CLP and cytotoxic activity per clone were measured by limiting dilution analysis as in Fig. 1, experiment 1 is the result from analysing this figure. The frequency was calculated using the method of Porter and Berry[20], the bracketed numbers after the entry giving 95% confidence limits. Experiment 2 was performed in an identical manner. In experiment 3, the added RNC.nu spleen cells were fractionated by velocity sedimentation[21] and either 3×10^5 unfractioned, or 3×10^5 (2–4.5 mm h^{-1}), or 3×10^5 (2–4.5 mm h^{-1}) plus 10^5 (4.5–9 mm h^{-1}) nude spleen cells tested for their ability to produce suppression.

What is the mechanism of the observed suppression? To obtain suppression, the added nude cells must carry the antigen against which the response is directed, H-2 in the case of an anti-H-2 response and TNP in the case of an anti-TNP response (Table 1). The reduction in cytotoxic activity results from a reduction in the number of CLP activated rather than the number of progeny CL produced per activated CLP (Table 2). Only a subpopulation of all the cells in nude spleen is capable of inducing the suppression (Table 2, expt 3 and ref. 9). The simplest explanation for these observations is that nude spleen contains a cell subpopulation which, when recognized by a CLP, sends a signal to the CLP which inactivates it. Whether the inactivation is reversible or permanent, that is, whether, using the terminology of enzymology, inhibition is competitive or non-competitive, is not firmly established at the present time although attempts to rescue inactivated CLP have so far been unsuccessful. Not all CLP can be inhibited. Although the cytotoxic activity developed in a primary MLR can be strongly inhibited, the inhibition is never complete and a secondary MLR cannot be inhibited at all (J. J. Rusthoven and R. G. M., unpublished observation). The inactivating signal could well be a factor although, if so, it must be short range or good fits would not have been obtained in the Poisson limiting dilution analysis (Fig. 1). In addition, attempts to isolate such a factor have so far been unsuccessful. The most novel feature of the model just outlined is the direction of recognition triggering the suppression: the CLP triggers its own suppression by recognizing the suppressor cell. An alternative point of view is that the suppressor cells have a repertoire of receptors capable of recognizing receptors which can recognize self antigens, that is, the suppression takes place through recognition of anti-self idiotypes[13]. Against this model is the observation (Table 1) that the suppressor cell can suppress an anti-self-TNP response only after the suppressor cell has been itself TNP-modified. It is

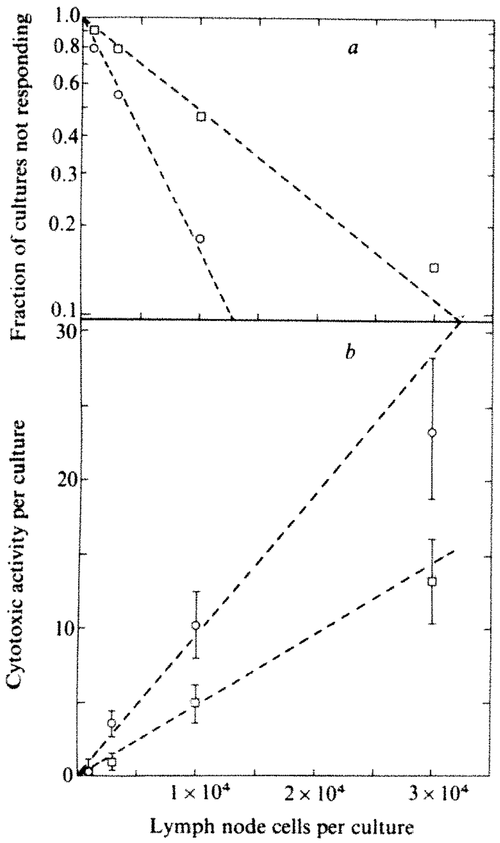

Fig. 1 Limiting dilution analysis of the RNC anti-RNC-TNP response in the presence of either RNC.nu (○) or RNC.nu-TNP (□) spleen cells. Groups of from 32 to 48 microcultures were set up and assayed as in Table 1. Each group contained RNC LN responder cells as indicated on the abscissa, 3×10^5 irradiated (1,500 rad) and TNP-modified RNC spleen stimulator cells, and 3×10^5 RNC.nu spleen cells either with or without TNP modification. The fraction of non-responding cultures as a function of the number of LN cells is plotted in *a*. A culture was scored as responding if the measured ^{51}Cr release was greater than the mean + 2 s.e.m. measured for a group of cultures from which LN responder cells were omitted. The mean cytotoxic activity per culture (including both responding and non-responding cultures) is plotted in *b* as a function of the number of LN responder cells cultured.

difficult to see how TNP modification could create a new receptor.

The unique properties of the suppressive activity described here are that the suppression is specific for antigens carried by the suppressive cell population and that the suppression is at the level of CLP activation in the responding cell population. Other tissues besides nude spleen have been screened for suppressive activity with the above properties. It is not seen in normal spleen[9,14] but is found in both normal bone marrow[14] and in thymus[15]. The suppressive activity found in bone marrow may represent a precursor population which seeds to thymus in a normal mouse but seeds to spleen in the athymic nude mouse. In the thymus, the suppressor cell could inactivate cells recognizing it before such cells are exported to the periphery. Such a mechanism is required in models for the somatic development of the specificity repertoire in which reactions against self antigens, particularly self H-2[16] are instrumental in driving the somatic variation of the repertoire. Cells reactive against foreign antigens might also be inactivated if the foreign antigens were incorporated on the surface of the suppressor cell.

I thank H. Derry, A. Hornby-Smith and D. Course for technical assistance; L.-M. Ching, A. J. Cunningham and R. A. Phillips for discussion and critical comments; and the MRC of Canada (MT 3017) for financial support.

Received 7 May; accepted 5 August 1980.

1. Burnet, F. M. *Cold Spring Harb. Symp. quant. Biol.* **32,** 1–8 (1967).
2. Cantor, H. & Gershon, R. K. *Fedn Proc.* **38,** 2058–2064 (1979).
3. Cunningham, A. J. *Transplantn Rev.* **31,** 23–43 (1976).
4. Claman, H. N. *Cell. Immun.* **48,** 201–207 (1979).
5. Borel, Y., Kilham, L., Kurtz, S. E. & Reinisch, C. L. *J. exp. Med.* **151,** 743–748 (1980).
6. Cerottini, J.-C. & Brunner, K. T. *Adv. Immun.* **18,** 67–132 (1974).
7. Bach, F. H., Bach, M. L. & Sondel, P. M. *Nature* **259,** 273–281 (1976).
8. Miller, R. G., Teh, H.-S., Harley, E. & Phillips, R. A. *Immun. Rev.* **35,** 38–58 (1977).
9. Miller, R. G. & Derry, H. *J. Immun.* **122,** 1502–1509 (1979).
10. Teh, H.-S., Harley, E., Phillips, R. A. & Miller, R. G. *J. Immun.* **118,** 1049–1056 (1977).
11. Shearer, G. M., Rehn, T. G. & Schmitt-Verhulst, A. M. *Transplantn Rev.* **29,** 222–250 (1976).
12. Doherty, P. C., Blanden, R. V. & Zinkernagel, R. M. *Transplantn Rev.* **29,** 89–123 (1976).
13. Jerne, N. K. *An. Immun.* **125C,** 373–389 (1974).
14. Muraoka, S. & Miller, R. G. *J. exp. Med.* **152,** 54–71 (1980).
15. Miller, R. G. (in preparation).
16. Jerne, N. K. *Eur. J. Immun.* **1,** 1–9 (1971).
17. Shearer, G. M. *Eur. J. Immun.* **4,** 527–533, 1974.
18. Teh, H.-S., Phillips, R. A. & Miller, R. G. *J. Immun.* **121,** 1711–1717 (1978).
19. Miller, R. G. & Dunkley, M. *Cell. Immun.* **14,** 284–302 (1974).
20. Porter, E. H. & Berry, R. J. *Br. J. Cancer* **17,** 583–595 (1964).
21. Miller, R. G. & Phillips, R. A. *J. cell. Physiol.* **73,** 191–201 (1969).

Intercellular communication patterns are involved in cell determination in early molluscan development

S. W. de Laat*, L. G. J. Tertoolen*,
A. W. C. Dorresteijn† & J. A. M. van den Biggelaar†‡

* Hubrecht Laboratory, International Embryological Institute, Uppsalalaan 8, 3584 CT Utrecht, The Netherlands
†Zoological Laboratory, State University of Utrecht, Padualaan 8, 3508 TB Utrecht, The Netherlands

The formation of specialized intercellular junctions, allowing the passage of low-molecular weight regulatory molecules, has been considered as a possible mechanism for regulating embryonic development[1,2]. No direct evidence for this concept has been found in early development. In the mollusc *Pattella vulgata* it was demonstrated that cell positioning and specific cellular interactions are key factors in the control of early development[3,4]. We have now investigated the pattern of intercellular communication during early development of this embryo by intracellular iontophoresis of the fluorescent dye Lucifer Yellow CH. We demonstrate that the formation of regional- and temporal-specific cell-to-cell coupling is correlated with the determination of the mesentoblast—the stem cell of the mesoderm—and the establishment of dorso-ventral polarity.

In the *Patella* embryo, bilateral symmetry is indicated from the 4-cell stage by the appearance of a distinct cross-furrow between the blastomeres B and D and a minimal one between the blastomeres A and C (Fig. 1)[3,4]. At the early 32-cell stage the macromeres of each quadrant (3A–3D) still have the capacity to develop into mesentoblast or to form entodermal structures. At this stage these macromeres protrude into the embryo after the withdrawal of the originally centrally placed second quartet cells. As a consequence of their relative positions only one of the cross-furrow macromeres (then denoted as 3D) is in contact temporarily with the overlying animal micromere quartet ($1a^{11}$–$1d^{11}$), and it is this event which determines that this macromere will form the mesentoblast and establishes dorso-ventral polarity perpendicular to the cross-furrow. Cell deletion experiments have demonstrated that such contact between the

---

‡ To whom correspondence should be addressed.

0028-0836/80/410546—03$01.00

macromere 3D and the micromeres $1a^{11}$–$1d^{11}$ is a prerequisite for these determinative events[4].

The intercellular transfer of low-molecular weight fluorescent dyes and intercellular electrical coupling are both considered as indicators for the presence of functional cell-to-cell pathways, structurally recognizable as gap junctions in the apposed junctional membranes[5,6]. Complex intercellular communication patterns can be easily recognized from intercellular transfer of fluorescent dyes. Lucifer Yellow CH (molecular weight 457.3) is extremely suitable for this purpose[7], and its intercellular transfer was found to be associated with the presence of gap junctions and electrical coupling[8,9].

As we were interested in the possible role of intercellular coupling in mesentoblast determination, we restricted the dye application to the vegetal macromeres, both cross-furrow and non-cross-furrow, from the 4-cell stage to the 32-cell stage. Because the dorso-ventral polarity of the embryo is absent at early cleavage stages, identification of the injected cell had to be made by the unequal cleavage pattern at the sixth cleavage[3]. In all cases Lucifer Yellow CH spread through the entire cell within 5 min. No effects were observed on subsequent cell division. Until the 16-cell stage initial dye spread was restricted consistently to the impaled cell, demonstrating the absence of functional intercellular communication pathways (Fig. 1*a*–*d*). This situation changed completely after the fifth cleavage. At the 32-cell stage, as the vegetal macromeres start to protrude into the embryo, intercellular junctions that allow the passage of Lucifer Yellow CH form between the vegetal macromeres and their neighbouring cells (Fig. 2*a*, *b*), with the exception of the junctional membrane between the macromere 3D and the blastomere $2d^2$, its neighbour on the future dorsal side (Figs 2*c*, *d* and 3). This communication pattern demonstrates the establishment of dorso-ventral polarity at the 32-cell stage. No dye transfer was observed from the macromeres 3A, 3B or 3C to animal cells. In contrast, the macromere 3D becomes exclusively coupled to the central animal micromere quartet $1a^{11}$–$1d^{11}$ at this stage (Fig. 2*e*, *f*). Although the non-central micromeres $1a^{12}$–$1d^{12}$, surrounding the central micromeres $1a^{11}$–$1d^{11}$, will come temporarily into contact with any of the macromeres at the early 32-cell stage, no dye transfer was observed between them. We conclude that only the central micromere quartet is able to become coupled to a macromere. By observing whole embryos we could not exclude the possibility that there is minimal dye transfer from the macromeres to their second neighbouring cells. However, histological sections of embryos fixed after dye injection confirmed that dye transfer from the macromeres is restricted to their neighbouring cells (Fig. 3).

Our results further demonstrate the binding of Lucifer Yellow CH to cytoplasmic components, as suggested previously[7]. With dye application at the 4-cell stage, fluorescence is only detectable in all daughter cells at later stages (Fig. 1*e*–*h*), in contrast to the dye spread observed immediately on dye injection into a macromere at the 32-cell stage (Fig. 2). From such considerations we estimated that cytoplasmic binding prevents further transfer of Lucifer Yellow CH in these embryos within about 30 min.

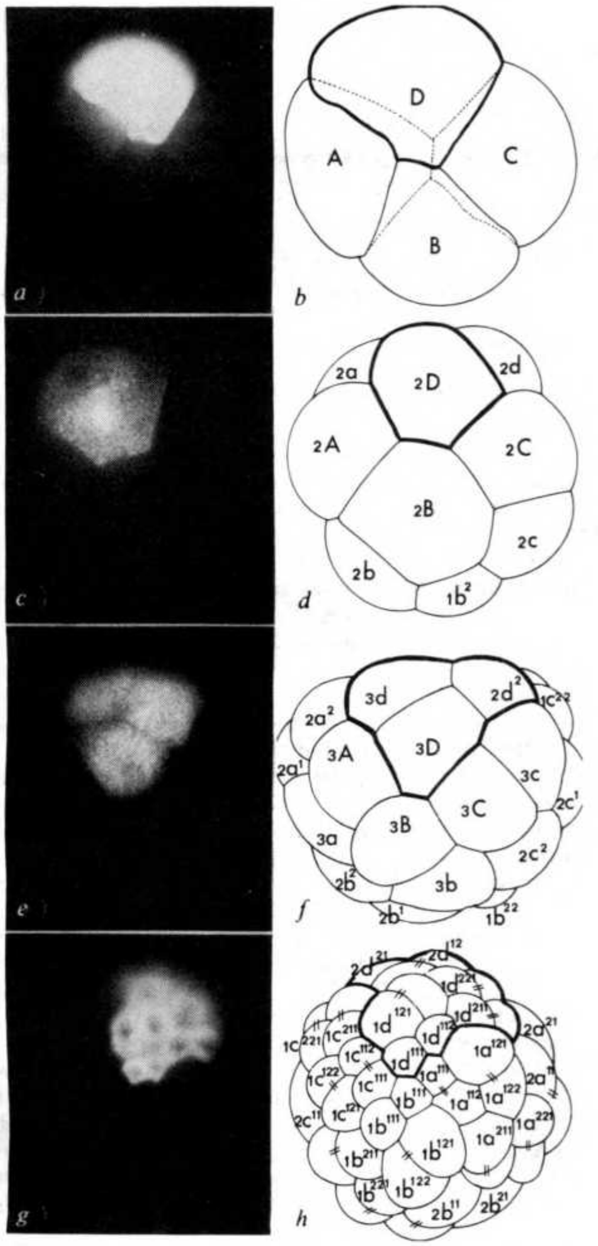

Fig. 1 Left column: micrographs of unfixed embryos of *Patella vulgata* after iontophoresis of Lucifer Yellow CH into one of the two cross-furrow cells at the 4- and 16-cell stage ×200. Right column: diagrams of the corresponding cell patterns. Before the mid 32-cell stage the two cross-furrow quadrants cannot be distinguished. For convenience the labelled quadrant has then been designated as D. *a*, *b*: 4-cell embryo 20 min after labelling of the D-cell; no dye transfer to adjacent cells. *c*, *d*: 16-cell embryo 20 min after labelling the macromere 2D; no dye transfer to adjacent cells. *e*, *f*: Vegetal view of the same embryo as in *a* at the onset of the 32-cell stage; only the progeny of D (3D, 3d, $2d^2$; others not visible) have received the dye. *g*, *h*: Animal view of the same embryo as in *a* at the 60-cell stage; only the micromeres of the injected quadrant have received the dye at successive cell divisions. *P. vulgata* used in this study were collected in the region of Point aux Oies, near Wimereux in France. Eggs were obtained, fertilized and cultured as described elsewhere[3]. The eggs were decapsulated by a brief treatment with acidified sea water, *p*H 3.8. Conventional glass microelectrodes were used for intracellular application of Lucifer Yellow CH. The tip of the micropipette was filled with a 3% aqueous solution of the dye whereas the remainder of the electrode system was filled with 3 M LiCl. Electrode resistances reached values greater than 200 MΩ. The dye was introduced iontophoretically into the cell by applying repetitive hyperpolarizing current pulses of 5 nA and 1.5 s with a time interval of 0.5 s for 3 min. The microelectrodes were connected to a high-impedance pre-amplifier equipped with a bridge circuit so that the membrane potential (−35 to −65 mV, depending on developmental stage) could be recorded as an indicator for proper cell penetration. During dye iontophoresis the embryos were observed in a dissecting microscope. The spread of fluorescence was observed in a Leitz Orthoplan epiluminescence fluorescence microscope with a ×32 objective (excitation: 450–490 nm; emission: >515 nm). Photomicrographs were taken on Kodak High Speed Ektachrome or Kodak High Speed Recording Film, with exposure times of 15–30 s.

The present results are the first demonstration that the formation of specific intercellular communication patterns is involved in cell determination in early development. In *P. vulgata* the interaction between the central micromere quartet and a macromere at the 32-cell stage results in the determination of this macromere as the stem cell of the mesoderm and of the dorso-ventral polarity in the embryo. The reported formation of intercellular communication pathways, probably via gap junctions, is exactly correlated in time and space with these determinative events. In this embryo the relative positions of the macromeres, together with the capacity of the cells along the animal–vegetal axis to become coupled at the 32-cell stage, determine bilateral symmetry.

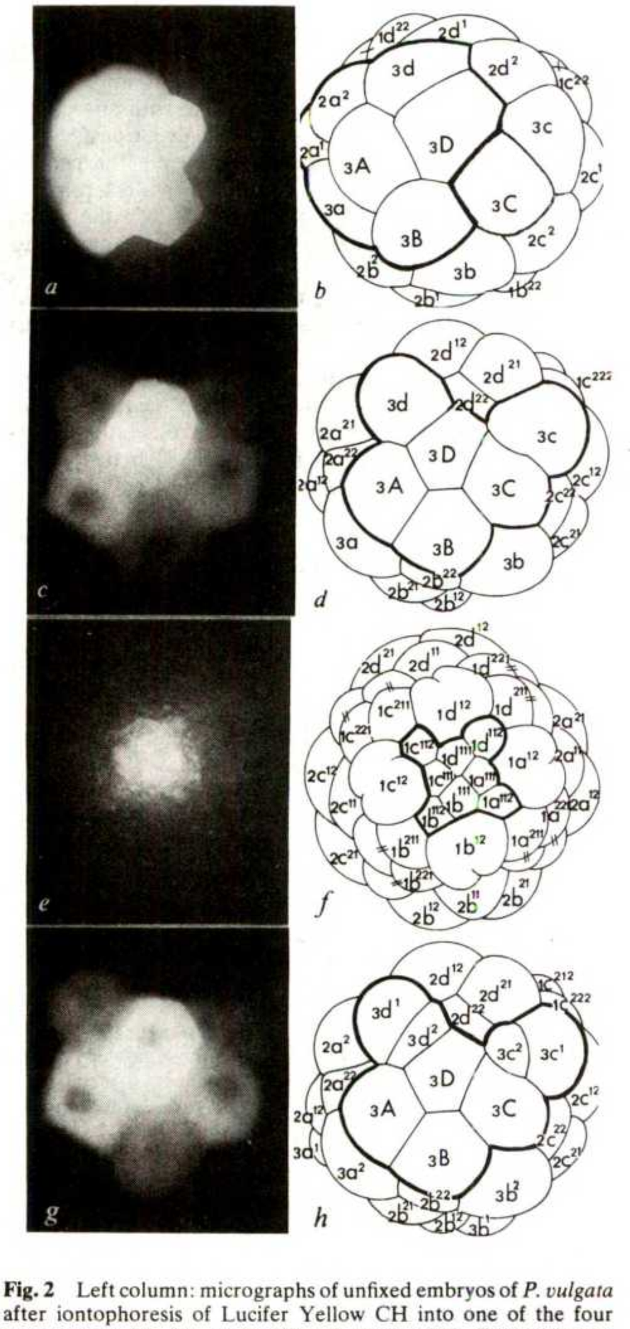

Fig. 2 Left column: micrographs of unfixed embryos of *P. vulgata* after iontophoresis of Lucifer Yellow CH into one of the four macromeres 3A–3D at the 32-cell stage ×200. Right column: diagrams of the corresponding cell patterns. *a*, *b*: Vegetal view of a 32-cell embryo after labelling macromere 3A; dye transfer is restricted to all adjacent cells. *c*, *d*: Vegetal view of a 32-cell embryo after labelling the macromere 3D; dye transfer is restricted to adjacent cells, except 2d^2. *e*, *f*: Animal view of the same embryo as in *c*, about 45 min later; dye transfer from the macromere 3D to the central animal micromeres. *g*, *h*: Vegetal view of the same embryo as in *c*, about 60 min later; no further transfer in comparison with *c*.

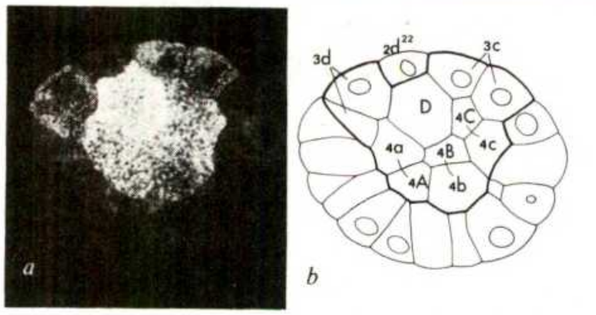

Fig. 3 *a*, Micrograph of an oblique section through an older stage of the same embryo as in Fig. 2*c*, *e*, *g* after fixation in 4% formaldehyde in 0.1 M cacodylate buffer, *p*H 7.4. Dye is only detectable in cells adjacent to the injected macromere 3D (3A, 3B, 3C, 3d, 3c) and their progeny, except its dorsal neighbour 2d^{22}. *b*, Diagram of the corresponding cell pattern ×200.

We thank Dr W. W. Stewart for his gift of Lucifer Yellow CH.

Received 19 May; accepted 18 August 1980.

1. Loewenstein, W. R. *Devl Biol.* **19**, Suppl. 2, 151–183 (1968).
2. Loewenstein, W. R. *Perspectives biol. Med.* **11**, 260–272 (1968).
3. Biggelaar, J. A. M. van den *J. Morph.* **154**, 157–186 (1977).
4. Biggelaar, J. A. M. van den & Guerrier, P. *Devl Biol.* **68**, 462–471 (1979).
5. Loewenstein, W. R. *Biochim. biophys. Acta* **560**, 1–65 (1979).
6. Unwin, P. N. T. & Zampighi, G. *Nature* **283**, 545–549 (1980).
7. Stewart, W. W. *Cell* **14**, 741–759 (1978).
8. Kater, S. B. & Galvin, N. J. *J. Cell Biol.* **79**, 20–26 (1978).
9. Spray, D. C., Harris, A. L. & Bennett, M. V. L. *Science* **204**, 432–434 (1979).

Pharmacological specificity of brain histamine H_2-receptors differs in intact cells and cell-free preparations

M. Dam Trung Tuong, M. Garbarg & J. C. Schwartz

Unité 109 de Neurobiologie, Centre Paul Broca de l'INSERM,
2ter, rue d'Alésia, 75014 Paris, France

Despite increasing evidence that histamine may be a neurotransmitter in brain, the functions of putative histaminergic neurones are just beginning to be known[1,2]. Both H_1- and H_2-receptors[3] seem to be present in brain[4–7] and histaminergic neurones might control arousal mechanisms or carbohydrate metabolism, via H_1-receptors[8–11]. The actions mediated by cerebral H_2-receptors are less clear mainly because available agonists and antagonists[3,12–15] do not cross the 'blood–brain barrier'. However, on a histamine-sensitive adenylate cyclase from guinea pig brain homogenates with pharmacological properties similar to those of H_2-receptors[16,17] compounds like tricyclic antidepressants or promethazine were extremely potent antagonists[18,19] suggesting that this might represent the molecular basis of clinical antidepressant activity[19]. Although electrophysiological[20] and behavioural[21] studies partially confirmed that one of these compounds, amitryptiline, could block cerebral histamine receptors in the living animal, their potency as H_2-antihistamines has never been precisely established in intact brain cell preparations. Histamine strongly stimulates cyclic AMP synthesis in brain slices but, in contrast with homogenates, both H_1- and H_2-receptors are involved[4,5,22]. As compounds like promethazine are potent H_1-antihistamines[7,8], we have developed a test specific for H_2-receptors consisting of the stimulation of cyclic AMP accumulation by impromidine, a potent and highly selective H_2-receptor agonist[14], in slices from guinea pig hippocampus and using it find that H_2-receptors differ considerably in their drug discriminatory properties from those mediating the stimulation of adenylate cyclase activity in homogenates.

0028–0836/80/410548—04$01.00

The involvement of both H_1- and H_2-receptors in the cyclic AMP response to histamine in hippocampal slices was shown mainly by the biphasic rightward shift of concentration–response curves to this amine in the presence of low concentrations of mepyramine, a pure H_1-antihistamine and the additive responses to H_1- and H_2-agonists[22]. This is further illustrated when considering the antagonism of histamine-induced accumulation of the nucleotide in slices of guinea pig hippocampus by promethazine, a potent H_1-antihistamine[23], also recently shown to inhibit the brain histamine-sensitive adenylate cyclase[19,24]. Thus the response to a fixed concentration of histamine (50 μM) is inhibited in a clearly biphasic manner by promethazine in increasing concentrations (Fig. 1). Approximately 50% of the response is inhibited with an IC_{50} of 0.13 μM whereas the remaining is abolished, after a plateau, for much higher concentrations (IC_{50} = 32.9 μM). A similar pattern of inhibition is obtained with cyproheptadine leading to IC_{50} values of 0.03 μM and 12 μM (not shown). Among the two components of the histamine response distinguished by promethazine, the first is likely to be mediated by H_1-receptors as proposed earlier[22], whereas the second is mediated by H_2-receptors as shown by the antagonism of highly selective agonists of these receptors. One of them, impromidine, is a particularly useful tool being 40–50 times as potent as histamine on a variety of biological responses mediated by H_2-receptors but having negligible potency on H_1-receptors[14]. As shown in Fig. 2a, this compound stimulates cyclic AMP accumulation in hippocampal slices with an EC_{50} value of 0.17 μM, that is, approximately 60 times lower than that of histamine and this effect is competitively antagonized by cimetidine, a H_2-antihistamine, with a K_i value of 0.95 μM similar to that found against histamine on peripheral H_2-receptors[13]. Thus, both its relative potency and the inhibition constant of cimetidine indicate that H_2-receptors mediate the stimulation elicited by impromidine. Promethazine antagonizes in a monophasic manner the response to impromidine with an IC_{50} of 22 μM (Fig. 1). This antagonism is of the competitive type as shown by the parallel rightward shift of the concentration–response curve to this H_2-agonist (Fig. 2a) and a K_i value of 6.2 μM is thus obtained. This value closely agrees with that (5.5 μM) obtained from the IC_{50} value regarding the second component of the response to histamine (Fig. 1). Again, as shown in Fig. 2b, a closely similar K_i value for promethazine (5.2 μM) is obtained regarding its apparently competitive antagonism of the response to dimaprit, another selective agonist of H_2-receptors possessing approximately 20% of the potency of histamine on peripheral biological systems[15].

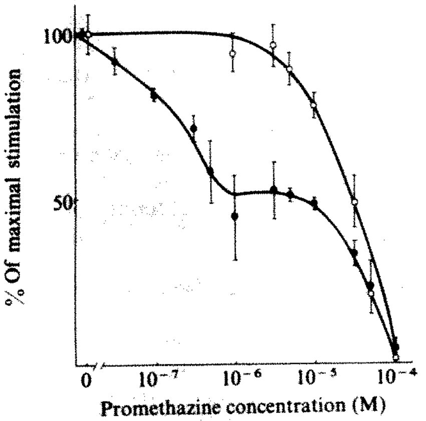

Fig. 1 Inhibition by promethazine of histamine- and impromidine-induced stimulation of cyclic AMP accumulation in slices from guinea pig hippocampus. Hartley guinea pigs were killed by decapitation and slices (250 μm thick) were prepared from hippocampus. Pooled slices from four animals were incubated for 30 min at 37 °C in Krebs–Ringer bicarbonate medium (40 ml per g of tissue) under a constant stream of O_2:CO_2 (95:5) in a Dubnoff metabolic shaker. Slices were then washed twice with fresh medium and 200 μl aliquots (about 500 μg protein) were distributed in incubation tubes containing promethazine. After 15 min at 37 °C under agitation, histamine or impromidine were added and a further 15-min incubation was performed. Incubations were terminated by sonication of the slices and heating for 10 min at 95 °C. Cyclic AMP concentration was determined by the protein kinase binding assay[39]. Results are expressed as per cent of stimulation elicited in the absence of promethazine. Each point represents the mean ±s.e.m. of six values obtained in two separate experiments. The accumulation of cyclic AMP (in pmol per mg protein) was 64.0±2.7 for 50 μM histamine and 39.7±2.2 for 1 μM impromidine. Basal levels (11.6±1.3 pmol per mg protein^{-1}) were not altered in the presence of promethazine in concentrations up to 100 μM. The IC_{50} values for promethazine, established by log-probit analysis, were 0.13 μM and 32.9 μM against histamine, and 22.0 μM against impromidine. Assuming competitive inhibition, the K_i values were calculated according to the equation[40] $K_i = IC_{50}/1 + S/EC_{50}$, where S represents the concentration of histamine or impromidine. The EC_{50} value of histamine was 10 μM (ref. 22) and that of impromidine, 0.16 μM (mean of values obtained in seven experiments similar to that of Fig. 2). K_i values were 0.022 μM against the first component of the response to histamine, 5.5 μM against the second component and 3.0 μM against impromidine. ●, Histamine (50 μM); ○, impromidine (1 μM).

Table 1 Comparison of the potency of several drugs on the histamine H_2-receptor-mediated stimulation of cyclic AMP formation in slices and homogenates from guinea pig hippocampus

	Inhibition constants (K_i, μM)	
Drugs	Slices	Homogenates
H_2-receptor antagonists		
Cimetidine	0.62	0.89* 0.60†
Metiamide	0.82	0.89* 0.87†
H_1-receptor antagonists		
Promethazine	3.0	0.030‡
Cyproheptadine	5.7	0.037§
Antidepressants		
Chlorimipramine	>10	0.053‡
Imipramine	>10	0.24† 0.14‡
Desmethylimipramine	>10	0.28‡
Amitriptyline	3.5	0.049* 0.036†
Mianserin	10.0	0.065*
Miscellaneous		
Chlorpromazine	5.9	0.041‡
Haloperidol	>10	0.081‡
Quinacrine	>10	0.26*

The antagonist potency on slices was determined against 1 μM impromidine as described in Fig. 1 legend. Drugs were added 15 min before impromidine in at least five concentrations and IC_{50} values obtained by log-probit analysis of mean data from sextuplate experiments. The EC_{50} mean value of impromidine in the absence of antagonist (0.16±0.02 μM) was determined from seven different concentration-response curves. None of the drugs modified the basal level or interacted with the kinase binding assay. The K_i values for homogenates are from: *, ref. 24; †, ref. 18; ‡, ref. 19; §, ref. 17.

Hence, the almost identical K_i values of promethazine regarding inhibition of the responses to histamine and to two H_2-agonists differing largely in chemical structure as well as in relative potency strongly support the conclusion that this compound has H_2-antihistamine activity. However, it is important to notice that its potency in the guinea pig hippocampal slice preparation is approximately 100-fold lower than on the histamine-sensitive adenylate cyclase of the cell-free preparation from the same region of guinea pig brain[19,24].

It was, therefore, of interest to determine the potency of other drugs that have been shown to strongly inhibit the cyclase in the cell-free preparation[18,19,24]. Most of the compounds listed in Table 1, including H_1-antihistamines, tricyclic antidepressants, antipsychotics and quinacrine, an inhibitor of histamine-N-methyltransferase, are significantly less potent on intact cells than on homogenates, the difference being, in most cases, more

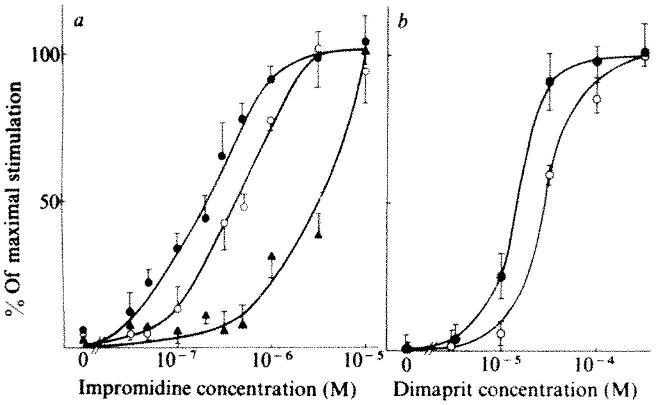

Fig. 2 Inhibition by promethazine or cimetidine of the stimulation of cyclic AMP accumulation in hippocampal slices elicited by two histamine H_2-receptor agonists. Promethazine and cimetidine were added 15 min before the agonists and incubations performed as described in Fig. 1 legend. Results are expressed as the per cent of maximal stimulation elicited in the absence of antagonist, that is, (in pmol of cyclic AMP per mg protein) 17.5 ± 1.1 for impromidine (*a*) and 16.2 ± 0.5 for dimaprit (*b*), the mean basal level being 5.9 ± 0.4. Mean ± s.e.m. of data from 3–6 values. The apparent dissociation constants of cimetidine, and promethazine were calculated according to the equation $K_i = A/(EC'_{50}/EC_{50} - 1)$ where A is the concentration of antagonist, and EC_{50} and EC'_{50} the concentrations of agonist required to give half-maximal response in the absence or in the presence of antagonist. The K_i values for cimetidine and promethazine inhibiting the response to impromidine were 0.95 μM and 6.2 μM, respectively. The K_i value for promethazine inhibiting the response to dimaprit was 5.2 μM. ●, Control; ○, promethazine (10 μM in *a*, 8 μM in *b*); ▲, cimetidine (5 μM).

than two orders of magnitude. However, this difference does not extend to the two H_2-antihistamines, metiamide and cimetidine, which have a similar effect on the two systems, with apparent dissociation constants in close agreement with those (0.75–0.96 μM) regarding inhibition of histamine effects on biological systems on which H_2-receptors have been initially defined, like the increase of contraction of guinea pig atrium or the inhibition of electrically induced contractions of rat uterus[13,25]. Hence it seems that the response to histamine on both systems can be considered to be mediated by H_2-receptors as in both cases several H_2-agonists exhibit the expected relative potencies and H_2-antagonists the expected affinities. However, compounds like the tricyclic antidepressants clearly discriminate between the 'H_2-receptors' from the two preparations, being much more potent than cimetidine on homogenates but less potent than this compound on intact brain cells.

The reasons for this discrepancy are not entirely clear at present but it is unlikely that the lower potency of compounds like promethazine or tricyclic antidepressants on the slice preparation results from their restricted diffusion into the intact tissue, for several reasons. First, their antagonist potency has been always determined following a 15-min period of preincubation to allow penetration into slices before the addition of histamine or agonists. Furthermore, we have observed for at least one compound, promethazine, that its potency was the same when it was added at the same time as histamine or impromidine. Second, promethazine has also a low potency (K_i of about 10 μM, as in hippocampal slices) regarding blockage of H_2-receptors mediating cyclic AMP accumulation in intact but isolated cells from stomach[26] or blood[27], that is, on preparations for which there is no diffusion problem. Indeed, as previously shown[22], the affinity of promethazine is also lower for H_1-receptors in slices compared to guinea pig ileum or ^3H-mepyramine binding sites, suggesting some nonspecific mechanism leading to a decreased potency of drugs at different receptor types in this preparation. But this is not the case for cyproheptadine which inhibits the response due to H_1-receptors in slices with an affinity (K_i, 0.005 μM) closely comparable to that found in other preparations[7] and nevertheless is 150 times less potent on H_2-receptors from slices than from homogenates.

It could be argued that, being highly lipophilic molecules, the relatively low potency of central nervous system (CNS)-active compounds like promethazine on the slice preparation might be related to extensive fixation on to 'sites of loss' like lipids. This seems unlikely because the concentration of ^3H-promethazine in the supernatant at the end of incubation is unchanged (data not shown).

It is also unlikely that the largely different potencies of these compounds on the two preparations reflect the interaction with two distinct subclasses of H_2-receptors. Thus the cyclic AMP response to histamine in homogenates parallels that in slices in various brain regions: for instance in the guinea pig (one of the few responsive species with both preparations) it is observed only in three regions which exhibit the same order of amplitudes (hippocampus > neocortex > striatum) for both preparations[16,28].

It seems more likely that the distinct pharmacology of H_2-receptors, when studied on a cell-free preparation as compared to intact cells, reflects modified drug discriminatory characteristics of these receptors which could be introduced either by the trauma of cell disruption or by the conditions required for optimal assay of adenylate cyclase activity. Several data already suggest that H_2-receptors on this test system may differ from those mediating physiological responses to histamine in intact organs, even when these responses may be triggered by cyclic AMP acting as second messenger. Hence promethazine and tricyclic antidepressants exhibit, as in brain, high affinities for the histamine-activated adenylate cyclase of homogenates from guinea pig heart[29,30] whereas both classes of agents seem to have inconsistent effects on the positive chronotropic and inotropic actions of histamine mediated by H_2-receptors in the intact organ[31,32].

One could postulate that the histamine-binding portion of H_2-receptors adopts a modified conformation when membranes which bear them are disrupted or when they are incubated in the presence of compounds like ATP, Mg^{2+}, GTP or EGTA which are required for optimal activation of the enzyme[33]. Selective modifications of the drug specificity of several classes of membrane receptors in the presence of guanylnucleotides or metal ions have already been evidenced in the last years by radioligand binding methods[34–36]. Alternatively, in the disrupted cell preparation some compounds might have access to regulatory or coupling units of the receptors that are normally hidden to them in the intact cell and thereby become potent inhibitors. Although this possibility seems *a priori* incompatible with the apparently competitive nature of the inhibition, established for most compounds[18,19,24], it cannot be entirely excluded in view of the complex interactions of histamine with the postulated allosteric sites for Mg^{2+} or nucleotides[33]. These various hypotheses may be checked when ^3H-ligands are available for studies of H_2-receptors.

Whatever the mechanism involved, note that a large difference in pharmacological specificity of striatal dopamine receptors mediating the stimulation of cyclic AMP formation in slices and homogenates, respectively, has recently been observed[37], whereas this does not seem to be the case of β-adrenergic receptors[38]. This suggests that the drug specificity of various types of receptors in cell-free systems has to be carefully compared to that in intact cell systems and that the idea that blockade of histamine H_2-receptors represents the common molecular basis of clinical activity of tricyclic antidepressants requires confirmation by other approaches.

Received 9 April; accepted 5 August 1980.

1. Schwartz, J. C. *A. Rev. Pharmac. Tox.* **17**, 325–339 (1977).
2. Green, J. P., Johnson, C. L. & Weinstein, H. in *Psychopharmacology: A Generation of Progress* (eds Lipton, M. A., Dimascio, A. & Killam, K. F.) 319–332 (Raven, New York, 1978).
3. Black, J. W., Duncan, W. A. M., Durant, G. J., Ganellin, C. R. & Parsons, M. E. *Nature* **236**, 385–390 (1972).

4. Baudry, M., Martres, M. P. & Schwartz, J. C. *Nature* **253**, 362–363 (1975)
5. Rogers, M., Dismukes, K. R. & Daly, J. W. *J. Neurochem.* **25**, 531–534 (1975)
6. Hill, S. J., Emson, P. C. & Young, J. M. *J. Neurochem.* **31**, 997–1004 (1978)
7. Tran, V. T., Chang, R. S. L. & Snyder, S. H. *Proc. natn. Acad. Sci. U.S.A.* **75**, 6290–6294 (1978)
8. Hill, S. J. & Young, J. M. *Eur. J. Pharmac.* **52**, 397–399 (1978)
9. Richelson, E. *Nature* **274**, 176–177 (1978).
10. Quach, T. T., Duchemin, A. M., Rose, C. & Schwartz, J. C. *Eur. J. Pharmac.* **60**, 391–392 (1979).
11. Quach, T. T., Duchemin, A. M., Rose, C. & Schwartz, J. C. *Molec. Pharmac.* **17**, 301–308 (1980).
12. Black, J. W., Durant, G. J., Emmett, J. C. & Ganellin, C. R. *Nature* **248**, 65–67 (1974)
13. Brimblecombe, R. W. *et al. J. Int. med. Res.* **3**, 86–92 (1975)
14. Durant, G. J. *et al. Nature* **276**, 403–405 (1978)
15. Parsons, M. E., Owen, D. A. A., Ganellin, C. R. & Durant, G. J. *Agents Actions* **7**, 31–37 (1977).
16. Hegstrand, L. R., Kanof, P. D. & Greengard, P. *Nature* **260**, 163–165 (1976)
17. Green, J. P., Johnson, C. L., Weinstein, H. & Maayani, S. *Proc. natn. Acad. Sci. U.S.A.* **74**, 5697–5701 (1977)
18. Green, J. P. & Maayani, S. *Nature* **269**, 163–165 (1977)
19. Kanof, P. D. & Greengard, P. *Nature* **272**, 329–333 (1978)
20. Haas, H. L. *Agents Actions* **9**, 83–84 (1979)
21. Nowak, J. Z., Bielkiewicz, B. & Lobrecht, U. *Neuropharmacology* **18**, 783–789 (1979)
22. Palacios, J. M., Garbarg, M., Barbin, G. & Schwartz, J. C. *Molec. Pharmac.* **14**, 971–982 (1978)
23. Marshall, P. B. *Br. J. Pharmac. Chemother.* **10**, 270–278 (1955)
24. Kanof, P. D. & Greengard, P. *J. Pharmac. exp. Ther.* **209**, 87–96 (1979)
25. Brimblecombe, R. W., Duncan, W. A. M., Owen, D. A. A. & Parsons, M. E. *Fedn Proc.* **35**, 1931–1934 (1976)
26. Batzri, S. & Gardner, J. *Molec. Pharmac.* **16**, 406–416 (1979)
27. Rudolph, S. A., Hegstrand, C. R., Greengard, P. & Malawista, S. E. *Molec. Pharmac.* **16**, 805–812 (1979)
28. Schwartz, J. C. *et al.* in *Histamine Receptors* (ed. Yellin, T. O.) 161–183 (Spectrum, New York, 1979)
29. Johnson, C. L., Weinstein, H. & Green, J. P. *Molec. Pharmac.* **16**, 417–428 (1979)
30. Kanof, P. D. & Greengard, P. *Molec. Pharmac.* **15**, 445–461 (1979)
31. Levi, R., Capurro, N. & Lee, C. H. *Eur. J. Pharmac.* **30**, 328–335 (1975).
32. Reinhardt, D., Wiemann, H. M. & Schümann, H. J. *Agents Actions* **6**, 683–698 (1976).
33. Kanof, P. D., Hegstrand, L. R. & Greengard, P. *Archs Biochem. Biophys.* **182**, 321–334 (1977).
34. Childers, S. R. & Snyder, S. H. *Life Sci.* **23**, 759–762 (1978)
35. Creese, I., Usdin, T. B. & Snyder, S. H. *Molec. Pharmac.* **16**, 69–76 (1979)
36. Wessels, M. R., Mullikin, D. & Lefkowitz, R. J. *Molec. Pharmac.* **16**, 10–20 (1979)
37. Saiani, L., Trabucchi, M., Tonon, G. C. & Spano, P. F. *Neurosci. Lett.* **14**, 31–36 (1979)
38. Williams, L. T. & Lefkowitz, R. J. *Receptor Binding Studies in Adrenergic Pharmacology* (Raven, New York, 1978)
39. Brown, B. L., Albano, J. D. M., Ekins, R. P. & Sgherzi, A. M. *Biochem. J.* **121**, 561–562 (1971)
40. Cheng, Y. C. & Prusoff, W. H. *Biochem. Pharmac.* **22**, 3099–3108 (1973)

Induction of experimental allergic encephalomyelitis in genetically resistant strains of mice

Zeev Lando, Dvora Teitelbaum & Ruth Arnon

Department of Chemical Immunology, The Weizmann Institute of Science, Rehovot, Israel

Experimental allergic encephalomyelitis (EAE) is an acute autoimmune disease of the central nervous system. It is elicited in various laboratory animal species by a single injection of either whole central nervous system tissue homogenate, or the purified basic encephalitogenic protein isolated therefrom. Clinical manifestations of hind leg paralysis usually occur 11–21 days after challenge, preceded by histological lesions of perivascular infiltration in the brain[1]. EAE has been intensively investigated both as a model for human demyelinating diseases and as a prototypic organ-specific autoimmune disease[1]. EAE is under genetic control in guinea pigs, rats and mice, and strains that are genetically susceptible or resistant to EAE have been demonstrated[2–4]. We have previously[4,6] investigated the genetic control of susceptibility to EAE in mice and demonstrated that the disease could be induced only in the SJL/J strain of mice, or in its crosses with various resistant strains. The resistance to EAE is not associated with genetic differences in the response of the various strains to pertussis vaccine, which is used as adjuvant in the induction of EAE in mice, as both the sensitive SJL/J strain and the resistant strains BALB/c, DBA/2 and C57BL/6J are responsive to pertussis[7]. A great difference was observed, however, in the sensitivity to EAE of the various F_1 hybrids of SJL/J. Thus, crossing the sensitive SJL/J strain with part of the resistant strains, such as NZB, BALB/c or its congenic strains BALB . B10 and BALB . C3H, led to fully susceptible hybrids, with even higher incidence of EAE than that observed in the parental SJL/J strain. On the other hand, crossing SJL/J with other strains, such as C57BL/6J or DBA/2, led to hybrids with very low susceptibility to EAE. These results suggested that in the crosses with the various resistant BALB strains and NZB strain, there is probably complementation with another gene. It was therefore postulated that in these resistant strains, the influence of the gene determining susceptibility to EAE is masked by the presence of naturally occurring suppressor cells. We present here experimental evidence which corroborates this assumption.

Mice of the resistant strain BALB/c were treated with various doses of cyclophosphamide (CY) 2 days before challenge with the basic protein (BE). This treatment, if carried out with appropriate low doses of CY, was previously shown to eliminate selectively suppressor cell population in several systems, resulting in depression of suppressive cell-mediated activity and augmentation of both cellular and humoral immune responses[8–11]. Figure 1 depicts the effect of CY on the susceptibility of BALB/c mice to the induction of EAE, showing that CY had a marked effect which is dose-dependent. At low doses (20 mg per kg), it drastically affected the resistance of the mice

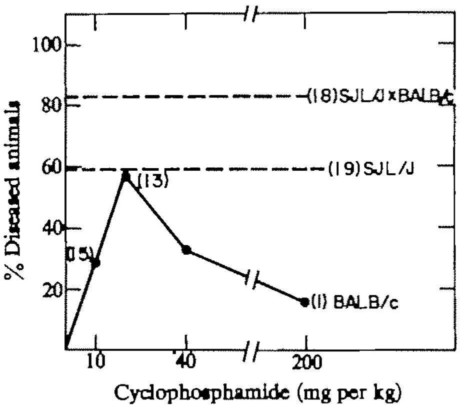

Fig. 1 Dose–response effect of CY on EAE induction in resistant BALB/c mice. EAE was induced by injecting 5 mg of dry lyophilized mouse spinal cord homogenate emulsified in 1:1 ratio in complete Freund's adjuvant supplemented with 4 mg ml^{-1} of *Mycobacterium tuberculosis* ($H_{37}Ra$) (Difco). The emulsion in total volume of 0.12 ml was injected in all four footpads. Immediately after and 48 h later, pertussis vaccine (*Bordetella pertussis*, Rafa Laboratories) 10×10^9 organisms, were injected intravenously. Mice were examined daily from day 11 post-induction for signs of EAE. Signs of disease were scored from 1 to 3 according to the clinical situation as follows: 1, loss of weight and loss of tail tonicity; 2, mild disease: paresis and paralysis of hind legs; 3, severe paralysis often leading to death. Animals were killed 18–24 days after injection and the whole brain and spinal cord were taken into 10% formalin solution for histological examination. Sagittal sections of brains and spinal cords, fixed in formalin and stained with Luxol fast blue, were examined microscopically for perivascular infiltration of mononuclear cells. The observations were done under code without knowledge of the injection regime. Solutions of CY (Polysciences), were freshly prepared by dissolving in minimal volume of ethanol and then diluted 100-fold in phosphate-buffered saline. CY was injected intraperitoneally 2 days before EAE induction. The numbers in the parentheses represent the mean score of disease signs. The broken lines represent the incidence of EAE in SJL/J and SJL/J × BALB/c mice without CY.

0028–0836/80/410551—02$01.00

to EAE—in these conditions BALB/c mice succumbed to the disease to the same extent and with the same severity as the susceptible strain SJL/J. Lower or higher doses of CY were less effective. High doses of CY (>200 mg per kg) affect the whole lymphoid system and suppress EAE induction altogether[12].

The effect of CY at its most effective concentration (20 mg per kg) was tested in additional resistant strains of various H-2 types. The results summarized in Table 1 demonstrate that in BALB.B10 and BALB.C3H, the congeneic strains of BALB/c, and to a lesser extent in the NZB strain, CY had a similar effect on the susceptibility to EAE to that demonstrated in BALB/c. On the other hand, in the other strains, such as C57BL/6J, DBA/2, AKR/J, ASW, B10.A and A/J, CY had no effect on the development of EAE. This phenomenon is therefore not linked to the H-2 type. It should be pointed out that in two of the these strains, C57BL/6J and B10.A, we have tested the effect of different doses of CY. No effect on EAE induction was observed at doses of 10, 20, 40 or 200 mg per kg. This experiment rules out the possibility that a non-optimal dose of CY was the factor responsible for the persistent unresponsiveness to EAE in those strains, and strengthens the conclusion that the involvement of suppressor cells in the resistance to EAE is not H-2 linked.

Similar effects to those demonstrated by CY on suppressor cells were also demonstrated in other systems by other immunosuppressive drugs, antilymphocyte serum, as well as by low-dose irradiation[8,11]. We therefore tested whether a similar effect to that demonstrated for CY on EAE induction could also be achieved using irradiation. BALB/c mice were exposed to whole body low-dose irradiation (200 R and 350 R) at various times before EAE induction. The results summarized in Table 2 demonstrate that when the mice were irradiated with 350 R 2 days before the encephalitogenic challenge, 50% of the otherwise resistant mice developed EAE.

It thus seems that there are two types of inbred strains that are resistant to EAE. Treatment with CY or low-dose irradiation can convert one type from resistant into susceptible, while it has no effect on the other type. It is suggested that in strains of the first type, a gene that is responsible for susceptibility to EAE does exist, but these strains probably maintain a natural high level of suppressor cells which prevent the manifestations of disease. Following treatment with CY, these suppressor cells are eliminated and disease is overt. In the F_1 hybrid, the balance between effector cells and suppressor cells is shifted towards the effector cell function, and therefore EAE can be induced. In addition, there is complementation of genes from the two parents and the resultant F_1 may be even.more sensitive. In rare cases, some animals of such strain may possess a lower level of suppressor cell, leading to the very low incidence of EAE in three resistant strains, even without CY treatment. In the second type of resistant strains, such as DBA/2, there is no Ir gene for EAE and therefore CY has no effect.

Table 1 Effect of low-dose CY on EAE induction

		Mice with EAE					
		Without CY			With CY		
	H-2 type	Clinical	Mean score	Histological	Clinical	Mean score	Histological
SJL/J	s	10/16	2.0	10/10	7/16	1.8	6/6
(SJL/J ×BALB/c)F_1	s/d	18/20	1.8	20/20	20/22	2.2	10/10
BALB/c	d	0/40		1/30	19/32	1.7	13/20
BALB.B10	b	1/28	1.0	1/5	4/11	1.3	4/10
BALB.C3H	k	2/20	2.0	1/11	4/8	1.8	4/8
C57BL/6J	b	1/19	1.0	2/19	0/18		1/8
NZB	d	0/7		0/5	2/8	2.0	5/7
DBA/2	d	0/6		0/6	0/5		0/5
AKR/J	k	0/19		0/9	0/17		0/8
B10A	a	0/7		0/7	0/9		1/8
ASW	s	0/11		2/6	0/10		0/7
A/J	a	0/6		0/6	0/6		0/4

EAE was induced as described in Fig. 1 legend. CY (20 mg per kg) was injected 2 days before disease induction.

Table 2 Effect of irradiation on EAE induction in BALB/c mice

Treatment	Mice with EAE	
	Clinical	Histological
None	0/7	0/7
200 R on day − 2	0/7	NT
350 R on day − 2	5/10	8/10
200 R on day 0	1/10	NT
350 R on day 0	3/10	3/6

NT, not tested.

[illegible] College
[illegible] Upper Circular Road
Calcutta

The results with CY and low-dose irradiation, although suggesting involvement of suppressor cells in regulation of sensitivity to EAE, do not provide unequivocal proof of the existence of such cells in resistant strains. However, we have recently demonstrated that CY eliminates suppressor cells involved in antigen-induced unresponsiveness to EAE[13]. In that study, protection against EAE[14] was induced in susceptible mice (SJL/J × BALB/c hybrid) by injection of an adequate protective antigen (spinal cord homogenate, BE or the synthetic polymer Cop 1) in incomplete Freund's adjuvant, before EAE induction. This unresponsiveness could be adoptively transferred by spleen T lymphocytes to normal syngeneic recipients. Low dose of CY (20 mk per kg) abrogated both actively induced and adoptively transferred unresponsiveness to EAE. It thus appears that in that system as well, the treatment with CY results in the elimination of suppressor cells, which interfere with the effector mechanisms responsible for EAE.

It is now well established that suppressor cells have a critical role in immune regulation, including maintenance of tolerance, antigenic competition and genetic control of immune responses[15]. It was also suggested that specific T-cell-mediated suppression could be one of the physiological processes of immune responsiveness against autoantigens[16]. In NZB mice it has been demonstrated that loss of effective suppressive T cell function can lead to autoimmune diseases[17]. The use of selective means for elimination of suppressor cells may assist in the elucidation of such activity in autoimmunity. Indeed, it was demonstrated that CY can induce a transient appearance of 'autoreactive' T lymphocytes in spleens of mice[18]. This accumulated information corroborates our present conclusion suggesting suppressor cell involvement in both natural and induced resistance to EAE.

Received 5 February; accepted 11 July 1980.

1. Paterson, P. Y. in *Textbook of Immunopathology* Vol. 1 (eds Misecher, P. A. & Muller-Eberhard, H. J.) 179–213 (Grune & Sratton, New York, 1976).
2. Stone, S. M. *Int. Archs Allergy appl. Immun.* **20,** 193–202 (1962).
3. Gasser, D. L., Newlin, C. M., Palm, J. & Gonatas, N. K. *Science* **181,** 872–873 (1973).
4. Bernard, C. C. A. *J. Immunogenet.* **3,** 263–274 (1976).
5. Teitelbaum, D., Lando, Z. & Arnon, R. in *Genetic Control of Autoimmune Disease,* 365–279 (Elsevier, Amsterdam, 1978).
6. Lando, Z., Teitelbaum, D. & Arnon, R. *J. Immunogenet.* **9,** 435–442 (1979).
7. Wardlaw, A. C. *Int. Archs Allergy appl. Immun.* **38,** 573–589 (1970).
8. Chiorazzi, N., Fox, D. A. & Katz, D. H. *J. Immun.* **117,** 1629–1637 (1976).
9. Askenase, P. W., Hayden, B. J. & Gershon, R. K. *J. exp. Med.* **141,** 697–702 (1975).
10. Rollinghoff, M., Starzinski-Powitz, A., Pfizenmayer, K. & Wagner, H. *J. exp. Med.* **145,** 455–459 (1977).
11. Chiorazzi, N., Fox, D. A. & Katz, D. H. *J. Immun.* **118,** 48–54 (1977).
12. Paterson, P. Y. & Drobish, D. G. *Science* **165,** 191–192 (1969).
13. Lando, Z., Teitelbaum, D. & Arnon, R. *J. Immun.* **123,** 2156–2160 (1979).
14. Alvord, E. C., Shaw, C. M., Hruby, S. & Kies, M. W. *Ann. N.Y. Acad. Sci.* **122,** 333–345 (1965).
15. Waldmann, T. A. & Broder, S. *Prog. clin. Immun.* **3,** 155–199 (1977).
16. Gershon, R. K. in *Autoimmunity* (ed. Talal, N.) 171–181. (Academic, New York, 1977).
17. Talal, N. *Transplantn Rev.* **31,** 240–263 (1976).
18. Lage-Stehr, J. & Diamanstein, T. *Eur. J. Immun.* **8,** 620–624 (1978).

Hormonal control of neurotransmitter choice in sympathetic neurone cultures

Keiko Fukada

Department of Neurobiology, Harvard Medical School, Boston,
Massachusetts 02115

Manipulation of the cellular and hormonal environment of cultures of dissociated primary neurones can be used to explore a neurone's developmental potential and to investigate the factors required for normal development. For example, developing adrenergic sympathetic neurones can be influenced to become cholinergic by both diffusible[1] and membrane-bound[2] factors from certain types of non-neuronal cells; when medium conditioned by incubation on heart cell cultures (CM) is placed on the neurones, they develop the ability to produce acetylcholine (ACh) and they form functional cholinergic synapses with each other[3]. Hormones could also contribute to the control of this transmitter choice[4], and McLennan *et al.*[5] recently reported that corticosterone treatment of whole superior cervical ganglia (SCG) greatly inhibited the cholinergic development of these ganglia in culture. It was not clear, however, whether the hormone acted directly on the neurones or indirectly via the non-neuronal cells. To study the role of hormones on this transmitter choice, I have now developed a serum-free medium (based on that of Sato and co-workers[6,7]) for the preparation of conditioned medium. The results obtained with this system show that glucocorticoids and epidermal growth factor (EGF) exert dramatic and antagonistic effects on the adrenergic–cholinergic transmitter choice and do so indirectly, by controlling the ability of heart cells to produce cholinergic CM.

Heart myocytes and heart fibroblasts (both simply called 'heart cells') were obtained by collagenase treatment of whole hearts from neonatal rats and grown in flasks containing 10% fetal calf serum (FCS, MA Bioproducts) in L-15 CO_2 medium[1]. After the cells had grown to confluency, they were either used for conditioning or were trypsinized and replated to be used as secondary cultures. To obtain conditioned medium, the flasks were washed with serum-free medium and incubated for 24 h with the medium to be conditioned. The CM was collected and frozen at −20 °C and the flasks were incubated for 24 h with the 10% FCS medium again. After washing, a second batch of medium to be conditioned was placed in the flasks for 24 h. This CM was collected and also frozen. Before addition to the neuronal cultures, the CM was thawed and mixed with an equal volume of fresh L-15 CO_2 medium containing, in addition to the usual components of the neuronal growth medium[8], 10% rat serum and 3 mg ml^{-1} Methocel. Control neuronal cultures received medium containing 5% rat serum and 1.5 mg ml^{-1} Methocel. In both cases, the medium was changed every 2 days. The neurones were mechanically dissociated from neonatal rat SCG and plated as previously described[8]. All neuronal cultures received control medium for the first 2 days and then experimental media until days 14–18, when they were assayed. Ganglionic non-neuronal cells were killed by treatment with cytosine arabinoside[8]. ^{3}H-ACh synthesis from ^{3}H-choline and ^{3}H-catecholamine (CA) synthesis from ^{3}H-tyrosine were assayed as previously described[1,9]. The ratio of synthesis of these transmitters, ACh/CA, is a sensitive indicator of the number of cholinergic as opposed to adrenergic neurones in this culture system[10].

Table 1 Effects of hormones on cholinergic induction

Additives	ACh/CA	ACh (pmol per dish)	CA (pmol per dish)
a BSA	0.03±0.01	0.20	7.26
EGF	0.18±0.03	1.22	6.53
EGF+BSA	2.47±0.10	12.53	5.07
EGF+BSA+insulin	7.53±0.71	25.25	3.38
EGF+BSA +transferrin	2.00±0.09	13.91	6.99
EGF+BSA+insulin +transferrin	9.09±0.15	32.86	3.62
EGF+insulin +transferrin	0.26±0.01	2.48	9.73
BSA+insulin +transferrin	0.04±0.01	0.51	11.98
Insulin+transferrin	0.04±0.01	0.44	11.12
b 5% Rat serum	4.20±0.09	18.56	4.41
5% Rat serum +hydrocortisone	1.57±0.12	8.40	5.33
EGF+BSA+insulin +transferrin	9.09±0.15	32.86	3.62
EGF+BSA+insulin +transferin +hydrocortisone	0.62±0.12	9.85	15.60
5% Rat serum+EGF +insulin+transferrin	6.00±0.88	24.14	4.08
5% Rat serum+EGF +insulin+transferrin +hydrocortisone	4.92±0.40	24.67	4.94

Confluent heart cells were incubated in L-15 CO_2 medium with various combinations of hormones and growth factors as substitutes for serum. The concentrations used were: BSA, 2.5 mg ml^{-1} (Sigma); EGF, 20 ng ml^{-1} (purified according to Savage and Cohen[13] or from Collaborative Research); hydrocortisone, 10^{-6}M (Sigma); insulin, 5 μg ml^{-1} (Sigma); selenium, 30 nM (Johnson Matthey, treated as in ref. 14); transferrin, 25 μg ml^{-1} (Sigma). Sympathetic neurones were grown in 50% CM from these cultures and transmitter synthesis was assayed on day 18.

Table 2 Identification of target of EGF action

	ACh/CA	ACh (pmol per dish)	CA (pmol per dish)
a Complete serum-free medium incubated in an empty flask	0.05±0.01	0.17	3.26
b Complete serum-free medium incubated on heart cells	3.66±0.25	12.57	3.44
c Serum-free medium, without hormones, incubated on heart cells, with fresh hormones added before placing on neurones	0.05±0.01	0.25	4.70
d Complete serum-free medium (−EGF) incubated on heart cells, with fresh EGF added before placing on neurones	0.05±0.01	0.19	3.90

Sympathetic neurones were grown for 14 days in 50% CM made by incubation in conditions *a* – *d*.

Heart cells were grown with various combinations of hormones and growth factors as substitutes for serum. CM from these cultures were tested for induction of ACh synthesis in neuronal cultures. The results of a typical experiment testing a variety of hormones are shown in Table 1*a*. CM from heart cells treated with medium containing bovine serum albumin (BSA) as the only additive gave the usual low ACh/CA ratio expected for medium with no additions at all. If EGF was used as the only additive, there was a significant increase in the ACh/CA ratio. This effect of EGF was greatly enhanced by the addition of BSA. Similarly, insulin had a synergistic effect on the transmitter ratio

0028–0836/80/410553—03$01.00

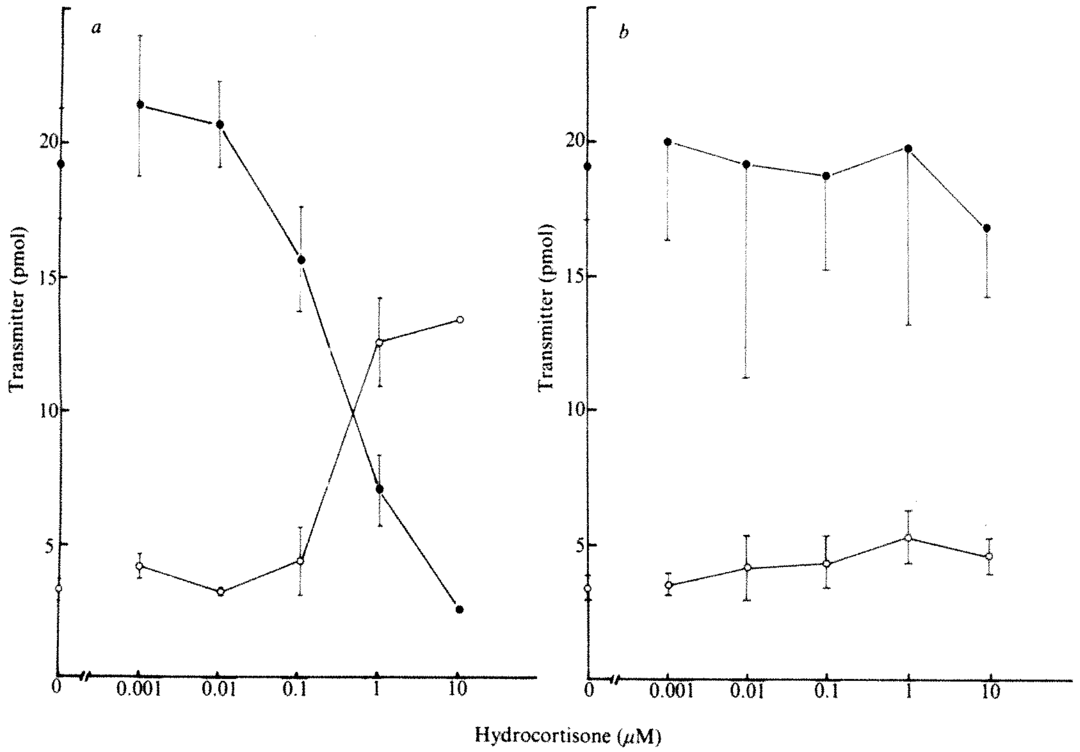

Fig. 1 *a*, Hydrocortisone was added at various concentrations to heart cells in complete serum-free medium for 24 h and the CM was tested for induction of neuronal ACh synthesis. *b*, Fresh hydrocortisone was added directly to neurones in complete serum-free medium conditioned on heart cells. The amounts of transmitters synthesized at day 17 (●, acetylcholine; ○, catecholamine) are expressed as pmol per dish. Points are means ±s.e.m. of triplicate cultures.

when added along with EGF, but had no effect in the absence of EGF. The effect of transferrin was variable and small. The most potent CM was consistently obtained using EGF, BSA, insulin and transferrin, and medium containing these additives is termed 'complete' serum-free medium.

In comparison, hydrocortisone had a striking inhibitory effect on the transmitter ratio. As shown in Table 1*b*, this hormone antagonizes the cholinergic effects of both the complete serum-free CM and CM containing the usual 5% rat serum. The 15-fold effect of hydrocortisone on the transmitter ratio in serum-free conditions is typical of the values seen in more than 10 such experiments. Other glucocorticoids (corticosterone, cortisone and dexamethasone) showed similar antagonistic effects on ACh induction. Both the cholinergic effect of complete serum-free conditioned medium and the antagonistic effect of hydrocortisone are reduced in the presence of 5% rat serum, suggesting that the complex mixture of hormones in serum obscures the effect of individual hormones.

Other hormones which showed small positive effects on the transmitter ratio were fibroblast growth factor (100 ng ml^{-1}, Collaborative Research) and relaxin (10 ng ml^{-1}) when added together with BSA, insulin and transferrin. Hormones showing little effect on the ratio were growth hormone (20 ng ml^{-1}), 3,3′,5-triiodothyronine (10^{-10} M, Sigma), prolactin (10 ng ml^{-1}), partially purified thyroid stimulating hormone (100 ng ml^{-1}) and follicle stimulating hormone (0.5 μg ml^{-1}), progesterone (10^{-9}M, Sigma), testosterone (5 × 10^{-9}M, Sigma), oestradiol (5 × 10^{-9}M, Sigma) and aldosterone (10^{-9}M, Sigma). Selenium, which is essential in some serum-free systems[7], had little effect on the transmitter ratio.

Do the hormones influence transmitter choice by acting directly on the neurones, or indirectly, by altering the ability of the heart cells to produce cholinergic CM? These possibilities were tested in the experiments shown in Table 2 and Fig. 1. Complete serum-free medium was incubated for 24 h in either an empty flask (*a*) or in one containing heart cells (*b*), and these CM were tested on the neurones. As expected, the heart cells were essential for the induction. Furthermore, if the hormones were added to serum-free conditioned medium (minus hormones, incubated on the heart cells) immediately before it was placed on the neurones (*c*), no cholinergic induction occurred. Addition of fresh EGF to complete (except for EGF) serum-free CM was similarly ineffective when added directly to the neurones (*d*). EGF had a very striking cholinergic inductive effect when added at 10 ng ml^{-1} on the heart cells, but had no effect when added directly to the neurones, even at higher concentrations (data not shown). Thus, the EGF effect on neuronal transmitter choice is an indirect one, via the heart cells.

When the same type of experiment was conducted with hydrocortisone, two different effects were seen (Fig. 1). When added to the heart cultures (Fig. 1*a*), this hormone antagonized the cholinergic effect of the complete serum-free CM, resulting in both lower ACh and higher CA production by the neurones. On the other hand, addition of hydrocortisone to the CM just before placing it on the neurones had little effect on cholinergic development, but may have slightly increased CA production (Fig. 1*b*). This latter effect has been observed before in this system (L. Chun, P. Walicke & P. H. Patterson, unpublished

Table 3 Effects of hormones on heart cells

	Labelled protein (c.p.m.)	Total protein (μg per dish)
a No hormones	7,951 ± 243	0.23 ± 0.04
EGF + BSA + insulin + transferrin	11,620 ± 448	0.26 ± 0.01
EGF + BSA + insulin + transferrin + hydrocortisone	10,732 ± 110	0.27 ± 0.04
5% Rat serum	12,850 ± 2,095	0.28 ± 0.01
5% Rat serum + hydrocortisone	13,708 ± 1,288	0.27 ± 0.01
		DNA (μg per flask)
b BSA + insulin + transferrin		26.2
EGF + BSA + insulin + transferrin		26.6
EGF + BSA + insulin + transferrin + hydrocortisone		30.7
5% Rat serum		34.3
5% Rat serum + hydrocortisone		32.9

a, Confluent heart cells were labelled with ^{3}H-leucine in L-15 CO$_2$ medium supplemented with hormones as indicated. After a 24-h incubation, the cells were washed with several changes of unlabelled medium for 30 min and then lysed with 2% SDS. The lysate was used for measuring both synthesized protein (total counts) and total protein (by Lowry's method[15]). *b*, The DNA content of heart cells in a similar experiment as in Table 1 was determined by pentose analysis[16].

results) and could be due to a NGF-mediated induction of tyrosine hydroxylase and dopamine-β-hydroxylase[11]. Thus, the dramatic effect of hydrocortisone on transmitter choice, like that of EGF, is primarily an indirect one, via the non-neuronal cells. Note that the concentrations of glucocorticoids which were effective in these experiments (10^{-7}–10^{-5}M) are similar to the plasma corticosterone level in neonatal rats (10^{-6}M)[12].

These results raise the question of whether the hormonal actions are due to nonspecific effects on growth or health of the heart cells. At the crudest level, EGF and hydrocortisone could have stimulatory and deleterious effects, respectively, on the number or growth of the heart cells. While this may be the case over extended periods of incubation, the 24-h incubation with hormones used in these experiments results in little alteration in the total DNA or protein content of the heart cell cultures (Table 3). Could the hormones be having effects on overall heart cell protein synthesis which was not reflected in the total protein content after only 24 h of incubation? This seemed unlikely as the hormones had little effect on ^{3}H-leucine incorporation into protein during the 24-h incubation (Table 3). Furthermore, in preliminary experiments, when ^{3}H-leucine-labelled protein secreted into the medium by heart cells was examined by SDS-gel electrophoresis, there were no gross differences in the patterns due to the presence of EGF or hydrocortisone (data not shown). The hormones thus appeared to have no obvious stimulatory or deleterious effects on the growth or health of the heart cells or on major proteins secreted during the 24-h incubation.

The results presented here suggest a further level of subtlety in the control of neurotransmitter choice in sympathetic neurones: specific hormones can act on non-neuronal cells to alter selectively the production or liberation of a factor (or factors) that induces neuronal cholinergic development and reduces adrenergic development.

Relaxin and the pituitary hormones were gifts of the NIH Hormone Distribution Program. I thank Dr Paul H. Patterson for his valuable discussions and encouragement throughout this work and for help in preparing the manuscript, Dr Izumi Hayashi for advice and information on serum-free culture systems, Dr Kathleen Sweadner for help in analysing the released protein from the heart cells, and Dr Edward Kravitz for the use of his equipment. This work was supported by a fellowship from the Muscular Dystrophy Association and an NINCDS grant to Paul H. Patterson.

Received 9 May; accepted 8 August 1980.

1. Patterson, P. H. & Chun, L. L. Y. *Devl Biol.* **56,** 263–280 (1977).
2. Hawrot, E. *Devl Biol.* **74,** 136–151 (1980).
3. Landis, S. C., MacLeish, P. R., Potter, D. D., Furshpan, E. J. & Patterson, P. H. *6th a. Meet. Soc. Neurosci.*, Abstr. **280,** 197 (1976).
4. Patterson, P. H. *Ann. Rev. Neurosci.* **1,** 1–17 (1978).
5. McLennan, I. S., Hill, C. E. & Hendry, I. A. *Nature* **283,** 206–207 (1980).
6. Hayashi, I. & Sato, G. *Nature* **259,** 132–134 (1976).
7. Bottenstein, J. *et al. Meth. Enzym.* **58,** 94–109 (1979).
8. Hawrot, E. & Patterson, P. H. *Meth. Enzym.* **58,** 574–584 (1979).
9. Mains, R. E. & Patterson, P. H. *J. Cell Biol.* **59,** 329–345 (1973).
10. Reichardt, L. F. & Patterson, P. H. *Nature* **270,** 147–151 (1977).
11. Otten, U. & Thoenen, H. *Brain Res.* **111,** 438–441 (1976).
12. Henning, S. J. *Am. J. Physiol.* **235,** 451–456 (1978).
13. Savage, C. R. Jr & Cohen, S. *J. biol. Chem.* **247,** 7609–7611 (1972).
14. McKeehan, W. L., Hamilton, W. G. & Ham, R. G. *Proc. natn. Acad. Sci. U.S.A.* **73,** 2023–2027 (1976).
15. Lowry, O. H., Rosebrough, N. J., Farr, A. L. & Randall, R. J. *J. biol. Chem.* **193,** 265–275 (1951).
16. Schneider, W. C. *J. biol. Chem.* **161,** 293–303 (1945).

A neuropeptide in mammalian tissues with physalaemin-like immunoreactivity

Lawrence H. Lazarus, R. Ilona Linnoila, Oscar Hernandez* & Richard P. DiAugustine

Endocrinology Group, Laboratory of Pulmonary Function and Toxicology and *Laboratory of Environmental Chemistry, National Institute of Environmental Health Sciences, Research Triangle Park, North Carolina 27709

Erspamer *et al.*[1-3] isolated several structurally related non-mammalian peptides, termed tachykinins[2,3], with biological activities similar to substance P (refs 2, 3). This similarity is due to a common COOH-terminal region[2,3], whereas the specific action of each member of the group depends on its unique NH_2-terminal sequence[3-6]. Based on these properties, parallel bioassays using numerous smooth muscle preparations and physiological parameters allow them to be generally distinguished[2,3,6]. However bioassays are time consuming and not highly specific. Thus, we developed a rapid physalaemin-specific radioimmunoassay that led to the initial discovery of a substance in mammalian tissues with an immunoreactivity resembling that of the original amphibian peptide[7]. We now present data on the distribution, localization and partial characterization of physalaemin-like immunoreactivity (PSLI) in tissues of several mammalian species.

Details of the preparation of the antiserum and the radioimmunoassay are described elsewhere[7]. Antiserum (PS-1) had a titre of 1:40,000 and specifically recognized the NH_2-terminal region of physalaemin with only minimal cross-reactivity with the other tachykinins (Table 1). Other bioactive peptides had negligible cross-reactivity ($<0.0001\%$)[7]. Antiserum PS-1 cross-reacted with uperolein $2.03 \pm 0.94\%$ (mean ± s.d., $n = 4$) (Table 1), but compared with physalaemin the displacement curve was nonparallel (the ratio of the slopes of physalaemin:uperolein = 2.10 ± 0.20; Fig. 1). The cross-reactivity of antiserum PS-1 using ^{125}I-uperolein yielded a complementary set of data: at a constant bound/free ratio (B/F) a lower antiserum dilution was required (1:6,000) and the sensitivity of the assay to physalaemin decreased fourfold to 29.8 ± 6.4 pg ($n = 4$) (Table 1); the cross-reactivity of physalaemin was also nonparallel relative to uperolein (ratio $= 2.43 \pm 0.88$, $n = 3$; Fig. 1); and 50% displacement by uperolein was 51.0 ± 14.2 pg (40.7 ± 11.3 fmol, $n = 4$; Fig. 1). As also shown in Fig. 1, a crude extract of guinea pig stomach and the peak material from either Bio-Gel P-4 or HPLC (Fig. 3) produced parallel displacement curves relative to the labelled peptide used. Thus, it appeared that PSLI in tissue extracts contained an amino acid sequence common to the NH_2-terminal region of both physalaemin and uperolein (-Asp-Pro-Asn-; Table 1). Predictably, the ratio between their slopes should be identical, and within experimental limitations this was the case. Although the concentration of immunoassayable substance would be higher by nearly an order of magnitude using ^{125}I-uperolein, PSLI was quantified on the basis of physalaemin as the antiserum was raised against this peptide.

PSLI was found throughout the gastrointestinal tract of all the mammalian species examined and exhibited parallel displacement to physalaemin (Fig. 1). The actual concentration in each region of the stomach varied considerably between species (Table 2), with the rabbit containing the highest levels[7]. Guinea pig stomach contained more PSLI than any other region of the gastrointestinal tract: it was higher in the duodenum than in either the jejunum or ileum and a similar quantity was found there to that in the pylorus and fundus (Table 2). In rabbit, the level of PSLI in the duodenum was considerably less than that found in the stomach. PSLI was also found in porcine oesophagus in the mucosal and muscle layers, and mucosa of the trachea, as well as in rabbit trachea. Inconsistent values and nonparallel displacement curves, similar to that produced by proteases, frequently occurred with extracts of brain, lung and plasma from rat and guinea pig.

The large amounts of PSLI in the gastrointestinal tract may indicate a functional role for this material. The detection of relatively small quantitites of PSLI in tissues containing a high

Table 1 Specificity of physalaemin antiserum PS-1 among the tachykinin group of polypeptides

		Molar cross-reactivity (%)	
Peptide	Sequence	^{125}I-physalaemin	^{125}I-uperolein
Physalaemin	pGlu-Ala-Asp-Pro-Asn-Lys-Phe-Tyr-Gly-Leu-Met-NH$_2$	100	174.0±38.9
Uperolein	——Pro——————Ala————————————	2.03±0.94	100
Phyllomedusin	pGlu-Asn—————Arg————————————	0.36±0.04	0.32
Substance P	Arg-Pro-Lys———Gln-Gln——Phe———————————	<0.00013	0.05
Eledoisin	——Pro-Ser-Lys-Asp- Ala——Ile————————————	<0.0001	NT
Kassinin	Asp-Val-Pro-Lys-Ser-Asp—Glu——Val———————————	0·013±0.003	NT

Cross-reactivity is derived from the 50% displacement values by unlabelled peptide and given as the mean±s.d. The sensitivity of antiserum PS-1 for physalaemin using ^{125}I-physalaemin is 6.79±1.98 pg (5.29±1.54 fmol, $n = 34$) and for uperolein using ^{125}I-uperolein (at a titre of 1:6,000 final dilution) 51.0±14.2 pg (40.7±11.3 fmol, $n = 4$). NT, not tested.

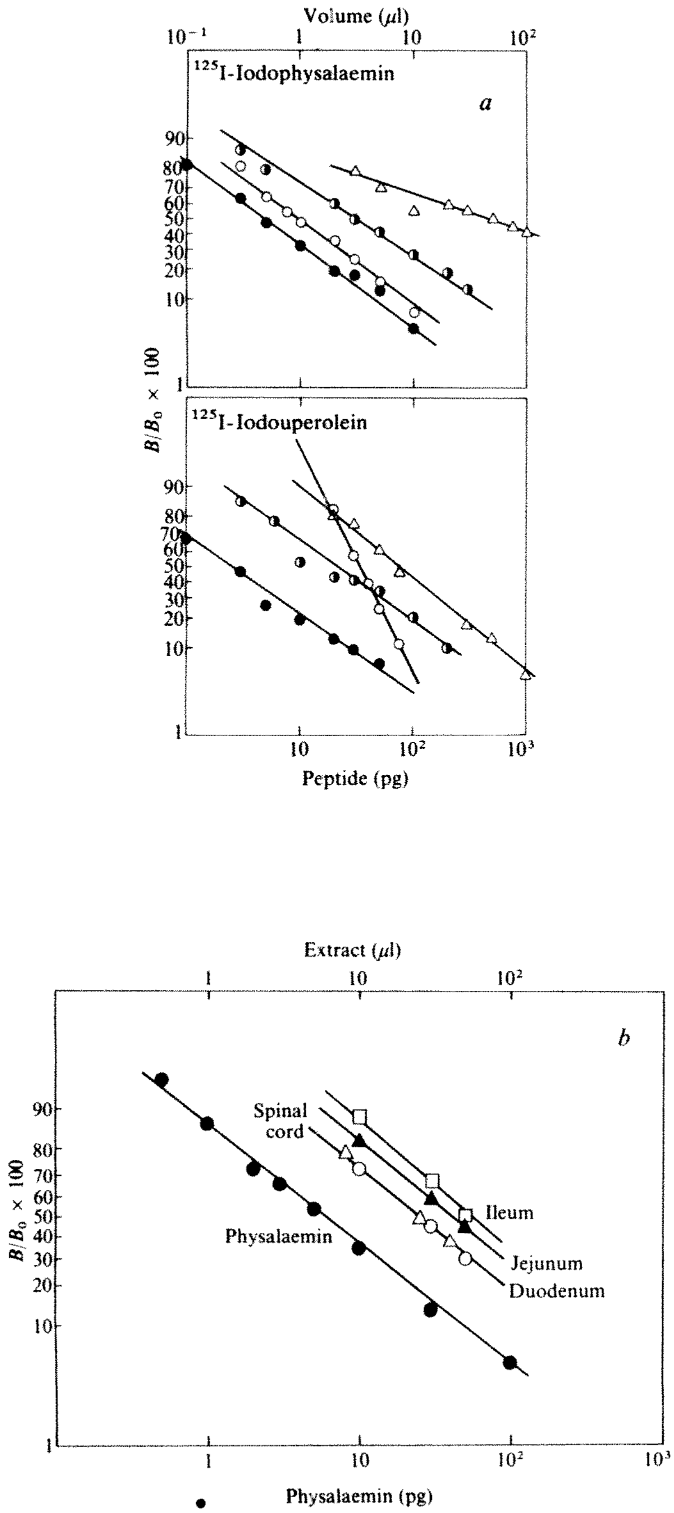

density of nerve fibres, for example, the sphincter areas of the stomach[8], may be masked by extraneous protein in the extract. On the other hand, subtle structural modifications may also affect its quantification: studies on amino acid variants of kassinin and physalaemin[6], charge differences in luteinizing hormone releasing factor[9] and vasoactive intestinal polypeptide (VIP)[10], and NH$_2$-terminally extended bombesin[11] and somatostatin[12] support this possibility. However, relatively small amounts of PSLI could exert profound effects as physalaemin is one of the most potent pharmacologically active peptides known[3].

Immunostaining was observed in both epithelial cells and nerve fibres in the gastrointestinal tract of guinea pig and rat. In guinea pig, the immunostaining can be summarized as follows: (1) scattered epithelial cells with PSLI in villi throughout the gastrointestinal tract; (2) the most conspicuous feature was the numerous, strongly immunostained cells in Brunner's glands[13] of the proximal duodenum (Fig. 2*a*); (3) submucosal glands of the ileum; (4) beaded, fibre-like structure, probably representing terminal and preterminal nerves in Meissner's and Auerbach's plexi in the duodenum; and (5) beaded fibres with PSLI among pancreatic acinar cells that are also lightly immunostained. In rat, immunostained cells were also widely distributed throughout the gastrointestinal tract, but scattered immunostained epithelial cells were most frequent in the colon (Fig. 2*b*). Also in rat, beaded fibres with PSLI were observed in the muscle layers of the gastro-oesophageal sphincter and surrounding unstained ganglion cells of Auerbach's plexus in the same region (Fig. 2*c*). The localization of PSLI in epithelial cells and nerve fibres of the gastrointestinal wall resembled that of substance P (refs 14–16), neurotensin[17–19], motilin[14], enkephalin[16,20],

Fig. 1 *a*, Specificity of the physalaemin raioimmunoassay. The assay contained 50 mM sodium cacodylate, *p*H 5.75, 1.0 mg bovine serum albumin, 4,000–5,000 c.p.m. ^{125}I-physalaemin or ^{125}I-uperolein, antiserum PS-1 (final dilution 1:40,000 with ^{125}I-physalaemin and 1:6,000 with ^{125}I-uperolein) and sample or standard peptide in a total volume of 100 μl. After incubation at 2–4 °C for 16 h, nonimmune rabbit serum and goat anti-rabbit antiserum (Cappel) were added to final dilutions of 1:2,000 and 1:50, respectively. The assays were incubated for 3 h at 22 °C, diluted with 1.0 ml buffer, centrifuged (2,500*g* for 30 min) and the residue counted[7]. Control tubes lacking antiserum PS-1 or in the presence of 60 pmol physalaemin had <1.0% of the total radioactivity. The plots contain standard curves for physalaemin (○), uperolein (△), an extract of guinea pig stomach (●) and the peak material from either Bio-Gel P-4 column or HPLC (Fig. 3) (◑). The upper panel shows the assay containing ^{125}I-physalaemin whereas the assay in the lower panel contains ^{125}I-uperolein. *b*, Physalaemin-like immunoreactivity in extracts of guinea pig tissue. Lyophilized tissues were powdered, then extracted in 10 volumes (wet weight) 1 mM EDTA-1 mM dithiothreitol at 98 °C. After cooling, they were acidified (1.0 M formic acid), homogenized (Polytron) and centrifuged (27,000*g* for 15 min at 4 °C). The pellets were re-extracted and the combined supernatants lyophilized[7]. The residue was dissolved in 50 mM cacodylate buffer, *p*H 5.75, and clarified before use. The data from a typical experiment are presented as the per cent *B*/*B*$_0$ against pg physalaemin (●), or volume of extract from duodenum (○), jejunum (▲), ileum (□) or spinal cord (△). The maximum variation between the slopes of the lines relative to physalaemin was 3%.

Table 2 Physalaemin-like immunoreactivity in mammalian tissue

Tissue	Amount in lyophilized tissue* (ng g^{-1})	
Guinea pig		
Fundus	17.64 ± 3.77	
Corpus	5.87 ± 3.80	
Pylorus	11.10 ± 3.22	
Duodenum	14.86 ± 2.54	
Jejunum	4.26(5.26, 3.26)	
Ileum	2.69(3.72, 1.65)	
Caecum	3.17(2.64, 3.69)	
Spinal cord	1.08(1.43, 0.73)	
Urinary bladder	1.86(1.16, 2.55)	
Pancreas	2.74(2.11, 3.36)	
Mouse†		
Fundus	5.59	
Pylorus	6.69	
Rat‡	Adult	Neonatal
Fundus	2.29 ± 0.68	3.89
Pylorus	5.53 ± 0.79	3.86
Small intestine	ND	2.45

ND, not determined.

* Dry weight constitutes 21.5 ± 2.8% of the wet weight. Values are mean ± s.d. ($n = 3$–4).

† These figures are from four Swiss-Webster mice.

‡ Data are from five adult male CD-2 rats and seven neonatal pups killed at 24 h postpartum.

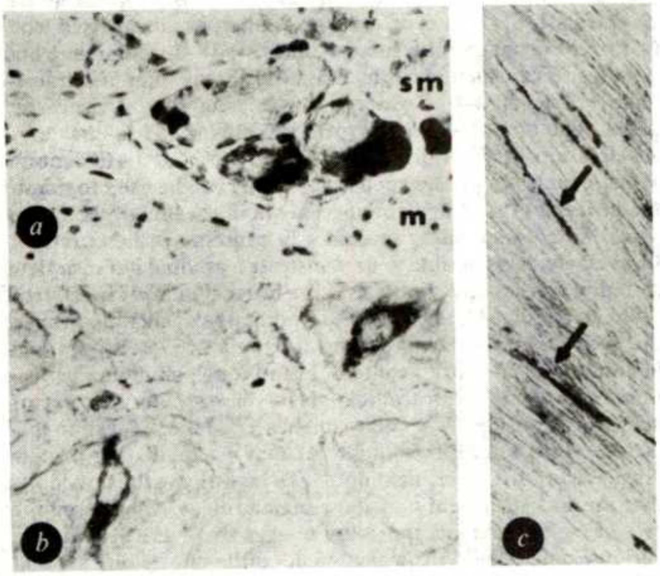

Fig. 2 Immunocytochemical localization of physalaemin-like immunoreactivity in the gastrointestinal tract. Immunostaining was carried out using the immunoperoxidase bridge technique[35]. The best results were obtained by freezing the tissue in 2-methylbutane at the temperature of liquid nitrogen, freeze-drying and fixing in the vapours of diethylpyrocarbonate[36]. Antiserum PS-1 gave satisfactory staining at a dilution of 1 : 1,000. Immunostaining was eliminated with the incubation of serial sections with either normal rabbit serum or antiserum PS-1 that was preadsorbed with 100 μg of physalaemin antigen. Immunostaining was not affected by preadsorption with 100 μg substance P or uperolein. *a*, Brunner's gland in the guinea pig duodenum showing dark, homogeneous staining (on the right side) in selected cells in the gland; sm = submucosa, m = muscle (circular layer). ×290. *b*, Two epithelial cells in rat colon; note that the nuclei are unstained. ×730. *c*, Beaded nerve fibres (*arrows*) with PSLI among the smooth muscle fibres of the gastro-oesophageal sphincter of the rat. ×290.

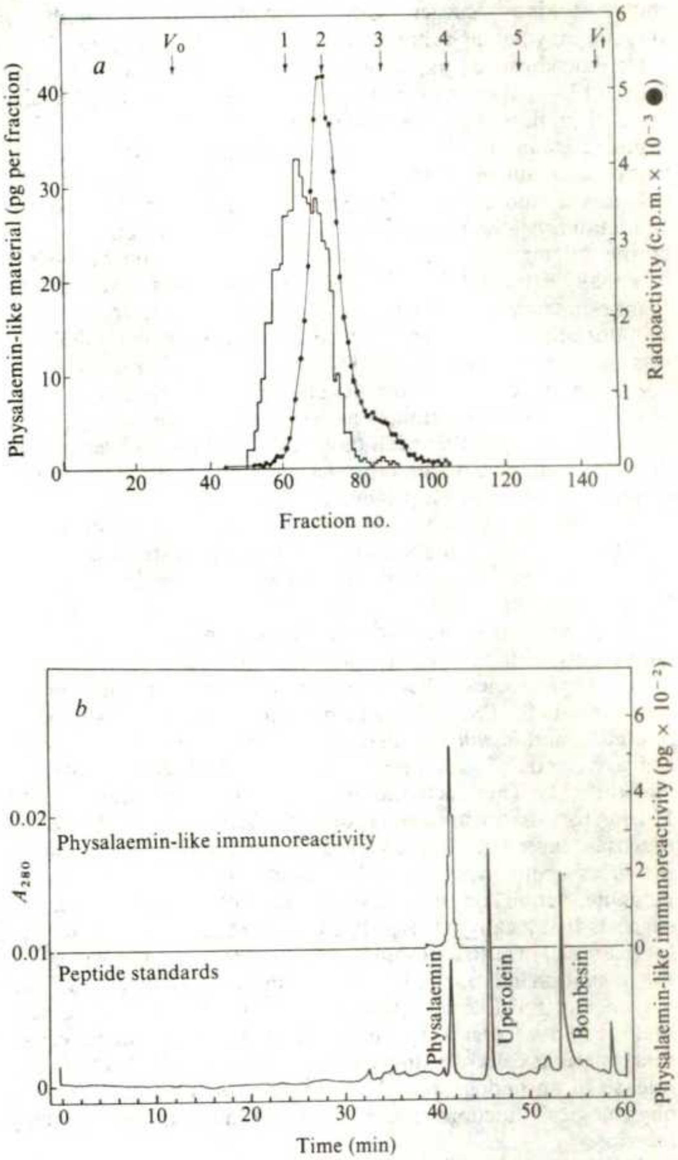

Fig. 3 *a*, Column chromatography of extracts of guinea pig stomach. Bio-Gel P-4 (100–200 mesh; Bio-Rad) columns (0.7 × 48.5 cm) were equilibrated and eluted with 0.1 M formic acid. Fractions (0.23 ml) were collected at a flow rate of 10.4 ml h^{-1} at a hydrostatic pressure of 100 cm. Each fraction was lyophilized and redissolved in 0.15–0.4 ml water or cacodylate buffer before assaying. Immunoreactivity (bar graph) and ^{125}I-iodophysalaemin (●) are presented. A physalaemin standard (determined by radioimmunassay) eluted in the same fractions as iodinated physalaemin due to variability in column chromatography: the s.d. in the peak is ±1.7 fractions[7]. The arrows indicate the position of the standards: V_0, Bovine serum albumin, 1, ^{125}I-[Tyr^8]-bombesin; 2, ^{125}I-physalaemin; 3, ^{125}I-[Des-Gly^9-Met-NH$_2$^{11}]-physalaemin; 4, ^{125}I-[des-pGlu^1-Phe^7]physalaemin; 5, ^{125}I-Tyr-Phe; and V_t, ^{125}I-Tyr or DNS–Ala. *b*, HPLC fractionation of the PSLI peak material from Bio-Gel P-4 columns. Fractions 55–75 were pooled, lyophilized, and the samples (100 μl) were fractionated on a Particil 5 ODS reverse-phase column (0.45 × 25 cm) (Whatman) in 10 mM Tris–phosphate, *p*H 7.05, and 20% methanol. Elution was carried out with a 20–65% linear methanol gradient in 45 min after an initial delay of 5 min at a flow rate of 0.8 ml min^{-1} (O.H. *et al.*, in preparation). Fractions were collected at either 0.1- or 0.2-min intervals, the methanol evaporated under N_2, lyophilized and dissolved in buffer. The lower tracing is the absorbance of a mixture containing 6 μg of physalaemin, uperolein and bombesin; the retention times of each were determined independently. The bar graph in the upper curve indicates PSLI.

somatostatin[14,16], VIP (refs 8, 13, 21, 22), bombesin[13,23,24] and cholecystokinin[25], suggesting that the mammalian form of physalaemin may belong to this diverse group of neuropeptides.

Column chromatography of extracts of guinea pig stomach on Bio-Gel P-4 columns ($n = 15$) gave only one symmetrical peak of PSLI (molecular weight 1,700) regardless of the area of the stomach examined. This was larger than any of the known tachykinins[6] and no other major peak with PSLI eluted from the columns. Cyanogen bromide digestion of the peak material gave an immunoreactive profile with the same elution volume as that of the original extract, suggesting that PSLI could be NH_2-terminally extended. This indeed was found for a mammalian bombesin-containing peptide[11], angiotensin from frogs[5] and somatostatin from porcine intestine[12]. Reverse-phase HPLC was used to resolve whether PSLI resembled physalaemin or uperolein: in acidic or neutral conditions, PSLI co-eluted with physalaemin several minutes earlier than uperolein (Fig. 3*b*). These data suggest that even though PSLI seemed to be larger than physalaemin, its ionic properties are very similar, if not identical, to those of physalaemin.

PSLI differs from substance P on the basis of several criteria: specifity of antiserum PS-1 (Table 1); tissue distribution and cellular localization[21]; substance P has not been localized in Brunner's glands[27] which contain cells immunopositive to the COOH terminus of gastrin[28] and bombesin[23]; and PSLI co-eluted only with physalaemin on HPLC (Fig. 3*b*).

The physiological effects of physalaemin may indicate a possible role for PSLI. Physalaemin affects mucous production *in vitro*[29], and *in situ* stimulates secretion of the lachrymal and salivary glands[3,30] with the secretion of K^+ and reabsorption of Na^+ (ref. 31). These activities may account for the presence of PSLI in tissues with mucous production, Brunner's glands and in mucosal layer of trachea and oesophagus. Physalaemin produces acute hypotension by vasodilation[2,3,6], and a spasmogenic action on extravascular smooth muscle[2,3] which suggests that locally released PSLI could regulate muscle tone; for example, in gastro-oesophageal sphincter[8] or enteric plexi[22] the relaxation induced by VIP may be antagonized by PSLI. The presence of PSLI nerves in the vicinity of acinar cells suggests that it could interact on specific physalaemin membrane receptors on acinar cells[32] leading to cellular secretion[32–34]. Thus the release of an endogenous PSLI may be involved in different physiological functions depending on its neuronal or cellular location.

We thank J. E. Rivier for physalaemin, J. Frushstick, C. Soldato, P. Merritt, M. Matherson, P. McLain and N. Peedin for technical assistance, R. Hester for literature retrieval, G. Jahnke and M. D. Erisman for their comments, and V. Erspamer for uperolein, phyllomedusin and kassinin and his encouragement.

Received 29 October 1979; accepted 1 August 1980.

1. Anastasi, A., Erspamer, V. & Cei, J. M. *Archs Biochem. Biophys.* **108,** 341–348 (1964).
2. Erspamer, V. & Melchiorri, P. *Pure appl. Chem.* **35,** 463–494 (1973).
3. Erspamer, V., Falconieri Erspamer, C. & Linari, G. in *Substance P* (eds von Euler, U. S. & Pernow, B.) 67–74 (Raven, New York, 1977).
4. Zappia, L., Molina, E., Sianesi, M. & Bertaccini, G. *J. Pharm. Pharmac.* **30,** 593–594 (1978).
5. Erspamer, V., Yasuhara, T. & Nakajima, T. *Adv. exp. Med. Biol.* **120A,** 7–13 (1979).
6. Falconieri Erspamer, G., Erspamer, V. & Piccinelli, D. *Naunyn-Schmiedebergs Archs Pharmak.* **311,** 61–65 ((1980).
7. Lazarus, L. H. & DiAugustine, R. P. *Analyt Biochem.* **107** (in the press).
8. Alumets, J. *et al. Nature* **280,** 155–156 (1979).
9. King, J. A. & Millar, R. P. *Science* **206,** 67–69 (1979).
10. Dimaline, R. & Dockray, G. J. *Life Sci.* **25,** 1893–1900 (1979).
11. McDonald, T. J. *et al. Biochem. biophys. Res. Commun.* **90,** 227–233 (1979).
12. Pradayrol, L., Jornvall, H., Mutt, V. & Ribet, A. *FEBS Lett.* **190,** 55–58 (1980).
13. Cochrane, W., Davies, D. V., Palfrey, A. J. & Stockwell, R. A. *J. Anat.* **98,** 1–10 (1964).
14. Yanaihara, C. *et al.* in *Gastrointestinal Hormones and Pathology of the Digestive System* (eds Grossman, M., Speranza, V., Basso, N. & Lezoche, E.) 269–283 (Plenum, New York, 1978).
15. Sundler, F., Håkanson, R., Larson L.-I., Brodin, E. & Nilsson, G. in *Substance P* (eds von Euler, U. S. & Pernow, B.) 59–65 (Raven, New York, 1977).
16. Polak, J. M. & Bloom, S. R. in *Gastrins and the Vagus* (eds Rehfeld, J. F. & Andrup, E.) 15–30 (Academic, New York, 1979).
17. Polak, J. M. *et al. Nature* **270,** 183–184 (1979).
18. Helmstaedter, V., Taugner, C., Feurle, G. E. & Forssmann, W. G. *Histochemistry* **53,** 35–41 (1977).
19. Sundler, F. *et al. Cell Tissue Res.* **178,** 313–321 (1977).
20. Linnoila, R. I., DiAugustine, R. P., Miller, R. J., Chang, K.-J. & Cuatrecasas, P. *Neuroscience* **3,** 1187–1196 (1978).
21. Bryant, M. G. *et al. Lancet* **i,** 991–993 (1976).
22. Jessen, K. R., Polak, J., van Noorden, S., Bloom, S. R. & Barstock, G. *Nature* **283,** 391–393 (1980).
23. Polak, J. M., Hobbs, S., Bloom, S. R., Solicia, E. & Pearse, A. G. E. *Lancet* **i,** 1109–1110 (1976).
24. Dockray, G. J., Vaillant, C. & Walsh, J. H. *Neuroscience* **4,** 1561–1568 (1979).
25. Dockray, G. J. *A. Rev. Physiol.* **41,** 83–95 (1979).
26. Nilsson, G. & Brodin, E. in *Substance P* (eds von Euler, U. S. & Pernow, B.) 49–54 (Raven, New York, 1977).
27. Hokfelt, T., Johansson, O., Ljungahl, A., Lundberg, J. M. & Schultzberg, M. *Nature* **284,** 515–521 (1980).
28. Larsson, L.-I. in *Gastrins and the Vagus* (eds Rehfeld, J. F. & Andrup, E.) 5–14 (Academic, New York, 1979).
29. Baker, A. P. Hillegass, L. M., Holdern, D. A. & Smith, W. *J. Am. Rev. resp. Dis.* **115,** 811–817 (1977).
30. Emmelin, N. & Lenniger, S. *Br. J. Pharmac. Chemother.* **30,** 676–680 (1967).
31. Coronea, M. T., Denniss, A. R. & Young, J. A. *Pflügers Arch. ges.* **381,** 223–230 (1979).
32. Jensen, R. T. & Gardner, J. D. *Proc. natn. Acad. Sci. U.S.A.* **76,** 5679–5683 (1979).
33. Gardner, J. D. *A. Rev. Physiol.* **41,** 55–66 (1979).
34. Erspamer, V., Melchiorri, P., Falconieri Erspamer, C. & Negri, L. in *Gastrointestinal Hormones and Pathology of the Digestive System* (eds Grossman, M., Speranza, V., Basso, N. & Lezoche, E.) 51–64 (Plenum, New York, 1978).
35. Petrusz, P., DiMeo, P., Ordronneau, P., Weaver, C. & Keefer, D. A. *Histochemistry* **46,** 9–26 (1975).
36. Pearse, A. G. E., Polak, J. M., Adams, C. & Kendall, P. A. *Histochem. J.* **6,** 347–352 (1974).

Dual ionic controls for the activation of protein synthesis at fertilization

M. M. Winkler, R. A. Steinhardt,* J. L. Grainger & L. Minning

Department of Zoology, University of California, Berkeley,
California 94720

The general metabolic activation of the sea urchin egg at fertilization is dependent on a release of intracellular stores of calcium and the subsequent transient elevation of intracellular Ca^{2+} (refs 1–3). However, this elevation does not by itself lead to increased macromolecular synthesis and development but initiates steps which result in a long-term elevation of intracellular *p*H (refs 4–6). Among the developmental processes dependent on the elevation of intracellular *p*H is the large acceleration in the rate of protein synthesis at fertilization[6]. Weak penetrating bases such as ammonia can be used to mimic the processes resulting in an increase in intracellular *p*H and so show the corresponding increases in protein synthesis rate[6–9]. Conversely, it is possible to demonstrate a gradual but complete shut down of protein synthesis if the intracellular *p*H is reduced to the unfertilized level with penetrating weak acids[6]. However, the rate of protein synthesis in ammonia-activated eggs lags behind that of fertilized controls even though ammonia activation can result in an intracellular *p*H increase greater than occurs in the fertilized egg[6,8,10]. This result has led to the suggestion that factors other than intracellular *p*H may be regulating protein synthesis following fertilization[6,10]. To investigate the possibility that the Ca^{2+} transient may have such a role, we measured the rate of amino acid incorporation in eggs that were activated in various ionic conditions which enabled the effects of Ca^{2+} and *p*H changes to be studied separately. Our results, reported here, show that if intracellular *p*H is elevated, increases in intracellular Ca^{2+} play an additional part in the activation of protein synthesis at fertilization.

Figure 1 shows the amount of ^{3}H-valine incorporated after activation in these different ionic conditions. Eggs were preloaded with ^{3}H-valine to circumvent problems of differential uptake of label in different experimental conditions. Fertilization typically results in a 10–30-fold stimulation of protein synthesis over the unfertilized rate. The variation between experiments stems from differences in both the basal unfertilized rate and the degree of stimulation resulting from activation.

Fertilization results in an increase of intracellular *p*H of about 0.45 *p*H units[5]. This seems to occur by a mechanism by which protons are released from the egg in the presence of external Na^+ (ref. 4). To determine how Ca^{2+} release in the absence of an

---

* To whom correspondence should be addressed.

0028-0836/80/410558—03$01.00

intracellular *p*H increase would affect the protein synthesis rate, eggs were activated with the Ca^{2+} ionophore A23187 in zero-sodium (0-Na^+) artificial seawater. The ionophore causes the release of intracellular Ca^{2+} and the discharge of the cortical granules, but in the absence of external Na^+ there is no intracellular *p*H increase[11], and the rate of protein synthesis is the same as in the unfertilized controls (Fig. 1*a*). Similarly, if eggs are fertilized in seawater and immediately transferred to 0-Na^+ artificial seawater before the onset of the Na^+-dependent H^+ efflux, there will be a Ca^{2+} release without an increase in intracellular *p*H. Protein synthesis remains at the unfertilized rate until Na^+ is added back and the intracellular *p*H increases (Fig. 2). Thus, a Ca^{2+} release in the absence of a *p*H rise does not stimulate protein synthesis.

Treatment with 10 mM NH_4Cl increases the intracellular *p*H by about 0.80 *p*H units and does so by an entirely different mechanism[5,9]. NH_4Cl in alkaline solutions will generate ammonia, which passively diffuses across the egg plasma membrane raising the intracellular *p*H, bypassing the transient intracellular Ca^{2+} release and not causing the discharge of the cortical granules. However, NH_4Cl in seawater containing Ca^{2+} does provoke a transient Ca^{2+} influx[12]. NH_4Cl activation in seawater or zero 0-Na^+ artificial seawater (both of which have the normal amount of Ca^{2+}) will result in similar stimulations of protein synthesis to levels less than those achieved by fertilization. If extracellular Ca^{2+} is present during NH_4Cl activation there will be a measurable influx of Ca^{2+}, which although insufficient to cause discharge of the cortical granules, does affect the level of protein synthesis. If protein synthesis is compared in eggs activated in 0-Na^+ seawater where Ca^{2+} influx can occur (Fig. 1*c*) and in 0-Ca^{2+} artificial seawater where there is no measurable Ca^{2+} influx, there is a significantly lower level of protein synthesis in the absence of the Ca^{2+} influx (Fig. 1*b*).

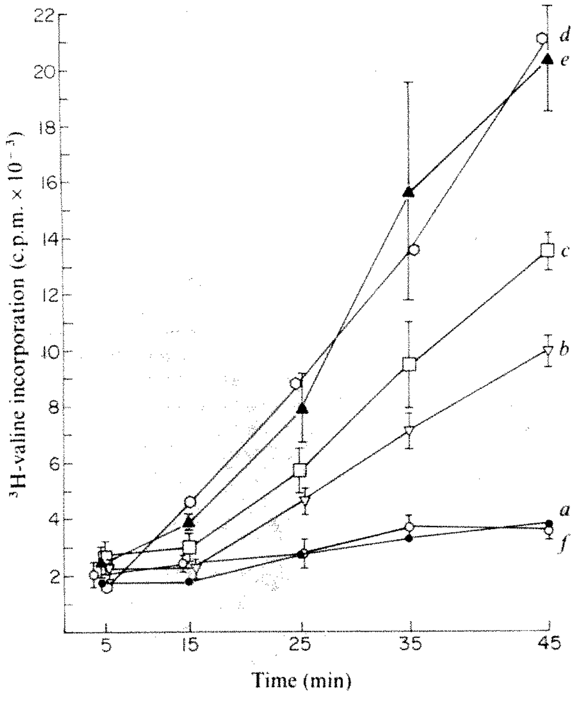

Fig. 1 Total ^{3}H-valine incorporation over a 45-min period starting 5 min after activation in various ionic media. The mean incorporation of label into unfertilized eggs from four experiments was determined for each time point. The ratio of this mean to the unfertilized rate in each of these four experiments was used to normalize the data presented for the different ionic conditions. The plotted data points represent the mean of the normalized incorporation data. The value shown represents the amount of incorporation ±s.e.m. for four repeats of this experiment testing five different conditions plus fertilization. The standard errors for fertilization have been omitted and the time points slightly spread out for clarity. *a*, Eggs activated by 2.5 μM A23187 in 0-Na^+ artificial seawater: intracellular Ca^{2+} release without an intracellular *p*H rise. *b*, Eggs activated by 10 mM NH_4Cl in 0-Ca^{2+} artificial seawater: a rise in intracellular pH without a Ca^{2+} release or influx. *c*, Eggs activated in 10 mM NH_4Cl in 0-Na^+ artificial seawater: an intracellular *p*H rise with some Ca^{2+} influx. *d*, Eggs activated in 10 mM NH_4Cl and 2.5 μM A23187 in 0-Na^+ artificial seawater: both an intracellular *p*H rise and a intracellular Ca^{2+} release. *e*, Eggs fertilized normally in natural seawater for comparison purposes. *f*, Unfertilized eggs in natural seawater. Artificial seawater: 484 mM NaCl, 10 mM KCl, 27 mM $MgCl_2$, 29 mM $MgSO_4$, 11 mM $CaCl_2$, 2.4 mM $NaHCO_3$, *p*H 8.0. 0-Na^+ artificial seawater had choline Cl substituted for NaCl and $KHCO_3$ for $NaHCO_3$. 0-Ca^{2+} artificial seawater had 16 mM NaCl substituted for $CaCl_2$ and 1 mM EGTA added. Eggs of the sea urchin *Lytechinus pictus* were obtained and preloaded as described previously[6]. Briefly, a 0.75-ml volume of packed dejellied eggs was preloaded in 15 ml of seawater containing 5 μCi ml^{-1} [2, 3-^{3}H]valine (Schwarz–Mann, 26 Ci $mmol^{-1}$) for 45 min. The eggs were then washed twice in seawater and once in the test solution before resuspending to a 0.1% concentration in the test solution. Aliquots (2 ml) were taken at 10-min intervals and processed for scintillation counting as described previously[6].

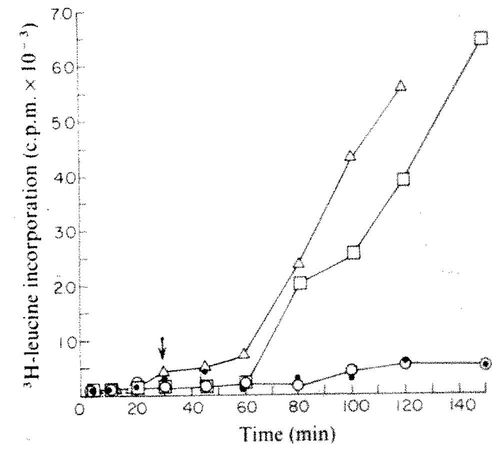

Fig. 2 Total ^{3}H-leucine incorporation over a 150-min period showing the effect of Na^+ on the acceleration of protein synthesis at fertilization. ●, Unfertilized eggs in seawater; ○, Eggs fertilized in normal seawater and completely transferred to 0-Na^+ seawater 50 s after fertilization; △, fertilized eggs in seawater; □, eggs fertilized in normal seawater and completely transferred to 0-Na^+ seawater 50 s after fertilization. At the arrow, 30 min after fertilization, eggs were transferred back to normal seawater. Eggs of the sea urchin *Strongylocentrotus purpuratus* were treated with 5 mM dithiothreitol (DTT), *p*H 8.5, until test aliquots showed that fertilization would not produce a fertilization envelope. Eggs were then preloaded with 5 μCi ml^{-1} [4, 5-^{3}H]leucine for 1 h. Aliquots (2 ml) of a 1% suspension of eggs were put into polylysine-coated Petri dishes, one for each time point. This treatment firmly attaches the eggs to the Petri dish where they will remain even if fertilized because the DTT treatment prevents the elevation of the fertilization envelope. These attached eggs could then be quickly and completely transferred in and out of the 0-Na^+ seawater. The attachment of DTT-treated eggs to polylysine-coated surfaces delays the response of protein synthesis to fertilization by 20 min in both the experimental and the control conditions. At each time point the seawater was removed and 5 ml of 10% trichloroacetic acid added to the Petri dish. At the completion of the experiment the eggs were scraped from the dishes using rubber policemen, collected on glass fibre filters and processed as described previously[6].

If eggs are treated with A23187 and 10 mM NH_4Cl in 0-Na^+ artificial seawater, there will be both an intracellular Ca^{2+} release caused by the ionophore and an intracellular *p*H increase caused by the NH_4Cl. The rate of protein synthesis approaches that of normal fertilized eggs (Fig. 1*d*). Thus, Ca^{2+} release and an increase in intracellular *p*H, although induced by mechanisms other than the normal ones used by the egg at fertilization, will lead to the fertilized level of accelerated protein synthesis. The higher levels of amino acid incorporation with both a Ca^{2+} and *p*H stimulation are unlikely to be due to a change in amino acid pools because pulse labelling experiments give an identical ordering of incorporation rates (unpublished results).

Thus, Ca^{2+} release in the absence of an intracellular *p*H increase does not stimulate protein synthesis. A *p*H increase in the absence of a Ca^{2+} release will yield a partial stimulation of protein synthesis. A small Ca^{2+} influx in the presence of a *p*H increase will yield higher levels of protein synthesis. Only in the presence of both an intracellular Ca^{2+} release and a *p*H increase will protein synthesis be maximally stimulated.

Brandis and Raff[10] have provided evidence for a increase in the peptide elongation rate associated with fertilization that is not seen with NH_4Cl stimulations. It is possible that the increased elongation rate is dependent on the Ca^{2+} release at fertilization. However, it is difficult to be sure of such an interpretation of the differences between NH_4Cl activation and fertilization because (1) the rate of protein synthesis is changing very rapidly, (2) it is affected by the cell cycle changes, and (3) extracellular Ca^{2+} enters during NH_4Cl activation in seawater. In our experiments, however, the magnitude of the response to NH_4Cl stimulation with varying amounts of Ca^{2+} entry or release clearly show that if the intracellular *p*H is elevated, Ca^{2+} plays an additional role in accelerating the rate of protein synthesis at fertilization.

This work was supported by NSF grants PCM 77–04260 and 79–04744 to R. A. S.

Received 28 April; accepted 18 August 1980.

1. Steinhardt, R. A. & Epel, D. *Proc. natn. Acad. Sci. U.S.A.* **71,** 1915–1919 (1974).
2. Chambers, E. L., Pressman, B. C. & Rose, B. *Biochem. biophys. Res. Commun.* **60,** 126–132 (1974).
3. Steinhardt, R. A., Zucker, R. S. & Schatten, G. *Devl Biol.* **58,** 185–196 (1977).
4. Johnson, J. D., Epel. D. & Paul, M. *Nature* **262,** 661–664 (1976).
5. Shen, S. S. & Steinhardt, R. A. *Nature* **272,** 253–254 (1978).
6. Grainger, J. L., Winkler, M. M., Shen, S. S. & Steinhardt, R. A. *Devl Biol.* **68,** 396–406 (1979).
7. Steinhardt, R. A. & Mazia, D. *Nature* **241,** 400–401 (1973).
8. Epel, D., Steinhardt, R. A., Humphreys, T. & Mazia, D. *Devl Biol.* **40,** 245–255 (1974).
9. Winkler, M. M. & Grainger, J. L. *Nature* **273,** 536–538 (1978).
10. Brandis, J. W. & Raff, R. A. *Nature* **278,** 467–469 (1979).
11. Shen, S. S. & Steinhardt, R. A. *Nature* **282,** 87–89 (1979).
12. Zucker, R. S., Steinhardt, R. A. & Winkler, M. M. *Devl Biol.* **65,** 285–295 (1978).

Mutagenic deamination of cytosine residues in DNA

Bruce K. Duncan*

Department of Microbiology, Johns Hopkins University School of Medicine, Baltimore, Maryland 21205

Jeffrey H. Miller

Département de Biologie Moléculaire, Université de Genève, Switzerland

Spontaneous deamination converts cytosine to uracil, which is excised from DNA by the enzyme uracil-DNA glycosylase, leading to error-free repair. 5-Methylcytosine residues are deaminated to thymine, which cannot be excised and repaired by this system. As a result, 5-methylcytosine residues are hotspots for spontaneous transitions, as demonstrated in the *lacI* gene of *Escherichia coli*. We show here that in bacteria which lack uracil-DNA glycosylase (Ung^-) and cannot excise uracil residues from DNA, the rate of spontaneous transition at cytosine residues is raised to the hotspot rate at 5-methylcytosine residues. These studies provide direct evidence that the deamination of cytosine is a significant source of spontaneous mutations.

The observation by Lindahl that potentially mutagenic cytosine deamination occurs at observable rates in *in vitro* physiological conditions led to the discovery of uracil-DNA glycosylase[1]. This enzyme initiates the repair of uracil from DNA by a 'base-excision' repair pathway[2,3]. *E. coli* uracil-DNA-glycosylase-deficient mutant strains[4] have been shown to have a weak G:C → A:T specific mutator phenotype[5]. Presumably, a G:U mismatched base pair resulting from cytosine deamination generates an A:U base pair after replication. Thus, one of the physiological roles of uracil-DNA glycosylase may be to repair such pre-mutational lesions resulting from deamination.

A more general description of the possible significance of cytosine deamination as an important mutagenic process comes from studies of the *E. coli lacI* gene[6–8]. Large numbers of independent *lacI* mutations have been characterized by genetic and biochemical methods. Of spontaneous base substitutions leading to nonsense mutations, approximately 75% arise by G:C → A:T transitions[6–8]. Two highly mutable 'hotspot' sites are conspicuous among 14 G:C → A:T amber mutation sites in the *lacI* gene; half of the observed amber transition mutations occur at these two sites. DNA sequence studies have demonstrated the presence of 5-methylcytosine residues at the hotspot sites[6]. It is clear that cytosine methylation increases the mutagenic susceptibility of a cytosine residue, presumably because of the inability of the cell to repair the deamination product, thymine.

Table 1 Frequency of spontaneous I^- mutants ($\times 10^6$)

Strain	Approx. I^- mutant frequency	% Amber mutants
GM1	2.5	1.0
BD1322	2.5	1.3
BD1323 (Ung^-)	2.5	4.6

I^- mutants were selected and screened against different suppressors to detect amber mutations, as described previously[7,8]. BD1322 is an Ung^+ derivative of the Ung^- strain BD1323. It is isogenic to GM1.

Table 2 Distribution of amber mutations in Ung^+ and Ung^- strains

		No. of occurrences		
Base substitution	Site	Ung^+ GM1	Ung^- BD1323	Ung^- BD1323 (2AP)
G:C → A:T	*A5*	0	2	0
	*A6**	51	4	39
	A9	8	18	4
	*A15**	37	0	29
	A16	9	1	2
	A19	11	2	1
	A21	8	2	0
	A23	8	7	2
	A24	10	1	5
	A26	6	2	2
	A31	1	2	3
	A33	5	4	1
	*A34**	12	3	11
	A35	1	2	0
Total G:C → A:T mutations		167	50	99
Transversions		55	4	0
Total amber mutations detected		222	54	99

Distribution of amber mutations in Ung^+ and Ung^- strains, showing the distribution found in GM1 and in BD1323 with and without 2-aminopurine (2AP). The number of occurrences refers to the number of mutations detected at a given locus in the collections of 222, 55 and 99 *lacI* mutations, respectively. The characterization of the GM1 amber mutations has been reported previously[6–8]. The I^- collection from BD1323 was analysed in the same manner.

* Presence of 5-methylcytosine at the mutational site[6].

We have studied the effect of the *ung* mutation, which results in the loss of uracil-DNA glycosylase activity, on the distribution of I^- nonsense mutations. The *ung-1* allele was inserted by P1 transduction into the *E. coli* GM1 used in previous studies of the *I* gene[6–8]. Table 1 shows that the frequency of amber mutations increased almost fourfold in the presence of the ung^- mutation. Thus, a deficiency of uracil-DNA glycosylase led to an increase in the frequency of mutations due to base substitutions. The I^- amber mutations were assigned to one of the known amber sites by deletion mapping and by examining the response to different amber suppressors, as described previously[7,8].

G:C → A:T transitions generate amber mutations at 14 different sites in the *lacI* gene. This represents 38% of the 37 characterized amber mutation sites in *lacI* which can be derived by a single base change. As Table 2 shows, 93% of the amber mutations detected in the Ung^- background arose by way of a G:C → A:T transition. In Ung^+ cells (GM1), 75% of all the amber mutations were G:T → A:T transitions, principally due to the 5-methylcytosine hotspots *A6* and *A15* (and to a lesser extent *A34*).

---

* Present address: Institute for Cancer Research, 7701 Burholme Avenue, Philadelphia, Pennsylvania 19111.

0028-0836/80/410560—02$01.00

A comparison of the distribution of the $G:C \rightarrow A:T$ mutations yields a more striking difference between *ung*$^+$ and *ung*$^-$ cells. The general increase of transition mutations in the *ung*$^-$ cells results from an increase in transitions at non-methylated cytosines, bringing them up to the level of the 5-methylcytosine sites. Thus, the 5-methylcytosine sites (*A6*, *A15* and *A34*) no longer appear as hotspots. Because uracil-DNA glycosylase has been shown to function in the base excision repair of uracil, these results demonstrate that cytosine deamination occurs *in vivo*; the failure to repair these lesions leads to an increase in the mutation rate.

Methylcytosine residues have also been shown to be hotspot loci when cells are mutagenized with 2-aminopurine (2AP)[6–8]. Could 2AP be stimulating the deamination of cytosine and methylcytosine residues? Perhaps the 2AP incorporation into DNA perturbs the structure of the DNA, making it more susceptible to cytosine deamination. Lindahl has shown that the DNA-cytosine deamination rate constant increases more than 100-fold when DNA is denatured[9]. This model does not necessarily assume the actual mispairing of 2AP with cytosine; formation of a 2AP:T base pair might also induce the deamination of nearest-neighbour cytosine residues. We have tested this hypothesis. The right-hand column of Table 2 shows that the *ung* mutation does not affect the mutability of methylcytosine residues compared with other cytosine residues in the presence of 2AP. Thus, with the Ung$^-$ strain, 80% of the 2AP-induced amber mutations are at the three methylated cytosines, which compares favourably with the wild-type Ung$^+$ (GM1) strain, in which 60% of the transitions resulting in amber mutations are at the methylated site, and with GM1+2AP[6–8], in which 85% of the amber mutations are at the methylated cytosines. These results argue that 2AP does not induce deamination.

This work was sponsored by a grant from the Swiss National Fund (FNS3.493-0.79) to J.H.M., a NSF Fellowship (SMI-12327) to B.K.D. and a short-term Visiting Scientist Fellowship from the European Molecular Biology Organization to B.K.D.

Received 10 March; accepted 1 August, 1980.

1. Lindahl, T. & Nyberg, B. *Biochemistry* **13,** 3405–3410 (1974).
2. Lindahl, T. *Proc. natn. Acad. Sci. U.S.A.* **71,** 3649–3653 (1974).
3. Tye, B. K., Chien, J., Lehman, I. R., Duncan, B. K. & Warner, H. R. *Proc. natn. Acad. Sci. U.S.A.* **75,** 233–237 (1978).
4. Duncan, B. K., Rockstroh, P. A. & Warner, H. R. *J. Bact.* **134,** 1039–1045 (1978).
5. Duncan, B. K. & Weiss, B. in *DNA Repair Mechanisms* (eds Hanawalt, P. C., Friedberg, E. C. & Fox, C. F.) 183–186 (Academic, New York, 1978).
6. Coulondre, C., Miller, J. H., Farabaugh, P. J. & Gilbert, W. *Nature* **274,** 775–780 (1978).
7. Miller, J. H., Ganem, D., Lu, P. & Schimitz, A. *J. molec. Biol.* **109,** 275–302 (1977).
8. Coulondre, C. & Miller, J. H. *J. molec. Biol.* **117,** 577–606 (1977).
9. Lindahl, T. *Prog. Nucleic Acids Res. molec. Biol.* **22,** 135–192 (1979).

Visualization of an unwound DNA duplex

Struther Arnott, P. J. Bond & Rengaswami Chandrasekaran

Department of Biological Sciences, Purdue University, West Lafayette, Indiana 47907

Certain dyes[1,2] and drugs[3,4] with planar aromatic components can intercalate these into stacks of base pairs and thereby bind tightly to DNA duplexes. Intercalation at one site usually precludes intercalation between the base pairs immediately adjacent[5]. This exclusion implies that two distinct nucleoside conformations are needed in the dinucleoside phosphates which include the intercalation site. The simplest distinction would involve no more than quantitative differences in the (usually *anti*) conformations at the glycosidic bonds[6]. This could be reinforced by additional, qualitative differences in the furanose ring puckerings (C-2′-*endo* and C-3′-*endo*)[7]. For the most pronounced difference there could be qualitative differences (*syn* and *anti*) in the conformations of the glycosidic bonds as well as in the conformations of the sugar rings. The model discussed here is an example of this most emphatic distinctiveness, as the nucleosides at the 5′ ends of the intercalation sites are C-3′-*endo* and *syn* and at the 3′ ends are C-2′-*endo* and *anti*. X-ray diffraction analysis suggests that a completely unwound allomorph of the DNA duplex can persist in oriented fibres when stabilized by certain platinum-containing intercalators. In the untwisting of (usually) right-handed DNA double helices, unwound duplexes are presumably fleeting intermediates.

Previous precise visualizations of intercalation in DNA came from extrapolatory modelling[6–9] inspired mainly[8,9], but not exclusively[6,7], by X-ray diffraction studies of crystals containing self-complementary dinucleoside monophosphate duplexes complexed with intercalators. The accuracy of particular models of intercalation into DNA itself can be determined[10,11] by X-ray diffraction studies of fibres of calf thymus DNA saturated with a variety of platinum derivatives. The fibres are uniaxially oriented and their diffraction patterns, of which Fig. 1 is an example, show a layer line with 10.2 Å spacing, in striking agreement, as the original authors[10,11] emphasized, with a neighbour exclusion model. This is exactly the length expected of a unit of structure involving an intercalator sandwiched between two base pairs (Fig. 2*a*) which are then directly stacked on the base pairs of the next intercalator sandwich (Fig. 2*b–d*). Also, some of the fibres are polycrystalline so that the layer lines on the diffraction patterns are populated with fairly sharp Bragg reflections. Their spacings and intensities are satisfactorily explained by a model whose molecular conformation and packing are rather different from those proposed earlier[10]. An important conclusion of our study is that the DNA duplexes in these complexes are completely unwound and therefore not double helices. We have therefore an unprecedented opportunity to visualize a most unusual allomorph of double-stranded DNA.

We have confined our detailed analysis to the diffraction pattern (Fig. 1) provided by the DNA · $[(\text{bipy})\text{Pt}(\text{en})]^{2+}$ complex; however, our interpretation of the patterns from the DNA complexes with the other platinum-containing intercalators would be essentially the same.

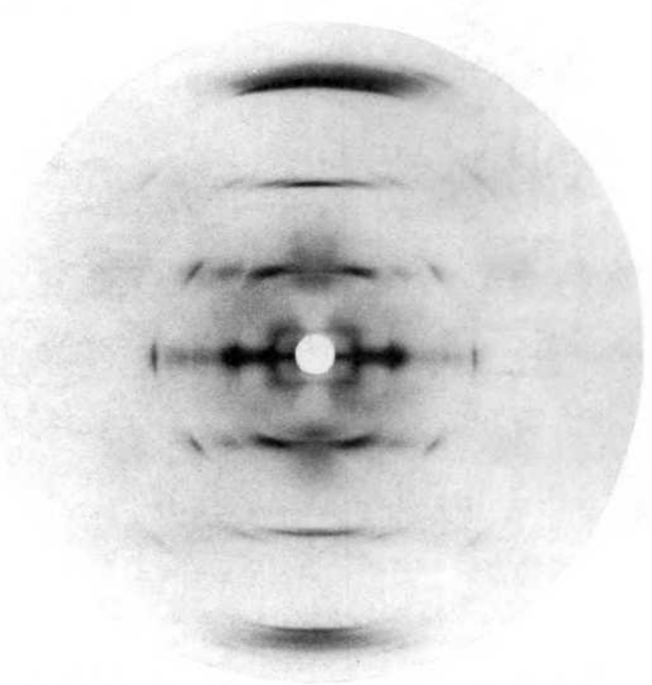

Fig. 1 The X-ray diffraction pattern from a uniaxially oriented, polycrystalline fibre of calf thymus DNA saturated with intercalating $[(\text{bipy})\text{Pt}(\text{en})]^{2+}$ cations. The layer line spacings indicate an axial repeat of 10.2 Å. The Bragg reflections can be indexed on the basis of a rectangular unit cell $11.5\times20.0\times10.2$ Å^3.

0028–0836/80/410561—03$01.00

Table 1 Comparison of the conformation angles of L DNA in the DNA · [(biby)Pt(en)]$^{2+}$ complex with those of S DNA

Conformation angle (deg)	L DNA		S DNA*	
	XpX†	XpX	CpG	GpC
θ(C4′–C3′–O3′–P)	−84	171	−72	−103
θ(C3′–O3′–P–O5′)	98	125	102	−91
θ(O3′–P–O5′–C5′)	82	−60	52	−110
θ(P–O5′–C5′–C4′)	−162	−133	−153	−168
θ(O5′–C5′–C4′–C3′)	180	−139	178	54
θ(C5′–C4′–C3′–O3′)	76	147	76	147
θ(O4′–C1′–N9–C4)†	26	167	89	—
θ(O4′–C1′–N1–C2)†	26	167	—	−159

L DNA is the trivial name we have given to the ladder-like structure, and S DNA is the polymeric version of the left-handed duplex.

* From ref. 14.

† X can be a purine or a pyrimidine.

The 30 independent Bragg reflections in Fig. 1 can be indexed adequately on the basis of a rectangular unit cell with dimensions (s.d.) $a = 19.95(15)$ Å, $b = 11.52(05)$ Å, $c = 10.20(05)$ Å. There are no reflections requiring the (six times) larger trigonal unit cell suggested earlier[10].

Clearly, the new unit cell cannot accommodate quasi-cylindrical DNA double helices with diameters at all like the traditional values of 21 ± 4 Å. This should not be surprising because the layer line spacings also are not compatible with a helical molecular structure. If successive, 10.2 Å-long units of structure were related by helical symmetry there should be layer lines with spacings $10.2(N/n)$ Å where N and n are integers and $N > 1$. In fact, $N = 1$ and all the layer lines have spacings $(10.2/n)$ Å, $n = 1, 2, 3 \ldots$, implying that the structural unit is repeated by simple translation along the chain axis.

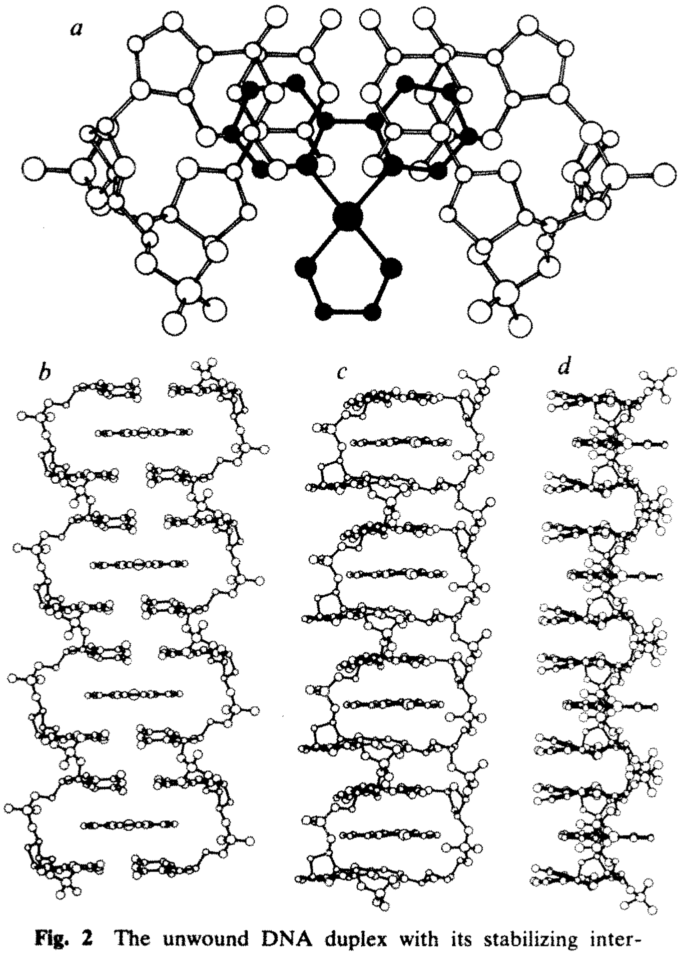

Fig. 2 The unwound DNA duplex with its stabilizing intercalators. *a* Shows the view parallel to the *c* axis of the stacking arrangement of an intercalator between two base pairs. Because this unit is repeated by simple translation along the *c* axis and the base pairs are almost perpendicular to this axis, the base pairs in the excluded site overlap one another in the same way as appears here; *b*–*d* contain three views perpendicular to the *c* axis, including the view down the diad axis (*b*) and views after successive rotations of 45° about *c*.

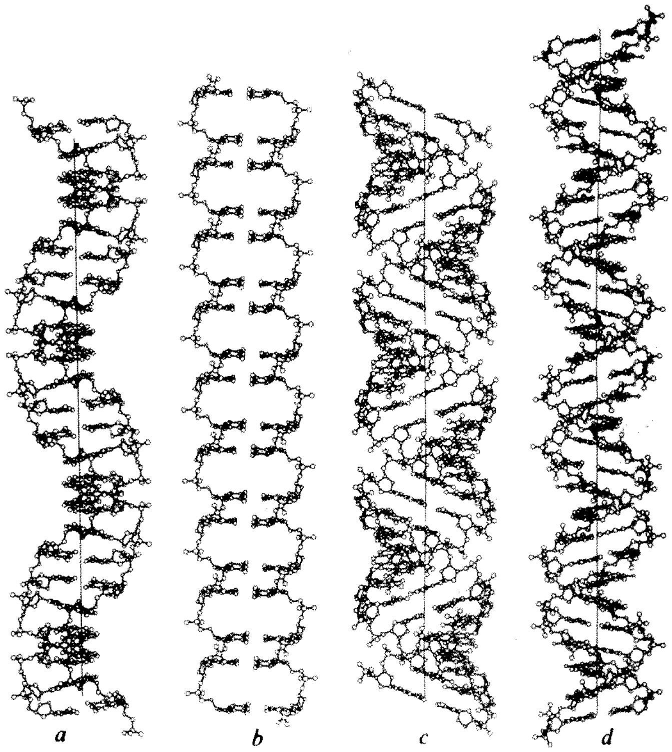

Fig. 3 Comparison of the morphologies of the most underwound (left-handed) DNA double helix (*a*), the unwound duplex (*b*), a right-handed double helix of the A family (*c*) and the most overwound (right-handed) double helix (which belongs to the B family) (*d*).

Bond *et al.*[10] were unable to build a stereochemically reasonable model duplex containing intercalated dinucleotide structure units except as N-fold helices with $N \geq 7$. In these experiments all glycosidic conformations were *anti*. By contrast, we have found that it is quite easy to construct a stereochemically acceptable model of the required '1-fold helix' if the glycosidic conformations along the polynucleotide chain are alternately *syn* and *anti*. The best arrangement associates a C-3′-*endo* furanose with the *syn* nucleoside and a C-2′-*endo* furanose with the *anti* nucleoside as in the left-handed screw structures observed with certain oligonucleotides[12,13] and DNA polymers[14]. Indeed, the segment involving stacked base pairs has the same kind of nucleotide conformations (see Table 1) as CpG in the left-handed (6_5) helical form of poly(dG-dC) · poly(dG-dC) (ref. 14). Not surprisingly, the GpC conformation in the 6_5 helix is not retained in the nucleotide which has to straddle the intercalation site. Extension of the chain and the achievement of no net winding after two nucleotides is contrived (see Table 1) by having *trans* conformations around C3′–O3′ (*gauche minus* in the 6_5 helix), P–O3′ (*gauche minus* in the 6_5 helix) and C4′–C5′ (*gauche plus* in the 6_5 helix).

In constructing the model of the DNA duplex in this complex, we assumed that the chains are antiparallel and conformationally identical. There are, therefore, diad axes half way between successive base pairs and perpendicular to the long axis of the molecule. We have further assumed that the diad axis within the [(bipy)Pt(en)]$^{2+}$ cation coincides with the DNA diad which is in the intercalation site. This leaves two possible dispositions for the intercalator. We find that the one which places the platinum atoms in the minor groove (Fig. 2*a*) seems to be preferable from both steric and diffraction considerations.

The small cross-section of the unit cell clearly shows that it can be traversed by no more than one intercalated duplex, oriented so that the minor groove is approximately bisected by the *b* axis. The diffraction pattern has some continuous intensity as well as Bragg reflections on each layer line, suggesteing a 'statistical' crystal structure[15]. The best arrangement we have found has rows of identically oriented molecules lined up along *a* 20-Å apart. About one-third of the rows separated by 11.5 Å in the *b* direction will also be mutually translated $c/2 = 5.1$ Å in the *c* direction and the molecules in the two rows mutually rotated by 30° about *c*. Such an arrangement would result in no steric anomalies and provide a good explanation of both the Bragg and the non-Bragg diffraction. For the Bragg reflections the conventional crystallographers' residual *R* has an encouragingly low value of 0.31 after a least-squares refinement[16] of the complex in which the polynucleotide chains are treated as a linked-atom system and the $[(\text{bipy})\text{Pt}(\text{en})]^{2+}$ intercalator as a rigid body free to move along and rotate about the diad axis which it is assumed to share with the DNA duplex.

In the refined structure the mean plane of each base pair of the DNA duplex is tilted 4° from being perpendicular to *c*. The bases in the base pairs are not coplanar but are 'propeller-twisted' with an angle of 22° between their planes. The intercalators are also tilted (in their case 5°).

Polynucleotide duplexes with Watson–Crick base pairs have quite polymorphic secondary structures (Fig. 3). Apparently this is not generally accepted because few of the many and varied allomorphs have been exploited in visualizing DNA and RNA duplexes in dynamic and interactive modes. Yet it is almost 30 yr since the identification[17] of A and B DNA indicated what a wide range of structure might be achieved by polynucleotide duplexes. A and B-DNA are helical structures with very distinct axial translations (h) and rotations (t) per nucleotide: $h, t =$ 2.56 Å, 32.7° in the former and 3.38 Å, 36.0° in the latter. Many allomorphs have now been trapped in oriented fibres and had their conformations defined[18]. All were right-handed double helices with $2.56\ \text{Å} \leqslant h \leqslant 3.38\ \text{Å}$ and $30.0° \leqslant t \leqslant 45.0°$. Recently, these ranges have been extended dramatically by the discovery of further wound right-handed helices[19] (with $t =$ 48.0°) and the underwound (left-handed) helices[14] (with $\langle t \rangle -$ 30.0°) anticipated by the NMR[20] and single crystal[12,13] studies of oligo(dG–dC) · oligo(dG–dC).

The present structure with $\langle h \rangle = 5.1$ Å and $\langle t \rangle = 0.0^{o}$ is a further example of the polymorphism of polynucleotide duplexes. Clearly, the partially stacked polynucleotide component of the complex could have only a brief lifetime in the absence of the stabilizing intercalator. Therefore, we have visualized one of the higher energy states available to DNA. In the present context this state has been exploited by a synthetic intercalator, but obviously it is a state which is available also for interaction with native molecules.

The structure of this complex also adds pointedly to the contention[6,8,9] that there is no single conformational strategy whereby polynucleotide duplexes contrive to accommodate intercalators. Further, the local unwinding resulting from intercalation can be much larger than is often supposed.

We thank Professor S. J. Lippard for materials and discussion. The research was supported by NIH grant GM17371 to S.A.

Received 18 June; accepted 8 August 1980.

1. Lerman, L. S. *J. molec. Biol.* **3,** 18–30 (1961).
2. Lerman, L. S. *Proc. natn. Acad. Sci. U.S.A.* **49,** 94–102 (1963).
3. Waring, M. J. *Biochim. biophys. Acta* **87,** 358–361 (1964).
4. Bauer, W. & Vinograd, J. *J. molec. Biol.* **47,** 419–435 (1970).
5. Crothers, D. M. *Biopolymers* **6,** 575–584 (1968).
6. Shieh, H.-S., Berman, H. M., Dabrow, M. & Neidle, S. *Nucleic Acids Res.* **8,** 85–97 (1980).
7. Sobell, H. M., Tsai, C.-C., Jain, S. C. & Gilbert, S. G. *J. molec. Biol.* **114,** 333–365 (1977).
8. Alden, C. J. & Arnott, S. *Nucleic Acids Res.* **2,** 1701–1717 (1975).
9. Alden, C. J. & Arnott, S. *Nucleic Acids Res.* **4,** 3855–3861 (1977).
10. Bond, P. J., Langridge, R., Jennette, K. W. & Lippard, S. J. *Proc. natn. Acad. Sci. U.S.A.* **72,** 4825–4829 (1975).
11. Lippard, S. J., Bond, P. J., Wu, K. C. & Bauer, W. R. *Science* **194,** 726–728 (1976).
12. Drew, H. R., Dickerson, R. E. & Itakura, K. *J. molec. Biol.* **125,** 535–543 (1978).
13. Wang, A. H.-J. *et al. Nature* **282,** 680–686 (1979).
14. Arnott, S., Chandrasekaran, R., Birdsall, D. L., Leslie, A. G. W. & Ratliff, R. L. *Nature* **283,** 743–745 (1980).
15. Arnott, S. *Trans. Am. Crystallogr.* **9,** 31–56 (1973).
16. Smith, P. J. C. & Arnott, S. *Acta crystallogr.* **A34,** 3–11 (1978).
17. Franklin, R. E. & Gosling, R. G. *Acta crystallogr.* **6,** 673–677 (1953).
18. Arnott, S. *1st Cleveland Symp. Macromolecules*, 87–104 (Elsevier, Amsterdam, 1977).
19. Leslie, A. G. W., Arnott, S., Chandrasekaran, R. & Ratliff, R. L. *J. molec. Biol.* (in the press).
20. Patel, D. J., Canuel, L. L. & Pohl, F. M. *Proc. natn. Acad. Sci. U.S.A.* **76,** 2508–2511 (1979).

Metallothionein occurs in roots of *Agrostis* tolerant to excess copper

Wilfried E. Rauser & Nester R. Curvetto*

Department of Botany and Genetics, University of Guelph, Guelph,
Ontario, Canada N1G 2W1

Metallothioneins have an important function in metal metabolism in animals[1]. These low molecular weight proteins have high contents of half-cystinyl residues (up to 33%) which can bind metals such as Zn, Cu, Cd, Hg or Ag in mercaptide complexes[1]. In normal conditions animal tissues have low concentrations of metallothioneins, but these increase on administration of metal[2–4], a reaction which is consistent with their suggested role in detoxification mechanisms[2,5,6]. Various plant genotypes exhibit tolerance to excesses of metals[7], and Jowett[8] proposed that such genotypes contain compounds capable of specific metal chelation. Metallothioneins could serve such a role. We report here that copper-thionein occurs in the roots of a clone of *Agrostis gigantea* Roth tolerant to excess copper[9]. This is the first unequivocal demonstration of a metallothionein in a vascular plant. These unusual proteins may have a role in metal metabolism in plants and could be important in the elucidation of the mechanism of metal tolerance.

Apical tillers of clone 4 of *Agrostis gigantea* were transplanted into tanks containing complete nutrient solution and allowed to develop roots for 3 weeks[9]. Plants were then exposed for 1 week to 16 μM $CuSO_4$ in the nutrient solution. Roots were harvested, washed three times in large volumes of cold deionized water and blotted with paper towelling. The roots were either used at once or frozen in liquid nitrogen for later use. All operations for extracting and isolating proteins were carried out at 0–4 °C with solutions purged with N_2 and in enclosures flushed with N_2. A typical separation of heat-denatured root extract on DEAE Biogel A is shown in Fig. 1. The protein was resolved into material not adsorbed to the ion exchanger (fraction A) and a prominent peak of copper-binding protein that was eluted only after adding NaCl (fraction B). Metallothioneins characteristically adsorb strongly to DEAE[3,10]. Fraction B from this and other isolations was purified by electrophoresis on 3-mm thick gel slabs of 10% w/v polyacrylamide with Tris-glycine *p*H 8.3 as electrode buffer[11]. In a typical run where 165 mg fraction B product was applied, a single dark brown band 5 mm wide was evident after migrating 10 cm. The dark brown material was eluted from the gel and analysed for molecular weight (MW), amino acid composition and metal content. Fraction B protein showed a major band at a MW of 14,400 and lesser bands at 9,800, 6,200 and 5,400 after SDS-polyacrylamide gel electrophoresis.

From the amino acid composition listed in Table 1 it is clear that fraction B protein has a high half-cystine content, a key feature of metallothioneins[1,2,10]. Acidic amino acids predominated and, along with cysteine, glycine and serine, accounted for 67.5% of the residues compared to 70.2% for yeast Cu-thionein[12]. The ratio of half-cystine to copper was 1.9–2.4 to 1 in accord with the stoichiometry found for Cu-thionein from

---

* Present address: Departamento Ciencias Agrarias, Universidad Nacional del Sur, Bahia Blanca, Argentina.

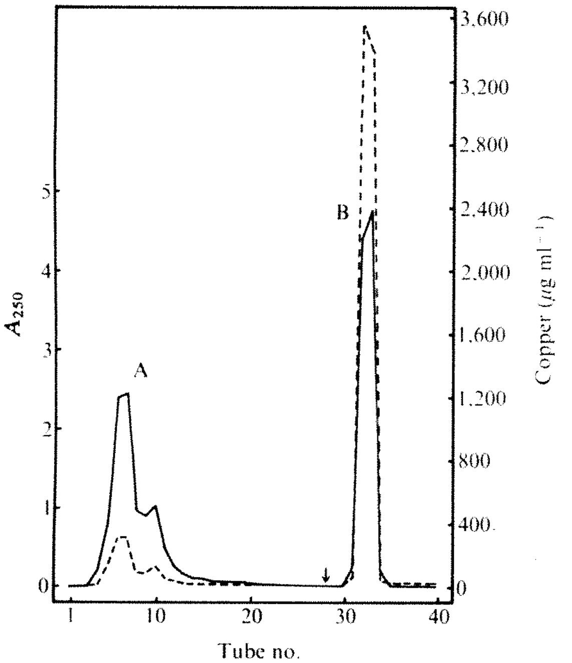

Fig. 1 Ion-exchange chromatography of copper-binding proteins from *Agrostis gigantea*. 60 g of frozen roots were homogenized with 60 ml 10 mM Tris-HCl, *p*H 8.0, 5 mM NaCl, 5 mM 2-mercaptoethanol in a mortar and pestle. The homogenate was strained through cheesecloth and centrifuged at 20,000*g* for 30 min. Heat denaturation of the supernatant was done by rapid heating at 60 °C for 3 min while stirring under a stream of N_2. The preparation was cooled in an ice bath and centrifuged at 20,000*g* for 30 min. The supernatant was concentrated to 5 ml by ultrafiltration on a Diaflo UM2 membrane (Amicon) and washed three times with a total of 50 ml 5 mM Tris-HCl, *p*H 8.6. The washed concentrate was applied to a DEAE Biogel A column (1.5 × 25 cm) equilibrated with 5 mM Tris-HCl, *p*H 8.6. Proteins were eluted with the same buffer at a flow rate of 70 ml h^{-1} with fraction volumes of 8 ml. At tube 28 (arrow) the elution buffer was changed to one containing 1 M NaCl. ——, Protein; --------, copper.

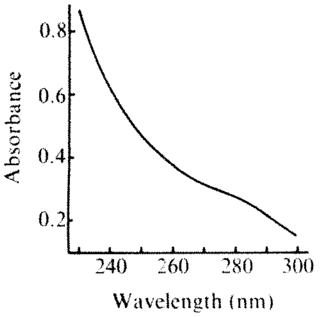

Fig. 2 UV absorption spectrum of fraction B protein in 5 mM Tris-HCl, *p*H 8.6.

Table 1 Amino acid composition of copper-binding proteins from *Agrostis gigantea*

	Fraction A	Fraction B
Half-cystine*	4.8	18.4
Aspartate	12.8	10.0
Glutamate	13.4	19.0
Glycine	11.7	11.9
Serine	8.6	8.2
Threonine	5.9	2.9
Proline	7.5	5.8
Alanine	9.0	6.0
Valine	6.4	4.2
Methionine	1.0	0.7
Isoleucine	3.6	1.5
Leucine	5.9	3.6
Tyrosine	1.1	0.6
Phenylalanine	2.0	1.5
Lysine	3.5	3.3
Histidine	1.4	0.8
Arginine	1.4	1.6

The material in fractions A and B from DEAE Biogel A separations was purified electrophoretically on slab gels, dialysed exhaustively against 5 mM Tris-HCl, *p*H 8.6, and then hydrolysed in N_2-saturated 6 M HCl at 110 °C for 24 h. Values are expressed as per cent of the total number of residues.

* Only 0.6–0.7 residue % was found as cysteic acid.

yeast[12], but markedly different from the sulphur to metal stoichiometry ratio of 3 : 1 known for Cd- and Zn-thioneins of animal origin. Fraction B protein contained copper and zinc, but copper comprised 93–98% of the bound metal. The low tyrosine and lack of tryptophan account for the low absorption at 280 nm (Fig. 2). This UV spectrum resembles that of chicken liver metallothionein fully loaded with copper[13]. The properties of thermal stability, low molecular weight, high half-cystine content, metal binding and UV spectrum are consistent with the designation of fraction B protein as a Cu-binding metallothionein as was done for the yeast protein[12]. The amino acid composition of fraction B protein resembles that of Cu-thionein from yeast[12]; however, both differ from equine Cd- and Zn-thioneins[14]. This divergence raises the possibility that the proteins binding copper might be set apart from the Cd- and Zn-thioneins even though they all have the unique function of binding abundant metal.

The nature of the Cu-binding material in fraction A is less clear. The amino acid composition of electrophoretically purified fraction A protein (Table 1) indicates that it is not an aggregate of Cu-thionein as has been suggested by others[13,15,16]. The copper content was much lower at a cysteine to copper ratio of 0.5 : 1, yet zinc comprised only 3–6% of the bound metal. Electrophoresis in SDS gels showed bands of 5,400, 11,600 and 52,300 MW against a background of Coomassie blue-staining material which reached the start of the gel.

Quantitative estimates of the amount of Cu-thionein in the roots of *Agrostis gigantea* were not possible. Protein estimations by either biuret or dye binding[17] methods were increasingly unreliable as the metallothionein was purified. Occlusion of material on the ultrafilter gave copper losses of 12–17% and there were even greater losses during dialysis of protein concentrates. More reliable methods are required to determine how much Cu-thionein occurs in the roots of *Agrostis gigantea* before any more can be inferred about its involvement in the mechanism of copper tolerance.

We thank Dr T. K. Smith for performing the amino acid analyses. This study was supported by NSERC grant A4921.

Received 11 January; accepted 25 April 1980.

1. Kojima, Y. & Kägi, J. H. R. *Trends biochem. Sci.* **3,** 90–93 (1978).
2. Nordberg, G. F., Nordberg, M., Piscator, M. & Vesterberg, C. *Biochem. J.* **126,** 491–498 (1972).
3. Premakumar, R., Winge, D. R., Wiley, R. D. & Rajagopalan, R. V. *Archs Biochem. Biophys.* **170,** 278–288 (1975).
4. Chen, R. W., Whanger, P. D. & Weswig, P. H. *Biochem. Med.* **12,** 95–105 (1975).
5. Leber, P. A. & Miya, T. S. *Toxic. appl. Pharmac.* **37,** 403–414 (1976).
6. Sabbioni, E. & Marafante, E. *Envir. Physiol. Biochem.* **5,** 132–144 (1975).
7. Antonovics, J., Bradshaw, A. D. & Turner, R. G. *Adv. ecol. Res.* **7,** 1–85 (1971).
8. Jowett, D. *Nature* **182,** 816–817 (1958).
9. Hogan, G. D. & Rauser, W. E. *New Phytol.* **83,** 665–670 (1979).
10. Kägi, J. H. R., Himmelhoch, S. R., Whanger, P. D., Bethune, J. L. & Vallee, B. L. *J. biol. Chem.* **249,** 3537–3542 (1974).
11. Davis, B. J. *Ann. N.Y. Acad. Sci.* **121,** 404–427 (1964).
12. Weser, U., Hartmann, H. J., Fretzdorff, A. & Strobel, G. J. *Biochim. biophys. Acta* **493,** 465–477 (1977).
13. Rupp, H. & Weser, U. *FEBS Lett.* **44,** 293–297 (1974).
14. Kojima, Y., Berger, C., Vallee, B. L. & Kägi, J. H. R. *Proc. natn. Acad. Sci. U.S.A.* **73,** 3413–3417 (1976).
15. Porter, H. *Biochem. biophys. Res. Commun.* **56,** 661–668 (1974).
16. Ryden, L. & Deutsch, H. F. *J. biol. Chem.* **253,** 519–524 (1978).
17. Bradford, M. *Analyt. Biochem.* **72,** 248–254 (1976).

MATTERS ARISING

Superheavy-element fission tracks in iron meteorites

BULL'S careful search[1] for superheavy element (SHE) fission tracks in silicate inclusions within iron meteorites seems to have given a null result. He finds an upper limit of 10^{-12} kg per kg for the original abundance of SHEs in the class 1A Odessa iron meteorite. As this is many orders of magnitude below what we postulated[2] from considerations of early heat sources in the Moon and from a highly speculative interpretation of elemental abundances in iron meteorites[3], Bull's result may be accepted as proof that superheavy elements either did not exist or did not play any part in the early Solar System. His observations therefore merit further study. His result refers to the date at which track retention becomes possible, that is when the temperature has fallen to ~200 °C. Now although the Rb–Sr, K–Ar dates of silicate inclusions in iron meteorites range up to ~4,600 Myr, they are not to be interpreted simply as the 'age' of iron meteorites nor are they the dates of the emplacement of the silicate grains. The process by which silicate inclusions get into iron meteorites is unknown: but they must certainly enter while the temperature of the iron is near to its melting point. Cooling rates of iron meteorites are determined by metallographic study and for the Odessa meteorite it is 1.5 °C Myr^{-1} in the range 700–300 °C. The meteorite might, therefore, only reach track retention temperatures 800 Myr after the emplacement of the silicate crystals. Taking the half life of SHEs determined from the decay of the ancient lunar magnetic field[4] as 100 Myr, the original abundance of SHEs in the iron would have decayed by nearly 3 orders of magnitude. This, of course, assumes that the rate of cooling at higher temperatures and at lower temperatures is the same. In fact if, as we suppose, SHEs have played a dominant part in the early thermal history of the parent bodies of meteorites, the cooling rates at higher temperatures may have been slower and the diminution in the abundance of SHEs at the time when track retention became possible greater than we have estimated here. Another possible explanation of Bull's results is, of course, that SHEs on the condensation of grains in the early Solar System were never fully taken up by the iron. This explanation seems probable in the case of the Odessa meteorite as IA iron meteorites have been interpreted as not originating in the iron core in a sizeable asteroid-like body. Probably only in a completely melted sizeable body would the molten iron, mixing with other crystals, dissolve the SHEs. The IA meteorites have reasonably been interpreted in terms of a model in which iron condenses from the nebula and forms small bodies within a much larger silicate parent body. If this model is correct, then the existence of ^{244}Pu fission tracks would have a simple explanation. Bull's studies ought to be done on the IIAB iron meteorites which are more reasonably assumed to come from the cores of entirely melted parent bodies, but the difficulty is that there are no silicate grains to record fission tracks. *Note added in proof*: We are, of course, aware that if the tracks inside the diopside crystals are due to the decay of Pu^{244}, synthesized with the other elements in stellar nucleogenesis processes just before the condensation of the primeval Solar System nebula, our first argument, that the presumed SHE tracks have disappeared due to annealing processes, collapses. But we wonder whether this identification, which, as Bull so clearly explains, is arrived at by a process of elimination, should be accepted without question. Extrapolation of the Periodic Table[1] does not show that all the SHE are siderophile and perhaps some of them, with longer half life, went into the mineral phase.

We agree that our suggested thermal history are necessarily speculative—as are all others—but the track retention temperatures of minerals, such as the quoted 400 °C for diopside, are based on laboratory annealing experiments.[5] But this extrapolation to 4,000 Myr assumes that the same excitation process can be assumed as in laboratory annealing; but it is characteristic of solid state physics phenomena that processes with different excitation energies are dominant over different ranges of temperature and time.

S. K. RUNCORN

School of Physics,
The University,
Newcastle upon Tyne NE1 7RU, UK

W. F. LIBBY
L. M. LIBBY

University of California at Los Angeles,
California 90024

---

1 Bull, R. K. *Nature* **282**, 393–394 (1979).
2. Runcorn, S. K., Libby, L. M. & Libby, W. F. *Nature* **270**, 676–681 (1977)
3 Libby, L. M., Libby, W. F. & Runcorn, S. K. *Nature* **278**, 613–617 (1979)
4. Runcorn, S. K. *Science* **199**, 771–773 (1978).
5 Fleischer, R. L., Price, P. B. & Walker, R. M. *Nuclear Tracks in Solids* (University of California Press, 1975).

BULL REPLIES—Runcorn *et al.* have proposed two explanations for the lack of superheavy element (SHE) fission tracks which I observed in silicates from the Odessa iron meteorite[1].

First, they point out that a thermal history for Odessa can be constructed in which the meteorite reaches track retention temperatures only after a time corresponding to many half lives for the SHEs (taken to be ~100 Myr) has elapsed. This explanation, however, fails to account for the large excess of fission tracks distributed throughout the diopside grains in Odessa. These exceed the number accruing through the decay of ^{238}U in the lifetime of the Solar System by a factor of ~100 and the most plausible source of this excess is the decay of ^{244}Pu which, significantly, has a half life which is very close to that assumed for the SHEs. This means that any cooling which was slow enough to allow most of the SHEs to decay would also result in the loss of most of the Pu and the very large excess of fission tracks in the diopside would be difficult to account for unless this mineral was very much enriched in Pu relative to U (an initial ratio of Pu/U of ~10 would be needed compared to values of ~0.01–0.1, inferred from fission Xe measurements on chondritic whitlockites[2]). As to the thermal history proposed by Runcorn *et al.*, I would point out that the track retention temperature of diopside is higher than 200 °C, probably nearer 400 °C and that there is considerable uncertainty as to the metallographic cooling rates.

The second explanation by Runcorn *et al.* is that the IA irons never took up many SHEs. This point may be valid in that the group IA meteorites are not typical irons and there is evidence that they were never melted. The pallasites, however, are believed to be fragments of a core boundary region and pallasitic metal probably represents core material. In Brenham the superheavy content of the metal was less than 10^{-15} kg per kg at the time of track retention but unfortunately we cannot as yet place firm constraints on when track retention occurred.

Finally, note that silicate inclusions are occasionally found in other iron meteorites groups and a study of these should provide further clues to the abundance of SHEs in the early Solar System.

R. K. BULL

Nuclear Power Company,
(Whetstone) Ltd, Leicester, UK

---

1. Bull, R. K. *Nature* **282**, 393–394 (1979)
2. Kirsten, T., Jordan, J., Richter, H., Pellas, P. & Storzer, D. *Meteoritics* **12**, 279–281 (1977).

0028–0836/80/410565—01$01 00

Grand unification theories and the large numbers hypothesis

BARROW[1] has recently used the large number hypothesis (LNH) in connection with the proton lifetime.

I wonder about the meaning of his result in light of the fact that he has based his computation on a closed Friedman universe, while Dirac has explicitly shown that "A model with a maximum size for the Universe is not permitted"[2], that is, is disallowed by the LNH.

V. CANUTO

Institute for Space Studies,
2880 Broadway,
New York, New York 10025

1. Barrow, J. D. *Nature* **282**, 698 (1979).
2. Dirac, P. A. M. *Proc. R. Soc.* **A338** (1974).

CURRENT ideas based on SU(5) gauge theory suggest the violation of baryon conservation. The proton lifetime, τ_p, is predicted to have various values between 10^{30} and 10^{37} yr. Barrow[1] has noticed that the dimensionless ratio of τ_p so predicted, to the Planck time $\tau_{p1} = (Gh/c^5)^{\frac{1}{2}}$, is not very different from the Universe baryon number $N \sim 10^{79}$. Assuming that the two numbers are equal, he can then assign to τ_p the more definite value of

$$(hc/Gm_p^2)^{\frac{1}{2}} H_0^{-1} \sim 10^{30} \quad \text{yr}$$

where m_p is the proton rest mass, H_0 the present Hubble 'constant', and factors of the order of unity have been omitted.

We consider instead of τ_{p1} a time unit that involves a property of the particle itself. The simplest choice is $\tau_m = h(m_p c^2)$ (so that for particles which remain massless $\tau_m \rightarrow \infty$). Intuitively, τ_m is, of course, the minimum lifetime of one proton before its inertial mass can be measured as $\geqq m_p$. Furthermore, we speculate on the lifetime τ'_p for its decay hypothetically to some unspecified particles of lower masses under gravitational interaction. The plausibility that all particles with rest masses have finite lifetimes has been considered[3]. All may eventually decay to gravitons on sufficiently long time scales for which charge conservation is violated; photons may not be massless. Maybe changeability is so prevalent in the physical world that all symmetries are ultimately broken spontaneously. Now, on dimensional grounds τ'_p may be expected to be given by a similar expression as τ_p, with the mediating boson mass replaced by the Planck mass $(hc/G)^{\frac{1}{2}}$ at which gravitational unification should occur, and with the coupling constant α_x substituted by another which is similarly of the order of 1/137. The result is $\tau'_p \sim 10^{50}$ yr.

We then find that τ'_p/τ_m is again of the same order as the baryon number in the Hubble sphere (or in the Universe). If $\tau'_p/\tau_h = fN$, where f is some factor such as $3^2/8\pi$ and numerically of the order of unity, then

$$\tau'_p \sim (hc/Gm_p^2) H_0^{-1}.$$

However, some of the cosmological coincidences, such as the above two, may really be coincidences and 'explicable' by the anthropic principle[2] or speculatively as 'historical' data[3]. This can be true although others are derivable (for example, the coincidences involving the Universe photon–baryon ratio: from SU(5) theory[4]). Future experimental verifications such as of the value of τ_p and excepting a decreasing G, therefore do not confirm the large number hypothesis. Some large dimensionless numbers may equal H_0^{-1}/τ_m or its square only in the present epoch. If the Universe is indeed closed, it has extremal scale factors which are unrelated to its age expressed in atomic units. Thus the hypothesis is inconsistent with[5] a closed Friedmann universe[1].

T. B. TANG

Darwin College,
Silver Street,
Cambridge, UK

1. Barrow, J. D. *Nature* **282,** 698 (1979).
2. Carr, B. J. & Rees, M. J. *Nature* **278,** 605 (1979).
3. Tang, T. B. *J. Br. Interplanet. Soc.* **32,** 84 (1979).
4. Yoshimura, M. *Phys. Rev. Lett.* **41,** 281 (1978).
5. Dirac, P. A. M. *Proc. R. Soc.* **A338,** 439 (1974).

BARROW REPLIES—A large numbers hypothesis (LNH) is not incompatible with a closed finite universe. The original statement of the LNH by Dirac[1] in 1938 was: "Any two of the very large dimensionless numbers occurring in Nature are connected by a simple mathematical relation, in which the coefficients are of the order of magnitude unity." To derive some predictions from this hypothesis one must accumulate a group of large dimensionless quantities of similar magnitude and equate them. The issue of whether or not a 'closed' universe is compatible with the hypothesis depends crucially on the type of large number that is chosen. Dirac's original[1] choice included the ratio of $e^2 m_e c^3 \sim 10^{-23}$ s, (the time for light to traverse the classical electron radius) to the presently inferred age of the Universe, $t_0 \sim 10^{17}$ s. This particular large number therefore incorporates an explicit time dependence through the changing value of t_0. The hypothesis that it be equal to other dimensionless collections of traditional constants with similar magnitude requires that one of the latter also possess an explicit time dependence. Dirac chose to incorporate the time dependence into Newton's gravitation 'constant', G. If the Universe were finite (either 'closed' or 'open' but with finite volume through topological identifications), then the LNH would also seem to require the total number of protons in the Universe ($\sim 10^{80}$) to increase as t^2 in violation of energy conservation. For this reason Dirac[1] required an open (infinite) cosmological model. However, it is only the choice of a 'large number' possessing an explicit time dependence that suggests such a conclusion, not the LNH itself.

If one chooses large numbers in a less anthropocentric fashion then one naturally replaces the time scale t_0 by t_m, the proper time to the expansion maximum in a closed universe. The quantity t_m, unlike t_0, is observer-independent and a fundamental cosmic time. Quantitatively this new choice leaves the value of the relevant large number virtually unchanged ($t_m m_e c^3/e^2 \sim 10^{40}$) because t_m is within an order of magnitude of t_0, but qualitatively its consequences are quite different: No varying 'constants', additional conformal degrees of freedom or unconventional physics become involved and a closed universe is actually necessary for consistency. Formulated in this manner the LNH simply claims that otherwise unrelated groups of constants possessing similar dimensionless magnitudes are actually equal. This is why I used the time t_m and a 'closed' universe in my formulation. It is, of course, equally legitimate to pursue the more speculative and complicated course that follows from choosing to incorporate t_0 into the large numbers. An 'open' universe would then be a necessary and testable prediction.

Tang derives an interesting estimate for the time scale of a possible gravitational decay of the proton, τ'_p. It depends linearly on the dimensionless gravitational coupling Gm_p^2/hc. A more natural candidate for this time scale might be provided by existing theory[2]—the time for a proton to quantum tunnel inside its own Schwarzchild radius, $R_s(p) \sim Gm_p/c^2$, and then evaporate into a state of zero baryon charge by the Hawking effect[3–5]. One might crudely estimate this time scale as $\tau''_p \sim [R_s^2(p)nc]^{-1}$ where $n \sim (h/m_p c)^{-3}$ is roughly the nuclear density. This estimate gives a decay time varying as the square of the gravitational coupling and considerably in excess of the lifetime suggested by grand unified gauge theories:

$$\tau''_p \sim \left(\frac{hc}{Gm_p^2}\right)^2 \left(\frac{h}{m_p c}\right) \sim 10^{48} \quad \text{yr}$$

JOHN D. BARROW

Berkeley Physics Department,
University of California,
Berkeley, California 94720

1. Dirac, P. A. M. *Proc. R. Soc.* **A165,** 199 (1938).
2. Hawking, S. W. *Nature* **248,** 30 (1974).
3. Zeldovich, Y. B. *Soviet Phys. Usp.* **20,** 945 (1977).
4. Barrow, J. D. & Tipler, F. J. *Nature* **276,** 453 (1978).
5. Barrow, J. D. *Surv. High Energy Phys.* **1**(3) (1980).

0028-0836/80/410566—01$01.00

BOOK REVIEWS

More uncertainty for the common man

J.S. Bell

Other Worlds: Space, Superspace and the Quantum Universe. By Paul Davies. Pp.208. (Dent: 1980.) £7.50.

THE aim of this book is to "face squarely the full impact of fundamental quantum theory on our conception of the world [and] not simply to review a notoriously difficult branch of modern physics, but to turn instead to broader issues. What is man? What is the nature of reality? Is the Universe we inhabit a random accident or the outcome of a delicate selection process?". And all this for a reader with "no previous knowledge of science or philosophy". Professor Davies does not lack ambition.

In fact, I doubt that the book will mean much to a scientific ignoramus; it is more for a reader whose mind is not quite blank before words like 'electromagnetic', 'atom', 'galaxy' and so on. But, with just a minimum of basic scientific culture, it will be possible to get from the book some idea of what quantum theory is, of what an enormous break it is seen to be with what went before, and of how physicists have not yet really digested it.

The first chapters take the reader for a race, a bit breathless, through some of the main ideas of classical mechanics, relativity and quantum theory. We are told of how physicists have come to think of the world as a "game of chance in which we are not merely spectators but players" — in that we now have fundamental laws which are indeterministic in character and whose formulation (in the orthodox contemporary view, in so far as it is coherent) seems to require reference to the observer; of the uncertainty principle and the exclusion principle; of the Dirac sea and the antiparticle; of how space-time itself must be subject to quantum fluctuations and be 'foamy' on a small scale. Repeatedly we are told how very bizarre and incomprehensible it all is.

In later chapters the story unfolds of the remarkable ideas advanced by remarkable physicists in trying to comprehend it all — Bohr's idea that we must renounce all attempts to visualize the atomic and subatomic world and must be content with a formalism that allows statistical predictions to be made about macroscopic events in macroscopic equipment; Wigner's concept that human consciousness plays an essential dynamical role in the world, in 'reducing the wave function'; Wheeler's idea that the very existence of the world, at any time, may somehow be caused by the existence of an observer at some time; the 'anthropic principle' of Dicke and Carter, that much in the observed world is fixed by the fact that it is being observed, because with even minor changes the world could not have produced observing creatures like us.

Above all we learn of the 'many-universes' interpretation of quantum mechanics, of Everett and De Witt, according to which all universes that might exist do exist. If they all exist, then the existence among others of relatively few tailored for our comfort is no mystery, and of course it is only in one of these few that we could find ourselves. Professor Davies is clearly attracted to the many-universes interpretation — and derives from it the title of his book — but correctly makes clear that it is taken seriously only by a handful of physicists. A final chapter dwells on the mystery of time, and especially the absence from our equations of anything corresponding to our impression of the passing of time. One must admire the intellectual intrepidity, and subtlety, of the author in "finding no reason to suppose that the future does not already exist, even though it is not yet determined, and even though the observer will have a hand in structuring it . . . ".

All this is vividly done. Perhaps even a little too vividly. Sometimes the confidence, even the complacency, of the assertions can be irritating. "We must acknowledge . . . " and "We have seen that . . . " really mean only that some qualitative considerations might suggest the entertainment of one possibility among others. But often the unqualified statement is modified a little later, or even has been qualified earlier — a distinction perhaps of little moment to one with such an Olympian view of time. In the closing sentences of his book the author allows that our subjective impression might be more reliable as regards time's passing than our equations. And his assertion that most scientists would agree that ". . . past, present, and future are merely linguistic conventions . . ." has been qualified already in the prologue, where it is said of such ideas that "most scientists live a sort of dual life, accepting them in the laboratory, but rejecting them without thought in daily life". Yes indeed.

On the whole the book gives a good impression of what is thought about these questions by physicists who consider them. But there is an exception, and it is a serious one. It concerns the views of Einstein in general and the Einstein–Podolsky–Rosen argument in particular. As regards Einstein's general reservations about quantum mechanics, Professor Davies propagates the view that they centred on indeterminism: "So unpalatable did this inherent chanciness seem to Albert Einstein that he refused to believe it throughout his life, dismissing the idea with the famous retort 'God does not play dice'". Perhaps the quotability of this famous retort is partly to blame for the fact that Einstein's more considered views are less well known. Compare the summing-up above with the following by Pauli. He is writing to Born in 1954:

> . . Einstein does not regard the concept of 'determinism' to be as fundamental as it is frequently held to be (as he told me emphatically many times) . . . he *disputes* that he uses as a criterion for the admissibility of a theory the question: — Is it rigorously deterministic? — . . . he was *not at all* annoyed with you, but only said you were a person who will not listen".

The Einstein–Podolsky–Rosen (EPR) argument comes up in Chapter 6: "So far we have deliberately been rather cavalier about notions like the real world. . . . In this chapter we shall face up squarely to the fundamental questions raised by the quantum revolution . . . ". In particular, we face up squarely to the possibility that "the apparently capricious and random fluctuations of microsystems do not represent an intrinsic indeterminacy in Nature, but are simply manifestations of a hidden level of structure . . . ". And then the EPR correlations are presented as the fundamental argument against such a possibility! While for EPR they were an entirely convincing argument for precisely such a possibility! The discussion exhibits the perplexity of one who refuses to contemplate the possibility that quantum mechanical description, of a photon in particular, is incomplete. It was the position of EPR that such perplexity could be relieved just by admitting the hypothesis in question. That Professor Davies misses the point not only of the original work, but of the renewed discussion and the associated experimental programme, is clear from the following: "The truly mind-boggling implications. . . are apparent if we use two parallely orientated polarizers . . . ". On the contrary, the mind is boggled only by polarizers which are not parallel. The results with parallel polarizers are easily explicable along Einsteinian lines. The results with off-parallel polarizers are not. That is the new point, unknown to EPR, which inspired the experimental programme of recent years to which the author seems to refer.

While I claim that Professor Davies is wrong on these points, it would certainly be unjust to pillory him on account of them. He makes these mistakes, if they are indeed mistakes, in the company of many other distinguished physicists. He could claim to be reporting a consensus! I enjoyed the book, despite all the reservations, and expect it to be enjoyed by many. The author provides a lively account, accessible with very little technical background, of what is being said about some momentous and inevitable questions. And if he sometimes leads into error, he does not lead into a minority. □

J. S. Bell is a physicist working at CERN in Geneva.

Data book on zinc

Roy M. Harrison

Zinc in the Environment. Edited by J. O. Nriagu. Part 1 *Ecological Cycling,* pp.453; Part 2 *Health Effects,* pp.480. (Wiley-Interscience: 1980.) Each volume £27.50, $59.85.

MOST non-specialists will probably associate the subject of metals in the environment with possible adverse human health effects; indeed in the cases of metals such as lead, cadmium and mercury the main stimulus for research has arisen from concerns over toxic symptoms arising from excessive environmental exposure. Zinc provides a very different case, however. Adverse health effects found in the general population result more often from zinc deficiency, rather than from toxicity due to elevated exposure. Indeed, despite the ubiquitousness of zinc in our environment, numerous well-documented cases of serious zinc deficiency syndrome have arisen amongst groups of people in many different parts of the world. Instances of zinc intoxication in humans are comparatively rare, arising only from extreme exposure conditions not normally experienced by the general population, and in some instances probably due to the cadmium impurity invariably present in technical-grade zinc.

The essentiality of zinc in mammalian metabolism coupled with its considerable toxicity, especially to aquatic biota, make the study of zinc in the environment an important matter which has been rather neglected in comparison with the intensive research efforts expended upon other environmental metals. This two-volume compilation by Nriagu may help to redress the balance; it is an extremely valuable collection of both factual information and numerical data on environmental zinc, and provides a useful source book.

Part I covers the production and uses of zinc, the environmental concentrations and pathways of the metal and its cycling within, and effects upon, near-shore marine, freshwater and forest ecosystems. Part II deals primarily with human health effects of zinc, but also includes the effects of zinc upon terrestrial and aquatic flora and fauna.

As in other recent books edited by Nriagu, the emphasis is upon detailed, but frequently uncritical reviews of the literature. Contributions are drawn from a large number of specialist authors and are fairly well up to date, with references up to 1978 included. The editor has imposed a fairly high degree of uniformity of style, and the book gives wide coverage of the topic with few omissions or overlaps. In these regards the book is of far greater value to the reader than the now-common review volumes cobbled together from the proceedings of a symposium and purporting to provide complete coverage of a topic.

Zinc in the Environment cannot be recommended as light reading for the individual requiring a brief overview of the subject. It will, however, be regarded as essential by many research workers in the field and will, in my view, represent an invaluable source of information for a good many years to come. □

Roy M. Harrison is a Lecturer in the Department of Environmental Sciences at the University of Lancaster.

En route to a classic of ornithology

Raymond O'Connor

Handbook of the Birds of Europe, the Middle East and North Africa: The Birds of the Western Palearctic. Vol.II. Edited by Stanley Cramp. Pp.695. (Oxford University Press: 1980.) £30, $85.

THIS is the second volume of *The Birds of the Western Palearctic*, the ambitious multi-volume work intended as the successor to Witherby's *Handbook of British Birds*, though with a wider geographical brief than the British Isles of the 1939 work.

The success of Vol.I testifies to the overwhelming acceptance of its general approach and format, and Vol.II follows the same pattern. The volume treats those species belonging to the Accipitriformes, Falconiformes, Galliformes and Gruiformes. Each species account begins with a general consideration of field characters followed by detailed discussion of the plumage characteristics of the recognizable age-classes. Sections on habitat, distribution, population, movements, food, behaviour and breeding follow, and each account is concluded with a listing of plumage and morphology data. The approach is entirely specific except for brief introductions to each family. The editors have rightly persisted with the format of Vol.I with only minor modifications, though I wish they would quote author initials when citing authors of the same surname. Another minor irritant is the failure to reproduce the explanatory material given in the first volume. As a reference work the *Handbook* should not require one to consult two hefty tomes to locate one's target information within Vol.II.

One general feature of this work is that its treatment of a topic is determined very much by the nature of the material available. For the kestrel, *Falco tinnunculus*, for example, nest site frequencies are tabulated for German and British studies, regional differences are described between northern and southern Britain, seasonal variation in clutch size is cited on the basis of a Swiss study, egg loss rates are quantified for Dutch and English populations, and breeding success to food supply correlations are mentioned for a Norwegian study. With the Western Palearctic as their geographical remit, the authors are entitled to their use of studies from different areas but I find two shortcomings in this approach. First, is the reader to assume that effects cited in a regional study are common to the whole region? The editors disclaim the validity of such assumption from the outset, correctly cautious but unhelpful to the reader. May we, for example, assume that British kestrels follow the Swiss pattern of a seasonal decline in clutch size or is it the case that the question has not been examined for the British population? Second, the absence of reference, for example to habitat differences in clutch and brood sizes, means what? — that there are no such differences or that there are no studies of this aspect of the species' breeding biology? With so much of the volume's layout standardized I regret the lack of systematic treatment of these finer points.

I also have mixed feelings about the treatment of species behaviour, mostly as to whether or not the text devoted to the subject is in keeping with that afforded more ecological topics. On diet, the authors have avoided the presentation of anecdotal data forced on Witherby, so thankfully the literature will be spared a further succession of notes of the 'Additional food items taken by the Greater Gas-bill' type. With behaviour, however, this danger has not been avoided as successfully. Having said this, I admit fully the usefulness of having the lucid descriptive accounts of what is known of the various species. Whilst some species have extensive coverage, for example seven full pages for the peregrine, *Falco peregrinus*, many run to only one or two columns of text and provide a valuable indication of the gaps in our knowledge.

The line drawings of C.J.F. Coombs illustrating the sections on behaviour are, on the whole, successful in providing schematic illustration of the behaviours of interest, without at the same time losing all of the natural 'jizz' of the birds. He deserves special credit for meeting a difficult task well. The colour plates are beautiful and for the game birds, especially, convey real expression. I was less taken by the plates illustrating perched raptors and was reminded by several of the 'in flight' illustrations of this group of nothing so much as of aircraft recognition charts. I personally would find the Peterson *Field Guide* (Collins, 1954) technique of pointers directed to the critical recognition features of help in using these illustrations, despite the reference rather than 'in field' purpose of this book.

If the work has a significant weakness, as opposed to the more trivial criticisms mentioned above, it is in relating the fieldwork and natural history to a broad theoretical background. Within its taxonomic scope this volume provides a magnificent synthesis of facts but not of knowledge. Examples abound. Female raptors are noted as taking a larger share of territorial defence as the nest cycle progresses from laying through to nestlings, but nowhere is there reference to the parental investment theories of Trivers nor to the study of Barash (*Wilson Bull.* **87**, 367–373; 1975) whose paper makes explicit the relevance of these theories to the nest defence pattern. Similarly, the parent–young bonds of the sparrowhawk, *Accipiter nisus*, are described as being typical of *Accipiter* in character and that of kestrels as "largely typical of falcons" but the reader is left to his own initiative to return to the family introductions to seek a description of these typical patterns. Even where general patterns are recognized as existing and deserving of theoretical explanation, as with the reversed sexual size dimorphism of the accipiters and falcons, the authors duck the question, giving references without even a hint of the nature of the theories to be found therein. This refusal to acknowledge that there is a 'Why' to the 'Whats' of bird-watching is, to my mind, the great weakness of this book. It undoubtedly reflects the composition of the editorial board for the *Handbook* and their individual interests, as well as the composition of the 'serious bird-watcher' market at which it is aimed. However, if ornithology has (as I believe to be the case) more to offer to the ecological and evolutionary sciences than has the study of any other single taxonomic group (with the possible exception of entomology) the replacement for Witherby's *Handbook* ought to display at least a nodding acquaintanceship with these sciences.

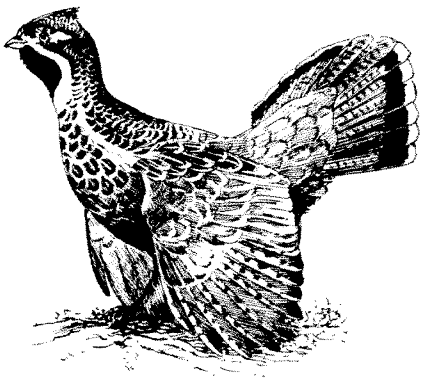

How easy it is to criticize! The volume lives up to the standards set by Vol.I and, in turn, by the Witherby classic. It brings so much information together that I could not be without a personal copy of this storehouse of avian natural history. Put alongside a copy of Welty's *Life of Birds* (W.B. Saunders, 1975) it will provide the serious bird-watcher with most of what he should know about the groups covered. My real regret is that at the present rate of writing (with three years between the publication of Vol.I and II) it will be 1995 before an authoritative compendium on the passerines is available. On their form to date Cramp and his colleagues will then have completed a classic of ornithological compilation. □

Raymond O'Connor is Director of the British Trust for Ornithology, Tring, Hertfordshire.

A plea for 2,4,5-T

Alastair Hay

The Science of 2,4,5-T and Associated Phenoxy Herbicides. By Rodney W. Bovey and Alvin L. Young. Pp.462. (Wiley: 1980.) £21.40, $46.90.

"Few agricultural chemicals have a longer safety record in the field than the phenoxy herbicides, including 2,4,5-T". This conclusion, stated baldly by the authors in the opening pages, sets the tone for this, the latest book on the subject.

As the authors note in their first chapter, the use of 2,4,5-T (2,4,5-trichlorophenoxy acetic acid) has been a controversial matter in many countries for the past ten years. That controversy has centred, in the main, on the presence in 2,4,5-T of an extremely toxic contaminant, 2,3,7,8-tetrachlorodibenzo-p-dioxin (dioxin). The dioxin contaminant, produced as an unwanted by-product in the manufacture of 2,4,5-trichlorophenol — from which 2,4,5-T is made — is a known teratogen and carcinogen in animals. However, dioxin is only present in most 2,4,5-T preparations in concentrations less than 0.1 ppm and in Britain, according to a recent government statement, in amounts less than 0.01 ppm.

Is all the fuss about 2,4,5-T justified? Bovey and Young think not. It is their view that much of the criticism of the herbicide is misinformed and based on biased, selective citation of reports. The authors consider many of these reports in some depth, and present evidence to show that allegations against 2,4,5-T are ill-founded. For example, two incidents linked to 2,4,5-T — an alleged increase in human illnesses in Globe, Arizona, and the deaths of reindeer in Lapland, both of which occurred in 1970 — were later shown to have no connection with the herbicide. Local doctors practising in the Globe area said that close investigation revealed no significant increase in illnesses linked to herbicide spraying. And the reindeer deaths in Sweden were eventually attributed to starvation rather than exposure to 2,4,5-T.

To support their argument the authors have provided a detailed review of the chemistry, toxicology and ecological effects of the compounds in question. The value of their work lies in its comprehensive coverage of the literature describing the properties of 2,4,5-T and the related herbicide 2,4-D (2,4-dichlorophenoxy acetic acid) in microorganisms, higher plants and animals, including human beings. Methods of detecting the herbicide in biological specimens are considered, as are the problems associated with its application.

Inevitably, authors of a book such as this must at some time make a decision when to stop reviewing the literature. Here, with coverage up to 1978, they have therefore missed some of the more important epidemiological studies on dioxin exposure in industry and silviculture.

Recently published studies of people exposed to dioxin in industry offer apparently conflicting evidence. The first investigation, of workers exposed to the chemical at the Monsanto company in West Virginia in 1949, clears dioxin — for the moment — of causing any increase in the mortality rate in the men; deaths in this group were in fact lower than would be expected. The second study, of workers exposed to dioxin in an accident in West Germany, suggests that the chemical could be the cause of an increase in gastro-intestinal cancer. A third survey, of workers employed in the forestry industry in Sweden, also claims that exposure to dioxin-contaminated 2,4,5-T could have increased the incidence of deaths from cancer. The authors of this study claim that silviculture workers exposed to 2,4,5-T have a six-fold higher incidence of soft tissue sarcomas (see *Nature* **283**, 613; 1980).

In their concluding chapters Bovey and Young detail the processes involved in registering new chemicals and list many suitable alternatives to phenoxy herbicides — although, as stated earlier, their view is that the phenoxy herbicides are not a great hazard. The economic consequences of dispensing with them is assessed as follows: an increase in farm production costs of $290 million, and the requirement of an additional 20 million hours of family labour to clear the foliage the herbicides keep down so effectively. However, it is not clear whether these figures are based on a situation where alternative herbicides are employed or one where no herbicides are used at all.

On phenoxy herbicide use for military purposes, the authors are quite explicit. Their use "in an armed conflict [in Vietnam] has jeopardised their continued use in world agriculture". The authors are not convinced that the use of 2,4,5-T in Vietnam — recognized to have had a dioxin content of 0.05–47 ppm — has caused birth defects among the general population, as has been claimed by Vietnamese scientists and doctors. However, Bovey and Young note that many scientists still hold different views on this subject and that more evidence is required before the issue can be resolved. The authors also claim that the incineration of the unused herbicide stocks from Vietnam means that "it is no longer an issue". Using herbicide destined for Vietnam may not be an issue — but the legacy of its use in that country is still very much in the public eye, following claims by former US veterans that the herbicide has damaged their health.

It remains to be seen whether reviews currently being conducted by government bodies in the UK and USA will come to the conclusion that the use of present formulations of 2,4,5-T also poses a health risk. Whatever the verdict, the authors make the plea that the suspension of 2,4,5-T and other products based on trichlorophenol "should not jeopardise other phenoxy herbicides". By all accounts the others are not in jeopardy. □

Alastair Hay is a Lecturer in the Department of Chemical Pathology at the University of Leeds.

Odours and vertebrate ecology

Vincent B. Wigglesworth

The Ecology of Vertebrate Olfaction. By D. Michael Stoddart. Pp. 234. (Chapman and Hall: 1980.) £15, $29.95.

THE purpose of this book was to put together an inclusive account of all the ways in which the lives of other vertebrates are guided by the richly scented world that is beyond our ken. Comparative anatomy of the olfactory system suggests that we differ from our more osmatic relatives in quantity rather than in quality; in the restricted area of our olfactory epithelium in comparison with the capacious chambers of other animals. As far as sensitivity is concerned, it sounds quite impressive to point out that the human female at the height of her sexual cycle can perceive the odour of synthetic musk at a concentration of 1 in 1,000 million; but this achievement fades beside the claim that the eel can detect β-phenylethyl alcohol at concentrations as low as 3×10^{-18}M, representing the dilution of 1ml of the alcohol in a volume of water equal to 58 times that of Lake Constance (Bodensee, the 60km lake on the Swiss–German border) — which will provide the eel with about three molecules in its olfactory sac at one time.

A survey of the chemistry of vertebrate scents reads like a catalogue of organic chemicals, but on closer analysis it seems that virtually all are refined waste products of metabolism and few or none are synthesized *de novo*. Moreover, although the glands from which they are liberated can be concentrated in many different parts of the body, they seem always to be modified, often scarcely modified, sebaceous glands, the secretory products of which are influenced by diet.

The book provides a detailed account of the multifarious roles of olfaction — the detection of food by herbivores and carnivores; the attraction of a mate and the advertisement of sexual state; the induction of oestrus and ovulation; the conduct of courtship and mating; the discrimination of families, populations and races (thus aiding sexual isolation between species); the maintenance of social hierarchy and territoriality; the detection of predators; the transmission of warning signals or active defence; and homing and navigation.

Olfaction is greatly involved in reproduction — in sexual attraction or the excitation of females by the rutting male, which may induce simultaneous oestrus in a wide group of females. In that most human of animals, the tortoise, the female in the early stages of courtship rubs her forearms against her chin glands and then proffers her perfumed arms to passing males. Even pregnancy may be upset by olfaction: in female mice the presence of a strange male or just his urine may prevent implantation of existing blastocysts in the female and may even terminate pregnancy more than half-way through gestation. Also, after birth, odour plays an essential role in forging the bond between mother and young. Olfaction can be important in the isolation of species: among mice the odour preference by the female seems to accord with sound genetic policy in that she prefers an unrelated male of the same stock, avoiding males of remote strains and rejecting siblings.

The author naturally devotes much attention to the marking of territory — a world of sense and a complex language which it is difficult for us to understand. It would seem, in general, that marking does not serve to keep intruders out but acts rather as a bond within the colony which boosts self-confidence and thus the ability to get the better of unwelcome intruders.

In a final chapter the author outlines some of the ways in which an understanding of the role of olfaction in the ecology of vertebrates may be utilized in improving husbandry or combating vertebrate pests. He does not claim too much. But in his eyes the grass looks greener on the other side of the fence; he gives a brief account of the use of pheromones in insect control which might fairly be described as optimistic.

This book is packed with information, well organized and fully documented with references. The author favours theories based on observational or experimental science. He is sceptical of conclusions based on anecdotes and pays only minimal attention to Freudian fantasies. He is therefore a good guide for the serious student of ecology. □

Sir Vincent B. Wigglesworth is Emeritus Professor of Biology in the University of Cambridge.

nature

16 October 1980

Towards less formal arms control?

What will happen to the cause of arms control if the Salt II treaty is never ratified? More than a year has now passed since the treaty, the product of seven years of negotiation, was signed by the Soviet Union and the United States. Since then, the treaty has languished in Washington, awaiting a fair wind in the US Senate where, like any other treaty, Salt II has to command a two-to-one majority before it can be ratified. The time has never been right. Faced with the prospect that the treaty would be thrown out by the Senate a year ago, the Administration let proceedings hang fire while lobbying for the support of individual senators. The Soviet intervention in Afghanistan was, ironically, a godsend for the treaty. The Administration was able to put the treaty on ice and thus to avoid the near-certainty of outright defeat. So far as can be told, the Soviet Union has been sympathetic. While Soviet spokesmen repeatedly complain at the delay in ratifying the treaty, none of these complaints has been coupled with the obvious threat that the treaty will be abandoned if the Senate does not quickly give its consent. Indeed Mr Brezhnev has gone so far as to suggest that Soviet ratification is by no means automatic, thus giving the impression that the US Senate is not the only cause of delay. Yet a treaty has no legal force if it is not ratified. As things are, either of the signatory governments could repudiate Salt II without turning a hair — and there are some in the United States who guess that precisely this will happen if Mr Ronald Reagan wins the election next month. What in the circumstances, should be done?

The first need is not, at this stage, to abandon hope. The outcome of the presidential election will be important but not decisive. Mr Carter's re-election would not by itself assure quick passage for the treaty; the re-election of the supporters of the treaty in the Senate — people like Senator Hart — could be more influential. On the other hand, if Mr Reagan is president of the United States in the new year, it is unlikely that he will act as intemperately as he was suggesting when he was still campaigning for the Republican nomination. Like all his predecessors, he would find that there is precious little room for manoeuvre. Given the widespread recognition in the United States that a continuing relationship with the Soviet Union is an indispensable component of national security, and public knowledge of the importance of Salt II in Soviet eyes, no new president is going to tear up the treaty. What might, with advantage, be done is to explore the possibility of modifying the treaty and, in the process, of improving it. Thus the expected five-year lifetime of Salt II is absurdly short. If it takes a decade or more to develop new strategic weapons, what sense can there be in a treaty which limits the numbers of missiles deployed only for a period of five years? Talks about improvement would help to get both Mr Carter and Mr Reagan off the hooks on which they are now impaled.

Even so, Salt II may remain in limbo. What would be the consequences for other initiatives in arms control? The most obvious dangers lie outside the strictly bilateral relationship of the Soviet Union and the United States. At the beginning of September, the signatories of the Non-Proliferation Treaty made loud complaints about the failure of the super-powers to ratify Salt II (see *Nature*, 11 September) — and even demanded that, pending ratification, the two governments should declare their intention of behaving as if ratification were a fact. (For the United States, such a course would be unconstitutional and, in any case, is prohibited by the US arms control legislation.) Most probably, the super-powers will be able to hold this ring. A more serious difficulty is that, hitherto, other items on this still thin agenda of arms control have been dependent on the conclusion of Salt II. This is why it is a hopeful sign that the Soviet Union and the United States seem willing to start talking about limitations of nuclear weapons in Europe — a process which West Germany in particular is keen to see begun. The main lesson seems to be that the frustrations of Salt II seems not to imply that other negotiations on arms control must be brought to a halt.

But what to talk about? In what forum? And what, in any case, would be the objectives? The negotiations about a comprehensive test-ban treaty are the most advanced, but the United States administration cannot realistically think of signing such a treaty until after the new Senate has had its say about Salt II. There is also an urgent need, not yet realized, for exploratory talks on the deployment of chemical weapons. After a ten-year moratorium on the manufacture of chemical weapons in the United States, the Department of Defense is now embarking on a programme for the manufacture of binary chemical weapons — devices in which two chemical components of a nerve gas are mixed together only when the shell or bomb that carries them is detonated. The decision has been influenced by the opinion that the Soviet Union is redeploying chemical weapons along the European border, but the evidence is only thin. Chemical weapons may not be central to strategic arms control, but they are powerfully symbolic. No harm but only good would come from bilateral negotiations on this subject.

Intermediate-range nuclear weapons, principally in Europe, are a harder problem for two different sets of reasons — political and technical. First, there is a serious dispute among the interested parties about the list of participants for Salt III. The Soviet Union has a simple line — negotiations about nuclear weapons in Europe must be conducted bilaterally between itself and the United States. No doubt it would be an embarrassment if the other members of the Warsaw Pact were allowed to have their say on matters which have hitherto been decided unilaterally by Soviet strategic planners. In the West, however, multilateralism is in the air. Nobody in Western Europe will be satisfied with a bilateral deal on non-strategic nuclear weapons between two super-powers which would not necessarily be in the front line if the weapons concerned were ever used in anger. Such a deal, arrived at without the consent of Western European governments, would probably turn Western Europe into a Gaullist citadel, more determined than at present to paddle its own canoe, both in planning for defence and in negotiations. Although the Soviet Union and the United States have this week (in Vienna) begun talking about the problem of the so-called Euromissiles, their talks will be mere chats if they do not devise some way of securing the open participation and consent of at least the Western European governments.

But what will these talks accomplish? Salt II was successfully negotiated only because limitations of long-range strategic weapons could be defined arithmetically. Each partner in the negotiations appears to be content with a fixed number of long-range missiles, based in silos and in submarines. (No doubt the knowledge that the quantity of nuclear explosives permitted is vastly greater than that needed for virtually total destruction of the other side has helped to make these limits acceptable.) The technical obstacles to a corresponding agreement on Euromissiles are more serious. What on one side is equivalent to what on the other? Will it be possible to distinguish between strategic and tactical delivery systems? What are the consequences of the geography of Europe? At this stage, nobody can tell whether

0028-0836/80/420571-02$01.00

these obstacles can be surmounted. In the end, an agreement on Euromissiles (if there is to be one) may have to be quite different in character from Salt II. It helps that the Soviet Union and the United States have at least begun flirting with the problems. It may not be a productive negotiation, but it cannot fail to be educative.

The outcome will not, however, be a formal treaty unless Salt II is ratified. The Soviet Union has made that plain. What, in the circumstances, can be the outcome of the Vienna talks (which are likely to drag on for years to come — unless Mr Reagan is ever in a position foolishly to put an end to them)? If the two sides merely understand each other's views of strategic weapons more fully, that will be worthwhile. In retrospect, it is clear that the negotiations ten years ago about anti-ballistic missles helped to persuade both sides that their deployment would be counter-productive, with the result that Salt I (with its limitation on anti-ballistic missiles) was something of a formality. Thus there is something in the view that in arms control negotiations the process may be as valuable as the product. This recognition has tempted some to go further and to argue that, in arms control, tacit understandings between the major powers are in some ways preferable to formal treaties. Mr McGeorge Bundy, adviser on national security to Presidents Kennedy and Johnson, was making this case only last week at a seminar at Massachusetts Institute of Technology. That tacit understandings might be more easily agreed, and even more ambitious, is beyond dispute. The snag is that almost by definition they cannot be policed or relied upon internationally. But if Salt II remains in limbo, or if Mr Reagan is elected and does his worst, they may be the best hope for arms control in the 1980s.

The space agency's neglect of science

The death last week on a climbing expedition in the Himalayas of Dr Thomas A. Mutch, associate administrator of the US National Aeronautics and Space Administration (NASA) will be widely mourned. In the past year, since his move from Brown University, Dr Mutch has helped to give NASA's support of scientific research a sense of greater civility than has often been the case in the past.

Sadly, however, Dr Mutch's death will inevitably prompt futher questions about the adequacy of NASA's general strategy on scientific research. From the beginning, the agency has lived in an uneasy and ambivalent relationship with the scientific community. For many people and groups, of course, it has been a source of unaccustomed and even unexpected largesse. But there has also been a constant grumble, from universities and other places where space vehicles are thought of as a means to an end, that the agency takes too short a view of its contribution to scientific research. There is a large stock of anecdotal evidence that it is far easier to wring from NASA quite large sums of money for putting things in spacecraft of various kinds than for the frequently less expensive task of making good use of the data which are eventually collected. What with one thing and another, but especially because of the way in which getting the space shuttle built is eating into NASA's budget, there is a nasty fear that science will be a conspicuous casualty of the years ahead.

The symptoms of present discontents are easily listed. The most evident is the prospect that, in the immediate future, there will be a dearth of Earth satellites and other spacecraft whose purposes are primarily scientific. Each interested party has a particular sense of grievance. Some most of all regret that projects like that to send a spacecraft to Halley's comet (due back within shooting range in 1986) may not get the funds they need in next year's budget. Others weep about the impending premature demise of the Einstein X-ray observatory, and the near certainty that there will not be a comparable instrument to replace it within this decade. The device known as a solar polar orbiter, the chief objective of which is to make measurements of the solar wind well away from the Sun's equator, survived only by the narrowest squeak the budgetary process earlier this year, largely because of the intervention of Dr Frank Press, the President's Science Advisor, and is probably now safe. It is also likely that the Large Space Telescope, the instrument confidently planned as the next big step forward in visual astronomy, will not now see its way into orbit until the second half of the 1980s. Some gloomy folk even fear that the cost of the telescope (likely to be more like $1,000 million than the original estimate of half as much) will itself turn out to be an internal pressure within the NASA budget.

The prospect that there will be a shortage of hardware in the remainder of this decade is, however, less alarming than that which faces the groups which have grown up in recent years and which are primarily concerned with the design of instruments carried on spacecraft and the interpretation of the results which they produce. NASA has rightly taken the view, since its earliest times, that one of its objectives should be the encouragement of research in universities and elsewhere. On several occasions, as for example when there was more Moon rock to be cut into specimens than there were suitably equipped investigators, NASA has glad-handed its dependants in an almost lavish way. Yet even where that huge (and expensive) harvest of material is concerned, the first flush of enthusiasm has not been matched by sustained effort. Although the Einstein satellite is reckoned in its truncated life to have produced so much data that those now working with it could be kept busy for six or seven years, there is a suspicion that the funds needed to make the most even of what exists will not be forthcoming. Certainly the data needed to make the most of the data which exist — and which, for example, may be especially important in making sense of variable X-ray sources — will not now be available until the next decade. One result is, that some of those who flocked into X-ray astronomy only a few years ago, when the Einstein satellite was being planned, are now flocking back again to their earlier fields of interest — wiser, perhaps, but also more cynical. People understandably have the sense that NASA as a whole is more interested in the ballyhoo that attends the launching and the operation of a major scientific satellite than in the more tedious but necessarily continuing task of making sure that the mission has been worthwhile.

To those responsible for NASA as a whole, views such as these may seem but evidence of base ingratitude on the eve of the close encounter of Voyager I with the system of Saturn and its rings, planned for 12 November. Between now and then, increasingly spectacular photographs of the planet and its satellites will no doubt be increasingly frequent in the daily newspapers. And in any case, the administrators will say, there is Voyager II, following six months behind, still to come. What on earth can be the complaint? The simple answer is that even at this late stage there is no confidence that there will be funds to support the continuing work of the groups now concerned with harvesting data from these encounters. People who have cut their teeth on these endeavours will find themselves looking for jobs elsewhere.

For NASA, the problem is one not merely of budgets but of procedures — or that, at least, is how the agency should set about putting its house in order. It is of course entirely understandable that an agency committed, wisely or otherwise, to a novel project such as the space shuttle should be unable to keep every programme intact when the costs turn out to be far greater than originally foreseen. It does not, however, follow that the agency has no choice but to sit back and accept the fate which Congress and the Office of Management and Budget decree when things go wrong. And if the need to accommodate the cost of the shuttle within the limits laid down by the Administration means that much valuable scientific data is literally wasted, NASA has not merely a right but a duty to tell its paymasters that money is being wasted. In short, if NASA shares the view that science is being needlessly neglected, it should say so. Otherwise, it should let the scientific community know more clearly where it stands.

0028-0836/80/420572-01$01.00

Another route to fusion to be explored

US looks hard at inertial confinement

Washington

The Department of Energy (DoE) is proposing to set up what one official describes as a "bluest of blue ribbon" review committee to look at the prospects of developing inertial-confinement fusion (ICF) techniques as a commercial source of nuclear power.

The decision to take a hard look at ICF comes close on the heels of a new bill signed into law by President Carter two weeks ago pledging support for a substantially expanded programme of research into magnetic confinement fusion, at present the front runner in the fusion race.

The Administration has been persuaded to back the Magnetic Fusion Bill by a report from the DoE's Energy Research Advisory Board. This says that results using magnetic confinement techniques at, for example, Princeton University's Plasma Physics Laboratory, are sufficiently impressive to justify the next stage of the development programme.

The bill proposes setting up a National Magnetic Fusion Engineering Center to look at the technical problems involved in scaling up laboratory experiments. It also requires DoE to produce a five-year programme for magnetic fusion detailing budget and research schedules.

The same committee, chaired by Dr Solomon Buchsbaum of Bell Laboratories, has now been asked to look at the progress and prospects of ICF. DoE's proposal is contained in a letter from Energy Secretary Mr Charles Duncan to the Office of Management and Budget, accompanying the department's budget request for the fiscal year 1982.

Department officials feel that, largely as the result of significant advances made during the past year or so, research on the civilian applications of ICF has progressed sufficiently to make it possible to evaluate the relative merits of different systems now under development.

Research on ICF has also been given a boost by a recent DoE decision to start declassifying previously secret information on high-energy X rays produced by the explosion of deuterium–tritium pellets — the source of fusion energy.

Three weeks ago, the department reported that it had decided that the following statement should no longer be considered a military secret: "In some ICF targets, radiation from the conversion of focused energy (such as laser or particle beam) can be contained and used to transfer energy to compress and ignite a physically separate component containing nuclear fuel".

DoE officials play down the impact of classification on the civilian programme, insisting that this has not prevented its own scientists from weighing the relative merits of different approaches. University scientists, however, have long argued that classification has been a barrier to their research; designs for ion drivers, for example, have required access to details of pellet behaviour in order to optimize beam/pellet interaction. "This is the news we have been waiting for", said one person on hearing DoE's decision.

The main problem now facing the ICF research community is how to choose the best technology for moving on to the logical next stage, the construction of a facility to probe the engineering difficulties that may lie ahead.

There is a general consensus that for magnetic fusion the Russian Tokamak design is still clearly the front-runner, but several options remain for the drivers needed to produce the energy that ignites the pellet for ICF. These include gas lasers, glass lasers and particle accelerators using light and heavy ions.

For the medium term, the best prospects seem to lie with either glass lasers or light-ion accelerators. Support for the former, in particular, has been increased by recent results from the University of Rochester, demonstrating that halving the wavelength of the light produces an ultraviolet laser beam that interacts much more efficiently with the pellet than does an infrared laser.

Dr Moshe Lubin, director of Rochester's Laser Energetic Laboratory, said last week that it was now possible to reach an efficiency of at least 80 per cent in converting the wavelength of the laser beam. This raises the possibility that crucial scaling-up experiments could be carried out much sooner than expected.

Further ahead, both glass lasers and light ions could face major difficulties. The lasers are difficult to cool, and it might therefore be hard to achieve tha high repetition rates necessary for the large-scale production of power. Light ions, although effective at close range, are difficult to focus accurately.

Here, two other options may come into their own — krypton fluoride lasers, now being developed at the University of California's Lawrence Livermore Laboratory, and heavy-ion beams, at present being squeezed for funding by a congressional preference for glass lasers with potential military applications, but eagerly supported by nuclear physicists as an extension of particle accelerator research.

DoE officials are more sceptical, suggesting that some of the claims of nuclear physicists have been over-optimistic and partly motivated by inter-laboratory competition for funds. Nevertheless, they admit that heavy ions are a serious contender for eventual commercialization, and hope that the new review committee will throw some light on where research priorities should lie.

David Dickson

Canada's uranium with strings attached

There is a prospect of a dispute between Canada and Euratom over uranium supplies. Canada is prepared to stop uranium supplies to Europe if Euratom states fail to comply with Canadian non-proliferation policy. But Euratom "is not going to surrender", according to Euratom and Canadian officials.

The confrontation will come to a head later this year, when an interim arrangement reached in January 1978 expires. And since Australia is taking a similar stance to that of Canada and the position of the United States — the other potentially large uranium supplier in the 1980s and 1990s — is clouded by the 1978 Non-Proliferation Act, uranium supply negotiations are becoming an increasingly sensitive element in the future growth of nuclear power.

Australia is furthest ahead in its negotiations with Europe. West Germany has a major share in the new Ranger mine, which will give the country 20,000 tonnes of uranium oxide in 1982–86 according to a recent agreement with the Australian government — provided Australia secures satisfactory non-proliferation agreements with Euratom. (Euratom currently negotiates safeguards with suppliers for its nine members, and must "approve" any bilateral supply deals. But its supra-national authority is under strong challenge from France — a further complication.

France also has a draft deal with Australia for the supply of 2,000 tonnes of uranium a year — a fifth of its estimated need in 1990 — but again that awaits an agreement between Australia and Euratom. The draft deal itself includes outline safeguards arrangements; but both sides have dodged giving them firm interpretation. Australia, mindful of the strong anti-nuclear lobby at home, has a public commitment (as does Canada) to ensure that none of its uranium is used for weapons building; so its policy is to require "prior consent" for re-transfers of its uranium outside Euratom states, for re-processing and for enrichment beyond 20

0028-0836/80/420573-02$01.00

per cent. According to Australia, the draft deal with France is in accord with policy; but according to French statements it offers no restrictions on reprocessing.

French industry minister André Giraud said recently that "we have no intention of using a single gramme of Australian uranium for our military programme" but, challenged on safeguards, said "we can say exactly where our power plants are and how Australian uranium will be used".

Hoping that such statements will satisfy the Australians, Euratom negotiators expect to tie up an accord soon, thus clearing the tables for Canada. Euratom fears Canada most; the US position is too uncertain to consider yet.

Canada — which already supplies 50 per cent of Britain's uranium (the rest comes from Namibia) — has the experience of India's 1974 nuclear test, which used Canadian uranium, to keep her resolution firm. The Indian test raised a storm of public protest; and although non-proliferation is no longer an election issue, it could become one if a similar incident occurred with Canadian involvement. And then uranium export might be halted. Thus, Canadian officials argue, it is in the interests of security of supply that Canada requires clear controls over its uranium.

Canada's position is ostensibly the same as Australia's — requiring prior consent for reprocessing, re-transfer and high enrichment. But, say Euratom states, such an arrangement would interfere with national sovereignty, complicate fuel management and give Canada unfair advance warning of impending international commercial deals. Canada, after all, with its fuel-efficient Candu reactors and heavy-water plants, is in the nuclear business as a whole, and not just in uranium exporting.

In the end, everything depends on exactly what is meant by "prior consent". Euratom could be expected to object strongly if it means that each sensitive step in the fuel cycle must first be cleared with Canada: for since fuel streams are inevitably mixed when fuel elements are fabricated and fuel enriched or reprocessed, any reporting of movements to Canada would involve reporting — and clearing — all steps in the cycle. France has stated openly that it would accept no restrictions.

On the other hand, Canada has indicated that it is prepared to interpret prior consent "more broadly". For example, Canada might accept an agreement which stated that its uranium was to be used only for energy, and specified the facilities at which the uranium was to be reprocessed. Canadian experts would still have to be satisfied that Euratom's uranium bookkeeping was effective, and that Canadian uranium could be "tracked" through the system.

And Euratom need be in no doubt about the firmness of Canada's commitment. "We stopped all uranium shipments in 1977 and we can do it again" said a Canadian nuclear official last week. Canada has already cancelled deals with India, Pakistan, and recently Switzerland — which objected to "prior consent". To cancel arrangements with Euratom would be more expensive (the UK needs contracts for another 2,000 tonnes of uranium per year by 1990, and France another 8,000 tonnes worth some $500 million dollars a year) but that appears not to frighten anyone in Canadian government. It does, however, frighten Europe. **Robert Walgate**

Swedish guidelines

Cloning committees

Stockholm

The regulation of hybrid-DNA research in Sweden is in a mess. Delegates to a recent microbiological conference at Umeå bemoaned the bureaucratic confusion foisted on them by a new regulatory system; and one firm has given up and is moving its activities abroad.

Since 1 January this year, any researcher wanting to work with hybrid DNA has been legally obliged to apply for permission under two existing laws: the Occupational Health and Safety Act (Arbetsmiljölagen) and the Law on the Protection of the Environment (Miljösyddslagen). The bodies that deal with the applications are the National Board of Occupational Safety and Health (NBOSH: Arbetarskyddsstyrelsen) and the Franchise Board for Environmental Protection (FBEP: Koncessionsnämnden förmiljöskydd), respectively. Both bodies are served by a Recombinant DNA Advisory Committee, set up in January under NBOSH. The committee's main task is risk classification. It has 17 members excluding its chairman (the director-general of NBOSH) and vice-chairman: four scientists, four members of parliament, five delegates from relevant authorities (National Board of Health and Welfare, Natural Science Research Council, etc.), three trades union representatives and one representative of industry and employers.

Both NBOSH and FBEP refer applications to the committee, which in turn passes them on to its working group on risk classification. If the application came from NBOSH, the working group classifies it and decides whether or not it is for new research (under the Occupational Health and Safety Act, only applications for new research have to be approved). The working group then makes its recommendation to the committee, which passes it on to NBOSH. The trouble with this is that nobody is quite sure what "new" research is. "It is difficult to interpret the meaning of this law", says Gustaf Brunius, who is in charge of DNA questions at NBOSH. "But *E. coli* K12 is a system that has been very thoroughly investigated, and if an application involves this system it is considered unnecessary to get permission for it unless the DNA sequences for toxins."

The procedure is even more complicated when the application comes from FBEP. FBEP sends the application not only to the committee, but also to 14 other bodies (including local government and health authorities and the Environment Protection Board), and asks for their comments. When all of them have replied — which takes months — FBEP holds a public meeting at which the application is publicly made and the various bodies which wish to comment publicly do so. FBEP then writes a judgement.

University researchers say they have not received any information about this system, and that they do not know how to apply. In practice, they are continuing their research without applying for permission at all, which technically makes criminals of them all. Only one firm has so far applied, and it is holding up its experience as an example of bureaucratic ineptitude. KabiGen which, in conjunction with Genentech Inc., owns the world rights for the production of human growth hormone, had applied for and been given permission to go ahead with developmental work under the old voluntary regulation system. When the new system was brought in, the firm made another application to use hybrid-DNA techniques to produce genes for human growth hormone, somatomedin B and human secretin. Six months later, permission was granted (in volumes of not more than 10 litres); but NBOSH specified P1 conditions, whereas FBEP specified P3. FBEP evidently did not take into account the revision in the National Institute of Health guidelines which occurred while it was considering the application. So KabiGen put in a new application to FBEP for permission to do the same work in P1 conditions. No decision has yet been made. The firm also applied again to NBOSH for a more general permission to do developmental work, and no decision has been made on that either. "We can do 10 litres here, but we want to do 400 litres", says KabiGen's research director, Dr Bertil Åberg. "It would take too long to get permission for that, and we'd lose too much money. We'll do it in England instead".

Some delegates to the Umea conference, which was organized by the Swedish Microbiological Association (universities) and the Foundation for Biotechnical Research (industry), suggested that the researchers themselves should take some of the blame for the present chaos. "There must be experts on the Recombinant DNA Advisory Committee, but they need not be in the majority", said Staffan Normark, Professor of Microbiology at Umeå University. "But everyone taking part in the committee's decisions must know what the research is about. We in the field haven't told them; and perhaps we should."

Wendy Barnaby

0028-0836/80/420574-02$01.00

Academic freedom

Promise for Poles

Poland is to introduce new legislation designed to meet the demands of the academic milieu for greater autonomy, according to Janusz Gorski, the Minister of Science, Higher Education and Technology. The first draft of the new bill should go before paliament in December, but many of its provisions regulating dealings between his ministry and the universities would come into force immediately. In particular, he said, the ministry would not appoint university rectors without prior consultation with the university senates.

Another development in the Polish academic world concerns the University of Warsaw, which has in the past couple of weeks had a sudden change of rector. The highly unpopular Dr Zygmunt Rybicki resigned shortly before the opening of the academic year, to be hastily replaced by historian Dr Henryk Samsonowicz. The significance of this change is not entirely clear — Polish academic life, like Polish life in general, is something of a melting pot at present. However, on 28 September, the university senate issued a statement which is, in effect, a blueprint for the restoration of academic autonomy.

The statement pays tribute to the new "self-governing" trade union movement, which has now spread to the university students, and makes a number of demands for the liberalization of society as a whole, including electoral and censorship reform. It then discusses the role of the universities which it says is, basically, to "carry out scientific research and to serve national culture and public education". Science, and the results of research, said the senate, should be implemented for the benefit of society a commission of experts should be established, and science should be involved in decision-making at all levels.

The statement advocates open and unhampered discussion and demands a basic reform of the higher education system. The main points of such a reform, said the Warsaw senate, should be:

(1) Self-governing and democratic status of universities and colleges of higher education, collegiate bodies, senates and faculties to decide on directions of research; secret elections of these bodies, with students and the working staff of the institution also represented; curricula to be decided in consultation with the relevant ministries.

(2) Free access to publications and sources of scientific information.

(3) Proper means and conditions of work guaranteed to students and staff.

(4) Freedom for students to organize their own lives.

(5) Academic appointments to be made on the basis of qualifications only.

(6) The Supreme Scientific Council to possess all necessary competence for shaping academic policy.

(7) The awarding of academic degrees to be the business of the collegiate bodies, faculties and senates, the Central Commission for Qualifications and the Council of State.

The question is, of course, how far these proposals will be implemented in the new legislation. Minister Gorski suggest that there will be some reforms in the awarding of higher degrees by the Central Commission for Qualifications.

However, the proposals announced for improvements in the student grant system have clearly met with less enthusiasm than Gorski had expected. The majority of Polish students, who have flocked to join the new "self-governing" student unions, appear more concerned with the lifting of censorship restrictions.

One good omen for the future, however: Miroslaw Chojecki, the young chemist dismissed in 1977 from the Swierk Nuclear Institute because of his membership of the then Workers' Defence Committee and on trial earlier this year for participation in the "independent" publishing movement, has been reinstated under the terms of the Gdansk accords. At least half of the Swierk staff, said Chojecki, personally endorsed his application for reinstatement.

Vera Rich

Endangered species

Mediterranean acts

The fifteen or so well-managed nature reserves around the Mediterranean are around ten times too few, the International Union for the Conservation of Nature (IUCN) is arguing at an intergovernmental meeting in Athens this week. Papers produced by IUCN for the meeting specify dozens of threatened species of mammals, amphibians, fish and plants.

The principal threat is tourism — expected to reach 200 million tourists a year by the year 2000 — with its demands for coastal hotels, marinas, and baubles such as coral, sponges and tortoiseshell.

The most endangered species is the monk seal, *Monachus monachus*. Besides one colony on the coast of Mauritania in West Africa, there are just 1,000 monk seals around Turkey, Greece, Yugoslavia and Tunisia, and numbers are falling by a hundred or so each year. Numbers are now so low, and groups so dispersed, that the seals are threatened by restricted genetic diversity. The marine turtle is in similar danger, as the beaches where it lays its eggs are turned over to tourism. Other species at risk include the Iberian midwife toad, the Mediterranean spur-thighed tortoise, the

---

Biggest radio telescope in the world

The Very Large Array radio-interferometer was inaugurated last week in New Mexico by Dr Frank Press, the President's Science Advisor.

The array, which consists of twenty-seven steerable parabolic dishes 82 feet in diameter, has been brought progressively into operation since October 1975. Individual dishes move along three double railway tracks at angles of 120 degrees — two of the tracks are 13 miles long and the third is more than 11 miles long. The array, operated as a national research facility by the National Science Foundation, is capable of greater angular resolution than any other instrument of its kind.

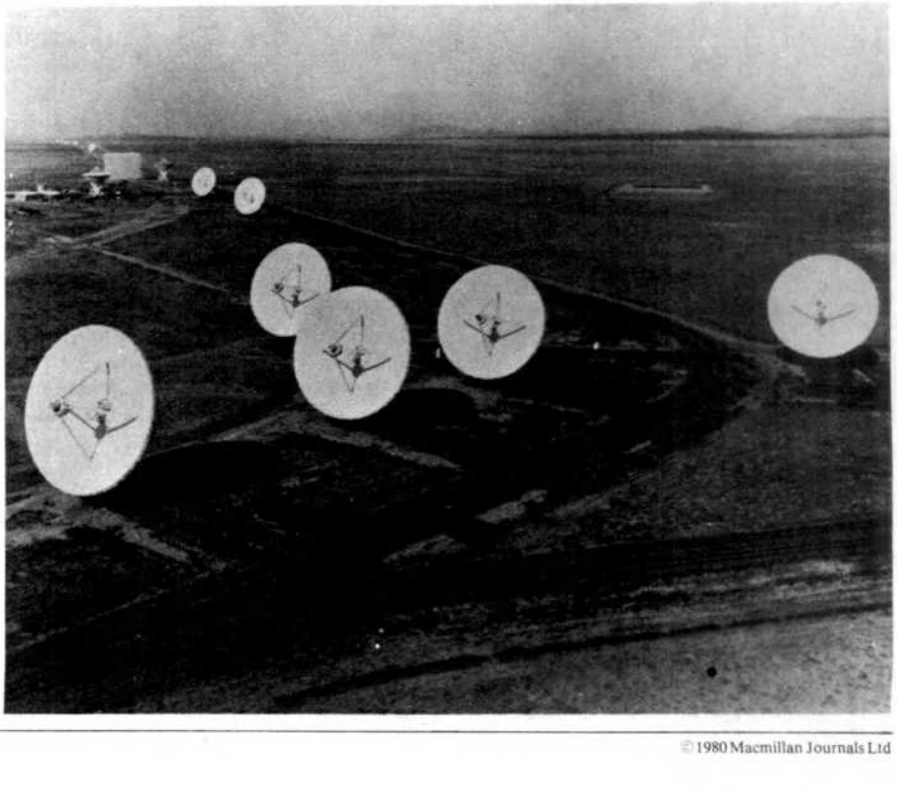

0028-0836/80/420575-02$01.00

La Scuola wall lizard, the Israel painted frog, the smooth snake, the meadow viper and the spectacled salamander.

But it is not just a question of protecting pretty animals, according to Dr Pierre Hunkeler, the Swiss ecologist who organized the scientific side of the Athens meeting Colonies of coastal plants and animals of great scientific interest need protection. Turkey and Greece have the richest coastal flora, followed closely by Morocco and Spain. Greece has 670 species of plants unique to the area (compared with Britain's 15) claim IUCN, and many of them are threatened.

Many of the ecosystems under attack are not yet well specified scientifically: in the wetlands, for example, like the protected Camargue (the Rhone delta), bird life is well understood but much less is known of the plants and water-dwelling animals. Ecologists and zoologists must have a chance to study these regions, argues Hunkeler, if only to give a baseline against which to measure the effects of pollution and development.

Representatives from ten Mediterranean nations had gathered in Athens by Monday: Greece and Turkey, France and Italy, Algeria, Libya, Tunisia, Israel, Yugoslavia and Malta were there. Representatives from Monaco and Cyprus were "on their way" from another meeting. The EEC was represented, but no sign had yet been seen of Spain, Morocco, Lebanon, Syria or Egypt.

The Athens meeting will avoid defining precise geographical regions to be protected. At that point, local political and development interests come into play, and costs and benefits must be worked out. If protected areas also mean protected fisheries, and increased amenities for the local populations and for tourists, then perhaps a deal can be reached which will satisfy both the ecologists and governments. But the Athens experts are leaving that to the politicians. **Robert Walgate.**

Plates in contact

Africa's slow movement towards Eurasia probably caused last Friday's 7.3-magnitude earthquake in El Asnam, Algeria, which destroyed 80 per cent of the city 20,000 killing perhaps people.

El Asnam, sits on a tectonic boundary between two plates — or so it appears, for the region is not seismically well characterized. The 1954, 6.7-magnitude earthquake in the same area, which killed 1.200, occurred before the world seismic monitoring network had been established. But measurements of magnetic anomalies between Africa and the United States, and between the United States and Eurasia, across the midatlantic ridge, indicate that the Africa–Eurasia boundary is closing.

The grisly event has one positive outcome: it will increase geological knowledge of the zone dramatically. Seismic stations can now pinpoint the epicentre to within 5 km, and by following the expected series of diminishing aftershocks (one of magnitude 6.2 occurred three hours after the main quake) determine the nature of the movement. This is expected to be a thrust, rather than strike-slip with Africa riding up over the Eurasian plate — the Atlas mountains themselves being part of the result.

Algerian authorities may not have a spot-on repeat of 1954; but they were criticized this week for not taking sufficient care to protect their buildings. The building codes for the El Asnam region call for stiffening to resist an extra 10 per cent weight static load, said Dr F.K. Farma of Imperial College, London, a civil engineer who made a study of the area. "But for that quake they needed 50 per cent". **Robert Walgate**

Electric cars

Win some, lose some

Washington

Plans for the development of a battery-driven electric car have taken one step forward and one step back. Scientists from the University of California's Lawrence Livermore Laboratory have announced the successful testing of a new aluminium-and-water battery which, they claim, can power cars for much greater distances than other batteries under development.

The announcement came only a few days after reports of tests by the Department of Energy (DoE) suggesting that Gulf and Western (G + W) may have been premature in some of the claims made for its new zinc-chloride battery, launched last June.

The Livermore results, presented at a meeting of the Electrochemical Society in Miami, are the products of research jointly sponsored by DoE and two large industrial corporations, Continental Group Inc. (working with the Lockheed Corporation) and the Diamond Shamrock Corporation.

The battery works by submersing an aluminium plate in a solution of sodium hydroxide. The reaction of the two with air produces an electric current and hydragillite, an aluminium compound which subsequently crystallizes out so that the aluminium can be recovered.

Unlike more conventional storage batteries which require overnight charging, the new battery is claimed to need only to be refuelled with tap water every 250–300 miles. The aluminium plates would be replaced every 1,000–3,000 miles, but the operation should take only 15–30 minutes.

One drawback is the cost. Operating the new battery — including in particular the need to replace the aluminium plates at regular intervals — would cost the equivalent of between $2 and $3 a gallon, about twice the present US price.

However, this may still be competetive with gasoline made from coal — and it would be as efficient to use coal for making the aluminium plates as for producing gasoline.

Meanwhile, a report in the *Wall Street Journal* that G + W is encountering technical problems in developing its zinc-chloride battery has raised questions about the extent to which the announcement was designed primarily as a publicity exercise. The newspaper quoted DoE reports that although G + W had claimed that the battery could power a standard car for 150 miles driving at 55 m.p.h., technical difficulties with charging the battery suggested that these figures were over-optimistic.

A spokesman for DoE, which has invested more than $15 million in the G + W project, accepted last week that the development of the battery had encountered several technical difficulties, and that as a result some of the claims made by the company last June were probably premature. But he denied that the department had lost enthusiasm for the programme. **David Dickson**

Nuclear wastes

Small disposals

Washington

Much to the relief of many east coast hospitals, universities and medical schools, the Nuclear Regulatory Commission (NRC) is proposing that liquid scintillation media used for detecting low levels of radioactivity in biological samples need no longer be buried in nuclear waste disposal sites.

At present, almost all scintillation media used in this way for biomedical research, as well as the carcasses of animals in which chemicals containing radioactive tracers have been studied, have to be transported in special drums 3,000 miles across the continent for disposal.

This expensive exercise — Harvard Medical School and its associated hospitals spent almost half a million dollars last year disposing of 3,000 drums in this way — has been necessary since the state of South Carolina announced a year ago that it was no longer prepared to accept low-level wastes from hospitals and research laboratories at its Barnwell storage site. Shortly afterwards, the nation's other two radioactive waste dumps at Richland in the state of Washington and at Beatty in Nevada announced that they too were closing their doors in protest at the poor way in which low level waste was being packaged and shipped.

Alarm spread quickly through the medical research community. Scientists said that many cancer research programmes would have to stop if liquid scintillation media and animal carcases containing trace amounts of radioactive elements could no longer be disposed of in this way. Some medical schools claimed that storage space was so tight that research

0028-0836/80/420576-02$01.00

could continue only for a few weeks if no action was taken.

Following this outcry, the contractor responsible for the Nevada and Washington sites announced that they would be reopened to receive laboratory wastes. However, the South Carolina site remains closed, and the two west-coast sites are being used by all major research laboratories which have not been able to obtain a licence for disposing of radioactive materials by other means.

Now NRC is proposing that liquid scintillation media and animal carcases containing less than μ0.05Ci of tritium or carbon-14 per gramme can be disposed of merely as toxic chemicals "without regard to their radioactivity".

The commission says that, since the potential dose to any individual exposed to these wastes would be less than 1 mrem a year, such a move would have a negligible effect on health aspects.

Using the same reasoning, it is also proposing that research laboratories and hospitals should be allowed to release up to 5 Ci of tritium and 1 Ci of carbon-14 a year into the sanitary sewage system, in addition to the present limit of 1 Ci per year for all radionuclides.

If these changes are approved, the commission estimates that research institutions and hospitals will save up to $13 million a year. Disposal of the wastes by more conventional means would cost only $3 million a year, compared with the $16 million it now costs to package and ship the materials to the west coast sites.

The proposed change in the rules is intended to conserve waste burial capacity that is already in short supply at nuclear dumps. At present, between 200,000 and 400,000 gallons a year of liquid scintillation media — mainly toluene containing heavily diluted radioactive tracers — has to be stored at these sites, taking up 400,000 cubic feet of space, with animal carcases taking up another 70,000 cubic feet.

Many university safety officers have welcomed the proposed changes in the rules. Others, however, are being more cautious, pointing out that the material will still have to be disposed of under strict federal, state and local regulations. Liquid scintillation media such as toluene are highly flammable and potentially carcinogenic — one of the reasons that South Carolina decided it no longer wanted to handle the wastes — and pose chemical and biological hazards which NRC says are a greater health problem than their radioactivity.

The result is that disposal will have to be carried out under strict new laws to deal with toxic wastes in general, such as the Resource Conservation and Recovery Act. The Environmental Protection Agency, however, has still to agree on how it intends to carry out the requirements of the act, and research laboratories are consequently uncertain of the new demands that they may have to meet. **David Dickson**

Soviet cosmonautics

Cuban went up

All the most interesting aspects of Cuban science have been reflected in the Soviet–Cuban space mission, according to Wilfredo Torres Yribar, President of the Cuban Academy of Sciences. Half of the 20 experiments planned for the flight, he said, reflect the interests of the Cuban economy.

Although space research began in Cuba "just five years after the victory of the revolution", Yribar admitted that the initial contribution had been "rather modest". In the beginning, he said, space research had not even come under the Academy of Sciences, but had been supervised by the Ministry of Communications. However, for the past ten years, Cuba had been making extensive use of data from meteorological satellites. At first this was only for weather forecasting, but now, he said, the Meteorological Institute was working out programmes for monitoring industrial pollution and studying the influence of the earth's climate on the ripening of sugar cane.

Many of the experiments performed in orbit by Cuban cosmonaut Arnaldo Tamayo Mendez and his Soviet crew-mate Yurii Romanenko, appear to be simple extensions of the regular Salyut programme. As usual, there was an experiment to grow semiconductor materials using the Soviet-designed Splav furnace, while Cuba, as the non-Soviet participant, provided the experimental capsule — in this case, the target substance was epitaxial aluminium-doped gallium arsenide — and an appropriate code-name "Caribba".

The MKF-6 camera and the Bulgarian-made Spektr-15 apparatus (so named because it can record 15 radiation channels) have been standard equipment on several Salyut missions, although on this occasion they were used in the "Tropika" experiment (photography and field observations of a defined area of Cuba) and in "Antilla" — an examination of the dynamics of the physical, chemical and biological characteristics of agricultural land and part of the surrounding seas.

Medical experiments, too, are a regular part of such missions. In this case, they included a Cuban-designed "coordinograph", which determined the accuracy and time characteristics of the cosmonauts' coordination of right and left arm movements. Another new medical experiment, "Cortex", was described by the Cuban back-up cosmonaut Jose Lopez Falcon on Moscow radio: the cosmonauts, he said, are fitted with bonnets which include sensors and electrodes; light and sound signals are transmitted, and the data recorded.

The most specifically "Cuban" experiments, however, were "Sakhar" and "Zona". These are designed to study the growth of sugar monocrystals in conditions of weightlessness — the first time an attempt has been made to crystallize an organic substance in orbit. Also of Cuban provenance is the "Support" experiment, which uses special Cuban-designed shoes that place a given load on the support areas of the feet. Returning cosmonauts, it seems, have a tendency to platypodia, and "Support" was intended to determine whether this change in the arch of the foot was a significant factor in post-flight posture disturbance. Although only Mendez wore the shoes on this occasion, they are to be worn by Soviet cosmonauts on future flights. **Vera Rich**

Forgotten martyrs

Perhaps the most interesting aspect of the Mendez–Romanenko flight is the light it throws on the early days of Soviet space research. Speaking last week on the twentieth anniversary of the Committees for the Defence of the Revolution, Fidel Castro paid tribute to the "scores of Soviet cosmonauts" who had paved the way for the Cuban flight. In particular, he recalled the "many who had died in their attempt to go into space or during their descent from space".

Those who died during descent are well known: Komarov in 1967 and the three crew-members of Soyuz 11 — Dobrovol'skii, Volkov and Patsaev — in 1971. It is less clear who he meant by those who died attempting to go into space. Yurii Gagarin died in a plane crash in 1968, while still officially on the space team, and a back-up cosmonaut, Seregin, was killed with him. Two other trainee cosmonauts are believed to have perished in high-altitude training missions. The Soviet space planners have always been highly reticent about such accidents, and the rumours of the early 1960s often complete with cosmonauts' names and family details, seem for the most part to have had little or no foundation. Even Gagarin's historic flight was rumoured to have been the back-up mission to a disaster the previous day — a story which seems to have been generated by a premature TASS announcement — although no signs of any launch were picked up by the US monitoring stations in orbit. (Just conceivably, of course, a spacecraft could have blown up on the launch pad.)

Castro referred to having visited a "gallery of martyrs" at, presumably, Baikonur, where he observed that the loss of life had been "relatively high" before space flights were "made safer". Since no westerner — except possibly Charles de Gaulle — has ever visited this gallery, Castro's remarks have renewed speculation as to just whom it commemorates.

0028-0836/80/420577-02$01.00

CORRESPONDENCE

Non-proliferation

SIR — The widespread use of nuclear power plants has caused concern regarding the proliferation potential of commercial plutonium. In a recent article (*Nature* 28 February)[1], Lovins concluded that "with modest design sophistication, high-burn-up plutonium from power reactors can produce powerful and predictable nuclear explosions".

The disadvantage of using even-plutonium isotopes in a nuclear explosive stems from different physical factors, which might be underestimated if considered separately. An example of this is the effect on the critical mass (neutron multiplication and balance)[2,4] or neutron generation time[3,4] of using even-plutonium isotopes in a nuclear explosive. However, by considering (1) the neutron multiplication factor, (2) the neutron generation time, (3) the subcritical multiplication by approaching the criticality and (4) the neutron background due to spontaneous fission, we have found that the explosive yield of a nuclear bomb is decreased rapidly by the presence of significant amounts of even-plutonium isotopes. Our analysis showed that it would not be possible to exceed an explosive yield of 1 kton or 100 ton TNT in the presence of 15 or 25% even-plutonium isotopes, resepectively, in the core of the critical assembly, even using high design sophistication.

However, even a low-yield fissile explosive can ignite a thermo-nuclear explosive. Also, the radioactive hazards of a low-yield nuclear explosive are substantial, as Lovins states[1]. Hence the problems of commercial plutonium with regard to proliferation remain.

The nuclear power countries will not be able to prevent the non-nuclear power countries from going ahead with the commercial exploitation of nuclear energy. The only way in which non-proliferation can be attained will be through a political decision by the non-nuclear power countries.

SUMER SAHIN

Laboratoire de génie atomique,
Swiss Federal Institute of Technology,
Lausanne, Switzerland

1. Lovins, A.B. *Nature* **283**, 817-823 (1980).
2. Sahin, S. *Automkernenegie* **27**, 23-26 (1976).
3. Sahin, S. *An. Nucl. Energy* **5**, 55-58 (1978).
4. Sahin, S. & Yalçin S. *Atomkernenergie/Kerntechnik* **36**, 139-140 (1980).
5. Sahin, S. & Ligou J. *Nucl. Technol.* **50**, 88-94 (1980).

Technical innocence

SIR — It seems likely that 37½ years in the Scientific Civil Service enables me to comment on your article (*Nature* 25 September, p.264).

Frustration and unease are not caused simply by the inability of administrators to comprehend the same "world-image" as we do; nor even is it just that they appear to take our advice or not according to lofty criteria that depend on the (? almost esoteric) concept of "policy" — which may sometimes not be within our own world-image, even though we may have been on more than one management course. Apart from these things we are human beings. Therefore we resent the fact that an administrative or management mandarin is, even when of "equal button", always "equal and above", as expressed in terms of money and in advancement-potential. Scientists, said the late Walter Elliott, should be "always on tap, but never on top". This cynical dictum still "rules" — but it is not OK, and never will be. It is not necessary to try to turn us into "managers" or "administrators" in order to value us as equals, of whatever button. This is the true "parity".

R. A. DAVIS

Tolworth Laboratory,
MAFF, Surrey, UK

Read the small print

SIR — I wish to draw attention to a potentially dangerous trend in the presentation of scientific papers. In a paper published in this journal almost a year ago (Meltzoff, A.N. and Borton, R.W. *Nature* **282**, 403-404, 1979) the widely publicized conclusion was that 1-month-old human neonates possess intermodal matching abilities. Although I feel that this conclusion, whether true or false, is derived by fallacious argument, my concern here is with a fault in the presentation of the paper; a fault which may account for the general acceptance of the paper's conclusion; and a fault encouraged in your "Guide to authors".

The authors of the paper use a modified version of a well tried, even "classical", experimental method in their investigation. Regrettably, they confine the description of their modifications to a densely printed figure legend, where it is embedded in the mass of relatively trivial detail intended for any who wish to repeat the experiment. More regrettably, the narrative of the paper carries what appears to be a complete account of an experimental method — the unmodified "classical" method — but it carries no hint whatever that this "classical" method has been modified by the manoeuvres which are mentioned only in the figure legend.

Thus, although all mention of certain heuristically significant experimental detail is omitted from the narrative of the paper, nothing suggests that the argument which is presented in that narrative, and which may impress the reader as being conclusive, fails to take account of all relevant factors.

When the description of experimental detail is fragmented as it is in this paper, there is a risk that fallacious conclusions may acquire an apparent but spurious validity, and a persuasive yet equivocal paper pass unchallenged into "the literature". There is, of course, no way of knowing how often the latter happens. Similarly, no amount of advice in a "guide to authors" can entirely eliminate its occurrence. But the practice of relegating experimental detail to figure or table legends is probably becoming more common; and the more common it is, the more dangerous: for readers learn to assume that authors *never*(!) displace heuretically significant detail from the narrative of a paper without due notice.

Authors cannot be prevented from inadvertently misleading readers, even referees; but perhaps your advice to them should be reconsidered: "Experimental detail vital to the paper yet which would interrupt the narrative is best placed in the figure legends." — Is it?

DAVID BELASCO

Swaffham,
Norfolk, UK

Generating costs

SIR — Richard Marshall's letter (*Nature* 18 September, p.184) on the Central Electricity Generating Board's published cost forecasts for new nuclear and coal-fired stations, requires some comment. First, the load factor on any station in any year is a function of two parameters — the availability of the plant and the proportion of total electricity demand which it is economic to allocate to that particular plant. Nuclear stations for most of their life and new coal stations early in their life will normally be operated economically to the limit of their available capacity. In later years they will come a time for both types of plant when, because of the construction of still newer capacity, their load factor will fall below the maximum permitted by availability. Since coal-fired stations have a much higher operating cost than nuclear stations this process will start earlier for coal-fired stations, which will therefore achieve a somewhat lower lifetime load factor than nuclear stations.

The load factor projections are therefore not arbitrary; they derive from a careful estimate of expected economic loading on each plant in each year. The load factors so far achieved on the Hinkley B advanced gas-cooled reactor (AGR) station reflect the fact that this is the first commercial AGR station ever built, still in its early years of experience. Inevitably its availability to date reflects teething troubles. Our projections of future availability are made on the reasonable basis that in due course new plant yet to be built would benefit from this experience.

We would therefore not expect coal to achieve a 70 per cent load factor while nuclear achieved only 50 per cent, but even if this were to happen, the cost projections quoted by Mr Marshall are still incorrect. Accepting for the sake of argument 50 per cent and 70 per cent load factors for new nuclear coal-fired plant respectively, the adjusted generation costs would be 2.6 and 3.1 pence per kWh, thus still retaining the cost ranking as predicted. These figures differ from Mr Marshall's because only the fixed component of the generation cost varies with load factor when working in pence per kWh.

F. P. JENKIN

Planning Department,
Central Electricity Generating Board,
London EC1, UK

0028-0836/80/420578-01$01.00

NEWS AND VIEWS

Nutrition and metabolism

from Mary Lindley

ON the top floor of the medical library at Johns Hopkins' University a modest display reminds visitors that last year was the centenary of the birth of E.V. McCollum, discoverer of vitamins A and D. After becoming professor emeritus at Johns Hopkins in 1944, they are told, he spoke out against the fortification of foods, arguing that a well balanced diet was the key to good health. The visitors might reflect that since then, as fads and fashions have dictated nutritional trends, it has not always been clear what a well balanced diet might be, and the answer does not seem to be at hand. Delegates to a recent symposium* at Johns Hopkins on the effects of nutrition on metabolism may well have departed thinking that only the bravest would recommend a universally healthful diet, when food can have such apparently profound influences on the body.

One influence that has been fully appreciated only in the past year centers around the role of brown fat, which, as J. Himms-Hagen (University of Ottawa) pointed out, is now seen to have a fundamental role in the body's thermogenic response to food as well as to the cold. During the past twenty-five years brown fat (otherwise known as brown adipose tissue) has been seen as a possible site of thermogenesis, producing heat, especially in animals waking from hibernation and in the newborn. The homeostatic mechanism that keeps babies warm can also be demonstrated in rats exposed to a cold environment. They develop the capacity to increase their metabolic rate and thus maintain body temperature, in response to noradrenaline released by the sympathetic nervous system, whenever re-exposed to the cold. Muscle has also been suggested as the site of this non-shivering thermogenesis and only in the past few years has brown fat been firmly acknowledged as the tissue responsible.

The most recent stage in the story of brown fat has been the clarification of its role in generating heat in response to overfeeding. As M.J. Stock (St George's Hospital, London) explained, studies of human subjects had shown that some individuals generate heat in response to excess energy intake, but further investigation had been hampered by the lack of a suitable animal model. Now Sclafani and Springer's cafeteria method has proved effective in inducing rats to supplement their diet of chow with delicacies such as bananas, biscuits and popcorn so that their voluntary energy intake increases by up to 80 per cent. Just like the human subjects, some of those rats do not become obese, but respond by generating heat. The site of this diet-induced thermogenesis turned out to be brown fat, pointing to a role for this tissue in energy balance as well as thermoregulation (Rothwell & Stock, *Nature*, 281, 31; 1979).

That idea has suggested a new way of looking at individuals who become obese in response to overeating. It is tempting to speculate that they have a defect in their brown fat and cannot dissipate the excess energy consumed. A hint that this may be correct is provided by the inability of obese animals to maintain their temperature in the cold, but, as W.P.T. James (Dunn Nutritional Research Laboratory, Cambridge) cautioned, a simple explanation of obesity is unlikely. Complications include factors such as thyroid hormone metabolism. E. Danforth (University of Vermont) explained that thyroid hormones regulate energy expenditure and are themselves regulated by diet; their metabolism is slow after a decrease in calorie consumption and accelerates after an increase.

The role of the sympathetic nervous system in the body's response to dietary stimulus is being investigated by L. Landsberg and J.B. Young (Harvard Medical School, Boston). They have measured noradrenaline turnover to show that sympathetic activity is suppressed in fasting rats and mice and stimulated when the animals are overfed by giving them access to sucrose in addition to their normal diet. The results indicate that the hypothalamus integrates those changes and that insulin may be an important link with the dietary stimulus. Landsberg suggested that such a system for controlling noradrenaline turnover, which is separate from the stimulatory effect of hypoglycaemia on the adrenal medulla, could be a mechanism to dissipate excess calories through thermogenesis and to conserve them when in short supply.

All this proved somewhat perplexing for the clinicians, who wanted to know what to do with their obese patients if a reducing diet would depress the activity of both thyroid hormones and sympathetic nervous system. Danforth advised them to complement dietary treatments with a programme of exercise; diet alone will never be effective in controlling obesity, he said.

During the past ten years the brain has also proved to be subject to dietary influence in spite of the blood-brain barrier, which, J.H. Growdon (Massachusetts Institute of Technology, Boston) explained, was long thought to isolate it from the rest of the body. Variations in concentrations of choline and amino acids in the plasma can be correlated with fluctuations in the brain's content of neurotrasmitters and their precursors. J. Fernstrom (Massachusetts Institute of Technology) explained that a diet containing largely carbohydrate and little protein stimulates the synthesis of serotonin, because its precursor tryptophan can enter the brain without competition from other amino acids, most of which are taken up by muscle. But when the diet is rich in proteins, competition from other amino acids prevents an increase in brain tryptophan, so that serotonin is not affected. The situation is different with tyrosine, the precursor of dopamine and noradrenaline. As C. Gibson (Massachusetts Institute of Technology) explained, tyrosine is more plentiful in food than tryptophan, and a diet rich in protein will supply sufficient of the precursor to enter the brain in spite of the competition and to influence the rate of synthesis of the two neurotransmitters.

A.J. Gelenberg (Massachusetts General Hospital, Boston) described how these three precursors are being used in clinical research as potential drugs to treat certain neurological disorders. Two examples are Alzheimer's disease, which involves recent memory loss and deficiency of choline acetyltransferase, and Parkinson's disease, a progressive motor disorder in which dopamine is deficient. Although it is not possible to assess the full therapeutic potential of neurotransmitter precursors, results so far have encouraged continuing studies.

As would be expected, malnutrition can have severe metabolic ramifications. The systemic immune response, for example, has often been shown to be subject to the vagaries of malnutrition, with T cells especially vulnerable. But N.F. Pierce

---

*The thirteenth Miles International Symposium, on Nutritional Factors: Modulating Effects on Metabolic Processes, was held at Johns Hopkins University, Baltimore on 18-20 June. It was organised by Dr R F Beers and the proceedings will be published by Raven Press.

Mary Lindley is an assistant editor of Nature.

0028-0836/80/420579-02$01.00

(Johns Hopkins University) said that less is known about the response to invading microorganisms although they can have a devastating impact, particularly in the developing world where diarrhoea and respiratory infections are common afflictions of childhood. Using immunonofluorescence to detect cells producing IgA, Pierce and his colleagues have examined the effect of protein malnutrition on the rat's mucosal immune response to cholera toxin. They found the response impaired in rats fed a diet containing 4 per cent protein compared with the usual 24 per cent.

F.B. Bang (Johns Hopkins University) reported that mice with a gene that normally makes them resistant to hepatitis will succumb to infection by that virus when maintained on a diet low in protein. In such cases malnutrition apparently affects the functioning of the macrophage system.

Malnutrition also influences infection by certain bacteria. E. Griffiths (National Institute for Medical Research, London) described how *Escherichia coli*, *Salmonella* and *Klebsiella* can sequester iron within their hosts. Those bacteria secrete enterochelin, which can remove iron from the binding proteins, transferrin in blood and lymph, and lactoferrin in mucosal secretions and milk. Once bound to enterochelin, the iron is taken up into the bacteria for their use. Of course the bacteria also have to contend with the host's immune system, which normally affords an effective defence. But children with the malnutrition syndrome kwashorkor, which depletes transferrin, and also impairs the immune system, will be extra susceptible to infection from bacteria that can thrive due to the increased availability of iron, especially if iron therapy is started during refeeding.

W.E.M. Lands (University of Michigan, Ann Arbor) introduced a fresh aspect to the debate over polyunsaturated fatty acids, already controversial for their proclaimed ability to lower plasma cholesterol. Some of them can inhibit the conversion of arachidonic acid to prostaglandins and thomboxane, and their prevalence in the diet may influence the amount of those two substances produced in response to the appropriate stimuli. J. Dyerbeg (Aalbrog Hospital, Denmark) provided epidemiological and experimental evidence to support that suggestion. The Eskimoes of Greenland, whose diet is rich in the polyunsaturated fatty acid eicosapentaenoic acid (EPA), a constituent of many marine oils, have a longer bleeding time and lower platelet aggregability compared with Caucasians. They also have a low incidence of myocardial infarction. In the experimental study, people given six grams of EPA per day for three weeks experienced a moderate decrease in platelet aggregation and prolongation of bleeding time. Dyerberg stressed, however, that the evidence so far does not justify recommendation of EPA as an anti-thrombotic agent.

Those who are brave enough to attempt to formulate guidelines for healthy living based on the disparate influence of diet on metabolism must also remember the influence of genetics. For example, A.M. Altschul (Georgetown University, Washington DC) pointed out that the evidence linking salt consumption with hypertension indicates that there is likely to be a positive correlation only for people with a family history of hypertension.

B. Childs (Johns Hopkins University) issued a warning by recounting his cautionary variation on the nursery rhyme — Jack Spratt could eat no fat, his wife could eat no lean. Mr Spratt apparently avoided the consumption of fat because he had hypercholesterolaemia and his father had died of a heart attack. Mrs Spratt, on the other hand, became dizzy and sick whenever she ate food rich in protein. Due to a mutant gene on one of her X chromosomes she had a partial deficiency of ornithine transcarbamylase, preventing the normal production of urea, and leading to the accumulation of toxic ammonia.

For Mrs Spratt and those with other defects of the urea cycle some hope seems to be offered by dietary manipulation facilitating the removal of waste nitrogen in some form other than urea; for example, supplementation with arginine increases the production of arginosuccinate, which is excreted by the kidneys. Although such examples represent the extreme of sensitivity, individual responses to dietary variation are likely to span a wide range, making the ideal diet impossible to formulate. □

Scanned image microscopy

from I. R. Smith and D. A. Sinclair

A recent conference* showed that new types of scanning microscope which promise unique imaging capabilities are rapidly being developed. As well as improved optical microscopes, X rays and acoustic waves are being used for high resolution scanned imaging and energy conversion techniques are being employed in the design of photo-acoustic and photothermal microscopes.

In a scanning microscope a tightly-focused beam is is scanned over the specimen and the transmitted or reflected energy is made to modulate the brightness of a scan-synchronized display to form an image. The resolution of the system is dependent upon the width of the beam (in general, comparable with the walelength of the radiation employed), whilst the image contrast depends upon the interaction of the radiation with the specimen. The development of new types of microscope is possible because the constraints upon the focusing elements of a scanning microscope are relaxed when compared with an imaging one. In particular, wide field performance is not required.

Scanned optical microscopes (SOM) are a factor of 1.4 times better in resolution than their imaging counterparts because of the use of a confocal lens arrangement in which the 'condenser' lens itself forms a diffraction limited spot upon the specimen (G. J. Brakenhoff, University of Amsterdam). Resolution may be further increased by the use of shorter wavelength ultra-violet radiation. Still higher resolution may be obtained in electron microscopes but these are unsuitable for imaging living cells. Scanning microscopes allow a great diversity of operating modes. One, demonstrated by T. Wilson (Oxford University), uses the SOM to probe semiconductor devices. The focused laser source of the SOM generates hole/electron pairs within the semiconductor, and these can be measured by monitoring the current in a p-n junction. The image shows how much current was generated over the device, and regions of low generation indicate the presence of electrically active defects, such as impurities, dislocations and grain boundaries, which can contribute to device failure.

X-ray microscopy has potentially very high resolution. At a wavelength of 3nm there is a large difference in the X-ray absorptivity of water and protein so it is possible that images of living cells can be obtained with both high resolution and contrast. Only synchrotron sources are currently bright enough for microscopy so widespread use must await the development of a compact, coherent X-ray source.

Above the 'soft' ultra-violet region, conventional refracting optical components become highly inefficient. Three solutions to this problem are being tried. In the first an unfocused X-ray beam passes through a very small (μm) aperture which is scanned over the object (H. Rarback, University of New York). The

I. R. Smith and D. A. Sinclair are Research Assistants in the Department of Electronic and Electrical Engineering, University College London.

---

*An international symposion on 'Scanned Image Microscopy' was held by the Royal Society, London, 22-24 September, 1980. The conference proceedings, edited by E. A. Ash will be published by Academic Press, November, 1980.

0028-0836/80/420580-03$01.00

Ash from Mt St Helens

from Robert A. Kennedy

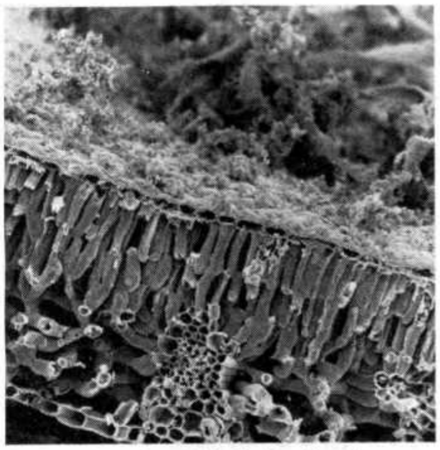

Cross section of apple leaf with ash on the upper epidermis.

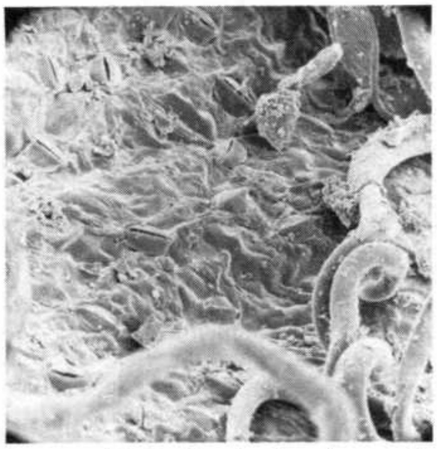

Lower apple leaf surface showing ash among the trichomes and stomata.

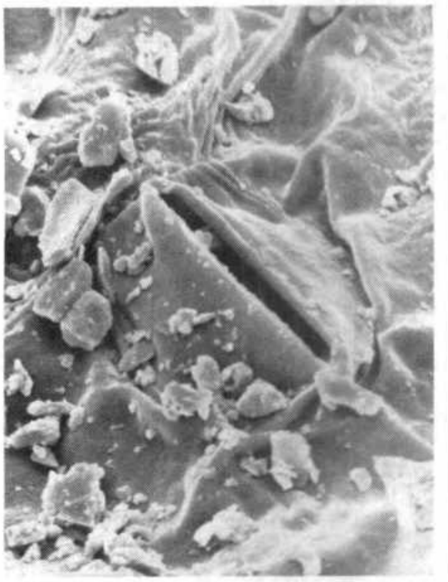

Ash inside a stoma on the lower epidermis of an apple leaf.

After the May 18th explosion of Mount Saint Helens ash fell on nearly seven million hectares of land in the State of Washington and in some places reached depths of 75cm. The pictures of plant leaves shown above were taken one and a half months after the explosion at Pullman, Washington, more than 250 miles from the volcano. Although over three inches of rain had fallen since the eruption large amounts of ash particles remain on the leaf surfaces, coating both the upper and lower epidermis and even finding their way into stomata.

The direct effect of the ash is to reduce light penetration; a one mm thick coating on the leaf absorbs 90 per cent of the light and virtually stops photosynthesis. More indirect and longer term effects may come from the presence in the ash (in concentrations of up to 10ppm) of the toxic element fluoride.

Robert A. Kennedy is associate professor in the Department of Horticulture and Landscape Architecture, Washington State University.

aperture defines the beam width, and hence the resolution. The second approach is the use of a Fresnel zone plate for focusing the radiation (G. Schmahl, University of Gottingen; N. M. Ceglio, Livermore Laboratories), a technique which has has resulted in 0.15 μm resolution. The third method uses a focusing mirror with multi-layer coatings to increase reflectivity (E. Spiller, IBM New York; R. P. Haelbich, University of Hamburgh) and seems likely to yield the highest resolution.

The development of scanning acoustic microscopy (SAM) has two main objectives; the attainment of at least sub-optical resolution and the determination of the object's elastic constants. A sub-optical resolution microscope implies the use of a low-velocity, low-loss acoustic coupling liquid. Lemons (1974) has defined a coefficient of merit, M, which normalises the resolution attainable with a particular liquid to that with water — the liquid conventionally used in the SAM. Cryogenic liquids, for example, Argon at 87K for which $M=3.7$ and Helium at 1.95K and 0.4K for which $M=3.7$ and 23 respectively offer potential improvements in SAM resolution. J. Heiserman (Stanford University) described a cryogenic reflection SAM designed to use these liquids and which currently works with liquid Helium down to 1.95K where the wavelength is 360 nm. The banded structure of human chromosomes has been clearly imaged with this system.

High pressure gases are, as pointed out by H. K. Wickramsinghe (University College, London), an attractive alternative to cryogenics since $M=4$ and 5 for Xenon and Argon at 40 and 250 atmospheres respectively. This suggests that resolutions just less than 100nm can be achieved. Room temperature operation is an additional advantage that will allow simple sample preparation techniques and the imaging of living cells.

To measure an objects elastic constants C. F. Quate (Stanford University) described a technique in which the output voltage, V, of a reflection SAM is recorded as a function of defocusing distance, z, at a single image point. The $V(z)$ curve obtained is a characteristic function of the elastic properties of the object surface. Both the density and the longitudinal velocity of the sample may, under certain conditions, be computed in this way.

The SAM has been used to image a wide range of objects. Coal may be characterised, as suggested by C. F. Quate, by its acoustic reflectivity. This technique should offer an increase in sensitivity of forty times over the comparable optical technique. He also showed using $V(z)$ techniques that the SAM is eminently suitable for detecting delaminations in thin films such as chrome on glass. The large impedance mismatch between the surface of a metallic object and the water coupling the lens to the object may be overcome by replacing the water with a liquid metal such as mercury or gallium. This and the use of shear waves in addition to the liquid metal coupling can provide improved resolution due to the decreased wavelength and reduced spherical aberration in the object (J. Attal, Universitie des Sciences et Techniques du Languedoc).

Interest in the photoacoustic effect, first demonstrated by Bell in the 1880's, has increased dramatically in the last decade with the development of several photoacoustic imaging systems capable of microscopic resolution. In what has become conventional photoacoustic microscopy (PAM) a modulated light beam is scanned across a solid surface. A microphone is used to detect the pressure waves generated in the gas above the surface by virtue of the periodic heating at the sample surface. Since a lock-in amplifier is normally used in the detection system both the amplitude and phase of the photoacoustic signal can be mapped out across the sample. A. Rosencwaig (University of California) and G. Busse (ZWE Physik) pointed out the components of the signal detected at different phases relate to information from different depths within the sample. The system resolution is determined partly by the optical spot size and partly by the thermal wavelength in the solid. This latter quantity is inversely proportional to the square root of the beam modulation frequency and affects the depth of penetration of the thermal wave in

0028-0836/80/420581-01$01.00

the solid.

G. Cargill (Watson Research Centre, IBM) and Rosencwaig showed that the beam in a SEM may also be used to generate a thermal wave in a sample. A piezoelectric detector bonded to the back surface of the sample collects the acoustic wave generated by the thermal expansion in the solid. In this technique of electro-acoustic microscopy much smaller spot sizes can be used to illuminate the sample and the resolution is then only limited by the thermal wavelength. Submicron resolution should be possible using 1-10 MHz modulation frequencies. Rosencwaig demonstrated the detection of a 2 micron crack beneath a solder pad in a ceramic substrate. By selection of the appropriate phase of the electroacoustic signal subsurface imaging is possible. He presented images showing phosphorous dopant regions in a Si substrate beneath a SiO$_2$ layer.

A technique related to PAM again uses a modulated light beam to illuminate the sample surface. An infrared detector is, however, used to directly, but remotely, monitor the sample surface temperature. The detector output is a function of both the optical and thermal properties of the sample. P. Nordal (Laser and Applied Optics Laboratories, Blindern) showed that this technique of photoinfrared microscopy was sufficiently sensitive to detect a single monolayer of aspartic acid in a chromatogram.

In conclusion, scanning microscopes offer higher resolution and a natural imaging environment for living cell cultures, whilst in the field of non-destructive evaluation, give information inaccessible to conventional techniques. □

Gluon fusion

from V. Barger

THE production of particles made of charm or b-flavor quarks has been under intensive study for several years. Of special theoretical interest in the production of these quark flavors is the large mass scales involved, which permit perturbative calculations of strong forces using the theory of quantum chromodynamics (QCD). Recent data from experiments with muon beams at CERN[1] and Fermilab[2] give evidence for copious production of charm and anticharm, which can be compared with QCD expectations. The successful description of these data was a major topic[3] at the XXth International Conference on High Energy Physics held at the University of Wisconsin-Madison in July.

A muon beam (μ^+ or μ^-) interacts with a nucleon target via the electromagnetic interaction through the exchange of a virtual photon. In the scattering of the virtual photon with a gluon constituent (g) of the nucleon, a charm-anticharm quark pair ($c\bar{c}$) can be created (Fig. 1). These quarks materialize with probability unity as charmed hadrons through the confinement force. The subsequent weak decays of the charmed particles can lead to additional muons (Fig. 2), which provide a clear experimental signature for charm events. On the average, the decays of a charm particle yield a muon about 10 per cent of the time, with a μ^+ originating from charm decay and a μ^- from anticharm decay. Counting the primary muon from the beam scattering, charm pair production results in dimuon and trimuon events. The muon emitted in charm decays is accompanied by a neutrino (ν), whose energy and momentum are unobserved. Thus multimuon events from $c\bar{c}$ production are characterized by missing energy.

Unlike the muon signals from charm decays, multimuon sources from other electromagnetic processes mediated by two virtual photons have zero or little missing energy. Fortunately, contributions from these non-charm sources can be reliably estimated.[4] By appropriate experimental cuts the charm signal can be isolated.

The theoretical calculation of photon-gluon fusion[5] (Fig. 1) depends on the strength of the gluon to $c\bar{c}$ strong interaction coupling, which is fixed by QCD analyses of other reactions. Another necessary ingredient is the probability density for finding a gluon carrying some fraction of the nucleon momentum. From inelastic electron scattering, it is known that gluons carry about half of the nucleon's total momentum. Using conventional theoretical prejudices about the shape of the gluon probability distribution,[6] the predictions of the photon-gluon fusion model are found to be in excellent agreement with the multimuon data.

The fusion approach also applied to the production of bound $c\bar{c}$ states, such as the ψ-particle. It is assumed[7] that ψ-production is proportional to the density of $c\bar{c}$ states produced near the ψ-mass. The model is in good agreement[8,9] with "elastic" ψ-production events[1,2] that have little accompanying hadronic energy. For inelastic ψ-production additional fusion diagrams enter, with an extra quark or gluon carrying away energy.[10].

In hadron-hadron collisions the creation of $c\bar{c}$ or $b\bar{b}$ pairs occurs via gluon-gluon fusion and via the fusion of light quarks q with their antiquarks $\bar{q}$ (Fig. 3). Data on the hadroproduction of the ψ and Υ particles allow the extraction of gluon distributions for pions, kaons, and nucleons. A consistent fusion description of the hadroproduction of heavy quark bound states emerges,[9] with the same gluon distribution for the nucleon as determined from virtual photoproduction.

These successes of the fusion model are somewhat clouded by the present situation concerning the hadroproduction of unbound charm, where the predicted rates are too small. One possibility is that yet to be calculated higher order QCD diagrams are important in hadron-hadron collisions. □

V. Barger is Professor of Physics at the University of Wisconsin-Madison.

Fig. 1

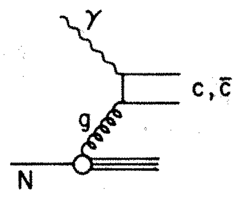

Fig. 2

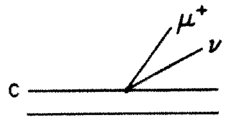

Fig. 3

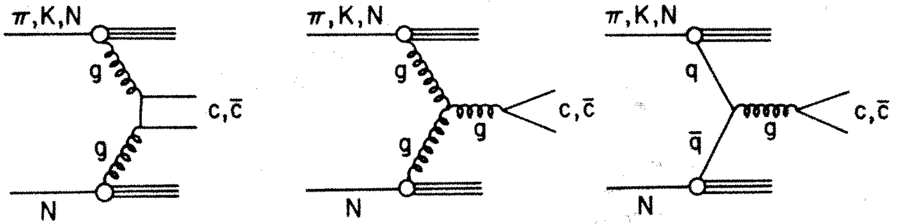

1. European Muon Collaboration, J. J. Aubert *et al. Phys. Lett. 89B,* 267; **94B**, 96, 101 (1980); CERN-EP/80-84.
2. Berkeley-Fermilab-Princeton Collaboration, A. R. Clark *et al. Phys. Rev. Lett.* **43**, 187 (1979); LBL-10747; LBL-10879; LBL-11009.
3. A comprehensive review of the phenomenology of new particle production was presented at this conference by R. J. N. Phillips and will appear in the conference proceedings; references to the extensive literature on this topic can be found therein.
4. See, for example, Barger, V., Keung, W. Y. & Phillips R. J. N. *Phys. Rev.* **420**, 630 (1979).
5. A detailed presentation of photon-gluon calculations can be found in J. P. Leveille & T. Weiler *Nucl. Phys.* **B147**, 147 (1979).
6. Farrar G.R. *Nucl. Phys* **B77**, 429 (1974).
7. Fritzsch H. *Phys. Lett.* **44**, 304 (1980).
9 Varger, V., Keung W. Y. & Phillips *Phys. Lett.* **91B** 235 (1980); *Z. Phys. C.* in the press.
10. Duke D. W. & Owens J. F., Florida State Univ. report HEP-800709.

0028-0836/80/420582-03$01.00

On the Lost Art of Seeing where Things are Going

from Simon Heywood

No one disagrees that one of the most important perceptual tasks to confront a sophisticated and mobile organism is the capacity to detect and discriminate movement, whether of itself or of other organisms or objects. It therefore seems obvious to devote research to the processes underlying the perception of movement, whether in terms of the psychological or phenomenonological characteristics of such processes or their putative realisation in neural machinery.

A recent NATO-sponsored symposium* called together some eighty workers in the area to review and to extend our knowledge of these processes. However, it must be admitted that simple as the problem of movement perception may sound, four days of conference served to illustrate that there remains considerable theoretical disagreement over what the proper object of study actually is. The explosion of "facts" unearthed by more or less ingenious physiological, psychophysical and psychological experiments has all too clearly not been parallelled by a development of theory to establish the meaning of such facts.

While it is obvious that we can and do perceive movement (just as we can and do perceive form or colour) it cannot be assumed that, therefore, the logic of investigating its physiological substrates is the same. Microelectrode studies reveal that a significant majority of visual cells in the cortex or the midbrain of animals respond to the movement of stimuli through their receptive fields; studies of great elegance classify the response types of these neurons in terms of stimulus velocity, or of their sensitivity to stimulus position change or of the position of their receptive fields and so on. But a moment's thought suggests that the relevance of these studies to the perception of movement is entirely unclear. In the great majority of visual environments, the predominating mass of visual objects and textures are actually stationary; a small subset moves. However, for any organism in motion (especially one with highly mobile eyes, like ourselves) the retinal images are constantly moving. The inescapable conclusion is that in order to interpret visually what is actually moving in the world we must first be able to establish the stability of the visible frame-of-reference within which and with reference to which that movement occurs. Single unit studies have (with a few notable exceptions) indicated only that cells respond to retinal stimulus motion, and hence fail to tell us whether such cells subserve the perception of movement or that of stability.

The simplest (and the oldest) solution is to argue that we establish stability by combining the retinal movement information with information about eye and head (and possibly body) movement. Thus perceived stability is achieved when the movement on the retina is matched and congruent with movement produced by the organism's oculomotor and neck musculature. In this case, the movement sensitive visual cells could at best only be understood in the context of other non-visual information, about whose distribution in the brain we are at present almost entirely ignorant.

Unfortunately two kinds of experimental results cast doubt on even this as a basis for the perceived stability (and hence perceived motion) of objects in the world. First, any such corollary signal from the eye and head moving systems to the perceptual apparatus appears to be far too "sloppy' to achieve the nicety of stabilisation that we perceive. Second, recent work, reported at the symposium, shows that high-level cognitive processes may be more important in assigning stability or movement than the exact relations between retinal image shift and eye/head movement. What is important, and dominant, in perception is the visual *relationship* between objects and frames-or-reference; it appears that the perception of movement in natural environments can be understood primarily as an object-relative phenomenon. This, of course, makes the interpretation of electrophysiological data even more problematic.

However, consensus does appear to be emerging on broad lines of how the visual perception of movement and stability may have to be structured; a number of speakers from quite different research backgrounds were echoing dichotomies first proposed in 1968 by Schneider, Trevarthen, Ingle and Held. There appear to be many ways of expressing these dichotomies and it is not yet clear how precisely they relate to each other and at what levels of description they operate, but three that were frequently mentioned were a) a distinction between a "movingness" (velocity-based) and a "displacement" (amplitude-based, hence perhaps related to position) system, using Claude Bonnet's terminology; b) a distinction between "central" and "peripheral" vision (which is not necessarily to be taken as an anatomical distinction, though there is clearly a spatial differentation between them), and c) a distinction between two modes of oculomotor activity, one designed to hold part of the retinal image still on the retina and assumed to be primarily driven by retinal image velocity, and the other designed to shift the retina fast underneath the retinal image and assumed to use primarily positional information. Such dichotomies are clearly interrelated and related to the dichotomies used elsewhere between sustained and transient channels, or ambient and focal vision, or *x* and *y* cell systems, or saccades and pursuit eye movement. Perhaps if we could devote the next symposium not to the presentation of many new facts, but to the elucidation of these concepts and their functional relationships, we should move closer to understanding not only our perception of movement but how such perception is related to the structure and control of our own activity. □

---

*Symposium on the Study of Motion Perception, Veldhoven, The Netherlands, 24–29 August 1980

Simon Heywood is in the Department of Psychology, University of Warwick.

Optical discs for information storage

from A. E. Bell

The high density optical disc may provide a new way of meeting the need for low cost information storage. A 12″ diameter optical disc can store as much as 10^{11} data bits, and recording rates up to 50 Mbits s^{-1} for a single channel have been demonstrated. By comparison to magnetic disc recording, optical recording increases the data packing density by about two order of magnitude, producing a much lower cost per bit stored.

The key component of the optical system is the recording medium and several possibilities, including an organic dye-in-polymer[1], generally satisfy the requirements of recording sensitivity and playback signal quality. Current research is now concentrated on improving the permanence of the information once stored as this is a key factor in the final selection of a suitable recording medium.

A typical high density optical recording system is shown in Fig. 1. The recording light source is a gas laser which emits a continuous, collimated and linearly polarised beam with a very well defined wavelength. The beam passes through a modulator to which the input data signal is applied and then via some optics and a polarising beam splitter/quarter-wave plate combination into the entrance pupil of the focusing lens. The lens focuses the intensity modulated beam to a spot on the recording medium, coated onto the surface

A. E. Bell is in the RCA Laboratories, Princeton, New Jersey.

0028-0836/80/420583-03$01.00

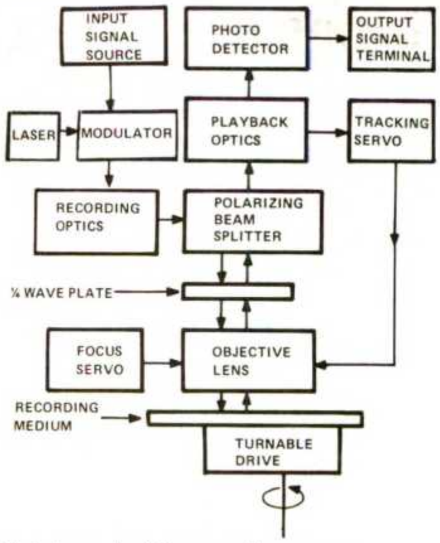

Fig 1 An optical disc recording system.

of the rotating disc substrate. Where the incident intensity is above threshold the recording medium is melted or vaporised so that the a record is made as a series of micronsized pits along the track (Fig. 2). These change the local reflectivity (or transmissivity) of the medium permitting optical playback of the recorded data.

To retrieve the data, the laser intensity is reduced below the recording threshold and a low intensity read spot is focused onto the information track. The intensity of the reflected beam is modulated by the pits and the reflected beam is collected by the focus lens and directed back towards the polarising beam splitter. As a result of the double passage of this read beam through the quarter-wave plate, the polarising beam splitter separates the read beam and directs it via the playback optics chain to a photodetector. The electrical output of the photodetector thus represents the original input data signal.

Three basic servo control are required by the optical recording system. The focus servo continuously adjusts the position of the focus (objective) lens to compensate for the uneveness of the disc substrate, and maintains the focused recording or readout spot in the plane of the recording medium. The tracking servo ensures that during playback the readout spot is centered on the information track of interest (the separation of tracks can be as low as two microns). The turntable servo controls the speed of rotation to preserve timebase information.

Fig 2 Scanning electron microscope image of melted pits recorded in a 30 nm thick tellurium film.

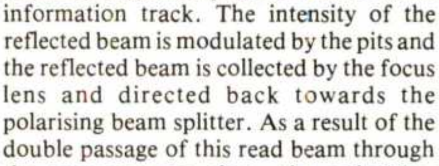

The simplest[2–4] recording medium is a disc substrate coated with a single vacuum deposited layer of metal (∼ 30-50 nm thick). As the recording mechanism consists of melting the coating to form a submicron diameter pit surrounded by a rim of resolidified material (Fig. 2), the quality of the playback data signal is largely determined by the geometrical regularity of the pit shape. The process by which the melted pit is formed is currently being investigated and while no complete detailed model exists it is clear that surface tension, viscosity and the presence of nucleation centres on the substrate can all play an important role.

The laser power required to melt the pit is determined by the thermal characteristics of the metal layer. The element, tellurium, which has unusually low thermal diffusivity and a melting point of 452°C, has been widely investigated.[4] Since the metal layer is so thin, even during the rapid recording pulse (a data rate of 10 Mbit s^{-1} corresponds to a 50 ns recording pulse) a significant fraction of the heat generated within the metal layer can be conducted into the substrate. To avoid this the thermal diffusivity of the substrate material should also be as low as possible. Low cost plastic substrates such as poly-(methyl methacrylate) or poly-(vinyl chloride) satisfy this requirement.

Of equal importance in determining the sensitivity of a recording medium is the fraction of the incident beam which is absorbed. As in single layer structures about 40 per cent of the beam may be reflected, antireflective coating configurations have been proposed[5] and investigated.[6,10] The bilayer structure, Fig. 3 *a* is most suited to moderately absorptive materials such as organic dyes, or organic dyes in polymer mixtures. A highly reflective aluminium layer is first vacuum-deposited onto the substrate. The recording medium itself is then deposited (by spin-coating or vacuum deposition) to a thickness of approximately one quarter-wavelength of the recording beam in the recording medium (that is, ∼ $\lambda/4n$) This thickness results[5] in a very low reflectivity with up to 90 per cent of the incident beam being absorbed in the recording medium. When the pit is formed, the interference condition is disrupted and the pit exhibits a very high reflectivity, as a result of the exposed, but unperturbed, aluminium layer. The bilayer approach thus gives a high sensitivity and a high playback signal contrast between the reflective pits and the antireflective lands in between.

Another approach which permits low reflectivities to be obtained even with strongly absorbing metallic recording media is the trilayer structure, Fig. 3*b*. The aluminium reflector layer is first coated with a transparent dielectric (such as silicon dioxide) and then a very thin layer (5-10 nm) of the highly absorbing recording medium. By manipulating the thicknesses of the dielectric and absorbing layers,[5], the phase and amplitude relationships required to produce destructive interference and thus low reflectivity, can be separately controlled. In a low reflectivity design up to 95 per cent of the incident beam is absorbed by the 5-10 nm thick layer of recording medium. Melting of the thin layer of recording medium disrupts the interference condition and results in a highly reflective pit. The reduced thickness of the metal absorber in the trilayer structure as compared to the single layer structure leads to improved signal-to-noise ratio (more uniform pit rims). Furthermore, the antireflection properties of the trilayer structure can be 'tuned' to a variety of recording wavelengths simply by adjusting the thicknesses of the dielectric and absorbing layers.

Some problems are common to any high density data disc design; these include the substrate preparation and the encapsulation of the recording medium to protect it from dust particles. Clearly, since the density of data storage is very high (∼10^8 bits cm^{-2}) even microscopic defects in the substrate disc can result in significant loss of data. Highly polished glass surfaces approach the level of perfection required, but they are both expensive and bulky. Low cost molded plastic substrates have a high level of surface imperfections and require surface improvement before use. The simplest procedure is to spin-coat the disc substrate with a thin layer (<20 μ) of liquid polymer resin which is then cured either by heat treatment or UV irradiation.

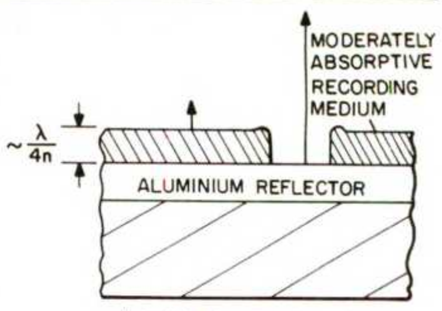
MODERATELY ABSORPTIVE RECORDING MEDIUM
$\sim \frac{\lambda}{4n}$
ALUMINIUM REFLECTOR

a.) BILAYER STRUCTURE

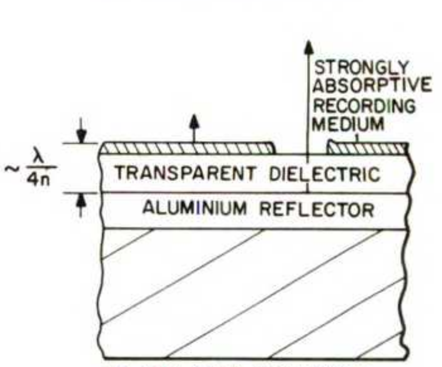
STRONGLY ABSORPTIVE RECORDING MEDIUM
$\sim \frac{\lambda}{4n}$
TRANSPARENT DIELECTRIC
ALUMINIUM REFLECTOR

b.) TRILAYER STRUCTURE

Fig 3 Antireflection structures for optical recording media.

The surface defects of the original substrate surface are filled in and the cured surface of the polymer layer can match or even exceed the surface quality of specially polished glass.

As dust particles falling onto the recording medium would rapidly introduce errors, the direct encapsulation of the recording medium with a relatively thick (180μ) layer of transparent polymer may be a valuable final step in the disc fabrication procedure. Dust particles will be on the outside surface of the encapsulation layer and out of focus.

High density optical recording may have very wide applications including the storage of computer, satellite, financial, X-ray and government statistics data, as well as video pictures. At the moment, the key problem is the permanence of the optical data as the minimum useful lifetime for most large volume applications is about 10 years. Of particular significance is the continuing development of relatively high power solid state diode lasers[9] and compatible media[10,11] since by comparison to the gas lasers these devices offer compactness, low power consumption, direct modulation capability and potentially increased reliability. □

1. Law, K. Y. *et al. Appl. Phys. Lett.* **36**, 11 (1980).
2. Maydan, D. *Bell Syst. Tech. J.* **50**, 1761 (1971).
3. Terao, M., M., Shigematsu, Y., Ojima, S. Taniguchi, Horigome S. & Yonezawa, S. *J. Appl. Phys.* **50** (11), 7881 (1979).
4. Bulthuis, K., Carasso, M. G., Heemskerk, J. P. J., Kivits, P. J., Kleuters W. J. & Zalm, P. *IEEE Spectrum* **16**, 26 (1979).
5. Bell A. E. & Spong, F. W. *IEEE J. Quantum Electronics* **QE-14** (7), 487 (1978).
6. Bell A. E. & Bartolini, R. A. *Appl. Phys. Letts.* **34** (4), 275 (1979).
7. Bell, A. E., Bartolini R. A. & Spong, F. W. *RCA Review* **40**, 345 (1979).
8. Kenney, G. C. Lou, D. Y. K., McFarlane, R., Chan, A. Y., Nadan, J. S., Kohler, T. R., Wagner, J. G. & Zernike, F. *IEEE Spectrum* **16**, 33 (1979).
9. Botez, D. *Appl. Phys. Letts.* **36** (3), 190 (1980).
10. Asbeck, P. M., Cammack, D. A., Daniele, J. J., Lou, D., Heemskerk, J. P. J., Kleuters, W. J., Ophey W. H. *Appl. Phys. Letts.* **34** (12), 835 (1979).
11. Bartolini, R. A., Bell, A. E. & Spong, F. W. *IEEE J. Quantum Electronics*, in the press.

Neuronal competition

from Dale Purves

ALTHOUGH the idea of competition between nerve cells during development is hardly new, it is enjoying a distict renaissance. There are several good reasons for this flurry of interest.

Early evidence for a competitive interaction between neurons came from the work of Hamburger and Levi-Montalcini[1]. They showed that about half of the nerve cells initially generated in some parts of the vertebrate embryo die during later development, and that the amount of this cell death is modulated by the neuronal target. Thus the vast majority of neurons in a population degenerate if their intended target (the limb, for example) is removed early in development and, conversely, the incidence of cell death is reduced if an additional target is provided (by implanting a supernumerary limb[2]). Taken together, these findings show that the death of some neurons is not a predestined affair, but depends on the ability of individual nerve cells to respond to some property of the limb. The importance of the target in regulating cell death by a mechanism that is, in a broad sense, competitive has been widely confirmed, most recently in a detailed study of the dependence of ciliary ganglion cells on the iris[3].

As with any idea that threatens to become a dogma, there has been some dissent, most recently expressed by Lamb[4]. He reported that when both right and left hindlimb motor neurons of the frog are made to project to a single limb at an early stage of development, the total number of surviving motor neurons in the relevant part of the spinal cord is greater than the number of neurons that normally survive to innervate that limb. He concludes that the "limb does not limit the number of survivors and therefore the hypothesis (of peripheral competition) is refuted . . .". Many neurobiologists, however, will take this result as an argument against a particular (one-to-one) conception of the neuron's dependence on its target, rather than an argument against competition as the basis of nerve cell death in normal development. Lamb's result suggests that the number of surviving neurons is not related to the amount of available target in a simple linear manner. A simple relation is not expected if neurons regulate the target property that they seek; a plausible notion since many properties of muscle fibers are regulated by the innervation they receive.

A central reason for renewed interest in the idea that neurons compete for some aspect of their target is that it seems likely that competition also regulates the number and arrangement of synaptic connections in the nervous system. Several phenomena in development and maturity have led to this view. For example, both muscle fibers and autonomic ganglion cells are innervated by more axons at birth than they are a few weeks later, indicating an extensive rearrangement of connections in early postnatal life[5]. In the central nervous system, a probable counterpart to the early elimination of some synapses in the periphery is a reduction in the number of climbing fibers innervating each cerebellar Purkinje cell in neonatal rats[6]. An especially intriguing example of central synapse elimination is the postnatal segregation of thalamic projections to the visual cortex of monkeys and cats[7]. At birth, axon terminals activated by one or the other eye are distributed throughout layer IV of the primary visual cortex, and may contact the same cortical neurons. During the subsequent weeks, however, the projections from the two eyes become separated so that cortical neurons in this layer are ultimately driven by either the left or the right eye. The axon terminals carrying information from the two eyes actually become segregated into domains that have the appearance of zebra stripes when mapped on the cortical surface. While the mechanism and purpose of this segregation in the brain remain a mystery, the underlying rearrangement of connections is in many ways similar to the winnowing out of some initial synaptic contacts in the periphery. In several parts of the nervous system, then, there is a gradual tuning of synaptic connections. These adjustments are competitive in the sense that the fate of particular terminals is not predetermined, but depends on an interaction with the target and with fellow axons.

The idea of a competitive balance of synaptic connections is by no means the exclusive province of developmental neurobiologists. It is well known that mature axons sprout and make additional synapses if their target is partly deprived on innervation, and, conversely, that adult axons can reduce the number of synapses they make on target cells under a variety of conditions[8]. These phenomena suggest that the number of synapses present in maturity continues to be regulated by interactions at the level of the target, much as competition between neurons for survival is regulated at an earlier stage of life.

What, then, is the relevant target property? A clue to the regulatory mechanism of both cell death and the ultimate equilibrium of maturing synaptic

Dale Purves is Professor of Physiology and Biophysics, Washington University School of Medicine.

1. Hamburger & Levi-Montalcini *J. Exp. Zool* **111**, 457 (1949).
2. Hollyday & Hamburger *J. comp. Neurol.* **170**, 311 (1976).
3. Pilar *et al. J. Neurophysiol.* **49**, 233 (1980).
4. Lamb *Nature* **284**, 347 (1980), see also *ibid* p305.
5. Redfern *J. Physiol.* **209**, 701 (1970); Bennett & Pettigrew *Cold Spring Harb. Symp. Quant. Biol.* **40**, 409 (1976); Brown *et al. J. Physiol.* **261**, 387 (1976); Betz *et al. J. Physiol.* **303**, 265 (1980); Lichtman *J. Physiol.* **273**, 155 (1977); Lichtman & Purves *J. Physiol.* **301**, 213 (1980).
6. Delhaye-Bouchaud *et al. C.R. Acad. Sci. (Paris)* **281**, 909 (1975); Crepel *et al. J. Neurobiol.* **7**, 567 (1976).
7. Sherman *et al. J. Comp. Neurol* **158**, 250 (1974); Hubel *et al. Phil. Trans. R. Soc.* **278**, 377 (1977); Rakic *Nature* **261**, 467 (1976); *Phil. Trans. R. Soc.* **278**, 245 (1977); LeVay *et al. J. Comp. Neurol.* **179**, 223 (1978).
8. See reviews by Purves & Nja *Neuronal Plasticity* (ed. Cotman, Raven Press, 1978).
9. Levi-Montalcini, Hamburger *et al. J. Exp. Zool.* **116**, 321 (1951); **123**, 223 (1953); Levi-Montalcini *et al. Cancer Res.* **14**, 49 (1954); Cohen *et al. Proc. natn. Acad. Sci. U.S.A.* **40**, 1014 (1954).
10. See review by Mobley *et al. New Eng. J. Med.* **297**, 1096 (1977); **297**, 1149 (1977).
11. Levi-Montalcini & Booker *Proc. natn. Acad. Sci. U.S.A.* **46**, 384 (1960).
12. Hendry & Campbell *J. Neurocytol.* **5**, 351 (1976); Hendry, *J. Neurocytol.* **6**, 299 (1977).
13. See review by Greene & Shooter *Ann. Rev. Neurosci.* **3**, 353 (1980).
14. Ebendal *et al. Nature* **286**, 25 (1980).
15. Nishi & Berg *Proc. natn. Acad. Sci. U.S.A.* 74, 5171 (1977); *Nature* **277**, 232 (1979); McLennan & Hendry *Neurosci. Lett.* **10**, 269 (1978); Bennett & Nurcombe *Brain Res.* **173**, 543 (1979); Ebendal, *et al. Neurosci. Lett.* **14**, 91 (1979); Adler *et al. Science* **204**, 1434 (1979); Obata & Tanaka *Neurosci. Lett.* **16**, 27 (1980).
16. Campenot *Proc. nant. Acad. Sci. U.S.A.* **74**, 4516 (1977).

0028-0836/80/420585-02$01.00

connections is the action of the protein called nerve growth factor (NGF). In the early 1950s, Levi-Montalcini, Hamburger, and their colleagues[9] extracted from a mouse tumour an agent that stimulates the growth of two types of mammalian neurons (sympathetic and dorsal root ganglion cells). Long considered a curiosity rather than a molecule of fundamental significance, NGF's biological importance has now been firmly established[10]. In brief, neonatal animals immunologically deprived of this agent grow to maturity with dramatically stunted sympathetic ganglion cells[11] while, on the other hand, neurons in ganglia surgically isolated from their target can be temporarily rescued from death by exogenous NGF[12]. These trophic effects are associated with NGF binding to specific receptors on the peripheral processes of sensitive neurons, and subsequent internalization and retrograde axonal transport[10]. The structure of the molecule is now known, and several groups have begun to unravel its mode of action[13]. Thus, for some neurons, there is considerable evidence that the object of competition in the struggle for survival is NGF produced at or near the ganglionic target. The weakest link in this argument for the function of NGF has been the inability (for technical reasons) to demonstrate in an unequivocal manner production of the protein by the usual targets of NGF-sensitive neurons. This part of the story has now been considerably strengthened by a report that at least one sympathetic target (the iris) does indeed produce NGF under appropriate conditions[14]. Since it is clear that NGF's influence is limited to a small proportion of neuronal types, a major effort is underway to discover agents presumed to operate in an analogous manner in other parts of the nervous system[15].

A further aspect of the effects of NGF suggests that a common mechanism may underlie a neuron's struggle for survival and the later competition between axons during synapse formation. Campenot[16] has shown that terminal processes of sympathetic neurons are influenced by local concentrations of NGF *in vitro* in a way that seems closely related to the proliferation and regression of synaptic connections observed *in vivo*. In Campenot's experiment a special culture chamber was used that allowed cell bodies and their processes to be exposed to media of different composition. When the neuronal processes were bathed in medium containing NGF they remained healthy; terminal processes regressed, however, when NGF was available to cell bodies, but absent in the vicinity of the processes. An attractive inference, therefore, is that competition of nerve terminals for trophic factors is also involved in the formation and maintenance of synaptic connections.

Neuronal competition is thus emerging as the common denominator of important processes (neuron death, neonatal synapse elimination both in the periphery and centrally, synapse proliferation and regression in maturity) that previously seemed unrelated. As such, it is likely to be one of the dominant themes in neurobiology for some time to come. □

---

100 years ago

The monster python which is kept alive in the Antwerp museum having had inflammation of the jaw, a Belgian doctor volunteered to enter its cage in order to cure it; but the brute attempted to suffocate the poor doctor, who was glad to escape with his life.

PHYSICS WITHOUT APPARATUS

Inertia may be demonstrated by the following trick: a number of the round wooden "men" used in playing the game of draughts are piled up in a column one upon another. If the lowest one of the pile is dextrously hit with the edge of a paper-knife or other suitable article it may be knocked away from under the others without overthrowing the others. The figure shows how the experiment is arranged, the narrow slip of wood which serves as the lid of the box being here used as the weapon. Beginners in science must not mistake the meaning of the term *inertia* as applied to matter. Matter is not in itself lazy or inert. But it possesses the property of *mass*, and to set mass in motion requires the expenditure of *energy*. If we skilfully spend the energy of the rapid blow upon the one draughtsman, it is knocked away before there is time for any considerable part of the energy to be imparted to the others that are piled upon it.

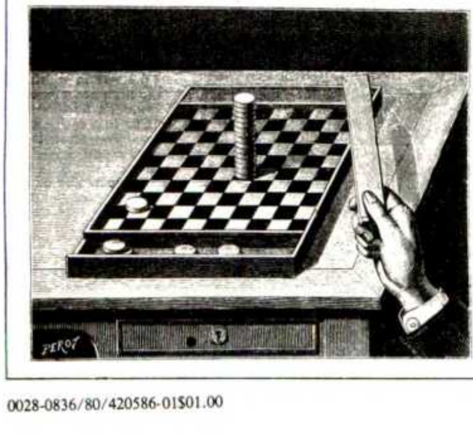

Another simple experiment, depending partly upon the inertia of matter and partly upon elasticity, is often show as an after-dinner trick. Upon a linen tablecloth is placed a threepenny-piece between two pennies or other larger and thicker coins. Over this an empty wine-glass is placed, and the puzzle is how to get out the smaller coin without touching the glass. The very simple operation of scratching with the finger-nail upon the cloth, as shown, suffices to accomplish the trick, for the little coin is seen to advance gently towards the finger until it has moved completely away from under the glass. The fibres of the linen cloth are elastic; when you scratch with your finger-nail they are drawn gently forward until the force of their elasticity becomes too great and they fly back, to be once more drawn forward, again to slip back, and so on. While the fibres are drawn forward slowly, they drag the coin with them to a minute distance. But when the slip occurs and they fly backward, they do so very rapidly, and slip back under the coin before there is time for the energy of their movement to be imparted to the coin to set it in motion. So the coin is gradually carried forward over the surface of the cloth.

We will next give a simple experiment which illustrates the principle that a substance which is very weak in one direction may be very strong in another. It is possible to lift a decanter full of water by means of a single straw. To do this the straw must be bent as shown, so that the weight comes longitudinally upon the straw. The straw is a very weak thing if it has to resist a force applied laterally. Lay a single straw horizontally, so that the two ends are supported, and then hang weights on to the middle of it: a very few ounces will break it across. But let the weights be fixed to one end of the straw, and the straw itself be hung downwards so that the pull is exerted along it, and it will support one or two pounds at least.

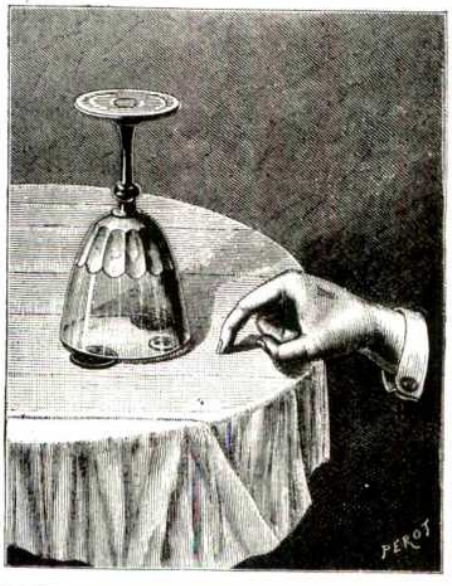

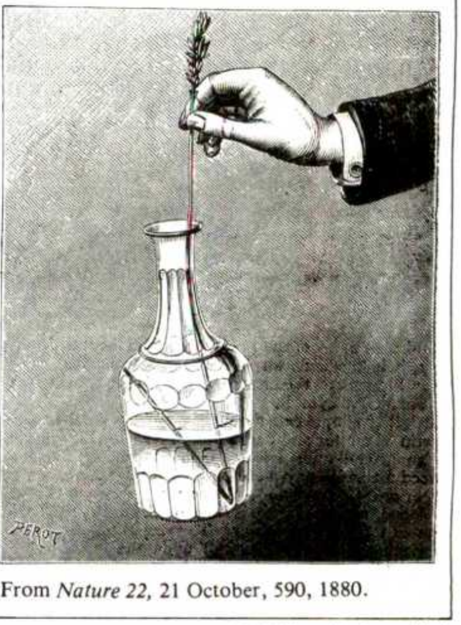

From *Nature 22*, 21 October, 590, 1880.

0028-0836/80/420586-01$01.00

Nature Vol. 287 16 October 1980

ARTICLES

A low velocity zone beneath Mount Etna and magma storage

A. D. L. Sharp*, P. M. Davis*† & F. Gray*

* University of Cambridge, Department of Earth Sciences, Bullard Laboratories, Madingley Rise, Madingley Road, Cambridge CB3 0EZ, UK
† University of California, Department of Earth and Space Sciences, 405 Hilgard Avenue, Los Angeles, California 90024

Travel time residuals and high frequency attenuation of regional and teleseismic events recorded at a seismic network around Mount Etna, Sicily, indicate the presence of a large volume of partial melt beneath the volcano. Petrographical evidence confirms that the anomaly is the main magma storage system and site of crystal differentiation beneath the volcano.

MOUNT ETNA, on the east coast of Sicily, is the largest and most active volcano in Europe. Hamilton[1] was one of the first to note that Etna did not have a simple, single eruptive site, but that the flanks of the volcano were covered with smaller eccentric cones. It was later[2,3] deduced that there has been a NW migration of the main eruption centre with time. Imbo[4] described Etna as having 266 eruptive systems, corresponding to the parasitic cones, spread over an area greater than 30 × 30 km on its flanks. This complex surface structure indicates large-scale subsurface features amenable to seismic investigation.

We installed a seismic network of short-period seismometers covering an area of 60 × 50 km around Mount Etna. The network was fully operational by the end of October 1977, and ran continuously until January 1978. The experiment used localized travel time delays of seismic waves from shots fired at sea, regional earthquakes and teleseisms, as well as waveform analysis to locate the source of Etna's lavas.

Background and geology

Mount Etna lies near the Calabrian arc and subduction zone, but on the side normally non-volcanic making its very existence surprising. The volcano is situated in a region of uplift on an E–W trending anticlinorium which is cut by the Messina–Comiso fault line. Parallel to this line are NNE directed normal faults having an easterly downthrow which suggests that E–W extension of eastern Sicily is responsible for the volcanic activity[5]. North of Etna, subduction beneath the Tyrrhenian Sea is demonstrated by the formation of the Aeolian Island arc. Chemically, however, Mount Etna is quite distinct from these island arc volcanoes, Etna being comprised of derivatives of true basaltic magmas (originating in the upper mantle) while the Aeolian Islands belong typically to the calc-alkaline series.

Petrological studies have revealed two main types of lava forming the volcano. The earliest etnean lavas are ~500,000 yr old, and are considered to be tholeiitic or transitional basalts, having a submarine character to the east, and a subaerial character to the west. These tholeiites are overlain by porphyritic differentiated alkali basalts which constitute the bulk of the volcano[6]. Although there have been periods of stronger differentiation, the overall composition of the differentiated alkali basalts has remained remarkably constant with time[6–10]. Study of single lava flows has also revealed some variation in composition. Chemical differences have been observed between the first and last parts of the 1971 eruption lava, with little variation throughout the intermediate parts of the lava flow[11]. This variation in chemistry of a single flow may indicate a secondary pneumatolytic differentiation within the feeding fissures in the upper volcanic layers before eruption[7,11]. However, the source and evolution of the differentiated alkali basalts are still undetermined. Rittmann[12] suggests that the chemical variation within single lava flows denies the existence of a single magma chamber beneath Etna, preferring a model of abyssal fissures in which crystal or pneumatolytic differentiation takes place, depending on the state of the vents as controlled by the movement of the surrounding crustal blocks. Cristofolini[7] argues that the porphyritic nature and general uniformity of the lavas indicate strong gravitational settling of crystals and mixing with fresh magma in relatively large batches at intermediate depth. Variations within single flows are then explained by compositional gradients in the feeding fissures immediately before an eruption or from tapping different levels of the same chamber, or from tapping different chambers.

There have been few previous geophysical studies capable of investigating beneath the surficial layers of the volcano. Machado[13] compared observed and theoretical seismic intensities of the Messina 1908 earthquake to obtain a large region of negative anomalies which were attributed to the absorption of seismic energy by a magma chamber under Etna. He deduced an approximately elliptical chamber, 40 × 100 km, assuming a mean depth of 5 km. No estimate of the vertical dimensions of the chamber could be made.

In 1968 a large refraction study was performed in northern Sicily[14], the eastern section of the line running just to the north of Etna. Interpretation of the later arrivals on the record sections showed the eastern Sicilian coast to have a typical continental crust, but with low velocity zones in the range 9–24 km. The low velocity zones were attributed to higher temperature gradients caused by deeper magma chambers under Etna. However, the nature of the linear refraction profile prevented the lateral bounds of the anomaly being determined accurately. There is, therefore, good evidence for a body with low seismic velocity beneath the volcano.

The experiment

To investigate further the three-dimensional structure and physical properties of this anomaly, the seismic network was installed on Mount Etna with configuration shown in Fig. 1*b*. The network comprised four arrays each consisting of a base with a 14-channel tape recorder and a three-component set of short-period seismometers, together with three or four radio-linked outlying stations. Each outlying station had a single vertical short-period instrument.

Four shots were fired at sea (Fig. 1*a*) from the RV Shackleton to determine a crustal model for the area. The composite record section constructed from the shots showed clear first arrivals to greater than 160 km, but no correlatable later phases except a strong T-phase associated with the water-wave to P-wave conversion at the Messina Scarp off the east coast of Sicily. As the profile was unreversed, a simple horizontal-layered model could

0028–0836/80/410587—05$01.00

be derived only, using the T-phase as a constraint on the uppermost layers. The crustal model so obtained is shown in Fig. 2, and is in good agreement with the simple structure derived from the reversed line of Cassinis *et al.*[14].

Travel time residuals

The 14 earthquakes which were the clearest regional and teleseismic events recorded by the network were chosen for analysis (Table 1). These events were well distributed in azimuth (329–171°), range (1–10°) and depth (10–485 km), to give a broad distribution of rays with widely varying azimuth and angle of emergence passing through the crust beneath Etna. The average frequency content of the P-waves was 1.5–2.0 Hz, giving a resolution limit of ~4 km in the lower crust.

Using P-wave arrival times to infer crustal structure beneath a seismic network has been successful in determining low velocity bodies beneath Yellowstone, Wyoming[15–17], and other geothermal areas[18,19]. By reducing the observed travel time $(t_i)_{obs}$ from an earthquake to a station by a theoretical travel time $(t_i)_o$, the residual

$$R_i = (t_i)_{obs} - (t_i)_o$$

is formed. These residuals depend on the total ray path (or total travel time), source location and origin time. For any set of residuals $\{R_i\}$ from a single event, these dependencies may be removed by subtracting the mean value $\bar{R}$ of the residuals from each residual, to give the relative residuals

$$r_i = R_i - \bar{R}$$

The need for a reference station is thus removed, and the residuals will depend only weakly on the source parameters.

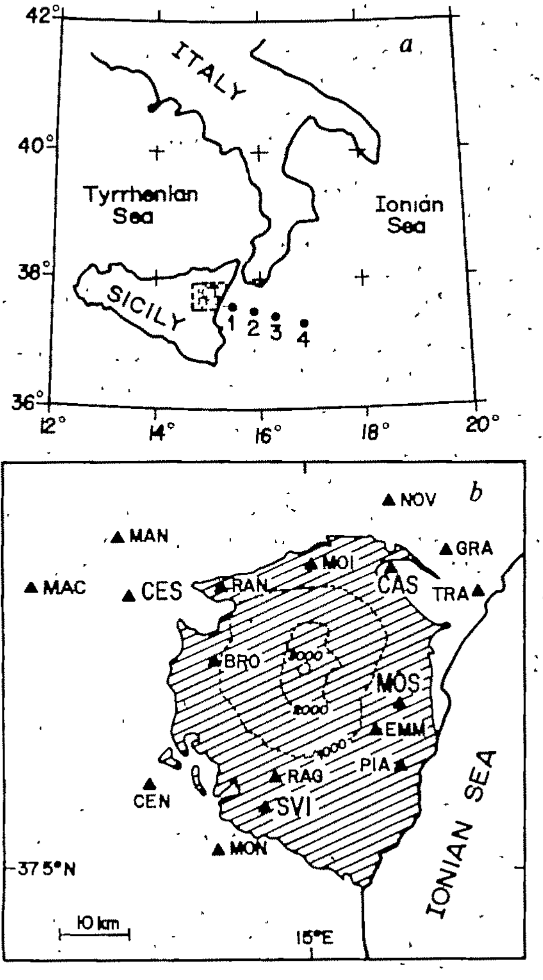

Fig. 1 *a*, Map of Southern Italy and Sicily showing the area covered by the seismic network (shaded), and shot positions (numbered). *b*, Seismic network configuration showing the four bases (CAS, MOS, SVI, CES) and the outlying stations. The shaded area defines the approximate extent of the etnean lavas.

The theoretical travel times were calculated using the US Geological Survey Preliminary Determination of Epicentre bulletins, bulletins of the Centre Seismologique Européo-Méditerranéen, and bulletins of the International Seismological Centre, to obtain source coordinates, and the travel time tables of Jeffreys and Bullen[20].

Wherever possible, the earthquake locations were compared with hypocentre redeterminations using Italian seismological observatory reports. A second set of residuals was obtained by subtracting from the arrival times the best fitting plane wave to the arrival times. The plane wave was calculated by the method of least squares with weighting dependent on the estimated accuracy of arrival time determination. The least squares residuals so obtained were generally in good agreement with those calculated from the theoretical travel times. Where the source location of an event was only poorly determined, the least squares residuals were used in the following analysis. Residuals from the arrival times of shots 2 and 3 were formed by calculating the theoretical travel times from the derived local crustal model.

Arrival times were obtained by visually measuring the first break of the P-wave from analogue records. Peaks, or later zero-crossing times[21,19], were not used as many signals showed increasing high frequency attenuation across the network. Such attenuation, due to lower Q paths, causes a relative broadening of the waveform which would give rise to errors in the timings of the peaks or zero crossings.

Examples of residuals are shown in Fig. 3. The shaded areas delineate approximately the areas of positive residuals (delays). All sets of residuals obtained exhibit similar features to those shown in Fig. 3, with the highest residuals always occurring on the opposite side of the volcano to the incident ray path, indicating the presence of a low velocity body beneath the array.

Several features of the low velocity anomaly may be qualitatively deduced from the general features of the delay patterns. The region of delay is of the order of tens of kilometres in lateral extent, and seems to be roughly ellipsoidal, elongated in a NNE direction. Also, the centre of each delay region seems to be displaced along the line of azimuth away from the centre of Etna, indicating that the anomaly lies at some depth beneath the volcano.

To quantify these observations, the low velocity anomaly was modelled as a tri-axial, ellipsoidal body centred at some depth and at some orientation beneath Etna, inverting for six parameters: ellipsoid axes, (a, b, c); depth to centre of ellipsoid, d; orientation, θ; and velocity reduction, δv (relative to the surrounding crustal velocity). Monte-Carlo inversion procedures are commonly used to invert nonlinear problems, but the random nature of the investigation may lead to poor sampling in parts of the parameter space. An organized grid search in the six-dimensional parameter space of the model was therefore adopted.

Over 20,000 models were tested by comparing the theoretical residuals with those observed. Theoretical residuals were calculated by ray-tracing through the combined crustal model and ellipsoidal anomaly structure for each ray, for each ellipsoidal model. As the velocity contrast was expected to be small, refraction effects at the boundaries of the ellipsoid were assumed to be negligible. The grid search was first performed with large grid intervals, then repeated with successively smaller intervals until the best model corresponding to the greatest reduction in the sum of squares of residual differences (observed – theoretical), $S(\phi)$, was obtained. The extent of the grid is given below, with the best model estimate in parentheses:

a	10–30	(22)	km
b	20–60	(31)	km
c	0–20	(4)	km
d	4–26	(20)	km
θ	5–40°	(13°)	
δv	−1.5–−0.3	(−1.15)	km s^{-1}

A sketch of the best model is shown in Fig. 2.

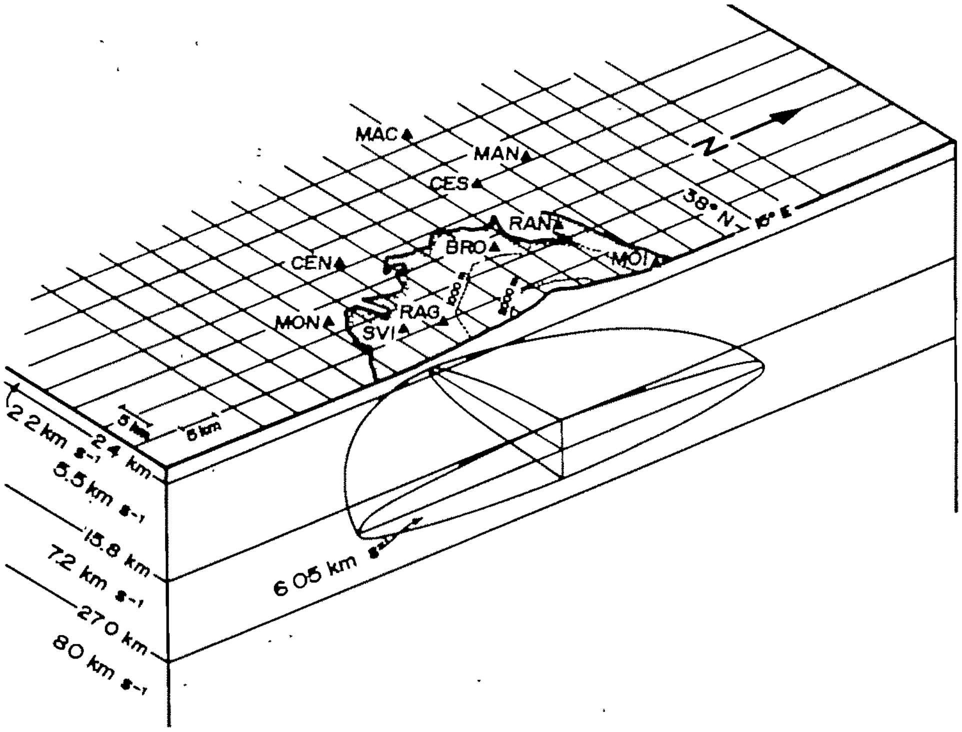

Fig. 2 Cut-away diagram of the crustal model and low velocity anomaly beneath Etna. Crustal layer velocities and depths are indicated. The ellipsoidal anomaly is shown centred beneath the volcano in the 7.2 km s^{-1} layer.

To estimate error limits on the best model, the criterion[22]

$$S(\phi) \leq S(\hat{\phi})\left\{1+\frac{m}{n-m}f(m, n-m, (1-\alpha))\right\}$$

was used, where n is the number of data and m the number of parameters. f is the value of the F-statistic for some confidence limit α, with m and $n-m$ degrees of freedom. $S(\phi)$ is the sum of squares of residual differences for a particular model, and $S(\hat{\phi})$ is the sum of squares of residual differences from the best model estimate. The six-dimensional parameter space surrounding the best estimate for all points satisfying the above criterion with $\alpha = 0.67$ was searched. The Hedgehog inversion procedure[23-25] was adopted to select the acceptable models, being ideally suited to determining the confidence regions of nonlinear problems. The search for acceptable ellipsoid models was constructed within the grid:

a	0	(5)	50	km
b	0	(5)	80	km
c	0	(2)	30	km
d	3	(4)	40	km
θ	0°	(5°)	60°	
δv	−4.0	(0.2)	−0.1	km s^{-1}

The above list shows the limits of the search, with the grid intervals in parentheses. Using the Hedgehog procedure, only those points in the neighbourhood of successful models were tested to give a singly-connected space of acceptable models. The set of acceptable models is shown in Fig. 4. Values for the a-axis and depth of the ellipsoid seem to be well constrained as no acceptable models were found with values for a and d other than $a = 22$ km and $d = 20$ km. Thus, only the variation of the other four dimensions need be examined. This variation is shown in the four-dimensional plot of Fig. 4. From each of the small sets of axes (c-axis versus δv), a trade-off between the height of the ellipsoid (c-axis) and the relative velocity reduction (δv) is seen. The large variation in values for the b-axis may be attributed to the network not being of sufficient extent in a N–S direction to cover the delay anomaly fully. This lack of resolution in the b-axis may also have caused some of the scatter in the determination of the orientation, θ, of the ellipsoid. The well resolved depth parameter confirms the existence of the deep low velocity zone of Cassinis *et al.*[14], and does not admit the possibility that the delay effects may be of upper crustal origin.

The above modelling has determined the ellipsoidal model, and associated error limits, which are the most consistent with the data. However, the single ellipsoidal model does not

Table 1 Shot and earthquake parameters

Date	Origin time (UTC)	Epicentre	Depth (km)	Distance (deg)	Azimuth (deg)	
1 November 1977	1238:15.2	37.47° N 15.86° E	0	0.7	112	(Shot 2)
1 November 1977	1538:20.5	37.37° N 16.27° E	0	1.1	110	(Shot 3)
8 November 1977	2144:46.4	34.55° N 15.59° E	10	3.2	171	CSEM
26 November 1977	1319:50.8	38.64° N 20.37° E	48	4.3	76	CSEM
28 November 1977	0259:10.0	35.96° N 27.79° E	74	10.4	96	ISC
3 December 1977	0539:29.5	40.25° N19.90° E	27	4.6	55	USGS
8 December 1977	0040:43.6	35.21° N 23.38° E	62	7.2	108	USGS
9 December 1977	1553:40.5	38.37° N 27.35° E	33	9.7	83	CSEM
15 December 1977	0806:10.8	34.92° N 23.08° E	47	7.1	111	USGS
16 December 1977	0737:32.3	38.45° N 27.36° E	36	9.7	82	CSEM
17 December 1977	0546:45.0	34.60° N 15.90° E	33	3.2	167	ISC
20 December 1977	2004:18.6	38.58° N 15.66° E	196	1.0	32	CSEM
25 December 1977	0211:12.5	40.38° N 12.95° E	485	3.1	329	CSEM
30 December 1977	1735:3.2	40.11° N 16.42° E	306	2.6	25	Relocated
30 December 1977	1808:51.3	39.97° N 16.00° E	270	2.5	19	Relocated
12 January 1978	2008:40.6	36.00° N 22.26° E	49	6.1	105	CSEM

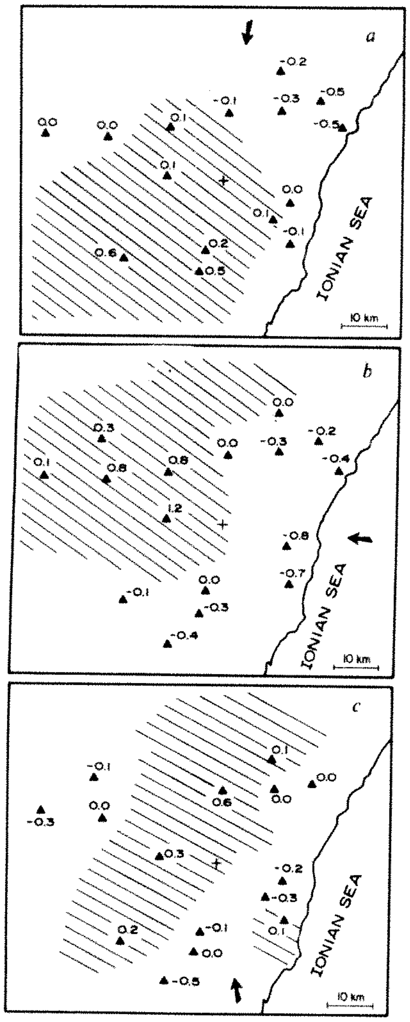

Fig. 3 Examples of travel time residuals from three earthquakes occurring: *a*, To the north, 30 December 1977 18 h 08 min; azimuth = 019°; $\Delta = 2.5°$; $d = 270$ km. *b*, To the east, 28 November 1977 02 h 99 min; azimuth = 96°; $\Delta = 10°$, $d = 74$ km. *c*, To the south, 8 November 21 h 44 min; azimuth = 171°; $\Delta = 3°$; $d =$ 10 km. Hatching shows areas of positive residuals. Arrows indicate the azimuths of the incoming waves as observed by the network.

completely fit some of the highest delays shown in Fig. 3. These large delays may indicate a secondary velocity anomaly or a non-uniformity in the present simple ellipsoidal velocity anomaly. But the present data are insufficient to resolve such finer structures.

High frequency attentuation

Many signals exhibited loss of high frequencies across the network. Figure 5 shows the P-wave arrival of the same earthquake as recorded by two stations. The waveform TRA has travelled from the source to the station without passing through the low velocity anomaly, whereas the waveform MAN has passed through the anomaly and has been attenuated in high frequency relative to TRA. Plotting the logarithm of the spectral ratio against frequency, the reduction in high frequency content of MAN is even more evident (Fig. 5). The gradient of the line may be related to the attenuation factor[26] Q. Assuming an average Q of 50 for the crustal layers surrounding the ellipsoid anomaly, a Q of 9 must be assumed for the anomaly itself to account for the high frequency attenuation.

Interpretation and discussion

Reduction in P-wave velocity may be caused by several factors (for example, a crack system, or simply a rigid body of lower seismic velocity). However, it is doubtful whether an open crack system can be maintained at depths of 20 km (equivalent to pressures of ~6 kbar). The large reduction of high frequencies (low Q) as shown by waveforms passing through the anomaly implies that the body is not completely rigid. This agrees with Machado's model of a magma chamber[13].

The simplest explanation of the observed results is that the ellipsoidal anomaly is the seismic manifestation of the main crustal magma storage region beneath Etna. The velocity reduction within the anomaly is 16% indicating that the ellipsoid is not completely molten. Assuming the body to be a partial melt composed of solid (7.2 km s^{-1}) and melt (3.0 km s^{-1}), the percentage of melt within the body is found to be 14%—corresponding to 1,600 km^3 of melt in a total of 11,424 km^3. Thus the magma chamber is not completely molten in the 'classical' sense, but rather it is likely to be formed by a complex series of veins (or fissures) of melt running through the ellipsoidal body.

Geological evidence supports these conclusions. The results of Cristofolini[7], and Romano and Sturiale[11] require that there must be a large magma storage system beneath Etna in which differentiation (gravitational crystal settling) takes place. Although Rittmann[12] argues that there is no single great magma chamber, his model of Etna does require differentiation of parental magma within "abyssal fissures". Thus the two geological models are not completely dissimilar, both requiring the temporary storage of magma at some depth.

The new geophysical model, although very approximate, demonstrates that there is a substantial quantity of magma stored beneath the volcano, and that the storage mechanism is more likely to be in a series of (interconnecting) fissures, rather that a single, completely molten chamber. The orientation and elongation of the geophysical model also agrees with the regional tectonic dislocations, N–S and NE–SW[6], supporting the hypothesis that etnean volcanism is related to lithospheric extension in that area[7–12,27].

Mineralogical studies[8,9] show that plagioclase is the dominant phenocryst material of the trachybasalts, having 20–30% by volume of plagioclase phenocrysts. Taking 'pyrolite'[28] as the parental material, Duncan[29] showed that fractional crystallization producing plagioclase phenocrysts must occur at depths less than 25 km. Hammill[30] also showed that differentiation trends in the fractional crystallization of high alumina clinopyroxene and titaniferous magnetite indicated differentiation at pressures of ~10 k bar. These findings agree well with the geophysical model of partial melt in the depth range 16–24 km.

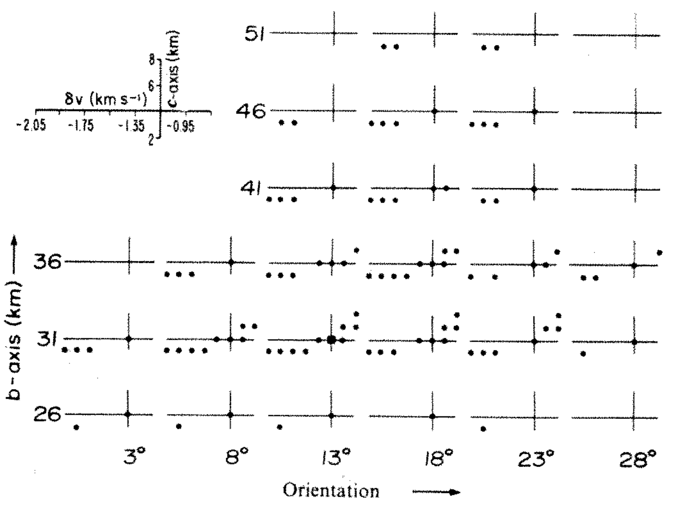

Fig. 4 Four-dimensional plot of all acceptable models from Hedgehog inversion. The small pairs of axes represent the velocity reduction δv (abscissa) and ellipsoid c-axis (ordinate), as shown in the inset. Each axes pair has an associated value of orientation θ, and ellipsoid b-axis which are given on the large horizontal and vertical axes, respectively. ■, The 'best' solution. As no acceptable model was found with a-axis and depth values other than $a =$ 22 km and $d = 20$ km these may be regarded as constants associated with each of the plots.

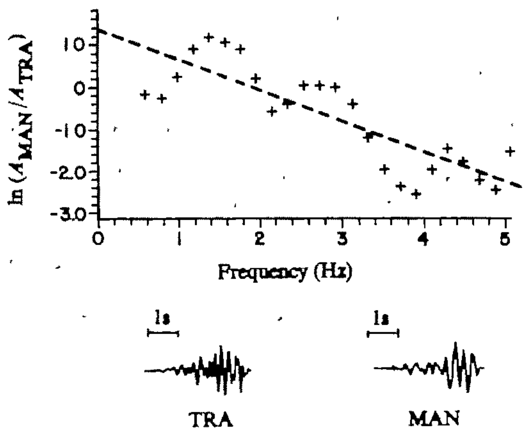

Fig. 5 P-wave arrivals from a single earthquake as recorded by two stations. The waveform TRA has not travelled through the anomaly, whereas the waveform MAN has passed through the anomaly and exhibits a loss in high frequency content relative to TRA. The plot shows the logarithm of the spectral ratio of the two signals, ln (A_{MAN}/A_{TRA}), plotted as a function of frequency. The average slope indicates a difference in the Q values of the two paths. Minor deviations from the average slope may be attributed to small differences in the crustal structure at the two stations.

It is also significant that the local etnean micro-earthquakes have a maximum depth[31] of ~12 km, suggesting that they occur in a brittle region overlying the volume of partial melt.

Conclusions

From a seismic network study of the etnean volcanic region, anomalous P-wave delays and high frequency attenuation of seismic signals have been observed. Simple three-dimensional modelling and inversion procedures show that the anomaly can be well represented by a triaxial ellipsoid of axes 22 km, 31 km (horizontal) and 4 km (vertical), at a depth of 20 km below Etna. The ellipsoid is elongated in a NNE direction, similar to the regional tectonic dislocations, and the velocity reduction of 16% indicates that the anomaly is most likely to be a series of fissures containing melt (14% by volume), rather than a completely molten chamber.

We conclude that lithospheric extension of eastern Sicily allows basic parental magma to rise from the upper mantle which is then trapped in a complex series of fissures at depths of 16–24 km, just beneath the 5.5/7.2 km s^{-1} discontinuity. Crystal fractionation, including some mixing with the parental magma, takes place within the fissures[7]. The differentiated magma then ascends into higher feeders, generally along the lines of tectonic dislocation, where secondary pneumatolytic differentiation takes place before eruption, causing minor fluctuations in the chemistry within individual lava flows[11].

Small variations in the differentiates with time may either be due to a change in the supply of parental magma with time, or a change in the time during which the magma is stored in the fissure system. The latter could be controlled by the tectonic movements of the surrounding crustal blocks[12].

We thank Dr D. H. Matthews for firing the sea shots, and for support, Dr H. M. Iyer for his help and encouragement, Dr G. C. P. King, I. Asudeh, G. Ballard, T. Owen, C. Soufleris and S. Morgan for help during the fieldwork. We thank the Istituto di Scienze della Terra and the Istituto Internazionale de Vulcanologia, Catania, for support, especially Mimmo Condorelli. Finally Dr J. K. Gardner is thanked for use of the Hedgehog inversion subroutines. This project was funded by the NERC a studentship for A.D.L.S. and a post-doctoral fellowship for P.M.D. The later stages of this work were also supported by US DOE grant AS03–76SF00034.

Received 30 June; accepted 19 August 1980.

1. Hamilton, Sir W. *Observations on Mount Vesuvius, Mount Etna, and other volcanoes* (The Royal Society, London, 1774)
2. Lyell, Sir C. *Principles of Geology*, 11th edn (Appleton, New York, 1877).
3. von Waltershausen, W. *Sartorius Der Aetna* Vols 1 & 2 (Engelmann, Leipzig, 1880)
4. Imbo, G. *Catalogue of the Active Volcanoes of the World including Solfatara Fields*, Part 18 (International Association of Volcanology, Rome, 1965).
5. Grindley, G. W. *Phil. Trans. R. Soc.* **A274**, 165–175 (1973).
6. Romano, R. *Prog. Fisal. Geodin.* **238**, 103–117 (1979).
7. Cristofolini, R. *Phil. Trans. R. Soc.* **A274**, 17–36 (1973).
8. Tanguy, J. C. *Phil. Trans. R. Soc.* **A274**, 45–54 (1973).
9. Duncan, A. M. *Geol. Mag.* **115**, 273–285 (1978)
10. Washington, H. S., Aurousseau, M. & Keyes, M. G. *Am. J. Sci.* **12**, 371–408 (1926).
11. Romano, R. & Sturiale, C. *Phil. Trans. R. Soc.* **A274**, 37–44 (1973)
12. Rittmann, A. *Phil. Trans. R. Soc.* **A274**, 5–16 (1973).
13. Machado, F. *Bull. volcan.* **28**, 375–380 (1965).
14. Cassinis, R. *et al. Boll. Geof. teor. appl.* **11**, 140–160 (1969)
15. Iyer, H. M. *Nature* **253**, 425–427 (1975).
16. Eaton, G. P. *et al. Science* **188**, 787–796 (1975).
17. Iyer, H. M. *Tectonophysics* **56**, 165–197 (1979)
18. Iyer, H. M., Oppenheimer, D. H. & Hitchcock, T. *Science* **204**, 495–497 (1979).
19. Reasenberg, P., Ellsworth, W. & Walter, A. *J. geophys. Res.* **85**, 2471–2483 (1980).
20. Jeffreys, H. & Bullen, K. E. *Seismological Tables* (British Association for the Advancement of Science, London, 1940).
21. Ellsworth, W. L. & Koyanagi, R. Y. *J. geophys. Res.* **82**, 5379–5393 (1977)
22. Jenkins, G. M. & Watts, D. G. *Spectral Analysis and its Applications*, 138 (Holden-day, San Francisco, 1968).
23. Keilis-Borok, V. I. & Yanovskaya, T. B. *Geophys. J. R. astr. Soc.* **13**, 223–234 (1967).
24. Valyus, V. P. *Vychislitel'naya Seismologiya* Vol. 4, 3–14 (Nauka, Moscow, 1968).
25. Knopoff, L. & Burrus, N. N. *Geophys. J. R. astr. Soc.* **36**, 515–539 (1974)
26. Bath, M. *Spectral Analysis in Geophysics*, 333–346 (Elsevier, Amsterdam, 1974).
27. Ghisetti, F. & Vezzani, L. *I.G.U.–U.N.E.S.C.O. Sicily Excursion in Italy* (in the press).
28. Green, D. H. & Ringwood, A. E. *Contr. miner. Petrol.* **15**, 103–190 (1967)
29. Duncan, A. M. *United Kingdom Research on Mount Etna 1975–1976*, 30–34 (The Royal Society, London, 1977)
30. Hammill, M. *United Kingdom Research on Mount Etna 1975–1976*, 37–42 (The Royal Society, London, 1977)
31. Sharp, A. D. L., Davis, P. M., Gray, F. & King, G. C. P. *United Kingdom Research on Mount Etna 1977–78* (The Royal Society, London, in the press)

Agulhas Basin magnetic bight

H. W. Bergh & D. M. Barrett*

Bernard Price Institute of Geophysical Research, University of the Witwatersrand, Johannesburg, South Africa 2001

The discovery of a magnetic bight in the Agulhas Basin places unique constraints on the relative motion between South America, Antarctica and Africa in the late Cretaceous.

RECONSTRUCTIONS of the predrift configuration of the three Western Gondwana continents (South America (SAM), Africa (AF) and Antarctica (ANT)) have relied heavily on the matching of selected bathymetric contours. Only in fitting AF against SAM and the northern edge of the Falkland Plateau has tightly constraining geophysical evidence been available. This sort of evidence (from fracture zone trends and recognition of linear magnetic anomalies) is only sparsely available for the separation history of the AF and ANT plates.

Well-documented Cretaceous and Eocene magnetic anomalies have been found[1] in the Mozambique Basin eastward of the Prince Edward Fracture Zone. A Mesozoic magnetic anomaly sequence in the Antarctic Basin[2] points towards a simple history of ANT–AF separation, while recently reported[3,4] Mesozoic anomalies in the northern Mozambique Basin provide evidence for the same simple manner of seafloor generation west of the Prince Edward Fracture Zone. No direct determinations have

---

* Present address: Esso Minerals (Africa) Inc., PO Box 78011, Sandton, Johannesburg, South Africa 2146.

0028–0836/80/410591—05$01.00

been made of past relative motion between SAM and ANT.

We describe here results from a geophysical survey of a small area of deep ocean south-west of the Agulhas Plateau (see inset, Fig. 1, for area location). Within this region we can clearly recognize an Upper Cretaceous magnetic bight at two points in time. The new data enable us to describe the behaviour of the triple junction SAM–AF–ANT at ~80 Myr ago. Previously unpublished data in the Antarctic Basin, combined with our new findings, are used to reconstruct the relative SAM–AF–ANT geometry at that time.

Magnetic bight data

Figure 1 shows total magnetic field anomalies plotted perpendicular to ship's track on a bathymetric chart of the survey area. The magnetic measurements were made from the MV RSA during October 1977. Bathymetric coverage on that cruise was supplemented by data from Lamont-Doherty Geological Observatory (Vema and Conrad) and by one Atlantis II track[5] run by the Woods Hole Oceanographic Institute.

Seafloor relief south-west of the Agulhas Plateau is generally small and sediment cover thin (between 0.0 and 0.5 s of two-way travel time). The slight elevation around 45 °S, 20 °E, called the Southwest Spur[6], appears to be partly due to raised basement and partly to increased sediment thickness. The deeper region between here and the Agulhas Plateau is heavily scoured, with scattered erosional outcrops hinting at a possible linear continuity of elevated basement.

The magnetic anomalies clearly delineate a chevron-shaped strip of negatively magnetized sea floor even where this is right-laterally offset in the south-east. The two limbs of this magnetic bight strike 150° (north-west limb) and 125° (south-east limb). We interpret these two limbs as being respectively related to relative motion between the plate pairs SAM–AF and ANT–AF. Correlation of the magnetic anomalies with the geomagnetic reversal time scale is based on the findings between Antarctica and Africa. Recent data between these two continents[7] show clearly that magnetic anomaly sequences are symmetric about the present spreading axis at 52.5 °S, 18 °E and almost complete out to anomaly 34 on either side. In Fig. 1 the northernmost anomalies are numbered, 30–34, of this complete sequence. The region with dotted negative anomalies corresponds to sea floor generated between anomaly 33 and 34 time. In terms of a recent reversal time scale[8] this refers to the period between 79.6 and 76.5 Myr ago. It corresponds to the A-section of the proposed type-section[9] from Gubbio in Italy.

Unique identification of magnetic anomalies on the north-west limb of the bight depends on their continuity with the same anomalies on the south-east limb as we are unable to recognize clearly identifiable anomalies immediately younger than 33 between South America and Africa. This is partly because of

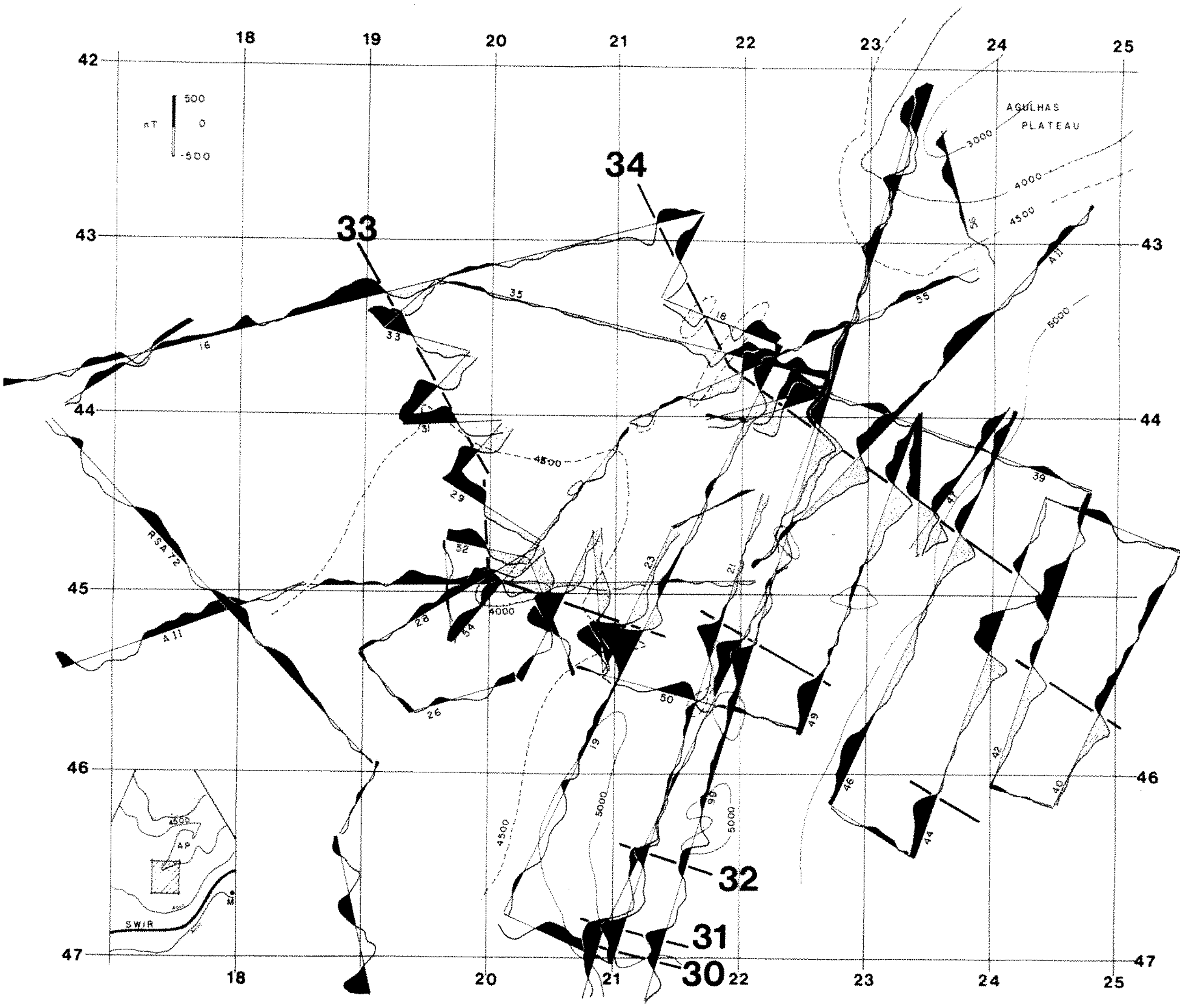

Fig. 1 Magnetic anomalies (total field minus IGRF 1975.0) plotted perpendicular to ship's tracks. Lines marked consecutively from 16 to 56 were run in October 1977 aboard the MV RSA. Lines 99 and RSA 72 were run between Antarctica and South Africa on the RSA in 1977 and 1972 respectively. AII is an Atlantis II track[5]. Positive magnetic anomalies are in black and the lines 34 and 33 refer to the end and beginning of the relevant polarity epochs. The inset shows the survey area in relation to southern Africa, the Agulhas Plateau (AP) and the Southwest Indian Ridge (SWIR). Bathymetry in metres.

poor data coverage but is also probably due to the complications of a westward ridge jump south of the Agulhas–Falkland Fracture Zone soon after anomaly 33 time. Such a jump has been postulated[10,11] to account for the present ridge offset across this fracture zone being ~1,150 km less than its probable offset at the initiation of relative motion between SAM and AF. The timing and nature of this ridge jump, or jumps, are still highly speculative.

Average spreading rates on the two limbs of the bight were determined for the negative polarity interval by projecting the magnetic anomalies perpendicular to their average strike (Fig. 2). In determining the latter parameter, the bight apex portion of anomaly 33 was neglected because it appears atypical of the general trend. We assume here that the anomalies are perpendicular to the spreading direction at their time of formation. This assumption seems to be appropriate[12,13] for spreading half-rates greater than about 30 mm yr^{-1}. Comparison of the projected profiles with suitable simulated profiles (Fig. 2) yields spreading half-rates of 40 mm yr^{-1} for ANT–AF and 55 mm yr^{-1} for SAM–AF.

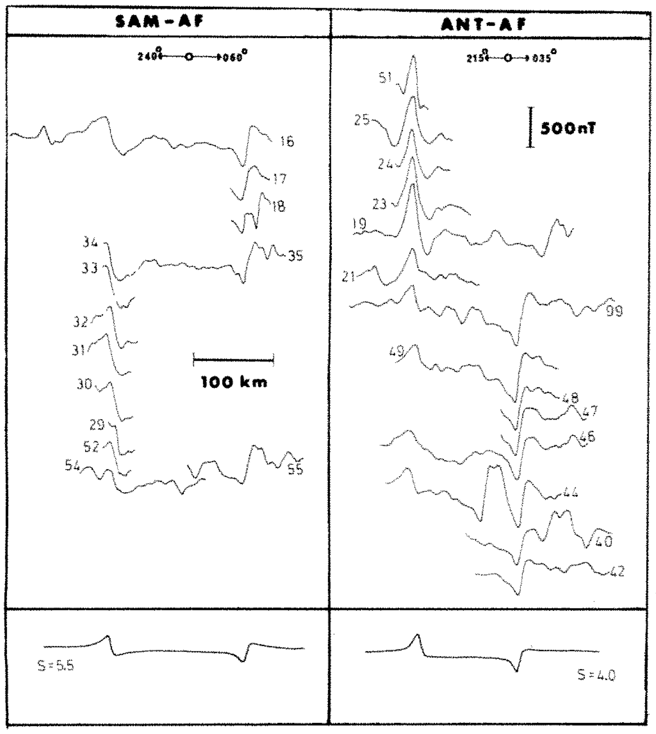

Fig. 2 Magnetic anomaly profiles projected perpendicular to the average strike of anomalies 33 and 34. The simulated profiles at the bottom give the spreading half rates S in cm yr^{-1} for the two plate pairs.

The ridge sections which generated the observed magnetic bight formed two arms of a triple junction at anomaly 34 time. For this junction to be stable the third arm must also have been a ridge. An RRF (ridge–ridge–fault) triple junction could only be stable if the two ridge segments were at right angles[14] or at least one ridge was very oblique to the spreading direction. From the velocity triangle (Fig. 3) we see that the SAM–ANT boundary was a ridge trending slightly east of north (with respect to a fixed AF) and having a half-spreading rate of 25 mm yr^{-1}.

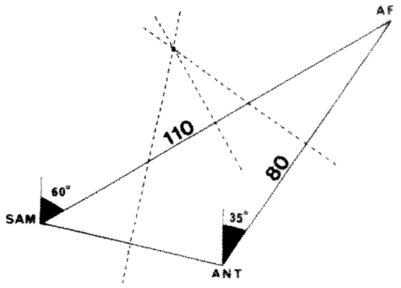

Fig. 3 Velocity triangle for the SAM–AF–ANT triple junction between anomaly 34 and 33 time Angles gives the azimuths of AF–SAM and AF–ANT relative motion and the total separation rate is shown in mm yr^{-1}.

80-Myr reconstruction

Figure 4 is our best reconstruction of the western Gondwana continents at anomaly 34 time. The position of South America relative to Africa differs insignificantly from published palaeolocations[15,16]. Antarctica's palaeoposition has been constrained by our recent findings in the Antarctic Basin and south-west of the Agulhas Plateau and agrees closely with that predicted by Norton and Sclater[17].

With Africa kept fixed, we have rotated South America to the Bullard *et al.*[18] fit and then applied a clockwise rotation of 28°, using the LePichon and Hayes[15] rotation pole at 22 °N, 14 °W. This rotation is only 2° more than theirs and is justified by the excellent matching of previously unpublished magnetic anomaly 34 findings in the Cape Basin with the corresponding anomalies[16] in the Argentine Basin. The Cape Basin anomalies, shown in Fig. 5*a*, are the best evidence we have for the location and strike of anomaly 34 immediately north of the Agulhas–Falkland Fracture Zone.

The Antarctic rotation pole was found by matching of anomalies 34 on either side of the Southwest Indian Ridge.

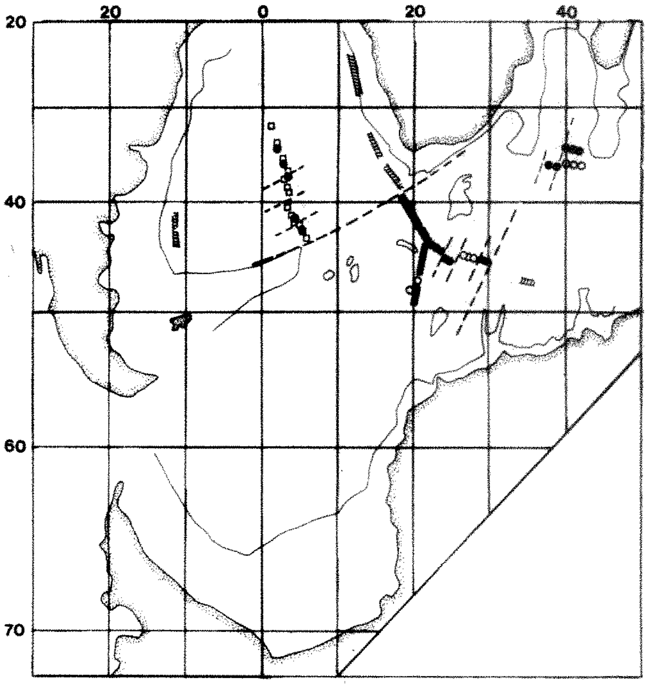

Fig. 4 80-Myr reconstruction of western Gondwana continents. Africa has been kept fixed. Anomaly 34 is shown as: ●, on African plate; ☐, rotated with SAM; ○, rotated with ANT. The rotations are described in the text; ANT has been rotated by 18° about a pole at 10° N, 40° W. Sea floor formed in the Mesozoic interval defined by anomalies M2 to M4 is hatched. Fracture zones are marked by dashed lines, the 3,000-m isobath by a thin solid line. No significance should be attributed to the retention of Madagascar in its present position.

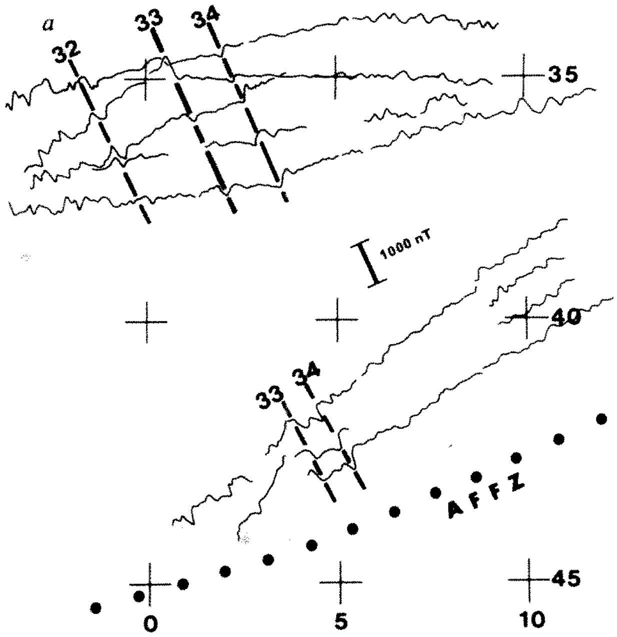

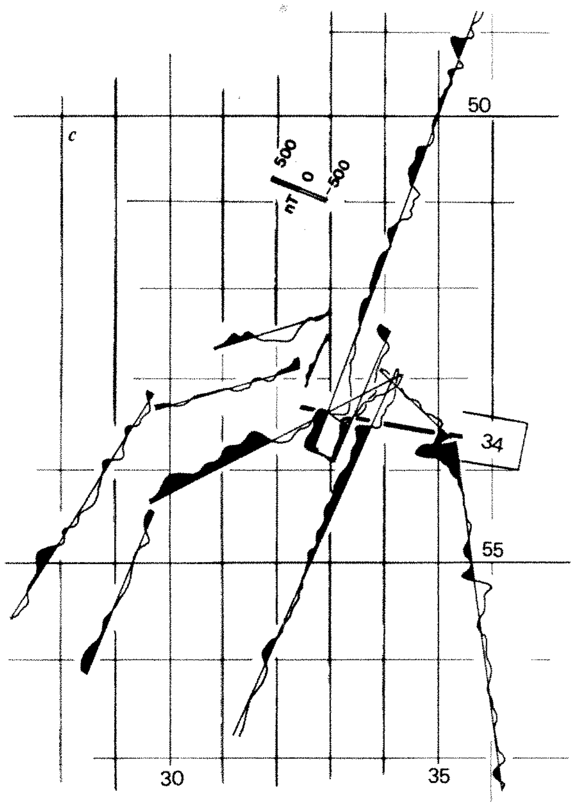

There is uncertainty over whether these conjugate anomaly pairs were formed at exactly the same section of spreading ridge. This need not be too serious a drawback as long as the relevant ridge segments did not have large offsets from one another. We used a very definite anomaly 34 north of Maud Rise (Fig. 5*b*) and a more tentatively identified one at 54 °S, 34 °E (Fig. 5*c*). The pole and angular rotation were adjusted to bring these into best coincidence with, respectively, the anomalies reported here and those in the Mozambique Basin[1].

The pole used for the Antarctic rotation is not much different from the present pole[19] and supports the suggestion[2] that the average ANT–AF pole since the Mesozoic closely approximates the present one. An interesting feature of Fig. 4 is that our questionable SAM–ANT spur of the anomaly 34 bight (Fig. 5*b*) rotates into the predicted position of the SAM–ANT ridge axis at the time of the reconstruction. More intense magnetic surveying is planned near Maud Rise to check on the inferred Antarctic Basin Bight.

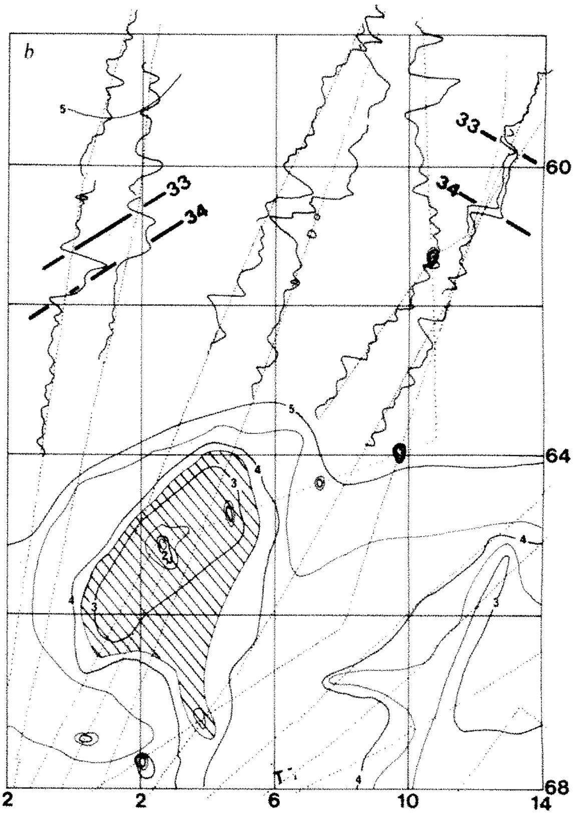

Fig. 5 Unpublished magnetic anomaly profiles obtained during voyages of the MV RSA: *a*, in the South Atlantic immediately north of the Agulhas Falkland Fracture Zone (AFFZ); *b*, north of Maud Rise; *c*, near 54 °S, 34 °E.

Discussion

We confine ourselves here to the evolution of the triple junction between anomaly 34 and 33 time and to possible changes in ANT–AF relative motion immediately after that period. The implications of the striking geometrical relationship between the Agulhas Plateau and the fossil triple junction will be considered elsewhere.

At anomaly 34 time the triple junction was probably a simple RRR with fast orthogonal spreading from all three limbs. By 33 time the ANT–AF half rate had commenced slowing down drastically to ~11 mm yr^{-1}, as determined from the spacing between anomalies 30 and 32. The simultaneous change in SAM–AF relative motion is well documented[16]. Changes in the vicinity of the triple junction seem to be dominated by the removal of the orthogonality constraint as the spreading rates were reduced. Two new transform faults were created and the ridge sections meeting at the triple junction rotated to reduce the lengths of these transforms, as seems to occur generally[12]. The azimuth of the ANT–AF ridge section immediately adjacent to the triple junction is preserved in later linear magnetic anomalies to the south. This incorporation of a persistent oblique spreading regime occurred at the same time in the Mozambique Basin[1] and thus seems to represent a stable mode for slow separation of two plates.

We recognize here that representative spreading rates are imprecisely determined from observations on one plate only of anomalies formed near a rapidly reorientated plate boundary. The problem is more severe near a triple junction, because three relative velocity vectors are changing sympathetically. The

SAM–AF velocity determined from the north-west limb of the bight is based on an assumption of orthogonal, symmetric spreading. The limb strikes very nearly at right angles to the Agulhas–Falkland Fracture Zone (AFFZ). However, assymmetric SAM–AF spreading in the late Cretaceous has recently been proposed[20] immediately south of this fracture zone, and is also apparent when the anomalies in Fig. 5*a* are compared with those near 45 °S on the South American plate[16]. We do not consider the variation in total SAM–AF separation rate to be sufficiently well known at that time to justify much discussion here. The effect of dominant accretion on the AF side of the SAM–AF boundary would have been to increase progressively the obliqueness of the SAM–ANT (ridge) boundary. The ANT–AF velocity seems to be on the high side as the Mozambique Basin half-rate[1] (at 90° from the rotation pole) is 35 mm yr^{-1} using the same time scale[8] as in the present paper. A more consistent half-rate (32 mm yr^{-1}) is obtained using the extreme south-east section of the bight. The effect on SAM–ANT spreading geometry, of taking this possible error into account, would be to make the ridge section more nearly north–south, with a slightly higher spreading rate.

The velocity triangle in Fig. 3 shows that the RRR triple junction will migrate northwards, with respect to ANT, along the SAM–AF rifting margin. Ridge jump proposals[11,20,21] have not considered the proximity of a triple junction to the AFFZ.

A stable RRF junction could possibly be formed if the RRR triple junction reaches this fracture zone. Such a junction with almost orthogonal SAM–ANT and AF–ANT ridges would move away from AF at half the SAM–AF velocity and so would not reduce the active transform length of the AFFZ. If oblique spreading is invoked, it would be possible for the RRF triple junction to migrate towards the SAM–AF ridge section north of the AFFZ, but not at sufficient speed to cause the large reduction in offset since the Cretaceous. Detailed surveying south of the AFFZ is still needed to resolve this problem.

This research was funded by the South African National Committee for Oceanographic Research. The cooperation of the late Captain E. Funk and crew of the MV RSA is gratefully acknowledged. The fine weather and technical expertise of George Knox and Jack Engelbrecht made the survey successful. We thank Frank Anderson, director of the National Research Institute for Oceanology, for equipment and technicians.

Received 19 June; accepted 12 September 1980.

1. Bergh, H. W. & Norton, I. O. *J. geophys. Res.* **81,** 5221–5239 (1976).
2. Bergh, H. W. *Nature* **269,** 686–687 (1977).
3. Segoufin, J. *C.r. hebd. Séanc Acad. Sci., Paris* **287,** 109–112 (1978).
4. Simpson, E. S. W., Sclater, J. G., Parsons, B., Norton, I. O. & Meinke, L. *Earth planet. Sci. Lett.* **43,** 260–264 (1979).
5. Uchupi, E. & Emery, K. O. *Woods Hole Inst. Ref.* No. 72–95 (1972).
6. Tucholke, B. E. & Carpenter, G. B. *Bull. geol. Soc. Am.* **88,** 1337–1346 (1977).
7. Bergh, H. W. & Norton, I. O. in preparation.
8. La Brecque, J. L., Kent, D. V. & Cande, S. C. *Geology* **5,** 330–335 (1977).
9. Alvarez, W. *et al. Bull. geol. Soc. Am.* **88,** 383–389 (1977).
10. Scrutton, R. A. *Earth planet. Sci. Lett.* **19,** 250–256 (1973).
11. Barker, P. F. & Dalziel, I. W. D. *et al. Init. Rep. DSDP* Leg **36,** 993–1014 (1976).
12. Atwater, T. & Macdonald, K. C. *Nature* **270,** 715–719 (1977).
13. Stein, S. *Earth planet. Sci. Lett.* **39,** 313–318 (1978).
14. York, D. *Nature* **244,** 341–342 (1973).
15. Le Pichon, X. & Hayes, D. E. *J. geophys. Res.* **76,** 6283–6293 (1971).
16. Rabinowitz, P. D. & La Brecque, J. L. *J. geophys. Res.* **84,** 5973–6002 (1979).
17. Norton, I. O. & Sclater, J. G. *J. geophys. Res.* **84,** 6803–6830 (1979).
18. Bullard, E. C., Everett, J. E. & Smith, A. G. *Phil. Trans. R. Soc.* A**258,** 41–51 (1965).
19. Norton, I. O. *Earth planet Sci. Lett.* **33,** 219–230 (1976).
20. La Brecque, J. L. & Hayes, D. E. *Earth planet. Sci. Lett.* **54,** 411–428 (1979).
21. du Plessis, A. *Nature* **270,** 719–721 (1977).

X-ray kinetic studies of microtubule assembly using synchrotron radiation

Eva-Maria Mandelkow, Arnold Harmsen & Eckhard Mandelkow
Department of Biophysics, Max-Planck-Institute for Medical Research, Jahnstrasse 29, D-6900 Heidelberg, FRG

Joan Bordas
European Molecular Biology Laboratory, c/o DESY, Notkestrasse, D-2000 Hamburg 52, FRG

The assembly of microtubules has been investigated by time-resolved X-ray diffraction using synchrotron radiation. The small-angle scattering becomes visible within seconds and thus enables study of the structural transitions of the protein aggregates during assembly from their subunits in solution. The X-ray pattern at 4 °C arises from a mixture of tubulin rings, dimers and some other species. Raising the temperature to 36 °C induces the breakdown of rings, followed by the growth of microtubules. The results suggest that microtubules may be formed from tubulin oligomers smaller than rings.

WE report here a study on tubulin polymerization and depolymerization *in vitro*, induced by variation of temperature and monitored by time-resolved X-ray scattering. The aims of our experiments were (1) to establish the usefulness of a new approach to the study of polymerization processes in general, and (2) to understand better the stages of microtubule assembly. We investigated the type of structural entities present in the several stages of assembly and disassembly, their time dependence, their dependence on chemical conditions, and the possibility of detection of intermediate states not previously encountered.

Equipment and method

The technique uses high flux of X-rays available from the positron storage ring DORIS at Hamburg, suitable X-ray optics, detector and data acquisition system[1–3] and offers the advantage of yielding not only the rate constants of the process under study, as for instance light scattering or turbidity measurements might do, but also time-resolved structural detail, comparable and/or complementary to that provided by static X-ray diffraction or electron microscopy. During the measurements the accelerator was running at 5 GeV with currents ranging over 10–25 mA. Typical fluxes on the specimens were of the order of 5×10^{10} photons s^{-1}. The wavelength of the radiation was 1.5 Å. Temperature control was achieved by containing the sample in a thermostatted cell around which circulation of a cold or warm fluid could be quickly selected by a system of switching valves.

The microtubule protein (tubulin and microtubule-associated proteins (MAPs)[4]) was prepared from porcine brain by temperature-dependent cycles of assembly and disassembly without glycerol[5].

0028-0836/80/410595—05$01.00

Experimental results

Figure 1 shows the behaviour of the system and corresponds to a three-dimensional plot, with the scattered intensity in the vertical axis, and the scattering angle and time course in the two horizontal axes.

We used temperature jumps from 4 to 36 °C and vice versa to induce protein assembly and disassembly. The half time of the jump was around 25 s (heating rate 0.6 °C s^{-1}). Two successive cycles of polymerization and depolymerization are depicted. The most prominent changes in the scattering patterns are in the region of the central scatter and in the positions and heights of the subsidiary maxima. The change of one type of scattering pattern into another, following the T-jump, is complete within ~150 s. In spite of the high flux of X-rays the polymerization properties are not affected noticeably by radiation damage during the course of an experiment. Thus the cycles of assembly and disassembly can be repeated several times as long as GTP is in excess of the GDP formed during assembly.

Figure 2 shows four scattering traces selected from Fig. 1. They correspond to the initial scattering from the cold solution, two intermediate states which appear shortly before the onset of microtubule formation, and the final pattern at high temperature. There is an overall decrease of the scattered intensity when going from the initial cold (Fig. 2*a*) to the first intermediate state(Fig. 2*b*). The subsidiary maxima around channels 12, 41 and 65 characteristic of the cold state are reduced. This is followed by a second intermediate state in which the subsidiary maxima are washed out and the central scatter increases again (Fig. 2*c*). The scattering of the final warm state (Fig. 2*d*) shows a marked increase near the origin as well as the appearance of new subsidiary maxima around channels 26 and 72.

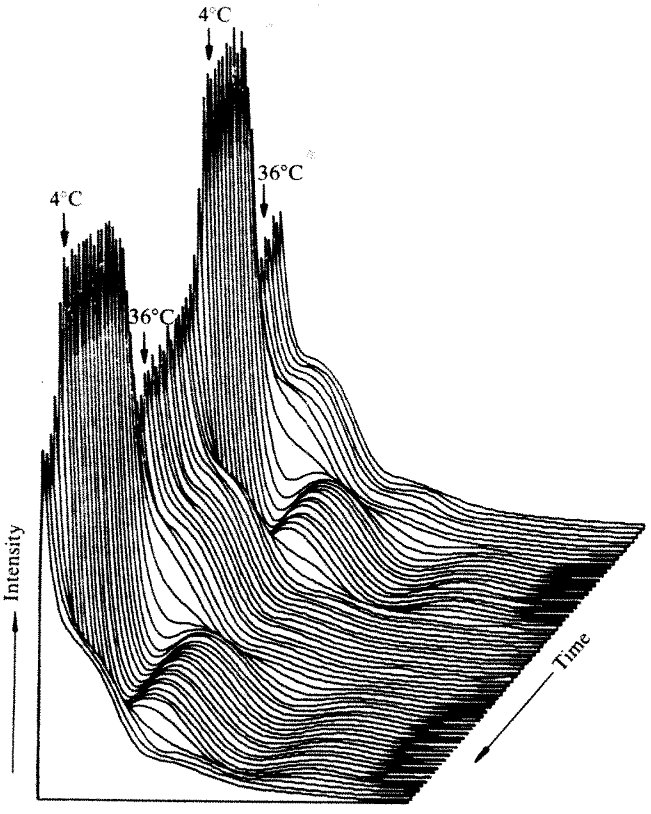

Fig. 1 Composite view of scattering traces obtained during two cycles of polymerization. Intensities were accumulated over time frames of 15 s, but only alternate frames are shown here. Temperature changes are as indicated. The half time of the T-jump is 25 s. Specimen–detector distance 320 cm, detector bin size 0.31 mm (80 mm per 256 channels). Note the changes in the height of the central scatter (left) and in the positions of the subsidiary maxima. The central scatter terminates abruptly due to a lead beam stop in front of the detector. The curves have been corrected for counter response, beam fluctuations, background, and splined to eliminate statistical noise. Microtubule protein was prepared from porcine brain following Borisy *et al.*[5]. The reassembly buffer was usually 0.05 M or 0.1 M PIPES, 1 mM each of GTP, dithiothreitol (DTT), EGTA, and $MgSO_4$, pH 6.94 at room temperature. After the second cycle the protein pellets were stored in liquid nitrogen. They were redissolved in reassembly buffer before use and either used directly or run through one additional cycle. Protein determinations were done by the Lowry assay. The efficiency of assembly was monitored turbidimetrically, and the protein composition was checked by SDS-polyacrylamide gradient gel electrophoresis and analytical ultracentrifugation.

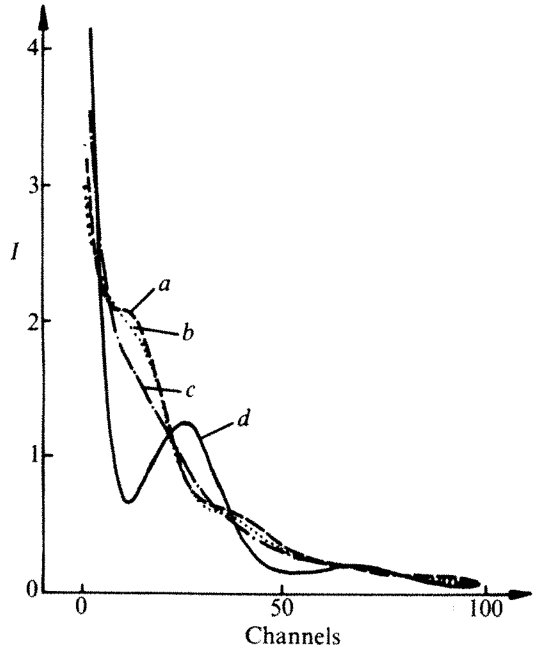

Fig. 2 Selected plots derived from Fig. 1. *a*, Initial cold solution, showing subsidiary maxima around channels 12, 41 and 65. *b*, 45 s after the temperature switch. At this point the temperature in the solution is about 27 °C. It corresponds to the bottom of the undershoot of Fig. 3*b*. The integrated intensity of the central scatter has decreased by about 8%, and the subsidiary maxima are reduced. *c*, 75 s after *T*-jump, corresponding to the recovery of the undershoot of Fig. 3*b*. The central scatter has increased about 8% over its initial value, and the subsidiary maxima have disappeared. *d*, Final warm solution, 225 s after T-jump. The central scatter has increased by 45% over the initial value. New subsidiary maxima appear further away from the origin, around channels 26 and 72.

Figure 3 shows the time course of the temperature in the specimen with the integrated intensities in several regions selected from Fig. 2. The central scatter (Fig. 3*b*) shows an undershoot which reaches its minimum value 45–60 s after the T-jump. This is followed by a sharp increase with a half time of ~100 s. The bottom of the undershoot corresponds to the intermediate scattering pattern shown in Fig. 2*b*. When the temperature is switched back from 36 to 4 °C, a continuous, biphasic, downward trend is observed.

The intensity integrated between channels 11 and 21 (first subsidiary maximum of the cold solution, Fig. 3*c*) decreases in a biphasic manner. The first phase coincides in time with the appearance of the undershoot in the central scatter, the second with its steep increase (Fig. 3*b*). The integrated intensity around channels 22–32 (first subsidiary maximum of the warm solution, Fig. 3*d*) follows a similar trend to the central scatter, but there is an additional lag of 30 s in the polymerization phase. During the depolymerization following the downward T-jump, the intensities return to their approximate initial values, but the lag and half times are shorter than for polymerization.

Figures 1–3 suggest that the assembling system responds to the temperature jump in at least two phases. The first is characterized by a general decrease of intensity throughout the angular range observed. During the second phase the intensity rises again in some regions (Fig. 3*b*, *d*) but continues to drop in others (Fig. 3*c*). This classification is probably oversimplified as the transition between the phases does not occur simultaneously in all parts of the pattern.

The difference between the two main phases may be demonstrated more clearly by reducing the heating rate to about 0.02 °C s^{-1}. In this case the system is much closer to equilibrium than in a T-jump experiment. Nevertheless, the time courses of the intensities are surprisingly similar in both conditions. Figure 4 shows initially a slow drop of intensity in all regions of the pattern with rising temperature. Around 25 °C there is an abrupt transition—the intensity in Fig. 4*b* and *d* rises again while that of Fig. 4*c* drops steeply.

Correlation with physicochemical experiments

The interpretation of X-ray scattering from proteins in solution usually depends on additional experiments to distinguish between different model structures. Gel electrophoresis shows the microtubule protein to consist of tubulin (α and β, $M_r \sim 55{,}000$), high molecular weight-associated proteins [$M_r \sim 270{,}000$ (refs 4, 5)] and several lower molecular weight components, among them the τ factor bands[6] of $M_r \sim 60{,}000$–$70{,}000$ (not shown). Analytical ultracentrifugation of the cold protein solutions yields two main components at 6S and 30S. 6S is the value of the α–β heterodimer of tubulin which constitutes the basic building block of microtubules. 30S is a ring-like structure made up of tubulin and MAPs[5]. The rings may be observed by negative stain electron microscopy (Fig. 4, left). Their apparent diameters vary from 320 to 430 Å. The polymerized microtubules are shown in Fig. 4, right. From the X-ray patterns of oriented gels[7] their mean diameter was determined previously to be ~220 Å.

The process of microtubule assembly is frequently monitored by UV light scattering or turbidity. The increase in the scattered intensity following the temperature jump is usually interpreted as microtubule growth, even though any assembly of tubulin into polymorphic forms produces very similar traces. Thus light scattering by itself is a nonspecific measure of overall aggregation. If the experiment is performed in the conditions of Fig. 1, we observe a decrease in turbidity before the onset of polymerization (not shown). This shows the correspondence between the time dependence of turbidity and the central X-ray scattering and emphasizes the additional information contained in the complete X-ray traces.

Interpretation of scattering curves

The changes in intensity and position of the X-ray scattering peaks could be used simply as indicators of the kinetics of assembly. However, the information above allows a structural interpretation using the theory of small-angle scattering[8]. In the approximation that all particles in solution scatter independently, one can express the intensity as

$$I(h, t) \propto \Sigma x_k(t)^* p_k(t)^* i_k(h)$$

where $h = 4\pi \sin \theta/\lambda$. The sum is taken over all aggregates k in solution. $x_k(t)$ is the fraction of subunits (tubulin dimers) incorporated into aggregate k; mass conservation can be expressed as $\Sigma x_k(t) = 1$. The degree of polymerization $p_k(t)$ expresses the number of subunits per aggregate k, and $i_k(h)$ is the characteristic scattering function of aggregate k normalized to unity at $h = 0$. It contains the structural information. At very small angles $i_k(h)$ approaches 1 so that $I(h, t)$ tends to $\Sigma x_k(t) p_k(t)$. Therefore the central scatter measures the overall aggregation of the system and corresponds to the intensity of scattered UV light. At larger angles the X-ray scattering reflects the overall shape of the aggregates, giving rise to a series of maxima.

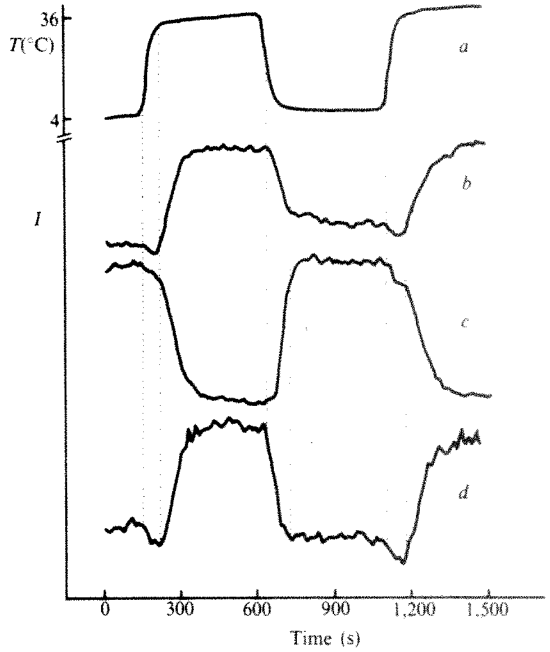

Fig. 3 Time dependence of selected regions of the scattering curves in a temperature jump experiment. *a*, Temperature, measured directly in the protein solution by means of a thermocouple. *b*, Channels 1–5 (central scatter). After the T-jump there is a lag of 45–60 s during which the intensity decreases (undershoot), followed by a sharp rise of half time 100 s. After the reverse T-jump to 4 °C there is a lag of 30–40 s during which the intensity stays constant. This is followed by a biphasic decrease of half times 50 s and 180 s. Depolymerization sets in when the temperature in the solution is about 15 °C. *c*, Channels 11–21 (first subsidiary maximum of the cold solution). The intensity drops steadily in a biphasic manner following the T-jump to 36 °C. The first phase corresponds to the undershoot of curve *b*, the second phase to the rise of *b*. *d*, Channels 22–32 (first subsidiary maximum of the warm solution). The increase in intensity is preceded by an undershoot whose minimum is reached 30–45 s after the one shown by the central scatter. Similarly, the increase in intensity lags behind that of the central scatter. Following the reverse T-jump the intensity decrease is monophasic and coincident with the first phase of the decrease of the central scatter (*b*).

By subtracting the first intermediate scattering pattern, obtained during the undershoot, from the initial cold one (Fig. 2), one obtains the trace of Fig. 5. The comparison with the model calculation shows that it corresponds to the scattering of rings in solution. In this experiment the best fit of the mean diameter is 375 Å. This value is somewhat larger than the mean diameters deduced from published figures based on electron micrographs (~350 Å, see ref. 9). The small discrepancy is probably due to shrinkage on the EM grid. The fact that the difference scattering curves are dominated by the scattering from rings proves that they are dissolved as the temperature is raised, before the formation of microtubules. Within the limits of the instrumental sensitivity the dissolution of rings seems to

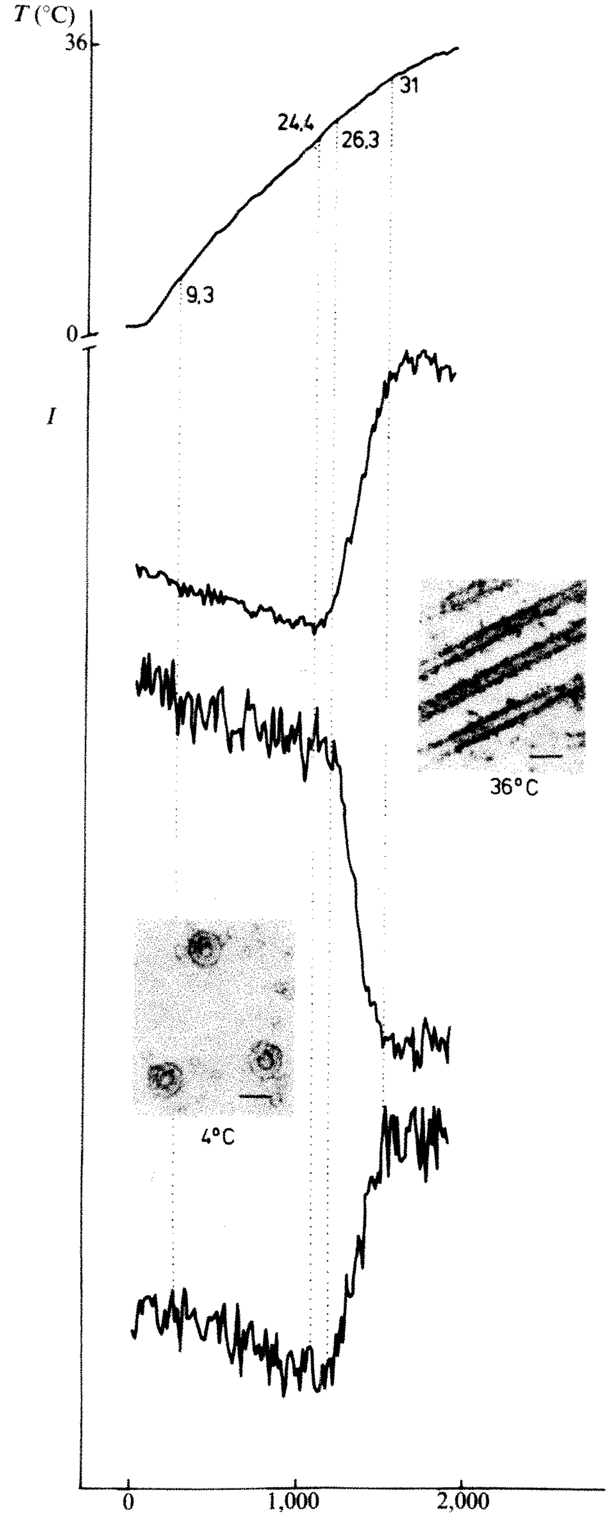

Fig. 4 Microtubule polymerization at a low heating rate. *a*, Temperature. *b–d*, Intensities in the regions corresponding to Fig. 3*b–d*. The central scatter decreases monotonously until 24.4 °C and then rises again (*b*). The region of the first microtubule peak behaves similarly, with the transition temperature displaced towards 26.3 °C (*d*). The region of the first ring peak/first microtubule node decreases monotonously. There is a slight change in rates around 9.3 °C. The second main phase sets in at 26.3 °C. At this point the contribution of rings to the X-ray pattern is below detectability (*c*). Polymerization of microtubules is complete around 31 °C. Insets, Electron images of negatively stained rings (left) and thin sections of microtubules (right). Bar = 500 Å. The cold solution shows single and double rings whose diameters vary between 320 and 430 Å. The warm solution contains microtubules of outer diameters around 250 Å.

be complete by ~60 s after the T-jump (Fig. 2*c*). The processes of ring break down and microtubule formation may be separated particularly well in conditions where the lag time is increased, for instance by raising the temperature slowly (Fig. 4). The transition temperature of about 25 °C coincides with a change in the thermodynamic parameters of the protein[10].

Removal of the contribution of rings from the cold pattern leaves a scattering curve which may be interpreted in terms of scattering from a mixture of dimers and other species smaller than rings. These could be MAPs and/or other tubulin oligomers whose structure is under study.

The scattering pattern of the high temperature state is essentially that of microtubules of mean diameters ~260 Å. We note that their sizes are greater than determined previously in different experimental conditions[7]. This is probably accounted for by the larger contribution of MAPs attached to the outsides of the microtubules (details elsewhere).

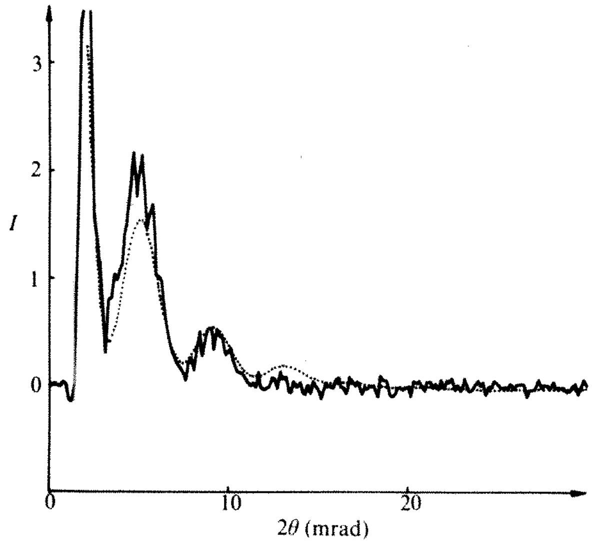

Fig. 5 Difference curve, obtained by subtracting the intensity at 45 s after the T-jump of Fig. 1 from the intensity of the initial cold solution. This plot is representative of the structures that are dissolved. The dotted trace is the calculated small-angle scattering of rings of mean diameter 375 Å, radial width 70 Å, and axial height 50 Å. The positions of the subsidiary maxima are essentially determined by the mean diameter while the width and height modifies mainly the relative amplitudes.

Summarizing the above arguments we may interpret the intensity changes qualitatively as follows: The central scatter ($h \leqslant 0.015$ Å^{-1}) indicates the average degree of polymerization. When rings break down its intensity (and that of the rest of the pattern) decreases. It increases again when microtubules are formed (Figs 3*b*, 4*b*). The region around $h \cong 0.02$ Å^{-1} corresponds to the first subsidiary ring peak. It decreases both absolutely and relative to the rest of the pattern when rings break down. The same region is also near the first subsidiary microtubule minimum. Therefore the intensity decreases even further when microtubules appear (Figs 3*c*, 4*c*). Around $h \cong 0.03$ Å^{-1} we observe the first subsidiary microtubule peak. The intensity decreases during the breakdown of rings and rises sharply with microtubule polymerization. These rules serve as a guide to assess the system's behaviour quickly (for example in Fig. 1), provided that they are backed up by a detailed comparison of the total scattering curves with model calculations such as Fig. 5. The delay between the intensity increases of the central scatter and the microtubule peak (Figs 3*b*, *d* and 4*b*, *d*) suggests that some transient structure is formed around 25 °C between the breakdown of rings and polymerization of microtubules (compare with Fig. 2*b*, *c*). This could correspond to the nucleating centre in the proper sense.

Implications for models of microtubule assembly

Published reports on microtubule polymerization contain a great variety of assembly models (reviewed in ref. 9). Although some of their differences may be due to preparative procedures we suspect that ambiguities inherent in the experimental data play an equally important role. The two main techniques used have been UV light scattering or turbidity and electron microscopy. Turbidity measures only overall polymerization without distinguishing between microtubules and other tubulin aggregates, let alone possible changes of effective diameters due to variations in protofilament number and/or MAP content. Electron microscopy records the structures distorted by drying and staining, it is biased towards large and visible aggregates and provides only snapshot views of the kinetic process. Thus the technique of time-resolved X-ray diffraction helps to bridge the gap between the two conventional approaches as it can be applied to solutions and yet contains structural information on aggregates of all sizes.

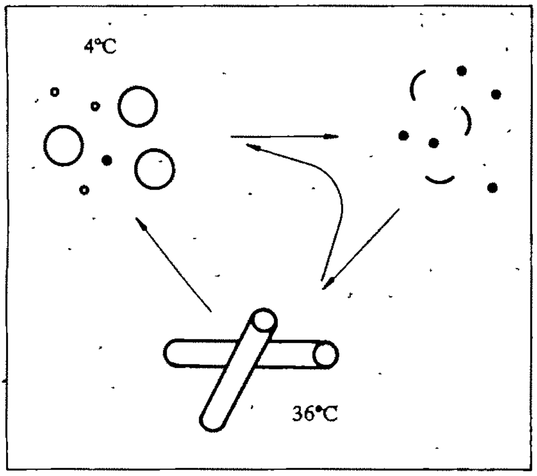

Fig. 6 Possible pathway of tubulin assembly. The initial cold solution contains tubulin dimers, rings, and other entities that are smaller than rings. After the T-jump to 36 °C the rings break apart into fragments which may be involved in the nucleation of assembly. The warm solution consists mainly of microtubules. Depolymerization may proceed either directly to the initial cold state, or via small oligomers.

The assembly models can be placed in three categories depending on the roles assigned to rings. Some assume that opened-up rings are responsible for nucleation and, together with tubulin subunits, contribute to the elongation of microtubules, possibly through intermediates such as sheets or twisted ribbons[11]. Others see a role of rings only in nucleation whereas elongation proceeds by end-on addition of 6S tubulin subunits[12]. Some authors have questioned the role of rings altogether as conditions of microtubule assembly can be found in the absence of rings[13]. There seems to be agreement, however, that brain microtubule assembly is most efficient when starting from a ring-containing solution.

The results presented here favour the view that rings do not directly participate in microtubule nucleation or growth as they tend to break down before microtubules appear. By implication, other intermediates seen in the electron microscope such as sheets or ribbons might also be formed from ring fragments and not by association of opened-up rings. These findings support those of Weisenberg[14] who demonstrated the breakdown of the 30S aggregate into smaller units before microtubule assembly.

During disassembly we observe a smooth transition from the scattering pattern of microtubules to that of rings. This could mean that the rings are formed directly as breakdown products of microtubules. Alternatively, if individual tubulin subunits or small oligomers dissociate from the microtubules they must rapidly reassociate into rings. Whatever the mechanism, the nearly parallel decrease of the central scatter and microtubule maxima (Fig. 3*b*, *d*) suggests that the tubules are largely depolymerized from their ends. The results are summarized in Fig. 6.

Main conclusions and future outlook

The main points to emerge from this study are the following: (1) A cold solution of microtubule protein mainly consists of rings, dimers and other entities made up of MAPs and/or tubulin dimers. (2) When the temperature is raised, either by a T-jump or gradually, rings dissolve into structures of lower degree of polymerization. (3) Within the sensitivity of the method the dissolution of rings is complete before the formation of microtubules. (4) There are at least two intermediate states which differ from both the initial cold and the final warm solution. The first corresponds to the dissolution of rings, the second to the appearance of a new structure just before microtubules begin to form. (5) It is possible to extract accurate sizes for rings and microtubules in solution. (6) Depolymerization is not the exact inverse of polymerization. (7) The cycles of assembly and disassembly can be repeated until the depletion of GTP. These conclusions apply for solutions of microtubule protein prepared in the absence of glycerol, with concentrations around 10–20 mg ml^{-1}

The aim of this experiment, to establish the use of this technique for monitoring the kinetic and structural transitions occurring during the assembly of macromolecules in solution, is fulfilled for microtubule assembly *in vitro*. The structures formed and their kinetics of polymerization do not seem to suffer significantly from radiation damage during the experiment. The extension of the technique to stopped-flow experiments at constant temperature may have a more direct relationship with physiological conditions. This might enable us to investigate the action of factors promoting assembly, especially that of microtubule associated proteins.

We thank Ursula Rühl for technical assistance with the protein preparations, the EMBL staff for help during the experiments, and Michel Koch and Zvi Kam for making available their data analysis and model building programs and for the many stimulating discussions on the subject of small-angle scattering.

Received 2 June; accepted 22 August 1980

1 Hendrix, J., Koch, M. H. & Bordas, J. *J. appl. Crystallogr.* 12, 467–472 (1979).
2. Gabriel, A. *Rev. sci. Instrum.* 48, 1303–1305 (1977).
3. Bordas, J. *et al. J. Phys. (C) Scient. Instrum.* (in the press)
4 Sloboda, R. D., Rudolph, S. A., Rosenbaum, J. L. & Greengard, P. *Proc. natn. Acad. Sci. U.S.A.* 72, 177–181 (1975).
5 Borisy, G. G., Marcum, J. M., Olmsted, J. B., Murphy, D. B. & Johnson, K. H. *Ann. N.Y. Acad. Sci.* 253, 107–132 (1975)
6 Cleveland, D. W., Hwo, S. Y. & Kirschner, M. W. *J. molec. Biol.* 116, 227–247 (1977)
7. Mandelkow, E., Thomas, J. & Cohen, C. *Proc. natn. Acad. Sci. U.S.A.* 74, 3370–3374 (1977).
8 Guinier, A. & Fournet, G. *Small-Angle Scattering of X-Rays* Engl. edn (Wiley, New York, 1955).
9 Kirschner, M. W. *Int. Rev. Cytol.* 54, 1–71 (1978).
10. Johnson, K. A. & Borisy, G. G. *J. molec. Biol.* 133, 199–216 (1979)
11. Kirschner, M. W., Honig, L. S. & Williams, R. C. *J. molec. Biol.* 99, 263–276 (1975)
12. Johnson, K. A. & Borisy, G. G. *J. molec. Biol.* 117, 1–31 (1977)
13. Lee, J. C. & Timasheff, S. N. *Biochemistry* 14, 5183–5187 (1975).
14 Weisenberg, R. C. *J. supramolec. Struct.* 2, 451–465 (1974)

Protein-linked RNA of poliovirus is competent to form an initiation complex of translation *in vitro*

Fred Golini*, Bert L. Semler, Andrew J. Dorner & Eckard Wimmer†

Department of Microbiology, State University of New York at Stony Brook, Stony Brook, New York 11794

*Present address: Department of Cellular Biology, Scripps Clinic and Research Foundation, 10666 North Torrey Pines Road, La Jolla, California 92037
†To whom correspondence should be addressed

Poliovirus RNA that had been labelled with ^{125}I in the 5′-terminal protein (VPg) was found competent to form an initiation complex of translation in a cell-free reticulocyte lysate. In conditions of ribosome binding, no cleavage occurred between VPg and RNA. We conclude that removal of VPg from poliovirus RNA is not a prerequisite for this RNA to initiate translation in vitro.

BOTH *in vivo* and in cell-free extracts, picornavirus RNA is a highly efficient messenger capable of initiating translation at a much faster rate than most host cell mRNAs[1,2]. Evidence from *in vitro* experiments indicates that picornavirus RNA is preferentially translated over cellular mRNAs by virtue of its ability to out-compete host cell mRNA for limiting amounts of a messenger discriminatory initiation factor[3]. The structural feature of picornavirus RNA responsible for its superior translation is not known. Unlike most cellular and viral messengers which require a 5′-terminal 7mG-containing 'capping group' for efficient translation, picornavirus RNA is not capped. Instead, the 5′ terminus of virion RNA is linked to the small virus-encoded protein, VPg (refs 4–8). In contrast, polio RNA isolated from polysomes lacks VPg and is terminated with a 5′ monophosphate[9].

Picornavirus RNA is accurately translated in the messenger-dependent reticulocyte lysate system. Processing of precursor polypeptides occurs to produce proteins which correspond to those seen *in vivo*[10]. Proteinase K treatment of polio virion RNA has been shown to degrade VPg proteolytically, leaving a few amino acid residues linked to the intact RNA molecule[6]. This treatment does not destroy the infectivity of the RNA[11]. Preliminary experiments showed that amino acid incorporation in the reticulocyte lysate was stimulated to the same extent and with identical kinetics by untreated and proteinase K-treated polio RNA. Furthermore, the proteins synthesized in response to both RNAs were indistinguishable when analysed by SDS-polyacrylamide gel electrophoresis (see below). Essentially the same results have been reported for mengovirion RNA treated with proteinase[12].

These results can be interpreted in two ways. In the first case, it may be that the presence or absence of VPg has no effect on the translation of picornavirus RNA. Alternatively, the cell-free system may be able to cleave VPg from RNA so efficiently that no apparent difference is seen in incubations programmed with the two messengers. An activity capable of removing VPg from RNA in extracts prepared from a variety of cells has been described[13]. However, as only a small proportion of the RNA

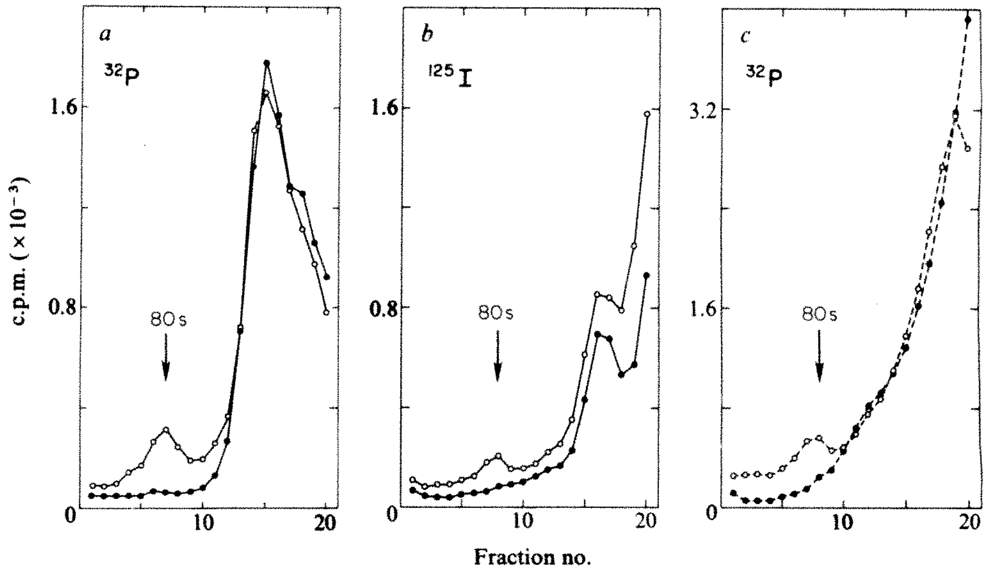

Fig. 1 Binding of polio RNA to reticulocyte ribosomes. Poliovirus ^{32}P-RNA and ^{125}I-VPg-RNA (from type I, Mahoney) were prepared as described previously[9,16]. The messenger-dependent reticulocyte lysate was prepared according to the method of Pelham and Jackson[20]. Incubation mixtures (100 µl) were assembled at 4 °C, containing nuclease-treated reticulocyte lysate (50 µl), creatine phosphokinase (10 µg), 10 mM phosphocreatine, 20 amino acids (0.1 mM each), 20 mM Tris-HCl, *p*H 8.2, 3 mM $Mg(OAc)_2$, 0.13 M KOAc, 2 mM dithiothreitol, reticulocyte ribosomal RNA (1 µg), 0.25 mM NAD, 0.1 mM sparsomycin, and 250 guinea pig L.D. per ml diphtheria toxin. After preincubation at 30 °C for 4 min, 0.1 µg labelled polio RNA was added and incubation continued for 4 min. An equal volume of 1% sodium deoxycholate, 1% Triton X-100 was added and 1 min later the incubation was terminated by chilling to 4 °C. Initiation complexes were resolved by sedimentation at 4 °C on 15–30% w/w sucrose gradients in buffer F (25 mM KCl, 10 mM NaCl, 1.5 mM $Mg(OAc)_2$, 10 mM Tris-HCl, *p*H 7.5 (ref. 14), supplemented with 0.5% sodium deoxycholate and 0.5% Triton X-100. Experiments containing polio ^{32}P-RNA (*a*, *c*) were centrifuged for 10 h at 29,000 r.p.m. in the Spinco SW41 rotor. For *b*, the incubation mixture was scaled up fivefold and programmed with ^{125}I-VPg-polio RNA. Centrifugation was for 10 h at 27,000 r.p.m. in the SW27 rotor. Radioactivity in sucrose gradient fractions was determined in a liquid scintillation counter after addition of one half-volume of H_2O and nine volumes of Biofluor (NEN). ○, Standard conditions; ●, preincubation mixture contained either 5 µg unlabelled polio RNA (*a*) or 10^{-4}M ATA (*b*, *c*). The S value of the ribosome complex was determined by incubating the lysate with ^{35}S-$tRNA^{met}$ and globin mRNA or poliovirus RNA in the same conditions as described for *a*, and sedimenting the initiation complex through a sucrose gradient[21].

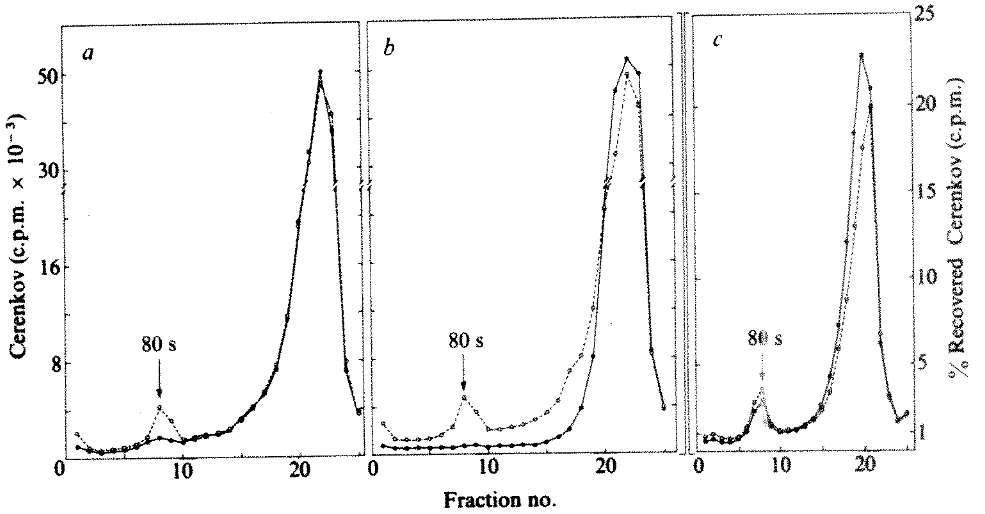

Fig. 2 Binding of polio RNA to reticulocyte ribosomes. Incubation mixtures of the messenger-dependent reticulocyte lysate were prepared as described in Fig. 1 legend. Standard condition reactions were programmed with virion ^{32}P-RNA at a final concentration of 2 μg ml^{-1}. Centrifugation was for 16 h at 21,000 r.p.m. in the SW27 on gradients as described in Fig. 1 legend. Radioactivity in gradient fractions was determined directly by Cerenkov counting. Proteinase K digestion of polio ^{32}P-RNA was done at 37 °C for 1 h[11]. The reaction mixture contained 10 mM Tris, pH 7.6, 100 mM NaCl, 1 mM EDTA, 0.5% SDS, proteinase K (500 μg ml^{-1}) and polio RNA (300 μg ml^{-1}). The mixture was phenol/chloroform extracted after the incubation and the RNA ethanol precipitated before use in the reticulocyte lysate. ○, Standard conditions; ●, preincubation mix contained pactamycin at a final concentration of: *a*, 4×10^{-6} M; *b*, globin mRNA at a final concentration of 400 μg ml^{-1}; *c*, the reaction was programmed with proteinase K-treated ^{32}P-RNA at a final concentration of 2 μg ml^{-1}.

added to *in vitro* cell-free systems is actually translated, the fate of VPg on those molecules which function as messenger was not ascertained. The approach we used to resolve this question was to isolate initiation complexes of ribosomes bound to polio RNA and then determine if VPg was retained on this fraction.

Characterization of initiation complex

Reticulocyte lysates supplemented with sparsomycin and diphtheria toxin allow the binding of ribosomes to mRNA and synthesis of the first peptide bond but block further elongation, permitting isolation of initiation complexes by sucrose gradient centrifugation as shown in Fig. 1 (ref. 14). Due to the large sedimentation coefficient of picornavirus RNA and its nonspecific association with cytoplasmic proteins, separation of ribosome-bound and unbound RNA is difficult. This problem can be overcome by the addition of deoxycholate and Triton X-100 to the incubation and gradient buffer. In the conditions described in Fig. 1 legend, 10% of the polio ^{32}P-RNA is found associated with ribosomes in a peak sedimenting at approximately 80S. The remaining RNA is recovered as a broad peak at 60S with a pronounced shoulder skewed towards the top of the gradient, an observation suggesting that ribonuclease degradation of the unbound RNA occurs. Several criteria have been used to establish that the more rapidly sedimenting peak in Figs 1 and 2 represents a true initiation complex. In control reactions kept at 0 °C, the 80S peak was not seen (data not shown). In Fig. 1*a*, it can be seen that preincubation with excess nonradioactive polio RNA saturates the capacity of the lysate and prevents subsequent binding of ^{32}P-RNA. The same effect was observed when the lysate was preincubated with nonradioactive globin mRNA (Fig. 2*b*). Addition of aurin tricarboxylic acid (ATA), an antibiotic which inhibits association of ribosomes with mRNA, or pactamycin, an inhibitor of initiation of translation[15], both prevent the appearance of the faster sedimenting peak (Figs 1*c*, 2*a*, respectively).

The initiation complex formed with polio ^{32}P-RNA has been further characterized by treatment with ribonuclease T1 and isolation of the ribosome-protected fragment. Analysis by polyacrylamide gel electrophoresis reveals that one major band about 40 nucleotides long is obtained (arrow, Fig. 3*a*, lane 2) together with other RNA bands. This band has been reproducibly observed in several independent experiments using intact virion RNA, or, as shown in Fig. 3*b*, lane 1, using autoradiolysed virion ^{32}P-RNA. The length of the other RNA fragments, however, changes from experiment to experiment (Fig. 3*b*, lane 1). The major band (arrow) is not generated when virion ^{32}P-RNA is bound to ribosomes, isolated without RNase T1 treatment, and analysed by acrylamide gel electrophoresis (Fig. 3*b*, lane 2). The major fragment protected by ribosome binding is capable of rebinding to ribosomes if the mixture of RNA fragments is subjected to a second cycle of ribosome binding (Fig. 3*a*, lane 3). We cannot rule out the possibility that more than one RNA species rebound to ribosomes because the amount of radioactivity in this lane was low.

The VPg moiety of polio genome RNA was specifically labelled with ^{125}I using the Bolton–Hunter reagent[16]. The results of ribosome-binding experiments with this RNA are shown in Fig. 1*b*. Approximately 5% of the labelled RNA is recovered in the initiation complex, showing that VPg is retained on a significant fraction of the polio RNA molecules bound to ribosomes. Formation of the complex is sensitive to ATA. The specific labelling of VPg has been confirmed by releasing ^{125}I-VPg from the initiation complex with RNase T2 and analysing it by gel electrophoresis as published previously[16]. The only radioactive product seen is VPg migrating to the same position as control VPg (data not shown). Unlike the results obtained using ^{32}P-RNA, the peak of unbound ^{125}I-VPg-RNA (in the right half of Fig. 1*b*) is relatively smaller and most of the radioactivity sediments more slowly. The reason for this is not understood.

Table 1 Determination of degree of cleavage of ^{125}I-VPg from ^{125}I-VPg-RNA in various incubations

	No inhibitors			+Sparsomycin +Diphtheria toxin			+ATA		
Time (min)	Aqueous phase (c.p.m.)	Organic phase (c.p.m.)	% Aqueous phase	Aqueous phase (c.p.m.)	Organic phase (c.p.m.)	% Aqueous phase	Aqueous phase (c.p.m.)	Organic phase (c.p.m.)	% Aqueous phase
0	3,473	152	96	3,421	154	96	3,181	125	96
10	3,436	177	95	3,372	192	95	3,253	211	94
20	3,333	243	93	3,331	239	93	3,212	244	93
30	3,116	465	87	3,088	565	85	2,929	488	86

Incubation mixtures (500 μl) were prepared as described in Fig. 1 legend with and without the inhibitors as indicated. At the times indicated, aliquots were removed and extracted with an equal volume of phenol/chloroform (1 : 1). Biofluor (NEN) was added to each of the samples and radioactivity was determined by scintillation counting.

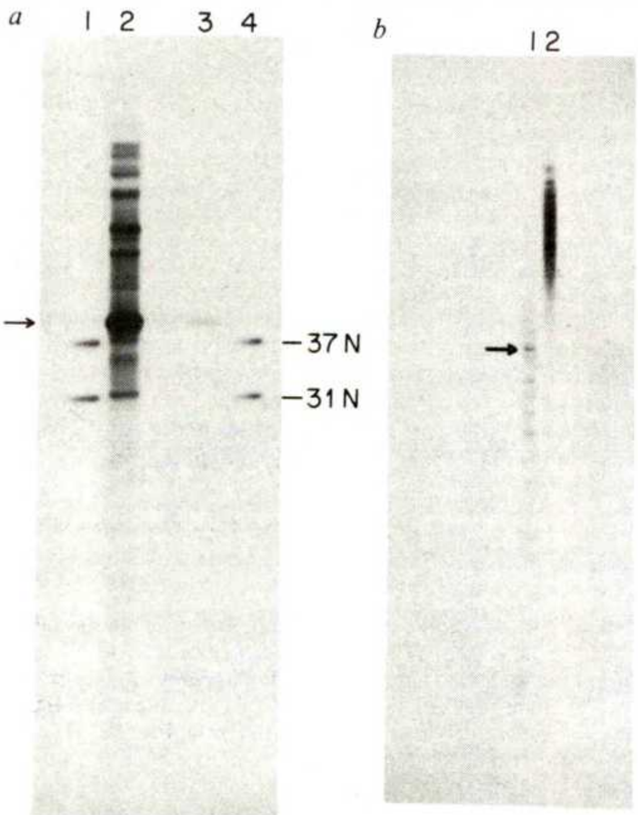

Fig. 3 Acrylamide gel electrophoresis of the ribosome-protected fragment(s) of ^{32}P-RNA from poliovirus. *a*, ^{32}P-RNA from poliovirus was bound to reticulocyte ribosomes as described in Fig. 1 legend. The peak fractions of the sucrose gradient (sedimenting at ~80S) were pooled. RNase T1 was added to 20 units ml^{-1} and incubated at 37 °C for 10 min. The mixture was then chilled on ice and diluted with an equal volume of ice-cold buffer F, containing 0.5% deoxycholate and 0.5% Triton X-100. The sample was pelleted through a 5-ml cushion of 15% sucrose (in buffer F) by centrifugation in the SW27 rotor at 27K r.p.m. (4 °C) for 12–14 h. The pellet was resuspended in 0.5 ml of column buffer (10 mM Tris-HCl, *p*H 7.5, 1 mM EDTA, 7 M urea) containing 0.1% SDS and extracted twice with phenol/chloroform (1 : 1). The aqueous phase was then applied to a small DEAE-cellulose column (0.5 × 4 cm) that had been equilibrated with column buffer. The column was washed with the same buffer containing an additional 0.15 M NaCl (5–10 ml). The presumptive ribosome-protected fragment(s) was eluted with column buffer containing 0.5 M NaCl. The solution containing the fragment(s) was divided. To one half, carrier (either tRNA to 20 μg ml^{-1} or purified oyster glycogen to 200μg ml^{-1}) was added and the sample was alcohol precipitated. This RNA was then analysed by gel electrophoresis on a 20% acrylamide slab gel containing 7 M urea (lane 2). Fragment(s) in the other half were subjected to a second cycle of the same binding and isolation experiments, and analysed by gel electrophoresis (lane 3). Lanes 1 and 4 are marker T1-oligonucleotides 1 and 3 from ^{32}P-RNA of poliovirus, 37 and 31 mucleotides long[22]. N, Nucleotides. *b*, Samples were prepared as described in *a*, except that autoradiolysed virion ^{32}P-RNA was used in the binding experiments and the DEAE cellulose column step was omitted. Lane 1, ribosome-protected fragments corresponding to lane 2 in *a*; lane 2, ribosome-protected RNA isolated without the RNase T1 treatment step.

Retention of VPg on virion RNA after initiation

In view of the activity in uninfected cell extracts that cleaves the linkage between polio RNA and VPg[13], we considered it possible that, by freezing the ribosome on the initiation site, we might prevent the removal of VPg subsequent to the initiation step. Three protein synthesis incubations were prepared containing ^{125}I-VPg-RNA and supplemented with no inhibitor, sparsomycin and diphtheria toxin, or ATA. Aliquots were removed at various times and the unlinking of VPg determined by the phenol extraction assay[13]. Similar results were obtained in the case of all three incubations: little cleavage of VPg from RNA was detected (Table 1). Thus, the retention of VPg on virion RNA reported here is not a consequence of blocking translation at the initiation step. The reason for the apparent discrepancies between our results of release of VPg from RNA and those of Ambros *et al.*[13] may be due to differences in the method of preparation of the reticulocyte extracts and conditions of incubation. A wash of HeLa cell nuclei[13], on the other hand, did remove 90% of VPg from [Tyr-^{3}H,^{32}P]VPg-RNA using the same phenol extraction assay (P. G. Rothberg and E.W., unpublished).

Role of VPg

If the presence of VPg on virion RNA did not prevent ribosome binding, it seemed possible that it might have at least lowered the efficiency of initiation complex formation. Therefore, we compared ribosome binding using VPg-RNA and virion RNA, the VPg of which was degraded proteolytically. As can be seen in Fig. 2*c*, both RNAs form the initiation complex to the same extent. Similarly, translation of VPg-RNA and proteinase K-treated RNA in the reticulocyte lysate leads to the same translat on products with similar yield (Fig. 4).

The role of VPg is not known but the appearance of protein-linked RNA during replication is a general feature of all

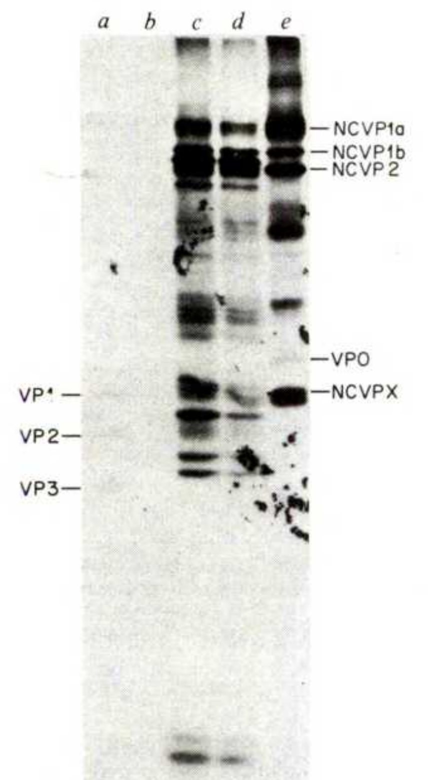

Fig. 4 Acrylamide gel electrophoresis of polio-specific proteins synthesized in the reticulocyte lysate. The messenger-dependent reticulocyte lysate was prepared according to the method of Pelham and Jackson[20]. Reaction mixtures (25 μl) contained 0.5 vol reticulocyte lysate, 20 mM Tris, *p*H 8.0, 2mM dithiothreitol, 100 mM KOAc, 1 mM Mg(OAc)$_2$, 0.5 mM spermidine, 80 μM amino acids except methionine, 50 μg ml^{-1} tRNA, 20 mM creatine phosphate, 100 μg ml^{-1} phosphocreatine kinase, 0.01 μg ml^{-1} rRNA, 60 μg ml^{-1} polio RNA and 400 μCi ml^{-1} ^{35}S-methionine (Amersham). Incubation was for 2 h at 30 °C. Aliquots (1 μl) of the reaction mixture were electrophoresed on 12.5% acrylamide gels containing 0.5% SDS according to the method of Laemmli[23]. The gel was subjected to fluorography according to the method of Bonner and Lasky[24] and exposed at −70 °C. Proteinase K-treated RNA was prepared as described in Fig. 2 legend. Lane *a*, ^{35}S-methionine-labelled capsid proteins isolated from purified virions; lane *b*, without added mRNA; lane *c*, polio virion RNA; lane *d*, proteinase K-treated polio virion RNA; lane *e*, *in vivo* lysate from poliovirus-infected HeLa cells labelled with ^{35}S-methionine. NCVP1a, NCVP1b, NCVP2, VP0 and NCVPX are polio-specific non-copied proteins.

picornaviruses examined[17]. Based on the observations that polio mRNA is infectious and that proteinase K-treated and untreated virion RNAs have equal specific infectivities in transfection assays, it seems that VPg is not essential for early events in replication[6,11]. The identification of VGp on nascent RNA molecules in molar yield implies that it is either a primer for RNA synthesis or is added to all growing chains very soon after initiation has begun[7,18].

We have suggested previously that cleavage of VPg from VPg-RNA may be a prerequisite for this RNA to function as mRNA[7,11]. Our data presented here argue against this hypothesis.

In view of the conclusion reported here that VPg does not interfere with translation *in vitro*, the cleavage of VPg from polysomal RNA *in vivo* is noteworthy. Polio mRNA is not packaged into virions[19]. It is tempting to speculate that retention of VPg may tag those RNA molecules which are to be encapsidated, and thus regulates whether newly synthesized RNA becomes mRNA or enters the pool of progeny genome RNA molecules[7,11,17]. Proof of such a function for VPg clearly awaits further experimental evidence.

We thank Corrado Baglioni for suggestions, Akiko Kitamura for technical assistance, Sandra H. Donaldson for manuscript preparation, Richard J. Jackson for his advice in preparing reticulocyte lysates, R. Hanecak for ^{35}S-methionine-labelled lysate of poliovirus-infected HeLa cells, and R. Rueckert and C. McLean for the gift of pactamycin. This work was supported in part by NIH grant AI 15122. F. G. was recipient of a traineeship from the NCI, grant CA 09176; B. L. S. is recipient of a post-doctoral fellowship, PF-1584, awarded by the American Cancer Society. A. J. D. is a member of the Molecular Biology Program of SUNY at Stony Brook.

Received 9 June; accepted 9 July 1980.

1. Jen, G., Birge, C. H. & Thach, R. E. *J. Virol.* **27,** 640–647 (1978).
2. Lawrence, C. & Thach, R. E. *J. Virol.* **14,** 598–610 (1974).
3. Golini, F. *et al. Proc. natn. Acad. Sci. U.S.A.* **73,** 3040–3044 (1976).
4. Lee, Y. F., Nomoto, A. & Wimmer, E. *Prog. Nucleic Acid Res. molec. Biol.* **19,** 89–96 (1976).
5. Lee, Y. F., Nomoto, A., Detjen, B. M. & Wimmer, E. *Proc. natn. Acad. Sci. U.S.A.* **74,** 59–63 (1977).
6. Flanegan, J. B., Pettersson, R. F., Ambros, V., Hewlett, M. J. & Baltimore, D. *Proc. natn. Acad. Sci. U.S.A.* **74,** 961–965 (1977).
7. Nomoto, A., Detjen, B., Pozzatti, R. & Wimmer, E. *Nature* **268,** 208–213 (1977).
8. Golini, F., Nomoto, A. & Wimmer, E. *Virology* **89,** 112–118 (1978).
9. Nomoto, A., Lee, Y. F. & Wimmer, E. *Proc. natn. Acad. Sci. U.S.A.* **73,** 375–380 (1976).
10. Shih, D. S. *et al. Proc. natn. Acad. Sci. U.S.A.* **75,** 5807–5811 (1978).
11. Nomoto, A., Kitamura, N., Golini, F. & Wimmer, E. *Proc. natn. Acad. Sci. U.S.A.* **74,** 5345–5349 (1977).
12. Pérez-Bercoff, R. & Gander, M. *FEBS Lett.* **96,** 306–312 (1978).
13. Ambros, V., Pettersson, R. F. & Baltimore, D. *Cell* **15,** 1439–1446 (1978).
14. Weber, L. A., Simili, M. & Baglioni, C. in *Meth. Enzym.* **60,** 351–360 (1979).
15. Stewart-Blair, M. L., Yanowitz, I. S. & Goldberg, I. H. *Biochemistry* **10,** 4198–4206 (1971).
16. Rothberg, P. G., Harris, T. J. R., Nomoto, A. & Wimmer, E. *Proc. natn. Acad. Sci. U.S.A.* **75,** 4868–4872 (1978).
17. Wimmer, E. in *The Molecular Biology of Picornaviruses* (ed. Pérez-Bercoff, R.) 175–190 (Plenum, New York, 1979).
18. Pettersson, R. F., Ambros, V. & Baltimore, D. *Virology* **27,** 357–366 (1978).
19. Baltimore, D. in *Biochemistry of Viruses* (ed. Levy, H. B.) 101–176 (Dekker, New York, 1969).
20. Pelham, H. R. B. & Jackson, R. J. *Eur. J. Biochem.* **67,** 247–256 (1976).
21. Darnbrough, C. H., Legon, S., Hunt, T. & Jackson, R. J. *J. molec. Biol.* **76,** 379–403 (1973).
22. Lee, Y. F., Kitamura, N., Nomoto, A. & Wimmer, E. *J. gen. Virol.* **44,** 311–322 (1979).
23. Laemmli, U. K. *Nature* **227,** 680–685 (1970).
24. Bonner, W. M. & Laskey, R. A. *Eur. J. Biochem.* **46,** 83–88 (1974).

Functional and non-functional joining in immunoglobulin light chain genes of a mouse myeloma

Werner Altenburger*, Michael Steinmetz‡ & Hans G. Zachau
Institute für Physiologische Chemie, Physikalische Biochemie und Zellbiologie der Universität München, FRG

Leader, variable (V) and joining (J) gene segments, and adjacent regions of two rearranged alleles of the same κ-chain producing mouse myeloma, comprising approximately 3,200 base pairs, have been sequenced. Sequence comparisons are reported. V–J joining in one of the alleles leads to a reading frame with a stop codon within the J-gene segment. Allelic exclusion is apparently realized in this tumour through the formation of such a non-functional allele.

IN germ-line DNA the information for leader, variable, joining and constant regions of immunoglobulin light chains is located on four separate gene segments called L, V, J and C. In differentiation to an immunocompetent cell, a V- and a J-gene segment are joined by a site-specific recombination process[1,2]. Generally only one type of immunoglobulin is expressed originating from one of the two alleles of the cell[3,4]; this has been termed allelic exclusion. In 15 of 30 mouse myelomas examined allelic exclusion seems to result simply from the fact that only one allele has undergone the V-gene rearrangement whereas the second allele remains in its germ-line configuration[5]. In other myelomas more than one allele was found to be rearranged[5-9]. In some, protein and/or genomic analyses clearly showed that one of the translocations was grossly aberrant[10-13]. However, in other myelomas it was not apparent that one translocation was aberrant or it was even shown that both translocations occurred in the J-gene cluster[14]. Assuming that allelic exclusion operates also in those myelomas one has to search for other reasons either in the translocation step or on the levels of transcription or translation.

Two rearranged κ light chain genes in one mouse myeloma have been previously described[8]. The cloning and restriction mapping of the two rearranged alleles on 14-kilobase[8] and 20-kilobase *Eco*RI fragments[14], respectively, were also reported. We used the myeloma from which the κ chain cDNA clone k38 was derived by Mach *et al.*[15] and which was thought to be identical to MOPC173. However, the sequence analysis described here shows that the V genes on k38 and on the two rearranged *Eco*RI fragments of the myeloma do not correspond to the amino acid sequences of MOPC173 (ref. 16) or other mouse myelomas[17]. Apparently a myeloma other than MOPC173 had been used for the isolation of the mRNA and the subsequent preparation of clone k38 (ref. 15). The same conclusion was reached in independent sequence work on the 14-kilobase fragment and the k38 clone by Fiori, Gorski and Mach (manuscript in preparation). To avoid introducing a new number into the notation before the myeloma is further

---

* Present address: Institut für Molekularbiologie II der Universität Zürich, Hönggerberg, 8093 Zürich, Switzerland.

† Present address: California Institute of Technology, Division of Biology, Pasadena, California 91125.

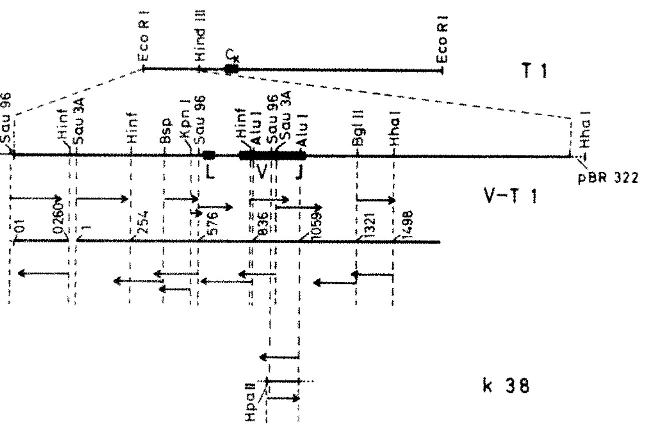

Fig. 1 Localization of the pBR322 subclone V-T1 on the 14-kilobase *Eco*RI fragment T1[14] and partial restriction map of V-T1. Digestions were as previously described[14]. DNA fragments were isolated by *Hha*I (or *Hpa*II) cleavage and separated from the small pBR322 fragments by isokinetic[31] sucrose gradient centrifugation (1 M NaCl, 20 mM Tris-HCl, 10 mM EDTA, *p*H 8.0; $C = 5\%$, particle density 1.89, rotor SW 27.1 for 40 h, 25,000 r.p.m., 20 °C, 1.5–2.0 mg DNA per tube). The fractions (taken from bottom to top) were tested on 1% horizontal agarose gels, pooled, precipitated with ethanol, and washed twice with 80% ethanol. 0.15–0.20 mg of the *Hha*I (or *Hpa*II) fragments (isolated in about 90% yield) were cleaved by one of the nucleases as indicated by dotted lines. Phosphatase treatment (67 °C) and the further steps of sample preparation were as in refs 18 and 32. Labelled fragments were purified by a DE52 step before chemical modification. All 90 °C steps were in siliconized capillaries. Direction and extent of the sequencing are indicated by the arrows. The sequencing strategy of the cDNA clone k38 (see text) is indicated in the bottom line.

characterized we called it tumour T (refs 14, 18, 19). Accordingly the 14- and 20-kilobase fragments are designated T1 and T2, respectively. A 5.3-kilobase *Eco*RI fragment called T3 which was cloned from the same tumour[18] is possibly related to the translocation of immunoglobulin gene segments.

Functional join of V-gene segment to J5-gene segment in one allele of tumour T

Our main interest here was to sequence the V gene segments of the two rearranged alleles and the adjacent L and J regions. We decided to extend the sequencing work both upstream and downstream of these regions for the following reasons. The upstream regions are interesting with respect to possible regulatory sequences and will be even more so as soon as comparison with analogous sequences of other immunoglobulin genes becomes possible. The region downstream of the J segments which extends into the intervening sequence (intron) between J and C_K gene segments is interesting with respect to a search for sites of possible aberrant recombinations[11–13].

As can be seen in Fig. 1, the L-, V- and J-gene sequences of the allele which is found on fragment T1 are located on the previously described subclone V-T1 (ref. 14). 1,800 base pairs have been sequenced (Fig. 2). As a starting point for orientation within the sequence we turn to nucleotides 1,029–1,067 which are identical to those of the J5 gene segment as it was sequenced in germ-line DNA[20,21] (designation as in ref. 20). The junction is within or to the right of the codon CCG, at positions 1,026–1,028. To check whether a V-gene segment is located upstream of the J5-gene segment, the sequence was examined for the presence of codons for the so-called invariant amino acids[17]. All characteristic amino acids were found in the expected positions (6, 16, 23, 26, 35, 44, 57, 59, 61, 62, 63, 64, 65, 73, 75, 86 and 88). The amino acid sequence of the V region as deduced from the nucleotide sequence of fragment T1 is not identical to any of the known[17] sequences of κ light chains. It differs from the published sequences within the 23 amino-terminal amino acids in more than four positions and therefore, by definition[22], cannot be assigned to any one of the known subgroups.

The L-gene segment was localized in fragment T1 at nucleotides 571–621 (Fig. 2) on the basis of the characteristic[23] amino acids at positions 1, 11, 12 and 17 in the leader sequence. Note that there is another possible start codon two codons upstream from the one of amino acid 1 of the leader sequence. The L gene is interrupted by an intron of 113 nucleotides with the probable splice signals AGGT at both ends (positions 618–

```
         10        20        30        40        50        60        70        80        90
GAATTCCCTTCATATTTGCACTTATCATAAAAGGAGTTGCAGTATGAATTTAGTATGTCTTCCCTTATGAAGTGTTTGGAGTAGGCATTTCATATGTAGA  0100
TATATTCTATCTTAACTAGTCAAACCTTTATGCTGAGAAACTGTGGGAAATAGTATTAAATGGCAGAAAAAAAGTAAAGCAAAATATGTAGGCACCCAAA  0200
CTGAGCAAAAGTTGTACCCATTTAGTTTGTAAGTAAGAAAGTCCTCCATTTTCACATGG.........................................

CAATGTGTTATATGTGCAACTCCTTTGTATTTCCTCTCTTTGAACTGTAGTTAGCAAAAGCAGTAGAACCTTATGTTTTTAATTCGGTGAAAATGTTTAT   100
GATAAATTCTCCTTTTAATTTCAACAAATGCCTACTCCAAACACTTCACTAGGGAGGAAATGCTATTTATTTTAGACAACCAAAGTAATTCTATTCGAGTG   200
AGTTAAAGATATAATAGTTTTTTCTTTGTTGTATATTCCCTGACAGCAGGGGATTCTTCTATATTTACCTTAGTATATCTTTGAAATATATTATTCAAAAT   300
AGAGACTACCTACAATAGAAATGACATCTATAATTATAAATCTTTGAAAAGAAATTCATTTTTCTGGAGATATTCAAGTGGTTTGACCTCAGTCATCTGGG   400
GACACTGGCCTTGAGTTAAGTGCTGACATGAGCAAGTCTTGCACCTGTGTCCAGCAATAACTGGTTCCCAATGATTTGCATGCTCTCACTTCACTGCCTT   500
GGGGACTTCTTCATATACCCGTCACACATGTACGGTACCATTGTCATTGCAGCCAGGACTCAGCATGGACATGAGGACCCCTGCTCAGTTTCTTGGAATC   600
                                                                (1) Met Arg Thr Pro Ala Gln Phe Leu Gly Ile  (10)
                   ↓
TTGTTGCTCTGGTTTCCAGGTAAAATGAACTAAAATGGGAATGTCACTGTGATTAGTGTTGATTGGCATTTGGGAGATTTTATCTTTTATGATGCTTACC   700
Leu Leu Leu Trp Phe Pro Gly
                                ↓
TATGTAGATACTCATTATGTCTCCATTCCTAGGTATCAAATGTGACATCAAGATGACCCAGTCTCCATCTTCCATGTATGCATCTCTAGGAGAGAGAGTC   800
          (-4) Gly Ile Lys Cys Asp Ile Lys Met Thr Gln Ser Pro Ser Ser Met Tyr Ala Ser Leu Gly Glu Arg Val  (19)
ACTATCTCTTGCAAGGCGAGTCAGGACATTAATAGCTATTTAACCTGGTTCCAGCAGAAACCAGGGAAGTCTCCTAAGACCCTGCTCTATCGTGCAAACA   900
Thr Ile Ser Cys Lys Ala Ser Gln Asp Ile Asn Ser Tyr Leu Thr Trp Phe Gln Gln Lys Pro Gly Lys Ser Pro Lys Thr Leu Leu Tyr Arg Ala Asn A  (53)
GATTGGTAGATGGGGTCCCATCAAGGTTCAGTGGCAGTGGATCTGGGCAAGATTTTTCTCTCACCATCAGCAGCCTGGAGTATGAAGATATGGGAATTTA  1000
rg Leu Val Asp Gly Val Pro Ser Arg Phe Ser Gly Ser Gly Ser Gly Gln Asp Phe Ser Leu Thr Ile Ser Ser Leu Glu Tyr Glu Asp Met Gly Ile Ty  (86)
                            ↓↓
TTATTGTCTTCAGTATGATGAGTTTCCGCTCACGTTCGGTGCTGGGACCAAGCTGGAGCTGAAACGTAAGTACACTTTTCTCATCTTTTTTTATGTGTAA  1100
r Tyr Cys Leu Gln Tyr Asp Glu Phe Pro Leu Thr Phe Gly Ala Gly Thr Lys Leu Glu Leu Lys Arg  (108)

GACACAGGTTTTCATGTTAGGAGTTAAAGTCAGTTCAGATAATCTTGAGAAAAATGGAGAGGGCTCATTTATCAGTTGACGTGGCATACAGTGTCAGATTTT  1200
CTGTTTATCAAGCTAGTGAGATTAGGGGCAAAAAGAGGCTTTAGTTGAGAGGAAAGTAATTAATACTATGGTCACCATCCAAGAGATTGGATCGGAGAAT  1300
AAGCATGAGTAGTTATTGAGATCTGGGTCTGACTGCAGGTAGCGTGGTCTTCTAGACGTTTAAGTGGGAGGATTTGGAGGGGATGAGGAATGAAGGAACTT  1400
CAGGATAGAAAAGGGCTGAAGTCAAGTTCAGCTCCTAAAATGGATGTGGGAGCAAACTTTGAAGATAAACTGAATGACCCAGAGGATGAAACAGCGCAGA  1500
TCAAAGAGGGG
```

Fig. 2 Nucleotide sequence of the L, V and J regions of fragment T1. Nucleotides are marked 01–0200 and 1–1,500 (interruption of about 40 base pairs between *Hinf* and *Sau*3A sites on the left of Fig. 1), amino acids in L, V, J are (1)–(10) etc. The splice and joining points are marked with vertical arrows. Overlaps with published sequences extend from position 1,028 to 1,356 (ref. 20; differences appear in positions 1,095, 1,119, 1,140, 1,209–1,211 and 1,028–1,118 (difference in position 1,092 with respect to ref. 21).

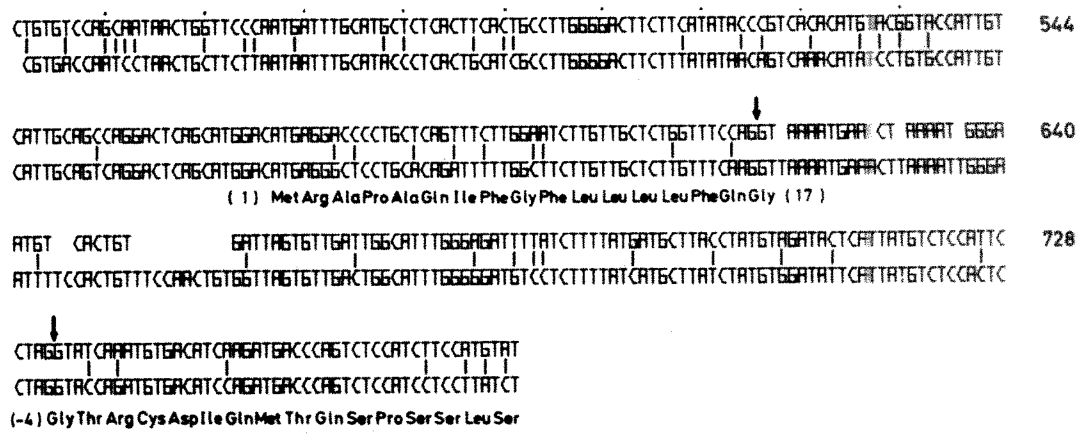
CTGTGTCCAGCAATAACTGGTTCCCAATGATTTGCATGCTCTCACTTCACTGCCTTGGGGACTTCTTCATATACCCGTCACACATG ACGGTACCATTGT
CGTGACCAATCCTAACTGCTTCTTAATAATTTGCATACCCTCACTGCATCGCCTTGGGGACTTCTTTATATAACAGTCAAACATA CCTGTGCCATTGT
544
CATTGCAGCCAGGACTCAGCATGGACATGAGGACCCCTGCTCAGTTTCTTGGAATCTTGTTGCTCTGGTTTCCAGGT AAAATGAA CT AAAAT GGGA
CATTGCAGTCAGGACTCAGCATGGACATGAGGGCTCCTGCACAGATTTTTGGCTTCTTGTTGCTCTTGTTTCAAGGTTAAAATGAAACTTAAAATTGGGA
640
(1) Met Arg Ala Pro Ala Gln Ile Phe Gly Phe Leu Leu Leu Leu Phe Gln Gly (17)
ATGT CACTGT GATTAGTGTTGATTGGCATTTGGGAGATTTTATCTTTTATGATGCTTACCTATGTAGATACTCATTATGTCTCCATTC
ATTTTCCACTGTTTCCAACTGTGGTTAGTGTTGACTGGCATTTGGGGGATGTCCTCTTTTATCATGCTTATCTATGTGGATATTCATTATGTCTCCACTC
728
CTAGGTATCAAATGTGACATCAAGATGACCCAGTCTCCATCTTCCATGTAT
CTAGGTACCAGATGTGACATCCAGATGACCCAGTCTCCATCCTCCTTATCT
(-4) Gly Thr Arg Cys Asp Ile Gln Met Thr Gln Ser Pro Ser Ser Leu Ser

Fig. 3 Comparison of leader and intron region sequences of T1 and MOPC41 (upper and lower line, respectively). Numbering is as in Fig. 2. The nucleotide and amino acid sequences of MOPC41 are according to ref. 2. Differences between the sequences are indicated as vertical lines.

621 and 731–734) corresponding to the sequence originally proposed by Breathnach *et al.*[24]. Nucleotides 733–743 downstream of the splice point apparently code for additional amino acids of the leader sequence.

In contrast to the V-gene segment, the L-gene segment on fragment T1 and the small intron show a remarkable similarity to a known sequence, that is, to the leader and intron sequences of the MOPC41 light chain gene (ref. 2 and Fig. 3). While the L-gene sequences are equal in length the optimal alignment of the introns requires the introduction of a few gaps in the first third of the T1 intron sequence. The overall difference is about 15% in the intron and the L-gene sequences of the two tumours, and also in the 75 base pairs upstream of the L genes; further upstream the difference increases to about 30% within the next 50 base pairs. Although according to the V-gene sequences, tumour T and MOPC41 clearly do not belong to the same subgroup, there seems to be a fairly close evolutionary relationship between them on the basis of the sequences of L-gene segments and small introns.

It is interesting that the nucleotide differences or exchanges between the T1 and MOPC41 L gene sequences in positions 611 and 617 seem to be correlated, because only if the nucleotides at these positions are complementary can the inverted repeat structures $\overline{\text{CTGG}}\text{TTT}\overline{\text{CCAG}}^{\downarrow}$ in the T1 and $\overline{\text{CTTG}}\text{TTT}\overline{\text{CAAG}}^{\downarrow}$ in the MOPC41 sequence be formed. Similar repeat structures are seen in an analogous position of fragment T2: $\overline{\text{CTGG}}\text{ATT}\overline{\text{CCAG}}^{\downarrow}$ (positions 846–856 in Fig. 5) and also in the K2 gene sequence[25]. The functional role of such structures on the DNA or RNA level is not known but their location immediately adjacent to a splice point makes it likely that they have one.

The sequences upstream of the L-gene segments of T1 and T2 were screened for the presence of regions similar to the 'Hogness box' TATAAATA which may have a promotor-like function[26]. In fragment T1 sequences centred around positions 0158!, 105, 169, 215!, 236, 264!, 291 and 335 show a fair degree of similarity to the above consensus sequence. The same holds for sequences around positions 215!, 230, 521, 551, 628, 678, 748! of fragment T2. (The exclamation marks indicate the sequences with the highest degree of similarity to the consensus sequence[26].) It cannot be decided at present whether any of these have a functional role. It should be mentioned that remarkably similar T-rich sequences are found in fragments T1 and T2 around positions 225 and 715, respectively, and also in the K2 sequence (around position 172, ref. 25).

To be sure that in myeloma T the T1 allele is transcribed, we sequenced part of the cDNA clone k38[15] (Fig. 1). The clone was found to contain a nucleotide sequence identical to the one of T1 from the middle of the V gene up to the J-gene segment (data not shown). After a stretch of about 30 C's the cDNA insert starts with nucleotide 905 forming a *Hpa*II restriction site; the sequencing was continued until position 1,055 (numbering as in Fig. 2). This proves that the clone k38 is derived from tumour T and that the T1 allele is transcribed into poly-(A) containing RNA.

In the other allele a V-gene segment is joined to J2 in a non-functional way

To sequence the L- and V-gene regions of the second rearranged allele of myeloma T, the previously described subclone V-T2 (ref. 14) was used. A partial restriction map and the sequencing strategy are shown in Fig. 4, the sequence itself in Fig. 5. The V-gene segment could again be identified by the codons for the invariant amino acids and the adjacent J-gene segment was found to be J2. The V-gene segment (nucleotides 1,072–1,358) runs to the codon CCA for Pro 95 but the J-gene segment (nucleotides 1,359–1,396) which is identical to the published one[20,21] does not start with the codon TAC for Tyr 96 but with AC only. Apparently the T has been lost in the V–J recombination event. To exclude experimental error the respective region was sequenced in both directions starting from two different cleavage sites each (Fig. 4). It is clear from the gels (Fig. 6) that between the CCA and the AC neither a T nor another nucleotide has been missed. It is unlikely that this deletion has occurred during the cloning in *Escherichia coli* because the same sequence was found in three independently isolated clones.

The deletion of one nucleotide in the V–J joining region has the important consequence that the reading frame is shifted such that a stop codon is encountered within the J region. In Fig. 5 the amino acid sequence of the presumed translation product, which is terminated after amino acid 105 is shown.

Recombination at the J2 segment may be somewhat more susceptible to mis-pairing than at the other J segments for the following reasons. In J2, but not in the other J's, the 5'-flanking sequence which is thought to pair with the 3'-flanking sequence of a V-gene segment, contains a remarkable stretch of alternating ACs and GTs: ACACCAGTGTGTGTAC[20,21], the terminal

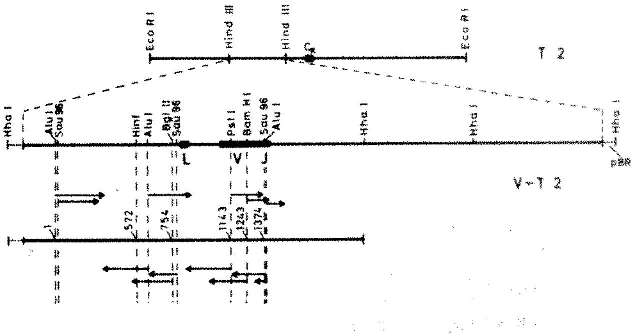

Fig. 4 Localization of the pBR322 subclone V-T2 on the 20-kilobase *Eco*RI fragment T2[14]. Partial restriction map and sequencing strategy. Details as in Fig. 1. For comparison the relevant *Hha*I fragment was also isolated from the fragment T2 containing Charon 4A DNA[14] of two different clones (centrifugation similarly as in the legend to Fig. 1). Sequencing over the V–J junction was from the *Bam*HI site.

```
        10        20        30        40        50        60        70        80        90
AGCTTGGTTATATGGACCACATGACAGGAACAACTGTTTCTTTTAATGGAACTGATAAAAAATTTCTCTCCTGATCTAGACTGCTGTGGTCTTTTAAGTA  100
GCATGAAAAACATCTGCTAAAGAAGGAATTAGTTTGAACATGCTAGAAATACATCTGTGATACTCTTCATCACTCTTGTTGGAAAGATATGCAAGAAGCA  200
CTATTTGGCTATTTATTTGGAAAGTGCTATAATGTATTTTGATATCTCAACCTCTGAAATTCTTCTGTATGTTGGCAGATTGTAAACTTTTATAAGGCTTT  300
CATTCTCTCTCTGGAGAAATATGTCTTTGTAGGCAATCCAGAATTTCTTATTTCTTGCTAATGAAATCTCCTCAGTGTGATATCACTTTAGTTTCATGTG  400
TTGTTATGCTTCATGTAATGTTAAGAAAGTTTTTGATNCTNCAATCCATATTGTAAGAAACATTCCAAGCCATGGAATAAGGCATGGATTTGAGATGCTC  500
TTTATTTCAAACTACTGAATATATCTTAGAGATTTCTTTAGACTGTGTTAAATATGTAACCATTTAAGTAGGAGTCAAGTCTCCTTTAAATCTCAACAGC  600
TCTTCAGGTAACCAACAAAAGGATAAATATTCTAATAAGTCACTAGGAGCATGCTCTTCTGACCAGGTCTTTCTTATAAGCAACATGAAGACAGTATGAT  700
TTGCATAAGTTTTTCTTTCTTCTAATGTCCCTGCCTCTTAGAGTATTTATAAGAAGATCTTTCTCAGGGATGTGTCATGGTCCACACAAACTCAGGGAAAG  800
                                                         ▼
TTTGAAGATGGTATCCACACCTCAGTTCCTTGTATTTTTGCTTTTCTGGATTCCAGGTATTGACTGTTTGGGTGTGGCAAAAAAGTGGAGATGTTATTTAA  900
   (1) Met Val Ser Thr Pro Gln Phe Leu Val Phe Leu Leu Phe Trp Ile Pro Gly (17)

ATACAAAATTTTCTTGCTTTATTTGGAAGCCAATGTCACATGGGAATTGACTTTCAGTTTAAAGAAATTGATACAATAAAAGTCATTTATTTTTCTAAGT  1000

                                                                      ▼
TGTTTAGAAGTGACTTTCATATTCAGTGTTGTGATCTACTAATGTATCTTCTATTTTTCCAGCCTCCAGAGGTGACATCTTGCTGACTCAGTCTCCAGCC  1100
                                                            (-1) Gly Asp Ile Leu Leu Thr Gln Ser Pro Ala  (9)
ATCCTGTCTGTGAGTCCAGGAGAAAGAGTCAGTTTCTCCTGCAGGGCCAGTCAGAGCATTGGCACAAGCATACACTGGTATCAGCAAAGAACAAATGGTT  1200
Ile Leu Ser Val Ser Pro Gly Glu Arg Val Ser Phe Ser Cys Arg Ala Ser Gln Ser Ile Gly Thr Ser Ile His Trp Tyr Gln Gln Arg Thr Asn Gly S  (43)
CTCCAAGGCTTCTCATAAAGAATGCTTCTGAGTCCATCTCTGGGATCCCTTCCAGGTTTAGTGGCAGTGGATCAGGGACAGATTTTACTCCTAGCATCAA  1300
er Pro Arg Leu Leu Ile Lys Asn Ala Ser Glu Ser Ile Ser Gly Ile Pro Ser Arg Phe Ser Gly Ser Gly Ser Gly Thr Asp Phe Thr Pro Ser Ile As  (76)
                                                         ▼
CAGTGTGGAGTCTGAAGATATTGCAGAATATTACTGTCAACAAAGTTATAGGTGGCCAACACGTTCGGAGGGGGGACCAAGCTGGAAATAAAACGTAAGT  1400
n Ser Val Glu Ser Glu Asp Ile Ala Glu Tyr Tyr Cys Gln Gln Ser Tyr Arg Trp Pro Thr Arg Ser Glu Gly Gly Pro Ser Trp Lys Term
AGCCTTCTCAACTCTTGTTCACTAAGTCTAACCTTGTTAAGTTGTTCTTTGTTGTGTGTTTTTCTTAAGGAGATTTCAGGGATTTAGCA
```

Fig. 5 Nucleotide sequence of L, V and J regions of fragment T2. Designations are as in Fig. 2. The position of non-functional joining is marked by an arrow, the respective stop codon in the J segment by underlining. Overlaps with published sequences[20,21] extend from position 1,359 to 1,489 (difference in position 1,403).

TAC being the one which codes for Tyr 96. Such alternating nucleotide sequences may be particularly apt to form stem structures in which non-fitting nucleotides are looped out. In the context of the non-functional joining found in fragment T2 it will be of interest to know the 3′-flanking sequence of the corresponding germ-line V-gene segment.

The amino acid sequence deduced from the V-gene segment of fragment T2 was compared with the known sequences[17] of myeloma light chains. Only one sequence showed a high degree of similarity, that is the one of a light chain from the NZB mouse myeloma PC3858, which was reported[27] up to position 23. The two sequences are identical except for the amino acid at position 10. This similarity bears on the general question of relatedness between BALB/c and NZB myelomas[27].

As on fragment T1, the L-gene segment was identified on fragment T2 by the codons for the four invariant amino acids. It extends from nucleotides 808 to 858 but an initiation at the ATG at position 769–771 cannot be excluded. The L gene on fragment T2, unlike the one on fragment T1, is not interrupted by an intron. Splicing must occur in this case between the 3′ end of the leader and the 5′ end of the V-gene segment, that is in the AGGT sequences at positions 855–858 and 1,070–1,073. Note that there is only about 60% homology with the L segment on fragment T1 and no striking similarities to other leader sequences were found.

Allelic exclusion in myeloma T may operate through non-functional joining on fragment T2

In contrast to the increasing number of reports on myelomas in which more than one allele is rearranged[5–13] Joho and Weissman[28] reported that, in mouse spleen cells, about 50% of the C_κ alleles are unchanged. This suggests that multiple rearrangements may occur in normal lymphoid cells either rarely or not at all. Considering, however, the difficulties in the quantification of blots[28], these experiments do not exclude the possibility that the multiple rearrangements found in myeloma cells occur also in normal lymphoid cells alone. It is possible that myelomas reveal only part of the repertoire of immunoglobulin genes[27] and that this part is enriched with respect to multiply rearranged alleles. It may also be that secondary rearrangements in general are more likely in long-lived or immortal cell lines such as myelomas or hybridomas[29] than in normal lymphoid cells. We believe that allelic exclusion can be effected by various mechanisms and that the mechanisms are basically the same in normal and malignant cells although those involving multiple and nonfunctional rearrangements occur more often in myelomas.

If the rearranged T2 allele of myeloma T is transcribed, translation would be terminated by the stop codon within the

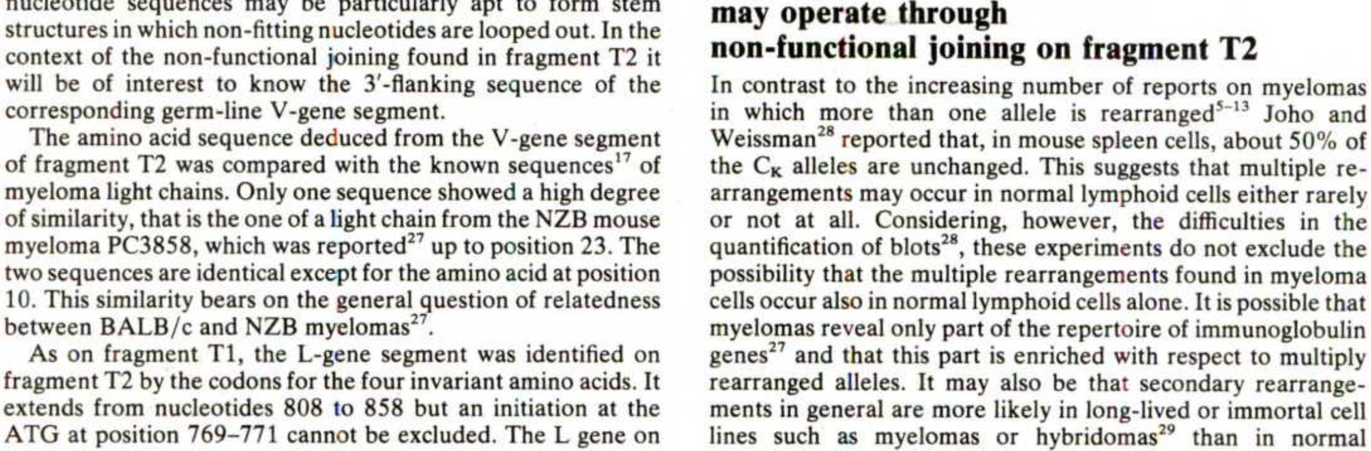

Fig. 6 Junction between the V- and J-gene segments in the V-T2 subclone. The autoradiogram of a 20% sequencing gel (see Fig. 2 legend) of the respective *Alu*I–*Pst*I fragment (Fig. 4) is shown. The complementary sequence to the one of Fig. 5 is indicated.

J-gene segment. Transcription[5] and even translation[10,30] of non-functional immunoglobulin genes have in fact been observed. It has been proposed that the recombination between V- and J-gene segments may occur at slightly different points thereby increasing the diversity of variable regions[20,21]. This flexible recombination mechanism may also lead to non-functionally recombined V-region genes. It is obviously of greater physiological significance to increase antibody diversity by junctional diversification than to generate a functional gene in every V–J joining step by a more stringent recombination mechanism.

Allelic exclusion may be the result of a multi-step process[5,30] with V-gene rearrangements taking place until one functional V–J junction has been formed and further rearrangements are inhibited by an unknown mechanism. The fragment T3 which was found in tumour T and in which 3′-flanking sequences of a V gene and 5′-flanking sequences of a J-gene segment are linked[18] may be the side product of an early translocation step either in the T1 or the T2 allele. Translocation(s) in the T1 allele eventually led to a functional gene while allelic exclusion was realized by a non-functional joining in the T2 allele.

We thank R. Gerl for assistance, and U. Hänggi and P. Neumaier for the computer programs. The work was supported by Bundesministerium für Forschung and Technologie. *Alu*I, *Bgl*II and *Hin*dII were from Boehringer Mannheim, *Bam*HI from T. Igo-kemenes, *Hpa*I from H. Feldman and other enzymes from R. E. Streeck.

Received 7 July; accepted 20 August 1980.

1. Bernard, O., Hozumi, N. & Tonegawa, S. *Cell* **15,** 1133–1144 (1978).
2. Seidman, J. G., Max, E. E. & Leder, P. *Nature* **280,** 370–375 (1979).
3. Pernis, B. G., Chiappino, G., Keleis, A. S. & Gell, B. G. H. *J. exp. Med.* **122,** 853–876 (1965).
4. Cebra, J. S., Colberg, J. E. & Dray, S. *J. exp. Med.* **123,** 547–558 (1966).
5. Perry, R. P. *et al. Proc. natn. Acad. Sci. U.S.A.* **77,** 1937–1941 (1980).
6. Lenhard-Schuller, R., Hohn, B., Brack, C., Hirama, M. & Tonegawa, S. *Proc. natn. Acad. Sci. U.S.A.* **74,** 4709–4713 (1978).
7. Davis, M., Early, P., Calame, K., Livant, D. & Hood, L. *ICN UCLA Symp.* **14,** 393–406 (1979).
8. Steinmetz, M., Zachau, H. G. & Mach, B. *Nucleic Acids Res.* **6,** 3213–3229 (1979).
9. Wilson, R., Miller, J. & Storb, N. *Biochemistry* **18,** 5013–5021 (1979).
10. Kuehl, W. M. & Scharff, M. D. *J. molec. Biol.* **89,** 409–421 (1974).
11. Rose, S. M., Kuehl, W. M. & Smith, G. P. *Cell* **12,** 453–462 (1977).
12. Schnell, H., Steinmetz, M., Zachau, H. G. & Schechter, I. *Nature* **286,** 170–173 (1980).
13. Seidman, J. G. & Leder, P. *Nature* **286,** 779–783 (1980).
14. Steinmetz, M. & Zachau, H. G. *Nucleic Acids Res.* **8,** 1693–1707 (1980).
15. Mach, B., Rougeon, F., Longacre, S. & Aellen, M.-F. *Miami Winter Symp.* **13,** 219–235 (1977).
16. Schiff, C. & Fougereau, M. *Eur. J. Biochem.* **59,** 525–537 (1975).
17. Kabat, E. A., Wu, T. T. & Bilofsky, H. *NIH Publ.* No. 80-2008 (1979).
18. Steinmetz, M., Altenburger, W. & Zachau, H. G. *Nucleic Acids Res.* **8,** 1709–1720 (1980).
19. Steinmetz, M., Höchtl, J., Schnell, H., Gebhard, W. & Zachau, H. G. *Nucleic Acids Res.* **8,** 1721–1729 (1980).
20. Sakano, H., Hüppi, K., Heinrich, G. & Tonegawa, S. *Nature* **280,** 288–294 (1979).
21. Max, E. E., Seidman, J. G. & Leder, P. *Proc. natn. Acad. Sci. U.S.A.* **76,** 3450–3454 (1979).
22. Potter, M. *Adv. Immun.* **25,** 141–212 (1978).
23. Burstein, Y. & Schechter, I. *Biochemistry* **17,** 2392–2400 (1978).
24. Breathnach, R., Benoist, C., O'Hare, K., Gannon, F. & Chambon, P. *Proc. natn. Acad. Sci. U.S.A.* **75,** 4853–4857 (1978).
25. Nishioka, Y. & Leder, P. *J. biol. Chem.* **255,** 3691–3694 (1980).
26. Gannon, F. *et al. Nature* **278,** 428–434 (1979).
27. Loh, E. *et al. Proc. natn. Acad. Sci. U.S.A.* **76,** 1395–1399 (1979).
28. Joho, R. & Weissman, I. L. *Nature* **284,** 179–181 (1980).
29. Wilson, R., Storb, U. & Arp, B. *J. Immun.* **124,** 2071–2076 (1980).
30. Alt, F. W., Enea, V., Bothwell, A. L. M. & Baltimore, D. *Cell* **21,** 1–12 (1980).
31. McCarty, K. S. Jr, Vollmer, R. T. & McCarty, K. S. *Analyt. Biochem.* **61,** 165–183 (1974).
32. Maxam, A. M. & Gilbert, W. *Meth. Enzym.* **65,** 499–560 (1980).

Phorbol esters and vasopressin stimulate DNA synthesis by a common mechanism

Phillip Dicker & Enrique Rozengurt
Imperial Cancer Research Fund, Lincoln's Inn Fields, London WC2A 3PX, UK

The potent tumour promoter 12-O-tetradecanoylphorbol-13-acetate (TPA) acts synergistically with all known mitogens to induce DNA synthesis in 3T3 cells. In contrast, the neurohypophyseal hormone vasopressin, which is mitogenic for 3T3 cells, fails to synergize with TPA to stimulate DNA synthesis, ornithine decarboxylase activity or 2-deoxyglucose uptake. Thus TPA acts through a pathway which converges with that used by vasopressin, and at least some of its biological effects occur through mechanisms normally utilized by specific hormones.

TUMOUR promoters constitute a family of compounds which, although not carcinogenic by themselves, drastically increase the incidence of tumours when applied repeatedly to animals that have received a sub-threshold dose of a carcinogen[1]. Tumour promotion is a phase in the development of many tumours including those that occur in humans[2,3]. Their mechanism of action is of considerable interest, with attention focusing on their biological effects in various types of cultured cells[2,4].

Studies of the cellular actions of 12-*O*-tetradecanoyl-phorbol-13-acetate (TPA), the most potent tumour promoter of the phorbol ester family[2], suggested that these compounds regulate a complex array of cellular activities, including mitogenesis, by using receptor–effector systems for a physiologically occurring material[5,6]. It has been suggested that the biological effects of TPA are mediated by the epidermal growth factor (EGF) receptor–effector system[7–9], but although TPA inhibits the specific binding of EGF to the cell, phorbol esters and EGF do not compete directly for the same receptors[10–12]. Further, TPA synergistically stimulates DNA synthesis when added in combination with most known mitogens including unfractionated serum[4,13,14], plasma[15], platelet-derived growth factor[15], multiplication-stimulating activity[15], fibroblast-derived growth factor (FDGF)[16], fibroblast growth factor[15], insulin[16] and EGF[6,10,15,16], indicating that TPA does not act identically to any of these growth factors. At least two alternative mechanisms of action of TPA can be envisaged. It may act in a fundamentally different way from hormones and growth factors by increasing cellular sensitivity to any growth factor in a non-selective fashion[15], or it may regulate biological activity through a specific hormonal pathway not yet identified[5,6].

We have found that the neurohypophyseal nonapeptide arginine vasopressin is a potent mitogen for Swiss 3T3 cells[17]. We were led to this finding when testing whether hormones and ionophores able to stimulate ion fluxes[18–20] could also regulate cell proliferation. The effect of vasopressin on DNA synthesis is synergistically potentiated by insulin, EGF and FDGF[17]. Similarities in the mitogenic properties of vasopressin and TPA prompted us to suggest that these chemically diverse factors stimulate DNA synthesis through an identical mechanism[6]. Based on the evidence presented here, we propose that the actions of TPA and vasopressin converge into a common

0028–0836/80/410607—06$01.00

pathway to stimulate DNA synthesis, 2-deoxyglucose uptake and ornithine decarboxylase activity in quiescent cultures of mouse Swiss 3T3 cells.

Equivalent mitogenic properties

A series of experiments demonstrated the equivalence of the mitogenic properties of TPA and vasopressin. Addition of saturating levels of either vasopressin or TPA to quiescent cultures of Swiss 3T3 cells stimulated identical increases in DNA synthesis when tested in combination with EGF, insulin, FDGF or low concentrations of serum (1.5–2.5%, Table 1), when DNA synthesis was measured either by ^{3}H-thymidine (^{3}H-TdR) incorporation into acid-insoluble material (Table 1) or by the percentage of labelled nuclei after autoradiography (results not shown).

We have found that exposure of cell cultures to vitamin A derivatives such as retinoic acid[21], or disruption of the microtubular network by colchicine[22], enhances the stimulation of DNA synthesis induced by growth factors in quiescent cells. To ascertain whether the mitogenic equivalence of vasopressin and TPA holds under those conditions of increased cellular responsiveness, cultures of quiescent 3T3 cells were exposed to vasopressin plus EGF or TPA plus EGF and to different concentrations of retinoic acid or colchicine. The dose-dependent enhancement of DNA synthesis produced by retinoic acid or by colchicine in the presence of TPA plus EGF is identical to that obtained in parallel cultures exposed to vasopressin plus EGF (Fig. 1). Thus vasopressin and TPA can substitute for each other in stimulating DNA synthesis in Swiss 3T3 cells in the presence of various agents, including EGF, FDGF, insulin, unfractionated serum (Table 1), retinoic acid and colchicine (Fig. 1).

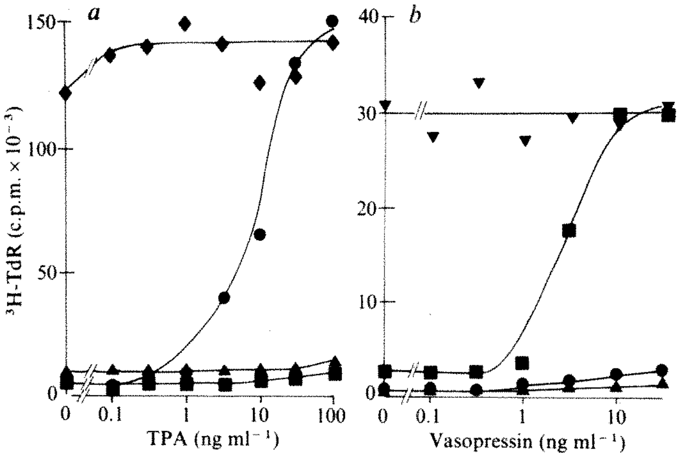

Fig. 2 Absence of synergistic interactions between the mitogenic effects of vasopressin and TPA, in the presence or absence of insulin or EGF. Cultures produced as in Fig. 1 legend were washed twice in DMEM, and incubated in 2 ml of a 1 : 1 mixture of DMEM: Waymouth medium containing ^{3}H-TdR plus the mitogens as indicated. After 40 h at 37 °C, cumulative ^{3}H-TdR incorporation into acid-insoluble material was measured. Conditions and measurements of ^{3}H-TdR incorporation were as in Fig. 1. Fetal calf serum (10%) induced incorporation of 156 × 10^3 and 105 × 10^3 c.p.m. in the experiments in *a* and *b*, respectively. Concentrations of mitogens were 1 μg ml^{-1}, 100 ng ml^{-1}, 10 ng ml^{-1} and 10 ng ml^{-1} for insulin, TPA, EGF and vasopressin, respectively. *a*; ◆, TPA plus insulin plus vasopressin; ●, TPA plus insulin; ▲, TPA plus vasopressin; ■, TPA only. *b*; ▼, vasopressin + TPA + EGF; ■, vasopressin plus EGF; ●, vasopressin plus TPA; ▲, vasopressin only.

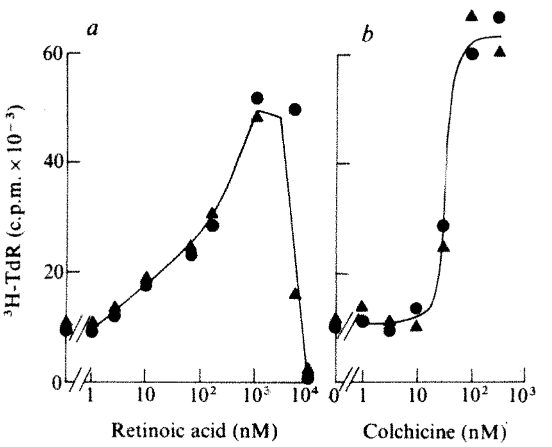

Fig. 1 Enhancement by retinoic acid and colchicine of ^{3}H-TdR incorporation induced by TPA plus EGF (●) or vasopressin plus EGF (▲) in Swiss 3T3 cells. Confluent and quiescent cultures of 3T3 cells were washed twice with Dulbecco's modified Eagle's medium (DMEM) at 37 °C to remove residual serum, then incubated in 2 ml of a 1 : 1 mixture of DMEM: Waymouth medium[43] containing ^{3}H-TdR (0.5 μCi ml^{-1}; 1 μM, Amersham) and mitogens as indicated. After 40 h at 37 °C ^{3}H-TdR incorporation into acid-insoluble pools was assayed as follows. Cultures were washed twice with ice-cold phosphate-buffered saline (0.15 M NaCl in 0.1 M K_2PO_4 buffer, *p*H 7.4) and acid-soluble radioactivity was removed by a 20-min treatment with 5% trichloroacetic acid (TCA) at 4 °C. Cultures were then washed twice in ethanol, cells were solubilized by a 30-min incubation with 0.1 M NaOH and 2% Na_2CO_3, and the radioactivity in the acid-insoluble pools was determined. Fetal calf serum (10%) induced incorporation of 155 × 10^3 and 198 × 10^3 c.p.m. when retinoic acid and colchicine (Sigma) were involved, respectively. TPA (Consolidated Midland, Brewster, New York), EGF or vasopressin (Sigma) alone induced incorporation of less than 2 × 10^3 c.p.m. Concentrations of mitogens were 10 ng ml^{-1}, 10 ng ml^{-1} and 100 ng ml^{-1} for vasopressin, EGF and TPA, respectively. All points are the average of duplicate plates. Stock cultures of Swiss 3T3 cells were maintained in DMEM plus 10% fetal calf serum, penicillin (100 U ml^{-1}), and streptomycin (100 μg ml^{-1}), in a humidified atmosphere of 10% CO_2 : 90% air at 37 °C. Cells were subcultured in 30- or 90-mm Nunc Petri dishes with medium containing 10% fetal calf serum, refed with the same medium after 2 d and used 5 d after the last change of medium. These cells were arrested in G_1 as judged by cytofluorometric analysis (Table 2) and by the fact that less than 1% of cells are autoradiographically labelled after a 40 h exposure to ^{3}H-TdR. Retinoic acid was dissolved in ethanol. Equivalent concentrations of ethanol were added to all controls and never exceeded 0.5% which was not toxic to our cells. Stock solutions of TPA (10 mg ml^{-1}) were made up in acetone and kept at −20 °C.

No additive or synergistic stimulation of DNA synthesis

The striking similarity in the mitogenic properties of TPA and vasopressin in Swiss 3T3 cells raises the possibility that they act through a common mechanism. If they stimulate DNA synthesis by an identical pathway, these chemically diverse factors should not interact either additively or synergistically in stimulating DNA synthesis when tested at saturating concentrations. We therefore tested their combined effect.

TPA caused a potent dose-dependent stimulation of ^{3}H-TdR incorporation into acid-precipitable material when tested in the presence of insulin (Fig. 2*a*). In contrast, addition of different concentrations of TPA in the presence of a fixed and saturating concentration of vasopressin (10 ng ml^{-1}), in either the absence

Table 1 Identical mitogenic properties of saturating concentrations of vasopressin and TPA

EGF (ng ml^{-1})	Insulin (μg ml^{-1})	FDGF (μg ml^{-1})	Serum % vol. : vol.	^{3}H-TdR (c.p.m. × 10^{-3}) No other addition	Vasopressin	TPA
—	—	—	—	1	1	1
10	—	—	—	1	46	52
—	1	—	—	5	164	172
—	—	11	—	6	180	188
10	—	3	—	18	153	178
—	1	3	—	18	208	214
—	—	—	2.4	9	152	138
10	—	—	1.5	45	195	196
—	1	—	1.5	104	196	214

Cultures produced as for Fig. 1 were washed twice in DMEM and incubated for 40 h at 37 °C in 2 ml of a 1 : 1 mixture of DMEM : Waymouth medium containing ^{3}H-TdR (0.5 μCi ml^{-1}; 1 μM) plus mitogens as indicated. Cumulative incorporation of ^{3}H-TdR was measured as in Fig. 1. Fetal calf serum (10%) induced incorporation of 208 × 10^3 c.p.m. Concentrations of vasopressin and TPA were 10 ng ml^{-1} and 100 ng ml^{-1}, respectively, which are saturating under these conditions (Fig. 2). FDGF was prepared as before[46].

or presence of insulin, did not alter stimulation of DNA synthesis (Fig. 2*a*). This lack of synergistic interaction between TPA and vasopressin was confirmed when both were added at submaximal concentrations together with insulin (results not shown).

Because the stimulation of DNA synthesis by saturating levels of TPA plus insulin or vasopressin plus insulin was frequently comparable to that promoted by fresh medium containing 10% serum (that is, maximal response), the possibility remained that a synergistic effect between TPA and vasopressin could be revealed in the presence of a third mitogen if DNA synthesis was stimulated submaximally. Figure 2*b* shows that in the presence of EGF the stimulation of DNA synthesis induced by saturating levels of TPA (a submaximal response) was not enhanced by increasing concentrations of vasopressin. Thus, vasopressin and TPA do not interact synergistically or additively in the presence or absence of a third mitogen.

The conclusions drawn from Fig. 2 are further substantiated by flow cytofluorometric analysis (Table 2). Vasopressin or TPA alone caused little increase in the percentage of the cell population moving from G_1 to $S+G_2+M$. Vasopressin and TPA together did not interact to increase cell exit from G_1. However, the addition of vasopressin or TPA together with insulin caused a striking increase in the proportion of cells in $S+G_2+M$ which was not further increased when the three mitogens were added together in the culture. These results agree well with those in Table 1 and Fig. 2.

Table 2 Equivalence of mitogenic effects of TPA and vasopressin demonstrated by cytofluorometry

Vasopressin	TPA	Insulin	Serum	Percentage of cells in $S+G_2+M$
−	−	−	−	9
+	−	−	−	13
−	+	−	−	12
+	+	−	−	14
−	−	+	−	12
+	−	+	−	78
−	+	+	−	76
+	+	+	−	71
−	−	−	+	87

Cell cultures (90-mm) produced as for Fig. 1 were washed twice in DMEM and incubated for 40 h at 37 °C in 10 ml of a 1:1 mixture of DMEM:Waymouth medium containing 2 μM colchicine (to arrest cells at mitosis) plus mitogens as indicated. Cells were then detached by minimal treatment with 0.025% trypsin and EDTA (0.16 mg ml^{-1}), suspended in DMEM containing 10% bovine serum, centrifuged at 1,000 r.p.m. for 2 min, washed twice with phosphate-buffered saline, suspended in 1 ml of saline and squirted rapidly through a 25-gauge needle into 3 ml of ethanol:saline (70:30). This suspension could be stored at 4 °C for 1–2 weeks. Immediately before a cytofluorometric assay, the ethanolic suspension was centrifuged at 1,000 r.p.m. for 2 min and the pellet was resuspended in 0.5 ml of a mixture containing mithramycin (50 μg ml^{-1}) in ethanol:H_2O (25:75) plus 15 mM $MgCl_2$. After 30 min DNA histograms were obtained with a fluorescence activated cell sorter. Two 90-mm cultures were used for each condition. Concentrations of mitogens were 10 ng ml^{-1}, 100 ng ml^{-1}, 1 μg ml^{-1} and 10% (volume:volume) for vasopressin, TPA, insulin and fetal calf serum, respectively.

In all the above experiments, cumulative DNA synthesis was measured after a 40-h exposure of cultures to mitogens. It is possible that vasopressin or TPA, in the presence of insulin and other agents, induce identical amounts of DNA synthesis but with different kinetics. The experiment shown in Fig. 3 rules out this possibility. Both the lag period preceding the onset of DNA synthesis (14 h) and the rate of entry into S phase were the same regardless of whether the cultures were exposed to TPA plus insulin, vasopressin plus insulin or TPA plus vasopressin plus insulin. Thus, with respect to the kinetics of stimulation of DNA synthesis as well as cumulative DNA synthesis, the effects of vasopressin and TPA are neither additive nor synergistic. Note that serum-stimulated cells enter S phase more rapidly than the parallel cultures treated with the tumour promoter and the hormones, indicating that potential additive or synergistic effects could be detected under our experimental conditions.

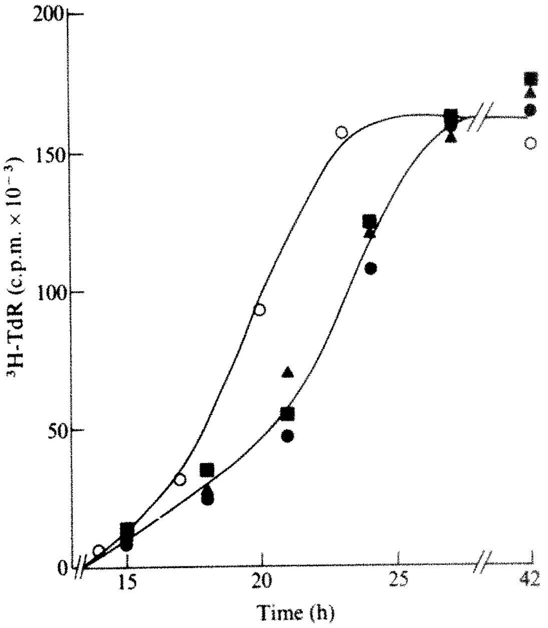

Fig. 3 Time course of ^{3}H-TdR incorporation into Swiss 3T3 cells stimulated by different combinations of TPA, vasopressin and insulin. Cultures produced as in Fig. 1 legend were washed twice in DMEM. Then 2 ml of a 1:1 mixture of DMEM: Waymouth medium containing ^{3}H-TdR plus mitogens as indicated was added (time 0), and the cultures were incubated at 37 °C. At the times indicated on the abscissa the incubation of duplicate cultures for each condition was stopped. The cumulative incorporation of ^{3}H-TdR into the acid-insoluble pools of these cultures was then determined. Conditions and measurements of incorporation were as for Fig. 1. Insulin, TPA or vasopressin alone induced incorporation of less than 15×10^3 c.p.m. of ^{3}H-TdR. Concentrations of mitogens were 10% (volume:volume), 10 ng ml^{-1}, 1 μg ml^{-1} and 100 ng ml^{-1} for fetal calf serum, vasopressin, insulin and TPA, respectively. ●, Vasopressin plus insulin; ■, TPA plus insulin; ▲, vasopressin plus TPA plus insulin; ○, serum.

The above evidence shows that vasopressin and TPA stimulate DNA synthesis by a common mechanism in Swiss 3T3 cells. However, TPA is a potent mitogen for several cell lines in which vasopressin is not active. For example, TPA stimulates DNA synthesis in quiescent 3T6 and hamster Nil-8 cells and synergistically stimulates DNA synthesis in the presence of other growth factors in BALB 3T3 cells[16,21]. Vasopressin when added to these cells fails to enhance DNA synthesis or elicit any early biological response either in the presence or absence of other growth factors (unpublished data). It seems likely that these cell lines possess receptors for TPA (see below) but not for vasopressin, which in turn suggests that TPA and vasopressin interact with distinct receptors in Swiss 3T3 cells.

Stimulation of ornithine decarboxylase activity and 2-deoxyglucose uptake

Do the actions of TPA and vasopressin converge before the initiation of DNA synthesis? When quiescent cultures of 3T3 cells are stimulated by serum or by defined growth factors, a complex array of biochemical events precedes the onset of DNA synthesis[23]. Two of these events—the induction of ornithine decarboxylase activity and of 2-deoxyglucose uptake—both of which peak 6 h after stimulation, are synergistically increased by combinations of growth factors. These events provide useful markers to determine whether the actions of TPA and vasopressin converge before the initiation of DNA synthesis, which occurs 14 h after mitogenic stimulation.

The activity of ornithine decarboxylase, a key enzyme in the biosynthesis of polyamines, rises markedly in different cell types stimulated by TPA[24–26] and the induction of this enzyme has been proposed as essential for tumour promotion[27].

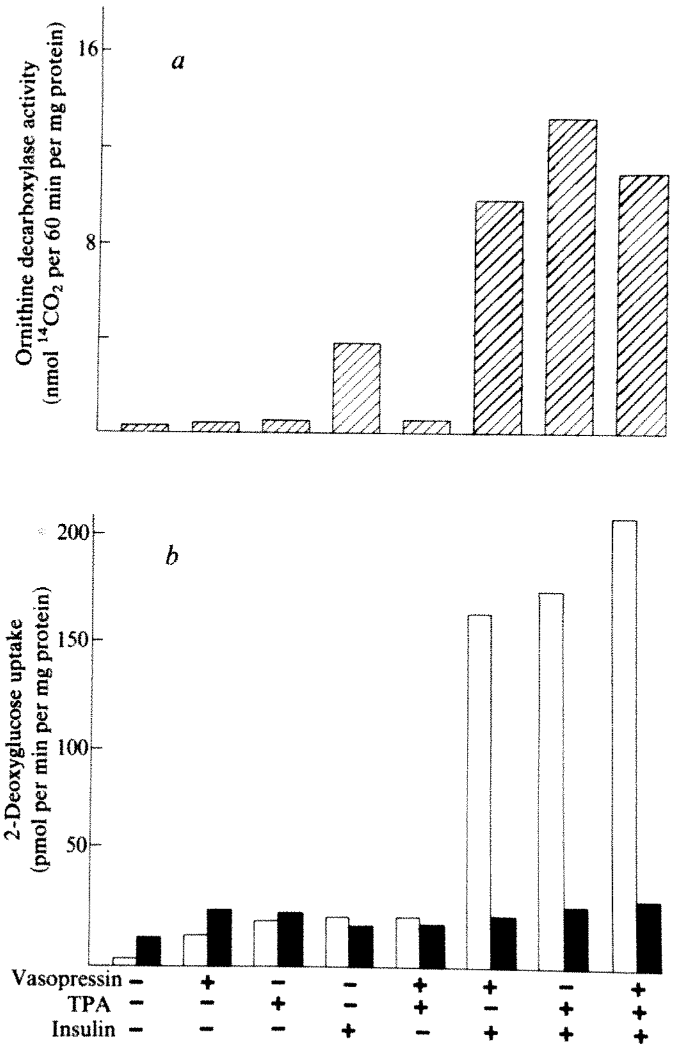

Fig. 4 Effect of TPA and vasopressin on ornithine decarboxylase activity (*a*) and ^{3}H-2-deoxyglucose uptake (*b*) in the absence and presence of insulin. *a*, Quiescent 90-mm cultures of Swiss 3T3 cells produced as for Fig. 1 were washed twice in DMEM and incubated for 6 h in 10 ml of a 1 : 1 mixture of DMEM : Waymouth medium plus TPA or the hormones as indicated. Cultures were then washed three times in ice-cold saline and cells were scraped off the dish with a rubber policeman. For each experimental condition, cells from three separate cultures (about 10^7 cells in total) were pooled, spun down, resuspended in 1 ml of saline, then spun down once more and stored at −40° until assayed. The assay used was similar to that of Hogan[44]. The cell pellet was frozen and thawed three times in 200 µl of the assay mixture. The final concentration of the various components in the enzyme assay was 0.1 mM EDTA, 0.05 mM pyridoxal phosphate, 5 mM dithiothreitol, ^{14}C-ornithine (0.2 µCi; 0.2 mH, Amersham) and 50 mM of HEPES, *p*H 7.1. The release of radioactive CO_2 in the assay was linear for at least 60 min of incubation at 37 °C and was also proportional to the amount of cell extract used. The amount released did not vary by more than 10% in duplicate samples and the values presented are the average of duplicate determinations. To ensure that the release of $^{14}CO_2$ from 1-^{14}C-ornithine was a valid measure of enzymatic activity, the formation of ^{3}H-putrescine (Amersham) from [5-^{3}H]ornithine was determined. Labelled putrescine was isolated from the reaction mixture and analysed by the method of Inoue and Mizutoni[45]. The amount of ^{3}H-putrescine formed was proportional to the amount of $^{14}CO_2$ released. Concentrations of mitogens were 10 ng ml^{-1}, 100 ng ml^{-1} and 1 µg ml^{-1} for vasopressin, TPA and insulin, respectively. *b*, Confluent quiescent 30-mm cultures produced as for Fig. 1 were washed twice in DMEM and incubated for 5.5 h in 2 ml of a 1 : 1 mixture of DMEM : Waymouth medium with the mitogens as indicated in the presence (black bars) or absence (plain bars) of 10 µg ml^{-1} cycloheximide. The cultures were then washed three times in DMEM minus glucose and incubated in DMEM minus glucose plus the mitogens as indicated with or without cycloheximide. After 30 min the cultures received ^{3}H-2-deoxyglucose (2.5 µCi ml^{-1}; 0.2 mM Amersham). After 15 min at 37 °C, cultures were washed rapidly four times with ice-cold saline. Acid-soluble radioactivity was measured by extracting for 20 min with 5% TCA at 4 °C. All values are the mean of duplicate determinations. Concentrations of mitogens were as for *a*.

Vasopressin, like TPA, increases the activity of ornithine decarboxylase[26]. Figure 4*a* shows that whereas addition of TPA or vasopressin to quiescent 3T3 cultures in the absence of other mitogens caused little increase in the activity of this enzyme, in the presence of insulin saturating concentrations of TPA or vasopressin synergistically induced identical levels of ornithine decarboxylase. When added together, the promoter and the hormone did not act synergistically in increasing enzyme activity in either the absence or presence of insulin. Thus the actions of vasopressin and TPA converge before the initiation of DNA synthesis.

The uptake of 2-deoxyglucose increases in a biphasic fashion[23,28–30] in quiescent fibroblasts stimulated to divide. In various types of cells TPA induces an increase in 2-deoxyglucose uptake[31,32]. In 3T3 cells TPA and insulin added together synergistically induced the cycloheximide-sensitive (second) phase of deoxyglucose uptake (Fig. 4*b*). Vasopressin could replace TPA in inducing the activity of this uptake system, acting synergistically with insulin. However, TPA and vasopressin together failed to act either synergistically or additively in the absence or presence of insulin. Thus, as with ornithine decarboxylase induction, TPA and vasopressin induce the second phase of 2-deoxyglucose uptake by a common mechanism.

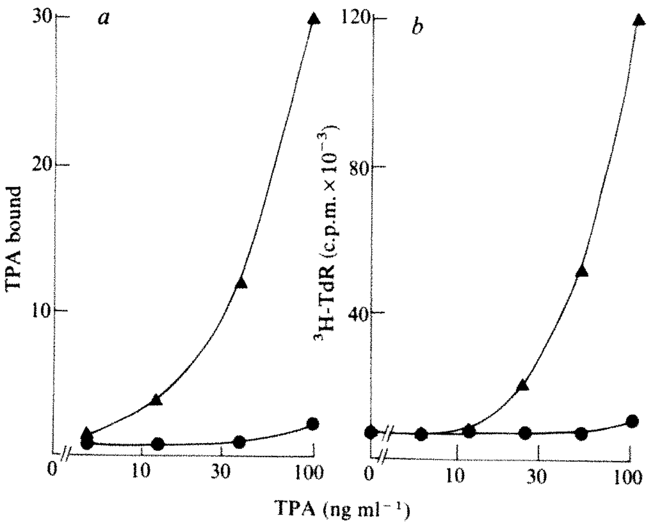

Fig. 5 Physical persistence of TPA (*a*) and the persistence of its mitogenic actions (*b*) are eliminated in parallel by BSA. *a*, 30 mm cultures produced as for Fig. 1 were washed twice in DMEM and incubated for 1 h at 37 °C in 2 ml of a 1 : 1 mixture of DMEM : Waymouth medium containing insulin (1 µg ml^{-1}) plus [20-^{3}H(N)]TPA (0.15 µCi ml^{-1}, NEN) at various specific activities. Cultures were then washed twice with DMEM at 37 °C and the amount of TPA bound (ng per culture) was determined from the remaining radioactivity extracted as described below (▲). Parallel cultures were exposed three successive times (45 min each) to 2 ml of recrystallized defatted BSA (10 mg ml^{-1}, Sigma) in a 1 : 1 mixture of DMEM : Waymouth medium supplemented with insulin (1 µg ml^{-1}), followed by three 10-min washes with the same medium without BSA (●). Radioactivity was extracted from the dish after two rapid washes with ice-cold 0.15 M saline followed by a 30-min incubation at 37 °C with 0.1 M NaOH and 1% SDS. Insulin was present in these incubations to maintain cell attachment. The number of cells per culture was the same after either treatment. The ^{3}H-TPA was dissolved in ethanol at a final concentration of less than 0.2% which had no effect on the cell cultures. *b*, Cultures were washed twice in DMEM and incubated for 1 h at 37 °C in 2 ml of a 1 : 1 mixture of DMEM : Waymouth medium containing insulin (1 µg ml^{-1}) plus various concentrations of TPA. Cultures were washed twice in DMEM and 2 ml of a 1 : 1 mixture of DMEM: Waymouth medium containing insulin (1 µg ml^{-1}) and ^{3}H-TdR (0.5 µCi ml^{-1}; 1 µM) was added either immediately (▲) or after the cultures had been washed with BSA solutions as above (●). After 40 h at 37 °C cumulative incorporation of ^{3}H-TdR into acid-insoluble pools was assayed as for Fig. 1. Addition of TPA (100 ng ml^{-1}) and insulin (1 µg ml^{-1}) to cultures pretreated with BSA or with cultures not pretreated with BSA, induced incorporation of 118×10^3 and 142×10^3 c.p.m. of ^{3}H-TdR, respectively, after a 40-h incubation. Thus treatment with BSA does not cause cells to become less responsive to the mitogenic actions of TPA plus insulin. Fetal calf serum (10%) induced incorporation of 185×10^3 c.p.m. in this experiment.

Table 3 TPA acts synergistically with each of a wide range of mitogens except vasopressin

Mitogens acting synergistically with TPA	Reference
Serum	4, 13
Depleted serum	14
EGF	10, 15, 16
Insulin	15, 16
FDGF	16
Fibroblast growth factor	15
Platelet-derived growth factor	15
Platelet-poor plasma	15
Multiplication-stimulating activity	15
Antitubulin agents	This report
Retinoids	21
Mitogens unable to act synergistically with TPA	
Vasopressin	This report

Transient exposure to TPA

The mitogenic effects of TPA persist after the removal of the TPA-containing medium (refs 15 and 16 and our unpublished data), but vasopressin must be in contact with cells continuously to stimulate DNA synthesis synergistically with insulin[17]. It has been suggested that mitogens such as TPA, which exert biological effects that persist after the medium containing the mitogen has been removed, act by inducing a cell to become 'competent'[33]. Mitogens such as vasopressin, which must be present throughout G_1 to cause entry into S phase[17], are postulated in this model to act in a fundamentally different fashion: they are said to allow a 'competent' cell 'to progress' through G_1 and into S phase[33]. According to this model TPA and vasopressin act by separate paths. This contradicts the evidence reported here. However, although the biological effects of TPA may be mediated by specific receptors (see below), it is also known that TPA associates tightly but nonspecifically with cell membranes[34], a phenomenon which may account for its persistent biological effects and has impeded the detection of specific binding of the molecule. The following experiments show that the mitogenic effects of TPA persist after the removal of the TPA-containing medium, merely because it binds tenaciously to cell cultures. Figure 5*a* demonstrates that the phorbol ester remains bound to cell cultures even after multiple washes with Dulbecco's modified Eagle's medium. About 30% of the ^{3}H-TPA added in a 1-h incubation remained attached to the culture after washing and this was not reduced by adding a vast excess of unlabelled TPA (that is, binding was nonspecific). TPA binds with high affinity to bovine serum albumin (BSA)[34], and the level of TPA remaining bound to cell cultures could be reduced considerably by repeated incubation with solutions of BSA (Fig. 5*a*). If the ability of TPA to exert its mitogenic effects after removal of the TPA-containing medium is due merely to its remaining bound to the cell culture, incubations with BSA solutions should prevent the persistence of the mitogenic effects of TPA. Figure 5*b* shows that this is indeed the case. The removal of TPA from cell cultures by BSA (Fig. 5*a*) parallels the elimination of the persistent mitogenic effects of TPA (Fig. 5*b*). Thus, as with vasopressin, a transient exposure to TPA is not sufficient to render the cells responsive to insulin in stimulating DNA synthesis. This is consistent with our data showing that vasopressin and TPA act as mitogens by identical mechanisms.

Conclusions and implications

Our study demonstrates that (1) TPA and vasopressin can substitute for each other in stimulating DNA synthesis, ornithine decarboxylase induction and 2-deoxyglucose uptake under various experimental conditions; (2) TPA and vasopressin added at saturating concentrations do not have additive or synergistic effects in eliciting these responses in either the absence or the presence of other factors such as EGF or insulin. The lack of synergistic interaction between TPA and vasopressin sharply contrasts with the synergistic interaction of TPA with practically all known growth-promoting polypeptides as summarized in Table 3. These findings indicate that vasopressin and TPA control cellular responses in mouse 3T3 cells by a common mechanism.

The effects on the induction of ornithine decarboxylase activity and 2-deoxyglucose uptake suggest that the common step occurs rapidly after TPA and vasopressin interact with the cell, possibly at the level of the cell membrane. There is considerable evidence that the membrane is an important target for the biological actions of TPA[31,35,36]. TPA can rapidly trigger ion fluxes in responsive cells (ref. 35 and our unpublished data) and similar findings have been made with vasopressin[37]. Another rapid and striking effect of TPA on the cell membrane is an alteration in the receptors for ^{125}I-EGF, which results in a profound inhibition of growth factor binding[8,10-12]. Recently we have found that vasopressin induces a potent, reversible and temperature-dependent change in the affinity of cellular receptors for EGF, again suggesting that the biochemical effects of TPA and vasopressin converge at the level of the plasma membrane[47].

Vasopressin and TPA could bind to specific receptors in 3T3 cells because their effects are elicited at low concentrations, are saturable and exhibit remarkable stereospecificity[16,17]. Indeed, specific binding of phorbol dibutyrate (a tumour-promoting phorbol ester) to membrane preparations of chick fibroblast has recently been reported[38] and there is physiological evidence for at least two classes of vasopressin receptors[39]. In theory, the lack of additive or synergistic interactions between saturating concentrations of TPA and vasopressin may result from (1) both agents binding to an identical cellular receptor; (2) both compounds binding to separate sites but interacting with a common effector system, or (3) TPA directly modulating the activity of a coupling protein[40] or an effector system that can interact with vasopressin receptors in those cells which possess such receptors. The lack of apparent chemical analogy between these agents and the fact that in several cell types TPA is mitogenic whereas vasopressin is biologically inactive (presumably because these cells do not express vasopressin receptors) renders the first possibility unlikely. More data are required to distinguish between the second and third alternatives, although it is interesting that TPA uncouples β-adrenergic receptors from adenyl cyclase in mouse epidermis[41,42]. Regardless of the specific details, the recognition that the phorbol ester tumour promoters act at least in part through a specific hormonal pathway is a prerequisite to understanding the mechanism of action of these important molecules.

Received 12 May; accepted 7 August 1980.

1. Berenblum, I. in *Cancer, A Comprehensive Treatise* Vol. 1 (ed. Becker, F. F.) 323–344 (Plenum, New York, 1975).
2. Slaga, T. J., Sivak, A. & Boutwell, R. K. (eds) *Mechanisms of Tumour Promotion and Cocarcinogenesis* (Raven, New York, 1978).
3. Miller, E. C. *Cancer Res.* **38,** 1479–1496 (1978).
4. Sivak, A. *J. cell. Physiol.* **80,** 167–174 (1972).
5. Weinstein, I. B., Wigler, M. & Pietropaolo, C. in *Origins of Human Cancer* (eds Hiatt, H. H., Watson, J. D. & Winston, J. A.) 751–772 (Cold Spring Harbor Laboratory, New York, 1977).
6. Dicker, P. & Rozengurt, E. *J. supramolec. Struct.* **11,** 79–94 (1979).
7. Lee, L. & Weinstein, I. B. *Nature* **274,** 696–697 (1978).
8. Lee, L. & Weinstein, I. B. *Science* **202,** 313–315 (1978).
9. Weinstein, I. B. *et al.* in *Biological Markers of Neoplasia, Basic and Applied Aspects* (ed. Ruddon, R.) 451 (Elsevier/North Holland, Amsterdam, 1978).
10. Brown, K. D., Dicker, P. & Rozengurt, E. *Biochim. biophys. Res. Commun.* **86,** 1037–1043 (1979).
11. Shoyab, M., De Larco, J. E. & Todaro, G. J. *Nature* **279,** 387–391 (1979).
12. Lee, L. & Weinstein, I. B. *Proc. natn. Acad. Sci. U.S.A.* **76,** 5168–5172 (1979).
13. Boynton, A. L., Whitfield, J. F. & Isaacs, R. J. *J. cell. Physiol.* **87,** 25–32 (1976).
14. Sivak, A. *In Vitro* **13,** 337–343 (1977).
15. Frantz, C. N., Stiles, C. D. & Scher, C. D. *J. cell. Physiol.* **100,** 413–423 (1979).
16. Dicker, P. & Rozengurt, E. *Nature* **276,** 723–726 (1978).
17. Rozengurt, E., Legg, A. & Pettican, P. *Proc. natn. Acad. Sci. U.S.A.* **76,** 1284–1287 (1979).

18. Rozengurt, E. & Heppel, L. A. *Proc. natn. Acad. Sci. U.S.A.* **72,** 4492–4495 (1975).
19. Smith, J. B. & Rozengurt, E. *Proc. natn. Acad. Sci. U.S.A.* **75,** 5560–5564 (1978).
20. Rozengurt, E. & Mendoza, S. *Ann. N.Y. Acad. Sci.* **339,** 175–190 (1980).
21. Dicker, P. & Rozengurt, E. *Biochem. biophys. Res. Commun.* **91,** 1203–1210 (1979).
22. Friedkin, M., Legg, A. & Rozengurt, E. *Proc. natn. Acad. Sci. U.S.A.* **76,** 3909 (1979).
23. Rozengurt, E. in *Surface Properties of Normal and Neoplastic Cells* (ed. Hynes, R.) 322 (Wiley, Chichester, 1979).
24. Yupsa, S. H. *et al. Nature* **262,** 402–404 (1976).
25. Kensler, T. W., Verma, A. K., Boutwell, R. K. & Mueller, G. C. *Cancer Res.* **38,** 2886–2899 (1979).
26. Sreevalsan, T., Rozengurt, E., Taylor-Papadimitriou J. & Burchell, J. *J. cell. Physiol.* (in the press).
27. O'Brien, T. G. *Cancer Res.* **36,** 2644–2653 (1976).
28. De Asua, L. G. & Rozengurt, E. *Nature* **251,** 624 (1974).
29. Bradley, W. E. C. & Culp, L. A. *Expl Cell Res.* **84,** 335 (1974).
30. Brownstein, B. L., Rozengurt, E., De Asua, G. L. & Stoker, M. *J. cell. Physiol.* **85,** 579 (1975).
31. Driedger, P. E. & Blumberg, P. M. *Cancer Res.* **37,** 3257–3265 (1977).
32. Lee, L. & Weinstein, I. B. *J. cell. Physiol.* **99,** 451–460 (1979).
33. Pledger, W. J., Stiles, C. D., Antoniades, H. N. & Scher, C. D. *Proc. natn. Acad. Sci. U.S.A.* **74,** 4481–4485 (1977).
34. Lee, L. & Weinstein, I. B. *J. Envir. Path. Toxicol.* **1,** 627–637 (1978).
35. Moroney, J., Smith, A., Tomei, L. D. & Wenner, C. E. *J. cell. Physiol.* **95,** 287–294 (1978).
36. Fisher, P. B., Flammi, M., Schachter, D. & Weinstein, I. B. *Biochem. biophys. Res. Commun.* **86,** 1063–1068 (1979).
37. Mendoza, S., Wigglesworth, N. & Rozengurt, E. *J. cell. Physiol.* (in the press).
38. Driedger, P. E. & Blumberg, P. M. *Proc. natn. Acad. Sci. U.S.A.* **77,** 561–571 (1980).
39. Michell, R. H., Kirk, C. J. & Billah, M. M. *Biochem. Soc. Trans.* **7,** 861–864 (1979).
40. Rodbell, M. *Nature* **284,** 17–22 (1980).
41. Grimm, W. & Marks, F. *Cancer Res.* **34,** 3128–3134 (1974).
42. Garte, S. J. & Belman, S. *Nature* **284,** 171–173 (1980).
43. Mierzejewski, K. & Rozengurt, E. *Expl Cell Res.* **106,** 394–397 (1977).
44. Hogan, B. L. M. *Biochem. biophys. Res. Commun.* **45,** 301–306 (1971).
45. Inoue, H. & Mizutani, A. *Analyt. Biochem.* **56,** 408–416 (1973).
46. Bourne, H. & Rozengurt, E. *Proc. natn. Acad. Sci. U.S.A.* **73,** 4555–4559 (1976).
47. Rozengurt, E. *et al.* (submitted).

LETTERS

Is PKS1921−29 a quasar with correlated radio and optical variations?

Gerard Gilmore

Royal Observatory, Blackford Hill, Edinburgh EH9 3HJ, UK

Although many quasars and related objects are variable at both optical and radio frequencies, the relationship, if any, between these variations is unclear. In particular, only three objects, OJ287 (ref. 1), 0235+164 (ref. 2) and 0420−01 (ref. 3), have shown well correlated radio–optical variability. The first two are BL Lac objects and showed little or no time delay between the radio and optical variations. The last object is a quasar, and underwent a radio flare some 2 years after a significant optical outburst. Optical observations of another quasar, PKS1921−29, which may also show correlated radio and optical variability are reported here.

Quasar PKS1921−29 has been monitored since 1975.6 at Mount John University Observatory of the University of Canterbury, New Zealand, as part of a larger quasar patrol programme[4,5]. All 27 observations available were taken with an unfiltered S20R photocathode image intensifier camera (effective $\lambda \approx 550$ nm). The plates were measured on a Becker iris photometer at the Royal Observatory, Edinburgh, and data reduced as described elsewhere[4]. The results are shown in Fig. 1. The object is also visible on two ESO Blue Sky Survey plates (fields 459, 460) and five UK Schmidt Telescope plates (IIIaJ+GG395). Magnitudes for the object and the comparison stars used in the iris photometry were visually estimated on these plates, and are also shown in Fig. 1. The fortuitous presence of the globular cluster NGC6809 near the centre of ESO/SRC Survey field 460 allowed the magnitude scale to be calibrated by comparison with the photometry of Harris[6]. Because of the different bandpasses, however, the possibility of both zero point and scale differences between the two data sets remains, and care should be taken in applying the magnitude scale of Fig. 1 to the Canterbury results.

The significant features of these results are the large flare($\gtrsim$1.5 mag) beginning near 1977.4, lesser amplitude activity in 1978, and the very bright state recorded during the single observation in 1979. By comparison, the object appears both fainter and less active during 1974–77, although few observations are available, and this may simply represent a sampling effect. Additionally, photoelectric observations on 9 May 1980 (UT) (not shown in Fig. 1) showed the object to have returned to near minimum level at $m_B = 16.8$ (P. Brand and C. Impey, personal communication).

Dent and Balonek[7] have recently reported radio flux observations from 1972 to 1980 at four frequencies between 7.9 and 89.6 GHz. These show a steady decline in radio flux from 1972 to 1976, a more rapid increase to 1979.4, and then a very rapid increase continuing at least to 1980.0. Superimposed on these trends are small (±25%) flares near 1975.3 (predominantly seen at 15.5 GHz) and 1977.5 (seen only at 31.4 and 89.6 GHz). Landau *et al.*[8] report 90 GHz data and note a factor of 2 decline in flux in only 2 days in December 1978 (see also ref. 9).

The coincidence of the increasing high frequency variability, and the optical variability may be evidence for a common origin of all activity. The significance of this cannot, however, be evaluated until the frequency of optical flaring, such as that in 1977, is better determined.

The optical burst beginning near 1977.4 is also significant. This may be correlated with the maximum of the high frequency activity (31.4 GHz and 89.6 GHz) reported by Dent and Balonek during 1977. In this case, however, the optical flare began near the maximum of the radio activity, and lasted for a significantly shorter time than the radio flare. Similar behaviour in the BL Lac type object AO0235+164 has recently been reported by Balonek and Dent[10].

Note that two possible identifications for this radio source have been published. Radivich and Kraus[11] suggested a 16.5 mag red star, while Peterson *et al.*[12] give a different identification. The Radivich and Kraus identification has shown no statistically significant variability on any of the plates measured here. The light curve in Fig. 1 refers to the Peterson *et al.* identification, and supports that object as the correct optical counter part to OV236. Final confirmation is provided by optical spectroscopy (ref. 13 and J. G. Bolton, personal communication) which provides a redshift $z = 0.352$ from two lines.

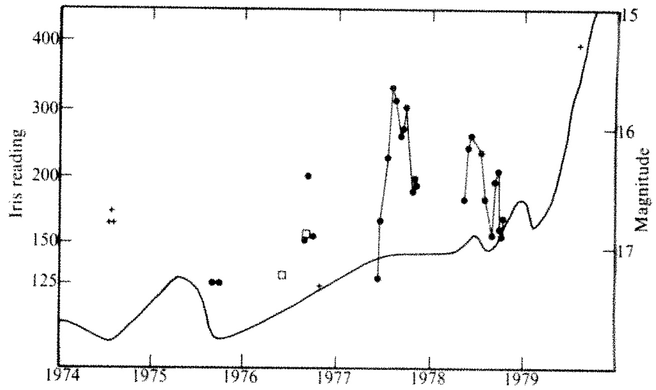

Fig. 1 Optical observations of PKS1921−29 at Mt John University Observatory (●, iris readings scale), on ESO B Survey plates (□) and UK Schmidt Telescope plates (+, magnitude scale). The magnitude scale is not accurately tied to the iris readings scale (see text). Photometric uncertainty is typically ±0.1 mag. The solid line is a smoothed representation of the 15.5 GHz radio data reported by Dent and Balonek[7].

0028-0836/80/410612—02$01.00

I thank Harold Corwin Jr for estimating magnitudes from the Schmidt plates, Peter Brand and Chris Impey for the photoelectric observation in April 1980, and John Bolton for data in advance of publication.

Received 23 June; accepted 19 August 1980.

1. Pomphrey, R. B. *et al. Astr. J.* **81,** 489 (1976).
2. Rieke, G. H. *et al. Nature* **260,** 754 (1976).
3. Dent, W. A. *et al. Astrophys. J. Lett.* **227,** L9 (1979).
4. Gilmore, G. F. *Mon. Not. R. astr. Soc.* **187,** 389 (1979).
5. Gilmore, G. F. *Mon. Not. R. astr. Soc.* **190,** 649 (1980).
6. Harris, W. E. *Astrophys. J. Suppl.* **29,** 397 (1975).
7. Dent, W. A. & Balonek, T. J. *Nature* **283,** 747 (1980).
8. Landau, R., Epstein, E. E. & Rather, J. D. G. *Astr. J.* **85,** 363 1980.
9. Epstein, E. E. *Bull. Am. astr. Soc.* **12,** 1 (1980).
10. Balonek, T. J. & Dent, W. A. Preprint (University of Massachusetts, 1980).
11. Radivich, M. M. & Kraus, J. D. *Astr. J.* **76,** 683 (1971).
12. Peterson, B. A., Bolton, J. G. & Shimmins, A. J. *Astrophys. Lett.* **15,** 198 (1973).
13. Bolton, J. G. *Computer Listing of the Parkes Radio Source Catalogue* (1978).

Star formation in a galactic wind

A. C. Fabian, P. E. J. Nulsen & G. C. Stewart

Institute of Astronomy, Madingley Road, Cambridge CB3 OHA, UK

Malin and Carter[1] have discovered giant shells of faint optical emission around several normal elliptical galaxies. We suggest here that these shells are composed of stars formed in shocked galactic wind material. Shocks might arise from relatively gradual increases in wind velocity, or from the collision of the wind with a tenuous intergalactic medium, and need not imply that cataclysmic events have occurred within the galaxy.

The evolution of the stars in an elliptical galaxy should produce a few $M_\odot\,\mathrm{yr}^{-1}$ of gas[2], mostly from giant stars and planetary nebulae. The lack of observable gas in most ellipticals has led to the suggestion[3,4] that the gas produced there is driven out of the galaxy in a wind powered by supernovae. Typical wind velocities are estimated to be several hundred kilometres per second.

The wind expands freely beyond the edge of the galaxy, so that its temperature falls rapidly and the flow becomes highly supersonic. Thus when it passes through a shock of velocity $v_s = 10^7 v_7\ \mathrm{cm\ s^{-1}}$ the gas is heated to a temperature

$$T_s = 1.3\times10^5 v_7^2 \quad \mathrm{K} \qquad (1)$$

The shocked gas is compressed to a density n_e electrons cm^{-3} and cools to $\lesssim 10^4$ K on a time scale

$$t_c = 1.4\times10^3 T^{1.6} n_e^{-1} \quad \mathrm{s} \qquad \text{(ref. 5)}$$

that is

$$t_c = 1.5\times10^8 R_{50}^2 \dot{M}^{-1} v_7^{4.2} \quad \mathrm{yr} \qquad (2)$$

behind a stationary shock at $R_s = 50\ R_{50}$kpc in a (spherical) wind of $\dot{M}M_\odot\ \mathrm{yr}^{-1}$. The pressure of the shocked gas is maintained at

$$n_e T = 8.4 R_{50}^{-2} \dot{M} v_7 \quad \mathrm{cm^{-3}\ K} \qquad (3)$$

by the ram pressure of the wind. The shock is easily confined by a very tenuous intergalactic (or circumgalactic) medium[6] (for example, at a temperature $\sim10^7$ K and density $\sim 8\times10^{-7}\ \mathrm{cm^{-3}}$, which is much less than the closure density of the Universe).

The total power in the wind is only $\sim 3\times10^{39}\ \dot{M}v_7^2\ \mathrm{erg\ s^{-1}}$ and will be converted into optical (mostly line) radiation with an efficiency which decreases with increasing v_7. Thus the cooling gas is unlikely to be visible.

The emission seen by Malin and Carter[1] is easily provided by $\sim 10^8 M_\odot$ of stars, each of $\sim 1 M_\odot$. Star formation can occur in the cooled gas if it is unstable to self-gravitation, that is Jeans unstable. To estimate whether this is possible we identify the likely length and mass scales that occur. The dense cooled gas is supported over lighter and more recently shocked gas against the pull of the galaxy. This situation is subject to the Rayleigh–Taylor instability which causes the shell to break into clouds of size r_c in a time

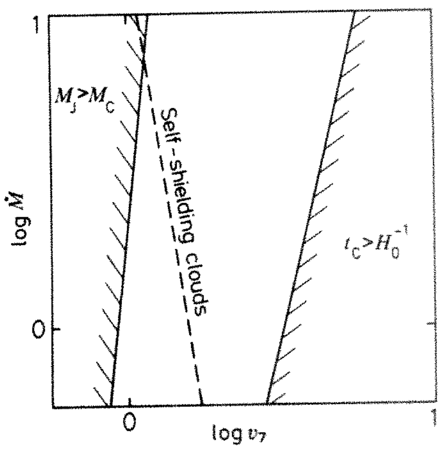

Fig. 1 $\dot{M}$ and v_7 are the mass loss rate and velocity of a galactic wind in $M_\odot\ \mathrm{yr}^{-1}$ and $10^7\ \mathrm{cm\ s^{-1}}$ respectively. Gas behind a shock in a wind at a radial distance of 50 kpc can cool within the age of the Universe provided that $\dot{M}$ and v_7 lie to the left of the rightmost line. The Rayleigh–Taylor instability causes cooled gas to form clouds of mass M_c, which exceed the Jeans mass M_J at 100 K and can thus collapse to form stars, if $\dot{M}$ and v_7 are to the right of the leftmost line. External shielding of quasar ionizing UV radiation is required if stars are to form below the dashed line.

$$t_{\mathrm{RT}} \simeq t_{\mathrm{ff}}(2/\pi)^{3/2}(r_c/R_s)^{1/2} \qquad (4)$$

where the free-fall time into a galaxy of mass $5\times10^{11}\ M\,M_\odot$,

$$t_{\mathrm{ff}} = 2.6\times10^8 R_{50}^{3/2} M^{-1/2}\ yr \qquad (5)$$

This fragmentation cannot proceed before the shocked gas has begun to cool, and leads to the size of a typical cloud forming at t_c being similar to the thickness of the shell of shocked gas (see ref. 7);

$$\begin{aligned}\Delta R &= \tfrac{1}{4} v_s t_c \\ &= 4 R_{50}^2 \dot{M}^{-1} v_7^{5.2} \quad \mathrm{kpc}\end{aligned} \qquad (6)$$

The corresponding cloud mass is then

$$M_c \simeq 1.6\times10^5 R_{50}^4 v_7^{14.6} \dot{M}^{-2} M_\odot \qquad (7)$$

The Jeans mass in neutral gas at a pressure given by equation (3) and a temperature $10^4\ T_4$ K is

$$M_J \simeq 5.0\times10^8 R_{50} \dot{M}^{-1/2} v_7^{-1/2} T_4^2 M_\odot \qquad (8)$$

which is less than M_c provided that the gas can cool still further to $T_4 \sim 10^{-2}$ and that

$$\dot{M} \lesssim 2.2 R_{50}^2 v_7^{10} M_\odot \quad \mathrm{yr}^{-1} \qquad (9)$$

The steep dependence on shock velocity means that gravitational collapse, and we presume star formation, can occur for almost any $\dot{M}$, provided that $v_7 \gtrsim 1$ (see Fig. 1).

An important step in the above process is the cooling of clouds from 10^4 K to $\sim 10^2$ K, so that the Jeans instability can occur. In the absence of any heat source in the clouds, this further drop in temperature can occur by radiative cooling due to the presence of heavy elements in the wind material. The only obvious heat source is ionizing UV radiation from quasars[8,9], which is poorly determined and may be shielded by gas at larger distances than are considered here. If no such external shield is present, the clouds at 10^4 K must shield themselves against the ionizing UV flux, assumed to be $10^4\ \Phi_4$ photons $\text{cm}^{-2}\ \text{s}^{-1}$, where $\Phi_4 \sim 1$ (refs 8, 9). This requires a cloud radius

$$r_{\text{UV}} \geqslant 39\ \Phi_4 R_{50}^4 \dot{M}^{-2} v_7^{-2}\ \text{kpc} \tag{10}$$

and we obtain $r_{\text{UV}} < r_c$ if

$$\dot{M} \geqslant 18 R_{50}^2 v_7^{-6.5} \Phi_4 M_\odot\ \ \text{yr}^{-1} \tag{11}$$

(Fig. 1).

The details of the process of star formation are not well understood. However, there is a substantial range in $\dot{M}$ and v_7 (Fig. 1) for which Jeans unstable clouds can arise. We propose therefore that shells of $\geqslant 10^8\ M_\odot$ of stars can sometimes form from galactic wind material at large distances from elliptical galaxies. The approximate spherical symmetry of the wind will be reflected in the distribution of the stars. To form a thin shell, the star formation must occur on a time scale which is short relative to the free-fall time. Patches of stars may form at several different radii following thermal instabilities in a thick region of shocked gas ($\Delta R \sim R$) or from velocity changes in the wind. These changes could be due to a cooling instability in the core of the galaxy[4], or to more dramatic events such as the accretion of a gas-rich companion or an outburst of the nucleus. Continuous star formation at a fixed radius gives the appearance of a thin shell, as the acceleration of the stars from rest under the influence of the galaxy gives a density profile $\rho_* \propto (R_s/R - 1)^{-1/2}$. Localized bursts of star formation in more peculiar galaxies might lead to small-scale wind shocks. The loop structures seen in Fornax A (NGC1316) could, in part, be due to this mechanism.

Star shells produced at large distances from a parent galaxy may remain roughly spherical for a reasonably long time scale $\sim t_{\text{ff}}$. This will be the approximate age of the component stars. We therefore expect the shells to appear bluer[11] than the parent galaxy (up to ~0.5 mag in $U-B$ and $B-V$) if the initial mass function is similar to that in the solar neighbourhood. Thereafter these high-velocity stars may contribute to the outer galactic envelope. Shocks in denser galactic winds at earlier epochs could have created substantial isothermal stellar envelopes to galaxies.

A.C.F. thanks the Radcliffe Trust for support.

Received 9 July; accepted 27 August 1980.

1. Malin, F. & Carter, D. *Nature* **285,** 643–645 (1980).
2. Tinsley, B. M. *Astrophys. J.* **186,** 35–49 (1973).
3. Johnson, H. E. & Axford, W. I. *Astrophys. J.* **165,** 381–390 (1971).
4. Mathews, W. G. & Baker, J. C. *Astrophys. J.* **170,** 241–259 (1971).
5. McKee, C. F. & Cowie, L. L. *Astrophys. J.* **215,** 213–225 (1977).
6. Fabian, A. C., Schwarz, J. & Forman, W. F. *Mon. Not. R. astr. Soc.* **192,** 135–142 (1980).
7. Gull, S. F. *Mon. Not. R. astr. Soc.* **171,** 263–278 (1975).
8. Rees, M. J. & Setti, G. *Astr. Astrophys.* **8,** 410–419 (1970).
9. Cowie, L. L. & McKee, C. F. *Astrophys. J. Lett.* **209,** L105–L105 (1976).
10. Schweizer, F. *Astrophys. J.* **237,** 303–318 (1980).
11. Larson, R. B. & Tinsley, B. M. *Astrophys. J.* **219,** 46–59 (1978).

Volcanic material from Mount St Helens in the stratosphere over Europe

M. Ackerman, C. Lippens & M. Lechevallier*

Institut d'Aéronomie Spatiale de Belgique, 3, Avenue Circulaire,
B-1180 Brussels, Belgium
*E.T.C.A., 16 bis, Avenue Prieur de la Côte d'Or,
F-94114 Arcueil, France

The two most recent balloon flights devoted to studying the stratospheric aerosol vertical structure by comparison with winds, temperature and ozone vertical structures took place on 7 May and on 5 June 1980. At 15.23 h GMT on 18 May Mount St Helens volcano (46 °N, 122 °W) erupted with a tremendous explosion, projecting ash into the stratosphere. An explosion of this size occurs only about once a decade[1]. This sudden introduction of material into the atmosphere offers the opportunity to study air motions both horizontally and vertically. The last such large-scale opportunity was offered by the Mount Fuego eruption which took place in 1974. In this latter case, the enhancement of stratospheric aerosols was observed by means of ground-based lidars and of balloon-borne particle counters. The time development of the aerosol event in 1974 and 1975 has been described elsewhere[2–4]. Mount St Helens material can now also be traced by various satellite-borne instruments. This new stratospheric aerosol event appears to be spectacular. As shown by the photographs discussed here, it leads in its early stage of development to an increase by a factor of three of the Earth limb reflectivity at 15-km altitude after a period of several years of low stratospheric aerosol content.

The new method[5] is based on the photographic observation from balloon altitude of the Earth limb in the azimuthal direction of the Sun at low solar elevation angles. Aerosols are known to scatter light mostly at small angles whereas, comparatively, Rayleigh scattering by air molecules occurs almost evenly at all angles. Our observational geometry favours aerosol detection.

At balloon altitude the camera lenses view the Earth limb below the horizontal line directly and the Sun above it through a neutral optical density ($D \cong 4$) screen which serves several purposes. It avoids penetration of straylight in the optics to obtain clean pictures of the Sun at various elevation angles providing an angular scale. It puts both the Sun and the Earth limb in the sensitive dynamic range of the film calibrated in relative units by means of a step wedge photographed before flight. The solar images provide the absolute scale. The gondola is Sun oriented so that the cameras have the Sun in the middle of the horizontal field of view. Colour (Kodak EPR 475) and black

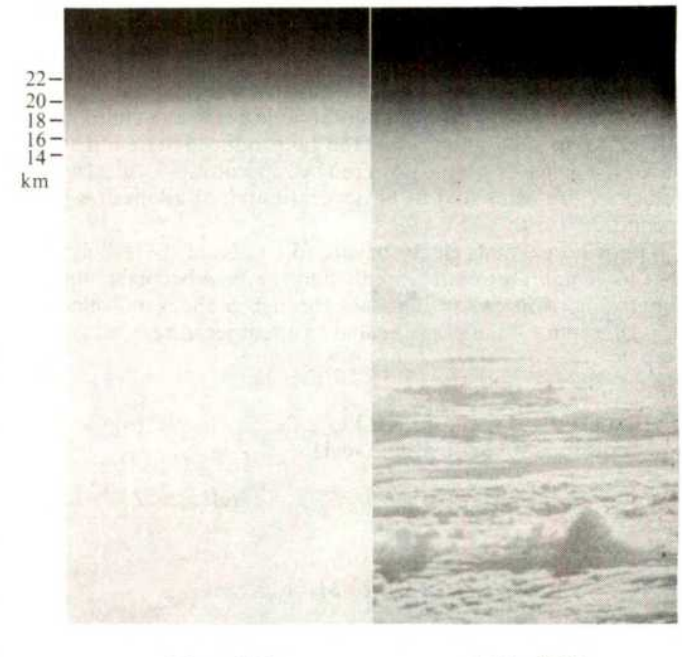

5 June 1980 7 May 1980

Fig. 1 Photographs of the Earth limb taken with identical exposure settings in the azimuth of the Sun at low solar elevation angles from balloon gondolas on 7 May and on 5 June 1980. The gondolas were at 37- and 35-km altitude respectively. An altitude scale of the grazing line of sight is shown in kilometres. Below the dark blue sky horizontally stratified aerosol layers are revealed by scattered sunlight. In the 5 June case, material from the Mount St Helens volcano has spread in the low stratosphere over a large horizontal extent. It enhances the brightness of the limb so that the cloud cover in the foreground can hardly be seen through the whitish veil. In contrast, the cloud cover is well visible on 7 May. Note that the grazing point at 16-km altitude is some 500 km away from the camera. An altitude difference of 1 km at that altitude corresponds to 7 arc min.

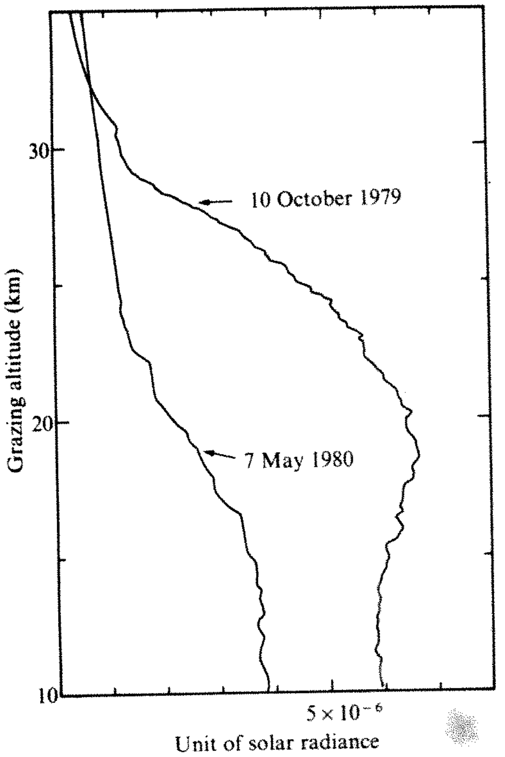

Fig. 2 Earth limb radiance in the azimuth of the Sun versus grazing altitude of the line of sight. The solar elevation angles were respectively 6.18° and 6.94° on 10 October 1979 and on 7 May 1980. The variation of the limb radiance versus altitude is relatively smooth in both cases. As most of the radiance observed is due to scattering by particles, their amount in the low stratosphere appears larger in October than in May where a low aerosol background had been reached. The situation at higher altitudes seems to be reversed. However, these aspects require confirmation from other flights and further interpretation of these raw data where ozone and air absorption should be taken into account. The uncertainties due to difficulties of the photographic photometry have also to be considered.

and white (Kodak Plus X Pan) 70-mm films are used. The results reported here were obtained in the red using Wratten filters nr. 25 set in front of the 80-mm focal length lenses of the Hasselblad EL500 cameras and without filter. The cameras are remotely operated from the ground. The telemetry return signal allows us to check their operation.

Three flights are considered here. The first two took place on the afternoons of 10 October 1979 and 7 May 1980 from Aire sur l'Adour in south-west France. To determine the geographical coordinates as accurately as possible, the tracking was performed by the CNES telemetry station and by radars located at the Centre d'Essais des Landes (Biscarosse). The altitude, longitude and latitude of the gondola at the time that the picture was taken were respectively 37 km, 1° E and 44° N. The third flight took place on 5 June 1980 from the other CNES range in the Alps. Radar tracking was performed in this case from Ile du Levant on the edge of the French Riviera. The coordinates were 35.2 km, 2° E and 44° N.

Inspection of limb pictures such as those shown in Fig. 1 reveals the presence of aerosol layers with a thickness ranging from 100 metres to several kilometres. The latter layers extend horizontally over the whole field of view whereas the thinner layers may have a smaller extension. The black and white photographs are analysed using a Jarrell–Ash densitometer. Grazing altitudes in the stratosphere are determined using the tables of Link and Neuzil[6], taking refraction into account.

The Earth limb radiance is deduced from the densitometric measurements. The radiance vertical profiles observed on 10 October 1979 and on 7 May 1980 in white light are compared in Fig. 2. These profiles are similar showing mostly smooth vertical structure. Figure 3 shows the vertical radiance profiles observed in red light on 7 May and on 5 June 1980. The abrupt radiance increase observed on 5 June between 15- and 16-km altitude is similar to the increase of particle amount observed shortly after the Fuego eruption[2–4]. The very sharp cutoff at the upper boundary of the layer is typical.

On the other hand, satellite-borne instruments have tracked at 16-km altitude material from the volcano crossing the east coast of the US on 23 May and moving towards Europe above the Atlantic Ocean on 27 May (M. P. McCormick, personal communication). The observation reported here is likely to have occurred shortly after the arrival over Europe.

Theory[7,8] predicts that a stratospheric aerosol increase reduces the amount of solar energy reaching the troposphere and the ground. Two main processes are involved: absorption in the aerosol layer and reflection to space of solar energy flux leading to small average temperature decreases in the troposphere[4,9]. The reflectivity data reported here will be augmented by further flights and together with other absorption data will hopefully improve the understanding of the problem and help to evaluate more precisely the possible impact of stratospheric aerosol events.

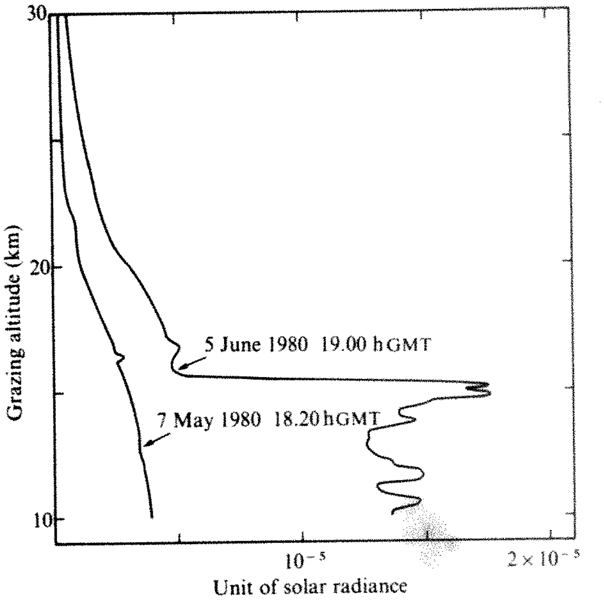

Fig. 3 Earth limb radiance in the azimuth of the Sun and in units of solar radiance versus altitude of the grazing line of sight. The solar elevation angles were respectively 6.94° and 6.26° on 7 May and on 5 June. The large and sharply cut radiance increase between 15.6 and 15.2 km is due to the stratospheric loading of volcanic material. The radiance increase at higher altitudes is thought to be partly due to the illumination increase of the upper levels by the lower levels. The thin layers (some 300-m thick) at some 16.5-km altitude seems to be a frequent feature of the mid-latitude stratosphere and is thought to be related with the height of the tropical tropopause.

We thank the French Centre National d'Etudes Spatiales balloon launching range for launches, tracking and recovery of the gondolas.

Received 9 July; accepted 14 August 1980.

1. *EOS* **61** (1980).
2. Hoffman, D. J. & Rosen, J. M. *J. geophys. Res.* **82**, 1435–1440 (1977).
3. McCormick, M. P., Swissler, T. J., Chu, W. P. & Fuller, W. H. Jr, *J. atmos. Sci.* **35**, 1296–1303 (1978).
4. Russell, P. B. & Hake, R. D. Jr *J. atmos. Sci.* **34**, 163–177 (1977).
5. Ackerman, M. & Lippens, C. *Aeronom. Acta* C n° 54 (1979).
6. Link, F. & Neuzil, L. *Tables of Light Trajectories in the Terrestrial Atmosphere* (Hermann, Paris, 1969).
7. *CIAP Monogr.* (US Department of Transportation, Springfield, 1975).
8. Pollack, J. B. *et al. J. geophys. Res.* **81**, 1071–1083 (1976).
9. Mass, C. & Schneider, S. H. *J. atmos. Sci.* **34**, 1995–2004 (1977).

Magnetic activity and variations in solar luminosity

E. A. Spiegel

Department of Astronomy, Columbia University, New York,
New York 10027

N. O. Weiss*

Harvard-Smithsonian Center for Astrophysics, Cambridge,
Massachusetts 02138

Attempts to detect changes in the solar luminosity suggest that the solar constant has been misnamed[1-4]. Although the Nimbus satellite data[4] show no significant fractional variations above 5×10^{-3} during the period 1975–78, results from recent balloon[5] and rocket[6] flights show changes of 4×10^{-3}. Intense magnetic fields in sunspots hamper convection locally[7] but active regions are believed not to be directly responsible for long term variations in luminosity of the Sun[8] or of RS CVn and BY Dra stars[9]. The cause of luminosity variations over spot cycles should be sought in more deep-seated global features. Here we indicate how strong magnetic fields at the base of the convective zone can alter the local convection. The resulting changes in thermal energy are large enough to produce variations of order 0.1% in the solar luminosity over the 11-yr sunspot cycle.

The magnetic field in the solar envelope is believed to be predominantly toroidal and generated by differential rotation[11,12]. Flux expulsion and magnetic buoyancy[11,12] will quickly sweep toroidal fields from the convective zone. Moreover, the observed large scales of coronal holes and complexes of solar activity point to a confinement of the toroidal field in the lower part of the convective zone[13]. We are led to a model in which the toroidal field is concentrated into a boundary layer at the base of the convective zone where there is relatively little motion. Flux expulsion and topological pumping[11] compress the fields into such a layer, and any flux tubes that stray into the main body of the convective zone will be brought up to the surface by magnetic buoyancy. Such a magnetic layer is deeply implicated in the solar cycle and is accordingly time dependent. We shall explore its influence on convective heat transfer.

Let T be the local temperature and $\bar{T}$ be its average over an equipotential surface, presumed spherical. Then $\bar{T}$ depends only on radius, r, and time. In the mixing-length treatment of stellar convection the heat flux is determined by the gradient of potential temperature,

$$G_p = \partial\bar{T}/\partial r - (\partial\bar{T}/\partial r)_{ad} \tag{1}$$

The adiabatic temperature gradient is given by

$$G_a = (\partial\bar{T}/\partial r)_{ad} = (\partial\bar{T}/\partial\bar{p})_{\bar{S}}\partial\bar{p}/\partial r = (\bar{\rho}C_p)^{-1}\partial\bar{p}/\partial r \tag{2}$$

where $\bar{S}$ is the horizontal average of the specific entropy. The radiative flux is fixed by the mean temperature gradient, $\partial\bar{T}/\partial r$.

From equation (2) and the hydrostatic relation,

$$\partial\bar{p}/\partial r = -g\bar{\rho} + \hat{\mathbf{r}}\cdot[\overline{(\boldsymbol{\nabla}\wedge\mathbf{B})\wedge\mathbf{B}}/(4\pi) - \overline{\boldsymbol{\nabla}\cdot(\rho\mathbf{uu})}] \tag{3}$$

where $\mathbf{u}$ is velocity and $\hat{\mathbf{r}}$ is a unit radial vector, it follows that G_a is directly affected by magnetic fields. Because the field $\mathbf{B}$ is solenoidal,

$$G_a = -g/C_p - (\bar{\rho}C_p)^{-1}\partial[\overline{(B_h^2 - B_v^2)}/(8\pi) - \overline{\rho w^2}]/\partial r \tag{4}$$

where B_h and B_v are the horizontal and vertical components of $\mathbf{B}$, and w is the vertical component of $\mathbf{u}$. In the nether regions of the convective zone $G_p \sim 10^{-6}$ K km^{-1} (ref. 10). The magnetic correction produced by a toroidal field occupying a layer of thickness d is

$$\delta G_a \sim \overline{B^2}/(8\pi\bar{\rho}C_p d) \tag{5}$$

with $\bar{\rho} \sim 0.1$ g cm^{-3} near the bottom of the solar convective zone. To estimate the variation in G_a during the solar cycle that results from the reversal of the toroidal field at sunspot minimum and the subsequent growth of magnetic flux with the approach of sunspot maximum, we need to focus on the magnetic layer that is formed between the radiative and convective zones by flux expulsion.

In standard mixing length theory, the bottom of the convective zone is well defined: motion is assumed to stop at the depth where $G_p = 0$. In reality, fluid slows down as it approaches this depth from above; then it overshoots and goes below it. A sublayer of mild convection forms in the lower part of which the toroidal field develops and whence it intrudes into the stably stratified radiative zone. In this magnetic intrusive region, $\partial B^2/\partial r > 0$. Hence the adiabatic gradient is modified in a way that causes the bottom of the convective zone slowly to recede. This helps stabilize the layer in which magnetic field is building up.

The field grows more rapidly than the stable layers can admit it by diffusion. Flux expulsion drives the magnetic energy density up to values comparable with the kinetic energy density at the base of the convection zone. Hence, in the reclaimed part of the convective zone, fields will grow to values comparable with the equipartition value of 10^4 G. Hydromagnetic convection theory indicates several possible instabilities, both linear and nonlinear, involving magnetic buoyancy. These will be of the 'double diffusive' type, with stable temperature gradient and unstable magnetic gradient. According to the rough criteria available these instabilities occur when d, the thickness of the magnetic layer, approaches the pressure scale height, $H_p \sim 5\times10^4$ km.

Instabilities driven by magnetic buoyancy produce ropes of magnetic flux, which rise up through the convective zone and emerge into the photosphere. As the subconvective fields become unstable, therefore, active regions appear more frequently at the surface and the sunspot cycle approaches a new maximum. The magnetic flux of a field of 10^4 G in a layer whose depth is of the order of H_p should, in this picture, be comparable with the flux that protrudes from the solar surface near sunspot maximum. This conclusion accords with observation[14].

The onset of the instability affects the toroidal field strength and hence modifies the adiabatic gradient. Thus it is accompanied by an increase in the convective intensity in the lower convective zone. We suggest that these changes will give rise to variations in the solar luminosity. To gauge their amounts we may use our estimates of $\overline{B^2}$ and d and find from equation (5) that $\delta G_a \sim 10^{-6}$K km^{-1}, which is comparable with G_p. Other terms of like magnitude also occur in the heat equation, through which G_p has a central role in the theory. None of these terms is included in the usual mixing length theory of stellar convection and their precise relative magnitudes and phases are not known. Moreover, fields of 10^4 G must exert dynamical effects on the motion. From the rate of work done against the Lorentz force we estimate that the potential temperature gradient may increase by as much as

$$\delta G_p \sim \overline{B^2}\,\bar{T}/(4\pi\bar{\rho}gd^2) = [\overline{B^2}/(4\pi\bar{\rho}\mathscr{R}d)](H_p/d) \tag{6}$$

where $\mathscr{R}$ is the gas constant. When $d \sim H_p$ this is comparable with the estimate of δG_a obtained above. Thus the alteration of the adiabatic gradient is one of several competing mechanisms which modify convective transfer through the action of strong magnetic fields arising at the base of the convective zone. These mechanisms have comparable numerical significance and we focus on one to estimate the order of magnitude of the resultant luminosity variation.

The convective zone itself adjusts to mild changes within a few turnover times of the largest eddies, that is months, but the underlying radiative zone requires much longer. In 11 yr thermal diffusion affects only a thin skin at the top of the radiative zone, whose thickness is 1,000 km and whose heat capacity is far smaller than that of the convective zone. Fluctuations in the convective zone do eventually influence a deeper region having a heat capacity comparable with its own, but that process takes

---

* Permanent address: Department of Applied Mathematics and Theoretical Physics, University of Cambridge, Cambridge, CB3 9EW, UK.

0028–0836/80/410616—02$01.00

10^5 yr (refs 15, 16). On the other hand, hydrostatic adjustments of the whole Sun occur within a few hours. We may therefore regard the convective zone as receiving a fixed flux from below, which it modulates during the 11-yr time scale of solar activity.

Whatever the precise dynamical details of such a modulation, its magnitude may be gauged from our estimate of δG_a. While the thermal state of the underlying radiative zone does not change much in the time of interest and the radiative flux from below remains nearly constant, the change in G_a must result in a change in convective flux in the deep convective zone as soon as the instability develops. This will be accompanied by a slight change in temperature at the base of the convective zone of the order of $\delta T \sim \delta G_a d \sim 0.05$K. The thermal energy involved in this change is of magnitude

$$\delta U \sim C_p M_c d\, \delta G_a \qquad (7)$$

where M_c is the mass of the convective zone. For the Sun, $M_c \sim 0.03 M_\odot$ and so $\delta U \sim 10^{39}$ erg. Locally the toroidal field rises from zero at reversal to its peak value in a time τ during which, by equations (5) and (7), the change in magnetic energy is comparable with δU. In the same period, there are slight changes in the Sun's structure, for even adiabatic processes allow exchanges among the potential, thermal and magnetic energy reservoirs.

These fluctuations affect the rate at which convection removes energy and conveys it to the solar surface. Such modifications of the convective flux reach the surface in a few months with consequent changes in the upper transition layer of the convective zone. Here, radiative transfer becomes the dominant heat transport mechanism. The energy carried up by convection is converted into local thermal energy and radiated into space, hence the temperature of this layer must be close to the effective temperature, T_e. We wish to estimate the amplitude of temperature variations in this layer that result from convective changes and to infer the magnitude of concomitant changes in solar luminosity.

Solar models, based on mixing length theory, indicate that the transition layer is quite thin: its depth is about one local scale height and its mass $m \sim 10^{-9} M_\odot$. Its thermal response time, $m C_p T_e/(4L)$, where L is the luminosity, is ~ 5 min. On this time scale this crucial layer adjusts itself to accommodate changes in the rate at which convection carries energy outward. The changes of interest here are of magnitude $\delta U/\tau$, and they are directly reflected in fluctuations in T_e and L. The former are given approximately by

$$\delta T_e \sim \delta U T_e/(4L\tau) \qquad (8)$$

and, for $\tau \sim 6$yr, this yields $\delta T_e \sim 2$K. Then, from equations (6) and (7), we find that

$$\delta L \sim M_c \overline{B^2}/(8\pi\bar{\rho}\tau) \qquad (9)$$

which does not depend on the thickness, d, of the magnetic layer. This gives a luminosity variation, $\delta L \sim 10^{-3} L_\odot$.

As we do not have an independent estimate of the radius variation, we cannot be explicit about the phases of the various changes. These enter through the familiar relation

$$\delta L/L = 4\, \delta T_e/T_e + 2\, \delta R/R \qquad (10)$$

In agreement with our estimates, a change of 0.1% in luminosity requires that $\delta T_e \simeq 1.5$K if R remains constant. The relevant measurements have been discussed elsewhere[17]: the best data indicate that T_e decreases[8] by about 6K from sunspot minimum to sunspot maximum and that R increases[19] by about 0.015% in the same time. These observations together with equation (10) point to the value $\delta L/L \simeq 4 \times 10^{-3}$, which agrees with the above estimate.

Magnetic corrections to G_a and G_p have therefore to be included in studies of variations of solar luminosity over the solar cycle. Although we cannot reliably predict the phases of such variations, application of the viral theorem[20], modified to allow for the fluctuations we are discussing here, suggests that an increase in luminosity accompanies a decrease in solar radius and *a fortiori* an enhancement of effective temperature. Livingston's measurements show a decrease in surface temperature as the sunspot cycle approaches maximum[18]; hence the solar luminosity ought to decrease in the intervals preceding sunspot maxima.

We thank S. Childress, D. O. Gough, R. Rosner and E. T. Scharlemann for comments, H. U. Schmidt, M. Schwarzschild, S. Shore and J. H. Thomas for discussion, and A. Arking for information on satellite data. This work was supported by the NSF under grant PHY77-27086 and by the Langley-Abbot program of the Smithsonian Institution.

Received 31 July; accepted 4 September 1980.

1. White, O. R. (ed.) *The Solar Output and its Variation* (Colorado Associated University Press, Boulder, 1977).
2. Herman, J. R. & Goldberg, R. A. *Sun. Weather and Climate* (NASA SP-426, Washington DC, 1978).
3. Eddy, J. A. in *The New Solar Physics* (ed. Eddy, J. A.) 11–35 (Wertman, Boulder, 1978).
4. Foukal, P. in *The Ancient Sun* (eds Eddy, J. A. & Pepin, R. O.) (Pergamon, Oxford, 1980).
5. Kosters, J. J. & Murcay, D. G. *Geophys. Res. Lett.* **6,** 382–384 (1979).
6. Wilson, R. C., Duncan, C. H. & Geist, J. *Science* **207,** 177–179 (1980).
7. Cowling, T. G. *Magnetohydrodynamics* (Hilger, Bristol, 1976).
8. Foukal, P. & Vernazza, J. *Astrophys. J.* **234,** 707–715 (1980).
9. Hartmann, L. A. & Rosner, R. *Astrophys. J.* **230,** 802–814 (1979).
10. Baker, N. H. & Temesvary, S. *Tables of Convective Stellar Envelope Models* (NASA, New York, 1966).
11. Moffatt, H. K. *The Generation of Magnetic Fields in Electrically Conducting Fluids* (Cambridge University Press, 1978).
12. Parker, E. N. *Cosmical Magnetic Fields* (Clarendon, Oxford, 1979).
13. Golub, L., Rosner, R., Vaiana, G. S. & Weiss, N. O. *Astrophys. J.* (in the press).
14. Galloway, D. & Weiss N. O. *Astrophys. J.* (in the press).
15. Dearborn, D. S. P. & Newman, M. S. *Science* **201,** 150–151 (1978).
16. Sofia, S., O'Keefe, J., Lesh, J. R. & Endal, A. S. *Science* **204,** 1306–1308 (1979).
17. Thomas, J. H. *Nature* **280,** 662 (1979).
18. Livingston, W. C. *Nature* **272,** 340–341 (1978).
19. Meyermann, B. *Astr. Nachr.* **279,** 45–46 (1950).
20. Cowling, T. G. in *Stellar Structure* (eds Aller, L. H. & McLaughlin, D. B.) 425–463 (University of Chicago Press, 1950).

Seasonal variation of oriental sunspot sightings

D. M. Willis & M. G. Easterbrook*

Rutherford and Appleton Laboratories, Ditton Park,
Slough SL3 9JX, UK

F. Richard Stephenson

Department of Geophysics, University of Liverpool, PO Box 147,
Liverpool L69 3BX, UK

An important, though inexact, index of past solar activity[1–3] is the frequency of unaided-eye sunspot sightings in the Orient[1,3–7]. When the glare of the Sun is reduced by a natural atmospheric filter, a single sunspot or compact group of sunspots located within the central part of the solar disk can be seen with the unaided eye if its area exceeds 0.5‰ of the Sun's visible hemisphere[8]. The oriental sunspot records represent one of the few available sources of solar data before the invention of the telescope[4,5]. The abundance of historical sunspot records from China and Korea must be attributed partly to the regular occurrence of atmospheric conditions suitable for the detection of sunspots[4–6]. Considerably diminished solar brightness, caused by, for example, atmospheric haze, dust storms, severe atmospheric absorption (for example, near sunrise or sunset) or reflection off still waters, is necessary to render sunspots visible to the unaided eye. Indeed, many of the oriental sunspot records explicitly mention reduced solar brightness[6] compatible with these conditions. We discuss here what information the dates of the oriental sunspot sightings provide on past atmospheric conditions in the Orient and hence on past solar activity.

---

* Present address: Laboratory for Planetary Atmospheres, Department of Physics and Astronomy, University College London, UK.

0028–0836/80/410617—03$01.00

Figure 1 shows the number of sunspot sightings that have been recorded in each month of the year according to a catalogue of pre-telescopic sunspot sightings (139 in all)[6] which is based on an independent search of official oriental dynastic histories. These sightings have been used to obtain the seasonal variation in the occurrence of atmospheric conditions favourable to the detection of sunspots with the unaided eye. Three sightings have been discarded because only the year of the sighting is known; a fourth has been omitted because it is the sole sighting recorded in Japan, where such phenomena seem to have attracted less attention.

The shaded part of the histogram in Fig. 1 shows the distribution of those dates (year, month and day) in the catalogue[6] that are specified without reservation. The unshaded part includes 12 dates for which either the day or month is uncertain; in such cases the most plausible historical date is used. In addition, each of the intervals within which the dates of eight other sightings lie has been contracted (from ~60 to 30 days) after re-examining the historical records. In these latter cases, which also contribute to the unshaded part of the histogram, the median day has been adopted as the date of the sighting. The probability of obtaining the shaded histogram by chance is less than 1 in 25,000, according to the χ^2 test[9] with the theoretically expected frequencies assumed to be proportional to the number of days in the month. If the unshaded part of the histogram is included, this probability is still smaller. Therefore the seasonal variation of oriental sunspot sightings is highly significant statistically and should not be affected appreciably by the sporadic nature of the sightings. A similar seasonal variation exists in the data before (70 sightings) and after (65 sightings) AD 1150, a convenient date that divides the data into two subsets containing approximately the same number of sightings. The seasonal variation also exists separately in the Chinese (103 sightings) and Korean (32 sightings) observations.

Figure 1 presents the composite seasonal variation of sunspot sightings arising from a combination of various atmospheric conditions occurring at different geographical locations. The probable places at which most of the oriental sunspot observations were made are shown in Fig. 2. Despite the diversity of locations, the main features of the seasonal variation can be explained in terms of known characteristics of the general climate of much of East Asia. Thus the marked spring maximum can be ascribed to the fact that dust storms and sand storms ('yellow winds') originating over central China occur most frequently during late winter and early spring, when aridity due to low winter rainfall and increased surface winds associated with cold fronts contribute to their occurrence[10–13]. The source of atmospheric dust and sand is the vast barren land comprising the Takla Makan, Gobi and Ordos Deserts and the Chinese loesslands[12]. Dust and fine sand carried into the lower troposphere by strong winds can be transported down-wind several thousand kilometres[12,13,15]. The resultant haze often obscures the horizon and causes deep red sunsets throughout China as far south as Hong Kong[16]. Airborne dust and fine sand over China and Korea acts as a natural filter that reduces the glare of the Sun, thus allowing fine detail to be perceived on the solar surface. Ho Peng Yoke[15] suggested that such atmospheric dust would produce favourable viewing conditions at sunrise and sunset, thereby making direct observations of the Sun possible. Furthermore, those sunspot sightings for which the oriental records quote a duration of several days[5] mostly occurred during winter or spring, which also supports the suggestion that dust storms produce favourable atmospheric viewing conditions.

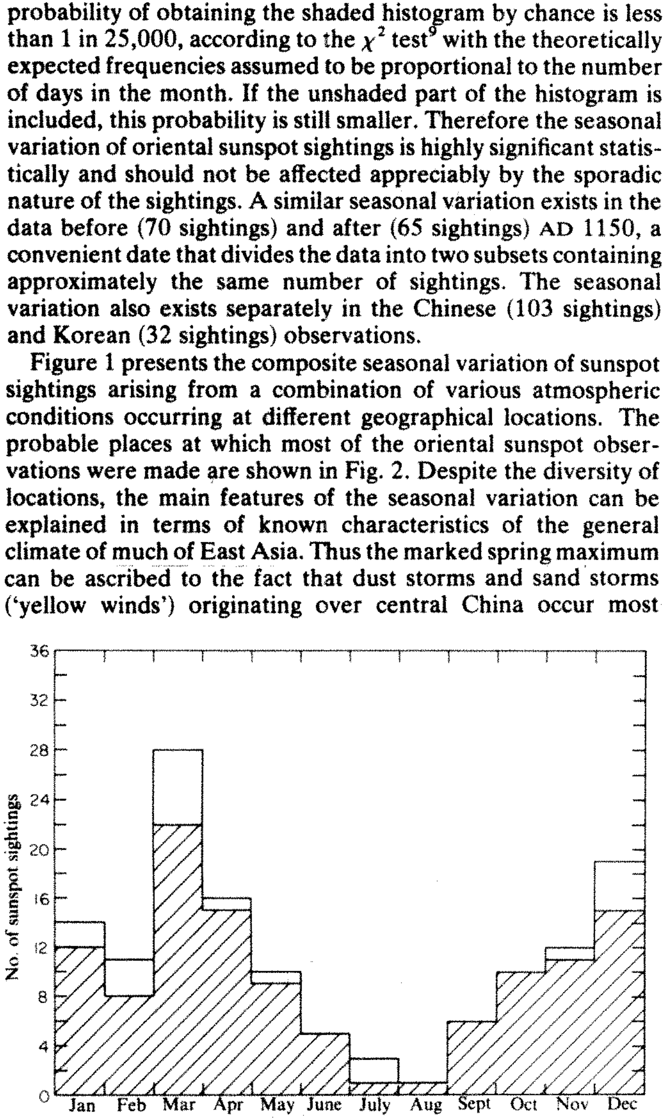

Fig. 1 Number of unaided-eye sunspot sightings recorded in each month of the year according to a catalogue of pre-telescopic sunspot sightings[6]. The date of the first sighting is 28 BC 10 May (Julian calendar) and that of the last sighting is AD 1604 25 October (Gregorian calendar). All dates have been corrected to the Gregorian calendar to allow for the gradual change in the dates of the seasons in the Julian calendar. The shaded part of the histogram refers exclusively to reliable dates, whereas the unshaded part includes dates for which the day or month is uncertain (see text).

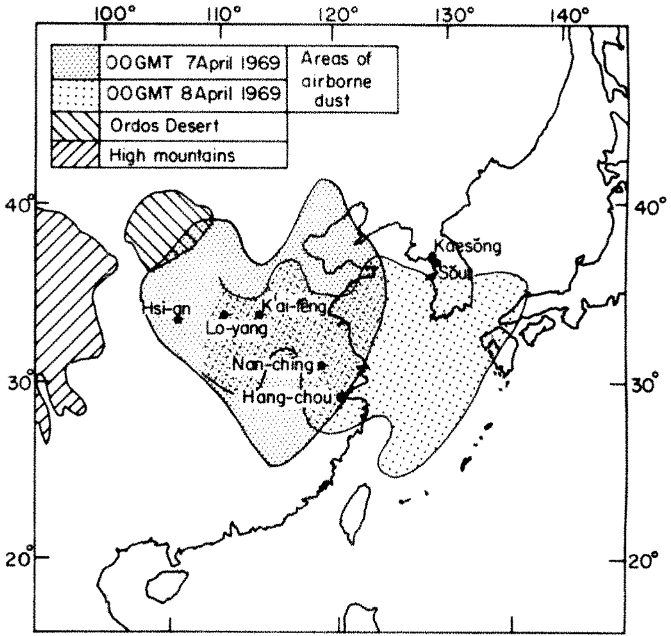

Fig. 2 The sites at which most of the ancient oriental sunspot observations were made. The areas affected by airborne dust or sand on two consecutive days during the large dust storm in April 1969 are shown for comparison. This storm was initiated by the passage of three successive cold fronts over the loesslands and Ordos Desert. The stippled areas define the regions within which meteorological stations reported blowing dust or sand: ESSA 9 satellite photographs confirm the large extent of this dust storm (after Ing[12]).

Colleagues who have travelled extensively in China have noted that a typical dust storm dims the Sun considerably but does not blot it out and may well provide the conditions necessary for observing fine detail on the solar surface with the unaided eye. During a typical dust storm the Sun appears a deep yellow colour. Several oriental sunspot records specifically mention that "the Sun was orange and had no brilliance"[6] and thus it seems likely that atmospheric dust in the lower troposphere was responsible for many of the oriental sunspot sightings.

An optically dense volcanic dust veil in the stratosphere would also dim and redden the Sun[17], but the residence times for such volcanic dust (or 'ash') are too long for the seasonal variation shown in Fig. 1 to be attributed to stratospheric dust. Although long-lived changes in atmospheric viewing conditions, resulting from changing amounts of volcanic dust in the stratosphere, may possibly have contributed to long-term changes in the frequency of oriental sunspot sightings, we show below that transient changes of dust in the lower atmosphere can probably account

Table 1 Number of severe winters per century in China (after Lamb[22]) and the corresponding number of oriental sunspot sightings (from Clark and Stephenson[6])

Century (AD)	6	7	8	9	10	11	12	13	14	15	16	17	Average	s.d.*
Severe winters	19	11	9	19	11	16	24	25	35	10	14	21	17.8	7.7
Sunspot sightings	12	0	0	6†	3	5	32	13	32	1	1	12‡	9.8	11.4

The correlation coefficient, $r = 0.89$, is significant at the 0·1% level§

* Standard deviation.

† The single Japanese sighting (AD 851 22 December, Julian calendar) has been omitted, as in Fig. 1.

‡ As Clark and Stephenson's catalogue[6] is confined to pre-telescopic sunspot sightings (sightings before AD 1611), the entry for the seventeenth century is based on the table presented by Cullen[25], which includes 12 Chinese sightings recorded in standard histories (*cheng shih*). If the 21 Chinese sightings found in local records (*fang chih*) are included, this number becomes 33. The correlation coefficient is then 0.83, but the significance level is unchanged.

§ According to Student's t-test[9]; the correction for autocorrelation is negligible.

for much of the variability in the number of sunspot sightings per century.

As an example, Fig. 2 shows the large area affected by airborne dust and sand for the dust storm generated over central China in early April 1969[12]; ESSA 9 satellite photographs have been combined with surface data from meteorological stations to track and identify the synoptic features of this dust storm. This particular storm was associated with the passage of three successive cold fronts over the loesslands and Ordos Desert. Such a large dust storm can obviously dim the Sun considerably and perhaps create propitious atmospheric conditions for viewing sunspots at all of the ancient observing sites. Smaller dust storms might produce the right atmospheric viewing conditions in more limited geographical regions.

The broad summer minimum shown in Fig. 1 can be attributed to greater cloudiness and precipitation during the rainy season[13]. The number of overcast days is highest in summer in both the Yellow River Basin (Hsi-an, Lo-yang and K'ai-fêng) and the Yangtze Basin (Nan-ching and Hang-chou)[18]; a similar situation prevails at the two observing sites in Korea (Kaesŏng and Sŏul)[19]. This explanation relies mainly on optically thick clouds obscuring the Sun and hence reducing the likelihood of sunspots being detected, particularly at sunrise or sunset, although optically thinner clouds or fog may occasionally favour the detection of sunspots. Heavy summer rainfall also washes dust out of the lower atmosphere, which results in maximum glare from the Sun on clear days. Owing to the greater cloudiness in summer[18,19], however, this 'clear sky' situation occurs on relatively few days per month. The small number of sunspot sightings recorded in July and August (see Fig. 1) can therefore be regarded as a summer base level determined by a combination of greater obscuration of the Sun on cloudy days and greater glare from the Sun on clear days, with the cloudy days outnumbering the clear days. The above discussion indicates that the detection of sunspots with the unaided eye depends sensitively on local atmospheric viewing conditions involving several meteorological variables. There are, however, considerable regional differences in climate within a geographical area as large as that shown in Fig. 2 and further research is required to clarify the seasonal variations of sunspot sightings in different localized regions.

Needham[4] has suggested that the Chinese may have viewed the Sun through pieces of semi-transparent jade, mica or smoky rock crystal. Further, Chu Wên-hsin[20] has described a method of observing solar eclipses and sunspots by looking at the reflection of the Sun in a basin of water blackened with Chinese ink, and very similar methods of observing the reflection of the Sun are actually mentioned in ancient Chinese astrological literature[21]. However, there is no convincing evidence that efficient artificial aids were used to dim the Sun systematically; indeed, from the viewpoint of the ancient observers, the use of such optical aids might negate any astrological predictions. Also, although many more sunspot sightings would have been recorded if an efficient artificial aid had been used, the seasonal variation might then be expected to depend on the duration (hours) of bright sunshine[18,19]. This inference is not substantiated by the seasonal variation shown in Fig. 1.

We conclude that atmospheric viewing conditions complicate the interpretation of the oriental sunspot sightings as an index of past solar activity. In particular, as dust storms in East Asia are associated with the passage of cold fronts over deserts and loesslands, more sunspot sightings should have been noted during cold winters and springs. Most of the oriental sunspot sightings were indeed recorded during those centuries for which the number of severe winters in China was above average[22], as indicated in Table 1; this association seems to be meaningful whatever the cause of the climatic changes in China. As the detection of sunspots with the unaided eye depends significantly on local atmospheric viewing conditions, the number of sunspot sightings in the Orient should not be compared with the severity of winters in geographical areas remote from China (such as Europe). However, if the frequency of the oriental sunspot sightings is still regarded as an approximate measure of past solar activity, rather than just an indicator of favourable atmospheric viewing conditions, the correlation ($r = 0{\cdot}89$) between severe winters and sunspot sightings presented in Table 1 conflicts with Eddy's claim[2] that cold climate coincides with low solar activity. It now seems more likely that the oriental sunspot records provide merely circumstantial evidence for excursions in solar activity[23] and that the radioactive isotope ^{14}C, preserved in the annual growth rings of trees , should be used as the prime guide to past solar activity. Nevertheless, the association between severe winters and sunspot sightings may help to elucidate the discovery in Chinese provincial historical records of six sunspot sightings during the 'Maunder minimum'[24,25], as the seventeenth century was one of the coldest in China[22].

Received 23 June; accepted 19 August 1980.

1. Eddy, J. A. *Science* **192,** 1189–1202 (1976); in *The Solar Output and its Variation* (ed. White, O. R.) 51-71 (Colorado Associated University Press, Boulder, 1977).
2. Eddy, J. A. in *Physics of Solar Planetary Environments* Vol. II (ed. Williams, D. J.) 958–972 (American Geophysical Union, 1976); *Climatic Change* **1,** 173–190 (1977); in *The New Solar Physics* (ed. Eddy, J. A.) 11–33 (Westview Press, Boulder, Colorado, 1978).
3. Eddy, J. A. *Scient. Am.* **236,** 80–92 (1977).
4. Needham, J. *Science and Civilisation in China* Vol. 3 (Cambridge University Press, London, 1959).
5. Stephenson, F. R. & Clark, D. H. *Applications of Early Astronomical Records* (Hilger, Bristol, 1978).
6. Clark, D. H. & Stephenson, F. R. *Q. Jl R. astr. Soc.* **19,** 387–410 (1978).
7. Wittmann, A. *Astr. Astrophys.* **66,** 93–97 (1978).
8. Bray, R. J. & Loughhead, R. E. *Sunspots* 229 (Chapman and Hall, London, 1964).
9. Weatherburn, C. E. *A First Course in Mathematical Statistics* 2nd edn (Cambridge University Press, London, 1952).
10. Gherzi, E. *The Meteorology of China* (Imprensa Nacional de Macau, 1951).
11. Watts, I. E. M. in *Climates of Northern and Eastern Asia* (ed. Arakawa, H.) 1–117 (Elsevier, Amsterdam, 1969).
12. Ing, G. K. T. *Weather* **27,** 136–145 (1972).
13. Boucher, K. *Global Climate* (English Universities Press, London, 1975).
14. Goudie, A. S. *J. Arid Envir.* **1,** 291–311 (1978).
15. Ho Peng Yoke *The Astronomical Chapters of the Chin Shu* 23 (Mouton, Paris, 1966).
16. Bell, G. J., Peterson, P. & Chin, P. C. *Meteorological Aspects of Atmospheric Pollution in Hong Kong* 2–3 (Royal Observatory, Hong Kong, Tech. Note No. 29, 1970).
17. Lamb, H. H. *Climate: Present, Past and Future* Vol. 1 (Methuen, London, 1972).
18. Chu Ping-hai *Climate of China* (Jt Publs Res. Serv., 41374, US Department of Commerce, Washington, 1967).
19. *Climatic Table of Korea Climatological Standard Normals (1931–1960)* Part 1 (Central Meteorological Office, Sŏul, 1968).
20. Chu Wên-hsin *Li-tai Jih-shih K'ao* 89 (Commercial Press, Shanghai, 1934).
21. Wang, P. K. & Siscoe, G. L. *Solar Phys.* **66,** 187–193 (1980).
22. Lamb, H. H. *Climate: Present, Past and Future* Vol. 2 (Methuen, London, 1977).
23. Clark, D. H. & Stephenson, F. R. *Nature* **284,** 592 (1980).
24. Xu Zhentao & Jiang Yaotiao *Nanjing Daxue Xuebao* (*Ziran Kexue Ban*) No. 2, 31–38 (1979).
25. Cullen, C. *Nature* **283,** 427–428 (1980).

Frequency sensitivity of the deep-sea climatic record

Thomas J. Goreau

Center for Earth and Planetary Physics, Harvard University,
Cambridge, Massachusetts 02138

Attempts to explain quasiperiodic glacial/interglacial transitions[1] in the Pleistocene ^{18}O deep-sea stratigraphic record have focused on spectral analysis of palaeoclimatic data and comparisons with Milankovitch-type calculations of variations in isolation caused by periodicities of the Earth's orbit around the Sun[2–6]. Periods close to those of orbital eccentricity (100 kyr), obliquity (41 kyr), and precession (22 kyr) can be identified in deep-sea cores, but their relative strengths are very different from those of solar insolation and other peaks are also present. Mixing of sediment by deposit-feeding infauna significantly perturbs stratigraphic boundaries in deep-ocean sediments[7]. Although mixing models[8–11] have been proposed to describe quantitative effects of bioturbation no formulation of the effect of this process on the spectrum of the climatic record has been presented. Using the signal processing model[11], the suppression of recorded climatic variation over the past 700 kyr is estimated. In the frequency range where changes in the Earth's orbital path affect incident solar radiation the results support an appreciably larger role for astronomical 'forcing' of climate than previously estimated.

Mixing is treated here as a process which filters input information arriving at the surface of the sediments from the overlying water. The mixing function, operating on the input, is the spatial distribution of an impulse input to the sediment surface after some period of mixing. Mixing proceeds by a series of stochastic events in which organisms overturn, ingest and excrete sediment while in search of food. On a sedimentation time scale huge numbers of such events occur.

The model evaluates the evolution of the profile through numerical solution of equations like:

$$O_\tau(x) = F_\tau(x)\frac{I_\tau}{S_\tau} + \int_0^{L_\tau} F_\tau(x) O_{(\tau-\Delta\tau)}(x - x'')\,\mathrm{d}x''$$

where x is the depth in the core at time τ; x'' a dummy variable; Δt the time integration step; L_τ the maximum mixing depth; S_τ the sedimentation rate; I the input time series; F the spatial mixing function; and O the distribution of the output in the mixing zone. Mixing functions, as shown in Fig. 1, were chosen to simulate the range of bioturbation patterns inferred from stratigraphic, geochemical and benthic ecological studies, as well as functions used in simple models[8,9]. The curves at the left of Fig. 1 show mixing functions of varying concavity and convexity, whereas those at right indicate the output following a long period of continuous mixing and burial following a pulse input. Profiles of deep-sea ash layers[18] and microtektites[19] resemble those of curve 3 (right) with maximum mixing depth of around 10 cm, whereas short-lived radionuclides have profiles peaked at the surface like Fig. 2*b* left, and a similar maximum depth. The impulse response displays transient behaviour until the input has been buried to a depth of ~4*L*, after which change in the shape of the output is negligible. This is convenient as deep downcore the output is a simple convolution integral of the input and asymptotic mixing function response[11], but it requires that treatment of recent inputs such as pollutants, ^{14}C, U–Th series daughter products, and even the last glacial–interglacial transition use the full recursive model. Mixing models lacking 'memory' of previous outputs applied to the glacial meltwater 'spike'[12,13] produce numerically unstable results which 'blow-up' the data (see, for example, ref. 14). The programme for recursive unmixing will be discussed elsewhere.

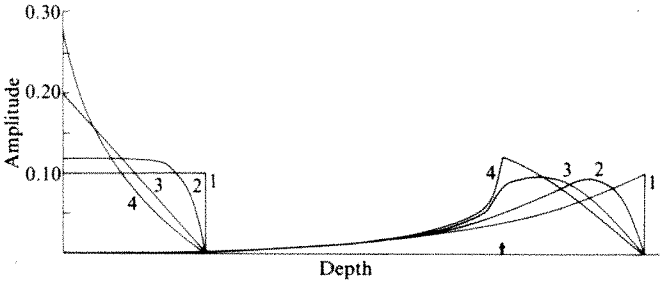

Fig. 1 Impulse response functions for mixing functions with the same maximum mixing depth but differing degrees of convexity and concavity. The curves at left show the 'instantaneous' (on a sedimentation time scale) response to a unit input at the top of the sediment, before burial. The curves at right show the output for unit inputs which have been delivered at the point shown by the arrow and subsequently mixed and buried. The impulse response function changes shape with increasing burial, but approaches asymptotic form after burial to about four mixing depths has occurred: only the initial and final shapes are shown. Amplitude reduction of unit inputs is sensitive to the shape of the mixing function near the surface, but almost insensitive to it after sufficient burial. Phase shifts between output and input are very sensitive to the shape of the mixing function. Deep-sea ash layer stratigraphy[18] and microtektites[19] give profiles of class 3, as do radionuclides such as ^{14}C. The first are deeply buried and the last are near surface inputs. Simulations using ^{14}C profiles show that they do not strongly constrain the shape of the mixing function.

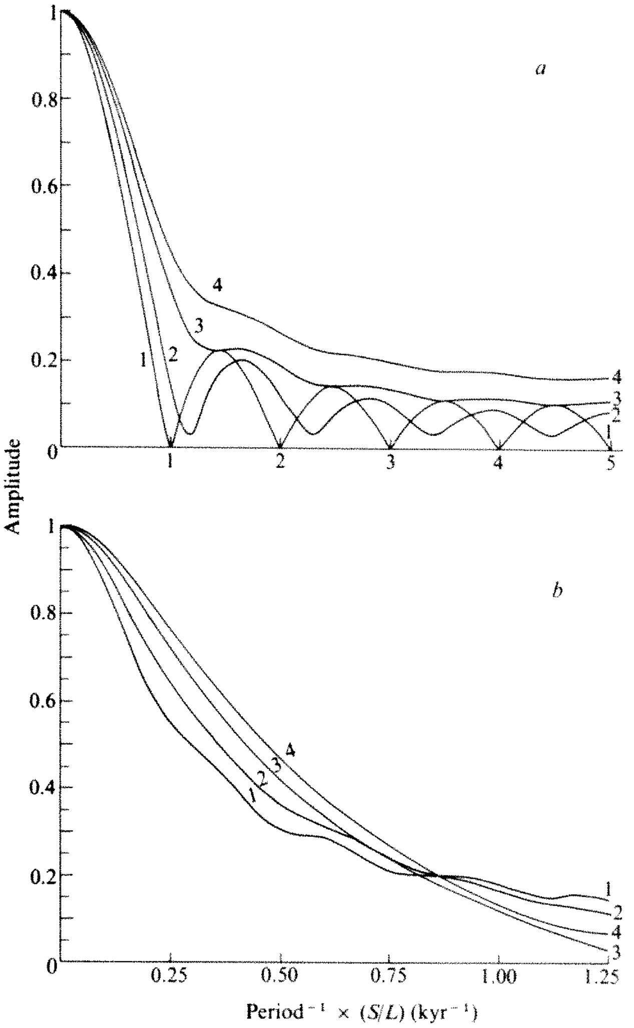

Fig. 2 *a*, The frequency response ('transfer') function for inputs to the surface before burial, calculated from the Fourier transform of the curves at the left of Fig. 1. Using curve 1 as a base for inverse filtering is numerically unstable because of the zeros in the curve. Frequency is scaled by the ratio of the sedimentation rate to the maximum mixing depth; a shape-dependent factor allows transformation to scaling by mean mixing depth, a convenient procedure when dealing with noisy data. *b*, Transfer functions following burial to asymptotic output shape under continuous mixing and burial. The curves of the right of Fig. 1 have been Fourier transformed as in *a* but note that the horizontal scales differ. The frequency band width of the bioturbation low-pass filter is about twice as wide before burial than after it so that high frequencies are somewhat better preserved at the very top of the core.

0028–0836/80/410620—03$01.00

Figure 1 shows the impulse response in the spatial domain. In the frequency domain the mixing transfer function, which indicates the fraction of input at any frequency seen in the output, can be obtained by Fourier transform of the curves of Fig. 1. This has been done by calculating the coefficients of the Fourier Series expansions. Figure 2*a* shows the frequency transfer functions for inputs before burial, and Fig. 2*b* shows the transfer functions of inputs so deeply buried that their transients have relaxed. For an input of known power spectrum, the power spectrum of the output is derived by multiplying the input power spectrum by the square of the transfer function at each frequency[15].

Climatic and other controls on local sedimentation rates introduce a non-linear filter that in the space domain is a measure of the uncertainty in the true age at each depth caused by variable sedimentation. This effect is particularly severe for high frequencies as small shifts in sedimentation alter apparent periodicities and suppress power. Present data on fluctuations of sedimentation rates are inadequate for quantitative treatment, although they limit the reliability of the record.

Curve *c* of Fig. 3 shows the power spectrum of Emiliani's[16] composite ^{18}O chronology for the past 730,000 yr (the late Pleistocene since the Brunhes–Matuyama magnetic reversal) computed from the periodogram determined by FFT[4]. Curve *b* shows the power spectrum of this climate record corrected for mixing by function 3 of Fig. 1 and appropriate values of L and S.

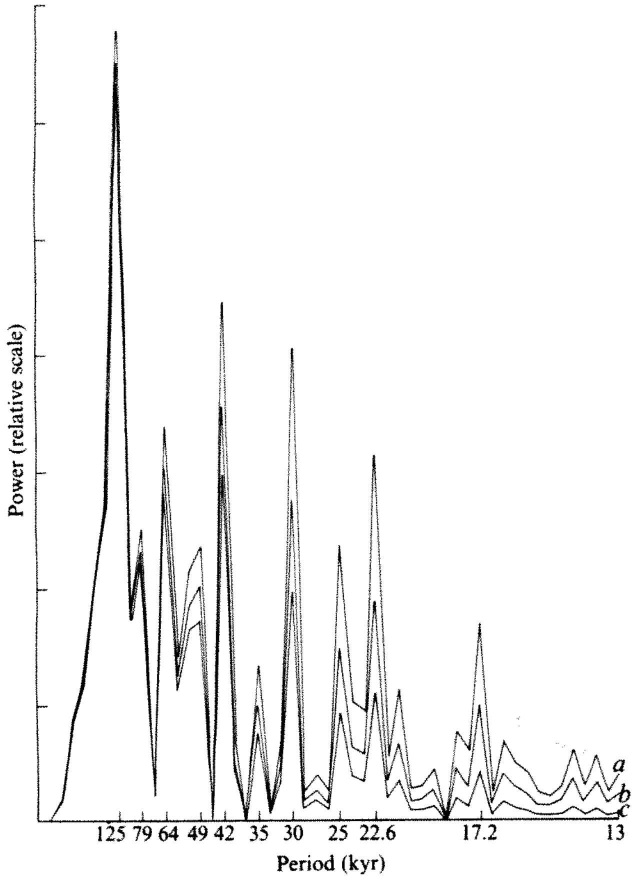

Fig. 3 Periodogram of observed climate variability of Emiliani's composite ^{18}O curve for the past 730 kyr (ref. 16) computed by FFT[4] (curve *c*). Curve *b* is the power spectrum unmixed by curve 3 and curve *a* for unmixing by curve 1 (note that the asymptotic form has been used, thus avoiding the numerical instability caused when the surface response is used to deconvolve the input). Bioturbation decreases the power at the precession frequency by a factor of two or more with respect to the power of the fundamental frequency, dependent on the shape of the mixing function. The non-Milankovitch frequencies at 64, 30, and 17 kyr^{-1} could be odd harmonics of the 125-kyr period produced by non-linear interactions but data are insufficient for statistical tests of this hypothesis without an underlying physical model (C. Wunsch, personal communication). The doublet at around 23 kyr results from splitting of the precession frequency by eccentricity modulation.

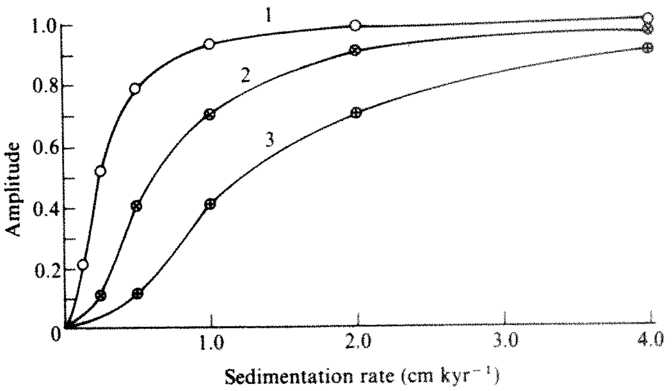

Fig. 4 Signal amplitude reduction at periodicities corresponding to those of the Earth's orbital eccentricity, obliquity, and precession for various sedimentation rates. These were calculated using curve 3 of Fig. 2*b* and S/L of 5 kyr^{-1}, a value consistent with the apparent sedimentation rates and mixing profiles of many deep-sea cores used in palaeoclimatic work. ○, 100 kyr; ⊗, 40 kyr; ⊕, 20 kyr.

Curve *a* shows the spectrum after correction for mixing pattern 1 of Fig. 1. Although such a pattern is atypical of deep-sea ash layers[18], it is similar to that assumed in most mixing models. These calculation suggest that the observed power at frequencies corresponding to orbital precession has been suppressed by a factor of about two. The actual amount may be greater because of possible variability in sedimentation rate. No attempt was made to 'tune-up' the record by making features cohere with expected precession and obliquity peaks as done by some workers without markedly changing the spectra[3,6].

Figure 4 shows the effect of sedimentation rate on amplitude suppression at 20, 40, and 100 kyr periodicities for a mixing curve of type 3 and a mixing depth of 10 cm. Increased depth of mixing shifts the curves to the right (greater attenuation of input), and reduced depth shifts them to the left. Analogous curves for attenuation and phase shift for mixing functions of differing shapes and S/L ratios are readily computed. Events of less than 10-kyr duration (such as the last glacial–interglacial transition) are strongly attenuated in all but very rapidly accreting cores. These results support Erez's suggestion that differences in glacial–interglacial ^{18}O amplitudes observed in cores from different oceans are greater than would be expected from mixing alone and are likely due to dissolution effects[20] or growth rate-dependent biological kinetic isotope fractionation during calcium carbonate deposition[21,22] superimposed on ice-cap volume and local temperature signals.

Energy-balance models have been developed to explain climate changes[23,24]. However, uncertainties in parametrizing atmospheric and oceanic heat transport, cloudiness, precipitation, albedo, and ice-cap growth as functions of insolation highlight the alternative approach: that of extracting as much information as possible from the historical record to estimate empirically climatic responses[3–6,16]. It has recently been suggested[5] that the observed climate spectrum is 'red' (power varying as the inverse square of frequency) in accordance with a climate model in which stochastic forcing at much higher frequency drives the lower frequencies seen in the deep-sea record[25]. When bioturbation is taken into account this interpretation is weakened: the astronomical frequencies explain a larger portion of the observed variance (as the coherence with insolation is proportional to responses at 20 and 40 kyr), and the spectrum is no longer 'red', dropping off as approximately the $-1/2$ power of frequency.

Deriving climate transfer functions for the astronomical theory of climate is made difficult by the narrow bandwidth of the forcing frequencies. At the high frequency end bioturbation limits the response, and at low frequencies it is uncertain whether the 100-kyr period is a sharply peaked or a non-linear response to eccentricity, an artefact of short data length, or generated by another process[3,4,23,24]. A linear climate model would require long response times: crustal rebound time scales[26] are too short, but some highly parameter-sensitive models have generated appropriate time constants for polar ice-cap growth[23,24,27]. The two processes are probably coupled[28]. Whatever mechanisms regulate climate on these time scales, detailed understanding of bioturbation is needed to estimate response time scales to external and endogenous forcing from the deep-sea record. This record contains more information than is apparent once the rules for its encoding are understood. Further work on particulate and chemical tracers of mixing[29–33] is needed to quantify the effects of bioturbation. Recent work on deep-sea ash layer stratigraphy[29,30] will further constrain the mixing function's spatiotemporal patterns in the deep sea and allow improved understanding of climate change.

I thank Cesare Emiliani and Henry Poor for data, discussion and encouragement; Carl Wunsch for stimulating comments; W. F. Ruddiman and W. H. Hutson for constructive suggestions.

Received 28 May; accepted 15 August 1980.

1. Emiliani, C. *J. Geol.* **63,** 538–578 (1955).
2. Kemp, W. C. & Eger, D. T. *J. geophys. Res.* **72,** 739–751 (1967).
3. Hays, J. D., Imbrie, J. & Shackleton, N. J. *Science* **194,** 1121–1132 (1976).
4. Rooth, C. G. H., Emiliani, C. & Poor, H. W. *Earth planet. Sci. Lett.* **41,** 387–394 (1978).
5. Kominz, M. A. & Pisias, N. G. *Science* **204,** 171–173 (1979).
6. Kominz, M. A., Heath, G. R., Ku, T.-L. & Pisias, N. G. *Earth planet. Sci. Lett.* **45,** 394–410 (1979).
7. McIntyre, A., Bé, A. W. H. & Preikstas, R. *Prog. Oceanogr.* **4,** 3–25 (1967).
8. Davis, R. B. *Limnol. Oceanogr.* **19,** 466–488 (1974).
9. Berger, W. H. & Heath, G. R. *J. mar. Res.* **26,** 134–143 (1968).
10. Guinasso, N. L. & Schink, D. R. *J. geophys. Res.* **80,** 3032–3043 (1975).
11. Goreau, T. J. *Nature* **265,** 525–526 (1977).
12. Emiliani, C., Rooth, C. G. H. & Stipp, J. J. *Earth planet. Sci. Lett.* **41,** 159–162 (1978).
13. Berger, W. H. *Nature* **269,** 301–304 (1977).
14. Berger, W. H. *Deep Sea Res.* **25,** 473–479 (1978).
15. Jenkins, G. M. & Watts, D. G. *Spectral Analysis and its Applications* (Holden Day, San Francisco, 1968).
16. Emiliani, C. *Earth planet. Sci. Lett.* **37,** 349–352 (1978).
17. Evans, D. L. & Freeland, H. J. *Science* **198,** 528–529 (1978).
18. Ruddiman, W. F. & Glover, L. K. *Bull. geol. Soc. Am.* **83,** 2817–2836 (1972).
19. Glass, B. P. *Earth planet. Sci. Lett.* **6,** 409–415 (1972).
20. Erez, J. *Nature* **281,** 535–538 (1979).
21. Erez, J. *Nature* **273,** 199–202 (1977).
22. Goreau, T. J. *Proc. R. Soc.* B**196,** 291–315 (1977).
23. Suarez, M. J. & Held, I. M. *J. geophys. Res.* **84,** 4825–4836 (1979).
24. Imbrie, J. & Imbrie, J. Z. *Science* **207,** 943–953 (1980).
25. Hasselman, K. *Tellus* **28,** 473–485 (1976).
26. Cathles, L. M. *The Viscosity of the Earth's Mantle* (Princeton University Press, 1975).
27. Birchfield, G. E. & Weertman, J. *J. geophys. Res.* **83,** 4123–4125 (1978).
28. Emiliani, C. & Geiss, J. *Geol. Rdsch.* **46,** 576–601 (1958).
29. Ruddiman, W. F. *et al. Sedim. Geol.* **25,** 257–276 (1980).
30. Hutson, W. H. *Geology* **8,** 127–130 (1980).
31. Peng, T.-H., Broecker, W. S. & Berger, W. H. *Quat. Res.* **11,** 141–149 (1979).
32. Krishnaswami, S., Benninger, L. K., Aller, R. C. & Van Dam, K. L. *Earth planet. Sci. Lett.* **47,** 307–318 (1980).
33. Fisher, J. B., Lick, W. J., McCall, P. L. & Robbins, J. A. *J. geophys. Res.* **85,** 3997–4006 (1980).

Dolomite formation in the seawater–freshwater interface

M. Magaritz & L. Goldenberg

Isotope Department, Weizmann Institute of Science, Rehovot, Israel

U. Kafri & A. Arad

Geological Survey of Israel, Jerusalem, Israel

The 'dolomite problem' long defied solution by geologists largely because it could not be resolved in experiments or by comparative studies with Recent sediments. Most of the known Pleistocene dolomites are from evaporative environments, whereas most of the ancient ones occur in rocks which show no evidence of intertidal or supratidal evaporative conditions. A possible environment for Recent formation of dolomites is the mixing zone between freshwater and seawater. We consider here dolomite formation in the interface mixing zone between freshwater and seawater and suggest that this type of dolomite formation is much more common than was previously indicated.

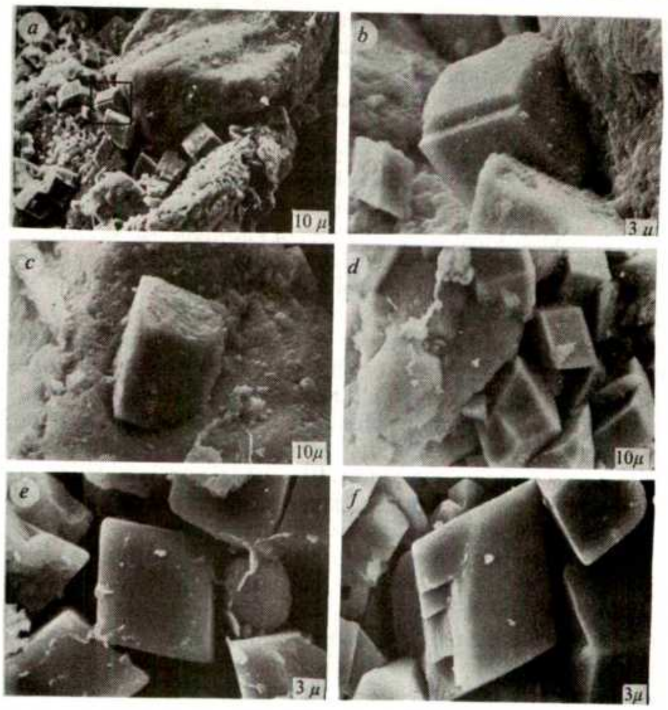

Fig. 1 *a*, Protodolomite rhombs cementing calcareous sandstone. Inset square is enlarged in *b*. *b*, *c*, Protodolomite rhombs attached to the surface of a quartz grain showing euhedral growth into the void. Imperfection of the euhedral form is found at the contact with the quartz grain. *d*, Protodolomite rhombs and calcite scalenohedron attached to bioclasts. Neither crystal shows evidence of replacement. *e*, Protodolomite cement and an unaltered coccolith. *f*, Subhedral protodolomite crystal.

Pleistocene to Recent dolomitization in hypersaline, evaporative environments has been reported by several authors[1–4]. In addition, dolomitization and precipitation of dolomite has been noted from freshwater karst systems[5]. Recent dolomite formation in brackish waters of the mixing zone between freshwater and either hypersaline or seawater has been postulated and described[6–8], particularly from carbonate coastal aquifers of the Caribbean region[8–10].

It seems that the latter phenomenon is more abundant than was previously recognized, little attention having been given to this process taking place in the diffusion zone between freshwater and seawater in coastal aquifers. This is probably partly related to the fact that most wells in coastal aquifers did not penetrate the diffusion zone.

Fortunately, the Mediterranean coastal aquifer of Israel is densely drilled and has been well sampled and documented to depths below the freshwater–seawater interface. This Quaternary coastal aquifer consists mainly of alternating calcareous sandstones (eolianites), claystones and siltstones[11,12]. The eolianites consist mainly of detrital quartz grains, transported from the Nile by longshore currents, together with 10% calcareous skeletal fragments. During exposure to meteoric water the bioclasts were recrystallized to coarse low Mg–calcite and calcitic cement was formed in the vadose zone[13,14].

Two groups of brackish water springs along the Coastal Plain of Israel, in the Zevulun Plain and southern Mt Carmel, were interpreted as mixtures of fresh aquifer water with intruding seawater[15,16]. Carbonate concretions which were precipitated from these brackish waters in the upper soil sequence were found to consist of magnesian calcites and some authigenic dolomite[17]. The ^{14}C age determination of the concretions from the Zevulun Plain was 3,200 ± 1,730 yr BP. (The age determination was carried out on magnesium-bearing calcite nodules which contain some protodolomite in the inner parts. The lack of

0028–0836/80/410622—03$01.00

available material meant that the gas for the counting had to be diluted, a process which increased the uncertainty of the age.)

Dolomite has been found in cores from the central and southern coastal aquifer of Israel, forming at the freshwater–seawater interface. Two horizons of protodolomite were detected in the cores, the upper one coinciding with the diffusion zone of the present-day freshwater–seawater interface and the lower one at a deeper level[18]. Note that the protodolomite occurrences were found only in these two specific horizons and not throughout the sequence.

Protodolomite which forms up to 90% of the total carbonate (sample 3K 108–109) has been studied using scanning electron microscope (SEM) (Fig. 1). Crystal size reaches 50 μm (Fig. 1*c*). Samples with a low protodolomite content are typically composed of smaller (1–15 μm) crystals. Some protodolomite rhombs form a cement around detrital grains (Fig. 1*a*), being attached to the grain at one point and showing euhedral growth into the intergranular void (Fig. 1*b*, *c*). This results in subhedral crystals (Fig. 1*f*). The protodolomite was formed in voids and is not pseudomorphing pre-existing $CaCO_3$. It precipitated directly from the solution and the sources of the Ca^{2+} and part of the CO_3^{2-} could be from dissolution of $CaCO_3$ somewhere in the aquifer. This can be seen in Fig. 1*a*, *b* where unaltered carbonate bioclasts are cemented by protodolomite. The crystals resemble closely the limpid protodolomites reported from schizohaline environments[8,19].

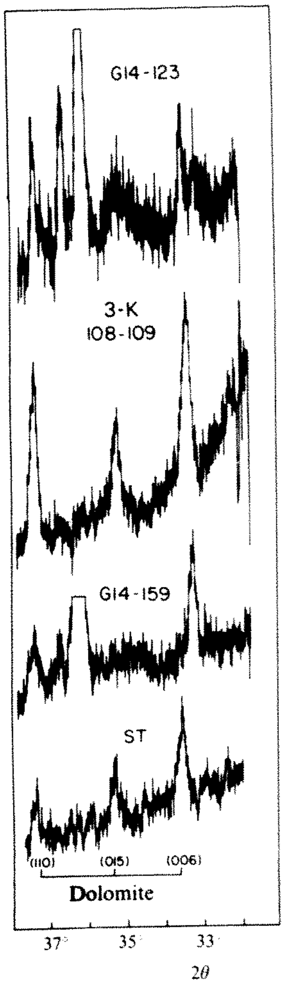

Fig. 2 X-ray diffraction traces showing variation in dolomite reflections in the studied samples compared to a standard ideal dolomite (ST). The ordering (015) reflection is broad and less intense than the non-ordering (110) peak. The 36.2° and 36.7° 2*θ* peaks are those of calcite and quartz.

All $CaMg(CO_3)_2$ minerals discussed here can be defined by X-ray diffraction and EDAX analyses as protodolomites[20]. The outer surfaces of the crystals are deficient with regard to Mg^{2+} compared with ideal dolomites. The EDAX analysis shows a Ca^{2+}/Mg^{2+} ratio between 6 and 7 (peak height) similar to some Florida limpid protodolomites[19], whereas this ratio in a normal dolomite is around 4. In addition, the X-ray diffraction (112) peak is shifted to the lower 2*θ* values typical of protodolomites with excess Ca^{2+}.

The degree of ordering of the protodolomites was determined by measuring the (015) ordering peak height and comparing it to another peak not directly associated with these alternating cation planes[21]. In the samples discussed the (015) ordering peak is either small (sample 3K 108–109) or almost non-existent (sample G 14-159) compared to the (110) non-ordering peak. The basal reflection (006) is slightly shifted compared to standard dolomite (Fig. 2).

The $\delta^{18}O$ and $\delta^{13}C$ values obtained for sample 3K 108–109 are $-1.3 \pm 0.1‰$ (ref. 22) and $-9.6 \pm 0.05‰$ respectively. These are similar to the results from Jamaican protodolomites precipitated from a mixture of seawater and CO_2 oversaturated groundwater[7]. The $\delta^{13}C$ values of these samples are similar to those obtained for the low Mg-calcite cement (−9 to −11‰) formed from meteoric water in the Israel Pleistocene coastal aquifer[14]. The $\delta^{13}C$ values of the dissolved carbonate in the aquifer near the coastline range between −10 and −12‰ and ^{14}C concentration range between 55 and 60 PMC (A. Kaufmann personal communication) indicating a mixed source for the dissolved carbonate (soil CO_2 and carbonate mineral dissolution). The $\delta^{13}C$ values of the protodolomite is −9.6‰ indicating an equilibrium between the protodolomite and the dissolved carbonate in the groundwater. The $\delta^{18}O$ of the protodolomite, however, differs by 4‰ from the calcitic cement. The same difference of 3–4‰ was experimentally obtained and has been attributed previously to isotopic fractionation between calcite and protodolomite[23].

The basic requirement for the dolomite depositing solution is that $[Mg^{2+}]/[Ca^{2+}] > 1$, and this ratio is reached at a chlorinity level[17] of 1,000 mg l^{-1}. As the cementing calcite and the protodolomite of the coastal aquifer discussed here are in isotopic equilibrium (having the same source of CO_3^{2-}) the solution must constitute more than 95% of the fresh groundwater. Dolomite formation is apparently proceeding in the subsurface of the Israeli Coastal Plain in a calcareous sandstone aquifer where the Mg^{2+} is mainly derived from seawater and where an isotopic equilibrium between calcite and protodolomite is reached.

We can now demonstrate that in addition to Recent dolomitization of an evaporative (supratidal) type, a non-evaporative dolomite precipitation is also currently occurring. This process seems to be more widespread than considered before, as it exists in a wide region where the mixing zone between fresh groundwater and intruding seawater occurs. In most of the known coastal aquifers, the contact between the two water bodies does not appear as a sharp interface, but as a wide diffusion zone occupied by brackish waters.

The existence of more than one level of dolomite precipitation in the sequence arises from the fact that the interface is not necessarily stationary. It moves vertically, shrinks and spreads with corresponding eustatic changes of sea level and seasonal fluctuations of the water table. Therefore, dolomites below the present-day interface might indicate 'palaeo-interfaces' or 'palaeo-diffusion zones' which were stationary during certain periods when lower sea levels prevailed, and are in agreement with the Quaternary history of the Mediterranean sea levels.

This continuous process of dolomite precipitation in the diffusion zone is responsible for the reported reduction of $[Mg^{2+}]/[Ca^{2+}]$ ratio[24] and it might also affect the reduction of permeability of some of the coastal aquifers by reducing their pore space.

We thank Dr A. Kaufmann for the ^{14}C age determination and M. Dvorachek and R. Knafo, for the SEM-EDAX analyses, and Dr D. J. J. Kinsman for his helpful comments.

Received 12 May; accepted 2 July 1980.

1. Alderman, A. R. & Skinner, H. C. W. *Am. J. Sci.* **255,** 561–567 (1957).
2. Kinsman, D. J. J. *Bull. Am. Ass. petrol. Geol.* **54,** 375 (1970).
3. Zenger, D. H. *J. geol. Educ.* **20,** 107–124 (1972).
4. Bathurst, R. G. *Carbonate sediments and their diagenesis: Developments in sedimentology* 12, (Elsevier, Amsterdam, 1975).
5. Thralkill, J. *J. Geol.* **79,** 683–695 (1971).
6. Hanshaw, B. B., Back, W. & Deike, R. G. *Econ. Geol.* **66,** 710–724 (1971).
7. Land, L. S. *Bull. mar. Sci.* **23,** 64–92 (1973).
8. Folk, R. L. & Land, L. S. *Bull. Am. Ass. petrol. Geol.* **59,** 60–67 (1975).
9. Hanshaw, B. B. & Back, W. *J. Hydrol.* **43,** 287–312 (1979).
10. Gebelein, C. D., Steiner, R. P., Hoffman, E. J., Garret, P. & Queen, J. M. *Bull. Am. Ass. petrol. Geol.* **63,** 457 (1979).
11. Issar, A. *Isr. J. Earth Sci.* **17,** 16–29 (1968).
12. Avnimelech, M. *Res. Counc. Isr. Bull.* **2,** 51–57 (1952).
13. Gavish, E. & Friedman, G. M. *J. sedim. Petrol.* **39,** 980–1006 (1969).
14. Magaritz, M., Gavish, E., Bakler, N. & Kafri, U. *J. sedim. Petrol.* **49,** 401–412 (1979).
15. Arad, A., Kafri, U. & Fleisher, E. *J. Hydrol.* **25,** 81–104 (1975).
16. Kafri, U. & Arad, A. *J. Hydrol.* **44,** 267–287 (1979).
17. Magaritz, M. & Kafri, U. *Chem. Geol.* **27,** 143–155 (1979).
18. Goldenberg, L. (in preparation).
19. Weaver, C. E. *Geology*, 425–428 (1975).
20. Gaines, A. M. *J. sedim. Petrol.* **47,** 543–546 (1977).
21. Füchtbauer, H. & Goldschmidt, H. *Geol. Rdsch.* **55,** 29–40 (1965).
22. Sharma, T. & Clayton, R. N. *Geochim. cosmochim. Acta* **29,** 1347–1351 (1965).
23. Fritz, P. & Smith, D. G. W. *Geochim. cosmochim. Acta* **34,** 1161–1173 (1970).
24. Nadler, A., Magaritz, M. & Mazor, E. *Geochim. cosmochim. Acta* **44,** 879–886 (1980).

---

^{243,244}Cm in Columbia River sediments

T. M. Beasley & L. A. Ball

School of Oceanography, Oregon State University,
Marine Science Center, Newport, Oregon 97365

Holm and Persson[1] have described the presence in lichens of ^{244}Cm resulting from the testing of nuclear devices. As the retention of transuranic radionuclides by lichens differs markedly as discussed by the above authors, integrated inventories of ^{244}Cm (mCi km^{-2}) resulting from fallout were not computed, nor were samples earlier than 1961–62 analysed to determine possible curium isotope production during testing in 1952–58. We have now measured ^{243,244}Cm as well as ^{238}Pu, ^{239,240}Pu and ^{241}Am in sediments from the Columbia River which show that (1) ^{243,244}Cm was produced in weapons tests before 1961, and (2) the total ^{243,244}Cm activity produced during testing was 1–3% that of ^{239,240}Pu. Even though the Columbia River received large amounts of radioactivity as a consequence of the operation of plutonium production reactors on the Hanford Reservation[2], we believe that the ^{243,244}Cm reported here is entirely derived from fallout and that our ability to detect these isotopes in river sediment is due to the concentrating effect of erosional processes on land which mobilize material containing ^{243,244}Cm (and other transuranic radionuclides) to the river, where they are subsequently sedimented.

The data presented here were derived from a sediment core raised from McNary Reservoir in August 1977. McNary Reservoir is located approximately 100 km downstream from the Hanford Reservation in Washington State and is formed by waters held by McNary Dam. It represents the first major accumulation site of fine-grained sedimentary material transported by the Columbia River after its confluence with the Snake, Yakima and Walla Walla rivers. On retrieval of the core, the sediment was extruded, sectioned and 0.5 cm trimmed from the outer rim to remove down-trained material. Each section was subsequently weighed, dried, homogenized and an aliquot dissolved in HNO$_3$ and HF. Calibrated amounts of ^{242}Pu and ^{243}Am were added before processing to quantify the recovery of Pu, Am and Cm isotopes. We have determined that our chemical procedures do not fractionate Am from Cm and therefore ^{243}Am can be used as a tracer for Cm isotopes. Our radiochemical procedures have been tested in blind intercalibration exercises[3] with excellent results. Except for the mass spectrometry data discussed below, all activities were determined by α spectrometry using silicon surface barrier detectors. Because the energies of the α particles emitted by ^{243}Cm and ^{244}Cm (5.79 and 5.82 MeV, respectively) are nearly identical, the relative percentages of the two isotopes cannot be distinguished by present-day α-spectrometry techniques. This becomes moderately troublesome where decay corrections are required owing to the different half lives of the two isotopes (^{243}Cm, $t_{1/2} = 28$ yr; ^{244}Cm, $t_{1/2} = 17.9$ yr). Therefore, the data reported here and those of Holm and Persson must be viewed with this constraint.

We will consider in turn our contention that curium isotopes were produced in weapons tests before 1961, that the curium isotopes we measure are derived from fallout rather than from the Hanford reactors and by inference, must be accumulating in environments similar to McNary Reservoir, and finally that by assuming identical mobilization from land for both Pu and Cm isotopes the total amount of curium isotopes deposited globally from weapons testing is 3–10 kCi.

Table 1 lists the activity concentrations of the transuranic radionuclides measured over the core length. The Pu and Am activities represent values at the time of collection; column 5 shows the curium isotope activities at the time of measurement (mid-1979) and column 6 the year represented by the respective sediment horizons. The sedimentation rate at this coring site ($\sim$1.8 cm yr^{-1}) was determined from the position of the ^{239,240}Pu subsurface maximum (identical to the subsurface maximum for ^{137}Cs) and the abrupt change in the ^{238}Pu/^{239,240}Pu ratio at 21 cm indicating the arrival of SNAP-9A ^{238}Pu in the Northern Hemisphere in mid-1966 (ref. 4). Our attempts to describe geochronologies using ^{210}Pb have been unsuccessful in McNary Reservoir because of the rapid sedimentation rates occurring there (2–5 cm yr^{-1}), the varying within-core textural qualities of the sediments, and the low activities of ^{210}Pb present (1–2 d.p.m. per g dry wt). All these conditions preclude the use of ^{210}Pb for establishing reliable sedimentation rates[5].

From the data of Table 1, we conclude that ^{243,244}Cm was produced in devices tested before 1961; unfortunately, low levels of activity present at depths >40 cm in our core prevented us fixing earlier production dates precisely. For the following reasons we do not believe the ^{243,244}Cm we measured in this core was derived from the operation of the various single-pass plutonium production reactors located at the Hanford complex which were in operation in 1944–71. First, from mass spectrometry measurements (T. M. Beasley, L. A. Ball and B. A. Blakesley, unpublished data), we have determined that the mean ^{240}Pu/^{242}Pu ratio observed in several cores raised from McNary Reservoir is 41 ± 9. Krey *et al.*[6] have reported a mean ^{240}Pu/^{242}Pu ratio of 40 ± 10 for global fallout on land. We consider that the agreement between these data sets suggests that release of Pu isotopes with mass numbers greater than 239 from the reactors did not occur and therefore the presence of their decay products (Am isotopes) could not have served as parent isotopes of ^{243,244}Cm through neutron capture and subsequent β decay.

Mass spectrometry results have also shown that approximately 25% of the ^{239,240}Pu radioactivity in McNary Reservoir sediments is reactor-derived. The mean ^{241}Am/^{239,240}Pu ratio from the data of Table 1, when corrected for this contribution, is 0.29. This is only slightly higher than the measured range of 0.22–0.25 characteristic of fallout-derived material as measured in the early to mid-1970s (refs 6, 7). Our values are somewhat higher due to the further decay through 1979 of ^{241}Pu ($t_{1/2} =$ 14.9 yr), the parent isotope of ^{241}Am. As the most probable event leading to direct introduction of ^{243,244}Cm to the river would have been fuel element rupture in the reactors, such events would most certainly have been accompanied by release of Pu isotopes and ^{241}Am. Because no excess ^{240}Pu appears in the sediments and because our ^{241}Am/^{239,240}Pu ratios are very near those of fallout, we think direct release of curium isotopes by the reactors unlikely.

To calculate integrated inventories of transuranics at the coring site (activity per unit area) the activity per g dry wt of sediment and the measured bulk dry density (g cm^{-3}) of each

0028-0836/80/410624—02$01.00

Table 1 Activity concentrations (d.p.m. per kg dry wt) of transuranic radionuclides in Columbia River sediments

Depth (cm)	^{238}Pu	^{239,240}Pu	^{241}Am	^{243,244}Cm	Year deposited
0–2	4.2±0.6	71±3	15.4±1.1	ND	
2–4	2.3±0.4	37±2	6.9±0.8	ND	
4–6	2.2±0.4	37±2	8.5±1.0	ND	
8–9	2.1±0.4	39±2	8.2±1.3	ND	
9–10	2.2±0.3	41±2	6.1±0.7	ND	
10–11	3.2±0.4	106±7	13.1±1.2	ND	
13–14	2.9±0.4	43±2	13.1±1.3	1.2±0.5	1970
14–15	3.0±0.4	51±4	9.4±0.6	0.6±0.2	
15–16	2.2±0.6	57±5	9.1±0.6	0.9±0.3	1969
16–17	3.4±0.5	73±3	16.3±0.6	0.8±0.2	
19–20	3.5±0.5	86±4	21.1±0.7	1.4±0.2	1967
22–23	3.6±0.5	105±4	28.7±2.2	1.4±0.2	
23–24	4.2±0.5	124±4	29.9±1.9	3.1±0.6	Mid-1964
24–25	3.9±0.5	117±4	29.3±2.1	2.9±0.9	
25–26	4.5±0.7	173±7	35.8±2.2	1.9±0.9	Mid-1963
26–27	4.0±0.6	147±6	32.4±1.8	1.6±0.4	
34–35	3.1±0.4	106±4	28.3±1.0	1.7±0.3	Mid-1958
39–40	1.9±0.4	79±3	18.1±1.2	0.8±0.2	1956
53–54	ND	4±0.7	ND	ND	
56–57	ND	0.16±0.08	ND	ND	

ND, not detectable. Errors represent 1 s.d. of the measurement determined from propagated counting errors.

section were plotted against depth through the core. The product of the mean activity per g dry wt and the mean bulk dry density over each 2.5 cm of core length was then summed to give the total activity per unit area. Errors through the summation process were propagated by standard techniques (1σ). We calculate integrated inventories of 19.4±0.5, 4.3±0.5 and 0.21±0.07 mCi km^{-2} for ^{239,240}Pu, ^{241}Am and ^{243,244}Cm, respectively, as of May 1979. Subtracting a 25% reactor contribution from the total ^{239,240}Pu activity gives a fallout-integrated inventory for these isotopes of 14.5 mCi km^{-2}, which is seven times the cumulative deposition that has been measured in undisturbed soils at 45° N latitude[8]. We have observed even higher cumulative deposits within the reservoir (>50 mCi km^{-2}), where both sedimentation rate and sediment texture lead to more rapid accumulation of fine-grained material. Clearly, erosional processes have mobilized the transuranic radionuclides from the landscape where they are then sedimented to the reservoir floor. Although the description of such processes is not novel, the degree of enrichment seen here for transuranic radionuclides is, we think, instructive.

Assuming ^{239,240}Pu and ^{243,244}Cm are mobilized by erosional processes to the same degree (a reasonable assumption based on our Am/Pu ratios measured), the amount of ^{243,244}Cm in our core was 1.4% that of the fallout ^{239,240}Pu in May 1979; considering the errors involved with individual inventory estimates, this percentage could be as low as 0.9% or as high as 1.9%. Were all the curium isotope activity due to ^{244}Cm (as was assumed by Holm and Persson for lichen), we calculate a decay-corrected total deposition of ^{244}Cm over the 14–40-cm interval of our core of 0.34±0.12 mCi km^{-2}, a value representing 2.3% of the total ^{239,240}Pu deposited (range 1.5–3.2%). As the half life of ^{243}Cm is significantly longer than that of ^{244}Cm, this latter calculation represents the maximum curium activity which could be present, and therefore we estimate that curium isotope deposition from fallout lies between 1 and 3% that of ^{239,240}Pu. As the ^{239,240}Pu inventory for global fallout has been reported at some 325 kCi (ref. 9), between 3 and 10 kCi of curium isotope activity has resulted from weapons testing.

We acknowledge support for this research from a contract with the Office of Health and Environmental Research, US Department of Energy.

Received 24 April; accepted 22 August 1980.

1. Holm, E. & Persson, B. R. R. *Nature* **273**, 289–290 (1978).
2. Foster, R. F. in *The Columbia River Estuary and Adjacent Ocean Waters*, 3–18 (University of Washington Press, Seattle, 1972).
3. Volchok, H. L. & Feiner, M. *EML-366*, 1–42 (Environmental Measurements Laboratory, US Department of Energy, 1979).
4. DeBortoli, M. C. & Gaglione, P. *Hlth Phys.* **16**, 197–204 (1969).
5. Nittrouer, C. H., Sternberg, R. W., Carpenter, R. & Bennett, J. T. *Mar. Geol.* **31**, 297–316 (1979).
6. Krey, P. W. *et al.* in *Transuranium Nuclides in the Environment, STI/PUB.410*, 671–678 (International Atomic Energy Agency, Vienna, 1976).
7. Livingston, H. D. & Bowen, V. T. in *Environmental Toxicity of Aquatic Radionuclides, Models and Mechanisms*, 107–130 (Ann Arbor Science, Ann Arbor, 1976).
8. Hardy, E. P., Krey, P. W. & Volchok, H. L. *Nature* **244**, 444–445 (1973).

Lower Cretaceous sediment from the East Antarctic continental shelf

Eugene W. Domack*, William W. Fairchild† & John B. Anderson*

* Department of Geology, Rice University, Houston, Texas 77001
† International Biostratigraphers Inc., 5933 Bellaire Blvd, Suite 108, Houston, Texas 77036

Except for a few localities along the Antarctic Peninsula, on Alexander and Livingston Islands (Fig. 1), there are no known outcrops of Cretaceous sedimentary rocks in Antarctica[1]. Thus, little is known concerning the palaeogeography and palaeoclimatology of Antarctica during the Cretaceous period. During Operation Deep Freeze 1979 to the George V–Adelie coast East Antarctica, a 40-cm long piston core, DF 79-38, was recovered which contains abundant palynomorphs of early Cretaceous age. Core 38 is an organic-rich siltstone believed to have been deposited in a non-marine setting. It represents the oldest known sediment recovered from the Antarctic continental margin and the first evidence for Cretaceous strata in East Antarctica. In addition, its exact location and sedimentary characteristics suggest an important correlation with similar sediments from the South Australian continental shelf.

Based on structural considerations, the probable existence of Cretaceous strata in Marie Byrd Land, West Antarctica (Fig. 1), was suggested by geologists of the New Zealand Antarctic Survey of 1958–59 (ref. 2). Cretaceous deposits are widespread on the South Australian continental shelf[3,4] and Kemp[5] discovered 'reworked' Lower Cretaceous palynomorphs in surficial glacial marine sediments collected off the West Ice Shelf, East Antarctica (Fig. 1). From this she suggests the local presence of sedimentary rock sequences of approximate Albian age. Reworked Cretaceous foraminifera have also been reported in Quaternary deposits from Taylor Valley, Transantarctic Mountains[6].

Core 38 penetrated a mono-lithological breccia which contains clasts of grey, organic-rich siltstone. Small flecks of carbonized organic matter and whispy laminations are conspicuous. Clasts are 0.5–4 cm in size and are highly angular. The breccia is clast-supported except for the upper 5 cm which contains a muddy matrix. Core 38 was taken at a depth of 1,407 m along the seaward flank of the George V Basin (67°44′ S, 146°51′ E Fig. 2). Based on available core coverage this unit is probably overlain by a relatively thick section of glacial and glacial marine sediments, some of late Quaternary age[7] (Fig. 2).

Five samples from the depths 8–10, 15–18, 24–29, 30–33, and 37–40 cm in Operation Deep Freeze Core DF 79-38 were processed for palynological study using standard maceration techniques. Each sample yielded abundant palynomorphs, comprising mainly spores with smaller amounts of saccate pollen. No significant differences were noted from top to bottom of the interval studied, suggesting that the entire interval was deposited in a single environment. The absence of marine microplankton (dinoflagellates) in these assemblages indicates deposition in a non-marine environment. Twenty-four species, listed in Table 1, were identified from core 38 samples, but the assemblages are so diverse and well preserved that many additional forms could undoubtedly be recognized with detailed study.

0028–0836/80/410625—02$01.00

Table 1 Palynomorphs recognized from DF 79-38

Aequitriradites spinulosus (Cookson and Dettmann) Cookson and Dettmann 1961
Alisporites grandis (Cookson) Dettmann 1963
Ceratosporites equalis Cookson and Dettmann 1958
**Cicatricosisporites australiensis* (Cookson) Potonie 1956
Classopollis classoides Pflug emend Pocock and Jansonius 1961
**Crybelosporites stylosus* (?) Dettman 1963
Cyathidites australis Couper 1953
**Cyclosporites hughesi* Cookson and Dettmann 1959
Foraminisporis wonthaggiensis (Cookson and Dettman) Dettmann 1963
Ischyosporites punctatus Cookson and Dettman 1958
Klukisporites scaberis (Cookson and Dettmann) Dettmann 1963
Stoverisporites lunaris (Cookson and Dettmann) Norvick and Burger 1975
Leptolepidites verrucatus Couper 1953
Lycopodiumsporites austroclavatidites (Cookson) Potonie 1956
Lycopodiumsporites circolumenus Cookson and Dettman 1958
Microcachrydites antarcticus Cookson 1947
**Murospora florida* (?) (Balme) Pocock 1961
Cepulina truncata (Cookson) Scultz 1967
Osmundacidites wellmanii Couper 1953
**Pilosisporites notensis* Cookson and Dettmann 1958
Schizoporis parvus Cookson and Dettmann 1959
Schizoporis reticulatus Cookson and Dettmann 1959
?*Trilobosporites trioreticulosis* Cookson and Dettmann 1958, maybe *T. purverulentus* (Verbitskaya) Dettmann 1963
Velosporites triquetrus (Lantz) Dettmann 1963

* The most stratigraphically useful species according to Dettmann and Playford[8].

An extensive review of Cretaceous palynology in Australia was presented by Dettmann and Playford[8]. They recognized four distinct spore–pollen zones as well as two subzones within the early Cretaceous. The oldest, *Crybelosporites stylosus* zone, was considered to be Neocomian; the *Cyclosporites hughesi* subzone as Neocomian to Aptian; the *Crybelosporites striatus* subzone as Aptian; and the youngest, *Coptospora paradoxa* zone, as Aptian to Albian. These zones have since been stratigraphically used in palynological studies in southern and eastern Australia. Most recently, Burger[9] found the zonation scheme of Dettmann and Playford[8] a workable one for Lower Cretaceous sediments of the Surat Basin in East Central Australia. In addition, Burger was able to correlate with faunal evidence and fix the age of his *Osmundacidites dubius* zone as Aptian[9]. Burger equates this zone with the middle and upper part of the *C. hughesi* subzone of Dettmann and Playford[8,9].

Many species identified in core 38 range throughout the Lower Cretaceous in Australia and elsewhere, and are thus of little value for precise age determinations. Five species in Table 1 are considered important stratigraphic indicators by Dettmann and Playford[8], most of these were also recognized by Burger[9]. A single specimen questionably identified as *C. stylosus* was noted in the sample from 37–40 cm. According to Dettmann and Playford this species is restricted to the *C. stylosus* zone, although Burger lists it as ranging up into the *O. dubius* zone[9]. *Murospora florida* and *C. hughesi* are found both in the *C. stylosus* zone and the *C. hughesi* subzone. *Pilosporites notensis* is also present in the *C. hughesi* subzone but ranges up into the *C. striatus* subzone as well. Comparison of the species identified in core 38 samples with those discussed by Dettmann and Playford[8] suggests that the assemblage present correlates fairly well with the *C. hughesi* subzone or the *O. dubius* zone of Burger[9], and that it is of early Cretaceous, Aptian age.

The continental margins of South Australia and East Antarctica, between 90° E and 150° E, represent classic passive-rifted margins[10,12]. The best morphological fit of the two continents before break-up seems to be that of Sproll and Dietz[10]; see also Weissel and others[13]. This fit is consistent with subsequent reconstructions of Australia–Antarctica with New Zealand, the Cambell Plateau, and other continental crust regions of the South-West Pacific margin of Gondwanaland[14]. According to their reconstruction, the continental shelf off the George V Coast, where core 38 was taken, lay directly south of the city of Adelaide and west of the Otway Basin, Australia (Fig. 3). Recent seismic profiling and exploratory drilling on the continental shelf of Australia has revealed a series of east–west trending normal faults[4,15]. Faulting occurred in the latest Cretaceous to earliest Tertiary, was associated with early rifting between the two continents, and produced a horst and graben structure typical of rifted margins[16]. Down-dropped blocks contain up to 2,500 m of Lower Cretaceous age sediments which are fluviatile-lacustrine in origin[15]. Transitional marine to marine sediments do not occur below the uppermost Cretaceous–Lower Tertiary stratigraphic interval, which unconformably overlies the Lower Cretaceous section.

The outer continental margin of East Antarctica, north of the shelf break, contains marginal rift structures similar to those developed along the southern Australian margin[17]. The George V Basin, of maximum depth[18] of 1,591 m, is one of several deep, inner shelf depressions which form a more or less continuous basin parallel to the coast of East Antarctica between 90 and 150° E (ref. 19). This feature is thought to represent a graben structure bounded by faults of Tertiary age[19]. Vanney and Johnson[20], in a more detailed analysis of the orientation of these basins, have also proposed a tectonic origin for these features.

The presence of Lower Cretaceous non-marine strata in the George V Basin implies a sedimentological and tectonic setting similar to that of the South Australian continental shelf during the Cretaceous. However, subsequent sedimentary and palaeoenvironmental conditions of the two regions have differed considerably, particularly with the development of a continental ice sheet on Antarctica, which is generally believed to have originated during the late Oligocene to mid-Miocene[5,21,22]. Unfortunately, early Tertiary sedimentary sequences from Antarctica are as limited as those of the Cretaceous period. With the discovery of early Cretaceous sediments from the East Antarctic continental shelf it seems likely that early Tertiary strata may be found in a similar setting. Future work should concentrate on coring of these marginal basins where a more complete sedimentary sequence may help clarify the palaeoclimatological setting of Antarctica.

This study was funded by NSF grants DPP77-26407 and DPP79-80242, and by grants from the Petroleum Research Foundation, administered by the American Chemical Society (PRF-1101-AC2 and PRF-2472-AC2). We thank officers and crew of the USCGC Glacier who provided the logistics for Operation Deep Freeze 1979, and Dennis Cassidy for help in obtaining samples.

Received 30 June; accepted 27 August 1980.

1. Craddock, C. *Geologic Map of Antarctica* (American Geographical Society, New York, 1970).
2. Cranwell, L. M., Harrington, H. J. & Speden, I. G. *Nature* **186,** 700–702 (1960).
3. Deighton, I., Falvey, D. A. & Taylor, D. J. *Aust. Petrol. Explor. Ass. J.* 25–36 (1976).
4. Boeuf, M. G. & Doust, H. *Aust. Petrol. Explor. Ass. J.* **15,** 33–43 (1975).
5. Kemp. E. M. *Mar. Geol.* **13,** 145–157 (1972); *Paleogeogr. Paleoclimat. Paleoecol.* **24,** 169–208 (1978).
6. Webb, P. N. & Neall, V. E. *Proc. Symp. on Antarctic Geol. and Solid Earth Geophys.* (SCAR/IUGS, Oslo, 1970).
7. Domack, E. W. thesis, Rice Univ. (1980).
8. Dettmann, M. E. & Playford, G. *Stratigraphy and Paleontology: Essays in honour of Dorothy Hill* 174–210 (ANU Press, Canberra, 1969).
9. Burger, D. *Palynological studies in the Lower Cretaceous of the Surat Basin, Australia Bull.* 189 (Australian Government Publications, Canberra, 1980).
10. Sproll, W. P. & Dietz, R. S. *Nature* **222,** 345–348 (1969).
11. Smith, A. G. & Hallam, A. *Nature* **225,** 139–144 (1970).
12. von der Borch, C. C., Conolly, J. R. & Dietz, R. S. *Mar. Geol.* **8,** 59–83 (1970).
13. Weissel, J. K., Hayes, D. E. & Herron, E. M. *Mar. Geol.* **25,** 231–277 (1977).
14. Griffiths, R. *Nature* **234,** 203–206 (1971).
15. Denham, J. I. & Brown, B. R. *Aust. Petrol. Explor. Ass. J.* **16,** 91–98 (1976).
16. Talwani, M., Mutter, J., Houtz, R. & Konig, M. *Geological and Geophysical Investigations of Continental Margins AAPG Mem.* **29,** 151–175 (1978).
17. Houtz, R. E. in *The Geology of Continental Margins* (eds Burke C. A. & Drake C. L.) 655–658 (Springer, New York, 1974).
18. Zhivago, A. V. *Proc. Soviet Antarct. Expd.* **21** (1961).
19. Holtedahl, O. & Holtedahl, H. *Bull. geol. Instn Univ. Uppsala* **40,** 183–187 (1961).
20. Vanney, J. R. & Johnson, G. L. *D. hydrogr. Z.* **32,** 39–88 (1979).
21. Hayes, D. E. & Frakes, L. A. *Init. Rep. DSDP* Leg **28,** 919–942 (1975).
22. Mercer, J. H. *INQUA Symp. Antarctic Glacial Evolution and World Paleoenvironment* 73–93 (1977).

Marine influence in the Triassic 'uplands'

John E. A. Marshall

Department of Geology, The University, Newcastle upon Tyne
NE1 7RU, UK

David I. Whiteside

Department of Geology, The University, Bristol BS8 1TR, UK

Several authors[1–4] have concluded that Mesozoic reptiles found in some fissures of the Bristol area belonged to a distinctive 'upland' fauna. We describe here a new fissure deposit recently found in the Carboniferous limestone near Thornbury which contains characteristic 'upland' reptiles associated with an assemblage of Rhaetian marine phytoplankton and land-derived palynomorphs. The marginal marine location of deposition deduced from the palynomorphs conflicts with the separation of late Triassic reptiles into 'upland' and 'lowland' regimens.

The new fissure is located 16 km north of Bristol in Tytherington quarry (ST 660 890). In 1975, before the level was flooded, several tons of fissure material were recovered and are now held in the University of Bristol.

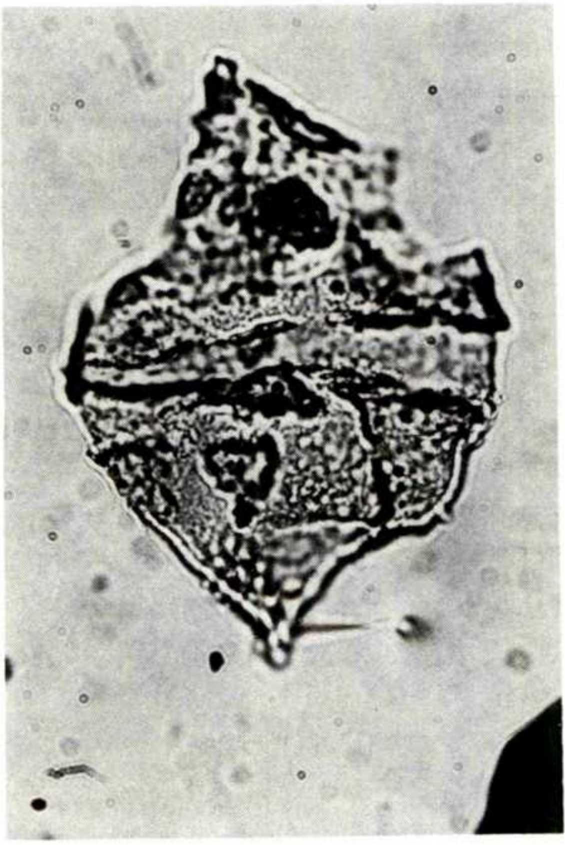

Fig. 1 The dinocyst *Rhaetogonyaulax rhaetica* (Sarjeant) Fisher and Van Helden, 1979 from the Tytherington fissure, ×1,000, transmitted light

Table 1 Palynomorph assemblage from the Tytherington fissure

	% of major elements (>1%)
Alisporites thomasii (Couper) Nilsson 1958	2
Cingulizonates rhaeticus (Rheinhardt) Schultz 1967	
Cingutrilites infrapunctus (Schulz) Morbey 1975	
Corollina torosus (Klaus) Cornet & Traverse 1975	9
Corollina zwolinskai Lund 1977	
Krauselisporites reissingeri (Harris) Morbey 1975	
Limbosporites lundbladii Nilsson 1958	
Lunatosporites rhaeticus (Schultz) Warrington 1974	
Ovalipollis pseudoalatus (Thiergart) Schuurman 1975	25
Rhaetipollis germanicus Schulz 1967	3
Riccisporites tuberculatus Lundblad 1964	18
Triancoraesporites ancorae (Rheinhardt) Schulz 1967	
Tsugaepollenites pseudomassulae (Madler) Morbey 1975	
Vesicaspora fuscus (Pautsch) Morbey 1975	4
Cymatiosphaera polypartita Morbey 1975	2
Dapcodinium priscum Evitt 1961	
Michystridium spp.	
Rhaetogonyaulax rhaetica (Sarjeant) Fisher and Van Helden 1979	19

The fissure material, composed of red and green marls, breccias and conglomerate, contains various terrestrial reptile bones, marine reptile fossils being entirely absent. Archosaur bones, such as those of *Thecodontosaurus*, are disarticulated and often in preferred orientation, but skeletal elements showing little sign of wear are frequently found associated; this suggests that transport has been very limited. Lepidosaur bones (including *Clevosaurus*), a few of which are water worn, occur widely distributed in the sediments. The reptiles include forms often termed as the Triassic 'upland' fauna[1–4] in contrast to the 'lowland' taxa with rhynchosaurs which are absent in the Bristol fissures.

The palynological assemblage was recovered from a grey siltstone. UV fluorescence studies[5] show that the palynomorphs were deposited in organic-rich laminae and have not been introduced in discrete reworked clasts. Furthermore, the assemblage itself is very well preserved. These findings therefore preclude any suggestion that the palynomorphs are derived from a Rhaetian deposit and reworked into the fissure in later times.

The palynomorph-bearing siltstone lies in a small pocket and although it borders an archosaur bone layer it has not itself yielded animal fossils. However, the nature of the enclosing fissure sediments (breccia, conglomerate and detritus-laden marls) and their chaotic bedform suggest a sedimentary episode of short duration. The most likely hypothesis is a cavern roof collapse with restricted pockets of silt forming in the spaces between the fallen rocks where the current flow would have been markedly reduced. In view of this situation and the finding of reptile remains from the same species in the marls enclosing the breccia and siltstone, we conclude that the palynomorphs and reptile bones were deposited penecontemporaneously.

The palynological assemblage (Table 1) has been compared with others of the European Rhaetian[6–8] and unequivocably equates with the *Rhaetipollis gemanicus* zone (phase 3). A comparison with other UK assemblages[9–11] shows that the sporomorph elements and proportions are consistent with a Rhaetian age from the Westbury or possibly lower Cotham Beds. Furthermore, the high percentage of the dinocyst *Rhaetogonyaulax rhaetica* is also consistent with this placing as there is a population acme for this species in the other British Rhaetian outcrops.

A further comparison with local British Rhaetian outcrops shows that the fissure palynomorphs have no distinctive elements which could be ascribed to an ecologically separate

0028–0836/80/410627—02$01.00

Table 2 Kerogen typing

Phytoplankton	4.5%	Total marine derived 51.5%
Amorphous kerogen	47%	
Wood	31%	
Cuticle	2.5%	Total terrestrial derived 48.5%
Spores/pollen	15%	

'upland' flora. The presence of acritarchs and dinocysts, well known from the nearby Rhaetian sections, indicate a marine input into the fissure. By analogy with the findings of Wall in some British Jurassic strata[12], the occurrence of the acritarch *Michystridium* sp. (as opposed to *Veryhacium*) suggests a near-shore (brackish?) environment and explains the absence of a stenohaline marine fauna. A morphological typing (Table 2) of the total kerogen shows that nearly half is amorphous organic material. Amorphous organic material is usually considered to have formed diagenetically[13] in marine conditions from algal biopolymers, through a monomer stage to give a condensed geopolymer. The high proportion of amorphous organic material in combination with the consanguineous Rhaetian dinocysts indicate a strong marine component and preclude any suggestion that the marine input was blown into an upland fissure by surface winds.

We postulate that the fissure was partly submerged under the transgressing Rhaetian sea. There is a patch of 'Rhaetic' (probably of the upper Westbury Beds) exposed 1 km south of the quarry and at a present-day altitude of over 20 m above the fossil-bearing cavern. This strengthens the suggestion that the lower fissure levels were flooded by saline waters; these would have brought in the organic-walled phytoplankton and provided the precursors for the formation of the amorphous organic material. At the same time, terrestrial vertebrates living around the entrance of the fissure and land-derived sporomorphs (showing no anomalous 'upland' elements) either fell or were washed into the cavern and were deposited with the marine palynomorphs.

This reconstruction of the environment exposes the anomaly of well preserved late Triassic 'upland' reptiles in a marginal marine deposit. Also, in the past, the difficulty of accurately dating 'upland' reptiles has meant that some 'lowland' taxa used for the comparison may not have been contemporaneous (for example, the last known record of a rhynchosaur is mid-Norian[14] whereas the Tytherington upland reptiles are Rhaetian). In view of these findings we suggest that the loose term 'upland' cannot prudently be applied to distinguish these fissure reptiles from those of other late Triassic sediments.

We thank Bob Savage and Geoffrey Warrington for encouragement and advice, and Mike Curtis for informing us of the find. Useful criticism and comments were also supplied by Keith Allen, Mike Benton, Sue Evans, Bernard Owens, Chris Cornford and Pete Smart. The Universities of Bristol and Newcastle-upon-Tyne and the NERC are thanked for financial aid.

Received 28 March; accepted 26 August 1980.

1. Robinson, P. L. *J. Linn. Soc.* (*Zool.*) **43,** 283–293 (1957).
2. Robinson, P. L. *Sci. Cult.* **33,** 169–173 (1967).
3. Tarlo, B. *New Scient.* No. 294, 32–34 (1962).
4. Halstead, L. B. & Nicoll P. G. *Studies in Speleology* Vol. 2, 93–102 (1971).
5. Ting, F. T. C. *Palynology* **1,** 27–32 (1977).
6. Morbey, S. J. *Palaeontographica* B**152,** 1–75 (1975).
7. Morbey, S. J. & Neves, R. *Rev. Palaeobot. Palyn.* **17,** 161–173 (1974).
8. Schuurman, W. M. L. *Rev. Palaeobot. Palyn.* **27,** 53–75 (1979).
9. Orbell, G. *Bull. geol. Surv. Gt Br.* **44,** 1–44 (1973).
10. Warrington, G. *Rev. Palaeobot. Palyn.* **17,** 133–147 (1974).
11. Warrington, G. *Bull. geol. Surv. Gt Br.* **57,** 40–43 (1977).
12. Wall, D. *Micropalaeontology* **11,** 151–190 (1965).
13. Welte, D. in *Advances in Organic Geochemistry* (eds Tissot, B. & Bienner, F.) 3–13 (1974).
14. Anderson, J. M. & Cruickshank, A. R. *Palaeont. afr.* **21,** 15–44 (1978).

0028-0836/80/410628—03$01.00

The first fossil cephalopod statoliths to be described from Europe

M.R. Clarke, Linda Maddock & E. Steurbaut

Marine Biological Association, Citadel Hill, Plymouth PL1 2PB, UK
Laboratorium Voor Paleontologie, Institute Gent, Belgium

Statoliths of cephalopods are small, hard calcareous stones which lie within the cartilaginous skulls of octopods, sepioids and teuthoids[1]. Fossil statoliths, clearly belonging to genera which are alive today, have previously been described from 11 Cenozoic deposits spanning from the Eocene to the Pleistocene in North America[2–5]. Such statoliths are of particular interest because they provide a means of studying the evolution of living cephalopod groups which have no calcareous shells, including the cosmopolitan and numerous teuthoids and octopods. Here, the first cephalopod statoliths to be recognized in European deposits are described and identified as *Loligo* sp. They are compared with the North American fossil *Loligo* species and statoliths removed from the two living *Loligo* species of Europe.

Cephalopod statoliths were found in two Burdigalian outcrops of the Southern Aquitanian Basin (early Miocene: age 20–16 Myr). Blue-greyish fine sand was sampled at the hamlets of Paillon, Poyartin (French geological map 1/50.000; XIV–43, Dax: coordinates $x = 342.100$, $y = 158.420$) and Jean Tic, Saubrigues (XIII–43, Saint-Vincent-de-Tyrosse: coordinates $x = 305.550$, $y = 152.050$), and each sample of 750 kg only yielded three statoliths. The deposits occurring at Paillon are considered to be synchronous with the Burdigalian stratotype deposits of northern Aquitaine, whereas those from Jean Tic,

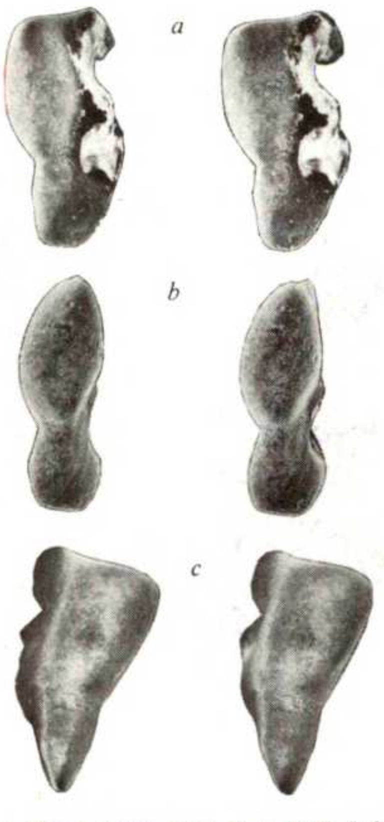

Fig. 1 *a–c*, Three stereo pairs of a fossil *Loligo* statolith (BM(NH) No. C46952) from a Miocene deposit in Europe photographed with a scanning electron microscope. These should be copied and suitably separated for obtaining a three-dimensional effect with a stereo viewer. Length of statolith = 1.75 m.

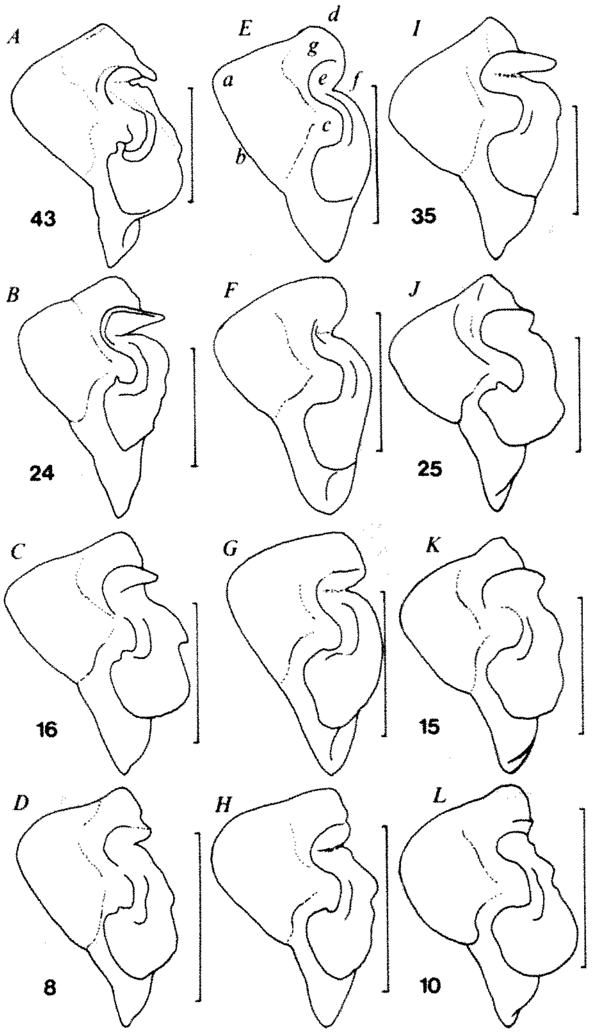

Fig. 2 Anterior views of *Loligo* statoliths. *A–D*, *L. vulgaris*; *E–H*, Miocene fossil statoliths from Europe (BM(NH) Nos. C46953–6). *I–L*, *L. forbesi*. Statoliths are shown as the same length to emphasize variation in form. Scales indicate 1 mm. The dorsal mantle length of the squids from which the statoliths were removed are indicated to the nearest centimetre. Drawings of statoliths *F–H* were reversed because they were the opposite side (left) to the others. Note that *E* and *F* are nearly the same length as *C*, *G* and *K*.

generally known as 'the Marls of Saubrigues', are certainly younger (? Upper or Post Burdigalian) and formed at greater depths[6].

The overall shape of these six statoliths is closely similar to statoliths removed from living *Loligo* species and clearly different from statoliths of cephalopods in other families. In particular, the lateral dome is broadest and rather pointed at its dorsal end (Figs 1, 2*a*), the lateral dome is not divided into superior and inferior lobes (Fig. 2*b*) and is oval from the lateral side and the spur is prominent and almost square (Fig. 2*c*). Other notable features are that the dorsal dome extends dorsally further than the lateral dome (Fig. 2*d*), the dorsal indentation (Fig. 2*e*) is smaller than the ventral indentation being both shorter and narrower, there is a distinct medial fissure (Fig. 2*f*) and the anterior surface of the dorsal dome is flat but not markedly deflected anteriorly (Fig. 2*g*). Although previous work shows that certain of these features distinguish between several *Loligo* species examined elsewhere and statolith shape varies between individuals and with growth (Fig. 2), when these variations are taken into account there are no other obvious features which distinguish between the fossil and the two living species of Europe *Loligo vulgaris* Lamarck 1799 and *Loligo forbesi* Steenstrup 1856. The North American fossil species are more easily distinguished from each other[3].

Comparison of these European fossils with North American fossil species shows that the European are closest in general shape to *Loligo mississippiensis* Clarke & Fitch 1979 from the Lower–Middle Oligocene deposit at Vicksburg, Mississippi[3]. They differ, however, from this species in having a less sharply pointed lateral dome which is more rounded anteriorly and ventro-laterally and has a deeper medial fissure.

To examine the species relationships further, nine dimensions of all the statoliths were used in a multiple discriminant analysis[4]. The measurements were defined previously[1,3,4] and are termed total length (tl), rostral length (rl), lateral dome length (ld), ventro-lateral length (vl), dorso-lateral length (dl), dorsal dome length (dd), dorsal-tip-to-spur length (dts), maximum width (w) and thickness (th). This analysis maximizes the differences between the species on the basis of combining all nine dimensions and extracting axes in decreasing order of importance. Thus, the first and second axes used here account for the greatest proportion of the total variance and give the best separation between the species.

The six European fossil statoliths fall into two size groups of three, corresponding to the two sites from which they were collected, and as the *L. vulgaris* and *L. forbesi* statoliths also both fall into two such size groups the analysis was run with nine groups, six for these three species and three American fossil species. The first two axes extracted accounted for 94% of the total variation between groups and were both significant at $P = 0.001$. All the scores on these two axes were standardized and the means and standard deviations of each of the nine groups are plotted (Fig. 3*A*).

Although there was some variation in the standard deviations between groups, the dispersions of the original variance–covariance matrices were not so different as to invalidate the discriminant analysis. The direction and magnitude of the effect

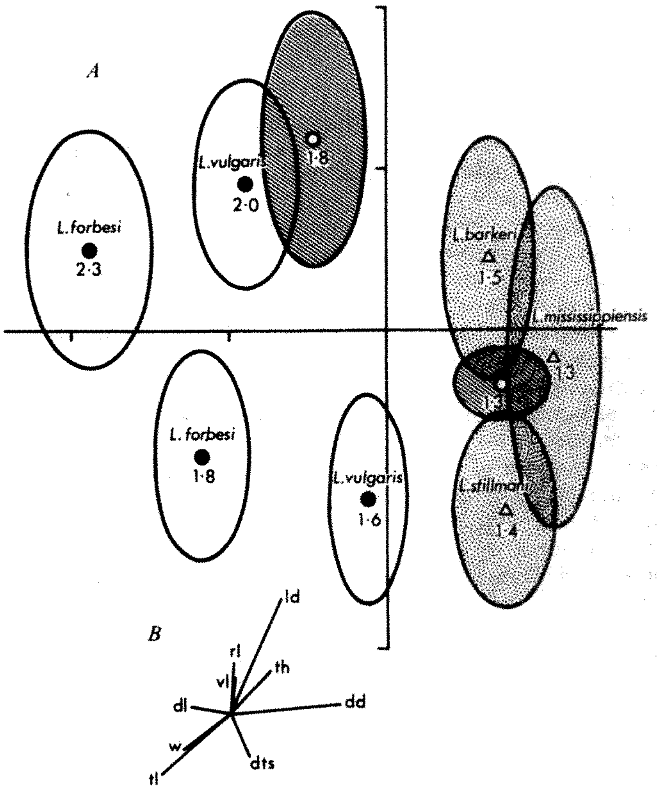

Fig. 3 *A*, Results of the multiple discriminant analysis of statoliths of three North American fossil species (stipled), one European fossil species (hatched) and two European living species of *Loligo*. The mean position of each species (or group) is plotted on the first two discriminant axes, with ellipses representing 1 s.d. for each group on each axis. The mean total length (in mm) of statoliths is given for each group. *B*, The relative weightings of the nine measurements on the axes. The measurements are identified as described in the text.

of each of the nine measurements on the separation of the species on the two axes are shown in Fig. 3*B*.

The spatial relationships between the groups of large and small statoliths of *L. forbesi*, *L. vulgaris* and the European fossil are very similar despite the fact that the fossil statoliths are smallest. This may suggest that the fossil species grew to a smaller adult than the living species. These fossils are approximately the same size as statoliths from *L. forbesi* and *L. vulgaris* individuals, with dorsal mantle lengths of 8.3–15.8 cm (Fig. 2). As the size of statoliths in the Loliginidae is closely correlated with the dorsal mantle length of the animals[5] it is likely that the fossil statoliths came from animals having mantle lengths of approximately 8–16 cm.

When the scores for all individual statoliths were plotted on the first two axes there was no overlap between *L. forbesi* and any of the fossils, whereas the larger *L. vulgaris* overlapped with the larger European fossils. The smaller *L. vulgaris* overlapped with *Loligo barkeri* and *Loligo stillmani* and the smaller European fossils overlapped with all three American fossils.

Thus, although differences between the species are rather too subtle to make identification possible between individual statoliths of *L. forbesi* and *L. vulgaris* or *L. vulgaris* and the large European fossils, discriminant analysis shows that there is a definite trend in form from the American fossils through the European Miocene fossil and *L. vulgaris* to *L. forbesi* (Fig. 3). Although the difference between the two size groups of the European fossil shown in Fig. 3 is probably a function of size, it might indicate a difference in species, because they come from different sites whose fauna show some differences. For example, the fish otoliths assemblage of Paillon, in which the smallest statoliths were found, differs from that of Jean Tic in having no mesopelagic representatives and in having many genera which are restricted today to the Indian Ocean. In addition, the association of Jean Tic contains some typical species recorded only from younger strata (ref. 6 and unpublished data). Such features are due to the difference in depth of deposition, but also reflect slight differences in age.

These data show that *L. vulgaris* or a closely similar species lived in European seas during the early Miocene. These seas were rather shallow (~ 30 m; the deepest parts, the canyon in which the Marls of Saubrigues were deposited, certainly did not exceed 300 m) and the climatic conditions were similar to those on the Atlantic coast of southern Morocco today.

Thus, the form of the statolith has remained virtually unchanged during a period of 20 Myr.

We thank Professors J. Z. Young and D. Donovan for helpful criticism. The fossils are housed in the British Museum (Natural History), London.

Received 14 August; accepted 9 September 1980.

1. Clarke, M. R. *J. mar. biol. Ass. U.K.* **58**, 701–712 (1978).
2. Clarke, M. R. & Fitch, J. E. *Nature* **257**, 380–381 (1975).
3. Clarke, M. R. & Fitch, J. E. *Palaeontology* **22**, 479–511 (1979).
4. Clarke, M. R., Fitch, J. E., Kristensen, T., Kubodera, T. & Maddock, L. *J. mar. biol. Ass. U.K.* **60**, 329–347 (1980).
5. Clarke, M. R. & Maddock, L. *J. mar. biol. Ass. U.K.* (in preparation).
6. Steurbaut, E. *Palaeontographica* **A166**, 1–3, 50–91 (1979).

Best shape for nature reserves

Margaret Game

Nature Conservancy Council, 19/20 Belgrave Square,
London SW1X 8PY, UK

The ideas of classical island biogeography[1] have been used[2–6] to derive rules for the optimal design strategy for nature reserves. For example, Diamond[3] states that, given limited (financial) resources, it is better to purchase a few large reserves rather than many small ones of equal total area; and that reserves should be as close to one another as possible. The validity of some of these rules has, however, been questioned[7–10]; for example it has recently been shown[9,10] that several small reserves may contain more species than a single one of equivalent area. These rules have nevertheless been accepted uncritically by others, including the IUCN[11]. Here, I examine Diamond's rule[3] that reserves should be as round as possible and conclude that in certain circumstances the optimal shape may be other than circular. There is no *a priori* reason for believing that these circumstances are unrealistic, and I know of no observational evidence to suggest whether they are found in nature or not. I also reason that the rule that reserves should be as close to each other as possible is inconsistent with the statement that they should be circular.

According to the tenets of island biogeography, the number of species inhabiting islands or isolated habitat patches (such as many nature reserves) is governed by the rates of extinction and immigration[1]; when these balance each other on average, the number of species is in equilibrium. If the extinction rate is higher than that of immigration, the island is supersaturated and the number of species will decline or 'relax' towards equilibrium. The rate of relaxation or net loss of species can be reduced by decreasing the rate of extinction or by increasing that of immigration and the purpose of Diamond's rules is to achieve both of these. For example, he states[3] that a large reserve is preferred to a smaller one because, amongst other things, it will have a lower extinction rate; and that reserves should be "as close to each other as possible ... to increase the immigration rates between reserves".

If immigration into nature reserves is indeed an important factor maintaining the total number of species, then it is questionable whether reserves should preferably be circular as this requirement implies the reduction of extinctions without reference to any simultaneous effects on immigration rate. To many dispersing organisms the apparent size of an island, and therefore the probability of colonization, must be more a reflection of the island's linear dimensions perpendicular to the direction of travel, that is the apparent width and height, rather than the area (J. L. Harper, personal communication). Therefore, immigration rate will depend on shape, not just area, whether the organisms are dispersed by voluntary or involuntary means. Thus, whereas departure from circularity may adversely affect extinction rate, this may be ameliorated by an increase in the immigrant population. The optimal shape for a reserve will depend on the balance between these two factors.

To investigate this quantitatively, define the dimensionless parameter R by[12]

$$R = \frac{p}{2(\pi A)^{1/2}}$$

where p is the island perimeter and A its area. R is a simple measure of shape; for any given area A, R may vary from unity for a circular shape to infinity for an infinitely long and narrow one. R is 1.1 for a square and 5.7 for a hedge 100 m long by 1m wide; the greater the departure from circularity, the greater is R.

Assuming that the effects of shape act independently of other influences, such as area and isolation, the average extinction and immigration rates, E and I, may be approximated by[1,4,13]

$$E = SVf(R)$$

$$I = (P - S)Ug(R)$$

where $f(R)$ and $g(R)$ are functions describing the effects of shape on E and I, S is the number of species present on the island at the given time, P is the total number of species in the species pool available for colonization, and V and U express the effects of other factors such as area, isolation, habitat diversity and such. To simplify the analysis, I ask: what value of R maximizes the equilibrium number of species, S_0? An alternative but qualitatively similar question would have been: what

0028–0836/80/410630—03$01.00

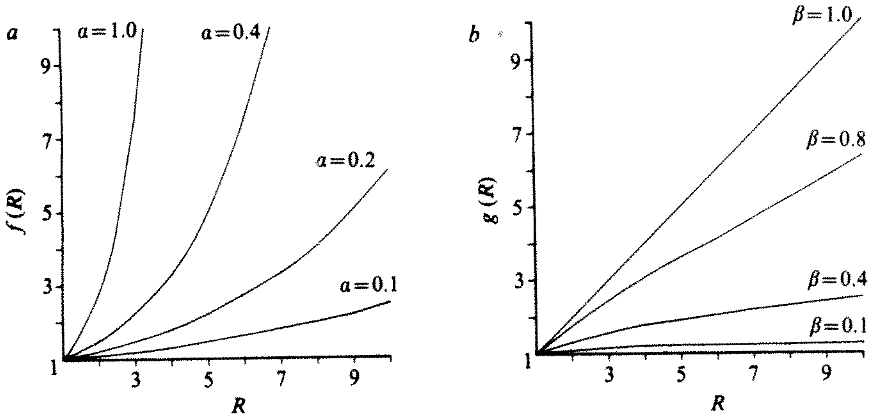

Fig. 1 *a*, Variation of $f(R)=C^{\alpha(R-1)}$ with α. *b*, Variation of $g(R)=R^{\beta}$ with β.

value of R minimizes the net extinction rate, $E-I$? At equilibrium, $I=E$, so that

$$S_0=\frac{PUg(R)}{Vf(R)+Ug(R)}$$

and this is maximum at constant U and V when

$$f(R)\frac{\partial g(R)}{\partial R}=g(R)\frac{\partial f(R)}{\partial R} \qquad (1)$$

I now ask what values $f(R)$ and $g(R)$ may reasonably be expected to take. It might be expected that the influence of shape on E is relatively slight when R is low (nearly circular reserves), but becomes severe at large R so that $f(R)$ would vary with R as shown in Fig. 1*a*. On the other hand, $g(R)$ might rise roughly linearly with R (which is proportional to perimeter length p) or level off towards some asymptotic value, as shown in Fig. 1*b*. Examples of functions with these general shapes, normalized to $f(1)=g(1)=1$, are:

$$f(R)=\exp\left(\alpha(R-1)\right) \text{ with } \alpha\geqslant 0$$

$$g(R)=R^{\beta} \text{ with } 0\leqslant\beta\leqslant 1$$

Substituting these functions in equation (1), the value of R which yields the highest value of S_0 is given by

$$R=\frac{\beta}{\alpha} \qquad (2)$$

(It is easily verified that this represents a maximum rather than minimum in S_0.) As $R\geqslant 1$, equation (2) only has a solution when $\alpha\leqslant\beta$.

The conclusion is: if extinction rate is not too dependent on shape (α is small) but immigration rate has a relatively stronger dependence on shape (β is not small), then the optimal shape for a reserve to maximize the equilibrium number of species is not circular. If these conditions are not met (that is, $\alpha\geqslant\beta$), so that a long boundary length affects the extinction rate more than the immigration rate, then the optimal shape is circular.

The above conclusion does not depend qualitatively on either the exact forms of f and g which were used or the equilibrium state being achieved. In general, if I depends relatively strongly on shape and E relatively weakly at least at low R, then there is no *a priori* reason to believe that a circular reserve will lead to the greatest number of species being conserved. However, this reuslt does depend on immigration contributing significantly to the maintenance of the total number of species.

There are several ways in which reserves may come into existence and this will influence whether immigration or extinction processes predominate. Perhaps the commonest mode of creation is the preservation of a remnant habitat patch while surrounding habitat is removed or degraded. However, reserves have also been created *de novo* by establishing habitats on a site where they had been destroyed or damaged. When existing habitat is being preserved, species extinctions are likely to dominate immigration if the reserve is either heavily supersaturated or has become relatively isolated. Supersaturation may occur through at least two processes. If habitat is destroyed, mobile creatures may concentrate in remaining patches. Alternatively, if the 'area-*per se*' hypothesis is correct[1,14,15] and the number of species increases with area because greater populations of each species cause a decrease in extinction probabilities, then if habitat area is suddenly reduced the site may be supersaturated for a time depending on the rate of relaxation. It is not known whether many reserves in Britain are supersaturated in this sense; Terborgh[2] and Diamond[16] believe that supersaturation occurs on some tropical islands and that it takes thousands of years for the avian fauna to relax to equilibrium, but this time scale is questioned by Abele and Connor[8].

Isolation of suitable habitat affects the ability of species to colonize. Many reserves in Britain are relatively remote from each other, reducing the probability of inter-reserve transfer. However, although species in need of conservation are often sedentary[17–19] this is not the case for migratory animals or for some plants such as orchids and bryophytes (M. O. Hill, personal communication). Therefore there are cases where immigration is an important factor even when long established habitat is involved. Immigration must certainly be of primary significance when new habitat is created. Note that where immigration is not an important factor, there is no need to locate reserves as close to each other as possible because the possibility of inter-reserve transfer of 'desirable' species is slight. Therefore Diamond's rules concerned with reducing mutual isolation of reserves are inconsistent with his statement that reserves should be as circular as possible: the first assumes that immigration is important and the second that it is not.

Finally, reserve shape may also affect other factors not explicitly accounted for in the above analysis. In particular, as J. L. Harper (personal communication) has pointed out, soil diversity and other habitat heterogeneities might be greater in long, linear reserves than in circular ones, and this might increase the number of species.

I thank J. L. Harper and Deborah Rabinowitz for useful discussions.

Received 7 July; accepted 26 August 1980.

1. MacArthur, R. H. & Wilson, E. O. *Evolution* **17**, 373–387 (1963); *The Theory of Island Biogeography* (Princeton University Press, 1967).
2. Terborgh, J. *Bioscience* **24**, 715–722 (1974); *Tropical Ecological Systems, Trends in Terrestrial and Aquatic Research* (eds Golley, F. B. & Medina, E.) 369–380 (Springer, New York, 1975).
3. Diamond, J. M. *Biol. Conserv.* **7**, 129–146 (1975).
4. Diamond, J. M. & May, R. M. *Theoretical Ecology, Principles and Applications* (ed. May, R. M.) 163–186 (Blackwell, Oxford, 1976).
5. Wilson, E. O. & Willis, E. O. *Ecology and Evolution of Communities* (eds Cody, M. L. & Diamond, J. M.) 522–534 (Harvard University Press, 1975).
6. Hooper, M. D. *The Scientific Management of Animal and Plant Communities for Conservation* (eds Duffey, E. & Watt, A. S.) 555–561 (Blackwell, Oxford, 1971).
7. Simberloff, D. S. & Abele, L. G. *Science* **191**, 285–286 (1976).
8. Abele, L. G. & Connor, E. F. *Proc. First Conf. sci. Res. in The nat. Parks* (ed. Linn, R. M.) Vol. I, 89–94 (1979).
9. Higgs, A. J. & Usher, M. B. *Nature* **285**, 568–569 (1980).
10. Gilpin, M. E. & Diamond, M. D. *Nature* **285**, 567–568 (1980).
11. Int. Union for Conservation of Nature and Natural Resources *World Conservation Strategy* (IUCN-UNEP-WWF, 1980).
12. Faeth, S. H. & Kane, T. C. *Oecologia* **32**, 127–133 (1978).
13. Gilpin, M. E. & Diamond, J. M. *Proc. nat. Acad. Sci. U.S.A.* **73**, 4130–4134 (1976).
14. Preston, F. W. *Ecology* **41**, 611–627 (1960); **43**, 185–215, 410–432 (1962).

15. Connor, E. F. & McCoy, E. D. *Am. Nat.* **113**, 791–833 (1979).
16. Diamond, J. M. *Proc. natn. Acad. Sci. U.S.A.* **68**, 2742–2745 (1971); *Proc. natn. Acad. Sci. U.S.A.* **69**, 3199–3203 (1972).
17. Pickett, S. T. A. & Thompson, J. N. *Biol. Conserv.* **13**, 27–38 (1978).
18. Diamond, J. M. *Ecology and Evolution of Communities* (eds Cody, M. L. & Diamond, J. M.) 342–445 (Harvard University Press, 1975).
19. Peterken, G. F. *Biol. Conserv.* **6**, 239–245 (1974).

Habitat selection maintains a deleterious allele in a heterogeneous environment

J. S. Jones & R. F. Probert

Department of Genetics and Biometry, University College London,
4 Stephenson Way, London NW1 2HE, UK

Little is known of how the large amount of genetic variation found in natural populations is maintained. Diversifying natural selection in a heterogeneous environment has great potential for promoting genetic polymorphism[1]. If one allele is favoured in one microhabitat and the alternative allele in another (which may be separated from the first by space or time), the disruptive effects of selection can maintain both alleles in the population. The limiting conditions of niche size, selective intensity and gene flow which could in theory maintain polymorphism in this way have been widely discussed[2,3]. This mechanism is much more effective in promoting genetic diversity if carriers of the alternative alleles are able to select the niche in which their fitness is greatest[4]. Here we explore the properties of a system in which two *Drosophila* eye colour alleles, known to show differences in fitness, are given the opportunity to select different microhabitats in a population cage. It seems that habitat selection in a heterogeneous environment can lead to the maintenance of polymorphism for an allele which is disadvantageous in either habitat when no opportunity for choice is available.

Eye colour mutants in *Drosophila* alter their carriers' response to light[5,6]. Wild-type (red-eyed) flies are in general positively phototactic, but are repelled by very bright light[7]. Flies lacking red screening pigment in the eye are more sensitive to light and tend to choose habitats in which light intensity is lower[8]. Wild-type flies are effectively blind in dim light (which is blocked by their screening pigment) whereas white-eyed flies (which lack this pigment) move towards dim red light as it is within their preferred range of hue and intensity. They avoid the bright white light selected by the wild type. White-eyed *Drosophila melanogaster* are considerably less fit than the wild type in white light, and are rapidly eliminated from polymorphic populations in cages[9].

Drosophila simulans (unlike *D. melanogaster*) mates less well in reduced light[10]. It is therefore possible that, in dim red light, white-eyed *D. simulans* might have a mating advantage over the wild type, as this is within their perceptual range but below that of the wild type. There is thus the opportunity to design a system in which lights of different hue and intensity cause flies of different genotype at the eye colour locus to select, because of their phototactic behaviour, an environment in which they are relatively fit. We describe here an experiment on the role of habitat choice and diversifying selection in a patchy environment on eye colour polymorphism in *D. simulans*.

Experimental populations were founded in cages of volume 8,750 cm^3 each of which was divided into two by a vertical partition having at its upper edge a 20 × 2-mm slit through which flies could pass freely. In the five white light controls, both halves of the cages were illuminated from above by a bright white light produced by three 80-W 'daylight' fluorescent tubes. The light in the five red light controls resulted from the attenuation of this by 10 thicknesses of red filter material to give a dim red light in both sections of the cage. In the five experimental cages, one half was illuminated by the bright white and one half by the dim red light. Each population was founded with 120 homozygous fertilized females from a wild-type strain, and the same number of fertilized female homozygotes from a white-eyed strain. The founding generation of flies was phased in over 3 weeks to reduce later population fluctuations. Cages were kept at 22–25° C and contained 200 ml of cornmeal–agar–molasses medium, one-third of which was replaced each week. Samples were taken by scoring the offspring of four sampling vials introduced to each side of the cage at 3-week intervals.

Figure 1 shows the course of gene frequency change. The frequency of the *w* allele drops rapidly in both white light and red light control cages; by week 30 its mean frequency in the white light controls is 0.01 and in the red light controls 0.06. However, although this allele is deleterious in both environments when no habitat choice is available, in the heterogeneous environment of the experimental cages the polymorphism is maintained for at least 30 weeks; the mean frequency of *w* in the patchy cages after this period is 0.32. Habitat selection (which may lead to an apportionment of resources between flies of different genotype) is maintaining polymorphism for an allele which in a uniform environment is lost from the population.

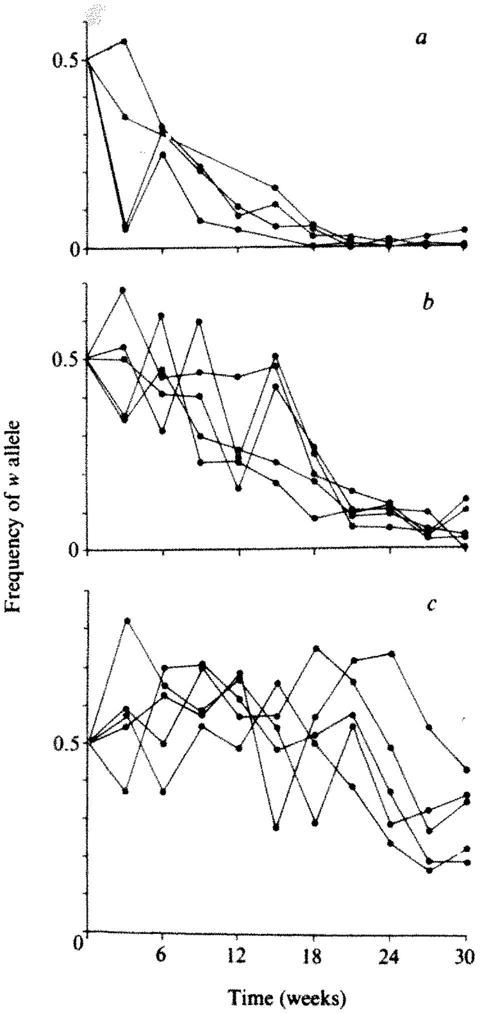

Fig. 1 Changes in the frequency of the *w* allele in *D. simulans* in: *a*, white light controls, *b*, red light controls and *c*, heterogeneous environments. One of the white light controls became extinct early in the experiment. Allele frequencies at this sex-linked locus were estimated using the weighted mean frequency in each sex. Although this does not provide an exact measure of allele frequency (as Hardy–Weinberg conditions do not hold) it is the most efficient estimate available.

0028-0836/80/410632—02$01.00

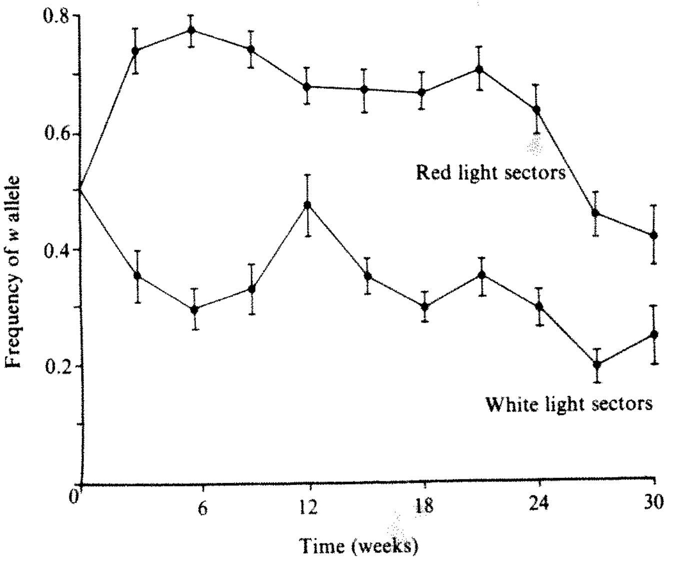

Fig. 2 Divergence in the frequency of the *w* allele between the red light and white light sectors of the experimental cages, summed over all cages.

There is considerable divergence in allele frequency between the two halves of the experimental cages (Fig. 2). To assess gene flow between red and white sectors two movement experiments were carried out. In the first, 12 vials containing *w* larvae were placed in the white light half of an experimental cage, and the same number of vials containing + larvae placed in the red light half. Flies emerged from the vials over the following 7 days and assorted themselves according to their habitat preference. The frequency of each allele among the offspring of the experimental flies was assessed by placing four sampling vials in each sector 1 week later. The frequency of *w* in the flies emerging from the sampling vials was 0.47 in the red light sector and 0.38 in the white light ($x_1^2 = 7.1$; $P < 0.01$). In the second experiment the 12 *w* vials were placed in the red light sector and the 12 + vials in the white light. Their offspring were sampled in the same way as in the first experiment; the frequency of *w* was 0.42 in the red light sector and 0.17 in the white light ($x_1^2 = 31.1$; $P < 0.001$). There is, therefore, the opportunity for substantial habitat selection by each generation between the environmental patches in the experimental cages. This is true whether or not the flies emerge into their preferred microenvironment, and must play a part in maintaining the differences in gene frequency between these patches shown in Fig. 2.

Associations between the extent of genetic polymorphism in natural populations and the ecological diversity of the habitats in which they live have often been reported. Populations of *Drosophila willistoni* living in florally complex environments have more inversion polymorphism than do those from simpler habitats[11] and there may be in some groups of animals a general association between niche breadth and morphological variation[12]. Similarly, *Drosophila* populations exposed to diverse environments in the laboratory retain chromosomal and molecular polymorphism to a greater extent than do those kept in stable conditions[13,14]. Natural and laboratory environments containing a variety of microhabitats offer the opportunity for genotypes to select those which are optimal. Differences in the tendency of individual members of natural populations to select particular microenvironments have indeed been found in *Drosophila*[15,16], and selection of the appropriate niche increases the relative fitness of, for example, melanic moths, cryptically coloured molluscs and lizards, and perhaps also of enzyme polymorphisms in *Asellus* and *Drosophila* exposed to a variety of foods[17–21].

Habitat selection can increase the fitness of an allele which is already advantageous. The experiments described here show that it can also lead to the maintenance of polymorphism for an allele which is otherwise deleterious to its carriers.

We thank Drs Derek Cosens, P. Hedrick, C. A. B. Smith and C. E. Taylor for useful discussions. R. F. P. was supported by a studentship from the SRC.

Received 3 March; accepted 15 August 1980.

1. Levene, H. *Am. Nat.* **87,** 331–333 (1953).
2. Maynard Smith, J. & Hoekstra, R. *Genet. Res., Camb.* **35,** 45–57 (1980).
3. Hedrick, P. W., Ginevan, M. E. & Ewing, E. P. *A. Rev. Ecol. Systematics* **7,** 1–32 (1976).
4. Taylor, C. E. *Genetics* **83,** 887–894 (1976).
5. Waddington, C. H., Woolf, B. & Perry, M. *Evolution* **8,** 89–96 (1954).
6. Markow, T. A. & Scavarda, N. J. *Behav. Genet.* **7,** 139–146 (1977).
7. Rockwell, R. F. & Seiger, M. B. *Am. Scient.* **61,** 339–345 (1973).
8. Chabora, P. C. & Kessler, M. E. *Behav. Genet.* **7,** 281–290 (1977).
9. Reed, S. C. & Reed, E. W. *Evolution* **4,** 34–42 (1950).
10. Grossfield, J. *Proc. natn. Acad. Sci. U.S.A.* **68,** 2669–2673 (1971).
11. Da Cunha, A. B. & Dobzhansky, Th. *Evolution* **8,** 119–134 (1954).
12. Van Valen, L. *Am. Nat.* **99,** 377–390 (1965).
13. McDonald, J. F. & Ayala, F. J. *Nature* **250,** 572–574 (1974).
14. Powell, J. R. *Science* **174,** 1035–1036 (1971).
15. Taylor, C. E. & Powell, J. R. *Genetics* **85,** 681–695 (1977).
16. Stalker, H. D. *Genetics* **82,** 323–347 (1976).
17. Boardman, M., Askew, R. R. & Cook, L. M. *J. zool. Res.* **172,** 343–355 (1974).
18. Giesel, J. T. *Evolution* **24,** 98–119 (1970).
19. Schoener, T. W. & Schoener, A. *Evolution* **30,** 650–658 (1976).
20. Christensen, B. *Hereditas* **87,** 21–26 (1977).
21. Cavener, D. *Behav. Genet.* **9,** 359–365 (1979).

Vesicle formation and acetylene reduction activity in *Frankia* sp. CpI1 cultured in defined nutrient media

John D. Tjepkema, William Ormerod & John G. Torrey

Cabot Foundation for Botanical Research, Harvard University, Petersham, Massachusetts 01366

It has been reported that certain species of free-living *Rhizobium* were capable of producing nitrogenase[1–5], thereby demonstrating conclusively that the *nif* genes reside in the bacterial component of the dinitrogen-fixing symbiosis between *Rhizobium* and leguminous host plants. In the comparable dinitrogen-fixing symbiosis between the actinomycete *Frankia* and the actinorhizal woody dicotyledons that serve as nodulated host plants, the endophytic filamentous bacteria have only recently been brought into culture[6–8]. We report here evidence that free-living *Frankia* sp. grown in appropriate nutrient conditions show nitrogenase activity (acetylene reduction) associated with a distinctive morphological structure formed in effective nodules and also developed in culture.

Frankia sp. CpI1 isolated from root nodules of *Comptonia peregrina* and grown in liquid yeast–extract nutrient medium[6] develops as a finely branching filamentous mat that produces enlarged intrahyphal or terminal sporangia of considerable size (up to 60 μm) and complexity containing numerous 1–2-μm diameter spores[9]. During the development of defined synthetic media for the culture of CpI1, it was observed that growth rates and morphological structures of the filamentous bacterium were affected by preparation procedures and chemical components of the medium. A defined medium was developed that elicited sporangium formation and also extensive formation of small spherical to ovoid structures borne terminally on short side branches, which we term vesicles, in agreement with earlier literature. Similar structures have been observed by others[10,11]. Under Nomarski interference phase optics, the vesicles show thickened walls (Figs 1, 2), in contrast to immature developing sporangia. Thus far, they have proved difficult to preserve and section for transmission electron microscopy.

In the yeast-extract medium[8], used for routine subculture, vesicles are not usually observed. Such cultures show no

0028–0836/80/410633—03$01.00

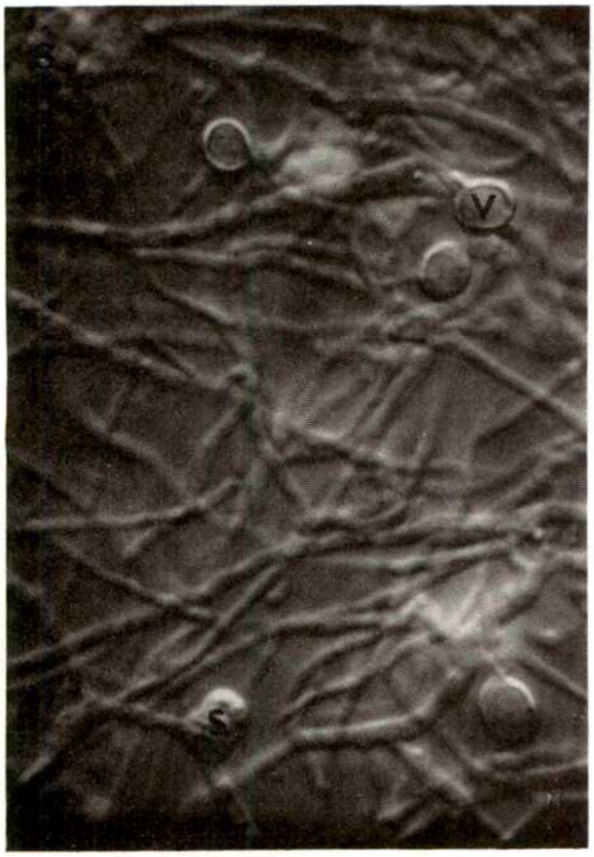

Fig. 1 A 4-week-old culture of *Frankia* sp. CpI1 grown in defined medium photographed with Nomarski phase interference optics. Branched bacterial filaments, enlarged sporangia (S) and a number of thick-walled vesicles (V) are visible. ×2,890.

acetylene reduction activity. The following procedure was used to elicit vesicle formation. The filamentous mat from yeast-extract medium was collected after 4–6 weeks of standing culture in flasks. The mat was homogenized in a Potter–Elvejhem homogenizer and then washed three times with mineral salt solution from the defined medium (see below) and its packed cell volume measured. A sample of known volume was resuspended in mineral salt solution and added to test tubes containing 5 ml of defined medium with the following composition. Mineral salt solution (gm l^{-1}): 1.0 KH_2PO_4, 0.1 $MgSO_4 \cdot 7H_2O$, 0.01 $CaCl_2 \cdot 2H_2O$, 0.01 FeNaEDTA; 1 ml l^{-1} of the following micronutrient stock solution (gm l^{-1}): 2.86 H_3BO_3, 1.81 $MnCl_2 \cdot 2H_2O$, 0.22 $ZnSO_4 \cdot 7H_2O$, 0.08 $CuSO_4 \cdot 5H_2O$, 0.025 $Na_2MoO_4 \cdot 2H_2O$; 1 ml l^{-1} of the following stock solution (mg per 100 ml): 10 thiamine HCl, 50 nicotinic acid, 50 pyridoxine HCl; and 1.2 gm l^{-1} succinic acid, *p*H adjusted to 6.8. Note that the only nitrogen-containing compounds in this medium are EDTA and the vitamins, and that they contain only very small quantities.

Table 1 Time course of nitrogenase activity by *Frankia* sp. CpI1 cultured in defined medium

Time (days)	No. of vesicles per tube ($\times 10^6$)	Acetylene reduction (nmol per tube per day)
0	0	0
5	1.67 ± 0.35	7.3 ± 0.4
7	1.85 ± 0.26	11.9 ± 3.0
14	2.73 ± 0.41	2.9 ± 0.7
	Defined medium plus 100 mg l^{-1} glutamic acid	
7	1.17 ± 0.41	6.6 ± 0.7

Values are ±s.e.m., $n = 5$.

In a typical experiment 0.8 ml packed cell volume of *Frankia* was used to inoculate 100 tubes (an inoculum of 8 μl packed cell volume per tube). Tubes were stoppered with cotton plugs and incubated at 25°C in the dark without agitation. For each sample used in time-course studies, five tubes were sampled for nitrogenase activity, using the acetylene reduction assay[12] with gentle agitation of the tubes. Vesicle counts were made by sonicating the contents of each tube for 30 s at 60 W and then counting in a Petroff-Hausser chamber under phase illumination.

Representative data are given in Table 1 showing the relationship between vesicle formation and acetylene-reducing activity over a culture period of 2 weeks. Cultures at the outset lacked vesicles and showed no acetylene reduction. Vesicle formation was first observed at 5 days and the number of vesicles per tube increased with time. Acetylene reduction occurred only in cultures with vesicles and this activity increased roughly in proportion with the number of vesicles formed between days 5 and 7. Nitrogenase activity decreased at 14 days, even though vesicle numbers continued to increase. The cause of this decrease is not known but may have been due to accumulation of inhibitory substances. The maximum activity recorded in any of these experiments was 44 nmol per tube per day. One experiment was conducted with *Frankia* sp. Ar13 from *Alnus rubra*[7] and this also resulted in vesicle formation and nitrogenase activity.

The nitrogenase activity observed is consistent with that of intact nodules, which is ~10 μmol $C_2H_4\ h^{-1}\ cm^{-3}$ of nodule volume. We estimate that vesicles make up about 1% of nodule volume; assuming that the vesicles are the site of nitrogenase, their activity would be 1,000 μmol $C_2H_4\ h^{-1}\ cm^{-3}$ of vesicle volume. Using a vesicle diameter of 2.5 μm, the highest activity we have observed (Table 2) is equivalent to 180 μmol $h^{-1}\ cm^{-3}$, or 18% of the value estimated for vesicles in nodules. For comparison, we calculate that bacteroids in legume nodules have a nitrogenase activity of ~100 μmol $C_2H_4\ h^{-1}\ cm^{-3}$ of bacteroid volume.

It is very unlikely that the nitrogenase activity of our cultures was due to contaminating organisms as activity was observed only in cultures with vesicles and was correlated with the number of vesicles. Further evidence is the lack of growth when CpI1 is inoculated into Difco nutrient broth, absence of turbidity in all cultures, and lack of growth and nitrogenase activity in anaerobic conditions.

Inoculum density was an important variable not easily controlled because of the difficulty in accurately measuring

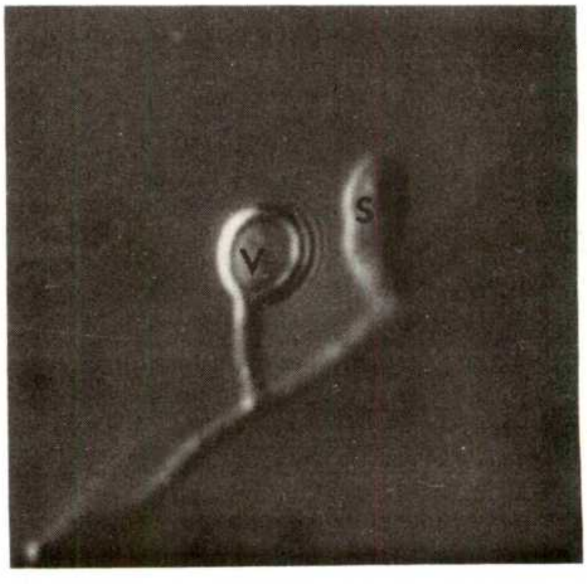

Fig. 2 A young culture of CpI1 showing a bacterial filament with an immature developing sporangium (S) side by side with a mature thick-walled vesicle (V). Nomarski optics. ×4,375.

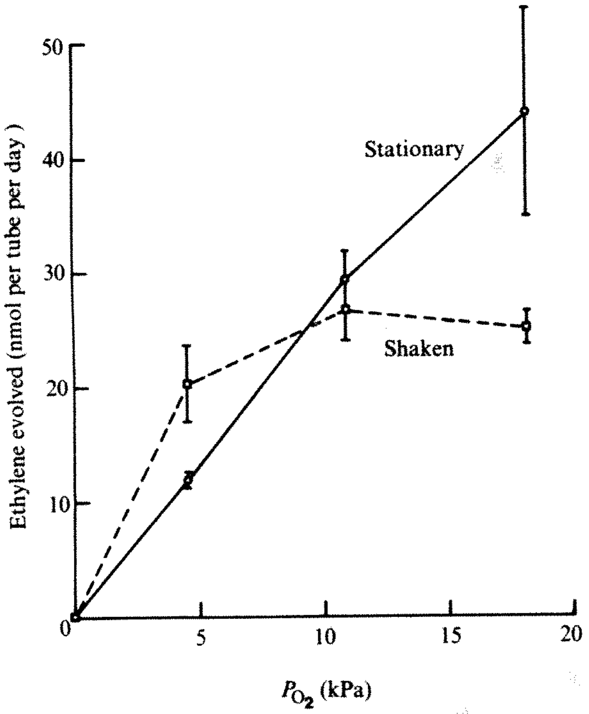

Fig. 3 Acetylene reduction by cultures of *Frankia* as a function of P_{O_2}. One set of tubes was shaken throughout the experiment and the other was stationary. From 0 to 19 days after inoculation, the tubes were incubated in air. They were then gassed with mixtures of air, N_2, and 10% C_2H_2. Vertical bars represent ±s.e.m.; $n = 5$.

actinomycete mass and growth. Positive correlations were found between inoculum density, vesicle number, and acetylene reduction activity (Table 2). Experimental differences in similar tests were probably most often attributable to variation in initial inoculum density.

In several series of experiments we tested the effect of additions of inorganic or organic components to the defined medium on acetylene reduction activity. Cellobiose added at 1% (w/v) completely inhibited vesicle formation and acetylene reduction over a period of 3 weeks. Glutamic acid added at 100 mg l^{-1} reduced the number of vesicles and nitrogenase activity by about half (Table 1). Ammonium chloride (54 mg l^{-1}) completely suppressed vesicle formation and acetylene reducing activity. From the experiments performed to date, medium additions which inhibit acetylene reduction activity do so by suppressing vesicle formation. We have no information to suggest that the ammonium chloride and glutamate inhibited nitrogenase activity *per se*.

Finally, in view of the known instability of the nitrogenase enzyme to molecular oxygen[13], we were interested in studying the effects of P_{O_2} on acetylene reduction activity in cultures of CpI1 in defined medium. As shown in Fig. 3, acetylene reduction by shaken cultures was little affected by the P_{O_2} values examined, while stationary cultures were oxygen limited. Apparently, the enzyme within the vesicle is protected from oxygen in some way, either by special metabolism within the vesicle or by the relative impermeability of the thickened wall. This suggests analogy with heterocyst formation and function in the blue-green algae.

Table 2 Effect of inoculum density on nitrogenase activity by *Frankia* sp. CpI1 cultured in defined medium

Time (days)	Inoculum density (%)	No. of vesicles per tube ($\times 10^6$)	Acetylene reduction (nmol per tube per day)
0	100	0	0
7	100	—	1.4±0.3
14	100	0.95±0.09	25.0±3.1
14	50	0.56±0.04	20.4±3.9
14	25	0.23±0.04	9.1±2.7
14	10	0.05±0.01	1.0±0.7

Values are ±s.e.m., $n = 5$.

These experiments establish several new and interesting facts. They give the first published evidence that free living *Frankia* sp. are capable of nitrogenase activity in appropriate nutrient conditions. The positive correlation between vesicle formation and acetylene reduction activity *in vitro* gives strong support to the already expressed view[8,13–17] that vesicles are the site of nitrogenase activity in actinorhizal plants. Our experiments further show that vesicle formation is elicited or made possible by the physico-chemical conditions which surround the microorganism *in vitro*, a fact which raises interesting questions about the lack of vesicle formation in certain incompatible cross inoculations[16,18]. These observations open up a new approach to the problems of structure and function in these important symbiotic nitrogen fixing relationships.

This research was supported in part by the Maria Moors Cabot Foundation for Botanical Research of Harvard University, by NSF grant DEB 77-2249 and USDA grant 5901-0410-8-0055-0.

Received 5 March; accepted 24 July 1980.

1. Keister, D. L. *J. Bacteriol* **123,** 1265–1268 (1975).
2. Kurz, W. G. W. & LaRue, T. A. *Nature* **256,** 407–408 (1975).
3. McComb, J. A., Elliot, J. & Dilworth, M. J. *Nature* **256,** 409–410 (1975).
4. Pagan, J. D., Child, J. J., Scowcroft, W. & Gibson, A. H. *Nature* **256,** 406–407 (1975).
5. Tjepkema, J. & Evans, H. J. *Biochem. biophys. Res. Commun.* **65,** 625–628 (1975).
6. Callaham, D., Del Tredici, P. & Torrey, J. G. *Science* **199,** 899–902 (1978).
7. Berry, A. & Torrey, J. G. in *Symbiotic Nitrogen Fixation in the Management of Temperate Forests* (eds Gordon, J. C., Wheeler, C. T. & Perry, D. E.) 69–83 (Oregon State University Press, 1979).
8. Baker, D., Torrey, J. G. & Kidd, G. H. *Nature* **281,** 76–78 (1979).
9. Newcomb, W., Callaham, D., Torrey, J. G. & Peterson, R. L. *Bot. Gaz.* **140,** Suppl. S22–S34 (1979).
10. Pommer, E. *Ber. dt. bot. Ges.* **72,** 138–150 (1959).
11. Lalonde, M. & Calvert, H. E. in *Symbiotic Nitrogen Fixation in the Management of Temperate Forests* (eds Gordon, J. C., Wheeler, C. T. & Perry, D. E.) 95–110 (Oregon State University Press, 1979).
12. Burris, R. H. in *The Biology of Nitrogen Fixation* (ed. Quispel. A.) 9–33 (North-Holland, Amsterdam, 1974).
13. Benson, D. R., Arp, D. J. & Burris, R. H. *Science* **205,** 688–689 (1979).
14. Akkermans, A. D. L. thesis, University of Leiden (1971).
15. Becking, J. H. in *Recent Developments in Nitrogen Fixation* (eds Newton, W., Postgate, J. R. & Rodriguez-Barrueco, C.) 551–567 (Academic, London, 1977).
16. Mian, S., Bond, G. & Rodriguez-Barrueco, C. *Proc. R. Soc.* B**194,** 285–293 (1976).
17. Mian, S. & Bond, G. *New Phytol.* **80,** 187–192 (1979).
18. Baker, D., Newcomb, W. & Torrey, J. G. *Can. J. Microbiol.* (in the press).

Complete reversal of antero–posterior polarity in a centrifuged insect embryo

Klaus-Gerhard Rau & Klaus Kalthoff

Department of Zoology, University of Texas at Austin, Austin, Texas 78712

Spatial pattern formation during embryogenesis is ascribed to differential gene expression, which in turn is thought to result in part from interactions of nuclei with cytoplasmic determinants[1]. In the chironomid midge *Smittia*, and probably in other dipterans as well, blastoderm cells seem to make an early decision as to whether they contribute to cephalic and thoracic or to abdominal (and possibly thoracic) structures[2]. Inactivation or translocation of cytoplasmic components involved in this antero–posterior decision could conceivably lead to duplications of head and thorax, or abdomen, or to complete but inverted embryos forming the head posteriorly and the abdomen anteriorly in the egg. Whereas the former two malformations have been described[3,4], completely inverted embryos are reported for the first time, to our knowledge, in this letter. Reversal of partial germ bands has previously been observed following combined ligation and cytoplasmic translocation in eggs of the leaf hopper, *Euscelis plebejus*[5].

0028-0836/80/410635—03$01.00

Smittia eggs were centrifuged during early intravitelline cleavage (stage P_2, two pole cells) for 20 min at 6,700*g* and 20 °C. During centrifugation, eggs were lined up, with their posterior poles pointing in the direction of the centrifugal force, in a tightly fitting groove between microscope cover slips[4]. Eggs recovered from the centrifuge were screened for proper stratification as shown in Fig. 1*i*; obliquely stratified eggs were removed. Out of 6,206 centrifuged eggs, 3,140 survived and formed analysable germ bands. Among these, we found 1,713 normal embryos (Fig. 1*d*, *f*), 1,341 double cephalons (Fig. 1*a*), 55 double abdomens (Fig. 1*b*) and 31 inverted embryos (Fig. 1*c*, *e*). As controls, 581 embryos were centrifuged with their anterior poles pointing in the direction of the centrifugal force. All of the 333 survivors developed into normal embryos. In similar experiments using higher centrifugal forces, centrifugation with the anterior pole pointing in the direction of the centrifugal force resulted in low yields of double cephalons and double abdomens[4].

Inverted embryos were identified using the following criteria: (1) the contour of the chorion (egg shell) is more pointed at the posterior and more blunted at the anterior pole (Fig. 1*a*–*f* and *i*); (2) the micropyle at the anterior pole is visible as a small but distinct dark area in transmitted light under the compound microscope (Fig. 1). With Nomarski optics, the micropyle region shows a bright blue coloration, depending on the position of the second Wollaston prism, and the angle between the polarisator plane and the plane tangential to the anterior pole of the embryo. Variation of this angle leads to appearance and disappearance of the blue colour in the micropyle every 90°; and (3) the stratification of yolk components in centrifuged embryos is maintained until after germ anlage formation; the gray and opaque proteid spheres accumulated centrifugally are easily distinguished from the lipid droplets in the centripetal region which have a brownish hue. In embryos of normal orientation, the head lobes formed in the lipid-containing region, while the 'Schwanzwulst' (posterior end of germ anlage) originated in the proteid-containing region (Fig. 1*f*). Conversely, the inverted embryos developed with their head lobes in the proteid and the Schwanzwulst in the lipid region (Fig. 1*e*). Application of criteria 1–3 led in no case to contradictory conclusions.

It is important to realize that the polarity inversions did not result from turning of the entire embryos inside their egg shells. This possibility is excluded by criterion (3) which indicates the orientation of the embryo relative to the yolk-rich endoplasm. The development of inverted embryos was also observed, in eleven cases, from the very beginning of germ anlage formation. The ensuing formation of amnion and serosa, embryonic rotations, germ band extension and contraction, dorsal closure, and spiralization of inverted embryos appeared normal or nearly so. More than half of the inverted embryos hatched and showed normal larval movements.

A hypothesis to explain the formation of four different segment patterns (normal embryos, double cephalons, double abdomens, and inverted embryos) after centrifugation is shown diagrammatically in Fig. 2. The hypothesis builds on a model developed earlier[6], according to which the potential for abdomen formation (p, p′) is present not only in the posterior but also

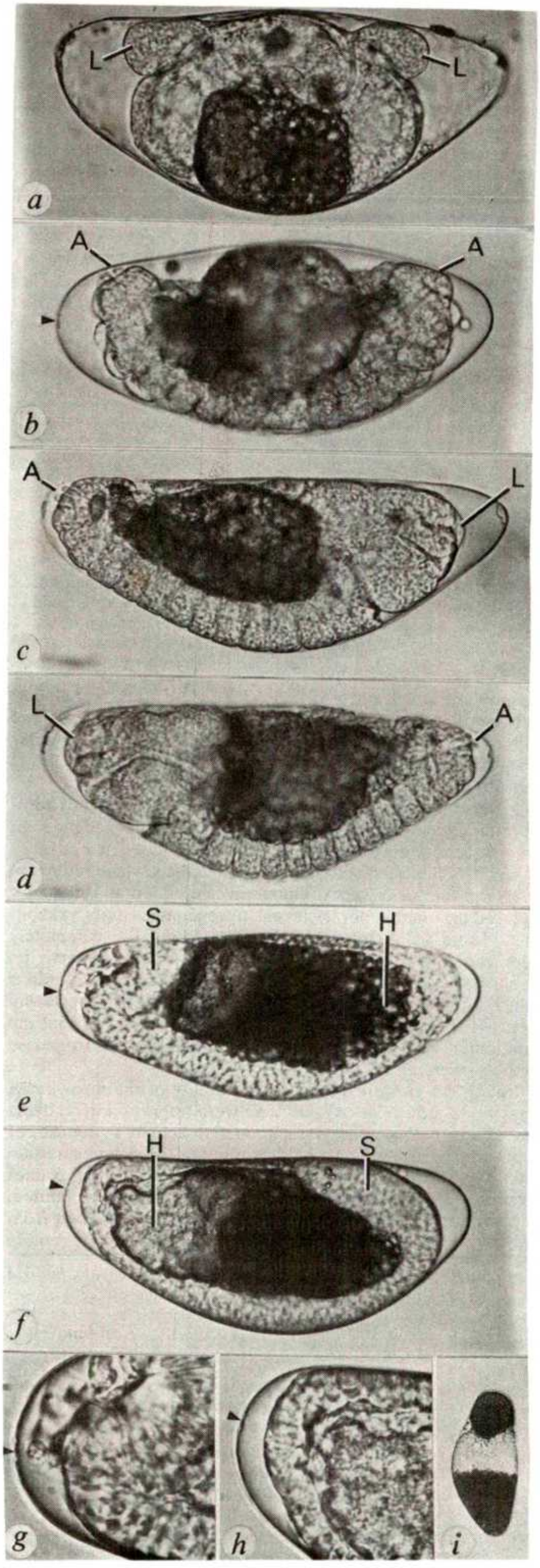

Fig. 1 Normal and abnormal segment patterns of *Smittia* embryos developing from centrifuged eggs. *a*–*h*, Ventral side down, anterior pole of egg shell to the left. *a*–*d*, Embryos after shortening of germ band, 53–78 h after deposition: *a*, double cephalon; *b*, double abdomen; *c*, inverted embryo; *d*, normal embryo. *e*–*h*, Embryos during formation of germ anlage, 18–19 h after deposition: *e*,*g*, inverted embryo; *f*,*h*, normal embryo; *i*, centrifuged egg, posterior pole (down) was facing in direction of centrifugal force. Note centrifugal accumulation of proteid spheres (at bottom in *i*, to right in *e* and *f*) and centripetal accumulation of lipid droplets. L, Labrum (anteriormost head structure); A, anal papillae marking abdominal end; S, Schwanzwulst (posterior bulge of germ anlage); H, head lobes, in lateral position, displacing yolk material in between; ►, micropyle at anterior end of egg shell.

in the anterior egg half. This is shown by the ability of isolated anterior fragments to form abdomens[7], and is also reflected in the synchronous and symmetrical development of double abdomens. The formation of head and thorax is ascribed to the superimposed activity of 'anterior determinants' which have been characterized as cytoplasmic ribonucleoprotein particles[6]. This is mainly based on the formation of double abdomens after application of RNase or UV light to the anterior pole region, on the action spectrum for UV-ray induction of double abdomens, and on the subcellular localization of the effective targets of UV light. Although the exact function of the anterior determinants remains to be elucidated, it is assumed that their activity in crucial regions of an embryonic half has to surpass a threshold level for head and thorax to be formed there. Sub-threshold levels of activity are thought to result in abdomen formation.

Centrifugation of *Smittia* eggs obviously causes stratification of yolk components (Fig. 1*i*) and probably of nuclei, and hence displacement of other egg components. In addition, disruption of some cytoskeletal structures and other less obvious consequences may occur. Redistribution of egg components after centrifugation involves disappearance of the intermediate layer of yolk-free cytoplasm within 4 h, and a somewhat abnormal blastoderm formation which seems to proceed from the egg equator to the poles[4]. These processes may lead, in the embryo, to various spatial distributions of anterior determinants whose activity may also depend on their intracellular environment and/or the time of their interaction with nuclei. As an overall result, one of the following four situations could arise with respect to anterior determinant activity. Above-threshold activity in both anterior and posterior halves (Fig. 2*c*), below-threshold activity in both anterior and posterior halves (Fig. 2*d*), above-threshold activity in the posterior half only (Fig. 2*e*), or above-threshold activity in the anterior half only (Fig. 2*f*). These situations, according to our model, should lead to formation of double cephalons, double abdomens, inverted embryos, or normal embryos, respectively. In fact, all of these segment patterns have been observed after centrifugation.

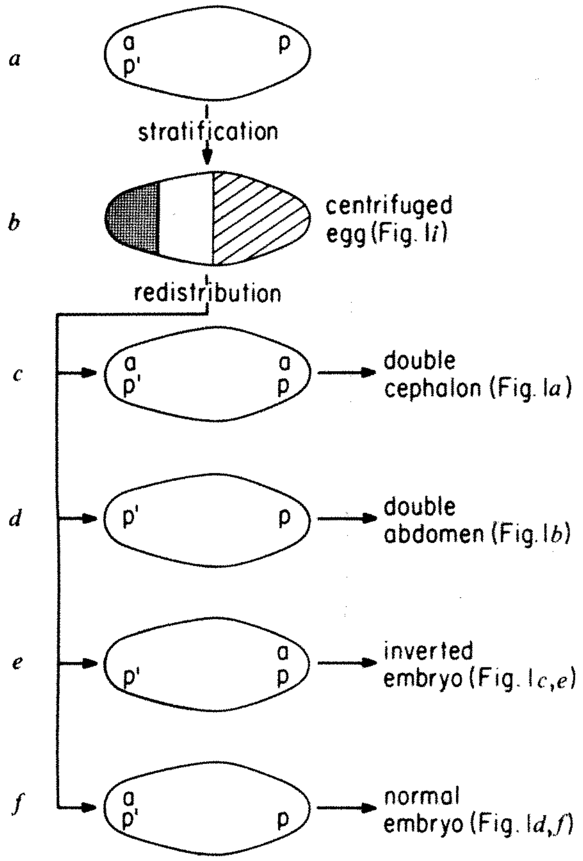
a
a
p'
p
stratification
b
centrifuged egg (Fig. 1*i*)
redistribution
c
a
p'
a
p
double cephalon (Fig. 1*a*)
d
p'
p
double abdomen (Fig. 1*b*)
e
p'
a
p
inverted embryo (Fig. 1*c*,*e*)
f
a
p'
p
normal embryo (Fig. 1*d*,*f*)

Fig. 2 Hypothesis explaining the formation of different segment patterns by different distributions of anterior determinant (a) activity after stratification and redistribution of egg material. p, p′, Posterior factors.

Moreover, this hypothetical explanation of our centrifugation experiments allows us to make four predictions as to the modifying effects of UV light (thought to inactivate anterior determinants) before or after centrifugation. (1) UV-ray irradiation of the anterior pole region before centrifugation should cause a major increase in the yield of double abdomens, and the disappearance of normal embryos, double cephalons, and inverted embryos; (2) UV-ray irradiation of the posterior pole before centrifugation should have little or no effect; (3) UV-ray irradiation of the anterior pole region after redistribution should reduce the yields of normal embryos and double cephalons, and enhance the yields of double abdomens and inverted embryos; and (4) UV-ray irradiation of the posterior pole region after redistribution should enhance the yields of normal embryos and double abdomens at the expense of double cephalons and inverted embryos. These predictions will be tested.

Incidentally, we expected and first discovered inverted embryos after centrifugation and subsequent UV-ray irradiation of the anterior pole region. In these conditions, they occurred more frequently than after centrifugation alone. Possibly they were also produced in earlier centrifugation experiments[4] but overlooked because they were not anticipated. *Note added in proof*: We have learned that inverted embryos have been generated earlier by centrifugation of *Chironomus samoensis* embryos[8].

Received 16 June; accepted 15 August 1980.

1. Davidson, E. H. *Gene Activity in Early Development* (Academic, New York, 1976).
2. Chan, L.-N. & Gehring, W. *Proc. natn. Acad. Sci. U.S.A.* **68,** 2217–2221 (1971).
3. Yajima, H. *J. Embryol. exp. Morphol.* **8,** 198–215 (1960).
4. Kalthoff, K., Hanel, P. & Zissler, D. *Devl Biol.* **55,** 285–305 (1977).
5. Sander, K. in *Cell Patterning* (Ciba Foundation Symposium 29, new series) 241–263 (Associated, Amsterdam, 1975).
6. Kalthoff, K. in *Determinants of Spatial Organization* (eds Subtelny, S. & Konigsberg, I. R.) 97–126 (Academic, New York, 1979).
7. Ritter, W. *Staatsexamensarbeit, Fakultät für Biologie*, Univ. Freiburg (1976).
8. Yajima, H. *Zool. Mag., Tokyo* **87,** 343 (1978).

Cytochalasin D does not produce net depolymerization of actin filaments in HEp-2 cells

Allen Morris* & Janet Tannenbaum†‡

* Department of Biology, Massachusetts Institute of Technology, Cambridge, Massachusetts 02139
† Department of Pathology, College of Physicians and Surgeons, Columbia University, New York, New York 10032

The altered morphology, disappearance or 'disruption' of actin filaments (microfilaments) in cells treated with cytochalasin[1] has sometimes been attributed to depolymerization of filamentous actin (F-actin) to its globular subunit (G-actin), but attempts to confirm that mechanism have been inconclusive. Treatment of purified actin filaments with cytochalasin B (CB) decreased their viscosity[2,3], consistent with depolymerization, which was not, however, revealed by electron microscopy[4], although the filaments appeared abnormal[5]. CB also increased the ATP-ase activity of F-actin, suggesting that it had been destabilized[3], while actin filaments in the acrosomal process were not depolymerized[6]. CB or cytochalasin D (CD) can dissolve actin gels (reviewed in ref. 7, see also refs 8 and 9) without depolymerizing their filaments. The 'disrupted' actin structures in CD-treated cells bound heavy meromysin[10], indicating that at least some of the cellular actin was filamentous. Using a rapid assay for G- and F-actin in cell extracts, based on the inhibition of DNase I[11], we have found that neither short-nor long-term exposure of HEp-2 cells to CD produce net depolymerization of actin filaments.

---

‡ To whom correspondence should be addressed.

0028–0836/80/410637—03$01.00

The human tumour cell line HEp-2 (ATCC CCL23) was grown in monolayers in minimal essential medium (Earle's salts) supplemented with 10% newborn calf serum, penicillin (100 U ml^{-1}), streptomycin (100g µl^{-1}) and Fungizone (0.25 µg ml^{-1}, Gibco). Cells were planted at a density of 5×10^5 per 60 mm plastic Petri dish (Falcon), incubated in a humidified atmosphere of 5% carbon dioxide–95% air at 37 °C, and used within 2–3 days (sub-confluent). CD (Sigma) was stored as a 1 mg ml^{-1} stock solution in DMSO and diluted into Earle's balanced salt solution (EBSS, Gibco) to prepare a working stock solution immediately before use. Treatment with CD was initiated by refeeding cells with fresh medium containing CD (or an equivalent amount of DMSO for controls). After incubation as indicated in Table 1, the monolayers were drained, rinsed quickly with warm EBSS and scraped into 0.3–0.4 ml of 5 mM potassium phosphate, *p*H 7.6, 150 mM NaCl, 2 mM $MgCl_2$, 0.2 mM dithiothreitol, 0.2 mM ATP, 0.5% Triton X-100 and 1 mM PMSF (added immediately before use). Samples of 10–20 µl of this cell lysate were used for the DNase I assay as described by Blikstad *et al.*[11]. Samples of lysate mixed with the guanidine hydrochloride depolymerizing solution[11] were sheared in a syringe with a 26-gauge needle to decrease viscosity. All other procedures were as described by Blikstad *et al.*[11]. Chemicals were reagent grade; highly polymerized calf thymus DNA (Sigma) and bovine pancreas DNase I (Sigma DN-Cl, lyophilized powder) were used. Protein concentration was estimated by the method of Bradford[12], using the Bio-Rad Protein Assay reagent and bovine gamma globulin or serum albumin standards.

HEp-2 cells treated with CD exhibited characteristic morphological effects, the protrusion of zeiotic knobs from the cell surface[13,14] at all three concentrations of CD tested. As Table 1 shows, short-(3.75 h) or long-term (24–27 h) treatment with CD did not result in a net depolymerization of actin. Although there was some variability in the results, the long-term effect of CD appeared to be a net decrease in the proportion of G-actin to total actin in the cell. Calculation of the total units of actin per µg of protein (Tables 1, 2) suggested that long-term treatment with CD resulted in an increased accumulation of actin in HEp-2 cells; this effect has been observed repeatedly in further experiments (unpublished data of J.T. and G. C. Godman). Addition of 1 µg ml^{-1} of CD (DMSO for controls) to the EBSS and the Triton-containing buffer used during collection and lysis of CD-treated cells (to prevent any possible reversal of the effects of CD during these steps) did not alter these results (Table 2).

Table 1 Effect of treatment with CD on proportion of G-actin and total actin in HEp-2 monolayers

Expt no.	Treatment	% G-actin	$\frac{\text{Units actin}}{\mu\text{g cell protein}}$
1	DMSO, 0.1% (3.75 h)	67.8 ± 16.4	ND
	CD, 0.5 µg ml^{-1} (3.75 h)	62.5 ± 5.8	ND
	CD, 1.0 µg ml^{-1} (3.75 h)	69.3 ± 13.5	ND
2	DMSO, 0.05% (24.0 h)	57.5 ± 5.4	ND
	CD, 0.5 µg ml^{-1} (24.0 h)	56.4 ± 7.4	ND
3	DMSO, 0.1% (26.75 h)	61.4 ± 4.4	ND
	CD, 0.5 µg ml^{-1} (26.75 h)	42.3 ± 9.0	ND
	CD, 1.0 µg ml^{-1} (26.75 h)	36.2 ± 4.7	ND
4	DMSO, 0.1% (27.0 h)	63.5 ± 5.0	2.2 ± 0.2
	CD, 0.2 µg ml^{-1} (27.0 h)	47.3 ± 6.7	2.6 ± 0.1
	CD, 0.5 µg ml^{-1} (27.0 h)	52.4 ± 6.3	2.7 ± 0.3
	CD, 1.0 µg ml^{-1} (27.0 h)	49.4 ± 5.3	2.8 ± 0.2

Replicate monolayers of HEp-2 cells were incubated with CD or DMSO solvent in medium as indicated (in experiments 1, 3, 4, all concentrations of CD were prepared in 0.1% DMSO). Cells were then collected and lysed as described in the text. Samples of lysate were assayed for their DNase I inhibitor activity before (a measure of G-actin) and after (a measure of total actin) addition of the guanidine hydrochloride depolymerizing buffer. For each determination, the amount of sample used was adjusted to produce inhibition of the DNase I within the linear range of the assay (30–70% inhibition). The percentage of G-actin was calculated by comparing the G-actin inhibitory activity with the total actin inhibitory activity for equal amounts of cell material. Data shown are each averages of three or four determinations per sample, ± s.d. Each experiment was performed with a separate set of replicate monolayers. In experiment 4, protein concentrations in the lysates were, in the order shown: 2.35, 2.25, 2.15 and 2.10 mg ml^{-1}. Values for units of actin per µg protein were calculated from the total actin in each sample (after guanidine hydrochloride depolymerization) for 10-µl volumes; 1 U inhibits 1% of the 1 µg of DNase in the standard assay. ND, not determined.

Table 2 Effect of continued exposure to CD during collection and lysis of CD-treated HEp-2 cells

Expt no.	Treatment	% G-actin	$\frac{\text{Units actin}}{\mu\text{g cell protein}}$
1	DMSO, *in vivo* and *in vitro*	80.0 ± 8.8	3.3 ± 0.2
	CD, *in vivo* (DMSO *in vitro*)	68.1 ± 10.0	4.1 ± 0.3
	CD, *in vivo* and *in vitro*	66.8 ± 4.2	3.9 ± 0.1
2	DMSO, *in vivo* and *in vitro*	86.0 ± 12.0	3.8 ± 0.3
	CD, *in vivo* (DMSO *in vitro*)	69.9 ± 6.3	4.6 ± 0.2
	CD, *in vivo* and *in vitro*	69.4 ± 10.8	4.5 ± 0.3

Replicate monolayers of HEp-2 cells were incubated with 0.1% DMSO or CD (1.0 µg ml^{-1}) in 0.1% DMSO for 17.0 h (experiment 1) or 19.5 h (experiment 2) (*in vivo* treatment). Cells were then rinsed and collected as indicated in the text, except that rinsing and lysing solutions contained 0.1% DMSO (cells exposed to DMSO '*in vitro*') or 1.0 µg ml^{-1} CD in 0.1% DMSO (cells exposed to CD '*in vitro*'). Thus, for cells treated with CD *in vivo* and *in vitro*, exposure to CD was continuous to prevent possible recovery from effects of the drug. All other details are given in the legend for Table 1. Separate stocks of HEp-2 cells were used in the experiments for Tables 1 and 2; possibly differences between these two stocks account for the higher % G-actin in Table 2 compared with Table 1. The values for units of actin per µg protein are not directly comparable between Tables 1 and 2, because different lots of DNase 1 and DNA substrate were used for each.

The approximate concentration of G-actin in the lysates can be determined from Table 1 and our estimate that 6.8% of the protein in DMSO-treated HEp-2 cells is actin (unpublished observations based on ^{35}S-methionine labelling of HEp-2 cells and isolation of actin by polyacrylamide gel electrophoresis). For the protein concentrations in experiment 4, we calculated that the lysates contained G-actin at a concentration of 102 µg ml^{-1} (DMSO control) and at 87, 94 and 90 µg ml^{-1} (respectively, for CD at 0.2, 0.5 and 1 µg ml^{-1}; all values were corrected for the increase in total actin per µg protein compared with DMSO controls). All these values are greater than the critical concentration reported for various non-muscle actins in similar conditions[15], possibly because the cellular G-actin is associated with inhibitors of polymerization such as profilin[16].

These results indicate that CD does not cause a massive net depolymerization of actin filaments *in vivo*. It should be noted, however, that the DNase I assay used does not distinguish the length of the actin filaments and therefore cannot test a proposed mechanism involving the scission of F-actin to shorter lengths of filament[17]. In addition, the data do not exclude the possibility that CD converts actin microfilaments to some other configuration rather than depolymerizing them.

Cytochalasins B, E and D have been reported to inhibit the *in vitro* induction of F-actin polymerization by a high molecular weight complex which binds dihydro-CB at high affinity[18]. Similarly, CD inhibited polymerization of actin nucleated by F-actin[19,20]. On the basis of these observations, it was suggested that cytochalasins might act by inhibiting polymerization of actin microfilaments in the cell. Because the actin in non-muscle cells probably undergoes cycles of polymerization and depolymerization (reviewed in ref. 21), this proposal implies that cytochalasin should eventually produce a net increase in the proportion of G-actin in the cell by inhibiting its repolymerization during the normal cycle. Our failure to detect such an increase, even after 27 h of treatment with CD at concentrations sufficient to alter cell morphology, tends to contradict this hypothesis. However, because the DNase I assay only determines the net balance of F and G-actin at the time the cells are collected, our experiments do not test the possibility that CD inhibited the nuclei-induced, rapid polymerization of actin in the cell but also allowed (and perhaps accelerated[22,23]) a compensating polymerization of this actin on to the more slowly growing end of actin filaments.

Our observation that CD does not cause a net depolymerization of actin filaments *in vivo* argues against any mechanism for the action of cytochalasin on cells which is based on the replacement of microfilaments by depolymerized actin. In particular, it suggests that normal levels of actin microfilaments would be available for participation in an energy-dependent contractile response of the cells to treatment with CD, as previously proposed[10,13,14,24,25].

In summary, treatment of live HEp-2 cells with CD did not cause a net depolymerization of filamentous actin. Rather, there seemed to be a small increment in the proportion of filamentous actin in cells treated for 27 h and an increase in the total content of actin. The possibility that an accumulation of F-actin in CD-treated cells corresponds to the actin-containing masses (reviewed in ref. 25) seen in such cells is being investigated.

This work was supported by grants from NIH, NSF and NASA to Dr A. Rich and an NIH grant to Dr G. C. Godman. J.T. was a Fellow of the Muscular Dystrophy Society of America and supported by NIH Grant 5T32 GM 07161-05.

Received 10 April; accepted 8 August 1980.

1. Tanenbaum, S. W. (ed.) *Cytochalasins Biochemical and Cell Biological Aspects* (Elsevier/North-Holland, Amsterdam, 1978).
2. Spudich, J. A. & Lin, S. *Proc. natn. Acad. Sci. U.S.A.* **69,** 442–446 (1972).
3. Löw, I. & Dancker, P. *Biochim. biophys. Acta* **430,** 366–374 (1976).
4. Forer, A., Emerson, J. & Behnke, D. *Science* **175,** 774–776 (1972).
5. Spudich, J. A. *Cold Spring Harb. Symp. quant. Biol.* **37,** 585–594 (1972).
6. Sanger, J. W. & Sanger, J. M. *J. exp. Zool.* **193,** 441–447 (1975).
7. Weihing, R. R. in *Cytochalasins Biochemical and Cell Biological Aspects* (ed. Tanenbaum, S. W.) 431–444 (Elsevier/North-Holland, Amsterdam, 1978).
8. Mimura, N. & Asano, A. *Nature* **272,** 273–276 (1978).
9. Ishiura, M. & Okada, Y. *J. Cell Biol.* **80,** 465–480 (1979).
10. Miranda, A. F., Godman, G. C. & Tanenbaum, S. W. *J. Cell Biol.* **62,** 406–423 (1974).
11. Blikstad, I., Markey, F., Carlsson, L., Persson, T. & Lindberg, U. *Cell* **15,** 935–943 (1978).
12. Bradford, M. M. *Analyt. Biochem.* **72,** 248–254 (1976).
13. Miranda, A. F., Godman, G. C., Deitch, A. D. & Tanenbaum, S. W. *J. Cell Biol.* **61,** 481–500 (1974).
14. Godman, G. C., Miranda, A. F., Deitch, A. D. & Tanenbaum, S. W. *J. Cell Biol.* **64,** 644–667 (1975).
15. Gordon, D. J., Boyer, J. L. & Korn, E. D. *J. biol. Chem.* **252,** 8300–8309 (1977).
16. Carlsson, L., Nyström, L.-E., Sundkvist, I., Markey, F. & Lindberg, U. *J. molec. Biol.* **115,** 465–483 (1977).
17. Hartwig, J. H. & Stossel, T. P. *J. molec. Biol.* **134,** 539–553 (1979).
18. Lin, D. C. & Lin, S. *Proc. natn. Acad. Sci. U.S.A.* **76,** 2345–2349 (1979).
19. Brenner, S. R. & Korn, E. D. *J. biol. Chem.* **254,** 9982–9985 (1979).
20. Brown, S. S. & Spudich, J. A. *J. Cell Biol.* **83,** 657–662 (1979).
21. Korn, E. D. *Proc. natn. Acad. Sci. U.S.A.* **75,** 588–599 (1978).
22. Dancker, P. & Löw, I. *Z. Naturforsch.* **34c,** 555–557 (1979).
23. Brenner, S. L. & Korn, E. D. *J. biol. Chem.* **255,** 841–844 (1980).
24. Tannenbaum, J. in *Cytochalasins Biochemical and Biological Aspects* (ed. Tanenbaum, S. W.) 521–559 (Elsevier/North-Holland, Amsterdam, 1978).
25. Godman, G. C. & Miranda, A. F. in *Cytochalasins Biochemical and Biological Aspects* (ed. Tanenbaum, S. W.) 277–429 (Elsevier/North-Holland, Amsterdam, 1978).

Lack of heterogeneity in anti-hapten antibodies of a phylogenetically primitive shark

O. Mäkelä

Department of Bacteriology and Immunology, University of Helsinki, SF-00290 Helsinki 29, Finland

G. W. Litman

Sloan-Kettering Institute for Cancer Research, Walker Laboratory, Rye, New York 10580

Individual mammals have the capacity to express at least one million distinct antigen binding specificities, implying a high degree of structural heterogeneity in the variable heavy and light chain (V_H and V_L) portions of the antibody molecules. Studies of higher vertebrate species suggest that this heterogeneity is created both through a sizeable repertoire of germ-line V_H and V_L genes[1] and through random rearrangements of V and joining genes[2–4]. Additional somatic mechanisms probably also contribute to the ultimate heterogeneity; one-third of murine plasmacytomas producing λ_1 immunoglobulin carry a somatically mutated Igl-V gene[5,6]. The relative contributions of these various mechanisms to the overall immunoglobulin variability are difficult to evaluate. The production of different antibodies to a defined determinant in different individuals of an inbred mouse strain [for example, (3-iodo-4-hydroxy-5-nitrophenyl) acetyl (NIP) in CBA mice[7]] suggests the involvement of somatic mutations or rearrangement but does not rule out the possibility that each individual CBA mouse expresses only a small random fraction from a large germ-line repertoire of V genes determining different anti-NIP binding sites. The opposite finding, that different individuals produce nearly identical antibodies to a defined determinant, would suggest the presence and expression of a limited number of germ-line genes without somatic alterations. Data presented here suggest that primitive sharks (*Heterodontus fransisci*)[8] produce such antibodies to the hapten furyloxazolone.

Heterodontus (0.2–0.5 kg) of estimated age 2–3 yr were maintained as described previously[9]. Intramuscular immunization with *Brucella abortus* to which 2-furyloxazolone (furyl Ox) was coupled[10] was carried out on day 0 and day 30. Inbred male rats of the SDK strain (0.34–0.43 kg) aged 3–4 months were immunized with the same dose and timing. Antibody to furyl Ox was measured by neutralization of bacteriophage T4 coupled with furyl Ox-aminocaproyl (furyl Ox-cap-T4)[10]. The shark antibody was found to reside in the high molecular weight serum fraction as judged by sensitivity to 0.1 M 2-mercaptoethanol and the 19S sedimentation constant of the phage neutralizing activity. Antibodies of rat sera were found in both high and low molecular weight fractions. However, in the experiments reported we have used the 19S fraction prepared by sucrose density gradient centrifugation, or for the day 9 sera, antibody remaining after elimination of IgG by incubation of 1.0 ml of 20% serum with 0.7 ml of packed protein A–Sepharose for 1 h at 20 °C (ref. 11).

The shark antisera discriminated between the structurally different haptens furyl Ox and azobenzene arsonate (Ars) in a manner comparable to rat antisera (Table 1). The anti-furyl Ox titres after immunization with furyl Ox were 170 times higher than the anti-Ars titres. The only anti-Ars serum that we tested exhibited a 56-fold difference in the reverse direction.

The affinity and fine specificity of the antibodies were characterized by the inhibition of the phage neutralization using seven structurally related haptens. The concentration of hapten required to reduce the antibody titre by 50% was termed the IC_{50}; a low IC_{50} value indicated a high affinity and vice versa[12].

Table 1 Anti-furyl Ox or anti-Ars titres of *Heterodontus* or rat antisera

	Anti-furyl Ox titres at various days post-immunization				Anti-Ars titres
Day	—	9	20	55	55
Heterodontus	1,300	—	18,000	143,000	270
Rat (whole sera)	—	4,600	12,000	386,000	160

The data are geometric mean titres of four *Heterodontus* and six rat sera. The antibodies were measured by neutralization of bacteriophage T4 coupled with furyl Ox–aminocaproyl[10] or BOC-ABA-tyrosine[16]. An anti-Ars serum obtained on day 180 of an immunization course with *B. abortus* coupled with azobenzene arsonate[9] was tested with the same phage conjugates; its anti-furyl Ox titre was 830 and anti-Ars titre 15,000.

0028–0836/80/410639—02$01.00

This analysis revealed three differences between shark and rat 19S antibodies (Fig. 1).

The shark antibodies had lower affinities for the immunizing hapten furyl Ox-cap (log mean IC_{50} 35 μM) than did rat antibodies (IC_{50} 0.82 μM). It might be argued that the IC_{50} values cannot be used to compare affinities because the degree of polymerization may differ in the rat and the shark IgM. Even if this were true, shark antibodies are likely to be less polymeric than rat antibodies. (Rat antibodies are pentameric, some fishes have tetrameric antibodies[13].) The true species difference of affinities would then be greater than the IC_{50} values indicate. The low affinity may be characteristic of all piscian antibodies[13].

Another difference between the two species is in the discriminating power of the antibodies. Shark antibodies had rather similar affinities for the immunizing hapten and all six analogues. The average relative affinities for the analogues only varied from 37% (styryl Ox-cap) to 150% (fluorophenyl Ox-cap), whereas rat antibodies discriminated strongly between furyl Ox-cap and some of the analogues. For example, the average affinity for nitrophenyl Ox-cap and styryl Ox-cap was less than 1/10th of the average affinity for furyl Ox-cap.

The third characteristic of shark antibodies which distinguishes them from rat antibodies was a constant pattern of relative affinities for the structural analogues of furyl Ox-cap. This species-specific pattern was exhibited by all eight sera representing four individual fish and two time points post-immunization. For example, the affinity for fluorophenyl Ox-cap was always ~150% and the affinity for styryl Ox-cap was always ~37% relative to the affinity for furyl Ox-cap. The greater vertical variations of rat values than shark values shown in Fig. 1 indicate that the rats showed no such species-specific pattern. Even more striking differences could be seen when comparing individual rats: thus, antibodies of one rat had a three times higher affinity for iodophenyl Ox-cap than for furyl Ox-cap whereas antibodies of another rat had a 40-fold difference in the reverse direction. A modest increase of affinities for furyl Ox-cap was observed in the rats from day 9 to day 55 but the differences were not statistically significant.

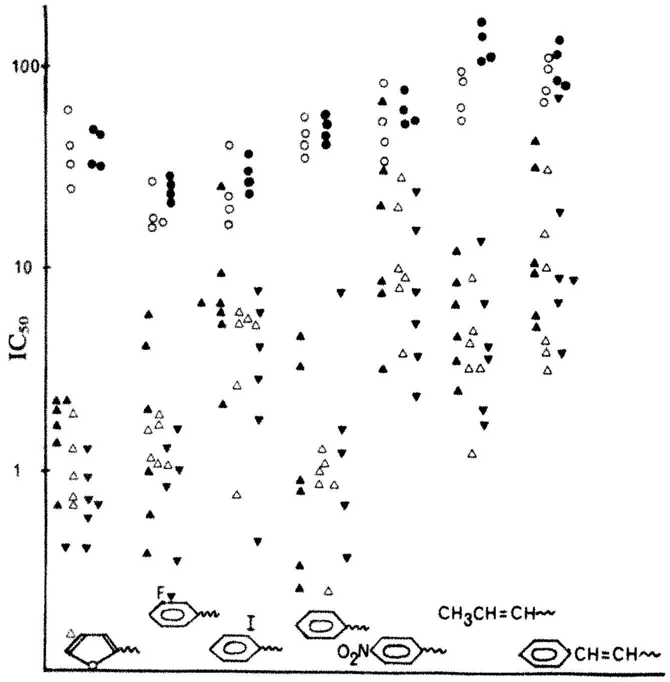

Fig. 1 Fine-specificity characteristics of *Heterodontus* and rat antibodies (19S). Relative affinities for seven different oxazolones were determined. Each symbol represents an IC_{50} value of an antiserum or its 19S fraction for the compound illustrated below the column. All compounds shared the oxazolone-ε-aminocaproyl (Ox-cap) structure. The structures illustrated were attached to the C-2 of Ox-cap. From the left the compounds are: furyl Ox-cap (closely resembles furyl Ox-lysine, the immunizing determinant), fluorophenyl Ox-cap, iodophenyl Ox-cap, phenyl Ox-cap, nitrophenyl Ox-cap, propyl Ox-cap and styryl Ox-cap. Circular symbols represent *Heterodontus* sera from day 20 (○) or day 55 (●). Triangles represent rat sera from day 9 (▲), day 20 (△) or day 55 (▼).

Thus, we found that furyloxazolone induced a similar low-affinity antibody population of limited discriminating capacity in four individual sharks and that this population did not change detectably over a 25-day period of immunization. By contrast, rat IgM antibodies elicited in response to immunization with the same bacterium–hapten conjugate had a high affinity for the immunizing hapten but a low affinity for some of its chemical analogues; differences between individual animals were large. These data are consistent with the presence in *Heterodontus* of a stable, limited repertoire of antibody molecules of probable germ-line origin, and expand preliminary structural observations which support this hypothesis[14,15]. *Heterodontus* may represent a valuable developmental model for examining the genetic processes which have been involved in the diversification of the variable-region gene pool during vertebrate evolution.

This work was supported by grants NIH CA-08748, NSF PCM-8001919 and A1-14454 (G.W.L.).

Received 28 April; accepted 20 August 1980.

1. Seidman, J. G., Leder, A., Nau, M., Norman, B. & Leder, P. *Science* **202,** 11–17 (1978).
2. Max, E. E., Seidman, J. G. & Leder, P. *Proc. natn. Acad. Sci. U.S.A.* **76,** 3450–3454 (1979).
3. Sakano, H., Hüppi, K., Heinrich, G. & Tonegawa, S. *Nature* **280,** 288–294 (1979).
4. Rao, D. N., Rudikoff, S., Krutzsch, H. & Potter, M. *Proc. natn. Acad. Sci. U.S.A.* **76,** 2890–2894 (1979).
5. Bernard, O., Hozumi, N. & Tonegawa, S. *Cell* **15,** 1133–1144 (1978).
6. Cohn, M. *et al.* in *The Immune System* (eds Sercarz, E. E. *et al.*) (Academic, London, 1974).
7. Kreth, H. W. & Williamson, A. R. *Eur. J. Immun.* **3,** 141–147 (1972).
8. Stahl, B. J. *Vertebrate History: Problems in Evolution,* 185 (McGraw-Hill, New York, 1974).
9. Litman, G. W., Scheffel, C. & Mäkelä, O. *Immun. Lett.* **1,** 213–215 (1980).
10. Mäkelä, O., Kaartinen, M., Pelkonen, J. L. T. & Karjalainen, K. *J. exp. Med.* **148,** 1644–1660 (1978).
11. Boyle, M. D. P. & Langone, J. J. *J. immun. Meth.* **32,** 51–58 (1980).
12. Sarvas, H. & Mäkelä, O. *Immunochemistry* **7,** 933–943 (1970).
13. Voss, E. W. Jr, Groberg, W. J. Jr & Fryer, J. L. *Immunochemistry* **15,** 459–464 (1978).
14. Kehoe, J. M., Sharon, J., Gerber-Jensen, B. & Litman, G. W. *Immunogenetics* **7,** 34–40 (1978).
15. Litman, G. W., Scheffel, C. & Gerber-Jensen, B. *J. Immunogenet.* **7,** 197–206 (1980).
16. Becker, M. J., Ray, A., Andersson, L. C. & Mäkelä, O. *Eur. J. Immun.* **5,** 262–266 (1975).

Phenypressin (Phe^2-Arg^8-vasopressin), a new neurohypophysial peptide found in marsupials

M. T. Chauvet, D. Hurpet, J. Chauvet & R. Acher

Laboratory of Biological Chemistry, University of Paris VI,
96 Boulevard Raspail, Paris 75006, France

Recent investigations on marsupial neurohypophysial hormones have revealed that species belonging to the Australian family Macropodidae and the American family Didelphidae have, apart from an oxytocin-like hormone, two vasopressin-like peptides which can be separated either by ion-exchange chromatography or chromatoelectrophoresis[1–3]. The major pressor hormone of two Australian species, the red kangaroo (*Macropus rufus*) and the tammar (*Macropus eugenii*), has been identified as lysine vasopressin by its amino acid sequence and its pharmacological properties[1,2]. We report here that the minor pressor hormone, which chromatographs on Amberlite CG-50 like arginine vasopressin[1,2], differs from it in sequence only at position 2 where phenylalanine replaces the tyrosine of arginine vasopressin[4].

The procedure described previously for isolation of lysine vasopressin[1,2] was used for the purification of the minor pressor hormone. Acetone-desiccated posterior pituitary lobes (oxytocic activity 0.7 U mg^{-1} and pressor activity 2.9 U mg^{-1} for red kangaroo, oxytocic activity 0.8 U mg^{-1} and pressor activity 2.3 U mg^{-1} for tammar) were extracted by 0.1 M HCl (1 ml for

0028-0836/80/410640—03$01.00

8 mg) for 4 h at 4 °C. Two experiments were carried out for each species with nine (42 mg) and 14 (67.7 mg) glands of red kangaroo and 24 (40.1 mg) and 33 (51 mg) glands of tammar. Supernatant solutions, separated by centrifugation, were subjected to molecular sieving on a column (1 × 120 cm) of Biogel P_4 equilibrated with 0.1 M acetic acid. Proteins were excluded and an oxytocic peak (yield in activity 78–83%) was separated from a pressor peak (yield in activity 77–87%). Fractions of each peak were pooled and solutions concentrated to a small volume by lyophilization. Materials were subjected to paper chromatoelectrophoresis in conditions described previously[5]. Regarding the pressor fraction, two pressor peptides having similar electrophoretic migrations (21 cm) but different chromatographic migrations (6–8 cm for lysine vasopressin, 10–12 cm for the new hormone) could be isolated. Spots, detected with dilute ninhydrin, were eluted with 0.1 M acetic acid. The yields in pressor activity were 27–36% for lysine vasopressin and 7–11% for the new hormone. Performic acid-oxidized or mercaptoethanol-added samples were subjected to hydrolysis (6 M HCl, 48 h, 105 °C *in vacuo*) and analysed with a Spinco 120B automatic analyser fitted with a high-sensitivity cell[6]. Results for the new hormone are given in Table 1. About 70 nmol of lysine vasopressin and 30–40 nmol of phenypressin were recovered from about 40 mg of acetone posterior pituitary powder.

For sequential studies, products purified from 14 glands of red kangaroo on one hand, and from 33 glands of tammar on the other, were used. In this case, spots were not eluted after chromatoelectrophoresis but Edman recurrent degradation was directly applied by using the paper-strip adaptation described by Chauvet and Acher[7]. Identification of phenylthiohydantoin (PTH) amino acids was carried out by thin-layer chromatography according to Edman and Henschen[8]. Spots were located by fluorescence and by reaction with ninhydrin which often gives characteristic colours[8]. About 100 nmol of pig lysine vasopressin and 50 nmol of ox arginine vasopressin were subjected, for comparison, to chromatoelectrophoresis and Edman degradation in the same conditions.

In the new hormone, Phe, Phe, Gln, Asn and Pro were identified in positions 2, 3, 4, 5 and 7 (Cys in positions 1 and 6 could not be seen because of the disulphide bridge). Comparison with arginine vasopressin or lysine vasopressin clearly showed PTH-Tyr in position 2 (lemon-yellow coloration) for these hormones instead of PTH-Phe (violet coloration after ninhydrin) for the new hormone. In contrast, PTH-Phe was found in position 3 for the three peptides. To characterize the residues in position 8 and 9 in the new hormone, after the eighth cleavage material was eluted from the paper strip with 0.1 M acetic acid and subjected to paper electrophoresis (0.1 M pyridine acetate buffer at *p*H 3.7, 50 V cm^{-1}, 35 min). PTH-Arg could be identified by a modified Sakaguchi reaction[9] (8.6-cm migration) and glycinamide with ninhydrin (20-cm migration). The two half-cystines, found as cysteic acid residues in performic acid-oxidized sample, were assigned to positions 1 and 6. A complete sequence is proposed for the new hormone in Table 2. We suggest the name *phenypressin* because of the substitution by phenylalanine of the second residue of arginine vasopressin, the classical pressor hormone of mammals[4]. On the other hand the biological properties resemble those of vasopressins.

Table 1 Amino acid composition of red kangaroo and tammar phenypressins

Amino acid	Red kangaroo (13 nmol)	Tammar (15 nmol)	Phenypressin (theoretical values)
Arg	0.88	0.93	1
Asp	1.00	1.00	1
Glu	1.06	1.08	1
Pro	1.03	0.71	1
Gly	1.15	1.22	1
Tyr	—	0.10	—
Phe	1.77	2.10	2
Cys*	1.18	1.33	2

Values are in molar ratios, using aspartic acid as reference.

* Half-cystines are determined as cysteic acid on a separate performic acid-oxidized sample. A partial destruction of cysteic acid is observed when hydrolysis is carried out with paper-eluted peptide.

Table 2 Amino acid sequence of phenypressin

Phenypressin	$\overset{1}{\text{Cys}}$-$\overset{2}{\text{Phe}}$-$\overset{3}{\text{Phe}}$-$\overset{4}{\text{Gln}}$-$\overset{5}{\text{Asn}}$-$\overset{6}{\text{Cys}}$-$\overset{7}{\text{Pro}}$-$\overset{8}{\text{Arg}}$-$\overset{9}{\text{Gly}}$ (NH$_2$)
Arginine vasopressin	$\overset{1}{\text{Cys}}$-$\overset{2}{\text{Tyr}}$-$\overset{3}{\text{Phe}}$-$\overset{4}{\text{Gln}}$-$\overset{5}{\text{Asn}}$-$\overset{6}{\text{Cys}}$-$\overset{7}{\text{Pro}}$-$\overset{8}{\text{Arg}}$-$\overset{9}{\text{Gly}}$ (NH$_2$)
Lysine vasopressin	$\overset{1}{\text{Cys}}$-$\overset{2}{\text{Tyr}}$-$\overset{3}{\text{Phe}}$-$\overset{4}{\text{Gln}}$-$\overset{5}{\text{Asn}}$-$\overset{6}{\text{Cys}}$-$\overset{7}{\text{Pro}}$-$\overset{8}{\text{Lys}}$-$\overset{9}{\text{Gly}}$ (NH$_2$)

Phe^2-Arg^8-vasopressin was synthesized, 18 years ago, by Huguenin and Boissonnas[10]. They compared the pharmacological properties of this analogue with those of arginine vasopressin. The substitution reduces the rat antidiuretic activity per μmol from 435 to 375 U and the rat blood pressure activity from 435 to 130 U. The intrinsic oxytocic activity is dramatically reduced from 17 to 0.2 U. From a limited number of measures, the rat blood pressure activity of natural phenypressin was found to range from 130 to 200 U, value in accordance with that reported for the synthetic peptide. Because of the small amount of material available and its very weak oxytocic activity, a reliable value could not be determined for this activity.

Examination by ion-exchange microchromatography[1] of six individual glands of red kangaroo collected either in Western Australia or in New South Wales, and of three individual glands of tammar, systematically revealed two pressor hormones. Duality was also found in individual glands of three other macropodid species (grey kangaroo, euro, quokka) and of two species belonging to the American family of Didelphidae (South American opossums)[3]. Apparently vasopressin duplication is current among marsupials. However, whether the pressor hormones of Didelphidae are identical with those of Macropodidae still needs clarification. Lysine vasopressin and phenypressin, characterized in two macropodid species, differ by two amino acid residues in positions 2 and 8. They are likely products of two distinct structural genes rather than two allelic forms of a single gene. Vasopressin dimorphism has previously been reported for some pig-like species (peccary, warthog, hippopotamus) without individual characterization[11,12]. It was assumed that the placental pressor hormones, arginine vasopressin and lysine vasopressin, were present, and because both hormones were not observed in all the glands examined, dimorphism was explained by heterozygosity[11].

Egg-laying prototherians are supposed to be the closest present-day mammals to the ancestral mammalian reptiles. The neurohypophysial hormones of an Australian prototherian, echidna, have been isolated and conventional mammalian peptides, oxytocin and arginine vasopressin, have been characterized[13]. All the non-mammalian tetrapods examined to date, including four reptile species, have mesotocin and arginine vasotocin[4] so that the change of arginine vasotocin into arginine vasopressin seems to have occurred early in mammalian evolution. In *Metatheria*, a duplication of the vasopressin gene occurred later and subsequent mutations might have produced lysine vasopressin on one hand and phenypressin on the other. Because neurohypophysial hormones are probably fragments of larger precursors in which they are bound to neurophysins[14] and because two types of neurophysins have been found in placental mammals[15], it will be of interest to establish whether the additional marsupial hormone is accompanied by an additional neurophysin.

We thank Professor C. H. Tyndale-Biscoe and Drs G. Byrne and F. N. Carrick for supplying pituitary glands. We also thank Mrs Danielle Thévenet and Miss Christine Jourdain for technical assistance. This investigation was supported in part by grants from CNRS (ERA no. 563 and ATP 3674), DGRST (no. 77-7-0290) and the Fondation pour la Recherche Médicale.

Received 18 July; accepted 28 August 1980.

1. Chauvet, M. T., Hurpet, D., Chauvet, J. & Acher, R. *Int. J. Peptide Protein Res.* (in the press).
2. Hurpet, D., Chauvet, M. T., Chauvet, J. & Acher, R. *Biochem. biophys. Res. Commun.* (in the press).
3. Acher, R., Chauvet, J., Chauvet, M. T. & Hurpet, D. *Sixth Int. Congr. Endocr., Melbourne* Abstr. **465** (1980).
4. Acher, R. *Proc. R. Soc. B* (in the press).
5. Acher, R., Chauvet, J. & Chauvet, M. T. *Eur. J. Biochem.* **17,** 509–513 (1970).
6. Spackman, D. H., Stein, W. H. & Moore, S. *Analyt. Chem.* **30,** 1190–1206 (1958).
7. Chauvet, J. P. & Acher, R. *Biochemistry* **11,** 916–926 (1972).
8. Edman, P. & Henschen, A. in *Protein Sequence Determination* (ed. Needleman, S. B.) 232–279 (Springer, Berlin, 1975).
9. Acher, R. & Crocker, C. *Biophys. biochim. Acta* **9,** 704–705 (1952).
10. Huguenin, R. L. & Boissonnas, R. *Helv. chim. Acta* **45,** 1629–1643 (1962).
11. Ferguson, D. R. *Gen. comp. Endocr.* **12,** 609–613 (1969).
12. Ferguson, D. R. & Pickering, B. T. *Gen. comp. Endocr.* **13,** 425–429 (1969).
13. Acher, R., Chauvet, J. & Chauvet, M. T. *Nature new Biol.* **244,** 124–126 (1973).
14. Brownstein, M. J., Russel, J. T. & Gainer, H. *Science* **207,** 373–378 (1980).
15. Acher, R. *Angewandte Chem. Int. Edn engl.* **18,** 846–860 (1979).

HCG stimulation of testicular LHRH-like activity

Richard M. Sharpe & Hamish M. Fraser

MRC Reproductive Biology Unit, Centre for Reproductive Biology,
37 Chalmers Street, Edinburgh EH3 9EW, UK

It is well established that the administration of high doses of luteinizing hormone (LH) or human chorionic gonadotropin (HCG) to animals can impair gonadal function in both the male and female^{1}. These effects can be duplicated by the administration of LH releasing hormone (LHRH) or its agonists to intact animals$^{2-5}$, including man^{6}. Somewhat surprisingly, recent results have demonstrated that similar impairment of gonadal function by LHRH and its agonists can be achieved in the absence of the pituitary (for review see ref. 7), and the demonstration of specific, high-affinity binding sites for LHRH and its agonists on ovarian luteal cells^{8} and on testicular Leydig cells$^{9-11}$, could mean that LHRH-like factors are involved in the local regulation of the gonads. A further intriguing finding is the striking similarity between the direct, inhibitory effects of LHRH and LH/HCG on the gonads^{7}; for example, both treatments reduce LH receptor numbers and the steroidogenic responsiveness of rat Leydig cells^{2,4,12,13}. We now offer a possible explanation for this similarity by demonstrating that HCG treatment stimulates the testicular production of a biologically active LHRH-like factor, suggesting that the inhibitory actions of HCG on the Leydig cell may be mediated by the local production of this factor.

We have utilized the receptor-binding ability of rat Leydig cells for LHRH and its agonists$^{9-11}$ to establish a robust and sensitive assay for LHRH-like activity present in testicular interstitial fluid (IF) (Fig. 1). Using this assay system, negligible activity was detectable in IF from saline-injected (control) rats whereas clearly detectable amounts were present 16 h after injection of 100 IU HCG. Interstitial fluid from such animals gave parallel displacement curves to unlabelled LHRH agonist (Fig. 1), and stimulated the release of pituitary LH from hemi-pituitaries *in vitro* (Table 1), establishing that the material was biologically active. Other factors present in high amounts in the IF, such as HCG^{14} and testosterone^{15}, did not contribute to this activity, as the addition of these hormones in large amounts (HCG up to 10^{-6} M, testosterone up to 10 μg ml^{-1}) to the receptor assay was without significant effect. Again, the inclusion of IF from control and HCG-injected animals in the rat LH radioimmunoassay was without detectable effect, thus demonstrating that the LH measured in hemi-pituitary incubation medium was derived from the pituitary tissue and not from the added IF.

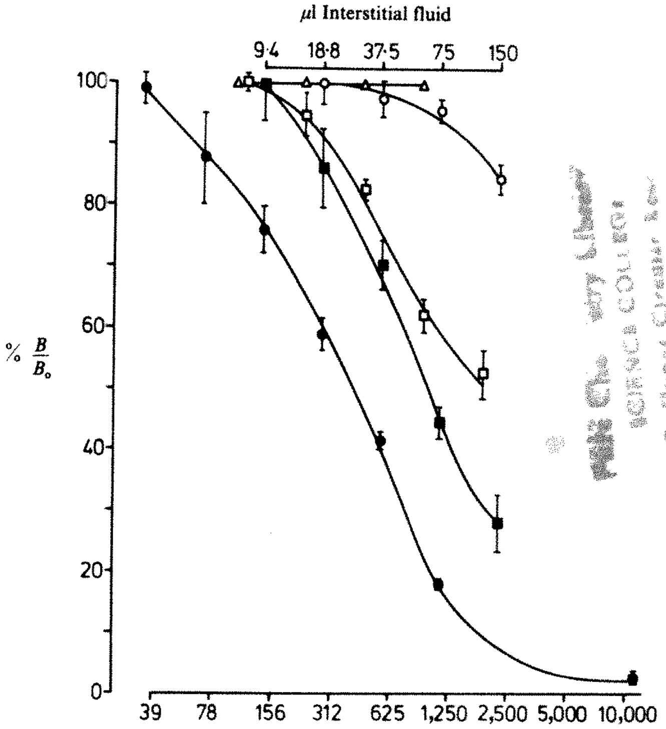

Fig. 1 Displacement of the binding of ^{125}I-LHRH agonist ((D-Ser-*t*-bu^{6}, *des*-Gly-NH$_2$^{10}) LHRH ethylamide) to dispersed Leydig cells by unlabelled LHRH agonist and testicular interstitial fluid from control and HCG-injected rats. Leydig cells were prepared by collagenase dispersion of decapsulated testes from adult (age ⩾90 days) Liverpool/Hooded rats, using techniques described previously^{11,19}. The dispersed cells were resuspended in Krebs–Ringer bicarbonate (KRB) solution (*p*H 7.5) containing 0.2% bovine serum albumin (BSA; fraction V, Sigma) and 200 μg ml^{-1} Bacitracin (Sigma). The volume of resuspension was equivalent to 1 ml per original testis and, for assay, aliquots (0.2 ml) of this cell suspension were dispensed into 63 × 11-mm polystyrene tubes. As determined by the staining of dispersed cells for 3β-hydroxysteroid dehydrogenase^{19}, each 0.2-ml aliquot contained approximately 5×10^{6} positively staining (Leydig) cells. The test materials or unlabelled LHRH agonist were added in a volume of 0.15 ml and ^{125}I-LHRH agonist (~150,000 c.p.m.) in a volume of 0.05 ml. Nonspecific binding was determined by parallel incubation in the presence of 10^{-6} M unlabelled LHRH agonist (see ref. 11 for details). All samples/standards were run in duplicate or triplicate and incubation was for 45 min at 21 °C. Incubation was ended by placing tubes on ice and immediately diluting the incubate with 1 ml ice-cold medium. Tubes were then centrifuged for 15 min at 1,000*g* and radioactivity in the pellet measured in a γ counter. LHRH agonist was labelled with ^{125}I using lactoperoxidase^{20} as described previously^{11} and, as determined by self-displacement in the receptor assay, had a specific activity of 1,200 mCi per mg. In eight successive assays the mean (±s.d.) binding of ^{125}I-LHRH agonist was 7.4 ± 1.5% of the total counts added, of which 32–40% was not displaceable by parallel incubation with 10^{-6} M unlabelled LHRH agonist, and was taken to represent the nonspecific binding; specific binding was 5.6 ± 1.3% of the total counts added. The sensitivity of the assay, defined as the concentration of unlabelled LHRH agonist required to suppress binding to 90% B/B_0, was 48 ± 16 pg ml^{-1}($n = 8$), and the intra-assay coefficient of variation was ± 5% for standards and ± 8.4% for interstitial fluid samples. Sprague–Dawley rats aged 70–80 days were injected subcutaneously with either 0.9% saline or 100 IU HCG (Chorulon) and killed with ether 16 h later. Testicular IF was collected as described previously^{14,15}, by allowing the fluid to percolate from the incised caudal end of the testis over a 16-h period at 4 °C; the fluid was then centrifuged for 5 min at 1,000*g* at 4 °C and the IF from 8–12 rats per treatment group was pooled before assay. The displacement curves for two such pools of IF from independent experiments are detailed in the figure. ●, Unlabelled LHRH agonist (standard); △, ○, interstitial fluid from saline-injected (control) rats; ■, □, interstitial fluid from HCG-injected rats. Results are plotted as the mean and range of duplicate determinations and, as determined by 2-factor analysis of variance (with replication), there was no evidence ($P > 0.05$) for non-parallelism of the displacement curves for standard and IF dilutions.

0028–0836/80/410642—02$01.00

We have used the receptor assay to quantify the LHRH activity in IF at various times after HCG injection (Table 2). In only 2 out of 12 samples from control rats (expts 1 and 2, Table 2) was there detectable LHRH activity, whereas high levels were found in all six samples from rats 16 h after injection of 100 IU HCG; at other times after this treatment, the frequency and level of detectable LHRH activity did not differ from controls. This effect of HCG on LHRH activity in IF at 16 h after injection was dose dependent (expt 2, Table 2), and a low dose of HCG (6 IU) was without detectable effect. As found previously[14,15], injection of HCG also increased the amounts of IF in the testis at 8–24 h after injection (Table 2), as a result of increased capillary wall permeability[16], and therefore calculation of the total amounts of LHRH activity in IF at 16 h after injection would exaggerate the difference from control levels.

Although we have shown that a factor present in IF from HCG-injected rats has LHRH-like activity *in vitro* at both the Leydig cell and pituitary levels, it seems most likely that any physiological effects of this factor are restricted to the testis. In support of this idea, we have preliminary evidence which suggests that the receptor-binding potency *in vitro* of this LHRH-like factor is considerably lower at the pituitary than at the Leydig cell level (H.M.F. and R.M.S., unpublished data). This may mean that there are differences in the type of degradative enzymes within the pituitary and the Leydig cell or that there are differences between the structures of hypothalamic LHRH and the LHRH-active factor produced by the testis. In this respect, the latter may correspond to the LHRH-active factor recently isolated from ovarian follicular fluid[17,18], which possesses LHRH-like biological activity but is immunologically distinct from native LHRH.

Table 1 Stimulation of pituitary LH release *in vitro* by LHRH and testicular IF from control and HCG-injected rats

Test material added to incubation medium	% LH released by test hemi-pituitary
10 ng LHRH	635 ± 192*
1 ng LHRH	101 ± 34
0.1 ml control IF	118 ± 50
0.01 ml control IF	76 ± 25
0.1 ml HCG + 16 h IF	357 ± 68*
0.01 ml HCG + 16 h IF	91 ± 15

Hemi-pituitaries from Sprague–Dawley rats aged 55 days were incubated at 37 °C *in vitro* for 4 h as described previously[21]. One-half of each pituitary was incubated in buffer alone (Krebs Ringer + 1 mg ml^{-1} glucose + 0.2% bovine serum albumin (BSA)) while the contralateral hemi-pituitary was incubated in the presence of one of the test materials listed. The incubation volume was 0.5 ml. LH in the incubation medium was determined by radioimmunoassay[22]. LH released in the presence of the test material is expressed as a % of that released by the (control) contralateral hemi-pituitary. For the two test materials which stimulated LH release, the basal and test-stimulated LH release (mean ± s.d.) were as follows—10 ng LHRH: basal, 2.45 ± 0.25 μg NIAMDD rat LH-RP-1 per hemi-pituitary; stimulated, 15.35 ± 4.68 μg; 0.1 ml HCG + 16 h IF: basal, 2.78 ± 1.05 μg; stimulated, 9.38 ± 1.59 μg. Results are the mean ± s.d. for three incubations.

* $P < 0.01$ (paired t-test comparison of control and test-stimulated LH release).

Table 2 The relationship between the dose of HCG injected and the time after injection on the levels of LHRH-active material in testicular interstitial fluid

					LHRH activity in IF (ng equiv. of LHRH agonist per ml)	
Expt	Treatment	Hours after injection	No. of animals	Interstitial fluid (μl per paired testes)	Detectable/ undetectable	Mean ± s.d.*
1	Saline	16	6	145 ± 19	1/5	1.24 ± 0.6
	100 IU HCG	2	4	123 ± 30	0/4	<1
		8	4	193 ± 21†	2/2	1.24 ± 0.2
		16	6	229 ± 44‡	6/0	5.48 ± 2.3‡
		24	4	213 ± 40†	0/4	<1
		40	4	130 ± 25	1/3	2.05 ± 1.8
2	Saline	16	6	107 ± 16	1/5	1.28 ± 0.7
	150 IU HCG	16	4	160 ± 7§	4/0	8.49 ± 4.0‡
	30 IU HCG	16	4	160 ± 14‡	4/0	5.29 ± 1.8‡
	6 IU HCG	16	4	138 ± 26	1/3	1.36 ± 0.6

Treatment of animals and collection of IF were as described in Fig. 1 legend, except that IF from individual animals was kept separate and not pooled. All the above samples were assayed together in 0.05-ml amounts in a single receptor assay, and the concentration equivalent of LHRH agonist in each sample was computed after log–logit transformation of the data. All samples were assayed in duplicate except for three control fluids for which only a single assessment was possible. The limit of detection of the assay (the level corresponding to 90% B/B_0) was equivalent to 1 ng LHRH agonist per ml for a 0.05-ml sample.

* All undetectable samples (<1 ng ml^{-1}) were assigned a value of 1 ng ml^{-1} to calculate the mean ± s.d. and assess statistical significance.

† $P < 0.02$; ‡ $P < 0.01$; § $P < 0.001$, in comparison with respective control group (Student's t-test).

In rats injected with high doses of HCG, impairment of the steroidogenic responsiveness of the Leydig cells and the loss of LH (HCG) receptors occur dramatically beyond 16 h after injection[14]. This time coincides precisely with the appearance of detectable levels of the LHRH-active factor in the interstitial fluid that bathes the Leydig cells. As LHRH agonists can themselves directly reduce LH receptor numbers and the steroidogenic responsiveness of the Leydig cells[12,13], it seems plausible that the inhibitory effects of HCG on the Leydig cell are mediated at least in part by the local production of this LHRH-active factor. Its origin is unknown but, as granulosa cells seem to be the site of production of an LHRH-active factor in the ovary[18], possibly the corresponding cell type in the testis, the Sertoli cell, is the site of production of the LHRH-active factor which we have detected. Certainly, the possibility that gonadotropins may affect gonadal function through locally produced LHRH-like substances opens exciting new dimensions for reproductive biology and its control.

We thank Drs J. Sandow and S. Dombey for supplies of LHRH and LHRH agonist, and the National Pituitary Agency, NIAMDD, US for materials for rat LH radioimmunoassay.

Received 15 July; accepted 26 August 1980.

1. Catt, K. J., Harwood, J. P., Aguilera, G. & Dafau, M. L. *Nature* **280,** 109–116 (1979).
2. Labrie, F. *et al. Int. J. Androl. Suppl.* **2,** 303–314 (1978).
3. Sandow, J., von Rechenberg, W., Baeder, C. & Engelbart, K. *Int. J. Fert.* (in the press).
4. Sharpe, R. M., Fraser, H. M. & Sandow, J. *J. Endocr.* **80,** 249–257 (1979).
5. Fraser, H. M. & Lincoln, G. A. *Biol. Reprod.* **22,** 269–276 (1980).
6. Bergquist, C., Nillius, S. J., Bergh, T., Skarin, G. & Wide, L. *Acta endocr. copenh.* **91,** 601–608 (1979).
7. Sharpe, R. M. *Nature* **286,** 12–14 (1980).
8. Clayton, R. N., Harwood, J. P. & Catt, K. J. *Nature* **282,** 90–92 (1979).
9. Labrie, F. *et al. Int. J. Fert.* (in the press).
10. Clayton, R. N., Katikineni, M., Chan, V., Dufau, M. L. & Catt, K. J. *Proc. natn. Acad. Sci. U.S.A.* (in the press).
11. Sharpe, R. M. & Fraser, H. M. *Biochem. biophys. Res. Commun.* **95,** 256–262 (1980).
12. Arimura, A., Serafini, P., Talbot, S. & Schally, A. V. *Biochem. biophys. Res. Commun.* **90,** 687–693 (1979).
13. Hsueh, A. J. W. & Erickson, G. F. *Nature* **281,** 66–67 (1979).
14. Sharpe, R. M. *Biol. Reprod.* **22,** 851–858 (1980).
15. Sharpe, R. M. *J. Reprod. Fert.* **55,** 365–371 (1979).
16. Sharpe, R. M. & Setchell, B. P. *Int. J. Androl.* abstr. (in the press).
17. Ying, S.-Y., & Guillemin, R. *C.r. hebd. Séanc. Acad. Sci., Paris* D**289,** 943–946 (1979).
18. Ying, S.-Y. & Guillemin, R. in *Progm. Abstr. Am. Endocrine Soc.* Abstr. 158 (June, 1980).
19. Sharpe, R. M. & McNeilly, A. S. *Molec. cell. Endocr.* **18,** 75–86 (1980).
20. Miyachi, Y., Chrambach, A., Mecklenburg, R. & Lipsett, M. B. *Endocrinology* **92,** 1725–1730 (1973).
21. Sharpe, R. M., Shahmanesh, M., Ellwood, M. G., Hartog, M. & Brown, P. S. *J. Endocr.* **65,** 265–273 (1975).
22. Fraser, H. M. & Sandow, J. *J. Endocr.* **74,** 291–296 (1977).

Gating charge immobilization and sodium current inactivation in internally perfused crayfish axons

R. P. Swenson Jr

Department of Physiology/G4, University of Pennsylvania,
Philadelphia, Pennsylvania 19104

The sodium permeability in nerve is regulated by two gating processes, activation and inactivation[1]. Their relationship to one another has been described as 'independent'[1] or 'coupled'[2,3]. An independent model, the Hodgkin and Huxley formulation, makes two testable predictions regarding gating current. First, as inactivation is voltage sensitive, it requires its own voltage sensor and might be expected to generate its own gating current. Second, gating current associated with activation should be unaffected by inactivation. Although charge movement associated with sodium activation is well characterized[4], no inactivation charge movement has been described. Instead, depolarizations long enough to produce sodium current inactivation were found to diminish the charge movement associated with channel closing[5]. Inactivation temporarily immobilized a substantial fraction of the gating charge. These observations suit a coupled model in which inactivation gains its voltage dependence by coupling to activation[3], and inactivation may in turn influence activation. However, the relative time course of the development immobilization (τ_{immob}) was found to be the same[3], the same in some voltage ranges[6] and slower than that for inactivation (τ_{inact}). In crayfish axons inactivation is roughly five times faster than in squid, providing an interesting opportunity to compare inactivation and immobilization. Further, inactivation is so rapid that inactivation gating current should be easily visible. No inactivation charge movement was found and τ_{immob} equals τ_{inact}.

Experiments were performed on internally perfused crayfish giant axons using an axial wire for voltage clamping the nerve. The solutions were prepared so that external sodium was the only permeant ion and gating currents were measured in the presence of tetrodotoxin (TTX). The relative time courses of inactivation in crayfish and squid nerve are compared in Fig. 1. The lower traces show that the sodium current (I_{Na}) decays with a time constant (τ_{h}) of 2.5 ms in squid and more quickly in crayfish, 0.45 ms at the same temperature and voltage. The upper traces in the figure show gating current recorded at the same voltage in the presence of TTX. The rapid time course of inactivation in crayfish should make it easy to resolve an additional component in the gating current due to inactivation, yet no such current is detectable at any potential.

Immobilization can be measured by integrating the gating current tails as the channels close at pulse termination (Q_{OFF}) and comparing them with the activation charge movement (Q_{ON}). The OFF gating currents diminish in both amplitude and area as the duration of the pulse was increased as shown in Fig. 2. After a depolarization of 10 ms (not shown), the OFF/ON ratio was 0.2; that is, 80% of the gating charge was temporarily immobilized and returned to its resting position too slowly to detect.

Table 1 Comparison of the time constants at 8 °C of sodium current inactivation (τ_{h} and τ_{tails}) and gating current immobilization (τ_{immob})

Potential	$\tau_{\text{h}}(n)$	$\tau_{\text{tails}}(n)$	$\tau_{\text{immob}}(n)$
−20 mV	0.55 ± 0.01 (4)	—	—
0 mV	0.46 ± 0.01 (4)	0.44 (1)	0.45 ± 0.04 (2)
+20 mV	0.39 ± 0.02 (3)	—	0.39 (1)
+40 mV	0.36 ± 0.01 (3)	0.31 (1)	0.38 (1)

n, Number of readings.

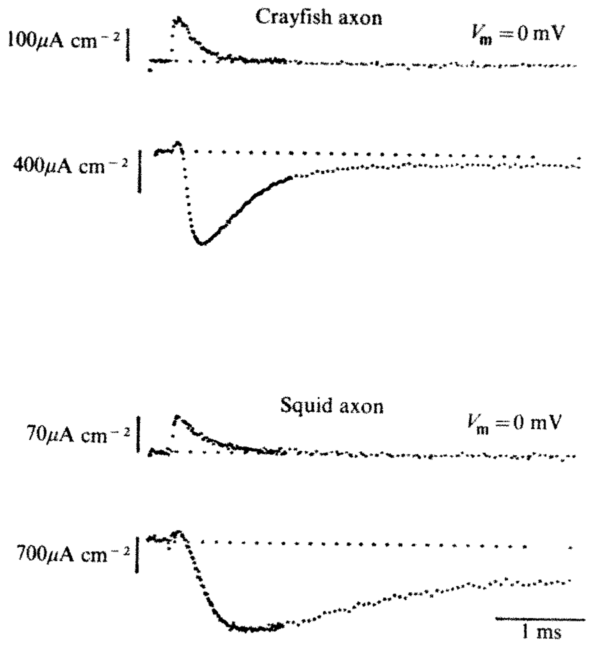

Fig. 1 Sodium and gating currents from crayfish and squid giant axon. Depolarizations to 0 mV from holding potentials of −80 mV (crayfish) and −70 mV (squid) elicit sodium currents of dramatically different time courses (lower traces). The ON gating currents (upper traces), are similar from the two nerves, and in neither is there a component with the time course of inactivation. Leakage and capacitive currents were subtracted using P/4 technique[5] from both I_{Na} and I_{g} records, and I_{g} represents the addition of 10 records. Crayfish currents were recorded with 70 mM NaCl, 140 mM Trizma (*p*H 7.0), and 20 mM $CaCl_2$ externally and 60 mM CsF, 60 mM Cs_3Citrate, and 120 mM mannitol internally. 10^{-7} M TTX was added externally to record I_{g} (axon Fe010Z). Squid currents were recorded in 112 mM NaCl, 378 mM Trizma (*p*H 7.0), 50 mM $CaCl_2$ externally and 150 tetramethylammonium (TMA) glutamate, 50 mM TMAF, and 650 mM sucrose internally (axon AU169Z). Temperature, 8 °C.

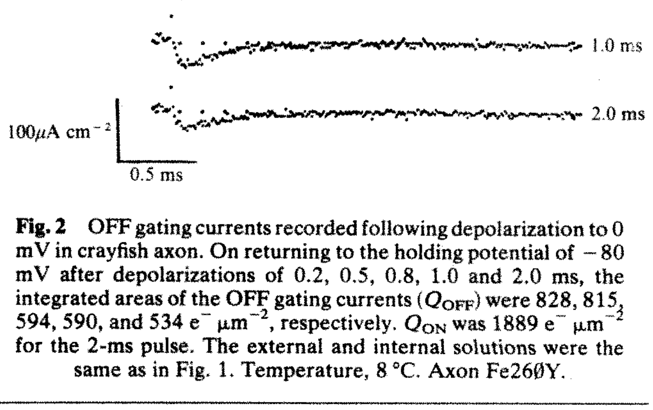

Fig. 2 OFF gating currents recorded following depolarization to 0 mV in crayfish axon. On returning to the holding potential of −80 mV after depolarizations of 0.2, 0.5, 0.8, 1.0 and 2.0 ms, the integrated areas of the OFF gating currents (Q_{OFF}) were 828, 815, 594, 590, and 534 e⁻ μm^{-2}, respectively. Q_{ON} was 1889 e⁻ μm^{-2} for the 2-ms pulse. The external and internal solutions were the same as in Fig. 1. Temperature, 8 °C. Axon Fe260Y.

0028-0836/80/410644—02$01.00

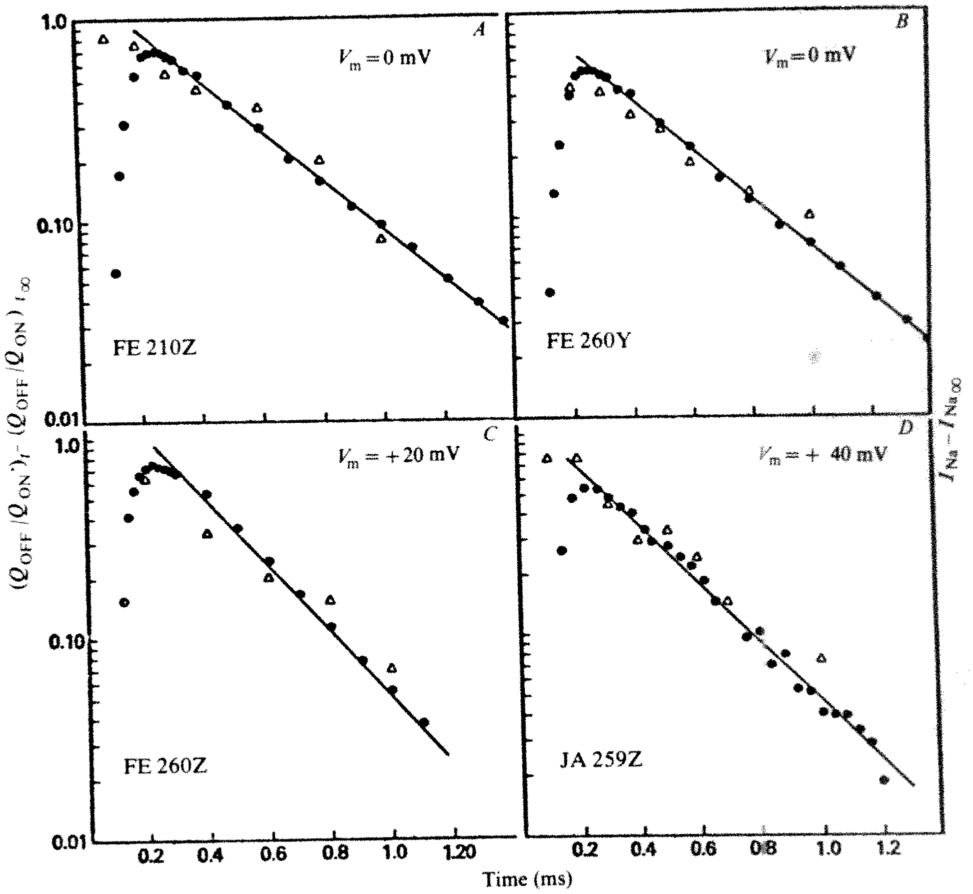

Fig. 3 Comparison of the rates of inactivation of the sodium current (●) and immobilization of the gating current (△) at 0, +20, and +40 mV in crayfish axon. ($I_{Na} - I_{Na\infty}$) is plotted where $I_{Na\infty}$ is the steady state sodium current. Axon Fe010Z. The sodium current in *a* and *b* is identical but slightly compressed on the vertical axis in *b*. Solutions as in Figs 1 and 2 without TTX. Peak amplitudes of the sodium currents were 0.84, 0.43, and 0.16 mA/cm^2 for 0, +20, and +40 mV, respectively. Superimposed on the sodium currents is the degree of immobilization (△) from four different axons measured from the area of the OFF gating currents after varying duration pulses. The OFF areas are plotted as the ratio of the integrated OFF gating current to ON gating current, $(Q_{OFF}/Q_{ON})_t$, minus a baseline correction, $(Q_{OFF}/Q_{ON})_{t\infty}$. t_∞ was 3.0 or 10.0 ms. *a*, Axon Fe210Z; *b*, Fe260Y; *c*, Fe260Z; and *d*, JA259Z. Solutions were the same as in Figs 1 and 2 with TTX. Temperature, 8 °C in all cases.

The temporal correlation between inactivation and immobilization is exemplified in Fig. 3, where sodium currents from one experiment are plotted on a semilogarithmic scale together with the OFF/ON ratio from other experiments. To allow for incomplete ON charge movement following brief pulses (0.5 ms), the OFF charge movement is normalized against the ON charge movement at various times ($[Q_{OFF}/Q_{ON}]_t$) and the baseline ($[Q_{OFF}/Q_{ON}]_{t\infty}$) was subtracted. Four experiments are shown, two at 0 mv, and one each at +20 and +40 mV. In all four, inactivation and immobilization agree closely in time course.

Table 1 summarizes the measurements of the time constant of immobilization (τ_{immob}), the time constant of inactivation of the sodium current measured from falling phase of the sodium current (τ_h), and the time constant of inactivation of the sodium current measured from sodium tail currents (τ_{tails}) at several potentials. The falling phase of the sodium current was well fitted by a single exponential. The two methods of measuring the rate in inactivation agree with one another, and were practically identical to τ_{immob}.

Although crayfish gating currents differ slightly in form from those measured in squid axons, the relatively fast rate of inactivation has allowed further evaluation of the relationship between the processes of inactivation and immobilization. The measurements reported here conform closely to the predictions of a coupled model: no inactivation gating current is visible in spite of the rapid time course of inactivation, and the time courses of inactivation and immobilization are identical. From these observations and others[3,6] it seems that inactivation of the sodium current and immobilization of the gating charge are in fact manifestations of the same underlying event. Following reorganization of the charged particles in the nerve which permits sodium conductance, a state develops which is characterized by both diminished conductance and a decreased ability of the charged particles to reprime. The development of this state can be followed either as inactivation of sodium current or immobilization of sodium gating current.

Received 19 May; accepted 15 August 1980.

1. Hodgkin, A. L. & Huxley, A. F. *J. Physiol., Lond.* **117,** 500–544 (1952).
2. Goldman, L. & Schauf, C. *J. gen. Physiol.* **59,** 659–675 (1972).
3. Armstrong, C. M. & Bezanilla, F. *J. gen. Physiol.* **70,** 567–590 (1977).
4. Armstrong, C. M. & Gilly, W. F. *J. gen. Physiol.* **74,** 691–711 (1979).
5. Bezanilla, F. & Armstrong, C. M. *Cold Spring Harb. Symp. quant. Biol.* **40,** 297–304 (1976).
6. Nonner, N. *J. Physiol., Lond.* 299–573–603 (1980).
7. Meves, H. & Vogel, W. *J. Physiol., Lond.* **267,** 377–393 (1977).
8. Bullock, J. O. & Schauf, C. L. *J. Physiol., Lond.* **286,** 157–171 (1979).

Are only α_2-adrenergic receptors present in bovine retina?

Helmut Bittiger, Jakob Heid & Niklaus Wigger

Research Department of the Pharmaceuticals Division of Ciba-Geigy Ltd, CH-4002 Basle, Switzerland

The retina represents a part of the central nervous system (CNS) with a well studied, geometrically defined structure and a specialized function—the processing of light signals[1]. Neurotransmitters such as glutamate,. aspartate, glycine[2–4], γ-aminobutyric acid (GABA), dopamine and acetylcholine[5–9] are considered to be involved in the neuronal activity of the retina. Receptors for acetylcholine[10,11], GABA[12], dopamine[13] and benzodiazepines[14,15] have also been demonstrated. Thus, the retina can be considered as a model for the study of neuronal processing in general, in which the input, light signals, can be selected and regulated in a defined way. We report here that α-adrenergic receptors in the bovine retina have been characterized using radioreceptor assays. ^{3}H-phentolamine (an α_1- and α_2-antagonist), ^{3}H-clonidine (a preferential α_2-agonist) and ^{3}H-WB 4101 [(2,6-dimethoxyphenoxyethyl)aminomethyl-1,4-benzodioxane, an α_1-antagonist[16]] were used as radioligands,

and WB 4101 and prazosin[17] (α_1-antagonists), tolazine (an α_2-antagonist)[18], yohimbine and its stereoisomers rauwolscine (preference for α_2-receptors) and corynanthine (preference for α_1-receptors)[19,20], were used as inhibitors of radioligand binding. Only α_2-adrenergic receptors[21,22] were found.

Figure 1*a* gives the saturation curve and corresponding Scatchard plot for ^{3}H-phentolamine binding. The dissociation constant (K_D) was found to be 3.4×10^{-10} M and the number of binding sites 437 fmol per mg protein. Nonspecific binding was defined in the presence of 10^{-6} M phentolamine and was only 5–10% of total binding. Association and dissociation were remarkably rapid in view of the low K_D values. At 20 °C and a concentration of 0.5 nM ^{3}H-phentolamine, half-saturation of binding was achieved within 2.5 min, and the half life of dissociation was 2.5 min (data not shown). ^{3}H-clonidine showed nearly identical binding characteristics (Fig. 1*b*), with a dissociation constant of 3.2×10^{-10} M and 341 fmol binding sites per mg protein. Association and dissociation had half lives of 1.5–2 min for a fast component, but there were, in addition, slower components with about 5–10-min half lives, which contributed about 20% of the total binding sites (data not shown). The binding characteristics of ^{3}H-WB 4101 are presented in Fig. 1*c*. Phentolamine, 10^{-6} M, was used to define nonspecific binding. The dissociation constant of 3.42 nM was higher but the number of binding sites of 378 fmol per mg protein comparable to those obtained with ^{3}H-phentolamine and ^{3}H-clonidine. The ratio of specific to nonspecific binding was much less favourable than with ^{3}H-clonidine and ^{3}H-phentolamine. Selected compounds were tested for their effects on ^{3}H-phentolamine, ^{3}H-clonidine and ^{3}H-WB 4101 binding in the retina and on ^{3}H-WB 4101 binding in the rat brain (see Table 1). The latter values are from own experiments or the literature[23]. Data from rat brain are usually similar to those from bovine brain[23,24]. Surprisingly, all compounds studied in the retina inhibited with about equal potency in all three radioreceptor assays. The somewhat lower IC$_{50}$ values in the ^{3}H-WB 4101 assay are probably due to the fact that the ^{3}H-ligand concentrat on of 1 nM was below the K_D of 3.42 nM, whereas those of ^{3}H-phentolamine and ^{3}H-clonidine were slightly above. Only agonists like noradrenaline, dopamine and clonidine were more potent in the ^{3}H-clonidine assay.

The order of inhibitory potencies of yohimbine and its stereoisomers in the retina was found to be rauwolscine > yohimbine > corynanthine, typical of α_2-receptors[20]. In the brain ^{3}H-WB 4101 assay, however (Table 1, last column), the reverse order, typical of α_1-receptors, was found[20]. Consistent with these findings, tolazoline, interacting preferentially with α_2-receptors, inhibited 140 times more potently in the retina

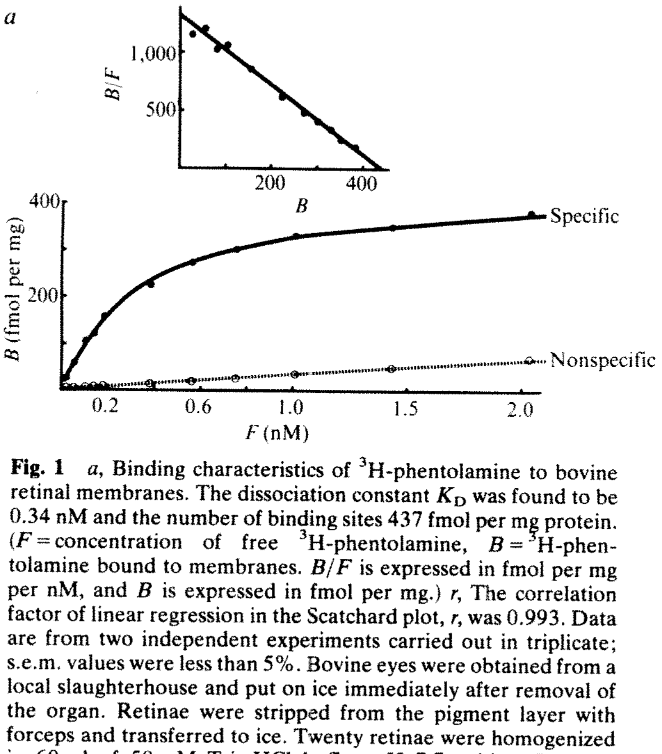

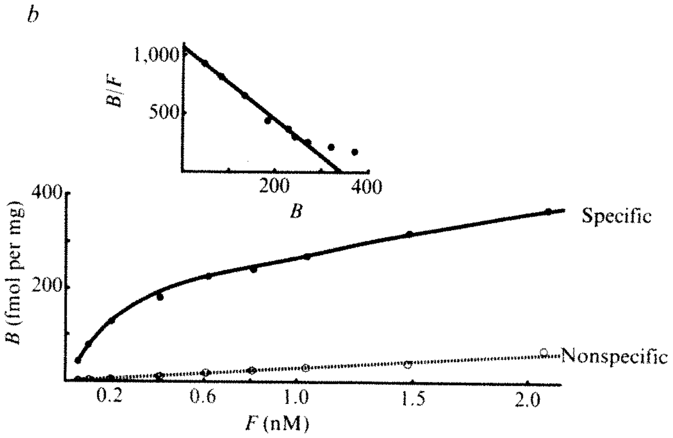

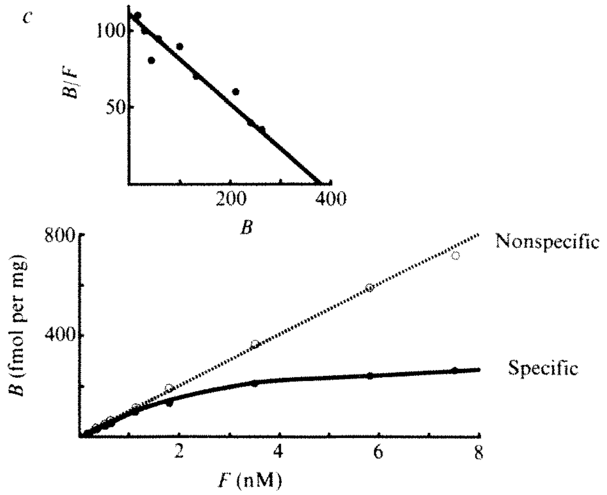

Fig. 1 *a*, Binding characteristics of ^{3}H-phentolamine to bovine retinal membranes. The dissociation constant K_D was found to be 0.34 nM and the number of binding sites 437 fmol per mg protein. (F = concentration of free ^{3}H-phentolamine, B = ^{3}H-phentolamine bound to membranes. B/F is expressed in fmol per mg per nM, and B is expressed in fmol per mg.) r, The correlation factor of linear regression in the Scatchard plot, r, was 0.993. Data are from two independent experiments carried out in triplicate; s.e.m. values were less than 5%. Bovine eyes were obtained from a local slaughterhouse and put on ice immediately after removal of the organ. Retinae were stripped from the pigment layer with forceps and transferred to ice. Twenty retinae were homogenized in 60 ml of 50 mM Tris-HCl buffer, *p*H 7.7, with a Polytron homogenizer (2 × 15 s, position 5) at 4 °C. The homogenate was centrifuged at 1,000*g* for 15 min and the resulting supernatant at 40,000*g* for 15 min. The pellet was resuspended in 50 mM Tris-HCl buffer, *p*H 7.7, and recentrifuged at 40,000*g* for 15 min. This step was repeated. The final pellet was suspended in about 100 ml buffer to give a final concentration of 1.5–2 mg protein per ml. The assay was carried out at 20 °C in 3 ml 50 mM Tris-HCl buffer, *p*H 7.7, containing 150–200 μg membrane protein and different concentrations of ^{3}H-phentolamine (20 Ci mmol^{-1}, prepared in the Ciba-Geigy radioisotope laboratories by halogen–tritium exchange in the aromatic ring, purity >98% as shown by pressure liquid chromatography and isotope dilution analysis). Incubation was for 15 min and was terminated by rapid filtration through Whatman glass fibre filters GF/B and three washes with 4 ml ice-cold buffer. Nonspecific binding was defined in the presence of 10^{-6} M phentolamine. Filter-bound material was digested in Soluene (Packard) and radioactivity was counted by addition of scintillator (Aquasol, NEN) in an Intertechnique liquid scintillation counter at an efficiency of 42%. *b*, Binding characteristics of ^{3}H-clonidine (NEN, 22.2 Ci mmol^{-1}) to bovine retinal membranes. The dissociation constant K_D was found to be 0.32 nM, the number of binding sites 341 fmol per mg protein and r 0.992. The experiments were performed as described in *a*. Nonspecific binding was defined in the presence of 10^{-6} M clonidine. *c*, Binding of ^{3}H-WB 4101 (NEN, 24.2 Ci mmol^{-1}) to bovine retinal membranes. Nonspecific binding was defined in the presence of 10^{-6} M phentolamine. The dissociation constant was found to be 3.42 nM, the number of binding sites 378 fmol per mg protein, comparable to those of ^{3}H-phentolamine and ^{3}H-clonidine, and r 0.948. To reduce nonspecific binding, retinae were osmotically shocked during the first homogenization in 1 mM Tris-HCl buffer and filtration was through GF/C glass fibre filters. Otherwise the procedure was as described in *a*.

Table 1 Radioligand inhibition of drug binding to retinal and brain membranes

	Retina			Brain	
Compound	^{3}H-phentolamine IC$_{50}$ (M)	^{3}H-clonidine IC$_{50}$ (M)	^{3}H-WB 4101 IC$_{50}$ (M)	^{3}H-WB 4101 K_i or IC$_{50}$ (M)	
Phentolamine	1.0×10^{-9}	1.0×10^{-9}	8.0×10^{-10}	1.0×10^{-8}	
Clonidine	6.4×10^{-9}	1.4×10^{-9}	3.6×10^{-9}	4.3×10^{-7}	(ref. 23)
WB 4101	2.0×10^{-8}	2.0×10^{-8}	1.6×10^{-8}	6.0×10^{-10}	(ref. 23)
Prazosin	5.8×10^{-6}	7.2×10^{-6}	2.0×10^{-6}	8.0×10^{-10}	
Tolazoline	5.0×10^{-8}	3.6×10^{-8}	6.4×10^{-8}	8.0×10^{-6}	
Yohimbine	5.0×10^{-8}	5.6×10^{-8}	3.6×10^{-8}	4.8×10^{-7}	
Rauwolscine	1.0×10^{-8}	1.6×10^{-8}	5.6×10^{-9}	1.0×10^{-5}	
Corynanthine	1.1×10^{-6}	1.1×10^{-6}	6.4×10^{-7}	3.0×10^{-7}	
Noradrenaline	2.6×10^{-7}	5.0×10^{-8}	2.2×10^{-7}	1.0×10^{-6}	(ref. 23)
Dopamine	2.0×10^{-6}	6.0×10^{-7}	1.6×10^{-6}	4.4×10^{-5}	(ref. 23)
Propranolol	$>10^{-5}$	$>10^{-5}$		6.9×10^{-6}	(ref. 23)

Assays were carried out as described in Fig. 1 legend. Drugs were added to the incubation medium at the same time as the radioligands. Concentrations of ^{3}H-phentolamine and ^{3}H-clonidine were 0.5 nM (slightly above K_D) and that of ^{3}H-WB 4101 nM (below K_D). IC$_{50}$ values were determined graphically from 8–10 different concentrations of drugs, each point performed in triplicate. Brain membranes were prepared as described in the literature[23] and the radioreceptor assays were carried out as described for retinal membranes.

than in the brain, whereas WB 4101 and prazosin, α_1-antagonists, were respectively, 30 and up to 2,000 times, more potent in the brain. Thus, the retinal α-receptors labelled by ^{3}H-phentolamine, ^{3}H-clonidine and ^{3}H-WB 4101 seem to be of the α_2-type and the brain receptors labelled by ^{3}H-WB 4101 of the α_1-type.

The retinal α-receptors seem to differ from α-receptors in all tissues or cells so far studied with these three radioligands. The K_D for ^{3}H-clonidine binding (0.32 nM) is much lower than that found in brain (5.6 nM)[23], although recently by using a special technique, a minority of high affinity ^{3}H-clonidine binding sites (0.5 nM) has been detected in brain[26]. ^{3}H-WB 4101, on the other hand, binds with much lower affinity to retinal (3.42 nM) than to brain membranes (0.35 nM)[23] and seems to label α_2-receptors in the retina and α_1-receptors in the brain. As seen in Table 1, prazosin seems to be more specific for α_1-receptors than is WB 4101. ^{3}H-phentolamine has a 35 times higher affinity for retinal α-receptors ($K_D = 0.34$ nM) than has been reported for α-receptors on human platelets ($K_D = 12$ nM)[25]. We have found that ^{3}H-phentolamine is not a suitable ligand for studying α-receptors in brain membranes, as very little specific binding can be detected. This may be due to the approximately 30 times higher dissociation constant in brain, as estimated from the inhibition constants in the ^{3}H-clonidine and ^{3}H-WB 4101 assays, which were of the order of 10^{-8} M (Table 1).

Retinal α-receptors seem to be peculiar in another respect. The relative inhibitory potencies of the agonists clonidine, dopamine and noradrenaline differ at most by a factor of five in the three radioreceptor assays. In the brain, however, these agonists are 60–180 times more potent in the ^{3}H-clonidine assay than in the ^{3}H-WB 4101 assay[23].

Receptors of the α_2-type have also been described on postsynaptic organs[27,28], so it cannot be concluded that the retinal α_2-receptors are functionally presynaptic. In marked contrast to the large number of α-receptors present in the retina, the concentration of noradrenaline is very low[8]. On the other hand, dopamine is found in retinae of different species[8]; binding to the retinal α_2-receptors and a functional interaction between the two cannot be excluded. Our studies do not reveal whether retinal α-receptors are functional or simply phylogenetic remnants.

In conclusion, the retina seems to be specific not only in geometry and function, but also in terms of neurotransmitter receptors. The specialization of α_2-receptors in the retina may have important consequences not only for the mechanism of signal processing in this part of the CNS, but also in a minority of receptors[26] for neuronal processing in other parts of the CNS.

Received 27 June; accepted 18 August 1980.

1. Dowling, J. E. *Invest. Ophthal.* **9**, 655–680 (1970).
2. Liebschütz, J., Airoldi, L., Brownstein, H. J., Chinn, N. G. & Wurtman, R. J. *Biochem. Pharmac.* **26**, 443–446 (1977).
3. Neal, M. J. *Gen. Pharmac.* **7**, 321–332 (1976).
4. Ehinger, B. & Lindberg-Bauer, B. *Brain Res.* **113**, 535–549 (1976).
5. Brandon, Ch., Lam, D. M. K. & Wu, J.-Y. *Proc. natn. Acad. Sci. U.S.A.* **76**, 3557–3561 (1979).
6. Kurijama, K. & Kirmua, H. in *GABA in Nervous System Function* (eds Roberts, E., Chase, T. & Tower, D. B.) 203–216 (Raven, New York, 1976).
7. Bonting, S. L. (ed.) *Transmitters in the Visual Process* (Pergamon, Oxford, 1976).
8. Da Prada, M. *Adv. biochem. Psychopharmac.* **16**, 311–319 (1977).
9. Massey, S. C. & Neal, M. J. *J. Neurochem.* **32**, 1327–1329 (1979).
10. Hruska, R. E., White, R., Azari, J. & Yamamura, H. I. *Brain Res.* **148**, 493–498 (1978).
11. Müller, E. W. *Neurosci. Lett.* **5**, 345–349 (1977).
12. Enna, S. J. & Snyder, S. H. *Brain Res.* **115**, 174–179 (1976).
13. Watling, K. J., Dowling, J. E. & Iversen, L. L. *Nature* **281**, 578–580 (1979).
14. Bittiger, H. in *Proc. 1st Int. Coll. Receptors, Neurotransmitters and Peptide Hormones*, Capri (Raven, New York, in the press).
15. Osborne, N. N. *Neurosci. Lett.* **16**, 167–170 (1980).
16. Kapur, H. & Mottram, D. R. *Biochem. Pharmac.* **27**, 1879–1880 (1980).
17. Greengrass, P. & Bremner, R. *Eur. J. Pharmac.* **55**, 323–326 (1979).
18. Delini-Stula, A., Baumann, P. & Büch, O. *Naunyn-Schmiedeberg's Archs Pharmak.* **307**, 115–122 (1979).
19. *The Merck Index* 9th edn, 1304–1305 (Merck, Rahway, New Jersey, 1976).
20. Weitzell, R., Tanaka, T. & Starke, K. *Naunyn-Schmiedeberg's Archs Pharmak.* **308**, 127–136 (1979).
21. Starke, K. *Rev. Physiol. biochem. Pharmac.* **77**, 1–124 (1977).
22. Langer, S. Z. *Br. J. Pharmac.* **60**, 481–497 (1977).
23. U'Prichard, D. C., Greenberg, D. A. & Snyder, S. H. *Molec. Pharmac.* **13**, 454–473 (1977).
24. U'Prichard, D. C., Greenberg, D. A., Sheehan, P. & Snyder, S. H. *Brain Res.* **138**, 151–158 (1977).
25. Steer, M. L., Khorana, J. & Galgoci, B. *Molec. Pharmac.* **16**, 719–728 (1979).
26. U'Prichard, D. C., Bechtel, W. D., Rouot, B. M. & Snyder, S. H. *Molec. Pharmac.* **16**, 47–60 (1979).
27. Timmermans, P. B. M. W. M. *Naunyn-Schmiedeberg's Archs Pharmak.* **311**, Suppl., R59 (1980).
28. Langer, S. Z. *Trends neurol. Sci.* **3**, 110–112 (1980).

Retrograde axonal transport of target tissue-derived macromolecules

I. A. Hendry & C. E. Hill

Department of Pharmacology, John Curtin School of Medical Research, Australian National University, PO Box 334, Canberra, Australia

Neurones depend on contact with their target tissues for survival and subsequent development[1–4]. The protein, nerve growth factor (NGF), can be selectively taken up by sympathetic nerve terminals and reaches the neuronal perikaryon by a process of retrograde intra-axonal transport[5], suggesting that its role *in vivo* is to act as a target tissue-derived trophic factor[6]. The development of the neurones of the chick ciliary ganglion requires the presence of structures derived from the optic cup[4]. Several studies *in vitro* have shown that media conditioned by non-neuronal cells contain factors that result in the survival of neurones from ciliary ganglia[7–11]. In particular, chick embryo iris, ciliary body and choroid contained large amounts of these factors indicating the presence of a target tissue-derived trophic factor for the cholinergic ciliary ganglion[12]. This study demonstrates that neurones of the ciliary ganglion accumulate, by retrograde intra-axonal transport, proteins synthesized and released by optic tissues in culture.

0028-0836/80/410647—03$01.00

The iris, ciliary body and choroid were dissected aseptically from 19-day-old chicken embryos, and material from one eye placed in 2 ml of Eagle's medium containing Hanks salts, 50 mM HEPES and 100 U ml^{-1} penicillin, and incubated at 37 °C in humid air. The ability of the conditioned medium to support parasympathetic neurones from 8-day-old chick embryos was assessed after 24 h in culture as previously described[13], and one trophic unit was defined by the volume of conditioned medium required to obtain a 50% neuronal survival[11,13].

The amount of neurotrophic activity in the medium increased with time and reached a level of 80 U ml^{-1} after 5 days. Parallel cultures containing ^3H-labelled amino acid mixture (Amersham, TRK 440) at 0.5 mCi ml^{-1} in place of the corresponding unlabelled amino acids showed a large accumulation of labelled protein in the medium; at 5 days 9% of the total radioactivity was precipitated by 5% trichloroacetic acid. The radioactive medium was dialysed against 154 mM NaCl to lower the labelled amino acid content and then 25-μl aliquots were injected into the right eye of either 1-day-old or 2-week-old chicks. After 16 h, right and left ciliary ganglia were removed, homogenized separately in 100 μl distilled water, and 20-μl samples counted in a scintillation counter. There was a significant accumulation of radiolabel in the ganglion on the injected side compared to the non-injected side indicating the retrograde axonal transport of material from the conditioned medium (Table 1). This accumulation of radioactivity was unlikely to be due to diffusion from the injection site, as an injection of 25 times the amount of ^3H-labelled amino acids in 154 mM NaCl did not result in a significant accumulation of radioactivity on the injected side (Table 1). This also demonstrates that the effect seen with the conditioned medium was not due to transport of residual labelled amino acids in the medium.

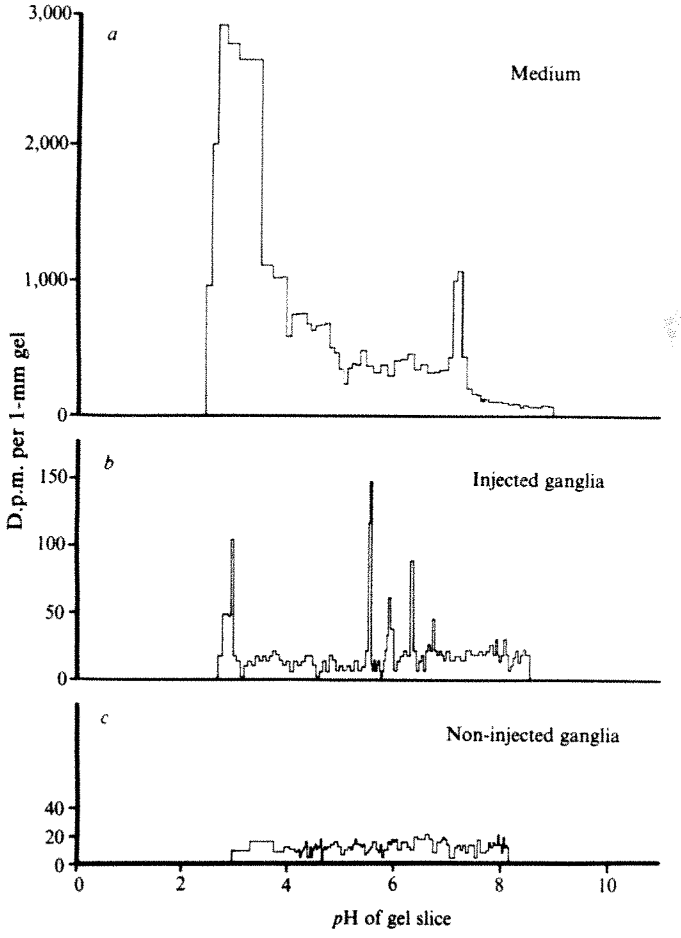

Fig. 1 Distribution of radioactivity after isoelectric focusing of: *a*, medium containing ^3H-labelled amino acids and conditioned by a 5-day exposure to optic tissues from 19-day-old chick embryos. *b*, Pooled homogenates of right ciliary ganglia from six 2-week-old chicks injected in the right eye with this conditioned medium. *c*, Homogenates of left ciliary ganglia from the same animals. In each case gels were cut into 1-mm sections which were eluted with 1 ml distilled water for radioactivity and *p*H measurements. The radioactivity (d.p.m.) is plotted against the *p*H of each gel slice.

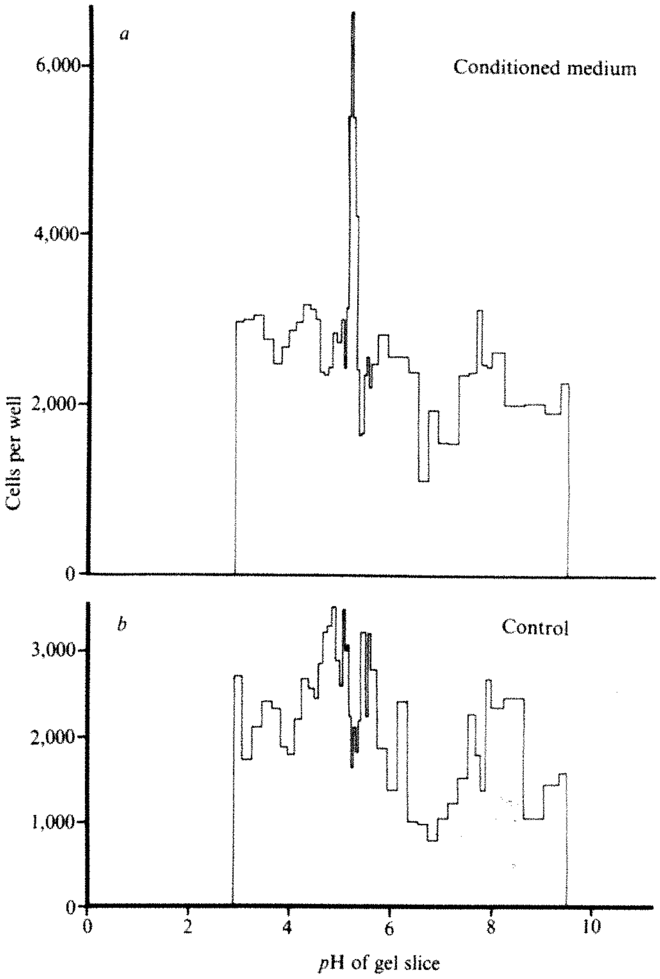

Fig. 2 Survival of parasympathetic neurones from 8-day-old chick embryos after 24 h in the presence of dialysed eluates of 1-mm slices from polyacrylamide isoelectric focusing gels. *a*, Medium conditioned by optic tissues. *b*, Control gel. The number of surviving neurones per 2-cm^2 well is plotted against the *p*H of each gel slice. In the absence of conditioned medium or gel eluates 900–1,500 cells per 2-cm^2 well survived.

To determine the selectivity of the retrograde transport, the macromolecules in the conditioned medium and in the pooled ciliary ganglion homogenates from the injected and non-injected sides were separated by polyacrylamide gel isoelectric focusing using *p*H 3.5–10 ampholines (LKB). There were many labelled macromolecules in the conditioned medium (Fig. 1*a*) but only five major labelled species were seen in homogenates of ciliary ganglia from the injected sides of 2-week-old chicks (Fig. 1*b*). Thus the retrograde axonal transport was selective for comparatively few of the macromolecules released by the cultured target tissues. There were no major radioactive peaks detected in the homogenates of the ciliary ganglia from the non-injected sides (Fig. 1*c*).

The ability of the conditioned medium to support parasympathetic neurones was assessed after polyacrylamide gel isoelectric focusing to see if any of the transported species might have neurotrophic activity. Conditioned medium was dialysed for 6 h against distilled water and the gels run for 3 h at 0 °C. Serial 1-mm slices were each eluted with 1 ml distilled water and the *p*H determined. The ampholines were then removed by

Table 1 Accumulation of radioactivity in chick ciliary ganglion after intraocular injection of radioactive conditioned medium or ^{3}H-labelled amino acids

	Age of injected chicks	Radioactivity (d.p.m. per ganglion)	
		Injected	Non-injected
Conditioned medium	1 day	2820 ± 630 (4)	15 ± 11 (4)
	2 week	6690 ± 645 (7)	90 ± 33 (7)
^{3}H-labelled amino acids	1 day	50 ± 10 (6)	33 ± 10 (6)
	2 week	9 ± 6 (6)	13 ± 5 (6)

The right eye was injected with 25 μl of either ^{3}H-labelled amino acids, 10 μCi or conditioned medium, 0.4 μCi. Sixteen hours later the right and left ciliary ganglia were removed and the radioactivity estimated. No. of ganglia in parentheses.

dialysis against 10 mM HEPES, *p*H 7.4, before the sample was mixed with medium for the determination of neurotrophic activity. Control gels were run similarly with distilled water in place of the conditioned medium. The component of the conditioned medium responsible for neuronal survival focused in the region of *p*H 5 (Fig. 2). One of the retrogradely transported radioactive proteins also focused in this region, suggesting that they may be the same.

In all neurones there must be a system for the retrograde transfer of information from the target cell to the innervating neurone. This information transfer can be accomplished by target tissues synthesizing and releasing proteins which are taken up by nerve terminals and *retro*gradely transported to neuronal cell bodies resulting in appropriate stimulation of metabolic pathways. It is likely that at least one of the retrogradely transported species described here is a retrophin (the *retro*gradely transported target tissue-derived neuro*trophic* factor) for neurones of the ciliary ganglia.

We thank Swee Lan Tan, Beverley Foote and Charles Claudianos for technical assistance and Dr I. S. McLennan, Mrs R. E. Bonyhady and Professor D. R. Curtis for helpful discussions. C.E.H. is a recipient of a Research Fellowship and a Grant-in-Aid from the National Heart Foundation of Australia. The name retrophin was first suggested by Professor G. A. R. Johnston.

Received 18 March; accepted 20 August 1980.

1. Hamburger, V. & Levi-Montalcini, R. *J. exp. Zool.* **111,** 457–501 (1949).
2. Prestige, M. C. in *The Neurosciences: Second Study Program* (eds Schmitt, F. O. & Worden, F. G.) 73–82 (Rockefeller University Press, New York, 1970).
3. Hamburger, V. *Neurosci. Res. Prog. Bull.* **15**, Suppl. April 1–37 (1977).
4. Landmesser, L. & Pilar, G. *Fedn Proc.* **37,** 2016–2022 (1978).
5. Hendry, I. A., Stöckel, K., Thoenen, H. & Iversen, L. L. *Brain Res.* **68,** 103–131 (1974).
6. Hendry, I. A. *Rev. Neurosci.* **2,** 149–194 (1976).
7. Helfand, S. L., Smith, G. A. & Wessells, N. K. *Devl Biol.* **50,** 541–547 (1976).
8. Nishi, R. & Berg, D. K. *Proc. natn. Acad. Sci. U.S.A.* **74,** 5171–5175 (1977).
9. Nishi, R. & Berg, D. K. *Nature* **277,** 232–234 (1974).
10. McLennan, I. S. & Hendry, I. A. *Neurosci. Lett.* **10,** 264–273 (1978).
11. Varon, S., Manthorpe, M. & Adler, R. *Brain Res.* **173,** 29–45 (1979).
12. Adler, R., Landa, K. B., Manthorpe, M. & Varon, S. *Science* **204,** 1434–1436 (1979).
13. Bonyhady, R., Hendry, I. A., Hill, C. E. & McLennan, I. S. *Neurosci. Lett.* **18,** 197–201 (1980).

Transmitter release from frog motor nerve terminals depends on motor unit size

A. A. Herrera & A. D. Grinnell

Department of Physiology, Jerry Lewis Neuromuscular Research
Center, Ahmanson Laboratory of Neurobiology, School of Medicine,
University of California, Los Angeles, California 90024

It has been postulated that the success with which a motor nerve terminal competes for synaptic connections[1,2] or the ability of an axon to maintain sprouts[3] may depend on the support each terminal receives from its soma, presumably in the form of some substance(s) synthesized there. The support received by each terminal may in turn depend on the total number of terminals maintained by that soma, namely, motor unit size. We show here that when motor unit size is experimentally decreased, transmitter release from the terminals is markedly enhanced. This is consistent with the view that the extent of support from the soma may also influence the effectiveness of synaptic transmission.

Eight to 12 weeks before acute experiments, the left sartorius nerve of adult *Rana pipiens* (body length 4.5–6.5 cm, anaesthetized in 0.2% tricaine methanesulphonate) was crushed near its entrance to the muscle. A lengthwise cut was made through the sartorius to remove muscle fibres in its lateral half. Thus when the motor axons regenerated, they encountered and re-innervated approximately half the normal number of fibres. Although there was repair of damaged muscle fibres at the cut edge, there was no evidence of substantial muscle regeneration. Control sartorius muscles, where the nerve was crushed but the muscle left intact, and normal muscles from unoperated frogs were tested for comparison. Samples were compared with the Mann–Whitney *U*-test unless otherwise noted. All data are presented here as mean ± s.e.m.

The number of increments in twitch tension produced by slowly increasing or decreasing the strength of a stimulus to the nerve was not significantly different ($P < 0.05$, Kruskal–Wallis *H*-test) in experimental (9.7 ± 0.5, $n = 14$), control (9.1 ± 0.9, $n = 7$) and normal (8.2 ± 0.35, $n = 13$) muscles suggesting that muscles in both operated groups become re-innervated by the same number of motor axons. Maximal twitch tension in experimental muscles (10.7 ± 1.4 g, $n = 15$) averaged approximately two-thirds that of controls (16.3 ± 2.0 g, $n = 7$), reflecting the removal of a substantial number of muscle fibres. In both whole and halved re-innervated muscles, the distribution of motor unit sizes, relative to the maximum tension that could be evoked, was essentially the same as normal. Mean motor unit size, expressed as a percentage of maximal nerve evoked tension, was not significantly different in experimental (10.1%), control (11.0%) or normal (12.2%) muscles. These observations suggest that most or all motor axons participated in re-innervation and that the size of the peripheral field of each motoneurone in the experimental case was indeed reduced.

Synaptic strength was tested in two ways, using previously described techniques[4]. In each case the degree of stretch of the muscle, known to affect synaptic strength[5], was carefully controlled. The first method, which estimates safety factors for junctional transmission, consisted of measuring the tension of twitches evoked by a single nerve stimulus while varying Ca^{2+} concentration in the Ringer's solution. When the Ca^{2+} concentration is lowered, twitch tension falls as transmission at the strongest junction on different fibres becomes sub-threshold[4]. At any particular low Ca^{2+} concentration, the extent to which tension has fallen is a measure of safety factors at junctions in that muscle. Using this approach, we compared safety factors in experimental, control and normal muscles by measuring the tension remaining after Ca^{2+} concentration was lowered from a normal value of 1.8 mM to 1.0 and 0.6 mM (Fig. 1). In Ringer containing 1 mM Ca^{2+}, tension in experimental muscles with reduced motor unit size fell only to 79% of the tension in normal Ringer. This was significantly more than the tension remaining in control or normal muscles (55% and 42% respectively, $P < 0.01$). Results from control and normal muscles were not significantly different ($P > 0.05$). In 0.6 mM Ca^{2+}, experimental muscle tension only fell to 22%, whereas control tension averaged 4% and normal tension 5%. Again, the differences between the experimental case and the other two cases were significant ($P < 0.02$).

The second method of testing synaptic strength was designed to determine if the increase in safety factor was due to a

0028–0836/80/410649—03$01.00

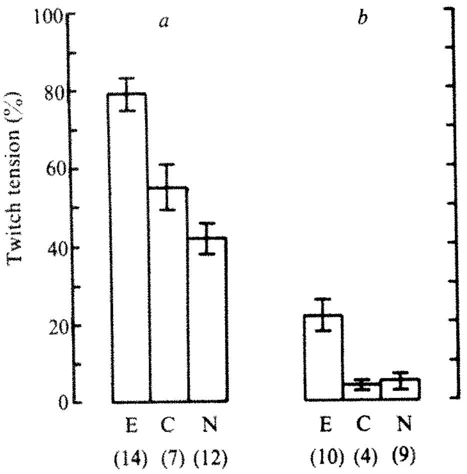

Fig. 1 The effect of lowered Ca^{2+} concentration (*a*, 1.0 and *b*, 0.6 mM) on twitch tension evoked by nerve stimulation. Tension is expressed as a percentage of the tension generated in normal Ringer containing 1.8 mM Ca^{2+}. At each concentration the mean, 2×s.e.m., and the number of muscles tested are shown for experimental (E, re-innervated half sartorius), control (C, re-innervated whole sartorius) and normal (N, unoperated sartorius) muscles. Experimental and control muscles were denervated by nerve crush 60–84 days earlier.

difference in the amount of transmitter release from nerve terminals in the experimental muscles. We measured end plate potential (e.p.p.) quantal content in Ringer containing 0.3 mM Ca^{2+} and 1 mM Mg^{2+}. For the operated muscles, junctions on regenerated muscle fibres in the area of the cut were not included in the quantal content analysis, nor were multiply innervated junctions, which were occasionally found but not at a frequency noticeably higher than in re-innervated whole muscle controls. As shown in Table 1, quantal content in muscles with reduced motor unit size was more than twice as great as that of control junctions (6.3 compared with 2.8) and three times greater than quantal content at normal junctions (2.1). The difference between experimental and control junctions was statistically significant ($P < 0.02$), but that between control and normal junctions was not. Miniature e.p.p. frequencies in the half muscles were also greater to approximately the same degree.

Because it has been shown that quantal content depends in part on nerve terminal size[6], the junctions from which recordings were made were marked by injection of a dye into the muscle fibre. These fibres were then identified in the light microscope and stained with the nitro blue tetrazolium (NBT) nerve terminal stain[7] and cholinesterase (ChE) stain[8]. Nerve terminal length was taken to be the sum of the individual lengths of NBT-stained processes located within the synaptic gutters outlined by ChE stain. As ChE activity persists for many weeks even in denervated gutters, we were able to observe that for both the re-innervated whole muscles and the undamaged fibres of the halved muscle, re-innervation occurred only at old endplate sites. No NBT-stained terminals were found without ChE and ChE deposits always looked normal in shape and size, unlike ectopic synapses seen in foreign nerve re-innervated sartorius muscles (A.D.G., unpublished data) or *de novo* synapses on cutaneous pectoris muscle fragments[9]. We conclude, therefore, that few if any ectopic synapses were formed. Using identified terminals that had been studied electrophysiologically, quantal contents were normalized to nerve terminal length. As shown in Table 1, terminals in muscles with reduced motor unit size released 1.89 quanta per 100-μm nerve terminal length. This was significantly higher than release per unit length in control (0.46) and normal (0.45) terminals (experimental versus control: $P < 0.002$; control versus normal: $P > 0.05$).

Table 1 Quantal content at sartorius junctions in Ringer containing 0.3 mM Ca^{2+} and 1 mM Mg^{2+}

	Quantal content	Quanta released per 100 μm
Re-innervated half sartorius	6.30 ± 0.84 (34)	1.89 ± 0.43 (21)
Re-innervated whole sartorius	2.79 ± 0.59 (19)	0.46 ± 0.09 (16)
Normal sartorius	2.07 ± 0.36 (25)	0.45 ± 0.09 (24)

Data shown are mean ± s.e.m. (*n*). For re-innervated muscles, the sartorius nerve was crushed 59–84 days previously.

Nerve terminals in experimental and control muscles were examined in the electron microscope to search for morphological correlates of this enhanced release. After processing the tissue as described previously[4], micrographs of randomly chosen transverse sections (×43,500) were examined for differences in: (1) the number of vesicles in a standard 0.528-μm² area just above the presynaptic membrane, (2) the number of mitochondria, (3) cross-sectional area, and (4) the width and character of the synaptic cleft. As shown in Table 2, neither vesicle density (possibly proportional to the number of readily releasable transmitter packets), nor the number of mitochondria (whose Ca^{2+}-sequestering activity may affect release[10]) differed significantly for experimental and control terminals. The cross-sectional area of control terminals did exceed that of experimental terminals by a marginally significant amount. We lack evidence for determining how such a difference could affect release. More relevant perhaps is our preliminary finding that control junctions show a higher incidence of interposition of Schwann cell processes between the pre- and post-synaptic membranes. Further observations on this point are in progress.

Table 2 Aspects of nerve terminal structure at experimental (re-innervated half sartorius) and control (re-innervated whole sartorius) junctions

	Experimental	Control	*P*
Vesicle density (no. vesicles per 0.528 μm²)	7.5 ± 0.5 (55)	7.0 ± 0.4 (34)	>0.05
No. mitochondria	3.0 ± 0.4 (65)	2.6 ± 0.4 (38)	>0.05
Cross-sectional area (μm²)	0.80 ± 0.06 (71)	1.10 ± 0.12 (38)	<0.05
% Junctions with interposed Schwann cell processes	18% (17/95)	36% (15/42)	
% Junctions with unobstructed synaptic apposition	82% (78/95)	64% (27/42)	

Data shown are mean ± s.e.m., with number of sections in parentheses.

It seems, therefore, that the process of transmitter release at frog neuromuscular junctions can show plasticity, with the size of the peripheral field of a motoneurone an important determining factor. If such variability in motor unit size occurs normally, it could help explain the relatively poor correlation that has been found between quantal content and nerve terminal size[4,6]. The dependence of release on motor unit size may, on the other hand, occur only as an experimental result in response to altered motor unit size. Further, it is not known if the increase in transmitter output per unit length is a permanent change.

Our data are consistent with the hypothesis that the level of transmitter output from a terminal may be related to the amount of material that that terminal receives from its soma. Production and/or transport of this material is fixed during development so that the supply is appropriate for the peripheral field of each motoneurone. If the field size is changed, the motoneurone may not compensate and one would expect to see a change in transmitter release. In the present experiments, for example, the original amount of this material would be distributed to a smaller number of terminals, resulting in enhanced transmitter release.

Further experiments are in progress to determine if an increase in the number of terminals per axon results in a decrease in transmitter release.

Received 14 April; accepted 21 July 1980.

1. Wigston, D. J. *J. Physiol., Lond.* (in the press).
2. Thompson, W. *Acta physiol. scand.* **103,** 81–91 (1978).
3. Brown, M. C. & Ironton, R. *J. Physiol., Lond.* **278,** 325–348 (1978).
4. Grinnell, A. D. & Herrera, A. A. *J. Physiol., Lond.* (in the press).
5. Turkanis, S. A. *J. Physiol., Lond.* **230,** 391–400 (1973).
6. Kuno, M., Turkanis, S. A. & Weakly, J. N. *J. Physiol., Lond.* **213,** 545–556 (1971).
7. Letinsky, M. S. & DeCino, P. A. *J. Neurocytol.* **9,** 305–320 (1980).
8. Karnovsky, M. J. *J. Cell Biol.* **23,** 217–232 (1964).
9. Ding, R. thesis, Univ. Calif., Los Angeles (1980).
10. Alnaes, E. & Rahamimoff, R. *J. Physiol., Lond.* **248,** 285–306 (1975).

Benzodiazepine recognition sites on GABA receptors

Moshe Gavish & Solomon H. Snyder*

Departments of Neuroscience, Pharmacology and Experimental Therapeutics, and Psychiatry and Behavioral Sciences, Johns Hopkins University School of Medicine, Baltimore, Maryland 21205

A role of γ-amino butyric acid (GABA) in benzodiazepine actions[1–3] is supported by the GABA stimulation of membrane-bound[4–8] and soluble[9,10] benzodiazepine receptors and preliminary evidence that GABA protects benzodiazepine receptors from heat inactivation[11]. We show here that the GABA receptors labelled by ^{3}H-muscimol possess a benzodiazepine recognition site, as benzodiazepines, in proportion to their pharmacological activity, protect ^{3}H-muscimol binding from inactivation by heat and the protein modifying reagent iodoacetamide. We also show that benzodiazepines and GABA act at apparently distinct sites to protect benzodiazepine receptors from heat and iodoacetamide.

Brain membranes were incubated with receptor 'protector' compounds, then were either heated or treated with iodoacetamide, and washed 15 times to remove the 'protectors'. In control membranes, seven washes restored ^{3}H-muscimol binding to control values after addition of GABA, while 15 washes were required to restore ^{3}H-flunitrazepam binding to control values after incubation with diazepam. The 15 routine washes used did not lower control binding of ^{3}H-flunitrazepam or ^{3}H-muscimol, presumably because any labile binding sites had already been degraded during the initial six washes used to remove endogenous GABA (Fig. 1).

GABA protects both ^{3}H-flunitrazepam and ^{3}H-muscimol binding from inactivation by heat or iodoacetamide (Fig. 1), but seems to be more effective in protecting ^{3}H-muscimol binding. Addition of 10 μM and 0.1 mM GABA apparently enhances ^{3}H-muscimol binding after heating. This may be due to the removal of factors[12] tightly bound to receptors by heating, which resembles the increased binding with freezing and thawing or with detergents[13]. Preliminary experiments with briefer periods of heating produced the same enhanced ^{3}H-muscimol binding in GABA-protected membranes.

The protection of flunitrazepam and muscimol binding by GABA reflects GABAergic synaptic actions, for diaminobutyric acid, structurally similar to GABA but devoid of GABAergic activity, fails to protect either ^{3}H-flunitrazepam or ^{3}H-muscimol binding from heat or iodoacetamide. In contrast, imidazoleacetic acid (IAA), which is slightly weaker than GABA in its synaptic effects, is somewhat less potent than GABA in protecting ^{3}H-flunitrazepam and ^{3}H-muscimol binding from heat inactivation.

4,5,6,7-Tetrahydroisoxazolo(5,4-*c*)pyridine-3-ol (THIP) competes strongly for ^{3}H-muscimol binding but does not stimulate benzodazepine receptor binding[14]; it acts as an antagonist at the GABA recognition site on benzodiazepine receptors to block GABA stimulation of ^{3}H-diazepam binding[15,16]. The finding that both THIP and the GABA antagonist bicuculline protect ^{3}H-flunitrazepam and ^{3}H-muscimol binding sites from heat inactivation indicate that occupancy by either agonist or antagonist can protect the receptor.

Benzodiazepines also protect both ^{3}H-flunitrazepam and ^{3}H-muscimol sites from heat and iodoacetamide. This effect reflects an affinity for benzodiazepine receptors, because Ro 5-6227, a benzodiazepine with a similar receptor affinity to diazepam, protects as well as does diazepam, whereas RO5-4964 and halazepam, benzodiazepines with low, weak benzodiazepine receptor affinity, do not protect ^{3}H-flunitrazepam and ^{3}H-muscimol binding.

In saturation analyses using 6–8 concentrations of ^{3}H-ligand, heat inactivation reduces numbers of binding sites (B_{max} in control and heated conditions, respectively, in fmol per mg protein are 440 and 142 for ^{3}H-muscimol and 600 and 190 for ^{3}H-flunitrazepam) for GABA and benzodiazepine receptors but has no effect on the dissociation constants (K_D: ^{3}H-muscimol 10.1 nM, ^{3}H-flunitrazepam 4.4 nM). Protection by GABA and diazepam involves changes in B_{max} values with no change in K_D. The increased values following heating observed for GABA-protected ^{3}H-muscimol binding also reflect increased B_{max} with unaltered K_D.

To explore the specificity of these protective effects we evaluated whether diazepam can protect dopamine or muscarinic cholinergic receptors from heat inactivation. Heating membranes at 55 °C for 30 min reduces ^{3}H-quinuclidinyl benzilate (^{3}H-QNB) binding to calf whole brain membranes (muscarinic receptors) and ^{3}H-spiroperidol binding to rat corpus striatal membranes (dopamine receptors) by 90%. Pretreatment with 10 μM diazepam in the same conditions that protected GABA and benzodiazepine receptors fails to protect dopamine and muscarinic receptor binding from heat inactivation. As an additional indication of specificity, chlorpromazine, haloperidol and phenothiazine pretreatment do not protect ^{3}H-muscimol or ^{3}H-flunitrazepam binding from heating.

To determine whether heat inactivation has similar effects on distinct GABA and benzodiazepine recognition sites on benzodiazepine receptors and whether protection by GABAergic and benzodiazepine compounds is exerted at both sites, we evaluated the influence of GABA (100 μM) on

Table 1 Interactions of GABA analogues and benzodiazepines in protecting ^{3}H-flunitrazepam and ^{3}H-muscimol binding sites from heat inactivation

Drug concentration (μM)	Per cent of unheated control ^{3}H-Flunitrazepam	^{3}H-Muscimol
—	15 ± 2	17 ± 1
GABA (10)	76 ± 8	128 ± 12
Diazepam (10)	48 ± 5	35 ± 3
Clonazepam (100)	45 ± 4	32 ± 3
IAA (100)	47 ± 6	80 ± 7
Bicuculline (100)	49 ± 5	47 ± 5
THIP (4,5,6,7-tetrahydroisoxazolo (5,4-*c*)pyridine-3-ol) (100)	38 ± 4	98 ± 8
GABA (10) + diazepam (10)	108 ± 9	194 ± 15
GABA (10) + clonazepam (10)	105 ± 7	188 ± 14
GABA (10) + IAA (100)	75 ± 6	130 ± 10
GABA (10) + bicuculline (100)	74 ± 5	135 ± 9
GABA (10) + THIP (100)	60 ± 4	109 ± 8
Diazepam (10) + IAA (100)	93 ± 8	140 ± 13
Diazepam (10) + bicuculline (100)	95 ± 8	79 ± 6
Diazepam (10) + THIP (100)	98 ± 8	140 ± 11

Methods were essentially as described in Fig. 1. Combinations of protecting substances were added simultaneously. Data are means ± s.e.m. for 8–10 determinations.

---

* To whom correspondence should be addressed.

0028-0836/80/410651—02$01.00

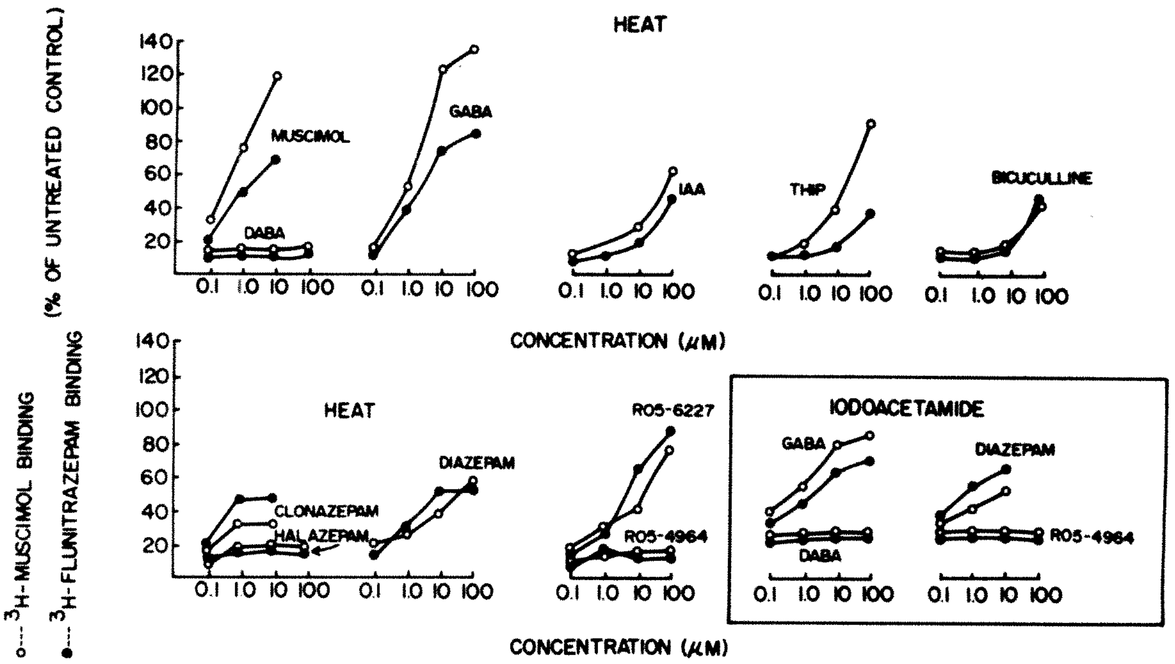

Fig. 1 Fresh calf brains were obtained from a slaughterhouse on ice within 30 min of death. Brains minus cerebella were homogenized with a Waring blender in 10 vol cie-cold 0.32 M sucrose and centrifuged 49,000*g* for 15 min at 4 °C. Pellets were resuspended in 2 vol 0.32 M sucrose and frozen for 18 h. After thawing, the tissue was washed five times by resuspension and recentrifugation with 40 vol 0.05 M Tris-HCl buffer (*p*H 7.4 at 4 °C) and refrozen for 18 h. After thawing, the tissue was washed once again by resuspension and recentrifugation with 40 vol 0.05 M Tris-HCl buffer. The pellet was then resuspended (70 µg protein ml^{-1}) in Tris-HCl buffer. The tissue was incubated for 30 min at 0 °C with different concentrations of drugs followed by either heat inactivation (30 min at 55 °C) or iodoacetamide treatment (0.1 M iodoacetamide 30 min at 37 °C). Samples were washed 14 times with Tris-HCl buffer and once again with 0.05 M Tris-citrate buffer (*p*H 7.1 at 4 °C). Incubation media contained 1.7 ml tissue (120 µg protein in Tris-citrate buffer), 0.1 ml ^{3}H-flunitrazepam (final concentration 0.4 nM), or ^{3}H-muscimol (final concentration 5.5 nM) and 0.2 ml of unlabelled drug (nonspecific binding) or H_2O (for total binding). To determine nonspecific binding incubations included 10 µM clonazepam (for flunitrazepam binding) or 100 µM GABA (for muscimol binding). After incubation (60 min at 0 °C) samples were filtered over GF/B filters and washed twice with cold Tris-HCl buffer. Filters were placed in vials containing 10 ml Formula 947 (NEN), shaken for 60 min and radioactivity was measured by liquid scintillation spectrometry. Data are means of 8–10 determinations. Protection from heating of both ^{3}H-flunitrazepam and ^{3}H-muscimol sites was significant ($P < 0.01$) for concentrations equal to or greater than 0.1 µM muscimol, 1 µM GABA, 10 µM IAA 10–100 µM THIP, 100 µM bicuculline, 1 µM clonazepam, 1 µM diazepam, 1 µM Ro 5-6227. Protection from iodoacetamide for ^{3}H-muscimol and ^{3}H-flunitrazepam was significant ($P < 0.01$) for concentrations equal to or exceeding 0.1 µM GABA and 0.1 µM diazepam. DABA, D,L-2,4-diaminobutyric acid.

^{3}H-flunitrazepam binding. In control unheated membranes as well as in heated membranes this concentration of GABA enhances ^{3}H-flunitrazepam binding about 60%. Moreover, half-maximal enhancement of ^{3}H-flunitrazepam binding occurs at 0.9 µM in both control and heated membranes. Additionally, in membranes treated with all the various protecting agents used in the present study, GABA (100 µM) uniformly enhances ^{3}H-flunitrazepam binding by 60%. Thus, GABAergic and benzodiazepine compounds protect the GABA recognition site of benzodiazepine receptors as well as their benzodiazepine recognition site.

Although GABA receptors clearly possess benzodiazepine recognition sites, we have failed to find stimulation or inhibition of ^{3}H-muscimol binding with 10 nM–10 µM clonazepam, an extremely potent benzodiazepine, and diazepam using Tris-citrate as well as Tris-HCl buffers.

To determine whether benzodiazepines and GABA protect the two receptors at the same or at different sites, we ascertained whether the effects of these substances were additive in protection experiments (Table 1). Maximal protection by GABA and IAA of ^{3}H-flunitrazepam and ^{3}H-muscimol binding is not additive, indicating that these substances act at the same sites. Might bicuculline or THIP antagonize GABA-elicited protection? Maximal protection of both ^{3}H-flunitrazepam and ^{3}H-muscimol sites by GABA and bicuculline is the same as with GABA alone, indicating no such antagonism. Protection by THIP and GABA for ^{3}H-flunitrazepam and ^{3}H-muscimol sites is slightly less than the maximal protection by GABA alone. In contrast to results with combinations of GABAergic substances, maximal effects of GABA and diazepam are even greater than the sum of the individual effects of these two compounds. Similarly, maximal effects of THIP and diazepam or IAA and diazepam are greater than the sum of the two substances acting separately. Thus, GABAergic agents and benzodiazepines exert their protective effects at distinct recognition sites both on the receptors labelled by ^{3}H-flunitrazepam and on those labelled by ^{3}H-muscimol. The synergistic interactions of GABA and diazepam in protecting these receptors suggest that the two sites are allosterically linked.

Our major finding here is that GABA receptors labelled by ^{3}H-muscimol possess recognition sites for benzodiazepines. Moreover, these sites have the same as or very similar drug specificity to benzodiazepine receptors. The findings that GABA receptors have benzodiazepine recognition sites and that benzodiazepine receptors have GABA recognition sites together with few differences in the chromatographic behaviour of the two purified receptors (M.G. and S. H. S., in preparation) indicates considerable structural similarity of the two receptor proteins.

This work was supported by USPHS grants MH-18501 and DA-00266, a grant of the McKnight Foundation and a Damon Runyon Fellowship. We thank Mr Gregory Mack for technical assistance.

Received 20 February; accepted 28 July 1980.

1. Costa, E., Guidotti, A., Mao, C. C. & Suria, A. *Life Sci.* **17,** 167–186 (1975).
2. Haefely, W. *et al. Adv. Biochem. Psychopharmac.* **14,** 131–152 (1975).
3. MacDonald, R. & Barker, J. L. *Nature* **271,** 563–564, (1978).
4. Tallman, J. F., Thomas, J. W. & Gallager, D. W. *Nature* **274,** 383–385 (1978).
5. Karobath, M. & Sperk, G. *Proc. natn. Acad. Sci. U.S.A.* **76,** 1004–1006 (1979).
6. Briley, M. S. & Langer, S. Z. *Eur. J. Pharmac.* **52,** 129–132 (1978).
7. Martin, I. L. & Candy, J. M. *Neuropharmacology* **17,** 993–998 (1978).
8. Wastek, G. J., Speth, R. C., Reisine, T. D. & Yamamura, H. I. *Eur. J. Pharmac.* **50,** 445–447 (1978).
9. Gavish, M. & Snyder, S. H. *Life Sci.* **25,** 783–790 (1979).
10. Gavish, M. & Snyder, S. H. *Life Sci.* **26,** 579–582 (1980).
11. Benson, D. L., Squires, R. F. & Klepner, C. A. *Soc. Neurosci. Abstr.* **5,** 1334 (1979).
12. Costa, E., Guidotti, A. & Toffano, G. *Br. J. Psychiat.* **133,** 239–248 (1978).
13. Enna, S. J. & Snyder, S. H. *Molec. Pharmac.* **13,** 442–453 (1977).
14. Karobath, M., Placheta, P., Lippitsch, M. & Larsen, P. *Nature* **278,** 748–749 (1979).
15. Braestrup, C., Nielsen, M., Krogsgaard-Larsen, P. & Falch, E. *Nature* **280,** 331–333 (1979).
16. Karobath, M. & Lippitsch, M. *Eur. J. Pharmac.* **58,** 485–488 (1979).

Uninfected avian cells contain structurally unrelated progenitors of viral sarcoma genes

Mitsuaki Yoshida*, Sadaaki Kawai† & Kumao Toyoshima†

* Department of Viral Oncology, Cancer Institute, Toshima-ku, Tokyo, Japan
† Department of Oncology, Institute of Medical Science, University of Toko, Minato-ku, Tokyo, Japan

A single gene, *src* of Rous sarcoma virus (RSV) coding for a protein of $pp60^{src}$, is responsible for the transformation of fibroblasts[1-3]. DNA sequences homologous to *src* (the endogenous *sarc*) are present in uninfected cells of chickens[4] and other vertebrates[5]. Endogenous nucleotide sequences have also been found in the putative transforming genes of MC29 (ref. 6) and avian erythroblastosis virus[7]. These viruses, however, induce different spectra of tumours in animals. From analysis of a new avian sarcoma virus, Y73, we present here evidence suggesting that multiforms of viral sarcoma genes originated from cellular genetic sequences, and that these viral genes are structurally unrelated, but have similar pathogenicities.

Y73, a strain of avian sarcoma virus newly isolated from a spontaneous tumour of White Leghorn[8], is a defective virus inducing fibrosarcoma in chickens but not any type of acute leukaemia, and contains 26S RNA as its genome[9]. To characterize the transforming gene (*yas*) of Y73, we prepared cDNA specific to 26S genome RNA (cDNA_{yas}) by transcribing 26S RNA into cDNA and selecting single-stranded cDNA after hybridization with a large excess of 35S genome RNA of Y73-associated virus (YAV). The specificity of the $^{32}\text{P-cDNA}_{yas}$ obtained was confirmed by the fact that the preparation showed no detectable hybridization with RNA of YAV or with 28S ribosomal RNA, which might contaminate the 26S RNA fraction owing to its similar size. This specific $^{32}\text{P-cDNA}_{yas}$ would represent about 2.5 kilobases of the middle portion of 26S RNA genome, because fingerprinting analysis of 26S RNA showed that 1–1.5 kilobases of both ends are common to 35S RNA of YAV leaving about 2.5 kilobases in the middle as specific sequence (manuscript in preparation).

The $^{32}\text{P-cDNA}_{yas}$ was hybridized with RNAs of various sarcoma and acute leukosis viruses in stringent conditions (Table 1). Most of the $^{32}\text{P-cDNA}_{yas}$ hybridized with 50–70S or 26S RNA of Y73, but not with the other virus RNAs tested (that is RNAs of avian myeloblastosis virus, avian erythroblastosis virus, MC29, the Prague strain of RSV, Fujinami sarcoma virus (FSV)[10] and PRCII sarcoma virus[11]). Hybridization of $^{32}\text{P-cDNA}_{total}$ indicated the presence of an appreciable amount of viral RNA and less than 1% of the viral RNA could easily be detected in the conditions used. These results clearly indicate that the Y73-specific sequences have no homology with the transforming sequences of known avian retroviruses. In particular, it should be emphasized that cDNA_{yas} is not structurally related to *src* of RSV or the transforming gene of FSV or PRCII. We also showed that cDNA_{src} of RSV did not cross-hybridize with the RNAs of Y73, FSV and PRCII (Table 1). Lee *et al.*[12] and Hanafusa *et al.*[13] recently reported that there is no sequence homology between *src* of RSV and FSV. These findings show that Y73 is a new type of avian sarcoma virus and that avian sarcoma viruses contain structurally distinct multiforms of sarcoma genes. The putative transforming genes of MC29 (ref. 6) and AEV[14], which can transform chicken fibroblasts *in vitro*, were reported to be distinct from *src* of RSV, but these viruses have different target specificity in animals. Our findings demonstrate that at least three structurally unrelated genes can induce similar fibrosarcomas in chickens.

As the *src* sequences of RSV were shown to be derived from host cell sequences[4,15], it was interesting to test whether the sarcoma sequences in Y73, which are unrelated to *src* of RSV, also originated from the avian genome. Thus, we analysed restriction fragments hybridizable with cDNA_{yas} by the blotting procedure of Southern[16]. DNA of uninfected chicken cells was digested with various restriction endonucleases and the fragments separated by electrophoresis in 0.8% agarose and fixed on a nitrocellulose filter. When the filter was hybridized with total $^{32}\text{P-cDNA}_{RSV}$, many bands of the endogenous viruses, as well as those of the endogenous *sarc*, were detected in digestions with *Eco*RI, *Hin*dIII, *Bgl*II and *Kpn*I (Fig. 1, *a* lanes). With $^{32}\text{P-cDNA}_{src}$ prepared from RSV, only a few bands representing endogenous *sarc* were detected in each digest (Fig. 1, *b* lanes). For example, in the digest with *Hin*dIII, two bands of approximately 12 and 28 kilobases were detected with $^{32}\text{P-cDNA}_{src}$ (lane *b*) and these bands corresponded to two of five bands detected with $^{32}\text{P-cDNA}_{RSV}$ (lane *a*). The fact that the three other bands could not be detected with cDNA_{src} showed that there was no significant contamination of the probe with other portions of the viral gene and thus that the fragments of 12 and 28 kilobases are those of the endogenous *sarc* sequences. Similar results were obtained with other enzyme digests, thus confirming the reliability of the method used.

When $^{32}\text{P-cDNA}_{yas}$ was used to hybridize the filter, only a few bands were detected in each digest (Fig. 1, *c* lanes) and the bands did not correspond to those of endogenous *sarc* in *b* lanes or those of endogenous viral gene in *a* lanes. These results unequivocally demonstrate that chicken DNA contains nucleotide sequences related to transforming gene of Y73 and that these endogenous DNA sequences (c-*yas*) are different from the endogenous *sarc* related to *src* of RSV and do not correspond to any endogenous viral sequences. Furthermore, the intensities of

Table 1 Absence of sequence homology of Y73-specific sequences with other avian sarcoma-leukosis viruses

RNA		^{32}P-cDNA (% hybridized)		
		cDNA_{yas}	cDNA_{src}	cDNA_{total}
Sarcoma viruses				
Y73	50–70S	91	4	98
Y73	26S	89	2	95
Y73-associated virus	35S	2	2	85
RSV(Pr-RSV-C)	39S	1	96	52
Y73	Cellular*	78	–	–
Fujinami virus	Cellular*	11	10	65
PRCII virus	Celullar*	10	9	53
Noninfected	Cellular*	9	5	6
Acute leukosis viruses				
AEV	30S	1	–	45
AMV	50–70S	3	–	65
MC29	Q8†			
	Cellular	11	–	21

Hybridization was carried out at 42 °C in buffer containing 0.6M NaCl, 50 mM Tris-HCl (*p*H 7.5), 1 mM EDTA and 50% formamide to a C_rt value of 15 mol s l^{-1} with purified virion RNAs or 600 mol s l^{-1} with total cytoplasmic RNA. The C_rt values (600 mol s l^{-1}) for cellular RNA were 50–70-fold in excess of C_rt for hybridization between cDNA_{total} and individual RNA preparation. $^{32}\text{P-cDNA}_{yas}$ and $^{32}\text{P-cDNA}_{total}$ were prepared as follows: the 26S RNA fraction of Y73 was transcribed into $^{32}\text{P-cDNA}_{total}$ with AMV reverse transcriptase in the presence of -[α ^{32}P]dCTP and random primer of calf thymus DNA digested with DNase I as described by Taylor *et al.*[17]. The $^{32}\text{P-cDNA}_{total}$ was hybridized with a large excess of 35S RNA of Y73-associated virus (YAV) to a C_rt of 100–150 mol s l^{-1} and single-stranded DNA, $^{32}\text{P-cDNA}_{yas}$, was separated on a hydroxyapatite column. $^{32}\text{P-cDNA}_{src}$ of RSV was prepared as described by Stehelin *et al.*[18] from the Prague strain of RSV and RNA of the transformation-defective mutant of the strain (td-RSV).

* Total cytoplasmic RNA was extracted from cells infected and fully transformed with the viruses and the contents of defective viral RNA were estimated to be more than 20% of the helper 35S RNA by the Northern transfer technique[19]; thus, if they have any homology, significant hybridization should be observed in the conditions used.

† Q8 is a nonproducer quail cell line[20].

0028-0836/80/410653—02$01.00

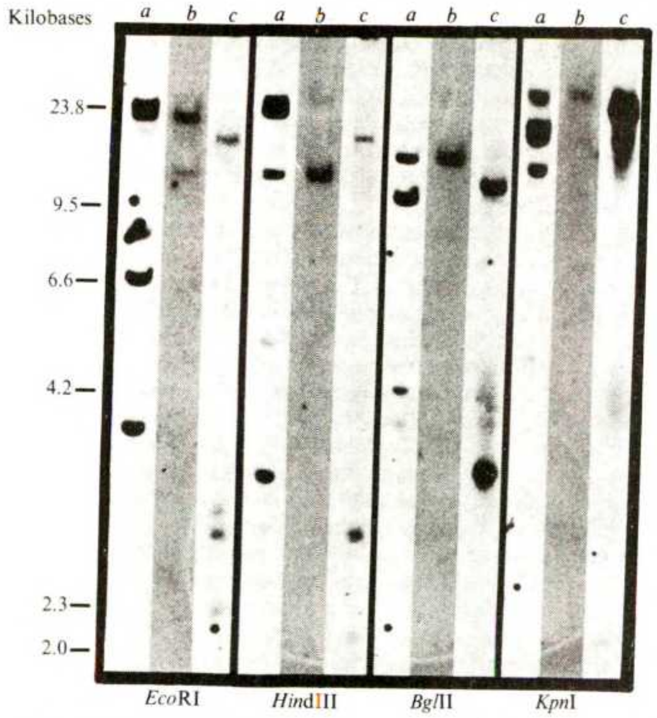

Fig. 1 Detection of nucleotide sequences homologous to the putative transforming gene of Y73 in uninfected chicken DNA and their comparison with endogenous *sarc* sequences related to *src* of RSV. DNA was extracted from uninfected chicken embryo fibroblasts and digested with *Eco*RI, *Hin*dIII, *Bgl*II and *Kpn*I respectively. Each digest was introduced into three slots in 0.8% agarose. The DNA fragments were separated by electrophoresis and blotted on to a nitrocellulose filter as described by Southern[12]. The three strips of the filter of each digestion were separately hybridized with total ^{32}P-cDNA$_{\text{RSV}}$ (*a*) ^{32}P-cDNA$_{yas}$ that had been prehybridized with RNA of td-RSV (*b*), and ^{32}P-cDNA$_{yas}$ that had been prehybridized with RNA of YAV (*c*), and autoradiograms were re-aligned. The marker for molecular size was λ DNA digested with *Hin*dIII.

the bands detected using ^{32}P-cDNA$_{yas}$ suggested that one or a few copies of c-*yas* sequences are present in chicken DNA. These findings strongly suggest that Y73 acquired the transforming gene from the c-*yas* sequences and that it belongs to a distinct class of avian sarcoma viruses. In preliminary results, the c-*yas* sequences are transcribed into RNA containing poly (A), suggesting that this RNA is translated into protein(s).

Our findings on the probable cellular origin of the putative transforming gene (*yas*) of Y73 indicate that the avian genome contains at least two copies of structurally unrelated progenitors of sarcoma genes of avian sarcoma viruses. These findings suggest that spontaneous or chemically induced sarcomagenesis might involve some modification and/or abnormally activated expression of one of these progenitor sequences, including as yet unidentified sequences. This hypothesis could be tested using a set of cDNAs specific to various classes of sarcoma genes.

We thank Dr H. Sugano for discussion and for critical reading of the manuscript, Drs H. Hanafusa and P. K. Vogt for gifts of FSV and PRCII virus, and Miss Y. Hirayama for technical assistance. This work was partly supported by a Grant-in-Aid for Cancer Research from the Ministry of Education, Science and Culture of Japan.

Received 21 May; accepted 7 August 1980.

1. Vogt, P. K. *Compreh. Virol.* **9,** 341–430 (1977).
2. Purchio, A. F., Erikson, E., Brugge, J. S. & Erikson, R. L. *Proc. natn. Acad. Sci. U.S.A.* **75,** 1567–1571 (1978).
3. Collet, M. S. & Erikson, R. L. *Proc. natn. Acad. Sci. U.S.A.* **75,** 2021–2024 (1978).
4. Stehelin, D., Varmus, H. E., Bishop, J. M. & Vogt, P. K. *Nature* **260,** 170–173 (1976).
5. Spector, D., Varmus, H. E. & Bishop, J. M. *Proc. natn. Acad. Sci. U.S.A.* **75,** 4102–4106 (1978).
6. Sheiness, S. & Bishop, J. M. *J. Virol.* **31,** 514–521 (1979).
7. Roussel, M. *et al. Nature* **281,** 452–455 (1979).
8. Itohara, S., Hirata, K., Inoue, M., Hatsuoka, M. & Sato, A. *Gann* **69,** 825–830 (1978).
9. Kawai, S., Yoshida, M., Sugiyama, H., Ishizaki, R. & Tosyoshima, K. *Proc. natn. Acad. Sci. U.S.A.* (in the press).
10. Fujinami, A. & Inamoto, K. *Z. Krebsforsch.* **14,** 94–119 (1914).
11. Carr, J. G. & Campbell, J. G. *Br. J. Cancer* **12,** 631–635 (1958).
12. Lee, W-H. *et al. Proc. natn. Acad. Sci. U.S.A.* **77,** 2018–2022 (1980).
13. Hanafusa, T. *et al. Proc. natn. Acad. Sci. U.S.A.* **77,** 3009–3013 (1980).
14. Stehelin, D. & Graf, T. *Cell* **13,** 745–750 (1978).
15. Hanafusa, H., Halpern, C. C., Buchhagen, D. L. & Kawai, S. *J. exp. Med.* **146,** 1735–1747 (1977).
16. Southern, E. M. *J. molec. Biol.* **98,** 503–517 (1975).
17. Taylor, J. M., Illmensee, R. & Summers, J. *Biochim. biophys. Acta* **442,** 324–330 (1976).
18. Stehelin, D., Guntaka, R. V., Varmus, H. E. & Bishop, J. M. *J. molec. Biol.* **101,** 349–365 (1976).
19. Alwine, J. C., Kemp, D. J. & Stark, G. R. *Proc. natn. Acad. Sci. U.S.A.* **74,** 5350–5354 (1977).
20. Bister, K., Hayman, M. J. & Vogt, P. K. *Virology* **82,** 431–448 (1977).

The *Agrobacterium tumefaciens* Ti plasmid as a host vector system for introducing foreign DNA in plant cells

Jean-Pierre Hernalsteens

Laboratorium voor Genetische Virologie, Vrije Universiteit Brussel, B-1640 Sint-Genesius-Rode, Belgium

Françoise Van Vliet, Marc De Beuckeleer,
Ann Depicker, Gilbert Engler, Michel Lemmers,
Marcelle Holsters, Marc Van Montagu & Jeff Schell*

Laboratoria voor Histologie en Algemene Genetika, Rijksuniversiteit Gent, B-9000 Gent, Belgium

The molecular basis of the neoplasmic transformation of plant cells by the crown gall bacterium *Agrobacterium tumefaciens* is the transfer to and stable maintenance of T DNA—a well defined segment of the bacterial Ti plasmid—in plant cells[1–4]. Transformed cells express new biosynthetic capacities, such as the synthesis of opines[5], of which octopine[6] and nopaline[7] are well known examples. Ti plasmids harbour genes enabling the bacteria to degrade opines and use them as carbon and nitrogen sources[8]. pTi-linked genes also determine the specificity of synthesis of opines in the plant tumour cells[8]. On this basis the Ti plasmid can be considered an unusual type of catabolic plasmid, which induces the synthesis of its substrate in transformed plant cells. This relationship, called genetic colonization[2], has opened prospects for the use of Ti plasmids as vectors for genetic manipulation of plants. To evaluate this possibility we inserted a well defined DNA segment, the bacterial transposon Tn*7* (ref. 9), into the Ti-plasmid DNA sequence that determines nopaline synthesis in *A. tumefaciens* strain T37 Noc$^{\text{c}}$1 (ref. 10). As we report here, the inserted Tn*7* DNA segment became part of the T DNA because the 9.6×10^6 molecular weight (MW) Tn*7* DNA sequence was transferred to, and maintained in, the DNA of tumour tissue cultures induced by this mutant strain.

Tn*7*, which encodes streptomycin, spectinomycin and trimethoprim resistance, was introduced into the chromosome of strain T37 Noc$^{\text{c}}$1. An RP4 :: Tn*7* plasmid[9], pGV1 (our isolate) was transferred from the auxotrophic *Escherichia coli* strain GV1000 (ref. 11) to strain T37 Noc$^{\text{c}}$1 by plate conjugation[12]. A transconjugant subsequently cured of its pGV1 plasmid was obtained by selection with the pilus-specific bacteriophage GU5 (J. P. H., in preparation). A culture of a transconjugant colony, exponentially growing in LB medium, was infected with a multiplicity of 5 plaque-forming units of GU5 per bacterium and plated after overnight incubation at 32 °C. About 15% of surviving cells were shown to have lost the carbenicillin, kanamycin and tetracycline resistance markers of RP4 but retained the spectinomycin (100 μg ml^{-1}) and trimethoprim (1,000 μg ml^{-1}) resistance markers of the Tn*7* transposon.

One such T37 Noc$^{\text{c}}$1 chr :: Tn*7* strain, GV15, was used for the isolation of Tn*7* insertions in the transfer-derepressed Ti plasmid of strain T37 Noc$^{\text{c}}$1 by selecting for the Ti-plasmid mediated conjugative transfer of the transposon resistance markers.

---

* Max Planck Institut für Züchtungsforschung, 30 Köln 5000, FRG.

0028-0836/80/410654—03$01.00

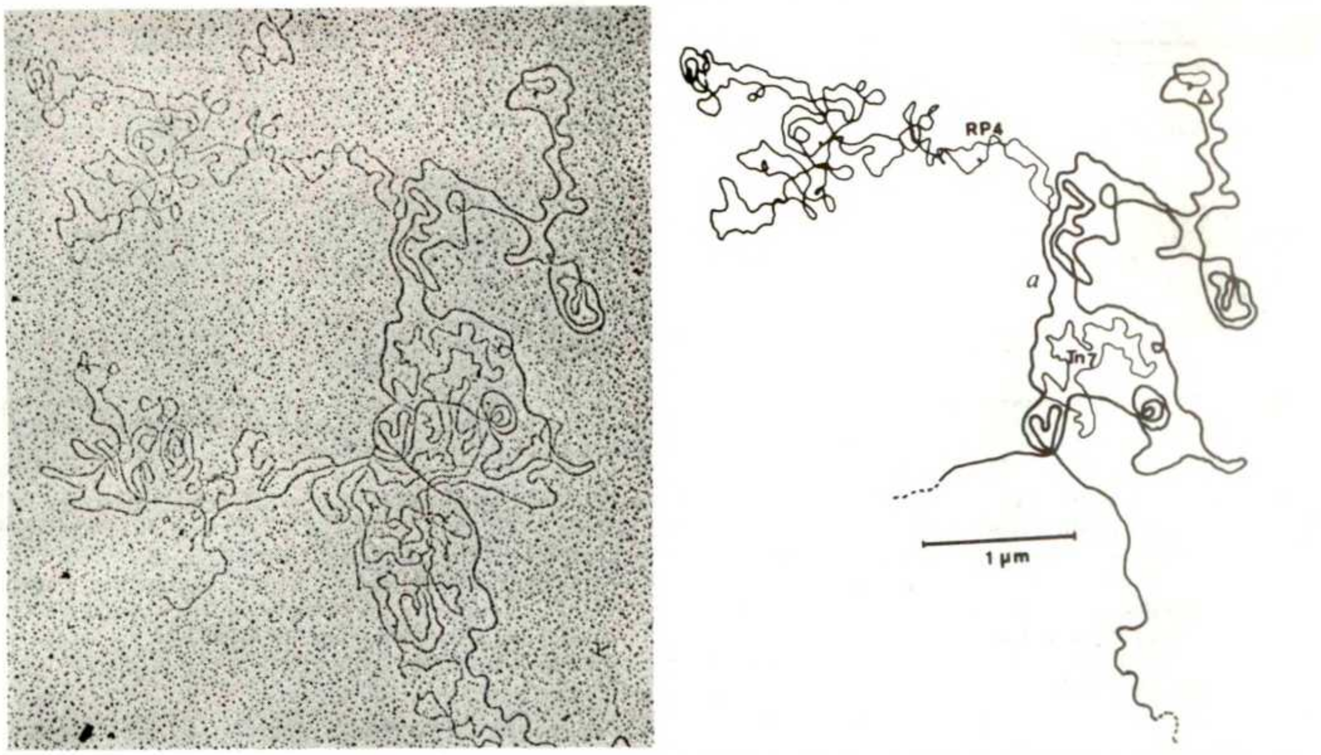

Fig. 1 Physical mapping of the Tn*7* insertion in a nopaline-synthesis deficient (Nos^-) mutant of pTiT37. pGV3106 DNA was prepared from strain GV3171 as described previously[12]. The Tn*7* insertion in pGV3106 was localized by electron microscopic analysis of heteroduplex molecules[20] formed by renaturation of single-stranded DNA molecules of pGV3106 and of pGV4000 (ref. 18), a co-integrate plasmid consisting of pTiC58 and the P plasmid RP4. The distance (*a*) between the Tn*7* transposon in pGV3106 and the RP4 insertion (at map position 130.4)[18] in pGV4000 is 1.3 ± 0.1 μm. The 0.5-μm deletion loop (Δ) in pTiT37 (ref. 4) and present in pGV3106 (at map position 124.3–125.3) (G. E., in preparation) was used as a reference point for the Tn*7* integration site. This mapping result agrees with the restriction endonuclease analysis (data not shown) of pGV3106.

Fig. 2 Analysis of Tn*7* and Ti-plasmid related DNA fragments present in restriction endonuclease digests of tobacco tumour DNA. W38T37::Tn*7*-1, a bacterium-free tumour tissue culture, was started from a tumour induced by strain GV3171 on *N. tabacum* cv Wisconsin 38, essentially as described previously[16]. After 5 months of *in vitro* culture on hormone-free medium, samples of the tissue were extracted with 25 ml buffer (Tris 50mM *p*H 8.2, EDTA 100 mM, diethylammonium diethyldithiocarbamate (DIECA) 100mM, triisopropyl naphthalene sulphonic acid 2%, diethylpyrocarbonate 0.1%) per g lyophilized tissue. The mixture was brought to 0.3 M NaCl and extracted with an equal volume of phenol and chloroform. The aqueous phase was brought to 0.5 M NaCl and re-extracted with the same organic phase. After precipitation with two volumes of ethanol the crude DNA was further purified by CsCl gradient banding (starting density 1.55). After dialysis it was concentrated to about 1 mg ml^{-1} by ethanol precipitation. The DNA was digested to completion with restriction endonuclease *Eco*RI. Digested DNA (20 μg) was separated by electrophoresis through a 0.8% agarose slab gel and transferred to a nitrocellulose filter[19]. The filter was hybridized by Southern's[19] method to cloned Ti-plasmid fragments derived from the T region of pTiC58 (ref. 17) and to ColE1::Tn*7* plasmid DNA, labelled *in vitro* with ^{32}P by nick-translation[21]. ColE1::Tn*7* plasmid DNA was used as a probe in lane *a*. The extent of the cloned pTi fragments used as probes for the hybridizations of lanes *b*, *c* and *d* is indicated on top of the physical map of the T region of pTiT37. Lanes *a* and *b* demonstrate the presence in the tumour DNA of the complete Tn*7* sequence integrated in a sequence homologous to the 9.4 × 10^6 MW *Eco*RI fragment of pTiT37. The localization of the integration site of Tn*7* in the T-DNA segment based on these data and confirmed by similar hybridization experiments with *Hin*dIII digests of the tumour DNA (data not shown), corresponds to the integration site of Tn*7* in pGV3106 (Fig. 1). Lanes *b*, *c* and *d* demonstrate that the T-DNA segment in this tumour line is identical, except for the *Eco*RI fragment of MW 9.4 × 10^6, to the T-DNA segment independently shown to be present in the BT37 tobacco tumour line induced by wild-type pTiT37 (ref. 4). Numbers adjacent to bands and numbers in each segment indicate MW(×10^{-6}).

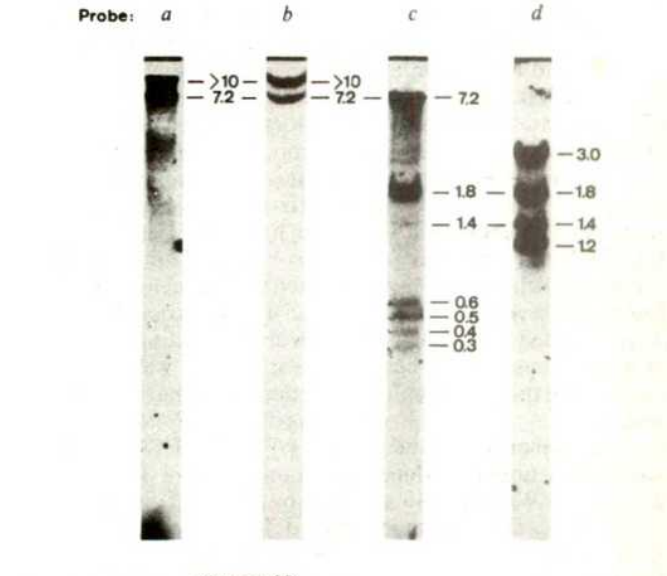

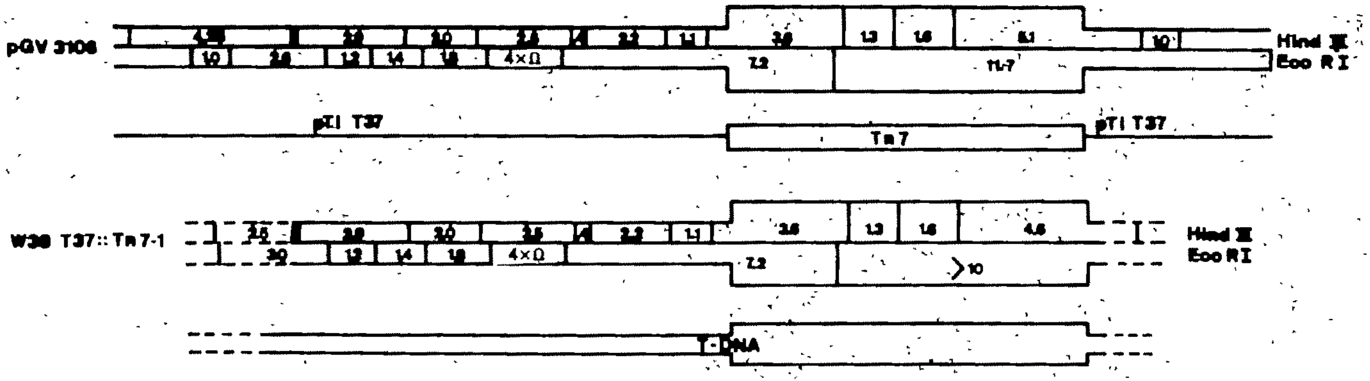

Fig. 3 The colinearity between the T region of the pTiT37::Tn*7* plasmid pGV3106 and the T-DNA segment in the tumour line W38T37::Tn*7*-1 induced by the *A. tumefaciens* strain GV3171 harbouring pGV3106. The figure is based on results obtained by Southern type DNA hybridizations as described in Fig. 2 legend.

GV15 was incubated for 24 h on minimal A[13] agar with the rifampicin- and erythromycin-resistant C58C1 derivative GV3102. Tn*7*-containing transconjugants were found at a frequency of 1.5×10^{-5} per recipient cell after plating on LB[13] medium supplemented with rifampicin (100 μg ml^{-1}), erythromycin (100 μg ml^{-1}) and spectinomycin (100 μg ml^{-1}). In 10% of these strains Ti plasmid could be demonstrated by its ability to degrade nopaline[8] and sensitivity to agrocin 84 (ref. 14). The remaining transconjugants expressed none of the Ti-plasmid markers and therefore probably harboured Tn*7* insertions in the cryptic conjugative plasmids of strain T37 Noc[r]1 (G. E., unpublished). Twelve transconjugants expressing both pTi and Tn*7* markers were inoculated on sunflower hypocotyl segments[15]. Nine were found to be pathogenic. Nopaline synthesis was demonstrated reproducibly by electrophoretic analysis[16] of the tumours induced by eight of these strains, but could not be detected in tumours induced by strain GV3171. The inability of strain GV3171 to induce nopaline synthesis was confirmed by analysis of tumours induced on potato, *Kalanchoë daigremontiana* and tobacco.

The Tn*7* insertion in strain GV3171 was localized on the mutant Ti plasmid (pGV3106) by restriction endonuclease analysis, and mapped in a DNA fragment homologous to the *Hin*dIII-23 fragment[17] of the standard nopaline Ti plasmid pTiC58 (data not shown). This localization was confirmed independently by electron microscopic heteroduplex analysis, which also showed that the Tn*7* inserted without detectable deletion (Fig. 1). This *Hin*dIII-23 fragment was subsequently shown to be homologous with the right-end border fragment of the T DNA[2,4] and thus to be part of the Ti-plasmid DNA segment which is normally transferred to plant cells. To confirm this result, several hundred Tn*1* and Tn*7* insertions in pTiC58 were screened for nopaline synthesis after induction of tumours. A single nopaline synthesis-deficient mutant was found and shown to be the result of a Tn*1* insertion in fragment *Hin*dIII-23 (ref. 18).

A bacterium-free tissue culture, W38T37::Tn*7*-1, was started from a tumour induced by strain GV3171 on *Nicotiana tabacum* cv Wisconsin 38. Analysis by Southern blot hybridizations[19] of a DNA sample isolated from this culture, using ColE1::Tn*7* (our isolate) DNA and various cloned segments of the nopaline plasmid pTiC58 as radioactive probes showed that the complete Tn*7* was present in the plant tumour genome, integrated at its original site in a normal-size T DNA (Figs. 2, 3).

Our results show that the Ti plasmid can be used as a vector for the experimental introduction and stable maintenance of foreign genes in higher plants. Furthermore, the demonstration that the Ti-plasmid DNA segment specifying nopaline synthesis in transformed plant cells is part of the T DNA, but not functionally required for the induction or maintenance of the neoplasmic state, supports the genetic colonization model of crown gall[2].

We thank Ruth Taimarchi for help. This work was supported by grants from the Kankerfonds van de ASLK, Instituut tot Aanmoediging van het Wetenschappelijk Onderzoek in Nijverheid en Landbouw (IWONL) (2841A), the Fonds Wetenschappelijk Geneeskundig Onderzoek (3.0052.78) to J. S. and M. V. M., and Fonds voor Kollektief Fundamenteel Onderzoek (2.0007.77) to M. Jacobs and M. V. M. M. H. thanks the Belgian NFWO for a fellowship and M. L. and M. D. B. thank the IWONL for financial support.

Received 5 June; accepted 8 August 1980

1. Chilton, M. D. *et al. Cell* **11**, 263–271 (1977).
2. Schell, J. *et al. Proc. R. Soc.* B**204**, 251–266 (1979).
3. Thomashow, M. F., Nutter, R., Montoya, A. L., Gordon, M. P. & Nester, E. W. *Cell* **19**, 729–739 (1980).
4. Lemmers, M. *et al. J. molec. Biol.* (in the press).
5. Petit, A., Dessaux, Y. & Tempé, J. *Proc. 4th int. Conf. Pl. Path. Bact.*, Angers, 143–152 (1978).
6. Ménagé, A. & Morel, G. *C. r. hebd. Séanc. Acad. Sci., Paris* **259**, 4795–4796 (1964).
7. Goldmann, A., Thomas, D. W. & Morel, G. *C. r. hebd. Séanc. Acad. Sci., Paris* **268**, 852–854 (1969).
8. Bomhoff, G. *et al. Molec. gen. Genet.* **145**, 177–181 (1976).
9. Barth, P. T., Datta, N., Hedges, R. W. & Grinter, N. J. *J. Bact.* **125**, 800–810 (1976).
10. Petit, A. *et al. Nature* **271**, 570–572 (1978).
11. Hernalsteens, J. P., De Greve, H., Van Montagu, M. & Schell, J. *Plasmid* **1**, 218–225 (1978).
12. Van Larebeke, N. *et al. Molec. gen. Genet.* **152**, 119–124 (1977).
13. Miller, J. H. *Experiments in Molecular Genetics*, 466 (Cold Spring Harbor Laboratory, New York, 1972).
14. Engler, G. *et al. Molec. gen. Genet.* **138**, 345–349 (1975).
15. Petit, A. & Tempé, J. *Molec. gen. Genet.* **167**, 147–155 (1978).
16. Aerts, M., Jacobs, M., Hernalsteens, J.-P., Van Montagu, M. & Schell, J. *Pl. Sci. Lett.* **17**, 43–50 (1979).
17. Depicker, A. *et al. Plasmid* **3**, 193–211 (1980).
18. Holsters, M. *et al. Plasmid* **3**, 212–230 (1980).
19. Southern, E. M. *J. molec. Biol.* **98**, 503–517 (1975).
20. Davis, R. W., Simon, M. & Davidson, N. *Meth. Enzym.* **21D**, 413–428 (1971).
21. Rigby, P. W. J., Dieckmann, M., Rhodes, C. & Berg, P. *J. molec. Biol.* **113**, 237–252 (1977).

Transforming genes of neoplasms induced by avian lymphoid leukosis viruses

Geoffrey M. Cooper* & Paul E. Neiman†

* Sidney Farber Cancer Institute and Department of Pathology,
Harvard Medical School, Boston, Massachusetts 02115
† The Fred Hutchinson Cancer Research Center, Seattle,
Washington 98104

Oncogenic avian retroviruses can be classified into three groups: sarcoma viruses, acute leukaemia viruses and lymphoid leukosis viruses (LLVs)[1]. Sarcoma and acute leukaemia viruses transform fibroblasts and/or haematopoietic cells in culture and induce tumours with short latent periods in infected birds. In contrast, LLVs do not transform cells *in vitro* and require long latent periods before formation of neoplasms *in vivo*. The most frequent neoplasm induced by LLVs is malignant lymphoma of the bursa of Fabricius, but LLVs also induce other neoplasms,

including sarcomas, nephroblastomas and erythroblastosis[2]. The genomes of both sarcoma and acute leukaemia viruses contain specific genes responsible for viral oncogenicity[1,3–5], whereas the genome of LLVs apparently includes only genes required for virus replication. The genetic basis for the low oncogenic potential of LLVs is therefore obscure. The present experiments indicate that LLV-induced tumours contain transforming genes that can be detected by transfection of NIH 3T3 mouse cells. These transforming genes are not linked to LLV DNA sequences, suggesting that oncogenesis by LLVs may result from indirect activation of cellular transforming genes.

DNAs used as donors in transfection experiments were extracted from seven different LLV-induced chicken tumours, from LLV-infected non-neoplastic tissues of tumour-bearing birds and from tissues of uninfected birds. The tumours included a nephroblastoma, three metastatic bursal lymphomas, a cell line established from such a lymphoma and two neoplastic bursal nodules, which are the presumed precursors to metastatic lymphomas. LLV DNAs in the tumours and LLV-infected normal tissues used in these experiments have been characterized by restriction endonuclease analysis[6]. The bursal nodules and the nephroblastoma appeared to contain single complete exogenous LLV genomes integrated at a different site in each tumour[6]. The advanced metastatic lymphomas and the derivative cell line contained variable numbers of LLV DNA integration sites, some of which corresponded to incomplete proviruses (ref. 6 and unpublished observations). In addition, recent studies using a probe homologous to the terminal sequences of LLV DNA (see below) revealed additional exogenous LLV DNA sequences in these tumour DNAs that were only detectable by this selective probe (unpublished observations). Red blood cells and normal bursal and kidney tissues from LLV-infected birds contained exogenous LLV genomes in quantities similar to LLV-induced tumours[6].

Table 1 Transformation by DNAs of LLV-induced tumours

Donor DNA (tissue-bird no.)		Total colonies/ total recipient cultures	Colonies per μg DNA
Salmon sperm		0/36	<0.002
Uninfected:			
Bursa	2407	0/4	<0.01
Erythrocyte	2407	0/5	<0.01
Total		0/9	<0.005
LLV-infected normal:			
Bursa	2993	0/5	<0.01
	2999	0/3	<0.02
	B7655	0/8	<0.01
Erythrocyte	2902	0/7	<0.01
	2993	0/4	<0.01
	2999	0/10	<0.005
Kidney	3000	0/4	<0.01
Liver	2993	0/4	<0.01
	2999	1/6	0.01
Total		1/43	0.001
LLV-induced tumours:			
Nodule	2993	5/4	0.06
	2999	54/3	0.9
Metastatic lymphoma	2902	2/6	0.02
	B7362	38/21	0.09
	B7363	5/7	0.04
Lymphoma line	LSCC-RP9	9/5	0.09
Nephroblastoma	3000	24/3	0.4
Total		137/49	0.14

DNAs were extracted from normal and neoplastic tissues of chickens infected with LLV strain 5938 (bird nos. 2902, 2993, 2999, 3000, B7655, B7362 and B7363), from normal bursa and erythrocytes of an uninfected chicken (no. 2407) of the same flock as chickens 2902, 2993, 2999 and 3000 and from an early (6th) tissue culture passage of a cell line (LSCC-RP9)[25] established from a transplantable bursal lymphoma (LSCT-RP6) induced by LLV strain Rous-associated virus-2. LLV infection of birds B7655, B7362 and B7363 was described by Neiman *et al.*[26] and LLV infection of birds 2902, 2993, 2999 and 3000 by Neiman *et al.*[6]. High molecular weight ($>20\times10^6$) DNAs were assayed by transfection of NIH 3T3 mouse cells as previously described[13]. Salmon sperm DNA was included as a control in all experiments. Recipient cultures were inoculated with 20 μg DNA per culture and were transferred into soft agarose-containing medium 7 d after exposure to DNA. Colonies of transformed cells were counted after 2–3 weeks of further incubation at 37 °C.

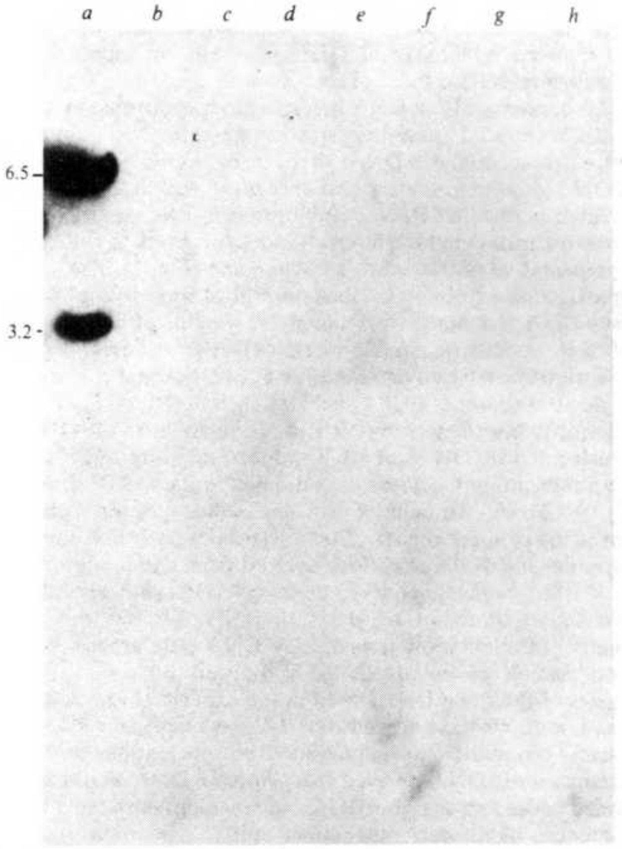

Fig. 1 Absence of LLV genomes in transformed NIH cells. DNAs of NIH cells transformed by Schmidt–Ruppin-D avian sarcoma virus DNA (lane *a*), NIH(BN-2993 DNA) cells (lane *b*), NIH(BN-2999 DNA) clone 1 cells (lane *c*), NIH(BN-2999 DNA)cl 2 cells (lane *d*), NIH(BN-2999 DNA) clone 3 cells (lane *e*), NIH(BL-B7362 DNA) cells (lane *f*), NIH(BL-LSCC-RP9 DNA) cells (lane *g*) and NIH 3T3 cells (lane *h*) were digested with *Hin*dIII, electrophoresed in 0.8% agarose gels and transferred to nitrocellulose filters as previously described[9]. Filters were baked and hybridized[10] to ^{32}P-cDNA (specific activity, $\sim4\times10^8$ cpm μg^{-1}) representative of the entire LLV genome which was synthesized by avian myeloblastosis virus reverse transcriptase from a template of Rous-associated virus-2 poly(A)-containing 35S RNA using oligomers of salmon sperm DNA as primers[27]. Filters were washed and exposed to X-ray film as previously described[10]. The molecular weights ($\times10^{-6}$) of LLV DNA-containing fragments are indicated.

The transforming activity of high molecular weight DNAs of tumours and normal tissues was assayed by transfection of NIH 3T3 cells, which have previously been shown to be transformable by DNAs corresponding to both viral and cellular transforming genes[7–13]. DNAs of all seven tumours, but not DNAs of either uninfected or LLV-infected normal tissues, induced transformation with efficiencies of 0.02–0.9 transformants per μg DNA (Table 1). These efficiencies were similar to the efficiencies of transformation by high molecular weight DNAs of cells transformed by avian sarcoma[9] and acute leukaemia[11] viruses and by DNAs of cells containing activated cellular transforming genes[12,13], but were 10–100-fold higher than the efficiency of transformation by fragments of normal cell DNA[13]. Thus, LLV-induced tumours, but not LLV-infected normal tissues, appeared to contain activated transforming genes that efficiently induced transformation of NIH 3T3 cells.

Several colonies of NIH cells transformed by LLV-induced tumour DNAs were grown to mass culture for further study. DNAs of these cells induced transformation in secondary transfection assays with similar efficiencies to the original efficiency of transformation by DNAs of LLV-induced tumours (~0.1 transformant per μg DNA) (Table 2) indicating they contained activated transforming genes. In contrast, transformation was not induced by DNAs of NIH 3T3 cells or spontaneously transformed NIH cells[9,13] (Table 2).

The content of LLV DNA in NIH cells transformed by DNAs of LLV-induced tumours was investigated by restriction endonuclease analysis. DNAs of the transformed NIH cells used as DNA donors in the experiments presented in Table 2 were digested with *Hin*dIII, electrophoresed in agarose gels, transferred to nitrocellulose filters[14] and hybridized to ^{32}P-cDNA representative of the entire LLV genome (Fig. 1). The sites of *Hin*dIII cleavage in viral DNAs are illustrated in Fig. 2. Two virus DNA fragments with molecular weights of 6.5 and 3.2×10^6 were readily detectable in *Hin*dIII-digested DNA of NIH cells transformed by avian sarcoma virus DNA and containing a single viral genome[9] (Fig. 1, lane *a*). In contrast, no LLV DNA sequences were detectable in any of the six lines of NIH cells transformed by DNAs of LLV-induced tumours (Fig. 1, lanes *b–g*), indicating that these cells did not contain LLV genomes.

LLV DNA contains a 300-nucleotide terminal repeat, consisting of approximately 200 nucleotides derived from the 3′ terminus and 100 nucleotides derived from the 5′ terminus of LLV RNA, which appears to be involved in synthesis, integration and expression of proviral DNA[15–18]. To determine whether terminal sequences of LLV DNA were associated with transforming genes of the LLV-induced tumours, *Hin*dIII digests of the same DNAs used in the experiment presented in Fig. 1 were also hybridized to ^{32}P-DNA of plasmid p53. This plasmid contains approximately 900 nucleotides of avian sarcoma virus DNA derived from *in vitro* DNA synthesis and cloned in the *Pst*I site of pBR322 and includes both the 3′ and 5′ sequences of the terminal repeat unit (K. Beemon, personal communications), and extends into the avian sarcoma virus *src* gene (unpublished observations, see Fig. 2). p53 ^{32}P-DNA hybridized to both *Hin*dIII fragments of DNA of avian sarcoma virus DNA transformed NIH cells (Fig. 2, lane *a*). Since the *Hin*dIII fragment of molecular weight 3.2×10^6 of this cell line is derived from the left-hand portion of avian sarcoma virus DNA and is homologous to p53 only at the terminal repeat unit (see Fig. 2), hybridization to this fragment shows the sensitivity of detection of these sequences. p53 ^{32}P-DNA also hybridized weakly to *Hin*dIII fragments of molecular weights 5.5 and 2.9×10^6 d in DNAs of all transformed cell lines (Fig. 2, lanes *a–g*) and in DNA of normal NIH 3T3 cells (Fig. 2, lane *h*). These fragments may represent normal mouse sequences homologous to *src*[19], since faint hybridization to these fragments was also detected with ^{32}P-cDNA representative of avian sarcoma virus RNA (unpublished observations). No additional LLV DNA sequences were present in NIH cells transformed by LLV-induced tumour DNAs (Fig. 2, lanes *b–g*), indicating that transforming genes of these cells were not associated with the terminal sequences of LLV DNA.

Thus, LLV-induced tumours contained cellular transforming genes, detectable by transfection of NIH 3T3 cells, which were not linked to LLV DNA. As transformation of NIH 3T3 cells was induced by DNAs of all seven tumours studied, including DNAs of two bursal nodules which represent an early stage of lymphoma development, it seems likely that activation of cellular transforming genes to a state in which they can be efficiently transmitted by transfection is significant in oncogenesis by

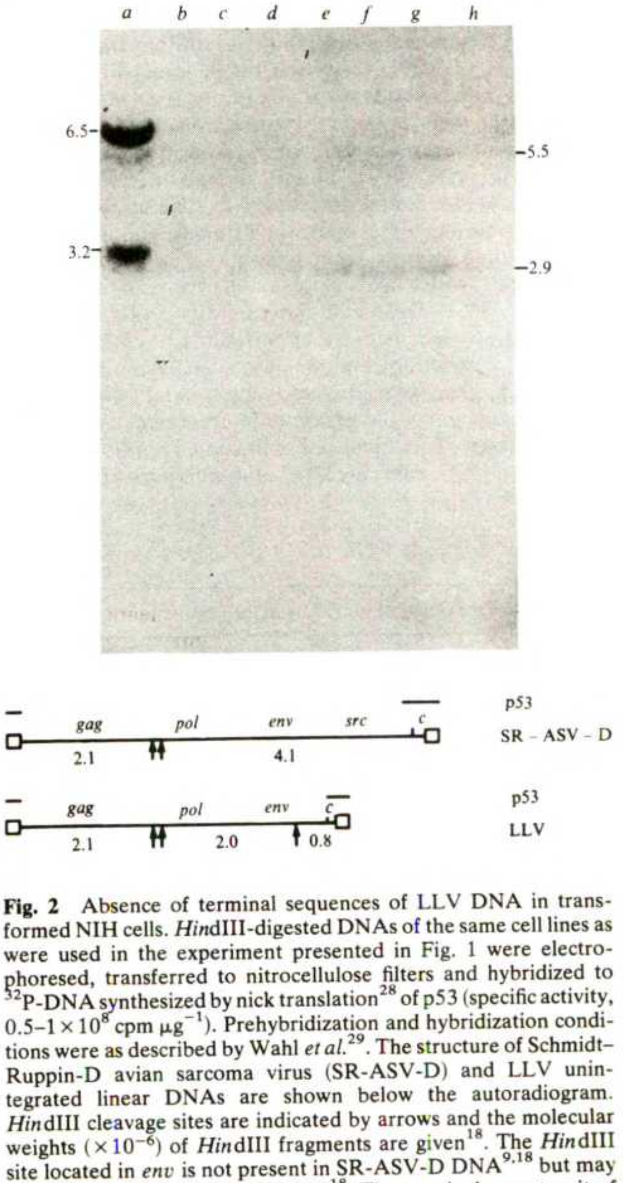

Fig. 2 Absence of terminal sequences of LLV DNA in transformed NIH cells. *Hin*dIII-digested DNAs of the same cell lines as were used in the experiment presented in Fig. 1 were electrophoresed, transferred to nitrocellulose filters and hybridized to ^{32}P-DNA synthesized by nick translation[28] of p53 (specific activity, $0.5–1 \times 10^8$ cpm μg^{-1}). Prehybridization and hybridization conditions were as described by Wahl *et al.*[29]. The structure of Schmidt–Ruppin-D avian sarcoma virus (SR-ASV-D) and LLV unintegrated linear DNAs are shown below the autoradiogram. *Hin*dIII cleavage sites are indicated by arrows and the molecular weights ($\times 10^{-6}$) of *Hin*dIII fragments are given[18]. The *Hin*dIII site located in *env* is not present in SR-ASV-D DNA[9,18] but may be present in some strains of LLV[18]. The terminal repeat unit of LLV DNA is shown as a box. The regions of viral DNA homologous to p53 are indicated above each map.

Table 2 Transformation by DNAs of transformed NIH cells

Donor DNA	Total colonies/ total recipient cultures	Colonies per μg DNA
Salmon sperm	0/28	<0.002
NIH 3T3	0/23	<0.002
NIH (spontaneous)	0/12	<0.005
NIH(BN-2993 DNA)	10/12	0.04
NIH(BN-2999 DNA)cl 1	23/18	0.06
NIH(BN-2999 DNA)cl 2	56/21	0.13
NIH(BN-2999 DNA)cl 3	48/16	0.15
NIH(BL-B7362 DNA)	17/15	0.06
NIH(BL-LSCC-RP9 DNA)	35/22	0.08

Salmon sperm DNA, NIH 3T3 cell DNA, DNA of spontaneously transformed NIH cells [NIH(spontaneous)] and DNAs of NIH cells transformed by DNAs of bursal nodule-2993 [NIH(BN-2993 DNA)], bursal nodule-2999 [NIH(BN-2999 DNA)clones 1, 2 and 3], bursal lymphoma-B7362 [NIH(BL-B7362 DNA)] and bursal lymphoma LSCC-RP9 ([NIH(BL-LSCC-RP9) DNA] were assayed as described in Table 1 legend.

LLVs. That transforming genes of LLV-induced tumours are not linked to LLV DNA suggests that oncogenesis by LLVs is not a consequence either of expression of an LLV transforming gene or of formation of recombinant transforming viruses and, furthermore, does not support the hypothesis that transformation results from viral promoters acting on adjacent cellular genes[20]. Instead, our results suggest that oncogenesis by LLVs may involve indirect activation of cellular transforming genes, possibly as a consequence of virus-induced mutations or gene rearrangements leading to abnormal gene expression. These events might be similar to those occurring in some chemically transformed mouse cell lines[12] or in the activation of potential transforming genes of normal cells during transfection with normal cell DNAs[13]. If the viral genome is not required for the maintenance of neoplastic change in LLV-induced tumours, the variability of LLV DNA in the metastatic bursal lymphomas, and the absence of detectable viral DNA in some lymphomas induced by analogous feline retroviruses[21], is not surprising.

The mechanism of activation of transforming genes in LLV-induced tumours is highly speculative. The pathogenesis of lymphomas induced by LLV suggests a process which includes several pre-neoplastic and neoplastic stages[22]. In addition, lymphomas pathologically identical to those induced by LLV occur at low frequency in the absence of exogenous LLV infection[23]. LLV may act thus at an early pre-neoplastic stage to expand the population of cells in which transforming events occur, which is consistent with the mechanism proposed by McGrath and Weissman[24] for induction of T-cell lymphomas by analogous retroviruses of the AKR mouse. LLV infection might also increase the frequency of genetic changes leading to transformation as a result of the activity of enzymes involved in integration of LLV DNA or by packaging transcripts of cellular genes in LLV virions followed by synthesis and integration of homologous DNAs in secondarily infected cells. Finally, the specificity of LLVs for transformation of bursal lymphocytes suggests that these cells provide a preferential site for LLV replication or that a bursal cell population provides a particularly sensitive target for genetic changes leading to transformation.

We thank K. Beemon for her gift of plasmid p53, W. Okazaki and L. B. Crittenden for the LSCC-RP9 cell line, S. Okenquist and L. Silverman for technical assistance, and D. M. Livingston for helpful comments on the manuscript. These studies were supported by grants CA21082 and CA20068 from the NCI.

Received 6 June, accepted 25 July 1980.

1 Hanafusa, H *Comprehensive Virol* **10**, 401–483 (1977).
2. Graf, T & Beug, H. *Biochim biophys Acta* **516**, 269–299 (1978)
3. Graf, T., Ade, N. & Beug, H *Nature* **275**, 496–501 (1978).
4 Duesberg, P H & Vogt, P K *Proc natn. Acad Sci. U.S A* **76**, 1633–1637 (1979)
5. Roussel, M *et al. Nature* **281**, 452–455 (1979).
6 Neiman, P., Payne, L. N. & Weiss, R A *J Virol* **34**, 178–186 (1980)
7. Andersson, P , Goldfarb, M P & Weinberg, R. A *Cell* **16**, 63–75 (1979).
8 Lowy, D. R , Rands, E & Scolnick, E M. *J Virol* **26**, 291–298 (1978).
9. Copeland, N. G , Zelenetz, A. D & Cooper, G. M *Cell* **17**, 993–1002 (1979)
10. Copeland, N. G , Zelenetz, A D. & Cooper, G. M. *Cell* **19**, 863–870 (1980).
11. Copeland, N G. & Cooper, G. M. *J Virol* **33**, 1199–1202 (1980).
12 Shih, C , Shilo, B -Z , Goldfarb, M P , Dannenberg, A & Weinberg, R. A. *Proc. natn Acad. Sci U S A.* **76**, 5714–5718 (1979)
13 Cooper, G M., Okenquist, S & Silverman, L. *Nature* **284**, 418–421 (1980)
14. Southern, E M. *J molec Biol.* **98**, 503–517 (1975)
15. Hsu, T W., Sabran, J L , Mark, G E , Guntaka, R V & Taylor, J M. *J. Virol* **28**, 810–818 (1978)
16 Hughes, S H. *et al Cell* **15**, 1397–1410 (1978).
17 Sabran J. L *et al J Virol* **29**, 170–178 (1979)
18 Shank, P. R. *et al Cell* **15**, 1383–1395 (1978)
19. Spector, D. H , Varmus, H. E & Bishop, J M *Proc natn Acad. Sci. U S A* **75**, 4102–4106 (1978).
20 Tsichlis, P N & Coffin, J M *J Virol* **33**, 238–249 (1980)
21 Koshy, R , Wong-Staal, F., Gallo, R C , Hardy, W & Essex, M *Virology* **99**, 135–144 (1979).
22. Neiman, P E , Payne, L N , Jordan, L & Weiss, R A *Cold Spring Harb Conf Cell Proliferation* (in the press)
23. Crittenden, L B , Witter, R L , Okazaki, W & Neiman, P. E *J natn. Cancer Inst* **63**, 191–200 (1979)
24 McGrath, M S. & Weissman, I L *Cell* **17**, 65–75 (1979)
25. Witter, R L *et al Avian Path.* **8**, 487–489 (1979).
26. Neiman, P E., Purchase, H G & Okazaki, W *Cell* **4**, 311–319 (1975).
27 Taylor, J M., Illmensee, R. & Summers, J. *Biochim biophys Acta* **442**, 324–330 (1976).
28 Rigby, P. W. S , Dieckmann, M , Rhodes, C. & Berg, P. *J molec. Biol* **113**, 237–251 (1977)
29 Wahl, G. M., Stern, M & Stark, G R *Proc. natn Acad. Sci U S A.* **76**, 3683–3687 (1979)

0028–0836/80/410659—02$01 00

Internal mobility of ferrocytochrome c

Scott H. Northrup*§, Michael R. Pear*,
J. Andrew McCammon*||, Martin Karplus†
& Tsunehiro Takano‡

*Department of Chemistry, University of Houston, Houston,
Texas 77004
†Department of Chemistry, Harvard University, Cambridge,
Massachusetts 02138
‡Department of Chemistry, California Institute of Technology,
Pasadena, California 91125

In the refinement of the X-ray diffraction structures of molecules, it is conventional to introduce atomic 'temperature factors' of the Debye–Waller form to characterize the widths of the electron density peaks corresponding to the atoms[1]. Although these factors are known to include a variety of contributions other than thermal fluctuations of the atomic positions[2], recent progress in the refinement of protein structures has led to inferences concerning atomic mobilities from the temperature factor data for several proteins[3–10]. Atomic position fluctuations can be calculated independently by the molecular dynamics method, in which the classical equations of motion for the atoms of an equilibrated protein are solved on a computer[11–16]. We now show that the X-ray diffraction and dynamical simulation methods yield similar pictures of the atomic mobility in tuna ferrocytochrome *c*.

The temperature factors used here are from a new refinement[17,18] of the X-ray diffraction data collected at 293 K (ref. 19); the final *R*-factor is 17% at a resolution of 1.5 Å. The simulation results are from a new dynamics calculation carried out as described earlier[14], but with the following modification to improve initial equilibration. After the 12 ps of warming from a partially relaxed structure, atomic velocities were randomly re-assigned from a 300 K maxwellian distribution every 0.2 ps for an 8-ps period. The calculation was then continued as before, with 12 ps of unperturbed equilibration followed by 16 ps of actual simulation at 301 K.

The results of the new dynamics calculation are very similar to those found without the additional velocity randomization[14], but the average structure is somewhat closer to the X-ray result and the fluctuations about the average structure are somewhat smaller. Relative to the 1.5-Å X-ray structure[17], the average deviation of C^α positions is 1.27 Å, whereas that for all heavy atoms is 1.54 Å; the corresponding deviations in the previous dynamics calculation[14] are 1.42 Å and 1.73 Å. All these deviations are 0.1–0.2 Å smaller than those relative to the 2.0-Å X-ray structure[19]. The r.m.s. fluctuations of the atoms about their average positions are typically 10–20% smaller than in the previous dynamics calculation[14], but the structural correlations are unchanged (see below). In part, this decrease reflects a corresponding decrease in large-scale fluctuations: the r.m.s. fluctuations in radii of gyration are 0.047 Å for C^α atoms and 0.041 Å for all heavy atoms; the corresponding fluctuations in the previous calculation are 0.055 Å and 0.047 Å.

To compare the atomic position fluctuations found in the dynamical simulation with those found in the X-ray diffraction study, it is necessary first to subtract from the atomic temperature factors a contribution due to disorder within the crystal[3,4]. The atomic temperature factors B are given by[1–4]

$$B = (8\pi^2/3)(\langle\Delta r^2\rangle_{av} + \langle\Delta r^2\rangle_{ld}) \qquad (1)$$

---

§ Present address: Department of Chemistry, Tennessee Technological University, Cookeville, Tennessee 38501.
|| To whom reprint requests should be addressed

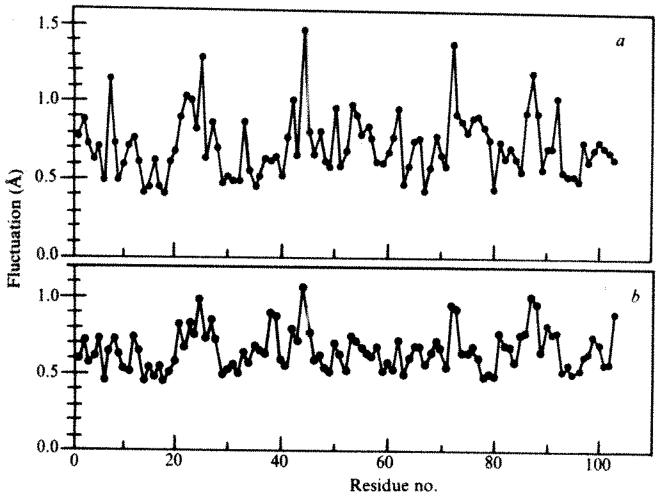

Fig. 1 Average r.m.s. atomic position fluctuation for each residue. *a*, Simulation result; *b*, X-ray result; the experimental values have been corrected uniformly for lattice disorder contributions (see text).

where $\langle \Delta \mathbf{r}^2 \rangle_{cv}$ is the mean-square dynamical fluctuation of the atomic position vector **r** due to conformational and vibrational motion, and $\langle \Delta \mathbf{r}^2 \rangle_{ld}$ is the mean-square fluctuation due to lattice disorder. With the simplifying assumption that only translational disorder need be considered, $\langle \Delta \mathbf{r}^2 \rangle_{ld}$ is the same for all atoms in the protein[4]. Here, $\langle \Delta \mathbf{r}^2 \rangle_{ld}$ was estimated by requiring that the average of $\langle \Delta \mathbf{r}^2 \rangle_{cv}$ over all interior atoms (that is, those atoms within 12 Å of the protein centre of mass)[14] obtained from the temperature factors be equal to the corresponding average of the mean-square position fluctuations in the simulation. The resulting value, $\langle \Delta \mathbf{r}^2 \rangle_{ld} = 0.22$ Å^2, is similar in magnitude to experimental estimates of this quantity for myoglobin crystals ($(\langle \Delta \mathbf{r}^2 \rangle_{ld} = 3\langle x^2 \rangle_{ld} = 0.14$ Å$^2)$[3,4]; the somewhat larger value found here is consistent with the fact that the myoglobin estimate is based only on iron atom data. The present comparison suggests that about half of the observed *B* factor value is contributed by thermal motion and half by other effects. In the following discussion, the r.m.s. position fluctuations $\langle \Delta \mathbf{r}^2 \rangle_{cv}^{1/2}$ calculated from equation (1) are compared with the r.m.s. position fluctuations from the dynamical simulation.

The magnitudes of the atomic position fluctuations derived from the X-ray temperature factors and from the dynamical simulation show the same correlations with the protein structure as were found in a previous simulation study[14]. The average r.m.s. fluctuations of the C^α positions are 0.58 Å (X ray) and 0.57 Å (simulation); the corresponding averages for all heavy atoms are 0.66 Å and 0.72 Å. To compare interior and exterior fluctuations, averages were calculated for atoms in spherical shells of 3-Å thickness centred at the protein centre of mass; the results are shown in Table 1. In the interior (shells with outer radii ≤ 12 Å)[14], the fluctuations are relatively small and increase slowly with shell size. In the exterior, the fluctuations increase more rapidly with increasing shell size; larger fluctuations occur in the simulation, reflecting the somewhat higher temperature and the neglect of the protein surroundings in the calculation. The atomic r.m.s. position fluctuations, averaged for each residue, are shown in Fig. 1; similar mobility patterns are evident, although the surface residues have larger fluctuations in the simulation. The most prominent differences are associated with the large peaks found in the simulation for exterior charged residues (for example, Lys), which are most strongly affected by the crystal and solvent environment.

Table 1 Average r.m.s. position fluctuations in shells of 3-Å thickness

Outer radius of shell (Å)	No. of atoms in shell	R.m.s. fluctuations X ray (Å)	R.m.s. fluctuations Simulation (Å)
6	41	0.54	0.51
9	148	0.56	0.53
12	284	0.60	0.61
15	262	0.71	0.83
18	96	0.85	1.09

The haem group is relatively rigid, with average r.m.s. fluctuations of 0.52 Å (X ray) and 0.46 Å (simulation). To assess the effect of the haem group on the mobility of nearby polypeptide atoms, a haem neighbourhood was defined by two cylindrical disks of 6-Å radius and 6-Å thickness lying on either side of the haem and coaxial with the iron[14]. The average r.m.s. fluctuations of the 61 heavy atoms in this neighbourhood are 0.54 Å (X ray) and 0.50 Å (simulation), compared with 0.60 Å (X ray) and 0.59 Å (simulation) for the other 374 heavy atoms of the protein interior. The average r.m.s. fluctuations are larger in the disk on the Met 80 side (0.57 Å, X ray; 0.52 Å, simulation) than in the disk on the His 18 side (0.51 Å, X ray; 0.49 Å, simulation). The additional flexibility on the Met 80 side may correlate with the larger structural changes observed on this side on oxidation of the protein[17].

Table 2 Average r.m.s. position fluctuations for various groups of atoms

Group	R.m.s. fluctuations X ray (Å)	R.m.s. fluctuations Simulation (Å)
C^α in helices	0.57	0.54
C^α not in helices	0.60	0.59
α atoms*	0.58	0.57
β atoms*	0.63	0.65
γ atoms*	0.72	0.78
δ atoms*	0.76	0.93

* Excluding proline residues.

Comparison of r.m.s. position fluctuation averages for other groups of atoms reveals additional correlations with the protein structure, as is seen in Table 2. In the backbone, there is somewhat less mobility in α-helical regions than in non-helical regions. In the side chains, the mobility tends to increase monotonically with increasing distance from the backbone.

The correlations of atomic mobility with structural features found here are in general agreement with simulation[11-13,15,16] and X-ray[4-10] results reported earlier for other proteins (compare with ref. 14). The detailed correspondence between the results from X-ray temperature factors and the molecular dynamics simulation for cytochrome *c* reinforces the view that valid information on the internal mobilities of proteins can be obtained from these complementary approaches.

This work has been supported in part by grants from the NSF, NIH and the Robert A. Welch Foundation. S.H.N. is an NIH Postdoctoral Fellow and M.R.P. is an NSF/NRC Postdoctoral Fellow. J.A.M. is an Alfred P. Sloan Fellow and the recipient of an NIH Research Career Development Award.

Received 14 July; accepted 26 August 1980.

1. Blundell, T. L. & Johnson, L. N. *Protein Crystallography* (Academic, London, 1976).
2. Willis, B. T. M. & Pryor, A. W. *Thermal Vibrations in Crystallography* (Cambridge University Press, 1975).
3. Parak, F. & Formanek, H. *Acta crystallogr.* **A27,** 573–578 (1971).
4. Frauenfelder, H., Petsko, G. A. & Tsernoglou, D. *Nature* **280,** 558–563 (1979).
5. Artymiuk, P. J. *et al. Nature* **280,** 563–568 (1979).
6. Huber, R. *Nature* **280,** 538–539 (1979).
7. Sternberg, M. J. E., Grace, D. E. P. & Phillips, D. C. *J. molec. Biol.* **130,** 231–253 (1979).
8. Artymiuk, P. J., Blake, C. C. F. & Oatley, S. J. *J. chem. Phys.* **76,** 813–815 (1979).
9. Sielecki, A. R. *et al. J. molec. Biol.* **134,** 781–804 (1979).
10. Watenpaugh, K. D., Sieker, L. C. & Jensen, L. H. *J. molec. Biol.* **138,** 615–633 (1980).
11. McCammon, J. A., Gelin, B. R. & Karplus, M. *Nature* **267,** 585–590 (1977).
12. McCammon, J. A., Wolynes, P. G. & Karplus, M. *Biochemistry* **18,** 927–942 (1979).
13. Karplus, M. & McCammon, J. A. *Nature* **277,** 578 (1979).
14. Northrup, S. H., Pear, M. R., McCammon, J. A. & Karplus, M. *Nature* **286,** 304–305 (1980).
15. Karplus, M. & McCammon, J. A. *CRC Crit. Rev. Biochem.* (in the press).
16. McCammon, J. A. & Karplus, M. *A. Rev. phys. Chem.* **31,** 29–45 (1980).
17. Takano, T. & Dickerson, R. E. *Proc. natn. Acad. Sci. U.S.A.* (in the press).
18. Jack, A. & Levitt, M. *Acta crystallogr.* **A34,** 931–935 (1978).
19. Takano, T. *et al. J. biol. Chem.* **252,** 776–785 (1977).

Economics down on the farm

R.C. Lewontin

Farm and Food Policy: Issues of the 1980s. By Don Paarlberg. Pp.338. (University of Nebraska Press: 1980.) $16.50, £9.90.

AGRICULTURAL economists stand out among students of the "dismal science" by being uniquely conscious of history. The paradigm of bourgeois economics is an equilibrium theory that sees the present forms of production and exchange as eternal and without historical roots. Agricultural economists, however, are acutely aware of the rapid changes that have taken place in world agricultural production and in the relations of the agricultural producers to other economic sectors. Their problem is to incorporate these changes into the conventionally accepted explanatory modes of economics and political science that are, by and large, designed to explain the supposed unchanging character of modern capitalism. The explanation invoked combines demographic change, the conflict between interest groups and the effect of technological developments. According to this theory, population growth, especially urban growth, has put increasing pressures on farmers to produce more food. The farmer has responded by adopting labour-saving technology which has resulted in a further displacement of population to cities, a drastic reduction in the relative size of the farm population and, as a consequence, the loss of political power by what was formerly a dominant pressure group in national policies. *Farm and Food Policy* follows this line of analysis and attempts to use it to predict changes in American agriculture during the next few decades.

According to Paarlberg, there have been three major stages in farm policy history (what he calls three "agendas"). The first, ending in 1933, was a period of strong reliance on public funding of research, technology and education in agriculture, by which means the farm sector succeeded in reaping the benefits of technological change that had been created at public expense. The second, ending in the 1960s, was the support of prices paid to the farmer, by means of various government commodity programmes, at the same time holding down farmer costs by exempting the agricultural sector from labour laws, trade laws and certain taxes. Both of these policy agendas were a consequence of the numerical, and therefore political, power of farmers to establish themselves as a unique sector of American business with unique privileges. The loss of this numerical and political power in the 1960s has resulted in the loss of agriculture's unique position and the imposition of a third agenda from outside the farm sector. This last agenda supports the interests of farm labour, consumers, conservationists — the non-farm sector at large. Paarlberg's conclusion is that an equilibrium will be reached in the next decades just as the producer–consumer, capital–labour tensions between interest groups have equilibrated in the rest of the economy to the benefit of all parties concerned.

The only trouble with the conventional view of the political history of agriculture in the United States is that it does not correspond very well with what has happened.

First, pure demographic superiority has never meant political power for farmers. In 1786 the farmers of Massachusetts rose in armed rebellion to prevent the sitting of the Courts of Common Pleas which were bringing judgements against them for debt. Farmers comprised over 90% of the population, but the legislature and executive power were in the hands of the merchants and bankers, who put down Shay's Rebellion in a few months and collected what was owed them. There has been no significant period in American history when farmers have succeeded in dominating the state.

Second, the decrease of the farm workforce since 1900, from 40% to 4% of the total labour force, grossly exaggerates the change in the political voice of the agricultural sector. A large part of the relative decrease in farm population is a consequence of the absolute increase in urban population. The non-farm labour force has increased by a factor of five in the USA, while the farm population has fallen by about a factor of three. Much of the reduction in farm labour has been in tenants, sharecroppers and farm labourers who were generally the poorest sector of the farm population and without political power. In 1900, of 5.7 million farms, 2 million were tenancies. By 1970, while there were only 2.7 million farms left, tenants accounted for only 350,000. Moreover, there has been an immense increase in those who service and sell to the farmer — the merchants of farm machinery, of seed and fertilizers, of consumer goods in market towns, the mechanics and servicemen. These are now two to three times as numerous as farmers and are an integral part of the agricultural sector of the economy. Thus, farmers and those who sell goods and services to them remain numerous and locally concentrated. Despite their lack of economic and political power nationally, the farm sector has, and still does, exert considerable pressure locally where their concentration is high. This local concentration is important because, for example, state funds account for two-thirds to three-quarters of the money spent on agricultural research and education.

Third, agriculture has not been alone in socializing the costs of research by displacing it to public institutions. The degree of the socialization of research costs depends in each case on the point at which such socialization interferes with exclusive private control over the product. The cost of drug research is socialized by having most basic research and chemical trials carried out in public institutions supported by tax money, or by tax-exempt contributions from individuals. Only when the final compounding of the trade-name product is to be done will the drug companies themselves — sometimes — spend research money. Most basic research in metallurgy, chemistry, electronics, transportation, information theory and so on is supported publicly by tax funds or by tax-exempt gifts. The situation is the same in agriculture. Public institutions do the basic breeding research and produce public lines. The seed companies then change them slightly, if at all, give them a brand name and make the profit.

Fourth, it is by no means clear who has received importent benefits from socialized research in agriculture. Farmers try to reduce their labour costs, at the same time increasing their control over the labour process. Both these ends have been accomplished by changing from a labour-intensive to a capital-intensive system of production. For farming this has been the result of three major technological changes, none of which was the product of agricultural research. The first, beginning in about 1850 and ending in 1900, was the introduction of labour-saving machinery such as new plough designs, mowers, reapers, harvester combines and the like. All of these were invented and improved by industrial entrepreneurs. Further advance was limited because of the lack of the flexible traction power needed to pull large gang ploughs and combines. Beginning in about 1910 and extending until the Second World War, developments in the automotive industry (gasoline and diesel

THEY WANT TO LIVE FREE...
BUT FIRST THEY HAVE TO LIVE.

The Afghan refugees need
more than our sympathy.
They need our support.
Please send
your contributions to:
Afghanistan Relief
Committee, Inc., P.O. Box 4855
Church Street Station
New York, N.Y. 10249

Photograph by Jim Sheldon/Contact

engines, the differential) gave the second great boost to labour productivity in agriculture. Finally, after 1945, the drop in the relative cost of fertilizers and other chemicals led to an immense increase in the use of agricultural chemicals. While none of these changes resulted from agricultural research, they all determined its direction. Plant breeding, for example, is largely devoted to making crop plants more responsive to fertilizers, and easier to harvest mechanically by reducing lodging, increasing morphological uniformity and making ripening simultaneous. The direction of agricultural research is determined by the existing forms of capital investment in production.

Who has benefited from these developments? Paarlberg assumes, conventionally, the consumer. His evidence is that Americans are spending, on the average, a decreasing proportion of their income on food, but this argument is spurious. As every economist (Paarlberg is one) knows, the demand for food, especially in prosperous countries, is virtually insensitive to income, so that as real incomes rise, food necessarily becomes a smaller and smaller proportion of expenditure. The real question is whether the price of food relative to the average price of other commodities has gone down. In 1913, the consumer price index of food relative to all other consumer items was 0.98; in 1967 (the base year) it was 1.00; and in 1979 it was 1.09. So much for cheaper food! Nor is it easy to show that farmers are better off. Paarlberg makes much of the increase in the value of farm real estate, but this is a paper increase that cannot be converted by the farmer into other assets because the market in farm real estate is a very thin one. In fact, the paper inflation of land value is a liability to the farm family because of the immense death duties that must be paid in cash that cannot be realized from continued farm operations. Like other small producers, most farmers consume all their surplus, so to the extent that farmers lead a better material life they have certainly profited. Driving an air-conditioned tractor is clearly better than sweating in the sun behind a mule. Yet the hours are just as long and the risks just as great. On the other hand, there is no doubt at all that the major beneficiaries of the technological revolution in agriculture have been the corporations that provide the farm inputs: chemical, seed and machinery companies, big grain merchants and those who lend money at interest.

Fifth, farmers cannot be treated as a homogeneous interest group sharing certain cultural features that arise from their unique way of life. Paarlberg portrays farmers as conservative, yet agriculturalists have been among the most politically radical groups in America, beyond such uprisings as Shay's Rebellion. In 1912 the Socialist Party had more paid members in Oklahoma than in New York, and Eugene Debs received more than 25% of the vote in the 23 counties of that state with highest tenancy levels and lowest incomes. The notion that mid-Western farmers are "conservative", despite their long record of populism, comes in large part from their rejection of the internationalist interventionist policies that were of clear advantage to industrial and banking capital and which were the hallmark of 20th century "liberalism". Tenant farmers who made up more than one-third of all American farm families until the Second World War cannot be lumped together with a 600-acre farmer who owns all his land and capital equipment. The political behaviour of farmers at any time reflects not some unique "way of life" but the way each farmer confronts the system of production and exchange of which he is a part.

Far from being unique, the history of agriculture in the United States is, in its main features, the history of American capitalist development. There has been a constant pressure to reduce labour costs and increase control over the labour process, a socialization, where possible, of the costs of technological development, a growth in the size of enterprises, a decrease in their number, and a growing monopoly control over production and exchange. Large corporations do not own the bulk of farmland and are not likely ever to do so because it is a poor use of capital, but that does not mean that agricultural production is any the less under the political and economic control of large capital concentrations. The forms are different, but the substance is the same. ☐

R.C. Lewontin is a Professor in the Museum of Comparative Zoology and the School of Public Health at Harvard University, and is a member of the World Agricultural Research Group.

NMR for experts

K.A. McLauchlan

NMR of Chemically Exchanging Systems. By Jerome I. Kaplan and Gideon Fraenkel. Pp.165. (Academic: 1980.) £11, $19.50.

THIS book does not provide an experimental account of rate processes studied by NMR, nor does it give simple recipes for extracting rate data from observations. Instead it constitutes an extensive account of the application of density matrix theory to chemically exchanging systems. Much prior knowledge of NMR theory is assumed, notably of the nuclear spin Hamiltonian, the properties of spin operators and the rotating frame. This approach is on occasions too demanding; for example, some of the important density matrix equations as applied to magnetic resonance are simply quoted rather than derived in their entirety.

To start with, the Bloch equation and

density matrix approaches are shown to yield similar results for a single absorption peak. This early section of the book is the least successful since it abounds with small errors, which make it difficult to follow. Cross-referencing is not always correct and symbols are confused: bold type is used sometimes for vectors and sometimes for operators (which also appear in script and in the text typeface). The density matrix is defined as an operator rather than as a representation of an operator and its usefulness and relevance is not established at an early stage. A student would be better advised to turn to C.P. Slichter's *Principles of Magnetic Resonance* (Springer-Verlag, 2nd edn 1978) for a clearer introduction.

Once into its stride, however, this is an immensely useful and unique book for anyone wishing to see in detail how to apply the theory to real systems. It covers relaxation theory (including quadrupole effects), chemical reorganizations of all descriptions in first-order and close-coupled situations, the lineshapes of exchanging systems at high and low RF fields, double resonance lineshapes (including with exchange) and, briefly, transient effects. Application of density matrices to 2D spectroscopy receives no attention. Each chapter concludes with a useful summary and bibliography.

This book is intended for "the serious student of NMR" who has a considerable understanding of his subject, and at that level will be of value. ☐

K.A. McLauchlan is a Lecturer in Physical Chemistry at Oxford University and a Fellow of Hertford College.

A holistic approach to the classification of behaviour

Susan D. and Leslie L. Iversen

Chemical Influences on Behaviour. Edited by K. Brown and S. J. Cooper. Pp.670. (Academic: 1980.) £39.20, $90.50.

THE editors of this volume have brought together a collection of review articles relating to the effects of 'chemicals' — including hormones, nutrients before and after birth, neurotransmitters and psychotropic drugs — on behaviour. The aim is to provide the student with an introductory discussion of chemical influences on growth and development of the CNS, neuro-endocrinology, behavioural homeostasis and the effects of chemicals on a range of sensory and cognitive functions. The preface states that "the coverage is not intended to be comprehensive but rather serves to introduce the field of chemical influences on behaviour by carefully chosen examples, and to illustrate the continuity in research methods and the common problems of interpretation". Unfortunately this continuity will not be immediately obvious to the student, but it would be a difficult goal to achieve in a text of this kind.

The range of material in the book is unusual, cutting across traditional barriers of specialized interest. Computer simulation of behavioural homeostasis (F.M. Toates) is an unusual bed-fellow for an ethological topic such as chemical communication between animals (K. Brown). Students should find this range of material fascinating. Efforts have been made in some chapters to discuss methodological and other problems in the design of experiments, and Cooper's chapter on drug interaction studies is particularly useful, as the problems of working with drug cocktails and combinations are rarely discussed.

Three chapters, by Booth, Toates and Blundell, and Latham are dedicated to an analysis of food and water homeostasis. They are all excellent, and when read together illustrate how a combination of research methods applied to a clearly defined problem can yield substantial advances in understanding the organization and control of behaviour.

For the past 50 years studies of eating and drinking have been dominated by efforts to find the brain centres controlling the behaviour. While it is clear that certain hypothalamic and limbic lesions dramatically disrupt such behaviour, these lesion models have, during the past 20 years, contributed little more to our knowledge. Fresh advances have come only relatively recently by paying meticulous attention to the whole physiological balance of the organism, where the brain lies on an axis of control and is not the 'genie in the lamp'. It is useful to compare studies of feeding with those on drinking, where physiologists have always been strongly represented in the research effort. The delicately balanced nature of water control mechanisms has forced experimentalists to consider the homeostatic balance of the whole organism. This approach has paid off handsomely in the elaboration of the extracellular dehydration control of thirst by Fitzsimons (reviewed here by Blundell and Latham). This concept has been extended, most successfully, to investigations of the chemical messengers involved and their sites of action in the brain. Similar research on the control of food intake is poised to follow, as Blundell and Latham illustrate.

Rodgers provides a useful review of aggression from the behavioural, neuroanatomical and neuropharmacological viewpoint. The relationship between the sensory and emotional responses to noxious stimuli, the pain/anxiety continuum, provides a challenge to research. The catecholamine and indolamine chemical transmitter pathways

New Studies in Biology

119 Medical Mycology
Mary P. English
The only undergraduate book on medical mycology which introduces the subject through a study of the interactions between fungus, host and environment in selected mycoses.
Paper £2.50 64 pages

120 The Respiration of Higher Plants
Helgi Öpik
A concise account of the biochemistry and physiology of the respiration of higher plants incorporating current ideas. Elementary concepts are explained and only a basic knowledge of biochemistry is assumed.
Paper £2.50 64 pages

121 Ecology of Insect-Plant Interactions
Peter J. Edwards and Stephen D. Wratten
This book describes the complex interactions between plants and animals that feed on them, and considers the ecological and evolutionary significance of these relationships.
Paper £2.50 64 pages

122 The Ecology of Streams and Rivers
Colin R. Townsend
An unusual description of the ecology of running waters focusing on the general principles which determine the distribution of organisms in streams and rivers.
Paper £2.50 72 pages

123 The Biochemistry of Pollution
J. H. Ottaway
A discussion on the biochemical theory underlying the causes of fresh-water, marine, atmospheric and terrestrial pollution.
Paper £2.50 64 pages

Edward Arnold
41 Bedford Square,
London WC1B 3DQ

Circle No. 26 on Reader Enquiry Card.

SCIENTIFIC BOOKSHOP

H. K. LEWIS can supply works in all branches of Pure and Applied Science. Catalogues on request. Please state interests.

SCIENTIFIC LENDING LIBRARY

Annual Subscription from £7.50.
(Available in U.K. only)

Reduced rates for multiple subscriptions.

Prospectus post free on request.

Quarterly List of New Books and new editions added to the Library sent post free to subscribers regularly.

H. K. LEWIS & Co. Ltd.

136 GOWER STREET,
LONDON, WC1E 6BS

Telephone: 01-387 4282
Telegrams: "Publicavit, London, WC1E 6BS."

Circle No. 20 on Reader Enquiry Card.

The ANS Journals

Your number One source for current information on the nuclear industry.

- NUCLEAR NEWS (NN)
- NUCLEAR SCIENCE & ENGINEERING (NS & E)
- NUCLEAR TECHNOLOGY (NT)
- NUCLEAR STANDARDS NEWS (NSN)
- NUCLEAR REPORT (NR)
- TRANSACTIONS (TR)
- REMOTE SYSTEMS TECHNOLOGY (RSTD)
- ANSPI (ANSPI)

(Write for our complete publications catalog)

Send To:

American Nuclear Society
555 North Kensington Avenue
La Grange Park, IL 60525 USA

Please send me information on....

☐ NN ☐ NS&E ☐ NT ☐ NSN
☐ NR ☐ TR ☐ RSTD ☐ ANSPI
☐ National Meetings
☐ Topical Meetings
☐ Individual Membership
☐ Corporation Membership
☐ Send me your free catalog

Name ______________________
Title ______________________
Organization ______________________
Address ______________________
City ______________________
State ______________ *Zip* ________

Circle No. 01 on Reader Enquiry Card.

of the hypothalamus and limbic system are involved in the emotional responses of aggression. But these same areas of brain have a high content of endogenous opioid transmitters, the endorphins. The endorphins in the brain stem are involved in the mediation of pain; their existence in forebrain may suggest a physiological axis of pain and anxiety. This is another area of research ripe for exploitation — the behavioural methods for studying responses to pain and aggressive responses are well developed; the chemical and anatomical axes of the spinal cord and brain are defined. It is now timely to ask what the functional relationships are between pain, anxiety and emotional behaviour.

In certain other areas there is less reason for optimism. If we consider the processes of learning and memory, it could be said that we are still struggling for the first rung of the ladder. Whilst it is recognized that there are methodological difficulties in studying memory — these can be overcome with appropriate controls (see Pilcher on state dependency) — there are more serious problems of interpretation: for example, in distinguishing deficits of retrieval from consolidation. We know that certain limbic areas are involved in the processing of information for memory storage, and we know that a wide range of endogenous and exogenous chemicals modify memory. But we still lack insight into the organization of the normal processes involved.

Much of the information in this volume could be found in a comprehensive textbook of physiological psychology, but there the material would be classified by brain site. The hypothalamus chapter, for example, would include eating, drinking and aggression. The achievement of this volume is that it provides another way of classifying behaviour: on physiological–chemical axes. This is not as novel as it seems; the terms pituitary–gonadal axis and pituitary–adrenal axis, used by Brain in his chapter titles, are traditional concepts in research related to sex hormones and behaviour, and to the relationship between ACTH, steroids and stress. But the same concepts could be applied to all behaviour. The brain and the body are inseparable and each possesses an integrated hierarchy of control. The endogenous neurotransmitter systems of brain and body provide a major force for integration. It is hardly surprising that so many chemicals modify behaviour since neural signalling depends so heavily on chemical relays, and it is with these tools and a conception of the whole organism that we may one day come to understand normal and abnormal behaviour. ☐

Susan D. Iversen and Leslie L. Iversen are Assistant Director of Research, Department of Experimental Psychology, and Director of the MRC Neurochemical Pharmacology Unit, University of Cambridge.

Asteroid revolution

D.E. Brownlee

Asteroids. Edited by Tom Gehrels. Pp.1181. (University of Arizona Press: 1979.) $19.95.

THE formation processes which created planets in the Solar System had at least one apparent failure. The failure occurred in the transition zone between the terrestrial and Jovian planets, and the surviving debris is known as the asteroid belt. Planetary formation was aborted at an early stage, presumably due to the proximity and rapid formation of Jupiter, the most massive planet in the Solar System. The majority of asteroids are believed to be composed of early Solar System materials which have been relatively well preserved for the age of the Solar System. They are the major source of meteorites and are a precious resource of information on the origin of the Solar System.

Ten years ago, measurable properties of asteroids were basically limited to orbits, broadband colours and brightness variations. Since then asteroid science has experienced a genuine revolution, with new observational techniques and new ideas producing a wealth of information relating to the composition and physical nature of asteroids as primitive Solar System bodies. The revolution is documented in this remarkable book, produced and edited by T. Gehrels and M.S. Matthews, with contributions from a significant fraction of the scientists active in asteroid research. The book is the product of a conference held in Tucson, Arizona, but by no means is *Asteroids* an ordinary proceedings volume. Instead of a loosely organized compilation of each participant's research results of the previous six months, this is a carefully created volume composed of review articles which cumulatively provide comprehensive and coherent coverage of existing knowledge of asteroids.

The book contains very few omissions, little repetition but extensive cross-

The Moss Flora of Britain and Ireland by A. J. E. Smith, first published in hardback in 1978, has been issued as a paperback by Cambridge University Press. Fully illustrated with line drawings by Ruth Smith, and containing an artificial key and full descriptions of taxa, the paperback edition costs £12.50.

referencing. Compilation of a 1181 page multi-author book with these attributes is obviously the result of careful planning and detailed iterative editing. Among the topics covered are orbital evolution, collisions, regolith development, reflectance spectroscopy, mineralogy, meteorite properties, formation from the solar nebula and possibilities for exploration by spacecraft.

Reading the volume, one is impressed by the diversity of techniques used to study asteroids. For example, asteroid diameters are now determined by measurement of polarization as a function of phase angle, the ratio of optical and infrared brightness, speckle interferometry, radar and occultations. Prior to 1970 diameters could only be estimated by visual telescopic observation. The most spectacular development described is the application of accurate spectral reflectivity measurements to reveal information on surface mineralogy. The measurements, combined with crystal field theory and laboratory data, have shown that asteroids are complicated bodies with diverse physical properties and surface mineralogy. One of the challenging goals for future theories on the origin of the Solar System will be to explain how such diversity could have been produced in what probably was only a small fraction of the solar nebula. Another exciting aspect of the reflectivity work is the attempt to identify specific asteroid parent bodies for various meteorite types.

Asteroids is a comprehensive and definitive book that will be of value to a variety of readers. For the specialist it will probably be the major reference source until future developments add a major increment to existing knowledge; such an advance will possibly not occur until a multi-asteroid spacecraft mission can be flown. For the newcomer to asteroid work the book will be invaluable because it contains numerous suggestions for future research. It also contains 140 pages of tabulated data for a large number of asteroids; this remarkable compilation contains information on orbital parameters, spectral reflectances, polarimetry, radiometry, light curves, magnitudes, diameters and discovery circumstances. In addition to active researchers, *Asteroids* will appeal to a much wider audience because of the review nature of the contributions. To smooth the mismatches that often occur in such an interdisciplinary field, a glossary is also included.

Although this is an excellent book it does, of course, have some shortcomings. Fortunately, these are of a relatively minor nature. A mineral defined in the glossary is misspelled and a few of the glossary definitions are not well thought out. In the text some of the material on meteorites is not as comprehensive as it could have been and does not reveal to the general reader the elements of controversy that exist in certain areas. In almost all other aspects, however, *Asteroids* is a real gem and remarkably enough for a book of its size is inexpensive enough to be a painless addition to one's personal book collection.

D.E. Brownlee is Associate Professor of Astronomy at the University of Washington, Seattle, and Associate in Geochemistry at the California Institute of Technology, Pasadena.

Children's skills with a difference

Peter Bryant

Beyond Universals in Cognitive Development. By David Henry Feldman. Pp.204. (Ablex: New Jersey, 1980.) $17.50

THERE is a character in Flaubert's short tale *A Simple Life*, who on being shown a map of America where her adopted son was at the time asked if she could see his house on the map and then if she could see him. Here is a dramatic if extreme illustration of the fact that people's skills with maps vary widely. This sort of variation between people is David Feldman's starting point and maps happen to be his main example.

His basic argument is impeccable. People's skills vary wildly. Some people play chess well, others are excellent gardeners and so on. Yet studies of the development of skills in children have concentrated on the few which virtually all adults possess. The understanding of number, the ability to make and understand logical inferences, even reading and writing are achievements which we take for granted in other adults, and yet these are at the centre of studies of child development. We spend very little time on studying how adults become so different from each other.

Feldman's approach is to look for similar variability among children, and he looks at two topics. The first is the way in which children draw maps. He divides this skill into a number of components and shows that different children forge ahead with different components. So much seems to be empirical fact. What causes this variability is still a matter for speculation, of which there is a great deal in this book.

His second example is creativity, but here because the measures of this elusive quality have been so unsuccessful Feldman's account is much less impressive. But he is right to point out that we have concentrated too much on universal features on human development and too little on the variations. □

Peter Bryant is Watts Professor of Psychology at the University of Oxford.

New Studies in Biology

124 Light and Plant Life
J. M. Whatley and
F. R. Whatley, FRS
An overall view of the effects of light on plant growth and development, from germination and seedling establishment, to flowering and senescence.
Paper £3.40 96 pages

125 Lipids and Polysaccharides in Biology
Anna J. Furth
This book describes exciting, new aspects of polysaccharide and lipid biochemistry, emphasizing the range of basic medical and biological problems that could be elucidated by structure-function studies of these somewhat neglected cell components.
Paper £2.60 72 pages

Coming in November:
126 Bioenergetics of Autotrophs and Heterotrophs
John W. Anderson
The book demonstrates that the principles of bioenergetics provide a unifying concept for understanding the metabolic activities of organisms, their interdependence and the cycling of elements by organisms.
Paper £2.50 64 pages

Coming in December:
127 Invertebrate Respiration
Rufus M. G. Wells
In this study, invertebrates are seen not as merely 'lower' animals, but as displaying control and regulatory capabilities which must cope with greater environmental exigencies than those of the vertebrates.
Paper £2.60 approx 72 pages

128 Immunobiology
Christopher J. Inchley
A concise introduction to the cellular basis of immune response in man and other animals, written from a biological viewpoint.
Paper £2.75 approx 88 pages

Edward Arnold
41 Bedford Square,
London WC1B 3DQ

Circle No. 27 on Reader Enquiry Card.

BOOKS RECEIVED

Biological Sciences

EDWARDS, P.J. and WRATTEN, S.D. Ecology of Insect–Plant Interactions. Institute of Biology's Studies in Biology No.121. Pp.60. Flexi ISBN 0-7131-2803-8. (Edward Arnold: 1980.) £2.50.

FERENCZY, L. and FARKAS, G.L. (eds). Advances in Protoplast Research. Proceedings of the 5th International Protoplast Symposium, Szeged, Hungary, July 1979. Pp.550. ISBN 0-08-02528-0. (Pergamon: 1980.) $73, £32.50.

FLORKIN, M., NEUBERGER, A. and VAN DEENEN, L.L.M. (eds). Comprehensive Biochemistry, Vol.19B, Part I. Pp.528. ISBN 0-444-80171-5. (Elsevier/North-Holland Biomedical: 1980.) $69.85, Dfl. 142.75.

GILBERT, L.E. and RAVEN, P.H. (eds). Coevolution of Animals and Plants. Symposium V, 1st International Congress of Systematic and Evolutionary Biology, Boulder, Colorado, August 1973. Revised edition. Pp.263. Flexi ISBN 0-292-71056-9. (University of Texas Press: 1980.) £6.

GLICK, J.L. Fundamentals of Human Lymphoid Cell Culture. Pp.157. ISBN 0-8247-6988-0. (Dekker: 1980.) Sw.Fr.52.

JOHNSON, J.A. and ANDERSON, R.R. (eds). The Renin–Angiotensin System Advances in Experimental Medicine and Biology, Vol.130. Pp.307. ISBN 0-306-40472-9. (Plenum: 1980.) $37.50.

JOHNSON, P.T. Histology of the Blue Crab *Callinectes sapidus*: A Model for the Decapoda. Pp.440. ISBN 0-03-056708-4. (Praeger: 1980.) $49.95

KERNAN, R.P. Cell Potassium. Transport in the Life Sciences, Vol.1. Pp.200. ISBN 0-471-04806-2. (Wiley-Interscience: 1980) £17.70.

POST, K.D., JACKSON, I.M.D. and REICHLIN, S. (eds). The Pituitary Adenoma. Pp.507. ISBN 0-306-40382-X. (Plenum: 1980.) $59.50.

PRATESI, R. and SACCHI, C.A. (eds). Lasers in Photomedicine and Photobiology. Proceedings of the Conference held at Florence, Italy, September 1979. Springer Series in Optical Sciences, Vol.22. Pp.235. ISBN 3-540-10178-0 (Springer-Verlag: 1980.) DM 50, $29.50.

PREZBINDOWSKI, K.S. Guide to Learning Anatomy and Physiology. Pp.361. Flexi ISBN 0-8016-4040-7. (Mosby: 1980.) £6.

RILEY, J.L. and McKAY, S.M. The Vegetation and Phytogeography of Coastal Southwestern James Bay. Life Sciences Contributions, Royal Ontario Museum, No.124. Pp.81. Flexi ISBN 0-88854-257-7. (Royal Ontario Museum: Toronto, Canada, 1980.) $5.50.

ROSSI, G.B. *In Vivo* and *In Vitro* Erthyropoiesis: The Friend System. Symposium of the Giovanni Lorenzini Foundation held in Urbino, Italy, October 1979. Pp.615. ISBN 0-444-80229-0. (Elsevier/North-Holland Biomedical: 1980.) $83, Dfl.170.

ROUTTENBERG, A. (ed.). Biology of Reinforcement: Facets of Brain-Stimulation Reward. Pp.174. ISBN 0-12-599350-1.,(Academic: 1980.) $16.

SARIN, P.S. and GALLO, R.C (eds). Inhibitors of DNA and RNA Polymerases. International Encyclopedia of Pharmacology and Therapeutics, Section 103. Pp.266. ISBN 0-08-024932-9. (Pergamon: 1980.) $60, £26.50.

SATTELLE, D.B., HALL, L.M. and HILDEBRAND, J.G. (eds). Receptors for Neurotransmitters, Hormones and Pheromones in Insects. Proceedings of the workshop held in Cambridge, September 1979. Pp.310. ISBN 0-444-80231-2. (Elsevier/North-Holland Biomedical: 1980.) $48.75, Dfl.100.

SCHEUER, P.J. (ed.). Marine Natural Products: Chemical and Biological Perspectives, Vol.III. Pp.229. ISBN 0-12-624003-5. (Academic: 1980.) $28.

SCHROEDER, W.A. and HUISMAN, T.H.J. The Chromatography of Hemoglobin. Clinical and Biochemical Analysis,, Vol.9. Pp.255. ISBN 0-8247-6941-4. (Dekker: 1980.) SwFr. 68.

TOWNSEND, C.R. The Ecology of Streams and Rivers. Institute of Biology's Studies in Biology No.122. Pp.68. Flexi ISBN 0-7131-2804-6. (Edward Arnold: 1980.) £2.50.

VAN RAMSHORST, J.D. (ed.) The Complete Aquarium Encyclopedia of Tropical Freshwater Fish. Pp.391. Flexi ISBN 0-7148-2156-X. (Phaidon: Oxford, 1980.) £12.50.

VORONTSOV, N.N. and Van BRINK, J.M. (eds). Animal Genetics and Evolution. Selected Papers of the XIV International Congress of Genetics, August 1978. Pp.383. ISBN 90-6193-602-0. (W. Junk: 1980.) Np.

WINTERBOTTOM, R. Systemics, Osterology and Phylogenetic Relationships of Fishes of the Ostariophysan Subfamily Anostominae (Characoidei, Anostomidae). Life Sciences Contributions, Royal Ontario Museum, No.123. Pp.112. Flexi ISBN 0-88854-252-6. (Royal Ontario Museum: Toronto, Canada, 1980.) $7.50.

ZIMEN, E. (ed.). The Red Fox: Symposium on Behaviour and Ecology. Biogeographica, Vol. 18. Pp.285. ISBN 90-6193-219-X. (W. Junk: 1980) DG 140, $73.50.

ZUCKERMAN, B. M. (ed.). Nematodes as Biological Models. Vol. 1, Behavioral and Developmental Models. Pp.311. ISBN 0-12-782401-4. (Academic: 1980) $35.

ZUCKERMAN, B. M. (ed.). Nematodes as Biological Models Vol. 2, Aging and Other Model Systems. Pp.306. ISBN 0-12-782402-2. (Academic: 1980.) $35

Applied Biological Sciences

BEGLEITER, H. (ed.). Biological Effects of Alcohol. Proceedings of the International Symposium held in Zurich, Switzerland, June 1978. Pp.832. ISBN 0-306-40349-8. (Plenum: 1980.) $75.

BENJAMIN, A. and HELAL, B. Surgical Repair and Reconstruction in Rheumatoid Disease. Pp.247. ISBN 0-333-24683-7. (Macmillan Press: London, 1980.) £25.

BROWN, A. C. and CROUNSE, R. G. (eds). Hair, Trace Elements, and Human Illness. Pp.360. ISBN 0-03-055441-1. (Praeger: 1980.) $41.95.

CARTER, N. (ed.). Development, Growth and Ageing. Pp.169. Hbk ISBN 0-085664-861-2; ISBN 0-85664-862-0. (Croom Helm: 1980.) Hbk £10.95; pbk £4.95.

CONNELL, J. J. *et al.* (eds). Advances in Fish Science and Technology. Papers presented at the Jubilee Conference of the Torry Research Station, Aberdeen. Pp.528. ISBN 0-85238-108-5. (Fishing News: London, 1980.) £39.50.

CONCEILLER, C. *et al.* Curares and Curarisation. XIth 1979. Pp.367. ISBN 9-0219-0443-8. (Elsevier/North-Holland: 1980.) Dfl. 140, —68.25.

CONSEILLER, C. *et al.* Liver anaesthesia and Critical Care. XIth International meeting of anaesthesiology and resuscitation, 1979. Pp 254. ISBN 90-219-0445-4. (Elsevier/North-Holland: 1980.) Dfl. 110, $53.75.

CORBIN, F. T. (ed.). World Soybean Research Conference II: Abstracts. Pp.124 ISBN 0-246-11-451-7. (Granada: St Albans, Herts, UK, 1980.) £8.95.

CORBIN, F. T. (ed.). World Soybean Research Conference II: Proceedings. Pp.897. ISBN 0-246-11-450-9. (Granada: St Albans, Herts, UK, 1980.) £20.

CROTTY, R. Cattle, Economics and Development. Pp.253. ISBN 0-85198-452-5. (Commonwealth Agricultural Bureaux: Slough, 1980.) £15.

DUMONT, J. E., MALONE, J. F. and VAN HERLE, A. J. Irradiation and Thyroid disease: Dosimetric, Clinical and Carcinogenic Aspects. Pp.255 Flexi ISBN 92-825-1715-2. (Commission of the European Communities: 1980.) Np.

ERIKSSON, K., SINCLAIR, J. D. and KIIANMAA, K. (eds). Animal Models in Alcohol Research. Based on the Proceedings of the Conference held in Helsinki, June 1979. Pp.496. ISBN 0-12-240650-8. (Academic: 1980.) $39.50, £17.

GAUGAS, J. M. (ed.). Polyamines in Biomedical Research. Pp.474. ISBN 0-471-27629-4. (Wiley-Interscience: 1980.) £30.

HARPSTEAD, M. I. And HOLE, F. D. Soil Science Simplified. Pp.121. Flexi ISBN 0-8138-1515-0. (Iowa State University Press: 1980.) $7.75.

HARRIS, K. F. and MARAMOROSCH, K. (eds). Vectors of Plant Pathogens. Pp.467. ISBN 0-12-326450-2. (Academic: 1980.) $48.

HORSFALL, J. C. And COWLING, E. B. (eds). Plant Disease: An Advanced Treatise. Vol. V, How Plants Defend Themselves. Pp.534. ISBN 0-12-356405-0. (Academic: 1980.) $49.50.

HUTCHINSON, J. and OWERS, A. C. Change and Innovation in Norfolk Farming Seventy Years of Experiment and Advice at the Norfolk Agricultural Station. Pp.72. ISBN 0-906527-04-X, (Packard Publishing: Funtington, Chichester, UK, 1980.) £3.

INTERNATIONAL IRRIGATION INFORMATION CENTRE. Irrigation Equipment Manufacturers Directory. 2nd Edn, IIIC Publication No 5. Pp. 312. ISBN 0-08-025512-4. (Pergamon: 1979.) $50, £22.50.

LEVINE, S. and URSIN, H. (eds). Coping and Health. NATO Conference Series. Pp.364. ISBN 0-306-40422-2. (Plenum: 1980.) $35.

LIEHR, H. and GRÜN, M. (eds). The Reticuloendothelial System and the Pathogenesis of Liver Disease. Proceedings of a Symposium held in Wurzburg, West Germany, September 1979. Pp.422. ISBN 0-444-80240-1. (Elsevier/North-Holland Biomedical: 1980.) $60, Dfl. 127.

McMULLAN, J. T. (ed.). Physical Techniques in Medicine, Vol 2. Pp.158. ISBN 0-471-27695-2. (Wiley-Interscience: 1980.) £15.

MOLINEAUX, L. and GRAMICCIA, G. The Garki Project. Research on the Epidemiology and Control of Malaria in the Sudan Savanna of West Africa. Pp.311. Flexi ISBN 92-4-156061-4. (WHO: Geneva, 1980.) Sw.Fr. 33.

NATELSON, S. and NATELSON, E A. Plasma Proteins in Nutrition and Transport. Principles of Applied Clinical Chemistry, Vol. 3. Pp.554. ISBN 0-306-40276-7. (Plenum: 1980.) $42 50.

NATIONAL COUNCIL ON RADIATION PROTECTION AND MEASUREMENTS. Management of Persons Accidentally Contaminated with Radionuclides. NCRP Report No. 65. Pp.205. Flexi ISBN 0-913392-49-9. (National Council on Radiation Protection and Measurements: Washington DC, 1980.) $8.

PAHLOW, M. Living Medicine. The Healing Properties of Plants. Pp.96. Hbk ISBN 0-7225-0605-8; pbk ISBN 0-7225-0592-2. (Thorsons Publishers: Wellingborough, Northamptonshire, 1980.) Pbk £2.95

POON, E.S. and KUO, T.T. Plant Pathology in Taiwan, Republic of China: A Case Study of Plant Pathology in Developing Countries of the Tropics and Subtropics. Pp.167 (National Science Council: Taiwan, 1980.) Np.

RICHTER, D Addiction and Brain Damage. Pp.305. ISBN 0-8391-4139-4. (Croom Helm: 1980.) £15.95

SANDLER, M. (ed.). Enzyme Inhibitors as Drugs. Report of a Symposium held in April 1979 at The Middlesex Hospital Medical School, London. Pp.285. ISBN 0-333-28984-6. (Macmillan Press: London, 1980.) £25.

SARBIN, R.S. and MANCUSO, J.C. Schizophrenia: Medical Diagnosis or Moral Verdict? Pp.250. ISBN 0-08-024613-3. (Pergamon: 1980) £12.50.

SEELIG, M.S. Magnesium Deficiency in the Pathogenesis of Disease: Early Roots of Cardiovascular, Skeletal, and Renal Abnormalities. Pp.488. ISBN 0-306-40202-5. (Plenum: 1980.) $39.50.

SMITH, R.A. and KIRKPATRICK, W. (eds). Ribavirin; A Broad Spectrum Antiviral Agent. Pp.237. ISBN 0-12-652350-9. (Academic: 1980.) $21.

SUMMERS, L.A. The Bipyridinium Herbicides. Pp 450. ISBN 0-12-676450. (Academic: 1980.) $69, £30.

SUTTER, V.L , CITRON, D.M. and FINEGOLD, S.M. Wadsworth Anaerobic Bacteriology Manual. 3rd Edn Pp.131. Flexi ISBN 0-8016-4848-3. (C V. Mosby 1980.) £5.50.

THOMPSON, C.I. Controls of Eating. Monographs in Pharmacology and Physiology, Vol.4. Pp.284. ISBN 0-89335-100-8. (MTP Press: Lancaster, UK, 1980.) £19.95.

nature

23 October 1980

How to change the Nobel Prize rules

It is never the right time to raise questions about the institution of the Nobel Prize. For much of the year, most people are uninterested. The Nobel committees, of course, beaver away throughout the year and it is just possible that there are some in the world outside who, after a hard day in the laboratory, allow themselves to drift to sleep wondering whether what they have just done will one day produce a telegram from Stockholm. For most people, however, the phenomenon of the Nobel Prize is a seasonal phenomenon — perhaps fittingly something to do with the run-up to Christmas. And this, of course, is the season when the telegrams go out.

The danger of raising questions about the institution of the Nobel Prize at this stage is that the entirely proper pleasure of the recipients may be undermined. It is therefore right and proper that last week's prizewinners and their friends should know that their awards have generated just as much pleasure, and deserve congratulation as wholehearted, this year as in the past. Indeed, last week's award to Dr Frederick Sanger should prove that it is possible to distinguish between the merits of the prizewinners and the merits of the scheme. There can be few who are not delighted that such a modest man, yet such an able and imaginative scientist, should have been awarded his second prize.

So what can be wrong with an institution capable of such enlightened decisions? Is there not inherent virtue in an organization whose doings stimulate the pursuit of excellence? Why should there be anxieties about the Nobel Foundation when, by the careful management of its endowment and the diligent pursuit of its procedures, it has become a conspicuous adornment of the scientific profession? And if the institution of the Nobel Prize has stimulated later benefactors to found charities whose work consists of the award of prizes in other fields, from mathematics to immunology, is that not a sign that the market for scientific prizes is buoyant — benefactors seem to like endowing prize funds and scientists to enjoy receiving prizes? There is force in all these implicit arguments. The doubts are harder to define.

One complication is that of envy. Especially in these egalitarian days, there are constant grumbles that the singling out of individuals, however distinguished, for special honour is offensive. Discovery, the argument goes, is often a matter of luck — of being in the right laboratory at the right time. And if it turns out that a person makes an outstanding contribution to the development of his field, might that not merely reflect the value of the groundwork done by his predecessors? After all, it was no less a person than Newton who confessed that "if I have seen further than others, it is because I have stood on the shoulders of giants".

This line of argument is sadly inappropriate, even discreditable. Nobody these days will deny the importance of the climate in which research is carried out in fostering discovery. Teamwork is important. So too is the way in which people brought together, apparently often by accident, in productive laboratories derive extra benefit from being there rather than in some relatively backward place. From the generality of the scientific profession (as of any other creative profession), some able men and women are distinguished by their creativity, clarity of mind and sheer drive. It is proper that these qualities should be recognized for what they are — disproportionately powerful stimulants of discovery. Prizes are one way of recognizing such outstanding qualities, and should be valued.

Such doubts as there are about the prize-giving system are thus largely second-order effects. The Nobel Prizes are most often discussed because they are known widely outside the profession and because they are commonly supposed to deal with the whole of science under the three rubrics of physics, chemistry and "medicine and physiology". (Peace, literature and economics are dealt with separately.) It is therefore important that the scope of the Nobel system is by no means as catholic as it is usually supposed to be. The gap left by the exclusion of mathematics from the terms of Alfred Nobel's will has now been more than amply filled by the annual Field Prize, but it remains an anomaly bordering on the nonsensical that, for example, David Hilbert would not have been awarded a prize under the present rules. It is stranger still that growing fields such as astronomy and the earth sciences should on the face of things be excluded. Although the appropriate committees have in the past few years found ways of counting as physicists Vine and Matthews (because they measured magnetic anomalies on the sea floor) and a number of radio-astronomers (no doubt because radioastronomy sprang from physics laboratories), it is hard to see the Nobel Foundation screwing up its courage to award a prize to, say, Hubble (the astronomer) or Napier (the meteorologist). Whether Darwin would have qualified is an open question.

On the face of things, these complaints are not complaints against Nobel Prizes as such but at the scope of the present system. There is more than that to be said, however. When Alfred Nobel wrote his will at the end of the nineteenth century, he and his advisers could not have known how the balance of science would shift in the succeeding years. They set out to define a set of prizes covering the whole of the science they knew. Their intentions have been overtaken by events. The result is that some fields of science are well covered and others only marginally. The consequences are potentially harmful for the reputation of the prizes which are awarded, if only because of the sense of fickleness that is engendered. By all accounts, the Nobel Foundation is aware of this problem but insists that it would be impossible to amend the terms of Nobel's will. Can that be so? Other charitable foundations are constantly having to change the terms of their trust deeds by applications to the courts so as to fulfil their founders' wishes more adequately. Why should the Nobel Foundation be prevented from following suit?

Modest reform along these lines would help make the Nobel Prize system seem more equitable, taking one field of science with another, but this is not the only respect in which the fairness of the system has been called into question. In the past few years, there have been several occasions when only one member of a small team responsible for some important development has been awarded a prize. This practice appears especially unfair when the team consists only of two people and the prize is awarded to the more senior. Some years ago, there was something of a public controversy in Britain about the award of a prize to Dr Anthony Hewish for the discovery of pulsating stars when his graduate student, Miss (as she then was) Jocelyn Bell went unsung. Both the principals came out of the affair with credit, as no doubt would emerge from any new controversy Dr W. Gilbert (one of this year's winners) and Dr A.M. Maxam (whose name is linked with that of Dr Gilbert in the scientific literature for their development of their novel nucleotide sequencing technique, but who has not his year been given a prize). Like judges in a beauty contest, the Nobel committee brings disappointment as well as pleasure. Strict fairness is unattainable, but there is a sense in which the growth of the practice of close collaboration between groups of scientists may be a threat to the credibility of the system.

A still more serious danger is that the Nobel committees will

0028-0836/80/430667-02$01.00

from time to time let their pent-up sense of mischief get the better of them. In other fields, and in the award of the literature prize in particular, they are prone to let rather temporal considerations get the upper hand. An award to a distinguished writer seems the more delicious (from Stockholm) if the result should be problems with an exit visa from, say, the Soviet Union. There could be just an element of that tail-twisting in this year's prize (shared with Sanger and Gilbert) to Dr Paul Berg of Stanford University, who is, of course, a molecular biologist of the highest standing and the first to join two pieces of DNA together synthetically and also a distinguished teacher. But Dr Berg has also been, perhaps unwillingly, one of the advocates of the regulation of genetic manipulation. Nobody will begrudge Dr Berg his prize, and nobody in his senses will deny that the progress of science is effected not merely by startling discoveries but also by the genial influence of men and women who help to ensure that a new subject is widely known, properly understood and regarded with enthusiasm. This, for what is is worth, was the late J. Robert Oppenheimer's influence in physics in the 1930s, but he died without a Nobel Prize. Nobel's will may be intact, but have the rules been subtly changed?

That such questions are asked of the Nobel Foundation is a measure of its success. For better or worse, the Nobel Prize has come to stay. The need now is to make sure that it creates more pleasure than grumbling disappointment. Broadening the terms of reference of the will would help. A more explicit statement of the reasons for making an award, and a more explicit recognition by the Nobel committees of the teamwork involved in novel discoveries, would often help to disembarrass those who are awarded prizes and who are frequently heard to say "It's not for me but for my lab". Indeed, there is even a case for thinking that the Nobel Foundation might itself give expression to that sentiment by making the award, as at present, to the distinguished scientist but sending the cheque to his institution.

Making British science policy by stealth

The present British government, noted for (and proud of) its empiricism, appears to have taken an axe (or at least a chopper) to the foundations of British science policy in the past decade without much caring what the consequences will be. Since 1971, the word Rothschild has been (among other things) the code word for a doctrine — that, in the planning of applied research, decisions about what to do and how to spend can sensibly be made only by the ultimate user of the results of the research. But who is the potential user of the results of publicly financed research? Constitutionally, Rothschild recognized, the strict answer must be the taxpayer. In theory, however, taxpayers' interests are represented by government departments. So what more natural than that government departments should be required to work out, between themselves and the Treasury, what proportion of their resources should be spent on research and then to arrange that the work should be undertaken by the contractor offering the best terms? This was the argument accepted by Mr Edward Heath's government in 1971. Different fractions of the budgets of the Agricultural and Medical Research Councils and the Natural Environment Research Council were transferred to the appropriate sponsoring ministries. (The budgets of the Science Research Council and of the Social Science Research Council were, for a supposedly provisional period, left untouched.)

Now (see opposite page) the system is beginning to break down. The Department of Health and the Medical Research Council appear to have decided that Rothschild's omelette had better be unscrambled. The attractions to both parties are clear enough. The department will rid itself of some tedious administration (and may in due course get rid of even more). The council will grow modestly in size (which is probably not an important consideration) and, more to the point, will know more accurately where it stands financially from year to year. Undoubtedly a great many things would, under the proposed transfer of funds, be carried out more efficiently than in the past. It is, for example, anomalous that the Department of Health should have commissioned the study of the side-effects of the use of pertussis vaccine directly from a group of academic physicians, while the council has on its staff or on its books a galaxy of distinguished epidemiologists better able to plan a study of the kind required than almost anybody else. Plainly, part of the weakness of the Rothschild doctrine has been that in some fields of enquiry there is not merely just one customer but just one contractor as well.

For the council, there is only one serious drawback in the proposed arrangements. If the department is planning to hand over at least half the money it now spends on applied medical research, it is only right that the council should accept the responsibility for deciding how these should best be spent. In other words, the council will have to work out for itself some way of identifying the needs of the department and ultimately of the National Health Service. For what it is worth, one of the council's weaknesses in the heyday of its growth in the 1950s and 1960s was its stolid disinclination to take responsibility for such problems. Now, plainly, its inclinations have changed. It is to be hoped that it will succeed. Certainly a failure to do so will mean further upheaval. On balance, however, there is every reason to hope that the council will be able to rise to the occasion and be the better for having part of its interest in the long-term development of applied research however untidy it may be.

The drawbacks, such as they are, will be found principally at the Department of Health but also in the principles on which public policy on research now rests. Evidently — this is the experience of the past decade — the Department of Health has been at a loss to know how to function efficiently as a customer for research. To use the Rothschild imagery, the department has had money to spend but has not known clearly what it wanted to spend it on. At this stage, it is probably too late to know whether the department has deliberately (or even unconsciously) dragged its feet in setting up the "strong" chief scientist's department that was an essential ingredient of the Rothschild prescription. It is, however, a curious turn-up for the book that the council should now be thinking of taking on responsibility for operational research in health care, apparently because the department does not keenly sense the operational need of the health services. Rothschild would say that that is precisely what is wrong. The trouble with the traditional departments is that they consider research to be a kind of commodity, like string or sealing-wax, that can be bought in from time to time as the fancy strikes the administrators and as the funds allow. Part of Rothschild's point was that government departments should be forced to take a more constructive interest in the potential of research. That battle is on the way to being lost.

The consequences of this new development for the British government's wider conduct of research are harder to foresee. No doubt the administration will be saying that the special arrangement for medical research does not mean that the Rothschild principle has been breached, but the members of the other research councils will be less than human if they do not now sense a quickening of ambition, a tendency towards what the Soviets call revisionism. The Minister of Health, when he comes to describe the new deal in the House of Commons, should therefore be asked to explain why medical research is such a special case. That may be more difficult than he thinks. For although agricultural research appears to have fitted well into the Rothschild framework, it has for some time been clear that the application of the principle to the affairs of the Department of Industry is far from satisfactory. The "requirements boards" intended to simulate customers for research are not a great success. The lack of an obvious contractor has been a serious drawback. Sadly, the time may be approaching for yet another inquiry into the management of research in Britain.

0028-0836/80/430668-02$01.00

[illegible] Upper Circular Road
CALCUTTA

Reorganization of UK medical research

MRC recovers funds from Rothschild?

A plan for reversing the Rothschild disposition of funds for British medical research is to be considered by the Medical Research Council (MRC) at its meeting today (23 October). The proposal, which has already been agreed by the Cabinet and was notified to the Advisory Board for the Research Councils on Monday of last week, may involve an increase of £12 million a year in the annual budget of the MRC, now running at £56 million a year.

Both the Department of Health and MRC at the official level appear to have arrived amicably at the proposal now being decided. One argument in its favour has been the difficulty experienced in the past several years in operating an effective Chief Scientist's Department within the Department of Health. Officials of MRC have also been swayed in the direction of the proposed arrangement by the recognition that, over the past decade, the funds available for contract work from the Department of Health and the Scottish Home and Health Department have been a declining proportion of the total budget for medical research in Britain.

The council will be expected at its meeting today to strike a balance between the benefits of a larger annual budget and the commitment it will now be expected to make to applied medical research. The proposal being considered involves no explicit strings, but representatives of the Department of Health will expect to be listened to more seriously in future if the council elects to take the funds now offered. If the council accepts, the Minister of Health intends to announce its decision next Tuesday in the House of Commons.

J.L. Gowans, MRC secretary

Formally, the Department of Health cannot off its own bat transfer funds from its own budget to that of MRC, which is dependent on the Department of Education and Science for its annual budget. This is why the feasibility of the proposed transfer of funds has had to be approved by the Cabinet before it could carry conviction with the council. But the redisposition of funds also entails an issue of principle — the abandonment of Lord Rothschild's "customer--contractor principle", at least as far as medical research is concerned.

The Rothschild doctrine, made public in 1971 and promptly accepted by the Conservative government of the day, recommended that 25 per cent of the then MRC budget should be progressively transferred to the Department of Health in the succeeding five years and that the department should use the funds concerned to commission research, not necessarily from the MRC.

One prominent feature of the Rothschild recommendations was the suggestion that each government department should be equipped with a "strong" chief scientist's department capable of making informed judgements of the department's need for research and of deciding how (and by whom) these objectives would best be met.

At the outset, MRC was more vigorous than the other research councils in its opposition to the Rothschild proposals. MRC also stands out among the research councils for the difficulties it has found in working out a smooth relationship with its sponsoring departments. Committees set up to suggest promising directions for applied medical research have been frustrated either by the lack of funds or the imprecision of their terms of reference. Research commissions by the Department of Health to MRC have generated uncomfortably large files of paper, while the council has been left with the sense that a substantial part of its annual spending is soft money.

At the Department of Health, difficulties have arisen because of the lack of full-time officials with a background in research. The chief medical officer has statutory responsibilities for the health of the population, and may find a conflict of interest between his day-to-day responsibilities and the planning of research. The National Health Service, presumably the prime customer in Rothschild's sense, is, however, administratively separate from the Department of Health proper.

An affirmative decision by the council at its meeting today will require that MRC equip itself to plan and execute programmes in applied medical research ranging from clinical research to the conduct of social surveys related to the effectiveness of medical care in Britian. The prize for success could well be a budget enlarged not merely by the £12 million of Rothschild money but a substantial slice of the further £14 million spent each year by the Department of Health and the Scottish departments on commissioned research with contractors other than MRC.

Genentech makes splash on Wall Street

Washington

"One of the most spectacular market debuts in recent history." That was how the *Wall Street Journal* described the first day of public trading in shares in Genentech, the San Francisco company which has been among the leaders of those aggressively pursuing the commercial exploitation of recombinant DNA technology.

Initially the company has proposed to offer one million shares at between $20 and $30 each. But demand was so great that an initial price of $35 was fixed for members of an under writing syndicate through which the shares were made public last week. An extra 100,000 shares were made available, providing the company with an investment — once brokerage commissions had been deducted — of $36 million.

During the day of frantic over-the-counter trading, in which more than half of the shares were resold by their original purchasers, the price rose at one point to $89 a share, eventually dropping back to $71. As the company has 7.5 million shares, this gives it a value of more than $500 million.

On paper, the Wall Street dealings have made multimillionaires of Genentech's two founders, Mr Robert Swanson, its president and chief executive, and Dr Herbert Boyer, vice-president and professor of biochemistry at the University of California, San Francisco.

Both own just under a million shares in the company. The principal shareholder is Lubrizol Incorporated of Cleveland, which previously bought 1.5 million shares in the company at $10 each. Kleiner and Perkins, an east coast venture capital firm, hold almost a million shares. The remainder are divided between directors and employees of the company.

Some employees have benefited from originally being paid in shares rather than cash. Robert Scheller, for example, a graduate research student at the California Institute of Technology, was given 15,000 for helping with research on human growth hormone four years ago. The stock is now worth more than $1 million.

The prices reached by the shares during the first day of public trading were con-

0028-0836/80/430669-02$01.00

siderably higher than most market analysts had anticipated. Two factors contributed. The first was a widespread expectation among investors that genetic engineering is the cornerstone of a future billion dollar industry, and Genentech is the only one of half a dozen small research companies to have gone public.

The second factor was a recent change in the tax law which has helped to restimulate the supply of venture capital. In 1969, Congress introduced legislation raising the effective rate of tax on long-term capital gains from 25 per cent to 48 per cent.

Many investors moved from the stock market to tax shelters, one result being a virtual drying up of new high-technology firms in the mid-1970s. In response, Congress cut the long-term capital gains tax back to 28 per cent in 1978, contributing significantly to the fact that the number of new companies is increasing rapidly again.

Thus, despite recent government warnings about declining investment in technological innovations, there was no shortage of bidders for other Genentech stock. Many brokerage houses were unable to obtain any shares at all in the initial allocation; others who had requested 50,000 or more only received a few hundred.

At the same time, federal officials have taken steps to try to prevent the shares from being oversold, frightened that a backlash could cause investment capital to dry up again. Thus the public offer of the Genentech shares was held up for several days, apparently after a ruling from the Securities and Exchange Commission that more details about the company's operations should be made public.

A revised prospectus issued by the company revealed that in the first half of 1980, Genentech had a revenue of $3.8 million, of which most came from research contracts, and earnings totalled only $80,000. Almost two-thirds of the contracts came from three pharmaceutical companies — A.G. Kabi of Sweden, Eli Lilly and Hoffman La Roche — with whom Genentech is working on human growth hormone, insulin and interferon respectively. The prospectus also revealed that the three companies will not be required to pay any royalties to Genentech after their research agreements expire. Although the agreements are described as "long-term", no further details are given.

Although several Wall Street analysts have claimed that the enthusiasm for the Genentech shares showed that the stock market was reviving, others added notes of caution. Half-way through the first day of trading, shares dropped from $80 to $74 following warnings from a senior partner of a major investment house that the explosive activity might be a "danger signal" and that "it will attract issues of lesser quality where an attempt will be made to create the same aura of scarcity".

• **David Dickson**

European universities

No room below

European universities seem uniformly to be heading for demographic trouble. According to a 15-nation study commissioned by the European Science Foundation (ESF), European universities have too many academics in the younger age groups and consequently too small a rate of recruitment to university staffs. To make things worse, there is a prospect of falling student numbers as a consequence of low birthrates since 1970.

The report urges "concrete corrective action" to avoid an "irreparable" loss of research talent in the immediate future and, in the longer run, a shortage of trained scientists for the economy. The rate of new recruitment to most university teaching and research staffs is estimated at less then half the 3 per cent per annum required to maintain a flat age distribution.

The decline of the European birthrate since 1970 is potentially a political threat to the universities. The report points out that unless a greater proportion of the age group elects for university education, enrolments will fall, teacher–student ratios will rise and governments will be tempted to cut university budgets.

Superficially, France may be the most seriously affected, with the most unbalanced age distribution among present academic staffs (see graphs). In 1977, 46 per cent of French uiniversity teaching staffs were aged 30–40, and retirement rates will average only 1.3 per cent a year over the next five years. But France is also among the most active in correcting the problem. In 1975, the Centre National de la Recherche Scientifique set itself a target of creating 3 per cent new posts a year within a staff of some 8,000 researchers. After a shaky start in 1978–79, recruitment seems likely to rise once more to 3 per cent, with consequent benefits for mobility among scientists.

Switzerland is at the other end of the spectrum. Retirements from the universities generate a 2.3 per cent annual demand for replacements in 1981–85, and thereafter more than 3 per cent.

In Germany, replacement demand is estimated at 1.5 per cent a year between now and 1985. The falling birthrate — down by 40 per cent in the period 1967-77 — will be especially troublesome. The "Heisenberg scheme" introduced in 1978 to increase the academic pool by 1 per cent a year, leaves much to be desired. Pay is relatively poor, contracts terminate after 5 years and in any case the most able get the few professorships on offer and leave the scheme.

Stock of permanent academic staff universities in seven European cou s.

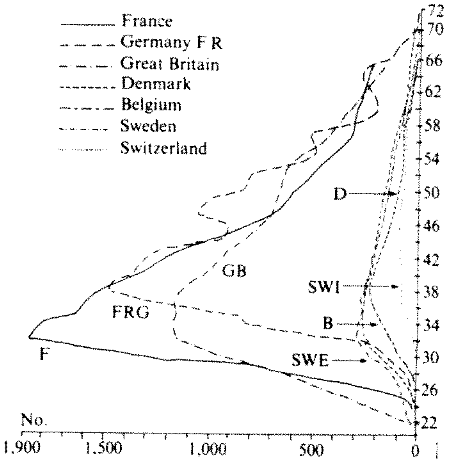

In the United Kingdom, the annual replacement rate is expected to be around 1.6 per cent, not reaching 3 per cent until the end of the century. Some 54 per cent of UK university staffs are between 30 and 45 years old. But, like France, the United Kingdom — and particularly the Science Research Council — has been at pains to do something about it. This year, the SRC is expected to make available 15 "Special Release Fellowships", which will pay professional salaries to senior academics — often burdened by administration — to return to full-time research, while the monies thus released to the university will be used to employ a larger number of young researchers.

Of other countries studied, Belgium is in a particularly difficult position: 43 per cent of its university scientific staff are on short-term contracts (compared with 61 per cent in government research institutions) and the majority of these are under 30 years old. Replacement demand for permanent positions is around 2 per cent, higher than most countries, but ESF has discovered no existing schemes in Belgium to tackle scientific unemployment. Denmark, with similar problems to most other countries, has proposals but no action; and Sweden,

Replacement demand for permanent academic staff in France by year.

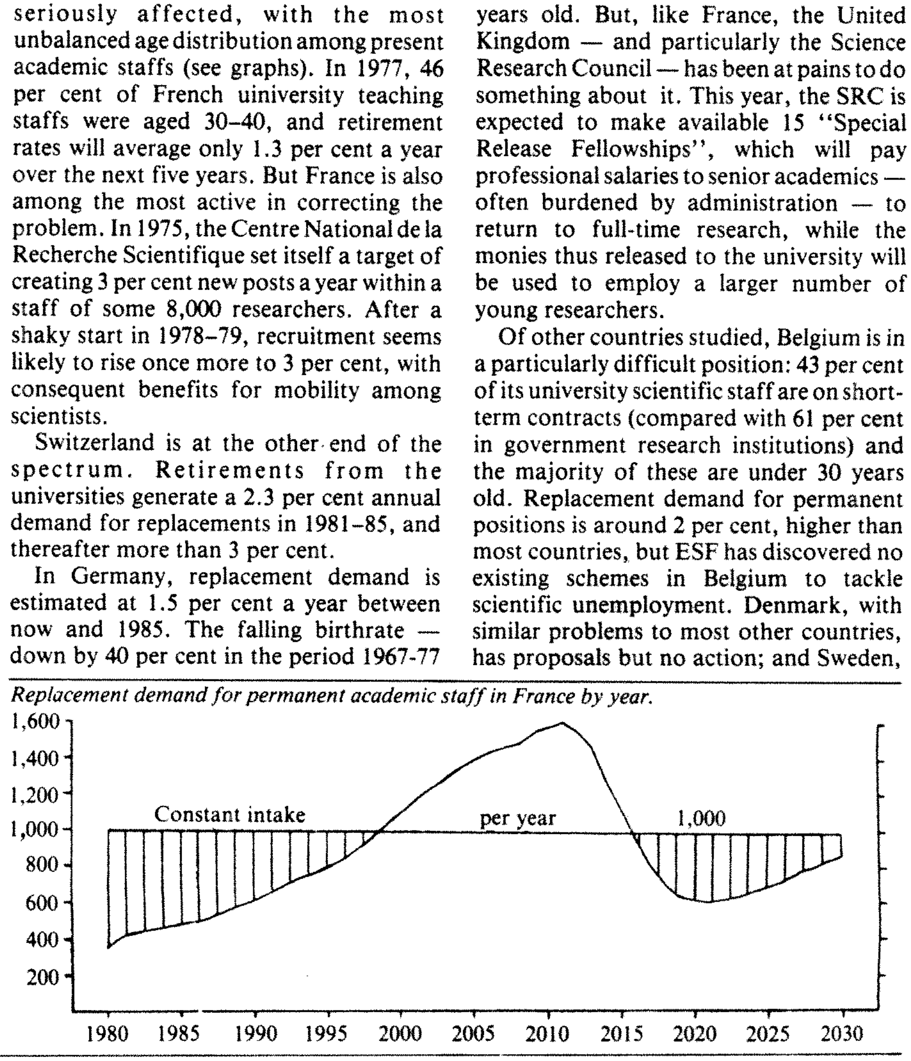

0028-0836/80/430670-01$01.00

Norway and Austria provided no information to ESF about the measures they were undertaking.

The net result must be a fair degree of pessimism about the future of academic employment in Europe. The report makes 19 recommendations, few of them novel. The report also makes it plain that scientific mobility is also very low in Europe compared with the United States. Anxiety about jobs seems to have kept people at home. In the United Kingdom, for example, successful applications for the Royal Society European Fellowship exchange scheme fell from 91 in 1976 to 61 in 1979 (although the reverse traffic has kept up at about 90). **Robert Walgate**

Carcinogen regulations

US labs exempt

Washington

Following protests from both university and industrial scientists, the Department of Labor's Occupational Safety and Health Administration (OSHA) seems to be softening its stand on the control of toxic substances in research laboratories. Until recently, OSHA had been insisting that laboratories should be treated no differently from other workplaces in which individuals are occupationally exposed to hazardous substances.

A case in point is OSHA's new cancer policy, which was introduced at the beginning of this year: once a substance has been classed as a carcinogen based on defined scientific criteria, measures must be taken to reduce exposure levels to the lowest that is technologically feasible — and eliminate them if possible.

Labour unions have supported OSHA's argument in the past that laboratories cannot be considered any safer than factory environments, and that the same regulations should therefore be applied to both. Union officials point to reports in the scientific literature which suggest that laboratory workers may be at increased risk with respect to carcinogens, and that cancer rates are high among certain professions, particularly chemists.

University scientists, however, have complained that regulations designed to reduce exposure to chemicals in an industrial environment may be inappropriate and unnecessarily expensive when applied to research laboratories using the same substance.

Additional problems arise from the fact that laboratory work may involve exposure to small quantities of many different chemicals, and that some of these might be difficult to subject to rigid classification.

Although OSHA's new cancer policy received much comment from the chemical industry when it was first proposed, little was heard from the scientific community until the public review process was well under way. (Many laboratories were unaware of the proposals' application to them.) As a result, when the revised policy was published in January, no specific attempt was made by the agency to exempt research laboratories from its scope. In a preamble to the policy, however, OSHA said that consideration would be given to setting separate standards for laboratories.

Now, under growing pressure from various agencies, including the National Science Foundation (NSF) and the Office of Science and Technology Policy (OSTP), the agency has begun to explore ways of moving in this direction. OSHA officials are working on a proposal, due to be published sometime in the new year, setting out possible procedures for the control of toxic substances in laboratories.

Their proposals are likely to conform closely to the recommendations of the *ad hoc* committee set up by the National Research Council of the National Academy of Sciences (NAS) to look at possible alternatives to the original OSHA cancer proposals as well as other aspects of handling toxic substances. Publication of the committee's report is expected soon.

The committee, initially financed by the American Chemical Society, the Alfred P. Sloan Foundation and the Manufacturing Chemists Association, with later federal support from the NSF, the National Institutes of Health (NIH) and the Environmental Protection Agency, is expected to propose that emphasis be given to developing general laboratory safety regulations rather than the substance-by-substance regulations favoured by OSHA for industrial settings. The committee has in particular been keen to explore approaches which would be more flexible and less costly than those required under OSHA's present regulations.

Also due for publication in the near future are new guidelines that have been prepared by NIH covering the use of potential carcinogens in in-house laboratories. According to Dr Emmet Barkley, director of NIH's new Office of Research Safety, the guidelines (which include provisions for safety plans and medical surveillance) would be triggered whenever either OSHA regulates a chemical or an institute determines that a chemical is a carcinogen.

NIH's guidelines could be used as a model for other research laboratories, if OSHA sticks to a substance-by-substance form of control. However if — as seems more likely — greater emphasis is placed on general laboratory safety guidelines, the NAS report would probably provide the starting point, since this strategy would be a major departure for OSHA.

Another idea on which OSHA is thinking of asking for public comment is the setting up of an advisory committee to comment specifically on the safety measures required in research laboratories. More controversial is likely to be the role played by labour unions, which have been minimally involved in negotiations so far.

David Dickson

1980 Nobel prizes

The Nobel Foundation has in the past two weeks announced in Stockholm the names of the recipients of Nobel Prizes as follows:

Chemistry

Dr Frederick Sanger (MRC Laboratory for Molecular Biology, Cambridge, UK) for the development of a technique for obtaining nucleic acid molecules.

Dr Walter Gilbert (Harvard University, Cambridge, USA) for the development of a different technique for obtaining the sequence of nucleic acid molecules.

Professor Paul Berg (Stanford University, California) for "research in nucleic acids and genetic manipulation".

The Sanger and Gilbert techniques have turned out to be complementary. Sanger uses a single DNA strand to synthesize random lengths of complementary DNA; Gilbert's technique entails the degradation of single strands of DNA in such a way as to generate a mixture of random polynucleotides always including some fixed recognition point.

Professor Berg is known to have been the first to use naturally occurring enzymes to synthesize composite DNA molecules in which two pieces of natural DNA were spliced together.

Medicine and physiology

The prize, which is shared three ways, was awarded for different aspects of the research leading to present understanding of the human histocompatibility gene system (HLA). The recipients are:

Dr George Snell (Jackson Laboratory, Bar Harbor, Maine), responsible for the recognition of the mouse analogue of the HLA system, known as H2, and for the development of appropriate strains of inbred mice.

Professor Jean Dausset, (University of Paris) whose chief contribution was the recognition of the human histocompatibility antigens.

Professor Baruj Benacerraf (an Argentinian working at Harvard University) was chiefly responsible for the identification of the system of genes responsible for the HLA antigens.

Physics

The 1980 physics prize has been awarded for the discovery of what is called "CP violation" to **Professor J.W. Cronin** (Chicago University) and **Professor Val Fitch** (Princetown University).

Their discovery was the experimental observation of the decay of a neutral meson into two charged pions (*Phys. Rev. Lett.* 13, 138; 1964). The outcome was the recognition that in the interactions or spontaneous transformations of elementary particles, parity (left or right-handed geometrical symmetry) need not be conserved.

0028-0836/80/430671-01$01 00

Almost 8,000 scientists, including 32 Nobel laureates, have signed a "personal moratorium" pledge in support of Andrei Sakharov, Yurii Orlov and Anatolii Shcharanskii, it was announced last week. The moratorium pledge was organized by the "SOS" campaign — original "Scientists for Orlov and Shcharanskii" but extended in January to include Sakharov on his exile to Gor'kii. All three were linked with the work of the Helsinki Watch Committee.

The pledge, which replaces an earlier "personal boycott", binds the signatories not to visit the Soviet Union nor to receive Soviet scientists in their laboratories from 15 May 1980 (the second anniversary of the Orlov trial) until the end of the forthcoming Madrid review conference on the progress of the Helsinki process — unless, in the meantime, Orlov and Shcharanskii are released from labour camp and Sakharov is restored to full liberty, including the right of residence in Moscow. A total of 6,100 scientists and engineers in 44 countries have signed the SOS pledge, while similar but independent pledges in France and Switzerland have so far attracted 1,200 and 600 signatures respectively.

Orlov tee-shirts on show

The organizers now plan to deliver an information dossier to the delegations of the 33 countries signatory to the Helsinki Final Act before the conference officially opens on 11 November.

According to Dr John Charap (Queen Mary College, London) who took the chair at a meeting in London last week to report progress, the moratorium and previous boycott pledges have significantly cut Soviet exchanges with the West. In 1979, he said, short-term US–USSR exchanges of personnel had numbered 783 US and 662 Soviet scientists. In the first half of 1980, partly as a result of the pledges, these figures had fallen to a mere 72 US and 117 Soviet scientists.

Since the pledges are essentially personal, it is impossible, of course, to stop Soviet scientists visiting Western establishments, even if there has been a large response to the campaign by the scientists employed there. CERN, for example, still receives a significant number of Soviet visitors, although a large number of the scientists there have organized and signed their own pro-Orlov moratorium. Here, the signatories to the pledge simply refuse to conduct the visitors around their laboratories. When such visitors are expected at CERN, laboratory walls and notice boards display posters bearing simply Orlov's photograph and name, while many staff don T-shirts with the slogan "Free Y. Orlov".

The organizers of the moratoria emphasize that they are not "cold warriors". Nobel laureate H. Christian Anfinsen of the US National Institutes of Health said last week "We have traditionally pushed for togetherness but now we are deciding to hold back because of our concern for human rights".

All moratoria so far have been partial. They do not bind the participants, for example, not to speak to Soviet scientists at international conferences outside the Soviet Union, or not to correspond with Soviet colleagues. Several signatories report tacit sympathy for the campaign among Soviet scientists.

What the organizers hope for is not, however, entirely clear. They stress the harm that Soviet science will suffer, although the Soviets, in their turn, stress that Soviet science is self-sufficient and that moratoria can only harm the West. Dr Charap said last week that the Soviet government needs Western contacts in order to build up its economy, and that such contacts and exchanges are dealt with under "Basket two" of the Helsinki accords. If the Soviet Union wishes to benefit under "Basket two", he said, it must be prepared also to implement "Basket three", which deals with human rights.

The Western attitude to the Helsinki Final Act has always been that the detente process is indivisible, while the Soviets have preferred to deal separately with the three "Baskets" and especially "Basket one" (arms control). The public speaking of the moratorium organizers is intended to stiffen the Western stand at Madrid on the human rights issue.

Last week's simultaneous meetings in London, Washington, Geneva and Paris were, however, timely for another reason. A few days before, Shcharanskii's mother, Mrs Ida Milgrom, reported that her son had collapsed on 23 September in his Perm labour camp and had been rushed to the prison hospital for emergency treatment of abdominal pains. And in London, John McDonald, QC, announced that Orlov had been put into the punishment area of his labour camp in the Urals, apparently for complaining that he was not receiving his mail and that the guards, drunk on duty, had beaten him up. His right to a visit from his wife this August was withdrawn, and she will not now be able to see him until August 1981. However, said Mr McDonald, Mrs Orlova is afraid that her 57-year-old husband will be unable to survive the present six months punishment regime. **Vera Rich**

Ariane failure known

A faulty fuel injector in one of four rocket motors led to the failure of the second launch of the European Ariane rocket on 23 May this year.

This is the conclusion reached by the European Space Agency, which said last week that the fault caused the rate of burning fuel in the engine to oscillate 2,000 times per second soon after the launching.

A review group of independent experts has recommended that the Société Européen de Propulsion (SEP), which built the engines, should make future injectors to finer tolerances, and select good ones by ground firing tests before they are fitted to a launch vehicle.

The injector mixes fuel with oxidant at the top of the engine. It consists of a cylinder equal in diameter to the engine, with 5-cm-thick walls pierced by hundreds of angled holes which direct streams of oxidant onto streams of fuel. Variations, within manufacturing tolerances, of the geometry of the holes seem to be capable of inducing instabilities in the burn – although the fluid dynamics of this is still not understood.

Experiments with engines at SEP in Vernon, near Paris, showed up the fault. Apparently, manufacturing tolerances have slipped since the 200 test firings, although with hindsight low amplitude oscillations have now been discovered in the data.

The third launch — with ground-tested injectors — is now scheduled for mid-March 1981. The fourth and last test flight would be in June 1981, and the first operational flight in October the same year, if all now goes well. The programme would then proceed with the dates planned before the failure of the second launch. **Robert Walgate**

Soviet science

Relations forsworn

Old wounds will be opened at the salt domes of Gorleben, Lower Saxony, early next year when a new inquiry begins on the disposal of spent nuclear fuel. But this time it will not be a staged confrontation, as happened last May, of nuclear and non-nuclear experts. Now the licensing authority, the Physicalisch-Technische Bundesanstalt of Braunschweig, will present the case from the platform and protesters will have to speak from the floor. And protesters will not be getting financial support from the state.

The previous inquiry led to the rejection of the proposals, for reasons which the prime minister of Lower Saxony, Herr Albrecht, insists were political, not technical. The plan then was for a final disposal facility for all West German nuclear waste, but this has now become a plan for the temporary storage of up to 1,500 tonnes of spent fuel in transport con-

0028-0836/80/430672-02$01.00

tainers, constantly cooled in a deep pit. A similar proposal is being made at Ahaus, 100 km from Gorleben, but the inquiry there will take place later.

Both proposals are backstops, not permanent solutions to the problem of nuclear waste in Germany. The spent fuel ponds of the existing 12 GW of nuclear power plants are full (allowing space for emergency core dumping), and spent fuel is being transferred to the French reprocessing firm Cogema. But that 500 times per year contract expires in 1984, when French capacity will be fully committed on domestic work.

One alternative being considered is what is called compact storage at existing ponds, using barium shields to absorb neutrons and to kill potential fusion chain reaction. The result could be a five- to sevenfold increase of storage capacity but only in the face of political opposition. As part of nuclear power station site construction (or modification), compact storage must be approved by public inquiry.

Compact storage has nevertheless been agreed for the six nuclear reactors now under construction, which will bring German nuclear power capacity to 21 GW by 1984, so that the issue is only relevant for existing reactors but is there critical. Legally, reactors whose fuel cannot be disposed of safely must be shut down. With the possible ending of the Cogema contract in 1984, West Germany may have to shut down 12 GW of nuclear power.

The sites of Ahaus and Gorleben are thus safety valves, and the planning process has been started in good time in deference to the inevitable opposition. At Gorleben, the chief opponent will be Helmut Hirsch, who organized the opposition at the previous inquiry. Backed by a consortium of environmental groups, he will be arguing that extended storage in transport casks is unsafe.

"The whole scheme is improvised" he said last week. Two years ago, he claimed, the nuclear industry had admitted that there was no recognized system of safe dry storage. In the new proposal, the fuel would become hotter in ponds, perhaps hotter even than in a reactor, and the mechanical stresses involved would lead to corrosion and collapse of the fuel cladding. Hirsch also emphasized that the containers will have to be actively cooled, so that safety will depend on the continuity of the power supply to the plant. The nuclear industry counters that Hirsch's scenarios are extremely improbable.

The long-term deep storage of reprocessed and glassified high active waste seems still a long way off. Indeed, the prospect has become even more uncertain since the last inquiry, for the East German government has now weighed in with complaints about the risks of siting a deep storage facility close to the border, where the prevailing winds would carry emissions to the East rather than the West.

Robert Walgate

Baltic oil pollution

Finns fight spill

Finland's Department of Environmental Protection is to set up a new marine biological research and rescue programme to deal with oil spills. This announcement by the Ministry of the Interior follows publication of a report on the damage caused by the oil slick from the *Antonio Gramsci*, which went aground in the Gulf of Riga in February 1979. Although the damage on this occasion was relatively slight, the report found Finnish preparations inadequate to deal with a major slick disaster. The new programme, which will cost an estimated FM 400,000 (£57,000) to implement, will include both oil-fighting and clean-up measures and longer-term research on toxic after-effects.

The oil from the *Antonio Gramsci* first entered Finnish waters at the end of March 1979, striking the edge of the sea ice just south of Utö. It then drifted away towards Sweden, but returned at the end of May and came ashore in the Aaland Islands until 4 June. After emergency clean-up measures, a survey was made during July and August on the impact of the oil on fish, seal and bird populations, and on the littoral and benthic ecologies.

Some 1,200 sea birds had perished in the disaster, and a further 500 were soiled. By the time the survey was made, fish life was found to be virtually unaffected. (The islanders had apparently continued to eat the fish without ill-effects.) However, ichthyologists found a significantly higher rate of abnormal tails in the fish examined, although it was not clear that this was the result of oil from the *Antonio Gramsci*.

There was, however, considerable benthic deposition of oil, with the consequent threat of accumulation in food chains. Six months after the incident, there were still traces of oil in mussels.

Finland's unpreparedness for post-spill rescue and clean-up measures is in remarkable contrast to its concern with pollution prevention. The pride of the Finnish passenger fleet, the *Finnjet* ice-breaker ferry, operates as a totally closed environment, with special port facilities for the discharge of sewage and bilges, while her onboard sewage treatment plant has been estimated to cost some £1,000 a day in lost cabin/cargo space alone.

Moreover, under the terms of the Helsinki Convention for the Protection of the Marine Environment of the Baltic Sea, Finland has special responsibility for pollution due to oil spills. Although the convention only came into force on 3 May 1980, there has been joint research and monitoring programmes between the participant countries for several years. A major programme for open-sea monitoring of biomass as an indicator of pollution is already under way. Finland, however, like all other participant countries, is experiencing some delays in getting started; in Finland's case, this is due to lack of carbon-determination facilities in institutes on the coast.

One country which is not taking part in the biomass monitoring programme, although it is a signatory to the Helsinki Convention, is the Soviet Union. The reason for this is mainly that the biomass working group needs to be able to meet at relatively short notice, shorter than the time needed for Soviet experts to obtain visas to attend. Therefore, when, at a working group meeting at the Gdynia Sea Fisheries' Institute last May, monitoring of the Baltic was partitioned between the participant countries, the Soviet offshore waters became the responsibility of Finland and the GDR.

It would seem, furthermore, that the Soviet Union is unable to meet its full commitment regarding damages from the *Antonio Gramsci* affair. The Finns set the total bill at some 15 million Finnmarks, but have agreed to settle for about 25 per cent of this sum, the one million rubles which is the maximum compensation permitted under Soviet law.

Vera Rich

Frosch moves on

Washington

Dr Robert Frosch, administrator of the National Aeronautics and Space Administration (NASA) since 1977, is the latest to join the exodus of science administrators from the federal government.

Following the departure in June of Dr Richard Atkinson, director of the National Science Foundation, and the widely expected appointment of the President's Science Advisor, Dr Frank Press, as president of the National Academy of Sciences (NAS), Dr Frosch has announced that he will become the first president of the American Association of Engineering Societies. on 20 January next year.

Before joining NASA he was associate director for applied oceanography at Woods Hole Oceanographic Institution, and has also been Assistant Secretary of the Navy for research and development. His three and a half years at NASA have seen the agency struggling increasingly against the escalating costs of the space shuttle programme, which is now biting deeply into the space research budget.

Dr Press's appointment is almost settled. His was the only name put forward by the academy's nominating committee, and no serious challenge is expected. Dr Press's appointment would have to be reviewed by a federal ethics committee, established last year to consider the exemption of science administrators from a new law forbidding an ex-government employee from accepting funds from his old agency for two years after leaving government service, but this is not expected to raise difficulties.

David Dickson

0028-0836/80/430673-02$01.00

CORRESPONDENCE

Science in Spain

SIR — The present status of science in Spain is unworthy of an advanced society that values its standing in the community of nations. It is incumbent upon a modern state to develop a balanced policy of support for basic and applied science; a policy for the advancement of science must be the concern of government as much as economic, educational, foreign and military policy. Unfortunately our administration is derelict of this obligation; it is disregarding the creative aspects of science in favour of short-term pragmatism, typical of a colonial society.

As a matter of intellectual dignity, of national prestige and of responsibility to future generations, this situation must not persist. As Spanish scientists we demand that the administration respect our right to pursue our scientific interests, and we assume the responsibility for generating a scientific establishment that is both of value to our society and a credit to our country.

The efforts committed to this endeavour will be justifiable only if the resulting science and technology are competitive at the international level. In order to be competitive, technology must be original, and because of its modern complexity it depends on complete and continuous access to basic research. It is impossible to generate a competitive technology without a parallel reinforcement of research in basic science.

The extent of the task that confronts us can be evaluated by examination of the commitment to science in other countries in the European Community. The initial investment required to approach their levels is modest, both in absolute terms and in comparison with the cost of other national programmes. However, this effort must begin immediately, because the deterioration of our scientific institutions, the demoralization of our scientists and the loss to other countries of the most able, especially among the young, increases daily.

In order to invigorate our science, the university departments must become centres of scientific excellence, with a balanced dedication to preparing new professionals and to research. Moreover, because of the complexity of modern scientific investigation it is necessary not only to reorganize and strengthen existing research centres, such as the Research Council, the Nuclear Energy Commission and the Agricultureal Research Institute, but even to create new ones.

Our country cannot be expected to reach a satisfactory level of cultural and economic development or a minimum of political independence, if we do not soon recognize that progress depends on knowledge. State administrators must become aware of the necessity of stimulating sound scientific research and of the historical responsibility they have in this endeavour.

The above *Manifesto* has been signed by, among others, 134 professors, 25 associate professors of the University of Madrid, 23 research professors and 14 investigators of the Spanish Research Council, heads of departments or institutes in the areas of humanities, natural sciences, medicine and technology in nineteen major cities of the country (Barcelona, Bilbao, Córdoba, Granada, La Laguna, León, Lérida, Madrid, Málaga, Murcia, Oviedo, Pamplona, Salamanca, Santander, Santiago, Sevilla, Valencia, Valladolid and Zaragoza) besides 21 investigators, heads of research groups in the Spanish Atomic Energy Commission and several medical institutions.

A GARCIA-BELLIDO

Centro de Biología Molecular,
Universidad Autónoma de Madrid,
Madrid-34, Spain

Nuclear electricity

SIR — The article 'Nuclear generating costs compared' (*Nature* 21 August, p.753) states that the analysis of relative costs given in the 1979/80 Report of the Central Electricity Generating Board (CEGB) "is likely to be much quoted in the months ahead, when plans are being laid for the further development of the British nuclear power programme". This is certainly true and it is therefore a pity that the report's figures were reproduced without question. In fact, for the purposes of comparison, the figures are almost totally misleading.

The apparent lower cost of nuclear (Magnox) electricity (1.30 pence per kWh against 1.56 pence per kWh for coal) is entirely an artefact of inflation. If currency had been stable over the lifetime of the Magnox stations (or if inflation had been corrected for in the accounts) the order would have been reversed. In 1980 prices the approximate corrected costs are 2.5 pence per kWh for electricity from nuclear stations and 1.9 pence per kWh from coal-fired stations[1].

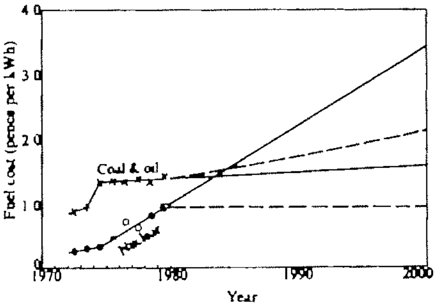

Fig. 1 Fuel costs from the 1979/80 CEGB Statistical Yearbook, Tables 9 and 10, from 1972/3 to 1979/80 in pence per kWh corrected to 1979/80 prices using the Retail Prices Index., Crosses, coal and oil combined, circles, nuclear 1980–2000 extrapolations. solid line, linear; dashed line, CEGB extrapolation for net effective cost calculations

The full calculation can only be undertaken when the CEGB decides that its present policy of withholding the data from which Table 1 in the *Nature* article was calculated is counterproductive, but all the indications are that the real cost of nuclear electricity in 1979/80 was well over 50 per cent greater than that from coal-fired stations.

When we come to future costs (Table 3 in the *Nature* article) the figures are calculated in 1980 £'s But here the figures are equally misleading for different reasons. Richard Marshall (*Nature* 18 September, p.184) has dealt with the CEGB's optimistic figures in the light of actual operating experience with regard to load factors. An equally optimistic view is taken of nuclear fuel costs relative to those of coal. Figure 1 shows the real costs of nuclear fuel for the last eight years. This rose quite rapidly for the first three years but then shot up at a rate of 0.12 pence per kWh per year to 0.94 pence per kWh in 1979/80. The increase shows no sign of slowing down and if it continues nuclear fuel costs will overtake those of coal in the mid 1980s.

It is significant in respect of future fuel costs that the 1979/80 CEGB Report records with satisfaction that an understanding has been reached with the National Coal Board to take 75 million tons of coal a year provided that the real price of coal does not increase for five years, but "the terms of a contract with British Nuclear Fuels Ltd for reprocessing oxide fuel from the advanced gas-cooled reactor (AGR) stations have yet to be negotiated".

It is extraordinary that the CEGB has nevertheless nowhere, either in its reports or in the evidence to the Select Committee, discussed the alarming increase in real nuclear fuel costs (over 10 per cent per year for the last five years) but has concentrated on postulated increases in the real price of coal up to the end of the century. This hypothetical increase is actually incorporated into Table 3. The figure of 2 38 pence per kWh for 'inclusive fuel costs' of a coal-fired station is composed of two parts. 1.36 pence per kWh is the approximate current fuel cost in March 1980 prices and the remainder, 1.02 pence per kWh, is entirely dependent on the assumption about increases in coal costs up to the year 2000. If real future costs for coal are assumed to remain stable this part would be zero.

No such addition to current costs occurs with nuclear fuel. The figure of 0.61 pence per kWh in March 1980 prices hardly covers the increase due to inflation from the 0.55 pence per kWh given for Hinkley Point B in 1979/80 average prices, let alone any allowance for the rapid rise in real costs. There is no provision for "present value of future real increases in the price of fuel" in the nuclear case and this means that it is assumed there will be no real increases in the price of nuclear fuel over the 25-year lifetime of the station.

It is on the basis of such wild assumptions that the net effectiveness cost calculations over the whole lifetimes of the stations have produced the apparently favourable results for nuclear power.

It is difficult to see why the CEGB did not present the obvious calculation — the estimated cost in pence per kWh for each station in its year of commissioning in 1980 costs and prices — and then make the various points relevant to possible alterations in these costs in the future. But then these considerations would have been explicit and generally understandable, whereas wrapped in the computer program for finding net effective cost they are almost immune from criticism.

J. W. JEFFERY

Birkbeck College,
Malet Street, London WC1, UK

---

1 Jeffery, J W *Energy Policy* (in the press)

0028-0836/80/430674-01$01 00

NEWS AND VIEWS

The economics and management of commercial fisheries

from Robert M. May

THE blockade of Channel ports by French fishing boats this summer will have forcibly reminded many unfortunate travellers that managing the fisheries of Northern Europe is no simple task.

As will be argued below, the major problems are economic, social and political rather than scientific. The scientific problems are, however, formidable. To begin, data for fish populations[1] and the intrinsic dynamical behaviour of the populations[2-4] are both subject to many kinds of stochastic effects. Thus, even when the millennium dawns and fisheries managers completely understand the biology underlying recruitment processes, predictions about stock densities and recommended catch levels are likely to remain probabilistic rather than deterministic statements[5,6]. This probabilistic character infuses much of the biological sciences[7], contrasting with the crisp determinism of most of classical physics and engineering; a contrast leaving many people with the uncomfortable feeling that such areas of biology are 'unscientific'.

The millennium lies a long way off for fisheries scientists, and many fundamental biological problems remain unsolved. One problem concerns the relation between stock and recruitment[1-8]. For whales, other marine mammals and some fish there is a rough — a very rough — understanding of the relation between the size and age composition of the population and the recruitment rate. But for most fish (including essentially all the commercially important species in the North Sea) recruitment appears to be approximately independent of stock density down to some threshold level, below which recruitment appears to collapse suddenly; at present, there is no *a priori* way of determining this threshold, although it may be (and this is debatable) that it has been discovered *post hoc* in 7 major clupeoid fisheries that have collapsed[9] (North Sea herring, Norwegian spring spawning herring, Hokkaido-Sakhalin herring, Pacific sardine, Far Eastern sardine, Southern African sardine, Peruvian anchovy). Another set of problems arises from the simultaneous harvesting of several different species that interact within a complicated ecosystem[1-10,11]; such problems are becoming more important with overfishing of many conventional fish species and the search for new kinds of food from the sea.

These scientific problems are the subject of several recent reviews[6,8,11,12]; the book edited by Gulland[1] is particularly good. The difficulties are often compounded by inadequate reporting of catch data. For instance, the International Council for the Exploration of the Sea (ICES) working group on hake stocks this year decided to double Spain's official figure for their hake catch (taken under license in EEC waters), on the basis of the number of unlicensed Spanish vessels sighted in the Bay of Biscay by the French authorities. Moreover, the agreed rules are not always obeyed: again to use hake as an example, French and Spanish fisheries in the Bay of Biscay in 1979 exceeded the total allocated catch (TAC) by some 10,000 tonnes, using small-meshed nets such that 80 to 90 per cent of the catch was below the internationally agreed minimum size of 25cm. Although the reasons given in defense of such infringement are often that the TAC set by ICES or other international bodies is not scientifically sound (even Le Monde[13] writes of "foreign competition (using) so-called scientific arguments, such as, for example, slashing quotas of catches in authorized fishing areas . . ."), the real reason lies in the economics and politics of the situation. To this I now turn.

In the past, most marine fish stocks have been exploited as 'common-property' resources; fishermen (unlike farmers, miners, or lumbermen) do not usually own the primary resource base from which their income is derived. In such common-property, open-access situations, there ensures what Hardin[14] has called a 'tragedy of the commons', as fishermen are forced to compete for their share of the catch taken from a finite resource stock. Even after the establishment of international management commissions which seek to prevent excess depletion of stocks (or rehabilitation of overexpolited stocks) by restrictions on fishing gear, closed seasons and areas, total catch quotas and so on, there remains a basic tension between[12] "the interests of the individual ('will an additional vessel make a profit') and of society as a whole ('will an additional vessel result in an increase in the value of total catch that is greater than the cost of the vessel')." In this way, competition within common-property fisheries has repeatedly led to overexpansion of fishing capacity and "dissipation of economic rent", even in those cases where management has succeeded in preventing depletion of the fish stocks.

With the introduction of 200-mile Exclusive Economic Zones (EEZ) by coastal states, most of the world's fish stocks are now susceptible to rational management; by the end of 1979, 99 per cent of all commercial fish catches were contained within the new EEZs. The UN Food and Agriculture Organization (FAO) has noted[12] that this global movement to patterns of national "sole ownership" marks "a time of fundamental change and tremendous opportunity . . . to move in an orderly way to develop processing capacity and markets based on a stable supply, and in general to look forward to great and continuing benefits from the resource". Partly motivated by these opportunities, there has been an upsurge in interest in methods for the economic regulation of commerical fisheries[12,15-19].

In particular, Clark[17] has analyzed models for fisheries, incorporating the microeconomic decisions made in the operation of individual vessels, in order to understand the consequences of various methods of regulation. These include total catch quotas, vessel licenses, taxes on catch (or effort) and transferable catch (or effort) quotas allocated to individual vessels.

Setting aside the technical problems associated with a licensing programme (who gets licenses, at what cost and under what limitations of transferability, etc.), it is important to realize that licensing by itself does not resolve the common-property problem of fisheries. The usual experience of licensing programmes has been that[20] "licensed vessels have been progressively replaced by larger, more powerful vessels with increased capacity for catching and storing fish on board." Such expansion in capacity typically necessitates additional regulation: the size and horsepower of vessels may be controlled, restrictions may be placed on gear or detection equipment, fishing grounds may be closed at specified times, and so on.

Similar problems beset regulation by

Robert M. May is Class of 1877 Professor of Zoology at Princeton University.

0028-0836/80/430675-02$01.00

total catch quotas. Both licenses and total quotas can prevent depletion of stocks, but they almost inevitably lead to the kind of overexpansion of fishing capacity that causes many of the problems in the North Sea. As Clark[20] summarizes it, "In practice, this process usually manifests iself in terms of a progressive shortening of the fishing season, with the entry of more and larger vessels, which become capable of capturing the annual quota in fewer and fewer days of fishing. When the regulation is by means of gear restriction, closed seasons, and the like, the resulting fleet expansion will tend to overcome the regulation, which will then have to be revised, initiating further expansion."

In short, any regulatory process that leads to fishermen competing for the catch may force individuals to act in ways contrary to the overall economic efficiency of the fishery.

A system that allocates quotas to individual vessels has the fundamental advantage of counteracting these competitive features. Clark notes that such allocated quotas are frequently used to manage other common-property resources, such as water supplies and grazing land[20]: "The owner of a quota knows that (barring unforeseen circumstances) he will be able to take his quota regardless of the activities of other users. On the other hand, he is prohibited from exceeding his quota. With this knowledge, it is then to his benefit to exploit his quota in the most economically efficient manner. The main incentives for wasteful expansion of fishing capacity and other inefficient activities are thus eliminated."

The quota certificates or licenses should, furthermore, be transferable. They would thus acquire a monetary value, keyed to fish prices and the costs of fishing, which would encourage efficiency and also would[20] "resolve the problem of permitting new entrants — although entry would of course be open only to those who could afford to buy up an existing quota license".

Clark[17] has also given a proof that taxes or royalties on catch or effort are formally equivalent to allocated quotas. In practice, however, this formal result should not be taken too literally; quotas by their nature provide a direct control over catches, and thence over stock density, whereas taxes act indirectly. Control of the total catch rate via taxes or royalties requires knowledge of the price of fish, the cost of fishing effort, and in general depends on the behavioural responses of fishermen, all of which are subject to serious imprecision and uncertainty.

For international fisheries, the allocated quota system may be extended by setting national quotas, which serve to divide fishing rights among the nations involved. Then each nation can apportion its quota, allocating fishing rights to individual fishermen or firms.

There remain, of course, many technical difficulties in the implementation of any scheme of allocated quotas. These include: the set of scientific problems noted above; problems in dealing with the intrinsic variability of many fish stocks; the management of multiple-purpose fishing fleets and multi-species catches; and the inevitable problems of enforcement. Further complexities enter when one gives explicit attention to the "concentration profile" characterizing the way a fish population is distributed in space or time[18]. Thus the economics and population dynamics of harvesting a stock that is uniformly distributed in the sea will differ from those for a stock that aggregates in a relatively few large schools; exploitation will always tend to follow the concentration profile, focusing first on the highest concentrations. Depending on the shape of the concentration profile, this can complicate the economics and management of the fishery.

In general, however, there appears to be a feeling[12] that the establishment of EEZs has provided a "finite opportunity — a window in time — in which the world community and the coastal states can work together to place these new national fisheries on a solid groundwork of management", and that the best available regulatory instrument is a system of transferable catch (or effort) quotas allocated to individual fishermen or vessels. □

---

1. Gulland, J. A. *Fish Population Dynamics*, (John Wiley, New York, 1977).
2. Doubleday, W. G. *Int. Comm. Northw. Atlant. Fish Sel. Pap.* **1**, 141 (1976).
3. May, R. M., Beddington, J. R., Horwood, J. W. & Shepherd, H. G. *Math. Biosci.* **42**, 219 (1978).
4. Shepherd, J. G., Horwood, H. W. *J. Cons Int. Explor. Mer* **38**, (1979).
5. Gulland, J. A. *J. Cons. Int. Explor. Mer* **38** 318 (1979).
6. Steele, J. H. (ed.) *Fisheries Ecology: Some Constraints That Impede Our Understanding.* (Natl. Acad. Sci., Washington, D. C., 1980).
7. Ghiselin, M. T. *The Triumph of the Darwinian Method* (Univ. Calif. Press, Berkeley, 1969).
8. Cushing, D. H. **Science and the Fisheries** (Edward Arnold, London, 1977).
9. Murphy, G. I. in Ref. 1, pp. 283-308 (1977)
10. May, R. M., Beddington, J. R., Holt, S. J., Laws, R. M. Clark, C. W. *Science* **205**, 267 (1979).
11. FAO *Fish. Tech. Pap.* **181** (1978).
12. FAO *Fisheries Report* **236** (1980).
13. Mathieu, G. in *Le Monde* section of *Manchester Guardian Weekly, Internl. Edn.* 7 Sept. 1980.
14. Hardin, G. *Science* **131** 1292 (1960).
15. Anderson, L. G. *The Economics of Fisheries Management* (Johns Hopkins Univ. Press, Baltimore, 1977).
16. Pearse, P. H. (ed.) *J. Fish. Aquat. Sci.* **37**, 1111 (1980).
17. Clark, C. W. *Can. J. Fish. Aquat. Sci.* **37**, 1111 (1980).
18. Clark, C. W. Inst. Appl. Math. Stat. Univ. B. C. Tech. Rept. **80** (1980).
19. Clark, C. W. *Mathematical Bioeconomics* (John Wiley, New York, 1976).
20. Clark, C. W. appendix 3 in Ref. 12, pp. 101-113 (1980).

Roles of RecA revealed

from Steve Sedgwick

AT first glance it seems improbable that a single protein can perform genetic recombination, regulate its own synthesis, and switch-on expression of several other operons. However it is now evident that the recA protein of *Escherichia coli* has all of these capabilities. Not surprisingly the activity and regulation of this protein are currently under intense scrutiny.

In a series of recent papers, groups led by C. M. Radding[1] and I. R. Lehman[2] have shown that purified recA protein will stimulate the formation of DNA structures resembling putative recombination intermediates. One such structure is the D-loop where a single DNA strand pairs with a complementary region in a locally denatured section of double stranded DNA. D-loops may represent an early stage in recombination where a single DNA strand invades a homologous duplex to initiate strand exchange. A series of partial reactions, all requiring recA, occur in D-loop formation. At low concentrations recA protein binds to single stranded DNA. At higher concentrations it binds to double stranded DNA using ATP as a cofactor. A three stranded complex then forms in which double stranded DNA is unwound. Finally ATP is hydrolysed and recA protein dissociates. If hydrolysis takes place at a region of homology between single and double stranded DNA a D-loop can form. Heterologous and homologous single strands stimulate unwinding, perhaps explaining how recA protein seeks for homology between DNA molecules. Unwinding occurs without topoisomerase (nicking-closing) activity and so requires a free DNA end or superhelical turns so that DNA strands can rotate around each other.

RecA protein will also join double stranded DNA circles to make figure-of-eight structures, provided that one of the circles has a single strand gap[3,4]. A joining reaction analagous to D-loop formation has been proposed where initial pairing occurs between an unwound section of duplex DNA and single stranded DNA in the gap of the second molecule[3]. Nevertheless, some uncertainty remains whether D-loop formation really reflects an event in recombination between duplex DNA. First, DNA crosslinking does not reduce the yield of figure of eight molecules even though it impairs strand separation and presumably, D-loop formation[4]. Second, binding of recA protein to gapped DNA is not restricted to single strand regions and extends into much of the double stranded portion of the molecule[5]. Howard-Flanders and colleagues suggest that duplex DNAs bound with recA protein can form four stranded synapsis structures[4].

Steve Sedgwick is in the Genetics Division, National Institute for Medical Research, Mill Hill, London.

0028-0836/80/430676-02$01.00

They refer to theoretical work showing that a helical arrangement of four DNA strands with four-square base pairing can be formed without strand breakage[6].

Indications that recA protein has a regulatory role, switching-on expression of its own and other genes, first came from observations on the physiological response of *E. coli* to DNA damaging treatments. It was found that the recA gene, and a second gene, lexA, were needed to induce synthesis of large amounts of recA protein and a variety of new physiological responses. The induced responses have been called SOS functions because some aid cellular recovery. Better known SOS functions are the induction of prophages to enter a cycle of lytic growth, induction of new DNA repair systems, induction of mutations, and induction of filamentous growth. Biochemically, λ induction is best understood and occurs by recA protein proteolytically cleaving the λ repressor protein[7]. The λ repressor is then unable to bind to λ operator sites and prevent transcription. It has been hypothesised that the recA gene, and genes for the other inducible processes, also have repressors sensitive to recA proteolysis.

Direct evidence for an array of operons regulated by recA and lexA has now been presented by Kenyon and Walker[8]. By using a specialized Mu-lac transducing phage developed by Casadaban and Cohen[9] they made random insertions of the *lac* structural gene into the *E. coli* chromosome. Bacteria were selected which became lactose positive after DNA damaging treatments. These bacteria presumably have a *lac* gene fused into a transcriptional unit whose expression is induced by DNA damaging treatments. So far five different loci have been identified where recA and lexA functions are needed for induction of gene expression. Surprisingly one of these loci appears to be the *uvr*A gene, a component of the exision repair process, long considered to be distinctly separate from recA and lexA pathways of repair.

Extensive genetic evidence indicates that expression of the recA gene is switched off by the product of the lexA gene, possibly acting as repressor. This is the regulatory state of a normal cell and provides a low basal level of recA protein sufficient to perform genetic recombination and recombinational DNA repair. Little *et al*[10] have shown that recA protein switches on expression of its own gene by inactivating the lexA protein. *In vitro* they found that lexA protein was proteolytically cleaved by purified recA protein in a reaction essentially identical to recA proteolysis of λ repressor. Lex A 3 mutants are unable to induce recA protein synthesis and have a lexA protein insensitive to proteolysis. It seems that recA protease activity is triggered by interaction with a signal molecule, possibly single stranded DNA or a short oligonucleotide, which accumulates in DNA damaged cells.

An additional twist to this story, described by Brent and Ptashne[11], is that lexA protein switches off transcription from the lexA promotor. Thus the lexA gene has negative autoregulation. Increased lexA protein levels also switch off expression of certain other genes such as those causing filamentous growth.

To summarise, evidence for the following control network is emerging. LexA protein represses expression of its own gene, the recA gene, and genes for some SOS functions. Other SOS functions are switched-off by their specific repressor molecules. DNA damage activates protease activity in the basal recA protein. RecA protease cleaves the lexA protein switching on expression of the recA gene and SOS genes under the direct control of lexA. Other SOS functions are derepressed by recA proteoysis of their specific repressors.

The structural basis of recA protease and recombinase activities has now begun to be examined. As a first step the amino acid sequence of the protein was determined from the nucleotide sequence of the recA gene, combined with partial sequencing of tryptic fragments[12]. The gene contains 1,059 coding bases specifying a 352 amino acid protein with a calculated molecular weight of 37,842. The nucleotide sequence contains several regions resembling 'vestigal' insertion sequences with characteristic direct repetition of 8-11 bases. An intriguing speculation is that the recA gene evolved through a process involving transposition. The amino acid sequence indicates the presence of central β sheet flanked by partially α helical segments. The amino terminus contains sequences of amino acids reminiscent of active sites of known serine proteases. It is worth noting that four recA mutations primarily affecting the induction of SOS functions were earlier mapped in this region[13]. The carboxy terminus of recA protein is rich in aromatic and basic amino acids believed to be important in DNA binding, and so might be concerned with recombination functions. A more detailed understanding of active site domains should come with the sequence analysis of different alleles of the recA gene. Finally, the announcement that recA protein has been crystallized and subjected to X-ray diffraction analysis promises an intimate dissection of this protein's structure in the near future[14]. □

1,2. For the latest in this series see Shibata, T., Das Gupta, C., Cunningham, R.P. & Radding, C.M. *Proc. natn. Acad. Sci. U.S.A.* **77**, 2606 (1980).
McEntee, K., Weinstock, G.M. & Lehman, I. *Proc. natn. Acad. Sci. U.S.A.* **77**, 857 (1980).
3. Cunningham, R.P., Das Gupta, C., Shibata, T. & Radding, C.M. *Cell* **20**, 223 (1980).
4. Cassuto, E., West, S.C., Mursalim, J., Conlon, S. & Howard-Flanders, P. *Proc. natn. Acad. Sci. U.S.A.* **77**, 3962 (1980)
5. West, S.C., Cassuto, E., Mursalim, J. & Howard-Flanders, P. *Proc, natn. Acad. Sci. U.S.A.* **77**, 2569 (1980).
6. Wilson, J.H. *Proc. natn. Acad. Sci. U.S.A.* **76**, 3641 (1979).
7. Roberts, J.W., Roberts, C.W. & Craig, N.L. *Proc. natn. Acad. Sci. U.S.A.* **75**, 4714 (1978).
8. Kenyon, C.J. & Walker, G.C. *Proc. natn. Acad. Sci. U.S.A.* **77**, 2819 (1980).
9. Casadaban, M.J. & Cohen, S.N. *Proc. natn. Acad. Sci. U.S.A.* **76**, 4530 (1979).
10. Little, J.W., Edmiston, S.H., Pacelli, L.Z. & Mount, D.W. *Proc. natn. Acad. Sci. U.S.A.* **77**, 3225 (1980).
11. Brent, R. & Ptashne, M. *Proc. natn. Acad. Sci. U.S.A.* **77**, 1932 (1980).
12. Sancar, A., Stachelek, C., Konisberg, W. & Rupp, D.W. *Proc. natn. Acad. Sci. U.S.A.* **77**, 2611 (1980).
13. Morland, P., Goze, A. & Devoret, R. *Molec. gen. Genet.* **157**, 69 (1977).
14. McKay, D.B., Steitz, T.A., Weber, I.T., West, S.C. & Howard-Flanders, P. *J. Biol. Chem.* **255**, 6662 (1980).

Charon's diameter

from David W. Hughes

OCCULTATION observations have been the mainstay technique for the measurement of planetary diameters for a considerable time now, and the discovery of such things as the Uranian satellite belt in 1977 and a binary asteroid in 1978 are obvious bonuses. The principle is simple. A planet passes in front of a distant star and blocks out the starlight for a specific time. Measurement of that time interval gives the angular size of the chord of the planetary disc in that direction. If this is done from a range of observatory positions on Earth the size and shape of the planetary disc perpendicular to the line of sight can be obtained. The method is technically quite difficult because it relies on extremely accurate knowledge of stellar and planetary positions and the use of highspeed photometers at the focal planes of large telescopes.

Whether or not an occultation of Charon, Pluto's satellite, would occur was difficult to predict. Gordon Taylor of the Royal Greenwhich Observatory reported that an occultation by Pluto or Charon of a 13th magnitude star in Virgo would possibly take place at about 0h on April 7, 1980. Subsequently it was predicted that Pluto would be about 1 arc sec away from the star and no occultation would be seen. Then it was noticed that Charon would be on the 'star side' of its orbit around Pluto and would be within about 0.2 arc sec of the track. As an error in the known position of Charon of ± 0.2 arc sec is quite possible Alistair R. Walker of the South African Astronomical Observatory decided to attempt the observation. His success is reported in a recent edition of *Monthly Notices of the Royal Astronomical Society*, **192**, 47P, 1980.

The occultation was monitored using a 100 cm telescope coupled to a pulse counting photometer which could operate at 1 ms per reading without difficulty. Twin

---

David W. Hughes in the Department of Physics, University of Sheffield.

0028-0836/80/430677-02$01.0(

channels were used, one looking at the star which was to be occulted, the other at a nearby reference star. The data was taken using an integration time of 2 sec. Sky conditions were excellent and the occultation took place at 23h 39m 28s on April 6, 1980 and lasted for 50 seconds. This duration corresponded to 0.055 arc sec or 1,200 km at the distance of Charon. Unfortunately, no other observations were made in the southern hemisphere (no occultation was observed from England) so the chord length of 1,200 km must simply be taken as a minimum value for the diameter.

Another clue to the size of Charon lies in the fact that it is 1.7±0.1 magnitudes fainter than Pluto. Unfortunately, the magnitude, which is a direct measure of the brightness, depends not only on the illuminated surface area but also on the reflectivity. There is no specific reason why the reflectivity of Pluto and Charon should be the same. Other satellites are not noted for having similar reflectivities to their planets.

The dominant constituent of the surface of Pluto is methane ice. By assuming that Charon has a similar covering and that its density is greater than 0.35 g cm^{-3} Walker concludes that its diameter lies in the range 1,350 to 1,800 km.

Pluto and Charon thus seem to form a 'double planet' with probable diameters of 3,600 and 1,650 km respectively. The mass ratio is about 10:1, an extremely low value for the ratio between the mass of a planet and its primary satellite. Whether this is significant or not is a matter for future conjecture but it does bring to mind a point stressed by R.A. Lyttleton (*Mon. Not. R. astr. Soc.*, **121**, 551; 1960) when discussing the origin of the solar system. The fissional break up of a rotating protoplanet results, according to Lyttleton, in two main fragments with equal densities, the mass ratio of these portions being at least 8:1, but not greatly more than this. Unfortunately, Lyttleton points out that the two fragments separate at more than the escape velocity and cannot remain gravitationally bound to each other. So the origin of the Pluto–Charon double planet is still a mystery. □

Opioid peptides: search for the precursors

from Michael J. Brownstein

In 1975 Hughes and his colleagues unraveled the structures of two opioid peptides — methionine-enkephalin and leucine-enkephalin — that they had isolated from brain extracts[1]. They pointed out that the amino acid sequence of methionine-enkephalin was contained within another larger peptide, β-lipotropin[2], and they suggested that the latter might be a methionine-enkephalin precursor. It is known that β lipotropin does give rise to at least one family of opioid peptides, the endorphins, but, although methionine enkephalin can be enzymatically liberated from the largest of the endorphins (β-endorphin), recent evidence suggests that both methionine- and leucine-enkephalin are produced by a quite different route.

Methionine-enkephalin and β-endorphin are found in separate populations of cells both in the central nervous system and the periphery. For example, β-endorphin, but not methionine-enkephalin, is found in high concentrations in the intermediate and anterior lobes of the pituitary where it is synthesized as part of a 31,000 molecular weight protein ('pro-opiocortin') that also gives rise to adrenocorticotropic hormone and α-melanocyte-stimulating hormone[5]. Again, very high levels of methionine-enkephalin and leucine-enkephalin, but not β-endorphin, are present in chromaffin cells of the adrenal medulla[6]. Finally, it is quite clear that leucine-enkephalin must be synthesized separately from β-endorphin because its amino acid sequence is not present in pro-opiocortin[7].

Table I. Opioid Peptides

Trivial Name	*Source*	*Structure*	*Ref.*
Methionine-Enkephalin Related Peptides			
Methionine-enkepahlin	pig brain	H-Tyr-Gly-Gly-Phe-Met-OH	1
Pro-methionine enkephalin	Pig hypothalamus, human adrenal medullary tumor	H-Tyr-Gly-Gly-Phe-Met-Arg-OH	12
—	bovine adrenal medulla bovine striatum	H-Tyr-Gly-Gly-Phe-Met-Arg-Phe-OH	9
Molluscan cardioexcitatory neuropeptide (FMRFamide)	clam ganglia	$H\text{-}Phe\text{-}Met\text{-}Arg\text{-}Phe\text{-}NH_2$	8
—	trypsinization of bovine adrenal medullary proteins	H-Tyr-Gly-Gly-Phe-Met-Lys-OH	10,11
—	trypsinization of bovine adrenal medulary proteins	H-Tyr-Gly-Gly-Phe-Met-Arg-Arg-OH	10,11
β-endorphin	camel pituitary	H-Tyr-Gly-Gly-Phe-Met-Thr-Ser-Glu-Lys-Ser-Gln-Thr-Pro-Leu-Val-Thr-Leu-Phe-Lys-Asn-Ala-Ile-Ile-Lys-Asn-Ala-His-Lys-Lys-Gly-Gln-OH	3
Leucine-Enkephalin Related Peptides			
Leucine-enkephalin	pig brain	H-Tyr-Gly-Gly-Phe-Leu-OH	1
α-neo-endorphin	pig hypothalamus	H-Tyr-Gly-Gly-Phe-Leu-Arg-Lys-Arg-Pro-$(Gly_1\ Tyr_2\ Lys_2\ Arg_1)$	15
Dynorphin-(1-13)	pig pituitary	H-Tyr-Gly-Gly-Phe-Leu-Arg-Arg-Ile-Arg-Pro-Lys-Leu-Lys-OH	16

In the years since the enkephalins were first described a number of peptides with opioid activity have been discovered. Most of these contain either the methionine-enkephalin sequence (H-Tyr-Gly-Gly-Phe-Met-OH) or the leucine-enkephalin sequence (H-Tyr-Gly-Gly-Phe-Leu-OH).

As shown in the table some of the unique enkephalin-related molecules are generated by incubating adrenal proteins in the presence of trypsin[10,11]. These include H-Tyr-Gly-Gly-Phe-Met-Lys-OH and H-Tyr-Gly-Gly-Phe-Met-Arg-Arg-OH. In addition, methionine-enkephalin, leucine-enkephalin, H-Tyr-Gly-Gly-Phe-Met-Arg-OH[12], and H-Tyr-Gly-Gly-Phe-Met-Arg-Phe-OH[9], are found in tryptic digests of adrenal medullary proteins. The larger molecules that give rise to the above peptide species are being isolated and analyzed. In the bovine adrenal two possible precursors with molecular weights of 3,000 to 5,000 have been already described[13] and are shown in Table 2.

Note that trypsin, which cleaves on the carboxy terminal side of basic amino acid residues, would liberate a single leucine-enkephalin molecule from the upper peptide and a single methionine-enkephalin molecule from the lower one. Trypsin would also release H-Tyr-Gly-Gly-Phe-Met-Arg-OH and H-Tyr-Gly-Gly-Phe-Met-Lys-OH from the upper and lower peptides respectively and methionine-enkephalin could be made from either of these molecules by removing

---

Michael J. Brownstein is in the National Institutes of Health, Bethesda, Maryland.

0028-0836/80/430678-02$01.00

the arginine or lysine by a carboxypeptidase B-like 'trimming enzyme'.

In human adrenal tumours there are two 2,000 molecular weight peptides that yield methionine-enkephalin when they are treated with trypsin and carboxypeptidase B (see ref. 11). The relationship of these two peptides to one another and to the 3,000-5,000 molecular weight bovine adrenal peptides described above is uncertain. It is clear, however, that 2,000 to 5,000 molecular weight human and bovine peptides are too small to be translation products themselves. They are more likely to be parts of a larger molecule; and, in fact, 8,000 to 50,000 molecular weight molecules have been detected in the brain and adrenal that either bind directly to opiate receptors or enkephalin antibodies or do so after treatment with trypsin[10,13,14].

Table 2: Two precursor molecules from the bovine adrenal gland which could give rise to enkephalins.

$\text{H-}\overset{1}{\text{Ser}}\sim\overset{\text{Lys}}{\text{Arg}}\text{-Tyr-Gly-Gly-Phe-Met-Arg}\sim\overset{\text{Lys}}{\text{Arg}}\text{-Tyr-Gly-Gly-Phe-}\overset{39}{\text{Leu}}\text{-OH}$

$\text{H-}\overset{1}{\text{Tyr}}\text{-Gly-Gly-Phe-Met-Lys}\sim\overset{\text{Lys}}{\text{Arg}}\text{-Tyr-Gly-Gly-Phe-}\overset{33}{\text{Met}}\text{-OH.}$

Recently, Lewis and his coworkers have isolated a 50,000 molecular weight protein from adrenal medulla that they think is an enkephalin precursor able to produce both methionine-enkephalin and leucine-enkephalin. The molecule contains methionine-and leucine-enkephalin sequences in a ratio of about 7 to 1, and could also contain α-neoendorphin[15] or dynorphin[16] (see Table 2), but (assuming that there is only one mole of leucine-enkephalin per mole of precursor) not both of them. It is also possible, of course, that α-neoendorphin, dynorphin, and methionine/leucine-enkephalin are all made in separate groups of cells and that there are precursors distinct from the postulated methionine/leucine-enkepahlin precursor. This could account for the report that there are separate leucine-enkephalin and methionine-enkephalin containing cell populations in the brain[17].

To establish a precursor-product relationship between the 'big' enkephalins that have been discovered and the small forms, pulse labeling studies will have to be undertaken. Workers in a number of laboratories have shown that radiolabeled amino acids can be incorporated into methionine-and leucine-enkephalin *in vivo* by the rat brain[18], and *in vitro* by striata slices[19], dissociated spinal cord cells[20], myenteric plexus explants[21], and adrenal medullary chromaffin cells[22,23]. In addition, Rossier and his colleagues[23] have shown that a 22,000 molecular weight methionine-enkephalin containing protein is synthesized in advance of methionine-enkephalin and may give rise to it. Much more work needs to be done to characterize the enkephalin precursor(s) and to show how they are metabolized into active peptides. The regulation of this process also needs to be studied in detail[22].

When the biochemistry, anatomy, and pharmacology of the various opioid peptides are better understood, the reason for their diversity may be more obvious. □

1. Hughes, J., Smith, T.W., Kosterlitz, H.W., Fothergill, L.A., Morgan, B.A. & Morris, H.R. *Nature* **258**, 577 (1975).
2. Li, C.H., Barnafi, L., Chrétien, M. & Chung, D. *Nature* **208**, 1093 (1965).
3. Li, C.H. & Chung, D. *Proc. natn. Acad. Sci. U.S.A.* **73**, 1145 (1976).
4. Austen, B.M., Smyth, D.G. & Snell, C.R. *Nature* **269**, 619 (1977); Knight, M. & Klee, W. *J. Biol. Chem.* **254**, 10426 (1979); Koida, M., Aono, J., Takenago, K., Yoskimoto, T., Kimura, T. & Sakakibara, S. *J. Neurochem.* **33**, 1233 (1979).
5. Mains, R.E., Eipper, B.A. & Ling, N. *Proc. natn. Acad. Sci. U.S.A.* **74**, 3014 (1977).
6. Schultzberg, M., Lundberg, J.M., Hökfelt, T., Terenius, L., Brandt, J., Elde, R.P. & Goldstein, M. *Neurosci.* **3**, 1169 (1978); Viveros, O.H., Diliberto, E.J., Jr., Hazum, E., & Chang, K.-J. *Mol. Pharmacol.* **16**, 1101 (1979); Yang, H.-Y.T., Costa, E., Diguilio, A.M., Fratta, W. & Hong, J.S. *Fed. Proc.* **38**, 364 (1979).
7. Nakanishi, S., Inoue, A., Kita, T., Nakamura, M., Chang, A.C.V., Cohen, S. & Numa, S. *Nature* **278**, 423 (1979).
8. Price, D.A. & Greenberg, M.J. *Science* **197**, 670 (1977).
9. Stern, A.S., Lewis, R.V., Kimura, S., Rossier, J., Gerber, L.D., Brink, L., Stein, S. & Udenfriend, S. *Proc. natn. Acad. Sci. U.S.A.* **76**, 6680 (1979).
10. Lewis, R.V., Stern, A.S., Kimura, S., Rossier, J., Stein, S. & Udenfriend, S. *Science* **208**, 1459 (1980).
11. Clement-Jones, V., Corder, R. & Lowry, P.J. *Biochem. Biophys. Res. Comm.* in the press.
12. Huang, W.Y., Chang, R.C.C., Kastin, A.J., Coy, D.H. & Schally, A.V. *Proc. natn. Acad. Sci. U.S.A.* **76**, 6177 (1979).
13. Kimura, S., Lewis, R.V., Stern, A.S., Rossier, J., Stein, S. & Undenfried, S. *Proc. natn. Acad. Sci. U.S.A.* **77**, 1681 (1980).
14. Childers, S.R. & Snyder, S.H. in *Central Nervous System Effects of Hypothalamic Hormones and other Peptides (eds. Collu et al.)* 253-260 (Raven, New York, 1979); Yang, H.-Y.T., DiGuilio, A.M., Fratta, W., Hong, J.S., Majane, E.A. & Costa, E. *Neuropharmacol.* **19**, 209 (1980); Yang, H.-Y.T., Fratta, W., Hong, J.S., Diguilio, A.M. & Costa, E. *Neuropharmacol.* **17**, 433 (1978); Lewis, R.V., Stein, S., Gerber, L.D., Rubenstein, M. & Udenfried, S. *Proc. natn. Acad. Sci. U.S.A.* **75**, 4021 (1978).
15. Kanagawa, K., Matsuo, H. & Igarashi, M. *Biochem. Biophys. Res. Comm.* **86**, 153 (1979).
16. Goldstein, A., Tachibana, S., Lowrey, L.I., Hunkapiller, M. & Hood, L. *proc. natn. Acad. Sci. U.S.A.* **76**, 6666 (1979).
17. Larsson, L.-I., Childers, S. & Snyder, S.H. *Nature* **282**, 407 (1979).
18. Clouet, D.H. & Ratner, M. in *Opiates and Endogenous Opioid Peptides* (ed. Kosterlitz, H.W.) 71-18 (Elsevier, Amsterdam, 1976); Yang, H.-Y.T., Hong, J.S., Fratta, W. & Costa, E. *Adv. Biochem. Psychopharmacol.* **18**, 149 (1978).
19. Hughes, J., Kosterlitz, H.W. & McKnight, A.T. *Br. J. Pharmacol.* **63**, 396P (1978).
20. Neale, J.H., McKelvy, J.F. & Barker, J.L. *Neuropeptides* in the press.
21. Sosa, R.P., McKnight, A.T., Hughes, J. & Kosterlitz, H.W. *FEBS Lett.* **84**, 195 (1977).
22. Wilson, S.P., Chang, K.-J. & Viveros, O.H. *Proc. natn. Acad. Sci. U.S.A.* **77**, 4364 (1980).
23. Rossier, J., Trifaro, J., Lewis, R.V., Lee, R.W.H. Stern, A., Kimura, S., Stein, S. & Udenfriend, S. *Proc. natn. Acad. Sci. U.S.A.* in the press.

Big eyes

from M.J. Disney

HISTORY shows that in astronomy, scientific advance rides on the back of technical progress. The last major step forward in optical telescope design was conceived in 1928 and completed in 1950 with the commissioning of the Hale 5-metre telescope on Palomar Mountain. Since then the emphasis has been on light detectors, which have improved 100 fold in sensitivity and which now respond to about 50 percent of the light collected. The scope for further significant improvement is therefore limited, for which reason interest has again turned to attempts to increase collecting areas. To that end a large workshop was held earlier this year at Kitt Peak National Observatory in Arizona.

Astronomers rely on optical spectroscopy to determine the redshift, distance, composition, luminosity, rotation-speed and temperature of sources. The spectral resolutions needed to supply these data require a light gathering capacity hundreds of times greater than that sufficient to merely detect the objects. To obtain detailed information from the clouds of faint galaxies that we can already see an ambitious increase in telescope size will be required. Many conference participants felt that a collecting area equivalent to a single 25 metre diameter mirror was a reasonable goal at which to aim.

Ideally, such a massive optical telescope should be placed in space where, free of atmospheric seeing problems, it would reach its diffraction limited performance. The 2.5-metre Space Telescope to be launched in 1983 will provide increased spatial resolution but its light gathering power may still not be sufficient for spectroscopic analysis of extended objects like galaxies. As the Space Telescope will cost 500 million dollars the launch of an even larger telescope seems out of the question.

The costs for conventional ground based instruments seems to increase approximately as the 2.6 power of diameter, so that more than 2 billion dollars would be needed for a 25 metre conventional telescope. However, technological developments, particularly

M.J. Disney is Professor of Astronomy at University College, Cardiff.

---

*The conference proceedings *Optical and Infra-red Telescopes for the 1990's*, will be published in 2 vols. by Kitt Peak National Observatory, ed. Hewitt.

0028-0836/80/430679-02$01.00

thin mirror construction, polishing of fast (that is highly curved) primaries, computer aided design and control, and the alt-azimuth concept with its favourable affects on dome size, will enormously decrease the costs of future telescopes per metre of aperture. A 2-metre for less than $2.5m complete is now a certainty and proposals for a 14-metre at the price of a conventional 4-metre are being discussed in detail.

With falling costs, single institutions may be able to contemplate a big telescope for themselves. The University of Texas is considering a thin mirror (20 cm) 7-metre monolith for less than 25 million dollars; the University of California, a segmented 10-metre mirror for somewhat more. Domes can prove expensive items in the budget: at 2 million dollars the rotating asymetric dome of the 3.6-metre equivalent Multi-Mirror Telescope, now in use on Mt Hopkins, is probably a realistic pointer towards the future.

The high cost of the conventional telescope springs largely from the mass needed to maintain optical rigidity. Very large telescopes must depart from this philosophy and rely instead on the active interrelation of light thin structures. The reflecting area will either be segmented or divided into a number of separate mirrors aimed at a common focus: lasers may be used for active alignment of the components (a scheme already being tested on the Multi-Mirror Telescope) although simpler, computer-based, electromagnetic linkages between segments now look quite adequate.

The dome costs, which are considerable, rise at something like the cube of the telescope length, so there is much more pressure to construct primary mirrors as fast as F/1.75 instead of the customary F/3. Such a trend will also help to shrink the starfield onto miniature modern detectors such as CCD's, but useful angular field of view will then also shrink due to aberrations. While opticians are now confident they can devise these fast mirrors using computer-controlled polishing machines, astronomers are uneasy at the loss in field of view. It is true that big telescopes are largely used for on-axis spectroscopy, in which field-size is unimportant. However, at the conference J.R.P. Angell (Steward Observatory) demonstrated the dramatic changes we can expect from optical-fibre techniques. He used fibres for the simultaneous conduction of light from 16 widely spaced cluster galaxies down the slit of his spectrograph; thus once again highlighting the usefulness of a wide field. The battle between the big-fielders and little-fielders has scarcely begun.

The alternative to a single large instrument of revolutionary design is an array of smaller ones, adding either their light or their post-detector signal. The problems of long horizontal light beams and multiple reflections probably make a light adding design suitable only for interferometry. Any array of small instruments must reduce unit costs to the point where a very large area can be operated at a reasonable price. To reach the goal of 25 m for around $150m the choice is either a fully instrumented 2-metre unit at $1m, or a 4-metre at $4m. The Kitt Peak proposal for an Advanced Technology Telescope of 2 metre size incorporates fast thin-mirror automatic setting and guiding for a projected cost around $1.7m. How far 'mass' production could bring this down further is still uncertain. In France, A. Labeyrie (CERGA, Grasse) is operating the first of his concrete, onion-shaped 1.5-metres, which, due to their weight do not need a dome and can cost a mere $120,000 per square metre of collecting area.

With infra-red astronomy making great strides it will obviously be sensible if infra-red and optical astronomers can contrive to share telescopes. There was much debate on this issue, but with no clear result, mainly because infra-red astronomers see the need for at least two different kinds of instrument. There seems to be no doubt that the diameter of the image is disturbed by atmospheric 'seeing' as a function of wavelength, following a $\lambda^{-1/5}$ law as predicted by the theory of homogenous turbulence. Given a telescope of sufficient diameter to be diffraction limited, the atmosphere will allow 0.5 arc second seeing at 10 microns.

This, combined with the long awaited infra-red imaging CCD's, calls for a single aperture telescope of 10-metres or more, whose structure does not radiate significantly into the beam. On the other hand, C. Townes (Bell Laboratories) and F. Low (University of Arizona) have demonstrated phase coherence at the same wavelengths for periods of up to an hour and want coherent arrays of smaller telescopes. It would seem that infra-red astronomy will now develop along the lines of radio astronomy with a request for both phased arrays and big single dishes.

The issues and questions raised by the conference come at an appropriate time. It does now seem likely that a 25-metre equivalent mirror can be built in any one of a variety of ingenious ways. It remains to be seen which is best and cheapest but astronomers will need to unite behind a single proposal before they approach governments for a sum that is likely to be nearer two than one hundred million dollars.

NATURE

100 years ago

ON THE SKIN-FURROWS OF THE HAND

A large number of prints have been taken by me from the fingers of people in Japan, and I am at present collecting others from different nationalities.

My method of observation was at first simply to examine fingers closely, to sketch the general trend of the curves as accurately as possible, recording nationality, sex, colour of eyes and hair, and securing a specimen of the latter. I passed from this to "nature-printing," as ferns are often copied.

A common slate or smooth board of any kind, or a sheet of tin, spread over very thinly and evenly with printer's ink, is all that is required. The parts of which impressions are desired are pressed down steadily and softly, and then are transferred to slightly damp paper. I have succeeed in making very delicate impressions on glass. They are somewhat faint indeed, but would be useful for demonstrations, as details are very well shown, even down to the minute pores. By using different colours of ink useful comparisons could be made of two patterns by superposition. These might be shown by magic lantern. I have had prepared a number of outline hands with blank forms for entering such particulars of each case as many be wanted, and attach a specimen of hair for microscopic examination. Each finger-tip may best be done singly, and people are uncommonly willing to submit to the process. A little *hot* water and soap remove the ink.

When bloody finger-marks or impressions on clay, glass, &c., exist, they may lead to the scientific indentification of criminals. Already I have had experience in two such cases, and found useful evidence from these marks. In one case greasy finger-marks revealed who had been drinking some rectified spirit. The pattern was unique, and fortunately I had previously obtained a copy of it. They agreed with microscopic fidelity. In another case sooty finger-marks of a person climbing a white wall were of great use as negative evidence. Other cases might occur in medico-legal investigations, as when the hands only of some mutilated victim were found. If previously known they would be much more precise in value than the standard *mole* of the penny novelists.

I have heard, since coming to these general conclusions by original and patient experiment, that the Chinese criminals from early times have been made to give the impressions of their fingers, just as we make ours yield their photographs. I have not yet, however, succeeded in getting any precise or authenticated facts on that point. That the Egyptians caused their criminals to seal their confessions with their thumb-nails, just as the Japanese do now, a recent discovery proves. This is however quite a different matter, and it is curious to observe that in our country servant-girls used to stamp their sealed letters in the same way. There can be no doubt as to be advantage of having, besides their photographs, a nature-copy of the for-ever-unchangeable finger-furrows of important criminals. It need not surprise us to find that the Chinese have been before us in this as in other matters. I shall be glad to find that it is really so, as it would only serve to confirm the utility of the method, and the facts which may thus have been accumulated would be a rich anthropological mine for patient observers.

HENRY FAULDS

Tsukiji Hospital, Tokio, Japan
From *Nature* **22**, 28 October, 605, 1880.

0028-0836/80/430680-02$01.00

REVIEW ARTICLE

Compound eyes: old and new optical mechanisms

M. F. Land

School of Biological Sciences, The University of Sussex, Brighton BN1 9QG, UK

Over the last twenty years classical views of how compound eyes work optically have undergone a series of overhauls. Exner's central concept of an optically inhomogeneous lens cylinder has survived, and such devices are now made commercially. He was wrong, however, about some crustacean eyes. They produce images by a mirror mechanism that was not discovered until 1975, and which now shows promise as an optical system capable of development.

IN 1891 Sigmund Exner produced a monograph[1] on the optical mechanisms of insect and crustacean eyes that was a landmark not only in biology, but also in optical theory. The problem at that time was that image formation in many animals with compound eyes was not comprehensible in terms of conventional spherical surface refraction, as in a simple lens. This is particularly true of aquatic insects and crustaceans, where there is only a negligible refractive index difference between external and internal media so that ray-bending by a curved cornea is minimal, and also in those eyes whose corneal surfaces are flat anyway—some mantids, for example[2]. Exner's solution was ingenious and unconventional. He proposed that the optical elements of many compound eyes behaved as 'lens cylinders', that is, cylinders with a graded refractive index, densest along the axis and declining in an approximately parabolic manner towards the outside. Such structures have the property that a non-axial ray, striking the end of the cylinder normally, will be refracted continuously towards the axis (Fig. 1*d*, *e*). In fact, if the gradient is right, all parallel rays will be refracted to the same point on the axis, and parallel rays at an angle to the axis will be focused in the same plane, but slightly to one side. In other words, an inhomogeneous flat-ended cylinder would behave very much like an ordinary converging lens in its image-forming properties.

Inhomogeneous lenses were not an entirely revolutionary proposal, even in Exner's day. Matthiessen[3] had already proposed that the lenses of fish eyes had a variable refractive index, highest in the centre. He used this to explain why fish lenses had a much shorter focal length than a homogeneous lens with the same central refractive index (this would be about 4 radii, whereas real lenses have a focal length of about 2.55 radii, a figure that has come to be known as Matthiessen's ratio). It also

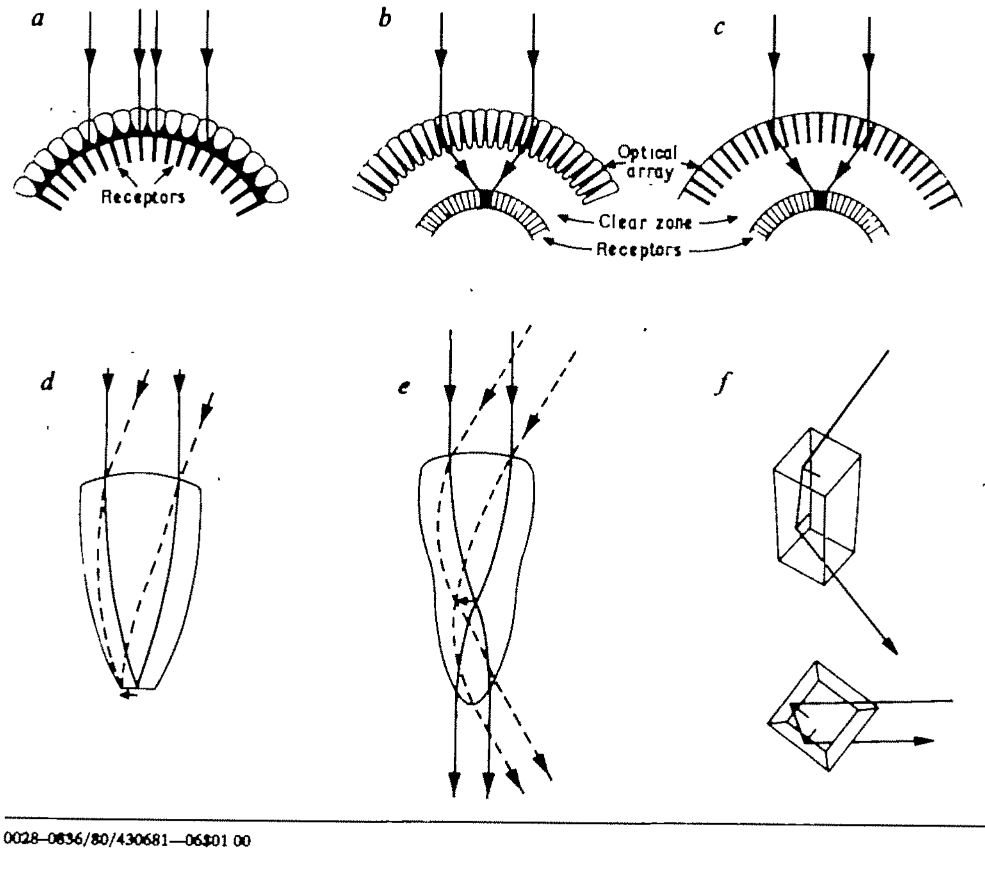

Fig. 1 Compound eye types and their optical components. *a*, Apposition eye; *b*, refracting superposition eye; *c*, reflecting superposition eye; *d*, apposition lens cylinder with focus at proximal tip; *e*, superposition (double length) lens cylinder; *f*, perspective and top view of ray path through a square cell in a reflecting superposition eye. *b*, *d*, *e* are based on Exner[1]; *c* is modified from Land[34], *f* from Vogt[37].

0028–0836/80/430681—06$01 00

explained why fish lenses are free of spherical aberration, which would otherwise be severe. Speculation about the properties of optically inhomogeneous media goes back to Maxwell[4], who "stimulated apparently by the contemplation of his breakfast herring" (ref. 5), devised a fish-eye universe with the alarming property that all rays emitted from a particular point returned to it, after passing through a conjugate image[4–6].

Much of Exner's work was based on two animals which he chose for their differences and experimental convenience. They are the king crab (Xiphosura) *Limulus*, and the glowworm *Lampyris*.

Limulus

Limulus has a smooth cornea behind which is a series of ingrowths of the cuticle (Fig. 2*a*), each of which abuts onto a cluster of receptors. Exner found that there was an inverted image at the tip of each such ingrowth (Fig. 2*c*), and because of the smooth cornea concluded that this had to be produced by lens-cylinder focusing. In one particularly telling experiment he cut a parallel-sided slice through one of these structures, and showed that this still acted as a converging lens, though of longer focal length. Exner's lens-cylinder explanation of *Limulus* optics was challenged recently by Levi-Setti *et al.*[7], who suggested that focusing might occur not by inhomogeneous refraction, but by reflection from the walls of each projection. They pointed out that the shape of the projections resembled that of an 'ideal collector', a reflecting device originally designed by Winston[8] for the collection of faint radiation. However, such devices produce erect, not inverted images, and furthermore, the refractive index gradient in the *Limulus* cornea, measured by interference microscopy (Fig. 2*b*), is precisely that required for lens-cylinder optics[9], so that Exner's mechanism survived the challenge.

Superposition images

Limulus has an apposition eye, that is, one in which each receptor cluster has its own private optics, and receives an image from a small solid angle of external space (Fig. 1*a*). Many nocturnal insects and crustaceans have eyes with a similar superficial appearance, but a quite different optical structure (Fig. 1*b*), known as superposition eyes. They are characterized anatomically by a wide zone of clear material between the superficial optics and the receptor layer, which usually forms a hemisphere with a radius of curvature about half that of the eye itself[10,11]. One group of insects with eyes of this kind are the glowworms and fireflies (Lampyridae) and these have the useful feature that the optical elements are physically part of the cornea, so that by simply cleaning out the interior of the eye the optics of the whole array can be studied. Exner did this, and found that instead of a series of inverted images at the cone tips there was just one erect image. This image was formed by the array as a whole and lay relatively deep, in approximately the position occupied by the retina. I have repeated Exner's observation (Fig. 3), as have others[12,13]. Unfortunately, it is not easy to see an image in most insect eyes with 'clear-zones', moths for example, because the optical elements (or crystalline cones) are separate from the cornea and the array does not survive the abuse of cleaning. In choosing *Lampyris*, and for that matter *Limulus*, Exner clearly knew what he was doing.

The explanation Exner gave for superposition image formation is shown in Fig. 1*b* and *e*. Essentially, parallel light entering many facets superimposes in the image region, and because the whole system is spherically symmetrical the overall result is an erect image. For superposition to occur it is clear that each optical element must behave as an inverter—a telescope with an overall magnification of −1. Parallel rays entering each element are redirected in such a way that the emergent beam makes the same angle with the element's axis as the entering beam, but, unlike the situation in a simple lens, the emergent beam lies on the same rather than the opposite side of the axis (Figs 1*e* and 3*b*, *c*).

There are two ways in which such a device could be made: as a conventional telescope made from two curved surfaces, with a focus in the middle, or from a pair of lens cylinders like those in *Limulus* but placed end to end. The former alternative is possible in theory[1] but in insects the refractive indices are too low and the curvatures inadequate for this to be the correct interpretation. Exner chose the double-length lens-cylinder explanation for *Lampyris*. Rays are brought to a focus by the first half of the element, then unfocused and inverted by the second half. The correctness of this interpretation has now been verified for fireflies[14], some other beetles[15], moths[16], skipper butterflies[17] and euphausiid crustaceans[18], in each case by examining sectioned crystalline cones using interference microscopy and confirming the existence of an appropriate refractive index gradient (Fig. 4).

Exner did, however, make one serious mistake. He generalized his mechanism to all eyes with a similar structure. Figure 1*b* admits of one other explanation and that is that the optical elements are simply plane mirrors (Fig. 1*c*). I shall return to this later.

Man-made lens cylinders

Commercial interest in inhomogeneous cylindrical lenses did not begin until the late 1960s, and the thrust was not to produce devices with compound eye-like properties, but to make optical fibres that transmitted images, as opposed to simply transmitting intensity. It is clear that an extended lens cylinder will keep imaging and re-imaging an object placed against its end at regular intervals along its length (Fig. 3*d*), and this ability could potentially be used to convey at least as much information per unit cross-sectional area as the alternative; this would be an expensive coherent light-guide array. The exact refractive index gradient that an image-transmitting lens cylinder should have was worked out in the mid-1950s by Fletcher, Murphy and Young[19] who, incidentally, also derived the refractive index gradient for a Matthiessen fish lens. They give the following relationship between distance between foci ($2F$), axial refractive index (n_0) and refractive index (n_r) at a radial distance (r) from the axis

$$n_r = n_0 \operatorname{sech}(\pi r/2F)$$

This expression can be expanded[20] to give

$$n_r = n_0\left(1 - \tfrac{1}{2}a^2r^2 + \tfrac{5}{24}a^4r^4 - \tfrac{61}{720}a^6r^6 + \cdots + \frac{En}{(2n)!}(ar)^{2n} \cdots\right)$$

where $a = \pi/2F$, and En are the Euler numbers. If one ignores all terms beyond the r^2 term, the refractive index gradient

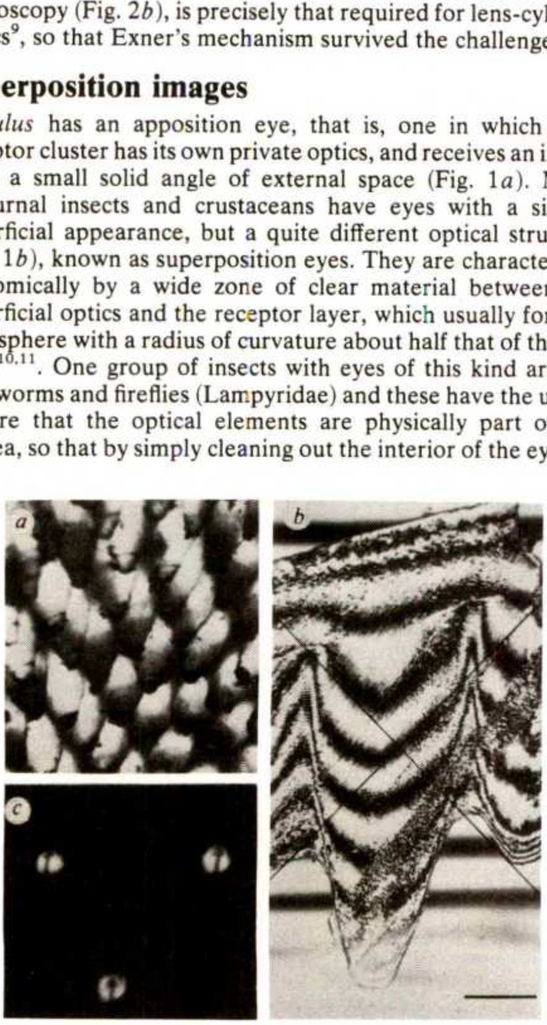

Fig. 2 Eye of *Limulus*. *a*, Crystalline cones projecting inwards from cornea. *b*, Interference micrograph of thin section of a cone. The fringe distortion is proportional to the local refractive index. Scale bar 100 μm. *c*, Inverted images of an arrowhead at the tips of the crystalline cones. (From Land[9].)

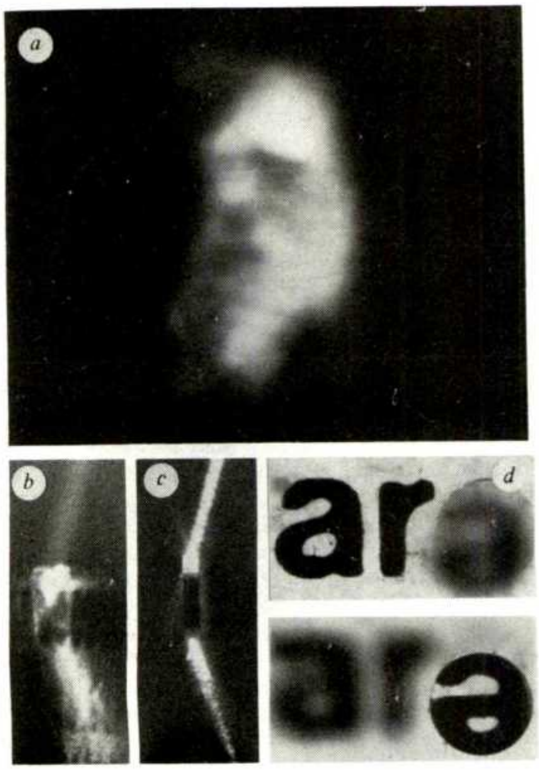

Fig. 3 Optics of refracting superposition eyes. *a*, Julia Cameron's portrait of Charles Darwin rephotographed through the cleaned cornea of a firefly. The eye was suspended in a hanging drop of water with the cornea in air. The image is erect, and the face is about 0.1 mm across. *b*, Bending of a light beam by a natural double length lens cylinder, a crystalline cone from a euphausiid crustacean. The beam is made visible with fluorescein and is 30 μm wide (from ref. 45). *c*, Light beam bent in a similar manner by a man-made SELFOC glass lens cylinder. Compare with the light paths in Fig. 1*b* and *e*. *d*, Lens cylinders also have the property of imaging an object at intervals of $2F$ (see text). The photograph shows the word 'are' with the same SELFOC as in *c* placed over the 'e'. The 'e' is re-imaged, inverted, at the upper end of the lens cylinder.

becomes a parabola, and it was this parabolic approximation that Exner's brother, Karl[21], derived in connection with biological lens cylinders (Fig. 4). Attempts to manufacture lens cylinders have also been made using diffusion processes which give rise naturally to parabolic gradients. In the 1960s attempts were made to use gas mixtures to produce lenses and waveguides[22]. Then in 1968 a glass lens cylinder (SELFOC) was produced and patented in Japan. It was made by heating a thallium-rich flint glass in a molten salt (KNO_3, at 500 °C) which leached out and replaced the heavy metal ions from the outside, thereby reducing the refractive index from 1.542 in the centre to 1.517 at the periphery[23,24].

More recently, plastic lens cylinders have been made by heating a high refractive index rod of soft polymerized plastic (diallyl isophthalate, $n = 1.57$) in a bath containing the monomer of a low index plastic (methylmethacrylate, $n = 1.49$)[25,26]. This gives a usable refractive index range that is similar to that of the glass lenses.

The future of man-made lens cylinders is unclear. They have good imaging properties over short distances—through one or two serial images (Fig. 3*d*)—but then aberrations of various kinds tend to degrade the image. The higher-order terms in the expansion for n, begin to become important, as does the fact that non-paraxial rays require a somewhat different index gradient from paraxial rays[20]. Chromatic aberration also accumulates, although this can be offset to some degree by a suitable choice of materials[26]. Given these problems, as well as those of manufacture, it is likely that aligned fibre bundles offer better prospects for long-distance image transmission than focusing lens cylinders. There should, however, be many other applications for versatile lens-like systems of very small dimensions.

Problems, and the light-guide heresy

During the 1960s, when commercial lens cylinders were at last being developed, their biological counterparts almost suffered extinction, as the following quotations show. Of lens cylinders: "It seems very doubtful if 'lens cylinder' properties will ever be found in a compound eye and therefore it would probably be better to discard the idea." (ref. 12). And of superposition optics: "There is no reason to suppose that this is true for any compound eye, and there are several reasons, given above, why the superposition image of the firefly is no more than an artifact of the cleaned retina." (ref. 27).

The revolt against Exner's principal ideas began with some careful observations by Kuiper[12], showing that in certain crustacean eyes there are no important refractive index variations in the crystalline cones, a conclusion subsequently verified by interference microscopy[28,29]. This would seem to rule out both lens-cylinder optics and superposition imagery. In their place Kuiper suggested that the important optical elements in this kind of eye were tracts or threads which crossed the clear zone, conveying images from lens systems in the region of the cornea to the deep-lying receptors. In support of this idea, he pointed out that these higher-index light-guide-like structures often became lined with pigment in the light-adapted eye, the function of which was to 'bleed' light out of the light guides by bringing high-refractive index material into contact with their sides. Effectively, Kuiper was suggesting that superposition eyes, in crustaceans at least, were really apposition eyes with a 'longitudinal pupil' mechanism for protecting the eye against high light intensities, rather than a superposition mechanism for increasing sensitivities at low intensities. Further support for this idea seemed to come from an interference microscope study by Allen[30], who claimed that in the hornworm moth the crystalline cones had a refractive index that was constant to less than 1%, and that the threads traversing the clear zone had an index of 1.523 (which would make them solid). These observations have not been confirmed, and indeed all subsequent work on insect superposition eyes[14–17], including moths, has led to opposite conclusions[11].

The present position is a satisfactory compromise. Most, if not all, insect eyes with clear zones do behave as proper Exner-type superposition eyes in the dark, with the threads that cross the clear zone interfering only minimally with the ray paths that contribute to the focused image. However, the effect of light adaptation is to cause pigment movement into the clear zone,

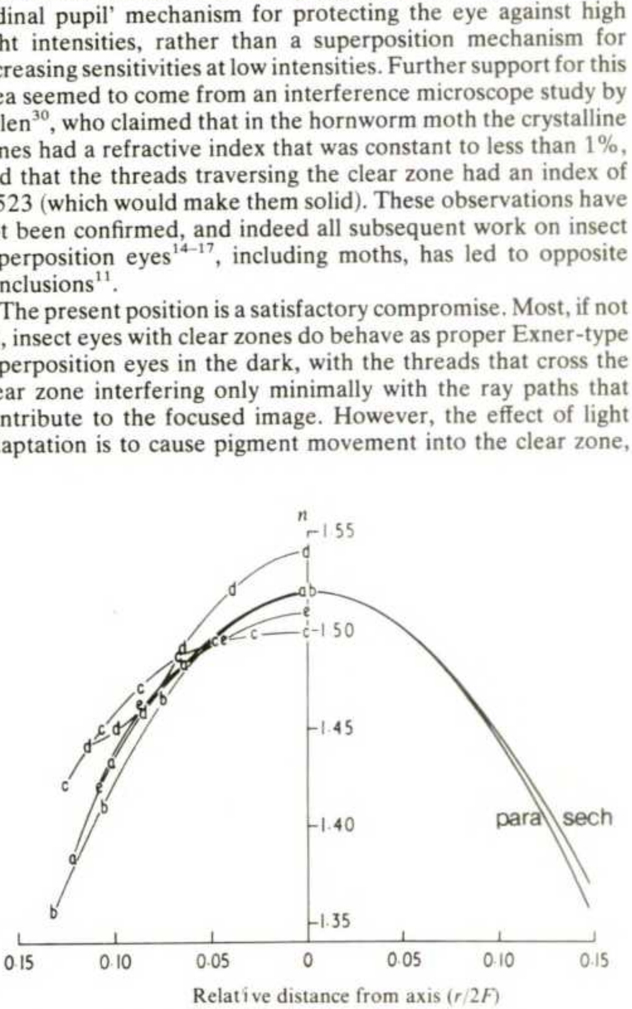

Fig. 4 Comparison of theoretical (right) and measured (left) refractive index distributions through crystalline cones. The theoretical curves show the difference between the Fletcher *et al.* equation[19] and Exner's parabolic approximation. Measured data are from: *a*, a euphausiid[18]; *b*, a firefly[14]; *c*, a moth[16]; *d*, a skipper butterfly[17]; *e*, *Limulus*[9]. The gradients have been normalized by taking the cone length as $2F$ for superposition eyes (a–d), and F in the case of the apposition eye of *Limulus* (e).

confining image-forming rays to the tract of thread joining each facet to its corresponding receptor bundle. Kuiper's light-bleeding mechanism, as well as simple pigment screening, probably both occur[31,32] and the net effect is that eyes with superposition optics at night have apposition optics by day. In moths one can watch this change happening. When suddenly illuminated in the dark, there is a large patch of 'glow' or eye-shine corresponding to the whole pupil of the superposition system, illuminated from within by light reflected from a tapetum behind the receptors (Fig. 5*d*). Exposure to light causes this patch to shrink to not much more than one facet, as pigment migrates inward and intercepts the oblique rays that would go to form the superposition image[32].

There remains, however, the problem that started the controversy. What happens in crustacean eyes without lens cylinders?

Reflecting superposition optics

Klaus Vogt provided the answer in a short note on crayfish eyes[33]. "Rays from an object point entering through different facets are superimposed not by refracting systems as in other superposition eyes but by a radial arrangement of orthogonal reflecting planes which are formed by the sides of the crystalline cones and purine layers surrounding them." Without being aware of Vogt's paper I reached the same conclusion about the eyes of a deep-sea shrimp[34]. If one looks at Exner's original figure[1,11] it is clear that the elements he drew could equally well be replaced by plane mirrors (Fig. 1*b*, *c*), and this is precisely what happens in certain crustacea, specifically the long-bodied decapods (shrimps, prawns, crayfish and lobsters, but not the true crabs). The structure of their eyes is very much like that of insect superposition eyes—a peripheral array of optical elements, a wide clear zone and a deep-lying hemispherical retina. They ought, anatomically, to be superposition eyes. The crucial difference is that the 'crystalline cones' are not crystalline—they are jelly-like with a refractive index of about 1.42—and neither are they conical. They are square in surface view (Fig. 5*a*, *d*), as shown perfectly accurately in Grenacher's plate of 1879 (ref. 35) (Fig. 5*b*).

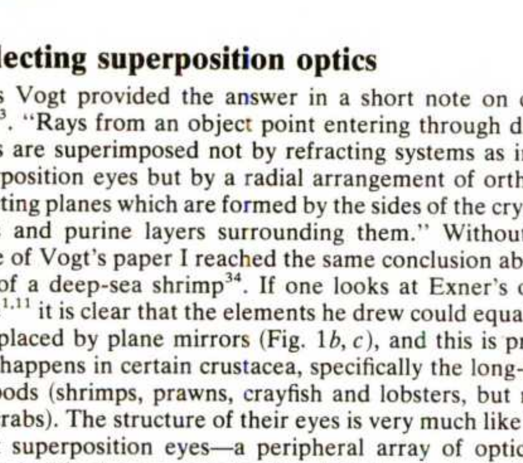

Fig. 5 Reflecting superposition optics. *a*, Surface of a crayfish eye showing the square array of mirrors; *b*, Grenacher's drawing[35] of an optical element from a shrimp; *c*, images formed by lenses in the cuticle of a crayfish eye, which prefocus the beams entering the mirror boxes[41]; *d*, adult eye of *Palaemonetes varians*, fully dark adapted, showing square symmetry and patch of eye-shine corresponding to the superposition pupil; *e*, 1st instar larva of *Palaemon serratus*, showing hexagonal symmetry and a small black pseudo-pupil characteristic of apposition eyes.

There is an elegant reason that eyes that use mirrors must have square facets. Figure 1*c* shows a two-dimensional diagram of an image-forming mirror array, but the question is: of what three-dimensional array would this be a section? One possibility is that it is a section of an axially symmetrical arrangement of tilted circular strips (Fig. 6*a*). Clearly, this will form an image of a distant point source located on the axis of the structure, but equally clearly it will not form an image of light originating from any other direction: the strips will not so much focus light as get in the way of it. What is required is an array that will behave like the strip arrangement, but for all directions. An array of square corners will do this. The reason is that a pair of mirrors at right angles to each other behave as though they were a single mirror that is always normal to the plane of the incident ray (Figs 1*f* and 6*b*): the complete angle through which the ray is reflected must add up to 180°. (One occasionally encounters corner mirrors in clothes shops—it is impossible to escape from one's image by moving around them.) Thus, provided most light entering the eye encounters two faces of each mirror box, all ray paths to the focus will be essentially identical to those of the two-dimensional diagram[29,36,37]. For a large-aperture eye like that of a crayfish each mirror box should be about twice as deep as it is wide, for the double reflection conditions to be met.

Not all eyes of the reflecting superposition type actually have mirrors. In the shrimp *Palaemonetes*, for example, reflection occurs at the faces of the mirror box by total internal reflection. With a refractive index of 1.41 inside the box, and a fluid outside with an index of about 1.33, the critical angle for total internal reflection is 71°, that is, rays making angles of up to 19° with the box wall will be reflected. This restricts the eye's effective pupil to about one-third of the eye diameter. To increase this the boxes are lined with a specular mirror in both crayfish and deep-sea shrimp. The mirrors are composed of a three-layer sandwich of one-quarter wavelength-thick plates alternating with tissue fluid[37], which is a common way for natural mirrors to be produced[38,39]. The nature of the material of the plates is not known in the crayfish, but in a pennaeid shrimp it is the pteridine isoxanthopterin[40].

A final refinement of the crayfish optical mechanism was found recently by Bryceson[41]. She noticed that each facet of the cleaned cornea is actually a long focus lens, with a focal length in water approximately equal to the distance from cornea to receptors (Fig. 5*c*). This has two implications. It means that the pencil of light passing through each mirror box is prefocused, so that it reaches the receptors as a fine beam, thereby improving image resolution. It also means that when the eye is in the light-adapted condition and each receptor only receives light from its 'own' facet[42], the focusing ensures a resolved image on that receptor and hence a narrow field of view. Interestingly, Kuiper had noticed inverted images in his original study[12].

Phylogeny and ontogeny

Mirror boxes with a hexagonal cross-section do not reflect light as shown in Fig. 1*f* and 6*b*, and so cannot be used in reflecting superposition eyes. Therefore, hexagonally faceted eyes do not use this mechanism, whereas square-faceted eyes probably do. Corneal geometry can thus be used as a reliable indication of an eye's optical type, and, since this is likely to be an evolutionary conservative character, of its ancestry as well[43,44].

An examination of the higher crustacea shows that square-faceted eyes are found only in the Decapoda, and there only in the long-bodies forms. The crabs (Brachyura) and hermit-crabs (Anomura), but interestingly not the squat-lobsters (also Anomura), have hexagonally faceted eyes of the apposition type, without a clear zone[43,44]. Equally interesting is the fact that the euphausiids, the shrimp-like krill usually grouped with the decapods in the super-order Eucarida, have both hexagonal facets and a clear zone. These eyes are very similar in their construction to the refracting superposition eyes of moths, and indeed their bullet-like crystalline cones bend light in the same way as in insect superposition eyes[45] and have a lens cylinder-

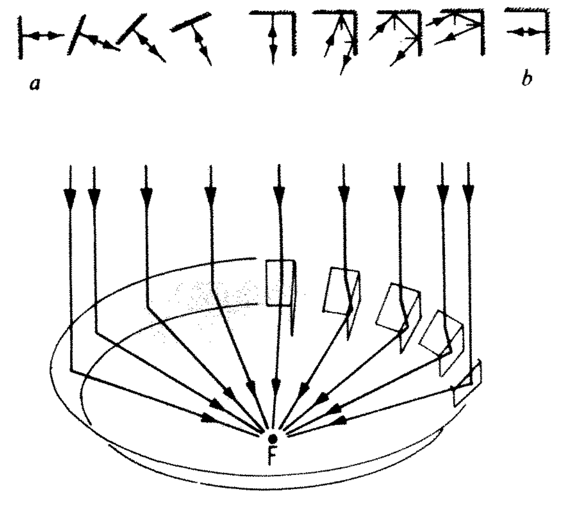

Fig. 6 A superposition focus can be formed either by set of tilted circular strips of mirror (*a*, left) or by a surface made of corner reflectors (*b*, right). Corner reflectors behave as though they are single mirrors at right angles to the plane of the incident ray (inserts above) so that the ray paths are almost the same as for the strips.

like refractive index profile[18]. The mysids (Peracarida), which look very much like euphausiids but differ from them in having a brood-pouch, also have refracting superposition eyes, although other peracaridans have apposition eyes. In the last century the euphausiids and mysids were grouped together as the Schizopoda, and my guess is that that grouping more accurately reflected their evolutionary affinity.

The decapods with reflecting superposition eyes do not start life that way (Fig. 5*e*). In their larval stages they have hexagonally faceted eyes with a typical apposition structure. In *Palaemonetes* it is not until about moult 15, when the animal is almost adult, that the facets square off and the superposition mechanism comes into operation. Presumably, the apposition type of eye is adequate for the upper ocean where the planktonic larvae live, just as it is in the light-adapted adults, but the deeper, dimmer waters the adults inhabit on maturity make it advantageous to use superposition optics, with their much greater light-gathering power. Larval crabs have eyes just like larval shrimps: the main developmental difference is that adult crab eyes retain the larval optical design. Again this makes sense, since most of them are shallow water or even terrestrial forms and would not need the superposition mechanism. It is as though the crab eye is derived from the crayfish eye by neoteny, the final developmental stage having been omitted.

This is somewhat perplexing for taxonomists. Eye structure links the mysids and euphausiids, which contemporary taxonomy does not. The reflecting superposition mechanism links all the long-bodied decapods, which are currently split between the Natantia and Reptantia[46] or the Dendrobranchiata and Pleocyemata[47]. It splits the galatheids (squat lobsters) from the pagurids (hermit crabs) and so divides the Anomura, and it suggests that the euphausiids and decapods are unrelated. Any one character is perhaps as fallible as any other as an evolutionary guide, but at least for eyes one can make the claim that once a design that works well has evolved it is most unlikely to be abandoned for an equally complicated but functionally equivalent one, as, for example, reflecting versus refracting superposition optics.

Although the decapods are alone among crustacea in possessing square-faceted eyes, there may be one possible parallel in insects. Horridge and Maclean[48] have described the eye of the Australian mayfly *Atalophlebia*, which has entirely square facets in its dorsal eye (in males the eyes are divided), square homogeneous crystalline cones and a wide clear zone. The optics are not well understood, but this ought to be a reflecting superposition eye. By contrast, the common European mayflies (*Cloeon*) have hexagonal facets and presumably refracting superposition optics. The Ephemeroptera are again a taxonomically difficult group, and it will be interesting to see whether eye structure is helpful here as well.

X-ray telescopes and other applications

Both types of superposition eye represent image-forming systems equivalent in many ways to conventional lenses and mirrors, but which have so far found few applications in optical technology. It is almost true to say that they have not properly been invented. In the case of refracting superposition devices it is clear that the task of making a large number of appropriate lens cylinders and aligning them accurately probably is not worth the effort, but for a reflecting system this is not necessarily true. One could imagine the construction of a reflecting array from strips of sheet metal, cut so as to interlock, or from a casting that was subsequently plated (there is a problem in trying to cover a sphere with squares—basically it cannot be done—but both geographers and lobsters have found ways round it). Such structures could have wide apertures, like crustacean eyes, and serve in applications like solar collectors, where condensing power rather than resolution is at a premium, or as emitters they could be useful for making large collimators, lighthouse lenses for example.

If the pupil is restricted, much higher resolution can be achieved, and it is this form that has produced the only important application so far, as an X-ray telescope[49,50]. X rays cannot be focused by refraction or by reflection at near normal incidence, which has meant that existing X-ray telescopes are all based on grazing incidence optics utilizing nested surfaces. Their design is basically similar to the tilted strips in Fig. 6*a*, and they suffer from the same drawback, a very narrow field of view. Angel[49] realized that the use of square cells as reflectors eliminates this problem, and has designed a telescope with a spatial resolution of 30 arc s. This degree of resolution is achieved by making the reflecting cells very long—about 100 times their width. Because they are reflecting devices, square-cell surfaces are usable over large parts of the electromagnetic spectrum, and provided the manufacturing problems can be overcome they should have a wide range of uses.

1. Exner, S. *Die Physiologie der facettierten Augen von Krebsen und Insecten* (Deuticke, Leipzig, 1891).
2. Horridge, G. A. & Duelli, P. *J. exp. Biol.* **80,** 165–190 (1979).
3. Matthiessen, L. *Pflügers Arch. ges. Physiol.* **21,** 521–528 (1886).
4. Maxwell, J. C. *Collected Works* **1,** 76–78 (1854).
5. Pumphrey, R. J. in *The Cell and the Organism* (eds Ramsay, J. A. & Wigglesworth, V. B.) 193–208 (Cambridge University Press, 1961).
6. Cornbleet, S. *Microwave Optics,* 121–132 (Academic, London, 1976).
7. Levi-Setti, R., Park, D. A. & Winston, R. *Nature* **253,** 115–116 (1975).
8. Winston, R. *J. opt. Soc. Am.* **60,** 245–247 (1970).
9. Land, M. F. *Nature* **280,** 396–397 (1979).
10. Horridge, G. A. (ed.) in *The Compound Eye and Vision of Insects,* 255–298 (Clarendon, Oxford, 1975).
11. Kunze, P. in *Handbook of Sensory Physiology* Vol. VII/6A (ed. Autrum, H.) 441–502 (Springer, Berlin, 1979).
12. Kuiper, J. W. *Symp. Soc. exp. Biol.* **16,** 58–71 (1962).
13. Eltringham, H. *Trans. R. ent. Soc. Lond.* **79,** 1–49 (1919).
14. Seitz, G. *Z. vergl. Physiol.* **62,** 61–74 (1969).
15. Meyer-Rochow, V. B. in *The Compound Eye and Vision of Insects* (ed. Horridge, G. A.) 299–313 (Clarendon, Oxford, 1975).
16. Hausen, K. *J. comp. Physiol.* **82,** 365–378 (1973).
17. Horridge, G. A., Giddings, C. & Stange, G. *Proc. R. Soc.* B**182,** 457–495 (1972).
18. Land, M. F. & Burton, F. A. *J. exp. Biol.* **82,** 395–398 (1979).
19. Fletcher, A., Murphy, T. & Young, A. *Proc. R. Soc.* A**223,** 216–225 (1954).
20. Rawson, E. G., Herriott, D. R. & McKenna, J. *Appl. Opt.* **9,** 753–759 (1970).
21. Exner, K. *Ann. phys. Chem.* **28,** 111–116 (1886).
22. Berreman, D. W. *Bell. Syst. Tech. J.* **43,** 1476–1479 (1964).
23. Uchida, T., Furukawa, M., Kitano, I., Koizumi, K. & Matsumara, H. *IEEE J. Quantum Electronics QE-6,* 606–612 (1970).
24. Koizumi, K., Ikeda, Y., Kitano, I., Furukawa, M. & Sumimoto, T. *Appl. Opt.* **13,** 255–260 (1974).
25. Ohtsuka, Y. *Appl. Phys. Lett.* **23,** 247–248 (1973).
26. Iga, K. & Yamamoto, N. *Appl. Opt.* **16,** 1305–1310 (1977).
27. Horridge, G. A. *Proc. R. Soc.* **B171,** 445–463 (1969).
28. Carricaburu, P. in *The Compound Eye and Vision of Insects* (ed. Horridge, G. A.) 236–254 (Clarendon, Oxford, 1975).
29. Vogt, K. *Z. Naturforsch.* **32**c, 466–468 (1977).
30. Miller, W. H., Bernard, G. D. & Allen, J. L. *Science* **162,** 760–767 (1968).
31. Walcott, B. in *The Compound Eye and Vision of Insects* (ed. Horridge, G. A.) 20–33 (Clarendon, Oxford, 1975).

32. Höglund, G. in *The Functional Organization of the Compound Eye* (ed. Bernhard, C. G.) 77–101 (Pergamon, Oxford, 1966).
33. Vogt, K. *Z. Naturforsch.* **30**c, 691 (1975).
34. Land, M. F. *Nature* **263,** 764–765 (1976).
35. Grenacher, H. *Untersuchungen über das Sehorgan der Arthropoden, insbesondere der Spinnen, Insecten und Crustacean* (Vanderhoeck & Ruprecht, Göttingen, 1879).
36. Land, M. F. *New Scient.* No. 1175, 10–13 (1979).
37. Vogt, K. *J. comp. Physiol.* **135,** 1–19 (1980).
38. Land, M. F. *Prog. Biophys. molec. Biol.* **24,** 75–106 (1972)
39. Land, M. F. *Scient. Am.* **239,** 126–134 (1968).
40. Zyznar, E. J. & Nicol, J. A. C. *J. exp. mar. Biol. Ecol.* **6,** 235–248 (1971).
41. Bryceson, K. *J. exp. Biol.* (in the press).
42. Kleinholz, L. H. in *The Physiology of Crustacea* Vol. II (ed. Waterman, T. H.) 133–169 (Academic, New York, 1961).
43. Land, M. F. in *Making Sense of Sense Organs* (ed. Laverack, M. S.) (Blackie, Glasgow, in the press).
44. Fincham, A. A. *Nature* **287,** 729–731 (1980).
45. Land, M. F., Burton, F. A. & Meyer-Rochow, V. B. *J. comp. Physiol.* **130,** 42–62 (1979).
46. Borradaile, L. A. *Ann. Mag. nat. Hist.* Ser. 7, **19,** 457–486 (1907).
47. Glaessner, M. F. in *Treatise on Invertebrate Paleontology* Part R., Vol. 2 (ed. Moore, R. C.) 399–566 (University of Kansas and Geol. Soc. Am., 1969).
48. Horridge, G. A. & McLean, M. *Proc. R. Soc.* B**200,** 137–150 (1978).
49. Angel, J. R. P. *Astrophys. J.* **233,** 364–373 (1979).
50. Hartline, B. K. *Science* **207,** 47 (1980).

ARTICLES

Guanine nucleotide-binding and autophosphorylating activities associated with the $p21^{\mathrm{src}}$ protein of Harvey murine sarcoma virus

Thomas Y. Shih, Alex G. Papageorge, Patricia E. Stokes, Maureen O. Weeks & Edward M. Scolnick

Laboratory of Tumor Virus Genetics, National Cancer Institute, National Institutes of Health, Bethesda, Maryland 20205

The purified $p21^{\mathrm{src}}$ protein of Harvey sarcoma virus shows a guanine nucleotide-binding activity and, in addition, at elevated temperature an autophosphorylating activity at a threonine residue using as phosphoryl donor GTP or dGTP but not ATP or dATP. These biochemical activities are unique among those associated with transforming proteins of RNA-containing or DNA-containing tumour viruses.

HARVEY MURINE SARCOMA VIRUS (Ha-MSV) is a replication-defective retrovirus with the potential to transform fibroblasts in cell culture and to induce solid tumours and erythroleukaemia in animals. It is a recombinant virus between genetic sequences of a helper-independent mouse type-C virus at both ends of the genomic viral RNA and inserted rat nucleic acid sequences[1-3]. Using antisera from rats bearing Ha-MSV-induced tumours, we have identified a 21,000-molecular weight (MW) protein (p21) coded for by the rat insert sequences in Harvey virus-transformed cells and in cell-free translation products of Ha-MSV virion RNA[4]. One form of p21 is phosphorylated in virus-transformed cells. Two major lines of evidence have led us to conclude that one of the forms of p21 is the transforming *src* gene product of Ha-MSV. First, the p21 encoded by a mutant (ts371) of the closely related Kirsten murine sarcoma virus (Ki-MSV), temperature-sensitive for the maintenance of transformation, is much more thermally labile than the p21 of the wild-type Kirsten virus[5]. Second, through transfection studies of the molecularly cloned Ha-MSV proviral DNA, its cloned subgenomic fragments and a series of Ha-MSV deletion-insertion mutants, the transforming *src* gene and the p21 encoding region have been localized to the 1,100-nucleotide rat sequences closest to the 5′ end of the viral genome[6-8]. The gene coding for an endogenous p21 also seems to be present in uninfected normal cells derived from a variety of vertebrate species. The antisera containing antibodies to the Ha-MSV p21 precipitated a smaller quantity of the 21,000-MW cellular homologue protein which is structurally and antigenically related to the Ha-MSV p21 and is itself highly conserved throughout evolution[9]. The major problem is, through what kind of molecular mechanism the p21 *src* transforms normal cells. Over 95% of the intracellular $p21^{\mathrm{src}}$ of a Ha-MSV-transformed MDCK dog cell has been localized to the inner surface of the plasma membrane by electron microscopic immunocytochemistry suggesting the cellular membrane to be a major site of action of this *src* protein[10]. Perhaps the most interesting property of the $p21^{\mathrm{src}}$ is its strong affinity for guanine nucleotides, implying that the transforming function of the $p21^{\mathrm{src}}$ may involve the metabolism of guanine nucleotides[11].

The $p60^{\mathrm{src}}$ gene product of Rous sarcoma virus (RSV)[12-15] and the T antigens of adenovirus[16] and polyoma virus[17] are associated in immunoprecipitates with an ATP-protein kinase activity which phosphorylates the immunoglobulin heavy chain. A tyrosine-specific phosphorylating activity has been found in immunoprecipitates of polyoma T antigens[18], Abelson murine leukaemia virus (MuLV) pl20 (ref. 19) and RSV $p60^{\mathrm{src}}$ (ref. 20). We report here a unique GTP-specific enzymatic activity of the partially purified Ha-MSV *src* protein which in solution without immunoprecipitation autophosphorylates the $p21^{\mathrm{src}}$ with $[\gamma\text{-}^{32}P]$GTP but not with $[\gamma\text{-}^{32}P]$ATP as phosphoryl donor. This enzymatic activity is clearly distinct from that of most of the other cellular protein kinases.

Purification of the p21 from NIH 3T3 cells transformed by Ha-MSV

Using antisera containing antibodies to the p21, a ^{3}H-GDP-binding assay specific to p21 has been developed[11]. Cellular extracts are incubated with ^{3}H-GDP and the antigen–antibody complexes precipitated by an absorbent, formaldehyde-fixed *Staphylococcus aureus*-containing protein A or protein A-Sepharose (Pharmacia). p21 in the immunoprecipitates is quantified by the ^{3}H-GDP bound to the p21 protein. This rapid assay allows purification of p21 from unlabelled cell extracts on a large scale. To preserve any enzymatic activity associated with p21, purification procedures used for most enzymes in

0028-0836/80/430686—06$01.00

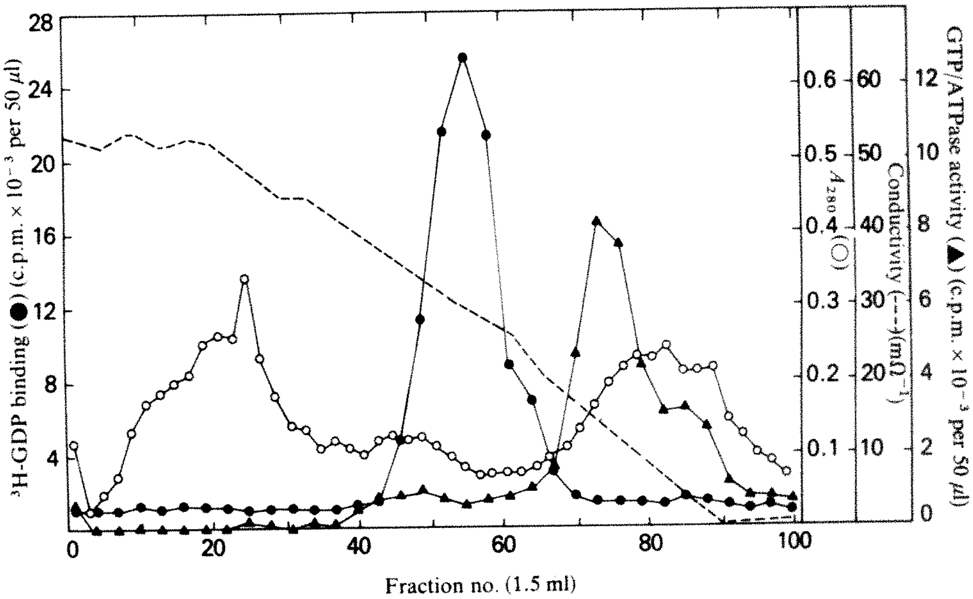

Fig. 1 Purification of the p21 by phenyl-Sepharose chromatography. 20 ml of hydroxyapatite-purified p21 (18 mg) in 0.09 M sodium phosphate, *p*H 6.8, was adjusted by adding 3.5 M ammonium sulphate to a final concentration of 0.8 M. It was loaded slowly on a small phenyl-Sepharose column (5 ml bed volume, Pharmacia) equilibrated with a starting buffer containing 0.8 M ammonium sulphate, 0.01 M sodium phosphate, *p*H 6.8, and 1 mM DTT at 4 °C. After washing in the sample with an additional 10 ml of the starting buffer, the column was eluted with 80 ml of a linearly decreasing ammonium sulphate gradient from 0.8 to 0 M in the same buffer at a flow rate of 0.2 ml min^{-1}. After completion of the gradient, the column was further eluted with 40 ml of the same buffer without ammonium sulphate and 1.5-ml fractions were collected. Immediately after measuring A_{280} and conductivity of the fractions, the fractions were dialysed against 50% glycerol in 0.01 M sodium phosphate, *p*H 6.8, and 1 mM DTT. The samples were stored at −20 °C, and no loss of p21 enzymatic activity was observed in this storage condition for at least 2 months. The p21 in column fractions was detected by a p21-specific ^{3}H-GDP binding assay as described in Table 1 using anti-p21 rat antiserum. In those conditions of assay, 7,300 c.p.m. represent 1 pmol of ^{3}H-GDP bound. As an illustration of the resolving power of the hydrophobic column, a cellular ATP/GTPase activity was also assayed by incubation with [γ-^{32}P]GTP across the gradient[34]. The ^{32}P-orthophosphate released by the enzyme reaction was extracted into the benzene/isobutanol organic phase as a silicotungstico-phosphomolybdate complex. In those assay conditions, 100 c.p.m. represents 1 pmol P_i produced in 20 min at 37 °C. ^{3}H-GDP-binding activity of the p21 (●); A_{280} (○); conductivity (- - -); ATP/GTPase activity (▲).

nondenaturating conditions were used. The membrane-bound p21 was solubilized by homogenizing cells in a buffer containing 1% Triton X-100. After high-speed centrifugation to remove nuclei and insoluble cell debris, the cell lysate was chromatographed on a hydroxyapatite column and eluted with a step-gradient of increasing sodium phosphate concentration. Most of the p21 was recovered in a fraction eluted between 0.005 and 0.09 M sodium phosphate. Essentially no detectable p21 was present in the flow-through material or fractions eluted with higher phosphate concentrations of 0.15 and 0.3 M. The specific binding activity of ^{3}H-GDP was increased 17-fold from the high-speed supernatant with a recovery of 172% total activity (Table 1). This increased activity was due to removal of substances interfering with the binding assay in crude extracts.

Hydroxyapatite chromatography is a valuable step in the purification scheme; it removes Triton X-100 and most other substances, such as lipid and nucleic acid. As p21 is mostly bound to membrane, chromatography based on hydrophobic interactions may be of particular value. Figure 1 shows the purification of p21 on a phenyl-Sepharose column. The hydroxyapatite fraction was applied to the column in 0.8 M ammonium sulphate and eluted with a decreasing gradient of ammonium sulphate which loosened the hydrophobic interaction. The p21 emerged as a single sharp peak at ~0.4 M ammonium sulphate at the minimum of the A_{280} profile. A cellular ATPase activity was detected at 0.2 M ammonium sulphate and was clearly separated from p21. As Table 1 shows, this step purified the specific GDP-binding activity of p21 by 16-fold. The overall purification from the high-speed supernatant of cell lysate was 265-fold with recovery of 93% total binding activity. To verify more directly that the purified GDP-binding activity represented the activity associated with the p21 protein, cellular proteins labelled in tissue culture with ^{35}S-methionine were purified by hydroxyapatite and phenyl-Sepharose chromatography. Both phosphorylated and non-phosphorylated forms of the p21 doublet were visualized by immunoprecipitation with antisera and SDS-gel electrophoresis from fractions eluted at 0.09 M sodium phosphate in the hydroxyapatite column and at 0.4 M ammonium sulphate in the phenyl-Sepharose column. The chromatographic profiles of the ^{35}S-methionine-labelled p21 on both columns were identical to that detected by the GDP-binding assay.

Table 1 Summary of p21 purification

Step	Total protein (mg)	Total GDP-binding activity (pmol GDP)	Specific binding activity (pmol mg^{-1})	Yield (%)	Step purification	Total purification
Total homogenate (50 g cells)	4,292	–	–	–	–	–
1. High-speed supernatant	2,523	2,291	0.9	100	1×	1×
2. Hydroxyapatite (0.09 M PO_4 fraction)	261	3,944	15.1	172	17×	17×
3. Phenyl-Sepharose (fractions 52–58)	9	2,131	241.0	93	16×	265×

All the purification procedures were performed at 4 °C. Approximately 50 g of Ha-MSV-transformed NIH 3T3 cells were lysed in 4 vol of lysis buffer containing 1% Triton X-100, 0.1 M NaCl, 0.005 M $MgCl_2$, 0.02 M Tris-HCl, *p*H 7.4, and 0.1 mM dithiothreitol (DTT). Cell lysis was assisted by two passages through an 18-gauge needle in a syringe. This is referred to as the total homogenate which was centrifuged at 150,000*g* for 30 min, and the pellets discarded. This fraction is the high-speed supernatant. For hydroxyapatite chromatography, the high-speed supernatant was dialysed overnight against the starting buffer (0.005 M sodium phosphate, *p*H 6.8, and 0.1 mM DTT) and was then loaded on a hydroxyapatite column (5 × 25 cm, Bio-Rad). The flow-through material was washed with the starting buffer until the A_{280} returned to the basal level. The fraction containing p21 was then batch-eluted with 0.09 M sodium phosphate, *p*H 6.8, and 0.1 mM DTT. The p21 was detected by a ^{3}H-GDP-binding assay[11]. Briefly, various amounts of column fractions were incubated at 4 °C with 10^{-5} M of ^{3}H-GDP (10 Ci mmol^{-1}) for 10 min in a final volume of 0.3 ml (1% Triton, 0.2 M NaCl, 0.005 M $MgCl_2$ and 0.02 M Tris-HCl, *p*H 7.4). Antisera or normal sera (7 µl) as controls were then added. After 90 min, the antigen–antibody complexes with bound ^{3}H-GDP were precipitated with 50 µl 10% (v/v) formaldehyde-fixed *S. aureus*. After several washings, the precipitates were dissolved by boiling in 0.30 ml of 2% SDS, 28 mM β-mercaptoethanol, 100 mM Tris-HCl, *p*H 7.8, 40% glycerol. ^{3}H-GDP dissolved in the supernatant was then counted. The ^{3}H-GDP binding activity of p21 was determined from the linear portion of the binding versus protein curves. The protein concentration was determined by the method of Lowry[33]. The hydroxyapatite fraction was stored in small aliquots at −170 °C, and subjected to only one cycle of freeze–thawing. Portions of this fraction were further purified by phenyl-Sepharose column detailed in Fig. 1 legend. The activity and yield shown above represent the total activity from the original 50-g cell pack.

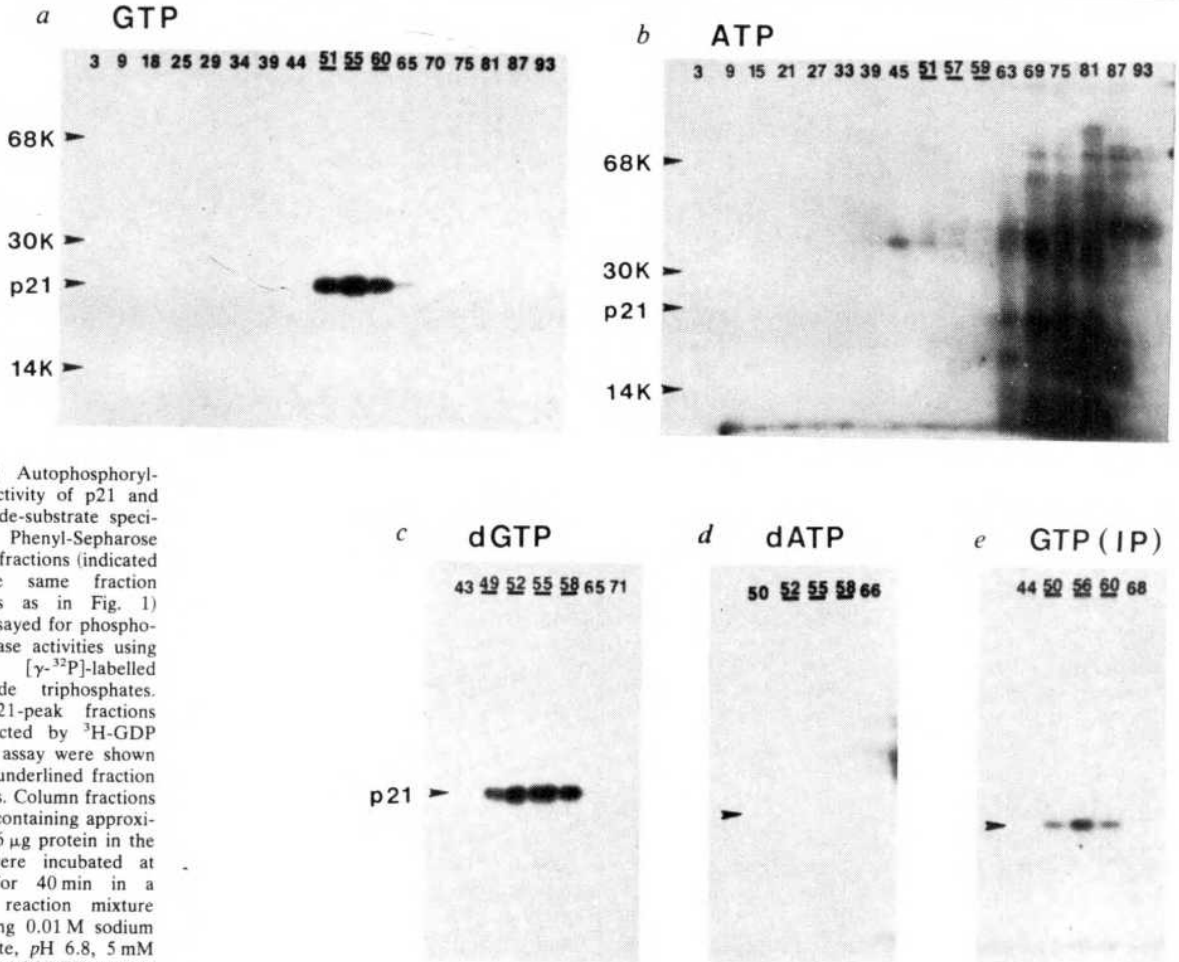

Fig. 2 Autophosphorylation activity of p21 and nucleotide-substrate specificity. Phenyl-Sepharose column fractions (indicated by the same fraction numbers as in Fig. 1) were assayed for phosphotransferase activities using various [γ-^{32}P]-labelled nucleotide triphosphates. The p21-peak fractions as detected by ^{3}H-GDP binding assay were shown by the underlined fraction numbers. Column fractions (40 μl) containing approximately 6 μg protein in the peak were incubated at 30 °C for 40 min in a 100-μl reaction mixture containing 0.01 M sodium phosphate, *p*H 6.8, 5 mM $MgCl_2$, 1 mM DTT, protein acceptors (5 mg ml^{-1}) as indicated, and various [γ-^{32}P]nucleotide triphosphates (~15 Ci mmol^{-1}) at a final concentration of ~4.7 μM. The exact condition for each experiment is indicated below. Except for the immunoprecipitation experiment (*e*), at the end of incubation the reaction was stopped by the addition of 0.5 ml cold 10% TCA. After standing at 4 °C for 60 min, the precipitated protein was pelleted by 10 min centrifugation in the Eppendorf microfuge. After being washed once more with 1 ml of 10% TCA at 4 °C, the pellets were dissolved by incubating at 95 °C for 3 min in 50 μl of 2% SDS, 0.2 M Tris-HCl, *p*H 8.0, 40% glycerol, 28 mM β-mercaptoethanol and 0.002% bromophenol blue. Proteins were separated by a 12% SDS-polyacrylamide gel electrophoresis (SDS-PAGE) as previously described[4]. The dried gels were autoradiographed for 18–72 h. The ^{14}C-labelled protein markers are bovine serum albumin (68K), carbonic anhydrase (30K) and lysozyme (14K). *a*, Column fractions were incubated with 2.7 μM of [γ-^{32}P]GTP (19 Ci mmol^{-1}, Amersham) in the presence of phosvitin (5 mg ml^{-1}, Sigma) which was visualized as a 40K band in Coomassie blue-stained gel. *b*, Column fractions were incubated with 5.6 μM of [γ-^{32}P]ATP (18 Ci mmol^{-1}, Amersham) in the presence of phosvitin (5 mg ml^{-1}). *c*, Column fractions were incubated with 1.8 μM of [γ-^{32}P]dGTP (25 Ci mmol^{-1}, ICN) in the presence of casein (5 mg ml^{-1}, Sigma) which revealed itself in the stained gel as a 25K band above the p21. *d*, Column fractions were incubated with 4.3 μM of [γ-^{32}P]dATP (10 Ci mmol^{-1}, ICN) in the presence of casein (5 mg ml^{-1}, Sigma). *e*, Column fractions were incubated with 9.3 μM of [γ-^{32}P]GTP (5 Ci mmol^{-1}, Amersham). After incubation, the p21 was immunoprecipitated by 7 μl of anti-p21 antiserum from tumour-bearing rats by a procedure previously described[4]. The immunoprecipitate was analysed by SDS-PAGE.

Nucleotide binding specificity of the purified p21

We have shown previously[11] that in crude cell lysates, the ^{3}H-GDP binding of p21 can be effectively inhibited by 20-fold excess of unlabelled GDP, GTP, dGTP, ppGpp, p[CH_2]ppG and to a lesser extent UTP but not by other nucleotide triphosphates, diphosphates, monophosphates and 3′,5′-cyclic phosphates. In crude extracts, the thermolability of the p21 encoded by the temperature-sensitive mutant of the closely related Ki-MSV can also be stabilized against thermal inactivation by 0.1 or 1 mM of GDP, GTP or dGTP. Using the purified p21 we examined the specificity by direct binding of ^{3}H-labelled nucleotides. As shown in Table 2, a constant amount of the p21 purified by phenyl-Sepharose was incubated with 4–12 μM of ^{3}H-labelled nucleotides; the bound nucleotides were immunoprecipitated as a complex with p21 by the antiserum. Only GTP, dGTP, GDP and to a lesser extent dATP demonstrate significant binding with normal serum. Nucleotides bound were approximately the same for GTP, GDP and dGTP, whereas dATP was only 24% of dGTP. Note that, in contrast to GTP, ATP gives no appreciable binding.

The nucleotide concentration for half-maximal binding was determined using p21 purified by phenyl-Sepharose in the ^{3}H-nucleotide concentration range from 2×10^{-9} to 10^{-7} M. In Mg^{2+}-containing buffer (5 mM $MgCl_2$, 0.2 M NaCl, 0.02 M Tris-HCl, *p*H 7.4), the concentration for half-maximal binding for GTP was observed at 8×10^{-9} M, for GDP at 7×10^{-9} M, and for dGTP at 9×10^{-9} M. The maximum amount of nucleotide bound was approximately the same for each of these three nucleotides. Although dATP gave appreciable binding, the concentration for half-maximal binding was ~5,000 times higher than that for dGTP. Contamination by dGTP of less than 0.02% could account for the dATP binding observed here. In buffers containing 5 mM EDTA and no added Mg^{2+} the same maximal extent of binding was observed but 100-fold higher concentrations of GTP were required for half-maximal binding.

These binding studies indicate that p21 is a quanine nucleotide-binding protein with strong affinity towards GTP, GDP and dGTP. Nucleotides of other bases and all monophosphates demonstrate much less significant binding to p21.

GTP-specific autophosphorylation of p21

The p21 immunoprecipitated from ^{35}S-methionine-labelled lysates of virus-transformed cells migrated as a doublet band in SDS-polyacrylamide gel electrophoresis; the lower band was a non-phosphorylated form of the p21, and the upper band was labelled with ^{32}P-orthophosphate *in vivo*. The high resolving power of the phenyl-Sepharose chromatography allowed us to study the possible enzymatic activities associated with p21. The guanine nucleotide-binding properties of p21 suggest that it may have enzymatic activity involving these nucleotide triphosphates. Small aliquots of the column fractions were incubated with various [γ-^{32}P]-labelled nucleotide triphosphates and the total proteins phosphorylated *in vitro* were then examined by SDS-polyacrylamide gels without prior immunoprecipitation. The results are shown in Fig. 2. Using [γ-^{32}P]GTP as a substrate (Fig. 2*a*), the only major protein phosphorylated across the column fractions is the ~21K band. This 21K band is most intense at the underlined fractions of numbers 51, 55 and 60, and coincides precisely with the p21 peak as determined by ^{3}H-GDP-binding assay seen in Fig. 1. That the 21K band is indeed the p21 protein is demonstrated by its immunoprecipitation with antisera containing antibodies to p21 (Fig. 2*e*) and its co-migration with the phosphorylated *in vivo* upper band of the p21 in SDS-gel electrophoresis (data not shown). It will be important to determine which form of the p21, the phosphorylated or non-phosphorylated, becomes autophosphorylated. In contrast to the results obtained with GTP, when [γ-^{32}P]ATP was used as phosphoryl donor, no p21 was phosphorylated at the peak fractions 51, 57 and 59 (Fig. 2*b*). The addition of 10 μM cyclic AMP had no effect on these patterns of phosphorylation. However, with [γ-^{32}P]ATP, extensive phosphorylation of various proteins are seen especially in fractions from 63 to 93, corresponding to the A_{280} peak seen in Fig. 1. This intense ATP-dependent protein kinase activity was well separated from the p21 peak in the phenyl-Sepharose chromatography. In Fig. 2*c*, it is seen that phosphorylation of p21 occurs at the same peak fractions by using [γ-^{32}P]dGTP as donor. The dGTP-dependent activity is similar to the GTP activity. The dATP-dependent reaction is also similar to ATP (Fig. 2*d*), and again no p21 phosphorylation is seen at the peak fractions. The lack of phosphorylation by [γ-^{32}P]ATP is not due to the phosphatase or pyrophosphatase activity in the preparation which selectively degrades ATP: most of the [γ-^{32}P]ATP or [γ-^{32}P]GTP remained intact after incubation with p21 for 80 min (Fig. 3). Compared with the control with no p21, very little ^{32}P-orthophosphate or ^{32}P-pyrophosphate was formed by incubation with the p21 preparation. Therefore, the phosphorylation reaction is very specific to GTP and dGTP and parallels the guanine nucleotide-binding specificity of the p21.

An important question is whether p21 phosphorylation is an autocatalytic reaction or p21 is simply a substrate for a contaminating protein kinase. Various commonly used protein kinase substrates were included in the reaction mixtures, for example phosvitin (40K) in Fig. 2*a* and *b* and casein (~25K) in Fig. 2*c* and *d*. No GTP/dGTP-dependent phosphorylation of these protein kinase substrates was seen at the p21 peak fractions. Also, the autophosphorylation reaction of the p21 *per se* was not affected by the presence of casein or phosvitin. No GTP-specific kinase activity of the p21 fractions was observed with calf thymus histones, protamine or a synthetic poly-L-tryosine-L-glutamate copolymer (data not shown). Other characteristics of p21 phosphorylation, such as relative insensitivity to EDTA, *N*-ethylmaleimide (NEM) and other agents, distinguish the autocatalytic reaction from most cellular protein kinases. Furthermore, the nucleotide specificity of the phosphorylation reaction is consistent with the nucleotide-binding specificity of p21. Thus it seems that GTP is a substrate for p21 and it is unlikely that p21 phosphorylation is due to a contaminating cellular protein kinase in the purified preparation.

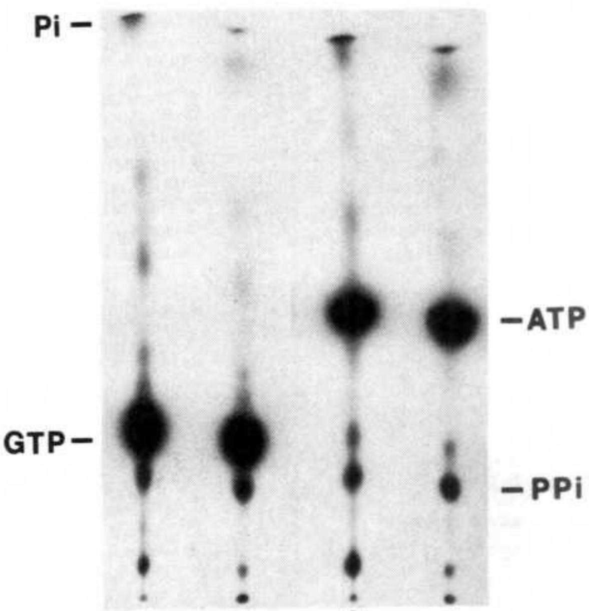

Fig. 3 Analysis of remaining [γ-^{32}P]GTP and [γ-^{32}P]ATP substrates after incubation with the purified p21. [γ-^{32}P]GTP (1.5 μM, 37 Ci mmol^{-1}, NEN) or [γ-^{32}P]ATP (2 μM, 22 Ci mmol^{-1}, NEN) was incubated at 30 °C for 80 min in the presence and absence of p21 purified by phenyl-Sepharose in conditons identical to those described in Fig. 4*A* legend. At the end of the reaction, 2 μl of each reaction mixture was spotted on a PEI-thin layer plate (Brinkmann). Ascending chromatography was in 0.75 M KH_2PO_4, *p*H 3.4. Authentic markers of GTP, ATP, P_i and PP_i were run on the same plate. Lane 1, [γ-^{32}P]GTP without p21; lane 2, [γ-^{32}P]GTP with p21; lane 3, [γ-^{32}P]ATP without p21; lane 4, [γ-^{32}P]ATP with p21.

Table 2 Nucleotide binding specificity of p21

^{3}H-labelled nucleotides	Bound pmol	
	Anti-p21 serum	Normal serum
GTP	2.00 ± 0.09	0.21 ± 0.01
ATP	0.11 ± 0.01	0.09 ± 0.01
UTP	0.09 ± 0.03	0.09 ± 0.00
CTP	0.05 ± 0.01	0.05 ± 0.01
dGTP	2.40 ± 0.09	0.14 ± 0.01
dATP	0.58 ± 0.05	0.06 ± 0.00
dTTP	0.08 ± 0.04	0.02 ± 0.00
dCTP	0.05 ± 0.03	0.03 ± 0.00
GDP	2.71 ± 0.33	0.24 ± 0.03
ADP	0.18 ± 0.04	0.16 ± 0.07
UDP	0.23 ± 0.09	0.24 ± 0.11
CDP	0.27 ± 0.13	0.22 ± 0.08
Cyclic GMP	0.05 ± 0.03	0.03 ± 0.00
Cyclic AMP	0.04 ± 0.01	0.03 ± 0.00
Cyclic CMP	0.03 ± 0.01	0.01 ± 0.00

The p21 purified by phenyl-Sepharose column (10 μg) was reacted with 7 μl of antiserum or control normal serum in ^{3}H-GDP binding assay conditions as described in Table 1 legend. The nucleotide concentration was at 4–10 μM at a specific radioactivity of 10–24 Ci mmol^{-1} (NEN). A triplicate determination was performed for each nucleotide and the average values and their standard deviations are listed.

Characterization of the p21 autophosphorylation reaction

Figure 4*A* shows the time course and temperature dependence of the autocatalytic reaction. The p21 band becomes more intense with incubation at 30°C for increasing periods of time. The reaction is relatively slow and persistent even after 80 min of incubation. Although nucleotide binding occurs readily at 4°C, autophosphorylation is strongly dependent on incubation temperature. Almost no phosphorylation reaction is seen at 4°C and the phosphorylation reaction rate is higher at 37°C than at 30°C. These characteristics are consistent with a *bona fide* enzymatic reaction. Band intensity was related to the amount of p21 protein, but the exact stoichiometry of phosphorylation is not yet determined. Figure 4*B* demonstrates the reaction rate as a function of [γ-^{32}P]GTP concentration. The p21 bands were cut off from the gels and the radioactivity counted. By double reciprocal plots of the incorporated c.p.m. against GTP concentration, the K_m for Mg^{2+}-GTP was estimated to be $\sim 2\times10^{-7}$ M

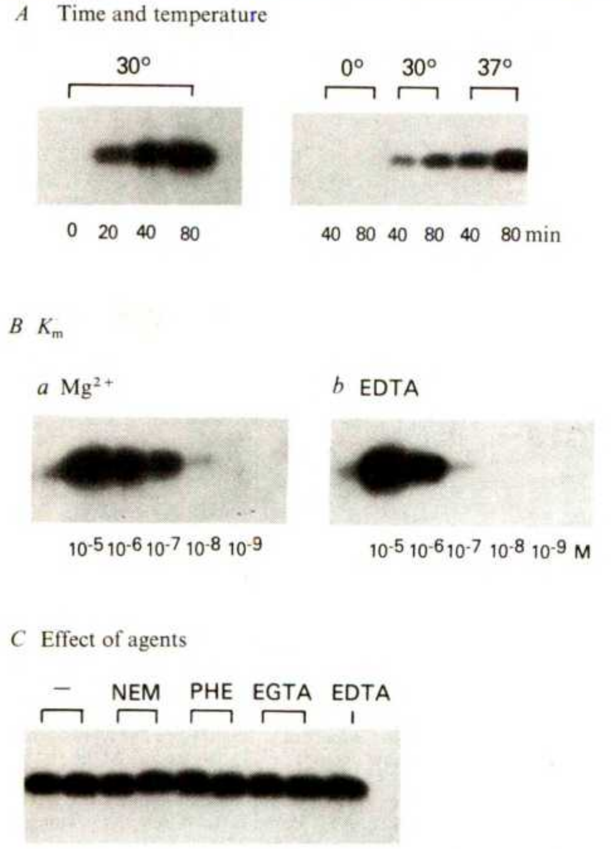

Fig. 4 Characterization of the p21 autophosphorylation reaction. *A*, Time course and temperature dependence of the reaction. The p21 peak fraction (1.5 μg) from the phenyl-Sepharose column was incubated at 30 °C for 0, 20, 40, or 80 min in the first experiment, and at 0 °C, 30 °C or 37 °C for either 40 or 80 min in the second experiment. The reaction mixture (50 μl) contained 5 mM $MgCl_2$, 0.01 M sodium phosphate, *p*H 6.8, 1 mM DTT and 0.5 mg ml^{-1} casein. The reaction was started by addition of [γ-^{32}P]GTP (37 Ci $mmol^{-1}$, NEN) to a final concentration of 1.5 μM. The reaction was stopped by 10% cold TCA. The precipitated protein was analysed by SDS-PAGE as described in Fig. 2 legend. Autoradiography was for 18 h with Dupont intensifying screen. Similar results were obtained if 0.01 M Tris-HCl, *p*H 7.5, was used instead of the phosphate buffer. *B*, Effect of [γ-^{32}P]GTP concentration. The purified p21 (0.8 μg) was reacted at 37 °C for 60 min with the following concentration of [γ-^{32}P]GTP (364 Ci $mmol^{-1}$, ICN): 10^{-5}, 10^{-6}, 10^{-7}, 10^{-8} and 10^{-9} M. *a*, Mg^{2+}-containing buffer of 5 mM $MgCl_2$, 0.01 M sodium phosphate, *p*H 6.8, and 1 mM DTT. *b*, Mg^{2+}-free buffer: the same composition without $MgCl_2$ and with 2.5 mM EDTA. *C*, The effect of various agents. The purified p21 (1.5 μg) was incubated in 50 μl of reaction mixture containing 0.01 M sodium phosphate, *p*H 6.8, 1 mM DTT, 0.5 mg ml^{-1} phosvitin and 1.5 mM of [γ-^{32}P]GTP for 80 min at 37 °C. In addition, various agents were added before incubation: *N*-ethylmaleimide (NEM, Sigma) at 2.5 mM or 5 mM; 1,10-phenanthroline (PHE, Sigma) at 2.5 mM or 5 mM; EGTA (Sigma) at 2.5 mM or 5 mM; EDTA at 5 mM.

and K_m for GTP in the presence of EDTA $\sim 2\times 10^{-6}$ M. No obvious Mg^{2+} optimum was observed between 0 and 10 mM in the absence of EDTA. The effect of various agents reactive to several protein functional groups is seen in Fig. 4*C*. The sulphydryl group reagent, *N*-ethylmaleimide (NEM), at 2.5 and 5 mM did not affect the reaction. At the GTP concentration used here, various chelating agents for metal ions at 2.5 mM or 5 mM also had little effect on the phosphorylation reaction, that is, 1,10-phenanthroline (PHE) which chelates Zn^{2+} and Fe^{2+}; EGTA which chelates Ca^{2+}; and EDTA which chelates Mg^{2+}, Mn^{2+} and Co^{2+}. If the enzyme requires these divalent cations at all, these metal ions must already be very tightly bound to the enzyme. These characteristics further distinguish the autocatalytic activity from most known protein kinases which require sulphydryl group and Mg^{2+} or Mn^{2+} for their activities, or in Ca^{2+}-dependent protein kinases, the Ca^{2+} for their activities[21]. Addition of $CaCl_2$ to the reaction mixture did not appreciably stimulate the p21 activity but is slightly inhibitory above 5 mM. The *p*H optimum has also been examined between *p*H 6.0 and *p*H 9.5. No sharp maximum was noted and phosphorylation decreased slightly above *p*H 8.5, perhaps due to alkaline lability of the phosphate linkage (see next section). The enzymatic activity was inactivated either by heating at 95 °C for 10 min or proteolytic degradation.

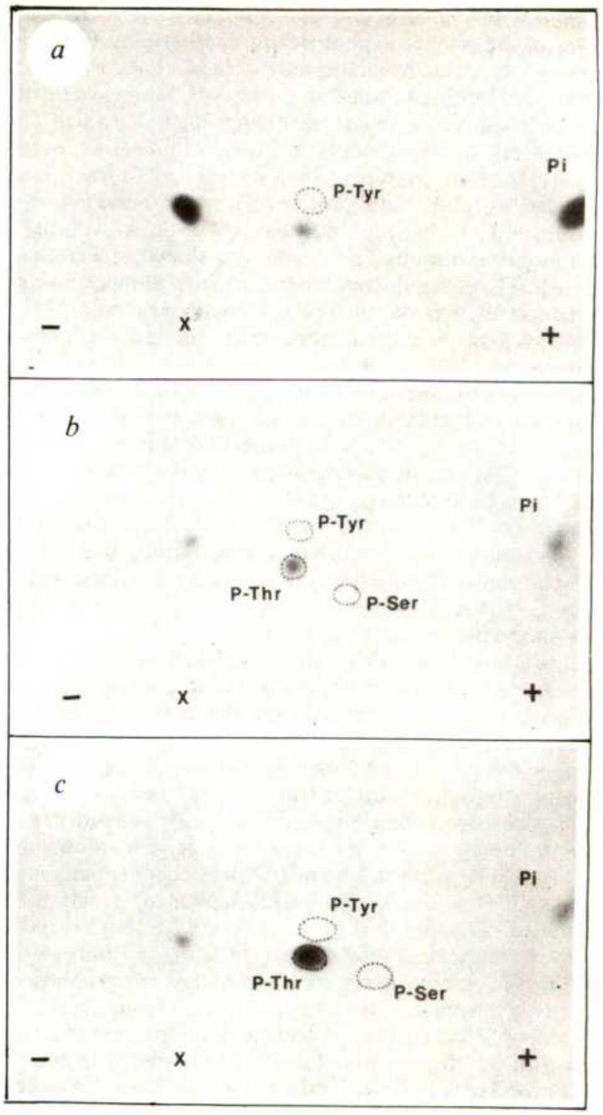

Fig. 5 Analysis of the phosphoamino acids of p21 phosphorylated *in vitro*. The purified p21 from phenyl-Sepharose column was autophosphorylated by incubation with [γ-^{32}P]GTP as described in Fig. 2*a* legend. The ^{32}P-labelled p21 was immunoprecipitated with anti-p21 serum and protein A-Sepharose (Pharmacia). The precipitated protein was solubilized with buffer containing SDS and β-mercaptoethanol. The solubilized protein was further precipitated with 20% cold TCA, washed with ethanol and hydrolysed with 6 M HCl at 100 °C at various time intervals. Approximately 4,000 c.p.m. of lyophilized sample was analysed by the two-dimensional method of Eckhart *et al.*[18] on the thin-layer cellulose plates. × marks the origin of samples. The first dimension at the horizontal direction was electrophoresis at 950 V for 90 min in *p*H buffer (glacial acetic acid : formic acid [88%] : H_2O, 78 : 25 : 897). The second dimension from bottom to top was chromatography in isobutyric acid : NH_4OH (0.5 M), 5 : 3. The phosphoamino acid markers, 5 μg each of phosphothreonine (Sigma), phosphoserine (Sigma) and phosphotyrosine (a gift of Dr Karen Beemon through Dr Gilbert Jay) were mixed with the ^{32}P-labelled samples and were spotted on the TLC plates. The radioactive spots were detected by autoradiography (6 days) with Dupont intensifying screen and the marker amino acids were visualized by ninhydrin spray. *a*, 4 h hydrolysis in 6 M HCl; *b*, 8 h hydrolysis; *c*, 15 h hydrolysis.

The phosphorylated amino acid residue

The p21 purified by phenyl-Sepharose was phosphorylated *in vitro* by [γ-^{32}P]GTP and the p21 was immunoprecipitated with the antiserum. The precipitated p21 was solubilized by SDS and β-mercaptoethanol and was precipitated with 20% trichloroacetic (TCA) acid at 4 °C. The precipitated protein was hydrolysed with 6 M HCl at 100 °C for various periods of time. The only ^{32}P-labelled amino acid was found to co-migrate with the *O*-phosphothreonine internal marker but not with *O*-phosphotyrosine or *O*-phosphoserine (Fig. 5). The spot moving more slowly towards the anode especially noticeable in the 4-h hydrolysate (Fig. 5*a*) seems to be an incomplete digestion product, as after longer hydrolysis of 8 h (Fig. 5*b*) and 15 h (Fig. 5*c*), the intensity of this spot decreases with concomitant increase in the phosphothreonine spot. Similar results were obtained by analysis of the p21 recovered from SDS-polyacrylamide gels or straight TCA precipitation of the reaction mixture. dGTP also appeared to phosphorylate the same amino acid residue as GTP. Consistent with the phosphorylated residue being phosphothreonine but not phosphotyrosine is the alkaline lability of the phosphate linkage. After treatment of the p21 phosphorylated *in vitro* with 0.1 M NaOH at 37 °C for 30 min, the phosphorylated p21 completely disappeared from gel electrophoresis.

In another experiment (data not shown), the p21 was labelled *in vivo* with ^{32}P-orthophosphate. After immunoprecipitation and SDS-gel electrophoresis, the p21 band was eluted and the amino acids analysed. The phosphorylated amino acid residue was threonine, similar to the *in vitro* product. Furthermore, a two-dimensional tryptic peptide map of the *in vitro* phosphorylated p21 was observed to be identical to a two-dimensional tryptic peptide map of the p21 labelled by ^{32}P-orthophosphate *in vivo* (unpublished observation). Several phosphopeptides were observed in each map and the maps were identical. However, as some of the phosphopeptide spots may represent incomplete trypsinization, the exact number of phosphorylation sites on each p21 molecule remains to be determined.

Discussion

The GTP-specific autophosphorylation of $p21^{src}$ observed here seems to be a unique enzymatic activity among those reported for many other transforming proteins. First, the nucleotide substrate specificity of the p21 reaction is more restrictive than the substrate specificity of either the $p60^{src}$ of RSV[12–15], the p120 of Abelson MuLV[19], or the T antigens of adenovirus[16], polyoma virus[17,18,22] or SV40 (refs 23–25). The protein phosphorylating activities associated with each of those transforming proteins use as phosphoryl donor ATP and in most cases also GTP, whereas p21 uses only GTP. Second, the protein kinase activity of the partially purified RSV $p60^{src}$ and the SV40 large T antigen has been demonstrated to phosphorylate exogenous protein acceptors such as casein, phosvitin or immunoglobulin heavy chain in soluble systems[23–27]. No such activity has been detected in reactions containing p21. Third, the phosphorylating enzymatic activities associated with $p60^{src}$, the Abelson MuLV p120 and the T antigens occur rapidly at 4 °C (refs 15, 19). Although binding of GDP or GTP to p21 can be observed at 4 °C, phosphorylation is markedly temperature-activated and proceeds linearly for up to 80 min at 37 °C. Finally, the amino acid residue phosphorylated with [γ-^{32}P]GTP in the p21 is a threonine residue, not a tyrosine residue as observed for the other proteins[18–20]. Thus at this point, it is not possible to assign a common denominator to the phosphorylating activities associated with transforming proteins. Comparing the results of p21 with other transforming proteins, note that p21 was purified by a GDP-binding assay that does not require the measurement of protein kinase activity. Thus it is possible that our binding assay and/or method of purification have allowed us to discern this novel GTP-specific autophosphorylating activity.

The question, then, is: what is the biochemical activity of p21 that is responsible for cell transformation? Two types of biochemical activities have now been associated with p21: (1) a binding activity in which either GDP or GTP will bind non-covalently to the p21; and (2) an autophosphorylating activity in which p21 is phosphorylated by the gamma phosphate of GTP. It is possible that the nucleotide-binding activity is the first step in the interaction of the p21 with GTP and that the subsequent phosphorylating activity is responsible for its transforming function. Within this model, autophosphorylation could be a phosphoenzyme intermediate which is a step in an enzymatic reaction which normally will go to completion *in vivo* and is trapped in the present *in vitro* condition due to the lack of suitable acceptors or cofactors for the catalytic turnover of the reaction. Alternatively, autophosphorylation of p21 may simply be an autoregulatory mechanism for some other activities of the p21 which may more closely reflect the transforming activity *per se*. The p21 may be activated or inactivated as a consequence of its phosphorylation and p21 activity may function in a way that does not *per se* require phosphorylating activity. Regulatory proteins which bind guanine nucleotides do exist and p21 could function as such a protein in a 'transforming reaction' which itself does not necessarily require phosphorylating activity. The regulatory G-protein of the adenylate cyclase system is an example[28,29]. Purified p21 and its phosphorylated product reported here may permit one to determine the missing components of its transforming activity. These may be protein substrates, other small or large metabolite molecules which simply bind to the p21–guanine nucleotide complex or actively participate in a unique phosphotransferase or even GTPase reaction. Recently, the Ha-MSV p21 and RSV p60 have been found to be located at the inner surface of the plasma membrane of transformed cells with the p60 being concentrated at gap junctions[10,30]; the Abelson MuLV p120 has a transmembrane subcellular location[31] and the polyoma middle T antigen is also membrane-associated[32]. The generally similar anatomical locations within cells of these transforming proteins suggest that the cell membrane may be a major site of action for transformation. Autophosphorylation of these proteins may have an important role in regulating normal membrane functions.

We thank Dr Harry Langbeheim for valuable discussion during this work.

Received 21 May; accepted 29 July 1980.

1. Scolnick, E. M. & Parks, W. P. *J. Virol.* **13,** 1211–1219 (1974).
2. Shih, T. Y. *et al. J. Virol.* **27,** 45–55 (1978).
3. Chien, Y.-H. *et al. J. Virol.* **31,** 752–760 (1979).
4. Shih, T. Y., Weeks, M. O., Young, H. A. & Scolnick, E. M. *Virology* **96,** 64–79 (1979).
5. Shih, T. Y., Weeks, M. O., Young, H. A. & Scolnick, E. M. *J. Virol.* **31,** 546–556 (1979).
6. Chang, E. H. *et al. J. Virol* **31,** 795–809 (1980).
7. Wei, C.-M., Lowy, D. R. & Scolnick, E. M. *Proc. natn. Acad. Sci. U.S.A.* **77,** 4674–4678 (1980).
8. Ellis, R. W. *et al. J. Virol* (in the press).
9. Langbeheim, H., Shih, T. Y. & Scolnick, E. M. *Virology* (in the press).
10. Willingham, M. C., Pastan, I., Shih, T. Y. & Scolnick, E. M. *Cell* **19,** 1005–1014 (1980).
11. Scolnick, E. M., Papageorge, A. G. & Shih, T. Y. *Proc, natn. Acad. Sci. U.S.A.* **76,** 5355–5359 (1979).
12. Collett, M. S. & Erikson, R. L. *Proc. natn. Acad. Sci. U.S.A.* **75,** 2021–2024 (1978).
13. Levinson, A. D., Oppermann, H., Levintow, L., Varmus, H. E. & Bishop, J. M. *Cell* **15,** 561–572 (1978).
14. Ruebsamen, H., Friis, R. R. & Bauer, H. *Proc. natn. Acad. Sci. U.S.A.* **76,** 967–971 (1979).
15. Richert, N. D., Davies, P. J. A., Jay, G. & Pastan, I. H. *J. Virol.* **31,** 695–706 (1979).
16. Lassam, N. J., Bayley, S. T., Graham, F. L. & Branton, P. E. *Nature* **277,** 241–243 (1979).
17. Smith, A. E., Smith, R., Griffin, B. & Fried, M. *Cell* **18,** 915–924 (1979).
18. Eckhart, W., Hutchinson, M. A. & Hunter, T. *Cell* **18,** 925–933 (1979).
19. Witte, O. N., Dasgupta, A. & Baltimore, D. *Nature* **283,** 826–831 (1980).
20. Hunter, T. & Sefton, B. M. *Proc. natn. Acad. Sci. U.S.A.* **77,** 1311–1315 (1980).
21. Krebs, E. G. & Beavo, J. A. *A. Rev. Biochem.* **48,** 923–959 (1979).
22. Schaffhausen, B. S. & Benjamin, T. L. *Cell* **18,** 935–946 (1979).
23. Griffin, J. D., Spangler, G. & Livingston, D .M. *Proc. natn. Acad. Sci. U.S.A.* **76,** 2610–2614 (1979).
24. Tjian, R. & Robbins, A. *Proc. natn. Acad. Sci. U.S.A.* **76,** 610–614 (1979).
25. Baumann, E. A. & Hand, R. *Proc. natn. Acad. Sci. U.S.A.* **76,** 3688–3692 (1979).
26. Mannes, P. F. *et al. Proc. natn. Acad. Sci. U.S.A.* **76,** 5028–5032 (1979).
27. Erikson, R. L., Collett, M. S., Erikson, E. & Purchio, A. F. *Proc. natn. Acad. Sci. U.S.A.* **76,** 6260–6264 (1979).
28. Limbird, L. E., Gill, D. M. & Lefkowitz, R. J. *Proc. natn. Acad. Sci. U.S.A.* **77,** 775–779 (1980).
29. Rodbell, M. *Nature* **284,** 17–22 (1980).
30. Willingham, M. C., Jay, G. & Pastan, I. *Cell* **18,** 125–134 (1979).
31. Witte, O. N., Rosenberg, N. & Baltimore, D. *J. Virol.* **31,** 776–784 (1979).
32. Ito, Y., Brocklehurst, J. R. & Dulbecco, R. *Proc. natn. Acad. Sci. U.S.A.* **74,** 4666–4670 (1977).
33. Lowry, O. H., Rosebrough, N. J., Farr, A. F. & Randall, R. J. *J. biol. Chem.* **193,** 265–275 (1951).
34. Das, A., Merril, C. & Adhya, S. *Proc. natn. Acad. Sci. U.S.A.* **75,** 4828–4832 (1978).

Molecular cloning and sequencing of cDNA encoding the precursor to the small subunit of chloroplast ribulose-1,5-bisphosphate carboxylase

John R. Bedbrook

Plant Breeding Institute, Maris Lane, Trumpington, Cambridge CB2 2LQ, UK
Division of Plant Industry, CSIRO, PO Box 1600, Canberra City, ACT 2601, Australia

Steven M. Smith & R. John Ellis

Department of Biological Sciences, University of Warwick, Coventry CV4 7AL, UK

Polyadenylated RNA from leaves of pea (Pisum sativum) *has been copied into DNA and cloned in the* Escherichia coli *plasmid pBR322. From these clones we have identified and sequenced DNA encoding the mRNA for the precursor of the small subunit of the chloroplast enzyme ribulose-1,5-bisphosphate carboxylase.*

CHLOROPLAST development requires the coordinated activities of both plastid and nuclear genetic systems. Some chloroplast polypeptides are encoded in the nucleus and synthesized in the cytosol, whereas others are encoded and synthesized in the chloroplast[1]. Recent data suggest that chloroplast polypeptides synthesized in the cytosol take the form of higher molecular weight (MW) precursors that are cleaved to the mature form on entry into the chloroplast[2]. One much studied chloroplast protein, which provides a model system for studying nucleus–chloroplast cooperation, is the stromal enzyme ribulose-1,5-biphosphate carboxylase (EC 4.1.1.39, also known as Fraction I protein, here abbreviated to RuBPCase). This enzyme is the most abundant chloroplast protein[3]. In higher plants it occurs as an oligomer of eight large subunits (MW 55,000) and eight small subunits (MW 14,000). The function of the small subunit is unknown, but the large subunit contains the catalytic sites for both the carboxylase and the oxygenase activities[4].

The large subunit is encoded in the chloroplast DNA[5,6] and synthesized inside the chloroplast[7]. The small subunit is encoded in nuclear DNA[8], and synthesized in the cytosol as a precursor of

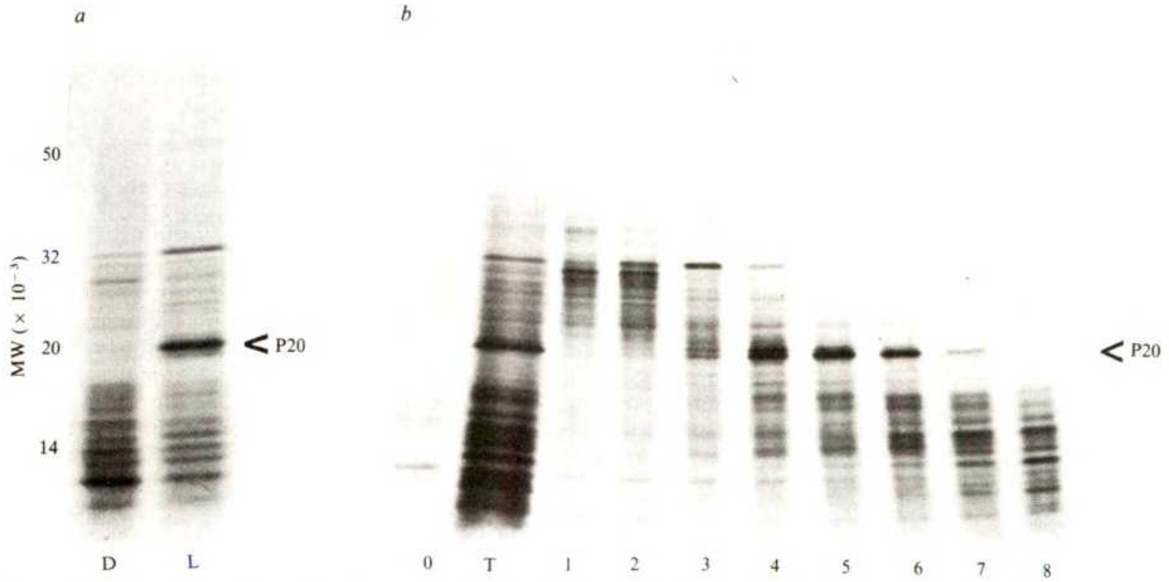

Fig. 1 Translation products of RNA preparations used in cloning and colony hybridizations. *a*, RNA from dark-grown and illuminated pea plants. Polysomal polyadenylated RNA was prepared from shoots of pea (*Pisum sativum*, var. Feltham First), translated in a wheat-germ protein-synthesizing system and the products analysed as described previously[10,12]. The photograph shows the autoradiograph of an SDS-polyacrylamide gel of the translation products. D, RNA prepared from pea plants grown for 9 days in darkness; L, RNA prepared from pea plants grown for 9 days in darkness followed by 48 h continuous illumination; P20, precursor to the small subunit of RuBPCase. Each sample contains an equal amount of trichloroacetic acid-precipitable radioactivity. *b*, Size-fractionated RNA from illuminated pea plants. Polyadenylated RNA from the leaves of illuminated pea plants (L, above) was fractionated by electrophoresis in a gel (17 × 17 × 0.3 cm) of 1.5% (w/v) agarose containing 0.1 × E buffer[26] (3 mM NaH_2PO_4, 3.6 mM Tris, 0.1 mM Na_2 EDTA) and 50% (v/v) deionized formamide. Electrophoresis was for 3 h at 30 mA after which the region of the gel containing RNA species between 0.1 and 0.7×10^6 MW was cut into eight equal fractions. Each gel fraction was cut further into 3-mm cubes and placed in a test tube. RNA was eluted from these gel sections (0.2 g each) by shaking at 4 °C with 0.25 ml 10 mM Tris-Cl *p*H 7.6, 0.4% (w/v) SDS, 1 mM EDTA and 400 mM LiCl. Elution was for a total of 20 h during which time the elution buffer was changed twice. Eluates for each fraction were pooled and the RNA precipitated with ethanol. The RNA was dissolved in 200 mM HEPES-KOH, *p*H 7.6, and centrifuged for 5 min in an Eppendorf 5412 microcentrifuge to remove any insoluble material. The RNA was ethanol-precipitated from the supernatant and finally reprecipitated once more from this buffer before being dissolved in sterile distilled water for translation and colony hybridizations (see Fig. 2). Translation and product analysis on a SDS-polyacrylamide gel were as described previously[10,12]. The photograph shows an autoradiograph of the translation products. O, No RNA added; T, unfractionated RNA; 1–8, RNA size fractions of decreasing MW; P20, precursor to the small subunit of RuBPCase.

0028–0836/80/430692—06$01.00

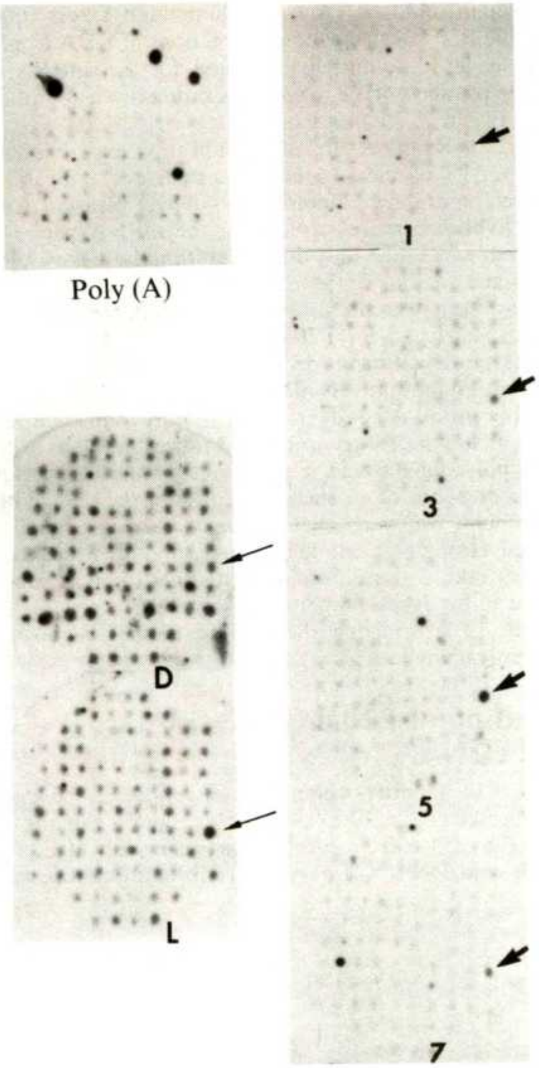

Fig. 2 Isolation and identification of cDNA clones. Polysomal polyadenylated RNA (10 μg) from illuminated pea leaves (see Fig. 1*a*) was used to direct the synthesis of cDNA using the method and buffers described by Myers and Spiegelman[27]. The reaction was carried out in 100 μl using 40 units of AMV reverse transcriptase. The cDNA was purified by phenol–chloroform extraction, and chromatography on Sephadex G-50 in a buffer containing 0.2 M sodium acetate and 1 mM EDTA. The cDNA fraction was concentrated by ethanol precipitation, dissolved in 70 μl H_2O, heated to 100 °C for 2 min and cooled in ice water. The denatured cDNA was converted to double-stranded DNA in a 100-μl reaction mixture containing 50 mM HEPES *p*H 6.9, 10 mM $MgCl_2$, 10 mM dithiothreitol (DTT), 0.5 mM deoxynucleotide triphosphates, 200 mM KCl and 10 units of fragment A polymerase I (Boehringer). The reaction mixture was incubated at 37 °C for 120 min, and the DNA purified by phenol–chloroform extraction and chromatography on Sephadex G-50, and concentrated by ethanol precipitation. The double-stranded DNA was treated with S_1 nuclease in a 100–μl reaction mixture containing 3 M NaCl, 0.3 M sodium acetate *p*H 4.5, and 1 mM $ZnSO_4$. The amount of S_1 nuclease required to remove the hairpin loop was determined empirically by titrating against double-stranded cDNA prepared from rabbit globin mRNA, and assaying the length of the product on denaturing polyacrylamide gels. The double-stranded cDNA was incorporated into the vector plasmid pBR322 (ref. 28) in two ways. (1) Using synthetic *Hin*dIII sequence linkers. Double-stranded cDNA obtained from 10 μg RNA was dissolved in 10 μl of a buffer containing 60 mM Tris-HCl *p*H 7.6, 8 mM $MgCl_2$, 10 mM 2-mercaptoethanol, 1 mM ATP and 0.2 mM deoxyribonucleotide triphosphates, and incubated with 1 unit of DNA polymerase I for 15 min at 15 C. 5′-Phosphorylated linkers (60 pmol) in 6 μl were added to the reaction together with 15 μl of 60 mM Tris-HCl *p*H 7.6, 8 mM $MgCl_2$, and an excess of DNA ligase. The mixture was incubated at 15 °C for an additional 4 h and the nucleic acid purified by phenol–chloroform extraction and chromatography on Sephadex G-200. The cDNA was recovered after ethanol precipitation and ligated to 1 μg of *Hin*dIII-linearized pBR322 DNA. The ligated DNA was used to transform the *E. coli* strain HB101 (ref. 29) to ampicillin resistance. (2) By homopolymer tailing of the double-stranded cDNA with dCTP, and *Pst*I-linearized pBR322 DNA with dGTP. The tailing reactions were as described previously[30]. Double-stranded cDNA from 5 μg RNA was reacted with 20 units of terminal transferase (PL Biochemicals) in a 100-μl reaction mixture containing 140 mM potassium cacodylate, 30 mM Tris-HCl *p*H 7.6, 1 mM DTT, 0.2 mM dGTP or 0.1 mM dCTP, 1 mM $CoCl_2$, and the plasmid DNA or the cDNA. The reaction was at 37 °C for 30 min. The tailed DNA was recovered by phenol–chloroform extraction and ethanol precipitation, and dissolved in 100 mM NaCl, 1 mM EDTA and 10 mM Tris-HCl, *p*H 8.0. The pBR322 and cDNA were mixed at approximately equal molar ratios, heated at 60 °C and annealed at 42 °C for 14 h. The annealed samples were used directly for transformation. Bacterial clones containing cDNA chimaeric plasmids produced by the linker method were detected by their sensitivity to tetracycline. Such clones were arrayed on Millipore filters, grown and prepared for nucleic acid hybridization. These filters were hybridized with RNA probes derived from RNA preparations described in Fig. 1 legend. Radioactive RNA probes were prepared using the 5′-phosphorylation procedure[31]. Samples of RNA (0.5 μg) were hydrolysed in 5 mM Tris-HCl *p*H 9.5, 10 mM EDTA and 0.1 mM spermidine at 95 °C for 5 min in a 17-μl reaction volume. The mixture was cooled, made to 50 mM Tris-HCl *p*H 9.5 and 10 mM $MgCl_2$, and added to a tube containing 30 μCi of dried [γ-^{32}P]ATP. After mixing, 4 units of T_4 polynucleotide kinase were added and the reaction mixture incubated for 30 min at 37 °C. RNA was purified from the reaction by phenol–chloroform extraction and ethanol precipitation. Before hybridization to probes, each filter was incubated for 6 h in 2 × SSC, 100 μg ml^{-1} *E. coli* tRNA, and 100 μg ml^{-1} polyadenylic acid at 60 °C. Hybridization to each 15-cm filter was carried out in 2 ml of 2 × SSC containing $\sim 4 \times 10^5$ c.p.m. of probe, 100 μg ml^{-1} tRNA, and 100 μg ml^{-1} polyadenylic acid at 60 °C for 16 h. After the incubation, the filters were washed in 2 × SSC, 0.1% (w/v) SDS at 60 °C, dried and exposed to X-Omat H X-ray film. The photographs show the results of hybridizing seven different RNA probes to the same 97 clones, the probes being: Poly(A), polyadenylic acid; D and L, polysomal poly(A)-containing RNA from dark-grown and illuminated leaves, respectively (see Fig. 1*a*); 1, 3, 5 and 7, size-fractionated poly(A)-containing RNA from light-grown leaves (see Fig. 1*b*). Clone 160 is indicated by an arrow.

MW 4,000–6,000 larger than the mature polypeptide[9–11]. This precursor (P20) enters isolated chloroplasts with cleavage to its final size by a mechanism which is independent of concomitant translation[10,11], and assembles in the stroma with the large subunit molecules into the holoenzyme[11,12]. The processing activity which cleaves P20 to small subunit is found in the soluble stromal fraction of the chloroplast[12]. These features establish a clear difference between the signal hypothesis advanced to explain the transport of secretory polypeptides across microsomal membranes[13] and the envelope carrier hypothesis proposed to explain the transport of polypeptides into chloroplasts[10].

The mechanism by which the expression of chloroplast and nuclear genomes is coordinated and the polypeptide transported into the chloroplast can be investigated using molecular cloning to elucidate the physical properties of the relevant genes. Specific hybridization probes can be used to obtain information on the structure and function of their RNA and polypeptide products. A cloned fragment of maize chloroplast DNA encoding the large subunit of RuBPCase has been used to show transcriptional control of the expression of this gene in maize leaf mesophyll cells[14]. Here we describe the isolation of cDNA clones of the mRNA for the small subunit of RuBPCase from pea (*Pisum sativum*). The cloned DNA has been sequenced to determine the amino acid sequence of most of the precursor polypeptide, and the sequence used to isolate and characterize P20 mRNA.

Light increases the amount of translatable P20 mRNA in polysomes

Light stimulates the accumulation of RuBPCase in pea leaves[10]. Polyadenylated RNA was prepared from polysomes isolated from leaves of pea plants grown in darkness for 9 days, and also from pea plants subsequently exposed to 48 h of continuous illumination. Translation of these RNA preparations in a cell-free protein-synthesizing system derived from wheat germ produced the polypeptides shown in Fig. 1*a*. A comparison of these translation products shows that the RNA from leaves of plants exposed to 48 h of light directs the synthesis of significantly more P20 than that from dark-grown pea plants. If plants are maintained in darkness for a further 48 h instead of being illuminated, this change does not occur (not shown). Thus, one result of illuminating etiolated pea plants is to cause an increase in the amount of translatable P20 mRNA in polysomes. The identity of P20 as the precursor to the small subunit of RuBPCase has been established previously[10].

Electrophoresis of these two RNA preparations in a polyacrylamide gel containing 7 M urea shows that the RNA from illuminated pea plants contains a ~900-nucleotide species which is not apparent in that from peas grown in the dark. A densitometer scan of a photograph of this gel indicates that this RNA species represents no more than 2% by weight of the total polyadenylated RNA. This RNA species was tentatively identified as the mRNA for P20 due to its co-electrophoresis (not shown) with a size class of polyadenylated RNA enriched with respect to translatable P20 mRNA (Fig. 1*b*, track 5). Figure 1*b* shows that RNA, fractionated by size on electrophoresis in an agarose gel containing formamide, is considerably enriched for P20 mRNA. Such enriched RNA fractions proved important in the identification of cDNA clones of P20 mRNA.

Identification of P20 cDNA clones using RNA probes containing different amounts of P20 mRNA

Clones were prepared from polysomal polyadenylated RNA derived from illuminated pea leaves as described in Fig. 2 legend. P20 cDNA clones were identified from the collection of clones by hybridization to RNA probes differentially enriched for P20 mRNA. Clones were arrayed on nitrocellulose filters and hybridized with ^{32}P-phosphate-labelled RNA probes using the method described by Grunstein and Hogness[15]. The probes included RNA from dark-grown leaves (low or devoid of translatable P20 mRNA), RNA from illuminated leaves (high in translatable P20 mRNA), and size fractions of RNA from illuminated leaves differentially enriched for P20 mRNA. The translation products of the RNA preparations used as probes are shown in Fig. 1.

Figure 2 shows the results of hybridization experiments carried out on 97 of the 278 clones tested, and indicates that different colonies show different levels of hybridization. Certain colonies hybridize more strongly to the mRNA probe from illuminated leaves than they do to that from dark-grown leaves (Fig. 2, D and L). One of these colonies (arrowed in Fig. 2) also hybridizes strongly to the probe derived from the size class of RNA most enriched for P20 mRNA (Fig. 2, 1–7). Colonies having the hybridization properties of the colony arrowed in Fig. 2 were therefore tentatively identified as P20 cDNA clones. To observe the probe-dependent differential hybridization shown in Fig. 2, it was necessary to pre-hybridize the filters with an excess of polyadenylic acid. The hybridization was also carried out in the presence of an excess of polyadenylic acid. Without this treatment, we found that clones containing poly(dT-dA) hybridized strongly to all the probes, and this masked the differences due to the differential amounts of coding mRNA sequences in the RNA preparations. Figure 2 [Poly(A)] shows the results of hybridizing the colonies with ^{32}P-phosphate-labelled polyadenylic acid.

Purification of P20 mRNA with cloned cDNA

To establish the identity of clones tentatively described above as containing P20 cDNA, the translation properties of the RNA hybridized by DNA from such clones was investigated. Supercoiled plasmid DNA was purified from liquid cultures of the

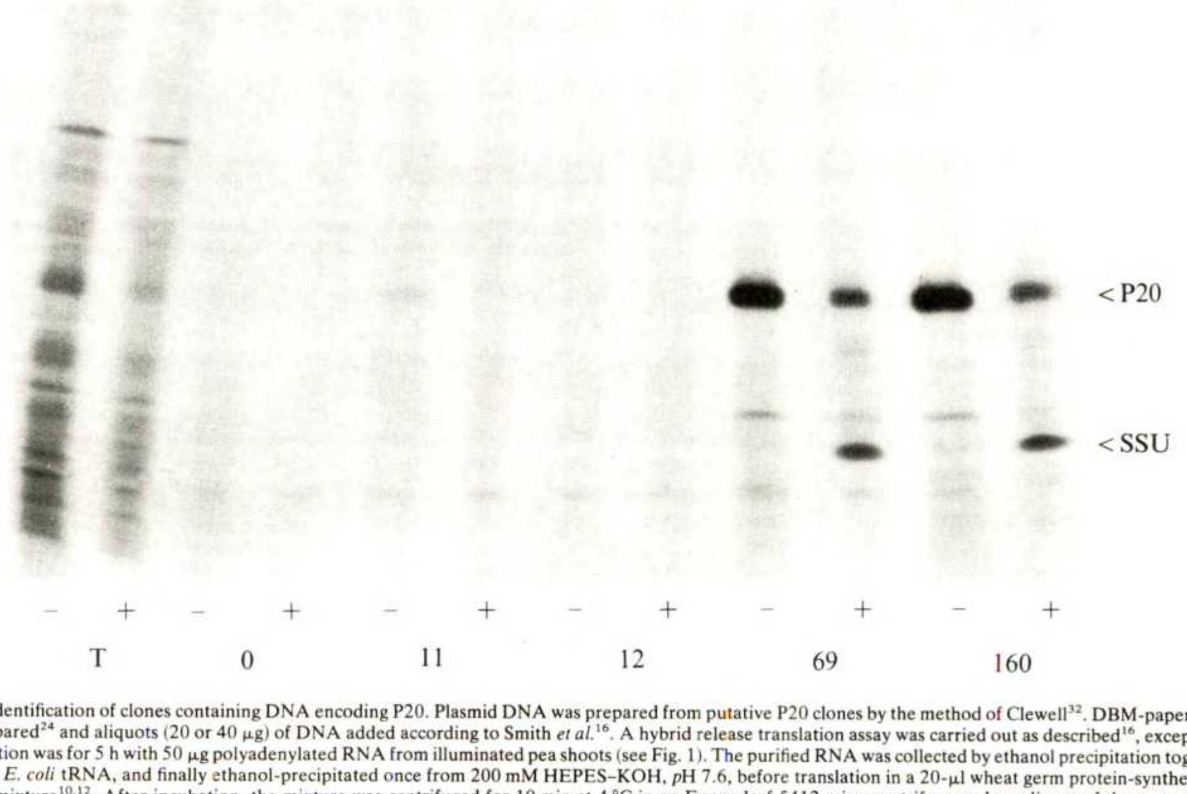

Fig. 3 Identification of clones containing DNA encoding P20. Plasmid DNA was prepared from putative P20 clones by the method of Clewell[32]. DBM-paper discs were prepared[24] and aliquots (20 or 40 μg) of DNA added according to Smith *et al.*[16]. A hybrid release translation assay was carried out as described[16], except that hybridization was for 5 h with 50 μg polyadenylated RNA from illuminated pea shoots (see Fig. 1). The purified RNA was collected by ethanol precipitation together with 6 μg *E. coli* tRNA, and finally ethanol-precipitated once from 200 mM HEPES–KOH, *p*H 7.6, before translation in a 20-μl wheat germ protein-synthesizing reaction mixture[10,12]. After incubation, the mixture was centrifuged for 10 min at 4 °C in an Eppendorf 5412 microcentrifuge and an aliquot of the supernatant solution removed for processing with isolated chloroplasts as described previously[12]. Translation products (9 μl) were incubated with 30 μl intact plastid buffer containing washed chloroplasts (6 μg chlorophyll), isolated from 10-day-old pea seedlings[12]. The non-processed control consisted of adding 9 μl translation products to an equivalent chloroplast preparation that had been denatured by boiling for 1 min in 1% (w/v) SDS. Products were analysed by SDS-polyacrylamide gel electrophoresis and autoradiography as described previously[10,12]. The photograph shows an autoradiograph of the products. T, Translation of total polyadenylated RNA; 0, no RNA; 11, 12, 69, 160, RNA complementary to the respective cloned DNA; −, non-processed control; +, post-translational processing with chloroplasts; P20, precursor to the small subunit of RuBPCase; SSU, small subunit of RuBPCase. The DBM-paper disc bearing DNA from clone 11 had only 20 μg DNA added to it, and had been used in two previous experiments. Other DBM-paper discs had 40 μg DNA added and were previously unused.

colonies and covalently linked to diazobenzyloxymethyl (DBM)-paper[16]. Polyadenylated RNA from leaves of light-grown plants was then hybridized to these DNA filters, and after removal of non-hybridized RNA by washing, the hybridized RNA was recovered for translation[16]. The translation of an RNA species purified by hybridization to cloned DNA encoding P20 would be expected to produce a single polypeptide of MW 20,000. To identify such a polypeptide as P20, a post-translational processing reaction with isolated chloroplasts[10,12] was carried out using an aliquot of the translation products. This treatment should process P20 to the mature small subunit of RuBPCase. Figure 3 shows the results of such experiments. DNA from clone 160 (arrowed in Fig. 2) hybridizes to a mRNA whose translation in the wheat-germ system produced a polypeptide of MW 20,000. We deduce that this polypeptide is P20 from the observation that on incubation with isolated chloroplalsts it is cleaved to a polypeptide which co-migrates with the mature small subunit of RuBPCase. Clone 12 provides a control for this experiment because it is shown to encode a minor polypeptide of MW ~29,000. We conclude from this experiment that clone 160 contains DNA encoding P20; this is confirmed by DNA sequence analysis (see below).

The translation products of the RNA purified by hybridization to the DNA of clone 160 includes other low molecular weight polypeptides in addition to P20. These other minor products have not been characterized because the identity of the cloned DNA was confirmed by nucleotide sequence analysis. However, we believe that they probably represent partial P20 polypeptide sequences generated as a result of RNA degradation during hybridization, or due to the infidelity of the wheat-germ protein-synthesizing system. The amount of polypeptide of about 15,500 MW decreases on incubation with isolated chloroplasts. After processing with isolated chloroplasts, an additional polypeptide of MW 18,000 is observed (Fig. 3). This product may represent either an intermediate in the processing of P20 to the mature small subunit or may arise from incorrect processing.

Several clones with properties identical to those of clone 160 were identified among the collection of clones prepared by the synthetic *Hin*dIII-linker procedure. Two clones (numbers 11 and 69) are included in the experiment shown in Fig. 3. The inserted sequence was purified from the plasmid of clone 160 (designated pSSU160) and used to screen for plasmids containing P20 cDNA in clone banks prepared by the homopolymer tailing method (see Fig. 2). The clones were used for sequence studies on the inserted cDNA.

DNA and polypeptide sequence determination

cDNA clones identified as P20 clones by the methods described above were used to determine the nucleotide sequence of P20 mRNA by the method of Maxam and Gilbert[17]. Both the physical map for P20 cDNA and the sequencing scheme are shown in Fig. 4*a*. The map was determined by a combination of hybridization methods[18], multiple digests with various restriction enzymes and the end-labelling procedure of Smith and Birnstiel[19]. Figure 4*a* illustrates the map position of some of the cDNA clones used in the sequencing. Figure 4*b* gives the determined nucleic acid sequence and the deduced amino acid sequence. The deduced amino acid sequence of the mature small subunit has been confirmed by sequence analysis, carried out directly on purified pea small subunit (I. A. H. Takruri, D. Boulter and R. J. Ellis, unpublished results). The molecule consists of 123 amino acids with a calculated MW of 14,480. The sequence shows considerable homology with that of the spinach molecule[20]; 89 residues are the same in both species. As the C-terminal amino acid codon is followed immediately by a termination codon (TAA), we conclude that the entire additional amino acid sequence of P20 is located at the N-terminus of the mature small subunit polypeptide. Schmidt *et al.*[21] have determined that the small subunit precursor in *Chlamydomonas*

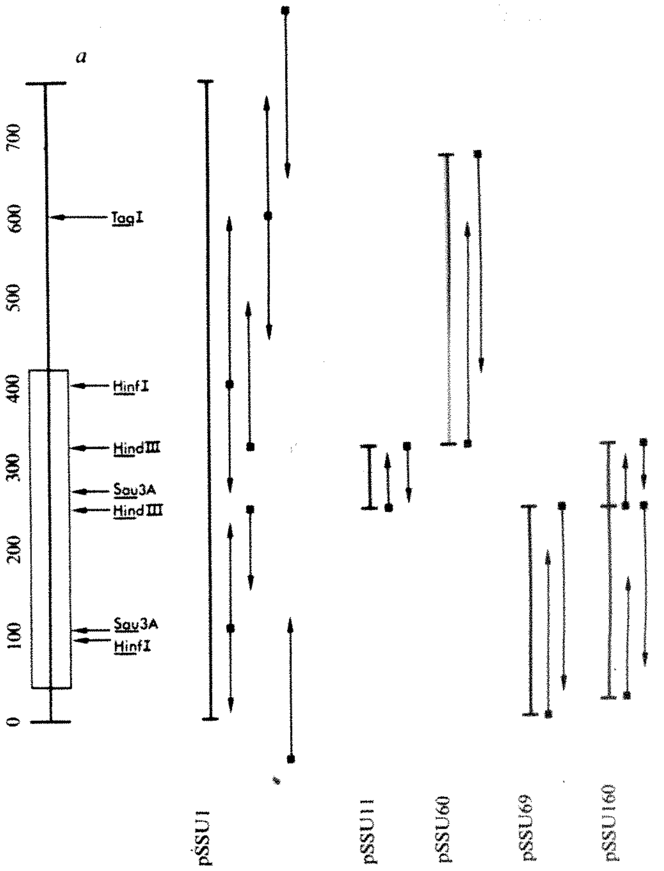

b

```
 N  T  D  I  T  S  N  G  E  R  V  K  C  M  Q  V  W  P  P  I  G  K  K  K  F
AACACTGACATTACAAGCAATGGTGAAAGAGTAAAGTGCATGCAGGTGTGGCCTCCAATTGGAAAGAAGAAGTTT
        10        20        30        40        50        60        70

 E  T  L  S  Y  L  P  P  L  T  R  D  Q  L  L  K  E  V  E  Y  L  L  R  K  G
GAGACTCTTTCCTATTTGCCACCATTGACGAGAGATCAATTGTTGAAAGAAGTTGAATACCTTCTGAGGAAGGGA
   80        90       100       110       120       130       140       150

 W  V  P  C  L  E  F  E  L  L  K  G  F  V  Y  G  E  H  N  K  S  P  R  Y  Y
TGGGTTCCATGCTTGGAATTTGAGTTGCTCAAAGGATTTGTGTACGGTGAGCACAACAAGTCACCAAGATACTAT
       160       170       180       190       200       210       220

 D  G  R  Y  W  T  M  W  K  L  P  M  F  G  T  T  D  P  A  Q  V  V  K  E  L
GATGGAAGATACTGGACAATGTGGAAGCTTCCTATGTTTGGCACCACTGATCCTGCTCAAGTCGTGAAGGAGGTT
  230       240       250       260       270       280       290       300

 D  E  V  V  A  A  Y  P  E  A  F  V  R  V  I  G  F  N  N  V  R  Q  V  Q  C
GATGAAGTTGTTGCCGCTTACCCCGAAGCTTTCGTTCGTGTCATCGGTTTCAACAACGTTCGTCAAGTTCAATGC
       310       320       330       340       350       360       370

 I  S  F  I  A  H  T  P  E  S  Y
ATCAGTTTCATTGCACACACACCAGAATCCTACTAAGTTCACTGCATTGGAGTTCCTATTTATATGTTATGCTTT
  380       390       400       410       420       430       440       450

TAAGTTCCTTTTGTTGTGTATTTTTATAATTTCTGTTTTTGGATTTCCAAATTGCAAATGGGATGTGTGTAAGAG
       460       470       480       490       500       510       520

TTAATGAATGATATGGTTAACTTTATTCCCAAGTTTACTTGGCGGTTTGTACTGTGTGGCTTTCGTTGTTCAGTG
  530       540       550       560       570       580       590       600

TTCGACATCTGTTGGTCCAAGTGGTAACACTGGCACAGGTACGTATTGGTCGGTGTTTGTGTATCCT-Poly A
       610       620       630       640       650       660
```

Fig. 4 Physical map and nucleotide sequence of P20 cDNA. *a*, The upper line gives the location of restriction enzyme targets used in sequencing experiments. The numbers refer to nucleotide base pairs. The blocked region between nucleotides 40 and 408 represents the coding sequence for the mature small subunit. The lower lines indicate the region of the map covered by specific clones. The homopolymer tailing procedure was used to obtain pSSU1 whereas pSSU11, 60, 69 and 160 were prepared using the *Hin*dIII-linker sequence procedure. The arrows under each of the clone maps indicate the start points and directions of sequence reading. The sequencing was carried out by the Maxam and Gilbert technique[17]. For pSSU1 the labelled 5′ ends of the various fragments were separated by cleavage with a second restriction endonuclease. For pSSU11, 60, 69 and 160 the labelled 5′ ends were separated either by strand separation or by cleavage with a second restriction endonuclease. *b*, The nucleotide sequence is that determined for the coding strand of the cloned DNA. The deduced amino acid sequence is indicated above the nucleotide sequence, in single-letter notation. The N-terminus of the mature small subunit is indicated by an arrow.

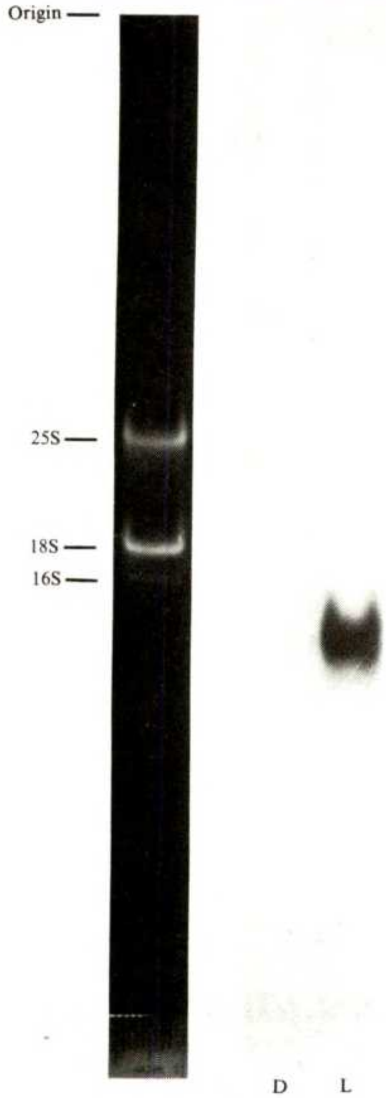

Fig. 5 Identification of P20 mRNA by hybridization with the cloned DNA probe. Samples (2.5 μg) of each of the two RNA preparations whose translation products are shown in Fig. 1*a* were glyoxalated according to McMaster and Carmichael[23]. This RNA was fractionated by agarose-gel electrophoresis, then transferred by blotting to DBM-paper[24] for subsequent hybridization to the cloned P20 DNA probe. Plasmid DNA was prepared from clones 60 and 160 (Fig. 4*a*) as described by Clewell[32]. DNA was digested with *Hin*dIII and fractionated by polyacrylamide-gel electrophoresis[33]. Gel pieces containing P20 DNA were excised and the DNA eluted at 37 °C for 10 h with 0.5 M $(NH_4)_2CH_3COOH$, 0.1 mM Na_2EDTA, 5 mM Tris-HCl *p*H 8.0. The purified DNA was collected by ethanol precipitation, and the different P20 DNA sequences were mixed in equimolar amounts. DNA was radioactively labelled by nick-translation[34] using [α-^{32}P]dCTP (Amersham) to a specific activity of 5×10^7 c.p.m. per μg DNA. Hybridization of this DNA to the RNA immobilized on DBM-paper was as described by Alwine *et al.*[24], using 10^6 c.p.m. per 100 cm^2 paper. After hybridization for 16 h at 42 °C, the paper was washed 3×30 min at 60 °C in $2\times$SSC, dried and exposed to X-omat H film (Kodak) with intensifying screens for 2 days. Shown here is a photograph of the autoradiograph. D, RNA from leaves of peas grown in darkness for 9 days; L, RNA from leaves of peas grown in darkness for 9 days followed by 48 h continuous illumination (see Fig. 1*a*). The electrophoretic mobilities of cytoplasmic ribosomal RNAs (25S and 18S) and 16S chloroplast ribosomal RNA are shown by the UV fluorescence photograph of a track of the same gel in which 2.5 μg total pea leaf RNA was fractionated and stained with ethidium bromide. Low molecular weight ribosomal RNAs are not seen in this RNA because its preparation involved precipitation from 2.5 M NaCl.

contains 44 additional amino acid residues at the N-terminus, but did not investigate the C-terminus. The available DNA sequence to the 5′ side of the ATG codon which specifies the N-terminal methionine residue of the mature small subunit encodes 13 amino acid residues. We deduce that these amino acid residues comprise part of a longer N-terminal extension. The elucidation of the complete sequence of this N-terminal extension awaits further molecular cloning.

Polyadenylated mRNAs from eukaryotes commonly contain the hexanucleotide 5′ AAUAAA 3′, about 20 nucleotides from the poly(A) tail[22]. Figure 4*b* shows that no such sequence occurs in the 3′ non-coding sequence of P20 mRNA. The 3′ non-coding sequence, including the translation termination codon, represents 260 nucleotides. The 3′ terminus of pSSU1 contains 98 A residues. Together with the deduced coding sequence of 408 nucleotides, our clones account for 766 residues of P20 mRNA.

Use of cloned DNA as a hybridization probe for P20 mRNA

The strategy for identifying cDNA clones encoding P20 depended on the assumption that the amounts of P20 mRNA in polyadenylated RNA preparations from dark-grown and illuminated pea leaves were reflected in the *in vitro* translation products of those RNAs. The success of this approach implies that our assumption is correct. The availability of cloned cDNA sequences enabled us to check this assumption. Further, we were able to determine the extent to which the size of the P20 mRNA molecule correlates with the cloned sequences which total 766 nucleotides (Fig. 4*a*). Equal amounts of the polyadenylated RNAs whose translation products are shown in Fig. 1*a* were denatured by glyoxalation and fractionated by agarose gel electrophoresis[23]. The fractionated RNA was transferred to DBM-paper and hybridized with the cloned P20 cDNA probe labelled by nick-translation[24]. The results of this analysis are shown in Fig. 5. The probe hybridizes to an RNA species of 900–1,000 nucleotide residues which is observed only in the RNA from illuminated leaf tissue. We conclude that this RNA species is P20 mRNA and that our cloned sequences encode most of this molecule.

The results presented here thus suggest various approaches for increasing our understanding of chloroplast development. We have predicted part of the amino acid sequence of the P20 polypeptide that is removed on entry into the chloroplast[10–12]. There is no apparent homology between this sequence and that of signal peptide sequences occurring in secreted animal proteins[25]. This is not surprising in view of the fact that a different mechanism is used to transport proteins into chloroplasts[2,10]. Furthermore, no significant homology is observed when comparing the pea P20 sequence with that from *Chlamydomonas*[21]. Again, this is not surprising because the *Chlamydomonas* polypeptide is not processed by pea chloroplasts[11]. Further sequence analysis with other cytoplasmically synthesized chloroplast polypeptides is necessary to determine whether any sequence rules are operating, and how they vary between species. The availability of cloned probes for the small subunit of RuBPCase will allow P20 to be prepared free from other labelled polypeptides, thereby facilitating investigation of its postulated interaction with proteins in the chloroplast envelope[10]. The nature of the control of P20 synthesis by light and the structure of the nuclear gene for this chloroplast polypeptide can also now be studied.

This work was supported by an EMBO long-term fellowship to J.R.B. and an SRC studentship to S.M.S. We thank Dr R. B. Flavell for laboratory facilities at the Plant Breeding Institute. Genetic manipulations were carried out under category II containment conditions as defined by GMAG (UK).

Received 10 July; accepted 21 August 1980.

1. Ellis, R. J., Smith, S. M. & Barraclough, B. R. in *Genome Organisation and Expression in Plants* (ed. Leaver, C. J.) 321–335 (Plenum, New York, 1980).
2. Chua, N-H. & Schmidt, G. W. *J. Cell Biol.* **81,** 461–483 (1979).
3. Ellis, R. J. *Trends biochem. Sci.* **4,** 241–244 (1979).
4. Jensen, R. G. & Bahr, J. T. *A. Rev. Pl. Physiol.* **28,** 379–400 (1977).
5. Coen, D. M., Bedbrook, J. R., Bogorad, L. & Rich, A. *Proc. natn. Acad. Sci. U.S.A.* **74,** 5487–5491 (1977).
6. Bedbrook, J. R., Coen, D. M., Beaton, A. R., Bogorad, L. & Rich, A. *J. biol. Chem.* **254,** 905–910 (1977).

7. Blair, G. E. & Ellis, R. J. *Biochim. biophys. Acta* **319,** 223–234 (1973).
8. Kawashima, N. & Wildman, S. G. *Biochim. biophys. Acta* **262,** 42–49 (1972).
9. Dobberstein, B., Blobel, G. & Chua, N. H. *Proc. natn. Acad. Sci. U.S.A.* **74,** 1082–1085 (1977).
10. Highfield, P. E. & Ellis, R. J. *Nature* **271,** 420–424 (1978).
11. Chua, N. H. & Schmidt, G. W. *Proc. natn. Acad. Sci. U.S.A.* **75,** 6110–6114 (1978).
12. Smith, S. M. & Ellis, R. J. *Nature* **278,** 662–664 (1979).
13. Blobel, G. & Dobberstein, B. *J. Cell Biol.* **67,** 835–851 (1975).
14. Link, G., Coen, D. M. & Bogorad, L. *Cell* **15,** 725–731 (1978).
15. Grunstein, M. & Hogness, D. S. *Proc. natn. Acad. Sci. U.S.A.* **72,** 3961–3965 (1975).
16. Smith, D. F., Searle, P. F. & Williams, J. G. *Nucleic Acids Res.* **6,** 487–506 (1979).
17. Maxam, A. M. & Gilbert, W. *Proc. natn. Acad. Sci. U.S.A.* **74,** 560–564 (1977).
18. Bedbrook, J. & Bogorad, L. *Proc. natn. Acad. Sci. U.S.A.* **73,** 4309–4313 (1976).
19. Smith, H. O. & Birnstiel, M. L. *Nucleic Acids Res.* **3,** 2387–2398 (1976).
20. Martin, P. G. *Aust. J. Pl. Physiol.* **6,** 401–408 (1979).
21. Schmidt, G. W., Devilliers-Thiery, A., Desruisseaux, H., Blobel, G. & Chua, N.-H. *J. Cell Biol.* **83,** 615–622 (1979).
22. Cheng, C. C. *et al. J. molec. Biol.* **107,** 527–547 (1976).
23. McMaster, G. K. & Carmichael, G. G. *Proc. natn. Acad. Sci. U.S.A.* **74,** 4835–4838 (1977).
24. Alwine, J. C., Kemp, D. J. & Stark, G. R. *Proc. natn. Acad. Sci. U.S.A.* **74,** 5350–5354 (1977).
25. Austen, B. M. *FEBS Lett.* **103,** 308–313 (1977).
26. Loening, U. E. *Biochem. J.* **113,** 131–138 (1969).
27. Myers, J. C. & Spiegelman, S. *Proc. natn. Acad. Sci. U.S.A.* **75,** 5329–5333 (1978).
28. Boyer, H. W. *et al.* in *Recombinant Molecules; Impact on Science and Society* (eds Beers, R. F. & Bassett, E. G.) (Raven, New York, 1977).
29. Boyer, H. W. & Roulland-Dossaix, D. *J. molec. Biol.* **41,** 459–472 (1969).
30. Roychoudhury, R., Jay, E. & Wu, R. *Nucleic Acids Res.* **3,** 101–116 (1976).
31. Maizels, N. *Cell* **9,** 431–438 (1976).
32. Clewell, D. B. *J. Bact.* **110,** 667–676 (1972).
33. Dingman, C. W. & Peacock, A. C. *Biochemistry* **7,** 659–668 (1968).
34. Rigby, P. W. J., Dieckmann, M., Rhodes, C. & Berg, P. *J. molec. Biol.* **113,** 237–251 (1977).

Cell cycle and experimental pattern duplication in the chick wing during embryonic development

J. Cooke & D. Summerbell

Division of Developmental Biology, National Institute for Medical Research, The Ridgeway, Mill Hill, London NW7 1AA, UK

Transient stimulation of cell division within chick wingbud mesenchyme is associated with the reorganization of limb pattern that follows insertion of a small graft from the posterior zone of limb polarizing activity into the anterior border of a host bud. This increase is initiated as an enhanced rate of entry to S phase, correlated with a decrease in packing density among mesenchyme cells, through much of the limb rudiment a few hours after the operations.

GROWTH CONTROL and pattern formation during embryonic development have been largely considered separately in recent years (but see refs 1, 2), because the spatial pattern for differentiation must be determined by direct cellular interactions during early stages, whereas growth has mainly been studied at much later (fetal) stages, where control through circulating hormones of varying degrees of target specificity has been documented[3,4]. There is, nevertheless, indirect evidence from stages of pattern formation for very local intercellular mechanisms, influencing the rate or amount of cell division in relation to the positional information or position value[5] that is determining which parts of patterns the cells concerned are to construct[6–10].

Relationships between intercellular signal systems controlling the cell cycle and those controlling pattern vary with stage of development. Determination of pattern up to gastrula stages in vertebrates and echinoderms is quite independent of the schedule of cell division which reflects the determination of the pattern rather than determining it[11–13]. By contrast, in regeneration of insect epidermal patterns after deletion of tissue, replacement and regulation of pattern occur very largely within new tissue specially grown as a response to the disturbance[6,7]. If generally circulating hormones and their cell-bound receptors mediate growth control in the differentiated and functioning body, while strictly local growth control via cell-bound positional codes is involved in pattern regeneration and the initial building of certain 'second-order' patterns[14] during post-gastrular development, we might expect at certain phases of embryonic life to observe signalling systems for growth which are intermediate between these extremes. We have studied the early wing rudiment in the chick as such a second-order embryonic field[14,15], in which pattern is actually being determined during extensive growth.

Within the chick wingbud, grafting a small piece of mesenchyme from a posterior limb-field region (the zone of polarizing activity, ZPA) into an anterior position leads to duplication of the wing pattern about its normal anterior border (Fig. 1)[16]. It has been suggested that an increase in the antero-posterior dimension, or width of the outgrowing bud, is a necessary accompaniment of successful duplication[17].

We have examined changes in the cell cycle within the host bud during the very early period after ZPA grafting, and compared this with the effect of a graft from an anterior donor position similar to the implantation site, an operation causing at most a small pattern disturbance (see later discussion) but usually resulting in quite normal development. The system is a sensitive one for cell cycle studies, as right and left buds are normally closely coordinated in their development[18], and equivalent populations of many thousands of cells can be scanned for uptake after labelling with ^{3}H-thymidine *in ovo*, and scored for mitotic incidence.

Hen's eggs after 3.5 days of incubation (a mixed local strain, Needle Farm, Hamburger & Hamilton, stage 19–20) were windowed and the right limb area of embryos exposed by removal of membranes. Operations grafting a piece of donor right wingbud mesenchyme with overlying ectoderm into a prepared anterior site were performed as described elsewhere[19]. In experimental cases the piece came from a posterior region known to possess polarizing activity (opposite somites 19/20, at stage 19), whereas in control operations it was from a donor position similar to the host site, opposite somite 16 at the same stage. Eggs were re-sealed with Sellotape and incubated for 4, 8 or 16 h before onset of ^{3}H-thymidine labelling. Figure 1*a* shows these operations in diagrammatic form, and Fig. 1*b* shows the morphogenesis that is finally seen after successful ZPA operations (about 90%) at 10 days of incubation.

The embryos were allowed to incorporate label for 1 h, then fixed. Figure 2 shows the appearances of typical fields within autoradiographs of sections through limb-bud mesenchyme (see legend for details of labelling, fixation, sectioning and staining). Whole buds were dissected free as right–left pairs during dehydration, embedded in Araldite and sectioned transverse to their own proximo-distal axes at 2 μm. All cells visible at each sectional level, distalwards from that where the graft–host junction was visible in the right limb, were scanned as sample populations for labelling index (proportion of nuclei in S phase at some time during the hour before fixation). This was done by dividing the mesenchyme outline concerned into four (or, at the tip, two) parts of equal antero-posterior extent (not equal area) to form boxes. The nuclear population within such boxes was usually between 500 and 1,100, and where fewer cells were transected near the bud tip, pairs of adjacent boxes in the proximo-distal sense were pooled. Data were collected directly with an electronic colony-counter (labelled + total nuclei) and by planimetry, from photographs of standard magnification. The

0028–0836/80/430697—05$01.00

data boxes are represented in grid plan form for each limb of the pairs shown in Fig. 2. Counts from replica photographs lie within 2% for both cell totals and labelling index, with the latter distributed around 35%. A typical cell packing density is 10,000 cells mm^{-2} of mesenchyme in these transverse sections.

Mitotic index (metaphases per 100 cells) as seen in the toluidine blue images was estimated for the whole population at each sectional level in some limb pairs, from the total cells visible per section (a large number with small relative variation among sections from a level) and the mitoses scored in four to six sections (a small number, of much greater relative variation as it records infrequent events). Estimates of mitotic index lie between 3 and 6% by this method, and are expressed here as % relative difference on the operated in relation to the left side (that is, a mitotic index of 6% is 100% enhancement over 3%). Even with effective samples at each level of 6–10,000 cells, only enhancements of around 25% or more on the right as compared with the left will reach statistical significance ($P < 0.01$), whereas much smaller relative differences in labelling incidence are significant with comparable sample sizes because the absolute incidence is so much higher.

Cell cycle stimulation spreads through host mesenchyme after ZPA grafts

We have analysed in detail two limb pairs labelled between 4 and 5 h after ZPA grafts (5-h limbs), two labelled between 8 and 9 h (9-h limbs) and one labelled between 16 and 17 h (by this stage, selection of visibly successful operations is possible because of the onset of width and shape changes that predict pattern duplication). A further visibly successful 17-h pair has been analysed for mitotic incidence only.

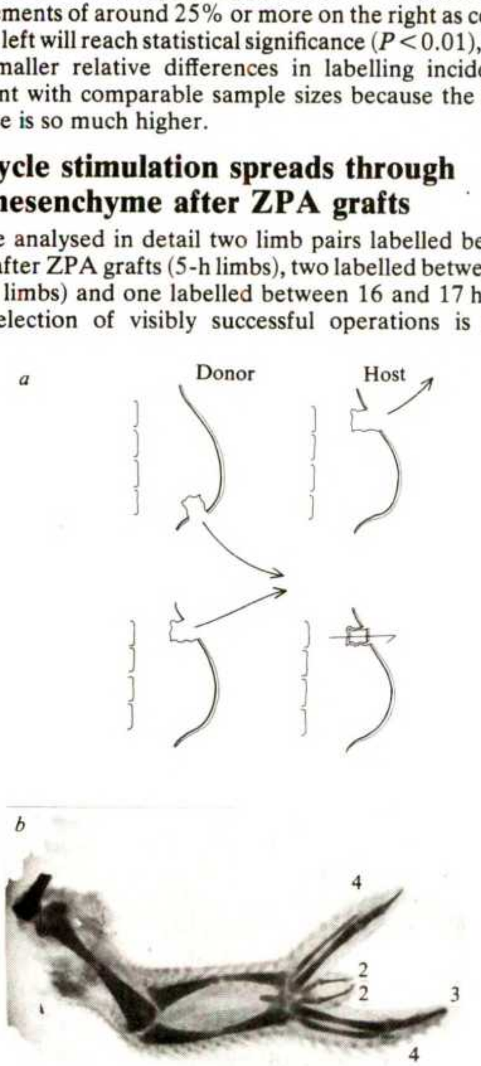

Fig. 1 The grafting operation. *a*, The diagram shows the graft site on the host, and the origin of the graft for ZPA and for sham operations. *b*, Typical result of a ZPA graft at 10 days of development, showing antero-posterior reduplication, together with contralateral control limb. The normal conventions of 2, 3, 4 (relative to a primitive pendadactyl limb pattern of 1–5) are observed for characterizing the digits. Scale bar, 1 mm.

Three anterior → anterior grafted (control) limbs and their left counterparts were examined for S-phase incidence and cell packing density after 8–9 h labelling, and two further 17-h pairs, one control-operated and one after an apparently unsuccessful ZPA graft (in view of lack of shape changes) were analysed for mitotic incidence only. Only host mesenchyme tissue is analysed, the boundary between host and small, discrete graft mesenchymal mass being still evident at these times. The large body of data collected per limb, and the magnitude in biological terms of the effects seen, assures us that our results document real events associated with ZPA implantation.

Figure 3 displays the spatial distribution of labelling index as determined within three of the experimental limb pairs and two of the control-operated pairs. It can be seen that a spatial pattern tends to exist in normal limb buds at these stages (around 21) whereby this index falls off from distal to proximal and from posterior to anterior borders within the mesenchyme. Variation in overall labelling incidence between embryos is unavoidable, probably because of biological variation and variation in precise conditions for ^{3}H-thymidine uptake during the experimental processing of groups of eggs. There is an enhancement of labelling index in ZPA grafted limbs, relatively local at 5 h, and widespread but concentrated on the anterior side at 9 and 17 h. The effect is not confined to the proximal level of the graft–host junction. A highly comparable sampling of the anatomy is made and 5–10,000 cells are involved in the grand total indices for each limb of each pair, so that the overall enhancements are highly significant ($P < 0.005$), even that within the 5-h pairs. Within individual data boxes, increases in labelling index of 8–10% over the left-hand equivalent (that is, 25–40% relative increase in S-phase entry over the hour, significant at $P < 0.01$) are typical within affected limb regions at each stage. The 9-h pair not illustrated showed an S-phase effect extremely similar on a quantitative and spatial basis to that in Fig. 3, whereas the other 5-h pair showed enhancement near the graft site comparable to that displayed, but could not be analysed spatially due to non-comparable planes of section in right and left buds.

None of the three control-operated 9-h pairs showed an S-phase effect on the right comparable with that seen after ZPA grafting to the anterior site. No overall enhancement was detectable even within the anterior half-mesenchyme total of right as compared with left side (28.4%, 31.6% and 33.9% right anterior half grand total labelling index, compared with 30.2%, 30.3% and 32.0% on left sides, respectively), whereas analysis of each 9-h ZPA pair reveals even posterior half-mesenchymal labelling index to be significantly enhanced within right limbs ($P < 0.01$). We deduce from this that the left is indeed an appropriate control for the right limb within individuals in terms of access of label, which would be essentially via the embryo's circulation. We consistently observe that mean grain density over labelled nuclei appears qualitatively greater in regions (especially in ZPA limbs) of highest labelling incidence among nuclei (see Fig. 2). The rate of DNA synthesis within S phase is probably correlated with the rate of cycle in cells that are susceptible to growth control (see below). The spread of stimulation of entry to S phase, through mesenchymal tissue, is therefore strongly associated with positional disparity between graft origin and implantation site within the rudiment, this disparity being itself generally necessary for the occurrence of new pattern formation as well as the morphological signs of early widening.

Full analysis reveals, however, in one out of the three control-operated cases (Fig. 3), a strong labelling enhancement in certain data boxes adjacent to the graft. This could reflect an effect on the cell cycle of local disturbance to the tissue integrity by the grafting operation, but it may occur because even an 'anterior-to-anterior' graft will induce some cell positional disparity, and any degree of such disparity triggers morphogenetic interactions to some extent (see below).

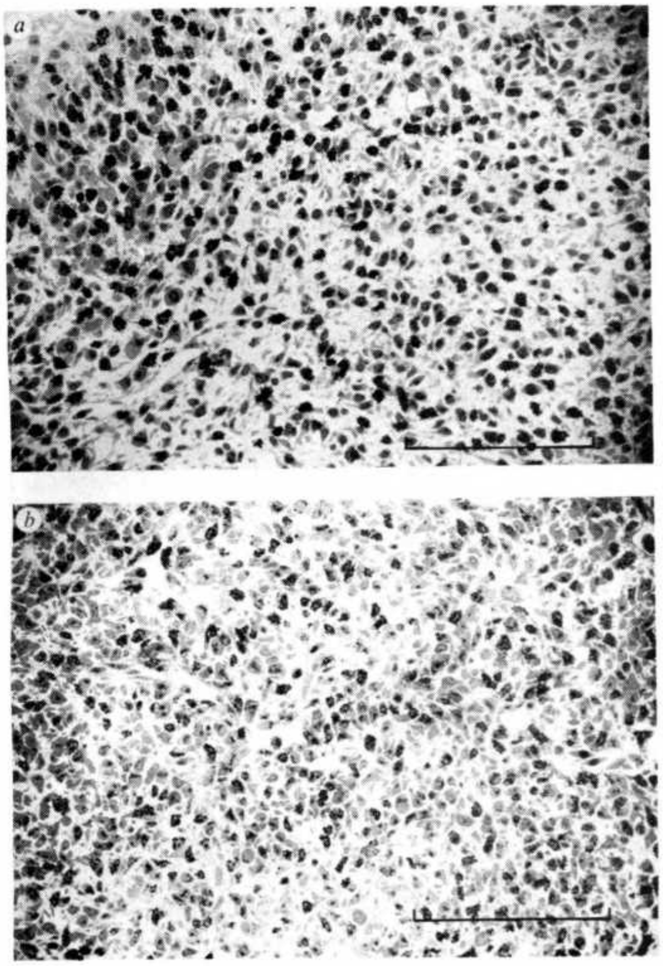

Fig. 2 Typical fields in autoradiographs of a 9-h limb pair. 500 KBq of ^{3}H-thymidine (TRK 120 [*Me*-^{3}H]thymidine, 720 GBq mmol^{-1}) in 100 µl of warm BSS were dropped into the opened amniotic cavity of each embryo. Eggs were resealed and incubated for 1 h at 38.5 °C. Embryos were then dissected off their chorio-allantoic membranes, removed from the egg and placed in warm BSS for 5 min, during which perfusion of the vascular system with BSS due to continued heart beat and the open circulation acted to lower background radioactivity. They were then fixed in half-strength Karnovsky fluid at *p*H 7.3, dehydrated in graded alcohols and propylene dioxide and embedded in Araldite. A small set of 2-µm sections from each limb of each pair, parallel to the embryo's long axis, was collected at each 50- or 100-µm interval along the proximo-distal axis, mounted on a subbed slide, dipped in Ilford K2 emulsion, exposed for 14 days, developed in Ilford D19 for 5 min at 20 °C, air dried and stained for 1 min in toluidine blue in 0.1% borax solution at 80 °C. This procedure strongly labels 25–50% of mesenchyme nuclei in various regions of control and experimental limbs, with very low background and no labelled mitoses. *a*, Anterior (pre-axial) region, labelled 8–9 h after ZPA grafting. Labelling index within the field is 32% and mean cell density 8,500 per mm^2. *b*, Anterior (pre-axial) region in the left, control limb for *a*. Labelling index is 23% and mean cell density 11,100 per mm^2. Scale bars, 100 µm.

Table 1 gives the relative mitotic incidence for the operated as opposed to the left side, in four ZPA grafted pairs and the two 17-h pairs acting as controls. Mitotic enhancement does not become significant before our 17-h time point, but is then dramatic, lying between 50 and 100% at various proximo-distal levels in the two ZPA grafted limbs examined. S-phase entry is responding at least as vigorously in both 9-h limbs (some 25% relative enhancement overall) as at 17 h, and has responded strikingly on a local level by 5 h. These data indicate that the signal caused by newly introduced positional disparity exerts a primary effect on the mesenchymal cell 'cycle' at a point near the passage from a G_1/G_0 condition into the determinate sequence that includes DNA synthesis and culminates in mitosis[20]. This resembles the situation found for conditions that control growth of cultured cells, and means that significant extra production of tissue would set in over the period (9–17 h post-operatively) when indeed width change is first observed. None of the control pairs (three 9-h, two 17-h) showed a trace of the massive mitotic effect seen in successful experimental limbs at 17 h.

The greater proportional enhancement of mitotic, as opposed to labelling, incidence seen at the peak of response can be understood by supposing that the actual time spent in mitosis is little changed during faster growth, whereas time taken by S may decrease in partial adaptation to a faster cell cycle[21,22]. Mitotic incidence might therefore be the more sensitive index of relative cycle time even though ^{3}H uptake reveals changes closer to the control point in the cycle.

Previous work has documented a general inverse, though complex relationship between mitotic index and cell packing density in normal early wingbuds. Our records of cell packing, in our control and experimental mesenchymes, both confirm this for S-phase and show that where the latter has been stimulated by the morphogenetic interactions we are studying, a correlated decrease of cell packing immediately occurs as exemplified in Fig. 2 (D.S. and J.C., in preparation).

Pattern formation and the control of size in wingbud mesenchyme

Our experiments suggest that, by contrast with a previously studied gastrular embryonic organiser[11], the ZPA region may control not only the spatial pattern of fates in limb tissue, but also the production of sufficient tissue to allow establishment of a normal version of pattern.

The postero-anterior decline in mesenchymal S-phase incidence, and the nonlinear aspect of the normal fate-map, whereby tissue whose fate is to form various parts of the structure is 'crowded' towards the posterior in the early bud (see Fig. 4 and refs 23, 24), are both consistent with the idea of a continuous, graded growth signal emanating from the posterior in normal development. However, the growth-stimulating effect of an anterior ZPA graft cannot simply be interpreted as an induction of 'posteriorness' in an anterior strip of tissue by

Table 1 Mitotic incidence at each proximo-distal level of right (operated) limb buds, expressed as % relative difference from the homologous left bud level, for five limb pairs

Limb pair	Level	Relative difference
Pair 623	1−	− 17%
Op. + 5 h	1+	+ 12%
	2	+ 14%
Pair 619	1	+ 26%
Op. + 9 h	2	+ 18%
	3	− 12%
	4	+ 12%
	5	+ 15%
Pair 634	2	+ 88%*
Op. + 17 h	3	+124%*
	4	+ 62%*
	5	+ 72%*
Pair 240	2	+ 56%*
Op. + 17 h	3	+ 52%*
	4	+ 49%*
	5	+ 65%*
Pair 632	2	+ 11%
Op. + 17 h	3	− 17%
failing to show width	4	− 8%
and shape change	5	+ 12%
Pair 633	2	− 13%
Sham op. + 17 h	3	+ 21%
	4	− 9%
	5	− 15%

Mitoses were pooled from four or six replica sections (toluidine blue, scanned at ×250) and related to the mean number of cells visible at each sectional level. Absolute mitotic index was ~3–6% in this work.

* Only differences between buds in pairs 634 and 240 were significant ($P < 0.01$).

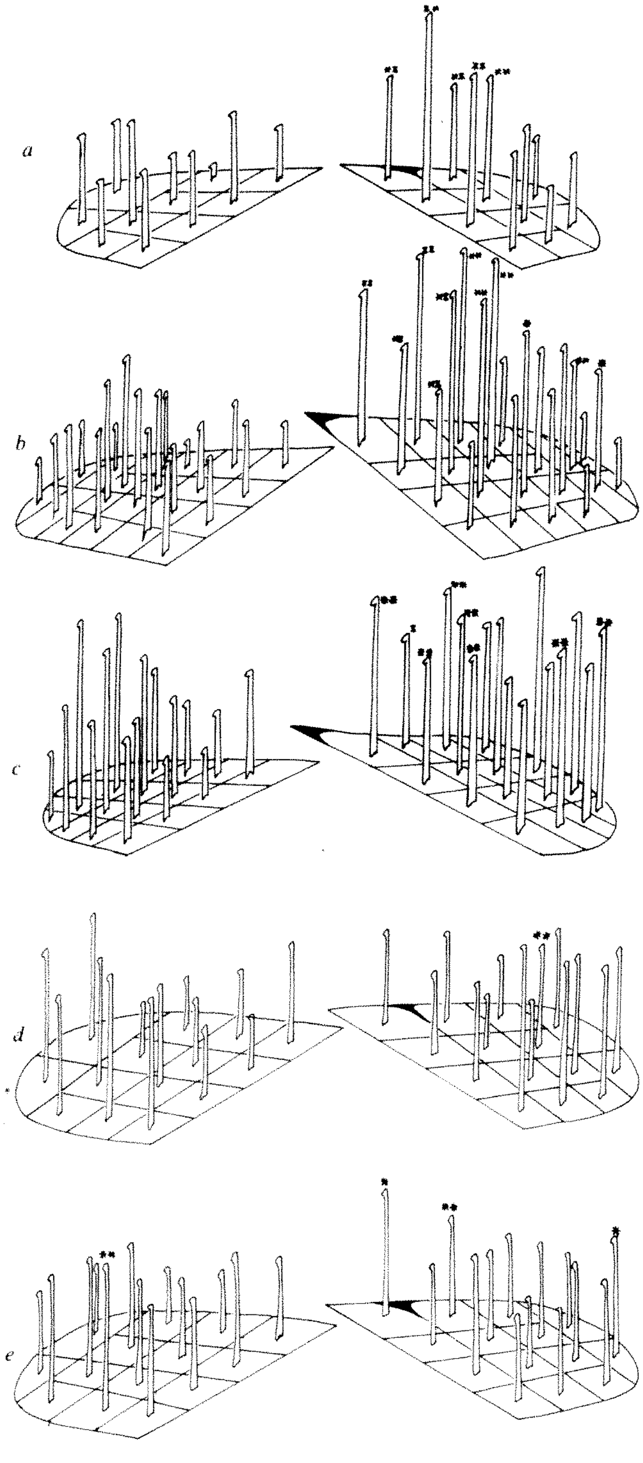

Fig. 3 Spatial variation in labelling index within limb pairs. Each outline represents a single limb-bud with dorsal surface viewed obliquely from the posterior, the (proximal) junction with the body towards the centre. They are arranged in pairs from single embryos, operated ones being on the right-hand side. Each box represents the cell population sampled in an area of mesenchyme derived by dividing the total cross-section visible at that proximo-distal level into four (or sometimes, distally, two) areas of equal antero-posterior width, and thus includes some 500–1,100 (usually around 800) nuclei. Solid corners anteriorly indicate those boxes where graft–host junction was visible. The column height in each box represents the labelling index there, in excess of an arbitrary baseline of 20% (the highest index shown being of 57%, in the 17-h experimental limb). Single and double asterisks above columns signify, respectively, an enhancement over the index of the homologous box in the control limb significant at $P < 0.05$ and $P < 0.01$. Lengths of the proximal baselines of each limb pair are drawn proportional to the total anterior-posterior widths of proximal cross-sections, but no attempt is made to depict the detailed shapes of bud outlines. *a*, Limb pair labelled from 4 to 5 h after a ZPA graft; *b*, limb pair labelled from 8 to 9 h after a ZPA graft; *c*, limb pair labelled from 16 to 17 h after a ZPA graft, where preliminary shape changes (indicating width increase) were visible externally in the right bud. *d,e*, Two limb pairs labelled from 8 to 9 h after an anterior → anterior (control) graft.

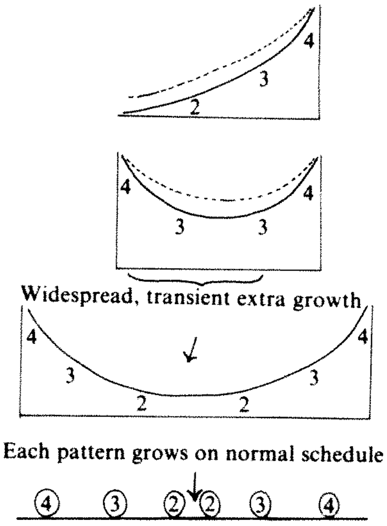
4
3
2
4
4
3
3
Widespread, transient extra growth
4
4
3
3
2
2
Each pattern grows on normal schedule
④ ③ ②②③ ④

Fig. 4 Outline model for relationship of limb pattern specification to early growth control. Pattern-controlling and growth-promoting signals in the system are seen as distinct entities, and perhaps only loosely correlated in profile at any time, although both organized from the ZPA and of a general gradient form. Cells may respond to the growth signal according to its 'rate of flux' as well as its absolute level, so that cycle stimulation is most pronounced locally soon after ZPA grafts, before the system reaches equilibrium (see, for example, Fig. 3*a*). The process of assigning a complete set of developmental programmes (that is, a whole pattern) to tissue is one that intrinsically occupies a particular space. There may be a stable gradient system of characteristic extent, and also perhaps a pre-pattern of spatial variables[28,29], requiring a standard size, for the detailed form. On this view, an anterior ZPA graft might be expected to lead initially to loss of anterior parts, centrally, in a mirror-image duplication. If complete duplication of distal—that is, later-determined[30]—pattern parts is ultimately found (see Fig. 1*b*), then the antero-posterior extent of territory across which pattern-forming events are occurring must have been appropriately increased by widespread, early response to the extra growth signal. Highly controlled size of the final limb is seen as a result of the constancy of the size at which patterns, for highly programmed growth as well as differentation, are initially laid down. The first three levels of the diagram represent the normal situation and then two time points within the first, say, 24 h after an anterior ZPA graft. The ordinate is the signal value at each location, the abscissa is the anterior (left) to posterior (right) tissue extent of the limb rudiment at each stage. – – – –, Profile of a signal influencing the cell cycle. ——, Profile of a signal assigning position value. 2, 3 or 4, levels of positional signal associated with formation of particular digits, but cell fate still labile (undetermined). ②, ③ or ④, local tissue determined as, or actually forming, particular digits. The bottom line in the diagram gives the proportions in the later (much larger) developing limb cross-section. Note that growth has been greatest for more posterior elements in the pattern.

pattern re-specification, with an early expression of that altered pattern in terms of intrinsic growth rate. Higher S-phase entry is seen, in regions where we would expect the most rapid changes of position value due to cell interactions at early times, than is found anywhere in the normal limb (for example, 53% labelling index, a 60% relative increase over the left bud as a whole, near a ZPA graft at 5 h after operation). This growth control effect, exaggerated by the unusual positional disparity initially involved in duplication after grafting, largely underlies the early antero-posterior widening whereby both the original and the newly induced limb pattern are able to be complete and to occupy normal amounts of tissue by the time of their specification.

Knowledge of the rate of spread of the growth signal and the kinetics of new tissue production is highly relevant to our understanding of normal and experimental pattern specification in this system. Recent modelling of the antero-posterior pattern control has conceived of the ZPA as source, and limb mesenchyme elsewhere as sink, for a morphogen substance giving a signal gradient of particular profile and spatial extent and hence, by cellular interpretation of local value, a specified differentiation pattern of particular size and proportions[17,19,24]. Despite recent suggestions that the cell interaction system may also have a component whereby any induced disparity of cell position value (that is, heterotopic grafting) produces some new pattern formation by local interaction[25], there is little doubt about the dominance and primary role of the ZPA in organizing large and potentially complete new patterns when grafted. Although the most pronounced local stimulation occurs very soon after operation (Fig. 3*a*), the widespread nature of the response thereafter effectively rules out the idea that the new pattern is produced solely in a local zone of special growth, and even makes it unlikely that the entire second pattern is formed within tissue derived from a very small ($\simeq$100-μm wide) region taken over by the new organizer. The present results support models of the general gradient form for pattern specification (regardless of molecular nature of the signal) and will help in improving their fit to some of the data.

Figure 4 gives the outline of a model for size control and pattern formation across the limb mesenchyme, which could be tested by future work and which seems most compatible with the data. The ZPA or organizing region is seen as emitting signals, both of essentially graded form but of separate molecular identities, one controlling the fates of cells in the pattern of differentiation, the other the rate and pattern of early growth which may ensure adequate tissue space for the complete specification of pattern by the first signal. The specified, normally sized and proportioned rudiment is then thought to grow according to its own endogenous programme to give the normal anatomy (see above and ref. 9). The ideas are treated further in Fig. 4 legend. Separate, correlated growth and position signals, although not the only tenable hypothesis (D.S., in preparation), would explain (1) the fact that we see widespread, considerable cellular response in growth within 9 h of grafting, whereas the grafted ZPA must be present for more than 10 h to produce any effect on pattern if excised again, and (2) the avoidance by the system of the loss of anterior pattern values (digit 2), between host and grafted ZPAs, expected on the simplest diffusion gradient models for specification.

Essentially all cells are cycling in the early wingbud[26], and the cycle time may be 6–10 h (refs 23, 27). Our data do not allow us to quantify the cycle shortening involved in our experiments but suggest that it is very considerable, and widespread (Fig. 3, Table 1). As total tissue mass only approaches a doubling in the most completely duplicated wings, and each limb pattern is believed to grow to a fixed schedule in late development, the growth stimulation must be very short-lived and followed by a return to equilibrium, perhaps within 24 or 36 h (two or three normal cycle times) of grafting.

We believe this to be the first report of an intercellular growth control system linked to morphogenetic processes in an early vertebrate embryo. Future work should be directed particularly at the question of whether the roles of the ZPA in pattern and in growth control utilize separate, correlated molecular signals, or reflect separate cellular responses to one positional signal system. We are now studying this by more complex experiments in which we attempt to separate the effects of possibly distinct growth signals from those of positional signals.

We thank Jasmail Jhite and June Colville for histology, and Beverley Block for assistance with computation. The work is supported by the MRC.

Received 5 February; accepted 1 August 1980.

1. Stoker, M. J. in *Paediatrics and Growth* (ed. Barltrop, D.) 5–14 (Fellowship of Postgraduate Medicine, London, 1978).
2. Edelman, G. M. *Science* **192,** 218–226 (1976).
3. Daughaday, W. H., Herington, A. C. & Phillips, L. S. *A. Rev. Physiol.* **37,** 211–244 (1975).
4. Bullough, W. S. *The Evolution of Differentiation* (Academic, London, 1967).
5. Wolpert, L. *Curr. Topics Dev.* **6,** 183–224 (1971).
6. Bohn, H. *Wilhelm Roux Arch. EntwMech. Org.* **165,** 303–332 (1970).
7. French, V. & Bulliere, D. *C. r. hebd. Séanc. Acad. Sci., Paris* **280,** 253–257 (1975).
8. Kieny, M., Mauger, A. & Sengel, P. *Devl Biol.* **28,** 142–161 (1972).
9. Lewis, J. H. & Wolpert, L. *J. theor. Biol.* **62,** 479–490 (1976).
10. Beach, D. & Jacobson, M. *J. comp. Neurol.* **183,** 625–632 (1979).
11. Cooke, J. *J. Embryol. exp. Morph.* **51,** 165–182 (1979).
12. Cooke, J. *Nature* **254,** 196–199 (1975).
13. Dan-Sohkawa, M. & Sato, N. *J. Embryol. exp. Morph.* **46,** 171–185 (1978).
14. French, V., Bryant, P. J. & Bryant, S. V. *Science* **193,** 969–981 (1976).
15. Cooke, J. *A. Rev. Biophys. Bioengng* **4** (1975).
16. Saunders, J. W. Jr & Gasseling, M. T. in *Epithelial-Mesenchymal Interactions* (eds Fleischmajer, R. & Billingham, R. E.) 78–79 (Williams and Wilkins, Baltimore, 1968).
17. Summerbell, D. & Tickle, C. in *Br. Soc. dev. Biol. Symp.* **3** (eds Ede, D. A., Balls, M. & Hinchliffe, M.) 41–53 (Cambridge University Press, 1977); Tickle, C., Summerbell, D. & Wolpert, L. *Nature* **254,** 199–202 (1975).
18. Summerbell, D. & Wolpert, L. *Nature* **244,** 228–230 (1973).
19. Summerbell, D. *J. Embryol. exp. Morph.* **32,** 227–237 (1974).
20. Smith, J. A. & Martin, L. *Proc. natn. Acad. Sci. U.S.A.* **70,** 1263–1267 (1973).
21. Graham, C. F. & Morgan, R. W. *Devl biol.* **14,** 439–460 (1966).
22. Wolfsberg, M. F. *Expl Cell Res.* **35,** 119–132 (1964).
23. Stark, R. J. & Searls, R. L. *Devl Biol.* **33,** 138–153 (1972).
24. Summerbell, D. *J. Embryol. exp. Morph.* **50,** 217–233 (1979).
25. Iten, L. E. & Murphy, D. J. *Devl Biol.* **75,** 373–385 (1980).
26. Summerbell, D. & Lewis, J. H. *J. Embryol. exp. Morph.* **33,** 621–643 (1975).
27. Cairns, J. in *Br. Soc. dev. Biol. Symp.* **3** (eds Ede, D. A., Hinchliffe, J. R. & Balls, M.) 123–138 (Cambridge University Press, 1977).
28. Turing, A. M. *Phil. Trans.* **B237,** 37–72 (1952).
29. Newman, S. A. *Science* **205,** 662–668 (1979).
30. Summerbell, D., Lewis, J. H. & Wolpert, L. *Nature* **244,** 492–496 (1973).

LETTERS

Ultraviolet spectra of asteroids

P. S. Butterworth*, A. J. Meadows*, G. E. Hunt†, V. Moore† & D. M. Willis‡

* Department of Astronomy, University of Leicester LE1 7RH, UK
† Department of Physics and Astronomy, University College London, Gower Street, London WC1E 6BT, UK
‡ SRC Rutherford and Appleton Laboratories, Slough SL3 9JX, UK

Spectra over the range 2,100–3,200 Å have been obtained for the three largest asteroids—Ceres, Pallas and Vesta—using the International Ultraviolet Explorer (IUE) satellite[1]. These represent the first detailed UV reflectivity data for asteroids. They extend the numerous measurements already carried out in the visible and IR[2,3] to shorter wavelengths, and so enlarge on previous studies of both the classification and the mineralogy of asteroids[4].

Table 1 lists basic information concerning the spectra we have analysed. Spectra labelled 'Arizona' were obtained by the University of Arizona: we have acquired them from the World Data Centre {Cl} at the Rutherford and Appleton Laboratories. Those labelled 'UK' were obtained by us at VILSPA, the European ground observatory located near Madrid.

The reduction and calibration of asteroidal spectra has presented a number of problems. In order to obtain the asteroidal contribution, it is first necessary to divide by the solar spectrum. Slight errors in the juxtaposition of wavelength scales in this process can lead to major errors in the residual asteroidal spectrum, and it has proved difficult to achieve exact coincidence. Partly to obviate this, the resolution of the original observations (6–8 Å) has been smoothed in our reduction program to an average resolution of 50 Å. This does not significantly affect our investigation, as solid-body absorption features are much wider than this.

The solar spectrum we have used in our reductions[5] was obtained in mid-1970, just after a solar maximum. Our spectra were obtained just before maximum. It is possible that this has introduced a systematic error in our results. However, from the data available on variations in the solar UV spectrum as a function of the solar cycle,[6] we estimate that the colour ratio λ 2,590/λ 3,075 should not differ by more than 5–10% between mid-1970 and the dates of our observations. Variations between spectra of the same asteroid (see Figs 1 and 2) taken at different times can be adequately explained by errors in the observational and reduction processes. There is no evidence that the results are affected by short-term changes in the solar UV flux.

0028–0836/80/430701—03$01.00

Table 1 Asteroidal spectra analysed

Object	Date observation	Image no.	Exposure time (min)	Aperture	Source
Ceres	28 July 1978	LWR 1890	10	Small	Arizona
Ceres	28 July 1978	LWR 1890	20	Large	Arizona
Ceres	12 November 1979	LWR 6107	10	Large	UK
Pallas	2 June 1978	LWR 1539	16	Small	Arizona
Vesta	21 May 1978	LWR 1532	5	Small	Arizona
Vesta	2 July 1978	LWR 1772	20	Large	UK
Vesta	12 November 1979	LWR 6106	120	Small	UK

The data obtained from IUE were next calibrated to transform them into geometric albedos. This involved four steps. First the radiometric visual albedos from the TRIAD database[7] were corrected to allow for new estimates of the diameters of Ceres, Pallas and Vesta[8]. Then the visual spectral reflectances of these asteroids (also from the TRIAD database)[9] were normalized to the absolute visual albedos. After this, the albedos obtained for the three asteroids with the OAO 2 satellite[10], which covered bands in both the visual and the UV, were normalized, over the appropriate wavelength region, to the visual spectral reflectance curves. Finally, our IUE spectra were normalized to the corresponding OAO 2 albedos at 3,075 Å. (One Vesta spectrum {LWR 6106S} was saturated at 3,075 Å and was therefore normalized to the average of the other two Vesta spectra.) These successive steps necessarily introduce uncertainties into the calibration process; as do uncertainties in the IUE calibration, itself[11]. We estimate that the cumulative random errors from all these sources are ±15%. Systematic errors, due especially to uncertainties in the original calibration of the OAO 2 observations, also almost certainly occur, and may be larger than the random errors.

Figure 1 shows our calculated geometric albedo values for Ceres and Pallas over 50-Å intervals. The corresponding values for Vesta are shown in Fig. 2. The estimated error bars are given for one set of measurements only for Ceres and Vesta to avoid confusion in the diagram. The set chosen is in each case the one for which the error estimates are largest. These errors have been derived from measurement of background noise along two strips parallel to, and on either side of, the UV spectrum strip as it appears on the image field recorded by the spectrograph camera. Some data points are missing from the Pallas spectrum, one Vesta spectrum and two Ceres spectra. These correspond to wavelength regions where the original UV spectra are saturated.

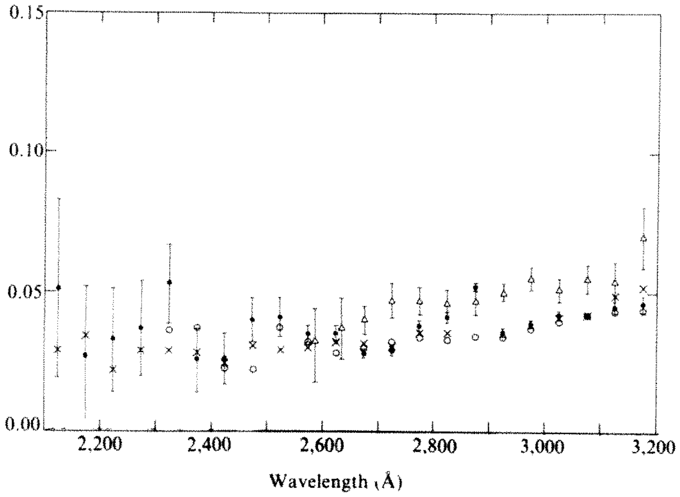

Fig. 1 Values for the geometric albedos of Ceres (●, ○, ×) and Pallas (△) over the range 2,100–3,200 Å. ●, LWR 6107 (large slot); ○, LWR 1890 (small slot); ×, LWR 1890 (large slot); △, LWR 1539 (small slot).

The results for Ceres presented in Fig. 1 suggest that its reflectivity near 3,200 Å is approximately 0.047. This is some 30% higher than the value obtained from ground-based measurements at 3,300 Å, which not only represents a large and sudden increase, but also goes against the trend of reflectivity in this wavelength region. It seems possible that the OAO 2 albedo at 3,075 Å, which we have used in our calibration, may be in error. D. L. Matson (personal communication) has unpublished data which suggest that the albedo of Ceres at 3,000 Å could be as low as 0.025. Use of this latter value—which corresponds to a lowering of the entire albedo for Ceres in Fig. 1 by a factor of 40%—would resolve the apparent discrepancy in values for the 3,200–3,300 Å region. The shape of the spectral curve for Ceres is not, of course, affected by such a shift: there is some indication of genuine dips centred on 2,425 Å and 2,650 Å.

The OAO 2 calibration for Pallas and Vesta gives results which agree better with ground-based observations. The Pallas spectrum shows no certain features, but there is some indication of a significant change in slope of the Vesta spectrum at about 3,000 Å. Unfortunately, coverage of this region of the Vesta spectrum is poor: further ground-based photometry is needed to define the slope longward of 3,000 Å more accurately.

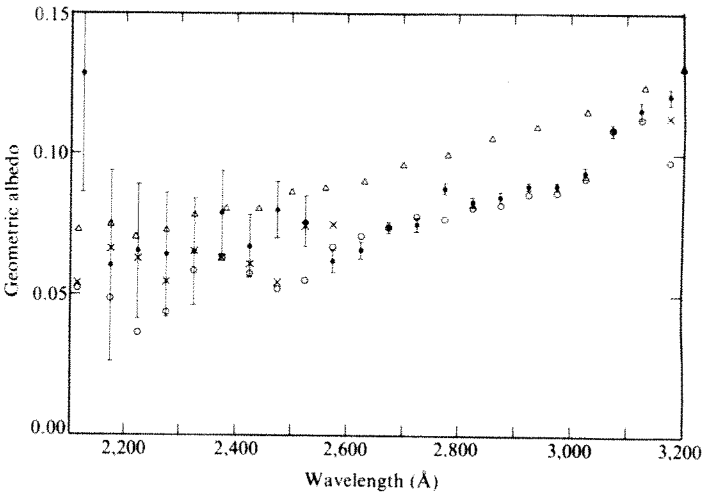

Fig. 2 Values for the geometric albedo of Vesta (●, ○, ×) over the range 2,100–3,200 Å. The spectral reflectance of the meteorite Kapoeta (△) over the same range is shown for comparison. ●, LWR 1532 (small slot); ○, LWR 1772 (large slot); ×, LWR 6106 (large slot).

Particular interest attaches to the UV spectrum of Vesta. At visible and IR wavelengths Vesta's spectrum shows considerable similarity to the spectra of the basaltic achondrite group of meteorites[4]. Laboratory measurements of UV reflectivity are available for the meteorite Kapoeta[12], a member of this group, and are plotted in Fig. 2 along with our results for Vesta. The values for Vesta are mainly smaller than those for Kapoeta, though the results for the two bodies suggest a generally similar trend with wavelength.

Systematic differences between the Vesta and Kapoeta spectra may well be attributable either to errors in our calibration procedure, or to differences between the surface texture of the meteorite samples and the asteroid. However, the Kapoeta measurements do not show a change in slope at 3,000 Å, as may occur in the Vesta observations. Confirmation of the existence of this feature might therefore be of importance for the study of the mineral assemblages present on Vesta.

We are currently examining the UV spectra of a number of other asteroids. The main limitation on reduction of this material is that albedo normalization data are only available for the three asteroids discussed above. However, our preliminary work suggests that the UV spectra of asteroids may be as distinctive as their spectra in the visible and near IR. To the extent that differences in spectral reflectance are due to differences in surface mineralogy, UV observations can therefore be used to extend the knowledge of asteroidal mineralogy already obtained from observations at longer wavelengths.

This work was supported by the SRC. We thank the resident astronomers at VILSPA for their unfailing assistance, and Drs D. L. Matson and M. J. Gaffey for their comments on the manuscript.

Received 27 June; accepted 15 September 1980.

1. Boggess, A. *et al. Nature* **275,** 372–377 (1978).
2. Chapman, C. R. & Gaffey, M. J. *Asteroids*, 655–687 (University of Arizona Press, Tucson, 1979).
3. Larson, H. P. & Veeder, G. J. *Asteroids*, 724–744 (University of Arizona Press, Tucson 1979).
4. Gaffey, M. J. & McCord T. B. *Asteroids*, 688–723 (University of Arizona Press, Tucson, 1979).
5. Broadfoot, A. L. *Astrophys. J.* **173,** 681–689 (1972).
6. Heath, D. F. & Thekaekara, M. P. in *The Solar Output and its Variation*, 193–212 (Colorado Associated University Press, Boulder, 1979).
7. Morrison, D. & Zellner, B. *Asteroids*, 1090–1097 (University of Arizona Press, Tucson, 1979).
8. Schubart, J. & Matson D. L. *Asteroids*, 84–97 (University of Arizona Press, Tucson, 1979).
9. Chapman, C. R. & Gaffey, M. J. *Asteroids*, 1064–1089 (University of Arizona Press, Tucson 1979).
10. Caldwell, J. *Icarus* **25,** 384–396 (1975).
11. Bohlin, R. C. *Astr. Astrophys.* **85,** 1–13 (1980).
12. Hua, C. T., Dollfus, A. & Mandeville, J. C. *Geochim. cosmochim. Acta* Suppl. No. 7, 2605–2622 (1976).

Discovery of intrinsic linear polarization in SS433

I. S. McLean*† & S. Tapia

* Royal Observatory, Edinburgh EH9 3HJ, UK
† Steward Observatory, University of Arizona, Tucson, Arizona 85721

The remarkable object[1] SS433 is the optical counterpart of a discrete variable radio and X-ray source[2–7] located in an extended radio-emitting region (W50) which may be a supernova remnant[8–11]. The best known attribute of SS433 is the 'moving' emission lines in the visible and near IR spectrum[12]. The displacements of the emission features have been shown to be due to Doppler shifts[12,13] arising from velocity variations with a period of $P \sim 164$ days; velocities up to +50,000 (0.17*c*) and −35,000 km s^{-1} are attained by the redshifted and blueshifted components respectively. A favourable configuration seems to involve two highly collimated, oppositely directed near-relativistic streams emerging from the central object. We report here new observations which reveal that the linear polarization of the optical radiation from SS433 exhibits a long-term variation as well as large night-to-night changes. This establishes that a substantial fraction of the observed polarization is intrinsic to SS433 whereas the remainder may be produced in the interstellar medium. As polarization is an indicator of physical and/or geometrical asymmetries in nature, this phenomenon can have a useful role in discriminating between contending configurations for SS433.

Early attempts to search for polarization of radiation from SS433, mainly as an indicator of magnetic fields and non-thermal processes in general, proved negative. Liebert *et al.*[13] found no circular polarization in red light, and Thompson *et al.*[14] found no significant linear polarization at 2.2 μm. Kemp[15] reported (3.1 ± 0.6)% linear polarization at $\theta = 3.1° \pm 3.0°$ in the blue-green region of the visible, and Shawl (personal communication) found (3.96 ± 0.41)% at $\theta = 4.1° \pm 3.0°$; these values were largely attributed to interstellar polarization. The linear polarization data presented here were obtained with the 2.3-m and 1.55-m telescopes of the University of Arizona Observatories. These measurements are an order of magnitude more accurate than the above and provide the first clear evidence of variations.

To maximize the signal-to-noise ratio, our observations were made with an unfiltered Ga–As photocathode covering the spectral region between 3,000 and 9,000 Å. As the bulk of the observed optical radiation from SS433 is concentrated at the red end of the spectrum, the characteristic wavelength of our unfiltered passband is near 7,000 Å and thus much redder than those of Kemp and Shawl. This is corroborated by a concordant measurement obtained with a filter having transmission only between 6,500 and 7,500 Å. The exceptional strength of the emission lines may have a small influence on the degree of polarization measured with our unfiltered passband but the effects of varying Doppler shift should be minimal. Also, the polarization at the rest wavelength of Hα (6,563 Å) was measured with a narrow passband (32 Å) in two consecutive cycles at times which were coincidentally near phase zero, that is when the emission lines cross the redshift of $z \simeq 0.04$.

Table 1 Optical linear polarization of SS433

Julian Day (2440000+)	(Phase (ϕ)	p(%)	θ(deg)
a, Unfiltered Ga–As, $\Delta\lambda \simeq 5{,}000$ Å			
3,964.99	2.496	2.64 ± 0.20	10.6 ± 2.2
3,966.98	2.508	1.97 ± 0.04	10.6 ± 0.6
4,114.70	3.409	2.18 ± 0.06	11.0 ± 0.7
4,126.64	3.482	1.87 ± 0.04	11.4 ± 0.6
4,127.75	3.489	2.13 ± 0.03	8.5 ± 0.5
4,146.625	3.604	2.03 ± 0.03	7.6 ± 0.5
4,194.585	3.896	2.33 ± 0.04	3.0 ± 0.5
4,217.579	4.036	1.92 ± 0.04	172.3 ± 0.7
4,218.579	4.043	2.15 ± 0.04	174.8 ± 0.5
4,339.986	4.783	2.32 ± 0.02	1.1 ± 0.3
4,349.972	4.844	2.48 ± 0.07	0.7 ± 0.8
4,369.949	4.965	2.41 ± 0.03	178.4 ± 0.4
4,383.944	5.051	2.24 ± 0.02	1.7 ± 0.3
4,384.944	5.057	1.80 ± 0.05	177.5 ± 0.8
4,385.944	5.063	1.47 ± 0.05	174.6 ± 1.0
b, $\lambda = 7{,}000$ Å, $\Delta\lambda = 1{,}000$ Å			
4,218.60	4.044	2.22 ± 0.09	176.1 ± 1.2
c, $\lambda = 6{,}563$ Å, $\Delta\lambda = 32$ Å			
4,217.60	4,037	2.65 ± 0.13	1.6 ± 1.4
4,218.599	4.043	2.61 ± 0.11	1.3 ± 1.2
4,383.944	5.051	2.69 ± 0.11	5.7 ± 1.2
4,384.944	5.057	2.47 ± 0.09	5.7 ± 1.0

The data are presented chronologically in Table 1 where p is the observed percentage of linear polarization and θ is the equatorial position angle. For comparison, ϕ is the 164-day phase[12]; the integer part of the phase is given to show the number of cycles observed. In these data the effects of instrumental polarization are negligible.

Because the observed continuum polarization is the vector sum of at least the intrinsic and the interstellar polarization, it is most instructive to plot the Stokes parameters defined by $Q = p\cos 2\theta$ and $U = p\sin 2\theta$, against time. Any constant interstellar polarization (Q_i, U_i) merely introduces an offset which still allows the intrinsic variations ($Q_*(t)$, $U_*(t)$) to be viewed directly because $Q_0(t) = Q_*(t) + Q_i$ and $U_0(t) = U_*(t) + U_i$. Thus Fig. 1 presents the phase dependence of the observed (continuum) Stokes parameters and shows that large variations in both Stokes parameters do indeed take place over the time scale spanned by the 164-day period but, as yet, the data are still too few to establish periodicity conclusively. The accuracy of our measurements is sufficient to reveal that very short time scale variations of the polarization are also present. In terms of our current knowledge of SS433 these short-term changes could originate in (1) the underlying binary period (13 days) or (2) stochastic (outburst-like) variations similar to the irregular departures of the radial velocity and light curve[16]. Obviously, such short-term variability will have to be averaged-out to enable variations following the 164-day cycle to be observed.

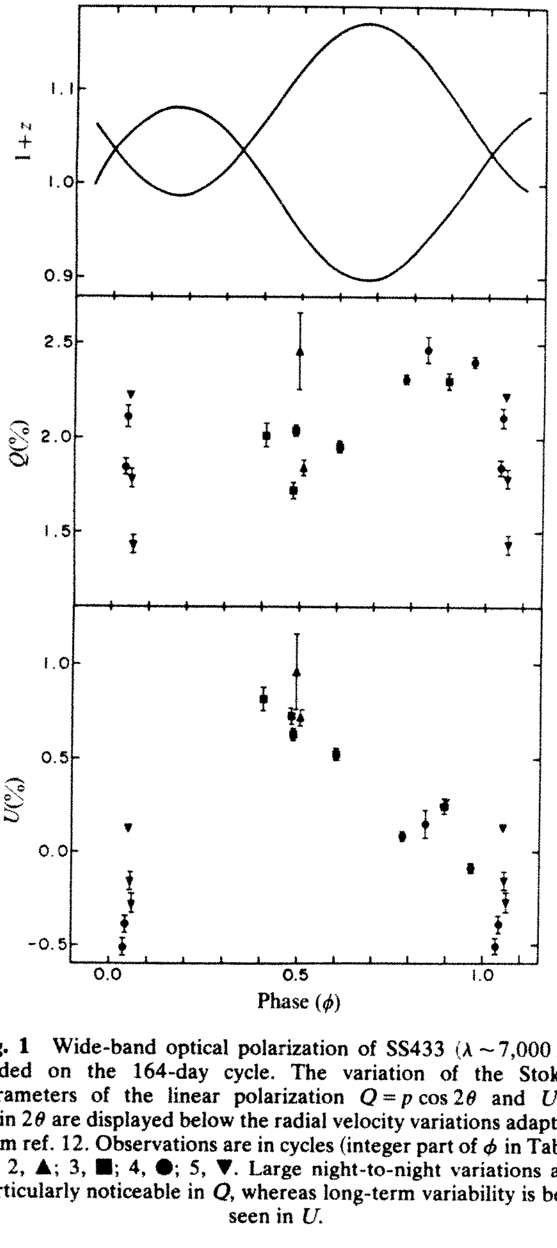

Fig. 1 Wide-band optical polarization of SS433 ($\lambda \sim 7{,}000$ Å) folded on the 164-day cycle. The variation of the Stokes parameters of the linear polarization $Q = p \cos 2\theta$ and $U = p \sin 2\theta$ are displayed below the radial velocity variations adapted from ref. 12. Observations are in cycles (integer part of ϕ in Table 1): 2, ▲; 3, ■; 4, ●; 5, ▼. Large night-to-night variations are particularly noticeable in Q, whereas long-term variability is best seen in U.

In Table 1 the observed degree of polarization at the wavelength of *Hα* is little different from that in the continuum. However, the difference between the position angles of the line and the continuum polarization exceeds the 3σ level. This rotation of the observed polarization at $\lambda 6{,}563$ can be thought of as an additional term in the expressions for the observed Stokes parameters: $Q_0 = Q_* + Q_{H\alpha} + Q_i$ and $U_0 = U_* + U_{H\alpha} + U_i$. However, without accurate values for the interstellar contributions it is not possible to assess whether the terms $Q_{H\alpha}$, $U_{H\alpha}$ are associated with an enhancement or a dilution of the polarization at $\lambda 6{,}563$.

From its reddening[2,17] ($0.75 < E(B-V) < 2.4$), albeit poorly determined, and location near the galactic plane, the allowed range of interstellar polarization (in the mid-visible) for SS433 is $2.25 > p_i(\%) < 7.20$. An upper limit (3σ) can be estimated using the 2.2-μm IR polarization of $(0.1 \pm 0.1)\%$ observed by Thompson *et al.*[14] at phase $\phi = 0.60$ if one assumes, *a priori*, no source of 2.2-μm polarization in SS433 and that the wavelength of maximum interstellar polarization is close to the normal value, $\lambda_{max} \simeq 0.55$ μm; the result is $p \lesssim 2.7\%$. (As the optical polarization mechanism is uncertain, a 2.2-μm polarization source in SS433 cannot be dismissed; however, the assumption is consistent with our discussion below.) An examination of polarization survey catalogues[18-20] suggests that, in the region of sky containing SS433, the mean position angle of interstellar polarization is $\theta_i \simeq 30° \pm 15°$. We have observed the broad band polarization of the uncatalogued stars in the 'diamond' pattern lying only ~2 arc min north-west of SS433. These data show that the northernmost component has no polarization, whereas the southernmost and westernmost components are polarized with $p = (1.54 \pm 0.09)\%$ at $35° \pm 2°$ and $p = (1.2 \pm 0.2)\%$ at $16° \pm 5°$ respectively. Thus a lower limit to p_i is ~1.5%. Until the interstellar polarization towards SS433 is known with accuracy comparable with the data in Table 1, it will be difficult to solve for the intrinsic polarization in the continuum and at Hα. However, for values of p_i in the range 1.5–2.7% at $\theta_i \simeq 30°$, the intrinsic polarization at $\lambda 6{,}563$ (continuum plus Hα) seems weaker than the continuum and at a position angle at least 15° larger. Because of the same difficulty one cannot yet derive the orientation of the intrinsic plane of polarization for comparison with that of the radio lobes in W50.

Several sources of intrinsic polarization in SS433 have been ruled unlikely. The lack of evidence for strong optical circular polarization (<0.1% in broad bands, <1% in emission lines) eliminates magnetic fields of $\sim 10^8$ G detected in degenerate dwarf stars[13]. Fields of $\lesssim 10^4$ G, found in Ap-type stars, may still be present[21] and could be detected with high resolution Zeeman spectropolarimetry. However, polarization in the continuum should be nil. Low degrees of linear polarization due to gyro radiation at radio frequencies are possible[21] but again with no detectable effects in the optical continuum.

Scattering processes commonly polarize optical radiation in many astrophysical scenarios. Milgrom[22] has suggested that light emitted by the regions producing the moving emission and rest-emission lines respectively can scatter from free electrons (Thomson scattering) in any of the other emitting regions and hence become polarized. Margon *et al.*[12], however, have searched for the predicted extra lines and find no conclusive evidence for them.

In the absence of any evidence for dust[14] and in view of the ionization levels expected in the line-emitting regions the most probable source of polarization in the optical continuum of SS433 seems to be electron scattering. Optically thick electron scattering could occur in a dense accretion disk. On the other hand, if the system includes a close binary undergoing mass transfer plus collimated, near-relativistic beams emerging in opposite directions, then optically thin electron scattering may occur in both regions[23], as in Be stars and some X-ray binaries. The continuum polarization would thus display two time scales of variation; one due to the binary period and a longer one due to the precession of the system. Differential changes in Q and U then provide information on the scattering geometry.

In terms of the models currently proposed[24-26] for SS433, the electron density (N_e) is sufficient to produce significant Thomson scattering. The corresponding optical depth τ needs to be equal to or larger than the fraction of polarized flux, that is $\tau \gtrsim 0.01$ according to the data in Table 1. Now, $\tau \simeq \sigma_T N_e L$, where L is the characteristic size of the scattering region. Then $N_e \gtrsim 1.5 \times 10^{22} L^{-1}$ cm^{-3}. If the scattering region and the source of radiation are close, L is approximately equal to the size of a typical circumstellar shell ($L \sim 10^{12}$ cm), as is known for Be-shell stars. In this case $N_e \gtrsim 1.5 \times 10^{10}$ cm^{-3}. However, for scattering blobs relatively distant from the star dilution effects are important and the characteristic length becomes $L \sim l^3/R^2$, where R is the distance to a scattering region of volume l^3. If such scattering regions can be identified with the emitting regions of the jets, then the estimated sizes[24,25] fall in the range $10^{12} \leq l \leq 10^{15}$ cm, with $R \gtrsim 20l$ for good collimation. Therefore, in this second case $10^9 \leq N_e \leq 10^{13}$. Optically thin electron scattering near the emitting regions is also consistent with the energy flow in the jets if this is less than 10^{40} erg s^{-1}.

These results emphasize the fact that polarization plays an important part in the search for a consistent model of SS433.

We thank J. C. Kemp, A. C. Fabian, M. J. Rees, G. V. Coyne, R. Williams and J. Liebert for helpful discussions, and H. S. Stockman for the polarization result on JD2444114.7. I. McL. acknowledges the support of NSF grant AST 77-08386 while a Research Fellow at the University of Arizona. Partial support for this work was also provided by NSF grants AST 79-23593, 78-21071 and NASA grant NSG-7574.

Received 2 July; accepted 28 August 1980.

1. Stephenson, C. B. & Sanduleak, N. *Astrophys. J. Suppl.* **33,** 459 (1977).
2. Clark, D. H. & Murdin, P. *Nature* **276,** 44 (1978).
3. Ryle, M., Caswell, J. L., Hine, G. & Shakeshaft, J. *Nature* **276,** 571 (1978).
4. Seaquist, E. R., Garrison, R. F., Gregory, P. C., Taylor, A. R. & Crane, P. C. *Astr. J.* **84,** 1037 (1979).
5. Seward, F. D., Page, C. G., Turner, M. J. L. & Pounds, K. A. *Mon. Not. R. astr. Soc.* **175,** 39P (1976).
6. Forman, W. *et al., Astrophys J. Suppl.* **38,** 357 (1978).
7. Marshall, F. E., Swank, J. H., Boldt, E. A., Holt, S. S. & Serlemitsos, P. J., *Astrophys. J. Lett.* **230,** L145 (1979).
8. Westerhout, G. *Bull. astr. Insts Neth.* **14,** 215 (1958).
9. Holden, D. J. & Caswell, J. L. *Mon. Not. R. astr Soc.* **143,** 407 (1969).
10. Velusamy, T. & Kundu, M. R. *Astr. Astrophys.* **32,** 375 (1974).
11. van den Bergh, S. *Astrophys J. Suppl.* **38,** 119 (1978).
12. Margon, B., Grandi, S. A. & Downes, R. A. *Astrophys. J.* (in the press).
13. Liebert, J., Angel, J. R. P., Hege, E. K., Martin, P. G. & Blair, W. *Nature* **279,** 384 (1979).
14. Thompson, R. I., Rieke, G. H., Tokunaga, A. T. & Lebofsky, M. J. *Astrophys. J. Lett.* **234,** L135 (1979).
15. Kemp, J. C. *IAU Circ.* No. 3379 (1979).
16. Kemp, J. C., Barbour, M. S., Arbabi, M., Leibowitz, E. M. & Mazeh, T. *Astrophys. J. Lett.* **238,** L133 (1980).
17. Margon, B. *et al. Astrophys. J. Lett.* **239,** L41 (1979).
18. Serkowski, K., Mathewson, D. S. & Ford, V. L. *Astrophys. J.* **196,** 261 (1975).
19. Mathewson, D. S. & Ford, V. L. *Mon. Not. R. astr. Soc.* **74,** 139 (1979).
20. Hall, J. S. *Publ. U.S. Naval Observatory*, 2nd Ser. Vol. XVII, Part VI (1958).
21. Collins, G. W., Newsom, G. H. & Boyd, R. N. Preprint (Ohio State University, 1980).
22. Milgrom, M. *Astr. Astrophys. Lett.* **78,** L17 (1979).
23. Brown, J. C. & McLean, I. S. *Astr. Astrophys.* **57,** 141 (1977).
24. van den Heuvel, E. P. J., Ostriker, J. P. & Petterson, J. A. *Astr. Astrophys.* **81,** L7 (1980).
25. Katz, J. I. *Astrophys. J. Lett.* **237,** L127 (1980).
26. Fabian, A. C. & Rees, M. J. *Mon. Not. R. astr. Soc.* **187,** 13P (1979).

Can galaxy warps be used to provide constraints on halo properties?

George Lake

Astronomy Department and Space Sciences Laboratory,
University of California, Berkeley, California 94720

James W.-K. Mark

Lawrence Livermore Laboratory, Livermore and Astronomy
Department, University of California, Berkeley, California 94720

The prevalence of flat rotation curves in external galaxies[1] strongly suggests an extensive but as yet unseen halo component. However, as direct observations of the implied matter distribution have proved very elusive, more indirect methods are needed to constrain its properties. At the same time, the explanation of observed warps in galaxies[3-7] has been intensively studied by dynamicists, resulting in the appearance of many rival mechanisms (see ref. 8 for a review). For galaxies with companions, the tidal interaction theory is the most attractive, but fails to account for the observed bending of our Galaxy "by a factor approaching 3" (ref. 9). The problem of the rapid kinematical disruption which results if one follows particle orbits in a self-consistent disk is avoided if one accepts the existence of a dominant spherical (halo) component in the region of the warps[8,10]. Here, we explore the consequence of separating disk and halo mass distributions using a recently developed theory of bending waves[2]. In this theory, the height of bending allows the functional form of the disk density distribution to be determined. With proper normalization this determination allows the halo density to be inferred from the rotation curve. We will discuss the warps in our Galaxy and in galaxies NGC2841 and M33, for which a relatively complete set of reduced data is available.

For many galaxies, the phenomena of warps start at moderate radii where the halo need not be the dominant contribution to the rotation curve. For these instances, Bertin and Mark[2] have developed an improved version of the earlier Kulsrud, Mark and Caruso[11] bending wave analysis and included disk–halo interactions in the manner of Mark[12]. This extended analysis is applicable to a wide range of disk-to-halo ratios. In this way, rather than instilling an initial bias towards dominant haloes, the theory may be used to constrain halo properties.

In the Bertin and Mark analysis, the transfer of angular momentum from disk to halo results in a destabilization of bending modes, much like a flag waving in the wind or the two-stream instability in a plasma. The resulting amplification can be large[2] and may explain the magnitude of the warp in our Galaxy, as well as the existence of warps in isolated spirals[5,7]. In this theory, the functional form of the warp is mainly dependent on the inertia (total surface density) of the disk $\Sigma(r)$,

$$H \sim \frac{1}{\Sigma(r) r^{1/2}} g(r) \qquad (1)$$

where r is the radial coordinate in the disk, H is the maximum vertical displacement at that radius and $g(r)$ is a smooth, weakly varying part of the amplitude. (For the following comparisons with observation, $g(r)$ may be assumed to be constant[2].)

The warp should be mostly observed in the outer parts of disks where the inertia is low. Frequently, in this region only the gaseous component is observed. Stellar disks are also observed to be warped[13,14], which is quite natural in the context of the theory of Bertin and Mark.

The theory as constructed by Bertin and Mark[2] has strong analogies with the theory of spiral structure[15]. As in any linear theory it is simple to calculate a relative amplitude as a function of radius, but the absolute normalization must be obtained directly from observations. However, equation (1) for the functional form of the amplitude provides a simple observational test which is independent of model parameters.

Figure 1*a* plots surface density against radius in our Galaxy as derived from equation (1) using the data of Henderson[4]. If we temporarily adopt a flat rotation curve with the circular velocity beyond the solar radius (R_0) equal to 250 km s^{-1}, we find the resulting points are well fitted by an exponential with a scale length of 3.4 ± 0.2 (R_0/10 kpc) kpc. This procedure is superior to determinations of the disk profile from fitting *HI* velocity profiles, because nothing is initially assumed about the mass distribution as a function of radius. (Of course, in both cases a rotation curve must be assumed or measured so as to derive distances from the observed line-of-sight velocities.) Assuming the same flat rotation curve, Knapp, Gunn and Tremaine[16] derive a scale length of 3.2 (R_0/10 kpc) kpc from such fitting of *HI* profiles with an assumed exponential mass distribution. Using the Oort limit[17] to normalize the density at R_0, we obtain a mass model close to that of Caldwell and Ostriker (in preparation). If we use the most recent rotation curve of Blitz, Fich and Stark[18], the scale length is 4.0 ± 0.2 (R_0/10 kpc) kpc, the disk mass integrated to 20 kpc is approximately 7.6×10^{10} $M_\odot$ (changing by ~10% depending on whether or not a central gap

0028–0836/80/430705—02$01.00

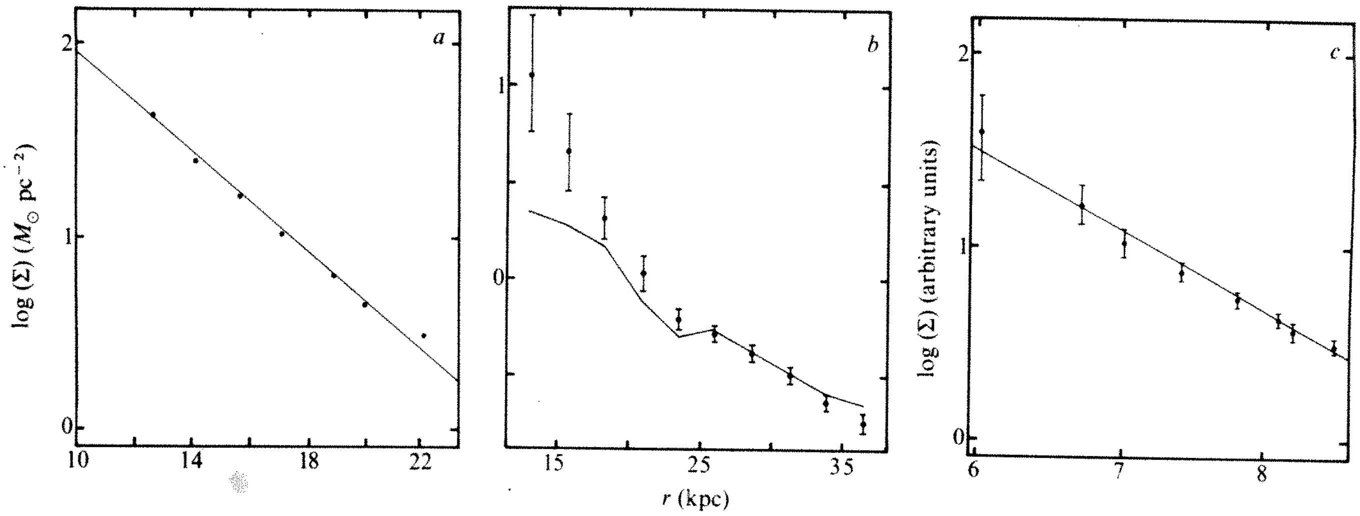

Fig. 1 *a*, The surface density $\Sigma(r)$ against radius in our Galaxy as derived from equation (1) using Henderson's[4] data for the warp. Distances are determined using a flat rotation curve with the circular velocity at the Sun equal to 250 km s^{-1}. The straight line is an exponential with a scale length of 3.4 kpc, normalized to the Oort limit[17] at the solar radius (10 kpc). Use of the rotation curve of Blitz, Fich and Stark[18] results in a computed scale length of 4.0 kpc. *b*, The surface density against radius for NGC2841 as derived from equation (1) using the data of Bosma[5] (H_0 is assumed to be 75 km s^{-1} Mpc^{-1}). The solid line is the observed neutral hydrogen surface density. The deviations at distances less than 20 kpc may be due to the contribution of the optical disk and (with more accurate data) may provide a method of measuring the mass-to-light ratio of the optical disk. *c*, The surface density against radius for M33 as derived from equation (1) using the data of Rogstad *et al.*[6]. The straight line is an exponential with a scale length of 1.1 kpc.

is included), and the combined mass of the halo and bulge out to 20 kpc is 3.1×10^{11} $M_\odot$. If this new rotation curve is used to recompute the halo component in the Caldwell–Ostriker model (leaving their bulge and disk parameters fixed), we find that the fraction of the gravitational force due to the halo at R_0, 1.5 R_0 and 2 R_0 is 17, 42 and 64%, respectively.

Next, we examine the galaxy NGC2841, which has been observed by Bosma[5]. Figure 1*b* compares the surface density of neutral hydrogen with the surface density derived from the observations of the amplitude of the warp, normalized to the *HI* surface density in the outer parts. (All distances in NGC2841 assume $H_0 = 75$ km s^{-1} Mpc^{-1}.) If there is no systematic variation of the mass-to-light ratio with radius in the observed optical disk and the mass-to-light ratio is less than 6 (twice the values obtained from stellar population models[19]), the surface photometry[20] suggests that the density of the optical disk is negligible in the region from ~20 to 30 kpc; this allows the normalization of the derived density from the warp to the *HI* surface density in the outer parts. However, the optical disk may be the source of the extra mass at radii less than 20 kpc. In any case, the agreement in the range ~20–35 kpc indicates that the *HI* surface density dominates the total surface density in this region. This is only ~1% of the local surface density needed to maintain the observed flat rotation curve[5], which implies that the mass density of the halo is inversely proportional to the square of the distance, as may be derived from the rotation curve in this region.

Although the bending wave results were derived with the assumption of small inclinations in the warp, it is encouraging that the theory gives a fairly reasonable description of the large inclinations in galaxy M33 (ref. 6). The derived density profile for M33 is shown in Fig. 1*c*. We calculate a scale length of 1.1±0.1 kpc, whereas the photometry yields a value of 1.6 kpc (ref. 21). This discrepancy might be attributed to the high degree of nonlinearity in the bend (the inclination angle of disk changes by 40° in the region from 5 to 9 kpc), but we feel that it is just as likely to be a problem in the photometry. The value of 1.6 kpc quoted by Freeman assumes an angle of inclination with respect to the sky of $i = 55°$, whereas Rogstad *et al.*[6] found $i = 50°$ and Sandage and Humphreys[14] found $i = 40°$, resulting in scale lengths of 1.4 kpc and 1.2 kpc, respectively. Furthermore, our length scale is derived from the radio data where the warp of the disk has been taken into account[6] in deriving the disk inclination as a function of radius. There, effects have not been included in the photometric determination of the length scale optical disk, which is observed to be warped in a manner consistent with the radio data[14]. Given these effects, our derived length scale of 1.1±0.1 kpc is quite reasonable.

For galaxies such as NGC2841, it may be possible with better data to measure a mass-to-light ratio in the disks of external galaxies using the bending wave theory. This measurement makes possible a computation of the core radius of the halo component, an important parameter for constraining theories of its origin and composition[22]. This is possible if the warp is measured over a range where it samples the mass distribution of the optical disk, and extends out to the region where the *HI* surface density dominates and provides the normalization. This project is ideally and uniquely suited for study with the VLA telescope, when accurate 21-cm line observations become possible.

We thank G. Bertin, L. Blitz, G. Efstathiou, A. Henderson, I. King, M. Roberts, P. Schechter, F. Shu and H. Visser for encouragement, advice or data in advance of publication. One of us (J.W-K.M.) has received support from the Department of Energy under contract W-7405-eng-48.

Received 19 May; accepted 1 August 1980.

1. Rubin, V. C. *IAU Symp.* **84,** 211 (1978).
2. Bertin, G. & Mark, J. W-K. *Astr. Astrophys.* (in the press).
3. Burke, B. F. *Astrophys. J.* **62,** 90 (1957).
Kerr, F. J. *Astrophys. J.* **62,** 93 (1957).
4. Henderson, A. P. *IAU Symp.* **84,** 493 (1978).
5. Bosma, A. thesis, Univ. Groningen (1978).
6. Rogstad, D. H., Wright, M. C. H. & Lockhart, I. A. *Astrophys. J.* **204,** 703 (1976).
7. Sancisi, R. *Astr. Astrophys.* **53,** 159 (1976).
8. Saar, E. M. *IAU Symp.* **84,** 513 (1978).
9. Hunter, C. & Toomre, A. *Astrophys. J.* **155,** 747 (1969).
10. Tubbs, A. D. & Sanders, R. H. *Astrophys. J.* **230,** 736 (1979).
11. Kulsrud, R. M., Mark, J. W-K. & Caruso, A. *Astrophys. Space Sci.* **14,** 52 (1971).
12. Mark, J. W-K. *Astrophys. J.* **206,** 418 (1976).
13. Tsikoudi, V. thesis, Univ. Texas (1977).
14. Sandage, A. & Humphreys, R. M. *Astrophys. J. Lett.* **236,** L1 (1980).
15. Bertin, G. & Mark, J. W-K. *Astr. Astrophys.* **64,** 389 (1978).
16. Knapp, G. R., Tremaine, S. D. & Gunn, J. E. *Astrophys. J.* **83,** 1585 (1978).
17. Oort, J. H. *Bull. astr. Insts Neth.* **15,** 46 (1960).
18. Blitz, L., Fich, M. & Stark, A. A. in *IAU Symp.* **87** (in the press).
19. Larson, R. B. & Tinsley, B. M. *Astrophys. J.* **219,** 46 (1978).
20. Houten, C. J. van Oort, J. H. & Hiltner, W. A. *Astrophys. J.* **120,** 439 (1954).
21. Freeman, K. C. *Astrophys. J.* **160,** 811 (1970).
22. Peebles, P. J. E. *Lecture notes for L'Ecole d'Eté de Physique Théoretique, Les Houches* (Gordon and Breach, London, 1979).

Identification of the anomalous 26.131-MHz nitrogen line observed towards Cas A

David H. Blake*, Richard M. Crutcher† & William D. Watson‡

* Electrical Engineering Department, University of Illinois
† Astronomy Department, University of Illinois
‡ Physics Department and Astronomy Department, University of Illinois, Urbana, Illinois 61801

Konovalenko and Sodin[1] recently reported the detection of an absorption line at a frequency of 26.131 MHz towards Cassiopeia A and attributed the line to the 26.127 MHz $F = 5/2 \rightarrow 3/2$ hyperfine transition of ^{14}N. The difference in frequency corresponds to a radial velocity of -40 km s^{-1}, which is compatible with the mean velocity of the Perseus arm H I absorption lines seen towards Cas A. However, to explain the strength of the line, Konovalenko and Sodin require $(N/H) = 8\times10^{-3}$ compared with the cosmic ratio of 1.2×10^{-4}. An anomalous abundance of this magnitude would have substantial impact on ideas about galactic nucleosynthesis. We suggest here that the line is a 631α recombination line due to neutral atoms of heavy elements—either carbon atoms in the H I clouds or possibly heavier atoms (Mg, Ca, Fe) in hot ($\sim10^4$ K) ionized gas along the line of sight to Cas A.

The C631α line lies at 26.126 MHz and the analogous lines of the heavier elements lie at 26.127 MHz. Because of the broadness of the observed line ($\sim$2 kHz), a unique line identification cannot be made on the basis of frequency alone. Radio recombination lines are normally seen in emission and not absorption. We discuss below how absorption can occur for transitions of very large principal quantum number n.

First consider carbon atoms in diffuse clouds. The strength of a recombination line will be:

$$T_L = \tau T_c(T_{ex}/T_c - 1)$$

where τ is the optical depth, T_{ex} is the excitation temperature, and T_c is the brightness temperature of the background continuum source. The optical depth is given by:

$$\tau = 1\times10^7 (f/n) b T_{ex}^{-1} T_k^{-3/2} \exp(157{,}800/n^2 T_k) E/\Delta\nu$$

where f is the oscillator strength ($f = 120$ for $631\alpha^2$), E (cm^{-6}pc) is the emission measure, $\Delta\nu$ (s^{-1}) is the linewidth, T_k is the electron kinetic temperature and b is the departure coefficient from local thermodynamic equilibrium (LTE). For the levels of interest, b is close to unity.

As carbon is primarily singly ionized in H I clouds, we use

$$E = \int n_e n_{C^+}\, dl = \overline{n_e} N_H(C/H),$$

where we will assume the cosmic abundance value $(C/H) = 3.7\times10^{-4}$. Neutral atomic hydrogen in the direction of Cas A has been studied by Griesen[3]. Using data of high spatial and velocity resolution he found H I column densities between 3 and 6×10^{21} cm^{-2}. Using these values for the H I column densities rather than the lower resolution data of Shuter and Verschuur[4], the N/H values required by Konovalenko and Sodin's interpretation range from 5 to 2.6×10^{-2}. Molecules such as H_2CO (ref. 5) and CO (ref. 6) have also been detected in this direction, indicating that there are diffuse clouds along this line of sight. Assuming that all electrons come for carbon we find $n_e = 0.1$ for a cloud of density 300 cm^{-3}. This yields $E = 0.07$ cm^{-6} pc for a H I column density of 5×10^{21} cm^{-2}. If the C631α line is formed in LTE at a temperature of 50 K then $S = 110\ E = 8$ s^{-1}. This compares well with the value of 6 s^{-1} reported by Konovalenko and Sodin. The following more detailed discussion is necessary to establish the plausibility of an excitation temperature near the LTE value.

At very large n, T_{ex} must approach T_k because the cross-sections for electron collisions which change n become large (proportional to n^6 in the regime of interest). For lower (but still large) n, the galactic radiation field becomes important in determining T_{ex}. At still lower n, these processes dominate less strongly and the excitation temperatures tend to become negative. The available calculations[7,8] extend only up to $n = 500$, but extrapolation to $n \simeq 631$ suggests that collisions and the galactic background control the excitation temperature provided the electron density exceeds 0.1 cm^{-3}. In this limiting case we have for $n \sim 631$:

$$T_{ex}^{-1} = (R/T_r + C/T_c)/(R + C)$$

Here, T_r is the brightness temperature of the galactic background, R is the absorption or stimulated emission rate ($R = 500$ s^{-1} for $T_r = 10^4$ K), and C is the rate for $n = 631 \rightarrow 632$ collisional excitations ($C = 1{,}670$ s^{-1} for $n_e = 0.1$ cm^{-3})[9]. For $T_k = 50$ K, $T_r = 10^4$ K and $n_e = 0.1$ cm^{-3}, the above equation yields $T_{ex} = 65$ K and the line will be in absorption against the hot ($T_c > 10^4$ K) background of Cas A. Using $T_{ex} = 65$K and $T_k = 50$K, we predict an integrated line strength of 6 s^{-1}, in agreement with the observed value.

The excitation temperature may be lowered and the line strength increased by the influence of a dielectronic-like recombination process involving the fine-structure states of ionized carbon. This effect has been incorporated into level population calculations for $n \leq 200$ (ref. 10) and shown to produce departure coefficients that can exceed unity for $n \sim 200$. At certain larger values of n, the derivative of the departure coefficients will then be negative, and the excitation temperatures will, therefore, be small and positive.

A remaining question is whether the expected breadth of the C631α line is compatible with that of the observed line. At typical cloud temperatures, and for $n_e > 0.03$ cm^{-3}, broadening by electrons dominates that due to other processes. We utilize the method of Griem[11] but use the more recent cross-sections of Gee *et al.*[9] for the n-changing collisions which are the dominant cause of broadening. The FWHM is:

$$\Delta\nu_e = \frac{1}{2\pi}\sum_{n'\neq n}\langle v\sigma(n\rightarrow n')\rangle n_e$$

$$\simeq 200\ \text{Hz}\ (n_e/0.03\ \text{cm}^{-3})(T_k/50\ K)^{3/2}.$$

Therefore, $n_e \leq 0.3$ cm^{-3} is compatible with the observed 2-kHz linebreadth.

The fact that the C631α line agrees so well in frequency, strength, and linewidth (without assuming any anomalies in abundance, excitation or other conditions) with the observations leads us to believe that it is the most likely identification for the 26.131-MHz line towards Cas A.

The physical processes relevant for the alternate possibility—that the line is due to heavier atoms in hot, ionized gases—have been analysed by Shaver[12] in a differerent context. At the higher temperatures, dielectronic recombination produces large population enhancements in the high Rydberg levels. The populations reach a peak at $n \sim 200$ and decline towards the LTE values for larger n. Very low, but positive, excitation temperatures then occur for $n \sim 631$ and will produce an absorption line when observed towards a strong ratio source. For $N_H = 10^{21}$ cm^{-2}, $n_e = 0.1$ cm^{-3} and cosmic abundance, Shaver's calculations indicate that an absorption line near the observed strength towards Cas A would be produced by a blend of Ca, Mg and Fe.

Collisions with electrons also dominate line broadening in this case. From Brocklehurst and Leeman[13] we take for temperatures near 10^4 K,

$$\Delta\nu = 30\ \text{Hz}\ (n_e/0.1\ \text{cm}^{-3})(10^4\ K/T_k)^{1/2}$$

hence, $n_e \leq 5$ cm^{-3} is compatible with the observed breadth.

Our suggestion that the line of Konovalenko and Sodin is a recombination line can easily be tested by searching for the 630α or 632α lines. ●

0028-0836/80/430707—02$01.00

Received 17 June; accepted 19 August 1980.

1. Konovalenko, A. A. & Sodin, L. G. *Nature* **283,** 360–361 (1979).
2. Menzel, D. H. *Astrophys. J. Suppl.* **18,** 221–246 (1969).
3. Greisen, E. W. *Astrophys. J.* **184,** 363–377 (1973).
4. Shuter, W. L. H. & Verschuur, G. L. *Mon. Not. R. astr. Soc.* **127,** 387–403 (1964).
5. Troland, T. H. & Heiles, C. *Astrophys. J.* **194,** 43–48 (1974).
6. Scoville, N. Z., Irving, W. M., Wannier, P. G. & Predmore, C. R. *Astrophys. J.* **216,** 320–328 (1977).
7. Shavers, P. A. *Astr. Astrophys.* **49,** 1–16 (1976).
8. Ungerechts, H. & Walmsley, C. M. *Astr. Astrophys.* **80,** 325–328 (1979).
9. Gee, C. S., Percival, I. C., Lodge, F. G. & Richards, D. *Mon. Not. R. astr. Soc.* **175,** 209–215 (1976).
10. Watson, W. D., Western, L. R. & Christensen, R. B. *Astrophys. J.* (in the press).
11. Griem, H. R. *Spectral Line Broadening by Plasmas,* 260 (Academic, New York, 1974).
12. Shavers, P. A. *Astr. Astrophys.* **46,** 127–130 (1976).
13. Brocklehurst, M. & Leeman, S. *Astrophys. Lett.* **9,** 35–36 (1971).

Electromagnetic spectral determination of the material composition of penetrable radar targets

G. C. Gaunaurd & H. Überall*

Naval Surface Weapons Center, R-31 White Oak,
Silver Spring, Maryland 20910

The resonance theory of scattering, recently developed for the diffraction of acoustic and elastic waves[1], is applied here to radar backscattering from penetrable targets in an attempt to solve the inverse scattering problem. This means the extraction of sufficient material-composition information from the electromagnetic scattering amplitudes of the returned echoes, to permit target identification. We illustrate the principle for the case of a conducting spherical target coated with a dielectric layer. The principle of our method is to use the resonances contained in each of the partial waves making up the radar cross-section for material characterization purposes. We demonstrate that in the high frequency region, the spacing between consecutive overtones becomes uniform, and is related to the dielectric constant of the coating. The width of these overtones is proportional to the coating thickness. The resonances, therefore, make up a code that we have deciphered to solve an inverse scattering problem for penetrable radar targets of known shape, but unknown material composition.

The electromagnetic situation described here is analogous to the elastic case we considered earlier[2] where the material composition of fluid fillers contained within cavities in elastic solids, was determined from the resonances in the elastic echoes returned by the filled cavity, as analysed in the light of the theory of resonance scattering[1].

Figure 1 shows a spherical conducting core covered with a layer of dielectric material of dielectric constant ε_1 and thickness δ which is illuminated by an incident plane wave of propagation constant $k_0 = \omega/c_0$. The far-field amplitude of the scattered electric field is given by[3]

$$\vec{E}_{sc} = E_0 \frac{e^{ik_0 r}}{r}\left[\hat{\varepsilon}_\theta S_1(\theta)\cos\phi - \hat{\varepsilon}_\phi S_2(\theta)\sin\phi\right] \qquad (1)$$

where

$$S_1(\theta) = -i\sum_{n=1}^{\infty}(-1)^n \frac{2n+1}{n(n+1)}\left(a_n \frac{P_n^1(\cos\theta)}{\sin\theta} - b_n \frac{dP_n^1(\cos\theta)}{d\theta}\right) \qquad (2)$$

$$S_2(\theta) = -i\sum_{n=1}^{\infty}(-1)^n \frac{2n+1}{n(n+1)}\left(a_n \frac{dP_n^1(\cos\theta)}{d\theta} - b_n \frac{P_n^1(\cos\theta)}{\sin\theta}\right)$$

and where the 'Mie coefficients' are

$$a_n = -\frac{xj_n(x) - iZ_n(xj_n(x))'}{xh_n^{(1)}(x) - iZ_n(xh_n^{(1)}(x))'}$$
$$b_n = -\frac{xj_n(x) - iY_n(xj_n(x))'}{xh_n^{(1)}(x) - iY_n(xh_n^{(1)}(x))'} \qquad (3)$$

and $x = k_0 a$, where ω is the circular frequency of incident wave; c_0 the light velocity in the outer medium (Fig. 1); c_1 the light velocity in the dielectric coating; θ, ϕ the spherical angles of the observer; $\hat{\varepsilon}_\theta$, $\hat{\varepsilon}_\phi$ the unit vectors in the θ, ϕ directions; E_0 the amplitude of the incident electric field.

Expressions for the modal impedances Z_n and admittances Y_n are given elsewhere[3–5]. The target eigenvibrations correspond to the zeros of the real parts of the denominators of a_n and b_n as follows

$$\frac{1}{iZ_n} = Re\left\{\frac{[xh_n^{(1)}(x)]'}{xh_n^{(1)}(x)}\right\} \quad \text{and} \quad iY_n = Re\left\{\frac{xh_n^{(1)}(x)}{[xh_n^{(1)}(x)]'}\right\} \qquad (4)$$

for the *TE* and *TM* modes, respectively. These characteristic equations can be solved for the real eigenfrequencies $x = x_{nl}^{TE}$ and $x = x_{nl}^{TM}$, respectively. The electromagnetic resonances are illustrated in Fig. 2 for a perfectly conducting sphere with a dielectric coating of relative thickness $\delta_r = \delta/a = 0.1$, and dielectric constant $\varepsilon_1 = 6$. The backscattering cross-section[3]

$$\frac{\sigma}{\pi a^2} = \left|\frac{2}{ka}\sum_{n=1}^{\infty}(-1)^n(n+\tfrac{1}{2})(a_n - b_n)\right|^2 \qquad (5)$$

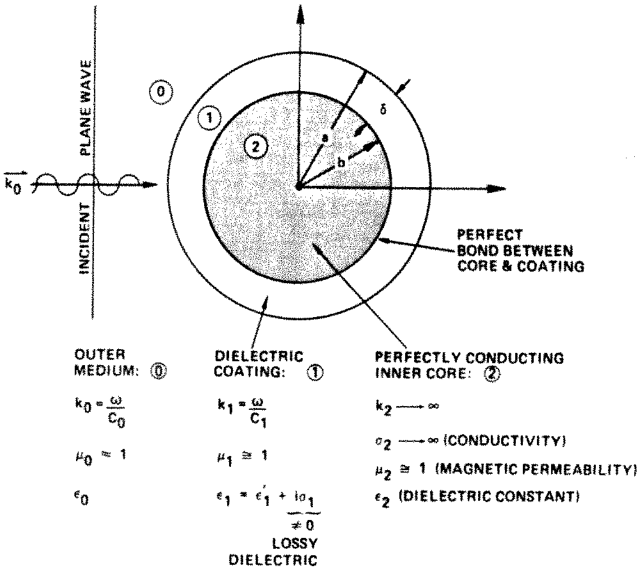
PLANE WAVE
INCIDENT
$\vec{k_0}$
⓪
①
②
a
b
δ
PERFECT BOND BETWEEN CORE & COATING
OUTER MEDIUM: ⓪
$k_0 = \frac{\omega}{C_0}$
$\mu_0 \approx 1$
ϵ_0
DIELECTRIC COATING: ①
$k_1 = \frac{\omega}{C_1}$
$\mu_1 \cong 1$
$\epsilon_1 = \epsilon_1' + i\sigma_1$
$\neq 0$
LOSSY DIELECTRIC
PERFECTLY CONDUCTING INNER CORE: ②
$k_2 \longrightarrow \infty$
$\sigma_2 \longrightarrow \infty$ (CONDUCTIVITY)
$\mu_2 \cong 1$ (MAGNETIC PERMEABILITY)
ϵ_2 (DIELECTRIC CONSTANT)

Fig. 1 The geometry of the problem. A perfectly conducting sphere coated with a layer of dielectric material under plane wave incidence.

is plotted in decibels against $k_0 a$ up to 25. We have identified the numerous rapid oscillations visible in Fig. 2 as *TE* or *TM* resonances by actually solving equations (4), and we have marked them by arrows and denoted them by (nEl) or (nMl) labels, respectively. This figure can be viewed as the 'characteristic resonance spectrum' identifying the target. We have also evaluated numerically some of the partial wave coefficients a_n and b_n which exhibit the (nEl) and (nMl) resonances for a given partial wave index n. For $n = 10$, Fig. 3 presents the *TE* (top) and *TM* (bottom) moduli $(2n+1)/n(n+1)|a_n|$ and $(2n+1)/n(n+1)|b_n|$ plotted against $k_0 a$, clearly exhibiting some of the resonances. Using the known forms for Z_n and Y_n and the asymptotic forms of the Bessel functions we can now solve the inverse scattering problem. We can show that for $x \gg 1$, one has

$$\frac{1}{iZ_n} \rightarrow (\varepsilon_1)^{1/2}\cot k_1\delta \quad \text{and} \quad iY_n \rightarrow -(\varepsilon_1)^{1/2}\tan k_1\delta \qquad (6)$$

where $k_1 = \omega/c_1 = k(\varepsilon_1)^{1/2}$. The asymptotic spacing Δ_l between

---

* Also at the Department of Physics, Catholic University, Washington, DC 20064.

0028–0836/80/430708—02$01.00

adjacent (*TE* or *TM*) resonances in this limit can be written as

$$\Delta_l \equiv x_{l+1}^{TE,TM} - x_l^{TE,TM} = \frac{\pi}{(1-\gamma)(\varepsilon_1)^{1/2}} \qquad (7)$$

where $\gamma = b/a$. A second equation for the two unknowns Δ_l and γ emerges from a consideration of the resonance widths. Our theory[1] gives these widths (for the *TE*-modes) as follows

$$\tfrac{1}{2}\Gamma_{nl}^{TE} = \lim_{x \to x_{nl}^{TE}} \frac{Im\left\{\dfrac{[xh_n^{(1)}(x)]'}{xh_n^{(1)}(x)}\right\}}{Re\left\{\dfrac{[xh_n^{(1)}(x)]'}{xh_n^{(1)}(x)}\right\} - \dfrac{1}{iZ_n}}(x - x_{nl}^{TE}) \qquad (8)$$

and when this expression is evaluated one halfwidth below any resonance (that is, at $x = x_{nl}^{TE} - \frac{1}{2}\Gamma_{nl}^{TE} \equiv X_{nl}^{TE}$) and we use the asymptotic expansion for the Bessel functions ($x \gg 1$) we find

$$(\varepsilon_1)^{1/2} = \tan\left[X_{nl}^{TE}(\varepsilon_1)^{1/2}(1-\gamma)\right] \qquad (9)$$

Substituting the value of $(\varepsilon_1)^{1/2}$ from equation (7) into equation (9) yields

$$\delta_r = \frac{\delta}{a} = 1 - \gamma = \frac{\pi}{\Delta_l}\cot\left(\pi\frac{X_{nl}^{TE}}{\Delta_l}\right) \qquad (10)$$

Substituting this value of $(1-\gamma)$ into equation (7) finally yields

$$(\varepsilon_1)^{1/2} = \tan\left(\pi\frac{X_{nl}^{TE}}{\Delta_l}\right) \qquad (11)$$

Equations (10) and (11) solve the inverse scattering problem, using our resonance formalism, for the dielectric constant and the thickness of the coating, from the uniform spacings Δ_l and widths X_{nl}^{TE} of the resonances in the high frequency region of the resonance spectrum.

A similar analysis may be carried out for targets of general shape but unknown composition. Shape information may be obtained, as in the case of nuclear photon scattering[6] from the splitting and relative weights of the resonances. The resonance frequencies of a penetrable prolate spheroidal target, for instance, are split into two different sets $f_{nm}^{(l)}$ and $f_{nm}^{(s)}$, corresponding to standing waves along a long or a short axis, respectively, with $f_{nm}^{(l)} < f_{nm}^{(s)}$. These two sets may be experimentally separated as follows. An incident polarized or unpolarized wave travelling along the long axis will excite only the $f_{nm}^{(s)}$ resonance. A wave incident along a short axis will excite the $f_{nm}^{(l)}$ or $f_{nm}^{(s)}$ resonances, depending on whether it is polarized either along the long or the short axis, respectively; if the wave is unpolarized it will excite both with equal weights. Incidence along any other direction will produce excitation of both sets of resonances with weights depending on the direction of incidence. This allows the lengths of the two axis and the target orientation to be determined. If both the shape and the composition of the target are unknown, these two types of analysis have to be combined.

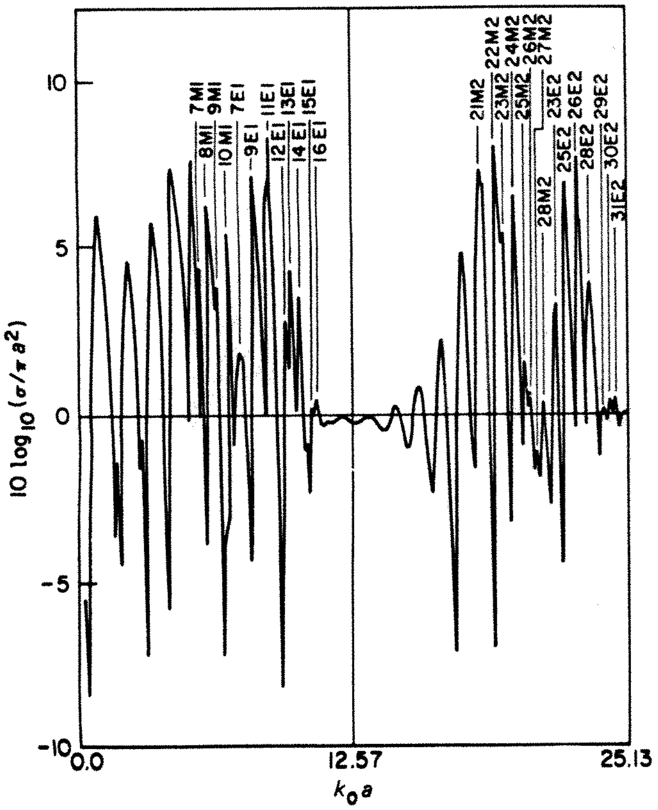

Fig. 2 Radar cross-section (in db) against k_0a for the coated target in Fig. 1 with $\varepsilon_1 = 6$ and $\delta_r = 0.1$. Numerous *TE* and *TM* resonances are identified and labelled using our theory[1].

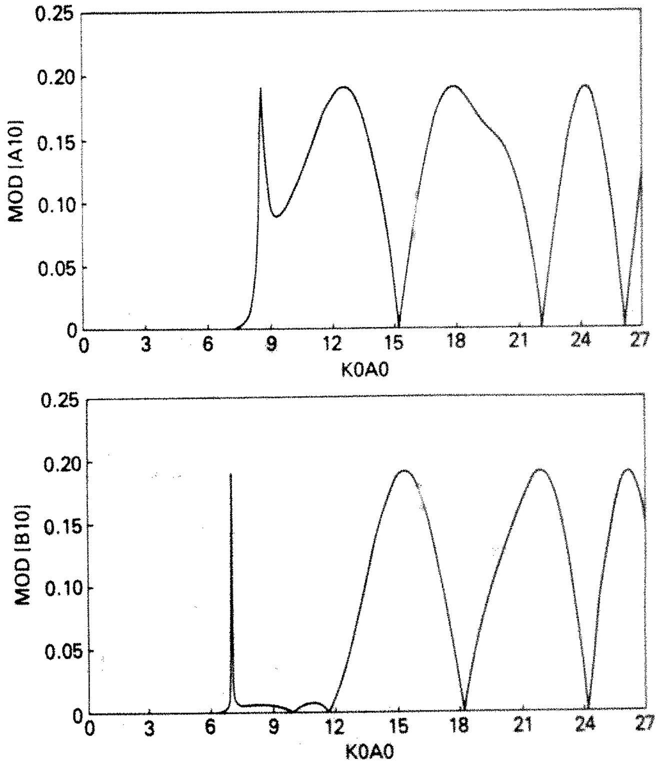

Fig. 3 Typical ($n = 10$) *TE* (top) and *TM* (bottom) partial-wave amplitude contained in the cross-section, clearly showing some of the resonances labelled in the (summed) radar cross-section of Fig. 2.

General areas where our resonance method of target characterization can be applied aside from radar backscattering have been given elsewhere[1,2]. Examples include the identification of radar targets (such as aircraft types) or of sonar targets (such as types of submerged objects); the identification of mineral or natural gas deposits in seismic prospecting; the characterization of flaws in elastic media by non-destructive evaluation, or of tumours in animal tissue (medical ultrasonics); or in the acoustic design of underwater sound absorbers, among others.

We conclude from the above example that the presence of resonances in the backscattered (radar) cross-section of simple targets can be used to solve material characterization problems in the light of the resonance theory of scattering as recently derived by us[1]. This example could be used as the start of a new scientific discipline of electromagnetic spectral analysis for more complex objects.

This work was supported by NSWC's Independent Research Board and by the Naval Air System's Command, Code AIR-310B.

Received 1 August; accepted 26 August 1980.

1. Flax, L., Gaunaurd, G. C. & Überall, H. *Phys. Acoust.* **15** (in the press).
2. Gaunaurd, G. C. & Überall, H. *Science* **206**, 61–64 (1979).
3. Ruck, G. T. *et al. Radar Cross Section Handbook* (Plenum, New York, 1970).
4. Helstrom, C. W. *Scattering of Electromagnetic Waves from Cylinders and Spheres Coated with Dielectric Material* (Westinghouse Research Labs, Res. Rep. 806-A800-R2, Pittsburg, 1961).
5. Rheinstein, J. *IEEE Trans.* AP-12, 334–340 (1964).
6. Danos, M. *Nucl. Phys.* **5**, 23–32 (1958).

Ground-based measurements of atmospheric NO_2 by differential optical absorption

B. B. McMahon & E. L. Simmons

Meteorological Office, Bracknell, Berkshire RG12 2SZ, UK

Nitrogen dioxide is important to stratospheric ozone chemistry[1]. The few observations of vertical distribution of the gas are reviewed elsewhere[2]. Most available data relate to ground-based measurements of the total amount in the vertical column. Such observations are ideally made from a high altitude site to avoid local tropospheric sources. Noxon[3] observed a mean value of 5×10^{15} molecules cm^{-2} from Fritz Peak Observatory. Pommereau and Hauchecorne[4] obtained much higher values, of a few $\times10^{17}$ molecules cm^{-2}, at Haute-Provence Observatory. Noxon *et al.* have reported latitudinal gradients[5,6] and response to stratospheric warmings[7], reporting stratospheric column values in the range $1-5\times10^{15}$ molecules cm^{-2}. During the past year, several series of observations have been made from a low altitude rural site in the UK. Values obtained for the vertical column were in the range $0.8-5.6\times10^{16}$ molecules cm^{-2}. In view of the tropospheric contribution expected at this site[8], these values represent an upper limit to the stratospheric NO_2 column and we show here that the values reported by Pommereau and Hauchecorne were anomalously high.

The technique[3,4,9] used exploits characteristic structure in the absorption cross-section of NO_2 in the spectral range 435–450 nm. Series of direct solar spectra were obtained on clear mornings from sunrise until noon, using a grating monochromator to scan repetitively across this range with 0.5 nm resolution. Partial compensation for changes in atmospheric turbidity during scanning was achieved by normalizing each spectral channel output with respect to a simultaneous broadband solar luminance signal. The ratios were recorded digitally for subsequent computer analysis. A spectrum recorded at high solar elevation near midday, when slant-path NO_2 should be at a minimum, was used as a reference. The difference between the logarithm of each individual spectrum and the logarithm of this reference spectrum contains the information needed to derive the difference in slant-path NO_2. Care was taken to compensate for wavelength drifts in the monochromator which, because of pronounced solar Fraunhofer structure in the observed spectral range, lead to spurious features in the difference spectra. Difference spectra were corrected for attenuation by atmospheric Rayleigh scattering and by ozone, the latter based on the total ozone amount for the day measured at the same site with a Dobson spectrophotometer. Possible water vapour absorption channels[10] were omitted from the analysis.

Attenuation due to particulate scattering may be assumed to vary linearly with wavelength[11–13] over the narrow spectral band used. A straight line was fitted to every difference spectrum by the least squares method and the deviation from this line was used as the corrected (difference) spectrum. Corrected spectra were regressed against a spectrum of NO_2 absorption also expressed as a deviation from the best fit line. The shape of this spectrum was determined using the same monochromator and spectral resolution with a carefully purified NO_2 sample, but was quantified by comparison with the absorption coefficients tabulated by Wilkerson *et al.*[14]. Regression coefficients thus calculated correspond to the difference in slant-path NO_2 between the times of each solar spectrum and the reference spectrum. A typical series of corrected spectra are shown in Fig. 1, in which successive spectra have had their origin shifted obliquely with respect to the first by an amount proportional to the time difference; the lowest curve is the NO_2 absorption spectrum. The resemblance confirms that NO_2 absorption is being observed. Some of the uncertainty associated with recognizing particular dips and peaks in the attenuated solar spectra[5,9] is avoided by making full use of the spectrum in this way. Full details of the technique will be published elsewhere.

Differences in slant-path NO_2 relative to the reference, were plotted against the atmospheric mass number, μ, given by the secant of the solar zenith angle at an assumed height for the centre of mass of the NO_2 distribution. Figure 2 is an example of such a 'quasi-Langley' plot, derived from the spectra in Fig. 1. If the NO_2 is constant in time and uniform horizontally, and the assumed height is correct, then the quasi-Langley plot should be a straight line with slope equal to the vertical NO_2 column. Rapid photolysis of NO_2 is believed to occur at sunrise, followed

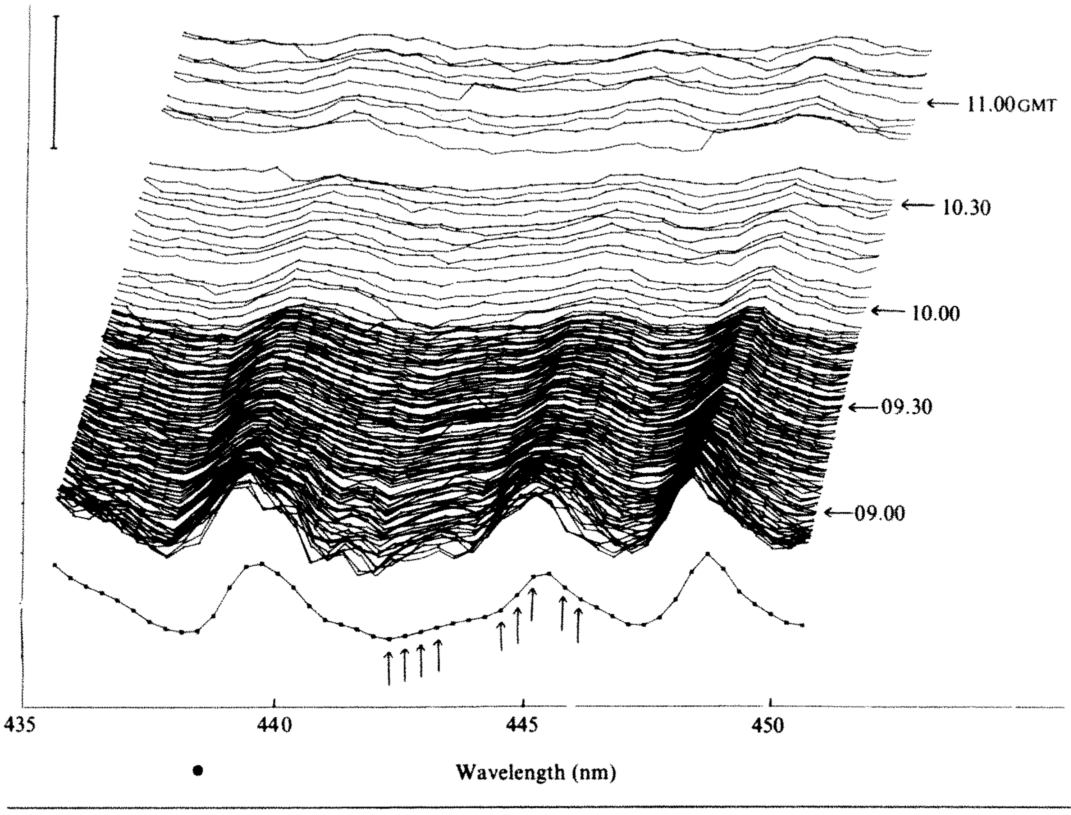

Fig. 1 Corrected spectra obtained using 21 December 1979 solar spectra. The bottom curve represents the NO_2 absorption spectrum used in the regression calculations, after suitable scaling to assist visual comparison with the corrected spectra. Solar spectra span the period 08.52–11.16 GMT on 21 December 1979; sunrise was at 08.06 GMT. Scale bar, optical depth of 0.1, relative to the reference. Note that the amplitudes of differential absorption decrease with time, indicating decreasing slant-path NO_2 during the morning. The smooth appearance of these spectra imply that good wavelength alignment of the solar spectra with the reference spectrum has been achieved. Arrows mark channels omitted from the analysis because of their susceptibility to H_2O absorption.

by a gradual increase in the daytime abundance due to slow N_2O_5 photolysis. Theoretical studies[15] of these processes predict that, by surface sunrise, the effect on slant-path NO_2 due to changes in the vertical NO_2 abundance is small compared with the effect of decreasing slant path, justifying the assumption of constant NO_2 at this time. However, because the above effects are predicted to become comparable near midday, solar spectra obtained within an hour of midday were ignored. Changes in slope were occasionally observed at relatively low μ-values, for which μ is insensitive to the assumed centre-of-mass height. This implies that significant advective changes in the NO_2 column were taking place, probably in the troposphere, which can lead to misinterpretation of the slopes. Consequently only those mornings were accepted on which the slope was essentially linear over a μ-range of at least 3. As our objective was to set an upper limit to the stratospheric NO_2 column, a stratospheric value[5] of 26 km was assumed for the centre-of-mass height. During episodes of high boundary-layer NO_2 this height would be much lower, so that our assumed mass numbers will be too low and our tabulated values will be an overestimate of the NO_2 vertical column. This source of bias error, which increases at low solar elevation, has been kept below 20% by ignoring solar spectra obtained at μ greater than 7. Noxon avoids this difficulty by using his twilight zenith sky technique[5]. We have not used this technique as we are not satisfied that in our viewing conditions it will yield valid results.

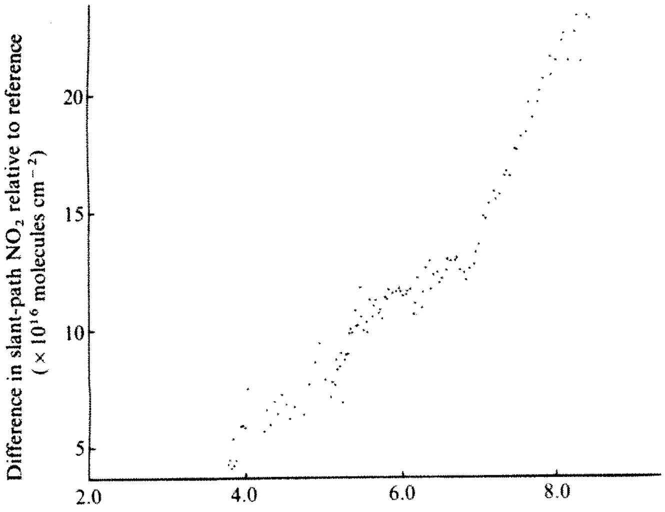

Fig. 2 Quasi-Langley plot for the corrected spectra of Fig. 1. Sunrise corresponds to $\mu = 11.1$. Some of the scatter in the points may be due to horizontal advection of boundary-layer NO_2 but the greater scatter exhibited towards midday (which was often found) may also be due to vertical convection of boundary-layer NO_2.

Estimates of the total NO_2 which were obtained, meeting the above criteria, are presented in Table 1, together with the μ-ranges and corresponding time intervals over which they were evaluated. Values are in the range $0.8\text{–}5.6 \times 10^{16}$ molecules cm^{-2}, which compare with Noxon's[3,5] findings of a mean total column value of 0.5×10^{16} molecules cm^{-2} and a mean stratospheric column value of around 0.25×10^{16} molecules cm^{-2}. If we subtract this stratospheric value from our totals and assume that the difference is uniformly mixed throughout a surface layer 1 km thick, then the mixing ratios are in the range 2–25 p.p.b. (parts per 10^9). These are within the range of surface mixing ratios (1–34 p.p.b.) reported[8] at Harwell which is less than 50 km from our measurement site. Noxon's relatively low total column value is understandable in view of the smaller tropospheric NO_2 component expected at his Fritz Peak site (3,000 m a.m.s.l.). However, it is difficult to explain the high values of a few 10^{17} molecules cm^{-2} reported by Pommereau and Hauchecorne[4], who observed from Haute-Provence Observatory (651 m a.m.s.l.).

Table 1 Values of the total vertical NO_2 column at Beaufort Park, Bracknell, Berkshire (51°23′ N, 0°47′ W, 70 m a.m.s.l.)

Date	Time interval (GMT)	μ-range	Total NO_2 estimated from slope (10^{16} molecules cm^{-2})
6 September 1979	06.10–08.39	1.9–7.0	0.9 ± 0.2
5 November 1979	07.56–08.57	4.0–7.0	0.9 ± 0.3
9 November 1979	08.07–10.44	2.8–6.8	0.9 ± 0.2
21 December 1979	09.11–10.58	3.9–7.0	3.0 ± 0.6
2 January 1980	09.13–10.03	4.0–7.0	1.9 ± 0.8
24 January 1980	09.01–11.12	3.1–6.4	1.7 ± 0.9
4 March 1980	07.29–08.40	3.4–7.0	5.6 ± 0.8
22 March 1980	07.01–08.31	2.6–5.8	0.9 ± 0.1
30 March 1980	07.47–10.00	2.0–5.5	$0.8 + 0.8 - 0.2$
20 April 1980	05.44–06.56	3.0–7.0	1.9 ± 0.4

The present apparatus and method of analysis have demonstrated the possibility of measuring the NO_2 total column at a site not having the best of viewing conditions, and have given some support to the relatively low values of NO_2 column reported by Noxon. A spectrophotometer system optimized for this type of measurement is being considered which could be used at a site well removed from continental tropospheric NO_2 sources.

We thank A. F. Tuck, S. A. Clough, A. E. Whittaker and other members of the Meteorological Office staff for assistance.

Received 14 July; accepted 19 August 1980.

1. Crutzen, P. J. *Q. Jl R. met. Soc.* **96,** 320 (1970).
2. Drummond, J. R. & Jarnot, R. F. *Proc. R. Soc.* A**264,** 237–254 (1978).
3. Noxon, J. F. *Science* **189,** 547–549 (1975).
4. Pommereau, J. P. & Hauchecorne, A. *C. r. hebd. Séanc. Acad. Sci., Paris.* B**288,** 135–138 (1979).
5. Noxon, J. F. *et al. J. geophys. Res.* **84,** 5047–5065 (1979).
6. Noxon, J. F. *J. geophys. Res.* **84,** 5067–5076 (1979).
7. Noxon, J. F. *et al. J. geophys. Res.* **84,** 7883–7888 (1979).
8. Cox, R. A. *Tellus* **29,** 356–362 (1977).
9. Harrison, A. W. *Can. J. Phys.* **57,** 1110–1117 (1979).
10. Curcio, J. A. *et al. Nav. Res. Lab. Rep.* 4669 (1955).
11. Kuznetsov, G. I. & Nigmatullina, K. S. *Izv. Fiz. Atmos. Okean.* **13,** 886–889 (1977).
12. Eldridge, R. G. *J. atmos. Sci.* **23,** 605–613 (1966).
13. Ahlquist, N. C. & Charlson, R. J. *Atmos. Envir.* **3,** 551–564 (1969).
14. Wilkerson, T. D. *et al. Tech. Note BN-784* (Institute for Fluid Dynamics & Applied Mathematics, University of Maryland, 1974).
15. Department of the Environment *Chlorofluorocarbons and Their Effect on Stratospheric Ozone* (Pollution Paper No. 15, HMSO, London, 1979).

A modified diabatic circulation model for stratospheric tracer transport

J. A. Pyle & C. F. Rogers

Department of Atmospheric Physics, University of Oxford,
Clarendon Laboratory, Parks Road, Oxford OX1 3PU, UK

The possible modifications of the ozone layer by various pollutants has created considerable interest in modelling of stratospheric minor constituents. A major limitation of such modelling work has been the treatment of eddy processes in one- and two-dimensional models. We now describe a two-dimensional model in which some problems associated with the cancellation of the mean and eddy terms in the species continuity equation are removed. If the eulerian mean meridional circulation is replaced by only that part of the circulation driven by the diabatic heating, part of the eddy transport term disappears, although the part associated with the chemistry of the transported species[1,2] must still be considered. The model explains the results of Prabhakara[3] who successfully used a modified diabatic circulation plus Fickian diffusion to model atmospheric ozone.

0028-0836/80/430711—04$01.00

In the usual eulerian mean approach zonal averages are taken at fixed points in space, defining a latitude–height grid. Thus, with $\overline{(\ )}$ the zonal eulerian mean operator $= 1/2\pi \int_0^{2\pi} (\ )\,d\lambda$, λ = longitude, and $(\ )'$ perturbation from the zonal mean, any variable χ can be written $\chi = \bar{\chi} + \chi'$. The zonally averaged continuity equation then contains terms involving just the zonal means and other terms (the eddies) involving zonal averages of the perturbation quantities. It has often proved useful to regard the stratosphic circulation as being composed of a zonally symmetric circulation plus eddies, or waves. The two-dimensional eulerian mean continuity equation for a species of mixing ratio χ is written

$$\frac{\partial \bar{\chi}}{\partial t} + \bar{v}\frac{\partial \bar{\chi}}{\partial y} + \bar{\omega}\frac{\partial \bar{\chi}}{\partial p}$$
$$= -\frac{1}{\cos\phi}\frac{\partial}{\partial y}(\overline{v'\chi'}\cos\phi) - \frac{\partial}{\partial p}(\overline{\omega'\chi'}) + \bar{S} \qquad (1)$$

where the first two terms on the right-hand side represent the eddy transport of χ. The velocities v and ω are in the y (northward) and p (pressure) coordinate directions respectively, ϕ is the latitude and $\bar{S}$ represents the net sources and sinks of χ.

The treatment of the eddy transport in equation (1) has traditionally followed the procedure of Reed and German[4] where the fluxes are written in terms of the mean gradients

$$\begin{aligned} \overline{v'\chi'} &= -K_{yy}\frac{\partial \bar{\chi}}{\partial y} - K_{yp}\frac{\partial \bar{\chi}}{\partial p} \\ \overline{\omega'\chi'} &= -K_{py}\frac{\partial \bar{\chi}}{\partial y} - K_{pp}\frac{\partial \bar{\chi}}{\partial p} \end{aligned} \qquad (2)$$

with $K_{yp} = K_{py}$. Equation (2) is then used for all quasi-conservative tracers with the same set of K values, generally derived from atmospheric statistics on rather shaky assumptions. Luther[5], for example, has determined Northern Hemisphere monthly mean values of K from heat flux data, and they have been widely used in modelling studies.

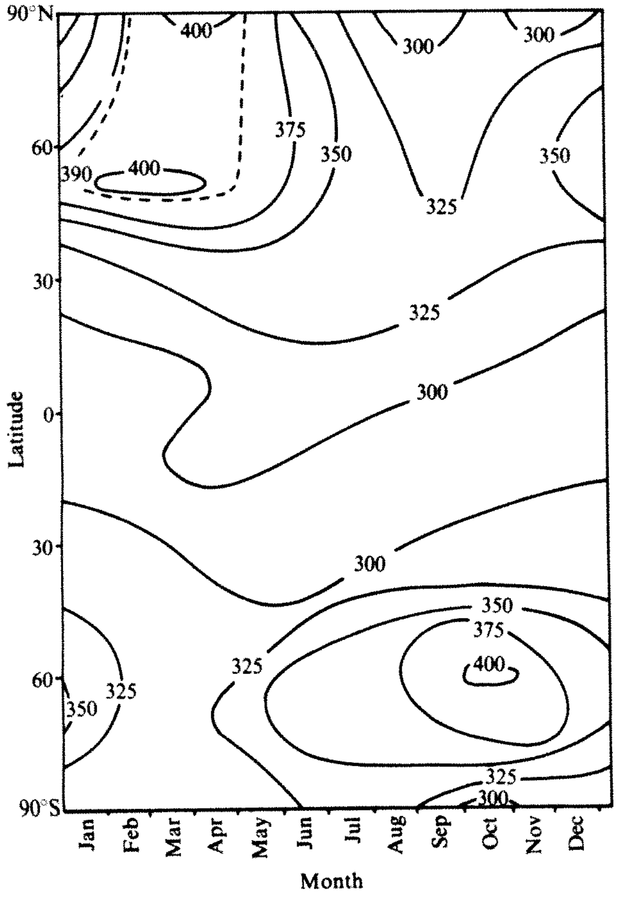

Fig. 1 Latitude–time section of total ozone (m atm-cm) from experiment 1.

Recent work has suggested improvements to two-dimensional models by using a more physically based K-theory[1,2,6–8]. By coupling a calculation of planetary wave propagation with solutions of the species perturbation continuity equation. We[2] have calculated tracer eddy fluxes and hence computed K fields. Of particular interest is that K varies between species, depending on their photochemical lifetimes. Matsuno[1] separated the K values into

$$\text{an anti-symmetric} \quad \begin{pmatrix} 0 & K'_{yp} \\ K'_{py} & 0 \end{pmatrix}$$

$$\text{and a symmetric} \quad \begin{pmatrix} K^{R}_{yy} & K^{R}_{yp} \\ K^{R}_{py} & K^{R}_{pp} \end{pmatrix} \quad \text{component.}$$

Note that $K'_{yp} = -K'_{py}$ but that $K^{R}_{yp} = K^{R}_{py}$. When the photochemical source is relatively weak, as, for example, with ozone in the lower stratosphere, the anti-symmetric component is independent of the species being transported, depending just on the wave structure: it is applicable to steady, conservative waves and an inert tracer. For photochemical tracers there is the additional symmetric component which depends on the photochemical lifetime, as well as the wave structure, and is, therefore, different for different species. Note that the symmetric component is large and can play a significant role. Matsuno[1] estimated that the anti-symmetric component dominated, but this was due to his choice of 100 days as a species lifetime.

A new approach to studies of tracer transport using a lagrangian framework has been suggested[9,10] in which the eddy terms apparently need not be calculated. Considering equation (1), in practice the mean and eddy flux terms almost cancel so that the small residual of two large terms must be found. The reasons for the cancellation are well understood in general theoretical terms[1,6–13]. For steady, non-dissipating waves (the eddies), an eulerian mean meridional circulation is induced which just cancels the effects of the eddies on the mean state. If, however, we consider a lagrangian description, the species continuity equation becomes particularly simple and no eddy terms appear:

$$\frac{\partial \bar{\chi}^{L}}{\partial t} + \bar{v}^{L}\frac{\partial \bar{\chi}^{L}}{\partial y} + \bar{\omega}^{L}\frac{\partial \bar{\chi}^{L}}{\partial p} = \bar{S}^{L}$$

where $\overline{(\ )}^{L}$ is some lagrangian average. (In a simple case this could be an average following an air parcel. Thus in a lagrangian frame we move with the flow; in a eulerian frame we observe the flow from a fixed point.) The problem now becomes one of finding $\bar{v}^{L}$ and $\bar{\omega}^{L}$ (and $\bar{S}^{L}$) rather than the eddies. Dunkerton[9] has identified the lagrangian mean circulation with that driven by the eulerian mean diabatic heating. Using the same approximations we can identify a 'residual meridional circulation' (the difference between the eulerian circulation and that part induced by the steady, non-dissipating waves)[13] as that circulation driven by the diabatic heating.

The cancellation of the eddy terms in equation (1) by an induced mean circulation is only exact in the case of steady waves, with no dissipation, away from critical lines and for an inert tracer. In these circumstances a mean circulation will be induced which will just cancel the transport modelled by the anti-symmetric K components[14]. There is, however, no cancellation of the chemically induced transport, modelled by the symmetric K values. The symmetric K component can be shown to be equivalent to the Stokes correction to the eulerian mean source, $\bar{S}$, where $\bar{S}^{L} = \bar{S}$ + Stokes correction. Thus in both the eulerian and lagrangian description this chemically induced transport must be considered. This is to be expected as they are simply different descriptions of the same physical process.

The three present model experiments all used the same ozone photochemical scheme but included different descriptions of the dynamical processes. All the experiments were carried out

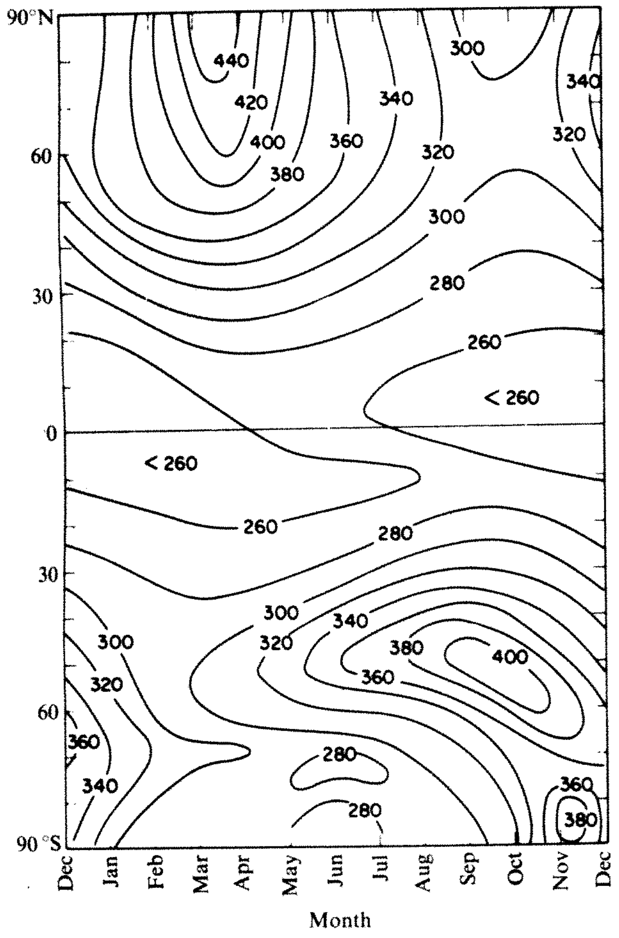

Fig. 2 Observed latitude–time section of total ozone (m atm–cm) after ref. 20.

within the framework of the University of Oxford two-dimensional model[15]. The photochemical scheme[16] included the effects of nitrogen and hydrogen compounds.

Figure 1 is a latitude–time section of total ozone from a run in which precomputed values of $\bar{v}$ and $\bar{\omega}$ were used, with the eddy transport calculated using Luther's[5] values of K. All the species use the same K fields and we assume that $K_{yp} = K_{py}$. Compared with the observed distribution in Fig. 2, Fig. 1 contains several satisfactory features with an equatorial minimum of total ozone and maxima at the spring pole in the Northern Hemisphere and at ~60° S in the Southern Hemisphere about seven months later. This asymmetry is reproduced using observed values of the eddy flux of angular momentum in calculating the $\bar{v}$ and $\bar{\omega}$ fields[17]. Although the broad features of the ozone distribution have been reproduced there are, however, important differences of detail. For example, the equatorial minimum should reach lower values whereas the Northern Hemisphere maximum should possibly be higher. This experiment is a typical example of present eulerian mean two-dimensional models.

In the second experiment the eddies were excluded, in both the calculation of the mean circulation and in the species continuity equations. Thus the calculated circulation is driven just by the radiative heating and the release of latent heat. The radiative heating scheme is described in Haigh and Pyle[18]. In the lower stratosphere, however, Rodgers[19] heating rates are used. The experiment can be considered from two viewpoints. The diabatic circulation can be considered as the residual circulation after the cancellation of the eddies and the ensuing induced circulation. Alternatively, Dunkerton suggested that the mass transport in the stratosphere is accomplished by the lagrangian mean circulation which he identified to a leading order with the eulerian diabatic circulation, which is used here.

Figure 3 shows the latitude–time section of total ozone from the run. The behaviour is mostly poor. Ozone is moved from equatorial to mid-latitudes where the modelled values are too large. The high latitude values, however, are too low, due to lack of eddy transport. Because negative mixing ratios can develop without any diffusion, the experiment was not run to a steady state. However, in a similar study including diffusion, Prabhakara[3] also failed to reproduce the polar maximum with low values of the diffusion coefficients. Maximum values occurred in middle latitudes. Failure to reproduce the observed ozone behaviour in this experiment is evidently not due to the omission of sub-grid scale diffusion.

The omission of eddies in the previous experiment is justified by the cancellation of the eddy circulation and the induced mean circulation. This cancellation does not occur if the waves are growing or decaying, near critical lines or when the tracer being transported is not inert. In a third experiment the uncancelled chemical eddy transport has been modelled. Thus, along with the diabatic circulation, the (chemical) symmetric part of the K-tensor is included. In lagrangian terms, this is equivalent to including the Stokes correction to the eulerian mean source to give the lagrangian mean source. Though we can calculate the symmetric K components[2], for simplicity we have used Luther's values, which are, of course, symmetric. Our calculated K values[2] are roughly similar in magnitude to Luther's values in the winter hemisphere, but much smaller in summer.

The total ozone distribution in this run is shown in Fig. 4. The behaviour is good with both an improved equatorial minimum and Northern Hemisphere polar maximum over those found in the first experiment (Fig. 1). By comparison with Fig. 3, the chemical eddy transport plays a major part in transporting ozone polewards.

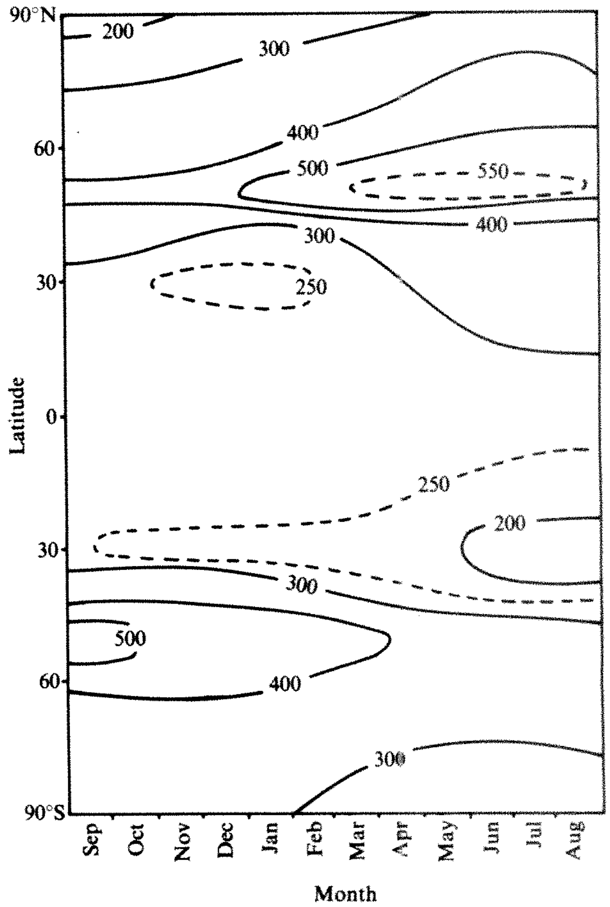

Fig. 3 Latitude–time section of total ozone (m atm-cm) from experiment 2.

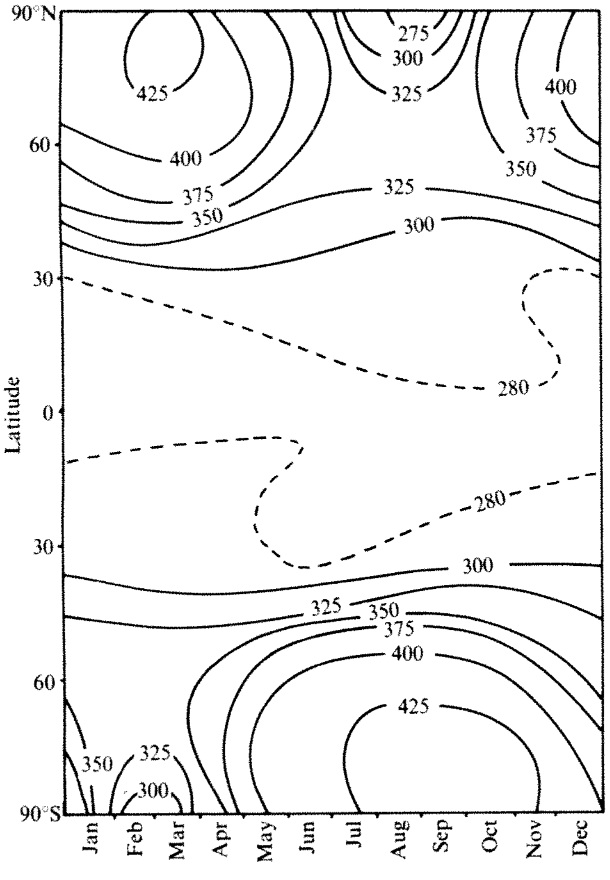

Fig. 4 Latitude–time section of total ozone (m atm-cm) from experiment 3.

The Southern Hemisphere is less well reproduced. Possibly because the eddy activity is less strong in the Southern Hemisphere, the *K* components should, therefore, be smaller there. Certainly the summer *K* in both hemispheres should be smaller than used here. In assessing the performance of the model, remember that *K* ought to vary with the species, whereas here the same *K* has been used for all species.

The above experiment is crude in that the *K* values are not calculated within the model. However, the results are encouraging and attempts at a more self-consistent calculation are in progress. An early indication is that the calculated *K* in winter high latitudes is not sufficient to account completely for the spring build up of ozone and an important role for wave transience is possibly indicated.

An advantage over the usual eulerian models is that the close cancellation between the eddies and the mean motions is removed. In models where the mean circulation is specified, problems of the compatibility of the chosen circulation and the eddy transport coefficients are also partly removed. Another advantage is that experiments with the radiative schemes, including possible perturbation experiments including radiative and hence dynamical feedbacks, are quite simple to perform in this model. Some knowledge of the eddy fields is, of course, still necessary but the model is simpler than the usual eulerian models. Furthermore, note that the cancellation of the eddy terms does not arise when the waves are transient or dissipating. However, because the modelled ozone distribution is quite good it suggests that the chemical eddy contribution may be the most important. Plumb[8] has shown that the tracer fluxes are oppositely directed during the growing and decaying phases of wave development (see also ref. 14). However, in explosive events like the sudden stratospheric warming we do expect wave transience to play a major part.

Finally, the model explains the success of a similar model by Prabhakara[3]. His success in a model which used the diabatic circulation was due to the inclusion of a large diffusion term in the ozone continuity equation. With small values of the diffusion coefficients, the behaviour was similar to that shown in Fig. 3. A good ozone distribution was obtained only with the larger values, comparable with the K_{yy} used in experiment 3. The transport modelled by Prabhakara's larger *K* values was of planetary scale, rather than a sub-grid scale diffusion, and is presumably mainly the chemical contribution discussed above.

The modelling work at Oxford is supported by the NERC.

Received 28 April; accepted 10 September 1980.

1. Matsuno, T. *Pure appl. Geophys.* **118,** 189–216 (1980).
2. Pyle, J. A. & Rogers, C. F. *Q. Jl. R. met. Soc.* **106,** 421–446 (1980).
3. Prabhakara, C. *Mon. Weath. Rev.* **91,** 411–431 (1963).
4. Reed, R. J. & German, K. E. *Mon. Weath. Rev.* **93,** 313–321 (1965).
5. Luther, F. M. *AIAA paper, 73-498, AIAA/AMS Conf.* Denver (1973).
6. Clark, J. H. E. & Rogers, T. G. *J. atmos. Sci.* **35,** 2232–2235 (1978).
7. Holton, J. R. *Phil. Trans. R. Soc.* A**296,** 73–85 (1980).
8. Plumb, R. A. *J. atmos. Sci.* **36,** 1699–1704 (1979).
9. Dunkerton, T. *J. atmos. Sci.* **35,** 2325–2333 (1978).
10. McIntyre, M. E. *Phil. Trans. R. Soc.* A**296,** 129–148 (1980).
11. Eliassen, A. & Palm, E. *Geophys. Publ.* **22** (1960).
12. Charney, J. G. & Drazin, P. G. *J. geophys. Res.* **66,** 83–109 (1967).
13. Andrews, D. G. & McIntyre, M. E. *J. atmos. Sci.* **33,** 2031–2048 (1976).
14. Hartmann, D. L. & Garcia, R. R. *J. atmos. Sci.* **36,** 350–364 (1978).
15. Harwood, R. S. & Pyle, J. A. *Q. Jl. R. met. Soc.* **101,** 732–748 (1975).
16. Pyle, J. A. *Pure appl. Geophys.* **118,** 355–377 (1980).
17. Harwood, R. S. & Pyle, J. A. *Q. Jl. R. met. Soc.* **103,** 319–343 (1977).
18. Haigh, J. D. & Pyle, J. A. *Nature* **279,** 222–224 (1979).
19. Rodgers, C. D. *Planetary Circulation Project* (Rep. No. A2, MIT, 1967).
20. Dütsch, H. U. *Adv. Geophys.* **15,** 219–322 (1971).

Chloride ions in aqueous solutions

S. Cummings*, J. E. Enderby§, G. W. Neilson & J. R. Newsome

H. H. Wills Physics Laboratory, University of Bristol,
Tyndall Avenue, Bristol BS8 1TL, UK

R. A. Howe, W. S. Howells† & A. K. Soper‡

Department of Physics, University of Leicester, University Road,
Leicester LE1 7RH, UK

In spite of much experimental and theoretical work during the past 80 yr, there is at present no generally agreed structural model for concentrated aqueous solutions, even for a relatively simple system like NaCl dissolved in H_2O (ref. 1). Aqueous solutions contain four chemical species and so require 10 pair correlation functions to describe the structure, thus complicating attempts to isolate, for example, ion–water correlations unambiguously from diffraction experiments. The combination of long-range Coulomb potentials, quantum-mechanical hydrogen bonding effects and the intractability of the liquid state has proved an obstacle to theoretical understanding. We have investigated the coordination of water molecules around Cl^- ions in aqueous solution by the isotopic substitution method. A range of counter-ions and concentrations was used to answer questions about the sensitivity of Cl^- hydration to the nature of the counter-ion and the ionic strength. We show here that Cl^- hydration is essentially independent of the cation and of ionic strength with the possible exception of a transition metal counter ion (Ni^{2+}). The insensitivity of Cl^- hydration to cation type should lead to a major simplification in the theory of solutions.

Present addresses: *L'Institut Laue-Langevin, B.P. 156 X, 38042 Grenoble Cedex, France; † Los Alamos Scientific Laboratory, New Mexico 87545; ‡ Neutron Division, Rutherford Laboratory, Chilton, Didcot, Oxon OX11 0X, UK.
§ To whom correspondence and reprint requests should be addressed.

0028-0836/80/430714—03$01.00

The unique role of neutron diffraction applied to aqueous solutions has been emphasized by two groups[2,3]. Narten *et al.*[2] demonstrated ion–water effects by comparing the neutron and X-ray scattering intensity from solutions of LiCl in D_2O. The Bristol/Leicester group[3–5] emphasized the use of isotopic substitution and showed that the coordination of water molecules around a given ion can be derived unambiguously from the algebraic difference, as a function of momentum transfer, $\hbar k$, of the absolute neutron-scattering cross-sections between two samples identical in all respects except that the isotopic state of the ion has been changed[4]. We have also shown that the recoil corrections which apply to neutron diffraction from aqueous solutions essentially vanish when this difference is used. Using this method the nature of the hydration of Ni^{2+} has been shown[5] to be concentration dependent, an unexpected result.

We now report on an investigation of the Cl^-–H_2O coordination (loosely referred to as hydration) in a range of different ionic solutions (Table 1) to establish the extent to which the geometry of ionic hydration is sensitive to the counter-ion. The parameters which define this geometry are shown in Fig. 1. This sensitivity has long been a controversial matter and has not previously been satisfactorily resolved either by theory[6] or experiment[7]. The experiments were carried out at the ILL Grenoble and a full account of the method has been given elsewhere[4].

For a given solution, two electrolytes $M^{35}Cl_n$ and $M^{37}Cl_n$ are dissolved in (heavy) water. The isotopic substitution made, $^{35}Cl \rightarrow {}^{37}Cl$, changes the Cl scattering length f from 11.7 fm to 3.50 fm. This yields[4] a first-order difference $\Delta_{Cl}(k)$ between two sets of diffraction data given by

$$\Delta_{Cl}(k) = A(S_{ClO}(k)-1) + B(S_{ClD}(k)-1) + C(S_{ClM}(k)-1) + D(S_{ClCl}(k)-1) \qquad (1)$$

where

$$A = \tfrac{2}{3}nc(1-c-nc)\,f_O(f_{Cl}-f'_{Cl})$$
$$B = \tfrac{4}{3}nc(1-c-nc)\,f_D(f_{Cl}-f'_{Cl})$$
$$C = 2nc^2 f_M(f_{Cl}-f'_{Cl})$$
$$D = n^2c^2(f^2_{Cl}-(f'_{Cl})^2)$$

c is the atomic fraction of cations, n is the cation valence and S_{ClO}, S_{ClD}, S_{ClM} and S_{ClCl} represent respectively the partial-structure factors related to chlorine–oxygen, chlorine–deuterium, chlorine–cation and chlorine–chlorine correlations. The numerical coefficients $A \ldots D$ are shown in Table 1 and the method exploits the fact that A and B are much larger than C and D. The Fourier transform of equation (1) yields[4] a weighted radial distribution given by

$$G_{Cl}(r) = A[g_{ClO}(r)-1] + [Bg_{ClD}(r)-1] + C[g_{ClM}(r)-1] + [Dg_{ClCl}(r)-1]$$

where $g_{\alpha\beta}(r)$ is the partial radial distribution function for β ions as seen from an α ion. However, A and B are much greater than C and D and because water is molecular in character, $G_{Cl}(r)$ gives the distribution of water around the Cl^- ion.

The characteristic form for $G_{Cl}(r)$ has been published previously for solutions of NaCl (ref. 4) and $CaCl_2$ (ref. 8) and turns out to be typical for all solutions studied. The significant results from these data are presented in Table 2, from which conclusions about the character of Cl^- hydration can be drawn.

(1) r_{ClO} falls in the range 3.20 ± 0.04 to 3.34 ± 0.04 Å. In general these distances are greater than those found in X-ray studies[7]—a consequence of the inherently poor discrimination of total X-ray patterns from solutions and the need to analyse the data in terms of a rather simple model[9]. They are in excellent

Table 1 Scattering lengths and sample parameters

Electrolyte solution	Isotopes	Abundance (%)	Scattering lengths (10^{-12} cm)	c	Molality	A (barns) 10^{-2}	B (barns) 10^{-2}	C (barns) 10^{-3}	D (barns) 10^{-3}
LiCl	^{35}Cl	99.35	1.17	0.598	9.95	1.66	3.83	−1.34	4.38
	^{37}Cl	90.4	0.35						
	^{35}Cl	99.35	1.17	0.023	3.57	0.695	1.60	−0.2	0.6
	^{37}Cl	90.4	0.35						
NaCl	^{35}Cl	99.35	1.17	0.0331	5.32	0.84	1.92	0.50	1.20
	^{37}Cl	90.4	0.35						
RbCl	^{35}Cl	99.35	1.17	0.0279	4.36	0.82	1.88	1.00	0.90
	^{37}Cl	90.4	0.35						
$CaCl_2$	^{35}Cl	99.35	1.17	0.0275	4.49	1.60	3.68	1.16	3.77
	^{37}Cl	90.4	0.35						
$NiCl_2$	^{35}Cl	99.35	1.17	0.027	4.35	1.57	3.63	2.40	3.60
	^{37}Cl	90.4	0.35						
$NiCl_2$	^{35}Cl	99.35	1.17	0.019	3.00	1.07	2.47	1.10	1.70
	^{37}Cl	90.4	0.35						
$BaCl_2$	^{35}Cl	99.35	1.17	0.00719	1.10	0.47	1.07	0.10	0.15
	^{37}Cl	90.4	0.35						

Table 2 Cl–water coordination

Solute	Molality	$r_{ClD(1)}$ (Å)	r_{ClO} (Å)	$r_{ClD(2)}$ (range) (Å)	ψ* (range) (deg)	Coordination no.
LiCl	3.57	2.25 ± 0.02	3.34 ± 0.04	–	0	5.9 ± 0.2
LiCl	9.95	2.22 ± 0.02	3.29 ± 0.04	3.50–3.68	0	5.3 ± 0.2
NaCl	5.32	2.26 ± 0.03	3.20 ± 0.05	–	0–10	5.5 ± 0.4
RbCl	4.36	2.26 ± 0.03	3.20 ± 0.05	–	0–10	5.8 ± 0.3
$CaCl_2$	4.49	2.25 ± 0.02	3.25 ± 0.04	3.55–3.65	0–6	5.8 ± 0.2
$NiCl_2$	4.35	2.29 ± 0.02	3.20 ± 0.04	3.40–3.50	6–11	5.7 ± 0.2
$NiCl_2$	3.00	2.23 ± 0.03	3.25 ± 0.05	–	0–6	5.5 ± 0.4
$BaCl_2$	1.10	2.24 ± 0.04	3.26 ± 0.05	–	0–6	6.2 ± 0.4

* Assuming that r_{OD} is 1 Å.

agreement with the recent quantum-mechanical calculation of Clementi *et al.*[10]. r_{ClD} spans the range 2.23 ± 0.02 to 2.29 ± 0.02 Å.

(2) The data favour the D-bond configuration (Fig. 1)[4] but with a tilt angle which is always less than 11°. Clearly the influence of the counter-ion on Cl-hydration is a second-order effect and this explains why it had not been unambiguously identified experimentally. Computer simulations based on the so-called ST2 potential predict significant counter-ion effects. Clearly, this widely used potential function needs critical re-examination and, indeed the alternative 'central force' model is also worth studying[11].

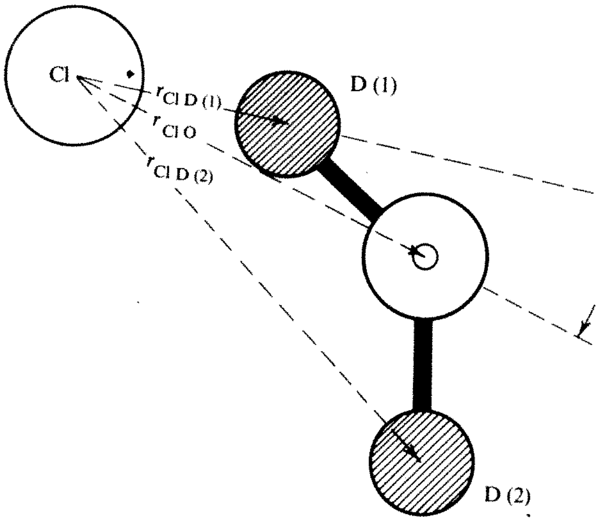

Fig. 1 The geometry of $\mathrm{Cl^-}$ hydration.

(3) The experimental uncertainty in r_{ClD} and r_{ClO} is such that all the solutions, except $\mathrm{NiCl_2}$ at high concentrations, could be characterized by $\psi = 0$. Whether the data for $\mathrm{Ni^{2+}}$ represent a general transition metal counter-ion effect must await further studies involving $\mathrm{Fe^{2+}}$ and $\mathrm{Co^{2+}}$

(4) The coordination number obtained by integrating G_{Cl} (ref. 2) over the first peak cannot necessarily be identified as a 'hydration' number[12]. This is because water molecules are entering and leaving the neighbourhood of a $\mathrm{Cl^-}$ ion on a time scale of $\sim 10^{-12}$ s (compared with cation–water residence times which are often $\sim 10^{-6}$ s (ref. 13) and where the equivalence of coordination and hydration is much clearer). Hence the conclusion that the 'hydration number' for $\mathrm{Cl^-}$ in solution may be concentration dependent needs care. The dynamical aspects of hydration have to be looked at in detail and such an experiment is in progress (Hewish and Howells, personal communication).

We conclude that the counter-ion effects are sufficiently small to be disregarded in a first-order theory and that quantum-mechanical calculations based on a single $\mathrm{Cl^-}$ surrounded by a small number of water molecules are the best guide to ion–water conformations in solution. The possibility that transition metal ions at high concentration may produce measureable counter-ion effects cannot, however, be ruled out.

This work was supported by the SRC. We thank the staff at the ILL, particular Hans Egger, Walter Knoll and Pierre Chieux for for their assistance.

Received 10 July; accepted 15 September 1980.

1. Franks, F. (ed.) *Water A Comprehensive Treatise* Vols 1–6 (Plenum, New York, 1972–79).
2. Narten, A. H., Vaslow, F. & Levy, H. A. *J. chem. Phys.* **58,** 5017 (1973).
3. Enderby, J. E., Howells, W. S. & Howe, R. A. *Chem. Phys. Lett.* **21,** 109 (1973).
4. Soper, A. K., Neilson, G. W., Enderby, J. E. & Howe, R. A. *J. phys. C Solid State Phys.* **10,** 1973 (1977).
5. Neilson, G. W. & Enderby, J. E. *J. Phys. C Solid State Phys.* **11,** L625 (1978).
6. Bopp, P., Heinzinger, K. & Jancsò, G. *Z. Naturf.* **32A,** 620 (1977).
7. Pálinkás, G., Radnai, T. & Hajdu, F. *Z. Naturf.* **35A,** 107 (1980).
8. Cummings, S., Enderby, J. E. & Howe, R. A. *J. Phys. C Solid State Phys.* **13,** 1 (1980).
9. Enderby, J. E. & Neilson, G. W. *Water, A Comprehensive Treatise* Vol. 6 (ed. Franks, F.) (Plenum, New York, 1979).
10. Kistenmacher, H., Popkie, H. & Clementi, E. *J. chem. Phys.* **61,** 799 (1974).
11. Bopp, B., Dietz, W. & Heinzinger, K. *Z. Naturf.* **34A,** 1424 (1979).
12. Neilson, G. W. *Chem. Phys. Lett.* **68,** 247 (1979).
13. Hertz, H. G. *Water, A Comprehensive Treatise* Vol. 3 (ed. Franks, F.) (Plenum, New York, 1973).

Chemical alkylation of lead (II) salts to tetraalkyllead (IV) in aqueous solution

I. Ahmad*, Y. K. Chau*, P. T. S. Wong*, A. J. Carty† & L. Taylor†

* Canada Centre for Inland Waters, Burlington, Ontario, Canada L7R 4A6
† Guelph-Waterloo Centre for Graduate Work in Chemistry, University of Waterloo, Waterloo, Ontario, Canada N2L 3G1

Methylation of lead in the environment would have serious consequences for water quality and for the well being of aquatic biota. As there is strong evidence that tetraalkylleads, the end products of lead alkylation, are considerably more toxic than lead (II) compounds[1,2], the elevated levels of inorganic lead now present in inland waterways and sediments as a result of industrial and motor vehicle emissions will pose a serious environmental hazard if mechanisms exist for the conversion to alkyllead (IV) species in aquatic systems. In the belief that the key to biological Pb(II) methylation lies in methyl transfer to Pb(II) from a carbonium ion donor (for example, *S*-adenosylmethionine), we recently initiated chemical and biological studies on the reactions of $\mathbf{CH_3^+}$ donors with neutral and anionic Pb(II) compounds. We describe here the unequivocal synthesis of volatile tetramethyllead and other tetraalkylleads from Pb(II) salts and simple chemical reagents in aqueous solution. The known occurrence of methyl iodide in natural waters[3] and our demonstration that $\mathbf{Me_4Pb}$ is readily synthesized from this reagent and Pb(II) salts in aqueous solution could have far reaching significance not only for the chemical synthesis of toxic organoleads but also for possible mechanisms of microbiological methylation.

Since the initial report by Wong *et al.*[4] of microbiological conversion of trimethyllead acetate ($\mathrm{Me_3PbOAc}$) and Pb(II) salts into tetramethyllead ($\mathrm{Me_4Pb}$) in active sediments and by pure strains of bacteria, it has been increasingly accepted that trimethyllead salts can be converted to tetraalkylleads via biological mechanisms in addition to disproportionation reactions (refs 5–8 and P. J. Craig and J. M. Wood, personal communication), even though the latter may be catalysed by the presence of sulphide ion[9]. For inorganic Pb(II), however, several questions concerning the facility and mechanism of the initial step to methylate a Pb(II) species remain unresolved. There are conflicting reports as to whether tetramethyllead can be formed from Pb(II) salts in aqueous systems. A report from Huber's laboratory[7] claimed formation of $\mathrm{Me_4Pb}$ from Pb(II) acetate with microorganisms cultivated in aquarium water, but workers from Ethyl Corporation (J. Bentz, M. Brandt, A. Pallay and G. Ter Haar, personal communication) failed to note increased levels of $\mathrm{Me_4Pb}$ above sediments enriched with Pb(II) nitrate. There was no reported reaction between Pb(II) and methylcobalamin in aerobic or anaerobic conditions[6,9,10]. In contrast, Witman and Weber[11] presented evidence for the demethylation of a synthetic $\mathrm{B_{12}}$ analogue by $\mathrm{Pb(ClO_4)_2 \cdot 3H_2O}$ in 2-propanol, implying synthesis of a transient methyllead (II) species. More recently, Harrison and Laxen[12] observed abnormally high alkyllead/total lead ratios in atmospheric samples in Morecambe Bay, UK, attributing these levels to natural methylation of inorganic lead in coastal/estuarine mud flats. An indirect pointer to the existence of a biological mechanism for Pb(II) methylation is the observation that 10–24% of fish from natural environments contain elevated levels of Me_4Pb in lipid fractions[13,14].

Of the potential mechanisms available for Pb(II) methylation in water, nucleophilic displacement of X^- in PbX_2 (where X is, for example, halide, acetate) by CH_3^- to generate $Me_2Pb(II)$ which could subsequently disproportionate to Me_4Pb and Pb(0) is rendered unfavourable by the extreme hydrolytic instability of Pb(II) alkyls[15]. Electrophilic attack by CH_3^+ on $Pb(II)X_2$ (PbX_3^-) is more attractive but the initial intermediate of the oxidative addition $(MePb(IV)X_2)^+$ has also been presumed unstable because no monomethyllead (IV) compounds have been characterized. Subsequent conversion of monomethyllead (IV) to tetramethyllead (IV) could occur either by disproportionation or by methylation by CH_3^- donors[6]. In our initial experiments we have attempted to demonstrate the feasibility of tetraalkyllead synthesis from simple carbonium ion reagents.

Table 1 Methylation of Pb(II) salts with methyliodide in water

Pb(II) salt	Pb as Me_4Pb (ng) *p*H 5–6	 *p*H 13*
$Pb(OAc)_2 \cdot 3H_2O$	65.4	370.5
$Pb(NO_3)_2$	90.1	176.8
$Pb(ClO_4)_2 \cdot 3H_2O$	72.7	261.9
$Pb(COO)_2$	2.3	147.2

Reaction conditions: lead salts, 1.0 mmol; water, 200 ml; MeI, 0.1 ml; reaction time, 5 days at 19 ± 1 °C.

* *p*H was adjusted by addition of 10 ml of 10% NaOH.

Lead (II) acetate ($Pb(OAc)_2 \cdot 3H_2O$) (1.0 mmol) was dissolved in 200 ml of deionized water in a 250-ml filtration flask fitted with an aluminium foil-wrapped stopper. Methyl iodide (0.1 ml, >1 mmol) was added and the flask was sealed with Parafilm. After 5 days at room temperature the head space gases above the solution were withdrawn through the side arm by means of a peristaltic pump and transferred to a U-tube containing 3% OV-1 at −70 °C. The trapped sample was then swept into a sensitive GC–AA system[16] for chromatographic separation and analysis. Tetramethyllead was positively identified by comparison with the retention time of an authentic sample and by molecular weight measurement using mass spectrometry. Standard samples consisting of $Pb(OAc)_2 \cdot 3H_2O$ alone in deionized water and methyl iodide in deionized water were also analysed to eliminate the possibility of artefacts.

The results summarized in Table 1 indicate that methyl iodide can methylate inorganic Pb(II) compounds in aqueous solution to produce various amounts of Me_4Pb. The lesser amount of Me_4Pb produced from $Pb(COO)_2$ might well be due to the slight solubility of the lead compound. With low concentrations of $Pb(OAc)_2 \cdot 3H_2O$ (0.001 and 0.002 mmol) in identical experimental conditions, 2.5 ng and 20.4 ng of Me_4Pb were produced, respectively. The amount of Me_4Pb produced in each case was increased when the reactions were carried out in highly basic conditions. A possible role for sodium hydroxide is to remove iodide ion, thus favouring tetraalkyllead formation over alkyllead iodides. In similar conditions, ethyl iodide (0.1 ml) also reacted with $Pb(OAc)_2 \cdot 3H_2O$ (1 mmol) to produce tetraethyllead (64.5 ng at *p*H 5–6 and 190.0 ng at *p*H 13) along with trace amounts of triethylmethyllead (Table 2).

Mixtures of methyl iodide and ethyl iodide in water without added base gave $MeEt_3Pb$ (1.5 ng) and Et_4Pb (12.0 ng) whereas at *p*H 13 Me_4Pb (1.3), Me_3EtPb (6.7 ng), Me_2Et_2Pb (97.1 ng), $MeEt_3Pb$ (231.4 ng) and Et_4Pb (349.1 ng) were obtained. In these competition experiments the amounts of tetraalkyllead produced thus increased with increasing ethyl substitution (Table 2). This may reflect different stabilities for initial $(RPb^{IV}X_{3-n})^{n+}$ intermediates (R = Me, Et) in the methylation sequence. It is interesting in this regard that the first examples of $EtPbX_3$ compounds have recently been described[17].

Table 2 Alkylation of $Pb(OAc)_2 \cdot 3H_20$ with different alkylating agents in water

Reagents	*p*H	Lead as tetraalkyllead (ng) Me_4Pb	 Me_3EtPb	 Me_2Et_2Pb	 $MeEt_3Pb$	 Et_4Pb
MeI	5–6	23.2	—	—	—	—
MeI	13*	224.3	—	—	—	—
EtI	5–6	—	—	—	0.2	64.5
EtI	13	—	—	—	14.5	190.0
MeI + EtI	5–6	—	—	—	1.5	12.0
MeI + EtI	13	1.3	6.7	97.1	231.4	349.1
$Me_3S^+I^-$	5–6	—	—	—	—	—
$Me_3S^+I^-$	13	1.9	—	—	—	—
$Me_3SO^+I^-$	5–6	0.1	—	—	—	—
$Me_3SO^+I^-$	13	3.4	—	—	—	—
$Me_3O^+SbCl_6^-$	5–6	0.2	—	—	—	—
$Me_3O^+SbCl_6^-$	13	0.1	—	—	—	—

Reaction conditions: $Pb(OAc)_2 \cdot 3H_2O$, 1.0 mmol; water, 200 ml; MeI, EtI, each 0.1 ml; $Me_3S^+I^-$, $Me_3SO^+I^-$, $Me_3O^+SbCl_6^-$, each 1.0 mmol; reaction time, 5 days at 19 ± 1 °C.

* *p*H was adjusted by addition of 10 ml of 10% NaOH.

Apart from alkyl iodides, other potential methyl carbonium ion donors react with Pb(II) salts in aqueous solution to generate Me_4Pb (Table 2). Trimethylsulphonium iodide, trimethylsulphoxonium iodide and trimethyloxonium hexachloroantimonate all yielded the volatile lead alkyl in similar conditions despite the precipitation of insoluble lead-containing compounds in these reactions.

Chemically, the synthesis of organoleads from inorganic reagents is traditionally carried out in strictly anhydrous conditions using, for example, Grignard, organolithium or organomercury reagents. We believe our observations that Pb(II) salts in aqueous solution can react with alkyl iodides to produce Me_4Pb to be unprecedented. It is interesting that the occurrence of methyliodide (3.1×10^{-7} g l^{-1}) in natural water has been reported[3]. We are investigating the possibility of chemical tetraalkyllead synthesis with such an environmental level of MeI and studying other mechanisms for the reactions, including catalysis by other metals.

We thank the Department of the Environment for support of this work through the Water Resources Support Program and the award of a visiting fellowship to I.A.

Received 23 June; accepted 29 August 1980.

1. Grandjean, P. & Nielsen, T. *Residue Rev.* **72,** 97–148 (1979).
2. Wong, P. T. S., Silverberg, B. A., Chau, Y. K. & Hodson, P. V. in *Biogeochemistry of Lead in the Environment* Vol. 1B (ed. Nriagu, J. O.) Ch. 17 (Elsevier, Amsterdam, 1978).
3. Lovelock, J. E., Maggs, R. J. & Wade, R. J. *Nature* **241,** 194–196 (1973).
4. Wong, P. T. S., Chau, Y. K. & Luxon, P. L. *Nature* **253,** 263–264 (1975).
5. Dumas, J. P., Puzdernik, L. R., Belloncik, S., Bouchard, D. & Villancourt, G. *Proc. 12th Can. Symp. Water Pollution Res.*, Canada, 91–100 (1977).
6. Ridley, W. P., Dizikes, L. J. & Wood, J. M. *Science* **197,** 329–332 (1977).
7. Schmidt, U. & Huber, F. *Nature* **259,** 157 (1976).
8. Chau, Y. K. & Wong, P. T. S. *Proc. Int. Experts Discussion on 'Lead – Occurrence, Fate and Pollution in the Marine Environment'*, Rovinj, 1977 (in the press).
9. Jarvie, A. W. P., Markall, R. N. & Potter, H. R. *Nature* **255,** 217–218 (1975).
10. Taylor, R. N. & Hanna, M. L. *J. envir. Sci. Hlth. Envir. Sci. Engng.* **A-11,** 201–211 (1976).
11. Witman, M. W. & Weber, J. H. *Inorg. Chem.* **15,** 2375–2378 (1976).
12. Harrison, R. M. & Laxen, P. H. *Nature* **275,** 738–739 (1978).
13. Sirota, G. R. & Uthe, J. F. *Analyt. Chem.* **49,** 823–825 (1977).
14. Chau, Y. K. *et al. Bull. envir. Contam. Tox.* **24,** 265–269 (1980).
15. Shapiro, H. & Frey, F. W. *The Organic Compounds of Lead* (Interscience, New York, 1968).
16. Chau, Y. K., Wong, P. T. S. & Goulden, P. D. *Analyt. chim. Ac[illegible]* **85,** 421–424 (1976).
17. Chobert, G. & Devand, M. *J. organometal. Chem.* **153,** C23–C24 (1978).

Kimberlites in the south-west Pacific

P. H. Nixon*

Geology Department, Box 4820, University PO, Papua New Guinea

Pipe-like bodies revealed by seismic refraction surveys over the Ontong Java Plateau (OJP), south-west Pacific, have characteristics of volcanic plugs[1,2]. The oceanic crust is old (Lower Cretaceous, possibly Jurassic) and unusually thick[3] (40 km), similar to that of some continental sections. The Island of Malaita, Solomon Islands, at the thinner periphery of the OJP contains several alnöite intrusions with suites of mantle inclusions, similar to those of the diamond-bearing rock, kimberlite, found in continental areas. Pyroxene geotherms calculated from the inclusions show alnöites to have formed in the Earth's mantle in warmer, shallower conditions compared with kimberlites[4]. However, by analogy with continental cratons, I suggest here that the thicker, northwestern parts of the OJP had lower geothermal gradients suitable for the formation of kimberlite pipes. These could be the bodies revealed by seismic prospecting.

The OJP occupies a 1,600 × 800-km area of the Pacific Ocean to the north-east of Bougainville Island (Papua New Guinea) and the Solomon Island chain, and is broadly defined by a water depth of less than 2,500 m (Fig. 1). Marine seismic studies[1,2] over the OJP have revealed the presence in the ocean-floor sediments of pipe-like bodies (Fig. 2) which Kroenke has suggested may be of igneous origin. They vary up to 2.5 km across[3] and show features which are similar to those produced experimentally by gas fluidization, in particular the presence of marginal faults and the development of crudely bedded conduit filling with inward dips and detached subsided blocks[5]. Such a mechanism operates in narrow vents and fractures within diatreme volcanoes, including diamond-bearing kimberlites, which could be produced phreatomagmatically, that is, by rising hot magma encountering groundwater[6]. Subsequent subsidence (caldera collapse) along concentric fractures may produce displacements up to 1,280 m (refs 7, 8). It is an important process in enlarging the vent and it also gives rise to a shallow crater or maar into which sediments are washed from a surrounding tuff ring. Progressive post-volcanic subsidence over an extended period may lead to deposition of water-laid sediments[7] ranging up to more than 300 m thick over the diatremes of some kimberlites and related volcanoes[9-11].

The seismic reflection profiles of the pipe-like bodies in the OJP also indicate collapse features (Fig. 2). Furumoto (personal communication) states that "none of these intrusives in the Ontong Java Plateau has penetrated the surface of the ocean floor. There are some cases where the intrusives have reached very close to the surface. In those cases the ocean floor dips downward directly over it, suggesting a collapse crater or depression".

The features are consistent with the idea that the pipe-like bodies are volcanic intrusions of the kind described above, but it is thought that they broke through to the ocean floor and were subsequently covered by pelagic oozes. Post-volcanic subsidence affected the oozes but with diminishing intensity. Several seismic profiles show a contraction of the disturbed zone overlying the pipe and fading displacements towards the top younger sedimentary layers. The long continued post-volcanic subsidence could be due to progressive solution of carbonate, or other soluble minerals, in the pipe tuffs at such times as they are below the ocean carbonate compensation depth (~4,000–5,000 m). There do not seem to be other deep oceanic volcanic centres with which these types can be readily equated (J. R. Cann, personal communication).

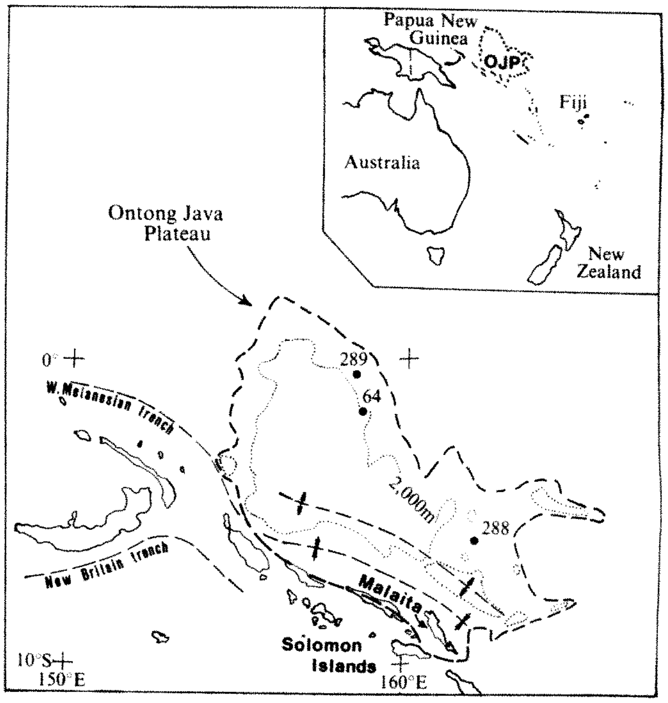

Fig. 1 The Ontong Java Plateau in relation to the islands of the south-west Pacific. The outline follows approximately the 2,500-m isobath, but the buckled southwestern margin is bounded by a thrust[15,22]. The main north-west trending structures on the OJP are: the Roncador Homocline–Stewart Arch[2], the North Solomon trench and (not shown) the Malaita Anticlinorium[2,12,21]. These resulted from collision of the Solomon Islands arc with a westerly moving OJP in late Tertiary times[16,20]. Deep Sea Drilling Sites 64, 288 and 289 are shown.

Kroenke[2] has pointed out similarities of the sedimentary succession of the OJP at Deep Sea Drilling Site 64 with that on northern Malaita (Fig. 1) mapped by Rickwood[12]. Subsequent mapping[13,15] and comparison with borehole cores at sites 288 and 289 (ref. 16) confirm that they are ocean-floor deposits ~1,500-m thick. They comprise pelagic foram-nannofossil oozes and chalk down to Oligocene beds, but below this there is an increasing amount of interbedded cherts and siliceous oozes. The oldest sediments encountered are Lower Cretaceous (Aptian). At site 289 and on the island of Malaita and neighbouring Santa Isabel to the north-west, the pelagites overlie, or are interbedded with, ocean-floor tholeiite basalts. These seem to be the topmost representatives of an extremely thick crustal succession of flood basalts which Kroenke[17] suggests mark the beginning of continent formation, that is, the OJP is a protocontinent. The age of the lower members is not known but could extend to the Jurassic.

Furumoto *et al.*[3,18] have demonstrated a crustal thickness of between 20 and 30 km in the trench and arched region north of Malaita (Fig. 1). The northwestern part of the OJP has an even greater crustal thickness of 35–42 km which is comparable with that of continents, for example, the Colorado Plateau area of North America. This part of the OJP also has a basal layer with a P-wave velocity range of 7.1–7.7 km s^{-1} immediately overlying the mantle[3,18]. From this, and the existence of a free air positive gravity anomaly[4] over the OJP, it has been suggested that burial metamorphism has produced a lower crustal granulite layer similar to that postulated for continents[19].

The southwestern portion of the Ontong Java Plateau, including Malaita, underwent deformation during the Pliocene[14]. This resulted in the northwesterly trending folds and the topographic low, the North Solomon trench, which now separate Malaita from the main portion of the OJP[2]. The

---

* Present address: Department of Earth Sciences, The University, Leeds LS2 9JT, UK.

0028-0836/80/430718—03$01.00

deformation was the response to the collision of westerly moving OJP into a structurally complex Solomon Island arc (Fig. 1) and the more usual subduction process was prevented, or arrested, due to the great thickness of the OJP[20,21]. The southwestern boundary of the Plateau and its island members—the Pacific Province of P. J. Coleman—is represented by the Korigole thrust[22] and associated upthrust mantle ultrabasic rocks[15,16]. To account for its tectonic behaviour not only the crust but the whole lithosphere of OJP must possess an unusual thickness and rigidity.

Until 1979 only one volcanic centre, at Babaru'u, with possibly a second related intrusion 2 km away, was known[23]. Another (Kwaikwai) has since been found and at least three more are indicated by 'shows' of heavy minerals in soils and stream gravels. These minerals include garnets, ilmenites and zircons which can be unusually abundant (Fig. 3). Zircons from two separate localities gave U/Pb ages of 33.9 Myr (ref. 24) and 34.1 Myr (Davis, personal communication). Further prospecting in the dense rain forests will reveal more outcrops.

Although field relationships are uncertain, and no crater sediments have been observed, the alnöites (biotite olivine melilitites) are important as they may be related to the intrusive features in the main part of the OJP described above. The tuffaceous textures and nucleated autoliths[23] are similar to those ascribed to gas fluidization and related phenomena of the olivine melilitite diatrems of the Swabian Alb, Germany[26]. The rounded, highly polished nature of some of the constituent minerals (Fig. 3) is further evidence of a gas-fluidized origin. From the zircon ages of the alnöites (Lower Oligocene) it is evident that eruptions took place before the folding of the leading edge of the OJP and emergence of Malaita, when the plate was east of its present position.

From stratigraphical considerations it can be seen that anything up to 1,000 m of pelagic oozes could have been laid down after intrusion and before the emergence of Malaita in Plio–Pleistocene times. Although fold movements and erosion have locally revealed the intrusions on Malaita, there is no reason why they should not also occur off-shore. Indeed, this is considered likely in view of the accumulating evidence for increasing numbers of occurrences in northern Malaita itself. There do not seem to have been any seismic reflection traverses in the vicinity of Malaita which could substantiate this claim; most of the pipe-like bodies have been recorded from the northwestern part of the OJP. However, it is this area where the crust is thickest, a factor which could have a profound influence on the kind of volcanicity produced.

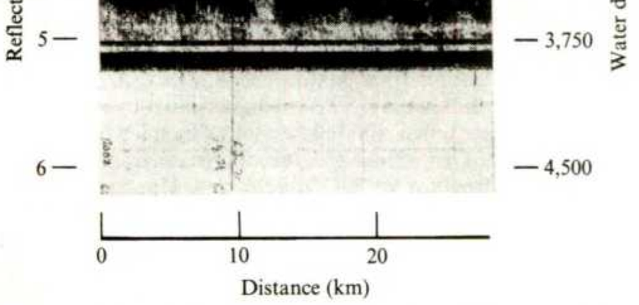

Fig. 2 Seismic reflection profile of a plug-like feature on the Ontong Java Plateau, taken from Kroenke[3] (Fig. 19, vertical exaggeration ~12:1. Location about 2°20′S, 161°45′E—slightly outside the OJP boundary as arbitrarily defined in Fig. 1). Note the apparent collapse of bedded vent material.

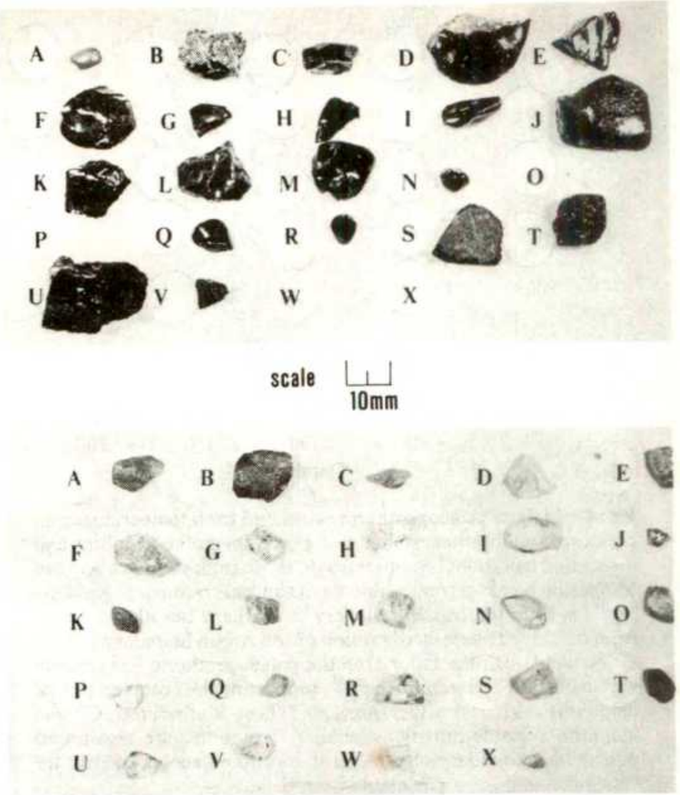

Fig. 3 Ilmenites (top) and zircons (bottom) from an alnöitic intrusion, North Malaita. Their rounded, highly polished nature is attributed to a gas-fluidized emplacement.

Although alnöites are mineralogically and chemically distinct from kimberlites[25] they contain similar suites of deep-seated garnet lherzolite (garnet, olivine, orthopyroxene, clinopyroxene) inclusions which give information about the composition and temperature distribution in the mantle at the time of eruption, and also the limiting depth of origin of the host volcanic rock itself[4,27]. Alnöite seems to have formed at depths[25] of ~120–130 km which are shallower than those for kimberlite.

The temperatures and depths of origin of the garnet lherzolites are estimated through the application of experimental and theoretical studies of relevant (Mg-rich) co-existing phases, the Mg orthopyroxene–clinopyroxene solvus for temperature determinations[28], and alumina solubility in Mg orthopyroxene for pressure (depth) determinations[29] as described by Boyd[30,31]. More recent experimental data do not significantly affect the results shown in Fig. 4 which are, therefore, used to provide a useful comparison with earlier determined curves from kimberlitic garnet lherzolites. The curves represent the Earth's temperature gradients (palaeogeotherms) below specific intrusions at the time of eruption. The Malaita plots show features which are intermediate between those of 'cool continents', where kimberlites are intruded, and 'hot oceanic' areas. The inflected steeper portion of the geotherms (Fig. 4) has been ascribed to shear heating at the base of lithospheric plate or to diapiric upwelling of asthenospheric mantle (review by Boyd[32]). Either interpretation, or combination of both, suggests that the point of inflection is a measure of depth to the base of the lithosphere. The lithospheric thickness calculated by this method in Malaita (southern OJP) is 110 km, which is thinner than that deduced by comparable methods for continents. It is, however, thicker than that in other oceanic areas determined by geophysical methods where values[33] usually average 50–70 km.

Even within a stable continental area (craton) mantle xenoliths from broadly contemporaneous kimberlite pipes indicate

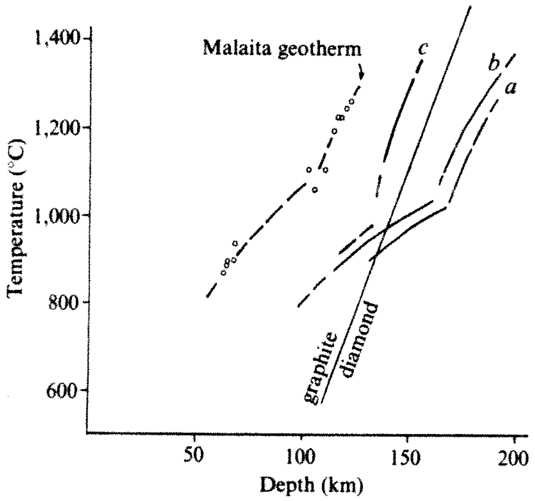

Fig. 4 Malaita palaeogeotherm calculated from temperature and pressure equilibration estimates of garnet lherzolite xenoliths and associated inclusions[4] compared with those from southern African kimberlite pipes: *a*, from within the Kaapvaal craton near Kimberley[34]; *b*, from the craton periphery in northern Lesotho[31]; and *c*, from outside the accepted position of the craton boundary in East Griqualand[35]. In the latter area the palaeogeotherm lies entirely within the graphite stability field[36], supporting the observed lack of diamonds within the inclusions and host kimberlites. Olivine melilitite volcanic intrusions, similar to alnöites, are also found outside the boundary of the craton but no palaeogeotherms are available from these.

lateral differences, notably increasingly higher palaeogeotherms (hotter for a given depth) towards the periphery, with an attendant decrease in lithospheric thickness and with lessening probability of diamond formation (Fig. 4) (refs 31, 34, 35).

If the OJP can be regarded as a proto-continent, then by analogy with cratons it could show similar variations in geothermal gradient and lithospheric thickness possibly reflecting the differences in crustal thickness. It follows that the thickest, coolest lithosphere is most likely to be found in the northwestern part of the OJP.

It is suggested that contemporaneously with the Malaita alnöites the thicker northernwestern OJP was also intruded by volcanic rocks represented by the pipe-like seismic reflection features. Although these could be alnöites the present evidence favours rocks of a deeper seated provenance, that is, kimberlites. If this is the case then diamonds may exist within the OJP.

I thank the Solomon Islands Government and officers of the Geological Survey, and Malaita Islands officials for facilitating research in the area. The work is part of a project being undertaken with F. R. Boyd whose suggestions (about drilling the plug-like features) inspired this paper. A. S. Furumoto, D. Erlandson and D. M. Finlayson provided seismic reflection profiles, M. E. McCallum and T. Woolsey, data on fluidization experiments, G. L. Davis, an unpublished zircon age and W. Manser, relevant S.W. Pacific literature. F. R. Boyd, A. S. Furumoto, V. Lorenz, C. McNulty, N. W. Rogers and J. Oliver provided helpful comments.

Received 30 June; accepted 3 September 1980.

1. Woollard, G. P. *et al. Rep. HIG-67-3* (Hawaii Institute of Geophysics, 1967).
2. Kroenke, L. *Rep. HIG-72-5* (Hawaii Institute of Geophysics, 1972).
3. Furumoto, A. S., Webb, J. P., Odegard, M. E. & Hussong, D. M. *Tectonophysics* **34**, 71–90 (1976).
4. Nixon, P. H. & Boyd, F. R. *Am. geophys. Un.* **2**, 400–423 (1979).
5. Woolsey, T. S., McCallum, M. E. & Schumm, S. A. *Phys. chem. Earth* **9**, 29–42 (1975).
6. Lorenz, V. *Phys. chem. Earth* **9**, 17–27 (1975).
7. Francis, E. H. *Bull. volcan.* **34**, 679–712 (1970).
8. Hearn, B. C. *Science* **159**, 622–625 (1968).
9. Hawthorne, J. B. *Phys. chem. Earth.* **9**, 1–15 (1975).
10. Edwards, C. B. & Howkins, J. B. *Econ. Geol.* **61**, 537–554 (1966).
11. Cornelissen, A. K. & Verwoed, W. J. *Phys. chem. Earth* **9**, 71–80 (1975).
12. Rickwood, R. K. *Colon. Geol. Miner. Resourc.* **6**, 300–305 (1957).
13. Coleman, P. J. *Solomon Islands Geol. Rec. III*, 1963–67, 53–58 (1968).
14. Hughes, G. W. & Turner, C. C. *Bull. geol. Soc. Am.* **88**, 412–424 (1977).
15. Coleman, P. J., McGowran, B. & Ramsay, W. R. H. *Bull. Aust. Soc. Explor. Geophys.* **9**, 110–114 (1978).
16. Packham, G. H. *et al. Init. Rep. DSDP* Leg **30** (1975).
17. Kroenke, L. W. *Eos* **55**, 443 (1974)
18. Furumoto, A. S., Wiebenga, W. A., Webb, J. P. & Sutton, G. H. *Tectonophysics* **20**, 153–164 (1973).
19. Nixon, P. H. & Coleman, P. J. *Bull. Aust. Soc. Explor. Geophys.* **9**, 103–107 (1978).
20. Coleman, P. J. & Packham, G. H. *Earth Sci. Rev.* **12**, 197–223 (1976).
21. de Broin, C. E., Aubertin, F. & Ravenne, C. *Int. symp. Geodynamics in SW Pacific* 37–50 Technip, Paris, (1977).
22. Stanton, R. L. *Overseas Geol. Miner. Resour.* **8**, 127–149 (1961)
23. Allen, J. B. & Deans, T. *Miner. Mag.* **34**, 16–34 (1965).
24. Davis, G. L. *Extended Abstr. 2nd int. Kimberlite Symp.* Santa Fe (1977).
25. Nixon, P. H., Mitchell, R. H. & Rogers, N. W. *Miner Mag.* **43**, 23–32 (1980).
26. Lorenz, V. *Am. Geophys. Un.* **1**, 354–363 (1979).
27. Delaney, J. S., Smith, J. V. & Nixon, P. H. *Contr. Miner. Petrol.* **70**, 209–218 (1979).
28. Davis, B. T. C. & Boyd, F. R. *J. geophys. Res.* **71**, 3567–3576 (1966).
29. MacGregor, I. D. *Am. Miner.* **59**, 110–119 (1974).
30. Boyd, F. R. *Geochim. cosmochim. Acta* **37**, 2533–2546 (1973).
31. Boyd, F. R. & Nixon, P. H. *Yb. Carnegie Instn Wash.* **72**, 431–445 (1973).
32. Boyd, F. R. *Yb. Carnegie Instn Wash.* **75**, 521–523 (1976).
33. Anderson, D. L. *A. Rev. Earth planet. Sci.* **5**, 179–202 (1977).
34. Boyd, F. R. & Nixon, P. H. *Geochim. cosmochim. Acta* **42**, 1367–1382 (1978).
35. Nixon, P. H. & Boyd, F. R. *Extended Abstr. 2nd Kimberlite Symp.* Cambridge (1979).
36. Kennedy, C. S. & Kennedy, G. C. *J. geophys. Res.* **81**, 2467–2470 (1976).

Sedimentological evidence for a stratigraphical break in the Durness Group

T. J. Palmer & W. S. McKerrow

Department of Geology and Mineralogy, University of Oxford,
Parks Road, Oxford OX1 3PR, UK

J. W. Cowie

Department of Geology, Queen's Building, University Walk,
Bristol BS8 1TR, UK

Around Durness north-west Scotland, the top of the Sailmhor Formation, Durness Group, is developed as a palaeokarstic surface deeply penetrated by breccia-filled fissures. Fossil evidence for the age of the Sailmhor Formation is equivocal, but we suggest here that the brecciated surface probably represents a break corresponding to the whole of the Middle and Upper Cambrian. Such a break is also seen in the contemporaneous carbonate successions in Greenland and Spitzbergen.

The limestones and dolomites of the Durness Group include both Lower Cambrian and Lower Ordovician (including Tremadoc or Lower Canadian) fossiliferous beds. It has been held that a continuous sequence of carbonates in north-west Scotland, spanning the whole of this time, is incompatible with contemporaneous deformation and metamorphism of the Dalradian rocks of the Grampian Highlands. As the Dalradian rocks extend from the Precambrian up into the Cambrian system, many authors have considered that the Grampian orogeny must have post-dated formation of the youngest Durness rocks. Strong evidence for the absence of Middle and Upper Cambrian sediments in the Durness sequence will now permit serious consideration of a major orogeny in the Grampian Highlands during this time. This break occurs above all known Lower Cambrian faunas and below rocks which we interpret to be exclusively of Ordovician age. It is not necessary to postulate diagenetic destruction of all Middle and Upper Cambrian fossils.

The Lower Cambrian age for the lowermost Ghrudaidh Formation, is based on the occurrence of *Salterella*[1–3]. Recently, Lower Cambrian microfossils have been recovered from cherts near the base of the succeeding Eilean Dubh Formation at Inchnadamph, 50 km south of Durness[4]. The ages of the following two formations (Sailmhor and Sangomore) are more doubtful. The lower (Sailmhor) is reported to have produced an age-diagnostic fauna at one locality. The species originally

0028–0836/80/430720—03$01.00

reported[1] included *Murchisonia* sp., *Euconia* (*Pleurotomaria*) spp., *Cyrotoceras* spp., ?*Orthoceras* sp., *Planolites* and *Asaphus* (*Isotelus*) *canalis*. Doubt has been thrown on the existence of the one specimen of the last-named species, as it is now missing[2]. The rest of the Sailmhor fauna suggests a Lower Canadian (Tremadoc) age[2]. Until now, no body fossils have been reported from the Sangomore Formation which are diagnostic of its age, but a new fossiliferous locality within the Balnakeil Bay outcrop of this unit (NC 3862 6887, see Fig. 1) has yielded *Murchisonia* sp., *Pleurotomaria* sp., and *Orthoceras* sp., suggesting a Lower Canadian (Tremadoc) age. The later formations of the Durness Group (in ascending order, Balnakiel, Croisaphuill and Durine) are of Arenig (and possibly Llanvirn) age[5,6].

The absence of Middle and Upper Cambrian calcareous fossils has been attributed to their destruction during the process of dolomitization[7]. It is more likely[3] that there is a major stratigraphic break comparable with that which occurs at approximately the same stratigraphical level in the carbonate successions in Ellesmere Island; north-west, north-east and east Greenland; and Spitzbergen[8,9].

We have examined the most complete section of the Durness Formation, which is that exposed along the southern shore of Balnakeil Bay (as spelt on the Ordnance Survey New Series 1:50,000 map), west of Durness, north-west Scotland (NC 374688–NC 390687). Rocks from the Eilean Dubh to the Balnakiel Formation are seen here with only minor tectonic disturbance. Our conclusions about the positions of the boundaries between the formations (Fig. 1) correspond to those shown on the 6 inch to 1 mile geological map deposited with the Institute of Geological Sciences in Edinburgh.

The transition between the whiter dolomites of the Eilean Dubh Formation and the darker dolomites of the Sailmhor Formation is gradational and does not suggest a major episode of non-sedimentation. The main changes are an increase in the number of beds with continuous or nodular horizons of chert, and an increase in the number of beds of black and white mottled dolomite. This mottling is almost certainly due to differential dolomitization in branching burrow systems of the *Spongeliomorpha paradoxica* type, such as have been described from other Lower Palaeozoic carbonate sequences[10,11]. In contrast, the junction between the Sailmhor and the overlying Sangomore Formation is sharp. The lowest beds of the latter form a low cliff between NC 3841 6887 and NC 3837 6886. Extending out from the base of this cliff is the upper surface of the Sailmhor. On close examination, it is immediately apparent that the upper part of the Sailmhor Formation is extensively brecciated, whereas this is not so in the base of the Sangomore Formation. The breccias occur, not in planar or lensoid units parallel or subparallel to bedding, but as the fillings of vertical fissures. These fissures dissect the Sailmhor Formation, descending from its top down to levels a considerable distance below. They are most abundant in the top 30 m, but at least two of them (Y in Fig. 1) seem to extend right down into the underlying Eilean Dubh Formation, and are, therefore, at least 150 m deep. They range in width from 4 m down to a few centimetres, merging below this range into cracks filled by growth of sparry dolomite. Most are of the order of half a metre to a metre or so wide, and trend in an east–west direction. Others trend north-west–south-east.

The breccias which form the fissure fills consist of angular and sub-angular clasts of dolomite, with subordinate chert fragments. The dolomites appear identical to those forming the beds of the Sailmhor Formation, and many of the fragments show the same burrow mottling. The size of the clasts ranges from sand size up to around 20 cm across. They are very poorly sorted, with the larger fragments being set at all angles in a matrix of the finer material. In some of the fissures, this finer-grained matrix is not present and the voids between the larger clasts has been filled with a crystalline dolomite cement. Towards the bottom of one of the deep fissures which penetrates the Eilean Dubh Formation, the sediment becomes much finer and shows bedding. To establish the density of the fissuring in the plane of bedding, we measured the proportion of fissures to country rock in a 65-m transect along a bedding plane about 40 m below the top of the Sailmhor Formation (A–B in Fig. 1); 18.2 m of this transect was accounted for by breccia-filled fissures, and the remainder consisted of undisturbed country rock and country rock with dolomite veins.

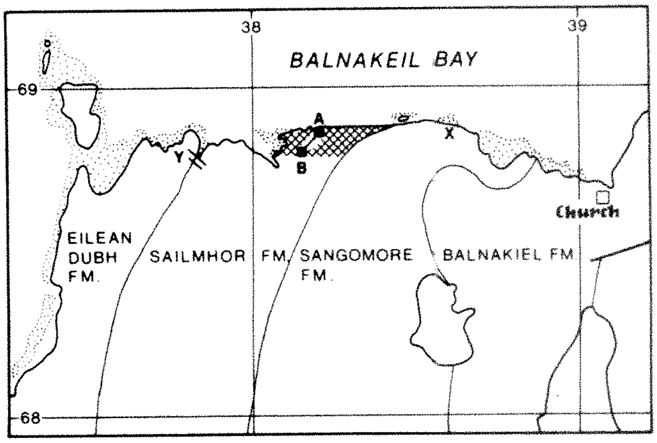

Fig. 1 Map of the south shore of Balnakeil Bay, west of Durness. The boundaries of the formations are after the Institute of Geological Sciences 6-inch geological maps, as modified by T. Robertson. X, Fossil locality; Y, fissures penetrating the top of the Eilean Dubh Formation; A–B transect showing 18.2 m of fissure-fill over a total distance of 65 m. Cross-hatching denotes area of maximum fissure development. Kilometre grid squares are indicated.

In view of the conspicuousness of the fissures with their breccia fills, and the thickness of sediment which they penetrate, why have they not been recognized previously? In fact, the breccias have been noticed, but have apparently always been ascribed to tectonism a long time after deposition. There are local fault breccias, usually of small width, which show displacement of the beds on either side. No vertical displacement at all occurs across the fissures that descend from the top of the Sailmhor Formation. There is also evidence of other sedimentary and diagenetic processes, which produce breccia horizons in the Durness Group as a whole. Young[12] has demonstrated the former presence of evaporite minerals in the Balnakeil Bay section, and locally there are horizontal breccia beds which closely resemble those formed by bed collapse after dissolution of evaporites in the Purbeck Broken Beds of Dorset[13]. Also seen are tepee structures resulting from interstitial cement growth during early diagenesis, and flake breccias which were produced by desiccation[14] and deposited either as horizontal beds or in the quiet micro-environments between stromatolite heads. Furthermore, in most of the other areas in Scotland where the Durness Group is seen (in contrast to the situation around Durness itself), it has been heavily affected by movement along the Moine Thrust zone. In these regions, tectonic brecciation and veining do become prominent. It seems, therefore, that brecciation has previously been regarded as a ubiquitous inconvenience whose effects have to be discounted before the rocks are interpreted.

The junction between the Sailmhor and the Sangomore Formations is well exposed only around Durness. The extensive development of breccia-filled fissures in the Sailmhor Formation is seen in the Balnakeil Bay section, in Durness village itself, and immediately inland. Elsewhere in north-west Scotland, we noted rare, small fissures of a similar type in the upper part of the Eilean Dubh Formation at Kishorn (NG 862443), but we have no way of telling if they originally descended from the top of the Sailmhor Formation.

This extensive and striking development of fissures suggests a major episode of non-deposition during which uplift and extensive erosion of the Sailmhor carbonates occurred. The top of the formation may be regarded as a major karstic surface. Petrographical details which might throw further light on the process are likely to have been destroyed by the extensive subsequent dolomitization and silicification[14,15]. The junction between the Sailmhor and Sangomore Formations represents a break corresponding to the Middle and Upper Cambrian. This break justifies the use of the terms Lower Durness Group for the Ghrudaidh, Eilean Dubh and Sailmhor Formations, and the Upper Durness Group for the Sangomore, Balnakiel, Croisphuill and Durine Formations. The non-sequence seems to correlate with those mentioned above from elsewhere in the Cambro–Ordovician of the North Atlantic region.

Our conclusion seems at first incompatible with the Lower Ordovician (Tremadoc) age assigned to the Sailmhor Formation on fossil evidence[1]. However, the diagnostic fauna only comes from a single locality, near the top of the Sailmhor. Its field relationships are unknown and we have not been able to relocate it. We feel that if this fauna does indeed come from below the Sailmhor/Sangomore boundary, then it represents material from the Upper Durness Group that has fallen into one of the fissures in the Lower Durness Group.

The timing of the Grampian Orogeny is still not definite, but it now seems probable that it occurred before the deposition of the late Tremadoc/early Arenig Lough Nafooey Group of western Ireland[16]. The early Ordovician rocks along the Highland Border (in Arran and near Aberfoyle) are perhaps (together with the Macduff Slates) younger than the main episodes of the orogeny. If this is so, the interval between the Lower Cambrian and Lower Ordovician (Tremadoc) rocks at Durness would correspond in time to the peak of the Grampian Orogeny.

We thank the Scottish Office of the IGS for access to the 6-inch field maps of Balnakeil Bay.

Received 19 June; accepted 8 September 1980.

1. Peach, B. N., Horne, J., Gunn, W., Clough, C. T. & Hinxman, L. W. *Mem. geol. Surv. U.K.* 1–668 (1907).
2. Cowie, J. W., Rushton, A. W. A. & Stubblefield, C. J. *Spec. Rep. geol. Soc.* **2,** 1–42 (1972).
3. Cowie, J. W. in *Cambrian of the British Isles, Norden, and Spitsbergen* (ed. Holland, C. H.) 123–155 (Wiley, London, 1974).
4. Brasier, M. D. *Nature* **268,** 719–720 (1977).
5. Whittington, H. B. *Spec. Rep. geol. Soc.* **3,** 1–74 (1972).
6. Higgins, A. C. *Proc. geol. Soc.* **127,** 295 (1971).
7. Gobbett, D. J. & Wilson, C. B. *Geol. Mag.* **97,** 441–456 (1960).
8. Cowie, J. W. in *Cambrian of the New World* (ed. Holland, C. H.) 325–383 (Wiley, London 1971).
9. Peel, J. S. *Rapp. Grønl. geol. Unders.* **88,** 29–39 (1979).
10. Kendall, A. C: *Bull Soc. petrol Geol.* **25,** 480–504 (1977).
11. Palmer, T. J. *J. Paleont.* **52,** 109–117 (1978).
12. Young, H. R. *Sedim. Geol.* **22,** 287–303 (1979).
13. West, L. M. *Proc. geol. Ass.* **86,** 205–225 (1975).
14. Swett, K. & Smit, D. E. *Bull. geol. Soc. Am.*:**83,** 3223–3248 (1972).
15. Swett, K. *J. sedim. Petrol.* **35,** 928–938 (1965).
16. Ryan, P. D. & Archer, J. B. *Can. J. Earth Sci.* **14,** 2453–1461 (1977).

Palaeoceanographic change in the Pacific at the Eocene–Oligocene boundary

L. D. Keigwin Jr

Graduate School of Oceanography, University of Rhode Island, Kingston, Rhode Island 02881

Oxygen isotopic studies both of benthic formanifera[1-5] and shallow-marine carbonates[6-8] have provided a useful monitor of marine palaeotemperatures. The Deep Sea Drilling Project (DSDP) has provided cores from many ocean basins to conduct detailed stable isotopic and palaeoceanographic studies of the Cenozoic and late Mesozoic. DSDP Sites 277 and 292, separated by ~60° latitude in Palaeogene times, each record an ^{18}O enrichment in benthic foraminifera of nearly 1‰ beginning at the Eocene–Oligocene boundary. Planktonic foraminiferal trends are similar to benthic trends in the high latitude south-west Pacific Ocean, but tropical planktonics show only a minor (~0.3‰) increase which may reflect a change in seawater composition. These results suggest a sudden cooling of Pacific deep waters and high latitude surface waters forms a useful stratigraphic marker for the Eocene–Oligocene boundary. This boundary is particularly important because of its association with several worldwide palaeo-oceanographic and biogeographic changes. These include a sudden drop in the calcite compensation depth of 1–2 km (refs 9, 10); a decrease in planktonic microfossil diversity[11-13]; a change in planktonic biogeographic patterns[12-14]; and increased erosion of deep-sea sediments over wide areas[15,16].

Most studies of the Eocene–Oligocene boundary (Table 1), based on coarse sampling, have revealed an early to middle Eocene temperature maximum in both surface and deep waters followed by cooling through the late Eocene into the early Oligocene. This is manifested as an oxygen isotopic enrichment of ~2‰ (equal to an 8 °C cooling) over a period of about 10 Myr. The temperature record at high latitudes reveals synchronous cooling in both surface and deep waters[3] whereas if low and middle latitudes were included the surface waters are shown to cool more gradually[5]. Most studies also record a benthic foraminiferal oxygen isotopic enrichment of ~1‰ (~4 °C cooling) at or near the Eocene–Oligocene boundary. Only in a detailed study[4] of this change at DSDP Site 277 is it shown to occur in the earliest Oligocene.

DSDP Site 277 was drilled in 1,214 m water depth on the Campbell Plateau in the south-west Pacific (52° 13.43′ S; 166° 11.48′ E). The Campbell Plateau is continental in origin[17] and plate tectonic reconstructions place it only a few degrees farther south 38 Myr ago[18,19]. Site 292 (ref. 20) is located at 2,943 m on the Benham Rise in the west Philippine Sea (15° 49.11′ N; 124° 39.05′ E). This is a tectonically complex region of anomalously shallow oceanic crust[21] which has been drifting northward since the early Palaeogene[22] so the location of Site 292 was tropical in Eocene–Oligocene times.

Microfossil ranges[23-27] of potential stratigraphic value shown in Figs 1 and 2. The biostratigraphic sequence at Site 277 is marked only by last appearances. The Eocene–Oligocene

Table 1 Summary of Eocene to earliest Oligocene stable isotopic studies

Site	Location	Ref.	Micro fossil type*	Bio-stratigraphic zone† in which change takes place	Approximate amount of isotopic enrichment
305	Shatsky Rise	37	N	P10 to P18	1.3
167	Central Equatorial Pacific	37	N	P18 to P19/20	0.9
167	Central Equatorial Pacific	2	B	P16 to P18	1.0
167	Central Equatorial Pacific	5	P	P14 to P17	1.0
44, 171	Central North Pacific	5	B	P16 to P18	1.0
44, 171	Central North Pacific	5	P	P13 to P18	0.5
277	Campbell Plateau	3	B & P	early to late Eocene‡	2.0
277	Campbell Plateau	4	B	earliest Oligocene‡	1.0
357	Rio Grande Rise	38	B	P14 to P17	1.0
357	Rio Grande Rise	38	P	P13 to P14	1.0
398	Off Portugal	39	B	P15 to P16	2.0
398	Off Portugal	39	P	P13/14 to P16	2.0

*B, Benthic foraminifera; P, planktonic foraminifera; N, nannofossils.
†Zones after Blow[23].
‡P zones not applicable.

0028–0836/80/430722—04$01.00

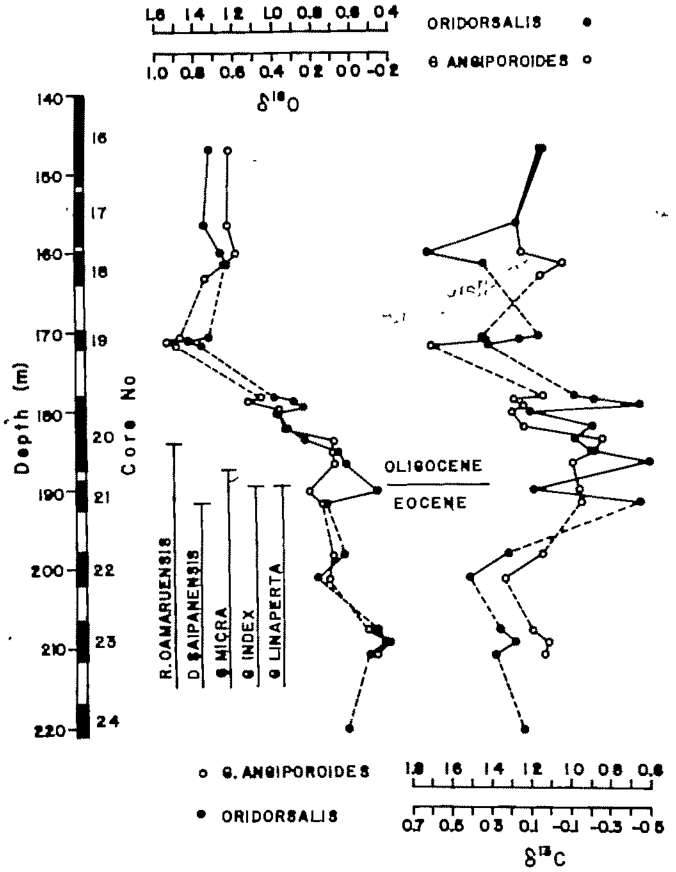

Fig. 1 Stable isotopic results (‰, PDB) at high latitude Site 277 on the Campbell Plateau, South-west Pacific Ocean Intervals of core recovery are in black along the vertical axis. Microfossil ranges are from refs 23, 24 Benthic and planktonic foraminiferal δ^{18}O suggests the entire water column at this location cooled by 3 to 4 °C beginning at the Eocene–Oligocene boundary.

boundary is defined in New Zealand by the last appearances of the planktonic foraminifera *Globigerapsis index* and *Globigerina linaperta* which are considered[28] to occur within planktonic foraminiferal zone P17. Nannofossil markers[24] place the Eocene–Oligocene boundary within a few metres of that defined by planktonic foraminifera (Fig. 1).

Although there are first and last appearances of taxa throughout the latest Eocene and earliest Oligocene at Site 292, several last appearances suggest that the Eocene–Oligocene boundary lies within core 35 (Fig. 2). Ujiie[25] places the boundary at the last appearance of the foraminifera *Globorotalia cerroazulensis* and *Hantkenina primitiva* (approximately equivalent to the top of zone P17). The base of zone P17 is defined by the last appearance of *Cribrohantkenina inflata*[28], so core 35 of Site 292 is probably time-equivalent to core 21 of Site 277. Ellis[26] finds important nannofossil markers (last appearances of *Discoaster barbadiensis* and *Discoaster saipanensis*) 8–13 m lower in the section. The presence of the short ranging latest Eocene radiolarian *Lophocyrtis jacchia* suggests that the sequence is nearly complete at this location[27].

Isotopic analyses followed standard procedures[29]. B-1 was used as a working standard and was calibrated to PDB using NBS-20 (Solenhofen limestone) as an absolute standard. For NBS-20 we take δ^{18}O = −4.18‰ and δ^{13}C = −1.07‰ with respect to PDB[30]. Eleven analyses of NBS-20 have been performed giving δ^{18}O B-1 = −4.12 ± 0.12‰ (1σ of the isotopic difference of samples run on a single day) and δ^{13}C B-1 = −1.71 ± 0.06‰. As a check we have run 10 samples of the standard TKL-1, giving δ^{18}O PDB = −4.43 ± 0.10‰ and δ^{13}C = −1.78 ± 0.28‰ which compare well with the mean isotopic compositions and standard deviations determined by 15 different laboratories of −4.26 ± 0.18‰ and −1.69 ± 0.13‰ for δ^{18}O and δ^{13}C respectively[30]. We have also run 11 Yule Marble samples as part of the CENOP intercalibration, giving δ^{18}O = −6.63 ± 0.08‰ and δ^{13}C = −2.30 ± 0.05‰ which compare well with −6.49, −2.28 and −6.57, −2.30 of J. Killingley (personal communication) and S. Savin (personal communication) respectively.

The benthic foraminifera *Oridorsalis* was chosen from the size fraction greater than 175 μm at both locations. There was no single abundant, long-ranging species of planktonic foraminiferal fauna common to each site that could be used for the isotopic analysis. Thus, *Globigerina angiporoides* was selected from Site 277 and *Globigerina ampliapertura* from Site 292. Both are from the 175–295 μm size fraction. I have assumed that both of these planktonic species previously inhabited near-surface waters and thus their isotopic composition mostly reflects variation in surface-water temperature.

Table 2 Stable isotopic results (‰, PDB) of the present study

	Depth	Site 277 *Oridorsalis* sp.		*Globigerina angiporoides*	
Sample	(m)	δ^{18}O	δ^{13}O	δ^{18}O	δ^{13}C
16-5, 140	147.4	1 33	0 05	0.63	1.11
17-5, 140	156.9	1.36	0.18	0 64	1.25
18-1, 140	160.4	1.28	0.63	0.60	1.23
18-2, 140	161 9	1.25	0 34	0.66	1 02
18-3, 140	163.4			0 76	1.13
19-2, 100	171.0	1.34	0 06	0.89	1 43
19-2, 140	171 4	1 45	0.16	0.96	1 41
19cc	172.0	1.38	0.32	0.91	1 69
20-1, 50	178.5	1.00	−0.12	0.47	1.12
20-1, 100	179.0	0.90	−0.22	0.54	1.27
20-2, 19	179 7	0 85	−0.45	0.38	1.22
20-2, 100	180 5	0.99	0.11	0.38	1 28
20-3, 140	182.4	0.93	−0 21	0 34	1.22
20-4, 140	183.9	0 84	−0 12	0.09	0.82
20-5, 140	185 4	0.67	−0 20	0.10	0.86
20-6, 140	186.9	0.63	−0.50	0.09	0.97
21-2, 140	190.4	0 47	0 09	0.22	0.94
21-3, 140	191.9	0.73	−0.45	0.15	0 93
22-1, 140	198.4	0 64	0.22	0.10	1.13
22-3, 140	201.4	0.78	0 42	0 12	1 32
23-1, 140	207.9	0.47	0 27	−0.08	1 18
23-2, 140	209.4	0.43	0.19	−0.19	1.10
23-3, 145	211.0	0 51	0.29	−0 13	1 12
24-3, 140	220.4	0.62	0.15		
		Site 292		*Globigerina ampliapertura*	
32-1, 100	292.50	1 60	0.44	−1 23	1.39
32cc	293.50	1.75	−0 12	−1 11	1.32
33-1, 24	301.24	1.61	−0.13	−1.18	1 39
33-2, 50	303.00	1.74	0.11	−1 07	1 57
33-2, 100	303.50	1.83	0.11	−1 16	1.40
33cc	304.50	1.98	0.51	−1.04	1.95
34-1, 52	311 02			−1 41	1.75
34-1, 99	311 49			−1 02	1 73
34-1, 148	311.98	1.92	0.62	−1.34	1.95
34-2, 50	312.50			−1.27	2.09
34-2, 99	312.99			−1.03	2.16
34-2, 148	313 48	2.26	0.56		
35-1, 87	320 87	1.04	0.23	−1.21	1 75
35-1, 99	320.99	0.95	0 26	−1.29	1 75
35-1, 141	321 41	1.20	0 23	−1 61	1.50
				−1.39	1.61
35-2, 36	321 86	0 85	0.48	−1 66	1.50
35-2, 101	322.51	1.01	0.25	−1.01	1 56
35-2, 141	322.91	0.96	0 01		
35-3, 95	323 95	0 71	−0 31	−1 52	
35-3, 147	324.47			−1 32	1 30
				−1.29	1.27
36-1, 89	330.39	0.87	−0.01		
36-1, 145	330.95	0.78	−0.10		
36-2, 59	331 59	0.82	−0.21	−1 42	1 43
36-2, 89	331.89	0.66	−0.25	−1 50	1.46
36-3, 117	333 67	1.04	0.09	−1.26	1 44
36-3, 136	333.86			−1.58	1.33
36-4, 116	335 16			−1 57	1.44
36-5, 85	336.35	0 92	0.03		
37-1, 88	339 88	1.01	0 24		
37-2, 100	341.50	1.40	0.24		
37-2, 148	341 98	1.01	0.08		
37-3, 50	342.50	1.06	0 23		

Benthic foraminiferal calcite becomes enriched in ^{18}O at both Sites 277 and 292 beginning at the Eocene–Oligocene boundary (Figs 1 and 2). At high southern latitude Site 277, the change in $\delta^{18}O$ between 170 and 190 m is about 1‰, whereas the average difference before and after the transition is slightly less (0.8‰). At Site 277 the planktonic and benthic $\delta^{18}O$ records are highly correlated. Site 292 also shows a large change in benthic $\delta^{18}O$ which is between 312 and 320 m, and is greater than the average difference below and above the transition (about 1.5 versus 0.9‰). The most important difference between the two sites is that unlike the high latitude site, at tropical Site 292 the planktonic foraminifera become gradually enriched in ^{18}O by about 0.3‰ over the interval examined. There is no abrupt change in Site 292 planktonic foraminiferal $\delta^{18}O$ at the Eocene–Oligocene boundary, but the average above and below the benthic transition are significantly different (0.28‰).

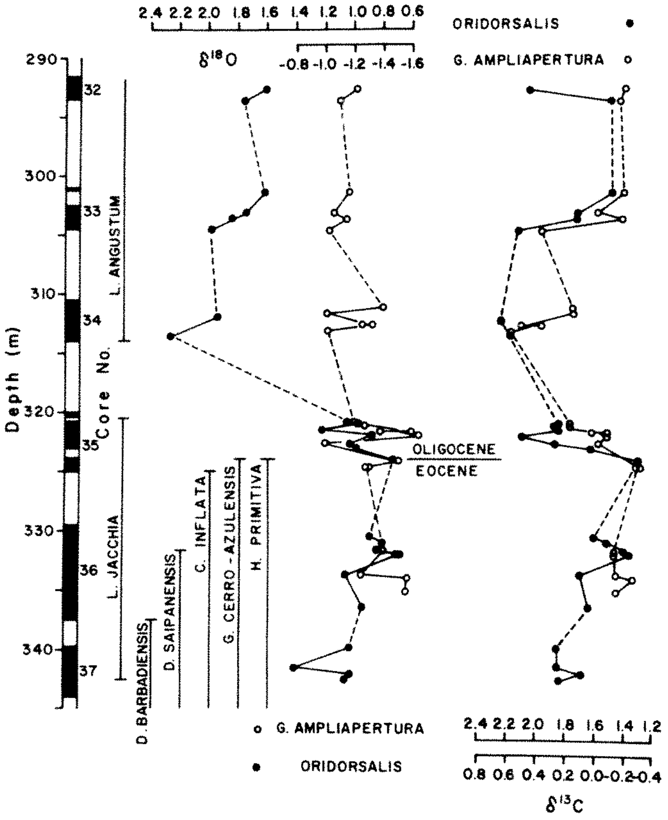

Fig. 2 Stable isotopic results (‰, PDB) at tropical Site 292 in the Philippine Sea. Intervals of core recovery are in black along the vertical axis. Microfossil ranges are from refs 25–27. Only benthic foraminiferal $\delta^{18}O$ suggests a 3 to 4 °C cooling beginning at the Eocene–Oligocene boundary. The slight enrichment in planktonic foraminiferal ^{18}O may record a minor change in seawater composition.

The $\delta^{13}C$ records of benthic and planktonic foraminifera appear subparallel at both locations (Figs 1 and 2). At Site 277 there is evidence that foraminiferal carbon across the Eocene–Oligocene boundary is lighter on average by a few tenths of a permil than before or after. Site 292 is marked by isotopically heavier foraminiferal carbon in the earliest Oligocene.

The oxygen isotopic results agree with an abrupt earliest Oligocene enrichment[4] in benthic foraminiferal ^{18}O (Figs 1, 2). My results differ from those of Kennett and Shackleton[4] for Site 277 in that the isotopic enrichment begins at the Eocene–Oligocene boundary and the transitional change is less by 0.2‰. This is due to my use of monogeneric samples (*Oridorsalis* sp.) compared with mixed benthics of Kennett and Shackleton[4]. This is important because the oxygen isotopic composition of different benthic foraminifera from the same sample may vary by nearly 1‰ (refs 31, 32). I have also used a closer sampling interval, especially in core 20; plotted core 19 at the top of the cored interval rather than the bottom; and used Jenkins'[23] range of *G. index* rather than that of the Site Report, Site 277 (ref. 17). The more accurate placement of the last appearance of *G. index* raises the boundary about 2 m from 192 to 189.6 m. I have checked samples between the two reported last appearance levels of *G. index* (21-2, 60 and 21 cc) and found it present in 21-2, 140 but absent from 21-3, 140. Thus its uppermost range is sporadic and partly leads to uncertainty in placement of the Eocene–Oligocene boundary.

The maximum duration of the oxygen isotopic transition may be estimated from published sedimentation rates. At Site 292 the late Eocene to early Miocene sedimentation rate is ~12 m Myr^{-1} (ref. 20), so the interval from the middle of core 35 to the base of core 34 represents a maximum duration of about 0.9 Myr. The sedimentation rate of Site 277 above core 21 is ~22 m Myr^{-1} (ref. 17). The $\delta^{18}O$ increase occurs over a maximum interval of ~18 m, giving a maximum duration of about 0.8 Myr, in good agreement with Site 292.

Three mechanisms which may account for the observed oxygen isotopic records, either singly or combined, are post-depositional alteration, a change in the isotopic composition of seawater, or a change in surface and bottom-water temperatures. Taken alone, the $\delta^{18}O$ record at Site 277 might be suggestive of diagenetic change or seawater compositional change because both benthic and planktonic foraminifera respond in the same way. Diagenetic effects at both sites are ruled out by scanning electron microscopic studies of foraminifera which show the fauna is well-preserved at both sites. Preservation of nannofossils is mostly 'moderate' between cores 16 and 25 at Site 277 (ref. 24), and although there are intervals of poor preservation at Site 292 (ref. 26), they bear no relation to the isotopic change.

A seawater compositional change could explain the shift in isotopic values of both planktonic and benthic species at Site 277, but Site 292 results argue against this. At the tropical location the benthics become markedly enriched in ^{18}O during the earliest Oligocene but the planktonics do not (Fig. 2). This suggests that the maximum seawater compositional change is the maximum enrichment in ^{18}O common to planktonics and benthics at both locations, ~0.3‰ between cores 32 and 36 at Site 292. Nevertheless, warming of tropical surface waters at the same time as a large oceanic enrichment in ^{18}O could produce the observed results and cannot be ruled out. Growth of continental ice is a possible mechanism of increasing $\delta^{18}O$ by 0.3‰. Evidence for Eocene–Oligocene continental ice in Antarctica is equivocal and is discussed by Mercer[33]. The sea level record based on seismic stratigraphy indicates a small Eocene–Oligocene regression relative to other Cenozoic changes[34]. If the ^{18}O enrichment in Site 292 planktonic foraminifera reflects an ice volume growth then the effect was to lower sea level by a few tens of metres.

Most oxygen isotopic studies of Cenozoic marine carbonates follow the interpretation that major Antarctic ice growth began in the middle Miocene, so pre-middle Miocene $\delta^{18}O$ values from well-preserved foraminifera essentially reflect seawater temperature[3]. Planktonic microfossils provide evidence of dramatic cooling from the Eocene to the Oligocene. Lipps[11] noted that, relative to the Eocene, Oligocene microfossil assemblages were marked by abundant cosmopolitan species of simple morphology. Subsequently Kennett[12] found planktonic microfossil diversity in the Southern Ocean during the Oligocene to be the lowest of the entire Cenozoic. Low faunal and floral diversity and abundant cosmopolitan species are inferred to reflect low marine temperatures in the earlier Cenozoic, as they do today.

If $\delta^{18}O$ changes are assumed to reflect only temperature changes rather than oceanic compositional changes, then the isotopic results of this study may be used to estimate latest

Table 3 Comparison of foraminiferal $\delta^{18}O$ data before and after earliest Oligocene cooling

	Benthic foraminifera n	Benthic foraminifera $\bar{x}$ (‰)	Benthic foraminifera σ	Planktonic foraminifera n	Planktonic foraminifera $\bar{x}$ (‰)	Planktonic foraminifera σ	Vertical isotopic contrast (‰)
Early Oligocene							
Site 277 (cores 16–19)	7	1.34	0.07	8	0.76	0.14	0.58†
Site 292 (cores 32–34)	8	1.84	0.22	10	−1.16	0.13	3.00†
latitudinal contrast					1.92*		
Late Eocene							
Site 277 (cores 21–24)	8	0.58	0.13	7	0.03	0.16	0.55†
Site 292 (below 35-3, 95)	10	0.96	0.20	6	−1.44	0.13	2.40†
latitudinal contrast					1.47*		

* Computed by subtracting Site 292 $\bar{x}$ from Site 277 planktonic foraminiferal $\bar{x}$.

† Computed by subtracting planktonic foraminiferal $\bar{x}$ from benthic foraminiferal $\bar{x}$.

Eocene and earliest Oligocene latitudinal temperature contrasts, and surface to deep-water temperature contrasts at a particular location (Table 3). Such reconstructions must assume that planktonic foraminiferal $\delta^{18}O$ largely reflects near-surface water temperature. It remains to be confirmed where *G. angiporoides* lived in the water column. An isotopic study of Oligocene planktonic foraminifera suggested *G. ampliapertura* inhabited intermediate-depth waters[35]. However, as *G. ampliapertura* does not show an earliest Oligocene $\delta^{18}O$ increase similar to the benthic foraminifera, I assume that its isotopic composition mostly reflects near-surface conditions.

Table 3 summarizes oxygen isotopic data from before and after the earliest Oligocene cooling. The vertical oxygen isotopic contrast between near-surface waters and the sea floor remained the same throughout the late Eocene and early Oligocene at Site 277, so it seems the entire upper water column chilled. At the lower latitude site (292) the vertical $\delta^{18}O$ contrast increased from 2.4 to 3.0‰, equal to an increase in the shallow to deep temperature contrast of ~2.4 °C. This increase is inferred to be mostly due to a temperature drop in deeper waters[4]. The latitudinal $\delta^{18}O$ contrast in near-surface waters increased from 1.5‰ in the late Eocene to ~1.9‰ in the early Oligocene, equal to a cooling of ~1.6 °C. This is due to a nearly 3 °C surface-water cooling in high latitudes, while low latitude near-surface waters cooled by only ~1 °C.

Two triggering mechanisms are proposed for the Eocene–Oligocene boundary event. Kennett and Shackleton[4] interpret the benthic foraminiferal oxygen isotopic enrichment to represent the sudden evolution of cold, thermohaline circulation (the 'psychrosphere'), perhaps in response to the opening of the Tasman Seaway and subsequent sea-ice accumulation around Antarctica. Thierstein and Berger[36] argue that this event may have been caused by the injection of water of greatly different density than normal seawater from an isolated basin to the open sea. In particular they propose that brackish water from a previously isolated Arctic Ocean rapidly spread across the surface of the world ocean and disrupted the heat exchange between the deep and surface waters. This is believed to have reduced the moderating influence of the ocean on climate, resulting in snow accumulation on Antarctica, northward migration of the polar front, and the subsequent production of cold bottom water.

The latter hypothesis[36] proposes Artic tectonic events (opening of the Greenland Sea passage) as the trigger of the Eocene–Oligocene cooling rather than the opening of the passage over the Tasman Rise[4]. Thierstein and Berger[36] stress the importance of carbon isotopic data: their 'injection event' hypothesis predicts isotopically light carbon in benthic foraminifera at the boundrary event and may be tested by detailed studies. At Site 277 benthic carbon is indeed lighter across the boundary (Fig. 1) but it is not so at Site 292 (Fig. 2). Data from more cores are necessary to evaluate mechanisms for the Eocene–Oligocene boundary cooling and the significance of $\delta^{13}C$ variability.

I thank M. L. Bender, W. A. Berggren, B. H. Corliss, J. P. Kennett, T. S. Loutit, T. C. Moore Jr., N. J. Shackleton and M. S. Srinivasan for assistance. Samples were provided through the DSDP by the NSF. This work was supported by NSF grant OCE79-14594 (CENOP).

Received 28 April; accepted 19 August 1980.

1. Emiliani, C. *Science* **119,** 853–855 (1954).
2. Savin, S. M., Douglas, R. G. & Stehli, F. G. *Bull. geol. Soc. Am.* **86,** 1499–1510 (1975).
3. Shackleton, N. J. & Kennett, J. P. *Init. Rep. DSDP* Leg **29,** 743–755 (1975).
4. Kennett, J. P. & Shackleton, N. J. *Nature* **260,** 513–515 (1976).
5. Savin, S. M. *A. Rev. Earth planet. Sci.* **5,** 319–355 (1977).
6. Dorman, F. H. *J. Geol.* **74,** 49–61 (1966).
7. Devereux, I. *N.Z. J. Sci.* **10,** 988–1011 (1967).
8. Buchardt, B. *Nature* **275,** 121–123 (1978).
9. van Andel, T. H., Heath, G. R. & Moore, T. C. Jr *Geol. Soc. Am. Mem.* **143,** 134 (1975).
10. van Andel, T. H. *Earth planet. Sci. Lett.* **26,** 187–194 (1975).
11. Lipps, J. H. *Evolution* **24,** 1–22 (1969).
12. Kennett, J. P. *Mar. Micropaleont.* **3,** 301–345 (1978).
13. Sancetta, C. *Mar. Micropaleont.* **4,** 363–398 (1979).
14. Haq, B. U. & Lohmann, G. P. *Mar. Micropaleont.* **1,** 119–194 (1976).
15. Kennett, J. P. *et al. Nature phys. Sci.* **239,** 51–55 (1972).
16. Moore, T. C. Jr *et al. Micropaleontology,* **24,** 113–138 (1978).
17. Kennett, J. P. *et al. Init. Rep. DSDP* Leg **29,** 1197 (1975).
18. Molnar, P. *et al. Geophys. J.R. astr. Soc.* **40,** 383–420 (1975).
19. Weissel, J. K., Hayes, D. E. & Herron, E. M. *Mar. Geol.* **25,** 231–277 (1977).
20. Karig, D. E. *et al. Init. Rep.*·*DSDP* Leg **31,** 927 (1975).
21. Louden, K. E. *Am. geophys. Un. Monogr.* **19,** 253–267 (1976).
22. Andrews, J. E. *Geology* **8,** 140–143 (1980).
23. Jenkins, D. G. *Init. Rep. DSDP* Leg **29,** 449–467 (1975).
24. Edwards, A. R. & Perch-Nielsen, K. *Init. Rep. DSDP* Leg **29,** 469–539 (1975).
25. Ujiie, H. *Init. Rep. DSDP* Leg **31,** 677–691 (1975).
26. Ellis, C. H. *Init. Rep. DSDP* Leg **31,** 655–676 (1975).
27. Ling, H. Y. *Init. Rep. DSDP* Leg **31,** 703–761 (1975).
28. Blow, W. H. *Proc. 1st int. Conf. Planktonic Microfossils* (eds Bronnimann, P & Renz, H. H.). 199–422 (Brill, Leiden, 1969).
29. Keigwin, L. D. Jr *Earth planet. Sci. Lett.* **45,** 361–382 (1979).
30. Blattner, P. & Hulston, J. R. *Geochim. cosmochim. Acta* **42,** 59–62 (1978).
31. Duplessy, J. C., Lalou, C. & Vinot, A. C. Science **168,** 250–251 (1970).
32. Erez, J. *Nature* **273,** 199–202 (1978).
33. Mercer, J. H. *Antarctic Glacial History and World Paleoenvironments* (ed. van Zinderen Bakker, E. M.) 73–93 (Balkema, Rotterdam, 1978).
34. Vail, P. R., Mitchum, R. M. Jr & Thompson, S. III. *Seismic Stratigraphy—Applications to Hydrocarbon Exploration* (ed. Payton, C. E.) 83–97 (American Association of Petroleum Geologists, Tulsa, 1977).
35. Boersma, A. & Shackleton, N. *Init. Rep. DSDP* Leg **41,** 957–962 (1978).
36. Thierstein, H. R. & Berger, W. H. *Nature* **276,** 461–466 (1978).
37. Douglas, R. G. & Savin, S. M. *Init. Rep. DSDP* Leg **32,** 509–520 (1975).
38. Boersma, A. & Shackleton, N. *Init. Rep. DSDP* Leg **39,** 911–924 (1977).
39. Vergnaud-Grazzini, C., Pierre, C. & Letolle, R. *Oceanol. Acta* **1,** 381–390 (1978).

Manganese nodule growth rates determined by fossil diatom dating

David Kadko & Lloyd H. Burckle

Department of Geological Sciences, Lamont-Doherty Geological Observatory of Columbia University, Palisades, New York 10964

We report here that a manganese nodule from the Central Pacific manganese nodule province has been dated by fossil diatoms found in mud scraped from near the nodule's centre. The nodule was taken at DOMES Site B from Core B55-56 at 11°50.3′N and 137°28.2′W in a water depth of 4,892 m. It was resting on the sediment surface, with about 1.5 cm of the nodule bottom (of a total nodule height of 4.2 cm) buried in the mud. The top surface of the nodule was covered with a smooth manganese coating, but the bottom had a very rough, crusty texture. It was found that recent mud had leaked in through cracks in the nodule bottom, but that there were no pre-Pleistocene diatoms in this material. The date obtained was compared with the growth rate determined by the ^{230}Th excess method and found to be in reasonable agreement. This study adds to the work of Harada[1,2] on the biostratigraphy (mainly coccoliths) of manganese nodules.

Figure 1 shows the results of the ^{230}Th dating of the nodule; these are consistent with growth rates found by others using this method for other nodules[3–5]. The nodule's top 3 mm indicate a growth rate of 3 mm Myr^{-1}, and the bottom yielded a rate of

0028-0836/80/430725—02$01.00

4.5 mm Myr^{-1}. (The bottom result is only an approximation as the ^{230}Th excess was quite low.) From the nodule's radius (normal to the sampled section) of 2.7 cm, and assuming a constant growth rate, an age of 9 Myr BP is suggested as the time of initial growth. However, we are aware that the constancy of growth has been questioned[5].

Two mud samples (B and C in Fig. 2) were taken from the nodule and examined for diatoms. One sample was from the nodule's centre and the other from 0.5 cm below the centre. Both samples contained many fragments of robust, well silicified diatoms. Essentially the only form that was identifiable was *Actinocyclus ingens* Rattray. This form is found sporadically in the early Miocene but is most common in the equatorial Pacific in the early middle and middle middle Miocene (~12–15 Myr BP, close to the ^{230}Th age). We also encountered occasional specimens (<1%) of the diatom *Pseudoeunotia doliolus* (Wall.) Grunow, an exclusively Pleistocene form.

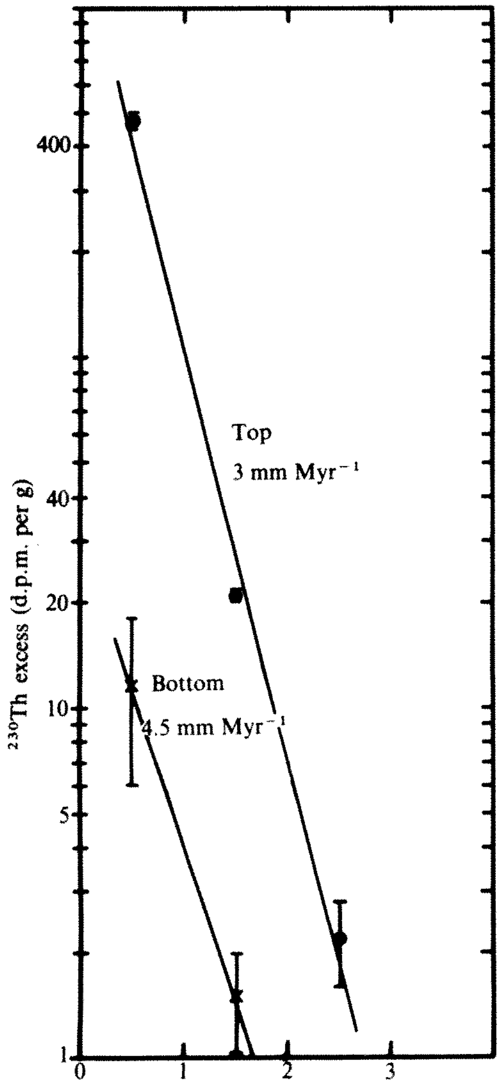

Fig. 1 A log-linear plot of ^{230}Th excess as a function of depth from the nodule's top and bottom surfaces.

To determine if the Miocene diatoms represented contamination from surface sediment, samples from the mud surrounding the nodule were also analysed for diatom species. The diatoms from 0–11 cm depth were representative of Pleistocene or Recent assemblages. The presence of *P. doliolus* indicates that this interval is younger than the Olduvai Event of the Matuyama Reversed Epoch (Pleistocene)[6]. Negative evidence, that is, the absence of such forms as *Rhizosolenia praebergonii* var. *robusta* Burckle, *Nitzschia reinholdii* Kanaya and Koizumi, or the silicoflagellate *Mesocena quadrangula* Bukry, suggests that this interval is younger than the Brunhes/Matuyama magnetic boundary. *A. ingens* was not present through this interval nor were there any other pre-Pleistocene forms.

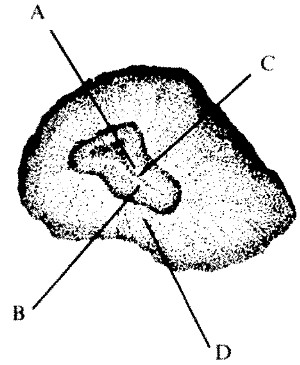

Fig. 2 Schematic diagram of the manganese nodule studied, with sample locations (see text).

Quinterno and Theyer[7] found several per cent of reworked Tertiary forms of radiolarians in surface Quaternary sediment of nearby cores. However, the percentage of reworked material varied markedly from core to core in their study, and in this core, to a depth of 9 cm, less than 1% of any pre-Pleistocene radiolarians were found. The complete absence of pre-Pleistocene diatoms in this interval is therefore not surprising, as diatoms are much more susceptible to corrosion than are radiolaria.

Mud within the nodule was also analysed for ^{230}Th. Figure 2 shows the sample locations of the mud taken from the nodule. The sample marked 'D' was 1 cm from the nodule bottom and had a ^{230}Th concentration of 150 d.p.m. per g. This corresponds to surface sediment and clearly shows that recent mud has leaked in through bottom cracks, and accounts for the presence of the few recent diatoms found in the nodule. Sample 'A', taken from the nodule centre, had only 44 d.p.m. per g, which indicates a mixture of older material with the surface sediment.

The ^{230}Th analysis and diatom data suggest that surface sediment with high ^{230}Th (but no Miocene fossils) reached the nodule's interior. The crusty nodule bottom, immersed in sediment, did have cracks where this material could have leaked in. However, material much older than surface sediment is at the nodule centre, and fossil diatoms there can indicate the approximate age of the nodule. This age should not be affected by contamination from recent sediment that probably leaked in through cracks at the nodule bottom.

This work was supported by US NSF grants OCE77-02871 (MANOP) and OCE78-20885. We thank W. Broecker and J. Morley for discussions.

Received 23 April; accepted 4 August 1980.

1. Harada, K. thesis, Kyoto Univ. (1977); *Mem. Fac. Sci. Kyoto Univ. Ser. Geol. Miner.* **45**, 111–126 (1978).
2. Harada, K. & Nishida, S. *Nature* **260**, 770–771 (1976).
3. Bender, M. L., Ku, T. L. & Broecker, W. S. *Science* **151**, 325–328 (1966).
4. Ku, T. L. & Broecker, W. S. *Deep Sea Res.* **16**, 625–637 (1969).
5. Krishnaswani, S. & Cockran, J. K. *Earth planet. Sci. Lett.* **40**, 45–62 (1978).
6. Burckle, L. H. *Quat. Res.* **7**, 330–340 (1977).
7. Quinterno, P. & Theyer, F. in *Marine Geology and Oceanography of the Pacific Manganese Nodule Province* (eds Bischoff, J. L. & Piper, F. F.) (Plenum, New York, 1979).

Deacidification in a plant with crassulacean acid metabolism associated with anion–cation balance

R. Phillips

Department of Biology, University of Stirling, Stirling FK9 4LA, UK

In plant tissues using crassulacean acid metabolism (CAM), malate accumulates during the dark and declines in the subsequent light period. The malate is an intermediate store of CO_2 which is fixed photosynthetically during the subsequent day and for CAM plants the amplitude of the fluctuation is significant for plant carbon assimilation[1]. Because they are so considerable, the maximum values for acid content aroused early comment[2]. The maximum seems to be related not just to the rate of acidification but also to internal factors which may include the water and cation content of tissues[3]. Changes in the distribution of cations have recently been linked to the diel fluctuation in malate[4]. I report here that the malate measured in leaves at the end of the day can be correlated with an imbalance between total cations and the organic acids other than malate in the leaves of *Kalanchoe daigremontiana*. There occurs a greater imbalance in leaves of plants grown in a long compared with a short day and this may explain the finding that leaves contain considerably more malate at the end of a long photoperiod.

K. daigremontiana was grown in Long Ashton culture solution until the plants were 9–12 weeks old as described previously[3]. The macronutrient composition of the solution was 4 mM KNO_3, 4 mM $Ca(NO_3)_2$, 1.5 mM $MgSO_4$ and 1.33 mM NaH_2PO_4. Although this supplied nitrogen largely as nitrate, the solution contained 1.86 mM ammonium added as hydroxide to bring its initial *p*H to 6.2. Plants were grown at 25 °C with either 16 h dark, 8 h light (short day); 8 h dark, 16 h light (long day); or 8 h dark, 8 h low light, 8 h light (pseudolong day). Light was provided by fluorescent and incandescent sources giving an intensity of 0.2 mE m^{-2} s^{-1} at midplant height, except during the period of low light in pseudolong days when the intensity was reduced to <0.02 mE m^{-2} s^{-1}. Leaves were removed at the end of the light period, divided in half and the midrib discarded. From one half organic acids were extracted and measured by gas chromatography[5]. The adjacent half was homogenized and centrifuged at 4,000*g* for 5 min. The *p*H of the supernatant was measured. The supernatant and pellet were separated and the pellet rinsed once with 25 cm^3 distilled water. After centrifugation at 40,000*g* for 20 min the supernatant was combined with the original supernatant and assayed for calcium, magnesium, potassium and sodium by atomic absorption spectrophotometry. This extraction consistently removed 99% of the monovalent and 90% of the divalent cations and allowance was made for this loss in calculations of the total cation concentrations.

The photoperiod markedly affected whether malate or isocitrate was the major component of the acid fraction of leaves at the end of the day (Table 1). In long days malate exceeded the sum of isocitrate and citrate whereas in pseudolong and short days the reverse was true. These differences occurred mainly because of large differences in the amount of malate. At the end of a long day leaves contained nine times more malate than after a short day. Several reports show that malate is at or close to its minimum during the diel fluctuation at the end of the photoperiod[6,7]. Clearly long days do not necessarily lead to low levels of malate in leaves by the end of the day.

Figure 1 shows that increasing amounts of malate occurred together with an increased excess of cations over the anions citrate and isocitrate. The slope of Fig. 1 is very close to unity. It is likely that virtually all the cations have been measured but the organic acids will represent only a component of the total anions in leaves. The intercept in Fig. 1 may provide an estimate of these unmeasured anions in which case this fraction is similar in all leaves at 64.1 μequiv. g^{-1}. A correlation like that shown in Fig. 1 would occur if *K. daigremontiana* deacidified to a limit determined by a particular balance between total anions and cations in the leaves.

Table 1 Amounts (μequiv. per g leaf water) of malate, citrate and isocitrate and the *p*H of extracts of leaves from node 7 (upper) and node 5 (lower) of *K. daigremontiana* analysed at the end of the photoperiod

	Malate	Citrate	Isocitrate	*p*H
Long day				
Upper	88.2±2.7	18.5±3.8	36.3±4.9	5.1±0.05
Lower	87.2±1.9	23.7±4.9	43.8±8.1	5.0±0.05
Pseudolong day				
Upper	46.2±6.0	26.0±1.5	53.1±5.3	5.9±0.01
Lower	26.4±0.8	32.0±3.0	95.0±8.8	6.0±0.05
Short day				
Upper	9.4±2.8	18.5±0.8	70.1±4.3	5.9±0.01
Lower	7.8±1.8	20.5±1.0	68.1±4.5	5.8±0.02

Results are shown as mean ±s.e. of at least three replicates.

The *p*H values recorded for leaf extracts were at least 5.0 and in most cases nearly 6.0 (Table 1). The published *pK* values for malate, citrate and isocitrate indicate that complete dissociation of these acids occurs at about *p*H 6.0 (ref. 8). The addition of small amounts of alkali to the extracts resulted in a rapid increase in their *p*H. Thus, by the end of the photoperiod, leaves have deacidified such that there is just sufficient malate to maintain electroneutrality in the leaves by organic acids anions rather than hydroxyl anions. This is very similar to the observation that higher plants generally redress any imbalance between inorganic cations and anions with organic acid, particularly malic acid[9].

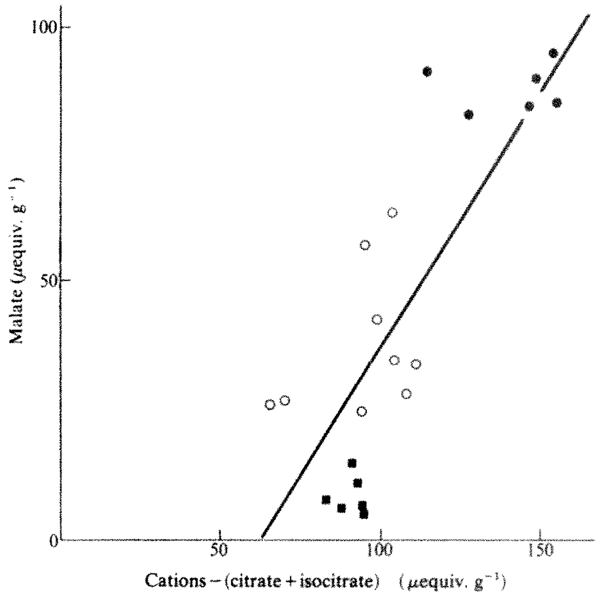

Fig. 1 The amount by which equivalents of cations exceeded citrate and isocitrate in leaves of *K. daigremontiana* and the equivalents of malate in the same leaves measured at the end of three different photoperiods. ●, Long day; ○, pseudolong day; ■, short day. $r = 0.81$, $P > 0.001$; $y = 1.02x - 65.4$.

0028–0836/80/430727—02$01.00

The results presented here suggest that the malate which fluctuates in CAM plants includes a component which is involved in charge balance and this fraction is not available for CAM.

Received 23 July; accepted 29 August 1980.

1. Osmond, C. B. *A. Rev. Pl. Physiol.* **29,** 379–414 (1978).
2. Ranson, S. I. & Thomas, M. *A. Rev. Pl. Physiol.* **11,** 81–110 (1960).
3. Phillips, R. D. & Jennings, D. H. *New Phytol.* **77,** 599–611 (1976).
4. Bloom, A. J. *Pl. Physiol.* **64,** 919–923 (1979).
5. Phillips, R. D. & Jennings, D. H. *New Phytol.* **77,** 333–339 (1976).
6. Nishida, K. *Pl. Cell Physiol.* **20,** 259–261 (1979).
7. Allaway, W. G., Osmond, C. B. & Troughton, J. H. *R. Soc. N.Z. Bull.* **12,** 195–202 (1974).
8. Martell, A. E. & Sillen, L. G. *Stability Constants of Metal-Ion Complexes Spec. Publ.* no. **17** (Chemical Society, London, 1964).
9. Raven, J. A. & Smith, F. A. *New Phytol.* **76,** 415–431 (1976).

Haplodiploid sex ratios and the mutation rate

R. H. Smith & M. R. Shaw*

Department of Zoology, University of Reading, Reading RG6 2AJ, UK

Deviations from a 1:1 sex ratio in species with haplodiploid genetics are well known and sociobiologists have produced various explanations[1–8], all of which ignore the effect of mutations on haploid viability. Lethal recessive mutations can significantly increase male (haploid) mortality and their effect should be estimated to provide the appropriate null hypothesis with which to compare observed sex ratios before considering any more complex, sociobiological hypothesis. Prospective maternal care[4] and local mate competition[1,2] will also affect sex ratio, but increased haploid mortality due to mutation rate is the only effect common to all haplodiploid species. Using emergence data for some parasitoid species, the rate of mutation to lethal recessives is estimated to be about 0.035 per genome per generation giving a differential haploid mortality of 10%.

The selective forces affecting sex ratio were first considered in detail by Fisher[9] who concluded that an equal investment by a parent in male and female offspring would be evolutionarily stable in a randomly mating population. In arrhenotokous (haplodiploid) species, the primary sex ratio is determined by mated females laying both fertilized (female) and unfertilized (male) eggs. Biased adult sex ratios are well known in groups such as the Hymenoptera and the Acarina; possible evolutionary explanations have included local mate competition[1,2], inbreeding with stochastic effects[3], and a variety of approaches based on asymmetrical relationships[4–8].

All of these explanations ignore a fundamental genetical feature of arrhenotoky which must always contribute to differential survival and hence to a biased sex ratio. A haploid male cannot survive if he carries a lethal recessive mutation and his viability will be severely reduced by non-lethal but deleterious recessive alleles. Mutation seems to have been ignored because the mutation rate per locus per generation is very small, but the mutation rate per genome per generation (m) is vastly greater. For instance, although there are difficulties in estimating m because of large amounts of redundant DNA, it is estimated that the total number of gene loci in man is about 3×10^4 with a mutation rate per locus of 10^{-5}, giving a rate per genome of around 0.3 per generation[10]. Data from consanguineous marriages give a comparable estimate of the mutation rate to lethals and lethal equivalents of 0.06–0.15 per gamete per generation[11]. An estimate of m which may be more relevant to haplodiploid arthropods than data from diplodiploid vertebrates has been obtained for sex-linked lethals in *Drosophila melanogaster*[12]. The mutation rate for recessive lethals is approximately 0.006 per X chromosome per generation or about 0.030 per haploid genome per generation, and the estimate of m is increased to 0.058 lethal equivalents per haploid genome per generation when deleterious recessives are taken into account. In the following discussion, m will be treated as though it refers entirely to lethal recessives.

If mutations occur randomly and independently of one another, the distribution per gamete will be Poisson and the probability that a haploid genome receives no new mutations will be $\exp(-m)$; thus the probability that a haploid male dies as a result of one or more new mutations is $1-\exp(-m)$. An unfertilized egg might also receive with probability 1/2 a lethal recessive present in the heterozygous state in the mother's genome. The probability that a female will not have received any new lethal mutation via either the maternal or the paternal gamete is $\exp(-2m)$. Summing over all previous maternal generations, the probability that a male receives one or more lethal mutations heterozygous in his mother's genome is:

$$(1-\exp(-2m))(\tfrac{1}{2}+\tfrac{1}{4}+\tfrac{1}{8}\ldots) = 1-\exp(-2m)$$

Thus, ignoring dominant lethal mutations which are assumed to be very rare, the probability that a male dies because of either a new mutation or the mutational load in the female genome is:

$$\begin{aligned} P &= (1-\exp(-m)) + (1-\exp(-2m)) \\ &\quad -(1-\exp(-m))(1-\exp(-2m)) \\ &= 1-\exp(-3m) \qquad (1) \end{aligned}$$

Equation (1) can be derived from more than one approach and represents a special case of the balance of selection and mutation for sex-linked recessives[13].

Maynard Smith (personal communication) has suggested that an intuitive interpretation of equation (1) is that the parents of a mixed brood suffer $3m$ new mutations per generation, on average, and all must be eliminated in males. Hence the survival rate of haploids relative to diploids is $\exp(-3m)$ simply as a consequence of the mutation rate, and an initially equal number of fertilized and unfertilized eggs will always lead to an average bias towards females in emergent adults. Numbers seem to be the appropriate measure of investment in the absence of maternal care[5] as there is no reason why fertilized and unfertilized eggs should represent different costs to the mother. Figure 1 shows the expected female : male ratio given an equal initial numerical investment in the sexes plotted against mutation rate per haploid genome m. The female bias obviously increases with m, and the logarithm of the sex ratio is linear in m. Note that the calculations assume that lethal recessive alleles cause no loss of viability in heterozygotes, and that the probability of homozygosity of a lethal allele is negligible (of the order of the mutation rate per locus per generation).

The importance of equation (1) is that it provides the correct null hypothesis against which any sociobiological explanation of a haplodiploid sex ratio should be tested; clearly a 1 : 1 ratio is not the expected consequence of an initially equal numerical investment. The difficulty which arises is that the appropriate

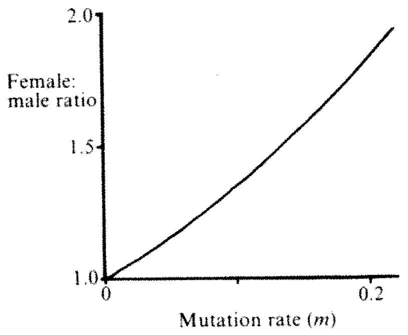

Fig. 1 Expected female : male ratio of adults, given an equal numerical investment in eggs, in relation to mutation rate per haploid genome per generation.

---

* Present address: The Royal Scottish Museum, Chambers Street, Edinburgh EH1 1JF, UK.

0028–0836/80/430728—02$01.00

Table 1 Differential haploid mortality and estimation of mutation rate (m) in gregarious *Apanteles* species

Species		*A. chares*	*A. ruficrus*	*A. abjectus*	*A. zygaenarum*	Total
All-male broods	Larvae	11	35	11	19	76
	Adults	7	33	8	8	56
Mixed broods	Larvae	6	51	169	335	561
	Adult males	1	4	43	124	172
	Adult females	3	46	103	117	269
Maximum likelihood estimate of haploid : diploid survival:			0.900			
95% confidence interval:			0.838 to 0.957			
Estimated mutation rate per genome per generation:			0.035			
95% confidence interval:			0.015 to 0.059			

Mortality of males and females is estimated using the total emergence data. The mortality considered here relates only to the time between parasite larvae leaving the hosts and emerging as adult parasites from their cocoons. Because mortality in earlier developmental stages has been ignored, m may well have been underestimated. Other mortality factors such as hyperparasitism or starvation have been assumed not to be differential. The maximum likelihood estimate was found by numerical exploration of the likelihood surface. The distribution of twice the log likelihood ratio is chi-squared, allowing the determination of a 95% confidence interval.

null hypothesis cannot be quantified without knowledge of the parameter m in any particular case. An approximate estimate of P can be obtained from the egg to emergent adult mortality in haploid broods of unmated females, but P would be overestimated if there were any mortality factors affecting both haploids and diploids. An unbiased estimate could, in principle, be obtained by cytological examination of eggs in mixed broods, giving a primary sex ratio for comparison with that of emergent adults. In either case it would be necessary to use sufficiently large numbers to obtain a reasonably precise estimate of P because differential mortality of haploids due to mutation is by nature stochastic and sex ratios will be very variable[8].

There seem to be no published data which allow estimation of P by comparing emergence in all-male and in mixed broods because entomologists generally eliminate data from broods where emergence is not close to 100%. However, one of us (M.R.S.) has collected data over a number of years on the emergence of broods of gregarious parasitoid species of the genus *Apanteles* (Hymenoptera: Braconidae) from hosts collected in the field and reared individually in the laboratory. Four out of 22 species produced large all-male broods as well as mixed broods and the data are given in Table 1, along with the consequent estimate of differential haploid mortality P and the mutation rate m. The 95% confidence interval for P shows clearly that haploids suffered significantly greater mortality than diploids. The maximum likelihood estimate $m = 0.035$ is remarkably close to Mukai's value[12] of 0.030–0.058 for *D. melanogaster*, which suggests that these figures are of the correct order of magnitude for haplodiploid arthropods. The consequent differential mortality of haploids relative to diploids is too large to be ignored and therefore the mutation rate is of some significance when formulating the correct null hypothesis associated with a primary sex ratio of 1:1.

It could be argued that factors other than the mutation rate might cause differential mortality in the two sexes (compare with ref. 14), but in haplodiploid species it is difficult to see how differential pre-emergent mortality in identical rearing conditions could be explained other than by lethal or strongly deleterious recessive alleles. Extreme female-biased ratios which cannot be explained by mutation alone are seen where inbreeding is combined with arrhenotoky[1], and any consequent local mate competition between brothers seems to be reduced by producing often only one or two males in a brood. In these circumstances a haploid male is effectively no more than his mother's gamete and fitness is defined as number of female offspring[1,3]. A full theoretical treatment of optimum sex ratios in inbred arrhenotokous species should include not only stochastic survival[3] but also differential haploid mortality as predicted by equation (1). It is interesting that inbreeding in haplodiploids will not increase female mortality through increasing homozygosity of lethal recessives because these are always eliminated in males. Similarly, because every female has a male parent and every male has a female parent, the increase in homozygosity of non-lethal but deleterious recessives will affect both sexes equally at equilibrium. Sex ratio arguments based on parental care[5] are unaffected by the effect discussed here only if differential mutational mortality occurs before the stage at which care is invested. Thus it is clear that mutations can have a significant effect and should therefore be taken into account by sociobiologists considering haplodiploid sex ratios.

We thank John Maynard Smith for noting an error in an earlier version of equation (1), and Roger Mead for advice on exploring messy likelihood functions.

Received 18 March; accepted 7 August 1980.

1. Hamilton, W. D. *Science* 156, 477–488 (1967).
2. Alexander, R. D. & Sherman, P. W. *Science* 196, 494–500 (1977)
3. Hartl, D. L. *Am. Zool.* 11, 309–325 (1971).
4. Pickering, J. *Nature* 283, 291–292 (1980).
5. Trivers, R. L. & Hare, H. *Science* 191, 249–263 (1977).
6. Macnair, M. R. *J. theor. biol.* 70, 449–459 (1978).
7. Charnov, E. L. *Am. Nat.* 112, 317–326 (1978).
8. Herbers, J. M. *Am. Nat.* 114, 818–834 (1980).
9. Fisher, R. A. *The Genetical Theory of Natural Selection* (Clarendon, Oxford, 1930).
10. Ohno, S. *Brookhaven Symp. Biol.* 23, 366–370 (1972).
11. Morton, N. E., Crow, J. F. & Muller, H. J. *Proc. natn. Acad. Sci. U.S.A.* 42, 855–863 (1956).
12. Mukai, T., Chigusa, S. I., Mettler, L. E. & Crow, J. F. *Genetics* 72, 335–355 (1972).
13. Haldane, J. B. S. *J. Genet.* 31, 317–326 (1935).
14. Trivers, R. L. in *Sexual Selection and the Descent of Man* (ed. Campbell, B.) 152 (Aldine, Chicago, 1972)

Eyes and classification of malacostracan crustaceans

A. A. Fincham

British Museum (Natural History), Cromwell Road,
London SW7 5BD, UK

During the past 100 yr various methods of classifying mysids, krill, prawns, shrimps, crabs and lobsters have been proposed, including the use of behaviour, gill type and the relationship of the carapace with the head and the thoracic segments. At least two factors have been ignored in all these schemes—larval characters and optical mechanisms. A survey of malacostracan crustaceans reveals three types of optical mechanism. The simplest uses apposition optics, often with hexagonal facets, and is found in all decapod larvae and most adult brachyuran crabs. Refracting, superposition eyes with hexagonal facets occur in mysids and euphausids, and reflecting, superposition eyes with square facets using mirror optics are found in adult prawns, shrimps, macrurans such as lobsters, and dromiid 'crabs'. Artificial relationships have been imposed on malacostracan crustaceans by a failure to incorporate eye structure in schemes of classification. Once evolved, eye structure is a stable character and provides evidence for the continued grouping together of penaeid, caridean and stenopid prawns and shrimps; it demonstrates their affinity with lobsters and other Macrura, and confirms the unity of a re-defined Brachyura and the weakness of the Anomura as a coherent taxon. •

0028–0836/80/430729—03$01.00

The classification of decapods has been based on adult characters. Boas[1] and Borradaile[2] used behaviour, Bate[4] and Burkenroad[3] gills, Laurent[5] structure of the head and its relationship with the carapace together with the degree of development before eclosion, and Guinot[6] the position of genital openings. It is difficult to frame diagnoses for larval groups using such frameworks of higher taxa based solely on characters of the adult. Larval characters have not been included in these schemes, yet ideally a natural classification should encompass both adult and larval stages[7].

Recent work on decapod development and larval adaptation[8–11] and optical mechanism in crustacean eyes[12–14] has led to a re-examination of decapod relationships. It was assumed that the compound eyes of crustaceans used the same refracting, superposition optical mechanism described by Exner[15] for nocturnal insects. Kuiper[16] pointed out that the peripheral optical elements in crustaceans did not have a sufficiently high refractive index and that they were too uniform to provide the continuous bending necessary. Vogt[17] and Land[12] independently discovered that superposition optics in certain Crustacea were achieved not by lenses but by mirrors and reflection. Grenacher[18] reported that individual facets were square in the compound eyes of prawns and shrimps and certain other groups of Macrura, but did not suggest that this was linked with a special optical mechanism. Square facets are, in fact, essential to the mirror mechanism[19,20]. Compound eyes in most malacostracans, including all decapod larvae and adult Brachyura, have hexagonal facets and the optical mechanism is one of apposition with no clear zone, a mosaic image being built up from indivdual ommatidia[21]. Syncarida, Hoplocarida and most Peracarida with well-developed compound eyes such as amphipods and isopods use apposition optics, but loose packing of the surface elements results in circular or irregularly shaped facets rather than closely packed hexagonal facets.

There are at least two exceptions to this usual apposition condition. The first includes mysids and euphausids, once classified together as the Schizopoda on the basis of biramous limbs retained throughout life. These groups are now placed respectively in the Peracarida (free posterior carapace when present and oostegites forming a marsupium) and Eucarida (carapace fused to all thoracic segments and often with a long planktonic development). However, Land[13] reported that mysids and euphausids both have refracting, superposition eyes in which the essential clear zone is present together with crystalline refractive cones and hexagonal facets. This may be a case simply of convergence by mysids and euphausids, but optical mechanism needs to be taken into account in future phylogenetic studies of these shrimp-like groups, especially in view of the suggestion[22] that mysid-like types may have given rise to euphausids and to decapods. The presence of a marsupium seems inadequate as evidence for the retention of such disparate orders as amphipods, isopods, cumaceans, tanaids and mysids together in the Peracarida.

Table 1. Eye structure and classification of selected recent Malacostraca

Taxon	Adult eye type
Subclass Malacostraca	
Series Eumalacostraca	
Superorder Peracarida	
Order Mysidacea	2
Superorder Eucarida	
Order Euphausiacea	2
Order Decapoda	
(Suborder Natantia)	
Section Penaeidea	3
Section Caridea	3
Section Stenopodidea	3
(Suborder Reptantia)	
Section Macrura	
Superfamily Eryonoidea	? (eyes reduced or absent)
Superfamily Scyllaroidea	3
Superfamily Nephropoidea	3
Superfamily Thalassinoidea	1 (eyes poorly developed or reduced)
(Section Anomura)	
Superfamily Galatheoidea	3
Superfamily Dromioidea	3
Superfamily Homoloidea	3 (see text for discussion)
Superfamily Paguroidea	1
Superfamily Hippoidea	1
Section Brachyura	
Subsection Gymnopleura	1
Subsection Oxystomata	1
Subsection Brachygnatha	
Superfamily Brachyrhynchoidea	1
Superfamily Oxyrhynchoidea	1

1, Apposition optics, hexagonal facets; 2, superposition refracting optics, hexagonal facets; 3, superposition reflecting optics, square facets. Taxa of dubious validity are given in parentheses.

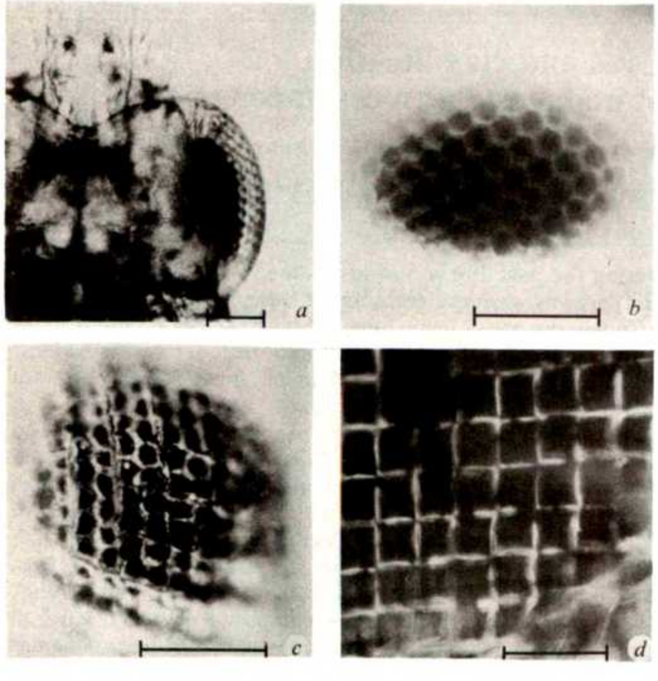

Fig. 1 *Palaemonetes* (*Palaemonetes*) *varians* (Leach, 1814). Stage 1 larva: *a*, dorsal view of compound apposition eye; *b*, surface view of hexagonal eye facets. Stage 5 post-larva: *c*, eye facets 'squaring off'. Adult: *d*, square facets of superposition reflecting eye. Bar scales represent 0.1 mm. (Photographs: Peter York BM(NH).)

The second exception to the usual apposition form of crustacean compound eye is superposition, represented by reflecting eyes with square facets which are found only in adult prawns and shrimps, Macrura and certain Anomura. The larvae of these groups begin their planktonic existence with hexagonal-faceted apposition eyes. There is such a great change in life style and morphology at metamorphosis that this would seem to be the most likely time to convert hexagonal facets to square facets on the surface of the compound eye in those groups which have this form in the adult. However, in the ditch shrimp *Palaemonetes* (*Palaemonetes*) *varians* (Leach, 1814) and other palaemonids[9–11], there is an hexagonal array in all larval stages (Fig. 1*a*, *b*) and the facets remain hexagonal until the fifth post-larval moult when the carapace is about 2.8 mm long. There is then a gradual 'squaring off' (Fig. 1*c*) of the hexagons until the juveniles reach a carapace length of about 5.8 mm. The facets are then perfectly square and arranged in an orthogonal matrix (Fig. 1*d*). The square-faceted eyes of the adult may still function as apposition eyes in well-lit conditions by migration of proximal and distal pigment cells across the clear zone (M. F. Land, personal communication).

Not all decapods develop mirror optics. Adult crabs retain hexagonal-faceted apposition eyes, in common with many other groups of crustaceans with compound eyes. An analysis of adult eye type of selected malacostracan groups held in the Crustacea collection at the British Museum (Natural History) is presented in Table 1. Natantia and Macrura with well-developed eyes have at least part of the compound eye composed of square facets. Those burrowing macrurans that have small or poorly developed eyes, such as members of the superfamily Thalassinoidea, have hexagonal facets. Section Anomura lies uneasily between the Macrura and Brachyura and contains a wide variety of forms. This is shown clearly by eye structure with square facets in superfamily Galatheoidea and hexagonal facets in superfamilies Paguroidea and Hippoidea. All Brachyura have hexagonal facets with the exception of the Dromiacea in which there are square facets distally with hexagons in the lateral field. This transference of Dromiacea from the Brachyura is strongly supported by larval evidence for the superfamily Dromioidea[7]. However, Rice[23] suggests, again on the evidence of larvae, that the Dromiacea are polyphyletic and that the homolid Dromiacea and raninids of the subsection Gymnopleura are closely related and near to the stem from which the higher Brachyura evolved. Homoloidea would therefore be alone among the Brachyura in having evolved independently square-faceted eyes.

The oldest decapod fossil material[24] comes from the Permo-Trias and includes *Antrimpos* Munster, 1839 of the natant family Penaeidae and *Protoclytiopsis* Birshteyn, 1958 of the astacid family Erymidae (Brachyura are not recorded until the Jurassic). Fossil evidence is equivocal about the structure of eyes as preservation is generally poor, but recent penaeids and lobsters have square-faceted eyes in the adult. Reflecting superposition eyes are found only in prawns, shrimps, long-bodied macrurans and some anomurans. Such an unusual eye type suggests a strong phylogenetic relationship and not simply convergence. As it is likely that this optical mechanism arose early in decapod evolution, eye structure will be useful as an indicator of affinity. This is turn provides a strong case for maintaining penaeid, caridean and stenopid prawns as a group, in contrast to recent proposals[5] for their division, and also emphasizes their link with the Macrura. Suborder Reptantia becomes an untenable taxon containing a mixture of eye types. Anomura has long been recognized as a taxon of convenience[7] rather than a natural grouping and its constituent groups should be redistributed (Table 1). On the basis of eye design the Decapoda should be divided into only two groups—Natantia, Macrura, Galatheoidea, Dromioidea and Homoloidea which have the unique reflecting superposition eye mechanism and the true Brachyura in which, together with the Paguroidea and the Hippoidea, the apposition eye present in the larva is retained throughout life.

I thank Drs R. W. Ingle, M. F. Land, A. L. Rice and D. I. Williamson for constructive criticism.

Received 12 May; accepted 31 July 1980

1. Boas, J E V *K. danske Vidensk Selsk Skr* Ser 6, 1, 25–210 (1880).
2. Borradaile, L A. *Ann Mag nat. Hist.* Ser 7, 19, 475–486 (1907)
3. Burkenroad, M D. *Tulane Stud Geol.* 2, 1–17 (1963).
4. Bate, C. S *Rep scient. Results Voy Challenger* 24, 1–942 (1888)
5 Laurent, M. de Saint *Bull. Off. natn Pêches Tunis* 3, 15–31 (1979)
6. Guinot, D. *Bull. biol Fr Belg.* 112, 211–292 (1978)
7. Williamson, D I *Thalassia Jugosl* 10, 401–414 (1974).
8. Knowlton, R E *Thalassia Jugosl* 10, 138–158 (1974)
9. Fincham, A W *Bull Br. Mus nat Hist (Zool)* 31, 1–28 (1977)
10. Fincham, A A. *Bull Br. Mus nat Hist. (Zool)* 34, 163–182 (1979).
11. Fincham, A A. *Bull. Br. Mus nat. Hist (Zool)* 37, 17–46 (1979).
12. Land, M F *Nature* 263, 764–765 (1976).
13 Land, M F., Burton, F A. & Meyer-Rochow, V. B. *J comp Physiol* 130, 49–62 (1979)
14. Land, M F *New Scient* 84, 10–13 (1979)
15 Exner, S. *Die Physiologie der Facettierten Augen von Krebsen und Insekten* (Deuticke, Leipzig and Wien, 1891).
16 Kuiper, J W *Symp Soc Exp Biol* 16, 58–71 (1962)
17 Vogt, K *Z Naturforsch* 30c, 691 (1975).
18. Grenacher, H *Untersuchungen über das Sehorgan der Arthropoden* (Vandenhoek und Ruprecht, Gottingen, 1879).
19. Vogt, K *Z. Naturforsch* 32c, 466–468 (1977).
20 Vogt, K *J. comp. Physiol* 135, 1–19 (1980)
21 Horridge, G. A. *Proc R. Soc., Lond.* B207, 287–309 (1980)
22 Waterman, T. H & Chace, F A in *The Physiology of Crustacea* (ed Waterman, T H) 1, 1–33 (Academic, New York, 1960).
23. Rice, A L *Trans zool. Soc., Lond.* 35, 271–424 (1980)
24 Glaessner, M. F in *Treatise on Invertebrate Paleontology* (ed. Moore, R C) Part R, Arthropoda 4, 2, 400–533 (Geological Society of America, 1969)

Modulation of lateral geniculate neurone excitability by noradrenaline microiontophoresis or locus coeruleus stimulation

Michael A. Rogawski & George K. Aghajanian

Departments of Pharmacology and Psychiatry,
Yale University School of Medicine and the Connecticut Health Center,
New Haven, Connecticut 06510

The dorsal lateral geniculate nucleus (LGNd) receives afferents from the brainstem which regulate its capacity to transmit visual information from the retina to the striate cortex[1]. One such pathway consists of noradrenaline (NA)-containing fibres originating in the locus coeruleus (LC). These provide a dense, uniform, noradrenergic innervation of the LGNd[2]. Electrical stimulation in the LC region has been reported to enhance the responsiveness of LGNd neurones to afferent excitation[3]. Although this effect was abolished when brain NA stores were pharmacologically depleted, it was not established as a direct action of NA on LGNd neurones because of the widespread distribution of LC fibres to many parts of the brain and the long latency of the response. Recently, we observed that NA, applied locally by microiontophoresis with low ejection currents, produced a delayed increase in the firing rate of most spontaneously active LGNd neurones, an effect selectively blocked by α-adrenoceptor antagonists[4]. We show here that microiontophoretic NA can mimic the ability of LC stimulation to enhance the synaptic excitation of LGNd neurones. As neither NA nor LC stimulation activated LGNd neurones in the absence of synaptic or glutamate-induced excitation, both appear to act through a neuromodulatory mechanism. The postsynaptic α-adrenoceptor antagonist WB-4101[5] blocks the facilitation produced by locally applied NA and by coeruleo-geniculate pathway stimulation, providing evidence for pharmacological identity of the two effects.

Extracellular recordings were obtained from single neurones in the LGNd of male albino rats anaesthetized with chloral hydrate. Microiontophoresis was carried out with blunt five-barrel micropipettes to which a fine glass recording pipette was cemented. The electrode assembly was positioned 4.0 mm anterior to lambda and 3.5–4.0 mm lateral to the midline and lowered approximately 4.0 mm below the cortical surface until the LGNd was recognized by cellular responses to movement of a light beam across the visual field. To activate LGNd neurones orthodromically, some animals had a stimulating electrode implanted in the optic chiasm. Further experimental details are given in Fig. 1 legend.

First we examined the effects of iontophoretically applied NA on the response of LGNd neurones to stimulation of the optic chiasm. Suprathreshold shocks usually evoked a single discharge with latency 2–4 ms followed by a period of inhibition typically lasting 70–230 ms. Late activity, consisting of bursts of up to four or five spikes at regular intervals following the inhibitory pause, was exhibited by most cells. This response pattern is characteristic of geniculocortical relay neurones (P-cells)[6].

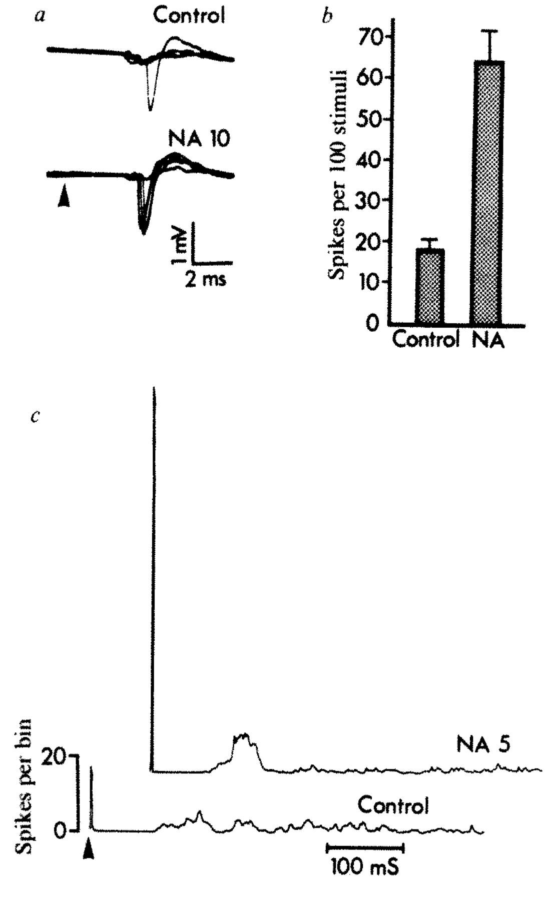

Fig. 1 NA facilitation of unitary action potentials in the LGNd evoked by optic chiasm stimulation. In *a*, subthreshold shocks were applied to the optic chiasm with a concentric bipolar stimulating electrode (SNE-100, Rhodes Medical Instruments) at a frequency of 1 Hz. The stimulus strength was adjusted so that approximately one out of five stimuli produced a short latency spike discharge (upper trace). For the cell shown, 0.5 mA peak to peak, 0.1 ms duration biphasic rectangular pulses satisfied this condition. The position of the stimulus is indicated on the storage oscilloscope record by an arrowhead. Shock artefacts were electronically blanked in these traces. During NA iontophoresis (10 nA, 60 s), four out of five stimuli produce spikes in identical stimulation conditions (lower trace). Five superimposed sweeps. Positivity is upward. *b*, Summary of data from five cells in four animals. The experimental procedure was as in *a* except that each unit was tested with 100 shocks before and during the iontophoresis of NA at 5–20 nA for 2–5 min and this was repeated 2–8 times per cell. Data are the mean ±s.e.m. of averages for each cell. *c*, Post-stimulus time histogram demonstrating the effect of NA on the early and late responses to optic chiasm stimulation. As well as facilitating the initial spike response (vertical line at left of each histogram), NA (5 nA, 50 s) causes a shift in the late activity to a peak of high probability firing immediately following the inhibitory pause (upper histogram). Histograms were generated with a Nicolet 1072 signal averager. Each histogram represents the summed responses to 100 stimuli delivered at 1 Hz. Stimulation parameters: 1 mA, 0.15 ms. Bin width: 2 ms. In this and subsequent experiments, Sprague–Dawley rats weighing 240–300 g were used. The animals were anaesthetized with chloral hydrate (400 mg kg^{-1}, intraperitoneally); additional anaesthetic injections were given as necessary. Core temperature (monitored with a rectal probe) was maintained above 36° C with a heating pad. Extracellular unitary action potentials were recorded using microelectrode assemblies consisting of a five-barrel micropipette array (15–25 μm in diameter) to which a fine single-barrel recording electrode (~1 μm tip diameter) was affixed with dental acrylic. The tip of the recording electrode extended 20–40 μm beyond the iontophoresis barrels. The recording electrode contained 2% pontamine sky blue in 2 M NaCl and typically had an impedance of 6–12 MΩ. Solutions used for microiontophoresis were: L-noradrenaline D-bitartrate (Regis), 0.1 M, *p*H 4; serotonin creatinine sulphate (Regis), 0.04 M, *p*H 4; L-glutamic acid monosodium salt (Sigma), 0.5 M, *p*H 8; picrotoxin (Sigma), saturated solution in 0.15 M NaCl, *p*H 4; and WB-4101 (2-([2′,6′-dimethoxy]phenoxyethylamino)methylbenzodioxan HCl; WB Pharmaceuticals), 0.1 M, *p*H 4. A retaining current of −10 nA was applied to the iontophoresis barrels between periods of ejection except when glutamate was used in which case the backing current was +10 nA. To minimize polarization artefacts, a balancing current was continuously passed through an electrode barrel containing 4 M NaCl. Electrode placement was verified by ejecting dye iontophoretically from the recording pipette and identifying the spot thus produced in brain sections prepared by routine histological procedures.

Local application of NA by microiontophoresis caused an increase in the probability of spike generation during the early phase of the response to chiasmatic stimulation (Fig. 1*a–c*). In addition, late spikes tended to occur at earlier times following the stimulus and frequently a peak of high probability late firing was observed immediately after the inhibitory pause (Fig. 1*c*). To obtain these effects, NA was applied with iontophoretic currents of 5–20 nA for periods of 1–5 min. (Low iontophoretic currents were exclusively used because recently[4] we found that higher currents may produce a loss of responsiveness or have weak depressant effects. This may, in part, account for the variable effects of NA noted by previous investigators[7–9].) In some cases the stimulus intensity was adjusted so that approximately 20% of the stimuli produced initial spikes. In these conditions, iontophoresis of NA resulted in a 255% increase in the frequency of spike generation (Fig. 1*a*, *b*). In contrast, in paired comparisons with NA, serotonin, another monoamine present within axon terminals in the LGNd[10,11], always depressed responses to optic chiasm stimulation (5–10 nA; six cells), as has been reported by others[7,8].

These results suggested that NA could facilitate the responsiveness of LGNd relay neurones to retinal ganglion cell excitation and ultimately enhance signal transfer from retina to visual cortex. To determine whether this was due to a direct excitatory action of NA or to an interaction of the amine with afferent synaptic activation, ongoing tonic excitation of the relay cells was suppressed by section of the optic nerve behind the globe of each eye[12,13]. Following this, NA generally failed to excite silent LGNd units although the same cells could be activated easily by iontophoresis of the excitatory amino acid glutamate. Thus NA, in contrast to glutamate, did not seem to be a direct excitant. However, low currents of NA (2–15 nA) were able to facilitate the excitatory action of the amino acid dramatically. Iontophoresis of glutamate at currents which produced little or no excitation before application of NA, resulted, with concurrent ejection of NA, in marked activation of firing (22 cells in 14 rats) (Fig. 2*a*). The effect of NA took 30–90 s to develop and lasted up to 6 min following cessation of the ejection.

The ability of NA to produce enhanced responsiveness to glutamate suggested that NA could facilitate the general excitability of relay neurones, presumably through a postsynaptic mechanism. However, it has been speculated that the facilitatory effects of conditioning LC stimulation are due to suppression of inhibitory interneurones[3] and it is possible that locally applied NA acts indirectly as well. Two populations of local inhibitory elements seem to synapse on P-cells: perigeniculate reticular (PGR) neurones located in the thalamic reticular nucleus[14] and intrinsic interneurones (I-cells)[15]. Arguments against the participation of PGR neurones in the facilitatory action of iontophoretic NA are: first, NA generally produced only a small decrease in the postexcitation inhibitory period believed to be mediated by PGR cells, yet the responsiveness, especially of the short latency spike, was markedly facilitated. Second, the activity of NA was independent of the proximity of the iontophoretic pipette to the reticular nucleus which is situated rostral to the geniculate, as much as 1.5 mm anterior to the caudal extent of the LGNd[14].

However, it is conceivable that I-cells could mediate the action of iontophoretic NA. Recent evidence suggests that γ-aminobutyric acid (GABA) is the neurotransmitter utilized by these cells[16]. Therefore, if the facilitatory action of NA on relay neurones was due to depression of I-cell firing or suppression of GABA release from presynaptic I-cell dendrites[17], blockade of GABA-mediated neurotransmission should produce a similar effect. In preliminary experiments, we found that the GABA antagonist picrotoxin was able to block GABA-induced depression of spontaneously active LGNd neurones when iontophoresed with currents of 15–20 nA for 1–5 min. Picrotoxin was then applied to 'silent' neurones in optic nerve-sectioned animals. Even with prolonged administration (up to 25 min), the GABA antagonist (15–50 nA) did not produce a facilitation of the response to glutamate (five cells) (Fig. 2*b*).

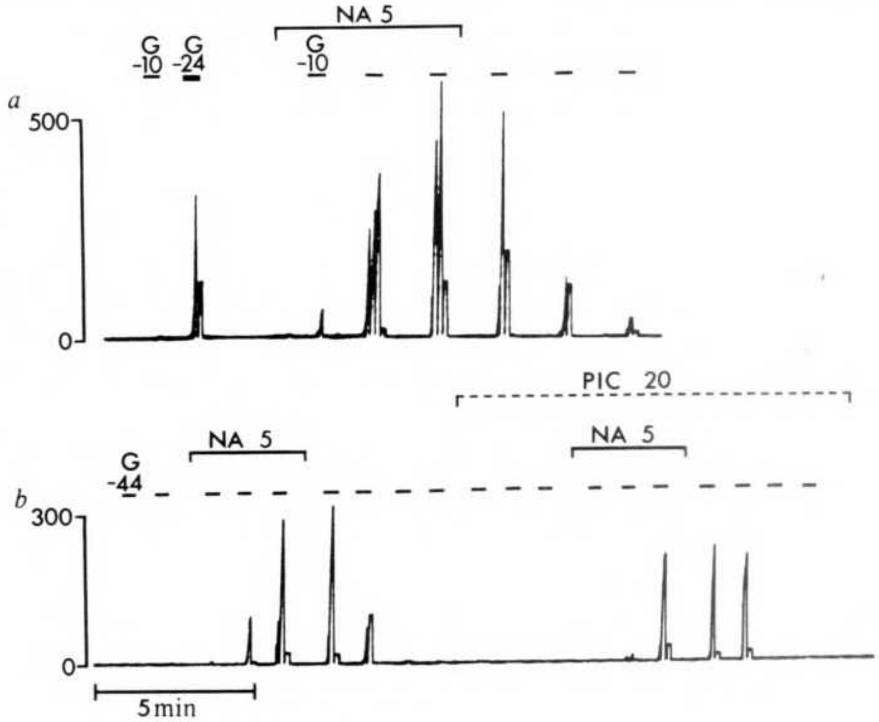

Fig. 2 NA facilitation of glutamate (G)-induced excitation in conditions of suppressed spontaneous activity. *a*, Constant current, 30-s pulses of G were applied to a 'silent' neurone in an acutely optic nerve-sectioned rat. NA causes a reversible potentiation of the response to subthreshold G. In this and subsequent examples, silent neurones were identified by optic chiasm stimulation or iontophoresis of G. Unit activity is expressed as an average rate histogram where the ordinate indicates the number of spikes per 10-s epoch. Duration of iontophoretic ejections are indicated by bars above each record. Numbers refer to iontophoretic currents in nA. *b*, Response of another cell demonstrating that NA but not picrotoxin (PIC) facilitates the action of G (20-s pulses). Note that during the PIC ejection the response to NA is slightly diminished rather than enhanced as would be predicted if the cell were under tonic GABA inhibition.

These observations suggest that the facilitatory action of NA is not mediated transynaptically via adjacent interneurones, although suppression of either class of inhibitory neurone could play a role in the overall physiological action of the coeruleo-geniculate pathway.

To confirm that activity in the coeruleo-geniculate pathway can produce similar effects on cellular excitability as iontophoretically applied NA, we examined the response of LGNd neurones to electrical stimulation in the region of the LC. Concentric bipolar stimulating electrodes were implanted in or

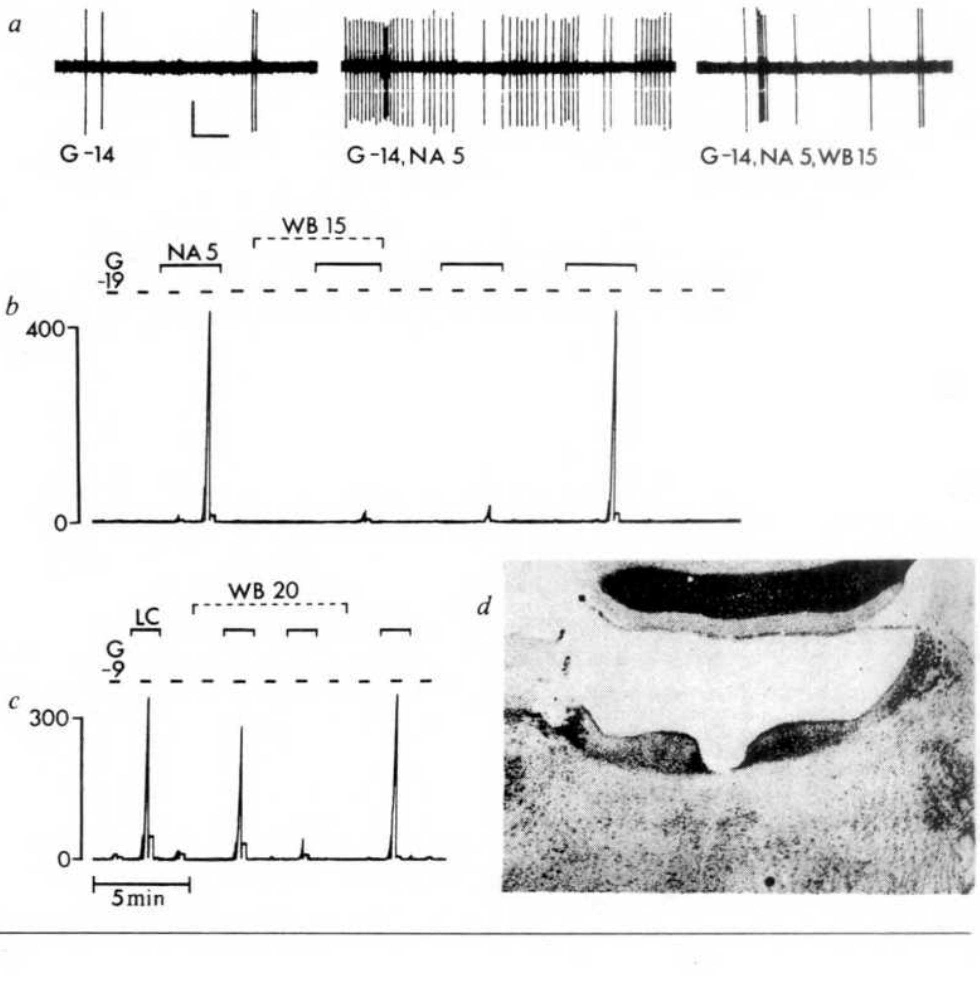

Fig. 3 Blockade by WB-4101 (WB) of the facilitatory actions of NA (*a*, *b*) and LC stimulation (*c*). *a*, Storage oscilloscope tracings of the extracellular spike records of a 'silent' unit in an acutely optic nerve-sectioned rat. The cell was activated by glutamate (G) (left panel) and this response was enhanced by NA (middle panel). WB applied for 16 min antagonized the effect of NA (right panel). Note that the spike amplitude is unaltered during prolonged application of WB. *b*, Rate histogram demonstrating the effect of WB on another cell. *c*, Blockade by WB of LC stimulation-induced facilitation of G in a third cell. LC stimulation does not activate the cell in the absence of G. Stimulation parameters: 0.5 mA, 1 ms, 10 Hz (NE-100 electrode, Rhodes Medical Instruments). *d*, Electrolytic lesion produced at tip of stimulating electrode (20 μA for 20 s) indicating typical placement in LC. Cresyl violet stained, 50-μm thick coronal section of formalin-fixed tissue. Position of the electrode tract is marked with an arrow. The arrowhead points to the contralateral LC. V, IVth ventricle. Calibration bar, 1 mm.

alongside the ipsilateral LC (Fig. 3*d*). Spontaneously active cells in normal animals invariably responded to trains of stimuli applied to the LC (1 ms duration, 10 Hz, 0.3–0.8 mA) with a dramatic increase in firing rate. As with NA iontophoresis, the effect of LC stimulation was delayed in onset (requiring 1–30 s to attain a peak response) and sustained beyond the duration of the stimulus (up to 20 s). In contrast to the effects on spontaneously active cells, 'silent' cells in optic nerve-sectioned animals were not activated directly by LC stimulation. However, as with iontophoretic NA, LC stimulation markedly enhanced the excitatory action of glutamate (five cells) (Fig. 3*c*).

For further evidence that LC stimulation and iontophoretic NA evoke identical postsynaptic actions, we examined whether the enhanced excitability each produced was sensitive to the α-adrenoceptor antagonist WB-4101. In four cells, WB-4101 at currents of 15–30 nA produced a blockade of the facilitatory action of NA (5 nA) (Fig. 3*b*). Spike amplitude was unaffected by WB-4101 (Fig. 3*a*) suggesting that local anaesthetic effects do not occur at the doses used. Similar iontophoretic currents also markedly attenuated the facilitatory action of LC stimulation (three cells) (Fig. 3*c*). As both the responses to LC stimulation and iontophoretic NA are antagonized by WB-4101, we conclude that the effects of stimulation of the LC are mediated by NA released from the terminals of noradrenergic fibres located in the vicinity of LGNd neurones.

These results support the concept that brain noradrenergic neurones act primarily to modify the responsiveness of their target cells to convergent inputs carried by other afferent channels[18]. This phenomenon has been termed 'neuromodulation' to distinguish it from the action of the conventional neurotransmitters which produce direct excitation or inhibition[19,20]. Modulatory transmitters typically have little effect on cellular activity in themselves and the changes in excitability they produce are usually slow to develop and prolonged in duration. The properties of NA action in the LGNd are those of neuromodulation and exemplify a common neuromodulatory role of monoaminergic neurotransmitters in invertebrate[21–25] and vertebrate[18,26–30] nervous systems. However, an understanding of the detailed cellular mechanisms mediating the facilitatory actions of NA on LGNd neurones requires analysis with intracellular recording techniques.

This work was supported by USPHS grants MH 17871, MH 14459 and GM 7324, and by the State of Connecticut.

Received 15 November, 1979; accepted 11 August 1980.

1. Burke, W. & Cole, A. M. *Rev. physiol. biochem. Pharmac.* **80,** 105–166 (1979).
2. Kromer, L. F. & Moore, R. Y. *Neuroscience* **5,** 255–271 (1980).
3. Nakai, Y. & Takaori, S. *Brain Res.* **71,** 47–60 (1974).
4. Rogawski, M. A. & Aghajanian, G. K. *Brain Res.* **169,** 11–27 (1980).
5. Kapur, H. & Mottram, D. R. *Biochem. Pharmac.* **27,** 1879–1880 (1978).
6. Burke, W. & Sefton, A. J. *J. Physiol.* **187,** 201–212 (1966).
7. Curtis, D. R. & Davis, R. *Br. J. Pharmac.* **18,** 217–246 (1962).
8. Tebēcis, A. K. & DiMaria, A. *Expl Brain Res.* **14,** 480–493 (1972).
9. Satinsky, D. *Int. J. Neuropharmac.* **6,** 387–397 (1967).
10. Fuxe, K. *Acta physiol. scand.* **64,** suppl. 247, 37–85 (1965).
11. Palkovits, M., Brownstein, M. & Saavedra, J. M. *Brain Res.* **80,** 237–249 (1974).
12. Freund, H.-J. in *Handbook of Sensory Physiology* Vol. VII/3B (ed. Jung. R.) 177-246 (Springer, Berlin, 1973).
13. Bishop, P. O., Burke, W. & Davis, R. *J. Physiol.* **162,** 409–431 (1962).
14. Sumitomo, I., Nakamura, M. & Iwama, I. *Expl Neurol.* **51,** 110–123 (1976).
15. Sumitomo, I. & Iwama, I. *Jap. J. Physiol.* **27,** 717–730 (1977).
16. Sterling, P. & Davis, T. L. *J. comp. Neurol.* **192,** 737–749 (1980).
17. Lieberman, A. R. *Brain Res.* **59,** 35–59 (1973).
18. Woodward, D. J., Moises, H. C., Waterhouse, B. D., Hoffer, B. J. & Freedman, R. *Fedn Proc.* **38,** 2109–2116 (1979).
19. Florey, E. *Fedn Proc.* **26,** 1164–1178 (1967).
20. Kupferman, I. *A. Rev. Neurosci.* **2,** 447–465 (1979).
21. Kupferman, I. *et al. Fedn Proc.* **38,** 2095–2102 (1979).
22. Evans, P. D., Talamo, B. R. & Kravitz, E. A. *Brain Res.* **90,** 340–347 (1976).
23. Evans, P. D. & O'Shea, M. *Nature* **270,** 257–259 (1977).
24. Swann, J. W., Sinback, C. N. & Carpenter, D. O. *Brain Res.* **157,** 167–172 (1978).
25. Berry, M. S. & Pentreath, V. W. *J. exp. Biol.* **65,** 361–380 (1976).
26. McCall, R. B. & Aghajanian, G. K. *Brain Res.* **169,** 11–27 (1979).
27. Libet, B. *Life Sci.* **24,** 1043–1058 (1979).
28. Wood, J. D. & Mayer, C. J. *J. Neurophysiol.* **42,** 582–593 (1979).
29. Foote, S. L., Freedman, R. & Oliver, A. P. *Brain Res.* **86,** 229–242 (1975).
30. Segal, M. & Bloom, F. E. *Brain Res.* **107,** 513–525 (1976).

ATP mediates rapid reversal of cyclic GMP phosphodiesterase activation in visual receptor membranes

P. A. Liebman* & E. N. Pugh Jr†

* Department of Anatomy and †Department of Psychology,
University of Pennsylvania, Philadelphia, Pennsylvania 19104

Weak or strong lights will activate visual receptor rod disk membrane (RDM) cyclic GMP phosphodiesterase (PDE) in the presence of GTP cofactor[1,2]. A similarly activated GTPase can exhaust small amounts of initially present GTP to deactivate the PDE. However, further additions of GTP reactivate PDE without more light, and deactivation by simple GTP depletion takes minutes or more, even at GTP concentrations 100 to 1,000 times lower than physiological levels[1,2]. A more rapid deactivation mechanism must exist if modulation of cytoplasmic cyclic GMP by light is to play a role on the time scale (seconds) of events in vision[3,4]. We report here that ATP is essential to such rapid control and that its presence permits multiple cycles of activation–deactivation. The complete control mechanism seems to involve gamma phosphate transfer from both ATP and GTP.

Bovine RDM suspensions were prepared from fresh or frozen retinas in IR light using standard procedures[5]. Cyclic GMP PDE activity was measured continuously using a fast recording *p*H meter to assay the stoichiometric production of protons[6], in the reaction

$$H_2O + cGMP^{-1} \rightleftharpoons 5'GMP^{-2} + H^+$$

A xenon photoflash equipped with calibrated attenuator filters was used to activate PDE. Light titration of the hydrolytic velocity with GTP cofactor showed saturation kinetics with half-maximal activation at bleaches of 1 part in 10,000–20,000. For all experiments reported here, the activating bleach was kept at 1 part per 50,000, within the linear range of the hydrolytic velocity response to the bleaching stimulus[3].

Figure 1, curve *a*, shows the formation of protons associated with cyclic GMP hydrolysis on flash activation in the presence of 60 μM GTP. Given sufficient substrate, cyclic GMP, the hydrolysis seen in curve *a* continues for more than 2 min while curves *b* and *c* show that a pulse of 8 μM ATP can arrest or 'quench' the activity within a few seconds anytime after the light activation. If this quenching effect were due to ATP competitive inhibition at the GTP binding site, one might expect ATP to be even more effective if added before the flash. This is not the case as seen in curve *d*. Activation takes place just as in the previous curves and is quenched with the same delay. Curve *e* shows that 8 μM ATP alone cannot support activation but that quenching has still occurred, as subsequent addition of GTP at times exceeding the characteristic quench delay shown in *b*, *c* and *d* can no longer produce activation. Yet after the GTP is available, a flash again produces a normal activation–quench cycle. Curve *f* and its derivative, *g*, show that this cycle can be repeated indefinitely.

In previous work, it was shown that the GTP analogues, GMP-PNP and GMP-PCP, are efficient cofactors of activation[1,2]. However, Fig. 2*A* shows that activation with GMP-PNP is not efficiently quenched by ATP (compare curves *a* and *e*). Nor is it possible to quench GTP-mediated activation using the ATP analogue, AMP-PNP (curve *b*). Instead, AMP-PNP competitively blocks the action of ATP (curve *d*).

Figure 2*B* shows that the efficiency of quench increases with ATP concentration. We find (Fig. 2*C*) that GTP alone can quench PDE activity, though both required concentration and maximum effectiveness show it to be a poor substitute for ATP. The quench process has a K_m of about 4 μM for ATP and about

0028–0836/80/430734—03$01.00

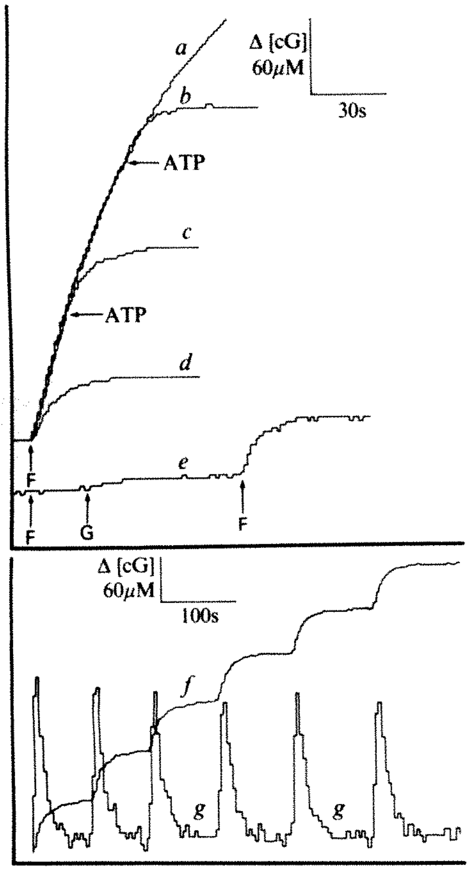

Fig. 1 Stoichiometric proton release with cyclic GMP hydrolysis following a flash, F, of 1-ms duration that bleaches 2.4×10^{-5} rhodopsin in presence of 60 µM GTP cofactor (*a–d*). Curves *b–d*, 8 µM ATP was injected at 25 s, 15 s or −5 s. Curve *e*, no GTP present until G, 23 s after flash, but ATP present at −5 s before flash. Curve *f*, cyclic GMP hydrolytic response to series of flashes in presence of 1 mM GTP/3 mM Mg-ATP. Curve *g*, derivative of trace *f* showing rise and fall of light-activated enzyme velocity. All traces from separate disk membrane samples containing 5 µM rhodopsin, 4 mM cyclic GMP, 2 mM $MgCl_2$, 150 mM KCl, 20 mM HEPES, 1 mM dithiothreitol, *p*H 7.9, $T = 32.4$ °C. Buffer limited *p*H change to 0.1 unit per 1 mmol H^+ added. 100 µM HCl or cyclic GMP gave equal deflections after hydrolysis of the latter in activated preparations. Membranes were from frozen retinas for this and subsequent figures. Fresh material gave nearly identical results.

1,400 µM for GTP. In addition, the V_{max} ratio of ATP to GTP in this process is about 2. Thus, the specificity V_{max}/K_m for quenching is about 700 times greater for ATP than for GTP.

It has been shown previously that rhodopsin is phosphorylated on bleaching in the presence of a membrane-bound kinase and ATP[7,8]. The K_m and specificity of this kinase for both ATP and GTP are close to those of the quenching process reported here[9]. No other protein is known to be phosphorylated on RDMs. We propose that the quenching process reported here, which terminates the potency of bleached rhodopsin to activate PDE, is opsin phosphorylation. A function for opsin phosphorylation has not been previously established.

The results of this and earlier work[2,3] suggest that light initiates a cycle of activation and deactivation of PDE according to the following scheme:

$$\text{Activation}\begin{cases}(1)\quad h\nu + \text{R} \rightarrow \text{R}^* \\ (2)\quad \text{R}^* + \text{D} \rightleftharpoons \text{R}^*\text{D} \\ (3)\quad \text{R}^*\text{D} + \text{GTP} \rightleftharpoons \text{R}^*\text{DGTP} \rightleftharpoons \text{R}^* + \text{D}^*\text{GTP}\end{cases}$$

$$\text{D}^*\text{GTP}\ \begin{matrix}\text{cyclic GMP}^{-1}\\ \searrow 5'\text{GMP}^{-2} + \text{H}^+\end{matrix}$$

$$\text{Deactivation}\begin{cases}(4)\quad \text{R}^* + n\text{ATP} \xrightarrow[\text{kinase}]{} \text{RP}_n + n\text{ADP} \\ (5)\quad \text{D}^*\text{GTP} \xrightarrow[\text{G'ase}]{} \text{D} + \text{GDP} + \text{P}\end{cases}$$

R* is the long-lived activator formed by the bleaching of rhodopsin, R. It can be quickly made inactive by phosphorylation [reaction (4)] as suggested by this report. While active, it can bind an inactive PDE molecule, D, and catalyse the binding of GTP to it or to a separate GTP-binding protein which in turn activates D by complexing with it to yield D*GTP (ref. 10). The active diesterase, D*GTP, then hydrolyses cyclic GMP until it also is deactivated by action of a GTPase that is specific for the bound form of GTP.

In this scheme, it is apparent why GTPase alone is not capable of deactivating D*, for the trigger molecule, R*, is still present and able to mediate activation again and again until it is deactivated by the kinase reaction. The gamma-phosphate lability of both GTP and ATP is required for fully reversible PDE activity: AMP-PNP does not permit R* to be phosphorylated and GMP-PNP does not permit GTPase to release the bound cofactor to terminate D* activity. After the activator, R*, is quenched, a GTPase specific for the bound GTP of the complex D*GTP

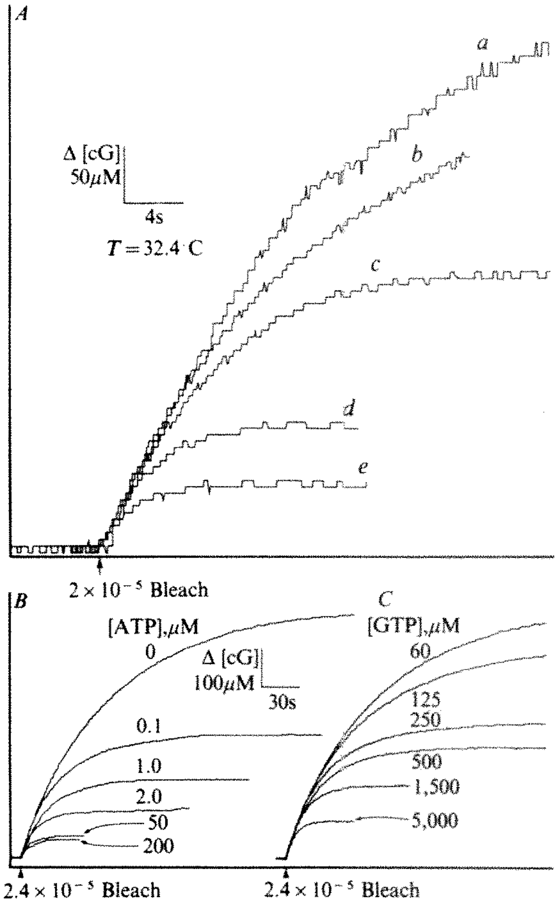

Fig. 2 *A*, Effect of ATP and GTP analogues on quench. Curve *a*, 500 µM GMP-PNP + 5 µM ATP; curve *b*, 50 µM GTP + 100 µM AMP-PNP; curve *c*, 50 µM GTP; curve *d*, 50 µM GTP + 5 µM ATP + 100 µM AMP-PNP; curve *e*, 50 µM GTP + 5 µM ATP. *B*, ATP titration of quench effect. The parameter labelling the curve is the concentration of ATP, in µM. 60 µM GTP present for all curves and ATP added 2 s before flash. *C*, GTP titration of quench effect (no ATP present). Flash F, as described in Fig. 1 legend.

could terminate activity even in the presence of large amounts of ambient but unbound GTP. Thus, the deactivator role of GTPase is not mediated via the cytoplasmic GTP depletion implied by previous work[1,2].

It is worthwhile to compare the mechanism proposed here with that of hormonally activated adenylate cyclase, also known to require GTP cofactor[11]. Both systems activate effectively in GMP-PNP[12] and neither can deactivate without the action of a membrane-bound GTPase[13]. As in RDM, however, it should not be possible for GTPase to deactivate the cyclase mechanism alone. The hormone–receptor complex needs to be deactivated as well. Reduction of blood hormone concentration alone might in some cases lead to adequate dissociation of the hormone–receptor complex to complete the deactivation on a time scale appropriate to needs for control. However, to achieve more rapid regulation, a hormone–receptor might be quenched by phosphorylation in a process similar to that which quenches the capacity of rhodopsin to activate RDM phosphodiesterase.

This work was supported by NIH grants EY00012, EY01583, RR07083 and EY00102.

Received 20 May; accepted 11 August 1980.

1. Wheeler, G. L. & Bitensky, M. W. *Proc. natn. Acad. Sci. U.S.A.* **74,** 4238–4242 (1977).
2. Yee, R. & Liebman, P. A. *J. biol. Chem.* **253,** 8902–8909 (1978).
3. Liebman, P. A. & Pugh, E. N. Jr *Vision Res.* **19,** 375–380 (1979).
4. Miller, W. H. & Nicol, G. D. *Nature* **280,** 64–66 (1979).
5. Hubbard, R., Brown, P. K. & Bownds, D. *Meth. Enzym.* **18,** 615–653 (1971).
6. Liebman, P. A. & Evanczuk, A. T. (in preparation).
7. Kühn, H. & Dreyer, W. J. *FEBS Lett.* **20,** 1–6 (1972).
8. Bownds, D., Dawes, J., Miller, J. & Stahlman, M. *Nature* **237,** 125–126 (1972).
9. Shichi, H. & Somers, R. L. *J. biol. Chem.* **253,** 7040–7046 (1978).
10. Shinozawa, T., Sen, I., Wheeler, G. & Bitensky, M. *J. supramolec. Struct.* **10,** 185–190 (1979).
11. Rodbell, M., Birenbaumer, L., Pohl, S. L. & Krans, H. M. J. *J. biol. Chem.* **246,** 1877–1882 (1971).
12. Pfeuffer, T. & Helmreich, E. J. M. *J. biol. Chem.* **250,** 867–876 (1975).
13. Cassel, D. & Selinger, Z. *Biochem. biophys. Res. Commun.* **452,** 538–551 (1976).

Localization of metabolites in animals using ^{31}P topical magnetic resonance

R. E. Gordon*, P. E. Hanley*, D. Shaw*, D. G. Gadian†, G. K. Radda†, P. Styles†, P. J. Bore† & L. Chan‡

* Oxford Research Systems, Ferry Hinksey Road, Oxford OX2 0DT, UK
† Department of Biochemistry, Oxford University, South Parks, Oxford OX1 3QU, UK
‡ Nuffield Department of Clinical Biochemistry, Radcliffe Infirmary, Oxford OX3 9OU, UK

High-resolution phosphorous (^{31}P)-NMR spectra of biological molecules provide detailed information about the metabolism of living systems[1–4]. Although the NMR method is non-destructive, all studies so far, with two exceptions[5,6], have been carried out on excised, perfused organs and tissues or have required some form of surgery[2] for *in situ* measurements. The use of 'surface' radiofrequency coils[5] does not require surgery but is best suited for tissues close to the surface of the animals. We describe here 'topical magnetic resonance'—a new, non-surgical method for acquiring ^{31}P-NMR spectra from a selected, localized place deep within an animal by modifying the main magnetic field, B_0, using only static-field gradients. The method is conceptually similar to one spin-imaging method[7] but primarily provides biochemical rather than spatial information. This new technique can be used in fundamental investigations into living systems, clinical diagnosis and the estimation of the efficacy of drug therapy.

To limit the volume from which the high-resolution ^{31}P-NMR signals are received, the effective homogeneous volume of B_0 must be reduced and centred on the region of interest. The topical magnetic resonance (TMR) technique consists of superimposing high-order, static magnetic field gradients on to B_0 via room-temperature magnetic field profiling coils mounted coaxially inside the bore of the magnet.

The magnetic field, $\beta(r, \theta)$, generated by a profile-coil system with azimuthal symmetry, can be described in terms of a Taylor expansion about the origin[8],

$$\beta(r, \theta) = \sum_{n=0}^{\infty} \beta_n r^n P_n(\cos\theta) \qquad (1)$$

where $\beta(r, \theta)$ is the magnetic field at (r, θ), $P_n(\cos\theta)$ are the Legendre polynomials of order n, and the field derivatives, β_n, are defined by the coil geometry and the d.c. current flowing through the coil system. A sensitive volume of homogeneous field can be delineated, centred on the origin and surrounded by inhomogeneous field gradients. A detailed discussion of the rationale of coil design will be given elsewhere.

The description of the magnetic field profile is simplified if only fields along the z-axis ($r = z$, $\theta = 0$) are considered. In a coil system of maximum order $n = 4$ where $\beta_0 = 0$ and β_4 is negative, the resultant profile along the z-axis produced by the sum of B_0 and $\beta(z)$ is shown in Fig. 1.

The inhomogeneity, ΔB, across the central region of axial extent, $2a$, is given by:

$$\Delta B = \frac{\beta_2^2}{2\beta_4} \qquad (2)$$

where

$$2a = 3.1\left(\frac{\beta_2}{\beta_4}\right)^{1/2} \qquad (3)$$

By varying β_2 and β_4 the sensitive volume can be adjusted to match that of the centrally placed region within any given object.

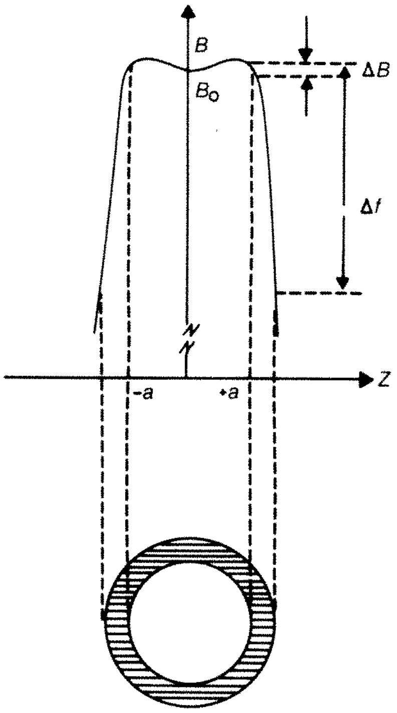

Fig. 1 The profile of the magnetic field along the z-axis in TMR. The inhomogeneity, ΔB, within the central region shown schematically in the projection below, is constrained to remain less than the typical ^{31}P linewidths. In the shaded region the ^{31}P lines will be broadened by the field gradients.

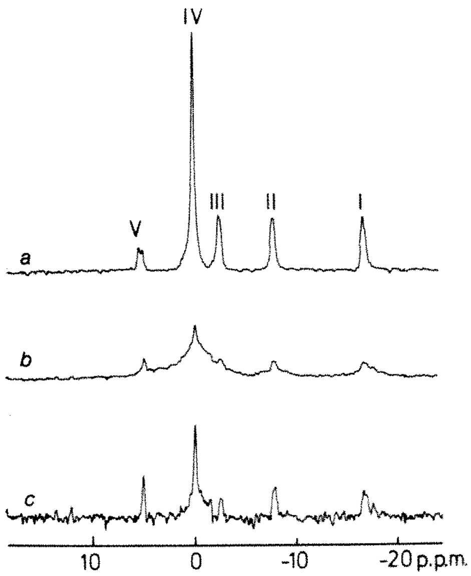

Fig. 2 ^{31}P-NMR spectrum of a two-compartment phantom containing ATP (signals I, II and III), phosphocreatine (IV) and inorganic phosphate (V). A single-turn saddle-shaped radiofrequency coil operating at 73.8 MHz was used in a standard wide-bore (89 mm) superconducting magnet. Profiling was obtained with a coil system designed to provide spatial localization across an internal volume ($2a \sim 15$–45 mm) whilst maintaining a homogeneity of ~ 0.1 p.p.m. at an operating B_0 field of 4.3T. The working bore of the system was 45 mm. The spherical compartment contained 4.65 mM ATP, 9.30 mM PCr and 3.72 mM P_i, and the cylindrical compartment contained 4.65 mM ATP, 18.60 mM PCr and 1.86 mM P_i. *a*, Spectrum (300 scans) in the absence of localizing fields. A 6-Hz line broadening exponential multiplication was used to enhance the signal-to-noise ratio. *b*, Spectrum (600 scans) with the axial extent reduced to 20 mm. The same line broadening was used as in *a*. *c*, Spectrum obtained on removing the broad component of spectrum *b* by convolution difference[9]. Line broadenings of 6 and 60 Hz were used and the vertical scale in the spectrum was multiplied by 4 for clarity of presentation. Chemical shifts are defined as positive in the high-frequency direction with phosphocreatine taken as an internal reference.

Adjacent to the sensitive volume lie regions where the magnetic field changes vary rapidly with position, causing broadening of the spectral lines. The radiofrequency coil will receive signals from the whole sample so the total signal will contain both the narrow, high-resolution lines and the inhomogeneously broadened lines which must be separated out to recover the high-resolution spectrum of the sensitive volume.

Experiments were carried out on a two-compartment test phantom consisting of a cylindrical compartment of diameter 30 mm surrounding a spherical compartment of diameter 20 mm, each containing ATP, phosphocreatine (PCr) and inorganic phosphate (P_i) (for concentrations, see Fig. 2 legend), dissolved in 150 mm KCl to simulate the electrical conductivity of tissue. The internal *p*H was adjusted to be 0.35 units less than that of the external *p*H, thereby producing a chemical shift difference between the P_i resonant frequencies of the two samples.

The spectrum of the sample was obtained with the axial extent set to 45 mm (Fig. 2*a*). The three ATP peaks and the PCr peak are unaffected by the difference in *p*H, whereas two clearly distinguishable P_i peaks appear. Using the PCr peak as a reference, the internal and external P_i peaks correspond to *p*H values of 7.10 and 7.45 respectively. The P_i concentration ratio measured from the peak areas is in good agreement with the expected value.

When the axial extent is reduced to 20 mm, a broad component at the base of each peak arises from the metabolites in the external compartment, which now lie in a region of inhomogeneous magnetic field (Fig. 2*b*). This broad signal is eliminated using the convolution difference technique[9] (Fig. 2*c*). The narrow peaks correspond to the metabolites present only in the spherical compartment, and the *p*H of the P_i peak in this spectrum is 7.10, in agreement with the position measured previously.

To demonstrate the potential of the method in animal experiments, we have studied the liver of a live rat. In the spectrum obtained from the rat in the absence of any localizing fields, the ATP and PCr peaks are readily identifiable, but the P_i and the sugar-phosphate region of the spectrum is less readily assigned because the 2,3-diphosphoglycerate from blood contributes two signals at ~ 5.0 and 6.5 p.p.m. and the first of these overlaps with the P_i signal (Fig. 3*a*). Blood contributes a negligible amount to the ATP peaks. Therefore the ATP signals arise primarily from liver and muscle tissue, the PCr arises exclusively from muscle, whereas the signals in the P_i and sugar-phosphate region may have contributions from liver, muscle and blood.

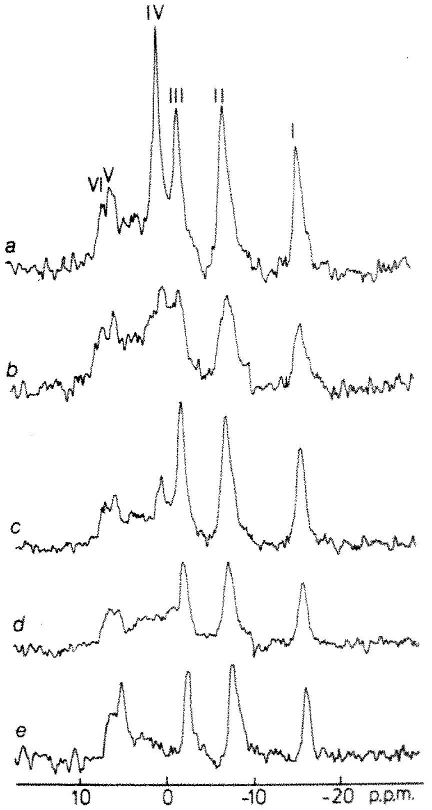

Fig. 3 Spectra *a–d* were obtained from an intact rat anaesthetized with pentabarbitol. 150-g male Wistar rats, starved for 24 h, were used for all experiments. Signal assignments are: I, II and III, the β-, α- and γ-phosphate, respectively, of ATP; IV, phosphocreatine; V, inorganic phosphate; VI, sugar phosphate, AMP and IMP. Peaks V and VI may also contain contributions from 2,3-diphosphoglycerate in the blood. Peak II contains a small contribution from ADP and peak III has contributions from ADP, NAD and NADH. *a*, Spectrum in the absence of localizing fields ($128 \times 90°$ pulses at 2-s intervals). *b*, The same as *a* with localization (axial extent 20 mm). *c*, Spectrum in the absence of localizing fields ($1{,}024 \times 90°$ pulses at 220-ms intervals). *d*, The same as *c* with localization (axial extent 20 mm). *e*, Spectrum of a perfused rat liver ($480 \times 90°$ pulses at 220-ms intervals). For clarity of presentation the spectra in *c* and *d* were divided by 4. The broad components were eliminated using the convolution difference technique[9] with line broadenings of 16 and 233 Hz. Chemical shifts are defined as positive in the high-frequency direction, and phosphocreatine is taken as an internal reference. Measurement of T_1, using progressive saturation technique[11], on the β-phosphate resonance of ATP gave a value of 0.14 s in the presence of localizing fields. This is characteristic of ATP in liver. The remaining small PCr signal in *b* is likely to arise from the diaphragm.

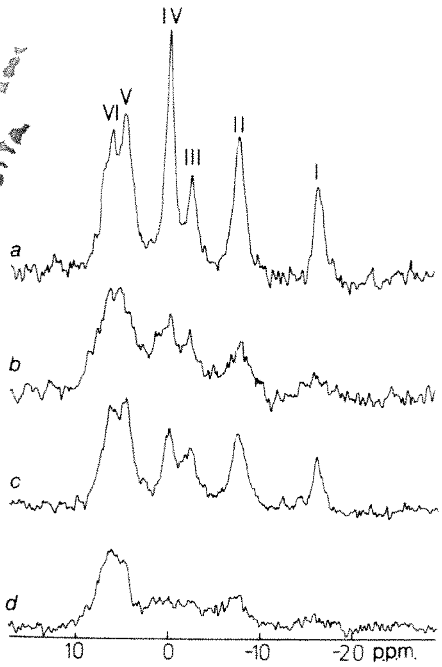

Fig. 4 ^{31}P-NMR spectra of a rat after surgery to cut off the hepatic blood supply. The spectrometer conditions were the same as in Fig. 3 legend. Spectra *a–d* are analogous to spectra *a–d* of Fig. 3.

The sensitive volume was reduced ($2a = 20$ mm) and the resulting TMR spectrum is shown in Fig. 3*b*. The smaller peak intensities indicate that now high-resolution signal is being acquired from a smaller volume, and as the spectra of Fig. 3*a* and *b* were obtained with the same spectrometer conditions, there will be an inevitable reduction in signal-to-noise ratio. Nevertheless, a change in the relative proportions of the metabolite resonances is apparent.

The spectra of Fig. 3*a* and *b* were obtained using a radiofrequency pulse interval of 2 s, which is typical for ^{31}P-NMR studies of whole tissue. Figure 3*c* shows a spectrum obtained with a pulse interval of 220 ms, in the absence of localizing fields. The PCr peak intensity is now significantly reduced in comparison with its intensity in Fig. 3*a*, because its spin–lattice relaxation time, T_1, is long (~ 3 s). The reduction in the ATP peak intensities is far less, as the ATP in tissues such as muscle has a rather shorter relaxation time (~ 1–2 s), and also because a significant percentage of the ATP is in the liver, and liver ATP has very short T_1 values (~ 100 ms)[10]. Figure 3*d* shows the spectrum obtained using the short pulse interval with the reduced sensitive volume ($2a = 20$ mm). This spectrum contains no PCr signal and is very similar to the spectrum of perfused liver shown in Fig. 3*e*, which was obtained using the same pulse interval of 220 ms. This suggests that the signals of Fig. 3*d* are predominantly from the liver. The improvement shown in Fig. 3*d* can only obtained using the localizing fields.

The P_i/ATP ratio is lower in the liver of the whole animal (Fig. 3*d*) than in the perfused liver (Fig. 3*e*). Previous NMR studies of the brain and skeletal muscle of whole rats also show remarkably low P_i levels[6].

By cutting off the hepatic blood supply of the animal using surgery, similar measurements were made on the same animal (Fig. 4). The marked reduction of ATP and increased levels of P_i after ligation (Fig. 4*b* and *d*) indicate unhealthy ischaemic liver, verifying the origin and interpretation of the previous TMR spectra. In contrast, the PCr signal intensity in Fig. 4*a* is very similar to that in Fig. 3*a* indicating that the metabolic state of the muscle is little affected by the operation.

Thus, we have identified *in vivo* liver tissue by the ^{31}P spectral characteristics and the relaxation time of the β-ATP resonance. Global liver ischaemia has been diagnosed in a non-invasive manner. The method is easily extended for the investigation of other organs of laboratory animals.

The work in the Department of Biochemistry was supported by the SRC and the British Heart Foundation. We gratefully acknowledge the work of J. R. Griffiths, R. A. Iles, R. Porteous and A. N. Stevens on perfused liver. Dr J. R. Griffiths provided the perfused rat liver spectrum.

Received 18 March, accepted 29 August 1980.

1. Radda, G. K. & Seeley, P. J. *A. Rev. Physiol.* **41,** 749–769 (1979).
2. Gadian, D. G., Radda, G. K., Richards, R. E. & Seeley, P. J. in *Biological Applications of Magnetic Resonance* (ed. Shulman, R. G.) 463–535 (Academic, New York, 1979).
3. Burt, C. T., Cohen, S. M. & Barany, M. *A. Rev. Biophys. Bioengng* **8,** 1–25 (1979).
4. *Phil. Trans. R. Soc.* B**289,** 379–559 (1980).
5. Chance, B., Nakase, Y., Bond, M., Leigh, J. S. & McDonald, G. *Proc. natn. Acad. Sci. U.S.A.* **75,** 4925–4929 (1978).
6. Ackerman, J. H. H., Grove, T. H., Wong, G. C., Gadian, D. G. & Radda, G. K. *Nature* **283,** 167–170 (1980).
7. Damadian, R., Minkoff, L., Goldsmith, M. & Koutcher, J. D. *Science* **194,** 1430 (1976).
8. Garrett, M. W. *J. appl. Phys.* **22,** 1091–1107 (1951).
9. Campbell, I. D., Dobson, C. M., Williams, R. J. P. & Xavier, A. V. *J. Magn. Reson.* **11,** 172–181 (1973).
10. McLaughlin, A. C., Takeda, H. & Chance, B. *Proc. natn. Acad. Sci. U.S.A.* **76,** 5445–5449 (1979).
11. Freeman, R. & Hill, H. D. W. *J. Chem. Phys.* **54,** 3367 (1971).

Excretion, isolation and structure of a new phenolic constituent of female urine

S. Roy Stitch*, Jack K. Toumba*, Marinus B. Groen†, Carel W. Funke†, Johannes Leemhuis†, Jan Vink† & Gilbert F. Woods‡

* Division of Steroid Endocrinology, Department of Chemical Pathology, University of Leeds, 26–28 Hyde Terrace, Leeds LS2 9LN, UK
† Scientific Development Group, Organon International, Oss, The Netherlands
‡ Scientific Development Group, Organon International, Newhouse, Lanarkshire, UK

The regular occurrence of a peak due to an unidentified substance (X) in the gas chromatographic traces obtained from phenolic extracts of urine from human pregnant and non-pregnant females has been reported[1]. The biphasic excretion of X with maxima in the luteal phase of the ovulatory cycle and relatively high levels in the first trimester of pregnancy were noteworthy and suggested that the substance may have a biological significance. Close similarities between the excretory pattern, the chemical and chromatographic properties of X and of those of the known phenolic steroids suggested initially that this compound was steroidal in nature. The same, or a similar, substance seems to be excreted in the vervet monkey (*Cercopithecus aethiops pygerythrus*)[2]. We now report the excretory pattern of X in more detail, the isolation of the pure compound from pooled pregnancy urine and the chemical structure. The structure determined by mass spectrometry, IR spectroscopy and NMR spectrometry is: *trans*-(±)-3,4-bis[(3-hydroxy phenyl)methyl]dihydro-2-(3H)-furanone (HPMF) and was confirmed by synthesis.

Sequential analyses were carried out on urine collected daily: (1) by volunteers throughout the normal ovulatory cycle; (2) when monitoring oestrogen excretion in patients who were being treated for anovulatory infertility following treatment with postmenopausal gonadotropin; and (3) when following the urinary excretion of oestrogens and of X from conception to term[3]. After acid hydrolysis of the urinary steroid and other conjugates, phenolic fractions were prepared, the extracts acetylated and analysed by gas liquid chromatography (GLC) using a Pye 104 gas chromatographic system[3]. Figure 1 shows

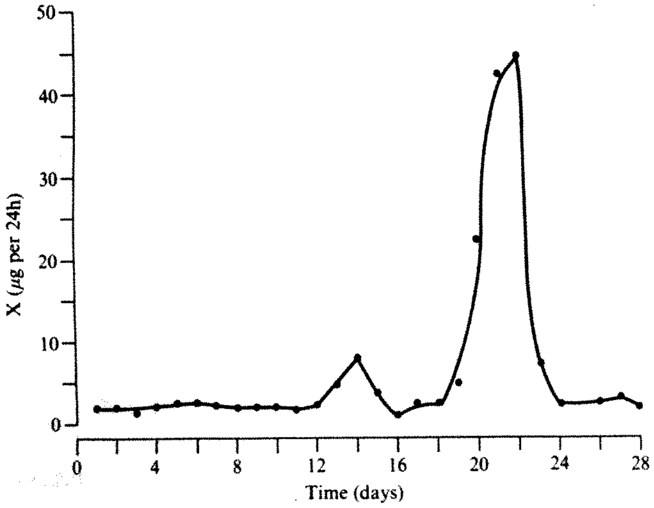

Fig. 1 Cyclic excretion of HPMF in a volunteer with normal ovulatory cycles. 24-h urine specimens were collected daily throughout the cycle and HPMF was extracted from each specimen as described in the text. The phenolic fraction was acetylated and subjected to GLC[3] on a Pye 104 gas chromatograph using a 1-m glass column packed with OVI on Gas Chrom Q Support (100–200 mesh). The oven temperature was maintained at 230 °C and the nitrogen carrier gas flow rate was 40 ml min^{-1}. Values obtained are uncorrected for losses which occurred during the chemical extraction and gas chromatography (~40%).

the biphasic excretion of X in a normal ovulatory cycle, maximum excretion being apparent in the luteal phase. In early pregnancy (Fig. 2) excretion of X exceeds that of oestrone, oestradiol or oestriol, but as pregnancy proceeds to term both the absolute excretion of X and the excretion of X relative to the steroidal oestrogens declines.

A purified sample of compound X (10 mg) was isolated for structural analysis from pooled urine (100 l) collected during the first trimester of normal pregnancies. The urine was processed in 2-l batches by passing through a column of XAD2 resin (BDH chemicals) and eluting first with distilled water and then with ethanol to give a fraction containing conjugates of the steroids and of compound X. The ethanol solution was evaporated to dryness under reduced pressure in a rotary evaporator, and the residue was heated on a steam bath for 1 h with aqueous hydrochloric acid (*p*H 1) to hydrolyse the conjugates. Saturated ammonium chloride was added, and the hydrolysed products were extracted into ether and washed with 8% sodium bicarbonate solution. The phenolic constituents were then extracted with 1 M NaOH solution which was acidified immediately with sulphuric acid. The crude phenolic product was extracted with diethyl ether and purified by chromatography on a column of Sephadex LH20 resin (Pharmacia) and elution with toluene : methanol (9 : 1, v/v). The fraction containing compound X was purified further by thin-layer chromatography on Kieselgel G (type 60, Merck) for 1.5 h with ethyl acetate : cyclohexane (1 : 1, v/v). Compound X (R_F 0.53) was located by spraying a test strip with Turnbull's blue solution (1% ferric chloride with 1% potassium ferricyanide [aqueous]), scraped from the plate, transferred to a small glass column and eluted with chloroform : methanol (1 : 1, v/v). The purity of the product was determined by GLC of a small sample after acetylation. From the IR, mass spectrometry and NMR spectra the structure of compound X was determined to be *trans*-(±)-3,4-bis[(3-hydroxyphenyl)methyl]dihydro-2-(3H)-furanone (HPMF, Fig. 3) on the following evidence.

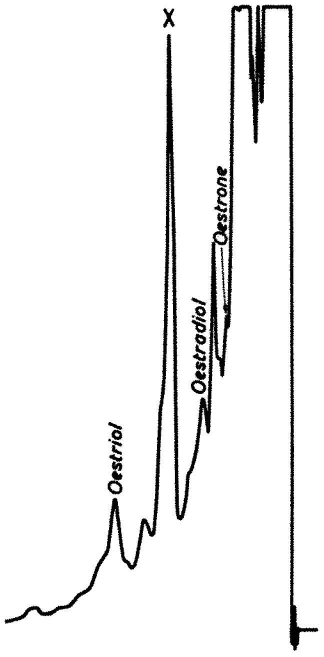

Fig. 2 HPMF was extracted from a 24-h urine specimen, obtained from a patient in the ninth week of pregnancy, as described in the text. The purified phenolic fraction was acetylated and subjected to GLC in the conditions described in Fig. 1 legend.

The formula $C_{18}H_{18}O_4$ was established from the mass spectrum by the parent peak at $m/e = 298.1193$ (calculated, 298.1205) and prominent peaks at $m/e = 107.0503$ (calculated for C_7H_7O, 107.0497) and 108.0583 (calculated for C_7H_8O, 108.0575) were indicative of $-CH_2C_6H_5OH$ groups. The presence of a γ-lactone (ν_{max} 1,770 cm^{-1}, C=O stretch) was evident from the IR spectrum. ^{13}C-NMR revealed signals characteristic of two similar but non-equivalent disubstituted aromatic rings (δ 113.9, 114.0, 115.7, 116.3, 121.1, 121.7, 130.0 and 130.0, aromatic =CH—). In the ^1H-NMR (200 mHz) spectrum, the aromatic region showed the presence of two non-equivalent *m*-hydroxyphenyl groups. In addition, the AB-parts of two ABX-systems centred at δ 4.0 ($J_{AB} = 9, J_{AX} \simeq J_{BX} \simeq 7$) and δ 2.96 ($J_{AB} = 14$, $J_{AX} = 5$, $J_{BX} = 6$) could be detected, arising from the partial structures $-OCH_2-CH\ R-$ and Ar CH_2CH-.

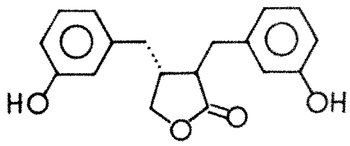

Fig. 3 Compound X; *trans*-(±)-3,4-bis[(3-hydroxyphenyl) methyl]dihydro-2-(3H)-furanone (HPMF).

The proposed structure (Fig. 3) is supported by ^1H-NMR data reported for closely related compounds and has been confirmed by synthesis (to be reported elsewhere)[4]. The racemic product (melting point 141–143 °C) was identical in all respects with the compound of natural origin. The absolute configuration and optical purity of the natural substance were determined by resolution of an intermediate (I) (Fig. 4) in the synthesis. The resolved compound (I) (Fig. 4) had $[\alpha]_D^{20} + 6.4°$ (1% in chloroform) and optically active HPMF prepared from it had a melting point of 125–129 °C and $[\alpha]_D^{20} - 38.4°$ (1% in chloroform). These values for the optical rotations compare favourably with reported values of +4.8° (ref. 5) and −34° (ref. 6) for the closely related compounds (II) and (III), respectively (Fig. 4). The specific optical rotations of samples of natural HPMF isolated from urine varied between 0° and −4° indicating an optical purity of ≤10%.

We have not detected HPMF in normal male urine and this, with the regularity of its cyclic excretion in women, leads to the conclusion that it is not of dietary origin. However, excretion of HPMF increases when anovulatory patients are treated with human menopausal gonadotropin. This and the pattern of its excretion during the menstrual cycle and in pregnancy suggest

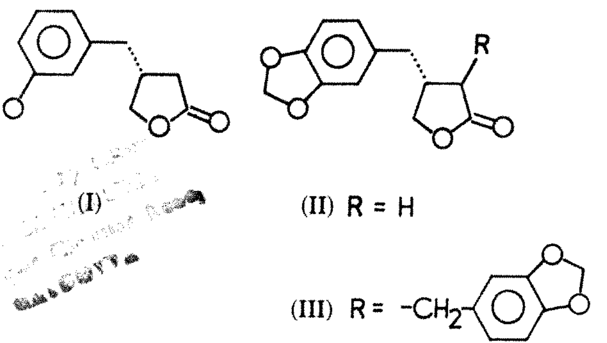

Fig. 4 Intermediate (I) and related compounds (II) and (III) in the synthesis of HPMF.

that there may be an ovarian source or stimulus for the production of HPMF. Investigations are now underway to establish the function and source of HPMF in the body and the biological properties of the synthetic substance. In this respect it is interesting that the same or a similar compound, and a substance with similar chemical and chromatographic properties seem to be excreted in the vervet monkey (*Cercopithecus aethiops pygerythrus*) during the reproductive cycle and in pregnancy[2].

Received 15 July; accepted 21 August 1980.

1. Stitch, S. R., Smith, P. D., Illingworth, D. & Toumba, K. *J. Endocr.* **85**, 23p (1980).
2. Setchell, K. D. R., Bull, R. & Adlercreutz, H. *J. Steroid Biochem.* **12**, 375-384 (1980).
3. Smith, P. D. & Stitch, S. R. *Clinica chim. Acta* **36**, 439-451 (1972).
4. British patent application nos 80.13.040, 21.4.80.
5. Kuhn, M. & von Wartburg, A. *Helv. chim. Acta* **50**, 1546-1565 (1967).
6. Grimshaw, J. in *Rodd's Chemistry of Carbon Compounds* Vol. IIID, 2nd edn (ed. Coffey, S.) Ch. 16, 258 (Elsevier, Amsterdam, 1976).

Lignans in man and in animal species

K. D. R. Setchell*, A. M. Lawson*, F. L. Mitchell*, H. Adlercreutz†, D. N. Kirk‡ & M. Axelson§

* Division of Clinical Chemistry, Clinical Research Centre,
Harrow, Middlesex, HA1 3UJ, UK
† Department of Clinical Chemistry, Meilahti Hospital,
University of Helsinki, Finland
‡ Department of Chemistry, Westfield College,
Hampstead, London NW3 7ST, UK
§ Department of Chemistry, Karolinska Institutet, Stockholm, Sweden

In our laboratories, for several years, two phenolic compounds have been detected during gas chromatographic–mass spectrometric analysis of urinary steroid extracts from human and animal species. Although features of the mass spectra of their trimethylsilyl (TMS) ether derivatives resembled those of oestrogens, they were atypical of steroids. The possibility that they were artefacts of the isolation procedures was discounted after careful studies with blanks, by varying the extraction method and because they were present almost exclusively as conjugates of glucuronic acid. Several of the general characteristics of the unknown compounds were reported[1,2] after one (referred to as compound 180/442) was found to have a cyclic pattern of excretion during the menstrual cycle of an adult vervet monkey (Fig. 1). An investigation of the nature and distribution of the compounds has shown them to be urinary constituents in humans, baboons, vervet monkeys and rats, and further related compounds have been detected, so far only in vervet monkey urine. We now report spectroscopic and chemical studies that show the two original compounds to be lignans, which have a 2,3-dibenzylbutane skeleton as their basic structure. Unlike all previously known natural lignans, invariably of plant origin, the two mammalian compounds carry phenolic hydroxy groups only in the *meta* position of the aromatic rings.

The two compounds are:

(I) 2,3-bis-(3′-hydroxybenzyl)-butyrolactone (referred to in previous reports[1,2] as compound 180/442).
(II) 2,3-bis-(3′-hydroxybenzyl)-butane-1,4-diol (referred to previously as compound 180/410).

Some related compounds subsequently found in the urine of the vervet monkey correspond to I and II but have additional methoxy substituents in one or both of the phenolic rings:

(III) 2-(3′-hydroxy-methoxybenzyl)-3-(3′-hydroxybenzyl)-butyrolactone.
(IV) 2-(3′-hydroxy-methoxybenzyl)-3-(3′-hydroxybenzyl)-butane-1,4-diol.
(V) 2,3-bis-(3′-hydroxy-methoxybenzyl)-butyrolactone.
(VI) 2,3-bis-(3′-hydroxy-methoxybenzyl)-butane-1,4-diol.

Several other compounds found in the urine of the vervet monkey appear from their physicochemical properties to be of related structure, but they have not been characterized.

The locations of the methoxyl groups in the phenolic rings of the relatively minor constituents (III–IV) remain to be established finally. In compound III the non-equivalence of the benzylic groups introduces uncertainty as to which aromatic ring contains the methoxyl function. Figure 2 illustrates the structural formulae of compounds I–VI. The evidence which led to the identification of I and II and the chemical synthesis which confirmed their structures are summarized here and will be described in detail elsewhere.

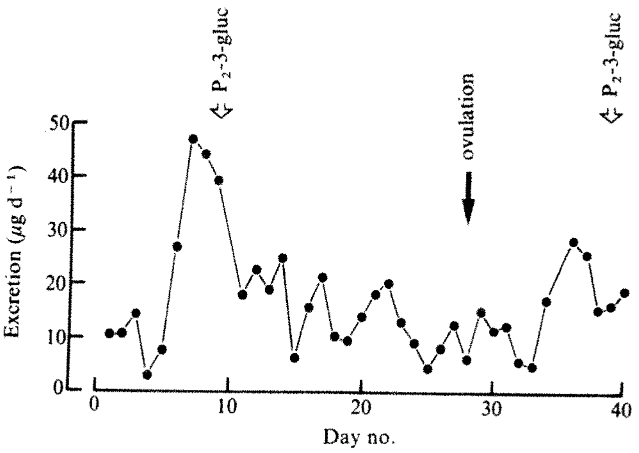

Fig. 1 Urinary excretion ($\mu g\ d^{-1}$) of 2,3-bis-(3′-hydroxybenzyl)-butyrolactone in a mature adult female vervet monkey (*Cercopithecus aethiops pygerythrus*) and its relationship to the time of ovulation and maximum corpus luteal activity determined from measurements of oestrone glucuronide and pregnanediol-3α-glucuronide (P_2-gluc), respectively[1].

Mass spectra of the TMS ether derivatives of compounds I and II isolated from human urine and those of chemically synthesized 2,3-bis-(3′-hydroxybenzyl)-butyrolactone and 2,3-bis-(3′-hydroxybenzyl)-butane-1,4-diol are illustrated in Fig. 3; they are identical. Some aspects of the fragmentation pattern of these spectra have been discussed previously[1]. The presence of the phenolic hydroxy group in the *meta* position is substantiated by the intense rearrangement ion at *m/z* 180. This ion is insignificant in TMS ether derivatives of *ortho* or *para* substituted lignan analogues and model compounds (work in preparation). The gas chromatographic (GC) characteristics of the TMS ether derivatives of the natural and synthetic compounds I and II on open-tubular glass capillary columns coated with silicone OV-1 were identical (retention times: (I, 27.50 methylene units (MU) and II, 27.70 MU). Accurate mass measurement of the molecular ions of the isolated compounds I and II showed their elemental composition to be $C_{18}H_{18}O_4$ and $C_{18}H_{22}O_4$ respectively in agreement with the structures shown in Fig. 2.

Nuclear magnetic resonance (NMR) spectra of the natural compounds I and II were compared with those of authentic

0028-0836/80/430740—03$01.00

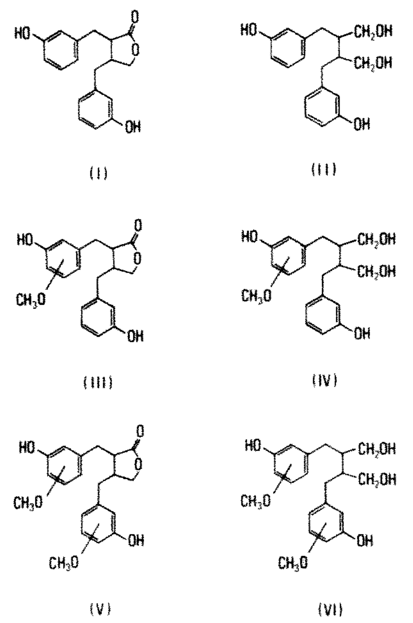

Fig. 2 Chemical formulae of newly identified lignans. Compounds I and II have been identified in the urine of humans, baboons, vervet monkeys and rats while III–VI have so far only been identified in vervet monkey urine[3]. All of these lignans have been identified in urine as glucuronide conjugates.

samples, respectively, of matairesinol dimethyl ether and dihydrocubebin (Fig. 4). The virtual identities of the high field regions of the pairs of spectra indicated the structures of the non-aromatic parts of the molecules I and II (Table 1). The aromatic regions of the spectra of I and II comprised complex multiplets split into two regions: a multiplet integrating for two protons, centred near 7.1 p.p.m., and a multiplet integrating for six protons, mainly between 6.6 and 6.8 p.p.m. A similar pattern found for some model *meta*-alkylated phenols indicated the location of the phenolic hydroxy groups in compounds I and II. The γ-lactone ring in compound I was further indicated by the infrared (IR) spectrum, with carbonyl absorption at 1,750 cm^{-1}.

Compounds I and II were synthesized by an adaptation of the traditional route to lignans of the 2,3-dibenzylbutane type[3,4]. A Stobbe condensation of 3-benzyloxybenzaldehyde (2 mol) with diethyl succinate (1 mol) gave bis-(3-benzyloxybenzylidene)-succinic acid. Catalytic hydrogenation, with simultaneous hydrogenolysis of the protecting benzyloxy groups, followed by reduction of the resulting 2,3-bis-(3'-hydroxybenzyl)-succinic acid with lithium aluminium hydride, and acidification, gave a mixture of products. Preparative thin layer chromatography (TLC) afforded samples which consisted essentially of 2,3-bis-(3'-hydroxybenzyl)-butyrolactone (I) and 2,3-bis-(3'-hydroxybenzyl)-butane-1,4-diol (II). The latter product appeared on the basis of GC and NMR data, to comprise a mixture of the *dl* and *meso* forms.

The TLC behaviour, and the IR spectra of the synthetic and natural compounds I and II, and the NMR spectra of the two samples of the dibenzylbutyrolactone (I), were indistinguishable. The NMR spectrum of the synthetic dibenzylbutanediol (II) contained all the features in the spectrum of the natural material, and some additional signals attributed to the presence of the *meso* isomer.

Compound I is of greatest interest at present because it is quantitatively the most important in human urine, plasma and bile and its daily urinary excretion is comparable to that of many steroid metabolites[2,5]. It is the most likely precursor of most of the other compounds in the series and can be reduced chemically to II. As indicated earlier it is present principally as a glucuronide conjugate[22], as are the other lignans identified in the series.

We found that the urinary excretion of the dibenzylbutyrolactone (I) increased significantly during the mid-luteal phase of the menstrual cycle and showed a marked surge in early pregnancy in humans[2,5] as well as the vervet monkey[1]. In four women the urinary excretion of I was at its minimum at the time of ovulation and then increased, reaching a maximum during the mid-luteal phase (Fig. 5). Furthermore, during pregnancy maximum excretion of dibenzylbutyrolactone occurs between weeks 14 and 22 of gestation[2,5]. A non-steroidal compound has been reported[6] to show similar urinary excretion patterns during the human menstrual cycle and in pregnancy.

The biosynthetic pathway of the lignans is not yet known, although their aromatic nature might suggest a dietary origin or formation by intestinal bacteria. Preliminary results, however, indicate that they may be ovarian in origin or that their production is influenced by ovarian function. For instance, in addition to the cyclic behaviour of compounds I and II[5], their excretion in a limited number of postmenopausal women studied was lower than in normally ovulating women, while in three ovariectomized/postmenopausal women excretion was approximately 5–10% of that in normal ovulating women. Because the compounds are barely detectable in the urine of newborn infants it seems that in pregnancy they are essentially maternal in origin.

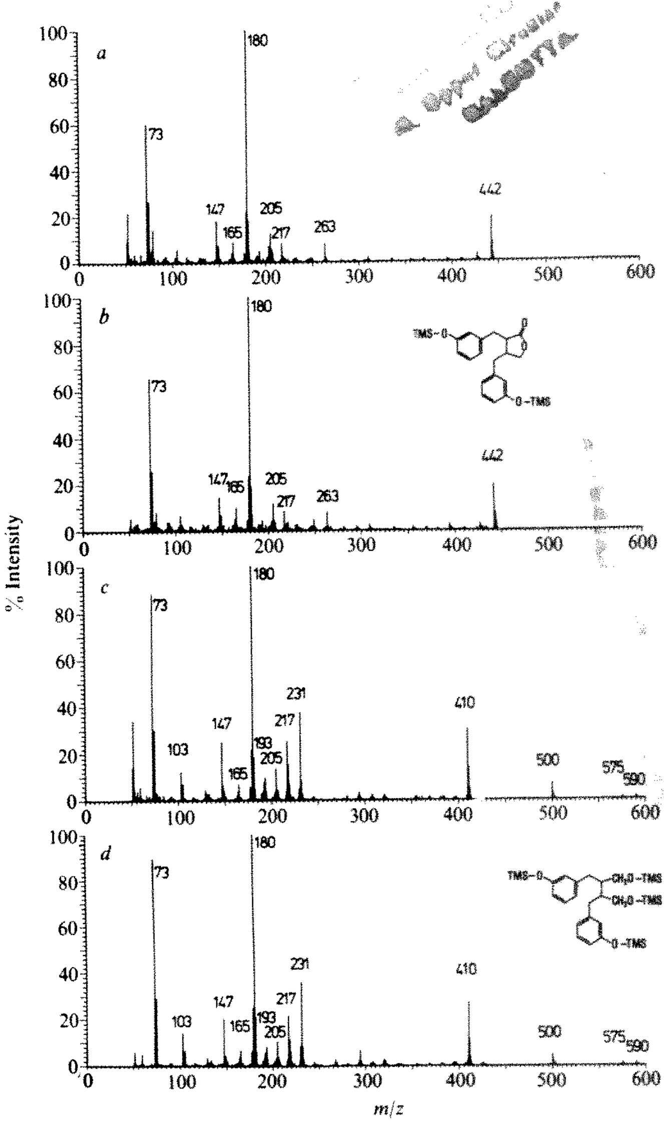

Fig. 3 Mass spectra of the TMS derivatives of: *a*, natural compound I; *b*, synthetic 2,3-bis-(3'-hydroxybenzyl)-butyrolactone; *c*, natural compound II and *d*, synthetic 2,3-bis-(3'-hydroxybenzyl)-butane-1,4-diol.

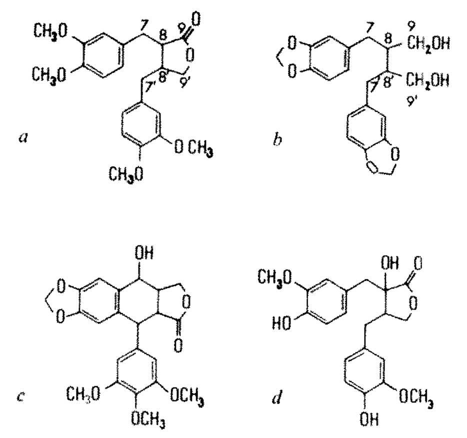

Fig. 4 Chemical structure of the lignans: *a*, matairesinol dimethyl ether; *b*, dihydrocubebin; *c*, podophyllotoxin; *d*, wikstromol.

Table 1 ^{1}H NMR spectra at 100 MHz in $CDCl_3$

Compound	H-7,7'*	H-8,8'*	H-9' or H-9,9'*
2,3-bis-(3'-hydroxybenzyl)-butyrolactone(I)	2.56 (8)	2.94 (9)	4.0 (about 34)
Matairesinol dimethyl ether	2.55 (8)	2.94 (9)	4.0 (about 30)
2,3-bis-(3'-hydroxybenzyl) butane-1,4-diol (II)	2.68 (10)	2.02 (about 10)	3.6–3.7 (br.m.)
Dihydrocubebin	2.66 (12)	1.82 (about 14)	3.63 (br.m.)

Δ Values are given in p.p.m. relative to the Me_4Si; $W_{1/2}$ is given in parentheses. The assignments of spectra are tentative: a detailed analysis of NMR spectra is in progress and will be published elsewhere. br.m., Broad multiplet.

* Numbering system in accordance with that used in ref. 7 (see also Fig. 4).

Compounds I and II were also found in adult males where their urinary excretion is quantitatively similar to that in the follicular phase of normal ovulating women. Although we have no information on the site of their production in men, the fact that they are almost undetectable in the urine of newborn infants[2,5] and in extremely low concentrations in children of both sexes suggests that their production is related to gonadal development.

The existence of lignans in humans, and preliminary observations on their disposition, pose questions as to their physiological and biological significance. The lignans are uncommon plant constituents which have been found so far only in higher plants of the orders Gymnospermophytina and Angiospermophytina. They have been investigated extensively by natural product chemists and various types of dibenzylbutane and related structures have been catalogued[7,8]. As far as we know, however, compounds with the substitution pattern reported here have not been identified in any plant species, presumably reflecting different pathways of biosynthesis or metabolism.

Lignans have been classified by the US National Cancer Institute[9,10] to be of 'high interest' as potential anticancer agents and several have been used in clinical trials to treat tumours[11–14]. Podophyllotoxin[15] (Fig. 4) is probably the best known lignan; it is derived from the roots of the Mayapple plant of the central USA. This lignan and a number of other less complex natural (for example, wikstromol, Fig. 4) and synthetic lignans, exhibits anti-mitotic activity and has been effective in treating several types of tumour in animals[16–20]. Whether or not the lignans of humans have similar activity remains to be determined although it is interesting that to be biologically active the plant compounds require a *trans* configuration of the benzyl substituents on the C_2-C_3 of the butane.

The diphenolic nature of compounds I–VI resemble many of the substances known either to exert oestrogenic action or to block oestrogen receptor sites[21]. The increased urinary excretion of the dibenzylbutyrolactone (I) in the luteal phase, a conspicuous feature of the menstrual cycles studied so far, suggests that this lignan, or a related compound, may be associated with luteolytic activity and the regulation of the length of the luteal phase of the cycle.

We thank Dr D. C. Ayres for matairesinol dimethyl ether, and Professors L. Crombie and R. Row for dihydrocubebin.

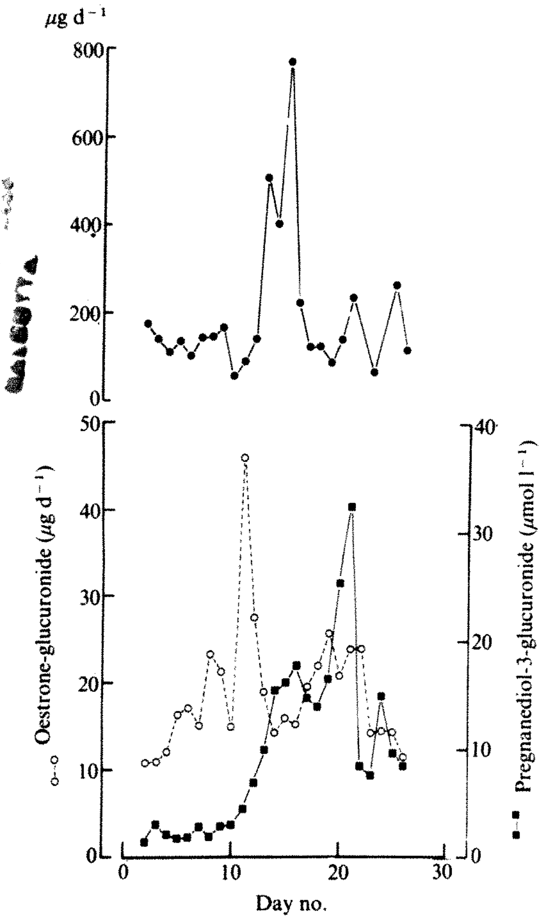

Fig. 5 Urinary excretion ($\mu g\ d^{-1}$) of 2,3-bis-(3'-hydroxybenzyl)-butyrolactone (upper) during the menstrual cycle of a normal ovulating woman. Oestrone–glucuronide and pregnanediol-3α-glucuronide were measured by radioimmunoassay and indicate the ovulatory and luteal phases of the cycle.

Received 29 July; accepted 27 August 1980.

1. Setchell, K. D. R., Bull, R. & Adlercreutz, H. *J. Steroid Biochem.* **12,** 375 (1980).
2. Setchell, K. D. R., Lawson, A. M., Axelson, M. & Adlercreutz, H. *Res. Steroids* **9,** 207 (1980).
3. Haworth, R. D. & Slinger, F. H. *J. chem. Soc.*, 1098 (1940).
4. Batterbee, J. E., Burden, R. S., Crombie, L. & Whiting, D. A. *J. chem. Soc.* (C), 2470 (1969).
5. Setchell, K. D. R. & Adlercreutz, H. *J. Steroid Biochem.* **12,** xv (1979).
6. Stitch, S. R., Smith, P. D., Illingworth, D. & Toumba, K. *J. Endocr.* **85,** 23P (1980).
7. Rao, C. B. S. *The Chemistry of Lignans* (Andhra University Press, 1978).
8. Ekman, R. *Holzforschung* **30,** 79 (1976).
9. Hartwell, J. L. *Cancer Treat. Rep.* **60,** 1031 (1976).
10. Barclay, A. S. & Perdue, R. E. Jr. *Cancer Treat. Rep.* **60,** 1081 (1976).
11. Savel, H. *Proc. Am. Ass. Cancer Res.* **5,** 56 (1964).
12. Greenspan, E. M., Colsky, J., Schoenbach, B. & Shear, M. J. *J. natn. Cancer Inst.* **14,** 1257 (1954).
13. Filler, R. M., Traggis, D. G., Jaffe, N. & Vawter, G. F. *J. pediat. Surg.* **7,** 136 (1972).
14. Dombernowski, P., Nissen, N. I. & Larsen, V. *Cancer Chemother. Rep.* **56,** 71 (1972).
15. Kelly, M. G. & Hartwell, J. L. *J. natn. Cancer Inst.* **14,** 967 (1954).
16. Torrance, S. J., Hoffmann, J. J. & Cole, J. R. *J. pharmac. Sci.* **68,** 664 (1979).
17. Stähelin, H. *Eur. J. Cancer* **9,** 215 (1973).
18. Weiss, S. G., Tin-Wa, M., Perdue, R. E. Jr & Farnsworth, N. R. *J. pharmac. Sci.* **64,** 95 (1975).
19. McDoniel, P. B. & Cole, J. R. *J. pharmac. Sci.* **61,** 1992 (1972).
20. Joland, S. D., Wiedhope, R. M. & Cole, J. R. *J. pharmac. Sci.* **66,** 892 (1977).
21. Lerclerq, G. & Heuson, J. C. *Biochim. biophys. Acta* **560,** 427 (1979).
22. Axelson, M. & Setchell, K. D. R. *FEBS Lett.* (submitted).

Endogenous digitalis-like substance in plasma of volume-expanded dogs

Kenneth A. Gruber, Janice M. Whitaker & Vardaman M. Buckalew Jr

Departments of Physiology and Pharmacology, Medicine and Microbiology and Immunology, Bowman Gray School of Medicine, Winston-Salem, North Carolina 27103

Considerable evidence supports the hypothesis that renal sodium excretion is partly regulated by a humoral agent released or activated by extracellular fluid volume (ECFV) expansion[1], including the demonstration of biological activities in extracts of plasma and urine which support the natriuretic hormone (NH) hypothesis[2–4]. NH is a low molecular weight peptide formed from a precursor in plasma[5], which inhibits sodium transport (anti-natriferic activity) in isolated toad bladder, an analogue of the distal renal tubule and collecting duct. Other evidence indicates that NH can inhibit renal $(\mathrm{Na^+ + K^+})$ATPase[6], which suggests that it might be an endogenous digitalis-like substance. Although an immunoreactive ouabain-like substance has been demonstrated in amphibian plasma[7], none has been reported in mammals. To identify an endogenous digitalis-like substance, we used an approach suggested by the work of Spector and his collaborators, who demonstrated that biological substances which bind to the same receptors as drugs, such as endogenous opioids[8] and benzodiazepines[9], may compete with antibodies specific for the drugs. Hough and Edwardson[10] showed that antibodies to thaumatin, a sweet-tasting plant protein, also bind non-protein sweet substances in a linearly related fashion to the sweetness of the compound, suggesting that the antibody binding site may be similar to the sweet taste receptor. Based on these observations, we postulated that if NH were an endogenous digitalis-like substance, it might bind to antibodies specific for digitalis glycosides. We report here the preliminary isolation of a substance in plasma of dogs which competes with digoxin for two specific digoxin antibodies and is an inhibitor of $(\mathrm{Na^+ + K^+})$ATPase activity. Increased amounts of this factor are found in plasma of volume-expanded dogs, suggesting it is the putative NH.

Blood was obtained from pentobarbital-anaesthetized, saline-expanded and hydropenic dogs. The procedures for acute saline expansion and the protocol for plasma processing have been published previously[5]. Deproteinized plasma extracts, representing an original plasma volume of 10 ml, were eluted by Diafiltration through Amicon UM-10 membranes (exclusion limit <10,000 molecular weight) with 0.05 M acetic acid. Four volumes per sample were eluted, freeze-dried and further purified by HPLC.

Figure 1*a* shows the chromatographic pattern obtained when a deproteinized plasma diafiltrate from a volume-expanded dog was chromatographed on a Partisil SCX (strong cation exchange) column (Whatman). Because we had previously shown that the anti-natriferic factor believed to be the active principle of NH eluted in the void volume on SCX[5], this fraction was tested for immunoreactivity with anti-digoxin antibodies. A substance showing binding to two anti-digoxin antibodies was demonstrated (Fig. 2). The dilution curve of the endogenous immunoreactive substance was similar to that of unlabelled digoxin standard. The two antibodies used were produced in different species to digoxin conjugated to either bovine serum albumin or human serum albumin. The apparent concentration of the endogenous substance in the SCX I sample shown in Fig. 2 was 355 pg digoxin equivalents per ml of plasma.

The SCX void volume fraction was further purified on reverse-phase chromatography (Lichrosorb-ODS; Fig. 1*b*). Salts emerged in the void volume followed by several, distinct fluorescamine-positive peaks. Each tube after the salt peak was assayed for immunoreactivity to the goat anti-digoxin antibody, and for $(\mathrm{Na^+ + K^+})$ATPase inhibitory activity with a purified hog brain ATPase preparation (Fig. 3). Immunoreactivity and ATPase-inhibitory activity eluted in two distinct peaks, the first coming immediately after the salt. These peaks of biological activity and immunoreactivity eluted at similar times, and corresponded to two distinct fluorescamine-positive peaks on ODS chromatography (Fig. 1*b*). Similar elution patterns were obtained with plasma extracts from both hydropenic and saline-expanded dogs. Most importantly, however, activity was higher in saline-expanded plasma samples. ATPase-inhibitory activity at the maximum of peak 1 from four saline-expanded plasma extracts was 185±46 pmol ouabain equivalents (equiv.) per tube compared with 66±25 pmol ouabain equiv. per tube at the maximum of peak 1 from four hydropenic dog samples ($P<0.03$). Similarly, at the maximum of peak 2, ATPase-inhibitory activity was 148±43 pmol ouabain equiv. per tube in four samples from saline-expanded dogs and 43±26 pmol ouabain equiv. per tube in four samples from hydropenic dogs ($P<0.03$). Comparison of peak heights indicates that saline-expanded samples are three times more active than hydropenic samples, but total differences are actually greater. Because the total amount of biological activity in the original samples is equal to the area under the curve for each peak, and because each sample has two approximately equal peaks, the total difference between the two groups would be the sum of the differences for each peak.

The quantitative difference in digitalis-like activity obtained between the radioimmunassay (RIA) and the ATPase activity is of interest (Fig. 3). In the sample shown in Fig. 3, immunoreactivity of peak 1 was 480 fmol digoxin equiv. per tube, whereas the ATPase inhibitory activity was 163 pmol ouabain equiv. per tube. As RIA is a function of numbers of molecules, it probably reflects the actual concentration of the endogenous digitalis-like substance more accurately. This indicates that the endogenous

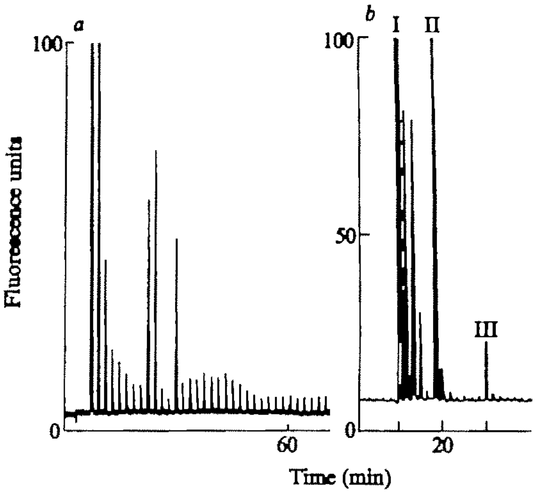

Fig. 1 *a*, Freeze-dried diafiltrate representing 10 ml of plasma was suspended in 400 μl of 10% formic acid and separated on Partisil SCX with a pyridine–acetate gradient[11]. The column flow rate was 400 μl $\mathrm{min^{-1}}$. The column effluent was monitored by a preparative fluorescamine monitoring system[12] which allows detection of primary amines (including peptides and amino acids) by automated, discontinuous sampling of the column effluent. Approximately 1–2% of the effluent was used for detection while the remainder was collected in a fraction collector at 4-min intervals. The discontinuous appearance of the chromatogram is a result of the monitoring system with each line representing one sampling period (2-min interval). The void volume peak (12–20 min), which contains all the plasma salts, was tested for immunoreactivity (Fig. 2) and purified further by reverse phase chromatography. *b*, Reverse-phase chromatography was performed on Lichrosorb ODS. The sample was eluted isocratically in 0.5 M pyridine titrated to *p*H 3 with formic acid, with a column flow rate of approximately 200 μl $\mathrm{min^{-1}}$. Fractions were monitored and collected every 2 min. The salt emerged in the void volume (ODS-I) and the next two fractions (ODS-II and ODS-III) were tested for immunoreactivity and $(\mathrm{Na^+ + K^+})$ATPase inhibitory activity.

0028-0836/80/430743—03$01 00

substance is about three orders of magnitude more potent an inhibitor of purified brain $(Na^+ + K^+)$ATPase than ouabain. This finding is in accord with our observation that 10^{-5} M ouabain is necessary to produce the same degree of antinatriferic activity (25% inhibition of short-circuit current) in toad bladder as that produced by an extract of 5 ml of plasma from volume-expanded dogs (W. C. Plunkett *et al.*, in preparation).

As a further demonstration that the digitalis-like immunoreactive substance is identical to the ATPase inhibitor, preliminary studies have shown that immunoprecipitation of plasma diafiltrates with the goat anti-digoxin antibody yields two peaks on ODS chromatography which are similar to those shown in Fig. 1*b*. Assay for ATPase inhibitory activity of these two peaks showed a similar difference between samples from volume-expanded and hydropenic dogs as shown in Fig. 3.

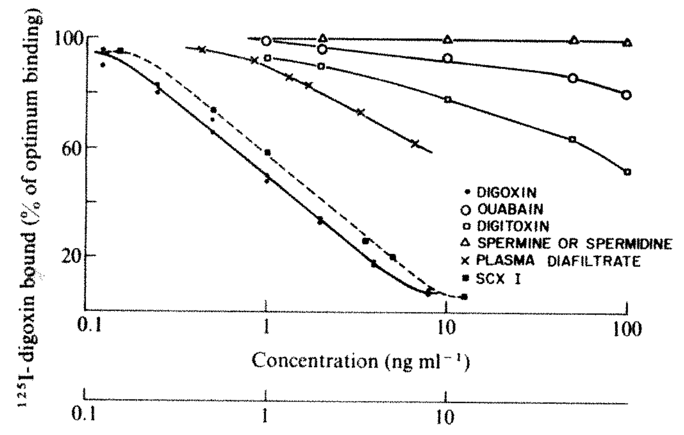

Fig. 2 Radioimmunoassay was performed on SCX fraction I and diafiltrates reconstituted in 500 μl of distilled water, adjusted to *p*H 7.6 with NaOH. Duplicate dilutions of these samples were assayed for cross-reactivity to either an ^{125}I-digoxin clinical radioimmunoassay kit (NEN) or an RIA for digoxin developed in our laboratories using a goat anti-digoxin antibody. The NEN antibody is produced in rabbits by immunization with a digoxin–human serum albumin conjugate, and shows less than 5% cross-reactivity with digitoxin, and essentially none with ouabain or any other steroid glycoside. For assay with the NEN kits, the antibody was incubated with samples or standards in the presence of ^{125}I-digoxin according to procedures provided. Separation of bound antigen from free antigen was accomplished either by charcoal adsorption, or by precipitation with a second antibody (sheep anti-rabbit γ-globulin). Although both separation techniques provided similar results, the double antibody precipitation technique was used routinely. A second, more sensitive RIA developed in our laboratories using an antibody produced in goats immunized with a digoxin–bovine serum albumin conjugate is demonstrated. The degree of cross-reactivity of this antibody with digitoxin, ouabain, spermine or spermidine (known ATPase inhibitors) is shown. Thyrotropin-releasing hormone and various amino acids including phenylalanine and proline were also tested and showed no cross-reactivity. For this RIA the anti-digoxin antibody was incubated for 2 h at 37 °C, *p*H 7.6 (phosphate-buffered saline) in the presence of ^{125}I-digoxin (Burroughs Wellcome) and duplicates of either samples or standards. Rabbit anti-goat γ-globulin was then added to the reaction mixture and incubated for an additional hour. Samples were then centrifuged at 3,000 r.p.m. for 30 min, the supernatant decanted and the pellet counted in a γ counter. Per cent bound was calculated by subtracting nonspecific background and comparing the results with 100% for optimum binding (tubes containing reaction mixture but no unlabelled standard or unknown sample). This immunoassay technique yielded a 10-fold increase in sensitivity over that of the clinical assay kits. Further details on this method will be presented elsewhere. The effect of various glycosides and polyamines on binding of ^{125}I-digoxin to its specific antibody is also shown. Aliquots (100 μl) of standard solutions of glycosides or polyamines were added to the reaction mixture containing buffer, ^{125}I-digoxin and antibody for a total volume of 400 μl. Concentrations of standards are calculated as ng ml^{-1} solution and plotted according to the concentration of the original stock solution. Aliquots (100 μl) of plasma extract from SCX I (void volume lyophilized, reconstituted in H_2O, *p*H 7.6 with NaOH) corresponding to plasma volumes ranging from 0.15 to 12.0 ml were also tested for their ability to compete with ^{125}I-digoxin for its antibody. The binding curve for SCX I is more nearly parallel to the digoxin standard than is the binding curve from the diafiltrate. Apparently, this is due to the removal of interfering substances during the purification procedure. Spermine or spermidine at 100 ng ml^{-1} show no cross-reaction with the antibody whereas similar concentrations of ouabain and digitoxin each show cross-reactivity of less than 1%. Points represent the mean of duplicates which show a variance of less than 5%. The data for plasma diafiltrates and SCX I samples are plotted as a function of original plasma volume; all other substances shown are ● plotted by concentration.

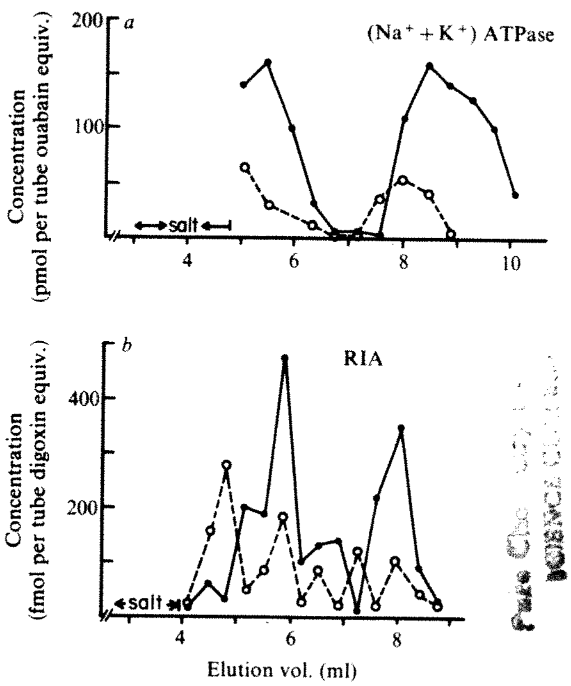

Fig. 3 Assays for $(Na^+ + K^+)$ATPase inhibitory activity (*a*) and digoxin immunoreactivity (*b*) were performed on each 2-min fraction (400 μl) of ODS column effluent. The solid line represents volume-expanded samples, while the dotted line represents hydropenic samples. ATPase inhibition was assayed using a purified $(Na^+ + K^+)$ATPase enzyme derived from hog cerebral cortex (Sigma). This enzyme was originally used in clinical assays for digoxin and digitoxin[13], and has also been used to assay for NH[14]. Ouabain or lyophilized HPLC samples were dissolved in an imidazole–HCl buffer (10 mM, *p*H 7.2) containing sodium (100 mM), potassium (5 mM), magnesium (1 mM) and EGTA (0.5 mM). After addition of enzyme solution the samples were incubated for 10 min in a shaking water bath at 37 °C. ATP was added to a final concentration of 1 mM. The total volume of each incubation tube was 1 ml. Blank tubes contained only ATP and the buffered ion solution, while control ATPase activity was determined in the absence of ouabain. After 15 min of incubation in the presence of ATP the reaction was stopped by the addition of 0.7 ml of cold 13% TCA. ATPase activity was determined as the amount of inorganic phosphate liberated by the method of Eibl and Lands[15]. The minimum sensitivity of this assay is approximately 10 pmol per ml of ouabain, while 100 nmol causes 100% inhibition of enzyme activity. The assay system was standardized with ouabain rather than digoxin because solubilization of digoxin requires an organic solvent which interferes with the assay. Although it is possible to aliquot and steam-dry digoxin[13], we preferred to avoid this rather cumbersome procedure. A dose–response curve for ouabain was generated for each set of unknowns and values for each unknown were calculated from the standard curve by computer program, and expressed as ouabain equivalents.

It is not clear from these studies why two peaks are recovered. However, we have previously reported two fluorescamine-positive peaks on ODS chromatography of the SCX void volume, both of which showed a high degree of correlation with anti-natriferic activity[5]. Thus, there appear to be two molecular species with similar biological activity that differ somewhat in their basic structure.

The evidence presented here suggests that the digitalis-like factors are peptides, as they can be separated by chromatographic protocols for small peptides, and elute in fluorescamine-positive peaks. In addition, we have found that treatment with concentrated HCl at room temperature for 30 min destroys all activity. This susceptibility to acid hydrolysis indicates that the ATPase inhibitory activity is not due to known endogenous ATPase inhibitors such as polyamines[16], vanadium[17] or bufotoxin-like steroids[18]. The initial studies on the use of Partisil SCX with biological samples[11] also demonstrated longer retention times for polyamines than is seen for SCX I.

Interestingly several investigators have reported data which in retrospect support our observations. Early attempts to measure

[illegible] Upper Circular Road
CALCUTTA

cardiac glycosides in plasma by the red blood cell ^{86}Rb uptake assay noted an endogenous interfering substance in patients with congestive heart failure or renal failure[19], which could be separated from cardiac glycosides by its water solubility[20]. The same enzyme preparation used in these studies was originally developed as an assay for digoxin by Burnett and Conklin[13], who also noted endogenous digoxin-like activity in normal non-digitalized controls, and in patients with fluid balance problems[13]. More recently, it has been reported[21] that RIAs for digoxin in patients with renal failure tend to overestimate plasma levels when compared with an HPLC method for the drug. If the factor demonstrated in our studies is the endogenous substance which interferes with clinical assays for digoxin, then its plasma level seems to be elevated in some pathological conditions.

We should mention that the observed plasma levels of endogenous digoxin-like factor would be toxic to an intact animal. This apparent discrepancy could be explained if NH circulated as an inactive precursor, as suggested previously by us[5]. As noted, the plasma isolation protocol used in this study includes a period of incubation to allow precursor breakdown. Alternatively, *in vivo* receptor binding of the endogenous substance for $(Na^+ + K^+)$ATPase could be much lower for all organs other than the target organ (presumably the kidney).

Thus, for the first time we have demonstrated and partially purified a circulating factor in mammals which is an inhibitor of $(Na^+ + K^+)$ATPase and possesses a structure which is recognized by antibodies to the cardiac glycoside digoxin. We have suggested that an appropriate name for this factor would be 'endoxin'[22]. Endoxin has a similar HPLC retention time as the previously demonstrated anti-natriferic factor[5], and both endoxin and the anti-natriferic factor are present in higher concentrations in volume-expanded than in hydropenic subjects. These data support the hypothesis that these several biological and immunoreactive activities are due to the same factor, that this substance is the putative NH, and that anti-digoxin antibodies can be used as an RIA for NH. Confirmation of this hypothesis will require the biochemical characterization of endoxin, which is now in progress.

Portions of this work were presented at the Conference of the Council for High Blood Pressure Research, American Heart Association Cleveland, Ohio (October 1979).

Received 11 April; accepted 21 July 1980.

1. de Wardener, H. C. *Clin. Sci. molec. Med.* **53,** 1–8 (1977).
2. Buckalew, V. M. Jr, Martinez, F. J. & Greene, W. E. *J. clin. Invest.* **49,** 926–935 (1970).
3. Clarkson, E. M., Raw, S. M. & de Wardener, H. E. *Kidney Int.* **10,** 381–394 (1976).
4. Favre, H., Hwang, K. H., Schmidt, W., Bricker, N. & Bourgoignie, J. J. *J. clin. Invest.* **56,** 1302–1311 (1975).
5. Gruber, K. A. & Buckalew, V. M. Jr *Proc. Soc. exp. Biol. Med.* **159,** 463–467 (1978).
6. Hillyard, S. D., Lu, E. & Gonick, H. *Circulation Res.* **38,** 250–255 (1976).
7. Flier, J. S., Marotos-Flier, E., Pallotta, J. A. & McIsaac, D. *Nature* **279,** 341–343 (1979).
8. Ginzler, A., Levy, A. & Spector, S. *Proc. natn. Acad. Sci. U.S.A.* **73,** 2132–2136 (1976).
9. Asano, T. & Spector, S. *Proc. natn. Acad. Sci. U.S.A.* **76,** 977–979 (1979).
10. Hough, C. A. M. & Edwardson, J. A. *Nature* **271,** 381–383 (1978).
11. Radhakrishnan, A. N., Stein, S., Licht, A., Gruber, K. A. & Undenfriend, S. *J. Chromatogr.* **132,** 552–555 (1977).
12. Bohlen, P., Stein, S., Stone, J. & Undenfriend, S. *Analyt. Biochem.* **61,** 438–445 (1975).
13. Burnett, G. H. & Conklin, R. L. *J. Lab. clin. Invest.* **78,** 779–784 (1971).
14. Raghaven, S. R. V. & Gonick, H. *Proc. Soc. exp. Biol. Med.* **164,** 101–104 (1980).
15. Eibl, H. & Lands, W. E. M. *Analyt. Biochem.* **30,** 51–57 (1969).
16. Ahmed, K. & Williams-Ashman, H. G. *Biochem. J.* **113,** 829–836 (1969).
17. Cantley, L. C. Jr *et al. J. biol. Chem.* **252,** 7421–7423 (1977).
18. Flier, J. S. *Nature* **275,** 285–286 (1978).
19. Lowenstein, J. M. *Circulation* **31,** 228–233 (1965).
20. Lowenstein, J. M. & Corrill, E. M. *J. Lab. clin. Med.* **67,** 1048–1052 (1966).
21. Gibson, T. P. & Nelson, H. A. *J. clin. Res.* **64,** 665A (1979).
22. Gruber, K. A., Whitaker, J. M., Plunkett, W. C. & Buckalew, V. M. Jr *Proc. Am. Soc. Nephrology*, Abstr. 47A (1979).

Unusual levels of $(ADP\text{-}ribose)_n$ and DNA synthesis in ataxia telangiectasia cells following γ-ray irradiation

Malcolm J. Edwards & A. M. R. Taylor

Department of Cancer Studies, The Medical School,
University of Birmingham, Birmingham B15 2TJ, UK

Poly (ADP-ribose) polymerase is a eukaryotic chromosomal enzyme which utilizes the ADP-ribose moiety of NAD to synthesize the nucleic acid homopolymer $(ADP\text{-}ribose)_n$ (ref. 1). The precise function of $(ADP\text{-}ribose)_n$ has not been fully established although it does covalently modify chromosomal proteins by ADP-ribosylation[2,3]. Here we demonstrate that γ-ray irradiation of lymphoblastoid cells from normal subjects results in depressed DNA synthesis and increased $(ADP\text{-}ribose)_n$ synthesis. Irradiation of lymphoblastoid cells from patients with the autosomal recessive disease ataxia telangiectasia (AT), however, failed to depress DNA synthesis and did not elevate $(ADP\text{-}ribose)_n$ levels. We have confirmed that $(ADP\text{-}ribose)_n$ is synthesized in response to DNA damage and we propose that this polymer may function in the recovery from DNA damage by suppressing DNA synthesis.

The synthesis of $(ADP\text{-}ribose)_n$ is increased by a variety of agents which cause DNA damage. Radiation[4–7], alkylating agents[8,9] and bleomycin, a radiomimetic antibiotic, increase $(ADP\text{-}ribose)_n$ synthesis and DNA repair synthesis in normal human lymphocytes[10]. The level of $(ADP\text{-}ribose)_n$ increases in normal lymphoblastoid cell lines after UV-irradiation, whereas this response is either absent or delayed in xeroderma pigmentosum (XP) cells[11], which are defective in the removal of UV-induced thymine dimers[12,13]. The synthesis of $(ADP\text{-}ribose)_n$ is increased in proportion to the number of DNA strand breaks induced by exogenous endonucleases[4].

We have investigated the synthesis of $(ADP\text{-}ribose)_n$ in lymphoblastoid cell lines from two ataxia telangiectasia (AT) patients. Patients with this disorder show a predisposition to cancer and enhanced sensitivity to X-ray or γ-ray irradiation as measured by colony survival[14].

Lymphoblastoid cell lines from two normal subjects (LIZ, DEW) and two AT patients (GM1525/AT2BI, GM1526/AT8BI) were irradiated with γ-rays (0–1,000 rad) at 4 °C. The synthesis of $(ADP\text{-}ribose)_n$ from both normal subjects increased in proportion to γ-ray dose. At a dose of 1 krad the synthesis of $(ADP\text{-}ribose)_n$ increased by 54–58% over mock irradiated normal cells. Lymphoblastoid cell lines from both AT patients showed a smaller (8–14%) increase in $(ADP\text{-}ribose)_n$ following the same dose of γ-rays (Fig. 1).

In all experiments the acid-insoluble product synthesized from ^{14}C-NAD was shown to be $(ADP\text{-}ribose)_n$ by the inability of DNase I ($100\ \mu g\ ml^{-1}$) and RNase I ($500\ \mu g\ ml^{-1}$) to hydrolyse the product, whereas 91% was hydrolysed into acid-soluble products by $600\ \mu g\ ml^{-1}$ snake venom phosphodiesterase (Table 1).

To investigate the possibility that poly (ADP-ribose) polymerase was deficient in AT cells, lymphoblastoid cell lines from a normal subject (LIZ) and an AT (GM1526/AT8BI) patient were permeabilized[15] and treated with exogenous DNase I ($100\ \mu g\ ml^{-1}$) and the synthesis of $(ADP\text{-}ribose)_n$ measured. Both the normal and AT cell lines synthesized $(ADP\text{-}ribose)_n$ in similar amounts in response to DNA damage introduced by exogenous DNase I (Table 1). This suggests that the inability of AT cells to synthesis $(ADP\text{-}ribose)_n$ was not due to an intrinsic defect in poly (ADP-ribose) polymerase.

It has been reported that NAD the substrate for $(ADP\text{-}ribose)_n$ synthesis caused decreased ^{3}H-TTP incorporation and template activity of chromatin in isolated rat liver nuclei[16,17] whereas this decrease was not observed in nuclei from

0028-0836/80/430745—03$01.00

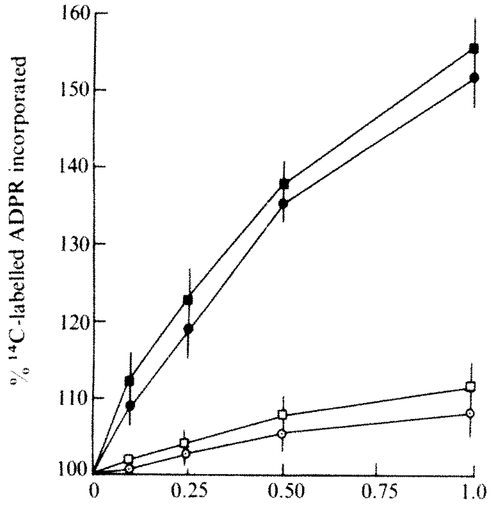

Fig. 1 Effect of increasing γ-ray irradiation dose on (ADP-ribose)$_n$ synthesis in permeable lymphoblastoid cell lines from normal subjects (LIZ ■, DEW ●) and AT patients (GM1525/AT2BI □; GM1526/AT8BI ○). Cell suspensions (7.8×10^5 cells per ml) in exponential growth (72 h) were resuspended in RPMI medium supplemented with 10% (v/v) fetal calf serum (FCS) and irradiated at 4 °C using a ^{60}Co γ-ray source at a dose rate of 200 rad min^{-1}. Irradiated and nonirradiated cell suspensions were centrifuged at 2,000g for 5 min, washed twice in Dulbecco A phosphate-buffered saline (containing 1.15 g l^{-1} Na_2HPO_4, 0.2 g l^{-1} KH_2PO_4, 0.2 g l^{-1} KCl and 8 g l^{-1} NaCl at pH 7.3), resuspended in permeabilizing buffer pH 7.8 (containing 10 mM Tris, 1 mM EDTA, 4 mM $MgCl_2$, 1 mM dithiothreitol and 0.05% (v/v) Triton X-100) for 15 min at 4 °C. 100 μl of cell suspensions were incubated at 30 °C with 10 μl of ^{14}C-NAD (final concentration 5 μl ml^{-1}, 100 μM) in the presence of 50 μl of assay buffer pH 7.8 (containing 50 mM Tris, 15 mM $MgCl_2$, 15 mM KCl, 10 mM NaF and 3 mM cyclic AMP). Triplicate samples were incubated for 10 min. The reaction was stopped with 0.2 ml of 20° (w/v) trichloroacetic acid (TCA). The samples were maintained at 4 °C for 2 h, filtered onto glass-filtre disks (Whatman GF/C) and washed with 10% (w/v) TCA containing 2% (w/v) $Na_4P_2O_7$ (5×10 ml). Protein[23] was determined and radioactivity on the filters was measured in Insta-gel (Packard). Enzyme activity (d.p.m. per μg of protein) is expressed as a percentage of the activity in mock-irradiated cells. Results are presented as the mean ±s.e.m. of three experiments each performed in triplicate.

lymphoma[18] and hepatoma[19] cells. Poly (ADP-ribose) polymerase activity is inversely related to DNA synthesis in rat cardiac muscle, and the synthesis of (ADP-ribose) has been implicated in the regulation of DNA synthesis[20]. We therefore measured DNA synthesis in these normal and AT lymphoblastoid cell lines in response to γ-ray irradiation. As previously demonstrated[21] an inhibition of [Me-^{3}H]thymidine incorporation into the DNA of both normal cell lines (LIZ, DEW) after treatment of cells with a γ-ray dose of 500 rad was observed (Fig. 2). However, no inhibition of [Me-^{3}H]thymidine incorporation into the DNA of either AT cell line (GM1525/AT2BI, GM1526/AT8BI) was observed at a γ-ray dose of 500 rad (Fig. 2). Control experiments demonstrated that the amount of [Me-^{3}H]thymidine transported into both normal and AT lymphoblastoid cells decreased by similar amounts after treatment with γ-rays.

These results confirm that γ-ray irradiation produces an inverse relationship between (ADP-ribose)$_n$ and DNA synthesis in normal human lymphoblastoid cells. It has been proposed that suppressed DNA synthesis and stimulation of (ADP-ribose)$_n$ are associated with the development of DNA strand breaks[22]. If this is correct the absence of an inverse relationship between (ADP-ribose)$_n$ and DNA synthesis in the two AT lines suggests one of at least two possible alternatives. First, the AT cells may have a lower number of strand breaks;

Table 1 Characterization of the acid-insoluble product synthesized from ^{14}C-NAD in permeable DNase I-treated lymphoblastoid cells from a normal subject (LIZ) and an AT patient (GM1526/AT8BI)

	Acid-insoluble radioactivity remaining after treatment with nuclease (d.p.m. per mg of protein)	
Treatment	Normal cells	Ataxia telangiectasia (GM1526/AT8BI)
100 °C control	12,922 ± 646 (3)	19,100 ± 947 (3)
Deoxyribonuclease (100 μg ml^{-1})	13,164 ± 661 (3)	19,100 ± 995 (3)
Ribonuclease (500 μg ml^{-1})	12,320 ± 610 (3)	18,038 ± 879 (3)
Snake venom phosphodiesterase (600 μg ml^{-1})	1,246 ± 58 (3)	1,380 ± 67 (3)

Cells (7.8–8.3×10^5 cells per ml) in exponential growth (72 h) were made permeable as described in Fig. 1 legend. Cell suspensions (4 ml) were incubated in the presence of DNase I (100 μg ml^{-1}) for 30 min at 37 °C. Aliquots (50 μl) were removed to measure total (ADP-ribose)$_n$ synthesis in 100 μl of poly (ADP-ribose) polymerase assay buffer, pH 7.8 and 10 μl ^{14}C-NAD added. Reactions were terminated at 100 °C for 5 min. Aliquots (0.3 ml) of the DNase I treated cell suspensions heated at 100 °C for 5 min were incubated at 37 °C for 30 h in the presence of DNase I (100 μg ml^{-1}), RNase I (500 μg ml^{-1}) or snake venom phosphodiesterase (600 μg ml^{-1}). Reactions were terminated with 0.2 ml of 20% (w/v) TCA containing 2% (w/v) $Na_4P_2O_7$. Acid-insoluble product was collected and radioactivity counted as described in the legend to Fig. 1. Results are presented as the mean ±s.e.m. of three experiments each performed in triplicate.

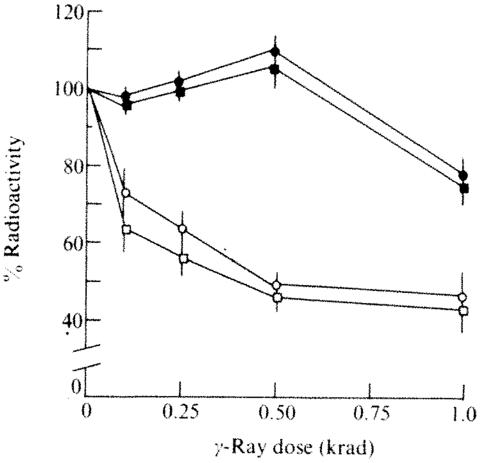

Fig. 2 Effect of increasing γ-ray radiation dose on DNA synthesis in lymphoblastoid cell lines derived from normal subjects (LIZ □, DEW ○) and AT patients (GM1525/AT2BI ■, GM1526/AT8BI ●). Cells in exponential growth (72 h) were resuspended in RPMI medium (7.4–8.3×10^5 cells per ml) supplemented with 10% (v/v) FCS and irradiated at 4 °C at the indicated dose using a ^{60}Co γ-ray source at a dose rate of 200 rad per min. Irradiated and non-irradiated cell suspensions were incubated after irradiation for 30 min at 37 °C and then 10 μl of [Me-^{3}H]thymidine (final concentration 10 μCi ml^{-1}, 10 μM) added. Triplicate tubes were incubated for 30 min at 37 °C. Cells were collected and washed twice in Dulbecco A phosphate-buffered saline, pH 7.3 at 4 °C (2×20 ml). Cells were resuspended in 1 ml of a buffer (containing 50 mM Tris, 4 mM $MgCl_2$ and 0.2 M NaCl at pH 7.4) and 0.2 ml of 20% (w/v) TCA added. The acid-insoluble product was washed in 10% (w/v) TCA (5×10 ml) and dissolved in 1 ml of 0.1 M NaOH. Protein was measured and radioactivity determined by liquid scintillation counting in Insta-gel. DNA synthesis (d.p.m. per μg of protein) in γ-ray irradiated cells is expressed as a percentage of mock irradiated (100%) control cells. Results are presented as the mean ± s.e.m. of four experiments each performed in triplicate.

there is, however, no evidence to support this[24]. Second, it might suggest that the damage produced by γ-rays in these cells is not translated into a signal which stimulates poly (ADP-ribose) polymerase. The synthesis of (ADP-ribose)$_n$ may have a role in the protection of DNA by suppressing DNA synthesis during states of DNA damage, and AT cells are hypersensitive to the effects of ionizing radiation for this reason.

We thank Professor D. G. Harnden and Dr C. Paraskeva of the Department of Cancer Studies for helpful criticism of the manuscript, Dr M. Steel of the Clinical and Population Cytogenetics Unit, Edinburgh, for the normal lymphoblastoid cell lines, the staff of the University of Birmingham Radiation Centre for the use of their facilities, Miss D. Williams for typing the manuscript and Miss Gillian Duckworth for technical assistance. This work was supported by the Cancer Research Campaign.

Received 30 July; accepted 19 September 1980.

1. **Hayaishi, O. & Ueda, K.** *A. Rev. Biochem.* **46,** 95–116 (1977).
2. **Nishizuka, Y., Ueda, K., Honjo, T. & Hayaishi, O.** *J. biol. Chem.* **243,** 3765–3767 (1968).
3. **Tsopanakis, C., Leeson, E., Tsopanakis, A. & Shall, S.** *Eur. J. Biochem.* **90,** 337–345 (1978).
4. **Benjamin, R. C. & Gill, D. M.** in *DNA Repair Mechanisms* **9,** 337–340 (1978).
5. **Campagnari, F., Whitfield, J. F. & Bertazzoni, U.** *Expl Cell Res.* **42,** 646–656 (1966).
6. **Scaife, J. F.** *Can. J. Biochem. Physiol.* **41,** 1469–1481 (1963).
7. **Hilz, H., Hlavica, P. & Bertram, B.** *Biochem. Z.* **338,** 283–299 (1963).
8. **Riott, I. M.** *Biochem. J.* **63,** 300–307 (1956).
9. **Davies, M. I., Shall, S. & Skidmore, C. J.** *Biochem. Soc. Trans.* **5,** 949–950 (1978).
10. **Berger, N. A., Sikorski, G. W., Petzold, S. J. & Kurohara, K. K.** *J. clin. Invest.* **63,** 1164–1171 (1979).
11. **Berger, N. A., Sikorski, G. W., Petzold, S. J. & Kurohara, K. K.** *Biochemistry* **19,** 289–293 (1980).
12. **Cleaver, J. E.** *Proc. natn. Acad. Sci. U.S.A.* **63,** 428–435 (1969).
13. **Setlow, R. B., Regan, J. D., German, J. & Carrier, W. L.** *Proc. natn. Acad. Sci. U.S.A.* **64,** 1035–1041 (1969).
14. **Taylor, A. M. R.** *et al. Nature* **258,** 427–429 (1975).
15. **Ghani, Q. P. & Hollenberg, M.** *Biochem. J.* **170,** 387–394 (1978).
16. **Burzio, L. & Koide, S. S.** *Biochem. biophys. Res. Commun.* **40,** 1013–1020 (1970).
17. **Burzio, K. & Koide, S. S.** *FEBS Lett.* **20,** 29–32 (1972).
18. **Lehmann, A. R. & Shall, S.** *FEBS Lett.* **26,** 181–184 (1972).
19. **Yamada, M., Nagao, M., Hidaka, T. & Sigimura, T.** *Biochem. biophys. Res. Commun.* **54,** 1567–1572 (1973).
20. **Claycomb, W. B.** *Biochem. J.* **154,** 387–393 (1976).
21. **Tolmach, L. J. & Jones, R. W.** *Radiat. Res.* **69,** 117–133 (1977).
22. **Berger, N. A., Petzold, S. J. & Berger, S. J.** *Biochim. biophys. Acta* **564,** 90–104 (1979).
23. **Lowry, O. H., Rosebrough, N. J., Farr, A. L. & Randall, R. J.** *J. biol. Chem.* **193,** 265–275 (1951).
24. **Fornace, A. J. & Little, J. B.** *Biochim. biophys. Acta* **607,** 432–437 (1980).

Defective DNA repair and increased lethality in ataxia telangiectasia cells exposed to 4-nitroquinoline-1-oxide

P. J. Smith & M. C. Paterson

Health Sciences Division, Atomic Energy of Canada Limited, Chalk River Nuclear Laboratories, Chalk River, Ontario, Canada KOJ 1JO

Ataxia telangiectasia (AT) is a rare autosomal recessive disorder in man characterized by progressive loss of muscular coordination (due to neurodegeneration) and permanent dilation of the small blood vessels of the eyes and skin[1,2]. AT patients also have repeated sinopulmonary infections, immune defects associated with thymus underdevelopment, and abnormal endocrine functions[1,2]. Affected patients are at high risk of developing malignancy, particularly lymphomas and lymphatic leukaemias[1], and there are clinical indications[3–5] that AT patients are hypersensitive to conventional radiotherapy administered for treatment of malignancy. Cultured diploid fibroblasts from AT donors are consistently hypersensitive to ionizing radiation[2,6,7], apparently due to defective enzymatic repair of radiogenic DNA damage[2,8]. We have determined the survival responses and DNA repair abilities of AT cells exposed to 4-nitroquinoline-1-oxide (4NQO), a chemical carcinogen whose DNA-damaging properties partially mimic those of ionizing radiation[9]. We report here that certain AT cell strains show hypersensitivity to inactivation by 4NQO and defective repair of 4NQO-induced adducts in DNA.

The mutant strains studied (Table 1) were selected on the basis of their *in vitro* DNA repair characteristics. AT2BE and AT3BI are defective in the excision repair of γ-ray-induced DNA base damage[2,8]; this is manifested in reduced levels of γ-ray-induced repair replication. The repair defects in AT2BE and AT3BI are genetically distinct, since the strains have been assigned to different complementation groups in cell fusion studies[10]. In the strain AT4BI[2,10], no anomalous repair of radiogenic base damage has been detected but it is possible that this strain is defective in the repair of a class of radiogenic DNA lesions that is simply not discernible in the repair assays used[2]. XP9RO was derived from a patient with the sunlight-sensitivity disorder xeroderma pigmentosum (XP). This strain (defective in the repair of UV-induced pyrimidine dimers in DNA[11,12]) is utilized as a sensitive control in repair experiments since XP cells are known to be sensitive to 4NQO[13] due to the defective repair of 4NQO-induced DNA base damage[14].

Figure 1 compares the survival responses of the cell strains to killing by 4NQO. Both AT4B1 and in particular AT2BE are abnormally sensitive to 4NQO, whereas AT3BI demonstrates a response similar to that of strains from two normal donors, GM 38 and GM 498. For example, when survival levels at 0.2 μM 4NQO are compared with those of the normal GM 38 control strain, then AT2BE, AT4BI and AT3BI yield ratios of survival values of 3.2-, 1.7- and 1.0-fold respectively. Compared with ionizing radiation, chemical agents induce a relatively narrow spectrum of lesions in cellular DNA[2]. Thus interstrain differences in the responses of AT cells to 4NQO and other radiomimetic chemicals[2,15,16] probably reflect the different DNA repair pathways in which AT strains are malfunctional.

The principal types of DNA damage induced by the active cellular metabolite of 4NQO are one stable adduct with adenine and two stable and one unstable adduct with guanine[14,17,18]. The

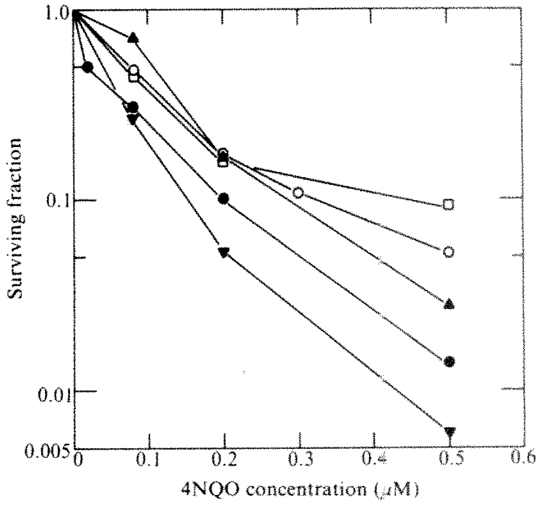

Fig. 1 Cell survival against 4NQO dose for normal and AT fibroblasts. Cells were collected from late logarithmic phase cultures and allowed to attach at 2×10^2–2×10^4 cells per 10-cm diameter plastic dish (Lux Scientific Corporation) containing growth medium at 37 °C for a period of 6 h. Attached cells were then washed with phosphate-buffered saline and incubated for 1 h at 37 °C with the indicated dilution of 4NQO in serum-free growth medium. Following the chemical treatment, the cultures were washed with growth medium and clonogenic potential was measured using the feeder layer technique previously described[7]. Data points represent the means of independent determinations (number in parentheses) for: ○, GM 38 [5; plating efficiency (PE) range, 7–21%]; □, GM 498 [1; PE, 6%]; ▼, AT2BE [3; PE range, 2–6%]; ▲, AT3BI [2; PE, 2% and 5%]; ●, AT4BI [4; PE range, 4–8%]. s.e. for each datum point was routinely ≤10%.

0028–0836/80/430747—03$01.00

Table 1 General description and *in vitro* DNA repair characteristics of diploid fibroblast strains

Strain	Details of donor			Repair of ionizing radiation damage*		
	Diagnosis	Age (yr)	Sex	Repair replication	Removal of base damage	Strand-break rejoining
GM 38	Normal	9	F	+	+	+
GM 498	Normal	3	M	+	NT	+
AT2BE	AT	7	F	−	−	+
AT3BI	AT	4	M	−	−	+
AT4BI	AT	6	M	+	+	+
XP9RO	XP	9	M	+	NT	+

Monolayer stocks of each fibroblast strain (whose origin was human skin) were cultured in Ham's F12 medium supplemented with 15% (v/v) heat-inactivated fetal bovine serum, 1 mM glutamine, 100 U ml^{-1} penicillin G and 100 μg ml^{-1} streptomycin sulphate (growth medium). All culture procedures have been described previously[7]. Solutions of 4NQO (K & K Laboratories) were prepared immediately before use by dissolving the solid in 100% ethanol at room temperature and diluting to the appropriate concentration in pre-warmed serum-free growth medium.

* Details of DNA repair characteristics for the normal strains (our unpublished data), AT strains[2,6,8] and the XP strain[25]: +, proficient; −, deficient; NT, not tested.

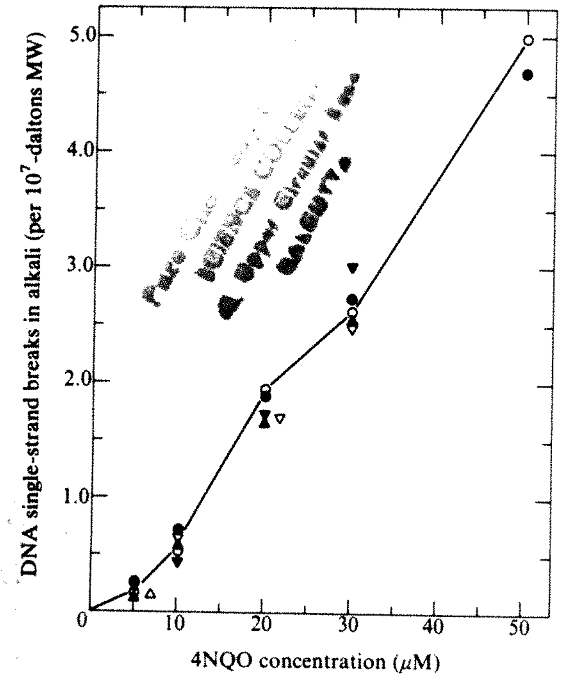

Fig. 2 4NQO dose-dependent induction of alkali-labile lesions in the DNA of normal, AT and XP fibroblasts. Cells were grown for ~48 h at 37 °C in medium containing either (*Me*-^{3}H]thymidine (1 μCi ml^{-1}; stock specific activity, 6.7 Ci/mmol^{-1}; NEN Canada) or [*Me*-^{14}C]thymidine (1 μCi ml^{-1}; 40.8 mCi mmol^{-1}; NEN). Tritium-labelled cultures (4 × 10^5–6 × 10^5 cells per 10-cm diameter dish) were exposed for 1 h to the appropriate concentrations of 4NQO as described in Fig. 1 legend. The ^{14}C-labelled control cultures were handled in a similar manner but not exposed to 4NQO. The parallel cultures were lysed and DNAs from the untreated control (^{14}C) and carcinogen-treated (^{3}H) cells were co-extracted with 0.5 M Tris-HCl (*p*H 8.0)-saturated phenol and dialysed against 0.05 M Na_2PO_4-1 mM EDTA buffer (*p*H 7.0). Co-extracted, radioactively labelled DNAs (100 μl) were incubated with unlabelled, sonicated calf thymus DNA (40 μl; 1 μg ml^{-1} stock; included to compete for any nonspecific nuclease activity) at 37 °C for 30 min followed by the addition of 1 M NaOH (100 μl). The DNAs were analysed by velocity sedimentation (40,000 r.p.m., 20 °C, 120 min in a Spinco SW-56 rotor driven by a Beckman L5-65 ultracentrifuge) in alkaline sucrose gradients (5–20%, w/v); 0.5 M NaCl, 0.2 M NaOH, 10 mM EDTA; *p*H adjusted to 12.5). After gradient fractionation and liquid scintillation counting, computer analysis of the gradient profiles yielded the number of strand breaks in alkali in the 4NQO-treated ^{3}H-DNA compared to the control ^{14}C-DNA. Data points represent arithmetic means of at least two separate determinations. ○, GM 38 (solid line); ▽, XP9RO (5 and 20 μM points offset for clarity); ▼, AT2BE, ▲, AT3BI; ●, AT4BI. s.e. for each datum point was ≤10%. MW, Molecular weight.

unstable guanine adduct appears to give rise to a DNA single-strand break in alkaline conditions[17,19,20]. The unstable 4NQO-guanine adducts are removed by a process(es) which may involve an ionizing radiation-like repair pathway(s)[9] and these defects are therefore candidates for the lethal lesions in the radiosensitive strains AT2BE and AT4BI. There is evidence in both bacterial[21] and mammalian cells[9,14] that the stable purine adducts are repaired by a UV-light-like excision repair pathway which leads to extensive DNA repair synthesis.

Figure 2 shows the 4NQO dose-dependent induction of single-strand breaks, detected in alkaline conditions, for several cell strains. The three AT strains examined all show similar levels of DNA damage to those of normal (GM 38) and XP (XP9RO) strains, despite their different sensitivities to the carcinogen.

Since the survival responses of AT strains to 4NQO could not be explained by differential susceptibility to DNA damage, we examined the repair kinetics of the alkali-labile lesions for the five strains (Fig. 3). In the normal strain (GM 38) and the AT strain of normal 4NQO sensitivity (AT3BI), fewer than 10% of the initial number of lesions remain 6 h after 4NQO treatment. Analysis of samples at incubation times longer than 6 h was sometimes complicated by anomalous sedimentation characteristics of the DNA preparations. For the two AT strains that

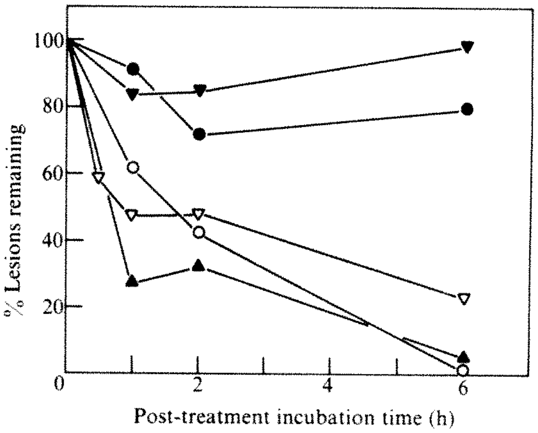

Fig. 3 Disappearance of 4NQO-induced alkali-labile lesions from the DNA of normal, AT and XP fibroblasts. The method is similar to that used to follow the repair of radiogenic single-strand breaks[8], and the protocol is detailed in Fig. 2 legend. Post-treatment incubation was in growth medium at 37 °C. Data points represent arithmetic means of multiple determinations indicated in parentheses: ○, GM 38 (6); ▼, AT2BE (4); ●, AT4BI (4); ▽, XP9RO (3); ▲, AT3BI (2). s.e. for each datum point was ≤15%.

are hypersensitive to 4NQO (AT2BE and AT4BI), more than 75% of the initial number of lesions remain 6 h after chemical treatment. This repair defect is also observed at lower 4NQO concentrations (data not shown). The XP strain displays an essentially normal rate of disappearance of this type of lesion. Thus, the cell survival responses of the three AT strains correlate with their ability to remove the carcinogen-induced alkali-labile DNA lesions.

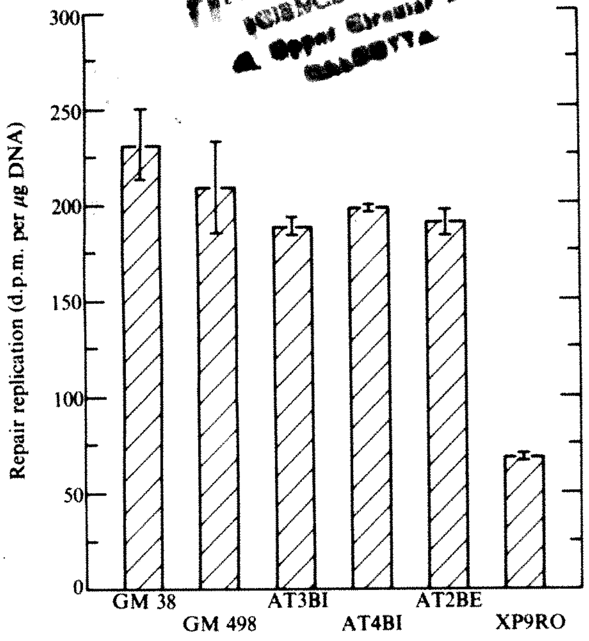

Fig. 4 DNA repair replication in normal, AT and XP fibroblasts exposed to 4NQO. The technique used was essentially that described for the measurement of γ-ray-induced DNA repair replication[8]. Repair replication is a measure of the incorporation of tritiated thymidine into non-replicating DNA during damage site repair. Growth medium was supplemented with 10% (v/v) dialysed calf serum rather than fetal bovine serum. Before 4NQO treatment, cultures (1×10^6–1.5×10^6 cells per 15-cm diameter dish) were incubated for 2 h in growth medium containing 6.5 μM 5-bromodeoxyuridine (BUdR) and 1 μM 5-fluorodeoxyuridine (FUdR). After exposure for 1 h to 30 μM 4NQO, repair was followed in the presence of 6.5 μM BUdR, 1 μM FUdR, 1 mM hydroxyurea and 10 μCi ml^{-1} [*Me*-^{3}H]thymidine (stock specific activity, 41 Ci mmol^{-1}; NEN) for 2 h at 37 °C. The labelling medium was then removed, and the cells were incubated for a further 1 h in medium containing 6.5 μM BUdR and 1 μM FUdR. DNA was then isolated for density gradient centrifugation by lysing the collected cells and extracting in chloroform–isoamyl alcohol. Neutral NaI gradients were prepared (6.2 ml containing 0.22 mM Na_2SO_3, 10–20 μg extracted human DNA, 0.1 mg ethidium bromide, 4.69 g NaI, adjusted to a final density of 1.54 g cm^{-3}) and centrifuged (33,000 r.p.m. at 30 °C; ≥60 h in a Spinco Type 40 rotor). The gradients were each fractionated into 18 tubes for the estimation of DNA concentration in a spectrofluorometer (Mk 1; Farrand Optical Co.). One rebanding of 'light' parental DNA was carried out to reduce contamination by 'heavy' DNA arising from semiconservative *de novo* DNA synthesis. Rebanding involved: (1) pooling six fractions containing light DNA per gradient; (2) dialysis overnight against 10 mM Tris-0.15 M NaCl-10 mM EDTA (*p*H 7.5) buffer; (3) preparation; and (4) centrifugation of NaI gradients as above. The rebanded samples were again fractionated and DNA concentration measured. Gradient fractions were transferred into ice-cold 10% trichloroacetic acid and 10 mM $Na_2P_2O_4$ and the precipitated, radioactive DNA collected on Whatman GF/C filter papers, and counted by liquid scintillation in toluene-Scintiprep 2 (Fisher Scientific). Histograms represent the arithmetic mean (background corrected) of two determinations for each designated strain with the range denoted by error bars.

Repair replication (a measure of repair synthesis) was measured for 2 h following exposure of cultures to 30 μM 4NQO. The results shown in Fig. 4 indicate that the technique clearly detects the defect in repair synthesis expressed by an XP cell strain[22–24]. However, there was no significant difference between the levels of repair in the two normal controls and the levels in the three AT cell strains. Since the expression of repair synthesis is considered to reflect largely the repair, by UV-like pathways, of the stable 4NQO-purine adducts[14], we conclude that such lesions are repaired with normal efficiency in AT strains. This view, that UV-like repair pathways are not defective in AT strains, is consistent with observations that far UV-induced repair synthesis is not reduced in AT strains[8,16] compared with normal cells.

As a DNA damaging chemical, 4NQO shows potential as a screening agent for DNA repair deficiencies in human cells. Its usefulness is facilitated in part by: (1) its dual UV-mimetic and radiomimetic properties, (2) its direct relevancy to carcinogenesis-related studies, and (3) the defined range of induced DNA lesions whose repair can be independently monitored.

Our data point to the presence in some AT cell strains of a defect in the repair of the unstable class of 4NQO–guanine adducts. We propose that the repair defect lies in the initial enzymatic release of the base adduct. Our results provide the first evidence of the nature of the putative DNA repair defect in AT4BI. Genetic heterogeneity in the repair abilities of AT strains following γ-ray or 4NQO treatment may be explained on the basis of deficiencies in either a pathway which handles γ-ray damage (for example, in AT3BI) or a pathway which handles γ-ray and 4NQO damage (for example, in AT2BE and AT4BI). Future research into the cellular and DNA repair properties of AT cells should provide a greater insight into the role of host and environmental factors in the process of neoplastic transformation and neurological degeneration.

P. J. S. was a Postdoctoral Fellow of the Natural Sciences and Engineering Research Council Canada.

GM 38 and GM 498 were from the Human Genetic Mutant Cell Repository, Institute for Medical Research, Camden, New Jersey; AT2BE (CRL 1343) was from the American Type Culture Collection; AT3BI was supplied by Dr A. R. Lehmann, AT4BI by Dr A. M. R. Taylor, and XP9RO (complementation group C[16]) was a gift from Dr D. Bootsma. Cell culture supplies were from Microbiological Associates.

Received 30 May; accepted 7 August 1980.

1. Kraemer, K. H. in *DNA Repair Processes* (eds Nichols, W. N. & Murphy, D.) 37–71 (Symp. Spec., New York, 1977).
2. Paterson, M. C. & Smith, P. J. *A. Rev. Genet.* **13,** 291–318 (1979).
3. Gotoff, S. P., Amirmokri, E. & Liebner, E. J. *Am. J. Dis. Child.* **114,** 617–625 (1967).
4. Morgan, J. L., Holcomb, T. M. & Morrissey, R. W. *Am. J. Dis. Child.* **116,** 557–558 (1968).
5. Cunliffe, P. N., Mann, J. R., Cameron, A. H., Roberts, K. D. & Ward, H. W. C. *Br. J. Radiol.* **48,** 374–376 (1975).
6. Taylor, A. M. R. *et al. Nature* **248,** 427–429 (1975).
7. Paterson, M. C., Anderson, A. K., Smith, B. P. & Smith, P. J. *Cancer Res.* **39,** 3725–3734 (1979).
8. Paterson, M. C., Smith, B. P., Lohmann, P. H. M., Anderson, A. K. & Fishman, L. *Nature* **260, 444–447** (1976).
9. Regan, J. D. & Setlow, R. B. *Cancer Res.* **34,** 3318–3325 (1974).
10. Paterson, M. C., Smith, B. P., Knight, P. A. & Anderson, A. K. in *Research in Photobiology* (ed. Castellani, A.) 207–218 (Plenum, New York, 1977).
11. Bootsma, D., Mulder, M. P., Pot, F. & Cohen, J. A. *Mutat. Res.* **9**, 507–516 (1970).
12. Smith, P. J. & Paterson, M. C. *Cancer Res.* (submitted).
13. Takebe, H., Furuyama, J.-I., Miki, Y. & Kondo, S. *Mutat. Res.* **15,** 98–100 (1972).
14. Ikenaga, M., Takebe, H. & Ishii, Y. *Mutat. Res.* **43,** 415–427 (1977).
16. De Weerd-Kastelein, E. A., Keijzer, W. & Bootsma, D. *Nature new Biol.* **23,** 80–83 (1972).
15. Hoar, D. I. & Sargent, P. *Nature* **261,** 590–592 (1976).
16. Scudiero, D. A. in *DNA Repair Mechanisms* (eds Hanawalt, P. C., Friedberg, E. C. & Fox, C. F.) 655–658 (Academic, New York, 1978).
17. Tada, M. & Tada, M. *Chem.-Biol. Interact.* **3,** 225–229 (1971).
18. Tada, M. & Tada, M. *Nature* **255,** 510–512 (1975).
19. Horikawa, M., Nikaido, O., Tanaka, T., Nagata, H. & Sugahara, T. *Expl Cell Res.* **59,** 147–152 (1970).
20. Walker, I. G. & Sridhar, R. *Chem.-Biol. Interact.* **12,** 229–239 (1976).
21. Ikenaga, M., Ichikawa-Ryo, H. & Kondo, S. *J. molec. Biol.* **92,** 341–356 (1975).
22. Stich, H. F. & San, R. H. C. *Mutat. Res.* **13,** 279–282 (1971).
23. Cleaver, J. E. *Cancer Res.* **33,** 362–369 (1973).
24. Stich, H. F., San, R. H. C. & Kawazoe, Y. *Mutat. Res.* **17,** 127–137 (1973).
25. Kleijer, W. J., Lohman, P. H. M., Mulder, M. P. & Bootsma, D. *Mutat. Res.* **9,** 517–523 (1970).

Dimeric tRNA precursors in yeast

Otto Schmidt*, Jen-i Mao*, Richard Ogden†, Jacques Beckmann†, Hitoshi Sakano†, John Abelson† & Dieter Söll*

*Department of Molecular Biophysics and Biochemistry,
Yale University, New Haven, Connecticut 06511
†Department of Chemistry, University of California, San Diego,
La Jolla, California 92037

Two DNA fragments, each containing a tRNA$_3^{Arg}$ and a tRNA^{Asp} gene in close conjunction, have been isolated from different genomic regions of *Saccharomyces cerevisiae*[1]. Nucleotide sequence analysis of the gene regions revealed that in both fragments the tRNA$_3^{Arg}$ coding region is located 5′-proximal to the tRNA^{Asp} coding region. They are separated by an identical spacer of 10 nucleotides. Although the 5′-flanking sequences are different in the two plasmids, some similarities are observed. To test the mode of expression of this gene configuration, we transcribed the DNA fragments in a *Xenopus* oocyte nuclear extract[2,3]. Specific transcription of the yeast tRNA genes took place in an RNA precursor which comprised both tRNA species. We report here that the precursor RNA was processed to the mature-sized tRNA molecules, indicating the presence of an enzyme activity in the *Xenopus* nucleus capable of cutting a dimeric tRNA precursor. This is the first observation of a eukaryotic dimeric tRNA precursor.

The tRNA genes of several eukaryotes have recently been shown to be organized in a variety of ways. In some cases, such as *Drosophila* and *Xenopus*, multiple copies of the same gene or a number of different genes are clustered[4–7]. On the other hand, in nematode[8], silkworm[9,10] and yeast[1], tRNA genes generally seem to be scattered throughout the genome. Pulse-chase experiments of RNA in mammalian cells[11] and UV-light mapping studies of transcription units in yeast[12] have shown that dimeric or multimeric tRNA precursors are very unlikely to exist. In addition, *in vivo* and *in vitro* transcription studies in the *Xenopus* system have determined that eukaryotic tRNA genes are organized as single transcription units[3,6–10,13–15].

The recombinant pBR313 plasmids pJB18u and pJB19f contain *Hin*dIII fragments of *S. cerevisiae* DNA[1]. Hybridization patterns of [5′-^{32}P]tRNA to Southern blots of different DNA fragments from these plasmids suggested that the coding sequences for tRNA$_3^{Arg}$ and tRNA^{Asp} are located in adjacent positions[16] and that they may be co-transcribed. The plasmid pJb18u contains, in addition, a tRNA^{Tyr} gene about 1 kilobase upstream of the tRNA$_3^{Arg}$ and tRNA^{Asp} genes[16]. The DNA around the tRNA$_3^{Arg}$ and tRNA^{Asp} position has been sequenced in both plasmids (Fig. 1). Up to position −12 the 5′ flanking sequences are almost identical, but further out differ considerably in the two plasmids. This confirms the results of restriction enzyme analysis that the *Hin*dIII fragments in pJB18u and pJB19f derive from unique sites in the *S. cerevisiae* genome. In both plasmids the tRNA$_3^{Arg}$ coding sequence is 5′-proximal to the tRNA^{Asp} coding sequence. They are separated by an identical 10-nucleotide spacer in pJB19f and pJB18u. The two plasmids contain the same tRNA coding sequences which are identical to the known tRNA$_3^{Arg}$ (ref. 17) and tRNA^{Asp} (ref. 18) sequences. As in most other eukaryotic tRNA genes, the 3′-flanking sequences in both clones contain an oligothymidylate sequence which is probably a transcription termination signal for RNA polymerase III[9,10,13,19].

The transcription of these tRNA genes was tested in a nuclear extract of *Xenopus* oocytes[2,3]. The radioactive RNA was separated by polyacrylamide gel electrophoresis as shown in Fig. 2. Four major products designated RNA-1, RNA-2, RNA-3 and RNA-4 were observed. Using yeast 5S, yeast 5.8S and tRNA precursors of known length[20] as markers, the length of RNA-1 was determined to be 170 ± 10 nucleotides.

The first evidence that RNA-1 is a precursor to the tRNA-sized transcripts came from a pulse-chase experiment. After incubation with [α-^{32}P]CTP for 1 h, an excess of unlabelled CTP was added and the reaction allowed to proceed for another 2 h (Fig. 2). It is evident that RNA-1 and RNA-2 are less prominent in the chase experiment, indicating a precursor–product relationship to RNA-3 and RNA-4. This result was confirmed by reincubation of isolated radioactive RNA-1 in GV extract, which led to formation of RNA-3 and RNA-4 (not shown).

The nucleotide sequence of these RNA species was established by conventional methods[21] and compared with the DNA sequence. The RNase T$_1$ fingerprint of RNA-1 displayed all the fragments expected for the two tRNAs (Fig. 3*a*, Table 1). In addition, the fragments CUUUG (fragment 4) and UUCUUCCG (in fragment 2) were present indicating that the spacer sequence between the two tRNA coding regions is transcribed. The fact that the mature 5′ end of the tRNA^{Arg} is not found in RNA-1 implicates additional nucleotides in the form of a leader sequence. RNA-4 contained all the RNase T$_1$ fragments of tRNA^{Asp} (Fig. 3*c*). Analysis of a separate [α-^{32}P]CTP-labelled RNA-4 revealed the mature ends to be pUCCG, which apparently co-migrates with CUUG (fragment 6), and CCA$_{OH}$ (Table 1). Additional evidence that the 3′ end contains the CCA$_{OH}$ oligonucleotide derives from the fact that the preceding RNase T$_1$ fragment (AG) is labelled in this RNA (Table 1)

SCIENCE COLLEGE
Upper Circular Road
CALCUTTA

Fig. 1 Nucleotide sequences of the anticoding strand of the tRNA$_3^{Arg}$–tRNA^{Asp} genes from plasmids pJB18u and pJB19f. They are aligned according to the tRNA coding sequences (boxed). The chemical degradation method of Maxam and Gilbert[24] was used for DNA sequencing. The pJB18u sequence was determined from a *Taq*I site at position 55 in opposite directions for ~110 nucleotides. The elucidation of the pJB19f sequence of a *Cla*I–*Hpa*I subfragment (440 base pairs) was done from the *Cla*I (position −235), the *Hpa*I (position 199), the *Hae*III (position −119) and the *Sau*3AI (position 127) site. The identity of each nucleotide was determined at least twice.

```
              -230      -220      -210      -200      -190      -180      -170
PJB 18U   5'-----------------------------------------------------------------------
PJB 19F   5'-ATCGATGTGTGTTATATGTACCTCTGCTTTGCAGTATAAGAAATTTACATTTATTTCTGACTAATAACACCTTG

          -160      -150      -140      -130      -120      -110      -100      -90
PJB 18U   --------------------------------------------------------------------------
PJB 19F   GTGCCCCAACGGTAAACAACTTGTATCAGTTCTCATAAGTGCGGCCATTTTATGCAATACAGGCTGCATTATTTCACCAG

           -80       -70       -60       -50       -40       -30       -20       -10
PJB 18U   ---------------------------AATTGGTGAAATCAAAGCATAGTTTACCTTTAATCCCAATCTTCCAACAAACA
PJB 19F   CCGTGAAAATCCGAAAATTGTAGTAATTGAAAGCGTAATTAGGTTTTACTATAATAAAGTAGTAAAACCTTCAACAAATA

             1 ARG 10        20        30        40        50        60        70
PJB 18U   GTA|GCTCGCGTGGCGTAATGGCAACGCGTCTGACTTCTAATCAGAAGATTATGGGTTCGACCCCCATCGTGAGTG|CTTTG
PJB 19F   GTA|GCTCGCGTGGCGTAATGGCAACGCGTCTGACTTCTAATCAGAAGATTATGGGTTCGACCCCCATCGTGAGTG|CTTTG

           80  ASP 90       100       110       120       130       140       150
PJB 18U   TTTCT|TCCGTGATAGTTTAATGGTCAGAATGGGCGCTTGTCGCGTGCCAGATCGGGGTTCAATTCCCCGTCGCGGAG|CTT
PJB 19F   TTTCT|TCCGTGATAGTTTAATGGTCAGAATGGGCGCTTGTCGCGTGCCAGATCGGGGTTCAATTCCCCGTCGCGGAG|ATT

          160       170       180       190       200
PJB 18U   TTTTT-----------------------------------------3'
PJB 19F   TTTTTGGCTACTCCTGTAGTTATTCTTCATTAATGCTTTGTTAAC-3'
```

0028-0836/80/430750—03$01.00

Table 1 Analysis of RNase T$_1$ fragments

Fragment		RNA-1		RNA-3			RNA-4		
No.	Sequence*	Labelled with [α-^{32}P]GTP†	Deduced‡	Labelled with [α-^{32}P]GTP*†	[α-^{32}P]CTP*†	Deduced‡	Labelled with [α-^{32}]GTP†	[α-^{32}]CTP†	Deduced‡
1	ACUUCUAAUCAG UUCAAUUCCCCG	AG, C	ACUUCUAAUCAG UUCAAUUCCCCG	AG	AAU, AC, U	ACUUCUAAUCAG	C	C, U	UUCAAUUCCCCG
2	UUUAAUG UUUCUUCCG	AAU, G, C	UUUAAUG UUUCUUUCCG	—	—		AAU, G	—	UUUAAUG*G*
3	AUUAUG	AU, G	AUUAUG*G*	AU, G	—	AUUAUG*G*	—	—	
4	CUUUG	U	CUUUG	—	—		—	—	
5	UAAUG	AAU, G	UAAUG*G*	AAU, G	—	UAAUG*G*	—	—	
6	UUCG, UCUG, CUUG	C, U	UUCG, UCUG, CUUG	C, U	G, U	UUCG, UCUG	U	—	CUUG
7	ACCCCCAUCG	C	ACCCCCAUCG	C	AC, AU, C	ACCCCCAUCG	—	—	
8	AAUG, AUAG	AAU, AG, G	AAUG*G*, AUAG	—	—		AAU, AG, G	—	AAUG*G*, AUAG
9	AUCG, UCAG	AG, G, C	AUCG*G*, UCAG	—	—		AG, G, C	AU, U	AUCG*G*, UCAG
10		AU	AUG§	AU	—	AUG§	—	—	
11	CUCG	C	CUCG	C	G, U	CUCG*C*	—	—	
12	UAG	AG	UAG	—	—		—	—	
13	UCG	C	UCG	—	—		C	G, U	UCG*C*
14	UG	G, U	UG, UG*G*	G, U	G	UG*C*, UG*G*	U	G	UG*C*
15	CAACG	AAC	CAACG	AAC	AAC, G	CAACG*C*	—	—	
16	CCAG	AG	CCAG	—	—		AG	C	CCAG
17	AAG	AAG	AAG	AAG	—	AAG	—	—	
18		AG	CAG§	AG	—	CAG§	—	—	
19	AG	AG	AG	AG	—	AG	AG	AG	AG*C*
20	CG	C	CG, CG*G*	C	—	CG	G, C	—	CG*G*
21	G	G	G	G	G	G	G	G	G
22	CCA$_{\mathrm{OH}}$	—	—	—	C	CCA$_{\mathrm{OH}}$	—	C	CCA$_{\mathrm{OH}}$

* From DNA sequence.
† Digested with RNase A.
‡ Bases in italics were deduced from nearest neighbour analysis.
§ These are overdigestion products of fragments 1 and 3.

although its nearest 3′ neighbour is A in the original transcript. An RNase T$_1$ fingerprint of RNA-3 (Fig. 3*d*) revealed all the oligonucleotides for tRNA$_3^{\mathrm{Arg}}$ (Table I) including the mature 5′ end (pGp). Furthermore, the CCA$_{\mathrm{OH}}$ oligonucleotide was found in a [α-^{32}P]CTP-labelled RNA (Table 1). Preliminary fingerprint analysis indicates that RNA-2 contains a mixture of the tRNA species and probably represents the cleavage product from the dimeric precursor. However, other events, such as transcription termination in the intergenic spacer region, cannot be ruled out.

Thus, the sequence analysis of the transcription products confirms the notion that the two RNA sequences are contained in a large transcription product including the spacer and probably flanking sequences. We suggest that dimeric tRNA precursors do exist in yeast, although they are not abundant. The dimeric transcript is processed in the nuclear extract to yield the

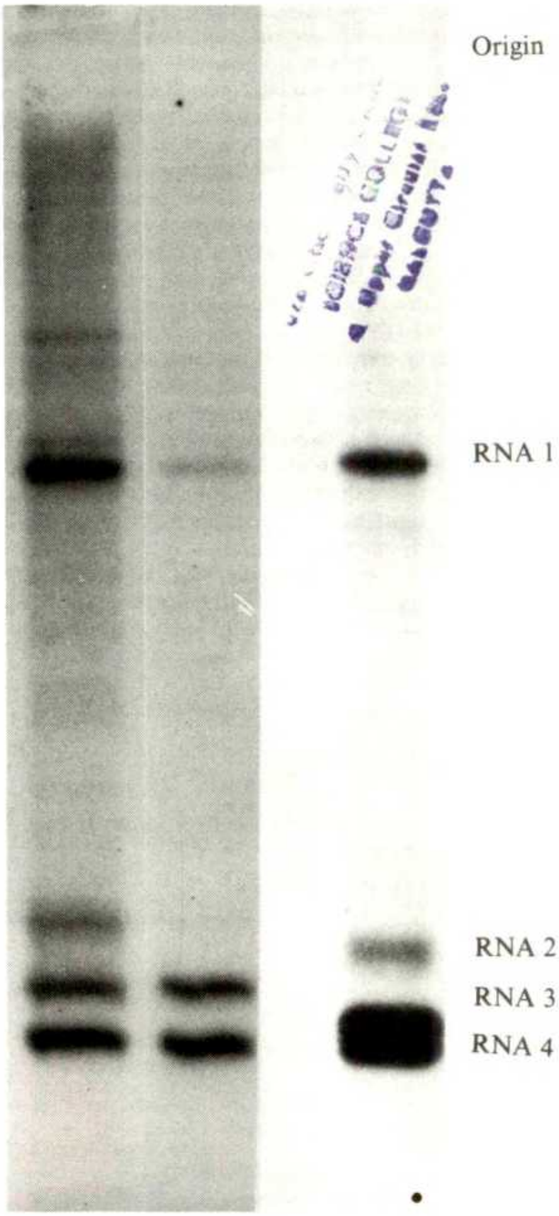

Fig. 2 Transcription and processing in *Xenopus* nuclear extracts. Autoradiograms of RNA transcribed from plasmids pJB18u and pJB19f in a variety of conditions separated on 10% polyacrylamide–4 M urea gels. The transcription reactions (40 µl) contained 30-µl GV extracts, 1 µg DNA, ATP, UTP, and GTP (0.03 mM each) and [α-^{32}P]CTP (0.01 mM, 40 Ci mmol^{-1}) in NH_4Cl (70 mM), $MgCl_2$ (7 mM), EDTA (0.1 mM), HEPES (10 mM, *p*H 7.4), dithiothreitol (2.5 mM) and 1% polyvinylpyrrolidone. After incubation at 22 °C for the specified length of time, the RNA was extracted[14] and separated by electrophoresis. Lane 1, pJB19f transcription for 1 h; lane 2, after 1 h in pJB19f transcription, reaction (lane 1) was supplemented with cold CTP and the incubation continued for a further 2 h; lane 3, pJB18u transcription for 1 h and separated on a different gel without urea.

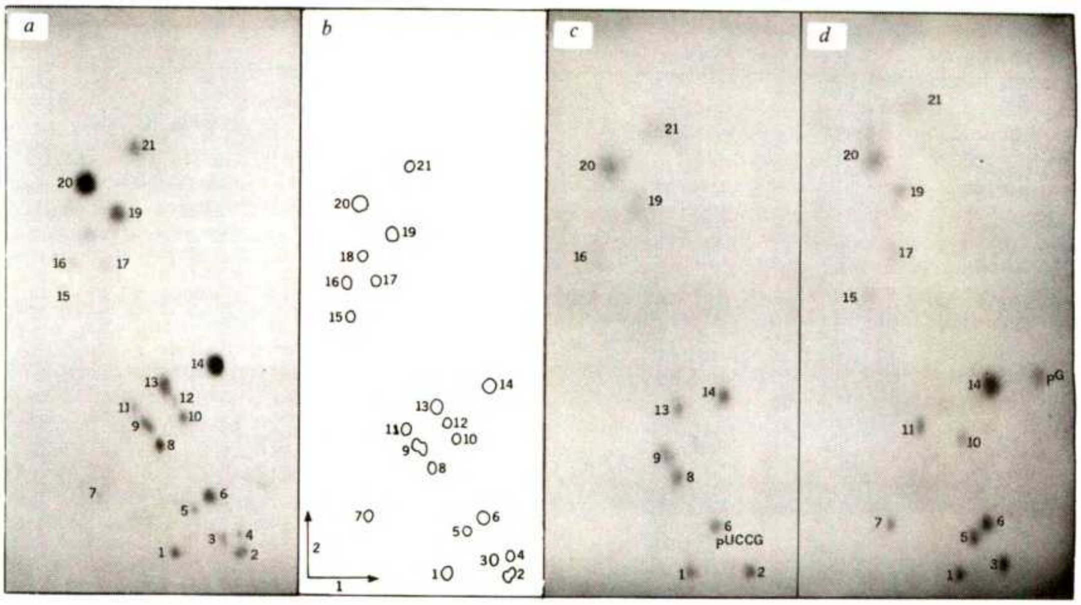

Fig. 3 RNase T_1 fingerprints of: *a*, RNA-1; *c*, RNA-4; *d*, RNA-3 of pJB19f DNA transcripts labelled with [α-^{32}P]GTP. *b* Is a diagram of a fingerprint of RNA-1. The numbering corresponds to that in Table 1. Standard RNA fingerprint separations were by electrophoresis on cellulose acetate at *p*H 3.5 (I) and on DEAE-cellulose at *p*H 1.7 (II).

Pure Chemistry Library
SCIENCE COLLEGE
92 Upper Circular Road
CALCUTTA

mature-sized tRNA molecules. A number of nucleotide modifications are also found in these RNA species. Analysis of C-labelled RNA-3 and RNA-4 revealed ψ and m^{1}A residues present in the position expected from the sequence of the mature tRNAs[17,18]. It is not known whether a specific endonuclease activity is required to cleave the dimeric precursor or whether the nucleases processing monomeric transcripts can perform this function. The analysis of a different dimeric tRNA precursor in *Schizosaccharomyces pombe* indicated an endonuclease activity to cleave at the 5′ end of the second tRNA[20]. This activity, together with the activities involved in the processing of the 3′-flanking sequences are present in the nuclear extract[9,10,17]. Therefore, these processing steps are likely to occur in the nucleus, which has also been shown by *in vivo* experiments[22].

As these experiments involved a heterologous system, the results need to be confirmed in a yeast transcription system or by Northern hybridization analysis[23] of yeast RNA. Our results agree with the existence of tRNA-related yeast RNA species of greater than 5S RNA size, which have been shown in short *in vivo* pulse-labelling experiments (R. M. Bock, personal communication).

We thank Frank Horodyski for initial mapping of pJB18u and Beverly Harrell for initial mapping of pJB19f. O.S. was a Postdoctoral Fellow of the Deutsche Forschungsgemeinschaft.

Received 14 April; accepted 22 July 1980.

1. Beckmann, J. S., Johnson, P. F. & Abelson, J. *Science* **196,** 205 (1977).
2. Birkenmeier, E. H., Brown, D. D. & Jordan, E. *Cell* **15,** 1077 (1978).
3. Schmidt, O., Mao, J., Silverman, S., Hovemann, B. & Söll, D. *Proc. natn. Acad. Sci. U.S.A.* **75,** 4819 (1978).
4. Yen, P. H. *et al. Cell* **11,** 763 (1977).
5. Hovemann, B., Sharp, S., Yamada, H. & Söll, D. *Cell* **19,** 889 (1980).
6. Tener, G. M. *et al.* in *Transfer RNA: Biological Aspects* (eds Söll, D., Abelson, J. & Schimmel, P.) 295 (Cold Spring Harbor Laboratory, New York, 1980).
7. Müller, F. & Clarkson, S. G. *Cell* **19,** 345 (1980).
8. Cortese, R., Melton, D., Tranquilla, T. & Smith, J. D. *Nucleic Acids Res.* **5,** 4593 (1978).
9. Garber, R. L. & Gage, L. P. *Cell* **18,** 817 (1979).
10. Hagenbüchle, O., Larson, D., Hall, G. & Sprague, K. *Cell* **18,** 1217 (1979).
11. Bernhardt, D. & Darnell, J. E. *J. molec. Biol.* **42,** 43 (1969).
12. Feldmann, H. *Nucleic Acids Res.* **4,** 2831 (1977).
13. De Robertis, E. M. & Olson, M. V. *Nature* **278,** 137 (1979).
14. Ogden, R. C. *et al. Cell* **17,** 399 (1979).
15. Telford, J. L. *et al. Proc. natn. Acad. Sci.* **76,** 2590 (1979).
16. Beckmann, J. S. *et al.* in *Nonsense Mutations and tRNA Suppressors* (eds Celis, J. E. & Smith, J. D.) 207 (Academic, New York, 1979).
17. Keith, G. & Dirheimer, G. *Biochem. biophys. Res. Commun.* **92,** 116 (1980).
18. Gangloff, J., Keith, G., Ebel, J. P. & Dirheimer, G. *Biochim. biophys. Acta* **259,** 210 (1972).
19. Silverman, S., Schmidt, O., Söll, D. & Hovemann, B. *J. biol. Chem.* **254,** 10290 (1979).
20. Mao, J., Schmidt, O. & Söll, D. *Cell* **20,** 589 (1980).
21. Brownlee, G. G. in *Laboratory Techniques in Biochemistry and Molecular Biology* (eds Work, T. S. & Work, E.) 67 (Elsevier, New York, 1972).
22. Melton, D. A., De Robertis, E. M. & Cortese, R. *Nature* **284,** 143 (1980).
23. Alwine, J. C. *et al. Meth. Enzym.* **68,** 220 (1979).
24. Maxam, A. M. & Gilbert, W. *Proc. natn. Acad. Sci. U.S.A.* **74,** 560 (1977).

The protein-coding sequence of the bovine ACTH-β-LPH precursor gene is split near the signal peptide region

Shigetada Nakanishi, Yutaka Teranishi, Masaharu Noda, Mitsue Notake, Yumiko Watanabe, Hitoshi Kakidani, Hisato Jingami & Shosaku Numa

Department of Medical Chemistry, Kyoto University Faculty of Medicine, Kyoto 606, Japan

The pituitary hormones corticotropin (ACTH) and β-lipotropin (β-LPH) are formed from a large common precursor[1–8]. Recently, we have elucidated the whole primary structure of the bovine ACTH-β-LPH precursor (designated alternatively as preproopiocortin) by determining the nucleotide sequence of cloned DNA complementary to the mRNA coding for the precursor protein[9]. The amino acid sequence assigned has disclosed a characteristic repetitive structure of the ACTH-β-LPH precursor. The repetitive units of the precursor protein each contain a melanotropin (MSH) sequence (α-, β- or γ-MSH) as well as other peptide components such as β-endorphin and corticotropin-like intermediate lobe peptide (CLIP). The repetitive units as well as their peptide components are each bounded by paired basic amino acid residues, which apparently represent the sites of proteolytic processing. Several studies[10] have confirmed the translational initiation site and protein structure assigned (see also ref. 11 and refs therein). In view of the recent knowledge about the organization of eukaryotic genes (see refs 12, 13 for reviews), it would be of particular interest to investigate the relationship between the repetitive structure of the ACTH–β-LPH precursor containing different functional components and the arrangement of the protein-coding sequence in its gene. We have now isolated and characterized bovine genomic DNA fragments encoding this precursor protein and have demonstrated that the protein sequence is encoded by two non-consecutive DNA segments. An intron (intervening sequence) of approximately 2.2 kilobase pairs separates the smaller exon (mRNA-coding sequence), which contains the gene sequence encoding the signal peptide, from the larger exon, which contains the gene sequence for most of the protein structure, including the known biologically active component peptides.

Calf thymus DNA was digested with various restriction endonucleases or their combinations and then subjected to agarose gel electrophoresis. DNA fragments containing an ACTH–β-LPH precursor gene sequence were identified by the Southern blotting method[14] with the cloned cDNA (*Pst*I-excised insert of plasmid pSNAC20[8]) as a probe. Three hybridization-positive *Eco*RI fragments of 0.9, 1.5 and 3.5 kilobase pairs were detected. For further characterization of these fragments, we used two additional probes produced by *Eco*RI digestion of the cDNA insert, which has a single *Eco*RI site corresponding to the carboxy-terminal amino acid residues of ACTH[9]. The cDNA segment representing the 5′ side of the mRNA (AL_L) hybridized exclusively to the 0.9 and 3.5-kilobase pair fragments, whereas that representing the 3′ side of the mRNA (AL_R) hybridized exclusively to the 1.5-kilobase pair fragment (for the AL_L and AL_R segments, see Fig. 1*e*). Further restriction patterns obtained with various endonucleases and their combinations enabled us to construct a restriction map of the ACTH–β-LPH precursor gene as shown in Fig. 1*a*. The 0.9- and the 1.5-kilobase pair fragments are adjacent to each other and are located on the left and the right side, respectively, of the unique *Eco*RI site present within the protein-coding sequence. The 3.5-kilobase pair fragment is positioned to the left of the 0.9-kilobase pair fragment.

To characterize the structural organization of the ACTH–β-LPH precursor gene, we isolated DNA clones carrying each of the three *Eco*RI fragments (for the cloning procedure, see Fig. 1 legend). Comparative restriction mapping with the Southern blotting technique confirmed that the cloned DNA fragments retained the sequence organization found in the cellular DNA. In addition, hybridization-positive calf thymus DNA fragments prepared by partial *Eco*RI digestion yielded DNA clones carrying a 5.9-kilobase pair insert which contains the 3.5-, 0.9- and 1.5-kilobase pair fragments oriented consecutively in this order.

Figure 1*c* and *d* compare the restriction patterns of the cloned 0.9- and 1.5-kilobase pair fragments with those of the cDNA segments AL_L and AL_R, respectively. There was a clear one-to-one correspondence between some of the restriction fragments derived from the 1.5-kilobase pair fragment and all restriction fragments derived from the AL_R segment, except the fragment that contains the site corresponding to the 3′ end (poly(A) addition site) of the mRNA (Fig. 1*d*, *e*). A one-to-one

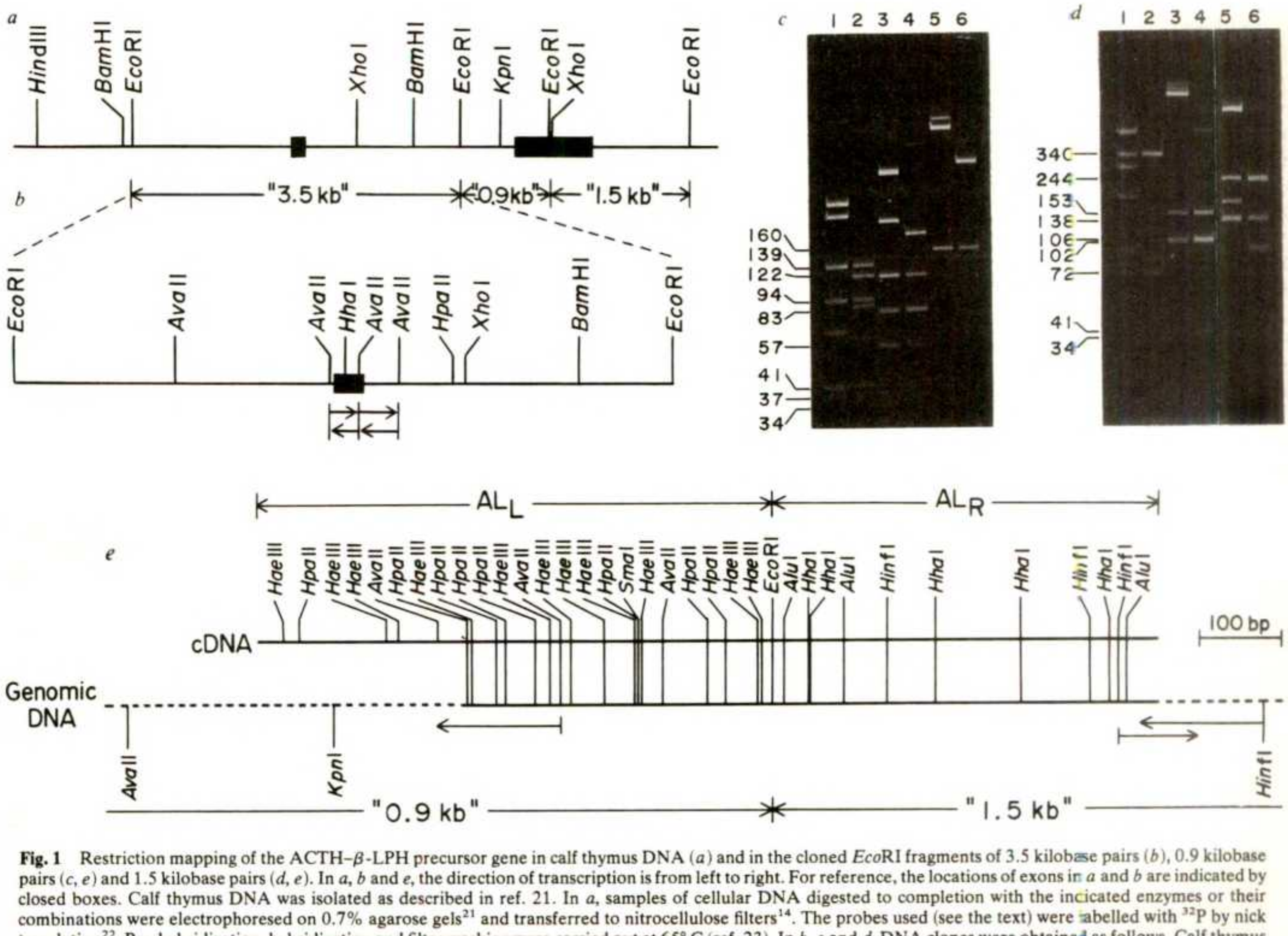

Fig. 1 Restriction mapping of the ACTH–β-LPH precursor gene in calf thymus DNA (*a*) and in the cloned *Eco*RI fragments of 3.5 kilobase pairs (*b*), 0.9 kilobase pairs (*c*, *e*) and 1.5 kilobase pairs (*d*, *e*). In *a*, *b* and *e*, the direction of transcription is from left to right. For reference, the locations of exons in *a* and *b* are indicated by closed boxes. Calf thymus DNA was isolated as described in ref. 21. In *a*, samples of cellular DNA digested to completion with the indicated enzymes or their combinations were electrophoresed on 0.7% agarose gels[21] and transferred to nitrocellulose filters[14]. The probes used (see the text) were labelled with ^{32}P by nick translation[22]. Pre-hybridization, hybridization and filter washing were carried out at 65° C (ref. 23). In *b*, *c* and *d*, DNA clones were obtained as follows. Calf thymus DNA fractions containing the *Eco*RI fragments of 3.5, 0.9 or 1.5 kilobase pairs were isolated by preparative agarose gel electrophoresis[21] and ligated to the purified *Eco*RI arms of bacteriophage λgtWES·λB (ref. 24). The recombinant DNA was packaged *in vitro* into viable phage[25], which were screened by hybridization with ^{32}P-labelled cDNA[26]. Each *Eco*RI fragment was isolated from these recombinant phage and subcloned in pBR322 (ref. 27). In *b*, samples of the 3.5-kilobase pair ("3.5 kb") fragment digested with the indicated enzymes or their combinations were electrophoresed on 5% polyacrylamide gels[9] or on 0.7% agarose gels[21] and were stained with 0.1% ethidium bromide. The *Ava*II sites were located by partial digestion of the *Eco*RI–*Hpa*II fragment on the left side; the *Hpa*II end was 5′-^{32}P-labelled. The horizontal arrows indicate the direction and extent of sequence determinations. In *c*, samples of the 0.9-kilobase pair ("0.9 kb") fragment (lanes 1, 3, 5) and the AL_L segment (lanes 2, 4, 6) were digested with *Hae*III (lanes 1, 2), *Hpa*II (lanes 3, 4) or *Sma*I (lanes 5, 6). The resulting restriction fragments were electrophoresed on 5% polyacrylamide gel[9] and stained as described above. Restriction fragments common between the cloned genomic DNA and cDNA are indicated on the left side of the electropherogram by their sizes in base pairs (bp). Faint bands observed in the upper region of the gel are due to incomplete digestion of the DNA. In *d*, samples of the 1.5-kilobase pair ("1.5 kb") fragment (lanes 1, 3, 5) and the AL_R segment (lanes 2, 4, 6) were digested with *Alu*I (lanes 1, 2), *Hha*I (lanes 3, 4) or *Hin*fI (lanes 5, 6). Other details were as described for *c*. In lane 4, the 3′-end-containing fragment was not separated from the fragments of 106 and 102 base pairs. In *e*, the restriction maps of the 0.9- and 1.5-kilobase pair fragments have been constructed on the basis of the data in *c* and *d* and the results of *Ava*II digestion. The dashed lines represent the regions where no correspondence between the restriction pattern of the cloned genomic DNA fragments and that of the cDNA was observed; in these regions, only the restriction sites used for DNA sequencing are shown. The horizontal arrows just below the line representing the genomic DNA indicate the direction and extent of sequence determinations. The portions of the AL_L and AL_R segments that correspond to the poly(dG)·poly(dC) tails and the poly(A) tail are not shown.

```
                                           Intron                       -131                                        -120
                                          <------|                      Met Pro Arg Leu Cys Ser Ser Arg Ser Gly Ala Leu
5'-----------------------------ATCTTGTTTGCCTCTGCAG AGCCTCAGCCTGCCTGGAAG ATG CCG AGA CTG TGC AGC AGT CGT TCG GGC GCC CTG
                                                 -413        -400

                                    -110                                    -100                                    -90
Leu Leu Ala Leu Leu Leu Gln Ala Ser Met Glu Val Arg Gly Trp Cys Leu Glu Ser Ser Gln Cys Gln Asp Leu Thr Thr Glu Ser Asn
CTG CTG GCC TTG CTG CTT CAG GCC TCC ATG GAA GTG CGT GGT TGG TGC CTG GAG AGC AGC CAG TGT CAG GAC CTC ACC ACG GAA AGT AAC
       -350                                                               -300

   -88                                                                         -87                         -80
    Intron                                                            Intron
Leu Leu |----->                                                      <------| Ala Cys Ile Arg Ala Cys Lys Pro Asp Leu Ser
CTG CTG GTACGTGGGCTGTGGCCGCCATCTTGATTT--------------------TCTGCCGCTCTCCGCAG GCG TGC ATC CGG GCC TGC AAG CCC GAC CTC TCC
    -262                                                                  -261        -250

                                                                   Poly(A)
Ala Glu Thr                                                           ↓
GCC GAG ACG──────────CTCTTAAAGCTGTCTGTAGTTAAGAAATAAAACCTTTCAAGTTTCACG AATATTGACTGGGTGAATTAAAAACG···········3'
       -220         530                 550                        577
```

Fig. 2 Nucleotide sequence of the exon and its surrounding regions in the 3.5-kilobase pair fragment, the exon–intron junction in the 0.9-kilobase pair fragment and the region corresponding to the 3′ end of the mRNA in the 1.5-kilobase pair fragment. 5′-End labelling of restriction fragments and DNA sequence analysis were carried out by the procedure of Maxam and Gilbert[28]. The sequencing strategy was as follows: for the 3.5-kilobase pair fragment, the two *Ava*II fragments containing the exon (see Fig. 1*b*) were labelled and denatured, and both strands of each *Ava*II fragment were sequenced (sequence between the two dashed lines); for the 0.9-kilobase pair fragment, the *Ava*II fragment containing the exon–intron junction was labelled and cleaved with *Kpn*I (see Fig. 1*e*), and the *Ava*II–*Kpn*I fragment containing the exon–intron junction was sequenced (sequence between the second dashed line and solid line); for the 1.5-kilobase pair fragment, the 3′-end-containing *Hin*fI fragment (see Fig. 1*e*) was labelled and denatured, and both strands were sequenced (sequence between the solid line and dotted line). The nucleotide sequence of the message strand is shown. Amino acid residues are numbered as in ref. 9. The numbers of nucleotide residues are those of the corresponding residues in the cDNA[9]. The solid line represents the exon sequence encoding the majority of amino acid residues and the 3′-noncoding segment of the mRNA. The dashed lines represent intron sequences, and the dotted line the 3′-flanking sequence. The exon–intron junctions indicated are positioned according to the GT/AG rule[16]. The redundant nucleotide residues at the exon-intron junctions and the residues corresponding to the ambiguous 3′ terminus of the mRNA are boxed. The nucleotide residues representing an inverted repeat are underlined.

correspondence was similarly observed between some of the restriction fragments derived from the 0.9-kilobase pair fragment and all restriction fragments derived from the AL_L segment that are located less than 0.37 kilobase pairs upstream from the unique *Eco*RI site (Fig. 1*c*, *e*). In contrast, the restriction fragments positioned further upstream in the AL_L segment were completely displaced by unidentical restriction fragments derived from the 0.9-kilobase pair fragment. In agreement with these results of restriction mapping, nucleotide sequence analysis located the 3′ end of the mRNA in the expected region of the 1.5-kilobase pair fragment, and an exon–intron boundary 373–374 nucleotide residues upstream from the right end of the 0.9-kilobase pair fragment (Fig. 2). We conclude, therefore, that one of the exons of the ACTH–β-LPH precursor gene is composed of 838–841 base pairs, which represent a major portion of the protein-coding sequence, specifying 221 amino acids from the alanine residue located 87 residues before the amino terminus of ACTH through the carboxyl terminus of the precursor protein, and the 3′-noncoding sequence of the mRNA. The site corresponding to the 3′ terminus of the mRNA cannot be uniquely defined because the first two residues of the poly(A) tail could be transcribed from the genomic DNA. The 10 nucleotide residues immediately preceding the poly(A) tail have 7 residues in common with the model sequence TTTTCACTGC proposed by Benoist *et al.*[15]. Note also the presence of an inverted repeat (a region of two-fold rotational symmetry) surrounding the 3′ end of the mRNA.

On the basis of restriction mapping of the cloned 3.5-kilobase pair fragment (Fig. 1*b*), a possible region containing the protein-coding sequence was located between 1.6 and 1.8 kilobase pairs upstream from the right end of this fragment. In fact, nucleotide sequence analysis of this region demonstrated a 156-base-pair sequence that corresponded precisely to the mRNA sequence starting 23 nucleotide residues upstream from the translational initiation codon (Fig. 2). Because the 3′-border sequence of this exon and the 5′-border sequence of the exon present in the 0.9-kilobase pair fragment form a consecutive sequence on the mature mRNA, we conclude that these two exons are separated by an intron of approximately 2.2 kilobase pairs on the genomic DNA. The border sequences of this intron exhibit a redundancy of two nucleotide residues. By appropriate selection of the splicing point, however, the intron follows the general rule proposed by Breathnach *et al.*[16]: it begins with a GT and ends with an AG dinucleotide.

Further mapping of the 3.5-kilobase pair fragment with restriction endonucleases known to cleave the region corresponding to the 5′-terminal sequence of the mRNA, in conjunction with the failure of the resulting restriction fragments to hybridize to a cDNA sequence in this region, indicated that the mRNA-coding sequence upstream from that of the smaller exon is not included in the 3.5-kilobase pair fragment. Our attempts to identify a DNA fragment(s) containing the 5′-terminal mRNA structure have been unsuccessful. This small mRNA-coding segment may have been missed due to the relative instability of the hybrid formed during the Southern filter analysis.

Our results on the structural organization of the ACTH–β-LPH precursor gene are summarized in Fig. 3. Comparison of the restriction sites and partial DNA sequence of the cloned genomic DNA fragments with the known structure of the cDNA has demonstrated that the protein-coding sequence of this gene is split into two portions by an intron of approximately 2.2 kilobase pairs. This intron is located within the region corresponding to the peptide structure that exhibits some homology to the hormone calcitonin (L. J. Deftos, personal communication and refs 11, 17) and thus separates the gene sequence encoding the signal peptide[18] from that encoding most of the protein sequence which includes different functional components corresponding to several biologically active peptides. A second intron is present within the region corresponding to the 5′-noncoding sequence of the mRNA as is the case for the ovalbumin gene[19]. Very recently, we have learned that Chang *et al.*[20] isolated a human genomic DNA segment containing a continuous sequence equivalent to the larger exon of the bovine ACTH–β-LPH precursor gene we identified.

This investigation was supported in part by research grants from the Ministry of Education, Science and Culture of Japan, the Mitsubishi Foundation and the Japanese Foundation of Metabolism and Diseases.

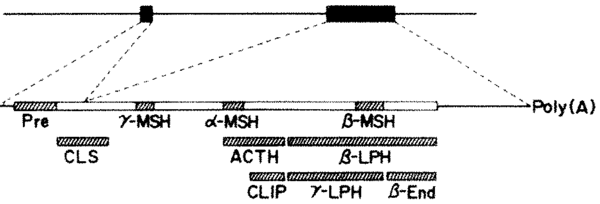

Fig. 3 Arrangement of the protein-coding regions in the bovine ACTH–β-LPH precursor gene. The exons are indicated by closed boxes on the upper line. For comparison, the topology of the mRNA is shown below. The shaded bars on and under the mRNA represent the regions coding for the component peptides of the ACTH–β-LPH precursor. Pre, signal peptide; CLS, calcitonin-like structure; β-End, β-endorphin.

Note added in proof: We have recently identified a third exon of 108 base pairs encoding the whole remaining 5′-terminal sequence of the mRNA by isolating additional bovine genomic DNA fragments and have thus confirmed the assigned position of the 3′ end of the proximal intron, which has a length of approximately 4 kilobase pairs.

Received 8 July; accepted 10 September 1980.

1. Nakanishi, S. *et al. Proc. natn. Acad. Sci. U.S.A.* **73,** 4319–4323 (1976).
2. Nakanishi, S., Inoue, A., Taii, S. & Numa, S. *FEBS Lett.* **84,** 105–109 (1977).
3. Taii, S., Nakanishi, S. & Numa, S. *Eur. J. Biochem.* **93,** 205–212 (1979).
4. Kita, T., Inoue, A., Nakanishi, S. & Numa, S. *Eur. J. Biochem.* **93,** 213–220 (1979).
5. Mains, R. E. & Eipper, B. A. *J. biol. Chem.* **251,** 4115–4120 (1976).
6. Mains, R. E., Eipper, B. A. & Ling, N. *Proc. natn. Acad. Sci. U.S.A.* **74,** 3014–3018 (1977).
7. Roberts, J. L. & Herbert, E. *Proc. natn. Acad. Sci. U.S.A.* **74,** 4826–4830, 5300–5304 (1977).
8. Nakanishi, S. *et al. Proc. natn. Acad. Sci. U.S.A.* **75,** 6021–6025 (1978).
9. Nakanishi, S. *et al. Nature* **278,** 423–427 (1979).
10. Nakamura, M., Inoue, A., Nakanishi, S. & Numa, S. *FEBS Lett.* **105,** 357–359 (1979).
11. Numa, S. & Nakanishi, S. *Biochem. Soc. Trans.* (in the press).
12. Crick, F. *Science* **204,** 264–271 (1979).
13. Dawid, I. B. & Wahli, W. *Devl Biol.* **69,** 305–328 (1979).
14. Southern, E. M. *J. molec. Biol.* **98,** 503–517 (1975).
15. Benoist, C., O'Hare, K., Breathnach, R. & Chambon, P. *Nucleic Acids Res.* **8,** 127–142 (1980).
16. Breathnach, R. *et al. Proc. natn. Acad. Sci. U.S.A.* **75,** 4853–4857 (1978).
17. Cooper, C. W., Peng, T. -C., Obie, J. F. & Garner, S. C. *Endocrinology* **107,** 98–107 (1980).
18. Blobel, G. & Dobberstein, B. *J. Cell Biol.* **67,** 852–862 (1975).
19. Gannon, F. *et al. Nature* **278,** 428–434 (1979).
20. Chang, A. C. Y., Cochet, M. & Cohen, S. N. *Proc. natn. Acad. Sci. U.S.A.* (in the press).
21. Polsky, F., Edgell, M. H., Seidman, J. G. & Leder, P. *Analyt. Biochem.* **87,** 397–410 (1978).
22. Weinstock, R. *et al. Proc. natn. Acad. Sci. U.S.A.* **75,** 1299–1303 (1978).
23. Jeffreys, A. J. & Flavell, R. A. *Cell* **12,** 429–439 (1977).
24. Leder, P., Tiemeier, D. & Enquist, L. *Science* **196,** 175–177 (1977).
25. Blattner, F. R. *et al. Science* **196,** 161–169 (1977).
26. Benton, W. D. & Davis, R. W. *Science* **196,** 180–182 (1977).
27. Lacy, E., Hardison, R. C., Quon, D. & Maniatis, T. *Cell* **18,** 1273–1283 (1979).
28. Maxam, A. M. & Gilbert, W. *Meth. Enzym.* **65,** 499–560 (1980).

Crystal structure analysis of a complete turn of B-DNA

Richard Wing*, Horace Drew, Tsunehiro Takano, Chris Broka, Shoji Tanaka, Keiichi Itakura† & Richard E. Dickerson

Division of Chemistry and Chemical Engineering, California Institute of Technology, Pasadena, California 91125

DNA is probably the most discussed and least observed of all biological macromolecules. Although its role in biology is a central one, with many examples such as operators and restriction sites where specific base sequences have control functions or interact with specific enzymes, the structures that DNA can adopt have been based until now only on sequence-averaged fibre diffraction patterns. Recent improvements in triester synthesis methods have made possible the preparation of sufficient homogeneous DNA of predetermined sequence for crystallization and X-ray structure analysis. We report here the first single-crystal structure analysis of more than a complete turn of right-handed B-DNA, with the self-complementary dodecamer sequence d(CpGpCpGpApApTpTpCpGpCpG) or CGCGAATTCGCG.

Two of the first crystal structure analyses of DNA prepared by the triester method, CGCGCG (ref. 1) and high-salt CGCG (ref. 2), produced variants of a totally unexpected left-handed zigzag or Z helix, of considerable structural interest but uncertain biological significance. The dodecamer sequence reported here was originally chosen to incorporate an *Eco*RI restriction endonuclease site, GAATTC, within ends related to the CGCG tetramer that was already being investigated in our laboratory. The discovery of the Z helix made this sequence potentially even more interesting as an example of two Z-compatible segments, CGCG, bracketing a Z-incompatible AATT. We fully expected the structure to contain left-handed Z ends and a right-handed or melted-out centre. Instead, we found a right-handed B helix with slightly more than 10 base pairs per turn.

Crystals were grown from a *p*H 7.5 solution of DNA with a 2:1 molar excess of magnesium acetate, and one spermine hydrochloride molecule per eight base pairs, by vapour diffusion from 20 to 30% 2-methyl-2,4-pentanediol (MPD). Crystals 3 mm × 0.7 mm × 0.5 mm could be grown in a matter of weeks. These were broken up and used for heavy atom soaking trials; more perfect small crystals were used for data collection.

The dodecamer crystallizes in space group $P2_12_12_1$ with cell dimensions $a = 24.87$ Å, $b = 40.39$ Å and $c = 66.20$ Å. An assumed crystal density of $1.5\ \text{g cm}^{-3}$ leads to one double-stranded dodecamer per asymmetric unit in a cell 47% DNA by weight. Assuming 22 negative backbone phosphate charges per dodecamer, the above unit cell dimensions indicate that the crystals are 2.2 M in negative charge even if no account is taken of possible anions contributed by magnesium acetate. Because all of these must be counterbalanced by spermine or other cations, the dodecamer crystals are fully as 'high-salt' in local DNA environment as are CGCG (2.0 M) or CGCGCG (2.6 M, see ref. 2). If there had been a significant tendency for CGCGAATTCGCG to adopt a partial Z-helical conformation, it should have done so in the crystal. Instead, a right-handed B helix is formed, with not even an indication of local structure irregularity in the CGCG regions.

The distribution of X-ray intensities on survey precession photographs suggests a cross pattern centred on the *c* axis and shows a cluster of very strong reflections at ~3.5 Å along the *c* axis, both implying that this is close to the direction of the DNA helix axis. Intensities remain strong in all directions out to 2.9 Å, and then exhibit a rapid decline until essentially no data can be obtained beyond 1.9 Å. Of the 5,691 possible reflections to 1.9 Å resolution, 2,818 were found to have an intensity greater than 2σ and were used in the analysis. Two isomorphous heavy atom derivatives were used: *cis*-dichlorodiamino platinum (II) obtained by diffusion, and a 3-Br derivative obtained by *de novo* synthesis of the dodecamer with 5-bromocytosine in the third position along each chain. The 1-Br derivative was crystallized but proved not to be isomorphous, and the 9-Br derivative was synthesized but not needed. Isomorphism in the *cis*-Pt derivative began to fail beyond 4-Å resolution, but the 3-Br derivative remains isomorphous to 2.7 Å.

The present report describes the partially refined structure obtained from multiple isomorphous replacement (MIR) analysis at 2.7 Å (mean figure of merit 57%), followed by Jack–Levitt refinement procedures[3] using 2,725 2σ intensities between 8.0 and 1.9 Å. The current residual error or *R* factor is 24.8% for a DNA molecule of 486 atoms and 9 initial water molecules. The structure of the DNA itself is essentially correct and is reported now because of its general interest. Refinement will continue with the addition of more solvent and spermine atoms, and some improvement in local nucleotide conformations.

A skeletal drawing of CGCGAATTCGCG is presented in Fig. 1, and a space-filling version from the same orientation in Fig. 2. The molecule is a Watson–Crick B helix with an average rise per residue of 3.4 Å, and 10.1 base pairs per turn. This is somewhat less than the 10.4 ± 0.1 base pairs per turn as measured in solution by Wang[4] or calculated by Levitt[5] from energy considerations.

The deoxyribose rings in our structure have been fitted to electron density in the MIR map and then allowed to refine; no attempt has been made to impose a uniform C2′-*endo* or C3′-*exo* geometry on them. At this intermediate stage of refinement they are about equally distributed between C2′-*endo* and the O1′-*endo* configuration that is related by rocking about the glycosyl bond, but no conclusions about sugar puckering should be drawn until refinement is completed. No sequence-dependent variations in the uniform B helix have been seen, but these will be watched for as refinement continues.

---

* Present address: Department of Chemistry, University of California at Riverside, Riverside, California 92521.

† City of Hope National Medical Center, Duarte, California 91010.

0028–0836/80/430755—04$01.00

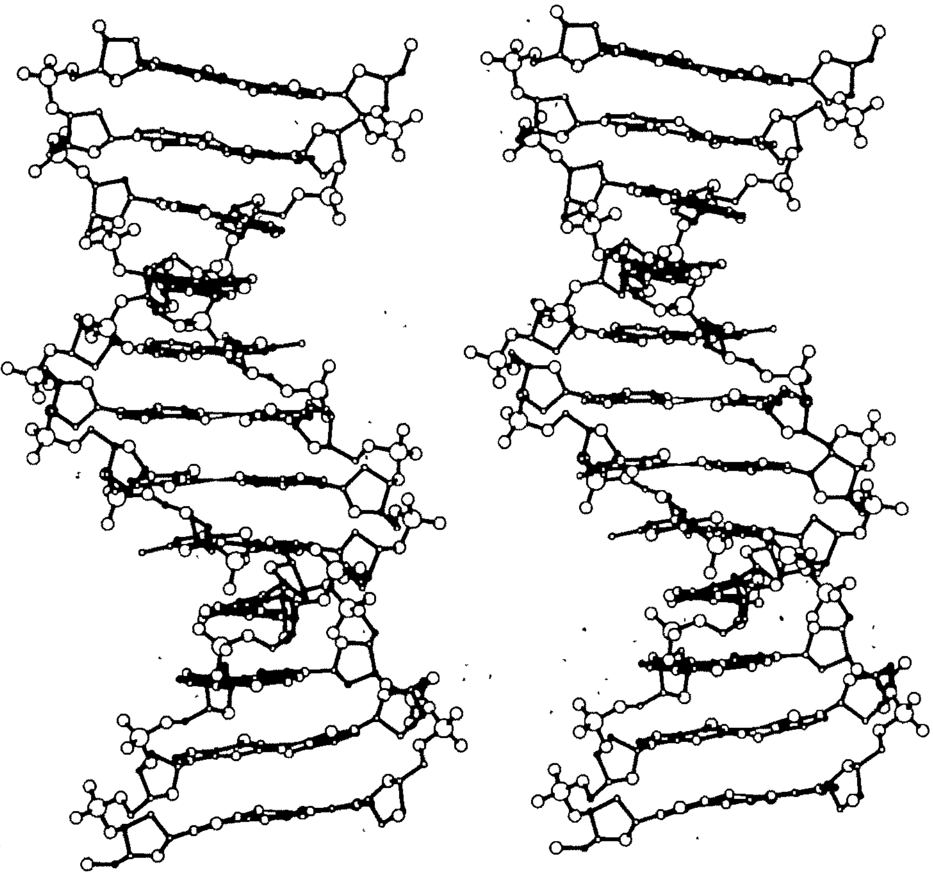

Fig. 1 Skeletal stereo drawing of CGCGAATTCGCG looking into the wide groove of the B double helix. Bases 1 and 24 are at the upper right and left in this view, and 12 and 13 are at the lower right and left. Note the uniform propeller twist in base pairs so as to maximize stacking contact with adjacent bases on the same strand, and the gentle curvature of the helix axis, concave to the right. For comments see text. Atoms in increasing order of size are C, N, O and P.

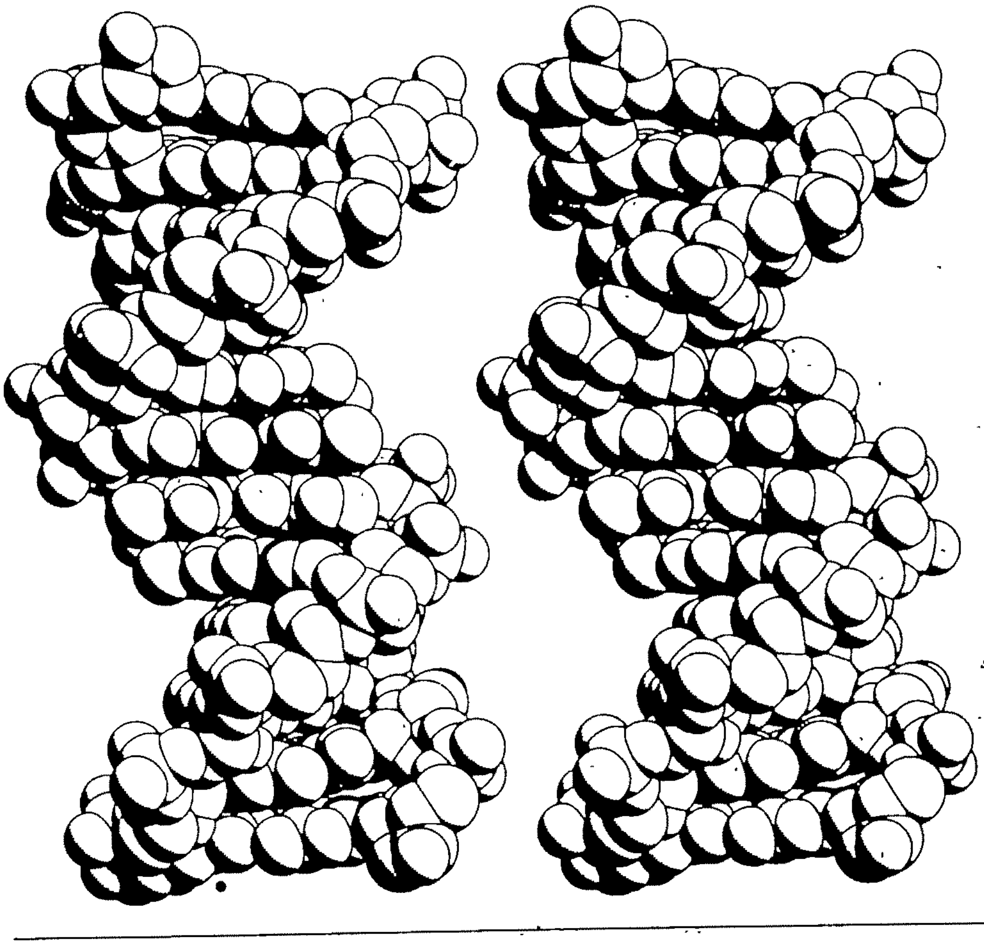

Fig. 2 Space-filling representation of CGCGAATTCGCG from the same viewpoint as Fig. 1. Atomic radii have been set at 85% of their true value for clarity. The advantage of propeller twist in maximizing adjacent base stacking can be seen in this packing drawing.

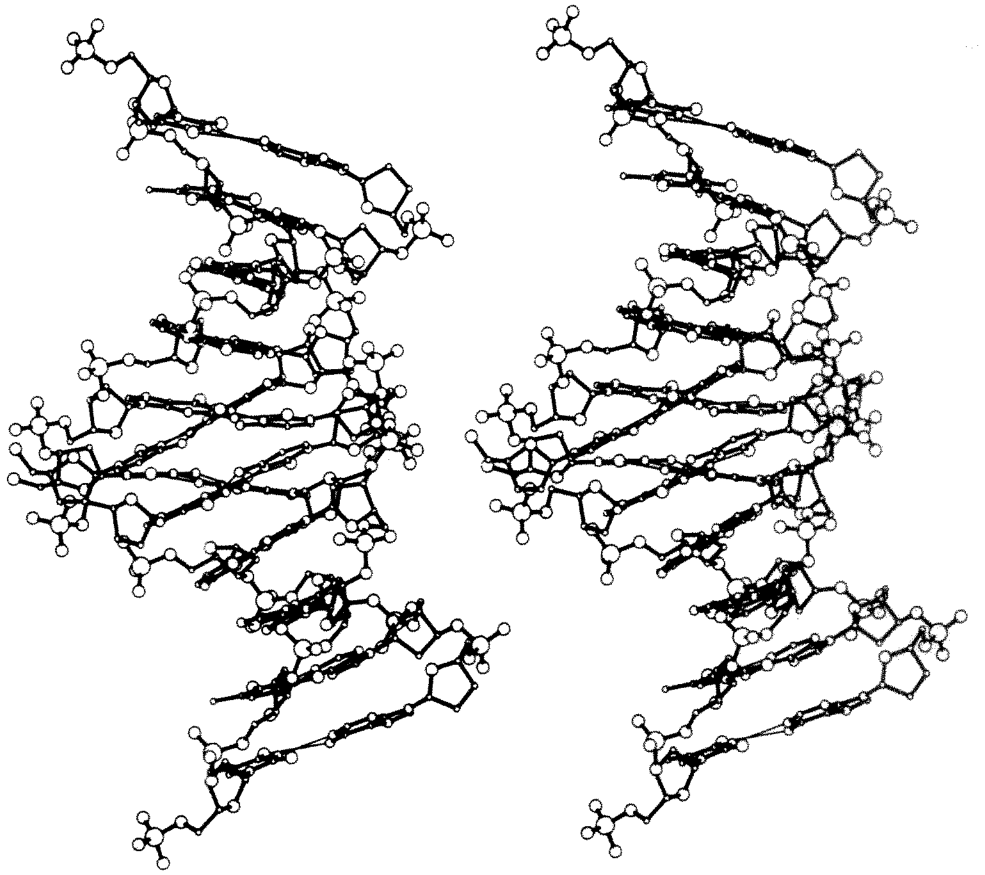

Fig. 3 Overlap of ends of molecules related by 2_1 axis along *c* (vertical). The upper half of one molecule (lower half not shown) sits in front of the lower half of another molecule (upper half omitted), with narrow grooves interlocked but with base planes tilted 35° to one another. The lower molecule shows bases 19–24 in front and 6–1 behind, and the upper molecule has bases 13–18 in front and 12–7 behind. The final base pair in each helix is packed parallel to, and in van der Waals contact with, the sugar–phosphate backbone of its neighbour. The narrow grooves at the ends of the molecules fit against one another like the palms of two cupped hands.

Even at this stage of the analysis, we can be confident about two interesting departures from classical B-helix geometry: each base pair has a propeller twist that increases the overlap between one base and its neighbours up and down the same chain, and the overall helix axis is slightly curved, concave to the right in Fig. 1. Levitt has proposed such a propeller twist in base pairs from energy calculations[5], and has found it to be persistent and not especially sensitive to the particular choice of energy parameters for minimization. Moreover, Hogan *et al.*[6] have found direct experimental evidence for propeller twist in solution from their transient electric dichroism measurements. This agreement gives us confidence that the DNA conformation we observe in the crystal is very close to that which occurs in solution.

The axis of the dodecamer helix bends by 19° over 11 base steps, for a radius of curvature of 112 Å. Moreover, the plane of bending does not contain the internal 2-fold symmetry axis of the base sequence; it is roughly 90° away from it (Fig. 1). This non-use of sequence symmetry means that equivalent positions in the two chains experience different local stresses, and suggests that the curvature is induced by external influences rather than being inherent in the molecule. Little energy would be required to produce such curvature. If the molecule is regarded as an

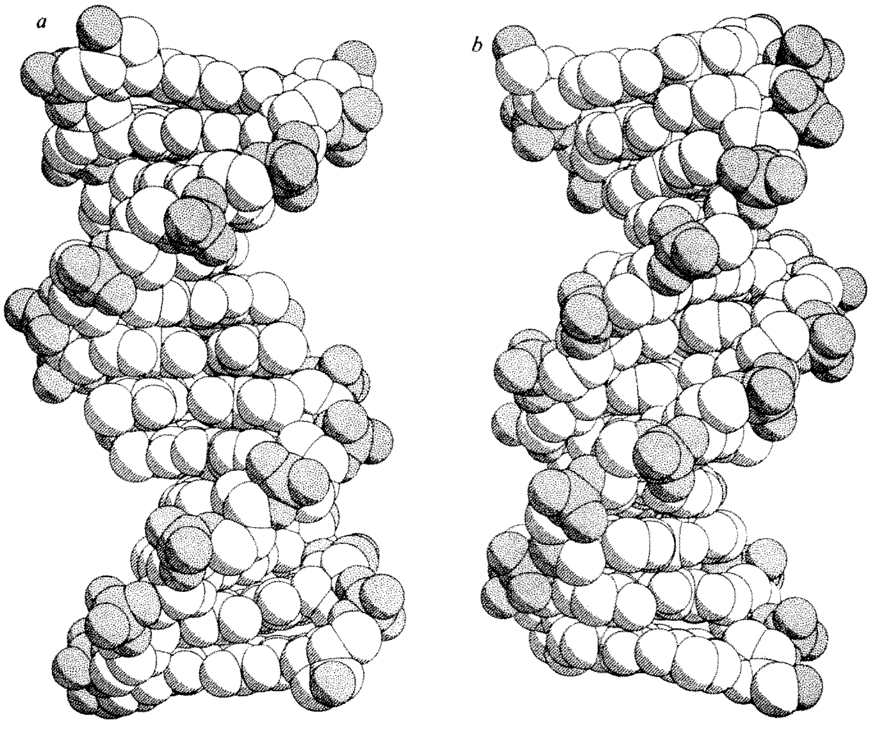

Fig. 4 Comparison of the wide groove (*a*) and narrow groove (*b*) in the B-DNA helix of CGCGAATTCGCG. Phosphate groups are shaded.

elastically deformable rod, the energy required for uniform bending is proportional to the rod length and inversely proportional to the square of the radius of curvature[7,8]. The proportionality constant can be evaluated from the persistence length of DNA in solution, and lies between 85 and 170 kcal Å mol^{-1} (refs 5, 8). This means that only 0.25–0.50 kcal of energy would be required per mol of dodecamer to produce the deformation seen in Fig. 1. As a comparison, the barrier to rotation about a single bond in ethane is nearly an order of magnitude greater, 3 kcal mol^{-1}. As crystal packing forces in proteins do frequently lead to different side-chain conformations in crystals where the asymmetric unit contains two molecules[9,10], such forces would be more than adequate to account for the observed curvature.

The probable origin of the crystal packing forces that produce the curvature is to be found in the association of neighbouring molecules up the 2_1 screw axis parallel to c as shown in Fig. 3. The molecules are not stacked on top of one another like cylindrical drums, instead they are staggered, with each molecule overlapping by three base pairs with its neighbours above and below. The overlap involves contact between minor grooves, with hydrogen bonds connecting ring N3 and amino N2 atoms in adjacent guanines from the two helices. (This pairing of guanines in the minor groove has been encountered in the structure of the complex of 9-ethylguanine and 1-methylcytosine[11], and has been proposed as a possible model for the recognition of guanine by asparagine or glutamine side chains of a protein (Fig. 3 of ref. 12).) Specifically, the N2 and N3 of guanine 14 in the upper molecule are hydrogen bonded to N3 and N2 of guanine 24 in the lower, and N2 and N3 of guanine 12 in the upper molecule are bonded to N3 and N2 of guanine 2 in the lower. However, base pairs in neighbouring molecules are sharply canted or tilted relative to one another by 35°, a tilt that brings the last base pair of one helix parallel to, and in packing contact with, the sugar–phosphate backbone of the other helix. The guanine N2 . . . N3 hydrogen bonds are twisted but not broken, and the tilted structure is locked into place by one more hydrogen bond—from the 3′-terminal OH of the upper helix in fig. 3 to the N2 of guanine 22 in the lower helix. The extra stability provided by these five bonds is more than enough to produce a 19° curvature in the helix axis. This interlocking of helix termini, a function of the CGCG sequences with which the molecule begins and ends, is probably also responsible for the unusual ease and rapidity with which crystals of CGCGAATTCGCG can be grown, in comparison with other DNA molecules whose crystallization has been attempted in our laboratory and elsewhere.

The contrast between major and minor from grooves can be appreciated from Figure 4, in which the molecule is viewed from diametrically opposed directions. The ratio of widths of major and minor grooves along the helix axis is almost exactly 7 : 4, and the minor groove gives, in this space-filling model, the impression of being quite constricted.

The mode of binding of *cis*-dichlorodiamino platinum (II) to DNA is of considerable medical interest because the complex shows promise as a carcinostatic agent in cancer chemotherapy[13,14]. The *cis*-Pt site in the dodecamer is in the vicinity of N7 and O6 of guanines 4 and 16 in the wide groove of the helix. As the *cis*-Pt complex is isomorphous with the native dodecamer only out to 4 Å resolution, it will be refined as an independent structural problem. The *trans*-Pt complex is even less isomorphous as judged by cell dimensions and intensity changes. All three refined structures will ultimately be reported, as a study of the mode of binding of platinum complexes to DNA.

CGCGAATTCGCG was originally synthesized as a substrate for the *Eco*RI restriction endonuclease. Its presence in solutions from which crystals of the endonuclease are being grown leads to a change in crystal form from that of the enzyme alone, fostering the hope that the crystals in the absence of Mg^{2+} contain an abortive binary complex of dodecamer and enzyme suitable for X-ray analysis. If Mg^{2+} is present, the dodecamer is cleaved well by the enzyme (J. Rosenberg, personal communication).

The B helix has been shown here to be the stable conformation of CGCGAATTCGCG in the crystalline state in salt conditions for which CGCG and CGCGCG adopt the left-handed Z configuration. Moreover, the value of 10.1 base pairs per turn and the propeller twist of bases indicate that this crystal structure is close to that which exists in solution. Although the bend in helix axis is probably induced by crystal packing, its presence illustrates the flexibility of the B-DNA structure, and the ease with which the molecule can be continuously deformed to wrap around objects such as the histone core in nucleosomes. Details of the hydration of B-DNA will be of interest as the transitions between B and other forms are generally considered to be a function of water activity[2]. These details, and any sequence-specific modifications of the uniform helix, will be matters of prime concern as refinement continues.

This work was supported by NIH grants GM-12121 and GM-24393, and NSF grant PCM79-13959. H. D. was also the recipient of an NIH Predoctoral Traineeship.

Note added in proof: Further refinement to an R factor of 17.8% has led to a regularization of the O5′-C5′-C4′-C3′ backbone torsion angles to a standard *gauche*$^+$ (about +60°) conformation.

Received 28 July; accepted 10 September 1980.

1. Wang, A. H.-J. *et al. Nature* **282,** 680–686 (1979).
2. Drew, H., Takano, T., Tanaka, S., Itakura, K. & Dickerson, R. E. *Nature* **286,** 567–573 (1980).
3. Jack, A. & Levitt, M. *Acta crystallogr.* **A34,** 931–935 (1978).
4. Wang, J. C. *Proc. natn. Acad. Sci. U.S.A.* **76,** 200–203 (1979).
5. Levitt, M. *Proc. natn. Acad. Sci. U.S.A.* **75,** 640–644 (1978).
6. Hogan, M., Dattagupta, N. & Crothers, D. M. *Proc. natn. Acad. Sci. U.S.A.* **75,** 195–199 (1978).
7. Schellman, J. A. *Biopolymers* **13,** 217–226 (1974).
8. Camerini-Otero, R. D. & Felsenfeld, G. *Proc. natn. Acad. Sci. U.S.A.* **75,** 1708–1712 (1978).
9. Tulinsky, A., Vandlen, R. L., Morimoto, C. N., Mani, N. V. & Wright, L. H. *Biochemistry* **12,** 4185–4192 (1973).
10. Takano, T. & Dickerson, R. E. in *Interaction Between Iron and Proteins in Oxygen and Electron Transport* (ed. Chien Ho) (Elsevier, Amsterdam, in the press).
11. O'Brien, E. J. *Acta crystallogr.* **23,** 92–106 (1967).
12. Seeman, N. C., Rosenberg, J. M. & Rich, A. *Proc. natn. Acad. Sci. U.S.A.* **73,** 804–808 (1976).
13. Khan, A. (ed. *Proc. 3rd int. Symp. Platinum Coordination Complexes in Cancer Chemotherapy*) Vols 1, 2 (Wadley Institutes of Molecular Medicine, Dallas, 1977).
14. Dorr, R. T. & Fritz, W. L. *Cancer Chemotherapy Handbook* (Elsevier, Amsterdam, 1980).

Corrigenda

The following acknowledgements should have appeared in the letter 'Endotoxin-induced uveitis in rats as a model for human disease' by J. T. Rosenbaum *et al. Nature* **286,** 611–613. 'This work was supported by grant AI 11313 from the NIH. J.T.R. was supported by a fellowship from the Arthritis Foundation.'

In the News and Views article 'X-ray astronomy with the Einstein laboratory' by J. L. Culhane *Nature* **284,** 509–510, reference was made to the 'Harvard Center for Astrophysics'. This should have read 'Harvard/Smithsonian Center for Astrophysics'.

In the News and Views article 'Between the galaxies' by M. G. Edmunds, *Nature* **284,** 213, it was erroneously suggested that the number of intergalactic hydrogen clouds discovered by Sargent *et al.* is considerably *higher* than for galaxies—the correct value was quoted, and the incorrect statement was based on an overestimate of the observed number density of galaxies. Nevertheless, the total mass of the clouds remains small compared with that in galaxies. The author apologises for this error.

In the article 'β-Chain contact sites in the haemoglobin S polymer' by R. L. Nagel *et al., Nature* **283,** 832–834, the credit for Fig. 2 was omitted. Figure 2 was modified from *The Structure and Action of Proteins* by R. E. Dickerson and I. Geis (Benjamin/Cummings, Menlo Park, 1969).

Errata

In the letter 'Oscillation of [Ca^{2+}]$_i$-linked K$^+$ conductance in bullfrog sympathetic ganglion cell is sensitive to intracellular anions' by K. Morita *et al., Nature* **283,** 204–205, the column headings for Table 1 should read: 0.5, 1.0 and 3.0 (mM caffeine), not –, 0.5 and 1.0 mM.

In the news item 'Distorting the epidemiology of cancer: the need for a more balanced overview' by R. Peto, *Nature* **284,** 297–300, the caption to the figure on page 299 should have read: Data plotting for 39 countries age-standardized breast cancer death versus total dietary fat (animal or vegetable).

MATTERS ARISING

Leaping dolphins

THE analysis of leaping dolphins by Au and Weihs[1] has some shortcomings. The expenditure of energy during shallow high-speed swimming is presumably correct, although one wonders why a dolphin would not spend at least some time at greater depths if a 4.5-fold decrease in drag can be obtained by going down a metre or so. However, the computation of energy loss during a leaping manoeuvre seems to be at fault. Neglecting spray effects initially, the extra energy required for jumping is given as WH which is the energy required to raise a dolphin of weight W to a height H. However, the energy expended in raising the dolphin against gravity is not lost, but is partially transformed into potential energy at the high point and back to kinetic energy on returning to water-surface level. The dolphin has the same total energy throughout the leap and re-enters the water with the same speed as it had when it emerged. The total loss of energy is zero.

The spray effect, for which an energy loss of mWH is given, has also been computed incorrectly. A dolphin of weight W carries along with it an additional weight of water mW and on leaving the water it leaves this behind in the form of spray. This does not in fact concern the dolphin until it re-enters, when it has to accelerate a similar mass of water up to its swimming speed (U), and so experiences a brief retarding force and a loss of kinetic energy. The loss of energy is clearly $\frac{1}{2}mWU^2/g$, where g is the gravitational constant, and is independent of the angle of the leap. Thus the total energy lost is $\frac{1}{2}m\rho_d VU^2$, where V and ρ_d are the volume and density of the dolphin, respectively, and not $\frac{1}{4}(1+m)\rho_d VU^2$ as the authors claim. They seem to have overestimated the energy loss by a factor of $(1+m)/2m = 3$.

Further, there are more general considerations which could significantly affect the result. It seems unlikely that the dolphin would swim close to the surface between leaps, one reason being the difficulty of launching itself upwards at an angle of 45° from this shallow position. This would require the application of large vertical forces by the fins, of a magnitude several times its own weight. It is more likely that the dolphin follows a sinuous path consisting of leaps out of the water interspersed by dives under the water of a similar shape, thus achieving a clean exit and entry, greatly reducing drag by going deeper while submerged, and presumably breathing while out of the water. It is this total 'flight path' which should be compared with steady shallow swimming in the no-leap case.

Finally, it is unlikely that a dolphin would leap at an elevation angle as great as 45° because of the resulting loss of speed. A dolphin leaping and diving at this angle reduces his forward speed to about 70% of his speed through the water. Reducing this angle has a small effect on the length of leap, which varies as sin 2α where α is the elevation angle, but gives a significant improvement in forward speed, which varies approximately as cos α. A better compromise seems to be about 30°, and this is more in accord with my recollections of leaping dolphins.

C. N. GORDON

General Research Corporation,
Santa Barbara,
California 93111

---

[1] Au, D. & Weihs, D. *Nature* **284**, 548–550 (1980).

Matters Arising

Matters Arising is meant as a vehicle for comment and discussion about papers that appear in *Nature*. The originator of a Matters Arising contribution should initially send his manuscript to the author of the original paper and both parties should, wherever possible, agree on what is to be submitted. Neither contribution nor reply (if one is necessary) should be longer than 300 words and the briefest of replies, to the effect that a point is taken, should be considered.

AU AND WEIHS' REPLY—Gordon's comments on the calculation of energy consumed during the leap, as well as the manner of leaping, are well taken. We originally considered a model such as his symmetric parabola, but adopted our model because we observed shallow, brief swimming between long leaps after the dolphins shifted to the running mode. Therefore, we treated the problem of comparing the cost of shallow swimming with a jump from and to a shallow depth. The potential energy of the leap would not be useful to the dolphin trying to maintain a shallow swimming depth and must be dissipated in the re-entry splash and turning forces necessary to maintain that depth. Our energy loss J is exactly that required to keep the animal from plunging deeper. We suggested that the shallow swimming was due to requirements of increased respiration. Gordon's treatment of the overall problem is relevant to the case of sinuous motion whereas our treatment is based on our observations of saltatory motion.

Gordon's approach to calculation of energy loss due to added mass is more accurate than ours. It would result in a 5% increase in the crossover speed U_c at most.

We believe the centre of mass during the leap approximates a parabola with 45° exit angle that maximizes leap length, both because of the great increase in leap length over that occurring during cruising speed and because photographs often suggest a 45° exit. There is often a steep rise out of the water followed by a flattening-over of the body angle once exited that may give the appearance of a lesser exit angle. The difficulty of leaping from, and returning to, a shallow subsurface depth is acknowledged, but we have not seen the kind of motion Gordon postulates. Perhaps the constant extension of the dolphin's pectoral fins during the entire leap, from exit to re-entry, is explained by the manner of locomotion we describe. The pectoral fins probably act as diving planes to redirect the body angle between leaps and this must contribute greatly to the characteristic splashing. We agree that our differences should be resolved with more careful observations and measurements of this difficult-to-observe behaviour.

Finally, we apologize for an error in the last equation of our letter[1] which should read: $U_c^2 = 65.3 V^{1/3}$.

D. AU

Southwest Fisheries Center, NMFS,
La Jolla, California 92038

D. WEIHS

Technion, Haifa, Israel

---

[1] Au, D. & Weihs, D. *Nature* **284**, 548–550 (1980).

Climatic warming of the West Antarctic ice sheet

IN our paper on the "Effect of climatic warming on the West Antarctic ice sheet"[1] we included an analysis of the state of equilibrium of the Pine Island and Thwaites glaciers, which drain the northern part of the ice sheet. Our conclusions concerning these glaciers were the result of our own analysis of available data, but we should point out that attention was first drawn to the Pine Island and Thwaites glaciers by Hughes[2,3]. Moreover, hypothetical Eemian collapse of the West

0028–0836/80/430759—01$01.00

Antarctic ice sheet[4] has been under investigation by Hughes, Denton and others as part of the CLIMAP experiments[5]. Results of their analysis were presented during the Symposium on the Dynamics of Large Ice Masses, held in August 1978 at Ottawa; where a review of our work was also presented.

We wish to acknowledge the work of Denton, Hughes and their colleagues concerning the Pine Island and Thwaites glaciers, and we do not claim priority in recognizing the existence of these glaciers, their importance as calving bays, and the possibility that they may currently be "surging".

ROBERT H. THOMAS

148 Main Street,
Orono, Maine 04473

TIMOTHY J. O. SANDERSON

Geophysics Department,
Imperial College,
London SW7 2BP, UK

KEITH E. ROSE

5 Upper Gwydir Street,
Cambridge CB1 2LR, UK

1. Thomas, R. H., Sanderson, T. J. O. & Rose, K. E. *Nature* **277**, 355–358 (1979).
2. Hughes, T. *Rev. Geophys. Space Phys.* **13**, 502–526 (1975).
3. Hughes, T. *Rev. Geophys. Space Phys.* **15**, 1–46 (1977).
4. Mercer, J. H. *Int. Ass. Sci. Hydrol. Publ.* No. 79, 217–225 (1968).
5. Denton, G. H. & Hughes, T. (eds) *The Last Great Ice Sheets* (Wiley-Interscience, New York, in the press).

Terminal Cretaceous catastrophe

THE statements of Smit and Hertogen[1] that the terminal Cretaceous extinctions were "extremely abrupt" (~200 yr), lacked "warning signal," and that "gradual extinction lose their credibility on more detailed inspection," require substantiation. Simultaneous geological-range terminations of numerous taxa in a stratigraphic section usually indicate a hiatus (missing strata). A terminal Cretaceous marine shallow-water $CaCO_3$ dissolution event is noted at most marine localities. Was it not operative at Caravaca? Such an event would have caused a terminal Cretaceous hiatus that, in itself, could have accounted for the simultaneous termination of ranges in the Caravaca section, creating the illusion of catastrophic extinctions. Certainly, the termination of ranges via a hiatus would lack a 'warning signal'. Until it is proved that a terminal Cretaceous hiatus does not exist in the Caravaca section, claims of a terminal Cretaceous 'catastrophe' cannot be accepted.

An instantaneous catastrophe phenomenon such as a meteorite impact would have caused synchronous land and marine extinctions. Smit and Hertogen's claims of "near synchronous extinction" conflicts with Butler *et al.*[2] and Lindsay *et al.*[3] who cast serious doubt on any simultaneity. The statement "the independence of the event from the known normal environmental processes going on in the latest Cretaceous", is unfounded; Smit and Hertogen fail to consider the global warming of deep and shallow marine waters across the Cretaceous–Tertiary boundary noted by Boersma *et al.*[4] and Margolis *et al.*[5] They also fail to explain why only planktonic $CaCO_3$-producing marine organisms were affected significantly by the extinctions. Our Cretaceous–Tertiary dinoflagellate studies along the eastern US—even across a terminal Cretaceous hiatus—record no notable terminal Cretaceous extinctions. Clearly, oceanic *p*H changes seem to have been a factor in the marine extinctions.

Smit and Hertogen have failed to integrate significant aspects of the geobiological record into their extraterrestrial extinction model. As such, their use of the term "holocaust" for the terminal Cretaceous extinctions is inappropriate.

DEWEY M. MCLEAN

Department of Geological Sciences,
Virginia Polytechnic Institute
and State University,
Blacksburg, Virginia 24061

1. Smit, J. & Hertogen, J. *Nature* **285**, 198–200 (1980).
2. Butler, R. F., Lindsay, E. H., Jacobs, W. L. & Johnson, N. M. *Nature* **267**, 318–323 (1977).
3. Lindsay, E. H., Butler, R. F., Johnson, N. M. & Jacobs, L. L. *Geology* **7**, 66–71 (1979).
4. Boersma, A., Shackleton, N., Hall, M. & Given, Q. *Init. Rep. DSDP* **43**, 695–718 (1979).
5. Margolis, S. V., Kroopnick, P. M. & Goodney, D. E. *Mar. Geol.* **25**, 131–147 (1977).

SMIT AND HERTOGEN REPLY—The hiatus assumed by McLean is the least likely explanation for extinctions at the Cretaceous–Tertiary boundary. McLean is confusing the sequence of the thermal events at the boundary and fails to consider the iridium peak, important evidence which we used to postulate a catastrophic (meteoritic) event.

McLean's postulated hiatus would have to be quite large to make it worldwide, and to let it wipe out any geochemical or other 'warning signals'. If such a large hiatus were operative, other taxa like benthic foraminifera and dinoflagellates should reflect a similar "illusion of catastrophic extinction", which is not the case. Further, the expected residual clay deposit from a dissolution event is not present either; a dissolution of the topmost 100 m of the Cretaceous at Caravaca would leave a 20-m thick clay deposit, but only one species would be added to the total of 55 planktonic species that became extinct. We have argued previously[1,2] that all stratigraphic subdivisions known to be connected with the boundary are present at Caravaca, including an additional interval, without signs of a hardground or dissolution. McLean needs to prove that a hiatus is present at Caravaca.

While synchronism of extinction is difficult to confirm, the results of Butler *et al.*[3] and Lindsay *et al.*[4] have been seriously questioned[5–7]. McLean also does not mention a similar magnetostratigraphic investigation by Lerbeckmo *et al.*[8,9], who favour synchronism. The problem has not been satisfactorily resolved and a claim of diachronism cannot yet be accepted.

The independence of the event from the normal environmental processes going on in the latest Cretaceous is inherent in the model and it certainly deserves further testing. McLean, however, is confusing cause and effect of the Cretaceous–Tertiary boundary event, when he brings a 'global warming' into the discussion as a normal terminal Cretaceous process. Data of Boersma *et al.*[10] and Margolis *et al.*[11] which indicate a warming, are exclusively Palaeocene and postdate the event. Rather a slight cooling is observed from the Cretaceous data only. The 'global warming' of Margolis *et al.*[11] indicates that the Cretaceous–Tertiary boundary occurred within a period of high global temperatures, lasting ~40 Myr from mid-Cretaceous to Lower Eocene, but as such there is no reason to relate these to the Cretaceous–Tertiary boundary event.

Lowermost Palaeocene warming[12] may well be a consequence of a large impact; either by direct heat generation or by a sort of 'greenhouse effect' (following oceanic impact) much in the same way as in the model of Alvarez *et al.*[13]. Dinoflagellates may escape the supposed suppression of sunlight by their cyst-forming abilities, as well as the dinoflagellate-like, $CaCO_3$ producing nannofossils *Braarudosphaera* and *Thoracosphaera*. However, we agree that the biological consequences of a very large impact are largely speculative at the moment.

JAN SMIT

Geological Institute,
Nieuwe Prinsengracht 130,
Amsterdam, Netherlands

1. Smit, J. & Hertogen, J. *Nature* **285**, 198–200 (1980).
2. Smit, J. *Cretaceous–Tertiary Boundary Event Symp.* **II**, 156–163 (1979).
3. Butler, R. F., Lindsay, E. H., Jacobs, N. M. & Johnson, N. M. *Nature* **267**, 318–323 (1977).
4. Lindsay, E. H., Butler, R. F., Johnson, N. M. & Jacobs, L. L. *Geology* **7**, 66–71 (1979).
5. Alvarez, W. & Vann, D. W. *Geology* **7**, 66–67 (1979).
6. Fassett, J. E. *Geology* **7**, 69–70 (1979).
7. Lucas, S. G. & Rigby, J. K. *Geology* **7**, 323–326 (1979).
8. Lerbeckmo, J. F., Evans, M. E. & Baadsgaard, H. *Nature* **279**, 26–30 (1979).
9. Lerbeckmo, J. F., Evans, M. E. & Baadsgaard, H. *Nature* **284**, 376 (1980).
10. Boersma, A., Shackleton, N., Hall, M. & Given, Q. *Init. Rep. DSDP* **43**, 695–718 (1979).
11. Margolis, S. V., Kroopnick, P. M. & Goodney, D. E. *Mar. Geol.* **25**, 131–147 (1977).
12. Thierstein, H. R. & Berger, W. H. *Nature* **276**, 461–466 (1978).
13. Alvarez, L. W., Alvarez, W., Asaro, F. & Michel, H. W. *Science* **208**, 4448, 1095–1108 (1980).
14. Emiliani, C. *EOS* **61**, 26, 505–506 (1980).

0028–0836/80/430760—01$01.00

BOOK REVIEWS

Hopes and fears for the Islamic world

Abdus Salam

The Future of Muslim Civilisation. By Ziauddin Sardar. Pp.288. (Croom Helm: 1979.) Hardback £14.95; paperback £4.95. Available from Biblio Distribution Centre, Totowa, New Jersey at $26.50.

THIS is a remarkable book written by a remarkable young author, not yet 30, addressed to Muslim scholars, intellectuals and scientists. Ziauddin Sardar's basic thesis is that, considering the present state of the Muslim world and of Muslim history of the past four centuries, as well as the urgency of the current global crises, it is imperative that Muslim peoples should think out and work for a planned, rather than an "aimless" future. As the argument develops, its two related dimensions emerge: "to operationalise a living, dynamic civilisation of Islam and to make a positive contribution to the Predicament of Mankind and the stabilisation of Spaceship Earth". In Sardar's view the two tasks are, in essence, one and the same; and both require intellectual boldness and courage.

Sardar starts with a critical look at the recent history of the Muslims. In his view, the Muslim civilization is the only civilization which still preserves something of its essence, and which has the potential to stand up to the dominant civilization of the occident. The tragedy, however, is that all attempts to adapt Western norms and values in the Muslim societies, from the eighteenth century Tanzimat reforms in the Ottoman Empire, to modern strategies of development, have failed to revive their dynamism. "The imitation of the West, has reduced the Muslim intellectuals to the status of voluntary mental slaves. It is now necessary for the Muslims to find solutions to their problems from *within* their own culture and traditional heritage."

In the long run, the author argues, Muslim people can discover their lost vigour and dynamism only by sustained research. He calls for a "Project Umran", an organized research programme to produce detailed conceptual maps and operational plans for alternative Muslim futures. The Muslims have not done their intellectual homework and the first aspect of his research programme calls for a new articulation of the age-old Muslim vision of the Medina State: the city established by the Holy Prophet after his migration from Mecca to Medina. "It is indeed a sorry reflection on the state of Muslim scholarship that almost all accounts of Medina State to date are almost as devoid of freshness and depth as they are of analysis." These are sentiments close to heresy in their boldness so far as traditional scholarship is concerned. And, in this context, Sardar's boldest suggestion is the outline of a modern methodology for the revivification of *ijtihad* (sustained reasoning) which was banned by traditional scholars some 600 years ago. This ban he asserts, was the chief reason for the decline of Muslim civilization. His ultimate picture is of a utopian future Muslim society, with the extended family as its base, the mosque as its focus, devising its own strategies of collective fulfilment, reaffirming commitment to Muslim traditions and values, maintaining elite and leadership accountability through the Islamic concept of criticism and self-criticism (*mahasbaah*), rediscovering the Islamic system of education based on personal contact and community awareness, and synthesizing Western and traditional modes of health care.

Mary Evans

Regarding science, Sardar is categorical: "bias-free observation is a myth", he declares. Contemporary science, he argues, is Western science, and only *a* science, and not *the* science.

> Nothing in perception is elementary, instantaneous, objective or strictly factual; it is all full of subconscious or indeed preconscious interpretations in the light of previous experience. The emotionally loaded word 'fact' has no place in science; it is a sign of either ignorance or dishonesty on our part if we believe that data gathered by science are wholly 'pure' and 'external', since they are always intermingled with our world-view and our perceptions [p.208–209].

The Muslims, in his view, must develop their own style of science and rediscover the spirit of science in Islam.

Whether one agrees or disagrees with him — and since I can see no distinction in spirit between, for example, the modern tradition in algebra and that of Omar Khayyam's, or the modern tradition in optics and that of Alhazen's, or Razi's observations on small-pox and their modern extensions, I certainly cannot subscribe to his views so far as *pure* science (as contrasted with goal-orientated technology) is concerned — Sardar's book does mark a sharp departure from conventional Muslim scholarship. He is intellectually demanding of the Muslims, and herein lies the importance of his work. As I indicated above, much of what he has said would spell heresy in some circles (both traditionalist and modernist). By itself, the extensive glossary at the end of the book testifies that his analysis has broken considerable new ground.

But nothing in this brief review can give an adequate idea of the remarkable felicity of Sardar's writing or its urgency and passion. There is his analysis of the "Parameters of Muslim Civilisation", including a historical survey of Muslim intellectual endeavour, an "Anatomy of Muslim Agony", a penetrating analysis of the history of the occidental world-view, and of the present world system.

And then there are the throw-away descriptions — for example of a new breed among Muslim intellectuals, "the professional Muslim" as he is called, whose first characteristic is

> . . . his self-appointed role as a contemporary bishop. The professional Muslim is always at every conference, whatever the theme, whether it is 'Muslim Education' in Mecca, 'Islam and the Challenge of New International Order' in London, 'The Third International Theory' in Tripoli, or 'Muslim Youth' (this despite the fact that he is usually over 45) in Kuala Lumpur.

In the same vein, and even more damning, is Sardar's assessment of the role of Muslim elites in their societies:

> . . . since the day of their independence, the Muslims have been ruled by elite minorities in the name of traditionalism, nationalism, socialism and democracy. These elites have acquired an unchallengeable sense of self-

> importance and omnipotence; they have transformed transient limited goals to universal imperatives. . . . They have sustained a value network characterised by materialism and vulgarity; [putting] blind imitation before critical inquiry, order before justice, obedience before responsibility, elitism and class before humanity, regionalism before universality, packaging before contents, . . . numbers before quality, efficiency before participation, expertise before wisdom, property before people, and economic and political gain before life.

But notwithstanding its power, the book, addressed as it is to the intellectual elites, has its (possibly self-imposed) limitations. There is little assessment of the contemporary Muslim political scene or of the fundamentalist politico-religious or spiritual movements which are currently shaping the Muslim world. It could be that Sardar believes in the transient, limited character of some of the current trends. But whatever these limitations of scope, are we witnessing with this work the emergence of a new, more analytical, impatient and aggressive breed of Muslim scholar? Regrettably, as things are at present in many Muslim countries, such scholars, if they do emerge, will be able to work and write only in the relatively freer atmosphere of the West. □

Abdus Salam is Director of the International Centre for Theoretical Physics at Trieste and Professor of Physics at Imperial College.

Muslim astronomers in the observatory at Istanbul, from a manuscript dated 1571.

The impact of volcanoes through human history

Alexander R. McBirney

Volcanic Activity and Human Ecology. Edited by Payson D. Sheets and Donald K. Grayson. Pp. 644. (Academic: 1980.) $52, £33.80.

Volcanism has recently received a new surge of attention, partly as a result of the eruption of Mount Saint Helens; *Volcanic Activity and Human Ecology* arrives, therefore, at an appropriate time. This book is the first of its kind, so far as I am aware, to attempt a comprehensive treatment of volcanic hazards and their effects on human activity, both modern and ancient. It can be divided into two parts: the first gives a brief summary of the main types of volcanic activity, hazards, tephra and volcanic soils; the second is a series of accounts of specific eruptions and how they affected different cultures.

The descriptions of volcanic activity by Fred Bullard and a chapter on tephra deposits and how they are studied, written by Larry Kittleman, are presented in a simple style easily comprehensible to the non-geologist. A contribution on volcanic soils by Ugolini and Zasoski provides a great deal of technical data, but would be far less tedious reading had it given less attention to chemical and mineralogical details and more to the practical aspects that interest most readers. Thorarinsson provides a fascinating account of the impact of eruptions in Iceland, and Warrick considers some of the general problems of dealing with volcanic hazards and their social consequences. The techniques of assessing volcanic risks in the Cascade Range are discussed in a paper that was written by Crancell, Mullineaux and Miller shortly before the eruption of Mount Saint Helens, and it makes interesting reading in the light of more recent events. On the whole, the authors fare quite well.

The topics dealt with in the second part of the book were more interesting to me, probably because they were less familiar. I was fascinated by two case studies by Hodge, Sharp and Marts, who describe the effects of recent eruptions on different cultures and economies, one in Hawaii and the other near Mount Baker in the state of Washington. The paper should be required reading for anyone responsible for assessing hazards and dealing with the public under conditions of stress and uncertainty. It shows quite clearly how people with different cultural backgrounds, economic interests and familiarity with a volcano perceive hazards and the restrictions imposed for their safety.

The eruption of Paricutin in Mexico between 1943 and 1952 is treated in considerable depth. Rees describes the impact on the physical environment, and Nolan gives a perceptive and thoughtful account of how five small communities reacted to the disruption of their lives and customs. The ways in which people responded varied widely, depending on the social structures of the communities, and it is particularly interesting to note that those that proved most resilient were people who had strong community ties and were subjected to the least amount of governmental assistance.

Several papers dealing with prehistoric eruptions in western North America address the question of how much importance can be attached to volcanic eruptions as agents affecting the migration, decline or ascendancy of primitive tribes. The contribution by Dumond on Alaska and the Aleutians is particularly notable for its clarity and readable style. The evidence seems to indicate that volcanism only rarely had the drastic impact on primitive cultures that has been attributed to it. But this is not necessarily true of more advanced societies, such as the classical civilizations of Central America and the Mediterranean. The effects of a huge eruption of Ilopango in El Salvador are shown to have had a profound effect on subsequent patterns of Mayan culture. The degree to which this was true of the eruption of Santorini in 1500 BC is still the subject of controversy. Renfrew discusses evidence for and against the hypothesis that the eruption accounted for the final demise of Minoan civilization, and, using evidence that volcanologists may find less than conclusive, he concludes that the eruption and the destruction of the community on Crete, dated within 50 years of each other, were coincidental.

No book on the effect of volcanism on civilized communities would be complete without a chapter on the eruption of Vesuvius in AD 79. Jashemski gives us a good summary of the eruption and its effects and explains some of the more recent archaeological work at Pompeii.

It is impossible to enumerate all the interesting facets of this volume. The editors deserve to be complimented on a splendid compilation of well-balanced papers, almost all of which are interesting, timely and well written. One of the most difficult tasks in a work such as this is keeping the papers on a level that will interest the average reader who is not concerned with details and the pet theories of individual specialists. The editors have managed to do this quite well. In short, the book is an unusually valuable contribution that will be useful to a wide range of readers. ☐

Alexander R. McBirney is at the Centre for Volcanology, University of Oregon, and specializes in the study of the volcanoes of the circum-Pacific region. He is co-author of Volcanology, *published last year by Freeman and Cooper.*

A star is born

F.D. Kahn

Star Formation. 10th Advanced Course of the Swiss Society of Astronomy and Astrophysics. By I. Appenzeller, J. L. Lequeux and J. Silk. Pp.222. (Geneva Observatory: Sauverny, Switzerland, 1980.) SwFr.30.

THE brightest stars in spiral galaxies line the insides of the spiral arms. The same regions are rich in interstellar gas, much of it ionized and made luminous by the stars themselves, and concentrations of the dust tend to occur nearby. But the spiral arms are manifestations of a wave-like disturbance that travels at some 100 km s^{-1} relative to the material in the galactic disk. The bright stars must therefore be short-lived, and be born and evolve during the time that the star-forming phase of the wave passes through the region. Stellar structure theory confirms that such stars do indeed consume their nuclear fuel in a relatively short time; the most luminous do so in as little as three million years. All this has been known for two decades or so.

These observations suggest that the diffuse interstellar material provides the source of matter for the new stars, and various theories have been proposed to describe how this might happen. But the sequence of events must be complex: the mean mass density is typically 24 orders of magnitude lower in interstellar space than it is in a star. The condensation process will consequently have various stages, each dominated by a different set of physical parameters. In addition, formidable problems are posed by the angular momentum content of the interstellar gas, and by the magnetic flux linked with it. There must be dissipative processes to reduce them both, otherwise star formation would be completely inhibited.

Many new observations have been made in the past few years which bear on these questions. The spatial and kinematical structure of molecular clouds has been revealed by spectroscopic observations at millimetre wavelengths. These clouds invariably contain much dust; any stars that form within them are therefore enclosed at birth within a cocoon of dust. The stars thus become initially detectable as infra-red sources, since it is possible only to observe the radiation from the heated dust that surrounds them, and obscures their surfaces. It seems to take some half a million years for this dust to clear away.

The 1980 Advanced Course at Saas Fee was devoted to this range of topics. As always three lecturers took part, and it is clear that this year each one saw his task in a different way. The first set of talks (I. Appenzeller) describes how to use a computer to simulate the process of condensation of matter into a star. The calculations are reasonably tractable if spherical symmetry is assumed. But should the description not be full three-dimensional? Can one even contemplate such a calculation for a system where some important lengths are as large as 10^{17} cm, and others as small as 10^{12} cm?

In the second group of talks, J. Lequeux sets out to establish some order among the large variety of observational data. He derives empirical formulae to connect the rate of star formation with the local density of interstellar matter, and to describe the distribution of masses (the initial mass function or IMF) among the newly formed stars. But is there an IMF which applies everywhere? Can the IMF for massive stars be reconciled with that for the lighter stars?

In the last group of talks, J. Silk presents a wide-ranging survey, with no less than 157 references, of recent observational and theoretical results. It is easy to appreciate, after reading his contribution, how complex star formation really is, and how many physical interactions are involved. Yet even so he leaves the impression that an acceptable theory will evolve before long.

The Saas Fee courses have deservedly become famous. The present text maintains their high standard, and provides an excellent guide to a very important subject. The book is well produced and the price most reasonable. But would the organizers be willing to consider a small suggestion? In future, when the three lecturers have spoken, might it not be worthwhile to have another speaker to provide a summary and put the different views in perspective? ☐

F. D. Kahn is Professor of Astronomy at the University of Manchester.

A summary of 30 years of solar radio astronomy

R. T. Stewart

Introduction to Solar Radio Astronomy and Radio Physics. By A. Kruger. Pp.330. (Reidel: 1979.) Hardback Dfl.95, $49.95; paperback Dfl.45, $23.50.

THE last monograph on this subject appeared in 1964, and since then a great number of significant radio observations of the Sun have been made from space and from large ground-based arrays. Considerable progress has also been achieved in theoretical aspects of plasma emission processes. Thus, the appearance of this volume in which the author attempts to summarize the work carried out during the past 30 years, is timely.

The book is divided into five chapters. In Chapter 1 a short history is given of the early attempts to detect radio emission from the Sun, leading to its discovery in 1942. This is followed by a brief description of the general properties and structure of the Sun. Chapter 2 is devoted to various types of instruments and techniques used in observational solar radio astronomy.

The great variety of radio emissions from the Sun is the subject of the next chapter, which contains many good illustrations. Recent kilometric and hectometric radio observations from spacecraft of type II and type III bursts are included in this account. Interpretation of these bursts in terms of plasma emission allows the determination of the electron density of the corona from near the Sun to near the Earth. Interpretation of millimetric and centimetric emissions in terms of thermal bremsstrahlung or gyro-synchrotron emission leads to estimates of electron temperatures, electron densities and magnetic field strengths in the chromosphere and low altitudes of the corona. Metric observations cover intermediate altitudes of the corona and give information on electron density, and the direction and strength of the coronal magnetic field. Hence radio observations cover most of the Sun–Earth environment.

The other important aspect of radio observations is the evidence they provide for non-thermal populations of energetic particles released by solar flares. The fourth chapter deals with the theory of solar radio emission and is divided into primary emission processes, such as thermal bremsstrahlung and gyro-synchrotron emission from accelerated particles, and secondary emission processes or wave-mode transformations such as Langmuir waves scattering into electromagnetic (plasma) radiation. Plasma instabilities such as the two-stream, velocity-anisotropy and tearing-mode instabilities are briefly discussed. The important question of amplification of radio waves is also mentioned but not considered in detail. The final chapter attempts to integrate solar radio astronomy with solar physics and solar terrestrial physics. The flare phenomenon is discussed, together with several possible mechanisms for the explanation of how particles are accelerated in the short time-scale of the flare and where the flare energy originates.

It is an ambitious undertaking to attempt to cover the entire span of the field in a single volume, but as an extensive review of the scientific literature the book is very successful and contains a useful list of references for the postgraduate student or research scientist. However, as an introduction to solar radio astronomy, it is less successful, being complicated by detail and lacking the highlights which give the reader an overall picture of an area of research. I feel that more emphasis could have been placed on the significant developments — instrumental, observational and theoretical — which have occurred in solar radio astronomy and that this would have led to a more readable account. However, I would recommend this book not only because of its uniqueness but also because it is an honest description of the work done in this field up until 1976. □

R. T. Stewart is a principal research scientist with the Division of Radiophysics of CSIRO, Sydney, Australia, and for the past 16 years has been closely involved with the interpretation of solar radio bursts observed by the Culgoora radioheliograph and other instruments.

Responses to arbitrary time schedules

J.T. Enright

Time in Animal Behaviour. By M. Richelle and H. Lejeune. Pp.273. (Pergamon: 1980.) Hardback £22, \$51; flexi £9.50, \$23.

Do not be misled by the title, the jacket and the foreward of this book. It does not treat general features of behavioural adjustment to time, but instead deals almost exclusively with the key- and lever-pressing performances of hungry rats, pigeons and a small number of other species. The introductory chapter led me to hope for an integration of biological-clock research (circadian and similar studies) with other broader aspects of temporal regulation, but, as one finally discovers on p.135: "In the almost total absence of [relevant biological-clock] experimental work, we shall content ourselves with defining the type of research that is strongly needed to fill the gap. . .".

The real intent of the authors is to introduce certain sorts of temporally programmed operant-conditioning experiments to the uninitiated. These experiments centre around one of two basic designs. On the "fixed interval schedule", the animal learns not to "emit responses" (I shudder) continually or randomly, but to wait, after a given success, for a major fraction of the imposed unrewarded interval before trying again, and then to try persistently until success finally comes. At the other extreme is "differential reinforcement of low rates", a programme in which any unsuccessful keypress resets the timer to zero; following a reward, the animal is required to wait for *at least* the pre-programmed interval before trying again. Granted proper shaping regimes, most animals can apparently master these schedules, as well as many complex variants. True enough, mastery of the programme usually involves only relatively imprecise indications that the animal has some sort of expectation in the time domain. Nevertheless, the evidence presented in this book clearly demonstrates that animals can evaluate and respond to arbitrarily chosen time intervals ranging from a few seconds to a few minutes.

The arbitrariness of the selected time intervals, based on their convenience in an operant-conditioning context, deserves emphasis. Most biologists are already familiar with certain other animal capacities to utilize time as a variable in an ecological context — matters of microseconds, as when an insectivorous bat uses sonar to home in on its prey, up to intervals of days, in time-training (*Zeitgedächtnis*) experiments with honeybees, and even weeks, in semi-lunar reproductive rhythms. Such aspects of temporal adaptation are presumably the intensely selected consequences of prolonged evolution. The animal skills considered in this book, on the other hand, seem to be completely devoid of any ecological relevance. To me, the impressive aspect of the results is that the animals show any capacity at all to deal appropriately with the arbitrary time schedules provided. These abilities are probably an evolutionary by-product, but the natural context in which they might originate remains obscure.

The general audience, for whom the book is intended, will encounter a number of stumbling blocks. It is easy to lose sight of the central questions when confronted with detailed results from yet another minor variant on the small number of standard experimental designs. A further difficulty lies in the authors' propensity for abbreviations which, once defined, the reader is expected to remember throughout subsequent chapters. The pages are peppered with FI, FR, FT, FI-FR, DRL 20s, DRL 60 LH 6, IRT, TO, RF/R and FRC, on through MULT FR 25 FI 7 min.

The authors emphasize (Chapter 6) that although brain lesions and certain drugs affect the response patterns, such results are fraught with ambiguity. I myself find the authors' attempts at overall interpretation (Chapter 9) to be equally ambiguous. For example, "We are dealing here with a relaxation phenomenon, and not a pendulum-type oscillatory system. . . Temporal regulation involves the buildup of some sort of tension that is suddenly discharged . . ." (p.222). That sort of conclusion seems to me to be inextricably tied up with the experimental designs; if the imposed timing schedule contains major elements of a relaxation oscillation (sudden reset to zero), how could the animals behave otherwise? What we have here, then, is a large body of experimental data which seem, at present, to be begging for adequate explanation at both the evolutionary and the neurophysiological level. The authors deserve our thanks for making these results accessible in a compact form for those — like myself — who have been unfamiliar with this body of empirical knowledge. □

J.T. Enright is Professor of Behavioral Physiology at the Scripps Institution of Oceanography, La Jolla, California.

BOOKS RECEIVED

Astronomy

HANES, D. and MADORE, B. (eds). Globular Clusters. Based on the Proceedings of a NATO Advanced Study Institute held at the Institute of Astronomy, University of Cambridge, August 1978. Pp.390. ISBN 0-521-22861-1. (Cambridge University Press: 1980.) £27.50.

ROSSANO, G.S. and CRAINE, E.R. Near Infrared Photographic Sky Survey: A Field Index. Astronomy and Astrophysics Series, Vol.8. Pp.202. ISBN 0-912918-11-X. (Pachart Publishing, Tucson, Arizona, 1980.) $38.

SZOKOLAY, S.V. World Solar Architecture. Pp.278. ISBN 0-85139-595-3. (Architectural Press: London, 1980.) £29.95.

Physics

ALCÀCER, L. (ed.). The Physics and Chemistry of Low Dimensional Solids. Proceedings of the NATO Advanced Study Institute held at Tomar, Portugal, August 1979. NATO Advanced Study Institutes Series C — Vol.56. Pp.436. ISBN 90-277-1144-5. (Reidel: 1980.) Dfl. 95, $50.

BARBE, D.F. (ed.). Very Large Scale Integration (VLSI) Fundamentals and Applications. Springer Series in Electrophysics, Vol.5. Pp.279. ISBN 3-540-10154-3. (Springer-Verlag: 1980.) DM52, $30.70.

BASS, R. Nuclear Reactions with Heavy Ions. Pp.410. ISBN 3-540-09611-6. (Springer-Verlag: 1980.) DM88, $52.

CROXTON, C.A. Statistical Mechanics of The Liquid Surface. Pp.345. ISBN 0-471-27663-4. (Wiley-Interscience: 1980.) £25.

EHRENREICH, H., SEITZ, F. and TURNBULL, D. (eds). Solid State Physics: Advances in Research and Applications, Vol.35. Pp.404. ISBN 0-12-607735-5. (Academic: 1980.) $39.50.

FISCHER, H. and HELLWEGE, K.-H. (eds). Magnetic Properties of Free Radicals. Atomic and Molecular Physics Vol.9. Pp.369. ISBN 3-540-09666-3. (Springer-Verlag: 1980.) DM 470, $277.30.

GRUBER, B. and MILLMAN, R.S. (eds). Symmetries in Science. Proceedings of the Einstein Centennial Celebration Science Symposium held at Southern Illinois University, February 1979. Pp.495. ISBN 0-306-40541-5. (Plenum: 1980.) $49.50.

HELLWEGE, K.-H. and HELLWEGE, A.M. (eds). Magnetic and Other Properties of Oxides and Related Compounds. Crystal and Solid State Physics, Vol.12. Pp.758. ISBN 3-540-09421-0. (Springer-Verlag: 1980.) DM 790, $466.10.

HULST, H.C. van de. Multiple Light Scattering. Tables, Formulas, and Applications, Vol.2. Pp.739. ISBN 0-12-710702-9. (Academic: 1980.) $46.50.

KUBO, R. and HANAMURA, E. Relaxations of Elementary Excitations. Proceedings of the Taniguchi International Symposium, Susono-shi, Japan, October 1979. Pp.285. ISBN 3-540-10129-2. (Springer-Verlag: 1980.) DM 72, $42.50.

LAITHWAITE, E.R. and FRERIS, L.L. Electric Energy: Its Generation, Transmission and Use. Pp.365. Flexi ISBN 0-07-084109-8. (McGraw-Hill: 1980.) £9.95.

LANDAU, L.D. and LIFSHITZ, E.M. Course of Theoretical Physics, Vol.9. Statistical Physics Part 2. Pp.350. Flexi ISBN 0-08-023072-5. (Pergamon: 1979.) $20, £9.

MANN, H.K. (guest ed.). Radiation Physics and Chemistry. Radiation Sterilisation of Plastic Medical Devices. Pp.124. Flexi ISBN 0-08-025067-X. (Pergamon: 1980.) £7.50.

MARLOW, W.H. (ed.). Aerosol Microphysics I: Particle Interaction. Topics in Current Physics, Vol.16. Pp.160. ISBN 3-540-09866-6. (Springer-Verlag: 1980.) DM54, $31.90.

MARTON, L. and MARTON, C. (eds.). Advances in Electronics and Electron Physics, Vol.51. Pp.455. ISBN 0-12-014651. (Academic: 1980.) $49.50.

MEZEI, F. (ed.). Neutron Spin Echo. Proceedings of a Laue–Langevin Institut Workshop, Grenoble, October 1979. Lecture Notes in Physics, Vol.128. Pp.253. Flexi ISBN 3-540-10004-0. (Springer-Verlag: 1980.) DM33, $19.50.

MOSS, T.S. (executive ed.), KNEÜBUHL, F. (guest ed.) CIRP 2. 2nd International Conference on Infra-red Physics. Papers presented at the Conference, Zurich, March 1979. Pp.506. Flexi ISBN 0-08-025055-6. (Pergamon: 1980.) £12.50.

NESBET, R.K. Variational Methods in Electron-Atom Scattering Theory. Pp.228. ISBN 0-306-40413-3. (Plenum: 1980.) $32.50.

OSTROVSKY, Yu. I., BUTUSOV, M.M. and OSTROVSKAYA, G.V. Interferometry by Holography. Springer Series in Optical Sciences, Vol.20. Pp.330. ISBN 3-540-09886-0. (Springer-Verlag: 1980.) DM89, $52.60.

PANKOVE, J.I. (ed.). Display Devices. Topics in Applied Physics, Vol.40. Pp.252. ISBN 3-540-09868-2. (Springer-Verlag: 1980.) DM89, $52.60.

RUDDEN, M.N. and WILSON, J. Elements of Solid State Physics. Pp.186. Hbk ISBN 0-471-27750-9; pbk ISBN 0-4741-27749-5. (Wiley: 1980.) Hbk np; pbk £5.95.

SANCHEZ-PALENCIA, E. Non-Homogeneous Media and Vibration Theory. Lecture Notes in Physics, Vol.127. Pp. 398. Flexi ISBN 3-540-10000-8. (Springer-Verlag: 1980.) DM41, $24.20.

SCHLENKER, M. *et al.* (eds). Imaging Processes and Coherence in Physics. Proceedings of a workshop held at Les Houches, France, March 1979. Lecture Notes in Physics, Vol.112. Pp.577. Flexi ISBN 3-540-09727-9. (Springer-Verlag: 1980.) DM59, $34.90.

SHANKAR, R. Principles of Quantum Mechanics. Pp.612. ISBN 0-306-40397-8. (Plenum: 1980.) $29.50.

SPRINGFORD, M. (ed.). Electrons at the Fermi Surface. Pp.541. ISBN 0-521-22337-7. Cambridge University Press: 1980.) £35.

SUBBARAO, E.C. (ed.). Solid Electrolytes and Their Applications. Pp.298. ISBN 0-306-40389-7. (Plenum: 1980.) $35.

SUPPES, P. (ed.). Studies in the Foundation of Quantum Mechanics. Pp.265. ISBN 0-917586-12-3. (Philosophy of Science Association: East Lansing, Michigan, 1980.) $6.

THOMPSON, G.H.B. Physics of Semiconductor Laser Devices. Pp.549. ISBN 0-471-27685-5. (Wiley: 1980.) £22.75.

Van de HULST, H.C. Multiple Light Scattering: Tables, Formulas, and Applications, Vol.1. Pp.299. ISBN 0-12-710701-0. (Academic: 1980.) $38.50.

VINNICHENKO, N.K. *et al.* Turbulence in the Free Atmosphere. 2nd Edn. Pp.310. ISBN 0-306-10959-X. (Consultants Bureau: New York and London, 1980.) $49.50.

WANG, K.Y. Acoustical Imaging, Vol.9. Visualization and Characterisation. Proceedings of the 9th International Symposium on Acoustical Imaging, held in Houston, Texas, December 1979. Pp.842. ISBN 0-306-40477-X. (Plenum: 1980.) $75.

WESSON, P. (ed.). Gravity, Particles, and Astrophysics: A Review of Modern Theories of Gravity and G-Variability, and Their Relation to Elementary Particle Physics and Astrophysics. Astrophysics and Space Science Library, Vol.79. Pp.276. ISBN 90-277-1038-X. (Reidel: 1980). Dfl.65, $34.

Chemistry

BANCE, S. Handbook of Practical Organic Microanalysis. Recommended Methods for Determining Elements and Groups. Pp.206. ISBN 0-835312-178-8. (Ellis Horwood: 1980.) £18.50.

BUNCEL, E. and DURST, T. (eds). Comprehensive Carbanion Chemistry. Studies in Organic Chemistry, Vol.5. Part A. Structure and Reactivity. Pp.400. ISBN 0-444-41913-6. (Elsevier: 1980.) $83, Dfl. 170.

CAZES, J. and DELAMARE, X. (eds). Liquid Chromatography of Polymers and Related Materials II. Chromatographic Science. Vol.13. Pp.272. ISBN 0-8247-6985-6. (Dekker: 1980.) Sw.Fr. 80.

CLEMENIT, E. Computational Aspects for Large Chemical Systems. Lecture Notes in Chemistry, Vol.19. Pp.184. Flexi ISBN 3-540-10014-8. (Springer-Verlag: 1980.) DM 29.60, $17.50.

CONDON, E.U. and ODABASI, H. Atomic Structure. Pp.658. Hbk ISBN 0-521-21859-4; pbk ISBN 0-521-29893-8. (Cambridge University Press: 1980.) Hbk £30; pbk £9.95.

De MAYO, P. (ed.). Rearrangements in Ground and Excited States, Vol.2. Vol.42 of Organic Chemistry. Pp.431. ISBN 0-12-481302-X. (Academic: 1980.) $77.

Technology

BREWER, G.R. (ed.). Electron-Beam Technology in Micro-electronic Fabrication. Pp.362. ISBN 0-12-133550-X. (Academic: 1980.) $36.50.

CHALMERS, B., CHRISTIAN, J.W. and MASSALSKI, T.B. (eds). Progress in Materials Science, Vol.23. Pp.267. ISBN 0-08-024846-2. (Pergamon: 1980.) £38.

COULTER, M.O. (ed.). Modern Chlor-Alkali Technology. Pp.289. ISBN 0-85312-184-2. (Ellis Horwood: 1980.) £27.50.

HAYES, W.C., Jr. (ed.). Space — New International Opportunities for International Ventures. 17th Goddard Memorial Symposium. Vol.49, Science and Technology Series. Pp.300. Hbk ISBN 0-87703-124-X; flexi ISBN 0-87703-125-8. (Univelt: San Diego, 1980.) Hbk $35; flexi $15.

LEE, W.R. (ed.) Current Research is Ophthalmic Electron Microscopy, 3. Transactions of the 7th Meeting of the European Club for Ophthalmic Fine Structure in Ystad, Sweden, April 1979. Pp.160. Flexi ISBN 3-540 09953-0. (Springer-Verlag: 1980.) DM 48, $28.40.

SCHRÖDER, J. Operator Inequalities, Vol.147 in Mathematics in Science and Engineering. Pp.367. ISBN 0-12-629750-9. (Academic: 1980.) $39.50.

VAN DEN BERG, P.J. and DE JONG, W.A. Introduction to Chemical Process Technology. Pp.308. Hbk ISBN 90-277-1099-6; pbk ISBN 90-277-1100-3. (Reidel: 1980.) Hbk Dfl. 50, $26;

Computer Science

GARSIDE, R.G. The Architecture of Digital Computers. Pp.365. Hbk ISBN 0-19-859627-8; pbk ISBN 0-19-859638-3. (Oxford University Press: 1980.) Hbk £25; pbk £12.50.

GIBSON, G. and LIU, Y. Microcomputers for Engineers and Scientists. Pp.479. ISBN 0-13-580886-3. (Prentice/Hall: 1980.) £16.20.

Earth Sciences

BANIN, A. and KAFKAFI, U. (eds). Agrochemicals in Soils. Selected Papers from a Joint Meeting of the Soil Chemistry, Soil Fertility and Soil Clay Mineralogy Commissions of the International Society of Soil Science, Jerusalem, June 1976. Pp.500. ISBN 0-08-025914-6. (Pergamon: 1980.) $68, £30.

BERNER, R.A. Early Diagenesis. A Theoretical Approach. Pp.24. Hbk ISBN 0-691-08258-8; pbk ISBN 0-691-08260-X. (Princeton University Press: 1980.) Hbk £13.70; pbk £5.25.

BUTT, C.R.M. and SMITH, R.E. (eds). Conceptual Models in Exploration Geochemistry, 4. Developments in Economic Geology, 13. Pp.286. ISBN 0-444-41902. (Elsevier: 1980.) $63.50, Dfl.130.

COLLINS, M.B. *et al.* (eds). Industrialised Embayments and their Environmental Problems: A Case Study of Swansea Bay. Proceedings of an Interdisciplinary Symposium held at University College, Swansea, September 1979. Pp.616. ISBN 0-08-023992-7-H. (Pergamon: 1980.) $75, £33.50.

EARNEY, F.C.F. Petroleum and Hard Minerals from the Sea. Pp.291. ISBN 0-7131-6298-8. (Edward Arnold: 1980.) £14.95.

EVANS, A.M. An Introduction to Ore Geology. Geoscience Texts, Vol.2. Pp.231. Hbk ISBN 0-632-00665-X; pbk ISBN 0-632-00574-2. (Blackwell Scientific: 1980.) Hbk £16; pbk £7.50.

FREEMAN, T.W. A History of Modern British Geography. Pp.258. ISBN 0-582-30030-4. (Longman: 1980.) £13.50.

METEOROLOGICAL OFFICE. Weather in Home Waters. Vol.III, The Waters around the Azores and off South-West Europe and off North-West Africa. Pp.370. Flexi ISBN 0-86180-032-X. (HMSO: 1978.) £35.

SEIDLER, G. and WOODS, J.D. (eds). GATE 1. Oceanography and Surface Layer Meteorology in the B/C Scale. Pp.294. DUING, W. (ed.). GATE 2. Equatorial and A-Scale Oceanography. Pp.356. ISBN 0-08-023983-8-H. (Pergamon: 1980.) 2 vol. set $100, £44.50.

TURNER P. Continental Red Beds. Developments in Sedimentology 29. Pp.562. ISBN 0-444-41908-x. (Elsevier: 1980.) $70.75, Dfl.145.

Psychology

BAUM, A. and SINGER, J.E. (eds). Advances in Environmental Psychology. Vol.2, Applications of Personal Control. Pp.208. ISBN 0-89859-018-3. (Lawrence Erlbaum: Hillsdale, New Jersey, 1980.) $19.95.

BLANKSTEIN, K.R., PLINER, P. and POLIVY, J. (eds). Assessment and Modification of Emotional Behaviour. Advances in the Study of Communication and Affect, Vol.6. Pp.225. ISBN 0-306-[illegible]02-4. (Plenum: 1980.) $25.

CARTLEDGE, G. and MILBURN, J.F. (eds). Teaching Social Skills to Children. Innovative Approaches. Pp.322. Hbk ISBN 0-08-024654-0; pbk ISBN 0-08-024653-2. (Pergamon: 1980.) Pbk £4.50.

COLE, R.A. (ed.). Perception and Production of Fluent Speech. Pp.576. ISBN 0-89859-019-1. (Lawrence Erlbaum: Hillsdale, New Jersey, 1980.) $29.95.

CUSTANCE, A.C. The Mysterious Matter of Mind. Pp.105. Flexi ISBN 0-310-38011-1. (Zondervan Publishing: Grand Rapids, Michigan/Paternoster Press: UK, 1980.) Np.

ELLIS, N.R. (ed.). Handbook of Mental Deficiency, Psychological Theory and Research. 2nd Edn. Pp.785. ISBN 0-89859-002-7. (Lawrence Erlbaum: Hillsdale, New Jersey, 1979.) $45.

FIELD, T.M. (ed.). High-Risk Infants and Children. Adult and Peer Interactions. Pp.387. ISBN 0-12-255550-3. (Academic: 1980.) $27.

GREENE, J. and LEWIS, D. The Hidden Language of Your Handwriting: The Remarkable New Science of Graphonomy and what it Reveals about Personality, Health and Emotions. Pp.252. ISBN 0-285-62449-0. (Souvenir: London, 1980.) £6.95.

HAMMOND, K.R., McCLELLAND, G.H. and MUMPOWER, J. Human Judgment and Decision Making. Theories, Methods, and Procedures. Pp.258. ISBN 0-03-057567-2. (Hemisphere: 1980.) $22.50.

HASTIE, R. *et al.* (eds). Person Memory: The Cognitive Basis of Social Perception. Pp.308. ISBN 0-89859-024-8. (Lawrence Erlbaum: Hillsdale, New Jersey, 1980.) $24.95.

RESNICK, L.B. and WEAVER, P.A. (eds). Theory and Practice of Early Reading, Vol.1. Pp.393. ISBN 0-89859-003-5. (Lawrence Erlbaum: Hillsdale, New Jersey, 1979.) $24.95.

RESNICK, L.B. and WEAVER, P.A. (eds). Theory and Practice of Early Reading, Vol.2. Pp.353. ISBN 0-89859-8. (Lawrence Erlbaum: Hillsdale, New Jersey, 1979.) $24.95.

RESNICK, L.B. and WEAVER, P.A. (eds). Theory and Practice of Early Reading, Vol.3. Pp.386. ISBN 0-89859-011-6. (Lawrence Earlbaum: Hillsdale, New Jersey, 1979.) $24.95.

TRIESCHMANN, R.B. Spinal Cord Injuries: Psychological, Social and Vocational Adjustment. Pp.250. Hbk ISBN 0-08-024661-3; flexi ISBN 0-08-025594-9. (Pergamon: 1980.) Hbk £10; flexi £6.

WEBSTER C.D. *et al.* (eds). Autism: New Directions in Research and Education. Pp.285. ISBN 0-08-025083-1. (Pergamon: 1980.) £11.25.

WILKENING, F., BECKER, J. and TRABASO, T. (eds). Information Integration by Children. Pp.320. ISBN 0-89859-015-9. (Lawrence Erlbaum: Hillsdale, New Jersey, 1980.) $24.95.

WITHEY, S.B. and ABELES, R.P. (eds). Television and Social Behaviour: Beyond Violence and Children. Pp.368. ISBN 0-89859-014-0. (Lawrence Erlbaum: Hillsdale, New Jersey, 1980.) $24.95.

Sociology

BARON, C.G. (ed.). Technology, Employment and Basic Needs in Food Processing in Developing Countries. Pp.384. ISBN 0-08-025228-1. (Pergamon: 1980.) $45. £20.

DENNIS, R. and CLOUT, H. A Social Geography of England and Wales. Pp.270. Hbk ISBN 0-08-021802; flexi ISBN 0-08-021801. (Pergamon: 1980.) Hbk $31.50, £14; flexi $13.50, £5.95.

EISINGER, P.K. The Politics of Displacement. Racial and Ethnic Transition in Three American Cities. Pp.223. ISBN 0-12-235560-1. (Academic: 1980.) $18.

GERGEN, K.J., GREENBERG, M.S. and WILLIS, R.H. (eds). Social Exchange; Advances in Theory and Research. Pp.306. ISBN 0-306-40395-1. (Plenum: 1980.) $24.50.

LEWENHAK, S. Women and Work. Pp.286. ISBN 0-333-29112-3. (Macmillan Press: London, 1980.) £12.

PERKINS, E.R. Education for Childbirth and Parenthood. Pp.180. ISBN 0-7099-0273-5. (Croom Helm: 1980.) £10.95.

History of Science

DERBOLAV, J. Von den Bedingungen gerechter Herrshcaft. Studien zu Platon und Aristoteles. pp.298. ISBN 3-12-915040-4. (Ernst Klett: 1980.) Np.

FIELD, H.H. Science without Numbers. A Defence of Nominalism. Pp.130. ISBN 0-631-12672-4. (Basil Blackwell: 1980.) £7.95.

GARFIELD, E. Essays of an Information Scientist, Vol.3. Pp.891. ISBN 0-89495-009-6. (ISI Press: Philadelphia, 1980.) Np.

Anthropology

CHARLESWORTH, B. Evolution in Age-structured Populations. Cambridge Studies in Mathematical Biology, 1. Pp.300. Hbk ISBN 0-521-23045-4; pbk ISBN 0-521-29786-9. (Cambridge University Press: 1980.) Hbk £18; pbk £5.95.

HERSHEY, D. and WANG, H.-H. A New Age-Scale for Humans. Pp.156. ISBN 0-669-03374-X. (Lexington Books: Farnborough, Hampshire, 1980.) £13.50.

KAULINS, A. The Phaistos Disc: Hieroglyphic Greek with Euclidean Dimensions. The "Lost Proof" of Parallel Lines. Studies in the History of Mankind and its Language, Vol.1. Pp.142. (Andis Kaulins: FRG, 1980.) Flexi Np.

KÖNIGSSON, L.-K. (ed.). Current Argument on Early Man. Proceedings of a Nobel Symposium held at Björkborns Herrgard, Sweden, May 1978. Pp.250. ISBN 0-08-024956-6. (Pergamon: 1980.) £27.

ORTON, C. Mathematics in Archaeology. Pp.248. ISBN 0-00-216226-1. (Collins: 1980.) £12.95.

WILLEY, G.R. and SABLOFF, J.A. A History of American Archaeology. 2nd Edn. Pp.313. Hbk ISBN 0-7167-1122-2; pbk ISBN 0-7167-1123-0. (W.H. Freeman: 1980.) Hbk £9.50; pbk £4.30.

General

BUSHA, C.H. and HARTER, S.P. Research Methods in Librarianship. Techniques and Interpretation. Pp.417. ISBN 0-12-147550-6. (Academic: 1980.) $19.50.

COLINVAUX, P. The Fates of Nations. A Biological Theory of History. Pp.384. ISBN 0-671-25204-6. (Simon & Schuster: 1980.) Np.

CROWLEY, M. (ed.). Energy: Sources of Print and Non print Materials. Pp.341. ISBN 0-918212-16-2. (Mansell: London, 1980.) £11.

DREW, C.J. Introduction to Designing and Conducting Research. 2nd Edn. p.356. ISBN 0-8016-1460-0. (YB Medical: 1980.) £9.

GOODGER, E.M. Alternative Fuels; Chemical Energy Resources. Pp.238. ISBN 0-333-25813-4. (Macmillan Press: London, 1980.) £14.

McHALE, V.E., HUGHES, B.B. and GRUNDY, K.W. Evaluating Transnational Programs in Government and Business. Pergamon Policy Studies on Socio-Economic Development. Pp.251. ISBN 0-08-025101-3. (Pergamon: 1980.) £13.75.

MOONEY, P.R. Seeds of the Earth. A Private or Public Resource? Pp.126. Flexi ISBN 0-9690149-3-7. (Inter Pares: Ottawa, 1980.) $6.52.

PARKIN, N. and FLOOD, C.R. Welding Craft Practice. Vol.2, Electric Arc Welding and Related Studies. 2nd Edn. Pp.176. Hbk ISBN 024260-X; flexi ISBN 024259-6. (Pergamon: 1980.) Hbk $15, £7.50; flexi $8, £3.75.

PARRINDER, P. Science Fiction: Its Criticism and Teaching. Pp.166. Hbk ISBN 0-416-71390-4; pbk ISBN 0-416-71400-5. (Methuen: 1980.) Hbk £5.95; pbk £2.75.

SINHA, P.B. and SUBRAMANIAN, R.R. Nuclear Pakistan. Atomic Threat to South Asia. Pp.156. (Vision Books: 36C Connaught Place, New Delhi 110001, India: 1980.) Rs.55.

SOBEL, L.A. (ed.). Energy Crisis, Vol.4 1977–1979. Pp.220. ISBN 0-87196-284-5. (Clio Press: Hinksey Hill, Oxford, UK, 1980.) £8.50.

SOIL CONSERVATION SOCIETY OF AMERICA. Resource-Constrained Economies. The North American Dilemma. Based on material presented at the 34th Annual Meeting. Pp.307. Flexi ISBN 0-935734-05-8. (Soil Conservation Society of America: Ankeny, Iowa, 1980.) $8.50.

STANDKE, K.-H. and ANANDAKRISHNAN, M. (eds). Science, Technology and Society: Needs, Challenges and Limitations. Proceedings of the International Colloquium, Vienna, Austria, August 1979. Pp.650. ISBN 0-08-025947-2. (Pergamon: 1980.) £50.

TANNENBAUM, P.H. (ed.). The Entertainment Functions of Television. Pp.272. ISBN 0-89859-013-2. (Lawrence Erlbaum: Hillsdale, New Jersey, 1980.) $19.95.

De VOLPI, A. Proliferation, Plutonium and Policy: Institutional and Technological Impediments to Nuclear Weapons Propagation. Pp.359. ISBN 0-08-023872-6. (Pergamon: 1979.) Np.

WELFARE, S. and FAIRLEY, J. Arthur C. Clarke's Mysterious World. Pp.217. ISBN 0-00-216536-8. (Collins: 1980.) £8.95.

WHYTE, A.V. and BURTON, I. (eds). Scope 15. Environmental Risk Assessment. Pp.157. ISBN 0-471-27701-0. (Wiley: 1980.) £12.

WILBERT, J. Carte Pédologique de France à 1/100.000. (Lesparre G-17). Pp.229. Flexi ISBN 2-85340-083-2. (Institut National de la Recherche Agronomique: Route de Saint-Cyr, 78000-Versailles, 1980.) 96F.

WORLD HEALTH ORGANIZATION. Manual of Basic Techniques for a Health Laboratory. Pp.487. Flexi ISBN 92-4-154145-8. (World Health Organization: Geneva, 1980.) Sw.Fr.30.

nature

30 October 1980

SCIENCE COLLEGE
4 Upper Circular Road
CALCUTTA

Why bother to rehabilitate Galileo?

The Vatican has been edging towards a posthumous reconciliation with Galileo Galilei for several years. Since the time of Pope Paul VI in the mid-1960s, commendations of Galileo have been customary in the Vatican. The present pope, John-Paul II, has been still more outspoken. He marked the centenary of Einstein's birth two years ago with a public declaration that Galileo was an honoured precursor. As yet, however, the Vatican has not gone as far as to acknowledge as mistaken Galileo's prosecution in 1633 by the Holy Office — the trial that led to Galileo's abjuration of his heliocentric heresy on 22 June that year. Some such development is now, however, on the cards. The synod of bishops was told last week in Rome of a plan to set up a commission of inquiry under Archbishop Paul Poupard to look into the circumstances of the trial of Galileo and, as they say in the civil service, "to report". It is unthinkable that the outcome can fall short of a public declaration that Galileo should not have been brought to trial, that he should not have been forced by the threat of torture to recant and that his book, *Dialogue of the Two Great World Systems*, might safely have been taken off the Vatican's list of prohibited books a little earlier than 1835.

No doubt the Church is hoping that it will then be able to deal straightforwardly with the criticisms that have been flung at it for the past three centuries. Doctrinally, it should not be too hard for the commission to reach such a position. By good fortune, Pope Urban VIII (once a friend of Galileo's) played no part in the proceedings in Rome in 1633, not so much by design as from indolence. So a re-examination of the history of this shabby affair will not undermine the notion that popes (even bad popes) are infallible. Indeed, with a little luck, the commission may be able to put the blame for Galileo's examination and forced recantation on the two Dominicans, Badino Nores and Augustino Mongardo, who kept the minutes of Galileo's first formal encounter with the Holy Office in 1616, and who appear to have left in the Vatican files a much sharper version of what was then asked of Galileo than he and even his inquisitor, Cardinal Bellarmine, afterwards recalled. In the event, in 1633, Galileo was hauled over the coals not merely for having published his great book but also for having broken his supposed earlier undertaking not to hold heliocentric views. As the past three centuries have amply shown, this would not have been the first or last occasion on which the minutes of an important meeting turned out to reflect more accurately the wishes of the minute-taker than the words spoken.

Certainly, if it chooses, the commission will also be able to convince itself that the root of the trouble with Galileo lay in a misunderstanding between him and the Holy Office about the terms in which Copernicans were allowed to describe their theories. From 1616 on, Galileo understood that the Church required of him merely that the Copernican theory should be advanced only as a "hypothesis", not described in any sense as the "truth". Galileo, in other words, was almost as free to talk about Copernicanism as would be a modern professional brought up in the spirit of Karl Popper. Is not a good hypothesis one that is by definition falsifiable? That was the licence that he indulged in the seventeen years between his first and second encounters with the Holy Office.

The commission will also conveniently discover that Galileo's own behaviour contributed to the dismal outcome. Although his reputation is chiefly that of a fierce controversialist, Galileo was also capable of extraordinary deviousness. Why else would he have written the *Dialogue* as a dialogue between a Ptolemaic and a Copernican, leaving it to his readers to decide to which to give the benefit of the doubt? Throughout his second trial, he lied consistently, denying Copernican inclinations. His final humiliation was his claim that the *Dialogue* had been written to demonstrate that Copernicus was wrong. Pathetically, he told the Holy Office that, in preparation for his examination, he had read the book again after an interval of three years and had been dismayed to discover that his literary intentions had gone awry: on reflection, he allowed, innocent readers might have been given the impression that Ptolemy and not Copernicus was mistaken. The cardinals of the Holy Office can hardly have believed their good fortune. For practical purposes, the trial was over before it had begun. Everybody present must have recognized that Galileo's repudiation of his own witty and incisive book would be a more serious penalty than any they could have dreamed up for him. Willingly, they accepted his lies at face value. The public confession he was required to read before being sent off to house imprisonment was almost a formality. The Holy Office had pulled off a huge success. To have made a heretic recant would have been a minor triumph, an everyday occurrence. To have so humiliated the source of an important heresy that it would afterwards be entirely discredited was a much greater victory.

Now, three centuries after the event, the new commission will be able to point out that Galileo was apparently a willing accomplice in the whole affair. The transcript of the proceedings is full enough for that to be plain. No doubt he was afraid, but does fear not make lying excusable? Indeed, the new commission may be able to proclaim, the events of 1633 might have taken a different course if only Galileo had been straightforward, sticking to his guns. He might even have been able to persuade his judges that the Earth goes round the Sun and not the Sun around the Earth. For much of his life, Galileo had indeed been trying to do just that. His first brush with the Holy Office in 1616 was provoked by a letter he wrote three years earlier in which he noted that "the holy scriptures cannot err" but went on to argue that over-literal interpretations of them might be misleading. In the last resort, he had found out, the Church, not he, held the master cards. The execution of Giordano Bruno in 1600 for a similar (if less cogent) proclamation of heresy would also have shown Galileo that on some important issues the Church was implacable. If Galileo had stuck to his heresy, the chances are high that even he would have followed Bruno to the stake. Then, the Poupard commission would have a much more difficult circle to square.

So why, if the humiliation of Galileo falls short of martyrdom, is it now thought necessary to reopen this old question? What the synod of bishops was told last week is that the trouble about Galileo still serves as a barrier between science and the Church, keeping potential believers away from the congregations to which they would otherwise belong. It is hard to think this can be a substantial consideration. Even those who have no allegiance to the Catholic Church now acknowledge that there have been substantial changes in the past three centuries. Willy-nilly, the old literal interpretation of the Bible has been watered down. Many distinguished clerics take a serious and constructive interest in what is happening in science. Many distinguished scientists are also believers. And if there is a gulf between science and the Church, its origin lies in contemporary issues, not those with which the seventeenth century was preoccupied.

That, indeed, is the reason why the new commission may have a harder task than its planners appear to be expecting. With the passage of all this time, the rehabilitation of Galileo is hardly more significant than the posthumous pardoning of a traffic

0028-0836/80/440767-02$01.00

violater who pleaded guilty in court. The new commission cannot expect to produce a persuasive report on Galileo without going thoroughly into the question of how the Church should make up its mind about scientific issues which are at present contentious. How will the Church make up its mind about Darwinism, for example? Hankerings after directed evolution still play too big a part in the Church's view of biology. What will happen if the Big Bang turns out not to be the cosmological convenience that the Church has leaped at? It is tempting to suppose that in these enlightened days the tragedy of Galileo could not be repeated. But is that so? What is to be made of the way in which the Church, by insisting on its views of how people should behave, frequently flies in the face of what is known about human behaviour? Only last Sunday, Pope John-Paul II, a charismatic publicist but an illiberal pope, was asking that remarried people should refrain indefinitely from sexual intercourse. The Church's views on birth-control, appropriate enough when the chances of newborn children reaching puberty were a good deal less than fifty per cent, are now a means of making millions small-time martyrs, pathetic contemporary analogues of Galileo. The Poupard commission will steer away from cans of worms like these. In doing so, it will fall far short of what seem to be its objectives.

Solutions for transatlantic universities?

Everybody agrees that higher education is important. Many people spend time worrying about its health. Almost nothing is being done. This, it seems, is the lesson to be drawn from the clutch of reports on higher education published in the past few days. The meeting organized by the European Community at Strasbourg last week (see page 773) was presented with a familiar analysis of what the future holds (see *Nature,* 23 October); immobile university teaching staffs unlikely to be renewed on a substantial scale for years ahead, indefinitely straitened budgets and declining student numbers. What the commission's working paper did was to extend to the whole of Europe the gloomy analysis of the future for British universities described just over two years ago when Mrs Shirley Williams was Secretary of State for Education and Science. According to temperament, some academics (and some of their well-wishers) will be heartened to know that misfortune is so widespread while others will be dismayed that the problem is so huge.

Yet the problem is also unchanging, or apparently so. This week's report from the House of Commons Select Committee on Education (see page 770) makes that plain. The committee is still urging action on issues that first became urgent years ago. Has the dual support system for research quite broken down, and if so why? Can something be done to make the Universities Grants Committee a better buffer between the universities and central government? What should be done to help universities deal with the inflexibility that demography has thrust upon them? The committee has some sensible and even original things to say. Whether they will evoke a response from government departments whose present concern is what it seems continuously to have been for the past several years — to find further economies in public spending — is another matter.

Only in the United States does it seem that optimism survives — and even that may be illusory. The report on science and engineering education put together for the White House by the National Science Foundation and the Department of Education (see page 769) is no doubt right to deny some of the wilder fears about the adequacy of higher education in the United States — the charge that the efficacy of United States defence may be jeopardized by the quality of graduates from the universities for example. Moreover, there is no substance in the wish that some sleight of hand by university administrators might of itself beat back the tide of imports from Japan and elsewhere. If the United States is slipping as an economic power, it is largely because its people have elected to enjoy more of the benefits of service industries than the people of states such as Japan (see *Nature,* 2 October). The White House report nevertheless discovers a number of points at which the university system is under stress. The difficulty of persuading engineers to teach other engineers is not an isolated problem but a sign that universities may chronically be least able to recruit the teachers whose services are most needed. And if the terms of reference of the study had been wider, it would probably have come to conclusions that echoed, perhaps less starkly, those of European commentators — ageing teaching staffs, too much immobility among them and the prospect of too few students. What on earth is to be done?

Times like the present, when most governments are preoccupied with serious financial problems, are not propitious for grand designs for reform. Radical and sweeping change is easiest when funds are plentiful. The most serious danger in the prolongation of present difficulties, however, is that university systems on both sides of the Atlantic will be further impoverished in their present pattern until change heralded by crisis is forced upon them. This is why, while waiting for the grand design, some of the common problems of these several university systems need to be tackled piecemeal and empirically.

The question of academic tenure is an obvious problem, with which American universities have grappled for several years. The House of Commons committee deals with the issue judiciously. Tenure is an essential ingredient of academic freedom, but there is no reason why a university that no longer needs a whole department should not invite the teachers concerned to leave, on terms regarded by their academic colleagues as equitable or even generous. Most European academics will resist this notion, familiar though it has unhappily become in the United States. Yet if the choice is between the health of a university and the discomfort of some of its academics, can lifelong tenure be justly held always to be beneficent? European universities are mostly too mealy-mouthed on this delicate subject — and too free with early tenure in any case.

Shortages of teachers in specialized subjects, identified in engineering by the White House report, are commonplace and also chronic. They are, however, by no means as novel as they seem — both in medicine and the law, most university systems have special devices for persuading high-earning professional people to devote themselves partly to the interests of students, their future competitors. In more novel fields, systems engineering for example, there has not been — and probably will not be — time for suitable inducements to be devised. Universities may have to manage indefinitely with unconventional solutions. Part-time teachers drafted in from industry may help but will not solve all the problems that abound. The general solution must however be more flexible and permanent. Is it not time that universities hard-pressed to teach students what only industries know and practise should, without shame, arrange to have their students taught vocational skills on the job?

Another conspicuous element of the common malaise is that universities are no longer as autonomous as they like corporately to pretend. Especially in Europe but also in parts of the United States system, external agencies have an increasing say in the development of policy. The explanation is simple — governments pay an increasing share of the costs, and expect an increased influence. Yet governments, however liberal, are less able to know what are the needs of individual universities than are the academics who work in them. In principle, academics are also best placed to judge their contribution to national needs, and their places in the university systems to which they belong. The precondition, however, is autonomy — the freedom to make decisions for themselves. In this sense, the demand that universities should be free from some of the shackles that at present bind them is not a demand for the right to irresponsibility but the opposite. More autonomy is certain to mean better universities.

0028-0836/80/440768-02$01.00

More commercial genetic manipulation

Harvard and Biogen establish Cambridge labs

Washington

Not to be outdone by West Coast colleagues, scientists from Harvard University and the Massachusetts Institute of Technology (MIT) are busy with their own plans for the commercial exploitation of research using recombinant DNA techniques.

The president of Harvard, Dr Derek Bok, is expected to announce shortly the university's decision to become a shareholder (although not an investor) in a company being set up to develop gene cloning techniques evolved in the university's laboratories. One candidate technique is Dr Mark Ptashne's methods of cloning human fibroblast interferon genes in *Escherichi a coli,* reported-in the latest issue of *Proc. natn. Acad. Sci. USA* (77, 5230; 1980).

At the same time, Biogen, the Swiss-based genetic engineering company whose board of directors includes Dr Walter Gilbert of Harvard and Dr Philip Sharp of MIT, is seeking permission to construct a $5.5 million research and manufacturing facility in East Cambridge.

Both schemes would make it easier for senior research scientists to maintain their university positions while working as consultants for the companies. In the case of Harvard — which 2 years ago agreed to license the rights to Dr Gilbert's insulin research to Biogen — the university would be able to invest its share of the profits from the new company in further research.

Inevitably, both plans have caused controversy. Harvard faculty members have been concerned about the potential conflict of interests between the goals of the proposed company and the university's commitment to basic research; Biogen's plans were the subject of a public meeting held on Tuesday before the Cambridge Biohazard Committee to discuss whether any conditions should be placed on the company's activities.

The Harvard plan was the brain-child of Dr Mark Ptashne, professor of biochemistry and molecular biology. Initially it had been proposed that the company would, at least temporarily, rent space in the university's biology laboratories; that postgraduate students might be able to work for the company while retaining university appointments; and that finance would be largely provided by the pharmaceutical company Eli Lilly, which had earlier bid unsuccessfully for the licence to Dr Gilbert's research.

Following an intense debate over the summer, various steps have been taken to keep the company, as one university official describes it, "very much at arm's length". For example, it has been agreed that, even if the university's involvement is approved, the company will seek separate premises.

In addition, although some Harvard scientists would be shareholders in the company and could be employed on a one-day-a-week basis as consultants — the generally accepted limit to outside commitments — direct overlap with university research staff would be minimal.

Financial support would probably come from outside sources of venture capital under a scheme being worked on by the Harvard Management Company, which manages the university's endowment.

The proposed organization of the company and its relationship to the university was discussed last week at a meeting of the faculty of arts and sciences. Although no formal decision was taken, Mr Daniel Steiner, Harvard's general counsel, said after the meeting that he saw "no overwhelming obstacles" to the plan being approved by Dr Bok, adding that the university "would not have gone as far as we have" if it had not been seriously interested in the project.

Ironically, the faculty meeting took place the day after Biogen had told the city council in Cambridge that it wished to build a research and manufacturing facilty in the city. At present, Biogen's main research facilities are in Geneva; and it is rumoured that one of the reasons for planning to build the new facility in Cambridge is the difficulty that has been experienced in obtaining Swiss work permits for US postdoctoral students.

Biogen's proposal was due to be presented on Tuesday to the Cambridge City Biohazard Committee, a subcommittee of the City Health Policy Council set up in 1976 after an intense local debate to monitor recombinant DNA research in the area.

More criticism was expected at the meeting. Ex-mayor Alfred E. Vellucci, who previously led an unsuccessful fight to ban all recombinant DNA research in Cambridge, was equally opposed to a "DNA factory" coming to Cambridge now.

Others thought that — particularly in the light of the investment fever that swept Wall Street two weeks ago over the public offer of shares in the San Francisco company Genentech — Biogen is unlikely to encounter substantial opposition.

If the Biogen facility gets the go-ahead, it is likely to be partly financed from a $20 million equity investment which the chemical company Monsanto is to make in the company. Also, the two other major equity holders — Shering Plough and International Nickel — have increased their equity by $8.8 million.

In a separate development, the Dow Chemical Company announced that it was making a $5 million investment in another small Massachusetts biotechnology company, Collaborative Research, of which Dr David Baltimore is chairman.

David Dickson

Few complaints on education

Washington

US science and engineering efforts are basically on an even keel, even if there are a few selective vacancies among the crew, the officers do not understand too much about how the engines work and the passengers occasionally question the course that is being followed.

This seems to be the main message of a long-awaited report on the state of US science and engineering education, requested by President Carter in February from the National Science Foundation and the Department of Education, and published in Washington last week.

The request, largely prompted by the President's Science Advisor, Dr Frank Press, responded to certain concerns expressed about aspects of educational policy in these two fields. These include a well documented decline in performance by US school-children in science-related subjects, difficulties faced by the armed forces in retaining technically trained recruits (much talked about after the failure of the attempt to rescue the hostages from Iran) and warnings of the dire consequences of apparent Soviet educational supremacy.

But whereas in the mid-1950s the launching of the Russian Sputnik was seen as a challenge which led to a massive injection of new funds to revitalize US efforts to improve scientific and technical skills, the new report implies that there is little need for general alarm — or any major investment of resources.

This time, the emphasis is on quality rather than quantity. The report concludes that the number of science and engineering graduates is likely to be adequate for the next couple of decades, apart from possible shortages in fields such as computer science.

Two main problems are identified: first, the increasing cost of providing a good engineering education, both in terms of employing good teachers and purchasing up-to-date equipment, and, second, evidence of a spreading "scientific illiteracy" which could have serious consequences in a world of increasing technical complexity.

It is the latter problem which provokes some of the strongest language in the report, with the claim that there is a

0028-0836/80/440769-02$01.00

"desperate need" for curricula for students who are not interested in professional scientific and engineering courses, and that "the current trend toward virtual scientific and technological illiteracy, unless reversed, means that important national decisions involving science and technology will be made increasingly on the basis of ignorance and misunderstanding".

The evidence used to support this contention — headlined in the US press coverage of the report — is scarce. However, various background studies are quoted. These reveal, for example, that in 1976–77 about 48 per cent of grade 9–12 students were enrolled in at least one science class. This compares with more than 59 per cent in 1960–61, the crest of the post-Sputnik science education boom.

Among the proposals aimed at tackling the growing gap between the two cultures is the setting up of a President's Council on Excellence in Science and Technology Education, to act as a possible vehicle for presidential statements about the need to raise science and mathematical requirements for all secondary school students. Other suggestions include a federal inter-agency coordinating committee of public understanding of science and technology, various regional conferences to help state and local administrators to discuss with teachers and educationalists ways of improving the quality and attractiveness of science courses, and various measures to increase awareness of the need to prepare for career opportunities in science and technology.

On the question of whether the current supply of science and engineering graduates is sufficient, the report is reassuring. In terms of scientists, a background "staff analysis" says that the present supply is adequate to satisfy demand except in a few sub-fields of physical and biological science, and that in 1990 the aggregate number of new science graduates at all degree levels should exceed the number able to find jobs in the broad fields in which they are trained.

In engineering, the picture is less optimistic. The same analysis indicates that there are current shortages of trained computer professionals and most types of engineers at all degree levels, and it says that for computer professionals in particular a shortage at all degree levels is likely to persist beyond 1990.

The general conclusion, however, is that the numbers of new engineering baccalaureates should be adequate to satisfy demand for the services, with neither a rapidly increasing defence budget nor a major programme in synthetic fuels creating significant additional demands.

Where the report does pinpoint a cause for concern is in the supply of engineering teachers and equipment. In the first case, it suggests that increased support for university-based research projects, and possibly salary increases for researchers approved by separate federal agencies, could reduce the rewards gap between industrial and academic careers.

In the second case, officials from the Office of Science and Technology Policy point out that the upgrading of university equipment is a principal objective of the extra $600 million in basic science support which President Carter pledged in his economic revitalization package announced in August.

The report's proposals are now being debated inside the White House to find those which, at a time of general budget austerity, can still be squeezed into the budget request for the fiscal year 1982. In a covering letter to the report, Dr Frank Press says that the Administration intends "to enhance the capabilities of our science and engineering programs for education and research".

However, following a report which throws lukewarm water on some of the more extreme claims and fears that have been expressed over the past year — nothing very dramatic is expected.

David Dickson

UK higher education

Commons take stock

British universities have at last found some friends in the House of Commons, to judge from the report (published earlier this week) of the inquiry by the Education, Science and Arts Committee into the funding and organization of higher education. Specifically, the committee sternly rejects the implications of the question raised by the Secretary of State for Education and Science, Mr Mark Carlisle, that the pattern of university courses should be tailored to the forecast needs of skilled manpower in the United Kingdom.

The committee has also sided with the universities in its urging that steps should be taken to encourage more potential students to go on to higher education, thus denying Mr Carlisle's statement that the present participation rate reflects market forces and should not be "artificially boosted". The question of participation rates is crucial for the universities, faced as they are with the prospect of a declining demand for university places for demographic reasons.

On the administration of institutions of higher education other than the universities (polytechnics, technical colleges and the like), the committee does not go the whole hog with radical opinion and recommend a committee analogous to the University Grants committee for channelling funds in their direction. Rather, it advocates a committee to be responsible for planning and advice in the non-university sector, saying that the local connections that have grown up between local authorities and the institutions which they maintain are valuable.

The committee links its opinion on the participation rate with the financial problems of higher education. It describes as "disappointing" Mr Carlisle's explanation of what is meant by "level funding" — the procedure by which the universities' budgets for the two coming years will "not be very different in real terms" from that for the present academic year. The committee says that the policy of "level funding" leaves no room for potential increases in the age participation rate, and that the government should instead devise a formula relating expenditure to student numbers.

The committee's approach to Mr Carlisle's delphic hope that there would be a "subject balance in broad terms in relation to the future of highly qualified manpower" was first to take advice on its meaning from his officials. For its pains, it won the supposed clarification that the objective was to translate "the very specific requirements of the market-place into very broad subject areas, grouping them in, for example, the technologies, the sciences and the arts subjects . . . to try to work out from such messages as can be derived . . . a subject profile which could be a guiding principle for the institutions of higher education".

While aspects of this opinion were echoed by others among the committee's witnesses, the committee says it found no agreement on what might be called the national need, and no workable suggestions as to how the task might be accomplished were put forward. The committee therefore recommends that the universities should indeed listen to such "messages" as they can hear, but that the suggestion that they should then attempt to work out "principles for higher education" should be rejected as impracticable.

The committee also asks that the University Grants Committee should be made more independent of the Department of Education and Science, perhaps by recruiting its own officials, not borrowing them from the department. It applauds the setting up of the Merrison committee, intended to look into the joint support of the University Grants Committee and the research councils for university research, and approves of the consideration now being given to the concentration of resources in those establishments where research is most vigorous.

For the rest, the committee gives its blessing to the department's present investigation of student loans, asks for a better definition of the problems of different fees for home and overseas students and suggests that the concept of tenure should be re-examined. The committee is judicious on the last point. It acknowledges that tenure is an important ingredient of academic freedom, but asks that it should not stand in the way of change. One solution, the committee suggests, would be for academics displaced from unwanted departments to be offered "fair redundancy".

0028-0836/80/440770-02$01.00

European Space Agency

Supposing stability

The European Space Agency (ESA) is hoping for a budget held steady for a decade, at a real £285 million a year from 1982. The sum is much less than ESA's current budget of £480 million, but it sets a floor below which ESA's rapidly falling spending should not fall.

This comes at a time when all is changing at ESA under Erik Quistgaard, the 58-year-old Danish industrialist who was appointed director-general of ESA in May. The current troubles come from the ending of the development programme for Ariane, ESA's launcher, and its transfer to the private company Arianespace, and the completion of Spacelab, due for launch on the space shuttle in 1983.

Last week Quistgaard presented his proposals to the ESA Council — the top decision-making body of ESA — in an unminuted restricted session of the Council "bureau", which consists of the top national delegates but takes soundings rather than decisions. It was this bureau session which agreed in principle to Quistgaard's budget. The bureau also supported his proposals for a 50 per cent increase over the next ten years in the mandatory science budget (which provides ESA's research satellites — 12 launched so far). This budget has been fixed effectively since 1971 at a level of £60 million a year (1980 prices), and is committed — all but £180 million — to 1990 on six projects.

These are a trip to Halley's comet in 1986 (a mission called Giotto), an astrometry satellite (Hipparcus), an X-ray observatory (Exosat), a 15 per cent involvement in the space telescope, an investigation of the solar corona outside the elliptic, and an experiment to measure the effects on the human body of controlled accelerations in space (SLED).

Whether the money materializes depends on decisions made nationally, and at subsequent meetings of ESA council (the next is this month). Agreement must be reached on the main technological programme of ESA — is it to be improvement of Ariane, Earth resources or communications satellites — against a tendency in France and Germany, opposed by smaller nations, to see ESA primarily as a research and development agency rather than a profit-making space multinational. And there are problems in both France and the United Kingdom over the procedure of contributing to ESA; so a ministerial meeting is being considered for the spring of next year.

In the United Kingdom, the problem is the division of contributions between the Department of Industry (for applications) and the Science Research Council (for research), so that a change in balance must be decided at ministerial level. In France, the problem is the competition between contributions to ESA and a growing national programme within the budget of a single agency, the Centre National pour les Etudes Spatiales — again a matter for cabinet-level decisions.

But whatever the remaining problems, Quistgaard himself scored a major personal success last week. Delegates came to Council prepared to take their pound of flesh — France, for example, wanted a 10 per cent cut in ESA staff — but in the end they applauded him. In his summing up Quistgaard told delegates "You nearly killed me — but I survived." More than that, he has streamlined ESA, getting Council to agree to eliminate the 40-strong directorate of future programmes and planning, and to set up a think tank of half the size which will report directly to Quistgaard; and to devolve power to the existing directors (now to be called the management team). **Robert Walgate**

Huxley for PRS

Sir Andrew Huxley, the neurophysiologist, is now almost certain to be the next President of the Royal Society in succession to Lord Todd, who comes to the end of his five-year stint at the anniversary meeting, to be held this year on 1 December.

The society's election procedures require that nominations of new council members and also of the new president should first be agreed by the Council, and then submitted to the membership of the society in the form of a single slate of candidates. Sir Andrew Huxley's name has apparently been agreed for several months, and it is known that several insititutions have already engaged him to speak at conferences or to officiate at centenary celebrations well into 1981.

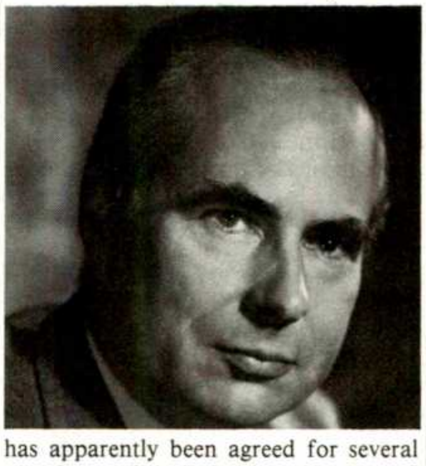

Now that Sir Andrew's nomination by the council is assured, the chances of his not being elected are vanishingly small. This could only happen if a majority of the members of the society were to strike out his name on the ballot paper and to substitute that of some other member.

Sir Andrew, who will be 63 at his election, has been a Royal Society Research Professor in the Department of Physiology, University College London, since 1969.

Indian laboratories

Back to GO

Bangalore

In what is considered to be a major step to tone up the state of Indian research, the government led by Mrs Gandhi has transferred back to the Council of Scientific and Industrial Research (CSIR) four laboratories which the previous Janata government had handed over to user ministries. The laboratories concerned are the Central Fuel Research Institute, Dhanabad; the Indian Institute of Petroleum, Dehra Dun; the Central Road Research Institute, New Dehli; and the Central Building Research Institute, Rourkee.

In April 1978, the Janata government, which under Morarji Desai was firm on "socially committed research", had dissociated these laboratories from CSIR and transferred them to user ministries on an experimental basis. Presumably this "delinking and transfer" was intended to foster a closer relationship between research and industry that would accelerate the country's scientific potential for industrial growth.

However, the decision proved to be counterproductive. Not only did it fail to achieve the desired goal but India's scientific community saw this step as a "vicious attack on scientific autonomy". For the past two years there has been a heated debate on the move in India's administrative and political circles. It was widely alleged that the decision was taken without considering the opinion of the scientific community.

The controversy surrounding the delinking had cast a shadow over scientific research in India. While the advocates of delinking called it an important measure to enhance industry — "research interaction" — the critics saw it as "a dark conspiracy of alien agents acting in collusion with their Indian masters" to subvert indigenous research efforts.

CSIR was established in the early 1950s to promote scientific research into the economic exploitation of India's vast resources. By Indian standards, CSIR is a giant covering four laboratories and research associations, and it has never been handicapped by the paucity of resources or dearth of skilled manpower.

The contribution that the CSIR laboratories have made to indigenous research for industrial development is difficult to assess. While the left-inclined high-technology advocates say that CSIR has been a trail blazer in easing India's poverty and backwardness through innovative research relevant to the socio-economic conditions of the country, pro-Gandhian, appropriate-technology proponents say that CSIR is a "colonial set-up subservient to the capitalistic research" that is alien to the Indian environment.

In recent years, CSIR technocrats have

been complaining that there are virtually no takers for the processes and technologies developed in CSIR laboratories. In fact, most public and private sector industries in India have favoured the wholesale import of foreign technology. This anomaly was said to be the motivation behind the handing over of the laboratories to user ministries. But the import of technology by the bureaucrats in the user ministries has continued unabated.

B. Radhakrishna Rao

NIH research grants

Trying new tricks

Washington

In an attempt to cut down on the amount of "time and effort" reporting required of scientists, the National Institutes of Health (NIH) are being urged to try a new mechanism for funding research grants that would make the researcher financially accountable to his or her university or research institution rather than directly to the funding agency.

At present, NIH project grants — whose total value is about $1,400 million, over half the total NIH research budget — are awarded on a "cost reimbursement" basis, under which the government agrees to cover all previously agreed costs that can be properly accounted for.

The proposal is to experiment with so-called "fixed obligation grants" (or "fixed price grants") where the research institution merely has to demonstrate to the funding agency that the scientific and technical goals of the research have been satisfactorily pursued.

"Time and effort" reporting is the most controversial of the strict new rules on accounting for research expenditures introduced last month by the Office of Management and Budget (OMB) in a document on cost principles known as Circular A-21.

These rules require all principal investigators to provide a semester-by-semester breakdown of the way they distribute their time between teaching, research, administration and other activities — and to report any change in this distribution to the federal government.

Federal auditors argue that this is necessary to ensure that money is being allocated and spent in the way agreed when a research grant is awarded. But scientists argue that in an over-zealous enthusiasm to minimize fraud and abuse — a popular target of congressional committees — the auditors are reducing the productivity of research laboratories for a minimal return.

Despite earlier protests, OMB had refused to delay the implementation of the new rules, the outcome of several years of negotiation. However, under continued pressure from universities, the agency is now prepared to discuss ways of reaching its accountability goals more effectively.

OMB has already agreed to experiment at ten universities where "time and effort" reporting will be on a statistical basis rather than professor-by-professor. What is now being suggested, however, is considered by NIH director Dr Donald Frederickson to be revolutionary — "as radical as *Finnegan's Wake*".

The outlines of the proposal were presented to the NIH Directors' Advisory Committee (DAC) by Dr Linda Wilson, Associate Vice-Chancellor for Research at the University of Illinois in Urbana, and Mr James Kelly, previously Executive Vice-Chancellor of the State University of New York and a long-time proponent of fixed-price contracts.

The general idea is that there would be no change in the present pre-award proposal process for the selection of research and determining the amount of an award. However, post-award administration would be changed to delegate most of the responsibility to the recipient institution and the principal investigator, in particular the emphasis of accountability would be shifted from the allowability of costs and the adequacy of documentation to criteria that indicate "reasonableness of technical progress".

Supporters of this new proposal, which comes out of a recommendation made in a recent report from the National Commission on Research for Experiments in Grant-in-Aid Support for Research Institutions, argue that it should still be possible to build in enough controls to ensure that public funds are not misused (such as spot auditing checks). The new system might eliminate some existing problems, but there could be new ones. For example, by shifting prime responsibility for the financial conduct of the grant from the federal government to the research institution, tensions between the government and the institutions could be replaced by tensions between the institution and its principal investigators.

Additional pressure would also be incurred on efforts to measure scientific accountability; Dr Wilson emphasizes that research grants should be treated as *assistance* rather than *procurement* funds, to avoid the rigid accountability — and hence loss of flexibility.

Mr Kelly told members of the DAC that there was little evidence that a new system for administering grants would save much money and that any increase in research productivity would not necessarily be measurable. The principal advantage, he said, was that the new approach might reduce tensions between universities and the federal government, currently running high in the wake of the introduction of Circular A-21.

Any experiments in this direction are likely to receive the approval of the Office of Science and Technology Policy (OSTP), whose associate director, Dr Denis Prager, told the committee that reducing non-budgetary constraints on research was one of OSTP's top priorities, particularly by encouraging forms of regulation based on performance.

Polish academy

Flexing muscle

Polish scientists wishing to travel abroad for professional purposes should in future find it considerably less complicated to obtain the necessary passport. Last week, Dr Jan Kaczmarek, Academic Secretary of the Polish Academy of Sciences, announced that the academy now has the right to decide such matters for its members.

This announcement marks a small, but significant step towards the greater academic autonomy widely demanded by Polish intellectuals in the wake of the Gdansk accords. It was made at an extraordinary general meeting of the Polish Academy of Sciences, which was called to discuss and re-evaluate the role of the academy, and of the scientific establishment generally, in the light of the recent changes in the country. The meeting, which participants reported had a warm and open atmosphere, made some sharp criticisms about the situation in Poland during the past few years, in particular, both the over-centralistic attitude of the authorities, which made it extremely difficult to get a

No stay for badgers

This will be a bad week for British badgers. Today (Thursday, 30 October) Lord Zuckerman's report on the practice of gassing badgers thought to be infected with bovine tuberculosis will be made public. This issue is contentious among conservationists because the Badger Act, carried through the British parliament with some emotion, which makes it a criminal offence to kill badgers even when they damage land and crops, provided an exemption for the Ministry of Agriculture, Fisheries and Food to allow the destruction of badger hides thought to be a reservoir of bovine tuberculosis.

Conservationists have since protested that the practice of gassing badgers for the sake of protecting cattle has been too widely licensed, and that it is in any case unnecessary or ineffective. Lord Zuckerman's report it thought to argue in an opposite direction.

0028-0836/80/440772-02$01.00

hearing for constructive criticism, and the consequent lack of responsibility. To remedy this situation, the academy called for clear limits to be set to the competence of anyone in authority and of rank-and-file functionaries.

A comprehensive system, the academy said, must be worked out for the proper functioning of the economy, based on the "broad utilization of all available and permissible self-regulating mechanisms". The authorities, it said, must show they trust the people. One obvious sign of such trust would be freedom of expression and the phasing out of censorship (except for the minimum needs of national security), which constituted a major point in the Gdansk accords.

A prominent speaker on this theme was Dr Jan Kielanowski, a leading nutritionist. He reminded the meeting that he and Dr Edward Lipinski had tried to raise the same issue of academic freedom and the abolition of the censorship at the academy's Annual General Meeting in May 1979 — but on that occasion, the motion was ruled out of order from the chair. Now, however, he observed, when the initiative came not from a couple of members of the academy, but from the broad masses of the Polish workers, the academy was prepared to listen.

The academy, in fact, had not waited until the extraordinary general meeting to take up the issue. Censorship and academic freedom had already been raised at the praesidium of the academy on 30 September. On that occasion, Professor Janusz Groszkowski, a former chairman of the academy, called for a detailed analysis of the situation in Polish research, including the moral and professional scrutiny of those researchers and scientists known to be letting down the intellectual integrity of their profession. Some researchers, said Groszkowski, are guilty of plagiarism, intellectual dishonesty, idleness and ignorance, while young people of genuine talent were given no opportunity to develop freely. "Hence", he concluded, "we have no great names and no great achievements." The academy, he said, must take the initiative in the reform and renewal of the scientific profession, without waiting for a lead; its deliberations should include possible changes in the legislation governing scientific research, the management of scientific institutes and the question of independent, trades unions for scientific research workers.

However, before this last proposal could be put to the general meeting of the academy, Poland's scientists had made their own decision: at the second delegate meeting of the new "Free Trade Union of Scientific, Technical and Educational Workers" (13 October), it was decided to terminate the existence of this body as a separate entity, and to transform it into a branch of the "Solidarity" confederation.

Vera Rich

European community

Research without end

Strasbourg

A meeting called by the European Commission here last week ended with a general air of expectancy among its participants. Next June, the commission will be proposing to the Council of Ministers a new research "enterprise". So far, however, it is not known how much the enterprise will cost, when it will start or even what it will do.

Commission officials nevertheless consider that last week's conference gave them a mandate to do something. And whatever it is, the cost will be added to the commission's present research budget, running at five per cent of the member states' research and development budgets.

The impetus for the initiative is twofold. First, there is a feeling in Brussels that there will be some slack in the EEC budget in the near future. Some think the Common Agricultural Policy will collapse, others that some part of agricultural spending will be put to other uses. All the community's directorates-general, including that for research, science and education, are eager to pick up the crumbs.

There is also a sense that something must be done to free posts and talent at the universities. As Sir Hermann Bondi put it last week, "the universities have been static for many years while other things are changing fast". He went on to advocate the setting up of research structures parallel to but in touch with the universities.

Most of those at Strasbourg agreed, but failed to provide the political wrapping or the precision that might lead to practical proposals to create scientific jobs or to improve mobility in Europe. In the end, the commission will work out its policy on the basis of background documents* prepared for Strasbourg, particularly those of Guy Denielou, president of the Technical University of Compiègne, Ilya Prigogine of the Free University of Brussels and Freddie Clarke, research director responsible for renewable energy at Harwell. Dr Günter Schuster, who heads the Brussels directorate-general for research, science and education, will now set up a task force to prepare proposals for June. There will be three scenarios, from ambitious to pessimistic, to cater for the unknown political climate nine months hence.

Schuster will rely largely on Denielou's proposals to define the "enterprise". But, says Denielou, the definition should concentrate on structure rather than topics. How the enterprise should function is more important, at this stage, than what it should do. The structure should not be academic, but like a business. It should be flexible, creating and closing teams as needs change. Its administration should be "very light". It should be cheap, probably based on existing laboratories.

A principal objective would be to foster mobility, for scientists are considered less free in Europe than in the United States. Research teams in the enterprise would therefore be drawn from across Europe. He proposes an experiment — three years, 50 teams of 30 scientists each, costs borne largely by the host laboratories.

To determine the subjects to be studied, the enterprise would need what Prigogine calls "an organ of perception" — something like the National Research Council in the United States — which would also select institutions and teams to investigate the chosen topics, using international referees. Brussels would thus be gaining an instrument for a centralized research policy — and a critical question for June will be what relationship such an instrument should have to the council, the supreme body in the community.

Robert Walgate

**"Towards a new undertaking in European research" by Guy Denielou and others; "Science and society in a changing Europe" by Ilya Prigogine; and "Community industrial research priorities for the early 1980s" by F. J. P. Clarke and others. (Commission of the European Communities (DG XII), Brussels.)*

China plays profit

Researchers at the Institute of Physics of the Chinese Academy of Sciences have recently been working on a new project — how to sell their results to industry.

It seems that until the recent economic reforms, what is now officially described as "a lack of communications" and "obstacles inherent in the system" prevented new scientific results from being applied to industry. New findings remained inaccessibly locked away in publications and festchrifts. Consequently, scientists had become upset and frustrated, while factories, unaware of new advances, were unable to modernize.

With the fall of the Gang of Four, however, factory managements were able to approach the scientists for advice on new results and how to apply them. So far, the Institute of Physics has worked out three possible cooperation procedures: (1) outright sale of the new technology, with technical assistance provided until the technology goes into production; (2) contracts for technological guidance, involving sending experts to the factories or training workers at the institute; with the onset of production, the institute is repaid on a sliding scale related to the profits from the new technology; for example, 20% in the first year, 10% in the second, 5% in the third; (3) provision of the new technology, for a decreasing percentage of its profits, for example, 5% the first year, 3% the second, and so on.

So far, the institute has signed contracts with 19 factories, many of which are already benefiting financially from such deals. **Vera Rich**

0028-0836/80/440773-02$01.00

Dangerous pathogens

New UK committee

The long-awaited reorganization of the British mechanism for regulating research with dangerous pathogens is planned for early in 1981. Last week the Department of Health and the Health and Safety Executive made public the terms of reference of a new regulatory body, to be known as the Advisory Committee on Dangerous Pathogens. The chairman and members of the group, which will replace the Dangerous Pathogens Advisory Group, have yet to be appointed.

The days of the existing advisory group have been numbered since the smallpox accident at the University of Birmingham in August 1978. Set up in 1975, the group was first responsible for drawing up lists of pathogenic organisms supposed to involve various degrees of hazard. The group also advised the Department of Health which laboratories should be licensed to work with organisms in the most hazardous category, category A. Control was voluntary.

The new system will be backed by the statutory requirement that laboratories planning to work with dangerous pathogens should first notify the Health and Safety Executive (HSE) of the people who will be involved and the experiments planned, giving at least 30 days' notice. The draft regulations published by HSE require more cursory notification of other listed pathogens.

Under the proposed arrangements, the new advisory committee will not scrutinize safety arrangements in individual laboratories, which will in future be the responsibility of officials of HSE. Instead, it will be responsible for advising the executive as well as the ministries responsible for health and agriculture on the classification of pathogens, the development of safety procedures and the opportunities for research.

One of the peculiar difficulties of the regulation of dangerous pathogens affects the working of medical diagnostic laboratories, which cannot know in advance whether a corpse on the slab has been laid low by, say, lassa fever. The proposed notification regulations will not apply to such laboratories, which will nevertheless be required not to carry out further work with schedule 1 organisms without going through the full procedure.

The composition of the new advisory group has been settled only in outline. There will be five employers' representatives drawn from universities, public health laboratories and the like, five representatives of employees' organisations and ten scientific members, together with a chairman.

For researchers in British laboratories, the chief consequences of the proposed arrangement will be that in future control will have the force of law. Failure to notify will be an offence, as will be failure to follow approved codes of practice.

Schedule 1 pathogens

Crimean haemorrhagic fever virus (Congo)
Ebola virus
Jumin haemorrhagic fever virus
Lassa fever virus
Machupo haemorrhagic fever virus
Marburg virus
Rabies virus
Simian herpes B virus
Smallpox virus
Venezuelan encephalitis virus

Soviet geophysics

Drilling deeper

Soviet geophysicists have had to rethink their models of the deep strata beneath the European part of the USSR, after processing the preliminary data from the super-deep borehole now being drilled on the Kola peninsula. And, according to Professor Vladimir V. Belousov, head of the Scientific Council on the Earth's Crust and Upper Mantle of the Department of Earth Sciences of the Soviet Academy of Sciences, two and possibly three more such holes will be started in the near future.

The Kola bore can advance at a rate of some 10–12 m per day, and has now passed a depth of 10,000 m. It is sited in an area thought to be geologically "dead", and without risk of earthquakes or volcanic activity. Core samples, however, have revealed that cracking extends to considerable depths, and at these levels, at a temperature of about 150°C, significant quantities of aqueous solutions, carbon dioxide and helium provide evidence of high geological activity.

This remarkable level of activity is not the only surprising result to have come from the Kola bore. It had been predicted that a transition from granites to basalts would be observed at a depth of about 7,000 m, and that, as the bore-hole went deeper, the angle of inclination of tilted strata would gradually flatten out. But so far it has been granite all the way, though of increasing density, and the angle of inclination of the strata remains constant.

The Kola bore has still another 5,000 m to go before it reaches its scheduled depth, but already some of the preliminary data are being used in planning prospecting for new mineral deposits. The other projected bores will also have their practical aspects — the Tyumen' bore will look for deep level oil and gas deposits in Western Siberia, while the Tagil bore will investigate the "foundations" of the Urals — an important range mineralogically.

The most exciting proposal under consideration would entail drilling a bore at the foot of the Avachinskaya Sopka — a large and active volcano in Kamchatka.

Vera Rich

Uranium deposits

France backs basics

Paris

A £1 million laboratory opened last week at Nancy seems intended to give France an incontestable world lead in uranium geology. Nicknamed CREGU, the laboratory will poach its director, Dr Bernard Poty, and five senior staff from the institute next door — the Centre de Recherche Pétrographique et Géochimique, which has already established a lead in using microscopic laser Raman spectroscopy to analyse fluid in inclusions in ore-bearing rocks. Such inclusions are expected also to give a clue to the formation of uranium ores — a complex process because of the extreme geochemical mobility of uranium, and the low concentrations of economically significant ores.

CREGU itself is a £400,000-a-year five-year experiment. Its £1 million buildings are a local enterprise, rented to the Commissariat à l'Energie Atomique and the five principal uranium prospecting firms in France. The Centre National de la Recherche Scientifique (which runs Poty's old lab) will pay the scientists' salaries. After five years, a council composed of members of the sponsoring organizations will decide whether the enterprise has been a success, and if it should continue.

To be successful, the new laboratory will not have to devise revolutionary methods for detecting uranium — though nobody denies this is the long-term aim of the investment. (In fact a proposal that CREGU should look at empirical methods of prospecting using magnetic anomalies was rejected by the laboratory's council.) Rather, it will attempt to extend the very sketchy existing knowledge of how the ore is formed. It is here that the fluid inclusions are significant, for they are relics of the fluids which deposited the ore — but they are so tiny that they have evaded detailed chemical analysis. CREGU, it is hoped, will solve this problem with its Raman techniques.

Other mining interests in France are watching the new laboratory carefully. It will help to train students and to retrain prospecting uranium geologists; and as ores of other minerals become economic at increasingly lower concentrations, greater and greater scientific subtlety is required in the detection of ores, and the judgement of the economic value of potential mines. So, it is believed in France, activities such as GREGU's, bridging basic science and industry, will become increasingly important.

Robert Walgate

The title **'Soviet science:** relations forsworn', *Nature* 23 October, p.672, should have appeared at the top of the left-hand column of the page, to head the article by Vera Rich. The article by Robert Walgate should have been entitled **'Nuclear waste:** West German problems'.

0028-0836/80/440774-02$01.00

NEWS AND VIEWS

Jupiter's magnetosphere

from S.W.H. Cowley

DIRECT observations by space probes over the past decade have shown that at least three planets in our solar system, in addition to the Earth, possess an intrinsic magnetic field. These are Mercury, Jupiter and Saturn. The solar wind, a tenuous proton-electron plasma blowing radially outwards from the Sun at speeds $\sim$ 400 km s^{-1}, confines this magnetic field to a cavity surrounding the planet forming a planetary magnetosphere from which the solar wind itself is largely excluded. Only Venus is known to be without a magnetic field although limited data suggests that this may also apply to Mars.

Of the four observed magnetospheres, that surrounding the Earth is, of course, the most thoroughly investigated and the best understood. Jupiter comes second, having been the subject of four fly-by encounters, by Pioneer 10 and 11 in 1973 and 1974 and by Voyager 1 and 2 in 1979. The Pioneer flights provided the first mapping of the Jovian magnetic field and the energetic charged particle radiation trapped on Jovian field lines. The Voyagers returned the first detailed data on the thermal plasma component and on plasma waves. Here we shall describe recently published Voyager results on low-energy Jovian plasma, setting them within the context of other major Voyager findings published in *Science* (**204**, 1979; **206**, 1979), *Nature* (**280**, 1979), and *Geophysical Research Letters* (**7**, 1980).

The properties of magnetospheric plasmas depend upon the nature of the plasma sources and sinks, and on the internal transport processes. In the Earth's magnetosphere transport is dominated by a large-scale convective flow driven by the solar wind (see Figure *a*). Since highly electrically-conducting plasmas and magnetic fields can be considered to be 'frozen' together we can equivalently describe the flow of field lines. Terrestrial field lines are transported by the solar wind flow from the dayside magnetosphere boundary at $\sim$ 10 R_E (1 R_E = Earth's radius $\sim$ 6,400 km) to the night side, where they are stretched out into a long $\sim$ 1,000 R_E magnetic tail. These flux tubes then flow back to the Earth through the 'centre' of the magnetosphere, heating entrained solar wind plasma and escaped ionospheric plasma up to $\sim$ 10 KeV energies as the tubes contract. A hot 'plasma sheet' is thus formed at the centre of the tail and a hot outer radiation zone around the Earth as shown in the Figure. Near the Earth, however, in a region usually extending to about $\sim$ 4 R_E in the equatorial plane, flows imposed by the Earth's rotation are more important than the solar wind driven convection. Here the flux tubes corotate with the Earth, their 'ends' being 'frozen' into the rotating ionosphere. This region then contains high density cold plasma from the ionosphere, and also, as a very minor constituent, energetic (Van Allen) radiation belt particles. The latter are transported into the region by radial diffusion from the outer radiation zone under the action of fluctuations in the external convection, rapidly gaining energy proportional to the field strength as they move inwards.

Sketch of (a) the terrestrial and (b) Jovian magnetospheres in noon-midnight meridian planes showing plasma flow within them. The Sun is to the left. Solid lines are field lines and the dashed line is the magnetosphere boundary. Flow in the Earth's magnetosphere is dominated by solar wind-driven convection, except near the Earth where corotation prevails and the flux tubes are filled with cold ionospheric plasma (heavy dots). In the Jovian magnetosphere corotation dominates, possibly resulting in a rotationally-driven planetary wind on the nightside. The sketches are not to scale. In linear dimension the Jovian magnetosphere is at least fifty times the size of the Earth's, and five times the size of the sun.

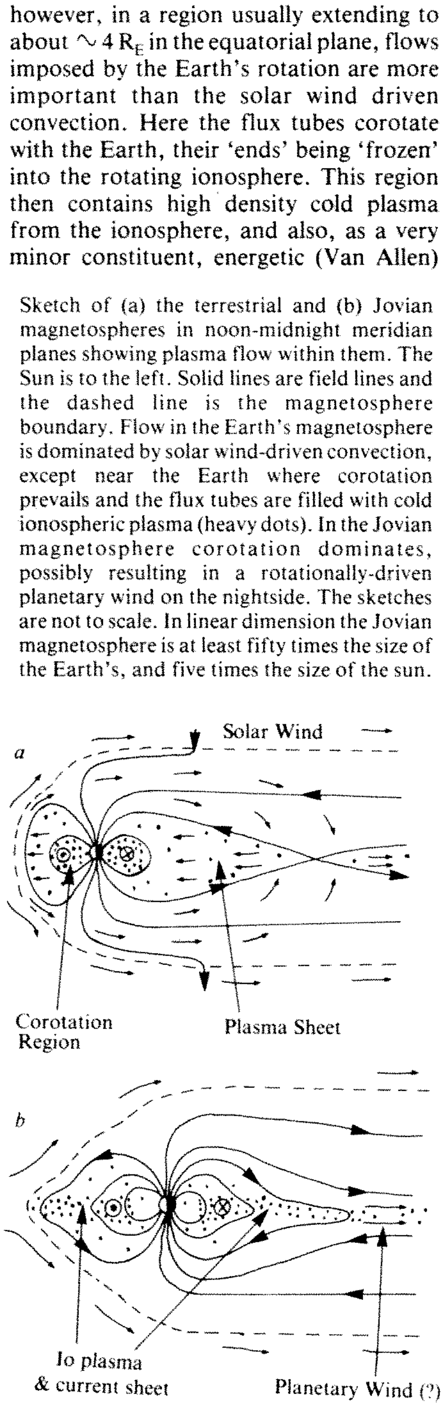

By contrast with the Earth, flow in the main part of the Jovian magnetosphere, extending some 50 R_J (1 R_J = Jupiter radius $\sim$ 71,400 km) on the dayside, is entirely dominated by corotation with the planet (Figure *b*), although this does not preclude the existence of a long (maybe $\sim$ 2 AU) magnetic tail on the night side arising from the solar wind interaction. Thus, like the Earth's corotating 'core' of field lines, the Jovian magnetosphere is dominated by cool plasma from internal sources, but also contains radially diffusing energetic particles of solar wind origin. The radial diffusion is probably driven both by turbulent Jovians atmospheric winds at ionospheric heights and by flux tube interchange motions arising from unstable density distributions of the low energy plasma.

The second important difference between the Earth's and Jupiter's magnetosphere is that the latter is so large that it encompasses the orbits of many of the moons. These bodies can then act both as absorbers of energetic particles, as the Pioneer results demonstrated, and as important sources of low energy plasma. Indeed, the Voyager results indicate that the dominant source of thermal plasma is not Jupiter's ionosphere as might have been expected, but the satellite Io, which orbits at a radial distance of 5.9 R_J, in the inner magnetosphere.

Voyager images show that Io is extremely volcanically active, probably due to intense internal tidal heating, thereby maintaining a tenuous atmosphere which appears to be composed mainly of sulphur dioxide. A small escape flux of this gas (small in relation to total volcanic outflow) followed by ionization then results in the formation of a dense corotating plasma torus in Io's vicinity composed mainly of sulphur and oxygen ions with energies several tens of eV. The torus has a thickness $\sim$ 1 R_J, the ions being retained near the rotation equator by centrifugal forces, and a sharp inner boundary at $\sim$ 5 R_J, where the temperature abruptly drops to a few eV. The latter

---

S.W.H. Cowley is a SRC Advanced Fellow in the Blackett Laboratory, Imperial College, London.

0028-0836/80/440775-02$01.00

observations indicate that inward radial diffusion of the ions towards Jupiter is rather slow, allowing time for the plasma to radiatively cool, thereby generating the considerable UV and optical emissions observed from the inner torus. The cooling plasma collapses towards rotation equator where the ions and electrons eventually recombine to produce relatively fast neutrals which fly off into the outer magnetosphere and solar wind.

By contrast, the outer part of the torus beyond the Io source appears to be unstable, the density gradient generating flux tube interchange motions which rapidly diffuse the plasma outwards into the magnetosphere. The plasma remains strongly concentrated at the equator, but the density rapidly drops with increasing distance due to the expanding flux tube volume as the field strength weakens. From values of several thousand cm^{-3} in the torus, the equatorial density falls to ~ 1 cm^{-3} at ~ 25 R$_J$ and to $\sim 10^{-2}$ cm^{-3} at 100 R$_J$ on the night side. In order to maintain rigid corotation, the Jovian atmosphere must continuously provide a torque on flux tubes in Io's vicinity where the plasma is created, since the coratation speed increases at a rate ~ 12.5 km s^{-1} R$_J{}^{-1}$ as the particles diffuse outwards. The torque is provided by atmospheric drag of ionospheric ions at the 'feet' of the flux tubes, but theoretical estimates (Hill *J. Geophys. Res.* **84**, 6554; 1979) indicate that the coupling may be too weak to maintain rigid corotation out to large distances. Voyager low energy plasma data indicates that is so, $\sim 20\%$ reductions below expected speeds being inferred at ~ 10 to 20 R$_J$. Indeed, even at ~ 40R$_J$ the azimuthal speed is reported as remaining near 200 km s^{-1}, less than half the corotation value. However, analysis of the angular anisotropies of higher energy ions shows good agreement with rigid corotation at such distances and beyond. The reason for this disagreement is currently unknown.

The most recent results on Jovian plasma flow (Belcher & Mc Nutt this issue of *Nature* p813) show that in addition to at least partial corotation, the low energy plasma also has comparably large flows along the field lines, directed toward the equator on the night side and away on the day side. As these authors point out, this flow most probably results from a day-night asymmetry in the magnetic field, which is compressed on the day side relative to the nightside by the dynamic pressure of the solar wind. As flux tubes rotate into the dayside sector they move closer to Jupiter and the plasma flows away from the equator due both to the field compression and to the decreasing centrifugal force. On the nightside the tubes expand and move outwards, the centrifugal force increase and the plasma collapses back toward the equator.

An important feature of a corotation-dominated magentosphere is that if the magnetosphere is large enough, and if corotation is maintained to large enough distances then the plasma kinetic energy density associated with the rotation will always reach and exceed the magnetic energy density at the equator at and beyond a certain distance. At this point the field can no longer retain the plasma, which will break away from corotation and flow rapidly outwards forming a 'planetary wind', a rotationally-driven analogue of the solar wind. Conditions on the dayside Jovian magnetosphere, confined to ~ 50 R$_J$ by the solar wind, seem somewhat marginal for planetary wind formation and no evidence for such an outflow was seen during the Voyager inbound passes near noon. On the nightside conditions are more favourable, and an antisunward flow which may be related to planetary wind formation was observed by Voyager 2 in a layer adjacent to the dawn magnetosphere boundary ~ 130 R$_J$ down-tail from Jupiter, as shown in Figure *b*. One particularly intense burst of such flow was found to consist mainly of heavy ions streaming at $\sim 2{,}000$ s^{-1}.

One final feature of Jupiter's magnetosphere which is receiving much attention is the considerable magnetic field distortions indicated in Figure *b*, due to an equatorial sheet of current carried by magnetospheric plasma in the azimuthal direction. These field distortions are most pronounced on the nightside, where they gradually take on the character of a magnetic tail at sufficiently large distances, but they are also observed on the day side as well. To produce the effects observed beyond ~ 10 R$_J$ the equatorial plasma pressure must be comparable to the field energy density. However, the pressure of the cool (~ 10 to 100 eV) Io torus plasma appears generally to be somewhat too small to account for the observed effects, thus indicating that a significant hot component is also present. Voyager observations at energies above ~ 30 keV show that such a component is indeed present with energies ~ 20–30 keV and an ion composition which includes protons, oxygen and sulphur as major constituents. The heavy ions must originate at Io, but how these particles become heated to such energies remains to be determined. It therefore seems that the Jovian magnetosphere contains at least two thermal plasma components, the cool Io torus plasma which may usually dominate the mass density, and a much hotter plasma also containing Io ions which often dominates the energy density. □

Iron deprivation as a biological defence mechanism

from Thomas Emery

OVER thirty years ago Schade and Caroline discovered that blood contains a specific iron-binding protein that inhibits the growth of pathogenic bacteria, such as *Shigella dysenteriae* (*Science* **104**, 340; 1946). They correctly concluded that the protein bound iron so tightly that the bacteria were deprived of that essential nutrient and were unable to grow. When it was subsequently discovered that the protein in question, transferrin, was responsible for mammalian iron transport, the significance of the bacteriostatic action was virtually forgotten. It now appears that deprivation of invading microbes of iron may be an important defence mechanism in both animals and plants.

Microorganisms excrete low molecular weight iron chelating agents, called siderophores, when they are deprived of iron (Neilands *Adv. in Chem.* **162**, 3; 1977). Siderophores are extraordinarily efficient iron chelators with binding constants of about 10^{30}, very close to the strength of transferrin. A microorganism invading the bloodstream is thus capable of competing with transferrin for the metal. If the microbe succeeds, a potentially fatal infection may result. This battle for iron is known to occur in other animal systems where bacterial growth might otherwise be especially favourable. Milk contains lactoferrin, a protein that binds iron in a manner very similar to transferrin. Lactoferrin is also found in human secretions associated with mucosal surfaces, and there is evidence that its iron binding properties offer bacteriostatic protection (Arnold *et al. Science* **197**, 263; 1977). Another iron-binding protein, conalbumin, is found in raw egg white, and Schade and Caroline were the first to suggest that conalbumin protects eggs from infection (*Science* **100**, 14; 1944). Protection by depriving infecting microorganisms of an essential nutrient has been called 'nutritional immunity' by Weinberg (*Science* **184**, 952; 1974).

It now appears that the plant world makes use of a similar strategy. Certain bacteria, called plant growth-promoting rhizobacteria (PGPR), significantly increase yields of potato, sugar beet and other plants when they colonize the roots. Work from the laboratory of Kloepper *et al.* reported in this journal (*Nature* **286**,

---

Thomas Emery is Professor of Biochemistry in the Department of Chemistry and Biochemistry, Utah State University.

885; 1980) demonstrates that PGPR in the soil produce extracellular siderophores which strongly complex iron and make it unavailable for growth of other potentially harmful microorganisms. A new siderophore, which the authors call pseudobactin, has been isolated from PGPR. *In vitro* experiments show that pseudobactin inhibits growth of the plant pathogen, *Erwinia carotovora,* by depriving the organism of iron. The effect was also demonstrated *in vivo* by greenhouse assays in which the addition of 10 μm pseudobactin in the water supply led to a more than a doubling of the weight of potato plants, attributed to a 74 per cent decrease in the number of pathogenic fungi found in the plant environment. Mutants of PGPR unable to produce pseudobactin did not show this effect.

A corollary to this work is that the plant itself must have a mechanism for utilizing siderophore iron lest it also be threatened by iron starvation. Virtually nothing is known about the possible importance of siderophores as a source of iron for higher plants. However, independent work reported in this journal has shown that siderophore type iron chelates are virtually ubiquitous in soils (Reid *et al.* see this issue of *Nature,* p833). Significant siderophore production was observed in extracts of all 57 soils surveyed. Of all iron binding agents tested, only siderophores proved to be efficient biological sources of iron in soil, and they conclude that microbial siderophores may be an important source of iron for higher plants, a function previously attributed to organic acids and polyphenolic humic material.

The role of siderophores in agriculture should be a subject of serious investigation. Each year many tons of synthetic iron chelates are used to ensure adequate iron supply to plants. Natural siderophores are apparently insufficient to supply this iron, possibly because very low levels of soluble iron are known to repress the excretion of siderophores by microorganisms. An interesting approach might be to produce mutants in the laboratory that are no longer subject to this negative control. Inoculation of solis with these organisms might increase the levels of soluble iron, as siderophore chelates, to a point where no additional supplementation would be necessary. This approach would have the added advantage of suppressing the growth of plant pathogens via iron deprivation. □

The development of animal segments

from Gerold Schubiger

IN this issue of *Nature* Nüsslein-Volhard and Wieschaus (see page 795) describe the isolation of mutations at 15 different gene loci that affect the pattern of segmentation in *Drosophila.* Segmentation is a phenomenon widespread in the animal kingdom; in annelids and arthropods blocks of cells become separated during development and then, within each block, the same components, such as ganglia, muscles and body cavities, differentiate. Even in the chordate embryo a metameric arrangement of some structures is obvious. Although similarity in appearance of metameric structures makes it tempting to conclude that they arise by a general developmental principle, there are still a great many unanswered questions.

We do not know if segmentation occurs by separating groups of cells from all the germ layers, or if one layer — ectoderm, neuroectoderm or mesoderm — first segments and then imprints its pattern on the other germ layers. The latter possibility is supported by observations of the leech, where the first signs of segmentation are seen in metamerically arranged mesodermal founder cells, and *Drosophila,* where the first cells to reveal a segmental pattern are the neuroblasts[1,2]. Normally, development of the insect embryo depends on similar inductive processes, such as the induction of mesodermal differentiation by the ectoderm (see ref. 3 for a review).

The mechanism which brings about segmentation is not understood. One possibility is that positional information is used to determine segment borders. Cells of the early *Drosophila* embryo are segregated into sub-populations or polyclones assigned to develop specific segments[4]. Cells of a polyclone are restricted: that is they can they can form only structures of their particular segments (see, for example, ref. 5). Such clonal restrictions have been found in the abdomen of *Oncopeltus*[6] and in the hypodermal segments of the adult *Drosophila*[7]. Restriction of clones in the hypodermis of the larva has been indicated but any clear compartmentalization of internal structure has not been documented.

It is also possible that development is primed from centres located in specific regions[8]. In some insects segmentation is first visible in the presumptive thorax region; more anterior and posterior segments boundaries arise later. In other insects, however, the role of such controlling centres is less obvious making it very difficult to generalize.

Experimental studies indicate that the segmental pattern in *Drosophila* is already determined in the blastoderm cells[9]. Embryonic fragments isolated before the blastoderm stage form a metameric pattern which is deficient in segment number indicating that different egg parts normally interact to form the full compliment of segments.

Searching for mutations and investigating their effects will tell us the extent to which segmentation is under genetic control. We already know that some genes (the homeotic) control the morphological character of segmental quality. Mutations in these genes transform patterns either within segments (for example, *engrailed*) or between different segments (for example *bithorax*)[10]. The mutation *bithorax* transforms the anterior metathorax into anterior mesothorax[11]. Homozygous *bx* clones have been induced in heterozygous animals during both embryonic and larval life and always express the transformed *bithorax* phenotype, showing that the expression of the normal phenotype requires continual activity of the *bx* locus. In such homeotic mutants the number of segments is not different from wild-type so it may be concluded that these genes control segment character and not number.

Abnormal segmentation may not be a direct consequence of gene mutation. For instance, mutations such as *rudimentary*[12] block pyrimidine synthesis and produce a generally sick embryo. The autophene (enzymatic block) is responsible for many allophenic characters such as abnormal segmentation[13]. Such mutations are obviously not helpful in understanding the genetic control of segmentation. Primary defects are more likely to be detected if the earliest developmental stages are analyzed, as has been done by Nüsslein-Volhard and Wieschaus with some of the mutations. It is important to realise that some genes may not be involved in primary segmentation, but may be responsible for maintaining the proper segmentation once it has formed. Analysis of mutants should also be extended to segmentally arranged structures other than the hypodermis, since there is good evidence that in *Drosophila* inductive processes are also involved in the development of segmentally arranged tissues. This will tell us if these mutations

---

Gerold Schubiger is in the Department of Zoology, University of Washington.

1. Poulson in *Biology of Drosophila* (John Wiley, New York, 1950).
2. Turner & Mahowald *Dev. Biol.* 37, 403 (1977).
3. Counce in *Developmental Systems: Insects* 2, (Academic Press, New York, 1973).
4. Crick & Lawrence *Science* **189**, 340 (1975).
5. Wieschaws & Gehring *Dev. Biol.* **50**, 249 (1976).
6. Lawrence *J. Embryol. Exp. Morph.* **30**, 681 (1973).
7. Lawrence, Green & Johnston *J. Embryol. Exp. Morph.* **43**, 233 (1978).
8. Sander *Adv. Ins. Phys.* **12**, 125 (1976).
9. Schubiger & Wood *Am. Zool.* **17**, 565 (1977).
10. Morata & Lawrence *Nature* **265**, 211 (1977).
11. Lewis in *The Role of Chromosomes in Development* (Academic Press, New York, 1964).
12. Norby *Heriditas* **66**, 205 (1970).
13. Counce *Z. für indukt. Abstammungsund Vererbungslehre* **87**, 462 (1956).

0028-0836/80/440777-02$01.00

interfere with induction rather than the process of segmentation.

Temperature-sensitive alleles of the most promising mutations that affect segmentation will enable us to find out when such genes are active during development. From studies of such a mutant (*patch*), Nüsslein-Volhard and Wieschaus were able to conclude that proper segmentation depends on early activity of the gene.

One mutation known to affect segmentation (*fused*) has a male-rescuable maternal-effect[13]. Homozygous mutant offspring from heterozygous mothers can develop normally. Moreover, heterozygous embryos from homozygous mutant mothers can be rescued by the *fused*$^+$ allele of the father. Thus, normal development requires the *fused* gene to be active either during oogenesis or in the zygote. This indicates that some genes that control normal segmentation are active during both oogenesis and early development. ☐

Cosmic spherules

from David W. Hughes

TAKE a kilogram of the sedimentary deposits from the floor of the deep oceans, wash and sieve it carefully and you will find, among a vast jumble of irregular particles, a collection of between a few hundred and a few thousand black 'stony' and 'iron' magnetic spherules with diameters between 30 and 200 μm. You don't even have to resort to deep-sea sediments; spherules can be found in arctic ice, manganese nodules, beach sands, ancient salt deposits and even on roof tops. They are a ubiquitous component of all terrestrial sediments.

The source of the spherules may be either terrestrial or cosmic, and it is the latter source that is of interest here. Collections removed from sediments laid down before the industrial revolution and its accompanying pollution make the selection process simpler but even then vulcanism is a major source of contaminants. The extraterrestrial nature of a specific spherule can be confirmed if it contains wüstite — a metastable iron oxide formed at high temperatures and low oxygen partial pressures. Wüstite slowly decomposes into α-iron and magnetite in most terrestrial environments and is thus almost unknown in nature. Having iron, nickel and cobalt in meteoritic ratios and free iron and nickel metals are also strong clues as is a low abundance of manganese, titanium and chronium.

Once a sample of cosmic spherules has been found and recognised we reach the major difficulty of deciding exactly where they come from. There are two classes of theory. The first postulates that cosmic spherules are molten spray from meteorites and meteoroids that have ablated as they decelerate in the Earth's atmosphere. The spray solidifies and drifts down to the surface. The second theory, advanced by Öpik nearly thirty years ago (*Irish Astr. J.*, **1**, 145; 1951), postulates that the spherules existed essentially as spherules in free space, entered the Earth's atmosphere in such a way that they survived evaporation and then fell earthward. D. W. Parkin, R. A. L. Sullivan and J. N. Andrews of the University of Bath, support the second theory and go even further in suggesting that cosmic spherules are condensed 'sparks' formed by collisions in the asteroidal belt. Their findings are published in a recent edition of the *Philosophical Transactions of the Royal Society of London*, **297**, 495; 1980.

From the qualitative standpoint both theories seem reasonable. A quantitative assessment is more stringent. Parkin *et al.* estimate that 5,000 tonnes of spherules fall to the Earth's surface per year. The dried clay sediment contains about one part per million by mass of cosmic spherules and the mass sedimentation rate is taken as 10 g of dry clay per square metre per year. Hughes (*Space Research*, **15**, 531; 1975) calculated that the total amount of interplanetary matter collected by the Earth each year is about 16,000 tonnes (upper and lower error limits being 30,000 and 8,000 tonnes respectively). So according to Parkin *et al.* spherules make up a considerable percentage of the total influx.

In 1976 Ceplecha (*Lecture Notes in Physics*, **48**, 385) suggested that most of the cosmic dust in the atmosphere (and by implication in sediments) came from the disintegration of meteoroids with in-space masses of between 10^5 and 10^9 g. The influx of these objects produce brilliant fireballs. Each day there will be about 4 of − 17 magnitude, 2 of − 18 magnitude and so on in the Earth's atmosphere. The mass flux is relatively uncertain simply because considerable disagreement exists as to the luminous efficiency of the incident bodies. Also the mass influx of large bodies to the Moon, measured by Apollo seismic stations, yield much smaller values than those predicted by Ceplecha.

Obviously, particulate matter is generated by fireballs. The massive injection of dust into the atmosphere following the Tunguska event in 1908 and the great daylight fireball of 1972 illustrate this. But what percentage of the fireball mass would end up as spherule-sized particles and what size distribution do these have? Complete ablation is common. Most fireball parents release the large majority of their mass at heights below 90 km and are still travelling at velocities above 4 km s^{-1} at the end of their luminous trails. Particles released at these low altitudes and high speeds are at least molten and in extreme cases completely vaporized. The liquid layer created at the front of the incident body by atmospheric friction will be carried round to the rear where sustained boiling may eject droplets in the vaccum wake behind the meteorite. The molten spray then cools by radiation but also undergoes considerable frictional power loading before retarding to free fall velocity. Whether this would produce a second melting or even complete evaporation would depend on the atmospheric density and particle velocity at emission. Meteorite parent bodies definitely undergo surface melting. Retrieved meteorites are covered with a millimetre or so of thick, black crust which may be either glassy (in stony meteorites) or composed of magnetic iron oxides (in iron meteorites).

Moving to the small-size end of the incident mass spectrum, it is rather remarkable how effective the Earth's atmosphere is as a collector of dust. Many incident microparticles are slowed down so gently that they remain virtually unaltered. The frictional power generated over the particle surface is low enough to be thermally radiated without the particle reaching it's melting point. However, the actual temperature that the particle reaches depends strongly on its initial velocity, size and entry angle. Particles larger than 100 μm usually melt even if their initial velocities are only slightly above the escape velocity of 11.2 km s^{-1} (the minimum velocity of an incident particle). 10 μm particles can enter at 45° to the vertical with an initial velocity of 15 km s^{-1} without melting. All particles moving faster than 50 km s^{-1} burn up.

Cosmic spherules straddle this size range, the Parkin *et al.* sample having sizes between 30 and 200 μm. They would melt at a temperature of 2,000 K. All can get through the atmosphere if they have low enough velocities and, for the larger particles, if they 'graze' into the atmosphere, arriving almost tangentially.

Parkin *et al.* go even further. From scanning electron microscope observations they are convinced that none of their collected spherules melted during entry. But some incident particles must melt. The authors suggest that these do not re-solidify. At best they evaporate and at worst they are blown to pieces by the sudden release of adsorbed solar wind gases. A 100 μm lunar soil grain exposed for about 1,000 y adsorbs about 10^{-4} mol per g of ^{4}He, sufficient to burst a molten spherule against surface tension.

David W. Hughes is in the Department of Physics, University of Sheffield.

We are left with the problem that too many spherules are found to be produced by meteorite or fireball parent body spalation alone. Indeed, according to Parkin *et al.* X-ray microprobe chemical analysis and examination with a scanning electron microscope indicate considerable differences between spherules and meteorite fusion crusts. To them the spherules seem to have survived the passage through the atmosphere relatively unscathed. Where did they come from?

The authors point to the asteroid belt and suggest that spherules are quenched sparks formed by colliding asteroids. They even went so far as to collect rounded, quenched grindwheel sparks from a wheel being used to grind a steel bar and to claim that there were distinct similarities to the deep sea spherules. Microdebris from asteroid collision would take about 10^6 y to spiral in to the Earth's orbit under the influence of the Poynting-Robertson effect, ample time to adsorb solar wind. It is even possible to imagine a temporary hot oxidising atmosphere at the collision site due to the abundance of hydrated minerals thus producing the requisite wüstite. But are asteroid collisions frequent enought to produce 5,000 tonnes of spherules per year?

Many people think that the asteroids have been around since the dawn of the solar system and that this permanence relies to a considerable extent on a collision rate which is decreasing with time. Individual collisions may produce swarms of spherules followed by long time periods when the production rate is much smaller. The beauty of core analysis is that, assuming a constant sedimentation rate, you have a perfect means of measuring the spherule influx rate as a function of time. In a note added in proof the authors claim to be able to see evidence for individual collision events. By considering the way in which spherule size varies as a function of core depth and the spiraling time varies as a function of particle size these events are placed in the asteroid belt.

Adherents to the first 'meteoritic ablation' theory are still not convinced. U-2 aeroplanes flying in the stratosphere at altitudes of 20 km collect many particles with meteoritic, extraterrestrial compositions. Brownlee, Blanchard, Cunningham, Beauchamp and Fruland (*J. Geophys. Res.* **80**, 4917; 1975) find that about 10 per cent of them are spherules. To them X-ray diffraction, mineralogy and texture all point to a very strong similarity between spherules and meteorite fusion crusts. It is possible that both theories are right and spherules can be formed either from ablation droplets or from quenched asteroid sparks. Indeed, still further sources are not ruled out — maybe comets contain spherules and maybe planetary cratering events produce spherules in the ejector. We have plenty of possibilities available. What is needed are more scientific investigators. ☐

Did the Santorini eruption destroy the Minoan world?

from Jörg Keller

THE recent report in *Nature*[1] of the discovery of volcanic ash from Santorini on the island of Rhodes raises once again the possibility that Minoan Crete was destroyed by the effects of a volcanic eruption.

Marinatos[2] was the first to postulate a direct connection between two of the most dramatic events in the early history of the Aegean area — the tremendously powerful eruption of the volcano of Santorini (Thera) early in the 15th century BC and the sudden and enigmatic decline of the flourishing Minoan civilization on Crete.

Seismic tidal waves, volcanic earthquakes and ash-fall were the physical effects considered most likely to have seriously damaged Minoan settlements all over Crete. A blanket of ash, thick enough to suffocate the agricultural economy on Crete, was widely thought to have fallen since deep-sea sediment cores drilled north and south of Crete had proved that the tephra had reached the island[3].

Since 1967, the settlement of Akrotiri has been excavated from underneath a thick pumice cover on the island of Thera (Santorini). An unexpectedly wealthy, cosmopolitan Minoan community has come to light. Countless examples of fine pottery, both of local manufacture and imported from Crete, and frescoes of incomparable beauty were found in three-storied houses and mansions[4]. The catastrophic dimensions of the Santorini eruption are very obvious. With increasing knowledge, however, the original idea of the direct physical destruction of Crete by volcanic phenomena has become more and more questionable[5,6].

Recent research in the Aegean area, both on land and in the deep sea has produced a distribution map for the Minoan ashfall[7,8], which shows an easterly dispersion away from the volcano towards Western Anatolia. Substantial fall-out must have affected the Eastern Aegean Sea and Western Anatolia (for example 30cm of tephra have been found on the Island of Kos[8]), but it is inferred that Crete received only a few centimeters of ash, too thin to account for the desertion of the Late Bronze age settlements.

The findings on Santorini also suggest that the volcanic destruction of the city of Akrotiri occured one stage earlier on the pottery-based time-scale of the archeologists than the devastation of Minoan cities and palaces on Crete. The Bronze age pottery style "Late Minoan IA" is fully developed in Akrotiri and the pottery record ends with this stage. In contrast, all over Crete LM IA is followed by pottery of Late Minoan IB, with its highly characteristic decoration showing marine subjects. It is thought that the time difference between the two substages is about 30-50 years. This suggests a date of 1500-1480 BC for the end of Akrotiri on Santorini and 1450 BC for the sudden end of the Minoan civilization on Crete.

Various ideas have been presented to account for the difference in the timing of the two events. Multistage volcanic activity, the possibility that the pottery might have been more old-fashioned in provincial Akrotiri, the destruction of Akrotiri by precursor earthquakes, or evacuation of the settlement some 30 years before the fatal eruption, have all been considered as explanations.

Only when Dorothy and Charles Vitaliano[9,10] found microscopic traces of Santorini tephra in archeological sites on Crete and Melos, and within strata believed to be uncontaminated Late Minoan IA did the possibility emerge that the climax of the Santorini eruption actually preceeded the end of the Minoan civilization by about 30 years.

This interpretation seems now to be fully supported by the new findings on Rhodes. The future investigations which Doumas and Papazoglou have announced will hopefully yield a complete pottery inventory from both below and above the tephra layer. They should characterize a possible LM IB destruction level. But already their conclusions appear to be inevitable: life continued without any significant break after the ash fall. The later destruction of Minoan Crete is once more an enigma. The influence of other civilizations especially neighbouring Mycenae, will certainly have to be re-evaluated. Whether a Mycenaean invasion and conquest of Crete happened during the aftermath of one of the most catastrophic volcanic eruptions known in the Mediterranean will only be revealed by continuing research. ☐

Jörg Keller is in the Geophysical Laboratory, Carnegie Institution of Washington.

1. Doumas, C & Papazoglou, L *Nature* 287, 322 (1980)
2. Marinatos, S *Antiquity* 13, 425 (1939)
3. Ninkovich, D & Heezen, B. C *Colston Papers* 17, 413 (1965).
4. Marinatos, S Excavations at Thera I-VII (1967-73)
5. Marinatos, S. (ed) *Acta Int Scient Cong Volcano of Thera (1971)*
6. *Doumas, C. (ed) Thera and the Aegean World* 1, (1978), 2, (1980)
7. Watkins, N D *et al* *Nature* 271, 122 (1978)
8. Keller, J *Thera and the Aegean World* 2, (1980)
9. Vitaliano, C J & Vitaliano, D B *Am J Archeology* 78, 19 (1974).
10. Vitaliano, C J & Vitaliano, D B *Thera and the Aegean World* 1, (1978)

0028-0836/80/440779-02$01 00

Global dendroclimatology in sight

from A. Barrie Pittock

Dendroclimatology, the systematic study of past climates using tree growth characteristics as proxy climate data, is a relatively young science. It is often confused with the much older and related science of dendrochronology, the dating of specimens by the use of tree-ring sequences. Dendroclimatology has only really developed as a science since the 1940s, primarily as a result of the pioneering efforts of workers at the Laboratory of Tree-Ring Research at the University of Arizona. Elsewhere, the serious application of dendroclimatic methods has only begun in the last five years or so.

It was, therefore, encouraging to find at a recent workshop* attended by 56 scientists from 14 countries that dendroclimatology is making great strides. Greater global coverage was reported in contributions from Europe, Asia, South America, South Africa and Australia, as well as eastern North America and the Arctic. A striking departure from early research in the semi-arid southwest United States was the documentation of useful climatic sensitivity in trees from other than obviously stressed environments. This was particularly well demonstrated for Southern Hemisphere rain forest environments by La Marche and co-workers, for the eastern United States by Cook and for Europe by several groups (Schweingruber, Eckstein, Baillie, Pilcher, and see Hughes *et al.* **272**, 606; 1978; Dunwiddie & La Marche *Naturer* **286**, 796; 1980; Garfinkel & Brubaker *Nature* **286**, 872; 1980). Major research groups (outside the western United States) now exist in several regions, including the United Kingdom, continental Europe and the eastern United States. Strong interest is also being shown in China (two workers were present at the meeting), Argentina, Australia and the Soviet Union. The Chinese plan to use tree-ring data in regions such as the northwest where historical data are not abundant.

Climatologists were also present at the conference and this led to a stimulating interaction between the potential users of dendroclimatic data and the data producers. It was suggested that attempts should be made to reconstruct a wider range of climatic variables, alongside temperature, precipitation and surface pressure and that sampling should be concentrated in regions which are climatologically important and/or where there are gaps in coverage from instrumental, historical or other proxy data. There is growing confidence that with some modification existing methods can extract useful climatic information from trees in many different parts of the world.

As dendroclimatology has expanded into new geographical areas over the last decade, techniques have been modified and refined. One example is the use of density as well as ring-width measurements for climate reconstructions. Density data have been used recently to reconstruct temperature data in Europe (Schweingruber *et al. Tree-Ring Bulletin* **38**, 61; 1978). Although basically similar, the climate-growth response appears simpler for density than ring width (Parker *Syesis* **9**, 163; 1976). New techniques take into account that growth in a particular year is influenced by growth in prior years, that growth is a function of tree age and that the climate-growth response may change as trees age. A recent innovation has been the use of selective filter techniques in calculating the response and transfer functions.

Of special interest were plans for European climate reconstructions put forward by one of the global data base working groups. The plans gave high priority to building up a dense network of chronologies back to at least 1750 covering the whole of Europe. Using instrumental data from 1880 to the present for calibration and earlier instrumental and historical data for verification, it should be possible to produce a detailed and continuous climate reconstruction from 1750. Because of the abundance of data for calibration and verification, this could prove the best continent-wide proxy climate data set in existence and Europe could become a test bed for refining dendroclimatic methods.

Five-hundred-year long chronologies are available already from living conifers in the Alps and at the northern tree-line and are expected from living oaks in Scotland, northern France and south-central Germany. These should allow the reconstructed record to extend back into the 15th century, and extension back for 1,000 years at a reduced spatial density is possible (see Serre *Tree-Ring Bulletin* **38**, 25; 1978). Abundant sub-fossil and archaeological material may be used to extend the chronologies still further. However, the use of such material poses methodological problems in matching series from dead wood with living trees, especially in a way which will not distort the low-frequency climatic information. Work on these problems is being actively pursued and its importance may be gauged from the potential development of several-thousand-year chronologies from various parts of the globe including Europe, North America and New Zealand. The application of densitometric and possibly isotopic methods may well overcome some of the more serious problems in using these long tree-ring chronologies. □

A. Barrie Pittock is in the Division of Atmospheric Physics, Commonwealth Scientific and Industrial Research Organization, Australia.

---

*The Second International Workshop on Global Dendroclimatology was held at the Climatic Research Unit, University of East Anglia, July 7-11, 1980. It was sponsored by the World Meteorological Organisations, the United Nations Enviroment Programme, the Scientific Affairs Division of NATO and the US National Science Foundation and was organised by M. K. Hughes (Liverpool Polytechnic), P. M. Kelly (University of East Anglia) and J. P. Pilcher (Queen's University, Belfast). A report on the proceedings will be published in 1980 and a book in 1981.

100 years ago

It is stated that at the National Exhibition to be opened at Milan next year there will be a captive balloon, on the model of the one which was so successful in Paris in 1878. It will measure not less than 180 feet in circumference, 84 feet in height, and contain 15,000 cubic feet of gas. To it will be attached a safe and solid car, capable of containing seats for at least eight persons. A steam-engine is to regulate the ascent and descent, and it will rise to a height of about 900 feet, affording a splendid view of Milan and the plains of Lombardy. The balloon will be constructed at Milan, m. Henri Beudet, the well-known and experienced aëronaut, having been sent for to direct the work.

THE *Boston Herald* gives the following account of an American experiment made on September 2: — "A novel exhibition of powerful electric lights was made last evening in the vicinity of the Sea Foam-house, Nantucket Beach, and the display was witnessed by quite a crowd of interested spectators. The Northern Electric Light Company have erected three wooden towers, each 100 feet high, and mounted upon each of these a circular row of twelve electric lights of the Weston patent, each light being estimated at 2,500-candle power. As these towers are but 500 feet apart and in a triangle, it will be seen that the light of 90,000 candles was concentrated within a limited territory. The design of the exhibition was to afford a model of the plan contemplated for lighting cities from overhead in vast areas, the estimate being that four towers to a square mile of area, each mounting lights aggregating 90,000-candle power, will suffice to flood the territory about with a light almost equal to midday. Last evening a motive power of thirty-six horses was used in generating the electricity from three Western machines, and the lights, with one single flicker, burned steadily and brilliantly all the evening. It is difficult to say whether the experiment proved anything or not. The claim put forward by the company is for an original plan of lighting cities and towns by grouping and elevating electric lights of any kind."

From *Nature* **22**, 28 October, 593 & 615, 1880.

0028-0836/80/440780-02$01.00

Nature Vol. 287 30 October 1980

REVIEW ARTICLE

Hormone families: pancreatic hormones and homologous growth factors

T. L. Blundell
Laboratory of Molecular Biology, Department of Crystallography, Birkbeck College, University of London, Malet Street, London WC1E 7HX, UK

R. E. Humbel
Biochemisches Institut der Universitat Zürich, Zürichbergstrasse 4, CH-8028 Zürich, Switzerland

The growing realization that biologically active polypeptides can be grouped in families, the members of which show structural and functional relatedness, is illustrated by the four families which are represented in the pancreas by the hormones insulin, glucagon, somatostatin and pancreatic polypeptide.

THE study of the origins of hormone-like activity is revealing great complexity in endocrine control systems, but a degree of simplicity in that most hormones belong to a family group. Members of any family are related in chemical sequence in a way which suggests their evolutionary relationships. In some cases members of a family retain common biological activities as a vestige of their common ancestry; however, for many the divergence of biological function is complete. Moreover these families are becoming extended with the inclusion of growth factors from the serum and neurotransmitters and neuroregulators from the central nervous system. These trends are well illustrated by examples drawn from the four families of peptide hormones represented in the pancreas by insulin, glucagon, somatostatin and pancreatic polypeptide.

Insulin

Porcine pancreatic insulin, shown schematically in Fig. 1, is a globular polypeptide. It has a hydrophobic core and two mainly hydrophobic surfaces which may be involved in intermolecular interactions stabilizing insulin dimers and 2-zinc insulin hexamers[1]. The sequences of vertebrate insulins[2] (Fig. 1) show that the residues of the hydrophobic core are conserved, and that all insulins might attain the same tertiary structure as porcine insulin. Although teleost fishes, reptiles, birds and most mammals have insulins which form dimers and hexamers[3], certain hystricomorph rodents such as the guinea pig and the casiragua, lack the zinc-building histidine at position B10 (Table 1) and have lost the ability to self-associate. The insulin of the primitive cyclostome, the hagfish, also lacks B10 histidine; it can form dimers but not zinc hexamers[4]. The sequence of proinsulin[5,6], the precursor of insulin, is shown in Fig. 1; a C-peptide connects B30 and A1. The probable structure of proinsulin is indicated in Fig. 2. The evidence for this structure[1] is indirect and is based on the similarity of proinsulin to insulin in circular dichroism, self-association, immunological studies and the ability of the two peptides to co-crystallize.

It has been recognized for some time that two species of rodents (rat, mouse) and at least one species of fish (toadfish) contain two different insulins, almost certainly derived from two nonallelic insulin genes[7]. Goodman and co-workers[8] have determined the sequence of the DNA for the rat insulins I and II and have shown that each contains an intervening sequence of 119 base pairs in a region corresponding to the 5′ untranslated portion of the mRNA. In addition, the rat insulin II gene contains a 499 base pair intervening sequence in the region of DNA coding for the C-peptide. More recently it has been shown that the human and chicken insulin genes resemble the rat II gene in having two intervening sequences, the second at exactly the same position in the C-peptide encoding region of the gene[9,10]. (Could the presence of the intervening sequence in the C-peptide region account for its being the most highly variant part of the proinsulin molecule in which deletions and additions also occur?) The similarity of the human chicken and rat II genes implies that their ancestral insulin probably contained two intervening sequences. Gene sequencing also suggests that there are two non-allelic insulin genes in humans which differ by at least one base pair[9]. This would be consistent with the report of an unusual insulin, which results in diabetes and hyperproinsulinaemia and which is produced in addition to a normal insulin, implying codominant expression of two alleles[11].

It is not known for certain whether the two rat insulins are synthesized by the same cell. Some indication that this might be the case comes from the electron microscopy of rat insulin storage granules within a single cell which show morphologies characteristic of both insulins[12].

Insulins bind to receptors from tissues of differing species in a way which reflects the origin of the hormone rather than the receptor. Hence, with the possible exception of hystricomorphs[13], there seems to have been evolutionary conservation of the insulin receptor. Studies of the potency and receptor binding of differing insulins and synthetic analogues have demonstrated that for full potency the general tertiary structure needs to be conserved[14-16]. Of the surface of the insulin molecule an extensive region around residues A21, B24 and B25, perhaps involving as many as eleven residues appears to be important in receptor binding.

Relaxin, a member of the insulin family?

For many years it was thought that insulin was not a member of a larger family of hormones. Recently, however, it has been suggested that relaxin, a polypeptide hormone from the corpus luteum and responsible for dilation of the symphysis pubis prior to parturition, may be a member of the insulin family. Relaxin has two chains (A and B) linked by disulphide bridges as shown in Fig. 1[17,18]. Model building shows that the backbones of the relaxin and insulin molecules may have similar conformations (see Figs 2 and 3), although the hydrophobic core of relaxin involves different side chains, close-packed into the same volume[19,20]. The absence of residues in relaxin equivalent to position A21 or to the B-chain C-terminal of insulin probably destabilizes the insulin fold but should not prevent its formation. The relaxin A-chain N-terminus has two extra residues and lies

0028-0836/80/440781—07$01.00

A Chains	−2	−1	1	2	3	4	5	6	7	8	9	10	11	12	13	14	15	16	17	18	19	20	21	22	23	24	25	26	27	28	29	30
Insulin																																
Bovine	—	—	Gly	Ile	Val	Glu	Gln	Cys	Cys	Ala	Ser	Val	Cys	Ser	Leu	Tyr	Gln	Leu	Glu	Asn	Tyr	Cys	Asn	—	—	—	—	—	—	—	—	—
Human	—	—	Gly	Ile	Val	Glu	Gln	Cys	Cys	Thr	Ser	Ile	Cys	Ser	Leu	Tyr	Gln	Leu	Glu	Asn	Tyr	Cys	Asn	—	—	—	—	—	—	—	—	—
Rat 1	—	—	Gly	Ile	Val	Asp	Gln	Cys	Cys	Thr	Ser	Ile	Cys	Ser	Leu	Tyr	Gln	Leu	Glu	Asn	Tyr	Cys	Asn	—	—	—	—	—	—	—	—	—
Rat 2	—	—	Gly	Ile	Val	Asp	Gln	Cys	Cys	Thr	Ser	Ile	Cys	Ser	Leu	Tyr	Gln	Leu	Glu	Asn	Tyr	Cys	Asn	—	—	—	—	—	—	—	—	—
Guinea pig	—	—	Gly	Ile	Val	Asp	Gln	Cys	Cys	Thr	Gly	Thr	Cys	Thr	Arg	His	Gln	Leu	Gln	Ser	Tyr	Cys	Asn	—	—	—	—	—	—	—	—	—
Casiragua	—	—	Gly	Ile	Val	Asp	Gln	Cys	Cys	Thr	Asn	Ile	Cys	Ser	Arg	Asn	Gln	Leu	Leu	Thr	Tyr	Cys	Asn	—	—	—	—	—	—	—	—	—
Coypu	—	—	Gly	Ile	Val	Asp	Gln	Cys	Cys	Thr	Asn	Ile	Cys	Ser	Arg	Asn	Gln	Leu	Met	Ser	Tyr	Cys	Asn	Asp*	—	—	—	—	—	—	—	—
Hagfish	—	—	Gly	Ile	Val	Glu	Gln	Cys	Cys	His	Lys	Arg	Cys	Ser	Ile	Tyr	Asn	Leu	Gln	Asn	Tyr	Cys	Asn	—	—	—	—	—	—	—	—	—
Insulin-like Growth factor																																
IGF 1	—	—	Gly	Ile	Val	Asp	Glu	Cys	Cys	Phe	Arg	Ser	Cys	Asp	Leu	Arg	Arg	Leu	Glu	Met	Tyr	Cys	Ala	Pro	Leu	Lys	Pro	Ala	Lys	Ser	Ala	
IGF 2	—	—	Gly	Ile	Val	Glu	Glu	Cys	Cys	Phe	Arg	Ser	Cys	Asp	Leu	Ala	Leu	Leu	Glu	Thr	Tyr	Cys	Ala	Thr	—	—	Pro	Ala	Lys	Ser	Glu	
Relaxin																																
Porcine	Arg	Met	Thr	Leu	Ser	Gln	Lys	Cys	Cys	Gln	Val	Gly	Cys	Ile	Arg	Lys	Asp	Ile	Ala	Arg	Leu	Cys	—	—	—	—	—	—	—	—	—	—

B Chains	−2	−1	1	2	3	4	5	6	7	8	9	10	11	12	13	14	15	16	17	18	19	20	21	22	23	24	25	26	27	28	29	30	31
Insulin																																	
Bovine	—	—	Phe	Val	Asn	Gln	His	Leu	Cys	Gly	Ser	His	Leu	Val	Glu	Ala	Leu	Tyr	Leu	Val	Cys	Gly	Glu	Arg	Gly	Phe	Phe	Tyr	Thr	Pro	Lys	Ala	—
Human	—	—	Phe	Val	Asn	Gln	His	Leu	Cys	Gly	Ser	His	Leu	Val	Glu	Ala	Leu	Tyr	Leu	Val	Cys	Gly	Glu	Arg	Gly	Phe	Phe	Tyr	Thr	Pro	Lys	Thr	—
Rat 1	—	—	Phe	Val	Lys	Gln	His	Leu	Cys	Gly	Pro	His	Leu	Val	Glu	Ala	Leu	Tyr	Leu	Val	Cys	Gly	Glu	Arg	Gly	Phe	Phe	Tyr	Thr	Pro	Lys	Ser	—
Rat 2	—	—	Phe	Val	Lys	Gln	His	Leu	Cys	Gly	Ser	His	Leu	Val	Glu	Ala	Leu	Tyr	Leu	Val	Cys	Gly	Glu	Arg	Gly	Phe	Phe	Tyr	Thr	Pro	Lys	Ser	—
Guinea pig	—	—	Phe	Val	Ser	Arg	His	Leu	Cys	Gly	Ser	Asn	Leu	Val	Glu	Thr	Leu	Tyr	Ser	Val	Cys	Gln	Asp	Asp	Gly	Phe	Phe	Tyr	Ile	Pro	Lys	Asp	—
Casiragua	—	—	Tyr	Val	Gly	Gln	Arg	Leu	Cys	Gly	Ser	Gln	Leu	Val	Asp	Thr	Leu	Tyr	Ser	Val	Cys	Lys	His	Arg	Gly	Phe	Tyr	Arg	Pro	Ser	Gln	—	—
Coypu	—	—	Tyr	Val	Ser	Gln	Arg	Leu	Cys	Gly	Ser	Gln	Leu	Val	Asp	Thr	Leu	Tyr	Ser	Val	Cys	Arg	His	Arg	Gly	Phe	Tyr	Arg	Pro	Asn	Gln	—	—
Hagfish	—	—	Arg	Thr	Thr	Gly	His	Leu	Cys	Gly	Lys	Asp	Leu	Val	Asn	Ala	Leu	Tyr	Ile	Ala	Cys	Gly	Val	Arg	Gly	Phe	Phe	Tyr	Asp	Pro	Thr	Lys	Met
Insulin-like Growth factor																																	
IGF 1	—	—	—	Gly	Pro	Glu	Thr	Leu	Cys	Gly	Ala	Glu	Leu	Val	Asp	Ala	Leu	Gln	Phe	Val	Cys	Gly	Asp	Arg	Gly	Phe	Tyr	Phe	Asn	Lys	Pro	Thr	—
IGF 2	Ala	Tyr	Arg	Pro	Ser	Glu	Thr	Leu	Cys	Gly	Gly	Glu	Leu	Val	Asp	Thr	Leu	Gln	Phe	Val	Cys	Gly	Asp	Arg	Gly	Phe	Tyr	Phe	Ser	Arg	Pro	Ala	—
Relaxin																																	
Porcine	Ser	Thr	Asn	Asp	Phe	Ile	Lys	Ala	Cys	Gly	Arg	Glu	Leu	Val	Arg	Leu	Trp	Val	Glu	Ile	Cys	Gly	Val	Trp	Ser	—	—	—	—	—	—	—	—

	1	2	3	4	5	6	7	8	9	10	11	12	13	14	15	16	17	18	19	20	21	22	23	24	25	26	27	28	29	30	31	32	33	34	35
Insulin																																			
Bovine	Arg	Arg	Glu	Val	Glu	Gly	Pro	Gln	Val	Glu	Ala	Leu	Glu	Leu	Ala	Gly	Gly	Pro	Gly	Ala	Gly	Gly	Leu	—	—	—	—	—	Glu	Gly	Pro	Pro	Gln	Lys	Arg
Human	Arg	Arg	Glu	Ala	Glu	Asp	Leu	Gln	Val	Gly	Gln	Val	Glu	Leu	Gly	Gly	Gly	Pro	Gly	Ala	Gly	Ser	Leu	Gln	Pro	Leu	Ala	Leu	Glu	Gly	Ser	Leu	Gln	Lys	Arg
Rat 1	Arg	Arg	Glu	Val	Glu	Asp	Pro	Gln	Val	Pro	Gln	Leu	Glu	Leu	Gly	Gly	Gly	Pro	Glu	Ala	Gly	Asp	Leu	Gln	Thr	Leu	Ala	Leu	Glu	Gly	Ser	Leu	Gln	Lys	Arg
Rat 2	Arg	Arg	Glu	Val	Glu	Asp	Pro	Gln	Val	Ala	Gln	Leu	Glu	Leu	Gly	Gly	Gly	Pro	Gly	Ala	Gly	Asp	Leu	Gln	Thr	Leu	Ala	Leu	Glu	Val	Ala	Arg	Gln	Lys	Arg
Guinea pig	X	X	Glu	Leu	Glu	Asp	Pro	Gln	Val	Glu	Gln	Thr	Glu	Leu	Gly	Met	Gly	Leu	Gly	Ala	Gly	Gly	Leu	Gln	Pro	Leu	—	—	Gln	Gln	Ala	Leu	Gln	X	X
Insulin-like Growth factor																																			
IGF 1	—	—	—	—	—	—	—	—	—	—	—	—	—	—	Gly	Tyr	Gly	Ser	Ser	Ser	Arg	—	—	—	—	—	—	—	—	—	Ala	Pro	Gln	Thr	—
IGF 2	—	—	—	—	—	—	—	—	—	—	—	—	—	—	—	Ser	Arg	Val	Ser	Arg	Arg	Ser	Arg	—	—	—	—	—	—	—	—	—	—	—	—

Fig. 1 The sequences of members of the insulin family of polypeptides (see ref. 2 for review). * The Asp at A22 may be incorrect; recent recalculation of amino acid composition by R. Horuk indicates one less Asp.

close to the B-chain C-terminus in the proposed structure. Preliminary sequence data from the laboratories of H. D. Niall and C. Schwabe indicate that similar structures may be assumed for rat and shark relaxins. Like insulin, relaxin is synthesized as a single chain precursor, prorelaxin. This molecule appears to be much larger than relaxin itself even though only a short connecting peptide of one or two residues would be necessary to allow the correct conformation of the hormone[21]. Although the tertiary structures of insulin and relaxin are most likely very similar, the surfaces of the two molecules are very different. It is therefore not surprising that they are not immunologically cross-reactive, and that relaxin shows neither insulin-like biological activity nor the ability to bind insulin receptors[22,23].

Would the similar tertiary structure of insulin and relaxin, if proven, amount to evidence of common ancestry and divergent evolution, given the low (~20%) sequence homology between the two peptides? If we begin with the assumption that there are only few stable structures for small proteins, then the folding of each structure implies restrictions on the residues if the secondary structure preference in a region is to be maintained. In particular, glycine residues alone give the unusual conformational angles that are found, for instance, at B8 and B20 of insulin, and only cystines could link the A and B chains. How significant, then, is the sequence similarity between relaxin and insulin, most of which comprises six homologous cystines and two homologous glycines? The need for a hydrophobic core further restricts the residues which can be accepted as evidence for divergent evolution. Insulin and relaxin therefore may share a similar structure, simply because it is one of comparatively few which are globular, contain disulphide bridges, and are formed by polypeptide chains of between 50 and 80 amino acid residues; the polypeptides might have converged to this structure. Nevertheless, it remains true that no molecule lacking hormone activity has been shown to have a similar structure, a fact which may be presented as evidence in favour of divergent evolution.

Insulin-like growth factors (somatomedins)

Recently, the insulin-like growth factors (IGFs) have also been added to the insulin family. Whereas insulin and relaxin are structurally distant relatives, giving no cross-recognition at the receptor level, insulin and the IGFs are structurally and functionally more closely related. IGFs or somatomedins are polypeptides purified from human serum and from media conditioned by cultured cells. The designation somatomedin was introduced by Daughaday[24] for substances fulfilling the following four criteria: their concentration in serum is regulated by growth hormone, they stimulate incorporation of sulphate into proteoglycans of cartilage, they have mitogenic activity in fibroblasts and they have insulin-like effects on adipose and muscle tissue. Four factors or groups of factors meeting these criteria have been described so far: non-suppressible insulin-like activity (NSILA)[25]; somatomedin A[26,27]; somatomedin C[28]; and multiplication stimulating activity (MSA)[29].

The concept that some or all of the four factors might be structurally related to insulin had been slowly emerging from numerous studies on their biological and chemical properties[30-32] and from the initial observation by Hintz *et al.*[33] that somatomedin-C competes with insulin for binding to the

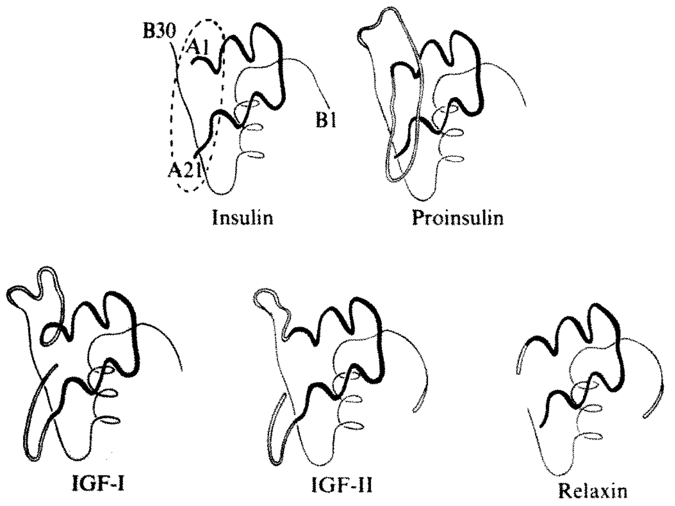

Fig. 2 Schematic diagrams showing the chain folding of insulin as derived from the X-ray analysis of insulin crystals[1] and proinsulin[1], IGF-I[42], IGF-II and relaxin[19] as proposed by model building experiments using the known sequences. The putative receptor binding region of insulin[1,14] is indicated.

insulin receptor on cell membranes. Eventually, the isolation of two homogenous polypeptides from purified NSILA[34] and the subsequent determination of their amino acid sequences[35,36] established unequivocally the long-suspected structural kinship of NSILAs to insulin and led to the new designation of insulin-like growth factors (IGFs) I and II[37].

A partial primary structure of somatomedin C has recently been shown to have considerable, although not complete, identity to IGF-I[38]. However, for somatomedins A_1 and A_2, the only data so far available are amino acid compositions[39] which do not suggest a structural relationship to insulin and the IGFs. The same is true of several forms of rat MSA which have been purified and have had their amino acid composition determined[40,41]. Thus out of the four groups of somatomedins, the IGFs and somatomedin C are clearly akin to insulin, whereas the putative structural relationships of somatomedin A and of the MSAs to insulin have yet to be shown.

The primary structures of IGF-I and -II in fact show more structural similarity to proinsulin than to insulin[35–37] (see Fig. 1). Like proinsulin IGF-I and -II are single-chain polypeptides with three intra-chain disulphide bridges. The regions of structural similarity in IGF are confined to the B- and A-chain part of proinsulin. An intermediary or connecting region between these A- and B-chain homologous parts consists of 12 and 8 residues compared to 35 in human proinsulin with little homology between these sequences. Also IGF-I and -II exhibit a carboxy-terminal extension of 8 and 6 residues, which is not present in proinsulin.

The structural similarity of IGF and proinsulin suggests a common ancestor from which these molecules diverged during evolution. From the number of identical residues between IGF and insulins from different species[2,36], the divergence between insulin and IGF can be surmised to have occurred before the appearance of the vertebrates provided that the rate of evolutionary change was similar in the two molecules. Likewise, the divergence between IGF-I and IGF-II can be timed at the appearance of the first mammals.

Based on the sequence similarity of IGF and insulin and the known three-dimensional structure of insulin, models have been constructed for IGF-I[42] and IGF-II (Figs 2 and 4). These indicate that the two growth factors can have an identical hydrophobic core and an identical conformation of those residues corresponding to the A- and B-chains of insulin. Their short connecting peptides are easily accommodated in the models although they cover less of the molecular surface than the C-peptide of proinsulin; this appears to be compensated by the extension of the A-chain termini in both IGF molecules. Part of the putative receptor-binding region of insulin described above is thus modified whereas the remaining region has many residues in common.

This structural model is entirely compatible with the notion that some effects of somatomedins may be due to an interaction with the insulin receptor. Earlier studies had demonstrated that impure preparations of NSILA-s inhibit the binding of ^{125}I-insulin to insulin receptors in direct proportion to their insulin-like activity[43]. However, the potency of IGF-I and -II as measured by the stimulation of the conversion of glucose to CO_2 in adipocytes is about 120 and 60 times, respectively, lower than that of insulin[44]. Interestingly, Piron and de Meyts[45] could show in lymphocytes that both IGF-I and -II induce, as insulin, negative cooperativity with potencies in perfect agreement with their apparent affinity for the receptor. More recently, compelling evidence for crossreactivity of somatomedins with insulin receptors has been obtained by the use of monovalent antibodies against the insulin receptor in adipocytes. These Fab fragments derived from a patient with extreme insulin resistance produced a 30-fold rightward shift in the dose response for stimulation of glucose oxidation by both insulin and MSA[46].

The discovery that somatomedins are recognized by the insulin receptor could not explain why the somatomedins have a relatively weak insulin-like metabolic effect, while their potency in promoting growth effects in fibroblasts is about 150 times the potency of insulin[44]. Since the initial studies of Morell *et al.*[47] it was therefore suspected that the metabolic effects of the somatomedins were secondary phenomena due to crossreaction with the insulin receptor, and that their main effects on growth parameters were due to an interaction with a second set of receptors of high affinity for somatomedins and a lower affinity for insulin. The studies of Van Wyk *et al.*[28] and Megyesi *et al.*[43] were the first observations of distinct somatomedin receptors.

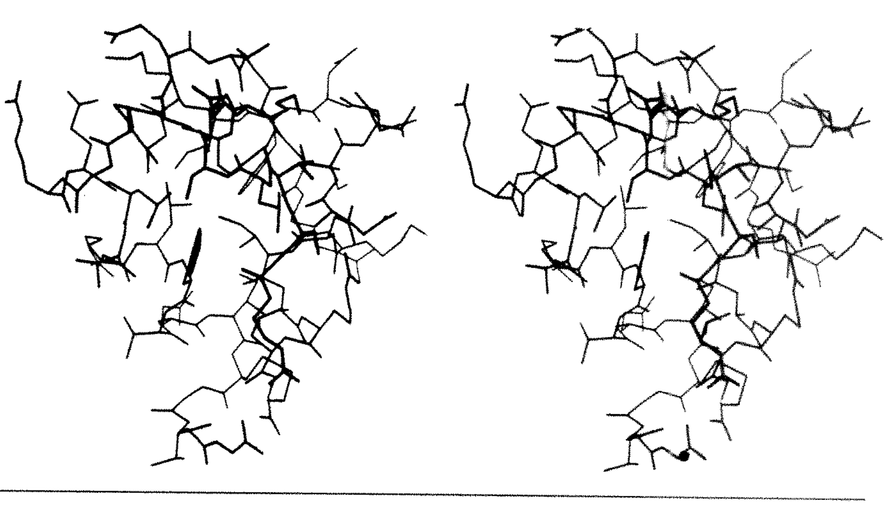

Fig. 3 Stereo view of the three-dimensional structure proposed for relaxin based on an assumed homology with insulin. (Reproduced with permission from *Nature* **270**, 449–451 (1977).)

Later, numerous other studies from several laboratories (see ref. 31) provided ample evidence for the existence of specific somatomedin receptors in several tissues. Of special interest is the observation that, relative to insulin, proinsulin is ten times more effective in binding to the MSA receptor than to the insulin receptor[48]. This observation is entirely compatible with the proinsulin-like structure of IGF-I[42]. The elegant studies of King *et al.*[46] demonstrate that blockage of the insulin receptor of cultured human fibroblasts does not abolish the effect of either insulin or MSA on thymidine incorporation into DNA. It appears, therefore, that interaction with the somatomedin receptor is responsible for the growth-promoting effect of somatomedins and of insulin.

On the basis of the model-building, IGF-II with its shorter connecting peptide is expected to bind insulin receptors with a greater affinity than either IGF-I or proinsulin, a prediction borne out by studies of Zapf *et al.*[44] on adipocytes and by preliminary results of de Meyts and co-workers[22] on lymphocytes. The question, however, remains whether more than one type of somatomedin receptor is present on target cells. Preliminary evidence for at least two receptors, one preferentially binding IGF-I, the other IGF-II and MSA has recently been obtained in several cell types by Rechler *et al.*[49].

In native serum, the somatomedins are bound to a large extent to at least one type of carrier protein[50] which also seems to be under the control of growth hormone[51,52] and to be released concomitantly with somatomedin from the liver[53,54]. The presence of such a specific and saturable binding protein in serum is unique among peptide hormones. Neither insulin[44] nor relaxin or nerve growth factor compete with the IGFs for binding. It may be speculated, therefore, that regions of the IGF molecules not homologous to insulin are making contact with the binding protein.

None of the somatomedins crossreacts with antibodies against insulin, despite the similar structures of the IGFs and of somatomedin C with insulin. However, the immunogenic region of insulin appears to be different from the receptor region and comprises residues mainly within the sequences B1–B10 and A8–A10 (refs 1, 55). The surface side chains in these regions of IGF molecules are quite different from those of any of the insulins, thus explaining the lack of cross-reactivity of the IGFs and of insulin with their respective antibodies. Antibodies against IGF-I crossreact 100-fold better with IGF-I than with IGF-II and antibodies against IGF-II 35-fold better with IGF-II than with IGF-I[56]. In radioimmunoassays for IGF-I and for somatomedin C, somatomedin-C behaves almost or completely identically to IGF-I[56,57], whereas somatomedin A and MSA are less than 5% as potent as somatomedin-C and IGF-I[57]. Surprizingly, in a radioimmunoassay for somatomedin A, IGF-I is 10 times more potent than somatomedin A[58], adding to the bewilderment about the identity of somatomedin A.

The recently developed radioimmunoassays for somatomedin C[59] and IGF-I and -II[56] have allowed the levels of these somatomedins to be determined in clinical conditions such as acromegaly and hypopituitary dwarfism. IGF-I seems to be stringently regulated by the levels of circulating growth hormones whereas the levels of IGF-II are only marginally influenced by growth hormone. Thus, *in vitro*, IGF-I and -II have qualitatively identical effects with some variation in potency, whereas *in vivo* a distinct difference in regulation suggests they play different roles. Further support for different physiological functions of IGF-I and -II comes from preliminary studies showing synthesis in chick liver cells of a somatomedin similar to human IGF-I, but not to IGF-II and the presence of IGF-II, but not IGF-I, in human cerebrospinal fluid. Thus, IGF-I and the somatomedins seem to be growth-hormone-dependent growth factors, whereas a physiological role for IGF-II has yet to be found.

The last-mentioned fact adds considerably to the deplorable semantic confusion in this field. Since somatomedins are defined as growth-hormone-dependent growth factors, IGF-I and somatomedins A and C qualify as true somatomedins, whereas IGF-II does not. Conversely, somatomedins such as somatomedin A or MSA cannot unreservedly be classified as insulin-like growth factors unless and until their structures can be shown to justify such a designation.

Nerve growth factor has also been proposed as a member of the insulin family on the basis of a suggested sequence similarity (see ref. 18 for review). However, the model of NGF that can be derived from its sequence does not contain a conserved hydrophobic close-packed core and deletions give rise to a different conformation of those residues equivalent to the B-chain helix of insulin. Definition of the degree of structural homology must await the determination of the three-dimensional structure[60]. It also appears that nerve growth factor is not able to compete with insulin for its receptor[22].

Glucagon

Compared to insulin, glucagon has a shorter polypeptide chain which is insufficient to allow a hydrophobic core to be shielded from the solvent. In dilute solution therefore, glucagon is flexible and many differing conformers are in equilibrium, with evidence for a stable interaction only between Val 23 and Trp 25 (ref. 61). At increasing concentrations (*p*H from 3.0 to 9.5) the molecules self-associate to α-helical trimers and higher oligomers[62]. An α-helical region exists between residues 6 and 27 resulting in the formation of two hydrophobic 'sticky' patches on the surface of each helix[63]. As with insulin, these hydrophobic patches are involved in self-association; glucagon trimers are formed. A similar hydrophobic interaction may account for the formation of α-helical conformers which occur in nonpolar solvents and in the presence of phospholipids[64].

All mammalian glucagons which have been sequenced are identical[2] and turkey and duck glucagon show only one and two conservative changes respectively from the mammalian sequence. It therefore appears that there are strong selective

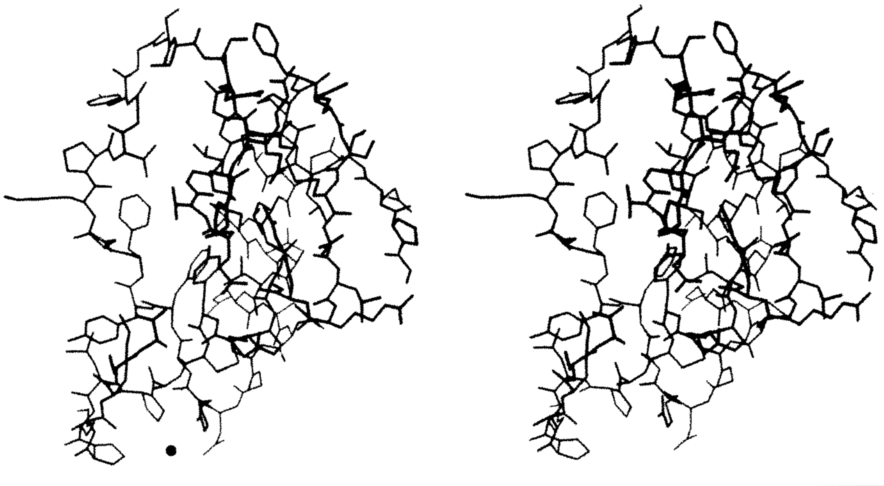

Fig. 4 Stereo view of the three-dimensional structure proposed for IGF-I based on an assumed structural homology with insulin. (Reproduced with permission from *Proc. Acad. Sci. U.S.A.* **75,** 180–184 (1978).)

	1	2	3	4	5	6	7	8	9	10	11	12	13	14	15	16	17	18
aPP	Gly	Pro	Ser	Gln	Pro	Thr	Tyr	Pro	Gly	Asp	Asp	Ala	Pro	Val	Glu	Asp	Leu	Ile
bPP	Ala	Pro	Leu	Glu	Pro	Glu	Tyr	Pro	Gly	Asp	Asn	Ala	Thr	Pro	Glu	Gln	Met	Ala
oPP	Ala	Ser	Leu	Glu	Pro	Glu	Tyr	Pro	Gly	Asp	Asn	Ala	Thr	Pro	Glu	Gln	Met	Ala
pPP	Ala	Pro	Leu	Glu	Pro	Val	Tyr	Pro	Gly	Asp	Asp	Ala	Thr	Pro	Glu	Gln	Met	Ala
cPP	Ala	Pro	Leu	Glu	Pro	Val	Tyr	Pro	Gly	Asp	Asp	Ala	Thr	Pro	Glu	Gln	Met	Ala
hPP	Ala	Pro	Leu	Glu	Pro	Val	Tyr	Pro	Gly	Asp	Asn	Ala	Thr	Pro	Glu	Gln	Met	Ala

	19	20	21	22	23	24	25	26	27	28	29	30	31	32	33	34	35	36	
aPP	Arg	Phe	Tyr	Asp	Asn	Leu	Gln	Gln	Tyr	Leu	Asn	Val	Val	Thr	Arg	His	Arg	Tyr	NH_2
bPP	Gln	Tyr	Ala	Ala	Glu	Leu	Arg	Arg	Tyr	Ile	Asn	Met	Leu	Thr	Arg	Pro	Arg	Tyr	NH_2
oPP	Gln	Tyr	Ala	Ala	Glu	Leu	Arg	Arg	Tyr	Ile	Asn	Met	Leu	Thr	Arg	Pro	Arg	Tyr	NH_2
pPP	Gln	Tyr	Ala	Ala	Glu	Leu	Arg	Arg	Tyr	Ile	Asn	Met	Leu	Thr	Arg	Pro	Arg	Tyr	NH_2
cPP	Gln	Tyr	Ala	Ala	Glu	Leu	Arg	Arg	Tyr	Ile	Asn	Met	Leu	Thr	Arg	Pro	Arg	Tyr	NH_2
hPP	Gln	Tyr	Ala	Ala	Asp	Leu	Arg	Arg	Tyr	Ile	Asn	Met	Leu	Thr	Arg	Pro	Arg	Tyr	NH_2

Fig. 5 The sequences of pancreatic polypeptides, PP (see ref. 23 for review). [a (avian), b (bovine), o (ovine), p (porcine), c (canine) and h (human).]

functional restraints on the glucagon molecule during evolution, although preliminary results on guinea pig, angler fish and shark glucagons indicate some divergence[65].

Study of the data on receptor binding and activity of glucagon on the glucagon-sensitive adenylate cyclase system of hepatocyte membranes led Rodbell *et al*[66] to suggest that almost the entire molecule is required for full biological potency. Their results and subsequent detailed studies by Epand *et al.*[64] have shown that modification at the COOH-terminal or NH_2-terminal regions and on polar groups invariably leads to decreased receptor potency, although modification of some nonpolar groups (such as tyrosine by iodination) can enhance activity, indicating the importance of the whole glucagon molecule to receptor binding. Des-His^1-glucagon and other glucagons modified at the N-terminus are partial agonists with reduced affinity for the glucagon receptor suggesting that this region might be involved in hormone action whereas the major part of the molecule, including the C-terminal hydrophobic region, might be responsible for enhancing receptor affinity[67]. Receptor binding studies of smaller N-terminal fragments of glucagon are consistent with this model[68]. Evidence that interaction with the receptor is entropy driven suggested a model in which a helical conformer, stabilized by hydrophobic interactions, is induced or selected at the receptor from a population of conformers[63].

Glucagon is a member of a large family of homologous polypeptides, found in the alimentary tract and elsewhere, including secretin[69], the first hormone to be discovered, vasoactive intestinal polypeptide[70] (VIP) and gastric inhibitory peptide[71] (GIP, now renamed glucose-dependent insulinotropic peptide) (see ref. 2 for review). Evidence for the existence of further homologous intestinal peptides[72] indicates that the family may be much more extensive.

Glucagon is more effective than either VIP or secretin in hepatic adenylate cyclase activation and appears to act through a receptor distinct from those for secretin and VIP[68,73]. Neither secretin nor VIP competes with ^{125}I-glucagon at the receptor on hepatocytes. In view of the close homology at the N-terminal region of glucagon, VIP and secretin, these observations might indicate that the C-terminal residues of glucagon are responsible for selecting the correct receptor. However, recent results indicate that the N-terminal region may also play a role in receptor selection since glucagon$_{1-6}$ is a partial agonist of glucagon, whereas the equivalent regions of secretin and VIP are not[74]. Secretin and VIP are both recognized by each other's receptors although each binds to its own receptor with greater affinity[75,76]. The results of these and many other comparative studies indicate that the secretin and VIP receptors, although perhaps not the glucagon receptor, have evolved from a common ancestor. Confirmation of this proposal must await chemical characterization of the receptors themselves.

Glucagon also has an ill defined relationship to glicentin, a 100-amino acid polypeptide isolated from the intestine. Glicentin is known to carry the immunodeterminants of glucagon and to account for most of the glucagon-like activity in the intestine[77]. Although it is tempting to believe that glicentin is the precursor of glucagon, particularly since it is found in the specific glucagon-containing granules of the pancreatic α-cell, recent evidence suggests that glicentin and glucagon are in topographically separated granules[78].

Pancreatic polypeptide and somatostatin

Two further peptides which may be classified as hormones are produced by specific cells of the islets of Langerhans. Pancreatic polypeptide[79,80] is a 36-amino acid peptide which appears to have gastrointestinal functions and may act as a satiety factor; it is released after a protein meal and leads to a decrease in weight of certain genetically diabetic mice[81,82]. Since Tatemoko and Mutt[72] find a homologous peptide in pig intestine, pancreatic polypeptide may be a member of a larger family of gastroenteric pancreatic hormones. All sequenced pancreatic polypeptides have amidated carboxytermini and there is close homology amongst the mammalian sequences[79,80] (Fig. 5). In contrast to glucagon, however, there are considerable differences between mammalian and avian pancreatic polypeptide sequences[79,80]. This is also reflected in the species specificity of immunological and some biological activities[80–82].

Although this polypeptide is only seven residues larger than glucagon, it appears to have a relatively stable tertiary structure[83–85] comprising a polyproline II-like chain segment folded against an α-helical region as shown in Fig. 6. In a similar way to insulin the molecules can self-associate to dimers. It seems that all mammalian and avian pancreatic polypeptides can attain this conformation and can dimerize; in addition the avian polypeptide, like insulin, can form higher oligomers in the presence of zinc.

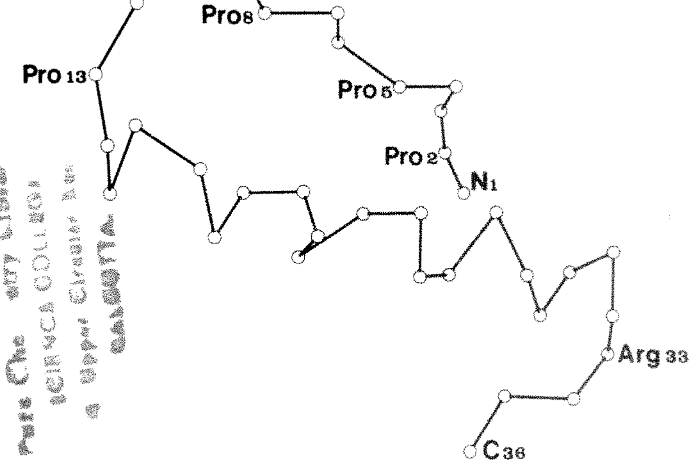

Fig. 6 The conformation of avian pancreatic polypeptide, PP, as determined by X-ray analysis. The α-helix and the polyproline-like helix pack together to give a compact structure. A similar structure may also be assumed by bovine pancreatic polypeptide, even though they are species specific in some of their biological activities. (Unpublished results of J. Pitts, S. P. Wood, I. J. Tickle and T. L. Blundell.)

Somatostatin[86] is the smallest of the pancreatic hormones. It contains 14 amino acids with one disulphide bridge; in fact an even smaller, relatively rigid peptide of residues 7–10 can be a potent agonist[87]. Somatostatin is widely distributed and was originally identified in the hypothalamus, although peptides in different organs and in different mammals (pig and sheep) seem to be identical. In general the peptide appears to act locally—in the pancreas it inhibits the release of insulin and glucagon; it is therefore strictly a local hormone or paracrine agent.

Evolution of pancreatic hormones and relation to gastroenteric and neuroendocrine systems

Finally, we consider whether pancreatic hormones or close relatives are also active in the nervous system. This question is being approached by the study of the developmental and evolutionary origin of hormone-producing cells and by attempts to localise and even extract the hormones from the central nervous system (see ref. 88 for a review).

Examples of pancreatic hormone-like activity are found in the alimentary tract (see ref. 89 for review) of both protostomian and deuterostomian lines of invertebrate evolution. For instance, an insulin-like substance which has a role in carbohydrate metabolism is found in the mucosa of the alimentary tract of molluscs[90]. Evidence for this insulin-like activity is derived from biological and radioimmunological assay, as well as ultrastructural, histological and histochemical techniques, but it has not yet been chemically characterized.

Van Noorden and Falkmer[89] have traced the movement of the four pancreatic hormones from the alimentary canal into the islets during vertebrate evolution. They have shown that the first hormone to be found in a well defined islet is insulin in cyclostomes such as the hagfish. Somatostatin also appears in the islet at that stage. Glucagon is the third hormone to reach the pancreas, being restricted to the gut mucosa in cyclostomes, but appearing in the pancreatic islets of the holocephalan cartilaginous fishes. In these fish pancreatic polypeptide immunoactivity is still located in the gut mucosa, but at the next evolutionary stage, the elasmobranchian cartilaginous fish, this molecule finally moves into the pancreatic islets.

Immunoreactive evidence of all pancreatic hormones has been observed in the central nervous system. Somatostatin is found immunocytochemically in the neurones of the N-paraventricularis of the hypothalamus and in other hypothalamic nuclei[91]. Insulin-like activity in the blowfly[92] has its origins in the median neurosecretory cells, and in the hookworm[93] an insulin-like molecule of the corpus cardiacum/corpus allatum capable of decreasing haemolymph trehalose, may also derive from neurosecretory cells. Much interest has been stimulated by the recent reports of Roth *et al.*[94,95] that insulin-like protein levels in many rat tissues including brain extracts are higher than in plasma. The marked similarity between this insulin-like activity and pancreatic insulin in radioimmunoassay, radio-receptor assay, and bioassay indicates that all tissues contain either genuine insulin or a very similar polypeptide rather than a proinsulin-like peptide or insulin-like growth factor. Roth *et al.*[94] find that genetically obese (*ob*/*ob*) diabetic mice in which circulating insulin is markedly increased, and insulin receptors in liver, fat and other tissues are severely depressed, have normal concentrations of insulin and insulin receptors in the brain. These and other related observations on rats made hypoinsulinaemic and diabetic by treatment with streptozotocin have been held to indicate the synthesis of insulin locally in the brain and other extrapancreatic tissues, and to suggest a possible role of insulin in neurotransmission, either as a neurotransmitter itself or as a neuromodulator. However, these reports have been disputed by Eng and Yalow who contend that insulin concentrations in the brain of larger animals never exceed plasma levels[96]. Much work remains to establish whether or not insulin is synthesized in the mammalian central nervous system; the high levels of insulin may well result from insulin which has crossed the blood–brain barrier, diffused through the brain and concentrated on brain receptor sites[96]. The discovery of many of the gastroenteric pancreatic hormones in the central nervous system of higher vertebrates indicates that neuronal peptide production may represent a primative capability. The explanation of this distribution of peptide hormones may lie in the APUD theory of Pearse[88,97] which proposes that the embryonic neuroectoderm of nerves and peptide hormone-producing cells have a common origin in the neuroendocrine-programmed cells of the ectoblast. The diffuse regulatory mechanism of the neuronal system may have become partially replaced by aggregation of cells of the endocrine system. These ideas do not preclude an even more primitive evolution of hormones and neurotransmitters from lysozomal proteases as suggested by Hales[98]. At the level of molecular evolution, duplication of ancestral genes—perhaps coding for neurotransmitters—must have given rise through natural selection of mutated sequences to a series of hormones and growth factors: families of molecules with homologous sequences.

We are grateful to many colleagues for helpful discussions and to Drs P. de Meyts, S. Falkmer, M. M. Rechler, S. Van Noorden and J. J. Van Wyk for making available unpublished results and reviews.

1. Blundell, T. L., Dodson, G. G., Hodgkin, D. C. & Mercola, D. A., *Adv. Prot. Chem.* **26,** 279–402 (1972).
2. Dayhoff, M. O. *Atlas Protein Sequence Struct.* **5,** 3 (1978).
3. Blundell, T. L. & Wood, S. P. *Nature* **257,** 197–203 (1975).
4. Falkmer, S. *et al. Am. Zool.* **15,** Suppl. 1, 255–270 (1975).
5. Lomedico, P. T., Chan, S. J., Steiner, D. F. & Saunders, G. S. *J. biol. Chem.* **252,** 7971–7978 (1977).
6. Steiner, D. F. & Oyer, P. E. *Proc. natn. Acad. Sci. U.S.A.* **57,** 473–480 (1967).
7. Humbel, R. E., Bosshard, M. R. & Zain, H. in *Handbook of Physiology*, Sect. 7 (eds Steiner, D. F. & Freinkel, N) 111–132 (Williams and Wilkins, Baltimore, 1972).
8. Lomedico, P. *et al. Cell* **18,** 533–543 (1979).
9. Bell, G. I. *et al. Nature* **284,** 26–32 (1980).
10. Perler, F. *et al. Cell* **20,** 555–566 (1980).
11. Tager, H. *et al. Nature* **281,** 122–125 (1979).
12. Wood, S. P. *et al. Archs Biochem. Biophys.* **186,** 175–183 (1978).
13. Horuk, R. *et al. Nature* **279,** 439–440 (1979); **286,** 822–823 (1980).
14. Pullen, R. A. *et al. Nature* **259,** 369–373 (1976).
15. De Meyts, P. *et al. Nature* **273,** 504–509 (1978).
16. Van Obberghen, E. *et al. Nature* **280,** 500–502 (1979).
17. Schwabe, C., McDonald, J. K. & Steinitz, B. G. *Biochem. biophys. Res. Commun.* **75,** 503–510 (1977).
18. Bradshaw, R. A. & Niall, H. D. *Trends biochem. Sci. Rev.* **3,** 274–278 (1978).
19. Bedarkar, S., Turnell, W. G., Blundell, T. L. & Schwabe, C. *Nature* **270,** 449–451 (1977).
20. Isaacs, N. *et al. Nature* **271,** 278–281 (1978).
21. Niall, H. *et al.* in *Insulin and Related Hormones* (eds Brandenburg, D. & Zahn, H.) 718–726 (de Gruyter, Berlin, 1980).
22. Piron, M. A. *et al.* in *Insulin and Related Hormones* (eds Brandenburg, D. & Zahn, H.) 371–391 (de Gruyter, Berlin, 1980).
23. Schwabe, C. *et al. Rec. Prog. Horm. Res.* **34,** 123–211 (1978).
24. Daughaday, W. H. *et al. Nature* **235,** 107 (1972).
25. Froesch, E. R. *et al. Rec. Progr. Horm. Res.* **23,** 565–616 (1967).
26. Hall, K. *Acta endocr.* Copenh. Suppl. **163,** 1–52 (1972).
27. Uthne, K. *Acta endocr.* Copenh. Suppl. **175,** 1–35 (1973).
28. Van Wyk, J. J. *et al. Rec. Prog. Horm. Res.* **30,** 259–318 (1974).
29. Pierson, R. W. Jr & Temin, H. M. *J. cell. Physiol.* **79,** 319–329 (1972).
30. Van Wyk, J. J. & Underwood, L. E. in *Biochemical Actions of Hormones* Vol. 5 (ed. Litwack, G.) 101–148 (1978).
31. Zapf, J., Rinderknecht, E., Humbel, R. E. & Froesch, E. R. *Metabolism* **27,** 1803–1828 (1978).
32. Humbel, R. E. *et al. Excerpta Med. Int. Congr. Ser.* **231,** 306–317 (1970).
33. Hintz, R. L., Clemmons, D. R., Underwood, L. E. & Van Wyk, J. J. *Proc. natn. Acad. Sci. U.S.A.* **69,** 2351–2353 (1972).
34. Rinderknecht, E. & Humbel, R. E. *Proc. natn. Acad. Sci. U.S.A.* **73,** 2365–2369 (1976).
35. Rinderknecht, E. & Humbel, R. E. *J. biol. Chem.* **253,** 2769–2775 (1978).
36. Rinderknecht, E. & Humbel, R. E. *FEBS Lett.* **89,** 283–289 (1978).
37. Rinderknecht, E. & Humbel, R. E. *Proc. natn. Acad. Sci. U.S.A.* **73,** 4379–4385 (1976).
38. Svoboda, M. E. *et al. Biochemistry* **19,** 790–797 (1980).
39. Fryklund, L., Uthne, K. & Sievertsson, H. *Biochem. biophys. Res. Commun.* **61,** 957–962 (1974).
40. Moses, A. C., Nissley, S. P., Short, P. A., Rechler, M. M. & Podskalny, J. M. *Eur. J. Biochem.* **103,** 387–400 (1980).
41. Moses, A. C., Nissley, P., Short, P. A. & Rechler, M. M. *Eur. J. Biochem.* **103,** 401–408 (1980).
42. Blundell, T. L., Bedarkar, S., Rinderknecht, E. & Humbel, R. E. *Proc. natn. Acad. Sci. U.S.A.* **75,** 180–184 (1978).
43. Megyesi, K. *et al. Biochem. biophys. Res. Commun.* **57,** 307–315 (1974).
44. Zapf, J., Schoenle, E. and Froesch, E. R. *Eur. J. Biochem.* **87,** 285–296 (1978).
45. Piron, M. A. & de Meyts, P. *2nd Int. Insulin Symp. Aachen*, Abstr. 121–122 (1979).
46. King, G. L., Kahn, C. R., Rechler, M. M. & Nissley, S. P. *J. clin. Invest.* (submitted).
47. Morell, B. & Froesch, E. R. *Eur. J. clin. Invest.* **3,** 119–123 (1973).
48. Nissley, S. P., Rechler, M. M., Moses, A. C., Short, P. A. & Podskalny, J. M. *Endocrinology* **101,** 708–716 (1977).
49. Rechler, M. M. *et al. Endocrinology* (in the press).
50. Zapf, J., Waldvogel, M. & Froesch, E. R. *Archs Biochem. Biophys.* **168,** 638–645 (1975).
51. Moses, A. C., Nissley, S. P., Cohen, K. L. & Rechler, M. M. *Nature* **263,** 137–140 (1976).
52. Kaufmann, U., Zapf, J. & Froesch, E. R. *Acta endocr.* Copenh. **87,** 716–727 (1978).

53. Moses, A. C., Nissley, S. P., Passamini, J., White, R. M. & Rechler, M. M. *Endocrinology* **104,** 536–546 (1979).
54. Schalch, D. S., Heinrich, U. E., Draznin, B., Johnson, C. J. & Miller, L. L. *Endocrinology* **104,** 1143–1151 (1979).
55. Blundell, T. L. *Trends biochem. Sci.* **4,** 51–54 (1979).
56. Walter, H., Humbel, R. E. & Schwander, J. *10th Cong. Int. Diabetes Fedn 1979* Abstr. No. 645.
57. Van Wyk, J. J., Svoboda, M. E. & Underwood, L. E. *J. clin. endocr. Metab.* **50,** 206–208 (1980).
58. Hall, K., Brandt, J., Ennberg, G. & Fryklund, L. *J. clin. endocr. Metab.* **48,** b71–278 (1979).
59. Furlanetto, R. W., Underwood, L. E., van Wyk, J. J. & D'Ercole, J. J. *Clin. Invest.* **60,** 648–657 (1977).
60. Wlodawer, A., Hodgson, K. O. & Shooter, E. M. *Proc. natn. Acad. Sci. U.S.A.* **72,** 777–781 (1975).
61. Boesch, C., Bundi, A., Oppliger, M. & Wüthrich, K. *Eur. J. Biochem.* **91,** 209–214 (1978).
62. Gratzer, W. B., Creeth, J. M. & Beaven, G. H. *Eur. J. Biochem.* **31,** 505–509 (1972).
63. Sasaki, K., Dockerill, S., Adamiak, D. A., Tickle, I. J. & Blundell, T. L. *Nature* **257,** 751–757 (1975).
64. Epand, R. M. & Jones, A. J. S. *Biochim. biophys. Acta* **491,** 296–304 (1977).
65. Sundby, F. *Metabolism* **25,** 1316–1321 (1976).
66. Rodbell, M. *et al. Proc. natn. Acad. Sci. U.S.A.* **68,** 909–913 (1971).
67. Lin, M. C., Wright, D. E., Hruby, V. J. & Rodbell, M. *Biochemistry* **14,** 1559–1563 (1975).
68. Wright, D. E. & Rodbell, M. *J. biol. Chem.* **254,** 268–269 (1979).
69. Mutt, V., Jorpes, J. E. & Magnusson, S. *Eur. J. Biochem.* **29,** 199–204 (1972).
70. Mutt, V. & Said, S. I. *Eur. J. Biochem.* **42,** 581–589 (1974).
71. Brown, J. C. & Dryburgh, J. R. *Can. J. Biochem.* **49,** 867–872 (1971).
72. Tatemoto, K. & Mutt, V. *Nature* **285,** 417–418 (1980).
73. Bataille, D., Freychet, P. & Rosselin, G. *Endocrinology* **95,** 713–721 (1974).
74. Wright, D. E. & Rodbell, M. *Proc. Am. Peptide Symp.* **6,** 1029–1031 (1980).
75. Taylor, D. P. & Pert, C. B. *Proc. natn. Acad. Sci. U.S.A.* **76,** 660–664 (1979).
76. Robberecht, P. *et al.* FEBS Lett. **103,** 229–233 (1979).
77. Moody, A. J., Jacobsen, H. & Sundby, F. in *Gut Hormones* (ed. Bloom, S. R.) 369–378 (Churchill Livingstone, Edinburgh, 1978).
78. Ravazzola, M. & Orci, L. *Nature* **284,** 66–67 (1980).
79. Kimmel, J. R., Hayden, L. J. & Pollock, H. G. *J. biol. Chem.* **250,** 9369–9374 (1975).
80. Floyd, J. C., Fajans, S. S., Pek, S. & Chance, R. E. *Rec. Prog. Horm. Res.* **33,** 519–570 (1977).
81. Malaisse-Lagae, R., Carpentier, J-L., Patel, Y. C., Malaisse, W. J. & Orci, L. *Experienta* **33,** 915–917 (1977).
82. Gates, R. J. & Lazarus, N. *Hormone Res.* **8,** 189–202 (1977).
83. Wood, S. P., Pitts, J. E., Blundell, T. L., Tickle, I. J. & Jenkins, J. A. *Eur. J. Biochem.* **78,** 119–126 (1977).
84. Pitts, J., Blundell, T. L. Tickle, I. J. & Wood, S. P., *Proc. Am. Peptide Symp.* **6,** 1011–1016 (1980).
85. Chang, P., Kimmel, J. R. & Noelken, M. E. *Int. Cong. Biochem.* **11,** 192 (1979).
86. Brazeau, R. *et al. Science* **179,** 77–79 (1973).
87. Veber, D. F. *et al. Nature* **280,** 512–514 (1979).
88. Pearse, A. G. E. *Med. Biol.* **55,** 115–125 (1977).
89. Van Noorden, S. & Falkmer, S. *Investigative and Cell Pathology* **3,** 21–35 (1980).
90. Plisetskaya, E., Kazakov, V. K., Solbitskaya, L. & Leibson, L. G. *Gen. comp. Endocr.* **35,** 133–145 (1978).
91. Brownstein, M., Arimura, A., Sato, H., Schnally, A. V. & Kizer, J. S. *Endocrinology* **96,** 1456–1461 (1975).
92. Lazarus, N. *Biochem. J.* **184,** 221–227 (1979).
93. Tager, H. S., Markese, J., Kramer, K. B. & Spiers, R. D. & Childs, C. N. *Biochem. J.* **156,** 515–520 (1976).
94. Havrankova, J., Schmechel, D., Roth, J. & Brownstein, M. *Proc. natn. Acad. Sci. U.S.A.* **75,** 5737–5741 (1978).
95. Rosenzweig, J. L. *et al. Proc. Nat. Acad. Sci. U.S.A.* **77,** 572–576 (1980).
96. Eng, J. & Yalow, R. S. *Diabetes* **29,** 105–109 (1980).
97. Pearse, A. G. E. *Proc. R. Soc.* **B170,** 71–80 (1968).
98. Hales, N. *FEBS Lett.* **94,** 10–15 (1978).

ARTICLES

Thermal history of the H-group of chondritic meteorites

[illegible] The [illegible] Library
SCIENCE COLLEGE
[illegible] Circular Road
Calcutta

R. Hutchison & A. W. R. Bevan
Department of Mineralogy, British Museum (Natural History), Cromwell Road, London SW7 5BD, UK

S. O. Agrell
Department of Mineralogy and Petrology, Downing Place, Cambridge CB2 3EW, UK

J. R. Ashworth
Department of Geological Sciences, The University of Aston, Gosta Green, Birmingham B4 7ET, UK

The Tieschitz unequilibrated H-group chondrite accreted at (800 ± 100) °C during rapid cooling[11]. *From their mineral chemistry, nine other H-group chondrites, exhibiting greater degrees of equilibration, also formed hot. Degree of equilibration is equated with slowness of cooling, especially below about 700 °C. If metamorphism is defined as change brought about by an increase in temperature, in the H-group chondrites it is recognized only in the localized effects of transient reheating, probably induced by shock.*

THE ordinary chondrites are stony types composed of silicate, metal and sulphide phases. Because of this mixture and because they were never completely melted, the ordinary chondrites are considered to represent primative, condensed matter of the early Solar System. Chemically they are subdivided into three groups. One of these, the high iron (H-) group, has a total iron content >24.5 wt% and iron-nickel metal generally in the range 12–21 wt%. Many members of this group have been unaffected by shock events which post-date crystallization and which caused veining, 'blackening' or brecciation in most members of the other two chemical groups[1–3]. The H-group, therefore, seemed most appropriate to re-investigate using modern techniques. Our work will be published in detail elsewhere[4,5]. Here, in summarizing our data, we favour a simpler early history for the H-group parent body (or parent bodies) than is currently accepted. Furthermore, we interpret for the first time the cooling history of all petrological types consistently in terms of the chemistry of both silicates and metal.

On a textural and mineralogical basis, Van Schmus and Wood[6] subdivided the chondrites into six petrological types. Types 1 and 2 do not occur in the ordinary chondrites. Type 3 refers to unequilibrated chondrites with prominent chondrules, sub-spherical masses of silicate, some of which are quenched liquid droplets, the remainder were fashioned from solid or plastic pre-existing rock[7,8]. In contrast, petrological type 6 applies to meteorites in which chondrules have crystallized and intergrown with the matrix. Types 4 and 5 exhibit integration of chondrules with matrices intermediate between that in types 3 and 6. The pyroxenes and feldspars of type 4 ordinary chondrites are partly chemically heterogeneous, but almost all of those in types 5 and 6 are not. In petrological type 3, metal and sulphide may form rounded droplets—metallic chondrules[9,10]—outside silicate chondrules, or they may occur separately or together as droplets within silicate chondrules. But in higher petrological types metal and sulphide are generally absent from silicate chondrules and occur as grains with irregular outlines

0028–0836/80/440787—04$01.00

indicative of partial to complete crystallization to fill the available spaces between the chondrules.

For our study, 10 H-group chondrites (named in Fig. 2) were chosen from the collection in the British Museum (Natural History) as unshocked or lightly shocked representatives of the different petrological types. The wavelength-dispersive electron microprobe at the British Museum (Natural History) was used for analysis of metal and sulphide; other phases were analysed using the energy-dispersive microprobe system at Cambridge. The 1-MV transmission electron microscope at Birmingham University provided information on the fine-structure of the chondrites.

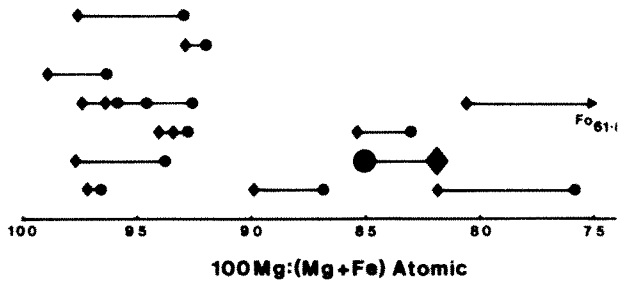

Fig. 1 Compositions of the 'cores' of co-existing phenocrysts of olivine (●) and low-calcium pyroxene (◆) in 12 Tieschitz chondrules. Except in one case (large symbols), pyroxenes are more magnesian than olivines. Because the plane of the section cuts each crystal at random, we cannot be sure that an analysis is representative of a crystal core; this accounts for the compositional differences shown. The vertical axis has no significance.

Silicate mineralogy

Tieschitz is the only highly unequilibrated chondrite among the 10 studied. In both olivines and low-calcium pyroxenes the molecular ratio of 100 Mg: (Mg+Fe) is variable within crystals and between crystals. In every zoned crystal studied the core is more magnesian than the rim, consistent with an earlier observation on the Sharps, H3 chondrite[7]; pyroxene cores are usually poorer in calcium than the rims[11]. Of some 40 chondrules, 12 contain phenocrysts of both olivine and low-calcium pyroxene. Of these, 11 have pyroxenes more magnesian than the co-existing olivine (Fig. 1). In Tieschitz the bias in favour of pyroxene in the partitioning of magnesium between pyroxene and olivine was undoubtedly the result of crystallization of chondrule liquids. In our sample of Bremervörde (H3/4) and in the chondrites of higher petrological type, on average, the 100 Mg: (Mg+Fe) ratio is ~2% higher in low-calcium pyroxenes than in the co-existing olivines; this is consistent with earlier data[12]. There is thus little difference in the partitioning of Mg between pyroxene and olivine among chondrites which exhibit different degrees of equilibration.

In Tieschitz and Bremervörde, low-calcium pyroxenes are typically of the polysynthetically twinned, monoclinic variety; they may have crystallized directly from chondrule liquids during rapid cooling but they are more probably inverted protopyroxene[5,13]. Most pyroxene cores contain <0.75 wt% calcium (Fig. 2), as do those in the remaining, more equilibrated chondrites. Although our calcium determinations broadly agree with those quoted by Dodd[12], we observe no correlation between calcium content of pyroxene cores and the increasing petrological type. Calcium-rich pyroxene occurs in both Tieschitz and Bremervörde as overgrowths of pigeonite on twinned, low-calcium pyroxene cores or as the minor phase in intergrowths with low-calcium, monoclinic pyroxene. Pigeonites exhibit exsolution on ~10 nm scale. Diopside has not been observed, but some chondrule mesostases are rich in normative diopside. In the two least equilibrated chondrites, crystallization of olivine or low-calcium clinopyroxene or protopyroxene resulted in the enrichment in calcium of residual chondrule liquids. Cooling was so rapid, however, that only pigeonite was able to crystallize on a pre-existing substrate of low-calcium pyroxene[5]. In the petrological type 4 and 5 chondrites the low-calcium pyroxene is typically the striated orthopyroxene which has been interpreted as "the disordered product of inversion from a high-temperature polymorph"[13]. In the H4 chondrites, low-calcium pyroxene cores may have overgrowths of pigeonite or even subcalcic augite; augite and diopside, however, were encountered only as components (normative) in chondrule mesostases, except in the TEM study of Quenggouk[5]. Here, some chondrule mesostases contain tiny crystallites of orthopyroxene, diopside, and plagioclase. The diopside lacks exsolution lamellae, even on the finest, sub-micrometre scale. It is evidence of slower cooling and a closer approach to equilibrium crystallization than by the pigeonites in Tieschitz and Bremervörde. In the two chondrites of petrological type 5, orthopyroxene or striated pyroxene often has overgrowths of augite or diopside which are resolvable by microprobe. Finally, in the H6 chondrites the low-calcium pyroxenes are represented by orthorhombic crystals only, and diopside occurs both as overgrowths and as individual, anhedral grains.

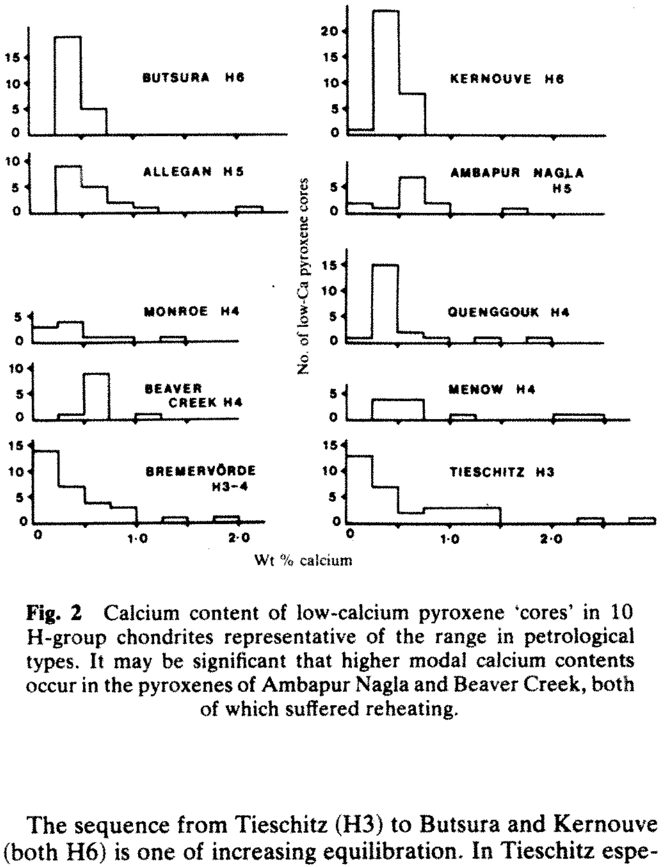

Fig. 2 Calcium content of low-calcium pyroxene 'cores' in 10 H-group chondrites representative of the range in petrological types. It may be significant that higher modal calcium contents occur in the pyroxenes of Ambapur Nagla and Beaver Creek, both of which suffered reheating.

The sequence from Tieschitz (H3) to Butsura and Kernouve (both H6) is one of increasing equilibration. In Tieschitz especially, but also in Bremervörde and the chondrites of type 4, olivines and monoclinic, low-calcium pyroxenes undoubtedly crystallized from chondrule liquids. Structurally, the 'striated orthopyroxene' of Allegan (H5) is intermediate between these monoclinic, low-calcium pyroxenes and the orthorhombic pyroxenes of Butsura and Kernouve. It is surprising that the low-calcium pyroxenes have uniformly low calcium contents throughout (Fig. 2). In addition, the partition of magnesium between olivines and pyroxenes always favours the latter. Had crystal–liquid and solid–solid equilibria been responsible for elemental partition between the phases at the respective extremes of the petrological sequence, systematic compositional differences should be evident. In their absence we conclude that, throughout the sequence, elemental partition was established by a single process acting in uniform physical conditions. In types 3 and 4, this process was undoubtedly crystallization from chondrule liquids; this must also be true for the type 6 chondrites which do contain relict chondrules. It seems, therefore, that in the H6 chondrites the partition of calcium between the pyroxenes was dominated by the crystallization of large amounts of very low-calcium clinopyroxene or protopyroxene from chondrule liquids. Subsequently, inversion to the orthorhombic form occurred. Had orthorhombic pyroxenes crystallized directly from liquids, the crystals should contain a higher calcium content or exsolution lamellae of calcium-rich pyroxene, as for example, do the bronzites of Bushveld type[14]. On the contrary, even on a sub-micrometre scale, no exsolution lamellae of calcium-rich pyroxene were found in the bronzites of Butsura or Kernouve.

Conventional mineral thermometers[15,16] are based on equilibrium partition of an element between two co-existing solid phases; a metamorphic environment has to be assumed. Our evidence indicates that these thermometers may not apply to the H-group chondrites, and this might also be true for the oxygen isotopic thermometer[17]. However, in addition to the above arguments based on the mineral chemistry of olivines and pyroxenes, we have observed chemical heterogeneity among the feldspars and chromites of Butsura. Thus, in at least one H6 chondrite, equilibration was not completely achieved; this conclusion was reached by Bunch and Olsen[15], who used data on pairs of crystals in contact for their assessment of the various mineralogical thermometers.

Metallography

It has been argued[10] that in Tieschitz, metallic chondrules and droplets in silicate chondrules cooled rapidly enough to preserve structural and chemical evidence of an origin by fractional crystallization from Fe–Ni–S melts. This is based on an interpretation of polycrystalline taenite as the relict of a solidification structure (Fig. 3*a*). In Tieschitz this does not seem to be in doubt because there is ample evidence of quenching in silicate chondrules and the meteorite is completely unshocked[5,11,18]. However, polycrystalline taenite occurs also in Bremervörde, Menow, Quenggouk, Butsura (Fig. 3*b*) and, rarely, even in Kernouve, the most equilibrated of our sample of H-group chondrites. Is then the polycrystalline taenite in H6 chondrites a relict solidification structure, or could it have formed in some other way? If the former is true, then the H6 chondrites could not have been metamorphosed during a reheating episode at a temperature above 700 °C, for this would have caused all metal to homogenize as the γ phase. Subsequent, slow cooling could not produce the crystal boundaries in the parent γ. Internal grain boundaries in γ crystals, if produced by deformation at high temperature, could be stabilized at low temperature only by quenching or by the widespread precipitation of α Fe–Ni along the crystal boundaries. Crystallites of α are very rarely observed in polycrystalline taenite. Finally, there is no evidence that polycrystalline taenite could have formed by brittle deformation of taenite below 700 °C.

We are forced to conclude that polycrystalline taenite in H6 chondrites is a relict solidification structure. For its preservation in Tieschitz, Bevan and Axon[10] state that cooling to below about 700 °C (entry of metal into the $\alpha + \gamma$ field) took days to weeks. In Butsura and Kernouve, polycrystalline taenite is rarer and more modified than in Tieschitz, indicating slower cooling in the case of the H6 chondrites; they may have taken weeks to months to cool from over 1,000 °C to below about 700 °C. However, the most important conclusion from these observations is that compositional variation in the metal of H-group chondrites was established at temperatures above 700 °C, and subsequently enhanced by the effects of solid-state diffusion at lower temperatures.

Discussion

Wood[9] modelled the development of nickel-distribution profiles in metal grains in the ordinary chondrites. He began, however, by assuming that above ~700 °C all metal was in the form of homogeneous γ crystals. On cooling into the $(\alpha + \gamma)$ field, α nucleated and grew at the expense of γ by solid-state diffusion of nickel. By computer modelling the build-up of nickel relative to grain-size in taenite (γ), Wood estimated the rates at which various ordinary chondrites cooled through about 500 °C. The presence of polycrystalline taenite in some of the H-group chondrites indicates that above 700 °C, in the γ field, metal was inhomogeneous and that initial nickel gradients had already been established by crystal–liquid fractionation. Therefore, Wood's model[9] must always underestimate the rate of cooling in the H-group chondrites, although for the type 6 meteorites it will produce a closer approximation to the true cooling rate than for the H3, Tieschitz.

Interpretation of polycrystalline taenite as a relict solidification structure parallels our conclusion that the

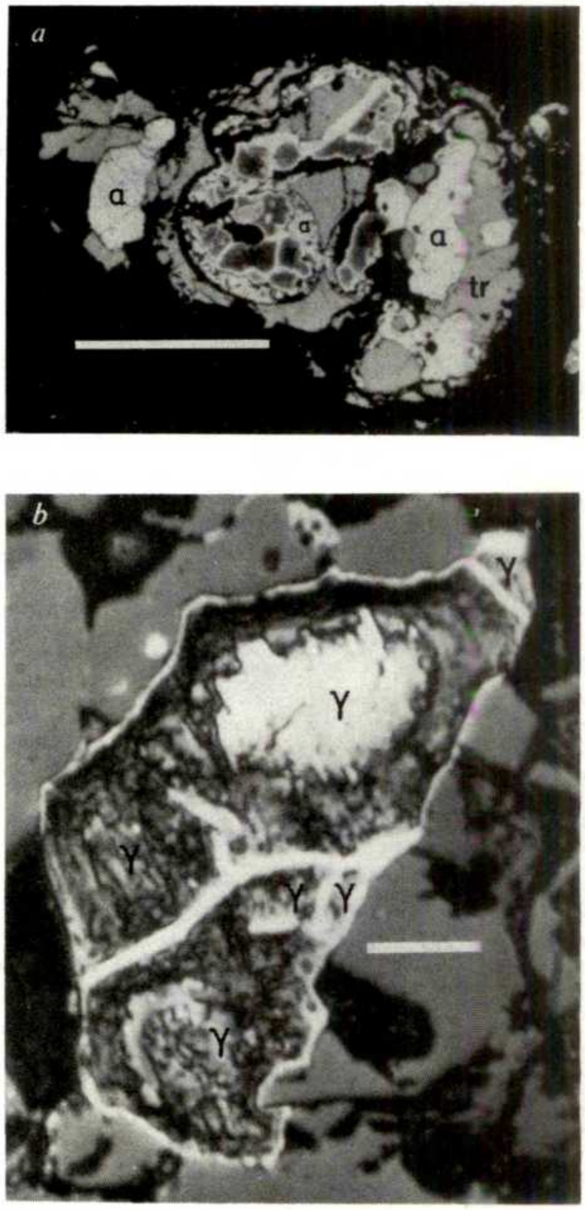

Fig. 3 *a*, Metal–sulphide chondrule in Tieschitz (H3). Scale bar, 100 μm. tr, troilite; α, kamacite; γ, taenite. Two adjacent crystallites of polycrystalline taenite (γ) are indicated; each has a dark-etching core and a rim of clear taenite. *b*, Polycrystalline taenite, Butsura (H6). Scale bar, 20 μm. Clear taenite (white) bounds the grain and wholly or partly delimits six crystallites (γ) each with a martensitic, dark-etching centre.

distribution of magnesium between olivine and low-calcium pyroxene, and of calcium between low-calcium and calcium-rich pyroxenes, was established by crystal–liquid equilibria during the crystallization of chondrule liquids. Moreover, survival of polycrystalline taenite and/or of monoclinic or 'striated' low-calcium pyroxene in H5 and H6 (refs 13, 19) chondrites indicates fairly rapid cooling to about 700 °C, after which there could have been no prolonged reheating at higher temperatures. 'Metamorphism' in the strict sense apparently then played no part in determining the major textural features in the H-group chondrites. Rather, we favour a model of hot accretion during cooling at various rates; H3 chondrites were rapidly cooled whereas H6 meteorites cooled more slowly, which allowed crystallization and some solid-state diffusion to occur by a self-annealing process. Based on textural and mineralogical observations, Fredriksson (see ref. 20) has argued against metamorphism in ordinary chondrites. However, the meteorites chosen are brecciated and, we believe, from Fredriksson's evidence, metamorphism followed by further chondrule formation cannot be ruled out. Dodd[12] favoured 'progressive metamorphism' as the process responsible for the varying degrees of equilibration exhibited by the ordinary chondrites. Our new interpretation of the cooling history of the metal and our observations on the uniformity of the calcium contents of the low-calcium pyroxenes remove Dodd's main objections to a self-annealing ('autometamorphic') model for the thermal history of the H-group chondrites.

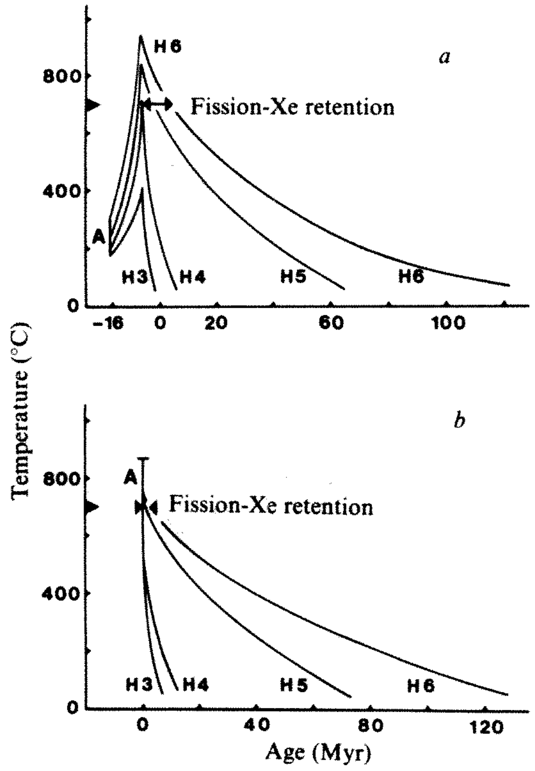

Fig. 4 Two schematic models of the cooling-history of H-group chondrites: *a*, metamorphic; *b*, self-annealing. 'A' indicates the approximate temperature of accretion. 'Fission-Xe retention' indicates the temperature at which half of the Pu-fission Xe is retained by phosphate during cooling; this temperature was attained by H4, H5 and H6 chondrites within 10 Myr (ref. 21). In both models zero time is set within this 10-Myr span. In the metamorphic model *a*, cold accretion may have taken place up to about 16 Myr before the final cooling through 700 °C. The time-limit is fixed by the content of iodine-correlated ^{129}Xe, which is released from specimens in the laboratory between 1,100 and 1,500 °C (refs 26, 27). Model *b*, inferred from the mineralogy, seems preferable because of its simplicity.

In Fig. 4 the generally accepted, progressive metamorphic model is compared with our preferred self-annealing model. The latter is favoured by the synchronous retention of plutonium-fission xenon, within 10 Myr, by H4, H5 and H6 chondrites; also in support are the revised plutonium-fission cooling rates[21] of H4, H5 and H6 chondrites. Furthermore, ^{39}Ar–^{40}Ar ages of H-group chondrites indicate that representatives of all petrological types began to retain radiogenic argon within a 60-Myr period from 4.51 to 4.45 Gyr ago, all ages being within experimental error of the mean[22]. Such synchronism seems less readily attainable if the history had been complex (that is, accretion at 200 °C followed by heating to metamorphic temperatures then slow cooling to gas retention temperature) rather than simple.

Support for the metamorphic hypothesis must now be based on the interpretation of the abundances of the volatile metals thallium, bismuth and indium. It has been argued that these elements were introduced into chondritic parent bodies as part of a low-temperature fraction which became mixed with a more abundant high-temperature fraction. Calculations based on the condensation of a gas of solar composition fix the temperature of accretion within a few tens of degrees of 200 °C (Fig. 4*a*) (ref. 23). However, the oxygen isotopic ratios favour 'condensation and accretion at high temperature'[24], and we have already argued that Tieschitz aggregated at higher temperature[11] and that an ambient gas was probably depleted in hydrogen relative to the solar composition. Uranium-lead systematics indicate that, at room temperature, chondrites become contaminated with lead from the terrestrial atmosphere[25]. We argue, therefore, that the H-group chondrites could have received their complement of volatile metals during cooling on a small, planetary body from ~700 °C, over 10^5–10^7 yr.

For either model of the thermal history our conclusions point unambiguously to a stratified parent body of the H-group chondrites. Slowly cooled, petrological type 6 material derives from greater depth than the near-surface location of type 3 which may have been within 20 m of the planetary surface[10]. As a corollary, this parent body could not have been externally heated after accretion of the H-group chondrite material.

We thank H. J. Axon for helpful discussion, and M. Christophe-Michel-Lévy and R. T. Dodd for helpful comments. Part of the work was supported by the NERC.

Received 24 June; accepted 26 August 1980.

1. Smith, B. A. & Goldstein, J. I. *Geochim. cosmochim. Acta* **41,** 1061 (1977).
2. Dodd, R. T. & Jarosewich, E. *Earth planet. Sci. Lett.* **44,** 335 (1979).
3. Fredriksson, K., Nelen, J. & Fredriksson, B. J. in *Origin and Distribution of the Elements* (ed. Ahrens, L. H.) 457–466 (Pergamon, Oxford, 1968).
4. Hutchison, R., Bevan, A. W. R., Easton, A. J. & Agrell, S. O. *Proc. R. Soc.* A (in the press).
5. Ashworth, J. R. *Proc. R. Soc.* A (in the press).
6. Van Schmus, W. R. & Wood, J. A. *Geochim. cosmochim. Acta* **31,** 747 (1967).
7. Dodd, R. T. *Contr. Miner. Petrol.* **31,** 201 (1971).
8. Dodd, R. T., Van Schmus, W. R. & Koffman, D. M. *Geochim. cosmochim. Acta* **31,** 921 (1967).
9. Wood, J. A. *Icarus* **6,** 1 (1967).
10. Bevan, A. W. R. & Axon, H. J. *Earth planet. Sci. Lett.* **47,** 353 (1980).
11. Hutchison, R., Bevan, A. W. R., Agrell, S. O. & Ashworth, J. R. *Nature* **280,** 116 (1979).
12. Dodd, R. T. *Geochim. cosmochim. Acta* **33,** 161 (1969).
13. Ashworth, J. R. *Earth planet. Sci. Lett.* **46,** 167 (1980).
14. Atkins, F. B. *J. Petrol.* **10,** 222 (1969).
15. Bunch, T. E. & Olsen, E. *Contr. Miner. Petrol.* **43,** 83 (1974).
16. Wells, P. R. A. *Contr. Miner. Petrol.* **62,** 129 (1977).
17. Onuma, N., Clayton, R. N. & Mayeda, T. K. *Geochim. cosmochim. Acta* **36,** 157 (1972).
18. Christophe-Michel-Lévy, M. *Earth planet. Sci. Lett.* **30,** 143 (1976).
19. Christophe-Michel-Lévy, M. *Bull. minér.* **102,** 410 (1979).
20. Fredriksson, K., Dube, A., Jarosewich, E., Nelen, J. A. & Noonan, A. F. *Smithson. Contr. Earth. Sci.* **14,** 41 (1975).
21. Pellas, P. & Storzer, D. *Proc. R. Soc.* A (in the press).
22. Turner, G., Enright, M. C. & Cadogan, P. H. *Proc. 9th Lunar planet. Sci. Conf.* **1,** 989 (1978).
23. Larimer, J. W. *Geochim. cosmochim. Acta* **37,** 1603 (1973).
24. Onuma, N., Clayton, R. N. & Mayeda, T. K. *Geochim. cosmochim. Acta* **38,** 189 (1974).
25. Unruh, D. M., Hutchison, R. & Tatsumoto, M. *Proc. 10th Lunar planet. Sci. Conf.* **1,** 1011 (1979).
26. Drozd, R. J. & Podosek, F. A. *Earth planet. Sci. Lett.* **31,** 15 (1976).
27. Jordan, J., Kirsten, T. & Richter, H. *Meteoritics* **13,** 506 (1978).

Measuring metamorphic history of unequilibrated ordinary chondrites

D. W. Sears & J. N. Grossman

Institute of Geophysics and Planetary Physics, University of California, Los Angeles, California 90024

C. L. Melcher[*] & L. M. Ross

McDonnell Center for the Space Sciences, Washington University, St Louis, Missouri 63130

A. A. Mills

Departments of Astronomy and Geology, University of Leicester, Leicester LE1 7RH, UK

A thermoluminescence sensitivity technique is used to give a new measurement of the degree of metamorphism of unequilibrated ordinary chondrites. Consequently the petrological assignment of these meteorites is modified.

THE wide range of textures in chondritic meteorites indicates a variety of metamorphic histories[1-4]. Most meteorites are metamorphosed and it is estimated that they have experienced maximum temperatures of around 1,200 °C (ref. 5). A few (described as type 3 in the scheme of Van Schmus and Wood[6]) have apparently experienced little or no metamorphic heating and their relatively unaltered state makes them interesting subjects for study[7]. We report here measurements which seem to enable the degree of metamorphism experienced by these unequilibrated ordinary chondrites to be quantified. Based on our findings, we propose a modification to the petrological type assignment of these meteorites.

We have used a thermoluminescence (TL) sensitivity technique, sensitivity being defined as the amount of TL induced in a sample by a standard radiation dose. Any previously accumulated TL is first drained by annealing the sample to ≥500 °C. The TL sensitivity, or TL per rad of absorbed radiation, is an intrinsic property of the luminescent mineral in the meteorite. It should not be confused with the level of natural TL, which is additionally governed by a complex interplay between the thermal and radiation environment of the meteorite.

This work was prompted by a study of H chondrites organized by Hutchison[29]. H chondrites are distinguished from the other ordinary chondrites (L and LL) on the basis of bulk chemistry, but the TL properties of the three ordinary chondrite classes are remarkably similar. This is presumably because TL is produced almost entirely by feldspar[12], which is present in the same proportions and has similar composition in each group[8]. When the results of our H-group study were available, it was decided to examine some type 3 meteorites. Most of the observed falls studied by Dodd *et al.*[9] were included (Table 1). Our measurements were made at the University of Leicester, UK[10] and at Washington University, St Louis[11]. Samples were lightly crushed and the metal and adhering sulphide removed with a hand-magnet. Three samples produced brown powders due to small quantities of terrestrial corrosion (Kernouvé, Butsura and Limerick). These were shaken for a few seconds in 10 M HCl to restore their normal grey colour, thus reducing an albedo effect which reduces TL[12]. The nonmagnetic portions of the chondrites were ground fine enough to pass through a 100-μm sieve and then heated to 500 °C to remove their natural TL. Leicester samples were given a test dose of 50 krad from a ^{60}Co γ source, whereas the St Louis samples were given a test dose of 25 krad with a ^{90}Sr β source. Samples of the Dhajala meteorite were run on both sets of apparatus and used for normalization to enable a comparison of data from the two laboratories. Using different test doses introduces a small error, but this is not thought to be significant in view of the large effects discovered. The TL sensitivity measurements are reproducible to within ±5%.

Results

Three plots of TL sensitivity against sample temperature ('glow curves') are shown in Fig. 1. These three curves demonstrate the range of shapes observed, although most meteorites produce glow curves which closely resemble those from Khohar. Variations in glow-curve shape are caused by the presence of several separate TL peaks whose relative contributions vary slightly. The shape variations seem unrelated to any of the factors considered here. We have also looked at the best method of extracting data from the curves; two possibilities are to measure the peak height or the area under the curve. We found no difference in the two approaches and present here the former. It also makes very little difference if the TL is measured at a given temperature rather than at the peak, as the glow curves are generally so similar and the effects discovered so large.

The thermoluminescence data are shown in Fig. 2 and listed in Table 1. The average TL sensitivity of the highly metamorphosed type 5 and 6 meteorites is appreciably higher than for the type 3 samples. Furthermore, the TL sensitivities range over a factor of ≤10 in samples of type 4–6 compared with a range of ~1,000 for type 3 chondrites.

A detailed examination of the accuracy of the TL sensitivity measurements for type 4–6 meteorites has been given else-

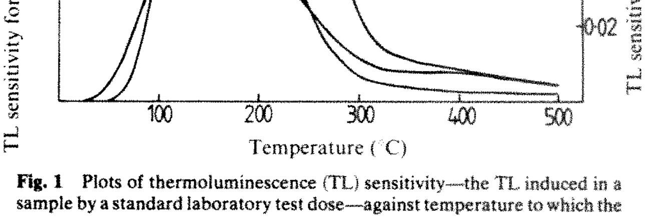

Fig. 1 Plots of thermoluminescence (TL) sensitivity—the TL induced in a sample by a standard laboratory test dose—against temperature to which the sample has been heated ('glow curves'). The TL is emitted mainly in a broad peak between 100 and 300 °C. Most chondrites studied here have glow-curve shapes resembling Khohar, but a few, like Manych and Ngawi, have shapes which differ in detail.

---

[*] Present address: W. K. Kellogg Radiation Laboratory 106-38, California Institute of Technology, Pasadena, California 91125.

0028-0836/80/440791—05$01.00

where[13]. The standard deviation in 10 different meteorites which were expected to have similar TL sensitivity was 21%. Type 3 meteorites are highly inhomogeneous and only small quantities were available for our measurements, so a second chip taken from a different location on the available sample was run. The root-mean-square deviation on the duplicate values is 48%. The error bars on Figs 3 and 4 are ±1 σ of the means.

Discussion

Several parameters for assessing the extent of equilibration in type 3 meteorites have been discussed, but none of them covers the range observed for TL sensitivity or is as free from ambiguity as TL (Fig. 3). The best indication of unequilibration available to Van Schmus and Wood[6] was the inhomogeneity of the silicates. This is expressed as the per cent mean deviation (PMD) shown by the fayalite content of the olivine or pyroxene. The olivine data of Dodd *et al.*[9] are compared with the TL data in Fig. 3*a*; the pyroxene data give a similar plot, but the range in pyroxene PMD is smaller. The inverse correlation indicates that as the meteorites equilibrate, TL sensitivity increases and the silicates become more homogeneous.

In an analogous way, the range of Co contents of the matrix kamacite becomes smaller as the meteorite becomes more equilibrated[7]; we have calculated the PMD of Co in the kamacite and added our own unpublished Tieschitz datum (Fig. 3*b*). Again, there is a clear negative relationship. Figure 3*c* compares our data with the percentage matrix recrystallization[14]. There is some uncertainty in this measurement because it is necessary to discriminate between chondrule fragments and other non-matrix components, but there is a trend in which TL sensitivity increases with the percentage of recrystallized matrix. Huss *et al.*[14] have shown that the FeO content of olivine in the matrix (normalized to the same parameter for the whole rock) decreases with equilibration. One possibility is that FeO is reduced out of the matrix and into the metal, consistent with the views of Wood[15] and Afiattalab and Wasson[7]. This parameter also shows an inverse correlation with TL sensitivity (Fig. 3*d*).

Changes in bulk chemistry can be related to metamorphism in ordinary chondrites, although the causes of these relationships

Table 1 Samples used in the present study, their TL sensitivity, and the laboratory at which the measurements were made

	Class†	Source and catalogue no.‡	Sample weight (g)	TL sensitivity (Dhajala = 1) Replicates	Mean	Lab. §
Kernouvé	H6	BM 43400	~0.100		25	L
Barwell	L5	BM 1965, 57	~0.100		16	L
Ambapur Nagla	H5	BM 81117	1.57		15	L
Appley Bridge	LL6	BM 1920, 40	3.86		14	L
Allegan	H5	BM 1920, 281	~0.100		8.6	L
Ogi	H6	BM 55256	~0.100		8.3	L
Jilin (Kirin)	H5	CAS	~0.100		7.7	L
Butsura	H6	BM 34795	0.69		7.5	L
Limerick	H5		~0.100		6.0	L
Quenggouk	H4	BM 33764	~0.100		6.0	L
Mangwendi	LL6	BM 1934, 839	0.450		6.0	L
Olivenza	LL5	BM 1925, 430	0.870		6.0	L
Beaver Creek	H4	BM 73646	0.995		2.6	L
Bremervörde	H3	BM 33910	0.880		2.6	L
Saratov	L4	BM 1956	~0.100		2.5	L
Monroe	H4	BM 25462	0.796		1.8	L
Dhajala	H3	PRL (T67)	0.30	1.0	1.0	L/SL
Mezö-Madaras	(L)3	HNM	0.030	1.3	0.9	SL
			0.037	0.96		
			0.027	0.82		
			0.031	0.51		
Hedjaz	(L)3	MHNP 2132	0.038	0.85	0.82	SL
			0.042	0.78		
Khohar	L3	ASU 623.1	0.032	0.30	0.44	SL
			0.039	0.58		
Parnallee	(LL)3	BM 34792	0.034	0.57	0.42	SL
			0.034	0.26		
Ngawi	(LL)3	USNM 2483(4)‖	0.029	0.16	0.25	SL
			0.025	0.34		
Tieschitz	H3/L*	BM 1975, M11		0.092		L
		NHMc 2140	0.038	0.20	0.23	SL
			0.039	0.23		
			0.034	0.27		
			0.035	0.22		
Chainpur	(LL)3	ASU 424.1(4)‖	0.032	0.061	0.078	SL
			0.058	0.078		
Sharps	H3	NHNM 640	0.039	0.044	0.071	SL
			0.032	0.098		
Manych	(L)3	AS 2331	0.032	0.061	0.070	SL
			0.058	0.078		
Bishunpur	(L)3/H*	ASU 618.8‖	0.030	0.0073	0.0054	SL
				0.0034		
Semarkona	(LL)3/H*	USNM 1805	0.032	0.0061	0.0045	SL
			0.036	0.0029		
Krymka	(L)3	AS 1707	0.032	0.0035	0.0027	SL
			0.053	0.0019		

† Ref. 6. The chemical classifications of type 3 chondrites are often uncertain. Those marked with an asterisk are based on Co content of kamacite (ref. 7, except our own unpublished value for Teischitz).

‡ BM, Dr R. Hutchison, British Museum (Natural History), London; PRL, Professor D. Lal, Physical Research Laboratory, Ahmedabad, Navrangpura, India; CAS, Drs Ouyang Ziyan and Lin Shunsheng, Chinese Academy of Sciences, Guiyang, China; AS, Academy of Sciences, USSR (through J. T. Wasson); ASU, Arizona State University, Tempe (through J. T. Wasson); HNM, Hungarian National Museum (through J. T. Wasson); NHM, Naturhistory Museum, Vienna (through J. T. Wasson); MHNP, Musée Histoire Naturelle, Paris (through J. T. Wasson);USNM and NHNM, Dr K. Fredriksson or Dr R. S. Clarke, Smithsonian Institution, Washington (through J. T. Wasson).

§ L, Leicester; SL, St Louis.

‖ Samples were powders taken from a larger reservoir of homogenized, nonmagnetic powder of unknown sample weight.

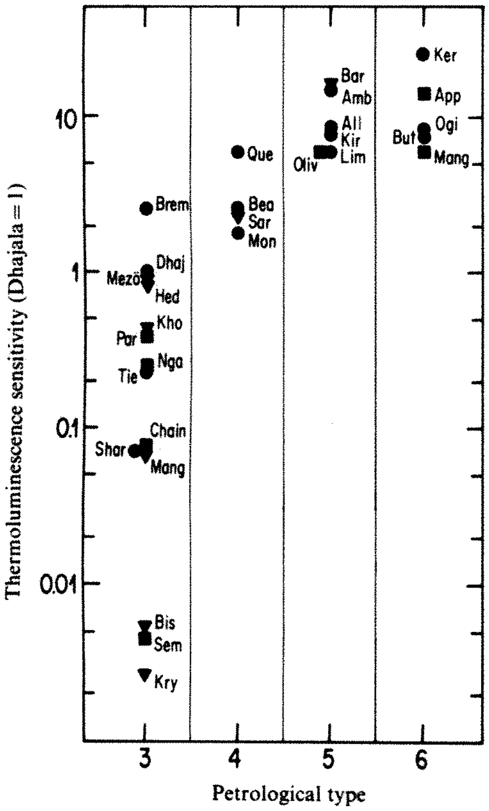

Fig. 2 Plot of TL sensitivity against petrological type for 29 meteorites, normalized to Dhajala. Note the much greater range displayed by type 3 compared with the other types. In this and Fig. 3, meteorites are identified by the first three letters of their names (see Table 1) or some simple variant. ■, LL chondrites; ▼, L chondrites; ●, H chondrites.

are debatable[4,16–18]. The carbon[6] and the primordial ^{36}Ar (ref. 19) contents of chondrites decrease with petrological type. These are compared with TL sensitivity in Fig. 4 (the sources of the ^{36}Ar and C data are given in the legend). These, too, display clear inverse relationships with TL sensitivity.

A relationship between TL sensitivity and petrological type was first suggested by Liener and Geiss[20], but their data fail to display such a relationship because only two of their 70 specimens are unequilibrated[12]. The relationship between TL sensitivity and petrological type is believed to be associated with changes in the crystalline structure of the phosphor, which in most ordinary chondrites is feldspar[21]. However, in unequilibrated ordinary chondrites, the feldspathic material is in the form of a glass[6]. Glasses are intrinsically poorer phosphors than crystalline substances of the same composition because the TL mechanism involves lattice defects or impurity ions in a crystal lattice[16]. The small TL sensitivity that glasses possess is probably due to localized areas of short-ranged order. The transition from glass to crystalline feldspar takes place in meteorites of type 3. In type 4, glass is generally absent, having been replaced by microcrystalline feldspar, although there may be occasional instances of turbid glass. In meteorites of type 5, glass is entirely absent and in type 6, the feldspar has grown to clear, coarse grains[6]. It seems reasonable, therefore, that TL sensitivity should be rather sensitive to the extent of equilibration in type 3 meteorites.

It has been proposed[22,23] that radiation damage will also cause changes in TL sensitivity. Evidence for this has long been sought[20,22,23], but the largest effects so far observed[24] are at most of the order of 25%. In fact, there is some evidence[12] that they may be zero for the TL emitted between 100 and 300 °C (Fig. 1).

The reheating and shock believed to have been suffered by the black chondrites causes a decrease in TL sensitivity comparable with the range observed here. The cause is similar to that responsible for the relationship between TL and petrological type; shock causes a vitrification of the feldspar[25]. The shock events required to affect TL are very large ($\gtrsim$250 kbar) and also cause loss of ^{40}Ar—reflected in K–Ar ages very much less than 4,600 Myr—and characteristic changes in the metallography. None of these meteorites are among those examined for shock effects by Heymann[24], although Wood[15] describes Manych as reheated and Huss *et al.*[14] mention shock effects in their descriptions of type 3 chondrites. Of the three meteorites with the lowest TL sensitivity in the present suite of specimens, ^{40}Ar data are available for two of them. Assuming a K content of 800 p.p.m., taking ^{40}Ar contents from ref. 26 and using the usual decay constants and other data, these meteorites have K–Ar ages of 4.060 Myr (Bishunpur) and 4,100 Myr (Krymka), where in each case the uncertainty is probably ±15%. It seems unlikely that these meteorites have had their TL appreciably lowered by a recent shock event of the magnitude responsible for the low TL sensitivities which have been observed in L chondrites[12]. However, we cannot rule out some complex relationship between very early shock and petrological type which also implicated TL.

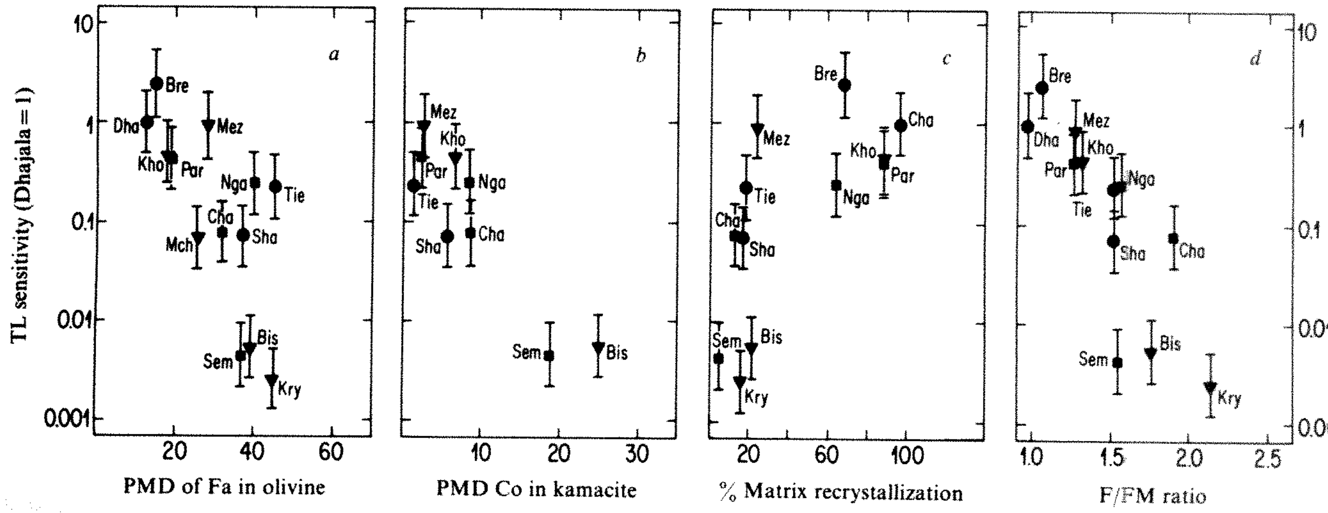

Fig. 3 Plots comparing the TL sensitivity of the type 3 meteorites studied here with literature data which attempt to measure the extent of metamorphic equilibration. *a*, Per cent mean deviation of the FeO content of the olivine[9]. *b*, Per cent mean deviation of the Co content of the kamacite (calculated from data in ref.7 with our own unpublished data for Tieschitz). These two parameters decrease during metamorphism as the silicate and metal compositions become more homogeneous. *c*, Per cent matrix recrystallization[14]. *d*, FeO/(FeO + MgO) in the matrix normalized to the same parameter for whole-rock[14]. This last parameter decreases with equilibration as FeO is apparently reduced out of the matrix. ■, LL chondrites; ▼, L chondrites; ●, H chondrites.

Table 2 Subdivision of petrological type 3

Type	Member*	TL sensitivity (Dhajala = 1)	PMD olivine†	PMD metal‡	Matrix recrystallization (%)§	F/FM ratio‖	C w/w%¶	^{36}Ar (10^{-8}cm^{3}STP g^{-1})#
3.9	*Clovis no. 1* *Prairie Dog Creek* *Carraweena* *Bremervörde*	2.2–4.6	5–15	<1.5	>60	<1.0	≤0.21	<4
3.8	Dhajala	1.0–2.2	15–20	1.5–2.5	>60	1.0–1.1	0.21–0.24	4–8
3.7	Mezö–Madaras Hedjaz	0.46–1.0	20–25	2.5–4.0	>60	1.1–1.2	0.24–0.27	8–13
3.6	Khohar Parnallee Ngawi Tieschitz	0.22–0.46	25–29	4.0–6.0	>60	1.2–1.3	0.27–0.30	13–18
3.5		0.10–0.22	29–33	6.0–8.0	~50	1.3–1.4	0.30–0.33	18–27
3.4	Chainpur Sharps Maynch	0.046–0.10	33–36	8.0–10	~20	1.4–1.5	0.33–0.38	27–35
3.3		0.22–0.046	36–38	10–13	10–20	1.5–1.6	0.38–0.43	35–45
3.2		0.010–0.022	38–40	13–17	10–20	1.6–1.7	0.43–0.50	45–55
3.1	Bishunpur	0.0046–0.0010	40–42	17–21	10–20	1.7-1.9	0.50–0.60	55–65
3.0	Semarkona Krymka	<0.0046	>42	>21	<10	>1.9	≥0.60	≥65

* Meteorites in italics were not examined by TL and their present assignment is tentative being based entirely on literature data.
† % mean deviation of fayalite in olivine[9].
‡ % mean deviation of Co in kamacite[7].
§ Ref. 14.
‖ FeO/(FeO + MgO) in the matrix normalized to the same quantity for the whole-rock[14].
¶ Ref. 27.
# Ref. 26.

Subdivision of petrological type 3

In many respects, and especially in their TL properties, the unequilibrated ordinary chondrites display a more excessive behaviour than shown by any other petrological type. For instance, Bishunpur bears as little similarity to Dhajala, another type 3, as Dhajala does to Kernouvé, a type 6 chondrite. To emphasize this point, we believe that some subdivision of petrological type 3 is desirable. There is no doubt that the metamorphism experienced by type 3 chondrites is gradational and shows no hiatuses. This is reflected in most of the data in Figs 2–4. (The only exception seems to be a possible discontinuity in matrix recrystallization.) This is also true of the more equilibrated meteorites. The sharpness of chondrule outlines and an olivine PMD of 5 are examples of parameters used to define higher petrological type boundaries (5–6 and 3–4 respectively), but neither is a sharp, single-temperature effect and both reflect gradational proceses. The lack of hiatuses in the equilibration parameters for type 3 chondrites, such as TL sensitivity, is not an argument against subdivision.

Afiattalab and Wasson have already proposed subdivision on the basis of metal homogeneity; they divided their nine unequilibrated ordinary chondrites into: four with 'high'; two with 'moderate'; and three with 'low' metal uniformity[7]. Huss *et al.* have proposed subdivision into four categories which they described with Roman numerals[14]. The utility of any subdivision scheme is governed not only by its necessity but also by its simplicity and consistency with existing schemes. Ideally, any subdivision should merge into existing schemes so naturally that it is largely self-explanatory. Terms like 'highly', 'moderate' and 'somewhat' unequilibrated are cumbersome; they cannot always be neatly incorporated into graphs or tables. Letter abbreviations, such as L3h, L3m and L3l, are confusing because current practice is to use letters for chemical class and numbers for petrological types. The simplest approach is to modify the present system by using decimal numbers. We propose that type 3 be considered to consist of 10 subdivisions going from type 3.0 to type 3.9. It might be logical to go from 2.5 to 3.4, so that the numbers round off to 3, but we believe our proposed range will be more popular.

Table 2 summarizes our proposed subdivision scheme for type 3 ordinary chondrites, based on the trends observed in Figs 3 and 4. Three of the subdivisions are unpopulated at present, but we see no obvious reason why these will not eventually be filled. One subdivision contains members which we have not examined, but literature data (mainly PMD olivine) suggest that they should be assigned to petrological type 3.9. They were included for the sake of completeness because they are more equilibrated type 3 members than those examined here. It is possible to assign a petrological subtype on the basis of each of the parameters in Table 2, and such assingments are generally in very good agreement with the TL sensitivity assignment. (We have arbitrarily chosen the upper value where data fall on the boundary between subtypes.) In general, most petrological subtype assignments are within ±0.1 of those listed in Table 2, and this is the uncertainty we would assign to the petrological

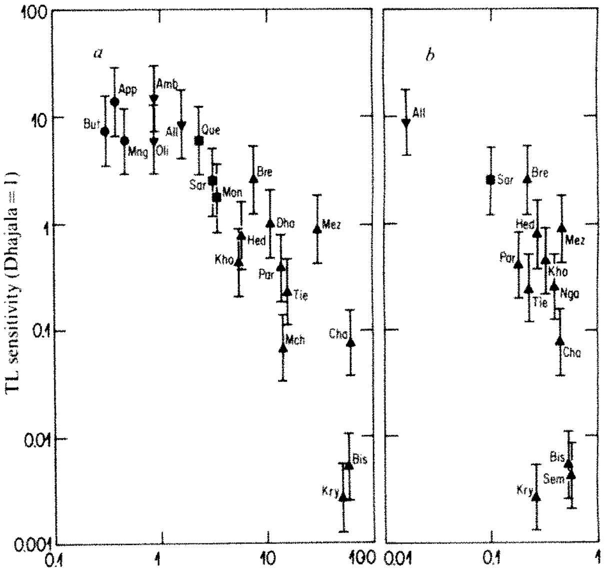

Fig. 4 Two bulk chemical parameters which are known to decrease with increasing equilibration during metamorphism, compared with TL sensitivity; *a*, primordial ^{36}Ar content, calculated from data in ref. 26 and unpublished supplements, assuming primordial ^{36}Ar/^{38}Ar = 5.6 and spallogenic ^{36}Ar/^{38}Ar = 0.65 (ref. 28); and *b*, carbon content. As with TL, the range of primordial ^{36}Ar and C contents is much greater in meteorites of type 3 than any other type. Types: ▲, 3; ■, 4; ▼, 5; ●, 6.

subtype of a given meteorite. There are only three meteorites for which the literature data assignments differ systematically from the TL assignment; the Mezö-Madaras subtype could be decreased by 0.1, the Parnallee value increased by 0.1 and the Semarkona value increased by 0.2. Clearly there would be no problem in assigning a petrological subtype in the absence of TL data, provided there were other good quality data available.

We thank the donors of meteorites listed in Table 1 and John Wasson for many discussions and encouragement; also Drs J. A. Wood, R. T. Dodd, and W. R. Van Schmus for advice, and Joanna Pai and Clare Marshall for technical assistance. This research is supported by NASA grant NGR 05-007-329 (at UCLA) and NSF grant EAR78-22440 (at Washington University).

Received 23 June; accepted 19 September 1980.

1. Wood, J. A. *Geochim. cosmochim. Acta* **26,** 739–749 (1962).
2. Dodd, R. T. & Van Schmus, R. *J. geophys. Res.* **70,** 3801–3811 (1965).
3. Van Schmus, R. *Earth Sci. Rev.* **5,** 145–184 (1969).
4. Dodd, R. T. *Geochim. cosmochim. Acta* **33,** 161–203 (1969).
5. Wasson, J. T. *Rev. Geophys. Space Phys.* **10,** 711–759 (1972).
6. Van Schmus, W. R. & Wood, J. A. *Geochim. cosmochim. Acta* **31,** 747–765 (1967).
7. Afiattalab, F. & Wasson, J. T. *Geochim. cosmochim. Acta* **44,** 431–446 (1980).
8. Van Schmus, W. R. & Ribbe, R. H. *Geochim. cosmochim. Acta* **32,** 1327–1342 (1968).
9. Dodd, R. T., Van Schmus, W. R. & Koffman, D. M. *Geochim. cosmochim. Acta* **31,** 921–951 (1967).
10. Mills, A. A., Sears, D. W. & Hearsey, R. *J. Phys* (*E*): *Sci. Instrum.* **10,** 51–56 (1977).
11. Melcher, C. L. (in preparation).
12. Sears, D. W. *Icarus* (in the press).
13. Sears D. W. *Meteoritics* **13,** 628–632 (1978).
14. Huss, G. R., Keil, K. & Taylor, G. J. *Geochim. cosmochim. Acta* (in the press); *Meteoritics* **13,** 495–497 (1978).
15. Wood, J. A. *Icarus* **6,** 1–49 (1967).
16. Garlick, G. F. J. *Luminescent Materials* (Clarendon, Oxford, 1970).
17. Larimer, J. W. & Anders, E. *Geochim. cosmochim. Acta* **31,** 1239–1270 (1967).
18. Laul, J. C., Ganapathy, R., Anders, E. & Morgan, J. W. *Geochim. cosmochim. Acta* **37,** 329–357 (1967).
19. Zähringer, J. *Geochim. cosmochim. Acta* **32,** 209–237 (1968).
20. Liener, A. & Geiss, J. in *Thermoluminescence of Geological Materials* (ed. McDougall, D. J.) (Academic, London, New York, 1968).
21. Lalou, C., Nordemann, D. & Labyrie, J. *C. r. hebd. Séanc. Acad. Sci., Paris* D **270,** 2104–2401 (1970).
22. Vaz, J. E. & Sears, D. W. *Meteoritics* **12,** 47–60 (1977).
23. Houtermans, F. G. & Liener, A. *J. geophys. Res.* **71,** 3387–3396 (1965).
24. Heymann, D. *Icarus* **6,** 189–221 (1967).
25. Binns, R. A. *Nature* **213,** 1111–1112 (1967).
26. Schultz, L. & Kruse, H. *Nucl. Track Det.* **2,** 65–103 (1976).
27. Moore, C. B. & Lewis, C. *J. geophys. Res.* **72,** 6289–6292.
28. Schultz, L. & Signer, P. *Earth planet. Sci. Lett.* **36,** 363–371 (1977).
29. Hutchison, R. *et al. Nature* **287,** 787–790 (1980).

Mutations affecting segment number and polarity in *Drosophila*

Christiane Nüsslein-Volhard & Eric Wieschaus

European Molecular Biology Laboratory, PO Box 10.2209, 69 Heidelberg, FRG

In systematic searches for embryonic lethal mutants of Drosophila melanogaster *we have identified 15 loci which when mutated alter the segmental pattern of the larva. These loci probably represent the majority of such genes in* Drosophila. *The phenotypes of the mutant embryos indicate that the process of segmentation involves at least three levels of spatial organization: the entire egg as developmental unit, a repeat unit with the length of two segments, and the individual segment.*

THE construction of complex form from similar repeating units is a basic feature of spatial organisation in all higher animals. Very little is known for any organism about the genes involved in this process. In *Drosophila*, the metameric nature of the pattern is most obvious in the thoracic and abdominal segments of the larval epidermis and we are attempting to identify all loci required for the establishment of this pattern. The identification of these genes and the description of their phenotypes should lead to a better understanding of the general mechanisms responsible for the formation of metameric patterns.

In *Drosophila*, the anlagen for the individual segments arise as equally sized subdivisions of the blastoderm, each segment represented by a transverse strip of about three or four cell diameters[1]. A cell lineage restriction between neighbouring segments is established at or soon after this stage[2]. Two basic types of mutation have been described which change the segmental pattern of the *Drosophila* larva. Maternal effect mutations like *bicaudal* lead to a global alteration of the embryonic pattern[3]. Bicaudal embryos develop two posterior ends arranged in mirror-image symmetry, and lack head, thorax and anterior abdomen. The *bicaudal* phenotype suggests that the initial spatial organisation of the egg established during oogenesis involves a morphogen gradient that defines antero-posterior coordinates in early embryonic pattern formation[3,4]. The subdivision of the embryo into segments is thought to occur by a differential response of the zygotic genome to the maternal gradient. Homeotic mutations (for example, *bithorax*[5,6]) seem to be involved in a final step of this response process. These mutations change the identity of individual segments; for example, *Ultrabithorax* transforms the metathoracic and first abdominal segments into mesothoracic segments. However, the homeotic loci do not affect the total number, size or polarity of the segments, nor do they point to any other step which might intervene between the maternal gradient and the final pattern of segments.

We have undertaken a systematic search for mutations that affect the segmental pattern depending on the zygotic genome. We describe here mutations at 15 loci which show one of three novel types of pattern alteration: pattern duplication in each segment (segment polarity mutants; six loci), pattern deletion in alternating segments (pair-rule mutants; six loci) and deletion of a group of adjacent segments (gap mutants; three loci) (Table 1, Fig. 1).

The segmental pattern of the normal *Drosophila* larva

Figure 2 shows the cuticular pattern of a normal *Drosophila* larva shortly after hatching. The larval body is comprised of three thoracic and eight abdominal segments. Although differences are observed in different body regions, all segments have certain morphological features in common. The anterior of each segment is marked with a band of denticles, most of which point posteriorly. The posterior part of each segment is naked. The segment borders run along the anterior margins of the denticle bands[7], they have no special morphological features. The polarity of the pattern is indicated by the orientation of the denticles and, in the abdomen, by the shape of the bands (Fig. 3). In the thoracic segments the bands are narrow with fine denticles whereas those in the abdominal segments are broader and comprised of thick pigmented denticles (for a detailed description of the cuticular pattern see ref. 1).

0028-0836/80/440795—07$01.00

Segment polarity mutants: deletions in each segment

Mutants in this class have the normal number of segments. However, in each segment a defined fraction of the normal pattern is deleted and the remainder is present as a mirror-image duplication. The duplicated part is posterior to the 'normal' part and has reversed polarity (Figs 1–3).

Six such loci have been identified. Three loci, *fused*[8], *wingless* (ref. 9 and G. Struhl, personal communication) and *cubitus interruptus*^{D}, were previously known whereas *gooseberry*, *hedgehog* and *patch* are new (Table 1). All the mutations in this class are zygotic lethals and the phenotypes are only produced in homozygous embryos. One of the loci, *fused*, also shows a maternal effect in that a wild-type allele in the mother is sufficient to rescue the mutant phenotype of the homozygous embryos.

In all mutants except *patch* the region deleted includes the naked posterior part of the pattern and the duplication involves a substantial fraction of the anterior denticle band. In mutant larvae, the ventral side of each segment is almost entirely covered with denticles, the posterior fraction of which point anteriorly. The segment identity seems to be normal, the denticles of the abdominal segments being large and pigmented whereas those of the thorax are short and pale (Figs 1, 2). The anterior margin of the region duplicated in these mutants coincides with the segment boundary in only two cases, *fused* and *gooseberry* (Fig. 3). In *wingless* and *hedgehog* it lies posterior to the boundary, such that these larvae apparently lack all segment boundaries.

The phenotype of embryos homozygous for *patch* contrasts with that produced by the five loci described above in that the duplicated region includes some naked cuticle anterior to each denticle band. The duplicated unit thus involves structures of two adjacent segments. *Patch* larvae, despite the normal number of denticle bands, have twice the normal number of segment boundaries (Figs 1, 3).

Despite these differences, the common feature of all mutants in this class is that a defined fraction of the pattern in each segment is deleted. This deletion is associated with a mirror image duplication of the remaining part of the pattern. We suggest that these loci are involved in the specification of the basic pattern of the segmental units.

Pair-rule mutants: deletions in alternating segments

In mutants of this class homologous parts of the pattern are deleted in every other segment. Each of the six loci is characterized by its own specific pattern of deletions (Table 1, Figs 1, 4). For example, in *even-skipped* larvae, the denticle bands and adjacent naked cuticle of the pro- and metathoracic, and the 2nd, 4th, 6th and 8th abdominal segments are lacking. This results in larvae with half the normal number of denticle bands separated by enlarged regions of naked cuticle (Figs 1, 4). In *paired* larvae the apparent reduction in segment number results

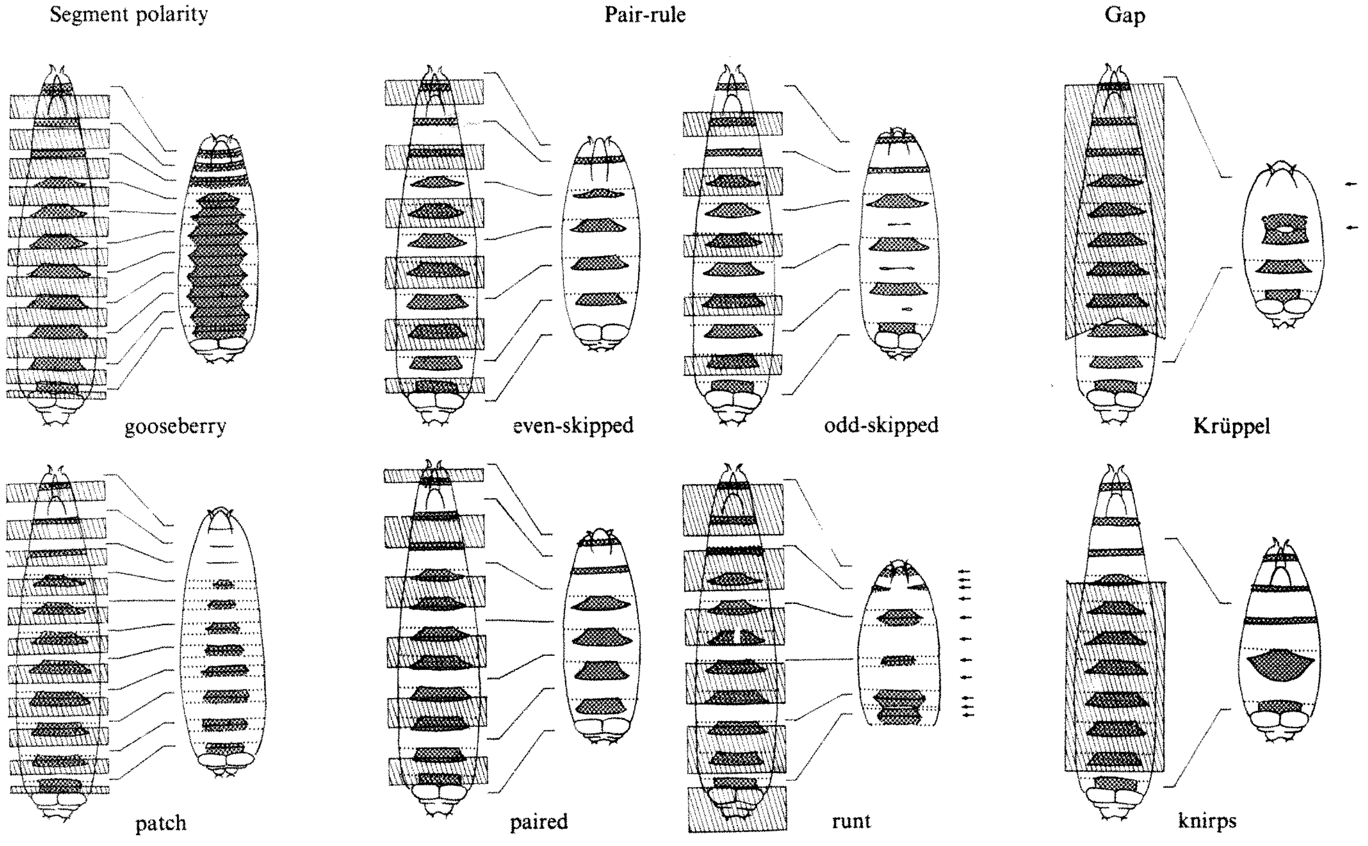

Fig. 1 Semi-schematic drawings indicating the regions deleted from the normal pattern in mutant larvae. Dotted regions indicate denticle bands, dotted lines the segmental boundaries. The regions missing in mutant larvae are indicated by the hatched bars. The transverse lines connect corresponding regions in mutant and normal larvae. Planes of polarity reversal in *runt* and *Krüppel* are indicated by the arrows. The two segment polarity loci *patch* and *gooseberry* are represented at the left. For indication of the polarity of the patterns, see Fig. 3. The patterns of *fused* and *ci*^{D} (not shown) look similar to the *gooseberry* pattern, whereas in *hedgehog* and *wingless* the deleted regions are somewhat larger, cutting into the denticle bands at either side. Four pair-rule mutants are shown in the centre. The interpretation of their phenotypes is based on the study of weak as well as strong alleles, combinations with *Ubx* (see text) and, in the case of *runt*, on gynandromorphs (unpublished). They probably represent the extreme mutant condition at the respective loci. The phenotypes of all known *barrel* and *engrailed* alleles (not shown) are somewhat variable and further studies are needed to deduce the typical phenotype. At the right, the two gap loci *Krüppel* and *knirps* are shown. Both patterns represent the amorphic phenotype as observed in embryos homozygous for deficiencies of the respective loci. The only known *hunchback* allele (not shown) deletes the meso- and metathorax.

COLLEGE Upper Circular Rd CALCUTTA

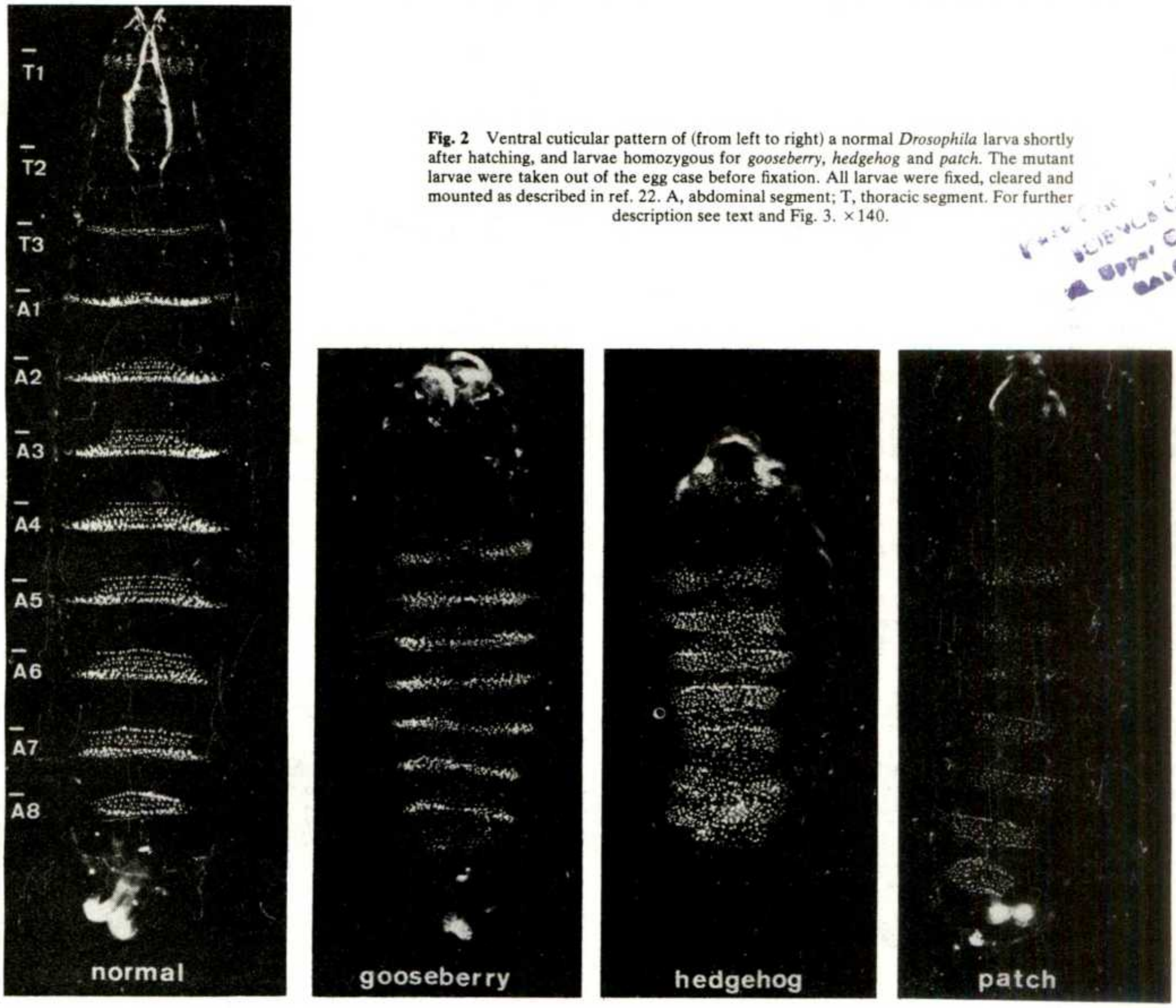

Fig. 2 Ventral cuticular pattern of (from left to right) a normal *Drosophila* larva shortly after hatching, and larvae homozygous for *gooseberry*, *hedgehog* and *patch*. The mutant larvae were taken out of the egg case before fixation. All larvae were fixed, cleared and mounted as described in ref. 22. A, abdominal segment; T, thoracic segment. For further description see text and Fig. 3. ×140.

essentially from the deletion of the naked posterior part of the odd-numbered and the anterior denticle bands of the even-numbered segments (Figs 1, 4). The double segments thus formed are composites of anterior mesothorax- and posterior metathorax, anterior first abdominal and posterior second abdominal segment, etc. The identification of the regions present or deleted in mutant larvae is based on the phenotypes produced by alleles with lower expressivity. In such embryos the deletions are in general smaller and variable in size. In a 'leaky' allele of *even-skipped*, the denticle bands of the even-numbered segments are frequently incomplete, whereas in *paired*^{2} (*prd*^{2}) the pattern deletions often involve only part of the naked cuticle of the odd-numbered segments, leading to a pairwise fusion of denticle bands (Fig. 4).

Further support for the composite nature of the segments in *prd* larvae was obtained in combinations with *Ultrabithorax* (*Ubx*), a homeotic mutation which when homozygous causes the transformation of the first abdominal segment into mesothorax[5]. In such *prd*; *Ubx* larvae, only the *denticle band* of the first double segment in the abdomen is transformed. The posterior margin of this band and the naked cuticle which follows remain abdominal in character and lack, for example, the typical mesothoracic sense organs. The composite nature of the segments in *paired* shows that the establishment of segmental identity does not require the establishment of individual segments as such.

The segmentation pattern in *prd*; *Ubx* larvae is typical of that of *paired* alone and is not affected by the *Ubx* homeotic transformation. Similarly, in *prd*;*Polycomb* larvae the naked cuticle of alternating segments is deleted just as it is in *paired* alone, even though in *Polycomb* embryos all the thoracic and abdominal segments have an 8th abdominal character[5]. These combinations, and similar ones with *even-skipped*, indicate that the observed grouping of segments in pairs depends on the position of segments within the segmental array rather than the segmental identity. These combinations thus provide evidence that mutations such as *paired* and *even-skipped* affect different processes from those altered in homeotic mutants.

Other mutants in this class show different deletion patterns. The phenotype of *odd-skipped* is similar to that of *even-skipped*. However, in this case it is the odd-numbered denticle bands that are affected. In *odd-skipped*, the deleted region is smaller and is restricted to a more posterior part of the segment than in *even-skipped* (Figs 1, 4). *Barrel* has a phenotype similar to *paired* although the pattern is often less regular (Fig. 4). *Runt*, on the X chromosome, is the only pair-rule mutant showing mirror-image duplications. *Runt* embryos have half the normal number of denticle bands, each a mirror-image duplication of the anterior part of a normal band (similar to the duplications found in *patch*). The bands in *runt* embryos, as well as the region of naked cuticle separating them, are of unequal sizes (Figs 1, 4).

To the list of pair-rule loci we have added the *engrailed*[10] locus. Lethal *engrailed* alleles[11] lead to a substantial deletion of the posterior region of even-numbered segments. In addition, the anterior margin and adjacent cuticle of each segment are affected. Thus, the defect pattern in *engrailed* shows repeats which are spaced at both one- and two-segment intervals.

Each of the six different pair-rule loci affects a different region within a double segmental repeat. In no case does the margin of the deleted region coincide with a segment boundary. When the deleted region corresponds in size up to one entire segment (*paired*, *even-skipped*) it includes parts of two adjacent segments.

The phenotypes of the pair-rule mutants suggest that at some stage during normal development the embryo is organized in repeating units, the length of which corresponds to two segmental anlagen.

Gap mutants: one continuous stretch of segments deleted

One of the striking features of the mutations of the first two classes is that the alteration in the pattern is repeated at specific intervals along the antero-posterior axis of the embryo. No such repeated pattern is found in mutants of the third class and instead a single group of up to eight adjacent segments is deleted from the final pattern. Three loci have been identified which cause such gaps in the pattern (Table 1, Figs 1, 5). *Krüppel* (*Kr*) was originally described by Gloor[12]. Embryos homozygous for *Kr* lack thorax and anterior abdomen. The posterior-terminal region with the abdominal segments 8, 7 and 6 is normal, although probably somewhat enlarged. Anterior to the 6th abdominal segment is a plane of mirror–image symmetry followed by one further segment band with the character of a 6th segment oriented in reversed polarity. The exact position of the plane of symmetry varies and does not usually coincide with a segmental boundary. A large part of the *Krüppel* pattern is reminiscent of the pattern observed in embryos produced by the maternal-effect mutant *bicaudal*, although no maternal component is involved in the production of the *Krüppel* phenotype (in preparation).

Table 1 Loci affecting segmentation in *Drosophila*

Class	Locus	Map position*	No. of alleles†	Ref.
Segment-polarity	*cubitus interruptus*^{D} (ci^D)	4-0	(2)	20
	wingless (*wg*)	2-30	6	9
	gooseberry (*gsb*)	2-104	1	This work
	hedgehog (*hh*)	3-90	2	This work
	fused (*fu*)‡	1-59.5	(9)	8, 20
	patch (*pat*)	2–55	8	This work
Pair-rule	*paired* (*prd*)	2-45	3	This work
	even-skipped (*eve*)	2-55	2	This work
	odd-skipped (*odd*)	2-8	2	This work
	barrel (*brr*)	3-27	2	This work
	runt (*run*)	1-65	1	This work
	engrailed (*en*)	2-62	6	11, 20
Gap	*Krüppel* (*Kr*)	2-107.6	6	12, 20
	knirps (*kni*)	3-47	5	This work
	hunchback (*hb*)	3-48	1	This work

* For the new loci (see last column) the map positions are based on recombination between the markers *S*, *Sp*, *Bl*, *cn*, *bw* for the second chromosome, and *ru*, *h*, *th*, *st*, *cu*, *sr*, e^S, *ca* for the third chromosome. For description of markers see ref. 20. The loci *runt*, *Krüppel* and *knirps* were further mapped using the breakpoints of deficiencies and duplications for the respective regions. All mutants were mapped by scoring the embryonic progeny of single recombinant males backcrossed to heterozygous females from the original mutant stocks.

† The numbers in parentheses refer to the alleles listed in Lindsley and Grell[20]. All other alleles, except the *runt* allele, three *Kr* alleles and one *knirps* allele, were isolated in a screen for embryonic lethal mutants on the second chromosome. 5,800 balanced stocks were established from individual males heterozygous for an ethyl methane sulphonate-treated *cn bw sp* chromosome using the DTS-procedure suggested by Wright[21]. 4,500 of the stocks had one or more new lethal mutations. Unhatched embryos from 2,600 putative embryonic lethal stocks were inspected for cuticular abnormalities[22]. Third chromosomal mutants discovered in the second chromosomal balanced lines were recovered after selection through individual females by balancing individual third chromosomes over TM3. Complementation tests were carried out between mutants with similar phenotypes whereby the occurrence of mutant embryos among the progeny of the crosses served as the criterion for allelism. Three new *Kr* alleles were isolated in a screen for lethals over the original *Kr* of Gloor[12], and one *knirps* allele of presumably spontaneous origin was discovered on a TM1 chromosome. The *runt* allele was isolated in a screen for X-linked lethals.

‡ *fused* is a male-rescuable maternal-effect locus[8]. Thus, the segment polarity reversal is observed in *fu*/*fu* embryos from *fu*/*fu* mothers. The progeny of *fu*/+ females show a normal embryonic pattern regardless of embryonic genotype.

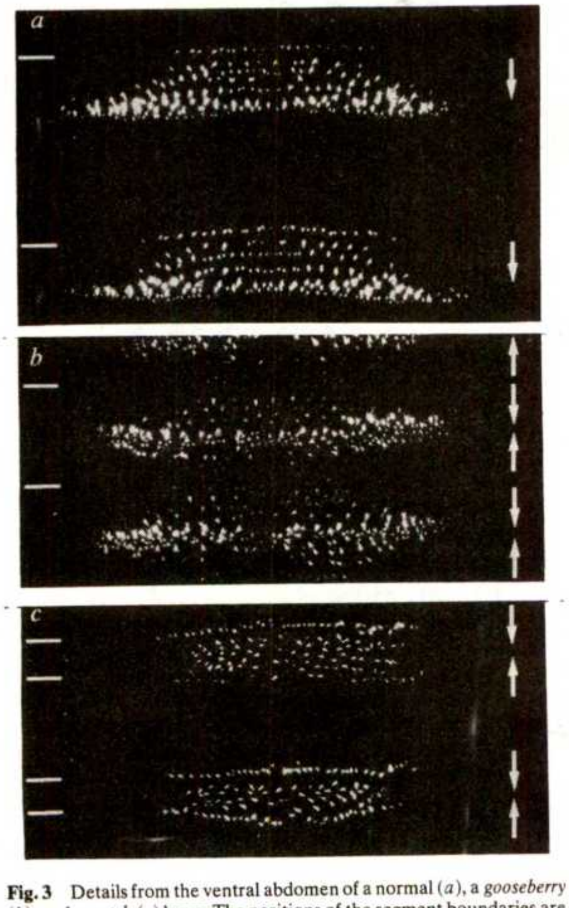

Fig. 3 Details from the ventral abdomen of a normal (*a*), a *gooseberry* (*b*), and a *patch* (*c*) larva. The positions of the segment boundaries are indicated at the left by the transverse lines. The arrows at the right indicate the polarity of the pattern as judged by the orientation of the denticles as well as the shape of the denticle bands.

In the other two loci of this class, the gap in the pattern occurs in specific morphologically defined subregions of the larval pattern, in the thorax and in the abdomen, respectively. In *hunchback*, the meso- and metathoracic segments are deleted. In embryos homozygous for *knirps*, only two rather than eight denticle bands are formed in the abdomen. The posterior-terminal region including the 8th abdominal segment seems normal whereas the anterior abdominal denticle band is considerably enlarged. The anterior margin of the denticle band is morphologically similar to the first abdominal segment but combinations with *Ubx* show that the band is a composite with more than one segmental identity.

All three loci are required for a normal segmental subdivision of one continuous body region. The lack of a repeated pattern of defects suggests that the loci are involved in processes in which position along the antero-posterior axis of the embryo is defined by unique values.

When are genes affecting segment number active?

The phenotypes described above are observed only in homozygous embryos, indicating that the loci identified by these mutations are active after fertilization and are crucial for the normal segmental organisation of the embryo. We have described the mutations in terms of their effect on the differentiated pattern. However, in many instances their effect can be observed much earlier in development. In normal embryos segmentation is first visible 1 h after the onset of gastrulation as a repeated pattern of

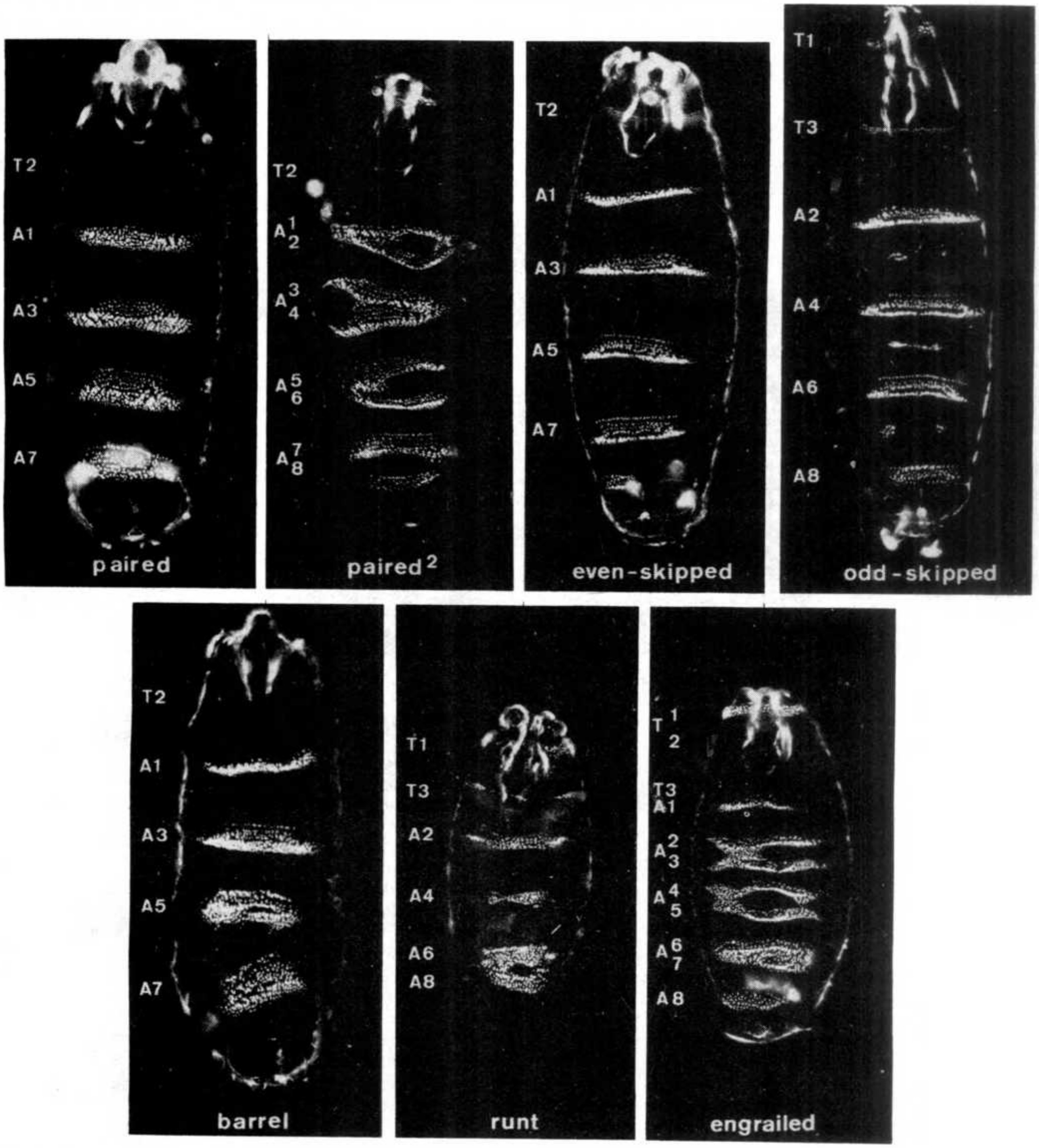

Fig. 4 Larvae homozygous for mutations at the six pair-rule loci. The segmental identity of the denticle bands is indicated at the left of each picture. A, abdominal band; T, thoracic band. For comparison with the normal pattern see Figs 1 and 2.

bulges in the ventral ectoderm (unpublished observations). In *paired* and *even-skipped* embryos the number of bulges is reduced and corresponds to the number of segments observed in the differentiated mutant embryos. *Krüppel*, *runt* and *knirps* embryos can be identified 15 min after the onset of gastrulation. All three mutations cause shorter germ bands, a phenomenon clearly related to the strong reduction in segment number observed in the differentiated larvae. Further evidence for an early activity at the *paired* locus was obtained using a temperature-sensitive allele. The extreme phenotype is only obtained when the embryo is kept at the restrictive temperature during the blastoderm stage. All these results indicate that the wild-type genes defined by the mutations are active before the end of gastrulation during normal development.

Discussion

Segmentation in *Drosophila* proceeds by the transition from a single field into a repeated pattern of homologous smaller subfields. Mutant alleles at the 15 loci we have described interfere with this process at various points. Although each locus has its own distinct phenotype, we were able to distribute the mutations in three classes. In one class only a single large subregion of the embryo is affected, whereas in mutants of the other two classes a reiteration of defects is produced with a

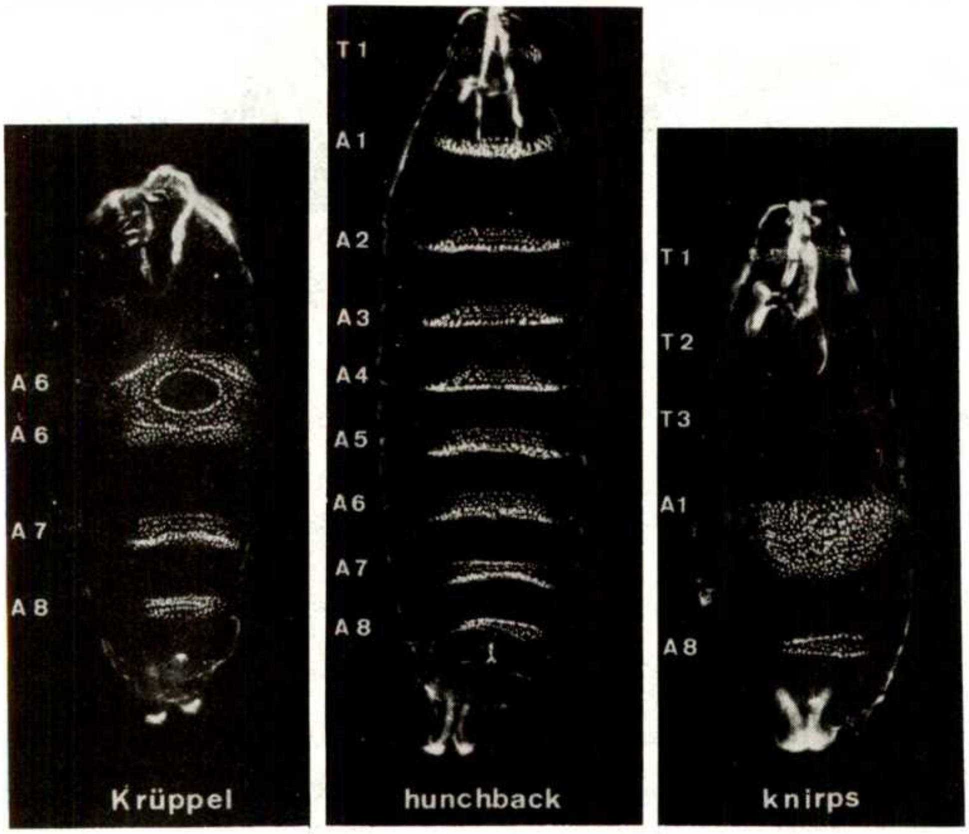

Fig. 5 Larvae homozygous for mutations at the three gap loci. A, abdominal segment; T, thoracic segment.

repeat length of one or two segments, respectively. This suggests that the process of segmentation involves three different units of spatial organization.

The organization of the egg is thought to be controlled by a monotonic gradient set up during oogenesis under the control of the maternal genome[3,4]. All the mutants we have described depend on the embryonic rather than the maternal genome. None of them alters the overall polarity of the embryo, the head always being at the anterior and the telson at the posterior end of the egg. The most dramatic alterations of the pattern are produced in the gap mutants and involve one large subregion of the egg. *Hunchback* and *knirps* affect the development of thorax and abdomen, respectively, and might be involved in the establishment of these large morphologically unique subregions of the embryo. The large mirror-image duplications found in the posterior pattern of *Krüppel* embryos are similar to those of *bicaudal*. The *bicaudal* phenotype has been interpreted as resulting from an instability in the maternal gradient[3,13], and thus *Krüppel* might be involved in the maintenance of elaboration of this gradient in the posterior egg region after fertilization.

The smallest repeat unit, the individual segment, is affected in mutants at the six segment-polarity loci. The pattern alteration consists of a mirror-image duplication of part of the normal pattern with the remainder deleted. In these mutants the deleted region corresponds in size to more than half a segment. Mutations causing smaller deletions in the segmental pattern do not lead to polarity reversals (unpublished observations). The mirror-image duplications produced by the pair-rule mutation *runt* are also associated with a deletion of more than half a repeat unit, that is, more than one segment. The tendency of partial fields containing less than half the positional values to duplicate is well described for imaginal disks in *Drosophila*[14], as well as for the larval epidermis in other insects[15,16]. On the other hand, the same types of pattern duplication are also produced in conditions which do not involve cell death and regeneration, but rather a reorganization of the positional information in the entire field[3,17]. More detailed studies of early development in mutant embryos may reveal which mechanism is responsible for the different mutant phenotypes.

Given the evidence for a homology between segments, the existence of a class of mutants affecting corresponding regions in each individual segment is perhaps not surprising. The discovery of a mutant class affecting corresponding regions in every other segment was not expected and suggests the existence at some time during development of homologous units with the size of two segmental anlagen. It is possible that the double segmental unit corresponds to transitory double segmental fields which are established early during embryogenesis and are later subdivided into individual segments. At the blastoderm stage the epidermal primordium giving rise to thorax and abdomen is only about 40 cells long[1]. An initial subdivision into double segments would avoid problems of accuracy encountered in a simultaneous establishment of segment boundaries every three to four cells. A stepwise establishment of segments implies that the borders defining double segments be made before the intervening ones. The mutant phenotypes do not definitely show which, if any, of the segment borders define a primary double segmental division in normal development. The mutant phenotypes which come closest to a pattern one would expect if the transition from the double segment to the individual segment stage were blocked are the patterns of *paired* and *even-skipped*. Both suggest the frame meso- and methathorax, 1st and 2nd, 3rd and 4th abdominal segment, etc.

It is also possible that the double segmental units are never defined by distinct borders in normal development. The existence of a double segmental homology unit may merely reflect a continuous property such as a wave with a double segmental period responsible for correct spacing of segmental boundaries (see, for example, refs 18, 19). We have not found any mutations showing a repeat unit larger than two segments. This may indicate that the subdivision of the blastoderm proceeds directly by the double segmental repeat with no larger intervening homology units. However, the failure to identify such larger units may reflect the incompleteness of our data.

Drosophila has been estimated to have about 5,000 genes and only a very small fraction of these when mutated result in a change of the segmental pattern of the larva. Some of the loci described here were known previously but only in the case of *Krüppel* has the embryonic lethal phenotype been recognized as affecting segmentation.[12] The majority of the mutants described here have been isolated in systematic searches for mutations affecting the segmentation pattern of the *Drosophila* larva. These experiments are still incomplete. Most of the alleles on the second chromosome were isolated in one experiment which yielded an average allele frequency of four or five alleles per locus (based on 42 embryonic lethal loci). From this yield and similar calculations for the third and first chromosomes, we estimate that we have identified almost all segmentation loci on the second chromosome and about 50% each of those on the third and first chromosome. Our sample of 15 loci should therefore represent the majority of the loci affecting segmentation in the *Drosophila* genome. Thus, in *Drosophila* it would seem feasible to identify all genetic components involved in the complex process of embryonic pattern formation.

We thank Hildegard Kluding for excellent technical assistance, Adelheid Schneider, Maria Weber and Gary Struhl for help during various parts of the mutant screens, Gerd Jürgens for stimulating discussion and our colleagues from the *Drosophila* laboratories in Cambridge, Freiburg, Heidelberg and Zürich for critical comments on the manuscript, and Claus Christensen for the photographic prints. Thomas Kornberg and Gary Struhl provided us with lethal alleles of *engrailed* and *wingless* respectively which facilitated the identification of our alleles. All mutants are available on request.

Note added in proof: All known *barrel* alleles fail to complement *hairy*[20], suggesting that the *barrel* mutations are alleles at the *hairy* locus.

Received 26 June; accepted 29 August 1980

1. Lohs-Schardin, M., Cremer, C & Nüsslein-Volhard, C. *Devl. Biol.* **73,** 239–255 (1979).
2. Wieschaus, E. & Gehring, W. *Devl. Biol.* **50,** 249–263 (1976).
3. Nüsslein-Volhard, C. in *Determinants of Spatial Organisation* (eds Subtelney, S. & Konigsberg, I. R.) 185-211 (Academic, New York, 1979).
4. Sander, K. *Adv. Insect Physiol.* **12,** 125–238 (1976).
5. Lewis, E. B. *Nature* **276,** 565–570 (1978).
6. Garcia-Bellido, A. *Am. Zool.* **17,** 613–629 (1977).
7. Szabad, J., Schüpbach, T. & Wieschaus, E. *Devl. Biol.* **73,** 256–271 (1979).
8. Counce, S. *Z. Induktive Abstammungs-Vererbungslehre* **87,** 462–81 (1958).
9. Sharma, R. P. & Chopra, V. L. *Devl Biol.* **48,** 461–465 (1976).
10. Lawrence, P. A. & Morata, G. *Devl Biol.* **50,** 321–337 (1976).
11. Kornberg, T., in preparation.
12. Gloor, H. *Arch. Julius-Klaus-Stift. VererbForsch* **25,** 38–44 (1950).
13. Meinhardt, H. *J. Cell Sci.* **23,** 117–139 (1977).
14. Bryant, P. J. *Ciba Fdn Symp.* **29,** 71–93 (1975).
15. Wright, D. & Lawrence, P. A., in preparation.
16. Lawrence, P. A. in *Developmental Systems: Insects* (eds Counce, S. & Waddington, C. H.) 157–209 (Academic, London, 1973).
17. Jürgens, G. & Gateff, E. *Wilhelm Roux Arch.* **186,** 1–25 (1979).
18. Meinhardt, H. & Gierer, A. *J. Cell. Sci.* **15,** 321–346 (1974).
19. Kaufmann, S. A., Shymko, R. M. & Trabert, K. *Science* **199,** 259–270 (1978).
20. Lindsley, D. & Grell, E. H. *Genetic Variations of Drosophila melanogaster* (Carnegie, Washington, 1968).
21. Wright, T. R. F. *Drosoph. Inf. Serv.* **45,** 140 (1970).
22. Vander Meer, J. *Drosoph. Inf. Serv.* **52,** 160 (1977).

Chemical synthesis of a polypeptide predicted from nucleotide sequence allows detection of a new retroviral gene product

J. G. Sutcliffe, T. M. Shinnick, N. Green, F.-T. Liu, H. L. Niman & R. A. Lerner

Department of Cellular and Developmental Immunology, Research Institute of Scripps Clinic, La Jolla, California 92037

We previously determined the nucleotide sequence of the 3′ end of Moloney leukaemia virus and discovered the potential coding region for an unknown protein, R. We now show that this region does encode a protein. A pentadecapeptide of R was chemically synthesized and antibodies raised against it. Antisera to the synthetic peptide recognize the R protein and the env *precursor polyprotein in infected cells. The strategy presented here should provide a general method for accessing proteins predicted by nucleotide sequences.*

THE accepted genetic structure of replication-competent murine leukaemia viruses, such as Moloney, Rauscher, Friend and AKV, includes three genes. These genes, *gag*, *pol* and *env*, are arranged, in respective order, along the single-stranded RNA genome. They are transcribed from the integrated double-stranded DNA provirus[1]. The protein products of these three genes are understood in considerable detail. The *gag* gene encodes a polyprotein of about 65 kilodaltons which is proteolytically processed to proteins, amino to carboxy terminal, of 15, 12, 30 and 10 kilodaltons, respectively[2]. These proteins are found in the core of the virion, and one, p30, has been associated with virus tropism[3]. The second gene, *pol*, is expressed as an apparent extension of the *gag* gene such that an approximately 180-kilodalton polyprotein containing both *gag* and *pol* components is observed. The polyprotein is processed to a 70-kilodalton protein which is the reverse transcriptase[4]. This enzyme is responsible for copying the single-stranded RNA genome of an infecting virus into the double-stranded DNA structure which can integrate into host DNA. The third gene, *env*, encodes a polyprotein which is glycosylated and processed into components gp70 and p15E (ref. 5). gp70 is the major envelope component and determines viral host range. It is sometimes found disulphide linked to p15E, a hydrophobic protein which may anchor gp70 to viral and cellular membranes[6]. Messenger RNA molecules have been described which can account for the expression of these three genes[7].

To understand fully the genetic structure of this class of viruses, we have been analysing their nucleotide sequences. We began our study at the 3′ end of Moloney murine leukaemia virus (Mo-MuLV) because of our particular interest in the *env* gene which was thought to be the most 3′-proximal gene. Surprisingly, we found an open reading frame which extended beyond the coding region for known viral products[8]. Even though we then had no evidence for a gene product, we provisionally named this the R-region because it is the coding region that is the furthest to the right in the genome. Here we report the detection of the R product. We chemically synthesized part of the R protein, raised antibodies to the synthetic peptide and detected immunologically cross-reactive material in infected cells.

The DNA sequence

For orientation purposes, several features of the previously reported[8] DNA sequence are presented here (Fig. 1). The DNA sequence was initially generated from an 1,108-base pair cDNA clone obtained by cloning the product of reverse transcription of purified detergent-disrupted Mo-MuLV. We have also sequenced most of this region of a full-length virus clone that can be demonstrated by transfection studies to carry all biologically active Mo-MuLV coding sequences. This new DNA sequence agrees with the original except for the differences described in Fig. 1 legend. We consider these differences to represent either variability in the population of biologically active genomes or artefacts due to the slight 'unfaithfulness' of the reverse transcriptase reaction (unpublished observations) which generated the clone we initially examined.

Proceeding from 5′ to 3′ along the DNA strand corresponding to genomic RNA, we see: the coding region for most of p15E (the carboxy-terminal *env* coding region); the origin of second-(positive) strand DNA replication; the inverted repeats, IR_L and IR_R, which flank the portion of viral sequences that are duplicated at the 5′ and 3′ ends of the integrated provirus (the so-called long terminal repeats, LTRs) and are responsible for the structure of the DNA of the virus resembling bacterial transposons[8,9]; and the poly(A) addition signal and presumptive 3′ ultimate nucleotides preceding the poly(A) tail[8]. Also indicated are features which are active at the 5′ copy of the LTR—the putative promoter for genomic expression and the first transcribed base[8].

A new protein predicted by DNA sequence

The new genetic region that we found can best be understood by considering what was previously thought to be the right-most coding region of the provirus—that for the viral protein p15E. The amino terminus of p15E can be positioned precisely by overlap between the protein sequence predicted by our DNA sequence and the protein sequence obtained by Copeland and Oroszlan (personal communication) (Fig. 1). The carboxyl terminus of p15E is not yet precisely defined. The apparent molecular size of p15E as determined on SDS gels is about 15 kilodaltons, a size estimate compatible with the mobility of a hydrophobic protein of about 100 residues. Surprisingly, we do not find a translational termination codon in this region. Instead, the open translational reading frame extends for a total of 196 triplets before encountering a stop. Thus we suspected that the primary *env* gene protein product in fact contained three peptides—gp70, p15E and the newly identified protein, R (positions ~100–196 in Fig. 1). Therefore, we looked for the R protein.

Chemical synthesis and detection of the R protein in infected cells

To detect and determine the cellular location of the R product, several peptides of the predicted Mo-MuLV R protein were synthesized by solid-state methods[10] and antibodies raised to these synthetic peptides. The predicted C-terminal peptides were synthesized because the N-terminus is not precisely known. Specifically, the C-terminal 15 residues (Leu-Thr-Gln-Gln-Phe-His-Gln-Leu-Lys-Pro-Ile-Glu-Cys-Glu-Pro) were attached to the carrier molecule keyhole limpet haemocyanin (KLH) and injected into six rabbits and four mice. We assayed the sera for the ability to precipitate immunologically a 36-residue synthetic substrate containing the 35 C-terminal residues of the R protein preceded by ^{125}I-tyrosine (^{125}I-Tyr-Ile-Leu-Asn-Arg-Leu-Val-Gln-Phe-Val-Lys-Asp-Arg-Ile-Ser-Val-Val-Gln-Ala-Leu-Val-Leu-Thr-Gln-Gln-Phe-His-Gln-Leu-Lys-Pro-Ile-Glu-Cys-Glu-Pro). Sera from all the immunized animals showed a positive response of 10–70-fold over normal serum (Table 1). We then looked for the R protein in lysates of MuLV-producing SCRF 60A cells that had been labelled by a 2-h ^{35}S-methionine pulse (the R protein contains no tyrosine and so was not expected to label with iodine). As can be seen in Fig. 2, an anti-R serum detects a protein with an apparent molecular size of approximately 80 kilodaltons in infected cells. All the individual immune rabbit and mouse sera detected proteins with the same molecular size. Additionally, no target molecules were observed in uninfected mouse lymphocytes, but the same band was seen after infection with Mo-MuLV (not shown). Because the nucleotide sequences showed that p15E and R were in the same reading frame, we expected that this molecule was, in fact, the *env* precursor. Antibodies to gp70, including an anti-gp70 hybridoma, detect a molecule with the same apparent molecular size as that precipitated by anti-R,

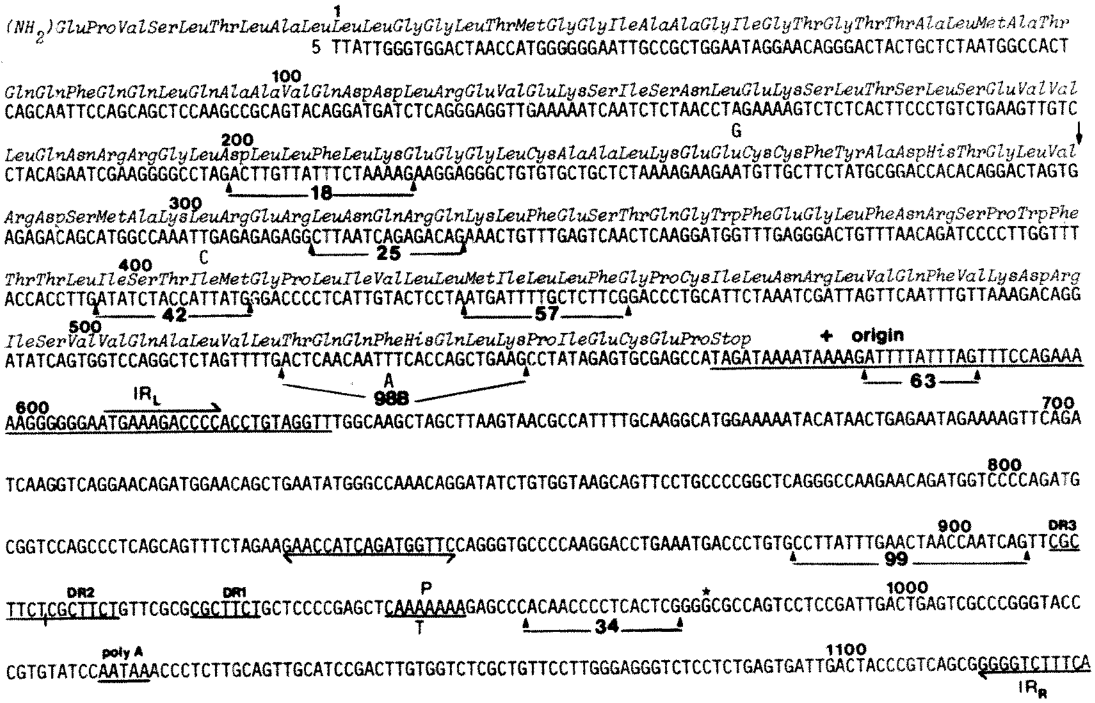

```
(NH2)GluProValSerLeuThrLeuAlaLeuLeuLeuGlyGlyLeuThrMetGlyGlyIleAlaAlaGlyIleGlyThrGlyThrThrAlaLeuMetAlaThr
                          5 TTATTGGGTGGACTAACCATGGGGGGAATTGCCGCTGGAATAGGAACAGGGACTACTGCTCTAATGGCCACT
GlnGlnPheGlnGlnLeuGlnAlaAlaValGlnAspAspLeuArgGluValGluLysSerIleSerAsnLeuGluLysSerLeuThrSerLeuSerGluValVal
CAGCAATTCCAGCAGCTCCAAGCCGCAGTACAGGATGATCTCAGGGAGGTTGAAAAATCAATCTCTAACCTAGAAAAGTCTCTCACTTCCCTGTCTGAAGTTGTC
LeuGlnAsnArgArgGlyLeuAspLeuLeuPheLeuLysGluGlyGlyLeuCysAlaAlaLeuLysGluGluCysCysPheTyrAlaAspHisThrGlyLeuVal
CTACAGAATCGAAGGGGCCTAGACTTGTTATTTCTAAAAGAAGGAGGGCTGTGTGCTGCTCTAAAAGAAGAATGTTGCTTCTATGCGGACCACACAGGACTAGTG
ArgAspSerMetAlaLysLeuArgGluArgLeuAsnGlnArgGlnLysLeuPheGluSerThrGlnGlyTrpPheGluGlyLeuPheAsnArgSerProTrpPhe
AGAGACAGCATGGCCAAATTGAGAGAGAGGCTTAATCAGAGACAGAAACTGTTTGAGTCAACTCAAGGATGGTTTGAGGGACTGTTTAACAGATCCCCTTGGTTT
ThrThrLeuIleSerThrIleMetGlyProLeuIleValLeuLeuMetIleLeuLeuPheGlyProCysIleLeuAsnArgLeuValGlnPheValLysAspArg
ACCACCTTGATATCTACCATTATGGGACCCCTCATTGTACTCCTAATGATTTTGCTCTTCGGACCCTGCATTCTAAATCGATTAGTTCAATTTGTTAAAGACAGG
IleSerValValGlnAlaLeuValLeuThrGlnGlnPheHisGlnLeuLysProIleGluCysGluProStop
ATATCAGTGGTCCAGGCTCTAGTTTTGACTCAACAATTTCACCAGCTGAAGCCTATAGAGTGCGAGCCATAGATAAAATAAAAGATTTTATTTAGTTTCCAGAAA
AAGGGGGGAATGAAAGACCCCACCTGTAGGTTTGGCAAGCTAGCTTAAGTAACGCCATTTTGCAAGGCATGGAAAAATACATAACTGAGAATAGAAAAGTTCAGA
TCAAGGTCAGGAACAGATGGAACAGCTGAATATGGGCCAAACAGGATATCTGTGGTAAGCAGTTCCTGCCCCGGCTCAGGGCCAAGAACAGATGGTCCCCAGATG
CGGTCCAGCCCTCAGCAGTTTCTAGAAGAACCATCAGATGGTTCCAGGGTGCCCCAAGGACCTGAAATGACCCTGTGCCTTATTTGAACTAACCAATCAGTTCGC
TTCTCGCTTCTGTTCGCGCGCTTCTGCTCCCCGAGCTCAAAAAAAGAGCCCACAACCCCTCACTCGGGGCGCCAGTCCTCCGATTGACTGAGTCGCCCGGGTACC
CGTGTATCCAATAAACCCTCTTGCAGTTGCATCCGACTTGTGGTCTCGCTGTTCCTTGGGAGGGTCTCCTCTGAGTGATTGACTACCCGTCAGCGGGGGTCTTTCA
```

Fig. 1 Nucleotide sequence of the 3′ end of the Mo-MuLV provirus. The sequence of the 1,123-nucleotide plus-strand from the 3′ LTR and carboxy-terminal virus coding region was determined from an 1,108-base pair long cDNA clone[8] and extended slightly by sequence from an infectious clone. The four differences in the infectious clone are indicated below the running sequence. The protein sequence translated from the DNA appears above the nucleotide sequence. The first 34 amino-terminal residues were determined by Copeland and Oroszlan and positions 10–34 match our sequence. The arrow at the end of the third line indicates the region of the carboxy terminus of p15E. The rest of the amino acid sequence is that of the R protein. The numbered oligonucleotides (25, 42, 57 and 98B) represent those corresponding to AKV virus and are shown in detail in Fig. 6. The underlined region downstream from the R coding region is the origin of plus-strand DNA synthesis. The regions marked IR_L and IR_R are the inverted terminal repeats which flank the LTRs. Within the LTR we recognize a 17-base long palindrome (underlined) and three direct repeats (DR 1, 2 and 3) which lie just upstream from the promotor Hogness box (p) for the 5′ end of the viral transcript(*). Further down the molecule is the poly(A) addition signal for the 3′ end of the transcript.

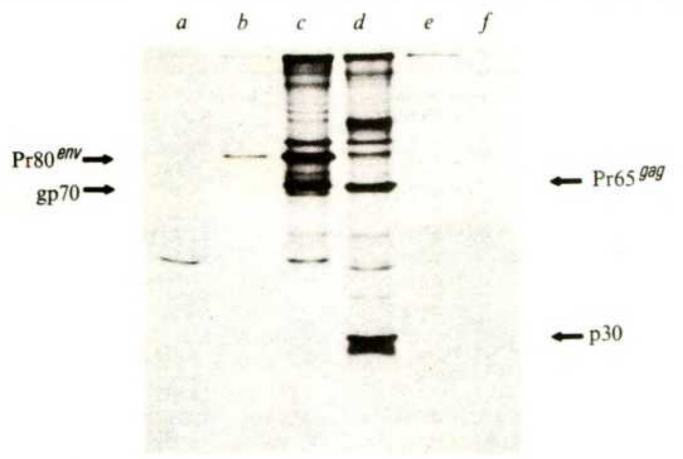

Fig. 2 Antibody to synthetic R peptide precipitates Pr80^{env}. Log-phase SCRF 60A cells, which produce a virus indistinguishable from Mo-MuLV[18], were grown in Eagle's minimal essential medium (MEM) with 10% fetal calf serum. The cells were labelled at 37 °C at 2×10^6 cells ml^{-1} for 2 h with ^{35}S-methionine (940 Ci mmol^{-1}, 100 μCi ml^{-1}) in Hank's balanced salts with 10% Eagle's MEM. Cells were chilled, washed with 0.15 M NaCl, 10 mM sodium phosphate *p*H 7.5, extracted with 0.15 M NaCl, 10 mM sodium phosphate *p*H 7.5, 1% NP40, 0.5% sodium deoxycholate, 0.1% SDS, 2% Trasylol for 20 min at 0 °C, then sonicated and spun at 12,000*g* for 5 min. The lysate was pre-cleared by reacting with 20 μl of normal rabbit serum and 20 μl of normal goat serum for 30 min at 0 °C, followed by the addition of formalin-fixed *Staphylococcus aureus* for 30 min and centrifugation for 15 min at 12,000*g*. Portions of the lysate were reacted with 5 μl of normal rabbit (*a*), rabbit anti-synthetic R pentadecapeptide (*b*), goat anti-gp70 (*c*), goat anti-p30 (*d*), normal goat sera (*e*), or anti-gp70 hybridoma (no. R1-16G07, ref. 19) (*f*) culture media for 1 h at 0 °C. Complexes were collected with *S. aureus* and after two washes with 500 mM LiCl, 100 mM Tris, *p*H 8.5, dissolved in loading buffer cleared of *S. aureus*, and loaded on an 11% SDS-polyacrylamide gel. The gel was soaked in Enhance (NEN) for 90 min, H$_2$O for 60 min, dried and exposed to film. The bands indicated have been identified previously in this laboratory and by others[20].

confirming that we are observing the *env* precursor. To rule out the possibility that these were two distinct molecules with a fortuitous correspondence in molecular size, we did two experiments. First, when the lysates are pre-cleared with anti-R sera, the 80-kilodalton radioactive target for anti-gp70 sera is removed. Conversely, clearing the lysate with anti-gp70 sera removes the R determinants. Second, proteolytic peptide fingerprinting of the two 80-kilodalton molecules precipitated by anti-R and anti-gp70 shows them to be identical (Fig. 3). Thus, we have identified the 80-kilodalton band as the complete *env* gene polyprotein product containing gp70, p15E (as shown by others) and R determinants.

Using different gel electrophoresis conditions, we were able to detect a protein of estimated molecular size 12 kilodaltons specifically precipitated by anti-R serum (Fig. 4). We tentatively identify this small protein as R although positive identification awaits N-terminal amino acid analysis. Also, we have observed, by indirect immunofluorescence, R protein determinants on the plasma membrane of SCRF 60A cells (to be published elsewhere), a result made more significant by the fact that the anti-R serum does not precipitate gp70 or p15E. Our experiments do not indicate at what time the p15E-R cleavage occurs and it is possible that the true gp70 membrane anchor is the 22-kilodalton protein containing p15E and R peptides. In that case, the proteolytic cleavage which generates p15E and R occurs during their isolation. We have not observed a 22-kilodalton protein with R determinants.

The R gene is present in another virus

Pederson and Haseltine[11] determined the nucleotide sequences of the large ribonuclease T$_1$ fragments of AKV virus, an endogenous leukaemia virus of AKR mice. By computer search we identified several of these fragments as having partial homologies to skeins of our Mo-MuLV sequence. Our defined order makes a reasonable match with the order obtained experimentally by Pederson, Crowther and Haseltine (personal communication). The matches within the R-region are indicated in Fig. 1 and detailed in Fig. 5. From these alignments we note first the matched fragments are not wholly conserved, which perhaps warns us as to what to expect from future comparisons of sequences of related viruses, and second, that matches within the R-region indicate that AKV probably encodes an R protein much like that of Mo-MuLV. Specifically, (1) none of the AKV differences introduces nucleotides which indicate a premature translational stop, (2) several (9) AKV/Mo-MuLV nucleotide differences are in third positions in triplets and do not alter the coded protein sequence, (3) some nucleotide differences do change R-protein amino acids, but the replacements tend to be conservative or synonymous (as indicated in Fig. 5), such as phenylalanine to tyrosine in spot 98B, Asn-Gln-Arg to Lys-Gln-Gln in spot 25, or Met to Leu in spot 57. All these substitutions are rated as positive correlations by the Dayhoff mutation matrix[13]. Additionally, a preliminary sequence obtained by Herr (personal communication) through 211 nucleotides of the R-region of AKV shows an open reading frame containing 51 nucleotide differences with our Mo-MuLV sequence. These 51 differences make only six amino acid alterations, all of which are synonymous. These observations indicate that the R-protein sequence is highly conserved in the two viruses.

Comments about the R protein

The entire amino acid sequence of the R protein does not correspond closely to any protein sequence in ref. 12. Some subregions of R, however, are reminiscent of subregions of known proteins such as dehydrogenases and proteases, perhaps

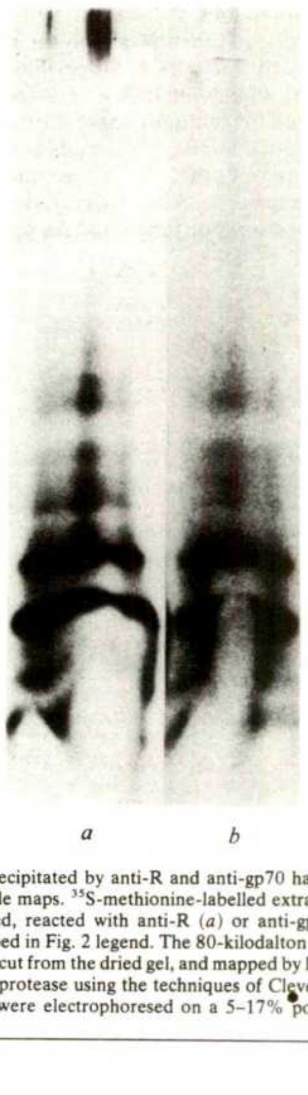

Fig. 3 Pr80^{env} precipitated by anti-R and anti-gp70 have the same one-dimensional peptide maps. ^{35}S-methionine-labelled extracts of SCRF 60A cells were prepared, reacted with anti-R (*a*) or anti-gp70 (*b*) sera, and analysed as described in Fig. 2 legend. The 80-kilodalton band precipitated by each serum was cut from the dried gel, and mapped by limited proteolysis with *S. aureus* V8 protease using the techniques of Cleveland *et al.*[21]. The reaction products were electrophoresed on a 5–17% polyacrylamide gel.

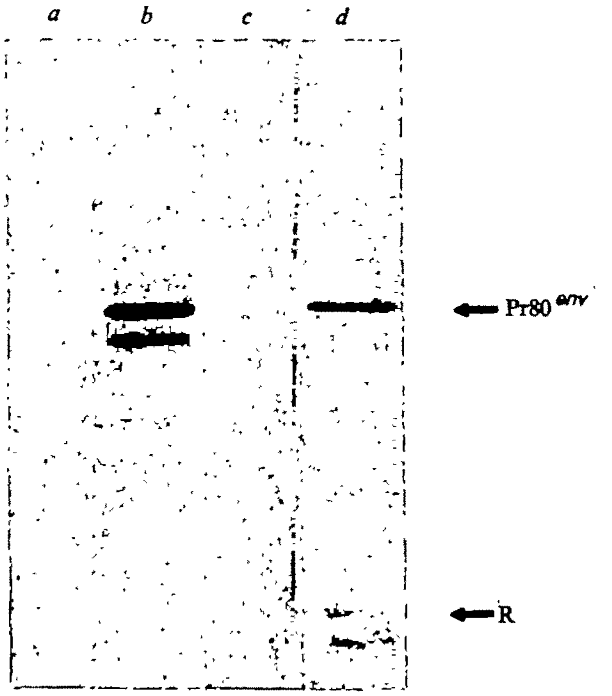

Fig. 4 Detection of the R protein. A ^{35}S-methionine-labelled lysate of SCRF 60A cells (as described in Fig. 2 legend) was divided into four equal portions and immunologically precipitated with normal goat (*a*), goat anti-gp70 (*b*), normal rabbit (*c*) or rabbit anti-R (*d*) serum, collected with *S. aureus* and electrophoresed on a 5–17.5% SDS–polyacrylamide gradient gel. The lower band in lanes *c* and *d* is usually seen with any normal rabbit serum and is thus not considered specific.

implicating domains of the R protein in nucleotide binding or protein–protein interactions.

The R protein might function simply as a structural viral protein. In this regard, the very hydrophobic domain between positions 32 and 61 suggest that R is inserted into cellular or viral membranes where it might serve to anchor other viral proteins. As mentioned above, we already have evidence from fluorescence microscopy that R is present in the plasma membranes of infected cells. Alternatively, the R protein might be involved in other sorts of functions. As originally noted by Fisher[14], genes and their regions of action seem to cluster. The R-region lies between the p15E coding region and the origin of positive-strand replication and LTR. It is, therefore, possible that R functions in replication or transposition (integration).

```
                  Mo-MuLV
Fragment            AKV

              ArgLeuAsnGlnArgGln
                GCTTAATCAGAGACAG
   25           GCTAAAACAACAACAG
                LeuLysGlnGlnGln

              LeuIleSerThrIleMet
                GATATCTACCATTATG
   42           GATATCCACCATCATG
                 IleSerThrIleMet

              LeuMetIleLeuLeuPhe
                AATGATTTTGCTCTTCG
   57           GTTAATTTTACTCTTTG
                 LeuIleLeuLeuPhe

              LeuThrGlnGlnPheHisGlnLeuLys
                GACTCAACAATTTCACCAGCTGAAG
   98B          GACTCAACAATATCATCAACTTAXG
                 ThrGlnGlnTyrHisGlnLeu
```

Fig. 5 Comparison of the R gene in two viruses. The oligonucleotide sequences determined by Pederson and Haseltine[11] for AKV were matched by computer to our Mo-MuLV sequence. Those matches within the R-region are shown, Mo-MuLV above AKV, with the corresponding translated amino acids. The numbers in the margin are those used by Pederson and Haseltine. Differences between the nucleotides are underlined. In fragment 98B, the phenylalanine codon in our cDNA sequence was a tyrosine codon in the infectious clone and is a tyrosine in AKV. The X in fragment 98B is an unsolved position for AKV[11].

Table 1 Precipitation of ^{125}I-synthetic peptide by sera from R-KLH-immunized rabbits and mice

	Immunization schedule	^{125}I-peptide precipitated (c.p.m.)
Rabbit		
1	None	432
2	*a*	4,867
3	*a*	15,359
4	*b*	21,200
5	*b*	18,436
6	*c*	5,548
7	*c*	19,799
Mouse		
1	None	553
2	None	521
3	*d*	18,522
4	*d*	20,282
5	*d*	28,890
6	*d*	38,497

The carboxy-terminal R pentadecapeptide (LTQQFHQLKPIECEP) was prepared and its acid hydrolysate was shown to be of correct composition. It was shown to be pure by TLC on both silica and cellulose in nBuOH/EtOAc/HOAc/H_2O (1:1:1:1) and electrophoresis in pyridine acetate, *p*H 5.6, on Whatman 3MM. The sample was visualized by reaction with ninhydrin reagent. It was conjugated to KLH through the cysteine sulphydryl. 63 μl of 15 mg ml^{-1} *m*-maleimidobenzoyl-*N*-hydroxysuccinimide ester[14–17] in *N,N'*-dimethylformamide was added dropwise with stirring to KLH (10 mg ml^{-1}) in 10 mM potassium phosphate, *p*H 7.0. After stirring for 30 min, the mixture was filtered and applied to a Sephadex G-25 column (0.1 M phosphate, *p*H 6.0). The activated protein (2.3 ml) was mixed with 0.1 ml of the R pentadecapeptide (10 mg ml^{-1} in 0.1 M potassium phosphate, *p*H 7.3, 5 mM EDTA) and the solution adjusted to *p*H 6.5, stirred for 4 h at room temperature and chromatographed on Sephadex G-100 (0.1 M ammonium bicarbonate, *p*H 9.5). The conjugated protein was collected and used directly for immunization of female New Zealand White rabbits (1.5–2.5 kg) or adult female G_{IX}^- mice (except mouse 1, which was BALB/c) as follows: Rabbits: 1 ml to hind footpads and subcutaneously at multiple sites along the back. Schedule *a*: 1 mg per kg in complete Freunds's adjuvant (CFA, 1:1), days 0, 7 and 14; blood days 21 and 28. Schedule *b*: 200 μg per rabbit in CFA on day 0; 50 μg per rabbit in incomplete Freund's adjuvant (ICF, 1:1) on day 7; 50 μg per rabbit in alum (4 mg per rabbit) intraperitoneally on day 14; bleed days 21 and 28. Schedule *c*: as schedule *b* except initial injection was 50 μg per rabbit. Mice were immunized intraperitoneally (schedule *d*) with 35 μg in CFA (1:1) on day 0, 35 μg with 500 μg alum intraperitoneally, day 14; bled day 21. ^{125}I-36-mer (5×10^6 c.p.m.) in immune precipitation buffer (0.15 M NaCl, 10 mM sodium phosphate *p*H 7.5, 1% NP40, 0.5% sodium deoxycholate, 0.1% SDS, 2% Trasylol) was incubated with 5 μl serum for 1 h at 0 °C, with formalin-fixed *S. aureus* for 30 min, then centrifuged for 15 min at 12,000*g*. Pellets were washed once in buffer, twice in 500 mM LiCl/100 mM Tris *p*H 8.5, then counted. *S. aureus* in the absence of serum bound, 528 c.p.m.

On the other hand, the R protein could have a role in viral transformation. A problem of the leukaemia viruses has been that, although they transform lymphoid tissues, they carry no apparent transforming genes. As a transforming protein, R could act directly or could interact with another protein. In either case, two important points must be explained: First, although they replicate in virtually all cell types of the mouse, these viruses only transform specific cells. Second, changes in the gp70 protein, which is encoded upstream from the R protein, are highly correlated with leukaemogenicity of various viruses, notably those called MCF (ref. 15). Therefore, we imagine either that gp70 and R interact directly (perhaps through disulphide linkage) and have, in the Moloney case, a T-cell-specific action or that gp70 triggers some cell-type-specific event which renders the T cell sensitive to the leukaemogenic effect of the R protein. What would cause the virus to maintain this gene is unknown.

The finding that Moloney and AKV, two viruses which cause T-cell lymphomas, have closely related R proteins, does not clarify the problem of specificity. We are now studying the R-region of other viruses such as Friend erythroleukaemia virus, which causes a disease of a different cell type, and a non-pathogenic xenotropic virus to determine whether the R protein is related to the pathogenicity and/or target tissues of the viruses.

We thank David Katz, Russell Doolittle and John Elder for helpful discussions, and Winship Herr, Stephen Oroszlan and William Haseltine and their collaborators for providing results before publication. This research was supported by a grant from the Pitman-Moore Company, Washington Crossing, New Jersey.

Received 24 June; accepted 1 September 1980.

1. Baltimore, D. *Cold Spring Harb. Symp. quant. Biol.* **39,** 1187–1200 (1974).
2. Oskarsson, M. K., Elder, J. H., Gautsch, J. W., Lerner, R. A. & Vander Woude, G. F. *Proc. natn. Acad. Sci. U.S.A.* **75,** 4694–4698 (1978).
3. Gautsch, J. W., Elder, J. H., Schindler, J., Jensen, F. C. & Lerner, R. A. *Proc. natn. Acad. Sci. U.S.A.* **75,** 4170–4174 (1978).
4. Jamjoon, G. A., Naso, R. B. & Arlinghaus, R. B. *Virology* **78,** 11–34 (1977).
5. Famulari, N. C., Buchhagen, D. L., Klenk, H. D. & Fleissner, E. *J. Virol.* **20,** 501–508 (1976).
6. Witte, O. N., Tsukamoto-Adey, A. & Weissman, I. L. *Virology* **76,** 539–553 (1977).
7. Fan, H. & Verma, I. M. *J. Virol.* **26,** 468–478 (1978).
8. Sutcliffe, J. G., Shinnick, T. M., Verma, I. M. & Lerner, R. A. *Proc. natn. Acad. Sci. U.S.A.* **77,** 3302–3306 (1980).
9. Shimotohno, K., Mizutani, S. & Temin, H. M. *Nature* **285,** 550–554 (1980).
10. Marglin, A. & Merrifield, R. B. *A. Rev. Biochem.* **39,** 841–866 (1970).
11. Pederson, F. S. & Haseltine, W. A. *J. Virol.* **33,** 349–365 (1980).
12. Dayhoff, M. O. (ed.) *Atlas of Protein Sequence and Structure* Vol. 5, Suppl. 3 (Natn. Biomed. Res. Fdn, Washington, DC, 1978).
13. Dayhoff, M. O., Schwartz, R. M. & Orcutt, B. C. in *Atlas of Protein Sequence and Structure* Vol. 5, Suppl. 3 (ed. Dayhoff, M. O.) 352 (Natn. Biomed. Res. Fdn, Washington, DC, 1978).
14. Fisher, R. A. *The Genetical Theory of Natural Selection* (Clarendon, Oxford, 1930).
15. Elder, J. H. *et al. Proc. natn. Acad. Sci. U.S.A.* **74,** 4676–4680 (1977).
16. Kitagawa, T. & Ailawa, T. *J. Biochem., Tokyo* **79,** 233 (1976).
17. Liu, F., Zinnecker, M., Hamaoka, T. & Katz, D. H. *Biochemistry* **18,** 690 (1979).
18. Lerner, R. A. *et al. Proc. natn. Acad. Sci. U.S.A.* **69,** 2965–2969 (1972).
19. Niman, H. L. & Elder, J. H. *Proc. natn. Acad. Sci. U.S.A.* **77,** 4524–4528 (1980).
20. Edwards, S. A. & Fan, H. *J. Virol.* **30,** 551–563 (1979).
21. Cleveland, D. W., Fisher, S. G., Kirschner, M. W. & Laemmli, U. K. *J. biol. Chem.* **252,** 1102–1106 (1977).

LETTERS

An extraordinary new celestial X-ray source

P. C. Gregory* & G. G. Fahlman†

* Physics Department
† Department of Geophysics and Astronomy, University of British Columbia, Vancouver, British Columbia, Canada V6T 1W5

The discovery of an extraordinary new X-ray source detected during a guest observer programme carried out with the Einstein X-ray Observatory is reported here. The object, designated G109.1 − 1.0, was found using the imaging proportional counter detector (IPC) on 17 December 1979. The IPC is sensitive to X-ray photons with energies between 0.1 and 4.5 keV. A longer exposure (3.6×10^3 s) IPC picture of a 1° field of view centred on the SNR was obtained on 8 July 1980 and is shown in Fig. 1. The picture shows a clear semicircular arc with an angular diameter of 36 arc min which appears to be the outer shell of the SNR. The resolution of the picture is 1 arc min. At the exact centre of the curvature of the shell is a strong compact source which we designate GF2259 + 586. The X-ray coordinates of GF2259 + 586 are RA = 22 h 59 min 02.5 s and dec = 58° 36′ 38″. The 1 arc min accuracy of the coordinates is limited by systematic calibration errors in the IPC detector. Emerging from the east side of the central source is a jet-like structure which curves northwards in another continuous arc smoothly joining the outer shell. On closer inspection, the jet appears to bifurcate with a second component continuing radially outwards from the central compact source. This very unusual structure has parallels with the W50 SNR with its central X-ray source SS433 and jet (F. D. Seward, personal communication).

The western half of the circular shell appears to be completely absent with the exception of a weak X-ray source located at 19 arc min from the central source and coincident in position with the bright Sharpless H II region[1] S152, which has an angular diameter of 2 arc min. The S152 X-ray source does not show up in Fig. 1 because of shadowing by a detector support rib, but does appear in the earlier exposure of 12 December. We note that S152 and GF2259 + 586 are accurately aligned along the axis of the X-ray jet. The Palomar red and blue prints fail to show any nebulosity associated with the X-ray shell. There are, however, two very faint filaments each ~2 arc min long located well inside the southern part of the shell at a distance of 12–13 arc min from the central source. Within the 1 arc min (radius) X-ray error circle of GF2259 + 586 there are about 50 possible optical counterparts to the limit of the Palomar red print, the brightest of which has a V magnitude of ~15. Also on the western side, adjacent to S152, is a second Sharpless H II region S153, which has an angular diameter of 5 arc min and is 17 arc min from the central X-ray source.

Radio emission was first detected[2] from this region (CTB 109)[2] in 1960 at 960 MHz. Their measured flux density of 75 Jy combined with a later integrated flux density measurement of 40 Jy at 3,200 MHz by RaghavaRoa *et al.*[3] indicate a nonthermal spectrum. The value of the spectral index $\alpha = -0.52$ (S proportional to ν^{α}) is typical of a SNR. One of us (P.C.G.) has obtained a differential radio map of this region at 6 cm with the NRAO 91-m telescope as part of a survey for variable sources in the galactic plane. The 6-cm map corresponds fairly closely with the X-ray emission including the jet-like feature but unfortunately there is a gap in the observations at the location of the central X-ray source. A scan through this location at 2.8 cm in June 1980, with the Algonquin Radio Observatory 46-m telescope, failed to detect a discrete radio source to a limit of 100 mJy. The 6-cm radio data indicate that the jet-like feature continues for a short distance west of the central source. There also seems to be emission extending to the north-west and there is strong radio emission from S152 and weaker emission from S153. On the western side there is no clear radio evidence for the continuation of the circular shell. The source has also been mapped at Westerbork at 50 cm. (V. A. Hughes, personal communication).

Although the true nature of the source is not entirely clear, certain aspects of the morphology suggest we may be dealing with a SNR. If so, a distance may be obtained by using the relationship of Clark and Caswell[4] between radio surface brightness and distance. The derived 408-MHz surface brightness (Σ) of 1.4×10^{-20} W m^{-2} Hz^{-1} s^{-1} using an angular diameter of 36 arc min falls close to a change in the slope of the Σ-D relationship. From their equations we arrive at a distance of 3.6 ± 0.4 kpc. Note that Crampton *et al.*[5] obtained a distance of 3.6 kpc for S152 and a distance of 4 kpc for S153. On the Palomar blue print S152 exhibits a curved tail which extends back towards GF2259 + 586. This and the alignment mentioned above suggest a possible relationship between the two objects. Hence the distance estimate is not dependent entirely on the SNR assumption.

At a distance of 3.6 kpc, the linear diameter of the shell is 38 pc, comparable to the Cygnus Loop and the Vela SNR[6].

A low energy cutoff is observed in the X-ray spectrum obtained from the IPC pulse height analyser (PHA) as expected for a ~3.6-kpc distance. However, actual spectral fits must await further IPC calibration analysis. One estimate of the X-ray absorption can be obtained from the reddening of the central stars of S152 and S153 which have $E(B - V) = 1.25$ and 0.75

0028-0836/80/440805—02$01.00

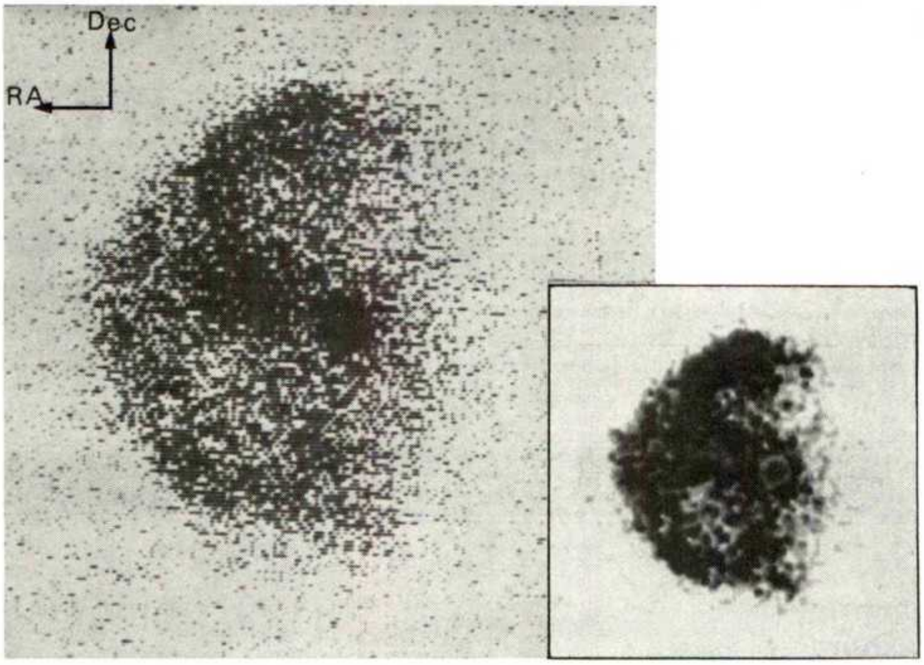

Fig. 1 IPC picture of a 1° field of view centred on G109.1–1.0. The inset shows the central core of the same object with better definition.

respectively[5]. These values can be converted to column densities of 0.85 and 0.51×10^{22} cm^{-2}, respectively, using the relationship of Ryter *et al.*[7]. We regard these as upper limits because of the possibility of dust in the H II regions themselves. Adopting a value of $N_H = 0.3\times10^{22}$ cm^{-2}, we estimate that the luminosity of the SNR, excluding the central source, is 2.7×10^{35} erg s^{-1}. If N_H is as high as 0.5×10^{22} cm^{-2} the corresponding luminosity is 4.9×10^{35} erg s^{-1}. Applying the theory of adiabatic blast waves as described in ref. 6, we find that the age of SNR is ~12,000 yr. The ambient interstellar density is ~0.1 cm^{-3} and the energy released in the supernova explosion is 3.8×10^{50} erg. The current shockwave velocity is predicted to be 600 km s^{-1}. The derived parameters are very similar to the Cygnus Loop and Vela SNR. By analogy with the Cygnus Loop we expect that the optical filaments noted earlier will have a much lower velocity than the predicted shock velocity.

If indeed this is a SNR, it is unusual because of its strong compact central source and jet-like feature which emerges on the eastern side of the central source. The PHA spectrum of the central source appears harder than the spectrum of the shell. Assuming thermal emission with $kT = 4$ keV, the corresponding luminosity of the central source is 3×10^{34} erg s^{-1}. The luminosity is uncertain by a factor of two but is of the same order as the X-ray emission from SS433. The most striking characteristics of this source are: (1) the semicircular shell which suggests a SNR; (2) a compact central X-ray source; and (3) a large-scale jet. These are also conspicuous features of the unusual object SS433 and its associated SNR, W50. Consequently, these two objects may be members of a new class of SNR. On the other hand, there are obvious differences in the morphology of the two objects. The spiral-like structure of the conspicuous X-ray jet and the hint of a similar feature to the south suggest that we may not be observing a SNR shell at all. The appearance may be the result of two jets which are being ejected from the central source and wound by rotation to give a shell-like structure. Alternatively, large-scale magnetic fields may be responsible for the observed geometry.

We thank Fred Seward of the Smithsonian Astrophysical Observatory for assistance. This research was supported by grants from the Canadian National Science and Engineering Research Council.

Note added in Proof: One of us (P.C.G.) recently obtained VLA observations of the source at 20 cm and 6 cm. A weak compact radio source was found 2 arc min from GF2259+586 but there is no optical counterpart to the limit of the Palomar Sky Survey.

Received 4 August; accepted 26 August 1980.

1. Sharpless, S. *Astrophys. J. Suppl.* **41,** 257–279 (1959).
2. Wilson, R. W. & Bolton, J. G. *Publ. astr. soc. Pacif.* **72,** 331 (1960).
3. RaghavaRoa, R., Medd, W. J., Higgs, L. A. & Broten, N. W. *Mon. Not. R. astr. Soc.* **129,** 159–168 (1965).
4. Clark, D. H. & Caswell, J. L. *Mon. Not. R. astr. Soc.* **174,** 267–305 (1976).
5. Crampton, D., Georgelin Y. M. & Georgelin, Y. P. *Astr. Astrophys.* **66,** 1 (1978).
6. Gorenstein P. & Tucker, W. H. *A. Rev. Astr. Astrophys.* **14,** 373–416 (1976).
7. Ryter, C., Cesarsky, C. J. & Audouze, J. *Astrophys. J.* **198,** 103 (1975).

Diffuse X-ray emission from the jets of SS433

F. Seward*, J. Grindlay*, E. Seaquist† & W. Gilmore†

* Harvard-Smithsonian Center for Astrophysics, Cambridge, Massachusetts 02138
† Department of Astronomy, University of Toronto, Toronto, Ontario, Canada M5S 1A1

The discovery of strong, variable emission lines[1], which are Doppler-shifted[2] from SS433, led to the development of a kinematic beam model[3-5] which explains the principal features of the time varying optical spectrum. In this model two opposed jets of material moving outwards from the central star at 0.258*c* precess with a period of 164 days, about an axis inclined 80° (or 20°) to the line of sight of the observer. The locus of the two beams forms a cone with an opening half angle of 20° (or 80°) (in the model an ambiguity exists between the inclination and cone angles, as the optical data alone cannot distinguish between the two possibilities). A 13-day period observed in the velocity of the 'stationary' lines from this object[6] shows that the system is binary. However, other models exist which also account for the

0028-0836/80/440806—03$01.00

time varying optical spectrum. For example, one model suggests that the Doppler-shifted emission lines originate in a ring of material orbiting a solitary massive black hole[7]. We now report the detection of large-scale X-ray 'jets' from SS433. The X-ray emission is diffuse, extending at least 30 arc min from SS433, and is exactly aligned with both SS433 and the bulges of the shell of the huge supernova remnant (SNR) W50. This detection now (1) directly confirms the existence of jets related to SS433, (2) shows the link between SS433 and W50, proving that SS433 is galactic, (3) establishes a minimum age of the jet phenomenon of ~10³ yr, and (4) offers an explanation of why W50 is so much larger than any other known SNR in at least one dimension. The morphology of the diffuse X-ray emission is strikingly similar to that of radio lobes of many extragalactic sources; either *in situ* heating or particle acceleration is required to explain the appearance of the diffuse X-ray emission.

The SS433 observations were made with the Einstein X-ray Observatory[8] using the high resolution imager (HRI) in April 1979, and the imaging proportional counter (IPC) during the period 5–22 October 1979. The HRI observations show that the compact central source is unresolved (⩽3 arc s) and has position (±5″) of RA(1950) = 19 h 09 min 21 35 s, dec(1950) = +04° 53′ 54.9″. This position is coincident with the optical and radio position of SS433 (ref. 9). The IPC observations were made in a series of 2,000-s observations so as to monitor variable X-ray and radio emission. Two simultaneous X-ray and radio flares were observed and will be described elsewhere[10]. Figure 1 shows the sum of all these short observations for the energy range 0.5–3 keV and with a total integration time of 17,000 s.

The morphology of the diffuse X-ray emission reveals several important points. To show the diffuse features in the 1° field more clearly, the data in Fig. 1 have been smoothed giving the contours shown in Fig. 2, which is somewhat distorted by the vignetting correction applied. The two diffuse features are aligned with the central source. A straight line passing through the centres of both diffuse features and the central source goes through position angle 98°—nearly identical to the position angle of the bulges of the shell of W50 (ref. 11) and also closely aligned with the position angle of extended small-scale (arc s) radio emission[12–14] Note that diffuse emission, including the radio features observed by Geldzahler *et al.*[11], is not detected elsewhere inside the remnant, nor from that portion of the shell which crosses the upper north-west portion of our field.

The detection of the extended X-ray emission thus directly confirms for the first time that diametrically opposed jets originate from SS433 and travel nearly a degree across the sky to the eastern and western extremities of W50 where they collide with the SNR shell and cause the observed bulges. Clearly, there is significant interaction along the way between the jets and the SNR W50. The validity of the 'beambag' hypothesis for the morphology of W50[15] is now confirmed. The X-ray data are quite consistent with 'beam models' involving twin processing jets and the ambiguity in these models between the inclination of the precessing axis and the opening half angle of the cone is removed. The X-ray morphology and the optical requirement that the angle between beam velocity and observer never be <60° fix the cone half angle at 20° and the inclination at 80°. If the beam velocity is ~0.258*c* across the whole remnant, this phenomenon has continued for at least ~10³ yr, assuming the distance is 3.7 kpc (refs 16, 17).

Examination of Figs 1 and 2 shows that the diffuse feature in the west appears to be stronger than that in the east. If real, this may be related to the asymmetries between the east and west halves of W50 as shown in the radio map of Geldzahler *et al.*[11] and may be due to slight long-term changes in the balance of the jets and/or different properties of the medium surrounding SS433. However, the most significant morphological feature of the observed diffuse emission is that the brightness increases outward from SS433, forming rather elongated lobes, somewhat reminiscent of the appearance of radio-emitting lobes in radio galaxies. It is not clear whether or not the diffuse emission is completely absent near the star. The angle subtended by this emission at the position of SS433 is significantly less than the full 40° cone angle expected if the outflowing gas followed a purely ballistic trajectory. Both characteristics indicate that the flow is influenced and confined by an external medium in the SNR. The interaction with this medium by some *in situ* process is probably the cause of the excitation in the lobes. To investigate this point further, we examined the physical state of the gas responsible for the X-ray emission.

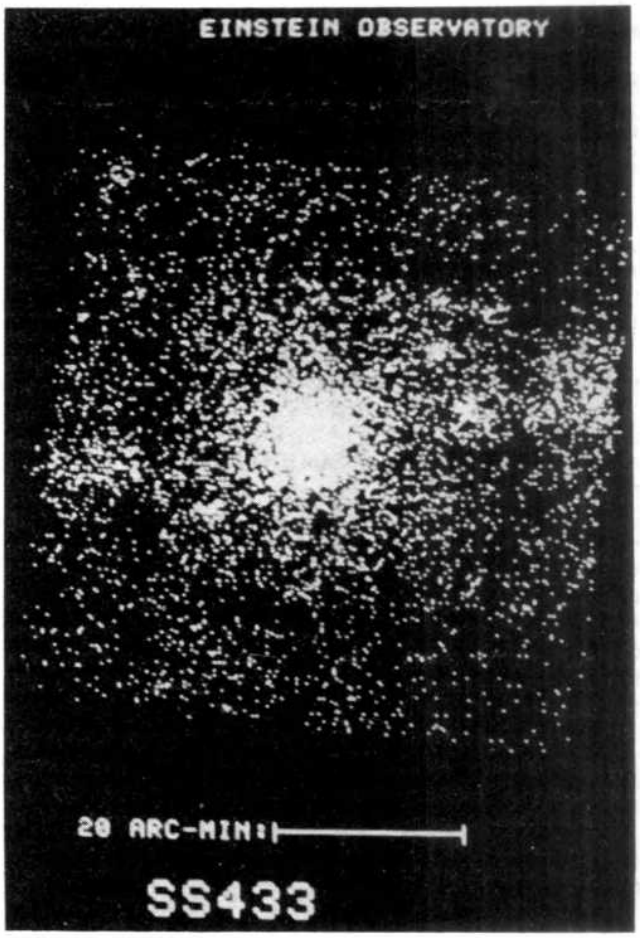

Fig. 1 X-ray emission from the central region of W50. The field of view is 1° × 1°. The bright central source is SS433. Diffuse X-ray emission is observed from a narrow region extending from east to west and roughly aligned with the central object.

The X-ray flux from the point source, SS433, is ~2×10^{-11} erg cm^{-2} s^{-1}. The X-ray flux from the diffuse source is ~3×10^{-12} erg cm^{-2} s^{-1}. At a distance of 3.7 kpc, these convert to luminosities of ~10^{35} and ~10^{34} erg s^{-1}, respectively. A factor of ~2 correction for low energy absorption (as expected for a ~3.7 kpc distance) has been applied. This is apparent in the X-ray spectra for both SS433 and diffuse emission, but actual spectral fits must await further IPC calibration analysis.

We consider two processes by which the beams might produce X-ray emission. First, the diffuse X rays could be produced thermally by hot plasma sustained by kinetic energy from particles in the beams. A possible mechanism for such heating is a shock generated by the beams interacting with the ambient medium (W. Tucker, personal communication). For an assumed X-ray spectral temperature of 10^7 K, the derived electron density is ~10^{-1} cm^{-3} and the total thermal energy contained in the plasma is 1×10^{49} erg. If the plasma has been built up over 10^3 yr, the required energy input for heating is 3×10^{38} erg s^{-1}, comparable in magnitude to the kinetic energy flow in the beams computed from the spectroscopic data[15]. Only 3×10^{-5} erg s^{-1} of this energy is required to account for the energy radiated as diffuse X rays. We conclude that the beam kinetic energy is sufficient to account for this plasma, and that a significant fraction of the beam kinetic energy might be dissipated in heating the plasma.

A second possibility is that the diffuse emission, which is detected at ~0.5–3 keV and may thus be relatively hard, is synchrotron radiation. The *in situ* production of relativistic particles by beams in regions distinct from a central compact source is clearly suggestive of the type of processes that have been invoked for double-lobed radio galaxies and QSOs. A self-consistent synchrotron model for the X-ray emission would require a magnetic field $B\approx10^{-5}$ G, 3×10^{42} electrons with Lorentz factors $\gamma\approx10^{8}$ and energy-loss lifetimes of $\sim10^{3}$ yr. Such electrons must have a total energy content of $\sim3\times10^{44}$ erg to account for the X-ray emission. Because the electron lifetime is comparable with its expected residence time in the beam (if $v\approx0.285c$), each relativistic electron radiates a significant fraction of its energy during the period of transit to the edge of the SNR.

As no clear radio counterpart to the X-ray beams is discernible above the radio background of the SNR, a lower limit of $\alpha\approx-0.8$ ($S\propto\nu^{\alpha}$) may be set for the spectral index α of the beam emission between the X-ray and radio region. Note that if $\alpha\approx-0.6$, similar to that in the radio for SS433 itself, the minimum energy in the form of relativistic electrons is 10^{47} erg, and could be as high as 3×10^{48} erg if the (unobservable) protons are included.

Regardless of which process is occurring, the internal co-moving energy density (or pressure) computed for the beams is within an order of magnitude of that resulting from relativistic particles and magnetic fields external to the beam and contained within W50, as known from the observed radio emission (see ref. 15). Thus, the beam may be confined laterally by the external medium within W50.

We have emphasized agreement with the kinematic jet model which is the model in best agreement with most data. Note that the X-ray data alone do not exclude other models. An accretion disk around a black hole, for example, could supply the high velocity material observed optically and also an axis of rotation along which escaping material might flow to form opposing 'jets' responsible for the diffuse X-ray emission.

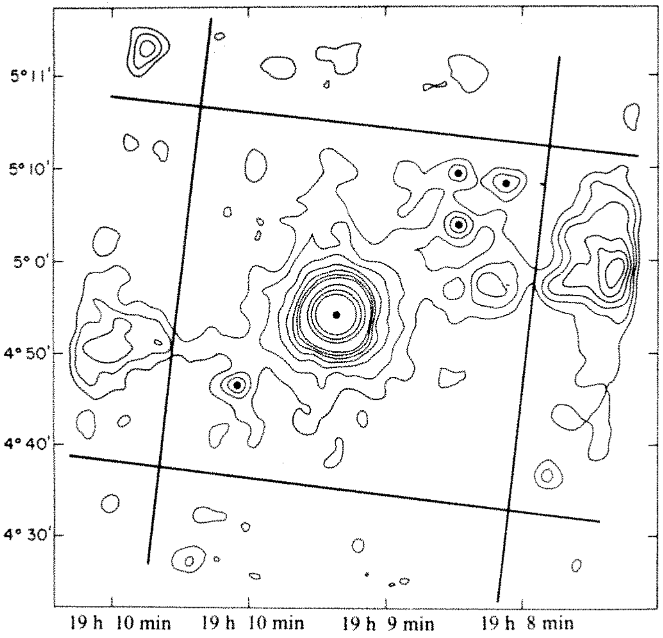

Fig. 2 Contours of constant X-ray brightness derived from data shown in Fig. 1. A correction has been made for vignetting in the telescope. Bars show detector window supports which shadow the diffuse emission. The positions of four other unidentified sources in the field are indicated. Contours showing diffuse emission are linear in increments of 5×10^{-15} erg cm^{-2} s^{-1} arc min^{-2}. Contours close to SS433 have larger increments and only show the instrument response to a strong point source.

Finally, we return to the above noted similarities between SS433 and mechanisms believed to occur in radio galaxies[5]. The similarity is in morphology but is seen in different spectral regions. In SS433, X-ray emission is seen and in the radio galaxies only radio emission is detected, that is, the ratio of X-ray to radio luminosity is very different. This fundamental spectral difference could be due to the enormous difference in size scale between the phenomena of SS433 and radio galaxies, although the primary acceleration processes may be the same. Given the same initial particle energy spectrum and assuming the X rays in the SS433 beams to be synchrotron in origin, the different ratio of X-ray to radio luminosity in these objects may be due to a different ratio of radiative lifetime to residence time in the emitting volumes. In radio galaxies, the particle residence times may be sufficiently long that we now predominantly see the radiation from the lower energy particles. In SS433, however, the radiative to residence times may be comparable; hence, we see more X-ray radiation.

This research was supported by NASA contract NAS 8-30751 and by the Einstein Guest Observer Program.

Received 11 August; accepted 7 October 1980.

1. Clark, D. & Murdin, P. *Nature* **276,** 44 (1978).
2. Margon, B. *et al. Astrophys. J. Lett.* **230,** L41 (1979).
3. Abell, G. & Margon, B. *Nature* **279,** 701 (1979).
4. Margon, B., Grandi, S. & Downes, R. *Astrophys. J.* (submitted).
5. Fabian, A. & Rees, M. *Mon. Not. R. astr. Soc.* **187,** 13p (1979).
6. Crampton, D., Cowley, A. & Hutchings, J. *Astrophys. J. Lett.* **235,** L131 (1980).
7. Ruffini, R. & Stella, L. *Nuovo Chim. Lett.* **27,** 529 (1980).
8. Giacconi, R. *et al. Astrophys. J.* **230,** 540 (1979).
9. Kaplan, G. H., Kallarkal, V. V., Harrington, R. S., Johnston, K. J. & Spencer, J. H. *Astrophys. J.* **85,** 64 (1980).
10. Gilmore, W., Seaquist, E. R., Grindlay, J., Seward, F. & Johnston, K. J. (in preparation).
11. Geldzahler, B., Pauls, T. & Salter, C. *Astr. Astrophys.* **84,** 237 (1980).
12. Spencer, R. E. *Nature* **282,** 483 (1979).
13. Gilmore, W. & Seaquist, E. R. *Astrophys. J.* (submitted).
14. Walker, R. C. *et al. Astrophys. J.* (submitted).
15. Begelman, M. C., Sarazin, C. L., Hatchett, S. P., McKee, C. F. & Arons, J. *Astrophys. J.* **238,** 722 (1980).
16. van Gorkom, J., Goss, W. & Shaver, P. *Astr. Astrophys.* **82,** L1 (1980).
17. van Gorkom, J., Goss, W., Gilmore, W. & Seaquist, E. R. (in preparation).

Light from electron avalanches and background rejection in X-ray astronomy

O. H. W. Siegmund, P. W. Sanford, I. M. Mason, J. L. Culhane & R. Cockshott

Mullard Space Science Laboratory, University College London, Dorking, Surrey RH5 6NT, UK

We have developed the parallel plate imaging proportional counter to register images of cosmic X-ray sources in the focal planes of X-ray telescopes[1,2]. An important factor determining the sensitivity of such an instrument, particularly for extended source studies, is the background count rate induced in the detector by the interaction of charged particles such as cosmic rays. This background in wire anode proportional counters can be reduced by applying risetime discrimination to the charge pulse[3]. We report here that a modified version of the parallel plate imaging proportional counter has been constructed as shown in Fig. 1*a*, to investigate the application of risetime discrimination to the scintillation pulses caused by the electron avalanche process[4]. We show that efficient background event rejection (>90%) is achieved and discuss an application of this system for X-ray astronomy.

An X-ray absorbed in the region between grid and the thin window produces a localized ionization cloud. The electrons in this cloud drift to the grid under the influence of a small electric field. A high electric field exists between the grid and the anode, accelerating the electrons to energies at which a Townsend avalanche occurs[5]. Light is emitted as a result of the ionizations and excitations which take place in this avalanche.

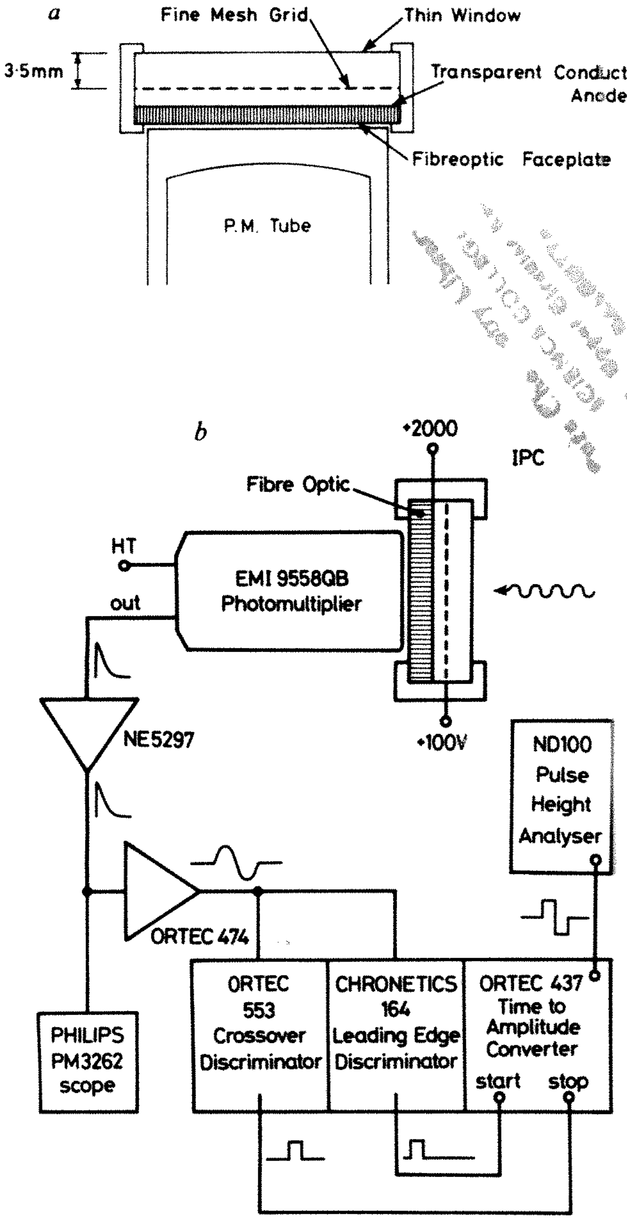
a
Fine Mesh Grid
Thin Window
3·5mm
Transparent Conductive Anode
Fibreoptic Faceplate
P.M. Tube
b
+2000
IPC
Fibre Optic
HT
out
EMI 9558QB Photomultiplier
NE5297
+100V
ND100 Pulse Height Analyser
ORTEC 474
ORTEC 553 Crossover Discriminator
CHRONETICS 164 Leading Edge Discriminator
ORTEC 437 Time to Amplitude Converter
start
stop
PHILIPS PM3262 scope

Fig. 1 *a*, Imaging scintillation proportional counter. *b*, Experimental configuration.

Figure 1*b* shows the experimental configuration used to investigate the risetimes of light pulses induced by X-ray and cosmic ray events. Light pulses are detected by an EMI 9558QB photomultiplier, which has an S20 photocathode and a minimum risetime of ~15 ns. The signals from the photomultiplier are then amplified and shaped to give a bipolar pulse. A measure of risetime is now obtained from the time interval Δt between the leading edge and crossover of the bipolar pulse. The risetime spectrum in terms of Δt was then calibrated against true risetime by direct observation of the photomultiplier signals by a fast oscilloscope (~3 ns minimum response).

The risetime spectra in Fig. 2 were obtained for Al K X rays (1.487 keV) and ^{60}Co γ rays over a limited pulse height band (1.2–1.8 keV). ^{60}Co was used because because it provides a reasonable simulation of 'in-flight' background for risetime discrimination systems[9]. Note that the events with risetimes faster than ~10 ns are due to noise.

For the gases used in this study the size of the electron cloud on reaching the grid is dominated by diffusion[2]. For Ar (90%)/CH$_4$ (10%) the maximum size (FWHM) of the electron cloud produced by an X-ray photon of a few keV is ~0.7 mm (ref. 6) (for a drift region 3.5 mm deep and a drift field of 300 V cm^{-1}). If the time development of the scintillation pulse is determined by the drift of the electron cloud across the grid, an estimate of the pulse risetime may be obtained by dividing the cloud size by the drift velocity. In Ar (90%)/CH$_4$ (10%) the drift velocity for the field of 300 V cm^{-1} is ~5 cm μs^{-1} (refs 6–8), giving a maximum pulse risetime of 14 ns. As this is comparable with the 15 ns minimum time response of the photomultiplier all the X-ray risetimes are centred on this value (Fig. 2). More recent investigations with a faster photomultiplier (EMI 9818 QBM, ~2 ns minimum response) have shown that the maximum risetime is ≲14 ns.

Relativistic charged particles such as cosmic rays or Compton electrons resulting from γ-ray interactions produce an extended track of low specific ionization in the drift region. Such particles may, therefore, give rise to energy pulses in the range of the X rays to be detected and will consequently contribute to the background. The scintillation pulses from these events will have risetimes up to a maximum given approximately by the total drift depth divided by the drift velocity. For a drift space of 3.5 mm and a drift velocity of 5 cm μs^{-1}, a maximum pulse risetime of ~70 ns results (Fig. 2). Both risetime distributions in Fig. 2 are consistent with the above estimates.

Figure 2 shows that charged particle rejection may be achieved by using risetime discrimination on the light pulse in a similar manner to that used for the charge pulse in proportional counters. Figure 3 demonstrates the ^{60}Co γ-ray rejection efficiency as a function of the X-ray rejection efficiency. It is possible to reject 91% of the γ-ray events for a loss of only 5% of the X-ray events. This represents a significant improvement over present parallel plate proportional counters[2] in which only ~50% of the γ-ray events may be rejected using charge pulse risetime discrimination. For X-ray astronomy this will result in a significant increase in instrument sensitivity. The sensitivity of an X-ray telescope of a fixed area is determined by the diffuse X-ray background, the cosmic ray background and the spatial resolution of the instrument (in the case of point sources). Rocket flight experience with a similar detector allows us to

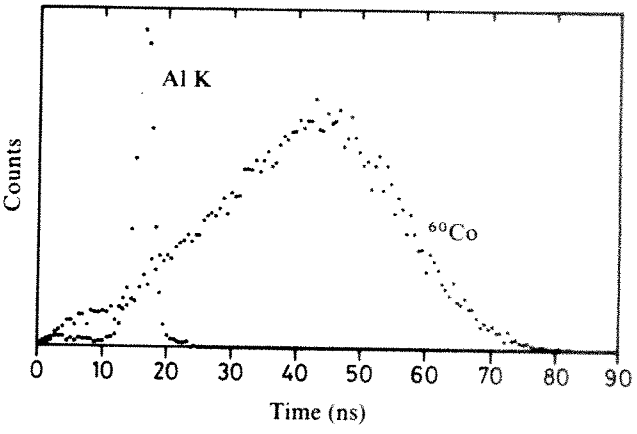

Fig. 2 Risetime spectra for a Al K X rays and ^{60}Co γ rays.

estimate the cosmic-ray background expected in flight. Taking an effective mirror area of 500 cm^2 for the range 0.1–2 keV we find that the count rate per pixel from the diffuse X-ray background is ~50% of the cosmic ray rate at low magnetic latitudes. Hence rejection of 90% of the cosmic ray background will allow the telescope sensitivity to be determined by the diffuse X-ray background, and independent of latitude variations in cosmic ray background, which can be as much as a factor of 3. This is especially important for studies of extended sources because the signal-to-background ratio is independent of the detector pixel size.

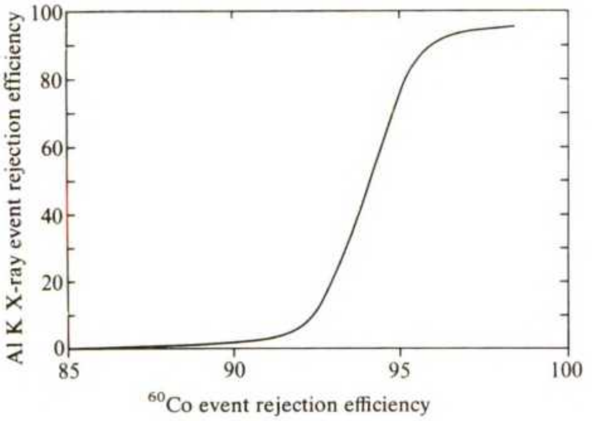

Fig. 3 ^{60}Co background rejection efficiency for risetime discrimination.

Note that for a geometrical X-ray telescope mirror area of 1,000 cm^2, a third magnitude star would result in 2×10^5 individual photon events s^{-1} in the photomultiplier, after attenuation by the counter window and anode. Most of these events will not be registered if a discriminator is used with a threshold set at a few photoelectrons equivalent pulse height. The background light from stars should not generally present a problem, however, because the density of stars brighter than third magnitude is only 2.5×10^{-3} deg^{-2}.

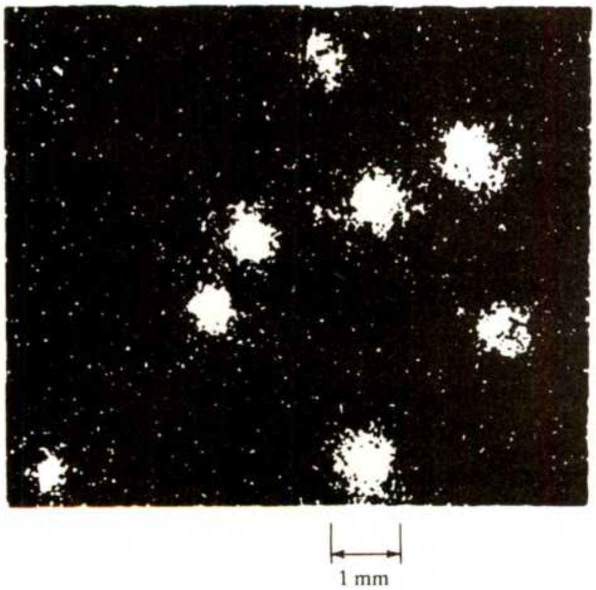

Fig. 4 Scintillation flashes produced by individual ^{55}Fe X rays in Ar (90%)–CH_4 (10%).

An investigation of the spectral distribution characteristics of the light emitted by Ar (90%)/CH_4(10%) has shown that there are two main emission bands centred on 750 nm and 420 nm, both bands having FWHM of ≤50 nm. The ratio of the intensity of the band at 750 nm to that at 420 nm is about 14 : 1. At a charge gain of 5×10^4 in Ar (90%)/CH_4 (10%) using Al K X rays a total of the order of 10^4 photons are produced for each X-ray photon event. Because the main emission band at 750 nm is reasonably narrow it should be possible to reduce the starlight background by factor of 15 using a narrow band filter transmitting between 700 and 800 nm.

Because most of the scintillation emission occurs within the last mean free path of the electrons in the avalanche region, it is possible to locate individual X-ray events from the scintillation pulse using a fibre optic faceplate and a transparent anode deposited on its surface. Figure 4 shows the localized flashes produced with Ar (90%)/CH_4 (10%) under irradiation by Mn K X rays (5.9 keV), recorded on film by means of an image intensifier. We are developing an optical detection system which will enable the centroid of each flash to be determined electronically. This work should lead to the development of a detector whose positional resolution is limited only by diffusion of the primary electron cloud in the drift space.

We thank Professor R. L. F. Boyd for helpful discussions, and H. Goddard and L. Goddard for construction of the detector. This work was supported by the SRC.

Received 12 June; accepted 12 September 1980.

1. Stumpel, J. W., Sanford, P. W. & Goddard, H. F. *J. Phys. E.* **6,** 397–400 (1973).
2. Sanford, P. W., Mason, I. M., Dimmock, K. & Ives, J. C. *IEEE Trans. Nucl. Sci.* **NS 26,** No. 1, 169–172 (1979).
3. Mathieson, E. & Sanford, P. W., *Proc. Inst. Symp. Nuclear Electronics, Paris,* **65** (1963).
4. Campion, P. J. *Int. J. appl. Radiat. Isot.* **19,** 219–234 (1968).
5. Townsend, J. S. *Electrons in Gases* (Hutchinson, London, 1947).
6. Paladino, V. & Sadoulet, B. *Nucl. Instrum. Meth.* **128,** 323–335 (1975).
7. English, W. N. & Hanna, G. C. *Can. J. phys.* **31,** 768–797 (1953).
8. Schultz, G. & Gresser, J. *Nucl. Instrum. Meth.* **151,** 413–431 (1978).
9. Cooke, B. A., Griffiths, R. E. & James, A. F., *Nucl. Instrum. Meth.* **106,** 147–155 (1973).

Distribution of cosmic-ray electrons in the Galaxy

M. R. Issa, P. A. Riley, A. W. Strong & A. W. Wolfendale

Department of Physics, University of Durham, South Road,
Durham DH1 3LE, UK

Although it seems that cosmic-ray electrons in the range 100–300 MeV are mostly generated in sources within the Galaxy (extragalactic electrons are kept out by the 2.7 K relict radiation) their distribution is not known. Studies of electron synchrotron radiation in the region of hundreds of MHz indicate that the synchrotron emissivity varies with position, generally decreasing as the galacto-centric distance, *R*, increases, but such dependence could be in either the electron flux, I_e, or the magnetic field strength, *H*, (emissivity $\propto I_e H^2$) or both. We examine here the distribution of I_e itself from studies of the γ-ray flux produced by electrons interacting in the interstellar medium by way of the dominant bremsstrahlung mechanism.

Using γ-ray data to find the distribution of cosmic rays has long been considered; for example, Dodds *et al.*[1] have reviewed the distribution of a mixed proton–electron component from analysis of γ rays above 100 MeV towards the galactic anticentre. Here, SAS 2 satellite data[2–4] is used in the energy range 35–100 MeV coupled with information on the distribution of target gas in the Galaxy.

In this energy range, the 1σ radius of the angular resolution function of the SAS 2 telescope for individual photons is 6°. Fichtel *et al.*[2] presented their data in the form of a number of photons observed in bins of equal solid angle (6.06×10^{-4} sr), each covering 2.5° in longitude, together with the relative sensitivity of the telescope for each bin. The above energy range is useful because the contribution to the γ-ray intensity from protons and heavier nuclei is small. Proton-induced γ rays come mainly from π^0 decay and the resulting γ spectrum has a peak at about 70 MeV ($m_\pi c^2/2$) whereas the spectrum of γ rays from electron bremsstrahlung falls continuously with increasing γ-ray energy. The overall spectral shape of γ rays indicates that π^0 and e-production do not become equal until ~170 MeV, leading to the conclusion that only ~10% of cosmic γ rays in the energy range 35–100 MeV result from π^0 decay. For γ rays in this energy range the corresponding electron energy is between about 70 and 300 MeV.

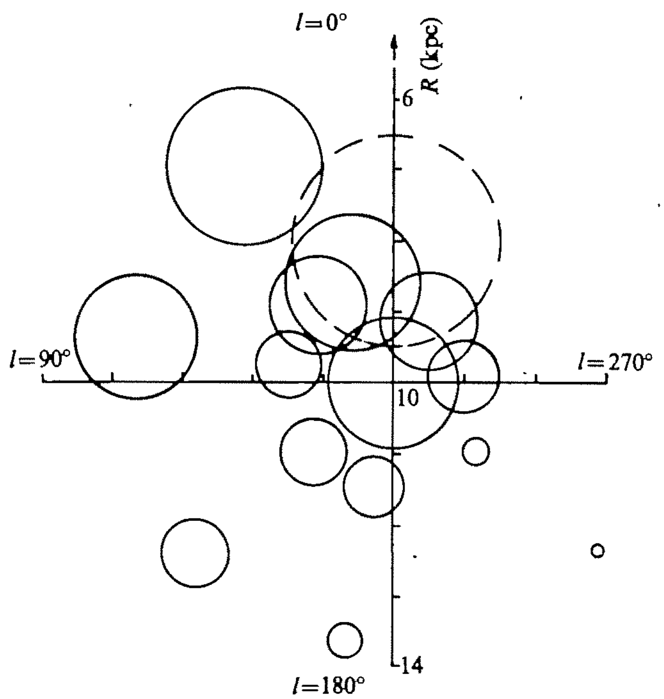

Fig. 1 Plan view of the Galaxy showing the intensity of cosmic-ray electrons in the region of several hundred MeV as a function of position in the local region. The electron intensity is proportional to the radius of the circle. Uncertainties in intensity are typically 30%. For absolute intensities see Fig. 2. The centres of the circles are the average positions to which the intensities refer; the positions are necessarily imprecise (uncertainty ~30% of distance to the Sun). The dotted circle relates to an attempt to allow for the contribution of discrete sources; the uncertainty is greater than for the other intensity estimates. The vertical scale is the distance from the galactic centre, *R*.

Previous analyses[5–7] have studied facets of this problem (although not in the present energy range) but here we examine the problem using recent data on gas densities and taking full recognition of various experimental factors (for example, the angular resolution function of the telescope). The object is to answer the specific question: how are energetic electrons distributed in the Galaxy?

We divide the γ-ray data into bands of longitude and latitude and for each find the value of $q/4\pi$ in the expression $I_\gamma = (q/4\pi)N_H + I_b$, where N_H is the volume density of target gas and I_b is the background (or more specifically, the component uncorrelated with the gas). q is proportional to the average electron intensity along the appropriate line of sight and, as a first approximation, can be taken to be proportional to $I_e(l, b, r)$ where r is the distance along the line of sight to a point $z(\frac{1}{2})$ above the galactic plane, $z(\frac{1}{2})$ being the half-thickness of the gas layer.

We have not tried to remove the contribution of 'discrete' sources from the data because we believe that many are due to molecular clouds irradiated by the ambient cosmic ray flux. As the sources CG184−5 and CG263−2 have been unambiguously identified with the Crab and Vela pulsars, however, data from within a few degrees of these sources are not used in this analysis.

This approach has several problems, the most important being that, of the gas constituents, only the atomic column densities are available for most of the range of l and b (here we adopt the Berkeley measurements[8]). The important H_2 column densities are readily available in restricted regions only, for example, $10° < l < 82°$, $b = 0°$ (±1°) (refs 9, 16) and from indirect analyses using galaxy counts[10–12] at $|b| > 10°$. The low counting statistics involved in the γ-ray results mean that a large area of the sky must be considered to obtain results with sufficient accuracy to be useful and such a wide coverage is not yet available in the case of the H_2 column densities. The H_2 column densities are, nevertheless, too large to be ignored completely. Gordon and Burton[9] presented measurements of the 2.6-mm line of CO which suggest that locally the surface densities of H I and H_2 (in atoms cm^{-2}) are about the same but their data for the local region (within 2 kpc of the Sun) may be too high, for two reasons. First, the quoted value for the local region is an average round the Galaxy at $R \sim 10$ kpc and most of the weight for the actual value comes from regions very remote from the Sun. The second point is that the formaldehyde results[13], Copernicus UV measurements[14], the analysis of Blitz and Shu[15] and our Galaxy count results favour values of N_{H_2}/N_{HI} in the range 0.25–0.5. The lack of detailed knowledge of the H_2 column density in the directions being studied can, however, be at least partially overcome if the correlation between H I and H_2 column densities can be shown to be small.

General arguments suggest poor correlation, mainly the fact that the molecular hydrogen occurs largely in dense clumps and the well-known observation that the thickness of the H_2 layer is only half that of the atomic hydrogen layer. A more detailed analysis gives the following. Galaxy count studies show a negligible correlation for the range $60° < l < 240°$ but a significant correlation for $10° < l < 60°$ (all for $|b| = 10$–$20°$). This negligible correlation for $60° < l < 240°$ would also be expected to apply for latitudes below 10°, largely because in the outer Galaxy the amount of H_2 decreases rapidly with increasing galacto-centric radius. Thus, we believe that the q-values derived from an I_γ, N_{HI} analysis give a good representation of the trend of I_e and R here, that is for $R \gtrsim 9$ kpc (we assume that the sum is at $R = 10$ kpc).

In the inner Galaxy the correlation between H I and H_2 causes more difficulty, but even here it is not insurmountable. Inspection of the CO and H I data at $b = 0°$ (summarized by Burton and Gordon[16]) show that both follow the same general decrease over the range $l = 10$–$65°$. However, large variations in the column densities of both components also occur on a smaller scale ($\Delta l \sim 1$–$5°$). These smaller-scale variations are sometimes of the order of 50% of the overall decrease in the range $l = 10$–$65°$ and the variations in CO seem uncorrelated with those in H I. If the longitude range is split into the two ranges $l = 10$–$35°$ and $l = 35$–$65°$, to be considered separately, then the smaller-scale variations are found to be large enough compared with the overall variation in column density to treat the H I and H_2 column densities as being effectively uncorrelated. The limited statistical accuracy of the data and the fact that the angular resolution is several degrees means that a rather large range of latitude must be considered (we take various regions, mainly with $|b| < 5.6°$ and $|b| = 2.4–12.8°$); thus, the contribution of H_2 will be much smaller than that at $b = 0°$ and the correlation effect even smaller. Considering $|b| < 12.8°$ the values of $(q/4\pi)$ are 3.4 ($l = 10–65°$), 3.8 ($l = 10–35°$), and 2.8 ($l = 35–65°$) × 10^{-26} s^{-1} sr^{-1} atom^{-1}. These indicate that there is very little correlation in this range, as correlation would cause the q value for $l = 10–65°$ to be bigger than for the divided ranges.

The data are analysed by plotting I_γ against N_{HI} (from ref. 8) and finding the maximum likelihood estimators of $q/4\pi$ and I_b in the expression $I_\gamma = (q/4\pi)N_{HI} + I_b$. If N_{H2} is uncorrelated with N_{HI} then the mean contribution of H_2 to the γ-ray flux in the region being considered will appear as a component of I_b, leaving $q/4\pi$ as the γ-ray emissivity of the atomic hydrogen gas. The present analysis differs from that of Fichtel *et al.*[6] in including the angular resolution of the SAS 2 telescope and in the more detailed analysis of the data in each longitude and latitude range.

Figure 1 shows the relative values of I_e; the radii of the circles are proportional to $q/4\pi$ at the position in the galactic plane (relative to the Sun) represented by their centres. The distance from the Sun to which each measurement of $q/4\pi$ refers is taken to be the distance along the line of sight to a point $z(\frac{1}{2})$ above the galactic plane. The goodness of fit of the lines to the data points gives an estimate of the uncertainty in the value of $q/4\pi$ and this is roughly 30%. Figure 1 shows a dispersion of intensities about a smooth dependence on galacto-centric radius such as corresponds to the estimated individual errors except for the intensities in the quadrant $l = 180°$ to 270° are singularly low. Such very intensities are probably real, however, and no doubt relate to the dearth in likely cosmic ray sources in this region (such as H II regions, and OB associations). The low values in general in the direction of the anticentre are particularly firm in view of their lack of contamination by the effects of molecular hydrogen.

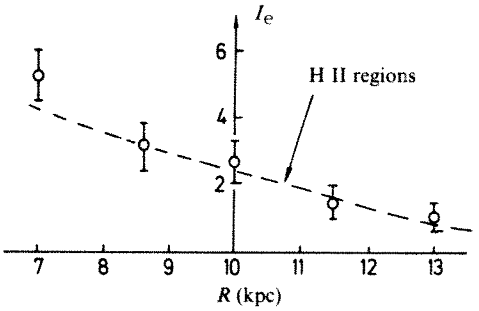

Fig. 2 Average intensity of cosmic-ray electrons as a function of galacto-centric radius, R, for the region covered by Fig. 1. I_e ($R = 10$ kpc) $\simeq 8 \times 10^3$ m^{-2} s^{-1} sr^{-1} GeV^{-1}. The dotted line is the average distribution of the number density of H II regions above a fixed threshold[15]. H II regions are not necessarily the sources of the electrons: many other astronomical objects have similar radial distributions, although it is interesting that the dearth of electrons at $R < 2$ kpc is mirrored by a deficit of H II regions (this is a difficult region in which to see the other objects) and the same situation arises for the region l, 180°–270°.

The data can be combined, assuming radial symmetry, to give the average radial distribution of electron intensity in the vicinity of the Solar System (within a few kpc of the Sun). Figure 2 shows the result.

The distribution of electrons nearer to the galactic centre than shown in Figs 1 and 2 can be studied using the unfolding technique to give the radial distribution of γ-ray emissivity; this is then divided by the gas density to give the electron intensity. Such unfoldings of the γ-ray data have been performed[17,18] and assume cylindrical symmetry of the γ-ray emissivity of the galactic disk to derive its radial distribution from the variation of the flux with galactic longitude. The method suffers because of large uncertainties in the amount of molecular gas in the inner Galaxy. Here, as no sophisticated analysis is possible, the earlier results are very doubtful.

New data on gas densities[19,20] have renewed interest in this method, however, at least for the central region of the Galaxy ($R \leq 2$ kpc). These data give a much higher mass of gas than previously suspected (and account for its non-observation previously). Specifically, Liszt and Burton[19] quote a mass of at least $10^9 M_\odot$ and Linke *et al.*[20] favour $8 \times 10^9 M_\odot$. These masses are high enough to derive important conclusions even allowing for some uncertainty in their magnitude.

We have made a new determination of the emissivity versus galacto-centric radius using the γ-ray line flux from Fichtel *et al.*[4] in the range 35–100 MeV. The γ-ray emissivity averaged within $R = 2$ kpc is $\sim 10^{40}$ γ's (35–100 MeV) kpc^{-2} s^{-1} (an essentially upper limit which does not depend at all sensitively on the unfolding assumptions), and the electron intensity required, using a mass of $8 \times 10^9 M_\odot$, is only 4% of the local value. Such a small value is difficult to explain in terms of exclusion of electrons from molecular clouds insofar as the gas seems to be rather smoothly distributed[17] rather than in clumps which could conceivably have associated excluding magnetic fields. If the gas data are correct it suggests that the electron intensity is very low (the arguments here relate to a region much larger than the 300-pc ring very close to the galactic centre for which different arguments apply[21]). Evidence on the deficit of likely sources of energetic electrons at $R < 2$ kpc is hard to come by; however, some data on H II regions (which are indicators of energetic phenomena) show a similar deficiency below 2 kpc (ref. 20). The most important feature is probably that not only are sources infrequent here but that diffusive motion is so small and the space is not filled with particles propagating from elsewhere.

Clearly there are significant variations in the intensity of cosmic-ray electrons over the Galaxy. A fall off at $R > 10$ kpc and a reduction by at least an order of magnitude, compared with the local intensity, for $R < 2$ kpc seem particularly firm.

We thank Professor W. B. Burton and Dr J. L. Osborne for useful discussions and Professor P. Thaddeus and Dr A. A. Stark for helpful correspondence.

Received 4 July; accepted 22 September 1980.

1. Dodds, D., Strong, A. W. & Wolfendale, A. W. *Mon. Not. R. astr. Soc.* **171,** 569 (1975).
2. Fichtel, C. E. *et al. NASA Tech. Mem.* 79656, GSFC, Greenbelt (1978).
3. Derdeyn, S. M. *et al. Nucl. Instrum. Meth.* **98**, 587 (1972).
4. Fichtel, C. E. *et al. Astrophys. J.* **198**, 163 (1975).
5. Stecker, F. N. *The Structure and Content of the Galaxy and Galactic Gamma Rays, Goddard Space Flight Center*, X-662-76-154, 357 (1976).
6. Fichtel, C. E., Simpson, G. A. & Thompson, D. J. *Astrophys. J.* **222,** 833 (1978).
7. Wolfendale, A. W. & Young, E. C. M. *Proc. 12th ESLAB Symp.* (eds Wills, R. D. & Battrick, B.) 157 (ESA, Frascati, 1977).
8. Weaver, H. & Williams, D. R. W. *Astr. Astrophys. Suppl.* **8,** 1 (1973).
9. Gordon, M. A. & Burton, W. B. *Astrophys. J.* **208,** 346 (1976).
10. Lebrun, F. & Paul, J. A. *Astr. Astrophys.* **65,** 187 (1978).
11. Strong, A. W. & Lebrun, F. *Astr. Astrophys.* (in the press).
12. Issa, M. R., Strong, A. W. & Wolfendale, A. W. *J. Phys. G.* (in the press).
13. Few, R. W. *Mon. Not. astr. Soc.* **187**, 161 (1979).
14. Bohlin, R. C., Savage, B. O. & Drake, J. F. *Astrophys. J.* **224**, 132 (1978).
15. Blitz, L. & Shu, F. H. *Astrophys. J.* **238**, 148 (1980).
16. Burton, W. B. & Gordon, M. A. *Astr. Astrophys.* **63,** 7 (1978).
17. Strong, A. W. *J. Phys.* **A8,** 617 (1975).
18. Caraveo, P. A. & Paul, J. A. *Astr. Astrophys.* **75**, 340 (1979).
19. Liszt, H. S. & Burton, W. B. *Astrophys. J.* **226,** 790 (1978).
20. Linke, R. A., Stark, A. A. & Frerking, M. A. *Astrophys. J.* (in the press).
21. Wolfendale, A. W. *Origin of Cosmic Rays IUPAP/IAU Symp.* No. 84 (eds Setti, G., Spada, G., & Wolfendale, A. W.) (Reidel, Dordrecht, 1980).

The dynamic expansion and contraction of the jovian plasma sheet

J. W. Belcher & R. L. McNutt Jr

Department of Physics and Center for Space Research, Massachusetts Institute of Technology, Cambridge, Massachusetts 02139

We report here that near noon in the magnetosphere of Jupiter, plasma is observed to flow away from the equatorial current sheet. The motion reverses near dusk, with a subsequent infall of plasma towards the sheet on the nightside. We associate this motion with the compression of magnetic flux tubes on the dayside and their subsequent expansion on the nightside due to the solar wind interaction with Jupiter. Such compression and expansion may be sufficiently rapid that the plasma in the sheet cannot reach quasi-static equilibrium. Dynamic motions at transonic velocities ensue.

The plasma instrument on board the Voyager spacecraft consists of four modulated-grid Faraday cups which measure positive ions and electrons with energies per charge in the range 10–5,950 V (ref. 1). Three of these cups are arranged in a cluster whose symmetry axis normally points towards the Earth. The fourth cup (the D cup) is situated so that its axis is perpendicular to the symmetry axis of the main cluster. The trajectory of Voyager 2, and the orientation of the sensor normals at various points along that trajectory, are shown in Fig. 1; the Voyager 1 trajectory and sensor orientations are qualitatively similar. Plasma flow in the jovian magnetosphere has a tendency to co-rotate with the planet, that is, to move azimuthally at the rotation rate of the planet. The D cup is orientated so that azimuthal flow moves almost directly into that cup on the inbound leg of the trajectory. Near closest approach, strictly co-rotating flow would move into the field of view of the main sensors, and after closest approach out of the field of view of all sensors.

The response functions[2] of the Voyager Faraday cups are broad, with 30% response at an angle of incidence of 60° to axes of cups in the main cluster, and 30% response at an angle of 40° to the side sensor axis. Over much of the inbound trajectory, there is at least one sensor for which the plasma flow velocity is within ~20° of the sensor normal. If, in addition, the plasma is reasonably supersonic (Mach $\geqslant 3$), the response function can be taken as unity. In such a situation, the analysis of the positive ion data from that sensor is relatively straightforward, although complicated by the fact that the jovian magnetospheric plasma consists of an admixture of many ionic species (H^+, S^+, S^{2+}, S^{3+}, O^+, O^{2+}, Na^+, SO_2^+). Such single sensor data have been exhaustively analysed since the Jupiter encounters for heavy ion densities and temperatures, as well as for the velocity component along the sensor axis[3–5]. However, only for a brief time near closest approach, and during isolated spacecraft manoeuvres, is the unit response assumption valid for more than one sensor. To obtain all three components of the plasma velocity, we must use information from at least three sensors; because two of the three are usually significantly oblique to the flow, it is necessary to use the full response functions of the sensors. The complete determination of the velocity is more complex and time consuming, and at present can only be done on a limited basis. We discuss some quantitative results from this analysis below.

First, however, we take advantage of the symmetry properties of two of the main cluster sensors with respect to the jovian equatorial plane to obtain some qualitative results about the plasma velocity component perpendicular to that plane. These qualitative results are quantitatively verified by our more sophisticated analysis below. When the attitude of the spacecraft is referenced to the star Canopus, the axes of the A and D cups are essentially in the jovian equatorial plane. The axes of the B and C cups, however, are inclined to that plane in a nearly symmetrical fashion, at angles of 18.6° south and 15.3° north, respectively, for Voyager 2. We compute the flux density in a given cup by taking the total current due to positive ions with energies per charge from 10 to 5,950 V, and dividing by the proton charge and the effective area of the sensor. Figure 2 shows the flux density of the B cup minus the flux density of the C cup, divided by the sum of the flux densities in the B and C cups for a portion of the Voyager 2 trajectory. Because of the orientation of the cups, this difference will be positive for flow towards the north and negative for flow towards the south. Figure 2 also plots the distance of the spacecraft above the magnetic dipole equatorial plane. We indicate at various points the local time, and the distance of the spacecraft from Jupiter, with perijove at 10.1 jovian radii (R_J) (9 July 1979 at 2230 h). We have only plotted data in Fig. 2 when the fluxes in the B and C sensors are high enough to allow a significant comparison, and when the spacecraft was on Canopus. Unfortunately, this means that we can use little data past 1400 h on 10 July 1979.

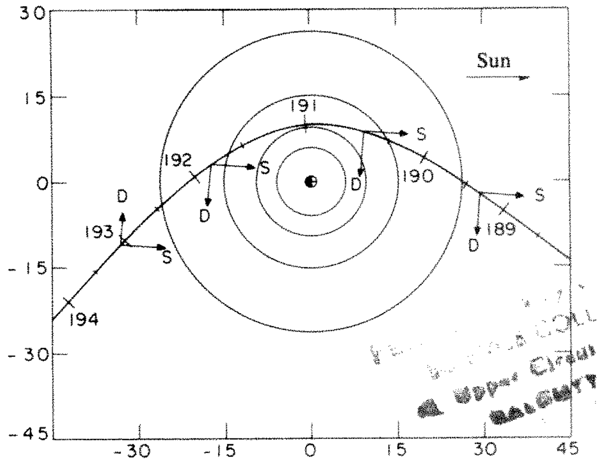

COLLEGE
Upper Circular Road
CALCUTTA

Fig. 1 The Voyager 2 trajectory projected onto the jovian equatorial plane. The line labelled S is the projection of the symmetry axis of the main cluster of Faraday cups, and the line labelled D is the projection of the D cup axis. The A and D cup axes are essentially in the jovian equatorial plane, with the A cup axis ~110° from the D cup axis. The B and C cup axes are inclined ~17° south and north of that plane, respectively, ~75° from the D cup axis. Tic marks along the trajectory are shown every 12 h, with day of year at the beginning of the day (day 190 is 9 July, 1979). The orbits of the four Galilean satellites are also shown. Distances are given in R_J.

Crossings of the magnetic dipole plane are reasonably accurate markers for crossings of the jovian current sheet, especially inside $20R_J$. From the Voyager 2 data in Fig. 2, and from similar plots of Voyager 1 data, it is clear that in the dayside jovian magnetosphere near noon, there is a marked tendency for plasma flow to be northward when the spacecraft is north of the magnetic dipole plane, and southward when the spacecraft is south of that plane—thus, the flow is away from the current sheet. This pattern is the same as that observed in Pioneer measurements of the anisotropies of MeV protons in the dayside middle magnetosphere[6,7]. The amplitude of the B–C difference decreases to zero with decreasing radius and increasing local time towards dusk. In the dusk to midnight sector, the B–C

0028-0836/80/440813—03$01.00

difference again increases with increasing radius and increasing local time towards midnight. However, in this sector the plasma flow tends to be northward when the spacecraft is south of the magnetic equator, and southward when it is north of the equator—that is, the flow is now towards the current sheet.

The flow pattern can also be seen in a detailed inspection of the positive ion spectra from the various sensors. Figure 3 shows a low-resolution scan of the positive ion flux density near the crossing of the magnetic equatorial plane near $20R_J$ on Voyager 2 inbound (see Fig. 2). The flux density spectrum in the D sensor is an unresolved superposition of H^+, O^{2+}, S^{3+} and S^{2+} (refs 4, 5). At this time, the B and C sensor normals are ~73° and ~67° from the rigid co-rotational flow velocity, with the D sensor normal only ~12° from that velocity. From these spectra, we conclude qualitatively that the flow velocity is mostly azimuthal at this time because the D sensor flux is much higher than fluxes in the main sensor. Moreover, the flow velocity must lie near the equatorial plane because of the near equality of the fluxes in the B and C cups. In contrast, Fig. 4 shows a low resolution scan of the positive ions during a dayside excursion of the spacecraft to $\sim 3.3R_J$ below the magnetic equatorial plane. The B and C sensor fluxes are comparable with those in the D sensor even though the sensor orientation is qualitatively the same as for the spectra in Fig. 3. This implies a significant component of velocity radially towards the planet during this interval. In addition, the C cup flux is larger than the B cup flux, implying a southward component of flow and thus a flow away from the current sheet. We also note that the main sensor is orientated such that there would be slightly more purely azimuthal flow into the C cup than the B cup on the inbound leg, and vice versa on the outbound leg. Thus even in the absence of any north/south flow, we qualitatively expect to see a negative signature in $(B-C)/(B+C)$ inbound and a positive signature outbound. In fact, the differences in Fig. 2 oscillate about a negative average value inbound and a positive average value outbound, as expected.

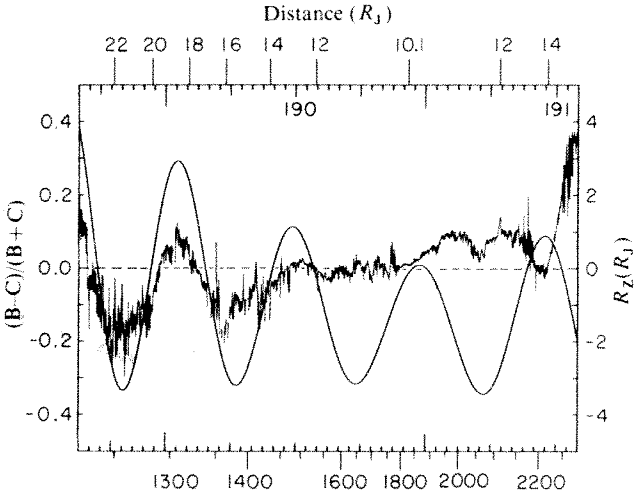

Fig. 2 The difference between the B and C cup fluxes divided by the sum of those fluxes, as a function of time during the Voyager 2 encounter, from 1600 h on 8 July, 1979 (day 189) to 1400 h on 10 July, 1979 (day 191). A positive value for this difference indicates northward flow. Also shown is the distance of the spacecraft above a magnetic dipole plane. Interior tic marks give spacecraft time at one hour intervals, with day of year given at 1200 h. We also indicate values of the local time and the radial distance from Jupiter.

This qualitative information on flow patterns is borne out by quantitative analysis of detailed measurements of the positive ion distributions in the various sensors. This analysis is essentially done in stages using an integration code which includes the full sensor responses. For example, we quote results obtained by Voyager 2 near 2009 h on 8 July 1979 (Fig. 4). The spacecraft was near noon, $21.6R_J$ from Jupiter and $-3.3R_J$ below the magnetic dipole plane. An analysis of the proton peak in the B, C and D sensors yields a density of 0.12 cm^{-3} and a thermal speed of 120 km s^{-1}. In a cylindrical coordinate system, where the z-axis is the rotation axis of Jupiter, the radial component of the proton velocity was -167 km s^{-1}, the azimuthal component was 264 km s^{-1} and the z-component was -95 km s^{-1}. These non-azimuthal velocity components should not be taken as typical, since for quantitative analysis, we must at present choose the most pronounced examples of the phenomenon. The azimuthal component here is slightly less than the 270 km s^{-1} velocity expected for rigid co-rotation[3]. In this interval, the plasma was flowing southward (away from the current sheet), in agreement with Fig. 2, and was also flowing radially towards Jupiter, a feature which cannot be deduced from Fig. 2. An analysis of spectra near midnight (at 1300 h on 10 July, 1979) yields similar results, except that the flow is now northward (towards the current sheet) and away from Jupiter.

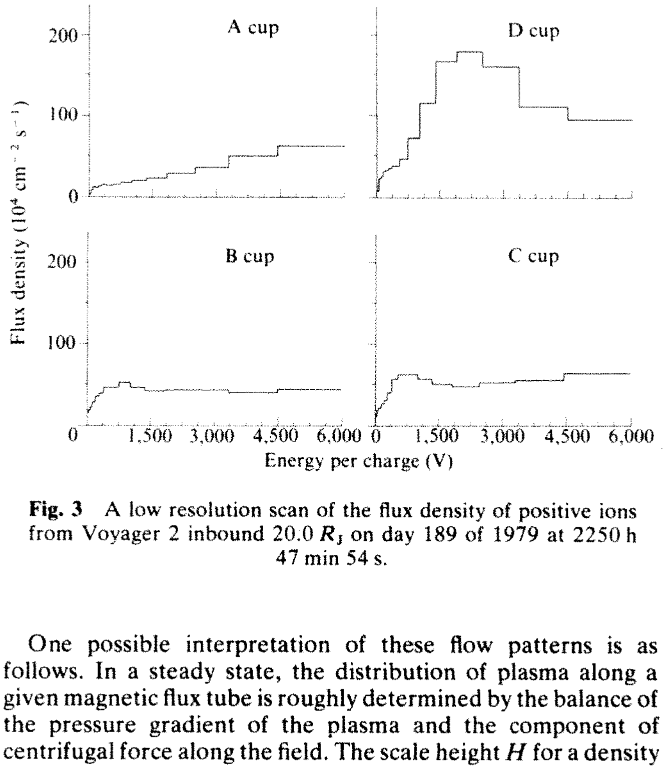

Fig. 3 A low resolution scan of the flux density of positive ions from Voyager 2 inbound 20.0 R_J on day 189 of 1979 at 2250 h 47 min 54 s.

One possible interpretation of these flow patterns is as follows. In a steady state, the distribution of plasma along a given magnetic flux tube is roughly determined by the balance of the pressure gradient of the plasma and the component of centrifugal force along the field. The scale height H for a density distributed in this way is the product of the sound speed C_s, the rotation period of the planet[8] and dimensionless factors of the order of $1/2\pi$. If this static situation is perturbed we still expect a quasi-static density distribution as long as the perturbation time scale is long relative to the dynamic time scale $2\pi H/C_s$. If the perturbation is short relative to this time scale, the plasma cannot adjust in a quasi-static fashion, and plasma motions with velocities up to C_s and beyond can result.

The dynamic time scale for the jovian plasma sheet is thus some fraction of the order of unity of the rotation period of the planet. However, the plasma sheet is perturbed on time scales of this order due to the compression of the dayside magnetosphere by the solar wind. Plasma will tend to move away from the plasma sheet as it moves into the dayside magnetosphere, because of both the compression and the decreasing component of centrifugal force along the field. Because of the rapid time scale, the adjustment of the plasma density distribution along the field line will not be quasi-static, and bulk motion along the field and away from the sheet can ensue. This motion will lead both to a north/south flow and a flow towards the planet on the dayside, as observed. At decreasing radial distances, the

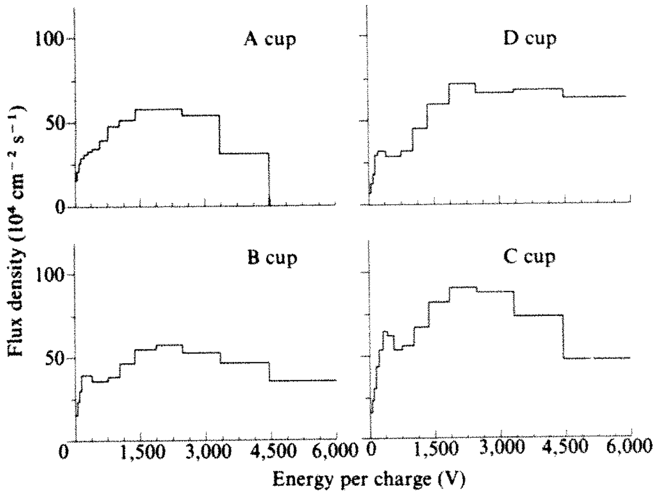

Fig. 4 A low resolution scan of the flux density of positive ions from Voyager 2 inbound 21.6 R_J on day 189 of 1979 at 2009 h 11 min 55 s.

perturbation associated with the solar wind is smaller and leads to a perturbed flow whose amplitude decreases with decreasing radial distance near noon, also in accord with observations (Fig. 2 and ref. 7). Past noon, the magnetic flux tube will begin to expand and move to larger distances. The expansion of the flux tube and the increasing component of centrifugal force will lead to a reversal of the plasma flow near dusk, and cause an infall of material at transonic (or supersonic) velocities in the nightside current sheet.

We note that this picture is very different from what would be expected from a quasi-static expansion and contraction of the plasma sheet due to the solar wind interaction. A quasi-static process would produce a sheet which was thickest at maximum compression (noon), and thinnest at minimum compression (midnight). Any small velocities associated with such a quasi-static process would be zero at noon and midnight, and maximal at dawn and dusk. In contrast, the dynamical velocity pattern described above, especially its phase, arises only in the absence of quasi-static equilibrium. The possibility of such a pattern depends on the fact that the solar wind interaction tends to perturb a given flux tube on the same time scale as it takes the plasma to come to static equilibrium.

These observations and our interpretation of them have two obvious implications for both theory and observation of the jovian magnetosphere. First, irreversible processes such as internal shocks or effective viscosities will lead to a net heating of the plasma as it expands away from and collapses towards the plasma sheet (that is, a fluid analogy of the acceleration mechanism of Goertz[9]). Second, theoretical models of the plasma sheet which assume quasi-static equilibrium, and interpretations of data based on such models, must be re-examined.

We thank H. S. Bridge and S. Olbert for discussions. This work was supported in part by NASA contract 953733.

Note added in proof: It has been suggested that the solar wind perturbation is slow enough to allow quasi-static solutions. This reasoning is based on a comparison of the solar wind perturbation time scale to the quasi-static equilibration time scale. Here we attempt to clarify our argument. In a plane parallel atmosphere,

$$\rho\frac{\partial \mathbf{v}}{\partial t} = -\nabla p - \rho g$$

where **v** is the plasma velocity, ρ the mass density, p the pressure, and g the gravitational (real centrifugal for Jupiter) acceleration. Taking a time derivative and using mass conservation

$$\rho\frac{\partial^2 \mathbf{v}}{\partial t^2} = +\rho C_S^2\frac{\partial^2 \mathbf{v}}{\partial z^2} + g\rho\frac{\partial \mathbf{v}}{\partial z}$$

where we have assumed that g and **v** are in the z direction, and we are only keeping terms of interest for order of magnitude (we have dropped many other terms). Assuming an $\exp(i(kz - \omega t))$ dependence for **v**, we have

$$\omega^2 = C_S^2k^2 - igk = k(kC_S^2 - ig)$$

The static or quasi-static solution is obtained by setting ω^2 to zero and obtaining $k = +ig/C_S^2$ and thus an $\exp[-z/H]$ falloff, with $H = C_S^2/g$. This solution will be valid as long as $\omega^2 \ll C_S^2k^2$, or $\omega \ll C_SH$. Thus, the angular frequency of any sinusoidal perturbation should be compared to C_SH to determine if the response of the system will be quasi-static.

At Jupiter, C_S/H is the angular rotation rate of the planet ($2\pi/10$ h), to factors of the order of unity ($\sqrt{2/3}$). The angular frequency of the solar wind perturbation is ($2\pi/10$ h). The similarity between these two frequencies is the basis for our contention that the quasi-static situation may not obtain. We have been rather sloppy in this derivation, but the overall conclusion remains even in a more careful consideration.

Received 15 June; accepted 1 August 1980.

1. Bridge, H. S. *et al. Space Sci. Rev.* **21,** 259 (1977).
2. Vasyliunas, V. M. in *Plasma Physics* Vol. 9B (ed. Lovbergs, R. H.) 49 (Academic, London, 1971).
3. McNutt, R. L., Belcher, J. W., Sullivan, J. D., Bagenal, F. & Bridge, H. S. *Nature* **280,** 803 (1979).
4. Bagenal, F., Sullivan, J. D. & Siscoe, G. L. *Geophys. Res. Lett.* 7, 1 (1980).
5. Belcher, J. W., Goertz, C. K. & Bridge, H. S. *Geophys. Res. Lett.* **7,** 17 (1980).
6. McDonald, F. B., Schardt, A. W. & Trainor, J. H. *J. geophys. Res.* **84,** 2579 (1979).
7. Northrop, T. G., Birmingham, T. J. & Schardt, A. W. *J. geophys. Res.* **83,** 3145 (1978).
8. Hill, T. W. & Michel, F. C., *J. geophys. Res.* **81,** 4561 (1976).
9. Goertz, C. K. *J. geophys. Res.* **83,** 3145 (1978).

Io control of jovian radio emission

Michael D. Desch

Department of Physics and Astronomy, University of Maryland,
College Park, Maryland 20742

The stimulation by Io of some fraction of the jovian decametre-wavelength radio emission was recognized in 1964[1]. Since then many observations have indicated that strong Io control is limited to frequencies between about 22 and 40 MHz (refs 2–4). At lower frequencies, that is 8–10 MHz, the degree of Io modulation declines markedly[5]. Recent low-frequency RAE 1 satellite[6], Voyager 1 (ref. 7), and groundbased[8] studies have shed some doubt on the conclusion that Io control predominates only at high frequencies. Data from the Earth-orbiting RAE 1 satellite[6] revealed a strong dependence of emission detection probability on Io orbital phase at frequencies in the range 6.5–2.2 MHz. These apparently conflicting results lead to two different conclusions: (1) Io control decreases markedly in the 10–20 MHz regime but reappears near 6 MHz, or, (2) observations above 8 MHz require[5] that the emission intensity be taken into account. We demonstrate here that the latter is the case and offer a reinterpretation of these data which is consistent with the recent low-frequency satellite and groundbased results.

Figure 1 shows the results of a two-year survey conducted at 26.3 MHz. These observations, a preliminary analysis of which was reported earlier[9], are unique in that they were made with an extremely sensitive antenna array consisting of 640 half-wave dipoles. Thus a large volume of very weak emission was detected for the first time. We divide the data into two approximately

---

Present address: Code 695, Planetary Magnetospheres Branch, Goddard Space Flight Center, Greenbelt, Maryland 20771.

0028–0836/80/440815—03$01.00

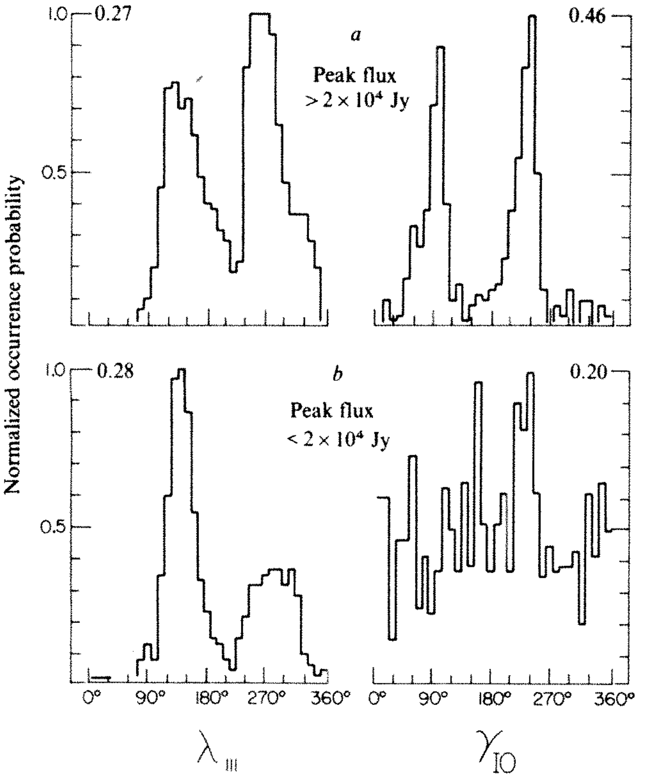

Fig. 1 A total of 151 h of 26.3-MHz jovian radio emission in which the occurrence probability is plotted as a function of the System III central meridian longitude (CML, 1965) and the geocentric phase of Io (γ_{Io}). In each case the data are divided into two components. One component (*a*), consisting of 83 h of activity is comprised of storms which exceeded a threshold intensity of 2×10^4 Jy (2×10^{-22} Wm^{-2} Hz^{-1}). The weaker component (*b*), consisting of 68 h of activity is made up of storms which did not exceed this same level. The observing period extended from 16 April, 1973 to 1 March, 1975 and contained 997 h of interference-free monitoring. The weak emission, while displaying strong modulation in CML, exhibits virtually no control by Io.

equal parts, one consisting of radio storms whose peak intensity exceeded a certain threshold and one component which did not exceed this threshold. Both the strong and weak components are plotted as separate functions of the System III (1965) central meridian longitude (CML) on Jupiter and the geocentric phase of Io (γ_{Io}). As anticipated from previous studies, the high intensity component (*a*) displays strong Io control, having occurrence probability peaks at the expected Io phase locations of 90° and 240°. The weak emission (*b*), however, shows no preferred Io phase. Instead it exhibits random fluctuations as a function of γ_{Io} and is, therefore, considered to be Io-independent emission. This latter result was entirely unexpected because large amounts of Io-independent emission had previously been observed only at relatively low frequencies, for example at 18 MHz and below. Reliable identification of these low-level Jupiter events is assured as can be inferred from the histogram (Fig. 1*b*) which shows the emission plotted as a function of CML. It displays the same dependence on CML as does the high intensity component.

Thus from the above observations alone it seems that there is not necessarily a strong frequency dependence to Io control. We hypothesize that, phenomenologically at least, Io control is a flux-dependent rather than a frequency-dependent phenomenon. We test this hypothesis by performing the same analysis as above at lower frequencies, where Io control is supposed to weaken and eventually disappear.

The results of such an analysis at 18 and 10 MHz are presented in Figs 2 and 3, respectively. The plots are identical in format to Fig. 1. In agreement with the 26.3 MHz results, there is strong Io control evident at both 18 and 10 MHz when the high intensity emission is isolated. The occurrence probability peaks are centred on the classical 90° and 240° Io-phase positions; only the relative amplitudes of the peaks differ. Note also that, just as was evident at 26 MHz, the low intensity emission is independent of Io phase. This is particularly striking at 18 MHz where the statistical reliability of the data is greatest. Both data sets retain modulation in the System III coordinate at both intensity levels, the absence of which might imply significant mistaken identification of Jupiter events.

We have shown that by isolating the high intensity radio emission at 26, 18, and 10 MHz the dependence of Io control on frequency disappears to first order. The explanation for apparent Io control in previous studies is now evident if one recalls that Jupiter's flux density spectrum peaks at ~8 MHz and falls off steeply at higher frequencies[10]. Thus, at the higher frequencies the radio emission is relatively weak and only the most intense, that is Io-controlled, events are detectable by the conventional low-gain radiometers. The weak, predominantly non-Io-controlled emission at these same high frequencies is generally undetectable, except by large antenna systems. On the other hand, at low frequencies, that is those nearer to the 8-MHz spectral peak, both the strong Io-controlled and weak non-Io emission can exceed the radiometer detection thresholds, leading to the specious conclusion that Io control has diminished. The apparent correlation between frequency and Io control is thus seen to result from a selection effect owing to the admixture of increasing amounts of non-Io emission as the observing frequency (and hence relative antenna detection threshold) is

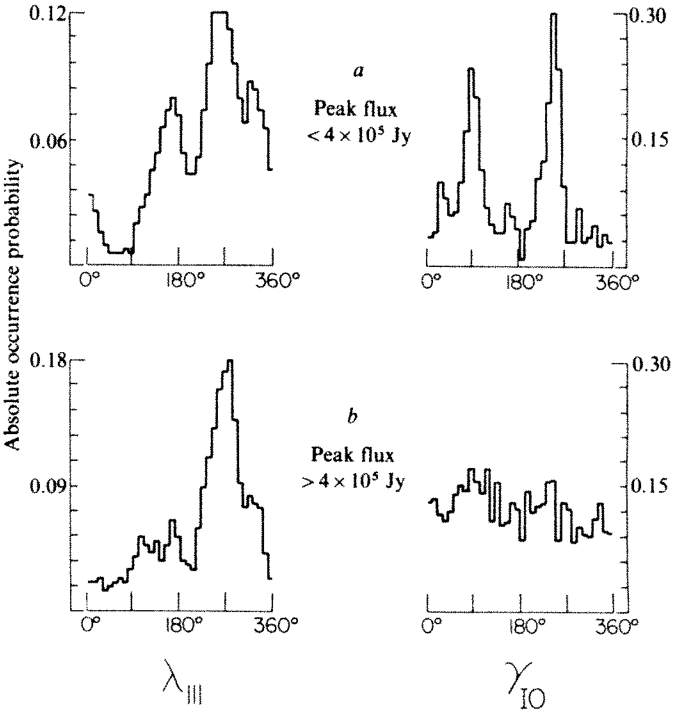

Fig. 2 A total of 491 h of 18-MHz jovian radio emission, organized as in Fig. 1, with high and low intensity components represented by *a* and *b*, respectively. Each component contains approximately equal amounts of activity. The intensity threshold in this case is 4×10^5 Jy. Observations were made at the University of Florida Radio Astronomy Observatory between 7 May 1964 and 8 May 1967, totalling 4,280 h of actual monitoring. As at 26 MHz, Io strongly modulates the high intensity emission, but the low intensity emission seems free of any Io control.

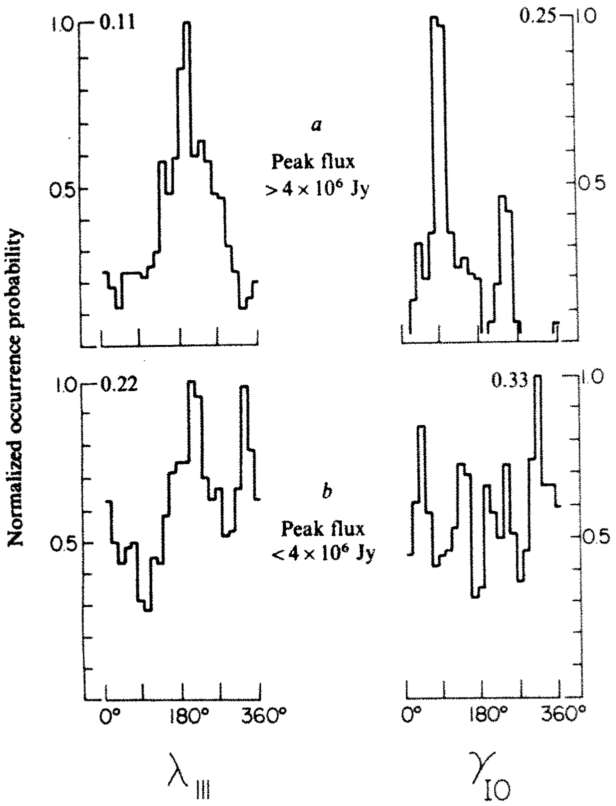

Fig. 3 A total of 138 h of 10-MHz jovian radio emission, organized as in Fig. 1. Here the low intensity component contains approximately three times as much activity as the high intensity component. The total observing time was 758 h. The observations at 10 MHz were made at the Maipu Radioastronomical Observatory in Chile in exceptionally good observing conditions between 18 May 1963 and 20 January 1964. The flux density threshold was set at 4×10^6 Jy. Qualitative agreement with the results at both 18 and 26 MHz is clear. Io modulation is evident in the case of the high intensity emission but nonexistent in the case of the relatively weak emission.

reduced. Primarily because the aforementioned low-frequency RAE 1 satellite observations were made with a relatively insensitive radiometer, it is not surprising that strong Io control was observed.

These results bear directly on the question of the radial extent of the Io-controlled source region. Those theories[11–14] which specifically address the problem of the stimulation mechanism itself generally postulate emission at or near the local electron gyrofrequency. Based on this assumption, an Io-controlled source location can be inferred from the Pioneer-modelled ambient magnetic field[15] and, most importantly, from the observed frequency range of the Io-controlled emission. The present study infers a contiguous Io-controlled source region which, rather than being limited to the near-surface planet, extends out several jovian radii along the Io flux tube. Detailed satellite studies are now being made to define more precisely the spatial extent of the source.

Received 1 April; accepted 19 August 1980.

1. Bigg, E. K. *Nature* **203,** 1008 (1964).
2. McCulloch, P. M. & Ellis, G. R. A. *Planet. Space Sci.* **14,** 347 (1966).
3. Wilson, R. G., Warwick, J. W. & Libby, W. F. *Nature* **220,** 1215 (1968).
4. Register, H. I. thesis, Univ. Florida (1968).
5. Dulk, G. A. & Clark, T. A. *Astrophys. J.* **145,** 945 (1966).
6. Desch, M. D. & Carr, T. D. *Astr. J.* **83,** 828 (1978).
7. Warwick, J. W. *et al. Science* **204,** 995 (1979).
8. Witham, P. S. *Nature* **272,** 40 (1978).
9. Desch, M. D., Carr, T. D. & Levy, J. *Icarus* **25,** 12 (1975).
10. Desch, M. D. & Carr, T. D. *Astrophys. J. Lett.* **194,** L57 (1974).
11. Goldreich, P. & Lynden-Bell, D. *Astrophys. J.* **156,** 59 (1969).
12. Wu, C. S. & Freund, H. P. *Astrophys. J.* **213,** 575 (1977).
13. Gurnett, D. A. *Astrophys. J.* **175,** 525 (1972).
14. Goertz, C. K. *Planet. Space Sci.* **21,** 1431 (1973).
15. Acuna, M. H. & Ness, N. F. in *Jupiter* (ed. Gehrels, T.) 830 (University of Arizona Press, 1976).

Si-rich Fe–Ni grains in highly unequilibrated chondrites

Ermanno R. Rambaldi, Derek W. Sears & John T. Wasson*

Institute of Geophysics and Planetary Physics, and Department of Chemistry, and * Department of Earth and Space Sciences, University of California, Los Angeles, California 90024

Some Fe–Ni grains in the Bishunpur L3 chondrite have Si contents in the range 1.3–4.5 mg per g (mole fractions of 0.003–0.009); the only previous report of Si in ordinary chondrite metal is a lower limit of 0.7 mg per g for metal in the Leighton H4 chondrite[1]. The Bishunpur Si contents are 1.1–4 times that found in a large metal grain in the Murchison CM2 chondrite[2]. As whole-rock systems both meteorites have high degrees of oxidation and consist of unequilibrated, essentially unmetamorphosed mineral assemblages. Thus the Si was not introduced into the metal during metamorphic reheating, but rather during nebular condensation[2]. Grossman *et al.*[2] calculated that the Si mole fraction of 0.0024 in the Murchison grain required a total nebular pressure $\geq 10^{-5}$ atm, which is higher than that generally inferred for the CM formation location. We show here that improvements in the Si activity coefficients and plausible constraints on the nucleation of mafic silicate condensates allow Si mole fractions of 0.003 at nebular pressures of $<10^{-6}$ atm. Thus such chondrites could have formed over a wide range of distances from the Sun.

Bishunpur is one of the three most unequilibrated chondrites[3–5] (Krymka and Semarkona are the others), and thus best preserves the record of processes occurring in the portion of the primitive solar nebula where the ordinary chondrites formed. Our data were obtained by electron microprobe; experimental details and Bishunpur's opaque phases are reported elsewhere[6]. All observations were made on polished thin sections 2359-1, 2359-2, and 2359-3 loaned by the Smithsonian Institution. Contrary to previous suggestions[2], we did not find that fluorescence of Si in adjacent silicates was a problem: (1) Si was below our detection limit of 0.4 mg per g in all metal grains except those listed in Table 1 and in two others having variable Si contents apparently reflecting the presence of Si-rich inclusions; (2) the problem is least where it is expected to be greatest, as regions of the Si-bearing metal that abut silicates have Si contents below our detection limit.

Figure 1 shows photomicrographs of three of our eight Si-bearing metal grains. Figure 1*a*, using transmitted light and partially crossed polars, shows an FeS–metal aggregate which is embedded in an olivine grain in the matrix (no. 39 in Table 1). The olivine grain, possibly a fragment of a chondrule, contains numerous opaque inclusions and it also displays undulatory extinction indicating distortion by shock. Not resolvable in this photomicrograph is a Ca–Al-rich glass having low Na and Fe concentrations. Such glass enriched in refractories is relatively common adjacent to Si-bearing metal, indicating that refractory materials are preserved within these chondrules. The large opaque inclusion is shown by reflected light in Fig. 1*b*. Its outer region is FeS and other minor phases and the interior is metal with a Ni content in the kamacite range. The sulphide gives the impression of having formed by corrosion of a metal grain.

Another FeS–metal assemblage (no. 19 and Table 1) is embedded in an olivine pyroxene chondrule that also contains

0028-0836/80/440817—04$01.00

two other Si-bearing metal assemblages and numerous small, uncorroded, spherical metal grains (Fig. 1*c*). We cannot detect Si in the uncorroded grains and the Si content of the corroded grain drops below the detection limit at those places where there is no FeS shield (upper right corner, near the dark embayment on lower right). Both the Si-bearing metal and the surrounding FeS contain numerous inclusions too fine to analyse. Some metal grains were not free enough of inclusions to be suitable for analysis. The areas whose compositions are listed in Table 1 were uniform in Si though an occasional point showed a high Cr content, perhaps reflecting the presence of $FeCrO_4$ or $FeCrS_4$. The Si we determined is probably in solid solution in the Fe–Ni, but we cannot completely rule out the presence of uniformly distributed submicroscopic grains of Si-rich phases such as perryite, $(Fe, Ni)_2(Si, P)_5$. As such a phase would have formed by low-temperature exsolution, its presence would not complicate the following discussion of how the Si was originally introduced into the metal.

Figure 1*d* shows the only Si-bearing metal that was not enclosed by olivine (no. 78 in Table 1). It is located in a thin layer of opaque, amorphous matrix with large porphyritic chondrules on either side. The entire assemblage is 480×320 μm, thus its area is about quadruple that of the largest of the grains embedded in olivine. The metal grains are more-or-less randomly distributed within the sulphide. They show little variation in Ni, Co, and Si, but Si drops below the detection limit at grain edges. As in the other assemblages, there is a Ca, P and Cr-rich layer between the metal and the sulphide. Unlike the grains within chondrules, this assemblage does not have a rounded outline, nor does it have the inner metal, outer sulphide configuration. Despite the differences, the compositional and petrological evidence indicates that this grain assemblage is genetically related to those found inside chondrules. It may have been freed of silicates before the chondrule melting process, or it may have been a fragment broken out of a chondrule. The preservation of reduced Si despite its siting in the matrix can probably be attributed to its large size.

Table 1 shows the compositions of the six Si-bearing Fe–Ni grains for which precise data could be obtained, and the Fe/(Fe+Mg) ratios in the host olivine. All grains are Cr-rich, but there is no correlation between Cr and Si or between these and other compositional parameters including olivine composition. One relevant observation is Cr zoning; Cr increased in concentration towards the grain edge. This implies that Cr was being reduced and diffusing into the grain before diffusion ceased. A possible interpretation is that Si was the agent reducing the Cr. All Ni concentrations are in a relatively restricted range of 34–40 mg per g, a composition that falls within the α stability field at temperatures between 550 and 1,100 K.

Summations in the FeS around the metal grains are often <980 mg per g reflecting the presence of the numerous fine inclusions mentioned above; even in areas of essentially pure FeS (Fe+S >980 mg per g), Ca, Cr, P and Si totalling 8–33 mg per g are observed.

Clearly, the FeS shell has either introduced the Si or preserved Si that entered the Fe–Ni at higher temperatures. As FeS cannot reduce silicates to Si, and because the only observed evidence for an oxidation–reduction reaction involves Si oxidation, we conclude that the latter is correct. We can think of two mechanisms by which the FeS shell could preserve the reduced state of Si during the mild metamorphism experienced by Bishunpur. It could either act as a barrier to diffusion of oxidant or Si, or it could act as a reducing buffer which consumed any oxidant (Fe^{2+}) released by the surrounding silicates. The reducing agent might have been $(Fe, Ni)_3P$ or Cr^{2+}. Diffusion at the low metamorphic temperatures experienced by Bishunpur probably limited any oxidant generation to very small amounts.

In unequilibrated chondrites the metal inside chondrules is significantly less equilibrated than the metal in the matrix[4]. Thus it is not surprising that seven of the eight Si-bearing grains that we observed are inside chondrules or inside olivine fragments that may have originated as chondrules. As the chondrules were either completely molten or high-degree partial melts, their temperatures at formation were surely $\gg$1,250 K, the FeS–metal eutectic temperature, it follows that the Si-bearing metal–FeS assemblages were also molten. It therefore seems probable that the concentric geometry (FeS as an exterior shell) and corroded appearance were produced during solidification and a very brief period of annealing. As the Si was not oxidized by FeO from the silicates during this process, it follows that the chondrules cooled very rapidly following formation.

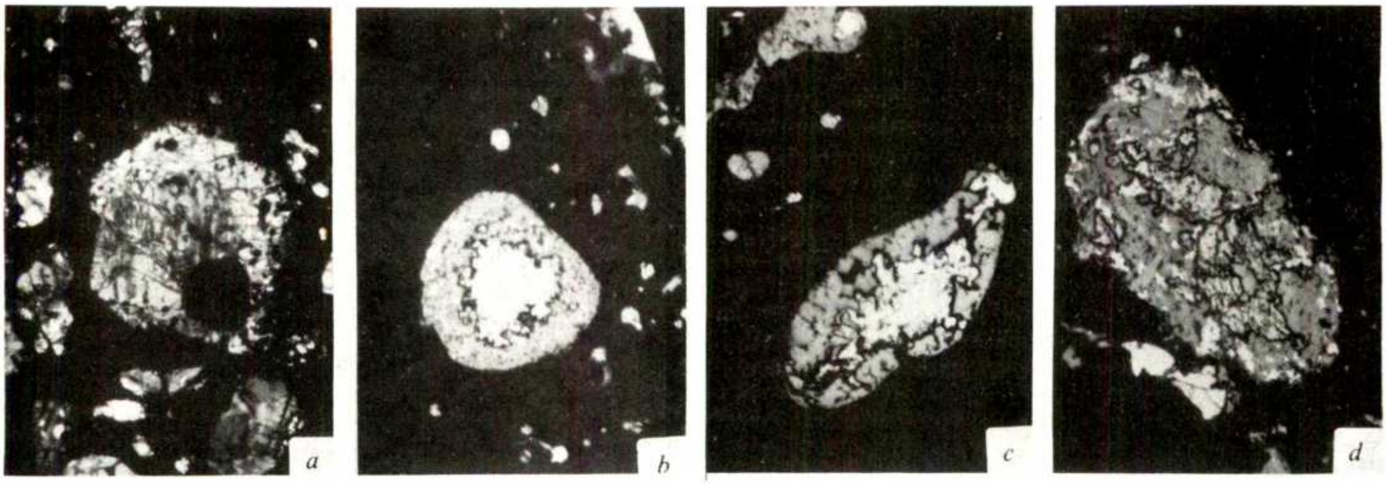

Fig. 1 Cr, Si-rich Fe–Ni grains in Bishunpur. *a*, Transmitted light photo showing a 760×950-μm olivine crystal. The olivine displays undulatory extinction, probably indicating shock, and it contains numerous glassy inclusions of variable composition, but all strongly enriched in Ca and Al. The small opaque inclusions are mainly metal; the large one (190 μm) is shown by reflected light in *b*. The white area is metal (no. 39 in Table 1) and the outer rim consists of FeS. The irregular outline of the metal suggests that the sulphide formed by corrosion of the metal. *c*, Reflected light view of a 97×310-μm metal–sulphide assemblage (no. 19 in Table 1) inside a chondrule. In the interior, the Si content is constant (3.7 mg per g) but drops below the detection limit near edges which are not coated in FeS. A fine-grained FeS-rich material, located between the metal and sulphide, is rich in Ca and P. The outer sulphide is relatively inclusion-free and contains Ca, Cr and minor P and Si. *d*, A large 320×480 μm metal–sulphide assemblage (no. 78 in Table 1) surrounded by a thin layer of matrix and sandwiched between two large porphyritic chondrules. In contrast to the other grains, the metal (white, irregular) is randomly distributed in the sulphide. The Si content drops below the detection limit at the edge of each metal grain.

Table 1 Compositions of Si-bearing metal and adjacent olivine in the Bishunpur L3 chondrite

Grain	Points	Fe (mg per g)	Co (mg per g)	Ni (mg per g)	Si (mg per g)	Cr (mg per g)	Olivine (mol % Fa)	Petrographical setting
19	5	954	4.6	38	3.7	8.6	3.6	Separate grains in chondrule
20	3	933	4.5	40	1.3	10.0		
27	3	941	4.2	36	2.9	6.7		
39	5	948	8.0	40	2.0	2.0	1.4	Olivine fragment
62	6	950	6.4	36	1.6	5.2	—	Chondrule
78	6	946	6.5	36	3.4	6.2	—	Matrix

The 250×360-μm metal grain from the Murchison CM chondrite[2] contained 1.2 mg per g Si; there is no indication that it was surrounded by a sulphide shell. Considered as whole-rock chemical systems both Bishunpur and Murchison are highly oxidized. In Bishunpur ~50% of the Fe is present in the +2 state as oxides; in Murchison about 75% is in the +2 and +3 state as oxides. At equilibrium Fe-rich silicates or magnetite will readily oxidize Si. The large amount of oxidized Fe and the highly unequilibrated nature of both chondrites are strong evidence that the Si-bearing metal did not form by reduction during metamorphism.

The more plausible mechanism for producing Si-bearing metal is to produce it during the condensation of the cooling solar nebula. In an unfractionated nebula the Si activity in Fe–Ni will be controlled by reactions of the sort

$$2\mathrm{MgSiO_3(s)} + 2\mathrm{H_2(g)} = \mathrm{Si(s)} + \mathrm{Mg_2SiO_4(s)} + 2\mathrm{H_2O(g)} \qquad (1)$$

if condensed silicates are the source of the Si. If gaseous SiO is the source of the Si the appropriate reaction is

$$\mathrm{SiO(g)} + \mathrm{H_2(g)} = \mathrm{H_2O(g)} + \mathrm{Si(s)} \qquad (2)$$

The chief hindrance to the accurate calculation of Si mole fractions during nebular condensation is the inadequacy of available activity coefficient (γSi) data[7]. Sears[8] used the function determined by Sakao and Elliott[9] at temperatures of 1,373–1,623 K:

$$\log(\gamma_{\mathrm{Si}})\alpha = 1.19 - \frac{7{,}070}{T} - \left(6.30 - \frac{18{,}300}{T}\right)X_{\mathrm{Si}} \qquad (3)$$

A study by Sakao *et al.*[10] yielded log γ values about 0.15 more negative. Grossman *et al.*[2] used the Sakao–Elliott function and one covering the temperature range 873–1,273 K obtained by Roberts[11], we have not used the latter because it does not cover the range of condensation temperatures for Fe–Ni. The Sakao–Elliott data were obtained for Ni-free α (body centred cubic) phase. The Fe–Ni that condenses from the nebula has the γ structure (face centred cubic) and a Ni content >50 mg per g. We cannot predict the effect of Ni, but there is evidence that $(\gamma_{\mathrm{Si}})_\gamma$ is lower than $(\gamma_{\mathrm{Si}})_\alpha$. Wai and Wasson[12] reported that Si concentrations in the γ phase of the Tucson iron are 1.3–1.5 times higher than those in the coexisting α phase. However, equilibrium was not achieved in Tucson. (There is no definite γ phase in other highly reduced meteorites that are more equilibrated than Tucson; Keil[13] found phases having 91–98 mg per g Ni in the Fe–Ni in EH Adhi-Kot and EL Hvittis, but the low Ni content of these grains leaves doubt that they are really γ.) The observed $\mathrm{Si}_\gamma/\mathrm{Si}_\alpha$ distribution ratio is probably a lower limit of that prevailing at the equilibration temperature of ~1,000 K; a plausible guess is that $(\gamma_{\mathrm{Si}})_\gamma$ is about three times lower than $(\gamma_{\mathrm{Si}})_\alpha$ at 1,000 K. Because γ should approach unity with increasing temperature, we will assume that the $\mathrm{Si}_\gamma/\mathrm{Si}_\alpha$ distribution ratio drops to 2 at 1,500 K. $\log(\gamma_{\mathrm{Si}})_\gamma - \log(\gamma_{\mathrm{Si}})_\alpha$ usually follows an $A + B/T$ relationship over moderate temperature ranges, so that equation (3) can be written:

$$\log(\gamma_{\mathrm{Si}})_\gamma = 1.24 - \frac{7{,}600}{T} - \left(6.30 - \frac{18{,}300}{T}\right)X_{\mathrm{Si}} \qquad (4)$$

the absolute change of log γ_{Si} is assumed to be the same for γ and α metal.

Figure 1 shows the nebular condensation of Si for two models: (1) the thick curves show the metal compositions if Fe–Ni and mafic silicates condensed heterogeneously as soon as temperatures fell low enough to make the condensates stable; and (2) the thin curves show the compositions if metal condensed heterogeneously, but the mafic silicates condensed homogeneously with amounts of required undercooling[14]. The thermodynamic data set is the same as that used by Sears[8], with the exception of the Si activity coefficient.

We suggest that the second model is the more appropriate one for the low-pressure regions of the nebula in which ordinary and carbonaceous chondrites formed. Evidence[15] indicates that CM chondrites formed at solar distances ≥2 AU where nebular pressures were probably $\leqslant 10^{-5}$ atm, and ordinary chondrites at ~1–3 AU at pressures $\leqslant 10^{-4}$ atm. Although Blander and Abdel-Gawad[14] and Blander[16] argued that at low nebular pressures ($\leqslant 10^{-4}$ atm) nucleation inhibitions should result in Fe–Ni nucleating at temperatures well below those at which enstatite and forsterite condense, the opposite must have occurred for the Si-rich grains. If supersaturation of metal led to condensation of Fe as silicates or FeS, subsequently condensed metal should have had a Ni/(Fe+Ni) atom ratio well above the solar ratio of 0.054; but the Murchison ratio (0.064) is only slightly higher, the ratios in Bishunpur (0.030–0.038) distinctly lower. Moreover, there is no way to condense metal having high Si contents after Si has largely (≥99%) condensed as silicates. If the nebula had a 'solar' $p\mathrm{H_2O}/p\mathrm{H_2}$ ratio of $\sim 5 \times 10^{-4}$, the Si concentration in subsequently condensed metal will be orders of magnitude lower than that observed in Bishunpur and Murchison. Thus, although we cannot rule out the condensation of other metal grains after silicate condensation, the evidence indicates that these Si-bearing grains condensed earlier than the bulk of the silicates. It has been proposed that refractory metal grains such as those embedded in refractory inclusions in CV chondrites could have served as condensation nuclei for Fe–Ni (ref. 17).

The carbonaceous and ordinary chondrite groups contain large quantities of Fe-rich silicates that probably either formed by direct condensation or by reaction of gaseous Fe with precondensed $\mathrm{MgSiO_3}$. Direct condensation avoids the need for mass-transport of Mg out of and Fe into these silicates, and may be more likely. Direct condensation implies a high degree of supercooling both for metal and silicates, consistent with our conclusion that most of the silicate condensation occurred at temperatures well below the equilibrium condensation temperature for Fe–Ni, and not inconsistent with the condensation of a minor amount of the metal at high nebular temperatures.

Figure 2 shows mole fractions of Si in Fe–Ni at nebular pressures of 10^{-4}, 10^{-5}, and 10^{-6} atm based on these alternative models. The positions are marked where $\mathrm{Mg_2SiO_4}$(Fo), Fe–Ni(M), and $\mathrm{MgSiO_3}$(En) become stable if equilibrium holds, and the point where silicate liquid (L) becomes stable in the constrained equilibrium model of Blander and Abdel-Gawad[14]. The heavy curves depict the Si/(Fe+Ni+Si) trajectories in equilibrium conditions. Maximum mole fractions reach 0.006, 0.002 and 0.001 at 10^{-4}, 10^{-5} and 10^{-6} atm, respectively. The results at 10^{-4} and 10^{-5} atm seem to agree with those of Grossman *et al.*[2]. The light curves show the Si mole fractions for metal grains condensing heterogeneously (in equilibrium conditions) while the condensation of the major silicates has not occurred because of nucleation constraints; the extensions of these curves below the estimated silicate nucleation temperatures (L) are shown dashed. If our second model is correct, then the Si/(Fe+Ni+Si) ratios of 0.012, 0.007 and 0.003 are reached before silicates condense at nebular pressures of 10^{-4}, 10^{-5} and 10^{-6} atm, respectively. If this is the correct model for the formation of Si-bearing grains, the Murchison grain could have formed at nebular pressures of 10^{-6} atm or slightly lower.

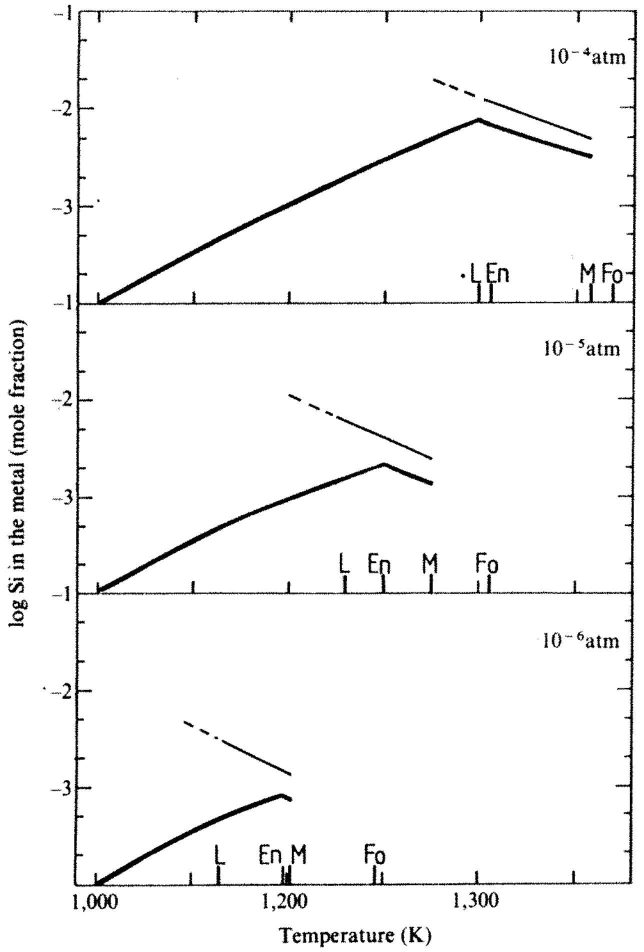

Fig. 2 Mole fraction Si in Fe–Ni condensing in a cooling nebula of solar composition at total (pH_2) pressures of 10^{-4}, 10^{-5} and 10^{-6} atm. The heavy curve shows the Fe–Ni composition if both Fe–Ni(s) and Mg_2SiO_4(s) condensed according to simple thermodynamic equilibrium. The light curve shows the Si content of the metal if the metal condenses according to the equilibrium calculations but silicates condense only after 70–85 °C of supercooling. Also indicated are the nucleation temperatures of Mg_2SiO_4(Fo), Fe–Ni(M), $MgSiO_3$(En) and a silicate liquid (L).

Is it reasonable that high Si contents could be preserved after mafic silicates start to condense? In some cases the Si was oxidized by H_2O(g) and entered silicates that nucleated on the surfaces of the metal grains. On the other hand, uncondensed SiO(g) is a more readily available source of Si, and rapid formation of silicates around a metal grain could remove the metal from contact with the gas and preserve its Si content, just as the refractory-rich metal grains are preserved in the inclusions of CV chondrites[17,18].

Studies of highly unequilibrated chondrites have taught us that if a phase can form in certain solar-nebula conditions it will probably eventually be found in these remarkable meteorites.

This research was mainly supported by NASA grant NGR 05-007-329. ●

Received 6 June; accepted 26 August 1980.

1. Wood, J. A. *Icarus* **6**, 1–49 (1967).
2. Grossman, L., Olsen, E. & Lattimer, J. M. *Science* **206**, 449–451 (1979).
3. Sears, D. W., Grossman, J. N., Melcher, C. L., Ross, L. M. & Mills, A. A. *Nature* **287**, 791–795 (1980).
4. Afiattalab, F. & Wasson, J. T. *Geochim. cosmochim. Acta* **44**, 431–446 (1980).
5. Huss, G. R., Keil, K. & Taylor, G. J. *Meteoritics* **13**, 495–497 (1978).
6. Rambaldi, E. R. & Wasson, J. T. *Geochim. cosmochim. Acta* (submitted).
7. Baedecker, P. A. & Wasson, J. T. *Geochim. cosmochim. Acta* **39**, 735–765 (1975).
8. Sears, D. W. *Icarus* (in the press).
9. Sakao, H. & Elliott, J. F. *Metall. Trans. A* **6A**, 1849–1851 (1975).
10. Sakao, H., Kubo, A. & Ishino, Y. *Proc. int. Conf. Sci. Technol. Iron and Steel*, 449 (1971).
11. Roberts, W. *Jernkont. Annlr.* **155**, 285–287 (1971).
12. Wai, C. M. & Wasson, J. T. *Geochim. cosmochim. Acta* **33**, 1465–1471 (1969).
13. Keil, K. *J. geophys. Res.* **73**, 6945–6976 (1968).
14. Blander, M. & Abdel-Gawad, M. *Geochim. cosmochim. Acta* **33**, 701–716 (1969).
15. Wasson, J. T. in *Comets Asteroids Meteorites: Interrelations, evolution and origins* (ed. Delsemme, A. H.) 551–559 (University of Toledo Press, 1977).
16. Blander, M. in *Asteroids* (ed. Gehrels, T.) 809–821 (University of Arizona Press, 1979).
17. Palme, H. & Wlotzka, F. *Earth planet. Sci. Lett.* **33**, 45–60 (1976).
18. Blander, M., Fuchs, L. H., Horowitz, C. & Land, R. *Geochim. cosmochim. Acta* **44**, 217–224 (1980).

Dead Sea Scroll parchments: unfolding of the collagen molecules and racemization of aspartic acid

Stephen Weiner*, Zina Kustanovich†, Emanuel Gil-Av† & Wolfie Traub‡

* Isotope Department, † Organic Chemistry Department, ‡ Structural Chemistry Department, Weizmann Institute of Science, Rehovot, Israel

The parchments of the Dead Sea Scrolls were prepared from the skins of animals, mainly sheep and goats[1,2]. They were copied and hidden between the beginning of the first century BC and AD 70[3]. Since then and until their discovery in the late 1940s by local Bedouins, they were located in caves close to the northwestern shore of the Dead Sea[4]. Having been handled by various intermediaries for periods of up to 8 yr, most of the intact scrolls are housed in the Israel Museum, Jerusalem. We have examined small pieces ($\leq$25 mm^2) from these scrolls, together with random fragments without any writing, to study some of the chemical changes which have occurred in the past 2,000 yr or so. Using X-ray diffraction and racemization analyses, we found that a major degradative change is due to the unfolding of the collagen molecules to form gelatin and that the degradation generally occurred many centuries ago.

Inspection of these parchments clearly differentiates lighter and darker areas (Fig. 1). The latter are generally located close to the edges and are obviously less well preserved. Under the scanning electron microscope, the damaged edges are generally seen to be more massive and gel-like than the better preserved areas, in which fibres can usually be identified. The IR spectra of Dead Sea Scroll fragments show a marked decrease of the 3,330-cm^{-1} amide A band absorption as compared with modern parchments, consistent with the interpretation of a loss of collagen structure[5].

We have developed a technique using X-ray diffraction to determine semiquantitatively the relative proportions of collagen and gelatin in parchment (Fig. 2). Only very small samples (a few mm^2) are required. The method is non-destructive and contaminating inorganic minerals generally do not interfere. In parallel, we have determined the ratios of the left-handed (L) and right-handed (D) isomers of aspartic acid, present in scroll fragment hydrolysates. Living tissues are generally composed of L-amino acids only. After death, conversion to the D-configuration slowly occurs to form eventually equilibrium mixtures of D- and L-isomers. Conditions influencing this process include the ambient temperature, the time elapsed, the pH, the protein amino acid sequence and the molecular conformations[6–8]. Thus, measurements of the D/L ratio may provide additional insight into the rates and conditions in which the chemical changes have occurred. Aspartic acid

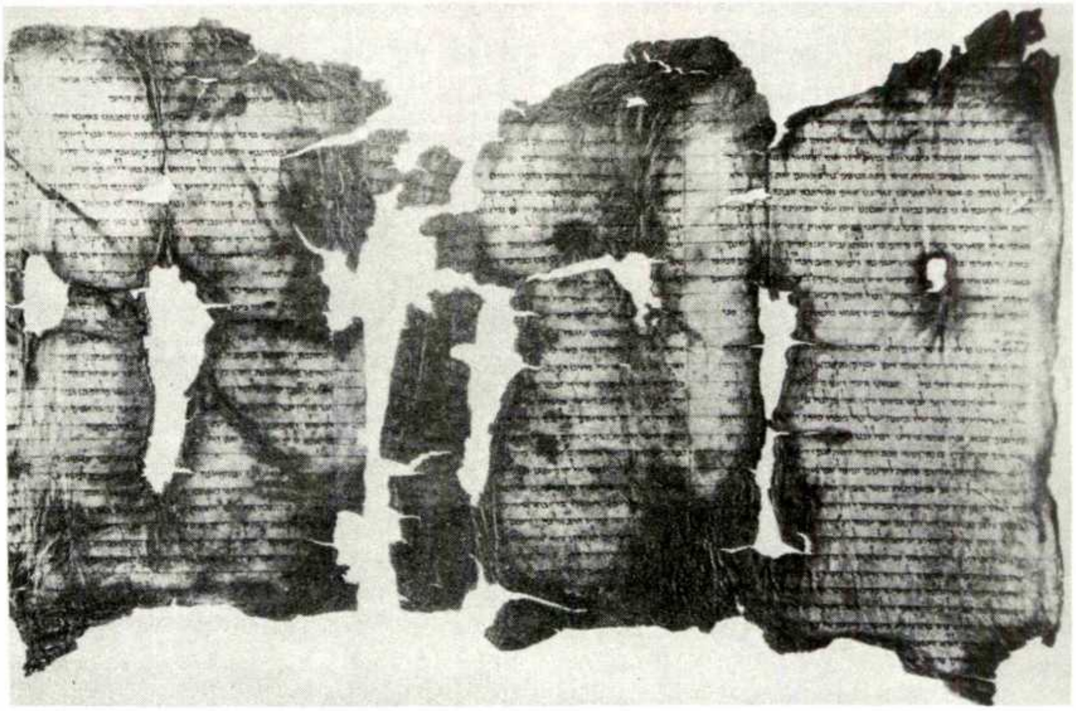

The Library COLLEGE Upper Circular Road CALCUTTA

Fig. 1. The Thanksgiving Scroll soon after unrolling.

undergoes racemization relatively rapidly[9] and is, therefore, well suited for this study.

The collagen to gelatin indices (C:G) and the ratios of D- and L-aspartic acid (D/L Asp) of the samples, are listed in Table 1 and plotted in Fig. 3. The C:G indices of Dead Sea Scroll parchments fall between the values for fresh rat tail tendon collagen and gelatin. On hydrolysis, both collagen and gelatin yield a small amount of D-aspartic acid, with gelatin showing more of the D form. Most of the scroll parchments, however, contain more D-Asp than is generated during the analytical procedure. The general distribution of the data in Fig. 3 shows that samples enriched in collagen contain only small amounts of D-Asp, whereas those enriched in gelatin have a range of D-Asp concentrations from insignificant to ~30%. In some cases, dark, poorly preserved edges were compared with lighter, better

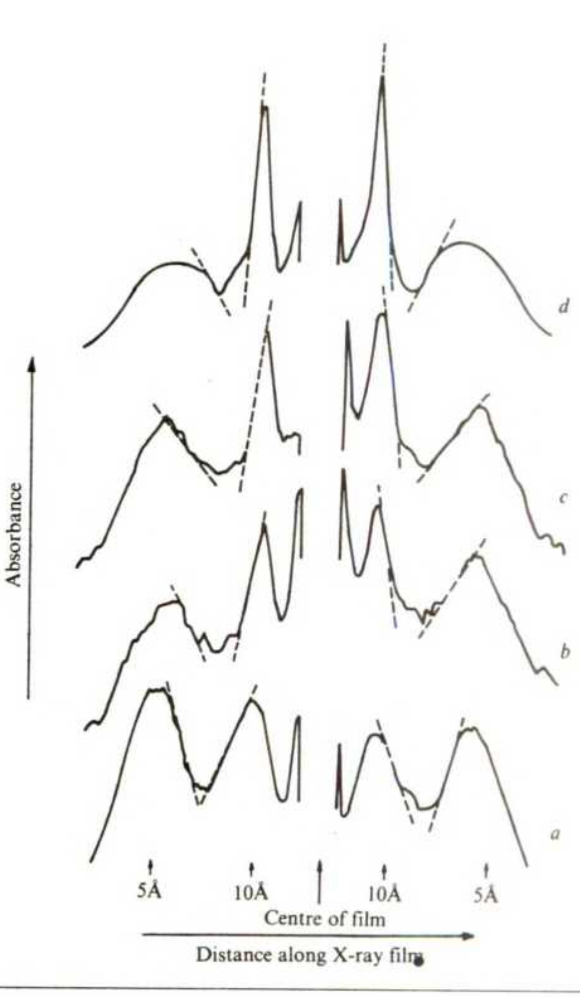

Fig. 2 Optical densitometer traces of X-ray diffractograms of collagen, gelatin and Dead Sea Scroll parchments. *a*, Gelatin; *b*, random fragment 32; *c*, random fragment 35; *d*, collagen. The parchment surfaces were mechanically cleaned and then X-rayed in a Debye–Scherrer camera for 8–24 h depending on the size of specimen. Optical densitometer traces through the centre of the film were made using a microdensitometer (Joyce, Loebl, model MKIII B) in standard conditions (slit width, 0.8 mm; sensitivity, 8; chart speed, 7; 0–1.0 absorbance wedge). The C:G indices were estimated by dividing the sum of the slopes for the 10-Å peak by the sum of the slopes for the 5-Å peak (the 10-Å peak is both higher and narrower in collagen than in gelatin, whereas the 5-Å peaks are quite similar for the two materials and provide an internal standard for each photograph, so that the C:G index does not depend on experimental conditions such as specimen size and exposure time). The standard deviation on repeat preparations of two samples (32 and 35; Table 1) is 0.4, but is probably much larger in samples composed predominantly of collagen, due to the difficulty of estimating the slope of the 10-Å peak. The results are not very dependent on exposure time, unless the film is either very light or very dark. Relatively fast scanning on the densitometer and a wide slit effectively results in a trace with minimal interference from the sharp mineral lines. The C:G index values are on a relative scale. Interpolation between collagen and gelatin curves indicates that 25, 50 and 75% collagen compositions correspond to ~1.4, 2.8 and 5.0, respectively, on the C:G scale.

Table 1 C:G index and D/L Asp of the samples analysed

Sample no.	Sample description	C:G	D/L Asp	Sample location and notes
1	Collagen	10.2	0.05, 0.04	Washed and dried rat tail tendon collagen
2	Gelatin	0.7	0.08, 0.09	Rat tail tendon denaturated at 100 °C for an hour in water
3	Modern parchments	9.9, 9.8, 12.5‡	trace	Different pieces prepared according to current Jewish rituals
4	17th century Dutch book cover	7.6	0.05	
5	Isaiah (St Marks) (representative)*	0.6	0.07	
6	Isaiah (St Marks)	1.0, 1.5‡	0.08	
7	Isaiah (St Marks) (repair patch)	3.5	0.14	Located on patch directly beneath sample 6
8	Isaiah (St Marks) (repair patch edge)	2.3	0.14	
9	Psalms (representative)	3.7	0.13	
10	Psalms	1.6	0.21	Located at dark edge a few cm from sample 9
11	War Scroll	1.6	0.12	Samples 11 and 12 located on first panel which is uniformly darker than other panels
12	War Scroll	1.1	0.18	
13	War Scroll	2.3	0.12	Located on second panel
14	War Scroll	0.6	0.13	Located on third panel
15	War Scroll	1.9	0.14	Located on last panel
16	Temple (representative)	1.9	0.25	Fragment that fell off during unrolling; scroll is backed with rice paper
17	Temple	1.3	0.29, 0.27, 0.31‡	Pieces taken from gelled top of scroll
18	Twelve Minor Prophets (ref. 17§, Pl. LXII) (representative)	3.1	0.08	
19	Twelve Minor Prophets (ref. 17, Pl. LXII)	2.0	0.31, 0.30†	Located 0.5 cm from sample 18
20	Twelve Minor Prophets (ref. 17, Pl. LXXI)	3.2	0.04	Best preserved area
21	Twelve Minor Prophets (ref. 17, Pl. LXXI)	2.1	0.15	Located a few cm from sample 21
22	Thanksgiving Hymns	1.4	0.22	5 samples span a 1.7-cm long section from a lighter area to a dark area
23	Thanksgiving Hymns	1.0	0.20	
24	Thanksgiving Hymns	1.2	0.20	
25	Thanksgiving Hymns	0.8	0.21	
26	Thanksgiving Hymns	1.6	0.22	
27	Fragment 891 (representative)	3.9	0.09; 0.11†	
28	Fragment 891	1.8	0.09	Located a few cm away from sample 30
29	Fragment 891	1.0	0.13	Dark edge adjacent to sample 31
30	Book of Jonah (fragment)	4.5	0.17	
31	Book of Jonah (fragment)	5.7	0.10	
32	Random fragment 4Q922C	3.8, 4.3, 3.6, 4.4‡	0.14, 0.11‡	
33	Random fragment 11Q988A	3.9, 3.4†	0.24	
34	Random fragment 11Q988B	2.0	0.17	
35	Random fragment 4Q920	5.5, 6.0, 6.4, 5.8, 6.6‡	0.08	
36	Random fragment	2.7	0.14	

* By visual criteria at least, samples designated 'representative' resemble the major portions of the total scroll.
† Two separate analyses of the same preparation.
‡ Separate preparations and analyses.
§ Ref. 17.

preserved areas from the same scroll. It was generally observed that the better preserved samples are enriched in collagen and contain less D-Asp (see, for example, samples 7 and 8; 9 and 10; 16 and 17; 20 and 21; 27, 28 and 29). In some cases, samples located within 1 cm of each other have D/L Asp ratios which span almost the entire range encountered (Table 1; Fig. 3).

Using different skins in one scroll and/or various parchment preparative treatments could conceivably influence the C:G index and the D/L Asp ratios. The first panel of the War Scroll, although uniformly darker than the other panels, is not significantly different from the rest of the scroll with respect to the two parameters measured (Table 1). The Isaiah Scroll had been repaired by the addition of a patch of parchment in one corner. In this case, the patch is enriched in collagen and contains more D-Asp than the main scroll parchment, which curiously shows no significant concentrations of D-Asp. Note also that the Temple Scroll, which has a light appearance and is relatively pliable, has surprisingly high concentrations of gelatin and D-Asp.

The unfolding of collagen to gelatin seems to be one of the major chemical changes which these parchments have undergone. The dark borders have suffered more than the light interior sections (Fig. 1). Furthermore, during unrolling it was observed that the inner sheets were better preserved than the outer sheets[10], suggesting that an external environmental agent, probably water, influences the conversion of collagen to gelatin. Collagen is more stable in drier conditions[11] and the low relative humidity in the area of the caves was probably a major factor responsible for the preservation of these materials. The micro-environment around the inner portions of the scrolls themselves was probably particularly dry as the outer layers probably trapped incoming water vapour. Extreme dryness also reduces the racemization rate of amino acids[12]. Fungal and bacterial activity may also have been absent for this reason. The sharp boundaries observed between light and dark areas are generally paralleled by marked variations in C:G proportions and D/L Asp ratios. This suggests that major water-accumulation events occurred sporadically during limited periods. Continual exposure to humidity would result in gradual variations in these two parameters due to a slowly expanding area in which collagen is unfolding.

It is easier to envisage racemization reactions and the consequent incorporation of D-amino acids occurring in gelatin, which has a largely disordered structure, than in the regular conformation of collagen. Indeed, the dominance of negative slopes for the connecting lines of Fig. 3 shows that, for different pieces of the same scroll, significantly higher proportions of D-Asp correspond to higher proportions of gelatin. Thus, the time of formation of gelatin from collagen should influence the ultimate D-Asp content measured. Some of the samples have accumulated considerable amounts of D-Asp (see Table 1 and Fig. 3). As fossil organic materials generally require hundreds

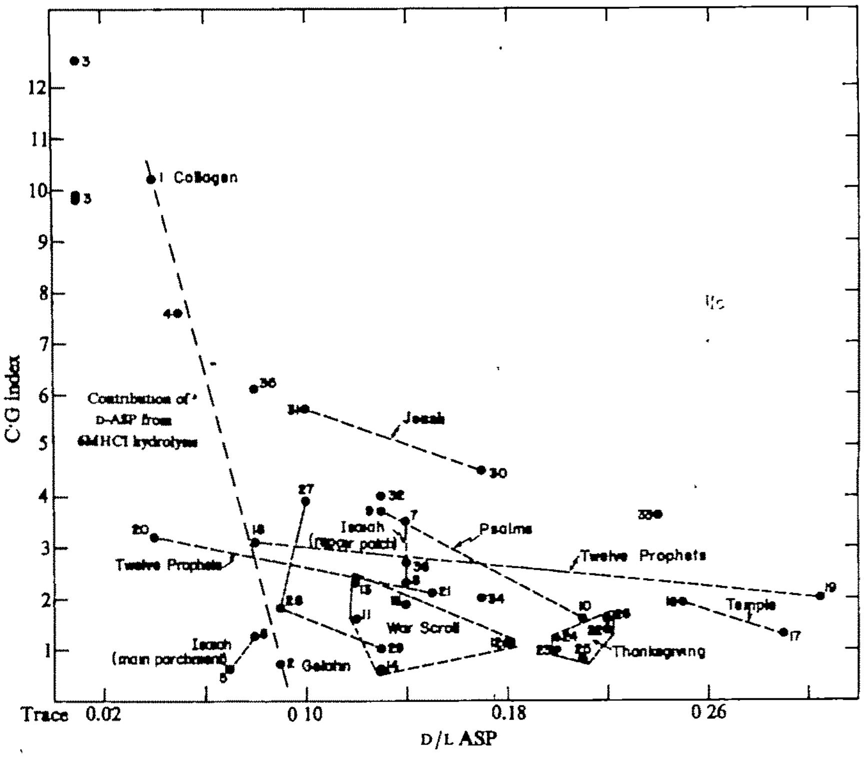

Fig. 3 The index plotted against D/L Asp of the samples analysed. For racemization analyses, ~2–5 mg of parchment were used. The parchment surfaces were mechanically cleaned, soaked in double distilled water for 2–3 h at room temperature and then transferred to 0.5 M acetic acid for 4 h at room temperature to remove the more soluble contaminants. The samples were hydrolysed in redistilled 6M HCl *in vacuo* at 150 °C for 40 min. Amino acid compositions of the random fragments closely resemble the amino acid composition of collagen. After extensive drying, the hydrolysates were derivatized to *N*-trifluoroacetyl isopropyl ester as described previously[15]. The samples were dissolved in ether and passed through a silica column (Merck, 200 mesh) in a Pasteur pipette. The aspartic acid enantiomers were separated by gas–liquid chromatography using a stainless capillary column coated with *N*-lauroyl-L-valine *t*-butylamide[16]. To confirm the identity of the D-Asp peak some of the samples were also chromatographed on the corresponding D-valine phase, which showed the expected peak reversal. Where large amounts of D-Asp were found, trace amounts of D-alanine and occasionally D-leucine, were also observed. The relative proportions of D- and L-Asp were measured by peak height. the reproducibility of the analyses is 5–10%. However, a significant portion of this variability may be due to sample heterogeneity. The ratios have not been corrected for the amounts of D-Asp generated during hydrolysis.

or thousands of years to accumulate significant amounts of D-Asp[6–8], it is reasonable to assume that most of the parchment fragments must have suffered collagen to gelatin denaturation many centuries ago, rather than in the comparatively short period since their removal from the caves. A careful visual comparison of photographs of scrolls taken soon after being unrolled 30 yr ago (Fig. 1) with the same scrolls in January 1980, revealed no noticeable differences in the distribution of light and dark areas. As at least the scroll fragments excavated by archeologists were found to be buried beneath sediments[4], the early damage may be due to the lack of a protective covering for some time after the scrolls were deposited in the caves or even, in part, be due to handling by the original readers. A corollary of our arguments might be that samples with relatively high gelatin but low D-Asp contents, such as the Isaiah scroll (see Fig. 3), were damaged more recently. However, this presupposes a more or less constant rate of racemization unaffected by differences in preparative treatments and microenvironmental conditions for different portions of the scrolls. The lower gelatin but higher D-Asp contents of the repair patch (see Fig. 3), which has presumably been attached to the Isaiah scroll for the past 2,000 yr, suggests that such factors probably do affect the rate of racemization.

Our study shows that the transformation of collagen to gelatin is one process which causes significant deterioration of the parchment. Optimal preservation conditions, which minimize the rate of transformation, should be established. As a guideline, the minimal melting temperatures of Dead Sea Scroll collagen[13], about 22 °C, and a relative humidity of 65% (above which uptake of moisture by collagen increases very rapidly)[14] should not be exceeded. The C:G index can be used in this regard to monitor any possible further deterioration, as well as to perform long-term simulation experiments.

Compared with various fossil materials, on which age determinations by racemization were made, parchment is a relatively well defined proteinaceous material. Nevertheless, our data show a wide range of D/L Asp ratios for different scrolls emanating from the same period and often even for different parts of the same scroll. Before attempting age determinations of parchment by the D/L Asp ratio, we need to understand better the mechanism of the changes involved and to develop an appropriate sampling procedure.

We thank Ms R. Yekutielli, for help and advice, also Drs A. Veis, M. Broshi and Y. Klibansky for assistance. This study was partly supported by a US–Israel Binational Science Foundation grant to S.W. and a grant by the Stiftung Volkswagenwerk to E.G.

Received 11 June; accepted 10 September 1980

1. Ryder, M. L. *Nature* 182, 781–783 (1958).
2. Poole, J. B. & Reed, R. *Technol. Cult.* III, 1–26 (1962).
3. Yadin, Y. *The Message of the Scrolls* 161–162 (Simon and Schuster, New York, 1957).
4. De Vaux, R. *Archaeology and the Dead Sea Scrolls* 95–96 (Oxford University Press, London, 1973)
5. Brodsky-Doyle, B., Bendit, E. G. & Blout, E. R. *Biopolymers* 14, 937–957 (1975)
6. Schroeder, R. A. & Bada, J. L. *Earth Sci. Rev.* 12, 347–391 (1976)
7. Dungworth, G. *Chem. Geol.* 17, 135–153 (1976).
8. Williams, K. M. & Smith, G. G. *Origins Life* 8, 91–144 (1977).
9. Bada, J. L. *Earth planet. Sci. Lett.* 15, 223–231 (1972)
10. Yadin, Y. *Bibl. Archaeol.* 30, 135–139 (1967)
11. Lennox, F. G. *Biochim. biophys. Acta* 3, 170–187 (1949)
12. Hare, P. E. & Mitterer, R. M. *Yb. Carnegie Instn Wash.* 67, 205–208 (1967).
13. Burton, D., Poole, J. B. & Reed, R. *Nature* 184, 533–534 (1959)
14. Gustavson, K. H. *The Chemistry and Reactivity of Collagen* 148 (Academic, New York, 1956).
15. Nakaparksin, S., Birrell, P., Gil-Av, E. & Oró, J. *J. Chromatog. Sci.* 8, 177–182 (1970).
16. Feibush, B. *Chem. Commun.* 544–545 (1971).
17. Benoit, P., Milik, J. T. & de Vaux, R. *Discoveries in the Judaean Desert* Vol. 11 (Oxford University Press, 1961).

High winter concentrations of SO_2 in the Norwegian Arctic and transport from Eurasia

Kenneth A. Rahn*‡, Einar Joranger*, Arne Semb* & Thomas J. Conway†

* Norwegian Institute for Air Research, Lillestrøm, Norway
† Graduate School of Oceanography, University of Rhode Island, Kingston, Rhode Island 02881

Since July 1977, the Norwegian Institute for Air Research has been studying trace gases and aerosols in the atmosphere at Bear Island, an Arctic site located at 74° N and 19° E. Although Bear Island lies well north of the Arctic Circle, the warm Norwegian Sea gives it an annual mean temperature of −1.8 °C, considerably warmer than at many other Arctic locations (Barrow, Alaska, for example, is 350 km farther south but has an annual mean of −12.2 °C). In summer, Bear Island is surrounded by open water; in winter there is open sea to the south and west and pack ice to the north and east. Atmospheric samples are taken 20 m above mean sea level and 2 m above local ground: high-volume filters are taken three times a week and analysed for various elements by atomic absorption, neutron activation and wet chemistry; sulphate and sulphur dioxide are measured daily by a method similar to that of Johnson and Atkins[1], using low-volume (16 m^3) prefilters for sulphate and KOH-impregnated afterfilters for SO_2. The collection efficiency of this method for SO_2 has been tested extensively[2]. Results for the high-volume samples have been reported[3]; here we discuss the SO_2 data, which seem to indicate that during winter there is efficient transport from Eurasian midlatitudes, due at least in part to long atmospheric residence times in and around the Arctic.

During summer, Bear Island has a narrow temperature range (typically 0–10 °C at noon) and persistently low concentrations of SO_2 (at or below the detection limit of 0.2 μg m^{-3}). For example, from May to October 1978 there were only 10 days with SO_2 concentrations >0.4 μg m^{-3}. During winter, however, the weather becomes more variable (temperatures range from 0 to −30 °C); SO_2 concentrations (and those of aerosol) often become much higher. For example, from November 1977 to April 1978 there were 65 days with SO_2 concentrations $>$ 0.4 μg m^{-3}. Concentrations of SO_2 are also highly episodic in winter, with about three to five irregularly spaced pulses per month. Pulse duration can vary from one day to more than a week. Between pulses, SO_2 concentrations are at the summer values, whereas daily mean concentrations in pulses reach 1–6 μg m^{-3}. Figure 1 records SO_2 concentrations from mid-December 1977 to mid-April 1978. *c* indicates probable contamination by the local diesel generator, deduced from wind observations every three hours.

Three of these pulses were associated with warm air from the south (0 to −5 °C), but 10 were associated with colder air (−10 to −30 °C). Wind direction during the cold-air episodes was typically northeastern at the surface and N–NE at 1,500-m elevation (which eliminated the possibility of local contamination from the north-west causing the high SO_2 values); wind speed was often high (>10 m s^{-1}) during cold-air episodes. During the period of Fig. 1, nearly every pulse of cold air at Bear Island had high SO_2 concentrations.

There is considerable evidence that this 'Arctic' SO_2 is derived from distant pollution sources, probably the Eurasian midlatitudes. (1) There is no correlation between the presence or elevation of local temperature inversions and SO_2 (or aerosol) concentrations, as would be expected if local sources dominated. With E–NE winds, there may be either ground-based temperature inversions or near-adiabatic profiles to a few hundred metres with an inversion above that. With W–SW winds there are usually surface-based inversions. (2) Aerosol species such as sulphate, vanadium and lead usually peak at the same time as SO_2, and have high enough concentrations (2–4 μg m^{-3}, 1–3 ng m^{-3} and 5–10 ng m^{-3}, respectively) to suggest that they have come directly from polluted areas. Of these, at least

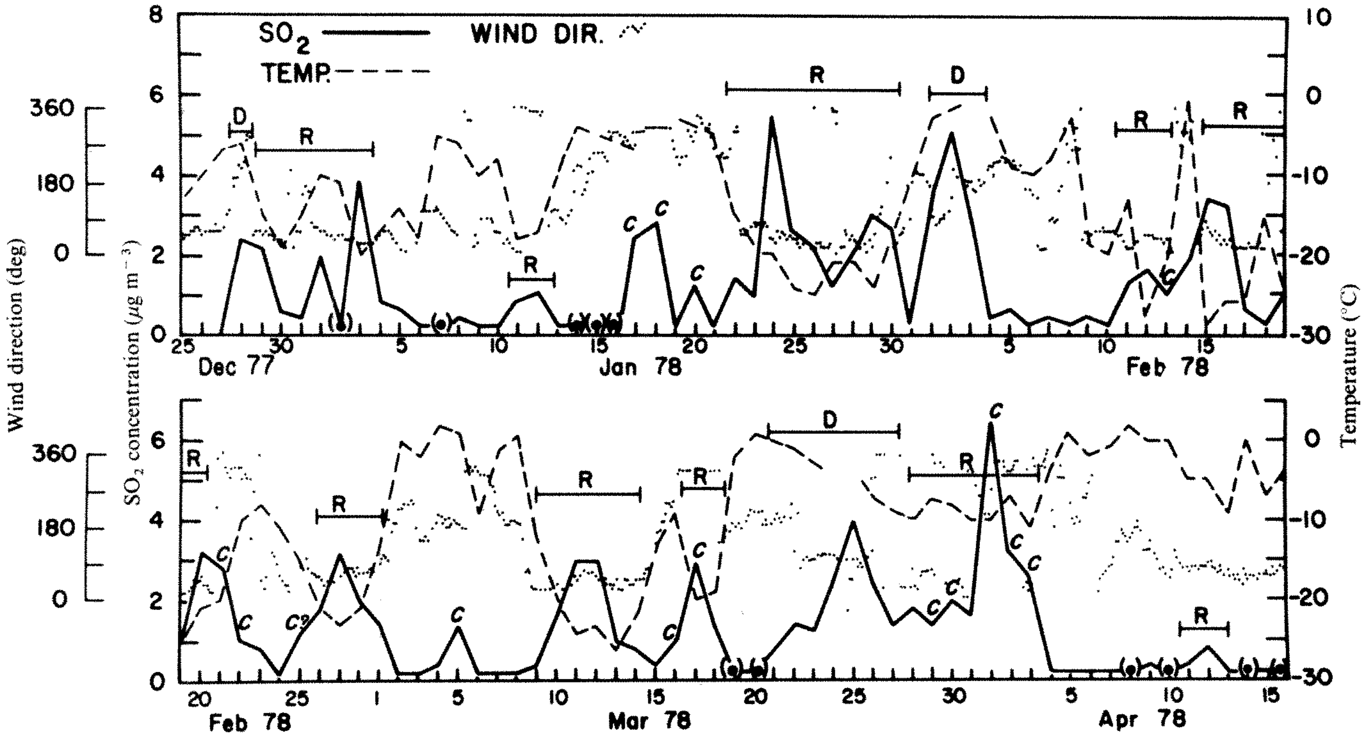

Fig. 1 Daily SO_2, temperature and wind direction at Bear Island, December 1977 to April 1978. D, Direct flow; R, return flow; *c*, probable contamination by local diesel generator.

---

‡ Present address: Graduate School of Oceanography, University of Rhode Island, Kingston, Rhode Island 02881

0028-0836/80/440824—03$01.00

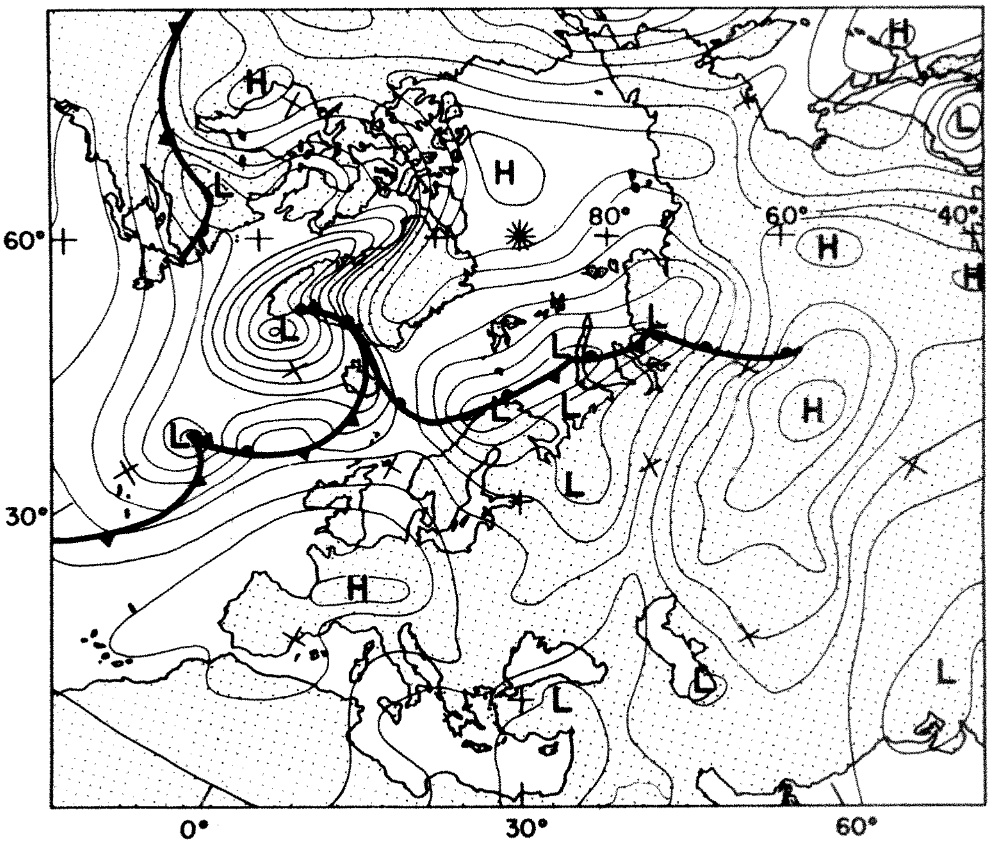

Fig. 2 Simplified surface synoptic situation for 10 March 1978, typical for cold-air episodes of SO_2 at Bear Island. H, High pressure; L, low pressure.

[illegible] Library [illegible] College [illegible] Chemistry [illegible]

vanadium has its main pollution sources in midlatitudes[4]. Occasionally, however, peaks of aerosol are not accompanied by peaks of SO_2. (3) Preliminary trajectory analysis indicates that during cold-air episodes, air flows to Bear Island around the eastward and northward sides of one or more low-pressure centres located over or just north of Scandinavia and the western USSR. A typical surface synoptic situation, for 10 March 1978, is shown in simplified form in Fig. 2. Surface-geostrophical five-day back-trajectories (which represent air flow between the surface and 1,500 m) for five high-SO_2, cold-air days at Bear Island during winter–spring 1978 are shown in Fig. 3. These trajectories, which are only rough guides to how the air masses could have travelled, indicate that for four of the five days, the air reaching Bear Island did seem to curve cyclonically around the low-pressure system, coming first from the region between Novaya Zemlya and the Taymyr Peninsula, and before that from farther south in the western USSR. Allowing for large-scale lateral diffusion, many of the densely populated areas of the western USSR and Europe are included within travel times of roughly 5–10 days. We call this the 'return-flow' pathway from Eurasia to the Norwegian Arctic.

A similar pathway to the Arctic was proposed earlier[4,5] for aerosol. The return-flow pathway is different from the 'direct-flow' pathway, where air flows northward from Europe to Bear Island, on the eastward side of a low-pressure centre located more to the south or west, and creates a warm-air episode[3]. In Fig. 1, these two types of air flow, as determined from surface meteorological maps, are indicated by 'R' and 'D', respectively.

The reason for the different character of the trajectory of 24 January 1978, which apparently came from the north, is not clear. The general synoptic situation at that time was similar to those for the other four cases of high SO_2; consequently, we think that the high SO_2 of 24 January came ultimately from the south as well. This illustrates the uncertainties of meteorological analysis in the Arctic, where weather stations are spaced widely.

The five trajectories for days of low SO_2 came from other directions. Three originated north and east of Bear Island, one came from North America via the North Atlantic, and one even came from Scandinavia and Europe. The trajectory of 6 February, which seemed to bring very low SO_2 from Europe, is another problem. It came a few days after a strong direct episode, but with considerably weakened pressure systems by the time it had reached northern Norway. Aerosol concentrations were still one-third to one-half of their values at the peak of the episode, but for some reason, SO_2 had decreased to more than an order of magnitude below its peak.

It seems, however, that rapid transport along the return-flow pathway from Eurasia to the Arctic is insufficient to explain the high winter SO_2 there; long atmospheric lifetimes also seem to be required. Transport times from Eurasia to Bear Island of 5–10 days, initial SO_2 concentrations of 30 $\mu g\ m^{-3}$ (mean winter values for the industrialized countries of Europe[6,7], probably an overestimate for Europe as a whole), dilution of the polluted air mass by a factor of four during transport (derived from simulations of aerosol transport to Bear Island, probably an underestimate), and a final SO_2 concentration of 3 $\mu g\ m^{-3}$ at Bear Island require that mean residence times during transport be 5–10 days. If the residence time increases during transport, as is likely, an initial value of 2–5 days at the source is still needed to explain the measured SO_2 concentrations. In contrast, currently accepted atmospheric residence times for SO_2 in Europe are 1–2 days[8–11]. Thus, winter residence times for SO_2 in Eurasia would seem to be up to five times longer than annual mean values, and in the Arctic of the order of weeks.

There are good physical and chemical reasons for these long residence times. In Eurasia, the residence time for SO_2 is determined primarily by the rate of dry deposition to the surface, secondarily by precipitation scavenging, and to a still lesser extent by the rate of oxidation to sulphate. In Arctic (or cold continental) winter conditions, all these rates should be very slow, because: (1) The rate of dry deposition decreases with increasing stability of near-surface air and surface smoothness; low values have been measured over snow[12]. (2) Wet deposition of SO_2 should be small during winter in the Arctic because of the slight precipitation there, typically only 5 mm per month. (3) Heterogeneous oxidation of SO_2 in Arctic cloud droplets ought

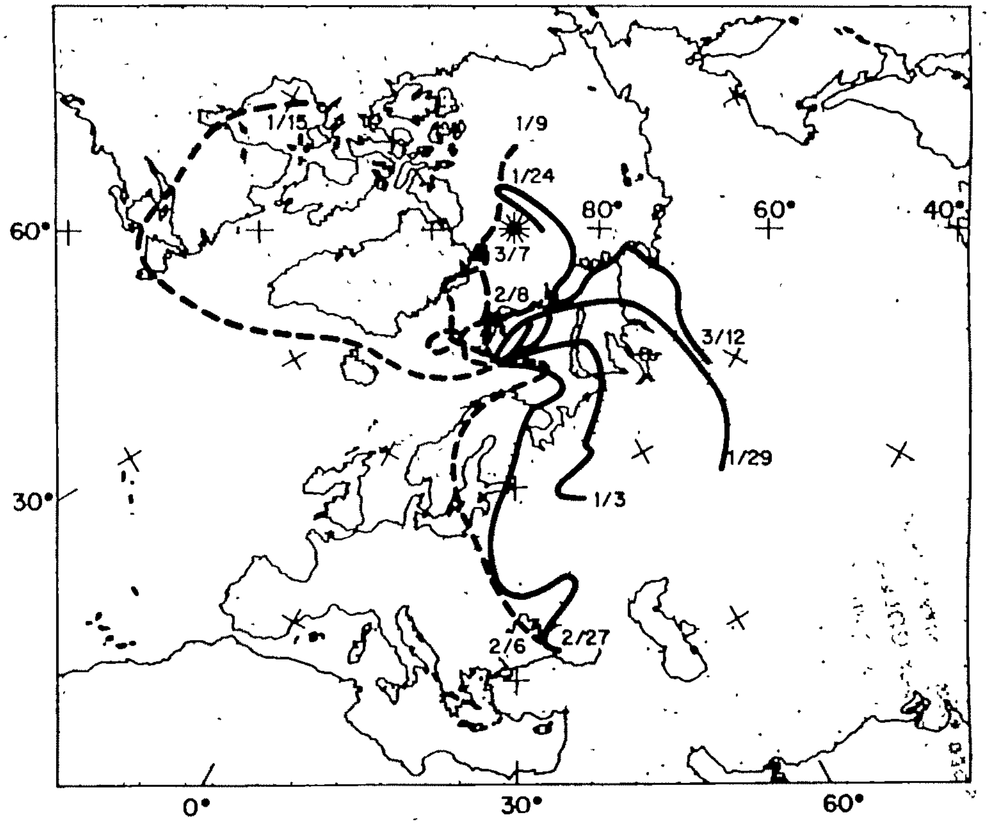

Fig. 3 Five-day surface geostrophic back-trajectories for cold-air episodes (solid line) and periods of low concentration (broken line) during winter 1977–78. Dates of arrival at Bear Island are indicated.

to be very slow because of the low temperatures, the low frequency of clouds, their restricted vertical extent, their small liquid–water content, and the meagre amounts of trace elements such as Mn and V available as catalysts (30–40 times less than in midlatitude air masses). This oxidation rate may decrease as an air mass ages, because acidity produced in the droplets limits the subsequent solubility of SO_2. (This decrease ought to be greatest over oceans and cold continents, where little NH_3 is available to neutralize the increasing acidity (C. Brosset, personal communication).) (4) Lastly, homogeneous oxidation of SO_2 by the OH radical ought to be extremely slow during the Arctic night because of the lack of direct solar radiation.

Similarly long lifetimes for aerosol in and around the Arctic have been deduced recently[4]. When combined with the long lifetimes for SO_2, they begin to explain how gaseous and particulate sulphur can be efficiently transported northward from midlatitudes during winter and dispersed over the entire Arctic.

This case illustrates just how sensitive the atmospheric rates of transformation and removal of the various forms of sulphur may be to climatic properties. In 1977 the Dubrovnik workshop on atmospheric sulphur[13] recommended that attention be given to these seasonal and regional variations for the sulphur system. Now that long-range transport of gases and aerosols through highly different climatic zones is known to be a regular feature of the atmosphere, such attention becomes mandatory, and should be extended to other species.

This work was supported jointly by the Norwegian Institute for Air Research, a fellowship to K.A.R. from the Royal Norwegian Council for Scientific and Industrial Research, the Office of Naval Research (contract N00014-76-C-0435), and NSF grant DPP77-27242. We acknowledge helpful discussions with B. Ottar and H. Dovland.

Received 3 June, accepted 28 August 1980.

1. Johnson, D. A. & Atkins, D. H. F. *Atmos. Envir.* **9**, 825–829 (1975)
2. Lewis, A. & Zachau-Christiansen, B. *Atmos. Envir.* 11, 861–862 (1977)
3. Larssen, S. & Hanssen, J. E. in *Pap. at WMO Tech. Conf. on Regional and Global Observation of Atmospheric Pollution Relative to Climate*, Boulder (WMO No. 549, Geneva, 1980) ●
4. Rahn, K. A. & McCaffrey, R. J. *Ann. N.Y. Acad. Sci.* **338**, 486–503 (1980)
5. Kerr, R. A. *Science* **206**, 290–293 (1979).
6. Ottar, B. *Atmos. Envir.* 12, 445–454 (1978)
7. Semb, A. *Atmos. Envir.* 12, 455–460 (1978).
8. Eliassen, A. *Atmos. Envir.* 12, 479–487 (1978)
9. Rodhe, H. *Atmos. Envir.* 12, 671–680 (1978).
10. Garland, J. *Atmos. Envir.* 12, 349–362 (1978)
11. Prahm, L. P., Torp, U. & Stern, R. M. *Tellus* **28**, 355–372 (1976)
12. Dovland, H. & Eliassen, A. *Atmos. Envir.* **10**, 783–785 (1976)
13. *Atmos. Envir.* 12, 7–23 (1978)

The UK wave energy resource

A. J. B. Winter

Energy Technology Support Unit, AERE Harwell,
Oxon, OX11 ORA, UK

Previous estimates[1,2] of wave energy around the United Kingdom have been made by extrapolating measurements from a few sites to the whole UK seaboard. Here directional wave spectra are used from a numerical wave model developed by the Meterological Office[3], to make estimates which are verified where possible by observation. It is concluded that around 30 GW of power is available for capture by wave energy converters: when estimates of converter spacing and efficiency are considered an average of about 7 GW of electrical power could be supplied. This resource estimate is smaller than previous ones, though consistent with them when factors such as the directional properties of waves and the likelihood that converters will be sited near coasts are included.

The first reliable wave measurements were made by weatherships at Ocean Weather Ship Station 'India' in the North-west Atlantic, 710 km west of the Outer Hebrides. The power density at this location has been estimated at between 80 kW m^{-1} (ref. 4) and 91 kW m^{-1} (ref. 2), to give a UK resource of about 120 GW (ref. 1). In 1976, the Institute of Oceanographic

Sciences[5] installed a waverider buoy 18 km west of South Uist, in 42 m of water. This has supplied the standard wave climate for evaluation of wave energy schemes[6,7], and the expected long-term average power density is 48 kW m^{-1} (ref. 6). In estimating the resource, account must be taken of the directional properties of waves: all the measurements referred to above have been of water-surface elevation at a point, and refer to the total power crossing a vertical cylindrical surface of 1-m diameter in the sea from all directions. Thus, the power density falling on a line of converters whose normal is at an angle θ to a given wave direction is $P \cos \theta$ where P is the power density measured by a non-directional instrument. Power usually arrives from a range of directions; this is referred to as a 'spread' sea. For a given orientation of a line of converters, the incident power per unit length is the integral of the product of the power flux in each directional component of the incident waves and their $\cos \theta$ factors. The ratio of this power to the non-directional power flux as defined earlier is termed the 'directionality factor', and is less than unity. The incident power density P crossing a line in the sea is then

$$P = p\delta \quad \mathrm{kW\,m^{-1}}$$

where

$$p = \int_{-\pi}^{\pi} p(\theta)\,\mathrm{d}\theta \quad \mathrm{kW\,m^{-1}}$$

is the incident power density from all directions and

$$\delta = \frac{1}{p}\int_{-\pi/2}^{\pi/2} p(\theta)\cos\theta\,\mathrm{d}\theta$$

is the directionality factor, usually integrated over waves crossing the line from one side only, as few wave energy converters absorb significant wave energy from behind. (This is not usually a significant restriction as near the coast few waves are generated travelling away from land.) If the converter line is oriented to intercept the maximum possible power (that is it faces the 'best direction'), then the directionality factor is a measure of the range of wave directions present. Off the Hebrides, for example, the best direction is close to west and the directionality factor is ~0.76.

Data used here are from the Meteorological Office depth-dependent wave forecasting model, developed by Golding[3]. In this model, surface winds over the sea are used to calculate wave spectra. Wind data are from the Meteorological Office 10-level atmospheric model, and wave fields are calculated on a 50-km grid covering the North Sea and most of the North Atlantic. The effects of energy loss and spreading mechanisms such as wave breaking, refraction and an idealized model of bottom friction are included. The resulting directional wave spectra are calculated every 30 min and archived every 12 h, and comprise spectral estimates at six frequencies (0.05–0.15 Hz) for each of 12 directions (that is, a 30° sampling interval) for every grid-point. The integrals referred to earlier have been calculated by summation over those directions. Results used here are from December 1977 to September 1979, the first two years of the model's operation. The gridpoints selected for analysis are

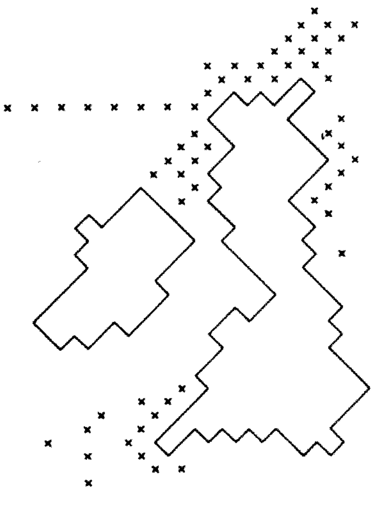

Fig. 1 The UK as it appears in the model. ×, Gridpoints where the archived wave spectra have been analysed; data for a gridpoint near OWSS 'India' have also been analysed.

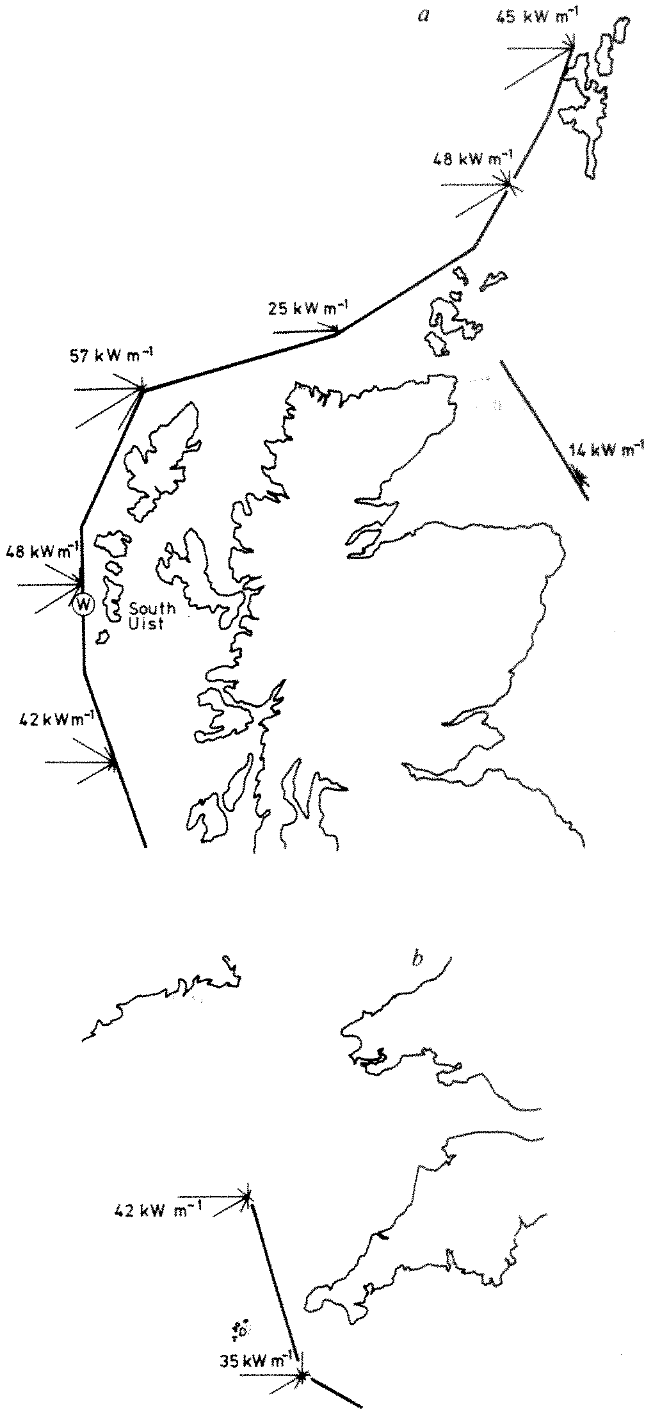

Fig. 2 *a*, Wave power at various gridpoints around the Scottish coasts. The numbers give average non-directional power density over the two years of data and the 'crows-feet' indicate the directional breakdown. The length of the direction bars in each crows-foot is proportional to the average power density arriving from a 30° sector centred on that direction. W, The location of the South Uist waverider. *b*, Wave power around the south-west of England. The heavy lines represent locations where it has been suggested that wave energy converters might be sited.

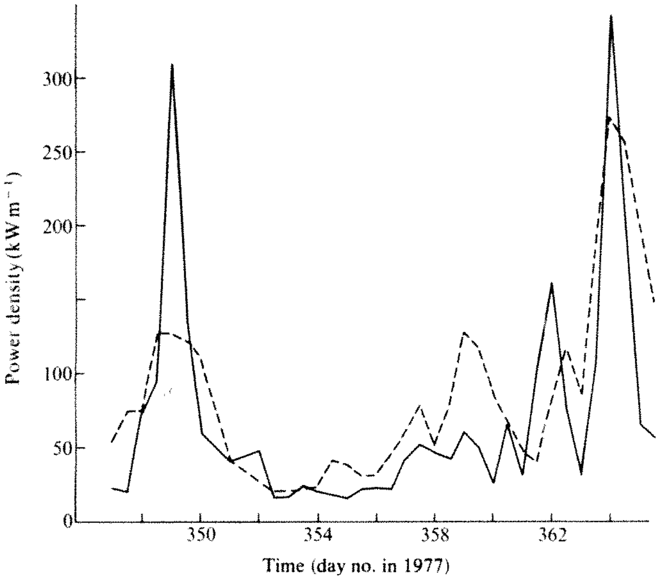

Fig. 3 Wave power density during part of 1977: measured by the waverider buoy at South Uist (solid line); results from the nearest model gridpoint (dotted line).

shown on Fig. 1. Evidently a 50-km gridpoint spacing is not fine enough to reproduce the convolutions of our coasts. To increase the accuracy of the model near the coast, the following procedure was adopted. Gridpoints were drawn on the 'real' maps (Fig. 2) at their correct positions where possible. If this was on land on the real maps (but in water in the model) or behind a real island which could not be reproduced in the model, then that gridpoint was displaced slightly when drawn on Fig. 2. In all cases, when calculating power levels the only directions used were those from which gridpoints as drawn on Fig. 2 could accept energy. This modification matches the coarse grid of Fig. 1 to the detailed coast shown in Fig. 2. It is applied after the wavefield has been computed, and does not affect refraction around headlands due to changes in bottom topography.

Figure 3 shows a time series of power for the South Uist waverider and the nearest model gridpoint, for 20 days in 1977. There are three points of interest. First, the model power levels are greater than the measured values in low-sea states, but less in high-sea states. Second, there is evidence of time shifts between the model and the waverider measurements, and finally high power levels develop sooner and die away more slowly in the model. These effects mean that when instantaneous model results are plotted against measured values they show a large scatter: this is reduced significantly if values for several consecutive time periods are averaged before being plotted. Figure 4 compares measured values and model results for South Uist. Each point represents the average power over a 2.5-day period: simultaneous observations and model results were available for 140 days in 1978. Figure 4 shows that the model gives slightly higher power levels than the waverider up to ~100 kW m^{-1}. Above this power level, the trend is reversed. The average power levels over the 140 days of the comparison were in very good agreement. The waverider measured 49 kW m^{-1} and the Meteorological Office model gave 52 kW m^{-1}. Note that the expected long-term average power level at South Uist is 48 kW m^{-1} (ref. 6), implying that the wave climate over the comparison period was representative of the long-term average. There are few other sites where direct comparisons are possible, because of the limited number of instrumental wave measurements made during 1978–79. If it is assumed that the wave climate in 1978–9 was representative of the long-term average, then the wave power at OWSS 'India' may be compared. Mollison *et al.*[2] give a weighted average power of 91 kW m^{-1} for this location: the nearest model grid point gives 96 kW m^{-1}. The Meteorological Office model is, therefore, accurate enough to determine the average power levels around the United Kingdom.

It should be emphasized that the power densities given below refer to power crossing the heavy lines in Fig. 2. For comparison, the power densities shown on various locations in Fig. 2 are omnidirectional power densities. The north-west line extends for 820 km from Islay, around the Hebrides to the Shetlands. The average power flux crossing the line is 24 GW, at a density of 29 kW m^{-1}. This value is lower than that suggested by non-directional measurements such as the 48 kW m^{-1} shown on Fig. 2*a* for South Uist: one reason is that a large fraction of the line (Cape Wrath to the Orkneys) does not face the best direction. In contrast, the section of the line around the Hebrides up to Lewis could provide 12 GW at a power density of 39 kW m^{-1}. This section faces approximately the best direction, and its directionality factor is 0.73, implying that most of the wave energy arrives from due west. The north-east line is often[4,7] drawn across the mouth of the Moray Firth, and is about 110 km long with an average power flux of 0.65 GW. The power density is only 6 kW m^{-1} and the directionality factor 0.52. These low values arise mainly from the absence of swell, which accounts for some 65% of the wave energy on the west coast[6]. Weather patterns in the North Sea are less consistent than in the North Atlantic, and the spread of wave directions is much larger in the North Sea. If the line were extended southwards by 340 km from Peterhead to Scarborough, the average power flux across the extension would be 1.9 GW, at a power density of 5.5 kW m^{-1}. The south-west line is 190 km long and the average power flux across it is 4.9 GW, at a density of 25 kW m^{-1}. This is comparable to the level off the Hebrides and supports the idea that a large fraction of the energy is received in the form of swell generated by depressions travelling across the Atlantic.

Wave power levels at OWSS 'India' are much higher than those at South Uist, close inshore. Figure 5 shows the variation of power with shore distance off the Hebrides. Curve *a* indicates total (non-directional) power density; curve *b* indicates the product of power times directionality factor, which is roughly constant over the whole range of distances. This suggests that the reason for higher power levels at OWSS 'India' is that the power arrives from a larger range of directions there, a conclusion supported by curve *c* which shows the power density arriving from directions centred on 240° ± 45°. This is actually

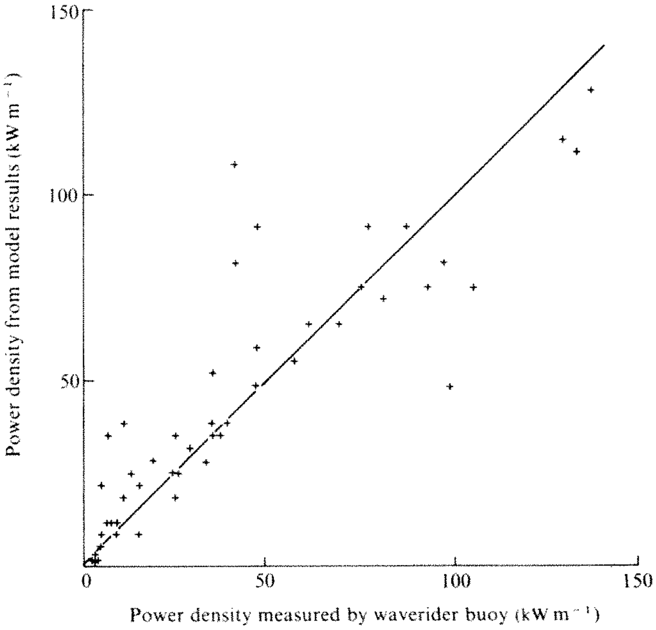

Fig. 4 Measured power densities plotted against model power densities. Each point represents the average values over a 2.5-day period, from a comparison of 140 days in 1978. The straight line has a slope of unity.

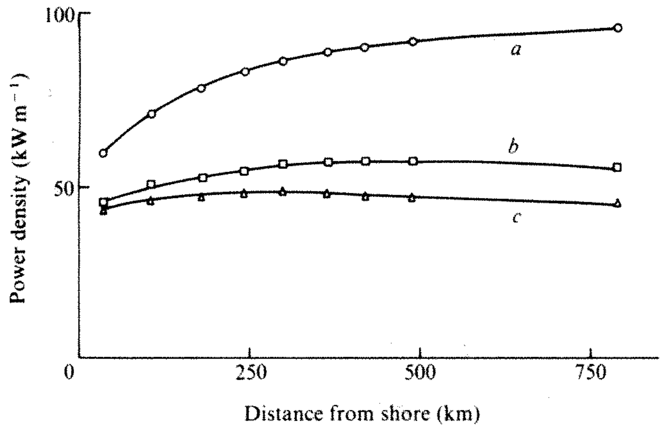

Fig. 5 Wave power as a function of shore distance, using the gridpoints extending westward from the Hebrides, shown in Fig. 1. Curves: *a*, the total power density from all directions; *b*, the product power times directionality factor; and *c*, the power arriving from directions centred on 240° ± 45°.

somewhat less at OWSS 'India' than at intermediate distances, probably because the westerly fetch for a typical depression is less there.

If ideal wave energy converters were sited on the lines shown in Fig. 2, the estimated wave energy resource would be 29 GW (annual average). Using this as an input figure, it is possible to estimate the contribution that such a scheme could make to the UK energy supply. There are two factors which would reduce the output of a large wave energy scheme. The first is that it would not be possible to install converters along the entire length of the lines shown in Fig. 2. Siting and mooring considerations imply that gaps must be left between individual converters; some parts of the lines could not be used as they intercept shipping lanes. It is difficult to quantify these factors at present. I assume here that 80% of the lines in Fig. 2 can be filled with converters.

The second factor arises from the low efficiency of converters. Most can capture 25% of the incident energy (averaged over a typical year), although it is possible that 30% can be achieved (S. Salter, personal communication). Taking values of 80% for the first factor and 30% for the second, the average power delivered would be 7 GW, ~25% of the CEGB's average power output. Siting converters further from the coast is unlikely to increase this substantially. As Fig. 5 shows, higher power further offshore comes from a larger range of directions; the power density crossing a line is largely independent of distance offshore. The suggestion that the resource could be significantly increased by deploying parallel lines of converters off the Hebrides is also debatable. Most of the wave power is in the form of swell, which would not be regenerated in a short fetch. The wind sea that might be regenerated could have a large directional spread, making capture less efficient because of the low directionality factor.

I thank Brian Golding, John Crabb and Technical Advisory Group 2 of the Wave Energy Steering Committee for helpful discussions, and the Department of Energy for permission to publish this paper.

Received 9 July; accepted 11 September 1980.

1. Glendenning, I. & Count, B. M. *Chem. Eng.* **604,** 595–600 (1976).
2. Mollison, D., Buneman, O. P. & Salter, S. H. *Nature* **263,** 223–226 (1976).
3. Golding, B. W. in *Proc. NATO Symp. on Turbulent Fluxes Through the Sea Surface, Wave Dynamics and Prediction* (Plenum, New York, 1977).
4. Leishman, J. M. & Scobie, G. *The Development of Wavepower* (EAU M.25. National Engineering Laboratory, East Kilbride, 1976).
5. Fortnum, B. C. H., Humphery, J. D. & Pitt, E. G. *IOS Rep. No. 71* (Institute of Oceanographic Sciences, Crossway, Taunton, 1979).
6. Crabb, J. A. in *Proc. Wave Energy Conf.* (ed. Quarrell, P. J.) (HMSO, London, 1978).
7. Dawson, J. K. *Energy Paper* No. 42 (HMSO, London, 1979).

North Pacific palaeoceanography: late Quaternary coiling variations of planktonic foraminifer *Neogloboquadrina pachyderma*

Peter R. Thompson

Lamont-Doherty Geological Observatory of Columbia University, Palisades, New York 10964

Nicholas J. Shackleton

Sub-Department of Quaternary Research, The Godwin Laboratory, Cambridge University, Cambridge CB2 3RS, UK

Intraspecific coiling variations of the planktonic foraminifer *Neogloboquadrina pachyderma* (Ehrenberg) form an important micropalaeontological technique for the palaeoclimatic interpretation of late Cenozoic mid-latitude marine sediments. In all the modern oceans, this species preferentially coils dextrally in subtropical to temperate latitudes and sinistrally in subpolar to polar latitudes[1,2]. Plankton[3–5] and surface sediment studies[6–20] of the North Pacific clearly associate sinistral populations with subarctic water masses and dextral populations with temperate-subtropical regions. Here we show that down-core ratios of sinistral to dextral coiling, when correlated with oxygen isotopes, indicate major late Quaternary southward advances of the subarctic boundary (polar front) and the Oyashio Current during oxygen isotope stages 2, 4 and 6.

Advective circulation of western boundary currents such as the Gulf Stream and the Kuroshio Current serves to transfer warm saline water (and the associated warm moist air) to temperate latitudes of the Northern Hemisphere. The Kuroshio is probably the most important ocean current influencing the climate of eastern Asia and, ultimately, of western North America. The deep-sea sediments of the north-west Pacific record the history of the major trends of this climate pattern as the responses of the marine organisms to the ambient temperature.

The planktonic forminiferal species *N. pachyderma* (Ehrenberg) is one of the most useful of such biostratigraphic tools for the interpretation of late Cenozoic marine sediments in high- and mid-latitudes. This species preferentially coils its test dextrally in subtropical to temperate latitudes and sinistrally in subpolar and polar seas[1,2]. The general plankton distribution of *N. pachyderma* is known for the North Pacific[3–5] and its occurrence in surface sediments has been mapped[6–19]. Here we describe the biogeographic distribution of the two coiling types for the northwestern Pacific from the total faunal analyses of more than 150 surface sediment samples[20] and the down-core coiling variations of 11 Quaternary piston cores (Table 1). The timing of the down-core coiling variations has been determined by correlation with the oxygen isotopic records of many of the cores and by the recognition of biostratigraphic datum levels in all of them.

Table 1 Cores used in the study

Core	N. latitude	E. longitude	Depth (m)	Isotopic refs	Palaeontological refs
V20-119	47°57′	168°47′	2736	23, 22	13, 20, 22
V21-146	37°41′	163°02′	3968	23, this work	14, 20
V28-294	28°26′	139°58′	2308	23	20
V28-304	28°24′	134°08′	2942	23, 25, this work	20, 25
V28-310	25°25′	125°38′	1579		20
V32-126	35°19′	177°55′	3870	This work	20
V32-128	36°28′	177°10′	3623		20
RC10-161	33°05′	158°00′	3587	23	17, 20
DSDP 310	36°52′	176°54′	3516		16, 18
DSDP 435	39°44′	143°48′	3401		24
DSDP 436	39°56′	145°34′	5240		24

0028–0836/80/440829—05$01.00

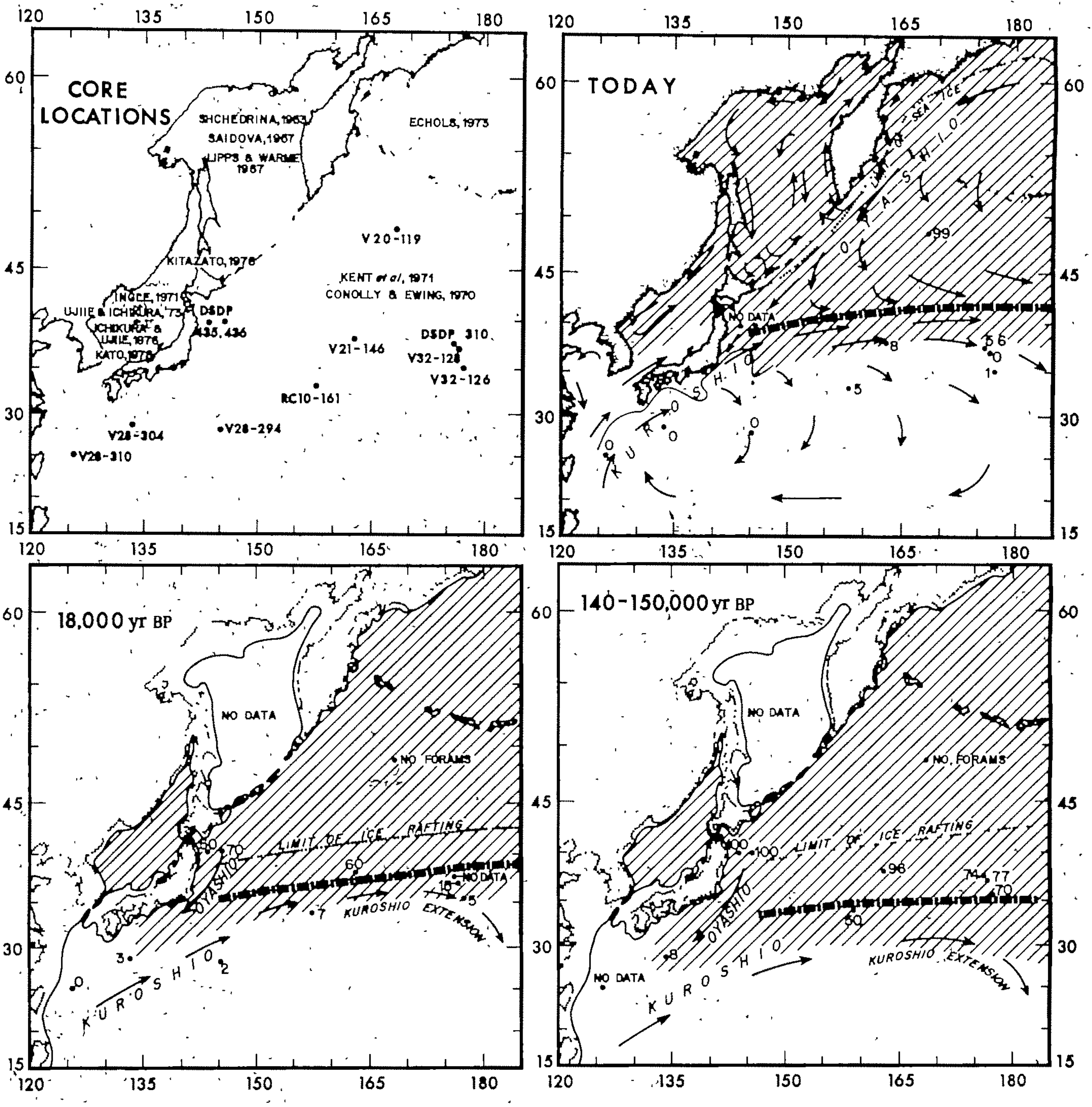

Fig. 1 Core locations and distribution of *N. pachyderma* in north-west Pacific. Upper left: core locations (see Table 1) and areas of previous study (refs 8–20, 33–36). Upper right: modern seabed percentage distribution of sinistral *N. pachyderma* relative to surface currents (arrows), position of subarctic boundary (heavy dashed line), and sea ice (dotted line). Lower left: 18,000-yr-BP position of subarctic boundary based on percentage of sinistral *N. pachyderma*, ice-rafted detritus[26] and sea-level drop of 120 m. Lower right: 140,000–150,000-yr-BP position of subarctic boundary.

The southern seabed limit of *N. pachyderma* is well defined along the western Pacific margin, where coring sites are closely spaced and the shallow depths of the locations minimize carbonate dissolution. The percentage frequencies of the species are very low at tropical sites, and frequencies do not exceed 1% south of 30° N. They account for 15–20% of the total fauna near Japan, however. Along the northern part of the Izu-Marianas Ridge and the area north of Taiwan, the dominant coiling mode is dextral. These individuals have 4.5–5 chambers in the final convolution forming a sub-rhomboidal outline; the surface of the test is non-spinose and coarsely reticulate. Dextrally coiled *Neogloboquadrina eggeri* (Rhumbler) (= *Neogloboquadrina dutertrei* of some authors) is also present in these sediments, but can be easily recognized as it has more than five chambers in the final whorl and an umbilical tooth in the apertural depression—*Neogloboquadrina pachyderma* has an apertural rim flush with the outer surface of the final chamber.

Near the confluence (about 35° N, 145° E) of the warm, saline and northward-flowing Kuroshio Current and the cold, low-salinity and southward-flowing Oyashio Current, small proportions (less than 2% of total fauna) of sinistrally coiled *N. pachyderma* first occur in surface sediments together with the more abundant dextral forms. Further east beneath the axis of the Kuroshio Extension (35–40° N, east of 155° E), central North Pacific populations are predominantly dextrally coiled and account for about one-third of the planktonic foraminiferal assemblage of the surface sediments.

North of latitude 40° N and along the continental shelf of

Japan north of about 36° N, populations of *N. pachyderma* are almost exclusively sinistral, and planktonic foraminiferal assemblages are often nearly monospecific. Individuals typically have four chambers in the final whorl, giving the shell a quadrate outline; about 1–2% of the *N. pachyderma* tests are dextrally coiled but have the quadrate, four-chambered arrangement of the sinistral type.

There is some difficulty in associating an exact temperature with the changeover from dextrally coiled to sinistrally coiled populations of *N. pachyderma.* Because of the wide seasonal contrasts of sea-surface temperatures in the western North Pacific in mid-latitudes[21], the changeover takes place where the annual range of temperature is 20 °C. There is no gradual shift of coiling direction, however, in the few sediment samples that have been recovered from this region: instead, there appears to be an abrupt switch from predominantly dextral coiling south of the subarctic boundary (polar front) to predominantly sinistral cooling north of it. Bradshaw[3] mapped the maximum plankton abundance of *N. pachyderma* (probably quadrate sinistral forms) as lying between 44 and 48° N, corresponding to an annual sea-surface temperature range of 2–15 °C. In the north-eastern Pacific between 44 and 48° N, Banerji[5] observed a change in plankton coiling directions at about 7–10 °C. These data are in good agreement with the observations of Bé[2] that the species is typically found in Antarctic seas between −1 and 8 °C, and most abundantly below 2 °C. Sea-surface temperatures in the region of dextrally coiled *N. pachyderma* have an annual range of 15–25 °C, clearly indicating two separate biogeographic populations that may be mixed only along a narrow region of the subarctic boundary.

Although temperature is a classically cited influence on the distribution and diversity of marine organisms, additional factors such as salinity, dissolved oxygen and nutrient availability, are also important. The physical boundaries for planktonic populations appear to be those of water masses characterized as large regions of fairly homogeneous properties. Thus it seems unwise to define a boundary between the coiling modes of *N. pachyderma* based on sea-surface temperature alone; rather, it is more useful (until plankton studies can be made at different seasons) to consider the coiling types as characteristic of the adjoining subarctic (sinistral) and subtropical (dextral) water masses. On either side of the subarctic boundary, coiling populations are distinct, as are the oceanographic properties of the water masses. The area of mixed coiling directions then represents a narrow transitional region where the two populations are mixed, perhaps seasonally or in response to the

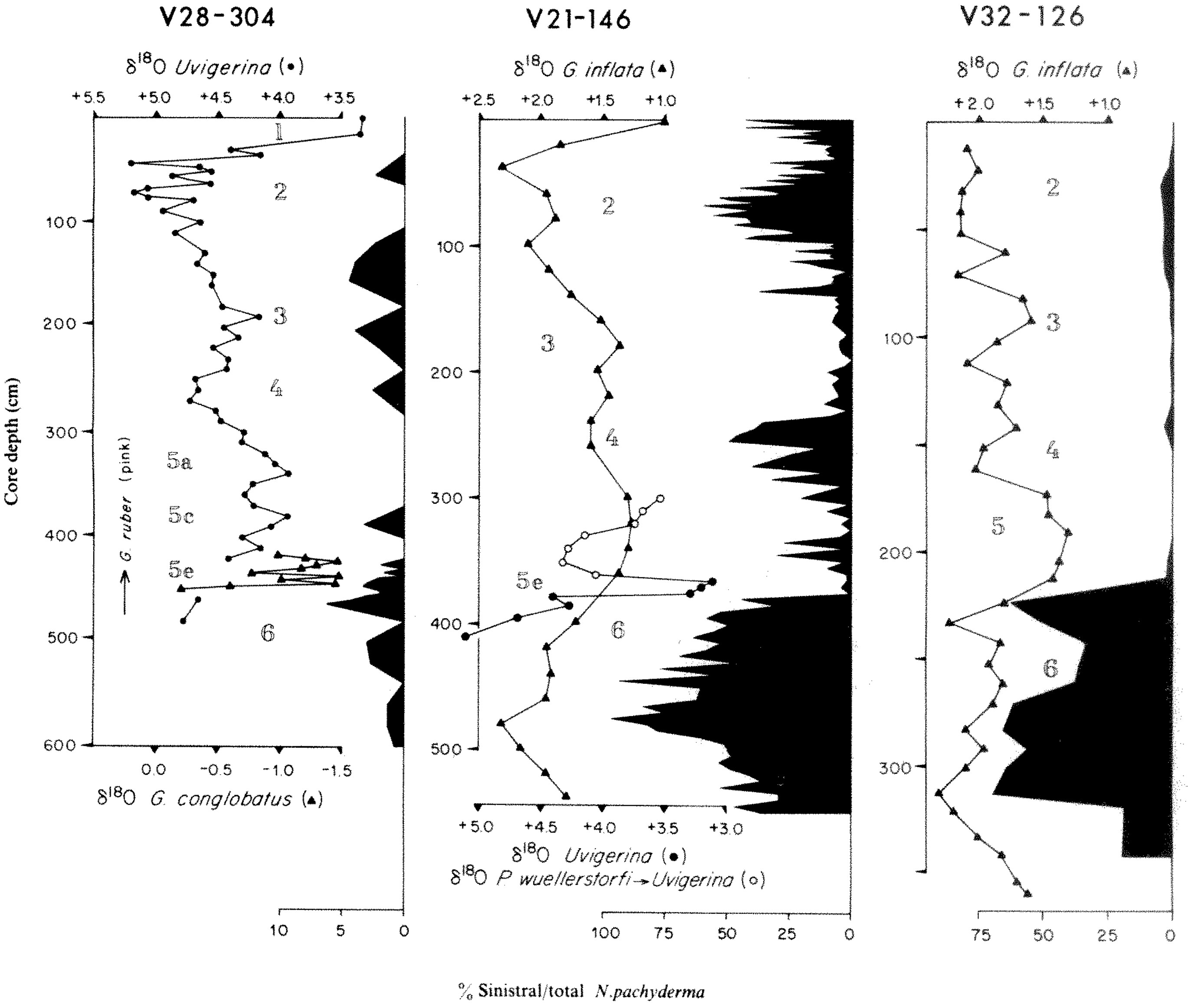

Fig. 2 Coiling ratio of sinistral to total *N. pachyderma* (shaded) versus oxygen isotopes (relative to PDB standard) for *Uvigerina* (solid circles), other benthic taxa (open circles) and planktonic taxa (solid triangles).

variable location of the many meanders and eddies along the confluence, and is further homogenized in the sediments by bioturbation over a long period of time.

Five of the six carbonate-rich piston cores (Table 1) were selected for both palaeontological and isotopic study because of their location on topographically positive features beneath the present-day axis of the Kuroshio Current and Extension; core V20-119 was retrieved from the Emperor Seamount Chain and represents a unique carbonate section available from the subarctic water mass[13]. Given the locations of the cores, we expected that down-core coiling variations of *N. pachyderma* could be interpreted as representing major fluctuations of flow within the Kuroshio gyre system, southward advances of the subarctic water mass or changes in carbonate preservation through time. (Total faunal analyses were made on plankton foraminiferal assemblages which will be described elsewhere.) Fluctuations of oxygen isotopic values are considered to monitor global ice volume[22,23] and are believed to be virtually isochronous within the time resolution of the sedimentary record.

Piston core V21-146 (ref. 14), located just north of the present southern limit of the subarctic boundary, contains the most detailed record of coiling variations (Fig. 2). The strong sinistral peaks at 70 cm (60% sinistral) and at 450 cm (96%) are associated with oxygen isotope stages 2 and 6 respectively, while dextral maxima are well defined in isotopic stages 1, 3 and 5. The topmost centimetres of the core show a return to sinistral coiling which may be interpreted as marking the period of recent climatic cooling since the Climatic Optimum at about 6,000 yr BP. Although the planktonic foraminiferan *Globorotalia inflata* was used throughout the core for isotopic analyses, benthic foraminiferal taxa were used to provide the details across the 5/6 transition, including *Uvigerina* and *Planulina wuellerstorfi* (corrected to *Uvigerina* by +0.64‰).

The piston cores located south of the present subarctic boundary [RC10-161 (Shatsky Rise)[17], V32-126, V32-128 and DSDP Site 310 (Hess Rise)[18]] are marked by dextral coiling interrupted by sinistral maxima. In these cores, the dramatic shift of the coiling dominance of *N. pachyderma* at the glacial intervals so prominant in V21-146 is not apparent. Only the major sinistral peak in V21-146 during oxygen isotope stage 6 can be widely recognized in cores south of the present polar front. The stage 2 sinistral peak seen in V21-146 is weak in the southern cores; the stage 4 sinistral peak, which is only moderate in V21-146, often cannot be located.

Along the western margin of the Pacific coast of northern Japan, DSDP Site 435 (ref. 24) has a moderate ratio of dextral to sinistrally coiled *N. pachyderma* near the top of the sequence, which gradually becomes entirely sinistral throughout the remainder of the downcore Pleistocene. Piston core V28-304, located beneath the axis of the Kuroshio south of Japan, shows very weak (< 10% sinistral) peaks (Fig. 2); the stage 6 peak can be identified only by its isotopic position. Here, the details of the 5e/6 transition were determined by analysis of *Globigerinoides conglobatus* because of the curious absence of *Uvigerina* in that part of the core. A weak sinistral peak correlated with stage 2 is present, but there are also several additional sinistral pulses during stage 3, which was expected to be dominantly dextral. Core V28-310, located south-east of core V28-304, has no isotopic record; correlation with core V28-304 using the extinction of pink-pigmented *Globigerinoides ruber* at 120,000 yr BP (ref. 25), did not reveal any sinistrally coiled *N. pachyderma* within the past 150,000 yr. Core V28-294, east of core V28-304, has a short stratigraphic record which does not extend to the pink *G. ruber* datum level and the oxygen isotope record identifies a weak sinistral peak in stage 2.

Core V20-119, from the centre of the subarctic water mass (Table 1), contains only sinistrally coiled *N. pachyderma* which vary in absolute abundance (Fig. 2) from over 70,000 tests per gramme near the top of the core to totally barren intervals. These barren sections, when correlated to the oxygen isotope record[22], are of glacial age. Although ice-rafted detritus is quite common in these same glacial sections[26], the sedimentation rate does not differ greatly from that of the interglacial intervals. Moreover, carbonate dissolution does not account for the absence of both planktonic and benthic foraminifera for there is no increase in fragmentation before or after the barren region; in any case, dissolution studies[27] indicate that carbonate dissolution is more intense in interglacial periods than in glacial stages. In this case, however, diatom abundances are increased in the glacial sections[28], suggesting a shift in the areas of diatom and planktonic foraminiferal production.

In the CLIMAP 18,000-yr-BP reconstruction[29], we noted that the sea-surface cooling at the last glacial maximum was small over most of the Pacific in comparison with the Atlantic, although in the region near the Pacific coast of Japan sea-surface temperature gradients were quite steep. The down-core distribution of sinistrally coiled *N. pachyderma* during isotopic stage 2 (as well as stages 4 and 6) supports the contention that the steepened gradient was the result of a southward advance of the polar front. In the modern ocean, the polar front overlies sediments containing 10–20% sinistral-to-total *N. pachyderma*; the water mass boundary (Fig. 1) for the past reconstructions has been drawn to correspond with such a ratio. Down-core increases in the sinistral-to-total ratio (Fig. 2) require that the subarctic boundary be moved to a location between 35–38° N during the stage 2 glacial and to about 32–35° N during the stage 6 glacial. South of Japan, core V28-304 marks the southernmost extent of the glacial advances of sinistral *N. pachyderma*, which implies drastic southward penetrations of the Oyashio Current (possibly as a submerged current[30]) along the coast of Japan. Mollusc[31] and pollen[32] records of the Pleistocene of Japan indicate a cold dry climate as far south as Tokyo. A eustatic closure of the Sea of Japan eliminated the warm Tsushima Current and glacial sections from the Sea of Japan contain only sinistrally coiled *N. pachyderma*[33–36].

The depositional centre of abundant sinistral *N. pachyderma* moved from near core V20-119 at about 50° N to about 45° N near core V21-146 during the late Pleistocene glacial advance (Fig. 2). The decrease in absolute abundances of both planktonic and benthonic foraminifera in core V20-119 and the accompanying increase of diatoms in glacial isotopic stages 2 and 6 may indicate substantial circulation changes in the subpolar gyre resulting in southward shifts in the locations of pelagic habitats. Species common to modern Sea of Okhotsk sediments such as *Globigerinita uvula* and *Turborotalita quinqueloba*[11] become prominent members of glacial faunas of cores V21-146, V32-126 and V32-128. The dominance of sinistrally coiled *N. pachyderma* at these sites is evidence for the prevalence of modern winter conditions over this area during most of the year.

In contrast, the interglacial maximum at isotopic stage 5e appears to have been somewhat warmer than today. As well as the dominance (up to 100%) of dextrally coiled *N. pachyderma* in both the tops and stage 5e of many cores (Fig. 2), there are many warm-water planktonic species in stage 5e samples, including *Globigerinoides conglobatus, Globorotalia truncatulinoides* and *Orbulina*. These species appear at low frequencies as far north as core V20-119, suggesting that the subarctic boundary may have been placed north of its present position, but the lack of foraminifera-bearing sediments precludes a firm conclusion.

We thank M. A. Hall for operating the mass spectrometer, and G. Wollin, W. Ruddiman and C. Sancetta for helpful discussions. P.R.T. was supported by CLIMAP (jointly funded by the NSF Office of Climate Dynamics and the International Decade of Ocean Exploration under grants OCE75-19627 and OCE77-22893) and N.J.S. by grant GR-3/1762 from the Natural Environment Research Council.

Received 16 June; accepted 8 August 1980.

1. Parker, F. L. in *Micropalaeontology of Oceans* (eds Funnell, B. M. & Riedel, W. R.) 289–307 (Cambridge University Press, 1971).
2. Bé A. W. H. in *Ocean Micropalaeontology* Vol. 1 (ed. Ramsey, A. T. S.) 1–100 (Academic, London, 1977).
3. Bradshaw, J. S. *Cushman Fdn Foram. Res.* Contr. **10,** 25–64 (1959).
4. Smith, A. B. *Cushman Fdn Foram. Res.* Contr. **14,** 1–15 (1963).

5 Banerji, R K , Schafer, C. T. & Vine, R *Atlantic Ocean Lab*, *Bedford Inst*, *Rep 1971-7* (1971)
6. Bandy, O L *Bull geol Soc. Am* **70**, 1708 (1959), *J. Paleont.* **34**, 671–681 (1960), in *Tertiary Correlations and Climatic Changes in the Pacific* (ed Hatai, K) 95–102 (11th Pacific Sci. Congress, Tokyo, 1967); *Palaeogeogr Palaeoclimatol Palaeoecol* **5**, 63–75 (1968).
7 Ingle, J. C. Jr, *Bull Am Paleont* **52**, 217 (1967), *Init. Rep. DSDP* Leg **18**, 517–567, 949–960 (1973).
8 Shchedrina, Z G *Akad Nauk SSSR*, *Trudy Inst. Zool* **13**, 12–32 (1953)
9 Saidova, Kh M *Dokl Akad Nauk SSSR* 14, 1302–1305 (1957).
10 Asano, K *Sci Rep Tohoku Univ 2nd Ser* **28**, 26 p. (1957)
11 Lipps, J H & Warme, J E *Cushman Fdn Foram Res.* Contr. **17**, 125–134 (1966).
12 Belyaeva, N V *Oceanology* **9**, 500–504 (1969)
13. Kent, D V., Opdyke, N D & Ewing, M *Bull. geol Soc. Am* **82**, 2741–2754 (1971).
14 Wollin, G , Ericson, D. B & Ewing, M. in *The Late Cenozoic Glacial Ages* (ed. Turekian, K. K.) 199–214 (Yale University Press, New Haven, 1971).
15. Echols, R J. *Init Rep DSDP* Leg **18**, 721–735 (1973)
16. Vincent, E *Init. Rep DSDP* Leg **32**, 765–801 (1975).
17 Maiya, S., Saito, T & Sato, T in *Progress in Micropaleontology* (eds Takayanagi, Y. & Saito, T) 395–422 (Micropaleontology Press, New York, 1976).
18. Keller, G *Mar Micropaleont* **3**, 97–119 (1978).
19. Kitazato, H *Geol Surv Japan*, *Cruise Rep* 11, 56–58 (1978)
20 Thompson, P R , thesis, Tohoku Imperial Univ (1977)
21. *U.S Naval Oceanographic Office*, *Spec Pub* 123 (US Government Printing Office, Washington, 1969).
22. Hays, J. D & Shackleton N J *Geology* **6**, 649–652 (1976)
23. Shackleton, N J *Phil Trans R. Soc.* B**280**, 169–182 (1977).
24 Thompson, P. R. *Init. Rep DSDP* Leg **56** (in the press)
25 Thompson, P. R , Bé, A W H., Duplessy, J C. & Shackleton, N J. *Nature* **280**, 554–558 (1979)
26 Conolly, J R & Ewing, M *Mem Geol Soc. Am.* **126**, 219–231 (1970)
27 Thompson, P R. *J. foram res.* **6**, 208–227 (1976).
28. Jousé, A P in *Micropalaeontology of Oceans* (eds Funnell, B. M. & Riedel, W. R.) 407–422 (Cambridge University Press, 1971)
29. CLIMAP *Science* **191**, 1131–1137 (1976)
30. Omori, M. *Deep Sea Res* **14**, 525–532 (1967)
31. Chinzei, K *Proc 1st Int Congr Pacific Neogene Stratigraphy* (eds Saito, T & Ujiié, H) 327–330 (Geological Survey of Japan, Tokyo, 1977)
32 Fuji, N *Proc. Jap Acad* **49**, 737–741 (1973).
33. Ujiié, H. & Ichikura, M *Trans. Proc. Palaeont. Soc. Japan* **91**, 137–150 (1973)
34. Ingle, J C Jr *Init. Rep. DSDP* Leg **31**, 693–701 (1975)
35 Ichikura, M. & Ujiié, H *Bull natn Sci. Mus*, *Tokyo* **C2**, 151–178 (1976).
36. Kato, M *Geol Surv Jap*, *Cruise Rep* **10**, 59–62 (1978)

Occurrence of hydroxamate siderophore iron chelators in soils

P. E. Powell*, G. R. Cline†, C. P. P. Reid† & P. J. Szaniszlo*

* Department of Microbiology, University of Texas, Austin, Texas 78712
† Department of Forest and Wood Sciences, Colorado State University, Fort Collins, Colorado 80523

Although iron is abundant in soils (1–6%), it is often unavailable to plants because its solubility is dependent on *p*H and controlled by the low solubility of ferric oxides. Iron availability to plant roots may thus depend on organic chelators which Lindsay reports would maintain an adequate iron supply by diffusion and mass flow at concentrations as low as 10^{-8} M[1,2]. Hydroxamate siderophores (HS), microbially produced, ferric-specific, iron transport molecules with stability constants[3] as high as 10^{32}, may represent the chelators which maintain these soil iron concentrations. Such peptide derivatives were shown to control iron availability in aquatic ecosystems[4], but little is known about their soil role beyond their function as microbial growth factors[5,6]. We report here the occurrence of HS in aqueous extracts of a variety of soils in concentrations (10^{-7} M–10^{-8} M after correction to 10% soil moisture) sufficient to affect plant nutrition[1,2].

Soil samples (0–10 cm deep) were collected from 57 sites representing numerous biomes and soil types. After extraction (1 : 1 H_2O : soil, w/w) at 4 °C for 1 h, samples were centrifuged, the supernatants dried (90 °C), and the residues rehydrated, filter sterilized, and bioassayed using the HS auxotrophic bacterium *Arthrobacter flavescens* JG-9. The initial survey used a diffusion plate method developed by P.J.S. as described by Estep *et al.*[7]. Nineteen survey soils, and other experimental materials, were assayed by a more sensitive turbidimetric, dilution-tube modification of the plate method. The mean values of quadruplicate samples were expressed as molar equivalents of the HS standard, desferrioxamine methanesulphonate (DFOM).

The specificity of any bioassay of complex natural substrates must be regarded cautiously. To verify the specificity of the *Arthrobacter*[8] we tested the natural chelators, citric acid, oxalic acid, 2,3-dihydroxybenzoic acid and the catechol siderophore, enterochelin, at concentrations of 4×10^{-3} M to 4×10^{-10} M. No growth stimulation was detected. A suspension of haemin was weakly stimulatory[9] in our assay and measured 7×10^{-9} M DFOM. Although the concentration of haemin in soil extracts is probably reduced during sample processing, stimulation by haemin or unknown compounds remains a possibility. The presence of secondary hydroxamates in highly concentrated soil extracts was demonstrated qualitatively by a positive Csaky test[10].

Hydroxamate siderophore concentrations in excess of 3×10^{-9} M DFOM equiv. were found in the extracts of all 57 preliminary survey soils. These soils were from grasslands, areas of mixed herbaceous vegetation, and coniferous and deciduous forests across the US. In extracts of 19 soils, representing a wide range of *p*H, diethylenetriaminepentaacetic acid-extractable iron (DTPA-Fe) and organic matter content, HS concentrations ranged from 3.4×10^{-8} to 2.7×10^{-9} M DFOM equiv. (mean, 1.2×10^{-8} M; median, 8.5×10^{-9} M). No simple relation between HS levels and either soil *p*H or DTPA-Fe was evident. However, HS concentration was directly correlated with per cent organic matter ($r = 0.868$, $n = 19$).

Significant adsorption of HS to soil surfaces was indicated by the low recovery (range, 0.3–17.3%; mean, 3.7%) of the model compound DFOM added at 1 μg per g dry wt of soil. Proof of a large reservoir of natural siderophores came from repeated extractions of an unamended soil sample (Fig. 1). The early extractions yielded nearly the same quantity of HS (~0.03 nmol g^{-1}), but yield subsequently declined to about 0.01 nmol g^{-1} per extraction. Total yield after 11 extractions was 0.18 nmol g^{-1}. DFOM added to a similar soil sample was more readily desorbed than was natural HS (Fig. 1). The decreasing yield of natural siderophores suggests that chemisorption on organic matter or migration to micropore sites occurs with time.

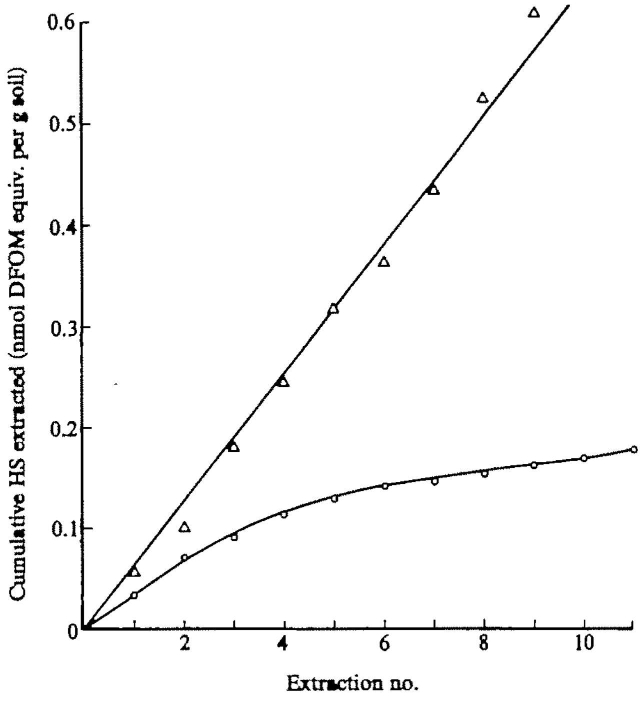

Fig. 1 Siderophore desorption (nmol per g soil) from soil (TC1) by the repeated extraction of amended DFOM at 1 μg per g dry wt soil (△) and natural HS (○).

0028-0836/80/440833—02$01 00

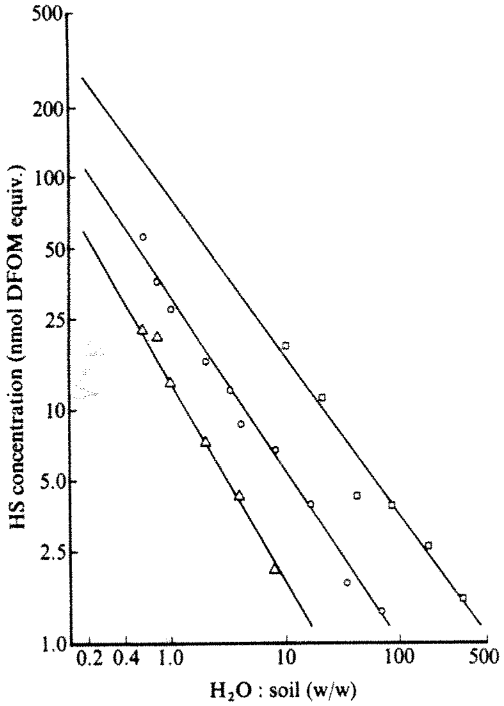

Fig. 2 Concentration (nmol) of natural HS in aqueous extracts of three soils at various H_2O : soil (w/w) ratios. (△), Soil TC9 with 2% organic matter, $\ln y = \ln 13.5 - 0.873 \ln x$; (○), soil TC1C with 10% organic matter, $\ln y = \ln 29.8 - 0.760 \ln x$; (□), Canadian sphagnum peat with 95% organic matter, $\ln y = \ln 80.2 - 0.686 \ln x$.

To estimate the solution concentrations of HS in realistic soil moisture conditions, we extracted several soils at various H_2O:soil ratios. Siderophore concentration in solution increased markedly as soil moisture decreased (Fig. 2) and was clearly a power function of per cent soil moisture. Slopes of the curves were inversely correlated with soil organic matter content, as would be expected if the chelators were adsorbed to soil organic matter. A conservative estimate of minimum siderophore concentrations at 10% soil moisture was extrapolated from the value for this 1:1 H_2O:soil extract using the slope value from sphagnum peat containing 95% organic matter (see Fig. 2 legend). Extrapolated values for 10% moisture varied from 1.7×10^{-7} M to 1.3×10^{-8} M DFOM equiv., entirely within the range theoretically necessary to maintain an adequate iron supply to roots[1,2].

The ecological significance of hydroxamate siderophores in ferric iron mobilization is apparent when their stability constants (for example, ferrioxamine B, log $K = 31$)[3] are compared with those of the less specific organic acids (for example, ferric citrate, log $K = 12$)[11], phenolates (for example, ferric p-hydroxybenzoate, log $K = 15$)[11] and several synthetic chelators. Although the synthetic chelate ethylenediaminetetraacetic acid (EDTA) has a log K of 26 for ferric iron, it cannot effectively retain iron in soil solutions above pH 6 because of competition from other cations[2].

We have shown that hydroxamate siderophores are present in a wide variety of soils in concentrations that significantly increase the availability of iron to plants. We have also presented evidence that large reservoirs of these compounds are adsorbed to soil organic matter. We believe that HS in soils perform many chelate functions previously attributed to organic acids and polyphenolic humic material.

This work was supported by grants DEB-77-00883 and DEB-79-11276 from the NSF. We thank W. L. Lindsay for encouragement and helpful suggestions and Janet Root for technical assistance.

Received 9 May; accepted 26 August 1980.

1. Lindsay, W. L. in *The Plant Root and Its Environment* (ed. Carson, E. E.) 507–524 (University Press of Virginia, Charlottesville, 1974).
2. Lindsay, W. L. *Chemical Equilibrium in Soils* (Wiley, New York, 1979).
3. Anderegg, G., L'Eplattenier, F. & Schwarzenback, G. *Helv. chim. Acta* **46,** 1400–1408 (1963).
4. Murphy, T. P., Lean, D. R. S. & Nalewajko, C. *Science* **192,** 900–902 (1976).
5. Lochhead, A. G. & Burton, M. O. *Soil Sci.* **82,** 237–245 (1956).
6. Waid, J. S. *Soil Biochemistry* Vol. 4 (eds Paul, E. A. & McLaren, A. D.) 65–101 (Dekker, New York, 1975).
7. Estep, M., Armstrong, J. E. & Van Baalen, C. *Appl. Microbiol.* **30,** 186–188 (1975).
8. Lankford, C. E. *Critical Rev. Microbiol.* **2,** 273–331 (1973).
9. Burnham, B. F. & Neilands, J. B. *J. biol. Chem.* **236,** 554–559.
10. Csaky, T. Z. *Acta chem. scand.* **2,** 450–454 (1948).
11. Bertin-Batsch, C. *Ann. chim. Fr.* **7,** 481–531 (1952).

Structure and function of mycorrhizal rhizomorphs with special reference to their role in water transport

J. A. Duddridge, A. Malibari & D. J. Read

Department of Botany, University of Sheffield, Sheffield S10 2TN, UK

Anastomosing systems of fungal rhizomorphs are found in association with mycorrhizal roots of trees in arid zones[1], in soils of temperate deciduous[2], coniferous[3] and humid tropical[4] forests, and even in mine spoils[5]. Although it is recognized that the fungus depends on the host for its carbon supply[6,7], the functional relationship between the partners has not been investigated fully. Transport of ^{32}P through rhizomorphs has been demonstrated[8], but their potential to absorb and transport water is not known. We have synthesized mycorrhizal rhizomorphs in association with pine, and preliminary experiments with tritiated water (^3H_2O) showed that the cut distal ends could absorb water which was transported to mycorrhizal roots and to seedling needles[9]. We have since developed a method for feeding ^3H_2O to the intact terminal portions of rhizomorphs in sealed vessels with negligible disturbance to the mycelial system, and we report here that mycorrhizal rhizomorphs can absorb water and facilitate its transport over ecologically significant distances. Electron microscopy shows that the rhizomorphs are differentiated structures with large central 'vessel' hyphae.

Mycorrhizas were synthesized in aseptic conditions in 250-ml Erlenmeyer flasks which contained a peat–vermiculite mixture (1:4 v/v) moistened with modified Melin–Norkrans (MMN) solution. The medium was inoculated with a disk of *Suillus bovinus* mycelium. After the fungus had become established, aseptically germinated seedlings of *Pinus sylvestris* were transferred to the flasks which were then maintained in a growth chamber. After mycorrhiza formation had been confirmed, seedlings were transferred to fresh non-sterile milled peat in Perspex chambers (15 × 17 × 1 cm) with detachable sides and base. Three seedlings were placed on the surface of the peat with most of their mycorrhizal roots visible on the upper surface. The wall was then replaced, the chambers were wrapped in aluminium foil to exclude light and replaced in the growth cabinet. Within 142 d the peat was extensively exploited by rhizomorphs, many of which formed on the wall of the chamber. A shallow Perspex cup (1 cm in diameter, 1 mm deep), its rim coated with anhydrous lanolin, and containing 4 μCi of ^3H_2O in 50 μl water, was attached to the lower surface of the chamber wall enclosing the terminal parts of a rhizomorph system. Cups were placed either near the upper peat surface and hence in close proximity to the seedlings, or at the base of the chamber at least 15 cm from the seedling needles (Fig. 1). After exposure to the isotope for 1 h the rhizomorphs emerging from the cup were cut, dissected away from the wall and peat, and traced backwards to mycorrhizal roots. They were then cut into 5-mm segments, which were placed in sealed scintillation vials

0028-0836/80/440834—03$01.00

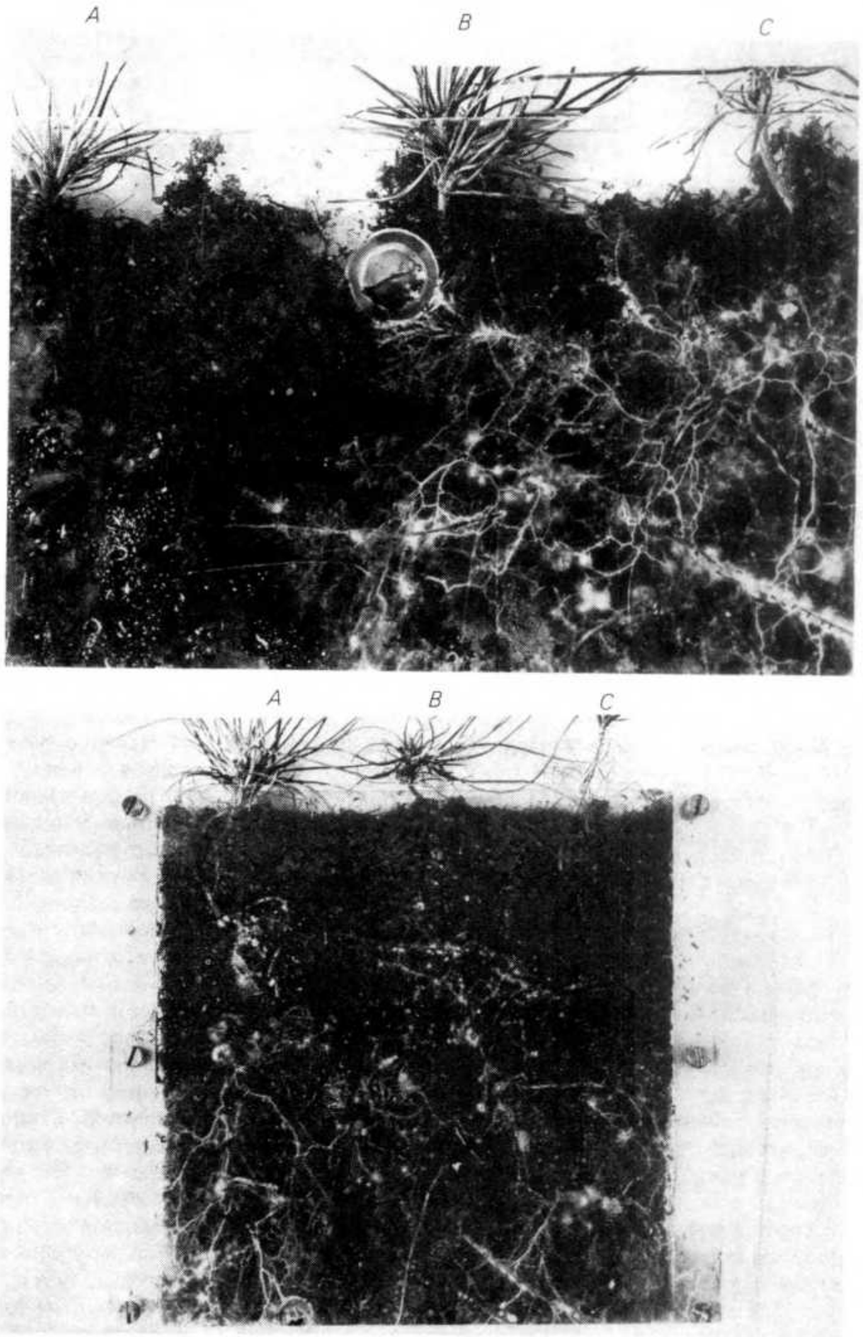

Fig. 1 *a*, Upper part of root chamber with source cup containing ^3H_2O attached by means of anhydrous lanolin to terminal parts of rhizomorph system. Position of seedlings *A*, *B* and *C* are shown relative to source (Table 1*a*). *b* Shows position of attachment of lower source cup and of seedlings analysed (Table 1*b*).

containing 1 ml of NCS tissue solubilizer (Amersham/Serle). These, together with vials containing peat, root and needle samples, were incubated at 50 °C for 48 h, cooled to room temperature, and hydrolysed with 0.4 ml of 5N HCl before radioactivity was determined by scintillation counting. Similar rhizomorphs from the chambers and from a pine plantation were cut into 2–3-mm lengths, fixed and processed for examination by transmission electron microscopy.

Within 1 h, ^3H_2O moved from both the upper (Table 1*a*) and lower (Table 1*b*) source cups, through rhizomorphs to mycorrhizal roots and shoots. In each case movement occurred to more than one of the seedlings in the chamber, indicating that, as would be expected from visual inspection of the rhizomorph system (Fig. 1), the route was irregular. Beyond the root, passage of label preferentially to young needles (plants *A* and *B*, Table 1*a*; plant *A*, Table 1*b*) suggests a polarity of movement along recently laid down conduits in the seedling. Seedling *A* (Fig. 1*a*), to which no rhizomorphs were attached, contained no label, demonstrating that water movement was dependent on the presence of a rhizomorph connection from source cup to seedling. Detection of counts in needles up to 27 cm from the source (Table 1*b*) indicates that a minimum rate of transport of 27 cm h^{-1} was obtained in these experimental circumstances. Such rates of transport, which are comparable with those frequently reported for xylem, suggest that the hydraulic conductivity of the pathway is high. It is likely that water moves through the rhizomorph along a gradient of water potential established by transpiration from the seedling.

Ultrastructural analysis reveals considerable differentiation in this type of rhizomorph. Transverse and longitudinal sections (Fig. 2) show that central hyphae of relatively large diameter, and which generally lack cytoplasmic contents, are surrounded by narrower densely cytoplasmic hyphae often with thick cell walls. These form a pseudoparenchymatous sheath around the central structures. Stages in the dissolution of transverse walls of the central hyphae, can be seen. At maturity these structures are analogous to the 'vessel' hyphae of *Serpula lacrymans*[10,11]. Their diameters are between 6 and 20 μm which, together with the absence of cross walls and cytoplasm, makes them structurally comparable with xylem vessels of higher plants. This helps to explain the low resistance to water movement through the rhizomorphs revealed by the tracer studies, and lends support to

Table 1 Transport of water through rhizomorphs to mycorrhizal pine seedlings as revealed by liquid scintillation counting of ^3H_2O extracted from rhizomorph segments, mycorrhizal roots and needles

a, Source cup attached to wall at top of chamber (Fig. 1*a*)

Material sampled	Distance of material from source (mm)	Counts (d.p.m.)
Rhizomorph segment (0.5 cm)	10	3,231
	20	800
	30	2,060
	40	2,610
Mycorrhizal root attached to rhizomorph	45	2,338
Young (extending) needle of plant *C*	60–70	1,004
Old (fully extended) needle of plant *C*	50–60	0
Young needle of plant *B*	60–70	3,577
Old needle of plant *B*	50–65	0
Young needle of plant *A*	70–80	0
Old needle of plant *A*	60–70	0
Peat below source	0	0

b, Source cup attached to wall at base of chamber (Fig. 1*b*)

Material sampled	Distance of material from source (mm)	Counts (d.p.m.)
Rhizomorph segments (0.5 cm)	10	1,476
	20	1,931
	30	1,019
	40	540
	50	689
	60	804
	70	913
Mycorrhizal root attached to rhizomorph	80	43,452
Lateral branch of rhizomorph	40	760
	50	851
Mycorrhizal root attached to lateral branch	80	25,661
Young needle of plant *A*	170–190	13,761
Old needle of plant *A*	160–170	458
Young needle of plant *B*	230–240	2,091
Old needle of plant *B*	180–220	1,641
Young needle of plant *C*	240–270	984
Old needle of plant *C*	200–230	0
Peat below source	0	0

the view that water moves apoplastically through the central vessels rather than symplastically through the narrow outer hyphae or through the cell walls. The accumulation of activity in the sheath region may reflect increased resistance to flow in this area, where presumably a considerable portion of the pathway must be through the symplast. Certain of these structural features would be expected to protect the vessel hyphae from collapse when under negative hydrostatic pressure. The parenchymatous sheath of the rhizomorph with its thick-walled members would supply external support, and the mycorrhizal sheath situated in the pathway between seedling and rhizomorph would supply a filtration resistance isolating the 'vessels' from the lowest seedling water potentials. The outer sheath of the rhizomorph also probably presents a high resistance to lateral movement of water which would explain the absence of isotope leakage into the peat (Table 1*a*).

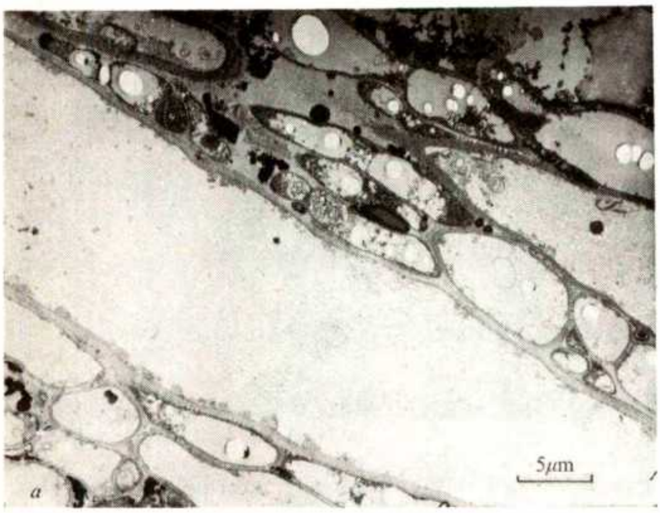

Fig. 2 *a*, Longitudinal section of rhizomorph from synthesized *Pinus sylvestris–Suillus bovinus* system. *b*, Transverse section of rhizomorph from the same system. *c*, Transverse section of rhizomorph attached to mycorrhizal root of *Pinus sylvestris* in the field. All tissues were fixed for 1.5 h in 2.5% phosphate-buffered glutaraldehyde, dehydrated in graded ethanol series and embedded in Spurr's resin.

Plants such as pine which are normally ecto-mycorrhizal have a relatively low root density compared to grasses and most other herbaceous plants[12–14]. Our observations indicate that the rhizomorphs of ecto-mycorrhizas may represent functional extensions of the root system. We have now synthesized mycorrhizas from which rhizomorphs grow to exploit moist soil while the soil around the seedling roots is allowed to dry progressively. In these circumstances seedling water balance has been maintained for several weeks by means of water transport through the rhizomorphs. During the same period control seedlings lacking rhizomorphs died.

Mycorrhizal fungi differ in their capacity to produce rhizomorphs and there may be structural and functional distinctions between rhizomorphs produced by different fungal symbionts. Such features are now being investigated with a view to selection of mycorrhizal associates which have the capacity to improve the performance of forest crops particularly in semi-arid areas.

We thank Dr B. C. Jarvis for advice on isotope extraction and counting procedures, and acknowledge receipt of financial support from the SRC, NERC and the Forestry Commission.

Received 12 June; accepted 16 September 1980.

1. Went, F. W. *Am. J. Bot.* **60,** 103–110 (1973).
2. Woods, F. W. & Brock, K. *Ecology* **45,** 886–889 (1964).
3. Zak, B. in *Ectomycorrhizas* (ed. Kozlowski, T.) 43–78 (Academic, New York, 1973).
4. Went, F. W. & Stark, N. *Proc. natn. Acad. Sci. U.S.A.* **60,** 497–504 (1968).
5. Schramm, J. R. *Trans. Am. Phil. Soc.* **56,** 1–194 (1966).
6. Harley, J. L. in *The Biology of Mycorrhiza* (Hill, London, 1969).
7. Reid, C. P. P. in *Mycorrhizae—Proc. First North American Conference on Mycorrhizae*, Misc. Publ. 1189, 222–227 (USDA Forest Service, Washington, 1971).
8. Bowen, G. D. in *Ectomycorrhizas* (ed. Kozlowski, T.) 151–205 (Academic, New York, 1977).
9. Read, D. J. & Malibari, A. *Proc. Int. Union Forestry Res. Org. Symp.*, Nancy (ed. Riedacker, A.) 410–424 (1978).
10. Falck, R. *Hauschwammforschungen* **6,** 1–405 (1912).
11. Butler, G. M. *Ann. Bot.* N.S. **22,** 219–236 (1958).
12. Kramer, P. J. & Bullock, H. C. *Am. J. Bot.* **53,** 200–204 (1966).
13. Newman, E. I. *J. appl. Ecol.* **6,** 1–12 (1969).
14. Andrews, R. E. & Newman, E. I. *Oecol. Plant* **5,** 319–328 (1970).

Maragheh: a classical late Miocene vertebrate locality in northwestern Iran

B. G. Campbell*, M. H. Amini†, R. L. Bernor*, W. Dickinson†, R. Drake‡, R. Morris*, J. A. Van Couvering§ & J. A. H. Van Couvering||

* Department of Anthropology, University of California, Los Angeles, California 90024

† Department of Geology, University of Colorado, Boulder, Colorado 80309

‡ Department of Earth Sciences, University of California, Berkeley, California 94720

§ American Museum of Natural History, New York, New York 10024

|| Museum, University of Colorado, Boulder, Colorado 80309

The fossil vertebrate localities of the Maragheh region in Azerbaijan, northwestern Iran, are among the most renowned late Miocene localities in Eurasia. The fossiliferous beds are found to the north and east of the town of Maragheh on the southern and eastern slopes of the Sahand massif and at an altitude of 1,450–1,900 m (Fig. 1). The first collection was made by Khanykof in 1840. Subsequent invertigators of the fauna[1–15], established Maragheh as the site of one of the principal 'Pontian' mammal faunas of Eurasia. Recently, Tobien[16], Erdbrink *et al.*[17], Takai *et al.*[18] and ourselves (the Lake Rezaiyeh Expedition) have concentrated on developing the geochronological and palaeoenvironmental aspects of the Maragheh fauna. The similarity of the Maragheh fauna to those of Samos, Pikermi, Saloniki and Mt Luberon, in particular, was recognized by most workers. The most significant results of the investigations reported here are that the Maragheh fauna spans an extended geochronological range, ~9.5–7 Myr, that the so-called 'Pontian' mammal communities are provincially distributed, and diachronic in their appearance, and finally that the absence of hominoid primates from this site and other late Miocene sites with similar savannah-like faunas strongly suggests their adaptation at this time to more forested environments which existed in Eurasia and Africa before and during the Maragheh interval.

The late Miocene deposits in the Maragheh Basin consist of a thick series of volcaniclastic and pyroclastic continental strata which underlie a broad pediplain on the southern and eastern sides of the Sahand volcanic massif. On the southern side of Sahand the strata are virtually undeformed, and very gently inclined to the west-southwest. The entire late Miocene section has previously been termed the Maragheh Formation[19], but we restrict this name to the volcaniclastic series, and distinguish a basal pyroclastic formation, the Basal Tuff, on lithological and stratigraphical grounds. South of Sahand the Maragheh Formation is eroded to a thickness of about 300 m and consists of strata made up exclusively of detrital fragments of hornblende, andesite lava and pumice, interbedded at widely spaced intervals with layers of pumice–lapilli tuff. These nominally andesitic beds are generally unlaminated, poorly sorted silty grits with cobble lenses of andesite and hard iron-stained pumice cobbles, in depositional units 1–3 m thick. The siltstone beds are the most fossiliferous and consist of massive poorly sorted volcaniclastic overbank deposits 3–10 m thick. We interpret each of the fining-upwards sequences as having been produced by a single flood event, or perhaps waxing and waning events within a single flood. The amount of sediment laid down in any particular flood is thus variable, but no major hiatuses have been found in the stratigraphic succession.

The interbedded pumice–lapilli tuffs are composed of soft, angular blocks and chips of snow-white andesitic pumice mixed to a greater or lesser extent with andesitic lava detritus. Laminated, upper parts of the pumice–lapilli tuffs obviously were reworked to a certain extent, but the basal pumicite zones are 'draped' over palaeotopographical relief (buried gullies) with constant thickness, indicating primary pyroclastic deposition.

The Basal Tuff is (apparently) a single airfall unit of rhyolite tuff with a local thickness of over 80 m. The unit is a uniform, unbedded, structureless deposit of white, devitrified ash with many randomly orientated flakes of mica and fresh crystal fragments of feldspar and quartz. The Maragheh Formation seems to rest on the Basal Tuff with a low-angle regional unconformity. The stratigraphical data, supported by the radiometric and biostratigraphical evidence, indicate that the

Table 1 Isotopic age determinations from the Basal Tuff and Maragheh Formation

Distance from LC (m)	Stratigraphic level	Amini (this work) Zircon FT		Drake (this work) Total-fusion K–Ar		Kamei *et al.*[19] Zircon FT		Erdbrink *et al.*[18] Total-fusion K–Ar	
+100	Korde-deh pumice Murdaq Chai					5.2	730-04		
+90 est.	Upper pumice Il'kchi	7.2 ± 0.4	R10	7.5 ± 0.4	R10pl				
+60 est.	Middle pumice Il'kchi	7.3 ± 0.5	R5	7.7 ± 0.5	R5pl				
			(R6)	7.2 ± 0.5	R6pl				
+15 est.	Lower pumice Il'kchi	7.4 ± 0.4/	R8/	7.9 ± 0.7	R8pl				
		7.0 ± 0.4	R8						
+(15) est.	Village pumice Il'kchi	5.2 ± 0.3/	R9/	5.5 ± 1.0	R9pl				
		5.3 ± 0.3	R9						
+7	Layered marker pumice Scholl'avand	7.6 ± 0.5	R2	8.3 ± 0.9	R2pl			8.1 ± 0.4	VIIWR
								6.2 ± 0.6	VIIhb
		7.7 ± 0.5	R12	6.4 ± 0.6	R12pl				
				6.9 ± 0.3	M5hb				
–	Loose chippings pumice Scholl'avand	7.8 ± 0.4	R11	7.4 ± 0.3	R11pl	6.6	730-19	8.7 ± 0.4	IIIWR
−50	Gürt Dareseh pumice Murdaq					6.5	730-17	14.4 ± 0.7	VWR
−110	Ignimbritic tuff Murdaq	10.6 ± 0.8	R3	8.8 ± 0.5	R3pl	7.0	730-10	12.9 ± 0.7	IWR
				8.9 ± 0.5					
	Basal Tuff Western area			11.2 ± 0.5	M1bi	7.2	730-20	10.1 ± 0.5	IXWR
								11.4 ± 0.5	IXbi
	Basal Tuff Il'kchi	11.2 ± 0.6	R4	10.1 ± 0.5	R4bi				
				9.3 ± 0.1	R4an				
		12.8 ± 0.5	R7	11.3 ± 1.0	R7bi				
				9.3 ± 0.1	R7an				

All fission-track ages are derived from separated zircon crystals. Total-fusion K–Ar age determinations were obtained from materials indicated as follows: pl, high-temperature plagioclase; hb, hornblende; bi, biotite; an, high-temperature anorthoclase; WR, whole-rock samples. Decay constants $\lambda\beta = 4.962\times10^{-10}\ \mathrm{yr}^{-1}$; $\lambda e = 0.581\times10^{-10}\ \mathrm{yr}^{-1}$; isotopic abundance: $^{40}\mathrm{K} = 0.01167\%$ of total K. Decay constants and isotopic abundance used by Erdbrink *et al.*[18] according to pre-1978 standards are slightly different, but do not change the computed values significantly. Kamei *et al.*[19] do not give their precision limits but state (p. 157) that these are "usually under 10%". Analytical details of new dating presented here are available from M.H.A. and R.D.

0028–0836/80/440837—05$01.00

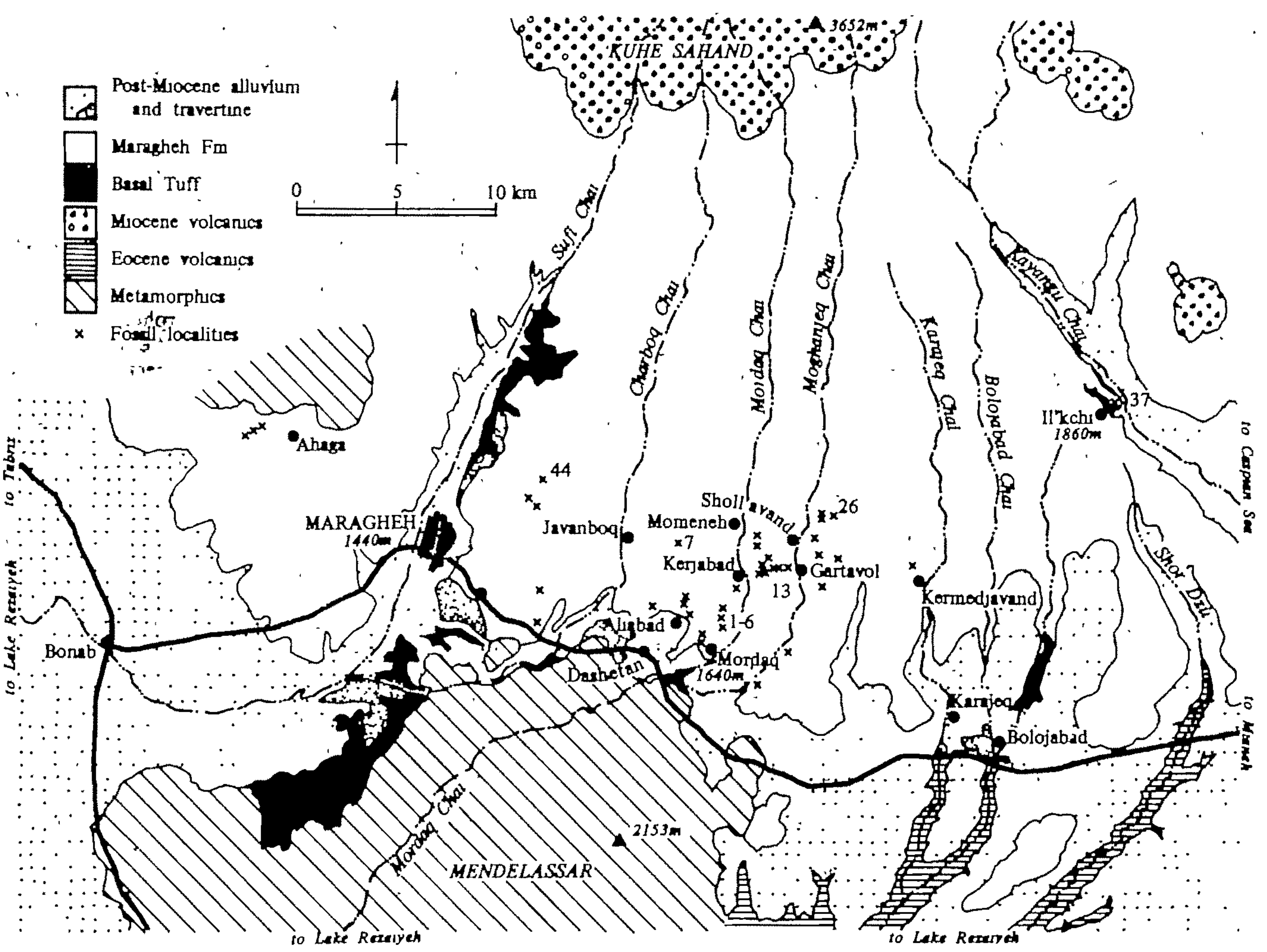

Fig. 1 Map of the southern part of the Maragheh Formation.

beds farthest to the west, and the fossils which they contain (at Kopran) were the earliest to have been deposited, and Il'kchi, the easternmost locality, seems to correlate with the youngest localities in the central area although it lies directly on the Basal Tuff. In the fossiliferous central area, the 'loose chippings' marker bed (LC), a distinctive and easily traced volcaniclastic breccia, was used as the key horizon for the allocation of Maragheh fossil localities to arbitrary 25-m stratigraphical intervals. The marker bed was also mapped over part of its exposures by Kamei[19] as the 'Scoria Bed', and it appears at the top of two of the sections measured by Erdbrink *et al.*[18] as 'trachytic breccia'.

We report here on 28 age determinations from the Basal Tuff and the Maragheh Formation in the fossiliferous district east of Maragheh. As summarized in Table 1 and Fig. 2, these determinations are based on 3 samples of the Basal Tuff and 10 samples from pyroclastic layers in the Maragheh Formation. Four of the five horizons dated by Erdbrink *et al.*[18], and three of the five horizons dated by Kamei *et al.*[19] from the same late Miocene sequence are represented in our samples. Our geochronology and that of Kamei *et al.*[19] are consistent with the stratigraphy described here, but the Kamei ages are systematically younger than ours at the same levels. The ages reported by Erdbrink *et al.*[18] on Maragheh pumicites are slightly to significantly older than ours from the same horizons, and are also inconsistent with the present stratigraphy, whereas their age analyses of the Basal Tuff are comparable with ours (see below).

As shown in Table 1, 11 of the 14 samples were dated both by fission-track (FT) analysis of pyroclastic zircons (M.H.A.) and by total-fusion K–Ar analysis of separated minerals (R.D.). Both biotite and anorthoclase were K/Ar dated in two Basal Tuff K–Ar samples. Of the 28 age determinations obtained, only one pair of FT and K–Ar ages (sample R3) were significantly different, and only one sample (R9) had an age that was clearly inconsistent with a simple superpositional interpretation. Furthermore, three horizons—Il'kchi middle pumice, layered marker pumice and Basal Tuff—were dated in at least two difference places, with good to moderate agreement.

The abundance of data, and the quality of the stratigraphy, nevertheless, clearly indicate problems in Maragheh geochronology that would not be apparent if there were only a few age determinations. There can be little question that the upper level of fossiliferous beds in the central area, and the isolated Il'kchi locality which we have correlated with this level, should be calibrated by the averages of 7.4 Myr respectively obtained on the directly superjacent pumicites in both areas. Unfortunately, the age determinations from the lower part of the section in the central area (for example, the ages obtained from the Murdaq 'ignimbrite' and the Gürt Dareseh pumicite) seem to be unreliable due to their large variation, and in addition two interpretations are possible from the dating of the Basal Tuff. We prefer to accept an age of 8.9 ± 0.5 Myr for the Murdaq ignimbrite as being both analytically satisfactory and stratigraphically consistent, the other, contradictory dates notwithstanding. We also conclude that the oldest Maragheh fossils are virtually certain to be younger than the cluster of FT and biotite K–Ar ages from the Basal Tuff, ~11 Myr, and may be younger than the age of the anorthoclase K–Ar age determinations of 9.3 Myr.

All the pyroclastic units in the Maragheh Formation contain accidental pebbles and grains of detrital andesite. For this reason, whole-rock age determinations on such units[18] must be regarded as dubious. Only the fact that the accidental contaminants are predominantly if not entirely derived from outcrops on the Miocene Sahand volcano, and not from even older rocks, gives such determinations an appearance of reliability. The Basal Tuff seems to contain no accidental fragments; on the other hand, whole-rock analysis would include the altered and devitrified matrix, from which some argon may have been lost. The discordantly young age reported by Erdbrink *et al.*[18] on a whole-rock sample may be erroneous for this reason. The lack of agreement between FT ages and anorthoclase K-Ar ages, as well as the discrepancy between biotite and anorthoclase K-Ar ages from the Basal Tuff is now under investigation.

The dating reported here gives a relatively unambiguous age for the upper limit of the Maragheh fossiliferous sequence of 7.4 Myr; preliminary and somewhat equivocal interpretations of the Basal Tuff samples suggest a maximum lower age limit of 11 Myr, but probably not more than 10 Myr. These limits are not limits of certainty, but represent the actual time-span of the Maragheh fossil fauna, interpreted here to be from about 9.5 to 7 Myr.

The biostratigraphy presented here (Table 2) combines the fossil mammal collections made by the Lake Rezaiyeh Expedition and Tobien's excavations, with information reported by Erdbrink *et al.*[18], Kamei *et al.*[19] and Bernor[20]. The Maragheh mammalian fauna is divided into three biostratigraphic intervals: lower Maragheh, extending from −150 m to −50 m below LC; middle Maragheh, extending from −50 m to −25 m below LC; and upper Maragheh, extending from −25 m to +25 m below/above LC.

In addition to the radiometric determinations cited above, detailed work on circum-Mediterranean East African late Miocene *Hipparion* evolution[21] has evaluated a recent analysis of *Hipparion* superspecific groups for use in provincial correlations between the Maragheh sites and several other Old World localities. These interpretations suggest that the Lower Maragheh *Hipparion* sp. 3 has a more primitive facial morphology than any of the *Hipparion* species from the Greek localities but compare closely with the early Vallesian *Hipparion* species *Hipparion catalaunicum*[22] and *Hipparion africanum*[23]. The Middle Maragheh *Hipparion H.* cf. *prostylum* occurs at Pikermi, Saloniki and Mt Luberon[24], and *Hipparion* cf. *mediterraneum* occurs at Pikermi, suggesting correlation of these localities with this Maragheh interval. In the Upper Maragheh, *H.* cf. *Hipparion dietrichi*, *Hipparion matthewi* and *H.* cf. *H. mediterraneum* are morphologically the most derived species of *Hipparion* in the sequence. These taxa, as well as *H.* cf. *Hipparion proboscideum* and *Hipparion 'minus'*, occur at Samos within a restricted chronological range (~0.5 Myr; N. Solounias, personal communication), suggesting correlation of Samos with Upper Maragheh, despite dating that indicates a relatively older age for the Samos material[25].

The biochronological interpretation of the Maragheh sequence given here broadly supports the radiometric determinations that refer it to an early Turolian to medial Turolian

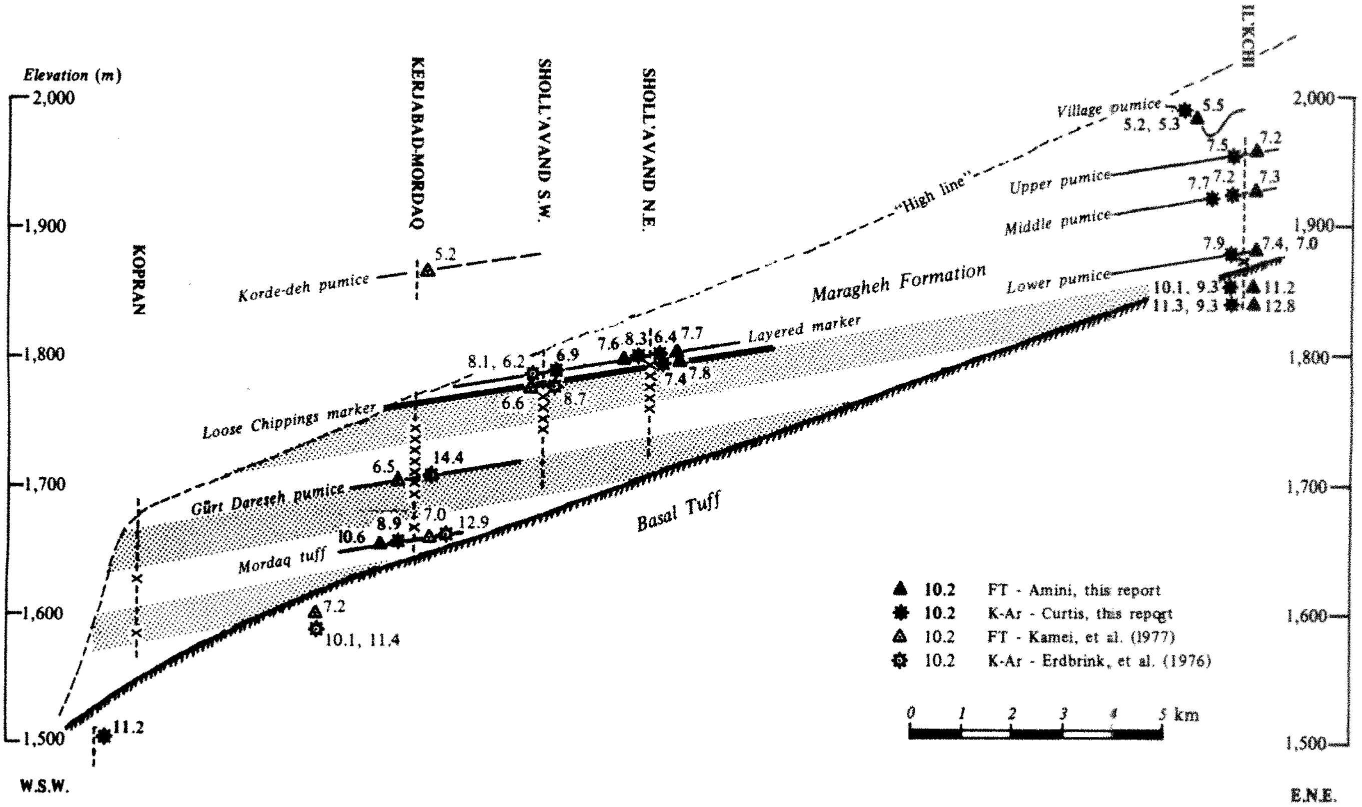

Fig. 2 Stratigraphical display of isotopic age determinations from the Maragheh Formation and Basal Tuff. See Table 1 for sample documentation. The FT and K–Ar ages obtained by Amini and Drake from the same samples are shown adjacent to one another. Repeat determinations, or determinations made on different materials from the same sample, are separated by commas. The sampling profiles on the line of section are generalized indications of the measured and studied thickness in the respective areas; portions shown by 'x' symbols represent intervals containing abundant mammalian fossils. Biostratigraphic subdivisions in 25-m increments from the plane of the LC marker are indicated by the stippled pattern. The 'high line' or interfluve maximum elevation is the residual thickness of the Maragheh Formation along the line of section inferred from the highest level of terrace deposits; thickness increases towards Sahand, where the Korde-deh tuff crops out.

Table 2 Stratigraphical ranges of Maragheh mammalian taxa

Distance above/below LC (m)	Stratiographical Positon of MMTT localities
+25	
	39 26 37 39
0	
	24, 32 38 22 16 47 27 29 15 49 49A 25 50 31 33 13 40 51 21
−25	
	7 14 6 18 19 20 34 1C 1B 2 11 4 17 35 3
−50	
	1A 5 8 42 45 23
−75	
	36 28
−100	
	44
−125	
	41 43 48
−150	

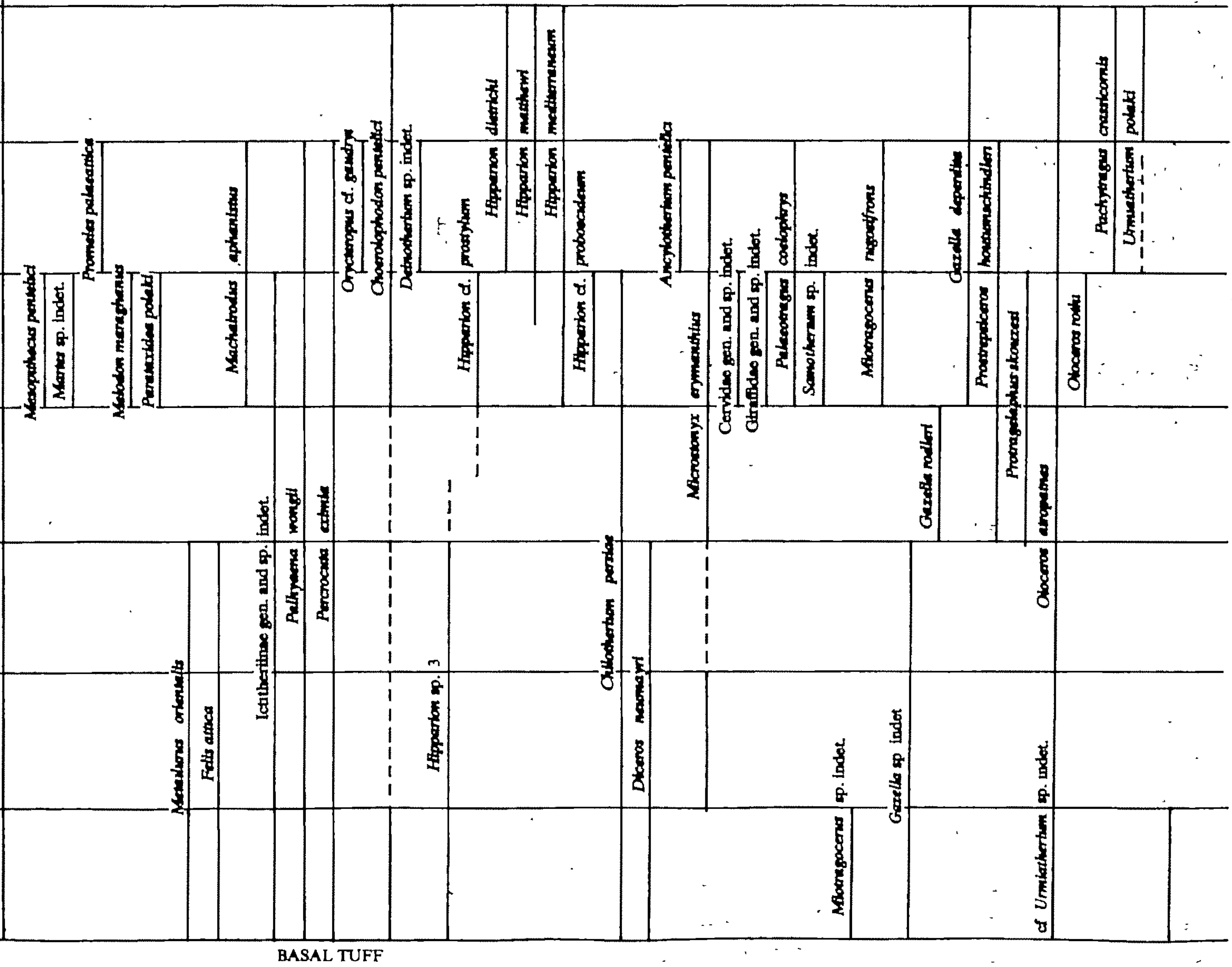

BASAL TUFF

age (MN 11 and 12, ref. 26). Pro-rated ages for the various Maragheh biostratigraphical intervals can be advanced here as: ~9.5–8.5 Myr for Lower Maragheh; 8.5–8.0 Myr for Middle Maragheh; 8.0–7.5 Myr for Upper Maragheh.

No complete, articulated skeletons were found. Taphonomic studies in a single quarry, MMTT-13, revealed 48% of the bones to be part of smaller, articulated units, predominantly distal limb segments. Skulls with mandibles and vertebral strings were also present, fragmented single bones and isolated teeth rare, complete or almost complete disarticulated limb bones and mandibular rami common. The bones showed no preferred orientation; few were of animals estimated to have weighed less than 10 kg. Taphonomic data support the interpretation that the fossils were incorporated in overbank deposits and either buried almost immediately or exposed long enough to allow removal of only a few elements by scavengers.

The Maragheh fauna has long been thought to be one of the typical Turolian savannah faunas of Eurasia. Preliminary studies of habitat spectra[27] suggest that the ecological diversity spectra are not typical of modern savannah, which is dominated by wooded grassland habitat, but are what would be expected in a savannah dominated by woodland with adjacent wooded grassland.

As shown in the East African record, the hominids did not join the savannah biome until the Pliocene, and the Maragheh ecological setting is too open and seasonal for the dryopithecines, sivapithecines (and related forms such as *Ramapithecus*)[28]. The presence of a single *Mesopithecus* from Maragheh demonstrates that these animals were in the vicinity even though the predominant fauna was probably derived from the more open woodland and wooded grassland habitat.

We thank the Trustees of the L. S. B. Leakey Foundation who sponsored this project, Gordon Getty for his generous financial help and Dr W. A. Akersten, Dr G. H. Curtis, Mr G. T. Jefferson, Dr C. W. Naeser, Dr Nikos Solounias and Dr M. O. Woodburne for assistance. Transportation, field equipment, support personnel, housing and laboratory facilities in Iran were provided by the National Museum of Natural History under the direction of Dr Hind Sadek-Kooros, and coordinated by Mr Paul Houshmast. Laboratory facilities and curatorial support were provided at the University of California, Los Angeles, and the University of California, Riverside.

Received 14 April; accepted 8 September 1980.

1. Abich, H. W. *Bull. cl. Phys.-Math. Acad. Imp. Sci. St.-Petersb.* **382,** XVI-22 Notes 27, 339–352 (1858).
2. Brandt, J. F. von *Denk. Natur.-ver. zu Riga, Her. An. Feirer 25-Jah.-best.*, 1–8 (1870).
3. Grewingk, C. *Verh. D. K. Geol. Reichsanstalt.* **15,** 296 (1881).
4. Pohlig, H. *Z. Geol. Ges.* **37,** 1022–1025 (1885).
5. Kittl, E. *Verh. Geol. Reichsanst.*, Vienna, 397–399 (1885).
6. Rodler, A. *Verh. Geol. Reichsanst.*, Vienna, 333–337 (1885).
7. Rodler, A., & Weithofer, K. A. *Denkschr. D. Kais. Akad. D. Wiss., Math.-Natur. Cl.* **42,** 753–772 (1890).
8. Schlesinger, G. *Denkschr. Naturhist. Mus. Vienna* **1,** 1–230 (1917).
9. Lydekker, R. *J. geol. Soc. Lond.* **42,** 173–176 (1886).
10. Forsyth-Major, C. J. *Proc. zool. Soc. Lond.* **1893,** 239–240 (1893).
11. Mecquenem, R. de *C. r. hebd. Séanc. Acad. Sci., Paris* **141,** 924–925 (1905).
12. Mecquenem, R. de *Nature, Paris* **24,** 10 (1906).
13. Mecquenem, R. de *Annls Hist. nat. Aisne* **1,** 27–29 (1908).
14. Mecquenem, R. de *Annls Hist. nat. Aisne* **1,** 81–98 (1911).
15. Mecquenem, R. de *Annls Paléont.* **13/14,** 135–160 (1924–25).
16. Takai, F. *Inst. Orient. Cult. Univ. Tokyo* **26,** 7–11 (1958).
17. Tobien, H. *Jb. Ver. Freunde Univ. Mainz*, 51–58 (1968).
18. Erdbrink, D. P. B. *et al. K. Ned. Akad. Wet. Proc.* **79,** 97–113 (1976).
19. Kamei, T. *et al. Mem. Fac. Sci. Kyoto Univ. Serv. Geol. Min.* **43,** 131–164 (1977).
20. Bernor, R. L. thesis, Univ. California (1978).
21. Bernor, R. L., Woodburne, M. O. & Van Couvering, J. A. *Geobios* **13,** 25–59 (1980).
22. Pirlot, P. L. *Mem. Commun. Inst. Geol. Barcelona* **14,** 1–222 (1956).
23. Arambourg, C. *Mem. Serv. Carte Geol. Algeria* no. 4 (1959).
24. Woodburne, M. O. & Bernor, R. L. *J. Paleont.* **54,** 1319–1348 (1980).
25. Van Couvering, J. A. & Miller, J. A. *Nature* **230,** 559–563 (1971).
26. Mein, P. *I.U.G.S. Comm. Strat. Bratislava*, 77–81 (1975).
27. Van Couvering, J. A. H. in *Fossils in the Making* (eds Behrensmeyer, A. K. & Hill, A. P.) 272–298 (Chicago University Press, Chicago, 1980).
28. Bernor, R. L. in *New Interpretations of Ape and Human Evolution* (eds Ciochon, R. L. & Corrucini, R.) (Plenum, New York, in the press).

Embryogenesis in a *Drosophila* mutant expressing half the normal segment number

K. Sander, M. Lohs-Schardin & M. Baumann

Institut für Biologie I (Zoologie) der Universität,
D-7800 Freiburg i.Br., FRG

Insect segments are seriated developmental subunits whose borders largely control intra-segmental patterning[1]. The individual segment owes its specific character to position-dependent instructions given to its early embryonic progenitor cells[2]. In *Drosophila*, the segment borders first become visible as a series of transverse infoldings on the surface of the germ band[3]. We describe here development in a mutant (prd^{FR1}) which forms half the normal number of transverse infoldings spaced at twice the normal distance, thereby subdividing the germ band into a series of giant domains (Fig. 1 *a–c*). Each domain develops the tracheal pits of two normal segments (Fig. 1*e*), thus revealing its composite origin, but the larva expresses only one segment border per domain and the cuticle between these borders is similar to the normal segment in both size and zonation (Fig. 2). We conclude that this course of development reflects a conflict between the seriated instructions specifying local segment character (see Fig. 1*b*) and controlling influences exerted by the abnormally spaced infoldings and later by the definitive segment borders.

The mutant we describe maps at 2-43 ± 0.7. It was obtained by EMS treatment of wild-type males with ethyl methane sulphonate and subsequently found to be allelic to the *paired* mutants[4]; the allele, which we designate as prd^{FR1}, is balanced over the CyO chromosome. In approximately 25% of the eggs, probably the homozygous fraction, gastrulation seems to be slightly delayed and the cephalic furrow either fails to appear or forms some time after the onset of germ-band extension. The maximum length of the extended germ band exceeds 90% of the normal value. When transverse epidermal furrows first become visible in the scanning electron microscope (Fig. 1), they are spaced at about twice the normal distance, demarcating six giant domains, each of which contains about as many cells as two segment anlagen in the same region of the normal germ band. The posterior domains develop tracheal pits in a rather peculiar way (Fig. 1 *d–f*). In wild-type embryos, the corresponding segments each form a single pair of pits which subsequently disappear in the anterior border furrow[3]. In the mutant, one pair of pits forms next to each furrow and slightly later another pair develops more posteriorly. The anterior pits then disappear, as occurs in normal development, but the posterior pits persist on the body flanks, and the ensuing tracheal system is severely disrupted. Within or just behind the anteriormost epidermal infolding, a pair of invaginations form (Fig. 1*e*, *f*); we consider these to be the anlagen for the salivary duct because they later fuse mid-ventrally as in wild type embryos[3]. After head involution the ventral rim of the pre-oral cavity produces the larval cuticle markers[5] characterizing the anterior border of the prothorax. The methods of observation used do not allow us to determine whether the transverse folds give rise to the definitive segment borders, as they do in normal development.

The larva moves in the egg case but fails to hatch. In its cuticle, segment length exceeds that of the wild type by a factor of 1.2–1.5. The cuticle of the oversized segments is zonated as in normal segments[5] (Fig. 2) but each zone expresses traits characteristic of two consecutive segments (hence 'paired'[4]). The traits of the anterior partner of each segment pair are restricted to a narrow anterior strip of cuticle[4]. A comparable reduction of the traits of the anterior segments occurs in the head and the caudal

0028–0836/80/440841—03$01.00

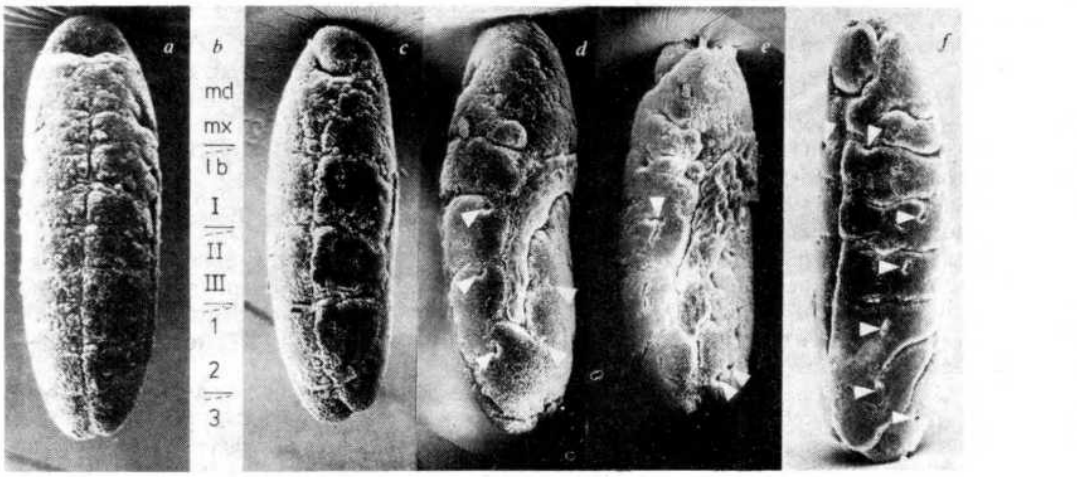

Fig. 1 Scanning electron micrographs of *Drosophila* embryos prepared by the technique of Turner and Mahowald[3]. *a*, *c*, Ventral views of normal-spaced and double-spaced patterns of epidermal infoldings at the stage of maximum germ band extension. Transverse lines link double-spaced infoldings in the mutant *paired* to the normal pattern. Embryo in *a* (possibly heterozygous for *paired*) is abnormal in showing a weaker expression of every second furrow (these are the furrows present in Fig. 1*c*). Lettering in *b* identifies segments in *a* but can also be taken to symbolize a prepattern specifying local segment character. Abbreviations: md, mandibular; mx, maxillar; lb, labial segments (head); I–III, thoracic segments; 1–3, anterior abdominal segments. A slight backward shift of the infoldings (dashed lines) is indicated by some observations and might account for the suppression of homologous cuticle elements in every second segment of the normal pattern[4]. *d–f*, Lateral views of germ band stages, ventral side at the left (negatives *d* and *e* were reversed to obtain this orientation). *d*, Onset of germ band shortening, to show anterior tracheal pits (arrows). *e*, Slightly later stage, posterior tracheal pits apparent and in most pairs linked to the anterior pit by a groove (one pair marked by arrows at bottom). The foremost anterior pit (top arrow) is about to enter the transverse furrow. *f*, The germ band is further contracted, posterior pits (horizontal arrows) persist on body flanks (albeit shifted anteriorly) and anterior pits have disappeared. Arrows at the top mark salivary duct pits also seen in *e*. *c–f* Represent typical specimens selected from more than 100 germ band stage embryos studied with the scanning electron microscope. Length of preparations varies between 0.33 and 0.4 mm.

complex. Here the H-piece (anterior part of the cephalopharyngeal skeleton) and the supra-anal tuft are markedly reduced; the former is derived from the labial segment[6], the latter from the rudimentary 9th abdominal segment[3]. The protuberances carrying the posterior spiracles and their atria (8th abdominal segment) are abnormally large and somewhat deformed, providing further evidence for the spatial prevalence of the posterior partner in the paired segments. Up to 45% of mutant embryos show holes in the larval cuticle and/or lateral (rarely ventral) fusion of adjacent denticle belts. No large-scale cell elimination which could account for these anomalies or for the reduction in segment number or segment size was noted.

The abnormal segmentation pattern in *paired* is not linked to a specific local segment character. This was shown by combining the mutant with an extreme *Ultrabithorax* allele which confers mesothoracic character on all segments between the mesothorax and the posterior spiracles[7]. The ensuing larvae (if not disorganized) exhibit thoracic transformation of all abdomen-type segments but retain the abnormal distribution of the epidermal infoldings and the reduced number of definitive segment borders.

Abnormal subdivision of the germ anlage as described here is a novel type of developmental anomaly. We propose to name it 'embryonic malpartitioning'. We assume that the mutation primarily affects the positioning of the transverse ectodermal infoldings thought to mark the boundaries between adjacent segments[3]. The resultant abnormal pattern of furrows (Fig. 1*c*) seems to act as an aberrant 'partitioning grid' imposed on a germ anlage which carries the normal set of instructions for individual segment character (shown diagrammatically in Fig. 1*b*). This view is based on the findings that (1) the incipient spatial pattern of transverse furrows is more abnormal than the pattern of other visible epidermal anlagen (tracheal and salivary duct pits, Fig. 1), and (2) the mutant generally maintains the normal spatial proportions of abdomen and thorax in the germ band and larval cuticle. In any case, the abnormal subdivision of the germ band must progressively influence subsequent patterning, because the tracheal pits appear in full number and nearly normal spacing (Fig. 1*e*) whereas the cuticle which forms later shows only half the normal number of segments. Despite their composite character these segments approach normal segment length, although not as closely as do the fused segments observed in the bug *Oncopeltus*[1].

Why the mutant should so exactly double-space the grid of epidermal infoldings (Fig. 1*c*) is a most intriguing question. To assume suppression of every second furrow of the normal pattern merely alters the problem because some wild-type patterned germ bands from our mutant stock partly suppress the alternative set of furrows (Fig. 1*a*). The double-spacing therefore probably reflects some basic property of the mechanisms responsible for the periodic positioning of epidermal infoldings in normal development. Mechanisms based on dissipative structures which can be envisaged as a spatial series of 'stationary waves'[8,9] could be inherently prone to this type of partitioning error; for instance, the mutant cells might recognize only the positive or the negative maxima (or zero transitions) whereas the wild-type cells could respond to both (possibly in succession). However, abnormal distribution of the periodic signals themselves cannot be excluded. Early anomalies like the defective cephalic furrow and subnormal germ band length might indicate changes in the geometrical boundary conditions which are critical for dissipative patterning and probably also for other spacing mechanisms. Whether the epidermal infoldings in the mutant initiate the full sequence of functions characterizing

Fig. 2 Phase contrast micrographs of ventral cuticle from the posterior thoracic region of *paired* (right) and wild-type (left) first instar larva. Note the typical transverse zonation of the mutant segment, and the increase in the number of denticle rows roughly proportional to the increase in segment length; a similar 'multiplication of elements'[13] has been described previously in oversized segments[14]. Arrows mark Keilin's sense organs. The band of denticle rows at the bottom is the anterior rim of the abdomen. Scale bar, 0.02 mm.

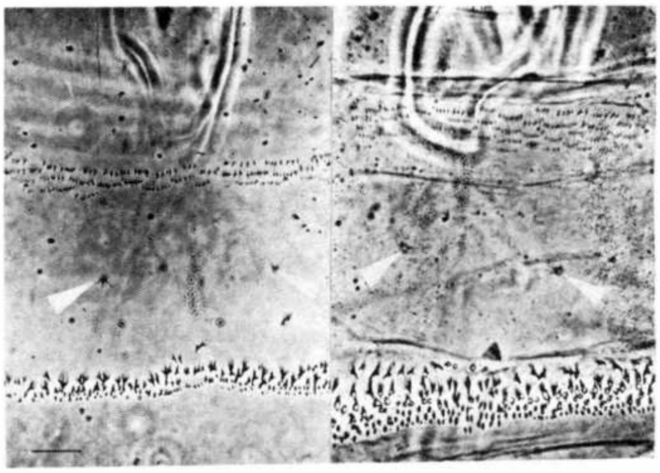

a typical segment border (including its function as compartment boundary[10]) is not known. It even remains to be shown (for example, by defect mapping[5]) whether the infoldings in the mutant harbour the progenitors of those hypoderm cells which subsequently express the cuticular segment borders. In the absence of proof for this, we can consider alternative possibilities. The most attractive of these is that the folds form across the prospective territory of the anterior segment of each pair (Fig. 1*b*) and that in this abnormal position they prevent some region of the prospective hypoderm from expressing its strip of the cuticular pattern. If the starting conditions for periodic patterning were liable to several kinds of disturbance, the transverse folds might be shifted to different positions (the 'floating grid' hypothesis). The resulting seriated cuticular defects should then affect different strips of the intra-segmental pattern. Several classes of mutant exhibiting such defects have been found[4] and observations on their early development may serve to test this assumption.

If, on the other hand, the infoldings represent functional segment borders, their aberrant distribution raises the question of how in normal development the pattern of segment borders is kept in register with the pattern of instructions specifying local segment character (Fig. 1*b*). One possibility is that both patterns develop independently on the basis of the same axial system of positional information, for instance, an axial gradient[2,11]. The mutant described here would then misinterpret this information when spacing its segment borders, but not when defining local segment character. Homoeotic mutants like *Ultrabithorax*, on the other hand, would misinterpret the same positional information with respect to local segment character[11,12]. The former error would result in aberrantly demarcated segments, the latter in assigning a wrong character to some correctly demarcated segments.

We thank Dr E. Gateff for supplying us with mutagenized flies, Drs Ch. Nüsslein-Volhard, E. Wieschaus, J. Campos-Ortega and C. M. Bate for valuable comments, Mrs M. Scherer and U. Zimmer for technical help, and the Deutsche Forschungsgemeinschaft for financial support (SFB 46).

Received 25 June, accepted 8 September 1980.

1 Lawrence, P. A. *Adv. Insect Physiol* 7, 197–266 (1970)
2. Sander, K. *Adv. Insect Physiol* 12, 125–238 (1976)
3 Turner, F R & Mahowald, A P *Devl Biol* 57, 403–416 (1977), 68, 96–109 (1979)
4 Nüsslein-Volhard, Ch & Wieschaus, E *Nature* 287, 795–801 (1980)
5. Lohs-Schardin, M., Cremer, Ch & Nüsslein-Volhard, Ch. *Devl biol* 73, 239–255 (1979)
6. Schoeller, J *Arch Zool exp gén.* 103, 1–216 (1964)
7 Lohs-Schardin, M *Drosoph Inf Serv* (in the press).
8 Nicolis, G & Prigogine, I. *Self-Organization in Nonequilibrium Systems* (Wiley, New York, 1977).
9 Kauffman, S A, Shymko, R M & Trabert, K *Science* 199, 259–270 (1978).
10 Szabad, J, Schüpbach, T. & Wieschaus, E *Devl biol* 73, 256–271 (1979)
11. Lewis, E. B *Nature* 276, 565–570 (1978).
12 Sander, K *Verh Dt. zool. Ges.* 67, 58–70 (1975)
13. Schubiger, G. *Devl biol* 26, 277–295 (1971)
14. Vogel, O *Wilhelm Roux's Arch. dev. Biol.* 182, 33–38 (1977)

Parathyroid hormone stimulates bone resorption via a Na–Ca exchange mechanism

Nancy S. Krieger & Armen H. Tashjian Jr*

Laboratory of Toxicology, Harvard School of Public Health, Boston, Massachusetts 02115 and *Department of Pharmacology, Harvard Medical School, Boston, Massachusetts 02115

Parathyroid hormone (PTH) stimulates the release of calcium from bone and is thought to initiate its action by a direct effect on the plasma membrane of bone cells[1]. Although specific membrane receptors for PTH have not yet been identified in bone, they have been characterized in kidney[2], and PTH does stimulate production of cyclic AMP in bone[3]. However, the mechanism by which PTH causes the release of Ca from bone is not understood. We have determined that several agents that alter ion transport across biological membranes inhibit PTH-stimulated bone resorption *in vitro*. These agents include ouabain, veratridine and certain monovalent cation ionophores, which transport monovalent cations selectively[4,5]. The inhibition of bone resorption is dose dependent and reversible within the first 24 h of treatment. All these compounds would be expected to increase intracellular sodium concentration in bone cells. Also, we find that decreasing the extracellular Na^+ concentration prevents PTH-stimulated resorption. Therefore, we propose that PTH acts on bone to stimulate Ca release by means of a Na–Ca exchange mechanism. Decreasing the Na gradient across the bone cell plasma membrane would prevent the Na–Ca exchange and thus inhibit the physiological response to PTH.

PTH stimulates the release of Ca from bone in organ culture, an action analogous to its physiological effect on the skeleton *in vivo*[1]. Studies in bone have demonstrated an early stimulated increase in Ca influx both *in vivo*[6] and *in vitro*[7]. A possible role for Na ions in hormonal stimulation of Ca release from bone has been postulated[8] but not demonstrated experimentally.

Our results using intact neonatal mouse calvaria in organ culture show that monovalent cations do play an important role in the release of Ca from bone that is enhanced by PTH. Bone resorption stimulated by 0.1 U ml^{-1} PTE (United States Pharmacopeia Parathyroid Extract, Eli Lilly Company) was inhibited by veratridine, ouabain and the monovalent cation ionophores, nigericin, monensin and X-206 (Table 1). Inhibition by ouabain was reversed almost completely by KCl (Table 1, Expt 2) whereas KCl had no effect on the inhibition produced by the monovalent ionophores (for example, Table 1, Expt 4).

Inhibition of stimulated bone resorption by nigericin was reversible within the first 24 h that the ionophore was present (Fig. 1*a*). However, after 48 h in the presence of both PTH and ionophore, the inhibition of bone resorption was no longer reversible (Fig. 1*b*). Similarly, if calvaria were pretreated with nigericin alone and then stimulated with PTE after washing out the ionophore, there was no subsequent response to PTE after prolonged (>24 h) pretreatment with ionophore. When similar experiments were performed with ouabain, the results were comparable; inhibition of stimulated resorption was reversible within the first 24 h of treatment, but not after 48 h of treatment with ouabain (N.S. K., unpublished observations).

To test directly for the role of monovalent cations in the PTH-stimulated Ca release from bone, experiments were performed in medium containing various concentrations of Na^+ and K^+ (Table 2). Decreasing the Na^+ concentration below the control level of 150 mM resulted in a dose-dependent inhibition of PTE-stimulated Ca release from the calvaria. Below 100 mM Na^+ there was no response to PTE. Removing K^+ from the medium had no significant effect on PTE-stimulated bone resorption nor on the inhibition of stimulated resorption produced by ouabain or nigericin. However, increasing the K^+ concentration above the control level of 5 mM blunted or reversed the inhibition by ouabain of PTE-stimulated resorption without altering the inhibition produced by nigericin.

All of the inhibitory agents used in this study alter monovalent ion fluxes across the plasma membrane and would be expected

0028–0836/80/440843—03$01 00

Table 1 Inhibition of PTH-stimulated bone resorption *in vitro*: effects of veratridine, ouabain and monovalent cation ionophores

Expt no.	Treatment	Medium calcium ($mg\ dl^{-1}$)
1	Control	6.2 ± 0.67
	PTE ($0.1\ U\ ml^{-1}$)	13.8*
	Veratridine (0.3 mM)	6.2
	PTE ($0.1\ U\ ml^{-1}$) + veratridine (0.3 mM)	6.3
2	Control	7.1 ± 0.88
	PTE ($0.1\ U\ ml^{-1}$)	12.8*
	KCl (15 mM)	8.0
	PTE ($0.1\ U\ ml^{-1}$) + ouabain (0.3 mM)	6.1
	PTE ($0.1\ U\ ml^{-1}$) + ouabain (0.3 mM) + KCl (15 mM)	10.4*
3	Control	8.0 ± 0.79
	PTE ($0.1\ U\ ml^{-1}$)	15.5*
	PTE ($0.1\ U\ ml^{-1}$) + nigericin (10^{-7} M)	7.5
	PTE ($0.1\ U\ ml^{-1}$) + monensin (3×10^{-7} M)	6.4†
	PTE ($0.1\ U\ ml^{-1}$) + X-206 (10^{-7} M)	8.1
4	Control	6.3 ± 0.46
	PTE ($0.1\ U\ ml^{-1}$)	9.4*
	KCl (15 mM)	7.2
	PTE ($0.1\ U\ ml^{-1}$) + nigericin (10^{-7} M)	6.0
	PTE ($0.1\ U\ ml^{-1}$) + nigericin (10^{-7} M) + KCl (15 mM)	5.7

Calvaria from 4–5-day-old neonatal mice were incubated at 37 °C in Dulbecco's modified Eagle's medium containing heat-inactivated (56 °C, 60 min) horse serum (15%) and fetal calf serum (2.5%)[15,16]. Treatment was begun at zero time with concentrations of each agent which were determined to be maximally effective by complete dose-response experiments. Cultures were gassed daily and the medium changed once at 24 h. Medium Ca concentrations were measured at 24-h intervals using an automatic fluorometric titration method. Values given are the mean of at least four bones per group at the end of a 72-h treatment period. By analysis of variance the s.e. was calculated from the residual error term for each experiment. Because the number of bones in each group in a given experiment was the same, the s.e. for each group was the same, and therefore for simplicity the s.e. is given only for the control group in each experiment.

* $P < 0.001$, † $P < 0.05$, compared to control cultures.

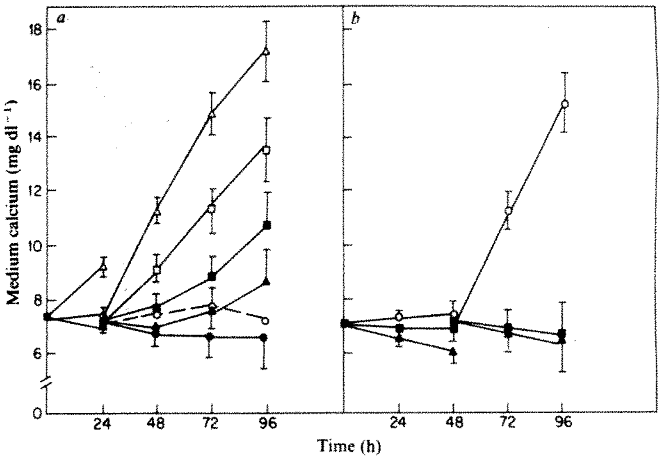

Fig. 1 Effects of pretreatment and reversibility of bone resorption inhibited by nigericin. *a*, Calvaria were cultured as described in Table 1 legend. Bones were treated with $0.1\ U\ ml^{-1}$ PTE without or with 10^{-7} M nigericin. Medium was changed at 24 h and fresh hormone and ionophore readded after washing each calvarium twice with 2 ml control medium. ○, Control; △, PTH alone; □, control medium for 24 h, then PTH; ■, PTH + nigericin for 24 h, then PTH alone; ▲, nigericin for 24 h, then PTH alone; ●, PTH + nigericin. *b*, Cultures were prepared and incubated in parallel with those in *a*, except that medium was changed and calvaria washed at 48 h. ○, Control for 48 h, then PTH; ■, PTH + nigericin for 48 h, then PTH alone; ▲, nigericin for 48 h, then PTH alone. Values are the mean ±s.e. for at least four bones per group.

to increase the intracellular concentration of Na^+. The cardiac glycoside, ouabain, is known to inhibit specifically the Na, K-dependent adenosine triphosphatase [($Na^+ + K^+$)ATPase], thereby preventing Na^+ efflux in exchange for K^+ influx[9]. Our observation that high K^+ reversed the inhibition by ouabain of PTE-stimulated bone resorption supports the argument that the ouabain effect described here is due to inhibition of ($Na^+ + K^+$)ATPase activity in bone. K^+ has been shown to compete in a complex manner with ouabain for binding to the ($Na^+ + K^+$)ATPase and to antagonize specifically the effects of cardiac glycosides in other target tissues[10]. Also, 0.3 mM ouabain maximally inhibited ($Na^+ + K^+$)ATPase-dependent ^{86}Rb uptake by calvaria (N. S. K., unpublished observations).

Monovalent cation ionophores allow fluxes of Na^+ and other monovalent cations along electrochemical gradients across the plasma membrane of the cell[4,5]. Ionophore-mediated Na^+ influx is unrelated to the influx that occurs via the voltage-dependent Na channel. However, veratridine binds directly to the Na channel, stabilizing it in the open conformation and thereby increasing Na^+ influx[11].

Once the intracellular Na^+ concentration is increased sufficiently to decrease the magnitude of the transmembrane Na^+ concentration difference, the Na^+ gradient across the plasma membrane would no longer be favourable for the Ca^{2+} efflux to occur that is coupled to Na influx[8,12]. If PTH-stimulated bone resorption requires Na–Ca exchange, inhibition of that exchange by increasing intracellular Na^+ would explain the common effects of the agents we used to inhibit bone resorption. Alternatively, ouabain, veratridine and the ionophores or high intracellular Na^+ concentrations might disrupt some other critical step in the mechanism of action of PTH by an indirect effect on cell metabolism. However, the findings given in Table 2 make this less likely. The transmembrane Na^+ concentration difference was decreased by lowering extracellular Na concentration. This manoeuvre had the same effect as increasing intracellular Na^+, providing strong evidence to support the necessity for a Na–Ca exchange mechanism in the PTH-stimulated release of Ca from bone. A recent model of how cardiac glycoside inhibition of the ($Na^+ + K^+$)ATPase affects Ca^{2+} levels in cardiac muscle cells proposes a similar coupling between a Na–Ca exchange mechanism and the action of the Na pump to regulate transmembrane cation movements[9].

Table 2 Effects of medium Na^+ and K^+ concentrations on PTE-stimulated bone resorption

Medium		Medium calcium ($mg\ dl^{-1}$)			
[Na^+] (mM)	[K^+] (mM)	Control	PTE	PTE + ouabain	PTE + nigericin
150	5	7.2 ± 0.38	10.4*	6.3*	6.7†
120	5	4.9 ± 0.25	6.4*	5.6†	ND
100	5	4.1 ± 0.25	4.7†	ND	ND
50	5	5.6 ± 0.36	6.0	6.0	6.2
150	0	6.4 ± 0.50	9.5*	4.7	5.4
150	10	5.6 ± 0.48	9.1*	7.5‡	5.5
150	30	7.0 ± 0.28	11.0*	8.4*	5.2*

Calvaria were cultured as described previously[9] except that the medium was made using an MEM-Select-amine kit (Grand Island Biological Co.) and salt concentrations were adjusted to the desired compositions shown. Isotonicity was maintained using choline chloride whenever the NaCl concentration was decreased below 150 mM. Bones were treated with $0.1\ U\ ml^{-1}$ PTE without or with 0.3 mM ouabain or 10^{-7} M nigericin and medium was changed once at 24 h. Values given are the mean ±s.e. of four bones per group after 72 h of treatment. As in Table 1, the s.e. for each different medium tested is presented with the control value. The concentrations of Na^+ and K^+ in unmodified medium are 150 and 5 mM, respectively. ND, Not determined.

* $P < 0.001$, † $P < 0.05$, ‡ $P < 0.01$, compared to control for each different medium.

The time dependence of the reversibility of nigericin (and ouabain) inhibition, and of the pretreatment effects on PTE-stimulated resorption are also consistent with a mechanism involving an increase in intracellular Na^+. Coupled transport of Na^+ and amino acids or sugars has been described[13]. Altering the Na^+ gradient would affect this transport system and, with prolonged treatment, such transport would decrease and cellular energy metabolism would be inhibited. This might explain the irreversibility of prolonged inhibition by the agents used. Such a general effect on cellular metabolism is unlikely to explain the inhibition of PTE-stimulated resorption, however, because the inhibition of resorption occurs more rapidly (within 6 h)[14] than the more long-term changes in metabolism.

The effects of pretreatment with nigericin and ouabain imply that their inhibitory actions are not the result of a direct competitive interaction at the level of the PTH receptor. This conclusion is supported by the ability of these compounds to inhibit bone resorption stimulated by prostaglandin E_2 and 1,25-dihydroxyvitamin D_3 as well as PTH[14]. Therefore, it seems that Na–Ca exchange may be the final common step in the mechanisms of action of several hormones that stimulate bone resorption.

We thank Dr Stanley Goldin and Ms Kut-Nie Tan for helpful discussions, and Mrs Elizabeth Moore for statistical analyses. This research was supported by the USPHS (AM 10206); N.S.K. received a NRS award (AM 05595).

Received 15 May; accepted 8 August 1980.

1. Raisz, L. G. in *Handbook of Physiology* Vol. 7, Sect. 7 (ed. Aurbach, G. D.) 117–136 (American Physiological Society, Washington, 1976).
2. Nissenson, R. & Arnaud, C. D. *J. biol. Chem.* **254,** 1469–1475 (1979).
3. Chase, L. R. & Aurbach, G. D. *J. biol. Chem.* **245,** 1520–1526 (1970).
4. Pressman, B. C. *A. Rev. Biochem.* **45,** 501–530 (1976).
5. Stern, P. H. *Clin. orth. rel. Res.* **122,** 273–298 (1977).
6. Parsons, J. A. & Robinson, C. J. *Nature* **230,** 581–582 (1971).
7. Dziak, R. & Stern, P. H. *Endocrinology* **97,** 1281–1287 (1975).
8. Hahn, T. J. *et al. J. clin. Invest.* **62,** 406–414 (1978).
9. Sweadner, K. J. & Goldin, S. M. *New Engl. J. Med.* **302,** 777–783 (1980).
10. Baker, P. F. & Willis, J. S. *Nature* **226,** 521–523 (1970).
11. Catterall, W. A. *J. biol. Chem.* **250,** 4053–4059 (1975).
12. Stallcup, W. B. *J. Physiol.* **286,** 526–540 (1979).
13. Schultz, S. G. & Curran, P. F. *Physiol. Rev.* **50,** 637–718 (1970).
14. Krieger, N. S. & Tashjian, A. H. Jr *Fedn Proc.* **39,** 729 (1980).
15. Tashjian, A. H. Jr & Levine, L. *Biochem. biophys. Res. Commun.* **85,** 966–975 (1978).
16. Ivey, J. L., Wright, D. R. & Tashjian, A. H. Jr *J. clin. Invest.* **58,** 1327–1338 (1976).

Disruption of optic fibre growth following eye rotation in *Xenopus laevis* embryos

Philip Grant & Eric Rubin*

Department of Biology, University of Oregon, Eugene, Oregon 97403

Eye rotation is an experimental paradigm used to study axial specification of the amphibian retina and its connections to the tectum[1–4]. Jacobson reported[4] that the naso-temporal and dorso-ventral axes are determined sequentially and independently between Nieuwkoop–Faber (NF)[5] stages 28 and 32 in *Xenopus*. Others claim, however, that both retinal axes are determined much earlier and not independently in *Xenopus* and *Rana*[6–8]. We now find that in *Xenopus* this operation can disturb the exit of optic fibres from the retina with the severity of disruption depending on the time of surgery. Eyes rotated 180° at NF stage 26–27, before any fibres develop, form aberrant retinal fascicle patterns in which the first optic fibres to differentiate (pioneer fibres), failing to exit from the eye, are deflected into circling instead of radial trajectories. Optic fibres appearing later follow these early misguided axons, creating circular bundles. Eyes rotated later (NF 32–34), after optic fibres differentiate, develop normal but inverted patterns because radial fascicles in the retina at the time of operation accurately guide all newly arising fibres to the optic nerve head. This stage-dependent sensitivity of retinal fascicle development must be considered when interpreting the results of rotation experiments.

While testing Sperry's hypothesis of neuronal specificity in *Xenopus*, Jacobson[4] claimed that after 180° rotation of the embryonic eye at NF stage 28, the retina regulated, and a normally ordered retinotectal projection developed, whereas rotation at stage 30 led to inversion of only the naso-temporal axis. Rotation at stage 32 produced a completely inverted retinotectal projection with both axes rotated. Others[7] find in *Xenopus*, however, that rotation of eye vesicles at stage 21–22 gave either rotated retinotectal maps or compound eyes, one normal and the other rotated. Likewise in *Rana*, at Shumway[9] stage 16–17 and at stage 26 in *Xenopus*, eye rotation resulted in inverted retino-tectal maps[6,8] with the map's orientation matching the position of the choroid fissure.

In such studies in *Xenopus*, ganglion cell fibres are assumed not to develop until stage 33 (refs 5, 10, 11). Hence, all eye operations before that stage are assumed to be completed before any optic fibres appear in the retina. We found, however, that optic fibres develop early in *Xenopus*[12–14]. Fibres appear as early as NF 28, before the retina completes invagination. They form bundles which enter the optic stalk and reach the brain by NF 32. These bundles organize into a stereotyped radial pattern within the early embryonic retina[12]. Evidently, optic fibres differentiate in the retina and form bundles precisely during those stages when the retina is assumed to undergo axial specification[4]. Thus eye rotation before or after the appearance of retinal fibres may have different effects on development of fascicle patterns and may, in turn, affect fibre outgrowth and connections in the brain. For example, the presence of degenerating axons in the optic stalk may guide regenerating axons to their targets in the brain[15].

To determine how the presence of optic fibres at the time of the operation affects development of fascicle patterns, embryonic eyes were rotated 180° at early stages (NF 26–28), before fibres had developed, and at later stages (NF 32–34), after optic fibres had entered the optic stalk and diencephalon. Control operations involved removal of the eye and replacement in normal orientation. When embryos reached tadpole stages 54–55, the operated eyes were removed and the retinas prepared as silver-stained whole mounts to reveal the fibre patterns[12,16]. A similar whole-mount technique has been used for the developing chick retina[17–19]. Silver-stained serial sections[20] of embryos fixed at hourly intervals after surgery were also prepared to determine how optic fibres emerge from rotated eyes.

A normal retinal fascicle pattern is shown in Fig. 1. A lesion at the dorsal pole of the eye identifies the dorsal quadrant. The long, thin fascicles in this quadrant are arranged in a distinctive arcuate pattern that differs from the pattern of shorter, thicker bundles in the ventral quadrant. Nasal and temporal quadrant fascicle patterns are very similar.

Twelve of 14 retinas in control eyes operated at early NF stages 26–28 gave rise to normal patterns (Table 1). On the other hand, 13 of 25 early rotated eyes were quite abnormal with bundles of circling axons (Fig. 2). Two retinas were normal in orientation and symmetry whereas eight eyes (one-third) exhibited 90°-rotated or 180°-rotated patterns (Fig. 3). Although some retinas possessed an optic nerve, those retinas exhibiting circling fibre patterns usually had no optic nerves or abnormally thin nerves.

The absence of optic nerves on some retinas indicates that optic fibres did not emerge. In silver-stained serial sections of early rotated eyes we found that a choroid fissure developed dorsally in most instances but no choroid or an abnormal choroid fissure developed in some embryos. Though some fibres exited through dorsally located fissures, others remained within the optic fibre layer or penetrated and grew in the receptor layer (Fig. 4) or over the cornea, sending branches into the dorsal head mesenchyme.

---

* Present address: Department of Physiology and Biophysics, Washington University School of Medicine, St Louis, Missouri 63110.

0028-0836/80/440845—04$01.00

Table 1 Retinal fibre patterns in 180° rotated eyes

			Normal patterns rotated through			Abnormal patterns		
Stage of operation	Series	No. eyes* stained	0°	90°	180°	Circling fibres	Crossing† fibres	Diffuse‡
Early (NF stages 26–28)	Control	14	12	0	0	2	—	—
	Experimental	25	2	1	7	13	1	1
Late (NF stages 30–33)	Control	12	11	0	0	—	—	1
	Experimental	18	0	4	13	—	—	1

Xenopus embryos reared at room temperature were anaesthetized in 100% Steinberg's solution containing MS 222 (1/3,000). The left eye was cut out of the orbit with tungsten needle and hair loop, then replaced in the orbit without rotation (controls) or rotated 180° (experimentals). Healing for 1 h was assisted by placing a small glass bridge over the eye. Animals were placed in 10% Steinberg's and allowed to develop to late-stage tadpoles (55–58) when they were re-anaesthetized. A lesion was made in the dorsal pole of the retina with a tungsten needle or a Biolaser beam. The animal was killed and the left eye removed from its orbit. After fixing in formol (10%)-sucrose (0.1M) for at least seven days, the lens, cornea, sclera and pigmented epithelium were carefully dissected away. The clean retina was then slit radially in four places and prepared as a whole flat mount. It was stained with silver according to a modified Bielchowsky precedure[16] and mounted in glycerol on a slide. Orientation of each retina was related to the position of the dorsal lesion. Each specimen was photographed in reflected light in a Zeiss Universal photomicroscope with a 4X Zeiss Epiplan HD objective and 6X eye piece. Kodak 4 × 5 Ektaplan negatives were prepared as contact prints giving a final magnification of almost ×40. To analyse bundle patterns the whole mounts were examined in photographs, under the stereomicroscope and under the light microscope using transmitted light.

* Data based on whole mounts of NF stage 55–58 tadpole retinas.

† A few fibres crossed others.

‡ Patterns stained too diffusely to interpret.

In eyes rotated at NF stages 32–34, 11 of 12 control eyes were normal, but most rotated eyes developed rotated patterns; 95% of fascicle patterns were approximately normal but rotated. Most of these (13/18) were inverted 180° whereas others were rotated only 90°. No normally oriented patterns were obtained although fascicle patterns in each retinal quadrant were normal for that quadrant. All retinas had optic nerves of normal thickness.

The emergence of fibres from eyes rotated at late stages was more normal. In serial sections of embryos examined 4–24 h after rotation, optic fibres emerged through a dorsal fissure. No fibres emerged through ectopic sites or grew into the receptor layer. In only one case did fibres remain in the head mesenchyme and collect into a thick neuroma. Otherwise, fibres leaving such a dorsally oriented fissure penetrated the region occupied by oculomotor nerves and eye muscles.

Thus, rotation of the embryonic eye anlage at early stages before fibres appear, and not the surgical procedure itself, affects development of retinal fascicle patterns. Most patterns are abnormal; the one-third normal but rotated patterns, resembling those obtained after late rotation, may have been older eyes (stage 28–29) with a few fibres already present at the optic nerve head[14]. Staging of early embryos is somewhat unreliable and such staging errors could occur[13]. Also, the two normal patterns may be partly due to errors in the operation or to derotation[19]—rotated eyes may return to a normal orientation during healing. Rotation at later stages, after fibres have emerged from the retina and entered the stalk, resulted in normally organized but inverted patterns. Of the combined 43 experimental eyes, only two yielded a normally oriented fascicle pattern.

We suggest that circling fibre patterns develop in eyes rotated early, before fibres are present, because axons that arise after the operation are unable to emerge and conseqently grow abnormally within the retina. This hypothesis is consistent with the observation that retinas with the most abnormal circling fibre patterns usually lack an optic nerve and it suggests that fibre outgrowth shortly after rotation is abnormal because the surgical procedure and tissue healing disrupt proper orientation of the first ganglion cell fibres. As the first ganglion cells

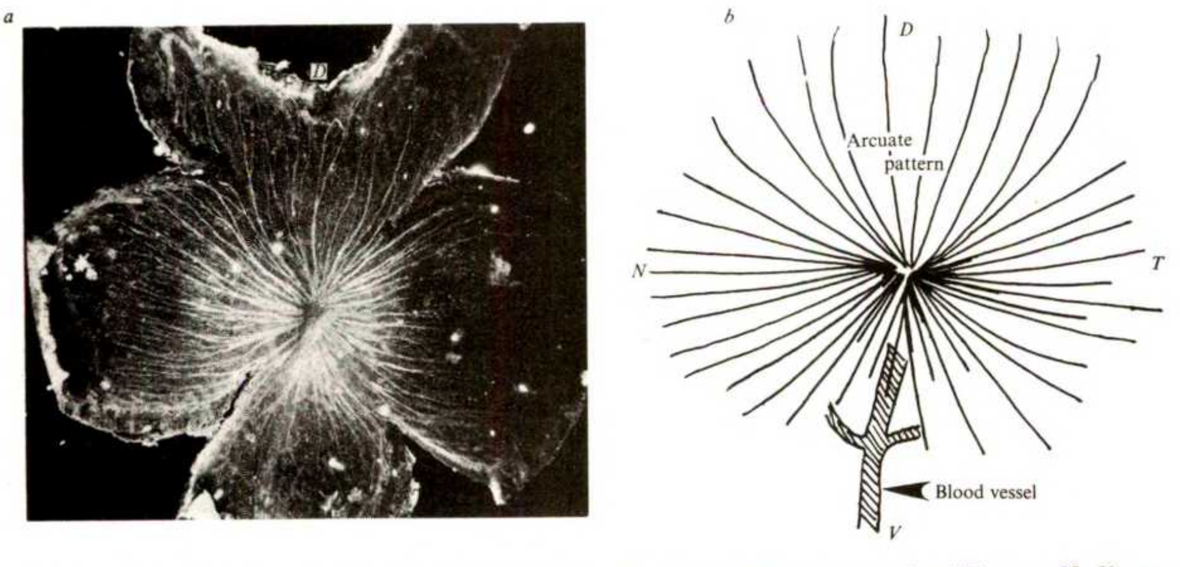

Fig. 1 *a*, Normal fascicle pattern in the optic fibre layer of a silver-stained whole mount of a NF stage 58 *Xenopus* retina. *b*, Diagram to assist identification of specific fascicle patterns. The characteristic thin, long, arcuate fascicles in the dorsal quadrant can be distinguished from the shorter and thicker bundles in the ventral quadrant. The nasal and temporal bundle patterns are mirror images of one another. The ventral blood vessel (hyaloid artery) in the retina is stained lightly and is useful as another orienting marker. Orientation is based on the notch (*D*) located at the dorsal pole of the retina. Magnification ×30. *D*, *V*, *N* and *T* refer to dorsal, ventral, nasal and temporal poles, respectively, corresponding to the position of the eye in the orbit.

differentiate, their axons are guided to the dorsally orientated fissure, if present, or randomly to some other retinal site, if the fissure is abnormal or absent. A few fibres may penetrate the stump of the optic stalk attached to the eye and enter the head mesenchymal space. If closure of the dorsal fissure is abnormal or delayed, or if the stump has healed over before fibres reach the fissure, then many of the earliest fibres do not emerge and grow within the retina instead. As newly differentiating axons at the margin of the growing retina follow pre-existing fibre bundles[12], only a few abnormally directed pioneering fibres appearing at early stages are sufficient to generate masses of circling fibres. Comparable circling fibre patterns have been noted in the regeneration of sensory fibres within the insect epidermis when regrowth of cuticle prevented fibres from returning to the central nervous system[21]. It remains to determine why the first fibres trapped in eyes form circular patterns, rather than random tangles.

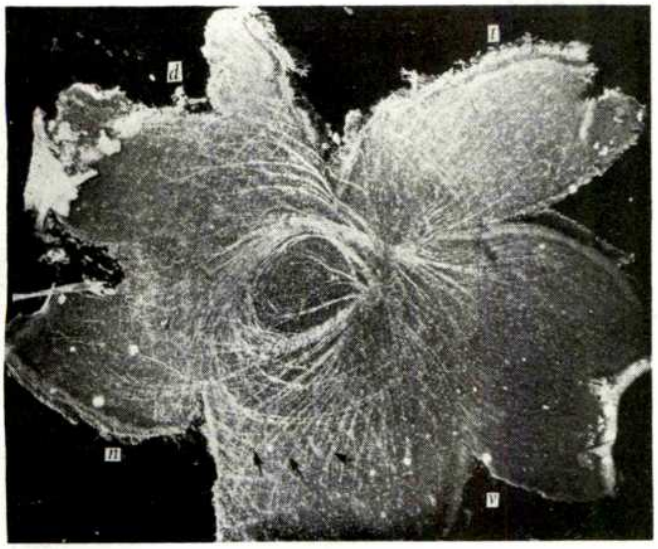

Fig. 2 Early rotation. Eye rotated 180° at stage NF 27/28 and prepared as a silver-stained whole mount at stage 56. Pattern of fascicles is highly abnormal with many fibres circling on themselves within the optic fibre layer of the retina. Some fibres do organize into radial fascicles (arrows) but their number and thickness is very much reduced. *d, v, n* and *t* refer to dorsal, ventral, nasal and temporal poles, respectively, corresponding to the position of the eye in the orbit. ×30.

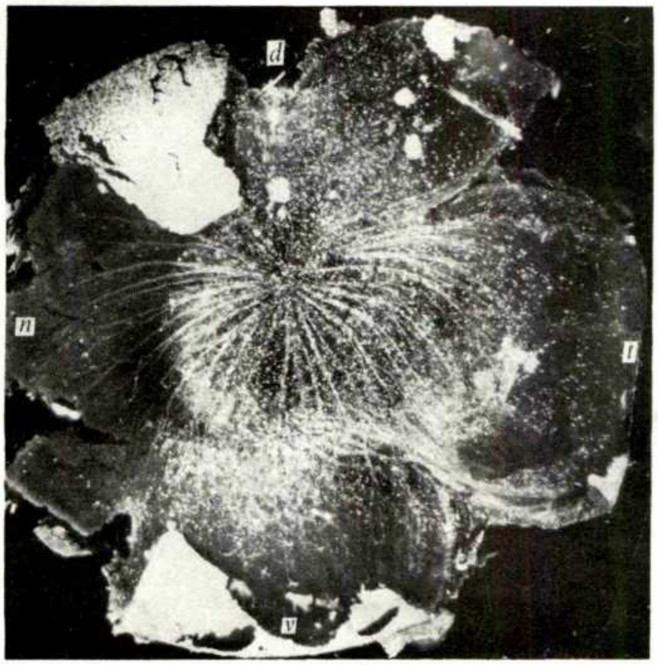

Fig. 3 Late rotation. Eye rotated 180° at NF stage 33 and prepared as a whole mount at stage 56. A normal but 180° inverted fascicle pattern is obtained. Arcuate fascicles characteristic of dorsal quadrant now oriented in opposite direction towards ventral pole. *d, v, n* and *t* refer to dorsal, ventral, nasal and temporal poles, respectively. ×40.

At later stages (NF 32), eyes have formed a normal fissure and fibres have already entered the optic stalk. Fibre pathways to guide ganglion cell axons to the optic nerve head and out of the fissure are thus established before the operation. After eye rotation, fibres in the proximal stump of the optic stalk grow out before wound closure and enter the head mesenchyme. All subsequent ganglion cell axons developing in the inverted eye are guided along the pre-existing fascicles to the optic nerve head, into the proximal stalk and out into the head mesenchyme. They reach the brain following aberrant pathways in most cases, usually along the oculomotor nerves or branches of the trigeminal nerve to the hind brain[22]. As quadrant-specific patterns of retinal growth are unaffected by eye rotation, a normal but inverted fascicle pattern develops within the retina.

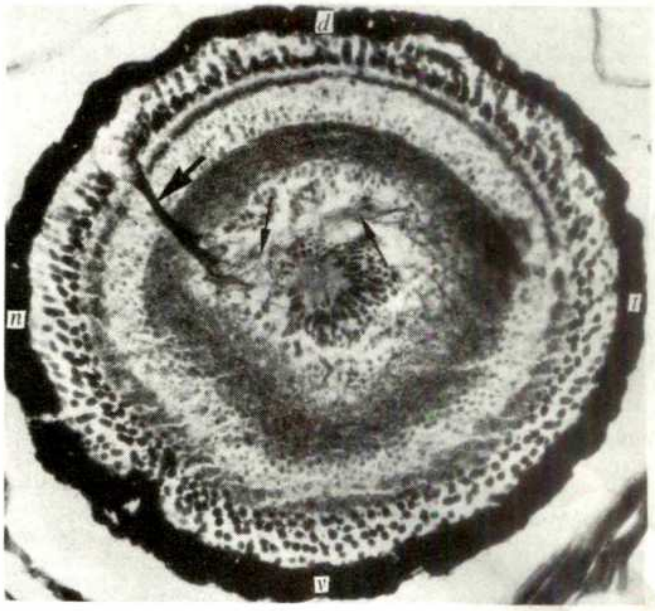

Fig. 4 Early rotation. Left eye rotated at NF stage 26/27 and fixed in aqueous Bouins at NF stage 48. Animal embedded in paraffin, sectioned in the sagittal plane, and stained with silver according to a modified Holmes stain[20]. Axons inside optic fibre layer of retina (small arrows) circle and collect into a large bundle (large arrow) which penetrates the receptor layer ectopically in dorso-nasal quadrant, at some distance from optic nerve head. Fibre bundle follows receptor layer at periphery when traced into more lateral sections. Some fibres eventually emerge abnormally and enter the dorsal mesenchymal space around the eye. *d, v, n* and *t* refer to dorsal, ventral, nasal and temporal poles, respectively. ×180.

These results are consistent with the idea that two processes govern the development of optic fibre fascicles in the retina: fibre following and the kinetics of annular ring growth at the retinal margin[12]. These rules are invoked in space–time models ordering growth and connection of retinal ganglion cell axons to visual centres in the brain[12,23]. It seems that most mapping experiments concerned with retinotectal connections and axial specification need to be re-examined in terms of the effects of surgery on development of retinal fascicle patterns and the emergence of optic fibres from the eye. Experiments correlating fascicle patterns and optic fibre pathways with retinotectal mapping from experimentally modified retinas are under way.

We thank Harry Howard and Carol Cogswell for assistance with photography, and Charles Kimmel and Charles Cima for criticisms. This research was supported in part by NSF grant BSN-75-23241 and grant EY 02646 from the National Eye Institute.

Received 27 May; accepted 3 September 1980.

1. Sperry, R. W. *J. Neurophysiol.* **7,** 57–70 (1944).
2. Sperry, R. W. *J. Neurophysiol.* **8,** 15–28 (1945).
3. Székely, G. *Acta biol. hung.* **5,** 157–167 (1954).
4. Jacobson, M. *Devl Biol.* **17,** 202–218 (1968).
5. Nieuwkoop, P. D. & Faber, J. *Normal Table of Xenopus laevis (Daudin)* (North-Holland, Amsterdam, 1956).
6. Sharma, S. C. & Hollyfield, J. G. *J. comp. Neurol.* **155,** 395–408 (1974).
7. Gaze, R. M., Feldman, J. D., Cooke, J. & Chung, S. H. *J. Embryol. exp. Morph.* **53,** 39–66 (1979).
8. Sharma, S. C., Hollyfield, J. G. *J. Embryol. exp. Morph.* **55,** 77–92 (1980).
9. Shumway, W. *Anat. Rec.* **78,** 139–148 (1940).
10. Fisher, S. & Jacobson, M. *Z. Zellforsch. mikrosk. Anat.* **104,** 165–177 (1970).
11. Grillo, M. A. & Rosenbluth, J. *J. comp. Neurol.* **145,** 131–140 (1972).
12. Grant, P. & Rubin, E. *J. comp. Neurol.* **189,** 671–698 (1980).
13. Grant, P., Rubin, E. & Cima, C. *J. comp. Neurol.* **189,** 593–613 (1980).
14. Cima, C. & Grant, P. *Devl Biol.* **76,** 229–237 (1980).
15. Murray, M. *J. comp. Neurol.* **168,** 175–196 (1976).
16. Rubin, E., Ma, P. M. & Grant, P. (in preparation).
17. Goldberg, S. & Coulombre, A. J. *J. comp. Neurol.* **146,** 507–518 (1972).
18. Goldberg, S. *Devl Biol.* **36,** 24–43 (1974).
19. Goldberg, S. *J. comp. Neurol.* **168,** 379–392 (1976).
20. Rowell, C. H. F. *Q. Jl microsc. Sci.* **104,** 81–87 (1963).
21. Wigglesworth, V. B. *Q. Jl microsc. Sci.* **94,** 93–112 (1952).
22. Grant, P. & Ma, P. M. *Soc. Neurosci. Abstr.* **5,** 161 (1979).
23. Horder, T. J. & Martin, K. A. C. *Symp. Soc. exp. Biol.* **32,** 275–258 (1978).

Aspartate and glutamate as possible neurotransmitters of cells in layer 6 of the visual cortex

Robert W. Baughman & Charles D. Gilbert

Department of Neurobiology, Harvard Medical School, 25 Shattuck St, Boston, Massachusetts 02115

Earlier work[1–8] has suggested that aspartate, glutamate and γ-aminobutyric acid (GABA) act as transmitters in the cerebral cortex. There is reasonable evidence for the identity of the cell population responsible for GABA release[9–12] but until now there has been little evidence concerning the sources for release of aspartate and glutamate. Here we have used two approaches to identify possible neurotransmitters used by cells in the visual cortex: measurement of the efflux of endogenous compounds in conditions of synaptic release and localization of these compounds to particular cell classes using neurotransmitter-specific histochemical techniques. Our results suggest that the acidic amino acids aspartate and glutamate may be cortical neurotransmitters, as shown by calcium-dependent release from endogenous stores and by uptake specific to pyramidal cells in layer 6 of the cortex. These substances may therefore have a role in the function of layer 6 cells, which are responsible for the recurrent projection from the cortex to the lateral geniculate nucleus and for the projection within the cortex from layer 6 to layer 4.

The release experiments were carried out with a tissue-slice preparation from rat visual cortex. An elevated potassium medium was used to induce synaptic release, and a similar medium with low calcium and high magnesium, which should block synaptic release, was used as a control. The release of endogenous compounds from slices incubated in each of these two media was measured using a HPLC system. The system used was capable of detecting compounds containing a primary amino group, with a detection limit of about 10 pmol. Its principal advantage in the present study was to enable us to analyse substances released from endogenous stores in the tissue. Rates of release for a series of amino acids measured in stimulated and control conditions are given in Table 1. To illustrate more clearly the changes in release between the stimulated and control media, the ratio of the rates of release for the two conditions are shown in Fig. 1. Marked increases were observed for aspartate (12-fold), glutamate (14-fold) and GABA (sixfold). The ratios for the other amino acids ranged from one- to twofold. These findings are consistent with previous work[1–8].

Autoradiographic localization based on uptake of ^{3}H-L-aspartate and ^{3}H-L-glutamate has been relatively unsuccessful for labelling of cell bodies, possibly because these substances are rapidly metabolized following uptake. The D-form of aspartate, which is not metabolized, is accumulated in brain tissue through the same high-affinity uptake system that transports the L-forms of both aspartate and glutamate and thus offers the possibility of labelling aspartate- or glutamate-accumulating neurones[13]. For this reason we used ^{3}H-D-aspartate to label the cortical cells that may be responsible for the previously demonstrated aspartate and glutamate release. Although it should be possible to label these cells at the site of injection, they may also be labelled by neurotransmitter-specific retrograde transport following injection at their distant efferent targets[14,15]. As cells in different cortical layers have distinct projections, we made injections in

Table 1 Release of various amino acids in stimulated and control conditions

	Release rate (pmol per mg wet wt per 5 min) Stimulated	Control
Taurine	49 ± 16	37 ± 15
Aspartate	206 ± 35	17 ± 4
Threonine	74 ± 14	34 ± 5
Serine	171 ± 54	88 ± 21
Glutamine	76 ± 29	63 ± 9
Glutamate	552 ± 171	38 ± 7
Glycine	98 ± 12	50 ± 10
Alanine	115 ± 22	54 ± 9
Valine	10 ± 2	12 ± 9
isoLeucine	21 ± 6	12 ± 3
Leucine	39 ± 14	21 ± 5
Tyrosine	6 ± 2	4 ± 1
Phenylalanine	10 ± 3	6 ± 1
beta-Alanine	5 ± 2	3 ± 2
GABA	111 ± 25	20 ± 6
Histidine	20 ± 4	14 ± 5
Lysine	19 ± 4	13 ± 6
Arginine	11 ± 6	7 ± 2

Blocks of visual cortex were sliced at 200-μm thickness with a tissue chopper. The tissue slices were suspended in an Earle's bicarbonate-buffered salt solution (143 mM Na^+, 5 mM K^+, 1.8 mM Ca^{2+}, 0.8 mM Mg^{2+}, 125 mM Cl^-, 26 mM HCO_3^-, 1.0 mM $H_2PO_4^-$, 0.8 mM SO_4^{2-}, 5.5 mM glucose) gassed with 5% CO_2/95% air at 37 °C. The slices were incubated in a series of buffers (5 ml of each) with changes every 5 min. For the stimulated release experiments, the slices were incubated with three consecutive 5-min changes of normal medium followed by a 5-min incubation (stimulated release) in high-potassium (50 mM K^+, 98 mM Na^+) medium. For the control release experiments, the slices were incubated with two 5-min changes of normal medium, followed by a 5-min incubation in low-calcium (0.1 mM Ca^{2+}, 10 mM Mg^{2+}, 132 mM Na^+) medium and a 5-min incubation (control release) in high-potassium, low-calcium (50 mM K^+, 0.1 mM Ca^{2+}, 10 mM Mg^{2+}, 87 mM Na^+) medium. All buffer solutions contained 1 μM *n*-leucine as an internal standard. At the end of the incubation series the sections were weighed, and the fractions from each buffer change were frozen in liquid nitrogen, lyophilized and desalted in 6 M HCl in acetone. The compounds present in the final extract were analysed on a HPLC, with a sulphonated divinylbenzene polystyrene cation exchange column (Dionex DC-5A resin in a 4 mm × 15 cm stainless steel column), and *o*-phthalaldehyde fluorescence detection[19]. This procedure detects compounds containing primary amino groups, such as amino acids and many peptides. Quantification was based on peak heights compared with the *n*-leucine internal standard.

0028-0836/80/440848—03$01.00

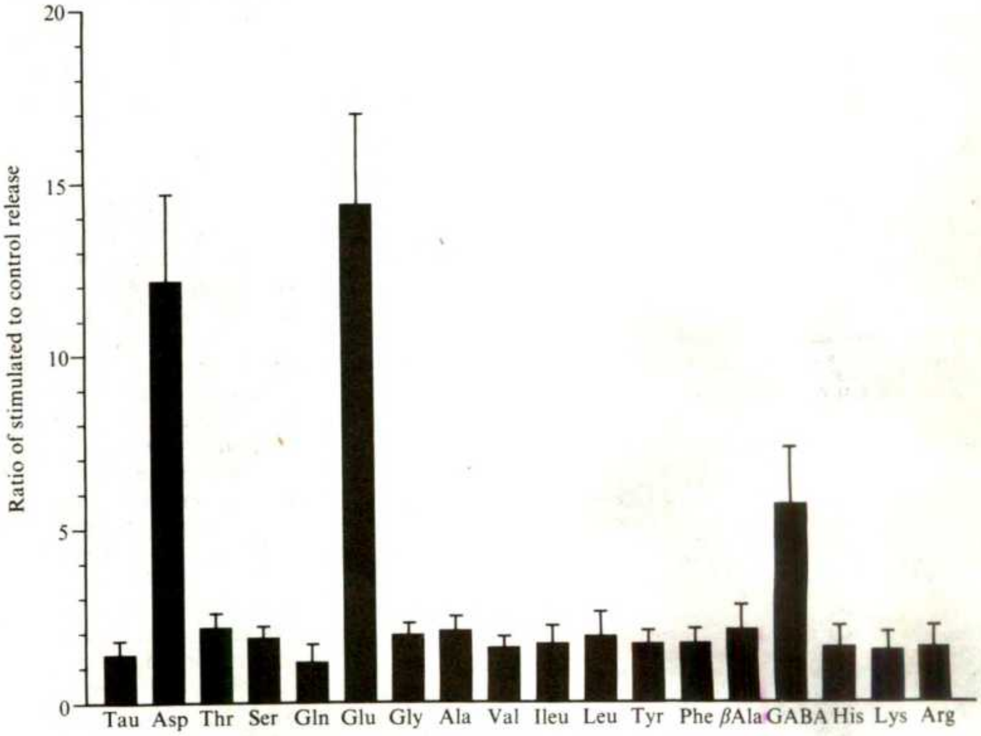

Fig. 1 Ratios of the rates of release of endogenous amino acids in stimulated and control conditions (from Table 1).

several areas to determine the population(s) capable of transporting the label retrograde from their terminals. These areas included the lateral geniculate nucleus (LGN), which receives input from cortical layer 6, the superior colliculus, which receives input from layer 5, and area 19, which receives input from layers 2 and 3 of area 17 (ref. 16). The most striking result was observed after the injections in the LGN (Fig. 2). Many cell bodies in layer 6 were labelled and a diffuse band of label was present in layer 4. No labelled cortical cells were seen after injections in the superior colliculus, and only a few were seen in area 17 after the injection in area 19. Following injections in area 17 the local pattern of cortical labelling was similar to that seen following retrograde transport from the LGN, that is, there was a diffuse band of label in layer 4 and many labelled cells in the deeper layers, especially layer 6. Thus within the visual cortex the ability to accumulate ^{3}H-D-aspartate seems to be particularly localized in layer 6 cells.

Following injections in the LGN, the cells in layer 6 are probably labelled by retrograde transport. The band in layer 4, however, could represent labelling either of geniculate terminals of the extensive plexus of collaterals of layer 6 cells which arborize in that layer[17]. Two lines of evidence support the latter: (1) at the injection site in the LGN the principal neurones are unlabelled, so it is unlikely that they take up the label and transport it to the cortex. (2) After cortical injections there was only a diffuse patch of label in the LGN at the topographically appropriate site, with no labelling of cell bodies. This is consistent with the idea that the geniculate neurones do not take up the ^{3}H-D-aspartate, and furthermore demonstrates that the layer 6 cells are capable of transporting the label anterograde to their terminals in the LGN. Thus the band of label in layer 4 seen after the injection in the LGN is probably the result of filling of collaterals of layer 6 cells.

Therefore, several results support the specificity of uptake of ^{3}H-D-aspartate by the layer 6 cortical cells. From the retrograde transport experiments we found that the layer 5 cells and the cells in the LGN, for example, do not take up and transport the label whereas the layer 6 cells do. Furthermore, after injections of label in the cortex the layer 6 cells are the predominant cell class responsible for uptake in the vicinity of an injection encompassing all layers. Previous studies, which have examined changes in high-affinity uptake of ^{3}H-D-aspartate and in endogenous content of aspartate and glutamate following cortical

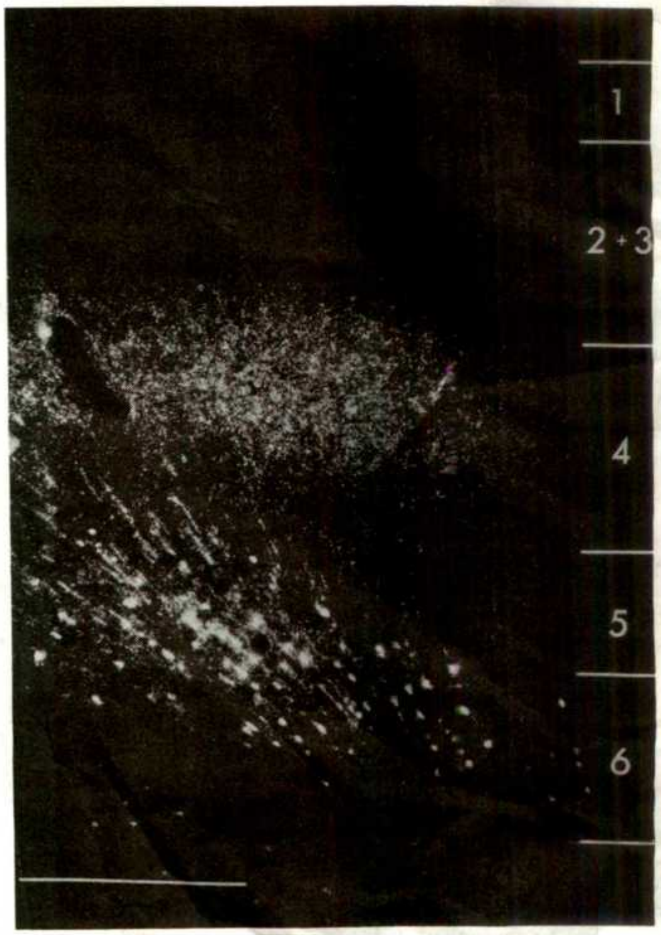

Fig. 2 ^{3}H-D-aspartate (50 μCi in 0.5 μl buffered saline) was pressure-injected from a recording pipette[20] into the LGN of the cat. The animal was resuscitated and, after 2 days, re-anaesthetized and perfused with a glutaraldehyde fixative. The brain was sectioned and the sections processed for autoradiography. The figure shows the pattern of labelling in the cortex, with labelled cells in layer 6 and a band of diffuse label in layer 4 (3-week exposure time). Bar, 500 μm.

ablation, have suggested that both the corticogeniculate and corticocollicular pathways are associated with aspartate and glutamate[18]. The present results suggest, however, that these compounds are only associated with the corticogeniculate pathway.

We have thus provided additional evidence based on release of endogenous compounds that aspartate and glutamate, as well as GABA, may act as neurotransmitters in visual cortex. The above results do not exclude the possibility, however, that aspartate and glutamate may be metabolites of the true transmitter. We have also shown that uptake of ^{3}H-D-aspartate is particularly associated with the cells in layer 6 that participate in the corticogeniculate pathway and that project to layer 4. These findings may be useful in determining the role of this cell class in cortical and geniculate function.

Received 10 June; accepted 3 September 1980.

1. Hayashi, I. *Keio J. Med.* **3,** 183–192 (1954).
2. Krnjevic, K. & Phillis, J. W. *J. Physiol., Lond.* **165**, 274–304 (1963).
3. Jasper, H. H. & Koyama, I. *Can. J. Physiol. Pharmac.* **47,** 889–905 (1969).
4. Logan, W. J. & Snyder, S. H. *Brain Res.* **42,** 413–431 (1972).
5. Bradford, H. F. & Richards, C. D. *Brain Res.* **105,** 168–172 (1976).
6. Clark, R. M. & Collins, G. G. S. *J. Physiol., Lond.* **262,** 383–400 (1976).
7. Nadler, J. V., Vaca, K. W., White, W. F., Lynch, G. S. & Cotman, C. W. *Nature* **260,** 538–540 (1976).
8. Storm-Mathieson, J. & Iversen, L. L. *Neuroscience* **4,** 1237–1253 (1979).
9. Hokfelt, T. & Ljundahl, A. *Expl Brain Res.* **14,** 354–362 (1972).
10. Chronwall, B. M. & Wolff, J. R. in *Amino Acids as Chemical Transmitters* (ed. Fonnum, F.) 297–303 (Plenum, New York, 1978).
11. Davis, T. L., Turlejski, K. & Sterling, P. *Invest. Ophthal. vis. Sci.* Suppl. (ARVO Abstr. 27, 1977).
12. Ribak, C. E. *J. Neurocytol.* **7,** 461–478 (1978).
13. Davies, L. P. & Johnston, G. A. R. *J. Neurochem.* **26,** 1007–1014 (1976).
14. Streit, P., Knecht, E. V. A. & Cuenod, M. *Science* **205,** 306–308 (1979).
15. Streit, P. & Cuenod, M. *Neurosci. Lett.* Suppl. **3,** S340 (1979).
16. Gilbert, C. D. & Kelly, J. P. *J. comp. Neurol.* **163,** 81–105 (1975).
17. Gilbert, C. D. & Wiesel, T. N. *Nature* **280,** 120–125 (1979).
18. Lund Karlsen, R. & Fonnum, F. *Brain Res.* **151,** 457–467 (1978).
19. Benson, J. R. & Hare, P. E. *Proc. natn. Acad. Sci. U.S.A.* **72,** 619–622 (1975).
20. Kelly, J. P. & Gilbert, C. D. *J. comp. Neurol.* **163,** 65–80 (1975).

Cell movements in *Xenopus* eye development

Christine Holt

Medical Research Council Cell Biophysics Unit, King's College,
26–29 Drury Lane, London WC2B 5RL, UK

The vertebrate eye develops morphological markers, such as the ventral choroid fissure, which define its anatomical polarity in relation to the body. Also, retinal nerve fibres behave as though regionally differentiated by forming ordered, topographical maps of the visual field in the brain[1–4]. It has long been held that these two features of eye polarity—its structure[5–10] and the neural specificity of the ganglion cells[11,12]—are labile in the early eye vesicle and become determined relative to body axes at a subsequent stage of development. Contrary to these earlier findings, recent experiments[13–15] show that the structure and connectivity of the eye are already determined by the time it first appears as a distinct eye vesicle; surgical construction of eye pigmentation chimaeras[14] suggested that normal tectal maps, previously reported after early eye rotations, may have arisen from neural retina cells recruited from the optic stalk after the operation. In agreement, using a radioactive tag which marks neural retina as well as pigment epithelium, I report here that during normal development in *Xenopus laevis*, cells in the ventral retina, where the choroid fissure forms, move into position from the optic stalk region during eye-cup formation. Depending on developmental stage, surgical eye rotations may intercept their movement and this provides a simple explanation of results previously taken to indicate a change from a labile to a determined state of eye polarity.

During development in *Xenopus*, the eye rudiment arises as a lateral protrusion of the neural tube and becomes a distinct eye vesicle at stage 22 (ref. 16). The vesicle, whose epithelium remains connected with the neural tube by the optic stalk until the eye-cup stage, then elongates dorsally leaving the stalk attached to its ventral pole. Before the outgrowth of optic nerve fibres, the vesicle invaginates on itself to form the double-walled eye cup. This inward movement, beginning dorsally at stage 27, brings the presumptive neural retina adjacent to the proximal wall of the vesicle, the presumptive pigment epithelium[17], which attenuates into a thin layer of flattened cells. The choroid fissure develops as a vertical cleft in the ventral part of the eye, beginning at stage 29 in the vesicle margin and elongating to completion along with retinal invagination at stage 32 (ref. 18). Its formation establishes continuity between the inner retinal surface and the optic stalk, thereby providing a direct pathway to the brain for pioneer ganglion cell fibres which begin to leave the eye through the apex of the fissure at stages 30–31 (refs 18, 19). An assumption implicit in the studies using eye rotation surgery to investigate the state of determination of eye polarity in embryos[5–12] has been that the boundaries of the eye vesicle define those of the newly invaginated eye cup. On this basis, the ventral fissure region should arise from cells already within the eye vesicle. The results presented here show this interpretation of eye morphogenesis, at least in *Xenopus*, to be erroneous.

To trace the cell movements involved in the morphogenesis of the eye cup between stages 22 and 32, a series of experiments was performed in which the whole or part of the *Xenopus* eye rudiment was excised, incubated in a droplet of operating medium containing ^{3}H-thymidine (^{3}H-TdR; 10^{-6} M, 46 Ci mmol^{-1}) for 10–15 min, then washed thoroughly in fresh medium (six changes) and replaced orthotopically in the original embryo. The operating medium was two-thirds strength Niu Twitty[20] solution containing 1:10,000 tricaine methane sulphonate (MS 222; Sandoz) at *p*H 7.6, and the animals were reared at 18–20 °C after the operations. They were fixed 12–48 h later (stages 36–42), serially sectioned at 1–4 μm thickness and prepared for light microscope autoradiography. As the eye, optic stalk and neural tube epithelia are continuous until later eye-cup stages, with no distinct boundaries between them, individual operations unavoidably included a variable number of cells from the optic stalk; however, cuts were made distally as close to the outlines of the vesicle as possible.

Ventral halves of eye vesicles from seven embryos (stages 24–27) were exposed to ^{3}H-TdR in this way. All the autoradiographs showed a labelling pattern similar to that shown in Fig. 1*a*, which is a stage 36 eye where ventral-half incubation was performed at stage 26. The fissure (arrow), which is prominent in this parasagittal section, divides the ventral retina into two lobes. The ^{3}H-TdR-labelled neural retina cells lie in a band dorsal to the ventral fissure. They do not occupy the ventral retinal lobes, the position expected if the cells within the early eye vesicle give rise to this region. There are sharp boundaries between the heavily labelled incubated cells and the retinal regions above and below. This shows that the sparse grains visible ventrally do not represent the outcome of serial dilution of label by normal cell division in the peripheral retina after the operation, but are due to background and possibly a small amount of diffusion at the time of surgery.

Further evidence for this proximo-distal movement of ventral neuroepithelial cells is presented in Fig. 1*b* and *c*. Whole eye vesicles were removed from six embryos during stages 22–28, incubated with ^{3}H-TdR and replaced. All the autoradiographs show label over the entire eye apart from an area of ventral neural retina (Fig. 1*b*) containing the fissure, except for one at stage 28, where surgery was judged to be deep, leading to label over the whole eye. When, in a 'negative' experiment, the eye vesicle is removed and the whole embryo incubated in ^{3}H-TdR, the autoradiographs show label confined to the ventral retina (Fig. 1*c*); brain cells are also heavily labelled (not shown). Further preparations of whole eyes labelled after the onset of cup formation at stage 27 gave rise to a progressively smaller

0028-0836/80/440850-03$01.00

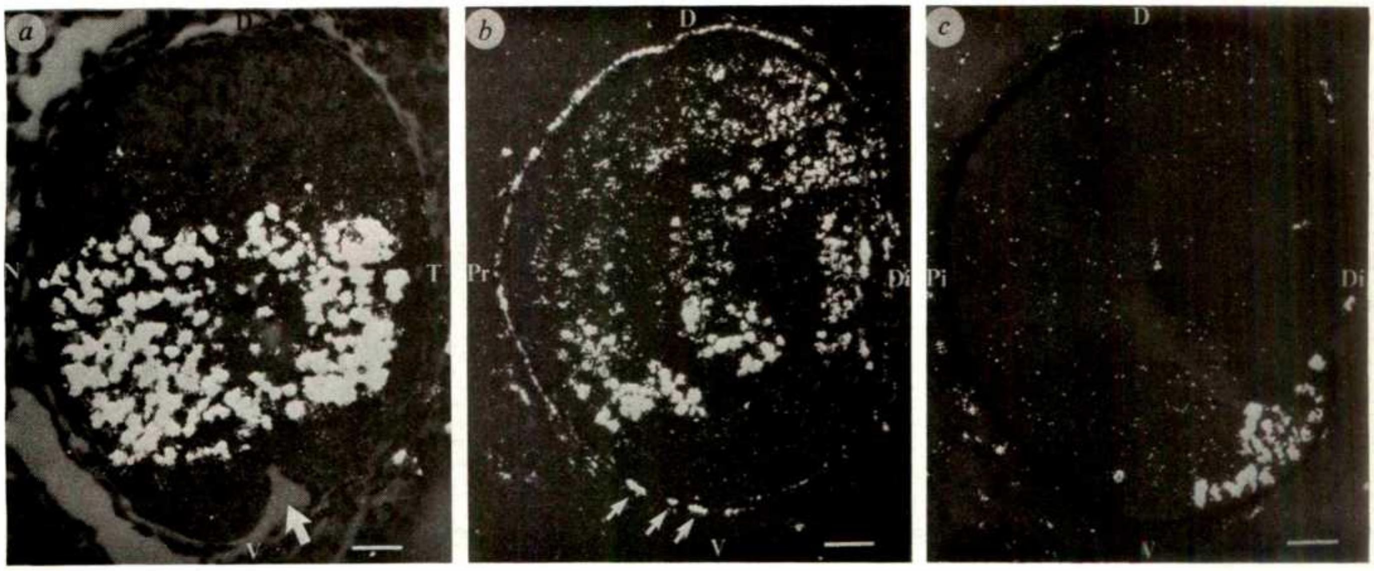

Fig. 1 Autoradiographs of *Xenopus* eyes, using combined light- and dark-field microscopy. Cells containing ^{3}H-TdR, following *in vitro* incubation in ^{3}H-TdR (see text), are strongly labelled with dense autoradiographic grains (white) above their nuclei. *a*, Parasagittal section of a stage 37 eye; the ventral fissure is indicated by an arrow. *b*, *c*, Transverse sections of stage 41 eyes from complementary experiments detailed in the text; the arrows in *b* indicate the ^{3}H-TdR-labelled pigment epithelial cells which are out of register with labelled neural retina (see text). D, Dorsal; V, ventral; ^{3}H-TdR incubation was performed at stage 26 in *a*, stages 22–23 in *b* and stage 24 in *c*. N, Nasal; T, temporal; Pr, proximal; Di, distal. Scale bars, 30 μm.

area of unlabelled cells occupying the ventral retina, with no such cells appearing after the fissure is fully formed. Therefore, cells positioned in the ventral margin of the eye vesicle do not define the ventral boundary of the newly invaginated eye cup, but are displaced dorsally by the late-arriving cells involved in ventral fissure formation.

Autoradiographs from whole eye incubations frequently show ^{3}H-TdR-labelled pigment epithelial cells in the otherwise unlabelled ventral region of the eye (Fig. 1*b*). This shows that neural retina and pigment epithelial cells move relative to each other and suggests that the boundaries of the pigment epithelial cell markers used in chimaeric eyes[14] may not reliably define the origin of the underlying neural retina.

As cells which come to comprise the ventral retina are in varying stages of transit from proximal to distal neuroepithelium, 180° eye rotation surgery, thought to reveal the time of polarization of the eye[5–10], could give rise to different fissure positions in the eye cup depending on when and where the cuts are made. Deep surgery at vesicle stages, or shallow surgery at early eye-cup stages (Fig. 2*c*) could translocate the entire population of presumptive ventral retina cells dorsally to give a dorsally positioned fissure, whereas shallow surgery at vesicle stages (Fig. 2*a*) might leave them still attached to the stalk, capable, providing healing is successful, of differentiating a normally positioned fissure. Double fissures, dorsally and ventrally located, would result if surgery divided this population of cells in two (Fig. 2*b*). These different patterns of anatomical polarity in the eye have been obtained after rotations at various stages in anuran[6], urodele[5,7,8] and chick[9,10] embryos, and the earliest stage at which dorsal fissures appeared was taken to represent the critical period at which the polarity of the eye becomes determined. As the origin of the fissure-forming cells was not considered in these experiments and was assumed to be in the eye at all stages of rotation, the 'labile' period can simply be explained by incomplete rotation of the whole eye rudiment at vesicle stages.

Jacobson[12] described a critical period during which he thought the polarity of the functional nerve connections from the eye become specified in *Xenopus* (stages 28–31). Although no anatomical evidence was presented, this functional polarization was determined separately from the anatomical polarization of the eye[21] (but see also ref. 11). However, Gaze *et al.*[14] and Sharma and Hollyfield[15] systematically failed to isolate a critical stage of polarization and found that even at early stages (stage 22), 180° rotation gave rise to either whole or partly rotated eye anatomy with functional connections of corresponding polarity. Using albino/wild-type chimaeras, Gaze *et al.* showed that eye vesicle rotations frequently result in eyes of compound origin with a rotated dorsal part (graft-derived) and a normally

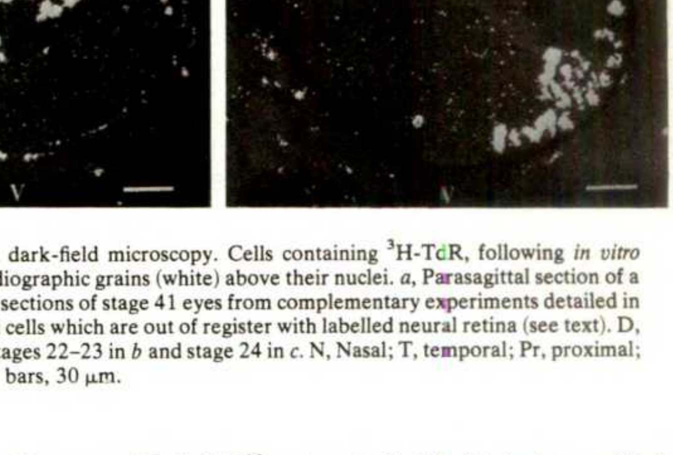

Fig. 2 Schematic representation of eye morphogenesis showing eye rotation surgery (dashed lines) in suggested relation to cell movements in the ventral neuroepithelium (striped region) drawn in transverse section. *a*, Optic vesicle stage (before stage 28 in *Xenopus*). The rotation surgery shown does not include future fissure-forming ventral retina cells. *b*, Invaginating eye at stage of ventral fissure formation (during stages 29–31 in *Xenopus*). The surgery shown divides the ventral cells. *c*, Newly invaginated eye cup (after stage 32 in *Xenopus*) in which the surgery shown includes the ventral retina and fissure. The resulting fissure positions and map ordering are explained in the text. nt, Neural tube; os, optic stalk; ov, optic vesicle; nr, neural retina; oc, optic cup; pe, pigment epithelium.

oriented ventral part (host-derived). They suggested that the unrotated eye tissue, derived from the optic stalk of the host, may have given rise to tectal maps interpreted as evidence for ocular respecification[9]. The present results favour this interpretation, but suggest that the origin of ventral retinal tissue outside the visible outline of the eye vesicle is a normal feature of development, rather than the outcome of cell proliferation stimulated by tissue mismatch caused in eye rotation surgery. The cell movements described here may be related to Hirose and Jacobson's observation[22], based on cell marking in early cleavage stages of *Xenopus*, that the ventral part of the eye apparently originates from the contralateral neural epithelium.

I thank Dr J. H. Scholes for his advice and assistance throughout, Drs W. R. Lieb and H. Saibil for helpful discussions, and Dr R. M. Gaze and his colleagues for advice and *Xenopus* eggs. This work was supported by an SRC studentship.

Received 25 July; accepted 17 September 1980.

1. Sperry, R. W. *J. Neurophysiol.* **7,** 57–70 (1944).
2. Sperry, R. W. *Proc. natn. Acad. Sci. U.S.A.* **50,** 703–710 (1963).
3. Gaze, R. M. *Q. Jl exp. Physiol.* **43,** 209–214 (1958).
4. Gaze, R. M. *The Formation of Nerve Connections* (Academic, New York, 1970).
5. Sato, T. *Wilhelm Roux Arch. EntwMech. Org.* **128,** 342–377 (1933).
6. Woerdeman, M. W. *Proc. ned. Akad. Wet.* **27,** 324–328 (1934).
7. Beckwith, C. J. *J. exp. Zool.* **49,** 217–259 (1927).
8. Stone, L. S. *J. exp. Zool.* **161,** 95–108 (1966).
9. Goldberg, S. *Devl Biol.* **53,** 126–127 (1976).
10. Goldberg, S. *J. comp. Neurol.* **168,** 379–391 (1976).
11. Szekely, G. *Acta biol. acad. sci. hung.* **5,** 157–167 (1954).
12. Jacobson, M. *Devl Biol.* **17,** 202–218 (1968).
13. Sharma, S. C. & Hollyfield, J. C. *J. comp. Neurol.* **155,** 395 (1978).
14. Gaze, R. M., Feldman, J. D., Cooke, J. & Chung, S-H. *J. Embryol. exp. Morphol.* **53,** 39–66 (1979).
15. Sharma, S. C. & Hollyfield, J. C. *J. Embryol. exp. Morphol.* **55,** 77–92 (1980).
16. Nieuwkoop, P. D. & Faber, J. *Normal Tables of Xenopus laevis* (North-Holland, Amsterdam, 1956).
17. Hollyfield, J. G. *Devl Biol.* **30,** 115–128 (1973).
18. Grant, P., Rubin, E. & Cima, C. *J. comp. Neurol.* (in the press).
19. Cima, C. & Grant, P. *Devl Biol.* **76,** 229–237 (1980).
20. Rugh, R. *Experimental Embryology* 3rd edn (Burgess, Minneapolis, 1962).
21. Jacobson, M. & Hunt, R. K. *Scient. Am.* **228** (2), 26–35 (1973).
22. Jacobson, M. & Hirose, G. *Science* **202,** 637–639 (1978).

Methyltetrahydrofolate is a potent and selective agonist for kainic acid receptors

A. Ruck, S. Kramer, J. Metz & M. J. W. Brennan*

Brian Research Group, Departments of Medical Biochemistry
and Haematology, School of Pathology of the University of the
Witwatersrand and South African Institute for Medical Research,
Johannesburg 2001, South Africa

Kainic acid, a dicarboxylic acid containing pyrrolidine, is a potent neuronal depolarizing agent in the mammalian central nervous system, being some 50 times more effective than the putative neurotransmitter L-glutamate[1–5]. As kainic acid is a structural analogue of glutamic acid, it has been proposed that the potent excitatory effects of kainate reflect its restricted conformation, which is optimal for interaction with excitatory glutamate receptors[2,4]. More recent studies, however, do not support this hypothesis. In invertebrates kainic acid has been found to be a rather weak agonist at excitatory glutamate receptor sites[6,7], whereas at the crustacean neuromuscular junction[8], on certain neurones of *Helix aspersa*[9] and in the mammalian cerebral cortex[3], kainic acid seems to act at receptors distinct from those which mediate the neuroexcitatory action of glutamate. In addition, the ionic requirements for kainate-induced neuronal depolarization differ from those for glutamate-induced depolarization in the mammalian brain[10], and glutamate-induced excitation of rat cortical neurones can be antagonized preferentially by drugs which are very weak in blocking kainate-induced depolarization[11]. Finally, the characteristics of binding sites for ^{3}H-kainic acid in rat brain are consistent with the existence of specific kainate receptors on neuronal membranes[12]. Thus, the kainate sites may represent receptors for an unidentified endogenous substance probably containing the glutamate structure. Here we report that the pteroylmonoglutamate compound methyltetrahydrofolate (MTHF) is a potent competitor for ^{3}H-kainic acid binding sites in rat cerebellar membranes. This action is specific in that MTHF is very weak or inactive at sites for ^{3}H-glutamate or ^{3}H-γ-aminobutyric acid (GABA) respectively. Electrophysiological studies in frog spinal cord suggest that MTHF is an agonist at the kainate receptors. The implications of these results are discussed.

In membranes prepared from rat cerebellum[13], ^{3}H-kainic acid labelled a single class of receptor sites having a dissociation constant (K_d) of 25 nM. Kainic acid and MTHF displaced 50 nM ^{3}H-kainic acid from these sites with apparent inhibition constants (K_is) of 0.08 μM and 0.88 μM, respectively (Table 1), and respective Hill coefficients calculated from the displacement data were 0.92 ($r = 0.97$) and 0.94 ($r = 0.99$). L-Glutamate was a relatively weak competitor for the ^{3}H-kainate site ($K_i = 28.3$ μM) and GABA (100 μM) was ineffective in displacing ^{3}H-kainic acid binding.

In the same membrane preparation, ^{3}H-glutamate labelled two populations of receptor. Mean K_d values of 314 nM and 1,850 nM were obtained for the high and low affinity sites, respectively. Binding of 100 nM ^{3}H-glutamate was displaced by glutamate ($K_i = 0.61$ μM) but not by kainic acid (100 μM) or GABA (100 μM). MTHF was a relatively weak competitor for the high affinity glutamate site ($K_i = 83.5$ μM) (Table 1). Binding of 10 nM ^{3}H-GABA to the membranes was displaced by GABA ($K_i = 0.069$ μM) but not by kainic acid, glutamate or MTHF at concentrations of 100 μM.

MTHF is the predominant form of folate in the blood and in cerebrospinal fluid (CSF)[14,15]. It is taken up into the brain by an active process[16], and subcellular fractionation studies have shown a high concentration in synaptosomal fractions[17]. Our data demonstrate that MTHF interacts specifically with kainate receptors on neuronal membranes. In this respect it is almost as potent as kainic acid itself (Table 1). In the frog spinal cord, MTHF induces neuronal depolarization followed by a long period during which the membrane is unresponsive to applied glutamate or electrical stimulation[18]. The depolarization induced by MTHF is not antagonized by glutamate diethyl ester, a drug which preferentially blocks glutamate responses[19], and is not effective in blocking kainate-induced excitation[11]. Thus, MTHF mimics the electrophysiological action of kainic acid in a vertebrate preparation. In addition, MTHF has convulsive properties in experimental animals[20,21], and administration of folates to epileptic patients is known to increase the frequency of fits. These observations are consistent with a neuroexcitatory action of MTHF. Thus, MTHF interacts specifically and with high affinity at one class of excitatory receptor sites and has agonist activity at these sites. These are characteristics expected of an endogenous, excitatory, neuromodulatory substance.

Recent studies have shown that *in situ* injection of kainic acid into brain produces a characteristic pattern of neuronal degeneration[22–25]. The microanatomical selectivity of these lesions together with structure–activity studies on kainate analogues suggest that the neurotoxicity of the compound may be related to its electrophysiological activity[26–28]. There is some evidence that MTHF is neurotoxic. In vitamin B_{12} deficiency, there is a marked accumulation of MTHF in the blood and CSF[29,30]. The occurrence of foci of neuronal destruction in the

---

* To whom all correspondence should be addressed at the Department of Medical Biochemistry, University of the Withwatersrand, Johannesburg 2001, South Africa.

0028-0836/80/440852—02$01.00

Table 1 Inhibition of kainate, glutamate and GABA receptor binding in rat cerebellar membranes

	K_i (×10^{-6} M)		
Agent	^{3}H-kainic acid binding	^{3}H-glutamic acid binding	^{3}H-GABA binding
Kainic acid	0.08 ± 0.009	≫100	≫100
L-glutamic acid	28.3 ± 3.60	0.61 ± 0.07	≫100
MTHF	0.88 ± 0.17	83.5 ± 10.62	≫100
GABA	≫100	≫100	0.069 ± 0.009
L-proline	—	≫100	—
Muscimol	—	—	0.020 ± 0.002

Cerebella from adult Wistar rats were homogenized in 15 vol ice-cold 0.32 M sucrose in a glass homogenizer and centrifuged at 1,000*g* for 10 min at 4 °C; the pellet was discarded and the supernatant centrifuged at 20,000*g* for 20 min. This pellet was resuspended in ice-cold distilled water, dispersed with a Brinkmann Polytron PT-10 (setting 6) for 20 s and centrifuged at 8,000*g* for 20 min. The supernatant fluid was collected and the pellet carefully rinsed to collect the upper layer. This suspension was then centrifuged at 48,000*g* for 20 min and the pellet washed once in distilled water. Synaptic membranes were stored at −20 °C until use (24–72 h). Frozen pellets were suspended by sonication in 0.05 M Tris-citrate buffer (*p*H 7.1), centrifuged at 48,000*g* for 10 min and resuspended in buffer (0.1–0.4 mg protein per ml) for binding assays. Solutions containing MTHF were prepared immediately before use, although the compound is stable for some 12 h at 4 °C. Binding of ^{3}H-kainic acid (2.4 Ci mmol^{-1}, Amersham)[12], ^{3}H-glutamate (21 Ci mmol^{-1}, Amersham)[33] and ^{3}H-GABA (65 Ci mmol^{-1}, Amersham)[13] was assayed in triplicate centrifuge tubes. Incubation of membranes (0.1–0.4 mg protein) in the presence of ^{3}H-kainic acid, ^{3}H-glutamate or ^{3}H-GABA was continued for 60 min at 4 °C, 15 min at 30 °C, or 5 min at 4 °C, respectively. After incubation, the reaction was terminated by centrifugation at 48,000*g* for 10 min. The pellets were superficially washed with two 5-ml aliquots of ice-cold buffer and then dissolved by incubating for 30 min at 55 °C in 1.5 ml Protosol (NEN). Dissolved pellets were counted in 10 ml Aquagel I liquid scintillant (Chemlab) in a Packard Tri-Carb 2660 spectrometer with automatic quench correction. Total specific binding of radioligand was defined as the difference between total binding and that in the presence of 0.1 mM unlabelled ligand. IC_{50} values were determined by log-probit analysis using at least five inhibitor concentrations, and apparent K_i values calculated from the equation $K_i = IC_{50}/(1 + [^3\text{H-ligand}]/K_d)$. K_d values of 25 nM, 314 nM and 22 nM (calculated from Scatchard analysis of saturation isotherms) were used for ^{3}H-kainic acid, ^{3}H-glutamic acid and ^{3}H-GABA binding sites, respectively. Each value is the mean ± s.e.m. of four experiments each done in triplicate.

brains and spinal cords of B_{12}-deficient patients might be explained on the basis of a neurotoxic effect of excess MTHF. It is interesting that the highest serum MTHF levels are indeed found in patients who have subacute combined degeneration of the spinal cord[31]. In addition, Brennan *et al.*[32] have recently demonstrated a selective reduction in high affinity GABA uptake in the brains of B_{12}-deficient fruit bats. This finding suggests a destruction of GABAergic neurones in the B_{12}-deficient state, which is consistent with a neurotoxic action of MTHF.

These studies were supported in part by grants from the South African MRC and the Atomic Energy Board of South Africa, M.J.W.B. is in receipt of a grant from the Loewenstein Research Foundation.

Received 20 June, accepted 10 September 1980

1. Shinozaki, H & Konishi, S *Brain Res* **24,** 368–371 (1970)
2 Johnston, G. A R., Curtis, D R., Davies, J & McCulloch, R M *Nature* **248,** 804–805 (1974)
3 McCulloch, R M., Johnston, G A., Game, C J & Curtis, D. R *Expl Brain Res.* **21,** 515–518 (1974).
4. Brun, N T., Puil, E & van Gelder, N M. *Gen Pharmac.* **7,** 5–14 (1976)
5. Polc, P & Haefely, W *Naunyn-Schmiedebergs Archs Pharmak* **300,** 199–203 (1977).
6. Constanti, A. & Nistri, A. *Br. J. Pharmac.* **57,** 359–368 (1976).
7. Clements, A N & May, T. E. *J. exp Biol* **61,** 421–422 (1974).
8. Shinozaki, H & Shibuya, I *Neuropharmacology* **13,** 1057–1065 (1974).
9 Walker, R. J. *Comp. Biochem. Physiol* **55c,** 61–67 (1976)
10. Evans, R. H, Francis, A A. & Watkins, J. C *Experientia* **33,** 246–248 (1977).
11. Hall, J. G., Hicks, T. P. & McLennan, H. *Neurosci. Lett.* **8,** 171–175 (1978).
12 London, E. D. & Coyle, J. T. *Molec. Pharmac* **16,** 492–505 (1979).
13. Enna, S. J. & Snyder, S. H. *Brain Res* **100,** 81–97 (1975).
14 Herbert, V., Larrabee, A. R. & Buchanan, J M *J clin. Invest.* **41,** 1134–1138 (1962)
15. Herbert, V & Zalusky, R *Fedn Proc.* **20,** 453 (1961)
16 Spector, R. & Lorenzo, A. V *Science* **187,** 540–542 (1975).
17. Bridgers, W. F. & McClain, L D. *Adv. Biochem Psychopharmac* **4,** 81–92 (1972)
18 Loots, J. M. *et al.* (in preparation).
19. Lowagie, C. & Gerschenfeld, H. M *Nature* **248,** 533–535 (1974)
20 Spector, R. G. *Biochem. Pharmac.* **20,** 1730–1732 (1971).
21 Hommes, O R. & Obbens, E. A. M T *J neurol. Sci* **16,** 271–281 (1972).
22. Olney, J. W, Sharp, L G. & de Gubareff, T *Neurosci Abstr.* **1,** 371 (1975)
23. Coyle, J. T & Schwarcz, R *Nature* **263,** 244–246 (1976).
24 Herndon, R. M. & Coyle, J. T. *Science* **198,** 71–72 (1977).
25 Coyle, J T, Molliver, M E & Kuhar, M J *J. comp. Neurol* **180,** 301–323 (1978)
26. Curtis, D R *et al* *Brain Res* **41,** 283–301 (1972).
27. Zieglgänsberger, W. & Puil, E. A. *Expl Brain Res* **17,** 35–49 (1973)
28 Schwarcz, R, Scholz, D & Coyle, J. T. *Neuropharmacology* **17,** 145–151 (1978)
29. Herbert, V. & Zalusky, R *J clin Invest* **41,** 1263–1276 (1962)
30. van Tonder, S., Metz, J. & Green, R. *Br. J. Nutr* **34,** 397–410 (1975).
31. Waters, A H & Mollin, D L *Br J Haemat.* **9,** 319–327 (1963).
32. Brennan, M. J. W. *et al.* *Brain Res.* (in the press).
33 Baudry, M. & Lynch, G. *Eur. J. Pharmac.* **57,** 283–285 (1979)

Lymphocyte activating factor promotes T-cell growth factor production by cloned murine lymphoma cells

Kendall A. Smith, Kevin J. Gilbride & Margaret F. Favata

The Immunology Program, Norris Cotton Cancer Center, Dartmouth–Hitchcock Medical Center, Hanover, New Hampshire 03755

Evidence has indicated that two soluble factors are essential for a T-cell proliferative response to antigen or lectin[1–3]. One such factor, thought to be of T-cell origin, is distinguished by its ability to initiate and maintain continuous T-cell growth (T-cell growth factor, TCGF)[4–6]. A second activity of macrophage origin augments lectin-initiated proliferative responses of thymocytes or adherent cell-depleted splenocytes (lymphocyte activating factor, LAF)[7]. Although it has been suggested that LAF promotes T-cell proliferation by facilitating the production of TCGF by T-cells[1–3], direct evidence supporting this hypothesis has been lacking. We describe here experiments with a murine thymic lymphoma which releases TCGF in response to lectin. In serum-free, defined medium, highly purified LAF promotes a concentration-dependent increase in TCGF release. Because the proliferation of T cells depends on the concentration of TCGF available[8,9], these results indicate that LAF and TCGF constitute an essential bimodal amplification system which ultimately determines the extent of T-cell clonal expansion.

To approach the functional relationship of LAF and TCGF, we sought LAF-responsive cells which could be cultured in a lymphokine-free medium. WEHI-7, an irradiation-induced Thy 1^+ lymphoma cell line of BALB/c origin[10] (Salk Institute Cell Distribution Center), was placed into culture with Iscove's modification of Dulbecco's modified Eagle's medium (IMDM) supplemented with bovine serum albumin, transferrin, cholesterol and soybean lipid[11,12]. The WEHI-7 cells were screened for TCGF production at multiple cell concentrations in the presence of concanavalin A (Con A) or phytohaemagglutinin (PHA) and LAF. No detectable TCGF activity was found in the culture medium in the absence of lectin stimulation, although both PHA- and Con A-elicited TCGF activity were found. LAF obtained from lipopolysaccharide (LPS)-stimulated human peripheral blood mononuclear cells did not cause detectable TCGF production, although LAF increased lectin-dependent TCGF production three- to fivefold. A typical experiment is shown in Fig. 1, where TCGF activity elicited by Con A in the absence and presence of LAF was assayed by the dose-dependent tritiated thymidine (^{3}H-TdR) incorporation of a TCGF-dependent cytolytic T-lymphocyte line (CTLL)[9].

0028-0836/80/440853—03$01.00

To investigate whether WEHI-7 was heterogeneous with respect to TCGF production, the cell line was cloned by limiting dilution in microtitre plates (0.3 cells per well, Poisson-calculated probability of co-fertile wells <0.05). Forty-one clones were obtained, and when tested for TCGF, 50% of the clones did not produce detectable TCGF activity regardless of whether lectin or LAF was present. In contrast, all of those clones which released TCGF on lectin stimulation also responded to LAF by at least a twofold increment in TCGF production. Thus, the WEHI-7 cells behaved similarly to normal T-cells: both lectin and LAF were required for optimal TCGF production[3].

In previous experiments it was observed that the extent of T-cell proliferation was TCGF-concentration dependent[8,9]. Therefore, if LAF augmented TCGF production, it seemed likely that LAF availability might be rate limiting in the ultimate T-cell proliferative response, especially if the effect of LAF on TCGF production was also concentration dependent. To examine this possibility, LAF partially purified by molecular gel chromatography and isoelectric focusing was added to TCGF-producing and nonproducing WEHI-7 clones in the presence of an optimal stimulatory concentration of Con A. As shown in Fig. 2, LAF clearly promoted a dose-dependent increase in TCGF release from one clone but not from the other clone.

The identification of a murine T-cell lymphoma that produces TCGF in response to lectin stimulation supports the impression that TCGF is T-cell derived. It was necessary to utilize cloned cells to provide such evidence as it was known that T-cell-enriched, normal cell populations required the presence of adherent cells for optimal TCGF production[2,3,13]: therefore the small amount of TCGF released by T-cell-enriched splenocytes could have been derived from residual adherent cells. As cloned thymic lymphoma cells were capable of producing TCGF in the absence of aherent cells and as LAF augments TCGF production, the data indicate that adherent cells contribute an early amplifying signal to T cells capable of TCGF production. Thus, the availability of a clonal population of cells, which can be studied in the absence of serum, provides the cellular system for detailed studies of the mechanism of LAF action and the molecular mechanism of TCGF production. Because both LAF and TCGF are essential for the T-cell proliferative response, such experiments will be important not only to investigate the nature of these lymphokines but also because information gained at the molecular level may increase insight into possible defects of lymphokine function which could underlie disease states.

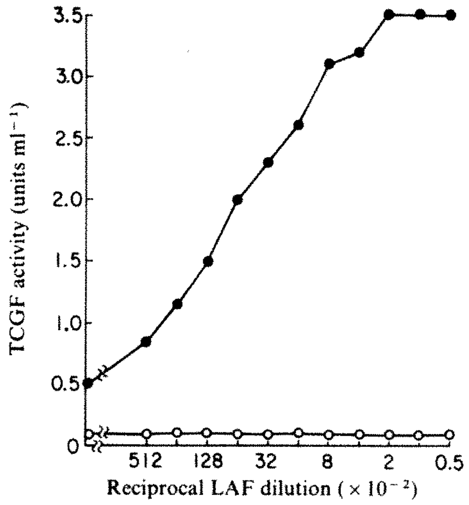

Fig. 2 LAF-concentration-dependent production of TCGF activity from WEHI-7 clone 49 (●) and clone 8(○). Clones were tested for TCGF production as described in Fig. 1 legend. The LAF preparation was partially purified by Sephadex G-75 chromatography (active fractions migrated with an apparent molecular weight of 20,000) followed by isoelectric focusing over a *p*H gradient of 3-10. LAF used for the experiment displayed was derived from the isoelectric focusing gradient, *p*H 6.85. Both the Sephadex G-75 fractions and the isoelectric focusing fractions which contained LAF activity displayed no detectable TCGF activity before addition to the WEHI-7 clones.

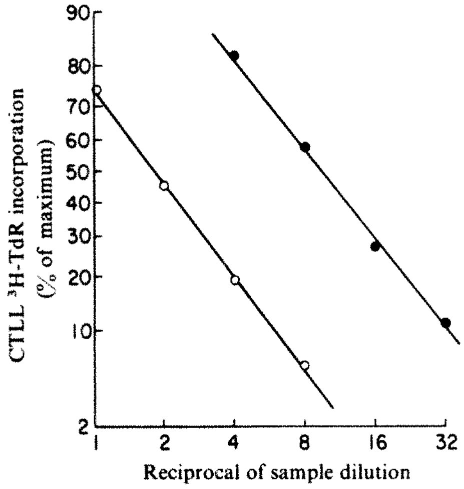

Fig. 1 TCGF activity elicited from WEHI-7 cells by Con A in the absence (○) and presence (●) of LAF. WEHI-7 cells (2×10^{6} cells ml^{-1}) were cultured for 24 h in IMDM[11,12] with Con A (2.5 μg ml^{-1}, Miles-Yeda). LAF was obtained from LPS (20 μg ml^{-1}, *Escherichia coli*, Gibco-stimulated human peripheral blood mononuclear cells cultured in serum-free RPMI 1640 medium (Gibco) for 48 h. Before use, the LAF-containing conditioned medium was concentrated 60-fold by passage through a YM-10 Amicon filter (Amicon), dialysed against 7,500 vol of saline, 500 vol of RPMI 1640, and assayed for LAF and TCGF activity as previously described[3,15]. No TCGF activity was detectable in the LAF preparation. The LAF preparation was added to the WEHI-7 cell cultures at a final dilution of 1:1,000. WEHI-7 conditioned medium was assayed for TCGF activity[3,15] using a TCGF-dependent cytolytic T-lymphocyte line (CTLL-2)[16]. The CTLL response to TCGF was quantified and displayed as the reciprocal of the sample dilution which resulted in 50% of the maximum CTLL ^{3}H-TdR incorporation elicited by a standard rat TCGF preparation[15]. ^{3}H-TdR incorporation was determined by the addition of 2 μCi ml^{-1} ^{3}H-TdR (specific activity 1.0 Ci mmol^{-1} Schwarz-Mann) during the last 4 h of a 24-h culture period as described previously[15]. In the experiment shown, maximum ^{3}H-TdR incorporation yielded 19,500 c.p.m. In the absence of TCGF the CTLL incorporated 75 c.p.m.

Because TCGF ultimately mediates T-cell proliferation and because the magnitude of TCGF elaboration is LAF-concentration dependent (Fig. 2), the data indicate that LAF and TCGF function in a bimodal amplification system which finally determines the extent of antigen- or lectin-initiated T-cell clonal expansion. Thus, it may be anticipated that physiological and pharmacological agents known to influence the immune response may do so by altering lymphokine function. Immunosuppressive agents which inhibit LAF-mediated TCGF production would have profound effects on the humoral and cellular immune response, as both cytolytic and helper T-cell proliferation is TCGF-concentration dependent[9,14]. For example, we have recently found that glucocorticoid hormones inhibit both the production and action of LAF which in turn results in a complete abrogation of TCGF production[3,5]. Similarly, immunoenhancing agents may function through the LAF–TCGF amplification network. As pointed out by Oppenheim *et al.*[7], many of the agents used as immunological adjuvants are also potent LAF inducers. As one can study separately the production and action of both LAF and TCGF, the mode of action of immunosuppressive and immunoenhancing agents may be amenable to experimental analysis.

This work was supported in part by NCI grants CA-17643, CA-23108, and NCI contract N01-CB-7414. K.J.G. is supported by NIH grant F32-CA06471.

Received 21 July, accepted 3 September 1980.

1 Smith, K A Gillis, S & Baker, P E in *The Molecular Basis of Immune Cell Function* (ed. Kaplan, J G. 223–238 (Elsevier, Amsterdam, 1979).
2 Larsson, E.-L., Iscove, N. N & Coutinho, A *Nature* **283**, 664–666 (1980)
3 Smith, K A, Lachman, L B., Oppenheim, J J & Favata, M. F *J. exp. Med* **151**, 1551–1556 (1980).
4. Morgan, D A., Ruscetti, F W & Gallo, R C *Science* **193**, 1007–1008 (1976)
5. Smith, K. A *Immun. Rev* **51**, 335–357 (1980).
6. Coutinho, A, Larsson, E -L, Gronvik, K. O. & Andersson, J *Eur. J. Immun* **9**, 587–592 (1979)
7. Oppenheim, J J, Mizel, S B & Meltzer, M S in *Biology of the Lymphokines* (eds Cohen, S., Pick, E. & Oppenheim, J. J) 291–321 (Academic, New York, 1979)
8 Smith, K A, Gillis, S, Baker, P E, McKenna, D T & Ruscetti, F W *Ann N.Y Acad Sci* **332**, 423–432 (1979)
9. Smith, K A. *Contemporary Topics Immunobiol* 11 (in the press).
10 Harris, A W, Bankhurst, A D, Mason, S & Warner, N L *J Immun.* **10**, 431–438 (1973).
11. Iscove, N. N & Melchers, F *J exp Med* **147**, 923–933 (1978)
12 Schreier, M. H *J exp Med* **148**, 1612–1619 (1978)
13 Smith, K. A., Baker, P E, Gillis, S & Ruscetti, F W *Molec Immun* **17**, 579–589 (1980)
14 Schreier, M. H., Iscove, N N, Tees, R, Aarden, L & von Boehmer, H *Immun Rev.* **51**, 315–336 (1980)
15. Gillis, S, Ferm, M M, Ou, W & Smith, K A *J Immun* **120**, 2027–2032 (1978)
16 Gillis, S & Smith, K A *Nature* **268**, 154–156 (1977)

Alloreactivity of an antigen-specific T-cell clone

Benjamin Sredni & Ronald H. Schwartz

Laboratory of Immunology, National Institute of Allergy and Infectious Diseases, National Institutes of Health, Bethesda, Maryland 20205

The apparent high frequency of alloreactive T cells has suggested that the two subpopulations—T cells specific for soluble protein antigens and alloreactive T cells—must overlap[1–3]. However, the existence of a set of germ-line genes encoding a family of anti-MHC (major histocompatibility complex) antigen-specific T-cell receptors has also been postulated to explain the high frequency of alloreactive clones[4–7]. In these latter models the two T-cell subpopulations are viewed as separate. Studies on whole T-cell populations have examined these two points of view by looking for cross-stimulation of alloreactive cells with antigen and vice versa[8–11]. Although significant cross-reactions have been reported, the problem of nonspecific recruitment made interpretation of results difficult. Recent developments in the cloning of antigen-specific T lymphocytes[12–16] have finally allowed investigation at the single-cell level where the results should be unambiguous. von Boehmer *et al.*[14] have isolated a cytotoxic clone specific for the H–Y antigen in conjunction with the syngeneic MHC antigens coded for by D^b. This clone was also cytotoxic for spleen cells bearing the alloantigens coded for by D^d in the absence of the H–Y antigen. However, because cytotoxic clones only grow in the presence of T-cell growth factor (TCGF) and because von Boehmer *et al.* were unable to stimulate or enrich for D^d-specific cytotoxic activity from bulk cultures initially stimulated with H–Y and D^b-bearing spleen cells[14], they hesitate to conclude that the same cell can respond to both foreign and alloantigens. We show here that a (dinitrophenyl-ovalbumin)(DNP-OVA)-specific T-cell clone from a B10.A mouse can be stimulated to divide (and propagate) *in vitro* with B10.S allogeneic spleen cells in the absence of DNP-OVA and B10.A antigen-presenting cells. Extensive recloning strongly suggests that a single T-cell clone is responding to two separate stimuli, a specific alloantigen and a soluble antigen in conjunction with self-MHC products.

B10.A mice were immunized with DNP-OVA and T-lymphocyte colonies prepared from the draining lymph nodes as previously described[12]. Most of the colonies tested were shown to be antigen specific, that is, their cells could be stimulated to divide with DNP-OVA but not other antigens such as GAT or purified protein derivative (PPD). One of these colonies was chosen to study alloreactivity as shown in Table 1. Cells from this colony could be stimulated to divide in the absence of DNP-OVA with either B10.S or B10.D2 irradiated spleen cells but not spleen cells from mice of six other independent halotypes. No change in the results was seen if syngeneic B10.A spleen cells were also added. This latter condition is essential for antigen stimulation although not sufficient by itself (Table 1). These results suggested that an antigen-specific cell could also manifest alloreactivity.

However, this conclusion depends on the colony being a true clone. Although all the colonies grew up completely isolated in the agar and were easy to pick independently of one another, whether each colony derived from a single cell is not clear as a large number of cells (2×10^6) were seeded in the agar allowing for the possibility of recruitment of nearby cells into the colony.

Table 1 Maintenance of alloreactivity on recloning

Source of spleen cells	Proliferative response (c.p.m. ± s.e.m.)		
	Colony	Clone 5	Subclone 5.6
B10.A	25 (±5)	150 (±95)	180 (±52)
B10.A + DNP-OVA	9,600 (±680)	14,700 (±2,300)	39,200 (±1,950)
B10	30 (±5)	130 (±55)	233 (±116)
B10.D2	9,100 (±600)	236 (±82)	410 (±35)
B10.M	10 (±2)	160 (±105)	46 (±8)
B10.P	10 (±1)	153 (±42)	230 (±41)
B10.Q	45 (±5)	190 (±150)	60 (±20)
B10.RIII	25 (±15)	107 (±18)	53 (±12)
B10.S	18,200 (±2,400)	15,900 (±2,000)	36,300 (±1,900)
B10.PL	15 (±5)	50 (±25)	80 (±39)

A colony of DNP-OVA-reactive proliferating T lymphocytes was derived from primed B10.A lymph node cells as previously described[12]. Small numbers of cells from this colony were cloned in soft agar with 80% plating efficiency. Of the 14 subcolonies which were picked and expanded, cells from one, clone 5, were again cloned in soft agar, this time with a 91% plating efficiency. Six of these colonies were picked and expanded. The table shows the antigen specificity and alloreactivity of the original colony, clone 5, and subclone 5.6. 10^4 T cells from the original colony and clone 5 or 2×10^4 T cells from subclone 5.6 were mixed with 10^4 irradiated (2,000 rad) spleen cells of various MHC haplotypes in the presence of 5% Con A supernatant. In the test for antigen stimulation, 10% Con A supernatant was used and 100 μg ml^{-1} of DNP-OVA was added. The cells were cultured for 6 days in RPMI 1640 plus 10% FCS with supplemental feeding at day 3 (ref. 12). At 16–18 h before collecting, the cultures were pulsed with 1 μCi of tritiated thymidine. The data shown are mean (c.p.m.) ± s.e.m. for triplicate determinations.

To investigate this problem, 200 cells from one colony were supplemented with 10^4 irradiated B10.A spleen cells and recloned in soft agar[12]. The use of a few T cells assured us that all colonies which developed would not have other T cells near them in the agar. Thus we could be sure that each of the colonies was derived from a single cell. After five days of incubation 160 colonies were observed in the agar for a plating efficiency of 80%. Of 15 of these colonies picked and expanded in liquid culture, 14 survived to test for antigen specificity; the remaining colony was lost because of microbial contamination. Cells from all 14 subcolonies showed an identical antigen specificity, responding to stimulation with DNP-OVA but not GAT or PPD (data not shown). Furthermore, as shown for a typical example in Table 1, cells from all 14 subcolonies responded to allo-stimulation with irradiated B10.S spleen cells. The dose-response curves shown in Fig. 1 indicate that the irradiated B10.S spleen cells could stimulate the B10.A T cells in the

0028-0836/80/440855—03$01 00

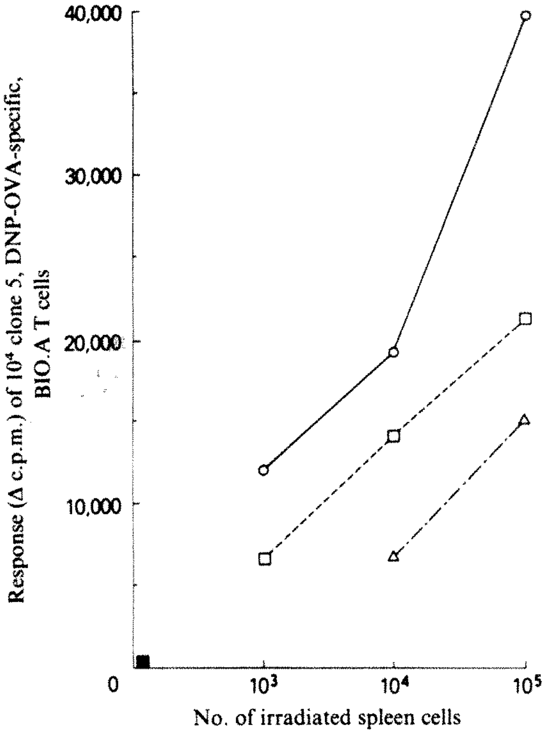

Fig. 1 10^4 T cells from B10.A clone 5 specific for DNP-OVA in association with B10.A spleen cells were stimulated with various numbers of irradiated allogeneic B10.S spleen cells in the absence of Con A supernatant (0% IL-2, △) or the presence of 5% (v/v) IL-2 (□) or 10% IL-2 (○). ■ indicates that no stimulation was seen with 10% IL-2 in the presence of 10^5 irradiated syngeneic B10.A spleen cells.

absence of any added growth factor in the culture (0% IL-2), provided that the T cells were cultured at a high enough density (10^4 per well) and a sufficient number of stimulator cells was added ($\geq 10^4$). However, addition of 5% or 10% concanavalin A (Con A) supernatant to the cultures improved the magnitude of the allogeneic proliferative response at all spleen cell doses, even though these concentrations of Con A supernatant were totally nonstimulatory in the presence of similar numbers of syngeneic B10.A spleen cells. The allostimulation of B10.S spleen cells was not due to a 'back-reaction', that is, recruitment into proliferation of the cloned T cells by alloreactive T cells in the irradiated spleen cell population, because cells from a B10.S macrophage colony were also capable of eliciting a response (data not shown).

Interestingly, none of the subcolonies responded to irradiated B10.D2 spleen cells. This suggests that the original colony was not a true clone but was contaminated with an alloreactive cell specific for H-2^d MHC antigens. The loss of reactivity against H-2^d antigens on recloning made us decide to reclone again to assure ourselves that the remaining alloreactivity for B10.S antigens was indeed associated with the same cells showing specificity for DNP-OVA. In this experiment the cells were recloned in the presence of 25% Con A supernatant in the bottom agar layer to improve the plating efficiency. The number of colonies observed ranged over 170–194 per 200 cells plated with a mean plating efficiency of 91 ± 2%. Six of these colonies were picked and expanded in liquid culture. All six could be stimulated with either DNP-OVA in the presence of syngeneic spleen cells or irradiated B10.S allogeneic spleen cells (Table 1, subclone 5.6). The failure to separate these two activities on recloning suggests strongly that the subcolonies were already true clones and that a single T cell possesses receptors for both specificities.

Previous studies with this B10.A T-cell clone had demonstrated that recognition of DNP-OVA was MHC restricted, requiring syngeneic B10.A irradiated spleen cells to present the antigen[12]. The gene(s) controlling this histocompatibility restriction was mapped to the I-A^k subregion of the MHC. Table 2 shows a similar type of genetic mapping experiment for alloreactivity. Data are shown for one clone but all 14 gave the same result—mapping of the gene(s) to the I-A^s or I-B^s subregion. Because the major lymphocyte-activating determinant (LAD) locus has been mapped to the I-A subregion[19], it is reasonable to conclude that the stimulating alloantigens in this case map to I-A^s. Thus, the same T cell which can respond to DNP-OVA in conjunction with I-A^k is also stimulated by I-A^s. The studies so far do not allow us to determine whether the same receptor or separate receptors account for the two specificities possessed by the clone.

These results have important implications for theories of T-cell recognition, as some of these theories[4,20] have postulated that alloreactive and antigen-specific T cells are separate subpopulations. Such models could account for the results presented here by postulating that we have identified a rare clone in which the receptor for the antigen, DNP-OVA, happens to cross-react with a determinant on the alloantigen, I-A^s. This is a testable hypothesis as it postulates that in this rare instance, the alloantigen is actually presented to the T cell like a foreign antigen, that is, in conjunction with I-A^k on the syngeneic antigen-presenting cell. As already mentioned, B10.S spleen cells will stimulate the clone in the absence of the additional B10.A spleen cells which are required for DNP-OVA presentation. However, it could be argued that sufficient B10.A spleen cells are present in the T-cell population, as a result of the feeding requirements for propagating the clone, to allow for the presentation of I-A^s antigens.

To test the possibility that I-A^s was recognized in conjunction with I-A^k, we grew one of the clones by stimulating it only with irradiated B10.S spleen cells in the presence of 5% Con A supernatant. At no time during the 39-day propagation were the cells exposed to DNP-OVA or B10.A spleen cells, even when the cultures were split. At the end of this time the cells were retested for specificity. As shown in Table 3, the cells retained their antigen specificity, responding to DNP-OVA and the carrier OVA but not to GAT or the hapten on another carrier, DNP-GLA. They also retained their allospecificity for B10.S and did not acquire any other alloreactivity. To reduce further the possibility that residual B10.A spleen cells remained in the T-cell cultures, the clone was propagated for another 29 days, this time in the complete absence of all spleen cells and antigen. This was done by increasing the concentration of the Con A supernatants (TCGF) to 50% (v/v). Again the clone maintained both its alloreactivity and antigen specificity (Table 3). Thus, after 68 days without adding B10.A spleen cells, presumably a time vastly longer than the lifetime of any irradiated spleen cells,

Table 2 Genetic mapping of allostimulation

Spleen cells		Clone 5
Strain	MHC haplotype	(c.p.m. ± s.e.m.)
B10.A + DNP-OVA	kkkkkdddd	14,700 (±2,300)
B10.A	kkkkkdddd	150 (±95)
B10.S	sssssssss	15,900 (±2,000)
B10.S (9R)	ss?kkdddd	15,700 (±800)
A.TL	skkkkkkkd	90 (±15)
A.TH	ssssssssd	15,700 (±2,300)

10^4 B10.A anti-DNP-OVA clone 5 T cells were stimulated with 10^4 irradiated (2,000 rad) spleen cells from various strains in the presence of 5% Con A supernatants. A 6-day tritiated thymidine incorporation assay was performed as described in Table 1 legend. The data are expressed as c.p.m. ± s.e.m. for triplicate determinations. The letters in the MHC haplotype column refer to the haplotype source of origin of the K, I-A, I-B, I-J, I-E, I-C, S, G and D regions of the murine MHC. The value for A.TH spleen cells was obtained in a separate experiment carried out in exactly the same conditions.

Table 3 Specificity of an alloreactive clone grown in the absence of antigen and syngeneic spleen cells

		Proliferative response (c.p.m. ± s.e.m.) of clone 5 expanded with:		
Antigen	Spleen cells	DNP-OVA and B10.A spleen	Allogeneic B10.S spleen	50% Con A supernatant
None	B10.A	90 (±29)	63 (±3)	120 (±6)
DNP-OVA	B10.A	15,700 (±1,000)	14,100 (±2,000)	14,000 (±1,200)
OVA	B10.A	13,700 (±1,200)	14,900 (±1,300)	14,300 (±1,170)
DNP-GLA	B10.A	143 (±70)	70 (±17)	50 (±12)
GAT	B10.A	150 (±55)	73 (±26)	50 (±21)
None	B10.S	15,900 (±2,015)	13,800 (±800)	13,100 (±400)
None	B10.D2	236 (±80)	60 (±15)	90 (±12)

DNP-OVA-specific B10.A T-cell clone 5, which is normally propagated by feeding every three days with 10^4 irradiated B10.A spleen cells and 100 μg ml^{-1} of DNP-OVA in medium containing 20% (v/v) Con A supernatant, was propagated with 10^4 irradiated B10.S spleen cells and 5% Con A supernatant for 39 days followed by propagation with 50% Con A supernatant alone for an additional 29 days. The table shows the antigen specificity and alloreactivity of the original clone (column 1), the clone after being grown with allogeneic spleen cells (column 2) and the clone after being grown with high concentrations of Con A supernatant (column 3). Antigen specificity was assessed in a 6-day thymidine incorporation assay using 10^4 T cells, 10^4 syngeneic, irradiated (2,000 rad) B10.A spleen cells, 10% Con A supernatant and 100 μg ml^{-1} of DNP-OVA, GAT and DNP-GLA or 300 μg ml^{-1} of OVA (see Table 1 legend). Alloreactivity was assessed by adding 10^5 irradiated B10.S or B10.D2 spleen cells in the presence of 5% Con A supernatant. The data are expressed as mean c.p.m. ± s.e.m. for triplicate determinations.

the alloreactivity of the clone was not diminished. These results strongly indicate that the T-cell clone is responding directly to I-A^s antigens and not to these antigens in conjunction with syngeneic I-A^k gene products.

Overall our data demonstrate that individual T cells do exist which can recognize and respond to both alloantigens and soluble protein antigens. This dual specificity can be explained in a number of ways. One could postulate two completely independent sets of receptors randomly expressed in all lymphocytes[2], alloantigen recognition through high affinity cross-reactions with the anti-self MHC receptor[3] or the antigen-specific receptor[6,7], or recognition through a combination of both the anti-self MHC and antigen-specific receptors[8,10]. Further studies are required with more T-cell clones to distinguish between these various models for T-cell recognition.

Received 5 June, accepted 3 September 1980.

1. Simonsen, M. *Cold Spring Harb Symp quant. Biol* 32, 517–523 (1967)
2. Wilson, D B in *Progress in Immunology* Vol 2 (eds Brent, L & Holborow, J) 145–156 (Elsevier, Amsterdam, 1974)
3. Janeway, C A Jr, Wigzell, H & Binz, H *Scand J. Immun.* 5, 993–1001 (1976).
4 Jerne, N. K *Eur J. Immun* 1, 1–9 (1971)
5. Blanden, R V & Ada, G L *Scand J. Immun* 7, 181–190 (1978).
6 Langman, R E *Rev physiol biochem. Pharmac.* 81, 1–37 (1978).
7 Cohn, M & Epstein, R *Cell Immun* 39, 125–153 (1978)
8 Burakoff, S J *et al J. exp. Med* 148, 1414–1422 (1978)
9 Lemonnier, F, Burakoff, S J., Germain, R N. & Benacerraf, B *Proc. natn Acad. Sci U.S.A.* 74, 1229–1233 (1977).
10 Bevan, M J *Proc natn. Acad Sci U S A.* 74, 2094–2098 (1977)
11 Haber-Katz, E & Wilson, D B *J. exp Med* 143, 701–706 (1976).
12 Sredni, B, Tse, H Y. & Schwartz, R H *Nature* 283, 581–583 (1980)
13 Schreier, M H. & Tees, R *Int Archs Allergy appl. Immun* 61, 227–237 (1980)
14 von Boehmer, H *et al Eur J Immun* 9, 592–597 (1979).
15 Watson, J *J exp Med.* 150, 1510–1519 (1979)
16 Baker, P E, Gillis, S., Ferm, M M. & Smith, K A *J. Immun* 121, 2168–2173 (1978)
17 Rosenberg, S A., Spiess, P J & Schwarz, S *J. Immun* 121, 1946–1955 (1978)
18 Schwuller, R, Rollinghoff, M & Wagner, H. *Scand J Immun* 11, 449–453 (1980)
19. Shreffler, D C. & David, C S *Adv. Immun* 20, 125 (1975).
20 von Boehmer, H, Haas, W & Jerne, N. K *Proc. natn Acad. Sci U S A* 75, 2439–2442 (1978)

A G_1 rate model accounts for cell-cycle kinetics attributed to 'transition probability'

LaRoy N. Castor

Institute for Cancer Research, Fox Chase Cancer Center,
7701 Burholme Avenue, Philadelphia, Pennsylvania 19111

Smith and his colleagues[1–4] have proposed that the duration of the cell cycle is determined by a random transition, analogous to the random decay of a radioactive nucleus, by which a cell passes from an 'A state' within the G_1 phase to a 'B phase' that includes the rest of the cycle. The experimental support for this transition probability hypothesis is the tendency of a cumulative plot of differences of cycle times of sibling cells (the β curve) to be exponential and parallel to the exponential tail of a cumulative plot of the cycle times themselves (the α curve). However, a close examination of four of the most extensive sets of experimental data now suggests that the two β curves with the steepest slopes may not, in fact, be exponential. These and all the other characteristics of the experimental curves are best matched by computer simulations using a cell-cycle model that will be termed here a G_1 rate model. This model is consistent with differences in cell metabolism, rather than a transition at an inherently unpredictable time, being the physiological basis for differences in cycle times within a cell population.

As cycle control occurs mainly in the G_1 phase, the formulation of any realistic model requires that the G_1 phase be treated separately from the remainder of the cycle. Monte Carlo simulations of α and β curves were performed using different combinations of exponential, reciprocal–normal, log–normal and normal distributions in two successive phases. Matches to the published curves were most readily obtained with normally distributed reciprocals of G_1 times (called G_1 rates by Sisken and Morasca[7]) and normally distributed times of passage through a second ($S+G_2+M$) phase. If t is the complete cycle time for a cell passing through the G_1 phase at a rate r_1 and through the remainder of the cycle in time t_2,

$$t = 1/r_1 + t_2$$

Let ω' and ω'' be random numbers from a normal distribution having zero mean and unit standard deviation, with ω' maintained the same in two sibling cells and ω'' generated separately for each of the siblings. The complete G_1 rate for a single cycle can be written as

$$r_1 = \bar{r}_1 + k_1[c_1\omega' + (1-c_1)\omega'']$$

in which $\bar{r}_1$ is the mean G_1 rate over the entire cell population and c_1 is a fraction determining the degree of sibling correlation. The value of k_1 is related to the standard deviation, σ_1, of the G_1 rate

$$k_1 = \sigma_1[c_1^2 + (1-c_1)^2]^{-1/2}$$

Similarly, using comparable notation and new random numbers, the complete time of the second phase is

$$t_2 = \bar{t}_2 + k_2[c_2\omega' + (1-c_2)\omega'']$$
$$k_2 = \sigma_2[c_2^2 + (1-c_2)^2]^{-1/2}$$

In Fig. 1, experimental α and β curves (individual points) are matched with computer simulations for 100,000 sibling pairs of cycles using the G_1 rate model (solid and dashed lines). The experimental data are from publications of the Smith group, except for set b (ref. 8), which has not been previously plotted as α and β curves. In the four sets of points a downward bend at the top of the β curve[9] is most pronounced for the steepest curve (a) and progressively less pronounced in the three other sets, left to right. The computer simulations for the G_1 rate model show the

0028–0836/80/440857—03$01 00

Table 1 Ability of G_1 rate and transition probability models to generate β curvatures found experimentally

Data	Pairs	β at midpoint	Experimental		G_1 rate model			Transition probability model		
			Slope	Curvature	Mean slope	Mean curvature	P^*	Mean slope	Mean curvature	P^*
a	37	0.70	−1.328	−0.691	−1.258	−0.476	0.22	−1.276	+0.002	0.02
b	256	0.25	−0.701	−0.288	−0.708	−0.368	0.67	−0.699	+0.005	0.06
c	107	0.35	−0.367	+0.147	−0.371	+0.108	0.58	−0.410	−0.099	0.85
d	24	0.40	−0.156	+0.242	−0.174	−0.069	0.74	−0.187	−0.145	0.78

For each model and each data set, 10,000 β curves were simulated using the same number of sibling pairs as was used experimentally (column 2). Parameters for the G_1 rate model were those of Fig. 1. For the transition probability model, β curves were generated for i cycles from the relationship $t_{ik} = (\ln N_i)/K$, with t_{ik} being the time spent in the A-state, K the measured slope of the experimental β curve, and N_i one of a set of random numbers, distributed uniformly between zero and unity. Each experimental and simulated curve was divided into upper and lower portions at a midpoint (column 3) chosen to delineate effectively the experimental curvature. Slopes (natural log units h^{-1}) were calculated by linear regression, using approximately 1,000 values at equal time intervals along line segments between the data points. Curvature was defined as the difference of the slopes of the upper and lower portions of a curve divided by its overall slope.

* Proportion of the 10,000 simulated β curves having a curvature more negative than the experimental curve.

same progression. For the simulations the major influence on the slopes of the α and β curves is the mean G_1 rate. Varying this parameter over a factor of 4.6 (with some adjustment of other parameters to give optimal matches to experiment) changes the slope of the β curve by a factor of 8. Other combinations of mean and standard deviation can also match the α and β curves. The correct combination could be determined if the mean G_1 time were known, but this was not measured for the experimental cell populations.

The two sibling correlation factors, c_1 and c_2, establish the slope of the β curve in relation to the slope of the α curve. The closeness with which a β curve approximates a straight line is enhanced when $c_1 \ll c_2$. This principle corresponds, to a rough approximation, with the assumption of no sibling correlation in the first phase of the transition probability model and perfect sibling correlation in the second phase[2-4]. However, the β curvature in set *b* was better matched with c_1 slightly greater than c_2, suggesting that there is no general rule that the G_1 phases of siblings are weakly correlated.

To examine the role of sampling error in determining β curvature, 10,000 simulations of each β curve were generated for each of the two models, using the same number of sibling pairs as was used experimentally. The proportion of the 10,000 simulated curves having a curvature more negative than the curvature found experimentally was then a measure of the frequency with which this curvature will be generated by the model. The repeated simulations (Table 1) show that the curvatures of all four sets of experimental data are within the range of values frequently attained with the G_1 rate model, as are the curvatures of sets *c* and *d* for the transition probability model. However, the transition probability model infrequently attains the curvatures of either set *a* ($P = 0.02$) or set *b* ($P = 0.06$). These data do not completely exclude the transition probability model as an explanation of cell-cycle control, but they suggest that a model that gives a slight downward curvature to steep β curves provides a more likely explanation.

These results with a model having a reciprocal–normal distribution in the G_1 phase are in contrast to those of Shields[4], who constructed α and β curves from 100 simulated cell cycles based on reciprocal–normal and log–normal models and concluded that neither model generated an exponential β curve. Aside from the problem of sampling error in such a small number of simulations, it is not reasonable to compare the two-phase transition probability model with a single-phase model, particularly as the major site of cycle control is known to be in the G_1 phase. By restricting the reciprocal–normal distribution to the G_1 phase, the G_1 rate model achieves higher coefficients of variation and brings the β curvature into a range that can accurately match the experimental β curves. Shields also concluded that only the transition probability model leads to

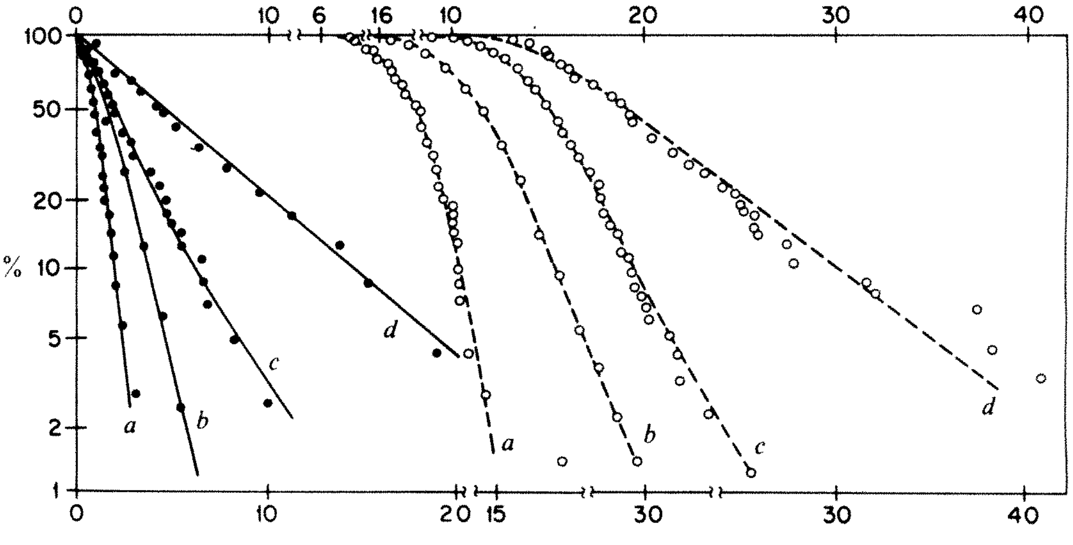

Fig. 1 Comparisons of published experimental data (●, ○) and Monte Carlo simulations using the G_1 rate model (—, ---) of the % of sibling pairs with a difference of cycle times $< t$ (β curves: ●, —) and the % of cell-cycle times $< t$ (α curves: ○, ---) against time, t. The simulations used 100,000 sibling pairs. They took into account the finite time a culture could be filmed (24, 125, 36, 60 h for *a*–*d*, respectively). Times between film frames were considered to be negligibly small except for *b*, which was 1 h. (These refinements had little effect on the simulated curves except for depression of both curves of *d*.) Numbers in parentheses are the six parameters ($\bar{r}_1, \sigma_1, c_1, \bar{t}_2, \sigma_2, c_2$) determining the simulated curves. *a*, Ref. 2, Fig. 2 (0.3, 0.03, 0.30, 7.3, 2.0, 0.70); *b*, ref. 8, Fig. 5 (0.131, 0.03, 0.68, 13.3, 2.0, 0.55); *c*, ref. 3, Fig. 1 (0.250, 0.11, 0.0, 10.5, 2.3, 0.70); *d*, ref. 3, Fig. 4 (0.065, 0.03, 0.40, 4.2, 1.0, 0.70). Measured correlation coefficients of simulated cycle times of siblings were: *a*, 0.83; *b*, 0.70; *c*, 0.36; *d*, 0.22.

parallel and exponential β curves when the data are divided into groups according to the shorter cycle time of each sibling pair. However, simulated β curves using the G_1 rate model have the same characteristic, within the sampling error of the experimental data (unpublished results).

Recent experiments using flow cytometry[10] have shown a 10% coefficient of variation in the RNA content of cells in early G_1 phase, comparable with the 10% coefficient of variation in the G_1 rate of set *a*, Fig. 1. The RNA content of individual cells was found to be correlated with the rate of progression through both the G_1 and S phases. Thus, much of the variation of cycle times within a population can be attributed to constitutive variations in the capacity of cells to synthesize protein. Theoretically, there could be a random transition in addition to the variation due to constitutive differences[5]. However, the present results show that the α and β curves can be accounted for completely without postulating such a transition, and there is no independent experimental evidence for one. The most reasonable hypothesis for interpreting the distribution of cycle times in a cell population is that it results from cell-to-cell variations in rates of metabolic reactions and in times required to complete essential steps in the cycle.

I thank Dr David Rigney for devising the original computer program and for many fruitful discussions. The simulations were performed on a PDP-11/70 computer (Digital Equipment Corp.), and the work was supported by DHEW grants CA-06927, CA-22780 and CA-24961 awarded by the National Cancer Institute and by an appropriation from the Commonwealth of Pennsylvania.

Received 27 June; accepted 10 September 1980.

1. Smith, J. A. & Martin, L. *Proc. natn. Acad. Sci. U.S.A.* **70,** 1263–1267 (1973).
2. Minor, P. D. & Smith, J. A. *Nature* **248,** 241–243 (1974).
3. Shields, R. & Smith, J. A. *J. cell. Physiol.* **91,** 345–356 (1977).
4. Shields, R. *Nature* **267,** 704–707 (1977); **273,** 755–758 (1978); **285,** 116 (1980).
5. Shields, R., Brooks, R. F., Riddle, P. N., Capellaro, D. F. & Delia, D. *Cell* **15,** 469–474 (1978).
6. Brooks, R. F., Bennett, D. C. & Smith, J. A. *Cell* **19,** 493–504 (1980).
7. Sisken, J. E. & Morasca, L. *J. Cell Biol.* **25,** No. 2, pt 2, 179–189 (1965).
8. Miyamoto, H., Zeuthen, E. & Rasmussen, L. *J. Cell Sci.* **13,** 879–888 (1973).
9. Pardee, A. B., Shilo, B.-Z. & Koch, A. L. *Cold Spring Harbor Conf. Cell Proliferation* **6,** 373–392 (1979).
10. Darzynkiewicz, Z., Evenson, D. P., Staiano-Coico, L., Sharpless, T. K. & Melamed, M. L. *J. cell. Physiol.* **100,** 425–438 (1979).

Cytosolic calcium ion activity in epithelial cells of *Necturus* kidney

Chin O. Lee, Ann Taylor & Erich E. Windhager

Department of Physiology, Cornell University Medical College,
New York, New York 10021

Calcium ions are believed to play an important role in the control of cellular function[1], and have recently been implicated in the regulation of sodium and water transport in epithelia[2–8]. In epithelial cells, as in excitable cells[1], low cytosolic free calcium levels may be maintained, in part, by a process of Na–Ca exchange across the plasma membrane[5,8–12]. In a recent model of transepithelial sodium transport in which a regulatory role for calcium ions was incorporated, it was assumed that cytosolic calcium ion activity of epithelial cells is similar to that of excitable cells[13]. However, no direct measurements of cytosolic calcium ion activity in epithelial cells in normal transporting conditions have yet been made. We report here the direct measurement with Ca^{2+}-selective microelectrodes of cytosolic calcium ion activity in proximal tubular cells of *Necturus* kidney. The results indicate that cytosolic calcium ion activity in these cells is ~10^{-7} M, and are consistent with the view that a Na–Ca exchange system, located at the basolateral cell membrane, plays a role in maintenance of low cytosolic calcium ion activity.

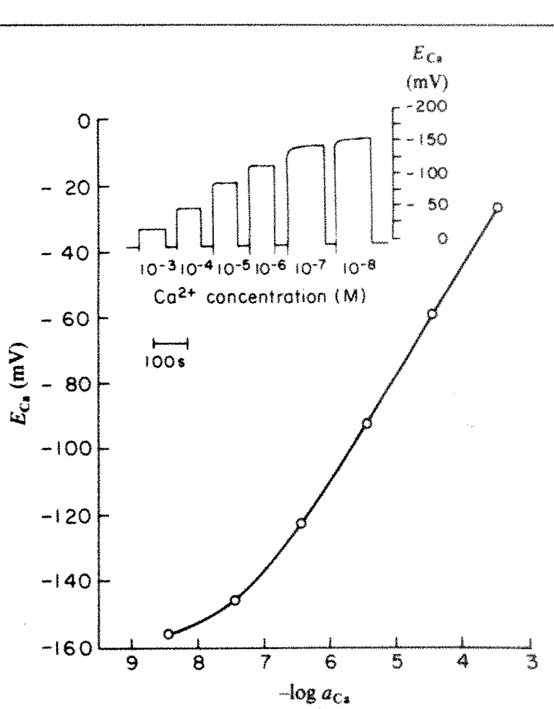

Fig. 1 Inset, microelectrode potentials measured at different calcium concentrations. Response times of the microelectrodes (time to reach a stable potential) were in the range of several seconds to one min. Main figure, microelectrode potentials plotted against $-\log a_{Ca}$. Solutions of 10^{-8}, 10^{-7}, 10^{-6}, 10^{-5}, 10^{-4} and 10^{-3} M Ca^{2+} concentration were used to calibrate the microelectrode. Those containing 10^{-8}, 10^{-7}, 10^{-6} and 10^{-5} M Ca^{2+} were made from a Ca^{2+} buffer containing EGTA. The Ca^{2+} concentrations of the solutions were calculated with the apparent stability constant of 4.90×10^6 M^{-1} for Ca-EGTA at *p*H 7.0. The solutions containing 10^{-4} and 10^{-3} M Ca^{2+} were made by dilution of 0.1 M $CaCl_2$ solution. All the solutions contained 100 mM K^+ and 1 mM Mg^{2+}, and had a *p*H of 7.0 The solutions have the same ionic strength, and hence probably the same activity coefficent of Ca^{2+}. In this study, the Ca^{2+} activity coefficient of 0.35, calculated by the extended Debye-Huckel equation[28] was used to obtain the calibration curve shown in the main part of the figure. This procedure is justified because calculated and measured Ca^{2+} activity coefficients at various ionic strengths are in reasonably good agreement[29,30]. The microelectrode potentials were not affected by *p*H changes in the range 7–8. In this study, the results are presented as activities, rather than Ca^{2+} concentrations, because: (1) many cell processes respond to ionic activities; (2) the microelectrodes measure potentials related to ionic activities; (3) expressing the results as ion concentration assumes that the activity coefficient of Ca^{2+} in the cytosol is equal to that of Ca^{2+} in the calibration solutions.

Experiments were performed on proximal tubules of doubly perfused kidneys of *Necturus maculosus*[14,15] using Ca^{2+}-selective microelectrodes. This preparation was chosen because of the relatively large size of the epithelial cells (~20 μm in diameter) and because the transport properties of this nephron segment have been reasonably well characterized[16,17]. Recently, Ca^{2+}-selective microelectrodes have been developed[18–20], which make measurements of cytosolic Ca^{2+} activities feasible. Ca^{2+}-selective microelectrodes were made employing a Ca^{2+}-selective liquid composed of 10% neutral ligand (*N*, *N'*-di(11-ethoxycarbonyl)undecyl-*N*, *N'* 4, 5-tetramethyl-3, 6-dioxaoctane diacid diamide), 1% sodium tetraphenylborate and 89% *o*-NPOE[21]. Glass micropipettes with tip diameters of ~1 μm or less were pulled from borosilicate glass capillaries (Corning Glass Works, code 7740). The inner surface of the micropipettes was silanized by exposure to dichloro-dimethylsilane gas. The micropipettes were first filled with 100 mM $CaCl_2$ solution; the Ca^{2+}-selective liquid was drawn up to 400–800 μm from the tip. Each microelectrode was calibrated before and after use by the procedure illustrated in Fig. 1. The inset shows the potential recordings measured in calibration solutions containing calcium ion concentrations of 10^{-8}–10^{-3} M (see

0028-0836/80/440859—03$01.00

Fig. 1 legend). At calcium levels $>10^{-6}$ M the potential changes corresponded to those predicted by the Nernst equation—a 29.6 mV change for a 10-fold change in calcium ion concentration. However, at calcium ion concentrations between 10^{-6} and 10^{-7} M, the potential changes varied from 10 to 25 mV; and between 10^{-7} and 10^{-8} M, from 5 to 15 mV. (The microelectrode characteristics have been considerably improved since our initial work[22].) In the main part of Fig. 1, the potentials recorded by the microelectrode are shown plotted against calcium ion activities, using an activity coefficient of 0.35 (see legend). Such a calibration curve was constructed for each electrode for the determination of intra- or extracellular calcium ion activites. Selectivity coefficients (k_{CaK}) of the microelectrodes against K^+ were in the range 1×10^{-6}–7×10^{-6}. Selectivity coefficients (k_{CaNa}) of the microelectrodes against Na^+ were in a range similar to or slightly greater than k_{CaK}. Considering the low cytosolic Na ion activities of *Necturus* proximal tubular cells[23], cytosolic Ca^{2+} activity measurements will not be significantly affected by changes in cytosolic Na^+ activity. (Detailed properties of the microelectrodes will be published elsewhere; C.O.L., in preparation.)

Figure 2 illustrates the measurement of basolateral cell membrane potential, V_M, and cytosolic calcium ion activity, a^i_{Ca}, in a proximal tubular cell of *Necturus* kidney. An epithelial cell was first impaled with a Ca^{2+}-selective microelectrode (see lower trace). When the intracellular potential recorded with this microelectrode had reached a stable value, a second cell of the same tubule was impaled with a conventional microelectrode (see upper trace). On this impalement, the potential recorded by the Ca^{2+}-selective microelectrode, E_{Ca}, fell by an amount equal to the peritubular cell membrane potential, and then reached another stable value. The rapid change in E_{Ca} represents the electronic subtraction of V_M from E_{Ca}. The E_{Ca} following the subtraction represents the cytosolic calcium ion activity. In 11 successful measurements on seven kidneys (out of a total of 52 experiments), the cytosolic calcium ion activity of *Necturus* proximal tubular cells averaged 116 ± 32 nM (mean ± s.d.), and the peritubular membrane potential was −56.6 ± 4.0 mV. Assuming that the activity coefficient of cytosolic Ca^{2+} is the same as that calculated for extracellular fluid (0.34), the cytosolic calcium ion activity of 116 mM is equivalent to a cytosolic free calcium ion concentration of 341 nM. (This assumption is justified if the cytosolic ionic strength is not too different from that of the extracellular fluid.) The value of 341 nM for cytosolic calcium ion concentration is in a range similar to that previously reported for other cell types[24].

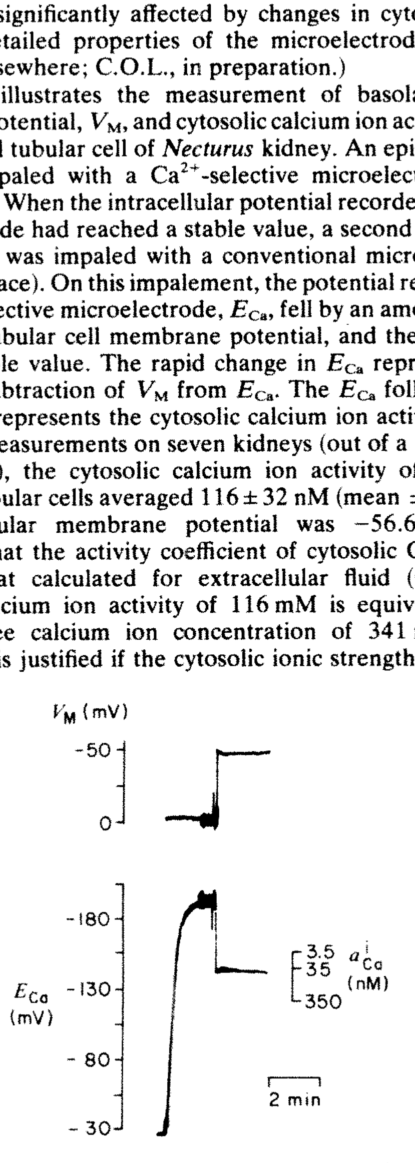

Fig. 2 Potential recordings obtained with a conventional microelectrode (upper trace) and a Ca^{2+}-selective microelectrode (lower trace) for determination of cytosolic Ca^{2+} activity. Experiments were performed on cells of proximal tubules of doubly perfused kidneys of *N. maculosus*. Both the aorta and the renal portal vein were perfused with a modified Ringer's solution[25] containing 100 mM Na^+. The kidney was also superfused with the same solution. The perfusion fluid was saturated with a gas mixture of 99% O_2 and 1% CO_2 to achieve a *p*H of 7.5–7.6. All experiments were carried out at room temperature (22–23 °C). Cells of the same tubule were impaled with the conventional microelectrode and the Ca^{2+}-selective microelectrode.

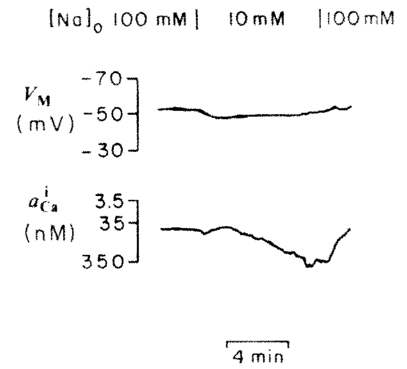

Fig. 3 Recordings of simultaneous measurements of peritubular cell membrane potential (V_M) and cytosolic calcium ion activity (a^i_{Ca}) during alteration of Na^+ concentrations in peritubular fluid. The low $[Na]_o$ solution was made by equimolar substitution of choline chloride for sodium chloride. The extracellular Ca^{2+} concentration was kept constant at 1.8 mM.

To measure the electrochemical gradient for calcium reabsorption by proximal tubular epithelium, calcium ion activities were measured in tubular and peritubular fluid of perfused kidneys. In 17 measurements on five kidneys, Ca^{2+} activity averaged 0.48 ± 0.07 mM in tubular fluid, and 0.61 ± 0.04 mM in peritubular fluid ($P<0.001$). In these tubules, the mean transepithelial potential difference was −5.6 ± 1.2 mV, lumen negative. Net fluid reabsorption was measured in separate experiments by the split-droplet technique[25]; the half time of reabsorption averaged 30.9 ± 10 min ($n = 7$), a value comparable to that obtained by previous investigators[25]. These results indicate that, in the process of calcium reabsorption, calcium ions may enter the cell passively across the luminal membrane, but must be extruded actively against a steep electrochemical gradient across the peritubular cell membrane.

Figure 3 shows simultaneous measurements of the basolateral membrane potential, and cytosolic calcium ion activity, in the control condition, and during reduction and subsequent restoration of the Na^+ concentration, $[Na]_o$, in the peritubular fluid. When $[Na]_o$ was reduced from 100 to 10 mM, the membrane potential depolarized by several millivolts. After the reduction of $[Na]_o$, cytosolic calcium ion activity increased slowly and reached a relatively stable level after 5 to 6 min. In eight successful measurements (out of 30 experiments), cytosolic calcium ion activity averaged 371 ± 59 nM ($P<0.001$) 6 min after the change in $[Na]_o$. In four experiments it was possible to extend the recording into the recovery period following restoration of normal $[Na]_o$. In these experiments, the membrane potential and cytosolic calcium ion activity returned to levels similar to the initial value; cytosolic calcium in activity averaged 376 ± 78 nM (±s.d.) 6 min after lowering $[Na]_o$ and had recovered to a mean value of 106 ± 22 nM (±s.d.; $P<0.001$) 2 to 3 min after restoring $[Na]_o$ to 100 mM. In individual impalements after restoration of normal $[Na]_o$, cytosolic calcium ion activities did not differ significantly from those in the initial control period; in the control period, cytosolic calcium ion activity averaged 115 ± 17 (±s.d.; $n = 6$), and after restoration of normal $[Na]_o$, 118 ± 47 ($n = 5$; *P*, not significant).

These results are consistent with the hypothesis that a Na–Ca exchange system operates across the peritubular cell membrane and plays a significant role in the maintenance of low cytosolic calcium ion activity in proximal tubular cells of *Necturus* kidney. These findings indirectly support the view[22] that the reported reduction in Na efflux from the lumen of isolated perfused rabbit proximal tubules in response to a decrease in contraluminal sodium concentration is associated with an increase in cytosolic calcium ion activity as previously postulated[8,13,26]. Likewise an elevation of cytosolic calcium ion levels may be causally related to the inhibition of net transport of sodium and of the hydro-osmotic response to vasopressin, observed in amphibian tight epithelia, on exposure to low serosal sodium concentrations[5,12,27]. We conclude that cytosolic Ca ion activity, regulated in part through a process of Na–Ca exchange across the basolateral cell membrane, may be important in the physiological regulation of sodium and water absorption by these epithelial tissues.

We thank Dr W. Simon for providing the neutral calcium ligand. This study was supported by NIH grants, USPHS HL 21136, AM 11489 and AM 19022.

Received 3 June; accepted 29 August 1980.

1. Scarpa, A. & Carafoli, E. (eds) *Ann. N.Y. Acad. Sci.* **307**, 1–655 (1978).
2. Taylor, A. *Fedn Proc.* **34**, 285 (1975).
3. Wiesmann, W., Sinha, S. & Klahr, S. *J. clin. Invest.* **59**, 418–425 (1977).
4. Ludens, J. H. *J. Pharmac. exp. Ther.* **206**, 414–422 (1978).
5. Grinstein, S. & Erlij, D. *Proc. R. Soc.* **B202**, 353–360 (1978).
6. Nielsen, R. J. *Membrane Biol.* **40**, 331–345 (1978).
7. Balaban, R. S. & Mandel, L. J. *Biochim. biophys. Acta* **555**, 1–12 (1979).
8. Figueiredo, J. F., Maack, T., Friedmann & Windhager, E. E. *Proc. 7th int. Congr. Nephrol.* Montreal, C-11 (1978).
9. Blaustein, M. P. *Rev. physiol. biochem. Pharmac.* **70**, 33–82 (1974).
10. Ullrich, K. J., Rumrich, G. & Klöss, S. *Pflügers Arch. ges. Physiol.* **364**, 223–228 (1976).
11. Gmaj, O., Murer, H. & Kinne, K. *Biochem. J.* **178**, 549–557 (1979).
12. Taylor, A., Eich, E. & Pearl, M. *Proc. 27th int. Congr. physiol. Sci.*, Paris 745 (1977).
13. Taylor, A. & Windhager, E. E. *Am. J. Physiol.* **236**, (6) F505–F512 (1979).
14. Giebisch, G. *J. gen. Physiol.* **44**, 659–678 (1961).
15. Boulpaep, E. L. in *Symp. Medical Hoechst. Electrophysiology of Epithelial Cells* (ed. Giebisch, G.) 31–118 (Schattauer, New York, 1970).
16. Windhager, E. E. *Micropuncture Techniques and Nephron Function* 90–92, 122 (Butterworths, London, 1968).
17. Boulpaep, L. E. *A. Rev. Physiol* **38**, 20–36 (1976).
18. Brown, H. H., Pemberton, J. P. & Owen, J. D. *Analyt. chim. Acta* **85**, 261–276 (1976).
19. Christoffersen, G. R. J. & Simonsen, L. *Acta physiol. scand.* **101**, 492–494 (1977).
20. Ashley, C. C., Rink, T. J. & Tsien, R. Y. *J. Physiol., Lond.* **280**, 27P (1978).
21. Simon, W., Ammann, D., Oehme, M. & Morf, W. E. *Ann. N.Y. Acad. Sci.* **307**, 52–70 (1978).
22. Sokol, H. H., Lee, C. O. & Lupo, F. J. *Biophys. J.* **25**, 143a (1979).
23. Spring, K. R. & Kimura, G. *Fedn Proc.* **38**, 2729–2732 (1979).
24. Rink, T. J., Tsien, R. Y. & Warner, A. E. *Nature* **283**, 658–660 (1980).
25. Berry, C. A. & Boulpaep, E. L. *Am. J. Physiol.* **228**, 581–595 (1975).
26. Friedman, P. A., Figueiredo, J. F., Maack, T. & Windhager, E. E. *Fedn Proc.* **38**, 1241 (1979).
27. Taylor, A., Eich, E., Pearl, M. & Brem, A. in *Hormonal Control of Epithelial Transport* 167–174, (INSERM, Paris, 1979).
28. Buttler, J. N. in *Ionic Equilibrium, A Mathematical Approach*, 428–468 (Addison-Wesley, Reading, Massachusetts, 1964).
29. Moore, E. W. & I. Ross, J. W. *J. appl. Physiol.* **20**, 1332–1336 (1965).
30. Schonhorn, H. & Gregor, H. P. *J. Am. chem. Soc.* **83**, 3576–3579 (1961).

Evidence for an adaptive DNA repair pathway in CHO and human skin fibroblast cell lines

Leona Samson & Jeffrey L. Schwartz

Laboratory of Radiobiology, University of California, San Francisco, San Francisco, California 94143

When *Escherichia coli* is chronically exposed to very low, nontoxic doses of a monofunctional alkylating agent (notably *N*-methyl-*N'*-nitro-nitrosoguanidine, MNNG), the adaptive DNA repair pathway is induced which enables the bacteria to resist the killing and mutagenic effects of further alkylation damage[1–3]. Mutation resistance in adapted bacteria is achieved, at least partly, by a greatly increased capacity of the cells to eliminate the minor DNA alkylation product O^6-methylguanine[4–6], which has been strongly implicated as premutagenic[7,8] and precarcinogenic[9]. We now show that the chronic treatment of a Chinese hamster ovary (CHO) and a SV40-transformed human skin fibroblast (GM637) cell line with non-toxic levels of MNNG renders the cells resistant to the induction of sister chromatid exchange (SCE) by further alkylation damage. CHO cells also become resistant to killing (GM637 cells have not yet been tested). Having ruled out explanations such as changes in cell cycle distribution, mutagen permeability and mutagen detoxification, we conclude that resistance is probably achieved by the cells becoming more efficient at repairing alkylation damage, analogous to the adaptive response of *E. coli*[1].

The existence of an inducible error-free mammalian DNA repair pathway, like adaptation, could significantly affect our approach to assessing the mutagenic and carcinogenic risk of chemicals in our environment. Chronic treatment of rats with the alkylating agent dimethylnitrosamine (DMN) has been reported to enable the livers of these animals specifically to avoid the accumulation of O^6-methylguanine[10,11]. Paradoxically, chronic DMN treatment is much more carcinogenic to the rat liver than a single high dose[12]. However, chronic DMN exposure also induces intense liver cell proliferation, which might obscure the role of the O^6-methylguanine lesion in hepatocarcinogenesis[10]. Thus, although there seems to be a biochemical analogue of adaptation in the rat liver, its biological effects such as carcinogenesis, cell killing and mutation, are either obscured or cannot be quantified. The aim of our study was, therefore, to determine whether adaptation can be observed in established mammalian cell lines which would be potentially much more versatile than the rat liver system.

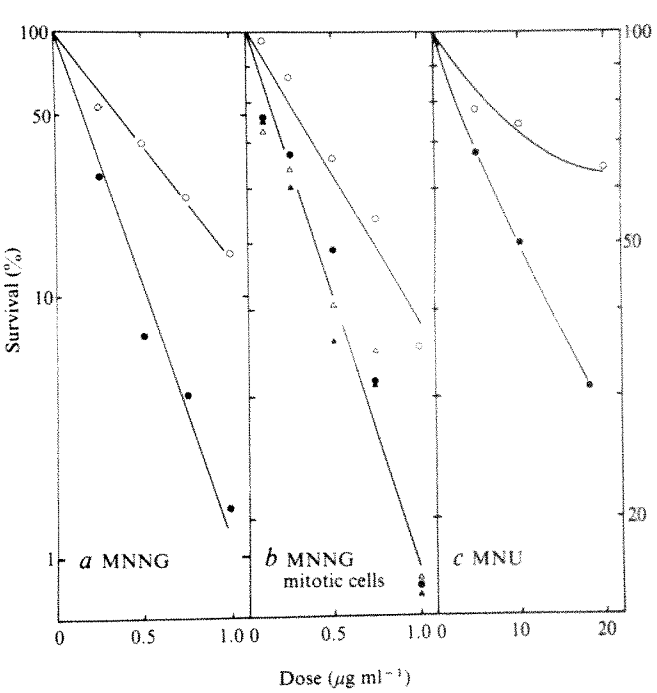

Fig. 1 The effect of MNNG pretreatment on the survival of CHO cells challenged with MNNG or MNU. Cells were grown for 48 h in Ham's F12 medium supplemented with 5% fetal calf serum, penicillin (100 U ml^{-1}), streptomycin (100 μg ml^{-1}) and L-glutamine (0.03%). Every 6 h, one set of cultures was treated with 0.01 μg ml^{-1} MNNG. Three hours after the final pretreatment dose, pretreated (○) and control (●) cells were either trypsinized (*a* and *c*) or synchronized by mitotic shake-off (*b*) and then plated into 100-mm Petri dishes. Each dish was challenged with either MNNG (0–1.0 μg ml^{-1}) or MNU (0–20 μg ml^{-1}). To measure the decay of resistance, cells that had been pretreated for 48 h (△) were grown for a further 24 h before mitotic shake-off and challenge (▲, 72 h control). After 10 days at 37 °C, the cultures were fixed and stained. Colonies were counted in duplicate dishes.

As an initial approach we have used cell survival and SCE as our endpoints. The bacterial studies had shown that the adaptive response could only be observed when both the low dose used to adapt the cells and the high challenge dose used to estimate the degree of resistance fell within critical boundaries[2,13]. Thus, to ensure the greatest chance of detecting adaptation in mammallian cells, a wide range of doses would have to be tested. As SCE induction has been correlated with mutation induction by simple alkylating agents[14] and with the persistence of O^6-methylguanine lesions in certain cell lines[15], we chose this far less time-consuming assay.

MNNG has a reported half life of between 14 min (ref. 16) and 80 min (ref. 17) in cell culture medium. Consequently, the

0028–0836/80/440861—03$01.00

nearest one can get to continuously exposing cells to MNNG is to deliver multiple doses over a prolonged period. (Only the most successful of several dose regimes tested will be dealt with here.) CHO cells received 0.01 μg ml^{-1} MNNG once every 6 h for 48 h. Pretreated and control cells were then challenged with various MNNG doses up to 100 times this concentration, and the resulting cell killing measured. At each challenge dose pretreated cells survived better than control cells, with about a twofold difference in the slopes of the survival curves (Fig. 1*a*, *b*). Similarly, CHO and GM637 cells that had been pretreated for 48 h and 72 h, respectively, were very resistant to the SCE-inducing effects of MNNG. Resistance to both killing (Fig. 1*b*) and SCE induction (Figs 2*a*, 3*a*) decayed when pretreatment was stopped.

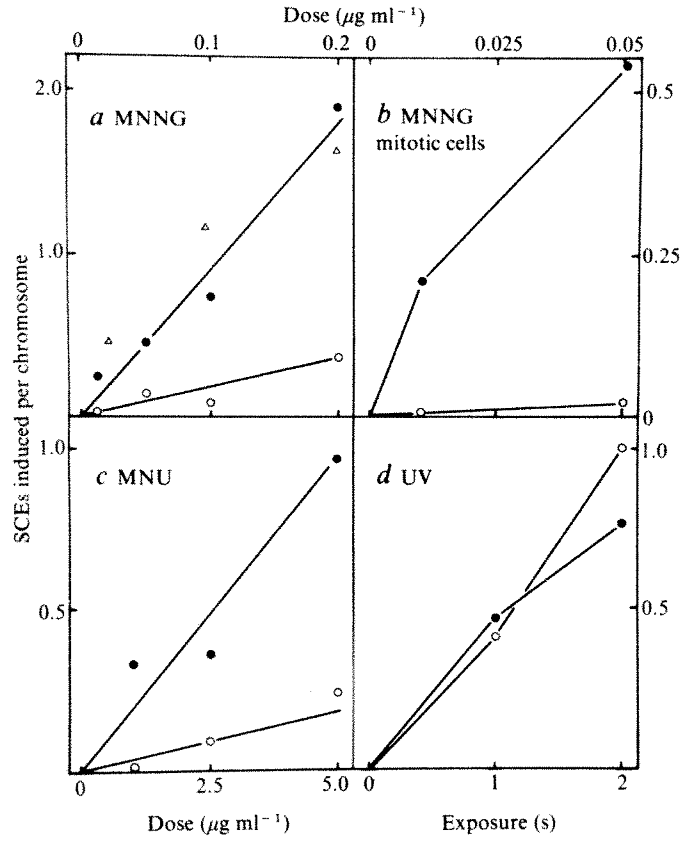

Fig. 2 The effect of MNNG pretreatment of CHO cells on the induction of SCEs. Cells were cultured as described in Fig. 1 legend. At 3 h (○) or 24 h (△) after the final adapting dose, pretreated (○, △) and control (●) cells were challenged with MNNG (0–0.2 μg ml^{-1}), MNU (0–5 μg ml^{-1}) or UV light (0–2 s, fluence rate 12 erg mm^{-2} s^{-1}), and then cultured for two rounds of DNA replication (26 h) in complete medium containing 10 μM bromodeoxyuridine. Colcemid (2×10^{-7} M) was present for the final 2 h. Mitotic cells were collected by shaking, treated with 0.075 M hypotonic KCl, then fixed in 3:1 methanol/glacial acetic acid. SCEs were differentiated by a modified fluorescence-plus-Giemsa technique[23], and at least 20 cells were counted per point. Induced SCEs were calculated by subtracting background levels (0.35–0.5 for control, 0.85–1.0 for pretreated cells) from the total SCE values.

Because the sensitivity of CHO cells to MNNG fluctuates throughout the cell cycle[18], a change in cell cycle distribution could generate an apparent change in the sensitivity of the overall population. However, pretreated and control CHO cells have approximately the same mitotic indices (1.25% and 1.4%, respectively) and proceed through the cell cycle at similar rates (Fig. 4*a*). Moreover, a cell cycle redistribution cannot account for increased MNNG resistance in CHO cells because homogeneous populations of mitotic cells also display differential sensitivity to MNNG killing (Fig. 1*b*) and SCE induction (Fig. 2*b*). An extended period in G1 might account for the observed increase in MNNG resistance[19], but G1 was shown to be the same in pretreated and control populations that had been challenged with 0.5 μg ml^{-1} MNNG (Fig. 4*b*).

We considered that resistance to MNNG could be achieved either by preventing alkylation from taking place or by dealing with alkylation damage more efficiently. As alkylation by MNNG is thiol stimulated, a reduction in cellular thiol levels could inhibit alkylation by this agent[17]. However, thiol depletion cannot explain our results because MNNG-pretreated cells were also found to be resistant to two alkylating agents which are unaffected by cellular thiol levels[20]; CHO cells were resistant to killing (Fig. 1*c*) and SCE induction (Fig. 2*c*) by methylnitrosourea (MNU) and GM637 cells were resistant to SCE induction by MNU (fig. 3*b*) and ethylnitrosourea (ENU) (Fig. 3*c*). Moreover, pretreatment does not alter the permeability of the cells to mutagen, because, for both CHO and GM637, the DNA purified from control and pretreated cultures that had been exposed to 2.5 μg ml^{-1} ^{3}H-MNU (120 Ci mol^{-1}) had similar specific activities. We therefore deduce that chronic MNNG exposure enables both CHO and GM637 cells to handle alkylation damage somewhat more efficiently and so become resistant to alkylating agents. This resistance seems to be specific for alkylation damage because MNNG-pretreated cells are not resistant to the induction of SCE by UV light (Figs 2*d*, 3*d*).

Thus, the response of two mammalian cell lines during continuous low-dose exposure to the carcinogen MNNG has, so far, exactly paralleled *E. coli* adaptation: a treatment which neither kills cells nor disturbs cell growth induces a resistance to alkylation damage, but not UV damage which decays once treatment is stopped. Furthermore the induced resistance in

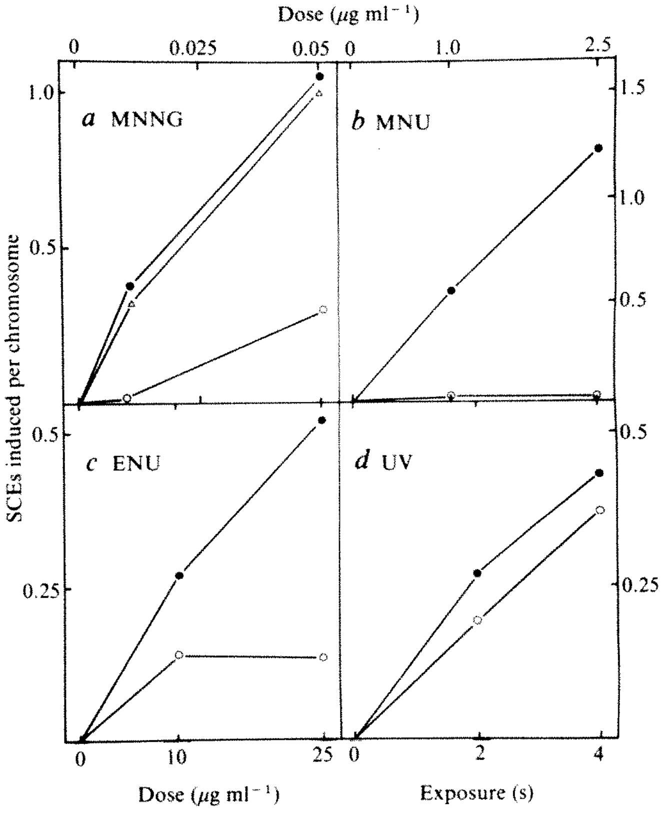

Fig. 3 The effect of MNNG pretreatment of GM637 cells on the induction of SCEs. GM637 cells were grown in minimum essential medium supplemented with 15% fetal calf serum, penicillin (100 U ml^{-1}), streptomycin (100 μg ml^{-1}), and L-glutamine (0.03%). Cells were treated and analysed as described in Figs 1 and 2 legends, except that the pretreatment regime lasted 72 h. The background SCE values were 0.26 SCEs per chromosome for controls (●) and 0.34 SCEs per chromosome for pretreated cells (○, △). Recovery (△) was measured 1 week after the final pretreatment.

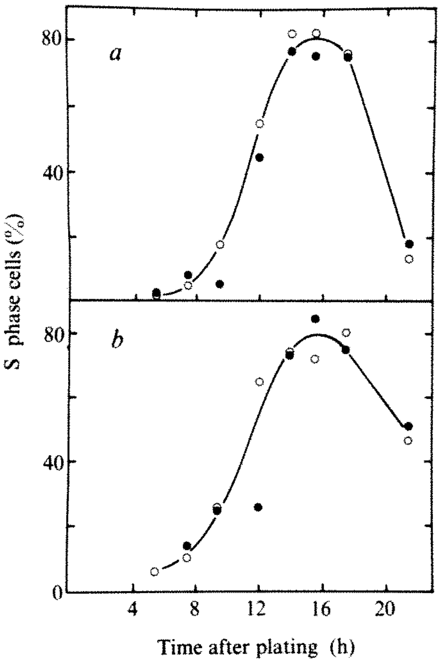

Fig. 4 The effect of MNNG pretreatment on the onset of DNA replication in synchronized CHO cells. Cells were pretreated as described in Fig. 1 legend. Three hours after the final adapting dose, pretreated (○) and control (●) cells were collected by mitotic shake-off (the mitotic index was about 0.95). Half of each group of cells were challenged with 0.5 $\mu g\, ml^{-1}$ MNNG (*b*), the other half remained unchallenged (*a*). The cells were plated into tissue culture slide chambers at a density of 10^3 cells per cm^2. At various times after plating, one set of slides was pulse labelled for 20 min with 10 $\mu Ci\, ml^{-1}$ ^3H-thymidine, then washed and fixed for autoradiography. For each data point 150–350 cells were counted.

mammalian cells becomes saturated at high challenge doses (GM637, Fig. 3*a*; CHO data not shown) with the same biphasic kinetics seen in bacteria[13]. It is improbable that our results could be attributed to the inducible error-prone DNA repair pathway reported to exist in mammalian cells because this pathway can act on UV damage[21,22]. However, it is not yet known whether the induced resistance to the killing and SCE-inducing effects of alkylating agents is accompanied by resistance to their mutagenic effects.

We thank John Cairns, James Cleaver, Regine Goth-Goldstein, Robert Painter and Sheldon Wolff for their interest and helpful advice, and Peter Tattersall for supplying the CHO cell line. L.S. was supported by a SRC postdoctoral fellowship, and the work was supported by the US Department of Energy.

Received 27 May; accepted 13 August 1980.

1. Samson, L. & Cairns, J. *Nature* **267,** 281–283 (1977).
2. Jeggo, P., Defais, M., Samson, L. & Schendel, P. *Molec. gen. Genet.* **157,** 1–9 (1977).
3. Jeggo, P., Defais, M., Samson, L. & Schendel, P. *Molec. gen. Genet.* **162,** 299–305 (1978).
4. Schendel, P. F. & Robins, P. E. *Proc. natn. Acad. Sci. U.S.A.* **75,** 6017–6020 (1978).
5. Robins, P. & Cairns, J. *Nature* **280,** 74–76 (1979).
6. Karran, P., Lindahl, T. & Griffin, B. *Nature* **280,** 76–77 (1979).
7. Loveless, A. *Nature* **223,** 206–207 (1969).
8. Gerchman, L. L., Ludlum, D. B. *Biochim. biophys. Acta* **308,** 310–316 (1973).
9. Goth, R. & Rajewsky, M. F. *Proc. natn. Acad. Sci. U.S.A.* **71,** 639–643 (1974).
10. Montesano, R., Bresil, H. & Margison, G. P. *Cancer Res.* **39,** 1798–1802 (1979).
11. Montesano, R., Bresil, H., Planche-Martel, G., Margison, G. P. & Pegg, A. E. *Cancer Res.* **40,** 452–458 (1980).
12. *IARC Monographs on the Evaluation of the Carcinogenic Risk of Chemicals to Humans* Vol. 1, 95–106 (International Agency for Research on Cancer, Lyon, 1972).
13. Schendel, P. F., Defais, M., Jeggo, P., Samson, L. & Cairns, J. *J. Bact.* **135,** 466–475 (1978).
14. Carrano, A. V., Thompson, L. H., Lindl, P. A. & Minkler, J. L. *Nature* **271,** 551–553 (1978).
15. Wolff, S., Rodin, B. & Cleaver, J. E. *Nature* **265,** 347–349 (1977).
16. Jensen, E. M., LaPolla, R. J., Kirby, P. E. & Haworth, S. R. *J. natn. Cancer Inst.* **59,** 941–944 (1977).
17. Lawley, P. D. & Thatcher, C. J. *Biochem. J.* **116,** 693–707 (1970).
18. Barranco, S. C. & Humphrey, R. M. *Mutat. Res.* **11,** 421–429 (1971).
19. MacRae, W. K. MacKinnon, E. A. & Stich, H. F. *Chromosoma* **72,** 15–22 (1979).
20. Wheeler, G. P. & Bowdon, B. J. *Biochem. Pharmac.* **21,** 265–267 (1972).
21. DasGupta, U. B. & Summers, W. C. *Proc. natn. Acad. Sci. U.S.A.* **75,** 2378–2381 (1978).
22. Sarasin, A. & Benoit, A. *Mutat. Res.* **70,** 71–81 (1980).
23. Wolff, S. & Rodin, B. *Science* **200,** 543–545 (1978).

Ca^{2+}-calmodulin-dependent phosphorylation and platelet secretion

Masakatsu Nishikawa, Toshio Tanaka & Hiroyoshi Hidaka

Department of Pharmacology, Mie University School of Medicine, Edobashi, Tsu 514, Japan

Protein phosphorylation may play a critical role in stimulus-coupled secretion of platelets. Some platelet proteins become phosphorylated on exposure to agents such as thrombin and collagen[1–5], and the smallest of these phosphoproteins (molecular weight 20,000), has been identified as a light chain of myosin[6–8]. Phosphorylation of myosin light chain increases the activity of actin-activated myosin ATPase[8] and the resultant contraction of the actomyosin presumably mediates the release reaction[6,9]. Platelet myosin light chain kinase has been identified as a calcium-dependent enzyme requiring calmodulin for its activity[10,11]. Calmodulin is a Ca^{2+}-binding protein with a molecular weight of ~18,000 which seems to be involved in a wide variety of cellular processes[12]. Although a growing body of evidence suggests that non-muscle actomyosin, such as that isolated from platelets, is regulated by Ca^{2+}-calmodulin-dependent light chain phosphorylation, the precise relationship between the phosphorylation and the function of platelets is not clearly established. We now present pharmacological evidence that a calmodulin-mediated system, such as Ca^{2+}-dependent myosin light chain phosphorylation, also plays an important role in the phenomenon of the release reaction. *N*-(6-aminohexyl)-5-chloro-1-napthalene-sulphonamide (W-7) (refs 13–15) is shown to bind selectively to calmodulin *in vitro* and inhibit its biological activity.

The effects of the calmodulin-interacting agent W-7 on human platelet aggregation and the ATP release induced by collagen (2 $\mu g\, ml^{-1}$), ADP (2 μM) and thrombin (0.1 $U\, ml^{-1}$)

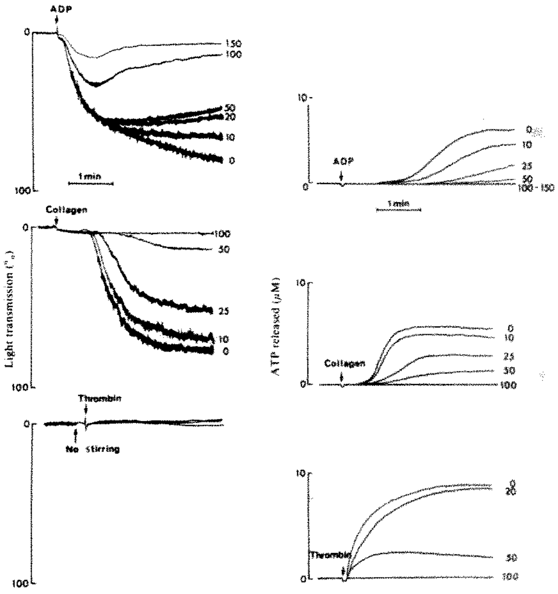

Fig. 1 Effect of W-7 on platelet aggregation and secretion induced by ADP (2 μM), collagen (2 $\mu g\, ml^{-1}$) or thrombin (0.1 $U\, ml^{-1}$). Secretion of ATP (right-hand traces) was measured by the firefly luminescence assay method and aggregation (left-hand traces) was determined simultaneously in the same cuvette turbidimetrically. The stirring motor was turned off to prevent aggregation in the experiment involving platelet stimulation by thrombin. The standard platelet reaction mixtures consisted of 0.4 ml of citrated platelet-rich plasma (PRP), 50 μl of Chrono-Lumi luciferase luciferin reagent, 50 μl of a dilution of W-7 (in saline), and aggregating agent. In experiments involving platelet activation by thrombin, 0.4 ml of washed platelet suspension ($4.0 \times 10^8\, ml^{-1}$) was used in place of PRP. The platelets were preincubated without (0) or with W-7 (the final concentration shown in μM by each curve) for 3 min before stimulation.

0028-0836/80/440863—03$01.00

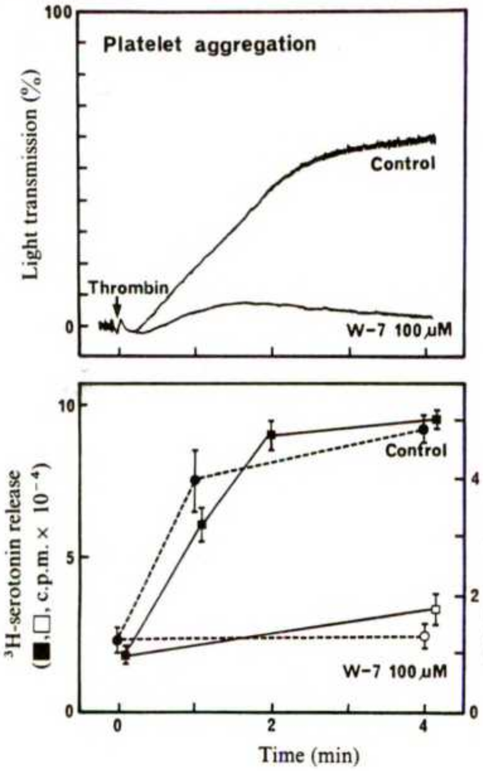

Fig. 2 Time course of platelet aggregation (top), and ^{3}H-serotonin release and 20,000-MW MLC phosphorylation (bottom) in response to thrombin (0.25 U ml^{-1}) amd the effect of W-7 (final concentration 100 μM) preincubation. Serotonin secretion and phosphorylation are shown as means ± s.e.m. ($n = 3$) ■, □, ^{3}H-serotonin release; ●, ○, MLC phosphorylation. Open symbols, W-7 100 μM; closed symbols, controls. *Method*: Human platelets suspension in 20 mM Tris-HCl pH 7.4, 150 mM NaCl, 0.1% glucose, 0.35% bovine serum albumin was incubated with ^{32}P-orthophosphate at 1 mCi ml^{-1} for 30 min at 25 °C. ^{3}H-serotonin creatinine sulphate at 1 μCi ml^{-1} was added, and the platelets suspension was incubated for another 30 min, then spun at 600g for 5 min and the supernatant discarded. The pellets were resuspended in the same buffer to give a platelet count of 5–10 × 10^8 per ml. The platelet reaction mixtures consisted of 1.8 ml of labelled platelets suspension, 0.2 ml of saline (control) or W-7 (concentration 100 μM) and thrombin (0.25 U ml^{-1}). The platelets were preincubated with saline or W-7 in the aggregometer (Rikadenki) for 3 min before stimulation with thrombin. The reaction was terminated with 1 ml of ice-cold 150 mM NaCl, 10 mM EDTA, 0.8 mM phenylmethylsulphonyl fluoride (PMSF), soybean trypsin inhibitor (0.2 mg ml^{-1}), then spun at 1,200g for 10 min at 4 °C. Samples of supernatant fluid (1 ml) were removed immediately and transferred into liquid scintillation vials. 10 ml of ACS II (Amersham) was added and the sample counted in a Beckman scintillation counter. Platelet pellets were frozen and extracted with a high ionic strength buffer containing 0.5 M KCl, 20 mM K_2PO_4 pH 7.4, 1 mM EGTA, 0.4 mM PMSF. The insoluble material was removed by centrifugation at 150,000g for 20 min at 4 °C. Each extract was electrophoresed on 1% SDS 10% polyacrylamide gel. The gels were stained with Coomassie brilliant blue, and photographed. ^{32}P content of 20,000-MW protein was determined by liquid scintillation counting of 2-mm gel slices.

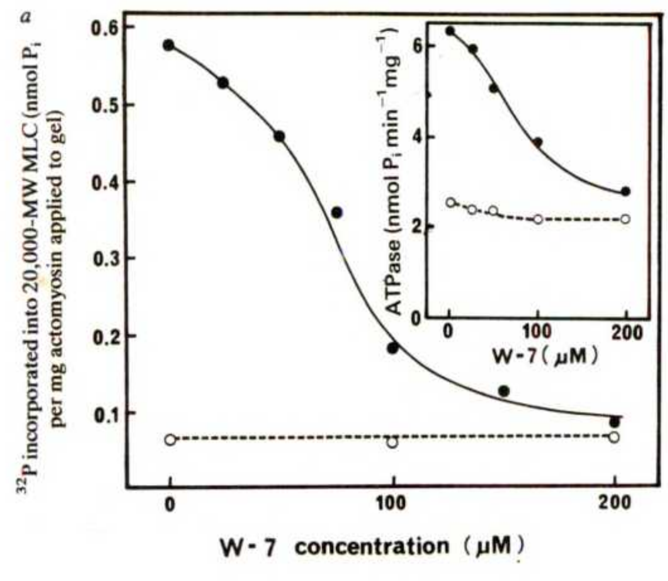

Fig. 3 *a*, Inhibition by W-7 of endogenous phosphorylation of the 20,000-MW MLC and actomyosin ATPase activity (inset) from human platelets in the presence of 100 μM Ca^{2+}(●) and in the presence of 2 mM EGTA (○). *b*, 8 M urea-gel electrophoresis (left) and its autoradiography (right) for detecting phosphorylation of the 20,000-MW MLC of platelet actomyosin. 1, Ca^{2+} 100 μM; 2, Ca^{2+} 100 μM + W-7 50 μM; 3, Ca^{2+} 100 μM + W-7 100 μM; 4, Ca^{2+} 100 μM + W-7 200 μM; 5, EGTA 2 μM. a, The unphosphorylated 20,000-MW MLC; a′, the phosphorylated 20,000-MW MLC. *Phosphorylation analyses*: The reactions were carried out at 25 °C for 10 min in 200 μl of reaction mixture containing 20 mM Tris-HCl pH 7.5, 125 mM KCl, 10 mM $MgCl_2$, 0.5 mM [γ-^{32}P]ATP (2 μCi per tube), platelet actomyosin (1.5 mg ml^{-1}), various concentrations of W-7, and 100 μM $CaCl_2$ or 2 mM EGTA. The reactions were initiated by the addition of ATP and terminated by the addition of 20 μl of 5% SDS containing 0.1 M 2-mercaptoethanol and 20% sucrose, *a*, The solution containing 60 μg protein was applied to SDS-polyacrylamide gel and electrophoresis was carried out using 10% acrylamide and 100 mM sodium phosphate buffer (pH 7.2). The gels were then stained with Coomassie brilliant blue, photographed and sliced into 2-mm portions from which the radioactivity was eluted. ^{32}P radioactivity was analysed by liquid scintillation spectrometer. *b*, Urea polyacrylamide slab gel electrophoresis was carried out by the method of Perrie *et al.*[18], using 10% polyacrylamide, 8 M urea, and 25 mM Tris-150 mM glycine buffer, pH 8.6. Samples of 60 μg of protein were applied to the gel. The gel was run, stained, destained and prepared for autoradiography. *ATPase assay*: ATPase activity was determined in 600 μl of medium containing 50 mM Tris-malate buffer pH 7.0, 50 mM KCl, 10 mM $MgCl_2$, 1 mM ATP, platelet actomyosin (0.4 mg ml^{-1}), various concentrations of W-7, and either 2 mM EGTA or 100 μM $CaCl_2$. Incubations were carried out for 30 min at 35 °C. The reaction was stopped by the addition of trichloroacetic acid to a final concentration of 10%. Inorganic phosphate was measured by the method of Allen[21].

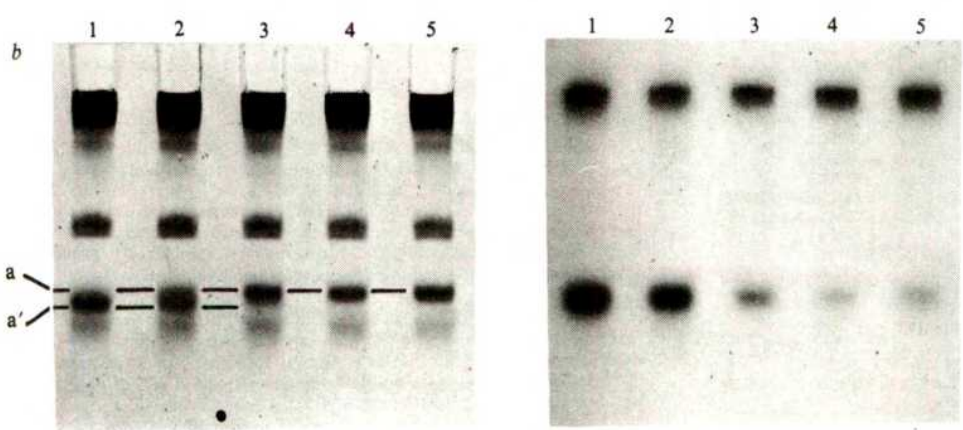

were studied in a Model 400 Lumi-aggregometer (Chrono-Log.), which simultaneously monitors aggregation and release of ATP[16,17]. A typical result is shown in Fig. 1. W-7 inhibited dose-dependently collagen-induced ATP release and aggregation. Two distinct phases of ADP-induced aggregation were evident and the inhibition by W-7 of the first phase was weaker than that of the second. The second phase of aggregation associated with ATP release was inhibited dose-dependently by W-7. Similar results were obtained when aggregation was induced by adrenaline, arachidonic acid or thrombin. When thrombin was added to the platelet suspension without stirring, ATP release occurred but there was no aggregation (Fig. 1). W-7 inhibited dose-dependently this thrombin-induced secretion of ATP, suggesting that the drug also inhibits stimulus-coupled secretion processes in platelets. W-7 had no effect on thrombin hydrolytic activity at concentrations as high as 200 μM.

To examine the effect of W-7 on protein phosphorylation in platelet aggregation and the release reaction, protein phosphorylation in platelets was measured by prelabelling with ^{32}P-orthophosphate and ^{3}H-serotonin and treating the stirred suspension of platelets with thrombin (0.25 U ml^{-1}). The platelet pellet formed after thrombin treatment was used for extraction of phosphorylated protein with a high ionic strength buffer, as described by Daniel *et al.*[6], and the supernatant was used for the assay of serotonin. Thrombin treatment of intact ^{32}PO$_4$-loaded platelets resulted in a four- to fivefold increase in phosphorylation of the 20,000-MW protein, when a high ionic strength extract was directly electrophoresed on SDS-polyacrylamide gel. The pattern of ^{32}P incorporation was similar to that described by Daniel *et al.*[6]. This 20,000-MW phosphoprotein was identified as the myosin light chain (MLC) by 8 M urea slab polyacrylamide gel electrophoresis[18]. The phosphorylated MLC migrates slightly faster than the unphosphorylated MLC in this electrophoresis system. The change in ^{32}P content of MLC correlated with the increased secretion of ^{3}H-serotonin rather than aggregation, as shown in Fig. 2. W-7 (100 μM) inhibited both the phosphorylation of 20,000-MW MLC and serotonin release from platelets.

We examined the effect of W-7 on calcium-dependent ^{32}P incorporation into the 20,000-MW MLC from [γ-^{32}P]ATP which constitutes the Ca^{2+}-sensitive regulatory mechanism of actin–myosin interaction. An actomyosin-rich fraction containing endogenous myosin light chain kinase and calmodulin (~50 units per mg protein) was prepared from human platelets by a modification of the method of Hathaway and Adelstein[11]. ^{32}P incorporation into the 20,000-MW MLC from [γ-^{32}P]ATP was observed in the presence of calcium ions (100 μM), and addition of EGTA to 2 mM inhibited ^{32}P incorporation into the MLC, indicating that this phosphorylation of MLC depends on calcium ions (Fig. 3*a*). Increasing the concentration of W-7 inhibited selectively the Ca^{2+}-dependent phosphorylation of the 20,000-MW MLC with an IC$_{50}$ value of 80 μM, as shown in Fig. 3*a*. Moreover, W-7 produced a concentration-dependent inhibition of Ca^{2+}-dependent ATPase of platelet actomyosin (IC$_{50}$ 100 μM) but did not inhibit Ca^{2+}-independent ATPase. Figure 3*b* demonstrates that the light chains of myosin have a greater electrophoretic mobility than other platelet proteins and that the Ca^{2+}-dependently phosphorylated 20,000-MW MLC migrates slightly faster than unphosphorylated MLC. Dose-dependent inihibition by W-7 of Ca^{2+}-dependent MLC phosphorylation was also demonstrated by using this urea gel electrophoretic analysis.

Calmodulin interacting agents such as W-7, N^{2}-dansyl-L-arginine-4-*t*-butylpiperidine amide (No. 233) and chlorpromazine inhibit Ca^{2+}-calmodulin-dependent enzymes, for example, myosin light chain kinase[14,15], cyclic nucleotide phosphodiesterase[13,19] and erythrocyte Ca^{2+}, Mg^{2+}-ATPase[20]. The pharmacological effects of calmodulin-interacting agents on platelets result from a combination of several types of molecular interactions and cannot be explained by a single mechanism. However, one of the important effects of calmodulin-interacting agents is the inhibition of calmodulin-dependent MLC phosphorylation. Our findings indicate that there is a calmodulin-mediated regulatory system in platelets similar to that in smooth muscle tissue. The calmodulin-interacting agent W-7 could be of interest clinically as it combines antithrombotic activity with vascular relaxant activity.

This work was supported in part by grant 448114 from the Ministry of Education, Science and Culture, Japan. We thank Y. Sasaki for his assistance and M. Ohara for criticism of the manuscript. W-7 was a gift from Banyu Pharmaceutical Co.

Received 13 May; accepted 13 August 1980.

1. Haslam, R. J. & Lynham, J. A. *Biochem. biophys. Res. Commun.* **77,** 714–721 (1977).
2. Haslam, R. J., Lynham, J. A. & Fox, J. E. B. *Biochem. J.* **178,** 397–406 (1979).
3. Lyons, R. M. & Atherton, R. M. *Biochemistry* **18,** 544–552 (1979).
4. Lyons, R. M. & Shaw, J. O. *J. clin. Invest.* **65,** 242–255 (1980).
5. Wallace, W. C. & Bensusan, H. B. *J. biol. Chem.* **255**, 1932–1937 (1980).
6. Daniel, J. L., Holmsen, H. & Adelstein, R. S. *Thromb. Haemostas.* **38,** 984–989 (1977).
7. Adelstein, R. S., Conti, M. A. & Barylko, B. *Thromb. Haemostas.* **40,** 241–244 (1978).
8. Adelstein, R. S. & Conti, M. A. *Nature* **256,** 597–598 (1975).
9. Lebowitz, E. A. & Cooke, R. *J. biol. Chem.* **253,** 5443–5447 (1978).
10. Dabrowska, R. & Hartshorne, D. J. *Biochem. biophys. Res. Commun.* **85,** 1352–1359 (1978).
11. Hathaway, D. R. & Adelstein, R. S. *Proc. natn. Acad. Sci. U.S.A.* **76,** 1653–1657 (1979).
12. Wolff, D. I. & Brostrom, C. O. *Adv. Cyclic Nucleotide Res.* **11,** 27–88 (1979).
13. Hidaka, H., Yamaki, T., Totsuka, T. & Asano, M. *Molec. Pharmac.* **15,** 49–59 (1979).
14. Hidaka, H., Naka, M. & Yamaki, T. *Biochem. biophys. Res. Commun.* **90,** 694–699 (1979).
15. Hidaka, H. *et al. Molec. Pharmac.* **17,** 66–72 (1980).
16. Feinman, R. D., Lubowsky, J., Charo, I. F. & Zabinske, M. *J. Lab. clin. Med.* **90,** 125–129 (1977).
17. Charo, I. F., Feinman, R. D. & Detwiler, T. C. *J. clin. Invest.* **60,** 866–873 (1977).
18. Perrie, W. T., Smillie, L. B. & Perry, S. V. *Biochem. J.* **135,** 151–164 (1973).
19. Levin, R. M. & Weiss, B. *Molec. Pharmac.* **12,** 581–589 (1976).
20. Kobayashi, R., Tawata, M. & Hidaka, H. *Biochem. biophys. Res. Commun.* **88,** 1037–1045 (1979).
21. Allen, R. J. L. *Biochem. J.* **34,** 858–865 (1940).

Optical properties of single elastin fibres indicate random protein conformation

B. B. Aaron & J. M. Gosline

Department of Zoology, The University of British Columbia,
2075 Wesbrook Mall, Vancouver BC, Canada V6T 1W5

In describing the properties of fibrous proteins it has been common practice to attribute the macroscopic mechanical properties to the organization at the molecular level. Hence, the high tensile stiffness of collagen and silk has been viewed as an inevitable consequence of their crystalline structure. For elastin, however, there has been considerable controversy and confusion in assigning a conformation to this rubber-like protein. The mechanical and thermodynamic properties of elastin are consistent with the kinetic theory of rubber elasticity[1–5], and this theory is based on an isotropic network of kinetically free, random-coil molecules. In contrast, numerous electron microscope studies of negatively stained elastins obtained by autoclave and alkali purification, as well as coacervates of the various soluble elastins, reveal a highly ordered (anisotropic) structure, consisting of 3- to 5-nm filaments that apparently run parallel to the long axis of elastin fibres[6–11]. These filaments have been accepted as evidence for an anisotropic molecular structure in elastin that is dramatically different from the random network of the kinetic theory. We have now used polarized light microscopy to distinguish these two types of structure. We find that both purified and unpurified, water-swollen, single elastin fibres are optically isotropic, in agreement with the predictions of the kinetic theory of rubber elasticity.

Polarized light microscopy is a useful technique because unlike electron microscopy it does not require any physical modification of the protein structure, and thus it reduces the chance of procedural artefacts. Further, the technique allows the evaluation of structure at two levels of organization: (1) at the molecular level as reflected by the intrinsic birefringence, and (2) at the submicroscopic level (that is, at the level of the 3- to 5-nm filaments) as indicated by the form birefringence. A

0028-0836/80/440865—03$01.00

general discussion of these types of birefringence is given by Bennet[12].

If elastin is totally isotropic, then this should result in a lack of both intrinsic and form birefringence. On the other hand, if elastin consists of isotropic filaments at the submicroscopic level, then it should exhibit an observable form birefringence. Finally, if these filaments are anisotropic at the molecular level, as is proposed in the anisotropic model of Urry[13], then there should be an intrinsic birefringence as well as a form birefringence. The determination of birefringence for test samples that are swollen in media of differing refractive index allows one to distinguish and quantify form and intrinsic birefringence[12]. Similar studies on collagen[14] and chitin[15] attest to the reliability of this type of analysis.

Single 6- to 8-μm elastin fibres were isolated from untreated bovine ligamentum nuchae and from ligament that had been purified by repeated autoclaving[16]. The fibres were viewed between crossed polarizers on a Wild M-21 polarizing microscope, and the retardation was determined at 546 nm using a Zeiss 1/30 wavelength rotary compensator. Birefringence was calculated by dividing the retardation at the centre of the fibre by the fibre diameter. The form birefringence curves were obtained from measurements on single elastin fibres and rat-tail collagen fibres swollen in liquids of known refractive index.

Both purified and unpurified single elastin fibres show an apparent positive birefringence of about 2×10^{-4} when swollen in distilled water ($n_m = 1.33$; see Fig. 1, solid square). The fact that autoclaved fibres show the same optical properties as unpurified ones argues strongly against the creation of any structural artefacts by this purification procedure. To put this low value of birefringence into perspective, curve *a* in Fig. 1 shows the birefringence expected for a system of parallel, isotropic cylindrical fibres swollen in a fluid medium of different refractive index, as predicted by an approximation of the Weiner equation derived by Stokes[17]. The volume fraction of the fibres ($v_f = 0.65$) used in this calculation has been selected to reflect the known water content of elastin and thus to provide a reasonable description of elastin structure if protein filaments separated by watery spaces actually exist. Clearly the birefringence of water-swollen elastin is many times smaller than the birefringence expected for a system of isotropic filaments.

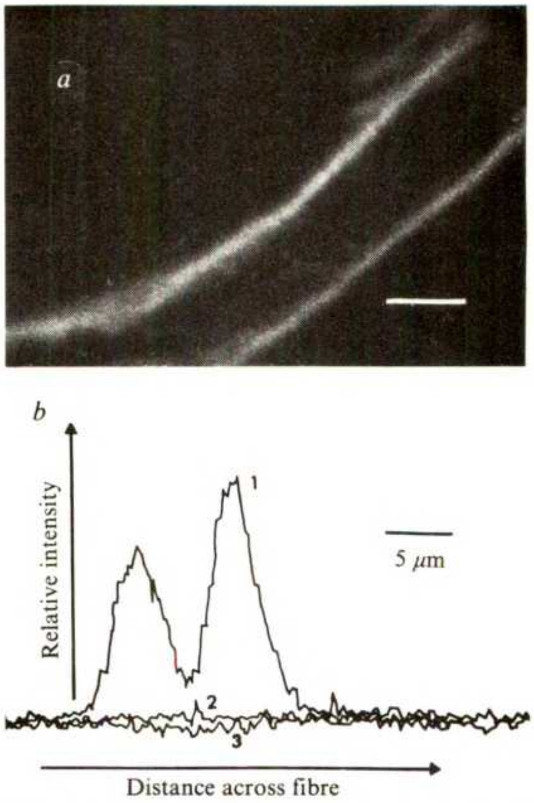

Fig. 2 *a*, Single elastin fibre ($n_f = 1.55$) in water ($n_m = 1.33$) photographed between crossed polarizers. Scale bar, 5 μm. *b*, Typical densitometer tracings for negatives of: 1, single elastin fibre in water; 2, water-swollen elastin fibre in immersion oil ($n = 1.52$); 3, control tracing of blank field.

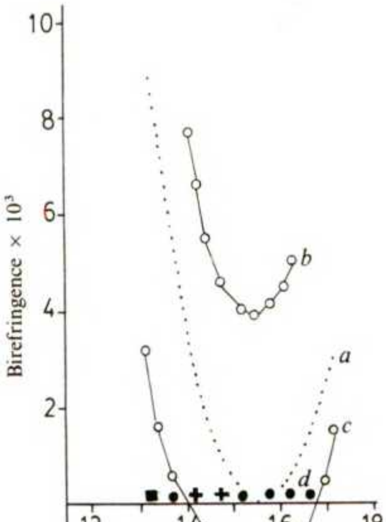

Fig. 1 (■) Birefringence of single, water-swollen elastin fibres, 2.5×10^{-4}. (●) Birefringence values for dry single elastin fibres immersed in organic liquids of different refractive index varying from $n_m = 1.36$ to 1.65. (+) Birefringence values measured for single elastin fibres swollen in ethelene glycol ($n_m = 1.43$) and glycerol ($n_m = 1.47$). Elastin swollen in these liquids retains its elastic properties. *Curve a*, Theoretical form birefringence for a system of parallel isotropic cylinders[17]: $B_F = (n_f - n_m)^2 v_f(1-v_f)/\bar{n}$, where B_F is the form birefringence, n_f and n_m are the refractive index of the fibre (1.55) and the medium (1.33 for water) respectively, with $\bar{n}$ being the value of their mean. v_f is the volume fraction of the fibres (0.65) (ref. 4). *Curve b*, Rat-tail tendon collagen fibres. *Curve c*, tannic acid-fixed collagen fibres[14].

If the small residual birefringence is actually inherent to the fibre, then one would expect the retardation to be proportional to the optical path length through the fibre and should therefore be highest at the centre of the fibre. Figure 2*a* shows a water-swollen elastin fibre (refractive index of elastin, $n_f \simeq 1.55$; refractive index of water, $n_m = 1.33$) between crossed polarizers. It is clear that the retardation, as indicated by the intensity, is greatest at the edges of the fibre. This suggests that the apparent birefringence at the centre of the fibre is not a property of the fibre itself, but results from the refractive index difference at the fibre–water interface. When this refractive index difference is reduced by suspending water swollen elastin fibres in immersion oil ($n = 1.52$) this apparent retardation virtually disappears (see the densitometer tracings in Fig. 2*b*). In fact the intensity (retardation) is indistinguishable from the background, suggesting that the true birefringence of elastin is actually zero or at least immeasurably small. We believe that this anomalous retardation created by the water–fibre interface is what has been measured by other workers[7] who have reported very high birefringence values for water-swollen elastin.

Although elastin appears to be completely isotropic, the possibility exists that the zero total birefringence is due to the summing of a positive form birefringence that is just equal to a negative intrinsic birefringence. This possibility is demonstrated in Fig. 1 for collagen fibres and tannic acid-fixed collagen fibres[14]. Collagen fibres, which are known to be anisotropic at both the molecular and the submicroscopic levels, show both positive form and positive intrinsic birefringence (Fig. 1, curve *b*). Tannic acid fixation reverses the sign of the intrinsic birefringence, and as a result of this, tannic acid-fixed fibres 'appear' to be isotropic (that is, show zero total birefringence) at n_m = 1.40 and n_m = 1.67 (Fig. 1, curve *c*). That the lack of birefringence in single elastin fibres does not occur as a result of this phenomenon is confirmed by the fact that elastin fibres swollen in a variety of solvents over a broad range of n_m show the same small birefringence as water-swollen fibres (Fig. 1, curve *d*). Thus, elastin shows neither intrinsic nor form birefringence, indicating an isotropic structure at both the molecular and the submicroscopic levels.

In conclusion, the extremely low residual birefringence values and the absence of any form birefringence leads us to believe that elastin does in fact possess a random conformation at the molecular level, similar to other known elastomeric materials. Although these data do not preclude the possibility that elastin contains randomly oriented filaments, there is clearly no evidence for the existence of the highly ordered, 3- to 5-nm filaments visualized by negative staining techniques in the electron microscope. We suspect that the filamentous organization seen for elastin may well be the result of drying elastin in the presence of the heavy-metal salts used for negative staining. It is also possible, however, that these filaments are cellulose contaminants, as suggested previously[18–20]. It is our opinion that the 120-nm subfibres which have been observed in the scanning electron microscope[21] are large enough to accommodate an isotropic random network structure, and thus are not in conflict with the idea of elastin being a typical kinetic rubber. However, the lack of form birefringence for elastin fibres suggests that these subfibres may only be due to a rough surface texture of the 6-μm fibres and may not extend through the entire thickness of the fibre. This interpretation is consistent with the appearance of elastin fibres seen in cross-section in the transmission electron microscope[22].

This research was supported by grants from the British Columbia Heart Foundation and the Canadian Natural Sciences and Engineering Research Council to J.M.G.

Received 16 April, accepted 11 August 1980.

1. Hoeve, C. A. J. & Flory, P. J. *Biopolymers* **13**, 677–686 (1974).
2. Dorrington, K., Grut, W. & McCrum, N. G. *Nature* **255**, 476–478 (1975).
3. Dorrington, K. & McCrum, N. G. *Biopolymers* **16**, 1201–1222 (1977).
4. Gosline, J. M. *Biopolymers* **17**, 677–695 (1978).
5. Volpin, D. & Ciferri, A. *Nature* **225**, 382 (1970).
6. Quintarelli, G., Bellocci, M. & Zito, R. *Histochemie* **37**, 49–60 (1973).
7. Serafini-Fracassini, A., Field, J. M. & Spina, M. *J. molec. Biol.* **100**, 73–84 (1976).
8. Serafini-Fracassini, A., Field, J. M. & Hinnie, J. *J. Ultrastruct. Res.* **65**, 190–193 (1978).
9. Gotte, L., Giro, M. G., Volpin, D. & Horne, R. W. *J. Ultrastruct. Res.* **46**, 23–33 (1974).
10. Cox, B., Starcher, B. & Urry, D. W. *J. biol. Chem.* **249**, 997–998 (1974).
11. Cleary, E. G. & Cliff, W. J. *Expl molec. Path.* **28**, 227–246 (1978).
12. Bennett, H. S. in *McClung's Handbook of Microscopical Techniques* 3rd edn (ed. McClung Jones, R.) 591 (Hoeber, New York, 1950).
13. Urry, D. W. in *Perspectives in Biology and Medicine* Vol. 21, 265 (University of Chicago Press, 1978).
14. Pfeiffer, H. H. *Arch. exp. Zellforschung* **25**, 92–98 (1943).
15. Diehl, J. M. & Iterson, G. *Kolloid Z.* **73**, 142–146 (1935).
16. Partridge, S. M., Davis, H. V. & Adair, G. S. *Biochem. J.* **61**, 11–21 (1955).
17. Stokes, A. R. *The Theory of the Optical Properties of Inhomogeneous Materials* (Spon, London, 1963).
18. Millward, G. R. *J. Cell Biol.* **42**, 317 (1969).
19. Fraser, R. D. B. in *Proceedings of the First Cleveland Symposium on Macromolecules* (ed. Walton, A. G.) (Elsevier, New York, 1977).
20. Fraser, R. D. B., Jones, L. N., MacRae, T. P., Suzuki, E. & Tulloch, P. A. in *Biomolecular Structure, Conformation, Function and Evolution* (ed. Srinivasan, R.) (Pergamon, Oxford, in the press).
21. Hart, M. L., Boydler, S. A. & Carnes, W. H. *Scanning Electron Microscopy* **2**, 21–25 (1978).
22. Ross, R. & Bornstein, P. *J. Cell Biol.* **40**, 366–381 (1969).

Motile flagellar axonemes with a 9+1 microtubule configuration

S. Marchese-Ragona & M. E. J. Holwill

Physics Department, Queen Elizabeth College, Campden Hill Road, London W8 7AH, UK

Electron microscope (EM) studies of the eukaryotic flagellum reveal that the organelle contains a 9+2 arrangement of microtubules, the axoneme, with nine doublets surrounding two singlets enveloped by a membrane which is continuous with that of the cell; various linkages and projections are associated with the microtubules[1]. Strong experimental evidence supports the idea that the forces required for bend formation on eukaryotic flagella are derived from active relative sliding of the peripheral doublets[2,3]. Dynein arms, which project from each peripheral microtubule and possess ATPase activity, interact with a neighbouring doublet and undergo conformational changes which induce sliding[4,5]. To form and propagate coordinated bends along a flagellum the sliding must be resisted in a controlled manner by structures within the axoneme. The regulatory mechanism responsible for the control of interdoublet sliding is not known in detail, but ultrastructural studies[6] suggest that interactions between the radial spokes attached to each doublet and the central complex of the axoneme may be involved. We report here the treatment of flagella with a 9+2 microtubular structure from the trypanosomid flagellate *Crithidia oncopelti* to produce motile axonemes with only one central microtubule. We conclude that the complete central complex is not involved in the conversion of microtubule sliding into axonemal bending, but may be both associated with the control of wave propagation and essential for bend initiation.

Cells from a 5–6-day old culture of *Crithidia* were demembranated by exposure to detergent using a procedure similar to that described by Holwill and McGregor[7], except that the chelating agents EGTA and EDTA were omitted from all solutions. Samples were removed from a particular preparation at periods of 1 min, 1 h and 4 h for structural examination by electron microscopy and for motility studies following reactivation with ATP. Samples were reactivated at room temperature on a microscope slide by gently mixing a drop containing demembranated cells with a roughly equal volume of reactivating solution containing 1 mol m^{-3} ATP. Reactivated cells were examined in a Zeiss WL Research microscope with stroboscopic illumination.

Structural studies of reactivated and non-reactivated cells were undertaken after an incubation period of 1 h; because no structural differences between the two preparations were detected, subsequent samples for electron microscopy were prepared without the addition of ATP. Transverse sections of axonemes were examined at the three sampling times specified above and classified according to the pattern of microtubules remaining. Four distinct categories could be recognized: 9+2, 9+1, 9+0 and A-microtubules held together in cylindrical arrays, presumably by nexin links (Fig. 1). The proportions of axonemes falling into these classes are presented in Table 1.

We have not established unequivocally which of the two central microtubules is removed first during the extraction process, but results obtained for other organisms suggest that it is probably CM3, as this microtubule is chemically less stable than CM8 (ref. 8). Because of their importance in motility the number of dynein arms in a section was determined and expressed as a percentage of the total expected. In practice, only the outer arms were scored, as these were solubilized before the inner arms and were easier to visualize. The results of these counts are presented in Table 1.

In assessing motility, only those cells which were propagating coherent bends were scored as motile; organelles with an oar-like or a local bending movement were considered to be non-motile. The proportions of motile cells observed in a typical experiment are shown in Table 1. In all cases, wave propagation was from base to tip, with the beat pattern similar to that described by Holwill and McGregor[7]. There were no major differences between the wave shapes displayed by flagella of a given sample, as judged by visual examination of the sample, but the beat frequency of motile cells was generally observed to

0028-0836/80/440867—03$01.00

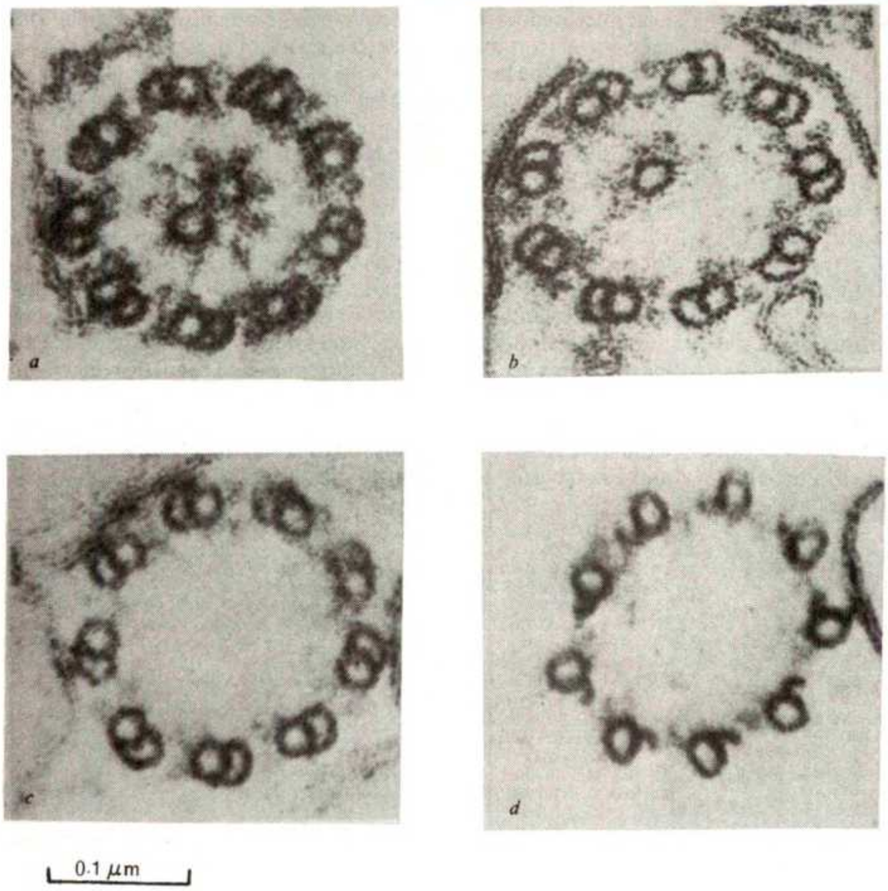

Fig. 1 Transverse sections of detergent-treated axonemes of *Crithidia oncopelti* showing the changes in microtubule arrangement which occur during degradation. *a*, Intact 9 + 2 axoneme; *b*, axoneme with one central microtubule missing; *c*, axoneme with both central microtubles missing; *d*, cylinder of A-microtubules. Membrane removal was performed at a ratio of 1 mg of cell protein (measured by the method of Lowry *et al.*[17]) to 1.0 cm^3 of 0.1% detergent solution, and the demembranated cells were incubated at 0 °C. The incubation periods for the axonemes represented by the sections shown were 1 h for *a* and *b* and 4 h for *c* and *d*. In preparation for electron microscopy, cells were fixed in 2.5% glutaraldehyde in phosphate buffer at room temperature, post-fixed in 1% osmium tetroxide, dehydrated and embedded in Spurr resin.

decrease with time. A detailed study of bend patterns is planned to determine whether subtle shape changes occur which may be attributed to variations in the axonemal structure.

Of particular interest in correlating structure with motility are the results obtained after 1 h of incubation. Whereas 83.2% of the sample was motile, only 15% of the axonemes examined had a 9 + 2 microtubular configuration. A large percentage of the axonemes with the 9 + 1 structure was therefore propagating bends at this time. After 4 h, the proportion of 9 + 1 axonemes in a sample is similar to that after 1 h, but the percentage motility has fallen by about 70. This decrease cannot be due to the 7% reduction in the number of dynein arms present at the later time, but could be due to a loss of functional integrity in these structures.

The fact that the axonemes with a disrupted central complex are capable of propagating bends leads to the question of whether any of the central complex is necessary for wave propagation. That 9 + 0 flagella may have been non-motile in the present study does not mitigate against this possibility, for structures other than the central complex could have been removed, without detection, during the treatment period, and this could be responsible for the lack of movement.

Although this is the first report of an axoneme which remains capable of activity after removal of a central microtubule, reports of undulating flagella with 9 + 0 (ref. 9), 6 + 0 (ref. 10) and 3 + 0 (ref. 11) microtubule configurations also indicate that central structures are not essential for movement. It may also be relevant that some insect spermatozoa have no central microtubules and yet are motile[12,13]; however, these spermatozoa have accessory components in addition to the nine doublets so that observations on these cells do not provide strong evidence that a cylinder of doublet microtubules alone is capable of coordinated bending activity.

That the integrity of the central complex may be important for motility is indicated by experiments on *Chlamydomonas* mutants which lack one or both of the central microtubules and seem to be incapable of bend formation and propagation[14,15]. Treatment of both mutant and wild-type flagella with trypsin, followed by ATP, induced identical disintegration processes which involved relative sliding of the peripheral microtubules, thus indicating that the dynein arms of the mutant organelles are able to generate shearing forces. Further observations which suggest that the central microtubules are necessary for bending movement have been made recently by Afzelius and Eliasson[16], who reported that spermatozoa from a man suffering from situs inversus lacked one of the central microtubules of the axoneme

Table 1 Results from a typical experiment to investigate motility of demembranated flagella of *Crithidia oncopelti*

	Microtubule configurations and associated outer dynein arms (D)* (%)									Sample size	
Incubation time (min)	9 + 2	D	9 + 1	D	9 + 0	D	A-cylinders	D	Motile cells (% + s.d.)	No. of EM sections	No. of cells observed in light microscope
1	79.2	100	19.5	100	0.0	—	1.3	0	93.9 ± 1.2	77	412
60	15	90.5	79.3	86.6	4.7	0	0.9	0	83.2 ± 2.3	213	286
240	4.0	93.3	78	79.6	9	48.9	9	0.8	13.9 ± 2.1	90	280

* The values for the outer dynein arms are percentages of the total expected for that particular microtubule configuration.

and were immotile, and by Baccetti, Pallini, Mazzini and Ranieri (personal communication), who find that human sperm lacking both central microtubules are immotile.

The motile properties of the 9+1 axonemes of *Crithidia* reported here are not shared by axonemes with a similar structure from *Chlamydomonas* mutants, which are characterized by paralysis. A possible explanation for the different behaviour observed in the two cases is that features other than the central complex which are important for motility are affected in the mutant system. Changes in such features may be too subtle for detection by electron microscopy, as can be seen from the results presented here for axonemes at 1 and 4 h. The 9+1 cross-sections prepared from both samples appeared identical, but, when the number of other microtubule patterns are allowed for, it is clear that some of the 9+1 sections taken at 4 h are from non-motile flagella.

The data relating to microtubule arrangement presented in Table 1 can be interpreted in two ways: either (1) the percentages quoted represent the sample fraction in which each flagellum in its entirety has a particular structure, or (2) each flagellum in a sample contains a particular microtubule configuration for the appropriate percentage of its length. For example, at 1 h, interpretation (1) would have 15% of the sample with a 9+2 arrangement and 79.3% with a 9+1 arrangement, whereas according to interpretation (2), 15% and 79.3%, respectively, of each flagellum would have the 9+2 and 9+1 configurations. We have attempted to distinguish between the two alternative interpretations by electron microscopic studies of sections and of whole mounts, but our results are inconclusive. For example, serial sections taken over a portion of the axoneme 350–450 nm long (about 2% of the total axoneme length) were examined for 15 organelles with the 9+1 structure and all were found to have the same appearance.

Whichever of the two structural interpretations is correct, it is clear that coordinated waves can be propagated by an axoneme with a disrupted central complex, so that the conversion into bending moments of the shearing forces developed by the sliding peripheral microtubules is probably not achieved through interactions between the radial spokes and the central complex. This conversion could be accomplished if, as is thought to be the case, microtubules are associated with structures at the flagellar base which prevent their free relative sliding.

From a purely mechanical viewpoint, therefore, bend propagation could occur in the absence of any interaction between the peripheral and central microtubules. The interaction between these structures which seems to occur in the *in vivo* 9+2 flagellum may therefore be associated with the control of wave propagation (perhaps in determining the direction of bend propagation or the plane of bending in *Crithidia*) and not be involved directly in the mechanics of the conversion of sliding into bending.

If each axoneme contains a varying microtubule pattern (interpretation (2)), it seems reasonable to suppose that degradation of the axoneme occurs in an ordered manner, say from the flagellar tip, so that the axoneme shows progressive structural deficiency from base to tip. One possible interpretation of our results would then be that the full 9+2 complement of microtubules is required for bend initiation (as all bend propagation was from the base), but that bend propagation can be maintained by regions of the axoneme with 9+1 or, possibly, 9+0 microtubule arrangements. This situation could explain the difference in behaviour between *Crithidia* flagella and the *Chlamydomonas* or sperm mutants, which presumably have the 9+1 configuration along their entire length. On this interpretation, the results presented here suggest that a minimum length (between 4% and 15%) of the axoneme should contain the 9+2 arrangement of microtubles for successful bend initiation to occur.

S.M.-R. thanks the SRC for a CASE award with Unilever, where some of the electron microscopy described here was performed. This work was supported in part by a research grant awarded by the SRC to M.E.J.H.

Received 17 June; accepted 10 September 1980.

1. Warner, F. D. in *Cilia and Flagella* (ed. Sleigh, M.A.) 11–37 (Academic, London, 1974).
2. Satir, P. in *Cilia and Flagella* (ed. Sleigh, M.A.) 131–142 (Academic, London, 1974).
3. Summers, K. E. & Gibbons, I. R. *Proc. natn. Acad. Sci. U.S.A.* **68,** 3092–3096 (1971).
4. Satir, P. in *The Spermatozoon: Maturation, Motility, Surface Properties and Comparative Aspects* (eds Fawcett, D. W. & Bedford, J. M.) 81–90 (Urban & Scharzenberg, Baltimore, 1979).
5. Zanetti, N. C., Mitchell, D. R. & Warner, F. D. *J. Cell Biol.* **80,** 573–588 (1979).
6. Warner, F. D. & Satir, P. *J. Cell Sci.* **12,** 313–326 (1973).
7. Holwill, M. E. J. & McGregor, *J. exp. Biol.* **65,** 229–242 (1976).
8. Jacobs, M., Hopkins, J. M. & Randall, J. *Proc. R. Soc.* **B173,** 61–82 (1968).
9. Baccetti, B., Burrini, A. G., Dallai, R. & Pallini, V. *J. Cell Biol.* **80,** 334–340 (1979).
10. Schrével, J. & Besse, C. *J. Cell Biol.* **66,** 492–507 (1975).
11. Prensier, G., Vivier, E., Goldstein, S. & Schrével, J. *Science* **207,** 1493–1494 (1980).
12. Philips, D. M. in *Cilia and Flagella* (ed. Sleigh, M. A.) 379–402 (Academic, London, 1974).
13. Baccetti, B. *Adv. Insect Physiol.* **9,** 315–397 (1972).
14. Witman, G. B., Fay, R. & Plummer, J. in *Cell Motility* (eds Goldman, R., Rosenbaum, J. & Pollard, T.) 969–986 (Cold Spring Harbor Laboratory, New York, 1975).
15. Witman, G. B., Plummer, J. & Sander, G. *J. Cell Biol.* **76,** 729–747 (1978).
16. Afzelius, B. A. & Eliasson, R. *J. ultrastruct. Res.* **69,** 43–52 (1979).
17. Lowry, D. H., Rosebrough, N. J., Farr, A. L. & Randall, R. J. *J. biol. Chem.* **193,** 265–275 (1951).

Expression of a transposable antibiotic resistance element in *Saccharomyces*

Antonio Jimenez* & Julian Davies

Department of Biochemistry, College of Agricultural and Life Sciences,
University of Wisconsin-Madison, Madison, Wisconsin 53706

Some eukaryotic genes can be expressed in bacteria but there are few examples of the expression of prokaryotic genes in eukaryotes[1]. Antibiotic G418 is a 2-deoxystreptamine antibiotic that is structurally related to gentamicin[2] but has inhibitory activity against a much wider variety of pro- and eukaryotic organisms. In bacteria, resistance to G418 can be determined by several plasmid-encoded modifiying enzymes[3] and, in view of the broad spectrum of activity of G418, we considered that this antibiotic might be useful as a selective agent for the introduction of these antibiotic resistance genes into a eukaryotic organism such as *Saccharomyces cerevisiae*. Additional impetus for these experiments came from the knowledge that certain of the G418-resistance determinants in bacteria are carried on transposable elements[4]; a study of the properties of these elements in eukaryotes would be intriguing.

We have transformed *S. cerevisiae* spheroplasts[5] with a mixture of DNA of the yeast *leu*2 cloning vector pYE13 (ref. 6) and a colicin E1 derivative (pA043) carrying the transposable element Tn*601(903)*[4]. The latter encodes aminoglycoside phosphotransferase-3′(I) (APH(3′)-I) that phosphorylates and inactivates a number of aminoglycoside antibiotics containing the 2-deoxystreptamine moiety, at the 3′-hydroxyl position. We chose to use co-transformation with pYE13 and pA043 because selection of the leu$^+$ phenotype provided a control for efficiency of transformation, and in addition, we anticipated that subsequent recombination would lead to the formation of a hybrid plasmid. Following regeneration, prototrophic transformants were selected and screened for resistance to G418; the frequency of resistant transformants was about 8% of the leu$^+$ progeny. The G418-resistant colonies were capable of growth in the presence of $>1\ \mathrm{mg\ ml^{-1}}$ antibiotic. The untransformed parent, or strains transformed with the yeast vector pYE13 alone, were sensitive to low concentrations of G418 (Fig. 1). In separate experiments we have shown that *S. cerevisae* mutants resistant to low levels of G418 ($150\ \mu\mathrm{g\ ml^{-1}}$) appear spontaneously at low frequency ($<10^{-5}$) and that this frequency is drastically diminished ($<10^{-7}$) when one selects for higher resistance levels ($500\ \mu\mathrm{g\ ml^{-1}}$) of G418, as assayed by plating on media containing the antibiotic.

The presence of APH(3′)-I activity in these transformants would show that the G418 resistance was due to the expression

---

* Permanent address: Instituto de Bioquimica de Macromoleculas, Madrid, Spain.

Table 1 Substrate specificity for the APH(3')I activity from G418-resistant yeast transformant

	c.p.m.	
Antibiotic tested	Yeast (JG13) extract	*E. coli* extract
Neomycin B	5,617 (100)	18,652 (100)
Lividomycin A	5,767 (102)	26,262 (140)
Butirosin	1,389 (25)	5,078 (27)
Tobramycin	353 (6)	30 (0)
G418	3,163 (56)	4,364 (23)

S. cerevisiae transformant JG13 was grown at 30 °C in 200 ml YEPD medium containing 200 μg ml^{-1} G418 to a density of 7×10^7 cells ml^{-1}. Cells were washed with water, resuspended in 0.7 ml 50 mM Tris-HCl, *p*H 7.6, 12.5 mM $MgCl_2$, 80 mM KCl, 1 mM dithiothreitol (DTT) buffer and disrupted by passing through a French pressure cell at 18,000 p.s.i. Cell extracts were centrifuged at 150,000 *g* for 2 h and the supernatant (0.5 ml) was passed through a Sephadex G-200 column (32 × 1.5 cm) using 10 mM Tris-HCl, *p*H 7.4, 10 mM $MgCl_2$, 1 mM DTT, 400 mM NaCl buffer. APH(3')-I activity eluted at a position corresponding to a protein of molecular weight ~60,000. *E. coli* KH802 carrying the plasmid pA043 was grown in 200 ml ML medium (1% tryptone, 1% NaCl, 0.5% yeast extract) to an A_{550} of 0.75. Cells were centrifuged, washed with saline, resuspended in 0.7 ml 10 mM Tris-HCl, *p*H 7.6, 1 mM $MgCl_2$, 0.15 mM EDTA and then disrupted as described above. The extract was centrifuged for 2.5 h at 150,000 *g* and the supernatant used as a source of APH(3')-I enzyme. APH(3')-I from the yeast transformant JG13 was assayed in 102-μl incubation mixtures containing, 14 mM Tris-HCl, *p*H 7.5, 32 mM NH_4Cl, 323 mM NaCl, 11.5 mM $MgCl_2$, 0.1 mM Na_2EDTA, 1 mM DTT, 0.06 mM [γ-^{32}P]ATP (Amersham, specific activity 10 Ci mol^{-1}), 80 μl of the peak fraction and 20 μg of the relevant aminoglycoside antibiotic. APH(3')-I from *E. coli* was assayed in 32-μl incubation mixtures containing 9 mM Tris-HCl, *p*H 7.1, 6 mM $MgCl_2$, 53 mM NH_4Cl, 0.2 mM DTT, 0.1 mM Na_2EDTA, 0.06 mM [γ-^{32}P]ATP, 60 μg ml^{-1} of the relevant antibiotic and 10 μl of *E. coli* KH802/pA043 extract. Reactions were incubated at 30 °C for 15 min and then 90- or 25-μl samples (for yeast or *E. coli* extracts, respectively) were spotted onto P-81 Whatman paper, washed with water and counted as described previously[7].

of the Tn*601(903)* gene. Accordingly, cell-free extracts from sensitive and resistant transformants were prepared and tested for their content of the enzyme using standard assay procedures[7]; the extracts were passed through Sephadex G200 before assay to remove ATPase activity that may limit the extent of aminoglycoside phosphorylation. Chromatography of extracts of G418-resistant transformants gave a peak of strong phosphotransferase activity. The substrate range of this enzyme activity corresponded to that of a typical APH(3')-I (Table 1). No such enzymatic activity could be detected in extracts of untransformed controls. Thus, we conclude that the phosphotransferase encoded on the element Tn*601(903)* can be introduced and expressed in yeast.

As confirmation of this we have established that G418-resistant transformants contain Tn*601(903)* sequences. Total cellular DNA was isolated from parental and transformed yeast strains, electrophoresed in an 0.7% agarose gel and transferred to nitrocellulose sheets according to the method of Southern[8]. The transferred DNA was hybridized to ^{32}P-labelled λ :: Tn*601* and pBR322 probe. As shown in Fig. 2*a*, the former probe, which has no homology with yeast, colicin E1, or pYE13 DNA, hybridizes specifically to DNA isolated from G418-resistant transformants.

Table 2 Stability of the G418-resistant phenotype in Tn*601* yeast transformants

	% No. of colonies			
Growth medium	YEPD	YEPD +G418	Minimal	Minimal +Leu
YEP	100 (340)	44 (150)	52 (176)	97 (330)
YEP + G418	100 (222)	70 (156)	73 (162)	96 (216)
Minimal	100 (316)	50 (158)	62 (196)	99 (312)
Minimal + leucine	100 (386)	61 (234)	67 (250)	108 (416)

Strain JG13 was grown for 10 generations in either YEPD or YEPD + 125 μg ml^{-1} G418 or for five generations in either minimal medium (0.76% Difco yeast nitrogen base w/o amino acids supplemented with 40 μg ml^{-1} histidine) or minimal supplemented with 40 μg ml^{-1} leucine. Serial dilutions of these cultures were plated onto selective media; numbers in parentheses represent total colonies scored on each medium.

The position of the sequences homologous to Tn*601* in the transformants is coincident with that of sequences hybridizing to pBR322 (Fig. 2*b*), which suggests that the transposable element Tn*601* is present in a hybrid pA043/pYE13 molecule. The intensity and the relative positions of hybridization of Tn*601* and pBR322 to DNA from JG13 and JG16 suggest that the putative chimaeras in the two transformants differ.

The G418 resistance of the yeast transformants is lost on growth in the absence of antibiotic (Table 2); this loss occurs at approximately the same frequency as loss of the leu^+ character encoded by pYE13, which suggests that *leu2* and Tn*601(903)* are associated. As confirmation of this, we have isolated recombinant pYE13/pA043 plasmid DNA from yeast transformants JG13 and JG16 and have used them for transformation of both *S. cerevisiae* and *Escherichia coli*, selecting either for leucine prototrophy or directly for resistance to G418. The plasmid DNAs from the two sources show differences in restriction digestion patterns, in agreement with the results of hybridization studies (A. J., unpublished observations).

The introduction of a bacterial resistance gene into yeast (as a transposable element) by direct selection of G418 resistance following transformation, raises some interesting possibilities for further study: (1) The control and expression of bacterial genes in eukaryotes; the use of the antibiotic modifying enzymes allows a simple assay for gene expression and could be used for the isolation of eukaryotic promoter sequences. (2) The expression and possible function of transposable elements: Tn5, for example, encodes aminoglycoside modification and several functions required for its own transposition[9]. It will be of interest to determine if these recombination capacities can operate in yeast and other eukaryotes. (3) G418 is an antibiotic with wide range inhibitory activity; it is a potent inhibitor of protein synthesis in cell-free extracts of bacterial, fungal, algae, plant and animal cells (S. Perzynski, unpublished). The combination of this antibiotic with any one of several bacterial resistance determinants should provide useful selection procedures for universal cloning vectors. Although, in principle, any of these

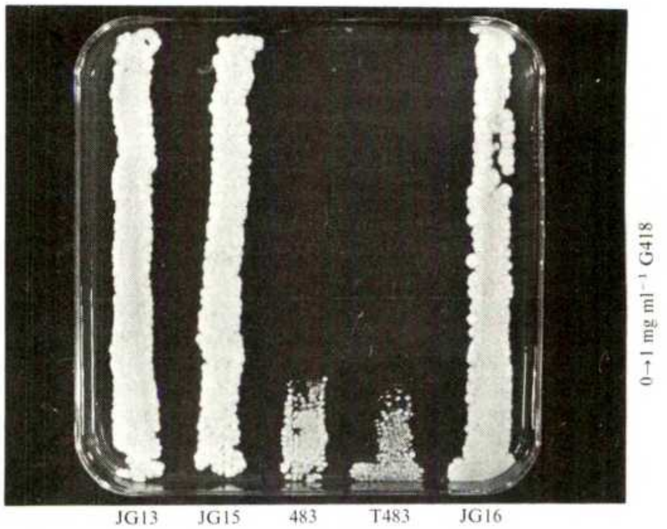

Fig. 1 Growth on G418 gradient plates of parental and transformed yeast strains. *S. cerevisiae* strain 483 (a, *leu2-3 leu2-112, his4, can1* was transformed as described by Hinnen *et al.*[5], using a mixture of 20 μg ml^{-1} each of pA043 (a Tn*601*-miniColE1 plasmid) and pYE13 (ref. 6) (a yeast-cloning vector containing the *leu2* gene), selecting for leucine prototrophy[5]. After 5 days incubation at 30 °C leu^+ transformants were streaked on YEPD plates containing 125 μg ml^{-1} G418 to screen for co-transformation of resistance to G418. About 8% of the leu^+ prototrophs were resistant to the drug. To examine levels of resistance, colonies were resuspended in YEPD medium at a density of 2×10^7 per ml and streaked onto an agar plate containing a gradient of antibiotic G418 from 0 to 1,000 μg ml^{-1}. JG13, JG15 and JG16 are G418-resistant co-transformants; T483 is the pYE13-transformed 483 strain and 483 is the *leu2-3* parental *S. cerevisiae* yeast strain used in the present work.

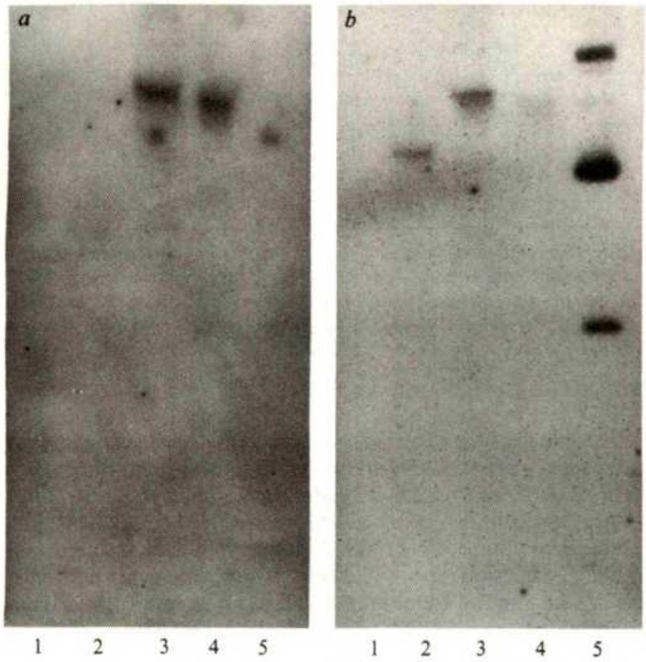

Fig. 2 Hybridization of total yeast DNA to ^{32}P-labelled (λ :: Tn*601* (*a*) and pBR322 (*b*) DNA probes. Yeast strains 483 (1) and T483 (2) were grown in YEPD medium and strains JGI3 (3) and JGI6 (4) were grown in YEPD medium containing 150 μg ml^{-1} G418. DNA was extracted from yeast spheroplasts, treated with α-amylase, pronase, pancreatic RNase and extracted with chloroform/isoamyl alcohol[10]. About 5 μg of each DNA sample was electrophoresed on two 0.7% agarose gels; well number 5 contained 0.2 μg pYE13 DNA. DNA was transferred from the gels to nitrocellulose paper by the blotting procedure of Southern[8] and was hybridized to ^{32}P-labelled λ ::Tn*601* (*a*) and pBR322 (*b*) DNA (provided by S. Stibitz). The filters were exposed to Kodak X-ray film for a suitable period of time, developed and scanned.

determinants could be used, we have found that, in yeast, the phosphotransferase of Tn*601(903)* is most effective. This may reflect some regulatory sequence peculiar to this gene. The resistance genes can be added to the appropriate plasmid or viral vector by transposition or by cloning (detailed restriction endonuclease maps are known for several of the G418-resistance determinants). For example, this could allow the cloning of replication origins by linkage to the resistance determinant.

The use of G418 for cloning vector selection should eliminate the necessity for special conditions (aerobic or anaerobic growth) or specially constructed recipients for transformation (auxotrophs); thus, this antibiotic resistance should be valuable in the genetic manipulation of industrial yeast strains. A wide variety of yeast species and genera are sensitive to G418 (unpublished observations).

We thank Dr Peter Daniels (Schering Corporation) for gifts of antibiotic G418 and many related compounds, and Gary Gray, Stephen Harford and Scott Stibitz for their help and advice. Dr Takeshi Oka provided an *E. coli* strain carrying pA043 and Dr J. Hicks provided both a source of the yeast vector pYE13 and the yeast strain 483. This work was supported by grants from the NIH (AI 12448) and the Comite Conjunto Hispano Norteamericano para la Cooperacion Cientifica y Tecnologica.

Note added in proof: Following submission of this manuscript, we were informed by C. P. Hollenberg (personal communication) that he had transformed *S. cerevisae* with a kanamycin resistance plasmid and had obtained kanamycin-resistant colonies.

Received 28 April; accepted 1 September 1980.

1. Cohen, J. D. *et al. Proc. natn. Acad. Sci. U.S.A.* **77,** 1078–1082 (1980).
2. Daniels, P. J. L., Yehaskel, A. S. & Morton, J. B. *13th Interscience Conf. Antimicrobial Agents & Chemotherapy*, Washington, Abstr. 137 (1973).
3. Davies, J. & Smith, D. I. *A. Rev. Microbiol.* **32,** 469–518 (1978).
4. Davies, J. *et al.* in *Topics in Infectious Diseases* Vol. 2 (eds Drews, J. & Högenauer, G.) 101–114 (Springer, Vienna, 1977).
5. Hinnen, A., Hicks, J. B. & Fink, G. R. *Proc. natn. Acad. Sci. U.S.A.* **75,** 1929–1933 (1978).
6. Broach, J. R., Strathern, J. N. & Hicks, J. B. *Gene* **8,** 121–133 (1979).
7. Haas, M. J. & Dowding, J. E. *Meth. Enzym.* **43,** 611–628 (1975).
8. Southern, E. M. *J. molec. Biol.* **98,** 503–517 (1975).
9. Rothstein, J. J., Jorgensen, R. A., Postle, K. & Reznikoff, W. S. *Cell* **19,** 795–805 (1980).
10. Cryer, D. R., Eccleshall, R. & Marmur, J. *Meth. Cell Biol.* **12,** 39–44 (1977).

Chelation of cadmium with BAL and DTPA in rats

M. George Cherian

Department of Pathology, Health Sciences Centre, University of Western Ontario, London, Ontario, Canada N6A 5C1

Cadmium is unique among non-essential metals in several of its toxicological effects because of its long biological half life, slow excretion and delayed action on the kidneys[1]. Although cadmium poisoning in humans is uncommon, there are reports of chronic cadmium poisoning in workmen[2–4] and also in others in certain polluted areas[5,6]. At present there are no suitable methods either to measure the body burden of cadmium or to treat cadmium poisoning[7]. The therapeutic effects of various chelating agents including 2,3-dimercaptopropanol (BAL) and its soluble glycosides have been studied without much success in acute cadmium intoxication[8–11]. However, those studies were done before anything was known of the specific binding of cadmium to metallothionein, an intracellular low molecular weight protein[12]. The potential role of this protein in the detoxification and toxicity of metals has been reviewed recently[13,14]. The induced synthesis of metallothionein has a marked effect on the pharmacokinetics of cadmium and other divalent metals[15,16]. Thus it is important to consider the intracellular binding of cadmium with metallothionein in developing a suitable chelation therapy for chronic exposure to cadmium[17]. The *in vivo* chelation of cadmium with BAL or BAL and diethylenetriamine pentaacetic acid (DTPA) from rats exposed to cadmium is reported here.

A group of male rats (150 g) was injected intraperitoneally (i.p.) with ^{109}CdCl$_2$ (1 mg Cd; 5 μCi) and kept in separate metabolic cages. Three days later they were divided into three groups and treated i.p. as follows for 5 d per week for 2 weeks: group 1 (11 rats) with BAL (50 mg per kg); group 2 (5 rats) with 50 mg each of BAL and DTPA, and group 3 (9 rats, control)

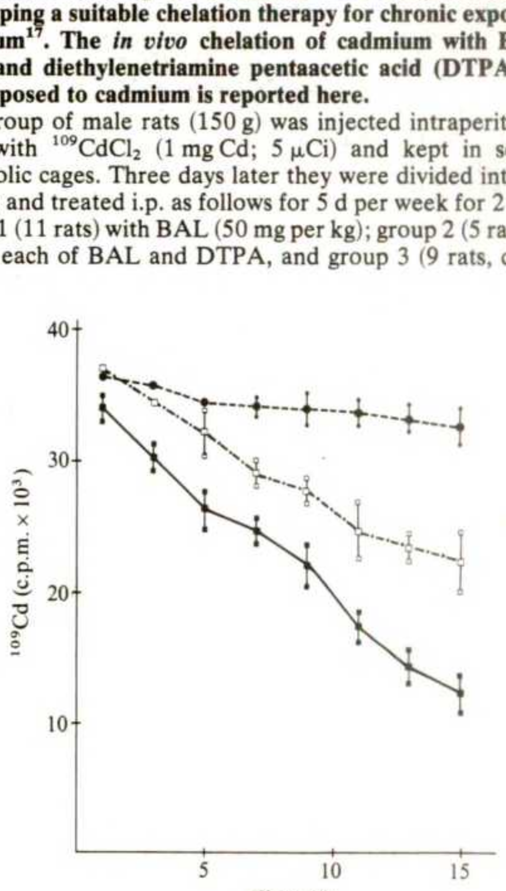

Fig. 1 Total body burden of cadmium. Rats were injected with ^{109}CdCl$_2$ (1 mg per kg; 5 μCi) and 3 d later were treated i.p. with BAL (group 1, □) or BAL and DTPA (group 2, ■) or saline (group 3, control, ●) for 2 weeks. The body burden of cadmium was determined from the whole body counting.

with normal saline. Urine and faecal samples were collected from each rat daily and the total excretion of cadmium was calculated from radioactivity. All rats were examined for ^{109}Cd radioactivity in a whole body counter[18] before and during the experiment.

Injections of BAL, both alone and in combination with DTPA, decreased the total body burden of cadmium in cadmium-exposed rats (Fig. 1), which retained only 57% and 40% of initial radioactivity, respectively. The control group on the other hand, retained about 92% of the cadmium. Thus the chelating agents effectively removed cadmium from the body when treatment started 3 days after injection of cadmium. In our previous *in situ* studies[17], BAL was the only chelating agent able to remove cadmium through the bile after the metal was bound to metallotheionein. Compounds such as 1,3-dimercaptopropanol and dimercaptosulphonic acid, which are structurally similar to BAL, had no effect. Therefore structural features, such as adjacent sulphydryl groups and lipophilic properties of chelating agents, are important for the chelation of cadmium from metallothionein *in vivo*.

Analysis of excreta for radioactive cadmium showed (Fig. 2) that the major route of excretion of cadmium after injection of chelating agents was in the faeces. The control group (group 3) excreted about 6% and 0.06% of the administered dose in faeces and urine, respectively, during the experimental 2 weeks. The group injected with BAL (group 1) excreted 28% in faeces and 1.4% in urine, while the group injected with a combination of BAL and DTPA (group 2) excreted 34% in faeces and 4.5% in urine. These results also suggested that the cadmium excreted through the bile after injection of BAL is not reabsorbed from the gut and is excreted in the faeces. Injection of DTPA with BAL increased both faecal and urinary excretion of cadmium.

The amount of cadmium in both liver and kidneys was significantly reduced after treatment with BAL or BAL and DTPA when compared with untreated rats (Table 1). The effect of BAL was more marked in the liver than in the kidneys. However, the mobilization of cadmium from the liver by BAL or BAL and DTPA together did not result in increased renal accumulation of the metal. In previous studies[8–11,17], when BAL was injected into animals before all the cadmium was bound to metallothionein, a major portion of cadmium associated with other bioligands was mobilized to the kidneys, increasing their content of cadmium. Thus the presence of metallothionein in the tissue may be an important factor in the effective therapeutic chelation of cadmium.

Our results provide the first evidence that BAL can be used successfully in proper conditions and at appropriate doses to mobilize cadmium from the liver without affecting its deposition in the kidneys, the critical organs in chronic cadmium toxicity. In reports from other laboratories[19,20] of chelation therapy for cadmium poisoning, chelating agents were administered within a short time of exposure to cadmium and the effect was measured by the rate survival of the animals. Those studies did not involve measurement of cadmium, and it was not clear whether the administered cadmium was either chelated or excreted from the body. One such study was later found to be invalid[21,22] and retracted[23]. Moreover, those studies do not have any relevance to the treatment of chronic poisoning. Our study reveals the potential use of BAL or BAL and DTPA together as a means of chelation of cadmium to remove it from the body without affecting the kidneys.

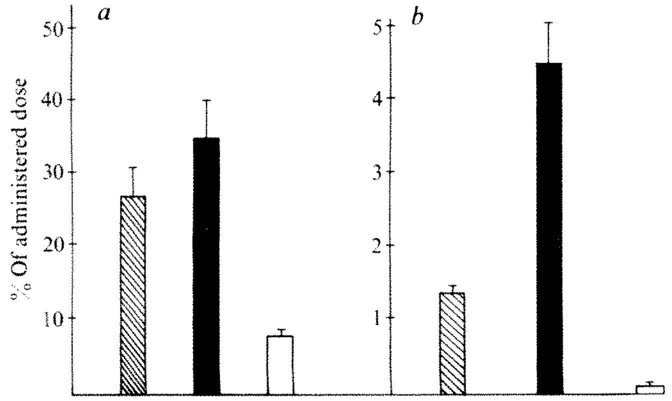

Fig. 2 Cumulative faecal (*a*) and urinary (*b*) excretion of cadmium in rats injected with $CdCl_2$ and treated with BAL (group 1, hatched columns) or BAL and DTPA (group 2, solid columns) or saline (group 3, open columns). Results are expressed as mean ± s.d.

Table 1 Tissue content of cadmium in rats injected with $CdCl_2$ and treated with saline or BAL and DTPA

Group	Concentration of Cd (μg mean ± s.d.)	
	Liver	Kidney
1	$2.95 \pm 0.4^*$	3.85 ± 0.3
2	$1.55 \pm 0.5^*$	$2.10 \pm 0.1^*$
3	9.30 ± 0.4	5.15 ± 0.6

All rats were injected with $^{109}CdCl_2$ (1 mg per kg; 5 μCi). Three days later they were injected i.p. with BAL (50 mg per kg, group 1) or BAL and DTPA (50 mg per kg, group 2) or saline (group 3) for 2 weeks. Rats were killed 2 d after the last injection and tissue concentration of cadmium was determined from radioactivity.

* $P < 0.01$.

This work was supported by grants from the International Lead and Zinc Research Organization, the Ontario Ministry of Labour and MRC, Canada. I thank Jane Collard, JoAnn St Louis and Karen Rodgers for technical assistance.

Received 25 June; accepted 29 August 1980.

1. Friberg, L., Piscator, M., Nordberg, G. F. & Kjellstrom, T. (eds) *Cadmium in the Environment* (Chemical Rubber Co., Cleveland, 1974).
2. Friberg, L. *Archs indust. Hyg. occup. Med.* **5,** 30–36 (1952).
3. Bernard, A. *et al. Int. Archs occup. envir. Hlth* **38,** 19–30 (1976).
4. Kjellstrom, T., Evrin, P. E. & Rahnster, B. *Envir. Res.* **13,** 303–317 (1977).
5. Hagino, T. *J. Jap. Ass. rural Med.* **7,** 288–292 (1959).
6. Friberg, L. *Lancet* **ii,** 823 (1979).
7. Nomiyama, K. *Sci. Total Envir.* **14,** 199–232 (1980).
8. Gilman, A., Philips, F. S., Allen, R. P. & Koelle, E. S. *J. Pharmac.* **87,** 85–101 (1946).
9. Tepperman, H. M. *J. Pharmac.* **89,** 343–349 (1947).
10. Tobias, J., Lushbaugh, C., Patt, H., Postel, S., Swift, M. & Gerhard, R. *J. Pharmac.* **87,** 102–112 (1946).
11. Dalhamn, T. & Friberg, L. *Acta pharmac. tox.* **11,** 68–71 (1955).
12. Vallee, B. L. *Metallothionein* (eds Kagi, J. H. R. & Nordberg, M.) 19–40 (Brikhauser, Basel, 1979).
13. Cherian, M. G. & Goyer, R. A. *Life Sci.* **23,** 1–10 (1978).
14. Nordberg, M. *Envir. Res.* **15,** 381–404 (1978).
15. Cherian, M. G. *J. Tox. envir. Hlth* **2,** 955–961 (1977).
16. Klaassen, C. D. *Am. J. Physiol.* **234,** E47-53 (1978).
17. Cherian, M. G. *Tox. appl. Pharmac.* **48,** A69 (1979); *J. Tox. envir. Hlth* **6,** 379–391, 393–401 (1980).
18. Cherian, M. G., Goyer, R. A. & Valberg, L. S. *J. Tox. envir. Hlth* **4,** 861–868 (1978).
19. Schubert, J. & Derr, S. K. *Nature* **275,** 311–313 (1978).
20. Jones, M. K., Weaver, A. D. & Weller, W. L. *Res. Commun. chem. Path. Pharmac.* **22,** 581–588 (1978).
21. May, P. M. & Williams, D. R. *Nature* **278,** 581 (1979).
22. Cantilena, L. R. & Klaassen, C. D. *Tox. appl. Pharmac.* **53,** 510–514 (1980).
23. Schubert, J. *Nature* **281,** 406 (1979).

Errata

In the article 'A low resolution structure for the histone core of the nucleosome' by A. Klug, D. Rhodes, J. Smith, J. T. Finch and J. O. Thomas, *Nature* **287,** 509–516, the third line of the equation displayed on the right-hand column of p. 514 should read

$$(H3)_2(H4)_2 + 2 \times H2A\ H2B$$

Also, in the same article, line 2 of the legend to Figure 7 should read 110° in place of 115° and 90° in place of 95°.

BOOK REVIEWS

The point of acupuncture

Patrick D. Wall

Celestial Lancets: A History and Rationale of Acupuncture and Moxa. By Lui Gwei-Djen and Joseph Needham. Pp.427. (Cambridge University Press: 1980.) £45, $97.50.

THIS extraordinary book is a syncopated side step in the long march of Joseph Needham's writing of *Science and Civilisation in China.* He has completed five of the seven volumes planned, but so widespread is the current interest in acupuncture that this book is issued as a footnote to the next volume on the life sciences. I think it is also related to the final volume on the social background because one of the crucial questions for me is why it is that acupuncture has so suddenly emerged into the Western daylight. As this book shows, it has been practised for 2,500 years in China and it is no fresh news to the West. Extensive accounts were published in Europe by de Bondt in 1658, Cleyer in 1682 and ten Rhijne in 1683, and we can enjoy here the beautiful illustrations of their books. These early reporters who took part in the Dutch drive to the East were as enthusiastic as those *Time* magazine journalists who went with Nixon on his expedition to China: "The results with acupuncture in Japan which I will relate surpass even miracles", wrote de Bondt.

This raises a double question: why has acupuncture suddenly reappeared in the West, and how could it be that the West forgot for 300 years that all sorts of awful diseases could be abolished by simply sticking needles into the skin?

I believe there are three answers to the first question. The Chinese themselves swung away from their own traditional medicine in the last century and attempted with hopelessly inadequate numbers of doctors to introduce Western medicine. After the liberation of 1948, faced with the atrocious state of the medical services, all available resources were mobilized and traditional and Western practitioners were brought together. For the first time, surgeons and acupuncturists cooperated and the startling practice of major surgery under acupuncture emerged. Second, the Western media, searching for something good to say about China, latched on to the "miracle" since they could hardly praise communism. Third, there are many in the West, disillusioned with our ways of thought, and with science in general and medicine in particular, who were delighted to accept that the pompous and ponderous academic establishment had been missing the point.

This book is divided into three parts. It starts by detailing the practice of acupuncture in the various schools with their historical developments and rationales. It is not intended as a clinical textbook but relates very clearly what is done and what were the ways of thinking about the body and disease. It also describes the less well-known treatment of moxa where the dried herb *Artemisia* is burned at the same points used for needling. This practice is also old and is widespread in many cultures, especially in the Arab and African worlds where localized cautery is used for the treatment of a wide variety of conditions from deafness to diarrhoea. The second part deals with physiological interpretations where an attempt is made to bring the old practices and explanations into an understandable framework in terms of modern physiology. Lastly, there is a section on the influences of other cultures which again emphasizes that the genius of China was never held in isolation for long periods. It dominated Korea, Vietnam and Japan, merged with Russian thought over a huge area and influenced the successive waves of Western colonization.

Turning now to my second question of why acupuncture so strangely appears and disappears in the West, one must obviously ask first if it works. On this question, this enormously scholarly and careful book is curiously silent. Statistics are given for surgical anaesthesia which are impressive and coincide approximately with the observations of many Western teams of specialist observers. What is not mentioned is that these figures are taken from a highly selected group of patients and that many of these had been given powerful additional medication.

We are faced here with a real but rare phenomenon not to be explained by the simple action of physiological mechanisms which we all possess in common. A fairly frequent pain complaint associated with tenderpoints in muscles, the myofascial syndrome, does seem to respond to needling of these spots, and it is interesting that a number of the acupuncture points for pain coincide with the common sites of

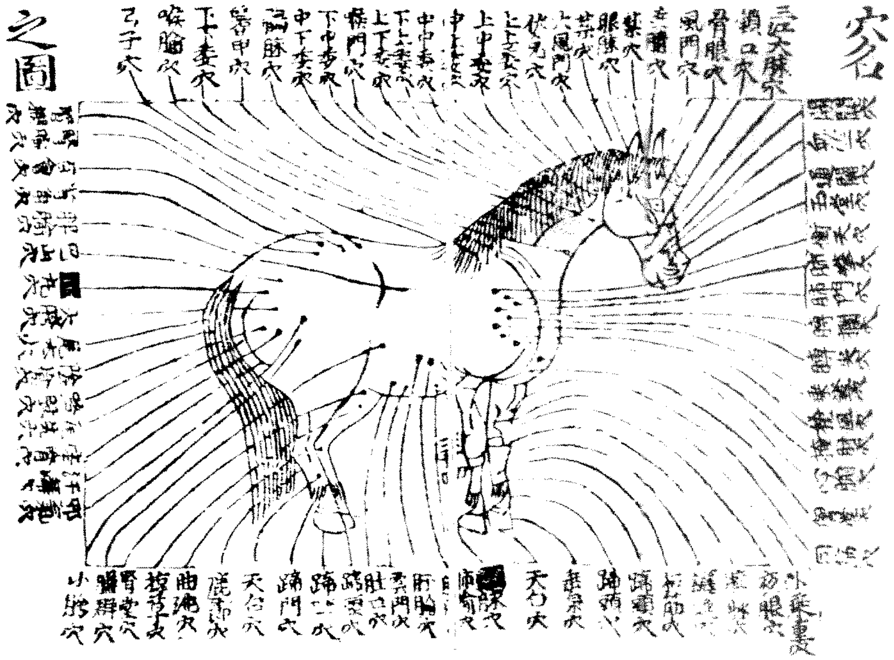

Veterinary acupuncture: points on the body of the horse. A drawing from the *Ma Niu I Fang* of + 1399.

these tender points. For other types of pain, the results of only two clinical trials have been published and they are both negative. Other disease treatments have not been subject to anything but a creeping barrage of anecdote.

Before attempting an explanation, we badly need clear statements of what it is we have to explain. Acupuncture is liable to disappear from sight once more, under a heap of dissatisfied patients and impatient doctors: I hope we will not have to await its next rennaissance before it is put to properly conducted trials which specify where and when it is effective. I hope this book with its careful description of "what" and "why" will encourage others to carry out those tests. ☐

Patrick D. Wall is Professor of Anatomy at University College, London, and co-author of the gate control theory of pain which is used widely in this book as an "explanation" of acupuncture.

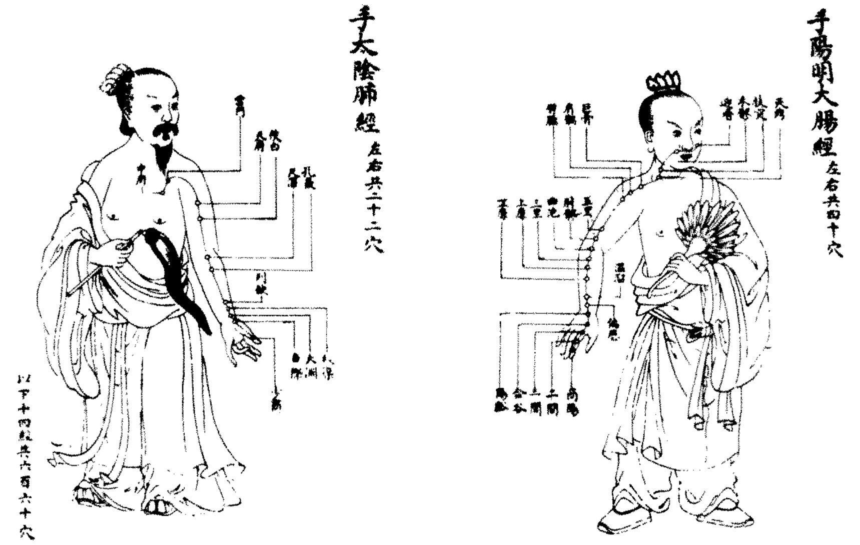
手太陰肺經
左右共二十二穴
手陽明大腸經
左右共四十穴
以下十四經共六百六十穴

The Cheirotelic pulmonic Thai-Yin acu-tract (left) and the Cheirogenic crasso-intestinal Yang-Ming acu-tract from Chang Chieh-Pin's *Lei Ching* of + 1624.

The fundamentals of chemical kinetics

C. F. Wells

Basic Chemical Kinetics. By H. Eyring, S.H. Lin and S.M. Lin. Pp.504. (Wiley-Interscience: 1980.) £19.15, $43.75.

I AM usually somewhat wary when I pick up a book with the word "basic" in the title, as I expect to find a highly simplified examination of the subject often without any pretence of rigour. This is very far from the case here, where "rigorous—fundamental" should be read for "basic".

After a brief introduction to rate equations and their integration, the authors devote their next chapter to potential energy surfaces. The dynamics of collisional processes are then considered, both from classical and quantum mechanical points of view. This is followed by a treatment of transition state theory, a theory to which Eyring has contributed so much, and of the theories of unimolecular reactions in the gas phase and their application to some experimental data. After a similar discussion of bimolecular reactions in the gas phase, the authors concentrate on photochemical reactions in condensed phases as well as in the gas phase. In the final chapter selected topics concerning kinetics in condensed phases are discussed. Four appendices complete the book: three devoted to an elaboration of mathematical treatments used earlier in the book, the fourth containing 79 problems covering aspects raised in all the chapters.

In one sense, this book is an extension and up-dating of the classic text, *The Theory of Rate Processes,* written by Eyring in collaboration with S. Glasstone and K. J. Laidler, and first published in 1941 by McGraw-Hill. This new book, too, should be of interest to all (particularly final-year undergraduates and research students) involved with the fundamentals of chemical kinetics. It will be invaluable to gas kineticists and to those concerned with photochemical kinetics, but perhaps has less direct application to the problems currently engaging solution kineticists. Chemists without an adequate mathematical background may find it hard going, and in this respect there are instances of undue compression of the text; for example l'Hôpital's Rule is referred to several times in Chapter 1 and is used in a problem in Appendix 4, yet nowhere is the Rule stated or defined.

Despite this reservation, the book is thoroughly recommended to all interested in the fundamentals of kinetic processes; it may well achieve "classic" status again for Eyring. ☐

C. F. Wells is Reader in Inorganic Chemistry at the University of Birmingham, and is especially concerned with the kinetics of inorganic reactions in solution.

The sinister phenomenon

Freda Newcombe

Neuropsychology of Left-handedness. Perspectives in Neurolinguistics and Psycholinguistics. Edited by J. Herron. Pp.357. (Academic: 1980.) $24.50, £13.80.

DEPARTURE from the usual pattern of right-handedness has often provoked annoyance, if not frank hostility, in the layman and has not inspired much in the way of scientific research until quite recently. There were occasional bursts of interest, ranging from a brief and hesitant question in a nineteenth-century anthrological journal ("is my parrot left-handed?") to the more unequivocal pronouncement of the venerable Dr Henschen on sighting the asymmetrical skull of a gorilla in University College Museum: "this gorilla was probably left-handed".

But these flashes in the dark, with their interesting implications of paw preference and morphological correlates, were not followed up by phenomenological studies or biological speculations until clinicians started to record anomalies of brain organization: speech disturbances due to damage to the *right* hemisphere of the brain, sometimes in left-handed patients. The work of Chesher, Penfield and Roberts, Subirana, and Luria developed the theme that the link between brain organization and handedness is less predictable in the non-right-handed members of the population: whereas some 98% of right-handed persons have speech functions represented in the left hemisphere, the proportion of left-handed people exhibiting this pattern is in the region of 60–66%. The remainder show the reverse pattern except for a very small minority that show bilateral representation. It is also suggested that a tendency to bilateral speech representation in the left-handed might be advantageous, in that the prognosis for recovery of speech after CNS damage may be better than that for the right-handed patient.

Despite this knowledge — provided both by neurological patients and by very large populations of ex-servicemen with focal brain-wounds — received wisdom and cultural prejudice are hard to eliminate. There are still members of the medical and teaching professions who believe that the functional organization of the brain of all left-handed people is the mirror image of that of the right-handed. Left-handedness, mixed handedness and 'crossed lateralization' have also become popular 'explanations' of such developmental disorders as dyslexia, stuttering and delayed language acquisition. Small-scale studies, based on biased clinical samples, appeared to buttress this notion until the more comprehensive investigations of Rutter, Tizard and Whitmore (*Education, Health and Behaviour.* Longman: 1970), and of Margaret Clark (*Reading Difficulties in School.* Penguin: 1970) cast doubt on its validity. It was clearly time to question the flimsy evidence available and to collect some hard data. Many neuropsychological studies in the past two decades have addressed this issue and most of them are at least referenced in this interesting book.

The chapters cover a wide range — historical, embryological and genetic, and experimental. Harris has a delightful contribution on the topic of early theories, facts and fancies; he has done the reader signal service in distilling the essence of an early literature that few of us have the time or energy to cultivate. Studies of neuroanatomical asymmetry are concisely reviewed by Witelson. There is an incisive critique of genetic models by Corballis, who accepts that of Annett as the most plausible; his conclusion that there is no convincing evidence to suggest that variations from the pattern of right-handedness and left cerebral control of speech "are due to anything other than environmental causes" is less compelling.

There are other contributions that illustrate the two strategies that determine much applied research in this area: the data-driven approach and the model-inspired design. The former has produced a quantity of perplexing material but at least illustrates a complex background to interpretation that must take into account both sex differences and developmental changes in hemispheric organization; studies by Herron, Kinsbourne and Kocel are apposite. Model-making is serving its heuristic purpose. Satz's theory of pathological left-handedness and Levy's biological and genetic speculations cannot be lightly dismissed although their empirical consequences lack — as yet — the support of consistent replication and large-scale studies. The search for a definitive genetic model must continue; and chapters by Boklage and by Springer and Searleman on embryological factors provide an important stimulus in this direction.

We continue to be handicapped by the impure quality of the data. 'Familial sinistrality' is probably an important variable but it is seldom defined in a way that permits the formulation of a rigorous genetic theory. Sample sizes are often inadequate and the criteria of handedness vary from study to study. For example, 'sighting' has been used as an index in this book despite Annett's evidence that one third of a large, right-handed 'normal' sample used the left eye for sighting.

This book does a service in fairly representing current work and thinking in the field. It reminds us that the programming of handedness may be sought in the embryo, that non-right handers are not a homogenous group, and that patterns of hand preference must be studied in the light of developmental change and gender differences. It provides a good source of reference material and it contains a reasonable supply of ideas for future research. It is not a definitive work but it is compulsory reading for neuroscientists with either theoretical or practical commitments in this field. □

Freda Newcombe is in the Neuropsychology Unit of the Department of Clinical Neurology, Radcliffe Infirmary, Oxford.

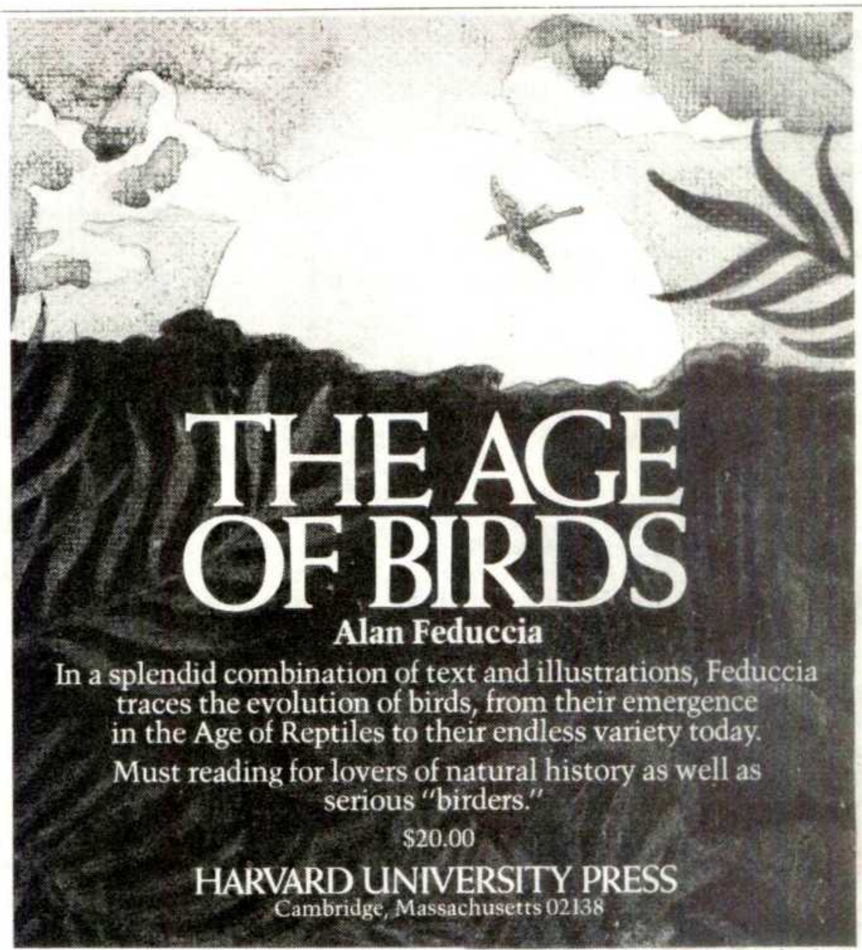

THE AGE OF BIRDS
Alan Feduccia
In a splendid combination of text and illustrations, Feduccia traces the evolution of birds, from their emergence in the Age of Reptiles to their endless variety today.
Must reading for lovers of natural history as well as serious "birders."
$20.00
HARVARD UNIVERSITY PRESS
Cambridge, Massachusetts 02138
Circle No. 04 on Reader Enquiry Card.

The inner alarm clock

Arthur T. Winfree

The Timing of Sleep and Wakefulness: On the Substructure and Dynamics of the Circadian Pacemakers Underlying the Wake–Sleep Cycle. Studies of Brain Function, Vol.3. By J.T. Enright. Pp.263. (Springer-Verlag: 1980.) Flexi DM49, $29.

THERE is a growing conviction among "clocks" physiologists that circadian behavioural rhythms in animals are generated in the central nervous system. It is also widely believed that in most organisms many different tissues independently determine circadian fluctuations of their individual function, and that the mechanisms may reside even in single cells. Add to this the astonishingly precise timing of some circadian rhythms, in the order of 3 minutes in a 23½-hour cycle for example, and you have arrived at J.T. Enright's stepping-off point for this monograph — the idea that thousands of nerve cells function as separate circadian "pacers" whose collective rhythmicity disciplines each one to enhanced regularity.

This is an old idea, going back at least to the first big "clocks" symposium at Cold

Spring Harbor in 1960. By 1970 the theoretical literature contained elaborate electronic mockups, computer simulations and mathematical analyses of such ensembles of mutually synchronizing, non-linear oscillators. What Enright ably brings to the discussion in 1980 is a detailed computer simulation, complete with noise statistics, built along lines suggested by his concept of pacemaker neurones. His "coupled stochastic systems" model, nicely summarized in Chapter 16, is distinguished from its forerunners by a curious feature: only the longer-period pacers actually synchronize; the others go their merry ways but in so doing provide a pool of potentially entrainable pacers whose contributions become important when the ensemble is exposed to stimuli that affect phases and periods. From this unique feature many of the observed peculiarities of vertebrate circadian rhythms seem to follow, but the extent to which they do so depends on a variety of adjustable quantities in the model. Enright is well aware of the implications of this:

> The weary reader may . . . begin to suspect that the model system under consideration shows embryonic symptoms of developing into an amorphous monster: one which can, like an amoeba, engulf and account for any set of data by modification of one parameter or another, but which thereby merely demonstrates its lack of backbone. Can any model with so many parameters lay legitimate claim to being a simple model?

He further argues that explanations that are simple in the sense of elementary physics simply would not be plausible in context of "the workshop of natural selection", which seems more likely to "assemble a reliable pacemaker out of components which are sloppy".

The reader will undoubtedly wonder whether sleep and wakefulness are really the same as rest and activity; whether circadian clocks really do function like pacemaker neurones, but a million times slower; and whether single cells do serve as independent clocks. But Enright's scepticism of his own model leaves little room for innovation by additional critics. Chapters 13 and 14 offer precise predictions for the outcome of feasible experiments which, if not fulfilled, will demand rejection or radical revision of the model. This detailed repartee between observation and interpretation is an edifying grace of Enright's monograph. In it we were treated to a thorough exposition of the present generalizations arising out of circadian physiology; and to a detailed exploration of the consequences of Enright's particular hypothesis.

What then is the upshot? Enright's model, based on observation of rest/activity cycles in birds and rodents, accounts for many of their peculiarities without having to resort to too many out-and-out *ad hoc* suppositions. It gives a reasonable vision of the kinds of mutual interaction among the pacers that would enhance their precision to the levels sometimes observed.

However, I suspect that much of the fitting to phase-resetting data and period-changing data could be managed with equal elegance by rather different models; there exists at present little of a factual nature to distinguish alternative visions of the internal organization of the central nervous system clock. Yet here we encounter what, from my present viewpoint among models of human circadian rhythms, seems a primary value of Enright's contribution. Research on sleep/wake rhythms is now in the midst of an explosive blossoming of discovery. Enright's model correlates definite facts and makes distinct critical predictions. This is just what we need, alongside the alternative visions of Wever, Kronauer and others, to catalyse the asking of sharp experimental questions.

Like almost all models in the behavioural sciences, Enright's is partly a fairy tale — in this case, a pleasing one, done with a sense of humour, but not frivolously. He remarks on p.249 that ". . . there is not the least doubt in my mind that the models as formulated will prove to be wrong; wrong because they are oversimplified; wrong because they have ignored one critical process or another; and wrong because some elements of the models arise from mistaken points of departure". But as Francis Bacon remarks in his *Novum Organum*, "truth will sooner come from error than from confusion". In my view, debate over Enright's facts and interpretations could take us a long way toward understanding one of the most conspicuous facts of human experience, the rhythm of sleep and wakefulness. ☐

Arthur T. Winfree is Professor of Biology at Purdue University, West Lafayette, Indiana.

With reference to variable stars

R. J. Tayler

Theory of Stellar Pulsation. By J. P. Cox. Pp. 380. (Princeton University Press: 1980.) Hardback £21.90, $50; paperback £7.50, $17.

FOR some time there has been a need for a new book on the theory of variable stars to consider the considerable developments in the subject that have taken place since the publication of Rosseland's *The Pulsation Theory of Variable Stars* (Oxford University Press, 1949). Now there are two new books: *Nonradial Oscillations of Stars* (Tokyo University, 1979) by Unno, Osaki, Ando and Shibahashi, which does not discuss the more widely studied and better understood radial oscillations, and the present book which covers the whole subject. J. P. Cox has written many review articles on variable stars and this, the book which has grown out of them, provides a thorough survey both of the foundations of the subject and of recent developments.

In 1949 it was clear that many intrinsic variable stars were pulsating radially, but important questions remained relating to the physical cause of the instability exciting the oscillation, to the observed phase relationships between light and velocity variations, to the processes limiting the instability to finite amplitude and to the evolutionary status of variable stars. The answers to all except the third of these questions are now reasonably clear. However, there is still considerable difficulty in deciding whether a star with a deep convective envelope will pulsate, because there is no good description of time-dependent convection, and there are arguments about whether the stellar masses required to give the correct pulsations agree with those implied by stellar evolution theory. Although there are clues to what produces the finite amplitude limitation of the instability, it is difficult to study the full non-linear problem without crude approximation. The study of non-radial oscillation is much more difficult than that of radial pulsation, but it is clear that non-radial oscillations are present in some stars and, indeed, convection is a non-radial oscillation of very high order. The study of non-radial oscillations has recently been stimulated by observations of small fluctuations in the properties of the Sun.

Cox gives a clear and detailed account of the subject, and this book is a very welcome addition to the literature. If I have any major criticism, it is that it is perhaps too detailed to be used as a textbook; for that purpose I would have omitted some references to topics which could not be discussed in detail. It will, however, be invaluable as a reference book. In particular, it contains a list of relevant papers which is more than 30 pages long. ☐

R. J. Tayler is Professor of Astronomy at the University of Sussex, author of three elementary astronomy textbooks and Managing Editor of Monthly Notices of the Royal Astronomical Society.

The British Museum (Natural History), in collaboration with John Wiley, have just published *Animal Identification: A Reference Guide* in three volumes. Each volume provides a listing of primary reference sources — Vol. 1 to marine and brackish water animals, Vol. 2 to land and freshwater animals (excluding insects), and Vol. 3 to insects — to assist non-specialists in identifying any animal. The three-volume set costs £31.

BOOKS RECEIVED

Mathematics

AHMAD, S. and KEENER, M. (eds). Differential Equations, Proceedings of the Conference held at Oklahoma State University, October 1979. Pp.278. ISBN 0-12-045550-1. (Academic: 1980.) $20.

BASAWA, I.B. and PRAKASA RAO, B.L.S. Statistical Inference for Stochastic Processes. Pp.435. ISBN 0-12-080250-3. (Academic: 1980.) $62, £26.80.

BOMFORD, D. Geodesy. 4th Edn. Pp.835. ISBN 0-19-851946-X. (Oxford University Press: 1980.) £49.

CHATTERS, A. W. and HAJARNAVIS, C. R. Rings with Chain Conditions. Research Notes in Mathematics, 44. Pp.197. Flexi ISBN 0-273-08446-1. (Pitman: 1980.) £8.

FENSTAD, J.E. General Recursion Theory. An Axiomatic Approach. Pp.225. ISBN 3-540-09349-4. (Springer-Verlag: 1980.) DM78, $46.10.

FIENBERG, S.E. The Analysis of Cross-Classified Categorical Data. 2nd Edn. Pp.198. ISBN 0-262-06071-X. (MIT Press: 1980.) $14.

GUMOWSKI, I. and MIRA, C. Recurrencies and Discrete Dynamic Systems. Lecture Notes in Mathematics, Vol.809. Pp.272. Flexi ISBN 3-540-10017-2. (Springer-Verlag: 1980.) DM 29, $17.20.

KAHN, D. W. Introduction to Global Analysis. Pp.336. ISBN 0-12-394050-8. (Academic: 1980.) $34.50.

MACFARLANE, A.G.J. (ed.). Complex Variable Methods for Linear Multivariable Feedback Systems. Pp.366. ISBN 0-85066-197-8. (Taylor & Francis: London, 1980.) £15.

ROUCHE, N. and MAWHIN, J. Ordinary Differential Equations: Stability and Periodic Solutions. Pp.260. ISBN 0-273-08419-4. (Pitman: 1980.) £22.

ROWEN, L.H. Polynomial Identities in Ring Theory. Pp.365. ISBN 0-12-599850-3. (Academic: 1980.) $39.50.

SAMOILENKO, A.M. and RONTO, N.I. Numerical-Analytic Methods of Investigating Periodic Solutions. Pp.183. Pbk ISBN 7147-1504-2. (Central Books: 14 The Leathermarket, London, 1980.) £1.95.

STÖER, J. and BULIRSCH. Introduction to Numerical Analysis. Pp.609. ISBN 3-540-90420-4. (Springer-Verlag: 1980.) DM 49.50, $27.80.

Physics

ASTARITA, G., MURRUCCI, G. and NICOLAIS, L. (eds). Rheology. Vol. 1, Principles. Proceedings of the 8th International Congress of Rheology, held in Naples, September 1980. Pp.421. ISBN 0-306-40465-6. (Plenum: 1980.) $50.

ASTARITA, G., MARRUCCI, G. and NICOLAIS, L. (eds). Rheology. Vol. 2, Fluids. Pp.677. ISBN 0-306-40466-4. (Plenum: 1980.) $55.

ASTARITA, G., MARRUCCI, G. and NICOLAIS, L. (eds). Rheology. Vol. 3, Applications. Pp.785. ISBN 0-306-40467-2. (Plenum: 1980.) $55.

BULLOUGH, R.K. and CAUDREY, P.J. (eds). Solitons. Topics in Current Physics, Vol.17. Pp.389. ISBN 3-540-09962. (Springer-Verlag: 1980.) DM 76, $44.90.

CLOSE, F.E. An Introduction to Quarks and Partons. Pp.481. Hbk ISBN 0-12-175150-3; pbk ISBN 0-12-175152-X. (Academic: 1980.) Hbk np; pbk £9.80, $23.

EMSLEY, J.W., FEENEY, J. and SUTCLIFFE, L.H. (eds). Progress in Nuclear Magnetic Resonance Spectroscopy, Vol.13. Pp.363. ISBN 0-08-026027-6. (Pergamon: 1980.) £34.

GOLDSTEIN, H. Classical Mechanics, 2nd Edn. Pp.672. Flexi ISBN 0-201-02969-3. (Addison-Wesley: 1980.) £9.95.

REICHL, L.E. A Modern Course in Statistical Physics. Pp.709. ISBN 0-7131-2789-9. (Edward Arnold: 1980.) £20.

SOCRATES, G. Infrared Characteristic Group Frequencies. Pp.153. ISBN 0-471-27592-1. (Wiley-Interscience: 1980.) £24.

WEBB, G.A. (ed.). Annual Reports on NMR Spectroscopy, Vol.10A. Pp.251. ISBN 0-12-505310-X. (Academic: 1980.) £28.50, $66.

WEBB, G.A. (ed.). Annual Reports on NMR Spectroscopy, Vol. 10B. Pp.511. ISBN 0-12-505348-7. (Academic: 1980.) £38.50, $89.

WINICH, H. and DONIACH, S. (eds). Synchrotron Radiation Research. Pp.754. ISBN 0-306-40363-3. (Plenum: 1980.) $65.

Chemistry

EYRING, H. and HENDERSON, D. (eds). Theoretical Chemistry Advances and Perspectives, Vol.5. Pp.267. ISBN 0-12-681905-X. (Academic: 1980.) $35.

GIDDINGS, J.C. *et al.* (eds). Advances in Chromatography, Vol.18. Pp.292. ISBN 0-8247-6960-0. (Dekker: 1980.) Sw.Fr. 88.

GOETHALS, E.J. (ed.). Polymeric Amines and Ammonium Salts. Invited Lectures and Contributed Papers Presented at the International Symposium on Polymeric Amines and Ammonium Salts, Ghent, Belgium, September 1979. Pp.424. ISBN 0-08-023941-2. (Pergamon: 1980.) £37.50.

HESS, H.-J. (ed.). Annual Reports in Medicinal Chemistry, Vol.15. Pp.346. Flexi ISBN 0-12-040515-6. (Academic: 1980.) $22.50.

HODGE, P. and SHERRINGTON, D.C. (eds). Polymer-supported Reactions in Organic Synthesis. Pp.484. ISBN 0-471-27712-6. (Wiley-Interscience: 1980.) £29.50.

KATRITZKY, A.R. and BOULTON, A.J. (eds). Advances in Heterocyclic Chemistry, Vol.26. Pp.247. ISBN 0-12-020626-9. (Academic: 1980.) $32.

KEYZER, H. and GUTMANN, F. (eds). Bioelectrochemistry. Proceedings of the US-Australia Joint Seminar on Bioelectrochemistry, held in Pasadena, California, July 1979. Pp.434. ISBN 0-306-40453-2. (Plenum: 1980.) $42.50.

LÖWDIN, P.-O., CALAIS, J.-L. and GOSCINSKI, O. (eds). Quantum Chemistry — A Scientific Melting Pot. Pp.423. International Journal of Quantum Chemistry Vol.XII, Supplement 1. Pbk ISBN 0-471-05248-5. (Wiley: 1980.) £14.50.

McLAIN, J.H. Pyrotechnics From the Viewpoint of Solid State Chemistry. Pp.243. ISBN 0-89168-032-2. (The Franklin Institute Press: Philadelphia, 1980.) $25.50.

PRINS, R. and SCHUIT, G.C.A. (eds). Chemistry and Chemical Engineering of Catalytic Processes. Pp.660. ISBN 90-286-0730-7. (Sijthoff & Noordhoff: 1980.) Dfl. 150, $75.

RATAJCZAK, H. and ORVILLE-THOMAS, W.J. (eds). Molecular Interactions, Vol.1. Pp.415. ISBN 0-471-27664-2. (Wiley-Interscience: 1980.) £28.

SAMSONOV, G.V. and VINITSKII, I.M. Handbook of Refractory Compounds. Pp.555. ISBN 0-306-65181-5. (IFI/Plenum: 1980.) $75.

SCOTT, A.F. (ed.). Survey of Progress in Chemistry, Vol.9. Pp.271. ISBN 0-12-610509-X. (Academic: 1980.) $35.

THIRSK, H.R. (senior reporter). Electrochemistry, Vol.7. A Review of Recent Literature. Pp.268. ISBN 0-85186-870-3. (The Chemical Society: London, 1980.) £24, $63.

VEPREK, S. and VENUGOPALAN, M. (eds). Plasma Chemistry I. Topics in Current Chemistry, Vol.89. Pp.143. ISBN 3-540-09825-9. (Springer-Verlag: 1980.) DM 88, $52.

VEPREK, S. and VENUGOPALAN, M. Plasma Chemistry II. Topics in Current Chemistry, Vol.90. Pp.121. ISBN 3-540-09826-7. (Springer-Verlag: 1980.) DM 88, $52.

VERMA, V.N. Spectroscopic References to Polyatomic Molecules. Pp.126. ISBN 0-306-65190-4. (IFI/Plenum: 1980.) $75.

WARREN, S.G., TSUJI, J. and SCHUDA, P.F. Syntheses of Natural Products. Topics in Current Chemistry, Vol.91. Pp.118. ISBN 3-540-09827-5. (Springer-Verlag: 1980.) DM 68, $40.20.

Biological Sciences

ALLEN, K. R. Conservation and Management of Whales. Pp.107. ISBN 0-295-95730-1. (Butterworths: 1980.) $12.50.

ANTHONY, C. P. and THIBODEAU, G. A. Structure and Function of the Body. 6th Edn. Pp.286. Pbk ISBN 0-8016-0287-4; hbk ISBN 0-8016-0273-4. (C. V. Mosby: 1980.) Pbk £6.25; hbk np.

BARANY, F.R., SHIELDS, R. and CAPRILLI, R. (eds). Gastrointestinal Emergencies, 2. Advances in the Biosciences, Vol.27. Proceedings of the 2nd International Symposium held in Rome, June 1979. Pp.184. ISBN 0-08-024927-2. (Pergamon: 1980.) $76.

BARRINGTON, E.J.W. Invertebrate Structure and Function. 2nd edn. Pp.765. Flexi ISBN 0-17-771041-1. (Thomas Nelson: 1980.) Np.

BROWN, D.S. Freshwater Snails of Africa and their Medical Importance. Pp.487. ISBN 0-85066-145-5. (Taylor & Francis: 1980.) £25.

CARAS, R. The Forest. Pp.178. Flexi ISBN 0-395-29611-0. (Houghton Mifflin: 1980.) $4.95.

CLEMENS, M.J. (ed.). Biochemistry of Cellular Regulation. Vol.1, Gene Expression. Pp.266. ISBN 0-8493-5454-4. (Blackwell Scientific: 1980.) £52.

CROWELL, M.R. Great Blue: The Odyssey of a Great Blue Heron. Pp.143. ISBN 0-8129-0905-4. (Times Books: 1980.) $10.95.

ESSMAN, W.B. (ed.). Neurotransmitters, Receptors & Drug Action. Pp.209. ISBN 0-85200-524-5. (MTP Press: Lancaster, UK, 1980.) £17.95.

HAYS, D.M. and KIMURA, K. Biliary Atresia. The Japanese Experience. Pp.218. ISBN 0-674-97325-8. (Harvard University Press: 1980.) £12.

HUGHES, M.J. and BARNES, C.D. (eds). Neural Control of Circulation. Research Topics in Physiology, 2. Pp.175. ISBN 0-12-360850-3. (Academic: 1980.) $24.

KOLB, B. and WHISHAW, I.Q. Fundamentals of Human Neuropsychology. Pp.502. ISBN 0-7167-1219-9. (W.H. Freeman: 1980.) $17.95.

KURTÉN, B. and ANDERSON, E. Pleistocene Mammals of North America. Pp.442. ISBN 0-231-03733-3. (Columbia University Press: 1980.) $53.10.

LAHLOU, B. Epithelial Transport in the Lower Vertebrates. Proceedings of the Symposium held at the Station Zoologique of Villefranche-sur-Mer, June 1978. Pp.366. ISBN 0-521-22748-8. (Cambridge University Press: 1980.) £25.

LAIRD, M. Bibliography of the Natural History of Newfoundland and Labrador. Pp.378. ISBN 0-12-434050-4. (Academic: 1980.) £25, $57.50.

LAMBE, D.W. Jr, GENCO, R.J. and MAYBERRY-CARSON, K.J. (eds). Anaerobic Bacteria: Selected Topics. Proceedings of the Symposium held at East Tennessee State University, April 1979. Pp.313. ISBN 0-306-40546-6. (Plenum: 1980.) $29.50.

LUCKETT, W.P. (ed.). Comparative Biology and Evolutionary Relationships of Tree Shrews. Pp.314. ISBN 0-306-40464-8. (Plenum: 1980.) $39.50.

MAY C.W. (ed.). Microbial Diseases: Notes, Reports, Summaries, Trends. Pp.322. Hbk ISBN 0-913232-85-8; pbk ISBN 0-913232-87-4. (William Kaufmann: Los Altos, California, 1980.) Hbk $14; pbk $7.95.

PETERSON, R.T. A Field Guide to the Birds East of the Rockies. 4th edn. Pp.384. Flexi ISBN 0-395-26619-X. (Houghton Mifflin: 1980.) $9.95.

ROSS, B. and GUDER, W.G. (guest eds). Biochemical Aspects of Renal Function. Proceedings of a Symposium held at Merton College, Oxford, September 1979. Pp.324. Flexi ISBN 0-08-025517-5. *(Pergamon: 1980.)* $55.

RUSSELL, P.J. Lecture Notes on Genetics. Pp.258. Flexi ISBN 0-632-00609-9. (Blackwell Scientific: 1980.) £6.80.

BARNES, R. K. and MANN, K. H. (eds). Fundamentals of Aquatic Ecosystems. Pp.229. Flexi ISBN 0-632-00014-7. (Blackwell Scientific: 1980.) £7.80.

BLOOM, F. E. (ed.). Peptides: Integrators of Cell and Tissue Function. Society of General Physiologists Series, Vol. 35. Pp.271. ISBN [illegible]-89004. (Raven: 1980.) $23.

BLOOMFIELD, J. A. (ed.). Lakes of New York State. Vol. III. Ecology of the Lakes of East-Central New York. Pp.[illegible]6. ISBN 0-12-10[illegible]5-3. (Academic: 1980.) $29.50.

BOURNE, G. H. and DANIELLI, J. F. (eds). International Review of Cytology, Vol. 66. Pp.374. ISBN 0-12-364466-6. (Academic: 1980.) $39.

BRICKELL, C. D., CUTLER, D. F. and GREGORY, M. (eds). Petaloid Monocotyledons. Horticultural and Botanical Research. Linnean Society Symposium Series No. 8. Pp.222. ISBN 9-12-133950-5. (Academic: 1980.) £26.80, $62.

DAVIES, D. D. (ed.). The Biochemistry of Plants: A Comprehensive Treatise. Vol. 2, Metabolism and Respiration. Pp.687. ISBN 0-12-675402-0. (Academic: 1980.) $65.

DE VICENTE, R. (ed.). Replies from Biological Research. Proceedings of the Symposium on Biology and Ethics. Pp.418. Flexi ISBN 84-00-04525-4. (Consejo Superior de Investigaciones Cientificas: Madrid, 1979.) Np.

DI BENEDETTA, C., BÁLAZS, R., GOMBOS, G. and PORCELLATI, G. (eds). Mulidisciplinary Approach to Brain Development. Proceedings of the International Meeting held in Selva di Fasano, Italy, April 1979. Developments in Neuroscience, Vol. 9. Pp.585. ISBN 0-444-80227-4. (Elsevier/North-Holland Biomedical: 1980.) $85, Dfl. 174.

DUMONT, H. G. and GREEN, J. (eds). Roataoria. Proceedings of the 2nd International Rotifer Symposium held at Gent, September 1979. Developments in Hydrobiology, 1. Pp.263. ISBN 906193754. (W. Junk: 1980.) Np.

DUNITZ, J. D. *et al.* (eds). Molecular Structure and Sensory Physiology. Structure and Bonding, Vol. 41. Pp.146. ISBN 3-540-09958-1. (Springer-Verlag: 1980.) DM 69, $40.80.

KIMBALL, F. A. (ed.). The Endometrium, Proceedings of the 8th Brook Lodge Workshop on Problems in Reproductive Physiology. Pp.350. ISBN 0-85200-525-3. (MTP Press: Lancaster, UK, 1980.) £15.95.

KITNEY, R. I. and ROMPELMAN, O. (eds). The Study of Heart-rate Variability. Pp.246. ISBN 0-19-857533-5. (Clarendon/Oxford University Press, 1980.) £25.

KLIEGEL, W. Bor in Biologie, Medizin und Pharmazie. Physiologische Wirkungen und Pharmazie. Pp.900. ISBN 3-540-93411-1. (Springer-Verlag: 1980.) DM 285, $168.20.

LAWRENCE, T. L. J. Growth in Animals. Pp.308. ISBN 0-408-10638-7. (Butterworths: 1980.) £20.

LURIA, A. R. Higher Cortical Functions in Man. 2nd Edn. (Basic Books: 1980.) $27.50.

MEZZICH, J. E. and SOLOMON, H. Taxonomy and Behavioral Science: Comparative Performance of Grouping Methods. Pp.178. ISBN 0-12-493340-8. (Academic: 1980.) $25, £10.80.

NAGORSEN, D. W. and PETERSON, R. L. Mammal Collectors' Manual. A Guide for Collecting, Documenting, and Preparing Mammal Specimens for Scientific Research. Pp.79. Flexi ISBN 0-88854-255-0. (Royal Ontario Museum: Toronto, Canada, 1980.) $6.50.

PFURTSCHELLER, G. *et al.* (eds). Rhythmic EEG Activities and Cortical Functioning. Developments in Neuroscience, Vol. 10. Proceedings of the International Symposium held in Schladming, Austria, September 1979. Pp.314. ISBN 0-444-80247-9. (Elsevier/North-Holland biomedical: 1980.) $48.75. Dfl. 100.

STEYN, P.S. (ed.). The Biosynthesis of Mycotoxins: A Study in Secondary Metabolism. Pp.432. ISBN 0-12-670650-6. (Academic: 1980.) $44.

STODDART, D.M. (ed.). Olfaction in Mammals. Symposia of the Zoological Society of London, No.45. Pp.364. ISBN 0-12-613345-X. (Academic: 1980.) £27.40 (UK only), $63.50.

TESTA, F. Leaves. Pp.28. ISBN 0-905478-74-6. (Andersen Press: London, 1980.) £3.50.

THOMAS, G., PODESTA, E.J. and GORDON, J. (eds). Protein Phosphorylation and Bio-Regulation. Friedrich-Miescher Institut and EMBO Workshop, Basel, December 1979. Pp.232. ISBN 3-8055-1168-X. (Karger: 1980.) SwFr.82. DM 98, $49.25.

WEINSTEIN, L. and FIELDS, B.N. (eds). Seminars in Infectious Disease, Vol.III. Pp.323. ISBN 0-913258-69-5. (Thieme-Stratton: New York, 1980.) $32.50.

Applied Biological Sciences

BASTENIE, P.A., BONNYNS, M. and VANHAELST, L. Recent Progress in Diagnosis and Treatment of Hypothyroid Conditions. Proceedings of the XVth International Congress of Therapeutics, Brussels, September 1979. Pp.155. ISBN 90-219-0448-9. (Excerpta Medica: 1980.) Np.

BOURNE, G.H., DANIELLI, J.F. and JEON, K.W. (eds). International Review of Cytology, Supplement 11A. Perspectives in Plant Cell and Tissue Culture. Pp.253. ISBN 0-12-364371-6. (Academic: 1980) Np.

BOURNE, G.H., DANIELLI, J.F. and JEON, K.W. (eds). International Review of Cytology, Supplement 11B. Perspectives in Plant Cell and Tissue Culture. Pp.257. ISBN 0-12-364372-4. (Academic: 1980.) $29.50.

CANTOR, C.R. and SCHIMMEL, P.R. Biophysical Chemistry, Part III. The Behaviour of Biological Macromolecules. Pp.524. Hbk ISBN 0-7167-1191-5; pbk ISBN 0-7167-1192-3. (W.H. Freeman: 1980.) Hbk £22.40; pbk £11.90.

COHEN, E.P. and KÖHLER, H. (eds). Membranes, Receptors, and the Immune Response. 80 years after Ehrlich's Side Chain Theory. Progress in Clinical and Biological Research, Vol.42. Pp.404. ISBN 0-8451-0042-4. (Alan R. Liss: New York, 1980.) $34. Available in Europe and the Middle East from European Book Service, Flevolaan, Holland, Dfl.102.

CROFT, L.R. Handbook of Protein Sequence Analysis: A Compilation of Amino Acid Sequences of Proteins with an Introduction to the Methodology. 2nd Edn. Pp.628. ISBN 0-471-27703-7. (Wiley: 1980.) £38.

CROFT, L.R. Introduction to Protein Sequence Analysis. Pp.157. Flexi ISBN 0-471-27710-X. (Wiley: 1980.) £4.95.

DAVIS, W., HARRAP, K.R. and STATHOPOULOS, G. (eds). Human Cancer: Its Characterization and Treatment. Advances in Tumour Prevention, Detection and Characterization, Vol.5. Proceedings of the 8th International Symposium on the Biological Characterization of Human Tumours. Pp.420. ISBN 90-219-0458-6. (Excerpta Medica: 1980.) $90.25, Dfl.185.

DAVISON, A.N. and CUZNER, M.L. (eds). The Suppression of Allergic Encephalomyelitis and Multiple Sclerosis. Based on the Proceedings of the Liversidge Symposium, held in October 1979. Pp.292. ISBN 0-12-206660-X. (Academic: 1980.) £14.80, $34.50.

ELLIS, G.P. and WEST, G.B. Progress in Medicinal Chemistry, 17. Pp.280. ISBN 0-7204-0669-2. (Elsevier/North-Holland: 1980.) $63.50, Dfl.130.

FRIEDLANDER, M. (ed.). Immunological Approaches to Embryonic Development and Differentiation, Part II. Current Topics in Developmental Biology, Vol.14. Pp.381. ISBN 0-12-153114-7. (Academic: 1980.) $39.50.

GREEP, R.O. (ed.). Recent Progress in Hormone Research. Proceedings of the 1979 Laurentian Hormone Conference, Vol.36. Pp.629. ISBN 0-12-57136-0. (Academic: 1980.) $54.

Psychology

HERSEN, M., EISLER, R.M. and MILLER, P.M. (eds). Progress in Behavior Modification, Vol.9. Pp.296. ISBN 0-12-535609-9. (Academic: 1980.) $29.50.

LANE, H. and GROSJEAN, F. (eds). Recent Perspectives on American Sign Language. Pp.170. ISBN 0-89859-053-1. (Lawrence Erlbaum: Hillsdale, New Jersey, 1980.) $16.50.

LEEDS, M. and MURPHY, G. The Paranormal and the Normal. A Historical and Theoretical Perspective. Pp.239. ISBN 0-8108-1278-9. (Scarecrow Press: Metuchen, NJ, 1980.) £9.45.

LEVI, I. The Enterprise of Knowledge. An Essay on Knowledge, Credal Probability, and Chance. Pp.462. ISBN 0-262-12082-8. (MIT Press: 1980.) $27.50.

MAGARO, P.A. Cognition in Schizophrenia and Paranoia: The Integration of Cognitive Processes. Pp.339. ISBN 0-89859-028-0. (Lawrence Erlbaum: Hillsdale, New Jersey, 1980.) $24.95.

O'CONNELL, A.O. and O'CONNELL, V.F. Choice and Change; the Psychology of Adjustment, Growth, and Creativity. Revised edn. Pp.543. Pbk ISBN 0-13-133066-7. (Prentice/Hall: 1980.) £9.05.

SARASON, I.G. (ed.). Test Anxiety: Theory, Research, and Applications. Pp.432. ISBN 0-89859-022-1. (Lawrence Erlbaum: Hillsdale, New Jersey, 1980.) $24.95.

ST. CLAIR, R.N. and GILES, H. (eds). The Social and Psychological Contexts of Language. Pp.338. ISBN 0-89859-021-3. (Lawrence Erlbaum: Hillsdale, New Jersey, 1980.) $27.95.

VAN DIJK, T.A. Macrostructures. An Interdisciplinary Study of Global Structures in Discourse, Interaction, and Cognition. Pp.317. ISBN 0-89859-039-6. (Lawrence Erlbaum: Hillsdale, New Jersey, 1980.) $24.95.

WALLER, T.G. and MACKINNON, G.E. Reading Research: Advances in Theory and Practice. Vol.1. Pp.262. ISBN 0-12-572301-6. (Academic: 1979.) $20.

WITTROCK, M.C. (ed.). The Brain and Psychology. Educational Psychology Series. Pp.423. ISBN 0-12-761050-2. (Academic: 1980.) $25.

General

DIN DEUTSCHES INSTITUT FUR NORMUNG E. V. Catalogue English Translation of German Standards 1980. Completed with December 1979 edition o 'DIN-Mitteilungen + elektronorm'. Pp.192. (DIN Deutsches Institut für Normung e.v.: 1980.) Flexi np.

DUFTY, W. Sugar Blues. Revised British Edition. Pp.218. ISBN 0-85626-179-3. (Abacus: Tunbridge Wells, UK, 1980.) £5.95.

FEINBERG, G. and SHAPIRO, R. Life Beyond Earth. The Intelligent Earthling's Guide to Life in the Universe. Pp.464. Hbk ISBN 0-688-03642-2; pbk ISBN 0-688-08642-X. (William Morrow: New York, 1980.) Hbk £14.95; pbk $7.95.

GASPARINI, I. Giornale Degli Economisti E. Annali Di Economia. Saggi in Onore di Giovanni Demaria. Pp.948. (Universita Commerciale Luigi Bocconi: 1979.) Np.

GORMAN, J. Hazards to Your Health. The Problem of Environmental Disease. Pp.70. Flexi ISBN 0-89766-024-2. (New York Academy of Sciences: 1979.) $4.

GORZ, A. Ecology as Politics. Pp.215. Pbk ISBN 0-89608-088-9; hbk ISBN 0-89608-089-7. (South End Press: Box 68, Astor Station, Boston 02123, 1980.) Np

HOLLANDS, C. Compassion is the Bugler. The Struggle for Animal Rights. Pp.201. ISBN 0-904265-35-8. (Macdonald Publishers: Midlothian, Scotland, 1980.) £6.95.

HUETING, R. New Scarcity and Economic Growth. More Welfare Through Less Production? Pp.269. ISBN 0-444-85400-2 (North-Holland: 1980.) Np.

INFELD, L. Quest — An Autobiography. Pp.361. ISBN 0-8284-0309-0. (Chelsea Publishing: New York, 1980.) $17.50.

KOREN, H. Handbook of Environmental Health and Safety. Principles and Practices. Parts 1 & 2. Pp.698. ISBN 0-08-023900-5 (Pergamon: 1980.) £47.50, $95.

LASZLO, E. *et al.* The Obstacle to the New International Economic Order. Pergamon Policy Studies on the New International Economic Order. Pp.144. Hbk ISBN 0-08-025110-2; flexi ISBN 0-80-025110-2. (Pergamon: 1980) Hbk £8.75; flex £3.55.

MABRO, R. (ed.). World Energy Issues and Policies. Proceedings of the Fir Oxford Energy Seminar, September 1979. Pp.367. ISBN 0-19-920119-[illegible] (Ox University Press: 1980.) £15.